Q
1
S3
V. 80-83
1977-80
SUB.
INDEX
CRY-GEO.
N/C
S.G.T

Physics Abstracts

Volumes 80-83 1977-1980

Cumulative Subject Index

Cry—Geo

28 July 1982

inspec
The Institution of Electrical Engineers

© 1981 The Institution of Electrical Engineers

CUMULATIVE SUBJECT INDEX 1977-80

Coverage

The present index provides a subject key to all papers abstracted in *Physics Abstracts* for the years 1977–80. It therefore comprises all relevant entries included in the six monthly subject indexes for the same period.

Subject Headings

In the course of the four years covered by this index the list of subject headings has been revised and new headings have been added. The present index uses the latest (i.e. 1980) version of the list. Entries for articles abstracted in the 1977, 1978 and 1979 volumes have been examined and, where appropriate, re-indexed under the new headings.

Arrangement

The subject headings are arranged in alphabetical order. The entries under each are prepared so that the most significant or 'key' words appear first and thus determine the position and grouping of entries in the alphabetical sequence under each heading.

Where the names of specific inorganic substances are significant under a given heading, the entries relating to them are found as a second alphabetical listing arranged by the chemical formulae of the particular elements or compounds.

Form of entry

The information contained in the subject index may be illustrated by an example.

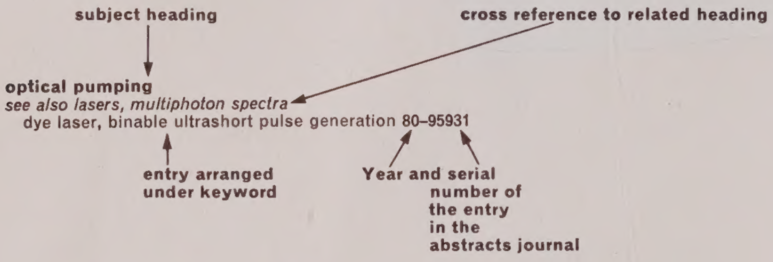
subject heading
cross reference to related heading
optical pumping
see also lasers, multiphoton spectra
dye laser, binable ultrashort pulse generation 80–95931
entry arranged under keyword
Year and serial number of the entry in the abstracts journal

How to use the index

The Subject index provides an alphabetical subject key to the articles included in the abstracts journal. Some general guidance on its use is given below:

1. Look in the index for the name of the specific subject in which you are interested. In most cases this name will be a heading in the index and you will find relevant articles listed under it. The majority of the subject headings fall into the following categories: property, phenomena, substance or named objects, instrument, device, theory, method, process, application, event.
2. Occasionally you will be directed from the subject heading chosen to a different heading under which the relevant or additional articles are listed.
3. If you do not find the subject heading you first chose, try a more general heading.
4. Each entry under the heading relates to an article appearing in the abstracts journal and gives the serial number of that article in the journal preceded by the last two digits of the current year, e.g. 78–12345; i.e. Abstract number 12345 in the abstracts journal for 1978.

   The language of the article, if it is not in English, is also indicated, e.g. optical fibre, three-wave stimulated Raman scattering (French) 0–78902.

   Each entry starts with a Keyword or Keyphrase considered to be most relevant to the heading. On sorting these Keywords, the qualifying prefixes are usually ignored (e.g. n-Ge is sorted under Ge).

   There are three main keyword lists; arabic numerals, alphabetical A–Z, and chemical symbols (organic substances are written and not given as chemical formula). More than one Keyword list may be present under each subject heading.

   For document on, say 'photoemission of silicon' at least two access points 'photoemission' and 'elemental semiconductors' are provided. Under the heading 'photoemission' the Keyword will be 'Si' and under 'elemental semiconductors' the Keyword will also be 'Si'.

   In a case like this, it is advisable and quicker to use the heading 'photoemission' and go straight to the chemical symbol list for 'Si' because there are few entries listed under 'photoemission'.

Printed by Unwin Brothers Limited, The Gresham Press, Old Woking, Surrey

Abbreviations and Acronyms

Abbreviations and acronyms are used in the modifiers in all INSPEC Cumulative Subject Indexes. Individual terms should be readily understood in the context of the subject headings. **Inorganic substances** are usually given by their chemical formulae. Iron and aluminium garnets appear in the formulae lists as MIG and MAG (where M is metal element, e.g. YIG and YAG); (Pb,La)(Zr,Ti)O_3 and $Ce_2Mg_3(NO_3)_{12}$ appear as PLZT and CMN respectively. **Organic substances** including **liquid crystals** are not given as formulae but common abbreviations are used.

ABS resin	acrylonitrile-butadiene-styrene
AC	alternating current
ACV	air cushion vehicle
A/D	analogue-to-digital
ADP	administrative data processing
AES	Auger electron spectra(oscopy)
AF	audio frequency
AFC	automatic frequency control
AFL	abstract family of languages
AGC	automatic gain control
AGR	advanced gas-cooled reactor
AM	amplitude modulation
ANS	Astronomical Netherlands Satellite
APACHE	accelerator for physics and chemistry of heavy elements
APR	acoustic paramagnetic resonance
APS	appearance potential spectra(oscopy)
APW	augmented plane wave
ATR	attenuated total reflection
ATS	applications technology satellite
ATWS	anticipated transients without scram
AVC	automatic volume control

BARITT	barrier injection transit time
BBEA	4-butoxybenzal-4'-ethylaniline
BCC	body centred cubic
BCD	binary-code decimal
BFO	beat-frequency oscillator
BWO	backward wave oscillator
BWR	boiling water reactor
BWT	backward wave tube

CAD	computer aided design
CAI	computer assisted instruction
CARS	coherent antiStokes Raman scattering (spectra)
CATV	community antenna TV
CB	citizen band
CBOOA	cyanobenzylidene octyloxyaniline
C-CD	charge-coupled device
CDI	collector diffusion isolation
CDM	code division multiplexing
CDW	charge-density wave
CEM	channel electron multiplier
CEPA	coupled electron pair approximation
CERN	Conseil Européen pour la Recherche Nucléaire
CESR	conduction electron spin resonance
CGTO	contracted Gaussian-type orbital
CHF	coupled Hartree-Fock
CI	configuration interaction
CIEH	charge iterated extended Huckel
CIHY	configuration interaction Hylleras
CNDO	complete neglect of differential overlap
COC	cholesteryl oleyl carbonate
COM	computer output to microform (fiche or film)
COOB	4,4'-cyano-octyloxy-biphenyl
CP	charge, parity
CPA	coherent potential approximation
CPSK	coherent phase shift keying
CPT	charge, parity, time
CRO	cathode ray oscilloscope
CRT	cathode ray tube
CS	coupled states
CSM	continuous slowing down models
CTR	controlled thermonuclear reactor
CVD	chemical vapour deposition
CW	continuous wave

D/A	digital-to-analogue
DBR	distributed Bragg reflector
DC	direct current
DDC	direct digital control
DDL	diode-diode logic
DECENT	distribution of exact classical energy transfer
DESY	Deutsches Electron Synchrotron
DF	Dirac-Fock
DFB	distributed feedback
DH	double heterostructure
DIL	dual-in-line
DITE	divertor in torus experiment
DLTS	deep level transient spectra(oscopy)
DM	delta modulation
DMSO	dimethyl sulphoxide
DMSS	Defence Meteorological Satellite System
DOBAMBC	p-decyloxybenzylidene p'-amino 2-methyl butyl cinnamate
DODS	different orbitals for different spins
DORIS	Dopple-ring-Speicher
DOVETT	double velocity transit time
DP	data processing
DPCM	differential pulse code modulation
DPPH	diphenylpicrylhydrazyl
DPSK	differential phase shift keying
DSC	differential scanning calorimetry
DTA	differential thermal analysis
DV-Xα	discrete variational Xα method

E1,E2	electric dipole, quadrupole
EAS	extensive air shower
EB	exponential Born
EBBA	4-ethoxybenzylidene-4'n-butylaniline
EBR	experimental breeder reactor
EBT	Elmo Bumpy Torus
ECC	emergency core cooling
ECELR	epithermal critical experiment laboratory reactor
ECG	electrocardiography (-gram)
EDA	ethylene diamine
EDP	electronic data processing
EDTA	ethylene diamine tetra-acetic acid
EEBAC	ethyl-4-(4'ethoxy-benzylidene-amino) cinnamate
EEG	electroencephalography (-gram)
EELS	electron energy loss spectra
EFM	extended Flygare method
EHD	electrohydrodynamics
EHF	extremely high frequency
EHP	electron-hole potential method
EHT	extended Huckel theory
EHV	extra high voltage
ELDOR	electron electron double resonance

ELF	extremely low frequency
EM	electromagnetic
EMC	electromagnetic compatibility
EMF	electromotive force
EMG	electromyography(-gram)
ENDOR	electron nuclear double resonance
EOS	earth observatory satellite
EPEN	empirical potential energy function based on interactions of electrons and nuclei
EPMA	electron probe microanalysis
EPR	electron paramagnetic resonance
ERG	electroretinography(-gram)
ERPS	extramolecular relaxation polarisation shift
ERTS	earth resources technology satellite
ESCA	electron spectroscopy for chemical analysis
ESCAR	experimental superconducting accelerating ring
ESFI	epitaxial silicon film on insulator
ESS	electronic switching system
EUV	extreme ultraviolet
EXAFS	extended X-ray absorption fine structure
FBR	fast breeder reactor
FCC	face centred cubic
FDM	frequency division multiplex(ing)
FDNC	frequency dependent negative conductance
FDNR	frequency dependent negative resistance
FEM	field emission microscopy
FET	field effect transistor
FFHR	fusion-fission hybrid reactor
FFT	fast Fourier transform
FFTF	fast flux test facilities
FIM	field ion microscopy
FM	frequency modulation
FPT	finite perturbation theory
FSK	frequency-shift keying
FSGO	floating spherical Gaussian orbitals
FTR	fast test reactor
GAMBIT	gate modulated bipolar transistor
GANIL	grand accelerateur national a ions Lourds
GARP	global atmospheric research programme
GATE	GARP Atlantic tropical experiment
GCFR	gas-cooled fast breeder reactor
GCM	generator coordinate method
GHF-NO-CI	generalised Hartree-Fock/natural orbital/ configuration interactions
GIAO	gauge-invariant atomic orbitals
GO	Gaussian orbitals
GOO	generalised Overhauser orbitals
GPM	ground potential model
GSO	general spin orbitals
GTO	Gaussian-type orbitals
GVB	generalised valence bond
HAM	hydrogenic atoms in molecules
HBAB	hexyloxybenzylidene-p′ aminobenzonitrile
HBT	N-(p-hexyloxybenzylidene)-p-toluidene
HCDA	hypothetical core disruptive accident
HCP	hexagonal close packed
HEED	high energy electron diffraction
HF	high frequency or Hartree-Fock
HFB	Hartree-Fock-Bogoliubov
HFER	hot fuel examination facility
HFIR	high flux isotope reactor
HFO	Hartree-Fock-Overhauser
HFS	hyperfine structure
HLW	high level waste (radioactive)
HMO	Huckel molecular orbitals
HOAB	heptyloxyazoxybenzene
HOBHA	p-n-heptyloxy-benzylidene-p-n heptylaniline
HOMO	highest occupied molecular orbitals
HORM	hybrid orbital rehybridisation method
HTGR	high temperature gas-cooled reactor
HV	high voltage
HVEM	high voltage electron microscopy
HWR	heavy water reactor
IAEA	International Atomic Energy Authority Agency
IBPBAC	isobutyl-4-(4′-phenylbenzylideneamino) cinnamate
IC	integrated circuit
ICDF	intermediate coupling Dirac-Fock
IDT	interdigital transducer
IEPA	independent electron pair approximation
IF	intermediate frequency
IGFET	insulated gate field effect transistor
IKO	Institute v. Kernph Ouder Amsterdam
I^2L	integrated injection logic
I^3L	isoplanar I^2L
ILS	instrument landing system
IMPATT	impact avalanche transit time
INDO	intermediate neglect of differential overlap
INDOR	internuclear double resonance
ING	intense neutron generator
INO	iterative natural orbital
INTELSAT	international telecommunications satellite consortium
I/O	input/output
IOC-ω	inclusion of the overlap charges in the omega
IR	infrared
IRDO	intermediate retention of differential overlap
ISABELLE	intersecting storage and acceleration
ISR	intersecting storage ring
ISX	impurity study experiment
ITEP	Institute of Theoretical and Experimental Physics
IU	Indiana University
IVO	improved virtual orbitals
JET	Joint European torus
JAERI	Japan Atomic Energy Research Institute
JINR	Joint Institute for Nuclear Research
KEK	Japan National Laboratory for High Energy Physics
KKR	Korringa-Kohn-Rostoker
LAMPF	Los Alamos meson physics facility
LC	inductance-capacitance
LCAO	linear combination of atomic orbitals
LCBO	linear combinations of (semi-localised) band orbitals
LCGO	linear combination of Gaussian orbitals
LCP	large coil program
LCRO	linear combination of Rydberg orbitals
LEC	liquid encapsulated Czochralski
LED	light emitting diode
LEED	low energy electron diffraction
LEP	large electron positron
LET	linear energy transfer
LF	low frequency
LMC	Large Magellanic Cloud
LMFBR	liquid metal fast breeder reactor
LMTO	linear combination of muffin tin orbitals
LOCA	loss of coolant accident
LOCE	loss of coolant experiment
LOFT	loss of flow test facility
LPE	liquid phase epitaxy
LSA	limited space charge accumulation

LSD	local spin density
LSI	large-scale integration
LTE	local thermodynamic equilibrium
LUMO	lowest unoccupied molecular orbitals
LV	low voltage
LWR	light water reactor
MADO	Mulliken approximation for differential overlap
M1,M2	magnetic dipole, quadrupole
MBBA	4-methoxybenzylidene-4'-n-butyl-aniline
MBE	molecular beam epitaxy
MBPT	many body perturbation theory
MCD	magnetic circular dichroism
MCPESCF	multiconfiguration paired excitation SCF
MCZDO	multi-centre zero differential overlap
MEDO	multipole expansion of diatomic overlap
MESFET	metal-semiconductor field effect transistor
MF	medium frequency
MFP	mean free path
MHD	magnetohydrodynamics
MIC	microwave integrated circuit
MIEHM	modified iterative extended Huckel method
MIM	metal-insulator-metal
MIS	metal-insulator-semiconductor or management information system
MIT	Massachusetts Institute of Technology
MMF	magnetomotive force
MNOS	metal-nitride-oxide-semiconductor
MO	molecular orbitals
MOCIC	molecular orbital constraint of interaction coordinates
MODPOT	model potential
MOS	metal-oxide-semiconductor
MOSFET	metal-oxide-semiconductor field effect transistor
MOST	metal-oxide-semiconductor transistor
MRD	multi-reference double excitation
MRINDO	modified Rydberg INDO
MSI	medium scale integration
MSR	molten salt reactor
MSU	Michigan State University
MTBF	mean-time between failures
MTF	modulation transfer function
MTXα	muffin-tin Xα
MUF	maximum usable frequency
MWH	Mulliken-Wolfsberg-Helmholz-semi-empirical method
NAL	National Accelerator Laboratory
NAND	not-and(logic)
NC	numerical control
NCMET	non-closed shell many electron theory
NDDO	neglect of diatomic differential overlap
NDT	nondestructive testing
NEMO	non-empirical molecular orbitals
NEVE	non-empirical valence-electron
NIC	negative impedance convertor
NMR	nuclear magnetic resonance
NNNDO	neglect of non-neighbour differential overlap
NOR	not-or(logic)
NPOST	non-perturbative open-shell theory
NPSO	non-paired spatial orbitals
NQR	nuclear quadrupole resonance
NRC	nuclear regulatory committee
NRM	natural remanent magnetisation
NTO	natural transition orbitals
OAO	orbiting astronomical observatory
OCR	optical character recognition

ODMR	optical detection of magnetic resonance
OER	oxygen enhancement ratio
OGO	orbiting geophysical observatory
OPHF	orbital polarised Hartree-Fock
OPW	orthogonal plane wave
OR	operations research
ORELA	Oak Ridge electron linear accelerator
ORNL	Oak Ridge National Laboratory
OSO	orbiting solar observatory
OTF	optical transfer function
PAA	paraazoxyanisole
PABX	private automatic branch exchange
PAC	perturbed angular correlation
PAHR	post accident heat removal
PAM	pulse amplitude modulation
PAMPUS	photons for atomic and molecular processes and universal studies
PAP	paraazoxyphenetole
PBF	power bursts facility
PBR	pebble bed reactor
PBX	private branch exchange
PC	printed circuit
PCAC	partially conserved axial currents
PCB	printed circuit board
PCGVB	pairwise correlated generalised valence bond
PCILOCC	perturbative configuration interaction using localised orbitals for crystal calculation
PCM	pulse code modulation
PCX	plasma confinement experiment
PDX	poloidal divertor experiment
PEP	positron electron proton
PETRA	positron electron tandem ringbeschleuniger anlage
PF	power factor
PFM	pulse frequency modulation
PHWR	pressurised heavy water reactor
PID(PI,PD)	proportional+integral+differential (derivative)
PLA	phase locked arrays
PLC	programmable logic control
PLL	phase locked loops
PLT	Princeton Large Torus
PM	pulse modulation
PMMA	polmethylmethacrylate
PMDR	phosphorescence microwave double resonance
PNDO	partial neglect of differential overlap
PNO-CI	pair natural orbital configuration interaction
POL	pair orthogonalised Lowdin
POPAE	protons on protons and electrons
POPOP	phenyl-oxazolyl-phenyl-oxazolyl-phenyl
POS	point of sale
PPDP/S	Pariser-Parr-Del Bene-Pople/Segal calculations
PPI	plan position indicator
PPM	pulse position modulation or parts per million
PPP	Pariser-Parr-Pople
PRDDO	partial retention of diatomic differential overlap
PRF	pulse recurrence (repetition) frequency
PROM	programmable read-only-memory or Pockels readout optical modulator
PS	proton synchrotron (CERN)
PSK	phase shift keying
PTFE	polytetrafluoroethylene
PTM	pulse time modulation
PVC	polyvinyl chloride
PWM	pulse width modulation
PWR	pressurised water reactor

QCD	quantum chromodynamics
QDMBPT	quasi-degenerate many-body perturbation theory
QED	quantum electrodynamics
QPSK	quaternary phase shift keying
RAM	random access memory
RBE	relative biological effectiveness
RC	resistance-capacitance
RCNDO	Rydberg CNDO
R & D	research and development
RF	radio frequency
RFI	radio frequency interference
RHEED	reflection high energy electron diffraction
RINDO	Rydberg INDO
RKKY	Rudermann-Kittel Kasuya-Yosida
RLC	resistance-inductance-capacitance
RMS	root mean-square
ROM	read-only memory
RPA	random phase approximation
RPM	relaxation potential model
SAMO	simulated ab initio molecular orbitals
SAS	small astronomy satellite
SAW	surface acoustic waves
SCF	self consistent field
SCL	space charge limited
SCPT	self consistent perturbation theory
SCR	silicon controlled rectifier
SDM	space division multiplexing
SDO	shielded diatomic orbitals
SEHF	spin extended Hartree-Fock
SEM	scanning electron microscope
SFE	solar flare effect
SGHWR	steam generating heavy water reactor
SHF	superhigh frequency
SHG	second harmonic generation
SIMS	secondary ion mass spectrometer
SIN	Swiss Institute of Nuclear Research
SINDO	scaled INDO
SISAM	spectrometer with interference selective amplitude modulation
SMC	Small Magellanic Cloud
SMS	synchronous meteorological satellite
S N	signal-to-noise
SOG	strongly orthogonal geminal
SOS	silicon on sapphire
SPA	separated pair approximation
SPC	stored program control
SPEAR	Stanford positron electron asymmetric ring
SPHF	spin polarised Hartree-Fock
SPIN-CIPSI	spin symmetry adapted generalisation of CIPSI
SPS	super proton synchroton (CERN)
SQUID	superconducting quantum interference device
SRMCASE	symmetry-restricted-multiconfiguration annihiliation of single excitations
SSB	single sideband
SSC	sudden storm commencement
SSI	supersonic transport
STD	salinity-temperature-depth or subscriber trunk dialling
STEM	scanning transmission electron microscopy
STO	Slater-type orbitals
STOL	short take-off and landing
STP	Slater-transfer Preuss
SUHFC	spin unrestricted Hartree-Fock with local approximation for correlations
SW	short wave
SWR	standing wave ratio
SXAPS	soft X-ray appearance potential spectrum
TBBA	terephthal-butylaniline
TCNE	tetracyanoethylene
TCNQ	tetracyanoquinodimethane

TCR	temperature coefficient of resistance
TDHF	time dependent Hartree-Fock
TDM	time division multiplex(ing)
TDMA	time division multiple access
TDPAC	time differential perturbed angular correlation
TE	transverse electric
TEA	transversely excited atmospheric
TEM	transverse electromagnetic or transmission electron microscopy
TEXT	Texas Experimental Tokamak
TFTR	Tokamak fusion test reactor
TGFB	triglycine fluoroberyllate
TGS	triglycine sulphate
TGSe	triglycine selenate
TJS	transverse junction stripe
TLD	thermoluminescent dosimeter(-ry)
TM	transverse magnetic
TMMC	tetramethylammonium manganese chloride
TOP	transient overpower accident
TNS	The next step
TRAPATT	trapped plasma avalanche triggered transit
TREAT	transient reactor test facility
TRM	thermoremanent magnetisation
TSC	thermally stimulated currents
TSEE	thermally stimulated exo-electron emission
TTF	tetrathiofulvalinium
TTL	transistor transistor logic
TTT	tetrathiotetracene
TUCA	transient undercooling accident
TV	television
TW	travelling wave
TWT	travelling wave tube
UCHF	uncoupled Hartree-Fock
UHF	ultra high frequency unrestricted Hartree-Fock
UHV	ultra high voltage
UKAEA	United Kingdom Atomic Energy Authority
ULF	ultra low frequency
UMD	unitised microwave devices
UPS	ultraviolet photoelectron spectra
US	ultrasonic
UV	ultraviolet
VB	valence bond
VCR	video cassette recorder
VDM	vector dominance model
VDU	visual display unit
VHF	very high frequency
VLBI	very long base line interferometry
VLF	very low frequency
VLSI	very large scale integration
VOR	VHF omnidirectional range
VPE	vapour phase epitaxy
VRC	visual record computer
VRDDO	variable retention of diatomic differential
VSB	vestigial sideband
VSEPR	valence shell electron pair repulsion
VSWR	voltage standing wave ratio
VTOL	vertical take-off and landing
VTR	voltage transformation ratio or video tape recorder
VUV	vacuum ultraviolet
VVER	water moderated water cooled reactors
WWER	water moderated water cooled reactors
XPS	X-ray photoelectron spectra
ZEBRA	zero energy breeder reactor assembly
ZGS	zero gradient synchrotron
ZPPR	zero power plutonium reactor

crystal atomic structure of inorganic compounds continued
- $FeSO_3.2^1/_2H_2O$, X-ray cryst. struct. determ. 80–88107
- α-$FeSO_3.3H_2O$, X-ray cryst. struct. determ. 79–60310
- β-$FeSO_3.3H_2O$, X-ray cryst. struct. determ. 80–15063
- $Fe(Sb_{1-x}Te_x)_3$ system cpds., prep., cryst. struct., elec. and mag. characteris. 80–108349
- $FeSc_2S_4$, prep. and X-ray cryst. struct. determ. *(French)* 79–60335
- $Fe_{0.85}Sc_{2.10}S_4$, prep. and X-ray cryst. struct. determ. *(French)* 79–60335
- $Fe_{1-x}Se$, phase relation 79–14926
- 3C-Fe_7Se_8, X-ray cryst. struct. study 79–55708
- γ-Fe_2SiO_4, electron density distrib. 77–35514
- Fe_2SiO_4, fayalite, Czochralski growth under controlled O_2 fugacity conditions 80–84843
- $FeSnO(OH)_5$, mag. props. and cryst. struct. 78–43574
- Fe_2SnS_4, cryst. struct. *(French)* 78–18595
- $(Fe_{0.5}Ta_{0.5})O_2$, rutile, cation distrib. and mag. ordering *(German)* 80–107116
- Fe_2TeO_5 and $Fe_2Te_3O_9$, evolution of coord. of Te IV and Fe III *(French)* 77–35537
- $FeTh_2S(Se)_5$, synthesis, cryst. characts. *(French)* 78–51517
- $FeThSe_3$, synthesis, cryst. characts. *(French)* 78–51517
- β-FeTiD, neutron diffr. exam. of struct. 78–47282
- $FeTiD_x$, γ-phase struct., neutron diffr. study 79–51085
- $FeTiNdO_5$, isomer shift, hyperfine field and distrib. of Fe^{3+} ions, Mossbauer spectrum 77–69747
- $FeTiO_3$, Fe_2TiO_4, influence of cryst. struct. on photoresponse of electrodes 78–43471
- $FeTiO_3$, ilmenite, lunar and terrestrial, cell dimensions and antiferromagnetism 77–21764
- Fe_2TiO_5, spin glass system, cation distrib. Mossbaeur spectra 80–71248
- $Fe_xV_{1-x}O_2$, X-ray diffr. obs. 77–27858
- $Fe_xV_{1-x}O_2$, $x\simeq0.25$, synthesis and cryst. struct. *(French)* 79–55713
- $FeV_2O_6H_{0.5}$, synthesis and cryst. struct. *(French)* 79–55720
- $FeYb_2S_4$, cryst. struct. determ. 79–77572
- $FeYb_2S_4$, structural study, X-ray diffr., Mossbauer spectroscopy 80–107159
- $Fe_{0.76}Yb_{2.16}S_4$, cryst. struct. determ. 78–26533
- $Fe_{1+x}Yb_{2-x}S_4$, X-ray and Mossbauer obs. 77–77132
- $Fe_2[As^{III}(As^VO_4)_3]$, cryst. struct., partial disorder of As^{III} atoms with linear order *(French)* 79–90600
- $Fe_3[Co(CN)_6]_2.12H_2O$ struct. dehydration fluorescence and IR studies 80–28976
- $Fe_2[PO_4]F$, synthetic, cryst. struct. determ. 79–14780
- GGG, GGG-ErGG, rare earth impurity, spectral probe of stoichiometry variations 77–85790
- Ga chalcogenides, cryst. struct. types 77–15392
- Ga-Ge-Te system, GaGeTe formation, peritectic decomp. and struct. *(French)* 77–85995
- Ga-Se system, phase diagram and cryst. struct. of phases *(French)* 80–93544
- GaAs, X-ray structure factors and Debye-Waller factor, from Bragg case diffr. curves 77–62509
- GaAs-AlAs system, diffuse scatt. of X-rays by single crysts. *(German)* 78–30517
- GaAs-GaP system, diffuse scatt. of X-rays by single crysts. *(German)* 78–30517
- GaAs-ZnSe system, heterovalent solid solns. of substitution, prep. and investig. 77–24553
- $GaCl_3$, cryst. struct., Zeeman split fine struct. lines, FT NQR obs. 80–54982
- $GaH(SO_4)_2.4H_2O$, cryst. parameters and X-ray powder diffr. data *(French)* 79–14765
- $Ga_xIn_{1-x}Se$, fabrication, struct., elec. and optical props. 80–44180
- $(Ga_xIn_{1-x})_2Se_3$, $1\geq x\geq0$, phases, lattice parameters and thermal expansion between room temp. and melting point 80–39031
- GaN, cryst. struct. refinement 77–84731
- $Ga_2Nb_2O_7$, and $Ga_2Nb_2O_{7.25}$, new phase of mixed oxide 78–59787
- β-Ga_2O_3, crystal structure, 2/m symm. deviation 77–35534
- α-GaOOD, powder neutron diffr. cryst. struct. exam. 78–2081
- GaP VPE layers, precision lattice parameter meas. by Umweganregung method 79–65047
- GaP:Te, VPE grown layers, precision lattice parameter determination 80–24429
- Ga_2S_3-PbS system, phase diagram and crystallographic study *(French)* 80–29937
- Ga_2S_2Te, single cryst. X-ray data, struct. determ. *(French)* 79–60316
- GaSe, exciton spectra at 4.2K rel. to layer struct. 77–16336
- GaSe, layer compounds, lattice instability, deformation dipole model 80–39249
- GaSe-SnSe system, phase diagram and lattice consts. of solid solns. 79–34014
- β-Ga_2Se_3 77–27862
- Ga_2Se_3-MnSe system, crystallographic study, phase diagram, DTA and X-ray diffr. determ. *(French)* 79–24506
- $GaSe_xS_{1-x}$, X-ray diffr. investig. of stacking sequences 77–43198
- Ga_6SnTe_{10}, cryst. struct. *(French)* 79–78946
- GaTe, cryst. struct., TEM and X-ray diffr. study 80–79757
- GaTe, cryst. struct. *(French)* 79–78946
- α-GaTe single crystals, Raman spectra, point group calc. 79–99883
- GaTe, X-ray cryst. struct. determ., direct method *(French)* 80–28956
- Ga_2Te_5, cryst. struct. *(French)* 79–78946
- Ga_2Te_5, struct. and bonding *(French)* 77–72589
- $GdAlO_3:Er^{3+}$, $^4S_{3/2}$ to $^4I_{9/2}$ transition laser action, optical and luminescence spectra 80–16082
- GdB_2, high press. synthesis 78–18608
- GdCa garnets, solid soln., mag. and cryst. chem. props. 77–16057
- $GdFe_2B_2$, compounds with $CeAl_2Ga_2$ structure type *(Ukrainian)* 79–32970
- $Gd_2Ge_3O_7(OH)_2$ 78–71714
- $Gd(IO_3)_3$, cryst. struct., X-ray diffr. obs. 77–84718
- Gd_3InO_6, high press. synthesis, cryst. struct. 77–68955
- $Gd_xMo_6S_8$, Chevrel phase, lattice instabilities, X-ray diffr. meas. 78–34491
- $Gd_2Ni_{12}As_7$, crystal. struct., X-ray diffr. obs. 79–1411
- $Gd_2O_3:Eu^{3+}$, luminesc., rel. to crystallographic data 79–33793
- GdPS, PbFCl-type struct. deriv. 77–80489
- Gd_2SiO_5, atomic positions, high resolution electron microscopy 80–100220
- $GdTiO_3$, cryst. struct. and cryst. chem. 80–1984
- $GdVO_3$, flux growth and chem. characts. 78–23595

crystal atomic structure of inorganic compounds continued
- Ge particles, grown in Ar gas, cryst. struct. and habit, electron microscope study 79–74071
- Ge-GaSb, metastable continuous solid solutions 79–8284
- Ge-In-Te system, homogeneity region, struct., electrophysical props. 78–44091
- Ge-Si system, diffuse scatt. of X-rays by single crysts. *(German)* 78–30517
- GeF_4, Raman spectra at 77K, scatt. angle, polaritons and space group 78–23439
- $Ge(HAsO_4)_2.H_2O$ 78–26552
- $Ge(HPO_4)_2.H_2O$ 78–26552
- Ge_2N_2O, pressure induced tetrahedral tilting and deform. 80–24415
- Ge_2N_2O, time-of-flight neutron diffr. study 79–19200
- $Ge_xNi_{1-x}O$, crystallographic and elec. props. 77–32011
- GeO_2, new high-pressure modification 78–75825
- GeO_2 particles used for optical fibre fabrication, struct. props. 80–89167
- GeS *(German)* 78–51484
- GeS, anisotropic EXAFS, cryst. struct. determ. 80–66323
- $GeSe_2$, struct. rel. with GeS_2 high temp. phase *(French)* 77–51359
- $Ge_xSn_{1-x}S(Se)$, lattice parameters, optical energy gap and IR refl. 78–23021
- GeTe, X-ray emission spectra, amorphous and cryst. struct. *(Russian)* 78–88385
- HCl, mol. cryst., angles of H-bonded mols., ab initio calcs. 78–6037
- $HCl.2ZnCl_2.2H_2O$, struct. refinement 78–51488
- $HCl.6H_2O$, cryst. struct., H bonds, X-ray determ. 78–83783
- HF, cryst., CNDO calcs., struct., binding energy, 4K 77–15338
- H_xMoO_3 ($0.3<x<2.0$), synthesis and phase characterisation 79–1416
- H_xMoO_3, structural anal. by neutron diffr. 79–65043
- H_3NSO_3, sulphamic acid, deformation electron density, X-ray and neutron diffr. 77–19941
- H_xNbS_2, struct., form. by cathodic reduction, neutron diffr. obs. 79–73150
- H_2O, ice, empirical potential model EPEN/2, parameterisation testing 79–54933
- $(H_3O)^+(HSeO_4)^-$, X-ray struct. anal., Patterson technique 80–1975
- $(H_5O_2{}^+)_3(PW_{12}O_{40}{}^{3-})$, struct. of Keggin's 'pentahydrate' from X-ray and neutron diffr. data 77–47382
- $(H_5O_2{}^+)_3(PW_{12}O_{40}{}^{3-})$, struct., X-ray and neutron diffr. study 79–42037
- $H_3PW_{12}O_{40}.21H_2O$, neutron diffr. 78–42977
- $H_2Pt(OH)_6$, platinic acid, X-ray cryst. struct. determ. 80–28967
- H_2SO_4, anhydrous, cryst. struct. refinement 80–19770
- HSO_3F crystal, indication of molecules existing as infinite chains *(French)* 80–989
- $HSbCl_6.3H_2O$, cryst. struct., cation $H_{14}O_6{}^{2+}$ *(German)* 80–107133
- H_xTaS_2, nonstoichiometric, incoherent neutron spectra, X-ray diffr. 78–42998
- $HUO_2AsO_4.4H_2O$ and $HUO_2PO_4.4H_2O$ layered cpds., struct. investigs. below antiferroelec. transition temps., H bond ordered structs. 80–107416
- $HUO_2PO_4.4H_2O$, H^+ ion cond., struct. mechanism, X-ray diffr. obs. 78–34651
- $HUO_2PO_4.4H_2O$, H^+ ion solid electrolyte, cryst. struct. 79–14759
- Hf-M-B systems (M=Rh,Ir), phase equilib. and cryst. structs. 80–15072
- Hf_3As, cryst. struct., X-ray diffr. pattern intensity profile 80–49201
- $HfNi_{1.8}Si_{3.2}$, X-ray obs. *(Russian)* 77–76361
- HfO_2, obtained by vapo-condensation, exam. of structure and phase props. *(French)* 79–19489
- HfO_2-CeO_2, solid solutions 77–16549
- $Hf_3Sc_4O_{12}$, cryst. struct. determ., powder X-ray diffr. exam. 77–4083
- HgA_2X_4 (A=Ga,In; X=S,Se), Fourier IR and Raman spectra, cryst. struct. and symm. *(German)* 79–24313
- $Hg_{3-\delta}AsF_6$, space group symmetry and phase ordering 80–6396
- $HgBi_2S_4$, X-ray cryst. struct. determ., rel. with pavonite homologous series 80–92487
- $HgCl_2$, X-ray cryst. struct. redeterm. and refinement 80–107140
- Hg_2Cl_2, calomel cryst., symmetry of low temp. phase 78–26544
- $HgCrO_4$, cryst. struct. determ. 78–63712
- $HgCr_2Se_4$, cryst., preparation, elec. cond., thermo EMF 77–8125
- HgF(OH), X-ray cryst. struct. refinement 79–46611
- $HgIn_2Se_4$, IR refl. spectra and cryst. struct. 79–56777
- $Hg_3In_2Te_6$, complex ordered-vacancy cpd., struct. and lattice dynamics 78–34496
- $HgLi_2(PO_3)_4$, cryst. struct. determ. *(French)* 77–4069
- β-$Hg_3O_2Cl_2$, single cryst. X-ray diffr. 77–31647
- $Hg_6O_4Cl_4$, cryst. struct. determ. 78–26516
- $Hg_4PO_4NO_3.H_2O$ *(French)* 78–42992
- HgS, habit variation of crystals of the $C3_12$-$C3_22$ space group 80–107090
- γ-$Hg_3S_2Cl_2$ order-disorder structures, desymmetrisation 80–38986
- $HgSO_4.H_2O$, X-ray and neutron diffr. study of struct. 80–33936
- HgSe-MnSe system, phase exam., solubility limit 77–36488
- $HgSeO_4.H_2O$, cryst. struct. determ. by neutron diffr. 78–55838
- $HoAlO_3$, Czochralski growth and props. 77–48335
- $Ho_4Ba_6(BO_3)_9$, flux growth and chem. characts. 78–23595
- $HoCoGa_5$, X-ray cryst. struct. determ. 80–1993
- Ho_2CoGa_8, X-ray cryst. struct. determ. 80–1993
- $HoCo_2Ge_2$, crystal and magnetic structure obs. 80–64976
- HoF_3, crystal structure by powder neutron diffr. study 80–15077
- $HoFe_2B_2$, compounds with $CeAl_2Ga_2$ structure type *(Ukrainian)* 79–32970
- $HoVO_3$, antiferromag., at. and mag. struct., neutron diffr. meas. 79–24142
- $I_{0.33}NbSe_4$, cryst. growth and struct. *(French)* 77–15375
- In chalcogenides, cryst. struct. types 77–15392
- In, face centred tetragonal, total cryst. energy with electronic screening effect, struct. stability 77–15345
- In_2BRCl_6, B=Li,Ag,Na, systematic structs., X-ray Guinier-Simon method *(German)* 80–44186
- InCl, red and yellow, X-ray structural anal. 79–4287
- $InCuAlO_4$, rhombohedral oxides, symmetry group *(French)* 80–84157
- InF_3-MF_1 (M=alkalines, Tl, NH_4), crystallographic study *(French)* 79–46631
- $InF_3.3H_2O$, cryst. struct. by X-ray diffr. 78–63729
- $InFe_{1.75}Si_{0.25}O_4$, rhombohedral oxides, symmetry group *(French)* 80–84157
- $In_2Ga_6Te_{10}$, X-ray cryst. struct. determ. *(French)* 79–23580
- $(In(H_2O)_2$-$(SO_4)_2)^-(H_5O_2)^+$, cryst. struct. *(French)* 79–73146

crystal atomic structure of inorganic compounds continued
  $InH(SO_4)_2.4H_2O$, cryst. parameters and X-ray powder diffr. data *(French)* 79−14765
  $In_xMo_6S_8$, Chevrel phase, lattice instabilities, X-ray diffr. meas. 78−34491
  $InMo_6Se_8$, X-ray cryst. struct. determ. 80−103299
  $In_2Mo_{15}Se_{19}$, X-ray cryst. struct. determ. 80−103299
  $In_{\sim 3}Mo_{15}Se_{19}$, containing isolated Mo_6 and Mo_9 clusters, single cryst. X-ray diffr. anal. 79−32952
  $In_xMo_{15}Se_{19}$, new ternary Mo(II) compounds, containing Mo_6Se_8 and Mo_9Se_{12} units, X-ray diffr. study 79−65056
  $InMo_3Se_3(Te_3)$, synthesis and struct. 80−92498
  InN, RMS dynamic displacements of atoms and struct. amplitudes 79−99154
  InNbS(Se), struct., X-ray powder diffr. meas 80−44175
  In_2O_3, defect chemistry and struct. stability, impurity incorporation 77−35552
  $In(OH)_3$, cubic, X-ray and neutron diffr. obs. 79−77568
  InP film, heteroepitaxial, deposited on GaAs substrate, X-ray analysis *(Czech)* 77−15710
  $InPS_4$, $In_4(P_2S_6)_3$, $In_4(P_2Se_6)_3$, struct. chem. 78−51482
  InSb, polymorphism and cryst. struct. at high temp. and press. 78−95026
  $InSb_{1-x}As_x$, cryst. struct. and far IR reflectivity 79−56752
  $InSb_{1-x}As_xBi_y$, far IR reflectivity 79−56752
  $InSbS_3(Se_3)$, prep., polymorphism, cryst. struct. 78−44002
  γ-InSe, 3R struct. type refinement 80−64962
  InSe (hexagonal), X-ray cryst. data redeterm. 80−19767
  InSe, large monocrysts., grown from nonstoichiometric melt, rhombohedral struct. X-ray anal. 77−55882
  InSe, layer compounds, lattice instability, deformation dipole model 80−39249
  InSe, X-ray crystallography, struct. determ. 77−4081
  InSe-SnSe system, phase diagram and lattice consts. of solid solns. 79−34014
  α-, γ-, δ-In_2Se_3 (hexagonal), X-ray cryst. data redeterm. 80−19767
  In_2Se_3, cryst. struct. determ. by X-ray diffr. *(French)* 78−26501
  α-, β-In_2Se_3, rhomobohedral, X-ray cryst. data redeterm. 80−19767
  InSeI, X-ray cryst. struct. determ. *(German)* 80−100214
  $In_2Si_2O_4$, high press. pyrochlore struct. 77−47426
  $InTa_{1-x}Nb_xO_4$ system, structural and luminescent props. 80−84769
  $In_3Ta_2O_7$, new phase of mixed oxide 78−59787
  InTaS(Se), struct., X-ray powder diffr. meas 80−44175
  In_2Te_3, low temp. ordered phase and transition state, TEM obs. 79−28095
  In_2Te_5 (II), cryst. struct. determ. 78−26510
  In_3Te_4, ordered state, cryst. struct. determ. 78−26499
  InTeBr, intermediate phase, cryst. struct. 80−100834
  InTeI, X-ray cryst. struct. determ. *(German)* 80−100214
  In_2TeO_6, crystal growth by high press. method, elec. and struct. props. 77−81206
  $In_2Te_3O_9$, isolated in In_2O_3-TeO_2 system, cryst. struct. anal. *(French)* 79−32977
  $InVO_4$, X-ray cryst. struct. determ. *(French)* 80−39019
  $In_{0.30}WO_3$, struct. anal. *(French)* 78−59786
  In_xWO_3 ($0.12<x<0.33$), structural evolution of bronze series *(French)* 79−73141
  Ir metal double oxides, elec. cond. and struct. 80−34438
  Ir ternary and quaternary oxides, prep., cryst. struct., and mag. props. 79−14771
  K triple orthoarsenates, $KM^{II}Cr_2(AsO_4)_3$, prep. by high temp. synthesis, and cryst. struct. 79−66028
  K-rare earth double sulphates, $K_{6+3n}R_{4-n}(SO_4)_9$, ($n\approx 0.4$), cryst. struct. 80−28985
  K-U-O system, cryst. chem. 77−39568
  K_3AgO_2, determ. of cryst. struct. X-ray diffr. *(French)* 78−95029
  $K_2Ag_4Se_3$, crystal struct., X-ray study *(German)* 78−83795
  $KAlCl_4$ 78−51487
  $KAl(CrO_4)_2.2H_2O$, cryst. struct. *(French)* 77−80478
  $KAlF_4$, single cryst., prep. and struct. *(French)* 80−79762
  $KAlSiO_4$ metastable polymorph, prep. by ion exchange with $RbAlSiO_4$, struct. 78−79585
  $KAlSi_3O_8$-$BaAl_2Si_2O_8$ hyalophane, natural and heat treated, cryst. struct. refinement 78−2072
  $K_4As_2O_7$, solid-state synthesis, X-ray powder data *(French)* 80−15079
  $K_5As_3O_{10}$, X-ray single-cryst. struct. determ., Patterson method 80−96484
  $K_2B_{12}H_{12}$ and $K_2B_{12}H_{12}.KX$, X=halogen cryst. growth from soln. and morphology 77−44145
  $KBO_2.4/3H_2O$, unusual hydrogen bonding 78−2058
  K_2BRCl_6, B=Li,Ag,Na, systematic structs., X-ray Guinier-Simon method *(German)* 80−44186
  $K(B_xW_{3-x})O_9$ (B=Na, Ca, Co, Ni, Cd, Ga, Bi, Nb, Ta) cryst. struct., temp. dielec. anomalies 80−1998
  $K_{6-2x}Ba_xTa_6Sl_4O_{26}$, struct. determ. *(French)* 77−27866
  $K_2Be_2Si_6O_{15}$, synthetic, epididymite group, X-ray diffr. struct. anal. 77−43204
  $K_{1.14}Bi^{III}{}_{0.64}Bi^{V}{}_{1.73}O_{5.85}(H_2O)_{0.97}$, cryst. struct. *(French)* 77−72596
  KBr, X-ray struct. study using synchrotron radiation and multichannel detector 78−47210
  $KBrO_2F_2$, struct. data, vibr. spectra 77−39563
  KC_8, intercalated graphite, electronic and cryst. struct. 80−44472
  β-K_2CO_3, cryst. struct. of high temp. monoclinic modification 77−11513
  $K_2C_2O_4(SbF_3)_2$, growth from soln. and X-ray diffr. study *(French)* 77−80481
  K_2CO_3Sr-CO_3 phase diagrams, evidence of new compound *(French)* 78−95033
  $KCaCl_3$, form. of equilib. pseudocubic phase from supersaturated solid soln. based on NaCl *(Russian)* 77−63681
  $K_2Ca(SO_4)_2.H_2O$, single cryst., X-ray cryst. struct. refinement 79−14781
  $K_2Ca[B_4O_5(OH)_4]_2.8H_2O$, synthetic, X-ray cryst. struct. study, H bond geometry 80−92509
  $K_2Cd_2(SO_4)_3$, ferroelastic phase transition, X-ray diffr. and dielec. temp. depend. meas. 79−55882
  $K_2Cd_2(SO_4)_3$, piezoelec. langbeinite-type, cryst. struct. and ferroelastic transform. 78−6036
  $K_2Cd_2(SO_4)_3$, piezoelectric, cryst. struct., near ferroelastic transition 78−42984
  $KCd_4(VO_4)_3$, cryst. struct., Patterson and Fourier calcs. 77−19916

crystal atomic structure of inorganic compounds continued
  $(K_{16}Ce(P_2W_{17}O_{61})_2).nH_2O$ (n=50), X-ray cryst. struct. determ. 79−94984
  $K_2CeSi_6O_{15}$, cryst. struct., X-ray diffr. meas. 78−18619
  $K_2CeSi_6O_{15}$, synthesis and X-ray structural anal. 78−2096
  KCl, exp. valence charge density calc., accuracy of one-term Gaussian representation 80−28952
  KCl, powder diffr. using synchrotron radiation, energy-dispersive technique 77−24245
  $KClO_3$, refinement of cryst. struct. 78−55850
  $KClO_4$, cryst. struct. determ. 77−80472
  K_2CoCl_4, cryst. structs. of orthorhombic and monoclinic modifications 77−15358
  $KCoCr_2(VO_4)_3$, synthesis and cryst. struct. 80−88114
  $K_xCr(Mn)(Co)O_2$, layer struct., elec. cond. behaviour *(French)* 78−26542
  $KCrO_2$, two-dimens. mag. props. rel. to cryst. struct. 80−75776
  α-K_2CrO_4, single crysts. electron density distrib. 79−7584
  K_2CrO_4-$CaCrO_4$, phase diagram determ., struct. of double salt 77−15543
  α-$K_2Cr_2O_7$, symmetry centres exam. by morphological methods 78−59796
  $K_2Cr_3O_{10}$, cryst. struct. determ. 79−23592
  $K_2Cr_3O_{10}$, X-ray powder cryst. struct. determ. *(French)* 79−32960
  $K_2CrTi(PO_4)_3$, cryst. data 77−39564
  $K_2Cr_2V_6O_{16}$, Hollandite type compound, synthesis, struct. and magnetic props. 79−11543
  $KCuCr_2(VO_4)_3$, synthesis and cryst. struct. 80−88114
  $KCuF_3$ crystals, with Jahn-Teller distortion, electron density distrib. X-ray diffractometry 79−69061
  K_2CuF_4, structural anal., X-ray diffraction meas. 79−86762
  KD_2PO_4, IR and Raman polarised spectra, rel. to crystal struct. 78−56489
  KD_2PO_4, phase transitions study, role of cryst. struct. determ. 80−75197
  $KD_3(SeO_3)_2$, phase transition, neutron diffr. 80−2158
  β-KEr_2F_7, crystal struct. *(French)* 80−107164
  β-KEr_3F_{10} *(French)* 78−51500
  $K_2Er(NO_3)_5$, cryst. struct. by X-ray diffr., cryst. binding 78−42988
  KF-ErF_3, phase diagram 80−92645
  KF-EuF_3 system, composition of phases determ. by DTA and X-ray crystallography *(French)* 77−68945
  KF-TbF_3 system crysts., X-ray struct. investig. 77−43187
  $KF.2H_2O_2$, cryst. struct., X-ray and neutron diffr. meas. 77−39569
  $KFe(CrO_4)_2$, cryst. struct., structural filiation with $KFe(CrO_4)_2.nH_2O$ series *(French)* 77−27855
  K_2FeF_5, crystal struct., single crystal diffr. 78−10002
  $K(Fe_{1.5}Mg_{0.5}Si_4O_{10})(OH)_2$, cryst. struct. refinement 78−26545
  $KFeO_2$, cryst. and mag. struct., neutron and X-ray powder diffr., and Mossbauer effect meas. 77−84722
  β-$K_5Fe_3O(SO_4)_6.10H_2O$, monoclinic struct. *(German)* 78−34473
  $KFe(PO_4)F$, crystal struct., interatomic distances, X-ray phase anal. 80−39053
  $KFeS_2$, cryst. struct. by X-ray diffr., isolated from colloid 79−43635
  $KFeS_2$, cryst. struct. and mag. ordering, neutron diffr. and mag. susceptibility meas. 80−54867
  $K_2Ga_2P_8O_{24}$, cryst. struct., atomic coordinates, anisotropic temp. corrections 80−33974
  $K_2HCr_2AsO_{10}$, X-ray cryst. struct. determ. *(French)* 79−14756
  $K_2HCr_2PO_{10}$, cryst. struct. data *(French)* 79−14756
  $KH_3(Ge_7O_{16}).3H_2O$, cryst. struct. determ. 79−90628
  $K_3H(H_2P_2O_7)_2$, single cryst., X-ray cryst. struct. determ., direct methods *(French)* 79−14742
  $KH(IO_3)_2$, cryst. struct. of new modification 77−80466
  $K_4(H_2I_2O_{10}).8H_2O$, cryst. struct., bond lengths 77−68956
  $K_x(H_2O)_yNbS_2$, cryst. struct. determ. 77−89416
  $K_x(H_2O)_yTaS_2$, cryst. struct. determ. 77−89416
  KH_2PO_4, ferroelec., tetragonal cryst. struct. determ., neutron diffr. meas. 77−7693
  KH_2PO_4, ferroelec. thin crysts., struct. investig. 79−27962
  KH_2PO_4, phase transitions study, role of cryst. struct. determ. 80−75197
  KH_2PO_4, single crystal neutron diffraction study at high pressure 80−92497
  $KHSO_4.KH_2PO_4$, cryst. struct. 80−75211
  $KHSi_2O_5$, cryst. struct., Patterson function anal., valency balance, hydrogen bonds 80−39051
  $K_8Hf(MoO_4)_6$, X-ray structural investigation 78−79597
  $KHgC_4$, and $KHgC_8$, intercalation cpds., synthesis and struct. 80−44183
  KIO_3, cryst. struct. 79−19234
  $KIO_3.HIO_3$, cryst. struct. 79−19230
  $KIO_3.HIO_3$, I atom electronic struct. in X-ray-neutron difference synthesis 79−90595
  $KIO_3.HIO_3$, new orthorhombic modification, X-ray cryst. struct. determ. 79−55723
  $KIO_3.KNO_3.2HIO_3$, cryst. struct. determ. 79−23591
  $K_2InCl_5.H_2O$, crystal structure and H-bonding 80−64978
  KIn_2F_7, cryst. struct. *(French)* 78−18590
  $KIn(SO_4)_2.4H_2O$, cryst. struct. 80−15082
  $(K_{0.5}La_{0.5})_xBa_{1-x}TiO_3$, cryst. struct., dielec. and IR spectral meas. 79−46614
  $KLi_3Ca_7Ti_2(Si_6O_{18})_2F_2$, baratovite, cryst. struct. determ. by X-ray diffr. 77−76382
  $KLi(Pt(CN)_4).2H_2O$, cryst. struct., polarised emission obs. 78−52538
  KM_gF_3, bond energy, equilib. distances and compressibility calcs. 80−70159
  $KM^{II}M^{III}F_6$, (M=1st row transition metal, Zn, or Mg), divalent and trivalent ion distribs., Mossbauer obs. 78−2777
  $K_2M(MoO_4)_3$, M=Zr, Hf, synthesis and struct. 77−36386
  $K_x(M_yTi_{2-y})O_4$, (M=Mg,Zn,Ni,Cu,Fe^{III},Mn^{III}), ($0.7\le x\le 0.9$), new layer struct. *(French)* 80−84149
  $KMgCl_3.nH_2O$, IR spectra and struct. features 79−15452
  $KMgCr_2(VO_4)_3$, synthesis and cryst. struct. 80−88114
  $K_3Mg_4LiSi_{12}O_{30}$, cryst. struct., X-ray diffr. and IR spectra *(French)* 80−107158
  $K_2Mg_3M_2Si_{12}O_{30}$ (M=Cu, Fe, Zn, Mg), cryst. struct., X-ray diffr. and IR spectra *(French)* 80−107158
  $K_2Mg(S_2O_3)_2.6H_2O$, isolation, struct., decomposition *(French)* 78−52506
  $K_{0.54}(Mn,Fe)F_3$, room temp., X-ray single cryst. struct. anal. and refinement 79−19195
  $KMnCl_3$, magnetic spiral struct., neutron diffr. study 80−39748

crystal atomic structure of inorganic compounds continued
$K_2Mn_2(SO_4)_3$, phase transition, X-ray diffr. study of high and low temp. phases 78−38832
$K_2Mn_5[Si_{12}O_{30}].H_2O$, synthetic Mn milarite, cryst. struct. 78−18618
K_2MoOCl_5, mol. and cryst. struct. from X-ray diffr. obs. 78−6046
$K_3(MoO_4)(ReO_4)$ *(French)* 78−47295
$K_2Mo_2O_7.H_2O$, cryst. and mol. struct. 77−76373
$K_2Mo_9S_{11}$, prep. and struct., Mo_{12} cluster in $Mo_{12}S_{14}$ unit 80−107168
$K_8Mo_4V_8O_{36}.12H_2O$, single cryst. X-ray cryst. and mol. struct. 79−99131
$K_7Mo_8V_5O_{40}.{\sim}8H_2O$, containing structurally new K-coordinated octamolybdopentavanadata anion, cryst. struct. 80−96479
KN_3, electron density distrib. by high-resolution X-ray diffr. 77−62505
KND_2, neutron diffr. exam. 31K *(German)* 77−62506
$K_2NH(SO_3)_2$, X-ray cryst. struct. refinement 79−69062
KNO_3, ferroelec. thin crysts., struct. investig. 79−27962
$KNO_3(II)$, Raman spectral study of struct. props., disordered groups 77−66486
$K_3N(SO_3)_2.H_2O$, X-ray cryst. struct. determ. 79−69062
$K_3N(SO_3)_3.2H_2O$, cryst. binding of H_2O, IR spectra 78−75620
$K_4Na_4(Al_8Si_8O_{32}).10H_2O$, amacite, cryst. struct. determ. 80−28961
$K_6Na(Fe,Cu,Ni)_{24\pm}S_{26}Cl$, jerfisherite, X-ray cryst. struct. determ. 80−92512
$K_3NaP_2O_7.4H_2O$ *(French)* 78−42961
$KNaSO_4$, X-ray cryst. struct. determ. 80−64963
$K_3Na(SO_4)_2$, X-ray cryst. struct. determ. 80−64963
$K_2Na[Co(NO4d2)_6]$, single cryst., X-ray deffrs. determ. of electron density distrib. 79−14746
$KNa[Pt(CN)_4].3H_2O$, neutron diffr. cryst. struct. exam., refinement by least squares 78−2079
$K_3Nb_3B_2O_{12}$, pentagonal tunnel struct. *(French)* 77−58985
$K_{12}Nb_{15.5}O_{35.5}F_{18.5}$, cryst. struct. determ. *(French)* 80−96489
$K_6Nb_{6.5}O_{14.5}F_{9.5}$, cryst. struct. determ. *(French)* 80−96489
$K_{10}(Nb_8O_{21})_2.Nb_6X_4O_{26}$, X=Si, Ge, cryst. struct. *(French)* 77−76378
$K_8Nb_{14}Si_4O_{47}$, struct. determ. *(French)* 77−27866
$KNbW_2O_9$, crystallography, polymorphism and phys. props. 78−79599
$K_3Nb_{8-x}X_xO_{21}$ (X=Nb, Ti, Cr, Fe, Ni, Mg, Zn), X-ray diffr., layer struct. *(French)* 77−15368
$K_5NdLi_2F_{10}$, X-ray cryst. struct. determ. and refinement 79−42030
$K_3NdSi_6O_{15}$, cryst. struct. determ. 78−34493
$KNd_9(SiO_4)_6O_2$, cryst. struct. determ. 79−90624
$K(Ni(CN)_2HN_2S_2)$, cryst. struct. determ. 78−63715
$KNiCl_3$, disorder as observed by electron diffr. 80−75213
$KNiCl_3$, X-ray cryst. struct. determ. at room temp. 80−33938
$KNiCr_2(VO_4)_3$, synthesis and cryst. struct. 80−88114
K_2NiF_4 structure, study by method of invariants, appl. to A_2BO_4 oxides *(French)* 80−33959
K_2NiF_4-type compounds, cationic radius ratio and formation 80−28992
$K_2Ni(MoO_4)_2$, X-ray cryst. struct. determ. 79−14782
$K_4NpO_2(CO_3)_3$, structure and bonding study 77−27868
KO_2, low temp. phase study, crystallographic domains and unit cell dimens. 78−63728
β-K_2O-Al O_3, cation distrib. 77−80487
K_2O-Ta_2O_5 mixed oxides, cryst. struct., electron microscopy study 78−91309
K_2O-Ta_2O_5 mixed oxides, cryst. struct., electron microscopy study 78−91310
$K_2O.3MoO_3.3H_2O$, fibrillar crysts., morphology and struct. 78−63959
$K_2O.5Ga_2O_3$, formation and ionic conductivity 77−4351
$K_3O.nWO_3$, n=4-20, X-ray diffr. 77−84726
$KOsO_3N$, interatomic distances of statistically oriented OsO_3N^- by radial distrib. analysis 77−15365
KPO_3F, cryst. struct. *(French)* 80−19762
$K_2P_2O_5F_2$ *(French)* 78−51501
$KPbI_3.2H_2O$, X-ray cryst. struct. determ. 80−64958
$K_2Pb[Co(NO_2)_6]$, X-ray cryst. struct. determ. 80−88106
$KPr(SO_4)_2$, X-ray cryst. struct. determ., least squares refinement 79−55725
$K_2Pt(CN)_4Br_{0.3}\times 3H_2O$, struct., neutron determ., Peierls distortion 79−46640
$K_2Pt(CN)_4Br_{0.3}.3H_2O$, struct. rel. to quasi one-dimensional elec. props. 78−14716
$K_2Pt(CN)_4Br_{0.3}.3H_2O$, quasi-one-dimens. conductor, Br^- distrib. long-range Coulomb interaction, effect on structure and CDW 79−7591
$K_2Pt(CN)_4Cl_{0.3}(Br_{0.3}).3H_2O$, struct., single cryst. neutron diffr. expts. 78−14321
$K_2(Pt(CN_4))(FHF)_{0.3}.3H_2O$, struct. determ., X-ray diffr. exam. 78−63711
$K_{1.75}Pt(CN)_4\times 1.5H_2O$, struct., neutron determ., Peierls distortion 79−46640
$K_{1.75}Pt(CN)_4.1.5H_2O$, struct., single cryst. neutron diffr. expts. 78−14321
$K_{1.75}Pt(CN)_4.1.5H_2O$, Pt chain distortion, X-ray obs. 78−14322
$K_{1.6}Pt(C_2O_4)_2\times 1.2H_2O$, sinusoidally modulated structure 77−84730
$K_{1.6}Pt(C_2O_4)_2\times 1.2H_2O$, struct., neutron determ. 79−46640
K_2PtI_5, synthesis and cryst. struct. *(German)* 78−79588
$KR(PO_3)_4$, R=Ho, Nd, Bi, Sm, Dy, Eu, cryst. struct. 77−43188
$KR(SO_4)_2$, R=La to Tb, unit cell parameters, thermal stability and decomposition 78−18613
K_2ReCl_6-K_2ReBr_2 solid soln., mixed ligand complexes 77−72585
K_2ReF_6 78−42971
K_2SO_4, anhydrous, struct. relationships w.r.t. fast ion cond. 80−107188
K_2SO_4, high temp. form, X-ray struct. redeterm. 80−54179
α-K_2SO_4, space group and cryst. struct., X-ray powder anal. 79−4275
K_2SO_4, thermal phase transition 80−19738
$K_2S_3O_6$, X-ray cryst. struct. redeterm. 79−99126
$K_2S_4O_6$, X-ray cryst. struct. determ. 79−99127
$KSbO_3$, cubic, K^+ ion ordering, electron microscopy 78−79550
$K_{0.51}Sb_{0.67}{}^{III}Sb_2{}^{V}O_{6.26}$, pyrochlore, cryst. struct. *(French)* 78−34470
$KSbSe_2$, cryst. struct. 77−43184
$K_4Sc_2(OH)_2Si_4O_{12}$, crystal struct., X-ray diffr. study 80−79763
K_2SeBr_6, rotational phase transitions, cryst. struct., X-ray diffr. study 80−70400
K_2SeO_4, SHG, hexagonal phase centrosymmetry 79−37684
K_2SnCl_6, high-tem=. phase, X-ray investigation 80−24409
K_2SnCl_6, structural phase transition exam. by neutron powder diffr. 78−55940
$K_2SnF_6.H_2O$, cryst. struct., Fedorov space group 77−89422
$K_2SnF_6.H_2O$, crystallographic characts. *(French)* 78−10011
$K_2Sn(NH_2)_6$, cryst. struct. determ. *(French)* 77−47384
$KSr(NH_2)_3$, cryst. struct. and cryst. chemistry *(German)* 79−51080

crystal atomic structure of inorganic compounds continued
$K_{10}(Ta_8, O_{21})_2.Ta_6X_4O_{26}$, X=Si, Ge, cryst. struct. *(French)* 77−76378
$K_3Ta_3B_2O_{12}$, pentagonal tunnel struct. *(French)* 77−58985
$K_{12}Ta_{15.5}F_{18.5}O_{35.5}$, X-ray cryst. struct. determ. 80−15059
$K_2Ta_4F_4O_9$, single cryst. X-ray struct. determ. *(French)* 79−99129
$K_3Ta_4F_7O_8$, X-ray cryst. struct. determ. 80−39018
KTa_5O_{13} structure, relationship to α-PbO_2 struct., crystallography data 78−42996
$K_{4+5x}Ta_{16-x}O_{42}$, (x=0.3), cryst. struct. 79−90611
$K_6Ta_{10.8}O_{30}$, cryst. struct., X-ray diffr. and electron microprobe meas. 78−34489
$K_2Ta_2O_3F_6$, Marignac's salt, X-ray diffr. study of cryst. struct. 77−89417
$K_2Ta_4O_9F_4$, NMR meas. on ^{19}F, localisation of F^- ions *(French)* 79−77579
$K_6Ta_{6.5}O_{14.5}F_{9.5}$, X-ray cryst. struct. determ. and refinement 79−42029
$K_8Ta_{14}Si_4O_{47}$, struct. determ. *(French)* 77−27866
$KTaWO_6.H_2O$, pyrochlore struct. and its relatives 79−14773
$K_{1-x}Ta_{1-x}W_{1-x}O_6.nH_2O$, composition, struct. and ionic conductivity 80−49410
KTb_3F_{10}, cubic packing of $[Tb_3F_{32}]^{14-}$ polyanions, X-ray diffr. obs. 78−10023
K_2TeCl_6, cryst. data from Guinier powder diagrams *(German)* 80−79751
$K_2TeO_3.3H_2O$, X-ray cryst. struct. determ. 78−95017
$K_2Te^{IV}Te^{VI}{}_3O_{12}$, cryst. struct., Te IV pentacoordination by O 78−63704
$K_2Te^{IV}Te_3{}^{VI}O_{12}$, mixed tellurate, cryst. chem. and elec. cond. *(French)* 80−107150
$KTh_2(VO_4)_3$, X-ray cryst. struct. determ., Fourier and Patterson method 80−19757
$KTiF_4$, X-ray cryst. struct. determ. and refinement *(French)* 79−69068
$K_{1-x}(Ti_{1-x}M_{1+x})O_5$, M=Nb, Ta, layer compound, cryst. struct., nonstoichiometry 80−64972
$KTiMO_5$(M=Ta, Nb), ion exchange props., synthesis and crystallographic props. *(French)* 80−28997
$K_2Ti_6O_{13}$, crystallographic study 77−72601
KTi_3SbO_9, X-ray cryst. struct. determ. *(French)* 80−107178
K_xTiSe_2 and K_xArSe_2 intercalation cpds. *(French)* 77−35536
$KTi_2Ta_5O_{17}$, chemically twinned rutile struct., X-ray study 80−107149
$K_{2.64}Tl_{2.36}Fe_3O(SO_4)_6.5H_2O$, X-ray cryst. struct. determ. 80−92483
$KTl(SeO_4)_2$, $K_3Tl(SeO_4)_3$, and $K_5Tl(SeO_4)_4$, cryst. struct. *(French)* 80−84148
$K_2(UO_2)_4O_2(OH)_2Br_4(H_2O)_6$, cryst. data 77−76366
$K_2(UO_2)_4O_2(OH)_2Cl_4(H_2O)_6$, cryst. data 77−76366
$K_2(UO_2)_4O_2(OH)_2Cl_4(H_2O)_6$, tetranuclear complex, struct. determ. *(French)* 77−80451
$K_6(V_2,Mo_{10})VO_{40}.13H_2O$, X-ray cryst. struct., electron spin resonance spectrum 80−88096
K_xVF_3 (x=0.25,0.19), cryst. struct. examination by electron diffr. using TEM 79−23583
KVO_3, X-ray determ. 78−6043
$K_{1.8}V_8O_{16}$, hollandite-type struct., synthesis and cryst. struct. 80−29003
$K_2V_8O_{16}$, hollandite-type struct., synthesis and cryst. struct. 80−29003
$K_{0.26}WO_3$, single cryst. X-ray and powder neutron diffr. studies 80−29001
$K_{0.27}WO_{(3+y)}$, struct. analysis 77−11510
$K_2W_4O_{13}$, twinned crystal, X-ray cryst. struct. determ. 79−7588
K_xWO_3, x=0.20 and 0.32, hexagonal W bronzes, X-ray cryst. struct. refinement 79−77577
$K_xWO_{(3+y)}$, direct imaging of ordering 77−11511
$KX(MoO_4)_2$, X=Sm, Eu, Gd, polymorphism investig. by X-ray diffr. and DTA 77−4091
β-KYb_3F_{10} *(French)* 77−15350
$K_3Yb(SO_4)_3$, X-ray cryst. struct. determ. 79−65058
$K_2Zn_2Be_2(SiO_4)(Si_2O_7)$, cryst. struct. determ. 80−88121
K_2ZnCl_4, modulated struct. in ferroelec. phase, X-ray obs. 80−64970
K_2ZnCl_4, X-ray cryst. struct. refinement 79−55705
$KZn_2H(PO_4)_2$, X-ray cryst. struct. determ. *(French)* 79−69080
$K_4Zn(MoO_4)_3$, cryst. struct., cohesion 77−31641
$K_2Zn(NH_2)_4$, cryst. struct. determ. *(French)* 78−79590
$KZn_4(PO_4)_3$, X-ray cryst. struct. determ. *(French)* 79−19205
$K_4Zn(WO_4)_3$, cryst. struct. and polymorphism 80−1996
$K_2Zn_3[Fe(CN)_6]_2.xH_2O$, X-ray cryst. struct. determ. and refinement *(French)* 80−28955
$K_8Zr(MoO_4)_6$, X-ray structural investigation 78−79597
$K_4Zr_5O_{12}$, cryst. struct., X-ray study 80−33957
$K_2ZrSi_2O_7$, second monoclinic modification, struct. determ. 77−84734
$K_2Zr[Si_3O_9]$, wadeite, cryst. struct. refinement, X-ray diffr. meas. 78−2091
$K[B(SO_3Cl)_4]$ 78−63701
$K_4[Bi_2Br_{10}].4H_2O$ 77−58988
$K_5[IMo_6O_{24}].5H_2O$, X-ray cryst. struct. determ. 80−54183
$K[InBr_4(H_2O)_2]$, X-ray cryst. struct. determ. 80−54186
$K_2[M(H_2O)_6](YO_4)_2$, Tutton's salts, M=Cu, Ni, Zn, Y=S, Se stereochem., neutron struct. determ. 78−18609
$K_6[MnMo_9O_{32}].6H_2O$, cryst. struct. 77−76374
$K[(OH)_{0.42}(O_2)_{0.50}]$, cubic solid soln., structural and mag. study *(French)* 80−107177
$K[OsNBr_4H_2O]H_2O$, mol. and cryst. struct. from X-ray diffr. obs. 78−6046
$K_2[Pd(SO_3)_2].H_2O$, X-ray cryst. struct. determ. and refinement, connexion modes 79−46608
$K_2[Pt(CN)_4]Br_{0.3}.3H_2O$, high press. structs. and phase transitions 80−107423
$K_2[Pt(CN)_4]X_{0.3}.3H_2O$, X=Br, Cl, X-ray and neutron diffr., 31K-room temp. 78−42964
$K_4[Ru_2Cl_{10}O]$, X-ray cryst. struct. determ. and refinement *(French)* 79−37670
$K_2[RuCl_6]$, X-ray cryst. struct. determ. and refinement *(French)* 79−37670
$K_3[SO_3ON(SO_3)_2].3/2H_2O$, struct. determ., X-ray and neutron diffr. 79−42038
$K_6[Si_2Te_6]$, cryst. struct. *(German)* 78−79569
$K_2[UF_2O_2(SO_4)].H_2O$, X-ray cryst. struct. determ. 80−54194
$K_2[(UO_2)_3F_8$-$H_20].3H_2O$, struct. determ. *(French)* 80−49193
$K_4[V(CN)_6(NO)].1/2KOH.1/2H_2O$, cryst. and molecular struct. 77−80469
$K_4(\beta_1$-$SiMoW_{11}O_{40}).9H_2O$, X-ray cryst. struct. determ. and refinement 80−28973
$Khu_3F_{10}:Eu^{3+}$, site occupancy from excitation and emission spectra *(French)* 77−81145

crystal atomic structure of inorganic compounds continued

- $KliFeS_2$, end product of $Li+KFeS_2$ electrochemical reaction, cryst. struct. 79−100397
- $LIFe_5O_8$, absolute struct. and space group determ. by electron microscopy 77−62454
- LI_2UO_4, energy transfer, cryst. struct. and chemical composition effect 80−108248
- $(La,Ca)_nTi_nO_{3n+2}$, (n=4.5,5 or 6), cryst. struct. determ. *(French)* 79−65039
- La, $(SO_4)_3.9D_2O$, soln. growth, struct., props. 77−77363
- La-Fe, liquid quenched, X-ray diffr. and Mossbaeur effect exam. of structure 78−76678
- La-H(D), lattice parameters 80−64982
- La-Ni-H compounds, prep. by gas absorpt. in La-Ni system, struct. 77−9078
- La_{1-x} Eu_x B_6 solid solutions, cryst. lattice defectiveness, mag. susceptibility and elec. conductivity 80−15083
- $La_{2-x}A_{1+x}Cu_2O_{6-x/2}$ (A=Ca, Sr), synthesis and characterisation *(French)* 80−104085
- $LaAg_xIn_{1-x}$, crystal struct., neutron diffr. obs. 80−49187
- LaB_6 film, structure, stoichiometry, elec. properties 78−60043
- LaB_2C_2, ordering of B and C atoms in struct. 80−96481
- $La_4Ba_6(BO_3)_9$, flux growth and chem. characts. 78−23595
- $LaCO_{1-x}M_xO_3$, M=Mg, Ti, cryst. struct., elec. and mag. props. 79−86748
- $La_{1-x}Ca_xVO_3$, struct., elec. and mag. props., temp. and conc. depend. *(French)* 77−4293
- $LaCoO_3$, synthesis and characterisation by powder X-ray diffr. 78−79580
- La_2CoO_4, synthesis and characterisation by powder X-ray diffr. 78−79580
- $La_4Co_3O_{10}$, cryst. struct., stability 80−24434
- $La_4Co_3O_{10}$, synthesis and characterisation by powder X-ray diffr. 78−79580
- $LaCrOS_2$, single cryst. X-ray diffr. struct. determ. *(French)* 79−23581
- $LaCrOS_2$, X-ray cryst. struct. anal. *(French)* 80−92484
- $LaCrS_3$, crystal atomic struct., X-ray diffr. analysis *(German)* 78−10003
- $LaCuO_3$, struct. rel. to phys. props., high-pressure series of perovskite-like oxides 78−51493
- LaF_3 single cryst., electron diffr., superlattice struct. 78−42993
- $LaFe_4P_{12}$, crystal growth and structure 78−14314
- $LaFe_4P_{12}$-type structure ternary arsenides, synthesis and cryst. struct. 80−84154
- $La_2Fe_{1.76}S_5$ *(French)* 78−51499
- $La_2Fe_2S_5$, $La_2Fe_{1.87}S_5$, struct. *(French)* 77−55277
- $La_{10}Ga_3Co_7$, X-ray cryst. struct. determ. 80−33977
- $LaGaOS_2$, cryst. struct. determ. *(French)* 78−79575
- $3La(IO_3)_3.HIO_3.7H_2O$, pyroelec., cryst. struct. 79−1410
- La_3InS_6, cryst. struct., four-circle diffractometer data and Fourier synthesis determ. *(French)* 79−14739
- $La_3Ir_3O_{11}$, prep. and cryst. struct. *(French)* 79−51084
- $LaKFe(CN)_6.4H_2O$, cryst. struct. determ. 78−55844
- $La_2Mg_3(NO_3)_{12}.24D_2O$, use of neutron time-of-flight technique for cryst. structs. investigation 79−19126
- $La_2Mg_3(NO_3)_{12}.24H_2O$, neutron diffr. obs. 78−18598
- $LaMnO_3$, orthorhombic lattice distortions, mag. props. rel. to prep. conditions 77−20592
- $La_{10}Mo_2O_{21}$, synthesis and X-ray characterisation of struct. *(French)* 79−99162
- La_2MoO_6, paramag. resonance and struct. 80−84162
- La_6MoO_{12}, synthesis and X-ray characterisation of struct. *(French)* 79−99162
- $La_6Mo_2O_{15}$, synthesis and X-ray characterisation of struct. *(French)* 79−99162
- $La_xMo_6S_8$, Chevrel phase, lattice instabilities, X-ray diffr. meas. 78−34491
- $LaNbO_4$, doped, modulated struct., characterisation in ABO_{4+x} phase 79−99148
- $LaNbO_4$, ferroelastic, cryst. struct. and twinning struct. 79−27965
- $LaNbO_4$, room temp. phase exam. 78−26536
- $LaNiC_2$, struct. determ. using X-ray diffraction *(Ukrainian)* 80−33949
- $LaNi_5D_6$, cryst. struct., neutron diffr. obs. 79−19221
- $LaNi_5H_6$ sponges, Al or Mn substitution, neutron diffr. 80−24427
- $LaNi_5H_x$ hydrogen storage system, $(0\leq x\leq 6)$, neutron scatt. obs. of static and dynamic props. 78−14323
- $LaNiO_3$, form. conditions and props. 80−21270
- $La_6Ni_6P_{17}$, synthesis and cryst. struct. 78−75634
- La_2O_3, cryst. struct., X-ray powder diffr. and electron diffr. study 80−107161
- La_2O_3, neutron diffraction study of high temp. struct. *(French)* 79−65050
- La_2O_3-Al_2O_3 system, alumina rich phase, X-ray obs. 79−29030
- $La(OH)_2Br$, hydrothermal phase equilib., cryst. struct. 78−35372
- $La_7(OH)_{18}Br_3(I_3)$, hydrothermal phase equilib., cryst. struct. 78−35372
- $La_7(OH)_{18}I_3$ 78−42968
- $La_2O_2S_2$, cryst. struct. determ. 79−51087
- $3La_2O_3.2WO_3$, X-ray charact. and thermal props. 77−43194
- $La_3Os_2O_{10}$, cryst. struct., Os_2O_{10} clusters with metal-metal bonds 79−86753
- $La_4Os_6O_{19}$, prep. and struct., metal-metal interaction exam. *(French)* 77−27865
- $La(PO_3)_3$, X-ray struct. characts. 80−54202
- LaP_3O_9, X-ray powder data 79−51079
- La_3ReO_8, cryst. struct. *(French)* 79−90614
- $La_6Re_4O_{18}$, X-ray cryst. struct. determ. Patterson and Fourier methods *(French)* 79−14745
- $LaRe_2Si_2$ 78−26551
- $LaRu_4B_4$, X-ray cryst. struct. determ. 79−32959
- $LaRu_xFe_{1-x}O_3$ perovskites, cryst. struct., elec., mag. and Mossbauer behaviour 77−55274
- La_3RuO_{11}, prep. and struct. study, metal-metal bonding *(French)* 78−91325
- $La_3Ru_3O_{11}$, crystal struct., X-ray diffr. study 78−67688
- $La_{3.5}Ru_4O_{13}$, perovskite-type cryst. struct., X-ray determ. *(French)* 80−75206
- $La_4Ru_6O_{19}$, prep. and struct., metal-metal interaction exam. *(French)* 77−27865
- $La_8Ru_4O_{21}$, mixed valence oxide of new hexagonal struct. type 78−51503
- LaS_2 *(French)* 78−34476

crystal atomic structure of inorganic compounds continued

- $La_2(SO_4)_3.9H_2O$, crystal struct. refinement 77−15369
- La_2Sb, X-ray cryst. struct. determ. 80−33943
- La_4Sb_3, X-ray cryst. struct. anal. 80−39013
- $LaSbO_3$, single crysts., hydrothermal synthesis and crystallographic characteristics 79−95916
- La_2Se_3, La_2Te_3, mutual solubility 77−21113
- $LaSiO_3F(Cl)(Br)$, phosphor host, luminesc. and struct. props. 78−48212
- $LaSiO_2N$, cryst. struct. 78−10017
- $LaSiO_2N$, cryst. struct. 78−10019
- $La_4Si_2O_7N_2$ single cryst. growth by floating zone method with SiO_2-Si_3N_4 additions 80−93481
- $La_{0.75}Sr_{0.25}CrO_3$, struct. refinement by X-ray powder diffr. profile analysis 77−84721
- $La_{1-x}Sr_xCrO_3$ system, phase relationships, cryst. struct. 77−69073
- $La_{2-x}Sr_xNiO_4$, $(0\leq x\leq 1)$, cryst. struct. and elec. props. 78−2088
- $LaTaO_4$, doped, modulated struct., characterisation in ABO_{4+x} phase 79−99148
- $LaTiO_3$, cryst. struct. and cryst. chem., cryst. showing complex twinning 80−1984
- $La_2Ti_2O_7$, crystal struct. and phase transitions, rel. to isomorphous crystals *(Japanese)* 80−49208
- $La_2V_{10}O_{28}.20H_2O$, cryst. struct., monoclinic unit cell parameters, X-ray anal. 79−86772
- $La_2V_{10}O_{28}.20H_2O$, X-ray cryst. struct. anal. 80−39060
- $La_2Zr_2O_7$-$La_2Hf_2O_7$ system, cryst. struct., phase diagram 78−83806
- $(Li,Na)VO_3$, struct. systematics 79−55719
- Li solid electrolyte materials, review of crystal and electrochem. props. 80−107524
- Li-Rh-H system, intermetallic cpds. and phase relationships, cryst. struct. 78−44084
- $Li_{0.5}$ $Fe_{2.5}O_4$, microwave material, mag. props., review 79−33504
- $Li_{0.5}Al_{2.5-t}Cr_tO_4$,$(0\leq t\leq 0.25)$, cryst. struct. 79−60319
- $LiAl_xFe_{5-x}O_8$, IR spectra, ionic ordering in absence of fine struct. 77−8583
- β-$LiAlO_2$, reindexing X-ray powder diffr. pattern 79−51069
- $LiAl_5O_8$, ordered single cryst., struct. determ. *(French)* 80−15074
- $LiAlSiO_4$, β-eucryptite one-dimens. fast ion cond., temp. depend. of cryst. struct. 80−107191
- α-$LiAmO_2$, prep. and crystallographic data *(French)* 78−47290
- Li_5B_4, cryst. struct., X-ray and neutron diffr., and NMR 79−23571
- $Li_4B_7O_{12}Cl$, cryst. struct. and ionic conductivity 77−84690
- $LiBa_3Nb_3(Ta_3)(Sb_3)Ti_5O_{21}$, insertion of Li, X-ray and neutron diffr. study *(French)* 78−91324
- $LiBaPO_4$, vibrational spectra and cryst. struct. 78−39536
- LiC_6 intercalation cpd., synthesis method and reflectivity spectrum 79−15600
- Li_2CaUF_8, X-ray single cryst. struct. determ. 79−77574
- $LiCdBO_3$, cryst. struct., X-ray determ. 79−19226
- $LiCdBO_3$ triclinic cryst. struct., X-ray and Patterson function anal. 80−39055
- $LiCdSiO_4$, X-ray cryst. struct. determ. 77−80458
- $LiClO_4.3H_2O$, absolute sign of piezoelec. d_{33} and pyroelectric p_3 coeffs. 78−43793
- $LiClO_4.3H_2O$, pyroelec. and piezoelec. coeffs., struct. refinement 78−18602
- β_{II}-Li_2CoSiO_4, disordered struct., twinning description 80−39017
- β_{II}-Li_2CoSiO_4, X-ray cryst. struct. determ. 80−15062
- $LiCr_xFe_{5-x}O_8$, IR spectra, ionic ordering in absence of fine struct. 77−8583
- $LiCrO_2$, two-dimens. mag. props. rel. to cryst. struct. 80−75776
- $Li_2Cr_2O_7.2H_2O$, cryst. struct. 79−32980
- $LiCsSO_3.2H_2O$, cryst. struct. *(French)* 80−24412
- $Li_2Cu_5(Si_2O_7)_2$, cryst. struct. and proposal of new values for effective ionic radii of Cu^{2+} 79−4276
- $LiEu(SO_4)_2$ 78−67695
- $Li_{0.5}Fe_{2.5}O_4$ milled ferrite powder, substruct. and sinterability 80−84894
- $Li_{0.5}Fe_{2.5}O_4$ Ru substitution effect on struct. and mag. props., and max. solubility determ. 80−75364
- $LiFePO_4$, cryst. struct. by neutron diffr. 78−43003
- $LiGaCr_4S_8$, 1:1 ordering on tetrahedral sites, IR spectra obs. *(German)* 78−6669
- $Li_{0.5}Ga_{2.5}O_4$-$CuCr_2O_4$ system, phase diagrams, IR spectra, Cu^{2+} electronic spectra *(French)* 78−51461
- $LiGaO_2.6H_2O$ *(French)* 78−42967
- $LiGaO_2.8H_2O_1$ X-ray powder diffr. data *(French)* 80−39033
- $Li_2Ge(GeO_3)_2(OH)_2$, cryst. struct. determ. 79−90629
- Li_4GeO_4, Mg_2GeO_4, Li_3PO_4, structural relns. *(French)* 77−47433
- LiH, density matrix, factor X-ray struct. factor 78−67692
- LiH, linear chain, ab initio calcs., cryst. orbital method 79−37659
- $LiHCd(Ge_5O_{15})$, cryst. struct. determ. by X-ray diffr. 77−76381
- $LiHCd_4(Ge_5O_{15})$, cryst. struct., comparison with natural rhodonite 78−30600
- $Li_{1-x}H_xIO_3$, cryst. growth from soln. and phys. props. 77−31634
- $LiHSeO_3$, X-ray cryst. struct. determ. 80−28966
- $LiH_3(SeO_3)_2$, ferroelec., absolute atomic arrangement and spontaneous polarisation, neutron diffr. study 80−59442
- $Li_{1-x}Hf_{2-x}Ta_x(PO_4)_3$, new solid ionic conductors 77−35953
- α- $LiIO_3$, crystal struct. refinement, corrected thermal parameters 77−4092
- α-$LiIO_3$, single cryst., opt. and physicochem. props. 77−8566
- α-$LiIO_3$ single crystal, enantiomorphism 79−95725
- $LiInCr_4S_8$, 1:1 ordering on tetrahedral sites, IR spectra obs. *(German)* 78−6669
- α-$LiIn(MoO_4)_2$, high-temp. form., X-ray cryst. struct. determ. 80−107183
- $LiInO_2$, prep., props. and struct. 80−35517
- $LiInS_2$, prep., props. and struct. 80−35517
- $Li_2K(IO_3)$ in $LiIO_3$-KIO_3 system, lattice parameter, equilib. and metastable phase diagram *(Chinese)* 80−7538
- $(Li_{0.5}La_{0.5})_xBa_{1-x}TiO_3$, cryst. struct., dielec. and IR spectral meas. 79−46614
- Li_2MgGeO_4, high temp. modif., struct. derivation *(French)* 77−47433
- $LiMn[BO_3]$, X-ray cryst. struct. determ. 79−42034
- LiN_3, evidence for N_3^- from static and dynamic props. 78−60465
- Li_3N, electron density study using Compton scattering 80−79750
- Li_3N, existence of N^{3-} ion in cryst. struct. 79−7583
- Li_3N, interstitial sites and anharmonic thermal vibrs. in cryst. struct., ionic cond. mechanism 80−107190
- Li_3N, ionic conductor, single cryst. defect struct. anal. data reduction and struct. refinements, 153-678K 79−32988

crystal atomic structure of inorganic compounds continued
Li_3N, superionic conductor, cryst. growth and struct., phys. props., book contrib. 79—42308
Li_6NBr_3, $Li_{13}N_4Br$, ionic transport 79—73336
$LiNH_4PO_3F$ *(French)* 78—34475
$LiNH_4SO_4$, atomic struct. exam. 79—37678
$LiNH_4SO_4$, low temp. antiferroelec. III phase, X-ray cryst. struct. determ. 79—42036
$LiNO_3.3H_2O$, neutron diffr. studies at 120 and 295K, H bond studies 80—88099
$Li(Na,K)CO_3$, therm. anal. and X-ray diffr. study *(French)* 79—46630
$Li_{0.04}Na_{0.1}Fe_{2.5}O_4$, $Li_{0.3}Na_{0.2}Fe_{2.5}O_4$, ferrites, form., X-ray, chem. and mag. anal. 77—36424
$LiNbO_3$, chemical, struct. and physical props., book contrib. 79—69783
$LiNbO_3$, Czochralski grown single crysts., cellular interface and struct. due to constitutional supercooling *(Chinese)* 79—51026
$LiNbO_3$, electric-field induced microscopic struct. changes, modulated X-ray diffr. detect. 78—47296
$LiNbO_3$:Na structure field stability limits, LPE film growth, SAW velocity 80—80102
$Li_x(NbO)_4Nb_{30}O_{90}$, struct. and ionic cond. 79—65246
$Li_3Nd_2(BO_3)_3$, cryst. struct., X-ray diffr. meas. 78—10028
$Li_2Ni_2Mo_3O_{12}$, struct. type systematics 77—72587
Li_2O, coexistence of rhombohedral and cubic form, X-ray study 80—1980
$(Li_2O)_{1-x}U_{1.4}W_{4.6}O_{18}$, $0\leq x\leq 0.4$, crystallographic identification, paramag. props. *(French)* 79—46633
$Li_2O.3MoO_3.5.7H_2O$, fibrillar crysts., morphology and struct. 78—63959
$LiPO_3$, cryst. struct. determ. *(French)* 77—4071
γ-Li_3PO_4, cryst. struct. of synthetic analog of lithiophosphatite 79—37688
Li_3PO_4, Li_4GeO_4, Mg_2GeO_4, structural relns. *(French)* 77—47433
$(LiPO_3)_x.H_2O$, existence of high- and low-temp. cryst. forms, X-ray diffr. data 79—19179
$LiPbPO_4$, vibrational spectra and cryst. struct. 78—39536
$Li_3Pr_2(BO_3)_3$, cryst. struct. 78—87655
$LiPr(SO_4)_2$, X-ray diffr. cryst. struct. determ. 79—14786
LiR $(WO_4)_2$, R=La-Sm, triclinic modification, cryst. struct. 80—33976
$LiRF_4$, R=rare earth, laser matrices prep. and characterisation 77—24945
$(Li_{0.5}R_{0.5})TiO_3$, distorted perovskite struct. 78—83791
$LiRbSO_4$, X-ray cryst. struct. determ. 80—33982
Li_2SO_4, high temp. fast ion cond. phases, neutron diffr. obs. of struct. 80—107512
$LiSO_3F$, cryst. struct. determ. 78—26509
$LiScS_2$, crystal struct. determ. by X-ray powder diffr. 80—49205
$Li_x(Si,Al)_{12}(O,N)_{16}$, α'-Sialon ceramics, prep. and characterisation 78—84750
$Li_{2.33}Si$, cryst. struct. and electrochem. anal. *(German)* 80—88132
Li_2SiO_3, Czochralski growth and charact. 79—91577
$(Li_2SiO_3)_x$ 77—35519
$Li_2Si_2O_5$, laminated cryst., IR spectra, dispersion anal. 77—1675
Li_4SiO_4, ordered, cryst. 80—19752
Li_4SiO_4-Li_3PO_4 solid solns., Li ion cond., unit cell parameters 77—89575
LiSiON, allotropes, powder diffr. obs. *(French)* 78—63726
$LiSrPO_4$, vibrational spectra and cryst. struct. 78—39536
$LiTaO_3$, crystallographic features and domain struct. 78—34498
$LiTaO_3$, quadratic optical susceptibility dispersion 79—18478
$LiTa_3O_8$, H-form cryst. struct. 79—60325
M-$LiTa_3O_8$, neutron diffr. obs. 78—18599
$Li_{1-x}Ta_3O_{8-x}F_x$ (x=0,0.25,0.5), structural studies by full profile refinements of Guinier-Hagg X-ray film data 79—23584
$LiTbS_2$, long and short range order 78—38667
$LiTe_3$, X-ray and neutron diffr., Te displacements 77—47399
Li_2TeO_4, X-ray obs. *(French)* 78—6041
Li_4TeO_5, crystl. struct. anal. by Patterson and Fourier synthesis *(French)* 79—4273
Li_3ThF_3, cryst. struct. comment on coordination polyhedra for ThF_9 group 79—69083
Li_3ThF_7 78—63702
$Li_2Th_5F_{22}.LiOH$, cryst. struct. determ. and refinement 79—73142
LiTi, substituted ferrite, cation distribution, Mossbauer, X-ray, neutron diffr. study 80—28975
$Li_2Ti_3O_7$, Li^+ ion conductor, X-ray cryst. struct. determ. 79—46604
Li_xTiS_2, alkali ion ordering, X-ray study 80—107165
Li_xTiS_2, Li ordering in intercalation battery, theory 79—77580
Li_2UO_4, cryst. struct., X-ray diffr. obs. 78—34485
$LiVO_3$, X-ray determ. 78—6043
$Li_xV_2O_5$ $(0.1<x<1.0)$, phase relationship in ambient temperature system 80—20912
Li_xVSe_2, intercalation cpds., electron chem., ionicity 80—89501
Li_2WO_4, Li sites determ., using method based on bond-strength calcs. 79—7514
Li_4WO_5, IR, Raman, luminesc. spectra meas., cryst. struct. investig. 77—52074
Li_xWO_3, electrochem. and chem. Li incorporation, cryst. struct. 80—88131
Li_xWO_3, Vegard relationships, lattice parameter versus composition, X-ray and chem. anal. 79—23582
$Li_2WO_4(IV)$, cryst. struct. rel. to wolframite-type struct. 80—92505
$Li_x(WO)_4W_{30}O_{90}$, struct. and ionic cond. 79—65246
Li_2W0_4, type II polymorph. crys. struct. determ. 80—15073
$LiYF_4$, elastic consts. and acoustic symm. 80—15182
$LiY(MoO_4)_2$, X-ray cryst. struct. determ. 80—107124
$LiYSiO_4$, cryst. struct. determ. 77—58997
$Li_6Yb(BO_3)_3$, cryst. struct. determ. 78—18621
LiZn, substituted ferrite, cation distribution, Mossbauer, X-ray, neutron diffr. study 80—28975
$Li_{0.5(1-x)}Zn_xFe_{2.5-0.5x}O_4$, neutron and X-ray diffr. obs. *(Russian)* 77—31645
$Li_{14}Zn(GeO_4)_4$, crystal struct. and ionic conductivity 78—51728
$Li_4Zn(PO_4)_2$, cryst. struct. determ. 77—15386
γ_{II}-Li_2ZnSiO_4, X-ray cryst. struct. determ. 80—15061
$Li_{14}ZnTa_4O_{18}$:Eu, fluorescence and cryst. symm. 77—24886
$LiZn[BO_3]$, X-ray cryst. struct. determ. 79—42034
$Li_2Zr(MoO_4)_3$, X-ray cryst. struct. determ. 80—88125
$Li_{1-x}Zr_{2-x}Ta_x(PO_4)_3$, new solid ionic conductors 77—35953
$Li_3[B_5O_8(OH)_2]$, interplanar distances atomic coordinates, temp. corrections 79—82192
$Li[Mn_2]O_4$ spinels, crystallographic, electronic and mag. props. *(German)* 79—60324

crystal atomic structure of inorganic compounds continued
Lisd4UO_5, energy transfer, cryst. struct. and chemical composition effect 80—108248
$LuAlO_3$, single crysts., prep. and phys. props., X-ray struct. anal. 79—4298
$LuAlO_3:Er^{3+}$, $^4S_{3/2}$ to $^4I_{9/2}$ transition laser action, optical and luminescence spectra 80—16082
$LuFe_2B_2$, compounds with $CeAl_2Ga_2$ structure type *(Ukrainian)* 79—32970
Lu_3InO_6, high press. synthesis, cryst. struct. 77—68955
LuOOH, $Lu(OH)_3$, growth from gel on ageing, X-ray diffr. patterns 80—24386
$Lu_2Si_2O_7$, crystal struct. of X form, polymorphism under press. *(French)* 77—47430
$Lu_2Si_2O_7$, polymorphism under press., cryst. struct. 77—35692
(Mg, Fe)SiO_3, orthopyroxenes, cation distrib., electronic and Mossbauer spectra 80—7370
Mg dichlorophosphate complexes, cryst. struct. ^{35}Cl NQR obs. 80—108108
Mg ferrite, crystal lattice defectiveness and degree of inversion, effect of synthesis temp. 77—11501
$Mg_3Al_2Si_3O_{12}$, pyrope, cryst. struct. and compressibility to 60 kbar 78—63718
$Mg_3Al_2Si_3O_{12}$, pyrope garnet-ilmenite transition 77—49063
$Mg_{9.10}An_{4.04}Mn_{1.89}(SO_4)_2(OH)_{26}.8H_2O$, mooreite, X-ray cryst. struct. determ. and refinement 80—92488
$MgAs_4$, X-ray diffr., coordination *(French)* 77—72583
$MgB_{12}H_{12}.10H_2O$, struct. dehydration, intermediate phases and thermooxidative degradation 80—33951
$MgB_{12}O_{19}.5H_2O=Mg[B_3{}^{\Delta}B_3{}^{t}O_7(OH)_5]_2$, cryst. synthesis and struct., bonding, X-ray study 80—33973
$MgB_6O_{10}.6H_2O$, cryst. struct. determ. 77—1116
$MgBr_2$-ABr (A=Cs, Rb, K, Na, Tl), thermochemical and struct. investigation *(German)* 79—1423
$Mg_2CO_3(OH)_2(H_2O)_3$, H bonding 78—18601
$Mg_5(CO_3)_4.(OH)_2(H_2O)_4$, cryst. struct., H bonding, X-ray diffr. meas. 77—47392
$MgCaH_{3.72}$, synthesis and struct. *(Japanese)* 78—84751
$MgCl_2$-alkali metal chloride system, solid and molten states, struct. props., Raman spectra 80—76011
$MgCl_2.nH_2O$, IR spectra and struct. features 79—15452
$MgCl_2.nH_20$, cryst. struct. *(German)* 80—1987
$(Mg_{0.776}Co_{0.224})SiO_3$, synthetic orthopyroxene 78—42970
MgF, single crysts., neutron diffr. study, least squares refinement 79—73147
MgF_2, cryst., atomic vibrs., anisotropy parameters, bonding 80—54195
$MgFeGe_2O_6$-$Ca(Mg_{0.5}Fe_{0.5})Ge_2O_6$, solid solns., phase equilibria, cryst. optical, X-ray struct. characts. 79—11577
$MgGeO_3$-$Ca_{0.5}Fe_{0.5}GeO_3$, solid solns., physicochem. props. 77—44223
Mg_2GeO_4, Li_4GeO_4, Li_3PO_4, structural relns. *(French)* 77—47433
Mg_2GeO_4 spinel, struct. refinement, neutron diffr. 77—72590
Mg_2GeO_4-Mg_2SiO_4 system, struct. similar solid soln. obs. and characts. 80—108403
$MgHPO_4.3H_2O$ and $MgDPO_4.3D_2O$, IR absorpt. and Raman spectra, vibr. assignments 80—97257
$MgHPO_4.3H_2O$, newberyite, struct. refinement and H bonding 80—15058
α-$Mg(IO_3)_2$, cryst. struct. using X-ray powder method *(Chinese)* 79—51059
$Mg(IO_3)_2.4H_2O$, crystal struct., unit cell, X-ray study 80—59447
$Mg(IO_3)_2.4H_2O$, struct. and phase transition using X-ray diffr. and thermal anal. *(Chinese)* 79—51059
$MgIn_2S_4$, cation distrib. and deform. parameter using Bertaut, Furuhashi and Baltzar methods 80—15041
$MgKPO_4.6H_2O$, struvite analogue, X-ray single cryst. struct. determ. 79—19190
$(Mg_{0.925}Mn_{0.075})SiO_3$, synthetic orthopyroxene 78—42970
$MgMo_2O_7$, cryst. struct. 78—18596
$MgMoO_4.5H_2O$, cryst. struct. determ. by X-ray diffr. *(French)* 77—47385
$Mg(NH_3)_6(ClO_4)_2$, phase transition, group theoretical anal. 80—65218
$Mg(NO_3)_2.6H_2O$, crystal structure changes due to substitution of Mg^{2+}, by Co^{2+} or Ni^{2+} *(German)* 80—24428
$Mg_{0.7}Na_{0.9}K_{2.0}Ca_{2.4}Al_{9.1}Si_{26.9}O_{72}.xH_2O$, erionite, cryst. struct. exam., stacking faults 78—2083
$MgNbF_7$, polymorphism, X-ray powder diffr. data *(French)* 80—19779
$Mg_3Nb_6O_{11}$, struct. determ. and refinement from X-ray 78—91319
MgO, at. charge densities, X-ray struct. factors 78—79566
MgO, electron diffr., dynamical effects for cryst. struct. determ. 78—83679
MgO, X-ray determ. of electron density distribs., atomic scatt. factors 80—15078
MgO-B_2O_3 system, glass and cryst. compd. struct. determ. by ^{11}B NMR 79—94905
$Mg_2(OH_2)CO_3$, cryst. struct. rel. to artinite topotactic thermal decomposition 77—68952
$Mg_3(OH)_2SO_4[B(OH)_4]_2$, sulphoborite, X-ray refl. data 77—15389
$Mg(OH)_2.2Mg_2SiO_4$, cryst. struct. determ. 77—47410
$Mg_{0.82}Pt(C_2O_4)_2\times 5.3H_2O$, struct., neutron determ. 79—46640
Mg_2Si, charact. X-ray temp. and thermal expansion coeff. 77—15599
$MgSiF_6.6H_2O$, orientational periodic antiphase *(French)* 80—15053
$MgSiO_3$, orthorhombic perovskite, contribution to crystal chem. 80—19777
$MgSiO_3$, perovskite, synthesis and cryst. chem. charact., rel. to mantle mineralogy 78—65266
$MgSiO_3$, perovskite struct., cryst. chem. 79—60336
$2Mg_2SiO_4.3Mg(OH)_2$, new high-press. struct. type, cryst. struct. 80—39028
$MgTaCuO_4$, cryst. struct., synthesis 78—83790
$MgTeMoO_6$, prep., cryst. struct., and catalytic props. 80—108709
$MgUO_4$, energy transfer, cryst. struct. and chemical composition effect 80—108248
$MgVO_3$, high-pressure modification, struct. and mag. props. 79—23727
$(MgV_2O_4)_c(FeFe_2O_4)_{1-c}$, struct. parameters, IR spectra, cluster-component analysis 77—47425
$Mg_{0.25}Zn_{0.75}Fe_2O_4$, ferrite, DC cond., dielec. props., lattice consts. 80—80272
$(Mn,Mg)Mg(OH)_2[ZnSiO_4]$, herstmannite, comparison with $Ca[ZnSiO_4].H_2O$, clinohedrite 79—19228
Mn aluminosilicate, ganophyllite, cryst. struct. 78—75633

crystal atomic structure of inorganic compounds continued

- Mn complex, $Mn(SCN)_2(C_2H_5OH)_2$, two-dimens. Heisenberg magnet, cryst. struct. and mag. props. 79−60337
- Mn complex, with 1,2,4-triazole, mag. susceptibility, 2-300K struct. 77−77045
- Mn dichlorophosphate complexes, cryst. struct. ^{35}Cl NQR obs. 80−108108
- Mn metallic perovskite, structural instability *(French)* 79−100123
- Mn-B system, microhardness and phase analytical studies 79−24502
- $Mn_3(BO_3)_2$, synthetic jimboite, X-ray cryst. struct. determ. 79−42035
- $(Mn_2(CO)_8\{GeMn(CO)_5I\}_2)$, X-ray cryst. struct. determ. 80−54190
- $MnCrF_5$ *(French)* 77−47403
- $Mn_xCr_{3-x}O_4$, cubic and tetragonal structs., neutron diffr. obs. 79−19369
- MnD_x, synthesized at high pressures, neutron diff. anal. of struct. 80−28977
- $MnGa_2S_4$, synthesis electrophys. props. 77−51747
- $Mn_{0.75}Ga_{2.17}S_4$, twinning and cryst. struct. determ. *(French)* 78−83798
- $MnGd_2S_4$, mag., struct. and Mossbauer effect study 78−51507
- $Mn(H_2PO_2)_2.H_2O$, X-ray cryst. struct. determ. and refinement, heavy-atom method 79−19194
- $Mn^{II}(H_2PO_4)_2.2H_2O$, cryst. and powder diffr. data *(French)* 80−24419
- $MnHPO_4.3H_2O$ and $MnDPO_4.3D_2O$, IR absorpt. and Raman spectra, vibr. assignments 80−97257
- $Mn^{2+}Mo^{4+}O_3$, defect spinel struct., elec. and mag. props. 80−70176
- $Mn_2N_{0.86}$, cryst. and mag. struct. at low temps. *(French)* 77−73003
- $Mn_2N_{0.86}$, crystal struct. determ. by neutron and X-ray diffr. *(French)* 77−80461
- Mn_6N_5 film, cryst. struct. and phase transform. exam. by electron diffr. 78−10189
- $Mn(NO_3)_2.H_2O$, coordination polyhedra, bonding 77−58980
- $MnNa_6(So_4)_4$, vanthoffite cryst. struct. lattice parameters and thermal behaviour 77−19929
- $Mn_{0.26}NbS_2$, intercalation compound, struct. and photoemission meas. 77−16453
- MnO, X-ray determ. of electron density distribs., atomic scatt. factors 80−15078
- $Mn_8O_{10}Cl_3$, cryst. struct., X-ray diffr. meas. *(French)* 77−47381
- $Mn_8O_{10}Cl_3$, preparation and props. *(French)* 77−4086
- $Mn(OH)SO_4.2H_2O$, cryst. struct. determ. from X-ray data, least squares refinement 79−37675
- $Mn(PO_3)_3$, cryst. struct. determ. *(French)* 78−55843
- $MnSb_2S_4$, synthesis, electrophys. props. 77−51747
- $Mn_{15}Si_{26}$, X-ray and electron probe analysis 79−100043
- Mn_5SiB_2, cell dimensions 79−24502
- $MnSiN_2$, 180°C Neel temp., mag. struct. and atomic coords., neutron diffr. meas. *(French)* 77−32168
- $MnSnO_3$, ordered ilmenite phase, cryst. struct. 78−47288
- Mn_2SnS_4, cryst. struct. refinement and mag. struct. determ. *(French)* 80−107131
- $MnTa_2O_6$, columbite struct., X-ray diffr., IR and Raman spectra *(French)* 78−63727
- $MnThSe_3$, synthesis, cryst. characts. *(French)* 78−51517
- $MnTiNdO_5$, distrib. of Mn^{3+} and Ti^{4+} ions, Mossbauer spectrum 77−69747
- $Mn_3(VO_4)_2$, X-ray powder diffr. and IR spectra 78−10016
- $Mn_{12-x}W_xP_7$, solid solns., prep., cryst. struct. *(French)* 78−63723
- $Mn_{23}Y_6D_x$, D atom location, neutron diffr. study *(French)* 80−24426
- MnZn ferrites, cationic distrib. and Curie temp. *(Russian)* 79−91232
- $Mn_4[AsSi_3O_{12}(OH)]$, cryst. struct. determ. and refinement 80−1970
- Mo complex, [triply bridged binuclear Mo (V) cation]$[MoOCl_4(H_2O)]^-$, struct. 77−76371
- Mo complex, halogenoxomolybdenum (V), cryst. and electronic struct., reactivity 77−76369
- Mo complex, $MoOCl_3.2Ph_2SO$, prep. and characterisation 78−30592
- Mo complex, $Na[Mo_2O_5(O_3(OH)C_6H_8(OH)_2)].2H_2O$, struct. determ. and refinement 78−2073
- Mo complexes, μ-oxo, di-μ-oxo, di-μ-oxo-μ-carboxylato bridged oxodimolybdates (v), structures 77−76370
- Mo complexes derived from electron-rich olefins, cryst. chem. 77−76372
- Mo cpds, chemistry and uses, conf., Oxford, Eng., Sep (1976) 77−77749
- Mo nitrido complex, with multiple Mo-N bonds, prep., struct. and reactivity 77−83758
- Mo-Si, film deposition by reactive sputtering, characteris. *(Japanese)* 80−93485
- Mo-Y(La)(Ce)-B, X-ray diffr., reciprocal lattice, crystal struct., phase equilibria 77−21122
- α-MoB, crystallographic relationship with CrB, UBC, ThBC 79−42025
- $Mo_6Cl_{10}S$, struct., dielec. and diamag. props. *(French)* 78−67691
- $Mo_6Cl_{10}Se$, struct., dielec. and diamag. props. *(French)* 78−67691
- $Mo_6Cl_{10}Te$, struct., dielec. and diamag. props. *(French)* 78−67691
- $MoCr_2O_6$, hydrothermal cryst. growth, 40 kbar, 873K, cryst. struct. *(French)* 78−35342
- MoO_3, Raman scatt. and struct. props. 77−55780
- MoO_3, thin cryst. obs. by convergent beam electron diffr. 78−38670
- MoO_3 topotactic transform into MoO_2, electron microscopy, X-ray anal. 80−107417
- Mo_4O_{11}, anodic dissolution, periodic phenomena 77−16735
- $MoRh_2O_6$, crystn. and cryst. struct., paramag. and elec. cond. props. *(French)* 77−80480
- MoS_2 intercalation compounds, reaction with alkali and alkali earth metals, band struct., superconductivity 78−26541
- MoS_2, molybdenite crystal, direct imaging of atom configuration projected onto the basal plane 80−64847
- MoS_2 on Mo, cryst. struct. and thermal stability 77−52539
- MoS_2, poorly crystalline ‘rag’ struct. 80−6391
- Mo_6S_8 Chevrel phases with group IIIa metals, Nb, Hg, Pb and Cu, synthesis, stability and characts. 80−71608
- $Mo_6S_6Br_2$, X-ray cryst. struct. anal. *(French)* 80−33965
- $MoSi_2$, integrated intensities and lattice parameters, X-ray anal. 78−63733
- Mo_5TeO_{16} *(French)* 77−72586
- $Mo_{1-x}W_xSe_2$, cryst. struct. parameters and growth conditions 79−86759
- $MuCl_2.nH_2O$, cryst. struct. *(German)* 80−1987
- $N(CH_3)_4GeCl$, cryst. and powder diffr. data 80−24422
- ND_3, cryst. struct. between 2-180K, neutron powder profile refinement 79−73134
- $(ND_4)_2BeF_4$, incommensurate-commensurate phase transition and spontaneous polarisation 77−40192
- $(ND_4)_2D_3IO_6$, neutron diffr. study 80−88098
- ND_4DSeO_4, crystals, struct., IR spectra, dielec. props. 80−75919
- ND_4NO_3, cubic, mol. orientation determ. by multipole anal. 79−73136

crystal atomic structure of inorganic compounds continued

- NH_4AlCl_4, crystal struct., X-ray, Raman, IR and NMR 78−63720
- NH_4AlF_4, single cryst., prep. and struct. *(French)* 80−79762
- $NH_4Al(OH)_2CO_3$, NH_4-dawsonite, cryst. struct., X-ray powder diffr. *(Japanese)* 79−69096
- NH_4AsO_2, struct. characterisation, monoclinic cell, $P2_{1/c}$ space group *(French)* 78−22697
- $(NH_4)_3AsO_4.3H_2O$, cryst. struct. 78−18600
- NH_3BF_3 and d_3, polycryst., for IR spectra, lattice vibrs., cryst. and mol. struct. interpret. 80−2771
- $(NH_4)_2BeF_2$, paraelec. phase 78−95025
- $(NH_4)_2BeF_4$, ferroelectric, cryst. struct., phase transition, X-ray study 79−28689
- $(NH_4)_2BeF_4$, paraelec. phase, X-ray and neutron diffr. cryst. struct. anal. 80−84159
- $(NH_4)_2BeF_4$, X-ray cryst. struct. determ. 79−69072
- NH_4Br, NH_4^+ rot. motion, quasielastic neutron scatt. obs. 80−96492
- NH_4CdCl_3, X-ray cryst. struct. refinement by blocked least-squares method 79−1404
- $(NH_4)Cd[PO_3OH](OH)$, cryst. struct. of second modification 77−1115
- $(NH_4)Cd_6[P_2O_7]_2[P_3O_{10}]$, with mixed anion radical, cryst. struct. by X-ray anal. 79−86771
- $(NH_4)Cd\{PO_4].H_2O$, B phase, cryst. struct. refinement, X-ray diffr. meas. 78−2095
- NH_4ClO_4, polymorphous phase transition mechanism 80−79737
- NH_4ClO_4, X-ray data collection and estimation of intensities variations 79−60312
- $NH_4^+ClO_4^-$, X-ray cryst. struct. refinement with multipole deformation density functions 79−60313
- $(NH_4)_2Cr_3O_{10}$, hexagonal form, cryst. data *(French)* 80−24418
- $(NH_4)_2Cr_3O_{10}$, X-ray cryst. struct. determ. *(French)* 80−28974
- $(NH_4)_2Cr_4O_{13}$, cryst. data *(French)* 80−28980
- $(NH_4)_2(Cu(H_2O)_6)(CuSO_4)_4$, cryst. struct. determ. by X-ray diffr. 78−55839
- NH_4F, cryst. struct., mol. wavefunction calcs. of struct. factors 77−62507
- $(N_2H_6)_2F_2[TiF_6]$, X-ray cryst. struct. determ. 80−54182
- $NH_4F.H_2O_2$ crystals, X-ray structural study 80−44188
- $(NH_4)_4Fe(CN)_6.1.5H_2O$, cryst. struct., and possible ionic transport mechanism 79−14758
- α-$NH_4Fe(CrO_4)_2$ *(French)* 77−47398
- NH_4FeF_4, mag. and Mossbauer obs. *(French)* 78−19389
- $(NH_4)_2GaF_5.H_2O$, crystal struct., water coordination by Ga, valence angles, cell parameters 79−77584
- $(NH_4)_2GeP_4O_{13}$, cryst. struct. determ. *(French)* 77−51358
- $NH_4H_2AsO_4$, H positions, paraelectric phase 79−19210
- $(NH_4)_4H_6(As_6V_4O_{13}).4H_2O$, cryst. struct. determ. by X-ray diffr. *(French)* 79−69076
- $(NH_4)_2HCr_3AsO_{13}$, X-ray cryst. struct. determ., existence of a new anion $(Cr_3AsO_{13})^{3-}$ *(French)* 79−4295
- $(NH_4)_2HCr_3AsO_{13}$, prep. and cryst. struct. *(French)* 79−1415
- $(NH_4)_2H_3IO_6$, neutron diffr. study 80−88098
- $NH_4H_2PO_4$, Mn^{2+}, Mn^{3+} and MnO_4^- ions effect on cryst. habit 77−58992
- $(NH_4)_3H(SO_4)_2$, room temp. phase 78−42965
- NH_4HSeO_4, cryst. struct., dielec. and ferroelec. props. 80−60528
- NH_4HSeO_4, ferroelec. props. rel. to struct. 80−71345
- $NH_4H_3(SeO_3)_2$, X-ray crystal struct. refinement at −150°C 77−4090
- $(NH_4)_6H_6W_{12}O_{42}.10H_2O$, X-ray cryst. struct. determ. *(French)* 79−77560
- $NH_4IO_3.2HIO_3$, dielec. constant, elec. cond. phase transition and cryst. struct. 80−1999
- $(NH_4)_3In(SO_4)_3$, low temp. form, cryst. and powder diffr. data *(French)* 80−28981
- $NH_4In(SO_4)_2.4H_2O$, cryst. struct. 79−19231
- $NH_4In(SO_4)_2.4H_2O$, H-bond system, X-ray diffr. obs. 80−6395
- $(NH_4)_2Mg(CO_3)_2.4H_2O$, cryst. and powder diffr. data 80−24420
- $(NH_4)_2Mg(S_2O_3)_2.6H_2O$, isolation, struct., decomposition *(French)* 78−52506
- NH_4MnCl_3, X-ray single crystal analysis, phase transitions, Mossbauer effect 79−19366
- $(NH_4)_4Mo_8O_{26}.4H_2O$, Lindqvist octamolybdate, cryst. and mol. struct. 77−76373
- $(NH_4)_4Mo_8O_{26}.4H_2O$, X-ray cryst. struct., Fourier and Patterson synthesis *(French)* 79−42032
- $(NH_4)_2MoS_4$, cryst. struct. refinement, X-ray diffr. meas. *(French)* 77−4076
- NH_4N_3, cryst. struct. determ. by neutron diffr. 78−79574
- NH_4NO_3, phase II, cryst. struct., neutron diffr. study, profile refinement method 79−60314
- NH_4NO_3, phase III, cryst. struct., neutron powder diffractometer study 80−107134
- $(NH_4)Na_2Cd(P_2O_7)_2Cl$, crystal struct. determ. 77−84732
- $(NH_4)_2Ni(BeF_4)_2.6H_2O$, X-ray cryst. struct. determ. 80−107137
- $(NH_4)_2Ni(CrO_4)_2.6H_2O$, X-ray single cryst. struct. determ. 79−19207
- $(NH_4)_{0.8}Ni_{1.1}PO_4.xH_2O$, ion exchange props., Cs^+ ion sorpt., struct., IR spectra 77−9121
- $(NH_4)_2Ni(SeO_4)_2.6H_2O$, X-ray cryst. struct. determ. 80−39027
- $NH_4P_3Be_2O_{10}$, cryst. struct., X-ray diffr. *(French)* 77−19920
- $(NH_4)_3PCr_4O_{16}$, cryst. struct., $(PCr_4O_{16})^{3-}$ anion geometry 80−107157
- $(NH_4)_2PO_3F$, H_2O, X-ray diffraction and Raman spectra struct. determ., external mode temp. depend. *(French)* 78−52507
- $(NH_4)_2PO_3F.H_2O$, cryst. struct. comparison with $(NH_4)_2SO_3.H_2O$ *(French)* 77−47404
- $(NHPO_2H)_4.2H_2O$, cryst. struct. determ. 77−24300
- $NH_4Pb_2Cl_5$, cryst. struct., X-ray diffr. 77−19923
- $NH_4PbI_3.2H_2O$, X-ray cryst. struct. determ. 80−64958
- $(NH_4)_2PtF_6$, X-ray cryst. struct. determ. 80−107125
- $(NH_4)_2PtI_5$, synthesis and cryst. struct. *(German)* 78−79588
- $(NH_4)_2ReCl_6$, neutron diffr. study of cryst. struct. 79−55701
- NH_4ReO_4, cryst. struct. at 295 and 135K 78−26521
- NH_4SCN, charge distrib., deform. density, cryst. struct. determ. by X-ray and neutron diffr. 77−47415
- NH_4SCN, polymorphous structural-kinetic transformations, phase orientational relation 79−90590
- $(NH_4)_2SO_4$-K_2SO_4 mixed crystal, cryst. struct., X-ray diffr. meas. 77−80484
- $(NH_4)_2S_2O_3$, cryst. and X-ray powder data 79−51074
- $(NH_4)_2S_2O_3$, X-ray crystal and powder diffr. data 79−14766
- $(NH_4)_2S_2O_3$, X-ray cryst. struct. determ. 79−77562
- $(NH_4)_2SO_3.H_2O$ S^{IV} lone pair, stereochem. role *(French)* 77−47404

crystal atomic structure of inorganic compounds continued
$(NH_4)_3Sc(SeO_4)_3$, cryst. struct. determ. 78-26524
$(NH_4)_3Sc(SeO_4)_3$, cryst. struct. 79-99122
$(NH_4)_2SeO_4$, X-ray obs. 77-24299
$(NH_4)_2Se_2O_5$, X-ray cryst. struct. determ. 80-54189
$(NH_4)_2SeO_4.2NH_4HSeO_4$ 78-71715
$(NH_4)_2SiP_4O_{13}$, cryst. struct. determ. *(French)* 77-4070
NH_4SnF_3 *(German)* 78-34480
$(NH_4)_2TcCl_6$, X-ray single cryst. struct. determ. 79-19197
$NH_4TeO_3(OH)$, cryst. struct., Patterson and Fourier synthesis *(French)* 80-33942
$(NH_4)_2TeO_2(OH)_4$, X-ray cryst. struct. anal. 79-77563
$(NH_4)_2Te_3O_8(OH)_4$, synthesis and crystallochem. study *(French)* 80-1990
$(NH_4)_2Te_2O_5.2H_2O$, crystal structure determination 78-91317
$NH_4Tl(SeO_4)_2$, $(NH_4)_3Tl(SeO_4)_3$, and $(NH_4)_5Tl(SeO_4)_4$, cryst. struct. *(French)* 80-84148
$(NH_4)_2(UO_2)_4O_2(OH)_2Cl_4(H_2O)_6$, cryst. data 77-76366
NH_4VO_3, X-ray determ. 78-6043
$(NH_4)_4[Bi_2Br_{10}].4H_2O$ 77-58988
$NH_4[TcO_4]$, X-ray cryst. struct. determ. 80-39016
$NH_4[Te^{IV}Te^{VI}O_5(OH)]$, 5 coordination of Te^{IV} atom by O atoms, cryst. struct. *(French)* 79-99130
$(NH_4)_2[VF_4O]$, X-ray cryst. struct. determ. 80-107128
$(NH_4)_2[ZnCl_4]$, X-ray cryst. struct. determ. 80-107138
NO_3^-, geometry in crystals *(French)* 79-65045
$(Na,Ca)_2Zr[Si_6O_{15}].3H_2O$, Mongolian elpidite, cryst. struct. 78-95038
$(Na,K)NbO_3$ solid solns., struct. transitions, neutron powder diffr. 78-38649
$(Na,K)(V,P)O_3$ system, cation substitutions, crystallographic studies 78-79581
Na orthophosphates and sulphates, anhydrous, struct. relationships w.r.t. fast ion cond. 80-107188
Na polysilicates, IR spectra, struct., crystallisation effects *(Russian)* 78-72528
Na triple orthoarsenates, $NaM^{II}Cr_2(AsO_4)_3$, prep. by high temp. synthesis, and cryst. struct. 79-66028
Na-Co strip-chain silicates, structural-composition inhomogeneities 80-88122
Na-Co-O system, synthesis and cryst. struct. determ. 80-107185
Na-graphite intercalates, preparation, struct. 80-103307
NaA zeolite, dielectric polaris., cation distrib. *(French)* 79-51903
$NaAl(CO_3)(OH)_2$, cryst. struct., IR spectral investig. 77-8567
$NaAlCl_4$, cryst. struct., charge distrib., X-ray, NMR and NQR meas. 77-11528
$NaAlCl_4$, crystal struct. refinement 79-73145
$NaAlCl_4$, Raman spectra, cryst. struct. *(French)* 80-60578
$NaAl(CrO_4)_2.2H_2O$, cryst. struct. *(French)* 77-80478
$Na_8Al_6Ge_6O_{24}(CO_3).3H_2O$, water molecule dynamics and hydrogen bonds, PMR spectra 79-90577
$Na_8Al_6Ge_6O_{24}(CO_3).3H_2O$, PMR anal. H_2O molecule orientation determ. 79-90631
$Na_8Al_6Ge_6O_{24}.CO_3.2H_2$, cryst. struct. 78-83805
$NaAlH_4$, X-ray cryst. struct. determ. 79-69081
$NaAl_{11}O_{17}$, β-alumina, local electroneutrality 79-65054
$Na_{0.91}Al_2(Si_{3.09}Al_{0.91})O_{10}(OH)_2$, paragonite 1M, cryst. struct. determ., electron diffr. 78-26547
$NaAlSiO_4$ (nepheline), high-press. to transform. to first silicate Ca ferrite isotype 77-64270
$NaAlSi_3O_8$, cryst., Al-Si order-disorder, electroneutrality effects in model 79-90593
$NaAlSi_2O_6.H_2O$, synthetic analcite, optical and crystallographic props. *(French)* 77-43183
$Na_3Al_3Si_3O_{12}.2H_2O$, cryst. struct. determ. 79-90625
$NaAsS_2$, infinite chains 77-35523
Na_3AsS_3 *(French)* 77-15347
$NaB_5O_6(OH)_4$, cryst. struct. determ. 78-26511
$Na_3B_5O_8(OH)_2.H_2O$, synthetic, cryst. struct. 78-18591
$Na_2B_4O_5(OH)_4.8H_2O$, borax, neutron diffr. cryst. struct. determ. 79-14740
$Na_2BeGe_2O_6$, crystal struct. by X-ray diffr. 77-1113
Na_2BeSiO_4, crystal struct. rel. to Na_2ZnSiO_4 77-1114
$Na_2Be[SiO_4]$, X-ray cryst. struct. determ., thermal vibration anisotropy allowance 80-92510
$Na_{0.5}Bi_{4.5}Nb_2WO_{15}$, cryst. struct. and dielec. const. 77-47428
$NaBrO_3$, optically active, remeas. 78-10009
$NaBr.2H_2O$, single cryst. struct. anal. by neutron diffr. 79-77561
$NaCN.2H_2O$, cryst. struct. determ. 78-75635
$NaCN.2H_2O$, electron density, 150K, X-ray crystallography expts. 77-24295
Na_2CO_3, disordered struct., 400°C neutron and X-ray powder diagrams 79-46625
$Na_2C_2O_4\ (SbF_3)_2$, growth from soln. and X-ray diffr. study *(French)* 77-80481
$Na_2CO_3.1^1/_2H_2O_2$, cryst. struct. 78-18588
$Na_2CO_3.1.5D_2O_2$, neutron profile refinement and deuterium positions 79-90602
$Na_2CO.2CaCO_3$, shortite, cryst. struct. and space group, pyroelec. effect 79-23573
$Na_{0.5}Ca_{0.5}Al_{1.5}Si_{2.5}O_8$, labradorite feldspars, lattice parameter determ. of exosolution structs. 77-84704
$Na_{7.5}Ca_{0.5}(AlSiO_4)CO_3.2H_2O$, cancrinite, proton-containing groups, PMR meas. 78-2094
$Na_6Ca_4(BeF_4)_6F_2$, cryst. struct. by X-ray diffr., cation distrib. *(German)* 78-43001
$NaCa_2Cu_2V_3O_{12}$, crystal struct. distortion due to cooperative Jahn-Teller effect *(Russian)* 77-1119
$NaCa(NH_2)_3$, cryst. struct. and cryst. chemistry *(German)* 79-51080
$Na_x(Ca_{3-x}Na_x)Al_2O_6$ series, powder diffr. data 79-94975
$Na_4Ca(SO_4)_3$, cryst. data and IR spectra 78-42986
$(Na_xCa_y)_2SO_4$, cryst. struct., form. 77-19928
$NaCa_2Si_4O_{10}F$, agrellite, new type of silicate double chain 78-51514
$Na_8Ca_3SiO_{1.5}[Si_2O_7][PO_4]_3$, synthesis conditions, cryst. struct. and IR spectra characts. 80-108335
$(Na_{1-x}Cd_x)Cd_2(PO_4)(PO_{3+x}(OH)_{1-x})$, cryst. struct. determ. 79-23589
$(Na_{1-x}Cd_x)Cd_2[PO_4][PO_{3+x}(OH)_{1-x}]$, cryst. struct. determ. 77-15387
$Na_2Cd_3Si_3O_{10}$, X-ray obs. 78-83801
$Na_4Cd_2[Si_3O_{10}]$, cryst. struct. determ. 79-14778
$Na_2Ce_2TiO_2[SiO_4](CO_3)_2$, tundrite, new crystal. struct. and formula 77-31648
NaCl dimer, electron diffr. study of mol. struct. 80-28951

crystal atomic structure of inorganic compounds continued
NaCl, powder diffr. using synchrotron radiation, energy-dispersive technique 77-24245
NaCl, struct. refinement at 32 kbar, using single-crystal diamond cell 78-67610
NaCl structure, evaluation of finite strain eqns. of state using lattice models 80-96620
NaCl, valence-electron charge density along nearest-neighbour axis 79-27944
$NaClO_3$, optically active, remeas. 78-10009
$NaClO_3$, X-ray diffr. determ. of ClO_3^- ion dimensions and libration correction 77-80462
$NaClO_4.H_2O$, cryst. struct. deform. refinement 80-107123
Na_2CoCl_4, cryst., chrysoberyl struct., neutron diffr. 77-19919
Na_2CoGeO_4, cryst. struct. determ. 79-90626
$Na_xCr(Mn)(Co)O_2$, layer struct., elec. cond. behaviour *(French)* 78-26542
$NaCrO_2$, two-dimens. mag. props. rel. to cryst. struct. 80-75776
$Na_3Cr_2(PO_4)_3$, crystallographic data, ionic conductivity *(French)* 80-88077
$Na_3Cr_2(PO_4)_3$, $Na_3Fe_2(PO_4)_3$, $Na_3Ti_2(PO_4)_3$ and $Na_3V_2(PO_4)_3$, synthesis and cryst. struct. *(French)* 79-32964
$Na_3Cr_3(PO_4)_4$, crystallographic data, ionic conductivity *(French)* 80-88077
$NaD_2AsO_4.D_2O$, crystal struct. determ. 77-80460
$Na_{0.6}(D_2O)_2VX_2$, X=S,Se, struct., chem. reactions, and hydration/dehydration process 79-46616
$NaEr(SO_4)_2$, cryst. struct. by X-ray diffr. *(French)* 78-42990
$Na_2Eu_3(NH_2)_8$, cryst. struct. and cryst. chemistry *(German)* 79-51080
NaF, X-ray diffr., electron distrib. determ. 77-84706
NaF, X-ray intensity, extinction wavelength depend. 79-27956
$Na_2(Fe,Mn)_5(PO_4)_4$, arrojadite, X-ray cryst. struct. determ. 80-39058
$NaFeF_2$, Mossbauer and low-temp. dilatometry study *(French)* 80-80662
β-$NaFe_2O_3$, struct. of single cryst. *(French)* 78-6033
α-$NaFe_2O_3$:$Mg^{2+}(Co^{2+})(Zn^{2+})$, substitution of Fe^{2+} *(French)* 78-95034
$Na_2Fe_3(PO_4)_3$, synthetic alluaudite 78-83802
$Na_3Fe_2(PO_4)_3$, crystallographic data, ionic conductivity *(French)* 80-88077
$Na_3Fe_2(PO_4)_3$, polymorphism and ionic conduction *(French)* 78-67678
$NaFeS_2$, cryst. struct. by X-ray diffr., isolated from colloid 79-43635
$Na_{0.56}Fe_{0.28}Ti_{1.72}O_4$, non stoichiometric, X-ray cryst. diffr. determ., heavy atom method 79-4293
$Na_2Fe_2Ti_6O_6$, freudenbergite, cryst. struct. determ. 78-26519
$Na_{0.70}Ga_{4.72}Ti_{0.29}O_8$, one-dimens. Na^+ ion cond., cryst. struct. and cond. meas. 80-107521
$NaGdSiO_4$, single cryst. data and ionic cond. 80-84158
$Na_5GdSi_4O_{12}$, ionic conductivity and struct. 78-18826
Na_2GeO_3 78-51489
$NaHAs_2O_6$, cryst. struct., and new type of bidimensional infinite anion $(As_2O_6)_n^{2n-}$ *(French)* 79-14757
$NaHCd_4(Ge_5O_{15})$, cryst. struct., comparison with natural rhodonite 78-30600
$NaHCd_2(Si_3O_9)$, synthetic cryst., refined struct. 79-86763
$Na_5HMo_5P_2O_{23}(H_2O)_{11}$, mol. and cryst. struct., X-ray diffr. anal. 79-32951
$Na(H_3O)(I(OH)_3O_3)$, pyroelec., cryst. struct. at room temp. 79-10835
β-$Na_2HPO_4.12H_2O$, dosorder of HPO_4^{2-} and H bonds 78-34471
$Na_2HPO_4.2H_2O$, crystal struct., coordination and H bond competition 78-14315
$NaH_2PO_2.4/5H_2O$, X-ray cryst. struct. determ., pseudo-symmetry and H_2 bonding 79-60315
α-$NaHSO_4$, cryst. struct. and hydrogen bonding 79-99128
$NaHSO_4$, struct. of new modification 78-34477
$Na_3H(SO_4)_2$, cryst. struct. refinement, short asymmetrical H bond, S-OH vs. O-H...O correlation 79-37663
$NaHSeO_3$, and $NaDSeO_3$, NMR of ^{23}Na and ^2D, hydrogen bonding 80-44190
$NaH_3(SeO_3)_2$, paraelec., neutron diffr. refinement of struct. 77-72584
$NaIO_3$, crystal struct. determ., anisotropic thermal vibr. parameters 80-88123
$NaInO_2$, prep., props. and struct. 80-35517
$NaInS_2$, prep., props. and struct. 80-35517
$Na_3In(SO_4)_3.3H_2O$, cryst. struct. by X-ray methods 80-6393
$NaIn(SeO_4)_2.6H_2O$, cryst. struct. by X-ray diffr., symm. 78-43004
$NaIn(SeO_4)_2.6H_2O$, X-ray cryst. struct. determ., H bond system 80-92511
$NaK_3(MO_4)_2$, (M=Mo, Se, W), cryst. struct., form. 77-19928
$NaKMg_3M_2Si_{12}O_{30}$ (M=Cu, Mg), cryst. struct., X-ray diffr. and IR spectra *(French)* 80-107158
$Na_{0.5}K_{3.5}(Te_2O_6(OH)_4).6H_2O$, cryst. struct. determ. 78-26520
$(Na_xKy)_2CO_3$, non-stoichiometric, cryst. struct. *(French)* 80-79761
$NaLO_3$, disorder of NO_3^- ions, rel. to Raman spectrum temp. depend. *(Russian)* 78-2099
$Na_3La(AsO_4)_2$, allotropes, prep. and cryst. struct. *(French)* 78-63724
$Na_2LaGeO_4(OH)$, cryst. struct. and refinement 77-65970
$Na_{5-x}Li_xErSi_4O_{12}$, solid electrolytes for Na/TiS_2 cells, synthesis, characts. and utilisation 80-107518
$Na_{2-x}Li_xSiO_3$, long-period superstructure 77-55269
$NaLiZrSi_6O_{15}$, zektzerite, silicate mineral with six-tetrahedral-repeat double chains 78-63719
$Na_5LuSi_4O_{12}$, cryst. struct. 79-32979
$Na_3M_2^{3+}Li_3F_{12}$ garnets, M=Al,Cr,Fe, synthesis from aq. soln., props. 77-44184
$NaMgF_3$, orthorhombic perovskite, contribution to crystal chem. 80-19777
$Na_3Mg_4LiSi_{12}O_{30}$, cryst. struct., X-ray diffr. and IR spectra *(French)* 80-107158
$Na_2Mg_3M_2Si_{12}O_{30}$ (M=Cu, Fe, Zn, Mg), cryst. struct., X-ray diffr. and IR spectra *(French)* 80-107158
$Na_3Mg_2P_5O_{16}$, cryst. and X-ray powder data 79-51072
$Na_3Mg_2P_5O_{16}$, new type of phosphate radical P_5O_{16} 79-94978
$Na_4Mg_2Si_3O_{10}$, powder diffr. cryst. data 80-19765
$NaMnCrF_6$ *(French)* 77-47402
Na_2MnFeF_7, trigonal weberite variant, X-ray and neutron diffr. *(German)* 78-51508
$Na_2Mn(SiO_3)_2$, X-ray diffr. anal. of cryst. struct. 77-35538
$Na_6Mn(Ti[Si_6O_{18}])$, Kazakovite, cryst. struct. determ. 80-19782
$Na_4Mo_{12}GeO_{40}(H_2O)_8$, X-ray diffr. cryst. struct. exam. 78-2075
Na_2MoO_4-Na_2SO_4, phase diag. and isomorphism 78-27486

crystal atomic structure of inorganic compounds continued

$Na_6Mo_5P_2O_{23}(H_2O)_{14}$, X-ray diffr. cryst. struct. determ., refinement 78–2074
$Na_6Mo_6V_2O_{26}(H_2O)_{16}$, X-ray cryst. struct. determ. 79–99132
NaN_3, electron density distrib., X-ray diffr. data 77–84705
$NaNH_4SeO_4.2H_2O$, crystal struct. in ferroelec. phase, nature of transition 77–43946
$NaNH_4SeO_4.2H_2O$, atomic struct. exam. and phase transition 79–37678
$NaNH_4SeO_4.2H_2O$, neutron-diffr. investigation 79–46638
$NaNO_2$, antiferroelec. phase, struct. anal. by neutron diffraction 80–24410
$NaNO_2$, ferroelec., electron distrib., X-ray and neutron diffraction study 80–24411
$NaNO_2$, ferroelec. thin crysts., struct. investig. 79–27962
$NaNO_3$, electron density distrib. *(German)* 80–92481
$Na_3Nd(AsO_4)_2$, allotropes, prep. and cryst. struct. *(French)* 78–63724
$Na_3Nd(PO_4)_2$, laser mat., cryst. struct. 78–79582
$NaNd(SO_4)_2$, cryst. struct. by X-ray diffr. *(French)* 78–42990
$NaNdSi_6O_{14}$, cryst. struct., X-ray diffr. meas. 77–15385
$NaNdSi_6O_{13}(OH)_2.nH_2O$, cryst. struct. determ. 78–63738
NaNdX, zeolite hydrated, ion exchange of Na for Nd, cryst. structs. 80–33979
$NaNiF_3$, X-ray diffr., perovskite type struct. 77–76362
Na_2NiFeF_7, weberite struct. refinement *(German)* 78–47294
Na_5NiO_4, crystallographic data *(German)* 78–63736
$Na_4NpO_2(O_2)_3.9H_2O$, structure and bonding study 77–27868
Na_2O-Al_2O_3-$SiO_2.xH_2O$, fibrous crystal growth in silica gel, X-ray, electron probe and IR spectra obs. 80–25541
Na_2O-Ga_2O_3 system, new superionic conductor *(French)* 78–14504
Na_2O-M_2O_3-TiO_2, (where M=Al, Cr, Fe or Mn) ternary systems, X-ray anal. 79–51067
Na_2O-MgO-Al_2O_3, β''''-alumina, high-resolution electron microscopy 80–75208
Na_2O-SiO_2-H_2O-FeO system, 'heavy phase', recrystallisation and struct. 78–2089
$Na_3PCr_3O_{13}.3H_2O$, cryst. struct. 80–107154
$NaPO_3$, Graham's, Kurrol's and Maddrell's salts, cryst. struct. and crystallinity 79–55721
$NaPO_3$-$NaAsO_3$ system solid solutions, four-mode type IR spectra 79–51942
Na_3PO_4, high temp. fast ion cond. phases, neutron diffr. obs. of struct. 80–107512
$Na_6Pb_4(BeF_4)_6F_2$, cryst. struct. by X-ray diffr., cation distrib. *(German)* 78–43001
$Na_2Pb_{11}F_{18}Br_6$, cryst. struct. determ., X-ray study 79–60320
$Na_3Pr(AsO_4)_2$, allotropes, prep. and cryst. struct. *(French)* 78–63724
$NaPrSi_6O_{14}$, cryst. struct., X-ray diffr. meas. 77–15385
$Na_2PrSiO_4(OH)$, cryst. struct. 77–65970
$Na_2Pt(CN)_4Br_2.2H_2O$, neutron diffr. determ. 77–24296
$NaRSi_6O_{14}$, R=La, Ce, Pr, Nd, new crystal-chemical group of rare-earth silicates 77–7703
$Na_5RSi_4O_{12}$ (R=Sm to Lu, Y, Sc), solid electrolytes, struct. characts. 80–1997
NaSCN, cryst. struct. and electron density determ., X-ray and neutron diffr. meas. 77–47414
$Na_2SO_4.10H_2O$, Glauber's salt, neutron diffr. cryst. struct. determ. 79–14740
$Na_2S_2O_6.2D_2O$, bonding in $[S_2O_6]^{2-}$, X-ray diffr. refinement and pictorial representation 80–54177
$Na_2S_2O_6.2D_2O$, X-ray diffr. cryst. struct. redeterm. 80–39014
$Na_2S_2O_6.2H_2O$ 78–42969
$Na_2S_2O_6.2H_2O$, bonding in $[S_2O_6]^{2-}$, X-ray diffr. refinement and pictorial representation 80–54177
$Na_2S_2O_6.2H_2O$, X-ray diffr. cryst. struct. redeterm. 80–39014
$4Na_2SO_4.2H_2O_2.NaCl$, cryst. struct. determ. 78–55841
$Na_2S_2O_3.5H_2O$ 77–47400
$Na_2S_2O_3.5H_2O$, cryst. struct. determ. by neutron diffr. 78–63714
$NaSbBrF_3.H_2O$, cryst. struct. *(French)* 78–18589
$NaSbClF_3.H_2O$, cryst. and mol. struct. *(French)* 77–43200
$Na_2Sb_4O_7$, cryst. struct., X-ray diffr. meas. *(French)* 77–47386
α-$NaSbS_2$, cryst. struct. and $\beta\rightarrow\alpha$ phase transform. features 80–33961
$Na_3SbS_4.9D_2O$, Schlippe's salt, H bonds and cryst. struct. refinement, by neutron diffr. 79–19191
$Na_3SbS_4.9H_2O$, Schlippe's salt, H bonds and cryst. struct. refinement, by X-ray diffr. 79–19191
$Na_3Sc_2(PO_4)_3$, X-ray cryst. struct. determ. 79–60341
$Na_3Sc_2P_3O_{12}$, superionic cond. synthesis, cryst. struct. and ionic cond. 80–107519
$NaScS_2$, crystal struct. determ. by X-ray powder diffr. 80–49205
Na_2SeO_4, cryst. struct., form. 77–19928
α-$Na_2Si_2O_5$, laminated cryst., IR spectra, dispersion anal. 77–1675
$Na_2Sr_3(NH_2)_8$, cryst. struct. and cryst. chemistry *(German)* 79–51080
$NaTaO_3$, high temp. structs. neutron powder diffr., comparison with $SrZrO_3$ and $NaNbO_3$ 80–88094
$NaTaO_3$, struct., X-ray powder diffr. 77–19912
$Na_{1+\alpha}(Ta_{1+\alpha}W_{1-\alpha})0_6$, synthesis by cation exchange, stability and struct. *(French)* 77–1110
Na_2TeO_3, chem. prep. and cryst. struct. *(French)* 80–79755
Na_2TeO_4, 3-dimens. X-ray struct. anal., Te(VI) and cation coord. *(French)* 78–18610
Na_2TeO_4, X-ray cryst. struct. determ. 77–80455
$Na_2Te^{IV}O_3.5H_2O$, crystallographic study *(French)* 79–69069
$Na_{0.9}Ti_{1.1}Fe_{0.9}O_4$, short period β-alumina type cpds., cryst. struct. and superionic cond. 80–107499
$Na_{16}Ti_{10}O_{28}$ structure determ. *(French)* 77–1108
$Na_2Ti_9O_{19}$, cryst. struct. anal. by 1 MV high-resolution electron microscopy 79–73137
$Na_2Ti_9O_{19}$, cryst. struct. 79–77573
$Na_2Ti_9O_{19}$, orthorhombic, unit-cell twinning of monoclinic $Na_2Ti_9O_{19}$, cryst. struct. 80–107155
$Na_xTi_4O_8$ bronze, hydrothermal prep., Na ion arrangement 80–75209
$Na(TiO)[SiO_4]$, revised cryst. struct. 79–32978
$(Na_2Ti_6O_{13})_n.(BaTi_4O_9)_m$, tunnel struct. intergrowth, electron, microscopy investigations 80–100218
Na_xTiS_2, alkali ion ordering, X-ray study 80–107165
Na_xTiS_2, electrochemically intercalated, ion ordering, X-ray diffr. meas. 80–44177
Na_xTiSe_2, intercalation cpds. *(French)* 77–35536
Na_2TiSiO_5 78–42976
$Na_2Ti_2Si_2O_9.Na_3PO_4$, lomonosovite, cryst. struct. determ. 78–51520
$Na_2TiZn_2(SiO_4)O_3$, cryst. struct. determ. 77–11522

crystal atomic structure of inorganic compounds continued

$Na_2TiZn_2[GeO_4]O_3$, cryst. struct. determ. 78–63734
δ-Na_2UF_6, X-ray single cryst. struct. determ. 79–55704
$Na_3UO_2F_5$, IR and Raman spectra, struct. *(French)* 79–11409
$Na_4UO_2(O_2)_3.9H_2O$, structure and bonding study 77–27868
$NaVO_3$, X-ray determ. 78–6043
$Na_6V_{10}O_{28}.18H_2O$, X-ray cryst. struct. determ. *(French)* 80–54191
$Na_xVS_2(Se_2)$, intercalation compounds, phys. props. 80–44179
Na_xVSe_2, synthesis and struct. determ. 78–26537
Na_xWO_3, $0.22<x<0.84$, low temp. struct., press. effects, NMR study 80–59443
$Na_6W_7O_{24}.14H_2O$, molecular struct. X-ray determ. 79–82188
NaX zeolite, hydrated, cryst. struct. at t=20 and −165°C 80–33978
$Na_6YSc[SiO_7]_2$, crystal struct., atom coordinates, X-ray study 80–59446
$NaYSiO_4$, crystal structure refinement, X-ray anal. 80–79764
$NaYSiO_4$, $Na_3YSi_2O_7$, $Na_3YSi_3O_9$ and $Na_5YSi_4O_{12}$, single cryst. data and ionic cond. 80–84158
$Na_{3(1+x)}Yb_{(2-x)}(PO_4)_3$, single cryst. preparation and X-ray cryst. struct. determ. 79–42028
$NaZn_{13}$, stella quadrangula as struct. building unit 80–15055
$NaZnCl_4$, cryst., chrysoberyl struct., neutron diffr. 77–19919
$Na_{2-x}Zn_xFe_3(PO_4)_2(OH)_{2-x}O_x$, x=0.1, X-ray struct. anal. 77–84733
$(Na_xZn_y)_2SO_4$, cryst. struct., form. 77–19928
Na_2ZnSiO_4, crystal struct. rel. to Na_2BeSiO_4 77–1114
$Na_2ZnSi_2O_8$ 77–47396
$Na_2Zn_2Si_2O_7$, cryst. struct. refinement 78–87652
$Na_2Zn_3(SiO_4)_2$, cryst. struct. anal. 79–19222
$Na_3ZnTh_6F_{29}$, X-ray cryst. struct. determ. *(French)* 80–19761
$Na_2Zn[Si_3O_8]$ crystal, phase A, refined cryst. struct. 79–19220
$Na_4Zr_2Ge_3O_{12}$, cryst. struct., X-ray diffr. 79–19224
$Na_2Zr(MoO_4)_3$, synthesis and cryst. struct. 80–39059
$Na_4Zr(MoO_4)_4$, synthesis and cryst. struct. 80–39059
$Na_4Zr_2Si_3O_{12}$, struct. analysis at 300 and 600°C, rel. to ionic cond. 80–107189
$Na_3Zr_2Si_2PO_{12}$, NASICON, phase transition, X-ray diffr., ionic cond. and sp. ht. meas. 80–19979
$NaZr[Si_2O_6OH]$, keldyshite, X-ray structural anal. 79–14779
$Na_2[B_4O_6(OH)_2]$ 78–51479
$Na_8[B_{12}O_{20}(OH)_4]$, X-ray cryst. struct. determ. and refinement 80–19753
$Na_2[B_2(O_2)_2(OH)_4].6H_2O$, X-ray cryst. struct. refinement 79–14749
$Na_2[Pt(CN_4)].3H_2O$, neutron diffr. 77–58990
$Na_8[Si_6Al_6O_{24}](OH)_2.1{:}7H_2O$, hydrosodalite, cryst. struct. by neutron diffr. 78–95039
$Na_6[Ti(Ti_{0.9}Nb_{0.1})_4(Si_6O_{17})_2(O,OH)_5].11H_2O$, zorite, X-ray cryst. struct. determ. 80–92513
$Na_3[V(NCS)_6].12H_2O$, single crysts., X-ray diffr. cryst. struct. anal. 78–95021
$Na_2[ZnSi_3O_8]$, synthetic 77–65968
(Nb,Ta)As, X-ray cryst. struct. determ. 79–69078
$(Nb,Ta)_8N_9$, cryst. struct. determ. *(German)* 80–107145
Nb chalcogenides and chalcogenide halides, geometrical struct. and metal-metal bonding 80–80172
Nb complex, $NH_4[NbO(C_2O_4)_2(H_2O)_2].3H_2O$, neutron diffr. obs. 77–24306
Nb complex, $NbOCl_3.2L$ (L=Ph_2SO, Ph_3PO and $(Me_2N)_3PO$), prep. and characterisation 78–30592
Nb-H system, NMR evidence for low temp. pseudo-cubic phase 78–80526
Nb-Ta family minerals, cryst. struct., X-ray powder diffr. study 80–107169
NbC coating on C steel and Armco Fe, deposition, struct. and props. 79–52462
NbC_x, static distortions and Debye temp. determ., neutron diffr. exam. *(Russian)* 77–80482
$Nb_xC_yO_z$, H solubility 80–34191
$Nb_xCr_{1-x}O_2$, cryst. prep. and struct., mag. props. 78–52198
$NbD_{0.04}$, neutron scatt. exam., press. depend. of superstruct. reflection 78–22696
$NbGa_2O_x$, O stabilised cpd., struct. determ. 80–103301
NbH_x, structural transform. rel. to order-disorder transform. 80–60858
NbH(D), structs. phase diagrams, morphologies, prep. methods, book contrib. 80–25675
NbO and NbO_2, H solubility 80–34191
$4NbO_{0.76}$ thin film, FCC cell struct. investigation 80–92796
$Nb_{10}O_{28}{}^{6-}$, mol. config. from cryst. structs. 77–71886
$Nb_{12}O_{29}$, high resolution lattice image, by HV electron microscope 77–15292
Nb_2O_5-TiO_2, splat cooled, crystallization and ordering 77–68953
Nb_2O_5-WO_3 system, TEM study of intergrowth of ReO_3 and tetragonal-type structs. 79–7580
Nb_2O_5-WO_3 system complex cpds. with TTB type subcells, HV superhigh resolution electron microscopy obs. of struct. 80–103311
$NbOAsO_4$ and $NbOAsO_4$ $4H_2O$, crystal growth, composition, struct. and crystallographic characts. 80–54198
$NbOI_2$, X-ray obs. 79–14770
$Nb(OR)_2Cl_3.L$, halo-alkoxide complex, prep. and props. 78–18605
$4Nb_2O_5.9WO_3$, cryst. struct. determ. by 1 MV TEM 79–7581
Nb_5Pt_3O, R phase of Nb-Pt‖O system, cryst. struct. 80–96495
NbS_2, high pressure polymorphs 78–51459
NbS_2 intercalate with tetraalkylammonium hydroxide, prep. and struct. 80–79752
NbS_2-$(pyridine)_{1/2}$ intercalation complex, superlattice struct., NMR meas. 80–70180
NbS_3, cryst. struct., X-ray diffr. obs. 79–1412
$NbS_2Cl_2(Br_2)(I_2)$, prep., struct. and props. 80–28994
$NbS(Se)_2$, polymorphism at high press. and temps., T_c and band struct. 78–26528
$NbS_3(Se_3)$, phase transitions and elec. props. 80–20178
$NbSbS_3$, synthesis and single cryst. growth and struct. 77–52234
$NbSc_5HfO_{12}$, cryst. struct. determ., powder X-ray diffr. exam. 77–4083
$Nb_{1.5}Sc_{5.5}O_{12}$, cryst. struct. determ., powder X-ray diffr. exam. 77–4083
$NbSc_6O_{11}F$, cryst. struct. determ., powder X-ray diffr. exam. 77–4083
$NbSe_2$, high pressure polymorphs 78–51459
$NbSe_3$ and related cpds. bands, bonds and charge density waves 79–95327
$NbSe_3$, CDW, cryst. struct., X-ray and electron diffr. studies 79–14768
$NbSe_x$, nonstoichiometric, thermodynamic props. and crystal struct. *(Japanese)* 78–11206
Nb_2Se_9, cryst. struct. from twin-crystal data 79–90599
$Nb_3Se_5Cl_7$, preparation, struct. and props. 79–65040

crystal atomic structure of inorganic compounds continued

$NbSe_2Cl_2(Br_2)(I_2)$, prep., struct. and props. 80—28994
Nb_3Si, A-15 struct. stability, atomic radii ratio *(Chinese)* 80—54393
$(Nb_{1-x}Ta_x)_2C$, modulated structs., periodic antiphase domains 79—94969
$NbTe_2$, high pressure polymorphs 78—51459
$Nb_{1-x}Ti_xO_2$, X-ray struct. anal. 80—28954
$(Nd,Ca)_nTi_nO_{3n+2}$, (n=4.5,5 or 6), cryst. struct. determ. *(French)* 79—65039
Nd complex, $(NdOP(NMe_2)_3)_6(ClO_4)_3$, X-ray struct. determ. 77—31646
Nd-Cr-B system, phase equil. at 800°C, boride lattice parameters *(Russian)* 78—31388
Nd-H(D), lattice parameters 80—64982
$NdAl_{2.07}(B_4O_{10})O_{0.6}$ nonstoichiometric, crystal struct. by X-ray spectral microanalysis 79—77582
$NdAs_2$, single-cryst. struct. refinement 78—63709
$Nd_{1-x}Ca_xVO_3$, solid solutions, elec. props. 80—96866
$NdCl_3$-$SnCl_4$-$POCl_3$, complex formation, struct. and comp. 77—89413
$NdCo_4B_4$, and its analogues, struct. determ. *(Ukrainian)* 78—91320
$NdCo(BO_2)_5$, cryst. struct. 78—63735
$NdCrOS_2$, single cryst. X-ray diffr. struct. determ. *(French)* 79—23581
$(NdCu_3)(Ti_3Fe)O_{12}$, synthesis, cryst. struct. and Mossbauer exam. 78—84505
$NdFeTiO_5$, magnetic props. and crystal growth 78—92185
$NdGa_3(BO_3)_4$ crystal structure by X-ray spectral microanalysis 79—46621
Nd_4GeO_8, crystal struct. by X-ray spectral anal., flame photometry, rhombic cell parameters 79—77583
$Nd_4In_5S_{13}$, chalcogenide cryst. struct., diffr. and Patterson function anal. 80—39056
$NdIr_3$, single cryst. X-ray diffr. struct. determ., new tetragonal phase 79—69064
$Nd_2(MoO_4)_3$-$Nd_2(SO_4)_3$ system, sulphatomolybdates and isomorphous substitution 80—19763
$NdNbO_4$, ferroelastic, cryst. struct. and twinning struct. 79—27965
$Nd_{1/3}NbO_3$, $NdNbO_4$, structural characteristics and residual polarisation 77—15361
Nd_2O_3, cryst. struct., X-ray powder diffr. and electron diffr. study 80—107161
Nd_2O_3, neutron diffraction study of high temp. struct. *(French)* 79—65050
$Nd(OH)_2Br$, hydrothermal phase equilib., cryst. struct. 78—35372
$Nd_7(OH)_{18}Br_3(I_3)$, hydrothermal phase equilib., cryst. struct. 78—35372
$Nd_2O_2S_2$, cryst. struct. determ. 79—51087
$3Nd_2O_3.2WO_3$, X-ray charact. and thermal props. 77—43194
$Nd_2O_3.4TiO_2$, growth from soln., struct. 78—83794
NdP_5O_{14} and $Nd_xLa_{1-x}P_5O_{14}$, large single crystal growth from H_3PO_4 and oxide, props. *(French)* 77—4723
$NdReSi_2$, cryst. struct. determ. 78—95037
$Nd_2(SO_4)_3$, anhydrous, cryst. struct. determ. 78—79598
$NdTiO_3$, cryst. struct. and cryst. chem. 80—1984
$Nd_2Ti_2O_7$, crystal struct. and phase transitions, rel. to isomorphous crystals *(Japanese)* 80—49208
$Nd_2V_{10}O_{28}.28H_2O$, cryst. struct. determ. 77—11523
$Nd_2V_{10}O_{28}.28H_2O$, X-ray cryst. struct. anal. 80—39060
$Nd_2Zr_2O_7$-$Nd_2Hf_2O_7$, struct., elec. cond. and melting point 80—54197
Ni complex, 1-(2-thiazolylazo)-2-naphtholato Ni (II), cryst. struct. 77—11536
Ni complex, $(Ni(C_2H_5NO)_6)(NO_3)_2$, field induced level crossing and cryst. struct. 79—47070
Ni complex, $(4\text{-methylpyridine})_4Ni(NCS)_2$, porosity 77—76364
Ni complex, bis-$(1,2\text{-benzoquinonedioximato})_2Ni.05I$, X-ray scatt. 77—1101
Ni complex, bis(L-isoleucinato)NiII dihydrate, struct. 78—18604
Ni complex, bis(N-benzylsalicylaldiminato) Ni (II), lattice consts. and space group 79—37680
Ni complex, di-(trichloroacetate).4n-para-anidine crystal struct., bond angles 79—86774
Ni complex, diaquo-bis-(acetylacetonate) nickel (II), cryst. struct. 80—100205
Ni complex, Ni (II)-substituted ethylenediamines and monocarboxylates, cryst. and mol. struct., X-ray diffr. obs. 79—82182
Ni complex, nickel di-(trichloroacetate).4n-toluidene complex, crystal struct., bond angles 79—82189
Ni complex, nickel di-(trichloroacetate).(aniline)4 complex, crystal struct., bond angles 79—82190
Ni complex, with 1,2,4-triazole, mag. susceptibility, 2-300K, struct., antiferromag. props. 77—77045
Ni complexes of N,N,N′,N′-tetramethylethylenediamine 78—34467
Ni intercalation compound, electron microscopy 80—84164
Ni-Co-Zn ferrite, exam. of electromag. characteristics 79—1409
NiAs, structure types, coordination 77—19913
$Ni_3B_7O_{13}I$, unit cell parameters and struct. transitions, 20 to 293K, X-ray diffr. study 80—24431
$Ni_{1-x}Cd_xFe_2O_4$, mag. props. rel. to ionic struct. 80—75756
$NiCl_2.nH_2O$, crust. struct. *(German)* 80—1987
NiD_x synthesized at high pressures, neutron diffraction anal. of struct. 80—28977
$NiFe_{2-x}Al_xO_4$, cation distrib. calc. from equilib. conditions 78—22701
$NiFe_{2-x}Mn_xO_4$, cell dimens. determ. 78—26526
$NiFe_2O_4$ milled ferrite powder, substruct. and sinterability 80—84894
Ni_2H, hexagonal type, cryst. struct. determ. by electron diffr. 79—55724
NiMoP, cryst. struct. determ. 77—80468
$NiMo_2Re_2S_8$, cubic structure, mixed tetrahedral cluster *(French)* 77—15372
$Ni(NH_3)_8(BF_4)_2$, phase transition, group theoretical anal. 80—65218
$Ni(NH_3)_6(ClO_4)_2$, phase transition, group theoretical anal. 80—65218
$Ni(NH_3)_6(ClO_4)_2$, structural phase transition, X-ray diffr. obs. 79—65023
$Ni(NH_4)_2(SO_4)_2.6H_2O$, electron density distrib., X-ray diffr. 78—95035
$Ni(NO_3)_2.4H_2O$, two spin ordered states under mag. field 79—15308
β-$Ni(NO_3)_2.4H_2O$, X-ray cryst. struct. determ. 80—28958
$NiNa_2H_8(PO_4)_4.4H_2O$, cryst. struct. determ. *(French)* 78—26504
$NiNa_6(SO_4)_4$, vanthoffite cryst. struct., lattice parameters and thermal behaviour 77—19929
$Ni_3Nb_2O_8$, $Ni_3NbB_3O_{15}$, flux growth and chem. characts. 78—23595
$Ni_{0.34}NbS_2$, intercalation compound, struct. and photoemission meas. 77—16453
NiO single crystals, growth by material transfer in DC arc, and X-ray anal. 79—52113
NiO, under controlled atmosphere, exam. of composition and temp. dependence, of lattice parameter *(French)* 79—19214

crystal atomic structure of inorganic compounds continued

NiO, X-ray determ. of electron density distribs., atomic scatt. factors 80—15078
NiO:Cr, effect of Cr additives on structure parameters *(Bulgarian)* 80—44319
NiO-Cr_2O_3-$MgSiO_3$ methanation catalyst, S-resistant, IR and Raman spectra 80—93290
NiO-TiO_2, solid soln. series, between rocksalt and spinel structure 78—51513
NiP_4O_{11}, formation in phosphoric acid melts 78—27394
$Ni_2P_2O_7$, new variety, crystalline struct. *(French)* 79—65051
NiS, X-ray diffr. obs., high press., diamond anvil camera method 77—4082
Ni_3S_2, hazelwoodite, X-ray cryst. struct. determ. 80—88105
$Ni(S_2N_2H_2)_2$, cryst. struct. determ., new β modification 78—63716
$NiS_2O_3.6H_2O$, cryst. data and mag. susceptibility 77—76368
$NiS_2O_3.6H_2O$, X-ray diffr. study, cryst. struct. determ. 79—4286
$Ni_{3\pm x}Te$, two-layer system, diffr. features 79—82187
$Ni_{3\pm x}Te_2$, long period superstruct., electron microscopy 79—86761
$Ni(UO_2AsO_4)_2.8H_2O$, prep. cryst. struct. characterisation 78—30589
$Ni_3V_2O_8$, flux growth and chem. characts. 78—23595
$(NiV_2O_4)_c(MgFe_2O_4)_{1-c}$, struct. parameters, IR spectra, cluster-component analysis 77—47425
$Ni_2V_2PbO_8$, flux growth and chem. characts. 78—23595
NiZn complexes with hydrazine, X-ray diffr. expts. *(Rumanian)* 79—73149
NiZn ferrite, ZrO_2 additions influence on sintering and physicochem. props. 80—108369
NiZn ferrites, comp., X-ray diffr. and saturation magnetisation obs. 78—18617
$Ni[B_6O_7(OH)_6].5H_2O$, cryst. struct. determ., X-ray diffr. 78—26546
$Ni[UO_2(SO_4)_2].4H_2O$, revision of crystallographic data 78—22699
$Np(VO_3)_4$, crystallographic data *(French)* 78—63725
$Np(VO_3)_4$, X-ray cryst. struct. determ. 79—99133
Os complexes, N-1-adamantylimido OsO_3, bis(N-tert-butylimido) OsO_2, cryst. struct., bonding, ligands π-donor capability 80—64969
Os metal double oxides, elec. cond. and struct. 80—34438
P_xAs_{1-x}, periodic structs. characts. determ. by means of satellite Bragg reflections 79—46510
PBr_3, low temp. struct. study *(French)* 79—32968
PBr_3, X-ray cryst. struct. determ. at 193K *(French)* 79—37667
PCl_3, low temp. struct. study *(French)* 79—32968
PCl_3, structural study at 123K *(French)* 80—88111
PCl_5, phase diagram, PCl_6^- ionising to PCl_4 and $2Cl^-$ under press. 79—82314
$P_xH_yH_z$, synthesis and struct. 80—54201
PON, synthesis and struct. 80—54201
α-P_4S_4 78—51486
Pa complex, protactinium tropolonate, synthesis, cryst. struct. parameters 80—33945
Pa metal double oxides, elec. cond. and struct. 80—34438
$PaAs_2$, Pa_3As_4, and PaAs, cryst. growth by chem. vapour transport, cryst. struct. 80—35066
$PaSb_2$ and Pa_3Sb_4, cryst. structs., mag. susceptibility *(French)* 79—65641
$(Pb,Ba)_5Ge_3O_{11}$ ferroelectric crystals, influence of Pb replacement by Ba on props. 79—87402
$(Pb, Sr)_5Ge_3O_{11}$, single crysts., growth and X-ray and dielec. investigations 80—88127
β-Pb hydride, electron diffr. investigation 79—65062
$PbAl_2Se_4$, X-ray cryst. struct. determ. *(German)* 80—107174
$Pb_2As_2O_7$, cryst. data, X-ray powder diffr. meas. 78—42987
Pb_5AsSb, isomertieite, fengluanite *(Chinese)* 79—1417
$Pb_{1-x}Bi_xF_{2+x}$, solid soln., struct. and ionic cond. correl., neutron diffr. study *(French)* 80—84324
$Pb_{46}Bi_{54}S_{127}$, carnizzarite, X-ray cryst. struct. determ. 79—23567
$PbBi_8Ti_7O_{27}$, cryst. struct. and dielec. const. 77—47428
$Pb_3Bi_2[\square|(GeO_4)_3]$, cryst. data 78—42985
$PbCl_2$, struct. comparison with Co_2Si, Co_2P, and SbSI *(French)* 80—84155
$PbCo_2(PO_4)_2$, mag. susceptibility, elec. cond. and optical refl. 79—56495
Pb_2CrO_5, flux growth and chem. characts. 78—23595
Pb_2CrO_5, thermal X-ray and dielec. investigations 79—47403
$Pb_3Cr_2(PO_4)_2$, synthesis and cryst. struct. 79—19218
$Pb_{1-p}Cr_2S_{4-p}(Se_{4-p})$, modulation of intergrowth struct. 79—94967
PbFI, X-ray studies 78—14320
Pb_2F_2O, X-ray obs. 77—89412
$6PbF_2.PbBr_2$, X-ray studies 78—14320
$6PbF_2.PbCl_2$, X-ray studies 78—14320
$Pb(Fe/Al/Ga)_{12}O_{19}$, solid soln., crystallographic charact. *(German)* 79—94972
$PbFeTi(PO_4)_3$ cryst. struct. and prep., rhombohedral lattice *(French)* 77—27856
$PbFe(_{2/3}W_{1/3})O_3$-$Pb(Co_{1/2}W_{1/2})O_3$ solid soln., crystallographic, dielectric, magnetic props., Mossbauer spectra 78—43807
$Pb_2Ga_2S_5$, X-ray cryst. struct. determ. and refinement *(French)* 80—107130
$PbGa_2Se_4$, X-ray cryst. struct. determ. *(German)* 80—107174
Pb_2GaTaO_6, transition from pyrochlore to imperfect fluorite struct. 80—19939
$PbGeO_3$, cryst. struct., dielec. and optical props. 77—1118
$PbGe_3O_7$, cryst. data and cryst. growth 78—47289
$Pb_{11}Ge_3O_{17}$, X-ray powder cryst. data, struct. rel. to Pb_6GeO_8 and PbO 80—84146
Pb_3GeO_5 antiferroelectric, cryst. struct. 79—19233
Pb_3GeO_5, cryst. struct. dielec. and optical props. 77—1118
Pb_3GeO_5, high temp. phase, cryst. struct. 80—1995
Pb_3GeO_5, single crystal, props., grown by hydrothermal method 79—11504
Pb_5GeO_7, cryst. data and cryst. growth 79—51076
Pb_5GeO_7, X-ray cryst. struct. determ. *(German)* 79—46603
$Pb_5Ge_3O_{11}$, struct. of paraelec. phase, neutron diffr. meas., rel. to phase transition mechanism 77—84720
Pb_6GeO_8, X-ray powder cryst. data, struct. rel. to $Pb_{11}Ge_3O_{17}$ and PbO 80—84146
$PbGe[Ge_3O_9]$, X-ray cryst. and powder data 80—19768
$Pb(HAsO_4)_2.H_2O$ 78—26552
$PbHPO_4$, phase transitions study, role of cryst. struct. determ. 80—75197
$Pb(HPO_4)_2.H_2O$ 78—26552
$Pb(HPO_4)_2.H_2O$, thermal stability, 20-1000°C, decomposition prod. struct. 79—11775

crystal atomic structure of inorganic compounds continued
$PbHfO_3$, X-ray cryst. struct. refinement 80—44189
PbI_2, 24-layered hexagonal polytype, growth in U-tube by silica gel method, struct. 77—4722
PbI_2 intercalated with organic donor mols., cryst. struct. and phys. props. 78—26543
PbI_2-$PbBr_2$ mixed systems, cryst. growth, struct. and optical props. *(German)* 80—96499
$PbIn_2S_4$, X-ray powder cryst. struct. determ. 80—66488
$Pb_4In_9S_{17}$, $Pb_3Tn_{6.67}S_{13}$ *(French)* 78—63707
$Pb_6In_{10}S_{21}$, X-ray powder cryst. struct. determ. 80—66488
$Pb_{0.27}K_{0.56}Nb_{0.91}Ta_{4.15}O_{15}$, coupled ferroelastic-ferroelectric props. 77—59543
$PbK_2(PO_3)_4$ 77—31638
$PbLaZrNbO_7$, dielectric with zero temp. coeff. of dielect. consts., electrophys. props. 77—52010
$PbLi(PO_3)_3$, cryst. struct. determ. *(French)* 77—80463
$Pb_2M_2^{III}Ge_2O_9$, (M^{III}=Fe,Mn,Sc,In), synthesis, X-ray diffr. and vibr. anal. 79—61360
$Pb_2M^{II}M^{IV}Si_2O_9$, (M^{II}=Mg,Ni,Co,Cu for M^{IV}=Sn; M^{II}=Co, Ni for M^{IV}=Ti), synthesis, X-ray diffr. and vibr. anal. 79—61360
$Pb(Mg_{1/3}Nb_{2/3})O_3$-$Pb(W_{1/2}Mg_{1/2})O_3$, struct. and dielec. props. 80—25312
$Pb(Mg_{0.5}W_{0.5})O_3$-$BiFeO_3$, dielec. props., cryst. struct. 78—84534
$Pb_3Mn_7O_{15}$ *(French)* 78—80525
$Pb_3Mn_7O_{15}$, X-ray cryst. struct. determ. *(French)* 79—14744
$PbMo_6S_8(Se_8)(Te_8)$, Chevrel phase correlation between struct. and supercond. transition temp. 80—7023
α-$Pb(N_3)_2$, neutron diffr. 78—10006
$PbNb_2O_6$, ferroelec., at. displacements, superstruct. *(French)* 77—72588
$Pb_xNb_yO_6$ pyrochlore phases, three odd superstructures *(French)* 77—68946
PbNbS(Se), struct., X-ray powder diffr. meas 80—44175
Pb_2NbYbO_6, X-ray structural investigation 79—65060
PbO, disordered photoconductor, dielec. props., temp. depend. anomalies 78—43765
PbO, X-ray powder cryst. data, struct. rel. to Pb_6GeO_8 and $Pb_{11}Ge_3O_{17}$ 80—84146
PbO-MoO_3-MO and PbO-WO_3-MO systems, M=Ca, Ba, Mg, Sr, perovskite type cpds. detection 80—108404
PbO-Nb_2O_5 system, pyrochlore block structs., cryst. struct. determ. *(German)* 80—70178
Pb_3O_4, cryst. struct., 5-240K, symm. change at 170K *(French)* 78—34618
Pb_3O_4, isomorphous with $ZnSb_2O_4$, cell parameters evolution with temp. *(French)* 78—75642
Pb_2OFBr, mimetic twinning, cryst. struct. determ. 79—23568
Pb_2OFCl, mimetic twinning, cryst. struct. determ. 79—23568
Pb_2OFI, mimetic twinning, cryst. struct. determ. 79—23568
γ-4PbO.SiO_2, synthesis and struct. 78—71716
15PbO.$3B_2O_3$.$2WO_3$, struct. and electrophys. characts. 77—84716
$Pb_3(PO_4)_2$, ferroelastic transformations and struct. as function of temp., neutron diffr. study 79—19188
$Pb_9(PO_4)_6$, X-ray cryst. struct. determ. and refinement 80—103300
$Pb_3(P_3O_9)_2.3H_2O$ *(French)* 77—15352
$Pb_3(P_xV_{1-x}O_4)_2$, ferroelastic phase transitions, lattice dynamics, dielec. and optical props. meas. 77—55334
$Pb_3(P_xV_{1-x}O_4)_2$, phase diagram and crystallography *(French)* 78—92252
$Pb_3Rh_7O_{15}$, struct. study, X-ray diffr. *(French)* 80—88100
$PbSO_4$, anglesite, crystal struct. and sulphate force consts. 78—83784
$Pb_4Sb_7S_{13}$, synthetic robinsonite, crystal struct., lattice constants by X-ray goniometry 79—77581
$(Pb_{0.66}Sb_{0.34})_6SnS_9$, garnet-like struct., synthetic, cryst. struct., X-ray diffr. study 79—19217
$Pb_xSn_{1-x}F_2$ solid soln., struct. evolutions *(French)* 80—96488
$Pb_{1-x}Sn_xSe$, single crystal and film, X-ray spectral investigation of solid solution 77—16477
$Pb_{1-x}Sn_xTe_{1-y}Se_y$, quarternary solid solns. with const. lattice parameter, cryst. growth and characts. 80—108332
PbTaS(Se), struct., X-ray powder diffr. meas 80—44175
PbTe film, struct. anal. and sensitisation 78—22982
PbTe-Bi_2Te_3 system cpds., powder pattern calcs. 77—43185
$PbTiO_3$, neutron powder profile refinement, temp. depend. 78—51476
$PbTiO_3$-La_2O_3.$3TiO_2$, struct. and dielec. props. 80—54200
$PbTiO_3$-$Pb(Fe_{1/2}Nb_{1/2})O_3$ based modified ceramics, struct. and elec. props. 79—87392
$PbTiO_3$-$Pb(Ni_{1/2}W_{1/2})O_3$ system, solid soln. form., struct., dielec. props. and thermal expansion *(Japanese)* 78—27501
$Pb_3(VO_4)_2$, ferroelastic, phase transitions, boundary walls 80—107419
$Pb_3(VO_4)_2$, low-temp. phase, cryst. data 77—39566
$Pb_8V_2O_{13}$, monoclinic lattice determ. and phase transitions *(French)* 79—99102
Pb_2WMO_6, M=Cd, Mg, synthesis, struct., phase transitions 77—84715
$PbWO_2$, IR and Raman multiphonon spectra, struct. 77—90143
Pb_xWO_3 ($0.01 \leq x \leq 0.28$), tetragonal and orthorhombic bronzes, cryst. chem. data 78—42997
$PbZnVO_4OH$, cryst. struct. refinement 79—42015
Pb(Zr, Ti)O_3 ceramics, low temp. sintering, elec. and mech. props. 80—71616
Pb(Zr,Ti)O_3:Mn, crystal struct. and electrophysical props., piezotransformer props. 78—43806
Pb_3ZrF_{10}, cryst. atomic struct. *(French)* 80—49203
Pb_3ZrF_{10}, X-ray cryst. struct. determ. *(French)* 80—33966
$PbZrO_3$, lattice distortion, X-ray diffr. profiles 79—55712
$PbZrS_3$, cryst. struct. refinement using neutron diffr. powder data 79—4294
$PbZr_{0.9}Ti_{0.1}O_3$, neutron powder profile refinement, temp. depend. 78—51475
$Pb_2[As_2O_5]$, paulmooreite, crystal struct., dimeric arsenite groups 80—84143
Pd complex, 1-(2-thiazolylazo)-2-naphtholato Pd (II), cryst. struct. 77—11536
Pd complex, bis(N-allylsalicylaldiminato)-palladium(II) cryst. and mol. struct. 79—32972
Pd complex, dichlorobis(N-methylimidazole)palladium(II), cis and trans, cryst. data 79—51078
Pd complex, tetrakis(N-methylimidazole)palladium(II), crystal data for the tetrachloropalladate 79—51077
Pd complex, tetrakis(imidazole)palladium(II), crystal data for the chloride 79—51077

crystal atomic structure of inorganic compounds continued
Pd complex di-μ-chloro-bis(2-methyl-allyl-3-norboryl)palladium, cryst. data 78—34484
Pd_2B, and other Pd_xB_y cpds., cryst. chem. 80—19769
Pd_2B, cryst. struct., X-ray diffr. study 80—54204
$PdBi_2O_4$, cryst. struct. *(French)* 78—51516
$PdD_{0.73}$, (1, 1/2, 0)-superlattice reflection splitting near 50K, neutron diffr. studies 80—70168
β-PdD_x, (1, 1/2, 0) superlattice reflection, neutron diffr. exam. 79—65038
PdF_2 flourite-type form, mag. props., structure studies *(French)* 80—34187
PdH_x, electronic props., H alloying effects, book contrib. 79—82522
PdP_3, cryst. struct. determ. *(German)* 77—89414
$Pd_3P_{0.8}$, pure and deuterated, cryst. struct., neutron diffr. study 80—84152
$Pd(PO_3)_2$, synthesis and struct. 79—90623
$PdPb(OH)_6$, cryst. struct. determ. *(French)* 77—47419
PdS_2, polymorphism at 75 kbars, 400-1350°C 79—82173
$Pd_{16}S_7$ *(German)* 77—11516
$PdSe_2$, polymorphism at 75 kbars, 400-1350°C 79—82173
$PdTe_2$, polymorphism at 75 kbars, 400-1350°C 79—82173
Pd_3Te_2, struct. and binding *(German)* 77—43192
Pr-Cr-B system, phase equil. at 800°C, boride lattice parameters *(Russian)* 78—31388
Pr-H(D), lattice parameters 80—64982
Pr_2C_3, cryst. struct., mag. struct. and props., 1.6 to 300K 79—11296
$PrCo_2Ge_2$, cryst. and mag. struct., neutron diffr. study 79—69059
$PrCo_2Ge_2$, crystal and magnetic structure obs. 80—64976
$PrCrOS_2$, single cryst. X-ray diffr. struct. determ. *(French)* 79—23581
$PrCr_{2.3}Ti_{2.3}O_9$, flux growth and chem. characts. 78—23595
$Pr_2(MoO_4)_3$-$Pr_2(SO_4)_3$ system, sulphatomolybdates and isomorphous substitution 80—19763
$PrNH_4P_4O_{12}$, cryst. struct., and isotypism with $NdNH_4P_4O_{12}$ *(French)* 77—24301
$PrNiC_2$, struct. determ. using X-ray diffraction *(Ukrainian)* 80—33949
$Pr_6Ni_6P_{17}$, synthesis and cryst. struct. 78—75634
PrO, high press. synthesis, struct. and lattice consts. *(French)* 80—29913
$Pr_{24}O_{44}$, beta phase, high resolution cryst. struct. images 78—42991
$Pr_{40}O_{72}$, ε-phase, defect cryst. struct. 79—90645
Pr_9O_{16}, ζ-phase, defect cryst. struct. 79—90645
$Pr(OH)_3$, cryst. struct. 80—24424
$Pr(OH)_2Br$, hydrothermal phase equilib., cryst. struct. 78—35372
$Pr_7(OH)_{18}Br_3(I_3)$, hydrothermal phase equilib., cryst. struct. 78—35372
$Pr(OH)_2NO_3$, cryst. struct., X-ray diffr. meas. 77—4068
PrOI, X-ray diffr. coord. parameter determ. 78—87656
$Pr_2O_2S_2$, cryst. struct. determ. 79—51087
Pr_2O_3.Si_3N_4, prep. by sintering and X-ray diffr. data 79—77570
$3Pr_2O_3$.$2WO_3$, X-ray charact. and thermal props. 77—43194
PrP_3O_9, X-ray powder data 79—51079
PrP_5O_{14}, chemical synthesis and crystal growth of laser quality 78—92184
$Pr_2(SO_4)_3.8H_2O$, crystal struct. refinement 77—15369
$PrSbO_3$, single crysts., hydrothermal synthesis and crystallographic characteristics 79—95916
Pt complex, $(C(NH_2)_3)_2Pt(CN)_4Br_{0.23}.H_2O$, pseudo-one-dimens. cpd., solitary wave excitations, and cryst. struct. 78—6307
Pt complex, bis(1,2-benzoquinonedioximato)platinum(II), rel. to intrinsic elec. cond. 78—6377
Pt complex, bis(1,2-benzoquinonedioximato)Pt(II), cryst. and mol. struct. 79—60327
Pt complex, tris[bis(1,2-diaminoethane)Pt(II)dichlorobis(1,2-diaminoethane)]Pt(IV)tetrakis[tetrachlorocuprate(I)], cryst. and mol. struct. 80—28964
Pt complexes, chain cpds., orientational antiphase struct., X-ray scatt. determ. 80—24435
Pt intercalation compound, electron microscopy 80—84164
Pt metal double oxides, elec. cond. and struct. 80—34438
Pt_4B, Pt_2B, and other Pt_xB_y cpds., cryst. chem. 80—19769
$PtBi_{1.6}Pb_{0.4}O_{3.8\text{-}4}$, cpd. with unidirectional linear chains of metallic atoms *(French)* 77—19934
PtGeSe, ferroelastic, cryst. struct. models 77—19927
$Pt_6(NH_3)_{10}Cl_{10}(HSO_4)_4$, chain struct. and elec. cond. 78—2469
Pt_5Se_4, cryst. struct. determ. *(German)* 77—89415
$Pt(SeC(NH_2)_2)_4Cl_2$, crystal and mol. struct. 78—59794
Pt(diethylenetriamine)(guanosine)$(ClO_4)_2$, crystal and molecular struct. 79—73157
Pu(C, N), PuC and PuN, lattice parameter variation at low temp., thermal expsn. 80—15046
PuGa, cryst. and powder diffr. data at room temp. 80—28982
PuO_2, struct. changes under self- and reactor irrad. 77—27927
PuP, lattice distortions in ferromag. phase, X-ray obs. 80—15774
$R_4Ba_6(BO_3)_9$, flux growth and chem. characts. 78—23595
Rb-U-O system, cryst. chem. 77—39568
Rb_2 $(CU(CO_3)_2)H_2O$, crystal struct., X-ray determ. *(French)* 79—99164
Rb_2AgI_3, cryst. struct. and polarised Raman spectrum 77—69813
$RbAg_3Se_2$, crystal struct., X-ray study *(German)* 78—83795
$RbAlCl_4$, solid state Raman spectra, 298-80K, vibr., struct. 79—28745
$RbAlF_4$, single cryst., prep. and struct. *(French)* 80—79762
β-$RbAlF_4$, struct. and irreversible and topotactic phase transition $\beta \rightarrow \alpha$ mechanism 80—107132
α-$Rb_5Al(MoO_4)_4$, cryst. struct. 79—19219
$Rb_4As_2O_7$, solid-state synthesis, X-ray powder data *(French)* 80—15079
RbAu, NMR line shape, Knight shift, X-ray diffr. study, struct. props. 78—68402
$Rb_2B_{12}H_{12}$ and $Rb_2B_{12}H_{12}$.RbX, X=halogen, cryst. growth from soln. and morphology 77—44145
Rb_2BRCl_6, B=Li,Ag,Na, systematic structs., X-ray Guinier-Simon method *(German)* 80—44186
$Rb(B_xW_{3-x})O_9$ (B=Na, Ca, Co, Ni, Cd, Ga, Bi, Nb, Ta) cryst. struct., temp. dielec. anomalies 80—1998
$Rb_2Be_2Si_2O_7$, X-ray obs. 77—24293
Rb_3Bi, cubic and hexagonal structs., transition 78—26480
Rb_3BiBr_6, cryst. struct. determ. 78—75638
$Rb_2C_2O_4(SbF_3)_2$, growth from soln. and X-ray diffr. study *(French)* 77—80481
$RbCaF_3$, struct., phase transitions, neutron diffr. study 80—33918
$RbCdBr_3$, cryst. struct., X-ray diffr. 77—19917

crystal atomic structure of inorganic compounds continued
$RbCdCl_3$, crystal struct., polarised Raman spectra and X-ray diffraction obs. 78−76443
$Rb_2Cd_2(SO_4)_3$, ferroelec., X-ray study on phase transition 77−85665
$RbCoCr_2(VO_4)_3$, synthesis and cryst. struct. 80−88114
β-$RbCrCl_3$, co-operative Jahn-Teller distorted struct. determ. 78−63713
γ-$RbCrCl_3$, cooperative Jahn-Teller distorted structure 79−90604
Rb_2CrCl_4, two-dimens. easy-plane ferromag., cryst. and mag. struct., temp. variation of moment 77−66255
$Rb_2Cr_3O_{10}$, hexagonal form, cryst. data *(French)* 80−28979
α-$RbCu_4Cl_3I_2$, solid electrolyte, cryst. struct. and anal. 79−82382
$RbCuCr_2(VO_4)_3$, synthesis and cryst. struct. 80−88114
$Rb_4Cu_{16}I_7Cl_{13}$ in CuCl-CuI-RbCl system, high Cu ion cond. solid electrolyte, elec. props. and powder X-ray diffr. anal. 80−15295
RbD_2PO_4, struct. at room temp., diffractometer study 80−1994
$RbD_3(SeO_3)_2$, ^2D NMR struct. anal. 80−2661
$RbDy(WO_4)_2$, cryst. struct. and refinement 77−65969
$Rb_5Er(MoO_4)_4$ 77−62510
$RbEu_3F_{10}$, crystal struct., X-ray studies *(French)* 80−33955
Rb_3EuF_6, Rb_2EuF_5, $RbEu_2F_7$, $RbEu_3F_{10}$, cryst. struct., X-ray diffr., equilib. in RbF-EuF_3 *(French)* 78−44107
$RbF.H_2O_2$, X-ray and neutron diffr. struct. determ. 78−67698
$Rb_2FeCl_5.H_2O$, cryst. struct., superconducting susceptometer mag. meas. 79−73717
$RbFeF_4$, Mossbauer spectra, struct. and hyperfine field 77−12266
Rb_2FeI_4, X-ray cryst. struct. determ. and refinement 79−69070
$Rb_5Fe_3O(SO_4)_6.5H_2O$, cryst. struct. determ. 80−92482
RbH_2PO_4, phase transitions study, role of cryst. struct. determ. 80−75197
RbH_2PO_4, tetragonal phase disordered struct. 78−42980
RbH_2PO_4, X-ray cryst. struct. refinement 79−14787
$Rb_2HPO_4.RbH_2PO_4.Te(OH)_6$, monoclinic, cryst. struct. *(French)* 80−33964
$RbHSeO_4$, ferroelec. props. rel. to struct. 80−71345
$RbHSeO_4$, X-ray cryst. struct. anal. 79−4292
$RbH_3(SeO_3)_2$, ferroelec., location of H atoms in cryst. struct., neutron diffr. meas. 78−2093
$RbH_3(SeO_3)_2$, low temp. struct., neutron diffr. 78−38669
$RbH_3(SeO_3)_2$, paraelec. phase, H bonding, neutron diffr. 77−47420
$RbHgC_4$, and $RbHgC_8$, intercalation cpds., synthesis and struct. 80−44183
$Rb_5I(I_3)(BiI_6)(H_2O)_2$ 77−58989
$RbIO_3.2LiIO_3$, crystal struct. refinement, Li atom localisation in I atom presence, cell parameters 79−77585
$RbIn_3F_{10}$, crystn. struct., unit cell parameters, coordination *(French)* 77−80485
$Rb_2In_3F_{11}$ *(French)* 78−42966
$RbIn(SO_4)_2.4H_2O$, refinement of cryst. struct., interatomic distances, bonds 80−59448
$(Rb_xK_{1-x})AgI_3$, cryst. struct. 77−51360
$(Rb_xK_{1-x})Ag_4I_5$, cryst. struct. 77−51360
$Rb_xK_{1-x}[GaSi_2O_6]$, partially ordered leucite-type struct. *(German)* 79−51088
$Rb_{12}M_{33}O_{90}.(12H_2O)$, cation exchanger with intersecting tunnel struct. *(French)* 78−20014
$RbMgCr_2(VO_4)_3$, synthesis and cryst. struct. 80−88114
$RbMnBr_3$, X-ray cryst. struct. determ. 80−54187
$RbMnCl_3$, cryst. struct., X-ray diffr., Weissenberg photograph 77−19922
Rb_2MnCl_4, cryst. struct. determ. 77−80473
$Rb_3Mn_2Cl_7$, cryst. struct. 78−79578
$Rb_3Mn_2Cl_7$, two dimens. double layer antiferromag., neutron diffr. exam. 77−8277
$Rb_2MnF_5.H_2O$, X-ray cryst. struct. anal. 79−4290
$RbNO_3$, high pressure phase V, X-ray struct. determ. 80−28953
$RbNO_3$, struct., high temp. phases, neutron diffr. study 80−79756
$RbNaMg_3M_2Si_{12}O_{30}$ (M=Cu, Fe, Mg), cryst. struct., X-ray diffr. and IR spectra *(French)* 80−107158
$Rb_{10}Nb_{29.2}O_{78}$, cationic exchanger with crossed tunnel struct., cryst. struct. *(French)* 78−83797
$Rb_{12.20}Nb_{33.56}O_{90}$, tunnel cryst. struct., X-ray diffr. 78−18611
$Rb_8Nb_{22}O_{59}$, cryst. growth from melt, and instability 78−35294
$Rb_4Nb_6O_{17}.3H_2O$, cryst. struct. by X-ray diffr. *(French)* 80−92503
$RbNbTeO_6$, pyrochlore struct. and its relatives 79−14773
$Rb_2Nb_6TiO_{18}$, X-ray obs. *(French)* 78−6040
$RbNdP_4O_{12}$, crystal struct. determ. 77−80459
$RbNiCr_2(VO_4)_3$, synthesis and cryst. struct. 80−88114
$RbNiF_3$, neutron scatt., automatic data processing *(Russian)* 80−54079
RbO_2, low temp. phase study, crystallographic domains and unit cell dimens. 78−63728
Rb_2O-Nb_2O_5 mixed oxides, cryst. struct., electron microscopy study 78−91309
Rb_2O-$Nb_2O_5(Ta_2O_5)$, phase equilib. relns. and crystal chemistry, structs. useful as ionic conductors 79−20033
Rb_2O-Ta_2O_5 mixed oxides, cryst. struct., electron microscopy study 78−91309
Rb_2O-Ta_2O_5 mixed oxides, cryst. struct., electron microscopy study 78−91310
$Rb_2O.SrO.4B_2O_3.12H_2O$, real Patterson function determ., method of rhombs. 78−5986
$RbPO_3$-$Mn(PO_3)_2$ system, $Rb_2Mn(PO_3)_4$ and $RbMnP_3O_9$ form. 79−78943
$RbPbI_3.2H_2O$, X-ray cryst. struct. determ. 80−64958
$Rb_2Pb[Co(NO_2)_6]$, struct. study 80−88106
Rb_2PtI_5, synthesis and cryst. struct. *(German)* 78−79588
$RbRF_4$, R=La, Ce, Pr, Nd, Sm, phase equilib. and cryst. struct. *(French)* 78−44107
$RbSbS_2$, cryst. struct., space groups 79−7592
$Rb_2Sn(NH_2)_6$, cryst. struct. determ. *(French)* 77−47384
$Rb_{10}Ta_{29.20}O_{78}$, tunnel struct. 80−107166
$Rb_{10}Ta_{29.2}O_{78}$, cationic exchanger with crossed tunnel struct., cryst. struct. *(French)* 78−83797
$Rb_2Ta_6TiO_{18}$, X-ray obs. *(French)* 78−6040
Rb_2Te_3, synthesis and cryst. struct. 80−88115
$RbTiMO_5$ (M=Ta, Nb), ion exchange props., synthesis and crystallographic props. *(French)* 80−28997
$Rb_{1-x}(Ti_{1-x}M_{1+x})O_5$, M=Nb, Ta, layer compound, cryst. struct., non-stoichiometry 80−64972
$RbTl(SeO_4)_2$, $Rb_3Tl(SeO_4)_3$, and $Rb_5Tl(SeO_4)_4$, cryst. struct. *(French)* 80−84148
$Rb_4(UO_2)_4O_2Cl_8(H_2O)_4$, cryst. data 77−76367
$Rb_2(UO_2)_4O_2(OH)_2Br_4(H_2O)_6$, cryst. data 77−76366

crystal atomic structure of inorganic compounds continued
$Rb_2(UO_2)_4O_2(OH)_2Cl_4(H_2O)_6$, cryst. data 77−76366
$Rb_{0.25}VF_3$, cryst. struct. examination by electron diffr. using TEM 79−23583
$RbVO_3$, X-ray determ. 78−6043
$Rb_{0.30}WO_3$, struct. anal. *(French)* 78−59786
$Rb_{22}W_{32}O_{107}$ 78−14313
$Rb_{20+x}(W_4O_6)_{1/3-x/12}W_{32}O_{108}$, struct. *(French)* 79−60321
$Rb_9(XeO_3Cl_2)_4Cl$, neutron and X-ray diffr. struct. determ., Xe-Cl bonding 78−30591
Rb_2ZnBr_4, average struct. determ. from neutron diffr. diagrams 79−32955
$Rb_2[C_2O_4].D_2O_2$, neutron profile refinement at 5K 80−88103
$Rb_2[Cu(H_2O)_6](SO_4)_2$, Tutton's salts, stereochem., neutron struct. determ. 78−18609
$Rb_2[MnBr_4]$, X-ray cryst. struct. determ. 79−32961
$Rb_2[Pt(CN)_4Br_2]$, neutron diffr. 77−35522
Re complex, $AsPh_4ReOCl_4$, cryst. and mol. struct. determ. 77−47390
ReO_3, coeff. of linear thermal expansion, 100-500K 79−10972
ReP_4, synthesis and cryst. struct. 79−99124
$Re_{12}P_{26}$, binary crystals containing plane Re_4 clusters *(French)* 80−19774
ReS_2, prep., struct. 79−38774
$ReSe_2(Te_2)$, high-press. modifications 77−51354
Rh metal double oxides, elec. cond. and struct. 80−34438
$RhBr_3$, bond distances exam. by EXAFS 78−26525
$RiRe_2O_6$, prep. and cryst. struct. 80−28991
Ru metal double oxides, elec. cond. and struct. 80−34438
Ru ternary and quaternary oxides, prep., cryst. struct. and mag. props. 79−14771
Ru_7B_3, stella quadrangula as struct. building unit 80−15055
SF_6, cryst., IR and Raman spectra at 9 and 97K, cryst. struct. 79−87427
SF_6, plastic phase, neutron diffr. obs. and theory 79−77533
$(SN)_x$, cryst. struct. by neutron diffr. 78−34488
$(SN)_x$, polymeric, shear transformation to orthorhombic phase 77−55257
S_4N_4, Raman scatt. and opt. absorpt., press. and temp. depend. 77−36227
$S_4N_4.AsF_5$, molecular adduct cyclotetra(azathiene), X-ray cryst. struct. determ. 80−54180
S_xSe_y, s=6-3, y=2-5, thermal behaviour 78−67813
Sb complexes, oxalate-fluoride and nitrate-fluoride cpds., NQR 77−12236
$SbCl_3$ complex, with (1,3,5-triacetylbenzene), single cryst., X-ray cryst. struct. anal. 79−14761
$SbCl_3$, cryst. struct., Zeeman split fine struct. lines, FT NQR obs. 80−54982
$SbCl_3$, X-ray struct. redeterm. 80−28970
$SbF_3.(NH_2)_2CS$ and $SbF_3.[(NH_2)_2CS]_2$, X-ray cryst. struct., IR spectrum *(French)* 78−87643
$SbFe_2Si_2O_8OH$, crystal struct., space groups by RHEED 78−47297
$Sb_{0.2(0.4)}MoO_{3.1}$, synthesis, struct. and oxidation state *(French)* 80−64971
$Sb_2Mo_{10}O_{31}$, X-ray cryst. struct. determ., Patterson method *(French)* 79−99125
Sb_2O_3, pyrochlore struct. and its relatives 79−14773
α-Sb_2O_4, cryst. struct., neutron diffr. study 77−47391
β-Sb_2O_4, X-ray powder patterns 77−7695
Sb_2O_5 hydrate, P_H phase, dehydration effects 77−35540
Sb_2O_5, single crysts., X-ray cryst. struct. full matrix least squares refinement *(German)* 79−37665
$Sb_4O_5Cl_2$, cryst. struct. refined 78−79572
$Sb_2(OH)_2(SO_4)_2.2H_2O$, X-ray cryst. struct. determ. *(French)* 79−4274
$2MASb_5O_7I$, polytype, crystal structure determination 78−91316
Sb_5O_7I polytypes, cryst. growth, struct., ferroelastic and ferroelec. props. 78−31309
$Sb_5O_{12}(OH).H_2O$, prep. and cryst. struct. *(German)* 79−32975
SbSI, crystal struct. in ferroelec. phase, displacive type transition 77−11515
SbSI, neutron diffr. obs. at −185, 16 and 100°C 77−43180
SbSI, struct. comparison with Co_2Si, Co_2P, and $PbCl_2$ *(French)* 80−84155
$Sb_2(S_2O_7)_3$, X-ray powder cryst. struct. determ. *(French)* 79−55703
Sc complex, $Sc(BH_4)_3$ with THF, synthesis and struct. 79−51068
Sc germanates and silicates, cryst. struct. and cryst. chemistry 77−39571
Sc-M-B systems (M=Rh,Ir), phase equilib. and cryst. structs. 80−15072
$ScB_{\sim 28}$, β-rhombohedral cryst. struct. by X-ray diffr. 78−34464
$ScCl_3$-NaCl-CsCl ternary system, cpd. form., thermographic investig. *(Russian)* 80−66490
ScCoSi, X-ray determ. of struct., new representative of struct. type TiNiSi 78−79595
$ScCo_{0.25}Si_{1.75}$, X-ray determ. of struct., new representative of struct. type $ZrSi_2$ 78−79595
Sc_2CoSi_3, X-ray cryst. struct. determ. and refinement 79−60343
$Sc_3Co_2Si_3$, X-ray cryst. struct. determ. and refinement 79−60343
ScF_3, metastable high press. phases, X-ray diffr. and IR absorpt. expts. 77−11499
$ScFe_{0.25}Si_{1.75}$, X-ray determ. of struct., new representative of struct. type $ZrSi_2$ 78−79595
$Sc_2Fe_3Si_5$, cryst. struct. determ. 78−18620
ScH_x:Er, ESP determ, of proton locations 80−34768
$Sc(H_2PO_4)_3$, synthesis, struct. and stability 77−47423
$Sc(HSeO_3)_3$ 78−51485
$ScH(SeO_4)_2.2H_2O$, single crysts., X-ray diffr. struct. anal. 78−95020
$ScH(SeO_4)_2.2H_2O$, $Sc(HSeO_3)_3$, cryst. struct. 79−99122
$Sc_{11}Ir_4(Os_4)(Ru_4)$, cubic struct. type described by cluster concept, X-ray determ. 80−33933
$ScMn_{0.25}Si_{1.75}$, X-ray determ. of struct., new representative of struct. type $ZrSi_2$ 78−79595
$Sc(NO_3)_3.4CO(NH_2)_2$, cryst. struct. determ. 79−23588
ScNiSi, X-ray determ. of struct., new representative of struct. type TiNiSi 78−79595
$ScNiSi_3$, cryst. struct., X-ray diffr. meas. 78−10027
$ScNi_{0.25}Si_{1.75}$, X-ray determ. of struct., new representative of struct. type $ZrSi_2$ 78−79595
$ScNi_2Si_3$, cryst. struct., X-ray structural anal. 78−95044
$Sc_2O_3+Sb(V)$ reaction, phase formation, structs. 77−84712
ScOF, ordering and structure, NMR and crystallographic determ. *(French)* 79−90618
ScO(OH), ScOF, and $Sc(OH)_3$, metastable high press. phases, X-ray diffr. and IR absorpt. expts. 77−11499

crystal atomic structure of inorganic compounds continued
Sc_2O_2S, cryst. atomic struct. determ. *(French)* 79—10837
$Sc(PO_3)_3$, cryst. struct. determ. from X-ray intensity data 78—95043
$Sc_4(P_4O_{12})_3$, cryst. struct. determ. *(French)* 78—55842
$Sc_2Re_3Si_4$, X-ray struct. determ. *(Russian)* 79—27958
$ScRu_4B_4$, superconducting and crystallographic data 80—33968
$Sc_2(SeO_4)_3$, cryst. struct. determ. 78—63708
$Sc_2(SeO_4)_3(.5H_2O)$ cryst. struct. 79—99122
$Sc_2Si_2O_7$, high press. pyrochlore struct. 77—47426
Se, cubic modification prepared by shock compression 78—34494
SeBr, X-ray diffr. study of crystalline modifications 77—89420
$SeBr_4$, X-ray diffr. study of crystalline modifications 77—89420
SeCl, X-ray diffr. study of crystalline modifications 77—89420
$SeCl_4$, X-ray diffr. study of crystalline modifications 77—89420
$SeMoOCl_7$, prep., cryst. struct., characterisation *(French)* 78—63722
$SeOCl_2$.dioxane, cryst. struct., secondary and multi-centre bonding 78—63751
Se_3S_5 78—42978
Se_4S_4, mol. chalcogenide, synthesis and struct. 79—33912
Se_2TiO_6, cryst. struct. *(French)* 78—95023
Si, crystn., electron density distrib. 80—49189
Si particles, grown in Ar gas, cryst. struct. and habit, electron microscope study 79—74071
Si-Al-O-N polytypes, direct lattice resolution using high resolution electron microscopy 78—38682
Si-Al-O-N system, phase analysis and TEM struct. obs. 80—108420
Si-C-Al-O-N and related systems, new materials 78—95159
Si_xB_y formed when Bi_2O_3 is diffused in Si, anal. study 79—19269
SiC, 126R polytype, struct. determ., use of lattice imaging in electron microscope 78—26498
SiC, $147R_{(b)}$ polytype, crystal structure, X-ray diffr. method *(Chinese)* 80—54206
SiC, extremely large-period polytypes, X-ray diffr. and TEM 77—31636
SiC, one dimensional disorder 78—51492
SiC, phys. props. and crystal growth, rel. to appl. in electrolum. devices, book contrib. 77—77299
SiC polytypes, contribution of ionic bonding to thermal stability 80—28946
SiC polytypes, lattice imaging studies on intergrowth structs. 80—107025
SiC polytypes, stacking sequences by high resolution electron microscopy 80—15054
SiC-2H, structure parameters and polarity, X-ray diffr. meas. 80—19781
SiF_4, Raman spectra at 77K, scatt. angle, polaritons and space group 78—23439
SiF_4, stella quadrangula as struct. building unit 80—15055
Si_3N_4, CVD, effect of deposition parameters 77—55272
α-Si_3N_4, lattice and atomic position parameters, neutron diffr. study 79—42040
Si_3N_4, N ion implantation synthesis, struct. and resonance mechanism of α-β transition during annealing 80—33981
Si_3N_4, pyrolytic, prep. by CVD, bulk and coatings, exam. of electrical, optical and physical props. 79—95935
α-Si_3N_4, stable phase in Si-Al-O-N system, cryst. struct. obs. using TEM 80—108421
β-Si_3N_4, X-ray cryst. struct. and refinement, struct. rel. to α-Si_3N_4 79—46605
β-Si_3N_4-AlN-Al_2O_3-MgO, insolubility of Mg in β-Si_3N_4 79—10953
Si_2N_2O, high-press. neutron diffr. exam. 77—51357
$Si_3N_4.Y_2O_3$ prepared by hot press, cryst. struct. 80—10534
SiO_2 (silicalite), new hydrophobic crystalline silica mol. sieve 78—30598
SiO_2, cristobalites and topologically related structures, cryst. struct. 77—7688
SiO_2, cryst. and vitreous, struct. sensitive expansivity 78—22873
SiO_2, low tridymite 78—36150
SiO_2, new high-pressure modification 78—75825
SiO_2, pseudopotential study of bonding and structure 78—75622
SiO_2, tridymite, non-integral phase from 150°-190° 79—99144
SiO_4 tetrahedra, mean Si-O bond lengths var. 78—63699
SiO_6 octahedra, var. of mean Si-O bond lengths 78—18577
SiP_2O_7, AIV, cryst. struct. refinement, phase with six coordinated Si 79—42018
Si_2Te_3, growth by Bridgman technique and sublimation, cryst. struct. 77—1106
Sm-Cr-B system, phase equil. at 800°C, boride lattice parameters *(Russian)* 78—31388
SmB_2, high press. synthesis 78—18608
$SmCrOS_2$, single cryst. X-ray diffr. struct. determ. *(French)* 79—23581
$Sm_8Cr_2Si_6N_2O_{24}$, apatite-like struct. study *(French)* 77—27854
SmF_2-SmF_3 system, four new compounds Sm_mF_{2m+5}, X-ray powder patterns, lattice parameters *(German)* 78—42999
SmFX mixed halides, synthesis and lattice parameters 78—30594
$Sm_4Ge_3O_9(OH_6)$, X-ray diffr. data 78—14330
Sm_3InS_6, X-ray struct. determ. *(French)* 77—80453
$Sm_xLa_{1-x}B_6$, solid solns., exam. of structure, elec. props. 80—39290
$Sm_3Ni_6Ga_2$, X-ray struct. determ. *(Russian)* 79—27959
Sm_3ReO_8, cryst. struct. determ. *(French)* 77—4073
SmS, semicond.-metal transition, phase struct. determ. 78—91618
Sm_3S_4, cryst. struct. and valence state of Sm *(German)* 78—75636
$Sm_2(SO_4)_3.8H_2O$, cryst. struct. refinement 77—89418
Sm_2SnS_5, X-ray cryst. struct. determ. *(French)* 80—19760
$Sm_xTb_{1-x}FeO_3$ orthoferrites, crystallo-optical props. 79—42027
$SmTiO_3$, cryst. struct. and cryst. chem. 80—1984
$Sn_2Br_{0.65}Cl_{3.35}.3H_2O$, X-ray cryst. struct. determ., Patterson synthesis *(French)* 80—28960
Sn_3BrF_5, cryst. struct. determ., environment of Sn (II) *(French)* 78—26508
$Sn_5Br_4F_6$, cryst. struct. determ. *(French)* 78—79591
SnClF *(French)* 77—15349
SnClI, X-ray cryst. struct. determ., Patterson synthesis *(French)* 80—96480
$SnCl_2.1.5H_2O$ single cryst., ^{35}Cl NQR, cryst. struct. 80—60449
SnF_2, cryst. struct. of β- and γ-phases 80—92500
α-SnF_2, crystallochemistry 80—28990
$SnF_2.AsF_5$, cryst. struct., X-ray diffr. 77—19921
$Sn_{0.225}Fe^{3+}{}_{0.575}Fe^{2+}{}_{1.465}Mg_{0.735}BO_3O_2$, hulsite, cation distrib., X-ray determ. 79—19225
$SnGa_6Te_{10}$, X-ray cryst. struct. determ. *(French)* 79—23580
$Sn(HAsO_4)_2.H_2O$ 78—26552
$SnHPO_4$, hydrogen-bonded dimers 77—15357
$Sn(HPO_4)_2.H_2O$ 78—26552

crystal atomic structure of inorganic compounds continued
$Sn(HPO_4)_2.H_2O$ and its alkali metal salts, struct. and vibr. spectra 80—39030
$Sn(HPO_4)_2.H_2O$, struct., vibr. spectra 79—15447
SnI_4, attachment energy as habit controlling factor 80—59421
Sn_2IF_3, X-ray cryst. struct. study using Patterson function *(French)* 79—4280
$Sn_{2.8}Li_{1.6}Mg_{1.6}O_8$, four layer close packing, cryst. struct. determ. *(French)* 80—28999
$Sn_{2.8}Li_{1.6}Zn_{1.6}O_8$, four layer hexagonal close packing, cryst. struct. determ. *(French)* 80—28999
$SnMo_6S_8$, cryst. struct., superconducting characts. changes 79—86773
$Sn_xMo_6S_8$, Chevrel phase, lattice instabilities, X-ray diffr. meas. 78—34491
$Sn_xMo_6S_8$, struct. anal. supercond. props. 80—97023
$SnMo_6S_8(Se_8)(Te_8)$, Chevrel phase correlation between struct. and supercond. transition temp. 80—7023
Sn(NCS)F, X-ray cryst. struct. anal. using Patterson functions *(French)* 79—4279
Sn(NCS)X, (X=F, Cl, Br or I), cryst. struct. *(French)* 79—51060
$SnNbS_2$, intercalate, cryst. struct. determ. 78—26534
SnNbS(Se), struct., X-ray powder diffr. meas 80—44175
SnO_2 fluorite isotype, implications for Earth's lower mantle 78—61371
SnO_2, transparent conductive film, prep. by magnetron sputtering and elec., optical and structural props. *(Japanese)* 79—8247
C-Sn_2O_3, electron diffr. 77—31650
$(Sn_2O_2F_4)Sn_2$, synthesis and cryst. struct., X-ray diffr. meas. *(French)* 77—47411
$Sn_3(PO_4)_2$ 77—58984
$Sn_2P_2S_6$, ferroelec. semicond., phase transition and lattice dynamics 80—60526
$Sn_2P_2S_6$ ferroelectric semicond., polarisation Raman scatt. spectra, X-ray struct. study 79—95778
SnS, single cryst. growth and struct. props. 79—52109
SnS-SnTe, solid solns., synthesis, Mossbauer spectra 77—24768
SnS_2 berndtite, cryst. struct. and compressibility at high press. 78—67685
SnS_2, effect of powdering on polytypic cryst. struct. 80—1979
SnS_2, polytypism, and cryst. struct. by X-ray methods 79—77542
SnS(Se), electron diffr. struct. anal. 80—44449
$SnS_{2-x}Se_x$ solid soln., resistivity, lattice parameter, comp. and temp. depend. 78—91693
$Sn_5Sb_2S_9$, cryst. struct. *(French)* 80—1991
SnSe-SnTe, solid solns., synthesis, Mossbauer spectra 77—24768
$SnSe_2$-$GeSe_2$, phase diag., electrophys. props. of solid solns. 77—52306
$SnTaS_2$ intercalate, cryst. struct. determ. 78—26534
SnTaS(Se), struct., X-ray powder diffr. meas 80—44175
SnTe, polymorphism, high press. and temp., X-ray diffr. study 80—54375
SnTe, struct. factors, rel. to temp.-depend. ^{119}Sn isomer shift 77—8457
SnTe-InTe, SnTe-In_2Te_3, solid soln. region, lattice constant variation 77—35697
$Sn_{10}W_{16}O_{46}$, cryst. struct. determ. 80—33934
$Sn_{10}W_{16}O_{46}$, struct. anal. and stereoactivity of Sn^{II} lone pair 80—33935
Sr Nb_2O_6, crystallography, polymorphism and isomerism, X-ray diffr. and DTA study 80—100216
$SrAg_2I_4.8H_20$, cryst. struct. 79—23575
$Sr_2Al_2GeO_7$, gehlenite struct., synthesis and physicochem. props. 79—43181
$SrAl_2O_4$, cryst. struct. with 3D framework 79—86766
$SrAl_2O_4$, X-ray powder diffr. data 79—51071
$Sr_4Al_4O_2[Al_{10}O_{23}]$ 77—31651
$SrAl_2SiO_8$, micro-crystal, appl. of method for indexing *(German)* 78—22608
$SrB_{12}H_{12}.10H_2O$, struct. dehydration, intermediate phases and thermooxidative degradation 80—33951
$Sr_3B_2O_6$, synthesis, struct. and mag. props. 77—89934
$SrBaNaNb_5O_{12}$, X-ray powder diffraction data determ. *(Chinese)* 80—70170
$Sr_{1-x}Ba_xZrO_3$, struct., X-ray powder diffr. study 80—1989
$SrBi_6Ti_3Nb_2O_{21}$, cryst. struct. and dielec. const. 77—47428
$SrBi_8Ti_7O_{27}$, mixed-layer compound, synthesis and struct. 77—35530
$Sr_2Bi(Y)RuO_6$, perovskites, prep., struct., emission control catalysts 77—68957
$SrBr_2$-H_2O, ^{79}Br NQR, cryst. struct. 78—27110
$Sr(Ca_{1/3-x}Sr_xNb_{2/3})O_3$, perovskite, X-ray and electron diffr. study *(French)* 79—99161
$SrCl_2$, orthorhombic, lattice parameters meas. 77—15382
$SrCl_2$, specific heat anomaly and sublattice disorder, neutron diffr. meas. 79—42238
$SrCl_2$, superionic, quasielastic neutron scatt. 78—79504
$SrCl_2$, valence-electron charge density along nearest-neighbour axis 79—27944
$SrCoO_{3-\delta}$, crystal struct. and mag. props., O vacancy effect 79—95587
$Sr_{1-p}Cr_2S_{4-p}(Se_{4-p})$, modulation of intergrowth struct. 79—94967
Sr_2EuAlO_5, X-ray cryst. struct. refinement 79—60318
Sr_2EuFeO_5, X-ray cryst. struct. refinement 79—60318
SrF_2-$(Y,R)F_3$, R=rare earth, phase equilibria, X-ray characts. of phases 79—61570
$SrF_{2-x}H_x$, synthesis and struct. determ. using neutron diffr. *(French)* 80—24425
$Sr_2Fe_xRu_{1-x}O_4$ solid soln., Mossbauer spectrosc. study 80—50235
$SrGa_{12}O_{19}$, single crystal growth, lattice const. meas. *(German)* 80—44159
$SrGa_2Si_2O_8$, ordered synthetic feldspar, cryst. struct. 78—34469
$SrGeO_3$, second modification 78—22702
Sr_2GeO_4-$Sr_3(PO_4)_2$, phase equilibria and struct. 77—85999
$SrHAsO_4$, weilite, cryst. struct. 78—38671
$Sr(H_2AsO_4)_2$, X-ray powder diffractometry, cryst. struct. determ. *(French)* 79—60317
α-$SrHPO_4$, triclinic, crystal structure determination *(French)* 78—91315
$SrIn_2Se_4$, cryst. struct. *(German)* 80—79760
$SrLaBO_4$, crystallographic and Pb^{2+} luminesc. data 79—32971
$SrLaCoO_4$, struct. and mag. props., electronic struct. of trivalent Co *(French)* 79—86760
$SrLaFeO_4$, mag. and cryst. struct. determ. *(French)* 80—54866
$SrLaFeO_4$, two-dimens. mag. props. rel. to cryst. struct. 80—75776
$Sr_{1+x}La_{1-x}MnO_4$, X-ray obs. *(French)* 78—6042
Sr_2MNbO_6, (M=Ti, Zr, Nb), perovskite struct., synthesis, lattice constants and elec. props. 77—21369

crystal atomic structure of inorganic compounds continued
$Sr_3M_6Si_4O_{26}$, M=Nb,Ta, IR spectra and cryst. struct. *(French)* 79−11418
$Sr_2MTa_5O_{15}$ (M=K, Rb, Tl, Cs), relative stability of struct. types, and piezoelec. props. *(French)* 80−49206
$Sr(ND_2)_2$, neutron diffraction exam. 31 to 570K, temp. depend. of lattice parameters *(German)* 79−69085
$Sr(NO_3)_2$, Raman and infrared spectra, structure of nitrate ion from space groups 78−43002
$Sr_{2.05}Na_{0.90}Nb_5O_{15}$, X-ray powder diffraction data determ. *(Chinese)* 80−70170
$SrNb_2O_6$-$NaNbO_3$-$LiNbO_3$ pseudo-ternary system, DTA, heat treatment and X-ray diffr. obs. *(Chinese)* 79−52175
$Sr_2Nb_2O_7$, crystal struct. and phase transitions, rel. to isomorphous crystals *(Japanese)* 80−49208
SrO, at. charge densities, X-ray struct. factors 78−79566
SrO-B_2O_3, ^{11}B NMR lineshape, BO_3^{-3} triangle, perfect trigonal symm. *(Korean)* 78−19367
4 $SrO.B_2O_3.SiO_2$, crystal struct., X-ray powder diffr. patterns *(Japanese)* 80−54209
α-$Sr_2P_2O_7$, Raman, IR spectra, factor group anal. and band assignment 78−35126
$Sr_5(PO_4)_3Cl:CrO_4^{3-}$, EPR, cryst. field parameters 79−87309
$SrRMnO_4$, (R=La,Nd,Sm,Gd), X-ray obs. *(French)* 78−6042
$Sr_3Re_2O_9$, cryst. struct., mag. and semicond. props. 79−10836
Sr_xReO_3 ($0.4 \leq x \leq 0.5$), cryst. struct *(French)* 79−65041
SrS_2, prep. at high press., cryst. struct. determ. by X-ray diffr. 77−4077
$SrSO_4$, celestite, crystal struct. and sulphate force consts. 78−83784
$SrSb_2O_5$, $SrSb_4O_9$, $SrSb_6O_{10}$, mixed valence cpds., prep., IR and X-ray investigation *(French)* 78−88292
$Sr_7Sb_2O_{12}$, prep. and cryst. struct. *(French)* 79−32967
$SrSi_2$, dimorphic, transform. of three-dimens. three-connected Si nets 78−42944
$SrSi_2$, high-pressure phase transform., cryst. struct. 77−35693
Sr_2SnS_4, $Sr_3Sn_2S_7$, prep., cryst. structs. *(French)* 79−34013
$SrTa_2O_6$, structural study X-ray diffr., IR absorpt. and Raman spectra *(French)* 80−107173
$Sr_2Ta_2O_7$, crystal struct. and phase transitions, rel. to isomorphous crystals *(Japanese)* 80−49208
$SrTeO_4$, powder diffr. cryst. struct. determ. 79−42020
$SrTiF_6.2H_2O$, cryst. struct. refinement 79−94979
$Sr_6Ti_2Nb_4O_{20}$, new class of layer ferroelectrics. X-ray anal. and permittivity meas. 77−16266
$SrTiO_3$, flame fusion growth, dislocation density, lattice const. and EPR spectra 78−11099
$SrTiO_3$, low temp. phase, X-ray cryst. struct. anal. at 77K 79−37683
$SrTiO_3$, mean square atomic displacement temp. depend., sublattice vibration anharmonicity 80−79890
$SrTiO_{3-x}$, anion deficiency and anion vacancy ordering 78−51532
$SrTiO_{3-x}$, struct. of anion-deficient compound 78−22708
$SrUO_4$, α to β transition, anomalous behaviour 78−10182
$Sr_3VTa_2O_9$, prep., characterisation and mag. props. 78−26535
Sr_5X_3, α, intermediate phases, cryst. struct. (X=IIb, IIIb, IVb, Vb element) 78−83793
$SrZrO_3$ 77−15351
$SrZrO_3$, high temp. phases, struct. determ., soft mode transitions 78−42942
$Sr_3Zr_2O_7.2H_2O$, cryst. struct. and thermal stability, X-ray characterisation 78−83796
$Sr[Fe(CN)_5NO].2H_2O$, cryst. and mol. struct. 78−91311
$Sr[Fe(CN)_5NO].4H_2O$, cryst. and mol. struct. 77−58982
Ta-Ga, at high press. polymorphism 80−88112
Ta_3As, X-ray cryst. struct. determ. 79−69078
TaC_x, static distortions and Debye temp. determ., neutron diffr. exam. *(Russian)* 77−80482
$Ta_2Co_4O_9$, flux growth and chem. characts. 78−23595
Ta_2D_{1+x}, atomic displacement of Ta determined by deuteron magnetic resonance 79−37701
Ta_2H, single cryst., X-ray diffr. study on H ordering 79−14736
TaH(D), structs. phase diagrams, morphologies, prep. methods, book contrib. 80−25675
$TaH_x(D_x)$, cryst. struct., phase diagrams, order-disorder transition 78−55836
$(TaI_5)_2$, X-ray cryst. struct. determ. *(German)* 80−19754
ε-TaN, cryst. struct. determ. by neutron diffr. exam. 78−26522
β-Ta_2N, growth by annealing Ta in N_2, cryst. struct. 77−35533
β-Ta_2N-εTaN, prep. by exothermic reaction and by zone melting, cryst. struct. 77−35533
Ta_3N_5, polycryst. film, electron diffr. *(French)* 77−76677
TaO_x film, optical const. var. with struct., ellipsometric meas. 77−63478
$2Ta_2O_3$ thin film, FCC cell struct. investigation 80−92796
Ta_2O_5 doped systems, struct. and ordering, high resolution TEM obs. 78−35378
Ta_2O_5, ε-modification, cryst. struct. and microstruct. 79−51083
Ta_2O_5, with hexagonal lattice in thin layers, atomic struct., electron diffr. 80−84160
Ta_xO_y deficient $Ta_{10}O_{18}$ struct., monoclinic, cryst. struct. by electron diffr. 77−39570
$Ta(OR)_2Cl_3.L$, halo-alkoxide complex, prep. and props. 78−18605
TaS_2 (1T) electron irradiated, lattice contraction 80−59520
TaS_2 (2H) intercalated with pyridine, ionic bonding model 79−65052
TaS_2, alkali metal and alkali metal hydroxide intercalates, lattice parameters, supercond. transition temps. 80−25029
TaS_2 intercalate with tetraalkylammonium hydroxide, prep. and struct. 80−79752
TaS_2/pyridine intercalated, struct. and bonding 78−91323
TaS_3, electron diffr. evidence for one-dimens. Peierls distortion 78−10024
TaS_3, monoclinic form, cryst. struct. determ., Peierls type transition obs. *(French)* 80−88109
TaS_3, one-dimensional compound, phase anal., X-ray and elec. meas. 79−51086
$TaS_2(NH_3)$ and $TaS_2(NH_3)_{1/3}(H_2O)_{2/3}$, incoherent inelastic neutron spectra 80−84163
$TaS_3(Se_3)$, phase transitions and elec. props. 80−20178
$TaS_3(1T)$, inequivalent lattice sites in charge density distorted phases 80−15835
$TaSe_2$ (4Hb), atomic displacements in CDW induced superstructure 80−10536
$Ta_xTi_{1-x}Se_2$, cryst. struct. and elec. props. 79−47133

crystal atomic structure of inorganic compounds continued
Ta_2WO_8, neutron powder diffr. study of cryst. struct., profile anal. 79−55706
$TbAsO_4$, cryst. struct. by X-ray diffr. co-operative Jahn-Teller transition 77−89411
$TbAsO_4$, cryst. struct. refinement at 77K and 5K by profile anal. from neutron diffr. powder data 79−37677
TbF_3, crystal structure by powder neutron diffr. study 80−15077
$TbFe_2B_2$, compounds with $CeAl_2Ga_2$ structure type *(Ukrainian)* 79−32970
$TbGa_3(BO_3)_4$, luminesc. spectra, local symmetry of rare earth ion determ. 80−16095
Tb_3InO_6, high press. synthesis, cryst. struct. 77−68955
$Tb_3In_5S_{12}$, crystal struct. determ. *(French)* 77−43179
$Tb(MoO_4)_3$ cryst. struct. in ferroelec., ferroelastic, antiferroelec. and paraelastic phases 80−75205
$Tb_2(MoO_4)_2$, ferroelectric-ferroelastic crystal, room temp. crystal struct., X-ray scatt. 80−28978
$Tb_2(MoO_4)_3$, lattice constants determ. in temp. range 296 to 503K 79−14943
$Tb(OH)_3$, neutron diffr. struct. exam. 78−2077
$Tb_2O_3.Si_3N_4$, prep. by sintering and X-ray diffr. data 79−77570
$Tb_4Si_2O_7N_2$, prop. and X-ray diffr. powder data 80−33944
Te complex, bis(pyridium) hexachlorotellurate(IV), cryst. struct. *(French)* 80−28965
$Te_3Nb_2O_{11}$, cryst. struct. 79−55715
TeO_2-BaO, cryst. chem. study, X-ray diffr. powder data *(French)* 80−15080
TeO_2-CaO, cryst. chem. study, X-ray diffr. powder data *(French)* 80−15080
TeO_2-CdO, cryst. chem. study, X-ray diffr. powder data *(French)* 80−15080
TeO_2-ZnO, cryst. chem. study, X-ray diffr. powder data *(French)* 80−15080
$Te(OH)_6$, X-ray diffr. cryst. struct. refinement 78−95022
$Te(OH)_6.Cs_2HPO_4$, cryst. struct. 80−64975
$Te(OH)_6.Cs_2HPO_4.2CsH_2PO_4$, cryst. struct. 80−64975
$Te(OH)_6.Na_2HAsO_4.H_2O$, synthesis and cryst. data *(French)* 80−33948
$Te(OH)_6.Na_2HPO_4.H_2O$, X-ray cryst. struct. determ. *(French)* 79−69077
$Te(OH)_6.Rb_2HAsO_4.Rb_2H_2AsO_4$, synthesis and cryst. data *(French)* 80−33948
$Te(OH)_6.2(NH_4)_2HAsO_4$, synthesis and cryst. data *(French)* 80−33948
$Te(OH)_6.2(NH_4)_2HPO_4$, X-ray cryst. struct. determ. *(French)* 79−69077
$Te(OH)_6$.diurea complex, cryst. struct. determ. 80−28971
$(Te_2O_3)SO_4$, cryst. struct., X-ray diffr. meas. 77−4078
Th-C-N system, existence of new β'ThCN' phase, struct. and thermodynamic study *(French)* 80−92499
ThBC, crystal struct. 78−55853
ThBC, crystallographic relationship with with CrB, α MoB, UBC 79−42025
$Th_3B_2C_3$, crystal struct. 79−14772
$Th(CO_3)_5^{6-}$, in Na and guanidinium salts, struct./props. correlation *(French)* 78−95032
$(ThCu_3)(Mn_2Fe_2)O_{12}$, synthesis, cryst. struct. and Mossbauer exam. 78−84505
Th_4D_{15}, cryst. struct. meas. by neutron diffr. with spallation neutron source 77−43190
ThF_4, monoclinic, lattice parameters and thermal contraction coeff., 25 to 83°C 77−47607
$Th_6F_{24}.H_2O$, X-ray cryst. struct. determ. and refinement 79−90603
$Th_4H_{15}(D_{15})$, massive, prep. and characts., supercond. props. 77−43768
$Th_{0.25}NbO_3$, cryst. struct., X-ray diffr. obs. *(French)* 79−1413
$Th_{0.25}NbO_3$-$xNaNbO_3$ solid soln., cryst. struct., perovskite-type phases, X-ray diffr. obs. *(French)* 79−1413
$Th(ReO_4)_4$-$M(KeO_4)$, (M=Na, K, Rb, Cs, Tl) crystallographic data for perrhenates of the actinides and their hydrates, thermal stability *(French)* 79−69091
α-$ThSi_2$-AlB_2 series, struct., symm. and rel. to other linear structs. 77−11525
$ThSiO_4$, huttonite and thorite polymorphs 78−51478
$Th(VO_3)_4$, crystallographic data *(French)* 78−63725
Ti complex, $Ti_2Cl_8(CH_3NO_2)_2$, single cryst., struct., IR and Raman spectra, X-ray diffr. 78−43000
Ti complex, $TiOCl[Co(cyclopentdienyl)_2]_{0.16}$, sxnthesis and struct. 80−44176
Ti garnets, synthetic, IR spectra, Ti struct. role 80−7346
Ti-N system, phase relations, struct. rel. to heat treatment 79−11552
Ti-N_2, condensate formed by plasma flow precipitation in vacuum, cryst. and surface props. *(Russian)* 80−100788
Ti-S, two novel polytype structs. in the system, 16H and 18H *(French)* 79−7582
26H Ti-S polytype, struct. determ. *(French)* 77−11509
TiC-TiN, physicochem. props., comp. depend. 80−55370
TiC-VC, mag. susceptibility, elec. cond. and thermoelec. props. 80−50033
TiC-ZrC, mag. susceptibility, elec. cond. and thermoelec. props. 80−50033
TiC_x, static distortions and Debye temp. determ., neutron diffr. exam. *(Russian)* 77−80482
$TiC_{1-x}N_x$, lattice distortion of ordered phase *(Ukrainian)* 78−68680
TiC_xN_y, neutron diffr. investig. 77−51355
TiC_xO_y, lattice completeness and period 78−22706
TiC_xO_y, structural mechanism of O inclusion into lattice 78−22707
$TiCuD_{0.90}$, neutron powder diffr. study for cryst. struct. refinement 78−95018
TiD_x, α- and β-phases, D-site occupancy, neutron diffr. study 79−42014
$TiFeH_x(D_x)$, struct., phase diagram, thermodynamics and diffusion *(German)* 79−56963
$Ti(HPO_4)_2 \times H_2O$, cryst. struct. 79−42023
$TiH(SO_4)_2.4H_2O$, cryst. parameters and X-ray powder diffr. data *(French)* 79−14765
TiN, synthesised in SHF discharge plasma, exam. of props. *(Russian)* 80−7524
TiN_x, cryst. and internal structs., electron diffr. and microscopy 77−27861
TiN_x, film, non-stoichiometry rel. to optical characts. 77−12456
$TiN_{0.32}H_{0.19}$, cryst. struct., neutron diffr. anal. *(Russian)* 80−64965
TiN_zO_y, cubic, concentration dependence of the degree of filling of unit cell 78−44063

crystal atomic structure of inorganic compounds continued
- TiN_zO_y, cubic, thermal expansion coeffs., Ti-Ti bond screening 79−10970
- TiN_zO_y, phase and structural features 77−48411
- $Ti_{0.5}NbSe_2$, cryst. struct., metallic cond., mag. and phys. props. *(French)* 80−33956
- TiO, ordered phase, vacancy-strain coupling 78−79549
- TiO, X-ray diffraction, cubic and monoclinic phases of Kelley's sample 77−51356
- $TiO_{0.3\text{-}0.5}$, O atom ordering, electron microscopy obs. 79−99150
- TiO_2, crystal structure, stability compared with CaF_2 *(Russian)* 80−64945
- TiO_2 film, electron diffr. exam. 78−79906
- TiO_2, hexagonal, implications for Earth's lower mantle 78−61371
- TiO_2, rutile, electron diffr. patterns and extinction distances 77−76363
- TiO_{2-x} reduced, crystallographic shear planes, dislocation struct. 80−107175
- TiO_y, thermal expansion of cubic phase at low temp. X-ray diffr. anal. 79−1514
- Ti_2O_3, $(Ti_{0.98}V_{0.02})_2O_3$, lattice parameters, temp. depend. 77−11855
- Ti_2O_3, electron density distrib., deform. density at 295K, X-ray anal. 80−107117
- Ti_2O_3, struct. changes at semicond.-metal transition 77−47397
- Ti_2O_3:$Sc_2O_3(Al_2O_3)$, struct. changes on Sc(Al) substitution 77−55276
- Ti_2O_3:V(Al)(Sc), crystal struct. and metal-metal distance, rel. to electronic struct. 77−47431
- Ti_4O_7 and $(Ti_{1-x}V_x)_4O_7$, metal-insulator transitions, EPR, elec. and mag. props. 80−2336
- Ti_5O_9, phase transitions, elec. cond., mag. susceptibility, sp. ht., EPR and struct. aspects 78−10526
- Ti_6O_{11}, electron-optical imaging, at 1.6 Å point-to-point resolution 79−46531
- TiO_yH_m, thermal expansion of cubic phase at low temp. X-ray diffr. anal. 79−1514
- $TiO_yN_zH_m$, m=0, 0.31-0.34, thermal expansion, H at. ordering 79−10971
- Ti_3P-type structures, atomic coord. and bonding 79−60330
- $TiS_{1.46}$, $(4H)_2$-4C type superstruct., high resolution electron microscopy determ. 79−69060
- $TiS_{1.5}$, $(4H)_3$-6C-type superstruct. revealed by high resolution microscopy 80−19755
- $Ti_{1+x}S_2$, polytypic struct., Ti ordering, two-dimensional model 79−14776
- $TiS_2(Se_2)$, and alkali metal intercalates, phys. props. 80−44179
- Ti_5Sb_3, struct. study, space groups *(French)* 77−68949
- $Ti_3Sc_4O_{12}$, cryst. struct. determ., powder X-ray diffr. exam. 77−4083
- $TiSi_2$, crystal atomic struct., X-ray diffr. exam., lattice parameters and integrated intensities 78−75647
- $TiSi_2$, struct. refinement and bonding 77−72592
- $Ti_{1-x}Ta_xO_2$, solid soln. formed in TiO_2-Ta_2O_5-Ta at 1100°C *(French)* 78−35375
- $TiTe_2$, struct. refinement by neutron diffr. 79−27967
- $Ti_{1-y}V_yH_x$, electronic props., H alloying effects, book contrib. 79−82522
- $(Ti_{0.9975}V_{0.0025})_4O_7$, metal-insulator transition, struct. aspects 79−86752
- $(Ti_{1-x}V_x)_2O_3$ solid soln., struct. changes comp. depend. 77−55275
- Tl chalcogenides, cryst. struct. types 77−15392
- Tl-Se-$TlInSe_2$, isomorphic pairs, struct. and growth peculiarities 79−1421
- Tl-V-S system, crystallographic data and phys. props of some phases *(French)* 79−99163
- $TlAlF_4$, single cryst., prep. and struct. *(French)* 80−79762
- $TlAsS_4$, struct. and soft mode behaviour 78−91327
- Tl_3AsS_4, crystal growth by Bridgman-Stockbarger method, exam. of props. 79−11506
- $TlAsTe_2$, local struct. changes on crystal-glass transition, Mossbauer spectra 77−36157
- $Tl_2B_{12}H_{12}$, cryst. growth from soln. and morphology 77−44145
- $TlBO_2$, X-ray single cryst. struct. determ. *(French)* 79−32974
- $Tl_2B_4O_7$, polymorphism *(French)* 78−6035
- $TlBO_2.xH_2O$, x=0, 0.5, 1 and 2 cryst. chem. *(French)* 78−18606
- Tl_2BRCl_6, B=Li,Ag,Na, systematic structs., X-ray Guinier-Simon method *(German)* 80−44186
- TlBS, synthesis, struct., optical, spectral props. 79−15631
- $Tl_4Bi_2S_5$, X-ray cryst. struct. determ. *(French)* 79−69063
- TlBr-VBr_2 system, cryst. struct., DTA investig. *(German)* 78−72766
- $TlCdI_3$, X-ray cryst. struct. determ. and refinement 79−69070
- $TlCoCr_2(VO_4)_3$, synthesis and cryst. struct. 80−88114
- α-Tl_4CrI_6, prep. and cryst. struct. determ. 80−28957
- $Tl_2Cr_2O_7$, $Tl_2Mn_2O_7$, pyrochlore type, synthesis and physical props. 80−33963
- $TlCuCr_2(VO_4)_3$, synthesis and cryst. struct. 80−88114
- Tl_2CuI_3, melting point, cryst. struct., DTA, X-ray diffr. *(French)* 77−84710
- $TlEr(MoO_4)_2$, polymorphic transition characts., temp. regions of stability 79−14785
- $TlGaTe_2$, multilayer cryst., lattice vibr. symm., IR absorpt. and Raman scatt. selection rules 80−39231
- $Tl_8Ge_5O_{14}$, X-ray cryst. struct. determ. and refinement *(French)* 79−46607
- $Tl_4Ge_2S_6$, cryst. struct. determ. *(German)* 78−79577
- $Tl_4Ge_4S_{10}$, cryst. struct., X-ray diffr. meas. *(German)* 77−4074
- $TlHF_2$, struct. and phase change 77−51996
- TlH_2PO_4, X-ray cryst. struct. refinement *(French)* 79−37666
- $TlH_5(PO_4)_2$, X-ray cryst. struct. determ., Patterson and Fourier methods *(French)* 79−14741
- Tl_2HPO_4, X-ray cryst. struct. determ. and refinement *(French)* 80−19756
- $TlH(SO_4)_2.4H_2O$, cryst. parameters and X-ray powder diffr. data *(French)* 79−14765
- $Tl_6I_6M_{2/n}{}^{n+}(I_4)^{2-}$, (M=Pb, Ag, Au, $(Bi_{0.5}Tl_{0.5})$), struct., rel. to phonon spectra 80−71425
- $TlInSe_2$-$TlPrSe_2$ system, struct., elec. cond., and thermoelec. props. 79−87119
- $TlInSe_2(Te_2)$, multilayer cryst., lattice vibr. symm., IR absorpt. and Raman scatt. selection rules 80−39231
- $TlLu(MoO_4)_2$, polymorphic transition characts., temp. regions of stability 79−14785
- $Tl_{12}M_{33}O_{90}(.12H_2O)$, cation exchanger with intersecting tunnel struct. *(French)* 78−20014
- $TlMgCr_2(VO_4)_3$, synthesis and cryst. struct. 80−88114
- Tl_2MoO_4, prep., characterisation 78−63731
- $Tl_2Mo_4O_{13}$, X-ray cryst. struct. determ. *(French)* 79−14748

crystal atomic structure of inorganic compounds continued
- $Tl_2Mo_8S_{11}$, X-ray cryst. struct. determ., Mo_{12} and Mo_6 isolated clusters *(French)* 80−92490
- $Tl_2Mo_9S_{11}$, prep. and struct., Mo_{12} cluster in $Mo_{12}S_{14}$ unit 80−107168
- $Tl_2Mo_6Se_6$, X-ray cryst. struct. determ., monodimensional clusters $(Mo_{6/2})^1\infty$ *(French)* 80−96482
- $TlMo_3Se_3(Te_3)$, synthesis and struct. 80−92498
- $Tl_{0.33}(NH_4)_{0.67}H_2PO_4$, X-ray crystallographic investig. *(French)* 80−49192
- $Tl(NO_3)_3(H_2O)_3$, cryst. struct. determ. 78−59790
- $Tl_3Na(SO_3)_2$, α-phase, IR and Raman spectra, order of cryst. struct. *(French)* 77−85718
- $TlNbO_3$ and $Tl_3Nb_{16}O_{41}$, new phase of mixed oxide 78−59787
- $TlNb_{3+x}O_{9-y}$, hexagonal bronze type with excess cations *(French)* 77−72591
- $Tl_{7.7}Nb_{54+x}O_{146-y}$, single crysts., synthesis and X-ray cryst. struct. determ. 79−69065
- $Tl_8Nb_{22}O_{59}$, synthesis and struct. *(French)* 77−24294
- $Tl_xNbO_{2+x}F_{1-x}$ $(0.5\leq x\leq 1)$, heavy ion location Tl^+, and struct. refinement *(French)* 79−73144
- $Tl_2Nb(Ta)_6TiO_{18}$, structs. with intersecting tunnels, Tl distrib. *(French)* 78−79586
- $TlNd(PO_3)_4$, cryst. struct. determ. 79−19216
- $TlNiCr_2(VO_4)_3$, synthesis and cryst. struct. 80−88114
- β-Tl_2O-Al_2O_3, cation distrib. 77−80487
- Tl_2O-GeO_2 system, structure of thallium I germanates *(French)* 80−79754
- Tl_3PSe_4, struct. and soft mode behaviour 78−91327
- $(Tl_{0.75}Pb_{0.25})_4Cl_5$, cation disordered phase, X-ray diffr. determ. of cryst. struct. 80−1985
- $TlR(MoO_4)_2$ (R=La to Ho), polymorphism, X-ray diffr., thermographic anal. 78−47269
- $TlRO_3$ (Ln=La, Nd, Sm, Eu, Gd), determ. of lattice parameters *(French)* 78−95031
- $(Tl_2S)_{3x}$-$(Sb_2S_3)_{1-x}$, phase equilibria and struct. of cpds. 77−85996
- Tl_5SbO_6, isomorphism with Tl_2SnO_3 *(French)* 78−10012
- $Tl_{0.51}Sb_{0.71}{}^{III}Sb_2{}^{V}O_{6.32}$, X-ray cryst. struct. determ. *(French)* 79−69079
- Tl_2SnSe_3, obs. in $SnSe_2$-Tl_2Se system, X-ray diffr. meas. *(French)* 77−51471
- Tl_2SnSe_3, preparation, Mossbauer spectra 77−28489
- Tl_2SnSe_3, X-ray cryst. struct. determ. *(French)* 80−107171
- Tl_4SnSe_4, preparation, Mossbauer spectra 77−28489
- $Tl_{4.62}Ta_{11.08}O_{30}$, cryst. struct. determ. *(French)* 79−69092
- $Tl_{1+x}Ta_{1+x}W_{1-x}O_6.nH_2O$, pyrochlore type, stoichiometry and ionic cond. 80−24648
- Tl_2TeO_3, $Tl_2Te_3O_7$, $Tl_2Te_2O_5$, Tl_2TeO_6, Tl_6TeO_{12}, synthesis, thermal stability, crystallographic data *(French)* 78−51518
- Tl_6TeO_6, solid, prep., thermal stability, cryst. parameters *(French)* 79−65037
- $TlTiMO_5$ (M=Ta, Nb), ion exchange props., synthesis and crystallographic props. *(French)* 80−28997
- $Tl_{1-x}(Ti_{1-x}Nb_{1+x})O_5$, layer compound, cryst. struct., nonstoichiometry 80−64972
- $Tl^ITl^{III}(SeO_4)_2$, $Tl_3{}^ITl^{III}(SeO_4)_3$, and $Tl_5{}^ITl^{III}(SeO_4)_4$, cryst. struct. *(French)* 80−84148
- $TlTm(MoO_4)_2$, polymorphic transition characts., temp. regions of stability 79−14785
- $TlUF_5$, X-ray cryst. struct. anal. *(French)* 80−54184
- $Tl_2U_yF_{x+4y}$, cryst. growth from flux, crystallographic characts. *(French)* 77−77364
- $Tl_{0.25}VF_3$, cryst. struct. examination by electron diffr. using TEM 79−23583
- $TlVO_3$, X-ray determ. 78−6043
- $TlVO_4$, synthesis and thermal props. *(French)* 80−97443
- $Tl_{1.74}V_8O_{16}$, hollandite-type struct., synthesis and cryst. struct. 80−29003
- TlV_5S_8, prep., props. and cryst. struct., metallic behaviour 77−27864
- Tl_3VS_4, cryst. struct., X-ray diffr. obs. *(French)* 79−14763
- $Tl_xV_6S_8$, prep., struct., props. 77−19935
- $Tl_{0.3}WO_3$, struct. anal. *(French)* 78−59786
- Tl_2WO_4, solid-state prep., cryst. struct. and props. 78−38673
- Tl_2WO_4, X-ray cryst. struct. determ. 79−99136
- $Tl_2W_4O_{13}$, tunnel struct., related to hexagonal tungsten bronze 80−28988
- $TlY(MoO_4)_2$, polymorphic transition characts., temp. regions of stability 79−14785
- $TlYb(MoO_4)_2$, polymorphic transition characts., temp. regions of stability 79−14785
- Tl_2ZnI_4, fast ionic cond., order-disorder transition, and cryst. struct. 79−99363
- $Tl_2[Fe(CN)_5(NO)]$, X-ray cryst. struct. determ., heavy atom method 80−92495
- $TmBO_3$, cryst. struct. reappraisal 77−47427
- TmFX mixed halides, synthesis and lattice parameters 78−30594
- $TmFe_2B_2$, compounds with $CeAl_2Ga_2$ structure type *(Ukrainian)* 79−32970
- $Tm(OH)_3$, cryst. struct. 80−24424
- Tm_xSe, low temp. props., effect of composition 77−80775
- $Tm_2Si_2O_7$, crystal struct. of X form, polymorphism under press. *(French)* 77−47430
- $Tm_2Si_2O_7$, polymorphism under press., cryst. struct. 77−35692
- U complexes, UT_5 and $UTCl_4$, (T=tropolone), synthesis, cryst. struct. parameters 80−33945
- U-C-N system, high temp. X-ray diffr. exam. of structure *(French)* 78−72765
- UAsSb, prep. and struct. 77−68951
- UBC, crystallographic relationship with with CrB, α-MoB, ThBC 79−42025
- UBr_5, cryst. struct. investig., powder neutron diffr. 78−91321
- UC 80−15046
- UC, fission dose depend. of lattice parameter changes 77−24333
- UCo_5Si_3, X-ray cryst. struct. anal. 79−60342
- UCr_2O_6, hydrothermal cryst. growth, 40 kbar, 873K, cryst. struct. *(French)* 78−35342
- β-UF_5, single cryst. struct., coordination of U^V 77−11512
- UFe_2O_6, hydrothermal cryst. growth, 40 kbar, 873K, cryst. struct. *(French)* 78−35342
- $UMnNiO_6$, hydrothermal cryst. growth, 40 kbar, 873K, cryst. struct. *(French)* 78−35342
- UMn_2O_6, hydrothermal cryst. growth, 40 kbar, 873K, cryst. struct. *(French)* 78−35342
- $U_2Mn_3Si_5$ 78−26550

crystal atomic structure of inorganic compounds continued
$UNi_{1.4}Si_{3.6}$, X-ray obs. *(Russian)* 77−76361
UNi_2Si_3, X-ray obs. *(Russian)* 77−76361
UNi_5Si_3, X-ray crystal struct. determ. 77−7701
UO_2, cluster-type fuel for ATR, lattice parameter meas. and neutron behaviour 77−46282
UO_2 fluorides, $M_2^I[M^{II}(H_2O)_6][(UO_2)_2F_8]$, M^I=K, Rb, or Cs and M^{II}=Mn, Co, Ni, Cu, Zn or Cd, struct. and IR spectra 77−35525
UO_2, neutron diffr. extinction, wavelength depend. 78−38588
UO_2 powder, temp. depend. of atomic thermal displacements, Rietveld profile-refinement procedure 80−49190
UO_2, reanal. of neutron diffr. data 80−15084
UO_2, single crysts., nucl. neutron diffr. intensity meas. analysis, extinction 79−27957
UO_2, single-cryst. neutron diffr. data, reanal. using third cumulants 80−100130
γ-UO_3, neutron powder profile obs. 77−15337
α-U_3O_8, cryst. struct. 78−6039
U_3O_{8-z}, thermal expansion, phase transforms. rel. to temp. 77−35721
UO_2Br, X-ray struct. determ., heavy-atom method *(French)* 77−80454
$(UO_2)_2Cl_3$, prep. and cryst. struct. 78−38674
$U_2O_2Cl_5$, prep. and cryst. struct. *(French)* 80−84150
α-UOF_4, neutron diffraction study 78−14327
$UOF_4.nSbF_5$ (n=1, 2 or 3), preparation and cryst. struct. *(French)* 79−51062
$UO_2(NH_2O)_2.2(NH_3O).2H_2O$, neutron diffr. cryst. struct. determ. 79−19206
$UO_2(NH_2O)_2.3H_2O$, low temp. neutron anal X-ray diffr. exam. 78−2068
α-$UO_2(NH_2O)_2.4H_2O$, low temp. neutron diffr. exam. 78−26518
β-UO_2SO_4, X-ray and neutron powder diffr. cryst. struct. anal. 79−14760
UO_2SeO_3 78−51490
UO_2SeO_4, α- and β-phases, X-ray and neutron powder diffr. cryst. struct. anal. 79−14760
UO_2TeO_3 78−51490
UOX_2 (X=Cl, Br, I) crystal struct., IR spectra, and mag. meas. *(French)* 79−60331
$(UO_2)_2[SiO_4](H_2O)_3$, synthetic soddyite cryst. stuct., powder photographs 80−39050
$UScS_3$, cryst. struct. determ. *(French)* 78−79576
$(U_xTh_{1-x})Te$, lattice parameters, room temp. obs. 77−20551
UZr_6FO_{14}, X-ray cryst. struct. determ. and refinement *(French)* 80−107122
V complex, α-α'-dipyridil iminodiacetato oxovanadium (IV), cryst. struct. 79−69086
V complex, VOCL $[Co(cyclopentadienyl)_2]_{0.16}$, synthesis and struct. 80−44176
V-C-O, phase relations 79−96012
V-O system, structure of γ-phase *(Ukrainian)* 79−51063
V-O system β phase BCT, X-ray diffr. study of additional scatt. effect *(Russian)* 80−10537
$V_{0.985}Al_{0.015}O_2$, struct. aspects of metal insulator transitions 78−18965
VC, damage sustained during neutron irradiation 77−1841
VC_x, static distortions and Debye temp. determ., neutron diffr. exam. *(Russian)* 77−80482
V_2C, X-ray determ. of rhombic modification *(Ukrainian)* 79−77564
VC_xN_y, superstructure induced by ageing, neutron diffr. obs. *(Russian)* 80−49195
$V(CO)_6$, cryst. and mol. struct., Jahn-Teller distortion, mol. vib. and librational correction 79−32949
VC_xO_y, conc. depend., of unit cell filling degree 80−54199
V_2Cg, struct. and orientation of rhombic modification *(Russian)* 77−55270
$(V_{1-x}Cr_x)_2O_{3+y}$, elec. props. and struct. 80−84494
V_2D, single crystal, superstructure modulation and long range order, X-ray obs. 78−71712
VF_2, prep., struct., heat capacity 5-300K, mag. ordering 79−86746
$V_{1-x}Fe_xO_{2-x}F_x$, $0<x<0.2$, phase diagrams, ^{57}Fe-Mossbauer spectra, X-ray diffr. studies *(German)* 80−29663
VH(D), structs. phase diagrams, morphologies, prep. methods, book contrib. 80−25675
$VH(SO_4)_2.4H_2O$, cryst. parameters and X-ray powder diffr. data *(French)* 79−14765
$V_{1-2x}M_x^{2+}N_x^{6+}O_2$, (M=Ni,Cu,Mn, N=W,Mo,Te) cryst. struct., transitions and thermal effects 77−68950
$V_{1-2x}M_x^{3+}Nb_xO_2$, (M=Fe,Cr) cryst. struct., transitions and thermal effects 77−68950
VN_{1-x}, vacancy ordered structure in cubic mononitride phase, transition entropy determ. 78−43011
β-V_2N, neutron powder profile-refinement cryst. struct. determ. 80−15060
$(V_{1-x}Nb_x)_2C$, modulated structs., periodic antiphase domains 79−94969
$V_{0.5}NbSe_2$, cryst. struct., metallic cond., mag. and phys. props. *(French)* 80−33956
$VO_{1.30}$, ordered phase, X-ray anal. of defect struct. 79−99177
VO_2, doped, morphology, structure and props. *(German)* 78−59823
VO_2-$CrNbO_4$, solid solns., synthesis and phase diagram 80−35171
VO_x, defect struct., local ionic arrangements in disordered phase 80−10532
VO_x, struct., model based on O vacancy superlattice 77−84707
$V_{13}O_{24}$ long-period Magneli phase as product of V_6O_{11}-V_7O_{13} periodic microsyntactic intergrowth 80−50618
V_2O, γ-phase, struct., O at. position 79−10834
V_2O_3, electron-density studies, deform. density at 295K, metal-metal bonds 80−107118
V_2O_4, struct. from electron microscopy of Tyep F-2 fibre 78−2087
V_2O_5 and lower oxides, electronic, optical, structural and surface props., review 80−88120
V_2O_5-Fe_2O_3 solid solution, Mossbauer investig. of cryst. props. *(French)* 77−4592
V_3O_5, low-temp. modification, cryst. struct. and valency distrib., importance of very weak reflections 80−92493
V_4O_7, cryst. atomic struct., 120K and 298K 78−34486
V_6O_{13}, low temp. phase 78−42979
$(VO)_2P_2O_7$, cryst. struct. determ. 80−15081
$VOSO_45H_2O$, single cryst. X-ray cryst. struct. determ., H_2 bonding *(French)* 79−73138
β-$VOSO_4.5H_2O$, X-ray cryst. struct. determ. and refinement *(French)* 80−107121

crystal atomic structure of inorganic compounds continued
$VOSO_4.6H_2O$, single-cryst. X-ray diffr. struct. determ. *(French)* 80−39021
$VOSb_2O_4$, synthesis and struct., stereochem. influence of lone pair *(French)* 77−15367
$VO[UO_2(SO_4)_2].6H_2O$, synthesis and crystallographic data 78−26532
V_4O(β-phase), X-ray study of precipitated phase *(Ukrainian)* 78−6928
VP, X-ray obs. 77−72594
$V(PO_3)_3$, cryst. struct., bond lengths, angles 77−80477
V_3S-type structures, α- and β-forms, atomic coord. and bonding 79−60330
$VS_2(Se_2)$, and alkali metal intercalates, phys. props. 80−44179
V_3Sb_2, struct. study, space groups *(French)* 77−68949
VSe_2 (1T), deform. modulated superstruct., electron diffr. expts. 78−51515
V_3Si, supercond. structure and properties *(German)* 80−93631
V_3Si-M, M=Hf, Nb, Ta, Mo, W, Ni, Ge, Sb, cryst. struct., supercond. T_c comp. depend. 78−51494
$V_xTi_{1-x}Se_2$, cryst. struct. and elec. props. 79−47133
$VaH_x(D_x)$, cryst. struct., phase diagrams, order-disorder transition 78−55836
β-W type (A-15 type) structure, double space group selection rules 77−39551
W-complex, $WOCl_4.Ph_3PO$, prep. and characterisation 78−30592
W-Y(La)(Ce)-B, phase equilib., struct. of crysts. 77−21122
WC_x, electrochem. separation from W alloys, phase anal. 78−60651
WCl_5, crystal structure determination 78−91318
W_3Fe_3C, pyrochlore struct. and its relatives 79−14773
WGe_2 and W_5Ge_3, synthesis at high pressure, cryst. struct. 79−77565
WO_2, struct. refinement by powder neutron diffr., profile anal. 79−99139
WO_3, hexagonal form, struct. study, X-ray powder diffr., electron diffr., and electron microscopy meas. 79−99157
WO_3, orthorhombic phase 77−24297
WO_3 polymorph, hexagonal, cryst. struct. imaging by high-resolution electron microscopy 80−103309
WO_3, trigonal 78−51483
WSe_2, lubricant, prep. by self-propagating high-temp. synthesis, technological characts. 78−35338
$WSeF_4$, cryst. struct., and preparation 78−63730
WV_2O_6, X-ray cryst. struct. refinement at 298 and 383K *(French)* 79−14747
XeF_2, stereochem. of structs. and valence bonds 79−69066
XeF_4, stereochem. of structs. and valence bonds 79−69066
XeO_3, stereochem. of structs. and valence bonds 79−69066
Y germanates and silicates, cryst. struct. and cryst. chemistry 77−39571
Y oxides, perovskite-like, synthesis, struct., elec. props. 80−65554
YA-$O_3{:}Er^{3+}$, pulsed laser action, $^4S_{3/2}$ to $^4I_{9/2}$ transition laser action, optical and luminescence spectra 80−16082
YAG, as substrate for $Er_3Al_{5-x}Ga_xO_{12}$ LPE film for solid laser 80−93419
YAG, neutron diffr. determ. of O coordinates 77−1117
YAG, rare earth impurity, spectral probe of stoichiometry variations 77−85790
YAG, simulated mol. images, point models and kinematical struct. amplitudes 80−103223
YAG single crystals, derivation of cryst. parameters and orientation by X-ray topography *(Chinese)* 79−46622
YB_{68}, melt grown, props. meas. 77−11518
YBO_3, cryst. struct. reappraisal 77−47427
$Y_{1.6}Bi_{1.0}Ca_{0.4}Fe_{4.4}In_{0.4}V_{0.2}O_{12}$, cation distrib. 79−19211
YCa garents, solid soln., mag. and cryst. chem. props. 77−16057
$Y_2Cr_2O_7$, $Y_2Mn_2O_7$, pyrochlore type, synthesis and physical props. 80−33963
$YD_{1.96}$, cryst. struct. by neutron diffr. 80−70179
YFe_2B_2, compounds with $CeAl_2Ga_2$ structure type *(Ukrainian)* 79−32970
YGG, YGG-ErGG, rare earth impurity, spectral probe of stoichiometry variations 77−85790
$Y_{10}Ga_3Co_7$, X-ray cryst. struct. determ. 80−33977
$Y_4GeO_6(OH, F)_4$, cryst. struct. 79−19229
$YH_{1.98}$, cryst. struct. by neutron diffr. 80−70179
YH_2, location of H, PMR rigid-lattice second moment meas. 80−71198
$YHfTaO_6$, powder X-ray diffr. data 79−99155
YIG, polarised neutron expts., extinction models 80−24322
YIG, single crystal., mag. domain Wall and cryst. struct. 77−16104
$Y_{3-x}La_xFe_5O_{12}$, mag. props. rel. to ionic struct. 80−75756
$Y_xLu_{1-x}Ir_4B_4$, supercond., magnetism and metastability 80−29501
Y_2MoO_6, growth from soln., struct., props. 77−28705
$YNO_3(Se_2O_5).3H_2O$, X-ray cryst. struct. determ. 80−1972
YNi_5Si_3, X-ray crystal struct. determ. 77−7701
Y_2O_3, translucent ceramic, prep. effect on struct. and props. 79−87601
Y_2O_3-$HfO_2(ZrO_2)$ systems, solid soln. form. mechanisms 79−11579
YOF, trigonal, NMR of F^{19} to detect paired formations 79−14788
$YOHCO_3$, cryst. struct., X-ray diffr. meas. 77−4079
YPo, X-ray struct. anal., FCC struct. and unit cell const. 77−15363
Y_3RB_7 and analogues, R=rare earth *(Ukrainian)* 77−31642
$Y(Rh_{0.85}Ru_{0.15})_4B_4$, mag. ordering and supercond. 78−14861
Y_5Ru_2, Mn_5C_2-type struct., X-ray cryst. struct. determ. 80−96483
YSeF, direct lattice imaging of polytypes 77−4087
YSeF, eight layer polytype *(French)* 78−10001
YSeF, orthorhombic polytype 140, struct. study *(French)* 80−88102
YSeF, ten-layer polytype 10M, cryst. struct., X-ray diffr. meas. *(French)* 77−47409
$Y_x(Si,Al)_{12}(O,N)_{16}$, α'-Sialon ceramics, prep. and characterisation 78−84750
$YSiO_3F(Cl)(Br)$, phosphor host, luminesc. and struct. props. 78−48212
$YSiO_2N$, X-ray obs., pseudowollastonite struct. 77−47427
YTa_7O_{19}, crystal struct., isomorphism with rare earth tantalates 77−7698
Y_3TaO_7, non-stoichiometric phase struct. 79−55716
$YThNbTiO_8$, synthesis and cryst. struct. *(French)* 78−83799
$YTiO_3$, cryst. struct. and cryst. chem. 80−1984
$YTiTaO_6$, powder X-ray diffr. data 79−99155
Y_6UO_{12}, energy transfer, cryst. struct. and chemical composition effect 80−108248
$Y_2V_{10}O_{28}.24H_2O$, cryst. struct. by X-ray diffr. 78−43005
$Y_2V_{10}O_{28}.24H_2O$, cryst. struct. determ. by vector subsystems method 79−60340
$Y_2V_{10}O_{28}.24H_2O$, X-ray cryst. struct. anal. 80−39060

crystal atomic structure of inorganic compounds continued
Y_2WO_6, new structural type, unit cell, space group, fluorescence spectra 79−1420
Y_2WO_6:Eu, noncontinuum model for energy transfer 79−33800
Y_2WO_6:Eu^{3+}, luminesc., rel. to crystallographic data 79−33793
Y_6WO_{12}:Eu^{3+}, crystal struct., fluorescence spectra, exam. 78−52558
$YbAlO_3$, single crysts., prep. and phys. props., X-ray struct. anal. 79−4298
YbB_{12}, mag. props., cryst. struct., valence of Yb *(Russian)* 78−60263
$YbBO_3$, cryst. struct. reappraisal 77−47427
YbC_6, intercalation cpd. with graphite, synthesis and struct. 80−44184
$Yb_{0.5}Eu_{0.5}Fe_2O_4$, rhombohedral oxides, symmetry group *(French)* 80−84157
YbFX mixed halides, synthesis and lattice parameters 78−30594
$YbFe_2O_4$, rhombohedral oxides, symmetry group *(French)* 80−84157
$Yb_3Fe_4O_{10}$, struct. image by a 1 MeV high resolution electron microscope 79−37671
$YbGa(In)_2X_4$, X=S,Se,Te, prep. and props. 77−85214
$YbMn_2As_2(Sb_2)$, pnictides with Ce_2O_2S-type struct. 79−65055
$Yb_4(P_4O_{12})_3$, X-ray struct. characts. 80−54202
$YbSi_{1.8}$, valence fluctuation cpd., X-ray anal., mag. susceptibility and linear expansion coeffs. 79−77569
Yb_3Si_5, valence fluctuation cpd., X-ray anal., mag. susceptibility and linear expansion coeffs. 79−77569
$Yb_2Si_2O_7$, crystal struct. of X form, polymorphism under press. *(French)* 77−47430
$Yb_2Si_2O_7$, polymorphism under press., cryst. struct. 77−35692
Zn complex, ZnS_2O_4.pyridine, cryst. struct., nature of S-S bonds 78−55847
Zn complexes, bis(methylammonium) tetrachlorozincate and bis(methylammonium) tetrabromozincate, cryst. data 77−39567
Zn-Li silicates, cryst. struct. and phase transform. 79−65036
Zn-Sb system, phase diagram, struct. and stability of phases *(German)* 78−60661
Zn-Ti-Fe-O, spinel solid solns. 77−48409
ZnA_2X_4 (A=Ga,In; X=S,Se), Fourier IR and Raman spectra, cryst. struct. and symm. *(German)* 79−24313
$ZnAl_2S_4$-$ZnCr_2S_4$, nonstoichiometric spinel solid solns., synthesis and cryst. chemistry 77−35526
Zn_2AsO_4OH, paradamite, X-ray cryst. struct. determ. H bond strengths 79−42016
$Zn_2(AsO_4)(OH)$, paradamite, crystal struct., anisotropic temp. factors 80−84145
ZnCaSO, struct. and phase analysis *(Russian)* 77−58995
$Zn_xCd_{1-x}S$, film for heterojunction solar cell 77−8208
$Zn_xCd_{1-x}S$ monocrystal, optical and nonlinear optical characts. *(Russian)* 79−98442
$Zn(ClO_2)_2.2H_2O$, X-ray cryst. struct. determ. 80−19759
$ZnCo_2O_4$, Mossbauer spectra and cryst. struct. determ. 79−56637
$ZnCrFeO_4$, ferrite spinel, unsupported and SiO_2 supported, structural and catalytic studies 80−44191
$ZnCr_2Se_4$, screw spin struct., neutron diffr. exam. 78−27019
ZnF_2, X-ray absorpt. spectrum polarisation depend. 80−104012
$ZnFeO_4$, ferrite spinel, structural and catalytic studies 80−44191
$ZnFe_2O_4$, cation distrib., preference energy determ. by neutron irrad. method 77−15384
$Zn_xFe_{0.85-x}O$, prep. and struct., mag. and semicond. props. *(French)* 78−51506
$Zn_2Fe(PO_4)_2.4H_2O$, phosphophyllite, chem., optical and X-ray data 77−15366
$ZnGa_2Te_4$, cryst. struct., melting point 78−35360
$ZnGeP_2$, P vacancies, lattice parameters, optical props. depend. on thermal treatment *(Russian)* 78−71729
$Zn(H_2PO_2)_2$, X-ray cryst. struct. determ. and refinement, heavy-atom method 79−19194
$Zn(H_2PO_2)_2.H_2O$, X-ray cryst. struct. determ. and refinement, heavy-atom method 79−19194
$ZnHPO_4.H_2O=(H_3O)ZnPO_4$, cryst. struct. determ. 78−63739
$Zn(HSeO_3)_2.2H_2O$, neutron diffr. cryst. struct. determ. 80−33983
$(Zn_{0.877}Hg_{0.116}Fe_{0.002})_{0.995}S$, unit cell dimensions *(Chinese)* 79−90616
ZnI_2, cryst. struct. determ., X-ray anal. *(French)* 79−7585
$ZnIn_2S_4$, IR refl. spectra and cryst. struct. 79−56777
$ZnK_4(P_3O_9)_2.4H_2O$, cryst. struct. determ. *(French)* 78−26503
$Zn_cM_{1-c}Fe_2O_4$, $M=Ni^{2+}$, Co^{2+}, Fe^{2+}, $Zn_cMFe_{2-c}O_{4-c}F_c$, $M=Ni^{2+}$, Co^{2+}, calc. of saturation magnetisation by cluster components 77−43817
$Zn_2Mg(PO_4)_2$, cation distrib. from X-ray profile-fitting refinement 77−76376
$Zn_xMn_{2-x}Sb$, anti-PbFCl type, cryst. struct. and ferromag. ordering 77−84723
$Zn^{2+}Mo^{4+}O_3$, defect spinel struct., elec. and mag. props. 80−70176
$ZnMo_2Re_2S_8$, cubic structure, mixed tetrahedral cluster *(French)* 77−15372
β-$Zn(NCS)_2$, cryst. struct. 77−65972
$ZnNH_4H_3(PO_4)_2.H_2O$, X-ray cryst. struct. determ. *(French)* 80−88104
$Zn_2NaP_3O_{10}.9H_2O$, cryst. struct. determ. *(French)* 77−47406
$ZnNa_6(SO_4)_4$, vanthoffite cryst. sruct., lattice parameters and thermal behaviour 77−19929
ZnO ceramics, nonohmic, cryst. phases 78−26530
ZnO, structure parameters and polarity, X-ray diffr. meas. 80−19781
ZnO-Cr_2O_3, crystal structure, valence of chromium ion rel. to variation of Cr/Zn ratio *(Rumanian)* 79−65057
ZnO-TeO_2, cryst. chem. study, X-ray diffr. powder data *(French)* 80−15080
$Zn_4O(B_6O_{12})$, skeletal cubic cryst., refinement of cryst. struct. 79−86765
ZnOHF (I), single cryst., X-ray cryst. struct. determ. 79−60344
$Zn_3O(SO_4)_2$ 77−27863
Zn_3P_2, high press. phase relns. and cryst. structs. 78−59792
$Zn_3(PO_4)_2.4H_2O$, hopeite, cryst. struct. redeterm. 78−75640
$Zn_3(PS_4)_2$, synthesis, structural and thermodynamic props. 77−24304
$Zn_4(P_2S_6)_3$ *(French)* 78−34474
$Zn_4(P_2S_6)_3$, monoclinic system *(French)* 78−59791
Zn_2PdO_4, cryst. struct. and mag. props. meas. *(French)* 77−15381
ZnS structure, evaluation of finite strain eqns. of state using lattice models 80−96620
ZnS:Ag, cryst. struct., electron traps and glow curves 79−61437
ZnS:Cu,Cl, exciton refl. spectra, hexagonal struct. 77−44021
ZnS-CdS:Ag(Cu), cryst. struct., electron traps and glow curves 79−61437
ZnS-ZnSe single cryst. grown from melt, anisotropy of mech. props. and struct. 77−24303

crystal atomic structure of inorganic compounds continued
$ZnSO_4$, cubic H-cristobalite struct. *(German)* 79−51089
$ZnS_{1-x}Te_x$, polytype single cryst. grown from melt 79−14762
$ZnSb_2O_4$, isomorphous with Pb_3O_4, cell parameters evolution with temp. *(French)* 78−75642
$ZnSc_2O_4$ spinel, X-ray obs. 79−32963
ZnSe, crystal, new polytype structure 78−14319
$ZnSiAs_2$, synthesis and layer growth by CVD in open flow system 78−15312
Zn_2SiO_4, willemite, cryst. struct. 78−83804
Zn_2SiO_4, Willemite, single crysts., X-ray evaluation of atomic parameters for study of optical props. 79−4283
$Zn_4(Si_2O_7)(OH)_2.H_2O$, calamine-hemimorphite, cryst. struct. determ. 77−76380
$Zn_4Si_2O_7(OH)_2.H_2O$, X-ray and neutron diffr. study 79−99159
$Zn_4Si_2O_7(OH)_2.H_2O$, hemimorphite, phase-angle determ. by anomalous X-ray scattering with 4-circle SSD diffractometer 80−49188
$ZnSiP_2$ crysts., imperfect struct. anal. using divergent X-ray beam technique 77−76259
$ZnSnCuO_4$, cryst., struct., mag. susceptibility obs. 78−2085
$Zn_2Ta_2O_6$, metastable orthorhombic variety, crystallographic characts. *(French)* 79−82185
$Zn(UO_2AsO_4)_2.8H_2O$, prep. cryst. struct. characterisation 78−30589
$ZnU_2.nH_2O$, cryst. struct. *(German)* 80−1987
$(ZnV_2O_4)_c(MgFe_2O_4)_{1-c}$, struct. parameters, IR spectra, cluster-component analysis 77−47425
Zn_3X_2, X=P,As,Sb, phys. props. 78−26527
ZnY_2O_4, cryst. struct. 80−100207
Zr double arsenates, $M^IZr_2(AsO_4)_3$, $M^{II}Zr_4(AsO_4)_6$, (where M^I=Li, Na, K, Rb, Cs and M^{II}=Ca, Sr, Ba, Mn, Co, Cu, Zn), cryst. characts. 79−55726
Zr double phosphates, $M^{II}Zr_4(PO_4)_6$, (where M^{II}=Ca, Sr, Ba, Mn, Co, Cu, Zn), cryst. characts. 79−55726
Zr hydrides, computed X-ray powder diffr. patterns and densities 77−43172
Zr-M-B systems (M=Rh,Ir), phase equilib. and cryst. structs. 80−15072
Zr-N_2, condensate formed by plasma flow precipitation in vacuum, cryst. and surface props. *(Russian)* 80−100788
$ZrB_{\sim 51}$, X-ray powder profile refinement 79−23574
$ZrC_{0.91}$, sintered, strength charact. effect of struct. and substruct. 80−16260
ZrC_x, static distortions and Debye temp. determ., neutron diffr. exam. *(Russian)* 77−80482
ZrC_x, x=0.99 to 0.13, elec. cond., supercond. state 78−43504
$Zr(Ca,Y)O_{2-x}$, local ionic arrangement, X-ray diffr. study 80−100203
$Zr(Ca,Y)O_{2-x}$, X-ray diffr. study of average struct. 79−99123
$ZrCo_5Si_3$, X-ray cryst. struct. anal. 79−60342
$ZrD_{1.82}$, and $ZrD_{1.96}$, struct. and phase equilib., neutron diffr. obs. *(Russian)* 78−92244
$Zr_3Er_4O_{12}$, cryst. struct. determ., powder X-ray diffr. exam. 77−4083
$Zr_2F_8(H_2O)_6$, cryst. struct. refinement 78−18592
ZrF_4-BaF_2 system solid phases, synthesis and characterisation *(French)* 80−92506
$ZrH_{1.9}$, neutron irrad. induced defects, nature and thermal stability 77−50246
ZrH_2, H positions by neutron quasi-elastic scatt. 79−42042
γ-$Zr(HPO_4)_2.2H_2O$, form. region and struct. model 79−46615
ZrI_4, X-ray cryst. struct. refinement, new AB_4 struct. type *(German)* 79−32950
$ZrIr_3Br_{\sim 4}$ 78−42963
$Zr(KPO_4)_2$, cryst., ionic cond., layered struct. 80−92710
$Zr(LiPO_4)_2$ cryst., ionic cond., layered struct. 80−92710
$Zr(NaPO_4)_2$, cryst., ionic cond., layered struct. 80−92710
$ZrNi_{1.4}Si_{3.6}$, X-ray obs. *(Russian)* 77−76361
ZrO_2, monoclinic, variation of lattice strains *(Japanese)* 77−72600
ZrO_2, obtained by vapo-condensation, exam. of structure and phase props. *(French)* 79−19489
α-ZrO_2, structure factor determ. using crit. voltage effect, comments 77−1102
ZrO_2, technical grade containing CaO, polymorphic transform. up to 1200°C 78−64539
ZrO_2 thin film, optical props. rel. to cryst. struct. 80−97357
ZrO_2-CaO system, fluorite related ordered compd. prep., struct. 77−68958
ZrO_2-UF_4, orthorhombic struct., X-ray and electron diffr. study *(French)* 78−67689
ZrO_2-Y_2O_3, stabilised, struct. of single crysts. 77−35527
ZrO_2-Y_2O_3, ZrO_2-CaO system, fluorite related ordered compd, prep., struct. 77−68958
$Zr_{11}Os_4$, cubic struct. type described by cluster concept, X-ray determ. 80−33933
$Zr(PO_3)_4$, modification I, X-ray refl. data 77−15390
$Zr_3Sc_4O_{12}$, cryst. struct. determ., powder X-ray diffr. exam. 77−4083
$Zr(SeO_4)_2.4H_2O$, cryst. struct., X-ray powder diffr. meas. 78−34483
$ZrSiO_4$, body centered matrix basis 80−79765
$ZrSiO_4$, zircon, cryst. struct. and compressibilty at high press. 79−82184
$ZrV_2D_{4.5}$, deuterated cubic Laves phase, D atom distrib., neutron diffr. anal. 80−29006
$Zr_3Y_4O_{12}$, δ-phase cryst. struct., X-ray diffr. 77−19925
$Zr_{0.8}Yb_{0.2}F_{3.2}O_{0.3}(MX_{3.5})$ anion excess ReO_3 phases, non-stoichiometry 79−60322
$Zr_3Yb_4O_{12}$, cryst. struct. determ., powder X-ray diffr. exam. 77−4083

crystal atomic structure of organic compounds
bis-(2-fluoro-2,2-dinitroethyl)nitramine, mol. density, depend. on ratio of intramolecular and intermolecular contacts 79−86781
2,4,6-tri-(3,5-di-ter-butyl-4-hydroxybenzyl)-mesitylene, cryst. and mol. struct. 79−86783
1,1′-Bis[phenylglyoxyloyl]-ferrocen, mol. and cryst. struct. *(German)* 80−10538
acetate-ferrileghemoglobin, X-ray struct. anal., 3D refinement at resoln. of 2.0 Å 80 104554
acetic acid, deuterated, neutron powder diffr. anal. at 4.2 and 12.5K 78−75649
acetic acid, hypothetical dimer-based cryst. struct. calc. 77−19940
acetic acid-d_0, -d_1, -d_4, cryst., IR spectra, H bonding 77−40217
3d-acetonitrile, cryst. struct., ^{14}N NQR free induction decay times meas. 80−54985
acridine-PMTA complex, cryst. struct. determ. 77−11535
actinium (III) axalate decahydrate, lattice consts. 78−2102

crystal atomic structure of organic compounds continued
- adamantane, order cubic $F\bar{4}3m$ phase, X-ray diffuse scatt. 78—38684
- 2-adamantanone, cryst. struct. in plastic phase 80—88065
- aggregate organic photoconductor, composition prep., struct. and optical props. 79—24006
- L-alanine, solid, H bonding, wide line NMR obs. 78—52362
- alaninium copper tetrahalides, exchange, mag. anisotropy, and spin diffusion contribs. to EPR linewidth 80—80597
- β- alaninium tetrachloroferrate (III), X-ray cryst. struct. determs. 79—90635
- p-n-alkoxybenzoic acids, mol. arrangement in cryst., nematic, and smectic C phases 79—32889
- alkylammonium compounds, intercalation of ions in $(TiNbO_5)^-$ layers 80—64985
- amide group molecules empirical pot. model EPEN/2, development, parameter testing 79—54935
- 5-amino-1-hydrogen-1,2,4-triazole, cryst. and mol. struct., X-ray study 79—55735
- 1-amino-2-phenyl benzocycloheptanol-hydrobromide monohydrate, cryst. struct., heavy atom method 78—79601
- p-aminobenzoic acid hydrochloride, X-ray cryst. struct. determ. 80—39063
- 4-aminopyridine hemiperchlorate, neutron diffr. and IR spectral obs. of strong asymmetric N-H-N hydrogen bond 80—92515
- ammonium benzoate, IR spectrum, cryst. struct. 78—19455
- ammonium hydrogen bisbenzoate, IR spectrum, cryst. struct. 78—19455
- ammonium hydrogen tartrate, struct. refinement using X-ray diffractometer equipped with Si(Li) detector 79—58855
- ammonium thiocyanate, testing aspherical atom refinements 79—7516
- ammonium uranyl formate, struct. determ. from X-ray diffr. and IR spectrum *(French)* 78—75653
- p-anisidine, crystal structure determination with DAR-UM+BESM-6 automatic system 77—76386
- anthanthrene, mol. cryst. images in electron diffr. patterns 80—103315
- anthanthrene, mol. imaging by high resolution electron microscopy 78—79600
- anthracene:tetracyanobenzene charge transfer complex, cryst. struct., temp. effects 80—96508
- anthracene, attachment energy as habit controlling factor 80—59421
- anthracene, metastable triclinic phase 80—59452
- anthracene crysts., mol. orientational disorder calc. vacancies, dislocations, photodimerisation 77—4915
- anthracene-phenanthrene-tetracyanobenzene, CT-cryst., mini-excitons and lattice dynamics, ESR, optical and Raman spectra 80—60406
- anthracene-tetracyanobenzene 1:1 charge transfer complex, low temp. phase 80—6397
- 9-anthraldehyde, struct. by TEM 80—79771
- 9-anthronitrile, struct. by TEM 80—79771
- L-arginine L-ascorbate, X-ray cryst. struct. determ. 80—35826
- 2-azanoradamantane N-oxyl, crystal-plastic transition, plastic crystal struct. exam. 78—2100
- azoxyphenetole, deuterated, cryst. and mol. struct. 79—86782
- barium acid oxalate, lacunary phase, thermodynamic and crystallographic characts. 79—55731
- barium beauvuricin complex, appl. of cryst. struct. refinement technique based on fast Fourier transform algorithm 78—91197
- barium methylsulphonate, X-ray powder cryst. data 80—59451
- Bence-Jones Rhe protein (1.9 Å), phase extension and refinement 79—99168
- benzene, cryst., orthorhombic, lattice energy and cell dimensions, spheroidal approx. 79—51041
- benzene, polycrystalline heteronuclear dipolar modulated chemical shift spectra, geometrical and orientational obs. 77—20750
- benzene rings, substituted, planar ring distortion, geom. constraints 78—18624
- benzenes, disubstituted, monosubstituted, effect of bonding electrons on molecular dimensions as determ. by X-rays 79—7595
- benzidine, cryst. struct. and lattice energy 79—37694
- benzil, crystallographic study of solid-solid phase transition *(French)* 78—55939
- benzil, structural transition model, cryst. symm. spontaneous strain components 80—2161
- benzoic acid, struct. refinement at room temp. 80—96502
- benzonitrile, 198K *(French)* 78—51524
- benzyl mercury chloride, cryst. struct. and absorpt. calcs. 80—84166
- 2-benzyl-5-benzylidenecyclopentanone, and substituted form, topochem. single-cryst.-to-single-cryst. photodimerisation 80—66819
- bie-solicylato-diaquo calcium (II), cryst. struct. 80—100222
- bilinear organic addition compound, cryst. struct. and cond., rel. to lateral elastic interaction between chains 77—39827
- biomembranes, radial autocorrelation function, significance in X-ray diffr. patterns 80—51048
- biopolymers, X-ray struct. study using synchrotron radiation and multichannel detector 78—47210
- biphenyl, three-dimensional cryst. struct. data and refinement, 203K 77—47439
- bis(diethylamino)dithiaboretane, cryst. struct., bond lengths and angs. X-ray diffr. obs. 78—18628
- β-bis(ethylammonium)tetrachloromanganate, cryst. struct. refinement, neutron diffr. 78—55858
- bis(n-butylammonium) tetrachloromanganate(II), X-ray cryst. struct. determ. at 294K 79—60346
- bis(p-toluene sulphonate)diacetylene, monomer and polymer, solid state phase transformation, far IR transmission spectra obs. 80—55077
- 4,4′-bis(pentyloxy)azoxybenzene, cryst. data 79—60347
- bis(propylammonium)tetrachlorocadmate, first-order phase transition, X-ray diffr. meas. 78—55826
- bis(tetrathiotetracene) triiodide, 1-D organic metal 77—59000
- boranes, $B_9H_{12}OCH_3S(CH_3)_2$, $C_2B_{10}H_{10}Br_2$, $B_{18}C_4H_{22}$, cryst. struct. *(Czech)* 78—87649
- boranes, $OCH_3(B_9C_2H_{10})_2Co$ and $(C_2H_5)_2Co_2CB_9H_{10}^-$, cryst. struct. *(Czech)* 78—87649
- bovine pancreatic trypsin inhibitor, struct. refinement by simultaneous minimisation of energy and R factor 79—7517
- bovine trypsinogen, low-temp. study, effect on flexibility, temp. factor, mosaic spread, extinction and diffuse scattering 80—54214
- 1-bromo-2, 4-dinitrobenzene, cryst., ^{79}Br NQR Zeeman effect 78—2765
- bromoacetic acid, cryst., films, polarised IR spectra, struct. 78—72502
- 4-bromobenzoyloxymethyl-trifluorosilane, cryst. struct., X-ray study 80—70187

crystal atomic structure of organic compounds continued
- bromocyanoacetylene, cryst., IR, far-IR and Raman spectra, vibr., struct. 77—63407
- bromoform, polycryst., cryst. struct., IR spectrum 77—44000
- 2-bromophenoxaycetyl-4-propylbenzene, cryst. and mol. struct., X-ray anal. 79—60349
- 4-bromophenoxyacetyl-4-ethylbenzene, single crystal, X-ray struct. determ. 79—1426
- 2-butyl-7-(1-oxopentyl)-9,10-dihydrophenanthrene, mesomorphous, cryst. struct. determ. *(French)* 77—4095
- cadmium formate, anhydrous, cryst. struct. 80—107195
- cadmium histidine, unique phase determination, two-wavelength Bijvoet pair method, reson. neutron scatt. 78—91201
- cadmium oxydiacetate trihydrate, monoclinic, cryst. struct. determ. and refined 77—47438
- caesium hydrogen tartrate, anomalous dispersion of Cs, refined struct. from modified least squares program 78—51522
- calcium bromide hexamethanol solvates, cryst. struct. *(French)* 78—34500
- calcium copper acetate hexahydrate, PMR at low temp., atomic position determ. 77—20728
- calcium di-DL-glycerate dihydrate, Ca binding, X-ray cryst. struct. determ. 79—46642
- calcium dipicolinate trihydrate, IR and Raman spectra, isotopic frequency shift, mol. vibr. obs., point groups determ. 80—89001
- α-calcium formate, neutron diffr., cryst. struct., 100 and 296K 77—59004
- calcium formate, polycrystalline, heteronuclear dipolar modulated chemical shift spectra, geometrical and orientational obs. 77—20750
- calcium hydrogen dihomophthalate pentahydrate, cryst. struct. 77—15395
- calcium malonate dihydrate 77—59003
- calcium phthalate monohydrate, single cryst., X-ray cryst. struct. refinement 79—14790
- calcium propionate monohydrate, cryst. struct. 77—76385
- carbamide phosphate, neutron diffr. 77—31652
- carbon tetrabromide, ordered, polymorphism 78—22700
- carbon tetrabromide, ordered phases, polymorphism obs. 80—54217
- carbon tetrabromide, phase I cryst. struct. 78—18626
- carbon tetrabromide, phase II cryst. struct. 78—18623
- carbon tetrachloride, and mol. struct. 79—77559
- carbon tetrachloride, ordered phases, polymorphism obs. 80—54217
- carbon tetraiodide, ordered phases, polymorphism obs. 80—54217
- carbonyl compounds, empirical pot. model EPEN/2, development, parameter testing 79—54934
- 3-carboxy-2,2,5,5-tetramethylpyrrolidinyl 1-oxyl system, enantiomer solid soln., cryst. struct. and phase diagram 79—86778
- carboxylic acids, crystals, empirical interatomic potential functions 79—7567
- catalase, electron microscope exam. of new cryst. form, Fourier transform. method 77—11447
- catalase, from the fungus penicillium vitale pidopl. et bilai, preliminary crystallographic investigation and props. 79—66444
- CBOOA, smectogenic, cryst. and mol. struct. determ. 78—2103
- celenious acid, rel. determ. of protons coordinates using moments of NMR spectra 79—60239
- cellulose triacetate I, mol. and cryst. struct., parallel chains 78—30548
- ceruloplasmin, human, calc. of rotation function for tetragonal. cryst. at 10 Å resoln. 80—108843
- chloro(2,4-dithiobiuret)copper(1)-N,N-dimethylformamide, cryst. and mol. struct. 79—99170
- trans-3-endo-chloro-4-(phenylthio)-9,10-cis-endo-bis(methoxycarbonyl)tricyclo[4,2,2,$0^{2,5}$]dec-7-ene, cryst. and mol. struct. 79—90639
- 6-chloro-α-pyridine anthraquinone, cryst. and mol. struct., X-ray diffr. meas. 77—43206
- o-chlorobenzoic acid, solid, H bonding, wide line NMR obs. 78—52362
- p-(N-chlorobenzylidene)-p-chloraniline, cryst., polymorphism, cryst. struct. rel. to mol. conform. 78—75611
- chlorocyanoacetylene, cryst., IR, far-IR and Raman spectra, vibr., struct. 77—63407
- 4-chlorophenoxyacetyl-4-propenyl benzene 78—63750
- cholesteryl acetate, cryst. struct. at 123K 79—46643
- cholesteryl acetate, long period obs. 77—62515
- cholesteryl alkanoates, mol. packing coeffs. 79—82195
- cholesteryl benzoate, crystallographic data, rel. to mesogenic state 79—77590
- cholesteryl bromide, cryst. and mol. struct. 79—82194
- cholesteryl chloride, cryst. and mol. struct. 79—82194
- cholesteryl chloroformate, crystal structure 78—91331
- cholesteryl ethyl carbonate, long periods in sol. state, X-ray diffr. study 80—96503
- cholesteryl laurate, X-ray cryst. struct. determ. at 298K 79—37692
- β-choline chloride, X-ray diffr. 78—55861
- choline phosphate calcium chloride tetrahydrate, struct., conformation, metal coordination, model for membrane surface interactions 80—15085
- α-chymotrypsin, Fourier phase refinement and dimeric struct. extension at 1.8 Å resolution by density modification 79—90634
- cis-3,5-dibromo-4-oxo-2,2,6,6-tetramethylpiperidin-1-yloxy, cryst. struct., secondary and multi-centre bonding 78—63751
- cobalt (III) diacetylmonoxime, Schiff base cryst. and mol. struct. 79—94998
- cobalt (III) diacetylmonoxime thiosemicarbazone, X-ray cryst. and mol. struct. 79—90641
- cobalt (III) methylhydrazinedithiocarboxylate, cryst. and mol. struct. 79—94998
- cobalt dimethyl glyoximate, molecular struct., cryst. structure 80—79769
- cobalt platino-oxalate, one-dimens. conductors, prep., struct. and elec. cond. 80—24900
- cobalt sulphate hexacarbamide, cryst. struct. 78—34507
- colchicine, cryst. struct., multiple soln. direct methods 78—34384
- collagne fibrils, rat tail tendon, quasi-hexagonal mol. packing model 80—30660
- conference, Crystal XII, Canberra, Australia (Jan.-Feb. 1980) 80—62388
- copper(II) methylphosphonate monohydrate, cryst. struct. *(French)* 79—99172
- copper 1,4-butanedisulphonate tetrahydrate, struct. 78—18630
- copper acetate mono-α-picoline, binuclear, cryst. and mol. struct. 79—99174
- copper benzoate di-(γ-picoline)hydrate, structural study using heavy atom method *(French)* 79—69098
- copper formate anhydrate, cryst. struct. and mag. props. 80—79768

crystal atomic structure of organic compounds continued
  copper formate tetradeuterate, deuterated, paraelec. and antiferroelec. phases, neutron diffr. obs. of struct. 79−87404
  copper iminodiacetate dihydrate, X-ray cryst. struct. and molecular struct. determ. 79−19237
  copper phthalocyanide, cryst. struct. sensitivity of band struct. 79−42444
  copper phthalocyanine, chlorinated, stacking disorder 78−34622
  copper phthalocyanine, molecule images, simulation by point models and kinematical struct. amplitudes 80−103223
  α'-copper phthalocyanine, struct. and susceptibility to radiation damage 79−32986
  copper platino-oxalate, one-dimens. conductors, prep., struct. and elec. cond. 80−24900
  copper sulphate tricarbamide, $CuSO_4.3CO(NH_2)_2$, cryst. struct. determ. 78−34506
  copper tetra-4-dimethylaminophthalocyanine intercalated with TaS_2, layered cpd., struct. and supercond. 78−84342
  cordycepin, X-ray cryst. struct. determ. 80−107198
  coronene, an ordered struct. 80−19786
  cortison, phase refinement, random approach to struct. determ. 79−10747
  coryol, crystal structure determ. using NQEST(x) function 80−64986
  γ-crystallin, calf-lens protein, single cryst., X-ray diffr. low resolution struct. anal. 79−16130
  cyanine dyes, low dimensional aggregate models from crystal struct. anal. 79−19241
  cyanoacetylene, and-d_1, cryst., IR, far-IR and Raman spectra, vibr., struct. 77−63407
  p-cyanophenol, X-ray obs. 77−24312
  cyanuric acid, electron-density matrix extraction from X-ray diffraction data 77−65930
  cyanuric acid, molecular charge distrib. refinement 79−55730
  cycasin, cryst. growth and struct. 78−18631
  cyclic olefin, ($C_{20}H_{19}ClN_2O_8S$), stressed, cryst. and mol. struct. X-ray anal. 79−86784
  cyclo-(glycine-tyrosine-glycine)$_2$, crystal struct. from packing anal. 77−2070
  β-cyclodextrin dimeric complexes as models for lipid bilayer diffusion transport 78−80838
  cyclohexadepsipeptide, refinements of mol. and cryst. struct. 77−39576
  cyclohexahydroxyisovaleryl, $C_{30}H_{48}O_{12}$, cryst. and mol. structs. 77−31653
  bis-π-cyclopentadienyltitanium dichloride, struct. parameter refinement 78−87660
  bis-π-cyclopentadienylzirconium dichloride, struct. parameter refinement 78−87660
  cytosine hydrochloride, cryst. growth, crystallographical parameters 78−14332
  cytosine monohydrate, deuterated, neutron diffr. cryst. struct. determ. 80−54215
  cytosol aspartate-transaminase, of chicken heart, prep. of orthorhombic crysts., X-ray determ. of unit cell 79−57577
  deuteromethane, crystalline, X-ray powder diff. study 80−96500
  1,2-di(N-piperidyl)ethane-bis-N-oxide tetrahydrate, synthesis, cryst. and mol. struct. obs. 79−32985
  di(tert. butylperoxy)triphenylantimony, X-ray cryst. struct. determ. 80−92517
  3,5-di-tert-butyl-4-hydroxybenzylidenemalononitrile, excited-state proton transfer, cryst. and mol. struct. 78−84630
  N,N′-diacetyl-1,2,1′,1′-tetrahydro-1,1′-diisoquinoline, cryst. and mol. struct. 78−2106
  diacetylene, single cryst., photopolymerisation, intermediate states, struct. changes 80−30235
  dialkyl ammonium manganese chloride, phases and structural phase transitions, DSC and X-ray diffr. meas. 77−47574
  dialkylammonium copper chloride, nearly 2-D ferromag., low temp. NMR 77−28455
  dialkylammonium manganese tetrachloride, lattice consts. and phase transition temps. 79−86779
  dianthronylidene ethane, luminescent excimer geometries, intermol. shift 78−27294
  2,7-diazanaphthalene, cryst. and mol. struct. 77−59002
  dibenzotetrathiafulvalene cation radical salts, cryst. struct. by X-ray anal., rel. to elec. props. 80−24436
  2,2-dibenzyl-1,3-dibromopropane, crystal structure and thermal motion 79−99173
  dibenzylmercury, cryst. struct. and conformation determ. 79−42045
  diborane, density distribution of bonding electrons, simple refinement 78−18574
  2,4-dibromo-1,5-diphenylpenta-3-one, cryst. struct., secondary and multi-centre bonding 78−63751
  dibromomaleic acid thioanhydride, mol. and cryst. structs., X-ray obs. *(German)* 80−44199
  p-dibromotetrafluorobenzene, neutron diffr. determ. of struct., constrained refinement 77−19839
  n-dibutyl(ethylene-1,2-dithiol)stannane, cryst. data 77−15400
  dicadmium dimethylammonium pentachloride dihydrate, X-ray cryst. struct. 79−77588
  1,5-dichloro anthracene, cryst. struct. calc., use of at.-at. pots. 79−46646
  2,6-dichloroacetanilide, NQR, cryst. struct., band character 78−6596
  β-9,10 dichloroanthracene, hole mobility anisotropy and cryst. struct., transient photocond. 78−95310
  p-dichlorobenzene, α, β and γ forms, cryst. struct. and pot. energy 78−38685
  p-dichlorobenzene, Cl-Cl interactions at 100K, isotropic pot. functions calcs. 78−18578
  4,4′-dichlorodiphenylsulphide, NQR line, Zeeman effect 77−59481
  dichlorodurene, order-disorder phase transition, struct. from neutron diffr. at 70K 78−55825
  p,p- diethoxythiocarbonylthiomethylaniline, cryst. and mol. struct. 79−94990
  diethyl tin dihalides, cryst. struct., secondary and multi-centre bonding 78−63751
  1,1′-diethyl-2,2′-cyanine iodide, sensitising dye 77−72602
  diethylammonium cadmium chloride, X-ray study of structural phase transition 78−2055
  3,3′-diethylthiatricarbocyanine iodide, cryst. and molecular struct. 78−26554
  5,10-dihydro-5,10-diethylphenozinium-iodide, average struct. 79−90636
  1,2-diidobenzene, vibr. spectra, packing calcs. and crystal structure investig. 80−28938

crystal atomic structure of organic compounds continued
  diiodomaleic acid thioanhydride, mol. and cryst. structs., X-ray obs. *(German)* 80−44199
  p-diiodotetrafluorobenzene, neutron diffr. determ. of struct., constrained refinement 77−19839
  diketomorpholine, cyclodepsipeptide, cryst. and mol. struct. 78−2104
  diketopiperazine, cryst. and molecular struct. determ. 77−11534
  5,7-dimethoxyindane-1-one, cryst. and mol. struct. 80−100223
  2,5-dimethyl-2-hexyn-2, 5-diol, deuterated, profile analysis, influence on struct. parameters and deformation density distribs. 79−73064
  2,5-dimethyl-3-hexyn-2,5-diol-d_{12}, cryst. struct. and electron density distrib., 90K 77−51362
  2-p-dimethylaminobenzylidene-1,3-indandione, X-ray cryst. struct. determ. 79−14793
  dimethylammonium cadmium tetrabromide, room temp. struct. 80−29000
  dimethylammonium manganese chloride, neutron diffr., 188K 77−47434
  dimethylammonium manganese chloride, neutron diffr., 404K 77−47435
  dimethyltin halides complexes with dimethyl sulfoxide and dimethylformamide, cryst. and mol. struct. 79−42047
  9,10-cis-endo-dimethyltricyclo[4,2,2,$0^{2,5}$]dec-7-ene, substituted molecular struct. 79−86785
  dinitrato[N,N′-propane-1,3-diylbis(salicylideneimine)]calcium(II), cryst. struct. anal. 79−99171
  m-dinitrobenzene, oriented film, intermol. vibr. coupling, polarised IR spectra 80−97264
  1,8-dinitronaphthalene, orthorhombic, X-ray obs., 22 and 97°C 78−6048
  2,4-dinitrophenol, cryst. and mol. struct. 77−15394
  DIP-trypsin, difference Fourier refinement using minicomputer, to 1.5 Å 77−58924
  diphenyl halonium compounds, X-ray struct. anal. and NQR, chem. bonding 77−12232
  diphenyl selenium halides, correlation between NQR spectra and cryst. struct. 77−12233
  diphenyl tellurium halides, correlation between NQR spectra and cryst. struct. 77−12233
  diphenyl tin sulphide trimer, cryst. data 77−15400
  N,N′-diphenyl-m-phenylenediamine, crystal and mol. struct., X-ray diffr. 78−47312
  N,N′-diphenyl-p-phenylenediamine, cryst. and mol. struct. 77−7706
  N-(4-diphenylamino) phthalimide, X-ray cryst. struct. determ. 79−42048
  9,10-diphenylanthracene, soln. grown, cryst. struct. by computational and X-ray study 79−37690
  diphenylmercury, cryst. struct. refinement 77−24310
  diphenylsilanediol, recrystallized, cell const. refinement precision powder data 79−10841
  dipicolinic acid, IR and Raman spectra, isotopic frequency shift, mol. vibr. obs., point groups determ. 80−89001
  dipotassium uridine 5′-diphosphate trihydrate, X-ray cryst. struct. determ. 79−57569
  dipyridinium copper bromide, $Py_2Cu_5Br_7$, Cu^+ ion conductor, cryst. struct. 78−51527
  distamycin A, analog cryst. and molecular struct. 79−88051
  dithiobismorpholine, cryst. data 77−35544
  DNA, cetavlon salt, cryst. struct., X-ray diffr. meas. 78−2105
  DNA, X-ray diffr. from side-by-side model 80−35835
  DNA cetavlon salt, struct., small-angle X-ray diffr. meas. 78−11609
  DNA double helical fragment intercalator complex, molecular struct. 79−16140
  DNA with heavy atom, X-ray struct. study using synchrotron radiation and multichannel detector 78−47210
  durene-p-dibromobenzene system, phase diagram and X-ray diffr. expts. 78−79774
  durene-para-dibromobenzene, binary mol. system, X-ray struct. anal. 79−55734
  EBBA, mol. and cryst. struct., X-ray diffr. study 80−88134
  electron microscopic approach to struct. and reactivities 79−73077
  enniatin B, DLLLLL-stereoisomer, molecular and cryst. struct. 78−25745
  enniatin B, Rb^+ complex of LDLLDL analog, struct. and conformation anal. 79−60348
  erbium triethyl sulphate, single cryst., H^+ coords., NMR 80−97152
  ethane, ordered cryst., Raman spectra, 74K 79−73942
  ethane, single cryst. X-ray struct. determ., plastic and monoclinic forms 78−63744
  p-(p′-ethoxybenzylidene)amino-benzonitrile, cryst. struct. rel. to liq. crystallinity 80−100225
  ethyl 4-(4′-methoxybenzylideneamino)cinnamate, mesomorphic compound, cryst. struct. and binding energy 77−80494
  (N-ethyl-o-phenanthrolinium)(TCNQ), cryst. and mol. struct. *(French)* 77−15396
  N-ethylacridone, cryst. and mol. struct. 80−33988
  ethylene, single cryst. X-ray struct. determ. at 85K 77−47440
  ethylene oxide, cryst. symmetry, X-ray diffr., far IR and Raman spectra 78−35123
  ethylene oxide deuterohydrate, cryst. struct. at 80K 77−72607
  ethylene-d_4, phases I and II, struct. determ. by neutron diffr. 77−27870
  eukaryotic initiator tRNA, cryst. struct. from electron density map 79−43813
  2-exo-acetoxy-7-anti-dinitrophenylthionorbornane, mol. and cryst. struct. 80−2007
  Fc-fragment crystals, low-temp. study, effect on flexibility, temp. factor, mosaic spread, extinction and diffuse scattering 80−54214
  ferrocene, mol. struct., ordered phase, 130K *(French)* 79−51093
  ferrocene, neutron diffr. study of cryst. struct. 79−55728
  ferrocene, new interpretation of disordered cryst. struct., X-ray anal. 79−65063
  ferrocene, ordered, disordered phases, structs. *(French)* 78−63749
  ferrocene, orthorhombic low-temp. cryst. phase, characterisation 80−96507
  ferrocene, triclinic, struct. anal. at 101, 123 and 148K 80−19785
  1,1′-ferrocenedicarboxylic acid, triclinic, X-ray and neutron cryst. and mol. struct. determ. at 78 and 298K 80−29008
  fluoroanthene, cryst. struct., X-ray and neutron diffr. meas. 77−47437
  2-fluoronaphthalene-2-naphthol system, phase relations, X-ray diffr. and DTA study 80−45287
  formamide, low temp. electron density distrib. 78−34502
  formic acid, cryst. struct. at 98K 78−26555
  formic acid, deuterated, neutron powder diffr. exam. at 4.5K 78−75650
  fructose, stereoviews and morphological data on microcrystals 78−18510

- **crystal atomic structure of organic compounds** continued
  - α-D-glucose, further struct. refinement based on neutron diffr. data 79—42043
  - L(+) glutamic acid halogen acid salts, crystallographic, optical and calorimetric meas., halide effect 78—34505
  - L(+)-glutamic acid hydrochloride, deuterium isotope effect, cryst. struct., IR spectra and SHG 77—46755
  - γ-glycine, cryst. struct. by neutron diffr. at 83K and 298K 80—35825
  - glycogen phosphorylase b activity, struct. of cryst. and complexes 78—80830
  - α-glycylglycine, cryst. struct. and deform. electron density, X-ray and neutron diffr. 79—86777
  - guanidinium uranyl sulphate trihydrate, X-ray diffr. 78—14331
  - guanido iodate, X-ray obs. 78—83807
  - guanyl ribonucleases of fungi, crystn. and X-ray diffr. 78—71718
  - gummosine, cryst. and mol. structs., and absolute config., X-ray expts. 78—79602
  - heparin, in soln., small angle X-ray scattering 80—14993
  - hexa-host inclusion compound, cryst. and mol. struct. 77—42436
  - hexabromobenzene, constrained refinement of neutron powder diffr. data 79—27970
  - hexachloroethane, orthorhombic, neutron struct. refinement 80—29009
  - hexadecachlorophthalocyanato-copper discrimination of individual atoms in mol. images 80—100226
  - hexamethylenetetramine-phenol mol. complexes, cryst. data 77—27871
  - hexamethylethane, crystal structures and phase transitions, X-ray diffr. study 79—73158
  - hexaphenylcarbodiphosphorane, cryst. struct., triboluminesc., polymorphism effects 79—61447
  - n-hexatriacontane, cryst., orthorhombic modification, vibr. spectra 80—50314
  - histidinedecarboxylase molecule, distance between heavy atom markers small angle X-ray scatt. determ. 79—55613
  - L-histidine.HCl.H_2O, photographic neutron diffr. by modified Laue method 77—66791
  - HOAB, cryst. and mol. struct. rel. to smectic C phase struct. 79—55732
  - homomolecular crystals, distrib. by chiral types and struct. classes 78—9986
  - hydrazinium hydrogen oxalate, electron and proton distrib. in the short O-H-O bond 79—14789
  - hydrazonium tartrate enantiomers, and deuterates, struct. and opt. props. 77—68954
  - N-hydro-N′-methylphenaziniumyl cation in HMP-ClO_4, mol. config. 78—62938
  - hydrocarbon crystal structure calc. by molecular packing analysis 78—14303
  - hydrocarbons, unsaturated, empirical potential model EPEN/2 parameterisation, testing 79—50103
  - p- hydroxy-trans-cinnamic acid, cryst. struct. basis for absence of thermal mesomorphism 80—96509
  - 3-hydroxymethyl-2,2,5,5-tetramethylpyrrolidinyl 1-oxyl system, enantiomer solid soln., cryst. struct. and phase diagram 79—86778
  - IBPBAC, cryst. struct. and struct. of ordered smectic phases, X-ray diffr. obs. 79—86780
  - idolalkylamines, conformational varieties in cryst. 78—10030
  - imidazole, cryst. struct. at 103K by neutron diffr. 79—37691
  - insulin, appl. of cryst. struct. refinement technique based on fast Fourier transform algorithm 78—91197
  - intercalation compounds, metal guests in chalcogenide hosts, struct., review 79—46627
  - iodide superionic conductors containing AgI, geometric struct. principles 77—89574
  - iodobenzene bis(dichloroacetate), cryst. struct., secondary and multi-centre bonding 78—63751
  - iodobenzene diacetate 78—63751
  - iodocyanoacetylene, cryst., IR, far-IR and Raman spectra, vibr., struct. 77—63407
  - N-iododimethylamine, polymeric, mol. struct. exam. *(French)* 78—2101
  - iodoxybenzene, cryst. struct., secondary and multi-centre bonding 78—63751
  - iron porphyrin chlorides, X-ray, EPR and mag. susceptibility obs., inter-mol. exchange interaction 78—10765
  - lanthanum bicarbamide acetate, cryst. struct. 79—19240
  - lanthanum nicotinate dihydrate:Nd^{3+} cryst., H coords., EPR and ENDOR determ. 77—59005
  - lanthanum nicotinate dihydrate, cryst., nucl. quadrupole interactions, D atom coords., ENDOR obs. 80—97161
  - layer 1st order interaction for polytypic crystals, statistical model 77—80436
  - layer distrib. of polytypic crystals, stochastic model 77—80435
  - lead triphenyl isocyanate, X-ray cryst. struct. determ. and refinement 79—51097
  - leghaemoglobin of Lupinus luteus, cryst. struct. of first component 78—27893
  - leghemoglobin, X-ray structural determ. at a resolution of 2.8 Å, electron density synthesis 79—42049
  - leghemoglobin minimisation of functions of many variables appl. to X-ray struct. anal. 80—3589
  - leucine aminopeptidase, 3D reconstruction by photosummation of projected functions 79—62183
  - liquid crystalline polymers, struct. and morphology, theory 79—69025
  - lithium formate monohydrate, Li sites determ., using method based on bond-strength calcs. 79—7514
  - lithium formate monohydrate, non-centrosymmetric struct., X-N and multiple deform. electron density maps 78—91328
  - lithium hydrogen phthalate monohydrate, X-ray cryst. struct. determ. 79—14791
  - lithium potassium tartrate monohydrate: Mn^{2+}, isomorphism with lithium ammonium tartrate monohydrate, EPR obs. 80—29607
  - lithium thallium tartrate monohydrate, paraelectric phase structure by neutron diffraction data 79—19238
  - lysozyme, binding to bacterial cell wall trisaccharide NAM-NAG-NAM, X-ray cryst. struct. anal. 80—35834
  - magnesium bromide hexamethanol solvates, cryst. struct. *(French)* 78—34500
  - magnesium platino-oxalate, one-dimens. conductors, prep., struct. and elec. cond. 80—24900
  - malononitrile, solid phases I-IV, vib. spectra 77—20840
  - manganese(II) propionate dihydrate, cryst. struct. determ. 77—80495
  - manganese (II) D-gluconate hydrate, X-ray cryst. struct. determ. 79—77587

- **crystal atomic structure of organic compounds** continued
  - manganese acetate tetrahydrate, neutron diffr. 77—47436
  - manganese adipate dihydrate, cryst. struct., H-bonding and O atom coordination 80—96506
  - manganese carboxylate, dodecanuclear mixed-valence, prep., struct., and mag. props. 80—107196
  - matrine, X-ray cryst. and mol. struct. determ 79—94993
  - matrine N-oxide, X-ray mol. and cryst. struct. 79—94997
  - MBPAA, nematogen, cryst. and mol. struct. 77—72604
  - melamine, electron density, exponent refinement 78—38579
  - metaquohemerythrin, difference Fourier refinement 79—8472
  - methane, crystalline, struct. and compression at high press., room temp. 80—107199
  - methane-d_1(-d_2,-d_3), solid, struct. of phase III from thermodynamic meas. 79—82193
  - α-methane-d_4, crystalline, X-ray powder diff. study 80—96500
  - methane-d_4, low temp. phase, X-ray study *(Russian)* 80—33985
  - methane-d_4, solid, lattice parameters and thermal expansion for different phases 78—51526
  - p-methoxy-p′-alkyltolanes, molecular arrangement in solid state *(French)* 77—51364
  - p-methoxy-XY-p′-alkyl tolanes, mol. struct., packing coeffs., and thermal stability 78—95046
  - p-(p'-methoxybenzylidene)amino-phenyl acetate, cryst. struct. rel. to liq. crystallinity 80—100225
  - p-methoxybenzylidene-cyanoaniline, mol. and cryst. struct., X-ray diffr. study 80—88134
  - methyl 2,3:4,5-di-O-isopropylidene-α-D-glucoseptanoside, struct. determ., X-ray and neutron diffr. study 79—42050
  - methyl ammonium compounds with $Nb_{10}O_{28}^{6-}$, mol. config. 77—71886
  - methyl fluoride, solid, IR and Raman spectra, cryst. struct., and deutero deriv. 77—36218
  - methyl meristotropate, mol. and cryst. struct. 78—95047
  - N′-methyl-N-β-D-xylosylurea 79—94995
  - N-methyl-piperidinium-acet-meta-chloro-anilide-iodide, crystallisation from water, X-ray exam. of cryst. struct., mol. config. *(German)* 79—51095
  - 9-methyladenine monohydrochloride hydrated salts, cryst. data 77—15398
  - 2-methylamino-1-(spiro[cyclopentane-1,1′-inden]-3′-yl)ethanol hydrochloride, triclinic cell parameters from Weissenberg photographs 79—7518
  - methylammonium hexahalometallates (IV), halogen NQR obs. of struct. phase transition 79—95673
  - methylammonium manganese trichloride dihydrate, cryst. struct. 77—51363
  - N-methylformamide intercalate, cryst. struct. determ. using film-scanned data 79—55729
  - methylzinc methoxide, tetrameric, X-ray cryst. struct. determ. 80—107197
  - molecular charge transfer complexes, mol. and cryst. struct. 78—62942
  - molecular crystals, use of atom-atom pots. in interpreting behaviour, book contrib. 80—84136
  - monoadipate-tetraquo-cobalt (II), cryst. struct., H-bonding scheme 80—96504
  - α-monochloroacetic acid, hydrogen-bond motifs 77—11529
  - β-monochloroacetic acid, hydrogen-bond motifs 77—15397
  - monocrotaline sulphite hydrochloride, struct., space groups from X-ray crystallography *(Chinese)* 80—49210
  - morphology of crysts. with two mols. in asymmetric unit cell *(German)* 80—24396
  - myoglobin, appl. of cryst. struct. refinement technique based on fast Fourier transform algorithm 78—91197
  - myoglobin, from Aplysia limacina, X-ray cryst. struct. determ. at 5 Å resolution 79—16131
  - N-(p-chlorophenyl) maleamic acid, cryst. struct. 79—65065
  - N-(p-tolyl)-maleamic acid, cryst. struct. 79—65064
  - naphthalene, lattice parameters, elastic consts., press. depend., neutron diffr. obs. 78—26558
  - naphthalene, quantitative structural studies by means of the energy-dispersive method with X-rays from a storage ring 80—24314
  - naphthalene, thermal diffuse scattering, errors in X-ray diffr. intensities and atomic parameters 79—73155
  - naphthalene, X-ray diffr. anal. of cryst. and mol. struct. at −150°C 77—7707
  - naphthalene-coumarin solid solution, struct. parameters and phase diagram 77—11532
  - naphthalene-d_8, struct. facators, time of flight neutron diffr. 78—47212
  - naphthoquinone series charge transfer complexes, cryst. and electronic structs. 79—73474
  - naphtho[1,8-cd:4,5-c′d′]bis[1,2,6]thiadiazine, mol., electronic, cryst. struct. 80—64984
  - nickel phthalocyanide, cryst. struct. sensitivity of band struct. 79—42444
  - n-nitro-n′-methylbenzylidene-aniline, triclinic, cryst. and mol. struct. 77—43205
  - p-nitro-p′-methylbenzylidene aniline, polymorphism 78—18633
  - o-nitrophenol, cryst. and mol. struct., H bond distance 78—51523
  - 4-nitrophenyl 4-n-octyloxybenzonate, space group unit-cell and crystallographic props. 80—6399
  - 2-nitroso-2-bromo-3,3-dimethyl-butane, cryst. data 78—67703
  - nitroxyl radical ($C_{13}H_{17}N_2O_2$), paramagnetic, deformation electron density *(Russian)* 79—90637
  - NMBA, monoclinic, cryst. struct. and nonlinear optical props. 78—26560
  - octadecyl hydrogen maleate, spectrometer cryst., 2d value determ. method 77—65933
  - octafluoronaphthalene, high press. struct., neutron powder diffr. 78—63743
  - octamethylcyclotetrasilazane, gas, liq., cryst., CCl_4 soln. IR and Raman spectra, assignments, struct. *(French)* 78—29790
  - one-dimensional conductors, struct. aspects, book contrib. 78—10429
  - organic dielectric layered structures quasi two dimensional conductors *(Russian)* 80—33989
  - organic molecules, saturated, empirical potential model EPEN/2, parameterisation testing 79—54933
  - organic ortho compounds, solid, H bonding, wide line NMR obs. 78—52362
  - organometallic transition metal hydride complexes, struct. geometry bonding, neutron diffr. studies 79—46641
  - organonitrogen derivatives of Si, Ge and Sn, prep. and props. 78—60456
  - organotin compounds, mol. and cryst. struct., X-ray diffr., NMR and Mossbauer spectra meas. 77—47441
  - orthocyanobenzyl bromide, lattice consts., space group, density, X-ray obs. 78—51525

crystal atomic structure of organic compounds continued
oxa-bis(t-butylperoxytriphenyl-antimony); X-ray cryst. and mol. struct. determ. 79−60350
oxalate cryst. struct. determ. by X-ray crystallography, relations with $Na_2C_2O_4$, $Na_2Sn(C_2O_4)_2$ *(French)* 80−2004
oxalic acid, theoretical deformation density, ab initio Hartree-Fock calcs. 79−32982
oxanilide, IR and Raman spectra, cryst. struct. and vibr. 79−42954
PAA, cryst. phase transitions, intermolecular motion, Raman and inelastic neutron scatt. spectra 80−2164
PAA, solid state polymorphism 78−42945
palmitic acid-choleic acid complex, cryst. struct. and van der Waals energy 80−64983
PAP, cryst. phase transitions, intermolecular motion, Raman and inelastic neutron scatt. spectra 80−2164
parabanic acid, charge density and cryst. struct. redeterm. by X-ray and neutron diffr. 79−46644
n-paraffins, cryst. struct., rel. to polyethylene, surface effects on core 79−23593
pentaphenylantimony, Coulombic interactions in anomalous structure 77−24285
perdeuteronaphtthalene, use of neutron time-of-flight technique for cryst. structs. investigation 79−19126
(phenacetin)$_2$.HI$_5$, cryst. struct. determ. using Patterson methods 79−46647
phenazine, charge carrier transport rel. to cryst. and band struct. 79−95403
phenoselenazine, cryst. struct. from X-ray automatic diffractometer data 77−4093
phenyl-trimethine-merocyanine, X-ray diffr. exam. of cryst. and mol. struct. 80−6398
p-phenylenediacrylic acid dimethyl ester, photopolymerisable cryst., struct. determ. 78−63747
phospholipid, 1,2-dilauroyl-DL-phosphatidylethanolamine, X-ray diffr. anal., crystallogrpahy, bond lengths 77−44590
phosphorylase A crystals, automated struct. determ., from micrographs 80−92425
phosphorylase b, structure factor moduli, estimates from negative intensity obs. 78−75486
phthalic anhydride derivative, quartet invariants in space group P1, least-squares analysis 77−84570
phthalocyanines, metal free, mol. cryst. images in electron diffr. patterns 80−103315
piezoelectrics, absolute config., bibliography 77−48129
piperazinium $Ag_{10}I_{12}$.4-dimethylformamide, exam. of electrical cond. and crystal structure 78−75871
PMMI-carbazole, 1:1 complex, X-ray cryst. struct. determ. 79−94991
PMTA-dibenzthiophene, 1:1 complex, X-ray cryst. struct. determ. 79−94991
poly(vinylidene fluoride) film, phase-III, IR study 80−20624
poly-bis-phenyl glutarate diacetylene, cryst., solid-state synthesis, struct. 79−15638
polyacetylene:I, NMR investigation of struct. 80−39011
polyacetylene:I, NMR struct. investigation 80−108082
trans-polyacetylene, bulk crystallinity, small-angle X-ray diffr. study 80−103263
polyamides containing 1,3-cyclohexane rings, cryst. struct. 80−103262
polyamine iodide-AgI solid electrolytes, elec. cond. and cryst. struct. 80−107537
polybis-p-toluene sulphate, single crysts., morphology 79−23594
polyethylene, chains extended struct. *(Chinese)* 79−51092
polyethylene, cryst. struct. struct., rel. to n-paraffins, surface effects on core 79−23593
polyethylene, linear, single cryst., surface melting, X-ray diffr. 77−31755
polymers, struct. classification, morphology and twinning *(French)* 79−51058
polyoma virion and capsid crystal structures 80−8011
polypeptides, cyclic, cryst. state conformations 79−24942
polyurethane elastomers, hard segment struct., model 79−64131
potassium acetate, thermal expansion 79−51280
potassium bis(oxalato)beryllate, cryst. struct. *(French)* 78−34499
potassium butyl xanthate, X-ray cryst. struct. determ. 80−33987
potassium formate, IR absorpt. spectra, sampling effects, Davydov splitting and struct. 78−52508
potassium formate, X-ray cryst. struct. determ. 80−107194
potassium hydroxymethanesulphonate, X-ray cryst. and mol. struct. determ. 79−32983
potassium oxalate, anhydrous, phase II, vibr. spectra and cryst. struct. 80−34901
potassium oxalate monohydrate, cryst., O-H bond lengths, H-O-H angles, corrections 79−32945
potassium p-chloranil, solvated with acetone, X-ray cryst. struct. determ. 80−39062
praseodymium tricarbamide acetate hydrate, cryst. struct., Patterson function anal. 80−79770
promethazine picrate, cryst. data and molecular packing 79−94988
p-propoxysalicylidene-p′-butylaniline cryst. and mol. struct., intramolecular bonding 80−44197
prostratin derivative, cryst. struct., overlapping Patterson peaks and direct methods 78−55779
protein, struct. analysis by electron diffr., single scatt. approx., domains of validity 80−101150
protein, X-ray struct. study using synchrotron radiation and multichannel detector 78−47210
protein data measured on oscillation camera, collection and reduction method 79−29672
protein structure factors from electron density, test on model crystal 78−47204
protein structure factors from electron density distrib., theoretical foundations 78−47203
Prussian blue analogues, Mossbauer spectra 80−15898
PTS, pyroelectric effect 78−95554
PTZ:PMDA, purification, growth, struct., optical and elec. props. 80−54216
pyrazine, cryst. phases, entropy changes and struct. implications 80−54397
pyrazine, phase transitions, sp. ht., X-ray diffr., LF vibr. spectra 78−43122
pyrene, cryst. struct., atom-atom pot. calcs., micro electron diffr. obs. 78−43007
pyrene, cryst. struct. calc., use of at.-at. pots. 79−46646

crystal atomic structure of organic compounds continued
pyrene picrate, crystal struct. oscill. and Weissenberg photographs 80−107200
pyridine-methylbenzene cyclic ring compound, $C_{13}H_{13}N_2I$, crystal struct. 77−35545
pyridinium manganese (II) chloride monohydrate, crystal struct. and mag. susceptibility 79−19239
pyrocalciferol, struct. determ. using Karle-Hauptman determinants 79−7513
pyromellitic acid dianhydride, cryst. struct., anisotropic proton mag. shielding 79−87326
pyromellitic acid diimide, cryst. struct. determ. 77−11533
pyromellitic N,N′-dimethyldiimide-anthracene, cryst. struct. determ. 78−2107
pyruvic acid, cryst. struct., X-ray diffr. 77−19942
quasi-one-dimensional organic conductor, chem. trends and stabilisation of nearly one-dimens. state, review 78−10328
quinolinium manganese (II) chloride monohydrate, crystal struct. and mag. susceptibility 79−19239
1:1quinone-hydroquinone complexes, struct. 79−73159
ribonuclease A, bovine, cryst. struct. determ. by X-ray and neutron diffr. 80−108841
ribosomal component, cryst. struct. at 2.6 Å resolution 80−97859
Rochelle salt, ferroelec. thin crysts., struct. investig. 79−27962
rubidium platino-oxalate, one-dimens. conductors, prep., struct. and elec. cond. 80−24900
satellite tobacco necrosis virus struct., detect. and idealisation procedures of non-crystallographic symmetry with phase refinement appl. 80−108840
scandium nitrate tetracarbamide, cryst. struct. determ. 79−23588
L-serine-L-ascorbic acid, X-ray cryst. struct. determ. 80−35827
silver iodide-N,N,N,N′,N′,N′-hexamethyl-1,3-propylenediomine diiodide, solid electrolyte, cryst. struct. determ. 77−7705
silver iodide-NNNN′N″N″N″-heptamethyl-N′-hydrodiethylenetriamine triiodide, cryst. struct. determ. 78−26553
silver methanedisulphonate, cryst. struct. and information determ. 79−90633
sodium acetate trihydrate, cryst. struct. and bonding 77−24309
sodium benzoylacetonate, dielec. props. and cryst. struct. 79−8099
sodium benzoylacetonate, unit cell dimensions, X-ray determ. 79−69097
sodium biphthalate, cryst. struct., X-ray diffr. meas. 77−39577
sodium biphthalate, water of crystn. detection, PMR 77−35546
sodium hydrogen oxalate monohydrate, neutron diffr. and deform. electron density analysis 78−10032
sodium oxalate, cryst. struct. rel. to those of $Na_2Sn(C_2O_4)_2$, SnC_2O_4 *(French)* 80−2004
sodium tin oxalate, cryst. struct. rel. to those of SnC_2O_4, $Na_2C_2O_4$ *(French)* 80−2004
squaric acid, cryst., neutron diffr., bond lengths and angles, vibr. modes 77−76384
squaric acid, neutron diffr. mol. and crystal struct. determ. 78−26557
squaric acid, struct. and Raman spectra 78−47311
trans-stilbene, disorder and degree of misorientation 78−38683
stramonin-B, X-ray cryst. struct. anal. 79−77589
streptomycin oxime selenate tetrahydrate, antibiotic, cryst. and mol. struct. 78−24028
strontium calcium tartrate tetrahydrate, crystals grown by ion diffusion through silica gels, exam. of preps. 79−52102
strontium maleate tetrahydrate, cryst. struct., H-bonding scheme 80−96505
strontium malonate 77−59003
strontium propionate monohydrate, cryst. struct. 77−76385
strontium uranyl tetraformate hydrate, struct. determ., orthorhombic unit cell, UR spectrum *(French)* 78−22705
D(+)-tartaric acid, absolute struct. factor determ. 77−65973
D-tartaric acid, cryst. struct., 35-295K, by X-ray diffr. 80−22369
tatrakis(ethyl isocyanide) platinum(II) tetracyanoplatinate(II), cryst. data, X-ray powder anal. 80−2003
TBBA, struct. at 20°C, butyl side chains disorder *(French)* 77−58998
TBBA, struct. at 20°C, comparison with smectic B *(French)* 77−58999
TCNQ:Rb, 3:2 complex, cryst. struct. at 113K 79−99169
TCNQ(perylene)$_2$, cryst. struct. determ. 78−75651
(TCNQ)$_2$, dimeric interactions, MO calcs., applicability to crystal struct. 80−75215
(TCNQ)$_2$ MEM, crystal struct. of 1:2 complex, at −160°C 78−10031
$(TCNQ)_5^{2-}(DBzPE)^{2+}$, cryst. struct., elec. cond. and thermoelec. power 77−72606
$(TCNQ)_5^{4-}(DEPA)_2^{4+}$, cryst. struct., elec. and mag. props. 77−72605
TCNQ 1:3 radical salt, $[Pt(dipy)_2]^{2+}[TCNQ]_3^{2-}$, cryst. struct. 78−63741
TCNQ complex, [1,2-bis(1-benzyl-4-pyridinio)ethane]^{24}$(TCNQ)_5^{2-}$, cryst. struct. and elec. cond. 79−19236
TCNQ complex salts, with pyridinium cations, cond. and structural studies 79−87087
TCNQ complex with 5-phenyl-[1-thiol]-3-selenol-2-thione, charge-transfer salt, cryst. and mol. struct. 80−33986
TCNQ complex with N-methyl-Z-ethylthiazoline, cryst. and mol. struct. 78−10034
TCNQ complex with o-phenanthroline, orientational disorder 77−72603
TCNQ complexes with ferrocenes, charge transfer type, struct. and mag. props. 80−24439
TCNQ derivatives, substituted, org. cond. with low-symmetric acceptors, cond. behaviour rel. to cryst. struct. 78−6365
TCNQ salt, (1,2,-bis(di-n-alkyl-4-pyridinium) ethene)$^{2+}$ $(TCNQ)_x^{2-}$, cryst. struct. and elec. props. 79−56209
TCNQ salt, (1,3,-bis(di-n-alkyl-4-pyridinium) propane)$^{2+}$ $(TCNQ)_x^{2-}$, cryst. struct. and elec. props. 79−56209
TCNQ salt, $(DEPE)^{2+}$ $(TCNQ)_4^{2-}$, semicond. form., cryst. struct., X-ray diffr. meas. 77−4094
TCNQ salt, (DEPE) (TCNQ)$_4$, semicond. phase 77−80497
TCNQ salt, $(TMA^+)_3(I_3^-)(TCNQ^-)_2(TCNQ^0)$, struct., phys. props. and lattice distortion evidence 78−6305
TCNQ salt, Ag.TCNQ, cryst. struct. 80−70186
TCNQ salt, bis(dipyridyl)platinum(II)-TCNQ, crystal struct. and EPR, TCNQ radical dimerisation 77−80490
TCNQ salt, DECA (TCNQ)$_2$, struct., phys. props. and irreversible phase transition 78−6273
TCNQ salt, HMTTF-TCNQ, Madelung energy, intermol. charge transfer, 1-dimens. disorder 79−7572
TCNQ salt, HMTTF-TCNQ, structure, metallic cond. and thermopower 77−8080

crystal atomic structure of organic compounds continued
TCNQ salt, K^+TCNQ^-, low and high temp. modifications 77−35541
TCNQ salt, K-TCNQ *(French)* 78−43006
TCNQ salt, N,N′-di(n-propyl)-4,4′-bipyridylium^{2+}(7,7,8,8,-TCNQ)$_4{}^{2-}$, cryst. struct., elec. props. 79−27971
TCNQ salt, NH_4-TCNQ, crystal structure and phase transition 78−91330
TCNQ salt, Rb^+TCNQ^-, new form 77−24311
TCNQ salt, tetramethylhexamethylenediammonium-TCNQ-iodine, elec. and mag. props., struct., specific heat 80−24898
TCNQ salt, $TTF_{1-x}TSeF_x$-TCNQ, mol. substitutional disorder 80−24438
TCNQ salt, [1,2-di(N-methyl-4-pyridinium)ethane]$^{2+}$(7,7,8,8-TCNQ)$_4{}^{2-}$, struct. and elec. cond. 77−80491
TCNQ salt, [1,3-di(N-pyridinium)propane]$^{2+}$(7,7,8,8,TCNQ)$_4{}^{2-}$, struct. and elec. cond. 77−80492
TCNQ salt, [1,4-di(N-quinolinium-methyl)benzene]$^{2+}$ (TCNQ)$_3{}^{2-}$, cryst. struct., elec. anisotropy 77−35542
TCNQ salt, $[Pt(NH_3)_4]^{2+}[(TCNQ)_2]^{2-}$ cryst. and mol. struct. and EPR props. 78−55860
TCNQ salts, (N-methyl pyridine) $(TCNQ)_Z$, struct. and cond., 280 to 340K 79−23955
TCNQ salts, lattice vibr. freezing, Kohn anomalies, lattice struct. 77−15401
TCNQ salts, microdomain model for struct. rel. to cond. 77−11902
TCNQ salts, spin density distribs., estimation from EPR fine struct. and cryst. data 79−11347
TCNQ-DTT, cryst. data 79−51094
TCNQ-TMTSF, conducting salt, cryst. and mol. struct. 77−24307
TCNQ-TMTTF, conducting salt, cryst. and mol. struct. 77−24308
tellurophene(-d_4), cryst., struct., phonon spectrum, exciton splittings, assignments 77−81088
TEM, appl. to organic solid-sate chemistry, review 79−60235
o-terphenyl, cryst. struct. determ. by neutron diffr. 79−42046
p-terphenyl, long range order at phase transition, neutron diffr. exam. 77−1228
1-(2,3,4,6-tetra-0-acetyl-β-D-glucopyranosyl)-2,3-(2R)-epoxypropane, molecular and cryst. struct. 78−25746
tetra-isoamyl phosphonium bromide hydrate, clathrate, cryst. struct., X-ray study 80−64987
2,3,4,5-tetraacetoxymercurithiophene, dark-field imaging, computer simulation 80−100151
tetrabromoethylene, cryst., IR spectra in polarised light, cryst. struct. 78−27223
tetrabromomethane, plastic phase, neutron diffr. obs. and theory 79−77533
tetrabutylammonium hexatungstate *(German)* 78−63740
1,2,3,5-tetrachlorobenzene, chemical perturbation of cryst. structs., Raman phonon spectra 78−26559
α1,2,4,5-tetrachlorobenzene, cryst. struct. and lattice vib. freqs. 77−19939
1,2,4,5-tetrachlorobenzene, exciton states in crystals and dimers 80−70620
tetrachloroethylene, cryst., IR spectra in polarised light, cryst. struct. 78−27223
tetracyanoplatinates, quasi 1d anion deficient, elec. and struct. props. 80−103683
tetracyclo[4,2,2,$O^{2,5}$,$O^{3,7}$] decane-10-carboxylic acid, lactone substituted, molecular, crystal struct. 79−90640
tetraethylammonium acetate tetrahydrate, stoichiometry and cryst. data 78−67702
tetraethylammonium chloride tetrahydrate, stoichiometry and cryst. data 78−67702
tetraethylammonium fluoride hydrate, stoichiometry and cryst. data 78−67702
tetraethylammonium sulphate monohydrate, stoichiometry and cryst. data 78−67702
tetrafluoromethane, intermolecular pot., lattice energy and heat of sublimation 80−38995
tetraiodoethylene, cryst. and mol. struct. at 4K 77−59001
tetraiodoethylene, disorder, neutron powder diffr. data refinement 78−34501
tetrakis(thenoyltrifluoroacetonato)thorium(IV), X-ray cryst. struct. determ. 79−37689
tetrakis-carbamide scandium (III) trinitrate, electron density distrib. from X-ray diffr. data 79−94994
2,2,5,5-tetramethyl-4-phenyl-3-imidazalin-3-oxide-l-oxyl, deform. electron density determ., X-ray diffr. 80−88135
2,2,2,6-tetramethyl-piperidino-oxy, cryst. growth and polymorphism 80−96645
tetramethylammonium hexafluorophosphate, X-ray cryst. struct. determ., full-matrix least-squares refinement 80−92514
tetramethylammonium manganese(II) tribromide, cryst. struct. at 235 and 115K 78−63745
tetramethylammonium mercury iodide, NQR spectra of ^{127}I and cryst. struct. 77−12230
tetramethylammonium salt of $[Me_2N(ICl)_2]^-$, cryst. struct., secondary and multi-centre bonding 78−63751
tetramethylammonium silicate, X-ray cryst. struct. determ. 79−94996
tetramethylammonium tetrachlorozincate, incommensurate phase study, ferroelectric-paraelectric phases *(French)* 80−88318
tetramethylammonium tetrachlorozincate, low temp. phases, superstruct., X-ray study 80−39065
tetramethyltetrathiofulvalene salts, complexes with anisotropic props. *(French)* 77−69307
tetraphenyldithiapyranylidene mixed valence polyiodides, crystalline struct. and optical props. 80−92516
tetrapotassium tetrakis(oxalato)zirconate (IV) pentahydrate, cryst. struct. determ. 78−63746
tetraselenatetracene cation radical salts, cryst. struct. by X-ray anal., rel. to elec. props. 80−24436
tetraselenotetracence chloride, cryst. and mol. struct. 79−94992
tetraselenotetracene chloride, quasi 1-D metal *(Russian)* 77−59281
tetraselenotetracene iodides, struct. and physical props., DC electrical cond. and EPR linewidth meas. 80−103312
tetraselenotetracene thiocyanate complex, X-ray struct. anal. 80−2006
tetrathiofulvalene-based salts, isomorphous series systematic investig. of solid-state props. 77−55517
tetrathiotetracenenickel bis(ethylene-1,2-dithiolene), one-dimens. cond., preparation and props. 77−85201
TETTF.$TCNQ_2$, cryst. struct. *(French)* 78−18625

crystal atomic structure of organic compounds continued
TGFB, ferroelec. and paraelec. phases, X-ray diffr. 79−86776
TGS, cryst. struct. exam. after X-irradiation/field treatment 77−11531
TGS, cryst. struct. exam. at low radiation doses 77−11530
TGS, deuterated, paraelec. phase, D atom positions 78−14334
$(theobromine)_2.H_2I_8$, cryst. struct. determ. using Patterson methods 79−46647
1-(2-thiazolylazo)-2-naphthol, cryst. struct. 77−11536
p-thiocyanatoaniline 78−71717
thiourea, bond charges, comparison of exptl. and theoretical X-ray scatt. curves 78−55782
thiourea, incommensurate phase, soft modes, condensation of even-order harmonics 80−103313
thiourea SbF_3, cryst. struct., single cryst. X-ray diffr. study, influence of secondary binding *(French)* 79−32987
thiourea-cyclohexane inclusion compound, crystal, low temp. diffr. pattern, atomic structure determ., phase transitions 78−31116
thorium phthalocyanine, phase contrast characteristics in STEM 80−100153
thulium phthalocyanine, mol. image in high resolution electron microscopy, radiation damage effect 80−107203
TMTSF-DMTCNQ, cryst. and mol. struct. 78−63742
$(TMTTF)_2BF_4$, organic conductor *(French)* 78−26556
$(TMTTF)_2Br$ *(French)* 78−34503
tolan-mercury diphenyl solid soln., anal. of diffusely scatt. intensity distrib. of X-rays 78−95048
2-(2-tosylaminophenyl)-4H-3,1-benzoxazine-4-one, cryst. and mol. struct. 80−84167
toxin, penicillum roqueforti, struct. and absolute configuration 80−39064
tri-(trimethylsilylmethyl) tin monoiodide, molecular and cryst. struct. 79−65068
tri-O-ethylamylose-solvent complexes, cryst. struct., chain conforms. 79−65067
s-triazine, charge density anal. 78−38578
s-triazine, structural transitions, low temp. phase 78−55943
bis-triazolopyridazines, conformation calcs. by mol. mechanics and CNDO/2 method 80−69079
bis-triazolyls, conformation calcs. by mol mechanics and CNDO/2 method 80−69079
tributyltin sulphate, cryst. struct. 78−18632
1,3,5-trichloro-2-bromobenzene, chemical perturbation of cryst. structs., Raman phonon spectra 78−26559
1,2,3-trichloro-5-bromobenzene, chemical perturbation of cryst. structs., Raman phonon spectra 78−26559
p-tricyanovinylphenyldicyanomethide ion, donor props., cyclic voltammetry and π-complex form. 80−88520
triethylamylose-solvent complexes, conform. and packing analysis 78−75654
triethylenediamine complexes, structural relationships *(French)* 80−54213
triindenylcerium pyridinate, X-ray cryst. struct. determ. 79−32984
trimesic acid, L-(or DL-) histidinium trimesate-$^1/_3$ acetone, X-ray cryst. struct. determ. 79−77586
N-trimethyl stannyl phthalimide, cryst. struct. refinement and determ., Sn atom position 79−90638
trimethylammonium cadmium chloride, $(CH_3)_3NHCdCl_3$, struct. phase transitions 79−1502
triphenyl telluronium pseudohalides, cryst. data 77−15399
triphenyl tin isocyanate, struct. determ. and refinement 78−67704
triphenyl-(triphenylgermanylperoxy)silane, cryst. and mol. struct. 80−39066
triphenylene esters, crystalline arrangement of disc like compounds 79−99175
triphenylgermanium isocyanate, X-ray crystal struct. determ. and refinement 77−7708
triphenyltin bromide, cryst. struct. determ. using Patterson and Fourier methods 79−42044
tris(2-cyanoethyl)phosphine selenide, X-ray cryst. data 79−94989
tris(2-cyanoethyl)phosphine sulphide, X-ray cryst. data 79−94989
tris(hydroxymethyl)aminomethane, crystalline and plastic structs. phase transforms. studied by X-ray diffr. 80−84130
triterpenes, isolated from Japanese Cimicifuga plants, cryst. struct. determ. 78−34504
trypsin, bovine, accuracy of two independent refined models 79−92128
tryptamine:1-thyminylacetic acid (1:1), cryst. and mol. struct. determ. using MULTAN 79−73156
$(TSeF)_x(TTF)_{1-x}TCNQ$, struct., cond., phase transitions 78−47770
TTF(MBDT) spin-Peierls transition, mag. exchange interactions, mag. props. 80−25138
$(TTF)_2$, dimeric interactions, MO calcs., applicability to crystal struct. 80−75215
$(TTF)_2(NiS_4C_4H_4)_3$, disordered solid soln. and struct. modulation obs. 79−94986
$(TTF)_7I_5$, superstruct. modulation, X-ray obs. 78−14333
$(TTF)Br_{0.74\text{-}0.79}$, lattice distortions 79−55733
TTF salts, physical props., Fermi energy scaling of metal-insulator transition temp. 77−8081
TTF-(2,5-diethyl)TCNQ, cryst. and mol. struct. temp. depend. 77−35531
TTF-DETCNQ, heat capacity, elec. cond., cryst. struct., metal-insulator transition 77−8077
TTF-TCNQ, and related cpds., lattice modulations, X-ray diffuse scatt. obs. 80−19787
TTF-TCNQ, dimeric interactions, MO calcs., applicability to crystal struct. 80−75215
TTF-TCNQ, organic metal, Van der Waals donor stacking 80−15037
TTF-TCNQ, struct. rel. to quasi one-dimensional elec. props. 78−14716
TTF-TCNQ, symmetry changes and phase transitions 78−6299
TTF-TCNQ analogues, TTTF-TCNQ and METTF-TCNQ, cryst. structs., X-ray anal. 80−19788
TTF-TCNQ and related compounds, cryst. struct., organisation, dimensionality, interchain disorder 80−19790
TTF-TCNQ complex, trans-diethyl-dimethyl TTF-TCNQ, one-dimens. cond. 80−96853
TTF-TCNQ series, cryst. struct., elec. cond., and EPR meas., steric factor effects 80−19789
$TTT_2{}^+.I_3{}^-$, cryst. and mol. struct. by X-ray study 79−51096
TTT^+Br^-, cryst. and mol. struct., X-ray method 80−107202
TTT, donor-acceptor system, physico-chemical studies *(Hungarian)* 80−75554
$(TTT)_2\ I_{3+\delta}$, struct., X-ray diffuse scatt. study 80−24437

crystal atomic structure of organic compounds continued
TTT cation radical salts, cryst. struct. by X-ray anal., rel. to elec. props. 80—24436
TTTF-TCNQ, crystal and molecular structure determination *(French)* 78—91329
urea, bond charges, comparison of exptl. and theoretical X-ray scatt. curves 78—55782
urea, bond electron density distrib., 123K, simple refinement 78—55857
urea, electron density distrib., multipolar expansion 80—96501
urea, quantitative structural studies by means of the energy-dispersive method with X-rays from a storage ring 80—24314
urea adducts, crystn., geometry of urea-cation bonding 80—39061
urea antimony fluoride, X-ray cryst. struct. determ. *(French)* 80—44196
urea-oxalic acid (1:1), X-ray cryst. struct. determ. and thermal expansion 79—46645
urea-uranyl sulphate, $UO_2SO_4.2CO(NH_2)_2$, lattice parameters, space groups, X-ray crystallography 78—59798
urea-uranyl sulphate, $UO_2SO_4.3CO(NH_2)_2$, lattice parameters, space groups, X-ray crystallography 78—59798
N-vinylcarbazole, polymerisable monomer, structural chemistry, cryst. struct. determ. 77—4096
X-ray diffraction powder patterns, standard, for 112 substances 79—60223
X-ray diffraction powder patterns, standard, for 87 substances 80—64839
2-zinc insulin, rhombohedral, cryst. struct. refinement, experience with fast Fourier least squares 78—92595
zinc malonate dihydrate, cryst. struct., X-ray refl. obs. 78—75652
$C_{12}A_7H$, X-ray powder diffr. patterns *(Slovak)* 79—69099
C_3AH_6, X-ray powder diffr. patterns *(Slovak)* 79—69099
Co II complexes, with tetradentate Schiff bases, synthesis, struct. and ESR obs. 80—80598
CsDNA of T2 phage, in classical crystn. B form, struct., amplitudes, synchrotron radiation diffraction 80—85335
Cu complex, bis(1,1-diisobutyl-3-benzoyl-selenoureato)Cu(II), single cryst. ESR, ^{77}Se hyperfine struct., bonding 77—77086
1,6-di-(N-carbazolyl)-2,4 hexadiin, cryst. struct., luminesc., γ-ray polymerisation 78—18629
Fe complex, $[Fe(2\text{-}pic)_3]Cl_2.EtOH$, struct. changes, spin phase transition mechanism 79—78380
FeOCl/ferrocene (cobaltocene) intercalation cpds., X-ray diffr. obs. 79—65066
Ni complex, cis-dichloro-bis(1,2,cyclohexadionedioxime) cryst. and mol. struct. 80—44198
p-phenylenediacrylic acid diphenyl ester, photopolymerisable cryst., struct. determ. 78—63748
Pt complex, $[2, 2', 2''\text{-terpyridine PtCl}]^+$, motion of Pt atoms, electron microscopy obs. 80—103314
TCNQ ion-radical salts, struct. disorder 79—99885
TCNQ salts, bond lengths and charge transfer *(French)* 77—80493
$(TMCHDT)_2ClO_4$, organic conductor, struct. study *(French)* 80—88133
B-trichloro-m-carborane, cryst. electrophilic chlorination of 9, 10-dichloro-m-carborane, cryst. and mol. struct. from X-ray diffr., cryst. struct. 78—9268
$UO_3.HCONH_2.0.5H_2O$, prep., cryst. struct. and charact 80—29010
W complex, $Li_4W_2(CH_3)_{8-x}Cl_x.4THF$, quadrupole bond stability, crystallographic investig. 77—58193

crystal binding
see also binding energy; lattice energy
bis-(2-fluoro-2,2-dinitroethyl)nitramine, mol. density, depend. on ratio of intramolecular and intermolecular contacts 79—86781
A15 struct., stabilized by crystal field distortion of exotic elements at chain sites 78—79555
A-15 compounds, radical plane construction appl. to effective atomic radii rerivation 79—99109
absolute stability limit *(Russian)* 77—47373
acetic acid, cryst. binding, ab initio MO SCF calc. 79—37657
N-acetyl-valine, NMR of solid, ^{14}N-^{1}H dipolar spectra, NH bond length 78—48055
acetylene, cryst., semiempirical atom-atom pots. appls. 80—100200
actinide compounds, BOA valence bonding with f-character 80—6790
actinide dioxides, electronic struct. and ionicity 80—10872
actinides, atomic volumes calc. 80—15042
alkali chalcogenides, electronic polarizabilities and ion sizes 80—59432
alkali chlorides, modified electronic charge density 78—79554
alkali halide, effective ionic charge and interionic separation, correl. 77—19896
alkali halide, exchange charge polarisation, dielectric const., Dick and Overhauser model 78—55832
alkali halide, hydride and deuteride, cryst. binding energy formula, halogen, H, D electron affinity 77—35501
alkali halide, interaction potential, Gruneisen parameter, compressibility 78—14304
alkali halide, interionic potentials, based on elastic consts. and equilib. eqns. 77—47374
alkali halide, lattice energy, binding, indeterminancy principle theory 78—59777
alkali halide, overlap repulsion and pot. energy function for Bohr-like atoms 77—15344
alkali halide, second-neighbour interaction potential 78—91298
alkali halide, strain polarisability parameter, evaluation 77—35617
alkali halide, Szigeti effective charge, temp. depend. 78—38653
alkali halide crystals, evaluation of van der Waals interaction energies 78—71705
alkali halide crystals, Szigeti effective charge parameter, strain derivative 79—7571
alkali halide solid solns., lattice parameter and heat of form. 80—79739
alkali halides, bond forces, parameterless calc. 78—47275
alkali halides, cohesive energy, atomisation energy 78—18576
alkali halides, compressibility, force const. and IR absorpt. freq. 77—27955
alkali halides, cryst. electronic polarisability, ion size and dielectric const., hydrostatic press. effects 78—26487
alkali halides, crystal binding, electronic delocalisation *(French)* 77—24286
alkali halides, exchange charge shell model analysis of strain derivatives of static polarisability, effective charge parameter 78—91296
alkali halides, interionic potentials, completely independent specification of Born-Mayer potentials 78—55828
alkali halides, interionic potentials, cryst. independent shell parameters and fitted Born-Mayer pots. 78—55827

crystal binding continued
alkali halides, ion sizes and short range repulsive interactions 79—37652
alkali halides, phenomenological potentials 79—37654
alkali halides, repulsive softness parameter anal. 80—107102
alkali halides, short range interactions, static polarisabilities 78—71702
alkali halides, static dielectric behaviour, vol. depend., many-body interactions effects 78—2786
alkali halides, static polarisability, vol. depend. 78—52428
alkali halides, three body interaction effects on cohesive props. 78—83770
alkali halides, vol. depend. of dielec. consts. and effective charge parameter, under hydrostatic press. 78—14689
alkali halides estimation of van der Waals dipole-quadrupole interactions 77—80441
alkali hydride, repulsion interaction 78—26488
alkali hydrides, bulk props. prediction from molecular behaviour 78—51468
alkali hydrides, crystal binding anal. interatomic force model, cohesive energy, compressibility, Debye temp. 79—65030
alkali metal, local Heine-Abarenkov-type model pot. 79—87031•
alkali metal binary intermetallic cpds., OPW calc. of struct., bonding and stability 77—43169
alkali metal chalcogenides, analysis in Born model of cohesion 78—38652
alkali metal chlorides, interionic pots. 77—47372
alkali metal halides, Born repulsive parameters 77—72579
alkali metal halides, interionic repulsive short-range interaction pot., lattice energy calc. 80—96466
alkali metal hydrides, bond forces, parameterless calc. 78—47275
alkali metal suboxides, thermal and struct. anal., elec. and optical props., photoelectron spectra 79—47587
alkali metals, effective ion-ion potential, compressibility and force consts. 80—70158
alkali metals, heavy, crystal structure, effect of Van der Waals forces 79—99111
alkali metals, partial pressure contributions to equation of state 80—107401
alkali metals, phonon dispersion binding energy, compressibility, elastic consts. electron screening and Ashcroft pot. calcs. 80—65174
alkali metals, vacancy formation energy calcs., electron density functional method 80—19801
alkaline earth chalcogenides, anal. of electronic polarisabilities of ions 78—30579
alkaline earth chalcogenides, analysis in Born model of cohesion 78—38652
alkaline earth chalcogenides, atomis. energy, electron affinity, mean amplitude of vibr. *(German)* 79—51045
alkaline earth chalcogenides, cryst. polarisabilities and ion sizes, calcs. 77—68941
alkaline earth chalcogenides, cryst. radii of ions 77—15340
alkaline earth chalcogenides, crystal parameters calcs. using repulsive interaction pot. 79—37795
alkaline earth chalcogenides, electronic polarisabilities and ionic radii of metal and chalcogenide ions in cryst. state 80—100198
alkaline earth chalcogenides, electronic polarizability of ions, effect of crystal potential 78—26490
alkaline earth chalcogenides, interionic repulsive short-range interaction pot., lattice energy calc. 80—96466
alkaline earth chalcogenides, ion sizes and short range repulsive interactions 79—37652
alkaline earth fluorides, vol. depend. of refr. index 78—88275
alkaline earth halides, electronic polarizabilities and ion sizes 80—59432
alkaline earth oxides and sulphides, dielec. behaviour 79—91343
alloy, AB type, equilib. props. by Markovian simulation 78—91302
alloy, variation in interatomic interaction and lattice parameters during ordering *(Russian)* 77—81255
alloy systematics, rel. to the long periodic table 79—37649
alloying and cpd. form. of later transition and early B subgroup elements, graphical rep. 77—19895
alloys, CsCl type, nearest neighbour distance and atomic props. 78—51465
alloys, ordering, atomistic approach 79—94947
alloys, ordering, improved variant of quasi-chemical theory *(Russian)* 78—22685
alloys, stability and structure, pseudopotential calcs. *(German)* 80—38913
aluminates, interdepend. between tetrahedral d(T-O) bond lengths, nonbonded d(T...T) separations and TOT angles (T=Al,Si,P), using regression anal. 79—19182
ammonium halides, cryst., H bonding, order-disorder phenomena 80—6379
Anderson-Gruneisen parameter for cubic crystals 78—79672
anharmonic crystal, lattice dynamics and stability, self-consistent phonon theory 79—51209
anthracene, attachment energy as habit controlling factor 80—59421
anthracene, electron diffr. of topochem. conversion and phase transition 78—83680
anthracene, exciton bands, dipolar lattice sums *(Japanese)* 77—43167
antimonates, columbite or trirutile struct., force fields rel. to cryst. struct. *(French)* 80—107104
atoms as structural components in metallurgy *(Dutch)* 80—96465
B-32 superstructure, instability in absence of many-particle interactions 77—58972
B-elements binary phase form., struct. groups characterisation 77—4066
BCC clusters, electronic props., cluster size effects, theory 79—94949
benzidine, cryst. struct. and lattice energy 79—37694
binary alloy, of simple metals, pseudopotential approach 80—44464
binary alloys, and intermetallic cpds., struct. and stability, ab initio pseudopot. calcs. 78—34460
binary compound, fast ion stopping, chem. bonding effects 77—27929
binary compounds, structural stability, nonlocal density-functional atomic pseudopot. method 80—49174
binary crystals, stability and average structure factors 78—91297
bond percolation in bounded geometries 79—93062
bond percolation in square, cubic, hypercubic lattice, probability renormalisation group method 80—31680
bond percolation problem in semi-infinite medium, Landau-Ginzburg theory 79—93068
bonding charge densities, determ. by electron diffr. 80—75125
borides, nature of chem. bond, book contrib. 78—47276
borides, proposed classification 80—19741
borides, spatial correls. of valence and external core electrons 80—10523

crystal binding continued
brass-like alloy phases, binding and cryst. struct., valence arguments 80—88081
bromobenzenes, intermol. forces in cryst. 77—76349
caesium halides press. depend. of effective ionic charge 80—96462
calcium di-DL-glycerate dihydrate, Ca binding, X-ray cryst. struct. determ. 79—46642
central pairwise potential alternative in computer simulation in materials science 78—30585
chalcopyrite compounds, $A^IB^{III}C_2^{VI}$, tetragonal distortion 79—32942
charge densities, X-ray form factors, and bonding props. 79—94950
charge numbers-bond orders determ. from diffr. data 78—14306
chloroaromatics, mol. crysts. Cl atom pot. energy calcs. 78—42948
cholesterol derivatives, mol. packing coeffs. and thermal stabilities 80—100201
combining X-ray and neutron diffr. for charge density distrib. obs., book contrib. 79—60227
compound semiconductor, electronic polarisability rel. to energy gap 80—10524
conference, International Crystallography Congress, Warsaw, Poland (Aug. 78) 79—23481
coordination number, quantifying concept for irregular coordination polyhedra 78—95008
coordination numbers in solids, Pearson diagrams 80—107103
copper halides, cryst. ionic radii and electronic polarisabilities 77—1091
corundum, attachment energy as habit controlling factor 80—59422
Coulomb systems, absence of long-range order with long-range potentials 80—70157
covalent and ionic solids, determ. of electronic struct. 78—2409
covalent bonding, pseudopot. theory 77—51345
covalent crystals, local Heine-Abarenkov model potential 78—42949
covalent elements, cohesion in condensed phases, corrections to simple Huckel approx. 78—59779
covalent elements, cohesion of σ and π bonds in condensed phases, simple Huckel approx. 78—59778
covalent radii, tetrahedral and octahedral 77—31632
covalent semiconductor, electronic and struct. energies calc. 78—59874
covalent semiconductor, structural props. using electron-ion Hamiltonian using density-fundamental methods 79—82177
covalent solid, struct. props. and valence force fields, non-empirical calc. 77—1096
density distribution of bonding electrons, simple refinement, method 78—18573
density distribution of bonding electrons, simple refinement, applic. to diborane 78—18574
depolarization correction for Coulomb lattice sums 79—10829
diamond, and isomorphic crysts., phonon dispersion relations, Born-von Karman study 79—86855
diamond, cluster, electronic struct. of deep levels, LCAO, SCF method 79—82555
diamond, ground-state, electronic properties, ground-state in local-density formalism 77—69223
diamond, relaxation about the vacancy 78—71722
diamond, tetrahedrally bonded valence crystals, SCF perturbation theory appl. 79—37658
diamond, two-phonon Raman peak linewidth, bond polarisability model 77—77212
diamond, two-phonon Raman spectrum, harmonic pot. and bond polarisability model 77—77213
diamond, Wigner-Seitz effective quasiparticle pot. 79—50160
diamond and zinc blende struct. bonding charges 77—76356
diamond clusters and corresponding saturated hydrocarbon ab-initio HF and PCILO calcs. 78—42951
diamond structure crystals, forbidden Bragg refl., electron distrib. 77—51265
diamond-like solids, laser irrad. effect on cohesion 80—50470
1,5-diazo-3,7-dithiabicyclo (3,3,1) nonane, molecular and cryst. struct. 78—51528
p-dichlorobenzene, Cl-Cl interactions at 100K, isotropic pot. functions calcs. 78—18578
diethylammonium manganese tetrachloride, IR active modes, interlayer and intralayer forces 77—59575
p-dihalobenzene series, cryst., chem. perturbation and lattice instability, X-ray and Raman scatt. 77—39654
dimethylammonium manganese tetrachloride, IR active modes, interlayer and intralayer forces 77—59575
dipolar crystal, surface local field effect, dipole moment, self consistent electric field calcs. 80—49178
dispersion force calculations, use of finite atomic radius 78—51467
effective atomic charge rel. to electronegativity and ionicity 77—24287
effective ion-ion interaction, third-order contrib., ang. forces, tetrahedral solids 78—67970
elastic dielectric, many-body theory, appl. to NaCl-structure 78—38805
electrical resistance alloys, oxidation mechanism, scale adherence *(Polish)* 79—79143
electron plasma of crystal, interactions of classical charges 78—79561
electronic polarizabilities of ions in doubly refracting crystals 78—79551
electronic structure and solid props., rel. to chemical bonding, book 80—86044
electronic system with two-fold degenerate band, free energy change due to electron-phonon coupling 79—42500
electrostatic lattice potentials, calcs. 77—39557
electrostatic potential of point charge lattice having lamina geometry 80—59433
electrostatic potentials, fields and field gradients 78—30578
EM field in crystalline slab 80—96463
EM field in finite cryst. 79—77546
EM potential in crystalline slab 79—77547
empirical potential methods derived from phonon data, reliability 80—39230
ethanol-$d_1(d_2)(d_3)$, glassy state, solvated electron geometry, electron spin echo modulation obs. 80—66009
fluoride crystals, rutile-type, interionic pots., cohesive energy, bulk modulus, calc. 80—79741
fluorides of alkaline earths and transition metals, high-press. melting systematics 77—51475
force constants, diamond and sphalerite struct. crysts. 78—91408
formic acid, cryst. binding, ab initio MO SCF calc. 79—37657
formic acid, lattice dynamics model to explain neutron scatt. data 79—86856
formic acid, lattice energy, non-empirical MO SCF calc. 79—37656

crystal binding continued
fragile lattice packing of spheres, in 3D space 80—49166
garnets, oxide and fluoride, relation between lattice parameters and ionic radii 80—1986
globular hydrocarbons, cohesive energy and Gruneisen parameter calcs. 79—19183
α-glycylglycine, cryst. struct. and deform. electron density, X-ray and neutron diffr. 79—86777
graphite, electronic struct. exact exchange HF calcs. 80—65438
graphite, valence charge density 77—84694
graphite, X-ray emission and absorption, XPS, electronic struct. 77—16431
graphite intercalation compound, elastic coherency strain 79—60306
graphite intercalation compound with halogens, ionisation 78—26489
graphite intercalation compounds, coherency strains and staging 80—44167
graphite intercalation compounds struct., elec. props. 78—27446
group IIIa dihydrides, structs. and stabilities 80—107146
group IV, V and VI elements, XPS, bond ionicity, struct. stability and charge transfer 77—44127
group IV semiconductors, cryst. binding and band struct. 80—24791
group V semimetals, cryst. binding and band struct. 80—24791
growth models, attachment energy as habit controlling factor 80—59420
guanadinium zinc sulphate:Cu^{2+}, EPR of Cu^{2+} at tetrahedrally coordinated Zn^{2+} sites 78—39388
halide, RX_2-type, positron annihilation ang. correl., bondind depend. 77—20951
Hartree-Fock theory, ab initio effective potentials 80—103290
heavy metal halides, atomis. energy, electron affinity, mean amplitude of vibr. *(German)* 79—51045
heterocyclic N-containing compounds, crysts., intermol. pots. calcs. 80—49169
hexamethyldialuminium, methyl group rotation and bonding, CW proton second moment and line shape studies 79—47346
hexamethylethane, crystal structures and phase transitions, X-ray diffr. study 79—73158
hydrazinium hydrogen oxalate, electron and proton distrib. in the short O-H-O bond 79—14789
hydrocarbon crystal structure calc. by molecular packing analysis 78—14303
hydrocarbons, Coulombic nonbonded interatomic pot. functions from vibr. freqs. 77—80587
ice, cryst. binding, H-bonding pot. function 79—32940
II-VI and III-V, ion effective charge parameter, electronic polarisability 78—51463
II-VI partially covalent crysts., vol. depend. of refr. index 78—88275
III-V crystals, ionicities 77—51342
III-V semiconductors, chemical shifts of NMR lines of Ga nuclei 78—88201
inert gas $A^{(2)}B^{(8)}$ compounds, hypothetical, stability 79—99110
inert gas cryst. struct., induction energies, FCC and HCP 77—15343
inert gas crystals, dispersion binding energy 77—76351
inert gas crystals, repulsive interaction energy, Born-Mayer parameters 78—26485
inert gas small clusters, three body interaction effects on thermodynamic props., comparison bulk props. 80—28128
inert gas solid, long range forces, book contrib. 77—51347
inert gas solids, cryst. struct., book contrib. 77—51348
inorganic compounds, rel. to Lindemann's theory for melting temp. 79—23702
inorganic crystal, bond lengths prediction 77—47371
interatomic potentials from experimental phonon spectra 78—75621
interionic repulsive force, and compressibility of ions 77—11500
intermetallic compounds valence bond test, for validity of structure 79—10830
intermetallic phases with $L1_2$ and $D0_{19}$ struct., atom incompressibility, lattice parameter approach 78—91294
ionic crystal, Compton profile interpretation to give ionic deform. and bonding 77—40301
ionic crystal, cryst. field due to piont charges, dipolar lattice sums *(Japanese)* 77—43167
ionic crystal, electronic dielectric const. first and second electronic dielectric const., effective charge parameters 80—29669
ionic crystal, electrostatic energy calc. by planewise summation method 79—23564
ionic crystal, quadrupole antishielding factors and polarisabilities 77—51346
ionic crystal, repulsion and struct. stability, appl. to alkali halides 79—65028
ionic crystals, binding forces and eqns. of state, inner electron contrib., calc. 80—64950
ionic crystals, compressibilities and radii 80—24397
ionic crystals, effect of Lundqvist's many body potential on phototelastic behaviour 77—63391
ionic crystals, eval. of 3rd order and press. depend. of 2nd order elastic consts. 79—77668
ionic crystals, interatomic forces, Gruneisen and Anderson-Gruneisen parameters 80—79904
ionic crystals, interplanar spacings near boundaries and repulsive forces between ions 79—99165
ionic crystals, model potentials 77—27845
ionic crystals, radii of simple and complex spherical ions, repulsion energy of ionic crysts. 77—62503
ionic crystals, relative stabilities of NaCl, CsCl and cubic ZnS structures 80—19745
ionic crystals, soft-core model, normal ionic salts and superionic conductors 80—49411
ionic crystals, van der Waals potentials 78—83767
ionic radii, limiting values, rel. to crystallochemical radii 79—14730
ionic radius, electronic polarisability and effective nucl. charge, correl. 78—63694
ionic solid, elec. potential in surface region, induced dipole contribs. 77—47882
ionic solids, deformation dipole model 78—72454
ionic solids, variation of shellwise s-electron density at nucleus 79—42507
ionic solids with NaCl struct., third order elastic consts. 77—35620
ionic systems, simple, stability and melting 78—71839
ionic-covalent crystal transition to plastic state 79—90717
ionicity, Pauling's and Phillips' comparison by empirical LCAO band theory 78—51464

crystal binding continued
ionicity and struct., interrelation, appl. to zincblende, rocksalt and wurtzite structs. and amorphous semiconductors 77—1093
isolated diatomic molecules, in inert gas matrix, cage size anal. 78—47397
IV-VI compounds, XPS, bond ionicity, struct. stability and charge transfer 77—44127
IV-VI semiconductors, crystal binding energy 79—37650
IV-VI semiconductors, transverse effective charge from one dimens. band struct. calc. 80—15038
IV-VI semiconductors, transverse effective charge from three dimens. band struct. calc. 80—15039
IV-VI semiconductors, transverse effective charges 79—37651
lattice oscillations and molecular oscillation, change in bond length and angles as cooridnates 80—107385
σ-αlattice stability, pair pot. model calc. 79—60305
lattice sums by Ewald method, dipolar and Coulomb energies in infinite lattices 77—68942
layered compound, rel. to anisotropy of lattice vibrs. 77—35642
layered crystals, optical phonon anisotropies and intralayer bonding forces 77—59573
ligand-metal overlap, rel. to ligand field and charge transfer interaction intensity 79—87067
melting and boiling points vs. Coulomb pot., parabolic behaviour 80—70375
metal, asymptotic ion-pair pots., contrib. to lattice energy, elastic consts., phonon dispersion 77—19898
metal, Dimple, temperature dependent multi-ion interactions 78—22691
metal, electronegativity scale 79—73129
metal, FCC, covalent component of electron density and energy *(Russian)* 80—28945
metal, interatomic potential determ. from phonon spectra 77—65962
metal, muon screening spherical solid model 79—56654
metal, valency electron density and total energy, weak pseudopotential calc. *(German)* 77—59241
metal clusters, distortions induced by finite size in regular clusters 77—35507
metal complexes, NQR spectrosc. appls. 80—54986
metal electronic and cohesive properties, review 80—44475
metal oxides, diffusion activation process, interatomic bonding energy *(Russian)* 80—54428
metal oxides, ESCA, Madelung pot. effects 80—104036
metallic cohesion, local-density approx. to exchange and correlation effects 77—47749
metallic compounds, cohesive props., augmented-spherical-wave calcs. 79—94952
metallic phases with AlB_2 and related struct. stability 79—46597
metallic radii, of group I, II, III and IV elements, rel. to ionic radii, based on pseudopotential method 79—86738
metals, electron-ion interactions 79—4377
metals, FCC, pair potentials calc., appl. to point defect props. 80—19798
metals, FCC, small vacancy clusters, structures and energies, computer simulation 80—39073
metals, ground state of solids, spin density functional method, binding energy, compressibility 80—65477
metals, interatomic potentials, from phonon spectra 80—33927
metals, interatomic potentials of Na, K, Al, Cu, Fe from phonon spectra 80—19744
metals, simple, interion interaction and interion force constants, effective pots. in nonlocal pseudopot. method *(Russian)* 78—22684
metals, tetragonal, electron-ion interactions 80—10527
metastable microalloys, equilib. form. criteria 78—30762
mica, layer deformation and cryst. energy, struct. models for 1M and $2M_1$ polytypes 79—19184
microcrystallites, LCAO-MO calcs, in HMO approx., influence of lattice distortion adsorption, absorpt. of gases *(German)* 78—30584
mixed crystals, 1D and 2D, ion distrib. statistics 80—49167
molecular crystal, impurity and vacancy, struct. disturbance and lattice relax. calc. 79—51099
molecular crystal, interatomic pot. parameter refinement 77—65961
molecular crystal, polarisation energy of localised charge, appl. to anthracene and naphthalene 80—15034
molecular crystals, Cl atom pot. energy calcs. 78—42948
molecular crystals, optimum packing in atom-atom approx., algorithm and computer program 80—1960
molecular crysts., symmetrised valence and relative motion coords. 80—84134
molecular solids, intermol. forces and eqn. of state, pseudoharmonic approx. calcs. 78—30731
momentum space formalism, total energy of solid, calc. 80—15468
Morse function, one-dimens. cryst. stability, for teaching 78—54134
Mulliken electronegativity scale, struct. stability 79—23562
niobates, columbite or trirutile struct., force fields rel. to cryst. struct. *(French)* 80—107104
niobates of divalent metals, bonding characterisation 78—38680
noble metal, cubic close-packed struct. anal., interplanar interactions from degenerate perturbation theory 77—58971
noble metals, interatomic potentials, from phonon spectra 80—33927
noble metals, Van der Waals contribution to binding energy 78—2062
one-dimensional system, two-body pot., min. pot. energy config. 78—30582
optical oscillator strengths and excitation energies in liquids, solids and mols. 78—6648
orbital calcs., deformation density transferable integrals 80—54581
orbital calculations, deformation density method, transferable integrals 80—38992
orbital calculations, deformation density method, transferable integrals, neutral atom pots. 80—38993
organic compounds, containing ^{14}N, NQR correl. anal. 77—12240
organic solids, one-dimens. conductor, dimer level splitting, hopping integral calc. using PPP Hamiltonian 80—24890
organometallics, intermolecular interaction, Mossbauer spectra 80—15899
orientational effects, average pot. *(Russian)* 78—47270
orthosilicates, determ. of electronic polarisabilities of ions 79—7570
oxalic acid, cryst. binding, ab initio MO SCF calc. 79—37657
oxide crystals, rutile-type, interionic pots., cohesive energy, bulk modulus, calc. 80—79741
oxides of alkalis and alkaline earths, O two electron affinity from cohesive energies 78—25736
p-orbital bands and crystal struct. stability 77—7691
Pauling electrostatic valence rule, anion-cation vibr. freq. 77—35641

crystal binding continued
penninite, one-layer triclinic chlorite, neutron diffraction study 80—84144
perchlorohydrocarbons, crystn., intermol. potential-function models 80—49168
percolation conductivity in anisotropic systems, infinite cluster struct. 79—93063
perovskite, ordered, $A_2^{II}BMO_6$ type, MO_6 octahedra, mean vibr. amplitudes *(German)* 80—54320
perovskite structure crystals, appl. of repulsion parameters of ions and radicals 79—32943
perovskites, form. entropy and tolerance factor 80—34204
α-perylene crystal, emission spectra, temp. variation and pair states 78—27300
phosphates, interdepend. between tetrahedral d(T-O) bond lengths, nonbonded d(T...T) separations and TOT angles (T=Al,Si,P), using regression anal. 79—19182
point defects in crystals, book 77—47442
polar flattening, non-spherical effective shapes of atoms in crysts. 79—73123
poly-m-phenylene isophthalamide-ε-caprolactam, complex polymer cryst. 78—9967
polycrystalline aggregates, Poisson's ratio, central-force interatomic pot. calcs. 77—15479
polyhedra coordination, identification in cryst. structs. 80—59431
potential energy parameters from crystalline state props. 79—73124
pyrene, cryst. struct., atom-atom pot. calcs., micro electron diffr. obs. 78—43007
pyroclore formation, structural characts. 80—54164
quantum static multipole polarisabilities 78—82859
quantum-defect theory of heats of formation and struct. transition energies 78—55830
quartz, crystal structure rearrangement due to neutron irrad. 80—64981
quartz, low, CC Si-O bond characteristics 80—84132
quartz, low, ionicity of Si-O bond 80—84133
quasi-continuous model for a crystal with ionic and electronic polarization 79—69053
radical radiation formation in solid organic compounds 80—85201
rare earth and actinide halides and oxides stability study, energy difference between trivalent and tetravalent metal states 78—79553
rare earth cobaltides, RCo_3type, hydride phase synthesis, thermal stability and struct. 80—59438
rare earth compounds, Curie constant rel. to valence bond strength 80—60251
rare earth hexaborides, obtained by melting, micromech. props., rel. to bonding 80—21082
rare earth hydrides, props., book contrib. 80—45291
rare earth intermetallics, valence, coordination no., polyhedral at. vols. 80—19742
rare earth metals, d-band occupancy rel. to cryst. struct. 77—35510
rare earth oxyphosphates, x Ln_2O_3.y P_2O_5, synthesis, characterisation and thermal stability 80—16256
rare gas crystals, three-body forces and third-order elastic consts. 79—51185
renormalised orbital radii 78—30583
repulsive short-range interaction pot., lattice energy calc. 80—96466
rutile-type compounds, crystal binding energies and electronic polarisabilities 80—75202
semiconductor, covalent, violation of Vegard's law 77—27847
semiconductor, diamond like, group IV elements, density of valence charge 78—34463
semiconductor, ionicity effects on O_2 sticking coeff., XPS expts. 77—85887
semiconductor, lone pair, defect chemistry 78—51935
semiconductor, ternary chalcopyrite, microhardness, empirical bond approach 77—69031
semiconductor, tetrahedral, bond orbital model on CNDO basis 77—47720
semiconductor, tetrahedral, lattice thermal cond., ionicity depend. 79—37884
semiconductor, tetrahedral, thermal expansion and MP, ionicity and bond length effects 77—47606
semiconductor, tetrahedrally bonded, microhardness, empirical bond approach 77—69030
semiconductor, valence electron crystal pot. and pseudopot. components determ. from X-ray scatt. factors 79—65032
semiconductor, zincblende type, building-up of covalent bonding, quadratic response of Fermi gas 77—28132
semiconductors, chem. bonding, struct., pseudopot. theory *(German)* 78—30581
short range atomic order, size effect in electron theory, static conc. waves approximation *(Russian)* 78—39049
shortened intermolecular contacts 78—63695
sigma phase structure, ionicity modified pair pot. model anal. 78—51466
silica, and silicate minerals, interdepend. between tetrahedral d(T-O) bond lengths, nonbonded d(T...T) separations and TOT angles (T=Al,Si,P), using regression anal. 79—19182
simple metals, volume forces 80—15178
spinel type cpds., normal, classification by ionic packing factor *(Japanese)* 79—46595
spinels, MCr_2O_4 and MV_2O_4, valency and ionicity rel. to magnetism 78—52229
stability and three-body interactions 80—79740
sulphides of nonmagnetic transition metals, semicond. props. rel. to at. vol. 78—64037
superconductors, high-temp., clustering hypothesis 78—26984
superlattices, bonding and diffr. 79—19535
tantalates, columbite or trirutile struct., force fields rel. to cryst. struct. *(French)* 80—107104
TCNE, lattice dynamics of both cryst. forms, '6-exp' pot. function 79—28055
TCNQ salt, $Cs_2(TCNQ)_3$, elec. cond. and elastic const., mol. bending *(Korean)* 78—23090
TCNQ salt, NMP-TCNQ, electronic struct., SCF calc., total energy polarisation effects 80—15469
teaching, coordinated polyhedra approach 77—78934
tellurium-thiourea compounds, Mossbauer investig. of ^{129}I, quadrupole interactions and bonding 77—48111
ternary alloys, A-15 phase, Cr_3Si type, atomic volumes deduced 78—22690
ternary compounds, variation of coordination numbers under polymorphic transitions 79—86737

crystal binding continued
tetragonal complexes, meas. of covalency 77—47781
tetragonal crystals, unstressed, for arbitrary interatomic interactions, simple proof for existence 80—79746
tetrahedral crystal, electron localisability by LCAO band theory, Pauling ionicity 77—47776
tetrahedrally coordinated solids, charge distrib., localised mol. orbitals 79—23560
rel. to thermal expansion correl. with MP 77—47604
thermochemical parameters, orbital model, quantum mech. theory 78—31675
thianthrene, heat of sublimation, cryst. lattice and polarisation energy 79—32941
titanates, Ti charge state, binding energy *(Ukrainian)* 77—68940
titanosilicates, Ti charge state, binding energy *(Ukrainian)* 77—68940
transition metal, 2^{nd} and 3^{rd} long period, covalence of atoms 78—47274
transition metal, band theory 78—34757
transition metal, eqn. of state, s- and d-contribs. 78—91633
transition metal 3d monoxides, specific vol. and mag. moment calcs. 80—65822
transition metal alloy, quantum theory of heat of formation 79—86907
transition metal alloys, binary, energy of formation 77—15341
transition metal alloys, cohesive properties and press.-vol. relation 80—92476
transition metal alloys, d-band hybridisation, electronegativities, structural stability 79—42007
transition metal carbides, Group IV-VI metals, thermal expansion coeff., rel. to bond energy 78—2266
transition metal carbides, nitrides, and borides, d-band contraction upon metalloid formation, resolution of bonding controversy 79—87041
transition metal compounds, closed electron shell occurrence, at. vol. additivity deviations 77—31630
transition metal cpds., rock salt struct., surface energy bands, Shockley surface states, bonding 80—92956
transition metal dichalcogenides, layered, electronic band struct. and bonding by atomic orbitals methods 79—15077
transition metal disilicides, chem. linkage, enthalpy, above 1200K 77—90324
transition metal hydride complex, struct. geometry bonding, neutron diffr. studies 79—46641
transition metal hydrides, interstitial solid soln., H coordination 77—24289
transition metal monoxides, metallic and insulating, binding and stability 77—76760
transition metal oxides, energy loss spectra, ion polarisability 78—68585
transition metal pnictides, atomic volume, semicond. props. 78—59780
transition metal valency in alloys 77—4288
transition metal-H dilute solns., pair potential anal., unrelaxed lattice model 79—65070
transition metalloids, t-matrix theory of thermal and nonstoichiometric softening 79—86788
transition metals, atomic volumes 77—68943
transition metals, interatomic forces, phonon spectra, from band structure charge densities 79—7662
transition metals, interatomic potentials, from phonon spectra 80—33927
transition metals silicides, atomic volume deviations and supercond. T_c 80—75203
transuranic compounds, 5f electrons delocalisation, crystal and mag. props. *(French)* 77—27857
triphenyl-(triphenylgermanylperoxy)silane, cryst. and mol. struct. 80—39066
TTF, heat of sublimation, cryst. lattice and polarisation energy 79—32941
TTF-TCNQ, deuterated, compressibility under hydrostatic press., neutron diffr. meas. 78—2197
TTF-TCNQ, nonbonding intermolecular forces 80—83443
TTF-TCNQ, organic metal, Van der Waals donor stacking 80—15037
two-electron bond-orbital model of tetrahedrally coordinated solids 77—8000
urea, density distributions of bonding electrons 78—75616
valence electron distribution and 'size of atoms' in crystals *(Russian)* 78—87644
van der Waals crystal, cohesive energy, many-body theory calc. 77—76348
water-water, pair pot. near H bonded equilib. config., amorphous and crystalline solid and liq. 80—64946
Wigner solid, electrostatic energy, correction to Fuchs' calc. 79—73130
wurtzite type crystals, bond ionicity anisotropy and spontaneous distortion 77—19900
zinc blende semiconductor, electronic charge density of valence electrons 77—1094
zincblende structure group IVA covalent crystals, Murnaghan parameter estimates from Morse pot. 78—95014
zone axis patterns, depend. on string integrals or number of bound states, HEED 77—84598
zone axis patterns rel. to projected cryst. pot, HEED 77—84597
Ag halide bonding LCAO-MO treatment 79—23561
Ag halides, anal. of cryst. binding and Anderson-Gruneisen parameters 80—15040
Ag halides, cryst., van der Waals coeffs. calcs. 80—96459
Ag halides, cryst. electronic polarisability and ion sizes 77—51341
Ag halides, localised MO treatment of fractional bonding 77—58970
Ag, phonon dispersion, binding energy, compressibility, pseudopot. calc. 77—4164
Ag, stability of FCC struct. collinear three-ion interaction 80—49173
$AgBF_4$, ionic radii and chem. shifts, correl. with electronegativity 80—66054
AgBr, exchange charge polarisation 78—92016
AgBr, interionic forces, cohesive energy, bulk modulus calcs. 79—82176
AgCl, exchange charge polarisation 78—92016
AgCl, interionic forces, cohesive energy, bulk modulus calcs. 79—82176
AgCl(Br)(I), static polaris. and effective charge parameters, Born-Mayer pot. 77—31628
AgF, interionic forces, cohesive energy, bulk modulus calcs. 79—82176
Ag_2HgI_4, XPES, lattice instability 79—33904
AgI, XPES, lattice instability 79—33904
$AgInSe_2(Te_2)$, far IR refl. spectra, ionic bonds 79—55695
Ag_2S, XPES, lattice instability 79—33904
Al, low-order Fourier coeff. of pot., modified thickness fringe method 80—75130
Al, model pot. calc., binding energy and compressibility 79—99650

crystal binding continued
Al, valence charge density calc. 78—6030
AlH_3, covalent nature of chem. binding, positron annihilation obs. 78—18581
α-Al_2O_3, charge distribution determ., SCF calc., Slater-type orbitals, Madelung type const. 80—107100
Al_2SiO_5, andalusite, phonon spectra and rigid-ion model calcs. 80—11391
alkali halides, interatomic forces, Born model anal. on US data 78—55833
Ar, solid FCC struct., temp. depend. of stability 77—35502
As_2O_3-SO_3, polarised Raman and IR spectra, force field calc. *(French)* 78—6674
Au, lattice vibr., electron press., central pair pot. model calc. 78—75749
Au, phonon dispersion, binding energy, compressibility, pseudopot. calc. 77—4164
Au, stability of FCC struct. collinear three-ion interaction 80—49173
Au_3Cd_5 and Au_5Ce_8.h, cryst. struct. and binding type *(German)* 79—86742
$B_{10}H_{14}$, molecular charge distrib. 78—26513
B_2H_6, mol., static electron densities 78—79552
BN, electronic struct., exact exchange HF calcs. 80—65438
BN tetrahedrally bonded valence crystals, SCF perturbation theory appl. 79—37658
$(BaF)_2[Zn_{1-x}Cu_xF_4]$, statistics of ion distrib. 80—49167
BaH_2, XPS spectra, crystalline potentials 77—77344
BaO, at. charge densities, X-ray struct. factors 78—79566
$BaTiO_3$, electrostatic energy calc. by planewise summation method 79—23564
$Ba_2V_2O_7$, cryst. struct. determ. and bond strength anal. 79—23576
Be, charge-density from X-ray structure factors 77—19893
Be, core electron distribution, X-ray diffr. and γ-ray Compton profile obs. 80—1958
Be, HCP metals, K-emission valence bands, structure and bonding 80—7438
BeH_2, ionic nature of chem. binding, positron annihilation obs. 78—18581
BeO, tetrahedrally bonded valence crystals, SCF perturbation theory appl. 79—37658
Ca, FCC, ground-state props. 78—75989
Ca metaborates, endogeneous, H bonds in cryst. structs. 80—33975
$CaBr_2.6H_2O$, cryst. struct. determ. 77—80474
$CaCO_3$, birefr. and electronic polarisabilities of constituent ions 80—7322
$CaCl_2.6H_2O$, cryst. struct. determ. 77—80474
$CaCu_5$-type structure, intermediate phase, relative stability and struct. characts. 77—58968
CaF_2 crystal structure, stability compared with TiO_2 *(Russian)* 80—64945
CaF_2:Nd^{3+}, Slater, Racah and Lande parameters, crystal bonding 80—16062
CaH_2, XPS spectra, crystalline potentials 77—77344
$CaNb_2O_6$, columbite, polarised Raman and IR spectra, normal coord. anal. 77—76500
CaO, at. charge densities, X-ray struct. factors 78—79566
CaO, crystalline pots. from XPS data 77—77344
CaO, electronic structure 80—2332
CaO, modified electron gas theory, high press. effect 77—19899
CaS, dielectric props., effective ionic change 79—65783
CaS(Se), crystalline pots. from XPS data 77—77344
Ca_2SiO_4-BaO, conditions and mechanism in cryst.-chemical stabilisation of unstable phases 80—39302
Ca_2SiO_4-FeO, conditions and mechanism in cryst.-chemical stabilisation of unstable phases 80—39302
Ca_2SiO_4-MgO, conditions and mechanism in cryst.-chemical stabilisation of unstable phases 80—39302
$CaWO_4$:Nd^{3+}, Slater, Racah and Lande parameters, crystal bonding 80—16062
Cd chalcogenides, electronic polarisabilities of ions 78—79559
CdI_2, interlayer interactions estimate from Raman and Brillouin scatt. 79—99884
$CdSiP_2$, bond strengths and bond lengths, thermal expansion coeff. meas. 78—87651
Cl_2, solid, electronic struct. of bonding, X-ray diffr. meas. 79—42006
Cl_2 solid, space group, anisotropic atom-atom forces 79—73127
CmO_2, band struct., cryst. binding and ESCA spectra, X_α cluster calc. 78—64443
Co complex, monofumaratotetraaquocobalt(II) monohydrate, cryst. struct. and cryst. binding 79—37681
$Co_3(AsO_4)_2$ polymorph, cryst. struct., closest packing 80—70174
$CoCr_2X_4$ (X=O,S), K absorpt. discontinuity chem. shift, bonding parameters 77—77318
$Co(NH_3)_6X_3$, (X=Cl, Br, I), internal and lattice vibr. normal coordinate anal. 79—69203
CoO, ab initio SCF and CI calcs. on d-d transitions, ${CoO_6}^{10-}$ cluster d-electron localisation 77—35897
$Co^{2+}[Fe(CN)_6]^{3-}$, struct. determ. 80—15901
Cr-Ni, high temp. strength, interatomic bonds ionic component correlation *(Russian)* 79—15761
Cs halides, rel. to dielectric behaviour and optic mode Gruneisen parameters 79—10907
$CsBF_4$, ionic radii and chem. shifts, correl. with electronegativity 80—66054
CsBr, evaluation of van der Waals dipole-dipole pot. 78—22692
$CsCdF_3$:Cr^{3+}, ENDOR exam. of electron spin transfer 77—48089
$CsCdF_3$:Fe^{3+}, ENDOR meas. on Fe^{3+}-F^--Cd^{2+} struct. 78—31122
CsCl, electrostatic energy calc. by planewise summation method 79—23564
CsCl, evaluation of van der Waals dipole-dipole pot. 78—22692
CsI, evaluation of van der Waals dipole-dipole pot. 78—22692
Cu complexes of amino acids and α-hydroxy acids, bonding effect on spin-orbit coupling 77—1399
Cu, cryst. pot. in electron diffr. and band theory 78—83677
Cu halides, anal. of cryst. binding and Anderson-Gruneisen parameters 80—15040
Cu, interatomic pot., vacancy form., migration energy from phonon dispersion curves 78—42950
Cu, interatomic potential from intermediate and low energy data 78—55829
Cu isoelectronic series, hard-core pseudopotentials and struct. maps 80—44168
Cu, lattice and force consts., pairwise atomic repulsions in cluster model 79—32939

crystal binding continued
Cu, stability of FCC struct. collinear three-ion interaction 80—49173
CuCl(Br)(I), static polaris. and effect charge parameters, Born-Mayer pot. 77—31628
$Cu_{0.5}Co_{0.5}Cr_{2-x}Rh_xS_4$, K absorpt. discontinuity chem. shift, bonding parameters 77—77318
$CuCr_2X_4$ (X=O,S,Se,Te), K absorpt. discontinuity chem. shift., bonding parameters 77—77318
Cu_2HgI_4, XPES, lattice instability 79—33904
$CuInSe_2(Te_2)$, far IR refl. spectra, ionic bonds 79—55695
$CuMn_2O_4$, comment on cryst. struct. determs. by neutron diffr. 79—23585
$CuMn_2O_4$, ionic config., re-exam. of expt. evidence 77—19897
$Cu(NH_3)_4PtCl_4$, $Cu(NH_3)_4^{2+}$ cation mol. orbital parameters 78—64011
Cu_2S, XPES, lattice instability 79—33904
D_2, intermolecular pair potential, from solid-state data 79—14727
Dy_2O_3, XPS, charging effects on core-level binding energies 79—24409
Er_2O_3, XPS, charging effects on core-level binding energies 79—24409
Eu intermetallic compounds, Mossbauer effect isomer shift, charge density at nucleus, trends 77—48112
α-Fe, BCC, stress-induced interaction and ordering 79—42057
Fe, conversion spectrum anal., outer-shell s-electron density, ACSEMP program 80—7208
α-Fe, interaction of He with C impurities, computer simulation calc. 79—99235
Fe, interatomic pots. choice rel. to melting temps. 79—74863
α-Fe, lattice and force consts., pairwise atomic repulsions in cluster model 79—32939
Fe oxides, interatomic interaction by XPS 80—7474
Fe, X-ray absorpt. spectra, effective co-ordination charges 80—84805
Fe-Sn compounds, type of binding *(German)* 77—35503
Fe_2O_3, X-ray absorpt. spectra, effective co-ordination charges 80—84805
Fe_3O_4, X-ray absorpt. spectra, effective co-ordination charges 80—84805
Fe_xO, X-ray absorpt. spectra, effective co-ordination charges 80—84805
Fe_3P-type structures, atomic coord. and bonding 79—60330
$FeTe_x$, Mossbauer spectra, 80 to 750K, quadrupole splitting and isomer shift 77—4590
Ga-La, energy band struct. and atomic radius 79—73434
GaAs, X-ray K absorpt. edge, effective ionic charge and bonding schemes 80—29827
$Ga_xIn_{1-x}P$:N, Delta lattice parameter model, correl. with electronic props. 78—91560
GaP, impurity distribution ratios, correl. with covalent and ionic radii 80—54276
GaP-based III-V solid solns., bonding and energy gap, mag. meas. 78—18580
GaS, mag. susceptibility anisotropy, chem. bonding *(Russian)* 79—61045
GaSb, anharmonic force consts. from third order elastic consts. at 300K 77—59074
GaSe, mag. susceptibility anisotropy, chem. bonding *(Russian)* 79—61045
GdIG, empirical formula for lattice const. calc. 79—27968
Ge, lattice stability, pseudopotential theory and problem of covalent bonding 77—55490
GeTe, crystal binding energy 79—37650
GeTe, interpretation of polymorphic transformations 80—15032
H linear chain, near Hartree-Fock limit study 79—32938
H, metallic, Coulomb crystal energy 78—91300
H, metallic, cubic structure, mechanical stability 77—4242
H, metallic, Hartree-Fock and correlation energies 78—34674
o-H_2, cohesive energy, non-additive term 79—50099
H_2, intermolecular pair potential, from solid-state data 79—14727
H_2, metallic, ground-state energies of liq. and solid phases, variational and Monte Carlo methods 80—70502
H_2, metallic and mol. crysts., X-ray scatt. factors, Hartree-Fock calc. 79—60219
H_2, metallic interion interaction *(Russian)* 78—91299
HBr, cryst. binding, H-bonding pot. function 79—32940
HCl, cryst. binding, H-bonding pot. function 79—32940
HCl crystals, orthorhombic and cubic, CNDO calcs. 80—6383
HCl, mol. cryst., angles of H-bonded mols., ab initio calcs. 78—6037
HF, cryst. binding, H-bonding pot. function 79—32940
HF, one-dimens. cryst., ground state energy PCILOCC method 79—10056
$HUO_2PO_4.4H_2O$, H^+ ion cond., struct. mechanism, X-ray diffr. obs. 78—34651
He, solid, theory and thermodynamic props., book contrib. 77—47646
Hg_2X_2, X=Cl, Br, I, acoustic props., cryst. lattice bonds 78—30700
Ho_2O_3, XPS, charging effects on core-level binding energies 79—24409
I_2, lattice dynamics, bond charge model 77—84858
InSe, mag. susceptibility anisotropy, chem. bonding *(Russian)* 79—61045
K isoelectronic series, hard-core pseudopotentials and struct. maps 80—44168
$KBO_2.4/3H_2O$, unusual hydrogen bonding 78—2058
KBr crystals, binding forces and eqns. of state, inner electron contrib., calc. 80—64950
KBr:Tl^{2+}, relation between bonding and g-shift 80—39492
KBr(Cl), positron ang. correl., cryst. orient. depend., positron states and ionic distortion 77—63484
KCl, TSM study of lattice statics and dynamics 79—82292
KCl:Tl^{2+}, relation between bonding and g-shift 80—39492
KCl-KBr mixed crystal, elastic consts. press. derivative 77—11619
KCl.Pb^{3+}, relation between bonding and g-shift 80—39492
K_2Cs, Laves phase, electronic charge density pseudopotential calcs. 79—77549
K_7Cs_6, μ-phase variant, chemical bonding, electronic charge density distrib. pseudopotential calcs. 79—77549
$K_2Er(NO_3)_5$, cryst. struct. by X-ray diffr., cryst. binding 78—42988
KF(Cl)(Br)(I), rel. to surface lattice dynamics 78—34693
$KIO_3.HIO_3$, I atom electronic struct. in X-ray-neutron difference synthesis 79—90595
K_2MnF_4, IR active modes, interlayer and intralayer forces 77—59575
$KMnO_4$, cryst., bond lengths and coordination numbers, EXAFS meas. 79—51043
$K_3N(SO_3)_3.2H_2O$, cryst. binding of H_2O, IR spectra 78—75620
KNa_2, binding energy and lattice const., nonparametric calc. *(Russian)* 78—51462
$K_2Na[Co(NO_2)_6]$, bond nature, X-ray diffr. determ. of electron density distrib. 79—14746

crystal binding continued
$KNbF_6$, NMR, quadrupole effects and struct. distortion 80—15809
$K_2Pt(CN)_4Br_{0.3}.2.7D_2O$, under hydrostatic press., compressibility, neutron diffr. 79—46742
$K_4Zn(MoO_4)_3$, cryst. struct., cohesion 77—31641
$K_2[MoO_{1-x}(OH)_{2x}(H_2O)_{1-x}O(MoO_4)_2].2H_2O$, proton NMR for chem. comp. at −195°C 78—38651
La, FCC, ground-state props. 78—75989
La-Co-O system, stability of ternary phases, nonstoichiometry 80—24434
La_3RuO_{11}, prep. and struct. study, metal-metal bonding *(French)* 78—91325
Li, binding energy and atomic radius calc., effect of nonlocalised charact. of pseudopot. *(Russian)* 78—18575
Li cluster, density functional calcs. 77—8031
Li intercalated atoms, host lattice strain effects 80—88082
Li isoelectronic series, hard-core pseudopotentials and struct. maps 80—44168
Li, phonon frequency, liquid electrical resist. and interionic pair potential 78—10140
Li sites, determ. in cryst. structs. using method based on bond-strength calcs. 79—7514
LiAl, NMR relax. investig. of ^7Li self-diffusion, evidence for covalent bonding 77—12217
LiF, Compton profile interpretation to give ionic deform. and bonding 77—40301
$Li_{0.5}Ga_{0.85}Cr_{1.625}O_2$ spinel, tetrahedral coordination of Cr^{3+} ion, electronic spectra, X-ray and neutron diffr. *(French)* 79—65031
LiH_2F hypothetical crystal, existence, total energy calc., pseudopot. calc. 78—2442
LiN_3, ionic nature, quadrupole splitting, mag. field depend., N^{3-} electron cloud deform., NMR 80—50210
$Li_2O.3MoO_3.5.7H_2O$, fibrillar cryst., IR and NMR investig. of water bonding 77—12370
Li_2SO_4, UPS, expt. methodology aspects 77—90245
LiX,(X=F,Cl,Br,I), UPS, expt. methodology aspects 77—90245
$Li_4Zn(GeO_4)_4$, ionic cond. 79—55922
Lu_2O_3, XPS, charging effects on core-level binding energies 79—24409
Lu_2S_3, XPS, binding energies 79—15586
Lu_3S_4, XPS, binding energies 79—15586
Mg, HCP metals, K-emission valence bands, structure and bonding 80—7438
$MgIn_2S_4$, cation distrib. and deform. parameter using Bertaut, Furuhashi and Baltzar methods 80—15041
$MgNH_4PO_4.6H_2O$, struvite crysts., periodic bond chains 79—41994
MgO, at. charge densities, X-ray struct. factors 78—79566
MgO, cryst. electronic polarisability, ion size and dielectric const., hydrostatic press. effects 78—26487
MgO, modified electron gas theory, high press. effect 77—19899
$Mg(OH)_2$:Fe, crystal field properties, Mossbauer spectra, isomer shift and quadrupole splitting 79—61278
Mn halogenides, optical spectra, metal-ligand bonds *(Russian)* 79—51986
$MnFeO_4$:^{57}Co, Mossbauer spectrum, 4s covalent bonding 80—20540
Mo, interatomic pot. from phonon spectra 77—76355
MoO_3-M_2O_3 system, M=trivalent metal, solid-state chem., review 77—24288
$MoS_2(2H)$, lattice dynamics, Coulomb and quasi-harmonic effects 80—39245
$MoSe_2(Te_2)$, IR and Raman spectra, lattice vibrs. interlayer bonding 80—40110
NH_4BF_4, ionic radii and chem. shifts, correl. with electronegativity 80—66054
Na cluster, density functional calcs. 77—8031
Na isoelectronic series, hard-core pseudopotentials and struct. maps 80—44168
Na, linear potential and phonons 79—82293
$NaAlSi_3O_8$, cryst., Al-Si order-disorder, electroneutrality effects in model 79—90593
NaCl, electrostatic energy calc. by planewise summation method 79—23564
NaCl, polarisation mechanism and lattice mechanics, microscopic approach 78—59888
NaCl, positron ang. correl., cryst. orient. depend., positron states and ionic distortion 77—63484
NaCl single crystals, screw dislocations, influence of interionic potentials on core configs. 80—34000
NaCl, UPS, expt. methodology aspects 77—90245
NaCl, valence-electron charge density along nearest-neighbour axis 79—27944
NaCl:H (Cl) interstitials repulsive parameters from electronic charge density overlap, diffusion 77—59006
NaF, UPS, expt. methodology aspects 77—90245
$Na_2HPO_4.2H_2O$, crystal struct., coordination and H bond competition 78—14315
$NaHSO_4.H_2O$ pseudo-symmetric crystal struct., hydrogen bonding 77—55258
$NaNO_2$, ferroelec., electric field gradient *(Korean)* 79—15419
$NaNbF_6$, NMR, quadrupole effects and struct. distortion 80—15809
NaOH, UPS, expt. methodology aspects 77—90245
NaSCN, and similar salts, Na atomic charge determ. by numerical integration 80—28944
$Na_2[MoO_{1-x}(OH)_{2x}(H_2O)_{1-x}O(MoO_4)_2].2H_2O$, proton NMR for chem. comp. at −195°C 78—38651
Nb, BCC, stress-induced interaction and ordering 79—42057
Nb_3Al, metallic bonding, electronic states calcs. 78—79916
$Nb_3Al(Ge)$, bonding, electronic charge distribs. and struct. transform. from self-consistent pseudopotentials 79—69054
Nb_3Au, A-15 struct. supercond., microhardness, bonding 78—76199
NbC, rock salt struct., surface energy bands, Shockley surface states, bonding 80—92956
Nb_3Ge, metallic bonding, electronic states calcs. 78—79916
Nb_3Ir, A-15 struct. supercond., microhardness, bonding 78—76199
Nb_3Sn, A-15 struct. supercond., microhardness, bonding 78—76199
Ni, band struct., cryst. pot. anisotropy effect *(Russian)* 80—88474
Ni complex, cis-dichloro-bis(1,2,cyclohexadionedioxime) cryst. and mol. struct. 80—44198
Ni complex, di-(trichloroacetate).4n-para-anidine crystal struct., bond angles 79—86774
Ni compound, $[Ni_3(CO)_6]_n^{2-}$, n=1,2, one-electron states in polynuclear carbonyls 79—95358

crystal binding continued
Ni, dynamic rearrangement of atomics in large cluster using Frohlich-Raimes method 78–30586
Ni intermetallics and oxide, interatomic interaction by XPS 80–7474
Ni, lattice and force consts., pairwise atomic repulsions in cluster model 79–32939
Ni-Al system, Mossbauer spectroscopy investigation *(Russian)* 80–20523
Ni-S(Se)(Te) mixtures, binding of phases, two-correl. model 77–80438
NiO, ab initio SCF and CI calcs. on d-d transitions, NIO_6^{10-} d-electron delocalisation 77–35896
$NiSi_x$, cryst. struct. of phase *(German)* 79–99119
O-containing anions of d-elements forming hydration-active phases, electron structs. and props. 79–42005
OHO bonds, O-H vs. O...O distance correlation and geometric isotope effect 78–75615
organometallic transition metal hydride complexes, struct. geometry bonding, neutron diffr. studies 79–46641
OsB_2, possibility of semicond. props., rel. to atomic volume 77–69317
P, black allotrope, orthorhombic bonding, up to 26.6 kbar, neutron diffr. obs. 79–99106
PCl_5, ^{31}P NMR of three solid phases, ionis. of PCl_6^- at high-press. 79–82882
PCl_5 III, Raman spectra of phase formed by high-press., PCl_6^- ionising dissoc. 79–82968
PCl_5, phase diagram, PCl_6^- ionising to PCl_4 and $2Cl^-$ under press. 79–82314
Pb, model pot. calc., binding energy and compressibility 79–99650
$PbCl_2$, binding, ionicity, covalent contrib., Madelung const., cohesive energy 78–79558
$PbCl_2$, single cryst., far IR refl. spectra, effective ionic charges 79–87430
PbI_2, single cryst., far IR refl. spectra, effective ionic charges 79–87430
PbS, mol. diamag. susceptibility, bonding types 78–31046
PbS(Se)(Te), crystal binding energy 79–37650
$Pb_{1-x}Sn_xTe$, lattice instability and phonon lifetimes, neutron scatt. 78–55932
Pd-S(Se)(Te) mixtures, binding of phases, two-correl. model 77–80438
Pd-Th, thermodynamic stability 79–55903
Pd-Zn system, struct. stability of B2 and $L1_0$ phases 78–26495
Pd_5As, cryst. struct. and cryst. binding *(German)* 78–42958
PdBi, rhombic, cryst. struct. determ. *(German)* 79–77556
Pd_5Bi_2, cryst. struct. *(German)* 79–51053
$Pd_{21}Ge_8$, cryst. struct. *(German)* 78–18586
Pd_5Ge, cryst. struct. and cryst. binding *(German)* 78–42958
PdPb.r, crystal structure *(German)* 80–96472
Pd_3Te_2, struct. and binding *(German)* 77–43192
Pd_9Te_4, cryst. struct. and binding *(German)* 78–51471
Pt compound, $[Pt_3(CO)_6]_n^{2-}$, n=1,2, one-electron states in polynuclear carbonyls 79–95358
Pt-S(Se)(Te) mixtures, binding of phases, two-correl. model 77–80438
$Pt_{13}In_9$, exam. of crystal structure, and phase diagrams *(German)* 78–83779
Pu, oxidation, binding energies, Auger and X-ray photoelectron spectra study 80–76550
$RbAg_4I_5$, Ag^+ ion pot. energy calcs. 79–10828
RbF(Cl)(Br)(I), chem. shift in X-ray absorpt. spectra, correl. with ion contrib. to bond 78–76559
$RbFeS_2^+$, ^{57}Fe Mossbauer hyperfine interaction, covalency effects, point charge model 78–39484
$RbICl_4$, ^{35}Cl NQR spectra, press. cond. temp. depend 80–20501
Rb_2MnCl_4, IR active modes, interlayer and intralayer forces 77–59575
$RbNiCl_3$, cryst., ^{35}Cl and ^{87}Rb NMR down to 1.3K 79–42848
ReB_2, electron struct., Fermi energy and surface, bonding 80–20076
ReB_2 possibility of semicond. props., rel. to atomic volume 77–69317
$Re_{12}P_{26}$, binary crystals containing plane Re_4 clusters *(French)* 80–19774
Ru-Sn compounds, type of binding *(German)* 77–35503
RuB_2, possibility of semicond. props., rel. to atomic volume 77–69317
α-S, attachment energy as habit controlling factor 80–59421
α-S, under hydrostatic press., deformable mol. lattice statics 80–49175
Sc alloying behaviour, C and B stabilising effect, lattice parameters and at. radius 77–36454
ScF_3, metastable high press. phases, X-ray diffr. and IR absorpt. expts. 77–11499
ScO(OH), ScOF, and $Sc(OH)_3$, metastable high press. phases, X-ray diffr. and IR absorpt. expts. 77–11499
Se, effective charge tensor, microscopic treatment 78–59879
Se, molecular cryst., Se-Se nonbonded pot. parameters derivation from heat of sublimation 79–27945
Se, monoclinic to trigonal conversion, thermodynamic stability and associated investigs. 80–24592
Si, bonding electron distribution 79–90594
Si, charge disturbance around neutral defect, simple new method, appl. to ideal vacancy 79–82554
Si, ductile-brittle transform. hypothesis and temp. depend. of charge bond *(Russian)* 78–35484
Si, lattice stability, pseudopotential theory and problem of covalent bonding 77–55490
Si noncrystalline film, struct., interatomic distances, SRO 80–107053
Si, phase transformation, lattice dynamics, microscopic theory 80–107387
Si, structural props. using electron-ion Hamiltonian using density-fundamental methods 79–82177
Si-Ge system, phase diagram, lattice const. var. effects 80–97470
SiC polytypes, contribution of ionic bonding to thermal stability 80–28946
SiC single crysts., polytypism obs. by high temp. oxidation expts. 78–59797
$Si_{1-x}H_x$, noncrystalline film, struct., interatomic distances, SRO 80–107053
SiO_2 different modifications, chem. bonding, struct. *(German)* 78–30581
SiO_2 polymorphs, CNDO/2 MO calc. 80–6386
SiO_2:B_2O_3 doped, IR spectra 79–78664
SiO_6 octahedra, var. of mean Si-O bond lengths 78–18577
SiO_x, electronic struct., random bonding model 79–82175
β-Sn, covalency of bonding, (202) almost forbidden reflection meas. 79–94953
α-Sn, lattice stability, pseudopotential theory and problem of covalent bonding 77–55490

crystal binding continued
SnI_4, attachment energy as habit controlling factor 80–59421
SnO_2, nonstoichiometric crystal, free electron density anal. 79–99108
SnO_2, point lattice electrostatic pot. calcs. *(Russian)* 80–15044
SnTe, crystal binding energy 79–37650
$SrCl_2$, valence-electron charge density along nearest-neighbour axis 79–27944
SrH_2, XPS spectra, crystalline potentials 77–77344
SrO, at. charge densities, X-ray struct. factors 78–79566
SrO, crystalline pots. from XPS data 77–77344
SrS(Se) crystalline pots. from XPS data 77–77344
TCNQ salts, bond lengths and charge transfer *(French)* 77–80493
Ta, BCC, stress-induced interaction and ordering 79–42057
Tb_4O_7, XPS, charging effects on core-level binding energies 79–24409
TcB_2, electron struct., Fermi energy and surface, bonding 80–20076
TcB_2, possibility of semicond. props., rel. to atomic volume 77–69317
Th, FCC, ground-state props. 78–75989
Th_3As_4, positron annihilation, mean ionic radius calc. 79–15550
ThO_4, prep., IR spectra and thermal exam. 77–89402
Ti, band struct., cryst. pot. anisotropy effect *(Russian)* 80–88474
TiC_xO_y, thermal expsn. coeffs. lattice spacing temp. depend. 77–69102
TiO_2 crystal structure, stability compared with CaF_2 *(Russian)* 80–64945
TiO_2, interionic repulsive short-range interaction pot., lattice energy calc. 80–96466
TiO_y, thermal expsn. coeffs., lattice spacing temp. depend. 77–69102
Ti_3P-type structures, atomic coord. and bonding 79–60330
$TiSi_2$, struct. refinement and bonding 77–72592
Tl (I)-O-M cpds., M=B,Tl,C,Si,Ti,Sn,Sb,P, lone pair position, electrostatic model *(French)* 78–34462
Tl halides, anal. of cryst. binding and Anderson-Gruneisen parameters 80–15040
Tl halides, cryst., van der Waals coeffs. calcs. 80–96459
Tl, halides, cryst. electronic polarisability and ion sizes 77–51341
TlBr, CsCl and NaCl phases, atomic interactions and lattice statics and dynamics 78–83889
TlBr-TlI, KRS-5, periodic strain anisotropy, optical and X-ray diffr. study 80–54167
TlCl(Br)(I), static polaris. and effective charge parameters, Born-Mayer pot. 77–31628
Tm_2O_3, XPS, charging effects on core-level binding energies 79–24409
TmSe, Curie constant rel. to valence bond strength 80–60251
U chalcogenides, electronic struct., relativistic single-site scatt. model 79–87040
U pnictides, electronic struct., relativistic single-site scatt. model 79–87040
UAs, U 4f ESCA spectra 80–16148
UAs_2, and U_3As_4, positron annihilation, mean ionic radius calc. 79–15550
UAsS(Se)(Te), positron annihilation ang. distrib., valence electrons and Fermi surface 77–28093
UAs(Se)(Te), positron annihilation, mean ionic radius calc. 79–15550
UF_4, 5f element fluoride bond length-strength anal. 80–54166
UN, U 4f ESCA spectra 80–16148
UP, U 4f ESCA spectra 80–16148
UP_2, positron annihilation, mean ionic radius calc. 79–15550
$UP_2(Sb_2)(As_2)$, positron annihilation ang. distrib., valence electrons and Fermi surface 77–28093
$U_xPu_{1-x}O_2$, theoretical study of electronic thermodynamic and valence props. 79–37655
US, U 4f ESCA spectra 80–16148
USb_2, positron annihilation, mean ionic radius calc. 79–15550
V, BCC, stress-induced interaction and ordering 79–42057
$V_{0.985}Al_{0.015}O_2$, insulating T-phase cation disproportionation and V-V pairing 77–62825
VC, energy band struct., chem. bonding 78–18958
V_3Ge, A-15 struct. supercond., microhardness, bonding 78–76199
VH_x, temperature limits for stable existence of hydrides, ionic state *(Russian)* 77–7690
VI_2, lattice dynamics and ionic charge 80–10615
V_2O_5 and lower oxides, electronic, optical, structural and surface props., review 80–88120
V_4O_7, cryst. atomic struct., 120K and 298K 78–34486
V_6O_{11}, metallic Magneli phase, electron state 79–94946
V_7O_{13}, metallic Magneli phase, electron state 79–94946
V_3S-type structures, α- and β-forms, atomic coord. and bonding 79–60330
V_3Si, A-15 struct. supercond., microhardness, bonding 78–76199
Xe, solid, high press. equation of state 79–37809
Xe(II, IV, VI and VIII) compounds, Mossbauer study 79–65772
YCo_3, hydride phase synthesis, thermal stability and struct. 80–59438
YIG, empirical formula for lattice const. calc. 79–27968
Yb_2O_3, XPS, charging effects on core-level binding energies 79–24409
Zn chalcogenides, electronic polarisabilities of ions 78–79559
Zn complex, ZnS_2O_4.pyridine, cryst. struct., nature of S-S bonds 78–55847
Zn, HCP metals, K-emission valence bands, structure and bonding 80–7438
Zn single crystal, EXAFS, using linearly polarised synchrotron radiation 78–2943
$ZnAs_2$, thermodynamic functions 79–10961
ZnO(S)(Se)(Te), cryst., ionic radii and electronic polarisabilities 77–1091
ZnSe, crystallographic polarity and etching behaviour 77–85030
$ZrS_2(Se_2)$, charge densities, X-ray form factors, and bonding props. 79–94950

crystal chemistry
see also crystallography
alkali metal halides, F-centre luminesc. rel. to cryst. chemical parameters 80–29780
alkali metal-transition metal oxide, AMO_2, stability rel. to coordination *(French)* 77–19933
alkaline earth oxides and fluorides, F-centre luminesc. rel. to cryst. chemical parameters 80–29780
alloying and cpd. form. of later transition and early B subgroup elements, graphical rep. 77–19895
alloys, criteria of chemical inhomogeneity 80–59670
alloys, CsCl type, nearest neighbour distance and atomic props. 78–51465

- **crystal chemistry** continued
  - aluminides of non-magnetic transition metals, atomic volumes deviation from additivity 79—82178
  - apatites with Ca deficiency, H atom stabilisation 78—23340
  - borides, B_{12}, cryst. chem. classification, book contrib. 78—47302
  - borides, nature of chem. bond, book contrib. 78—47276
  - borides, proposed classification 80—19741
  - borides with ReB_2 and Mo_2IrB_2 type structures 78—42995
  - bytownite, quenched from 1723K, X-ray single cryst. struct. anal. and refinement 79—19193
  - cation-deficient close-packed structures, combinatorics 79—23558
  - ceramic, rational molecular engineering 78—11179
  - chemical formulae symbolism, for simple inorganic cryst. structs. 80—33910
  - chromite natural samples of Brazilian, Philippine origin, chem. comp., Mossbauer spectroscopy 80—103901
  - compound semiconductor, nonstoichiometry and carrier conc. control in MBE 79—95941
  - conference, solid state chem., Strasbourg, France (Feb. 1978) 79—46506
  - crystal density, liquid mixture, comment on simple method of measuring by determ. of refractive index 79—51014
  - di-o-thymotide, cryst. chem. study and morphology *(French)* 79—46576
  - disordered multicomponent solid solutions conc. fluctuation waves, microscopic theory 80—44327
  - excess component concentration, appl. to conc. determ. in nonstoichiometric appls. 78—43131
  - feldspars, superplastic flow and cryst. chemistry changes 79—79831
  - ferrite, synthetic, inhomogeneity, nonstoichiometry and lattice defects 77—35547
  - ferrite systems, thermodynamic stability, dissociation and phase relations *(Japanese)* 80—55378
  - fluorite-related phases, Ln_3MO_7, (Ln=rare earth, Y or Sc), (M=Nb, Sb or Ta) 79—46619
  - fluoroapatite, IR spectra, H motion in nonstoichiometric cryst. 78—35125
  - graph theoretical basis, trivalent graphs with 10 vertices 78—38644
  - halide compounds, cryst. chem. and structs. of type $A_2B^+B^{3+}X_6$ 79—46639
  - halide compounds ABX_3 with perovskite struct., cryst. chem., X-ray diffr. anal. 78—95042
  - hydroxylapatites, IR spectra, H motion in nonstoichiometric cryst. 78—35125
  - intercalation, review *(Japanese)* 77—68930
  - intermetallic phases, struct. description *(German)* 80—88090
  - layer structures, raster scanning depth profiling 77—16441
  - metal, Bloch-Simon struct. index, chem. bond geometry interpretation 77—35508
  - metal ionic radius and oxide structure chart 79—73152
  - metal oxides, boundary conditions of formation of primary nonstoichiometry 77—21115
  - metal-boron systems, correlation of phase equilibria, with boride crystal chemistry 79—11562
  - metavanadates, MVO_3, (M=Li,Na,K,NH_4,Tl,Rb,Cs), struct. variation in series 78—6043
  - mica, crystal chemistry, review 79—46612
  - molecular charge transfer complexes, mol. and cryst. struct. 78—62942
  - molybdates, nonstoichiometric, IR spectra rel. to vacancy struct. *(French)* 78—43867
  - non-stoichiometric compound with ionised punctual defects, Gibbs-Duhem eqn. 77—31786
  - nonstoichiometric solid solutions, ordering 78—87794
  - nonstoichiometry and dielectric props. 78—43135
  - nontransition metals, electron density, bulk and surface props. relation 80—103609
  - order-disorder structures, desymmetrisation 80—38986
  - order-disorder structures, layer stacking 80—38981
  - oxides, ABO_4 type, high press. phase transforms. and struct. types, cryst. chem. aspects 80—79940
  - oxides, stoichiometry meas. and control 78—51694
  - oxides, surface microphases investigation by X-ray electron spectral anal. 79—51269
  - phase diagram interpret. using cryst. chem. formulae 77—81251
  - phlogopites, mica, Fe^{2+}, F^-, and OH^- distrib. in octahedral sheet, NMR study 79—82183
  - phosphates, condensed, survey 79—86745
  - photoluminescence activation conditions for binary inorganic crystals 78—10394
  - plane nets 80—49157
  - point defect chemistry, book contrib. 78—10044
  - pyrochlores of charge-coupled type, form. in comps. $A^{2+}A^{4+}Ti_2O_7$ and $A^+A^{3+}B^{4+}B^{6+}O_7$ 80—92504
  - pyroclore formation, structural characts. 80—54164
  - rare earth alloys, book 80—36785
  - rare earth alloys with Cu_3Au lattice, cryst. chemistry and supercond. crit. temp. 79—86744
  - rare earth antimonates, $RSbO_4$ (R=Nd-Lu or Y), high temp. modifications, cryst. chem. identification X-ray anal. 79—65059
  - rare earth antimony oxides, $RSbO_4$, low temp. form, prep., cryst. chem. identification 78—47300
  - rare earth cobaltides, RCo_3type, hydride phase synthesis, thermal stability and struct. 80—59438
  - rare earth compound properties, periodicity at atom props. 80—96586
  - rare earth intermetallic cpds., cryst. chemistry, book contrib. 80—39010
  - rare earth metal orbital radii, quantum-mech. calcs. rel. to inner series contraction 77—83514
  - rare earth molybdates, cryst. growth, cryst. chem., and phys. props., book contrib. 80—44194
  - rare earth oxymolybdates and oxytungstates, R_2MO_6, spectroscopic props. and crystallochem. laws 77—36215
  - rare earth oxyorthotitanates, crystallochem. classification 80—107142
  - rare earth perovskites and garnets, prep. and props. book contrib. 80—44193
  - rare earth theoretical chemistry, book contrib. 80—42919
  - rare earth thiosulphate, IR and Raman spectra, possibility of nonexistence of cpd. of given formula *(French)* 77—24279
  - rod packings 78—9981
  - semiconducting alloys, comp. profile, second derivative wavelength modulation 80—103967
  - semiconducting binary compound, third component solubility 78—43124
  - semiconductor alloy, for appl. in IR detector arrays, comp. control 80—31872

- **crystal chemistry** continued
  - SiAlON X-phase, X-ray diffr. data 80—49198
  - silicates, layered, not containing Al, synthesis and cryst. chem. 78—51495
  - silicates, plane Si-O rings with max. number of tetrahedra 78—18622
  - solid electrolyte materials chemistry problems 80—96680
  - spinels, ligand field stabilisation evaluation using Mossbauer determ. cation distrib. 78—31126
  - spinels, oxo and sulpho, boundary conditions for existence 78—23684
  - steel, inclusion chemistry control for machinability enhancement 80—85067
  - sulphosalt minerals, exam. of crystal chemistry and morphology 79—10838
  - superconductor, A_3B cpds. with A-15 lattice, cryst. chemical laws 78—34914
  - superconductors, A-15 compounds, homogeneity range 80—2172
  - ternary compounds, defect chemistry 79—90648
  - ternary metal borides, struct. chem. 79—14769
  - tetrahedral structures, related to wurtzite type (B4), non-bonded interactions and cryst. chemistry 79—14743
  - transition metal chalcogenides, stability criterion between spinel- and defect NiAs-type structs. 77—84696
  - transuranic chalcogenides and pnictides, prep. and cryst. chem. 80—16255
  - zeolites, coordination of Al and Si from X-ray spectra 78—11021
  - $(2CdTe)_x$-$(In_2SnTe)_{1-x}$, x=0.25, 0.5, 0.75, tetrahedral semiconductor, chem. interaction of Sn atoms, Mossbauer study 80—39977
  - $ABCl_3$ cpds., basic struct. types and polymorphisms 78—79583
  - $AgNO_2$, high-pressure phase behaviour, crystal chemistry of univalent nitrites 78—30749
  - $Ag_xNa_{2-x}Te_2^{IV}Te_3^{VI}O_{14}$, (x=0,4), mixed tellurate, cryst. chem. and elec. cond. *(French)* 80—107150
  - β-Ag_2S, electrogalvanic and elec. props., and range of existence *(French)* 78—43175
  - $Ag_8S_3SO_4$, new cryst. data 79—37685
  - β-$Ag_xW_yV_{2-y}O_5$ bronzes, β-phase existence range, elec. cond. and Ag diffusion 78—35373
  - AlBi, possibility of existence with sphalerite struct. 80—33950
  - Al_2O_3-SiO_2, sillimanite, lattice defects, crystallo-chemical model, TEM obs. *(French)* 78—26570
  - Al_2SiO_5 polymorphs (sillimanite-andalusite-kyanite), thermal expansion and high-temp. cryst. chemistry 80—39319
  - AuF_3, ^{19}F NMR chemical shift, crystal chemistry 78—87645
  - B, and borides, cryst. chem., struct., book contrib. 78—47278
  - B_4C, thermal cond., nonstoichiometry effect 78—63887
  - $BaCuO_{2+x}$ $(0 \leq x \leq 0.12)$, study of mag. and elec. props. rel. to the nonstoichiometry *(French)* 78—95051
  - BaF_2-NiF_2-CrF_3, X-ray crystallography study, phase identification at 700°C, cryst. symm. *(French)* 78—95733
  - $Ba_2M_{II}M_{III}'F_9$, (M_{II}=Fe, Co, Ni, Zn; M_{III}'=V, Cr, Fe), solid state synthesis and cryst. chem. study *(French)* 79—41988
  - $Ba_3(M_4Ti_4)O_{21}$, M=Nb, Ta, Sb, effects of Sb substit., synthesis and cryst. chemistry 77—76379
  - $BaMnO_{3-x}$, O_2 deficiency induced polymorphs 78—26531
  - BaO-TeO_2, cryst. chem. study, X-ray diffr. powder data *(French)* 80—15080
  - $BaTiO_3$, defect chem., elec. cond. obs. 77—4097
  - $BaTiO_3$, single cryst., elec. cond., 800-1200°C, nonstoichiometric disorder 78—51989
  - $Ba_3WFe_2O_9$ and $Ba_3WFe_2O_{8.42}$, crystallographic and mag. props., comparative study 80—103303
  - Ba_xWO_3, $(0.01<x<0.33)$ series form. 79—65046
  - Ca-water interactions, in crystalline hydrates, geometry 80—39024
  - $Ca_xGd_{2-x}Sn_{2-x}Sb_xO_7$, pyrochlorate struct. form. 80—92504
  - CaS:Nd phosphors, X-ray powder diffr. anal. 80—100204
  - Ca_2SiO_4, K_2NiF_4-type structure, high pressure synthesis, crystal chemical and geophysical implications 79—69089
  - $CaWO_4$:Gd, site occupation 79—28608
  - Cd compound with XO_4 tetrahedral, complex, var. of cation coordination numbers 79—86768
  - $CdAs_2$, synthesis, microstruct., hardness and elec. cond. 79—51268
  - $CdCr_2S_4$, single crystal ferromagnetic semiconductor, vapour-liquid transport growth method 77—21013
  - $Cd_xHg_{1-x}Te$, carrier lifetime, effect of comp. fluctuations and second-phase inclusions 80—80294
  - $CdK_4(P_3O_9)_2.2H_2O$, cryst. chemistry and cryst. struct. determ. *(French)* 78—26505
  - CdO-TeO_2, cryst. chem. study, X-ray diffr. powder data *(French)* 80—15080
  - $Cd_3P_2(As_2)$, cryst., gas phase growth, morphology 79—10821
  - CdS, rock-salt type high-press. phase synthesis using metal sulphide additives 80—104084
  - CdSe, nonstoichiometry, Cd and Se press. meas., up to 1400K 78—87664
  - $CeNbO_4$, cryst. chemistry exam. 78—38678
  - Ce_3NbO_x, $CeNbO_x$ and $CeNb_3O_x$, redox processes, elec. resist., phase anal., mag. suscept., thermogravimetric meas. 78—34482
  - CeO_2-La_2O_5 system, surface microphases investigation by X-ray electron spectral anal. 79—51269
  - CeO_2-PrO_x system, mixed cryst. phase characterisation 79—14936
  - CeO_{2-x}, $1.5<O/Ce<2$, physicochemical equilibria, statistical thermodynamics model *(French)* 78—38688
  - CeO_{2-x}, small polaron mobility, elec. cond. and nonstoichiometry meas. 78—47785
  - $CeTaO_4$, $CeTa_7O_{19}$, cryst. chemistry exam. 78—38678
  - $CeTi_2O_6$, cryst. chemistry exam. 78—38678
  - CfO_x-O_2 system, for $1.50<O/Cf<1.72$, temp., press. and stoichiometry depends. 77—28009
  - CoSb, cryst. growth from nonstoichiometric melt, and cryst. chem 78—35286
  - γ-CoSe, d-electron deficit model, electrochem. meas. of free enthalpy *(French)* 78—30605
  - $Co_2Ti_{2-2x}Fe_{2x}O_{6-x}$ solid solution, extended defect model, X-ray diffr. and electron microscopy *(French)* 77—47446
  - CrO_2 and tetravalent Cr oxide derivatives, metallic, chem. and phys. props. review 78—31069
  - $CsAuF_4$, ^{19}F NMR chemical shift, crystal chemistry 78—87645
  - $CsN_{1-x}Mn_xF_3$, hexagonal perovskites, struct. evolution and mag. props., effects of high pressure 79—41987
  - $CsSbF_6$, high press. phase relations, vibr. spectra, and cryst. chemistry 80—108200

crystal chemistry continued
$Cs_{1-x}(Ti_{1-x}Nb_{1+x})O_5$, layer compound, cryst. struct., nonstoichiometry 80−64972
$Cs_2[M(CN_4)].H_2O$, M=Pt,Pd,Ni, cryst. data 79−51070
Cu-Te system, cryst. chem., Mossbauer investig. 77−16220
$CuGaSe_2$ crystals, electron probe microanal., correction procedure 80−2171
$CuInS_2$, homogeneity region and intrinsic dopant mechanism 78−34630
$CuInSe_2$ crystals, electron probe microanal., correction procedure 80−2171
$Cu_3P_2H_3(NO_3)(OH)_2.H_2O$, likasite, comp. and struct. *(French)* 77−47405
$Cu_{2-\delta}S$, Cu chem. diffusion, and nonstoichiometry, 400°C, electrochem. determ. 79−28132
$Cu_{2-\delta}(S+Se)$ solid soln., deviation from stoichiometry, effective hole mass 77−31775
$Cu_{1.8}Se$, I-V characts., switching effects, nonstoichiometry effects *(Russian)* 78−84266
$Cu_{1.7}Te$, and Cu_2Te, I-V characts., switching effects, nonstoichiometry effects *(Russian)* 78−84266
Eu^{3+}, symmetry group from sign inversion of MCD spectrum in aq. soln. 77−34669
Fe-Ni-C, single cryst., singularities of distrib. of Ni and C *(Russian)* 77−77467
$FeBO_3$-MBO_3 solid soln., (M=Mn, Cr, Al, Ga, In), synthesis, crystal chem. and mag. props. 78−31058
$FeCo_2O_4$, spinel, cation distrib., Mossbauer spectra meas. 78−31127
$Fe_{0.5}Co_{2.5}O_4$, spinel, cation distrib., Mossbauer spectra meas. 78−31127
$Fe_{1-x}O$, wustite, crystals of various stoichiometries, growth in arc furnace 80−25545
$Fe_{1-x}O$, wustite phase, surface elec. props. 78−76133
α-Fe_2O_{3-x}, nonstoichiometry effect 77−47583
Fe_3O_4, magnetite, nonstoichiometry, depend. on prep. conditions *(German)* 78−3081
δ-FeO(OH) and its solid solns. synthesis, X-ray diffr. and TEM studies 80−29891
FeS, structural chem., influence of itinerant 3d electrons and valence-band holes 79−23563
$Fe_{1-\delta}S$ chemical diffusivity and nonstoichiometric props. 78−10217
$Fe_{1+\delta}Sb$, nonstoichiometry influence on mag. props. *(Russian)* 80−65813
n-GaAs, melt-grown, stoichiometry, photolum. obs. 78−72583
GaAs, stoichiometry meas. by 15 MeV He^{2+} backscattering 79−99330
GaBi, possibility of existence with sphalerite struct. 80−33950
$GdPt_x$, $Gd_{1-x}A_xPt_2$ (A=Sc, La), Laves phase alloy, NMR, nonstoichiometry 77−63298
$GdTiO_3$, cryst. struct. and cryst. chem. 80−1984
HfV_2, C15 Laves phase, supercond. and stoichiometry 78−39245
Hg-Tl, metastable system, prep. by quenching, phase struct. 78−52762
$Hg_{1-x}Cd_xTe$, for appl. in IR detector arrays, comp. control 80−31872
Hg_2Cl_2, calomel cryst., symmetry of low temp. phase 78−26544
$Hg(NH_3)_2Br_2$, $Hg(NH_3)_2Cl_2$, thermodynamic study of disorder 79−28109
$HuO_2P(As)O_4.4H_2O$, water deficiency, enthalpy of dehydration, thermogravimetric anal. 80−65251
InAs, intrinsic point defects, nature and influence on electrophys. props. 78−79609
InAs, obtained by liquid-seal method, deviation from stoichiometry 77−40345
InBi, possibility of existence with sphalerite struct. 80−33950
$In_{1-x}Ga_xP$, quantitative characterisation of chemical disorder from wavelength-modulated no-phonon absorpt. 79−15482
InI, InI_2 and InI_3, far-IR spectra, valence states in InI_2 79−47435
$InSbSe_3$, cryst. prep. and props. 79−15601
$In_{1.8}Sb_{0.2}Se_3$, cryst. prep. and props. 79−15601
$In_2Te_3O_9$, isolated in In_2O_3-TeO_2 system, cryst. struct. anal. *(French)* 79−32977
$K_2Cu_{1-x}Mn_xF_4$ system, ($0 \leq x \leq 0.2$), prep., cryst. chem., and ferromag. props., X-ray and neutron diffr. study 79−24162
$KLiSO_4$:Cr; optical activity characts. cryst.-chem. exam. 78−95569
$K_2Mg_4Mo_4O_{16}(OH)_2(H_2O)_2$ study of non-stoichiometry *(French)* 78−30604
K_2NiF_4-type compounds, cationic radius ratio and formation 80−28992
K_3PO_4-$M_3(PO_4)_2$, M=Ca, Sr, Ba, Zn, Cd, high temp. stabilisation of phases *(French)* 77−44235
$K_2Pt(CN)_4Br_{0.3}.3H_2O$, one-dimensional cond., phys. props. *(Japanese)* 78−30916
$KSr(NH_2)_3$, cryst. struct. and cryst. chemistry *(German)* 79−51080
$K_2Te^{IV}Te_3^{VI}O_{12}$, mixed tellurate, cryst. chem. and elec. cond. *(French)* 80−107150
$K_{1-x}(Ti_{1-x}M_{1+x})O_5$, M=Nb, Ta, layer compound, cryst. struct., nonstoichiometry 80−64972
$K_2[MoO_{1-x}(OH)_{2x}(H_2O)_{1-x}O(MoO_4)_2].2H_2O$, proton NMR for chem. comp. at −195°C 78−38651
LI_2UO_4, energy transfer, cryst. struct. and chemical composition effect 80−108248
$(La_{0.8}Ca_{0.2})MnO_{3+y}$, non-stoichiometry and lattice consts. 80−100212
$LaMnO_3$, O_2 environment, phase stability and nonstoichiometric behaviour, 1200°C 78−43134
La_2O_3, cryst. struct., X-ray powder diffr. and electron diffr. study 80−107161
La_xS_y, stoichiometry and opt. props. during hot pressing 78−23653
$LaTiO_3$, cryst. struct. and cryst. chem., cryst. showing complex twinning 80−1984
$LiNbO_3$ crystals, composition determ. from parametric scattering spectra *(Russian)* 77−15595
$LiNbO_3$, ref. index, stoichiometry effects 77−59549
$LiNbO_{31}$ Li_2O diffusion for chemical control of laser induced optical damage 78−46693
$(Li_2SiO_3)_x$, bond length variations, mol. orbital study 78−26500
Li_4WO_5, IR, Raman, luminesc. spectra meas., cryst. struct. investig. 77−52074
$Lisd4UO_5$, energy transfer, cryst. struct. and chemical composition effect 80−108248
$(Lu_{1-x}Sc_x)_2V_2O_7$, prep., cryst. chem. and chem. anal. 79−41986
$Lu_2V_2O_7$, prep., cryst. chem. and chem. anal. 79−41986
$(Lu_{1-x}Y_x)_2V_2O_7$, prep., cryst. chem. and chem. anal. 79−41986
MgO-Al_2O_3 system, surface microphases investigation by X-ray electron spectral anal. 79−51269
$MgSiO_3$, othorhombic perovskite 80−19777
$MgSiO_3$, perovskite struct., cryst. chem. 79−60336

crystal chemistry continued
$MgUO_4$, energy transfer, cryst. struct. and chemical composition effect 80−108248
$MnFe_2O_4$, valency states, NMR 77−51987
$Mn_{1-x}Fe_{2+x}O_{4+\delta}$, ferrites, homogeneity region, cluster component model 78−35367
$MnFe_2(PO_4)_2(OH)_2.6H_2O$, strunzite, cryst. chem., Mossbauer study 80−39975
MnSb, cryst. growth from nonstoichiometric melt, and cryst. chem 78−35286
MnZn ferrite, natural, intrasite cation ordering and clustering 77−12259
MnZn ferrites, form. of comp. heterogeneity during high-temp. sintering 80−60818
$Mn_{0.510}Zn_{0.417}Fe_{2.073}O_{4+\delta}$ relationship between magnetic permeability and stoichiometry 79−42799
Mo complexes, dinuclear, chem. and spectroscopic props. 77−77239
Mo complexes derived from electron-rich olefins, cryst. chem. 77−76372
Mo_2BC, planar intergrowth defects and nonstoichiometry 78−2145
MoO_3, ultrafine crystals, exam. of reduction using electron microscopy *(Russian)* 79−29394
MoO_3-M_2O_3 system, M=trivalent metal, solid-state chem., review 77−24288
$(NH_4)_2Te_3O_8(OH)_4$, synthesis and crystallochem. study *(French)* 80−1990
$NaAl_2O_4$-$MgAl_2O_4$ spinel solid solns., activities rel. to cation distrib. 77−15377
$NaCa(NH_2)_3$, cryst. struct. and cryst. chemistry *(German)* 79−51080
$Na_2Eu_3(NH_2)_8$, cryst. struct. and cryst. chemistry *(German)* 79−51080
β-$Na_2HPO_4.12H_2O$, dosorder of HPO_4^{2-} and H bonds 78−34471
$(Na_xKy)_2CO_3$, non-stoichiometric, cryst. struct. *(French)* 80−79761
$NaMgF_3$, orthorhombic perovskite 80−19777
$NaPF_6$, high press. phase diagram, vibr. spectra 78−60446
Na_3PO_4-$M_3(PO_4)_2$, M=Ca, Sr, Ba, Zn, Cd, high temp. stabilisation of phases *(French)* 77−44235
$NaRSi_6O_{14}$, R=La, Ce, Pr, Nd, new crystal-chemical group of rare-earth silicates 77−7703
$Na_4R(WNb_2)O_9F_5$, (R=Y, Nd, Eu, Gd, Dy, Lu), synthesis, cryst.-chem. and dielec. study *(French)* 80−108164
$Na_2Sr_3(NH_2)_8$, cryst. struct. and cryst. chemistry *(German)* 79−51080
$Na_2[MoO_{1-x}(OH)_{2x}(H_2O)_{1-x}O(MoO_4)_2].2H_2O$, proton NMR for chem. comp. at −195°C 78−38651
Nb-Pd constitution diagram, metallographic and X-ray diffr. anal. 80−89204
NbC_x, stoichiometric and defective phases, electronic energy spectrum and physical props. *(Russian)* 77−35868
Nb_4Ga_5, cryst. struct. and homogeneity range 78−42957
$Nb_{28}O_{70-x}$, O diffusion, rel. to Nb_2O_5 nonstoichiometry *(French)* 78−47583
$Nb(OR)_2Cl_3.L$, halo-alkoxide complex, prep. and props. 78−18605
Nd_2O_3, cryst. struct., X-ray powder diffr. and electron diffr. study 80−107161
$NdTiO_3$, cryst. struct. and cryst. chem. 80−1984
Ni-Fe-Ti-O spinel phase, single-phase region and cryst. chem. characts. 77−52301
NiSb, cryst. growth from nonstoichiometric melt, and cryst. chem 78−35286
β-NiSe, d-electron deficit model, electrochem. meas. of free enthalpy *(French)* 78−30605
Np_6Fe, existence and cryst. chemistry 77−51349
O-containing anions of d-elements forming hydration-active phases, electron structs. and props. 79−42005
P-O compounds, inorganic, exam. of crystal chemistry 79−1406
$Pb_2Fe_2O_5$, IR absorpt., Mossbauer spectra, Neel temp., cryst. cell *(French)* 79−42759
$Pb_xMo_6S_{8-y}$, phase relns., stoichiometry, T_c 78−15378
Pb_3O_4, tetragonal to orthorhombic transition, heat capacity meas. 80−20929
$Pb_{1-x}Sn_xTe$ p-n heterostructure, VPE, struct. and electrophysical characts. 78−10547
$Pb_xSn_{1-x}Te$, for appl. in IR detector arrays, comp. control 80−31872
Pb_xWO_3 ($0.01 \leq x \leq 0.28$), tetragonal and orthorhombic bronzes, cryst. chem. data 78−42997
Rb_2O-$Nb_2O_5(Ta_2O_5)$, phase equilib. relns. and crystal chemistry, structs. useful as ionic conductors 79−20033
$Rb_{1-x}(Ti_{1-x}M_{1+x})O_5$, M=Nb, Ta, layer compound, cryst. struct., nonstoichiometry 80−64972
S atom, van der Waals radius, mean statistical value 77−83515
Sc germanates and silicates, cryst. struct. and cryst. chemistry 77−39571
Se_2TiO_6, cryst. struct. *(French)* 78−95023
Si-O bonds, cryst. chem. at high press., rel. to Earth mantle mineralogy 79−48470
$Si_6O_{15}^{6-}$ double chain anion containing anhydrous silicates, synthesis, cryst. chem. 80−59444
SmS, cryst. struct. in homogeneity region 78−91334
$SmTiO_3$, cryst. struct. and cryst. chem. 80−1984
α-SnF_2, crystallochemistry 80−28990
SnO_2:Sb, and pure cryst., microstruct., X-ray diffr., optical and electron microscope studies 78−79619
Sr Nb_2O_6, crystallography, polymorphism and isomerism, X-ray diffr. and DTA study 80−100216
Sr-Ti-O system, perovskite oxides, nonstoichiometry rel. to dielectric const. 77−80628
SrO-Fe_2O_3 system, non-existence of single phase $SrFe_2O_4$, Mossbauer expts. 80−29178
$Sr_{1-x}Pb_xTeO_3$, ferroelec. soln., prep. at room temp. *(French)* 79−43190
SrS:Ho phosphor, prep. methods, X-ray diffr. appraisal 77−51350
$SrTiO_{3-x}$, anion deficiency and anion vacancy ordering 78−51532
TLP, possibility of existence with sphalerite struct. 80−33950
$Ta(OR)_2Cl_3.L$, halo-alkoxide complex, prep. and props. 78−18605
TeO_2-BaO, cryst. chem. study, X-ray diffr. powder data *(French)* 80−15080
TeO_2-CaO, cryst. chem. study, X-ray diffr. powder data *(French)* 80−15080
TeO_2-CdO, cryst. chem. study, X-ray diffr. powder data *(French)* 80−15080
TeO_2-ZnO, cryst. chem. study, X-ray diffr. powder data *(French)* 80−15080
Ti-Ni (48 to 53 at.%), heat treatment and deviation from stoichiometry 80−104192
TiO_2-Ta_2O_5 system, surface microphases investigation by X-ray electron spectral anal. 79−51269

crystal chemistry continued
- Ti_nO_{2n-1}, cryst. growth and characterisation 78—31311
- TlAs, possibility of existence with sphalerite struct. 80—33950
- TlBi, possibility of existence with sphalerite struct. 80—33950
- TlSb, possibility of existence with sphalerite struct. 80—33950
- Tl_2TaO_6, Tl I lone pair stereochem. activity rel. to ferroelectricity 78—15131
- Tl_2TeO_3, $Tl_2Te_3O_7$, $Tl_2Te_2O_5$, Tl_2TeO_6, Tl_6TeO_{12}, synthesis, thermal stability, crystallographic data *(French)* 78—51518
- $Tl_{1-x}(Ti_{1-x}Nb_{1+x})O_5$, layer compound, cryst. struct., nonstoichiometry 80—64972
- $Tm_{1-x}Eu_xSe$, semicond. with valence instabilities, cryst. chem. considerations 80—100213
- TmSe and its mixed crysts., valence instabilities, phase diagram 80—70651
- Tm_xSe, low temp. props., effect of composition 77—80775
- $TmSe_{1-x}Te_3$, semicond. with valence instabilities, cryst. chem. considerations 80—100213
- $Tm_2V_2O_7$, prep., cryst. chem. and chem. anal. 79—41986
- U-O system, phase equilibrium, thermal, X-ray and cond. meas. 78—35371
- UCo_2, cubic Laves phase, prep. and stoichiometry 79—24459
- UFe_2, nonstoichiometry effects on Curie temp., susceptibility obs. 80—25131
- $UO_2S_2O_3.H_2O$, IR and Raman spectra, possibility of nonexistence of cpd. of given formula *(French)* 77—24279
- $US_xN_yO_z$, neutron diffraction exam. of structure 78—79777
- V_nO_{2n-1}, cryst. growth and characterisation 78—31311
- VSe_2 phase, stability and Se equilib. vapour press., homogeneity range 78—43133
- Y germanates and silicates, cryst. struct. and cryst. chemistry 77—39571
- YCo_3, hydride phase synthesis, thermal stability and struct. 80—59438
- $YTiO_3$, cryst. struct. and cryst. chem. 80—1984
- Y_6UO_{12}, energy transfer, cryst. struct. and chemical composition effect 80—108248
- $Yb_2V_2O_7$, prep., cryst. chem. and chem. anal. 79—41986
- $ZnAl_2S_4$-$ZnCr_2S_4$, nonstoichiometric spinel solid solns., synthesis and cryst. chemistry 77—35526
- ZnO, single crystal, excess Zn atom conc. and elec. cond. determ. 78—3435
- ZnO-TeO_2, cryst. chem. study, X-ray diffr. powder data *(French)* 80—15080
- Zn_3P_2, stoichiometry deviation from phase diagram 80—35164
- ZrC_x, change in lattice const. in region of homogeneity 77—25029
- ZrI_3, disproportionation 77—89546
- ZrO_2-Y_2O_3-Nd_2O_3, spectral determ. of crystal stabilisation 78—27203
- $ZrOS_2O_3.8H_2O$, IR and Raman spectra, possibility of nonexistence of cpd. of given formula *(French)* 77—24279
- $ZrS(Se)_2$, nonstoichiometry 78—75841
- $Zr_{0.8}Yb_{0.2}F_{3.2}O_{0.3}(MX_{3.5})$ anion excess ReO_3 phases, non-stoichiometry 79—60322

crystal classes *see crystal symmetry*

crystal cleavage
- Admiralty Metal, transgranular stress corrosion crack propag. 80—89402
- alkali halide, brittle fracture of single crysts. and active struct. of cleavage surfaces 79—28039
- alkali halides, surface step struct. 77—31853
- crack propag. due to dislocation tilt wall splitting 78—91377
- device for cleaving rocksalt for clean surface prep. 77—13738
- fracture, ionisation wave generation, microbreakdown mechanism 79—33032
- graphite, ion bombarded, light gases, structural study using TEM 80—92570
- guanidinium aluminium sulphate hydrate, ferroelec., decoration patterns on cleavage surface, domain obs. 80—97218
- guanidinium uranyl sulphate hydrate, ferroelec., decoration patterns on cleavage surface, domain obs. 80—97218
- ionic crystal, dislocation mechanism of electrification during cleavage 77—24353
- mechanoelectron emission mechanism following cleavage 80—7482
- metal, classical cleavage energy, layer summation method 77—85287
- mica, emission of high-energy electrons during cleavage 79—56917
- mica surfaces, interaction forces at small separations in polar and non-polar liquids 80—39458
- polyethylene, oriented chain-extended, Young's modulus, fracture and compression behavior 80—11747
- quartz, habit variation of crystals of the $C3_12$-$C3_22$ space group 80—107090
- stearic acid, microscopic obs. of cleaved surface 79—95248
- steel, C, heterogeneous structure, fracture characts. 79—38961
- steel, C, martensites, fractography, facets classification *(Slovak)* 79—20173
- steel, Mn-Mo-Ni-Cr, bainitic, microstruct. and mech. props. *(French)* 80—16362
- steel, structural, second phase particle effects on impact strength 80—108581
- strontium calcium tartrate tetrahydrate, crystals grown by ion diffusion through silica gels, exam. of preps. 79—52102
- TGS, cleavage surface, electron microscopy using shadow decoration technique 77—7955
- TGS, ferroelec., vacuum cleaved, charge compensation 80—60510
- TGS, ferroelec. cleavage surface microscopic struct. by electron microscopy 79—51403
- TGS, morphology of Au and AgCl films on complementary cleavage planes 79—15031
- TGS, vacuum-cleaved cryst., charge compensation, ferroelec. field effect obs. 78—95556
- triglycine sulphate, ferroelec., decoration patterns on cleavage surface, domain obs. 80—97218
- As, (111) surface, freshly cleaved, vaporisation, surface morphology changes obs. 77—80612
- $BaSO_4$, single cryst., neutron bombard. effect on struct. 78—63793
- $Ba_xSr_{1-x}Nb_2O_6$, growth defects 78—38640
- Be, polycryst., plasticity and cleavage, yield and flow stresses 80—44249
- Be, polycryst. plasticity, cleavage strength, ductility transition temp. 80—44250
- Bi-Sb (5-12 at.%), single cryst. cleavage plane, microhardness parameters depend. 78—35486
- CaF_2 crystals, mirror chips, in contact with liq. phase, ellipsometric investigation 80—11516
- Eu_2O_3, large single crystals, production and props. rel. to structural anisotropy *(French)* 77—36396
- Fe-Si (2.6 wt.%) single cryst., crack propag., controlled plastic crack tip opening rate 80—60943
- GaAs (110), comparison of LEED intensities for chemically polished and cleaved surfaces 78—18884
- GaAs (110), double-dangling-bond defects and band bending 79—69411
- GaAs wafers, for semicond. lasers, cleaving process 78—37915
- GaP, cleaved (110) surface, electron surface props. 80—11067
- Gd_2SiO_5, atomic positions, high resolution electron microscopy 80—100220
- HgS, habit variation of crystals of the $C3_12$-$C3_22$ space group 80—107090
- InP (110) surfaces, cleaved and polished-sputtered-annealed, LEED and AES study 80—103550
- Ir, fracture mechanisms, and cleavage criteria 79—74253
- KCl, spontaneous cleavage, step line propag., macroscopic defects 78—87662
- LiF, cleaved cryst., electrification mechanism 78—19126
- LiF crystals, mirror chips, in contact with liq. phase, ellipsometric investigation 80—11516
- LiF, dislocation mechanism of electrification during cleavage 77—24353
- LiF, electrification of crystals by cleavage 78—60189
- LiF, plasic deform., cleavage-crack propag., X-ray topography 77—39625
- $LiNbO_3$, cleaved, crystallographic and electrooptic props. 80—59575
- $LiNbO_3$, wedge fabrication for line acoustic wave propag., using cleavage method 78—30818
- $LiNbO_3$:Ti in-diffused optical waveguide fabrication 79—76892
- $LiTaO_3$ monocrystal lapping and precision machining characteristics *(Japanese)* 79—80593
- MgO surface, electron beam cleaved, characterisation by Au decoration 77—47657
- Mg_2SiO_4 crysts., dislocations configuration and cleavage steps dissoln. 80—107250
- Mg_2SiO_4, single cryst., (010) cleavages, etch patterns and dislocations, interferometric obs. 78—2127
- Mo, single cryst., δ_R criterion for brittle fracture *(Russian)* 78—56732
- MoS_2, angular loss studies on natural surfaces by low-energy electron spectroscopy, surface cleavage influence *(French)* 79—56898
- $Na_2Al_2Si_3O_{10}.2H_2O$, natrolite, cleavage etching in acidic and neutral media 80—6407
- NaCl, cleavage faces, evaporation pattern determ. by decoration method in electron microscopy *(German)* 80—107626
- NaCl, cleavage ledges and interface dislocations on Suzuki phases 79—90659
- NaCl cleavage step decoration, nucleation and growth of metallic thin films 77—69200
- NaCl, high density of dislocations meas., new etchant 78—43019
- NaCl, investigation of fast electrical processes 79—24045
- NaCl, mechanoluminesc. peaks, microbreakdown mechanism, generation of ionisation waves 79—33032
- NaCl, plastic deform., cleavage crack propag., X-ray topography 77—39625
- NaCl, single crystal, surface markings, left by unsteady cleavage crack propag. 79—46746
- NaCl:Ca crystals, surface recrystn., moisture effect 80—84950
- NaI crystals, used in nuclear medicine, determ. of cause of breakage 80—98077
- Sb, cleavage faces, evaporation pattern determ. by decoration method in electron microscopy *(German)* 80—107626
- Sb_2Te_3, cleavage faces, evaporation pattern determ. by decoration method in electron microscopy *(German)* 80—107626
- Se, habit variation of crystals of the $C3_12$-$C3_22$ space group 80—107090
- Se surface, $(10\bar{1}0)$ and $(1\bar{2}10)$, LEED study *(French)* 79—14991
- Se_{90}-Te_{10} alloy crystals, growth and cleavage 78—88421
- Si, (111) cleavage, Kikuchi pattern, 40 keV incident electrons, electron energy loss spectra *(French)* 78—87594
- Si, near (111), fracture by painted indenter, SEM study 80—71734
- Te, habit variation of crystals of the $C3_12$-$C3_22$ space group 80—107090
- W bicrysts., crack propag. across grain boundaries, crack speed meas. technique appl. 80—108575
- Y_2O_3 fused single crystals, struct. 80—19804
- ZnS:Ag, struct. and mech. props. 78—22753
- $ZrH_{1.92}$, plasticity 77—36569

crystal defects
- *see also Cottrell atmospheres; crowdions; crystal inclusions; crystal microstructure; defect electron energy states; disclinations; dislocations; grain boundaries; impurity-defect interactions; phonon-defect interactions; point defects; stacking faults; twinning*
- γ-ray diffractometry, extinction, correction 77—19850
- A15 compounds, T_c reduction due to defects, gap anisotropy mechanism 77—43773
- A15 supercond. with defects 78—76183
- A-15 compound, defect influence on T_c 80—20345
- A-15 compounds, supercond. transition temp., correl. with resist. anomalies and defect struct. 77—47920
- A-15 superconductors with defects, transition temp. 78—14857
- accelerator irradiation, heavy ion irradiation damage 80—100291
- actinide carbides, lattice defects and rel. to phys. props., review 77—27874
- adsorbed layers, commensurate-incommensurate transitions, substrate defects effect 80—75437
- β''-Al_2O_3, Mg- and Li-stabilized, high electron microscopy images of defects 79—73135
- alkali halide:alkaline-earth cations, defect structs. examined by methods based on Mott-Littleton techniques 80—59487
- alkali halide, excitonic mechanism of defect form. 77—47737
- alkali halide, irradiated crystal, recombination of radiation defects *(Russian)* 80—39151
- alkali halide adsorbate motions and reactions at surface defects, mol. beams 77—59205
- alkali halide crystals, defect state change during electrolysis 78—95057
- alkali halide surfaces, adsorbate binding energies and struct. at surface defects 77—59206
- alkali halides, laser induced breakdown, 10.6 μm, reproducibility 77—62023
- alkali halides, sputtering, thermal effects, review 80—35033
- amorphous solids, crystallography tentative description 80—6360
- anharmonic lattice with defects 78—73937

crystal defects continued
anharmonic system, generalisation of CPA 78−75783
anthracene, γ-irradiation influence on defects, luminesc. study *(Russian)* 80−55185
anthracene, orientationally disordered cryst., lattice relax. effect 80−107278
anthracene, structural defect, photolum., γ-irrad. and temp. depend. *(Russian)* 79−28797
anthracene crysts., Frenkel exciton dissoc. near charged defect 77−51669
atomic scale computer simulation of lattice defects, stress tensor determ. 78−30602
benzophenone, cryst., phosphoresc. spectra and decay time, temp. depend. 79−87479
boundary conditions for textures and defects 78−26561
γ-brass type alloys, faulted defects, nature determ. by image matching technique 78−63777
brass wire, US inspection, immersion method 80−66757
1-bromoadamantane, orientationally disordered, γ-irrad. free radical defects, positron probe obs. 79−23647
burst noise, physical sources 79−24033
carrier scattering by lattice defects, nonlinear optical props. 80−29399
cavity nucleation, by plastic deform. 79−29127
cavity stability at high temps. 77−76388
central-force interatomic pot. construction from whisker deform. data 79−56103
ceramic characteristics *(Japanese)* 80−15075
ceramic fission reactor fuels, high temperature chemistry, nonstoichiometry, review 77−14238
chalcogenide glass-like semiconductors, defect model, neutral diamagnetic quasimolecules, excess orbital bonds *(Russian)* 80−70647
channelling studies of surfaces and defects 79−4358
classification, systemisation, taxonomy *(German)* 77−39578
classification according to influence on radiative diffraction *(Russian)* 80−70189
clustering of irradiation defects, HV electron microscope study 77−1891
clusters of defects, nucleation and growth due to energetic particle radiation, chemical rate reaction theory, computer program 80−49263
coherent-optical materials testing for vibration pattern and defect discrimination *(German)* 80−30181
collision cascades, fast charged particle bombard., of solid. defect prod. *(Russian)* 77−89492
computed electron micrographs, use in defect identification 79−69101
conference, International Crystallography Congress, Warsaw, Poland (Aug. 78) 79−23481
conference, Krusevac, Yugoslavia, Sept. 1978 79−56104
copper phthalocyanine, cryst. growth from vapour, hollow cryst. form, mechanism *(German)* 77−55252
α' copper phthalocyanine and chlorinated derivative mol. crysts., radiation damage in electron microscope 80−107328
corundum, defect cryst. struct. study 80−103316
coupling of clusters in linear chain 79−51144
crossing of defects in ordered media and topology of 3-manifolds 78−2108
dating method with digital ESR 80−86542
defect structure near phase transition pt., effect on solid props. *(Russian)* 79−37838
deformed crystalline struct., two-dimens. model 77−78940
determination from initial slopes of Fourier coeff. v. order curves for X-ray diffr. 77−7710
diamond:B, variable-range hopping cond., effect of electron irrad. induced compensating centres 77−43599
diamond, accelerator irradiation, heavy ion irradiation damage 80−100291
diamond, form. by shock compression of graphite, cryst., surface struct. 78−44060
diamond, laser beam drilling process mech., thermal stresses, elec. surface forces *(Dutch)* 77−7759
diamond, natural type Ia, dechannelling and nature of defect structures 80−49282
diamond, natural type IB, thermal conductivity anomaly, defects obs. 77−85003
diamond, platelets, giant, on cube planes, electron microscopy 77−84765
diamond, polarised cathodoluminescence in near IR, from platelet defects 77−48253
diamond, type I$_a$, phonon scatt. by platelets, N-decorated stacking fault model 77−4173
diamond, type I, defects of platelet nature, TEM study 79−37719
diamond, ultradisperse, ESR, particle size and lattice microdistortions 80−97140
diamond powders, EPR of defect centres 77−66423
1,4-dibromonaphthalene, optical props., struct. disorder effects 78−52525
(1,4)-dibromonaphthalene, triplet exciton scatt., absorpt. spectra 78−6696
dickite, unusual crystal habit, structural disorder 80−59445
dielectric solid, absorpt. of laser radiation by defects in surface layer *(Russian)* 80−25497
diffraction contrast and defect symm. 80−79778
diffusion, chemical, highly defective solids, steady-state computer simulation method for lattice gas 80−49401
diffusion layer, method for determining dopant and defect distribs. using polishing agent 79−37727
diffusion-controlled defect recombination, incorporating Coulomb interaction and annihilation 78−23044
diffusion-limited reactions between defects 77−1147
diffusive release of gas from solid in presence of traps using linear tempering schedule 77−69187
dilatation centres, elastic interaction, nonlocal elasticity theory 79−46743
dimension determination by acoustic emission 80−104381
direct observation and characterisation 78−88617
dislocation internal friction in impure cryst. *(Russian)* 77−73297
dislocation segments, pinned, effects of viscosity on quantum motion *(Russian)* 80−44207
displacive phase transitions, localised modes, central peak, influence of defects 78−83905
displacive transformation, defect cell and neutron scatt. central peak 77−15531
dual elastic continuum model of media with quasicracks, tensional medium with mobility effects 77−72153
early work on imperfections in crystals, and forerunners of dislocation theory 80−62450
effective annealing time determ. using analogue computer 78−88475

crystal defects continued
Einstein-Kanzaki model of static and dynamic lattice relax. 78−34676
elastic interaction of defect clusters with arbitrary strain fields in an anisotropic continuum 79−60397
elastic interaction of defects in crystal under high hydrostatic press. 80−96512
elastic interaction of point defects and volume defects near interfaces 79−65115
elastic wave scatt. theory for anal. and design of flaw characterisation expts., long-wavelength limit 79−83408
electron diffraction, in high lattice defect density specimens, statistical theory 78−14250
electron diffraction contrast and defect symmetry, theory 80−96418
electron diffraction contrast for lattice defects, analytical calcs. in two-beam case 80−100134
electron microscope diffr. contrast 78−83700
electron microscope dynamical image contrast, small lattice defects 77−15422
electron microscope imaging 80−88006
electron microscopy, imaging and diffraction from localised defects and disorder 80−100152
elemental semiconductors, group IV, Mossbauer spectroscopy of defects, radiation damage and deep levels 80−59533
EM wave diffraction, Ewald dynamical theory 77−65928
entropy of formation, of defects or inhomogenities, validity of eqn. 80−79960
epitaxial film/substrate interface in injection lasers *(Russian)* 77−54712
Euclidean invariance, spontaneous breaking, long range ordered media, defect, config. classification 78−59748
exoelectronic emission, crystal defects effects *(Russian)* 77−55872
extended defect system, phase transform., critical props. 80−103455
extended growth defect characterisation, review 78−30649
fast neutron bombardment, influence of temp. on defect form. *(Russian)* 77−65992
ferrite, synthetic, inhomogeneity, nonstoichiometry and lattice defects 77−35547
ferroelectrics, properties near phase transition point, influence of defects 79−42918
ferromagnet, domain wall motion, pinning by lattice defects, magnetisation 80−71079
ferromagnet, uniaxial, coercive force associated with domain boundary pinning on plane defects *(Russian)* 78−6543
ferromagnetic crystal with defects, domain boundary displacement and magnetisation discontinuities, statistical theory *(Russian)* 79−51800
ferromagnetic domain wall pinning, planar defects, coercive force and correl. length, soliton theory 78−31092
ferromagnetic domain wall pinning rel. to coercive force 77−1561
ferromagnetic film, mag. anisotropy and defect distrib. *(Russian)* 77−59434
film, liquid-phase epitaxial growth on (100) and {111} substrates, 'tears' occurrence reduction *(Slovak)* 79−15037
film defect growth and nucleation, electron microscopy and diffraction exam. *(French)* 80−59824
finite sample, mag. rearrangements near surface 80−11240
fluid inclusion formation mechanism *(Chinese)* 79−73160
foil, preparation apparatus, for X-ray diffr. study of lattice defects 79−37585
formation energy of defects, Gibbs free energy 78−91332
p-GaAs:Zn, diffusional doping, photoluminesc. in mag. field 77−16384
Gaussian TEM$_{00}$ mode laser beam scatt. from surface defect, normlaization 80−48313
geometrical theory of structural defects *(German)* 80−88136
graphite, artificial, electrophys. props. 77−51745
graphite, ground natural, Raman spectra, grinding influence 79−42956
graphite, neutron irrad., porosity changes, neutron small angle scatt. investig. 78−34544
graphite, pyrolytic, thermal expansion coeff. rel. to temp. 78−43147
graphite, synthetic materials, radiation defects, review 77−47494
graphite intercalation compounds struct., elec. props. 78−27446
hard magnetic material, coercive field, planar defect influence 77−24710
heteroepitaxial structures based on III-V compounds, appl. in optical electronics, defect form., review 78−23160
homogeneous material, 2D defects, interface problems 79−46674
ice:HF, I$_c$, anelastic relax., Bjerrum defects *(French)* 78−6122
ice, dielectric const., Onsager-Slater theory and unit model, Bjerrum defects 80−11310
ice, two-dimens. square, correl. function calcs., approx. methods, Bjerrum fault conc. effects 80−10513
II-VI compounds, hollow crysts., morphology, review 77−11494
II-VI semiconductors, lattice defects, X-ray diffr. and electron microscopic study 80−15088
III-V compounds and alloys, MBE process and problem areas, review 80−10815
III-V multilayer structure, as-grown, assessment of defects by differentiated cathodolum. topography 80−59819
III-V oxide interface state and Schottky barrier form., unified mechanism 80−44724
III-V semiconductors, radiative recomb., optical evaluation review 80−60647
ill-condensed matter, summer school, Les Houches, France (July-Aug. 1978) 80−82561
images produced by piezobirefringence, simulation 78−30521
imperfect solids, positron-defect interaction and annihilation characts., book contrib. 79−99978
inelastic interaction of crystal lattice defects, estimate of interaction energy 79−69154
inhomogeneous solid solutions with conc. expansion, thermodynamics, energy defect diffusion calcs. 80−24618
insulating crystals, conf., Gatlinburg, USA (Oct. 1977) 78−63755
insulator, wide-gap, damage by UV laser radiation 80−76110
insulators, neutron activated β-emitters, hyperfine interactions 78−39070
interaction of defects, radiation physics *(Russian)* 79−46702
interface interaction of point defects and volume defects 79−14843
intergrowths, regular, investigation with Laves-Ernst compensator 79−96843
intermetallic phase with B2 structure, relationship between enthalpy of form. and disorder parameter 77−7878
intermetallic phases, B2 struct., substitutional and triple defects, enthalpies of formation 80−96520
internal stress fields caused by lattice defects, entropy 80−39067

crystal defects continued
interstellar oxide grains, surface defects rel. to mol. prod. 79—25690
ion channelling, defect anal. 79—95063
ion trapping and gas release effects in cryst. lattices, thermal desorption spectrometry, review 77—43262
ionic crystal surfaces, defect struct. 79—19439
ionic crystalline materials, radiational stability *(Russian)* 77—80539
ionic crystals, defects, computer modelling, review 80—107205
ionic crystals, electronic excitation decay into radiation defects, review 78—47420
ionic crystals, evaluation of association parameters of quadrupoles 77—43365
ionic crystals, influence of defect interaction upon their recomb. 80—84206
ionic crystals, lattice defects, conference, Canterbury, England (Sept. 1979) 80—105420
ionic crystals, thermodynamics and kinetics of lattice defects 77—84738
ionic crystals, transport phenomena, appl. to solid state devices 78—55976
IR cathodoluminescence topography, imaging methods 78—22201
IR crystals, optical imaging of growth defects 80—64988
isotropic solid, strain energy associated with extended defect 79—14821
itinerant ferromagnet, effect of planar defects on electronic struct. and mag. ordering 79—99672
laser crystal evaluation, testing and meas. instrument 77—7226
lattice defect information from diffusion studies *(Dutch)* 80—96681
lattice defects, high resolution microscope images, calc. and interpretation 79—73075
lattice defects and diffusion processes in solids, book 80—107207
lattice deformation determ. from X-ray Pendellosung fringes 78—18499
lattice dynamics, harmonic chain with molecular defect, exponential transformations 77—84872
lattice fringe imaging theory 80—103225
lattice image calculations for imperfect crysts., superlattice approach 80—107030
lattice images of defects, computer simulation of high resolution images 80—107208
lattice imaging by high resolution electron microscopy 79—77467
Laue reflections splitting and defects image contrast form. *(Russian)* 80—64833
LEED, defects in surface structure 80—44402
light scattering near phase transition points, cryst. defect effects 79—15415
light scattering near phase transitions, review 80—29752
line defects, X-ray topography *(French)* 78—79502
macroscopic defects, ordered regions and percolation phase transform. *(Russian)* 80—92665
magnetic domain wall pinning simulation, coercive force, susceptibility, defect depend. 77—16103
magnetic field, technical-saturation approx. 80—87262
magnetic resonance line broadening effects associated with cryst. imperfections, theory 78—35021
many-beam lattice images from thicker crystals 80—88004
metal, blister formation due to the ion irrad. 80—65072
metal, FCC He ion irrad., He gas bubbles lattices obs. 79—14858
metal, induced elastic interaction of dilatation centres with grain boundaries *(Russian)* 80—84205
metal, neutron activated β-emitters, hyperfine interactions 78—39070
metal, plasticity, dynamic, governing relations, elastic energy 79—43328
metal, positive muon spin depolarisation, defect study 78—47314
metal, positron annihilation study of neutron damage, review 78—71769
metal, positron lifetime spectra, anal. errors 78—19591
metal, positron trapping at defects, positron-phonon scatt. effect 77—89736
metal, pure, with max. of cryst. lattice distortion, struct. and strength props. *(Russian)* 80—89234
metal crystal radiation defect research using field-emission microscope 78—333
metal crystl, anisotropy of electron radiation damage 77—84796
metallographic observation *(Japanese)* 79—82130
metals, atom probe time-of-flight field-ion microscope, appl. 77—82645
metals, cryst. defects, positron annihilation method, review *(German)* 77—44082
metals, defects in structure of lattice 78—88617
metals, FCC, plane shock wave loading, microdistortion X-ray anal. *(Russian)* 77—52399
metals, gases accumulation at lattice defects, trends in modern anal. *(Russian)* 80—15123
metals, irrad., multiple atom displacements 79—46701
metals, lattice defects, positron annihilation study, book contrib. 79—99977
metals, muon trapping by defects and impurities 80—20573
metals, plane lattice defects contrib. to elec. resist. *(Russian)* 80—49688
metals, positron annihilation, localised probe of lattice defects 80—55224
metals, positron trapping by defects influence of positron-phonon and electron-phonon interactions *(Russian)* 80—93425
metals, radiation defect treatment at annealing stages V and VI *(Russian)* 80—71676
metals, radiation effects, ion beam study, review 79—10883
metals and alloys, positron annihilation, theoretical and expt. techniques, book 79—99975
metals and alloys, sulphidation mechanism, review *(Polish)* 80—45413
metrological defectoscopy, US materials testing refinements *(German)* 78—15638
mica, defects effect on epitaxial film struct. 78—26794
mica substrate of Au film, surface defects on heterogeneous nucleation and growth 78—47684
microbiomechanics, crystal defect theory approach 80—3687
minerals, high-resolution TEM obs. 80—72517
minority carrier recombination 80—65591
misfit boundary, X-ray diffr., general soln. 78—51562
misfit boundary, X-ray diffr., special cases 78—63776
model, unit cell construction with polystyrene balls on rods 77—60882
modulated structures, extended defect ordering and formation energetics 79—95034
modulation operations and derived structs. 79—94930
molecular crystals, low freq. Raman spectra, defects and lattice vibr. 78—31194
molecular crystals, optical props., struct. disorder effects 78—52525
molecular crystals, struct. disorder effect on optical props. 77—90165

crystal defects continued
molecular single crystal, librational Raman spectra polaris., temp. depend. 79—1760
morphological stability, cube grown from soln., affected by defects 77—51333
Mossbauer effect appl., conference, Kyoto, Japan (Aug.-Sept. 78) 80—7199
multicomponent solid solutions, defect formation in heteroepitaxial structures 78—83825
muon probes study 79—56700
muon spin rotation method, review *(Polish)* 80—88901
muscovite mica, annealing of latent tracks of heavy ions *(French)* 79—19290
naphthalene:2-fluoronaphthalene(2-chloronaphthalene), triplet state X-traps, ENDOR obs. 79—33561
naphthalene, cryst., low freq. Raman spectra, defects and lattice vibr., 80-320K 78—31194
negative activation volumes calc. 80—92518
nephrite jade, struct. irregularities, electron microscope obs. 77—19969
neutron diffraction topography, domain and cryst. defect studies, results 79—46520
NMR and dielectric relaxation, defect diffusion models 79—15375
non-metals, low-temperature strong enhancement of diffusion and defect generation 79—28149
non-stoichiometric solids, correl. between dielectric const. and defect struct. 77—85638
nonlinear water soluble crystals, characts. of laser pulse damage 79—45987
nonstoichiometric compounds preparation probability thermodynamic approach 77—31611
nuclear fuel element model for cladding performance during power changes, strain defects 78—58359
nylon 6, relationship between morphology and dynamic mech. props. 79—4992
observation by X-ray reflection topography *(Chinese)* 80—44074
one dimensional wave function for the effective Hamiltonian of non-local potential 80—46847
optical, of laser active materials, ruby and garnet, influence on energetic effectiveness obs. *(Czech)* 78—79022
optical data storage, requirements and attainable bandwidths *(Russian)* 77—10841
ordered media, classification of topologically stable symm. defects 77—62516
ordered media containing defects, gauge-like variables 79—88889
organic solids, electron microscopic approach to struct. and reactivities 79—73077
oxidation resistance, effect of P cpds., metal impurities and struct. defects 77—81331
oxide, defect struct., nonstoichiometry and elec. cond., pentavalent oxide dopant effect 80—24442
oxides, sputtering, thermal effects, review 80—35033
p-terphenyl, positronium and thermal defects 80—24496
paracrystal theory appl. to cryst. struct. investig. *(German)* 77—39552
paraelectric defect relaxation process, quantum interference and multilevel aspects 79—95109
parametrically excited waves, interaction with defects exhibiting internal structure 80—7173
Permalloy, FCC, mag. anisotropy induced by cold rolling 80—11188
Permalloy, high-permeability, influence of grain struct. and non-mag. particles on mag. props. *(German)* 77—16112
perovskite structure crystals, Jahn-Teller effect for surface impurities 78—47744
perovskite type oxides, long period structures *(French)* 78—26395
phase transitions, defect influence on solid props. 80—75334
photoconductivity, electronic nonequilibrium behaviour 80—44667
plane Ising lattice, local magnetisation depend. on linear defects *(Russian)* 80—2595
plastic behaviour in terms of defect motions 78—95104
point defect trapping and migration, calcs., in presence of rare gases and dislocations 79—77834
point-force array description 78—18646
Polirit polishing ability and physicochemical props. 79—72730
poly-[1,2-bis-(p tolylsulphonyloxymethylene)-1-butene-3-inylene], defect imaging 77—15418
polycrystals, models for constrained cavity growth 80—44251
polyethylene, crystal, dielectric α-relax., soliton as crystal defect 80—45004
polyethylene, crystalline, steric struct. modelling of end defects 80—6371
polyethylene, crystalline, twist disclination formation and longitudinal motion of defects 80—19810
polyethylene, melt crystallised, chain defects distrib. and microstruct. 79—10818
polyethylene, shish-kebab crystals, core struct. 80—38945
polyethylene, solid, nucl. spin-lattice relax. time, freq. depend. defect diffusion, 77-373K 78—72428
polyethylene crystal, thermal creation of defects, dielec. evidence 80—44151
polymer crystal, conformational energy calcs., appl. to defect props. 80—54154
polymers, crystalline, with lattice defects, exam. of plastic deformation for 2-d models 78—68747
polyoxymethylene copolymers, solid, mol. motions, 4-315K, dynamic-mech. study 79—4258
pore velocity, due to surface diffusion under temp. gradient, finite thermal conductivity correction 80—15428
powder, lattice defect effect on mixing 79—73313
precipitation kinetics, effect of particle solubility and inhomogeneities 78—27530
properties of solids, review of influence of defects 77—7709
pseudo-groups applied to symmetry and defects ordered media 80—10541
pulsed irradiation, annealing and accumulation of defects 78—47419
pyrazine, PMDR due to single defect species, vibronic structs. 78—19535
pyrene, positronium and thermal defects 80—24496
quantum solid behaviour, defect and impurity diffusion, review 77—7945
quartz, appl. of cathodolum. microscopy and spectrometry 77—69919
quartz, electron pulse irrad. effect on defect formation 80—15155
quartz, synthetic, as-grown and etched cobbled Z-surfaces, SEM obs. *(French)* 80—24719
quartz, synthetic, crystallisation and defects *(Chinese)* 79—69041
α-quartz, synthetic, growth, defects induced by seed orientation 80—96454

crystal defects continued
quartz, synthetic, growth spirals on prism faces, electron and optical microscope obs. 77—7723
quartz, synthetic, line defects, etch tunnels and X-ray topography 77—76406
quartz radiation defects, effect of annealing on absorpt. spectrum *(Russian)* 77—47495
quartz synthetic crystals, observation of growth defects by light scatt. tomography 78—71743
quinoxaline, in p-dibromobenzene, ^{81}Br, elec. field grad. distortion near defect sites, optically NQR 79—38409
radiation damage, defects and surfaces in bulk metallic, covalent and ionic systems, review 80—34049
radiation damage, imitation by action of shock waves *(Russian)* 78—95107
radiation damage, mechanisms, in semiconductors and insulators, review 80—107315
radiation damage in crystals, computer modelling methods 77—7760
radiation damage probing using low energy light ions 77—43260
radiation induced, book 77—39615
radiation induced, X-ray diffraction study, review *(Japanese)* 80—15152
rare earth molybdates, cryst. growth, cryst. chem., and phys. props., book contrib. 80—44194
Rayleigh and hyper-Rayleigh light scatt. 78—60478
resonant defect enhancement of laser elec. field 77—63499
review of lattice defects *(Chinese)* 79—69100
Rochelle salt, paraelectric-ferroelectric phase transition, relaxing defects effects 79—61320
rutile: Ga, Mg, intersecting defect structures, TEM study 79—51123
scattering phaseshifts and resonances for line defects 78—51953
SEM, crystalline materials observation using diffr. effects, bibliography 78—22612
SEM, electron channelling imaging 80—10471
SEM, energy filtering, backscattered electrons *(French)* 77—74558
SEM channelling patterns, review 77—55217
SEM electron beam induced conductivity obs. of semicond. using Schottky barriers 78—34898
SEM observation of single defects using electron channel imaging 80—64848
semi-infinite isotropic elastic medium, reson. scatt. of Rayleigh waves by mass defect 80—20025
semiconductor, apparent ageing, caused by defect migration, dark and photocond. 79—11169
semiconductor, defect electronic structure and lattice config., MO approaches 80—65495
semiconductor, defect state microscopy, review 79—94856
semiconductor, defect struct., double cryst. spectrometer *(German)* 77—72527
semiconductor, flow detection using IR laser defectograph 78—3299
semiconductor, kinetics of defect cluster annealing 80—84209
semiconductor, localised defects, theory of SEM charge-collection imaging 79—1374
semiconductor, model describing removal and scattering of charge carriers by defect clusters 78—76069
semiconductor, radiation damaged, residual defects rel. to back reaction annealing kinetics 78—3161
semiconductor, screened interaction of charged defects 78—39042
semiconductor, SEM charge-collection images, contrast formation 80—70087
semiconductor, SEM in EBIC mode vs. HVEM images 78—9923
semiconductor, spatial resolution of SEM electron beam induced conductivity images 80—6327
semiconductor, threshold energy for displacement of atoms 78—47428
semiconductor characterisation and analytical techniques *(Japanese)* 77—84735
semiconductor crystal defect obs. by TEM *(Japanese)* 77—84752
semiconductor crystals, role of nonequilibrium state in radiation treatments 80—39152
semiconductor defect birefringence detection by polarisation IR microscopy 79—83405
semiconductor devices, appl. of STEM 78—23155
semiconductor impurity distrib. and defect structure analysis by charge collection SEM 78—9924
semiconductor injection lasers, defect-induced pulsations, theory 80—91793
semiconductor laser, atom displacement as result of nonradiative recomb., defect form. mechanism 79—10308
semiconductor laser crystals, defect-forming resonance electron capture, theory 80—14341
semiconductor laser diodes, degradation, lattice defects *(Japanese)* 77—34889
semiconductor materials, noise models for investigation of defects *(German)* 78—87661
semiconductor physics, conf., Edinburgh, Scotland (Sept. 1978) 79—95303
semiconductors, charge collection microscopy, surface barrier method, for defect investig. 79—37598
semiconductors, cryst. defects induced by radiation, review 79—55776
semiconductors, defect processes, electronic stimulation 80—24665
semiconductors, defects and radiation effects, conf., Nice, France (Sept. 1978) 80—22140
semiconductors, ion irradiation produced amorphisation, disorder-ion fluence functions, disorder mechanisms 80—29090
semicorductors, elemental and binary, under subthreshold irrad. conditions, defect formation ionisation mechanism possibility 80—6430
p-Si, anodic etching for discriminating between elec. active and inactive defects 80—108605
p-Si, interstitial Fe and thermal defects, Hall effect and resist. meas. 79—82200
n-Si, recombination centres and carrier lifetimes after γ-irrad. 80—60004
Si, single cryst. characteris. by SEM using Schottky barrier charge collection microscopy 77—4444
simple cubic lattice, localised vibrs., isotopic defects effects 79—86862
solar cells, defects, rel. to elec. parameters, SEM electron beam induced current investig. 79—43772
spectroscopic techniques, anal. with STEM for electronic anal. and obs. of defects in semiconductors 79—14812
stationary lattice defects as sources of elastic singularities 78—59800
stationary lattice defects as sources of elastic singularities in micropolar media 80—107206
stearic acid, microscopic obs. of cleaved surface 79—95248

crystal defects continued
stearic acid, single cryst., characterisation *(Japanese)* 79—46587
steel, C, machined, microdefects on surface 80—16607
steel, classification of hydrogen traps 80—19792
steel, Cr-Mo-V, high temp. steam pipe weld, defect distrib. and growth 80—25979
steel, high-speed, powder, atomised, microdefects in particles 77—28753
steel, square parts, surface inspection, defect depth meas., eddy current method 79—29307
steel, stainless, low energy D implanted, microstruct. 78—95073
steel, stainless, Type 316, neutron irrad. effects on tensile props. and microstruct. 80—65059
steel 120Kh3G3, lattice defects during $\gamma \rightarrow \alpha \rightarrow \gamma$ transform., electron microscopy obs. *(Russian)* 79—47681
steel 12X18H10T, microdefect behaviour at point of contact of coolants *(Russian)* 80—19793
steel wire, US inspection, immersion method 80—66757
steels, C, H_2 embrittlement after patenting and cold deform. *(Russian)* 79—29175
STEM, structural and chemical analysis, appls. 80—88003
STEM microdiffraction patterns, effect of cryst. defects 78—22610
structural defects, effect on dynamical scatt. of X-rays *(Russian)* 79—64960
structural phase transitions, crit. dynamics and quasi-elastic scatt. 80—92641
structure determination, light interference, diffraction and scattering 80—103316
substitution order-disorder, study by X-ray and electron diffr., book contrib. 79—68983
superconductivity, electron-hole, influence of struct. defects 77—20489
superconductors, A-15 type defects 77—47927
surface, Rayleigh wave scatt. from mass defect. 77—20177
surface defects, investigation via low-energy proton beams, instrumentation aggregate 77—76266
surface defects, review 78—14551
swirl defects in single crysts. 80—44200
synthetic metals, anisotropy of elec. props. rel. to chem. bond struct. 80—24888
TCNQ salt, Qn(TCNQ)$_2$, defect depend. of dielec. permeability and cond. 79—78608
TEM, appl. to organic solid-sate chemistry, review 79—60235
TEM, high-resolution imaging techniques 78—34400
TEM diffraction contrast of defects causing strain and struct. factor contrast simultaneously 77—24253
temperature spikes stochastic analysis, contribution towards component damage exposed to nuclear radiation environment 79—7627
p-terphenyl, positronium form. at elevated temps. 77—89473
textural defects 80—49158
TGS:Cr single cryst., lattice defect influence on critical behaviour 80—25315
TGS, γ-irrad., lattice defect effects on ferroelec. dispersion 79—51904
TGS, polarisation reversal, cryst. defects effect 78—27156
TGS, static crit. phenomena, lattice defect influence 80—71336
TGS, US propag. and vel. rel. to growth defects 79—28049
TGS, with radiation defects, dielec. dispersion 79—42882
theory, and defect processes, review 80—2009
theory, rate eqns., chemical rules 80—33990
theory of defectsin solids, review 80—6400
thermoelectric alloys, phase diagrams, and imperfection chemistry 80—108422
topography settings, white beam X-ray, for cryst. defects, synchrotron radiation 2-axis spectrometer 78—67619
topological solitons graded Lie algebras, appl. to obstructions for crossing defect hypersurfaces 79—42062
topological theory of defects in ordered media 79—93072
transition metal carbonitrides, physicochem. props., comp. depend. 80—55370
transition metal oxides, extended defects, review 78—63753
transparent solid optical materials, laser damage statistics rel. to structural defect statistics 80—91829
tris-sarcosine calcium chloride:Mn(Fe), influence of cryst. defects on ferroelec. transition, EPR 79—38466
TTF-TCNQ, and related compounds, low temp. irrad. effects 80—24906
TTF-TCNQ, phase transitions and CDW state, controlled disorder effects 80—15507
TTF-TCNQ, phase transitions and CDW state, induced defect depend., transport and mag. studies 80—24980
TTF-TCNQ, X-ray irrad., transverse cond. 80—6432
TTF-TCNQ crystals, X-ray topographic study of cryst. perfection 80—96525
$TTT_2I_{1.5-x}Br_x$, chem. impurities and neutron irrad. induced defects, effects on DC cond. 80—49699
TTT_2I_3, chem. impurities and neutron irrad. induced defects, effects on DC cond. 80—49699
type II superconductor influence of structure defects on resistive and Hall effects *(Russian)* 79—33419
US testing, automatic *(German)* 79—83406
1-vinyl-o-carborane, orientationally disordered, γ-irrad. free radical defects, positron probe obs. 79—23647
weak beam calculations, effects of column approximation, in electron microscopic studies 79—32863
Wiener filtering appl. to nondestructive evaluation 79—11732
X-ray anal., conf., Denver, USA (Aug. 1976) 77—70382
X-ray and neutron section topography, cryst. dislocation and planar defect images, book contrib. 78—42863
X-ray characterisation of single crystals for devices with multiple crystal arrangement 78—83651
X-ray diffraction analysis, broad beam technique with increased resolution 79—86650
X-ray diffraction by close-packed crysts., chaotic subtraction packing defects, general soln. 80—92422
X-ray diffractometer attachment for large-crystal structural imperfection control 79—68975
X-ray line breadth calculations, convolution relations 78—51394
X-ray reflection section topography, technique to determine kinematically reflecting region depths, use in crystal defect obs. 79—50945
X-ray scanning with widely divergent beam for investig. of imperfection cryst. 77—7634
X-ray scattering from small defects in very perfect crysts. 78—47395
X-ray topography, contrast of images of defects, book contrib. 79—68979
X-ray topography, developments, review 80—64836

crystal defects continued
X-ray transverse topographs, defect contrast numerical calc. 77—84572
zero-gap semiconductors, lattice defects and chemical bonds *(Japanese)* 79—73161
Ag film, annealing study of elec. resist. and defect density 78—76167
Ag film, vac. deposited, defect density and activation energy depend. on deposition rate 80—29294
Ag, oriented crystallisation on active amorphous C centres, growth of nuclei at defects 79—7762
Ag thin films, spike effects of heavy ion sputtering 80—35034
Ag-Cu, highly deformed eutectic composite wire, anomalous props., fibre diameter and foreign atom effects *(German)* 77—36566
α-Ag-Zn, electron irrad., atomic mobility enhancement by defects, dynamic characts. 79—37871
AgBr-AgCl, mixed crystals, pure and I doped, lattice defect parameters, Frenkel defect form. energy, ionic cond. 80—44359
$AgGaS_2$:Fe, EPR of Fe-associated defect 80—60412
AgI, defects rel. to elastic behaviour near phase transitions with negative dP/dT 78—83885
Ag_3Mg, ordered alloy, projected pot. image of defect obs. 79—99176
(Al,Ga)As injection lasers, pulsations and adsorbing defects 79—94234
Al alloy, AK4-1, dispersion-hardening, US effects on ductility and thermal resist. *(Russian)* 77—32582
Al bimetal film with Cu, Ti(V,Ni) and alloy MLT(RS-3710), struct. and macroscopic defects *(Russian)* 79—1555
Al, compression, effect of press. on lattice defects up to 90 kbar *(Japanese)* 77—72654
Al, defects due to neutron irrad., muon probes study 79—56701
Al, defects formed during cryst. growth or by plastic deform., X-ray transmission topography obs. *(Russian)* 80—25761
Al, dynamic defect annealing during plastic deform. 78—88478
Al, high purity single cryst., etch pit morphology and their correl. with microstruct. *(French)* 79—69106
Al, quenched, irradiated, anisotropic electron scatt. on defects 79—95397
Al-Ag, type-II superconductor, torque oscillations in mag. field *(Russian)* 80—103800
Al-Al_2O_3-metal capacitor, capacitance and power factor rel. to voltage and temp. changes 80—54802
Al-SiO_2, Al-SiO_2(SiO)-Si, solid-state reaction mechanism 77—52623
Al-Ta_2O_5-Al, healing of defects in dielec. film by anodisation 80—65406
AlGaAs-GaAs lasers, defects and degradation *(Japanese)* 79—31899
$Al_xGa_{1-x}As$, DH, defect generation in active regions at high optical excitation rates 79—23845
$Al_xGa_{1-x}As$:Sn(Te)(Ge), anneal-induced defects, photoluminesc. obs. 79—61422
Al_2O_3, β- and β''-phases, defect struct. obs. by high resolution TEM, battery ageing relevance 80—107501
α-Al_2O_3, crystal defects from X-ray irradiation, F-centres, X-ray luminesc. obs. 80—55176
Al_2O_3, gamma irradiated single crystal, defect centres 79—65117
α-Al_2O_3, ion bombard., vol. expansion, annealing compaction, surface props. 78—67748
α-Al_2O_3, unintentionally doped, defect struct. 79—60755
α-Al_2O_3:Er(Cr), crystal defects from X-ray irradiation, F-centres, X-ray luminesc. obs. 80—55176
α-Al_2O_3:Mg, defect. struct., cond. and optical absorptiob 77—55279
Al_2O_3-Ca_3SiO_5, solid solution, exam. of lattice defects 79—95167
β-Al_2O_3-Na_2O, fracture stress, effect of microstruct. defects 77—44338
β''-Al_2O_3-Na_2O, spinel formation, TEM obs. 77—76423
β''-Al_2O_3-Na_2O-MgO, blocking defects observed by high resolution electron microscopy 78—55879
As, amorphous, optical, vibr., transport and defect-related props., review 79—51935
Au, positron annihilation, 4.2-500K, Doppler broadening meas. 78—43957
Au thin films, spike effects of heavy ion sputtering 80—35034
B fibre, US inspection, immersion method 80—66757
BN, structural changes occurring during shock compression in presence of H_2O 80—16301
BP, epitaxial, CVD on Si substrate, cryst. imperfections 78—10294
BP:Zn(Se)(Cd), epitaxial layers, ion implantation, defects and lattic locations, channelling obs. 80—88179
Ba ferrite powder, effect of lattice defects on coercivity *(German)* 79—24194
BaF_2:Er^{3+}, fluoresc., importance of defect clustering 79—33827
BaF_2:La^{3+}, thermal depolarisation of La^{3+}-F_i^- defect dipoles 80—75926
Ba_2MoO_5, Ba_3MoO_6, electrophys. props., effects of thermophys. props. of medium in synthesis 77—48375
$Ba_xSr_{1-x}Nb_2O_6$ crystals, defects and their characteristic features 80—88138
$Ba_xSr_{1-x}Nb_2O_6$, growth defects 78—38640
BaT:O_3:Mn, ferroelec. domain stabilisation by bulk ordering of defects 79—42925
$BaTiO_3$, polarisation switching, influence of charges arising from defects 79—69796
$BaTiO_3$, polycrystalline, X-ray diffraction, Curie temp., lattice defects, phase changes 79—99830
$Ba_{1-x-y}U_xCe_yF_{2+2x+y}$, solid soln., ionic cond. 79—99356
Be, blisters due to He irrad., proton backscatt. study 80—75273
Bi film, evaporated, lattice distortion spectrum, elec. resistance temp. variation 80—54806
Bi film, surface defects and struct., electron microscopy and elec. props. *(French)* 80—15415
$Bi_{12}GeO_{20}$, single crysts. optical homogeneity depend. on growth conditions 78—95007
δ-Bi_2O_3, thermoelectric power rel. to fast ionic conduction 80—107549
δ-$(Bi_2O_3)_{1-x}(Y_2O_3)_x$, thermoelectric power rel. to fast ionic conduction 80—107549
C, diamond like, graphitisation, elec. resist. meas., 30-550°C *(Russian)* 77—39676
$CaCO_3$, Iceland spar, polarizing prism, struct. defects effect 78—18065
$CaCO_3$ single crystals, effect of defect struct. charact. on X-ray diffr. 79—65089
$CaCO_3$, with and without inversion centres, nonlinear susceptibilities *(Russian)* 78—13750
$CaCO_3$:Li, synthetic calcite, $(CO_3Li)^{2-}$-Li^+ defect after X-irrad., EPR study 80—75852
CaF_2:Er, defect structure, quenching effect, dielec. relax. and optical absorption 80—65031
CaF_2:Er^{3+}, fluorite, defect equilibria cluster control 79—99231
CaF_2:ErF_3, clustering, defect struct., NMR study 78—80229

crystal defects continued
CaF_2:Eu, Mn, cathodoluminescence SEM appl., stroboscopic 80—70088
CaF_2:La^{3+}, thermal depolarisation of La^{3+}-F_i^- defect dipoles 80—75926
CaF_2:Tb, spectra of radn.-induced defect form. 80—2801
CaF_2:YbF_3, clustering, defect struct., NMR study 78—80229
$Ca_2(Mg,Fe)_5(Si_4O_{11})_2$-$(OH)_2$, amphibole nephrite, planar defects termination, high resoln. electron microscopy 80—79772
$(Ca_{0.15}Mn_{0.8}Fe_{0.05})SiO_3$, rhodonite lattice imaging of struct. defects 80—49240
$CaMoO_4$, electrical cond. and ionic transport number meas., defect struct. model 80—2388
$Ca_{1-x-y}U_xCe_yF_{2+2x+y}$, solid soln., ionic cond. 79—99356
Cd, film, freshly deposited, 77K, refl., annealing effect, thickness depend. 77—16413
Cd, lattice defects studied by gamma ray angular correlation 79—51895
Cd, positron annihilation, 4.2-500K, Doppler broadening meas. 78—43957
$Cd(ClO_3)_2$ irradiated single crystal, ESR and annealing, trapped defect centre 80—55141
$CdCr_2Se$, nonstoichiometric native defects from P-T phase diagram 77—63636
Cd_xHg_{1-x} Te, elec. characts., impurity effects 80—92890
$Cd_{0.2}Hg_{0.8}Te$, annealing in saturated Hg vapour *(German)* 79—43447
$Cd_xHg_{1-x}Te$, comp. determ. by electroreflection method 77—52708
$Cd_xHg_{1-x}Te$, single cryst. homogeneity and molar conc. determ. with electron microprobe *(German)* 78—2109
CdS, 200 keV electron induced defects, low temp. annealing 77—80796
CdS, defect struct., dark-field microscopy, anal. of decoration patterns 79—23506
CdS, defects formed by laser radiation of subthreshold intensity, bulk photo-EMF investigation 79—91098
n-CdS, growth from Te soln., photocond. and cryst. perfection 79—99579
CdS:Cu,Pb reflectivity of Ni-salt coated powder, pre-irrad. effect on defect form. 79—27973
CdSb single crystals, surface layer melting and recrystallisation due to laser irradiation *(Ukrainian)* 79—46699
CdSb-Ag, thermoelectric, thermal defect relax., elec. cond. and thermo-EMF effects *(Russian)* 78—14749
CdSe:Li, pure and doped, reson. Raman and Brillouin scatt., elastic exciton-defect scatt. 80—80788
p-$CdSiAs_2$, electron irrad. elec. props. annealing, lattice defects 80—100465
CdTe and CdTe:Cl, grown by travelling heater method, EPR defect charact. 77—40125
CdTe, melt-growth review, including liquid encapsulation method, defect charact. 77—40350
CdTe, nearest-neighbour hopping cond., effect of electron irrad. induced compensating centres 77—43599
CdTe, properties and appls., conf., Strasbourg, France (Jun-Jul 1976) 77—39832
CdTe:As(P), ion implanted, elec. props. 80—65021
$CdWO_4$ single cryst., melt growth, defects and growth mechanism 80—29933
CeO_2:CaO(Y_2O_3), oxygen ion cond. and defect struct. 80—107553
$CoFe_2O_4$ synthesis, chem., thermal histories rel. to fine cryst. struct. 79—43186
CoGa, defect struct. model 79—46648
Co_3Pd epitaxial films, multiray dynamic theory of diffr. contrast to explain defects nature 79—64962
Cr, film, defects and mechanical stability, different deposition methods *(Bulgarian)* 80—44438
Cr, films, vac. deposited, defects *(Russian)* 79—33203
Cr-Fe-Ni alloys, cryst. struct. and defects, high resolution electron microscopy obs. 79—94961
Cr-Si(GaAs) Schottky barriers, interfacial structural defects effect on avalanche breakdown 79—42644
CsI, mechanical props., effect of impurities 77—69034
CsI:Tl, crystallophosphor, luminesc. characts., temp. and conc. depend. 80—55175
CsI:Tl single crystal gamma-optical converting screens, factors influencing relative afterglow intensity 79—8173
Cu, blisters due to He irrad., proton backscatt. study 80—75273
Cu complex, bis-(alkylammonium) (11) tetrachloride, perovskite, lattice perfection 78—87633
Cu, defect annealing around stage III, $\gamma\gamma$ ang. correlation expt. 79—14846
Cu, deformed, defects, thermal relaxation, positron experiments *(German)* 80—50455
Cu, deformed, positron lifetimes, trapping model 77—15451
Cu high purity, grain boundaries as dislocation sources in premacroyield strain region 79—34096
Cu, high purity crystal, resistivity changes with deform., subsequent recovery 77—52397
Cu, irradiation with O_2 ions, defect production and annealing 80—88214
Cu, polycryst. magnetoresist. due to crystal defects 78—56128
Cu, self ion irrad., determ. of the nature of defect clusters by Rutherford backscatt. of He ions 79—4342
Cu, stress removal during annealing after hydrostatic extrusion 79—83215
Cu-Ag (Au), dil., dose depend. of impurity detrapping stages after electron irradiation 78—51582
Cu-Al-Ni(Mn), duplex shape memory effect after nonuniform plastic deform. *(Russian)* 80—25759
Cu-Fe (0.2 at.%), quenched, Fe dimers and defects 80—40007
α-Cu-Ga (3.4-15 at.%) cold-worked, lattice imperfections, X-ray obs. 77—55291
Cu-Ge(Sn)(Sb) alloys, stress removal during annealing after hydrostatic extrusion 79—83215
Cu-Ni, clean surface, surface segregation and growth process of altered layer *(Japanese)* 80—24720
Cu-Zn(30 at.%), electron irrad., positron annihilation, defect recovery 79—74018
Cu_3Au, displacement cascades prod. by Cu^+ bombardment 79—99251
Cu_3Au, neutron irrad., displacement cascades, direct obs. method 80—107335
$CuFeS_2$, natural chalcopyrite, defect struct., TEM 77—62535
Cu_2O, growth by melting, photocond. spectra 78—52029
Cu_2O, photoconductivity in 1S excitonic line 80—34366
$Cu_{2-x}S$, single cryst., as p-component of heterojunction, props. 77—39926

crystal defects continued
Cu_2S(Te), microstructure, work hardening in polymorphic transform. and subsequent annealing effect 79—52199
$Cu_{2-x}Se$, single cryst., as p-component of heterojunction, props. 77—39926
Cu_2TE, annealing and deform. of defects induced by phase work hardening during thermal cycling 79—52230
CuTe, Cu_2Te and $Cu_{2-x}Te$ alloys, struct., electron diffraction investigation 79—51066
Cu_2Te, microstructure, work hardening in polymorphic transform. and subsequent annealing effect 79—52199
$Cu_{2-x}Te$, single cryst., p-component of heterojunction, props. 77—39926
$CuWO_{4-x}$ prod. from $CuO+WO_3$ solid state reaction 80—66796
EuO, quadrupole coupling due to lattice imperfections 78—76347
$EuO_iF^-_{8-2i}$ defect structure, stabilisation of Eu^{2+} in fluorites 79—56649
EuS films, mag. and elec. props. rel. to stoichiometry and defects 80—97122
Fe, deformed, defects, thermal relaxation, positron experiments *(German)* 80—50455
Fe, ductile RE inoculated, black spots *(Chinese)* 77—72628
Fe:C, neutron irradiated at low temp., mag. disaccommodation 80—44881
Fe-Al, hyperfine field meas. using muon-spin-rotation method 80—10933
Fe-Al (40 wt.%), defect elimination by laser irradiation *(French)* 79—65960
Fe-Co films, ordered and disordered, Mossbauer study, role of lattice defects 79—24241
Fe-Cu (0.34 wt.%), neutron irradiated, field-ion microscope detection of ultra-fine defects 79—42116
Fe-Mn(Ni) systems, struct. defects effect on interdiffusion 80—15314
Fe-Mo alloys, cryst. struct. and defects, high resolution electron microscopy obs. 79—94961
Fe-Mo quenched alloy, electron microscope exam. of planar defects 79—79000
Fe-Ni-Mn-steel 48, struct. defects effect on interdiffusion 80—15314
Fe-Si (2-8 wt.%), single crysts., growth striations, X-ray studies 80—79774
Fe-Si (3 wt.%), polycrystal in mag. field, stress induced magnetisation, synchrotron Bragg refl. topography obs. 80—50139
$Fe_{80}B_{20}$, amorphous, cold neutron scatt., local and extended defects 80—84089
Fe_2O_3, haematite, annealing of nonequil. defects 79—43283
Fe_3O_4, magnetite, defect content, gas-phase comp. effects 77—43336
Ga, film, freshly deposited, 77K, refl., annealing effect, thickness depend. 77—16413
GaAS-AlGaAs LPE layers, defects formed by oxygen in ambient gas *(Japanese)* 77—70009
GaAlAs DH, optically-pumped, degradation at elevated temps. 79—50295
GaAlAs DH laser diodes, catastrophic degradation 79—50290
$Ga_{1-x}Al_xAs$ laser, DH, rel. to enhanced localised degradation and anomalous emission spectra 77—680
$Ga_{1-x}Al_xAs$ visible diode lasers, degradation 80—43330
$Ga_{1-x}Al_xAs$ visible diode lasers, degradation mechanisms 80—64026
GaAs cleaved (110) face, interaction with O_2, influence of cleavage defects, AES study 80—66684
GaAs, deep radiation centres from heat treatment, γ-irrad., deform., probability of nonradiative electronic transitions 80—50408
GaAs, defect cluster annealing, pot. barrier height determ. 80—84209
GaAs, defect clusters induced by γ-rays and neutrons, effect on elec. props. 80—29408
GaAs, defects produced by O_2 chemisorpt., influence on Fermi level pinning 79—60637
n-GaAs, epitaxial film, defect clusters, charge-carrier mobility temp. depend. anal. 80—54701
GaAs, epitaxial multilayer, electron irrad. defect study by transient capacitance 79—99241
GaAs, epitaxy by metallorganic and chloride depositions, defect characterisation at growth interface 80—59817
GaAs, gas-phase epitaxy, step stopping centre form. kinetics 80—65407
GaAs LPE layers, X-ray topographic studies of defects 77—62772
GaAs layers, electroepitaxy and thermal LPE growth, defect struct. and electronic characts. 80—2290
GaAs single crystals, laser damage statistics rel. to structural defect statistics 80—91829
GaAs, structural defects in single crysts., first order distribs. eval, *(German)* 78—6049
GaAs tunnel diode, electron beam bombard. induced defects, influence on excess current *(Russian)* 77—4424
GaAs:Cd, lattice defects caused by quenching, elec. cond. 79—56160
GaAs:Cr, Be^+ implantation, atomic conc. and defect density profiles after annealing 80—39123
GaAs:Si, IR absorpt. bands, localised modes, Si-related defects 80—76054
GaAs:Si, pulsed laser annealing of implanted layers, defect structure and Hall effect meas. 79—69118
GaAs-AlGaAs DH laser, rapid degradation caused by process-induced defects 77—71985
GaAs-$Ga_xAl_{1-x}As$ laser, degradation, TEM obs. 77—51625
$GaAs_{1-x}P_x$, structural defects, optical props. effect 80—55208
GaInAsP diode lasers, self-sustained pulsations in light output 80—64012
GaP, LEC growth of dislocation-free crysts., microdefects and striations 78—9974
GaP:Te, struct. imperfections, prep. and doping effects 77—89451
Gd, electron irradiated, relation of defect densities to Rayleigh parameters 77—62517
$Gd_3Ga_5O_{12}$ crystal growth from melt, X-ray topography meas. *(Hungarian)* 80—11556
$Gd_3Ga_5O_{12}$, planar defects, X-ray topography obs. *(French)* 80—2008
Ge, compensated by thermal defects, recomb. and optical props. 80—64989
Ge film, amorphous, influence of deposition parameters on e.p.r. 77—1586
Ge foil, [110] oriented, seven-beam lattice images of defects 80—107209
Ge, lattice disorder influence on optical spectra in interband transition region 79—43006
Ge, lattice images of defects and radiation damage applics. 80—107210
Ge, microdefect distrib. due to dislocation injection, selective etching 78—2122
Ge, microflaw vol. conc. determ., etching method 79—24688

crystal defects continued
Ge, p-type, and n-type converted to p-type by irradiation at 77K, defect form. mechanism 79—23651
Ge, quenched, defect annihilation process near 100°C 79—95047
Ge US absorpt., high temp. peak due to surface defects 79—69197
p-Ge:Ga, cryst. defects due to γ-irrad., annealing 79—55779
Ge:Ga, cryst. defects due to neutron irrad., elec. cond. and annealing 79—55789
Ge:P(Sb), growth atm. effect on struct. microdefect form. 80—20779
p-Ge:Sb, cryst. defects due to γ-irrad. 79—55779
Ge-Si(GaAs) heterodiodes, interfacial structural defects effect on avalanche breakdown 79—42644
GeTe, antistructural disordering 77—15402
$GeTe_x$ cermet specimens, density, 25 to 412°C, depend. on nonstoichiometry and annealing temp. 77—25004
^3He, solid, mag. transition, defect-melting model 79—28172
^3He, two-dimens. solid, melting mechanism 80—10643
HfO_2 single crystals, Y_2O_3 stabilised, optical props., impurities and annealing conditions influence 79—52399
HgCdTe, cryst. and photodiode, imperfections and surface conditions using electron induced current technique 79—67385
HgI_2, imperfections determ. by thermally stimulated currents method 77—54413
In, film, freshly deposited, 77K, refl., annealing effect, thickness depend. 77—16413
In, positron annihilation, 4.2-500K, Doppler broadening meas. 78—43957
InAs(P), electron irrad. at 50 MeV, elec. and optical props. 77—47486
InGaAsP-InP DH LED, high temp. aged, dark-spot defects, TEM obs. 80—66300
$In_{1-x}Ga_xAs_yP_{1-y}$, DH laser material, spatially resolved photolum. characterisation and optically induced degradation 79—47486
$In_{1-x}Ga_xAs_yP_{1-y}$-InP DH laser, 10000 h continuous CW operation, dark-line and dark-spot defects 79—98384
$In_{1-x}Ga_xP_{1-z}As_z$ DH laser diode, defect and phonon assisted tunnelling 78—13708
$In_{1-x}Ga_xP_{1-z}As_z$:Zn, x∼0.12, z∼0.26, LPE, DH lasers, tunnelling involving defects 77—65594
In_2O_3, thin film, sputter deposition form., optical and elec. props. 80—60123
n-InP, heat treatment in controlled P vapour 80—88137
InP substrate, thermal damage suppression by adding Ar in H_2 atmosphere 79—100275
InP-S(Te)(Zn), dislocation-free, TEM study of microdefects 79—82213
InSb, high-purity, electron irradiation effects on transport props. 79—23650
InSb, low defect crystal growth by InN doping, IR detector appl. 80—20780
$In_xSi_yO_z$, thin film, sputter deposition form., optical and elec. props. 80—60123
K ternary halides, A_2MX_6 type, radiation induced lattice defects and solid state reactions *(German)* 79—42101
KBr crystal, cordlike defects and countermeasures 79—72636
KCl, growth, supersaturation rel. to cryst. characts. 79—52101
KCl, pure and Ba doped, symm. of elastic fields due to defect displacements, diffuse X-ray scatt. 80—70256
KCl, single cryst., liq. inclusion movement in stress gradient field 80—44370
KCl, spontaneous cleavage, step line propag., macroscopic defects 78—87662
KCl, undoped and Pb- or NO_3^--doped, colloid centre formation, absorpt. spectra, 300-1000 nm 79—78710
KCl:Ba, defect struct., dark-field microscopy, anal. of decoration patterns 79—23506
KCl:Eu^{2+}, lattice defect equilib. optical absorpt. and cond. studies 80—29767
KCl:Pb, photoluminesc. induced by Suzuki-like occlusions, ionic thermocond. 79—33808
KCl:TlCl, lattice defects, X-ray line profile obs. 80—24455
$KClO_4$:CrO_4^{2-}(SO_4^{2-}), AC electrical conductivity meas. between temp. range 25-325°C, automated technique 80—59699
KH_2PO_4, real structure influence on optical strength 79—7187
KH_2PO_4, with and without inversion centres, nonlinear susceptibilities *(Russian)* 78—13750
$K_2Pt(CN_4)Br_{0.3}.3H_2O$, anisotropic radiation damage in electron microscopy, diffr. spot fading rate obs. 80—107329
$K_2SO_4.Al_2(SO_4)_3.24H_2O$, stirring effect on crystalline quality of soln. grown crystals 78—91281
LaB_6 crystals, zone refined, chem. characterisation 80—93821
$LaCoO_3$, reduction, direct obs. using high voltage TEM 77—63817
$LaPO_4$ catalyst crysts., high resolution electron microscopy, morphological characts. rel. to catalytic activity 80—107193
LiF, defects of electron irradiated single crystals *(Russian)* 77—47488
LiF, single crystal, neutron and gamma irradiation, SEM and Bragg profile anal. 80—15158
LiF:Mg(Eu)(Co)(Si)(O), cation sublattice, defect struct., elec. cond. 79—7709
$LiIO_3$, crysts., spontaneous parametric scattering of light by defects 80—34936
α-$LiIO_3$, defects decorated by space charge, X-ray topography study *(Chinese)* 80—107204
$LiIO_3$, nonlinear light scatt. on cryst. defects 78—5527
$LiIO_3$ single crystal, DC field effect, neutron diffr. enhancement *(Chinese)* 80—44077
α-$LiIO_3$, single crysts., light diffr. under DC field 80—11367
α-$LiIO_3$, surface defect layer struct. due to mechanical working *(Russian)* 80—100238
Li_3N, ionic conductor, single cryst. defect struct. anal. data reduction and struct. refinements, 153-678K 79—32988
Li_3N, optical absorpt. coeffs., exciton creation, optical anisotropy 79—95796
$LiNb_{1-y}Ta_yO_3$, Czochralski growth and basic props. 77—63556
Li_2O, neutron irrad. effects, optical absorpt. spectra 80—75271
Mg and Mg-Fe films, defect energy distrib., elec. resist. meas. during annealing 80—54808
$Mg_cFe_{1-c}O_{1+\delta}$ cluster component method calc. of lattice params., composition, imperfection 77—25031
MgO, criteria for assessing activity 79—11820
MgO, evidence for field induced trapping of defect dipole, thermally stimulated depolarisation 79—99820
MgO:Al^{3+}(Fe^{3+}), defect struct., shell model calcs. 79—99180

crystal defects continued
MgO:Fe^{3+}, defect structure, and oxidation reduction behaviour of Fe 79—99181
Mo crystals, joined by compression during heating, structural changes *(Russian)* 80—108513
Mo, diffusion of H(D), trapping at ion implantation induced defects 77—47622
Mo, electron irrad., anisotropic damage prod. 80—2071
Mo wire, US inspection, immersion method 80—66757
Mo-Co-Si alloys, cryst. struct. and defects, high resolution electron microscopy obs. 79—94961
Mo-Zr-C-B, dilute, electron microscope obs. of planar defect diffr. contrast patterns 77—43227
Mo_3CoSi, TEM study, planar defects 79—51047
$(Mo_{0.6}Ru_{0.4})_{82}B_{18}$, supercond. metallic glass, neutron irrad. effects 80—29060
MoS_2, lattice images of defects and radiation damage applics. 80—107210
n-Si, ion implantation causing surface defects, electroreflectance 79—19274
N_2 matrix N-N stretching vibr., IR activation, guest mol. depend. 80—60570
$NH_4H_2PO_4$, α-particle bombard. effects, circular crater form. 77—59051
Na-Co strip-chain silicates, structural-composition inhomogeneities 80—88122
$NaAl_3(PO_4)_2(OH)_4$, EPR of at. H caused by X-rays 79—28614
NaCl, damage caused by CO_2 laser radiation 77—90222
NaCl, defects of electron irradiated single crystals *(Russian)* 77—47488
NaF, γ-irradiated cryst., relaxational damping of elastic waves and activiation energy of motion of defects 79—14891
NaF:Li, pulsed double nucl.-nucl. reson. *(Russian)* 78—10804
Na_xWO_3 bronzes ($0.4<x<1$), domain, surface and substrate structs. 80—34281
Nb, blisters due to He irrad., proton backscatt. study 80—75273
Nb, defect annealing in 7 MeV-irrad. samples, positron annihilation obs. 80—24497
Nb, defects due to neutron irrad., muon probes study 79—56701
Nb, diffusion of H(D), trapping at ion implantation induced defects 77—47622
Nb, diffusion of N, alloying additions and struct. defects effect 79—55938
Nb film, bias sputtering prep. 79—1826
Nb films electron beam evaporated, struct. defects *(German)* 77—76684
Nb, neutron bombarded, defect size distrib. influence on hardening *(Russian)* 80—10580
Nb-H system, temp.-stimulated acoustic emission, hydride precip. 80—3044
Nb-Ni-Al alloys, cryst. struct. and defects, high resolution electron microscopy obs. 79—94961
NbH, H impurity screening, lattice deformation, dipole force tensor component calcs. 79—77611
$Nb_{12}O_{29}$-Nb_2O_5, oxide defect structures of stable and metastable phases, 800 to 1100°C 79—46651
$NbSe_x$, $x=1.48$-2.0, thermodynamic props., defect struct. anal. 79—74139
$Nd_{1-x}Ca_xVO_3$, solid solutions, elec. props. 80—96866
Ni, Czochralski growth conditions rel. to cryst. imperfections, mag. domain walls 77—68937
Ni, H diffusion in imperfect lattice, annealing and cold rolling effect 80—49425
Ni, lattice defects, formation kinetics, work hardening and resistivity study *(Russian)* 80—10557
Ni-Al alloy, solid phase reaction kinetic parameter calcs., defect formation *(Russian)* 80—54399
Ni-Cr (2 wt.%), role of hydrostatic pressure on sintering of creep cavities 79—28980
Ni-NbC (10 wt.%) eutectic alloy, directional solidification and struct. *(Russian)* 80—84922
Ni-steel U8 system, struct. defects effect on interdiffusion 80—15314
Ni-Ti(Fe), neutron irradiated, thermally activated deform. 80—6438
Ni-Zn ferrites, comp., lattice imperfections, sintering 78—3080
$Ni_{0.5-x}Co_xZn_{0.5}Fe_2O_4$ ferrospinal solid solutions, cryst. lattice defects and props. 80—19796
NiGa, defect struct. model 79—46648
NiO, thin films with spinel-type defect structure, FMR study 80—39877
NiO, transport number and cationic cond. *(French)* 80—15297
β-Ni_3S_2, defect struct. 78—63754
PLZT ceramics, electro-optic; defect struct. and prop. 79—42910
Pb film, monocryst., heteroepitaxial growth, struct. defects, and elec. props. *(Russian)* 80—84403
Pb, penetration field and magnetisation curve, lattice defect effects 77—28292
Pb, supercond., mag. hysteresis meas., pinning due to defects *(French)* 77—4463
$PbCO_3$, neutron diffr. topographic study of growth defects 78—91282
PbF_2, acoustic phonon modes up to high temps., neutron scatt. meas., time averaged defect struct. 79—33052
$Pb_5Ge_3O_{11}$, growth defects and polarisation switching 78—48132
$PbMo_6S_6$, cold-worked core-wires, supercond. transition temp. and lattice instability 78—6469
$PbSe_xS_{1-x}$, comp. depend. of density, effect of defects 77—11538
$Pb_{1-x}Sn_xTe$ layers, LPE, phase diagram rel. to lattice const., distrib. coeffs. 79—37925
PbTe, effect of pressing and sintering, study of induced defects by SEM 80—59983
PbTe film, ion-implantation-induced lattice defects 77—68985
Pd, film with defects, field-induced resist. min. 80—11050
$Pd_{1-x}Ag_xH_n$, positron annihilation examination of electronic structure *(German)* 77—69931
Pd_2MnSb, ferromag. Heusler alloy, mechanical and heat treatment effects 79—78582
Pt thin films, spike effects of heavy ion sputtering 80—35034
β_1-PtZn, defect struct., lattice parameter meas. 78—43009
Pu and other actinides, conf., Baden-Baden, Germany (Sept. 1975) 77—19807
$(SN)_x$, cryst. struct. by neutron diffr. 78—34488
$(SN)_x$, deform. and defects, lattice strain, fibrillation 80—3139
$(SN)_x$, struct. defects, nature and origin 77—24313
p-$Sb_xBi_{2-x}Te_3$ *(German)* 79—51618
Se, photoconductive film, field instability, Ar^+ ion irrad.-induced defects 78—87997

crystal defects continued
Si, annealed, photoluminesc. anal. of defects 80—80836
Si, annealing during Czochralski growth, influence on defect density 80—60769
Si, As-doped, effect of elec. and struct. parameters on avalanche breakdown localisation 77—11926
Si, blistering due to 400 to 1800 keV $^4He^+$ ions, modal range determ. 80—100289
Si, compensated by thermal defects, recomb. and optical props. 80—64989
Si, compression, effect of press. on lattice defects up to 90 kbar *(Japanese)* 77—72654
Si, crucible grown, virgin and implanted, laser irradiation effects on surface structure 80—92768
Si crystal, Czochralski grown, enhanced Borrmann effect 80—70191
Si crystal growth, for electronic devices 80—66419
Si, crystal growth conditions effect, on microdefect distrib. 80—50549
Si, Czochralski cryst., hillock etching of microdefects, TEM obs. 78—87678
Si, Czochralski crystals, O microsegregation, swirl defect distrib., growth rate depend. meas. 80—39295
Si, Czochralski-grown cryst., swirl defect formation and defect migration 77—76405
Si, Czochralski-grown crysts., thermally induced microdefects, annealing temp. and starting material effects 80—49141
Si, defect annihilation depth by pulse laser annealing 80—16128
Si, defect crystal structure 80—103316
p-Si, defect form. due to multiple N^+ and B^+ irrad. 79—90706
Si, defect generation and annealing by intense subthreshold electron beam bombardment 79—51149
Si, defect storage kinetics during neutron irrad. 80—24505
Si, defects, electrically active, correl. of electrolytic etch and surface photovoltage methods 79—77929
Si, defects detect. by EPR superheterodyne spectrometer 77—43885
Si defects in surface due to oxidation, exam. using double crystal back reflection topography *(German)* 79—51098
Si, dendritic film growth on alumina, solar cell appls. 77—77432
Si, devices and starting material, high voltage TEM obs. 78—10037
Si, diffusion of Ni below 475°C, role of defects 79—51319
Si dislocation free, quantitative determ. of microdefect density by preferential chem. etching 80—65001
Si, dislocation structure, effect of induction heating *(Russian)* 77—21180
Si, dislocation-free, defect formation, high temp. treatment, growth-band influence *(Russian)* 79—4299
Si, disorder depth distrib. prod. by N^+ irrad. 79—73227
Si dosimetry diode, irrad. by γ-rays and fast neutrons, lattice defect annealing *(Czech)* 79—45570
Si, electron irradiated, positron annihilation 78—87713
Si, electron irradiation induced displacement defects 77—80543
Si, electron-hole droplets nucleation at swirl defects 79—15095
Si, epitaxial growth on ion-implanted Si:As 78—6243
Si, epitaxial layer, growth mechanism from ion-molecular beams 80—2299
Si film, on sapphire, etching method 78—7070
Si, float zone, process-induced effects on carrier lifetime and defects 80—81216
Si, foreign interstitial atoms rel. to thermal intrinsic defects 80—29018
Si, growth and melting processes, origin of swirl defects 77—76407
Si, growth conditions rel. to cryst. struct. perfection *(Russian)* 80—38971
Si, heat treated, minority carrier lifetime, effect of swirl defects 77—39868
Si, heavily implanted, lattice defects and strains after high temp. annealing 78—10077
Si, heavy ion induced disorder in surface and at shallow depths 80—59535
Si, high-dose Ar implantation, X-ray topographic obs. of strains and damage 80—59496
Si, IR absorption spectra, Si-H bonds, crystal defects *(Chinese)* 80—55073
Si integrated circuits, effects of introduction, review 78—88547
Si, ion bombardment induced defect distrib., IR and electron diffr. study 80—65074
Si, ion irrad., temp. and dose depend. of defect profiles 80—29097
Si, ion-implanted layers, crystalline-to-amorphous transition, radiation defect prod. 78—87696
Si, ion-implanted polycrystalline film, defect build-up efficiency 80—2054
Si ion-implanted structure annealing, defect behaviour obs. *(Russian)* 80—49281
Si, lattice images of defects and radiation damage applics. 80—107210
Si, lattice parameters and perfection *(Japanese)* 79—4300
Si, microdefect distrib. due to dislocation injection, selective etching 78—2122
Si, microdefects, diffuse X-ray scatt. obs. 80—34014
Si, microdefects, X-ray topography 79—86797
Si, n^+-p diode, γ-radiation defects, annealing and recomb. props. 80—65045
Si, neutron transmutation doping, at. displacement effects 80—19852
Si, P^+ implantation, induced disorders. 80—6422
Si p-n junction solar cells, photon degradation effects 79—92078
Si p-n junctions, avalanche breakdown anisotropy 80—70811
Si, photoluminescence of annealed cryst., defect anal. 79—87500
Si, polycrystalline, large grain size, gross defects effect on effective carrier lifetime 77—80793
Si polycrystalline film, effect of defects/grain boundaries on photovoltaic mech. 80—93883
Si, RTR ribbon, impact of defects on photovoltaic potential 79—11186
Si, residual stress and defects induced by scribing 80—60990
Si, single cryst., electrolytic buffing using non-abrasive electrolyte *(Japanese)* 77—4862
Si, single cryst., heterogeneities meas. *(Japanese)* 77—35549
Si single crystals, laser damage statistics rel. to structural defect statistics 80—91829
Si single crystals, swirl defect formation model 79—94999
Si, single-crystal, grown-in structural defects 79—10860
Si, small-diameter cryst. grown by pedestal technique, investigation of microdefects using X-ray topography 79—55683
Si solar cells, capacitance transient spectra of processing- and radiation-induced defects 80—61340

crystal defects continued
- Si, sputter cleaning using Ar^+ ions, temp. depend. of residual damage, 25 to 800°C 77−48558
- Si surface, thermal oxidation induced defects, origin and growth *(Chinese)* 80−66681
- Si, swirl defects, gettering effects, obs. by photoluminesc. meas. 78−84623
- Si, technology and physics, review 80−34353
- Si, thermally induced microdefect form., C and O role 80−11439
- Si, vapour-liq.-solid growth, using Pt and Au liq. forming agents, struct. perfection 78−42936
- Si, wafer, Cu-decoration technique for lattice imperfection characterisation *(Japanese)* 79−65069
- Si wafers, etched in HCl, exam. of bunch formation 78−68831
- Si wafers, floating-zone, etch struct. on microdefects as affected by dopants and surface treatment 80−79773
- Si:As, implanted, residual defects after one- and two-step annealing 78−6083
- Si:As^+ sheet resistivity rel. to isochronal annealing and defect structures 77−76443
- Si:As(B), ion implanted, pulsed laser annealing appl. to device fabrication 79−73180
- Si:B, ion implanted, structure defects formation and behaviour under annealing in various ambients 80−65033
- Si:B, ionisation-assisted annealing 79−23628
- n-Si:B,P, radiative recombination at thermal defects, luminescence centre electron struct. 79−91496
- Si:B implanted wafers, ionis. assisted annealing and effects 80−100257
- Si:H,Li, amorphous, photoluminescence obs. 80−66280
- Si:H(D), H-related defects, channelling and IR meas. 80−25422
- Si:In, gradient transport soln. growth, IR monitoring, 950-1300°C 79−100040
- Si:Na, quantitative analysis of residual impurities with SIMS 78−87688
- Si:O, Czochralski crystal, oxygen striation and thermally induced microdefects 80−100275
- Si:P, Cu(Au) radiation-doped, influence of growth defects on elec. props. 79−69144
- p-Si:P, defect energy levels, ion implantation effects, Hall coeff., sheet resist. meas. 77−85173
- Si:P, doped by neutron transmutation, lattice defects 80−34018
- n-Si:P, fast neutron irrad., defect clusters and defect build-up kinetics 79−33019
- n-Si:P, secondary defects produced by high-temp. electron irrad. 79−33017
- Si:P, through-oxide implanted samples, anomalous residual defects after annealing 77−76432
- Si:P polycrystalline layer, role in lattice defect reduction assoc. with P predeposition 80−70229
- Si:P spherical defect cluster and dislocation loop analysis 78−14356
- Si:Sb, high dose Sb ion implantation, buried layer appls. 80−88186
- Si-H, amorphous, plasma-deposited, H evolution and defect creation 80−44914
- Si-Li(Au)(Cu), diffusion-induced defects, X-ray triple cryst. diffractometry 80−2213
- Si-SiO_2, ion implantation through SiO_2 film, recoil implantation of O, EPR study 80−88180
- Si-SiO_2, oxide defect density depend. on appl. elec. field and thickness 80−19791
- Si-SiO_2 interface, light induced reson. centres, photocond. reson., EPR obs. 80−50184
- Si-SiO_2 interface in MIS structs., effects of crystal defects on generation process 80−65702
- Si-SiO_2 system, structural defect formation rel. to thermal oxidation kinetics *(Russian)* 78−43478
- SiC (6H) (000$\bar{1}$), Ar^+ ion bombard., defect form., LEED obs. 79−69165
- SiC, surface defect annealing, following Ar ion and electron irrad. 80−7603
- SiC, surface defects due to Ar ion bombardment, 100-1000 eV 80−6445
- SiC:Al^+ p-n junctions, elec. props., defect effects 80−15594
- α-SiC(6H), electron bombardment, formation of defects on (000$\bar{1}$) surface 80−19844
- SiC(6H), ion-implanted, laser-induced recrystallization and defects 80−44221
- Si_xGe_{1-x}-Si(GaAs) heterodiodes, interfacial structural defects effect on avalanche breakdown 79−42644
- Si_3N_4:C film struct., oxidation, defects 79−51455
- SiO_2, amorphous and cryst., neutron irrad. and unirrad., intrinsic defect photolum. 80−50401
- SiO_2 crystal and amorphous modifications, structural defect model 80−38915
- SiO_2 films, growth on Si, role of defect structure 80−65403
- SiO_2 surface defects, influence of adsorbed O_2 EPR spectra 80−7163
- SiTe:Ge(Sn), substitution of Si, thermoelectric props. *(Russian)* 80−11023
- SiTe-GaTe, thermo-EMF, elec. cond. and solubility 77−20346
- $(SiTe)_{1-x}(ATe)_x$, A=Ge, Sn, Pb, solid soln. with small substitution, mag. susceptibility *(Russian)* 80−70933
- $SmCo_5$ single crystals subjected to shock waves, magnetisation, creation of high-coercivity state *(Russian)* 77−66384
- Sn, supercond., mag. hysteresis meas., pinning due to defects *(French)* 77−4463
- SnO_2, cassiterite, appl. of cathodolum. microscopy and spectrometry 77−69919
- SnO_2 films, cohesive energy, free electron density effect 79−60655
- $Sn_{1-x}Pb_xTe$, film, production under quasi-equilibrium conditions 80−45241
- SnTe-PbTe solid solns., defects from susceptibility meas. 77−84737
- SrF_2:La^{3+}, thermal depolarisation of La^{3+}-F_i^- defect dipoles 80−75926
- Sr_3MoO_6, electrophys. props., effects of thermophys. props. of medium in synthesis 77−48375
- $SrTiO_{3-x}$, planar defects in anion-deficient compound 78−22708
- $Sr_{1-x-y}U_xCe_yF_{2+2x+y}$, solid soln., ionic cond. 79−99356
- TMMC, antiferromagneric chain, 3-D ordering temp. controlled by solitons and defects, mag. field depend. 80−60275
- TTF-TCNQ, pure and irrad., nonlinear transport, ESR study, 1.2-4.2K 80−20167
- TaS_2, 1T and 1H polytypes, fast neutron irrad., defect prod., effects on resist. and charge density waves 80−65060
- $TbVO_4$, Jahn-Teller phase transition, γ-ray diffractometry 78−91205
- ThO_2, lattice defects and irrad. damage, review 77−27873

crystal defects continued
- Ti alloy, BT22 quenched from 850-1200°C, X-ray study of structure *(Ukrainian)* 80−24402
- Ti alloy, corrosion cracking resist. of type VT3-1 containing artificial defects *(Russian)* 79−52436
- Ti, neutron irradiated, relation between microstructure and recovery behaviour 77−15456
- Ti, pure (0.9998), positron annihilation study of defects 80−3281
- TiC-Mo_2C-TiN-Co, fracture toughness, effect of microstructural defects *(Japanese)* 77−56087
- TiC-TiN, physicochem. props., comp. depend. 80−55370
- TiN_x, film, non-stoichiometry rel. to optical characts. 77−12456
- TiO_2, K^+ implantation, extended defects and precipitates 80−49251
- TiO_2, OH^- adsorption on defect site, electronic struct. 79−47150
- TiO_2 powder, radiation induced defects 77−62562
- TiO_2, rutile, defect struct. and elec. cond. at 1273K 80−44604
- TiO_2, slightly vacuum-reduced, {312} planar defects, TEM obs. 78−22736
- TiO_2:$Ta_2O_5(Nb_2O_5)$, rutile, defect struct. and elec. cond. at 1273K 80−44604
- TiO_x, anomalous difference between theoretical and expt. densities, non-vacancy character 79−90630
- Ti_6O_{11}, electron-optical imaging, at 1.6 Å point-to-point resolution 79−46531
- $(U,Pu)O_2$, lattice defects and irrad. damage, review 77−27873
- U, anomalous thermal prop. behaviour at low temp. interpret. 77−28018
- UO_2, lattice defects and irrad. damage, review 77−27873
- UO_{2+x}, configurational entropy of defect complexes, Mayer cluster theory calcs. 79−77591
- UO_{2+x}, defect complexes model, rel. to lattice gas virial coeffs. 79−97308
- ^{238}U complex, α-induced defects, vibronic luminesc. band fine struct. 79−87489
- VN powder, defect struct., thermal and elec. props. 77−59286
- V_2O_5, wedge shaped cryst., electron lattice image interpret. 80−103319
- $V_{2-x}Sb_xO_4$, defect struct. exam., temp. depend. 78−18635
- V_3Si, He irrad., computer simulation of channelling 79−55800
- V_3Si, lattice defect, high voltage electron microscopy *(French)* 79−27993
- ^{48}V positron source prep. for annihilation radiation lineshapes, positron lifetimes meas., crystal defect studies 80−876
- W (110) stepped surface, electron stimulated desorption of O, atomic steps and defects influence 80−80091
- W (110) surface defect. exam., LEED obs. 79−82421
- W, defect recovery following neutron irrad., annealing effect 79−77642
- W wire, US inspection, immersion method 80−66757
- WC, hexagonal, meas. of mean square shift of atoms in micron powders *(German)* 78−47313
- WC-Co cemented carbide, carbide grain size effect on strength rel. to structural defects 77−32689
- WO_3, reduction, defect role, in situ HVEM obs. 80−81323
- YAG:$Ce^{3+}(Tb^{3+})$, emission from unrelaxed and relaxed defect state 79−61443
- $Y_3(Al,Fe)_5O_{12}$, optical anisotropy and stress birefringence assoc. with growth striations 79−42940
- $Y_3Al_3O_{12}$ crystal growth from melt, gas bubble capture theory 80−64941
- $Y_3Fe_{5-x}Ga_xO_{12}$, mag. domains and cryst. defects 80−75789
- YIG, film, photoinduced mag. surface anisotropy spin wave reson. 77−4560
- YIG, optical detection of scatt. of homogeneous precession of magnetisation by defects 79−69728
- Y_2O_3 film in Y-Y_2O_3-Au junction, defect struct. and local conduction 78−26970
- $(YSmLuCa)_3(GeFe)_5O_{12}$, LPE low defect density films, prep. for mag. bubble device fabrication 79−87590
- YSmLuCaGeIG, mag. props. and defects, depend. on B_2O_3 conc. on growth in PbO-B_2O_3 solvents 78−68321
- Zn, neutron irradiated, recovery of c-axis spacing and elec. resist. 80−34081
- Zn, positron annihilation, 4.2-500K, Doppler broadening meas. 78−43957
- Zn-Cu system, sputtering during atomic diffusion, UPS meas. 78−92159
- ZnO, crystallising in double HCP lattice, TEM and electron diffr. obs. 77−31655
- ZnO, growth by recrystallisation of ZnO in H_2O vapour and H_2 77−85913
- ZnS, Bridgeman growth under pressure, macroscopic inclusions and defects 80−45226
- ZnS, defect struct., dark-field microscopy, anal. of decoration patterns 79−23506
- ZnS film, defect form. and development 80−96759
- ZnS, sphalerite, appl. of cathodolum. microscopy and spectrometry 77−69919
- $(ZnS)_{0.2}(CdS)_{0.8}$, elec. props. effect of wurtzite-sphalerite boundary 77−55531
- ZnSe, Bridgeman growth under pressure, macroscopic inclusions and defects 80−45226
- ZnSe, elec. props. efect of wurtzite-sphalerite boundary 77−55531
- ZnSe electron irradiation induced displacement defects 77−80543
- p-$ZnSiAs_2$, electron irrad. elec. props. annealing, lattice defects 80−100465
- ZnTe:B^+ native and implant-created defects 77−76446
- Zr, elastically deformed, positron annihilation, Doppler broadening study 79−69900
- Zr, H(D) implanted, superconductivity enhancement obs. 80−70884
- Zr-Nb solid solutions, BCC, direct imaging of linear defect using diffuse scatt. 78−22726
- ZrO_2, doped, ionic cond., theoretical model 80−107552
- ZrO_2 single crystals, Y_2O_3 stabilised, optical props., impurities and annealing conditions influence 79−52399

crystal dislocations *see dislocations*

crystal electron states *see electron energy states (condensed matter)*

crystal energy *see lattice energy*

crystal etching *see etching*

crystal faces
- birefringent crystal faces, meas. method of growth and dissoln. rates 80−79719
- coatings, textured, crystallites faces determ. 80−64846
- cubic crystals, growth-layering effect on optical symmetry 80−88072

crystal faces continued
geometric, and kinetic features of cryst. face growth, analytical method for determ. 79—86728
growth, modification control 80—49150
growth models, attachment energy as habit controlling factor 80—59420
holohedral varieties of simple forms of crystals 79—94940
ice, monolayer ledges on basal surfaces 77—35809
ice disc growth from vapour, cryst. habit change mechanism 80—84117
ionic crystal, stability of polar surface planes 77—39554
jellium metal, work function changes on single crystal planes 79—99604
kinetic stability of plane-faced crystal growth forms 78—47259
laser alignment of crystal face perpendicular to axis of rot. 77—15283
Mg (0001) face, incipient oxidation, EELS and LEED studies 80—81237
NaCl crystals, air cleaved, anisotropy of round evaporation spirals, electron microscopy study 79—73300
nucleation rate equation, generalisation of nucleus shape depend. parameters 78—84765
optical crystallography, book 80—12862
organic crystal, struct. and habit correspondence, mol. centre of gravity determ. *(German)* 79—32934
pyramids of different slopes, growth on cryst. face at const. supersaturation, model interpret. 78—2050
quartz, cultured, hydrothermal growth, prism face develop. rel. to microcryst. form. 77—72572
quartz, cultured, prism faces growth and development, attached microcrystals role 77—31612
quartz, hydrothermally grown single crystals, real struct. investig. of rhombohedral faces *(German)* 78—2348
quartz, microtopographical obs. of 2nd order prism faces, hydrothermally-grown crysts. 80—54481
quartz natural microcrystals, elementary growth layers on faces 78—14634
sapphire, growth angle determ. from cryst. lateral face shape and solidified separation drops 80—103282
sapphire, profiled growth, struct. perfection 78—68621
steel, C, martensites, fractography, facets classification *(Slovak)* 79—20173
symmetric Belov subclasses for homologous series of bases of structural minals 79—19176
triglycine sulfate crystal, nematic liquid crystal behaviour on cleavage face 79—94899
X-ray goniometer, for producing accurately oriented cryst. faces 79—37591
Ag, electrodeposit, on (111) face, habit modification caused by Cl^- 80—71600
Ag surface, optical photoemission, high index faces, angle of incidence variation 79—100024
Ag vacuum deposition on GaAs (001), perfect and facetting growth 79—47632
Al vacuum deposition on GaAs (001), perfect and facetting growth 79—47632
Al_3Ni dendrite facets, determ. cryst. direction by SEM *(French)* 78—87893
Au film, detection of faceting on (h,k,0) surfaces by diffr. in electron microscope at 100 kV 78—43273
Au particles, small single cryst., habit plane characterisation 80—79733
Bi, single crystal from Bridgman's method, triangular facet formation 80—28933
$Ca_3Al_2Si_3O_{12}$-$Mg_3Al_2Si_3O_{12}$, synthetic garnet, soln. grown, surface features 78—2346
$CaCO_3$, calcite, gel grown crysts., spirals on rhombohedral faces 80—7486
$CaHPO_4.2H_2O$, brushite, obs. of etch pits on as grown faces 79—73169
CdS, $(10\bar{1}0)$ face, deformed zones around microimprints 78—23812
CdS, cryst. growth from vapour by one-dimens. nucleation on (110) singular surface, model 78—2048
CdS, epitaxial layers on Ge, morphology and six-pointed optic figures obs. 78—2390
Cu, (100) and (111) faces, response function with d orbital effects on electronic screening 77—62977
Cu complex, bis-(alkylammonium) Cu(11)tetrachloride, perovskite, face struct. and growth rate 78—87634
ErAG, facet formation 78—63687
GaAs-AlGaAs DH laser with buried facet 78—55373
$Ga_xIn_{1-x}P_yAs_{1-y}$, 111-A and 111-B faces, defect struct., etching and X-ray diffr. obs. 80—2026
GaSb, pulled crystal, microfacet obs. near irregularly remelted surfaces 78—91278
Ge, (111) cleavage face, struct. changes, LEED and Auger spectroscopy study 79—95249
InP, and InP_xAs_{1-x}, 111-A and 111-B faces, defect struct., etching and X-ray diffr. obs. 80—2026
InSb, crystal growth from melt, facets and twin formation obs. *(Chinese)* 80—59409
InSb, growth angle determ. from cryst. lateral face shape and solidified separation drops 80—103282
KCl crystal, surface elementary steps interaction with Au particles 80—39400
KH_2PO_4 crystals, rel. between selective and total soln. 80—39103
KH_2PO_4 single crystal evidence for spiral growth on pyramidal faces 80—84120
$NH_4H_2PO_4$ single crystal evidence for spiral growth on pyramidal faces 80—84120
$Na_3Al_2Li_3F_{12}$ garnet, cryolithionite, hydrothermal growth 79—43123
NaCl, evaporating cryst. surfaces, successive monatomic step trains with different density 80—29254
Pt, stability and struct. of high Miller index forces in vacuum and with adsorbed C and O 77—76651
Sb-crystals, in binary or ternary alloys, shapes on solidification *(German)* 80—3020
SbSI, vapour phase growth on seeds, prismatic faces 78—11090
Si, dissolution rates in KOH, orientation effect 77—36674
W, incoherent twin boundary microfaceting on annealing, field ion microscope determ. 79—77608
W, surface energy anisotropy and faceting behaviour in vac. and in H_2 77—7961
YAG, facet formation 78—63687
YAG, influence of facial growth effect on Yb ion incorporation 79—10822
$YAl_3(BO_3)_4$, cryst. growth rate determ. 79—86731

crystal field interactions
see also crystal hyperfine field interactions
A15 struct., stabilized by crystal field distortion of exotic elements at chain sites 78—79555
A-15 superconductors, transition temp., d band relative displacement *(Chinese)* 80—103770
acetylene cryst., lattice energy, spheroidal multipolar expsn. for intermol. energy 79—14726
actinide intermetallic cpds., cubic, var. from localised to itinerant magnetism 77—20534
actinides, ligand field theory 77—59269
actinides, ligand ordering parameters, nephelauxetic and spectrochem. series 77—76777
adatoms on metal surface, photoelectron angular distrib. from cryst. field split levels 77—63533
additive models for effective parameters 79—33269
adsorbed layer, classical octupoles on triangular lattice, orientational phases 80—2263
alkali bromide-VBr_2 systems, cryst. struct., DTA investig. *(German)* 78—72766
alkali chloride: V^{2+}, phonon induced zero field splitting 78—39073
alkali halates, NQR freq. temp. depend., phonon spectra interpretation 77—12226
alkali halide:Eu^{2+}, spin-Hamiltonian parameters, superposition model calcs. 80—96830
alkali halide:Eu^{2+} , spin Hamiltonian, cryst. field consts. calcs. 79—51537
alkali halide:Ga^+,In^+,Tl^+, cryst. field effect on spectral characts. 77—24880
alkali halide:Sn^{2+}, V_c^--centres, vacancy induced splitting of excited states, Sn^{2+} structure 78—51931
alkali halides: cation with s^2 ground-state configuration, absorption bands assignment 80—97310
alkali halides, three-body interactions, effect on electronic polarisabilities and photoelastic behaviour 79—47382
alkali metal halides, crystal properties, cohesive energy, bulk modulus and press. depend., interionic force model 80—15035
alkali metal-hexamethylphosphoramide, low temp. glass, EPR of solvated K, Cs and Rb 78—91927
alkali sulphates, SO_4^{2-} optical and spectroscopic props., cryst. environment effect 77—40224
alkaline earth chalcogenides, electronic polarizability of ions, effect of crystal potential 78—26490
alloys, magnetic anisotropy, influence of local symmetry *(Russian)* 80—93109
ammonium hydrogen oxalate hemihydrate, single cryst., DNMR obs., elec. field gradients, reorientation 77—85618
amphiboles, Mg and Mn rich, Mossbauer spectra 79—38412
aniline, in p-xylene host cryst., phosphoresc. triplet state, ESR and MIDP obs. 80—66077
aniline-chlorophenol complexes, ^{35}Cl NQR, inter- and intramol. interactions 80—63666
anthracene:tetracene, electronic absorpt. spectrum, host-cryst. field effect 80—100669
anthracene, fluoresc., site selection spectroscopy, 2-300K 77—1731
antiferrimagnet, vivianite type spin structure model, mol. field approx. 77—66232
antiferromagnet, uniaxial S=1, effect of cryst. field anisotropy 77—28344
antiferromagnetic garnet, absorpt. and luminesc. spectra, cryst. field and exchange interactions 77—73154
antiferromagnetic semiconductor, magnon-plasmon interaction and its effect on Raman scatt., theory 78—56302
benzene, derivatives, calc. of second-order susceptibility, using electronic spectra data 80—29756
benzene/benzene-d_6, cryst., X-trap phosphoresc., ODMR, 1.3K, triplet state struct. 77—20902
p-benzoquinone(-d_4), n-π^* excited states, distant intramol. interaction between identical chromophores 78—90203
Berthollides, chaotic mag. states 78—56330
biological systems, containing Fe, electronic and mag. struct., semiempirical MO cluster calcs. 78—62733
biotites, optical absorpt. bands 80—7371
biphenyl:tetracene, electronic absorpt. spectrum, host-cryst. field effect 80—100669
biphenyl crystals, electronic and vib. states, cryst. field mixing, two-photon spectra 77—59603
boracite, single cryst. prep. and phys. props. 80—100763
borate glass: Ni, absorption spectra, mag. props., coordination behaviour *(German)* 80—40147
calcium formate, intermolecular shielding contributions, proton mag. shielding 80—34783
calcium tartrate tetrahydrate:Cr^{3+}, optical absorpt. spectrum, cryst. field parameters 80—16067
calcium tartrate tetrahydrate:Cu^{2+}, spin-orbit coupling, optical absorpt. spectra 80—45120
calcium tartrate tetrahydrate:Ni^{2+}, optical absorpt. spectrum 78—84610
calcium tartrate tetrahydrate:VO^{2+}, optical absorption spectrum, cryst. field parameters determ. 78—6713
carbazole:tetracene, electronic absorpt. spectrum, host-cryst. field effect 80—100669
carbazolyl substituted diacetylene monomer cryst., ODMR and triplet state kinetics 78—76355
CdS:Cu, V, photoluminescence spectra 79—83027
cerium ethylsulphate, elec. susceptibility evidence for electronically driven lattice dilation 77—76781
chalcogenide, charge transfer, influence of cryst. field 79—99516
charged defects, Holtsmark elec. field sitribs. and assoc. broadening effects 79—1584
chemical state effects in AES 78—92566
chloroanisoles, ^{35}Cl NQR, inter- and intramol. interactions 80—63666
chlorophenols, ^{35}Cl NQR, inter- and intramol. interactions 80—63666
chromocene, mag. props., complete ligand field theory 78—31048
chromocene, mag. suscept., zero-field splitting, ligand field, 1-303K 77—89924
classical solid solutions, beyond-mean-field approx. 77—20039
Clausius-Mossotti relation, modified, for lattice of finite ions 79—42503
close-packed metals, elec. field gradients, vol. and struct. depend. 78—64014
cobaltocene, mag. props., complete ligand field theory 78—31048

crystal field interactions continued
complex compounds, calc. of probability of electronic excitation energy transfer 79—69478
compressed D_{4h} cluster, g_{zz}-g_0 value 77—80756
conference, group theory and application to spectroscopy, Nova Scotia, Canada (Aug. 1978) 80—41947
cooperative Jahn-Teller T-systems dynamics vibronic excitation branches 80—10934
copper porphin, Zeeman expt. on phosphoresc. triplet and quartet states 79—33786
copper porphine, $X\alpha$ multiple scatt. calcs., EPR and electronic spectra 78—13426
core level ligand field splittings in photoelectron spectra 80—43106
Coulomb interactions of electrons, modifications by polarisable atoms 77—11879
cryst. with defects 78—60478
cubic complexes, weak-field coupling scheme 80—92866
cubic crystal E state ion in tetragonal cryst. field, static Jahn-Teller effect 77—24539
cubic crystals, local field factors, electric dipole approx. calcs. 80—54661
cubic crystals, pseudo-tetragonal APR spectra 80—88861
cubic ionic structures, cryst. field coeffs., geometric struct. factors 77—43547
cubic metal:Gd, influence of cryst. field on EPR 78—52346
cubic metallic structures, cryst. field coeffs., geometric struct. factors 77—43547
$d^{3,7}$-configurations, weak field energy matrices calcs. with nonzero spin-orbit coupling 78—76029
d^3-configuration in trigonal field, Trees correction *(Russian)* 77—46556
$d^{4,6}$-configurations, weak field energy matrices calcs., spin-orbit coupling effects 78—76030
d^5-configurations, weak field energy matrices calcs. 78—76031
d^6-complexes and oxides, spin-state transitions, PES study 79—100014
deep oxide acceptor, intra- versus inter-small-polaron transitions 78—30874
di(ethylene diamine $H_2)_2$ zinc hexachloride, single crystals, EPR parameters for Mn^{2+} 79—56607
di(methylamino) zinc tetrachloride, single crystals, EPR parameters for Mn^{2+} 79—56607
diacetylene, single cryst., EPR of low-temp. photoproducts, photopolymerisation 78—85175
diagrammatic Green function technique appl. to cryst. field systems with exchange 78—68130
dialkylammonium copper chlorides, mag. and struct. transitions, IR absorption 77—52097
diamond, local field, microscopic electronic polarisation 80—25283
diatomic molecule, electron correlations, cryst. field interactions, Hubbard calc. 80—75530
p-dibromobenzene, in p-dichlorobenzene cryst., absorpt. spectra, mol. clusters static interaction 78—15198
dielectric response of solids, approxs. for treatment of local field effects 79—47033
dihydroporphin free base, in n-octane cryst., zero-field optically detected mag. reson., triplet state kinetics 78—42103
dilute local moment local magnetisation, Kondo-like deviations from free spin behaviour 80—44800
dilute magnetic alloy, random collinear states, Gaussian internal mol. field distrib. 77—16016
dilute magnetic alloys crystal fields for mag. ions from itinerant electrons 80—39537
dimethyl cadmium, photoelectron spectra, 4d spin-orbit splitting, crystal field and band-broadening effects, CNDO calcs. 78—76577
trans-dimethyl organometallic moieties, nuclear elec. quadrupole moment from elec. field gradients 80—29371
dimethyl zinc, core level photoelectron spectra, electric field gradient splittings 77—88494
dimethyl zinc, valence band and Zn 3d levels, electric field gradients 77—88495
dimethylbenzaldehydes in durene single crysts., ZFS D-parameters 77—55731
diphenylanthracene, fluoresc., site selection spectroscopy 2-300K 77—1731
dipolar crystal, surface local field effect, dipole moment, self consistent electric field calcs. 80—49178
disclination, force-free, motion, dynamic field theory *(German)* 77—1127
disordered solids, nonresonant paramagnetic absorption, quantum theory 79—69712
displacive phase transition, S ion spin Hamiltonian parameter dependence on order parameter 80—70356
doublet-triplet mag. system, dipolar and quadrupolar ordering 79—8004
effective field models in magnetism, unifying theory 77—32136
electric field gradient, calc. using point-charge approx. 78—19010
electric field gradient sign, possibility of obtaining from combined TDPAC and Mossbauer meas. 78—24907
electric field gradient sign, possibility of obtaining from combined TDPAC and Mossbauer meas. 78—24908
electronic system with two-fold degenerate band, free energy change due to electron-phonon coupling 79—42500
energy matrix checking, method 79—56173
enneaaquo rare-earth ethyl sulphates, cryst. field parameters, angular overlap model 79—56171
EPR parameters for orbital singlet of d^1 ion in cryst. 78—10751
EPR quintet transition, exact axial reson. fields calc., rel. to powder spectra 80—2622
EPR transitions for ions with $S=3/2$, small distortions of cubic cryst. field 77—51941
f^n-electron system, paramag. principal susceptibilities, calcs. using ang. overlap model 77—32158
ferric myoglobin compounds, single crysts., Mossbauer spectrum in small mag. field 79—100571
ferrimagnetic spinel, magnetostriction effects from Mn^{3+}, Co^{2+} and Fe^{2+} ions 79—91277
ferroelectric transition, displacive, effect of strong cubic anisotropy of lattice anharmonicity, mol. field theory 77—52026
ferromagnet, anisotropic, spin one, Callen's decoupling approx. 77—8258
ferromagnet, dynamic magnetic field on fast charged traversing particle 79—38423
ferromagnet, easy-plane, magnetic anisotropy, temp. and field depend., classical model 80—71008
ferromagnet, internal fields, positive muon investigation 78—68438

crystal field interactions continued
ferromagnet, singlet-triplet dynamics, spectral density method 79—73652
ferromagnetic, anisotropic, Green-function theory 77—16025
ferromagnetic BCC and HCP crystals, anisotropy of dipole fields, at interstitial sites 79—33584
ferromagnetic resonance, line width, inhomogeneous broadening, magnon scatt. 78—35043
fluorene, lowest singlet state, exciton band struct. calc. 78—63983
fluorite type crystal; $Tm^{2+}(Yb^{3+})$, axial g-values of $4f^{13}$ ions with trigonal symmetry *(Korean)* 79—24135
fluorite type crystal, Ti^{2+} doped, electronic struct. and EPR of Ti^{2+} 78—76034
garnet:^{57}Fe, electric field gradient, Mossbauer exam. 79—1732
garnet:Nd^{3+}, doped, Schottky specific heat and mag. susceptibility calcs. 79—51759
garnet:Nd^{3+}, spectral, structural regularities, anal. 78—51948
garnet, Fe^{3+} ligand field spectrum 79—78701
garnet, magnetostriction effects from Mn^{3+}, Co^{2+} and Fe^{2+} ions 79—91277
garnet, spin Hamiltonian and mag. anisotropy, appl. to $3d^4$ and $3d^6$ ions 79—99669
garnets, superexchange operator and cryst. field interactions 80—59931
graphite, adsorbed o-H_2 (p-D_2), NMR, orientational behaviour, weak crystal field 78—75935
guanidine aluminium sulphate, lattice charge contribution to coordination polyhedron cryst. potential 80—103651
guanidine aluminium sulphate hexahydrate:Cr^{3+}, ESR spectra fine struct. 80—93169
guanidinium aluminium sulphate hexahydrate:Cr^{3+}, EPR, 295.5, 78.45, 1.61K, zero field splitting 78—68359
guanidinium aluminium sulphate hexahydrate:Mn^{2+}, NMR 78—91939
guanidinium vanadium sulphate hexahydrate, singlet ground state system, low temp. mag. props. 80—44843
Hamiltonians of small perturbations, cluster model 77—24538
heat magnetization in the singlet-triplet model 78—64211
Heisenberg, ferromagnet, spin-one, uni- and biaxial anisotropy, RPA and mol. field approx. 78—34989
Heisenberg Hamiltonian, generalisation for crystal with allowance for orbital degrees of freedom 79—4644
Heisenberg system, ordered phase, reaction field approx., anisotropy presence 79—61030
high spin/low spin transition, model including lattice dynamics 77—63202
high temperature series expansion for complicated level systems 77—51863
hindered rotational energy levels of a linear ion in octahedral and tetrahedral crystalline fields 78—59767
Hubbard, half-filled band model, local field correction to plasmon freq. 80—24823
hydrates, solid, electric field gradient tensors at deuterons, and vibr. motion 77—71792
1-hydronaphthyl radical, in naphthalene single cryst., anisotropic oscill. strength 78—50591
hydrostatic pressure shifts of Van Vleck susceptibilities and Knight shifts, appl. of parametrisation 78—72120
II_3V_2 semiconductors, spin-orbit and cryst. field splittings of valence band 78—63980
II-IV-V_2 semiconductors, electronic band struct., general model pseudopot. 78—39020
III-V semiconductors, deep centres, many-electron effects 79—15117
impurity molecules in crystals, exclusion rules for librational-tunnelling states 78—84174
impurity spectrum, anisotropic condensed system, dipole-inductive interactions *(Russian)* 78—31225
induced moment paramagnet, singlet ground state, mag. fluctuations 77—4482
induced-moment singlet-triplet model, high-temp. series expansion 79—73653
induced-moment singlet-triplet model, rel. between ground-state moment and crit. temp. 79—78282
inert gas cryst. struct., induction energies, FCC and HCP 77—15343
inert gas crystals, intermediate-radius excitons *(Russian)* 79—11068
insulators, charge transfer processes influence on cryst. field 80—92865
intercombination transition intensities in strong crystal fields, symmetry reduction method 78—84175
Invar effects in weak and strong ferromagnets 79—56484
ion channelling, coherent excitation 79—46727
ion with d^N config., level splitting in trigonal and tetragonal cryst. field symm. 78—51949
ionic crystal, cryst. field due to piont charges, dipolar lattice sums *(Japanese)* 77—43167
ionic crystals, surface F centres, electronic struct., numerical soln. of one electron Schrodinger eqn. 78—64091
ions, closed-shell cryst. field and self-consistency effects on dipole and quadrupole polarisabilities 79—87072
ions in $^6S_{5/2}$ ground state, ESR line with 3.33 isotropic g-factor 80—15787
iron (II) formate dihydrate, mag. sp. ht., $S_z{}^4$-term 79—61127
irreducible tensor operator methods in strong-field coupling 79—7811
Ising ferromagnet, with transverse single-ion anisotropy, phase transitions 78—19259
Ising model, arbitrary spin, space renormalisation group calc. 78—27046
Ising spin gass, glass, Edwards-Anderson order parameter instability 80—71043
IV-VI semiconductor, Cr^{2+} doped, Jahn-Teller interaction energy calc. 78—2455
Jahn-Teller system, octahedral T_1, ligand trajectories 78—76028
Kramers doublets strong spin-lattice coupling, due to Jahn-Teller effect 77—85181
Kramers ions, virtual phonon exchange, field theoretic formalism 80—20137
lanthanide, trivalent, hypersensitive transitions, intensity parameters, charge transfer mixing 77—55498
lanthanide ions, finite ligand size and Sternheimer antiscreening 79—19561
lanthanide ions in $4f^N$ electronic config., correlation cryst. fields 77—76785
lanthanide shift reagents, pseudocontact shift, temp. depend. 79—95659
lanthanides, ligand ordering parameters, nephelauxetic and spectrochem. series 77—76777

crystal field interactions continued
lanthanum ethylsulphate:Gd^{3+}, zero-field splitting, contributory mechanism 80−80231
lattice sums by Ewald method, dipolar and Coulomb energies in infinite lattices 77−68942
layer materials, SXAPS interpret., cond. band self-convolution model, cryst. field splitting 78−23558
lead formate, intermolecular shielding contributions, proton mag. shielding 80−34783
ligand field calculations for arbitrary point groups in strong field coupling, energy diagrams, plotter routines 77−76778
ligand field spin-orbit coupling calcs. for d^7, d^8, d^9 five coordinated complexes 77−18781
ligand field theory, energy matrices checking method *(Russian)* 78−72123
ligand-metal overlap, rel. to ligand field and charge transfer interaction intensity 79−87067
lithium potassium tartrate monohydrate: Mn^{2+}, isomorphism with lithium ammonium tartrate monohydrate, EPR obs. 80−29607
local electric field, impurity centre dipole transitions *(Russian)* 78−34811
magnetic 3d impurity in non-magnetic metal, effective ion Hamiltonian 78−64016
magnetic field induced phonon splitting of cryst. field levels 80−13110
magnetic form factor meas. by inelastic neutron scatt. 78−52221
magnetic symmetry and spin-wave Hamiltonian struct. 78−84373
magnetic system with cryst. field pots., Green's function theory and high temp. series expsn. 80−15673
magnetically ordered crystals with orbital degenerated impurities, single- and two-magnon absorpt. by localised excitations *(Russian)* 77−69858
magnetically ordered singlet ground state system, nucl. spin Hamiltonian 79−28496
magnetism, conference, Munich, Germany (Sep. 1979) 80−56997
magnetoelectronic density of states for model cryst. 79−77978
magnets, EPR line shape 78−91926
manganese minerals, photoluminesc., cryst. field theory *(Russian)* 78−84654
matrix isolated atoms, matrix influence, theory 78−46288
matrix shifts of HFS consts. of Cu, Au and Ag atoms 77−42254
metal:D, dynamic quadrupole nuclear spin relax., α or α' phases 77−48085
metal:magnetic ion, ESR, book 77−48037
metal, μ^+ SR, localisation and diffusion, rel. to H 80−50248
metal, antishielding effects and temp. depend. of field gradients 78−51951
metal, conduction electron coupling with moments of 3d and 4f ions 78−60090
metal, cubic, effect of impurities on electric field gradient 78−23061
metal, elastically strained, elec. field gradients on nuclei, calc. *(Russian)* 78−60096
metal, elec. field gradient at nucleus, antishielding theory 77−4316
metal, non-cubic, electric field gradient, press. and temp. depend. 77−8057
metal, noncubic, possibility of isotopic mass effect on quadrupole coupling consts. 78−43725
metal, spherical solid model for muon and H in metals 79−78601
metal hexafluorides, $MF_6(M=W,Re,Os,Ir,Pt)$, ionisation energies and optical spectra in Dirac-Slater model 77−83488
metallic actinide compounds, localised cryst. field states, neutron inelastic scatt. obs. 78−14697
metallic systems with rare earth impurities, US attenuation in mag. field, absorpt. mechanisms 79−15336
metallic Van Vleck pnictide, ESR of non S-state ions 77−43881
metals, close-packed, elec. field gradients, vol. and struct. depend. 78−51947
metals, electronic transport eqns., optical cond., number conserving relaxation time approx. calcs. 80−49681
metals, inelastic neutron scatt. cross-section, effect of cryst. field 79−65642
metals, Kondo effect, Anderson hamiltonian 80−60187
metals, non-S-state impurities, coupled ESR 79−47326
metamagnetic tricritical point, effective exponent β 80−71045
methane:O_2, crystal field, O_2 catalysis of spin-species conversion 77−51706
methane, solid, orientational order of molecules in phase III 79−51042
methyl substituted antimony chlorides, $(CH_3)_xSbCl_{3-x}$, lone pair electrons, ^{121}Sb Mossbauer spectroscopy study 80−39984
micas, Mg and Mn rich, Mossbauer spectra 79−38412
microcrystals, magnetically ordered, high temp. behaviour 78−84456
minerals, physical theories for origin of colour 78−69323
molecualr energy level clustering, qualitative theory of irreducible tensor operators spectra 80−28001
molecular crystal, calc. of second-order susceptibility, using electronic spectra data 80−29756
molecular crystal, quadrupole ordered phase, thermodynamic props. *(Russian)* 79−82353
molecular crystal, spheroidal multipolar expsn. for intermol. energy 79−10824
molecular crystals, Stark splitting ang. depend. dipole moment and polarisability effects 77−51711
molecular orbital theory connections, field parameter expressions from electron charge density 80−29514
molecule, tetrahedral, in cryst. field, torsional ground state splitting, appl. to methane and $(NH_4{}^+)_2SnCl_6{}^{2-}$ 80−15019
Mossbauer ^{57}Fe spectra, ferrous charact., cryst. field interactions 80−108133
Mossbauer effect appl., conference, Kyoto, Japan (Aug.-Sept. 78) 80−7199
Mossbauer quadrupole splitting calcs. using cryst. field model, applic. to ferrous complexes 77−32301
muon trapping in Cu(V)(Nb)(Ta), Knight shift, rel. to H interstitials 80−50247
muonium quadrupole moment, cryst. elec. field influence on spin relax. 78−19404
$N_2H_5[Fe(N_2H_3COO)_3].H_2O$, elec. field gradient at Fe^{2+}, perturbation theory calcs. 78−19002
naphthalene:tetracene, electronic absorpt. spectrum, host-cryst. field effect 80−100669
naphthalene pair $(C_{10}H_8)$ in $C_{10}D_8$ host, mini-exciton obs., electron spin echo and ODMR 77−4559

crystal field interactions continued
1,4-naphthoquinone, $T_1 \leftarrow S_0$ transition, elec. and mag. field spectra 78−88322
neodymium ethyl sulphate, electronic spectra Stark pattern, crystal elec. field and mag. props. 77−12084
nephelauxetic effect interpretation 77−43548
neutron scattering and magnetism, conference, Julich, Germany (Aug. 79) 80−41934
nickel oxalate, electronic struct. from Huckel calcs., optical props. and reactivity 77−89741
niobates, Lorentz elec. field, and short-range Nb-O interactions 77−43941
noble metal, matrix-isolated, matrix-induced changes in opt. spectra 77−57913
noncubic metals, conduction electron electric field gradient, effect of orthogonalisation 78−26832
noncubic metals, elec. field gradients, nuclear electric quadrupole interaction 79−65420
nonlinear σ model, rel. to classical Heisenberg ferromagnet 77−4489
nontransition metals, calculated contribs. to elec. field gradients 78−39079
NQR, steady-state, basic principles 78−76349
NQR pressure sensitivity, vol. depend. of elec. field gradient and lattice vibrs. 77−12225
NQR spectra, crystal symmetry determ. and elec. effects 77−11450
NQR spectroscopy, elec. field gradient tensor parameters 78−72432
octahedral ions and molecules of 2nd and 3rd row metals, force consts. 77−54548
octahedral symmetry, unitary group treatment of strong crystal field *(Chinese)* 79−51534
organic compound containing ^{35}Cl, NQR, crystal splitting, bonding effects 77−12221
organic solids, charged excitonic complexes, coupled states, exciton interaction with charge carriers study 80−20090
palladium porphin, in n-alkane crystal, Zeeman and crystal field effects, absorpt. vibr. anal. 80−7372
palladium porphin, triplet state, optically detected EPR and Zeeman meas. 79−19809
palladium porphin, Zeeman expt. on phosphoresc. triplet and quartet states 79−33786
palladiumporphin, in n-alkane, $S_1 \leftarrow S_0$ absorpt. spectrum, vibronic coupling and avoided crossing, field splitting 78−84613
paramagnetic impurity centre interaction with external elec. field 77−89727
paramagnetic ion, eigen-value problem in crystalline and mag. field 79−7954
parametrisation of crystal induced correlation between f-electrons 78−19004
parametrisation of temp. depend. of splitting of axial ^8S state ions 78−91652
permutation symmetry, geometrical approach 78−21001
phonon scattering by paramag. ions with $S=1$ in cryst. field of uniaxial symm. 77−76496
phosphate glass: Ni, absorption spectra, mag. props., coordination behaviour *(German)* 80−40147
phosphorescent triplet state, spin-lattice relax. mechanism *(Russian)* 78−68542
phthalocyanine film, surface photovoltage, central ligand effect 79−78231
plagioclase:$Mn^{2+}(Fe^{3+})$, ligand field bands of impurity luminesc. centres and their site occupancy 78−88350
pnictides, charge transfer, influence of cryst. field 79−99516
polyethylene, crystal split fundamentals, resolution by Raman difference spectroscopy 79−95373
praseodymium oxydiacetate crystal, opt. rot. dispersion 77−36193
pryromellitic and dianhydride, intermolecular shielding contributions, proton mag. shielding intermolecular shielding contributions, proton mag. shielding 80−34783
pyrite type dichalcogenides, ^{57}Fe isomer shift, quadrupole splitting, Mossbauer study 80−15832
pyrochlore compounds, EFG and Mossbauer quad. splitting calcs. 77−62877
quadrupole spin echo envelope EFG tensor axisymmetry in mag. field 80−20497
quantum mechanics, use in magnetism and crystal field theory, review 78−76215
quartz, single-cryst., Fe^{2+} absorpt. spectra in polarised light and struct. position 79−43007
quinoxaline, in p-dibromobenzene, ^{81}Br, elec. field grad. distortion near defect sites, optically NQR 79−38409
quinoxaline in durene (naphthalene) crystal, Stark effect, space charge, local field tensor and dipole moment 77−28601
radiative transitions, proximity effects, role of vibronic coupling and static crystal field interactions model 80−69126
rare earth, hydroxides, cryst. field parameters, ang. overlap model calcs. 77−89738
rare earth alloys, cryst. field effect on EPR and NMR 78−56391
rare earth alloys, cryst. field effects on thermal props. 77−12072
rare earth alloys, line width of cryst. field excitations 77−85183
rare earth alloys, magnetic properties, impurity effects, CPA calc. 80−44784
rare earth alloys, R_2Co_{17}, formation of mag. anisotropy role of rare earth ions *(Russian)* 78−76238
rare earth alloys, vol. magnetisation, point charge cryst. field model 77−63254
rare earth alloys and compounds, book 80−36785
rare earth amorphous alloys, antiferromagnetism, mol. field approx. 78−80142
rare earth and actinide ions, corrections to cryst. field Hamiltonian 79−33268
rare earth and rare earth intermetallic hydrides, magnetic properties, effect of hydrogenation 78−68210
rare earth chalcogenides, cryst. field splitting, press. depend. 80−24852
rare earth chlorides, doubly degenerate E-phonons, mag. field splitting 77−43297
rare earth chromates (lanthanide series), paramag. state, crystalline elec. field calcs. 78−39074
rare earth cobaltites, ^{59}Co NMR, quadrupolar and hyperfine interactions 79−15366
rare earth compound, crystal field and Slater parameters and coordination 78−6771

crystal field interactions continued
rare earth compounds, cryst. field effects on EPR and NMR *(Japanese)* 77−43879
rare earth compounds, cryst. field effects on EPR and NMR *(Japanese)* 77−43880
rare earth compounds, cryst. field effects on EPR and NMR 79−4736
rare earth compounds, hexagonal, cryst. field effect in thermal expansion 80−49390
rare earth compounds, Kramers, temp. renormalised spectrum of mag. excitations, cryst. field level ordering 77−20516
rare earth compounds, multipolar interactions, evidence and origins 80−59935
rare earth compounds, neutron inelastic mag. scatt., book contrib. 77−89944
rare earth cpds., with cryst. field splitting mag. inelastic neutron scatt. cross-section 77−55659
rare earth dihydrides and dideuterides, electronic and mag. props. 80−25260
rare earth garnets, anisotropy due to cryst. elec. field and exchange 77−69543
rare earth garnets, appl. of superposition model to cryst. field 78−68132
rare earth garnets, cryst. field depend. on coordination of dodecahedron 79−73475
rare earth impurity, ESR, exchange induced broadening in low lying crystalline field system 80−108062
rare earth intermetallic, cubic, direct coulombic contrib. of cond. electrons to cryst. elec. field 79−91005
rare earth intermetallic, cubic direct Coulomb contrib. of cond electrons to crystalline elec. field 77−76784
rare earth intermetallic compounds with Cu_3Au structure, crystal field splitting 80−54663
rare earth intermetallic cpds., cryst. field effects rel. to mag. props. 80−59933
rare earth intermetallics, cubic, exchange coulombic contrib. of cond. electrons to cryst. elec. field 79−95376
rare earth intermetallics, cubic, magnetic order effects on cryst. field parameters 77−40019
rare earth intermetallics, magnetostriction and struct. distortion 77−63248
rare earth intermetallics, quadrupole interactions, magnetoelasticity 80−15489
rare earth intermetallics, RAl_2, cryst. field volume magnetostriction calc. 79−8029
rare earth intermetallics, RAl_2-Gd(Er)(Dy)(Nd), dil., (R=La, Yb, Lu), EPR and mag. susceptibility 80−15797
rare earth intermetallics, $RFe_{5-x}Ni_x$, giant intrinsic mag. hardness 78−56354
rare earth intermetallics, RGa, mag. props., 4.2-350K 77−63230
rare earth intermetallics, RPt, (R=Gd, Tb, Dy, Ho, Er, Tm), structs. and mag. props. 80−50069
rare earth ion, spin correlation effect calc. 78−23058
rare earth ion energy separation, $4f^N$-$4f^{N-1}$ nl, host depend. 80−49676
rare earth ion spectra, crystal field integral parameters, spin-orbit interaction 80−100447
rare earth ions, energy transfer rates, unified method using standard tensor calc. *(French)* 78−79965
rare earth ions, orbit-lattice interaction empirical parameter determ. 78−38799
rare earth ions in crystals, electric dipole transitions intensities 79−78062
rare earth ions in cubic field, anal. of absorption spectra $4f^{N+1} \rightarrow 4f^N5d$-6s 80−7382
rare earth iron garnets, contribution of Fe ions in noncubic magnetostriction from crystal field model 78−43622
rare earth iron garnets, level intersection and instability of mag. struct. *(Russian)* 77−43816
rare earth iron garnets, mol. field coeffs. 77−1544
rare earth Laves phase compounds, $R_xR_{1-x}Fe_2$, magnetostriction, anisotropy energy 80−25177
rare earth metal, conduction electron interactions, anisotropic 80−15492
rare earth metal, screening effects on cryst. electric fields 79−78058
rare earth metal S-states in metals, anomalous cryst. field splittings 79−19563
rare earth metallic systems, linewidth of cryst. field excitations 78−67988
rare earth metals, EFG produced by conduction electrons, mag. ordering effects 77−40020
rare earth metals, mag. excitations, neutron inelastic scatt., review 79−47265
rare earth metals, two- and single-ion mag. anisotropy 77−63164
rare earth metals and alloys 78−84177
rare earth molybdenum selenides, supercond., mag. props., 0.7 to 295K 77−32113
rare earth orthoferrites, mag. anisotropy in cryst. field approx. 80−60241
rare earth oxyhalides: Eu^{3+}, fluorescence spectra obs. *(French)* 80−89042
rare earth perrhenates, $(ReO_4)^-$ ion vibrs. rel. to static field, Raman investig. *(Russian)* 78−76470
rare earth perrhenates, Raman spectra, $(ReO_4)^-$ ion normal vibrs. rel. to static field 79−65858
rare earth pnictide, effective cryst. field 77−63050
rare earth pnictides, cryst. field splitting, press. depend. 80−24852
rare earth pnictides, prep. and props., book contrib. 80−54212
rare earth pseudobinary intermetallic compounds, ESR studies 80−108064
rare earth salts, phonon field contrib. to g-shift, symm. restrictions 77−55500
rare earth series, variation of fourth and sixth order cryst. field parameters 78−72122
rare earth sesquisulphides, $RS_{1.5}$ (R=La,Ce,Pr,Nd,Gd,Tb,Dy,Ho,Er,Tm,Lu) sp. ht. between 2 and 20K 79−60518
rare earth systems, book contrib. 80−39540
rare earth systems, crystal field effects 78−67987
rare earth systems, mag. field depend. of polaritons 79−33246
rare earth trichloride hexahydratee Gd^{3+} EPR, linear point charge model predictions 80−25200
rare earth trihydrides, light, low-temp. sp. ht., mag., elec., and cryst. field splitting effects 80−49379

crystal field interactions continued
rare earth zinc intermetallics, RZn, rel. to magnetoelastic consts. 78−15005
rare earth-Ag alloy, amorphous, model calcs., of mag. props. 80−84616
rare earth-Al, RAl_2, spontaneous cell distortion due to cryst. field, magnetoelastic consts. 77−63255
rare earth-Al Laves phase intermetallics, RAl_2, R=Gd, Ho, Dy, Tb, cubic Laves phase compounds, exchange striction determ. 80−44895
rare earth-Co, RCo_2:^{57}Fe, easy magnetisation directions, Mossbauer meas. and cryst. field calc. 77−63168
rare earth-Co, RCo_5, high anisotropy origin, cryst. field contrib. 77−73020
rare earth-Co, RCo_5, mag. moment orientation, anisotropic mol. field model 77−89950
rare earth-Co alloy, mag. anisotropy origin 79−38319
rare earth-Co amorphous alloys, mag. compensation temp. 77−66277
rare earth-copper intermetallic cpds., RCu_2, metamag., mag. props. 79−87242
rare earth-copper intermetallic cpds., RCu_2, metamag., mag. props. 79−87243
rare earth-Cu intermetallic compds. single crysts., mag. props. 80−54892
rare earth-Fe-Al alloys, RFe_4Al_8, mag. props. 78−52250
rare earth-nonmagnetic metal intermetallic cpds., struct. and props., review 79−95377
rare earth-transition metal alloys, RM_5 78−43339
rare earths, spin waves and excitations 78−84407
rare earths, trivalent, 5d states charge transfer and intershell spectra, separation and overlap 78−10966
rare earths in metallic environment, mag. moments 78−6515
rare-earth compounds, antiferromag., mag. props., cryst. field theory 78−27006
rare-earth compounds, antiferromag., mag. props., cryst. field theory 78−27007
rare-earth ion spectra, effect of coordination polyhedron struct. 77−55807
rare-earth ions, charge transfer and crystal field theory 80−70654
rare-earth-Ni alloy, RNi_2 (R=Gd, Tb, Dy, Ho or Er), Mossbauer effect of ^{57}Fe 77−69743
reduction symmetry method 77−66141
reduction symmetry method in crystal field theory 80−70656
relativistic quadrupolar contrib. in systems with nonvanishing orbital magnetism 78−43338
ruby:Cr^{3+}, ESR saturation, dynamical mag. susceptibility increase in zero mag. field 77−40122
ruby, luminesc., ground state of Cr(III) pair 79−33782
ruby, Raman ^{2}E and phosphorescence transitions, line widths, time correl. study 80−20621
SCF theory, boson transform. 77−80430
scheelite-type species, magnitude of cation fields 78−80111
screening of fields of static distortions 80−6797
semiconductor, cryst. field coeff. of point defect 77−43537
semiconductor, diamond structure, plasmon line shape, local field effects 78−76011
semiconductor, heavily doped, perturbation potential distrib. and density of states 79−47052
semiconductor, impurity levels of transition metal ions in cryst. field 78−23059
semiconductor, recombination radiation mag. depolaris., spin level quadrupole splitting of lattice nuclei *(Russian)* 79−38666
semiconductor, zinc-blende structure, plasmon line shape, local field effects 78−76011
semiconductors, magnetic moment spin splitting 79−56175
sigma phase structure, ionicity modified pair pot. model anal. 78−51466
simple jonic crystals, ion transport 78−63878
singlet ground state system in mag. field, anisotropic exchange interaction effect on props. 79−91224
singlet-doublet model of induced moment system, surface magnetism near Curie point 77−1530
sodium acetate trihydrate, press. depend. of methyl tunnelling motion 80−10603
solid state theory, 1926-33 80−57067
spectroscopy, finite symmetry adaptation 80−43032
spin echo, rot., in solids, anisotropic interaction recovery 78−68410
spin glass, Ising, cryst. field effects 77−85460
spin relaxation in photo-excited triplet states via vibronic excitation: rotation of spin axes 79−78503
spin system with double electron exchange order-order transitions 77−4522
spin-lattice relax. 79−15337
spin-lattice relax. times in crystals, anisotropy 79−15374
spin-state transitions in solids, two-phonon model 79−56170
spinels, ligand field stabilisation evaluation using Mossbauer determ. cation distrib. 78−31126
Sternheimer valence shielding-antishielding factor including exchange, ions of interest in Mossbauer spectra 77−85182
strongly anisotropic magnets, canonical transform. method 77−85404
strontium formate dihydrate:Cr^{3+}, optical absorption spectrum 80−50380
strontium formate dihydrate, EPR and optical absorption spect. of VO^{2+} ion 77−40112
strontium tartrate tetrahydrate Co^{2+} electronic absorpt. spectrum 78−92098
superconductor with crystalline-field-split mag. impurities, free energy and thermodynamical crit. field 77−32127
superconductors with paramag. impurities, NMR theory in singlet state 79−28445
superexchange interactions in cryst. with many-electron paramag. ions and strong cryst. field 77−59402
superposition model 77−28149
superposition model of g-shift of S-state ions 77−72838
terbium ethyl sulphate, mag. and thermal props. 79−7971
ternary semiconductor, struct. effects on energy band struct. 78−39021
p-terphenyl host, breakdown of anisotropic Lorentz approximation 78−5276
tetrachloroaurates and tetrachloroiodates, ^{35}Cl NQR freqs., correl. with crystallographic data 79−33559
tetraethyl lead, core level photoelectron spectra, electric field gradient splittings 77−88494
di-(tetraethylammonium)tetrahalomanganate, mag. circular and linear dichroism obs. 80−29725

crystal field interactions continued
tetrahedral molecule, hindered rot. energy levels in trigonal field 77−7678
TGS:Cr^{3+}, EPR obs. of ferroelectric monocrystals, fine struct. EHT-SCCC-MO calcs. 79−19769
TGS crysts., effects of radiation induced defects on internal bias field 80−88941
three open shell configs., inter electron repulsion integrals 77−55499
thulium ethyl sulphate, Van Vleck paramag., mag. reson. on uniaxial and uniform compression *(Russian)* 79−61243
tin containing organic compounds, $[R^{I}R^{II}R^{III}PO]_2SnR_nCl_{4-n}$, $[R^{I}R^{II}R^{III}PO]SnR_3Cl$, Mossbauer spectra, isomer shift and quadrupolar splitting *(Russian)* 79−61285
titanates, Lorentz elec. field, and short-range TiO interactions 77−43941
TMNB, ferromag. chains with easy-plane anisotropy, exchange const., anisotropy const. and g-value 77−80927
TMNC, ferromag. chains with easy-plane anisotropy, exchange const., anisotropy const. and g-value 77−80927
transition metal, 3d, cryst. field potential calc. 77−59366
transition metal $^6S(d^5)$ ions in tetragonal and rhombic symm., zero-field splitting 77−1390
transition metal alkali metal halide, A_nCY_6, spectra by cryst. field theory 79−4820
transition metal complex ions, $MY_4{}^{n-4}$, $MY_6{}^{n-6}$, alkali metals and alkaline earth outer-sphere cations, spectroscopic splitting parameters 78−39075
transition metal complexes, A_2MX_6, d-electron config., effects on phase transitions 77−35687
transition metal complexes, acetylacetonates, mag. susceptibility and optical reflection spectra 77−59381
transition metal complexes, octahedral substituted, ligand-fluid splittings, accidental degeneracy origin 80−10932
transition metal compound, superexchange interaction, effective spin-orbital Hamiltonian 80−70998
transition metal compound, superexchange interaction, multielectron theory 80−70997
transition metal compounds, intensity of Laporte forbidden transitions, ligand polarisation model 78−64378
transition metal compounds, Jahn-Teller induced high spin-low spin transitions 79−69676
transition metal compounds, pd^N (N=7,8,9) electron system in cubic crystal field, energy matrices *(Japanese)* 79−42504
transition metal compounds and dil. alloys, mag. ordering phenomena in high mag. fields 80−50075
transition metal dihalides, crystal field stabilisation energies, lattice energies 80−38994
transition metal halides and oxides, cryst. field stabilisation and lattice energy 80−75201
transition metal hydrides, isotope effects on supercond. props. 79−65580
transition metal hydrides, supercond., isotope effects, depend. on cryst. field energies 79−56353
transition metal intercalates of Ni and Ta dichalcogenides, magnetic susceptibility, function of temp. 80−39756
transition metal ion 3d→4s transitions in crystals, obs. and interpretation 78−6339
transition metal ion pairs, simply reducible symmetry group crystal fields, kinetic exchange theory 80−39541
transition metal ion system, multiplet and cryst. field split photoemission spectra 77−66577
transition metal ions, 3d^N, in crysts., Slater parameters and 3d-4s excitation energies 78−33433
3d-transition metal ions, s-doublet struct., appl. of exchange correlation mass operator approx. 80−106266
transition metal ions in amorphous compounds, crystal field theory and mag. props. 78−72318
transition metal ions in crysts., two-centre exchange interactions between orbitally degnerate ions 79−15126
transition metal ions in HCP hosts, energy splittings 78−67989
transition metal oxides, crystal field effect on isothermal bulk moduli 78−61364
transition metal oxides, crystal field stabilisation energies, lattice energies 80−38994
transition metal oxides, pressure-induced high-spin-low-spin transitions 78−85549
transition metal systems, ESR studies, polarised absorption, ligand field model, group theory applications 80−43077
transition metal trinuclear carbonyl complexes, electronic structures. and spectra 79−59480
transition metals, theory of ferromagnetism involving spin-orbit and cryst. field interactions 80−2541
1,3,5-trichlorobenzene, ^{35}Cl NQR, high press. behaviour 79−33560
trimethyl gallium, core level photoelectron spectra, electric field gradient splittings 77−88494
trimethylammonium manganese chloride dihydrate, optical absorpt. spectrum, 300K, 90K, cryst. field parameters 78−27253
triphenyl phosphonium ytterbium chloride, Yb^{3+}(4f^{13}) absorpt. spectrum, cryst. electric field splitting 77−73151
Tutton salt:Mn^{2+}, EPR, 298K, spin-Hamiltonian parameters, cryst. fields 78−27086
type II antiferromagnet with bilinear and biquadratic coupling, magnetic excitons in cubic cryst. field 79−78353
Yang-Lee edge singularity and ϕ^3 field theory 78−65882
YIG, energy location of mag. Fe levels, spin polarised photoemission 79−24413
zinc formate dihydrate, Co^{2+}-doped, EPR spectrum, g-factor anisotropy for A- and B-sites 77−77089
Zn-Mn(Cr), dil., mag. anisotropy below 1K, low field magnetisation meas. 80−20382
Ag, deformation potentials for isotropic strains 79−42506
Ag, electron density at nucleus, press. depend., Hartree SCF calcs. 78−56411
Ag halides, quadrupolar deformability theory by tight binding method 80−10614
Ag host, impurity effect on electric field gradient 78−23061
Ag-Al(Ga) electric field gradient temp. depend., nearest neighbour impurity mass effect, TDPAC meas. 78−6612
Ag-Dy, dil., Schottky effect, sp. ht. meas. 78−34633
Ag-Dy, dil., thin films, ESR spectra, stress effects 80−39866
Ag-Dy(Er), dil., cryst. field and spin exchange parameters, susceptibility and ESR expts. 77−40129

crystal field interactions continued
Ag-Gd(Tb)(Tm), dilute, thermopower, crystal field and interaction effects 77−66158
Ag-Pd, dil., elec. field gradients due to Pd near neighbour configs., TDPAC obs. 78−19391
$Ag_{0.5}Cd_{0.5}$, Cd 4d band apparent splitting, cryst. field and d-d overlap influence XPS obs. 79−78825
AgCl, electronic contact charge density of ^{107}Ag, core and overlap contrib. 79−78064
AgCl(:AgBr), intrinsic ODMR spectrum mechanism, doping effect 78−43682
$AgClO_3$, ClO_2 spin Hamiltonian 78−60326
AgF, -Z 79−78064
$AgFeO_2$, EFG tensor, nucl. quadrupole coupling const., O^{2-} polarisability 77−72844
Ag_3SbS_3, NQR elec. field effect, temp. depend. near ferroelec. transition 77−77121
Ag(111), valence band struct. along Λ, angle resolved photoemission spectra 79−95316
Al, electron-irrad., NQR, EFG around vacancies and interstitials 78−88220
Al, muon diffusion at low temp., effect of nuclear elec. field gradients 77−52005
Al:^{12}B, relax. mechanism for polarised implant 78−87693
Al/AlO_x/La-rare earth metal tunnel junctions, cond. meas., cryst. field effects 80−88694
Al-Al oxide-$Bi_{1-x}Pr_x$ tunnel junction, cryst. field struct. obs. in conductance 78−84358
Al_2Ce, Al_3Ce, nucl. orientation exam. of Ce ground state at very low temp. 78−67999
$Al_{2x}Ga_{2(1-x)}O_3$:Cr^{3+}, luminesc., lifetime, 77 and 4K, struct., energy transfer 79−28798
$AlNH_4(SO_4)_2$:Cr^{3+}, optical spectral, crystal field, spin orbit and exciton interactions 80−34958
Al_2O_3, 3d^4 ion study by cross-relaxation 79−99755
Al_2O_3, zero field ground state splitting of Fe group ions, phonon spectroscopy 79−90738
Al_2O_3:Cr^{3+}, shock compression, absorpt. spectra 80−20675
Al_2O_3:Fe^{2+}, phonon spectroscopy using superconducting tunnel junctions 78−91389
AmB_2 (B=Al, Co, Fe, Rh, Ru), hyperfine fields at Am site 77−27851
AmO, and AmO_2, electronic struct. and chem. bonding and XPS line shape calcs. 79−33264
Ar:H_2, nuclear spin relax. of H_2, crystal field meas. 79−51875
Au-Ag-Cd, γ-ray PAC of ^{111}Cd, nearest neighbour contrib. to elec. field gradient 77−36161
Au-Co, dil. alloy, crystalline electric field and spin-orbit splitting, NMR results 77−32274
Au-Fe, dil., contact charge density, internal conversion meas. 79−56630
Au-Gd, dil., crystal-field splitting of localised Gd^{3+} moments, ESR obs. 79−82869
Au-Gd(Tb)(Tm), dilute, thermopower, crystal field and interaction effects 77−66158
Au(111), Λ-line valence bands, angle-resolved photoemission determ. 80−108323
$BaCl_2$:Gd^{3+}(Eu^{2+}), EPR, electrostatic versus superposition model 78−23337
BaClF:Sm^{2+}, energy levels, optical props. 78−84631
$Ba(ClO_3)_2.2H_2{}^{17}O$, fine struct. in quad. reson. of ^{17}O, DNMR 77−8453
Ba_2EuNbO_6, luminescence Raman spectra, means for localisation of binding energy levels *(German)* 78−88304
Ba_2EuTaO_6, luminescence Raman spectra, means for localisation of binding energy levels *(German)* 78−88304
BaF_2:Gd^{3+}-m$^+$ complex, cryst. field parameters, EPR 78−10768
BaF_2:Tb^{3+}, cubic Tb^{3+} centres, energy level and cryst. field parameters 77−52181
BaF_2:Tm^{2+}(Yb^{3+}), trigonal centres, point-charge approx. 78−39072
$BaMgF_4$:Mn^{2+} ferroelec., EPR and ENDOR study, cryst. field tensor 80−71162
$BaMo_4$, M=Mo,W, EPR spectrum, temp. depend. of zero field splitting 79−15346
$Ba(NO_3)_2$, electric field gradient, quadrupole coupling consts. 77−89740
$Ba_4NbRu_3O_{12}$ and $Ba_4TaRu_3O_{12}$, $(Ru_3O_{12})^{13-}$ cluster obs. in presence of orbital degeneracy and spin-orbit coupling *(French)* 80−70655
BaO:Mn^{2+}, impurity pot. well shape calcs. 78−87950
$BaTbO_3$, perowskite struct., Tb^{4+} EPR obs., cryst. field parameters determ. *(Italian)* 78−52350
$Ba[Fe(CN)_5NO]_2.2H_2O$, NMR, H_2O orient. *(French)* 78−52366
Be, electric field gradient, magnitude and sign 77−80755
Be, noncubic crystal, temp. depend. of elec. field gradient 79−99515
Be, quadrupole interaction for ^{100}Rh, ^{111}Cd, and ^{181}Ta, temp. depend. TDPAC obs. 77−20772
Be_2SiO_4:P, EPR and ENDOR 78−76295
$Bi_4Ge_3O_{12}$ crystals, doped with Dy^{3+}, Ho^{3+}, Er^{3+}, Tm^{3+}, Yb^{3+}, growth, spectral and laser props. 80−45115
BkO, and BkO_2, electronic struct. and chem. bonding and XPS line shape calcs. 79−33264
$CaCo_2(PO_4)_2$, reflection spectrum and mag. susceptibility meas. 77−59586
CaD_2, neutron diffr., NMR 77−15378
CaF_2:Co^{2+}, designation of optical transitions near 5.40 nm, temp. evolution of absorption spectra meas. 77−55806
CaF_2:Dy^{3+}, cubic cryst. field effects 80−2368
CaF_2:Dy^{3+}, cubic sites, Γ_7 state energy, e.p.r. 77−1590
CaF_2:Dy^{3+}, Γ_8 quartets, orbit-lattice interaction, e.p.r. under stress 77−1591
CaF_2:Dy^{3+}, spin-lattice interaction in Γ_8 quartets, models tested for EPR data 78−23336
CaF_2:Dy(Tm), overlap and covalency contribs., orbital calc. 77−1397
CaF_2:Eu^{2+}, nuclear spin diffusion barrier, ^{19}F NMR Obs. 78−64282
CaF_2:Fe^{2+}, electronic props., Mossbauer and far IR spectroscopy 79−99803
CaF_2:Fe^{2+}, relax. meas., Mossbauer spectroscopy, 10-30K 80−44977
CaF_2:Gd^{3+}, effect of strain on cryst. field, EPR longitudinal and shear strain parameters 77−90027
CaF_2:Gd^{3+}, Eu^{2+}, natural, EPR study of impurity centres 78−19318
CaF_2:Gd^{3+}, Li$^+$(K$^+$), elec. field gradient at nuclei on orthorhombic sites, vs. elec. zero-field splitting 79−87070
CaF_2:Gd^{3+}, S-state splitting, investigation by ESR and ENDOR at high pressure 78−52345
CaF_2:Gd^{3+}-m$^+$, complex, cryst. field parameters, EPR 78−10768

crystal field interactions continued
$CaF_2:Nd^{3+}$, crystal field splitting 79—65418
$CaF_2:Nd^{3+}$, crystal field study, absorption spectra 80—20668
$CaF_2:Nd^{3+}(Yb^{3+})$, cryst. field at O_h sites 77—35899
$CaF_2:Np^{3+}(U^{3+})$, cryst. field splittings, ab initio MO calcs. 77—20520
$CaF_2:Pr^{2+}$, EPR data interpretation for octahedral Γ_8 state in cubic cryst. field 80—2634
$CaF_2:Tb^{3+}$, cubic Tb^{3+} centres, energy level and cryst. field parameters 77—52181
$CaF_2:Tm^{2+}(Yb^{3+})$, trigonal centres, point-charge approx. 78—39072
$CaF_2:Tm^{3+}$, 8.2 keV excited state, mag. props., Schottky ht. capacity, nucl. quadrupole splitting 78—76037
$CaF_2:U^{5+}$, charge compensation, struct. 79—15124
$CaF_2:YB^{3+}(Ce^{3+})$, point-charge approx. of tetragonal centres 77—47778
CaF_2+Yb^{3+}, Stark level Zeeman energies, mag. susceptibiltiy, Schottky specific heat, crystal field splitting 78—26831
$CaHfO_3:Ta$, electric field gradient temp. depend., TDPAC 77—20768
$CaMO_4:Mn^{2+}$, M=Mo,W, EPR spectrum, temp. depend. of zero field splitting 79—15346
$CaMoO_4:Fe^{3+}$, single crystals, structure and kinetics, EPR meas. 79—99760
$CaO:Cr^{2+}$ Jahn-Teller system, APR spectrum, zero strain site energy level diagram 79—99756
$CaO:Eu^{3+}$, influence of crystal field on luminesc. *(Russian)* 80—80834
$CaO:Mn^{2+}$, impurity pot. well shape calcs. 78—87950
$Ca(OH)_2:Ni^{2+}$ single cryst., X-irrad., Ni^+ EPR, g-factors and point-charge model 80—2626
$Ca(PO_3)_2:Eu^{3+}$, amorphous, phonon-assisted site-to-site electronic energy transfer, fluoresc. line narrowing obs. 77—81140
$Ca_2PO_4Cl:MnO_4^{3-}$, polarised electronic spectrum 77—52137
$Ca_5(PO_4)_3F:Nd^{3+}$, optical fluorescence intensity and cryst. field parameters 78—52570
CaV_2O_6, elec. field gradient at ^{51}V, NMR meas. and ionic model calcs. 78—19370
$CaWO_4:Er^{3+}$, magnetocaloric behaviour, cryst. field theory 77—4520
$CaWO_4:Fe^{3+}$, EPR, spin Hamiltonian parameters from anal. of Kramers' doublets 79—28595
$CaWO_4:Mn^{2+}$, polycryst., EPR spectra calc. using Bir's method, compared with expt. 79—1707
$CaWO_4:R^{3+}$, X=rare earth, cryst. field parameters, ang. overlap model 79—60772
Cd complex, bis(thiosemicarbazide) Cd II sulphate, elec. field gradients, γ-ray PAC spectrosc. 79—65773
Cd complex, dichlorobis (pyrazole) cadmium:Cu(II), ESR, compressed tetragonal symmetry 78—6568
Cd complexes, dithiocyanato(diethylenetriamine) Cd(II) and dithiocyanato(pentamethyldiethylenetriamine) Cd(II), Cu^{2+} doped, ESR 80—108059
Cd, electric field gradient, magnitude and sign 77—80755
Cd, electric field gradient press. depend., lattice vibrs. effect, PAC expts. 79—61267
Cd, electron density at nucleus, press. depend., Hartree SCF calcs. 78—56411
Cd, field gradients, temp. depend., electronic and lattice contribs., ab initio study 79—42501
Cd, noncubic crystal, temp. depend. of elec. field gradient 79—99515
Cd, nuclear quadrupole interaction, theory 78—10412
Cd, nuclear quadrupole interaction theory using first-principles pseudopotential 79—73482
Cd, photoelectron spectra, 4d spin-orbit splitting, crystal field and band-broadening effects, CNDO calcs. 78—76577
$CdBr_2:Co^{2+}$, ground-state g-value, EPR meas. 77—16159
$CdBr_2:Eu^{2+}$, layered, temp. depend. of consts. in ESR Hamiltonian, 16-300K *(Russian)* 77—32254
$CdBr_2:Mn^{2+}$, layered, pressure effect of ESR on axial field const. of spin Hamiltonian *(Russian)* 77—32254
$CdCl_2:Co^{2+}$, ground-state g-value, EPR meas. 77—16159
$CdCr_2Se_4$, energy structure, magnetooptic effects 80—71394
$CdF_2:Eu(Gd)(Nd)$, semicond., symmetry of optical centres, optical and elec. props. 77—59592
$CdGa_2Se_4$, thermoreflectance and visible absorpt. spectra, energy gap, cryst. field splitting 80—34945
$CdInGaS_4:Er^{3+}$, cryst. field parameters, thermal and mag. props. calc. 77—20540
$CdIn_2S_4:Cr$, absorpt. and photoluminesc. spectra, Cr conc. depend. 79—78712
$CdIn_2S_4:Cr$, ligand field induced photocond. and photoluminesc. 77—28214
$CdIn_2S_4:Er^{3+}$, cryst. field parameters, thermal and mag. props. calc. 77—20540
$CdMoO_4:Mn^{2+}$, EPR spectrum, temp. depend. of zero field splitting 79—15346
$Cd(NH_3)_6(BF_4)_2:Ni^{2+}$, EPR of $[Ni(NH_3)_6]^{2+}$, temp. depend. at phase transition 77—20685
CdS, surface photovoltage in exciton absorpt. range 78—19119
$CdS:Ni^{2+}$, config. interaction and cryst. field theory 77—39811
$CdS_{1-x}Se_x$ mixed crystals, free excitons, disorder effects 80—34365
CdTe, NMR, dipole-dipole coupling between ^{111}Cd, ^{113}Cd and ^{125}Te 79—91305
$CdTe:Cr^{2+}$, absorpt. and luminesc. of $Cr^{2+}(d^4)$, cryst. field theory interpretation 79—83000
$CdTm_2Se_4$, mag. susceptibility meas. 4.2 to 300K cryst. field approx. 77—66246
$(Ce, La)In_3$, heat capacity and elec. resist. 80—71049
Ce compounds, rocksalt type, low temp. thermal props. 78—84445
Ce compounds with group V elements, antiferromag., temp.-renormalised longit. mag. excitations 77—51862
Ce dilute alloys, cryst. field and Kondo effect 77—43809
Ce impurity Kondo system, crystal field effects on thermopower and Kondo effect 77—66163
Ce, inelastic neutron scatt. cross-section, effect of cryst. field 79—65642
Ce monochalcogenides, cryst. field effects, phase transitions 80—24853
Ce monopnictides, cryst. field effects, phase transitions 80—24853
Ce^{3+}, local symmetry in frozen aq. solns., EPR and linear electric field effect 77—16169
Ce-alloys, dil., elec. resist. in presence of external mag. field 78—19022
CeAg(Mg)(Zn), magnetic struct. and cryst. field, neutron diffr. exam. 78—72328
$CeAl_2$, Anderson lattice system, thermal expansion meas. 1.5 to 10K 79—37860
$CeAl_2$, dynamic Jahn-Teller effect, neutron energy loss obs. 79—78060

crystal field interactions continued
$CeAl_2$, mag. anisotropy, transition, crystal field splitting 78—52243
$CeAl_2$, mag. behaviour 2.5 to 300K, neutron scatt. meas. 77—63110
$CeAl_2$, magnetoelasticity, rot. invariance and magnetoacoustic birefringence 79—87304
$CeAl_2$, NMR, cryst. field effects and mag. order in low temp. phase 78—68391
$CeAl_2$, resistivity and volumetric meas., phase diagrams, comparison with CeS 80—107789
$CeAl_2$, skew scatt., evidence of cryst. field effect, Hall effect meas. 78—2466
$CeAl_3$, cryst. field effects, inelastic neutron scatt. meas. 77—51710
$CeAl_3$, inelastic neutron scatt. meas. 79—47066
$Ce_{30}Au_{20}$, amorphous, cryst. field effects and mag. interactions, magnetisation and transport props. meas. 78—68191
CeBi, lattice distortion modes and mag. structural transitions 79—78325
CeBi, magnetoelastic effects, anisotropic mag. behaviour 80—25176
CeBi(Sb), anisotropic mag. ordering and mag. structural transitions 79—78324
CeBi(Sb), enhanced lattice-displacement effects on cryst. field and anomalous mag. anisotropy 79—73477
$CeBi_xSb_{1-x}$, mag. props. and press. effects 80—71026
$CeCl_3$, doubly degenerate phonon states, mag. field dependent splitting 77—16320
$CeCl_3$, mag. field depend. of polaritons 79—33246
$CeD_{2.12}$, neutron cryst.-field spectroscopy 80—14967
CeD_x, $1.94 \leq x \leq 2.74$, Ce^{3+} ground state crystal field splitting from inelastic neutron scattering 79—99517
CeD_x, (x=1.94 to 2.75), phonon dispersion, crystal field splitting, neutron scatt. study 79—60452
$CeFe_2Si_2$, CeFeSi, absence of effective mag. field at Fe nuclei *(Russian)* 78—19397
$CeH_{2.70}$, sp. ht., 2 to 260K, second-order phase transitions and cryst. field splitting 79—82355
$(Ce_{1-c}Ho_c)Ru_2$, superconducting, mag. props., neutron scatt. study 80—44808
$Ce(In, Sn)_3$, heat capacity and elec. resist. 80—71049
$Ce_{1-x}La_x$ alloy, thermoelectric power 79—78080
$Ce_{1-x}La_xAl_2$, extraordinary Hall effects, 4.2-300K, cryst. field interaction 78—79980
$(Ce_xLa_{1-x})Al_2$, inelastic neutron scatt. cross-section, effect of cryst. field 79—65642
$Ce_xLa_{1-x}Al_3$, Kondo system, mag. susceptibility, 1.5 to 20K 79—78310
$Ce_{0.9-x}La_xTh_{0.1}$, mixed valence state, static and dynamic mag. response 80—103816
$Ce_x(La_{0.76}Y_{0.24})_{1-x}Bi$, mag. phase diagrams 79—56535
$CeO_2:Yb^{3+}$, ENDOR, evidence for covalency 78—80247
$CeO_2:Yb^{3+}$, trigonal centres, point-charge approx. 78—39072
CeP(As), single crystals, low temp. thermal, electrical and mag. props. meas. 78—27051
$CePd_3$-Gd, ultralow interaction temp. and cryst. field effects for Gd impurities 79—61100
$CePt_5$, mag. susceptibility, 4.2 to 295K *(German)* 79—47233
CeS, mag. props., sp. ht. and thermal expansion 78—60292
CeS, resistivity and volumetric meas., phase diagrams, comparison with $CeAl_2$ 80—107789
CeSb, cryst. field splitting of Ce^{3+} and microwave resist. meas. 77—4383
CeSb, crystal field effect in thermal expansion 78—19305
CeSb, ferromag., mag. excitation spectrum, inelastic neutron scatt. obs. 79—78352
CeSb, mag. excitations dispersion 80—25121
CeSb, magnetoelastic effects, anisotropic mag. behaviour 80—25176
$CeSb_XAs_{1-x}$, mag. props. and press. effects 80—71026
CeSe, mag. props., sp. ht. and thermal expansion 78—60292
$CeSn_3(Pb_3)(In_3)$, crystalline elec. field parameters, exchange and Coulomb contrib. 77—20278
CeTe, mag. props., sp. ht. and thermal expansion 78—60292
$Ce_{0.8}Th_{0.2}$, inelastic neutron scatt. meas. 79—47066
$CeTl_3$, mag. susceptibility, magnetisation, neutron diffr., elec. resist., and sp. ht. meas. 80—75733
CeX (X=P, As, Sb, Bi), neutron inelastic scatt. expts. 80—19674
$Ce_{0.08}Y_{0.92}Sb$, dilute f-electron system in cluster regime, crystal field and exchange splittings 80—97062
CeZn, cryst. field and exchange effects, inelastic neutron scatt. study 80—24855
CeZn, mag. struct. and cryst. field effects 78—52223
Cl_2^-, in ion pairs with metals, ESR, in AR matrix, V-centre theory 77—16172
CmO, and CmO_2, electronic struct. and chem. bonding and XPS line shape calcs. 79—33264
Co complex, Co(III) five coordinate, paramagnetic behaviour 79—15276
Co, dipole field anisotropy, at interstitial sites, lattice-deformation effects 79—33584
Co, ferromag., local mag. field at positive muon 77—12295
Co, muon resonance meas. of local mag. dipole field at interstitials 79—95699
Co, single crystal, muon spin rotation expt. results 77—12294
Co^{2+} in crystal, Racah parameter 78—56110
Co^{3+} d^6-complexes and oxides, spin-state transitions, PES study 79—100014
$CoAl_2O_4$, electron density distrib. 78—51481
$Co_3(AsO_4)_2.8H_2O$, optical absorpt. spectra, spin orbit splitting and cryst. field parameters 79—38560
$CoCO_3$, antiferromag., Raman spectra, 2-300K 77—32380
$CoCl_2$, electronic absorpt. spectra and coord. in cryst., soln. and melt 79—38570
$CoCl_2.2H_2O$, phonons and electronic transitions, Raman spectra 79—28761
Co(III) compounds, XPS exam., struct. of 2p lines 78—19631
$CoK_2(SeO_4)_2.6H_2O:Mn^{2+}$, Tutton salt, EPR exam. of cryst. field parameters 78—39394
$Co_{1/3}NbS_2$, intercalate, metallic cond., Hall effect and mag. props. 77—76789
CoO, ab initio SCF and CI calcs. on d-d transitions, CoO_6^{10-} cluster d-electron localisation 77—35897
CoO, valence band struct., cryst. field anal., photoelectron data 79—47007
Co_3O_4, crystal field calcs. for normal spinel struct., teaching approach 77—13554
Cr, μ^+ depolarization and diffusion 77—59500

crystal field interactions continued
Cr^{3+}, electronic states interactions with crystal odd vibrs., R-lines vibr. recurrences 78–84639
Cr^{3+} impurity spectra anal. with Trees' correction 78–68539
CrAs, high press. paramag. antiferromag. transitions, elec. props., band model development *(Russian)* 80–60277
$CrBr_3(Cl_3)$, two-dimensional mag. insulator, cryst. field splitting, spectroscopic g-factors 79–47059
$CrBr_3(Cl_3)$, two-dimensional mag. insulators, cryst. field spectra, mag. circular dichroism 79–47058
CrF_6^{3-}, spectra, cryst. field least squares fitting interpretation 80–44548
CrO_3^{-} radical in K_2CrO_4 and $KCrO_3Cl$, g-factor anisotropy 78–67994
Cr_2O_3, UV absorption spectra from reflectivity meas. 78–2879
Cs halides, elec. field gradient at F_{Z1} electron site 78–22713
CsBr:CrO_4^{2-}, coupling and fine struct., IR electronic and vibr. spectra obs. 80–45118
CsBr:Cu^{+}, off-centre, optical absorpt. meas., cryst. field splittings 79–33740
$CsCdCl_3$ and $CsPbCl_3$, NQR investig. of press. induced phase transition 77–12224
$CsCdCl_3$:Co^{2+}, ground-state g-value, EPR meas. 77–16159
$CsCoBr_3$, ID Ising antiferromagnet, spin dependent Raman scattering from phonons and electronic excitations 80–103948
Cs_2CoCl_4, paramag. mag. exchange rel. to low temp. mag. characts. 77–55669
$CsFeCl_3$, linear chain cryst., quadrupole and mag. reson., rel. to $RbFeCl_3$ 79–38403
$CsFeCl_3$, single cryst. mag. susceptibility meas. 77–20560
$CsFeS_2$, crystal ligand field theory, band assignment, absorpt. spectra study 80–20657
CsH_2PO_4, NMR of ^{133}Cs, elec. field gradient 78–15034
$Cs_4Hf(C_2O_4)_4.nH_2O$, electric field gradient at metal site, γ-ray perturbed ang. correlation meas. 78–52380
CsI:CrO_4^{2-}, coupling and fine struct., IR electronic and vibr. spectra obs. 80–45118
CsI:Tl, crystallophosphor, luminesc. characts., temp. and conc. depend. 80–55175
Cs_2KPrF_6, Raman spectrum and cryst. field *(German)* 79–51940
$Cs_2KTmBr_6(Cl_6)(F_6)$, Cs_2NaTmF_6 and Cs_2RbTmF_6, mag. behaviour 2.9 to 251.3K, cryst. field levels, ang. overlap model *(German)* 80–29520
Cs_2KYbF_6, mag. behaviour, 3.5-251.3K *(German)* 80–50041
$CsMF_3$:Mn^{2+}, (M=Ca,Cd), zero-field splitting of Mn^{2+}, superposition model *(French)* 79–15267
$CsMHoF_6$, (M=Na, K, Rb), mag. behaviour *(German)* 80–65774
$CsMn_{1-x}Co_xF_3$, ferrimag., mag. props. and cryst. struct. 77–77056
$CsMn_{1-x}Ni_xF_3$, ferrimag., mag. props. and cryst. struct. 77–77056
$Cs_2NaCe(III)Cl_6$ high symmetry complex, low temp. Raman spectrum CF splitting, paramag. susceptibility temp. depend. *(German)* 77–12380
$Cs_2NaErCl_6$, mag. susceptibility and IR and Raman spectra meas., crystal field splitting determ. 80–100652
$Cs_2NaEuCl_6$, luminescence Raman spectra, means for localisation of binding energy levels *(German)* 78–88304
$Cs_2NaEuCl_6$, mag. dipole transitions $^5D_3 \rightarrow {}^7F_4$, interpretation 79–42505
Cs_2NaRCl_6 (R=Ce, Nd), tetragonal distortion from cubic symm., magnetisation and NMR meas. 80–34403
Cs_2NaRCl_6 (R=rare earth), low-temp. Raman spectra meas., cryst. field parameters calc. *(German)* 77–36228
Cs_2NaRCl_6, R=Pr^{3+}, Eu^{3+}, Tb^{3+}, Tb^{3+}, crystal field, ligand polarisability contributions 80–39536
$Cs_2NaTbCl_6$, emission spectra, mag. dipole transitions assignments 78–23505
$Cs_2NaTbCl_6$, Tb^{3+} $^5D_4 \rightarrow {}^7F_J$ transitions, mag. and elec. dipole intensities 78–76033
$Cs_2NaTmCl_6$, UV absorpt. spectra, mag. circular dichroism spectra, vibr. obs. 80–29758
Cs_2NaYCl_6:^{249}Cf, mag. susceptibility of Cf^{3+} in octahedral site 77–12089
Cs_2NaYCl_6:Tb^{3+}, emission spectra, mag. dipole transitions assignments 78–23505
$Cs_2NaY_{0.99}Eu_{0.01}Cl_6$, cryst. field parameters of Eu^{3+} ion 77–31983
$Cs_2NaYbBr_6$, mag. behaviour, 3.5-251.3K *(German)* 80–50041
$Cs_2NaYbCl_6$, electronic struct., paramag. susceptibility and electronic Raman spectrum, cryst. field parameters *(German)* 77–63072
Cs_2NaYbF_6, mag. behaviour, 3.5-251.3K *(German)* 80–50041
$CsNiF_3$, demagnetising effects on antiferromag. reson. 80–15803
$CsNiF_3$, single cryst. mag. susceptibility meas. 77–20560
$CsNpF_6$, cryst. field splittings for Np^{5+}, ab initio MO calcs. 77–20520
$CsPr(MoO_4)_2$, energy levels and mag. props. of Pr^{3+} ion *(Russian)* 79–7810
Cs_2RbYbF_6, mag. behaviour, 3.5-251.3K *(German)* 80–50041
$Cs_2ReF_6(-Cs_2GeF_6)$ cryst., $ReF^{-2}{}_6$ ion electronic absorpt. spectra, Raman, visible, IR and UV, liq. H and room temps. 77–77193
$CsTmO_2$, mag. props. of normal-temp. form, 2.9-251.3K *(German)* 79–91205
$CsUF_6$, D_{3d} distortion on octahedral UF_6^- complex 77–47779
$CsUF_6$, D_3d distortion on octahedral UF_6^- complex *(French)* 78–84173
$Cs_2UO_2Cl_4$, electronic struct. of cryst., theory of uranyl ion 79–73476
$CsUO_2(NO_3)_3$, electronic struct. of cryst., theory of uranyl ion 79–73476
$CsYbO_2$, normal-temp. form, mag. props. *(German)* 80–54864
Cs_2ZrCl_6:Np^{4+}, EPR data interpretation for octahedral Γ_8 state in cubic cryst. field 80–2634
Cu complex, strong antisymmetric exchange 78–34976
Cu complex, substituted Cu(II) acetates, exchange interactions, EPR, struct. 79–42829
Cu complexes, with tridentate Schiff bases, exchange interactions, EPR, mag. susceptibility 78–23324
Cu, deformation potentials for isotropic strains 79–42506
Cu, muon diffusion at low temp., effect of nuclear elec. field gradients 77–52005
Cu^{2+} complexes, ground state wave functions, g-factor anisotropy, lattice structs. 77–24536
Cu^{2+}, dopant, ground state wavefunctions and Δg 78–64012
Cu^{2+}, g-anisotropy and ground state wave functions in crysts. *(German)* 78–23065
Cu^{2+} ions, ground state wave functions, cryst. field effect, ESR data anal. 78–23060
Cu-based dilute alloys, nonmagnetic, electric field gradient tensor 77–72843
Cu-Cr, dil. alloy, Knight shift temp. depend., electronic struct. 78–84488

crystal field interactions continued
Cu-Pd, dil, perturbed angular correlation exam. of Pd impurity, ^{111}Cd probe 79–78588
Cu-Te system, cryst. chem., Mossbauer investig. 77–16220
Cu-transition metal, alloys, satellite NMR study, lineshifts and splitting 80–34786
$CuAlS_{2x}Se_{2(1-x)}$, excitonic structure, spin-orbit and cryst. field splittings 78–2872
$CuCl_4^{2-}$ anion, [g] tensor calcs. 77–28343
$CuCl_4^{2-}$, charge distrib. and ligand field splitting calc. 77–62879
$CuFeO_2$, EFG tensor, nucl. quadrupole coupling const., O^{2-} polarisability 77–72844
$CuGaS_2$, tetragonal distortion, crystal field splitting, temp. depend. 79–47060
$CuGaS_{2x}Se_{2(1-x)}$, excitonic structure, spin-orbit and cryst. field splittings 78–2872
$CuGaTe_2$ and $CuInTe_2$, electroreflectance data, direct gap obs., cryst. field splitting and hybridisation degree 78–39557
$Cu(NH_3)_4PtCl_4$, $Cu(NH_3)_4^{2+}$ cation mol. orbital parameters 78–64011
CuO-MgO system, Cu ions valence states, electronic refl. spectra 78–35168
$CuSiO_3.2H_2O$, chrysocolla, electronic absorpt. spectra 78–92087
DBr, orientational phase transitions, effective field approx. calcs. 77–24404
Dy, magnetic anisotropy and ^{161}Dy Mossbauer effect 78–92001
Dy, magnetocrystalline anisotropy, perturbation theory 78–2675
Dy, μSR in ferro- and antiferromag. phases, local fields 78–43763
Dy-Cu amorphous mag. alloy, linear sp. ht. due to single-ion excitation 78–91874
$DyAl_2$, sp. ht. and thermal props., 5 to 300K 77–43342
$Dy_3Al_5O_{12}$:Ca^{2+}, optical absorpt. spectrum, strong crystal field of tetragonal symm. 77–32410
$DyCo_2$, cryst. field parameters from ^{57}Fe Mossbauer spectroscopy results 77–63328
Dy_4Co_3, cryst. field effect on mag. moment direction, neutron diffr. meas. 78–80132
DyD_2, cryst. elec. field transition, neutron energy loss spectra meas. 79–78059
$Dy_3Ga_5O_{12}$, crystal field effect on paramag. props. of Dy^{3+} ion 80–50040
$Dy_2Ge_2O_7$, opt. absorpt. spectra, cryst. field parameters 77–48196
DyH_2, mag. and electronic props., ^{161}Dy Mossbauer spectroscopy 78–80262
$Dy_{1-x}Ho_xNi_2$, cryst. field quenching of Dy^{3+} 4f shell, Mossbauer effect meas. 78–39480
DyIG, magneto-optical absorption, near IR 80–40094
DyIG, mol. field coeffs., magnetisation and mag. susceptibility anal. 78–95406
$DyNi_2$, single cryst. mag. props. 77–24684
$DyNi_5$ crystal, basal plane anisotropy, torque meas. 80–65857
DySb, biquadratic exchange interactions, magnetisation above Neel point 77–69533
$Dy_{1-x}Y_xAl_2$, cryst. field quenching of Dy^{3+} 4f shell, Mossbauer effect meas. 78–39480
Er^{3+}, local symmetry in frozen aq. solns., EPR and local electric field effect 77–16169
$ErAl_2$, crystal field study rel. to $La_{0.9}Er_{0.1}Al_2$ 78–76036
$ErAl_2$, sp. ht. and thermal props., 5 to 300K 77–43342
$Er_cCe_{1-c}Pd_3$, cryst. field spectra, neutron scatt. study 80–50047
$ErCo_2$, cryst. field parameters from ^{57}Fe Mossbauer spectroscopy results 77–63328
$ErCo_2$, mag. excitation spectrum, neutron inelastic scatt. obs. 79–78351
Er_4Co_3, cryst. field effect on mag. moment direction, neutron diffr. meas. 78–80132
$ErCrO_3$, spin-reorientation, optical obs. 77–63201
ErCu, cubic antiferromag., mag. excitations inelastic neutron scatt. meas. 78–72341
$ErFe_2$, crystal field interaction contribution to specific heat 80–39788
$ErFe_2$, excited state spin waves inelastic scatt. meas. 78–76234
$ErFe_2$, Laves phase, cryst. field effects on spin wave dispersion relations 78–84408
$ErFe_3$, 47K magnetic anomaly, point charge crystal field model 77–20517
$ErFe_3$, mag. anomalies at 47 and 131K 77–63134
$Er_6(Fe_{1-x}Mn_x)_{23}$, mag. props. and mol. field coeffs. 78–39319
$ErFeO_3$, far IR spectra 78–88303
$ErFeO_3$, low-temperature spin reorientation 79–65683
ErGa garnet, Er^{3+} ion behaviour in tetragonal field 77–8259
$Er_2Ge_2O_7$, opt. absorpt. spectra, cryst. field parameters 77–48196
ErH_3, cryst. fields and mag. props. 78–68181
ErH_3, Mossbauer spectra of Er^{3+}, gyromagnetic ratios and cryst. field parameters determ. 78–19388
$Er_{1-x}Ho_xRh_4B_4$, mag. and supercond. transitions, cryst. field effects 80–107950
$Er_xLa_{1-x}Be_{13}$, mag. sp. ht. and ESR, cryst. field interactions 80–60290
$ErMo_6Se_8$, crystal field excitations, inelastic neutron scatt. obs. 79–78321
$ErMo_6Se_8$, mag. supercond., neutron scatt. obs. 80–70952
$ErNi_5$, cryst. field parameters in ferromag., paramag. states, susceptibility meas. 77–63139
$ErRh_4B_4$, superconducting and normal state props. 79–73632
ErSb, cryst. field effects on transport props. 78–72133
ErSb, crystal field effect in thermal expansion 78–19305
Er_2Te_3, magnetic susceptibility meas., cryst. field interpretation 80–11156
$Er_{1-x}Tm_xRh_4B_4$, mag. and supercond. transitions, cryst. field effects 80–107950
$(Er_xY_{1-x})Al_2$, cryst. field splitting, inelastic neutron scatt. data 80–44551
Eu complex, $(Et_4N)_3$ $[Eu(NCS)_6]$, Eu^{3+} ion site symm. 78–84656
Eu double metaphosphates with alkali metals or H, luminesc. props. 80–100675
Eu piperidinium salts, emission spectra, ligand field symmetries 79–61413
Eu pyrochlores, $Eu_2Z_2O_7$, (Z=Ti, Ru, Ir, Mo, Sn, Zr, Pb, Pt and Hf), elec. field gradient, Mossbauer expt. 79–8077
Eu^{2+}, ground state fourth-order spin-Hamiltonian parameters 77–69278
Eu^{2+} impurities in cubic crystals, 5d$\rightarrow$4f radiative transition probability calc. 80–71474
$EuCl_3.6H_2O$:Gd^{3+}, EPR spectrum, g-tensor and zero-field splitting 77–55706

crystal field interactions continued

- $Eu_xLa_{1-x}Al_2$, cryst. fields and exchange parameters, ESR meas. 80−71175
- $Eu_2Mg_3(NO_3)_{12}.24H_2O$, Zeeman effect in ahsorpt. spectrum 77−63402
- EuO, cryst. field parameters due to $4f^{N-1}5D$ configs. 80−80230
- Eu_2O_2S, cooperative optical absorption obs. in luminesc. excitation spectra 78−27308
- EuP_5O_{14}, 4f-level press. depend., fluorescence exam. 77−72841
- $Eu_2(SO_4)_3.8H_2O$, mag. props., thermal var., cryst. field reduced matrix elements 77−51875
- $(EuX_6)^{3-}$, (X=Br, Cl), spectral hypersensitive intensity, ligand polarisability contrib. 78−51946
- Fe $(H_2O)_6^{2+}$, in crystals and aqueous soln., asymmetrical quadrupole spectra 80−44974
- Fe complex, $^{57}Fe(2\text{-aminomethylpyridine})_3Cl_2.C_2H_5OH$, temp. depend. spin state, ^{57}Fe Mossbauer emission spectroscopy 80−39980
- Fe complex, Fe (II) pseudo-tetragonal high-spin cpds., paramag. susceptibility amd Mossbauer quadrupole splitting 78−26834
- Fe complex, $Fe_4[Fe(CN)_6]_3$, $Fe_3[Fe(CN)_6]_2$ and oxidised $Fe[Fe(CN)_6]$, electron structs. and refl. spectra 77−55813
- Fe complex, Fe^{2+} chelate of hydrazinecarboxylic acid, Mossbauer effect, cryst. field splitting 79−78591
- Fe complex, $Fe(Br)[S_2CN(C_2H_5)_2]_2$, 3-D Ising ferromag., cryst. susceptibility, 1.5-20K 80−20390
- Fe complex, $Fe(Cl)[S_2Cn(C_2H_5)_2]_2$, 3-D Ising ferromag., cryst. susceptibility, 1.5-20K 80−20390
- Fe complex, Fe(III) tris diseleno chelates, sextet doublet Boltzmann equilib. Mossbauer spectra 78−60366
- Fe complex, Fe(II) and Fe(III) cyanides-3d transition metal, mag. suscept., reflectivity spectra, cryst. field 79−56808
- Fe complex, $Fe(5\text{-methylpyrazole})_4X_2$, X=Cl, Br, I, mag. susceptibility, mag. saturation; Mossbauer and ligand field spectra, single model interpretation 78−23064
- Fe complex, $Fe(pyrazole)_4X_2$, X=Cl, Br, I, mag. susceptibility, mag. saturation; Mossbauer and ligand field spectra, single model interpretation 78−23064
- Fe complex, iodobis(morpholyldithiocarbamate), allotropes, intermol. exchange interactions 77−8455
- Fe complex, tetraphenylporphynate iron III bromide, mag. props., zero-field splitting 80−34584
- Fe complexes, electronic and mag. struct., semiempiricial MO cluster calcs. 78−62733
- Fe complexes, rhombic, g-values and zero-field splitting 79−78061
- Fe, $muon^+$, 40 MeV, traversing magnetised plates, dynamic mag. fields 79−38422
- Fe, single crystal, muon spin rotation expt. results 77−12294
- Fe, spin 3/2, in strong crystal field, axial and rhombic symmetry, EPR parameters 79−28591
- Fe^{2+} d^6-complexes and oxides, spin-state transitions, PES study 79−100014
- Fe^{2+}, nuclear quadrupole interaction, theory, including many-body effects 78−34813
- Fe^{2+}, singlet ground state high-spin, in complexes with rhombic distortions, spectroscopic props. 77−51861
- Fe^{3+}, crystalline spherical pot., effect on Fermi-contact term 80−20140
- Fe^{3+}, cubic spin-Hamiltonian parameters in inorganic compounds, superposition model anal. 80−20367
- Fe^{3+}, zero-field splittings, correl. with axial site distortions, superposition model 80−93168
- Fe-Co, Mossbauer investig. of order-disorder and α-γ transitions 77−48110
- Fe-Ni film, $\alpha \to \gamma$ transition, Mossbauer effect *(Russian)* 77−40154
- Fe-Ni Invar alloys, Mossbauer spectra, heat treatment effect 80−15855
- Fe-O compounds, MO cluster calc. of charge densities and elec. field gradients 77−76783
- Fe-Si (3 wt.%), elec. field gradient by trigonal and tetragonal distortions 77−8474
- Fe^{3+}-doped crystals, mag. susceptibility, cryst. field calc. 78−76035
- $FeBO_3$, Mossbauer coherent scatt. polaris., rel. to cryst. mag. struct. *(Russian)* 79−11368
- Fe_3BO_6, Mossbauer exam. of electric field gradients 77−40163
- $FeBr_2$, optical props. around Neel temp. 79−78658
- $FeCO_3$, siderite, Fe^{2+} Mossbauer spectrum, ligand field theory 77−16212
- $Fe(CO)_2(PF_3)_3$, ^{31}P and ^{19}F NMR, 25 to −100°C axial and equatorial ligand interchange 77−73091
- $Fe(CO_3)(PF_3)_2$, ^{31}P and ^{19}F NMR, 25 to −100°C, axial and equatorial ligand interchange 77−73091
- $FeCl_2$, optical props. around Neel temp. 79−78658
- $FeCl_2$, reorientation of mag. moments under mech. stresses at 0K 80−93153
- $Fe(ClO_4)_2.6H_2O$, single cryst. polarised opt. spectra 77−48188
- $FeCl_2.2D_2O$, magnon-phonon coupling 78−72530
- $FeCl_2.2H_2O$, also deuterated, electronic transitions in Raman spectra 78−80337
- $FeCl_2.2H_2O(2D_2O)$, phonons and electronic transitions, Raman spectra 79−28761
- $FeCl_2.4H_2O$, antiferromag., Mossbauer exam. 77−16221
- $Fe_{1-x}Cr_x$, Mossbauer exam. 77−16222
- FeF_2, antiferromagnet, fourth-order spin Hamiltonian terms for Fe^{2+} 78−10628
- FeF_2, electronic struct., charge density and elec. field gradient, MO cluster calc. 77−51704
- FeF_2, theory of Raman scattering, coupled phonon-magnon excitations 78−72531
- FeF_3, canted antiferromag., spin echo spectra of ^{57}Fe and ^{19}F nuclei 80−2662
- $FeGe_2$, antiferromag., biquadratic exchange 80−2371
- $Fe(H_2O)_6.SiF_6$, pressure-induced orbital ground state inversion, Mossbauer study 80−39979
- Fe(III) Laeme complex, EPR g-value anal. 80−30657
- $Fe_xMg_{1-x}SO_4.7H_2O$, EFG tensor evaluation, ^{57}Fe single crystal Mossbauer meas. 78−88237
- $Fe_{3-x}Mn_xSi$, struct., magnetisation, and spin echo expts., rel. to local environment model 77−20518
- $Fe(NH_4)_2(SO_4)_2.6H_2O$, Fe^{3+} EPR, tetragonal cryst. field 77−51946
- $Fe_{1/3}NbS_2$, intercalate, metallic cond., Hall effect and mag. props. 77−76789
- Fe_3O_4, 3d-photoelectron spectrum, final state effects, compared with Fe_xO 77−69964
- Fe_3O_4, magnetite, Mossbauer spectra of Fe^{2+} 79−91319

crystal field interactions continued

- Fe_3O_4, Mossbauer spectra at 80K, Fe electronic states and hyperfine interactions *(Russian)* 78−43696
- Fe_3O_4, Mossbauer spectra above Verwey transition 78−68415
- Fe_3O_4, polar Kerr effect invisible and near IR spectral regions 80−108187
- Fe_3O_6, O_2 annealed, optical absorpt., spin struct., polaronic absorpt., cryst. field transitions 78−68493
- Fe_xO, wustite, width of d-level final-state struct. obs. in XPS 78−19633
- $FeOHSO_4$, mag. props., Mossbauer spectra meas. 79−19824
- α-$FeOOH.nH_2O$, hydrogoethite, Mossbauer spectra, Neel point, Fe^{3+} config. 77−32310
- FeS, structural chem., influence of itinerant 3d electrons and valence-band holes 79−23563
- $Fe^{3+}(^6S)$ paramagnetisations, spin lattice relaxation Mossbauer study, dynamic spin Hamiltonian formalism 80−97173
- $Fe_{0.996}S$, $Fe_{0.93}S$, determination of quadrupole splitting sign, ground state appl. 78−76363
- α-FeSe, quadrupole splitted Mossbauer spectrum 79−24239
- $FeSiF_6$, phase transform. and relax., EFG and quadrupole spectra 77−51995
- $Fe_{3-x}V_xSi$, struct., magnetisation, and spin echo expts., rel. to local environment model 77−20518
- $Fe_{1-x}Zn_xF_2$, dil. antiferromag., electronic and mag. props., Raman scatt. and optical absorpt. study 80−108207
- $(Fe^{3+})d^5$ config. in C_{4v} and C_{2v} symmetries, appl. to ferrihaemoglobins 78−39071
- GaAs, nucl. spin levels, elec. induced shifts 80−34408
- GaAs:Co, neutral state of Co impurities, optical absorption and mag. susceptibility 78−39578
- $GaAs{:}Co^{2+}$, piezoabsorption meas. tunnel splitting and Jahn Teller effect in $^4T_1(P)$ state 79−15494
- GaAs:Cr, impurity electron states by $X\alpha$ scattered wave cluster method, electron-electron interactions 80−6767
- $GaAs{:}Cr^{2+}$, cluster calcs. of Cr^2 electronic states 79−87064
- GaAs:V, ion implanted, luminesc., level splitting 80−97338
- GaP:Co, optical spectra and Zeeman anal. of Co $3d^7$ state 80−66247
- $GaP{:}Fe^{2+}$, absorpt. and luminesc. spectra 77−16388
- GaP:Mn, ENDOR of cubic $^{55}Mn^{2+}$ 79−69749
- GaP:Ni, optical and EPR study of two-electron-trap state 79−73806
- Gd compounds, ionic, elec. field gradients 79−91004
- Gd, dipole field anisotropy, at interstitial sites, lattice-deformation effects 79−33584
- Gd, in polycrystalline cubic metallic cpds., cryst. field effects 77−77096
- Gd, optical conductivity, direct interband transitions 80−15488
- Gd^{3+}, ground state, fourth-order spin-Hamiltonian parameters 77−69278
- Gd^{3+}, spin correlation effect calc. 78−23058
- Gd-Fe(Co), mag. interactions, exchange fields, mol. field model 77−4498
- Gd^{3+}-doped crystals, mag. susceptibility, cryst. field calc. 78−76035
- $GdCl_3$, crystn. field parameter of Gd^{3+} 80−10930
- $GdCl_3.6H_2O$, cryst. field parameters computation using Ewald method lattice sums 79−91003
- $GdCo_{5c}Ni_{5-5c}$, intrinsic coercivity, anisotropy, exchange and cryst. field interactions 80−75806
- $GdCrO_3$, magnetisation, appl. of molecular field theory 79−4637
- $Gd_3Ga_5O_{12}{:}Nd^{3+}$, cryst. field anal. 78−64013
- $Gd_xLa_{1-x}Al_2$, cryst. fields and exchange parameters, ESR meas. 80−71175
- $Gd_2(MoO_4)_3$, cryst. field parameters for Gd^{3+} 77−66142
- $Gd_2(MoO_4)_3{:}Nd^{3+}(Dy^{3+})$, cryst. field parameters 77−66142
- $GdVO_4{:}Eu^{3+}$, ligand field parameters, computed from fluoresc. and absorption data 78−2453
- $(Gd_{0.5}Y_{0.5})Ni$, FeB struct., cryst. field effects on mag. struct. 78−52226
- Ge, local field, microscopic electronic polarisation 80−25283
- $GeFe_2O_4$, single crysts., elec. and mag. props, optical absorpt. spectra 80−54719
- $GeO_2{:}V^{4+}$, crystal field splitting from ESR and optical absorpt. results 79−47063
- Ge_xTe_{1-x}, amorphous, struct., quadrupole splitting of $^3/_2$ spin state of ^{125}Te calc. 77−65950
- H linear chain of atoms, electronic struct. calc. 78−79969
- p-H_2, local strain effects for isolated pairs of o-H_2, calc. 79−65419
- H_2, molecular, interact. with solid matrix. 80−80229
- o-H_2 molecules in solid nonmagnetic host, nucl. spin lattice relax. times calc. 80−20483
- H_2 monolayer, on triangular lattice, orientational phases 78−75934
- p-H_2, solid, cryst. field energy for o-H_2 impurities, NMR studies 80−15331
- H_2, solid, nuclear spin-lattice relaxation, crystal and mag. field effects 79 -42865
- p-H_2, solid cryst. field for ortho-H_2 impurities 77−72839
- p-H_2:o-H_2, solid, cryst. field interactions, impurity effects 79−82562
- HfO_2, chem. induced elec. field gradient, perturbed ang. correl. obs. 78−80257
- $HfO(H_2PO_4)_2.H_2O$, chem. induced elec. field gradient, perturbed ang. correl. obs. 78−80257
- HfP_2O_7, chem. induced elec. field gradient, perturbed ang. correl. obs. 78−80257
- $HfSiO_4{:}U^{4+}(U^{5+})$, opt. spectra 78−88334
- Ho-Ag(Cu)(Mg)(Zn), crystal field parameters from neutron spectra, ordered state mag. props. 77−43546
- $HoAl_2$, Ho moment reorientation, polarized neutron diffr. study 79−42761
- $HoAl_2$, magnetisation and neutron diffr. meas., cryst. field and exchange 77−63163
- $HoCo_2$, cryst. field induced spin rot., Mossbauer meas. 77−16227
- $HoCo_2$, ground state spin excitations, inelastic nneutron scatt. study 80−50077
- $HoCo_2$, mag.excitations, neutron inelastic scatt. meas. 80−60231
- $HoCo_2$, vol. magnetostriction, point charge cryst. field model 77−63254
- Ho_4Co_3, cryst. field effect on mag. moment direction, neutron diffr. meas. 78−80132
- $HoCrO_3$, cryst. field levels and mag. interactions, inelastic neutron scatt. study 77−69277
- $HoFe_2$, crystal field interaction contribution to specific heat 80−39788
- $HoFe_2$, spin wave and cryst. field excitations, neutron scatt. 78−68196
- HoIG, mol. field coeffs., magnetisation and mag. susceptibility anal. 78−95406
- $HoMo_6S_8(Se_8)$, mag. supercond., neutron scatt. obs. 80−70952

crystal field interactions continued
$Ho_{1.2}Mo_6Se_8$, crystal field excitations, inelastic neutron scatt. obs. 79–78321
Ho_2Ni_{17}, ferrimag. struct., neutron diffr. expt., cryst. field calcs. 77–73001
$HoRh_4B_4$, ferromag., mag. struct., neutron diffr. obs. 79–78323
$HoRh_4B_4$, low temperature magnetic properties 80–88728
$Ho_xTb_{1-x}Fe_2$, single crystals, continuous spin orientations, magnetisation easy direction 78–84453
$HoVO_4$, first excited doublet, zero field splitting 77–20870
$Ho_xY_{1-x}F_3$, calc. of $Ho^{3+} \rightarrow Ho^{3+}$ energy transfer rates *(French)* 78–79966
$Ho_xY_{1-x}Sb$, mag. props. 80–34634
HoZn, mag. excitations near spin rot. temp., neutron scatt. study 79–19731
^{181}Ho-^{181}Ta, dil., elec. field gradient at impurity, anomalous temp. depend., host 4f levels, γ-γ correls. 78–95272
In, electric field gradient, magnitude and sign 77–80755
In, electron density at nucleus, press. depend., Hartree SCF calcs. 78–56411
In inorganic and organometallic cpds., photoelectron spectra, valence bands, ligand field broadening 77–63525
In-Ag, dil., TDPAC technique appl. to diffusion model 79–78589
InSe, spin orbit split off valence bands, exciton transitions, Hopfield's quasicubic model, visible absorpt. spectrum 80–50370
IrF_6, in mixed crysts., Jahn-Teller effect, $\Gamma_{8g}(t_{2g})^3$ state, 6800 Å 78–76032
IrO_2, electronic struct., XPES obs., rel. to TiO_2, RuO_2 78–52632
K, elastic constants, cryst. equilib. and electronic contrib. 79–73243
$K_5Bi_{1-x}Nd_x(MoO_4)_4$ solid soln., growth, spectroscopic and laser props. 78–2901
$KBr:Eu^{2+}$, spin Hamiltonian cryst. field consts. calcs. 79–38035
KCN_x-KCl_{1-x}, finite-freq. local field catastrophe with appl. to spectra 79–51491
$K_4CdCl_6:Co^{2+}$, ground-state g-value, EPR meas. 77–16159
$KCdF_3:Gd^{3+}$, EPR, spin Hamiltonian parameters 79–65725
KCl, cluster expansion of density matrix and crystal energy 78–87952
$KCl:Eu^{2+}$, spin Hamiltonian cryst. field consts. calcs. 79–38035
$KCl:Pb^{2+}$(0.005% Pb), A band fine structure, electron-phonon interaction 78–60491
$KCl:V^{2+}$, EPR spectrum temp. depend., crystal field theory 77–16163
$KCl(Br)(I):Eu^{2+}$, single cryst. optical absorpt. spectra 80–45117
$K_3Co(CN)_6$, ^{59}Co quadrupole coupling const., temp. depend. 80–44557
$KCoF_3$, magnon-phonon interaction mechanism 77–20019
K_2CoF_4, pseudo Ising antiferromag., inelastic light scatt. by mag. excitons 80–11377
$KCr_xAl_{1-x}(SO_4)_2.12H_2O$, EPR of single crystals, zero-field splitting of Cr^{3+} 80–66015
$K_2Cr_5F_{17}$, monocrystal, cryst. field and mag. props., EPR and optical absorpt. spectra 79–19773
$K_2CuCl_4.2H_2O$, and isomorphous cpds., mag. interactions of H and D nuclei, NMR obs. 79–87251
KF(Br)(Cl)(I), K^+3p core excitons, refl. spectra study, low temp. 80–29759
$K_3Fe(CN)_6$, electronic struct., electron density, elec. field gradient, mag. susceptibility and g-tensor 79–91006
$K_4Fe(CN)_6.3H_2O$, internal field and ferroelec. ordering 78–76406
K_2FeF_4, two-dimensional antiferromag., cryst. field effects, Mossbauer spectroscopy 80–71254
K_2FeF_5, one dimensional antiferromagnet, Mossbauer effect, mag. and electric field gradient axes 79–78587
$K_3Fe_2F_7$, two-dimensional antiferromag., cryst. field effects, Mossbauer spectroscopy 80–71254
$KFeS_2$, crystal ligand field theory, band assignment, absorpt. spectra study 80–20657
$KH_2PO_4:VO^{2+}$, EPR spectra, Hamiltonian parameters, ferroelec. transition 78–39387
KH_2PO_4;Tl, UV absorption bands obs. 78–27266
$K_4Hf(C_2O_4)_4.nH_2O$, electric field gradient at metal site, γ-ray perturbed ang. correlation meas. 78–52380
$KI:Tl^+$, pre-resonant enhancement of Raman scatt. 80–7354
$KLu_3F_{10}:Eu^{3+}$, crystal field and spin-orbit parameters 78–30892
$K_2MF_4:Mn^{2+}$, (M=Mg,Zn,Mn), zero-field splitting of Mn^{2+}, superposition model *(French)* 79–15267
$KMgF_3:Cr^{3+}$, trigonal centres, EPR lines, pseudo-Stark splitting 78–68367
$KMgF_3:Eu^{2+}$, f-f transition, cryst. field parameters calc. 77–15805
$KMgF_3:Fe^{2+}$, super hyperfine struct., Zeeman splitting and dynamic Jahn-Teller effect 77–85555
$KMgF_3:Ni^{2+}$, absorpt., MCD and emission spectra 79–51953
$KMgF_3:Sm^{2+}$, absorpt. spectra and Zeeman effect, 3000-12000 Å, 4.2-295K 79–24341
$KMgF_3:Yb^{3+}$, cryst. field parameters, optical, EPR spectra, spin-lattice relax. time 77–51950
$K_3Mn(CN)_6$, low-spin mag. studies 79–95582
$KMnF_3$, Mossbauer effect in ^{57}Fe, quadrupole splitting near struct. and mag. transitions 77–20779
$KMn_{0.1}Zn_{0.9}F_3$, exchange interaction determ. by neutron scatt. 79–47274
$K_2NaGaF_6:Cr^{3+}$, magneto-optical study of $^2T_{1g}$, $^4T_{2g}$, ^2E_g-$^4A_{2g}$ transitions 80–71384
$KNbF_6$, NMR, quadrupole effects and struct. distortion 80–15809
$KNiF_3$, electronic struct. and spectrum of NiF_6^{4-} complexes, scattered wave method calc. 77–15807
K_2O-BaO-$SiO_2:Nd^{3+}$ glasses, absorption and fluoresc. spectra, density 80–25417
$K_2PdBr_4.2H_2O$, visible and UV absorpt. spectra, 10-295K 79–38572
K_2PdCl_4, visible and UV absorpt. spectra, 10-295K 79–38572
$K_2Pd(SCN)_4$, visible and UV absorpt. spectra, 10-295K 79–38572
K_2PtBr_4, visible and UV absorpt. spectra, 10-295K 79–38572
K_2PtCl_4, visible and UV absorpt. spectra, 10-295K 79–38572
$K_2Pt(SCN)_4$, visible and UV absorpt. spectra, 10-295K 79–38572
$KY_3F_{10}:Eu^{3+}$, cryst. field parameters and intensity parameters, J-mixing effects 80–59932
$KY_3F_{10}:Eu^{3+}$, crystal field and spin-orbit parameters 78–30892
$KY_3F_{10}:Eu^{3+}$, fluoresc. intensity, 77 to 4K, cryst. field parameters of Eu^{3+} 78–72580
$KY_3F_{10}:Eu^{3+}$, fluoresc. decay, radiative and nonradiative transition probabilities 78–72581
$KZnF_3:Eu^{2+}$ f-f transition, cryst. field parameters calc. 77–15805
$KZnF_3:Gd^{3+}$, EPR, spin Hamiltonian parameters 79–65725

crystal field interactions continued
$KZnF_3:Ni^{2+}$, absorpt., MCD and emission spectra 79–51953
$KZnF_3:Yb^{3+}$, cryst. field parameters, optical, EPR spectra, spin-lattice relax. time 77–51950
(La,Er)Al_2, cryst. field parameters, inelastic neutron scatt. study 79–23937
(La, Nd)Sn_3, cryst. field effects, normal and supercond. props. 79–60973
(La,Nd)Sn_3, reverse Kondo effect in presence of crystalline elec. field splitting 80–103684
La, ground state, two band Hubbard model, for almost mixed valence system 78–84171
La-Pr, superconductive tunnelling, cryst. field effects 78–88085
La_{1-x} Pr_xSn_3, Kondo effect from excited cryst. field levels, elec. resist. 78–14723
LaAg, Tb and Pr substituted, superconductors, cryst. field transitions linewidths 80–24854
$LaAl_2$, cryst. field splitting and spin-spin interaction of Eu^{2+} and Gd^{3+}, ESR meas. 78–68370
$LaAl_2$, doped with Tb, Nd, or Pr, crystal field effects, tunnelling within mK range 80–70907
$LaAl_2$, Tb and Pr substituted, superconductors, cryst. field transitions linewidths 80–24854
$LaAl_2:Gd^{3+}(Eu^{2+})$, cryst. field parameters, relax. rates 78–84482
$LaAl_3$-Ce, dil., linewidth of cryst. field excitations 78–67988
$LaBe_{13}$:Er, ESR, appl. of exchange induced broadening in low lying crystalline field system 80–108062
$LaBe_{13}$:Er(Dy)(Gd), ESR, crystalline field single ion effects 78–84481
$LaBe_{13}$-Er(Dy), dil., ESR, crystalline elec. field splitting, exchange parameters 78–52348
$La_2Be_2O_5:Nd^{3+}(Pr^{3+})$, cryst. growth, spectral and laser properties in $^4F_{3/2} \rightarrow {}^4I_{11/2}$ and $^4F_{3/2} \rightarrow {}^4I_{13/2}$ transitions 80–80853
$LaBr_3:Np^{3+}$, energy level anal., polarised absorpt. and fluoresc. spectra 80–76056
$LaCl_3:Gd^{3+}$, EPR spectra, linear-electric-field effect 79–73808
$LaCl_3:Ho^{3+}$ parametric energy level anal. 78–18991
$LaCl_3:Np^{3+}$, energy level anal., polarised absorpt. and fluoresc. spectra 80–76056
$LaCl_3:Pr_1$ optical absorpt. and Zeeman spectra, zero mag. field splitting 79–91482
$LaCl_3:Pr^{3+}$, crystal field parameters using multiple-scatt.-X_α method 78–95271
$LaCl_3:Pr^{3+}$, satellite lines in optical absorpt. spectra, Zeeman effect 79–65911
$LaCl_3:R^{3+}$, cryst. field parameters, angular overlap model calcs. 78–26830
$LaCl_3:U^{3+}$, cryst., spectrum anal., cryst. field parameters 80–76057
$La_{0.9}Er_{0.1}Al_2$, crystal field study rel. to $ErAl_2$ 78–76036
LaF_3:Ce, cryst. field parameters, optical transitions and g-factor determ. 78–2456
$LaF_3:Ho^{3+}$, site symmetry and selection rules 78–60514
$LaF_3:Pr^{3+}$, ultraslow optical dephasing 80–58648
LaF_3:Pr(Nd)(Sm)(Eu)(Gd)(Dy)(Ho)(Er)(Tm), cryst. field anal. of triply ionised ion spectra 80–2796
$LaF_3:R^{3+}$, R=rare earths, crystal field anal., intensity calcs. 80–100670
$La_2Li_{0.5}Co_{0.5}O_4$ phase, intermediate electronic configuration 80–80226
$La_2Mg_3(NO_3)_{12}.24D_2O:Mn^{2+}$, ESR spectra and non-diagonal cryst. field paremters 77–55705
$La_2Mg_3(NO_3)_{12}.24H_2O:Mn^{2+}$, ESR spectra and non-diagonal cryst. field parameters 77–55705
(LaNd)Sn_3, containing Nd impurities, supercond. and normal state props. 80–49967
$LaNi_5$, crystal field investigation from inelastic slow neutron scatt. expts. 80–39538
$(La_2O_3)_{0.95}(CeO_2)_{0.05}:Mn^{2+}$, X-band EPR study 80–60409
$LaPb_3$, doped with Tb, Nd, or Pr, crystal field effects, tunnelling within mK range 80–70907
$LaPb_3$, Tb and Pr substituted, superconductors, cryst. field transitions linewidths 80–24854
$LaPd_3$, Γ_5 and Γ_2, states at Pr^{3+} site, creation by cryst. field 79–28547
$(La_{1-x-y}Pr_xA_y)Cl_3$ (A=Ce, Gd, Y), satellite lines in optical absorpt. spectra, Zeeman effect 79–65912
$La_{1-x}Pr_3(Sn_3)$, superconducting, cryst. field excitations, inelastic neutron scatt. obs. 80–15653
$La_{1-x}Pr_xSn_3$, singlet ground-state system, mag. susceptibility 78–19215
$La_{1-x}Pr_xSn_3$, supercond., 0.6 meV cryst. field transitions, neutron spectroscopy 78–67991
$La_{1-y}Pr_ySn_3$, neutron spectroscopy of 0.6 meV cryst. field transitions 78–30894
$(La_{1-x}Pr_x)_3Tl$, mag. props., simple phenomenological model 77–16041
$LaPt_5$, cryst. field effects on transport props. 78–72133
LaSb, cryst. field effects on transport props. 78–72133
$LaSn_3$, doped with Tb, Nd, or Pr, crystal field effects, tunnelling within mK range 80–70907
$LaSn_3$, Tb and Pr substituted, superconductors, cryst. field transitions linewidths 80–24854
$La_{1-x}Tb_xAg$, supercond., 0.6 meV cryst. field transitions, neutron spectroscopy 78–67991
$La_{1-y}Tb_yAg$, crystal field effects, normal and superconducting states 78–2621
$La_{1-y}Tb_yAg$, neutron spectroscopy of 0.6 meV cryst. field transitions 78–30894
$La_{1-x}Tb_xAg(Sn_3)(Al_2)$, paramag. anisotropy of Tb^{3+} in cubic cryst. field 80–15687
$La_{1-x}Tb_xAl_2$, supercond., 0.6 meV cryst. field transitions, neutron spectroscopy 78–67991
$La_{1-y}Tb_yAl_2$, neutron spectroscopy of 0.6 meV cryst. field transitions 78–30894
$La_{1-x}Tb_xSn_3$, supercond., 0.6 meV cryst. field transitions, neutron spectroscopy 78–67991
$La_{1-y}Tb_ySn_3$, neutron spectroscopy of 0.6 meV cryst. field transitions 78–30894
LiAl, NMR relax. investig. of ^7Li self-diffusion, electric field gradients of defects 77–12217
$Li_3AsO_4:CrO_4^{3-}$, EPR, 4.2K, cryst. field parameters 79–28586
$LiErF_4$, spectroscopic anal. Er^{3+} polarised absorpt. spectra, cryst. field parameters 79–95756
$LiF:U_3O_8$, X- or γ-irrad., cryst. field model for U^{5+} luminesc. molecular centre 77–48224
$Li_{0.5}Fe_{2.5-x}Cr_xO_4$ press. depend. of anisotropy consts. 80–65865

crystal field interactions continued
$LiHoF_4$, spectroscopic anal., Ho^{3+} polarised absorpt. spectra, cryst. field parameters 79−95756
α-$LiIO_3$:$Cr^{3+}(Fe^{3+})$, zero-field splitting const. calc. 77−51709
α-$LiIO_3$:$Cr^{3+}(Ni^{2+})(Mn^{3+})$, absorption spectra, impurity environments 78−27275
Li_3N, Watson sphere model, Madelung energy calc. 79−99112
$LiNbO_3$, optical damage effects 77−40186
$LiNbO_3$:Co, optical props. 78−64383
Li_3PO_4:CrO_4^{3-}, EPR, 4.2K, cryst. field parameters 79−28586
$LiRF_4$, (R=Tb, Dy, Ho, Er, Yb), paramag. phase props., basal plane anisotropy and cryst. field parameters 77−69486
$LiRF_4$ (R=Tb,Ho,Er), cryst. field parameters, mag. susceptibility meas., 0.3 to 100K 80−60214
$LiSO_4.H_2O$:Cr^{3+}, single cryst., EPR and optical absorpt. spectra 80−39855
$LiTbF_4$, Tb^{3+} absorption spectra, 4000 to 25000 cm^{-1} 78−72550
$LiTmF_4$, ^{169}Tm NMR spectrum, hyperfine field parameters, and cryst. field calcs. 77−12213
$LiTmF_4$, spectroscopic anal., Tm^{3+} absorpt. spectra, cryst. field parameters 79−95757
$LiTmF_4$, Van Vleck paramag., mag. reson. on uniaxial and uniform compression *(Russian)* 79−61243
$LiTmF_4$:rare earth, EPR spectra, elec. field effects, cryst. field interactions 80−71176
Li_3VO_4:CrO_4^{3-}, EPR, 4.2K, cryst. field parameters 79−28586
$LiYF_4$:Er^{3+}, magnetocaloric behaviour, cryst. field theory 77−4520
$LiYF_4$:Pr^{3+}, polarized absorpt. and fluoresc. spectra, 10 to 300K, energy levels and live intensities 79−95836
$LiYF_4$:Pr^{3+}, spectroscopic determ. of ground config. energy levels 80−34969
$LiYF_4$:rare earth, EPR spectra, elec. field effects, cryst. field interactions 80−71176
$LiYF_4$:Tm^{3+}, cryst. field parameters, appls. 77−20277
α-Sn, local field, microscopic electronic polarisation 80−25283
Lu-rare earth, dil., cryst. fields 78−80127
Lu-rare earth, dil. alloy cryst. field determ. 78−10651
Lu-rare field, dil. alloy, cryst. field parameter determ. 78−10650
LuAG:Nd^{3+}, cryst. field anal. 78−64013
$LuAl_2$, sp. ht. and thermal props., 5 to 300K 77−43342
$LuBe_{13}$:Er(Dy)(Gd), ESR, crystalline field single ion effects 78−84481
$LuBe_{13}$-Er, dil., ESR, crystalline elec. field splitting, exchange parameters 78−52348
$LuFe_2$, crystal field interaction contribution to specific heat 80−39788
$Lu_3Ga_5O_{12}$:Nd^{3+}, cryst. field anal. 78−64013
$LuPO_4$:Sc, Gd^{3+}, EPR spectrum, satellite resonances, cryst. field splitting 78−2734
$LuRh_4B_4$, superconducting and normal state props. 79−73632
$LuVO_4$:Eu^{3+}, ligand field parameters, computed from fluoresc. and absorption data 78−2453
Mg, electric field gradient and Knight shift, temp. depend., OPW calcs. 78−56387
Mg-Mn, dil., cryst. field and spin parameters, transmission ESR obs. 77−40130
Mg-Mn, dil., mag. props., EPR meas. 79−73804
Mg-rare earth dilute alloy, mag. susceptibility and magnetisation 80−15689
Mg-Tb(Dy)(Ho)(Tm), dil., macroscopic shape effect due to quadrupole orientation, magnetostriction and thermal expansion meas. 80−60396
$MgCl_2$:Co^{2+}, ground-state g-value, EPR meas. 77−16159
$MgCl_2$:Co^{2+}, Zeeman electronic Raman scatt. spectra 79−42962
$MgCr_2O_4$, magneto-electric splitting of crystal field Γ_2-level of Cr^{3+} ion, neutron spectroscopic obs. 79−19562
$MgCs_2(SeO_4)_2.6H_2O$, EPR, crystal field and hexahydrate distortion 78−91938
$Mg_{1-x}Er_x$, dil., cryst. field interactions, neutron scatt. spectra 80−50048
MgF_2:$Co^{2+}(Mn^{2+})$, Coulomb and exchange interaction consts. optical spectra line assignment, new technique 80−45124
$MgIn_xFe_{2-x}O_4$ and $MgSc_xFe_{2-x}O_4$, Mossbauer spectra, elec. and mag. props. *(Russian)* 77−69737
$MgK_2(SeO_4)_2.6H_2O$:Mn^{2+}, EPR, crystal field and hexahydrate distortion 78−91938
Mg_6MnO_8, EPR in magnesium-manganese spinel *(Russian)* 78−91936
MgO, local field, microscopic electronic polarisation 80−25283
MgO:$Cr^{2+}(V^{2+})$, coupling of T_{1u} and T_{2u} vibr. to $^2E_g \rightarrow {}^4A_{2g}$ transition 77−63453
MgO:Cr^{3+}, axial centres, EPR and fluoresc. meas. 78−2731
MgO:Cr^{3+}, ODMR study, Cr^{3+} ions in tetragonal symm. sites 80−88892
MgO:Cr^{3+}, strain modulated ESR 78−88175
MgO:Cr^{3+} (Mn^{2+}) spin Hamiltonian parameters, lattice expansion and vibr. effects 80−24851
MgO:Er^{3+}, Γ_8 quartets, orbit-lattice interaction, e.p.r. under stress 77−1591
MgO:Er^{3+}, spin-lattice interaction in Γ_8 quartets, models tested for EPR data 78−23336
MgO:Fe^{2+}, phonon-induced transition interf. in EPR and IR spectra, ion-lattice coupling 77−51945
MgO:Mn^{3+}, ground state exam., thermal conductivity meas. 79−42497
MgO:Ni^{2+}, config. interaction and cryst. field theory 77−39811
MgO-Ti^{3+}, orthorhombic distortion, Jahn-Teller effect 77−66140
$Mg(OH)_2$:Fe, crystal field properties, Mossbauer spectra, isomer shift and quadrupole splitting 79−61278
$Mg(OH_2)_6(NO_3)_2$:Mn^{2+}, EPR spectra, crystal field symm. and strength 77−69674
MgS:Ce^{3+} phosphors, emission and excitation spectra *(French)* 80−93380
MgS:Eu^{2+} phosphors, anal. of absorption spectra $4f^{N+1} \rightarrow 4f^N5d$-6s 80−7383
$MgSiF_6$, phase transform. and relax., EFG and quadrupole spectra 77−51995
Mg_2SiO_4:$Fe^{3+}(Mn^{2+})(Cr^{3+})(Mg^{2+})$, elec. field gradients, asymmetry parameters 80−54660
$MgTe_2$:Mn, pyrite phase, strong axial cryst. field of Mn^{2+}, EPR meas. 78−27081
Mg_2TiO_4:Cu(Ni), ESR of Cu^{2+} and Ni^{3+} 80−97131
Mn complex, $[Mn(urea)_6](UO_4)_2$, thermal expansion coeff., crystal field parameters, phosphoresc., absorv., excitation spectra 78−43932
Mn complex, $MnCl_2$.3,5-lutidene hydrochloride complex, photoluminesc. and photoexcitation 78−92106

crystal field interactions continued
Mn complexes, with pyridine, excitation luminesc., ligand field effect 77−48213
Mn^{2+}, crystalline spherical pot., effect on Fermi-contact term 80−20140
Mn^{2+}, cubic spin-Hamiltonian parameters in inorganic compounds, superposition model anal. 80−20367
Mn^{2+}, in polycrysts., EPR spectra calc. using Bir's method 79−1707
Mn^{2+}, zero-field splittings, correl. with axial site distortions, superposition model 80−93168
$MnBr_2$, vibr. struct. in cryst. field electronic transitions 78−59895
$MnCl_2$, vibr. struct. in cryst. field electronic transitions 78−59895
$MnCl_2$-lutidine HCl complex, photoexcitation, photoluminesc. 78−27301
$MnCl_4$, fine struct. of Mn^{2+} lines 79−33780
$MnCl_2.2H_2O$, magnetisation and mag. resonance 79−11349
$MnCl_2.2H_2O$, phonons and electronic transitions, Raman spectra 79−28761
$Mn_{1-x}Cu_xCr_2S_4$, phase relationships and mag. phase diagram 79−78374
MnF_2, zero-field splitting of Mn^{2+}, appl. of complete d-electron calc. 77−15799
MnF_2:Fe^{2+}, temp. depend. of magnon pair-mode energies, Raman scatt. meas. 77−20577
$Mn_{1/3}NbS_2$, intercalate, metallic cond., Hall effect and mag. props. 77−76789
MnO, optical absorpt. spectra fine struct. 77−32393
MnO-Al_2O_3-SiO_2 glass, spin freezing, muon spin depolarisation, superparamag. domain model 78−68272
MnO-B_2O_3, polycryst. cpds., mag. susceptibility and ^{11}B NMR 79−8056
MnO_4^{m-} chromophore, tetrahedral, electronic spectra 77−58032
$MnSiF_6$, phase transform. and relax., EFG and quadrupole spectra 77−51995
$MnSiF_6.6H_2O$, optical absorption spectra, 77-300K, assignments 77−36259
$(Mo_xV_{1-x})_2O_5$, mag. and spectroscopic investigation 80−25206
N_2 complex, $NiC(C_6H_5NO)_6(NO_3)_2$, singlet ground-state systems, field induced mag. long range order 80−60266
α-N_2, solid, $w^1\Delta_u$-$X^1\Sigma_g^+$ intensity and band shape 79−47427
N_2:N, dynamically induced electronic transitions of matrix isolated atom 78−63825
NH_3-^{57}Fe, solid, Mossbauer study of iron bonding to solid ammonia and its photofragments 80−15833
NH_4 compounds, tunnelling frequency of NH_4 ion in crystals, cubic and noncubic 78−38633
NH_4^+, hindered rot. energy levels in trigonal field 77−7678
$(NH_3$-$(CH_2)_2$-$NH_3)Cd_{1-x}Mn_xCl_4$, Mn^{2+} single ions, clusters and layers, ESR study 79−78507
$(NH_4)_2Cd_5Fe_3Al(SO_4)_{12}.18H_2O$, crystal field splitting of Fe^{3+}, EPR expts. 78−10762
NH_4ClO_4:Co^{2+}, optical absorpt. spectra 77−66523
$(NH_4)_2Co(SeO_4)_2.6H_2O$:$Mn^{2+}$, EPR 77−90017
$(NH_4)_4Hf(C_2O_4)_4.nH_2O$, electric field gradient at metal site, γ-ray perturbed ang. correlation meas. 78−52380
$(NH_4)_xTl_{1-x}Al(SO_4)_2.12H_2O$:$Cr^{3+}$, zero field splitting, g-values, EPR spectra obs. 80−50169
$(NH_4)_2Zn(SO_4)_2$:Ni^{2+}, optical absorpt. spectrum, room and liq. air temp. 79−15499
$NaBF_4$, electric field gradient, quadrupole coupling consts. 77−89740
$NaCeS_2$, mag. susceptibility, 3.7 to 297K, extended mol. field model 79−87227
NaCl, local field, microscopic electronic polarisation 80−25283
NaCl:Cu^+, X-irrad. at room temp., ESR of Cu^{2+} centres 78−52343
NaCl:Eu^{2+}, single cryst. optical absorpt. spectra 80−45117
NaCl:Eu^{2+}, spin Hamiltonian cryst. field consts. calcs. 79−38035
NaCl:K_3IrCl_6 electron irrad., ligand field anal., EPR obs. 80−29612
NaCl:Mn^{2+}, CN^-, EPR spectrum rel. to Mn^{2+}-vacancy-CN complex 80−54942
NaCl:V^{2+}, EPR and optical absorpt. spectrum temp. depend., crystal field theory 77−16163
$NaCrS_2(Se_2)$, EFG tensor, S and Se dipolar contribution 77−31984
NaF:K^+, γ-irradiated, H_A(K) centres, EPR obs. 77−69689
α-$NaFeO_2$, EFG tensor, nucl. quadrupole coupling const., polarisability 77−72844
$NaHSO_4$:Mn^{2+}, EPR 79−24215
$Na_4Hf(C_2O_4)_4.nH_2O$, electric field gradient at metal site, γ-ray perturbed ang. correlation meas. 78−52380
$NaInS_2(Se_2)$, EFG tensor, S and Se dipolar contribution 77−31984
$NaMgF_3$:Sm^{2+}, absorpt. spectra and Zeeman effect, 3000-12000 Å, 4.2-295K 79−24341
$NaNO_2$, electric field gradient, quadrupole coupling consts. 77−89740
$NaNO_3$, electric field gradient, quadrupole coupling consts. 77−89740
$NaNO_3$, pure cryst., NO_3^- singlet-triplet absorption, Stark effect obs. 79−8153
$NaNbF_6$, NMR, quadrupole effects and struct. distortion 80−15809
NaO_2, physical mechanisms of phase transitions 80−6381
Na_2O-BaO-SiO_2:Nd^{3+} glasses, absorption and fluoresc. spectra, density 80−25417
$Na_3Pr(C_4H_4O_5)_3.2NaClO_4.6H_2O$, absorpt., circular dichroism, and mag. circular dichroism spectra 80−97243
Na_2S:Gd^{3+} crystal field splitting, parametrisation of temperature dependence 78−91652
$NaXO_2$ (X=In, Cr, Ti, Tl, Al, Sc), electric field gradient tensor, dipolar contribs. 77−51707
Nb, isotope effects for H_2 diffusion, crystal field stabilisation 80−59728
Nb, muon diffusion at low temp., effect of nuclear elec. field gradients 77−52005
$NbSe_2$-Fe, layered supercond. quenching of Kondo anomaly by cryst. anisotropy field 79−60972
Nd, complex, Nd^{3+}-hexakis-antipyrine triiodide single crysts., polarised absorpt. spectra 78−10922
Nd^{3+} auto-extinction, fundamental mechanism and predicative criterion *(French)* 79−59702
Nd^{3+}, local symmetry in frozen aq. solns., EPR and linear electric field effect 77−16169
Nd^{3+}:scheelite-type crysts., magnetic, thermal properties, cryst. field calcs. 78−91875
Nd-Co alloys, NMR of ^{143}Nd and ^{145}Nd 78−19343
$NdAl_2$, elastic constants, 4.2K to 280K, crystal field effects 77−11615
$NdAl_2$, mag. excitation spectrum, neutron inelastic scatt. 78−10673
$NdAl_2$, mag. excitations, cubic cryst. field and isotropic Heisenberg exchange models 77−63154
$NdAl_3$, cryst. field effects, inelastic neutron scatt. meas. 77−51710
Nd_2C_3, cryst. struct., mag. struct. and props., 1.6 to 300K 79−11296

crystal field interactions continued
$NdCo_2$, cryst. field induced spin rot., Mossbauer meas. 77−16227
$Nd_{1-x}La_x$ alloy, thermoelectric power 79−78080
$Nd_{0.25}La_{0.75}Mg$, cryst. field, neutron diffr. meas. 78−34810
$Nd_{0.2}La_{0.8}Zn$, cryst. field, neutron diffr. meas. 78−34810
Nd_2O_3, A-type, optical absorpt. spectrum and paramag. susceptibility 79−56811
Nd_2O_3 and Nd_2O_2S, electrostatic cryst. field parameters including induced dipole contribs. 80−80233
Nd_2O_3, electrostatic cryst. field parameters, quickly converging calc. method 77−39809
$Nd(OH)_3$, heat capacity from 10 to 350K, lattice and Schottky contribs. 80−84300
NdP-UP solid soln., cryst. field parameters 80−10927
NdP_5O_{14}, laser site-selection time-resolved spectroscopy 78−76524
NdSb, mag. excitation spectrum, neutron inelastic scatt. 77−63152
NdSi mag. struct. and mag. moments, neutron diffr. meas. 77−85424
$NdSn_3$, elec. cond., cryst. field effect, spin disorder contrib. 80−65540
$NdSn_3(In_3)(Pb_3)(Pd_3)$, crystalline elec. field parameters, exchange and Coulomb contrib. 77−20278
$Nd_2Ti_2O_7$, Nd_2TiO_5, mag. susceptibility meas. 1.6 to 70K, cryst. field splitting of Nd^{3+} ground state 78−10649
$(NdX_6)^{3-}$, (X=Br, Cl, I), spectral hypersensitive intensity, ligand polarisability contrib. 78−51946
Ni complex, hexa(pyridine-N-oxide)$(ClO_4)_2$, field-induced mag. ordering in S=1 singlet ground-state 78−23288
Ni complex, $Ni(C_5H_5NO)_6(ClO_4)_2$, field induced antiferromag., magnetocaloric effect 80−29551
Ni complex, Ni(5-methylpyrazole)$_4X_2$, (X=Cl, Br, I), mag. props., EPR, ligand field calcs. 77−62880
Ni complexes hexamethylamine nickel halides, Ni^{2+} EPR in high pulsed mag. field, zero field splitting parameters 80−71160
Ni, Si ion projectile bound s electron polaris. rel. to transient mag. fields 79−33023
Ni Tulton salts, cryst. field spectra in visible and near IR regions, solid dilution effect 80−100666
Ni-Cu, ferromag., mag. moment, local environment effects, HF CPA cluster calc. 80−65817
$Ni(BF_4)_2.6H_2O$, EPR, cryst. field symmetry 79−28593
$NiBr_2$, photoconductivity spectrum meas. using rate of charge method, transport props. 78−60160
$NiBr_2$, vibr. struct. in cryst. field electronic transitions 78−59895
$NiCl_2$, vibr. struct. in cryst. field electronic transitions 78−59895
$NiCl_4^{2-}$, charge distrib. and ligand field splitting calc. 77−62879
$Ni(ClO_4)_2.6H_2O$, EPR and IR spectra, 98-298K, phase transition at 224K 78−84477
NiF_6^{4-}, spectra, cryst. field least squares fitting interpretation 80−44548
$NiI_2.6H_2O$, disordered linear chain mag., ESR, mag. susceptibility and NMR meas. 77−20688
$Ni(NO_3)_2.6H_2O$, rhombic cryst. field, spin ordering in mag. field 77−77058
$Ni_{1/3}NbS_2$, intercalate, metallic, cond., Hall effect and mag. props. 77−76789
NiO, ab initio SCF and CI calcs. on d-d transitions, NIO_6^{10-} d-electron delocalisation 77−35896
$Ni(OH_2)_6(NO_3)_2$:Mn^{2+}, EPR spectra, crystal field symm. and strength 77−69674
$NiPtCl_6.6H_2O$, singlet-ground-state magnets, ESR at low temps. 80−97132
$NiSiF_6$, dilute, single-spin cross-relax. calcs. 80−97129
$NiSiF_6.6H_2O$, and hexadeuterate, optical absorption spectrum, 300 and 80K 79−73966
$NiSiF_6.6H_2O$, single cryst., EPR, 77-300K, Debye temp. 77−85551
$NiSnCl_6,6H_2O$, singlet-ground-state magnets, ESR at low temps. 80−97132
NpO, and NpO_2, electronic struct. and chem. bonding and XPS line shape calcs. 79−33264
NpO_2, mag. transition at 25K, Kramers doublet as cryst. field ground state 80−59936
$POCl_3$-$SnCl_4(ZrCl_4)(TiCl_4)$, splitting of Sm^{3+} near IR absorpt. bands 80−2750
^{231}Pa Mossbauer resonance, elec. field gradient 80−15927
Pb glazes, Cu^{2+} doped, alkaline substitution, crystal field modifications, EPR study 79−95634
Pb, inorganic and organometallic cpds., photoelectron spectra, valence bands, ligand field broadening 77−63525
Pb, supercond., internal mag. field meas. by μ^+ method *(Russian)* 79−33391
$Pb_{1-x}Ba_xZrO_3$, electric quadrupole interaction meas., by PAC 77−4591
PbF_2:Gd^{3+}, EPR and ENDOR of Gd^{3+} at cubic sites 80−7161
PbF_2:Mn^{2+}, superionic, cryst. field fluctuation dynamics, EPR 78−23328
PbF_2:Tb^{3+}, cubic Tb^{3+} centres, energy level and cryst. field parameters 77−52181
PbF_2:Tb^{3+}, ESR spectrum of ions in cryst. field of cubic symmetry 79−38378
PbFCl:$Gd^{3+}(Eu^{2+})$, crystal field splitting, parametrisation of temperature dependence 78−91652
$PbF_2(Cl_2)(Br_2)$ 78−72082
$PbMo_4$, M=Mo,W, EPR spectrum, temp. depend. of zero field splitting 79−15346
$PbMoO_4$, doped and undoped single crysts., polarisation of luminesc. and assignments 80−76069
$PbMoO_4$:Fe^{3+}, single crystals, structure and kinetics, EPR meas. 79−99760
$PbMoO_4$:Nd^{4+}, optical absorpt. intensities, 300, 550 and 4.2K, expt. and Judd-Ofelt theory 77−20894
$PbMo_6S_8$:Gd^{3+}, powder EPR spectra, cryst. field, supercond. energy gap 80−34769
$Pb_3(PO_4)_2$:Gd^{3+}, EPR near ferroelastic transition point 79−15350
$Pb_3(PO_4)_2$:$Gd^{3+}(Eu^{2+})$, EPR spectra of α- and β-phases 80−11261
$Pb_{1-x}Sn_xTe$:^{119}Sn, symm. breaking of Sn local environment, Mossbauer splitting obs. *(Russian)* 77−40166
$PbWO_4$, doped and undoped single crysts., polarisation of luminesc. and assignments 80−76069
Pd-Co, dil., breakdown of ferromag. order, magnetoresist. obs. 80−71046
$Pd_{1-x}Pr_x$ (x=0.02 and 0.03), dil. alloy, min. resist. around 20K 79−19583
$Pd_{100-x-y}Si_xFe_y$, amorphous, ^{57}Fe Mossbauer spectra, X-ray diffr., ageing behaviour 79−28651

crystal field interactions continued
Pr compounds, Van Vleck paramagnets, mag. props., anisotropy from NMR anal. 80−54862
Pr intermetallic compounds, singlet ground state magnetism, hyperfine enhnaced nuclear cooling *(Japanese)* 79−51744
Pr ion in free state and in crystal, change of spectra 79−33271
Pr, mag. scatt., effect of cryst. field levels 77−62904
Pr, magnetic excitations, exchange, crystal field and magnetoelastic interactions 80−2563
Pr, magnetisation and magnetostriction in pulse fields from 3-78K 79−99747
Pr pnictides and chalcogenides, press. depend. of cryst. field splitting 78−68392
Pr^{3+} aquo ion spectra, MCD of $^3P_0 \leftarrow {}^3H_4$ transition 80−7331
Pr^{3+}, configuration interaction contrib. to correlation cryst. field 78−56111
Pr^{3+} hexa-antipyrene triiodide, single cryst., polarised absorpt. spectra 77−77234
Pr-Nd (5%), impurity modes and mag. ordering 78−84422
$PrAl_2$, cryst. field interpretations of inelastic neutron scatt. meas. and mag. props. 79−56174
$PrAl_2$, cryst. field splitting of Pr^{3+}, inelastic neutron scatt. exam. 77−20275
$PrAl_2$, crystal field splitting, inelastic neutron scatt. study 79−47067
$PrAl_2$, elastic constants, 4.2K to 280K, crystal field effects 77−11615
$PrAl_3$, crystal field splitting of Pr^{3+}, inelastic thermal neutron scattering 78−67996
$PrAl_3$, crystal-field effects, inelastic neutron scatt. meas. 77−8268
Pr_3Al, crystal field splitting, inelastic neutron scatt. study 79−47067
$PrAl_{2-x}Ag_x$, cryst. field and exchange interactions 77−63076
PrAs, crystal field press. depend., negative point charge model representation 79−42502
PrAs(Bi)(P)(Sb):Gd, EPR relax. of impurity in Van Vleck paramag., host ion fluctuation spectra 77−48049
PrB_6, metallic, elec. resist., aspherical Coulomb and exchange scatt. of cond. electrons 77−51725
PrBi, crystal field press. depend., negative point charge model representation 79−42502
$PrCl_3$, one and three dimensional antiferroelec. ordering 77−4607
$PrCo_2$, cryst. field parameters from ^{57}Fe Mossbauer spectroscopy results 77−63328
$PrCu_2$, cryst. field transitions near cooperative Jahn-Teller transition 78−84178
$PrCu_5(Pt_5)$, cryst. field effects on transport props. 78−72133
PrD_2, neutron scatt. and cryst. fields 78−79970
$PrD_{2.5}$, neutron scatt. and cryst. fields 78−79970
PrF_3, crystal field split levels, inelastic neutron scatt. study 79−47065
$PrFeO_3$, crystal field splitting, inelastic neutron scatt. study 79−47067
$PrGaO_3$, crystal field splitting, inelastic neutron scatt. study 79−47067
PrH_2, cryst. field splitting, reciprocal susceptibility, book contrib. 79−82754
$PrH_{2.65}$, sp. ht., 2 to 260K, second-order phase transitions and cryst. field splitting 79−82355
$PrIn_3$, nucl. orientation of ^{144}Pm in singlet ground state, exchange interaction and cryst. field splitting obs. 80−71275
$PrIn_3$:Gd, EPR relax. of impurity in Van Vleck paramag., host ion fluctuation spectra 77−48049
$Pr_{1-c}La_cAl_2$, mag. props. 79−65658
$Pr_xLa_{1-x}Al_3$, cryst. elec. field 80−24856
$Pr_xLa_{80-x}Au_{20}$, amorphous, low temp. excitations, specific heat 80−100337
$Pr_{0.25}La_{0.75}Mg$, cryst. field, neutron diffr. meas. 78−34810
$Pr_{0.25}La_{0.75}Zn$, cryst. field, neutron diffr. meas. 78−34810
$PrMg_3$, cryst. field study, inelastic neutron scatt. and sp. ht. meas. 80−59939
$Pr_2Mg_3(NO_3)_{12}$, sp. ht. and elec. susceptibility 77−85642
$Pr_2Mg_3(NO_3)_{12}.24H_2O$:$Gd^{3+}$, EPR X-band, fine struct., low field lines 79−15351
PrN, compressibility, mag. susceptibility and NMR freq. shift meas. 77−85595
$PrNi_5$, crystal field investigation from inelastic slow neutron scatt. expts. 80−39538
$PrNi_5$, crystal-field effects, comparison of calcs. with expts. 79−87071
$PrNi_5$, nucl. cooling agent, relax. and exchange, EPR and NMR study 80−25237
$PrNi_5$-Gd, dil., single crystal, ESR study 80−75850
Pr_2O_3:Gd^{3+}, EPR, zero-field splitting 79−51850
$Pr(OH)_3$, low temp. heat capacity, thermophys. props. optical spectra, anal. of Schottky contributions, review 80−24611
PrP, nonstoichiometric, with singlet ground state, induced van Vleck ferromag. spin glass 77−66378
PrP, sp. ht., 20-300K, cryst. field effects contrib. 77−16092
PrP(Sb)(Bi), singlet ground state paramag. system, microwave resist. meas. 77−20353
$PrPd_3$, Γ_5 and Γ_2 states at Pr^{3+} site, creation by cryst. field 79−28547
PrSb, compressibility and NMR freq. shift 77−85595
PrSb, crystal field effect in thermal expansion 78−19305
PrSb, crystal field press. depend., negative point charge model representation 79−42502
PrSb, mag. excitations, press. depend., inelastic neutron scatt. meas. 78−10699
PrSb(Bi), Gd ESR, Gd-Pr exchange, conduction electron effects 79−69719
PrSe, crystal field press. depend., negative point charge model representation 79−42502
$Pr_3Se_4(S_4)$, induced ferromagnet, mag. props. under hydrostatic press. 80−60395
PrSi, mag. struct. and mag. moments, neutron diffr. meas. 77−85424
$PrSn_3$, inelastic neutron scatt. spectra, cryst. elec. field effects 78−43336
$PrSn_3(Pb_3)(In_3)(Pd_3)$, crystalline elec. field parameters, exchange and Coulomb contrib. 77−20278
PrTe, crystal field press. depend., negative point charge model representation 79−42502
Pr_3Tl, induced ferromag., mag. props. under hydrostatic press. 78−56315
Pr_3Tl, linewidth of cryst. field excitations 78−67988
Pr_3Tl, microwave resist. meas., rel. to singlet ground state paramag. systems 77−20353
Pr_3Tl, resistivity and sp. ht. near threshold 79−78399
$PrVO_4$, energy levels, opt. and NMR meas. 78−80226
Pt porphin in n-alkane single cryst. ^3E_u-$^1A_{1g}$ transition, Zeeman expts. at 4.2K 80−78645

crystal field interactions continued
Pt-Fe, dil., breakdown of ferromag. order, magnetoresist. obs. 80—71046
$Pt_{0.72}Fe_{0.28}$, isomer shift and effective mag. field at ^{57}Fe, press. depend. 77—16232
Pt(111), Λ-line valence bands, angle-resolved photoemission determ. 80—108323
PuO, and PuO_2, electronic struct. and chem. bonding and XPS line shape calcs. 79—33264
Rb, elastic constants, cryst. equilib. and electronic contrib. 79—73243
$RbCaF_3$:Gd^{3+}, O_h^1-D_{4h}^{18} struct. transition, ESR obs. 80—50178
$RbCdF_3$:Gd^{3+}, O_h^1-D_{4h}^1 struct. transition, ESR obs. 80—50178
RbCl:Mn^{2+}, spin-Hamiltonian parameters anal., superposition model applicability 79—28592
RbCl:V^{2+}, EPR spectrum temp. depend., crystal field theory 77—16163
RbCl(Br):Eu^{2+}, single cryst. optical absorpt. spectra 80—45117
$RbCoF_3$, mag. space group and Raman tensors in antiferromag. phase 79—82760
Rb_2CoF_4, pseudo Ising antiferromag., inelastic light scatt. by mag. excitons 80—11377
$Rb_2Cu(SO_4)_2.6H_2O$, single cryst., fine struct., mag. dipole coupling, EPR obs. 78—68360
$RbFeCl_3$, linear chain cryst., quadrupole and mag. reson., rel. to $CsFeCl_3$ 79—38403
$RbFeCl_3$, singlet ground state 1-D ferromag., far IR Zeeman spectra 77—52098
$RbFeS_2$, crystal ligand field theory, band assignment, absorpt. spectra study 80—20657
$RbH_3(SeO_3)_2$, ^{87}Rb NMR, elec. field grad. temp. depend. 79—78536
$Rb_4Hf(C_2O_4)_4.nH_2O$, electric field gradient at metal site, γ-ray perturbed ang. correlation meas. 78—52380
$RbICl_4$, ^{35}Cl NQR spectra, press. cond. temp. depend 80—20501
$RbMF_3$:Mn^{2+}, (M=Mn,Cd,Ca), zero-field splitting of Mn^{2+}, superposition model *(French)* 79—15267
$ReCl_6^{2-}$ doped in various host lattices, luminesc. spectra and vibr. struct. 79—43024
ReF_6, cryst., Raman and absorpt. spectra, Jahn-Teller effect 78—6675
Ru complexes, $K_{\alpha1}$ lines chem. shift, donor-acceptor capacity of ligands 79—33867
RuO_2, electronic struct., XPES obs., rel. to TiO_2, IrO_2 78—52632
SF_6, IR rot. spectra, orbital level splitting in octahedral symmetry, high J levels 77—69815
SF_6, IR rot. spectra orbital level splitting in octahedral symmetry, high J levels 77—69816
SRF_2:Er^{3+}, laser excitation of single ion and clustered ion sites 77—69879
^6S state ions, overlap and covalency contrib. to zero field splitting, LCAO-MO calc. 80—24850
Sb complexes, dithiocarbamates, lone pair electrons, ^{121}Sb Mossbauer spectroscopy study 80—39984
Sb, electron density at nucleus, press. depend., Hartree SCF calcs. 78—56411
Sb inorganic and organometallic cpds., photoelectron spectra, valence bands, ligand field broadening 77—63525
Sc-rare earth, dil. alloy, cryst. field parameter determ. 78—10650
Sc-rare earth, dil. alloy, cryst. field determ. 78—10651
$ScAl_2$-Er(Dy)(Nd), dil., EPR and mag. susceptibility 80—15797
Si, local field, microscopic electronic polarisation 80—25283
Si two-step impurity diffusion, effect of internal elec. field 77—76624
Si:Fe, ESR, cryst. field under stress, C_{11} and C_{44} meas. 77—12194
SiC, (6H), radiation damaged, luminesc. 80—25462
Sm,$(Co,M)_{17}$, (M=Fe, Mn, Cr), exchange and crystal field parameters, anisotropy meas. 77—69535
Sm intermetallics temp. depend. of Sm^{3+} magnetisation, exchange and cryst. field effects 77—8302
Sm^{3+} in magnetically ordered Sm compounds, crystal-field effects on crossover temp. of magnetisation 79—69656
Sm^{3+} in ordered compounds magnetisation temp. depend., exchange and cryst. field effects 77—51890
$SmAl_2$, exchange and cryst. field effects 80—24857
SmAs, low temp. props. 79—28528
SmBi, low temp. props. 79—28528
$SmCo_5$, exchange and cryst. field effects 80—24857
$SmCo_5$, single crysts., mag. props. study and role of anisotropy effects of cryst. field *(French)* 79—38356
$SmCo_5$, temp. depend. of Sm^{3+} magnetisation, exchange and cryst. field effects 77—8302
$SmCo_5$, temp. depend. of Sm mag. form factor, polarized neutron expts. 79—78329
$SmCo_3B_2$, high coercive forces, ferromag. ordering and saturation moments 77—24711
$SmCo_{3.5}Cu_{1.5}$, single crysts., mag. props. study and role of anisotropy, effects of cryst. field *(French)* 79—38356
$Sm_2(Co_{1-x}M_x)_{17}$, magnetocryst. anisotropy 77—40054
SmH_2, low temp. sp.ht., antiferromag. ordering and cryst. field splitting effects 78—84439
$SmH_{2.84}$, sp. ht., second-order phase and cryst. field splitting effects 79—87279
SmN, magnetic props., neutron diffr. and mag. susceptibility meas. 80—50036
SmO, cryst. field parameters due to $4f^{N-1}5D$ configs. 80—80230
SmP, low temp. props. 79—28528
Sm_2S_3, mixed valence compound, mag. and thermal props. 79—78400
Sm_3S_4, mixed valence compound, mag. and thermal props. 79—78400
SmSb, crystal field effect in thermal expansion 78—19305
SmSb, low temp. props. 79—28528
Sm_3Se_4, mixed valence compound, mag. and thermal props. 79—78400
$SmSn_3$, NMR Knight shift, extension to low temp. 77—20735
$Sm_xY_{3-x}Fe_5O_{12}$, magnetostriction comp. depend., 78 to 300K 77—77082
$Sm_2Zn_3(NO_3)_{12}.24H_2O$:$Gd^{3+}$, EPR X-band, fine struct., low field lines 79—15351
Sn, electric field gradient, magnitude and sign 77—80755
Sn, electron density at nucleus, press. depend., Hartree SCF calcs. 78—56411
Sn inorganic and organometallic cpds., photoelectron spectra, valence bands, ligand field broadening 77—63525
$SnCo_2O_4$ spinel, mag. props. 77—1543
$SnMo_6S_8$:Gd^{3+}, powder EPR spectra, cryst. field, supercond. energy gap 80—34769
$SnO_2(F_4)$, elec. field gradient at Sn^{4+} site, Mossbauer quadrupole splitting and anionic polarisability calc. *(French)* 79—15384
SrCl:Mn^{2+}, shape of potential well, calc. 78—87951

crystal field interactions continued
$SrCl_2$:$Fe^{2+}(Co^{2+})$ electronic absorption spectra in far and middle infrared 78—68537
$SrCl_2$:Gd^{3+}, Na^+, elec. field gradient at nuclei on orthorhombic sites, vs. elec. zero-field splitting 79—87070
$SrCl_2$:Gd^{3+}-m^+ complex, cryst. field parameters 78—10768
$SrCl_2$:$Mn^{2+}(Co^{2+})$, cubic impurity EPR spectra, elec. field effect, mechanism 78—68361
SrF_2:Ce^{3+}, cryst. field energies 80—59941
SrF_2:Gd, cryst. field parameters calc. and model of tetragonal Gd^{3+} centres 79—28328
SrF_2:Gd^{3+}, cryst. field parameters calc. 77—8048
SrF_2:Gd^{3+}, $Na^+(Kr^+)(Rb^+)(Ag^+)$, EPR of orthorhombic Gd^{3+}-univalent metal ion complexes 80—11262
SrF_2:Tb^{3+}, cubic Tb^{3+} centres, energy level and cryst. field parameters 77—52181
SrF_2:$Tm^{2+}(Yb^{3+})$, trigonal centres, point-charge approx. 78—39072
$SrLaCoO_4$, struct. and mag. props., electronic struct. of trivalent Co *(French)* 79—86760
$SrMo_4$, M=Mo,W, EPR spectrum, temp. depend. of zero field splitting 79—15346
SrO:Mn^{2+}, impurity pot. well shape calcs. 78—87950
SrO_2:$Fe^{2+}(Fe^{3+})$, EPR spectra, evidence for off-centre displacement of Fe^{2+} 78—72398
$Sr_5(PO_4)_3Cl$:CrO_4^{3-}, EPR, cryst. field parameters 79—87309
$Sr_5(PO_4)_3Cl$:CrO_4^{3-}, polarised absorpt. spectra, visible and IR, ligand field transitions 79—95812
$SrRFeO_4$, R=La, Pr, Nd, Sm, Eu, Gd, Mossbauer effect, Neel temp. and internal mag. field 77—12284
$SrTiO_3$:Cr^{5+} Jahn-Teller system, EPR, electric field effects 79—28599
TaS_2(1T) pure and doped, electrical, structural and mag. props. 79—78141
Tb complex, in $Cs_2NaTbCl_6$, f-f transitions, mag. dipole intensities, vibronic coupling model 80—25404
Tb, magnetocrystalline anisotropy, perturbation theory 78—2675
Tb^{3+} in YF_3 struct. cryst., optical spectra 78—19563
Tb-Sn, effective field at diamag. Sn impurities, 4.2 to 235K *(Russian)* 77—69549
$TbCo_2$ cryst. field parameters from ^{57}Fe Mossbauer spectroscopy results 77—63328
$TbCo_2$, spontaneous distortion, mag. props. due to cryst. field, exchange field, magnetoelastic energy 79—61096
Tb_4Co_3, cryst. field effect on mag. moment direction, neutron diffr. meas. 78—80132
TbD_2, mag. struct., neutron diffr. study 77—85421
TbD_2, sublattice magnetisation, cryst. elec. field effects 78—39295
$TbFeO_3$, ortho-ferrite, electron spin relax. time temp. depend. 77—90026
$TbFeO_3$ static effective mag. field acting on ^{160}Dy nucleus 77—90074
$Tb_{0.5}Ho_{0.5}$, ferromag. and helical phase, spin wave dispersion relations 79—24149
TbIG, appl. of superposition model to cryst. field 78—68132
TbIG, magnetisation and mag. susceptibility meas. along (111) direction, 4.2-295K 77—80917
TbIG, mol. field coeffs., magnetisation and mag. susceptibility anal. 78—95406
$(Tb_cLa_{1-c})Be_{13}$, mag. struct., cryst. field effects, neutron diffr. study 80—65789
$Tb_{1.2}Mo_6Se_8$, crystal field excitations, inelastic neutron scatt. obs. 79—78321
TbP, magnetic Γ_1-Γ_4 exciton, inelastic neutron scatt. study 80—11159
$TbPO_4$, zircon struct., cryst. field analysis 80—80232
$Tb_pY_{1-p}AsO_4$, crystallographic, mag. phase transition as function of temp. and Tb conc. 78—43334
$Tb_cY_{1-c}Sb$, elec. resist., cryst. field and exchange interaction contribs. 80—39556
TbZn, mag. excitations meas. 80—70979
Te, electron density at nucleus, press. depend., Hartree SCF calcs. 78—56411
Te, trigonal, nucl. elec. field gradient ellipsoid, extended Huckel approx. calc., comparison with Mossbauer spectra 77—55736
$ThBe_{13}$:Er(Dy)(Gd), ESR, crystalline field single ion effects 78—84481
$ThBr_4$:U^{4+}, single cryst., absorpt. and emission spectra 77—90174
ThH_2:Er^{3+}, EPR of Er localised electron mag. states, Kondo effect 80—25202
Th_4H_{15}:Er^{3+}, EPR of Er localised electron mag. states, Kondo effect 80—25202
ThO_2:Np^{4+}, cryst. field splittings, ab initio MO calcs. 77—20520
ThO_2:Yb^{3+}, trigonal centres, point-charge approx. 78—39072
ThOS:Gd^{3+}, EPR study, g-factor and cryst. field parameters 80—25204
$ThSiO_4$:$U^{4+}(U^{5+})$, opt. spectra 78—88334
TiO_2, core levels, cryst.-field splitting, X-ray emission study 80—66328
TiO_2, electronic struct., XPES obs., rel. to RuO_2, IrO_2 78—52632
TiO_2:Ru^{4+}, rutile, EPR and cryst. field const. 80—60415
TlBr-VBr_2 system, cryst. struct., DTA investig. *(German)* 78—72766
$TlCdF_3$:Mn^{2+}, zero-field splitting of Mn^{2+}, superposition model *(French)* 79—15267
TlCl, band structure and optical spectra, local field and exchange effects 80—24798
$(Tm,La)Al_2$ disordered alloys, cryst. field transitions, inelastic neutron scatt. obs. 80—50055
Tm, magnetisation, uniaxial anisotropy, mean field model 78—2660
Tm_4Co_3, cryst. field effect on mag. moment direction, neutron diffr. meas. 78—80132
$TmCu_5$, crystal field level scheme, neutron inelastic scatt. and specific heat meas. 79—51536
$Tm_{1-x}Eu_xSe$, semicond. with valence instabilities, cryst. chem. considerations 80—100213
TmN(P)(As)(Sb), singlet ground state paramag. system, microwave resist. meas. 77—20353
TmSb, cryst. field effects on elasticity, rot. and higher order interactions 77—63251
TmSb, cryst. field effects on transport props. 78—72133
TmSb, crystal field effect in thermal expansion 78—19305
TmSb, Gd ESR, Gd-Pr exchange, conduction electron effects 79—69719
TmSe, first obs. of negative elastic const. 80—103409
TmSe, intermediate valence cpd., susceptibility, single-ion approach 80—70935
TmSe, mixed valence systems, spin dynamics and mag. ordering 78—68162
TmSe, paramag. intermediate valence cpd., single ion approach to susceptibility 79—61042

crystal field interactions continued
Tm_2Se_3, mag. susceptibility meas. 4.2 to 300K cryst. field approx. 77–66246
$TmSe_{1-x}Te_3$, semicond. with valence instabilities, cryst. chem. considerations 80–100213
TmTe, crystal field effect in thermal expansion 78–19305
TmZn, cooperative Jahn-Teller effect 78–67998
TmZn, magnetic-ion-lattice interactions, cryst. elec. field 77–4540
U complex, cyclopentadienyl-U-halides, paramag., U IV ligand interaction, mag. susceptibilities, 1-300K *(German)* 79–15279
U complex, $U(acac)_4$, cryst. fields, mag. susceptibility, chem. shift *(French)* 78–84179
U monopnictides, mag. props. 78–43554
U^{3+}, screening factors *(French)* 78–72119
U^{4+}, cryst. field effects and screening factors *(French)* 78–72119
UAs and UPd_4, localised cryst. field states, neutron inelastic scatt. obs. 78–14697
U_3As_4, ferromag., mag. field induced phase transitions 80–65887
U_3As_4, heat capacity, 5-300K, ferromag. transition obs. 80–88769
U_3As_4, magnetisation in strong fields, 4.2 to 200K anisotropy and exchange forces 80–54886
UAs(Sb), anisotropic mag. ordering and mag. structural transitions 79–78324
$U(BH_4)_4$, in $Hf(BH_4)_4$, excited state assignments and E-symmetry ground state, near IR MCD obs. 80–66153
UBr_3, cryst. field levels, neutron scatt. determ. 80–65509
UCl_4, cryst. field transitions obs. by neutron spectroscopy 77–47780
UCl_5, IR absorpt., ground config. splitting, spin-orbit coupling 77–55778
UCl_5, mag. susceptibility, ESR and g-value, crystal field model anal. 79–91292
UD_3, crystalline elec. field studies using neutron inelastic scatt. at NRCN 80–10931
UF_4, crystalline elec. field studies using neutron inelastic scatt. at NRCN 80–10931
UF_6, matrix isolated, vibronic fine struct. in fluoresc. spectrum 80–83406
$UF_4(Cl_4)(Br_4)(I_4)$, paramag., U IV ligand interaction, mag. susceptibilities, 1-300K *(German)* 79–15279
UGeS(Se)(Te), mag. props., 4.2-300K, cryst. field parameters 78–10667
$U_2N_2As(P)(S)(Se)$, susceptibility, 4.2-1000K, cryst. field and exchange interactions 77–20569
UO_2, crystalline elec. field studies using neutron inelastic scatt. at NRCN 80–10931
UO_2, electronic transitions, crystal field effects and phonons, phase transition 80–97303
UO_2, mag. ordering lattice internal rearrangement transition, theory 80–20402
UO_2, optical props. and electronic struct. 78–68527
UO_2, uranyl cpds., X-ray photoemission spectra obs. of electronic struct. 77–28695
UO_2^{2+}, electronic struct., secondary ligands effects, Dirac-Slater model 77–411
$U(OH)_2SO_4$, antiprismatic crystal field, paramag. susceptibility, 4.2 to 300K 79–1655
$U(OH)_2SO_4$, cooperative Jahn-Teller effect, mag. susceptibility meas. 78–72121
$U_6O_4(OH)_4(SO_4)_6$, antiprismatic crystal field, paramag. susceptibility, 4.2 to 300K 79–1655
UPb_3, crystal field energy levels, magnetisation and susceptibility, neutron spectra obs. 80–50064
UPd_3, anomalous behaviour in low temp. props. 79–28108
UPd_3, crystalline elec. field studies using neutron inelastic scatt. at NRCN 80–10931
UPd_3, crystalline electric field levels of U, neutron scatt. exam. 78–60267
$U(SO)_2.4H_2O$, antiprismatic crystal field, paramag. susceptibility, 4.2 to 300K 79–1655
USb, antiferromag., neutron diffr. exam. of ordered state 77–20557
USb, neutron inelastic scatt. meas., phonon spectra, mag. response, anisotropy 80–50065
U_3Si, crystalline elec. field studies using neutron inelastic scatt. at NRCN 80–10931
$USiO_4$, cryst. field parameters, paramag. susceptibility, 2-500K 77–55658
USn_3, crystalline elec. field studies using neutron inelastic scatt. at NRCN 80–10931
V (d^3) in II-VI semiconductors, absorption and luminesc. spectra 78–15203
V, isotope effects for H_2 diffusion, crystal field stabilisation 80–59728
V^{4+}, cryst. field effect on ESR parameters 77–36116
VO_2, V_2O_3, film, absorption spectra, semicond.-semimetal transition 78–19512
V_2O_5, core levels, cryst.-field splitting, X-ray emission study 80–66328
V_3Si, EFG and band struct. 77–35861
$W(CO)_6$ dissolved in oriented compensated nematic mixture, distortion of cubic mol., linear dichroism obs. 79–95797
α-$W_xV_2O_5$, paramag. defect study by ESR 80–103881
$(Y,Er)Al_2$, cryst. field parameters, inelastic neutron scatt. study 79–23937
Y-Cd, dil., electric field gradient, γ-ray ang. correl. meas. 79–56632
Y-Fe(Co), mag. interactions, exchange fields, mol. field model 77–4498
Y-rare earth, dil., cryst. fields 78–80127
Y-rare earth, dil. alloy, cryst. field parameter determ. 78–10650
Y-rare earth, dil. alloy, cryst. field determ. 78–10651
YAG, Yb^{3+} crystalline field, Schottky specific heat, paramagnetic susceptibility temp. depend. 77–11882
YAG:Ce^{3+}, photoluminescence excitation energy, crystal field and temp. effects 80–11460
YAG:Cr^{3+}, optical absorption, cryst. field pot. expansion 77–36268
YAG:Er^{3+}, crystal field theory, Er^{3+} behaviour in tetragonal field 77–8259
YAG:Eu^{3+}, reson. fluoresc. spectra, showing multiple Eu^{3+} sites 80–2812
YAG:Ho^{3+}, low-lying cryst. field levels 79–91007
YAG:M^{3+}, ESR absorption spectra, line broadening of Fe^{3+}, Cr^{3+}, Gd^{3+} 78–91940
YAG:Nd^{3+}, cryst. field parameters calc., exchange charge model 78–47747
YAG:Nd^{3+}, cryst. field anal. 78–64013
YAG:Nd^{3+}, multiplet splitting, effective ligand point-charge model calcs. 77–76779

crystal field interactions continued
YAG:Nd^{3+} and free Nd^{3+} ion, energy levels, absorption spectra 79–11076
YAl_2-Er, dil., EPR, $Er^{3+}\Gamma_8$ ground state 80–15798
YAl_2-Er(Dy)(Nd), dil., EPR and mag. susceptibility 80–15797
$YAlO_3$:Cr^{3+}, fluorescence R-lines anisotropy, effective Hamiltonian parameters 77–16368
$YAlO_3$:Er^{3+}, free-ion-model cryst.-field calc. 77–43545
$YAlO_3$:Tm^{3+}, cryst. field parameter determ. 77–15800
$Y_3Al_5O_{12}$:Nd^{3+}, single crystal, $^4F_{3/2}$ level splitting and spectra dependence on press. *(Russian)* 77–52183
$Y_2(Co_{1-x}M_x)_{17}$, magnetocryst. anisotropy 77–40054
$Y_{1-x}Er_x$, dil., cryst. field interactions, neutron scatt. spectra 80–50048
$Y_xEr_{1-x}Al_2$, paramag. anisotropy 80–39737
YF_3, crystal field parameters acting on rare earth ions 79–69475
$YFeO_3$, mag. anisotropy in cryst. field approx. 80–60241
YGa garnet, Yb^{3+} crystalline field, Schottky specific heat, paramagnetic susceptibility temp. depend. 77–11882
$Y_3Ga_5O_{12}$:Ho^{3+}, low-lying cryst. field levels 79–91007
$Y_3Ga_5O_{12}$:Nd^{3+}, cryst. field parameters calc., exchange charge model 78–47747
$Y_3Ga_5O_{12}$:Nd^{3+}, cryst. field anal. 78–64013
YH_3:Er, Mossbauer spectra of Er^{3+}, gyromagnetic ratios and cryst. field parameters determ. 78–19388
YIG, superexchange and applied field depend. of Faraday rot. induced by elec. dipole transitions 77–36206
YIG, thermoreflectance spectra 80–20616
YIG:Si(Ge), Fe^{2+} spectroscopic props., nontrigonal cryst. field effects 80–44553
Y_2Ni_{17}, ferromag. struct., neutron diffr. expt., cryst. field calcs. 77–73001
Y_2O_3:Eu^{3+}, absorpt. spectra, fluoresc., electron beam excitation 78–92093
Y_2O_3:Eu^{3+}, cubic, laser-induced polarised fluoresc., Stark levels and cryst. field parameters 79–95838
YPd_3-Gd, ultralow interaction temp. and cryst. field effects for Gd impurities 79–61100
$Y_3Sc_2Al_3O_{12}$:Nd^{3+}, cryst. field parameters calc., exchange charge model 78–47747
$Y_{1-x}Tb_xPd_3$, magnetisation, magnetostriction, and inelastic neutron spectra 80–65998
YVO_4:Eu^{3+}, absorpt. spectra, fluoresc., electron beam excitation 78–92093
YVO_4:Eu^{3+}, laser site-selection spectroscopy investigation 78–68556
YVO_4:Eu^{3+}, ligand field parameters, computed from fluoresc. and absorption data 78–2453
YVO_4:Nd^{3+}, absorption and fluoresc. spectra of laser states 77–38900
YVO_4:Nd^{3+}, zircon struct., cryst. field analysis 80–80232
YVO_4:Tm^{3+}, cryst. field parameters, appls. 77–20277
Yb impurity Kondo system, crystal field effects on thermopower and Kondo effect 77–66163
YbAG, cryst. field parameters calc., exchange charge model 78–47747
$YbFe_2$, cryst. elec. field and exchange interac., ^{170}Yb Mossbauer obs., magnetostriction contrib. 80–108124
YbGaG, mag. props. between 44-600 mK 80–80517
YbO, cryst. field parameters due to $4f^{N-1}5D$ configs. 80–80230
$YbS_{1.387}$, magnetic and thermal props. 80–34586
ζ-Yb_2Se_3, mag. susceptibility and cryst. field parameters 80–65510
Zn, core levels, cryst.-field splitting, X-ray emission study 80–66328
Zn, EFG sign at ^{69m}Zn site 77–59492
Zn, electric field gradient, magnitude and sign 77–80755
Zn, field gradients, temp. depend., electronic and lattice contribs., ab initio study 79–42501
Zn, noncubic crystal, temp. depend. of elec. field gradient 79–99515
Zn, nuclear quadrupole interaction, theory 78–10412
Zn, nuclear quadrupole interaction theory of ground state of ^{67}Zn nucleus 79–73481
Zn-Cr, dil., mag. anisotropy, 0.001 to 2K 78–68157
Zn-Mn(Cr), dil, mag. anisotropy, Hartree-Fock calcs. 80–11162
$Zn(BF_4)_26H_2O$:Ni, phase transition study, EPR of diluted Ni^{2+}, 98-298K 80–75846
$ZnCl_2$, UPS, cryst. field splitting 79–83103
$ZnCr_2O_4$, antiferromag. spinel, absorpt. and luminesc. spectra 80–66225
$ZnCs_2(SO_4)_2.6H_2O$:VO^{2+}, optical absorpt. spectra obs. 80–40146
ZnF_2, 93.3 keV Mossbauer transition in ^{67}Zn, isomer shifts 80–39978
ZnF_2, UPS, cryst. field splitting 79–83103
ZnF_2:Mn^{2+}, zero-field splitting, appl. of complete d-electron calc. 77–15799
$ZnIn_2S_4$:Er^{3+}, cryst. field parameters, thermal and mag. props. calc. 77–20540
$Zn_{0.8}Mn_{0.2}Fe_2O_4$, spin interaction, neutron diffr. and Mossbauer effect meas. 77–4501
ZnO, light sensitivity rel. to local internal fields *(Russian)* 78–49932
ZnO:Co^{2+}, polarised optical absorpt. spectrum, crystal field transitions 77–48206
ZnO:Ni^{2+} tetrahedral ion config. interaction and crystal field spectra intensity 78–43335
ZnO(S)(Se)(Te), 93.3 keV Mossbauer transition in ^{67}Zn, isomer shifts 80–39978
Zn_3P_2 bulk and thin film, UV reflectivity spectra, photovoltaic effects, optical consts. 80–25472
ZnS:Co^{2+}, spin-lattice relax., phonon heating effect *(Russian)* 78–19317
ZnS:Cr^{2+}, Cr^{2+} $^5T_2$ and ^5E states, Jahn-Teller effect calcs. 80–39539
ZnS:Cr^{2+}, excitation spectrum of IR emission 77–12421
ZnS:Cr^{2+}, Jahn-Teller interaction energy calc. 78–2455
ZnS:Fe^{2+}, relax. meas. from Mossbauer absorber and source expts. 80–39956
$ZnSO_4.7H_2O$:VO^{2+}, single cryst., struct., EPR 78–15014
ZnS(Se)(Te):Ag^{2+}(Cu^{2+}), absence of EPR spectra due to strong spin-lattice coupling of Kramers doublets 77–85181
ZnS(Se)(Te):Cr^{2+}, absorpt. and luminesc. of Cr^{2+}(d^4), cryst. field theory interpretation 79–83000
ZnSe:Co, effect of in-band position of states on photoelec. props. 78–23132
ZnSe:Cr^{2+}, Cr^{2+} $^5T_2$ and ^5E states, Jahn-Teller effect calcs. 80–39539
ZnSe:Cr^{2+}, excitation spectrum of IR emission 77–12421
$ZnSiF_6.6H_2O$, spin-phonon interaction between Ni^{2+} ions, phonon bottleneck effects, splitting parameters *(Russian)* 80–15796
$ZnSiF_6.6H_2O$:Ni^{2+}, cryst. field, uniaxial compression method *(Russian)* 78–35027

crystal field interactions continued
  $ZnSiF_6.6H_2O:V^{2+}$, paramagnetic impurity ion spin multiplet initial splitting parameter, immediate environments distortion influence on sign 79–65720
  $ZnTe:Cr^{2+}$, Cr^{2+} $^5T_2$ and ^5E states, Jahn-Teller effect calcs. 80–39539
  ZrClH, ^1H NMR shielding anisotropy 80–20466
  $(Zr_{1-x}Er_x)_3Rh$, amorphous, influence of mag. ordering on supercond. props. 80–29511
  $(ZrO_2)_{0.9}(Y_2O_3)_{0.1}$:Cr, Mn, stabilised single crystal, EPR of Mn^{2+} and Cr^{3+} obs. 80–66024
  $ZrSiO_4:U^{4+}(U^{5+})$, opt. spectra 78–88334
crystal field splitting *see crystal field interactions*
crystal field theory *see crystal field interactions*
crystal fields *see crystal field interactions*
crystal filters
  30th Annual Frequency Control Symposium, Atlantic City (1976) 77–37852
  220 MHz acoustic bulk wave resonator and filter realisation 78–59245
  acoustic bulk wave resonators and filters with fundamental mode >100 MHz 77–42671
  AT quartz plate resonators and filters, discrete element model 79–55297
  backward-wave-mode thickness vibration energy trapping by piezoelectric reaction control 79–56728
  band stop suing periodically corrugated piezoelec. cryst., Bleustein-Gulyaev waves behaviour 80–96115
  frequency control 32nd Annual Symposium, Atlantic City (1978) 79–54100
  HF, using $Pb(Zn_{1/3}Nb_{2/3})O_3$-$PbTiO_3$-$PbZrO_3$ and $Pb(Mg_{1/3}Nb_{2/3})O_3$-$PbTiO_3$-$PbZrO_3$ *(Japanese)* 80–60507
  hybrid IC monolithic crystal filter 77–39171
  ion beam etching, for SAW refl. struct. fabrication, role of redeposition 77–56123
  monolithic, overtone analysis 77–39170
  piezoelectric thin film unidirectional SAW transducer and filter 78–46879
  quartz, 40-channel filter spectral analyser, RF spectrometer appl. *(Russian)* 77–22566
  quartz filter resonators with energy trapping, optimum design 78–32663
  quartz temperature-stable shallow bulk acoustic wave devices 79–55293
  rectangular electrode and array dimensioning on AT-cut quartz crystals 77–39169
  SAW in-line chirp filter applications 78–59207
  ST-quartz SAW resonators and coupled resonator filters 77–39174
  two-pole monolithic crystal filters, overtone mode anal. 78–30142
  two-port quartz SAW resonator construction and performance 77–39145
  $LiNbO_3$, monolithic filter operating at 220 MHz 77–42671
  $LiNbO_3$ UHF SAW filters using group-type unidirectional interdigital transducers 78–59252
  $LiTaO_3$ crystals for commercial SAW TV IF filters, fabrication 80–80961
  $LiTaO_3$ monocrystal lapping and precision machining characteristics *(Japanese)* 79–80593
  $LiTaO_3$, monolithic filter operating at 230 MHz 77–42671
  $LiTaO_3$ temperature-stable shallow bulk acoustic wave devices 79–55293
  $Pb(Zr_{0.53},Ti_{0.47})O_3$, piezoelec. ceramic, HF filter appl. *(Korean)* 79–27472
  SbSI single crysts., nonlinear dielec. effects and microelectronic applics. 77–43944
crystal growth
  see also crystal growth from melt; crystal growth from solution; crystal growth from vapour; crystal purification; crystallisation; dendrites; epitaxial growth; nucleation
  actinide metal preparation and refining 78–84705
  alkali halide single crystals, high purity, prod., purification characts. *(Hungarian)* 77–52229
  alkaline earth uranates, struct., phys. and chem. props., preparation methods, review *(Japanese)* 79–14764
  n-alkanes, monoclinic, polygonized spiral growth patterns on {001} faces *(Italian)* 79–23559
  n-alkenes, n even, interaction energy at twin boundary, dihedral reentrant, salient angle effect on growth morphology 78–55876
  anthracene and dianthracene, phase equilib. in photocondensation *(Russian)* 79–7561
  apatite crystal growth in skeletal tissues 80–94181
  assessment by X-ray topography using synchrotron radiation 77–84586
  asymmetrisation in the growth process, sectorial struct. and structural ordering 79–90581
  benzene, rot. motions and cryst. growth, Monte Carlo calcs. 79–46577
  bibliography, cryst. growth of inorganic materials, book pt.A 80–22168
  bibliography, cryst. growth of inorganic materials, book pt.B 80–22169
  binary alloy, normal growth on an atomically rough boundary 79–94934
  binary alloy single crysts., dilute, morphological stability of unidirectional growth, thermodynamic study *(French)* 79–86727
  book, cryst. growth bibliography, pt.A 80–22168
  book, cryst. growth bibliography, pt.B 80–22169
  book, macroscopic equilib. and transport concepts 80–27054
  computer simulation, Monte Carlo calc. 78–26463
  conference, 3rd international summer school on cryst. growth, New Hampshire, USA (July 1977) 80–57008
  conference, Cambridge, MA, USA (July 1977) 78–27388
  conference, International Crystallography Congress, Warsaw, Poland (Aug. 78) 79–23481
  conference, Lancaster, England, Sept. 1979 80–62369
  crystal face, growth behaviour in presence of screw dislocations 80–103276
  crystal growth-disorder models and Ising models 79–46585
  crystal size distribution prediction, modelling size dispersion 78–9971
  crystallite growth on curved metal surface, fragmentation *(Russian)* 78–22676
  cubic crystals, growth-layering effect on optical symmetry 80–88072
  cubic single crystal, orientation determ. method using optical microscope 79–52482
  dendrites, growth models, steady state, exam. 78–72052
  dendrites, growth theory, replacement of maximum velocity principle, by stability criteria 79–11049
  dendrites, growth theory, surface tension effects 79–11051
  dendrites, Ivantsov needle crystal model, with zero capillarity and small Peclet number, stability analysis 79–11050
  dendritic growth rates, evidence for a universal law 79–4496
  device technology, an introduction *(Korean)* 80–49136
crystal growth continued
  diamond, nucleation and growth, 55 kbar and 1450K 79–99087
  diamond, obs. and interpretation of spirals for spiral growth 80–15027
  diamond, synthesis with Ni catalyst, growth mech. *(Japanese)* 77–60122
  diamond, synthetic, history and present status 79–33906
  diamond, with rhombic dodecahedral faces, growth using catalyst metal 77–48339
  diamond internal structure by electrostatic charging technique, growth history revealed 80–10468
  diamond with garnet inclusion, expt. crystallisation conditions study 80–46172
  diffusional crystal growth mechanisms 80–3059
  directory of crystal growth and solid state materials production and research 79–65988
  disorder, solution for two-dimensional model 77–76342
  disorder growth model in 3-dimens., with cubic symmetry 79–73118
  disorder models by symmetry imposition 77–31614
  dynamic computer models 80–103284
  electron microscopy, decoration method, rel. to crystal growth *(German)* 80–103222
  electronic materials 80–66405
  elemental layered material prep. and growth, book contrib. 78–19647
  endotaxy, chemical problems, book 77–12524
  extended growth defect characterisation, review 78–30649
  face effect, with paraboloidal or ellipsoidal isotherm effect 80–107085
  faces, geometric and kinetic features of growth, analytical method for determ. 79–86728
  fast volume diffusion, vacancies 79–99352
  Fe-N system, fine particles growth, prep. by reactive gas evaporation technique, lattice consts. and habit study 79–56919
  film, growth mode and growth kinetics of dislocation free interfaces 77–85103
  film, transition from island to layer growth, a Monte Carlo simulation 77–85104
  garnets, prep. and imperfections, rel. to props. 79–100031
  generalised kinetic equation, growth spiral in chem. pot. gradient 78–87631
  generalized kinetic eqn., 2- and 3-D problems 77–55249
  graphitisation and crystal growth, review 80–89165
  growth disorder, 3D model, rel. between Ising models 79–51025
  ice, Antarctic, cryst. size and climatic record down to last ice age 80–94544
  ice, crystal growth rate in subcooled pure water 77–80431
  ice, monolayer ledges on basal surfaces 77–35809
  ice Ih, dislocations, effect on physical and mechanical props. *(French)* 77–55287
  III-V semiconductors, point defects and deep traps, thermodynamic history, model 80–59908
  imperfect faces, Monte-Carlo growth rates 77–11493
  inorganic hydrate, solidification, heat transfer processes *(Japanese)* 80–6372
  inorganic materials, cryst. growth bibliography, book pt.A 80–22168
  inorganic materials, cryst. growth bibliography, book pt.B 80–22169
  instabilities and pattern formation, review 80–35064
  insulating crystals, growth mechs., practical techniques, review 77–69975
  interfacial roughening transition, renormalisation group theory 79–2734
  ionic crystal and liquid, trace element partitioning 78–47255
  IV-VI compound layered materials, prep. and growth, book contrib. 78–19651
  kinetic coefficient of two-phase transitional region between A+B melt and crystalline bulk phase A 80–96455
  kinetic theory equation, binary system crystallisation 80–88071
  kinetics, microscopic and phenomenological theories, book contrib. 79–69340
  layer-by-layer crystal growth, step motion kinetics 77–4063
  layered materials, book 78–19646
  layered structures, single-crystal growth methods, review 77–59680
  layerwise growing crystals, face profiles calcs. 79–60290
  Lennard-Jones (100) crystal-liquid interface, structure 78–91284
  Lennard-Jones system, cryst. nucleation kinetics 77–62615
  linear macromolecular crystals 78–30561
  localized, morphology analysis 79–99089
  low gravity environment, cryst. growth 78–31306
  low gravity experiment possibilities in electronic materials growth technology 79–47606
  magnetic applications, crystals for, book 79–69967
  magnetic halide, method of growing low-dimensional single crystal *(Japanese)* 80–50539
  material processing facilities and expts. on Spacelab. 78–36431
  materials processing in Spacelab 78–35295
  materials science, current topics, book 79–69966
  materials science and technology, space flight appl., conf., Gaithersburg, USA (April 1977) 79–47881
  materials science in space, crystal growth, prod., and rare earth synthetic mag. materials *(French)* 79–83111
  melt crystallisation in self-excited vibr. regime 80–103275
  membranes appl., cellulose acetate, vector mass transport appl. 79–96360
  metal hydroxide layered materials, prep. and growth, book contrib. 78–19649
  metal whisker, growth axes determ., rapid X-ray technique 77–11830
  model, correspondence to Ising model, disorder points 77–47366
  models, high-field expansion constraints 77–58964
  models, zero field susceptibilities and correlations 78–34454
  Monte Carlo computer simulations, of cryst. surfaces and cryst. growth 79–14710
  Monte Carlo simulation, review, book contrib. 79–80532
  Monte Carlo simulation nucleation, comparison with normal growth theories 77–68932
  Monte Carlo simulation of crystal surface structures, appl. of statistical tests, cryst. growth 77–4060
  nitrides, structs. and cryst. growth 80–29865
  nonstoichiometric compounds preparation probability thermodynamic approach 77–31611
  nucleation kinetics for non-spherical nuclei, and high pressure effects 80–19730
  nucleation models, 2D, computer simulation of cryst. growth 79–73116
  one-dimensional Stefan problem, expansions in time 80–64354
  organic eutectics, surface nucleation parameters 79–19163

crystal growth continued
orientation density function of single crystals from growth selection experiments 79—90589
phase boundaries in first-order phase transitions, dynamics stability 80—107403
phase diagrams and crystal growth 80—66407
phase transition in 3D growth-disorder model 78—26462
polar materials, appl. to SAW and other devices 80—66114
polytypism, some aspects in crystals, rel. to growth 78—83764
preparatory experiments for first Spacelab flight 78—88414
pyramids of different slopes, growth on cryst. face at const. supersaturation, model interpret. 78—2050
quartz, dissolution of grown synthetic quartz inside the autoclaves 78—63911
quartz, high-grade low-temp. impurity band IR absorption spectra 79—56825
quartz, synthetic, growth boundary between −X and Z sectors 78—59775
quartz, synthetic, growth sector boundary between −X and Z sectors 78—59774
quartz, synthetic, growth spirals on prism faces, electron and optical microscope obs. 77—7723
quartz, twinned crystals, after Japan Law, investigation of regrowth 80—54162
rare earth halides, prep. and props., book contrib. 80—54211
rare earth iron garnets, site ordering and magnetostriction 77—90007
rare earth metals, preparation methods and properties, review 79—69969
review, morphology of crystals *(French)* 79—4266
rough interfaces growth rates 79—86730
roughening models, step free energies, and correlation functions in X-Y models 78—67675
roughening transition, self-consistent calc. of statics and dynamics 79—27939
roughening transition dynamics, appl. to crystal growth rate 78—45574
roughening transition in crystal growth theory, rel. to spin glass transition 78—27045
roughening transitions of finite order 80—38975
sealed ampoule of fused SiO_2 for cryst. growth, thermal transmission function 80—84731
secondary nucleation theory, error in surface area estimation 77—89396
semiconductor lasers, recent progress, review 78—17938
semiconductors, appl. of analytical techniques for observation 80—73546
semiconductors, in zero gravity, Polish expts. in space *(Polish)* 79—56920
single crystal growth in two phase region *(Chinese)* 79—74070
single crystals, growth simulation 80—88069
size dependent crystal growth, two parameter kinetic equation 79—65016
size dependent growth systems, effective nucleation rate 80—38972
size-dependence, surface integration kinetics 77—4057
snow, growth by droplet accretion 80—41495
snow, growth mechanism with specific grain boundary 79—23547
solid on solid model rel. to XY model and Coulomb gas 77—84684
solid phase growth expts. *(Hungarian)* 80—7491
solid state growth techniques, review 77—85935
solid state physics, conf. Munster, Germany (March 1979) 80—41941
solid-on-solid model, screw dislocations, rel. to correl. in X-Y model 78—63691
space environment, future research 79—47607
space laboratory, crystal growth, techniques *(Hungarian)* 79—47603
space microgravity environment 79—47605
Spacelab, crystal growth expts. 78—52647
Spacelab, past and future cryst. growth in space 78—80462
Spacelab crystal growth expts. 78—52648
step motion, in the presence of a mobile impurity, computer model 79—14713
step trains, modes of vibr., rhythmical bunching, expt. obs. to show periodicity in step patterns 79—41996
stochastic models, anal. treatment, comparison of two interface dynamics 77—89397
stress, and dislocations, creation during crystal growth *(Russian)* 80—103277
stress in growing crystals, effects of radial and axial temp. gradients *(German)* 78—67672
surface reconstruction as source of growth steps 77—55251
surface self-diffusion consts. from growth or evaporation spiral evolution kinetics, appl. to NaCl and KCl 79—65301
surface steps, thermodynamic props., solid on solid model 77—7683
surface-dynamics of growing crystals 80—44160
symmetric models of crystal growth disorder graphical solns. for correlations 79—1401
temperature field for crystal growing, electrical analogue model *(German)* 78—63688
thermohydrodynamic equations for two-phase polydisperse medium with phase transformations and size distrib. 79—41743
topological modelling of crystal growth 80—59418
transients in cryst. growth rate 80—84118
transition metal dichalcogenides prep. and growth, book contrib. 78—19650
transition metal hydrides and deuterides, $MH_x(D_x)$, M=gp. V metal, single cryst. prep. and characterisation 79—95910
transition metal silicides, growth and characterisation 80—66408
TTF-TCNQ crystals, X-ray topographic study of cryst. perfection 80—96525
two-component crystal growth, analytic theory 79—82168
two-dimensional, simulation using kinetic Ising model 80—54156
zero-gravity crystal growth, Spacelab project, review 77—29619
zincblende type crystal, atom clustering and stacking formations in interfaces 77—19884
Ag-Sn, dil., high perfection single crysts., strain-anneal technique 78—44010
AgBr, activation parameters of mass transfer process by radiochemical meas. *(German)* 80—38974
AgBr emulsion, model system, Ostwald ripening obs. 77—2707
AgBr melts, surface energy and surface tension coeffs., effect on photographic emulsion microcryst. growth rate *(Russian)* 80—47132
AgCl, activation parameters of mass transfer process by radiochemical meas. *(German)* 80—38974
AgCl melts, surface energy and surface tension coeffs., effect on photographic emulsion microcryst. growth rate *(Russian)* 80—47132
$Ag_2H_3IO_6$ crystal, growth, specific heat, antiferroelec. transition 77—69781

crystal growth continued
α-Ag_2S, growth by solid-state phase transition 78—22846
α-Ag_2S, growth of single crysts. in solid/vapour system 77—85907
$Ag_2S(Se)$, ionic-electronic mixed conductor, solid state controlled growth using cryst. rotation 78—31338
α-$Ag_2S(Se)$, single cryst. growth through capillary tube 80—108331
α-Ag_2Se, growth of single crysts. in solid/vapour system 77—85907
β-$(Al,Be)B_{12}$, prep. and struct., book contrib. 78—47277
Al, dislocation density, prep. of high-purity cryst. by strain-anneal method 78—48314
$Al_2Be_4(Si_6O_{18})$, beryl single crysts., growth defects study using X-ray topography *(French)* 79—37710
AlN whiskers, strength rel. to growth conditions using vapour-liquid-solid method 79—11052
$Al_2(SO_4)_3(NH_4)_2SO_4$ or $AlNH_4(SO_4)_2.12H_2O$, size dependent growth systems, effective nucleation rate 80—38972
alkali earth uranates, struct., phys. and chem. props., preparation methods, review *(Japanese)* 79—14764
Au decoration technique, TEM and SEM study of localisation of decorating crystallites *(French)* 80—10470
B and borides, conference, Varna, Bulgaria (Oct. 1978) 80—12842
BN, artificial production of growth twins 78—30641
BN, cubic, water catalysed form. 78—53199
$(Ba_3Nb_6Si_4O_{26})_n.Ba_3Nb_4Ti_4O_{11}$, n=3/2 to 29/2, intergrowth series, electron microscope obs. *(French)* 78—83762
BeB_{12}, prep. and struct., book contrib. 78—47277
Be_4TeO_7, cryst. growth by solid-state reaction and struct. *(German)* 78—18603
CaF_2, fluorite crystals, surface struct., growth mechanism 79—99096
$Ca_2Nb_2O_7$, crystal struct. and phase transitions, rel. to isomorphous crystals *(Japanese)* 80—49208
$Cd_xHg_{1-x}Te$, IR detector appls., prep., elec. props. *(German)* 78—86332
$Cd_{14-x}P_4S_{24-2x}I_{2x}$, icosahedral structs., synthesis and characts. 77—1107
$CdSnO_3$, crystal growth by high press. method, elec. and struct. props. 77—81206
Co-Fe, double hexagonal alloys, crystalline and mag. props. *(Japanese)* 79—73132
$Cr_{12-x}W_xP_7$, solid solns., prep., cryst. struct. *(French)* 78—63723
Cu whisker, H_2 reduction of CuI, growth mechanism 78—30853
$CuIn_{11}S_{17}$, defect spinel, cryst. growth, search for new superionic cond. cpds. 78—31307
$CuInSnS_4$, spinel, cryst. growth, search for new superionic cond. cpds. 78—31307
$Cu_2S(Se)$, ionic-electronic mixed conductor, solid state controlled growth using cryst. rotation 78—31338
Fe, high purity large single crystal sheet prep. method *(French)* 77—77375
α-Fe single crystal whiskers, controlled growth by H reduction of ferrous halides, X-ray and SEM exam. of crystals 78—60554
Fe, solid state recrystn., twinning, growth length *(French)* 77—12523
Fe, whisker growth, added C black effect 78—30852
Fe whisker growth, on wustite, Wagner's mechanism 80—10847
Fe_3C, cementite spherol crystals, morphology and growth 78—18567
FeS, hollow particle growth by sulphuration of Fe 77—68934
$Fe(Sb_{1-x}Te_x)_3$ system cpds., prep., cryst. struct., elec. and mag. characteris. 80—108349
GaAs, structural defects in single crysts., first order distribs. eval. *(German)* 78—6049
GaAs synthesis, Ga+As reaction temp. determ. 77—24978
$Gd_3Ga_5O_{12}$, single cryst. growth for mag. appls., book contrib., review 79—69968
Ge, amorphous Ge contact for electron or hole blocking 77—54400
Ge detector; high-purity, effect of crystal growth direction on energy resolution 79—45541
HfB_2, single crystal growth *(Japanese)* 79—65987
In_2TeO_6, crystal growth by high press. method, elec. and struct. props. 77—81206
$K_2Cu_{1-x}Mn_xF_4$ system, $(0 \leq x \leq 0.2)$, prep., cryst. chem., and ferromag. props., X-ray and neutron diffr. study 79—24162
$K_5La(WO_4)_4$, formation possibility 77—36392
$K_2Mo_9S_{11}$, prep. and struct., Mo_{12} cluster in $Mo_{12}S_{14}$ unit 80—107168
$La_2Ti_2O_7$, crystal struct. and phase transitions, rel. to isomorphous crystals *(Japanese)* 80—49208
$LiNbO_3$, single cryst. growth and phys. props. *(Japanese)* 79—65018
$LiNbO_3$ single crystals grown by automatic diameter control, power striations *(Chinese)* 80—81080
$LiNbO_3$-$Ca(NbO_3)_2$, cryst. growth in baked mixture, Seignettoelec. phase *(Russian)* 79—47395
$LiNdP_4O_{12}$ laser material, optical props. and crystal growth *(Japanese)* 79—27259
$LiTaO_3$, single cryst. growth and phys. props. *(Japanese)* 79—65018
Mg-Al single crystal growth, specimen for tensile testing in corrosive medium *(Russian)* 80—20774
Mn chalcogenides-II-VI compound solid solutions, cryst. growth and physicochem. props. 79—14711
$Mn_{12-x}W_xP_7$, solid solns., prep., cryst. struct. *(French)* 78—63723
$MoSi_3$ crystalline layers, diffusion growth kinetics at 1700°C under influence of direct elec. current 79—52112
Mo_5Si_3, layer electrotransfer of Si 80—92708
$NH_4H_2PO_4$, {100} faces cryst. growth kinetics, low supersaturations range, dislocations 79—56047
$NH_4H_2PO_4$, cryst. growth, pH effect, H_3O^+ inclusions 79—55682
$NaAlSi_2O_6.H_2O$, synthetic analcite, optical and crystallographic props. *(French)* 77—43183
$NaBrO_3$, dislocation struct. inhomogeneity rel. to growth rate 77—47456
NaCl, activation energy for mass transfer, quantum theory calc. *(German)* 79—51031
Nb_3Ge, superconducting, high crit. temp., prep. *(Japanese)* 79—78914
γ-NbN, single crystal growth by annealing, NbN in nitrogen gas pressure 79—8246
Nd, single crystal prep. by solid state electrotransport 78—84709
$NdLaP_5O_{14}$, large crystal growth technique *(Chinese)* 79—24418
NdP_5O_{14}, large crystal growth technique *(Chinese)* 79—24418
$Nd_2Ti_2O_7$, crystal struct. and phase transitions, rel. to isomorphous crystals *(Japanese)* 80—49208
NiO single crystals, growth by material transfer in DC arc, and X-ray anal. 79—52113
Pb ternary oxides, antiferroelec., growth and props. 79—38461
PbI_2, 24-layered hexagonal polytype, growth in U-tube by silica gel method, struct. 77—4722

crystal growth continued
PbI_2-$PbBr_2$ mixed systems, cryst. growth, struct. and optical props. *(German)* 80—96499
$PbMoO_4$, single crystal growth in Na_2SiO_3 gel 77—77351
$PbNb_2O_6$, surface (001), microstruct. obs. by optical, etching, and interferometric techniques 79—11399
Pr, single crystal prep. by solid state electrotransport 78—84709
Sb_2S_3, phase transitions and improper photoconductivity, effect of growth conditions *(German)* 78—39515
$SeMoOCl_7$, prep., cryst. struct., characterisation *(French)* 78—63722
Si crystal growing technology *(Korean)* 80—50538
Si, dislocation free crystal growth 79—100030
Si_3ON_2 needle crystal growth by nitriding Si-SiO_2 system in powder compacts *(Japanese)* 78—68609
Sn polymorphic transformations ($\beta \rightarrow \alpha$), effect of impurities, exam. 80—7557
$Sn_xPb_{1-x}Te$ mixed cryst., cryst. growth and assessment 78—80463
$SrGa_{12}O_{19}$, single crystal growth, lattice const. meas. *(German)* 80—44159
$Sr_2Nb_2O_7$, crystal struct. and phase transitions, rel. to isomorphous crystals *(Japanese)* 80—49208
$Sr_2Ta_2O_7$, crystal struct. and phase transitions, rel. to isomorphous crystals *(Japanese)* 80—49208
β-Ta_2N, growth by annealing Ta in N_2, cryst. struct. 77—35533
β-Ta_2N-εTaN, prep. by exothermic reaction and by zone melting, cryst. struct. 77—35533
TiB_2, single crystal growth *(Japanese)* 79—65987
$Tl_2Mo_9S_{11}$, prep. and struct., Mo_{12} cluster in $Mo_{12}S_{14}$ unit 80—107168
W, monocryst. particles and whiskers, reduction of vap. deposited WO_3 77—52249
$YAl_3(BO_3)_4$-$NdAl_3(BO_3)_4$, substitution of Nd for Y in $YAl_3(BO_3)_4$, exam. 80—11551
YIG, prep. and imperfections, rel. to props. 79—100031
ZnS, (110) cleavage stratigraphic etch patterns, displacements 77—7680
ZnSe, growth centres, crystallographic parameters and etching patterns study *(French)* 79—41998
ZnSe, single crysts., opt. band gap and Mn^{2+} EPR, effects of prep. conditions 77—47730
ZrB_2, single crystal growth *(Japanese)* 79—65987

crystal growth from gel
lead tartrate, single cryst. growth in gel, dendrite form. and self-regulation 77—77352
modified gel technique improved design to grow larger more perfect single crysts. 80—84842
sodium tartrate tetrahydrate, gel-grown single crysts., charact. 77—90261
strontium calcium tartrate mixed crystal, growth in silica gel 77—48325
strontium calcium tartrate tetrahydrate, crystals grown by ion diffusion through silica gels, exam. of preps. 79—52102
strontium calcium tartrate tetrahydrate, gel grown mixed single crystals, defect characterisation 80—2027
transition metal oxalates, growth in silicate gel, X-ray diffr. and i.r. spectrum 77—4724
AgBrI photographic emulsion prep., double-jet nucleation turbidimetry 79—100446
AgCl crystal growth in gelatin soln. 80—64942
AgCl, crystal growth modification in aq. gelatin by incorporation of Br^- and I^- ions 77—5946
AgI, growth, elec. and optical props. 79—77805
AgI large single crysts., gel and soln. growth and props. 80—35071
Ag_2SeO_4 single crystal growth in SiO_2 79—95915
$BaCO_3$, growth in silica gel medium in test tube 77—36379
$BaMoO_4$ crystals, growth in SiO_2 gel under influence of elec. field 80—93469
$BaMoO_4$, growth in silica gel medium in test tube 77—36379
$BaMoO_4$, growth kinetics from silica gel, habit modification, morphology, crystallisation 80—20777
$BaWO_4$, flux- and gel-grown, comparative microtopography 77—31852
$CaC_2O_4.2xH_2O$ ($0<x<5$ zeolite water fraction), weddellite, growth morphology, PBC analysis 80—24388
Cs_2PdCl_4 and $Cs_2PtCl_4.H_2O$, single cryst. growth and gel and soln., morphology 77—77360
$CsSn_2I_5$, surface props., Auger study, elec. cond. meas., photochem. study 80—66339
$KClO_4$, cryst. growth from gelatin gels, exam. of growth and morphology 80—7488
$KClO_4$, single cryst. growth in silica gel 77—63549
$KClO_4$, single crysts., growth by modified gel technique 78—72711
KH_2PO_4, dendritic growth in silica gel 80—35072
KH_2PO_4, ferroelectric, crystal growth in silica gel, effect of pH and gel ageing 78—48301
KH_2PO_4, growth from gel and aqueous soln., oriented inclusions 80—15023
LuOOH, $Lu(OH)_3$, growth from gel on ageing, X-ray diffr. patterns 80—24386
$MnCO_3$ crystals, gel. grown, Ca^{2+}, Ni^{2+} impurity influence, SEM study 80—20778
Na_2O-Al_2O_3-$SiO_2.xH_2O$, fibrous crystal growth in silica gel, X-ray, electron probe and IR spectra obs. 80—25541
$PbCO_3$, cryst. growth, Liesegang ring form., pH effect 80—49140
$PbCO_3$ whiskers, growth kinetics in silica gel 78—75971
$PbHPO_4$, ferroelectric, sp. ht., effects of growth method 79—19853
PbI_2 crystal, gel-grown AgI impurity effects on struct. transformations during growth 77—76339
PbI_2 single crystal growth, modified gel technique improved design 80—84842
$PbMoO_4$, cryst. growth from gel soln., habit modifications 78—2043
$PbMoO_4$, hollock growht origin in gel growth 80—49139
Rb_2PdCl_4 and Rb_2PtCl_4, single cryst. growth from gel and soln., morphology 77—77360
$SrWO_4$, flux- and gel-grown, comparative microtopography 77—31852
TlI, growth in silica hydrogels at 25°C, mechanism 78—35287
ZnS, cubic, expt. conditions 78—68614
γ-$Zr(HPO_4)_2.2H_2O$, form. region and struct. model 79—46615

crystal growth from melt
see also liquid phase epitaxial growth; zone melting
accelerated crucible (and crystal) rotation technique, for cryst. pulling 80—64935
actinide metals and their refractory cpds., synthesis from oxides and single cryst. growth 80—16229
$Al_5(BO_3)O_6$ synthetic, interplanar distances, struct. 79—86775

crystal growth from melt continued
alkali halide crystals, optical components, melt growth conditions 78—50955
alkali halides, growth shape stability, dendrite and prominences appearance *(Hungarian)* 80—7489
alkali-trihalogeno-plumbates, $M[PbX_3]$, cryst. growth struct. and spectra *(German)* 79—90632
alkaline earth fluorides, cryst. growth in reactive atmosphere 80—80962
alkaline earth fluorides, using CF_4 and C_2F_4 as reactive atmos. processing agents 77—8747
n-alkanes purification and single cryst. growth 80—71589
alloy melt, impurity conc. field model, growth by Czochralski method *(Russian)* 80—75191
alloy melt, temperature distribution during cryst. growth by Czochralski method *(Russian)* 80—75192
alloy powder, plasma remelting, spherical monocrystals for X-ray work obtained 78—47205
alloys, type A15 struct. Czochralski growth, supercond. behaviour 79—74080
anorthite, growth rates meas. 77—16489
anthracene, liq. chromatography, sublimation, zone refining, exciton fluoresc., mobility meas., melt grown crystal 79—38736
anthracene, prep. and growth of single cryst. 78—64463
anthracene crystals, growth in melts of cholesteryl-caproate-anthracene system 80—2943
apparatus for growing low-temp. single crysts. 79—4908
aromatic hydrocarbons, growth rate from melt *(Japanese)* 78—23605
atomic kinetics and supercooling influence on crystn. front and growing cryst. radius 79—94937
Automatic crystal puller for the Czochralski technique *(German)* 78—23602
automatic diameter control system 77—1797
azobenzene, foreign particle behaviour 78—47264
benzil cored fibres, void-free cryst. growth, X-ray diffr. and optical microscopy study 80—71586
benzophenone, kinetics, determ. using IR radiometric microscopy 78—34453
binary alloys, directional solidification, theory of dendritic growth 80—70145
binary alloys, initial transient segregation during unidirectional solidification in a furnace with thermal damping 80—70146
binary crystal, computer simulation 78—9979
binary melt-crystal phase transformation kinetics, stat. modelling of cryst. growth mechanism 80—24389
binary systems, crystallisation of solid particles due to concentration fluctuations 80—24391
borides, hexa- and tetra-, prep., struct., elec., mag. props., book contrib. 78—47303
Bridgman-Stockbarger technique, influence of insulation on stability of interface shape and position 80—59412
brittle crystal, residual stress rel. to dislocation density 78—2042
2-bromo-4-nitroaniline, for possible electro-optic appl., cryst. growth in glass capillary 77—44150
bronzes, Na-W, cubic crysts., orientation relation of nucleation and growth 79—55687
bubble domain memory material, Czochralski-type cryst. growth system 79—91581
Burton-Prim-Slichter equation, interpret. of diffusion boundary layer thickness 78—87636
bytownite megacrysts., study of trapped basaltic melts, petrogenetic process study 78—95688
capillary phenomena during solidification 78—30564
capillary shaper, crystn. from melt, stability 78—2037
capillary shaper under conditions of weightlessness 78—2038
capillary shaping, boundary conditions, expt. results for sapphire 77—47364
capillary shaping, boundary conditions, theory 77—47363
capture of foreign particles by cryst. growing from melt containing impurities 78—2051
carbon tetrabromide, cryst. growth from melt, dissolution morphology *(German)* 77—24283
carbon tetrabromide, inherent moisture as purity probe *(German)* 77—85933
$Cd_xHg_{1-x}Te$, vertically grown crysts., effects of growth speed on comp. variations 79—55684
cd CdTe, growth from In solvents, self-compensation 77—28144
chalcogenide cubic compounds, physical properties, application as lens or laser window materials 79—98450
chalcopyrites, for electrolum. device appl., props. and technology, book contrib. 77—73175
Chevrel type compounds, single crystals, growth, stoichiometry, elec. resist. 78—92187
p-chloronitrobenzene-p-bromonitrobenzene system, growth rate depend. of solid soln. supersaturation 77—1804
chondrules, experimental reproduction of textures 80—94763
cold crucible, design and construction 79—66001
composite material, matrix impurity distrib. in melt crystallisation *(Russian)* 80—100277
composition control of crysts. grown in elec. and mag. fields 79—33920
computer built random model for simulation of cryst.-melt interface 77—20165
convection caused by cryst. rotation in crucible, computational results 80—84116
convection control, future fluid flow research, space environment possibilities 79—47622
convection in melts, and cryst. growth under large inertial accelerations 80—66421
core boundary growth rate oscills. calcs. *(German)* 78—30570
corundum, growth of large crystals of high opt. quality 77—34916
corundum, shaped crystal, grown from melt, struct. perfection 78—3021
corundum, Verneuil growth, directional depend. of crystallisation *(German)* 77—35496
corundum large optical crystal production with zero orientation 79—50457
corundum shaped crystal growth, Stepanov method 78—3013
corundum single crystals, stress relax., cracking during growth 78—47263
countercurrent melt crystallisation, ultra-pure substance prep. 80—100779
crystal growth, from liquids at high temps., review 79—15602
crystallisation process, controlled from binary melt *(Polish)* 79—14708

crystal growth from melt continued
crystallising bar, oscillations, EM excitation 80—84845
cylindrical pores growth, numerical calcs. 80—92471
Czochralski and related methods, diameter control, review 78—31328
Czochralski based method for single crystals with high temp. phase transform. 78—23599
Czochralski crystal growth, automatic, weighing method 77—85929
Czochralski crystal growth, automatic, weighing method 77—85930
Czochralski crystal growth, heat, mass and fluid flow, computer simulation 80—104055
Czochralski crystal growth, temp. distrib. 79—60288
Czochralski crystal-pulling process, digital simulation of flow patterns 78—15304
Czochralski growth, effects of crucible and crystal rotation, model 79—99091
Czochralski growth, fluid flow changes, depth depend. 77—69981
Czochralski growth, macroscopic model, theoretical and expt. study 79—74081
Czochralski growth model, transient phenomena 80—84125
Czochralski growth simulation, influence of crystal rotation rate 77—85931
Czochralski growth system, time-depend. cryst.-melt interface shape 77—24280
Czochralski method, automatic crystal diameter control *(Hungarian)* 80—45228
Czochralski method, modified, variations of impurity distrib. 80—88193
Czochralski method, temp. distrib. in growth of semi-transparent crysts., theory 79—65017
Czochralski method, thermal conditions effect in temp. distrib. 78—3019
Czochralski-grown crystals, cracking 78—31323
dendrite, interface kinetics effect on growth rate 79—90927
dendrite growth, steady-state models, validity 78—34732
dendrites, Monte Carlo simulation of growth from melt 80—15427
dendritic crystal, growth, stability effects 78—26802
diamagnetic solids cyrstallised from melt, mag. fluid effect on props. 79—37815
diamond, polycryst., growth at high temp. and press., morphology 77—11495
dibenzyl-tolane, single cryst. growth from melt, influence of supercooling and impurity conc. on growth rate of faces 79—14714
dilute binary alloy monocrystal, thermodynamics of growth, model *(French)* 78—87635
m-dinitrobenzene, electrooptic cryst., growth in monomode optical fibres 80—55288
m-dinitrobenzene, for possible electro-optic appl., cryst. growth in glass capillary 77—44150
m-dinitrobenzene cored fibres, void-free cryst. growth, X-ray diffr. and optical microscopy study 80—71586
diopside, growth rates meas. 77—16489
disjoining pressure repulsion of macroscopic particle ahead of crystn. front. 78—95005
docosane, purification and single cryst. growth 80—71589
dopant distribution in cryst. growing from lightly doped melt 78—2039
durene-p-dibromobenzene system, phase diagram and X-ray diffr. expts. 78—79774
edge-defined film-fed growth of controlled shape crysts. 78—31327
edge-defined film-fed growth process, invention and appl. to sapphire 80—104057
eicosane, purification and single cryst. growth 80—71589
eutectic crystal-melt system, interphase boundary struct., Monte Carlo method study 80—1950
faceted to nonfaceted growth transition 79—95922
faceting transition in melt grown crystals 78—30565
flow method, simple and economical apparatus *(Italian)* 80—80960
fluctuation of growth velocity for growth with rot. seed and solidification interface *(German)* 78—2049
fluor-richterite crystal, habit, growth in oxide-fluoride mixtures, statistical study *(German)* 78—38639
fluoramphibole fibres, synthesis by unidirectional crystn. 80—2941
foreign particle behaviour on growing face 78—47264
foreign particle trapping during solidification, anomalous influence of body force 78—2045
formyl-nitrophenyl hydrazine, for possible electro-optic appl., cryst. growth in glass capillary 77—44150
garnet, Stockbarger-grown, impurity capture and distrib. 77—28713
garnet film, Bi substituted, LPE growth 77—1798
garnet growth, Czochralski bulk flow 80—38979
garnets, chemical site preference of rare earth ions 77—68936
gas evolution and gas bubbles at crystallisation front when growing crystals from melt 78—9980
gemstones, synthetic, cryst. growth, review *(German)* 79—33926
glass forming melts, crystn. kinetics processes 80—64905
glass forming systems, cryst. growth mechanism 78—30555
glass-forming melts, nucleation and cryst. growth 78—2016
graphite, single crystal, from Fe-C melt, morphology 78—42932
growth affinity, a driving force for crystallisation 79—23554
growth limitation by thermal activation barriers 79—69040
growth rate influence, on radius of cryst. 79—94935
halides, physical properties, application as lens or laser window materials 79—98450
heat resistant monocrystal growth apparatus, heat regimes, crystallisation *(Russian)* 80—107071
helical impurity distrib. produced by hydrodynamic instability, vertical solidification 78—30567
high pressure chamber, for cryst. growth, temp. field distrib. determ. 78—82001
high temperature reaction cell for microscopic obs. 78—64457
high-melting metal multicrystal hollow ingot growth 79—69978
high-meniscus ribbon growth, thermal balancing via distributed inert gas streams 78—31329
homogeneous solid solution crystallisation crucible 80—45224
horizontal crystal ribbon growth, meniscus stability 80—103281
horizontal ribbon growth from melt, forced convection heat flow effects 80—107079
horizontal ribbon growth from melt, theoretical anal. 78—75604
ice, dendritic growth in supercooled water, natural convection effect 77—7999
ice, droxtals grown from supercooled water droplets, morphology 79—24426
ice-water interface struct., fluctuations during solidification 78—59935

crystal growth from melt continued
II-VI and IV-VI semiconductors, optimal synthesis conditions for single cryst. growth 80—100776
II-VI compounds, hollow crysts., morphology, review 77—11494
II-VI semiconductors, dependence of mass losses upon press., Bridgman method 80—25547
II-VI semiconductors, high intensity US effects on synthesis and growth 77—819
II-VI semiconductors, optimal synthesis methods for single cryst. growth 80—100764
III-V quaternary alloys, melt and soln. growth of bulk single crysts. 80—35079
III-V semiconductors, methods *(Czech)* 80—89131
III-VI compound layered materials, prep. and growth, book contrib. 78—19661
impurity distrib. ratios, kinetic depend. 78—43044
impurity distribution, kinetic factor effects 78—52656
impurity incorp., effect of crystallisation front oscills. 78—52657
inclusion capture, growth front shape, crit. growth rate 77—31615
inorganic hydrates, applicability to heat storage material of latent heat type *(Japanese)* 78—23606
interface temperature monitoring, thermoelec. method, appl. to Czochralski growth of InSb 78—31331
kinetic equation theory of multi-component crystal growth 80—75194
kinetics, determ. using IR radiometric microscope 78—34453
lamp image type floating-zone furnace for cryst. growth *(Japanese)* 79—74085
leucosapphire, crystal growth by Kyropoulous method, temp. effect on structural and optical quality 80—20784
leucosapphire, large cryst., UV transmittance 77—88876
leucosapphire large crystals, anomalies in block struct. formation 80—9972
liquid encapsulated Czochralski crystal growth, pressurised chambers 78—64459
low-melting point materials, appl. of Czochralski method 78—76599
macroparticle capture by growing cryst., influence of particle thermal cond. 78—79543
magnetic bubble materials, props. and preparation models, review *(Rumanian)* 80—93149
magnetic field effect *(Russian)* 79—37641
magnetic garnet, comp. anal. by AAS 78—92585
magnetic spinel single crystals, by Bridgman technique, book contrib. 79—69977
magnetoelectric composite, gas bubble form. ahead of solidification front 79—29044
Marangoni number, critical, for the onset of oscillatory flow in crystal growth melts 79—23555
materials processing in space 78—35296
materials processing in Spacelab 78—35295
melt flow during Czochralski growth, computational simulation 78—48306
melt surface boundary, mass transfer, influence on crystal habit during growth 79—14712
metal halide layered materials, prep. and growth, book contrib. 78—19648
metal refractory single crystal growth by plasma heating *(Russian)* 78—35292
metallic one component systems, normal cryst. growth fluctuations theory 80—15025
metallic systems, in-situ obs. of solidification interfaces with 1 MeV electron microscope 79—87574
metals, crystal growth, electrochem. Czochralski method, growth rate limitations 78—88433
metals, ingots, controlled crystn. using Bridgman method, modernisation of OKB-8093 unit 79—24425
methane-d$_4$, quantum crystal, growth from melt at low temps. 78—31319
microsegregation in crystals, anal. 80—59410
mirror furnace at Czochralski growth 80—60766
multi-component growth, kinetic equation theory 80—79721
naphthalene, charge separation during cryst. growth, Costa Ribeiro effect 80—7316
naphthalene-adipic acid system, V-ΔT and V-λ relations 80—19734
natural mineral crystal growth characts. 78—32072
m-nitroaniline single crystal fibre waveguide core, melt growth and characts. 77—34965
nondecane, purification and single cryst. growth 80—71589
nucleation on supercooling, inter-nuclear separation distrib. function *(German)* 77—19885
one-dimensional polycrystalline structure, computer simulation *(German)* 77—68935
optical crystal component blank production 79—72725
organic compounds grown by Czochralski technique, assessment of perfection 78—64460
oriented single crystal growth using vacuum intake method *(Russian)* 77—4732
oxide and related single crystals, melt growth, review 78—31322
oxide crystals flow transitions and interface shapes in Czochralski growth 77—24949
oxide single crystals, Czochralski grown, thermoelastic stresses 78—55822
oxides, use of Xe-lamp imaging furnace *(Japanese)* 80—50547
particle trapping in cryst. growing from melt at variable rate 78—67676
partition coefficients, theoretical calc. of isovalent impurities with due regard for excess entropy of mixing in solid soln. and melt 79—65015
periodic regrowth during cryst. growth 78—30566
phthalic anhydride, dendritic growth 78—18936
phthalic anhydride, single crystals growth and perfection 79—78869
phthalic anhydride spherulites, cryst. growth from melt 79—32930
plane front stability in single component system 77—31616
poly(ethylene-oxide), isothermal growth, thickening, melting, bilayer crysts. and chain end effects 80—38939
polyethylene oxide, melt grown single crystal, isothermal growth, thickening and melting 78—51432
polymer, row nucleation, phenomenological model 78—14301
pyridinium cuprous bromide, solid electrolyte 78—64462
rare earth arsenates, RAsO$_4$, flux growth and characterisation by X-ray topography 78—48311
rare earth gallium borates, high temperature crystallisation, composition, struct., props. 80—40253
rare earth garnet substrate crystals, substituted, and LPE films, for magneto-optic appls. 78—31351

crystal growth from melt continued
- rare earth molybdates, cryst. growth, cryst. chem., and phys. props., book contrib. 80—44194
- rare earth orthoaluminates, effects of Co and Ti ions on cryst. growth 77—28711
- rare earth oxides, binary, struct. and props., book contrib. 80—45292
- rare earth perovskites and garnets, prep. and props. book contrib. 80—44193
- rare earth titanates, $R_2Ti_2O_7$, synthesis and phys. props. 79—43128
- rare earth $Zr_{1-x}O_{2-x/2}$ growth from skull melting, directional solidification 78—60567
- rare earth-3d transition metal amorphous alloys, crystallisation behaviour 80—49116
- rare earth-Al_2, cubic Laves phases, prep. and phys. props. *(German)* 78—23075
- rare earth-Sn-X, X=Rh, Ir, Ru, Co, cryst. growth and cryst.-chem. invest, supercond./mag. ternary cpds. 80—100777
- rare erath oxytungstate, growth from soln. in melt 77—1806
- rate determination, graphical method *(German)* 77—36389
- refractories, single crystal growth, techniques 80—108341
- refractories, synthesis and cryst. growth by RF melting 79—70032
- refractories, use of Xe-lamp imaging furnace *(Japanese)* 80—50547
- refractory compounds, high temp. cryst. growth, appl. of Stober technique 77—28709
- repulsion of macroscopic particles by gas layer at crystallisation front 78—18568
- review *(Japanese)* 79—4915
- ribbon growth by EFG method, dynamics and control of meniscus height 80—107081
- ribbon growth using scanned focused CO_2 laser beams 80—66417
- ribbon-form material, rapid quenching from melt *(Japanese)* 78—92210
- rotating container melt growth, crystallisation parameters calcs. 80—103285
- ruby, cryst., optical properties, effect of annealing near melting point 78—90419
- ruby rod, EPR study, comparison of Verneuil and Czochralski grown crystals 78—91945
- sapphire, capillary shaping, expt. results 77—47364
- sapphire, Czochralski crystals, formation of low angle grain boundary macrostruct. 78—47392
- sapphire, edge-defined film-fed growth process 80—104057
- sapphire, growth angle determ. from cryst. lateral face shape and solidified separation drops 80—103282
- sapphire, profiled growth, struct. perfection 78—68621
- sapphire, rel. between growth angle and shape of lateral surface 79—94936
- sapphire, shaped single crystals, porosity, microstruct. 78—2125
- sapphire, Stepanov's growth method, axial temp. distrib. 80—103280
- sapphire flat films for SOS LSI/VLSI technology *(German)* 79—95918
- sapphire growth and slicing developments 77—77371
- sapphire ribbon crystal, interface growth feature rel. to voids 78—34456
- sapphire ribbon crystals, EFG growth and charact., voids, grain boundaries and dislocations 80—103283
- sapphire ribbon crysts., grown by edge-defined film-fed growth technique, X-ray topography study of dislocations 79—4305
- sapphire ribbon EFG prod., substrate for heteroepitaxial Si 80—108342
- sapphire ribbon microvoid distribution control in edge-defined film-fed SOS growth 77—77370
- sapphire rod, crystn. from melt, capillary conditions 78—3020
- secondary nuclei birth and growth rate in single-seeded batch crystalliser 78—83759
- segregation, fluctuating growth rates effect, backmelting 80—59413
- segregation, fluctuating growth rates effect, no backmelting 80—54161
- segregation, reformulation of Burton Prim and Slichter model during cryst. growth from melt 79—4909
- semi-transparent crystals, temp. distrib. in crysts. grown by Czochralski method, theory 79—65017
- semi-transparent crystals, temp. distribution in growth from Czochralski method 79—65998
- semi-transparent single cryst. temp. distrib. during Czochralski pulling, thermal emission 77—66584
- semiconducting crystals, with toxic and/or highly voltaile components, improved system for Bridgman growth 79—47620
- semiconducting solid solution, growth of homogeneous single crystals 77—12518
- semiconductor, crystn. in constant electric field, thermoelectric parameters 77—44146
- semiconductor, Czochralski bulk flow, digital simulation 78—31320
- semiconductor alloy, for appl. in IR detector arrays, comp. control 80—31872
- semiconductor shaping problem, Stepanov method 78—3012
- semiconductor single crystals, melt grown, dislocation creation by thermal stresses 78—83825
- semiconductors, crucible shape effect on crystallisation front 80—16173
- semitransparent shaped components, temp. and thermal stress patterns 78—2035
- semitransparent single crystals, temp. distrib. during Czochralski pulling, thermal field anal. 77—66585
- shape former, pulling method for desired cross-section *(Japanese)* 79—15603
- shape stability theory 77—4058
- shaped crystal growth from melt, meniscus-controlled process 80—107075
- Si:In growth by Czochralski crystal pulling, characterisation for extrinsic IR detectors, focal-plane arrays 80—76168
- single crystal, techniques 80—108341
- single crystal permanent magnet, industrial technology and equipment for manufacturing process 80—35075
- solid solution, single cryst. growth from melt, role of composition fluctuations 79—8239
- solid-liquid interface shape, effect on temp. distrib. in cryst. growth from melt 79—61513
- solidification, stability analysis, interfacial surface entropy effect in heat balance 78—26464
- solute redistribution during crystallisation, interface field effects 80—84119
- spherical particle growing from stirred melt, stability 77—47365
- stability during capillary shaping, general theory of capillary and thermal stability 80—107076
- stability during capillary shaping for arbitrary small perturbations 80—107077
- statistic model 77—15332

crystal growth from melt continued
- steel, with high temp. phase transform. Czochralski based method 78—23599
- step free edge energy, estimation from growth kinetics 79—46586
- Stepanov's method, for controlled profile crysts. 78—31326
- Stepanov's method, of growing profiled optically transparent crysts., temp. fields 79—55688
- Stepanov method, liq. mixing in shaper hole, simulation device 78—3022
- Stepanov method, physical problems in shaped cryst. growth 80—103279
- Stepanov method, rel. between growth angle and shape of lateral surface of growing cryst. 79—94936
- Stepanov method with wetted and unwetted shapers 78—3018
- striated impurity distrib. calc. in melt-grown crystals 80—24488
- succinonitrile, growth kinetics and shapes 77—31617
- succinonitrile, low entropy of fusion plastic crystal, dendritic growth, expt. test of theory 77—35842
- sulphides, use of Xe-lamp imaging furnace *(Japanese)* 80—50547
- temperature field, method of investigation *(Russian)* 79—78866
- ternary semiconductor crystals for nonlinear optical applics., review 78—33782
- thermal conditions effect on stability 77—76343
- thermal stresses and struct. defects 78—2041
- thermic screen translation 79—95921
- thermoelastic and thermoplastic stress form., dislocation density estimation *(German)* 80—15022
- thermoelastic stress distribution in single cryst. pulling by Czochralski technique 78—63681
- thermoelastic stresses in thin rod, asymptotic calc. method 78—2031
- 4-m-toluylene diamine, single crysts., conditions of growth and heat treatment influence in dislocation struct. 79—95020
- transition metal borides, refractory, single cryst. prep. methods and characterisation, book contrib. 78—48296
- transition metal phosphates, MH_2P_2O and $M_2P_4O_{12}$, formed by oxide reactions with phosphoric acid melts 77—12517
- travelling solvent method, heat flow, diffusion and convection 77—39549
- trimethylacetic acid, large ultra-pure single crysts., grown by modified Bridgman technique 77—55883
- trivalent metal phosphates, condensed, synthesis in polyphosphoric acid melts, physicochem. equil. considerations 80—97419
- two component systems, multilayer solid-on-solid interface model 80—28935
- vapour-liquid-solid growth mechanism *(Russian)* 80—107074
- Verneuil technique, powder feeder for crysts. of large diameter 79—33925
- vertical directional crystallisation device, heat transfer, analytical investig. *(Russian)* 78—52654
- wide ribbon growth by multiple inert gas jet thermal profile control 78—64458
- zone melting crystn. parameters optimisation using temp. distrib. calcs. *(German)* 79—43140
- Ag and dil. alloys, Bridgman growth, distrib. of growth directions 79—33924
- Ag chalcogenides, single-phase, preparation 78—35293
- Ag, dendrite growth from supercooled melt 77—51628
- AgBr, prep. of high purity cryst. with <3 ppb I 77—69982
- AgBr single-crystal IR optical fibres, growth from melt 80—53449
- AgCl, cryst. growth by Stepanov's method 78—23600
- AgCl oriented single crystal, Kyropoulos growth using NaCl seed crysts. 78—11102
- AgCl, Stepanov growth, oriented plates, rods and tubes 78—3023
- AgCl:Cd, large sheet single cryst. prep. *(German)* 77—32516
- $AgGaS_2$, optical quality, grown from melt, EPR characterisation 78—64260
- $AgGaSe_2$, growth by Bridgman method, optical characts. 77—69980
- $AgGaSe_2$, seeded Bridgman growth of crack-free crysts., thermal expansion coeff. 78—11101
- $AgGa(Se_{1-x}S_x)_2$, crystal growth, phase studies, optical props. 78—48305
- AgMg two phase bicrystal, growth by solid state diffusion couple method 80—60773
- $(Ag_{x/2}Pb_{1-x}Bi_{x/2})Te$ solid solution, preparation and thermoelectric props. 77—47839
- Al bicrystals, isoaxial, fatigue crack initiation in grain boundary affected regions *(Japanese)* 80—89338
- Al, defects formed during cryst. growth or by plastic deform., X-ray transmission topography obs. *(Russian)* 80—25761
- Al, perfect single crystal growth from melt, different orientations of crystallisation front *(Russian)* 77—55881
- Al single crystals, relation between axial orientation rotating and deform. banding 80—104206
- Al-Mn profiled alloy components pulled from melt, physicomech. props. 78—3175
- $AlBeB_{24}$, and β-$(Al,Be)B_{12}$, prep. and struct., book contrib. 78—47277
- $Al_xGa_{1-x}As$, growth of high-resistivity layers by liquid-phase epitaxy 79—70008
- $Al_2In_{12}S_{21}$, preparation, struct. and elec. props. 77—59685
- α-Al_2O_3 CVD and Czochralski grown crysts., imperfection anal. comparison 79—78868
- Al_2O_3, corundum, cryst. growth by Verneuil method, effect of thermal conditions on quality 77—44152
- Al_2O_3, corundum, γ-irrad., colour centres, growth method effect 77—1710
- Al_2O_3, Czochralski bulk flow, in microgravity, digital simulation 80—28934
- Al_2O_3, influence of cooling rate on nucleation *(German)* 78—38638
- Al_2O_3 sapphire, ribbon crystal growth by edge-defined film-fed growth technique *(Japanese)* 78—27396
- Al_2O_3:$Cr_2O_3(Ti_2O_3)$, dopant influence on struct. and mech. props. 80—24471
- Au, spherical crystal, drop grown from melt, RHEED obs., superstructs. 78—43225
- B modifications, polymorphism, cryst. chem., struct., growth, book contrib. 78—47278
- β-B, rhombohedral, single cryst. growth, modified Verneuil method *(French)* 78—44005
- B-Si alloys, B-rich, prep., anal. and cryst. growth *(French)* 80—104091
- $BaAl_{12}O_{19}$, single crysts., Czochralski growth, Al_2O_3-BaO phase diagram, cryst. quality 79—24428
- BaF_2:Y^{3+},Gd^{3+} production and mech. props. 79—72638
- $(BaF_2)_{1-x}(YF_3)_x$, crystal growth and struct. 77—12520
- $(BaF_2)_{1-x}(YbF_3)_x$ and $(BaF_2)_{1-x}(NdF_3)_x$, crystal growth and struct. 77—12520

crystal growth from melt continued

- $Ba_2LiNb_5O_{15}$, Czochralski growth, crystn. 80−35081
- $BaM_2(PO_4)_2$, M=Ni, Co, Mg, melt growth, optimal crystn. conditions 77−59683
- $Ba_2Na(Nb,Ti)_5O_{15}$, prep. and electro-opt. props. 78−76432
- $Ba_2NaNb_5O_{15}$ crystal, high optical quality, and optical absorption coeff. meas. 78−30036
- $Ba_2NaNb_5O_{15}$, Gd substitution, effect on linear thermal expansion, possible BSN replacement 78−43153
- $Ba_2NaNb_5O_{15}$, growth layer form., crystallization conditions effect, light diffr., Curie temp. 80−100778
- $Ba_{2.09}Na_{0.72}Nb_{5.02}O_{15}$, cryst. growth, monodomenisation, detwinning, optical homogeneity, composition, dielec., spectral props. 77−44151
- $Ba_xSr_{1-x}Nb_2O_6$ crystals, optical defects and edge dislocation distributions 80−19806
- $Ba_xSr_{1-x}Nb_2O_6$, growth defects 78−38640
- $Ba_2TiGe_2O_8$-$Ba_2TiSi_2O_8$, pseudobinary system, pyroelectricity and related props. 78−95553
- $BaTiO_3$, crystallisation from melt, nucl. and final cryst. sizes 77−24951
- $BaTiO_3$, pure and doped, cryst. growth and chemical composition 77−40349
- $BaTiO_3$:Nb, ferroelec. and paraelec. phases, props. 79−42919
- $Ba_2Ti_9O_{20}$ single crysts., prep. and unit-cell parameters 80−103302
- $Ba_2TiSi_2O_8$, fresnoite, Czochralski growth and phys. props. 78−3026
- $BaWO_4$, single cryst. growth by Czochralski method and U incorporation, effective distrib. ratios, luminesc. characts. 79−42094
- Ba_2ZnS_3, prep. by solid state reaction and melt growth, X-ray anal. 77−73226
- $BaZrO_3$, cryst. growth and thermoluminesc. *(Russian)* 78−23604
- Bi and Bi-Sb (12 at.%), impurity distrib. control by electrotransfer method *(Russian)* 80−66418
- Bi, growth of single cryst. wires with high resistivity ratios 78−68622
- Bi, single crystal from Bridgman's method, triangular facet formation 80−28933
- Bi thin single-crystal filaments in glass insulation 77−44147
- Bi:Sb, solid soln. struct., growth rate effects 77−52246
- Bi-MnBi eutectic, directional crystallisation and microstruct. *(Russian)* 77−55915
- Bi-Sb (1.2-7 at.%) solid solns., microhardness of single crystals 77−28886
- $Bi_3B_5O_{12}$, crystal growth from melt, exam. of growth kinetics 78−72717
- $Bi_{12}GeO_{20}$, Czochralski single crystal growth 79−1823
- $Bi_{12}GeO_{20}$, single crysts. optical homogeneity depend. on growth conditions 78−95007
- $Bi_4Ge_3O_{12}$ crystals, doped with Dy^{3+}, Ho^{3+}, Er^{3+}, Tm^{3+}, Yb^{3+}, growth, spectral and laser props. 80−45115
- α-Bi_2O_3, single cryst. growth and refractive indices 77−21018
- Bi_2O_3-$SiO_2(GeO_2)$, metastable phases form., crystn. conditions, melt viscosity and density effects 80−35167
- $Bi_{12}SiO_{20}$, growth of single cryst. thin plates by EFG method 80−97423
- $Bi_{12}SiO_{20}$, optical quality, Czochralski growth 78−31324
- $Bi_{12}SiO_{20}$, pulling large crystals 79−11507
- Bi_2Te_3 single crystals, melt grown, structural perfection 80−15101
- Bi_2Te_3-Bi_2Se_3 solid solns., bladed cryst. growth, electrophysical props. 78−43387
- Bi_2Te_3-Bi_2Se_3 solid solns., single cryst. growth and thermocouple construct. 80−104056
- BiTeI, Bridgman method modified for excess iodine, elec. props. 79−4907
- BiTeI, melt and vapour grown, optical props. 80−84746
- $Bi_2Te_{2.88}Se_{0.12}$, solid soln., single cryst. growth and doping, thermoelec. efficiency and Hall coeff. 79−33921
- $Bi_4Ti_3O_{12}$, $Bi_2Ti_2O_7$, $Bi_2Ti_4O_{11}$, crystal growth from melts in Bi_2O_3-V_2O_5-TiO_2 system 78−19659
- $Bi_4Ti_3O_{12}$, thick single cryst. growth from Bi_2O_3-B_2O_3-TiO_2 77−8746
- $BiVO_4$, cryst. growth and struct. 80−35078
- $Ca_{12}Al_{14}O_{33}$, piezoelectric material, cryst. growth and characterisation 79−99825
- $CaAl_2Si_2O_8$-$NaAlSi_3O_8$ (anorthite-albite) system, crystal growth rates and processes 80−4010
- $Ca_{0.2}Ba_{0.8}TiO_3$:Nb, conductive single cryst. growth by Verneuil method 77−85928
- $CaCO_3$, crystallization inhibition by phosphate and glycerophosphate ions 78−23593
- $CaCo_2(PO_4)_2$, growth by Bridgman method, crystn. speed depend. 77−59684
- CaF_2:M^{3+}, M=activator ion, redox processes during growth 77−85924
- CaF_2:U single crystal, Czochralski-Kyropoulos grown, U ion localization 79−91580
- CaFz crystals, grown from synthetic raw materials, quality, effect of impurities, composition 78−79083
- $Ca_3Ga_2Ge_3O_{12}$, appl. as substrate for mag. bubbles 77−28418
- $CaGa_2O_4$, Czochralski grown, and CaO-Ga_2O_3 phase diagram 80−29934
- $CaLa_4(SiO_4)_3O$:Nd, laser rod, minimisation of Ir inclusions 77−68246
- $CaMoO_4$, single crystal, growth and characterisation 77−36467
- CaO, single cryst. growth from molten $CaCl_2$ in wet atmosphere, habits 80−55287
- 12CaO.7Al_2O_3, single cryst. growth from melt 79−47614
- $CaSiO_3$, fibrous, controlled crystallisation and anisotropy 80−59425
- $CaTiO_3$, crystallisation from melt, nucl. and final cryst. sizes 77−24951
- $CaWO_4$, Czochralski grown, distrib. coeffs., cavity form., cellular struct. 77−11492
- $CaWO_4$, single cryst. growth by Czochralski method and U incorporation, effective distrib. ratios, luminesc. characts. 79−42094
- $CaYAl_3O_7$, type of melting, crystallisation from melt 77−12515
- ω-Cd-Hg alloy, melt-growth, morphology of single crysts. 78−64464
- $Cd_xCa_{1-x}MoO_4$, growth and props. 80−71588
- $CdCr_2Se_3$:Ga, synthesis and photoferromag. effect 77−51936
- $CdCr_2Se_4$, ferromagnetic semiconductor, single cryst. growth *(Japanese)* 79−47612
- $Cd_3Ga_5O_{12}$ melt, simulation of fluid flow 78−31321
- CdGeAs, vertical Bridgman growth with control of interface shape and orientation 80−66420
- $CdGeAs_2$, cryst. growth and elec. props. *(French)* 77−59682
- $CdGeAs_2$ crystals, Bridgman grown, optical props. rel. to O_2 content of starting materials 80−81213
- $CdGeAs_2$, optical and elec. props. 79−19590
- $CdGe(As_{1-x}P_x)_2$, crystal growth, phase studies, optical props. 78−48305
- $CdGeP_2$ synthesis and cryst. growth 79−87577
- Cd_xHg_{1-x} Te, elec. characts., impurity effects 80−92890
- $Cd_xHg_{1-x}Te$, cast-recrystallise-anneal growth 79−91578

crystal growth from melt continued

- $Cd_xHg_{1-x}Te$, high-speed quenching of melt *(German)* 79−65997
- $Cd_xHg_{1-x}Te$, homogeneous mixed crysts. with large segregation tendency, Bridgman growth *(German)* 79−33923
- $CdIn_2S_4$ single crystal growth by two-zone horizontal Bridgman technique 78−27400
- $Cd_xMg_{1-x}Se$ single crystals, melt grown, struct. and microhardness anisotropy 79−86836
- CdS, cryst. grown from melt under press., microstruct. 77−59019
- n-CdS, growth from Te soln., photocond. and cryst. perfection 79−99579
- CdS, single cryst., effects of annealing in Cd or S vapour on photoelectric props. 77−16370
- CdS single cryst., melt growth, improvement of elec. characts. 79−38734
- CdSb, monocrystalline film, prep., elec. props. 79−43159
- CdSe, grown from melt, SEM exam. of dislocation boundaries 80−24456
- $CdSnP_2$, single cryst. growth, by means of temp. gradient 79−56927
- $CdSnP_2$-InP, n-n heterojunctions, growth, elec. characts. 77−11992
- CdTe and CdTe:Cl, grown by travelling heater method, EPR defect charact. 77−40125
- CdTe, growth by travelling heater method in Te solvent 77−40360
- CdTe, growth from Cd rich soln. by solvent evaporation 77−40355
- CdTe, growth from Te soln. by slow cooling or travelling heater method, Te inclusions 77−40352
- CdTe, growth from Te-rich soln. by travelling heater method, cond. and luminesc. 77−40351
- CdTe, growth from Te-rich soln. in vertical Bridgman furnace 77−40354
- CdTe, high-resistivity, grown by modified travelling heater method, trapping parameters 77−39871
- CdTe, low temp. themal cond., growth parameter influence 80−92725
- CdTe, melt-growth review, including liquid encapsulation method, defect charact. 77−40350
- CdTe, purification, efficiency for extraction of Cu and Ag impurities, impurity scatt. meas. 77−8749
- CdTe, undoped, high-resist., grown by travelling heater method, characterisation 77−39801
- CdTe:Cl, gamma-ray detector growth, travelling heater method improvement 77−40353
- CdTe:Cl, grown by travelling heater method, carrier homogeneity investig. 77−39848
- CdTe:Tl, growth by travelling heater method, elec. and optical characterisation 77−40356
- CdTe-ZnSe pseudobinary system, phase diagram and equil., Bridgman single cryst. growth method 79−43213
- $Cd_2Ti_2O_5F_2$, single cryst. growth and props. 79−100046
- $CdWO_4$ single cryst., melt growth, defects and growth mechanism 80−29933
- $Cd(WO_4)_{1-4}(MoO_4)_x$, growth and props. 80−71588
- $Cd_{1-x}Zn_xCr_2Se_4$, synthesis Curie pt., photomag. effect 77−51937
- CeB_6, crystal preparation, elec. resistance, phase transitions 80−97427
- $CePd_3$ single crystal Czochralski growth and characterisation 80−60767
- $CoAl_2O_4$, cryst. growth by Verneuil method 77−1805
- CoB_{12}, growth from melt and phys. props. 80−20782
- Co_2GeO_4, crystal growth by Czochralski method under 4 atm N_2 77−77368
- $Co_{1-x}O$, single cryst. growth by skull melting 80−84844
- $CoSi_2$, interface struct. and growth mechanism from melt 79−14715
- CrB_2, crystal growth by floating-zone method, elec. and mag. props. 77−1801
- Cr_2O_3, cryst. growth from decomposition of $K_2Cr_2O_7$ melt 79−43131
- $Cs_5Bi(MoO_4)_4$, synthesis, X-ray and thermal investigations 77−36390
- $Cs_2NaLn(III)Br_6$, single crysts. grown by Bridgemann-Stockbarger method, charact. by X-ray powder diffr. *(French)* 79−43135
- Cs_2NaYCl_6:Bi^{3+}, luminesc., cryst. growth, Stockberger method 79−8174
- $Cs_8Nb_{22}O_{59}$, growth and struct., dielec. and optical characterisation 78−35294
- $CsR(MoO_4)$ R=Dy, Ho, Er, permittivity temp. depend., polymorphic transition 80−92670
- Cu chalcogenides, single-phase, preparation 78−35293
- Cu, dendrite growth from supercooled melt 77−51628
- Cu, dislocation-free, growth conditions 78−3025
- Cu, growth method for large oriented single crystal plates 77−90267
- Cu, meas. of contact angle between melt and cryst. during Czochralski growth 77−28708
- Cu, preferred crystallographic orientation of melt grown single crystals *(Czech)* 79−43134
- Cu, single crystal growth, new technique for prep. from bulk using four pts., RHEED anal. 79−8240
- Cu single crystal growth from melt 78−48308
- Cu, thermal stress role in dislocation form. during growth from melt 80−6374
- Cu-Al spherical crysts. grown from drop of melt, topography 80−84353
- Cu-Al(Si), preferred crystallographic orientation of melt grown single crystals *(Czech)* 79−43134
- Cu-Ge (5 at.%), single crystal, Bridgman growth, neutron diffraction topographic obs. of layer substructure 79−27938
- Cu-In eutectoid, directional eutectoid decomposition growth, crystallography 80−29874
- Cu-Nb, supercond. wire, directional solidification of melts, supercond. ionisation temp. *(Russian)* 78−76596
- Cu-Ni, Monte-Carlo method modelling, surface roughness *(Russian)* 79−77536
- $CuAl_5S_8$, cryst. growth, struct., and fluoresc. 77−48328
- $CuCl_2$, anhydrous, single crysts., prep. 77−85932
- $CuCr_2Se_4$, crystal growth from melt, exam. of props. 80−55283
- $CuInSe_2$, large single crystals growth by iodine transport and Bridgman methods 78−35300
- $CuInSe_2$, melt-grown, EPR characts. 78−35030
- $CuInTe_2$ single crystals, directional freezing growth and doping, resist. changes on annealing 80−60768
- $Cu_4Mn_2S_4(Se_4)(Te_4)$ spinel, prep. and elec. props., 100 to 650K 79−43127
- $Cu_xMo_6S_8(Se_8)$, prep., metallurgical and supercond. props. 77−32102
- Cu_2O, growth by melting, photocond. spectra 78−52029
- Cu_3P, single crystal, prep. and props. 80−40250
- $CuSbS_2$ crystals, growth and characterisation 80−60770
- DyAG, single cryst. growth by Czochralski method 78−95690
- $Dy_3Al_5O_{12}$, Czochralski growth, interface shape transitions 78−59772
- DyF_3, crystal growth by Bridgman-Stockbarger method and Czochralski method 78−52660
- $Dy_2(MoO_4)_3$, cryst. growth and props. 79−55727

crystal growth from melt continued
ErAG, facet formation 78−63687
$Er_3Al_{5-x}Ga_xO_{12}$, LPE, spectroscopic props. 80−93419
ErB_4, Czochralski crystal growth 79−95920
ErF_3, crystal growth by Bridgman-Stockbarger method 78−52660
$ErFe_2$, Czochralski growth, and cryst. quality determ. 77−8742
$ErFeO_3$:Co, Ti, effects of Co and Ti ions on cryst. growth 77−28711
$EuGa(In)_2X_4$, X=S,Se,Te, prep. and props. 77−85214
EuO, single crystal enriched in ^{17}O, growth from melt in sealed Mo crucible 77−4734
Eu_2O_3, large single crystals, production and props. rel. to structural anisotropy *(French)* 77−36396
Fe-Ge intermetallides, melt struct. rel. to growth mechanism 77−84681
Fe-Ge system, cryst. growth forms and interface struct. 79−61515
Fe-Mn-O melts, formation of oxide inclusions, cryst. pulling, Bridgeman tests *(German)* 80−35074
Fe-Ni (31 wt.%) alloy, Bridgman grown, cellular to dendritic crystn. transition, morphology and microstruct. *(Russian)* 79−14709
Fe-Ni alloy, Bridgman growth, distrib. of growth directions 79−33924
Fe-Ni alloy, cellular-dendrite struct., effect of temp. gradient and crystallisation rate on morphological singularities *(Russian)* 78−3115
Fe-Si intermetallides, melt struct. rel. to growth mechanism 77−84681
$Fe_{23}B_5C$, growth by heat treatment of Fe-B-C system, struct. 77−28779
$FeBO_3$, $FeBO_6$, magneto-optical materials, single cryst. growth *(Japanese)* 79−47612
$FeGe_2$, interface struct. and growth mechanism from melt 79−14715
$FeGe_2$, single cryst. perfection depend. on growth rate and direction 80−55284
$Fe_{1.76}Ge$, interface struct. and growth mechanism from melt 79−14715
$Fe_{1-x}O$, single cryst. growth by skull melting 80−84844
Fe_3O_4, magnetite crysts., skull melter growth 79−24430
Fe_3O_4, single cryst. growth by melt transport in DC arc 77−8745
FeP_4, twinned cryst., synthesis and cryst. struct. 79−4278
α-$FeSi_{2.33}$, interface struct. and growth mechanism from melt 79−14715
Fe_2SiO_4, fayalite, Czochralski growth under controlled O_2 fugacity conditions 80−84843
$FeTiO_3$, Fe_2TiO_4, Fe_2TiO_5, prep. and Czochralski cryst. growth 77−21017
Ga, contact angle meas. between melt and crystal during Czochralski growth 78−64461
Ga, cryst. growth from melt, dissolution morphology *(German)* 77−24283
Ga, Czochralski growth, heat transfer during drawing *(French)* 78−48309
Ga, effect of small Cu additives 77−32515
Ga, single cryst. growth by pulling, thermal parameters governing purity *(French)* 78−2046
Ga single crystals, rate equations for dislocation-free and dislocation-assisted growth 79−4262
$Ga_{1-x}Al_xSb$, melt growth and elec. props. 79−65999
GaAs, concs. of C and O_2 in LEC grown cryst. determ. 77−39612
GaAs, cryst. prod. in strip and rod form., Stepanov method 78−3017
GaAs crystal growth, thermal and elastic const. evaluation 80−92586
n-GaAs, crystal growth by Czochralski method kinetics, total emittance determ. 80−75193
GaAs, crystal pulling of semi-insulating material, liquid encapsulated compounding and Czochralski growth 79−43136
GaAs, Czochralski grown, pure and doped, elec. props. 80−10989
GaAs, Czochralski growth, melting and regrowth, inclusion density and dislocation generation 77−21016
GaAs, grown-in dislocation density, impurity effect 78−51543
GaAs, LEC growth using pyrolytic BN crucibles 78−6841
GaAs, large dislocation-free single crystal growth 80−25550
n-GaAs, melt-grown, stoichiometry, photolum. obs. 78−72583
GaAs, single crystal growth by liq. encapsulated Czochralski technique using B_2O_3 80−11554
GaAs, synthesis in pyrolytic BN boat 78−6840
GaAs, travelling heater method growth, dislocation elimination 77−7684
GaAs:B, incorporation of B during growth 80−93471
GaAs:Cu melt grown, 1.36 eV band luminescence studies, edge emission 79−87510
GaAs-$Ga_{1-x}Al_xAs$ laser, low threshold room temp. embedded DH, fabrication and characts. 77−681
GaAs-ZnSe, solid solution crystals, grown by Bridgman method, exam. of resistivity and Hall effect 79−95919
$GaBO_3$:Fe^{3+}, ESR spectra, lattice parameters 80−93170
GaInAsP-InP DH lasers made by melt-back method, operating characteristics 80−48287
$Ga_xIn_{1-x}P$, real struct. exam. by electron microscopy and channelling 78−2143
$Ga_xIn_{4-x}PyAs_{1-y}$, In rich bulk single crysts. growth from melt via gradient freeze method, and characterisation 78−68618
$Ga_xIn_{1-x}Sb$, Ga-rich, prep. by Czochralski technique 80−60771
$Ga_xIn_{1-x}Sb$ p-n junction photodiode fabrication, sensitivity as 1 to 2.5 μm detectors *(Japanese)* 80−52311
GaP, cryst. growth for green luminesc. diode manuf. 77−40346
GaP electroluminescent diode struct. prep. by SSD and Czochralski methods, dynamic props. *(Czech)* 80−97425
GaP, facets on pulling under concave interface conditions 78−23601
GaP, growth conditions rel. to dislocation structure 80−88151
GaP, growth of dislocation free crysts. from stoichoometric melt. 77−81212
GaP, impurity behaviour during crystallisation from melt 77−84772
GaP, LEC growth of dislocation-free crysts., microdefects and striations 78−9974
GaP:Cr_2O_3, growth, dopant distribution, elec. resist. 78−34531
GaP:Te, struct. imperfections, prep. and doping effects 77−89451
$(GaP)_x(ZnSe)_{1-x}$, solid solution, reaction of Zn with Se during Czochralski growth and LPE 79−8238
GaSb, LEC growth, Hall coeff. 80−89133
GaSb LEC single crystal growth, novel encapsulant material 80−93475
GaSb, pulled crystal, microfacet obs. near irregularly remelted surfaces 78−91278
GaSe, basal plane orientation determ. in vertical Bridgman grown single crysts. 78−19658
GaSe, growth of crysts. with natural facets at large angles to layers 78−15305
p-GaSe, resist. and Hall-mobility meas. at 77-850K 77−59295
$\alpha(\beta)$-Ga_2Se_3, cryst. growth, optical, X-ray diffr. and SEM study 80−71587
GaTe, single cryst. prep. and electroabsorpt. spectra investig. 80−103968

crystal growth from melt continued
Gd-Ga garnet growth, effect of buoyancy parameter of Czochralski bulk flow 79−61512
GdB_6, crystal preparation, elec. resistance, phase transitions 80−97427
GdF_3, crystal growth by Bridgman-Stockbarger method 78−52660
GdGa garnet, Czochralski grown, substrate material dislocation propagation 78−59771
$Gd_3Ga_{5-x-y}Mg_xZr_yO_{12}$, cryst. growth, coupled substitution of Ga by Mg and Zr 78−31325
$Gd_2Ga_5O_{12}$, cryst. growth by Czochralski technique, dissociation products calcs. 79−47615
$Gd_3Ga_5O_{12}$ crystal growth from melt, X-ray topography meas. *(Hungarian)* 80−11556
$Gd_3Ga_5O_{12}$, Czochralski grown, effect of melt flow phenomena on perfection 78−88419
$Gd_3Ga_5O_{12}$, grown by automatic diameter control, growth striae 77−69979
$Gd_3Ga_5O_{12}$, growth of 3″ diameter crystals 78−68616
$Gd_3Ga_5O_{12}$:Nd^{3+}, growth, stimulated emission, spectral props. 78−95593
$Gd_2(MoO_4)_3$, and isotypes exam. of crystal growth, and defect generation 78−68617
Ge, contact angle meas. between melt and crystal during Czochralski growth 78−64461
Ge, crystal growth, O equilib. between Ge and gas over melt 80−2938
Ge, crystal growth and segregation under zero gravity 79−43130
Ge, Czochralski growth system, time-depend., cryst.-melt interface shape 77−24280
Ge, fast and slow quenching defects 78−39052
Ge, growth conditions and doping level influence on impurity distrib. ratio 77−12516
Ge, hydrogen multivalent acceptor complexes 77−55491
Ge, large shaped single cryst. prod., Stepanov method 78−3014
Ge, melt grown single crystals, preferred growth directions and perfection 79−77537
Ge ribbon single crysts. grown from melt, dislocation struct. form. under thermal stress 80−107082
Ge, shaped crystals, grown by Stepanov method, struct. perfection 78−2123
Ge shaped single crystal, Stepanov method growth, temp. distri b. 78−2032
Ge, single cryst. growth, supercooling needed for Czochralski and Stepanov methods 78−3015
Ge single crystal of circular cross section, thermoelastic stresses 78−2033
Ge single crystals, constitutional supercooling growth conditions, structural and chem. inhomogeneities 80−93473
Ge strips grown by Stepanov method, thermoelsatic stress calc. 78−2034
Ge:B, single crystals, grown by Czochralski method, exam. of B distribution ratio and diffusion coeff. 79−95042
Ge:Ba, heavily doped, second phase inclusions on melt growth 78−22751
Ge:Be single crystals, grown by Czochralski method, exam. of Be distribution ratios and solubility 79−95043
Ge:Ga, appl. of heat pipe to Czochralski growth, segregational behavior 79−61511
Ge:Ga, effects of destabilising vertical thermal gradients on cryst. growth and segregation 78−52659
n-Ge:O, Czochralski growth, O content rel. to props., IR, Li precipitation determs. 77−15445
Ge:O, IR absorpt. at low temp. *(Chinese)* 80−108228
Ge:P(Sb), growth atm. effect on struct. microdefect form. 80−20779
Ge:Sb, Czochralski growth, orientation depend. of impurity distrib. coeff. 79−69976
Ge:Sb, dopant distrib. rel. to direction of cryst. growth 77−51400
Ge-Ga, segregation of Ga due to barometric mol. diffusion in gravitational, centrifugal fields 78−14472
Ge-Si system alloys, growth by Czochralski method, morphology 77−15329
Ge-Si-Sb, segregation of Si,Sb due to barometric mol. diffusion in gravitational, centrifugal fields 78−14472
GeTe, nonstoichiometric, homogenisation 78−44004
^3He, quantum crystal, growth from melt at low temps. 78−31319
^4He, quantum crystal, growth from melt at low temps. 78−31319
$Hg_{1-x}Cd_xTe$, for appl. in IR detector arrays, comp. control 80−31872
$Hg_{1\ x}Cd_xTe$, grown from melt, Kirkendall and Frenkel effects 80−100365
$Hg_{1-x}Cd_xTe$, high-pressure reflex growth technique, IR detector appl. 77−40347
$Hg_{1-x}Cd_xTe$, homogeneous single cryst., growth by modified Bridgman technique 78−39682
$HgGa_2S_4$, melt growth, optical props. and SHG, HgS-$HgGa_2S_4$ phase diagram 80−50548
HgI_2, soft γ-ray detector fabrication and props. 77−3208
HgSe, Bridgman growth at hydrostatic press. to 3 kbar, free electron conc. and mobility 77−52245
HgSe-CdSe pseudobinary alloy, phase diagram and cryst. growth 78−68620
HgTe-CdTe, distrib. ratios of components during crystn. of melt 77−16485
HgTe-MnTe, growth from two-phase melts, crystallisation characts. 77−36393
$HoAlO_3$, Czochralski growth and props. 77−48335
HoF_3, crystal growth by Bridgman-Stockbarger method and Czochralski method 78−52660
$HoFe_2$, Czochralski growth, and cryst. quality determ. 77−8742
InAs, obtained by liquid-seal method, deviation from stoichiometry 77−40345
InAs:Cd,Te interaction between impurities, effect on elec. props., Hall effect. 80−19832
n-InAs:Cr, Czochralski growth of high-resist. single crysts. 77−66587
InAs-FeAs, eutectic, growth from melt, electrical props. 77−11911
$InBO_3$:Fe^{3+}, ESR spectra, lattice parameters 80−93170
In_2Bi-In, thin lamellar eutectic strips, unidirectionally solidified, morphologic and crystallographic study *(French)* 77−55264
$In_xGa_{1-x}Sb$, vertical Bridgman Stockbarger growth, magnetic field effect 78−60565
InP, concs. of C and O_2 in LEC grown cryst. determ. 77−39612
InP, Czochralski grown, etch pit obs., produced by new etchants HBr/HF or HBr/CH_3COOH 79−60370
InP, grown-in dislocation density, impurity effect 78−51543
InP, growth and props. 79−1822
InP growth from soln. and LEC, photolum. and elec. meas. 79−87575

crystal growth from melt continued
p-InP, LEC growth 77—81211
InP, LEC growth of dislocation free crystals 80—89134
InP, LEC growth using pyrolytic BN crucibles 78—6841
InP, liq.-seal growth, protective props. of B_2O_3 flux 77—12519
InP, liquid encapsulated Czochralski cryst. growth, X-ray study 79—47619
InP substrate, LEC-grown, defect evaluation by cathodoluminescence 80—2866
InP, synthesis solute diffusion grown, elec. props., photoluminesc., etch pit profiles 79—4914
InP, twin-free, prep. using liquid encapsulated Czochralski growth 80—50546
InP:S, SSD growth of low dislocation density crystals 80—89135
InP-GaP, solid soln. crystallization from stoichiometric melt, solidus construction 77—85927
InSb, convection in melts, and cryst. growth under large inertial accelerations 80—66421
InSb, Czochralski growth, thermoelec. monitoring of interface temp. 78—31331
InSb, dislocations due to thermal stress, single and composite crysts. 78—2124
InSb, facets and twin formation obs. *(Chinese)* 80—59409
InSb, growth angle determ. from cryst. lateral face shape and solidified separation drops 80—103282
InSb, low defect crystal growth by InN doping, IR detector appl. 80—20780
InSb, morphological instability under constitutional supercooling during cryst. growth from melt and stabilising thermal gradient 79—4910
InSb, periodically doped cryst. prod. by Peltier effect, helicon diagnostics *(German)* 77—48338
InSb:Te, cryst. growth from melt, pulling method, US effects on facet growth 80—76169
InSb:Te, Czochralski cryst. growth, strain configuration study using X-ray anomalous transmission topography 79—23552
$InSbS_3(Se_3)$, prep., polymorphism, cryst. struct. 78—44002
$InSbSe_3$, cryst. prep. and props. 79—15601
$In_{1.8}Sb_{0.2}Se_3$, cryst. prep. and props. 79—15601
InSe, large monocrysts., grown from nonstoichiometric melt., comp. and photovoltaic substrate 77—55882
InSe, layered crystalline slabs, growth by Czochralski method 78—68619
In_6Se_7, single cryst. prep. and electrophys. props. 79—43129
β-In_3Sn, crystn., decomp. and superconductivity 79—91579
$K_5Bi_{1-x}Nd_x(MoO_4)_4$ solid soln., growth, spectroscopic and laser props. 78—2901
KBr bicrystal, grown from melt, interfacial substructure, impurity effects 77—4263
KBr crystal, cordlike defects and countermeasures 79—72636
KBr, IR laser window appl., crystal growth, polishing and optical absorpt. 77—7102
$K_2Cd_2(SO_4)_3$, melt growth and ferroelastic transition, and K_2SO_4-$CdSO_4$ phase diagram 78—31335
KCl, crystals, grown by Czochralski method, effect of growth rate on defect generation 79—51032
KCl, Czochralski-grown, creep and struct. changes, 77-300K *(German)* 77—28862
KCl, Czochralski-grown, dislocation subboundary characts. 78—67718
KCl, spiral growth, screw dislocation mechanism, phase-contrast microscopy obs. 78—87637
KCl, zone refined single crystal growth for high power CO_2 laser optics 78—22181
KCl:Ca(Ba), effect of doping on dislocation distrib., in melt grown cryst. 80—6410
KCl:RbCl, $SrCl_2$, IR window material, cryst. growth and props. 78—31333
KCl(Br)(I), Czochralski growth, dynamical aspects, use of optical diameter controller 78—31332
$K_2Co_2(SO_4)_3$ polycryst., growth and phase transitions 79—33918
K_2CuF_4, single crysts., cryst. growth by Brigman-Stockbarger technique 79—52107
K_2CuF_4-K_2ZnF_4, solid soln., cryst. growth by Brigman-Stockbarger technique 79—52107
KI:Tl, crystallisation from melt by various methods, impurity distrib. 77—4733
$K_5La(WO_4)_4$, formation possibility 77—36392
$KMn_{1-x}Me_xF_3$ (Me=Mg^{2+}, Fe^{2+}, Co^{2+} and Ni^{2+}) Bridgman growth, 80—60764
KN_bO_3, single domain crystal growth, SHG with Nd:YAG laser 78—74954
$KNbO_3$ crystals, growth from melt 79—100041
$KNbO_3$ single crystals, preparation of pure, Fe doped, and reduced crystals 78—60564
$KNbO_3$:Fe, large single domain cryst., growth and prep. for optical storage 77—1799
$KZnF_3$ single crystal growth, Czochralski method 80—97421
LaB_6, synthesis and props., review *(Japanese)* 80—40255
$La_2Be_2O_5$:Nd^{3+} (Pr^{3+}), cryst. growth, spectral and laser properties in $^4F_{3/2}\rightarrow{}^4I_{11/2}$ and $^4F_{3/2}\rightarrow{}^4I_{13/2}$ transitions 80—80853
$LaNbO_4$, single cryst., grown by Czochralski method, props. 77—52247
La_3NbO_7, synthesis and cryst. growth 80—71590
7LiAl, cryst. growth, Stockbarger method, struct. and homogeneity 80—89137
LiAl single crystals, growth by Tamman technique 80—66422
$LiBO_2$, $Li_2B_4O_7$, Czochralski growth 78—19657
LiB_4O_7, crystal growth from undercooled melt 77—52248
$Li_2B_4O_7$, heat low controlled growth during crystallisation 79—65014
LiC_6 intercalation cpd., synthesis method and reflectivity spectrum 79—15600
LiCl:Na (K,Rb,Cs,Ag), theoretical and experimental study of partition coeffs. of isovalent impurities 79—65111
$LiGd_3(MoO_4)_5$, single crysts., cryst. growth, optical props. 80—60763
$Li_2Gd_4(MoO_4)_7$, Czochralski growth, struct. and optical props. 78—27397
Li_2GeO_3, melt-grown single crysts., polar twins, piezoelec. meas., etching behaviour 79—32999
$LiHoF_4$ crystal melt growth, comparison of Czochralski and Bridgman-Stockbarger methods 80—60765
$LiInS_2$, single cryst. growth by directional solidification, photoluminescence meas. 79—61514
Li_3N single crystals, Czochralski growth, exam. 78—56574

crystal growth from melt continued
Li_3N, superionic conductor, cryst. growth and struct., phys. props., book contrib. 79—42308
$LiNbO_3$, Czochralski grown single crysts., cellular interface and struct. due to constitutional supercooling *(Chinese)* 79—51026
$LiNbO_3$ Czochralski grown single crystals, facetted and nonfacetted growth sections, growth striae *(Chinese)* 80—64940
$LiNbO_3$, growth from melt and characts. *(Chinese)* 80—54155
$LiNbO_3$ single crystals, growth from melt, Czochralski method *(Chinese)* 80—76171
$LiNbO_3$ single crystals, wetted-die technique 80—97426
$LiNbO_3$:Rh, Czochralski-grown oxide crystals, fluid-flow effect on gas-bubble entrapment 80—84121
$LiNb_{1-y}Ta_yO_3$, Czochralski growth and basic props. 77—63556
$LiNdP_4O_{12}$ laser material, crystal growth and optical props. 79—41386
$LiNiO_3$, surface dendrite occurrence, growth condition-depend. 80—2316
Li_2O, single crystal synthesis using vacuum fusion technique 80—71585
$LiRF_4$, R=rare earth, laser matrices prep. and characterisation 77—24945
Li_2SiO_3, Czochralski growth and charact. 79—91577
Li_2SiO_3, melt-grown single crysts., polar twins, piezoelec. meas., etching behaviour 79—32999
$LiTaO_3$ crystals for commercial SAW TV IF filters, fabrication 80—80961
$LiTaO_3$, Czochralski technique, light guide prod. by Nb diffusion *(German)* 80—20783
$LiTaO_3$, Czochralski-grown oxide crystals, fluid-flow effect on gas-bubble entrapment 80—84121
$LiTaO_3$, single cryst. prep. for surface acoustic wave device appls. *(Japanese)* 80—60772
$LiTaO_3$, single crysts., Czochralski growth for SAW device appl. 79—33922
$Li_2Ti_3O_7$ growth by Bridgman-Stockbarger technique 80—25548
LiV_2O_5, needle cryst. form. by reduction of molten Li_2O-V_2O_5, semicond. props. *(Japanese)* 78—3030
$LiY_{0.416}Er_{0.5}Tm_{0.067}Ho_{0.017}F_4$, Stockbarger single cryst., charact. of solidification behaviour 77—24948
$LiYF_4$, prep. and crystal grwoth for laser appls. 77—55879
Li_2ZnGe, single cryst. growth, by normal freezing method, X-ray diffr. study 79—28908
$LuAlO_3$, single crysts., prep. and phys. props., X-ray struct. anal. 79—4298
$LuBO_3$:Fe^{3+}, ESR spectra, lattice parameters 80—93170
Lu_2O_3-K_2O_3 (K=Ho, Er, Tm, Yb, Y), crystn. by Verneuil method 80—40254
Mg, melt grown by Bridgeman method, X-ray topography 78—59770
MgF_2:Ni, growth by vertical gradient freeze method, in self-sealing graphite crucibles 78—31334
MgO, melt-grown cryst., direct evidence for brucite precip. 77—28712
MgO, single cryst. growth using modified plasma torch furnace, doping *(Japanese)* 79—95923
Mg_2SiO_4, grown by Czochralski method, trivalent ion distrib. between melt and single crystals 78—9972
(Mn,Ni,Zn) ferrite single cryst., flame fusion cryst. growth, conc. change 77—77369
Mn chalcogenides-II-VI compound solid solutions, cryst. growth and physicochem. props. 79—14711
MnB_{12}, growth from melt and phys. props. 80—20782
γ-MnCu crystals, antiferromag. Czochralski growth 80—97420
$Mn_{1-x}O$, single cryst. growth by skull melting 80—84844
MnSb, pulling with seed from nonstoichiometric melt 77—16488
$MnSi_{\sim 1.73}$ crystal growth and characterisation 80—93474
$Mn_{15}Si_{26}$, growth by Bridgman method and chemical transport, X-ray structural analysis 79—100043
Mn_5Si_3, elastic moduli, phase transitions, ultrasonic velocity 80—92589
Mn_5Si_3, interface struct. and growth mechanism from melt 79—14715
Mn_2SiO_4-MnO eutectic composite, EFG die-top geom. effect on solidification interface shape 77—48420
MnZn ferrite, combined Bridgeman-zone levelling cryst. growth technique 80—35076
MnZn ferrite single cryst., high temp. phase transform. characts., growth techniques *(Chinese)* 79—33927
MnZn ferrite single cryst., Bridgman growth and appl. *(Chinese)* 79—33928
MnZn ferrite single crystals, growth by Bridgman technique, book contrib. 79—69977
Mo, C and Ir impurities in single cryst. growth, effect on fine struct. *(German)* 77—28714
NaBr:Ho^{3+},Eu^{2+}, single cryst. synthesis, rel. to purification methods 77—8744
NaBr:Tl, impurity segregation with Kyropoulos growth 78—9977
Na_2CO_3, single cryst. growth from melt, thermal expansion meas. 79—4913
NaCl Czochralski crystal growth for large CO_2 laser windows 80—74525
NaCl, Czochralski growth, temp. distrib. near crystn. front 78—2036
NaCl:Ca, light scattering coeff., effect of growing condition 78—55418
NaCl:LiCl, melt, semiperiodic closed growth lamellae on crystal-melt interface 78—67668
NaCl:$PbCl_2$ crysts., melt grown, Pb distrib. determ., UV spectrochem. anal. 78—40101
NaCl-KCl novel encapsulant for LEC growth of GaSb single crystals 80—93475
NaCl-LiCl mixed crystals, Au decoration study of solid-melt interface, phase separation 80—15026
β-Na_2O-Al_2O_3, isomorphous replacement of Al^{3+}, solubility of Cr^{3+}, Ti^{3+}, Fe^{3+} 77—85926
β-Na_2O-Al_2O_3, single cryst. Czochralski growth 77—77367
Na_2O-Ga_2O_3 system β and β″ phases, fast ion cond., prep. and phase comp. 80—59716
$Na_2O.2SiO_2$, nucleation kinetics, temp. depend. 78—26467
Na_2S single cryst. grown by Bridgman-Stockbarger method 79—100044
β-$Na_xV_2O_5$, Bridgman and Czochralski single cryst. growth 79—47618
Nb, impurity conc. monitoring during single cryst. production, use of nuclear phys. methods 78—31337
Nb, influence on degree of perfection of rate of cryst. growth *(Russian)* 77—43162
Nb single crystals, growth by pulling from a melt on a pedestal, charact. arrangement of dislocations 79—4911
NbC single crystals, synthesis and impurities 80—55329
Nb_2O_5-TiO_2, splat cooled, crystallization and ordering 77—68953

crystal growth from melt continued
Nb_3Si, A-15 type, growth by levitation melting, transition temp. meas. *(Chinese)* 79–24424
Nb_3Sn, Zr alloy element effect on growth kinetics *(Chinese)* 79–90579
Nd:YAG, grown from melt, in Mo crucibles, laser props. 80–48261
$NdAl_3[BO_3]_4$, single phase crystallisation region from solvent melt 80–38977
$Nd_xLa_{1-x}P_5O_{14}$, crystal growth, laser generation characts. 80–38020
$NdNbO_4$, cryst. growth rel. to investig. of $PbO\text{-}KF\text{-}B_2O_3\text{-}PbNdTiNbO_7$ cross section 77–86004
$NdNbO_4$, single cryst. grown by Czochralski method 77–52247
Ni, Czochralski grown single cryst., X-ray topography, mag. domains 77–12147
Ni, Czochralski grown single crystal, crystal perfection 78–47252
Ni, Czochralski growth conditions rel. to cryst. imperfections, mag. domain walls 77–68937
Ni, growth direction orientation effect on impurity distrib. 78–47261
Ni-Co alloy, Bridgman growth, distrib. of growth directions 79–33924
Ni-Zn-Mn-Fe spinel, crystn. from soln. in melt 80–2945
NiF_2, growth in induction furnace, using enclosed graphite crucible 77–4735
Ni_2MnSn, large single cryst. growth by Czochralski and Kyropoulous method 79–47613
$Ni_2Mn_{1-x}V_xSn$, large single cryst. growth by Czochralski and Kyropoulous method 79–47613
NiO, oriented bicrystal growth by floating zone and Verneuil's method *(French)* 78–92186
$NiO\text{-}Al_2O_3$, Verneuil-grown crysts., phase comp. 77–66586
NiP_4O_{11}, formation in phosphoric acid melts 78–27394
$Ni_xZn_{1-x}Fe_2O_4$, crystal growth from $BaO\text{-}B_2O_3\text{-}ZnO\text{-}NiO\text{-}Fe_2O_3$ melt, exam. of crystal props. 80–40249
P, white, high purity, cryst. growth morphology 77–15330
$(Pb, Sr)_5Ge_3O_{11}$, single crysts., growth and X-ray and dielec. investigations 80–88127
$Pb_xCa_{1-x}MoO_4$, growth and props. 80–71588
PbFBr(Cl), dehydration, zone refining and Bridgman cryst. growth 77–36395
PbFCl(Br), single crystal ionic cond., deviation from molecularity, effect of O_2 impurities 79–51305
$Pb_3(Ge,Si)_2O$, growth from melt, struct. and dielec. props. 77–44148
$PbGeO_3$, cryst. struct., dielec. and optical props. 77–1118
$PbGe_3O_7$, cryst. data and cryst. growth 78–47289
Pb_3GeO_5, cryst. struct. dielec. and optical props. 77–1118
Pb_5GeO_7, cryst. data and cryst. growth 79–51076
$Pb_5Ge_3O_{11}$, Czochralski-grown oxide crystals, fluid-flow effect on gas-bubble entrapment 80–84121
$Pb_5Ge_3O_{11}$, formation of secondary phases during growth 78–3027
$Pb_5Ge_3O_{11}$, growth defects and polarisation switching 78–48132
$Pb_5Ge_3O_{11}$, single crystal, ferroelec., Czochralski growth 78–3024
$Pb_5Ge_3O_{11}$ single crystals, switching behaviour and hysteresis 80–40077
$Pb_{0.97}Hg_{0.03}Te$ photovoltaic detector produced by Sb^+ ion implantation 80–82821
$Pb_xMo_6S_{8-y}$, phase relns., stoichiometry, T_c 78–15378
$Pb_xMo_6S_8(Se_8)$, prep., metallurgical and supercond. props. 77–32102
$PbNdTiNbO_7$, rel. to investig. of $PbO\text{-}KF\text{-}B_2O_3\text{-}PbNdTiNbO_7$ cross section 77–86004
PbO orthorhombic crystals grown from melt, followed by quenching 79–100038
PbSe-flux, boundary interfacial tension, rel. to Czochralski growth 77–35797
PbSe(Te), reaction kinetics in binary melts of KCl, NaCl and $PbCl_2$ 77–16486
$Pb_5(SiO_4)(VO_4)_2$ cryst. growth and elastic props., appl. in acousto-optical devices 78–19660
$Pb_{1-x}Sn_xSe(Te)$ single crystals, Bridgeman grown, X-ray exam. 79–56926
$Pb_{1-x}Sn_xTe$, cryst. growth rel. to IR detector fabrication 77–85911
$Pb_{1-x}Sn_xTe$, segregation during solidification by Bridgman technique 79–38735
$Pb_xSn_{1-x}Te$, for appl. in IR detector arrays, comp. control 80–31872
$Pb_{1-x}Sn_xTe_{1-y}Se_y$, quarternary solid solns. with const. lattice parameter, cryst. growth and characts. 80–108332
PbTe-flux boundary, interfacial tension, rel. to Czochralski growth 77–35797
PbTe-SnTe solid solns., directional solidification 77–44149
$PbWO_4$, growth by Czochralski method, props. 78–60566
$PbWO_4$, single cryst. growth by Czochralski method and U incorporation, effective distrib. ratios, luminesc. characts. 79–42094
$Pb(WO_4)_{1-x}(MoO_4)_x$, growth and props. 80–71588
$Pb(WO_4)_{1-x}(MoO_4)_x$ mixed crystal, growth by Czochralski method, props. 78–60566
$Pd(PO_3)_2$, synthesis and struct. 79–90623
Rb_2CrCl_4, cryst. growth by Czochralski technique 77–28710
$Rb_8Nb_{22}O_{59}$, growth and instability 78–35294
$(Sb,Bi)_2(Se,Te)_3$ profiled crystalline ingot continuous elongation 79–69975
$Sb_2O_4\text{-}NaSbO_3(KSbO_3)\text{-}NaF$, phase equilibria and crystal growth 77–70035
SbSI, crystal growth from SbI_3 flux 79–66000
$(Sb_2Se_3)_{0.7}(Bi_3Se_3)_{0.3}$, solid soln., prep. and elec. properties of layered crystals 80–70762
Sb_2Te_3, $Sb_{1.5}Bi_{0.5}Te_3$, Te- and Se-doped cryst. growth and elec. props. 77–48334
$Sb_2Te_3\text{-}Bi_2Te_3$, low-temp. thermoelectric mats., growth of microhomogeneous crysts. 77–48337
$Sb_2Te_3\text{-}Bi_2Te_3$ solid solns., bladed cryst. growth, electrophysical props. 78–43387
$Sb_2Te_3\text{-}Bi_2Te_3$ solid solns., single cryst. growth and thermocouple construct. 80–104056
$ScBO_3:Fe^{3+}$, ESR spectra, lattice parameters 80–93170
$Sc_2(WO_4)_3:Er^{3+}$, growth, solubility, absorption spectrum and thermal expansion meas. 77–36391
$Se_{90}\text{-}Te_{10}$ alloy crystals, growth and cleavage 78–88421
Se_xTe_{1-x}, growth of single crystals by Czochralski method 80–66423
Si 80–44200
Si (111), growth and etching vectors, adsorption and step reconstruction 79–23548
Si, annealing during Czochralski growth, influence on defect density 80–60769
Si, as-grown Czochralski crystal, multiple p-n junction structure obtained by heat treatment, appl. to solar cells 80–101099

crystal growth from melt continued
Si, carrier lifetime degradation at room temp. 78–95301
Si continuous polycrystalline films on C substrates 78–64490
Si, cooling rates of large diameter crysts. 78–35291
Si, crack free ingots, by directional solidification using heat exchanger method 79–8242
Si, cryst. growth, float zone, low ohmic seeds and dislocations 78–27398
Si crystal, high O_2 content, Czochralski growth parameters related to epitaxial stacking faults 79–4314
Si, crystal defects in integrated circuits, review 78–88547
Si crystal growth, for electronic devices 80–66419
Si, crystalline sheets production, low cost, crystal growth techniques comparison 80–35083
Si, Czochralski cryst. growth, faceted and nonfaceted, Sb microsegregation 80–45227
Si, Czochralski crystal growth and charact., oxidation induced stacking faults 79–47621
Si, Czochralski crystal growth, low O content 80–40251
Si, Czochralski crystals, O microsegregation, swirl defect distrib., growth rate depend. meas. 80–39295
Si, Czochralski grown, dislocation free, swirl defect form., doping effect 80–92519
Si, Czochralski grown, inhomogeneous O precip. and stacking fault form. 79–14820
Si Czochralski grown, O distrib. meas. 77–11580
Si, Czochralski grown crystal, radial impurity distrib. improvement 77–73225
Si, Czochralski grown crystal, O precip., nucleation behaviour and dislocation loop form. *(Japanese)* 80–59664
Si, Czochralski grown crystals, swirl-type defect obs. 80–100236
Si, Czochralski growth, drop form. and crystn. rel. to dislocation struct. 78–2030
Si, Czochralski growth, equilib. of dissolved C and O with CO in ambient atm. 80–1949
Si Czochralski growth, large crystal, convection and segregation 78–6843
Si, Czochralski growth and characterisation *(Japanese)* 79–43125
Si, Czochralski growth from heavily Sb doped melt, interface morphological instability 80–2939
Si, Czochralski growth of dislocation-free (110) crystals 79–100042
Si, Czochralski growth with automatic diam. control 78–52658
Si Czochralski wafer intrinsic gettering by oxide precipitate induced dislocations 78–6092
Si Czochralski wafer oxidation-induced stacking faults correl. with bulk defects 77–76428
Si Czochralski wafer oxide precipitate-dislocation complex characterisation 78–14357
Si, Czochralski-grown, oxide precip. form. process 80–49364
Si, Czochralski-grown cryst., swirl defect formation and defect migration 77–76405
Si, Czochralski-grown crysts., thermally induced microdefects, annealing temp. and starting material effects 80–49141
Si, deformed crystal, Czochralski and float zone growth, Luder's bands 79–79025
Si, dendritic film growth on alumina, solar cell appls. 77–77432
Si dendritic web growth, correlation of solute and interface partition coeffs. 79–24427
Si, dendritic web growth processes for solar cells, computer modelling 79–11508
n-Si, dislocation free, process induced cryst. defects 80–24392
Si, dislocation-free crystal point defect condensation 78–6026
Si, dislocation-free Czochralski-grown, detection of microamounts of O *(German)* 78–26592
Si, doping impurity distrib., during cryst. growth by Czochralski method *(Russian)* 80–100276
Si, EFG ribbon, characterisation by ion beam tech. 80–79833
Si, effect of C on dissolution of quartz in liq. Si, rel. to melt growth 80–70414
Si, failure in strong melt grown single crysts. 78–3205
Si, fivefold twinned crystals grown in Al-Si (16 wt.%) melt 80–2942
Si, from Al-Si-Cu melt, faceted cryst., cellular hole growth 77–4061
Si, growth and melting processes, origin of swirl defects 77–76407
Si, growth in vac., origin of SiC impurities 80–2940
Si, growth mechanisms of single crysts. with and without dislocations 77–89395
Si growth technology, erosion of graphite and vitreous C in molten Si 78–3244
Si, heteroepitaxy, refractory oxides as substrates *(French)* 77–44181
Si, high capacity arc heater production for solar cell manufacture 79–11509
Si, high-meniscus ribbon growth, thermal balancing via distributed inert gas streams 78–31329
Si, inclusion type defects removal from bulk of single cryst. by elec. fields 79–43126
Si, influence of imperfections on microplasma formation in p-n junctions 77–8177
Si ingots, polycrystn., growth and characterisation from metallurgical grade source material 79–87576
Si, interstitial swirl defect form. in dislocation free floating zone cryst. 77–7682
Si, introduction of defects during growth and processing 79–95925
n-Si, irrad. with 1.2 GeV electrons, form. of radiation defects 79–51156
Si, large single crystal production, using directional solidification tech. 78–35298
Si, laser annealing, nonequilib. incorporation of impurities during rapid solidification 80–55286
Si, liquid, interaction with die material during edge defined film fed growth 80–104060
Si low angle boundary formation, in single crysts., effect of impurities on cryst. growth conditions 80–11555
Si, low cost production for solar cells, growth from melt 78–3028
Si, melt and vapour growth for integrated circuits and solar cells 79–47609
Si, melt grown crysts., impurity incorporation, calcs. 80–79718
Si, metallurgical grade, purification and charact. 78–56573
Si, metallurgical-grade, fabrication by epitaxial growth or direct diffusion 80–101104
Si monocrystalline sheet fabrication for solar cells, CLF Czochralski furnace and enhanced slicing technology 80–93476
Si multicrystalline solar cell material prep., fast-pulled float zone, CZ and cast ingot and foil methods 80–93483

crystal growth from melt continued
Si, multiple ribbon growth by EFG 79−8245
Si on ceramic, coating with inverted meniscus (SCIM) technique, solar cell appl. 80−89163
Si on ceramic, for solar cell appl. 79−11511
Si plate prod. by Stepanov method, stability analysis *(Russian)* 78−52655
Si, polycryst. film, ion plating on Al, growth from eutectic melt 77−8765
Si, polycryst. layers, ribbon-against-drop pulling process 79−8241
Si, polycryst. manufacturing methods for photovoltaic energy prod., solar cells, grain growth from melt *(Dutch)* 78−52661
Si polycrystalline, low cost conversion into sheet by heat exchange method and fixed abrasive slicing technique 80−93479
Si, polycrystalline, ribbon to ribbon, using laser scanning, solar cell appl. 78−35299
Si, preshaped single crystal prep. by pendant drop method *(French)* 78−64466
Si, rapidly grown RTR sheet, props. and solar cell processing 79−100048
Si, reaction of rare earth impurities with carbon during cryst. growth 79−38733
Si ribbon, crystal characterisation, growth with dies 78−76598
Si ribbon, dendritic web growth, solar cell prod. and characterisation 77−77366
Si ribbon, dendritic web growth from melt, solar cell module fabrication 80−93478
Si, ribbon, edge-defined film-fed grown, orientation depend. of defect struct. 77−1134
Si ribbon, edge-defined film-fed growth, solar cell prod. and characterisation 77−77365
Si ribbon, edge-defined film-fed growth, melt temp. distrib. 79−52108
Si, ribbon, impurity distrib. in EFG 78−91280
Si ribbon, low angle sheet growth technique, direct shaping characts. 80−93480
Si ribbon crystal growth, 10 cm wide, temp. distrib. meas. in die 80−104059
Si ribbon crystals, edge-defined film-fed growth technique for solar cells 80−89633
Si, ribbon edge-defined film-fed growth control using C-CD imagers 78−68623
Si ribbon growth, ribbon-to-ribbon process, thermal environment control 80−35116
Si ribbon growth, Stepanov technique, recent develop. 79−11510
Si ribbon growth by capillary action shaping technique 80−29888
Si ribbon growth by EFG, thermal sensitivity and stability 80−107080
Si, ribbon growth by edge-defined film-fed process, morphology, stability 77−24947
Si ribbon growth from melt, monitoring device for width and thickness uniformity 80−35077
Si, ribbon growth via RTR technique, process update and material characterisation 78−76597
Si ribbon parallel twinned structure development by shaped crystallisation 78−64465
Si ribbon-graphite in-situ thermocouple, calibration and meas. accuracies manufacture 79−97386
Si ribbons, capillary action shaping tech., lifetime charact. 78−34847
Si ribbons, dendritic web for solar cells 80−89634
Si ribbons, edge-defined film-fed growth technique for solar cells 80−89138
Si ribbons grown by capillary action shaping technique, surface quality and impurity distrib. 80−108343
Si, ribbons produced through capillary action shaping, elec. and struct. characts. 78−47804
Si sheet casting for solar cells 80−89139
Si sheet edge-defined film-fed growth, for photovoltaic cells 79−61982
Si, single cryst. growth in clear SiO_2 crucibles, heat exchanger method 79−33919
Si single crystal, improved horizontal ribbon growth technique 80−108345
Si single crystal growth, Czochralski method, small-angle dislocation boundary form. anal. 80−89136
Si single crystal growth advances 78−6842
Si single crystal growth by heat-exchanger casting 78−11104
Si single crystal ingot growth from metallurgical grade Si, inhomogeneities 80−59416
Si, single crystal ribbon growth, thermal anal. 78−3029
Si, single crystal sheets grown from melt require no slicing or polishing 79−74079
Si, small defects in Czochralski grown and zone-floated monocrystals, TEM identification 79−95001
Si solar cell, transition metal doped Czochralski and web crystals, measurement of impurity effects 78−35297
Si solar cell fabrication from multiple ingots using melt replenishment Czochralski method, cell anal. 80−93477
Si solar cells, capacitance transient spectra of processing- and radiation-induced defects 80−61340
Si solar cells, crystal growth, heat exchanger method, fixed abrasive slicing technique 80−35082
Si, solar grade, advances in Dow Corning process 79−8243
Si, solar grade, Czochralski growth, solar cell efficiency vs. metallic impurity conc. 78−31330
Si, solar grade, directionally solidified using C crucibles, TEM study 79−47617
Si solar power cell production by capillary action shaping technique 79−34431
Si, solar-grade, directional solidification in carbon crucibles 80−45663
Si, square single crystals, Czochralski growth 80−97422
Si strips, growth by Stepanov's method 79−78867
Si, swirl type defects in float-zone and Czochralski single crysts. 79−27992
Si, temp. distrib. in working zone of composite heater, heat transfer calc. 78−3016
Si thin ribbon grown at high speed, thermal stresses, reduced thermal buckling 80−107078
Si tube growth by EFG process 80−108344
Si wafers, Czochralski, gettering of surface and bulk impurities 78−64456
Si wide ribbon, high speed edge-defined film-fed growth 80−104058
Si, wide ribbon crystal growth apparatus 78−48307
Si:Al ribbon, edge-defined film-fed growth, Al redistrib. 80−29873

crystal growth from melt continued
Si:B(Sb)(P), microdefect formation depend on doping, Cu decoration, X-ray transmission topography, preferential etching 79−69120
Si:C(O)(Sb), striated impurity distributions calc. 80−24488
Si:O, C, impurity conc. profiles and process-induced defects 78−6094
Si:O, IR absorpt. at low temp. *(Chinese)* 80−108228
Si:P, Czochralski growth, dopant evaporation coeffs., resistivity distrib. 77−16487
Si:P Czochralski crystal donor homogenisation by thermal neutron irradiation 78−6108
Si:Sb, dopant microsegregation rel. to crystal and crucible rotation 78−11106
Si:Sb crystal Czochralski growth, radial microsegregation analysis 78−11105
SiAs, cryst. growth from melt, elec. props. 80−76170
β-SiC, polytype stability, $\alpha \rightarrow \beta$ phase transformation during growth 78−6028
SiC:Al(B)(Ga), 4H-, 6H- and 3C-polytypes, melt growth and photoluminesc. 77−24885
α/β-Si_3N_4, phase yields during form., influencing factors 80−108408
β-Si_3N_4, single cryst., growth from Si melt in N_2 atmosphere, growth mechanism 79−24429
Si_2Te_3, growth by Bridgman technique and sublimation, cryst. struct. 77−1106
SmB_6, crystal preparation, elec. resistance, phase transitions 80−97427
Sn, crystn., mechanism of influence of soluble impurities 78−71692
Sn white crystals grown by Bridgman method, dislocation density, cryst. width 79−100045
$Sn_xMo_6S_8(Se_8)$, prep., metallurgical and supercond. props. 77−32102
SnS, single cryst. growth and struct. props. 79−52109
SnS_2, crystal growth and optical props. in visible and IR regions 77−52114
SnSe, single crysts., growth by Bridgeman technique, electron diffr. anal., lattice consts., carrier conc. 79−47616
SnTe, annealed, iodide method of prep., props. meas. 80−71591
$Sr_{0.75}Ba_{0.25}Nb_2O_6$, large cryst. growth, control of opt. defects 78−76595
$Sr_{1-x}Ba_xNb_2O_6$, and Nd doped growth of low dislocation density cryst., dislocation struct. 77−40348
$Sr_{1-x}Ba_xNb_2O_6$ crysts., defect-free growth 80−108346
$SrCoO_{2.70}$, growth and props. 78−48310
$Sr_4NaLiNb_{10}O_{30}$, single cryst. growth, Czochralski method *(Chinese)* 79−74078
4 $SrO.B_2O_3.SiO_2$, crystal struct., X-ray powder diffr. patterns *(Japanese)* 80−54209
$SrTiO_3$, crystallisation from melt, nucl. and final cryst. sizes 77−24951
$SrTiO_3$, defects grown by Verneuil method 77−51390
$SrTiO_3$, flame fusion growth of optical quality crysts. 78−11099
$SrWO_4$ cryst. growth, from Na_2WO_4 melts, thermodynamic props. 80−107084
$SrWO_4$, single cryst. growth by Czochralski method and U incorporation, effective distrib. ratios, luminesc. characts. 79−42094
Tb-Y, single crystal growth from melt, X-ray obs., props. *(Russian)* 78−95689
TbB_4, Czochralski crystal growth 79−95920
TbF_3, crystal growth by Bridgman-Stockbarger method 78−52660
Te, Czochralski growth of single crystals 79−4912
Te, growth of single crystals by Czochralski method 80−66423
Te, single crysts., Czochralski growth, etch pit orientation study 79−43133
TeO_2, Czochralski-grown oxide crystals, fluid-flow effect on gas-bubble entrapment 80−84121
ThO_2 single crystals, crystal growth, using crucibleless skull melting technique 78−39681
TiC single crystals, synthesis and impurities 80−55329
TiO_2, crystal growth from melts in Bi_2O_3-V_2O_5-TiO_2 system 78−19659
TiO_2, plasma growth, photoelectronic props. 78−52662
Ti_2O_3, cryst. growth by chem. transport and tri-arc methods, and characterisation 78−3003
Ti_nO_{2n-1}, cryst. growth and characterisation 78−31311
Tl single crystals, growth and polishing procedure for (0001) face 79−78870
Tl_3AsS_4, crystal growth by Bridgman-Stockbarger method, exam. of props. 79−11506
TlBr-TlI crystals, Pb halide impurity distribs. for various cryst. orientations 79−51135
$Tl_2U_yF_{x+4y}$, cryst. growth from flux, crystallographic characts. *(French)* 77−77364
$Tl_2V_2S_6$ single crystal growth, Bridgman-Stockbarger technique 80−89132
Tl_3VS_4, growth of inclusion free crystals, for surface wave and bulk wave acoustic devices 80−25549
$Tm_{1-x}Y_xTe$, ($0 \leq x \leq 1$), single cryst. growth and characts. 78−23603
$^{235}UO_2$ single crystals, electrochemical prep. 78−37478
V_nO_{2n-1}, cryst. growth and characterisation 78−31311
V_3Si, chemical composition effect on phase transition and transition temp. 78−14860
V_3Si, Czochralski growth, supercond. behaviour 79−74080
W, high purity, zone-refining growth, radial distrib. of structural defects *(Russian)* 79−19250
WB_{12}, growth from melt and phys. props. 80−20782
WO_3, struct. transforms. during crystallisation from P_2O_5-WO_3-CaO 77−40343
$(Y,Sm)_3(Ga,Fe)_5O_{12}$ films, growth from melt, growth property control 78−27395
$(Y,Gd,Yb)_{3-x}Bi_x(Fe,Al)_5O_{12}$ film growth on $Gd_3Ga_5O_{12}$ substrates 79−78623
YAG, Czochralski grown crystals, interface shape change 78−83760
YAG Czochralski grown crysts., growth of facets and vicinal interfaces *(Chinese)* 79−90578
YAG, facet formation 78−63687
YAG, influence of facial growth effect on Yb ion incorporation 79−10822
YAG, molten, complexity in solidification behaviour, SEM electron images 79−43229
YAG single crystal growth, by vertical directed crystn., thermal characts. 80−2944
YAG, single crysts., melt growth using heat exchange method 79−52106
YAG:Ce phosphors, luminesc. efficiency, prep. and dopant effects 80−45151
YAG:Ho^{3+}, spectroscopy, stimulated emission 80−93374

crystal growth from melt continued
YAG:Nd, laser cryst., dislocations density and propag., rel. to Czochralski growth *(Chinese)* 77—11552
YAG:Nd, single crysts., melt growth using heat exchange method 79—52106
YAG:Ti, growth conditions from melt 79—95924
$YAl_3(BO_3)_4$, and $(Y,Er)Al_3(BO_3)_4$, crystallisation and growth characts., density and composition 80—35080
$YAl_3(BO_3)_4$, solubility in fused potassium trimolybdenate and seeded cryst. growth 77—43330
$YAlO_3$, cryst. growth with $Y_3Al_5O_{12}$ by flux method 77—24950
$YAlO_3$, $YAlO_3$:Nd, colour centre form. rel. to growth conditions, absorpt. spectra 79—90652
$Y_3Al_3O_{12}$ crystal growth from melt, gas bubble capture theory 80—64941
$Y_3Al_5O_{12}$, cryst. growth with $YAlO_3$ by flux method 77—24950
YB_4, Czochralski crystal growth 79—95920
YB_{68}, melt grown, props. meas. 77—11518
YIG, growth from molten soln., improved crucible shapes *(German)* 77—1800
YIG, single cryst. growth by floating zone method 78—19656
YIG:Ga, growth by high-resolution induced striation method, mass transport 77—1802
Y_2O_3, cooling rate in melt-growth effect on struct. perfection 77—85925
Y_2O_3, dislocation density depend. on crystal pulling rate 77—81210
Y_2O_3-R_2O_3, (R=La,Nd,Sm,Gd and Dy to Yb), cryst. growth by Verneuil method 77—1803
Y_2WO_6, growth from soln. in melt 77—1806
$YbAlO_3$, single crysts., prep. and phys. props., X-ray struct. anal. 79—4298
$YbGa(In)_2X_4$, X=S,Se,Te, prep. and props. 77—85214
Zn, bicrystals grown by modified Bridgman technique 78—60563
Zn, growth from melt, conditions influencing dislocation struct. *(Russian)* 80—97424
Zn, highly perfect crysts., Bridgman growth, dislocation density rel. to annealing *(Japanese)* 80—40252
Zn, shaped single crystal prod., twinning 78—2040
$ZnGeP_2$, synthesis, characts., applic. to laser windows *(French)* 78—80467
$Zn_{1-x}Mg_xTe$ alloy, model explanation of liquidus surface *(French)* 77—21019
ZnO-Nb_2O_5 system, Czochralski growth, phase relations and cryst. data 78—9975
Zn_3P_2, single crystal, growth, electronic and device props. 80—25551
ZnS, Bridgeman growth under pressure, macroscopic inclusions and defects 80—45226
ZnS, cryst. grown from melt under press., microstruct. 77—59019
ZnS, low resistivity, prep. and characterisation for blue LEDs 77—81209
ZnS, single cryst., RF heated, impurity distrib. coeffs. 77—55298
ZnS-MgS, solid solution, prep. of single crystals with wurtzite structure, exam. 79—1821
$ZnS_{1-x}Te_x$, polytype single cryst. by Bridgman's method 79—14762
ZnSe, Bridgeman growth under pressure, macroscopic inclusions and defects 80—45226
ZnSe, Bridgman growth under Ar press., temp. distrib. in furnace 78—11100
ZnSe, single crysts., grown from melt under Ar pressure, defects form. 79—4312
ZnSe, twinning on melt-growth under pressure 77—80515
ZnSe:Ag(In)(Cu), melt growth, dopant partition coeffs. 79—14837
$ZnSe_xS_{1-x}$, melt grown, 10K, band edge photoluminesc. 78—84628
$ZnSiAs_2$, cryst. growth and elec. props. *(French)* 77—76815
$ZnSnP_2$, characts. of Zn-Sn-P phase diag. 77—44225
ZnTe, growth from In solvents, self-compensation 77—28144
ZrC single crystals, synthesis and impurities 80—55329
$ZrSiO_4$, single cryst. growth from soln. in melt, solvent system selection 80—55285

crystal growth from solution
see also crystal growth from gel; liquid phase epitaxial growth
actinide metals and their refractory cpds., synthesis from oxides and single cryst. growth 80—16229
adenine hemisulphate hydrate, single cryst. growth from soln., props., cryst. parameters, X-ray anal. 79—32929
adenine sulphate, single cryst. growth from soln., props., cryst. parameters, X-ray anal. 79—32929
adsorbed film of soln. on cryst. surface, NMR investig. 77—8426
adsorption, localised in one layer, on cryst.-soln. interface, using Bragg-Williams monolayer model 79—46582
$AgBi(CrO_4)_2$, synthesis, thermolysis, crystallography *(French)* 80—33946
alkali metal compounds, $MAlF_4$, (M=K, Rb, Cs), hydrothermal growth method in presence of hydrofluorhydric acid *(French)* 80—25543
alkaline earth compounds, $MB_{12}H_{12}.xH_2O$, M=Ca,Sr,Ba, cryst. growth from soln. and morphology 77—44145
n-alkane, adsorption energy of mols. on long-chain even n-alkane crysts., rel. to cryst. growth kinetics 78—42933
alternating mixing, electronic device 80—25546
amethyst, natural form. conditions and optimum artificial growth conditions *(French)* 79—33911
amethyst large cryst. growth from hydrothermal fluoride soln. 78—11098
p-anisidine, single cryst. growth from cyclohexane-water immiscible system 80—40244
anthracene, substrate prep. for selective epitaxial growth of anthracene 77—63558
benzoic acid, single cryst. growth from nitrobenzene-water immiscible system 80—40244
birefringent crystal faces, meas. method of growth and dissoln. rates 80—79719
bisphenol-A-epichlorohydrin copolymer, single cryst. aggregate growth 77—27842
Burton-Cabrera-Frank surface diffusion model. 80—59415
$CaCO_3$, calcite, linear growth rate by pH-stat method *(German)* 79—74073
calcite, crystal intergrowth condensation-crystallisation contact bridge, between dissimilar crystals 79—65332
calcium phosphates, seeded growth, effect of solid/soln. ratio, calcification 78—15303
camphor crystals, investigation of structural formation and growth kinetics 79—47610
capillary tube crystn., grain diameter distribs. 79—41999

crystal growth from solution continued
cellulose, shish kebab-like structures 77—62485
cellulose II, preparation and crystal growth, electron diffr. obs. 78—91285
chalcopyrites, for electrolum. device appl., props. and technology, book contrib. 77—73175
m-chloronitrobenzene, crystal growth from soln., obs. of surface steps using cine camera 77—76341
citric acid monohydrate, crystallisation and cryst. growth rate 78—87638
colloidal crystals, single, prod. technique 79—99097
complex oxide crystal flux growth, starting comp. prediction 77—48331
convection effects, holographic interferometic obs. 80—77565
corundum, bladed crystals, morphology and struct. 77—84680
corundum single cryst. growth from Na_3AlF_6-xLi_3AlF_6 system fluxes 78—11094
Coulter counter technique, new method to follow cryst. growth rate in precipitating systems 79—52100
cryolite, hydrothermal synthesis of large synthetic single crystal, props. 78—19654
crystal frequency distribution, simulation taking nuclei distrib. into account 80—100184
crystal growth, from liquids at high temps., review 79—15602
crystal size distribution, from cascade of mixed tanks 78—39678
crystal-solution interfacial tension, from crystn. meas. 79—69045
crystallisation systems, and their mathematical models 80—100186
crystalliser, with precision control of supersaturation 78—80465
CTA-DNA crystal growth and morphology 80—26198
cube growing from infinite quiescent soln., diffusion about cube 77—47361
cubic crystal growth, from soln., numerical soln. 80—88074
cycasin, cryst. growth and struct. 78—18631
cytosine hydrochloride, cryst. growth, crystallographical parameters 78—14332
cytosine monohydrate, cryst. growth from aq. soln., elec. props. 78—3007
cytosine monohydrate single crystal growth, effect of pH 79—34473
dendrite growth on ion emitters for field desorption mass spectroscopy 79—2873
dialkylammonium compounds, $(C_nH_{2n+1}NH_3)_2MX_4$, cryst. growth solubility, and props. 78—43999
diamond, crystallisation in C-metal system, kinetic peculiarities of transport processes 77—15331
diamond, metastable overgrowths in dissoln. medium in Ni presence at atm. pressure 79—51030
diamond, polycrystal growth under ultra high pressure *(Chinese)* 79—78863
diamond solid-fluid interface roughening transition, Monte Carlo simulation 79—99088
p-dichlorobenzene, contact nucleation 77—52661
diffusion apparatus, modified, for growth of single crystals 78—35290
diffusion coefficients in water soln., holographic interferometry control 78—39680
diffusion controlled constant growth rate with nonequilibrium interface conditions 77—72571
diffusion kinetics, crystallisation of salts from supersaturated solns. 79—23553
diffusive crystal growth, numerical soln. accounting for growth rate and surface tension anisotropy 80—33912
diffusive mass transfer in crystal growth, exam. 78—67669
diglycine nitrate, cryst. growth, dielec. and electromech. props. 80—2701
dipropylammonium manganese chloride, layer perovskite, step bunching obs. by compound holographic microscopy 78—63682
discontinuous growth, effect of equilib. segreg. at boundaries 77—51336
DNA-cetavlate crystal growth and morphology 77—66583
electrolyte, binary, cryst. growth kinetics during precipitation 80—49149
equilibrium form of crystal *(Japanese)* 80—24395
evaporative vacuum crystallizers, modified design 77—81204
far IR thin crystal pyroelectric detector development 77—37994
ferromagnetic semiconductors, cryst. growth, review 77—85923
fluorite, crystal intergrowth condensation-crystallisation contact bridge, between dissimilar crystals 79—65332
flux growth, crystn. conditions expt. method *(French)* 77—63552
flux growth, melt column shape 78—3006
flux growth, modification of starting composition effects 78—48298
flux process for large cryst. growth 78—31316
1-formyl 2(4-nitrophenyl) hydrazine, preparation, optical and electro-optical props. 77—36201
free convection about rectangular prismatic cryst. growing in soln. 80—19382
garnets, magnetic, cryst. growth from high-temp., solns., book contrib. 79—69973
germanates, growth from PbO-GeO_2 flux 77—16484
glutamic acid hydrochloride, L(+), single cryst., soln. growth and characterisation, SHG 77—24943
glutamic acid hydrochloride, L(+), solution growth of large single crystals, using cylindrical seeds 78—60556
glyceryl tristearate, surface entropy factor calc. 78—42934
grow rates, random processes theory to study fluctuations 79—55689
growth, and dissoln. of crysts. in suspension, kinetic expts. anal. 80—59414
growth affinity, a driving force for crystallisation 79—23554
growth curves, growth affinity presentation, for growth from soln. 79—27936
growth dispersion 80—49148
growth rate studies 80—100188
growth rates determination, in batch fluidized beds 80—100187
gypsum, crystal intergrowth condensation-crystallisation contact bridge, between dissimilar crystals 79—65332
habit, modification control in growth 80—49150
helical impurity distrib. produced by hydrodynamic instability, vertical solidification 78—30567
hexachloroparaxylene, crystn. from heptane, optimising purification 80—100774
hexamethylene tetramine, cryst. growth kinetics from soln., role of solvent-solute interactions 77—24282
hexamethylene tetramine crystals, growth from aqueous and ethanolic solns., (110) surface struct. 77—76338
hexamethylene tetramine in water-acetone soln., crystal growth kinetics 78—30554
hexatricontane, growth kinetics of (001) faces from soln. 79—52098
α-HgS, cryst. growth from soln. at low temps. 80—7487
high compression crystal growth system 80—66415

crystal growth from solution continued
C-,D-$Ho_2Si_2O_7$, single cryst. flux growth, polymorphic forms study by X-ray methods 79—52097
hollandites, cryst. growth and structural props. 80—89129
homogeneous solid solution crystallisation crucible 80—45224
L(+) hydrazonium tartrate, soln. growth and cryst. morphology 79—33914
hydrodynamic conditions, on second order surface reaction cryst. growth 80—49152
hydrodynamic environment effects review *(French)* 80—29872
hydrothermal growth, physicochemical aspects 78—3011
hydrothermal synthesis, kinetics of crystal growth on seeds, quality of crystals 80—16169
hydrothermal synthesis and growth, selection of mineralisers 78—72715
8-hydroxy quinoline, single cryst. growth from cyclohexane-water immiscible system 80—40244
III-V compound crystal growth from solution, computer simulation 77—51332
III-V quaternary alloys, melt and soln. growth of bulk single crysts. 80—35079
III-V semiconductors, crystal growth by travelling heater method 80—11553
impure, and pure systems, cryst. growth 80—49145
impurity incorporation into vicinal faces, interface model 80—84127
impurity role, in crystn. 80—49146
industrial crystallisation, progress in cryst. growth from soln. 80—49147
interface reaction const., correl. with elementary surface process 78—63683
ionic crystal growth, fast growth of ordered AB crystals, Monte Carlo simulation 79—19165
ionic crystals, precipitation from aq. solns., induction period 80—50882
ionic crystals, solvent effects and growth kinetics 79—19169
irreversible process anal., mutual interf. of heat and material flow 77—47367
kinetic stability of plane-faced crystal growth forms 78—47259
kinetics, soln. pH effect 79—99095
lamellar-spiral growth hillocks, kinetics and morphology 78—18566
lecithin cryst. growth rel. to mol. bilayer props. 78—31780
leucosapphire single cryst., W grid reinforced, growth 77—16530
lithium formate, isotope exchange during crystallisation from aqueous solns. 78—18569
low gravity growth 78—84706
lysozyme effect of pH on dimorphic crystal growth 79—14728
magnetic bubble materials, props. and preparation models, review *(Rumanian)* 80—93149
magnetic oxides, hydrothermal crystallisation, for mag. appl., review book contrib. 79—69974
manganese carboxylate, dodecanuclear mixed-valence, prep., struct., and mag. props. 80—107196
materials processing in space 78—35296
materials processing in Spacelab 78—35295
mechanical stresses caused by growth centres 80—19735
mechanism, equil. props. of crystallising systems, theoret. interpret. *(Rumanian)* 80—88073
mechanism, role of solvent-solute interactions, surface entropy factor 77—24281
metal halide layered materials, prep. and growth, book contrib. 78—19648
metal ion adsorption, nucleation effects *(German)* 78—68635
metallic systems, in-situ obs. of solidification interfaces with 1 MeV electron microscope 79—87574
N-methyl-piperidinium-acet-meta-chloro-anilide-iodide, crystallisation from water, X-ray exam. of cryst. struct., mol. config. *(German)* 79—51095
monostearine crystals, spiral growth from organic soln. 80—93467
morphological stability, cube grown from soln. without convection 77—51333
morphological stability of plane interface, electrocrystallisation from molten salts 77—35497
morphology analysis in crystal dissolution 79—99089
multisection continuous crystalliser, process control 80—2935
naphthalene crystals, investigation of structural formation and growth kinetics 79—47610
natural mineral crystal growth characts. 78—32072
$NH_4H_2PO_4$, cryst. growth from aqueous solns., dislocation groups in (100) faces, kinetics 79—74072
nosean identification, in sodalite and conversion of nosean sodalite 80—84907
Nylon 6, solution crystallization 79—86719
octacosane crystals, complex growth polytypism and periodic polysynthetic twins 77—47360
organic compounds, recrystallisation, solvent selection, student experiment 79—84917
organic crystals, computer simulation 78—30558
paradibromo benzene crystals, investigation of structural formation and growth kinetics 79—47610
periodic mass crystn., kinetics and max. supersaturation *(German)* 79—41997
(perylene)$_3$TCNQ, prep. and spectra, electron-mol. vib. coupling 77—16290
phlogopite, solubility in basic aqueous solns. under hydrothermal conditions 78—43127
phloroglucinol dihydrate crystals, growth characts., X-ray diffr. and optical microscopic study 79—19986
phthalic anhydride, dendritic growth 78—18936
poly(trans-1,4-butadiene), crystals in suspension, epoxidation kinetics 79—61861
poly-m-phenylene isophthalamide-ε-caprolactam, complex polymer cryst. 78—9967
polyacrylonitrile, single cryst. formation, during soln. polymerisation, struct. determ. 80—38938
polyethylene, shish kebab structure, formation mechanism 78—14286
polyhedral crystal growth from soln., morphological stability 78—26466
polymer, row nucleation, phenomenological model 78—14301
polymer nucleation, bundle-like and longit. growth of fibrillar crystal from flowing soln. 78—51433
α,ω-polymethylene diammonium metal (II) tetrahalides, cryst. growth, solubility and props. 78—43999
polystyrene, soln. grown isotactic crystals, degree and distrib. of crystallinity, thermal stability 78—9964
polystyrene, solution grown isotactic crystal, thermal change kinetics study by X-ray diffr. 78—9965

crystal growth from solution continued
precipitation processes, study by particle site anal. 80—50883
programmable temp. controller for crystal growth expts. 77—24944
proteins, effect of protein conc. and solubility on nucleation rate 78—87632
proteins, globular, cryst. growth kinetics 80—35823
PVC:Fe(Cu) film, struct. and optical props., soln. growth technique 78—51837
pyrophosphatase, inorganic, of yeast, cryst. growth, derivatives formation, heavy atoms positions 80—108842
quartz, crystal growth in fluoride environment, growth features and props. 80—6373
quartz, crystal intergrowth condensation-crystallisation contact bridge, between dissimilar crystals 79—65332
quartz, cultured, hydrothermal growth, prism face develop. rel. to microcryst. form. 77—72572
quartz, hydrothermal cryst. growth, appl. of O isotope doping technique 77—28706
quartz, hydrothermal crystallisation, role of soln. density 80—10516
quartz, hydrothermal crystn., new natural nutrient sources 77—8738
quartz, hydrothermally grown single crystals, real struct. investig. of rhombohedral faces *(German)* 78—2348
quartz, microtopographical obs. of 2nd order prism faces, hydrothermally-grown crysts. 80—54481
quartz, optical quality, culturing process 79—81494
quartz, synthetic, as-grown and etched cobbled Z-surfaces, SEM obs. *(French)* 80—24719
α-quartz, synthetic, growth, defects induced by seed orientation 80—96454
quartz, synthetic, growth forms and interface molecular group waviness correlation *(Chinese)* 79—51027
quartz, synthetic, metallic impurity incorporation 79—19167
quartz, synthetic single crystal, impurity content 77—11583
quartz crystal manufacture, Z-plate, Japanese technology 79—91575
quartz crystals, synthetic, using large autoclaves with 400 kg/batch capacities 79—91576
α-quartz dislocation free and low dislocation, prep. by hydrothermal crystallisation 78—72712
quartz single cryst., mech. Q depend. on soln. growth rate 78—9978
quartz synthetic, lattice spacing and orientation variation with growth sectors 79—52099
quartz synthetic crystals, observation of growth defects by light scatt. tomography 78—71743
quasi-one and -two dimensional materials *(Japanese)* 80—35073
rare earth gallium garnet, growth of crystals from $50PbO.40PbF_2.10B_2O_3$ flux 77—21014
rare earth garnet prep., novel Li_2MoQ_4-$R_2(MoO_4)_3$ flux system 77—48359
rare earth garnets, prep. and props. book contrib. 80—44193
rare earth germantes, flux-grown, X-ray topography 80—64939
rare earth oxides, binary, struct. and props., book contrib. 80—45292
rare earth oxymolybdates, growth from soln., struct., props. 77—28705
rare earth potassium molybdates, flux growth of $RKMo_2O_8$, R_2MoO_6 and R_6MnO_{12} in R_2O_3-K_2O-MoO_3 system 78—35289
rare erath oxytungstate, growth from soln. in melt 77—1806
(rare-earth) $Fe_3(BO_3)_4$, cryst. growth from soln.-melt, props. 80—108337
rare-earth-Ti_2O_7, flux growth 79—83113
rate constant of reaction, determ. from overall crystal growth coeff. 78—59773
review, sparingly soluble single crysts. from soluble complexes 80—29868
roughening transition of crystal surface, exactly solvable model 77—47368
rubidium acid phthalate, solution growth of large single crystals, using cylindrical seeds 78—60556
salol crystals, investigation of structural formation and growth kinetics 79—47610
seawater, unusual cryst. growth 80—26516
silicate gardens, growth morphology, mechanisms 80—100765
silicates, growth from PbO-SiO_2 flux 77—16484
sillimanite-mullite intermediate phase, crystallisation under hydrothermal conditions 77—44137
size dependent crystal growth, new empirical kinetic equation 78—38637
sodalite, crystallisation process, effect of solid and liq. boundary layers, SEM 79—23544
sodalite, hydrothermal growth on seed crysts. covered with boundary layers, growth mechanism 78—30571
sodalite single crystals, exam. of growth mech. in hydrothermal method, using SEM 79—52105
sodium acetate trihydrate, whisker growth on membrane in aq. soln. 78—30854
sodium aluminium tartrate, β-particle effects on crystallisation from aq. solns. 77—36387
solution concentration, interconversion during crystn. 80—100773
sparingly soluble salts, aqueous supersaturated solutions, scale formation, biological mineralization 79—43119
stability criterion of polyhedron and infinite plane face rel. to various types of perturbations 77—11497
stearic acid, grown from benzene soln., etch pit obs. of dislocations 78—87676
stearic acid, large single cryst. growth from organic soln. 78—31314
stearic acid, single cryst., characterisation *(Japanese)* 79—46587
stearic acid, single cryst. growth mechanism 78—30562
stearic acid crystals grown from solution, spatial correlation between growth spirals and inclusions 80—96527
succinonitrile, undercooled, analysis of dendritic growth 78—75970
sucrose, mathematical model of crystn. rate in pure solns. 80—49151
sucrose crystal formation, and growth, effect of same metallic impurities 80—100768
supersaturated soln., shape stability of growing cylindrical particle due to diffusion and interface kinetics 80—79720
supersaturation evaluation, in cryst. growth from soln. 79—46584
surface entropy factor calc. 78—42934
suspension concentrates, physical stability criteria, review 80—45562
TCNQ solids, quasi-one and -two dimensional materials crystal growth *(Japanese)* 80—35073
tetraoxane crystals, growth and perfection by evaporation of solns., X-ray topography 79—61510
tetrathiotetracenenickel bis(ethylene-1,2-dithiolene), one-dimens. cond., preparation and props. 77—85201
TGFB, deuterated, single cryst. growth from soln. and props. 79—24422
TGS, crystallisation by epitaxial germination *(French)* 77—21040

crystal growth from solution continued
TGS, deuterated, undoped and alanine-doped, growth by rotating disc method and elec. props. 79−47611
TGS, effect of aniline in aqueous crystal growing soln. on physical props. 78−43810
TGS, epitaxial growth method from soln., on Ag layer 77−32536
TGS, growth from solution containing aniline, dielec. and pyroelec. props. 78−6639
TGS, growth of large area, doped and undoped crysts. by rotating disc method 78−19652
TGS, orientation depend. of l-alanine incorporation 78−42938
TGS, pure and Cu doped, growth from soln., dislocation density 79−52096
TGS, soln. growth of large single crystals, using cylindrical seeds 78−60556
theory, review *(Chinese)* 80−66414
thermodynamics of adsorbed layers, Gibbs formulation 77−76336
TMTTF-TCNQ crystals grown from several organic solvents 80−25544
transition metal borides, refractory, single cryst. prep. methods and characterisation, book contrib. 78−48296
transition metal fluorides, flux growth 79−65991
transition metal oxalate hydrates, powders, precipitation from aq. solns., cryst. numbers, sizes 77−44143
transition metal oxides cryst. growth, using $K_2S_2O_7$ as flux material 80−71582
triglycine fluoberyllate, deuterated, dislocation line defect X-ray topographic analysis 80−59465
triglycine fluoroberyllate, solution growth of large single crystals, using cylindrical seeds 78−60556
TTF-TCNQ-d_8, large single cryst. platelet growth by diffusion method 78−3010
two-step mechanism, anal. and identification 80−100190
unsaturated solutions, crowded ripening 77−62492
urea mixed and adsorption mixed crystals and epitaxial growth from solns., tracht and habit *(German)* 80−38973
urea monocrystals from aq. soln., growth kinetics 79−99092
uric acid occurrence, growth morphology of $C_5H_4N_4O_3$ anhydrous monoclinic modification 80−84123
vapour, SiC cryst. growth from soln. in Si, temp. gradient method 78−35301
viscosity, rel. to temp. 80−100189
vitamin B_{12b}:B_{12r}, cryst. growth, orientation, ESR obs. 79−34486
water thermostat, linear thyristor control and thermistor sensing *(Japanese)* 77−90264
YIG, cryst. growth from high-temp. soln., book contrib. 79−69973
zinc oxalate, isothermal crystallisation from soln. 80−108336
Ag, crystal (100) faces, polynuclear growth mechanism during electrocrystallisation *(German)* 78−18562
Ag, electrocrystn., screw dislocation free (100) face growth kinetics 78−30557
Ag filaments, cryst., electrolytic growth in Teflon capillaries, differential-capacity meas. 77−40552
Ag growth in Ag-Bi and Ag-Pb melts, transition from round to face forms *(Russian)* 79−28906
Ag halide emulsion crystal growth, complex solubility computation 79−83516
Ag halogenide, grain form. and growth in metastable soln. *(Russian)* 77−34048
Ag, single crystal, adsorption of metal ions on (111) and (100) surfaces *(German)* 78−68636
AgBr, crystal growth behaviour, influence of Gibbs-Thomson effect 78−24883
AgBr monosize emulsion growth 79−79312
AgCl microcrystals in sol., cryst. growth, optical absorpt. 77−12835
$Ag_xHg_ySI_2$, prep. of mixed sulphide iodides, photochromism 77−36385
AgI large single crysts., gel and soln. growth and props. 80−35071
AgI nascent hydrosol absorption spectra and microcrystal growth 79−100449
AgI precipitations, effects of pAg on crystal growth 79−19172
$AgNbO_3$, cryst. growth and phase transitions 80−40243
$AgNbO_3$, single crysts. flux growth, space group determ. 80−55282
$AgTaO_3$, single crysts. flux growth, space group determ. 80−55282
Al-Ga-Sb system, ternary phase diagram and appl. to soln. growth 79−74135
AlB_{12}, preparation of single crystal 78−43997
$Al(HSeO_3)_3$, synthesis under hydrothermal conditions 77−85918
$Al_2In_{12}Se_{21}$, cryst. growth from melt, elec. props. 79−56922
$AlK(SO_4).12H_2O$, growth and dissoln. rates 80−50545
$AlM_xH_{1-x}(SeO_3)_2.nH_2O$, M=alkali metal, hydrothermal crystallization, thermal decomp. 77−90265
$Al_3Mg_2[Si_5AlO_{18}]$, cordierite cryst., effect of face symmetry on structural ordering of Al 78−22703
Al_2O_3, corundum, growth mechanism in cryolite flux 78−30563
$AlPO_4$, hydrothermal synthesis 78−48297
$AlPO_4$ hydrothermal synthesis 78−60562
$AlPO_4$ solubility, in H_3PO_4 hydrothermal soln., conditions for cryst. growth *(French)* 79−77539
α-Al_2S_3, prep. by direct sulphidation, chem. vapour transport and AlI_3 flux growth 79−43118
$Al_2(SO_4)_2$ $(NH_4)_2SO_4.24H_2O$, crystn. kinetics in an MSMPR crystalliser 80−100185
$Al_2(SO_4)_3$ $K_2SO_4.24H_2O$, formation, survival and growth of nuclei from secondary nucleation 80−50540
$Al_2(SO_4)_3K_2SO_4.2H_2O$, growth and growth dispersion 80−49148
$Al_2(SO_4)_3K_2SO_4.2H_2O_7$ small cryst. growth 80−50543
$Al_2(SO_4)_3K_2SO_4.24H_2O$, secondary nucleation rate under agitation 80−50541
$Al_2(SO_4)_3.K_2SO_4.24H_2O$, spirals, growth and dissolution from liq. state 80−15027
AlSb, gravitational influences on liquid-state homogenisation and solidification 79−78864
$Al_2(SeO_3)_3.6H_2O$, synthesis under hydrothermal conditions 77−85918
Au film, chem. deposition on Si, form., struct. 78−34723
α-B, rhombohedral, prep. methods, book contrib. 78−48295
BN, cubic, press. and temp. stability region in presence of ammonium borate 77−85922
BN prep. by water solvent, electron microscope charact. 78−47253
BP, cryst. growth from Cu-fluxed melt, and characterisation 77−85920
(Ba,Gd)TiO_3, flux growth and chem. characts. 78−23595
BaB_6, (La,Ba)B_6, (Ea,Ba)B_6, single crystal growth for thermionic emission 78−92183

crystal growth from solution continued
BaBrF, reacted flux growth, dislocation density, dielec. const. and loss, IR spectra 77−36214
$BaCl_2.2H_2O$, artificial production of growth twins 78−30641
$BaCrO_4$, precipitation from aq. soln., cryst. growth kinetics 77−72574
BaFBr, single cryst. growth by flux method, dislocation etch pits on dissoln. 79−56925
$BaFe_{12}O_{19}$, discontinuous growth, effect of equilib. segreg. at boundaries 77−51336
$Ba_2Fe[Ge_2O_7]$, hydrothermal growth, struct. and opt. props. 77−65971
$BaMoO_4$, precipitation from neutral equivalent solns., cryst. numbers, final morphology and sizes 78−23597
$Ba(NO_3)_2$, isomorphous crysts., growth defects, X-ray topography 80−70188
$BaO.Al_2O_3.2SiO_2$, hydrothermal synthesis, phase transitions 77−48378
$BaSO_4$, crystal growth, effect of nitrilotri (methylenephosphonic acid) adsorption 78−88417
$BaSO_4$, crysts., coagulative growth from a strongly supersaturated aq. soln. 80−2937
$BaTiO_3$, crystn. from melts, comparison of different prospective oxy-anion solvents 80−71583
$BaTiO_3$, pure and doped, cryst. growth and chemical composition 77−40349
$BaWO_4$, crystallization kinetics from saturated Na_2WO_4 solns. 79−99093
$BaWO_4$, flux- and gel-grown, comparative microtopography 77−31852
BeO, flux process for large cryst. growth 78−31316
$Bi_{3-2x}Ca_{2x}Fe_{5-x-y}In_yV_xO_{12}$, single crystal by flux method *(Chinese)* 77−40056
$Bi_{3-2x}Ca_{2x}Fe_{3-x}V_xO_{12}$, crystallization in $Bi_{0.7}Ca_{2.3}Fe_{3.85}V_{1.15}O_{12}$-$Bi_2O_3$-PbO 77−48330
BiOCl, exam. of crystal structure and morphology, as function of growth conditions, using electron microscopy 79−52103
25 $Bi_2O_3.P_2O_5$, hydrothermal growth, vib. spectrum 77−63555
$Bi_2(SeO_4)_3$, single cryst. growth in silica gels, X-ray diffr., IR and emission spectroscopy study 79−74075
$BiTaO_4$, cryst. growth. hydrothermal method 77−8736
Bi_2Te_3-based solid solns., decomp. kinetics under flux layer 77−81205
Bi_2WO_6, hydrothermal and flux growth 80−76166
Bi_2WO_6, layer-like ferroelec., cryst. growth 78−23598
Bi_2WO_6 single crystal, growth from flux in Bi_2WO_6-Na_2WO_4, below transformation temperature 78−72713
CC GaP, improvements in synthesis, solute diffusion (SSD) growth 79−65992
Ca salts, biological mineralization mechanism . 78−31764
Ca_2 $Mn(PO_4)_2$, hydrothermal synthesis and cryst. growth 80−60762
$Ca_3Al_2Si_3O_{12}$-$Mg_3Al_2Si_3O_{12}$, synthetic garnet, soln. grown, surface features 78−2346
$Ca_{2x}Bi_{3-2x}V_xFe_{5-x}O_{12}$ ferrogarnet, magnetis. distrib., correl. with morphological habit 79−42802
$CaCO_3$, acceleration of growth of particles, Lorentz forces, electric and mag. field effects 78−51455
$CaCO_3$, calcite, gel grown crysts., spirals on rhombohedral faces 80−7486
$CaCO_3$ crystallisation from aqueous solutions, kinetic study 80−59419
$CaCO_3$, precipitation from Mg^{2+} containing soln. *(French)* 77−85915
CaF_2, whiskers and crysts., flux growth and charact. by morphology and fracture strength 79−19987
$Ca_3Fe_2(Mn_2)Ge_3O_{12}$, single magnetic sublattice antiferromagnetic garnets 78−52652
$CaHPO_4.2H_2O$, cryst. growth in silica gel, etch pits obs. on as grown faces 79−73169
$CaHPO_4.2H_2O$, gel grown crysts., quality study by X-ray topography 79−87572
$CaLn_4(SiO_4)_3O$ silicate oxyapatites, prep. and props. of single crystals 77−28704
$Ca_{18}M_2H_2(PO_4)_{14}$, (M^{2+}=Mn, Co, Ni, and Cu), hydrothermal synthesis and cryst. growth 80−60762
$CaMoO_4$, precipitation from neutral equivalent solns., cryst. numbers, final morphology and sizes 78−23597
CaO and CaO:Gd^{3+}, crystal growth from molten solvent LiF-20 mole % CaF_2 77−77358
$Ca_{10}(PO_4)_6(F,OH)_2$, apatite, cryst. growth and habit, F ion conc. effect 78−30560
$Ca_{10}(PO_4)_6(OH)_{2-2x}O_x\square_x$ polycryst. sintered bodies, prep. and thermal props. 80−25624
$CaSO_4$, cryst. growth kinetics at heated metal surfaces, thermal cond. morphology and crystn. 80−29867
$CaSO_4$ crystallisation, from liq. solns. as heat-transfer surface 80−100772
$CaSO_4$:Bi, cryst. growth, luminesc. props. 77−58993
$CaSO_4$:Dy, using Na_2SO_4 charge compensator, thermoluminesc. 79−56923
$CaSO_4.2H_2O$ crystals, linear growth rates in presence of additives 80−10515
$CaSO_4.2H_2O$, gypsum, at 298 and 313K, with and without mag. field influence *(Russian)* 78−9973
$CaSO_4.2H_2O$, gypsum, cryst. growth rates and nucleation *(French)* 80−80959
$CaSO_4.2H_2O$, supersaturated soln., nucleation induction time 79−69042
$CaSO_4.2H_2O$, thermodynamic expression for crystal growth and dissolution affinity 80−24385
$Ca_6Si_6O_{18}.4H_2O$, tobermorite synthetic crysts., hydrothermal growth, TEM and X-ray diffr. characterisation 79−43122
$CaSo_4$, growth on CaF cryst. face etched in H_2SO_4, etch pit morphology 80−6408
$CaWO_4$, cryst. growth from solns. in melts, kinetics parameters and thermodynamic props. 80−59424
$CaWO_4$, crystal growth from soln. in Na_2WO_4 melts, by continuous cooling, growth kinetics exam. 78−48303
$CaWO_4$, crystn. from solns. in $NaWO_4$ melts, kinetics obs. by DTA 80−40246
$CdCr_2Se_4$, crystn. from high temp. soln., $CdCr_2Se_4$-$CdCl_2$ phase diagram 78−3009
$Cd_xGe_yO_2$, hydrothermal crystallisation at 300°C 77−52241
$CdGeP_2$, growth from melt solution in Cd, microhardness 77−44139
$Cd_xHg_{1-x}Te$, crystallisation from solution in Hg 77−19883
CdI_2 crystals, growth conditions effect on polytypism, X-ray diffr. study 80−28942
CdI_2, soln. grown, rotation twinning, arcing and polytypism 78−51557
$CdIn_2O_4$, crystal growth from flux, elec. and struct. props. 77−81206

crystal growth from solution continued
$CdNd_4(SiO_4)_3O$, synthesis, cryst. struct. 78—87653
CdS, crystallisation and stability in high-temp. alkaline solns. 77—52240
CdS, film prep. from aqueous soln. of thiourea 77—8767
CdS films, chemically deposited, phase comp. and photoelec. props. 77—40394
CdS, hydrothermal crystal growth on seeds of various orientations 77—4730
CdS, solution growth, using Te solvent 79—65993
$CdSnO_4$, crystal growth from flux, elec. and struct. props. 77—81206
$CdSnP_2$ crystal growth, DTA obs. of Cd-Sn-$CdSnP_2$ phase diagram 80—24394
$CdSnP_2$-$CdSnAs_2$, and $CdSnP_2$-$CdGeP_2$, solid solution form. and elec. characterisation 78—43125
CdTe cathodic deposition from aqueous electrolytes 78—64484
CdTe, growth by travelling heater method, high resistivity charact., γ-ray detector appl. 78—84707
CdTe, growth from soln. in fused $CdCl_2$ 77—44138
CdTe, high purity crystal, growth from soln., γ-ray detector appls. 77—14310
CeB_6, single crystal growth for thermionic emission 78—92183
$Ce_2(SO_4)_3.9H_2O$, grown from solution, exam. of Raman spectra and physical props. 79—52104
$CoCO_3$, monocryst. solubility under hydrothermal conditions 77—12512
$CoCO_3$, spherocobaltite, complexing during cryst. growth, electron diffr., neutron diffr. and spectroscopic obs. 77—44144
Co_2GeO_4 hydrothermal growth from CoO-GeO_2-H_2O 77—48329
$CoNb_2O_6$, flux growth 77—21015
CoO, hydrothermal growth from CoO-GeO_2-H_2O 77—48329
$Co(OH)_2$, hydrothermal growth from CoO-GeO_2-H_2O 77—48329
CoSb, cryst. growth from nonstoichiometric melt, and cryst. chem 78—35286
Cr_2O_3 crystals, flux growth from $K_2Cr_2O_7$-K_2CrO_4-$K_2B_4O_7$ mixture *(Japanese)* 80—108339
Cr_2O_3 crystals, growth by decomposition of $K_2Cr_3O_7$ melt *(Japanese)* 80—108338
Cr_2O_3 flux growth from $K_2Cr_2O_7$-K_2CrO_4-$K_2B_4O_7$ mixture 79—100037
$CsAlSiO_4$, prep. and X-ray characterisation 78—39728
$Cs_2B_{12}H_{12}$ and $Cs_2B_{12}H_{12}$.CsX, X=halogen cryst. growth from soln. and morphology 77—44145
$Cs_2C_2O_4(SbF_3)_2$, growth from soln. and X-ray diffr. study *(French)* 77—80481
$CsCuCl_3$, phys. props. 77—62511
$Cs(D_xH_{1-x})_2AsO_4$, isotope exchange during crystallisation from aqueous solns. 78—18569
$Cs(D_xH_{1-x})_2AsO_4$, two-step process for taper free cryst. growth 78—11095
$Cs(D_xH_{1-x})_2PO_4$, D distrib. during crystallisation from aq. soln. 77—11496
$Cs(D_xH_{1-x})_2PO_4$, isotope exchange during crystallisation from aqueous solns. 78—18569
CsH_2PO_4, single cryst. growth, struct. and elec. props. 78—71693
CsI, selective etching, growth and dissolution in alcohols 78—71739
CsI, Wulf habits, ideal forms of soln. of crysts. 79—14718
$CsNO_3$, anhydrous, kinetics of crystallisation 77—43164
Cs_2NpBr_6, prep., cryst. struct. and enthalpy of formation 78—10014
Cs_2PdCl_4 and $Cs_2PtCl_4.H_2O$, single cryst. growth and gel and soln., morphology 77—77360
$CsSnX_{3(5)(6)}$ (X=Cl, Br, I), single cryst. gel growth, X-ray diffr. study 80—29870
$CsVF_4$, flux growth of crystal 79—78861
Cu complex, bis-(alkylammonium) (11) tetrachloride, perovskite, lattice perfection 78—87633
Cu complex, bis-(alkylammonium) Cu(11)tetrachloride, perovskite, face struct. and growth rate 78—87634
Cu, electrochem. nucleation and growth on Te and Al, TEM 80—104451
Cu electrocrystallisation, multiple twin form. 77—39750
Cu electrocrystallisation from $CuSO_4$ solns., current density under stationary surface diffusion *(Russian)* 79—8237
Cu electrocrystallisation from $CuSO_4$ solns., current density/overvoltage curves *(Russian)* 79—8236
Cu electrocrystallisation from $CuSO_4$ solns., exptl. methods *(Russian)* 79—8235
Cu electrocrystallisation from $CuSO_4$ solns., expt. and slow surface diffusion theory *(Russian)* 79—11505
Cu electrolytic form. by electrodeposition, structural defects 77—39749
Cu ferrites, crystallisation of monocrystals from high temp. soln. 78—60561
Cu, in acid $CuSO_4$, ridge growth on (110) face 77—11807
CuI, single crysts., growth and optical props. 80—93470
$(CuInTe_2)_{1-x}$-$(2ZnTe)_x$, phase diagram and cryst. growth of $CuZn_2InTe$ from $ZnCl_2$ flux 80—16287
$CuO.Al_2O_3.2SiO_2$, hydrothermal synthesis, phase transitions 77—48378
$CuSO_4.5H_2O$, secondary nucleation and growth in a fluidized bed 80—50542
Dy_2O_3, soln. in $K_2O.2(3)MoO_3$, rel. supersaturation and supercooling 80—40245
$DySbO_3$, single crysts., hydrothermal synthesis and crystallographic characteristics 79—95916
E-$Dy_2Si_2O_7$, single cryst. flux growth, polymorphic forms study by X-ray methods 79—52097
$ErFe_3(BO_3)_4$, solubility in Bi_2O_3-B_2O_3 melt and crystallisation 80—19736
$ErOHCO_3$, synthesis of rare earth carbonates under hydrothermal conditions 78—72714
C-,D-$Er_2Si_2O_7$, single cryst. flux growth 79—52097
(Eu, Pb)MnO_3, flux growth 79—83113
EuB_6, (La,Eu)B_6, (Eu,Y)B_6, (Eu,Ba)B_6, single crystal growth for thermionic emission 78—92183
EuB_6, growth by soln. method, struct., mech. and elec. props. 80—16168
Eu_2O_3, monoclinic, growth from molten NaF solvent 78—19653
Fe hydroxylboracite, hydrothermal crystallisation 77—85917
$(Fe_{1-x}M_x)_2O_3$, yH_2O, M=Cr,Cu,Ni, characterisation by Mossbauer spectroscopy, mag. meas. and electron microscopy *(French)* 80—80655
$Fe_2NaBa_6Ge_8O_{24}.4(OH,H_2O)$, growth and struct. 77—65971
$FeNb_2O_6$, flux growth 77—21015
$Fe_{1-x}O$, wustite, crystals of various stoichiometries, growth in arc furnace 80—25545
α-Fe_2O_3 crystal flux growth, solubility and relative supersaturation in Fe_2O_3-PbO-V_2O_5 fluxed melt system 80—64934
Fe_3O_4, hydrothermal growth in Au capsule in presence of H_2 77—1793
Fe_3O_4, magnetite, hydrothermal crystal growth 80—66411

crystal growth from solution continued
FeO_2H, growth in alkaline solution, phase composition *(Chinese)* 80—108334
FeOOH, crystal growth in $FeSO_4$ solution with NaOH or NH_4OH as precipitant, phase diagrams *(Chinese)* 80—44158
FeS_2, cryst. growth, literature review 78—31318
$FeSiO_4$, hydrothermal growth, effect of NaOH soln. conc. and O_2 fugacity on morphology 79—65996
Ga-YIG, accelerated crucible rotation technique effect on cryst. growth by induced striation method 77—63553
GaAs, cryst. growth from large Ga:As solns., critical cooling rate 80—64938
$GaCO_3$, calcite, hydrothermal growth processes revealed by defects 77—55250
GaInAsP/InP, DH laser, low threshold current density, 1.3 μm emission 79—94249
$Ga_xIn_{1-x}Sb$, computer simulation of growth from In soln. 77—51332
β″-Ga_2O_3-Na_2O, single cryst. growth by Na_2O evaporation from molten Na_2O-Ga_2O_3 77—44141
n-GaP, cryst. growth, synthesis solute diffusion method, elec. characts. *(Korean)* 78—52653
GaP LPE layers, low temp. growth from In solvent 79—56924
GaP, soln. growth of bulk crysts., luminesc. and elec. props. 78—92181
GaSb, single crysts., grown by vertical and horizontal travelling heater method, growth parameters and cryst. quality 79—24421
$GdFe_3(BO_3)_4$, solubility in Bi_2O_3-B_2O_3 melt and crystallisation 80—19736
$Gd_3Ga_5O_{12}$, flux growth and nucleation temp. determ. *(Chinese)* 80—60761
$GdOHCO_3$, $Gd_2O_2CO_3$, synthesis of rare earth carbonates under hydrothermal conditions 78—72714
$GdVO_3$, flux growth and chem. characts. 78—23595
Ge-Sn-M, M=Cu, As, Sb, formation of Ge-based solid solns. during crystallisation 77—80625
GeO_2 hydrothermal growth from CoO-GeO_2-H_2O 77—48329
HIO_3:Cr(Ni)(Fe)(Mn), growth and struct. perfection, effect of impurity ions 77—12514
HgI_2, cryst. growth from soln., doping rel. to elec. cond., phase transitions 77—55880
α-HgI_2, single cryst. growth from iodomercurate complexes 80—35069
α-HgI_2, single cryst. growth from dimethylsulfoxide complexes 80—35070
HgI_2, soft γ-ray detector fabrication and props. 77—3208
HgI_2, soln. grown crystals, low-energy gamma-ray cond. type detectors 80—97418
HgI_2, thermally stimulated current meas. 78—41896
$Hg_{1-x}Mn_xS$, phase studies and hydrothermal synthesis 77—48333
α-HgS, crystn. in NaHs solutions 77—8740
α-HgS, hydrothermal synthesis 77—48333
HgTe, high purity cryst. grown from soln. by travelling heater method 77—52243
$Ho_4Ba_6(BO_3)_9$, flux growth and chem. characts. 78—23595
Ho_2O_3-GeO_2-NaOH-H_2O, hydrothermal crystallisation 77—40344
$In_{1-x}Ga_xP$, homogeneous bulk, growth from soln. with predetermined cryst. comp. 78—11097
In_2O_3, grown from Sn-In melt, Sn solubility 77—11697
InP, crystal growth by synthesis solute diffusion method 78—64454
InP growth from soln. and LEC, photolum. and elec. meas. 79—87575
InP, high-purity bulk, prep. from soln. 78—6839
InP, large size single crysts., synthesis, solute diffusion technique 79—33917
p-InP:Cd(Zn), single cryst. growth by temp. gradient method 79—28907
InSb, single crysts., grown by vertical and horizontal travelling heater method, growth parameters and cryst. quality 79—24421
IrP_2, prep. and characterisation 78—39679
$K_2Al_2(SO_4)_4.24H_2O$, growing in aqueous solution, observation of secondary nuclei production 78—68613
$K_2B_{12}H_{12}$ and $K_2B_{12}H_{12}$.KX, X=halogen cryst. growth from soln. and morphology 77—44145
$KB_5O_8(D_xH_{1-x})_2O$, isotope exchange during crystallisation from aqueous solns. 78—18569
KBr, avalanche type crystal formation *(Hungarian)* 80—11552
KBr:PbI_2, single crysts. grown from aq. soln., growth striations obs. 77—1089
$K_2C_2O_4(SbF_3)_2$, growth from soln. and X-ray diffr. study *(French)* 77—80481
KCl, agglomeration of crystals from aqu. soln. 79—90580
KCl crystal growth in fluidised bed, comparison to dissoln. *(French)* 80—16167
KCl, crystal growth rate in cooling soln., nucleation and supersaturation 77—76337
KCl crystallites, nucleation, oriented growth on amorphous SiO_2 using square-wave surface relief grating 78—47672
KCl, growth, supersaturation rel. to cryst. characts. 79—52101
KCl, influence of collisions on cryst. growth and secondary nucleation under conditions of meas. crystn. 80—50544
KCl solution, thermodynamic driving force, for crystallisation at 298K 79—37643
KCl, spirals, growth and dissolution from liq. state 80—15027
KCl:Pb crystals, development of mechanical stresses during growth 80—19735
$KClO_4$ crystal growth and nucleation in SiO_2 gels 78—48299
$KClO_4$ single crystals, gel growth, temp. effects etching 79—78862
$KCoF_3$, $KFeF_3$ and $KNiF_3$, crystal growth from flux, degree of perfection and dislocation density 77—77359
$K_2Cr_2O_7$, growth and growth dispersion 80—49148
$K_2Cr_2O_7$, role of metastable β-phase in cryst. growth 79—32931
α-$K_2Cr_2O_7$, symmetry centres exam. by morphological methods 78—59796
$K(D_xH_{1-x})_2PO_4$, D distrib. during crystallisation from aq. soln. 77—11496
$K(D_xH_{1-x})_2PO_4$, isotope exchange during crystallisation from aqueous solns. 78—18569
$K(D_xH_{1-x})_2PO_4$, monoclinic and tetragonal forms, existence in aq. soln. 78—47262
KDP, growth in soln., nucleation rate, supersaturation and temp. depend. 77—4728
KD_2PO_4, X-ray topography of single crysts. grown on KDP seeds 78—23594
KFe_2F_6, flux growth of crystal 79—78861

crystal growth from solution continued
$K(H,D)_2PO_4$ crystals, effect of isotopic replacement on growth kinetics 78-95006
$KH_{2(1-x)}D_{2x}PO_4$, X-ray topographic study of growth strains in single crystal 78-91279
KH_2PO_4, cryst. growth, splitting due to colloidal inclusions 77-7681
KH_2PO_4, cryst. regeneration of z-cut plates, effect of impurities 79-43120
KH_2PO_4 crystals, mechanism of growth in presence of impurities 79-1403
KH_2PO_4, growth and dissolution kinetics, temp. and pH effect 80-88070
KH_2PO_4, growth from gel and aqueous soln., oriented inclusions 80-15023
KH_2PO_4, kinetics of crystn. from soln., activities, interfacial energy and solubility 77-76340
KH_2PO_4, kinetics of growth from aqueous soln. 78-6838
KH_2PO_4, liq. inclusion formation during large cryst. growth 78-64455
KH_2PO_4, liquid inclusion form., hydrodynamics and supersaturation role 78-30559
KH_2PO_4 single crystal evidence for spiral growth on pyramidal faces 80-84120
KH_2PO_4, spirals, growth and dissolution from liq. state 80-15027
KH_2PO_4, supersaturated solution, nucleation rates meas. from induction period 79-23549
KH_2PO_4:cation impurities, growth domains 79-99224
$KHSO_4$:Co^{2+}(Fe^{3+}), impurity effect on growth habit from saturated soln. 77-4059
$K_2M(MoO_4)_3$, M=Zr, Hf, synthesis and struct. 77-36386
$KMnF_3$, flux growth of crystal 79-78861
KNO_3, cryst. growth rates, random processes theory to study fluctuations 79-55689
$(K_xNa_{1-x})NbO_3$ single crystals, growth and phase transitions 79-33915
$KNbO_3$, growth from soln. in melt and characterisation of optical quality cryst. 77-8741
$KNbO_3$, layer growth, optical and electron microscopy 77-59021
$(K_2O)_x.TiO_2$ fibres, flux growth reactions 80-16171
$K_2PbX(NO_2)_6$, (X=Cu, Ni), single cryst. growth in gel *(German)* 79-74076
$K_2Pt(CN)_4X_{0.3}$, X=Cl,Br, electrochem. growth of highly conducting inorganic complexes 77-8739
$K_{1.75}Pt(CN)_4.1.5H_2O$, electrochem. growth of highly conducting inorganic complexes 77-8739
$K_{1.64}Pt(O_2C_2O_2)_2.2H_2O$, electrochem. growth of highly conducting inorganic complexes 77-8739
$K_xRb_{1-x}TiOPO_4$, new nonlinear optical material 77-14784
K_2SO_4, continuous multi-particle crystal growth in vertical cone 77-69978
K_2SO_4, growth rate characts. in fluidised bed crystalliser 79-19164
K_2SO_4, kinetics of crystn. from soln., activities, interfacial energy and solubility 77-76340
K_2SO_4 solution, thermodynamic driving force, for crystallisation at 298K 79-37643
$K_2SO_4.Al_2(SO_4)_3.24H_2O$, stirring effect on crystalline quality of soln. grown crystals 78-91281
$K_2Ti_6O_{13}$ fibres, synthesis by the hydrothermal dehydration method 79-43121
$(La,Cs)B_6$, single crystal growth for thermionic emission 78-92183
$(La, Pb)MnO_3$, flux growth 79-83113
$(La,Y)B_6$, $(Eu,Y)B_6$, single crystal growth for thermionic emission 78-92183
La, $(SO_4)_3.9D_2O$, soln. growth, struct., props. 77-77363
$LaAlO_3$:Cr^{3+} enriched in ^{17}O isotope, flux growth 79-87573
LaB_6, $(La,Eu)_6$, $(La,Y)B_6$, $(La,Ba)B_6$, $(La,Cs)B_6$, single crystal growth for thermionic emission 78-92183
LaB_6, growth by soln. method, struct. mech. and elec. props. 80-16168
$LaBO_3$, flux growth 79-38732
$La_4Ba_6(BO_3)_9$, flux growth and chem. characts. 78-23595
$LaFe_4P_{12}$, single crystals grown from Sn flux, struct. 78-14314
La_2O_3-P_2O_5-H_2O, solubility, regions of crystallisation, 100-500°C 77-16483
$LaOHCO_3$, $La_3Cl(CO_3)_4$, synthesis of rare earth carbonates under hydrothermal conditions 78-72714
$LaSbO_3$, single crysts., hydrothermal synthesis and crystallographic characteristics 79-95916
β-$LiAlSiO_4$, cryst. growth from high temp. LiF-AlF_3 soln. 78-31317
$LiCoPO_4$, flux growth 79-83113
$Li_{1-x}H_xIO_3$, cryst. growth from soln. and phys. props. 77-31634
α-$LiIO_3$, cryst. growth of high piezoelec. and optical quality 78-31313
α-$LiIO_3$, cryst. growth by conc. convection of soln. 78-72716
α-$LiIO_3$, dislocation struct. 77-1132
$Li_xM_yF_z$, (M=U, Th), flux growth 77-85919
LiN_3, low temp. method for single cryst. growth 79-74077
$LiNO_3.3H_2O$, crystallisation kinetics 79-4264
$LiNbO_3$, crystallisation from solution in borate, vanadate and tungstate melts 79-1820
$LiNd(PO_3)_4$, crystallisation from $LiPO_3$ flux, exam. of optical props. *(German)* 79-11401
$LiNdP_4O_{12}$, grown by top seeded pulling technique, possible laser material 80-25542
$LiNdP_4O_{12}$, single crysts. flux growth and cryst. morphology, solubility curve 79-43124
$LiNdP_4O_{12}$ single crystal growth, study of Li_2O-Nd_2O_3-P_2O_5 phase diagram 80-25668
$LiYF_4$, prep. and crystal grwoth for laser appls. 77-55879
γ_{II}-Li_2ZnSiO_4, flux growth *(Japanese)* 79-95917
Mg hydroxylboracite, hydrothermal crystallisation 77-85917
$MgAl_2O_4$ crystals, flux grown, artificial spinel twin form. by $BeAl_2O_4$ addition 80-96542
$MgNH_4PO_4.6H_2O$, struvite crysts., growth morphology and cryst. habit 79-41994
$Mg(OH)_2$, cryst. growth from aq. soln. at 60°C, pH effects 78-23591
$Mg(OH)_2$, cryst. growth from MgCl+$Ca(OH)_2$ in brine 78-23592
$MgO.Al_2O_3.2SiO_2$, hydrothermal synthesis, phase transitions 77-48378
$MgSO_4$, rate constant of reaction, determ. from overall crystal growth coeff. 78-59773
$MgSO_4.7H_2O$, cryst. regeneration and growth in contact nucleation 79-23545
$MgSO_4.7H_2O$, growing in aqueous solution, observation of secondary nuclei production 78-68613

crystal growth from solution continued
$MgSO_4.7H_2O$, relation between soln. and growth rates of cryst. faces 79-14716
$MnFe_2O_4$, discontinuous growth, effect of equilib. segreg. at boundaries 77-51336
$MnNb_2O_6$, flux growth 77-21015
MnS, γ and α phases, hydrothermal syntheses 77-48333
MnSb, cryst. growth from nonstoichiometric melt, and cryst. chem 78-35286
NH_4Cl, cryst. nucleation, growth rates from organic media, outline meas. technique 79-38730
NH_4Cl, dendrite growth at very low supersaturation 78-43277
NH_4Cl soln., crystal growth under press. *(Korean)* 77-73266
$(NH_{4(1-x)}D_{4x}H_{2(1-x)}D_{2x}AsO_4)$, crystal growth of para- and antiferroelectric phases 78-48300
$NH_4Fe_2F_6$, NH_4AlF_4, hydrothermal growth method in presence of hydrofluorhydric acid *(French)* 80-25543
$NH_4H_2PO_4$, cryst. growth in presence of Mn ions 80-93468
$NH_4H_2PO_4$, crystal growth kinetics, in situ X-ray topography study 80-76167
$NH_4H_2PO_4$ single crystal evidence for spiral growth on pyramidal faces 80-84120
$NH_4H_2PO_4$, solution growth mechanism investig., growth spiral interactions 77-58963
$NH_4H_2PO_4$, unstable growth features and mechanisms of inclusion formation 79-99090
$(NH_4)_2SO_4$, single crystal growth from aq. soln. *(Japanese)* 78-92182
$(NH_4)_2SO_4$:Cu^{2+}, ESR parameters, effect of pH of mother soln., trapping sites 80-15791
NaA and NaX zeolite crystals, crystn. study in presence of triethanolamine, Na_2O and SiO_2 content influence 79-65995
$Na_3Al_2Li_3F_{12}$ garnet, cryolithionite, hydrothermal growth 79-43123
$Na_2Al_2Ti_6O_{16}$ bronze, synthesis in $NaBO_2$, growth conditions *(French)* 78-43998
$NaBO_2.H_2O_2.3H_2O$, crystallisation from aq. soln., nucleation rates with surfactant 78-91276
$NaBO_2.2H_2O_2.3H_2O$, crystallisation from aq. soln., growth kinetics with surfactant 78-91277
$Na_2C_2O_4$ $(SbF_3)_2$, growth from soln. and X-ray diffr. study *(French)* 77-80481
$Na_8Ca_3SiO_{1.5}[Si_2O_7][PO_4]_3$, synthesis conditions, cryst. struct. and IR spectra characts. 80-108335
NaCl, prep. of fine crysts. demonstrated by electron microscopy 78-48302
NaCl solution, thermodynamic driving force, for crystallisation at 298K 79-37643
NaCl:Pb^{2+} crystals, grown from aq. soln., flotation study 80-39144
NaCl-KCl mixed crystal, growth, X-ray exam. and microstruct. 78-44001
NaCl-NH_3-CO_2-H_2O system, $NaHCO_3$ crystn. 80-100771
$NaClO_3$, cryst. growth from soln., selective etching technique for observation of dislocations 79-19251
$NaClO_3$, cryst. growth from soln., convection phenomena 79-74074
$NaClO_3$, crystallisation, composition of heat carrier heating aqueous solution system 77-12513
$NaClO_3$, dislocations rel. to growth mechanism from aq. soln., X-ray topography 80-59464
$NaClO_3$, effect of i.r. radiation on growth rate 77-1794
$NaClO_3$, growth and dissolution kinetics, diffusion and convection regimes 78-63684
Na_2CoGeO_4 hydrothermal single crystals, X-ray topographic study of growth defects rel. to growth conds. 79-19166
Na_2CoGeO_4, single cryst. growth and study of their piezoelec. and elastic props. 79-4906
$Na_2Fe_2Ti_6O_{16}$ bronze, synthesis in $NaBO_2$, growth conditions *(French)* 78-43998
$Na_4Ge_9O_{20}$, Na_2CoGeO_4, $Na_2GeO_3.H_2O$ hydrothermal growth from CoO-GeO_2-NaOH-H_2O 77-48329
$Na_2Nd_2Pb_6(PO_4)_6Cl_2$, laser material, flux growth *(French)* 78-35288
$Na_2NiTi_7O_{16}$ bronze, synthesis in $NaBO_2$, growth conditions *(French)* 78-43998
Na_2O-Al_2O_3-GeO_2-H_2O system, hydrothermal synthesis 77-36388
$Na_2O.Al_2O_3.10TiO_2$, crystallized bronze, chem. comp., morphology, optical and thermal props. *(Japanese)* 80-16172
$Na_2S_2O_3.5H_2O$, solidification, heat transfer processes *(Japanese)* 80-6372
$Na_3Sc_2P_3O_{12}$, superionic cond. synthesis, cryst. struct. and ionic cond. 80-107519
Na_2SiF_6, precipitation from H_2SiF_6 soln., mechanism, kinetics, habit 77-44142
$Na_{2(4)}Zr(MoO_4)_{3(4)}$, synthesis and cryst. struct. 80-39059
$Na_20.3MoO_3$, nucleation of fibrillar crystals, effect of surface layer, growth on air bubbles 78-60559
$Na_20.3MoO_3.3H_2O$, nucleation and growth from soln. 77-84682
NbO_2, continuous coating crystallite, electrocrystallisation from molten fluorides containing oxide contamination 79-24423
NbO_2 hollow needles, electrocrystallisation from molten fluorides containing oxide contamination ,79-24423
$NbOAsO_4$ and $NbOAsO_4$ $4H_2O$, crystal growth, composition, struct. and crystallographic characts. 80-54198
(Nd, Pb)MnO_3, flux growth 79-83113
$NdAl_{2.07}(B_4O_{10})O_{0 6}$ nonstoichiometric, crystal struct. by X-ray spectral microanalysis 79-77582
$Nd(C_2H_5SO_4)_3.9H_2O$, large single crystal growth 77-4729
$NdFe_3(BO_3)_4$, solubility in Bi_2O_3-B_2O_3 melt and crystallisation 80-19736
$NdFeTiO_5$, magnetic props. and crystal growth 78-92185
$NdNbO_4$, cryst. growth rel. to investig. of PbO-KF-B_2O_3-$PbNdTiNbO_7$ cross section 77-86004
$Nd_2O_3.4TiO_2$, growth from soln., struct. 78-83794
NdP_5O_{14} and $Nd_xLa_{1-x}P_5O_{14}$, large single crystal growth from H_3PO_4 and oxide, props. *(French)* 77-4723
NdP_5O_{14} single crystals used in microlaser 79-98377
NdP_5O_{14} single crystals grown from polyphosphoric acids, morphology control 80-15395
$Nd_xR_{1-x}P_5O_{14}$ (R=La, Y: $0.1<x<1$), laser quality cryst. growth, morphology 80-66412
$Nd_xY_{1-x}P_5O_{14}$, NdP_5O_{14}, laser materials, flux evaporation growth, dislocation etch tunnels 77-35560
$NiCO_3$, crystal growth by counterflow diffusion and temp. drop hydrothermal synthesis 77-4731

crystal growth from solution continued

$Ni(H_2V)_2(H_2O)_2$, synthesis and characterisation *(French)* 80—45225

$Ni(NH_4)_2(SO_4)_2.10H_2O$, precipitation, supersaturation, cryst. size distrib. changes 77—72573

$Ni(NH_4)_2(SO_4)_2.6H_2O$, precipitation from equimolar aqueous solns., kinetics study 80—7848

$NiNb_2O_6$, flux growth 77—21015

$Ni_3Nb_2O_8$, $Ni_3NbB_3O_{15}$, flux growth and chem. characts. 78—23595

$NiSO_4$, spirals, growth and dissolution from liq. state 80—15027

NiSb, cryst. growth from nonstoichiometric melt, and cryst. chem 78—35286

$Ni_3V_2O_8$, flux growth and chem. characts. 78—23595

$Ni_2V_2PbO_8$, flux growth and chem. characts. 78—23595

Pb-S-I-X-H_2O, (X=solvent) crystallisation conditions 78—80466

$Pb(Bi_{1/2}Nb_{1/2})O_3$, single cryst. growth from PbF_2-PbO-B_2O_3 77—48336

$PbCl_2$, large needles and single crysts., gel cryst. growth 80—29869

$PbCrO_4$, cryst. growth kinetics and particle size in precipitating K_2CrO_4-$Pb(NO_3)_2$ mixed soln. 78—26472

Pb_2CrO_5, flux growth and chem. characts. 78—23595

Pb_3GeO_5, single crystal, props., grown by hydrothermal method 79—11504

$PbHPO_4$, ferroelectric, sp. ht., effects of growth method 79—19853

$PbHPO_4$, single cryst., growth, optical props., ferroelec. transition 78—35285

$Pb_{1-x}Hg_xS$, variable gap film for i.r. detector 77—1796

$Pb_{0.27}K_{0.56}Nb_{0.91}Ta_{4.15}O_{15}$, coupled ferroelastic-ferroelectric props. 77—59543

$PbLaZrNbO_7$, dielectric with zero temp. coeff. of dielect. consts., electrophys. props. 77—52010

$Pb_2Li_{1/2}Nb_{3/2}O_6$, antiferroelec. cryst. growth and props. 77—36189

$Pb_3MgNb_2O_9$, crystal growth procedure, meas. electro-optic and dielectric props. 78—88418

$Pb_3MgTa_2O_9$, crystal growth procedure, meas. electro-optic and dielectric props. 78—88418

$PbMoO_4$, colour origin 77—85921

$PbNdTiNbO_7$, rel. to investig. of PbO-KF-B_2O_3-$PbNdTiNbO_7$ cross section 77—86004

PbO mixtures with various oxides, solvents for garnet growth, cryoscopic study 80—24393

PbO tetragonal crystals, top-seeded soln., growth method from 6% TiO_2-PbO soln. 79—100038

γ-4PbO.SiO_2, synthesis and struct. 78—71716

PbS, crystallisation and stability in high-temp. alkaline solns. 77—52240

PbS film, form. by chem. spraying, elec. and optical props. 78—2588

PbS, film prep. from aqueous soln. of thiourea 77—8767

PbS, thin film comp. and struct. rel. to precip. by allyl thiourea 77—48356

$Pb_5S_2I_6$, ferroelec., synthesis and hydrothermal growth 79—38731

$Pb_{1-x}Sn_xTe$ single crystals, selection using travelling solvent method *(German)* 80—2936

$Pb_{1-x}Sn_xTe$, Te-rich growth by ingot nucleation method, laser fabrication 77—77362

Pb_2WO_5, phase transformation study by high temp. X-ray diffr. and differential scanning calorimetry 79—43244

$Pb(Yb_{1/2}Nb_{1/2})O_3$, single cryst. growth from PbF_2-PbO-B_2O_3 77—48336

$PrCr_{2.3}Ti_{2.3}O_9$, flux growth and chem. characts. 78—23595

Pr_2MoO_6, flux growth 79—83113

PrP_5O_{14}, chemical synthesis and crystal growth of laser quality 78—92184

$PrSbO_3$, single crysts., hydrothermal synthesis and crystallographic characteristics 79—95916

$R_4Ba_6(BO_3)_9$, flux growth and chem. characts. 78—23595

RPO_4-$Pb_2P_2O_7$, R=Tb-Lu, solubility curves for high temp.-melts for growth of single crysts. 78—95687

$RbAg_4I_5$, cryst. growth from soln. 79—33916

$Rb_2B_{12}H_{12}$ and $Rb_2B_{12}H_{12}$.RbX, X=halogen, cryst. growth from soln. and morphology 77—44145

$Rb_2C_2O_4(SbF_3)_2$, growth from soln. and X-ray diffr. study *(French)* 77—80481

$Rb_2Cd_2(SO_4)_3$ single cryst., growth and phase transitions 79—33918

$Rb(D_xH_{1-x})_2PO_4$, D distrib. during crystallisation from aq. soln. 77—11496

$Rb(D_xH_{1-x})_2PO_4$, isotope exchange during crystallisation from aqueous solns. 78—18569

$RbMF_3$ (M=V, Mn), flux growth of crystal 79—78861

$RbMF_4$ (M=Ti, V), flux growth of crystal 79—78861

$RbNO_3$, anhydrous, kinetics of crystallisation 77—43164

$RbNbW_2O_9$ crysts., growth and props. 80—104054

Rb_2PdCl_4 and Rb_2PtCl_4, single cryst. growth from gel and soln., morphology 77—77360

$RbSnX_{3(5)(6)}$ (X=Cl, Br, I), single cryst. gel growth, X-ray diffr. study 80—29870

RbV_2F_6, flux growth of crystal 79—78861

RuP_2, prep. and characterisation 78—39679

$SbNbO_4$, ferroelec., synthesis and hydrothermal growth 79—38731

$SbNbO_4$ single crystals, pure and doped, growth and pyroelec. and ferroelec. props 80—40248

$SbNbO_4$:CoO(Fe_2O_3)(TiO_2), growth, pyroelectric and ferroelectric props. 79—73886

Sb_2S_2O, kermesite, synthesis, controlled precipitation and crystn. 77—48332

$SbTaO_4$, ferroelec., synthesis and hydrothermal growth 79—38731

Sc germanates and silicates, hydrothermal synthesis, cryst. struct. and cryst. chemistry 77—39571

Sc_2O_3-GeO_2-KF-H_2O system, scandium germanates crystallisation in high temp. aq. solns. 77—24942

Se, trigonal, cryst. growth from CS_2 soln. 78—23596

Se_4S_4, mol. chalcogenide, synthesis and struct. 79—33912

Si:In, IR monitoring of In, O_2, C concs., 950-1300°C 79—100040

SiC, phys. props. and crystal growth, rel. to appl. in electrolum. devices, book contrib. 77—77299

SiO_2, coesite, crystn. from soln. at high press. and temp. *(Japanese)* 77—72556

$SmB_4(B_6)$, growth by soln. method, struct. and mech. props. 80—16168

SnO_2, grown from Sn-In melt, In solubility 77—11697

SrClF, SrBrF, reacted flux growth, dislocation density, dielec. consts. and losses IR spectra 77—36214

$Sr(Fe_{0.766}W_{0.234})O_3$, cryst. growth, mag. and Mossbauer studies 79—42743

$SrMoO_4$, precipitation from neutral equivalent solns., cryst. numbers, final morphology and sizes 78—23597

crystal growth from solution continued

$Sr(NO_3)_2$, isomorphous crysts., growth defects, X-ray topography 80—70188

$Sr(NO_3)_2.4H_2O$, crystallisation kinetics 79—4264

Sr_2RAlO_5 (R=La, Pr, Nd, Sm, Eu, Ga, Tb), monocrystals growth by flux method 80—20776

Sr_2RFeO_5 (R=Nd, Sm, Eu, Gd), monocrystal growth by flux method 80—20776

$SrSO_4$, mass transfer in precip. from mixed solvents *(German)* 78—67674

$SrWO_4$, flux- and gel-grown, comparative microtopography 77—31852

SrW_20_4, kinetics of crystal growth from solns. in $Na_2W_20_4$ melts, by continuous cooling 80—11550

Sr[$Al_2Si_2O_8$], hydrothermally grown, cryst. morphology study 79—46590

TGS, deuterised, growth in form of oriented blocks, domain struct. obs. 77—90266

TaB_2, single cryst. growth, floating zone and Al soln. methods 79—86729

$Ta_2Co_4O_9$, flux growth and chem. characts. 78—23595

$Tb_2Ge_2O_7$, flux-grown, X-ray topography 80—64939

Te, single cryst. growth by hydrothermal method *(French)* 78—11096

$Te(OH)_6.Na_2HAsO_4.H_2O$, $Te(OH){\longrightarrow}_4 6.Rb_2HAsO_4.Rb_2H_2AsO_4$ and $Te(OH)_6.2(NH_4)_2HAsO_4$, synthesis and cryst. data *(French)* 80—33948

$TlAlF_4$, hydrothermal growth method in presence of hydrofluorhydric acid *(French)* 80—25543

$Tl_2B_{12}H_{12}$, cryst. growth from soln. and morphology 77—44145

$Tl_2BNi(NO_2)_6$, (B=Cd, Hg), single cryst. growth in gel *(German)* 79—74076

$Tl_2B[Co(NO_2)_6]$, (B=Pb, Ba), single cryst. growth in gel *(German)* 79—74076

$Tl_2Cd_2(SO_4)_3$ single cryst., growth and phase transitions 79—33918

$Tl_{7\,7}Nb_{54+x}O_{146-y}$, single crysts., synthesis and X-ray cryst. struct. determ. 79—69065

$Tl_2PbX(NO_2)_6$, (X=Cu, Ni), single cryst. growth in gel *(German)* 79—74076

Tl_2WO_4-$In_2(WO_4)_3$, cpd. formation and single cryst. growth 77—86010

Tl_2WO_4-$Sc_2(WO_4)_3$, cpd. formation and single cryst. growth 77—86010

$Tm_2Ge_2O_7$, flux growth 79—83113

Tm_2O_3, mineraliser effect on growth morphology 78—91283

C-$Tm_2Si_2O_7$, single cryst. flux growth 79—52097

USb_2, crystallisation from U-Sb-Sn, U-Sb liquid solutions 80—15024

VO_2-$VO_{2.5}$-H_2O system, hydrothermal exam. *(French)* 77—52244

VO_2(:Al,W), layers, liq. phase prep., resist.-temp. behaviour *(German)* 77—77435

$VOPO_4$, prep. of cryst. from H_3PO_4 and V_2O_5 80—35068

WO_3, struct. transforms. during crystallisation from P_2O_5-WO_3-CaO 77—40343

Y germanates and silicates, hydrothermal synthesis, cryst. struct. and cryst. chemistry 77—39571

YAG, crystallization kinetics and growth mechanism on oriented seeds in melt-solns. 79—14717

YAG, high temp. soln. growth using accelerated crucible rotation 79—100039

YAG single crystal growth by flux method *(Japanese)* 78—19655

YAG, single crysts., kinetic characts. of growth from melt-solns. on oriented seeds 79—14719

YAG solution, in PbO/PbF_2/B_2O_3 solvent systems, density, surface tension and expansivity data, effect of B_2O_3 conc. 79—19985

$YAl_3(BO_3)_4$, cryst. growth rate determ. 79—86731

$YAl_3(BO_3)_4$, crystallisation from solution in a melt, solvent composition 80—38976

$Y_{3-x}Bi_xFe_{5-y}Ga_yO_{12}$-PbO-$B_2O_3$-$Bi_2O_3$ system, crystn. fields 78—43996

$Y_2(CO_3)_3.nH_2O$, tengerite, single cryst. hydrothermal growth 80—97417

$YFe_3(BO_3)_4$, solubility in Bi_2O_3-B_2O_3 melt and crystallisation 80—19736

$YFeO_3$, hydrothermal synthesis, mag. struct. 77—47972

$YFeO_3$, solubility in aq. KOH under hydrothermal conditions 77—39677

$Y_3Fe_5O_{12}$, growth rel. to physicochem. investig. of $Y(OH)_3$-α-FeOOH system 77—40418

YIG crystals, bulk growth from high temp. solns., props. 80—66413

YIG, single cryst. growth from high temp. soln. 78—31315

YIG single crystal growth in Na_2O-B_2O_3 flux system in air 77—81207

YIG single crystals, liq. flux growth, obs. 80—66416

YIG:La film, for microwave applics., growth and ferromag. reson. meas. 78—3008

YIG:Si single crystals, liq. flux growth, obs. 80—66416

Y_2MoO_6, growth from soln., struct., props. 77—28705

Y_2O_3-Lu_2O_3-Eu_2O_3-CaO-GeO_2-Fe_2O_3-PbO-B_2O_3 system, garnet crystn. fields 78—43995

$Y(OH)CO_3$, ancylite like phase, hydrothermal cryst. growth *(French)* 80—108340

$YOHCO_3$, synthesis of rare earth carbonates under hydrothermal conditions 78—72714

Y_2O_2S:Eu phosphor, particles of different sizes, prep. by flux method 77—44140

YPO_4-$Pb_2P_2O_7$, solubility curves for high temp.-melts for growth of single crysts. 78—95687

YSmLuCaGeIG, mag. props. and defects, depend. on B_2O_3 conc. on growth in PbO-B_2O_3 solvents 78—68321

Y_2WO_6, growth from soln. in melt 77—1806

$Yal_3[BO_3]_4$, impurity incorp. on growth from soln. 77—52242

YbB_6, growth by soln. method, struct. and mech. props. 80—16168

Yb_2O_3-GeO_2-NaOH-H_2O, hydrothermal crystallisation 77—40344

$ZnC_2O_4.2H_2O$, crystn. kinetics by precipitation 80—50884

$ZnGa_2O_4$, flux growth, for appl. as nonmag. substrate in LPE 78—44000

$Zn_{1-x}Mg_xTe$ alloys, high purity, metallurgical and analytical methods of prep. 80—40247

ZnO, wurtzite structure, hydrothermally grown exam. of thermal expansion coefficient 78—75854

ZnO:Li, effect of LiOH mineraliser on struct. and optical props. 77—8737

ZnS cubic single crystals, growth by double decomposition reaction in melt 78—60557

ZnS, solution growth, using Te solvent 79—65993

$ZnSO_4$, rate constant of reaction, determ. from overall crystal growth coeff. 78—59773

ZnS.CdS, flux growth, processes accompanying roasting of CdS+NaCl 78—23590

ZnSe, near band edge photoluminescence, electron-hole recombination 80—80835

ZnSe, solution growth, using Te solvent 79—65993

$ZnSiF_6.6H_2O$, aq. soln growth 77—63554

crystal growth from solution continued
$ZnSiP_2$ crystal growth, DTA obs. of Sn-Zn-$ZnSiP_2$ phase diagram 80—24394
$ZnSiP_2$, effect of crystal growth method, on physical props., effect of doping on physical props. *(German)* 79—52094
$ZnSnP_2$, characts. of Zn-Sn-P phase diag. 77—44225
$ZnSnP_2$-$ZnSiP_2$, heterocombination simultaneous crystallisation 78—60560
$ZrMF_6$ (M=Fe, Cr, Ni, Co, Mn, V), flux growth of crystal 79—78861
ZrO_2, crystallisation from $Zr(OH)_4$, influence of water vapour *(Japanese)* 79—78865
ZrO_2, hydrous, prep. from $ZrOCl_2$ soln. and cryst. texture determ. *(Japanese)* 77—89398
ZrO_2, optical layer form. from $ZrOCl_2$ in alcoholic soln. 77—88877
ZrO_2, Y_2O_3 stabilised, hydrothermal growth 78—15302

crystal growth from vapour
see also vapour phase epitaxial growth
acetylene, spherical cryst. grown in situ for low-temp. X-ray work 78—68612
actinide dioxides, cryst. growth by chem. transport 80—16166
actinide metals and their refractory cpds., synthesis from oxides and single cryst. growth 80—16229
adamantane, growth rate from vapour, variability under const. conditions 78—34452
adamantane crystals, vapour grown, temp. depend. of morphology of initial growth forms 79—47608
alkali halide, morphology of growth and evaporation surface 78—79544
alkali-trihalogeno-plumbates, $M[PbX_3]$, cryst. growth struct. and spectra *(German)* 79—90632
n-alkane, adsorption energy of mols. on long-chain even n-alkane crysts., rel. to cryst. growth kinetics 78—42933
binary compound crystals, growth mechanism *(Japanese)* 77—47369
binary crystal, growth mechanism, dissoc. adsorption effect 78—26465
boracite, single cryst. prep. and phys. props. 80—100763
carbon tetrabromide, vapour deposition for optical studies, Raman spectra 78—64451
CdSe whiskers, growth in H_2 80—15425
chalcogenide magnetic semiconductors, spinal-type, closed tube vapour transport method *(Japanese)* 80—25539
chalcopyrites, for electrolum. device appl., props. and technology, book contrib. 77—73175
chemical transport reactions in gaseous phase 80—44161
copper phthalocyanine, cryst. growth from vapour, hollow cryst. form, mechanism *(German)* 77—55252
β-copper phthalocyanine, large single crystal growth from vapour *(German)* 77—32513
β-copper phthalocyanine, single cryst., equilib. shape, growth shape, vapour phase growth *(German)* 77—43163
crystalline film growth reactor, gasdynamic problems 79—83130
diamond, homogeneous formation in gas phase, laser beam effects *(Russian)* 80—104052
dichalcogenides, layered, thermodynamic considerations for growth by vapour transport processes 79—4903
diffusion field calcs. *(German)* 77—31613
diffusionless vapour transport 79—78859
diphenyl crystallites, changes in face growth rate from vapour phase 79—55686
ethane, spherical cryst. grown in situ for low-temp. X-ray work 78—68612
ethylene spherical cryst. grown in situ for low-temp. X-ray work 78—68612
ferromagnetic semiconductors, cryst. growth, review 77—85923
frost growth rate prediction eqn. for cooled surfaces 78—87248
frost properties, rel. to frost formation types 77—80614
GeO_2, hexagonal needle crystals, vapour growth 78—52651
growth affinity, a driving force for crystallisation 79—23554
heterogeneous reactions, modified entrainment method appls. 79—23551
hexachloroethane, surface roughening transition in vapour phase growth 78—2044
ice, diffusion eqn. theory 80—12489
ice crystal growth in vapour at high saturation, thermodynamic anal. 77—1088
ice crystal morphology, vapour growth, influence of vapour diffusion and heat diffusion 80—64933
ice crystals, epitaxial, influence of environmental saturation and elec. field on growth and evaporation 79—42408
ice crystals, freely falling, produced by two different seeding methods, mass growth meas. 79—87570
ice crystals, vapour-grown, appearance of non-singular surfaces 79—60297
ice dendrite formation from vapour phase, morphology, sizes and growth rates 78—10313
ice disc growth from vapour, cryst. habit change mechanism 80—84117
II-VI compounds, hollow crysts., morphology, review 77—11494
II-VI semiconductors, optimal synthesis methods for single cryst. growth 80—100764
III-V compounds, vapour growth, element incorporation 78—30556
III-VI compound layered materials, prep. and growth, book contrib. 78—19661
IV-VI compounds, mixed, morphology and transport rates, in microgravity 77—77353
kinetics, impurity capture 78—26468
lamellar-spiral growth hillocks, kinetics and morphology 78—18566
metal, BCC, fine particles formed by gas-evap. technique, cryst. struct. and habit 79—27935
metal crystallites, polyhedral, growth in inactive gas, review 79—27934
metal halide layered materials, prep. and growth, book contrib. 78—19648
metal oxide smoke particles, prep. by burning metal in Ar-O_2 gas, electron microscope obs. 77—52238
metal ultrafine crystallites, form. by gas evaporation technique, crystal habit 77—52239
metallic multi-point field emission source, prep. by cathodic growth 80—100758
methane-d_4, solid, sound velocity meas., 4-77K 78—75734
microgravity environment, benefits and constraints 79—83131
minerals, vapour growth and epitaxy, comparison of growth methods 79—23856
molecular processes on surfaces 80—34339
natural mineral crystal growth characts. 78—32072

crystal growth from vapour continued
nucleation kinetics, at high supersaturations on (111) faces of crysts. with diamond struct. 80—84128
phthalic anhydride, whisker crystals, vapour growth and morphology 77—35841
phthalic anhydride, whisker growth in closed cryst.-vapour system 78—34734
physical vapour transport method for low dislocation density crysts. 78—43992
PTZ:PMDA, purification, growth, struct., optical and elec. props. 80—54216
rare earth orthophosphates, gas transport reactions 79—1819
rare earth pnictides, prep. and props., book contrib. 80—54212
simulation 78—31312
stochastic models, diffusion and relax. kinetics 79—37642
surface migration of small crystallites, Monte Carlo calc. with continuous time 78—26783
surface step, thermodynamic props., excess energy 78—47254
surface steps, statistical props. 78—47648
synthetic crystals, vapour growth and epitaxy, comparison of growth methods 79—23856
2,2,2,6-tetramethyl-piperidino-oxy, cryst. growth and polymorphism 80—96645
thermomolecular fluid flow effects in low-g 79—73117
transition metal borides, refractory, single cryst. prep. methods and characterisation, book contrib. 78—48296
whisker crystal growth, radial periodic instability mechanism *(Russian)* 80—107682
whisker growth by vapour-liquid-solid mechanism, book contrib. 79—69383
XX HgI_2, cryst. growth by multiple vacuum sublimation 80—7485
Ag on Si and W substrates, UHV-SEM studies of Stranski-Krastanov growth 80—79722
Ag, small particles prep. by evaporation in clean Ar atm., cryst. morphology 77—62494
Ag-Se system, formation of FCC thin films *(French)* 77—4267
$AgIn_5S_8$, crystal growth by I_2 vapour transport, using temperature variation method 78—68610
α-Ag_2S whiskers, growth in VLS system, SEM and X-ray diffr. anal. 79—46989
$Ag_2S(Se)(Te)$, thermodynamic props., growth of single cryst. by chem. transport reaction 77—36380
Ag_2Te, growth by chem. transport *(Russian)* 79—38728
Al, small particles prep. by evaporation in clean Ar atm., cryst. morphology 77—62494
AlF_3, single crysts., vapour phase chem. transport prep. *(French)* 79—69971
AlN, condensates, growth from vapour, morphological comparison with, ZnO, MgO 78—34450
AlN, crystn. from reactive pulse plasma 78—31308
AlN, precipitation from gas phase 78—6025
AlN, single cryst. growth by sublimation-recondensation technique 78—31310
$Al_{10}N_8O_3$, sublimation growth, cryst. struct. determ. 80—19751
$Al_9N_7O_3$, sublimation growth, cryst. struct. determ. 80—19751
γAl_2O_3, crystn. from reactive pulse plasma 78—31308
Al_2O_3 single crystal, vapour-grown, self-diffusion coeff. of O 78—30792
Al_2O_3, whiskers growth by hydrolysis of AlF_3 79—28260
α-Al_2S_3, prep. by direct sulphidation, chem. vapour transport and AlI_3 flux growth 79—43118
$As_2(Se_{1-x}S_x)_3$, crystal growth and at. struct. 79—60289
Au crystallites, formation in flowing Ar system, density, size distrib. and size dispersion 78—88415
Au, film growth on mica substrate, surface defects and heterogeneous nucleation 78—47684
AuBr, I and P forms, growth by vap. transport, cryst. struct. 78—38676
B, CVD, structure of deposits-process relations 78—27410
B, CVD from impinging jets, mass transfer, equilib. and kinetics 78—27409
B modifications, polymorphism, cryst. chem., struct., growth, book contrib. 78—47278
α-B, rhombohedral, prep. methods, book contrib. 78—48295
B, tetragonal, phase I, prep. and struct., book contrib. 78—47277
B_6As, single crysts., prep. by chem. transport reactions 79—100032
B_4C, morphology and struct. of vap. grown crysts. 79—7562
$B_{50}C_x$, x=1 to 2, prep. and struct., book contrib. 78—47277
BN, cubic, cryst. growth in systems containing H_2 80—55279
BN, polymorphic modifications form. under low and high press. 79—15597
$B_{50}N_x$, x=1 to 2, prep. and struct., book contrib. 78—47277
BP:Ni pillar crystal growth from vapour 80—60758
BiOCl, cryst. growth, Raman and IR spectra *(German)* 77—21012
BiTeI, melt and vapour grown, optical props. 80—84746
C microneedles, grown on W wires under intense elec. fields, X-ray diffr. and AES 80—54580
C, polymorphic modifications form. under low and high press. 79—15597
Cd, vapour grown crystal, morphology and growth mechanism, Bi impurity effects 79—23546
$CdAs_2$, thermoelec. props., anisotropy 80—34470
Cd_3As_2 platelet, single vap.-grown cryst., passive annealing, Fermi energy variation 80—45223
Cd_3As_2, single cryst. platelet growth, X-ray topographic obs. of perfection 78—9976
$CdBr_2$, vapour grown crystals, polytype formation, effect of mode and conditions of growth 78—72709
$CdBr_2(I_2)$, vapour growth crystals, decomposition, electron microscope study 78—92268
$CdCr_2S_4$ magnetic semiconductor crystal growth, structural defects, physical properties 80—60759
$CdCr_2S_4$, single cryst. prep. and elec. props. 79—38727
$CdCr_2Se_4$, single cryst. growth by chem. transport reactions 80—16163
$CdGa_2S_{4(1-X)}Se_{4x}$, solid soln., crystallographic studies 78—15301
$CdGeP_2$, crysts., prep. by chem. vapour transport 80—55280
$CdGu_2S_{4(1-x)}Se_{4x}$, opt. absorpt., elec. cond., spectral response, thermopower 77—72862
CdI_2 polytypes, vapour growth mechanism 80—84124
CdI_2, sublimed films, preparation, struct. 77—24491
CdI_2, vap. growth and cryst. struct. 77—72570
$CdI_{2-x}Br_x$, vapour grown mixed cryst., growth and polytypism 79—69044
$CdIn_3Se_4$, cryst. growth, photoresponse and optical props. 78—39165

crystal growth from vapour continued
CdP_2, large tetragonal single cryst. growth 77−69976
CdP_4 single crystal growth 80−35065
CdS, CdSe, growth rate, sublimation rate and etching behaviour along polar axis 80−24387
CdS, cryst. growth from vapour in sealed silica tubes, emission and mass spectra 79−43117
CdS, crystal growth from vapour phase, model for interface kinetics 77−76335
CdS crystal growth from vapour, preferential deposition, elec. field effects 80−84122
CdS crystal growth with strong long-lived polarisation echoes 79−43113
CdS, grown from vapour, SEM exam. of dislocation boundaries 80−24456
CdS, one-dimens. nucleation on (110) singular surface, model 78−2048
CdS, oriented single cryst. growth method from vapour 77−8734
CdS, seeded growth from vapour of large single crystals 78−64449
CdS, single crystal, growth by modified Piper-Polich method, props. *(Japanese)* 79−100036
CdS single crystal growth by sublimation *(Japanese)* 78−11093
CdS single crystals, grown from vapour, analysis of static method 79−52092
CdS smoke particle growth, prep. by evaporation in inert gases 77−24938
CdS, vap. phase grown cryst., stoichiometry control, elec. cond. 79−100034
$CdS:I_2$ system, interface kinetics and vapour phase mass transport 80−19732
CdS:In whisker prep. 78−75969
CdS-CdSe solid solns., bladed crystal prep. from gas phase 77−16478
CdTe, growth by sublimation travelling heater method 77−40360
CdTe, growth by vapour phase chem. transport in I_2 77−40342
CdTe, laser window material, vap. deposition 78−27391
CdTe, single cryst. sublimation growth, X-ray topographic characterisation 80−29866
CdTe, static method in closed vessel, optimal growth conditions 77−24936
$CdTl_2Se_4$, single cryst., preparation, elec. cond. 77−24554
$CoAs_3$, prep. and characterisation 77−77356
$CoCl_2(Br_2)(I_2)$, prep. using chem. transport via gas complexes *(German)* 79−15599
CoO on Co_3O_4, oriented growth following Co_3O_4 pyrolysis 78−80739
CoP_3, prep. and characterisation 77−77356
$CoSb_3$, prep. and characterisation 77−77356
Cr whisker cryst., growth incorporated with field electron emission 80−44458
Cr_xC, cathodic needle growth, at lower electric fields from $Cr(CO)_6$ vapour 80−76161
Cr_2O_3, thin plate single crystal, vapour phase growth 78−64450
$CrPr_2S_4$, synthesis, single crystal growth, mag. and elec. props. 79−78857
$CrPr_2Se_4$, synthesis, single crystal growth, mag. and elec. props. 79−78857
Cr_2S_3, single crystal, exam. of unit cell structures by interference contrast microscopy 78−67670
$CrWO_4$, cryst. growth and struct. *(French)* 77−43202
$(Cu,Ag)_2Se/(Bi, Sb)_2Te_3$, P type selenide segmented element fabrication, thermoelectric props. 80−107835
Cu, electrodeposition and formation of crystallised layers on Ni(111) surface, twinning 77−24495
Cu, thin single cryst. films, new technique for prep. employing two stages of evaporation 79−33932
$CuAl_5S_8$, cryst. growth, struct., and fluoresc. 77−48328
$CuCl_2(Br_2)(I_2)$, prep. using chem. transport via gas complexes *(German)* 79−15599
$CuGa_xIn_{1-x}Se_2$, CVD, elec. and optical props., use as heterojunction solar cell absorber 79−52095
$CuGaS_2$, crystal growth and luminesc. *(Japanese)* 78−23515
$CuGaS_2$, crystal growth by I_2 vapour transport, using temperature variation method 78−68610
$CuGaS_2$-$CuGaSe_2$ system, forbidden-band width 78−35280
$CuGaSe_2$ single crystals, electrical and photovoltaic props. 80−92940
$CuInS_2$, crystal growth by I_2 vapour transport, using temperature variation method 78−68610
$CuInS_2$ crystals, growth, struct., and elec. props. 79−38729
$CuIn_5S_8$, single crystn. phase, CVD prep., X-ray cryst. struct. determ. 79−65990
$CuInS_2(Se_2)(Te_2)$, film, electron and X-ray diffr. 77−11819
$CuInSe_2$, large single crystals growth by iodine transport and Bridgman methods 78−35300
Cu_5MTe_4, M=Gd, Tb, Dy, single cryst. growth by chem. transport reaction 77−52231
Cu_2O, CVD from Cu-O-H-Cl-N system, thermodynamic anal. 78−39676
Cu_2S-Ga_2S_3 alloys, cryst. growth, struct. and fluoresc. 77−48328
Cu_2SnSe_3, single cryst. growth and morphology 77−85908
$EuSb_4S_7$, single cryst. growth, and X-ray anal. 79−100033
$EuSb_2Se_4$, single cryst. growth, and X-ray anal. 79−100033
Fe whiskers grown from $FeCl_2.4H_2O$, exam. of growth morphology 78−72051
Fe-S system, chemical transport of non-stoichiometric phase 79−69972
Fe_3BO_6, weak ferromag., growth of bulk single crysts. by vapour phase reaction 77−24939
$Fe_3B_2O_{13}I$, boracite single cryst., nucleation control density growth 80−80955
$FeCl_2(Br_2)(I_2)$, prep. using chem. transport via gas complexes *(German)* 79−15599
$(Fe_xCr_{1-x})_2O_3$ corundum-type solid solution single crystal growth, chem. vapour transport 80−93465
$FeCr_2S_4$, ferrimag. semicond., elementary step growth on surface of vapour grown cryst. 77−76649
$FeCr_2S_4$, single crysts., vapour grown, growth of triple unit cell steps on surface 79−19984
$FeCr_2S_4$, struct. and stoichiometry, X-ray fluoresc. anal. 79−4263
$FeCr_2S_4$, vapour grown, step growth by elementary steps and multi-steps 78−27392
$FeCr_2S_4$, vapour grown, growth mechanism of multisteps on surface 78−75605
FeF_3, single crysts., vapour phase chem. transport prep. *(French)* 79−69971
FeI boracite single crystals, dielectric, pyroelectric props., vapour phase transport growth 80−80673

crystal growth from vapour continued
FeS_2, pyrite, single cryst. growth by chem. vapour transport, surface struct. and morphology 79−23550
Fe_2TiO_5, pseudobrookite, single cryst. growth by chem. transport 78−80464
GaAs (100), VPE, role of Cl, LEED, RHEED, and AES obs. 77−1327
GaAs, whisker growth by thermal decomp. 77−55875
GaAs-AlAs, epitaxial struct. with alternate layer comp. modulation, fabrication and characterisation 77−1322
$GaAs_{1-x}P_x$, chemical transport and crystal growth in closed tube *(Japanese)* 78−39673
$Ga_xIn_{1-x}P$ solid solutions, single cryst prep. and props. 80−16162
GaN, growth and morphology of crystals *(Japanese)* 80−11548
GaN:Mg, and undoped, epitaxial growth from vapour, orientation, elec. props. 77−4740
GaP, chem. vapour growth in closed system 78−35283
GaP ribbon waveguide, vapour-grown, phase-matched SHG 80−48339
GaP-ZnS, solid solns., microstruct. investig. 78−2128
GaS, optimisation of crystal growth conditions by I_2 vapour transport 78−68611
GaS(Se), growth by I_2 vapour transport using temp. oscill. method 77−77355
GaS_xSe_{1-x}, grown by iodine vapour transport, X-ray struct. studies 79−4411
GaSe, optimisation of crystal growth conditions by I_2 vapour transport 78−68611
Ga_2Se_2, sublimation growth, closed tube, mass flow and press. meas. 77−63550
$GdAs_2$ single crystals 78−88416
$Gd_2Se_3/PbTe$, N type selenide segmented element fabrication, thermoelectric props. 80−107835
Ge chalcogenides, screw dislocations in layer crystal growth from vapour *(Russian)* 80−1953
Ge, thin single crystal, (110) orientation, preparation technique 79−95930
Ge, ultrafine multiply twinned particles, form. by gas-evaporation technique 78−63685
Ge, ultrafine particles prep. by gas evaporation in Ar 78−34455
$GeAs+Cl_2(Br_2)(I_2)$, high temp. Raman spectra, cryst. growth mechanism *(French)* 79−26999
GeS, gas-phase single-cryst. growth, photoelec. props. 77−36381
GeS, growth parameter meas. during cryst. growth from vapour in closed ampules 79−19168
$GeSe_2$, single cryst. growth 77−52305
HfO_2 crystallite growth from oxide plasmas, growth morphology 80−59417
HfS_2, growth by I_2 vapour transport using temp. oscill. method 77−77355
Hg, condensation, two-dimensional, on W 80−107666
$Hg_{1-x}Cd_xTe$, mixed crystals, crystn. by chemical transport 80−20775
$HgCr_2Se_4$, vapour growth using $AlCl_3+Cl_2$ as transport components 78−35282
$HgCr_2Se_4$:Cd, precipitations during growth by chem. transport method 80−55409
HgI_2 detectors, recent improvements 78−37507
HgI_2 detectors, state-of-art crystal growth and nucl. spectroscopic evaluation 78−41895
HgI_2, doped, vap. growth by temp. oscill. method 78−39674
HgI_2, single crystal growth in small opened ampoules using dynamic sublimation technique 79−4904
HgI_2, soft γ-ray detector fabrication and props. 77−3208
HgI_2, thermally stimulated current meas. 78−41896
HgI_2, vap. growth by temp. oscill. method in horizontal furnace 78−39675
Hg_2I_2, cryst. growth by multiple vacuum sublimation 80−7485
HgS, cinnabar, chem. vapour growth in closed system 78−35283
HgSe, CVD crysts., electrophys. characts. 77−85910
HgTe single crystals, crystn. from vapour phase, thermodynamical conditions 79−33908
$HoPO_4$, single crystal, conditions for transfer and formation 77−12507
$I_{0.33}NbSe_4$, cryst. growth and struct. *(French)* 77−15375
$In_{1-x}Ga_xAs_yP_{1-y}$, vapour grown, alloy comp., thermodynamic calc. 79−99094
In_2O_3 smoke particles prepared by gas evap., morphology and coalescence growth 80−97738
$In_{2/3}PSe_3$, cryst. growth and characterization 77−77357
In_2Se_3, chem. transport reactions with I, single cryst. growth 77−16480
KBr, appl. of physical vapour transport method for low dislocation density crysts. 78−43992
KCl, appl. of physical vapour transport method for low dislocation density crysts. 78−43992
$K_{0.27}WO_{(3+y)}$, struct. analysis 77−11510
LaB_6, chemical vapour growth of whiskers, and single crystals 78−72710
LaB_6 film, structure, stoichiometry, elec. properties 78−60043
MgO, condensates, growth from vapour, morphological comparison with, ZnO, AlN 78−34450
$MgTe:Cr^+$, cryst. growth and EPR 78−39393
$MnCl_2(Br_2)(I_2)$, prep. using chem. transport via gas complexes *(German)* 79−15599
MnS(Se)(Te), CVD crystal growth, role of Mn-Al-Cl complexes 80−84840
$Mn_{15}Si_{26}$, growth by Bridgman method and chemical transport, X-ray structural analysis 79−100043
Mo, film, formation by reduction of $MoCl_5$, influence of electric field 80−93491
Mo whisker cryst., growth incorporated with field electron emission 80−44458
Mo_xC, cathodic needle growth, at lower electric fields from $Mo(CO)_6$ vapour 80−76161
MoO_2, crystn. from gas phase in presence of I_2 79−52090
MoO_2, MoO_3 and Mo_xO_{3x-1} single cryst. growth by chem. transport, elec. resist. meas. 77−59681
MoO_2, needle-shaped crystals, by vapour phase transport in I_2, 800 to 1000°C *(French)* 77−4725
MoO_2:V, growth by VO_2 transfer reacts. 79−43116
MoO_3, smoke particles, coalescence growth by gas-evaporation 78−47256
MoO_3 smoke particles prepared by gas evap., morphology and coalescence growth 80−97738
MoO_{3-x}, single cryst. growth and vapour phase transport 79−28903

crystal growth from vapour continued
MoS_2, synthetic molybdenite single crystals, growth from vapour, elec. props. 80—34446
$MoSe_2$, single cryst., growth, struct. obs. 79—90607
$MoTe_2$, pure and V doped, single cryst. growth and vapour phase transport 79—28903
$Mo_{0.5}W_{0.5}Se_2$ single cryst. vapour growth, characterisation 80—93466
$Mo_{1-x}W_xSe_2$, cryst. struct. parameters and growth conditions 79—86759
NH_4Cl, surface roughening transition in vapour phase growth 78—2044
$Na_2Mg_6Si_8O_{22}F_2$, fluoramphibole, fibrous, crystn. from gas phase, mechanism 78—34451
$Nb_xCr_{1-x}O_2$, ($x \geq 0.5$), cryst. growth by chem. transport and phase transitions 78—35281
$Nb_xCr_{1-x}O_2$, cryst. prep. and struct., mag. props. 78—52198
Nb_3Ge, CVD, hysteretic losses, precipitates and deposition temp. effects 77—28319
NbN, Nb_4N_3-NbN, Nb_2N-Nb_4N_3, Nb_2N, cryst. growth parameters and morphology of chem. vapour deposition, X-ray diffr. and SEM study 79—23861
NbO, cryst. growth and microstructure 79—95913
NbO, single cryst. growth by chem. transport reactions 77—12508
NbO_2, chemical transport with $TeCl_4$, exam. of deposition and crystal morphology 79—52093
NbO_2, cryst. growth and microstructure 79—95913
$NbO_{2.417}$, chemical transport with $TeCl_4$, exam. of deposition and crystal morphology 79—52093
$NbO_{2.417}$ to $NbO_{2.5}$, equilib., chem. transport with $TeCl_4$ 80—2934
$Nb_{12}O_{29}$, cryst. growth and microstructure 79—95913
Nb_2O_5, cryst. growth and microstructure 79—95913
Nb_2O_5, single cryst. growth by chem. transport reactions involving $TeCl_4$ 77—36382
$NbSbS_3$, synthesis and single cryst. growth and struct. 77—52234
$NbSe_2$, I_2 vapour phase transport kinetics *(French)* 78—11092
$NbSe_x$, $x=1.48$-2.0, nonstoichiometric, press.-comp.-temp. rel. determ. by annealing 79—74139
$Ni_3B_7O_{13}Br$, boracite single cryst., nucleation control density growth 80—80955
NiBr boracite single crystals, dielectric, pyroelectric props., vapour phase transport growth 80—80673
$NiCl_2(Br_2)(I_2)$, prep. using chem. transport via gas complexes *(German)* 79—15599
NiFe ferrite, prep. of single crystal by chem. transport with $TeCl_4$ 80—104051
$NiFe_2O_4$, single cryst. prep. by chem. transport 78—23589
Ni_2SiO_4, single crystals, chem. transport prod. mechanism and thermodynamics *(German)* 77—36383
NiZn ferrite, prep. of single crystal by chem. transport with $TeCl_4$ 80—104051
NpO_2, cryst. growth by chem. transport 80—16166
NpO_2 single crystal growth, gas phase chemical transport method *(French)* 80—60760
$PaAs_2$, Pa_3As_4, and PaAs, cryst. growth by chem. vapour transport, cryst. struct. 80—35066
Pb whiskers, grown from metallic vapour phase, whisker resist. 78—47686
PbS, sublimation growth, using liq. encapsulation zone-refined source material 78—27399
$Pb_{0.93}Sn_{0.07}Se$ crysts., sublimation growth, controlled carrier concs. for IR lasers and detectors 77—52237
$(Pb_{1-x}Sn_x)Te$, growth by sublimation technique *(German)* 77—73224
$Pb_{1-x}Sn_xTe$, large non-seeded single cryst. growth by sublimation method, and characterisation 79—78860
$Pb_{1-x}Sn_xTe$, large single crystal growth, on quartz surface, non-seeded 78—48293
$Pb_xSn_{1-x}Te$, grown by vap. transport in closed system, quality improvement 77—40341
$Pb_{1-x}Sn_xTe_{1-y}Se_y$, quarternary solid solns. with const. lattice parameter, cryst. growth and characts. 80—108332
PbTe single crystals, growth from vapour phase under micro-gravity conditions 80—80957
$PdCl_2(Br_2)(I_2)$, prep. using chem. transport via gas complexes *(German)* 79—15599
$(SN)_x$ cryst., synthesis and elec. cond. *(Japanese)* 77—69308
$(SN)_x$, preparation and properties 78—27389
Sb, filamentary crystal growth 77—40339
$Sb_4O_5Cl_2$, single crysts., prep. and props. 80—35067
Sb_5O_7I polytypes, cryst. growth, struct., ferroelastic and ferroelec. props. 78—31309
SbSI, crystallisation from vapour phase, morphology 77—4726
SbSI, on seed, constant temp. gradient and reversal gradient methods 78—11090
Sc, CVD, open-tube technique 80—89128
ScH_2, CVD 79—24420
Se-Te whisker crystals, growth 79—99464
$(Se)_x$, crystn. and melting 80—40241
Si (111), growth and etching vectors, adsorption and step reconstruction 79—23548
Si crystal growth, for electronic devices 80—66419
Si, crystallisation in Si-H-Cl system, adsorpt. layer comp. 77—15697
Si fibre, growth by thermal decomp. of SiH_4 79—69970
Si, filamentary, grown by chem. transport reaction method, banded struct. 80—38978
Si filamentary crystals, grown from vapour, electron probe microanal. 79—77538
Si, mechanism of cryst. growth during chemical reactions in Si-H-Cl system 78—2392
Si, melt and vapour growth for integrated circuits and solar cells 79—47609
Si monocrystalline rod growth from gas phase 78—64453
Si, solar grade, by silane pyrolysis, process design and economics 79—8234
Si, strip-type crystals, growth mechanism, morphology 79—7559
Si, ultrafine particles prep. by gas evaporation in Ar 78—34455
Si, vapour-liq.-solid growth, using Pt and Au liq. forming agents, kinetics and morphology 78—42935
Si, vapour-liq.-solid growth, using Pt and Au liq. forming agents, struct. perfection 78—42936
Si:P, doping during growth from gas phase, thermodynamic analysis 80—59489
Si-Ge-Br, heterogeneous system, equilib. gas phase composition, Si-Ge cryst. growth appl. 79—10820

crystal growth from vapour continued
Si-Ge-Br system, diffusion mass transfer 80—33911
$SiAs+Cl_2(Br_2)(I_2)$, high temp. Raman spectra, cryst. growth mechanism *(French)* 79—26999
SiC (2H), vapour grown, growth and deform. faults, X-ray obs. 78—30650
SiC, cryst. growth on oriented seeds by sublimation 78—35279
β-SiC, cryst. temp. variation during growth 77—40340
SiC, crystal growth from gas phase role of Si in mass transfer 79—8233
β-SiC crystals, wetting by Si and growth by vap.-liq.-solid mechanism 78—3005
SiC, determ. of size and conc. of crit. clusters in vapour phase in homogeneous nucleation process 79—94951
SiC, eccentric growth spirals 78—26470
SiC, fibre growth kinetics in laser-heated system 77—81203
β-SiC, film prep by RF sputtering 77—44164
β-SiC, gas phase comp. effects on growth kinetics 77—52233
β-SiC, growth kinetics by Van Arkel method 77—16479
SiC, monocryst., and epitaxial layer growing, temp. distrib. study in high temp. furnaces 79—65989
SiC, monocrystalline bars, grown from gas phase, exam. of growth process 79—95912
SiC, N doping inhomogeneities due to growth conditions 78—22741
SiC, phys. props. and crystal growth, rel. to appl. in electrolum. devices, book contrib. 77—77299
α-SiC, single cryst. growth rel. to polarity 77—52235
SiC, single cryst. ingots, growth using seeds, 1800-2600°C 78—43993
SiC:Be, gas-phase equilib. comp., thermodynamic analysis rel. to cryst. growth and doping 77—85909
Si_xGe_{1-x} multitip photofield emission cathode, fabricated by crystn. from vapour, emission characts. 78—2975
α-Si_3N_4 single crysts., growth, morphology, hardness and slip system 79—83112
Si_2NO_2, needle crystals, formation and growth rate, nitridation of Si-SiO_2 powder compacts *(Japanese)* 79—91574
SiO_2, crystobalite form. in evacuated silica ampoules, cryst.-amorphous transform. 77—68933
SiO_2, transfer in quartz capsule 79—4902
Si_2ON_2 needle crystals, growth by nitridation of Si-SiO_2 powder compacts *(Japanese)* 79—56921
Si_2Te_3, growth by Bridgman technique and sublimation, cryst. struct. 77—1106
Sn chalcogenides, screw dislocations in layer crystal growth from vapour *(Russian)* 80—1953
SnO_2, cryst. growth by chem. transport method 78—3004
SnO_2, crystal growth habits *(Japanese)* 78—95686
SnO_2 film, pure and Sb doped, transparent cond., prop., characts., stability, struct. *(Japanese)* 78—47889
SnO_2:Cr(Sb), cassiterite, gas phase growth on seed 77—24937
$Sn_{1-x}Pb_xTe$, film, production under quasi-equilibrium conditions 80—45241
SnS_2, cryst. growth, photoconductivity 77—85912
SnS_2, growth by I_2 vapour transport using temp. oscill. method 77—77355
SnS_2-SnI_4, and SnS_2-I_2, systems, transport props. and thermodynamical calcs. 79—32928
$SnS_{2\ x}Se_x$ solid soln., resistivity, lattice parameter, comp. and temp. depend. 78—91693
SnS_xSe_{2-x}, growth by I_2 vap. transport, cryst. struct. 77—73223
SnSe, sublimation growth, deviation from stoichiometry, elec. props. 78—76594
$Sn_xZr_{1\ x}Se_2$, growth by I_2 vap. transport, cryst. struct. 77—73223
TaS_xSe_{2-x}, growth by I_2 vap. transport, cryst. struct. 77—73223
Te film, vacuum deposited, growth and morphology of crysts. 80—96766
Te-Se-Cd, sandwich structure, fabrication and characteristics 80—60089
Th_3As_4-U_3As_4, cryst. growth by chem. vap. transport 78—23588
ThO_2 crystallite growth from oxide plasmas, growth morphology 80—59417
Th_3P_4, cryst. growth by chem. vap. transport 78—23588
$ThSb_2$, Th_3Sb_4, cryst. growth by chem. vap. transport 78—23588
$ThSiO_2$, single crysts. prep. by vapour phase reaction 79—28905
Ti crystal bar, prep. by iodide process 77—55878
TiB_2, chemical vapour growth by modified hot wire method 78—60555
TiB_2, crystal growth by chem. vapour transport 80—16164
TiC single crystals, growth from vapour by modified hot wire method, temp. effect on habit 79—61509
TiC whiskers, growth rate for CVD 77—47704
TiF_3, single crysts., vapour phase chem. transport prep. *(French)* 79—69971
TiN, gaseous phase, crystallisation, effect of temp., vapour-gas mixture conc., and deposition time 79—33910
TiN(C) whisker growth in CVD 80—59843
TiO_2, anatase, influence of Al_2O_3, Ga_2O_3 or In_2O_3 to polymorphic crysts. in vapour 79—78858
TiO_2, anatase, single cryst. growth by chem. transport reactions 77—36384
TiO_x, thermodynamic of chem. transport systems 78—27393
Ti_2O_{2x-1}, prep. by chem. transport method, equilib. comp. of TiO_2-Ti-Cl_2 gas phase 80—21317
Ti_2O_3, cryst. growth by chem. transport and tri-arc methods, and characterisation 78—3003
Ti_4O_7, controlled growth by chem. transport reactions 77—90262
Ti_nO_{2n-1}, cryst. growth and characterisation 78—31311
TiP-I_2, exam. of equilibrium gas-transport reaction 79—95911
TiS_2, chem. transport rate effects on stoichiometry 77—90263
TiS_2, growth by chem. vapour transport using press.-temp.-comp. diagram 77—59764
TiS_2, nonstoichiometric, chem. transport reaction mechanism 77—8735
TiS_2, V addition effect on chemical transport 79—24419
UAs, U_3A_5, cryst. growth by chem. vap. transport 78—23588
UO_2, cryst. growth by chem. transport 80—16166
UO_2 crystallite growth from oxide plasmas, growth morphology 80—59417
UO_2, growth by chem. vapour transport, using $TeCl_4+Ar$ 78—35284
USb, USb_2, U_3Sb_4, cryst. growth by chem. vap. transport 78—23588
USb_2, crystal growth by chemical vapour transport 80—15024
$U_{1-x}Th_xO_2$, solid solution, single crystal growth by chemical transport reactions 78—72708
V-O system, chemical transport of non-stoichiometric phase 79—69972
$(V_{1-x}Cr_x)_2O_3$, vapour phase transport, single cryst. growth *(French)* 77—24940

crystal growth from vapour continued
V_3Ga, single crystal prep. by iodine transport, supercond. T_c meas. 78−48294
VI_2, single crysts., growth from vapour phase 80−66410
V_2O_3, vapour phase transport, single cryst. growth *(French)* 77−24940
V_3O_5 single crysts., prep. by chem. transport reacts. props. 79−43115
V_nO_{2n-1}, cryst. growth and characterisation 78−31311
V_nO_{2n-1}, microsyntactic intergrowth 79−1402
Vo_2, crystal growth by I_2 vap. transport 79−43116
W needle crystal growth, discharge-induced decomp. of hexacarbonyltungsten mols. 80−84414
W needles, mechanism of cathodic growth, decomp. of $W(CO)_6$ under high field conditions 80−76162
W needles produced by $W(CO)_6$ decomp. 79−95302
W whisker cryst., growth incorporated with field electron emission 80−44458
WO_2, chem. transport conditions influence on morphology and quality 79−43114
WO_3, smoke particles, coalescence growth by gas-evaporation 78−47256
WO_3 smoke particles prepared by gas evap., morphology and coalescence growth 80−97738
WS_2, single crysts., growth by direct vapour transport method, X-ray and electron diffr. study 79−28904
WSe_2, chem. vapour transport growth, microstruct. develop. 80−103278
WSe_2, single cryst. growth by sublimation method 78−11091
YbSe, chem. transport reaction with I_2 77−24935
$ZnAs_2$ single crystals 78−88416
Zn_3As_2:Cu(Te), single crysts., gas phase growth, elec. props. 79−15598
Zn_2GeO_4 single crystals, vapour growth 79−87571
$ZnGeP_2$ dissoc. press., vapour comp. and press., thermodynamic characts. 77−24934
$ZnIn_2S_4$ film, photoluminesc. and photocond. 78−52677
ZnO, c-direction cryst. growth and crystallographic polarity 79−28902
ZnO, condensates, growth from vapour, morphological comparison with, MgO, AlN 78−34450
ZnO, growth by recrystallisation of ZnO in H_2O vapour and H_2 77−85913
ZnO, hollow crystals, growth by oxidation of ZnSe vapour, mechanism 78−34733
ZnO, precipitation from gas phase 78−6025
ZnO, single cryst., photo- and thermoluminescence 80−66311
ZnO, single cryst. growth in ZnO-H_2-H_2O-O_2 vapour, morphology, electrophys. and opt. props. 78−52649
ZnO, ZnS, growth rate, sublimation rate and etching behaviour along polar axis 80−24387
ZnP_2, large tetragonal single cryst. growth 77−69976
Zn_3P_2 large crystal growth, vapour transport perforated capsule technique, prototype solar cell appls. 80−93464
Zn_3P_2 photovoltaic material and Schottky diode characteristics 78−64066
$Zn_3P_2(As_2)$, cryst., gas phase growth, morphology 79−10821
ZnS, single cryst. vap. growth by sublimation and chem. transport 78−27390
ZnS vapour grown crystals, morphology and structure 78−42937
ZnS, Zn(S,Se), large single crystals, vapour growth and defect characterisation 80−25540
ZnS(Se)(S_xSe_{1-x}), growth of cubic single crystal by I_2 transport 79−91572
ZnSe, crystal, new polytype structure 78−14319
ZnSe, single cryst. vap. growth by sublimation and chem. transport 78−27390
ZnSe, vapour phase single crystal growth 79−91573
ZnSe:I crystals, I vapour transport prep. 79−100035
ZnSe:In, single crysts., new vapour phase growth method, elec. cond. props. and photoluminesc. spectra 79−19982
ZnSe-GaAs solid solns., chem. transport cryst. growth, struct. 78−43991
$ZnSiAs_2$, cryst. growth and elec. props. *(French)* 77−76815
$ZnSiP_2$, conc. profiles during gas phase transport *(German)* 78−64452
$ZnSiP_2$, crystallisation from gas phase *(German)* 77−69977
$ZnSiP_2$, effect of crystal growth method, on physical props., effect of doping on physical props. *(German)* 79−52094
$ZnSiP_2$, growth under nonstoichiometric conditions in gas phase, microanalytical investig. *(German)* 79−33909
Zn_2SnO_4, form. by vapour phase method, form. reaction, effect of starting materials *(Japanese)* 77−32514
Zn_2SnO_4, needle cryst. growth from ZnO-Sn mixture 77−12509
ZnTe, cryst. growth under thermodynamically controlled conditions 77−48327
ZnTe growth from vapour, growth interruption 80−97416
ZnTe high-purity single cryst. growth by sublimation travelling heater method 79−28901
ZnTe, low temp. vapour growth, closed tube transport technique 77−85914
ZnTe, single cryst. vap. growth by sublimation and chem. transport 78−27390
ZrC, single cryst. growth by modified hot-filament method, cryst. morphology and microhardness 79−19983
ZrN(C) whisker growth in CVD 80−59843
ZrO_2 crystallite growth from oxide plasmas, growth morphology 80−59417

crystal hyperfine field interactions
β-ray spectra of recoil nuclei polarised by fast polarised beams 77−28502
N-acetyl-L-cysteine, X-irrad., ^{33}S nucl. coupling and nature of free radicals 77−52743
actinyl complexes, hyperfine interactions 80−10928
L-alanine:Cu(II), EPR and ligand-ENDOR measurements 80−44907
alkali bromide (chloride):V^{2+}, electron spin transfer 78−87949
alkali dithioferrates (III), electronic struct. and hyperfine interactions, Xα calcs. 80−100448
alkali fluorides, ESR study of interstitial atomic H centres 79−56609
alkali halide:Hg, EPR and optical props. 78−91933
alkali halide:Tl^+-like ions, triplet state lifetime, hyperfine interaction 80−2844
alkali halides, ^{14}N impurities, molecular point defects, EPR isotropic hyperfine triplets 80−2636
alkali halides, F-centres, optical pumping, spin-orbit and hyperfine coupling 77−16360
alkali halides, implantation of ^{57}Fe, conversion electron Mossbauer spectroscopy technique 80−40012

crystal hyperfine field interactions continued
alkali metal halides, analysis of spin-Hamiltonian parameters of heteronuclear XY^- defects 80−88509
alkali metal salts, NMR spectra of alkali metal nuclei, shielding and quadrupole coupling consts. 78−84487
alkali metavanadate:Cr^{5+}, study of ESR spectra 80−80601
alkaline earth fluoride:Gd^{3+}, ligand ENDOR, spin Hamiltonian and hyperfine parameters 77−43903
alkaline earth fluoride:$Gd^{3+}(Eu^{2+})$, model of ligend hyperfine interaction 80−6792
allowed β-γ angular correlations induced by mag. interactions 78−68419
alloy, elec. field gradient analysis 78−51950
alloys, dil., Kondo coupling, hyperfine and exchange interactions 79−65647
alloys and semiconductors, Mossbauer spectrometry *(French)* 80−80660
amidinium salts, ^{14}N NQR spectra, H^+ relax. times 80−60448
anisotropic HFS tensors for double zeta functions with applic. to neutral radical proton interactions 77−35903
anthracene:rhodamine, triplet exciton density, isotope substitution effect, in weak mag. field 77−90184
antiferromagnet, local field at positive muon 78−92010
antiferromagnets, low anisotropy, nuclear spin waves spectra, relaxation, parametric excitation, NMR dynamic shift *(Russian)* 80−11180
arabinose, X-irradiated single crystal, intermol. electron trapping, hyperfine ESR pattern 79−39166
aromatic molecular crystals, optical nuclear polarization by optically excited triplet states 79−19804
L-asparagine.H_2O, X-irrad. at room temp., ESR and ENDOR 77−40131
atomic hyperfine coupling consts., calc. 77−39810
9-aza-bicyclo (3,3,1)nonan-3-one-9-oxyl, dimerisation, ESR, NO radical pair exchange 78−19330
BCC metal, heavy ion implanted, vacancy annealing stage, Mossbauer meas. 78−39463
benzophenone, high resolution ODMR and optically detected ENDOR 79−19811
benzophenone $^3(n,\pi^*)$, and isotopic forms, in 4,4′-dibromodiphenylether, level anticrossings, ODMR obs. 78−2772
2,1,3-benzothiadiazole, EPR of phosphorescent state 77−8405
biotite, elec. field gradient Mossbauer absorption 77−85629
α-bromofluoro alkyl pi-radical, signs of hyperfine and quadrupole couplings, ESR determ. 80−97141
N-bromosuccinimide, X-irrad., ESR study of Br and σ^* radical 80−66037
CDW phase excitations 78−43317
charge transfer complexes, doped, excited cryst., fine and hyperfine struct., ESR 77−12188
chromocene, solid, Raman transition assignments, mag. susceptibility, mag. moment 78−43861
conference on hyperfine interactions, Madison, NJ, USA (Jun 1977) 78−39076
contact hyperfine interaction, influence of exchange hybridisation of impaired s electron with ligand electrons 77−15806
copper acetate monohydrate, pure quadrupole reson., covalency 77−16205
copper diethyldithiocarbamate single crystal, EPR exchange coupled pairs, low temp. hyperfine anomaly 77−90021
core polarisation hyperfine interactions, unrestricted Dirac-Fock theory 78−19005
crystal lattice electron energy spectrum depend. on external electric field *(Russian)* 80−34498
cubic alloys, anisotropic hyperfine interactions, Mossbauer spectra 80−15854
cubic fluoride lattice, π-electron spin density due to Cr^{3+} ion 80−49683
cubic metals, ferromag., mechanisms for elec. field gradients 78−43340
diamagnetic lattice, EPR parameters of V^{4+}, cryst. field effects 78−64263
diamagnetic perovskites, AMF_3, Fe^{3+}-O^{2-} pair EPR probe for struct. phase changes 77−36113
diamond:^{111}In, ion implanted, intrinsic limitations of doping 80−34019
diamond:Xe, quadrupole interaction of implanted Xe 79−61279
diamond, electric quadrupole sum rules rel. to optical consts. 79−38036
diamond, implanted ^{129m}Xe, lattice location, combined Mossbauer and IPAC meas. 78−43733
diamond type crystals, polarization of μ^+ in muonium atom *(Russian)* 78−39492
diamonds, natural, N3 centre, EPR obs. 79−51842
dibenzenechromium-dibenzenevanadium, proton HFS data, ENDOR obs. 80−66073
p-dibromobenzene, cryst. nucl. spin polarisation, cross relax. study 80−29647
dichloromethane-d_2, spectral densities determ. from spin-lattice relax. and spin-echo decay rates 80−75877
diethylammonium copper tetrachloride, ^{63}Cu NMR, hyperfine interactions 80−54956
dil. impurity hyperfine fields, comparison with models 78−14954
dilute alloys, point defect electric field gradient, anisotropic screening effect 79−56177
dimethyl stannous chloride di(pyridine 1-oxide), ^{119}Sn Mossbauer spectra, elec. field gradient 80−15909
dimethyl tin diisothiocyanate, ^{119}Sn Mossbauer spectra, elec. field gradient 80−15909
dimethylammonium iron chloride, two-dimens. antiferromag., ^{57}Fe Mossbauer obs., sublattice magnetis. 77−66443
dimethylbenzaldehydes, in durene single cryst., zero-field splitting, guest and host isotope effects 80−107752
diphenylhaloselenium radical trapped in single crysts., FSR, struct. 80−44919
disordered matrix, effect of quadrupole coupling on electron spin echo modulation patterns 77−85571
distorted cubic metals, elec. field gradient, temp. depend. 78−39481
doublet-triplet mag. system, dipolar and quadrupolar ordering 79−8004
DTGS:VO^{2+}, ENDOR 79−99791
dulcitol, X-irradiated single crystal, intermol. electron trapping, hyperfine ESR pattern 79−39166
dynamic polarisation of nuclei, nonlinear effects on time taken to establish steady state 80−11293
electric quadrupole interaction, special feature of integral perturbed ang. correlation method 79−11364
electric quadrupole interactions measured by nuclear orientation and NMR on oriented nuclei, review 80−92868

crystal hyperfine field interactions continued
electron gas, spin-polarised, self-consistent screening of positive muon 78—47714
electron spin echo envelope modulation effect, powder pattern behaviour, hyperfine coupling consts. determ. 79—33524
electron-nuclear systems, forbidden transitions 77—12254
ENDOR, forbidden transitions, hyperfine interactions, theory 80—50226
enzyme, nucl. quadrupole interaction parameter related to structure-function 77—8472
EPR of heteropairs with strong exchange coupling, hyperfine struct. 78—72395
EPR of triplet excitons, model Hamiltonian, Kubo-Tomita approximation 77—24734
EPR spectra, angular var. calc. 80—54940
EPR spectra, hyperfine structure, low symmetry effects, calc. 80—50165
EPR spin Hamiltonian, perturbation treatment, M=0 electronic state, HFS of triplet state EPR 80—25185
ferric haeme complex of low spin, Mossbauer spectra, crystal field parameters 80—26203
ferric myoglobin cpds., single cryst., Mossbauer studies 80—8016
ferrimagnet, indirect hyperfine and superexchange interactions 77—69537
ferromagnet:Ra, hyperfine field determ. 77—85622
ferromagnet, amorphous and crystalline, evaluation of complex Mossbauer spectra 78—60370
ferromagnet, local field at positive muon 78—92010
ferromagnet, metallic, correl. of temp. anomalies of hyperfine field and thermal expansion of lattice 80—20400
ferromagnet, nuclear magnetisation motion, hyperfine field microscopic inhomogeneity, NMR freq. shift *(Russian)* 80—80623
ferromagnet, one-dimensional localised nuclear magnon modes 80—93098
ferromagnetic alloys, hyperfine field 77—24537
ferromagnetic alloys, hyperfine field systematics of nonmag. ions 78—60093
ferromagnetic metal, magnetisation density in vacancies, μ^+ probe, theory 77—28504
ferromagnetic metal, temp. depend. of hyperfine fields at impurities 79—15300
ferromagnetic metal-rare earth, dil., hyperfine fields 78—87947
ferromagnetic metallic glass, hyperfine field and spin wave excitations, $T^{3/2}$ depend. 78—10672
ferromagnetic metals, muon spin rotation; freqs., and relax. rates 80—55006
ferromagnetic phase transitions, nucl. spin dynamics in anisotropic systems 80—11205
ferromagnetic phase transitions, nucl. spin dynamics in isotropic systems 80—11204
ferromagnetic semiconductors, Raman scattering of light on plasmon excitations 80—2738
ferromagnetic transition metal, Fano effect and hyperfine field of non-transition impurity 80—25128
ferromagnets, hyperfine field at positive muon 80—40029
ferromagnets and antiferromagnets, mag. impurity levels, standard basis operator method *(Russian)* 80—11192
ferrous oxalate dihydrate, Mossbauer spectrum, hyperfine fields 78—39483
ferrous tetraphenylporphyrin, Mossbauer effect, mag. hyperfine interaction 79—24236
fluorene:acridine, EPR of excited triplet state complex 79—19767
fluorene:acridine (phenazine)(anthracene), optical nuclear polarisation, non-crossing rule, guest-host complex 77—42339
fluorene crystal, doped, photochemical hydrogen abstraction, proton hyperfine structure via optical nuclear polarisation 80—63659
fluorides, electric field gradient, time-differential-angular-distrib. method 80—60463
$Ga_xAl_{1-x}As$, optically oriented electron, nuclei spin instability *(Russian)* 80—70660
gamma-ray absorption, multipole transition, Hermitian intensity matrix 77—43911
gamma-ray linear polarisation, elec. quadrupole interaction effects 77—12265
gamma-ray perturbed ang. correls. with quadrupole interactions, geometrical coeffs. 80—73109
garnets, mag. props. of V^{4+} ion, effect of covalency 78—64010
generalised spin precession eqn., elec. quadrupole interaction sign 78—43744
group IV elements, ^{57}Fe isomer shift, quadrupole coupling and interat. distance correl. 78—52408
guanadinium zinc sulphate:Cu^{2+}, EPR of Cu^{2+} at tetrahedrally coordinated Zn^{2+} sites 78—39388
guanidinium aluminium sulphate hexahydrate:Mn^{2+}, NMR 78—91939
halides, NMR spectra of halogen nuclei, shielding and quadrupole coupling consts. 78—84487
halogens, solid, intermolecular bonding influence on nucl. quadrupole interaction tensor 77—62882
HCP metal, naive model for electric field gradient, numerical results for Zn 78—91650
Heisenberg ferromagnet, nuclear spin quantum mechanical behaviour 77—51872
Heisenberg ferromagnets, BCC, with $K_2CuCL_4.2H_2O$ struct., ^{17}O transferred hyperfine interactions 78—39439
heme-proteins, general spin Hamiltonian for determ. of ligand nucl. Zeeman and hyperfine interactions 77—85617
Heusler alloy, Mn-containing hyperfine field and magnetic behaviour 79—78360
Heusler alloy with nonmagnetic impurity, transferred hyperfine field using volume overlap model 79—78054
Heusler alloys, hyperfine fields and mag. interactions, NMR spectra 78—88222
Heusler alloys, hyperfine fields at sp sites, spin echo NMR meas. 78—19371
hexaaquo-magnesium dihydrogen EDTA:VO^{2+}, single cryst., ESR spectra and spin Hamiltonian parameters 80—75845
hexacyanobenzene-naphthalene, charge transfer triplet states, electron distrib., ESR 77—3388
high speed rot., spin diffusion, NMR spin lattice relax. obs. of D 80—66056
high spin/low spin transition, model including lattice dynamics 77—63202
hippuric acid, X-irrad. single cryst., ^{14}N and ^{1}H ENDOR study; 80—71240

crystal hyperfine field interactions continued
Hirshfeld type deformation functions, and elec. field gradients calcs. by Fourier series 79—73479
hydrazinium iron tri(hydrazoformate) monohydrate single cryst., effective EFG tensor, Mossbauer spectra obs. 79—56628
I-III-VI_2 semiconductors, nucl. quadrupole coupling consts. and struct. parameters 79—42509
II-VI semiconductor:Mn^{2+}, superhyperfine struct. tensor and g-shift 78—39056
III-V semiconductors, electric field gradient-elastic tensor components, acoustic NMR obs. 80—25229
impurity ion effect on covalency, hyperfine interaction 78—23063
insulator, exchange-coupled, interference effects in NMR, with anisotropic hyperfine interactions 77—81022
insulators, neutron activated β-emitters, hyperfine interactions 78—39070
interdoublet EPR spectrum ang. depend. for ions with arbitrary electron and nuclear spins in strong axial cryst. field 80—93164
intermediate state perturbation in low temperature nuclear orientation 80—97168
Invar, deformed, magnetism and temp. depend. of effective field on ^{57}Fe *(Russian)* 79—24234
Invar, effect of deform. by cold rolling, Mossbauer expt. 77—48556
Invar, mag. inhomogeneity, ^{57}Fe and ^{61}Ni NMR 79—19803
ionic compounds, amorphous, Mossbauer study, frozen mag. state and hyperfine interaction *(French)* 80—80661
ionic crystal, Sternheimer antishielding factors of F^-, Cl^-, Br^- and I^-, approx. free- and cryst.-ion pot. influence 80—39544
ionic crystals, Sternheimer quadrupole shielding-antishielding function for F^-, Cl^-, Br^-, and I^- 80—80236
ionic iron group compounds, nuclear quadrupole interactions, role of antishielding effects 78—47748
ionic lattice $ABCL_3$ systems, covalency parameters estimation from nucl. quadrupole coupling 80—25246
Ising model lattice, impurities and probe independence of hyperfine crit. exponents 79—87267
Ising system, local crit. behaviour at impurities 77—48001
K-capture probability depend. 77—18480
Kondo system, comparison of nuclear orientation and magnetisation expt. 77—63297
lanthanum nicotinate dihydrate, cryst., nucl. quadrupole interactions, D atom coords., ENDOR obs. 80—97161
lattice isolation of impurities from hyperfine interaction and channelling results 78—43731
liquid crystals, lyotropic, ^{23}Na NMR quadrupole splittings, elec. double layers 78—76345
luminescence thermal quenching for linear and derivative nucl. operators 77—8631
macroradical, electron spin echo spectra, instantaneous and conventional spectral diffusion 79—15355
magnetic cooling, hyperfine enhanced nucl., using Pr alloys 79—1674
magnetic critical phenomena, hyperfine expts., selective review 78—43722
magnetic dipole-dipole hyperfine integrals for Slater-type orbitals 79—11095
magnetic insulator, supertransferred hyperfine interaction 77—85403
magnetic insulators, indirect exchange interactions, polar model study 78—88110
magnetic insulators, perovskite-like struct., supertransferred hyperfine interaction 78—14913
magnetic materials, μSR meas. 79—56660
magnetic materials with nonmagnetic impurities, conduction electron polarisation and mag. hyperfine fields 77—63174
magnetic metals, hyperfine mag. fields at ^{119}Sn nuclei 80—60248
magnetic semiconductor, helicon wave propag., hyperfine interaction effect 80—80307
magnetic semiconductors, long-range exchange interactions 77—69531
magnetic spin rotation in presence of weak quadrupole interactions 78—43345
magnetically ordered cryst., indirect nuclear spin interactions 80—103847
magnetically ordered crysts., mag. pendulum beats in Mossbauer scatt., theory 79—69760
matrix isolated metal atoms, matrix influence, theory 78—46290
metal, antishielding effects and temp. depend. of field gradients 78—51951
metal, correlation of annealing temp. for radiation damage fields to melting point in DPAD expts. 78—43737
metal, elec. field gradient analysis 78—51950
metal, electron mediated nucl. spin-phonon interaction 77—1604
metal, heavy ion implantation, site population model 77—80518
metal, interstitial, quadrupole effect on dipolar field width 78—2457
metal, lattice sums with screened potentials 78—43341
metal, muon screening spherical solid model 79—56654
metal, neutron activated β-emitters, hyperfine interactions 78—39070
metal, non-cubic, electric field gradient, press. and temp. depend. 77—8057
metal, noncubic, charge screening enhancement of quadrupole shielding factors 78—43342
metal, noncubic, conduction-electron elec. field gradient, probe valence effects 78—47749
metal, noncubic, possibility of isotopic mass effect on quadrupole coupling consts. 78—43725
metal, physics of radiation damage 78—38752
metal hydrides, rare earth and intermetallic, electronic and mag. props., Mossbauer study 80—34830
metals, ferromagnetic, nonmagnetic impurity hyperfine field temp. depend. 80—34402
metals, fraction of ions in unique sites, following ion implantation 77—15438
metals, sp, elec. field gradient at ^{111}Cd, effects of high press., TDPAC meas. 80—25266
metastable polarised crystals, decay kinetics, exchange magnon-phonon interactions *(Russian)* 80—7060
methyl-d groups, reorienting or tunnelling spin-lattice relax. 80—97156
methylammonium chromium alum, single cryst., Cr^{3+} EPR, g-factor, hyperfine splitting 78—2729
1-methylimidazole complexes, with ferriporphyrins, PMR obs. 77—12214
molecular crystals, chem. shielding, spin-lattice, quadrupole interactions, ^{2}D NMR spin echo spectroscopy 80—34817
monochloroacetic acid single crystal, Zeeman and ^{35}Cl NQR investig. 80—66066

crystal hyperfine field interactions continued
  Mossbauer ^{57}Fe spectra, ferrous charact., cryst. field interactions 80—108133
  Mossbauer diffraction, combination type maxima, hyperfine interactions on nuclei 80—25263
  Mossbauer effect-time dependent PAC technique, theory of combined method 79—28645
  Mossbauer isomer shift measurement, book contrib. 79—87349
  Mossbauer lines, polarisation analysis in presence of relax. 78—10813
  Mossbauer quadrupole splitting calcs. using cryst. field model, applic. to ferrous complexes 77—32301
  Mossbauer scattered radiation, perturbed ang. correl., hyperfine field determ. 77—81032
  Mossbauer spectra, struct., electronic and mag. props. 79—91320
  Mossbauer spectra of E2 transitions, interference effects 77—59491
  Mossbauer spectroscopy, effect of neighbours on hyperfine field 80—39931
  Mossbauer spectroscopy at ultralow temps. 78—43742
  muon probes, state-of-the-art 77—63351
  muonium, two-frequency precession determ. of hyperfine splitting 77—28505
  met-myoglobin:Cu^{2+}, single cryst., EPR, conform. changes 77—73505
  myoglobin-O_2(CO), elec. field gradient tensor, Mossbauer meas. 80—8017
  nitrosodisulphonate ion salt dimerisation, ESR of dimers in triplet state *(French)* 77—12791
  NMR linewidth, RF field effect in system with nonequidistant spectrum 78—10788
  noble metal-Eu, dil., hyperfine fields of rare earth impurity, calc. 80—15486
  noble metal-Gd, dil., hyperfine fields of rare earth impurity, calc. 80—15486
  noncubic metals, ^{178}Hf Mossbauer transition, electric quadrupole interaction 80—39928
  nonmetallic crystals, ENDOR of impurity centres 80—25249
  nuclear elec. quadrupole coupling const. sign determ., appls. 77—12291
  nuclear electric field gradient splittings calc. using ligand splittings in photoelectron spectra 80—43106
  nuclear electric hexadecapole interactions, in solids 80—65513
  nuclear inelastic channel suppression, nuclear reson. and electronic scatt. of γ-quanta, hyperfine transitions 78—60361
  nuclear orientation and NMR of oriented nuclei, appl. to solid state magnetism, review 80—44928
  nuclear spin echo in the NMR and FMR overlap region 79—24229
  optical nuclear polarisation, field and orientation depend., non-crossing rule, perturbation anal. 77—42337
  optical nuclear polarisation, the non-crossing rule, electronic relax. perturbation anal. 77—42338
  organometallics, Mossbauer spectra of spin crossover 80—15903
  paramagnetic centres, quadrupole relaxation transitions due to carrier exchange scattering 79—73803
  paramagnetic systems, NMR shifts calc. using nonmultipole expansion method 80—2651
  pentamethylbenzene-TCNB, charge transfer triplet states, electron distrib., ESR 77—3388
  periodic structure, electron-exciton complex auto ionisation *(Russian)* 80—49611
  Permalloy, proton radiation effects, Mossbauer obs. 80—40008
  phenanthrene-d_{10}, oriented in biphenyl, triplet zero-field splittings, conc. depend. 78—2773
  phenanthrene-pyromellitic acid dianhydride, single cryst., EPR, delocalised and localised charge transfer excitons 77—85545
  phosphoranyl radicals, magnetic hyperfine tensor, quadrupole coupling tensor, g tensor, ESR study 79—56611
  2,5-piperazinedione, X-ray damaged, ENDOR, δ proton hyperfine interaction 77—9103
  polarised ferromagnetic media, decelerating ion, transient field phenomena 78—72445
  polyacrylic acid:Fe^{3+}, electron state of Fe^{3+}, Mossbauer and magnetisation obs. 79—73872
  polycrystals, hyperfine interaction determ. from Mossbauer spectra in applied mag. field 77—28497
  potassium halides, F-centres, optical pumping, spin-orbit and hyperfine coupling 77—16359
  praseodymium ethyl sulphate, one-dimensional X-Y model, hyperfine contrib. to specific heat 79—1678
  press. depend. of effective mag. fields on ^{57}Fe nuclei 78—52383
  protocatechuate 3,4-dioxygenase, reduced, Mossbauer effect zero field splitting 79—24955
  PTS polydiacetylene single cryst. reflection spectra, exciton site splitting 78—31211
  pyrochlore compounds, EFG and Mossbauer quad. splitting calcs. 77—62877
  quadrupole splitting-isomer shift linear rel., elec. field gradient sign 77—1624
  quanidinium aluminium sulphate hexahydrate:Fe^{3+}, EPR, zero-field splitting 77—8395
  α-quartz:^{57}Fe, anomalous hyperfine splitting 80—103650
  α-quartz:Ag^{2+}(Cu^{2+}), γ-irradiated, stabilisation of impurity atoms 79—8047
  quartz, muonic atoms, hyperfine splitting frequency *(Russian)* 79—91332
  quartz, muonium hyperfine splitting meas., muon spin rot. technique 80—50246
  α-quartz, muonium precession, quadrupole splitting 79—42879
  rare earth, heavy, elec. field gradient, at ^{111}Cd impurities, temp. depend. 79—28642
  rare earth alloys, $R(Fe_xRh_{1-x})_2$, mag. props., Mossbauer spectra 80—25108
  rare earth alloys, RAl_2, RZn, ordered, NMR determ. of hyperfine fields 78—84180
  rare earth alloys, RFe_4Al_8, cryst. struct. mag. props. and hyperfine interactions 78—87648
  rare earth alloys, $RIn_3(Sn_3)$, ^{111}Cd quadrupole coupling consts. and valence states, PAC meas. 77—48102
  rare earth cobaltides, R_2Co_{17}, ^{59}Co NMR obs. of hyperfine fields and mag. moments 77—20726
  rare earth ethyl sulphate nonahydrates:Gd^{3+}, $g_{\parallel}$, EPR obs. 78—35031
  rare earth ferromagnet, mag. hyperfine field interaction, ^{197}Au Mossbauer effect 77—8463

crystal hyperfine field interactions continued
  rare earth ferromagnet, polarisation in external mag. fields, TDPAC 77—8462
  rare earth garnets: $^{154}Gd^{3+}$, hyperfine interactions, PAC 77—43909
  rare earth intermetallic compounds, NMR anal. of indirect mag. interactions 80—71193
  rare earth intermetallics, AB_2, (A=Y, La, Ce, Lu; B=Ir, Rh) 77—85564
  rare earth intermetallics, R_xFe_y, conc. depend. of Fe moments 78—56413
  rare earth intermetallics, RAl_2, exchange modification of cond. bands 79—82568
  rare earth intermetallics, RFe_2 and $R(Co_{0.98}\,Fe_{0.02})_2$, magnetostrictive material, changes in vibr. modes near mag. phase transition 79—90736
  rare earth ions, Dirac-Fock exam. of electronic props. 79—56106
  rare earth iron intermetallics, R_2Fe_{17} and $R_2Fe_{17-x}Ni_x(Co_x)$, mag. anisotropy and hyperfine interactions 77—8298
  rare earth metal, alloy and cpd., static and dynamical aspects of hyperfine interaction, NMR investigation 79—91299
  rare earth metals, heavy, NMR exam. of electric field gradient 78—52363
  rare earth monochalcogenides, 4f-6s excitation energy, metallic and insulating elec. props. 80—44603
  rare earth nonmetallic compounds, indirect spin-spin coupling, models 80—80238
  rare earth nuclei in cubic cpds., self polarisation field calc. 80—15487
  rare earth orthochromite, Sn^{4+}-doped, indirect Sn^{4+}-$O_2^-Cr^{3+}$ interactions 77—11887
  rare earth orthoferrite, Sn^{4+}-doped, indirect Sn^{4+}-O^{2-}-Fe^{3+} interactions 77—11887
  rare earth orthoferrites, hyperfine interaction anisotropy, NMR study *(Russian)* 80—66052
  rare earth phosphates, RPO_4, ^{13}P NMR exam. of transferred hyperfine effects 79—61241
  rare earth rhodium borides, RRh_4B_4, NMR and sp. ht. in supercond. and mag. ordered phases 80—7037
  rare earth systems, NMR, EPR, and Mossbauer effect, book contribs. 80—39883
  rare earth tellurides, electron density distrib. from Mossbauer spectra 78—23374
  rare earth trichloride hexahydrate:Gd^{3+}, EPR meas. 78—15017
  rare earth-Al_2(Zn), mag. coupling mechanism 79—4655
  rare earth-Au, dil., Mossbauer exam. of mag. hyperfine field at ^{197}Au impurity 78—88244
  rare earth-Fe alloy, RFe_2 (R=Tb, Dy, Ho and Y) crit. phenomena, Mossbauer exam. 78—52403
  rare earth-transition metal alloys, $RM_2Si_{2-x}Ge_x$ and $RM_{4+x}Al_{8-x}$, magnetism and hyperfine interactions, magnetisation and Mossbauer effect studies 80—75892
  rare-earth alloys, quadrupole scatt. anisotropy, magnetically ordered material 78—64034
  rare-earth impurities in s-p hosts, self-polarization hyperfine fields 79—33456
  rare-earth vanadates, transferred hyperfine effects, ^{51}V NMR studies 79—82893
  relativistic quadrupolar contrib. in systems with nonvanishing orbital magnetism 78—43338
  relaxation phenomena and magnetic hyperfine fields of isolated Ce ions in liquid and solid metals 80—108137
  RF discrete saturation, effects of dipole reservoir 79—56626
  rhamnose, single cryst., X-irrad. at 4.2K, trapped electrons and electron traps characts. 79—78037
  ruby, echo intensity depend on mag. field, Cr^{3+} and ^{27}Al nuclei superhyperfine interaction 79—68419
  ruby, ENDOR of Cr^{3+} ions, elec. field effect *(Russian)* 79—8071
  ruby, EPR spectrum, temp. depend., cryst. field parameters determ. 78—15016
  ruby, optical free induction decay modulation and absorpt. line struct. due to superhyperfine interaction 80—33091
  ruby, photon echo, modulation in μs pulse separation regime 78—30029
  scheelites, zero-field splitting of Mn^{2+} ions 80—75531
  semiconductor with transition metal impurity states, EPR linewidth calc. 80—80599
  Si:Sb(P)(As), shallow donor states with strong central cell perturbation theory 78—51933
  sodium nitroprusside, isomeric molecular states generated by polarised light, Mossbauer resonance obs. 77—20781
  sodium oxalate:Cu^{2+}, anhydrous spin Hamiltonian and bonding parameters and orbital-reduction factors 80—60408
  spin correlated crystalline elec. field effective operators 80—59938
  spin Hamiltonian, higher order hyperfine terms, transition metal ion in octahedral symmetry field 78—79967
  steel, Cr-Ni-Mo-V, Mossbauer austenitometry and mag. props. 80—40003
  stochastic theories for hyperfine spectra in presence of relax. 78—43743
  stroboscopic resonance meas. of nucl. quadrupole interaction 77—85621
  succinamic acid, X-irrad., primitive radn. damage, ESR, ENDOR 78—3352
  sucrose, single cryst., X-irrad. at 4.2K, trapped electrons and electron traps characts. 79—78037
  sulphides, mag. interactions of Fe group ions 79—99753
  superhyperfine and hyperfine interaction parameters, ENDOR determ. *(Russian)* 79—47064
  superhyperfine structures, paramagnetic impurity, ligand nuclei interaction, calcs. 78—80195
  symmetry of lattice with hyperfine interactions at atomic nuclei 78—67677
  TCNQ salt, N-n-butyl-quinolinium $(TCNQ)_2$, ESR spectrum fine struct. splitting 80—44904
  TCNQ salt, quinolinium $(TCNQ)_2$, mag. chain double resonance study, deuteration 80—25250
  TDPAC pattern depend. on principal axis orientation 80—39898
  tetrabutylammonium iron tetraiodide, structural and mag. props., ^{57}Fe and ^{129}I Mossbauer spectra 79—61282
  tetraethylammonium iron tetraiodide, structural and mag. props., ^{57}Fe and ^{129}I Mossbauer spectra 79—61282
  tetraethylammonium neptunium hexachloride, Mossbauer spectra and mag. susceptibility meas. 80—108140
  tetramethylammonium cadmium chloride, EPR of Mn^{2+} meas. 77—59452
  tetramethylammonium neptunium hexachloride, Mossbauer spectra and mag. susceptibility meas. 80—108140

crystal hyperfine field interactions continued
TGS:VO^{2+}, single cryst. H^2 ENDOR investig. 79−99791
$[TMPD^+]_2[Cu_xNi_{1-x}(mnt)_2]$, ESR obs. of triplet excitons and Cu(II) ions, mag. interactions 79−95633
transient ESR line profiles, $S=I={}^1/_2$ system, calcs. 78−88170
transition d element, hyperfine field on nucleus, mag. moment and electron struct. 77−62883
transition elements, higher types, electronic config. and nucl. quadrupole interaction, atomic SCF Hartree-Fock calcs. 79−60777
transition metal 3d, spin-orbital interaction effect on NMR, g-factor anisotropy *(Russian)* 77−24752
transition metal complexes, discrete variational $X\alpha$ cluster calcs. 80−15444
transition metal diiodides, (V, Cr, Mn, Fe, Co, Ni, Cd), Mossbauer spectrum, electronic and mag. props. 77−32302
transition metal octahedral $(MeF_6)^4$, fluorine ion Sternheimer antishielding, PAC 78−10818
transition metal salts, antiferromag., ^{111}Cd hyperfine fields, PAC meas. 77−48104
transition metal-rare earth dil. alloy, hyperfine field of rare earth impurity 79−1588
transition metal-rate earth alloy, dil., hyperfine fields, theory 78−68226
transition metals, HCP, elec. field gradient 78−14698
triglycine calcium bromide:Cu^{2+}, ESR studies 80−97136
trimethyl ammonium cobalt chloride dihydrate, antiferromag., ^{59}Co NMR 77−77124
trimethyl tin cyanide, ^{119}Sn Mossbauer spectra, elec. field gradient 80−15909
trimethylenemethane, ground state triplet, HFS, EPR obs. 80−50188
trinuclear exchange clusters, Dzyaloshinsky coupling effects in Mossbauer spectra *(Russian)* 80−108142
triphenylantimony, single crystal, irrad. by UV, diphenylantimony radical prod., ESR 78−31662
triphenylstannyl radical, EPR in single cryst. matrix, ^{119}Sn hyperfine coupling tensors 78−23346
TTF-TCNQ electronic props., PMR 78−2763
Tutton salts:Mn^{2+}, EPR, 300K 79−51848
vacancy induced hyperfine interaction detected by γ-ray PAD 77−43913
van der Waals crystal, cohesive energy, many-body theory calc. 77−76348
vanadyl bisacetylacetonate, frozen soln., proton ENDOR, ligand hyperfine tensors 79−99792
ytterbium ethyl sulphate, crystal field effects on mag. and hyperfine props. of Yb^{3+} 80−97101
$3d^5$-ions, variation of hyperfine splitting consts. with interatomic distance 80−97133
$\{Cu(NH_3)_4\}^{2+}$ complex, superhyperfine interaction 79−91284
Ag alloy, dil., temp. depend. of elec. field gradient, impurity mass and conc. effects 78−48085
Ag, and Ag^+, solvation in deuterated-ice matrices, electron spin echo obs. 80−15780
Ag, correlated radiation damage, TDPAC of ^{109}Cd and ^{113}Sn 78−43739
Ag, elec. field gradient generated by nearest-neighbour impurity atoms 79−42510
Ag host, electric field gradients created at ^{111}Cd nuclei by near neighbour impurities 78−39450
Ag, spin rotation amplitudes for ^{107}Cd and ^{109}Cd, comparison of temp. depend. 78−43738
Ag:^{111}Cd, hyperfine interaction, dose-rate depend. and annealing props. rel. to PAC obs. 77−27920
Ag-^{112}In, dil., ^{112}In nucl. alignment, radiation damage, γ-ray spectra 78−19398
Ag-Cd, dil., DPAD meas. on ^{107}Cd and ^{109}Cd, nucl. Larmor precession meas., role of hyperfine interactions 79−47363
Ag-Cu(Au)(Zn)(In)(Sn)(Bi), dil., elec. quadrupole interactions on ^{111}Cd probe nuclei, time differential PAC meas. 78−15066
Ag-Cu(Sn), dil. alloys, EFGs at impurities, ^{111}Cd TDPAC 77−16213
Ag-In, dil., interaction between recoil implanted impurities and lattice defects, TDPAC meas. 78−39467
Ag-Mn, dil., nuclear orientation expts. 78−43713
Ag-Pd, dil., elec. field gradient, conc. and temp. effects 78−68416
Ag-Pd(Pt), dil., electric field gradient temp. depend., TDPAC meas. 78−39451
Ag-Pd(Pt), dil., electric field gradient meas. by TDPAC method 78−39452
Ag-Pd(Pt), dil., TDPAC exam. of radiation damage 78−39464
Ag-Sn, dil., electric quadrupole interaction of ^{111}Cd probe nuclei, time depend. PAC 77−16229
AgBr:Pd, EPR of Pd^+ ions 78−27087
AgCl:Ni, double quantum EPR transition, superhyperfine struct. 80−7154
AgCl:Pd^+, ESR spectra, superhyperfine struct. lines 77−12197
$AgClO_3$, ClO_2 spin Hamiltonian 78−60326
$AgFeTe_2$, Mossbauer parameters in phase-transition region 80−11308
$AgNa(NO_2)_2$, ^{23}Na elec. field gradient tensor from NMR satellite lines near phase transition 80−71191
$AgNa(NO_2)_2$, ferroelec. transition, ^{23}Na elec. field gradient tensor, NMR meas. 79−4777
Al, hyperfine interactions of implanted Fe, conversion electron Mossbauer spectroscopy 78−52391
Al:^{111}In, electron irrad., defect trapping at impurities 78−55892
Al-Co, electron irradiated, quadrupolar relaxation effect in Mossbauer effect 78−39459
Al-Dy, dil., ion implanted, crystal hyperfine field interaction, Mossbauer spectroscopy study 80−44968
Al-Er, dil., lattice location of ^{169}Er ions after implantation, Mossbauer effect of ^{169}Tm 78−39460
Al-In, dil., vacancy trapping and detrapping at ^{111}In, PAC spectra 78−39461
Al-Y, dil., hyperfine interactions, $^{87}Y^m$ nuclear orientation meas. 78−43715
$Al(NO_3)_3.9H_2O$:Fe^{3+}, nucl. level hyperfine struct., reson. RF field effect, Mossbauer effect *(Russian)* 77−77133
Al_2O_3, transition metal ion doped, phonon spectroscopy using freq. crossing techniques 79−42193
α-Al_2O_3:Co,H, Co and proton ENDOR, IR and optical spectra charge compensator nature and defect struct. 80−44956
α-Al_2O_3:$Cr^{4+}(V^{3+})$, ground state spin Hamiltonian parameters and electric field effect 77−15801
Al_2O_3:Mo^{3+}, zero field splitting study by ESR 80−7159

crystal hyperfine field interactions continued
Al_2O_3:V^{3+}, frequency crossing signals of V^{3+} ions, conc. depend. study using thermal phonons 78−95115
Al_2O_3:$V^{3+}(Fe^{2+})$, hyperfine splitting and magnetoelastic consts., freq. crossing spectroscopy 80−107392
β-Al_2O_3-$(Na,Li)_2O$, first-order quadrupole NMR obs. of cation distrib. and ion motion 80−108113
Al_2O_3-Fe_2O_3:Cr^{3+}, dil. paramag. system, Cr^{3+} conc., effect on cross relax. 79−15387
Al_2O_3-Fe_2O_3(:Cr^{3+}) paramag. system, cross relax. temp. and mag. field effects on Mossbauer spectra 79−33576
β-Al_2O_3-Na_2O, anomalous Na behaviour obs. using pulsed and CW NMR 80−108095
β-Al_2O_3-Na_2O, ENDOR meas. of defects 80−66074
β''-Al_2O_3-Na_2O, NMR of ^{23}Na, elec. quad. interaction, 185 to 419K, ion motion obs. 80−108110
AlP, multiple pulsed double NMR and nucl. spin dynamics 77−16208
$AlPO_4$, low quartz struct., charge density refinement, use of elec. field gradient calcs. 79−73480
^{241}Am, α-radiation self-damage effect on hyperfine interaction and Debye-Waller factor, Mossbauer meas. 80−7230
^{40}Ar:^{41}K, matrix isolation model system 78−45722
As_2Se_3, effect of Cu and I, investigated by Mn^{2+} EPR spectra 77−73075
$As_2Te_{3-x}Se_x$, ^{125}Te Mossbauer expts., comparison of amorphous and cryst. samples 78−88232
Au (I) compounds, electronic config. and nucl. quadrupole interaction, atomic SCF Hartree-Fock calcs. 79−60777
Au complex, paramag., ^{197}Au mag. and elec. hyperfine interactions 78−39471
Au complexes, electronic config. and elec. field gradient, relativistic HF method 80−54664
Au lattice location in Zn, gamma-spectral study 80−80227
Au-Dy, dil., hyperfine interaction of Γ_8 quartet, Mossbauer expt. 78−43718
Au-Dy, dil., hyperfine interaction, Mossbauer study, Kramers quartets 80−66083
Au-Fe ion implanted alloy, Mossbauer conversion electron scatt. 80−88898
Au-Gd, dil., fine struct. splitting, magnetisation meas. 79−56498
Au-Mn, dil., nuclear orientation of recoil implanted ^{52}Mn 78−43716
Au-Te, elec. field gradients and charge transfer, Mossbauer spectra 80−25268
Au-Y, dil., hyperfine interactions, $^{87}Y^m$ nuclear orientation meas. 78−43715
Au-Yb alloys, dil., nucl. reson. of ^{173}Yb local moments 79−65763
Au_2MnAl, Heusler alloy, Mossbauer, determ. of Au hyperfine field 77−4586
AuMnSb, ferromag. Heusler alloy, mag. hyperfine fields at Au and Sb sites, Mossbauer spectra 77−32303
BMn, ferromag., ^{55}Mn magnon-induced pseudoquadrupole processes 79−19802
$BaCO_3$, electric quadrupole interaction, TDPAC meas. 78−39455
$Ba(ClO_3)_2.2H_2{}^{17}O$, fine struct. in quad. reson. of ^{17}O, DNMR 77−8453
BaF_2, mag. hyperfine const. and lattice distortion of V_k-centre 77−62864
BaF_2:Cd^{2+}, X-irrad., ESR of Cd^+ centres 77−59459
BaF_2:Eu^{2+}, ENDOR of ^{19}F ligands, under uniaxial stress 77−16207
BaF_2:U^{3+}, single crystal, superhyperfine interaction of tetragonal centres 79−42834
$BaFe_{12}O_{19}$, high field Mossbauer effect on ^{57}Fe at room temp. and 4.2K 79−24238
$BaGeF_6$, Group IV hexafluoride anion radical γ-irrad., EPR spectra 78−72411
$Ba(NO_3)_2$, electric field gradient, quadrupole coupling consts. 77−89740
BaO-B_2O_3-SiO_2:Ti^{3+}, optical absorpt. spectra 78−72564
$BaPbF_6$, Group IV hexafluoride anion radical γ-irrad., EPR spectra 78−72411
$BaSO_4$, electric quadrupole interaction, TDPAC meas. 78−39455
$BaSO_4$, single cryst., $SO_4{}^{2-}$ vibr. levels, cryst. field effects, laser Raman spectroscopy 78−43847
$BaSr_xCa_{1-x}Fe_4O_8$, substituted hexagonal ferrites, mag. split Mossbauer spectra obs. and X-ray struct. data 80−71250
$BaTiO_3$:^{89}Zr, electron capture decay lifetime, struct. environment effects 77−28523
$BaTiO_3$:Hf, crystal field distortion by stacking faults, PAC meas. 80−11306
BaV_2O_6:Cr, EPR spectra temp. depend., paramagnetic ion point symm. 80−71166
$BaVS_3$, mag. transition and hyperfine interaction, neutron spin-flip scatt. obs. 80−97093
$BaVS_3$:Fe, Mossbauer and mag. studies, electronic state of Fe 80−108130
Ba_2XRuO_6(X=La,Eu), ^{99}Ru Mossbauer spectra and other techniques 80−29659
Be, electric field gradients of recoil-implanted ^{19}F via $^9Be(^{12}C, np)^{19}F$ 77−8471
Be, electronic struct., NMR study 80−108085
Be, quadrupole interaction of ^{12}B and ^{12}N 78−47750
Be:$^{100}Rh(^{111}Cd)(^{181}Ta)$, quadrupole interaction temp. depend. 77−8466
Be-Au, dil., quadrupole interactions and lattice location, ^{197}Hg TDPAC and Mossbauer expts. 78−43726
Be-Ir, dil., elec. field gradient, Mossbauer meas. 80−80665
Be-Ru, dil., quadrupole interactions at ^{99}Ru, TDPAC meas. 78−91996
BeF_2, radiation induced defects, nuclear Hanle effect 78−43734
BeNi, dil., electronic struct., NMR study 80−108085
BeO, ceramic and single cryst., EPR-ENDOR study of [Li]° centre 77−85569
Bi, quadrupole interaction of ^{69}Ge, TDPAD expts. 78−48089
Bi-Mn, dil. liq. alloy, static and dynamic props. of localised Mn moments 79−82755
BiMn, ferromag., nucl. orientation of Bi isotopes 78−13010
$Bi_9Ti_3Fe_5O_{27}$, combined hyperfine interaction 79−28663
C_2O_3:$^{125}Te^{6+}$, mag. hyperfine interactions, Mossbauer study *(French)* 79−24247
$CaCO_3$:Mn^{2+}, calcite, on axis half-field forbidden lines, numerical prediction 77−16161
CaF_2, (n,γ) induced lattice defects, struct., polarised ^{20}F NMR 77−20724
CaF_2, (n,γ) induced lattice defect annealing, polarised ^{20}F NMR 77−20725

crystal hyperfine field interactions continued
CaF_2, mag. hyperfine const. and lattice distortion of V_k-centre 77—62864
CaF_2, radiation induced defects, nuclear Hanle effect 78—43734
CaF_2: Ni crystals, X-irradiated, EPR study of Ni^+ and Ni^{3+} 80—75849
$CaF_2:Cd^{2+}$, X-irrad., ESR of Cd^+ centres 77—59459
$CaF_2:Ce^{3+}$, ENDOR meas. on Ce^{3+} photochromic centre 78—19372
$CaF_2:Ce^{3+}$, Na^+, ^{23}Na ENDOR meas. 77—69730
$CaF_2:Dy^{3+}$, Mossbauer obs. 78—64303
$CaF_2:Eu^{2+}(Gd^{3+})$, ENDOR of ^{19}F ligands, under uniaxial stress 77—16207
$CaF_2:Gd^{3+}$, ligand ENDOR cubic centres, elec. field effect *(Russian)* 78—60357
$CaF_2:PrF_3$, EPR of cubic Pr^{3+} 79—28607
$CaF_2:Tm^{2+}$, ultra-low nuclear spin temp., low field behaviour, EPR study 80—100614
$CaF_2:Tm^{2+}(Yb^{3+})$, evidence for covalency 77—85180
CaF_2:U, U^{5+} centres, nonoctahedral symmetry 80—11266
$CaF_2:U^{4+}$, EPR hyperfine struct. 80—15781
$CaF_2:U^{5+}$, trigonal centres, hyperfine parameters, EPR 78—43643
$CaF_2:U^{5+}$, trigonal EPR spectrum 78—15021
$CaFe^{3+}Fe_2{}^{2+}(Si_2O_7)O(OH)$, ilvaite, electronic struct., press. and temp. depend. of ^{57}Fe Mossbauer spectrum 80—108129
$Ca_3Fe_2Si_3O_{12}$, andradite, hyperfine parameters, Huckel theory calc. 80—39542
$CaO:Bi^{3+}(Pb^{2+})$, impurity centres vibronic spectra, lattice dynamics and electron-phonon interactions 80—7396
$CaO:Fe^{2+}$, octahedral symm., vibronic effects from Zeeman field induced Mossbauer spectra 77—8477
$CaO:Gd^{3+}$, quadrupole hyperfine interaction, ENDOR 78—23370
CaO:Ir, quadrupole interactions and static Jahn-Teller effect in EPR spectra 77—72842
$CaO:Mg^+$, EPR exam., hyperfine const. determ. 77—8388
$CaO:V^{3+}$ orbital triplet, intermediate Jahn-Teller effect, APR 80—34758
$CaSO_4$, anhydrite and gypsum, phonon spectroscopy, lattice dynamical calc. 80—19889
$CaSO_4(.2H_2O)$, single cryst., $SO_4{}^{2-}$ vibr. levels, cryst. field effects, laser Raman spectroscopy 78—43847
CaSe:Pb, luminesc. and EPR props. of Pb centres 80—55168
$CaSe:Sn^{3+}$, EPR study of octahedral Sn^{3+} centres, 4 to 290K *(Russian)* 80—84637
$Ca_{1-x}Sr_xFeO_3$, Mossbauer spectra, charge disproportionation 80—15891
$Ca_{1-x}Sr_xFeO_3$, Mossbauer spectra, charge disproportionation 80—20542
CaV_2O_6:Cr, EPR spectra temp. depend., paramagnetic ion point symm. 80—71166
$CaV_2O_6:W^{6+},Mo^{5+}$, g-factors and hyperfine coupling parameters of V^{4+}, ESR 77—12196
Ca_2XRuO_6 (X=Y,La,Eu), ^{99}Ru Mossbauer spectra and other techniques 80—29659
Cd, nuclear quadrupole antishielding effects, ab initio theory 78—34814
Cd, quadrupole hyperfine interaction of ^{111}Cd, effect of radiation defect annealing 78—43741
Cd, quadrupole interaction of ^{107}Cd $11^-/2$ states 77—8468
Cd, quadrupole interaction for ^{129}I, ^{131}I, and ^{132}I, PAC expts. 78—48087
Cd:^{113}Sn, quadrupole interaction temp. depend. 77—8469
Cd:^{116}Sn, quadrupole interaction, radiation damage effects 78—43752
Cd:^{11x}Sn, (x=3-6,8), γ-ray spectra, quad. interaction, spin-rot. spectra 77—26571
Cd:^{67}Ge, elec. quadrupole interaction temp. depend., PAC meas. 79—42877
Cd:^{67}Ge, quadrupole interaction temp. depend. 77—12264
Cd:^{67}Zn elec. quadrupole interaction temp. depend., PAC meas. 79—42877
Cd:^{99}Ru, quadrupole interaction temp. depend., PAC method, electric field gradients 77—73105
Cd-Hg, dil., anomalously high elec. field gradients below 0.05K 78—72442
Cd-perovskites, $CdXO_3$ (X=Ti,Zr,Hf,Sn), electric field gradient temp. depend. 78—39454
Cd-Sb, dil., loss of nucl. alignment of ^{115}Sb by radiation induced defects 78—43344
$CdF_2:Gd^{3+}$, investigation of superhyperfine struct. in EPR spectra 79—51851
$Cd_{1-x}Fe_xCr_2S_4$, Fe II electronic struct., Mossbauer spectra 80—15876
$Cd_xFe_{3-x}O_4$, collective electron states, ^{57}Fe Mossbauer meas. 77—69748
$Cd_xFe_{3-x}O_4$, cond. mechanism, collective electron description 77—4588
CdHg, electric field gradient temp. depend., TDPAD meas. 79—56647
$CdI_2:M^{2+}$, M=V, Mn, Co, EPR 78—68362
$CdIn_2S_4:Cr^{3+}$, ESR and ENDOR 77—20692
$Cd_2Nb_2O_7$, Mn^{2+} ESR, hyperfine interaction const., ferroelectric domain orientation 80—54943
CdNi ferrite, quadrupole interaction, cation distrib. influence 78—2776
$Cd_{0.8}Ni_{0.2}Fe_2O_4$ ferrite, Fe spin relaxation Mossbauer study, mag. hyperfine struct. *(Russian)* 80—15932
$Cd_xNi_{1-x}Fe_2O_4$, mag. behaviour, Mossbauser meas. 78—52390
$CdS:Mn^+$, cryst., X-band ESR 78—2730
$CdS:Ti^{2+}$, superhyperfine interact., ENDOR study at 4.2K 80—80639
$CdSiP_2$, PAC examination of deuteron irrad. damage, annealing effects 78—47446
$CdSiP_2$:Fe, EPR and optical absorpt. of Fe^+, Fe^{2+}, Fe^{3+} and Fe^{4+} on tetragonal sites 77—8397
CdY_2S_4:Fe (Mn), superhyperfine interaction of Mn and Fe, ESR spectra 77—63271
^{111}Cd, nucl. orientation coeffs. with axially symm. elec. field gradient 80—97168
Ce compounds, Kondo coupling, hyperfine and exchange interactions 79—65647
$CeAl_2$, NMR, cryst. field effects and mag. order in low temp. phase 78—68391
$CeAl_2$, specific heat between 0.02 and 1K 79—1680
$Ce_{0.73}Ho_{0.27}Ru_2$, superconductors, mag. correlations and crystal-field levels 80—34547
$Ce_{0.73}Ho_{0.27}Ru_2$:Co, spontaneous mag. order below superconducting transition temp., Mossbauer study 80—39701
$CeM_2:Nd^{3+}$, M=Ru, Rh, Ir, ESR investigation 79—78514
$CeO_2:Yb^{3+}$, ENDOR, evidence for covalency 78—80247
$CeO_2:Yb^{3+}$, trigonal sites of Yb^{3+}, ENDOR meas. 79—95677
CeO_2-$LaCrO_3$, and CeO_2-La_2O_3, quadrupole interactions and moments, ^{137}La Mossbauer obs. 78—27121
$CeSn_3$, valence instabilities 79—78546

crystal hyperfine field interactions continued
$(Ce_xY_{1-x})Fe_2$, mag. susceptibility and Mossbauer meas., lattice parameters 80—97068
Co alloys, ferromag., 4d and 5d impurities, hyperfine fields 78—31133
Co based amorphous alloy, mag. ordered, hyperfine field distribs., NMR meas. 78—68409
Co based Heusler alloys, ferromag., hyperfine fields meas. by NMR 77—63315
Co complex, bis-(β-diketonato) Co(II) dihydrate, Fe chem. states, Mossbauer emission 80—15917
Co complex, $CoCl_2(indazole)_2$, linear chain ferromagnetism 79—56519
Co complex, $CoCl_2(pyrazole)_2$, linear chain ferromagnetism 79—56519
Co complex, $Co(C_3H_4N_2)_6(NO_3)_2$ and $Co(C_{11}H_{12}ON_2)_6(ClO_4)_2$, paramag., hyperfine sp. ht. 77—55683
Co complex, diimine complexes with ^{57}Co II, ^{57}Fe II anomalous spin states, Mossbauer spectroscopy 77—12261
Co complex, diimine complexes with ^{57}Co (II), Mossbauer spectra, temp. depend. 77—12262
Co complex, Werner complexes, ^{57}Fe partial quadrupole splitting, emission Mossbauer spectra 80—15919
Co complexes, 1,2-bis(diphenylphosphino)-ethane in-plane ligand ^{31}P hyperfine interaction, ESR obs. 77—77087
Co, crystal hyperfine fields and neutron scatt. 79—56172
Co, FCC single-crystals, NMR freq. depend. on interatomic distances 79—69748
Co, ferromag., HCP, electronic struct. calcs., mag. hyperfine field 78—39080
Co, ferromag., hyperfine fields at positive muons 78—43758
Co, ferromagnetic, calc. hyperfine fields and their press. derivations 80—6796
Co, ferromagnetic, temp. depend. of μ^+ hyperfine field 78—43761
Co, HCP, ferromag., anisotropic hyperfine interactions, NMR expt. 78—43658
Co host, dil. impurity hyperfine fields, comparison with models 78—14954
Co, hyperfine mag. fields at ^{67}Ge, TDPAC meas. 78—43701
Co, impurity hyperfine fields 79—99518
Co, NMR enhancement of modulating field due to anisotropic component of hyperfine field 77—55729
Co, NMR-ON meas., mag. hyperfine splitting const. of ^{60}Co, ^{52}Mn and ^{90}Nb 78—43651
Co, nucl. orientation on implanted ^{114m}In 79—47345
Co Schiff base complex, N,N′-ethylene-bis (salicylideniminato)-Co II pyridine doped in Znsalenpy crystal, ENDOR, EPR studies 80—34819
Co^{2+}, doped ion in divalent metal cpds., correl. between Szigeti charge and hyperfine coupling consts. 80—96832
Co:^{129m}Xe, mag. hyperfine field determ. by Mossbauer effect 77—8460
Co:^{41}K hyperfine field calc. by gamma ray ang. corr. method 78—6340
Co:Ga(Ge)(As), temp. anomalies of hyperfine fields 78—23265
Co:Lu, nuclear orientation meas., hyperfine field 77—32308
Co:Ra, hyperfine field determ. 77—85622
Co-^{48}V, nucl. orientation of ^{48}V, γ-ray anisotropy obs. 80—97169
Co-3d transition metal alloys, hyperfine field and mag. perturbation distrib., NMR spectra meas. 79—61263
Co-based Heusler alloys, Co_2TAl, (T=Ti, Zr, Hf), paramag. state NMR and susceptibility meas. 79—65643
Co-Cd, dil. alloy, impurity hyperfine interactions 78—84416
Co-Fe, dil., effective mag. field at ^{59}Co, impurity conc. depend., spin echo expts. 78—48080
Co-Mn, dil., hexagonal hyperfine field at ^{54}Mn, nucl. orientation meas. 79—8057
Co-Ni, dil., effective mag. field at ^{59}Co, impurity conc. depend., spin echo expts. 78—48080
Co-Ru, dil., mag. hyperfine fields, TDPAC meas. 78—43702
Co-Sn, dil., ferromag., temp. anomalies of Sn mag. hyperfine field and thermal expansion 79—33270
Co-Sn, dil., hyperfine field, press. depend., Mossbauer spectra meas. 79—95375
$(Co_xFe_{1-x})_5Ge_3$, Mossbauer investig. of hyperfine field at Fe nuclei 77—20776
$CoFe_2O_4$, mag. hyperfine fields, Mossbauer spectra 80—108139
Co_2HfAl, hyperfine fields of Fe impurities, Mossbauer spectra 80—71255
Co_2HfSn-Fe, dil., Heusler alloy, Fe hyperfine fields, Mossbauer obs. 78—68424
$Co_2Mn_xFe_{1-x}M$, (M=Ga,Ge,Si,Sn), hyperfine fields of Fe impurities, Mossbauer effect meas. 78—31130
Co_2MnSi, ferromag. Heusler alloy, spin echo NMR meas. 77—63319
$Co_{2-x}(Ni,Fe)_xTiSn$, Heusler alloy, positive contribs. to hyperfine fields, magnetisation and NMR meas. 78—43654
CoO, antiferromagnetic, ^{59}Co NMR and hyperfine field 77—77109
CoO, paramag. shifts of ^{19}F at O 78—43719
Co_3O_4:^{119}Sn, hyperfine field exam., Mossbauer meas. 77—69753
CoS_2, hyperfine parameters and quadrupole splitting determ., ^{57}Fe Mossbauer spectra 77—77131
$CoSe_2$, hyperfine parameters and quadrupole splitting determ., ^{57}Fe Mossbauer spectra 77—77131
Co_2TiAl, ferromag., ^{59}Co NMR 78—2760
Co_2TiAl, hyperfine fields of Fe impurities, Mossbauer spectra 80—71255
Co_2TiSn, Heusler alloy, positive contribs. to hyperfine fields, magnetisation and NMR meas. 78—43654
Co_2TiSn-Fe, dil., Heusler alloy, Fe hyperfine fields, Mossbauer obs. 78—68424
CoV alloys, phase dependent MNR spectra 80—108114
Co_2VAl, hyperfine fields of Fe impurities, Mossbauer spectra 80—71255
Co_2VGa, ferromag. Heusler alloy, spin echo NMR meas. 77—63319
CoV_2O_4:Fe, spinel, prep. and Mossbauer spectra 79—28660
Co_2ZrSn-Fe, dil., Heusler alloy, Fe hyperfine fields, Mossbauer obs. 78—68424
^{57}Co, Mossbauer absorpt. and emission spectra, hyperfine struct. and relax. effects 80—71279
$Co^{2+}[Fe^{III}(CN)_6]^{3-}$, time depend. linewidth of Mossbauer spectrum 80—15911
Cr, antiferromag., mag. and non-mag. impurities, hyperfine interactions, ^{181}Ta and ^{100}Rh TDPAC meas. 78—43704
Cr chalcogenide spinels, $ACr_{1.9}Sn_{0.1}X_4$, Sn hyperfine interactions 80—15485
Cr, hyperfine interactions on ^{111}Cd-probe nuclei, TDPAC meas. 80—75904
Cr, μ^+ depolarization and diffusion 77—59500
Cr, spin density waves detected by Ta mag hyperfine field meas. 78—60364

crystal hyperfine field interactions continued
Cr-Fe, antiferromagnetic, effect of press. on hyperfine mag. fields at Fe nuclei *(Russian)* 80—15936
Cr-Fe (20 to 30 at.%), Mossbauer spectra temp. var. and ferromag. props. 77—81037
Cr-Rh, dil., hyperfine fields meas. 79—47056
Cr-Ru, dil. absence of mag. hyperfine field, TDPAC meas. 80—50237
Cr-Ta, mixed SDW and Zeeman hyperfine interactions, TDPAC calc. 79—99797
$Cr_xFe_{3-x}O_4$, spin and charge density oscillations due to impurities *(Korean)* 80—20565
CrI_3, ferromagnetic, origin of magnetic hyperfine field transferred at iodine 78—92000
$Cr_{1-x}Mn_xO_2$, hyperfine mag. fields at ^{119}Sn, Mossbauer study 80—71260
Cr_2O_3:$^{119}Sn^{4+}$, Mossbauer spectra *(French)* 79—24248
Cr_2TeO_6, CC ^{57}Fe Mossbauer spectrum, hyperfine field, Neel temp. 79—56636
$CrTiRO_5$, R=Pr,Nd,Sm,Eu,Gd,covalency contribs. to Mossbauer spectra 78—10808
$CsAsF_6$, γ-irrad., EPR spectra, hyperfine interactions and g-value determ. 77—81416
$CsCdF_3$:Cr^{3+}, ENDOR exam. of electron spin transfer 77—48089
$CsCdF_3$:$Cr^{3+}(Fe^{3+})$, ligand polarisation and transferred hyperfine interactions 79—51535
$CsCdF_3$:Fe^{3+}, ENDOR meas. on Fe^{3+}-F^--Cd^{2+} struct. 78—31122
CsCl, impurity and defect sites, elec. field gradient calc. 79—78034
CsCl(Br)(I), F-centre ESR in relaxed excited state, isotropic superhyperfine interaction consts. 79—65733
$CsCoCl_3$, antiferromag., ^{59}Co NMR spectrum obs. by spin echo method 79—51881
$CsCoCl_3$, covalency parameters estimation from nucl. quadrupole coupling 80—25246
$CsCrI_3$, Mossbauer spectra, struct., electronic and mag. props. 79—91320
$CsCuCl_4.2H_2O$, hyperfine and super-exchange interactions 80—103654
$Cs_2CuCl_4.2H_2O$, Bloch-wall NMR, anisotropic hyperfine interaction 79—51864
$Cs_2CuCl_4.2H_2O$, ferromag., hyperfine and exchange interactions, NMR study 80—50208
$CsFeCl_3.2H_2O$, rectangular Ising cpd., Mossbauer meas. 80—71252
$CsFeCrF_6$, $CsFeVF_6$, crystal struct., Mossbauer hyperfine spectra 78—52381
Cs_2HfCl_6:Mn^{2+}, ESR of mol. jumps, zero-field splitting tensor 77—51944
Cs_2IrCl_6, hyperfine spectra of mag. ordered state at very low temp., Mossbauer meas. 77—69744
$CsMgCl_3(Br_3)$, quadrupole interaction meas. by NMR spin-echo modulation 77—85615
$CsMi_3$, (M=V, Cr, Mn), Mossbauer spectra, struct., electronic and mag. props. 80—15908
$CsMnF_3$, NMR saturation, nuclear spin wave excitation, large freq. shifts *(Russian)* 80—50207
Cs_2NaRCl_6:$Er^{3+}(Gd^{3+})$, R=lanthanide, EPR parameters and interpret. 77—59456
Cs_2NaYCl_6:Ce, ENDOR evidence of noncubic distortion 79—11357
$CsNiCl_3(Br_3)$, quadrupole interaction meas. by NMR spin-echo modulation 77—85615
$CsNiF_3$, ^{19}F NMR, spin fluctuation suppression 78—91970
Cs_2NpCl_6, Mossbauer spectra and mag. susceptibility meas. 80—108140
$CsSbF_6$, γ-irrad., EPR spectra, hyperfine interactions and g-value determ. 77—81416
$Cs_3VCl_6.4H_2O$, magnetisation of ground state, field-induced level crossing 79—47068
$CsVI_3$, Mossbauer spectra, struct., electronic and mag. props. 79—91320
$CsVO_3$, polycryst., quadrupole coupling const., asymmetry parameter, chem. shift, NMR computer calcs. 78—6584
Cs_2ZrCl_6:Mn^{2+}, ESR of mol. jumps, zero-field splitting tensor 77—51944
Cs_2ZrCl_6:Np^{4+}, EPR obs. 79—33526
Cu complex, $(CH_3NH_3)_2Cu(Cl_{1-x}Br_x)_4$, ferromag., Br NMR mas. 80—29642
Cu complex, bis(1,1-diisobutyl-3-benzoyl-selenoureato)Cu(II), single cryst. ESR, ^{77}Se hyperfine struct., bonding 77—77086
Cu complex, $Cu(H_2O)_6{}^{2+}$, ligand hyperfine interactions, orbital angular momentum contrib. 80—96833
Cu, implanted ^{222}Rn TIPAC measurements 78—43732
Cu, muon spin rot., EFG, site of localisation 78—2785
Cu, radiation damaged, elec. field gradient, temp. depend. 78—39481
Cu, radiation damaged, temp. depend. of elec. field gradient, DPAC expt. 78—43727
Cu, screening charge density round $\Delta Z=-1$ impurities, vacancies, NQR study 80—103897
Cu^{2+} ion, ground state wavefunctions and ESR parameters 80—88868
Cu^{2+} ions, ground state wave functions, cryst. field effect, ESR data anal. 78—23060
Cu:$^{69}Ge(^{67}Zn)$, nucl. alignment temp. depend. rel. to radiation damage during PAC obs. 77—27919
Cu/Ni coherent modulated structures, electronic struct. and magnetism 80—103620
Cu-Ag, electron density change during Cu decay 79—99519
Cu-Fe, dil., powder, transferred orbital hyperfine field on near neighbours, NMR meas. 78—27098
Cu-In, dil., point defect trapping after ion implantation, DPAC meas. 78—43728
Cu-Mn Kondo system, ^{54}Mn nucl. orientation 78—68421
Cu-Ni(Pd)(Pt), dil., screening charge density round $\Delta Z=-1$ impurities, vacancies, NQR study 80—103897
CuBr(Cl)(I), electric field gradient-elastic tensor components, acoustic NMR obs. 80—25229
CuCr(Fe)(Mn), dil., anisotropic hyperfine coupling, NMR study 80—65784
$CuCr_{2-x}Fe_xO_4$, charge transfer, Mossbauer spectroscopy 80—15836
$CuCr_2O_4$-$CuFe_2O_4$ (2 mol.%), Mossbauer expts., existence of Fe^{2+} 78—43721
$Cu^{2+}F^-$ and $Cu^{2+}F^-Cu^{2+}$, transferred hyperfine interactions 80—70659
$CuFe_2O_4$, Jahn-Teller type crystal distortions 80—103904
$CuFeS_2$, antiferromag., NQR local mag. field effects 80—71234
$Cu_2Mn_{0.98}Al_{1.02}$, Heusler alloy, hyperfine fields at sp elements, spin echo NMR meas. 78—84496
$Cu_2MnAl_{1-x}Sn_x$, Mossbauer effect study 80—60473
$Cu_2MnIn_{1-x}Sn_x$ alloy, compositional SRO, hyperfine interactions 80—71065

crystal hyperfine field interactions continued
$Cu_2MnSn(In)$, Heusler alloy, hyperfine field at ^{111}Cd, TDPAC meas. 78—43705
DIO_3, cryst., NQR coupling const. and field gradient tensors 79—73828
Dy, crystal hyperfine fields at positive muons 79—56662
Dy:$^{111}Cd(^{177}Hf)$, polycryst. ferromag., impurity hyperfine field polarisation, TDPAC and IPAC 77—73106
Dy:^{181}Ta, ferro- and antiferromag. phases, temp. depend. of mag. hyperfine field, TDPAC obs. 77—36165
Dy-Fe_xNi_{1-x} system, mag. hyperfine field, influence of lattice struct. and substituent 77—8058
Dy-Sc, magnetic relax. phenomena 79—33579
Dy-Sn alloy, hyperfine fields acting on diamag. impurities and anisotropic exchange, Mossbauer spectra 77—1625
Dy-Ta, dil., elec. field gradient at ^{181}Ta, temp. depend., TDPAC meas. 79—95689
DyAG, electrostatic model of cryst. field 80—59945
$DyAl_2$, conduction electron spin and orbital polarisation effects 78—80228
$DyCo_3$, mag. and quad. interactions, Mossbauer spectra 77—12267
Dy_2Co_{17}, hyperfine interactions and cryst. field effects, Mossbauer spectra 80—2369
DyF_3, transferred hyperfine interaction, NMR study 78—68393
$DyFe_2$, hyperfine interactions 80—44549
Dy_2Fe_{17}, hyperfine interactions and cryst. field effects, Mossbauer spectra 80—2369
$Dy_2(Fe_{1-x}Co_x)_{17}$, hyperfine interactions, Mossbauer spectra 78—2780
$Dy(Fe_xNi_{1-x})_2$, mag. behaviour, susceptibility and Mossbauer expts., 4.2-1300K 78—52235
$Dy_2(Fe_{1-x}Ni_x)_{17}$, hyperfine splitting, constant Fe moment evidence 78—6614
Dy_2FeSbO_7, supertransferred hyperfine mag. fields and relax. of Dy^{3+} ions by Mossbauer spectroscopy of ^{57}Fe 77—59494
$Dy_{1-x}Gd_xAl_2$, ordered alloys, ^{163}Dy NMR, hyperfine field 78—10801
$Dy_{1-x}Gd_xAl_2$, ordered alloys, hyperfine field, anomalous con. depend. NMR 80—75868
DyH_2, mag. and crystal field props. from ^{161}Dy Mossbauer studies 79—95692
DyH_3, mag. and crystal field props. from ^{161}Dy Mossbauer studies 79—95692
DyIG, noncrystalline, Mossbauer and magnetisation data 80—34828
$Dy_{0.9}M_{0.1}Al_2$, (M=Sc, Y, La, Lu), hyperfine field, NMR spectra 80—15811
Dy_2Ni_{17}, hyperfine interactions and cryst. field effects, Mossbauer spectra 80—2369
Dy_2O_3, ^{161}Dy hyperfine parameters for C_2 and C_{3i} site symmetries, Mossbauer obs. 77—20770
$Dy(OH)_3$, Mossbauer spectra, cryst. field and mag. props. 80—15873
DyO_2X, X=S,Se,Te, mag. and quadrupole hyperfine interactions 77—63336
DySb, quadrupole interactions above T_N 79—78304
DySb, quadrupole scatt. anisotropy, magnetically ordered material 78—64034
$Dy_2Sn_2O_7$, supertransferred hyperfine mag. fields and relax. of Dy^{3+} ions by Mossbauer spectroscopy of $^{119}Sn^m$ 77—59494
$DyVO_4$, electric field influence on elastic props., electron state initial splitting 80—34123
$Dy_{1-x}Y_xAl_2$, ordered alloys, ^{163}Dy NMR, hyperfine field 78—10801
Er-Ta, dil., elec. field gradient at ^{181}Ta, temp. depend., TDPAC meas. 79—95689
Er-Ta, dil., mag. hyperfine field determ., TOPAC meas. 79—91330
$ErAl_2$, conduction electron spin and orbital polarisation effects 78—80228
ErF_3, single cryst. ^{19}F NMR, ligand hyperfine field interactions 77—48067
$ErFe_3$, H_2 sorption, mag. and struct. props. of hydrides 80—34831
$ErFe_3$, Mossbauer and magnetisation investig. of 47K mag. anomaly, atomic rearrangement 77—20766
$ErFe_2H_{3.65}$, $ErFe_2H_{4.12}$, Mossbauer spectra, electronic and structural studies 80—15860
$Er_{1-x}Gd_xAl_2$, effective mol. field at ^{167}Er, NMR meas. 80—71197
$Er_{1-x}Gd_xAl_2$, nuclear hyperfine field, quadrupolar splitting, NMR study 80—39888
$Er(OH)_3$, g-values and hyperfine interaction parameters, calc. for Er^{3+} 79—15123
$Er(OH)_3$, Mossbauer spectra, cryst. field and mag. props. 80—15873
$ErRh_4B_4$, superconducting, magnetic dilemma 80—75680
Eu intermetallic compounds, hyperfine interactions, high press. Mossbuaer expts. 78—43714
Eu, Mossbauer isomer shift and magnetic hyperfine field, press. effect 78—52386
Eu-Cd compounds, Mossbauer effect, mag. props. and lattice consts. 77—36164
Eu_xCa_{1-x}, mag. ordering temp. conc. depend., Eu mag. hyperfine field temp. depend. 78—14971
$EuCu_5(Pt_2)(Pd_2)$, indirect exchange, spin echo NMR meas. 80—15822
$EuCu_2Si_2$, valence fluctuation and temp. depend. of Cu nuclear quadrupole interaction 80—15818
EuIG, noncrystalline, Mossbauer and magnetisation data 80—34828
$Eu_xLa_{1-x}Al_2$, dil. EPR, cryst. fields and effective exchange interaction 80—66029
$EuLiH_3$, transferred hyperfine fields at Eu nuclei, NMR meas. 80—71195
EuM_2Ge_2, M=Mn, Fe, Co, Ni, Cu, magnetism and hyperfine interactions 78—76228
$EuMg_2H_x$, Mossbauer effect exam. 78—48094
$EuNi_xCu_{5-x}$, mixed valency of Eu, Mossbauer expts. 78—52407
$EuNi_5H_x$, Mossbauer effect exam. 78—48094
$EuNi_xZn_{5-x}$, mixed valency of Eu, Mossbauer expts. 78—52407
EuO, quadrupole coupling due to lattice imperfections 78—76347
EuO:Sm^{3+}, hyperfine field at Sm, TDPAC meas. 80—93215
EuO-RN solid soln., (R=Nd,Eu,Gd), ^{151} Mossbauer spectroscopy 78—6610
EuO(S)(Se)(Te), Heisenberg ferromag. semicond., hyperfine and exchange interactions 77—69530
$EuPd_2$, elec. field gradient, spin echo NMR meas. 80—20509
$EuPt_2$, elec. field gradient, spin echo NMR meas. 80—20509
EuS, hyperfine field and magnetisation temp. depend., NMR meas. 77—8422
EuS, transferred hyperfine interacs. 77—69741

crystal hyperfine field interactions continued
- EuS:Sn^{2+}, Mossbauer spectra, Sn^{2+} transferred hyperfine fields 80—15887
- $EuSe_{1-x}Te_x$, transferred hyperfine fields at Eu nuclei, NMR meas. 80—71195
- $Eu_zSn_{1-z}Mo_6S_y$, supercond., mag. props. 77—69447
- $(Eu_{1-x}Sn_x)S$, high press. Mossbauer exam. of Curie temp. and transferred hyperfine field 79—56643
- $(Eu_{1-x}Sn_x)Se$, high press. Mossbauer exam. of Curie temp. and transferred hyperfine field 79—56643
- $Eu_xSr_{1-x}S$, mag. ordering temp. conc. depend., Eu mag. hyperfine field temp. depend. 78—14971
- $(Eu_xSr_{1-x})S$, transferred hyperfine fields, NMR 80—71196
- $Eu_xSr_{1-x}SO_4$, mag. ordering temp. conc. depend., Eu mag. hyperfine field temp. depend. 78—14971
- EuTe, Neel temp. and hyperfine interactions, press. depend. up to 60 kbar, ^{151}Eu Mossbauer obs. 77—63181
- EuTe:Sn^{2+}, Mossbauer spectra, Sn^{2+} transferred hyperfine fields 80—15887
- EuX_5, X=Cu, Zn, Ag, Au, cond. electron spin polarisation effects 77—63136
- Fe, ^{155}Tb sources produced by recoil implantation, ^{155}Gd Mossbauer transition 80—40009
- Fe, ^{56}Fe recoil, PAC, enhanced transient fields 77—15802
- Fe alloys, ferromag., 4d and 5d impurities, hyperfine fields 78—31133
- Fe, BCC, high field Knight shift and hyperfine anisotropy of ^{57}Fe 80—71205
- Fe based amorphous alloy, mag. ordered, hyperfine field distribs., NMR meas. 78—68409
- Fe complex, $[Fe(S_2C_2O_2)_2X]^{2-}$, (X=Cl,Br,I), Mossbauer effect, EPR, mag. susceptibility 79—11366
- Fe complex, dithiocyanato bis(4-methyl-1, 10-phenanthroline) iron, Mossbauer effect and magnetism down to 0.98K 77—28490
- Fe complex, Fe $(alkyldithiocarbamate)_2X$, X=Cl, I, mol. orbital calc., hyperfine fields, elec. field gradient 80—39981
- Fe complex, $Fe(dithiocarbamate)_2X$, X=NCS,Cl,Br,I,NO, elec. field gradient, HMO calc. 80—39543
- Fe complex, ferrous pseudo-tetrahedral compounds, paramag. relax., Mossbauer spectra 80—15869
- Fe complex, iodobis(morpholyldithiocarbamate), allotropes, intermol. exchange interactions 77—8455
- Fe complex, perchlorato(meso-tetraphenylporphinato) iron (III), mag. props., Mossbauer study 79—99802
- Fe complex, pyridine-n-oxide perchlorate, Mossbauer spectra, site distortions enhanced by grinding 80—15883
- Fe complex, tris(monothio-β-diketonato) Fe (III), spin equilib., Mossbauer spectra 80—15910
- Fe complex (2, 9-dimethylphenanthroline) sulphate, mag. props., Mossbauer spectra 80—66081
- Fe complexes, Fe (III) bis(dithiocarbamato) iodides, transferred hyperfine interactions and mag. ordering 77—20759
- Fe complexes, tris and bis dithiocarbamates, quad. splitting, Mossbauer obs. 77—59489
- Fe complexes with dimethylformamide, dimethylthioformamide, Mossbauer and mag. props. 80—39974
- Fe, conversion electron meas. of core polarisations 80—20530
- Fe, crit. fluctuations, Mossbauer obs. 78—43724
- Fe, crystal hyperfine fields and neutron scatt. 79—56172
- Fe dicyclopentadienyl-dibenzenevanadium, coalescence temps., full proton HFS tensor, ENDOR obs. 80—66073
- Fe dilute alloys, itinerant 3d electron spin density oscills. around solute atoms 77—72978
- Fe dilute alloys, with s-p elements of third or fourth periods, Mossbauer spectra meas. 77—63344
- Fe, effective mag. fields near ^{238,240}Pu and ^{248}Cm, PAC obs. *(Russian)* 77—4593
- Fe epitaxial film, Mossbauer effect, depth profiling of mag. hyperfine field 80—11295
- Fe, ferromag., hyperfine fields at positive muons 78—43758
- Fe, ferromagnetic, calc. hyperfine fields and their press. derivations 80—6796
- Fe, ferromagnetic, hyperfine fields; SCF calcs. 77—8061
- Fe, ferromagnetic, temp. depend. of hyperfine fields for F 80—20141
- Fe film, antiferromagnetic ordering, Mossbauer spectroscopy 78—14990
- Fe film, ultra-thin Mossbauer spectroscopic studies of mag. props. 80—44970
- Fe film coated by MgO, Mossbauer spectra, mag. hyperfine field 80—7221
- Fe foil, hyperfine interactions of implanted reaction products 78—48093
- Fe halides, electronic charge and spin distrib. from interpretation of hyperfine interactions 79—60776
- Fe, heavy impurity implanted, relation between hyperfine field and lattice-location meas., influence of radiation damage 80—6794
- Fe, hyperfine field and diffusion of μ^+ 77—52006
- Fe, hyperfine field at Hg, Larmor-precession frequencies 78—506
- Fe, hyperfine field at nonmagnetic impurities 80—25129
- Fe, hyperfine fields at impurity sites 77—66297
- Fe, hyperfine fields at impurities in ferromag. metal 78—52244
- Fe, hyperfine fields for transition metal impurities 80—80237
- Fe, hyperfine mag. fields at ^{67}Ge, TDPAC meas. 78—43701
- Fe, impurity hyperfine fields 79—99518
- Fe, mag. hyperfine field at ^{129}I, press. depend., nucl. gamma reson. 80—71256
- Fe, mag. hyperfine field of K, Ca and Ti, TDPAD meas. 78—52389
- Fe, magnetic hyperfine fields of Zr, DPAD meas. 80—39901
- Fe, magnetic transient fields at N and O nuclei recoiling in external mag. field 77—12263
- Fe, magnetisation, spin wave and Stoner contribs. 77—73017
- Fe, Mossbauer energy shift near Curie temp. 78—52388
- Fe, $muon^+$ spin precession and relax., hyperfine field temp. depend. 77—63350
- Fe, $muon^+$ spin rotation meas., local hyperfine field temp. depend. 77—63349
- Fe, non-mag. impurities, size effects on mag. hyperfine fields 78—43586
- Fe, noncrystalline, mag. hyperfine data from Mossbauer spectra 78—39477
- Fe, nuclear orientation and NMR/ON on implanted ^{114m}In 79—47345
- Fe, polarised, high vel. ion recoil, transient mag. fields 77—43910
- Fe, positive muon spin precession, effect of press. 80—40030
- Fe, screening of non-transition element impurities, model 77—4312

crystal hyperfine field interactions continued
- Fe $SiF_6.6H_2O$, phase transform., temp. depend. of Mossbauer parameters 77—73102
- Fe, transient mag. field, vel. and atomic number depend. 78—91999
- Fe, transient magnetic low velocity field 80—80642
- Fe, ultrathin film, mag. hyperfine field, temp. and thickness depend. 78—39478
- α-Fe, uniaxial stress effect on Mossbauer spectrum 80—71244
- Fe^{2+} compounds, Mossbauer spectra, spin-lattice relax. effects 80—50239
- Fe^{2+}, in octahedral symm., vibronic effects from Zeeman field induced Mossbauer spectra 77—8476
- Fe^{3+} in crystals, quadrupole hyperfine struct., screening coeffs., Mossbauer spectra 77—52000
- Fe:^{119}Sn, pressure dependence of effective magnetic fields 78—52382
- Fe:^{110}In, nucl. orientation, nucl. mag. moment, γ-ray spectra 77—28485
- Fe:^{116}Er, hyperfine interaction of impurities, Mossbauer spectra 77—48105
- Fe:^{119m}Te, mag. moment, nucl. orientation, γ-ray spectra 77—28486
- Fe:^{129m}Xe, mag. hyperfine field determ. by Mossbauer effect 77—8460
- Fe:^{129}Cs, implanted atom sites and hyperfine interactions, Mossbauer obs. 77—20753
- Fe:^{129}Te, implanted atom sites, Mossbauer obs. 77—20756
- Fe:^{129}Tm, implantation below 15K, in situ Mossbauer obs. 77—20754
- Fe:^{129}Xe, implanted atom sites, NMR/ON 77—20723
- Fe:^{129}Xe, implanted atom site populations, Mossbauer, NO and NMR/ON obs. 77—20755
- Fe:$^{12}C(2_1{}^+)$, PAC meas. of transient mag. fields 79—99800
- Fe:^{131}Xe, negative parity states, nucl. orientation, γ-ray spectra 77—28487
- Fe:^{169}Tm(^{175}Lu), radiation-damage evolution influence on hyperfine interaction 80—6793
- Fe:^{169}Yb, hyperfine field of implanted Yb, annealing temp. depend., PAC meas. 77—48100
- Fe:^{172}Yb, hyperfine mag. field, TDPAC meas. 78—52394
- Fe:^{198}Hg, combined lattice-location hyperfine-interaction expt. on implanted Hg 77—20752
- Fe:^{199}Au, quad. interaction, orbital mag. hyperfine field by NMR/ON 77—12250
- Fe:^{220}Rn(^{222}Rn), combined elec. quad. and mag. interaction, PAC 77—16214
- Fe:^{60} Co, nucl. orientation-pulsed NMR obs., γ-radiation anisotropy 77—59490
- Fe:^{60}Co, elec. quad. interaction, single passage NMR/ON 77—16204
- Fe:^{71}As(^{72}As), nucl. mag. moment by NMR/ON 77—12251
- Fe:^{82}Br, nucl. orientation 77—59486
- Fe:^{83}Rb, implanted atom sites and hyperfine interactions, Mossbauer obs. 77—24765
- Fe:^{93,94}Tc, γ-ray spectra, nucl. mag. moment determ. 77—28484
- Fe:^{95}Nb NMR 77—59482
- Fe:Ar(K), implantation perturbed ang. distrib. 78—12969
- Fe:F, lattice location of implanted F rel. to mag. hyperfine fields 77—59041
- Fe:I, ^{131}I NMR, vacancy associated impurity sites 78—91964
- Fe:K(Ar), mag. hyperfine interaction, temp. depend. 78—68420
- Fe:Lu, nuclear orientation meas., hyperfine field 77—32308
- Fe:Ra, hyperfine field determ. 77—85622
- Fe:Xe, gyromagnetic ratios of first 2^+ states in Xe, implantation PAC 78—12966
- Fe:Yb,^{18}O, interaction between implants 77—27921
- Fe-^{48}V, nucl. orientation of ^{48}V, γ-ray anisotropy obs. and NMR meas. 80—97169
- Fe-Al, dil. alloy, temp. depend. of ^{27}Al hyperfine field 78—47972
- Fe-Al, hyperfine field meas. using muon-spin-rotation method 80—10933
- Fe-Al(Si)(Ga)(Ge)(As)(Sn)(Sb) dil. alloys, mag. hyperfine fields, Curie temps. and Mossbauer meas. 77—63190
- Fe-alloys, Mossbauer isometric effects *(Dutch)* 79—1731
- Fe-B, amorphous, short-range order, Mossbauer meas. 80—44986
- α-Fe-based dil. solid solutions, electronic struct., hyperfine interactions 78—79968
- Fe-C, martensite, struct., Mossbauer meas. 80—40000
- Fe-Co, equiatomic, atomic order, Mossbauer study *(French)* 78—27135
- Fe-Co, hyperfine field, variation with atomic order 79—7953
- Fe-Co, hyperfine field distrib., temp. and press. depend. 78—91651
- Fe-Co-Cd(Sn), mag. hyperfine fields at Fe, Cd and Sn sites, Mossbauer and TDPAC meas. 78—60363
- Fe-containing minerals, in coals, mag. hyperfine fields meas. 78—88234
- Fe-containing minerals in coals, magnetic hyperfine fields meas. 78—68427
- Fe-Cr, disordered, mag. order, Mossbauer study 80—39992
- Fe-Cr, hyperfine magnetic fields, Mossbauer spectra 80—97165
- Fe-Cr, influence of annealing on hyperfine interaction parameters, Mossbauer effect 80—71263
- Fe-Cr (1.20, 3.63, 7.98 wt.%), Mossbauer spectra shape depend. on deformations 79—61272
- Fe-Cr alloy, mag. moments and Fe site hyperfine fields, magnetis. obs. 78—76276
- Fe-Cr-Co, mag. alloys, Mossbauer spectra 78—19386
- Fe-Cr-Co alloy, Mossbauer exam. of spinodal decomposition 77—69742
- Fe-Cu metastable dil. alloy film, hyperfine interactions 78—52398
- Fe-Dy, dil., implanted impurity hyperfine interaction 78—68417
- Fe-Eu, dil., hyperfine interaction of ^{153}Eu, Mossbauer effect meas. 78—43703
- β-Fe-Ge, mag. props. from X-ray, magnetisation and Mossbauer meas. 79—42755
- Fe-In, dil., hyperfine field of In, clustering effect, nucl. orientation obs. 77—16188
- Fe-Ir, hyperfine field distrib., spin echo NMR meas. 78—76351
- Fe-K(Ca)(Ti), dil., mag. hyperfine field, TDPAC meas. 78—43699
- Fe-Mo, hyperfine field distrib., spin echo NMR meas. 78—76351
- Fe-Ni, hyperfine field distrib., temp. and press. depend. 78—91651
- γ-Fe-Ni, Mossbauer exam. 79—56640
- Fe-Ni alloy, anisotropic hyperfine interactions, Mossbauer spectra 80—15854
- Fe-Ni Invar, Mossbauer exam. 79—56639
- Fe-Ni-Cr, Invar alloy, Mossbauer obs. *(Russian)* 78—19381
- Fe-Ni-Mn, Invar, RF collapse and thermal effects, Mossbauer study 80—100624
- Fe-Ni(41.3 at.%) Invar alloy, asymmetric Mossbauer spectra 77—63346
- Fe-nonmagnetic impurity, transferred hyperfine field using volume overlap model 79—78054

crystal hyperfine field interactions continued
Fe-P-B, amorphous alloy, Mossbauer effect and short-range order 80−2675
Fe-P-C, amorphous alloy, Mossbauer effect and short-range order 80−2675
Fe-Pd alloy, uniaxial ferromag., anisotropic component of localised mag. field, Mossbauer meas. *(Russian)* 79−15382
Fe-Pt, Invar type, strong ferromagnetism, mag. props. 78−64197
Fe-Pt, Mossbauer exam. 79−56639
Fe-Pt-Ir, Mossbauer effect of ^{193}Ir and ^{57}Fe, hyperfine field, isomer shift 78−15072
Fe-Pu, dil., effective mag. fields, temp. depend. *(Russian)* 78−43587
Fe-rare earth, dil., contact contribution to mag. hyperfine interaction of rare earth impurities 77−80932
Fe-Rh, hyperfine field distrib., spin echo NMR meas. 78−76351
Fe-Rh(Os), mag. hyperfine interactions Mossbauer effect meas. 77−66442
Fe-Ru (30-60 at.%) alloy, mag. ordering, Mossbauer obs. 77−4585
Fe-Ru(Os), CC hexagonal phase, ^{57}Fe Mossbauer study, saturated hyperfine fields and Neel temp. determ. 79−91321
Fe-Ru(Os) alloys, antiferromag. ordering, hyperfine fields 80−15867
Fe-Si, hyperfine fields, Mossbauer meas. 80−40024
Fe-Sn, dil., ferromag., temp. anomalies of Sn mag. hyperfine field and thermal expansion 79−33270
Fe-Ta, nuclear mag. moment of ^{182}Ta NMR-ON study 80−78139
Fe-V alloys, hyperfine fields at solute and solvent sites rel. to mag. moments 77−8461
Fe-V alloys, Mossbauer study, hyperfine field effect on formation of local moments 78−27134
Fe-X-Sn dilute alloy, Mossbauer meas. of Sn interaction with solute atoms 80−15856
Fe-Y, dil., hyperfine interactions, $^{87}Y^m$ nuclear orientation meas. 78−43715
Fe-Zn, stable and metastable alloys, order-disorder, mag. interactions and corrosion behaviour 78−68422
Fe_3Al, exam. of hyperfine field variations with order state 80−6800
Fe_3B, distinctness of magnetic hyperfine fields associated with structurally unique Fe sites 77−63330
Fe_3B, mag. props., ^{57}Fe Mossbauer spectra meas. 79−95693
$Fe_{80}B_{20}$, amorphous ferromagnet, Mossbauer hyperfine fields, mag. struct. 80−75894
$Fe_{80}B_{20}$, binary amorphous ferromagnet, Mossbauer spectra 79−4749
$Fe_{80}B_{20}$ Metglass, Mossbauer spectra line broadening 78−52400
Fe_xB_{100-x}, amorphous, mag. props., ^{57}Fe Mossbauer spectra and magnetisation meas. 79−95693
$Fe_{84}B_{16-x}C_x$, amorphous, hyperfine interaction and Curie temps., Mossbauer meas. 79−73858
$FeBO_3$, parametric echo, magnetoelastic NMR excitation *(Russian)* 80−66072
$FeBr_2$, hyperfine interaction, ^{57}Fe Mossbauer expts., mag. transition obs. 78−43720
FeC_x ($x \leq 0.05$), splat-quenched, struct., elec. and mag. props. 77−21187
$FeCO_3$, Mossbauer quadrupole splitting of ^{57}Fe, vibronic effects 79−19813
$FeCO_3$, siderite, Fe^{2+} Mossbauer spectrum, ligand field theory 77−16212
$FeCO_3$, vibronic coupling at Neel temp. 80−15491
$FeCl_2$, adsorbed monolayers, gamma-ray reson. 77−8478
$FeCl_2.4H_2O$, pressure effects on hyperfine interaction in single crysts. in mag. field 77−16211
FeCo disordered alloys, Mossbauer spectra, hyperfine mag. field distrib., Curie temp. 80−7198
$FeCoCrO_4$, ^{57}Fe Mossbauer spectra, cation distrib. 80−15879
$Fe_{3-x}Co_xO_4$, charge transfer, ion distribs., Mossbauer effect 77−20767
$(Fe_{0.2}Co_{0.8})_{80}P_{17}Al_3$, Mossbauer spectra, isomer shift, mag. hyperfine field 80−11301
$FeCo_2Si$, Heusler type materials, mag. props. 77−40042
$Fe_{3-x}Co_xSi$, structural, mag. moment, and hyperfine field behaviour, local environment model 79−65762
$Fe_{1-x}Co_xSn$, transferred hyperfine fields at ^{119}Sn, Mossbauer spectroscopy 79−33582
$FeCr_2S_4$, ionic distrib. and band struct., Mossbauer study 80−80646
FeF_3, antiferromag. Mossbauer spectrum, effect of mag. hyperfine struct. at low temps. 79−28662
FeGe, hyperfine interactions of ^{119}Sn atoms, Mossbauer spectra *(Russian)* 80−29665
$Fe_{1.67}Ge$, Mossbauer and X-ray expts. 79−1734
Fe_3Ge, ^{119}Sn mag. hyperfine interaction, Mossbauer spectra *(Russian)* 79−38420
Fe_3Ge, mag. props. of cubic and hexagonal phases 77−8475
Fe_xGe_{1-x} amorphous alloys, high field mag. meas. 79−82765
$Fe(H_2O)_6^{3+}$, in frozen aqueous soln., Mossbauer spectrum, hyperfine struct. 77−77130
FeI_2, hyperfine interaction, ^{57}Fe Mossbauer expts., mag. transition obs. 78−43720
$Fe_{1.2}Mg_{1.4}Ti_{0.4}O_4$, mag. ordering, Mossbauer effect in external mag. fields 80−71257
$Fe_{3-x}Mn_xSi$, evidence for the ang. depend. of the hyperfine interactions 78−76241
$Fe_{3-x}Mn_xSi$, struct., magnetisation, and spin echo expts., rel. to local environment model 77−20518
$Fe_{1-x}Mn_xSn$, transferred hyperfine fields at ^{119}Sn, Mossbauer spectroscopy 79−33582
Fe_2MoO_4, ^{57}Fe Mossbauer spectra, cation distrib. 80−15879
$(Fe_xMo_{1-x})_{75}P_{16}B_6Al_3$, amorphous, effects of Mo on mag. props., Mossbauer meas. 79−73859
$FeNb_2O_6$, low temp. Mossbauer exam. 79−28659
$Fe_{0.33}NbS_2$, lattice dynamics and hyperfine interactions, Mossbauer spectra study 80−108135
$Fe_{0.65}(Ni_{1-x}Co_x)_{0.35}$, Mossbauer spectra, ^{57}Fe hyperfine field distrib. 80−20533
$Fe_{0.65}(Ni_{1-x}Mn_x)_{0.35}$, Mossbauer spectra, ^{57}Fe hyperfine field distrib. 80−20533
$Fe_{3-x}Ni_xO_4$, low temp. Mossbauer spectra, electron transfer and spin density distribution 78−52404
$Fe_{40}Ni_{40}P_{14}B_6$, amorphous ferromagnet, Mossbauer hyperfine fields, mag. struct. 80−75894
$Fe_{40}Ni_{40}P_yB_{20-y}$, amorphous, mag. props. effect of metalloid elements 79−28658
$(Fe_xNi_{1-x})_{80}P_{14}B_6$, amorphous, hyperfine field distrib., ^{57}Fe Mossbauer spectra 79−11367

crystal hyperfine field interactions continued
$(Fe_{1-x}Ni_x)_{80}P_yB_{20-y}$, local struct. disorder and crystallisation, Mossbauer exam. 79−1728
$Fe_{0.5}Ni_{0.5}S_2$, hyperfine field at ^{57}Fe, Mossbauer effect *(Japanese)* 77−43916
$Fe_{1-x}Ni_xSn$, transferred hyperfine fields at ^{119}Sn, Mossbauer spectroscopy 79−33582
FeO_4^{2-} ion, electronic struct., hyperfine interactions, SCF Xα calcs. 79−37951
Fe_2O_3, amorphous, temp. depend. of hyperfine field, Mossbauer spectroscopy 78−84508
β-Fe_2O_3 film, hyperfine interactions below and above mag. ordering temp., Mossbauer obs. 77−69745
γ-Fe_2O_3, hyperfine mag. field at ^{119}Sn, Mossbauer expt. 80−50232
α-Fe_2O_3, muon spin rotation above and below Morin transition 78−43762
Fe_2O_3, nuclear quadrupole interactions, role of antishielding effects 78−47748
γ-Fe_2O_3 small particles, hyperfine field below superparamag. blocking temp., Mossbauer obs. 78−19392
α-Fe_2O_3:Sn, Mossbauer investig. of mag. hyperfine interactions 77−32306
Fe_2O_3-Bi_2O_3 system, mag. props., hyperfine parameters, Mossbauer spectrum 77−69746
Fe_3O_4, hyperfine field temp. depend., Mossbauer meas. near Verwey transition 77−69749
Fe_3O_4, hyperfine fields and spin densities below 20K 78−52405
Fe_3O_4, hyperfine mag. field at ^{119}Sn, Mossbauer expt. 80−50232
Fe_3O_4, low temp. phase, Mossbauer spectra *(Japanese)* 77−43917
Fe_3O_4, magnetite, Mossbauer spectra of low temp. phase 80−20541
Fe_3O_4, magnetite, valence instabilities, Mossbauer effect 80−20543
Fe_3O_4, magnetite Mossbauer spectra, mag. dipolar and elec. quadrupole effects 80−20544
Fe_3O_4, Mossbauer spectra at 80K, Fe electronic states and hyperfine interactions *(Russian)* 78−43696
Fe_3O_4, Mossbauer spectra above Verwey transition 78−68415
Fe_3O_4, NMR exam. of low temp. phase 78−56401
Fe_3O_4, NMR of low temp. phase, electron ordering anal. 78−56402
Fe_3O_4:^{119}Sn, hyperfine field exam., Mossbauer meas. 77−69753
Fe_3O_4:Sn, hyperfine field temp. depend., Mossbauer meas. near Verwey transition 77−69749
FeOCl, Mossbauer spectra, lattice dynamics, hyperfine interactions 80−44985
$Fe_3O_{4-x}F_x$, low temp. Mossbauer spectra, electron transfer and spin density distribution 78−52404
α-FeOOH, goethite small particles, mag. hyperfine field, bulk and surface contribs. 77−69758
β-FeOOH, Mossbauer investigation of the quadrupole splitting 78−76370
$Fe_{1-x}P_x$ dilute alloys, electronic struct., mag., elec. and struct. props. 79−37971
Fe_2P:Cu, Mossbauer spectra, mag. transition 80−50240
$Fe_2(PO_4)Cl$, Mossbauer study of mag. ordering and local co-ordination 80−39972
$Fe_3(PO_4)_2(OH)_2$ synthetic barbosalite, temp. depend. quadrupolar and mag. hyperfine interactions 80−25255
Fe_3Pt, Invar alloy, elastically stressed, ^{57}Fe effective field, anomalous behaviour, Mossbauer obs. *(Russian)* 77−8485
Fe_3Pt, non-linear local environment effect, Mossbauer effect of ^{57}Fe and ^{195}Pt 80−39910
$Fe_2Pu(Np)(U)(Zr)(Tm)$, Mossbauer diffr., combination type maxima, hyperfine interactions on nuclei 80−25263
FeS, quadrupole splitting and ground state, Mossbauer spectra 80−29657
FeS_2, electric field gradient and mean-square displacement of Fe sites 79−95690
FeS_2, Mossbauer effect in mag. field, absence of mag. moment 77−12288
FeS_2, pyrite, elec. field gradient, Mossbauer spectrum 80−15493
$FeSO_4$, anhydrous, γ, β and γ-phases, Mossbauer spectra, polymorphism 77−12287
$Fe_2(SO_4)_3$, Mossbauer isomer shift in rhombohedral and monoclinic forms 78−6609
$Fe(SO_3F)_2$, Mossbauer and electronic spectra, cryst. field splittings, mag. hyperfine interactions 77−48096
$Fe_{1+x}Sb$, hyperfine interactions of ^{57}Fe, room temp. Mossbauer meas. 79−47374
$FeSb_2O_4$, Mossbauer spectra, molecular field effects 78−91997
FeSi, hyperfine fields about μ^+ 79−56664
Fe_2Si-transition metal alloys, Heusler type materials, mag. props. 77−40042
Fe_3Si, 3d transition metal substituted, limits of solubility, mag. props. and electron conc. 78−10670
Fe_3Si, transition metal impurities, hyperfine fields 77−59365
Fe_3Si-based alloy, dil., cond. electron polarisation and moment perturbations 78−68224
Fe_3Si-based dil. alloys, conduction electron polarisation, moment perturbations 78−68225
$Fe_3Si_{1-x}Al_x$, hyperfine interactions and structural disorder, spin echo, X-ray and magnetisation meas. 77−32289
$Fe_3Si_{1-x}Al_x$, hyperfine-field distrib. 79−69732
$Fe_3Si_xAl_{1-x}$-Co, dil., site preference of ^{57}Co impurities, Mossbauer study 80−39999
$FeSiF_6$, phase transform. and relax., EFG and quadrupole spectra 77−51995
$FeSn_2$, hyperfine mag. fields at ^{57}Fe, ^{119}Sn nuclei, under press. *(Russian)* 78−39486
Fe_3Sn_2, ^{57}Fe anisotropic hyperfine field variation 79−11294
Fe_3Sn_2, magnetic properties, ^{119}Sn Mossbauer study 79−91323
Fe_3Sn_2, Mossbauer effect and magnetisation meas. 78−31132
Fe_xSn_{1-x}, amorphous film, struct. and mag. props. 80−65972
$Fe_{3-x}Sn_xO_4$, mag. hyperfine fields, ^{57}Fe and ^{119}Sn Mossbauer spectra 80−39944
1T-$Fe_{0.1}Ta_{0.9}S_2$, mag. modulation of lattice electric field gradient 77−85628
$Fe_{1+x}Te$, ^{129}I transferred hyperfine field, Mossbauer spectroscopy study 80−44972
Fe_2TeO_6, CC ^{57}Fe Mossbauer spectrum, hyperfine field, Neel temp. 79−56636
$FeTiNdO_5$, isomer shift, hyperfine field and distrib. of Fe^{3+} ions, Mossbauer spectrum 77−69747

crystal hyperfine field interactions continued
Fe_2TiO_5, spin glass system, cation distrib. Mossbaeur spectra 80—71248
$FeTiRO_5$, R=Pr,Nd,Sm,Eu,Gd,covalency contribs. to Mossbauer spectra 78—10808
Fe_xTiS_2, lattice dynamics and hyperfine interactions, Mossbauer spectra study 80—108135
$Fe_xV_{1-x}O_2$, mag. props. and Mossbauer spectra meas., exchange-coupled Fe^{3+} clusters at lower temp. 78—31136
$Fe_{3-x}V_xSi$, Fe hyperfine fields 79—78055
$Fe_{3-x}V_xSi$, struct., magnetisation, and spin echo expts., rel. to local environment model 77—20518
$Fe_{3-x}Zn_xO_4$ low temp. Mossbauer spectra, electron transfer and spin density distribution 78—52404
$FeZrF_6$, phase transition at 212.3K, Mossbauer, EPR study, quadrupole splitting, Jahn-Teller effect *(German)* 78—68430
^{57}Fe, hyperfine fields in Xe matrix, Mossbauer spectroscopy, Hartree-Fock calcs. 78—43749
^{57}Fe, hyperfine interactions in implanted metals, Mossbauer spectra 80—108141
^{57}Fe implantation in metals, electric hyperfine interactions, conversion electron Mossbauer meas. 80—7241
^{57}Fe, implanted in 3d, 4d and 5d metals, conversion electron Mossbauer spectra 77—12286
^{57}Fe interstitial cpds. and solid solns., Mossbauer spectra 80—20557
^{57}Fe, Mossbauer absorpt. and emission spectra, hyperfine struct. and relax. effects 80—71279
^{57}Fe, Mossbauer effect-time dependent PAC technique, theory of combined method 79—28645
$FrCr_2S_4$, second-order phase transition, Mossbauer spectra 80—20569
Ga, orthorhombic, quadrupole interaction of $9^+/2$ states of ^{71}As and ^{73}As 77—8467
GaAs, valence band fine struct. from light mod. with nonequilib. opt. phonons 78—39568
GaAs-AlAs mixed crystals, valence charge distrib. and elec. field gradients 80—80239
GaP, electron irrad., EPR of antisite-impurity defect 80—25211
GaP:Ge, ENDOR study, superhyperfine interactions 80—93210
GaP:S, ENDOR meas., symmetries, hyperfine parameters 78—72435
GaP:Te, ENDOR meas., hyperfine interactions and elec. field gradient 79—42869
GaP:Zn, isolated Ga vacancy due to electron irrad., EPR study 78—95519
$GaP\text{-}Ni^{3+}(Co^{2+})(Fe^+)$, EPR assessment of $3d^7$ transition metal impurity state 78—48031
Gd, ^{161}Dy TDPAC, hard core correl. 78—10809
Gd alloys, ferromag., 4d and 5d impurities, hyperfine fields 78—31133
Gd alloys, hyperfine fields, Mossbauer meas. 77—85635
Gd, crystal hyperfine fields at positive muons 79—56662
Gd, ferromag., hyperfine fields at positive muons 78—43758
Gd, ferromag., transient mag. fields at stopping nuclei, stopping power 78—34555
Gd, ferromag., vel.- and Z-depend. of transient mag. fields 78—43698
Gd, ferromagnetic, temp. depend. of μ^+ hyperfine field 78—43761
Gd, ferromagnetic, temp. depend. of hyperfine fields for F 80—20141
Gd host, dil. impurity hyperfine fields, comparison with models 78—14954
Gd host matrix, hyperfine interaction of ^{188}Os, temp. depend. 78—48102
Gd, hyperfine interaction of ^{197}Au, Mossbauer obs. 77—20773
Gd, impurity hyperfine fields 79—99518
Gd, magnetic transient hyperfine fields, IMPAC obs. 77—8464
$Gd{:}^{160}Tb$, hyperfine interaction for ^{160}Tb *(Russian)* 77—63347
$Gd{:}^{177}Hf$, polycryst. ferromag., impurity hyperfine field polarisation, IPAC 77—73106
$Gd{:}^{75}As$, mag. hyperfine field determ. by PAC 77—8459
Gd:Ra, hyperfine field determ. 77—85622
Gd-Dy(Er)(Tb)(Tb), magnetic and electric hyperfine fields at Gd, NMR spin echo 77—77123
Gd-Hg, dil., mag. hyperfine field, TDPAC meas. 78—52414
Gd-Ir, dil., hyperfine interaction of ^{193}Ir, Mossbauer effect meas. 78—52413
Gd-Sc, dil. alloy, ferromag. hyperfine field determ. 77—43919
Gd-Ta, dil., elec. field gradient at ^{181}Ta, temp. depend., TDPAC meas. 79—95689
Gd-Ta, dil., mag. hyperfine field and elec. field gradient at ^{181}Ta impurities, TDPAC meas. 79—47361
Gd-Yb(Ir), dil., ferromag., mag. hyperfine fields of ^{170}Yb and ^{193}Ir, Mossbauer effect meas. 79—24242
GdAG, electrostatic model of cryst. field 80—59945
$GdAl_2$, hyperfine fields, ferromagnetic coupling between rare earth spins, NMR study 80—39880
$GdAl_2$, spin reorientation, NMR features rel. to preferred magnetisation direction change 77—63213
$Gd(Al_xFe_{1-x})_2$, intermetallic compounds, pseudobinary, Mossbauer studies 80—75887
$GdAlO_3$, ^{155}Gd excited states, determ. of nuclear parameters using Mossbauer effect 79—28646
$GdAlO_3$, canted antiferromagnetic, Mossbauer meas. 80—97171
$Gd_xCe_{1-x}Ru_2$, magnetic ordering by ^{155}Gd Mossbauer spectroscopy 78—27139
$GdCo_2$, ^{59}Co hyperfine field, temp. depend. splitting 77—8447
$Gd(Fe_xCo_{1-x})_2$, Mossbauer effect at 78 and 300K, ^{57}Fe hyperfine fields 80—2677
$Gd_2(Fe_{1-x}Co_x)_{17}$, hyperfine interactions, Mossbauer effect 78—2780
$Gd_2(Fe_{1-x}Ni_x)_{17}$, hyperfine splitting, constant Fe moment evidence 78—6614
$Gd_{0.99}Ho_{0.01}(Rh_{1-x}Fe_x)_2$, spin echo meas. on ^{165}Ho, quenching effect of Fe substitution 78—48079
$Gd_{0.1}La_{0.9}Ni_5H_x$, $Gd_{0.1}La_{0.9}Co_5H_x$, ^{155}Gd Mossbauer spectra 77—63340
$Gd_{1-x}La_xRh_2$, NMR, contribution of Gd neighbours to Gd hyperfine field 77—8423
GdM_x, M=3d transition metal, hyperfine interactions 78—19401
GdM_2Ge_2, M=Mn, Fe, Co, Ni, Cu, magnetism and hyperfine interactions 78—76228
Gd_2O_3, ^{161}Dy TDPAC, hard core correl. 78—10809
$GdPt_x$, $Gd_{1-x}A_xPt_2$ (A=Sc, La), Laves phase alloy, NMR, nonstoichiometry 77—63298
$(Gd_{1-x}R_x)(Co_{1-y}M_u)_5$, R=rare earth, M=Cu, Ni, Pt, origin of hyperfine fields acting on Gd, Mossbauer study 80—44967
$GdRh_2H_x$, $GdRu_2H_x$, struct. and mag. props., Mossbauer and magnetisation meas. 80—71271
$Gd_{1-x}Sc_x$, Mossbauer spectra, hyperfine interactions 80—15923

crystal hyperfine field interactions continued
$GdVO_4$, ^{155}Gd excited states, determ. of nuclear parameters using Mossbauer effect 79—28646
$GdVO_4$, hyperfine field and exchange interactions, Mossbauer meas. 79—47370
$Gd_{1-x}Y_x$, Mossbauer spectra, hyperfine interactions 80—15923
$Gd_xY_{1-x}Co_2$, ferrimag., ^{155}Gd Mossbauer effect and ^{165}Ho NMR expts. 77—63339
$GdZrFe_2$, hyperfine field at Gd, TDPAC meas. 80—93214
$Gd[Co_xFe_{1-x}]$, NMR, hyperfine fields, conc. depend. 77—43902
Ge, anomalous muonium states 80—34841
Ge, deep and shallow levels of muonium, electronic struct. 78—39051
Ge, electric field gradient-elastic tensor components, acoustic NMR obs. 80—25229
Ge, electric quadrupole sum rules rel. to optical consts. 79—38036
Ge, polarisation of implanted ^{12}B 78—43653
Ge, spin Hamiltonian and anomalous muonium states 80—71286
$Ge{:}^{125}I(^{125}Te)$, implanted atom sites and quadrupole interaction, Mossbauer spectra 77—20758
$Ge{:}^{57}Co$, ion-implanted, Mossbauer study, annealing effects 80—7231
$Ge{:}^{57}Fe$, quadrupole interac. 78—92005
Ge:Fe, recoil implantation Mossbauer expt. in presence of external mag. field 80—44981
Ge_2FeGa, and Fe_2CoGa, site preference and local environment effects, Mossbauer and NMR expts. 78—43710
GeO_2:Al, Ga, EPR, transferred hyperfine interactions of impurity-related trapped hole centres 77—85568
$GeO_2{:}Sc^{3+}(Y^{3+})(In^{3+})$, trapped-hole centres, ESR meas. 79—77597
$GeO_2{:}V^{4+}(Cr^{3+})$, direct mechanism in supertransferred hyperfine interaction 79—23936
GeTe, degenerate semiconductor, EPR experiments on Mn^{2+} 79—11339
H atom lattice impurity, H atom confined to spherical box with penetrable walls, Schrodinger eqn. 79—84987
H, trapped in inert gas matrix, anisotropic hyperfine interactions 79—65728
$\alpha\text{-}HIO_3$, HI_3O_8, I_2O_5 and deuterated cpds., crystalline, ^{127}I NQR, bonding and mol. dynamics 80—39889
Hf-Ir, dil., elec. field gradient at ^{193}Ir, Mossbauer meas. 80—66090
HfC:Ta, perturbed ang. correlation spectra, elec. quadrupole interaction 80—15916
$HfCo_2$:Ta, perturbed ang. correlation spectra, elec. quadrupole interaction 80—15916
$HfFe_2$:Ta, perturbed ang. correlation spectra, elec. quadrupole interaction 80—15916
$Hf(Fe_{1-x}Co_x)_2$, mag. props., Mossbauer spectra and magnetisation meas. 80—39948
$HfFe_{2-x}Si_x$, Mossbauer spectra, hyperfine interactions 80—15862
$HfGeO_4$, nuclear quadrupole interactions, TPDAC meas. 79—82902
HfNi, hyperfine critical exponents, TDPAC meas. of bulk meas. 77—8465
$Hf(SO_4)_2$, elec. quadrupole interaction, TDPAC technique, coincidence system 80—93216
$HfV_2O_7{:}^{181}Ta$, EFG temp. depend., TDPAC 77—59488
Hg electric field gradients at different Be lattice sites, gamma-spectral study 80—80224
Hg, quadrupole interactions in Zn, lattice location, gamma spectral study 80—80227
$HgSe{:}Mn^{2+}$, temp. depend. of EPR of ^6S state ions 80—80593
Ho, ^{111}Cd impurity electric quadrupole interaction temp. depend. 80—39900
$Ho{:}^{119}Sn$, mag. hysteresis of hyperfine field, compensation in mag. field *(Russian)* 77—81039
$^{165}Ho{:}^{166}Ho^m$, gamma-ray emission from oriented nuclei in multiaxis nucl. spin system 79—82905
Ho-Au, dil., hyperfine interaction of Ho^{3+}, nuclear orientation expts. 78—43717
Ho-Sn, dil. alloy, hyperfine interaction of ^{119}Sn, Mossbauer meas. 78—91998
Ho-Ta, dil., elec. field gradient at ^{181}Ta, temp. depend., TDPAC meas. 79—95689
Ho-Ta, dil., mag. hyperfine field determ., TOPAC meas. 79—91330
$HoAlO_3$, electronic and nucl. mag. ordering, mol. field approx. 80—60157
$HoAlO_3$, neutron diffr. at 0.04K, mag. ordering *(French)* 78—10653
HoF_3, ^{19}F NMR, ligand hyperfine interaction, shift tensor determ. 78—48056
$Ho(Fe_xNi_{1-x})_2$, mag. behaviour, susceptibility and Mossbauer expts., 4.2-1300K 78—52235
HoGa garnet, mag. ordering induced by hyperfine interaction, neutron diffr. meas. 77—66265
$Ho_3Ga_5O_{12}$, hyperfine interac. induced antiferromag. order *(French)* 77—59392
$Ho_{0.01}Gd_{1-x}Y_xNi_2$, spin echo meas. on ^{165}Ho, limited quenching of Ho moment by cryst. field 79—73851
$Ho(OH)_3$, Mossbauer spectra, cryst. field and mag. props. 80—15873
HoSb, quadrupole scatt. anisotropy, magnetically ordered material 78—64034
$HoVO_4$:Gd, indirect superhyperfine interaction, EPR line width meas. 80—2633
$Ho_xY_{1-x}(Fe_{0.1}Co_{0.9})_2$, ^{57}Fe hyperfine interaction, mag. props., Mossbauer study 80—39951
In, nuclear quadrupole alignment of $^{114}In^m$ 78—48090
In, quadrupole interaction of ^{69}Ge, TDPAD expts. 78—48089
In, two stage nuclear demagnetization experiments 79—65644
$In{:}^{67}Ge$, elec. quadrupole interaction temp. depend., PAC meas. 79—42877
In-Te, elec. field gradient, at ^{111}Cd probes, temp. depend. 79—28643
InAs, fine struct. of diamag. excitons, oscillatory magnetoabsorpt. obs. 78—18971
InP, recoil damage obs. by PAC with ^{111}Cd 77—89484
InP, valence band fine struct. from light mod. with nonequilib. opt. phonons 78—39568
$InP{:}Fe^{3+}$ (Cr^{2+}), EPR, symm., spin Hamiltonian parameters 78—10759
InSb, recoil damage obs. by PAC with ^{111}Cd 77—89484
$InSb{:}Mn^{2+}$ nondegenerate semicond., mag. impurity indirect interaction *(Russian)* 80—34591
^{111}In, nucl. orientation coeffs., nucl. mag. moment 80—97168
$Ir_{1.07}Mn_{1.07}Sn_{0.88}$, ferromag. Heusler alloy, ^{193}Ir and ^{119}Sn hyperfine fields 79—78581
$K_2Al_2(SO_4)_4.24H_2O$, temp. depend. curves of quadrupole interaction parameter for $^{27}Al^{3+}$ 77—55727

crystal hyperfine field interactions continued
KBr, F-centre spin-lattice relax., theory and MCD meas., phonon-modulated HFS 77—43883
KBr, H-centre struct., hyperfine interactions 78—79611
KBr:Na, U-centres, HFS and g-factor, EPR spectra 80—39869
KBr(I):Co, coloured and uncoloured, Mossbauer effect, inhomogeneous hyperfine fields 77—32307
KCl, ENDOR of F-centres, sign of ^{41}K elec. quadrupole moment 80—34820
KCl, F-centre hyperfine interaction parameters, press. shifts 77—8043
KCl, H-centre struct., hyperfine interactions 78—79611
KCl, press. shifts of F-centre hyperfine interaction parameters 78—79957
KCl:Ag, Br, EPR spectra of $Ag^0(Br_1)$ paramag. centres *(French)* 79—11346
KCl:Au, EPR and optical absorpt. 78—39397
KCl:Ga(In), ESR of impurity centres, impurity optical absorpt. bands 80—29618
KCl:H, dynamical superhyperfine interaction 80—2663
KCl:H, ENDOR and ESR study of anion sites 80—108118
KCl:$K_4Os^{II}(CN)_6$, electron irrad., EPR, ligand hyperfine struct. 78—60335
KCl:Li,H optical and EPR exam. of H centre, $(LiH)^+$ absorpt. spectra 79—99920
KCl:PO_2^-, ODMR spectra at 2K, HFS tensor of P 79—87333
KCl:PO_2^-, triplet state, level anticrossing and pseudonuclear Zeeman effect, microwave ODMR 80—39896
$KCoF_3$, antiferromag., ^{59}Co NMR exam. 78—76332
$K_2Cr_2O_7$ single crystals, X-irrad., EPR spectra 80—2638
$K_2CuCl_4.2H_2O$, Bloch-wall NMR, anisotropic hyperfine interaction 79—51864
$K_2CuCl_4.2H_2O$, ferromag., hyperfine and exchange interactions, NMR study 80—50208
$K_2CuCl_4.2H_2O$, hyperfine and super-exchange interactions 80—103654
$K_2CuCl_4.2H_2O$, paramag. single cryst., PMR temp. depend., hyperfine const. and exchange interaction *(Korean)* 80—29630
$K_2CuCl_4.2H_2O$ structures, BCC Heisenberg ferromags., transferred hyperfine interactions of ^{1}H, ^{2}D and ^{17}O 77—69725
$KCuF_3$, hyperfine interactions of ^{19}F nuclei, n.m.r. meas. 77—12209
K_2CuF_4, hyperfine interactions of ^{19}F nuclei, n.m.r. meas. 77—12209
$KD_3(SeO_3)_2$, D NMR above and below ferroelec. transition, H-bond behaviour 78—52460
KF, self-trapped exciton, ODMR spectra, anisotropy of hyperfine interaction 79—28286
KF+Eu^{2+}, cryst., hyperfine splitting, EPR 78—2733
$(KF)_n$-FeF_3, antiferromagnetic systems, dimensionality and spin reduction effects, Mossbauer study 80—39947
$K_3Fe(CN)_6$, electronic struct., elec. field gradient tensor 80—15483
K_2FeF_4, antiferromag., Mossbauer study of mag. ordering 79—28655
K_2FeF_5, Mossbauer spectra, 1D antiferromag. 80—15886
K_2FeF_5, one dimens. antiferromag., zero point spin reduction 77—85456
K_2FeF_5, one-dimens. antiferromag., single cryst. Mossbauer spectra 78—23376
K_2FeF_5, one-dimensional antiferromag. systems, Mossbauer studies 80—71266
KFe_2O_3, β''' phase, mag. props., hyperfine interactions, Mossbauer study 80—20524
$KFeS_3$, quadrupolar and mag. hyperfine anisotropy, Mossbauer meas. 78—56408
KH_2PO_4:KH_2AsO_4, X-irrad., EPR 77—32257
KH_2PO_4:$NH_4H_2PO_4$, EPR of arsenic and phosphorus oxyradicals 77—77102
K_3HfF_7:^{181}Ta, elec. quad. interac., DPAC 77—32299
K_2IrF_6, hyperfine spectra of mag. ordered state at very low temp., Mossbauer meas. 77—69744
$KMgF_3$, F-centre, superhyperfine interaction, g-factor, symmetry, ENDOR obs. 80—39893
$KMgF_3$, F-centre ENDOR study 80—108117
$KMgF_3$:Fe^{2+}, octahedral symm., vibronic effects from Zeeman field induced Mossbauer spectra 77—8477
$KMgF_3$:Fe^{2+}, transferred hyperfine interactions, EPR exam. 78—31105
$KMgF_3$:Ti^{3+}, ESR and ENDOR spectra, superhyperfine interaction parameters 77—40121
$KMgF_3$:V^{2+}, ^{51}V ENDOR meas., spin Hamiltonian parameters 79—28638
$KMgF_3$:Yb^{3+}, ^{19}F hyperfine interaction, anisotropic Fermi and isotropic dipolar interactions 79—78056
$KMgF_3$:Yb^{3+}, perovskite type cryst., ENDOR meas. 80—80638
$KMgF_3$:Yb^{3+}, transferred hyperfine interaction of Yb^{3+}, ENDOR meas. 78—19375
$KMg_3[AlSi_3O_{10}].F_2$ with excess Al, synthetic fluorphlogopite, radiation-induced paramag. O^- centres 80—60417
$KMnO_4$, ^{55}Mn NMR second-order quadrupole splitting, asymmetry parameter 77—63312
KN_3, ab initio calcs. of elec. props. of N_4^- 79—95363
KPF_6, temp. depend. hyperfine interactions of trapped pyramidal radicals 80—44918
K_2SO_4:$(NH_4)SO_4$, X-irrad., EPR of NH_3^+ 80—11272
K_2SnF_6, Group IV hexafluoride anion radical γ-irrad., EPR spectra 78—72411
$KZnF_3$, exchange interactions of transition metal ions in orbitally degenerated excited states 80—65512
$KZnF_3$:V^{2+}, ^{51}V ENDOR meas., spin Hamiltonian parameters 79—28638
$KZnF_3$:V^{2+}, calc. of t_{2g} antibonding mol. orbital in $|VF_6|^4$, rel. to ESR 80—50174
$KZnF_3$:Yb^{3+}, perovskite type cryst., ENDOR meas. 80—80638
$LaAlO_3$, exchange interactions of transition metal ions in orbitally degenerated excited states 80—65512
$LaBr_3$:Pr^{3+}, laser-induced fluoresc. line-narrowing, hyperfine struct. and Zeeman effect 77—85789
$LaCl_3$:Gd^{3+}, ^{139}La ENDOR, hyperfine and elec. quadrupole interactions 77—20749
$LaCl_3$:Pr^{3+}, hyperfine Zeeman effects, fluorescence line-narrowing technique 77—62881
$LaCl_3$:Pr^{3+}, Zeeman second-order effects, fluoresc. line narrowing technique 80—16103
LaF_3:Nd^{3+}, spin echo envelope modulation exam. 79—61212
LaF_3:Pr^{3+}, $^1D_2$ metastable state, hyperfine splittings, enhanced and saturated absorpt. spectra 78—43694
LaF_3:Pr^{3+}, 2K, optically detected coherent transients in nuclear hyperfine levels 79—19806

crystal hyperfine field interactions continued
LaF_3:Pr^{3+}, hyperfine splitting of $^1D_2$ metastable state, RF optical double reson. 78—35067
LaF_3:Pr^{3+}, nuclear hyperfine interactions, photon echo relax. obs. 79—59771
LaF_3:Pr^{3+}, nuclear quadrupole interaction, optical-RF double reson. meas. of ground electronic state 77—48092
LaF_3:Pr^{3+}, optical line narrowing by nuclear spin decoupling, photon echo meas. 80—48353
LaF_3:Pr^{3+}, spectroscopic and relaxation character of $^3P_0$-$^3H_4$ transition, photon echo 80—39897
$LaFe_{1-x}D_xO_3$:Sn, D=Al, Ga or Sc, Mossbauer effect, hyperfine mag. fields at Sn 77—24772
$LaFeO_3$, doped, effect of doping on hyperfine fields, supertransfer model 79—47057
$LaFe_{12}O_{19}$, high field Mossbauer effect on ^{57}Fe at room temp. and 4.2K 79—24238
LaM_2:Nd^{3+}, M=Ru, Rh, Ir, Pt, ESR investigation 79—78514
$LaNi_{1-x}Fe_xO_3$, magnetisation meas. and ^{57}Fe Mossbauer studies 80—93217
$LaNi_{1-x}Mn_xO_3$, ^{55}Mn NMR study, magnetisation meas., ferromag. and Pauli paramag. components 80—7191
La_2O_3:Mn^{2+}, position and intensity of forbidden hyperfine lines, ESR spectra 79—19775
$LaRh_2$:Nd^{3+} cubic metallic host, spin-lattice relaxation, ESR obs. 79—1710
$La_{0.98}Sn_{0.02}Mo_6Se_8$, Chevrel phase supercond., hyperfine interaction, microscopic study 79—56650
$La_{1-x}Tb_xAl_2$, competing paramag. anisotropy from cryst. field and indirect quadrupolar coupling 80—60180
$La_{1-x}Y_x$ alloys, PAC obs. of hyperfine field fluctuation at ^{140}Ce, Kondo effect interpret. 77—20761
^{137}La, possibility of obs. of Mossbauer effect 78—39457
Li-Zn ferrites, (Li, Zn, Ti, Cr substituted), Mossbauer spectrometry, effect of supertransferred hyperfine fields and relaxation *(French)* 80—80654
$LiBaF_3$:Mn^{2+}, having inverse periodic struct., ENDOR study 80—97162
LiCl, press. shifts of F-centre hyperfine interaction parameters 78—79957
$LiCuCl_3$-$2H_2O$, ^{7}Li NMR lineshape 77—48061
$LiErF_4$, EPR studies, lowest levels of rare-earth ions, submillimetre freq. 80—39865
LiF, self-trapped exciton, ODMR spectra, anisotropy of hyperfine interaction 79—28286
LiF:Mg(Ag), electron spin-lattice relax. of V_k-centre 78—95518
LiF:Na^+ H_A-centre struct., hyperfine interaction 78—79611
LiF:OH, neutron irrad., interstitial H-centres, ESR obs. 80—93175
LiF:Ti, EPR exam., superhyperfine interactions 78—31107
LiF:U, Mn, EPR of Mn^{4+} centre, g-values and hyperfine struct. 77—12192
$LiFeO_2$, quadrupole splitting in Mossbauer ^{57}Fe spectrum, geometric anal. and computer simulation 79—1730
$LiFeS_2$, magnetic hyperfine interactions, Mossbauer spectra and mag. susceptibility meas. 80—29658
$LiHoF_4$, EPR studies, lowest levels of rare-earth ions, submillimetre freq. 80—39865
$LiHoF_4$, NMR shift tensors, temp. and field depend. 79—38391
α-$LiIO_3$:$Cr^{3+}(Fe^{3+})$, hyperfine interactions, RF discrete saturation of EPR lines 78—48032
α-$LiIO_3$:Fe^{3+}, local environment and superhyperfine interactions by RF discrete saturation 77—85554
$Li_2IrCl_6.xH_2O$, hyperfine spectra of mag. ordered state at very low temp., Mossbauer meas. 77—69744
$LiNbO_3$:$^{57}Fe^{2+}$ Mossbauer spectra, EFG axis 77—20760
$LiNbO_3$:Fe, electron spin relaxation study, Mossbauer effect, mag. and crystal field effects 80—39902
$LiRF_4$, R=Dy, Er, Ho, Tb, NMR rotation spectra, transferred hyperfine interaction 77—85590
$LiTaO_3$, electric field gradients and isomer shift ^{181}Ta 78—39453
$LiTbF_4$, EPR studies, lowest levels of rare-earth ions, submillimetre freq. 80—39865
$LiTbF_4$, NMR shift tensors, temp. and field depend. 79—38391
LiTi ferrite, Mossbauer study, relax. and supertransferred hyperfine fields 80—39941
$LiTmF_4$, ^{169}Tm NMR spectrum, hyperfine field parameters, and cryst. field calcs. 77—12213
$LiVS_2$, intercalation cpd., NMR 77—90048
$LiYF_4$:Pr, NMR meas. of hyperfine const. of Pr^{3+} excited state 80—88895
LiZn ferrite, Mossbauer study, relax. and supertransferred hyperfine fields 80—39941
Lu, electric field gradient, at ^{181}Ta substitutional atoms, pressure dependence 78—52385
Lu, nuclear quadrupole alignment of ^{177}Lu 78—48090
Lu-Ir, dil., elec. field gradient at ^{193}Ir, Mossbauer meas. 80—66090
LuAG, electrostatic model of cryst. field 80—59945
$LuIr_2$-Nd^{3+}, dil., ESR, hyperfine crysts. of ^{143,145}Nd, g-factor, crystalline field splitting 78—52349
$LuPO_4$:Pb^{3+}, EPR, hyperfine interactions 80—108050
$LuRh_2$-Nd^{3+}, dil., ESR, hyperfine crysts. of ^{143,145}Nd, g-factor, crystalline field splitting 78—52349
Mg, quadrupole interaction of ^{12}B and ^{12}N 78—47750
Mg, quadrupole interaction of ^{181}Ta, gamma-spectral study 80—80228
Mg:^{12}B ions, decoupling of hyperfine interactions by external mag. field 77—24756
$MgFe_2O_4$, Mossbauer study 79—47375
$Mg(NH_4)_2(SO_4)_26H_2O$:$VO(H_2O)_5^{2+}$, proton ENDOR meas. used to determine hyperfine coupling tensors 80—66075
$Mg(NH_4)(SO_2)_4.6H_2O$:$Cu(H_2O)_6^{2+}$, ^{1}H ENDOR 79—73854
MgO, ^{25}Mg superhyperfine struct. of V-type defects, ENDOR 77—66439
MgO, transition metal ion doped, phonon spectroscopy using freq. crossing techniques 79—42193
MgO:Cr^{3+}, cubic centre, high resolution ESR, superhyperfine interaction 77—16162
MgO:Cr^{3+} (Mn^{2+}) spin Hamiltonian parameters, lattice expansion and vibr. effects 80—24851
MgO:Ir^{2+}, quadrupole interactions and static Jahn-Teller effect in EPR spectra 77—72842
MgO:Ir^{2+}, superhyperfine struct. of ^{25}Mg in EPR spectra of Ir^{2+} 77—69683

crystal hyperfine field interactions continued
$MgO:Rh^{2+}$, EPR of Jahn-Teller ions, ^{17}O superhyperfine structure 77-32253
$MgSiF_6$, phase transform. and relax., EFG and quadrupole spectra 77-51995
β-Mn alloys, weakly antiferromag., hyperfine fields, NMR meas. 78-39441
Mn $TiRO_5$, R=Pr,Nd,Sm,Eu,Gd,covalency contribs. to Mossbauer spectra 78-10808
Mn^{2+} compounds, strongly exchange coupled, solid and liq. states, EPR and NMR, 300-1450K 77-73077
Mn^{2+} doped EPR powder samples, hyperfine line intensities and axial cryst. field 79-78511
Mn^{2+}, doped ion in divalent metal cpds., Szigeti charge and correl. with hyperfine coupling const. 80-96831
Mn-Tb, dil., hyperfine interactions, nuclear orientation 80-15929
Mn^{2+}-Cu^{2+} coupled pair, ESR spectrum, strong isotropic exchange model 80-29606
$MnCO_3$, NMR saturation, nuclear spin wave excitation, large freq. shifts *(Russian)* 80-50207
$MnCl_2.4H_2O$, antiferromagn., nucl. orientation 78-43652
$Mn_{1-x}Co_xSb$, ferromagnetic, NMR exam. 79-24228
$Mn^{2+}F^-$ and $Mn^{2+}F^-Mn^{2+}$ systems, transferred hyperfine interaction at F^- site 80-70657
$Mn_{1-x}Fe_xCr_2S_4$, Fe II electronic struct., Mossbauer spectra 80-15876
$MnFe_2O_4:Sn$, hyperfine mag. fields at ^{119}Sn and ^{57}Fe nuclei, influence of press. 79-99811
$(Mn_{1-x}Fe_x)_5SiC$, magnitude of quadrupole splittings, Mossbauer study 78-43747
$Mn_4N_{0.8\text{-}1}$, NMR of ^{55}Mn, reson. curve fine splitting, spin echo meas. 78-2768
MnO, ^{19}F isomer shift, time differential PAD 77-12280
MnO, paramag., μ^- spin rotation at O site 77-20785
$Mn_3O_4:^{119}Sn$, hyperfine field exam., Mossbauer meas. 77-69753
MnSb, ^{119}Sn Mossbauer obs. 77-40160
MnSb, hyperfine interactions at ^{57}Fe and ^{119}Sn, Mossbauer spectroscopy 78-23375
Mn_2Sb, domain and domain wall resons. in ^{55}Mn NMR spectrum 80-25219
Mn_2Sb, hyperfine fields of ^{121}Sb in several mag. phases 79-28650
Mn_2Sb, large anisotropy in mag. hyperfine field at ^{121}Sb, Mossbauer spectra meas. 77-73101
MnSi-CoSi solid solution, mag. props. 78-56403
$MnSiF_6$, phase transform. and relax., EFG and quadrupole spectra 77-51995
$MnTe_2$, Mossbauer spectra, hyperfine field 80-15866
Mo-Co Kondo alloy, Co impurity susceptibilities, Knight shift 80-88721
MoO_3, electric quadrupole interaction, TDPAC meas. 78-39455
N_2, solid, exciton-phonon coupling in strong coupling limit, temp. depend. 80-92616
$ND_4Cl:Cu^{2+}$, high-press. EPR, order-disorder transitions 78-19310
$ND_4D_2AsO_4$, ND_4 role in antiferroelec. transitions, D NMR 77-52025
$(ND_4)_2Zn(SO_4)_2.6D_2O:Cu^{2+}$, EPR exam. 77-24735
$(NH_4)_2$ $Zn(SO_4)_2.6H_2O:VO^{2+}$, γ-irradiated $NH_3{}^+$ ESR, N hyperfine coupling tensor 79-69722
$NH_4Cl:[MoOCl_5]^{2-}$, single cryst., struct. investigations 77-66524
NH_4ClO_4, γ-irrad. single cryst., $NH_3{}^+$ EPR obs., g-tensor hyperfine splitting 78-2739
$(NH_4)_2CuBr_4.2H_2O$, ferromag., hyperfine and exchange interactions, NMR study 80-50208
$(NH_4)_2CuBr_4.2H_2O$, hyperfine and super-exchange interactions 80-103654
$(NH_4)_2CuCl_4.2H_2O$, Bloch-wall NMR, anisotropic hyperfine interaction 79-51864
$(NH_4)_2CuCl_4.2H_2O$, ferromag., hyperfine and exchange interactions, NMR study 80-50208
$(NH_4)_2CuCl_4.2H_2O$, hyperfine and super-exchange interactions 80-103654
$(NH_3)_2FeF_5$, one-dimensional antiferromag. systems, Mossbauer studies 80-71266
$(NH_3)_2FeF_5$, quasi two-dimens. antiferromagnet, Mossbauer study 80-39947
NH_4FeF_4, mag. and Mossbauer obs. *(French)* 78-19389
$N_2H_6FeF_5$, Mossbauer spectra, 1D antiferromag. 80-15886
$N_2H_6FeF_5$, one-dimensional antiferromagnetism, Mossbauer study 80-65872
$(NH_4)_2HAsO_4$, Zeeman perturbed NQR spectra, EFG tensors and antiferroelectric ordering 77-43898
$NH_4HC_2O_4$, hemihydrate, ^{14}N NMR, high resolution spectra, elec. field gradient tensor 77-81018
$(NH_4)_2HPO_4:KH_2AsO_4$, EPR of arsenic and phosphorus oxyradicals 77-77102
$(NH_4)_3HfF_7$, longitudinal decoupling of quadrupole interaction 78-39456
$(NH_4)_6MnMo_9O_{32}.8H_2O$, mag. susceptibility, rel. to EPR, zero field splitting parameter 77-36122
NH_4ReO_4, quadrupole coupling, cation electric field gradients 78-35060
$(NH_4)_2SO_4$, ferroelec. transition, EPR study 79-38472
$(NH_4)_2SO_4$, paraelectric, N-quadrupole coupling meas. by proton-N double resonance 80-60459
$(NH_4)_2SO_4:SeO_3{}^-$, γ-irrad., hyperfine interaction, ferroelec. transition effects, EPR expt. 78-15024
$(NH_4)_2SO_4.Al_2(SO_4)_3.24H_2O$, temp. depend. curves of quadrupole interaction parameter for $^{27}Al^{3+}$ 77-55727
NH_4VO_3, polycryst., quadrupole coupling const., asymmetry parameter, chem. shift, NMR computer calcs. 78-6584
$Na_8(Al_6Si_6O_{24})Cl_2$, sodalite, electronic struct. of F-centre 80-2356
$NaBF_4$, electric field gradient, quadrupole coupling consts. 77-89740
NaCl, electric field gradients near dislocations, resulting NMR lineshapes 80-75225
NaCl, press. shifts of F-centre hyperfine interaction parameters 78-79957
NaCl:Au, EPR and optical absorpt. 78-39397
NaCl:Ga(In), ESR of impurity centres, impurity optical absorpt. bands 80-29618
NaCl:Li, U-centres, HFS consts., g-factor, EPR spectra 80-39869
$NaCrS_2$, intercalation cpd., NMR 77-90048
$NaCrS_2(Se_2)$, EFG tensor, S and Se dipolar contribution 77-31984
NaF, self-trapped exciton, ODMR spectra, anisotropy of hyperfine interaction 79-28286

crystal hyperfine field interactions continued
$NaF:U^{5+}$, U isotope abundance determ. by EPR hyperfine struct. 79-91296
$NaF+Eu^{2+}$, cryst., hyperfine splitting, EPR 78-2733
$Na_2(Fe,Mg)_5Si_8O_{22}(OH)_2$, riebeckite, low temp. Mossbauer obs. of oriented single cryst. behaviour and mag. props. 80-84674
$NaFeF_2$, Mossbauer and low-temp. dilatometry study *(French)* 80-80662
$NaFeS_2$, mag. hyperfine fields and covalency, Mossbauer effect meas. 77-90077
$Na_2HPO_4.7H_2O:KH_2AsO_4$, EPR of arsenic and phosphorus oxyradicals 77-77102
$NaInS_2(Se_2)$, EFG tensor, S and Se dipolar contribution 77-31984
$NaNO_2$, ^{23}Na elec. field gradient tensor from NMR satellite lines near phase transition 80-71191
$NaNO_2$, electric field gradient, quadrupole coupling consts. 77-89740
$NaNO_2:Ag^+$, optical and MODR spectra, anion states spin-orbit perturbation 79-19908
$NaNO_3$, electric field gradient, quadrupole coupling consts. 77-89740
$NaNo_3$, ^{23}Na satellites in nuclear double resonance interferometric spectroscopy 79-4745
Na_2O-Al_2O_3-B_2O_3-SiO_2:Ag, photochromic glass, EPR of Ag^0 and $Ag_2{}^+$ centres 77-24741
$NaReO_4$, quadrupole coupling, cation electric field gradients 78-35060
Na_3RuO_4, ^{99}Ru Mossbauer spectra, antiferromag. order, mag. relax. 80-50234
$NaTaO_3$, electric field gradients and isomer shift ^{181}Ta 78-39453
$NaVO_2$, polycryst., quadrupole coupling const., asymmetry parameter, chem. shift, NMR computer calcs. 78-6584
$NaVS_2$, intercalation cpd., NMR 77-90048
$Na_2Zn(SO_4)_2.4H_2O:Ag^{2+}$, EPR, Ag^{2+} dimeric struct., hyperfine and fine struct. tensors 77-51949
$Na_2Zn(SO_4)_2.4H_2O:Ni$, optical absorp. and EPR obs. 78-76501
Nb, spin polarised μ^+ meas., localisation and thermal diffusion 78-39489
$NbS_2.Sn$, $NbS_2.Sn_{1/3}$ intercalation cpds., lattice dynamics, hyperfine interactions 79-61273
Nb_3Sn, proton and γ-irradiated, lattice dynamics from ^{119}Sn Mossbauer studies 78-39458
^{90}Nb, decay rate perturbation by implantation in metals 77-22944
$Nd^{3+}:LaCl_3$, laser-induced fluoresc., hyperfine structs. 80-100677
$Nd^{3+}:LaCl_3$, laser-induced fluoresc. energy transfer effects 80-100678
Nd-Co alloys, NMR of ^{143}Nd and ^{145}Nd 78-19343
$NdAl_2$, conduction electron spin and orbital polarisation effects 78-80228
$NdFe_2$, Curie temp., elec. quadrupole couplings, Mossbauer study 80-39949
$NdFe_2$, high field Mossbauer study 80-75893
Ni, ^{155}Tb sources produced by recoil implantation, ^{155}Gd Mossbauer transition 80-40009
Ni (111), Mossbauer effect emission spectroscopy and AES 79-91329
Ni alloys, dil., hyperfine field distribs., DPAC meas. 80-93222
Ni alloys, ferromag., 4d and 5d impurities, hyperfine fields 78-31133
Ni complex, $[Ni(OCH_3)\ (acac)\ (CH_3OH)]_4$, sp. ht., 0.4-285K, methyl group internal rotation 78-47531
Ni complex, hexamethylphosphorotriamide Ni (II), paramagnetic, pulsed NMR, substitution reaction *(French)* 78-10793
Ni, critical exponent β for hyperfine fields, PAD techniques 78-19403
Ni, crystal hyperfine fields and neutron scatt. 79-56172
Ni, ferromag., hyperfine fields at positive muons 78-43758
Ni, ferromag., hyperfine field of positive muon 79-47378
Ni, ferromag., Knight shift of hyperfine field at positive muon 77-43925
Ni, ferromag. hyperfine fields on ^{12}B, NMR obs., near T_c 77-28476
Ni, ferromagnetic, calc. hyperfine fields and their press. derivations 80-6796
Ni, ferromagnetic, electronic struct. and hyperfine field of nonmag. impurities, calc. 80-70658
Ni, ferromagnetic, temp. depend. of hyperfine fields for F 80-20141
Ni, ferromagnetic zero point motion effect on hyperfine field at interstitial positive muon site 80-2681
Ni host, dil. impurity hyperfine fields, comparison with models 78-14954
Ni, hyperfine field and magnetisation, press. and temp. depend. 80-6795
Ni, hyperfine field of μ^+, calc. 77-40167
Ni, hyperfine interactions on implanted ^{12}B, crit. behaviour near T_c 78-43663
Ni, hyperfine mag. fields at ^{67}Ge, TDPAC meas. 78-43701
Ni, impurity hyperfine fields 79-99518
Ni, lattice defect symmetry, time differential PAC meas. 78-15069
Ni, mag. hyperfine field at ^{140}Ce, TDPAC meas. 79-11363
Ni, magnetic hyperfine fields of Zr, DPAD meas. 80-39901
Ni, magnetisation spin wave and Stoner contribs. 77-73017
Ni, magnetisation temp. depend. exam. using ^{61}Ni NMR 77-73089
Ni, muon hyperfine field, cluster calc. 79-56661
Ni, $muon^+$ spin rotation, hyperfine field determ., 0.12 to 300K 77-24775
Ni, $muon^+$ spin rotation meas., local hyperfine field temp. depend. 77-63349
Ni, paramag., μ^- relax. 77-24776
Ni, positive muon spin precession, effect of press. 80-40030
Ni quadrupole interaction of vacancy associated with Te impurity, β-γ TDPAC meas. 78-43730
Ni, self implantation damaged, crit. behaviour, perturbed ang. distrib. meas. anal. 80-60476
$Ni:^{111}In$, ion implantation damage, DPAC obs. 77-59052
$Ni:^{116}Er$, hyperfine interaction of impurities, Mossbauer spectra 77-48105
$Ni:^{119}Sn$, 78-52382
$Ni:^{129m}Xe$, Mossbauer obs. of mag. hyperfine field 77-8460
$Ni:^{129}Te$, implanted atom sites, Mossbauer obs. 77-20756
$Ni:^{12}B(^{12}N)$, hyperfine field determ. by NMR 77-8418
$Ni:^{172}Yb$, hyperfine mag. field, TDPAC meas. 78-52394
$Ni:^{192}Ir$, NMR/ON, resonant freq. shift with applied field 77-28462
$Ni:^{83}Rb$, implanted atom sites and hyperfine interactions, Mossbauer obs. 77-24765
$Ni:^{86}Y$, mag. hyperfine field determ. by DPAC 77-8458
Ni:B, impurity electronic struct. calc., ^{12}B NMR data anal., magnetisation decrease 79-47046
Ni:B(N), hyperfine interactions, recoil-implanted β-NMR method *(Japanese)* 79-51865

crystal hyperfine field interactions continued
- Ni:F, ion-implanted, mag. hyperfine field, anomalous temp. depend., PAC meas. 79—4754
- Ni:F, lattice location of implanted F rel. to mag. hyperfine fields 77—59041
- Ni:Lu, nuclear orientation meas., hyperfine field 77—32308
- Ni:Ra, hyperfine field determ. 77—85622
- Ni-As, dil., temp. depend. of hyperfine field, TDPAD meas. 78—43700
- Ni-b, hyperfine interactions from 6 to 730K, ^{12}B NMR 80—29372
- Ni-Co, local mag. field on μ^+ 79—56665
- Ni-Cr, dil. alloy paramag., μ^- relax. 77—24776
- Ni-Cu, local mag. field on μ^+ 79—56665
- Ni-Cu(Zn)(Ga)(Ge)(As)(Se)(Br)(Kr), dil., ferromagnetic, hyperfine field and relax. time obs. of impurity heavy nuclei 80—75533
- Ni-Cu(Zn)(In), implantation damaged, crit. behaviour, perturbed ang. distrib. meas. anal. 80—60476
- Ni-Dy, dil., implanted impurity hyperfine interaction 78—68417
- Ni-Fe-Mo, K-effect, Mossbauer study 80—39998
- Ni-H, implanted film, resistivity and TDPAC meas. 78—39229
- Ni-In, dil., symmetry of lattice defect, DPAC meas. 78—43729
- Ni-In, dil., uncorrelated radiation damage, TDPAC meas. 78—43343
- Ni-In, elec. field gradient, at ^{111}Cd probes, temp. depend. 79—28643
- Ni-Pu, dil., effective mag. fields, temp. depend. *(Russian)* 78—43587
- Ni-Ta, dil., crit. behaviour, ^{181}Ta PAC expt. 78—43723
- Ni-Ta, dil., crit. behaviour of local magnetization, PAC and magnetisation meas. 78—48098
- $Ni_{1-x}Au_x$-Co, dil., hyperfine field and isomer shift, precip. process, Mossbauer expts. 80—25267
- $Ni_{1-x}Au_x$-Co, dil., Mossbauer effect, mag. hyperfine field 80—20528
- $Ni(ClO_4)_2\ 6H_2O$, sp. ht. between 2 and 17K 78—47532
- NiCr, hyperfine fields about μ^+ 79—56664
- $NiCr_2O_4$, ^{61}Ni Mossbauer effect studies of hyperfine interactions, mag. dipole and elec. quadrupole 78—43746
- $NiCr_2O_4$, sign of net mag. hyperfine field, ^{61}Ni Mossbauer study 80—39946
- NiFe disordered alloys, Mossbauer spectra, hyperfine mag. field distrib., Curie temp. 80—7198
- Ni_3Fe, atomic order, Mossbauer effect obs. 77—69736
- Ni_3Fe disordered alloys, Mossbauer spectra, hyperfine mag. field distrib., Curie temp. 80—7198
- Ni_3Fe, Mossbauer spectra, long range order 78—10810
- Ni_3Fe, Mossbauer spectra, order-disorder transition 78—10811
- Ni_3Fe, non-linear local environment effect, Mossbauer effect of ^{57}Fe 80—39909
- $Ni_{73}Fe_{27}$, order-disorder transition, Mossbauer study 79—95163
- $NiFe_{2-x}Al_xO_4$, ^{57}Fe and ^{61}Ni Mossbauer spectra 80—39940
- $Ni_{0.6}Fe_{2.4}B_7O_{13}I$, boracite, mag. hyperfine interactions, Mossbauer study 80—39935
- $Ni_{0.98}{}^{57}Fe_{0.02}S_{1.0}$, quadrupole splitting and ground state, Mossbauer spectra 80—29657
- $Ni_2Mn_{0.9}Fe_{0.1}Sn$, Fe site hyperfine field and mag. moment, Mossbauer effect meas. 78—76365
- $Ni_2Mn_xM_{1-x}Sn$ (M=Ti,V) mag. hyperfine fields, ^{119}Sn Mossbauer spectra study 80—55003
- NiMnSb, hyperfine mag. field at Cd impurity, TDPAC study 80—39906
- $Ni_{1+x}MnSb$, mag. hyperfine field on ^{111}Cd, TDPAC obs. 78—43709
- Ni_2MnSn, Heusler alloy, mag. interactions and cond. electron polarisation, spin echo NMR meas. 77—77125
- Ni_2MnSn(In)(Sb), Heusler alloy, hyperfine field at ^{111}Cd, TDPAC meas. 78—43705
- $Ni_2Mn_xTi_{1-x}Sn$, Mossbauer spectra, mag. hyperfine field 80—15857
- NiO, paramag. shifts of ^{19}F at O 78—43719
- NiO:^{67}Zn, perturbed ang. correl. 78—95535
- NiS_2, hyperfine parameters and quadrupole splitting determ., ^{57}Fe Mossbauer spectra 77—77131
- $NiSe_2$, hyperfine parameters and quadrupole splitting determ., ^{57}Fe Mossbauer spectra 77—77131
- $NiSe_2$, paramag. props., NMR, mag. susceptibility 80—60175
- Np intermetallics, NpM_2Si_2, (M=Cr, Mn, Fe, Co, Ni, Cu), Mossbauer and magnetization expts. 78—31138
- $NpCo_2Si_2$ and $NpFe_2Si_2$, itinerant magnetism obs. 77—28406
- $NpFe_{2-x}Co_xSi_2$, mag. and hyperfine props. 79—51887
- $NpFe_{2-x}Co_xSi_2$, mag. and hyperfine props. 80—7247
- NpM_2Ge_2 (M=Cr, Fe, Co, Ni, Cu), Mossbauer and magnetisation meas. 77—1555
- $(Np_{1-x}U_x)Fe$, Mossbauer spectra, magnetism and hyperfine interactions 80—20529
- Os, Mossbauer meas., elec. field gradients at ^{186}Os nuclei 79—47373
- Pa, Mossbauer resonance, electric field gradient 79—19823
- ^{231}Pa Mossbauer resonance, elec. field grad. 80—7207
- Pb, perturbed angular distribution of ^{208}Po, temp. depend. 78—43735
- Pb, perturbed γ-ray angular distrib. of ^{210}Po, temp. depend., radiation damage effects 78—43736
- PbF_2, gamma-ray and neutron irrad. at low temps., EPR of Pb^{3+} ions 77—63262
- $PbF_2:Gd^{3+}$, EPR and ENDOR of Gd^{3+} at cubic sites 80—7161
- $PbF_2:Yb^{3+}$, superhyperfine interaction, ENDOR and RF discrete saturation expts. 79—73856
- $Pb_5Gd_3O_{11}$, trigonal Gd^{3+} centre structure 79—69720
- $Pb_5Ge_3O_{11}$, ESR of Fe^{3+} ions 79—95639
- $Pb_5Ge_3O_{11}:Gd^{3+}$, discrete saturation of ESR, due to superhyperfine interaction 77—28440
- $Pb_5Ge_3O_{11}:Gd^{3+}$, EPR hyperfine struct. 79—82867
- $PbHfO_3$, elec. field gradient, crit. behaviour, DPAC meas. 78—80303
- $PbHfO_3$, elec. quadrupole interaction, temp. depend., DPAC meas. 79—51884
- $PbI_2:M^{2+}$, M=V, Mn, Co, EPR 78—68362
- $PbZr_{1-x}Hf_xO_3$, crystal field distortion by impurities, PAC meas. 80—11306
- $PbZrO_3$:^{89}Zr, electron capture decay lifetime, struct. environment effects 77—28523
- Pd, muon depolarisation, hyperfine anomaly 77—28503
- Pd:^{111}Cd, radiation damage in DPAD expts., quad. interaction 77—27917
- Pd-Co, dil., Mossbauer emission spectra, fast relaxation regime, ^{57}Co hyperfine field 78—60362
- Pd-Co, Mossbauer effect under press. for ^{119}Sn impurity atoms and hyperfine mag. field model *(Russian)* 77—55742
- Pd-Co, very dil., Mossbauer emission spectra of ^{57}Co, relax. effects 80—29656

crystal hyperfine field interactions continued
- Pd-Er, dilute alloy, EPR spectrum, effect of fine and hyperfine interactions 78—19323
- Pd-Fe, del. alloy, Mossbauer obs., 0.018-300K 77—69740
- Pd-Fe, highly dil., mag. behaviour, 0.06-300K, Mossbauer expt. 78—43711
- Pd-Fe, Mossbauer effect under press. for ^{119}Sn impurity atoms and hyperfine mag. field model *(Russian)* 77—55742
- Pd-Fe, Mossbauer spectra, scatt. and transmission geometries, differences in crit. behaviour near T_c 78—76367
- Pd-Fe, Pd-Fe-H and Pd-Fe-D, Mossbauer effect, internal hyperfine field temp. depend. 77—12283
- Pd-Fe, very dil., Mossbauer emission spectra, relax. effects 80—66084
- Pd-Fe alloys, dil., spin polarisation effect on hyperfine interactions, anal. of Mossbauer meas. *(Russian)* 79—47055
- Pd-H-Fe, Mossbauer effect, hyperfine field, effect of changing spin susceptibility 77—20494
- Pd-Ni, local susceptibilities, ^{61}Ni Mossbauer spectroscopy 78—95536
- Pd-Rh, dil., hyperfine anomaly between bound negative muon and Rh nucleus 79—56707
- $(Pd_{1-x}Au_x)_{0.99}Co_{0.01}$, mag. hyperfine interaction for impurity Co atoms *(Russian)* 80—7078
- Pd_3Fe, hyperfine interactions during atomic ordering, Mossbauer obs. *(Russian)* 78—56630
- PdH_x-Fe, dil., Kondo system, local moment hyperfine studies, Mossbauer expt. 80—39908
- $PdH_xFe_{0.003}$, Kondo system, local moments, hyperfine fields, Mossbauer study 80—80478
- PdHg-Rh, dil., quadrupole interaction of ^{100}Rh 79—99520
- Pd_2MnIn (Sn)(Sb), Cd impurities, hyperfine field meas. 78—15074
- $Pd_2MnIn_{1-x}Sb_x(Sn_x)$, Heusler alloy, Mossbauer effect exam., mag. coupling 79—69755
- $Pd_2MnIn_{1-x}Sb_x(Sn_x)$, Heusler alloy, Mossbauer effect exam., hyperfine interactions in ferromag. phase 79—69756
- $Pd_2MnIn_{1-x}Sn_x$-Cd, dil., Heusler alloy, hyperfine mag. field on Cd, TDPAC obs. 79—8075
- PdMnSb, Heusler alloy, hyperfine fields of 5sp shell impurities substituting Sb, Mossbauer spectra 78—80261
- PdMnSb, hyperfine field at ^{125}Te, Mossbauer expts., compared with Jena-Geldart model 78—43707
- PdMnSb, Pd_2MnSb, Heusler alloys, ^{129}I mag. hyperfine struct., Mossbauer meas. 79—33580
- $Pd_{1+x}MnSb$ Heusler alloys, magnetic hyperfine fields on ^{111}Cd, TDPAC and magnetisation meas. 80—93219
- Pd_2MnSb and PdMnSb, Heusler alloy, hyperfine field at ^{111}Cd, TDPAC meas. 78—43705
- Pd_2MnSb, Heusler alloy, hyperfine fields of 5sp shell impurities substituting Sb, Mossbauer spectra 78—80261
- Pd_2MnSb, mag. hyperfine field of ^{129}I, Mossbauer spectra 78—43706
- Pd_2MnSb:^{119}Sn, ferromag., mag. hyperfine structure, Mossbauer obs. 77—32309
- Pd_2MnSn, Heusler alloy, mag. interactions and cond. electron polarisation, spin echo NMR meas. 77—77125
- $Pd_2Mn_{0.95}Sn_{1.05}$, hyperfine mag. fields, Mossbauer spectra 80—15870
- $Pd_2Mn_{0.98}Sn_1In_{0.02}$, Heusler alloy, hyperfine fields at sp elements, spin echo NMR meas. 78—84496
- $Pd_2MnSn_{1-x}Sb_x$, Heusler alloy, Mossbauer effect exam., hyperfine interactions in ferromag. phase 79—69756
- $PdPb_2$-Rh, dil., quadrupole interaction of ^{100}Rh 79—99520
- PdSb-Rh, dil., quadrupole interaction of ^{100}Rh 79—99520
- $Pd_{80-x}Si_{20}Fe_x$, amorphous, low x, hyperfine interactions and mag. ordering temp. 79—15303
- PdTe-Rh, dil, quadrupole interaction of ^{100}Rh 79—99520
- Pr, soft mode excitation behaviour under press., long range order 80—39838
- $PrAlO_3$, tetragonal, mag. props. 77—90052
- $PrBe_{13}$, hyperfine enhanced nuclear mag. cooling 79—63216
- $PrCl_3$, one-dimensional X-Y system, far IR absorpt. spectra, cooperative spin excitations 78—95584
- $PrCl_3$, rare earth ion overlap in crystal field theory, configuration interaction 80—44552
- PrEu(Gd), magnetic interactions, Mossbauer spectra quadrupole splitting, crystal field parameters 80—39907
- $PrFe_2$, Curie temp., elec. quadrupole couplings, Mossbauer study 80—39949
- $PrFe_2$, high field Mossbauer study 80—75893
- $PrFe_2$, Laves phase, mag. props., Mossbauer spectra, crystalline field mag. anisotropy 80—65851
- $PrIn_3$, two stage nuclear demagnetization experiments 79—65644
- $PrIr_2(Pt_2)(Rh_2)(Ru_2)$, hyperfine sp. ht. and magnetisation meas. at 4.2K 80—75775
- $PrNi_5$, two stage nuclear demagnetization experiments 79—65644
- Pr_3Tl, hyperfine interactions, sp. ht. and magnetisation meas. 79—28531
- $PrVO_4$, NMR of ^{141}Pr and ^{51}V 77—77110
- Pt:^{181}Ta, lattice defect induced elec. field gradient, PAC meas. 79—42878
- Pt-Fe, very dil., Mossbauer emission spectra, relax. effects 80—66084
- Pt-In, dil., damage induced quadrupole interactions, DPAC exam. 78—39465
- Pt-In, dil., radiation damage heating, TDPAC exam. 78—39466
- Pt-Mn dilute alloy, cubic foil, Mn spin behaviour, nuclear orientation technique 78—27044
- Pt-Mn-Sn alloy, mag. hyperfine fields 79—1737
- PtMnSb, hyperfine mag. field at Cd impurity, TDPAC study 80—39906
- PtMnSn, ^{197}Au and ^{119}Sn hyperfine fields, Mossbauer expt. 78—72439
- PtMnSn(Sb) Cd impurities, hyperfine field meas. 78—15074
- α-quartz:Ge,Ag^+, Ag-compensated Ge centre, EPR meas. 77—77098
- α-quartz:P, X- and γ-irradiated, EPR studies of phosphoric ion 77—63263
- RM_4Al_8 (M=Cr, Mn, Fe, Cu), magnetism and hyperfine interactions 80—25256
- $RbAl(SO_4)_2.12H_2O$, spin-Hamiltonian with trigonal S^3I terms for describing $^{57}Fe^{3+}$ ENDOR spectra 80—75885
- $RbCdF_3$, Fe^{3+}-O^{2-} pair EPR probe for struct. phase changes 77—36113
- RbCl, F-centre ESR in relaxed excited state, isotropic superhyperfine interaction consts. 79—65733
- RbCl:Au, EPR and optical absorpt. 78—39397
- RbCl:H, dynamical superhyperfine interaction 80—2663
- RbCl:Na, U-centres, HFS consts., g-factors, EPR spectra 80—39869
- Rb_2CrCl_4, NMR of ^{53}Cr 78—10798

crystal hyperfine field interactions continued
$Rb_2CuBr_4.2H_2O$, ferromag., hyperfine and exchange interactions, NMR study 80−50208
$(Rb)_2CuBr_4.2H_2O$, hyperfine and super-exchange interactions 80−103654
$Rb_2CuCl_4.2H_2O$, BCC Heisenberg ferromag., transferred hyperfine interactions of ^{1}H, ^{1}D and ^{17}O 77−69725
$Rb_2CuCl_4.2H_2O$, Bloch-wall NMR, anisotropic hyperfine interaction 79−51864
$Rb_2CuCl_4.2H_2O$, ferromag., hyperfine and exchange interactions, NMR study 80−50208
$Rb_2CuCl_4.2H_2O$, hyperfine and super-exchange interactions 80−103654
$Rb_2CuCl_4.2H_2O$, NMR spectra, second-order effects of mag. hyperfine interaction, pseudoquadrupole interaction 79−78540
$Rb_2Cu(SO_4)_2.6H_2O$, single cryst., fine struct., mag. dipole coupling, EPR obs. 78−68360
$Rb_2CuX_4.2H_2O$, (X=Cl, Br), fine struct. due to indirect coupling of nuclear spins 79−78541
$RbF+Eu^{2+}$, cryst., hyperfine splitting, EPR 78−2733
$(RbF)_n$-FeF_3, antiferromagnetic systems, dimensionality and spin reduction effects, Mossbauer study 80−39947
$RbFeCl_3.2H_2O$, rectangular Ising cpd., Mossbauer meas. 80−71252
$RbFeF_3$, Mossbauer spectra, mag. phases 80−15878
$RbFeF_4$, Mossbauer spectra, struct. and hyperfine field 77−12266
Rb_2FeF_5, 1D antiferromagnetic system, Mossbauer investigation 78−95533
Rb_2FeF_5, Mossbauer spectra, 1D antiferromag. 80−15886
Rb_2FeF_5, one-dimensional antiferromag. systems, Mossbauer studies 80−71266
$RbFeS_2^{+}$, ^{57}Fe Mossbauer hyperfine interaction, covalency effects, point charge model 78−39484
$RbGa(SO_4)_2.12H_2O$, spin-Hamiltonian with trigonal S^3I terms for describing $^{57}Fe^{3+}$ ENDOR spectra 80−75885
Rb_2IrCl_6, hyperfine spectra of mag. ordered state at very low temp., Mossbauer meas. 77−69744
$RbMnF_3$, nuclear spin waves spectra, relaxation, parametric excitation, NMR dynamic shift *(Russian)* 80−11180
$RbNiFeF_6$, pyrochlore, Mossbauer spectra in paramag. and mag. ordered states 77−52003
$RbReO_4$, quadrupole coupling, cation electric field gradients 78−35060
Re, Mossbauer meas., elec. field gradients at ^{186}Os nuclei 79−47373
Re:Ir, electric quadrupole orientation of $^{186,188\text{-}190}$Ir 80−78140
Re-Hg, dil., anomalously high elec. field gradients below 0.05K 78−72442
$ReNCl_4^{-}$, EPR in $Ph_4As[RuNCl_4]$, hyperfine splitting and spin Hamiltonians 78−64272
Rh_2CoSn, ferromag., crit. exponent of ^{119}Sn hyperfine field, Mossbauer obs. 78−92008
Rh_2CoSn, ferromag., mag. hyperfine fields of ^{119}Sn, Mossbauer meas. 78−10816
Rh_2CoSn, ferromag. Heusler alloys, hyperfine fields, spin echo meas. 77−63314
Rh_2CoSn, hyperfine mag. fields at ^{119}Sn, under press., Mossbauer expts. 79−99812
Rh_2FeSn, ferromag., mag. hyperfine fields of ^{119}Sn, Mossbauer meas. 78−10816
Rh_2FeSn, ferromag. Heusler alloy, hyperfine fields, spin echo meas. 77−63314
Rh_2FeSn, Heusler alloy, Sn and Fe hyperfine field, Mossbauer exam. 77−43920
Rh_2FeSn, hyperfine mag. fields at ^{119}Sn and ^{57}Fe, under press., Mossbauer expts. 79−99812
Rh_2MnGe, ferromag. Heusler alloy, hyperfine mag. field meas. by TDPAC technique 79−78580
$Rh_2MnGe(Pb)$, hyperfine mag. field at Cd impurity, TDPAC study 80−39905
Rh_2MnPb, hyperfine fields, ferromag., NMR and Mossbauer effect studies 80−71259
Rh_2MnSb, hyperfine fields, ferromag., NMR and Mossbauer effect studies 80−71259
Rh_2MnSn, ferromag. Heusler alloy, hyperfine fields, spin echo meas. 77−63314
Rh_2MnSn, ferromag. Heusler alloy, hyperfine mag. field meas. by TDPAC technique 79−78580
Rh_2MnSn, Heusler alloy, Sn hyperfine field, Mossbauer exam. 77−43920
Rh_2MnSn, mag. hyperfine fields at Rh and Sn sites, and their temp. depend. 78−43708
Rh_2MnSn, Rh_2NiSn, Heusler alloys, hyperfine mag. field at Sn 78−39482
Ru_2FeSn, ferromag. Heusler alloys, hyperfine fields at nonmagnetic atoms in various sites, Mossbauer effect and NMR meas. 80−66089
Ru_2FeSn, hyperfine mag. field, Mossbauer spectra 80−15865
Sb compounds, Mossbauer effect, isomer shifts, quadrupole splitting, CNDO/II calcs. 77−24766
Sb, quadrupole interaction of ^{69}Ge, TDPAD expts. 78−48089
Sb:^{111}Cd, quad. interac. temp. depend. 77−59487
Sb:^{111}Cd,In, elec. field gradient, TDPAC expts. 80−55002
Sb-Hg, quadrupole interaction, time differential perturbed ang. correl. and nucl. orientation 79−24250
SbSn, ^{120}Sb elec. quadrupole interaction, temp. depend. 78−19399
Sc, electric field gradient of ^{181}Ta substitutional atoms, press. depend. 78−52385
Sc-Fe(ru)(Au), dil., elec. field gradient, Mossbauer meas. 80−80665
Sc-Ir, dil., elec. field gradient at ^{193}Ir, Mossbauer meas. 80−66090
Sc-Ru, elec. field gradient and temp. depend. TDPAC meas. 80−60477
$ScFe_2$, Mossbauer effect of ^{57} Fe 80−75903
$ScFe_2H_2$, Mossbauer effect of ^{57}Fe 80−75903
Sc_3In, itinerant electron ferromag., NMR and relax. 78−6586
Si, deep and shallow levels of muonium, electronic struct. 78−39051
Si, divacancy, hyperfine interactions from ENDOR meas. 79−42868
Si, electron irradiated, EPR of C-O divacancy complex 77−69691
Si, extended Huckel theory calc. of hyperfine interactions of positive divacancy 77−89742
Si, extended Huckel theory calculations for positive divacancy 78−87938
Si, hyperfine interaction of divacancies, ENDOR meas. 77−4579
Si, implanted ^{222}Rn TIPAC measurements 78−43732
Si, muon state, muon spin rot. exam. 78−60373
Si, μSR, spin Hamiltonian and anomalous muonium states 80−71286
Si:^{119}Te(^{119}Sb), implanted atom site changes with time, Mossbauer obs. 77−20757

crystal hyperfine field interactions continued
Si:^{57}Co, ion-implanted, Mossbauer study, annealing effects 80−7231
Si:^{57}Fe, quadrupole interac. 78−92005
Si:Au, EPR spectrum, strong nucl. quadrupole effect 80−93172
Si:P, heavily doped, EPR spectra of electron irradiation induced defects 77−81008
Si:P(Sb), electron-nucl. interaction under optical pumping, ^{29}Si optical polarisation meas. 79−95680
Si:Sb(P)(As), shallow donor electrons, hyperfine interactions, reply to Onffroy's calcs. 78−51934
Si:Sn, Mossbauer study of defects due to ^{119}In implantation 80−80641
Si_3N_4:Fe, α- and β-phases, Mossbauer and Raman obs. of state of Fe 79−33572
SiO_2, g-tensor and ^{29}Si hyperfine tensors of E_1'-centre for model of O^{-} vacancy 79−19777
SiO_2, glass, ^{29}Si hyperfine struct. of E′ centre, microwave saturation props. 80−7165
SiO_2, glass, irrad., EPR of Al E_1' centres 80−11268
SiO_2, implanted ^{222}Rn TIPAC measurements 78−43732
SiO_2, vitreous, irradiated, EPR exam. of H_2 hyperfine spectra 79−28611
Sm-Al(Fe)(Co)(Pt), hyperfine field exam. by NMR spin echo 78−23365
Sm-Eu alloy, dil., mag. and elec. hyperfine interac., TDPAD obs., paramag. behaviour, exchange integral 80−103908
$SmAl_2$, hyperfine fields, ferromagnetic coupling between rare earth spins, NMR study 80−39880
$SmFe_2(Co_2)(Ni_2)$, hyperfine interactions and exchange fields acting on Eu^{3+}, Mossbauer obs. 77−63338
$Sm_{1-x}Gd_xAl_2$, hyperfine fields, ferromagnetic coupling between rare earth spins, NMR study 80−39880
Sn, ^{69}Ge TDPAD, search for isotopic mass effect on quadrupole coupling consts. 78−43725
β-Sn, anisotropy of Mossbauer effect and quad. splitting 77−12268
Sn complex containing P, $L_2Sn(CH_3)_nCl_{4-n}$, Mossbauer parameters, quadrupole splittings *(Russian)* 78−76362
Sn compounds, Mossbauer effect, isomer shifts, quadrupole splitting, CNDO/II calcs. 77−24766
Sn, elec. field gradient on Cd, press. depend., TDPAC expts. 78−48092
Sn, electric field gradients of recoil-implanted ^{19}F via ^{9}Be(^{12}C, np)^{19}F 77−8471
Sn, electric field gradient, Debye model calc. 80−49682
Sn, quadrupole interaction of ^{69}Ge, TDPAD expts. 78−48089
Sn:^{117}In, quadrupole interaction temp. depend. 77−8470
Sn:^{120}Sb, elec. qudrupole interaction, perturbed ang. distrib. method 79−99799
Sn:^{67}Ge, elec. quadrupole interaction temp. depend., PAC meas. 79−42877
Sn:^{67}Ge, quadrupole interaction temp. depend. 77−12264
Sn:^{99}Ru, quadrupole interaction temp. depend., PAC method, electric field gradients 77−73105
$SnMo_6S_8(Se_8)$ Chevrel phase supercond., hyperfine interaction, microscopic study 79−56650
$SnO_2:Mo^{5+}$, hyperfine and superhyperfine interactions, EPR 77−8398
$SnO_2:V^{4+}(Cr^{3+})(Mo^{5+})(Nb^{4+})(Re^{4+})$, direct mechanism in supertransferred hyperfine interaction 79−23936
$SnO_2:W^{5+}$, EPR parameters, g hyperfine and superhyperfine tensors 77−85560
$SnO_2(F_4)$, elec. field gradient at Sn^{4+} site, Mossbauer quadrupole splitting and anionic polarisability calc. *(French)* 79−15384
$Sn_{1-x}Pb_xSe(Te)$ films, Mossbauer effect of ^{119}Sn, spectral characts., conc. depend. 80−103903
$SrCl_2:Gd^{3+}$, hyperfine interaction, X-band ENDOR 80−60457
$SrCoO_3:Fe^{4+}$, ferromag., sign of Fe^{4+} hyperfine field, spin struct., Mossbauer study 80−39933
$SrEu_2Fe_2O_7$, ferrite, Mossbauer effect study of hyperfine interactions, spin reorientation 78−19383
SrF_2, mag. hyperfine const. and lattice distortion of V_k-centre 77−62864
$SrF_2:Cd^{2+}$, X-irrad., ESR of Cd^{+} centres 77−59459
$SrF_2:Eu^{2+}$, ENDOR of ^{19}F ligands, under uniaxial stress 77−16207
$SrF_2:Eu^{2+}$, superfine struct. in EPR obs. 77−1593
$SrF_2:Tb^{3+}$, mag., thermal and hyperfine props. 80−29368
$SrF_2:Tm^{2+}$, modulation magnetooptic spectroscopy of cross-relaxation resonances 79−15381
SrF_2:Yb, superhyperfine interaction of trigonal Yb^{3+} centres 78−27117
$SrFe_{12-x}Cr_xO_{19}$, effects of substitution of Fe by Cr, Mossbauer spectra 80−2674
$SrFe_{12-x}Cr_xO_{19}$, hexagonal ferrite series, Mossbauer study 80−71258
Sr_2FeEuO_5, ^{57}Fe Mossbauer study 80−39976
$Sr_{1-x}La_xFeO_3$, Mossbauer spectra, charge disproportionation 80−20542
SrO, neutron-irradiated single cryst., F^{+} centres, ENDOR obs. 80−15824
$SrO:Ni^{+}(Cu^{2+})$ noncentral Jahn-Teller ion, coupled polar-tetragonal strains 80−44555
$SrO:Pb^{2+}(Bi^{3+})$, impurity centres vibronic spectra, lattice dynamics and electron-phonon interactions 80−7396
SrO-Fe_2O_3, EMF meas. with solid state cell, Mossbauer effect and magnetic props. *(Korean)* 77−28493
$SrTb_2Fe_2O_7$, ferrite, Mossbauer effect study of hyperfine interactions, spin reorientation 78−19383
$SrTb_2Fe_2O_7$, Mossbauer spectra, hyperfine parameters, ordering temp. 77−90079
$SrTiO_3$:^{181}Ta, quadrupole interaction, $\gamma\gamma$ cascade PAC meas. 77−81042
Sr_2YRuO_6, ^{99}Ru Mossbauer spectra and other techniques 80−29659
Ta, nucl. acoustic reson. determ. 79−51868
TaS_2 intercalated with NH_3, charge transfer, PAC meas. 78−76366
TaS_2, TDPAC meas., CDW, structural and charge transfer effects 78−39468
TaS_2(1T)(2H), nucl. quadrupole interactions, high press. effects 78−35072
TaS_2.Sn, intercalated, Mossbauer effect, hyperfine interaction, lattice dynamics 77−8473
1T-$TaSe_2$, CDW obs. by ^{181}Ta Mossbauer effect 78−39469
Tb, ferromagnetic, mag. dipole and elec. quadrupole hyperfine fields, NMR obs. 80−34791
Tb-Al(Ag), hyperfine field exam. by NMR spin echo 78−23365
Tb-Ta(Cd), elec. quadrupole interaction, temp., and press. depend., TDPAC meas. 80−60469
$TbAl_2$, conduction electron spin and orbital polarisation effects 78−80228
TbF_3, ^{19}F NMR, ligand hyperfine interaction, shift tensor determ. 78−48056
TbF_3, transferred hyperfine interaction, NMR study 78−68393

crystal hyperfine field interactions continued
TbGa garnet, mag. ordering induced by hyperfine interactions, neutron diffr. meas. 77–66265
$Tb_3Ga_5O_{12}$, hyperfine interac. induced antiferromag. order *(French)* 77–59392
$Tb_{1-x}Gd_xAl_2$, effective mol. field at ^{159}Tb, NMR meas. 80–71197
TbO_2:Dy^{3+}, mag. hyperfine interaction, PAC expt. 78–35069
$Tb(OH)_3$:Er^{3+}, g-values and hyperfine interaction parameters, calc. for Er^{3+} 79–15123
$TbSi_2$, γ-γ ang. correl. obs. of polymorphic transition, 200-900°C 80–29653
Tc:^{51}Fe, dilute, quadrupole splitting and isomer shift 78–48096
Tc-Fe alloy, Mossbauer spectra, hyperfine field 80–20526
Te complexes of thiourea, Mossbauer spectra 80–15914
Te, quadrupole interaction for ^{129}I, ^{131}I, and ^{132}I, PAC expts. 78–48087
Te, quadrupole interaction of 81 keV state of ^{133}Cs and 247 keV state of ^{111}Cd, TDPAC expts. 78–48088
Te, quadrupole interaction at ^{181}Ta, TDPAC meas. 80–20521
Te, trigonal, ^{129}I Mossbauer obs. at high press. 80–55005
Te:^{111}Cd, quad. interac. temp. depend. 77–63324
Te:^{125}Te, PAC, quad. moment of $9/2^-$, 321 keV level of $_{52}{}^{125}Te_{73}$ 77–28488
TeSn, ^{115}Te elec. quadrupole interaction, temp. depend. 78–19399
Th_4D_{15}, NMR relax. expts., diffusion processes and hyperfine fields 79–8066
ThO_2:Gd^{3+}, ENDOR, nuclear mag. moment and HFS, stress-induced splitting 77–51990
ThO_2:Yb^{3+}, trigonal sites of Yb^{3+}, ENDOR meas. 79–95677
$ThRu_2$:Nd^{3+}, supercond. state, ESR investigation 79–78514
Ti^{2+}, doped ion in divalent metal cpds., correl. between Szigeti charge and hyperfine coupling consts. 80–96832
Ti:^{57}Fe, quadrupole interaction, Mossbauer and PAC meas. 77–48101
Ti-Ir, dil., elec. field gradient at ^{193}Ir, Mossbauer meas. 80–66090
TiO_2:$Mn^{2+}(Mn^{4+})$, anatase single cryst., ESR spectra at 77K, 300K 78–10764
TiO_2:Mo^{5+}, interstitial EPR, g-tensor and hyperfine tensor 80–84647
Tl, quadrupole interaction of ^{69}Ge, TDPAD expts. 78–48089
Tl-Cd, dil., quadrupole interaction, γ-γ ang. correl. meas. 79–56629
Tm-3d transition metal intermetallics, ^{169}Tm Mossbauer effect 80–71261
TmAG, Mossbauer study of crystal field props. 80–66082
$Tm_3Al_5O_{12}$:Yb^{3+}, g-shift meas., EPR 78–56376
$Tm_3Ga_5O_{12}$, Mossbauer study of crystal field props. 80–66082
TmH_3, ^{169}Tm Mossbauer study 80–44976
TmTe, hyperfine struct. of Tm^{2+}, Mossbauer spectra 78–76368
$TmVO_4$, type crystals with cooperative Jahn-Teller effect, acoustic NMR *(Russian)* 77–28460
$TmZn_2$, Mossbauer effect meas. in antiferromag. and paramag. states 80–71265
U complex, $U(acac)_4$, cryst. fields, mag. susceptibility, chem. shift *(French)* 78–84179
U, electric field gradient, of ^{181}Ta substitutional atoms, press. depend. 78–52385
U tetragonal compounds, mag. props. 80–15704
U^{3+}, U^{4+}, shielding factors, cryst. field effects 80–10926
UH_3, hyperfine splitting of proton determ. by inelastic neutron scatt. 77–43814
V^{2+}, doped ion in divalent metal cpds., correl. between Szigeti charge and hyperfine coupling consts. 80–96832
V^{4+}, cryst. field effect on ESR parameters 77–36116
V^{4+} ion complexes in diamagnetic crystals, ground state wavefunctions, hyperfine interaction parameters, EPR meas. 78–19311
V^{4+} on tetragonally distorted tetrahedral sites, Jahn-Teller effect and hyperfine parameters 77–69276
$V^{2+}F^-$, $V^{2+}F^-V^{2+}$ π-electron systems, transferred hyperfine interaction, HF calc. 80–24859
VO_2, electronic struct., quadrupole coupling, Mulligen-Wolfsberg-Helmholtz calcs. 78–87948
V_2O_{3+x}, nonstoichiometric, microscopic mag. props., NMR and inelastic-spin-flip neutron scatt. 79–38323
V_2O_5-TeO_2 glasses, ESR spectra 78–10755
V_3O_7, hyperfine interactions, inelastic spin flip neutron scatt. 77–28372
V_3O_7, microscopic mag. props., NMR 80–7177
V_4O_7, sublattice magnetisation temp. depend., ^{51}V NMR 79–91301
$mV_2O_5.(100\text{-}m)P_2O_5$, (m=100-2), V(IV) complexes conc., absorpt. and ESR spectra 78–64266
V_3S_4, antiferromag. order, ^{51}V NMR spectrum 79–56625
V_5S_8:Fe, Mossbauer and mag. studies, electronic state of Fe 80–108130
V_3Se_4, antiferromag. order, ^{51}V NMR spectrum 79–56625
WC recoil implantation damage, PAC obs. 77–85620
WO_3, recoil implantation damage PAC obs. 77–85620
WO_3, single cryst. and amorphous film, ESR of defects 78–10770
Y-Co, hyperfine fields, NMR spin echo 77–63318
Y-Ir, dil., elec. field gradient at ^{193}Ir, Mossbauer meas. 80–66090
Y-Ru, elec. field gradient and temp. depend. TDPAC meas. 80–60477
YAG, electrostatic model of cryst. field 80–59945
YAG:Gd^{3+}, EPR absorpt. spectrum 78–76305
$YAlO_3$:Pr, hyperfine interaction in lowest levels of $^3H_4$ and $^1D_2$ states 79–78065
$(Y_{3-x}Ca_x)(Fe_{2-x}Sn_x)(Fe_3)O_{12}$, long and short range magnetic order 79–38419
$Y_{3-x}Ca_x[Fe_{2-x}Sn_x]Fe_3O_{12}$, Mossbauer spectra, Sn hyperfine mag. field 80–15893
YCo_5, NMR enhancement of modulating field due to anisotropic component of hyperfine field 77–55729
Y_xCo_y, NMR meas. of ^{59}Co 77–85585
$YCrO_3$, antiferromag., mag. domain walls, ^{53}Cr NMR study 79–11327
$Y_{1-x}Dy_xCo_5$, NMR meas. of ^{59}Co 77–85585
YFe_3, NMR investig. of Y hyperfine field temp. depend. 77–4567
Y_2Fe_{17}, Mossbauer effect, 5 to 300K 77–85634
$Y(Fe_{1-c}Al_c)_2$, mag. and Mossbauer study, local environment effects 78–27033
$Y(Fe_xAl_{1-x})_2$, Mossbauer spectra and mag. props. 80–39950
$Y(Fe_{0.022}Co_{0.978})_2$ mag. props., Mossbauer expts., 0.15-4.2K 78–43712
$Y(Fe_{1-x}Co_x)_2$, mag. hyperfine field, conc. depend., Mossbauer expts. 77–63337
$Y(Fe_xCo_{1-x})_2$, $0.5 \geq x \geq 0.2$, Mossbauer effect meas., 5 to 300K *(German)* 77–24771
$Y(Fe_xCo_{1-x})_2$, Mossbauer effect at 78 and 300K, ^{57}Fe hyperfine fields 80–2677
$Y_2(Fe_{1-x}Co_x)_{17}$, hyperfine interactions, Mossbauer effect 78–2780

crystal hyperfine field interactions continued
$Y(Fe_{1-x}Ir_x)_2$, magnetisation, mag. hyperfine field 80–20531
$Y_2(Fe_{1-x}Ni_x)_{17}$, hyperfine splitting, constant Fe moment evidence 78–6614
$Y_{1-x}Gd_xCo_2$, NMR meas. of ^{59}Co 77–85585
$Y_{1-x}Gd_xCo_2$, NMR of ^{59}Co 78–52376
$(Y_{1-x}Gd_x)_2Co_{17}$, ^{59}Co NMR, hyperfine fields and contrib. of 4f electrons 77–20727
$Y_{1-x}Ho_xCo_5$, NMR meas. of ^{59}Co 77–85585
YIG, Al substituted, transferred hyperfine fields, Mossbauer effect meas. 79–1726
YIG, electrostatic model of cryst. field 80–59945
YIG, hyperfine parameters, Huckel theory calc. 80–39542
YIG octa- and tetra-sublattices, anisotropy of effective mag. field at ^{57}Fe *(Russian)* 80–10929
YIG, press. depend. of effective mag. fields on ^{57}Fe nuclei 78–52383
YIG:Gd^{3+}, mag. relax., hyperfine field interactions, PAC expts. 78–27128
YIG:Si(Ge), effects of nontrigonal cryst. field on spectroscopic props. of Fe^{2+} ions 80–92864
YM_2:Nd^{3+}, M=Rh, Ir, Pt, ESR investigation 79–78514
YM_4Al_8 (M=Cr, Mn, Fe, CU), magnetism and hyperfine interactions 80–25256
$Y(OH)_3$:Er^{3+}, g-values and hyperfine interaction parameters, calc. for Er^{3+} 79–15123
YPO_4:Pb^{3+}, EPR, hyperfine interactions 80–108050
YbAG, electrostatic model of cryst. field 80–59945
$YbAl_3$, Mossbauer effect obs. of induced hyperfine field 78–52396
$YbAl_3$, valence instabilities 79–78546
YbCuAl, intermediate-valent, nucl. reson. and relax. 79–78550
$YbCu_2Si_2$, valence fluctuation and temp. depend. of Cu nuclear quadrupole interaction 80–15818
$YbFe_2$, Curie temp., elec. quadrupole couplings, Mossbauer study 80–39949
$YbFe_2$, high field Mossbauer study 80–75893
$YbFe_2$, Mossbauer spectra, cryst. elec. field and exchange interaction 79–47368
$Yb_2Ti_2O_7$, cryst. field props., Yb^{3+} hyperfine spectra, Mossbauer effect meas. 78–67990
$Yb_2Ti_2O_7$, crystal field props., ^{170}Yb Mossbauer spectroscopy 79–4750
^{170}Yb in some metal and metal-like compounds, Mossbauer study, isomer shift and intermediate valence state 79–33569
Zn, EFG sign at ^{69m}Zn site 77–59492
Zn, elec. field gradient on Cd, press. depend., TDPAC expts. 78–48092
Zn, electric field gradients of recoil-implanted ^{19}F via ^{9}Be(^{12}C, np)^{19}F 77–8471
Zn, Mossbauer spectra, quadrupole interaction 80–7206
Zn, naive model for electric field gradient 78–91650
Zn, nuclear quadrupole alignment of $^{69}Zn^m$ 78–48090
Zn, nuclear quadrupole antishielding effects, ab initio theory 78–34814
Zn, quadrupole interaction, ^{67}Zn Mossbauer expt. 78–27120
Zn, quadrupole interaction of ^{67}Ge and ^{71}Ge, TDPAC meas. 78–43740
Zn, quadrupole interaction of ^{12}B and ^{12}N 78–47750
Zn, quadrupole interaction for ^{129}I, ^{131}I, and ^{132}I, PAC expts. 78–48087
Zn, quadrupole interaction at ^{181}Ta, TDPAC meas. 78–52392
Zn:^{115}In, 828 keV state, elec. quadrupole interaction meas. 77–8484
Zn:^{67}Ge, elec. quadrupole interaction temp. depend., PAC meas. 79–42877
Zn:^{67}Ge, quadrupole interaction temp. depend. 77–12264
Zn:^{69}Ge, quad. interac., rad. damage effs. during PAC obs. 77–27918
Zn:^{99}Ru, quadrupole interaction temp. depend., PAC method, electric field gradients 77–73105
Zn-Ag, dil., elec. field gradient, temp. depend. 78–39481
Zn-Hg, dil., anomalously high elec. field gradients below 0.05K 78–72442
$ZnAl_2S_4$:Fe(Mn), superhyperfine interaction of Mn and Fe, ESR spectra 77–63271
$ZnCO_3$:Fe^{2+}, electronic relaxation, Mossbauer effect 78–19385
$Zn_xCu_{1-x}Fe_2O_4$, mag. props., Mossbauer spectra 79–87344
ZnF_2:Co^{2+}, Raman tensor calcs. of isolated impurity in diamagnetic matrix 80–76025
$Zn_xFe_{3-x}O_4$, collective electron states, ^{57}Fe Mossbauer meas. 77–69748
$Zn_xFe_{3-x}O_4$, cond. mechanism, collective electron description 77–4588
$Zn_{0.3}{}^{2+}Mn_{0.7}{}^{2+}Mn_y{}^{3+}Fe_{2-y}{}^{3+}O_4$, Mossbauer hyperfine field meas. 77–81033
$Zn(NH_3)_4(ClO_4)_2$:Mn, EPR study of Mn^{2+} detection of structural transition 79–87308
$Zn_xNi_{1-x}Fe_2O_4$, Mossbauer spectra, mag. hyperfine struct. 80–15877
ZnO:Cu,H, motional effects in EPR spectra 78–80207
ZnS:Co Mossbauer source, Fe^{2+} abnormal populations and vibronic props. 80–15912
ZnS:Mn^{2+}, $^4T_2$ level, Zeeman splittings, Jahn-Teller effect 80–40141
ZnS:Mn^{2+}, cubic, EPR, ENDOR 77–77093
ZnSe:Mn^{2+}, ligand HFS calcs., EHT-SCCC, scattered-wave, LCAO methods, comparison with expt. 77–55501
ZnSe:Ti^{2+}, EPR meas. 80–80594
ZnSe+Mn^{2+}, LCAO calc. of d-orbital splitting 77–28148
$ZnSiF_6.6H_2O$:Co, influence of hydrostatic press. on Co^{2+} EPR spectrum 78–27084
ZnTe:Mn^{2+}, forbidden transitions of Mn^{2+} induced by hyperfine interactions 80–60458
$(Zr,Hf)Fe_2$, mag. hyperfine field at Hf sites, TPDAC meas. 79–82901
ω-Zr, electric field gradients at substitutional Ta atoms, TDPAC high-pressure study 78–52384
Zr-Ir, dil., elec. field gradient at ^{193}Ir, Mossbauer meas. 80–66090
$Zr(Fe_{1-x}Al_x)_x$, transition region, spin glass or long range mag. order 80–44841
$Zr(Fe_{1-x}Co_x)_y$, transition region, spin glass or long range mag. order 80–44841
$Zr_{0.9}Fe_{0.1}V_2$, NMR and mag. susceptibility 78–95527
$ZrH_{1.97}$, FCT, elec. quadrupole interaction at ^{181}Ta, TDPAC obs., 20-588K 79–33574
ZrH_x:Er, (x=1.5 and 1.85), Mossbauer spectra 80–20527
$Zr_{1-x}Nb_xZn_2$, microscopic mag. props., NMR investigation 80–15807
ZrO_2:^{89}Zr electron captive decay lifetime, struct. environment effects 77–28523
ZrO_2-CaO:Mn^{2+}, EPR spectra, impurity substitution behaviour in various phases 77–16160
$Zr_{0.99}Pt_{0.99}V_2$, NMR and mag. susceptibility 78–95527
$ZrSiO_4$, natural, radiation defect centre, EPR obs. 80–75853
ZrV_2, NMR and mag. susceptibility 78–95527

crystal imperfections *see crystal defects*

crystal inclusions
200 to 500 MHz A-scan defect characterisation 79−47873
alkali halides, cryst., optical emission following pulsed 10.6 μ irrad. 79−28847
alkali halides, radiolysis, growth of colloidal metal inclusions 78−92493
Allende mineral grain inclusion, excess ^{129}Xe meas., chronological information 80−67675
alloy, disperse state formation *(Russian)* 78−52757
alloy with dispersion precipitate of ordered phase, yield limit theory surmountable pair mech. *(Russian)* 77−1855
Alnico 5 alloy, S and Ti additions effect rel. to non-metallic inclusions, coercive force and grindability 80−89375
anisotropic continuum theory 79−73162
anisotropic elastic medium, elastic energy of plate inclusion 78−38687
anisotropic ellipsoidal inclusion, polynomial eigenstrain problem 78−83808
anisotropic media, elastic strain energy of precipitates, and periodic distrib. inclusions 78−84810
baryta crystal gas-liquid inclusion meas. with microscope heating stage 80−76967
α-brass, with few inclusions, shear mode of ductile fracture 77−36652
brittle composite, local crack-driving force, elastic and thermal mismatch 78−7017
brittle materials, influence of structural parameters on fracture toughness 79−96133
butt welded joint dynamic strength, partial penetration and slag inclusion effects 79−83288
carbon tetrabromide, inherent moisture as purity probe *(German)* 77−85933
ceramic composite, toughening by oriented nucleation of microcracks 77−8921
cleanliness assessment by US *(French)* 80−104411
composite material models, three phase sphere and cylinder models soln. for effective shear props. 80−25749
crystal defects and the mechanism of fluid inclusion formation *(Chinese)* 79−73160
cylindrical, motion in dislocation strain field, diffusion theory *(Russian)* 78−18676
Debonding of circular second phase particles 78−5688
deformability of inclusions, during processing, effects on directionality 80−55345
deformation field of misfitting inclusion 77−73276
deformation field of misfitting inclusion 77−77488
diamond, epitaxial synthesis by C-ion deposition at low energy, and struct. 79−1559
diamond, olivine inclusion epitaxy 77−78173
diamond, polycryst. sintered under ultra high press., binary inclusion content effect on thermal stability *(Chinese)* 80−66453
diamond, synthetic, semiconducting, X-ray exam. of inclusion 77−84788
diamond, synthetic monocrystals, inclusions phase comp., radiographic method 80−100978
diamond, thermal cond. at low temp., correl. with IR absorpt. features 80−49435
diamond with garnet inclusion, expt. crystallisation conditions study 80−46172
dielectric, transparent, laser-induced damage, role of absorbing microinclusions, passive methods 79−31969
diffusion motions of macroscopic inclusions in nonuniform compressive stress fields *(Russian)* 80−88351
diffusional motion and distortion of macroscopic inclusions under influence of elastic stresses *(Russian)* 77−66676
dilatation energy of extended defects of arbitrary shape and size near solid surfaces 78−34508
ductile fracture, quantitative study of inclusions taking part in process 78−27630
ductile fracture process, quantitative study method of inclusions 80−35318
Duralumin, fatigue cracks development, intermetallic inclusion influence 79−38962
elastic media, flaw characts. from ultrasonic scatt. data 79−79188
elastic stress field shape change kinetics depend. on inclusion-edge dislocation interaction 79−86815
elastic wave scatt. by thin inclusions 80−65151
elastic wave scatt. from localised defects in solids, long-wavelengths 79−87794
elastic wave scattering, Born approx. 77−79984
electric field distribution, form of inclusions of second phase *(Russian)* 77−55504
electron diffraction contrast of misfitting inclusions, precip. close together on dislocation 77−27886
eutectics, single grained, directionally solidified, anisotropic yielding behaviour 80−103412
fatigue testing, statistical analysis of inclusion effects *(French)* 77−73379
Fe, ingot, cast, exam. of nonmetallic inclusions, size freq. distrib. 78−39989
ferroelectric phase formation energy in inhomogeneous inclusion under press. 77−12338
ferromagnet, interaction energy of domain wall with spherical cavity 77−8335
ferromagnets, hardening by non-mag. inclusions, meas. of coercivity 79−38841
fibre reinforced composites, bond stresses of isotropic body with elastic inclusions 78−30180
fluorite crystal gas-liquid inclusion meas. with microscope heating stage 80−76967
fluorophosphate and fluoroberyllate glass laser damage thresholds and solid inclusions 80−33054
gas-liquid inclusions, in crysts., movement in temp. field gradient 79−55942
α-glycine crystal, Cu(II) impurity complex, ligand ENDOR spectra 79−65765
grain boundary migration in presence of grain-boundary coalescence of inclusions *(Russian)* 78−26579
grain boundary sliding and intercrystalline fracture in high temp. creep *(Czechoslovakian)* 77−32642
graphite, from reactor, quantitative microanalysis by laser emission spectroscopy 80−81384

crystal inclusions continued
graphite, spheroidal, presence of magnesium studied with electron probe microanalyser *(Ukrainian)* 80−26072
growth from melt, capture of inclusions 77−31615
guanidine aluminium sulphate, lattice charge contribution to coordination polyhedron cryst. potential 80−103651
heterogeneous matrix systems, calc. of thermal cond. coeff. *(Russian)* 77−24455
hydrogen embrittlement due to H-inclusion interaction 78−30664
identification using computed electron micrographs 77−51383
impurity incorporation into vicinal faces grown from dil. solutions 80−84127
inhomogeneous materials, with ellipsoidal inclusion, and polycrystals, elastic deform. 78−15451
interaction of disperse inclusions of soluble phase, with grain boundaries, theory *(Russian)* 77−80513
interaction with point defects near solid surface, energy *(Germany)* 78−38750
isotropic body containing rigid plate-like inclusions, antiplane deform. *(Russian)* 77−27476
isotropic homogeneous medium, elastic wave scatt. by circular cylindrical flaws and inclusions 79−86369
isotropic medium, elastic wave scatt. from flaws, long-wave approx., appl. to ellipsoidal voids and inclusions 79−86368
laser beam interaction with inclusion defects in isotropic solids 79−76741
laser impact on transparent dielectric, shock wave dissipation from imperfections 79−69925
laser materials with inclusions, thermal stresses 77−729
leucosapphire crystals, gaseous inclusions 78−2151
light diffraction by absorbing inclusions 77−79757
liquid inclusion migration, nonequilib. morphology 78−38882
liquid inclusion migration in temp. gradient field 78−18842
liquid inclusions, thermal migration, dislocation drag 77−7911
long elastic wave scatt., inverse problem 79−55819
macroscopic defects, ordered regions and percolation phase transform. *(Russian)* 80−92665
macroscopic inclusion motion due to field of struct. inhomogeneity 77−89569
martensitic steel, fatigue crack nucleation, rotating beam determ. of true min. stress *(French)* 77−25122
metal, dissolved species in cracks, linear differential eqn. problem 79−51316
metal, ductile, hard inclusion effect on plastic strain distrib., model meas. 77−59062
metal, ductile fracture mechanism, theoretical and expt. investigation *(German)* 77−70142
metal ingots, cast, nonmetallic inclusions, size frequency distrib. determ. 78−39989
metal-C system, spheroidal graphite formation, role of high angle boundaries *(Russian)* 80−81065
metallography, quantitative methodology *(French)* 80−30205
metals, gas-forming impurities in crystal inclusions, trends in modern anal. *(Russian)* 80−15123
metals and alloys, BCC lattice, crit. embrittlement temp., struct. parameters effect *(Russian)* 80−66618
mica, proton induced giant halos round α-emitting inclusions containing water 77−51420
microhardness anisotropy 80−21079
misfitting inclusion deformation field 77−36505
monazite, PIXE aval. in search for superheavy elements 79−79845
monazite inclusions in mica, proton-induced X-ray emission, evidence for primordial superheavy elements 77−9429
motion, equation of 80−75387
non-metallic materials, flaw detection by tomodensitometry *(French)* 79−20295
nuclear fuel, quantitative metallographic anal., computer program, QMA 79−15951
nuclear fuel shell inspection, mag. method for detecting ferromag. particles 80−66746
oblate spheroidal inclusion, internal stress, misfit, inhomogeneity and plastic deform. 78−60701
paramagnetic matrix with ferromagnetic inclusions, mag. susceptibility determ. 79−97407
parelastic force on homogeneous cryst. inclusion, theory 80−79777
particle trapping in cryst. growing from melt at variable rate 78−67676
periodic elastic inclusion-rectilinear crack system in isotropic medium 79−41619
Permalloy, 50NP, and 79NM, magnetic properties and structure, environment effect during annealing 80−60366
Permalloy, high-permeability, influence of grain struct. and non-mag. particles on mag. props. *(German)* 77−16112
photoimaging system based on photopolymerisation in cryst. coatings 80−40716
physical chemistry of some microstructural phenomena 79−11550
PMMA, optical strength rel. to surface defectiveness 77−28665
PMMA, thermochem. instability at Pt sphere inclusions caused by CW laser beam 80−29689
point source modelling for extended source stresses 77−72609
pores in system with excess vacancies extraneous inclusion role in nucleation *(Russian)* 79−73164
porous rigid-plastic material containing rigid inclusions, yield function, plastic potential, void nucleation 78−64612
purification, inclusion emersion in vertical zone refining 78−52663
quartz, cultured, prism faces growth and development, attached microcrystals role 77−31612
quartz, from alpine fissures, fluid inclusions, reln. to metamorphism *(German)* 77−25677
quartz, synthetic, annealed, light scatt. centres 77−11586
α-quartz, synthetic, growth, defects induced by seed orientation 80−96454
quartz, synthetic influence of hydrostatic pressure on precip. of structure-bound water in microinclusions 78−75838
quartz inclusion morphology for thermolum. dating, effect of HF etching 78−70240
radiographic detection, eval. of detectability in welded joints 80−81266
rare earth garnets, preparation, substrate and epitaxial layer surface quality control, X-ray topography *(German)* 77−55432
refractory metals, technique for investigation of nonmetallic inclusions 77−52587
ruby, optical strength rel. to surface defectiveness 77−28665

crystal inclusions continued
second phase particle, diffusional relaxation 80—60898
semiconductor, enhanced electrodiffusion purification in mag. field, GaAs epitaxial film appl. 80—66409
semiconductor doping, thermomigration method, using molten wires, nonequilib. morphology of migrating liq. inclusions 78—38882
shear stresses induced by hydrostatic pressure near the surface of an inclusion 78—75074
solid surface, point defects, inclusion and separation zones, elastic energies determ. *(German)* 78—95054
Somigliana dislocations and pure inclusions, internal stresses 78—30615
spherical strain fields, caused by inclusions, S-matrix theory calcs. 80—100133
stearic acid crystals grown from solution, spatial correlation between growth spirals and inclusions 80—96527
steel, 12X2H4A, nonmetallic inclusion effect on plasticity and impact strength *(Ukrainian)* 78—92296
steel, 18% Ni maraging, fatigue strength, effect of soln. treatment and inclusions 78—23805
steel, AISI 4340, sulphide inclusion behaviour during thermomechanical treatment 78—3151
steel, AISI 4340, thermomechanical treatment, sulphide inclusion behaviour 79—11647
steel, Al semikilled, $(Fe_xMn_{1-x})O.Al_2O_3$ inclusions, deoxidation, thermodynamic conditions 80—60830
steel, Al-Cr, $FeO.(Al_xCr_{1-x})_2O_3$ inclusions, thermodynamics 80—60831
steel, anisotropic rolled plate, torsional fatigue in middle and high cycle fatigue ranges *(Japanese)* 77—12691
steel, austenitic, Cr-Ni, nonmetallic inclusions modification using rare earth metals *(Russian)* 80—40369
steel, austenitic stainless, blister initiation inclusion, heat treatment and thermomechanical treatment effects *(French)* 80—35224
steel, austenitic stainless, deformation induced cavitation, exam. 79—43363
steel, austenitic stainless Ni-Cr, heat resist. and comp. of non-metallic inclusions, effect of La, Nd, Pr and Ce 80—76315
steel, ball bearing, fatigue damage, influence of dispersed phases in martensitic matrix 80—108549
steel, BN extraction, and identification, IR anal. 80—85254
steel, C, 35, low-temp. fracture toughness, non-metallic inclusions influence *(Russian)* 79—52346
steel, C, hydrogen attack, steelmaking effects 79—100076
steel, C, inclusions, influence on toughness and fatigue props. 80—40533
steel, C, quenched and tempered, ductility, effect of hydrostatic press. 78—44190
steel, carbon type, hydrogen press. effect on morphology of hydrogen attack 80—85052
steel, cast, nonmetallic inclusion size frequency distrib. determ. 78—39989
steel, cast high-strength, local integranular fractures, formation mechanism *(Russian)* 78—95795
steel, Cr, high C, ingot, macrostruct., effect of diffusion annealing, solidification condition *(Chinese)* 78—15429
steel, Cr-Mn, non-metallic inclusions anal. with increased N content *(Bulgarian)* 79—82259
steel, Cr-Mo:P (2.25, 1 wt.%), stress relief cracking, effect of P segregation 80—89324
steel, Cr-Mo-V, cast, creep resistant, rare earth addition effect on deoxidation, nonmetallic inclusions and mech. props. *(German)* 79—66067
steel, Cr-Ni-Al, intergranular crack investigation by etching *(Chinese)* 79—43457
steel, Cr-Ni-Mo, 'light spots', fractographic anal. 79—29204
steel, dimple fracture, relation between inclusions and morphology *(Chinese)* 79—74231
steel, ductile fracture in presence of elongated sulphides *(French)* 80—45394
steel, ductile structural, crack resistance and cohesive strength 80—50722
steel, free cutting, with MnS inclusions, tensile flow and fracture 78—11290
steel, free-cutting type, inclusion investigs. using EPIQUANT automatic structure analyser 80—55609
steel, fully killed, nonmetallic inclusions, microprobe and metallographic exam. 80—30196
steel, high C, pearlitic, non-metallic inclusion effect on threshold behaviour of fatigue 79—91786
steel, high-C, boriding, boride case struct. 79—24665
steel, homogenisation of sulphide inclusions 77—32605
steel, inclusion, grain boundaries and H_2 attack, fracture analysis 77—32695
steel, inclusion behaviour investigations using SEM 78—23916
steel, inclusion chemistry control for machinability enhancement 80—85067
steel, inclusion cleanliness, US meas. 80—25978
steel, inclusion content, sampling in quantitative image analysis *(French)* 77—28961
steel, inclusion content, ultrasonic method of determination *(French)* 79—52555
steel, inclusion effect on cold formability 80—29975
steel, inclusions, rapid microprobe analysis using energy dispersive spectrometer and minicomputer *(German, English)* 79—92038
steel, inclusions effect on distrib. of local microheterogeneous deform. *(Russian)* 78—80586
steel, large forging, mech. props. 77—4797
steel, leaded, resulphurised, deform. index of MnS inclusions 77—66683
steel, low alloy, fatigue crack nucleation under high cycle fatigue and uniaxial loading 79—79060
steel, low alloy, quenched and tempered, formation of stony fracture during forging 79—79059
steel, low C, hot rolled and cold deep drawn, nonmetallic inclusion distrib. in microcavities *(Russian)* 79—52265
steel, low C, nucleation and increase of discontinuities in environment of non-metallic inclusions *(Polish)* 79—79022
steel, low C, structurally free cementite formation 78—23697
steel, low C, Ti inclusion nucleation, effect on crack formation *(Czech)* 79—91782
steel, low C, type 08Yu, influence of nonmetallic inclusions on microfailures, during strain *(Russian)* 79—34128
steel, low C and medium C, high-temp. heating effect on oxide inclusions 79—96051
steel, low-alloy pipe, low-cycle fatigue in H_2-evolving media, S content and sulphide inclusion effects *(Russian)* 78—11398

crystal inclusions continued
steel, maraging, Ni (18 wt.%), fatigue crack initiation and propag. in earlier stage *(Japanese)* 77—8937
steel, maraging, Se microalloying, machinability improvement 80—21116
steel, mild, nonmetallic inclusion effect on pitting 80—35381
steel, molten, deoxidised, reaction with oxidising gas bubbles 78—88438
steel, molten deoxidised, reaction with oxidising gas bubbles 78—84739
steel, non-metallic inclusions 80—84839
steel, nonmetallic inclusion, effect on hot ductility 80—29999
steel, nonmetallic inclusion segregation during cooling *(Russian)* 80—100330
steel, nonmetallic inclusions effect on ductility 80—30042
steel, nonmetallic inclusions effects on low-temp. fracture *(Russian)* 77—59895
steel, oxide inclusions 78—23648
steel, plate, thickness and rolling ratio influence on inclusion behaviour 80—16340
steel, powder forged, fatigue, surface treatment effect 80—85048
steel, powder forged, impact strength and fatigue strength, slag inclusion effects 77—21271
steel, process induced matrix inclusion separation 77—28818
steel, railway, oxidation by Fe-Si-Ca-V complex alloy, nonmetallic inclusions *(Russian)* 80—93685
steel, rare earth addition effects and behaviour, review *(Chinese)* 79—43257
steel, rimmed, metallographic method of cleanliness eval. 77—52562
steel, rimming, continuously cast, nonmetallic inclusion distrib. *(Russian)* 78—80534
steel, rolled, anisotropic, fatigue fracture surface obs. *(Japanese)* 80—108546
steel, rolled, effect of inclusions on torsional fatigue 78—92314
steel, SiO_x inclusion formation on introduction of solid SiO into molten steel *(Russian)* 78—80530
steel, stainless, Cr-Ni (18, 8 wt.%) average inclusion size and contents exam. measurements using optical microscopy and Br-Methanol methods *(Korean)* 79—66080
steel, stainless, deoxidation in melting with Si *(Korean)* 78—19947
steel, steam turbogenerator rotors, fatigue crack initiation and growth, from macroscopic slag inclusions 78—64681
steel, structural, addition of solid SiO, effect on ductile fracture 80—16465
steel, structural, impurity effect on crack initiation, dynamical loading *(Czech)* 80—60955
steel, structural, second phase particle effects on impact strength 80—108581
steel, thermal fatigue, effects of inclusions 80—81183
steel, transformer, formation of perfect cubic texture in thin sheets *(Russian)* 78—80557
steel, types 60G, ShKh15, structural changes near holes and inclusions due to pulsed currents *(Russian)* 80—108459
steel 30L, critical size of nometallic inclusions in fracture 79—83322
steel austenitic stainless, pitting corrosion susceptibility, non-metallic inclusion effect 80—11816
steel creep resistant, rare earth metal effect on inclusion charact. *(Czech)* 77—86134
steel inclusions, SiO_2, Al_2O_3, FeS, effect of high temp. heating on size, number and distrib. 78—44145
steel inclusions and plasticity, crystn. conditions influence *(Russian)* 80—20923
steel morphology changes obs., during heating, influence on ductile fracture *(Spanish)* 80—25744
steel sheet, hot and cold rolled, cold formability, notched tensile test and stretch bend test *(German)* 80—61031
steel wire, US inspection, immersion method 80—66757
steels, mechanism of H_2 entry in acid environments 79—39023
stress concentration due to oblate spheroid inclusion, exam. 78—71281
stress concentration due to spheroidal inclusion *(Japanese)* 80—16320
superconductor, type II, with normal inclusions, current density distrib., theory 80—80461
surface, point defects, inclusion and segregation zone, elastic energies *(German)* 78—95049
surfaces and interfaces, elastic energy of point defects and inclusions 80—73272
tetrabrommethane, monoclinic and cubic polymorphs, vapour inclusions and surface melting 77—76648
thermal conductivity of solid containing gas-liq. inclusions *(Russian)* 78—22908
thermoelastic condition of a body containing a heat-evolving inclusion *(Russian)* 78—9563
thermoelastic inclusion energy in semi-infinite solid 80—14565
thermoelastic interference, between two neighbouring ribbon-like inclusions *(Japanese)* 77—68423
transparent dielectric, laser destruction, impact mechanism diverting energy from absorb. inclusions 78—43962
transparent dielectric, laser induced fracture *(Russian)* 77—51406
transparent dielectrics, with inclusions, laser-induced stresses 79—28012
transparent medium with random absorbing inclusions, laser heating statistics *(Russian)* 77—28666
transparent object, testing for bubbles and light scatt. inclusions 77—88973
triglycine fluoberyllate, deuterated, dislocation line defect X-ray topographic analysis 80—59465
type II superconductor, flux-line lattice instability due to planar imperfections 78—23218
US testing, automatic *(German)* 79—83406
zeolite A, synthetic, with salt inclusions, elec. and thermal props. 79—55925
zeolite inclusion complexes, $LiA.LiNO_3$ and $LiX.LiNO_3$, ^7Li NMR motional line narrowing 79—56618
Al alloy, fracture of large second phase particles 78—7010
Al alloy, fracture toughness and struct. *(Russian)* 77—25134
Al alloy, void form. in defeated targets 77—15403
Al alloys, inclusions, oriented distrib. metallography and effects on anisotropy *(Russian)* 78—80589
Al alloys, preliminary forging effects on struct. and mech. props. of extruded sections *(Russian)* 78—80564
Al-Bi(Cd)(Pb)-Ti, containing low-melting pt. inclusions, mech. props. 80—93632
Al-Cu, isothermal coarsening of liquid inclusions 77—21166
Al-Ni-Si sintered SAS-1 alloy, struct. *(Russian)* 79—52135

crystal inclusions continued

- Al-Pb alloys, with isolated liq. phase inclusions, recrystn. *(Russian)* 80—20970
- Al-Pb(Bi)(Cd), containing low melting point inclusions, impact props., temp. depend. 78—60792
- Al-Zn-Mg alloy, TEM characteris. of precipitates 80—104166
- Al-Zn-Mg alloys, role of dispersed transition metal intermetallic compounds 79—96088
- Al_2O_3-B_2O_3 system, phase comp. and sorption props., Al salts chem. nature influence 79—51426
- Al_2O_3-ZrO_2 dispersed system, fracture toughness, inclusion induced microcracking effect 78—11296
- Al_2SiO_5:Fe^{3+}, spin lattice relax. 77—73076
- Au-Co, electroplated, 'polymer' inclusions, chem. identity obs. 79—37931
- B fibre, US inspection, immersion method 80—66757
- B fibre reinforced Al, interaction between fibre and matrix 80—10712
- Be, fracture and strength properties, dynamic ageing effects 80—81202
- Be ingot, high-purity, TEM obs. of BeO dispersion 80—104165
- Be, sintered, physicomech. props. anisotropy, BeO inclusions effect 80—60804
- Bi:Sb, solid soln. struct., growth rate effects 77—52246
- C fibre, structural and mech. characts. 77—28737
- $CaCO_3$, Iceland spar, polarizing prism, struct. defects effect 78—18065
- CaF_2-rare earth trifluoride, characts. of ordering of solid solns. 79—14725
- $CaLa_4(SiO_4)_3O$:Nd, laser damage initiating inclusions 77—68246
- $Cd_xHg_{1-x}Te$, carrier lifetime, effect of comp. fluctuations and second-phase inclusions 80—80294
- CdS film, inhomogeneities responsible for residual cond., microinclusions 77—28269
- CdS films, amorphous and polycrystalline, microinclusion distrib. of high resist. phase and residual cond. 80—7008
- CdS films, growth, residual cond., inclusions 78—43492
- CdTe, growth from Te soln., Te inclusion density 77—40352
- CdTe, laser window material, absorbing Te inclusions, damage threshold 77—46749
- CdTe, window material with absorbing inclusions, damage thresholds 77—38971
- Co-Al alloys, deformed, mag. props., positron annihilation *(Russian)* 77—85416
- $CoAl_2O_4$, single crysts., pt. defects type determ. involved in reactions of form. and decomp. of inclusions 79—95003
- Cr effect on carbon steel weld metal hot cracking resistance 79—79061
- Cu cathode, electroluminesc. from semicond. impurities on surface 77—90200
- Cu complex, bis-(alkylammonium) (11) tetrachloride, perovskite, lattice perfection 78—87633
- Cu, continuously cast, O free, effect of nonmetallic inclusion on microstruct. and props. 77—81280
- Cu, fatigue behaviour effect of Zn, Au diffused coatings 78—72850
- Cu glow discharge sputtering redeposition, in noncond. compound chem. anal. 77—77860
- Cu ingot, cast, nonmetallic inclusion size frequency distrib. determ. 78—39989
- Cu, with Al_2O_3 inclusions, breakdown and emission props., effect of inclusions 79—87389
- Cu-Be-Co, cuboid (Co, Cu, Ni, Fe)Be inclusions, metallography, ageing effects 80—11645
- $CuCrS_2$, domain struct. and superstructure, TEM obs. 80—79779
- Cu_2O, Cu inclusions and annealing, optical and IR absorpt. obs. 80—60630
- EuS, defect struct., etch pitting and electron microscopic obs. 79—27989
- Fe, Armco, grain size and strength depend. on nonmetallic inclusions *(Russian)* 80—100894
- Fe, cast, electron probe determ. of traces of modifying agents in spheroidal graphite 79—52814
- Fe, cast, innoculated with Ce-Mg-Fe master alloy, struct. and props. 80—100843
- Fe, cast, Mg, despheroidising effect of Bi, Sn on graphite in alloy 78—56670
- Fe, cast, Mg-modified, scale for shapes eval. of graphite inclusions 78—35609
- Fe, cast, modified with Al and S, nonmetallic inclusion effects, electron microscope obs. *(Russian)* 77—65987
- Fe, cast, P and Ce effect on struct. *(Russian)* 79—52224
- Fe, cast, US study of sections undergoing deform. or thermal cycling 80—104285
- Fe, cast alloyed, struct., props., heat treatment 77—16623
- Fe, grey cast, P effect on distrib. of alloying elements 77—12634
- α-Fe, interaction of He with C, computer simulation calc. 79—99235
- Fe, powder forged, impact and fatigue strengths, slag inclusion effects 77—21271
- Fe, pure, ductile fracture, effect of nonmetallic inclusions 78—64660
- Fe-Al, sintered and worked alloy, nonmetallic inclusion identification by quantitative metallography 77—77701
- Fe-C-Fe_xO_y, cleavage initiation by ductile tearing 78—64656
- Fe-Cr, high-C, sulphide inclusion distrib. obs. 79—74168
- Fe-Mn-O melts, formation of oxide inclusions, cryst. pulling, Bridgeman tests *(German)* 80—35074
- Fe-Mn-S, thermodynamics, solubility of S and Mn in γ-Fe, 1100 to 1300°C 79—47662
- Fe-N (0.03 at.%), single cryst., stress distrib. around spherical inclusion, TEM study 79—34038
- Fe-Ni, coercive force depend. on grain struct. and inclusions 77—20635
- Fe-Ni-Al (10, 0.1 wt.%), clustering of Al_2O_3 inclusions 79—83205
- Fe-Si (3 wt.%), behaviour of disperse inclusions, influence of recrystn. processes *(Russian)* 80—66519
- Fe-Si (3 wt.%), grain growth inhibition by MnS spherical particles with size distrib. 80—35218
- Fe-Si (3 wt.%), grain-oriented, effect of forsterite coatings in domain struct. 78—23293
- Fe-Si-Mn-C, east, Ce additions, nonmetallic inclusions *(Russian)* 78—19710
- Fe-SiO_2, slowly and rapidly solidified, coarsening of SiO_2 77—86023
- $Ga_{0.7}Al_{0.3}As$ epitaxial film, inclusion-generated dislocation clusters 77—89445
- GaAs, autoepitaxial layer, local impurity inhomogeneities *(Russian)* 79—23854
- GaAs, cylindrical and spherical localised inhomogeneities in mag. field, anomalous to elec. props. calcs. 80—44621

crystal inclusions continued

- GaAs, Czochralski growth, melting and regrowth, inclusion density and dislocation generation 77—21016
- GaAs, migration of liquid inclusions, effect of DC current and temp. 77—7910
- GaP, containing matrix metal inclusions, internal friction study 79—42145
- GaP:Cu, elec. and optical props., rel. to doping and heat treatment 80—16056
- GaSb, migration of liq. inclusions, effect of DC current and temp. 77—7910
- GaSb:Mn, oriented $Mn_{0.6}Ga_{0.4}Sb$ inclusion form., elec. props. 77—15869
- p-GaSe, single cryst., negative photocond. induced by elec. field 79—19623
- Gd, nonmagnetic inclusions, effect on easy direction 77—77052
- $Gd_3Ga_5O_{12}$ crystal growth from melt, X-ray topography meas. *(Hungarian)* 80—11556
- $Gd_3Ga_5O_{12}$ dislocation anal. at inclusions by repeated etching technique 80—29024
- $Gd_2(MoO_4)_3$, and isotypes exam. of crystal growth, and defect generation 78—68617
- Ge, composition of inclusions, single cryst. 77—15441
- Ge, heavily-doped single cryst., macroinclusions, annealing in elec. field 77—47474
- Ge, second-phase inclusions after O_2 treatment, electron microscope obs. 77—43238
- Ge:Ba, heavily doped, second phase inclusions on melt growth 78—22751
- Ge:Cu, displacement of Ge-Cu inclusions in const. elec. field, 700-850°C *(Russian)* 77—15634
- H_2 transport by dislocations to fracture initiation sites, inclusions, microvoids 77—21263
- HfO_2 single crystals, y_2O_3 stabilised, optical props., impurities and annealing conditions influence 79—52399
- α-HgS, synthetic cinnabar, morphological, optical and X-ray studies *(French)* 77—43223
- InAs, migration of liq. inclusions, DC current and temp. effects 77—7910
- n-InAs:Cr, Czochralski growth of high-resist. single crysts. 77—66587
- InSb-NiSb two-phase system, photomag. effect, orientational depend., 90-300K *(Russian)* 78—2524
- InSb-NiSb two-phase system, electron scatt. mechanism *(Russian)* 78—6373
- $KCaCl_3$ impurity in NaCl cryst., precipitation and dissolution 79—42259
- KCl, migration of brine inclusion, nonequilib. morphology 78—38882
- $KClO_4$, cryst. growth from gelatin gels, exam. of growth and morphology 80—7488
- KH_2PO_4, cryst. growth, splitting due to colloidal inclusions 77—7681
- KH_2PO_4, growth from gel and aqueous soln., oriented inclusions 80—15023
- KH_2PO_4, liq. inclusion formation during large cryst. growth 78—64455
- KH_2PO_4, liquid inclusion form., hydrodynamics and supersaturation role 78—30559
- LaB_6, single crysts., growth by laser heated floating zone method 77—81213
- Mg, inclusions, types and size distrib. *(German, English)* 80—97492
- Mg-Cu-Mn-Ni-Fe-O, UHF ferrites, synthesis, physicochem. state, mag. and dielec. parameters 79—11536
- MgO, implanted K aggregates, TEM and optical spectra obs. 78—83838
- MgO:Fe, Fe^{2+} oxidation and Fe^{3+} reduction kinetics, EPR obs. 79—70399
- MgO:Li^+, quenched, elec. polarisation, thermal depolarisation and dielectric loss meas. 79—1738
- MnSb, cryst. pulling with seed from nonstoichiometric melt 77—16488
- Mo wire, US inspection, immersion method 80—66757
- Mo-He, Born-Mayer interaction potentials derived from He desorption expts. 79—99409
- $NH_4H_2PO_4$, cryst. growth, pH effect, H_3O^+ inclusions 79—55682
- $NH_4H_2PO_4$, unstable growth features and mechanisms of inclusion formation 79—99090
- NaCl single crystals, thermomigration of brine inclusions, eval. of radioactive waste repositories 80—99251
- NaCl:Sr, solubility of free and assoc. Sr by elec. cond. and ionic thermocond. meas. 77—62645
- Nb alloys, non-metallic inclusion form. during quenching from liquid state 78—95766
- Nb-W-X-C, X=Ti, Zr, Hf, quenched from liquid state, formation of non-metallic inclusions *(Russian)* 79—57007
- Nb-Zr-C welding solid solutions, ageing kinetics, influence of inclusion elements *(Russian)* 80—100853
- Ni alloy, ZhS6K, diffusion layer form. on Nb addition, struct., comp. *(Russian)* 78—56814
- Ni, ductility and fracture, nonmetallic inclusions effect 80—104221
- Ni, electrodeposit, linear defect obs., TEM study 79—4304
- Ni, high temp. plasticity, oxide inclusion effect 80—50681
- Ni-ceramic coating structure, influence of micropowder inclusion *(Russian)* 80—59820
- Ni-Cr alloy, Kh20N80, inclusions and plasticity, crystn. conditions influence *(Russian)* 80—20923
- Ni-Cr-W-Co-Ti, thermal fatigue, effects of inclusions 80—81183
- Ni-Fe (36 to 50 wt.%), initial permeability, domain struct. model 80—88811
- Ni-Fe oxidised film, extraordinary viscous wall motion at extreme vel. 78—14997
- Ni-ZrO_2, dispersed inclusions, effect on recovery and recrystallisation 77—25064
- NiO, Hall effect anomaly, sign reversal at 600K 80—100471
- $Pb_{1-x}Sn_xTe$ (x=0.15 to 0.20), SEM study, dislocation density, and carrier density and mobility 79—69107
- $Pb_{1-x}Sn_xTe$, large non-seeded single cryst. growth by sublimation method, and characterisation 79—78860
- $Pb(Zr_{0.42}Ti_{0.58})O_3$, hot-pressed piezoelec. ceramic, effect of nonferroelectric phase 77—43936
- Se electrophotographic films, ageing effects on structure and properties 77—47699
- Si, amorphous, scanning TEM studies of cryst. inclusions 80—79699
- Si, annealing in elec. field, behaviour of second phase inclusions *(Russian)* 79—23779
- Si, composition of inclusions, single cryst. 77—15441
- Si epitaxial layers, temp. dependence of P dopant inclusion in gas phase deposition *(German)* 79—52127

crystal inclusions continued
Si, inclusion type defects removal from bulk of single cryst. by elec. fields 79—43126
Si, nondestructive monitoring using X-ray diffraction and IR microscopy methods 79—55749
Si single crystal ingot growth from metallurgical grade Si, inhomogeneities 80—59416
SiC-B eutectic alloys, struct. of crystallising graphite 79—38829
Si_3N_4, Wiener filtering appl. to nondestructive evaluation, defect charact. 79—11732
$Si_xO_yN_2$ film, opt. props. rel. to reactive sputter prep. conditions 77—81165
$SmCo_5$ magnetic alloys, pressed, sintering rel. to mag. props., cryst. struct. 78—60600
$SmCo_5$, sintered, high coercivity, microstruct. and mag. props. 77—69629
$Tb_2Ge_2O_7$, flux-grown, X-ray topography 80—64939
Ti, deform. and H_2 inclusion effect on annihilation γ-ray ang. correl. curve shape 78—31273
Ti sintered, struct. stability, effect of dispersed refractory compound inclusions 77—28825
Ti-B, binary inclusions, interaction with diamond in polycryst. diamond sintering *(Chinese)* 78—80484
Ti-Cr, sintered, friction and wear, structural factors 78—60843
Ti-Cr-TiC, sintered, friction and wear, structural factors 78—60843
Ti-Si, binary inclusions, interaction with diamond in polycryst. diamond sintering *(Chinese)* 78—80484
Ti-TiC system, sintered, friction and wear, structural factors 78—60843
α-U, strain rate effect on flow and fracture 80—100887
W, elastic wave scatt. from oblate spheroidal WC inclusion 80—65151
W wire, US inspection, immersion method 80—66757
YAG crystals, dislocations and inclusions, birefringence topography obs. 80—107248
$Y_3Al_5O_{12}$, laser cryst., struct. inhomogeneity obs. by vac. decoration 77—35701
Zn-In alloy, solid-liq. equilib. roughening transition 80—96630
ZnS films prepared by thermal evaporation in vac., nature of defects 80—10835
ZnS single crystals, O content determ. by fast neutron activation anal 80—15142
ZnSe(:Ga)(Al), effect of thermal treatment and doping on elec. props. 77—85223
ZnTe, elec., SEM and TEM studies of impurity segregation during long annealing 80—30001
ZnTe:Li, Li in Te precipitates, diffusion during thermal anneal 80—39358
ZrB_2, oxidation in O_2 atmosphere, exam. 80—11814
ZrO_2 single crystals, Y_2O_3 stabilised, optical props., impurities and annealing conditions influence 79—52399

crystal internal fields *see crystal field interactions*

crystal interstitials *see interstitials*

crystal lattice structures *see crystal atomic structure*

crystal microphones *see microphones*

crystal microstructure
for microstructural changes, see also phase transformations, hardening, heat treatment, metalworking
see also crystal defects; crystal inclusions; crystallites; dendritic structure; domain boundaries; domains; electron microscope examination of materials; eutectic structure; grain boundaries; grain size; Guinier-Preston zones; mosaic structure (microstructure); noncrystalline state structure; precipitation; segregation; subboundary structure; superlattices; texture; X-ray diffraction examination of microstructure
acoustic wave analysis of material structure 80—65163
alite paste, mature, microstructure study by SEM, TG and X-ray diffr., corrosion 78—92381
alloy, lamellar multiphase, struct. and spatial comp. variation, analytical STEM 78—24011
alloy, two phase microstrct. revealed by selective sublimation 79—24698
alloys, definition for arbitrary duration and expt. temp. 79—51267
alloys, fracture toughness rel. to microstruct. characts., alloy design 79—43423
alloys, industrial, stacking fault energy rel. to mech. props. *(French)* 79—43339
alloys, two-phase, coarse microstructs., structural approach to yield strength 80—7634
Alnico 5 alloy, S and Ti additions effect rel. to non-metallic inclusions, coercive force and grindability 80—89375
Alnico alloy, C addition effects on struct. and mag. props. 78—23835
anthracene, stable monoclinic phase, (001) planar faults 79—69115
anthracene, ultrathin films on fused quartz and sapphire 80—59812
austenite, hot-worked, struct., post-deform. ht. treatment effects *(Russian)* 77—8859
automatic microstructure analyser, construction and operation, optical mechanical scanning advantages *(German, English)* 77—77697
binary eutectic system, steady state lamellar solidification, self consistent theory 77—70041
biotite deformation, comparison with muscovite from optical microstruct. 80—26507
black chrome solar selective absorber, microstruct., chemical comp. and reflective props. 80—7959
bone china body, MgO effect on vitrification mech. props. *(Japanese)* 79—78922
boride coatings, high temp. resist. and struct. 79—39008
borosilicate, anisotropic glasses, birefringence and microstruct. 77—8541
brass, 70:30, rolled, nucleation and annealing texture development 80—45320
β-brass, spinodal decomposition, electron microscope and diffr. study 79—78930
brass, two-phase α/β bicrystal, diffusion induced twins in α-phase 79—46967
brass, two-phase α/β bicrystal, morphology and crystallographic relationships between phases 79—46966
brass LMtsSKA 58-2-2-1-1, heat treatment, struct. and props. 79—83239
brittle model mats., porous and nonporous, strength and struct. 77—4849
calcite microstructure, geological aspects 79—57933
calcite rocks, experimentally deformed, texture development 79—83230
cavitation erosion, observation of eroded surface by SEM 78—15536
cellular microstructure, 3-dimens. anal. by computer simulation 78—87640
cellular phase separation rate, extremum condition 80—2137

crystal microstructure continued
ceramic, ferrimag. or ferroelec., microstructure and physical props. 78—72756
ceramic, plastic deformation, grain and grain boundary processes 77—4814
ceramic science application of high-resolution TEM 78—35397
ceramics, automatic structure analyser, EPIQUANT, quant. microscopic meas. 79—83409
ceramics, fracture mech. appl. 79—43426
ceramics, microstructure dependence of mechanical behaviour 78—88533
ceramics, polycrystn., strength-grain size relations 79—79081
ceramics, US attenuation 78—67772
cermet film, as solar selective absorbers, production, struct. and optical props. 79—29485
cermet layers deposited by silk-screen printing, microscopic struct. obs., cond. matrix form. mechanism *(Czech)* 77—48386
chalcedonies, structural disorder by IR spectroscopy 79—87450
charcoal, active, heat-treated, spiral growth structs. *(German)* 78—44141
chondritic meteorites, severely reheated, metallic microstruct. and thermal history 78—12167
coherency loss in modulated structures, approx. criterion 77—48391
coherent domain structures from crystal transitions with related space groups 79—42002
coherent interphase boundary energy anisotropy between cubic-type crystals 80—54252
coke, metallurgical, microstruct., using refl. light microscopy and image anal. 80—66732
cold rolling, texture form., model *(French)* 78—68705
composites, two phase, depend. of texture and microstruct. on yield stresses of components 79—91697
corundum, corrosion resist. in fused Li rel. to phase and microstruct. changes 77—44378
corundum, crystallization during bauxite reduction at 800-1800°C 77—86296
corundum, growth of large crystals of high opt. quality 77—34916
corundum, subjected to thermal shock, study of substruct. and surface morpholoy 79—43292
corundum ceramic, high-temp. treatment, powder medium effect on microstruct., comp., strength and dielec. props. 79—33984
creep and growth, radiation induced, fundamental mechanisms 80—92596
crystallites with step displacement, particle sizes and distortion determ., by means of X-rays *(German)* 80—14960
Debye-Sears cell lattice, basis determ., general analytical method 77—7739
deep-drawing curves, cryst. microstruct. during deform. *(French)* 79—20066
defect theory and processes, review 80—2009
development over 50 years, microscopic particles, microscopic struct. of matter *(Chinese)* 77—68929
devitrificates, quantitative charact. of microstruct., electron microscope study *(Polish)* 79—100311
devitrificates, quantitative charact. of microstruct. *(Polish)* 79—91889
diamond, form. by shock compression of graphite, cryst., surface struct. 78—44060
diamond, natural, polycryst., distinctive features of struct. 79—92530
diamond, synthetic grits, crystal morphology of cyclic twins 80—2037
diamond, ultradisperse, obtained by high temp. synthesis in explosion, struct. 79—29003
diamond tool, metallic binder, microstruct. charact. by electron probe anal., SEM obs. *(Rumanian)* 79—74114
diffraction-profile Fourier analysis, determ. of microstruct. parameters 80—49042
diffusion welded joints, creep deformation effect on characts. 80—25806
dual-phase microstructure *(German)* 80—45280
Duralumin, effect of alloy purity and ageing on fracture mechanism, and resultant toughness 79—5049
earth reentry exposure, simulated, effect on mech. props., oxidation of ThO_2 dispersion hardened alloys, Haynes 188 and Hastelloy X 79—5086
electron microscope appl. to metals research, steel microstructure determ. *(German)* 80—15089
electron microscopy, developments in high resolution imaging 80—99001
electron probe microanalysis use for microstruct. determ. of thin surface layers *(German, English)* 77—56204
electronics microstructure analysis by SEM 79—80723
enantiomorphic crystals, electron microscopy 77—84602
eutectic alloy, dendrite growth—the coupled zone 80—97489
fatigue resistance, in metals 80—94907
feldspars, superplastic flow and cryst. chemistry changes 79—79831
ferrite, microstruct. depend. of props. and applics., review 78—88548
ferrite, orientation in pearlite, rel. to austenite *(Russian)* 80—81072
ferrite, transform. kinetics, grain size, alloying element effect, carbide precip. 80—93560
ferrite film, prop. by plasma jet spraying microstruct. and magnetic props. 78—6546
ferrites, polycryst., dynamic mag. susceptibility rel. to ferromag. reson, grain struct. effect *(Russian)* 77—66267
ferrous metals, banded structure determ., automatic structure analyser 78—39973
film, evaporated at oblique incidence, columnar grains inclination angle 80—75468
films, elec. and galvanomag. props., microstruct. 80—70859
fine fragmented crystals, complex struct. analysis by electron microscopy 80—104416
fluoropolymers, determ. of microstruct. by secondary emission mass spectrometry *(Russian)* 77—31604
friction surfaces microstructure, during tribotechnical processes *(German)* 78—15540
fusion reactor materials, microstruct. development in simulated irrad. 80—34072
fusion reactor materials, microstructure evolution under irradiation 80—34041
gamma-ray diffraction applications 80—14972
gamma-ray diffractometry, phase transitions, domain structures, twinned texture studies 80—19678
garnet:Nd^{3+}, spectral, structural regularities, anal. 78—51948
glass, sheet, laminated struct., effect of prod. method 79—61555
glass, sheet, laminated struct. and homogeneity, mech. agitation effect 79—61554

crystal microstructure continued

- glass, sheet, striation form. mechanism, luminous point method meas. 79—61751
- glass fibre reinforced Al alloy, formed by hot extrusion, mech. props. 77—24987
- glass fibre reinforced plastics, microstructure rel. to mech. props. 80—11685
- glazes, opaque, with ZnO, microstruct. 79—60281
- grain coordination in plane sections of polycrystals 79—78984
- grain disorientation angles, density and distrib. in non-cubic cryst. systems 79—61560
- graphite, polycryst., reactor-grade, neutron irradiated, isothermal annealing obs., by ESR *(Japanese)* 77—43254
- graphite, pyrolytic, thermal expansion coeff. rel. to temp. 78—43147
- graphite intercalation cpds., struct. and order-disorder transforms. 78—71710
- graphites, strength and struct., conf., Bath, London, England (Apr. 1979) 80—82566
- graphitic Ceylon and California, occurrence carbyne forms of C, X-ray and SEM anal. 79—77450
- graphitised PAN fibre layered compounds with metal chlorides 79—91600
- Hastelloy X, grain size effect. creep and creep-rupture *(Japanese)* 80—16382
- Hastelloy X, mech. props. effect of solidification substruct. 77—25040
- high resolution TEM, role in structure research, C, W_xO_y and mineral examples *(Hungarian)* 77—76267
- high strength structural mats., microstruct. influences on fatigue and fracture resist. 78—56728
- homogeneous nucleation and growth processes, computer simulation 78—30764
- I_2-IV-VI_3 cpds., tetrahedral phase stability 77—48415
- II-VI semiconductors, electron microscopic investigations 79—32864
- Incoloy 800, exam. of mech. and microstructural props. 79—5022
- Incoloy 903, microstruct. and effect of H_2 charging 77—86143
- Inconel 617, microstruct., mech. props., thermal ageing effect 77—36557
- interface composition during diffusion controlled precipitate growth, model for ternary systems 77—36513
- ion implantation, metastable phases in metals, review 80—49254
- jade, fracture parameters and crack propag. resist., rel. to fibrous microstruct. 77—8908
- Johnson-Mehl and cellular microstructure, comparative analysis, computer simulation 80—54392
- lath martensite, habit plane and morphology 77—8823
- layered materials, struct. changes rel. to CDW, TEM, electron diffr., dichalcogenides appl. 80—39042
- local control methods 79—91655
- lunar soil 15081,2, adsorpt. of methanol and water, microcrystallinity determ. 77—87292
- magnetic materials, psarks rel. to pseudo-single domain behaviour 78—65274
- Magnico alloy, with Si, Nb, Ti effect of Ub on mag. props. and grindability 77—63811
- martensite crystals, orientation relationship definition, anal. method 78—60670
- martensite layers, external stress effects on equilibrium morphology, thermodynamic model *(Russian)* 78—52804
- martensitic transformation, internal stress relax. effect on microstruct. and kinetic features 77—44250
- massive transformations, free energy, microstruct., growth and nucleation 77—4776
- materials props. depend., book 78—88470
- materials under load, durability and accumulation of damage *(Russian)* 77—59892
- mechanical properties, influence of microstructure 77—7302
- metal, grain neighbourhood relationships *(French)* 77—77694
- metal, microstructural evidence supporting SIPA creep mechanism 79—61679
- metal, microstructure and strength *(German)* 77—70138
- metal, pure, with max. of cryst. lattice distortion, struct. and strength props. *(Russian)* 80—89234
- metal, thin sheet, tensile instability and limit strains, growth of surface roughness 77—86084
- metal alloys, microstructural instabilities, review 78—35348
- metal foams, solidification in space environment, fluid flow effects 79—47674
- metal powder, method for TEM study 80—84038
- metallic materials, crack propag. mech. and fracture toughness, microstruct. effects 78—19859
- metallography, quantitative methodology *(French)* 80—30205
- metals, cubic, heavily deform., development of lattice curvature 80—81136
- metals, effect on bulk material props. 80—34004
- metals, FCC, small vacancy clusters, structures and energies, computer simulation 80—39073
- metals, recrystallisation during hot deform. 78—68714
- metals, structural state and physical similarity criteria *(Russian)* 79—52298
- meteorite, Kirin, fusion crust microstruct. from SEM study *(Chinese)* 79—2525
- MgO-ZrO_2 ceramic reinforced with filamentary crystals, mech. and thermal props. 80—45262
- mica, metamorphic white, surface microtopography 80—54493
- microstruct. and tensile props. 80—34077
- muscovite deformation, comparison with biotite from optical microstruct. 80—26507
- naphthalene-adipic acid system, crystal growth from melt, V-ΔT and V-λ relations 80—19734
- NASICON solid electrolyte, processing and phys. props. 80—60820
- nearest-neighbour size correlation with grain size *(French)* 77—8843
- Nimonic, IN100, γ' precipitates, casting conditions effect on morphology 80—7548
- nuclear fuel, quantitative metallographic anal., computer program, QMA 79—15951
- nuclear reactor materials, radiation damage, fast breeder and fusion reactors *(Japanese)* 79—81011
- opal, ordered arrangements of SiO_2 spheres of two different sizes 78—87658
- oxide eutectics, directionally solidified, crystallography and microstruct. 79—78950

crystal microstructure continued

- oxides, fluorite and ReO_3, n-beam struct. images, expt. observations and computer calc. 78—38593
- Permalloy, high-permeability, influence of grain struct. and non-mag. particles on mag. props. *(German)* 77—16112
- petrographic method of determ. of quantitative relation between phases in microcryst. structs. 78—35608
- phase connectivity in two-phase microstruct., Monte Carlo calc. of topological and percolation props. 78—30765
- plastic deforms ands rupture mechanisms, depend on B additives *(Russian)* 79—61650
- poly-phase microstructures, quantitative metallography, review 79—15925
- polyethylene, chain-extended, deform. of lamellar microstruct. on drawing five-fold 77—21220
- polyethylene, high density, film, melt growth, cryst. superstruct., small angle light scatt. 77—31602
- polyethylene, pyramidal crysts., soln.-grown, collapse mechanics 78—76713
- polyethylene, single, polycryst., ^{60}Co-γ irrad., effect on melting behaviour 77—15548
- polyethylene, single cryst. and spherulites, microstruct., deform. micromechanisms 78—83758
- polyethylene films, hard elastic, deform. mechanism 77—32652
- polyethylene spherulites, high density, microstruct. and mech. props. 78—42921
- polyethylene terephthalate, mech. props., influence of cryst. arrangement and noncryst. region struct. 78—76707
- polyfluorvinylide, determ. of microstruct. by secondary emission mass spectrometry *(Russian)* 77—31604
- polymer, crystalline, crystallisation, morphology rel. to props. 77—39546
- polymer, drawing properties, role of interfibrillar tie mols. 78—76706
- polymer, recrystallisation during drawing 78—76658
- polymer, soln.-grown cryst., diffr. line-broadening, bending contrib. 78—75574
- polymer microstructure morphogenesis, book contrib. 78—83757
- polymers, crystalline formations study, light refl. from untreated surface 77—28945
- polymers, microtoming for structure analysis 80—40665
- polymers, solid, orientation effects, conf., Budapest, Hungary (April 1976) 78—75557
- polypropylene, cold-drawn isotactic bars and thin films, microstruct. and annealing 78—95760
- polytrifluorclorethylene, determ. of microstruct. by secondary emission mass spectrometry *(Russian)* 77—31604
- Portland cement, hydration mechanism 78—35349
- portland cement paste, microstructure study by SEM, TG and X-ray diffr., corrosion 78—92381
- powder metallurgy superalloy, wrought, phase relations and microstruct., C and Hf conc. effect 77—44218
- property relations 77—36378
- pyrographite, Si-containing, high-temp. treatment effects 77—40429
- quartz, microtopographical obs. of 2nd order prism faces, hydrothermally-grown crysts. 80—54481
- quartz, resonator, X-ray double crystal topographic assessment of defects 79—50943
- quartz, synthetic, annealed, light scatt. centres 77—11586
- quartz fibres, polar orientation, stereospecific twisting 78—42930
- quartz grains in Moine thrust zone, deformation-induced microstructs. rel. to differential stress 80—85652
- quartz overgrowths, on quartz, cathodoluminescence and microstruct., SEM exam. 79—25239
- quartz porcelain fast fired, development of microstruct. *(German)* 78—60625
- quartz-feldspar mylonite, microstruct. and fabric development 78—96201
- quartzite, naturally deformed, textural and microstructural development, metallurgical approach 79—83228
- quartzites, intracrystalline deform. comparison in natural and exptl. deform. 79—79830
- Raman microprobe-microscope appl., molecular optical laser examiner 80—62737
- rare earth-Cd double tungstates, with scheelite structure 78—44103
- rare earth-Co permanent magnets, microstruct., TEM obs., magnetisation 78—91901
- rectorite, stacking and ordered interstratification, high-resolution TEM obs. 80—109140
- refractory alloys, creep mechanism and struct. changes *(Russian)* 79—52299
- refractory fusion reactor materials, neutron irrad., microstruct., voids, nucleation TEM study 80—29065
- refractory wear-resistant coatings, composite struct. develop., props. 77—63618
- resistive layer microstructure on superconducting Al surface *(Russian)* 80—34567
- SAP (Al_2O_3-Al) alloy, effect of high He^+ and H_2^+ conc. on microstruct. 80—34098
- sapphire, profiled growth, struct. perfection 78—68621
- satellite, hardness and erosion resistance to aqueous SiO_2 slurry, microstruct. obs. 79—43441
- SEM channelling contrast technique for material deform. obs. 78—23917
- semiconductor, flow detection using IR laser defectograph 78—3299
- semiconductor film, polycrystalline, modified carrier model *(German)* 80—7012
- semiconductor junction, ion implanted, elec. props. correl. with n^+ region microstructure 77—76916
- simulation of micrographs, based on optical, electron and field-ion microscopy 80—19679
- sintering, liquid phase, microstructural evolution, coarsening 77—70014
- sintering, liquid phase, microstructural evolution 77—70013
- Sn coated Cu, fine struct. in diffusion zone and mech. props. 77—11739
- solid state chemistry problems, appl. of electron microscopy and diffr. 79—46527
- spinodal alloys characterisation techniques, props. and appls., review 80—50588
- steatite ceramic, sintering and crystn., depend. on original powder state 79—61527
- steel, 0.2 to 0.8% C, ferrite-pearlite transformation, tensile strength, cooling rate effect 80—7549
- steel, 0.7% C, welded zone, fatigue strength and microstruct. *(Japanese)* 80—89339
- steel, 08Yu, annealing effect on texture, microstruct., and mech. props. 78—44138

crystal microstructure continued
- steel, 0Kh12G14N4Yu2, struct. after deformation under conditions of superplasticity 80−21031
- steel, 12Cr1MoV, thermal fatigue and creep effect in fracture 80−104297
- steel, 12Kh1MF, structural changes during creep tests 77−63746
- steel, 20Kh, warm extrusion effects on struct. and mech. props. 77−44311
- steel, 24Kh2NMFA, weldments, heat-affected zone struct. 79−24552
- steel, 34KhN1MAR structural heterogeneity of 70 ton ingots γ to α transform, in dendritic section 77−70047
- steel, adhesive wear, heat treated load effect 78−11344
- steel, Al and Cr coated, structural transformations oxidation effect in Kh25N20S2 steel 79−57154
- steel, alloy, 300M, fracture toughness and strength, effect of heat treatment on microstruct. 78−15436
- steel, alloy, low C, effects of pre-treatment on graphitisation behaviour *(Japanese)* 78−84860
- steel, alloy, maraging, 18% Ni, effect of solution and ageing treatments, on microstruct., tensile props., fracture toughness 78−80648
- steel, alloy, medium and low C, quenched and tempered, fracture resist., nonmartensitic transformation products effect 79−96054
- steel, alloy, Mn-Si-C, exam. of fracture toughness for sheets, using linear elastic fracture mechanics 78−56762
- steel, alloy, transform. kinetics of supercooled austenite in 12Kh1MF, structural method 78−52801
- steel, alloy, type 52100, exam. of microstruct. and fracture, as function of austenitising in temp. range 800 to 1100°C 78−76673
- steel, alloy, type AISI 4340, martensitic transformation, TEM study 80−3043
- steel, alloy, type Kh16N11M3, struct. changes during thermocyclic working, dislocation struct. *(Russian)* 80−54243
- steel, alloy, U20Kh6T2D, structural transformations during heat treatment, and wear resistance 78−88484
- steel, alloy, ultrahigh-strength, near threshold fatigue crack propag., microstructure effects 77−86168
- steel, alloy, V-W-Mo-Cr, exam. of carbide transformation 80−16299
- steel, alloy type 25KhN3MFA, tempering of bainitic structure 80−20983
- steel, austenite, abnormal decomposition kinetics and mechanism *(Russian)* 80−55344
- steel, austenite hot deformation influence on phase transformations 80−7606
- steel, austenitic, 40Kh13N8G8, dissolution kinetics of carbide $Cr_{23}C_6$ *(Russian)* 78−48369
- steel, austenitic, AISI 4340, effect of step quenching on microstruct. and fracture toughness 78−84834
- steel, austenitic, fracture state in creep *(Czech)* 80−30081
- steel, austenitic, Kh12N20T3R, ageing, submicroscopic struct. role in dispersion hardening *(Russian)* 78−64549
- steel, austenitic, low-C, transform. kinetics rel. to temp., deform., struct., mech. props. 79−24519
- steel, austenitic, substructure change in hot deform. process *(Russian)* 77−16617
- steel, austenitic and austenitic ferritic, welds, rel. between solidification and microstructs. 79−61579
- steel, austenitic and duplex 308 stainless, mech. of intergranular corrosion and pitting corrosion 79−91846
- steel, austenitic and martensitic, structural sensitivity of Bauschinger effect *(Russian)* 79−52303
- steel, austenitic stainless, ferritic, single phase ferritic solidification in welds, exam. 80−7546
- steel, austenitic stainless, He role in neutron induced microstruct. evolution 80−29064
- steel, austenitic stainless, mech. props. correl. methodology development for fusion environments 80−29068
- steel, austenitic stainless, microstructural effects on US attenuation 78−11455
- steel, austenitic stainless, microstructure and transient creep 79−61675
- steel, austenitic stainless, precipitates and grain orientation by non aqueous electrolyte potentiostatic etching method *(Japanese)* 80−15102
- steel, austenitic stainless, type 304, exam. of continuous cooling sensitization 79−29098
- steel, austenitic stainless, unlubricated, friction, wear and microstruct. of types 304, 316 and Nitronic 60 80−108589
- steel, austenitic stainless, welded explosively, induced martensites morphology 80−104153
- steel, austenitic stainless, welds, exam. of austenitic solidification mode 80−7545
- steel, austenitic stainless type 304, time-depend. fatigue, mechanistic model 80−100925
- steel, C, bainitic, microstruct. and cleavage resistance 77−52481
- steel, C, fatigue crack propagation in sheet, influence of struct. of ferrite-pearlite bands *(French)* 80−76338
- steel, C, fracture, effect of cementite *(Russian)* 78−7037
- steel, C, fretting fatigue damage, SEM exam. 78−88541
- steel, C, microstructural inhomogeneity, influence on formability and fracture 80−11682
- steel, C, quenched, restoration of austenite grains during rapid heating *(Russian)* 80−76272
- steel, C, type S15CK, tufftrided, fatigue strength at elevated temp., under reversed axial strength *(Japanese)* 78−84980
- steel, C, weldable, ferrite-pearlite, Widmanstatten structs., resist. to fracture 79−29203
- steel, carbide cracking as source of acoustic emission 78−19872
- steel, carbide formation, microscopic exam. aided by rating charts *(German)* 79−61805
- steel, carbide structure, quantitative analysis using Epiquant analyser *(German)* 80−3284
- steel, carburised, microstruct. and fracture 79−24658
- steel, case-hardened cast, contact endurance rel. to austenizing *(Russian)* 78−56805
- steel, cast, high speed, solidification, $(Fe,Mo)_6C$ form., struct. 79−24514
- steel, cementite coarsening in type 1080 in a temp. gradient 78−88486
- steel, cementite phase evolution during annealing *(Russian)* 77−32836
- steel, chemicothermal treatment quality control by fractographic method 79−39080
- steel, comp. and processing effects on microstruct. and props. rel. to low temp. applic. 77−52365
- steel, Cr, influence of ultrasound on tempering processes *(Russian)* 78−52827

crystal microstructure continued
- steel, Cr, post-hotforming recrystallisation condition, use of NEOPHOT 2 and EPIQUANT 80−84949
- steel, Cr (12wt.%), mech. props, carbide phase struct. 79−15702
- steel, Cr plated, factors influencing durability 80−108643
- steel, Cr-Mo, annealed, microstructural effects on creep-rupture behaviour 79−57120
- steel, Cr-Mo (2.25, 1 wt.%), damage accumulation and microstruct. changes during creep 80−3129
- steel, Cr-Mo (2.25, 1 wt.%), in high temp. Na, heat treatment and metallurgical struct. effects 77−16619
- steel, Cr-Mo (2.25, 1 wt.%), small changes effect in impurity elements, creep life 80−25790
- steel, Cr-Mo (9, 1 wt.%) microstructural instability during creep, heat treatment effects 78−48472
- steel, Cr-Mo-(V), microstruct. effect on high-temp. props. *(Czech)* 80−89300
- steel, Cr-Mo-V, creep, effect of microstruct., heat treatment, transform. temp. 78−11248
- steel, Cr-Mo-V, creep fracture, microstruct. effects 78−64668
- steel, Cr-Mo-V, medium strength, correlation between crack initiation, propag. and microstruct. 78−60787
- steel, Cr-Mo-V (0.5, 0.5, 0.25 wt.%), creep crack growth in notched bend test, microstruct. effect 77−21261
- steel, Cr-Mo-V (0.5, 0.5, 0.25 wt.%), heat treated, microstructure effect on threshold region fatigue 78−56757
- steel, Cr-Mo-V pressure vessel, microstruct. parameters and yielding rel. to plastic deform. 80−89318
- steel, Cr-Ni, microstructural distrib. of cathodic H_2, autoradiography *(French)* 79−99234
- steel, Cr-Ni-Mo, combined B and rare earth metal additions effect on microstruct. impact strength and hardness 79−38963
- steel, Cr-Ni-Mo-V, magnetic induction, struct. dependence *(Czech)* 80−50141
- steel, Cr-Ni-Mo-V, quenched, morpholgoy, structural constitution after austenite form. by heating *(Russian)* 78−68709
- steel, Cr-Ni-Ti-B, grain size effect on mech. and struct. props. *(French)* 80−45361
- steel, Cr-V (1.5, 0.5 wt.%), ferritic, effect of temp. and microstruct. on creep damage 79−5023
- steel, crack propagation, struct. effects 79−52370
- steel, cracking resistance of high-strength 40Kh and 35KhGSA, tempering temp. influence *(Russian)* 79−52252
- steel, CrMoV, creep resistant, quantitative struct. parameter use in props. prediction *(Czech)* 80−108481
- steel, dual phase, improved etching technique for percent martensite determ. 80−16624
- steel, ductile fracture under cold metal forming conditions, metallurgical struct. influence 79−34125
- steel, fatigue fracture after Fe and Ce diffusion coating, microstruct. investigation *(Russian)* 79−52446
- steel, fatigue life, structural parameters and chem. comp. effects, rel. to test parameters 77−59928
- steel, Fe-C martensite, quenched, and heated to 293K, struct., Mossbauer obs. *(Russian)* 77−59784
- steel, ferrite-pearlite, cyclic behaviour, fatigue, chem. comp. and microstruct. effects 78−60833
- steel, ferritic, low alloy, effect of microstruct. on creep fracture 78−80640
- steel, ferritic and austenitic, microstruct. study by means of replicas taken from components at 100°C 80−81256
- steel, ferritic stainless, Cr-Mo (12,1wt.%) microstructure influence on localised corrosion behaviour 80−61018
- steel, ferritic stainless, embrittlement 80−85041
- steel, Hadfield, containing Ni, carbide precipitation, heat and cold work effects *(Korean)* 77−77484
- steel, heat-resistant, martensitic, Kh12NMFB weldability 80−20987
- steel, heat-treatment furnace trays, in service embrittlement, microstruct. and props. changes 77−63784
- steel, heating effect on phase composition, microstruct. and mech. props. 80−100859
- steel, high C, thermomech. treated, strengthening factors 77−8862
- steel, high Mn mandrels, wear resist., surface layer chem. comp. influence *(Russian)* 79−52444
- steel, high Mn-Cr, austenitic struct. stability and low-temp. toughness *(Japanese)* 80−76356
- steel, high purity, low S content, for tough semi-finished products in nuclear power plant *(German)* 80−45393
- steel, high strength weld metal, fractography, microstructure and reheated zone toughness effects *(Japanese)* 80−108543
- steel, high-speed, eutectic carbide structure, determ. by SEM 78−85075
- steel, high-speed, fracture toughness, carbides influence *(French)* 80−108559
- steel, high-speed, N effects on struct. and props. 77−59799
- steel, high-speed cutting, struct. and props. Co addition effects *(Russian)* 77−21177
- steel, hot rolled, low C, low alloy, bainitic alloying addition effects on microstruct. and props. 77−36546
- steel, hypereutectoid, austenite dissociation depend. on strain at intercritical temps., pearlite transform. *(Russian)* 80−40362
- steel, hypereutectoid, thermomech. treatment, Fe_3C distrib. and yield point *(German)* 79−52243
- steel, hypereutectoid type HF-1, microstruct. effects on fracture toughness, ductility, strength 79−74255
- steel, hypoeutectoid, singularities of cryst. geometry of pearlite *(Russian)* 77−21093
- steel, Kossel patterns, small area 79−1375
- steel, large forging, mech. props. 77−4797
- steel, low alloy, B, quenchability and microstructure *(French)* 79−47727
- steel, low alloy, C-Ni-Cr-Mo (0.36 wt.%), impact toughness rel. to microstruct. *(Korean)* 77−21188
- steel, low alloy, creep crack growth, microstruct., fatigue effects 80−7672
- steel, low alloy, eutectoid pearlitic, exam. of microstructures dominating ductility *(Japanese)* 78−84917
- steel, low alloy, exam. of fatigue crack growth, and Paris Law parameter relationship 78−92343
- steel, low alloy, exam. of microstructure, in type PZhK-1000 soldered joint by metallography 79−52257

crystal microstructure continued
- steel, low alloy, high strength, correlation between fracture toughness, tensile props., fracture morphology 78−60789
- steel, low alloy, microstruct. effects on fatigue at intermediate and high crack growth rates 79−74247
- steel, low alloy, pearlite block, exam. of crystallographic features, formation processes *(Japanese)* 78−84799
- steel, low alloy, reactor pressure vessel, effect of Mn and C content on irrad. response 79−20196
- steel, low alloy, sintered, isothermal transformations, porosity effects 80−3032
- steel, low alloy and C, bainite morphology 78−68682
- steel, low alloy Cr-Mo, heat fatigue, effect of technical factors 79−79058
- steel, low C, $\gamma \rightarrow \alpha$ transform., martensitic mechanism *(Russian)* 79−47682
- steel, low C, C content effects in corrosion fatigue in nitrate solns. *(Russian)* 78−56811
- steel, low C, high strength, thermomech. treatment, microstruct. 79−57015
- steel, low C, hot rolling effects on struct. *(Russian)* 78−19793
- steel, low C, Mb-Nb, reheated, quenched, tempered, microstruct. 77−36550
- steel, low C, microalloyed, heat treatment, mech. props. 79−24551
- steel, low C, Mn, laws of banding structure form. *(Slovenian)* 78−83776
- steel, low C, Mn-Nb, quenched and tempered, microstruct. and props. 77−36549
- steel, low C, Nb-V microalloyed, Nb, V effect on impact and toughness props. 78−15515
- steel, low C, normalised, plastic deform., using microhardness and grain strain meas. 77−4810
- steel, low C, quenched, hardening during explosive forming 79−87650
- steel, low C, quenched, struct. and props. after plastic deform. and tempering 78−23734
- steel, low C, struct. changes during decarburisation in intercritical temp. interval *(Russian)* 77−25075
- steel, low C, structurally free cementite formation 78−23697
- steel, low C, tempered, lath martensite, Ni (5 wt.%), microstruct./yield strength relationship 77−21234
- steel, low C, tufftrided, fatigue strength ahd microstructure change by reversed stressing *(Japanese)* 78−15511
- steel, low C, type AISI 1018, microstruct. effects on fatigue crack growth 79−61718
- steel, low-alloy, bearing, mech. props., carbide behaviour effect *(Korean)* 80−93615
- steel, low-alloy structural 16G2 and 16GFR, struct. and props. after quenching and tempering 80−76280
- steel, low-C, fully pearlitic, struct. and mech. characts. rel. to cooling conditions *(French)* 80−40425
- steel, low-C, preliminary thermomech. treatment, cold deform. effect on struct. and props. 79−38847
- steel, low-C, transformed by cooling in ferritic-pearlitic range, relations between cooling rate, struct. and mech. props. *(French)* 77−32570
- steel, lower bainite, struct. changes during tempering *(Russian)* 77−21178
- steel, maraging, heated to high temperatures, γ to δ transformations 80−20930
- steel, maraging, steady state unidirectionally solidified, austenite reversion and determ. 77−25118
- steel, martensite, brittle fracture resistance, struct. after quenching effects, tempering effects 79−57104
- steel, martensite, partially disintegrated X-ray anal., appl. of method of moments 79−52223
- steel, martensite-ferrite combined microstructure, two-phase, tensile fracture strength 78−60783
- steel, martensitic, ageing, thermal recovery 77−56011
- steel, martensitic, fatigue crack form. associated with cyclic slip deform. along prior austenite grain boundaries 78−60831
- steel, martensitic transform., orientation relationships *(German)* 77−25050
- steel, medium C, type 35 laser treatment effect on struct. and mech. props. 79−39041
- steel, microalloy V-Nb, V, Nb effects on strength and formability of cold rolled sheets 77−55979
- steel, microstructure control in flash butt welding 79−91715
- steel, microstructure of 0Kh16N15M3B after creep tests in BR-10 reactor, electron, microscope invest. *(Russian)* 80−92531
- steel, mild, annealed, fatigue crack init., microstructure and strain ageing effect 77−86162
- steel, mild, semi-killed, tempering, effect of microstruct. and hardness 77−21184
- steel, mild, Ta coating at atm. press. using CVD method 80−55591
- steel, mild, yield strength and fracture toughness, microstruct. effect, heat treatment 78−27615
- steel, mild explosively welded, 0.1% C tube to 0.2% C plate, microstructure 77−70221
- steel, Mn, as rolled bainitic, tensile, impact and machinability props., transport appl. 78−88503
- steel, Mn, influence of ultrasound on tempering processes *(Russian)* 78−52827
- steel, Mn (16 to 20 wt.%) metallographic analysis method 80−50791
- steel, Mn-Mo-Nb, high strength, ductile, acicular ferrite struct. 77−21191
- steel, Mn-Mo-Ni-Cr, bainitic, microstructures and mechanical properties *(French)* 80−16362
- steel, Mn-Sn(-Nb), extra low C, shear transformation struct. *(German)* 80−60873
- steel, Mo-V, creep rupture strength, rel. to microstruct. *(German)* 78−35467
- steel, Ni, cryogenic fracture toughness enhancement through grain refinement 77−36651
- steel, Ni, microstruct., plastic zone size and crack propag. 78−60790
- steel, Ni and W, recrystallisation mech. during laser treatment 80−50658
- steel, Ni-B, B effect on temperability and microstructure 79−15710
- steel, Ni-C, martensitic, microstructural distrib. of cathodic H_2, autoradiography *(French)* 79−99234
- steel, Ni-Cr-Ti, thin bands, cold working, props. and struct. of 36NKhTYu 79−78994

crystal microstructure continued
- steel, Ni-Mn-Al-V, nonmagnetic, ageing, dispersion hardening, microstruct., phase comp., mech. props. *(Russian)* 79−34046
- steel, pearlitic, fatigue, metallographic aspects 78−60828
- steel, pearlitic, heat treatment effects on mech. props. and microstruct. *(German)* 77−8857
- steel, pearlitic, strength, fracture, microstructure effect 77−40449
- steel, pearlitic, wear behaviour rel. to basic material props. 80−108592
- steel, perforated bent sections, microstruct. near holes 78−23725
- steel, plain C, quench ageing avoidance, critical cooling rate *(German)* 79−52244
- steel, plain C having ferrite-martensite mixed structs., microstructural parameters effect on fatigue strength *(Japanese)* 80−71735
- steel, plasticity of two-phase, coarse microstruct.-material *(German)* 77−59882
- steel, precipitation hardening, strength and struct. *(German)* 79−47701
- steel, quenched and tempered, microstructure effect on cleavage fracture toughness 79−74252
- steel, railway, oxidation by Fe-Si-Ca-V complex alloy, nonmetallic inclusions *(Russian)* 80−93685
- steel, Rheocast, struct. and props. 77−28804
- steel, SAE 1045, permeation meas. of H trapping, rel. to cryst. microstruct. 80−84328
- steel, Si(3 wt.%) grain oriented, high permeability obs. 77−1881
- steel, Si (3 wt.%), struct. and preferred orientation, annealing parameters influence *(Czech)* 80−89248
- steel, Si-Mn, ferrite-pearlite structs., fatigue crack propagation *(Russian)* 79−34126
- steel, spheroidized AISI 1095, ductile fracture of U-notched bend specimens 79−24616
- steel, spring alloy, microstruct. and props. at low temps. 77−44286
- steel, stainless, AISI 304, dislocation struct., carbides, deform. mech. map 77−16650
- steel, stainless, alloyed with C, magnetron-sputtered, microstruct., and cryst.-amorphous transition 80−19719
- steel, stainless, austenitic, explosively welded, orientation relationship in martensitic transform. 80−104158
- steel, stainless, austenitic, microstructural distrib. of cathodic H_2, autoradiography *(French)* 79−99234
- steel, stainless, austenitic, precipitation hardening and N_2 effects obs. *(Rumanian)* 77−55973
- steel, stainless, C heterogeneities demonstration by high-resolution autoradiography *(French)* 77−66729
- steel, stainless, Cr-Ni (18, 9 wt.%), cold rolled, struct. 79−83214
- steel, stainless, depth distrib. of swelling, TEM exam. 80−15165
- steel, stainless, fatigue crack morphology of type 304 cycled at const. stress amplitude at elev. temps. 78−64671
- steel, stainless, ferrite to austenite decomp. 80−93554
- steel, stainless, ferritic, BCC cryst., fagigue cracking rel. to cryst. orient. *(French)* 79−20178
- steel, stainless, filament produced by glass coated melt spinning, new metastable tetragonal struct. 79−20072
- steel, stainless, irradiation creep and swelling, microstructural modelling 77−52407
- steel, stainless, Kh18N10T, substructure after high-temp. thermomechanical treatment with high deformation rates *(Russian)* 78−76657
- steel, stainless, low energy D implanted, microstruct. 78−95073
- steel, stainless, maraging, Cr-Co, effect of ageing on microstruct., TEM and neutron diffraction exam. 78−84867
- steel, stainless, martensitically ageing, techniques for revealing microstruct. characts. 79−70241
- steel, stainless, neutron irradiated, stress effects on microstruct. 77−47490
- steel, stainless, orthopaedic fixation devices, failure, SEM exam. of fatigue crack surfaces and microstructure 78−77156
- steel, stainless, stress corrosion testing, slow strain rate, elevated temp. and high press. study 80−97615
- steel, stainless, sulphide stress corrosion cracking resistance, improvement by heat treatment 78−7076
- steel, stainless, Type 316, neutron irrad. effects on tensile props. and microstruct. 80−65059
- steel, stainless, with Ni base filler metals, brazed joint strength *(Japanese)* 80−16636
- steel, stainless 304, metallurgical factors on the corrosion and mass transfer in liq. Na *(Japanese)* 80−71804
- steel, stainless AISI 316, fatigue crack growth, effect of grain size on threshold stress intensity 78−44216
- steel, stainless Kh15N9Yu, elastic limit, effect of microstruct. and heat treatment 79−83251
- steel, stainless type 304 attack morphology of stress corrosion cracking, TEM study *(French)* 79−83368
- steel, stainless type 316 welds, post weld heat treatments on struct., composition and ferrite amount 80−29992
- steel, structural, CrN-modified, tempering and quenching effects on struct. and props. 77−59835
- steel, structural, lithoidal fracture surfaces *(Russian)* 77−8905
- steel, surface Si reinforced type U8, metastable phase, composition, struct. *(Russian)* 80−92599
- steel, tempered martensitic, type AISI 410, role of C in embrittlement phenomena 80−93652
- steel, thermal etching displaying hardening structure 77−40487
- steel, tool, cutting blades, heat treatment in fluidised bed, hardening 79−20087
- steel, tool, M2, laser surface melted, heat treatment effects on struct. 79−70086
- steel, tool, NC6, carbide lattice, kinetics of its destruction *(Polish)* 78−92280
- steel, tool, quenching procedure effect on distortion, tool life 80−50657
- steel, tool and high speed samples, emission spectral and X-ray fluorescence anal., SEM microstruct. obs. *(Japanese)* 79−43232
- steel, transformer, EM losses, influence of charact. of substruct. distrib. *(Russian)* 78−7058
- steel, type 1Kh18N9T, neutron irradiated, microstruct. and mech. props. *(Russian)* 80−24503
- steel, type 52100, heat treatment effect on microstruct. and mech. props. 80−29993
- steel, type Kh13N9D2MT martensitic aged, struct. and mech. props. *(Russian)* 80−93600
- steel, ultrahigh strength, near-threshold fatigue crack propagation, load cycle and cyclic strength effects 78−11331
- steel, V, carbide eutectic presence, solidification and struct. 80−50624

crystal microstructure continued
steel, W alloy, microstruct. and hardness, splat quenching effect 80—76293
steel, W-Mo-V-Cr(6,5,2,4 wt.%), 56-5-2, microstruct. produced by melting and powder metallurgy *(German, English)* 77—63591
steel, Zn coated, cold rolling influence on struct. and deform. of diffusional layer *(Russian)* 80—55465
steel, Zn coated strips, plastic deform. influence on struct. and quality *(Russian)* 80—40377
steel 0Kh16N15M3B, neutron irradiated, kinetics of nucleation and growth of vacancy pores and dislocation loops *(Russian)* 77—51408
steel 12Kh18N10T, struct. and mech. props. after prolonged working at −183°C 77—55988
steel 30Kh2NMFA, microstructure of cup and cone fracture surface, effect of size of disperse phase particles *(Russian)* 78—68762
steel 45, acoustic-emission signals, rel. to struct. 79—52297
steel 45 microstruct. and hardness after electron bombardment 79—38956
steel fibre reinforced Ag, exam. of recrystallisation behaviour *(German)* 78—84849
steel hardfaced, effects of quenching on structure and wear resist. 77—21175
steel plates, fatigue substructures after high cycle vibrs. 77—8945
steel tool, martensitic plate arrangement following austenisation 77—40420
steel U8, hydrogenation effects on fatigue crack propag. *(Russian)* 78—56800
steels, C, quenched and tempered, struct.-prop. relationships 80—7599
steels, high-purity and commercially based, containing 10 wt.%W or 5 wt.%Mo, tempering behaviour 80—7600
steels, hot forming property and struct. *(German)* 80—25730
steels, tool, type U10A and R6M5, phase comp. and phys. props. after hydrostatic extrusion 79—96053
steels 60, 18Kh2N4MA, 17GSND, and 12Kh21N5T structure after high-speed cold plastic deformation 80—76316
STEM, fine microstructural details, characterisation 80—24328
structural materials, radiation effects, review 80—49267
structural steel, microstruct. and brittleness, rel. to austenizing and heat treatments 77—56091
styrene-butadiene block polymers, multiphase systems, struct., props. 77—31600
subgrain imaging, in bulk specimens to study localised plasticity using SEM 80—66609
submicroscopic struct. determ. using very-slow-neutron transmission 77—62448
subsurface structure detection by scanning photoacoustic microscopy 80—6323
sulphide minerals, superstructure and modulated struct. 79—99146
superalloy, microstructure resulting from alloying and heat treatment, effect on creep, fatigue, fracture strength 78—11246
superconducting composites, bronze process, metallurgy 80—3004
superstructure involving inversion domains, large scale incommensurate structs. 79—95174
surface microstructure determ. and microanalysis by ultrahigh vacuum field emission gun SEM 80—96423
sylvite powder, compression in smooth faced rolling presses, preferred orientation *(German)* 79—33959
tetrafluorethylene-ethylene copolymer, determ. of microstruct. by secondary emission mass spectrometry *(Russian)* 77—31604
tetrakaidecahedra as grain models 78—51458
thin films, magnetic anisotropy rel. to columnar microstruct., calc. 80—39822
thin films and interfaces, analytical techniques, review 80—80120
Ti alloy, VT22, hot deform., microstruct. form. and mech. props. *(Russian)* 77—28830
$\alpha+\beta$ Ti alloys, prior β grains and α platelet morpholgoy, exam. 78—76679
Tishomingo Fe meteorite, microstructural study 79—16898
titanomagnetites, domain struct. var. with temp. 78—65272
transition metal, amorphous struct. microcrystalline model 79—14733
transition metal alloys, deformation and solute-induced microstructural effects on superconductivity 79—7925
transition metal alloys, domain struct. of diffuse ω-phase formed in quenching, 1D model 78—27523
transition metal carbides and nitrides, M_2X, struct. and phase transitions 79—70051
transition metals and alloys, high-melting-point, fast cooling from melt, cooling rate influence on struct. *(German)* 79—43287
turquoise, crystalline, Nogales Mexico, SEM and TEM study 79—29760
two-phase interfaces, differential geometry 77—51388
Udimet 500, microstructural instability in industrial gas turbine engine vane 77—28833
Udimet 520, Nicralloy-coated, microstruct. degradation, influence of corrosioin protective coating 80—40611
Udimet 700, microstruct. of resolidified zones formed by laser melting single crysts. 79—78953
Udimet 700, superalloy, melted by laser beam, microstructure and topography exam. 79—69919
upset forgings, grain flow structure 79—38872
vacuum deposited metal film, elec. field effect on residual struct. 78—51836
vapour deposited film, columnar microstructure, shadowing mechanism 78—22987
VT3-1, HTMT effects on struct. and props. 78—23740
welded joint, microstructural and chemical heterogeneity 79—29096
welded joints, flash, fatigue strength obs. 79—15760
white Fe castings, morphology of eutectic M_3C and M_7C_3 80—108427
X-ray laser holography, possible appl. to crystal and biological microstructure 78—55322
YIG, hot spraying to give fine, free flowing, sinterable powder 80—20865
Zircaloy, deformed, positron annihilation and electron microscopy 77—8898
Zircaloy tubes, grain struct., texture, dislocation density effect on irradiation creep, X-ray diffr. and optical microscopy anal. 79—74208
Zircaloy-4, PWR tubes, ZrO_2 scales formed in steam, microstruct. 77—6524
Zircaloy-4, resistance-welded, microstruct. of weld region 80—66549
Zircaloy-4, stress relaxation specimens, thermally induced strain recovery causing microstruct. changes 77—25057

crystal microstructure continued
zircon, dissociated, form. in plasma furnace, comp. and microstruct. 77—36429
Ag chalcogenides, single-phase, preparation 78—35293
Ag film, ion plated, on AT-cut quartz crystal, crystallographic structure obs. 80—2280
Ag film, vacuum deposited on NaCl, microstructure and orientation, surface condition influence 79—82486
Ag-Cu (6.6% at.wt.), melted by laser beam, microstructure and topography exam. 79—69919
Ag-Cu alloy filaments, prod. by glass coated melt spinning, microstruct. and tensile strength 79—91667
Ag-Cu flex leads, microstruct. study of corrosion 80—76406
Ag-Cu surface alloyed films, laser melt quenched, microstruct. 80—76423
Ag-Zn (2 to 12 wt.%) containing several metals, internal oxidation *(Japanese)* 80—16570
$AgAsS_2$-$AgSbS_2$ system, thermal, microstructural X-ray phase anal. 77—32565
AgBrI photographic grains, TEM investig. of morphology and crystallography 77—57418
AgCdO, powder metallurgy production, for switchgear in power engineering 80—104094
$Ag_2S+Ln_2S_3$, powdered mixtures, reaction rate, production of ionic semiconductors 80—93741
$AgZr_2(PO_4)_3$ system, phase charact. at different temps. 80—29936
Ag—(100)InP, metal-semicond.cathode contact, metallurgical, physical, chemical processes 80—107911
Al alloy, fracture toughness and struct. *(Russian)* 77—25134
Al alloy, sheets, type 7004, asymmetrical solidification structures, fluid flow, in W arc welds 78—84794
Al alloy 2219-T851, fatigue crack initiation, effect of intermetallic comp. and microstruct. 79—5054
Al alloy 7075, precipitation hardening, toughness and microstruct. *(Japanese)* 78—15509
Al alloy D16AT, fatigue life, struct. and microhardness, working conditions effect 80—55525
Al alloy D16T, acoustic-emission signals, rel. to struct. 79—52297
Al alloy V96Ts, superplasticity 79—52326
Al alloys, effect of melt treatment with granules *(Russian)* 77—44190
Al alloys, laser generated stress waves, effect on microstruct., hardness and strength 79—69192
Al alloys, microstruct. effects on strength, fracture toughness, fatigue cracks 79—43434
Al alloys, optical contrast enhancement by vacuum deposited ZnTe layers 78—44301
Al alloys, preliminary forging effects on struct. and mech. props. of extruded sections *(Russian)* 78—80564
Al alloys, stress corrosion cracking protection, by $\gamma_1 Al_2O_3$ anodic film 78—95836
Al and Al alloys, plastically deformed, influence of microstruct. on energy stored 78—84894
Al bronze, plasticity of two-phase, coarse microstruct. material *(German)* 77—59882
Al cell structures produced by cycling and monotonic creep 80—55452
Al coating, plasma sprayed on steel substrate, microstructural investigation and oxidation effects 78—11426
Al, cold neutron small angle elastic scatt., microstruct. exam. 77—84736
Al, condensed film, phase and struct. nonuniformity *(Russian)* 80—54536
Al, deformed in uniaxial and equibiaxial tension, dislocation arrangements 80—108516
Al, deformed surface layer, block misorientation 79—99405
Al, perfect single crystal growth from melt, different orientations of crystallisation front *(Russian)* 77—55881
Al, solidification, high press. effects 80—66499
Al, structure sensitive props., temp. hysteresis after melting and crystallisation *(Russian)* 79—29036
Al, trial cuts at low speeds in relation with traction trials *(French)* 80—24448
Al, wire, appl. of subgrain control 77—86060
Al, work softening, microstruct. interpretation 77—32593
Al-Al_3Ni eutectic, temp. gradients, microstructural changes 80—84971
Al-Al_6Fe, fibre reinforced eutectic, deformation behaviour by rolling, TEM and SEM study 79—29129
Al-alloy plates, type VAD23, thermomech. parameters effect on struct. and props. 80—20988
Al-Bi-(Fe), directionally solidified monotectic, growth parameters for aligned microstructs. 79—43236
Al-Bi(Cd)(Pb)-Ti, containing low-melting pt. inclusions, mech. props. 80—93632
Al-Cr, rapidly solidified, crystalline and amorphous structures 77—44274
Al-Cr(Mn), cold-worked and homogenised, precip. kinetics, impurity resist. and TEM meas. 77—16596
Al-Cu, effect of alloy purity and ageing on fracture mechanism, and resultant toughness 79—5049
Al-Cu (4 wt.%), AE during deform., effect of ageing at 170°C 78—64597
Al-Cu (4 wt.%), effect of semicoherent precipitation on void swelling, when neutron irradiated, microstruct. obs. 79—42115
Al-Cu (4 wt.%) alloy, high temp. cyclic deform., θ' particle dissolution obs. 80—108515
Al-Cu (4.5 wt.%) alloy, controlled electropotential corrosion in NaCl soln., microstruct. exam 78—39948
Al-Cu alloys, quenched rapidly, microstruct. 78—56668
Al-Cu thin films, microstruct. rel. to electromigration 80—44355
Al-Cu-Mg, type 2036, deformation at ageing temp., effect on struct. and props. 80—7605
Al-Cu-Mg alloy, extruded, press forming in liquid/solid coexisting state, mech. props., Mg effects 78—11151
Al-Cu-Mg-(Ag), effect of addition on fatigue microstructure relationships 80—40483
Al-Cu-Ni, directionally solidified, exam. of struct. of two phase alloys 78—80537
Al-Cu-Ni, vacancy ordering, electron microscope and electron diffr. obs. 79—27954
Al-Cu-Si, Al rich, unidirectionally solidified, microstruct. 79—34021
Al-$CuAl_2$, eutectic system, interlamellar spacing meas. 77—36492
Al-$CuAl_2$ eutectics, microstruct. after solidification, heat pipe influence 80—76243
Al-$CuAl_2$ lamellar composite, creep, microstruct. obs. 79—8331

crystal microstructure continued

- Al-Cu(0-10 wt.%) sintered compacts, mech. props. rel. to sintering 80−76210
- Al-Fe-Si(0.5, 0.2 wt.%), cast, phase determ. 77−70032
- Al-In alloys within miscibility gap, agglomeration in space environment 79−47672
- Al-Mg alloy AMg6, US vibr. during superplastic deform. effect on struct. 79−38911
- Al-Mg alloy Al27-1, corrosion cracking behaviour and fine struct. *(Russian)* 79−52438
- Al-Mg alloys, relationship between props. and nonequilib. phase diagram 79−96000
- Al-Mg cold drawn wires with FCC lattice, texture and structure 77−70067
- Al-Mg-Be, solid soln. decomposition, metallographic study 77−16577
- Al-Mg-Li alloy, metastable S′-phase, struct. *(Russian)* 80−103291
- Al-Mg-Li-Zr alloys, struct., mech. props. 79−24498
- Al-Mg-Ti(Zr), struct. and factors determining brittle intermediate compound form. 78−52817
- Al-Mg-(Ag), effect of addition on fatigue microstructure relationships 80−40483
- Al-Mn, splat cooling and heat treatment effect on struct. and props. *(Russian)* 77−48456
- τ-Al-Mn-C, permanent magnetism and microstruct. 80−75811
- Al-Mn-Fe(Co)(Ni)(Cu), permanent magnetic materials, grain struct. effect *(Rumanian)* 79−73773
- Al-Ni (3-18wt.%), gun-quenched from melt, struct. 80−76225
- Al-Ni(Cd)(Fe)(Si), cold worked, struct. and props. 80−71666
- Al-Ni(Pt)(Zn), rapidly solidified, twinned dendrites 80−70572
- Al-Si, hypereutectic silumins, P and Na modification 78−84792
- Al-Si, inoculated with NaCl+KCl+NaF, effect on morphology of eutectic columns *(Russian)* 79−15684
- Al-Si, unidirectionally solidified eutectic alloy grow at different rates, Vickers hardness 77−36654
- Al-Si (25.4 wt.%), solidification, high press. effects 80−66499
- Al-Si eutectic, Na, Sb and Sr alloying addition effects on microstructure *(French)* 78−64548
- Al-Si_xNyO_z-Al systems, mechanism of current transfer *(Russian)* 77−69427
- Al-SiO_2 interface, stress and microstruct. via TEM 78−26797
- Al-Ti-B alloys, phase comp. and distrib. of components, X-ray obs. *(Russian)* 79−52164
- Al-Zn, comparison between very-slow-neutron transmission and small-angle neutron scatt. expts. 80−19677
- Al-Zn (38 at.%), TEM study of precipitation processes or different microstructures during ageing 80−93561
- Al-Zn (6.8 at.%), synchrotron radn. use in X-ray scatt. *(French)* 79−47723
- Al-Zn alloy coated mild steel, interface struct. 79−52466
- Al-Zn-Mg, effect of microstruct. on localised shear failure 78−52996
- Al-Zn-Mg, plastic deform. influence on structural transform. and mechanical props. *(Russian)* 80−7623
- Al-Zn-Mg, weldable, microstruct. and intercrystalline fracture 77−48550
- Al-Zn-Mg (6,3 wt.%) high-strength alloy, dislocations distrib., corrosive environment influence *(Russian)* 79−52442
- Al-Zn-Mg alloy, microstruct. obs. by optical and electron microscopy *(German, English)* 77−52601
- Al-Zn-Mg alloys, role of dispersed transition metal intermetallic compounds 79−96088
- Al-Zn-Mg and Al alloy 7050, age hardenable, microstruct., effect of monotonic and cyclic straining 77−36633
- Al-Zn-Mg type 7N01-T4, weld, SCC in NaCl-H_2O_2 soln. *(Japanese)* 80−108631
- Al-Zn-Mg/Al-Mg filler welds, weld fusion boundary structure 80−39459
- Al-Zn-Mg-Ti, Ti effect on microstructure during ageing 78−64568
- Al-Zn-Mg-(Zr) alloy, microstruct. effect on fatigue crack growth 80−3164
- AlB_2 flake reinforced composites, prep., props. rel. to aspect ratio, book contrib. 78−48366
- Al_4C_3-Be_2C-SiC system, phase analysis and TEM struct. obs. 80−108420
- $Al_4C_3.3Be_2C$, X-ray difr. and TEM study 80−14973
- $Al_xGa_{1-x}As$ epitaxial film, microstruct., effect on elect. characts. of Schottky diode *(Russian)* 80−107671
- AlN film, oriented c-axis, low temp. deposition by reactive magnetron sputtering 80−76180
- α-Al_2O_3, CVD-grown, cryst. perfection by transmission X-ray diffr. topography 79−65337
- Al_2O_3, corundum ceramic, effects of Na_2O, CaO additions on sintering struct., props. 79−15630
- Al_2O_3, defect microstructure due to ion bombardment, TEM study 80−34100
- Al_2O_3, derived from boehmite, phase transformations and microstruct. 80−60857
- Al_2O_3, derived from gels, sintering behaviour, microstruct. 80−20875
- Al_2O_3 films obtained by pyrolysis of Al acetylacetonate, struct. and props. 77−85098
- α-Al_2O_3, growth and adhesion on Pt-Al alloys 77−8994
- Al_2O_3, high-purity, modulus of rupture, expt. test of Weibull scaling theory 77−21258
- Al_2O_3 plasma-sprayed, struct. and thermal diffusivity 79−86932
- β-Al_2O_3, polycryst. with preferred grain orientation, hot pressing of gibbsite and Na_2CO_3 *(Japanese)* 79−56948
- Al_2O_3, polycrystalline, fracture toughness and acoustic emission rel. to microstructure, temp. depend. 80−11745
- Al_2O_3 substrate, notched, grain struct., SEM study *(German)* 80−33860
- β- Al_2O_3 type compounds, microsyntactic intergrowth 79−99149
- Al_2O_3:Cr_2O_3(Ti_2O_3), dopant influence on struct. and mech. props. 80−24471
- Al_2O_3-B_2O_3 system, phase comp. and sorption props., Al salts chem. nature influence 79−51426
- Al_2O_3-Cu composite, dispersion-strengthened, hardness, tensile strength and struct. 77−70063
- Al_2O_3-glass mixture, microstructural changes and shrinkage during sintering 80−25640
- β- Al_2O_3-Na_2-CaO, microstruct. and ionic resistivity 80−44357
- β-Al_2O_3-Na_2O, AC impedance, microstruct. and strength 80−100349
- β-Al_2O_3-Na_2O, fracture stress, effect of microstruct. defects 77−44338
- Al_2O_3-Na_2O, syntaxy between β and β'' structures, TEM 77−20075
- β''-Al_2O_3-Na_2O solid electrolyte, processing and phys. props. 80−60820

crystal microstructure continued

- β-Al_2O_3-Na_2O:Mg, ionic cond., effect of microstruct. and phase composition 78−67859
- β-Al_2O_3-Na_2O:Mg, with and without Co co-doping, ionic cond. and cryst. struct. 78−26723
- β-Al_2O_3-Na_2O-SiO_2, solid electrolytes, exam. of microstruct. ionic resistivity 78−80566
- Al_2O_3-SiO_2 heat insulating refractories, prep., physical, thermal, structural props. 78−68662
- Al_2O_3-SiO_2-Fe_2O_3-CaO-MgO-TiO_2, refractory, corrosion and mech. behaviour correlations 80−40563
- Al_2O_3-SiO_2-TiO_2-RO (where R=Ca, Sr, Ba) system glass-crystal material, elec. cond. 79−60876
- Al_2O_3-ZrO_2, microstructure effect on friability 78−64515
- γ- AlOOH, boehmite, dehydration to γ-Al_2O_3 80−21277
- Al-AlOOH, disapore, superstructure form. on dehydration, electron microscopy obs. 80−3327
- Al_xVO_2, reduced, microstruct., crystallographic shear planes, electron microscope obs. 79−1443
- Au, grain boundary struct. anal. by HVEM *(Japanese)* 80−15109
- Au-Al system, influence of current on phase form. in diffusion layer *(Russian)* 78−52826
- AuCu II, periodic antiphase struct. *(French)* 79−14937
- Au_4Mn, fully ordered, microstruct., high resolution electron microscopy 79−1439
- Au_4Mn, high resolution dark field electron microscopy exam. of ordering 79−7615
- Au_5Mn_2, monoclinic, ordering, high resolution electron microscopy 79−43290
- Au_5Mn_2, variants in domain struct. 77−43224
- B fibre, US inspection, immersion method 80−66757
- B-B_4C materials, hot-pressed, elastic modulus and flexural strength rel. to grain size and porosity 79−79018
- B-transition metal thin films, amorphous to cryst. transformation 80−7563
- BC, sintered, struct. and props. 80−104181
- BN structure after high temp. shock compression 80−39220
- B_2O_3-SiO_2, optical waveguide glass, sintering kinetics 80−84898
- $BaFeO_{2.79}$, 6H polytype, perovskite related phase, electron microscope obs. 77−51391
- $Ba_5Nb_4O_{15}$, 5H polytype, perovskite related phase, electron microscope obs. 77−51391
- BaO-Nd_2O_3-TiO_2-Bi_2O_3 system ceramics, high stability low loss dielectric preparation 80−81008
- $Ba_{0.1}Sr_{0.9}MnO_{2.96}$, 4H polytype, perovskite related phase, electron microscope obs. 77−51391
- $BaTiO_3$ ceramic, PTC-type, voltage contrast imaging for low and high Ti excess 77−28183
- $BaTiO_3$ ceramic, semiconductive sintering 77−36430
- $BaTiO_3$, donor doped, exam. of heterogeneous microstructure *(German)* 79−24632
- $BaTiO_3$ powder, US dispersed, SEM study *(German)* 80−33860
- $BaTiO_3$, single crysts., electron microscope study of domain and defect structs. 79−15425
- $BaTiO_3$:$BaTi_3O_7$, dielec. props. and microstruct. 80−60481
- $Ba_{100}Ti_{101-x}Sn_x$+0.3 at.%Sb, intergranular capacitor, effect of microstructure on electrical props. 79−34160
- BamSrmPb hexaferrites, prep. by cernet procedure, mag. props. 77−32174
- Be, cast, crystallographic orientation of columnar grains 77−59774
- Be, ultra fine-grained, recrystn. after deform. 79−52239
- Bi-MnBi eutectic composites, microstructure and mag. props., annealing effect 79−82827
- Bi-Pb-Sn, eutectic alloys, struct. instability and absence of superplasticity *(Russian)* 77−8882
- $Bi_2CaNa_{n-2}Nb_nO_{3n+3}$, intergrowth, IMV high-resolution electron microscopy 80−107436
- $Bi_{100-x}Sb_x$, chem. microhomogeneities, topographical and electron beam microanalysis obs. 79−65206
- $Bi_{0.52}Sb_{1.48}Te_3$, microstructure rel. to thermoelec. props. 77−85249
- Bi_2Te_3-Sb_2Te_3, Bi:Sb=1:2, 2:1, solid soln. deviation from stoichiometric cross section 79−43221
- Bi_2Te_3-Sb_2Te_3 solid soln., deviation from stoichiometric cross section 78−35362
- $Bi_2Te_{3-x}Se_x$, microstructure rel. to thermoelec. props. 77−85249
- $Bi_4Ti_3O_{12}$ ceramics, ferroelectric, hot-forged, grain orientation and dielectric props. 80−40076
- C fibre, structural and mech. characts. 77−28737
- C fibre reinforced Al, factors affecting struct. formation and some props. 78−15346
- C graphitic, imperfectly ordered ultramicrostruct. characts. direct imaging feasibility by high resolution electron microscopy 79−77463
- C materials, conf., Baden-Baden, Germany (June 1976) 78−43990
- C, microscopic features of carbons obtained from aromatic hydrocarbons using carbonisation catalysts 77−66597
- C, obtained from aromatic hydrocarbons using $AlCl_3$ catalyst. 77−63572
- C pyrolytic, paracrystn. nature, bimodal statistics anal. 79−77451
- C, pyrolytic, spiral growth rel. to temp., press., flow conditions, dislocations, props. *(German)* 78−42931
- C, strength and struct., conf., Bath, London, England (Apr. 1979) 80−82566
- C-C composites, existence diagram and properties *(French)* 78−64517
- $C_{12.6}AuCl_3$, intercalation compound, struct. *(French)* 78−42982
- Ca Mg $(CO_3)_2$ (dolomite), modulated struct. 79−100832
- $Ca_2(Al,Fe,Cr)O_5$ solid soln., planar interfaces, TEM obs. 80−65008
- $CaCO_3$, thermal decomp. in vacuo, ultrastruct. and crystallography 78−71864
- $Ca_3Ga_2Ge_3O_{12}$, substrate, electron examination of microstruct. and microsegregation 78−67919
- $CaMnO_3$, microstruct., elec. cond., thermoEMF 78−23084
- CaO-SiO_2/GeO_2-H_2O system, phase relations, influence of Si/Ge isomorphous substitution 79−52180
- $Ca_{10}(PO_4)_6(OH)_2$, synthesis and characterisation in dense polycryst. form 77−4749
- β-Ca_2SiO_4, stabilisation, IR and Raman spectra 79−42265
- Ca_3SiO_5, P containing, hydrated, microstruct. and IR struct. 79−29074
- $CaTiO_3$-$LaAlO_3$ solid soln., phase redistrib. during roasting in H_2 78−52735
- $CaWO_4$, Czochralski grown, distrib. coeffs., cavity form., cellular struct. 77−11492
- $CaZrO_3$-$CaHfO_3$, solid soln. formation obs. 77−86003

crystal microstructure continued
Cd-Sn, eutectic alloys, struct. instability and absence of superplasticity *(Russian)* 77–8882
Cd-Sn alloy, superconductivity and microstructure 80–107949
Cd-Zn eutectics, microstruct. after solidification, heat pipe influence 80–76243
$CdAs_2$, synthesis, microstruct., hardness and elec. cond. 79–51268
$Cd_{0.1}Hg_{0.9}Te$, polycrystalline thin film, correlation between structure and 1/f noise 78–39234
$Cd_xHg_{1-x}Te$ compressed sintered slabs, Hall coeff. and microstructure obs. *(Russian)* 78–10475
$Cd_xHg_{1-x}Te$, X-ray topographic assessment 79–37716
CdI_2, hexagonal-rhombohedral polytypic transformation, electron diffr. and X-ray diffr. obs. 80–49163
CdS, cryst. grown from melt under press., microstruct. 77–59019
CdS film, precipitation from solns., form. characts. 79–11524
CdS films, photosensitive, growth by reactive RF sputtering, props. *(French)* 78–35308
CdS, polycryst. films, microstruct. and X-ray cond. 79–56336
CdS, polycrystn. films, recrystn. accompanying annealing *(Russian)* 80–20948
CdS-based phosphor, microstruct. and luminesc. efficiency 78–10959
CdTe, laser window material, vap. deposition, mech. props. 77–46776
CdTe, laser window material, vap. deposition 78–27391
CdTe-Co(Mn) systems, reaction of components, DTA, microstruct. and microhardness obs. 79–38804
Co, deformed, microstruct. singularities in pre-transform. temp. range *(Russian)* 80–45347
Co film, evaporated, texture and columnar struct. 80–54566
Co, sputtered film, high coercivity and high hysteresis loop squareness 79–91259
Co-base superalloy, machine thixocast, mech. prop. deficiencies 79–74244
Co-C-TaC directional eutectic, high-strength, interphase boundaries *(Russian)* 79–38812
Co-Cr recording films, perpendicular mag. anisotropy, hysteresis loop, microstruct., TEM obs. 78–95491
Co-Cr-Nr-TaC eutectic alloys, fatigue, microstructure effects 78–23803
Co-Cu-Fe-Sm magnet, microstruct. exam. after ageing, TEM meas. 77–48555
Co-Fe alloys, transformation induced microstructs. extended total dislocations, TEM study 79–42073
Co-Mo-Cr-Si, plasma and detonation coatings, Laves- and carbide-strengthened, comparative props. 78–15562
Co-P electroless film on Al base disc substrate, microstruct. rel. to mag. props. 78–68304
Co-Re, sputtered film, high coercivity and high hysteresis loop squareness 79–91259
Co-Sb-Te ternary system, crystn., heat treatment and phase equilib. 79–52156
(Co-Ni)-$Cr_{23}C_6$ eutectic alloy, directionally soldified, microstruct. and crystallography 78–48390
Co(-Re) sputtered films, mag. props. and microstructures 79–82837
Co(Cr,Ni)-TaC fibrous eutectic, deformed, thermal stability of microstruct. *(Russian)* 79–1895
$CoOOH \rightarrow Co_3O_4$, morphology, topotaxy, comparison with $Co(OH)_2 \rightarrow CoOOH$ 77–16817
Co_5Sm crystals, microstruct., homogeneous precip. and nucleation 80–104160
Cr and Cr alloys, structural changes during low-temp. phase transform. *(Russian)* 79–52202
Cr bronze Sn, recrystn. props., hot rolling, annealing, polygonisation *(Russian)* 80–55419
Cr coatings, electrodeposition, conditions rel. to H_2 conc., internal stresses 77–1933
Cr, columnar struct. rel. to deposition conditions 78–52675
Cr effect on carbon steel weld metal hot cracking resistance 79–79061
Cr, electrodeposits, relation between preferred orientation and microstructure *(Korean)* 77–28733
Cr foil, laser irradiated, low-angle X-ray scatt., angular block misalignment and hardness *(Russian)* 80–103413
Cr, interaction with dense stream of N ions, metallography, microhardness, specific volume *(Russian)* 80–15169
Cr steel, austenite, abnormal decomposition kinetics and mechanism *(Russian)* 80–55344
Cr/Au layered films, microstruct. and interdiffusion during ageing, 423 to 573K 79–46965
Cr-Ce-N, Ce and N effects in ductile-brittle transition, microstruct., hardness, *(Russian)* 78–35497
Cr-Co-Fe, for telephone receiver mag. use 80–45318
Cr-Co-Fe permanent magnet anisotropic alloys, plastic deform., ageing, particle alignment temp. 80–35254
Cr-Fe, with Si and Ta additions, metallurgical and mechanical characterisation *(Italian)* 77–66674
Cr-Fe (30 wt.%) alloys, refined fine comminution 78–60598
Cr-Fe microstructural changes, heating and cooling cycles 79–78956
Cr-N, N_2 absorpt. by molten chromium, cryst. microstruct. after quenching *(Japanese)* 79–43201
Cr-Ni VKh-4 alloy, deformation and fracture mechanism investigation *(Russian)* 80–11738
CrC-Ni-(P), hard alloys, sintered, fracture props., P addition effects 78–60610
Cr_2O_3-Al_2O_3-$ZrSiO_4$, exam. of microstructure by optical microscopy 79–29073
Cr_2O_3-Cr black, solar collector coating, microstruct., FIM and SEM obs. 80–26166
$Cr_3Si_2(C_2)$, sputtered films, microstruct. and wear props. 78–64733
$Cs_2O.Al_2O_3.4SiO_2$ (pollucite) for long term-storage of $^{137}CsCl$ 80–37467
Cu based materials, sputter deposited at high rate, microstruct. and props. 78–22988
Cu chalcogenides, single-phase, preparation 78–35293
Cu, cold neutron small angle elastic scatt., microstruct. exam. 77–84736
Cu complex, bis-(alkylammonium) (11) tetrachloride, perovskite, lattice perfection 78–87633
Cu, explosive loading, depend. of struct. on deform. *(Russian)* 78–3177
Cu foil, laser irradiated, low-angle X-ray scatt., angular block misalignment and hardness *(Russian)* 80–103413
Cu, He gas-bubble superlattice form. 80–2086
Cu ion-plated coating, grain structure 79–28249
Cu, polycryst., grain size and high-temp. yield strength 80–7641
Cu, polycrystn., strain localisation during hot deform. 80–104195

crystal microstructure continued
Cu rich dental amalgams, SEM and energy dispersive X-ray analysis 78–24184
Cu, virgin surface, contact formation and cohesion, influence of multiple contacting *(Russian)* 80–40548
Cu-Al, two-phase Cu-rich alloy, influence of microstruct. on stress-strain behaviour 80–7631
Cu-Al (15 at.%), rolled single crysts., metallographic study of deformation struct., orientational change, shear bonds *(Japanese)* 79–24582
Cu-Al-Fe (11, 2 and 1 wt.%), Fe effects on microstruct. and mech. props. *(Korean)* 77–28807
Cu-Al-Ni (14.5, 3 wt.%), fatigued, polycrystn., pseudoelastic, dislocation and martensite substructs. 79–82223
Cu-Al-Ni-Fe, (10, 5, 5 wt.%), cast microstruct. 78–80535
Cu-Al-Si, Si effect on mech. props. and microstructure *(Korean)* 79–38903
Cu-Al-Sn system, coexistence of different and brass like phases 80–89206
Cu-Al-Ti, formation of modulated structure rel. to barrier nucleation of new phase *(Russian)* 77–32580
Cu-Be (6.2, 9.3, 13.4 at.%), cell growth of discontinuous precipitation *(Japanese)* 79–24525
Cu-Be-Co, discontinuous reaction, analytical TEM 80–100842
Cu-Cr(Nb), formation of two phase microstructure, during volumetric, and directional crystallisation *(Russian)* 79–29040
Cu-Fe system, ageing and reversion phenomena study 80–89274
Cu-Ge (5 at.%), single crystal, Bridgman growth, neutron diffraction topographic obs. of layer substructure 79–27938
β-Cu-In, directionally transformed eutectoid, morphology exam. by metallography *(German)* 78–92257
Cu-In eutectoid, coarsening at 829K 79–1885
Cu-mild steel explosively welded interface, SEM examination *(German, English)* 80–96746
Cu-Mn-Al, constricted hysteresis loop rel. to microstruct. 78–19273
Cu-Mn-Al alloys, displaced hysteresis loop and microstructure obs. 80–84613
Cu-Nb (7 wt.%), solidification microstruct., SEM 77–12611
Cu-Nb alloy, chill casting, consumable arc melting, ingot prep. techniques 80–84879
Cu-Ni (10 at.%), struct. changes during deform. *(Russian)* 78–19818
Cu-Ni-Cr, microstruct. behaviour and mechanical hardening 78–47281
Cu-Ni-Cr (28, 2.8 wt.%), spinodal alloy, microstruct. and tensile props. 78–39858
Cu-Ni-Cr system, coarsening in the $(\gamma_1+\gamma_2)$ region, metallographic study 78–84762
Cu-Ni-Fe, spinodal alloy, heat treatments for improved mech. props. 79–5024
Cu-Ni-Nb-Al, formation of γ' and γ'' precipitates 78–76655
Cu-Ni-Sn (9, 6 wt.%), decomposition, initial stages, TEM study 80–2992
Cu-Ti, internally oxidised, morphology, struct., particle precipitation singularities *(Russian)* 79–70067
Cu-Ti (3.5%), coherent precipitates, US irrad. effect on struct. and hardness *(Russian)* 77–48446
Cu-Ti (4 wt.%), combined recrystallization and precipitation 79–29072
Cu-Ti (4 wt.%), isothermal transformation, electron and optical microscopy obs. of microstructure 80–16307
Cu-Ti-Cr(Fe), internally oxidised, morphology, struct., particle precipitation singularities *(Russian)* 79–70067
Cu-V-Ga dil. alloys with V_3Ga particles, supercond. props. and microstruct. 78–39278
Cu-Zn, interface sliding of FCC and BCC boundaries 80–104240
β-Cu-Zn-Al (27.5, 4.0 wt.%), strain induced martensite, exam. of structure, microstructure 80–7648
Cu_3Ga, interpretation of diffuse contours in electron diffr. *(French)* 79–19377
Cu_3Ga, transition state between long range order and short range order, model, computer simulation *(French)* 80–49371
$CuGaS_2$-$CuGaSe_2$ system, forbidden-band width 78–35280
$(CuGaTe_2)_{1-x}$-$(2CdTe)_x$, phase diagram and microstruct. DTA and X-ray diffr. 77–59762
$Cu_{0.5}In_{2.5}Se_4$, transition state and domain struct. by electron microscopy and diffr. studies 80–15095
$(CuInTe_2)_{1-x}$-$(2ZnTe)_x$, phase diagram and cryst. growth of $CuZn_2InTe$ from $ZnCl_2$ flux 80–16287
$Cu_xMo_6S_8(Se_8)$, prep., metallurgical and supercond. props. 77–32102
Cu_xNbS_2 and Cu_xTaS_2, electron diffuse scatt., microstruct., of transition state 77–31771
Cu_2O, creep substruct. under compression, X-ray diffr. study 78–95785
$Cu_2S+Ln_2S_3$, powdered mixtures, reaction rate, production of ionic semiconductors 80–93741
Cu_xS-CdS solar cell, p-n junction shape and struct. 77–55599
Cu_2Te-$Ge(Sn)Te_2$, phase equilib., microstructural, DTA investigs. 77 16560
Fe alloy, cast, Young's modulus and microstructure *(German)* 77–25090
Fe alloy YuNDK35T5, mag., solidification, direct elec. current effect 79–78954
Fe alloys, anisotropic precipitation struct. in external mag. field *(German)* 78–72785
Fe alloys, influence of plastic deform. on twinned martensite struct. *(Russian)* 78–88493
Fe, Armco, microstruct., effect of strain rate on change, due to tension-compression 78–80614
Fe, Armco, microstruct. and hardness after electron bombardment 79–38956
Fe, Armco, microstructure in quasibrittle and plastic fracture 77–1863
Fe, cast, eutectic solidification, expt. study by quantitative metallography 79–24516
Fe, cast, flake and nodular, heterogeneous nuclei and graphite chemistry 79–55896
Fe, cast, flaky graphite, damping capacity 77–8869
Fe, cast, grey, solidified in oscillatory and rotating moulds, metallographic study 80–89213
Fe, cast, high Cr, phase composition, mech. props. rel. to heat treatment 79–29108
Fe, cast, homogenization of property difference due to mass effect by repeated heat treatment *(Japanese)* 79–38857
Fe, cast, innoculated with Ce-Mg-Fe master alloy, struct. and props. 80–100843

crystal microstructure continued
Fe, cast, malleable, with divorced pearlite, structural strength improvement by annealing 79−96049
Fe, cast, Mn, wear resist. and hardening, struct. effect 79−87734
Fe, cast, rare-earth-Mg nodular, fracture toughness and fatigue *(Chinese)* 78−95791
Fe, cast, wear mechanism of friction couples 79−83329
Fe, cast-Ni, 78−44086
Fe, columnar struct. rel. to deposition conditions 78−52675
Fe, dislocation struct. at tip of fatigue crack 77−4107
Fe film, evaporated at oblique incidence, columnar grain struct. using anisotropy field meas. 77−59231
Fe, foil, fatigue crack, low growth rate, microstruct. round top 77−16674
Fe, grain struct., multifeature mass analysis utilising digital image processing, Fe anal. appl. 79−43684
Fe, granular film, microstructure using X-ray, electron diffr. and TEM 79−65344
Fe, grey cast, P effect on distrib. of alloying elements 77−12634
α-Fe, high temp. deform. and substruct. *(Japanese)* 77−21226
Fe, interaction with dense stream of N ions, metallography, microhardness, specific volume *(Russian)* 80−15169
Fe, nitrided wire, magnetic charact. and microstruct. *(Korean)* 78−19277
Fe one raw material, sintered, ionic etching as new method of struct. investigation 77−52588
Fe oxides, phase equilibrium and microstructure interpretation 80−60847
Fe, penetration of H_2, influence of microstruct. changes induced by cold working *(Russian)* 77−20182
Fe, polycryst. whisker, microstruct. SEM and TEM 77−39755
Fe, pure, nitrided layers obtained by ion bombardment, microstruct. exam. *(French)* 78−15581
Fe, pure, splat-quenched, martensite morphology, SEM study 80−7547
Fe, sintered, produced by dynamic hot pressing, recrystn. diagram 79−70017
α-Fe, TEM on struct. round fatigue cracks 77−12699
Fe, whiskers, high strength, polycrystalline, microstruct. obs. 79−33214
Fe-Ag, three-dimensional microstruct. analysis, appl. of basic topological concepts 77−59739
Fe-Al powder cpds., prep. in low-temp. plasma, struct. props. 77−44192
Fe-Al-C steel, singularities of struct., electron microscope and electron diffr. analysis *(Russian)* 77−77476
Fe-Al(Cr)(V)(Ti), hardness after nitriding, metallographic, electron microscopic and microprobe anal. 78−51608
Fe-Al(24.3 at.%)-C alloy, magnetic permeability disaccommodation, 260-400K 80−93144
Fe-B, rapidly solidified, metastable phases *(German)* 79−29045
Fe-Be (16.5 or 19.5 at.%), four-phase model of struct. in initial ageing stages *(Russian)* 78−48430
Fe-C (0.64 wt.%), quasicleavage during fatigue crack propag., pearlitic microstruct. effect 79−11702
Fe-C (1.2 wt.%), Mossbauer study of early stages of tempering 80−16342
Fe-C (30 at.%), production of Fe_7C_3 at high press., morphology and microstruct. *(Russian)* 79−38828
Fe-C system, effect of microstruct. on fatigue crack propagation 79−79097
Fe-C-Cr-Mo(Ni)(V), white cast, effect of abrasion on carbide microstructure *(German)* 78−88540
Fe-C-Si, effects of Si on matrix struct. of spheroidal graphite cast iron *(Korean)* 78−60666
Fe-C-Ti (0.2 to 1.8, 0.1 to 1.7 wt.%), crystallisation and microstruct. *(Russian)* 77−66632
Fe-Co-V(2%) alloy, correl. of resistivity with microstructure 78−72896
Fe-Co-W-C steel, M_6C carbide behaviour during ht. treatment *(Russian)* 77−66658
Fe-Cr, microstructural study of oxidation, selective etching 78−44245
Fe-Cr-C, austenite to ferrite+precipitate reaction, TEM/STEM study 80−3075
Fe-Cr-C (10,0.2 wt.%), isothermally transformed, precipitate orientations 80−50640
Fe-Cr-C (10,0.2 wt.%) isothermally transformed, carbide distrib., microstruct. development 80−3076
Fe-Cr-Co, magnetic domain walls, Lorentz microscopy 80−103854
Fe-Cr-Co (31 wt.%, 23 wt.%), microstruct. and mag. props., ageing and thermomag. treatment effects 78−76769
Fe-Cr-Co ductile magnet, with high $(BH)_{max}$, processing, mag. props., and microstruct. 77−8957
Fe-Cr-Co hard-mag. alloys, fine cryst. struct. *(Russian)* 77−66706
Fe-Cr-Co permanent magnet system, miscibility gap, microstruct. and mag. props. obs. 80−76228
Fe-Cr-Co-Al (27.5, 17.5, 0.5) alloy, rel. to mag. props. 78−72367
Fe-Cr-Co-Mo, microstruct., hardness, mag. props., influence of isothermal tempering and heat treatment 79−79129
Fe-Cr-Co-Mo high energy permanent magnets, mag. props. 80−97119
Fe-Cr-Mo alloy castings, thick-section, factors affecting 80−108374
Fe-Cr-N (5.9, 0.5 wt.%), martensitic, tempered, fine struct. 77−25079
Fe-Cr-Ni austenitic alloys, environment sensitive cracking, metallurgical variables effect 80−35391
Fe-Cr-Ni-C (17.2, 7.34, 0.2 wt.%) alloy, twin related laths, fracture elongation, TEM study 79−29192
Fe-Cr(W)-M, (M=Si,Mo,Ni,Mn,P,Cr), cellular growth of S-pearlite formed by carburisation 80−108486
Fe-Cu, lath martensite habit planes, TEM study 80−84942
Fe-Cu, modulated microstruct., continuous cooling effect, hardness and electron microscope obs. 79−87665
Fe-Cu (75 ppm), internal oxidation, local struct. determ. by EXAFS 80−25916
Fe-Cu-Ni, austenite to ferrite+precipitate reaction, TEM/STEM study 80−3075
Fe-Cu-Ni (2,2 wt.%), isothermally transformed, precipitate orientations 80−50640
Fe-Cu-Ti, improvement of irradiation-enhanced Cu embrittlement by Ti addition 79−43393
Fe-Cu-glass ternary multiphase composite, microstruct. and props. *(German)* 77−90314
Fe-Cu(-C), alloyed with graphitising elements, geometrical thermodynamics *(Russian)* 79−52261
Fe-M, (M=Cr,W,Mo,V,Ti), morphology and growth kinetics of δ-pearlite formed by carburisation 80−108485

crystal microstructure continued
Fe-Mn (15(24)(30)wt.%), high hydrostatic pressure influence on stress-strain curve 80−25805
Fe-Mn alloys, quantitative phase anal., correction factor for texture 79−52528
Fe-Mn-C, cast iron and steel, Mn effects on struct. 78−23696
Fe-Mn-C, structural var. during warm deform. in $\gamma \rightarrow \varepsilon$ transform. region *(Russian)* 77−81293
Fe-Mn-Mi, martensitic, morphology and substruct. study 77−70059
Fe-Mn-Si-C, cast, Mn effect on struct. during solidification 79−83191
Fe-Mo alloys, carburised, austenite-carbide colonies struct. *(Russian)* 79−52449
Fe-N crystal, orienting $Fe_{16}N_2$ particles by external magnetic field *(German)* 77−25058
Fe-Nb (3.1 wt.%), semihard mag. alloy, Recalloy, mag. props., elec. cond. *(Japanese)* 78−10723
Fe-Ni, alloy 20N24, martensitic, exam. of structure after laser treatment, and recrystallisation *(Russian)* 79−11608
Fe-Ni, $\alpha \rightarrow \gamma$ conversion, electron microscope and X-ray spectral microanal. 79−78966
Fe-Ni, secondary recrystn. and mag. props. 80−89247
Fe-Ni (23 wt.%), struct., composition changes during α to γ transform., martensite plastic deformation influence *(Russian)* 80−11642
α-Fe-Ni (3-12 wt.%), structure and $\gamma \rightarrow \alpha$ polymorphic transform. kinetics 80−71645
Fe-Ni (31%) alloy, deformed by slip, misaligned zones in $\{259\}_A$-martensite crysts. *(Russian)* 77−59850
Fe-Ni (32.86, 30.65 wt.%), characts. of quenched struct. formed in textured sheets, TEM and optical microscopy study 79−34084
Fe-Ni-C, C effect on recrystallisation and reversion *(French)* 77−81282
Fe-Ni-C (31, 0.28 wt.%), crossings of thin plate martensites, TEM obs. 80−25756
Fe-Ni-C (31.9, 0.02 wt.%) alloy, hardness of martensite-austenite mixtures 80−60959
Fe-Ni-C (31.9,0.02 wt.%), determ. of number and size distrib. of martensitic plates 80−76255
Fe-Ni-C alloy, external stress effects on equilibrium morphology, thermodynamic model *(Russian)* 78−52804
Fe-Ni-C alloy, N31, austenite state in premartensitic temp. interval *(Russian)* 78−56634
Fe-Ni-Co alloys, struct., appl. of mag., thermomag. methods *(French)* 79−20318
Fe-Ni-Co-C, substruct. effect in mech. props. 80−30086
Fe-Ni-Cr, pulsed HVEM irrad., effect on microstruct. evolution 80−34053
Fe-Ni-Cr (20, 15 wt.%), single and dual ion irrad., microstruct. studies 80−29077
Fe-Ni-Cr (35, 15 wt.%) superalloy, stress rupture and tensile props., C and B additions effect *(Chinese)* 80−104244
Fe-Ni-Cr-Al-Y, oxidation mechanism, Y addition effect on kinetics and oxide adherence 80−97623
Fe-Ni-M alloys, (M=C, Ti,Mn), habit plane and morphology of lath martensites 77−8823
Fe-Ni-Mn (20, 5 wt.%), rel. orientation between adjacent martensite laths 80−76254
Fe-Ni-P, interface composition during diffusion controlled precipitate growth 77−36513
Fe-Ni-Ti, undeformed metastable alloy, cellular decomposition of austenite during ageing *(Russian)* 79−100178
Fe-Ni-V, nitrided austenitic alloys, modulated substitutional interstitial solute atom clustering 79−74160
Fe-Ni-V-C alloy, reverse α to γ transformation, previous deformation influence on struct. and props. *(Russian)* 79−100139
Fe-Si, grain oriented sheet, grain struct. by computer mapping 80−88168
Fe-Si (3 wt.%), grain oriented, MnS precipitate distribution, electron microscope observation *(Chinese)* 78−95751
Fe-Si (3 wt.%), single crystal, colour etching of striations 77−70253
Fe-Si (3.1 wt.%), anisotropy of electromigration of substructure of polygonisation *(French)* 77−28047
Fe-Si (3.5 wt.%), microstructure inhomogeneity testing using Barkhausen noise strain depend. 77−12155
Fe-Si alloys, recrystn. while carburising, interphase boundaries movement 79−52208
Fe-Si sheets, grain oriented, with insulating coating, nondestructive grain identification methods *(Slovak)* 79−5090
Fe-Si single crystals with cube-on-edge orientation, iron-loss-domain-struct. correls. *(Japanese)* 80−7534
Fe-Ta alloy, mech. drawn and aged, exam. of electrical resistivity, hardness, microstruct., and mag. props. *(Japanese)* 78−48545
α-Fe-Ti, ion implanted, with C impurity, microstruct. of TiC precips. 80−66513
α-Fe-Ti, ion-implanted and annealed, microstruct. evolution 80−15132
Fe-Ti-C, rapidly quenched by splat-cooling 80−84923
Fe-Ti-(Mn)(O), exam. of interrelations between phase diagrams and hydriding props. 79−8277
Fe-V-C, austenite to ferrite+precipitate reaction, TEM/STEM study 80−3075
Fe-VC alloys, struct. and mech. props. 79−52171
Fe-WO_3 system, struct. phase exam. by optical microscopy and X-ray diffr. 78−31389
Fe-X-C (X=Cr, Mo, W), quenched rapidly from melts, nonequilib. phases *(Japanese)* 80−71630
Fe-Zn, crystallographic relations by X-ray diffr. 80−24408
Fe-Zn, quenched, martensite struct. and hardness, electron microscope exam. *(Russian)* 80−66619
FeB_x coatings on steel, formed by B diffusion, pack cementation process, microstruct. and mech. props. 78−15592
FeCoC, unidirectionally transformed eutectoid, crystallography of herringbone pearlite, TEM obs. 78−31399
$Fe_{0.5}Co_{0.5-x}Cr_x$ films, vacuum-deposited cryst. and mag. struct. *(Russian)* 80−93081
FeNiCrAlLi alloy, γ' hardened, noncellular mech. for form of lamellar η phase morphology 77−28824
$Fe_{1-x}O$, wustite, crystals of various stoichiometries, growth in arc furnace 80−25545
γ-Fe_2O_3, microstruct. and magnetisation 80−44875
Fe_2O_3 reaction with NiO, ZnO, and (Ni,Zn)O solid soln., microstruct. 79−87834
γ- Fe_2O_3-Fe_3O_4, lodestone, microstructure and mag. props., source of mag. hardening 79−82828

crystal microstructure continued
Fe_3O_4 briquettes, porous, struct. changes during reduction 77−21064
Fe_3O_4, magnetite, defect content, gas-phase comp. effects 77−43336
Fe_3O_4, orientation on α-Fe_2O_3 after low-temp. reduction, X-ray texture analysis *(French)* 77−39738
β-FeOOH, akaganeite, struct. changes due to radiation damage 79−28014
β-FeOOH, lattice imaging and pore struct., high resolution electron microscopy obs. 80−103310
α-FeOOh, goethite, superstructure form. on dehydration, electron microscopy obs. 80−3327
Fe_3Pt, plastically deformed, struct. inhomogeneities, positron annihilation meas. 79−33859
Fe_xVO_2, reduced, microstruct., crystallographic shear planes, electron microscope obs. 79−1443
Fo-Fe-Nb, cold-worked and aged, mag. props. and microstruct. 80−34690
GaAs epitaxial film, microstruct., effect on elect. characts. of Schottky diode *(Russian)* 80−107671
GaAs:Au, back surface gettering 80−10758
GaAs:Si, Li, IR absorpt., microstruct., charge compensation 80−107565
$GaAs_{1-x}P_x$, mol. beam epitaxial growth, cryst. quality, composition investig. *(Japanese)* 77−55895
Ga_2O_3-Na_2O, syntaxy between β and β'' structures, TEM 77−20075
GaP, cryst., characterisation by light scatt. *(Japanese)* 77−35498
GaP, mol. beam epitaxial growth, cryst. quality composition investig. *(Japanese)* 77−55895
GaP-ZnS, solid solns., microstruct. investig. 78−2128
GaSb:Mn(Sm), struct., thermo EMF, galvanomag. props. rel. to dopants, eutectic $Mn_{0.6}Ga_{0.4}Sb$ form. 77−15869
Ga_xVO_2, reduced, microstruct., crystallographic shear planes, electron microscope obs. 79−1443
Gd films, electrical props. correlation with microstructure 80−97009
Gd-Co(Fe) amorphous films, microstruct. and mag. anisotropy 79−82838
Gd-Fe-Si, phase diagram 79−52158
$Gd_3Ga_5O_{12}$, substrate, electron examination of microstruct. and microsegregation 78−67919
Ge-Sn-As system alloys, microstruct., X-ray phase and thermal anal. 77−32564
Ge-Te system, microstruct. in phase transform. region 79−52177
GeTe, low temp. alloys, microstruct. obs. *(Russian)* 78−19768
Hf-V, superconductivity and metallurgy of C15 materials 79−4610
HfC, etchant for revealing microstructure 80−85097
Ho_xCo_{1-x} amorphous films, microstruct. and mag. anisotropy 79−82838
In-Sb-Bi system, solid solns., solubility limits, microhardness, microstruct. investig. 78−35368
InAs-CdTe quasi-binary system, temp.-comp. diagram, physicochem. and thermodynamic analysis 80−104127
$In_xGa_{1-x}Sb$, influence of annealing on microstruct., exam. 78−56669
InP, microstructs. assoc. with hardness indentations 78−80627
InP, transferred electron device, effect of grain struct. on microwave performance and I-V characts. 80−6981
InP-Au contacts, conditions of fabrication that control interfacial microstruct. 79−42643
In_2Te_3-PbTe system, phase diagram, elec. props. 78−35361
Invar alloys, plastically deformed, struct. inhomogeneities, positron annihilation meas. 79−33859
KCl microcrystal boundary influence on IR spectrum 77−40243
KCl:Ba(Ca)(Sr), microstruct. and hardness, impurity distrib. effects 79−24529
KCl(Br)(I), single cryst., quenched, microstruct. around indentations 80−7628
KH_2PO_4, ferroelectric, crystal growth in silica gel, effect of pH and gel ageing 78−48301
$KNbO_3$, layer growth, optical and electron microscopy 77−59021
$K_2Pb(MoO_4)_2$, and isomorphs, domain struct. and phase transition *(Russian)* 78−6159
$LaAlO_3$ perovskite electrolytes for high-temp. fuel cells 79−29467
$LaAlO_3$, Pm3m to R3c or R$\bar{3}$c phase transitions, TEM method for domain identification 80−14980
LaB_6 film, structure, stoichiometry, elec. properties 78−60043
Li-Al-Mg alloy electrodes, polarisation behaviour and struct. 79−43588
$LiFe_5O_8$, hysteresis and other mag. props. rel. to microstruct., TEM investig. 77−20636
$LiFe_5O_8$, vacuum annealed, tetragonal γ-phase obs. with TEM 80−11661
$Li_{0.5}Fe_{2.5}O_4$, effects of low-melting additive on struct. and dielec. props. 77−85494
$Li_{0.5(1-x)}Mn_x\ Fe_{2.5-0.5}O_4$, rectangular hysteresis loop, microstruct. form. 77−12718
LiO_2 pellets, sintered, exam. of microstructure 78−72749
$Li_2O.2SiO_2$, ceramic, prep. of oriented microstructure by unidirectional solidification of melts 80−71614
Mg ferrite, sintered, cation redistribution, microstructural effects 77−55356
Mg-Al-Zn (9wt.%Al), sand cast, preferred orientation and mechanical props. *(Japanese)* 80−20979
Mg-Er (<25%) alloys, struct. and props. 79−96001
Mg-Y-Zn-Nd-Cd alloys, influence of Zr addition on struct. and mech. props. *(Russian)* 80−40370
$Mg_{(x+2)/3}\ T_{(x-2)/3}O_x$ (T=Si, Mg), 145 Å superstructure 79−99143
$MgAl_2O_4$, composition rel. to ceramic microstruct. form., light transmission 79−43188
$MgAl_2O_4$, corrosion resist. in fused Li rel. to phase and microstruct. changes 77−44378
$Mg_{1.86}Al_{1.67}Si_{2.47}O_{3.19}N_{3.81}$, 12H polytype, intergranular phases and compositional variations 80−79645
Mg_3Cd, lattice imaging of B19 ordering transform. and interfacial struct. 77−36495
$MgFe_2O_4$ ferrite form. mechanism in mixture of metallic oxide powders 77−63609
MgO, corrosion resist. in fused Li rel. to phase and microstruct. changes 77−44378
MgO, fused periclase, sintering and struct. characts. 78−23652
MgO, hot-pressed, elasticity props. of polycrystals and single crystals 80−54301
MgO, sintering, effect of Ca compound additions *(Japanese)* 80−55340
MgO-Al_2O_3-SiO_2, exam. of microstructure and crystallisation kinetics 78−80501

crystal microstructure continued
MgO-$Al_2O_3(Cr_2O_3)(Fe_xO_y)$-CuO, phase relations and microstruct. 79−74140
$MgSi_2$, laser irrad. induced form., cryst. microstruct. 80−35011
Mg_2SiO_4, forsterite, decorated dislocations 80−54245
Mn-Al-C, ferromag., transform. kinetics 80−34627
Mn-Si (62.5 to 63.8 wt.%), phase anal. and cryst. struct. *(Japanese)* 80−15049
MnSi-Si system, striations and cryst. struct. of matrix 80−103292
MnZn ferrite, appreciable SiO_2 content, origin of core losses, microstructure and mag. props. 78−64225
MnZn ferrite, microstructure and initial permeability, presintering process effect 80−89367
MnZn ferrite powders, reactive, mag. materials obtained by compaction 80−89182
MnZn ferrites, impurity induced exaggerated grain growth 78−92222
Mo alloy, long-term ageing effects on ductility and microstruct. 77−44348
Mo, BCC, struct. singularities rel. to solid solution behaviour *(Russian)* 77−11696
Mo, cellular structure, initial stages of formation in rolled single crystals 79−23611
Mo, fragmented struct. formed during plastic deform., TEM investig., dislocation model *(Russian)* 77−32634
Mo, impurity interactions with C, N, and O, struct., mech. props. and purification 79−52277
Mo, macroscopic heterogeneity of plastic deform., metallographic examination *(Russian)* 79−100210
Mo, microstruct., swelling induced by ion bombard., He injection effects 80−29083
Mo, secondary recrystallisation grain structure, effect of conditions of annealing *(Russian)* 78−6945
Mo, structure of large single crystals produced by electron beam spot welding *(Russian)* 77−44136
Mo-Al-Ge, phase equilibria, X-ray and microstructural anal. 80−93536
Mo-C (0.07 wt.%), two-phase alloy, fracture and deform. characts., struct. depend. *(Russian)* 77−32635
Mo-Mn alloy, plasticity, fracture, strength depend. on C content *(Russian)* 80−35257
Mo-N system, phase diagram of solid and liq., high and low press. 78−44083
Mo-Ni-Fe-Co-Zn alloys, Ni, Fe, Co and Zn distrib. using neutron-activation anal. 79−52531
Mo-O crystals, electron microscopy study 80−28889
Mo-Ru-C, deformed, singularities of fragmented structs. *(Russian)* 77−44289
Mo-Zr-C, deformed, singularities of fragmented structs. *(Russian)* 77−44289
Mo-ZrC, internal oxidation, struct. formation law, microstruct. examination 78−84836
Mo_2C coatings, phase and struct. transformations on heating 79−96206
MoS_2 hydrotreating catalysts, Co, Fe and Ni effects on microstruct., TEM, SEM and EPMA obs. 79−52762
$MoSi_2$, sputtered films, microstruct. and wear props. 78−64733
NH_4Br, dislocation influence on phase transition and light scatt. *(Russian)* 80−59648
Na-rich plagioclase microstructure and exsolution 80−72501
Na_2-SiO_2 glass, prep. by metallic-organic derived method, phase separation 78−56610
NaCN, struct. domains, NMR determ. 80−50204
Na_2CO_3, quasicrystalline state, incommensurate phase transformation 79−99310
NaCl, deformed surface layer, block misorientation 79−99405
$NaCl:Eu^{2+}$, oriented growth and cryst. struct. of precipitated phases 80−24303
NaCl-KCl mixed crystal, growth, X-ray exam. and microstruct. 78−44001
$NaNbO_3$-$SrNb_2O_6$, phase diagram, props. meas. 79−11576
Na_2O-B_2O_3-SiO_2 glass, phase separated, HCl leaching rate and microstruct. 79−29242
$Na_2O.Li_2O.Al_2O_3$, comp. and props. for use in Na-S battery 79−87745
Nb alloys, long-term ageing effects on ductility and microstructure 77−44348
Nb, BCC, struct. singularities rel. to solid soln. behaviour *(Russian)* 77−11696
Nb film sputtered onto Cu substrate, microstruct. and supercond. props. 77−85370
Nb, neutron irrad., microstruct. and tensile props. 80−34077
Nb-C alloys, alloyed with Mo, Ti, and Zr, phase comp. and precip. after heat treatment 79−57020
Nb-Ge, compounds with A15 structure, films, TEM study *(French)* 80−80135
Nb-Ge-Si, compounds with A15 structure, films, TEM study *(French)* 80−80135
Nb-Mo, BCC, struct. singularities rel. to solid solution behaviour *(Russian)* 77−11696
Nb-Nb_2C eutectic composites, directionally solidified, growth crystallography and lamellar to rod transition 77−32569
Nb-Nb-Al-(Cr), γ/γ'-δ type eutectic, fatigue, effect of composition and microstruct. 78−48520
Nb-Si, compounds with A15 structure, films, TEM study *(French)* 80−80135
Nb-Si liquid quenched alloy, metastable A-15 and amorphous phases, interstitials 80−54394
Nb-Zr-C, (1, 0.1 wt.%) alloy, mech. characts. structral sensitivity in strained state *(Russian)* 79−52301
NbC coating on C steel and Armco Fe, deposition, struct. and props. 79−52462
NbC, etchant for revealing microstructure 80−85097
Nb_3Ge, CVD, impurity doping effect on supercond. crit. props. 78−52174
Nb_3Ge films, correl. between crit. current density and microstruct. 79−38277
NbO, cryst. growth and microstructure 79−95913
NbO_2, cryst. growth and microstructure 79−95913
NbO_2, slightly substoichiometric, microstructure 77−47584
$Nb_{12}O_{29}$, cryst. growth and microstructure 79−95913
Nb_2O_5, cryst. growth and microstructure 79−95913
Nb_2O_5-V_2O_5-P_2O_5, glasses and glass ceramics, elec. cond., struct. 80−84466
Nb_3Si, A-15 struct. stability, atomic radii ratio *(Chinese)* 80−54393

crystal microstructure continued
Nb_3Sn, alloying agent influence on struct. and supercond. props. *(Russian)* 80−39698
Nb_3Sn, electron beam deposited, microstruct., rel. to supercond. props. 79−37935
Nb_3Sn film formation, solubility, precipitating processes *(Russian)* 80−92792
Nb_3Sn, supercond., AC losses, low field behaviour morphology depend. 77−24655
Nb_3Sn-Al_2O_3 composite, electron beam deposited, microstruct., rel. to supercond. props. 79−37935
Nb_3Sn-Cu multifilamentary composite wire, Nb_3Sn filament morphology and grain size 80−100855
Nb_3Sn-Cu superconducting composite, electron beam co-evaporated, TEM study 79−28247
NbZr(Hf)-C(N) alloys, phase comp. after casting and annealing, precip. 79−56983
Ni alloy, IN-100, aluminised, microstruct. degradation, influence of corrosioin protective coating 80−40611
Ni alloy EhI698, new etchant for revealing microstructure 80−25934
Ni alloys, recrystallised, grain boundary inheritance and props. 77−59816
Ni alloys EhP539L, heat-resist., heat treatment effect on props. and hardening phase morphology 80−29995
Ni base superalloy IN 100, corrosion resistant intermetallic coating, microstruct. effect on mech. props. 78−85058
Ni base superalloy Nimonic 80A, microstruct. anal. by high-resolution electron microscopy 80−76459
Ni, cold neutron small angle elastic scatt., microstruct. exam. 77−84736
Ni, deformed by filing, fine struct. obs. *(Russian)* 77−21309
Ni, dislocation structure evolution after hydroextrusion *(Russian)* 80−96530
Ni, He gas-bubble superlattice form. 80−2086
Ni, neutron irrad., microstruct. and tensile props. 80−34077
Ni, polycryst., hydrogenation rel. to fine struct. 78−59950
Ni powder, porous, relationships between mech., physical, and microstructural characts. 80−20846
Ni single crystal, stretched, electron microscope exam. of deformation cell structure during polygonization *(German)* 80−7651
Ni solar collector coating, microstruct., FIM and SEM obs. 80−26166
Ni, solidified from supercooled condition, Si conc. influence on struct. *(Russian)* 77−16567
Ni sputtered coating microstructure on mechanically activated cathode *(Russian)* 79−91586
Ni superalloy, cast, microstruct. and microanalysis 78−35393
Ni-Al, (2 and 6 wt.%), oxidation, α-Al_2O_3 growth, microstruct., precip. 80−108626
Ni-Al (0.5 wt.%), microstruct. formation during internal oxidation, effect of additional microalloying *(Russian)* 77−80650
Ni-Al-Cr alloy IN 100 powder, rapidly solidified, effect of high melt superheat on microstructure 79−52195
Ni-Al-Cr(Ti), ageing kinetics and γ'-phase particles spatial distrib. under applied load *(Russian)* 77−32598
γ-αNi-Al-Mo eutectic, γ' precipitation 77−12629
Ni-Al-Ti(Nb), heat-resisting dispersion-hardening alloys, props. and struct., γ'-phase comp. influence *(Russian)* 80−20943
Ni-Al(Cr)(Ti), ion irradiation induced void swelling and defect microstructs., TEM obs. 79−51164
Ni-base alloy, age hardened, stress corrosion cracking resistance, plastic deform. and microstruct. relation 77−63829
Ni-base superalloy, IN-738, microstruct. changes during isochronal heat treatment, 773-1467K 78−27531
Ni-ceramic coating structure, influence of micropowder inclusion *(Russian)* 80−59820
Ni-Co-Al alloys, continuous precip., SEM, TEM, X-ray diffr. study 80−89220
Ni-Cr, wrought, fatigue at high temp., microstruct. assessment 79−29208
Ni-Cr alloy, ÉI 437B, vibrocreep at normal and high temps. 77−4824
Ni-Cr alloy (20 wt.%), on steel, plasma-sprayed coating 79−96222
Ni-Cr alloys, method of etching in Br-methanol reagent 77−90516
Ni-Cr machine steel, austenite grain size effects on mech. props. *(Russian)* 77−44292
Ni-Cr-Al, oxidation, NaCl vapour effects on microstruct. 78−44274
Ni-Cr-Al-TaC, eutectic composite, microstructure, fatigue props. 80−85038
Ni-Cr-Co-Mo-Al-Ti alloys, Waspaloy, Astroloy, exam. of microstruct. effect on crack growth 78−52977
Ni-Cr-Fe Alloy 600, stress corrosion cracking in high purity water, effect of microstruct. 77−66713
Ni-Cr-Fe-Mo-Co (21.41, 19.28, 8.64, 2.16 wt.%), Hastelloy alloy X, exam. of thermal stability 78−84865
Ni-Cr-Ta-Ti-Si, EP557 precipitation hardening alloy, mech. props., heat treatment effect 80−60877
Ni-Cr-TaC directional eutectic, high-strength, interphase boundaries *(Russian)* 79−38812
Ni-Cr-W (20, 10 to 40 wt.%), phase composition, struct. and props. 80−21034
Ni-Cu-Al(Si), spinodal decomposition, morphology of microstructure, elastic strain energy anisotropy effect 78−15354
Ni-Cu-X (X=Sn, Nb, Ti), spinodal decomp. alloys, linear expansion coeff. influence on morphological anisotropy *(Japanese)* 80−70431
Ni-Fe-Ce superalloy, vacuum melted, Ce effects on microstruct. 77−36552
Ni-Fe-Cr superalloy type 718, heat treatment effect on room temp. and elevated temp. fracture toughness response 80−100922
Ni-ferrite powders, form. in presence of Li_2SO_4-Na_2SO_4 molten salts, prep. and characts. 80−84869
Ni-Mo (20.8 wt.%), order, heat treatment effects 80−40406
Ni-Mo (5.8-24 at.%) solid soln. struct. and strength characts. *(German)* 79−4975
Ni-Mo-Al eutectics, unidirectional solidification 77−4769
Ni-Mo-Cr-Si, plasma and detonation coatings, Laves- and carbide-strengthened, comparative props. 78−15562
Ni-NbC (10 wt.%) eutectic alloy, directional solidification and struct. *(Russian)* 80−84922
Ni-Ni_4Mo system, deformation microstruct. 80−93591
Ni-Si solid solution alloys, γ phase precipitation under irrad. 77−1839
Ni-Ti, near equiatomic alloy, TEM exam. of austenite-martensite interface 78−51401
β-NiAl, oxidation, α-Al_2O_3 growth and microstruct. 80−108627

crystal microstructure continued
$Ni_{66}B_{34}$, morphological, structural and phys. props. *(French)* 80−44444
$Ni_{0.5-x}Co_xZn_{0.5}Fe_2O_4$ ferrospinal solid solutions, cryst. lattice defects and props. 80−19796
NiFe, single and multilayer thin films, strip domains, inplane magnetisation 80−103866
$NiFe_2O_4$ ferrite form. mechanism in mixture of metallic oxide powders 77−63609
$NiFe_2O_4$, hysteresis and other mag. props. rel. to microstruct., TEM investig. 77−20636
$NiFe_2O_4$, microstruct. and magnetic props., electron microscope obs. 79−87290
$Ni_xFe_{3-x}O_4$, DC and low freq. cond. and influence of microstruct. 80−70699
Ni_4Mo alloy, high temp. oxidation, oxide layer growth, struct., mech. behaviour 78−44269
Ni_4Mo, domain struct. on annealing, and dislocation struct. during deform. *(Russian)* 77−16640
NiTaC eutectic superalloy, casting, furnace atm. effects 80−84880
NiTiCu, shape memory alloys, electron microscope and X-ray diffr. study of struct. 79−82179
NiZn ferrites, nonstoichiometric, initial susceptibility and microstruct. 80−84591
$Ni_{0.32}Zn_{0.68}Fe_2O_4$ ferrite, effects of silica content, sintering temp. and sintering time obs. 79−87746
Pb, high purity microstructural investigation by etching with aqueous $HClO_4$ 77−56205
Pb, structure sensitive props., temp. hysteresis after melting and crystallisation *(Russian)* 79−29036
Pb, virgin surface, contact formation and cohesion, influence of multiple contacting *(Russian)* 80−40548
Pb:O, thin film, microstruct. and thermal stress, doping effects 80−88458
Pb-Ag eutectic alloy, microstruct. coarsening under isothermal and temp. gradient conditions 79−20079
Pb-Bi, peritectic reaction, microstruct. changes 78−52753
Pb-Sn, directionally solidified lamellar eutectic, deform. induced microstruct. instability 77−32623
Pb-Sn, eutectic alloys, struct. instability and absence of superplasticity *(Russian)* 77−8882
Pb-Sn eutectic, directionally solidified, perfection and stability of lamellar struct. *(French)* 77−77468
Pb-Sn-Ca alloy sheet, continuously cast, for battery grids, ageing behaviour 77−16603
Pb-Sn(20 wt.%), partially remelted interdendritic fluid flow 77−4771
$Pb_{0.94-x/2}Ba_{0.6}Nb_xZr_{1-x}O_3$, Nb dopant morphology effect on microstructure 80−81005
$Pb_xMo_6S_8(Se_8)$, prep., metallurgical and supercond. props. 77−32102
PbO-B_2O_3-SiO_2, glass enamel, heat treated, exam. of microstructure and chemical durability 79−29254
PbO-B_2O_3-SiO_2-Li_2O-MgO(CaO)(ZnO)(Al_2O_3)(TiO_2)(ZrO_2), glass enamel, heat treated, chemical durability, MgO, CaO, ZnO, Al_2O_3, TiO_2, ZrO_2 addition effects 79−29255
PbO-B_2O_3-SiO_2-Li_2O-ZrO_2-CdO(CoO)(CuO), glass enamel, chemical durability, microstruct., CuO, CdO and CoO addition effects 79−29256
PbTe thermoelectric materials, microstructure anal. using SEM X-ray microanalysis 80−107211
Pb(Zr,Ri)O_3:Ni-silicon rubber flexible composite pyroelectric, dielectric props. 80−80704
Pb($Zr_{0.42}Ti_{0.58}$)O_3, hot-pressed piezoelec. ceramic, effect of nonferroelectric phase 77−43936
$PbZr_xTi_{1-x}O_3$ ceramics, morphotropic phase boundary 80−81035
Pr_7O_{12}, n-beam struct. images, expt. observations and computer calc. 78−38593
β_1-PtZn, defect struct., lattice parameter meas. 78−43009
Pu, $\beta \rightarrow \alpha$ and $\gamma \rightarrow \alpha$ transforms., microstructures and kinetics 77−25048
239PuO_2, stoichiometric, high-temp. deformation 80−81111
$^{239}PuO_2$, hypostoichiometric, high temp. deformation rel. to cryst. microstruct. 79−79041
Rb_2ZnBr_4, quasicrystalline state, incommensurate phase transformation 79−99310
Re film, electrodeposition on Cu, packing defects, X-ray diffr. 77−1333
ReO_3 related oxides, elastic strain energy of matrix between shear planes, array microstruct. 78−43033
Sb_2Te_3-Bi_2Te_3, low-temp. thermoelectric mats., growth of microhomogeneous crysts. 77−48337
$Sc_{(x+2)/3}\,T_{(x-2)/3}O_x$ (T=Si, Mg), 145 Å superstructure 79−99143
Se, Fourier-transformed Compton profile as microstruct. probe 77−59636
Si, (100) and (110), anisotropic etching for fabrication of 3-D microstructures 79−15826
Si, amorphous, hydrogenated film, struct. determ. using electron microscopy 80−10806
Si, autoepitaxy, displacement of microrelief 80−2307
Si crysts., deformed, strain distrib. characterisation, annealing response 77−70140
Si film, polycryst., grain struct. and surface roughness, TEM study 80−70556
Si films, electron-beam-deposited on W substrates, growth and struct., AES and SEM obs. 79−46972
Si ion damage critical gettering microstructures 78−6098
Si, polycryst. with columnar struct., crystn. using casting technique and microstruct., book contrib. 79−43137
Si, polycrystalline structure stability, stacking defects, twins grain struct. *(Russian)* 80−100248
Si solar cells, polycrystalline, from recrystallized plasma deposited thin films 80−104509
Si, solar grade, directionally solidified using C crucibles, TEM study 79−47617
Si:Ar, ion-implanted, epitaxial regrowth by laser annealing, microstruct. 80−84404
Si:Fe(Cu), impurity segregation and microstructural changes by pulsed laser irrad. 79−82254
Si:O, Czochralski crystal, oxygen striation and thermally induced microdefects 80−100275
Si-Al-O-N ceramic, single-phase, prep. by hot-pressing, microstruct. investig. 77−8792
Si-Al-O-N polytypes, hot-pressed, microstruct. 80−3023
Si-Al-O-N system, phase analysis and TEM struct. obs. 80−108420
SiC, appl. of replica electron fractography 79−60237
SiC, $\beta \rightarrow \alpha$ transformation, interfacial energetics 79−8296

crystal microstructure continued
- SiC, $\beta \rightarrow \alpha$ transformation, microstructural aspects 79–8295
- SiC, CVD, microstruct. obs., optical and TEM 79–7560
- SiC, CVD film growth, morphological, chem. and cryst. struct. investig. 77–40385
- SiC fibre reinforced Ni-Cr alumina coated fibres, hot pressed, annealed, IR study 78–60623
- β-SiC, fluidised bed deposited coatings for nucl. fuel granules, microstructural obs. by SEM 77–14233
- β-SiC powder compact, microstruct. changes and β to α transform., Si vapour influence 78–19738
- SiC pyrolytic coatings for HTGR fuel particles, props. rel. to deposition conditions 79–31088
- SiC, reaction bonded, microstruct. characterisation 78–48353
- SiC, reaction sintered, microstruct. *(Japanese)* 77–1825
- SiC, reaction sintered, TEM exam. of recrystallisation, phase transformation 78–80567
- SiC, reaction-bonded , 'REFEL', microstruct. characterization 80–97490
- SiC, self-bonded, microstruct., electrical props., sintering effects 77–1822
- α-SiC, sintered, influence of B, C additives on microstructure, SEM exam. 79–8262
- SiC, subjected to thermal shock, study of substruct. and surface morpholoy 79–43292
- SiC, uncommon mode of morphological development among coherent phases, optical and electron microscope exam. 78–80544
- SiC-AlB_2 (0.61 to 1.2 wt.%), hot pressed, microstruct. 80–93563
- SiFe sheets, grain-oriented, stray field meas. 80–88775
- Si_xFe_{100-x} polycryst. ribbon, prep. by rapid quenching, and props. 80–75803
- Si_3N_4, CVD, struct., optical and mech. props. 77–1816
- Si_3N_4, hot pressed, effect of powder composition and sintering temp., on phase transformation kinetics, microstructure and mech. strength *(German)* 79–4939
- Si_3N_4, hot pressed, Y_2O_3 fluxed, microstruct. 78–64512
- Si_3N_4, hot-pressed, impurity phases, TEM obs. 79–8260
- Si_3N_4, reaction bonded, effect of Si powder grain size on microstructure, and mech. props. *(German)* 79–4998
- Si_3N_4, reaction bonded, fracture mech. pararucters, microstmet. amd temp. effect 79–24598
- Si_3N_4, reaction bonded, pore size and distrib. effect on strength 79–29165
- Si_3N_4, reaction sintered, microstruct. charact. 80–35145
- Si_3N_4, reaction-bonded, microstructural analyses 77–8782
- Si_3N_4, reaction-bonded, struct., form. mechanisms and kinetics 77–4760
- Si_3N_4-based refractories, strength and microstruct. rel. to sintering 77–63610
- Si_3N_4-MgO (5 wt.%), microstructural changes during gas pressure sintering *(Japanese)* 77–12589
- Si_3Ni_4, hot pressed, subcritical crack growth boundaries at internal fracture origins 80–11748
- SiO_2 phase equilibrium and microstructure interpretation 80–60847
- SiO_2, sitall coating, control of phase composition, microstruct. and props. 77–32545
- SiO_2-Al_2O_3, mullite, sintering behaviour and microstruct. 80–20876
- $Sm(Co,Cu)_z$, precip.-hardened, mag. and metallographic props. 77–8339
- $SmCo_5$ magnetic alloys, pressed, sintering rel. to mag. props., cryst. struct. 78–60600
- $SmCo_5$, sprayed magnet, microstruct. and mag. props. between 650°c and 800°C 79–82829
- $Sm(Co_{0.87}Cu_{0.13})_{7.8}$, coercivity and microstruct. 79–56569
- $Sm_2Cu_{1.6}Zr_{0.16}Fe_{3.3}Co_{12}$, enhancement of mag. props. 79–82825
- Sn, molten rotating stream, vortical filament generation during solidification *(Russian)* 78–88460
- Sn/graphite particulate composite, prep. using vacuum infiltration, microstruct., anal. 79–20005
- Sn-Pb, eutectic system, interlamellar spacing meas. 77–36492
- Sn-Pb eutectic, struct. and plasticity, thermomech. treatment effects *(Russian)* 78–60686
- $Sn_xMo_6S_8(Se_8)$, prep., metallurgical and supercond. props. 77–32102
- SnO_2 CVD coating on glass, elec. resist. rel. to cryst. microstruct. 80–84520
- SnO_2, crystal growth habits, CVD method *(Japanese)* 78–95686
- SnO_2:Sb, and pure cryst., microstruct., X-ray diffr., optical and electron microscope studies 78–79619
- $Sn_{1-x}Pb_xSe(Te)$ films, oxidation rel. to annealing temp. and time, Mossbauer spectra, X-ray and microstruct. obs. 80–104311
- SnSe-Sb_2Se_3 system, phase diagram, differential thermal, microstruct., X-ray phase and microstructure anal. 77–16555
- $SnSe_2$-$GeSe_2$, phase diag., electrophys. props. of solid solns. 77–52306
- $SrFe_{12}O_{19}$, microstruct. and magnetic props., electron microscope obs. 79–87290
- $SrZrO_3$ ceramic, high-temp. corrosion resist. *(Polish)* 79–52409
- TC-Co, nearest-neighbour size correlation with grain size *(French)* 77–8843
- Ta, bamboo struct., wire, high-temp. rheology 77–1851
- Ta film sputtered onto Cu substrate, microstruct. and supercond. props. 77–85370
- TaC, etchant for revealing microstructure 80–85097
- $Tb_{0.27}Dy_{0.73}Fe_2$, vertically zoned, magnetomechanical coupling and magnetostriction 80–65999
- Te, evaporated film epitaxial and amorphous-crystalline phase transition growth and struct. 79–51449
- Te film, evaporated, predeposited Ag, Sn, Bi, Al and Se nucleation centres effect on grain growth 77–4739
- Te film, microstructure 80–103598
- (Ti,V)C, activated reactive evaporation deposited films, annealing study, microstructure 80–24762
- α-Ti alloy, crystallographic texture, importance in characterization 77–28821
- α-β Ti alloy, fracture toughness rel. to microstruct. 77–16673
- Ti alloy, microstruct. and mech. props., room and elevated temps. 77–36554
- Ti alloy, microstructure resulting from heat treatment, alloying, effect on creep, fatigue, fracture strength 78–11246
- Ti alloy, VT3-1 mech. props. and low-temp. creep 77–44314
- Ti alloy VT20, phase composition and structure effect on mech. props. 79–38958
- $\alpha+\beta$Ti alloy VT3-1, drop forgings, grain orientation and props., combined mech. working, hardening and high-temp. heat treatment influence *(Russian)* 80–20973

crystal microstructure continued
- Ti alloys, domain struct. of diffuse ω-phase formed in quenching, 1D model 78–27523
- Ti alloys, H_2 diffusion at room temp. 79–51312
- Ti alloys, toughness and behaviour under dynamic loads *(French)* 80–45383
- Ti alloys fracture toughness-mech. props. interrelations 77–86154
- Ti, fatigue fracture surface microstruct., electron microscope obs. 78–60834
- Ti, neutron irradiated, relation between microstructure and recovery behaviour 77–15456
- Ti-11, unstable shear modes in fatigued β-annealed specimens 78–84984
- Ti-(Al)-Zr-Si (5, 0.5 wt.%), creep 77–36595
- Ti-Al, phase diagram in Ti rich region *(Russian)* 77–25013
- Ti-Al, structural and phase changes due to annealing *(Russian)* 80–55440
- Ti-Al (27.3 wt.%), arc melted, microstruct. 79–61577
- Ti-Al diffusion coatings on C steel, struct. and props. 79–57156
- Ti-Al-Cr-Mo (6, 2.0, 2.5 wt.%), microstructural changes and mech. props. 77–25080
- Ti-Al-Cr-Mo system, VTZ-1 alloy, microstruct. influence on fatigue characts. 80–3195
- Ti-Al-H, H effect on mech. props. and lattice constants 80–21036
- Ti-Al-Mo, type Ti-6242S, irrad. induced creep 80–39163
- Ti-Al-Mo (31, 13 wt.%), transform. microstruct. 78–48394
- Ti-Al-Sn, type Ti-5621S, irrad. induced creep 80–39163
- α-βTi-Al-Sn-Zr-Mo (6, 2, 4, 6 wt.%), interface struct. 77–44212
- α-βTi-Al-Sn-Zr-Mo (6, 2, 4, 6 wt.%), deformation associated with surface cracks and α particles 79–79107
- Ti-Al-V, (6,4 wt.%), single and dual ion irrad., microstruct. studies 80–29077
- Ti-Al-V, irrad. induced creep 80–39163
- Ti-Al-V (4.7, 2 wt.%) pseudo alpha alloy, laminar struct. singularities, β to α transformation *(Russian)* 80–7552
- Ti-Al-V (6, 4 wt.%), annealed and rolled plate, elevated temp. plastic anisotropy 79–61663
- Ti-Al-V (6, 4 wt.%), deform. charact. under isothermal forging conditions 77–36600
- Ti-Al-V (6, 4 wt.%), stress corrosion cracking, composition, microstruct. and texture effects 79–11725
- Ti-Al-V (6,4 wt.%), α/β interface phase influence on tensile props. 80–30034
- Ti-Al-V (6,4 wt.%), cyclic stress-strain response 77–21170
- Ti-Al-V (6,4 wt.%), effects of grain size on superplasticity, deformation mechanisms, microstructural characteristics 79–52323
- Ti-Al-V (6,4 wt.%), heavy ion irrad. effect on microstructure 79–10884
- Ti-Al-V (6,4 wt.%) alloy foil, substrate temp. effect on struct. 80–7497
- Ti-Al-V-Cr-Mo-Zr (3,8,6,4,4 wt.%), beta-C, microstruct. effect on mech. props. 78–27577
- Ti-Al-V(Sn) alloys, plastic deformation and fracture characts. at low temps. *(Russian)* 80–7624
- Ti-Al-(V) (6,4 wt.%), hot salt stress corrosion susceptibility, microstruct. effects 77–36688
- Ti-alloy, IMI-685, unstable shear modes in fatigued β-annealed specimens 78–84984
- Ti-Fe, corrosion, effect of microstruct. caused by casting, annealing, beating *(Russian)* 79–57140
- α-βTi-Mn (4.3 wt.%), interface phase struct. 77–44212
- Ti-Mo (5 at.%) based alloy, supercond. transition temp. enhancement by varying struct. state 77–20483
- Ti-Mo-Zr-Sn (11.5, 6.0, 4.5 wt.%) alloy, struct. as affected by processing history 80–84972
- Ti-Nb alloys, Fe, Mo, V, Ta alloying additions on microstruct. after combined treatment *(Russian)* 77–59826
- Ti-Nb-W, 20 to 1000°C, isothermal section, X-ray anal., microstruct., hardness, cond., transform. *(Russian)* 77–55947
- Ti-Ni-Mo (1.5, 2 wt.%), Mo effect on microstructure 77–36536
- Ti-V-Cr, type Ti-15-333, irrad. induced creep 80–39163
- Ti_3Al-Sn-Zr, alloy, Sn and Zr alloying influence on creep and scaling resist. *(Russian)* 79–52302
- TiB_2 coatings, CVD, electron microprobe, SEM, X-ray diffr. characterisation *(French)* 78–43271
- TiC, activated reactive evaporation deposited films, annealing study, microstructure 80–24762
- TiC single crystal, vapour deposited on Mo and W wires, electron microscope study 77–1795
- TiC-steel alloys, structure formation during sintering 77–59732
- TiC_x, fused material, microstruct. 78–44115
- TiC_xN_y, fused material, microstruct. 78–44115
- TiN-AlN composites, struct. and props. 77–40413
- TiO_2-Ga_2O_3 system, phase relations and microstructs. 78–3107
- Tl-Bi-Sb-Te system, peritectic reactions in $TlBiTe_2$-$TlSbTe_2$ cross section, crystn. character 80–108406
- TlI, on KCl, epitaxial growth habit rel. to optical scatt. 77–50738
- $(U,Pu)O_2$, ceramographic exam. of Dounreay PFR fuels, data bank storage 79–49811
- U, anomalous thermal prop. behaviour at low temp. interpret. 77–28018
- U film, for bombardment targets, prod. techniques 77–389
- U-Mo (2 wt.%), depleted, effect of microstruct. on mech. props. 80–108497
- U-Mo-Nb-Zr-Ti (0.75, 0.75, 0.75, 0.5 wt.%), heat treatment effect on microstruct. and mech. props. 78–23729
- UO_2, commercial fuel pin, irradiation induced volume changes, comparison with model 78–78465
- UO_2 fuel pellet, bending strength, fabrication and microstruct. effect 80–2986
- UO_2, high temp. irradiation, effect on microstruct. and unstable fission products 78–33250
- UO_2, microstructure in rods operated above critical heat flux 77–42098
- UO_2 pellet fuel, radiation induced densification 77–6519
- UO_2-U_4O_9, thermal cond., effect of microstruct. and microcracking 79–97810
- V, ion implanted with 2 MeV He under pulsed conditions, microstructure obs. 80–29088
- V-N, BCC solid soln., superperiodicity of lattice in quenched ordered struct. *(Russian)* 78–56662
- VC, damage sustained during neutron irradiation 77–1841
- V_2Cg, struct. and orientation of rhombic modification *(Russian)* 77–55270
- V_3Ga, superconducting transition temp., metallurgical processing, struct. 77–63019

crystal microstructure continued
VO_2, reduced, microstruct., crystallographic shear planes, electron microscope obs. 79—1443
V_2O_5 cathode, used in Li-V_2O_5 reserve cells, microstruct. optical reflectance, elec. cond. meas., chem. anal., SEM obs. 79—43752
V_2O_5-based glasses, amorphous and crystallized electronic cond. and related props. 79—99547
V_6O_{11}, microsyntactic intergrowth 79—99149
V_7O_{13}, microsyntactic intergrowth 79—99149
(W, Mo)C, hard-facing applications, effect of Mo on struct and hardness of WC 80—108474
W, BCC, struct. singularities rel. to solid soln. behaviour *(Russian)* 77—11696
W, creep in monocrystal at 0.57 T_m *(Russian)* 77—1856
W, drawn wire, microstruct. effect on fracture 80—3177
W, evaporated coatings, produced by carbonyl method, struct. *(Russian)* 77—43441
W fibre, KSiAl doped, recrystallisation, Li diffusion effects, hardness, strength, microstructure meas. *(German)* 78—64644
W, impurity interactions with C, N, and O, struct., mech. props. and purification 79—52277
W, SEM expts., anomalous patterns *(Chinese)* 80—59349
W, substruct. stability of single crysts. on high temp annealing *(Russian)* 77—66666
W, wire, doped, heavily drawn, recrystallisation 77—16609
W wire, incandescent, motion and growth of K bubbles *(Hungarian)* 77—48460
W, with different microstructs., temp. depend. of yield strength 80—16404
W, with impurities, grain boundaries, effect on high temp. plasticity *(Russian)* 79—79057
W-Ni, liquid phase sintering 80—25613
W-Ni system, grain growth and densification during liquid phase sintering 79—38760
W-Re alloy, substruct. stability of single crysts. on high temp. annealing *(Russian)* 77—66666
W-Re fibre-reinforced Ni-base refractory alloy, struct. and props. *(Russian)* 77—59721
W-ThO_2 composite, struct., lamination tendency, effects of method of manuf. 78—68653
WC, plasma sprayed coating 78—68835
WC-Co, cemented carbide sintered, appl. of dihedral angle meas. to microstruct. 78—39716
WC-Co, exam. of effect of continuous carbide phase, on hardness, and deformation 78—52974
WC-Co, nearest-neighbour size correlation with grain size *(French)* 77—8843
WC-Co, rupture stress, microstructure and other effects 77—73343
WC-Co, STEM anal. of grain boundaries 80—79644
WC-Co, sintered, obs. of spinel particles by TEM 78—95714
WC_x formation during pyrolysis of WCl_6 and toluene, coating props. 77—36682
$W_xNb_yO_7$ ordering of atom string, cluster model 77—68959
WS_2, single cryst., growth by direct vapour transport, pit density determ. by etching 79—28904
WSe_2, chem. vapour transport growth, microstruct. develop. 80—103278
Y-Fe-Si alloy, phase diagram 79—52158
YAG Czochralski grown crysts., growth of facets and vicinal interfaces *(Chinese)* 79—90578
Y_xFe_{1-x} amorphous films, microstruct. and mag. anisotropy 79—82838
Y_2O_3, corrosion resist. in fused Li rel. to phase and microstruct. changes 77—44378
Y_2O_3 fused single crystals, struct. 80—19804
Zn based alloys, preferred crystal orientations, rot. mill device investig. 79—57006
Zn film, vac. deposited, X-ray diffr. study of microstruct. 78—26796
Zn, film, vac. deposited, X-ray diffr. study of microstruct. 78—75966
Zn particulate composite, mech. props., microstruct. correlation, at low and high temps. 77—32624
Zn, preferred crystal orientations, rot. mill device investig. 79—57006
Zn, structure sensitive props., temp. hysteresis after melting and crystallisation *(Russian)* 79—29036
Zn-Al eutectoid superplastic alloy, fatigue, microstruct. obs. and frequency effect 77—36659
Zn-Al(22 wt.%), alloy sheet, superplastic, cold-rolling effects on mech. props. and microstructure *(Japanese)* 80—71671
Zn-Cd, three-dimensional microstruct. analysis, appl. of basic topological concepts 77—59739
ZnO based varistors, evolution and role of chem. constituents rel. to prep. method, influence on elec. props. *(French)* 78—31367
ZnO ceramics, heat treatment effect on cryst. phases, microstruct. and elec. props. 79—100268
ZnO, crystallising in double HCP lattice, TEM and electron diffr. obs. 77—31655
ZnO crystals, SEM study *(German)* 80—33860
ZnO, sintered, impurity ion effects on crystalline state *(Japanese)* 77—28768
ZnO-Al_2O_3-SiO_2, transparent glass-ceramics, EPR obs. of glass crystallisation 78—80507
ZnO-Al_2O_3-SiO2, transparent glass ceramics, heat treatment effect on microstruct. 78—56667
ZnO-$Al_2O_3SiO_2$, transparent glass-ceramic, microstruct., physical props., crystallisation ht. treatment depend. 78—80506
ZnO-based ceramic microstructure and nonlinear props., B diffusion effects *(Russian)* 80—49423
ZnO-Bi_2O_3-Sb_2O_3-Co_2O_3-MnO_2-Cr_2O_3, nonohmic ceramic, microstruct. exam. 78—47292
ZnO_2, polycrystn., determ. of crystallographic orientation of grains 79—69049
ZnS, cryst. grown from melt under press., microstruct. 77—59019
ZnS, laser evaporated film, microstruct. TEM obs. 79—82479
ZnS:Ag, struct. and mech. props. 78—22753
ZnS-based phosphor, microstruct. and luminesc. efficiency 78—10959
ZnS-MgF_2 dielectric film, laser irrad. and microscopic inhomogeneities 78—2157
ZnS-SrF_2 dielectric film, laser irrad. and microscopic inhomogeneities 78—2157
ZnTe:Cu, precipitates, electron microscopic investigation 80—45312
ZnTe-CdSe solid solutions phase equilibria *(Russian)* 79—43224
ZnTe-Ga_2Te_3, phase diagram 78—35360

crystal microstructure continued
Zr alloys, domain struct. of diffuse ω-phase formed in quenching, 1D model 78—27523
Zr alloys, H_2 diffusion at room temp. 79—51312
Zr alloys, irradiation growth, influence of microstructure and test conditions 80—92561
Zr, irradiation growth, influence of microstructure and test conditions 80—92561
Zr, microstructure exam. by electron microscopy, oxide film appl. 79—70243
Zr-Al (4.6 wt.%), microstruct. effect on mech. props. 79—20080
Zr-Dy dil. alloys, plastically deformed, mech. props. and microstruct. *(Russian)* 79—20112
Zr-Nb (2.5 wt.%), cold-worked, pressure tubing, metallography and mech. props. 80—89269
Zr-Nb (2.5 wt.%), seam welding tubing, microstruct. in weld region 79—61621
Zr-Nb (2.5 wt.%) alloys, microstruct investigation by electron microscopy using oxide films 79—70243
Zr-Ru, alloy Zr rich, Ru solubility, eutectic decay, $\alpha\rightleftarrows\beta$ transform., struct. *(Russian)* 80—65227
Zr-V, superconductivity and metallurgy of C15 materials 79—4610
Zr_3Al, cold worked, annealing effects 77—36535
ZrB_2, pure, vacuum hot-press sintering and microstruct. *(Japanese)* 78—23649
ZrB_2-Ta composite, vacuum hot-press sintering and microstruct. *(Japanese)* 78—23649
ZrC-C, CVD, microhardness and microstruct. 77—8916
ZrH_x, laser irrad. effect on interstitial phases, metallographic obs. 79—37734
$Zr(HPO_4)_2.H_2O$-Kynar membranes, struct., ion mobility 78—76915
ZrN-AlN composites, struct. and props. 77—40413
ZrO_2, MgO partially stabilized, microstruct. development during ageing 79—91710
ZrO_2, optimum sintering characts., density, X-ray diffr., IR spectrum, UV spectrum obs. 78—76617
ZrO_2 stabilised with Y_2O_3, ultrafine grained, fabrication and flexural strength 77—1829
ZrO_2-W, eutectic microstruct. 78—27499
ZrO_2-Y_2O_3 monocrystalline solid solutions, struct. and phase form. 79—52188
ZrO_2-Y_2O_3-CaO(MgO), long term firing effect at 2100 to 2200°C on solid soln. conc. and microstruct. 77—90309
$Zr_3Sc_4O_{12}$, n-beam struct. images, expt. observations and computer calc. 78—38593
$ZrSiO_4$, plasma dissociated, quenching rate effect on microstruct. 79—38854

crystal morphology
adamantane crystals, vapour grown, temp. depend. of morphology of initial growth forms 79—47608
alkali halide, morphology of growth and evaporation surface 78—79544
n-alkanes, monoclinic, polygonized spiral growth patterns on {001} faces *(Italian)* 79—23559
n-alkenes, n even, interaction energy at twin boundary, dihedral reentrant, salient angle effect on growth morphology 78—55876
Antarctic ice core, ice crystal size and shape *(Japanese)* 77—81944
austenitic stainless steel, 18 Cr-11 Ni, directly aged, nucleation of $M_{23}C_6$ carbides *(Polish)* 78—52806
barium oxalate, lacunary phase form., morphological and kinetic characts. 79—60299
binary alloy, morphological stability, discrete lattice theory, appl. to interfacial zones 78—3133
binary alloy single crysts., dilute, morphological stability of unidirectional growth, thermodynamic study *(French)* 79—86727
boracite, single cryst. prep. and phys. props. 80—100763
brass, morphological stability of α/β phase interface, interface moving direction effect 77—15700
β-brass, spinodally decomposed, morphology and characts. 80—60863
brass, two-phase α/β bicrystal, morphology and crystallographic relationships between phases 79—46966
camphor crystals, investigation of structural formation and growth kinetics 79—47610
carbon tetrabromide, cryst. growth from melt, dissolution morphology *(German)* 77—24283
conference, International Crystallography Congress, Warsaw, Poland (Aug. 78) 79—23481
copper phthalocyanine, cryst. growth from vapour, hollow cryst. form, mechanism *(German)* 77—55252
β-copper phthalocyanine, single cryst., equilib. shape, growth shape, vapour phase growth *(German)* 77—43163
cordierite glass-ceramic, effect of crystn. on thermal diffusivity, TEM, X-ray anal. 79—33127
corundum, bladed crystals, morphology and struct. 77—84680
corundum, subjected to thermal shock, study of substruct. and surface morpholoy 79—43292
crystal face, growth behaviour in presence of screw dislocations 80—103276
crystal surface morphology development during sputter erosion 80—88414
crystalline polymer, epitaxial crystallisation on surface of drawn polytetrafluoroethylene 78—14626
crystallisation kinetics, review, book contrib. 77—39550
CTA-DNA crystal growth and morphology 80—26198
cube from soln. without convection, morphological stability 77—51333
cubic single crystal, orientation determ. method using optical microscope 79—52482
cytosine monohydrate, cryst. growth from aq. soln., elec. props. 78—3007
di-o-thymotide, cryst. chem. study and morphology *(French)* 79—46576
diamond, form. by shock compression of graphite, cryst., surface struct. 78—44060
diamond, polycryst., growth at high temp. and press., morphology 77—11495
diamond, synthetic, external crystal morphology, SEM obs. 79—73078
diamond, synthetic disorientation of crystallite subgrains *(German)* 77—68939
diamond, synthetic grits, crystal morphology of cyclic twins 80—2037
dickite, unusual crystal habit, structural disorder 80—59445
diphenyl crystallites, changes in face growth rate from vapour phase 79—55686
DNA-cetavlate crystal growth and morphology 77—66583

crystal morphology continued
- electrocrystallisation from molten salts, morphological stability of plane interface 77—35497
- electrolytic Fe based composite metal-powder coating structure *(Russian)* 79—83170
- Fe-N system, fine particles growth, prep. by reactive gas evaporation technique, lattice consts. and habit study 79—56919
- film, morphology and morphological changes 78—72043
- film, ultrathin, effort of optical radiation on growth and struct. 78—72045
- fluor-richterite crystal, habit, growth in oxide-fluoride mixtures, statistical study *(German)* 78—38639
- fructose, stereoviews and morphological data on microcrystals 78—18510
- graphite, single crystal, from Fe-C melt, morphology 78—42932
- graphitic carbons, particle emission rel. to morphological changes during sublimation 77—47566
- growth and dissolution, crystal shapes encountered 79—99089
- habit, modification control in growth 80—49150
- habits, graphical presentation, programmable method 79—32935
- heteroepitaxial surface morphologies and misalignments *(Japanese)* 80—15411
- hexachloroethane, surface roughening transition in vapour phase growth 78—2044
- hexatricontane, growth kinetics of (001) faces from soln. 79—52098
- L(+) hydrazonium tartrate, soln. growth and cryst. morphology 79—33914
- ice, droxtals grown from supercooled water droplets, morphology 79—24426
- ice crystal morphology, vapour growth, influence of vapour diffusion and heat diffusion 80—64933
- ice crystals, vapour-grown, appearance of non-singular surfaces 79—60297
- ice dendrite formation from vapour phase, morphology, sizes and growth rates 78—10313
- icicle crystallisation phenomenon, growth mechanism, structure and shape 80—59423
- II-VI compounds, hollow crysts., review 77—11494
- interfacial angles of small crystals meas. using SEM, sample holder 77—27792
- intergrowths, regular, investigation with Laves-Ernst compensator 79—96843
- ionic crystal, stability of polar surface planes 77—39554
- lamellar-spiral growth hillocks, kinetics and morphology 78—18566
- lath martensite, habit plane and morphology 77—8823
- liquid crystalline polymers, struct. and morphology, theory 79—69025
- macroscopic metal catalysts, morphology and etching processes, review 80—7856
- martensite crystal, struct. X-ray diffr. study 78—79565
- martensite layers, external stress effects on equilibrium morphology, thermodynamic model *(Russian)* 78—52804
- MBBA, liq. crystal, morphological changes and electro-optical characts. appl. laser light modulation 77—20826
- MBBA, solid, NMR and thermal behaviour, cooling and mag. field effects 78—76336
- metal crystallites, polyhedral, growth in inactive gas, review 79—27934
- metastable crystal forms, crystallisation behaviour 79—86733
- microclusters, electric viewpoint of morphology, energy spectrum of single electron states 78—10327
- monostearine crystals, spiral growth from organic soln. 80—93467
- naphthalene crystals, investigation of structural formation and growth kinetics 79—47610
- Nimonic, IN100, γ' precipitates, casting conditions effect on morphology 80—7548
- 4-nitrophenyl 4-n-octyloxybenzonate, space group unit-cell and crystallographic props. 80—6399
- nucleation rate equation, generalisation of nucleus shape depend. parameters 78—84765
- nylon-6, pressure-crystallised, morphology and structure 77—84669
- optical crystallography, book 80—12862
- organic crystal, struct. and habit correspondence, mol. centre of gravity determ. *(German)* 79—32934
- organic crystals, morphology of crysts. with two mols. in asymmetric unit cell *(German)* 80—24396
- paradibromo benzene crystals, investigation of structural formation and growth kinetics 79—47610
- phloroglucinol dihydrate crystals, growth characts., X-ray diffr. and optical microscopic study 79—19986
- phthalic anhydride, whisker crystals, vapour growth and morphology 77—35841
- phthalic anhydride spherulites, cryst. growth from melt 79—32930
- point groups, basis functions for irreducible representation, appl. to morphic effects on IR and Raman spectra *(Japanese)* 79—4265
- poly(chlorotrifluoroethylene) films, crystalline superstruct., mol. orientation, X-ray diffr., depolarised light scatt. 78—71685
- poly(p-phenylene terephthalamide), crystallised during polymerisation, morphology *(Japanese)* 77—51328
- poly(p-phenylene terephthalamide), quiescent and strain induced crystallization from H_2SO_4 soln. 79—90571
- poly-γ-methyl-D-glutamate, α-helical form, annealing effect, morphology 79—14702
- trans-polyacetylene, bulk crystallinity, small-angle X-ray diffr. study 80—103263
- polybis-p-toluene sulphonate, single crysts. 79—23594
- polycaprolactam, fibre, struct. change when used as resin reinforcement *(German)* 77—21091
- polydiacetylene, extended-chain crysts., struct. and morphology 79—82165
- polyethylene, {110} twinning mode, X-ray obs. 77—35572
- polyethylene, crosslinked networks, stress-induced crystallisation, theory 77—24277
- polyethylene, fibre, phase structure and molecular mobility, broad-line NMR spectroscopy 78—14290
- polyethylene, high density, environmental stress cracking and morphology 78—68834
- polyethylene, obtained from heterogeneous Ziegler-Natta catalysts, cryst. morphology and growth 80—38941
- polyethylene, single crystal, electron microscopy study 80—103273
- polyethylene, stress crystallised, melting behaviour 77—47554
- polyethylene fibre, high-strength high-modulus, morphology and tensile prop. relations 80—103264
- polyethylene films, hard elastic, deform. mechanism 77—32652

crystal morphology continued
- polyethylene oxide, peculiarities of struct. form. near below the melting point 80—54150
- polyhedral crystal growth from soln., morphological stability 78—26466
- polymer, crystalline, crystallisation, morphology rel. to props. 77—39546
- polymer, Raman spectra, cryst. morphology, longitudinal acoustic mode 78—43859
- polymer, Raman spectra, longitudinal acoustic mode 78—43858
- polymer, semicrystalline, mol. morphology 78—38631
- polymer film, crystallisation induced by biaxial stretching during manufacture 79—82164
- polymer morphology and lamellas in bulk and oriented linear high polymer 78—51434
- polymers, crosslinked networks, stress-induced, crystallisation, theory 77—24277
- polymers, crystallisation under extreme temp. and press. gradient 79—82163
- polymers, struct. classification, morphology and twinning *(French)* 79—51058
- polystyrene in tetrachloroxylene and tetrachlorobenzene, morphology of crystallized additives 79—99082
- polystyrene-tetrachloroxylene(tetrachlorobenzene) glassy solns., additive morphology rel. to mech. props. 79—65007
- polyvinylidene fluoride, melt-solidified, crystn. and morphology 80—103461
- Portland cement mortar, micromorphology and interfacial zone around aggregates, SEM obs. 79—61598
- pyramids of different slopes, growth on cryst. face at const. supersaturation, model interpret. 78—2050
- quartz, cultured, prism faces growth and development, attached microcrystals role 77—31612
- quartz, twinned crystals, after Japan Law, investigation of regrowth 80—54162
- rare earth mixed molybdates, $R_2(MoO_4)_3$, $R_{2(1-x)}R'_{2x}(MoO_4)_3$, cryst. growth and crystallographic data 79—43132
- (rare-earth) $Fe_3(BO_3)_4$, cryst. growth from soln.-melt, props. 80—108337
- review, morphology of crystals *(French)* 79—4266
- review of controlling factors *(Japanese)* 77—55256
- salol crystals, investigation of structural formation and growth kinetics 79—47610
- sapphire, profiled growth, struct. perfection 78—68621
- selective epitaxial growth and morphology control 77—77378
- SEM, automation of comparative morphological analysis 79—23509
- semiconductor, electronic properties, rel. to chem. bonding and lattice dynamics 80—44169
- silicate minerals Raman spectra, microscopic samples molecular analysis 80—57391
- slip morphology in dispersion hardened materials 77—4785
- sodalite, hydrothermal growth on seed crysts. covered with boundary layers, growth mechanism 78—30571
- sodium acetate trihydrate, whisker growth on membrane in aq. soln. 78—30854
- solid-solid interface chemistry, characterisation, theory 80—75448
- SOS early growth, island coalescence model 77—76704
- SOS early growth, transmission electron microscope obs. 77—76703
- spherical particle, growing from a binary alloy melt, morphological stability 80—29943
- sputtering induced topography on solids, energetics and kinetics 80—88220
- stearic acid, single cryst. growth mechanism 78—30562
- steel, cast, high speed, solidification, $(Fe,Mo)_6C$ form., struct. 79—24514
- steel, dimple fracture, relation between inclusions and morphology *(Chinese)* 79—74231
- steel, low C rimming, effect of addition of Al to Zn on phase composition and morphology *(Polish)* 78—53014
- steel, metastable alloys, singularities of $\alpha \rightarrow \gamma$ transform. and hardening *(Russian)* 79—52210
- steel, non-metallic inclusions changes due to heating obs., influence on ductile fracture *(Spanish)* 80—25744
- steel, Si, lower bainite morphology *(Czech)* 79—78959
- steel, Si killed, effect of Al addition to Zn on phase composition and morphology of products of Fe-Zn reaction *(Polish)* 78—85021
- steel, stainless, $\alpha+\gamma$ phase, tensile deform. induced α' martensite, morphology 78—44122
- steel, stainless, martensite formation, in situ obs. 80—25692
- steel, weld, morphology, effect of ferrite content 77—36521
- step trains, modes of vibr., rhythmical bunching, expt. obs. to show periodicity in step patterns 79—41996
- step-step interaction on clean surfaces, morphological changes 78—14552
- stereoviews and morphological data on microcrystals 78—18510
- succinonitrile, crystn. kinetics and shapes 77—31617
- sulphosalt minerals, exam. of crystal chemistry and morphology 79—10838
- tetrakaidecahedra as grain models 78—51458
- triglycine fluoberyllate, deuterated, dislocation line defect X-ray topographic analysis 80—59465
- tris (3-mercapto-1, 3-diphenyl-2-propen-1-onato) Co(III), multiple twinning 80—100250
- turquoise, crystalline, Nogales Mexico, SEM and TEM study 79—29760
- twinned crystals, re-entrant corner effect, re-investigation 79—73177
- urea mixed and adsorption mixed crystals and epitaxial growth from solns., tracht and habit *(German)* 80—38973
- uric acid occurrence, growth morphology of $C_5H_4N_4O_3$ anhydrous monoclinic modification 80—84123
- Wulf habits, ideal forms of soln. of crysts. 79—14718
- Ag, electrodeposit, on (111) face, habit modification caused by Cl 80—71600
- Ag electrodeposition, on (100) face of single crystal Ag in presence of sulphadiazine 80—89161
- Ag electrodeposits, dendritic growth inhibition by tartaric acid and tartrates *(French)* 78—87894
- Ag, small particles prep. by evaporation in clean Ar atm. 77—62494
- Ag-Zn (38 at.%), morphological and struct. studies of thermoelastic martensites 77—63669
- AgBr emulsion, model system, Ostwald ripening obs. 77—2707
- AgBr emulsion crystal habit transitions 79—100447
- AgBr, influence of Cd ions on crystal shape 79—19235
- AgBrI photographic grains, TEM investig. of morphology and crystallography 77—57418
- AgCl film, on complementary cleavage planes of TGS, morphology, electron microscope obs. 79—15031

crystal morphology continued

AgCl, habit modification by incorporating of Br^- and I^- ions during growth in aq. gelatin 77—5946
AgCl particles suspended in photochromic glasses, shape rel. to photosensitivity 78—31223
AgMg two phase bicrystal growth, orientation, interface struct. 80—60773
$AgNO_3$, centre of symmetry and cryst. perfection *(French)* 80—107089
α-Ag_2S whiskers, growth in VLS system, SEM and X-ray diffr. anal. 79—46989
Al film, ion plated, morphology exam. by SEM 79—28251
Al, small particle prep. by evaporation in clean Ar atm. 77—62494
Al-Al_4Ca, eutectic alloy, unidirectionally solidified, exam. of growth and crystallography 78—72771
Al-Cd hypomonotectic alloy, rapid solidification and decomposition 80—50638
Al-Cu (4 wt.%), non IPS geometric surface relief effects associated with diffusional phase transform. 77—32575
Al-Cu-Zn alloy, ageing, X-ray and electron diffr. meas. *(Russian)* 78—39806
Al-Ti alloys, growth crystallography and morphologies of Al_3Ti primary dendrites 79—43230
$Al_{0.3}Ga_{0.7}As$:Te(SN), impurity effects on interface morphology of LPE films on corrugated GaAs substrates 78—88435
AlGaAsSb LPE growth, lattice-matched to GaSb, characterisation 80—60794
AlN, condensates, growth from vapour, morphological comparison with, ZnO, MgO 78—34450
Al_3Ni, cryst., theoretical morphology and comparison with observed habits *(French)* 80—79732
Al_2O_3, alumina, whiskers growth by hydrolysis of AlF_3 79—28260
Al_2O_3, crystallite size and lattice distortion, determination using X-ray line broadening analysis, appl. to ceramic powders 79—8261
α-Al_2O_3, growth and adhesion on Pt-Al alloys 77—8994
Al_2O_3, layer, obtained by reactive evap., surface struct. and morphology *(Polish)* 79—28242
Al_2O_3, translucent, fabrication by high press. sintering 78—11167
Al_2O_3-TiO_2 powder, plasma-prepared, morphology and phase constitution 80—100833
Au film, chem. deposition on Si, form., struct. 78—34723
Au film, on complementary cleavage planes of TGS, morphology, electron microscope obs. 79—15031
Au fine particles, vacuum deposited, morphological features using TEM weak-beam dark-field technique 80—15410
Au thin films, cryst. ripening rel. to heat treatment *(German)* 80—3109
Au vapour deposited particles, with pentagonal profiles struct. by TEM imaging techniques 79—77566
Au, vapour deposited particles, with hexagonal profile, struct. determ. using TEM imaging 79—77567
$AuSn_4$-Sn, eutectic struct., faceting and morphological regularity 79—61573
B, tetragonal, phase I, prep. and struct., book contrib. 78—47277
BN external crystal morphology, SEM obs. 79—73078
BN, high pressure synthesis, exam. of relationship between synthesis condition, and crystal shape, size *(Japanese)* 79—20018
BP:Ni pillar crystal growth from vapour 80—60758
$BaCO_3$, grown in silica gel medium in test tube 77—36379
$BaMoO_4$ crystals, growth in SiO_2 gel under influence of elec. field 80—93469
$BaMoO_4$, grown in silica gel media in test tube 77—36379
$BaMoO_4$, single crystals, habit modification, growth kinetics in silica gel 80—20777
BiOCl, exam. of crystal structure and morphology, as function of growth conditions, using electron microscopy 79—52103
$Bi_2(SeO_4)_3$, single cryst. growth in silica gels, X-ray diffr., IR and emission spectroscopy study 79—74075
C, columnar and laminar forms, deposition on polycrystalline Ni foils 78—63943
C, morphology and growth mechanism of carbons formed by Ni-catalysed decomp. of hydrocarbons 78—35679
C, pyrolytic, spiral growth rel. to temp., press., flow conditions, dislocations, props. *(German)* 78—42931
$CaAl_2Si_2O_8$-$NaAlSi_3O_8$ (anorthite-albite) system, crystal growth rates and morphologies 80—4010
$Ca_{2x}Bi_{3-2x}V_xFe_{5-x}O_{12}$ ferrogarnet, magnetis. distrib., correl. with morphological habit 79—42802
$CaC_2O_4.2xH_2O$ ($0<x<5$ zeolite water fraction), weddellite, growth morphology, PBC analysis 80—24388
CaF_2, etching behaviour in HCl vapour 78—59812
CaF_2, whiskers and crysts., flux growth and charact. by morphology and fracture strength 79—19987
$CaHPO_4.2H_2O$, brushite, obs. of etch pits on as grown faces 79—73169
CaO, single cryst. growth from molten $CaCl_2$ in wet atmosphere, habits 80—55287
$Ca_{10}(PO_4)_6(F,OH)_2$, apatite, cryst. growth and habit, F ion conc. effect 78—30560
$CaSO_4$, cryst. growth kinetics at heated metal surfaces, thermal cond. morphology and crystn. 80—29867
Ca_3SiO_3, hydrated, composition and morphology 78—26755
$Ca_6Si_6O_{18}.4H_2O$, tobermorite synthetic crysts., hydrothermal growth, TEM and X-ray diffr. characterisation 79—43122
Cd, vapour grown crystal, morphology and growth mechanism, Bi impurity effects 79—23546
ω-Cd-Hg alloy, melt-growth, morphology of single crysts. 78—64464
$CdBr_2.4H_2O$, cryst. struct. determ. *(French)* 78—26502
$CdCl_2 . 2.5H_2O$, rel. between theoretical and obs. morphology *(French)* 80—70148
CdI_2, vap. growth and cryst. struct. 77—72570
CdS, epitaxial layers on Ge, morphology and six-pointed optic figures obs. 78—2390
CdS smoke particle growth, prep. by evaporation in inert gases 77—24938
CdS/Cu_2S solar cells, polycryst. thin film photovoltaic materials, photon loss anal., expt. determ. 80—93888
CdSe film, effect of growth conditions on electrophysical properties 78—44024
Ce_3NbO_x, $CeNbO_x$ and $CeNb_3O_x$, redox processes, elec. resist., phase anal., mag. suscept., thermogravimetric meas. 78—34482
Co-Fe, morphology and certain props. of α-and η-phase martensite *(Russian)* 77—1838

crystal morphology continued

(Co-Ni)-$Cr_{23}C_6$ eutectic alloy, directionally soldified, microstruct. and crystallography 78—48390
$(Co_{1-x}Ni_x)O$, single crysts., morphology change during compressive creep testing 79—29144
$CoOOH \rightarrow Co_3O_4$, morphology, topotaxy, comparison with $Co(OH)_2 \rightarrow CoOOH$ 77—16817
25Cr-20Ni stainless steel dendritic solidification, growth morphology and solute redistrib. *(Japanese)* 80—81045
CrO_2 and CrO(OH), fine particle obs. of cryst. morphology and topotaxy 80—65969
CrO_2, synthesis and morphology 79—24481
Cr_2O_3, cryst. growth from decomposition of $K_2Cr_2O_7$ melt, morphology study 79—43131
Cr_2O_3-Cr film, electrodeposited, optical degradation rel. to surface morphology, SEM and AES obs. 79—79401
$Cr_{2.8}V_{0.7}Fe_{3.4}C_3$, stacking fault study, morphology, comp. and struct. 80—84190
$CsCuCl_3$, phys. props. 77—62511
CsH_2PO_4, single cryst. growth, struct. and elec. props. 78—71693
Cs_2PdCl_4 and $Cs_2PtCl_4.H_2O$, single cryst. growth and gel and soln., morphology 77—77360
Cu and α-Cu-Zn alloy, whisker growth in Zn reduction, morphological change to dendrites 79—28261
Cu, cementation, on Fe, deposit struct., reaction rates, SEM 80—104421
Cu corrosion, by COS, kinetic and morphological study *(French)* 79—43488
Cu, deposits on Cu (110) electrode, morphology and crystal growth 79—47644
Cu electrodeposits, collagen and chloride additions effects obs. 78—51852
Cu-Al-Ti-Zr, internally oxidized, morphology of precipitates and dispersion hardening *(Russian)* 79—52217
Cu-Cd, structure, electrolytic deposition on monocrystalline Cu cathodes *(Polish)* 80—44435
Cu-Cr, eutectic, effect of comp. and solidification conditions on microstruct. *(Russian)* 79—29037
Cu-Ni crystals, growth, H_2 reduction of CuI-$NiBr_2$ mixture, habit study by X-ray difr., optical and SEM 79—60665
Cu-W composite powder, prod. by H_2 reduction of $CuWO_4$ 79—20006
Cu_2S-CdS thin film solar cells, Cu_2S layer separation, struct. 79—95282
$CuSO_4.5H_2O$, dehydration into trihydrate obs. using monocryst. platelets, product domains shape 80—71905
Cu_2SnSe_3, single cryst. growth and morphology 77—85908
$Dy_2(MoO_4)_3$, cryst. growth and props. 79—55727
Fe, cast, white, prep. and morphological obs. *(French)* 79—43168
α-Fe crysts. growing in $Fe_{80}(C_{1-x}B_x)_{20}$ glass, morphology 80—70129
Fe epitaxial growth on Au single crystals, substrate temp. effect on morphology 78—26798
Fe, high purity, boriding with cryst. B powder 80—84951
Fe whiskers, cryst. morphology and dislocation struct. study using optical and SEM, X-ray diffr. topography 79—23876
Fe-B-C system, phase composition, morphology after heat treatments, $Fe_{23}B_5C$ struct. 77—28779
Fe-C(0.47 wt.%) austenite, obs. of morphology and crystallography of proeutectoid ferrite 77—8837
Fe-Cr-C alloy, bainitic struct. morphological changes, due to external stress, plastic deform. 78—44120
α-Fe-Cr(V)(Ti)(Mo)(W), morphology and growth kinetics of δ-eutectoid produced by carburisation 77—16618
Fe-Ni, strain energy controlled shape of cryst. forming due to martensite transform. or decomposition 78—38648
Fe-Ni (23.1 wt.%), α to γ transformation, struct., conc, changes, heating rate, residual austenite influence *(Russian)* 79—83194
Fe-Ni (29.3%), N29, martensitic tranform. kinetics and morphology, ordering role 77—63673
α-Fe-Ni (3-12 wt.%), structure and $\gamma \rightarrow \alpha$ polymorphic transform. kinetics 80—71645
Fe-Ni (31 wt.%) alloy, Bridgman grown, cellular to dendritic crystn. transition, morphology and microstruct. *(Russian)* 79—14709
Fe-Ni alloy, cellular-dendrite struct., effect of temp. gradient and crystallisation rate on morphological singularities *(Russian)* 78—3115
Fe-Ni alloy, solid solution, vibr. analogue of Bain deform. and morphology of martensite in 78—2224
Fe-Ni single crystal, pseudo-Kossel study of fibrous substruct. 77—1835
Fe-Ni-C alloy, external stress effects on equilibrium morphology, thermodynamic model *(Russian)* 78—52804
Fe-Ni-M alloys, (M=C, Ti,Mn), habit plane and morphology of lath martensites 77—8823
Fe-Ni-Mn (20, 5 wt.%), surface martensite, crystallography and morphology 80—40354
Fe-Ni-Ti (30, 6 wt.%), austenitic, discontinuous coarsening of lamellar cellular precipitates, morphology 79—78967
Fe-Ni-Ti-Al, martensite, nature of tetragonality 79—32936
Fe-Pt, crystallography and morphology studies, lenticular thin plate transition, thin plate morphology 79—1862
$Fe^{2+}Cr_x{}^{3+}Al_{2-x}{}^{3+}O_4{}^{2-}$, finely divided, oxidation kinetics 80—50848
$FeCr_2S_4$, single crysts., vapour grown, growth of triple unit cell steps on surface 79—19984
α- Fe_2O_3, mutual orientations and morphology obs. *(French)* 79—37647
Fe_3O_4 particles, nonstoichiometric, morphology and enhanced coercivity, Mossbauer meas. 80—7132
δ-FeO(OH) crystallites, TEM imaging investigation 80—39096
FeOOH crysts., prep. by hydrolysis, struct. and reactions with silica 78—35678
FeS, hollow particle growth by sulphuration of Fe 77—68934
FeS_2, pyrite, single cryst. growth by chem. vapour transport, surface struct. and morphology 79—23550
$FeSiO_4$, hydrothermal growth, effect of NaOH soln. conc. and O_2 fugacity on morphology 79—65996
Ga, cryst. growth from melt, dissolution morphology *(German)* 77—24283
Ga-Al, effect of Al on solidification kinetics, and morphology of Ga 78—56628
GaAs, back etching and growth by liq. phase epitaxy, surface morphology obs. 80—29287
GaAs, polycrystalline, for solar cells 78—11124
GaAs surface morphology during etching with H_2O vapour 80—39094
GaAs, VPE growth, surface morphology study by optical microscopy 79—60651
GaAs, whiskers grown by thermal decomp. from vapour 77—55875

crystal morphology continued
GaAs:Si LPE layers, surface morphology, substrate misorientation, initial supercooling effects 80—34329
n-GaAs-n-GaN, diffusion growth kinetics, morphology and electrical properties 80—20294
$GaAs_xSb_{1-x}$ solid solution epitaxial layer, morphology and defect structure 77—1330
GaN, growth and morphology of crystals *(Japanese)* 80—11548
GaN single crystals, growth by three methods *(Japanese)* 79—43112
GaN:Zn LED, electrolum. centres, rel. to growth morphology, Zn conc. and etch patterns 77—1733
Ge particles, grown in Ar gas, cryst. struct. and habit, electron microscope study 79—74071
Ge, thin crystal, SEM, contrast features, variation of specimen thickness 79—23508
Ge-Sb, eutectic alloy, exam. of morphology during solidification *(Russian)* 79—34022
Ge-Si system alloys, growth by Czochralski method, morphology 77—15329
HfO_2 crystallite growth from oxide plasmas, growth morphology 80—59417
$Hg_{1-x}Cd_xTe$, mixed crystals, crystn. by chemical transport 80—20775
HgI_2, doped, vap. growth by temp. oscill. method 78—39674
α-HgI_2, single cryst. growth from iodomercurate complexes 80—35069
α-HgI_2, single cryst. growth from dimethylsulfoxide complexes 80—35070
α-HgS, synthetic cinnabar, morphological, optical and X-ray studies *(French)* 77—43223
HgTe single crystals, crystn. from vapour phase, thermodynamical conditions, cryst. habit 79—33908
In_2Bi-In, thin lamellar eutectic strips, unidirectionally solidified, morphologic and crystallographic study *(French)* 77—55264
$In_{1-x}Ga_xAs$, LPE on InP substrate, comp. latching phenomenon and lattice mismatching effects 79—28961
InGaAsP, LPE growth on InP, influence of lattice mismatch on surface morphology 79—1553
InGaAsP, LPE grown, impurity effect on surface morphology 80—29291
In_2O_3 smoke particles prepared by gas evap., morphology and coalescence growth 80—97738
InP, LPE grown, impurity effect on surface morphology 80—29291
InP, LPE grown, surface morphology 77—62771
InP:S, SSD growth of low dislocation density crystals 80—89135
$K_2C_2O_4.H_2O:Cu^{2+}$, ESR and isomorphism of Cu^{2+} 77—32252
KCl, growth, supersaturation rel. to cryst. characts. 79—52101
$KClO_4$, cryst. growth from gelatin gels, exam. of growth and morphology 80—7488
α-$K_2Cr_2O_7$, symmetry centres exam. by morphological methods 78—59796
$K_2O.3MoO_3.3H_2O$, fibrillar crysts., morphology and struct. 78—63959
$KTh_2(VO_4)_3$, optical goniometry morphology study 80—19757
$LaPO_4$ catalyst crysts., high resolution electron microscopy, morphological characts. rel. to catalytic activity 80—107193
$LiNbO_3$, Czochralski grown single crysts., cellular interface and struct. due to constitutional supercooling *(Chinese)* 79—51026
$LiNbO_3$ Czochralski grown single crystals, facetted and nonfacetted growth sections, growth striae *(Chinese)* 80—64940
$LiNdP_4O_{12}$, single crysts. flux growth and cryst. morphology, solubility curve 79—43124
$Li_2O.3MoO_3.5.7H_2O$, fibrillar crysts., morphology and struct. 78—63959
$MgNH_4PO_4.6H_2O$, struvite crysts., growth morphology and cryst. habit 79—41994
MgO, condensates, growth from vapour, morphological comparison with, ZnO, AlN 78—34450
MgO-Al_2O_3-SiO_2, exam. of microstructure and crystallisation kinetics 78—80501
$Mg(OH)_2$, cryst. growth from aq. soln. at 60°C, pH effects 78—23591
$Mg(OH)_2$, cryst. growth from $MgCl+Ca(OH)_2$ in brine 78—23592
Mg_2SiO_4 crystals, morphology and dislocation etch pits, (010) surface 80—24457
MnAs, single cryst. whiskers, morphology and cryst. orientation, SEM and X-ray diffr. study 79—60664
$MnCO_3$, crysts., Ca^{2+} and Ni^{2+} conc. influence on habit in growth from gel 80—20778
$Mn_2NaSi_3O_8(OH)$, serandite, synthesis, struct., physicochem. props. 79—43187
MnSb, cryst. pulling with seed from nonstoichiometric melt 77—16488
Mo-O crystals, electron microscopy study 80—28889
MoO_2, crystn. from gas phase in presence of I_2 79—52090
MoO_3 smoke particles prepared by gas evap., morphology and coalescence growth 80—97738
MoO_3, ultrafine crystals, exam. of reduction using electron microscopy *(Russian)* 79—29394
MoS_2 film, sputtered, solid lubricant, morphological growth 77—35825
MoS_2, poorly crystalline 'rag' struct. 80—6391
NH_4Cl, surface roughening transition in vapour phase growth 78—2044
NH_4ClO_4, polymorphous phase transition mechanism 80—79737
$(NH_4)_2Cr_2O_7$ crystal hypomorphism and hypermorphism 80—59427
$NH_4H_2PO_4$, cryst. growth in presence of Mn ions 80—93468
$NH_4H_2PO_4$, crysts., mechanism of habit change due to Fe^{3+}, Mossbauer study 79—19821
$NH_4H_2PO_4:{}^{57}Fe$, Mossbauer study, Fe^{3+} effect in habit 80—100627
NH_4NO_3, elastic growth of cryst. during IV to x polymorphic transitions 79—46593
NH_4SCN, polymorphous structural-kinetic transformations, phase orientational relation 79—90590
$NaCaPO_4$-Ca_2SiO_4 partial system, phase diagram 78—35364
$NaCaPO_4$-$Ca_3MgSi_2O_8(CaO)$ systems, phase diagrams of partial system 78—35369
$NaCaPO_4$-Ca_3SiO_5 partial system, phase diagram 78—35365
$NaCl:BaCl_2$, oriented growth of $BaCl_2$ phases, platelet-matrix interface structure and energy 78—87793
NaCl:Ca crystals, surface recrystn., moisture effect 80—84950
NaCl-$BaCl_2$ 1%, oriented growth of $BaCl_2$ phases, morphology 77—80627
NaCl-LiCl mixed crystals, Au decoration study of solid-melt interface, phase separation 80—15026
$Na_2O.Al_2O_3.10TiO_2$, crystallized bronze, chem. comp., morphology, optical and thermal props. *(Japanese)* 80—16172
β-$Na_xV_2O_5$, Bridgman and Czochralski single cryst. growth 79—47618
Nb alloy SVMTs, high-temp. ageing, struct. and morphology of hardening phases *(Russian)* 80—40390

crystal morphology continued
NbH_x, supercond. T_c and low temp. resistivity, morphology 77—72940
NbN, Nb_4N_3-NbN, Nb_2N-Nb_4N_3, Nb_2N, cryst. growth parameters and morphology of chem. vapour deposition, X-ray diffr. and SEM study 79—23861
NbO, single cryst. growth by chem. transport reactions 77—12508
NbO_2, chemical transport with $TeCl_4$, exam. of deposition and crystal morphology 79—52093
$NbO_{2.417}$, chemical transport with $TeCl_4$, exam. of deposition and crystal morphology 79—52093
Nb_2O_5, single cryst. growth by chem. transport reactions involving $TeCl_4$ 77—36382
Nb_3Sn film, electron beam codeposited, growth morphology and tensile props. 78—10301
NdP_5O_{14} single crystals grown from polyphosphoric acids, morphology control 80—15395
$Nd_xR_{1-x}P_5O_{14}$ ($R=La$, Y: $0.1<x<1$), laser quality cryst. growth, morphology 80—66412
Ni, electrocrystallisation, reaction mechanism, appl. of impedance meas. *(French)* 80—103597
Ni, fine particles, prep. by vacuum evaporation, crystal habits 78—88437
Ni sulphide ores from Kambalda, W.Australia, sulphide fabrics 78—77229
Ni-Al (15 wt.%) single crystals, morphological changes of γ' precipitates during uniaxial stress-annealing 79—83236
$Ni_{66}B_{34}$, morphological, structural and phys. props. *(French)* 80—44444
Ni_4Mo alloy, high temp. oxidation, oxide layer growth, struct., mech. behaviour 78—44269
${}^{237}NpO_2$ powder, oxalate based, prep. and charact. 78—11166
P, white, high purity, cryst. growth morphology 77—15330
Pb, underpotential adsorption, cathodic deposition, on Ag(111) and (100) *(German)* 80—108363
Pb-Sn, lamellar eutectic stability and growth struct., fault formation 79—96019
Pb-Sn directionally solidified eutectic alloy, morphology and crystallography 77—90340
$Pb_{0.94-x/2}Ba_{0.6}Nb_xZr_{1-x}O_3$, Nb dopant morphology effect on microstructure 80—81005
PbS, chem. deposited thin film, effect of morphological struct. on photosensitivity 80—70760
PbTe, VPE, on $LiNbO_3$, struct. and morphology obs. 80—54561
Pd crystallite morphology, surface struct., electron microscopy obs. 80—29257
Pd growth on MoS_2, reorientation of small particles 78—84103
Pt crystallite morphology, surface struct., electron microscopy obs. 80—29257
Pt-Co, magnetically hard, struct. and morphology, electron microscope study 79—82171
$Pt_{0.7}Ni_{0.3}Fe$, magnetically hard, cryst. morphology and mag. domain struct. 77—69615
Rb_2PdCl_4 and Rb_2PtCl_4, single cryst. growth from gel and soln., morphology 77—77360
$(SN)_x$, synthesis and prep., TEM study 79—65004
Sb-crystals, in binary or ternary alloys, shapes on solidification *(German)* 80—3020
Si, amorphous, hydrogenated film, struct. determ. using electron microscopy 80—10806
Si, electronic properties, rel. to chem. bonding and lattice dynamics 80—44169
Si, electrophysical props. of single crysts. with and without dislocations 77—47812
Si epitaxial thin film growth on sapphire and spinel by MBE 80—76186
Si, heteroepitaxial early growth island morphology rel. to deposition conditions 78—6245
Si particles, grown in Ar gas, cryst. struct. and habit, electron microscope study 79—74071
Si, ribbon growth by edge-defined film-fed process, morphology, stability 77—24947
Si, strip-type crystals, growth mechanism, morphology 79—7559
Si, surface, morphology and electronic struct. 79—78194
Si, vapour-liq.-solid growth, using Pt and Au liq. forming agents, kinetics and morphology 78—42935
Si, vapour-liq.-solid growth, using Pt and Au liq. forming agents, struct. perfection 78—42936
Si whiskers, radial growth rates anisotropy, steps on {112} faces 79—60666
Si:Cu, precipitate morphology, IR microscopy study *(Chinese)* 80—103539
Si-Ge heteroepitaxial system, imperfections and morphology, electron microscope and electron diffr. obs. 79—42420
Si-SiO_2, interface, morphology and electronic struct. 79—78194
Si-SiO_2 interface, thermal SiO_2 sputter induced roughness, Auger sputter profiling study 80—75424
α-SiC, epitaxial layer, impurity macroincorporation, distrib. of Al, B, N and P 77—69192
SiC, reaction sintered transform. interface morphology 78—31364
SiC, subjected to thermal shock, study of substruct. and surface morpholoy 79—43292
β-Si_3N_4, growth mechanism 79—55685
α-Si_3N_4 single crysts., growth, morphology, hardness and slip system 79—83112
SiO_2-Al_2O_3 based minerals, phase equilib., struct., comp. *(French)* 78—60659
SnO_2 film, transparent cond. support for ZnS:Mn films, effect of morphology 79—56092
$SrSo_4$ epitaxy, on $BaSO_4$ from aqueous solns. mechanisms of growth 79—56093
$Sr[Al_2Si_2O_8]$, hydrothermally grown, cryst. morphology study 79—46590
Te film, vacuum deposited, growth and morphology of crysts. 80—96766
Te, vacuum deposited on NaCl, crystallite growth and morphology, electron microscopy 80—65401
ThO_2 crystallite growth from oxide plasmas, growth morphology 80—59417
Ti film, ion plated, morphology exam. by SEM 79—28251
Ti-Mo-Zr(-Al) (15, 5 (3) wt.%), quenched and aged metastable β-phase, crystallography, morphology and decomposition 80—76262
TiC single crystals, growth from vapour by modified hot wire method, temp. effect on habit 79—61509
TiC whiskers, CVD growth on various metals and refractory oxides, SEM examination 79—33211

crystal morphology continued
TiN, gaseous phase, crystallisation, effect of temp., vapour-gas mixture conc., and deposition time 79—33910
TiN(C) whisker growth in CVD 80—59843
TiO$_2$, sintered ceramic, props. rel. to additives, impurities 78—35329
Tl, underpotential adsorption, cathodic deposition, on Ag(111) and (100) *(German)* 80—108363
Tm$_2$O$_3$, mineraliser effect on growth morphology 78—91283
C-Tm$_2$Si$_2$O$_7$, single cryst. flux growth, morphology 79—52097
UO$_2$ crystallite growth from oxide plasmas, growth morphology 80—59417
VO$_2$, doped, morphology, structure and props. *(German)* 78—59823
V$_3$O$_5$ single crysts., prep. by chem. transport reacts. props. 79—43115
WC$_x$, electrochem. separation from W alloys, phase anal. 78—60651
WO$_2$, cryst. growth, chem. transport conditions influence on morphology and quality 79—43114
WO$_3$ smoke particles prepared by gas evap., morphology and coalescence growth 80—97738
YAG Czochralski grown crysts., growth of facets and vicinal interfaces *(Chinese)* 79—90578
Zn, electrocrystallisation, reaction mechanism, appl. of impedance meas. *(French)* 80—103597
Zn electrodeposition, from high purity industrial acid sulphate electrolyte, effects of Cd contamination obs. 79—56091
Zn electrodeposits, electrode kinetics and inhibition mechanisms 79—56089
Zn electrodeposits morphology and orientation, Pb contamination effects obs. 79—56090
ZnO, condensates, growth from vapour, morphological comparison with, MgO, AlN 78—34450
ZnO, growth by recrystallisation of ZnO in H$_2$O vapour and H$_2$ 77—85913
ZnO microcrystals, morphology, formed by Zn anodic electrocrystn. 77—80432
ZnO, rate of deposition and morphology 78—84719
ZnO, single cryst. growth in ZnO-H$_2$-H$_2$O-O$_2$ vapour, morphology, electrophys. and opt. props. 78—52649
Zn$_3$P$_2$(As$_2$), cryst., gas phase growth, morphology 79—10821
ZnS cubic single crystals, growth by double decomposition reaction in melt 78—60557
ZnS vapour grown crystals, morphology and structure 78—42937
Zr-Cr (1.9 wt.%), β-quenched and tempered, optical and TEM study 79—66061
ZrC, single cryst. growth by modified hot-filament method, cryst. morphology and microhardness 79—19983
ZrC, whiskers, CVD on Ni, catalytic effect 78—51865
ZrN(C) whisker growth in CVD 80—59843
ZrO$_2$ crystallite growth from oxide plasmas, growth morphology 80—59417
ZrO$_2$-CaO(MgO)(YO$_{1.5}$), partially stabilised, growth morphology of tetragonal phase 79—4968

crystal orientation
analyser optical alignment for X-ray fine spectral structure study 77—18148
average potential for orientational effects *(Russian)* 78—47270
biotite at Fleurieu Peninsula, South Australia, crystallographic alignment rel. to slaty cleavage development 80—21735
brass, orientation distribution function anal. by superposition of Gauss type scattering functions 79—86735
bronzes, Na-W, cubic crysts., orientation relation of nucleation and growth 79—55687
channelling patterns, selected area, cryst. orientation determ. method 80—70092
correction when calculated adjustment exceeds allowed movement on one arc 78—18495
corundum large optical crystal production with zero orientation 79—50457
corundum optical crystal block structure 79—72637
cubic crystal orientation determ. from meas. sound vels. 79—55691
cubic single crystal misorientation angle determ. by US speed meas. 80—54315
cubic single crystals, rapid crystallographic orientation determ. method using US vel. anisotropy 78—6027
decahedral particles, high symmetry orientations, HEED and TEM study 79—86732
diamond, synthetic disorientation of crystallite subgrains *(German)* 77—68939
distribution determ. from incomplete pole figures, computer program 78—64804
distribution function, approx. determ. 79—86736
distribution function anal. by superposition of Gauss type scattering functions 79—86735
distribution function anal. in maximum shear planes 79—82172
distribution function generalisation using rotation matrix 80—11665
doubly rotated crystal frequency and temp. coeff. angular dependence 77—39142
electrode, effect on iodide ion adsorption on Au surface 79—15020
electron diffraction patterns, computer anal. 77—1049
epitaxial film, X-ray topographic measurement, local variations in spacing and orientation of lattice plane *(Japanese)* 78—38585
epitaxial layers, on monocrystn. supports, degree of disorientation, determ. by interferometry *(Russian)* 80—24748
ESR line profile, depend. on cryst. orientation 80—15786
FCC crystal-melt interfaces, mol. dynamics simulation 80—79913
films, orientation effects in quantitative X-ray microanal. 80—85259
grain boundary characterisation, zone axis method *(French)* 80—44215
habits of crystal construction 78—26477
hematite, multiple orientation relationships between magnetite, TEM study 79—60298
heteroepitaxial surface morphologies and misalignments *(Japanese)* 80—15411
HF quartz crystal unit frequency/temp. and activity/temp. anomalies 77—39139
high-melting metal multicrystal hollow ingot growth 79—69978
ice, c-axis alignment, Arctic Alaska coast 80—67375
ice, preferred orientations in fast sea ice along Arctic margins 79—16486
ice crystals at base of Ross Ice Shelf, alignment rel to subglacial ocean currents 80—101393
icicles, examination between crossed polarizers, growth mode determination, cryst. orientation 79—41995

crystal orientation continued
isocahedral particles, high symmetry orientations, HEED and TEM study 79—86732
Kossel technique in SEM for crystallographic orientation 80—75133
large monocrystal orientation using X-ray camera 78—22600
laser alignment of crystal face perpendicular to axis of rot. 77—15283
lattice images of defect, misorientation effects 80—107210
Laue method, computer calc. *(Chinese)* 79—32853
Laue patterns, cylindrical, flat transmission or flat back-reflection Laue photographs, calc. of crystal orientation 80—19670
Laue patterns and stereographic projections, Laue back-reflection techniques, plot program PLOMAC 80—19669
Laue photograph indexing and monocrystal orientation determination by computer, new approach *(Chinese)* 80—79636
liquid crystal, orienting action of US related to theorem of min. entropy prod. 79—77498
low quartz crystal setting, enantiomorphism 78—79496
magnetite, multiple orientation relationships between hematite, TEM study 79—60298
metal whisker, growth axes determ., rapid X-ray technique 77—11830
metals and alloys, HCP struct., relative orientation of cryst. lattices 80—84181
mica solid state particle track detectors, fission fragment ranges rel. to cryst. orientation 80—91408
microhardness anisotropy 80—21079
nonlinear optical polarisations, second and third order, general effects of cryst. symmetry and orientation 77—19358
nuclear quadrupole spin-lattice relaxation time in single crysts., orientation depend. 79—95666
orientation density function of single crystals from growth selection experiments 79—90589
orientation distribution function, calc. of odd part 80—20954
polycrystalline specimen, orientational distrib. function calc. methods 79—86734
polycyclic aromatic quinone, epitaxy on alkali halides, adsorbed water effect 79—28239
polypropylene, isostatic, uniaxially oriented, Raman spectra *(French)* 80—60557
preservation in crystal transfer, rapid and precise method 77—76257
PVDF dielectric, piezoelec. and pyroelectric props. rel. to crystalline forms 80—15982
quartz, ⟨a⟩ axes preferred orientations in tectonites, flow kinematics 78—96200
quartz, c-axis fabrics anal. via photometric method 80—101456
quartz, handedness determination for electron diffr. convergent beam patterns 78—34498
quartz, synthetic local variations meas. in spacing and orientation of lattice plane, X-ray anal. 79—52099
quartz c-axis orientation in Saxony Granulites, petrofabric anal. by optical and X-ray diffr. studies 80—21740
quartz in shear zone from Castell Odair, Scotland, orientation reinvestigation 78—77216
rock thin sections, microprocessor controlled photometric analyser 80—41560
schreibersite, platelike, in hexahedrites, habit planes 78—65572
SEM determination using electron back-scatt. patterns 77—76268
shear wave polarisation, cryst. orientation error 77—35006
single-crystal diffractometry, peak searching, crystal setting and determining automatic cell constants 80—6319
snow pack metamorphosing states *(Japanese)* 77—86948
solid-solid interface chemistry, characterisation, theory 80—75448
steel, 50N29 type, self-consistent junctions and spatial relative organisation 80—19750
steel, Cr-W(Mo), quenched, carbide reactions during tempering 80—89229
steel, electrical, crystal orientation and dimension determ. by magnetic method 79—70278
steel, mild, orientation distribution function, representation of texture and slip directions 80—11665
steel, P, deep-drawing, spatial orientation distrib. of crystallites in cold-rolled and in annealed sheets 80—81079
STEM specimen orientation modes 78—34406
temperature compensated materials with high piezoelectric coupling 77—40184
texture anal., three dimensional, computer simulation of errors 78—64805
texture study, use of crystallographic orientation distrib. function 79—52228
thermoelectric convertor error due to crystallographic misorientation anisotropy 78—77904
vacuum deposited film, orientation axis tilt rel. to vapour angle of incidence 80—88456
water supercooled droplets, on ice substrate after low speed collision, freezing behaviour, cryst. struct. 80—29152
X-ray diffractometrical sub-structure analysis *(German)* 77—68894
X-ray goniometer, for producing accurately oriented cryst. faces 79—37591
zone axis method, appl. to grain boundaries, TEM 80—103226
Ag epitaxial growth, on W-ribbon substrate, in UHV, cryst. orientation determ. by etching *(German)* 79—65994
Ag film, vacuum deposited on NaCl, microstructure and orientation, surface condition influence 79—82486
Ag, plasmons, influence of cryst. orientation on intensity, electron energy loss meas. *(German)* 79—23921
Ag, single cryst. film, cryst. orientation effect on EELS 78—80442
AgMg single crystals, orientation and temp. depend. of slip 78—87682
AgMg two phase bicrystal growth, orientation, interface struct. 80—60773
Al, anodisation, influence of substrate orientation 78—88581
Al crystal, lattice rotation during tensile deform., X-ray diffr. meas. 80—49231
Al, flow mechanism in cutting, crystal orientation effects in single crystal 79—100300
Al, galvanostatic anodising of high purity sheet, galvanolum. obs., cryst. orientation effect 77—90489
Al, isoaxial bicrystal, Moire investigation of mechanical behaviour 77—16647
Al-Al$_3$Ni eutectic, cryst. struct., orientation, electron microscopy, computer calcs. *(German)* 77—72582
Al$_4$Ca, phase transformation, struct. and orientation relationships 79—78963

crystal orientation continued
$Al_xGa_{1-x}As$, epitaxial growth, orienting substrates effects 77—43444
AlN films on glass substrate, prep. by reactive DC magnetron sputtering technique, c-axis orientation 80—89146
β-Al_2O_3, polycryst. with preferred grain orientation, hot pressing of gibbsite and Na_2CO_3 *(Japanese)* 79—56948
Au, effect of intermittent deposition on nucleus formation and growth on alkali halide substrates 79—23853
AuMn alloy, ordered, vacuum deposited epitaxial films, orientation control by external stress 80—100426
BaF_2 and fluorite large crystal, block orientation determ. from light scatt. pattern 79—50964
C precipitates with preferred orientation [100], from dissoc. of n-xylene *(Russian)* 80—45484
Cd, dislocation internal friction, orientation depend., for single crysts. 78—52882
$Cd_xHg_{1-x}Te$, crystallisation from solution in Hg 77—19883
CdS layers, by vacuum evaporation, formation mechanism of preferred orientation 79—56094
CdS, polycrystn. films, recrystn. accompanying annealing *(Russian)* 80—20948
Co-P films with various preferred orientations, mag. props. 80—100604
CoO on Co_3O_4, oriented growth following Co_3O_4 pyrolysis 78—80739
Cu, crystalline reorientation following ion bombard. 80—70269
Cu crystals, floating zone method growth, X-ray diffr. study of preferred growth 80—7490
Cu, electrolytic epitaxial nucleation and growth, on (111) Ag 80—104081
Cu, implanted with Cu^+, effect on cryst. orientation, Kr penetration meas. 80—88174
Cu, influence of cryst. orientation on work function, with and without adsorbed S *(French)* 78—76134
Cu Laue X-ray back reflection pattern solving, algorithm and statistical error analysis 79—99030
Cu, range of Ni^+ ions, increase due to ion bombardment induced crystalline reorientation 78—26611
CuAu alloy, ordered, vacuum deposited epitaxial films, orientation control by external stress 80—100426
β-CuZn, yield stress and operative slip systems, orientation depend. 77—48498
Fe epitaxial growth on Au single crystals, substrate temp. effect on morphology 78—26798
Fe films, evaporated at oblique incidence, columnar struct. and texture 79—77967
α-Fe single crystal whiskers, controlled growth by H reduction of ferrous halides, X-ray and SEM exam. of crystals 78—60554
Fe zone refined crystals, cryst. orientation and distrib. of stray grains 80—70509
Fe-Mn-C, atomic interaction structure in carbides 78—42955
Fe-Ni, reversibility of crystal orientation in reverse martensitic transformation 79—83199
Fe-Ni-Ti-Al-Nb, struct. mechanism for inverse α→γ transform. *(Russian)* 80—40351
Fe-Si (3 wt.%) locally deformed, EM loss depend. on cryst. struct. and orientation *(Russian)* 80—7694
Fe-Si (6.5%) alloy, struct. and rolling texture 79—79006
Fe_3Al, slip geometry and pseudoelastic behaviour, effect of crystal orientation *(French)* 78—87681
α- Fe_2O_3, mutual orientations and morphology obs. *(French)* 79—37647
Fe_2O_3/Fe_3O_4 transformation matrices, higher-order orientation relationships 80—100846
FeS_2, (pyrite), angle-independent Mossbauer effect 80—20570
Ga_2O_3 on spinel and sapphire, VPE and orientation *(Japanese)* 77—51611
GaP, growth conditions rel. to dislocation struct. 80—88151
$GaP_{0.9}As_{0.1}/GaP$, heteroepitaxial structs., refined formulation of relative orientation criterias 80—44448
GaSe, basal plane orientation determ. in vertical Bridgman grown single crysts. 78—19658
Ge, ionisation rates, cryst. orientation depend. 80—103700
Ge, melt grown single crystals, preferred growth directions and perfection 79—77537
Ge, volume plasmon, cryst. orientation influence 80—80921
Ge:Sb, Czochralski growth, orientation depend. of impurity distrib. coeff. 79—69976
p-H_2, solid, NMR spectrum of isolated o-H_2 pairs 80—15332
^{3}He crystals, nucleation and orientation 80—84339
Hg_2Cl_2, calomel, birefractive cryst., light spreading *(German)* 77—77168
KCl crystallites, nucleation, oriented growth on amorphous SiO_2 using square-wave surface relief grating 78—47672
KNO_3 calcite-type crystals, topotaxial decomp. TEM obs. 80—108710
KNO_3, orientations and twinning in the struct. transform. aragonite-type to calcite-type 77—24284
$K_2PbCu(NO_2)_6$, uniaxial stress, EPR meas. 80—20455
LaB_6, cathode, brightness, cryst. orientation and purity effects 77—12483
LaB_6 cathodes, single crystal, of <100> and <110> orientations, brightness meas. from 1500 to 1950K 80—62808
Mg, dislocation internal friction, orientation depend., for single crysts. 78—52882
MgO film, vacuum deposited on NaCl-type alkali halides, struct. characterisation 79—82490
MgO, spherical particle impact damage, effect of crystallographic orientation 79—79135
MgO-CdO, interface, coincidence-site-lattice relations 80—103588
MgO.1.1 Al_2O_3 spinel, high temp. deform., cryst. orientation effect 80—107263
Mn-Al-C anisotropic permanent mag., cryst. orientation and form., X-ray diffr. anal. 79—82778
MnAs, single cryst. whiskers, morphology and cryst. orientation, SEM and X-ray diffr. study 79—60664
Mo single crystal, effect of prior ultrasonic working on hardness, crystal orientation and creep resistance *(Russian)* 79—34056
Mo single crystals, orientation and alloying effect on mech. props. *(Russian)* 80—71706
Mo-Nb-C, mech. props., effect of alloying and Mo cryst. orientation *(Russian)* 80—71706
$Na_2(Fe,Mg)_5Si_8O_{22}(OH)_2$, riebeckite, low temp. Mossbauer obs. of oriented single cryst. behaviour and mag. props. 80—84674
Nb, surface oxide softening, anisotropy 78—60716
Ni electrodeposits, struct., electrolyte anions influence 80—20056

crystal orientation continued
Ni, substrate surface effects on C deposition 77—28721
Ni sulphide ores from Kambalda, W.Australia, sulphide fabrics 78—77229
Pb film, thermal strain, depend. on cryst. orientation 78—10311
PtSi, epitaxial film, cryst. perfection and thermal stability, channelling and backscatt. meas. 79—99255
$Rb_2PbCu(NO_2)_6$, uniaxial stress, EPR meas. 80—20455
Sb, thin layer, amorphous to crystalline phase transition *(German)* 77—69196
Sb:Te vapour saturation, diffusion zone struct. crystallisation orientation *(Russian)* 80—54438
Si, dissolution rates in KOH, orientation effect 77—36674
Si, plasmons, influence of cryst. orientation on intensity, electron energy loss meas. *(German)* 79—23921
SiC single crystals, friction, deform., and fracture, crystal orientation effect 79—96150
α-Si_3N_4, hardness anisotropy 78—95804
$SmCO_5$ based permanent magnets, props. and cryst. orientation *(Russian)* 80—20431
$SmCo_5$ alloy powders, orientability and texture, milling time effect 79—100168
Ta-N, domain configurations of new phase *(French)* 78—56648
Ti-Al-V (6,4 wt.%), strongly textured, influence of crystallographic orientation on tensile behaviour 80—7633
V-C(N) system, mutual phase orientation, X-ray diffr. exam. *(Russian)* 77—62498
V-Ti-C, high temp. carbide form., electron microscopy study 80—89228
W spheres, in liq. Ni, sintered, coalescing, crystallographic orientation, SEM study 80—45249
W/α-Al_2O_3, heteroepitaxial structs., refined formulation of relative orientation criterias 80—44448
W/α-Al_2O_3 heteroepitaxy, orientation relationships, X-ray diffr. study 79—60661
W_2C, oxidation, oriented struct. transform. to W, FEM and TEM obs. 80—30124
$(Y,Gd,Yb)_{3-x}Bi_x(Fe,Al)_5O_{12}$ film growth on $Gd_3Ga_5O_{12}$ substrates 79—78623
$Y_3Fe_5O_{12}$ LPE growth on $Gd_3Ga_5O_{12}$ substrates, substrate orientation effect 80—66438
Zn, dislocation internal friction, orientation depend., for single crysts. 78—52882
Zn electrodeposition, from high purity industrial acid sulphate electrolyte, effects of Cd contamination obs. 79—56091
Zn electrodeposits morphology and orientation, Pb contamination effects obs. 79—56090
Zn film, vac. deposited, X-ray diffr. study of microstruct. 78—26796
$ZnGeP_2$, Br_2-methanol etching soln. for crystallographic axes determ. 78—35541
ZnO RF sputtered films, post deposition annealing behaviour 80—100416
ZnO_2, polycrystn., determ. of crystallographic orientation of grains 79—69049
ZnS, crystals with stacking faults, Laue method study 79—94847
ZnS, single electron excitation study, cathodoluminescence image contrast using STEM 80—89072
ZnSe, epitaxial growth, orienting semiconductive substrate effects 77—47688

crystal oscillators *see crystal resonators*

crystal properties
see also crystal chemistry
oxides, struct. and props. 79—27964
thermodynamic theory for cryst. props. behaviour near structural transitions *(German)* 78—38809

crystal purification
see also zone refining
alkali halide single crystals, high purity, prod., purification characts. *(Hungarian)* 77—52229
alkali metals, distiller for purification, construction, operation 78—80490
anthracene, liq. chromatography, sublimation, zone refining, exciton fluoresc., mobility meas., melt grown crystal 79—38736
carbon tetrabromide, inherent moisture as purity probe *(German)* 77—85933
inclusion emersion in vertical zone refining 78—52663
magnetic halide, method of growing low-dimensional single crystal *(Japanese)* 80—50539
metal refining by crystallisation and reflux, three component Raoultian behaviour 77—28799
polypropylene, change of crystn. forms during purification 77—55934
PTZ:PMDA, purification, growth, struct., optical and elec. props. 80—54216
recrystallisation *(Russian)* 77—24946
semiconductor, doping reduction using zone recrystn. with temp. gradient 80—104062
semiconductor, enhanced electrodiffusion purification in mag. field, GaAs epitaxial film appl. 80—66409
AgBr, prep. of high purity cryst. with <3 ppb I 77—69982
Al_2O_3, commercial, Na_2O impurity removal and modifier in corporation 79—43183
B, β-rhombohedral, purification by electron beam melting and CVD 80—20781
BaF_2 purification for laser components, selective ion filter design and construction 79—14051
$BiTaO_4$, cryst. growth. hydrothermal method 77—8736
CdTe, purification, efficiency for extraction of Cu and Ag impurities, impurity scatt. meas. 77—8749
Cu-Ag (Pb)(Bi), evaporation of Ag, Pb, Bi in vacuum induction melting 77—28742
Cu-Ag(Bi)-O, evaporation of Ag, Bi in vacuum induction melting 77—28742
Dy, recrystallisation *(Russian)* 77—24946
Fe, high purity, single crystal prep., by strain-anneal technique *(German)* 77—48326
Fe, high purity prep. by electron beam floating zone melting under ultra high vacuum 77—28751
Fe, purification, recrystn. temp. and elec. resistivity *(Japanese)* 80—100780
GaAs, bulk purification by chemical vapour transport 79—24437
Gd, fused salt electrorefining, evaluation of electrolytes 78—92215

crystal purification continued
Ge, second-phase inclusions after O_2 treatment, electron microscope obs. 77—43238
HgI_2, soln. grown crystals, low-energy gamma-ray cond. type detectors 80—97418
InP, LPE, high purity, use of baking to reduce Si contamination 78—72744
InSb, charact. and phys. props., review *(Japanese)* 80—39576
KBr, IR laser window appl., crystal growth, polishing and optical absorpt. 77—7102
KBr purification for laser components, selective ion filter design and construction 79—14051
KBr(Cl), prep. of crysts. containing impurities of specified amounts *(Russian)* 80—66424
LiCl-KCl eutectic mixture, purification, effect of impurity ions *(Japanese)* 78—40108
Mo, impurity interactions with C, N, and O, struct., mech. props. and purification 79—52277
$NaBr:Ho^{3+},Eu^{2+}$, single cryst. synthesis, rel. to purification methods 77—8744
Nd solid-state electrotransport 77—59679
Si, inclusion type defects removal from bulk of single cryst. by elec. fields 79—43126
Si, metallurgical grade, impurity gettering of polycrystalline solar cells 80—81441
Si production from rice husk ash for solar cells 79—62008
Si purification, plasma melting zone technique *(French)* 80—89141
Si purification, plasma melting zone technique, optimisation *(French)* 80—89142
Si:P, Au gettering by P diffusion and P-induced dislocations 78—91346
SrF_2 purification for laser components, selective ion filter design and construction 79—14051
Te, pure, prep. by combined method, vacuum distillation and double condensation 79—33956
Ti crystal bar, prep. by iodide process 77—55878
V, purification and plastic props. 80—25810
W, impurity interactions with C, N, and O, struct., mech. props. and purification 79—52277
n-ZnSe, purified by annealing in molten Zn, Hall mobility and polaron coupling 77—85243

crystal resonant gamma-ray interactions *see Mossbauer effect*

crystal resonators
see also piezoelectric oscillations
1 MHz crystal anharmonic AT modes, holographic displacement amplitude meas. 79—54097
31st Annual Frequency Control Symposium, Atlantic City (1977) 78—57905
32.768 kHz X-Y flexure watch crystal as pressure-force transducer 78—57934
300 MHz oscillators using SAW resonators and delay lines 78—59255
acoustic bulk wave resonators and filters with fundamental mode >100 MHz 77—42671
AT quartz plate resonators and filters, discrete element model 79—55297
AT-cut crystal resonance frequencies, finite element analysis 79—56732
AT-cut quartz plate vibration anal. using light modulated oscillator 78 71255
atomic reference frequency stability transfer to quartz crystal oscillator 79—54108
biconvex circular AT-cut plate thickness-shear vibration mode analysis 77—39144
circular plate thickness-shear resonance frequencies, acceleration effects 77—39136
clocks and watches, accuracy setting and control *(Czech)* 79—40541
coupled, depend. of interresonator coupling coeff. on orientation of electrodes *(Czech)* 77—46860
crystal tuning fork development and biography of Jurgen Staudte *(German)* 79—30182
digital quartz crystal thermometer principle and technical parameters *(Polish)* 78—24791
digital thermometer appl. 77—82514
digital thermometers using quartz crystal oscillator high accuracy achieved 78—65932
doubly rotated crystal frequency and temp. coeff. angular dependence 77—39142
electrode deposition from nozzle beam type metal vapour source 77—40376
equivalent cct. parameters meas., high-accuracy bridge instrument 77—10056
force-frequency measuring gauge based on oscillating quartz crystal 80—31727
frequency control 32nd Annual Symposium, Atlantic City (1978) 79—54100
HF quartz crystal unit frequency/temp. and activity/temp. anomalies 77—39139
high-performance quartz crystal oscillators, systems approach 79—54109
horizontal-shear surface wave grating resonators 78—59249
immunity to acceleration fields in any shock/vibration environment 80—91953
impacting oscills. simulation of resonator with vibrating wall *(Japanese)* 78—9483
intrinsic Q estimation of quartz 80—43578
ion beam etching, for SAW refl. struct. fabrication, role of redeposition 77—56123
large amplitude behaviour, 3rd order elasticity coeff., maximum loading determ. *(German)* 78—31158
liquid atomisation, using US piezoelectric resonators *(German)* 79—66359
metal-oxide system characterisation by high-resolution electron spectroscopy 77—40624
micro-resonators, high flux, for X and γ-ray lasers 79—7151
microwave Q-factor meas. system 78—54396
orientation of industrially cut alpha quartz AT plates 80—92008
oscillating quartz crystal stress distribution meas. by laser probe 77—20803
overtones of coupled thickness shear and thickness twist, anal. 79—81673
parabolic frequency/temp. characteristic compensation 79—55294
periodic grating oscillator performance 77—39190
phase and frequency instabilities in precision frequency sources, characterisation and mathematical models 79—2750
piezoceramic disc resonators, dispersion of thickness vibrs. 78—22237

crystal resonators continued
piezoceramic elastic compliance and mechanical Q-factor at high drive levels 78—60395
piezoceramic planar Poisson ratio variation with poling conditions 79—11391
piezoelectric, phase-metric readings of RF phase bridge 80—4732
piezoelectric ceramic plate energy trapping methods of thickness extension and thickness shear modes 80—15980
piezoelectric ceramic platelets, geometry effect, effect on props. of flexural oscillator *(German)* 79—32168
piezoelectric ceramic resonators, eigencoupling state space vector representation 80—2697
piezoelectric plate HF vibrations, two-dimensional eqns. 77—39143
Pioneer Venus Programme stable quartz oscillator 77—41288
planar piezoresonator shear vibration mode for viscosity meas. 77—19643
planoconvex AT-cut quartz resonator vibration displacement meas. by laser interferometry 77—37976
plasma etched SAW resonator ageing effects 77—39148
polarisation effects, in piezoelectric resonators executing longitudinal vibs. 79—1741
polyvinylidene bimorph cantilever vibrator, resonant type, air flow generation, theory 79—87391
polyvinylidene fluoride fan, electromech. conversion efficency and high field dielec. loss 79—82926
quartz, acceleration, sensitivity, influence of cryst. supports *(French)* 77—87753
quartz, appl. to optical film monitoring 78—5592
quartz, AT-cut resonator operating at 270 MHz 77—42671
quartz, AT-cut resonators, temp. depend. of oscillation freq. between resonance and antiresonance freqs. 79—46749
quartz, doubly rotated plates, angle-of-cut goniometry 79—54098
quartz, electroded doubly-rotated thickness-mode resonators, temp.-induced frequency 79—55298
quartz, electron irrad., optical absorpt. 77—8609
quartz, electron irradiated, optical and anelastic absorptions and resonator freq. 78—64385
quartz, for laser damage determ. to metal film 78—31286
quartz, freq. spectrum determ. 78—23402
quartz, growth sector boundaries 77—39595
quartz, inductive gauge 79—63189
quartz, irradiated by alpha particles, frequency change 77—16253
quartz, mag. field effect on fundamental and overtone modes 77—12182
quartz, plane-convex AT cuts, Ag electrodes, used as film thickness monitor 78—11116
quartz, resonator, X-ray double crystal topographic assessment of defects 79—50943
quartz, SAW resonator transverse modes, SEM obs., phase effects 79—68452
quartz, second-order phenomena and polarising effect with plates of orientation 78—72463
quartz, SEM surface patterns obs., energy trapping appl. 80—71323
quartz, stable exciting electrode preparation, by ion plating of Ag film on AT-cut quartz crystal 80—2280
quartz, synthetic, growth boundary between $-X$ and Z sectors 78—59775
quartz, synthetic, growth sector boundary between $-X$ and Z sectors 78—59774
quartz, transfer of freq. stability from atomic freq. standards 80—17927
quartz, weak anharmonic modes detection, multicryst. reson. freqs. 77—81061
quartz acoustic bulk wave resonators using AT-cut crystals, tolerance effects 80—53601
quartz cryst., piezoelec., coated, detection of HCl gas in ambient air 78—92532
quartz crystal, characts., operation mode and struct. *(German)* 79—61306
quartz crystal, influence of tabs thickness and resonating props. 78—18140
quartz crystal, oscill. props., mag. field effects 77—59516
quartz crystal impedance and admittance bridge development 77—37944
quartz crystal microbalance, reson. freqs., influence of mass loading outside electrode area 77—82491
quartz crystal oscillator checking against standard frequencies in LF/VLF ranges 77—74372
quartz crystal resonator nonlinear analysis 79—55299
quartz crystal thermometer with 10^{-4}°C resolution *(Polish)* 79—40562
quartz crystal US vibrations, SEM obs. 79—56733
quartz filter resonators with energy trapping, optimum design 78—32663
quartz fused, refractive index distrib. normal to polished surface, ellipsometric meas. 79—86965
quartz gravitational wave antenna, Q-factor 79—35623
quartz oscillator microbalance, high resolution, appl. to Al oxidation 77—70219
quartz oscillator plate, surface treatment by 100 keV B ion implantation *(Japanese)* 78—59826
quartz plate, bevelled AT-cut, thickness-shear vibrations 79—90166
α-quartz plate frequency changes rel. to electroelastic tensor and second-order phenomena 78—60398
quartz plates, surface irregularities due to mechanical, chemical treatment *(Polish)* 80—89380
α-quartz plates vibrating in thickness, doubly rotated, zero polarizing effect 80—55038
quartz rectangular AT-cut plates with patch electrodes, vibration modes 79—55295
quartz resonator, large mag. field effect on rate of time 80—27195
quartz resonator, low-freq. heat-sensitive, characts. 79—30475
quartz resonators, anisotropic circular plate initial stress effect calc. 79—55300
quartz resonators, freq. instability rel. to time scales *(Italian)* 79—17400
quartz resonators, parameter calc. with energy trapping *(Russian)* 78—30141
quartz resonators, thickness-mode, thermal stress effects on reson. freq., theory 80—50272
quartz SAW oscillator higher-order temp. coefficients 79—55291
quartz SAW resonator deep etching 78—59248
quartz SAW resonator design with Al metallisation 77—39147
quartz SAW resonator tuning by shorted reflector opening 78—59246
α-quartz twinning and tailored domain patterns 77—40197
quartz wafer, use in simultaneous mass and temp. determ., optimised cryst. cut improvement 79—49205

crystal resonators continued
quartz wafer surface contaminant estimation methods, cleaning processes appl. *(Polish)* 80—89381
rectangular AT-cut quartz resonator frequency rel. to mass loading and electrode geometry 77—39140
regulation by atomic time receiver of Rugby 60 kHz transmission, quartz watches, clocks. appl. 78—4597
SAW, 1.56 GHz operating freq. 80—87687
SAW, 310 MHz, with Q at material limit, design and fabrication 78—5608
SAW, as stress sensor, freq./stress sensitivity 77—2645
SAW, characts. from Fabry-Perot cavity anal. 77—39131
SAW, resonator transverse modes, effects of anisotropy 78—5609
SAW 300 MHz resonator oscillator close-in phase noise rel. to vibration 79—55289
SAW deeply-etched resonators, long-term aging improvement 79—55290
SAW devices props. and appl., ZnO thin-film, for HF range *(Japanese)* 80—53598
SAW oscillator quartz cuts for improved temp. stability 79—55292
SAW resonator filters 79—55283
SAW resonator optical waveguide model 77—39146
SAW resonators, comparison of metal strip and waffle iron arrays 78—51030
ST-quartz SAW resonators and coupled resonator filters 77—39174
stress compensated quartz resonator calculations 77—39137
surface-skimming bulk wave controlled quartz crystal oscillator 78—59250
temperature stable oscillators employing parallel-connected SAW resonators 80—74615
thickness-extensional trapped energy resonators, mode coupling 80—74655
thin film thickness measurements, instrumentation system 78—89436
thin film thickness monitor, temp.-controlled, voltage readout 77—24953
tourmaline, electroelastic constants, elec. field induced freq. shift study 80—20597
trapped-energy ceramic resonator with improved response characts. *(Japanese)* 78—9522
tunable variable bandwidth/frequency SAW resonator 78—59247
tuning fork for HF operation, second-mode, finite element anal. and expts. 80—102980
two-port quartz SAW resonator construction and performance 77—39145
unplated piezoceramic plate frequency response meas. 78—248
vibration analysis, combined plate eqn. and finite element method 79—55296
$Bi_{12}GeO_{20}$, piezoelec. resonator, electroelastic coeffs. 77—52020
CdS, flexural waves in resonator platelets, synchronous amplification and generation 78—84527
$Gd_2(MoO_4)_3$, variable frequency SAW resonator on ferroelectric-ferroelastics 78—33977
$LiNbO_3$ microwave resonators, for optical radiation modulation 77—27353
$LiNbO_3$, piezoelectric plate resonator, acoustic correl. 79—76929
$LiNbO_3$ SAW resonator design with Al metallisation 77—39147
$LiTaO_3$, piezoelectric resonator characterisation 78—95550
$LiTaO_3$ thin plate temperature characteristics 77—39141
$LiTaO_3$-SiO_3, temp. compensated SAW device fabrication 79—76923
$NH_4H_2PO_4$, rods, longitudinally vibrating, polarizing effect and electrostatic tensor 77—7278
$Pb(Mg_{1/3}Nb_{2/3})O_3$-$PbTiO_3$-$PbZrO_3$, piezoceramics for high frequency use 78—95555
$PbTiO_3$, piezoceramics for high frequency use 78—95555
$Sr_xPb_{1-x}(Zr_{0.545}Ti_{0.455})O_3$, piezoelec. resonator, preparation and props. *(Rumanian)* 80—28402

crystal structure
see also crystal atomic structure; crystal microstructure; crystal morphology; crystal orientation; crystal symmetry; crystallography; granular structure; polymorphism
classical octopolar solid, temp. effect, Monte Carlo calc. 78—75598
device technology, an introduction *(Korean)* 80—49136
electron microscope imaging 80—88006
graphite-like materials, exam. of preferred functions 80—1945
Kevlar fibres, effect of crystallinity and orientation on mech. props. *(Japanese)* 79—38952
metal ultrafine crystallites, form. by gas evaporation technique, crystal habit 77—52239
molecular model building, computer program MMB 80 *(Japanese)* 79—36793
NBS reactor, summary of activities, (July 1976 to June 1977) 78—82435
orthosilicate chloritoid, layered, disordered, electron microscopic and X-ray anal. 78—75511
planetary system evolution from preplanetary gas disc, rel. to crystallisation and cryst. struct. *(German)* 78—93129
snow, crystalline forms rel. to cloud source thermodynamics *(Rumanian)* 77—33169
tilted perovskites, influence of ionic radii on transition temp. 80—24590
water supercooled droplets, on ice substrate after low speed collision, freezing behaviour, cryst. struct. 80—29152
Al-Mg-Si, dil. alloy, Mn additions and heat treatment effect on $\beta \rightarrow \alpha$ transformation 80—7566
Au vapour deposited particles, with pentagonal profiles struct. by TEM imaging techniques 79—77566
Au, vapour deposited particles, with hexagonal profile, struct. determ. using TEM imaging 79—77567
CrC, plasma sprayed coating 78—68835
α-Fe, nitrided, aging at room temp. 80—71679
H metal, superconductivity and crystal struct. *(Hungarian)* 78—38659
$Li_6In_2O_6$, ionic cond. rel. to cryst. struct. 79—77810
Li_7LO_7 (L=Nb, Ta), ionic cond. rel. to cryst. struct. 79—77810
Li_8MO_6 (M=Zr, Sn), ionic cond. rel. to cryst. struct. 79—77810
$LiNO_3.3H_2O(D_2O)$, crysts. and melts, density, mol. vol., thermal coeff. of expansion, rel. to struct. 80—15270
Sb_2S_3, spherulitic crysts., struct. revealed by direct resoln. of lattice by TEM 79—94982
Si-Al-O-N ceramic systems, layer struct. 80—6382

crystal surface and interface vibrations
absorbed atoms, vibrational modes 77—69172
adatom lattice instability and fluctuation of field emission current 79—15024

crystal surface and interface vibrations continued
adatom on transition metal surface, vibr. model using pair interactions 80—15357
adatom-surface interaction potential, vibr. spectrum 80—103581
adsorbate vibrations, large-angle inelastic electron scatt., theory 80—75427
adsorbed diatomic molecule, coupled-harmonic-oscillator model for vibr. modes 79—82461
adsorbed gas films on grafoil, neutron scatt., lattice gas *(Japanese)* 77—47685
adsorbed layers, normal modes of vibr. obs. by neutron scatt. 79—19443
adsorbed molecule, angle-resolved and variable impact energy electron vibr. excitation spectroscopy 80—76119
adsorbed molecule on metal, vibr. energy relax. 79—42362
adsorbed molecule vibr. excitation due to plastic deform. accompanying fracture 77—15488
adsorbed molecules, electron-impact vibr. excitation, specular selection rule 80—80051
adsorbed molecules, IR frequency shifts, coverage dependence 79—19464
adsorbed molecules on metal surface, vibr. excitation due to electron impact 79—46912
adsorbed molecules on metal surfaces, enhanced Raman scattering, calc. 79—99882
adsorbed species, neutron scatt. obs., book contrib. 77—89505
adsorbed surface structure and dynamics, neutron scatt. studies, review 79—60639
alkali chlorides, thin film, crystal-vacuum (100) surfaces, mol. dynamics computer simulation 80—34288
alkali halides, absorpt. in molecules, clusters and microcrystals 78—80363
alkali halides, thin films, crystal-vacuum (110) interfaces, mol. dynamics computer simulation 80—34289
alkali metal chemisorbed on metallic surface, vibr. freq. 77—7975
amorphous film, tunnelling states, at low temps., thermal and acoustical props. 77—24500
amorphous solid, surface phonons, tunnelling states and propagation characts., low temps. 79—69337
anisotropic multilayer solids, macroscopic fields anal. 77—89547
anthracene, surface polaritons, attenuated total refl. 77—63423
atom, chemisorbed on solid, diffusional motion, microscopic anal. 79—4467
atom scattering from solid surface, multiphonon theory, tetradic scatt. formalism 79—56905
atom-solid surface scattering, quantum theory 78—27357
atom-surface in-plane scattering, 2- and 3-dimens., rainbow struct., energy spectra, surface temp. influence 79—38699
atom-surface scatt., lattice dynamics effects 80—2909
atom-surface scattering, quantum theory, Debye-Waller factor 80—7459
atomic beam scattering by surface and bulk phonons 77—73209
benzene, adsorbed at metal surface, obs. of vibrational modes 80—6649
benzene, deuterated and chemisorbed on glass, vibr. bands, Raman scatt. study 80—84737
bicrystal interface vibrational props., different-interface phonons and low-temp. sp. ht. 77—76656
Brillouin scattering by Stoneley waves, elasto-optic and surface ripple mechanisms 80—71435
butane, adsorbed on graphite, struct. and dynamics, empirical interatomic pots. 79—99417
charged particles surface excitation system, ground-state energy 80—15462
chemisorbed atom, electronically adiabatic vibr. state lifetime 77—72768
chemisorbed atoms, inelastic tunnelling spectra 78—47664
chemisorbed atoms and mols., vibrational motion dynamics, infrared absorpt. line shape 78—51814
chemisorption systems, IR spectral linewidth and sticking coeffs., non-adiabatic effects 80—39423
clean metal surface physics, review 77—15659
conference on lattice dynamics, Paris, France (Sept. 1977) 78—59869
corrugated hard wall, elastic and inelastic scatt. of neutral 79—46899
crystal growth kinetics, microscopic and phenomenological theories, book contrib. 79—69340
cubic crystal, new type of long-wavelength surface vibrs., Green's function method study 78—26758
cubic crystals, anisotropic, surface Green function matching anal. 80—70518
damped surface polaritons at a boundary between isotropic crystals 80—2346
Debye-Waller factor rel. to He at. scatt. 77—63516
degenerate semiconductor, with surface depletion layer, surface polaritons, hydrodynamical model 80—6752
density response, transition-metal slab 78—71930
desorption, laser stimulated, quantum theory 78—79876
desorption, multiphonon processes, quantum-statistical theory 80—107641
desorption, thermal, one-phonon at. scatt., 3-dimens., continuum model 78—87860
desorption kinetics, Kramers-Langevin stochastic eqn., heavy-adatom limit, adatom-phonon coupling 78—84065
desorption rates, stochastic description 77—20184
diamond, optical surface modes calc. 77—59200
diamond (111) surfaces, relax. and reconstruction using C_4H_9 clusters, MINDO/3 calc. 79—42356
p-dibromodiphenylether surface, normal and ultra-Brewster refl. spectra 80—25400
dichalcogenide layer compounds, interface plasmon-phonon interactions, transverse cond. 80—49641
dielectric films, transition layer vibrs., resonance region auxiliary surface polaritons *(Russian)* 80—2347
dielectric slab, electronic polarisability effect on electron-phonon interaction 77—35651
dielectric-metal interface, boundary conditions for phonon hydrodynamics *(Russian)* 77—80692
disordered surfaces, lattice dynamics 79—60616
displacive phase transitions in surface layers, surface phonons 79—65167
dye crystal, CTIP, exciton surface polaritons detect. by ATR spectra at 295K 79—4818
dynamical properties of solid surfaces, analytic approach 78—71929
effective-modulus approximation for surface-vibration modes 79—19446
Einstein model, anharmonic surface vibration, 1-D self-consistent model 78—14563
Einstein model, self consistent, penetration of surface vibr. and melting 79—33171

crystal surface and interface vibrations continued
elastic approximation, vibr. and mag. props. of interface and planar defect *(French)* 77−72767
elastic continuum theory of surface atom mean-square displacements 77−76655
elastic surface waves at hexagonal surface and interface, thermodynamic and dynamical props. 79−69338
elastic surface waves in crysts., special surfaces, directions 80−92604
electron energy loss spectroscopy, book contrib. 77−63509
electron-plasmon and electron-phonon interactions in bulk and near surface, Kikuchi patterns 78−26759
electrons in surface phonon field 80−107885
ethane, adsorbed on graphite, struct. and dynamics, empirical interatomic pots. 79−99417
exceptional surface waves in triclinic crysts., existence problems, general props. 80−92603
exciton polaritons, review, book contrib. 80−49623
far IR surface polariton obs. by attenuated total reflection 77−39790
FCC, self-consistent Einstein model of anharmonic surface vibr. 78−75920
ferroelectrics, surface sound waves on domain boundaries, low temp. sp. ht. 78−71937
ferromagnetic nonmetallic film, stand exchange mode determ. 80−2565
film, light scatt. from interface, polaritons 79−8202
film, surface backscatt. phonon pulse time delay, heat-sensitive detector obs. 78−22927
fine particles melting, model, surface phonon softening effect 79−99297
finite harmonic oscillator chain with surface impurity, dynamics 80−59776
fluorite and antifluorite structs., (110) surface vibr. modes, dynamics and adiabatic potential 80−6613
fluorite type struct., impurity defect interaction in boundary layer, adiabatic approx. 80−6614
force constant changes near surface 77−85047
gas-solid desorption, lattice motion effects, RRKM model 78−2367
gas-solid energy transfer, test of first order distorted wave Born approx. 77−85876
gas-solid processes, generalised Langevin theory, continuum elastic treatment of surface lattice dynamics 80−6612
gas-surface scattering, energy transfer in laser field 79−69941
glass film on substrate, Brillouin scatt. from surface phonons, SAW vel. and attenuation 78−95587
graphite, with physisorbed Xe monolayer, dynamical and thermal props. 80−34292
graphite particles, small, adsorption of butane, struct. and dynamics, appl. of neutron scatt. 79−4481
graphite with adsorbed butane, intramol. surface vibr. modes, inelastic neutron scatt. obs. 77−72780
Green's function and generalised phase shift for surface and interface problems, Green's function and generalised phase shift 79−60895
Green's function calculation, surface atom freq. spectrum, mean correl. displacements *(French)* 78−2206
Green's function for surface physics, partial differential eigenvalue eqn. 80−6929
Green's function generating coeffs., appl. to FCC lattice 77−1185
Green function method for electronic struct. and vibr. modes calc. at surfaces 78−88012
hard corrugated surface, one phonon scatt. of atoms 79−47577
hemicylinder-air-quartz system, semi-infinite crystal, dispersion of surface phonon polaritons 78−71939
hexagonal crystal, bulk and surface-atom mean square displacements, elastic continuum theory 77−7795
hexagonal crystal, surface contrib. to low temp. sp.ht. 77−1233
high frequency phonon, at interface, coupling mech. 79−28189
high resolution electron energy loss spectrometer for surface vibrational studies 80−2260
ice, I_h, water monomer on basal plane, static interaction model 78−18891
ice, intrinsic surface order near melting point 79−14986
incommensurate two-dimensional crystal, ground state, spectrum, phase diagram 79−19458
inelastic scattering of low energy electron beams by surface vibrs., nature of image force 78−91527
inert gas absorbate-substrate system, surface phonons, superstructures 77−15676
inert gas atom-solid surface beam-scatt. spectroscopy in eV range, nucl. channel, formal theory 79−78820
interface specific heat at low temp., vibr. contribution, elasticity theory 77−1234
interface three-phonon processes, Kapitza conductance and pulse expt. applications 80−2261
interface-atom mean-square displacements, elastic continuum theory 77−89632
ion reflection, surface semichannelling effects 79−46728
ion scattering, medium and high energy, two-atom model for surface blocking calc. 79−4886
ionic conductor, interfacial polarisation effects 79−60538
ionic crystal, phys. adsorption of nonpolar gases, localised and mobile phases, hopping adsorbates 80−24739
ionic crystal, surface lattice dynamics, Green function approach 77−31865
ionic crystal, surface vibrational properties, review 78−71928
ionic crystal, with rocksalt struct., vibr. modes of (001) unrelaxed face, shell model 77−43420
ionic crystal, zero point energy contrib. to adsorpt. energy 80−24738
ionic crystal plate, line widths in spectrum of surface vibr. 79−33174
ionic crystal plate, surface vibrations, energy level widths 80−6617
ionic crystal spheroids, IR spectra, calc. using point matching method 77−32377
ionic crystal-degenerate semiconductor interface, localised plasmon-optical phonon coupled modes 78−38930
ionic crystal/degenerate semiconductor interface, localised plasmon-optical phonon coupled modes 77−28071
ionic crystallite, on substrate, IR active modes 77−1667
ionic crystals, surface polaron 78−60020
ionic crystals, surface rumpling at finite temps, Verwey model 79−51402
ionic crystals, vibrational surface modes, vibrational contributions to surface thermodynamic functions 77−47659
ionic solids, surface phonon-plasmon coupling (surface plasmarons) 80−54497
isotropic solid bounded by free surface, correlation function 77−7960

crystal surface and interface vibrations continued
Kapitza resistance, axiomatic acoustic mismatch theory, with loss 79−33132
Kapitza resistance and phonon refl. between solids and liq. He 79−86941
Langevin theory for atom-surface scatt. 77−8701
Langevin theory for gas-solid processes 77−8700
lattice force constant determination 78−71933
lattice soliton, scatt. by mass interface, reductive perturbation method 78−18889
layered structure, surface polaritons, dispersion relations, recursive soln. 77−69390
LEED, anisotropic vibr. effects 78−71650
light atom-solid surface scatt., diffractive and inelastic, unified model 79−87553
light interaction with semiinfinite crystal, phonon approach 77−83811
linear chains, monatomic, anharmonicity in surface and size effects in sp. ht. 77−1236
localised, resonant and antiresonant modes *(French)* 78−71938
low-energy electrons, interaction with surface lattice vibrs. 78−30820
magnetic film, surface state swapping effect 77−90040
melting, as surface-initiated process 80−10644
metal, adsorbate vibrational excitation by inelastic electron scatt. 77−43428
metal, change in refl. on adsorption of molecular monolayer 79−65877
metal, energetics of chemisorption, book contrib. 80−24740
metal, irradiated, surface plasmon modes of voids 79−60617
metal, light scatt. from surface acoustic phonons 78−76484
metal, rel. to low energy atom scatt., theory 78−39648
metal, spin scattering and spin-orbit coupling 80−29369
metal, surface relax. from LEED, Fourier transform-convolution method 79−4459
metal, surface relaxation determ. from LEED via transform method, appl. to W 77−43419
metal surface, adsorbed molecule vibration excitation low energy electron scatt. 78−18910
metal surface, electron-phonon coupling in image-potential bound states 80−54752
metal surface, rough, anomalous low-freq. Raman scatt. from localised acoustic vibrs. 80−93307
metal surface, sticking coeff. and transmission problem, quadratic phonon coupling effects 80−39424
metal surface, sticking rate, transmission problem, model Hamiltonian 80−107640
metal-air interface, far IR propag. distances of surface EM waves 79−42616
metal-liquid He interface, thermal boundary resistance, determ. in transport approach 78−51815
metallic fine particles, anharmonic lattice vibr. theory, Einstein model appl. 78−18714
metallic fine particles, theory of melting in the Percus-Yevick limit, appl. to particles on SiO_2 and C substrates 80−20060
metallic surfaces covered with adsorbed species, vibrs., electron impact spectrometer appl. *(French)* 78−41380
metals, chemisorption of CO, electronic struct., vibr. spectra, and chem. 79−42390
metals, lattice surface relaxation, electrostatic model 80−49488
microcrystal slab, surface phonon modes 79−65303
MIS device, polar-optical phonon interaction with two-dimens. electron gas 79−82434
MIS structure, optical phonon-electron gas interaction, high freq. cond. 80−6888
mixed quantum model for gas-solid energy transfer 78−35235
molecular complex, adsorbed on metal, charge transfer model of Raman intensity enhancement 79−13720
molecular monolayers, IR absorpt. enhancement by thin metal overlayers, ATR technique 80−88995
naphthalene, surface dynamics, calc. 80−92772
optical surface modes of lattice vibrs. 77−59199
phonon processes, investigation using spectrometry of low energy Ne atomic beam 77−28670
phonon transmission from incoherent radiator into cryst., anisotropic continuum acoustics 77−47521
phonon transport in bounded systems, influence of size effect and surface roughness 79−46849
phonon-polariton modes for freq. chirped optical pulse compression 78−46689
phonons, interaction with external probes, scatt. expts. 80−10772
piezoelectric crystal, surface polaron states, polaron-phonon interactions 80−70790
piezoelectric semiconductor film, surface phonon amplification 77−31864
piezoelectric semiconductors, acoustoelectric surface phonon-conduction electron interaction 79−42360
piezoelectric semiconductors, surface phonon acoustoelectric interaction, elastic anisotropy effects 80−6610
piezoelectric substrate, surface-skimming bulk wave excitation, analysis using Green's function formulation 80−53519
plasmarons, effect of finite thickness of accumulation layer, theory 80−103636
polar crystals, cryst. surface effect on lattice vibrs. induced by polarisable impurity 79−90737
polar dielectric interface, phonon-polariton modes 77−24474
polar dielectrics interface, phonon-polariton damping 77−51587
polar semiconductor, optical phonon-magnetoplasmon interface oscills. 78−43467
polar semiconductor crystalline thin films, surface vibr. states, IR absorpt. spectra obs. *(Russian)* 80−60606
polar semiconductors, phonon-plasmon-polariton mode propag. at interface 79−60731
polariton frequency shift, cryst. surface and dielec. function depend. 80−44522
polariton generation through grating couplers 77−85153
polariton interaction with periodic surface struct. 77−47879
polariton scatt. at order parameter fluctuations, phase transition investig. *(Russian)* 77−20179
polariton scattering by order parameter fluctuations near phase transition 77−35981
polaritons, bulk and surface, nonlinear spectroscopy 77−50730
polaritons, semi-infinite crysts., review 77−89827
polaritons, stimulated Raman scatt. *(Russian)* 77−38993
polaritons, surface, obs. by two-photon absorption 77−51676

crystal surface and interface vibrations continued

- propane, adsorbed on graphite, struct. and dynamics, empirical interatomic pots. 79—99417
- propiolic acid, adsorbed in thin film tunnel junctions, hydrogenation and deuteration, IETS obs. 80—45547
- pyrazine absorbed on electrode, surface enhanced Raman spectra, symmetry and polarisability changes 80—50310
- quantum effects of lattice elastic surface waves 77—1290
- quartz, amorphous and crystalline, surface polaritons and splitting of optical frequencies 78—72090
- α-quartz, Au film coated, surface polariton dispersion, IR spectra obs. 78—48249
- α-quartz as substrate in thermal phonon radiation 79—42363
- Raman scattering by surface polaritons 77—12391
- response functions for cryst. and surfaces, appl. to surface scatt. 78—72669
- roughness effects on dynamical props. 78—75923
- Rutherford backscattering and LEED for surface struct. 79—82419
- sapphire-^{4}He interface, transmission of ballistic longitudinal and transverse phonon pulses at 0.25K 79—51416
- sapphire-LiF film system, ATR, substrate surface polaritons reson. effect *(Russian)* 77—32384
- sapphire-Pb interface, heat transfer coeff. meas., 2-80K 80—88419
- sapphire-superfluid ^{4}He interface, ballistic-phonon-pulse transmission at 0.25K 79—95229
- sapphire-vacuum interface, phonon refl. 80—15358
- semi-infinite solid, elementary excitations in surface region 79—60618
- semiconductor, degenerate, surface optical phonons 80—70520
- semiconductor, opaque, light scatt. from surface acoustic phonons 78—76484
- semiconductor, surface Brillouin scattering from acoustic phonons 80—55113
- semiconductor, surface reconstruction, dynamical theory 80—10773
- semiconductor-dielecltric interace, surface polaritons of LO-phonon-plasmon coupled modes 79—7792
- semimetallic film, Wigner crystal in high magnetic field 79—73456
- silica, amorphous surface, phonon spectrum effect on adsorbed NH_3 Raman scatt. 80—11948
- slab or semi-infinite solid, electronic contributions to lattice vibr. 78—71932
- solid-liquid He, interface, Kapitza resist. and phonon scatt. 79—55983
- solid-solid interface, existence conditions and energies for optical phonons 80—20027
- spectroscopy using stimulated Raman scatt. 80—38062
- step trains, modes of vibr., rhythmical bunching, expt. obs. to show periodicity in step patterns 79—41996
- Stoneley waves at (001) interface between cubic symm. cryst. 80—100388
- substrate-adparticle system, phonon instabilities 79—90861
- subsurface atoms, dynamic characts. with account for changes in interatomic interaction *(Russian)* 77—31862
- superconducting film, acoustic matching to substrates 80—15652
- superconductor, possibility of surface polaritons at interfaces 77—24639
- superstructures rel. to surface phonons 77—62731
- surface backscattering yields, effects of correlated lattice vibrs. 79—69942
- surface Brillouin scattering, from acoustic phonons, general theory 80—34932
- surface polaron in mag. field 79—23912
- thermal resistance calc., acoustic-mismatch theory 77—89631
- thermodynamics props. of adsorbed monolayer, vibr. contrib. *(French)* 77—4261
- thin film on substrate, normal Brillouin scatt. by acoustic phonons 80—20648
- three-phonon processes and anomalous interfacial energy transport 79—46913
- tight binding metal, vibr. freq. of atom normal to surface, Einstein model 79—51412
- Toda lattice, surface impurity localised mode vibr. 79—60462
- transition metal, surface lattice dynamics 78—95224
- transition metal, tight-binding model, surface atom vibrations, self-consistent calc. 80—103560
- transition metals, FCC, surface relax. and force consts. 80—39404
- transition metals, surface phonons calc., rel. to superstructures 77—1291
- two-dimensional crystal boundary, oscill. propag. 78—63924
- two-dimensional Wigner-crystal-liquid-surface system, eigenmodes and instability of charged liq. surface 80—10896
- vibration entropy and mean square atomic displacements due to defects in crysts. *(French)* 79—28064
- vibrational states, calc. *(Russian)* 77—51588
- water, chemisorbed on Pt (111), EELS spectra, vibr. freqs. 80—80920
- waves and surface thermodynamics 78—6207
- zeolites, type 13X, acetylene adsorption, inelastic neutron scatt. 78—14584
- Ag, (111) surface, He impact, energy transfer isotropic Debye model 77—16443
- Ag (111) surface phonon dispersion, He atom scatt. meas. 80—75426
- Ag, adsorbed CN monolayer, vibr. spectra, picosec. Raman gain technique 80—91859
- Ag film, Raman scatt. from adsorbed CO 79—78672
- Ag, with adsorbed Cl monolayer, enhanced Raman intensity 79—95766
- Ag/organic dye, excited mol. decay near metal surface, energy transfer to plasmon surface polaritons 80—50440
- $Ag+H_2(D_2)$, energy transfer, quantum mech. theory 77—8699
- AgBr surface, vibr. freq. of adsorbed Ag atom, LCAO-MO calc. *(Russian)* 79—2866
- Al, Brillouin spectra, light scatt. cross section for surface ripples 80—71434
- Al-Al oxide-Pd tunnel junctions, exposed to H_2, inelastic electron tunnelling spectra 80—20327
- Ar adsorption on graphite, orientational epitaxy in self-consistent phonon approx. 79—95261
- Ar, monolayer adsorbed on graphite, lattice dynamics 78—75946
- Ar-graphite system, effects of dynamic coupling 80—10771
- $BaTiO_3$, electron energy loss spectra, 0.02-2 eV 78—39642
- BeO, small crystal, surface phonon modes, IR transmission spectra 80—11398
- CN monolayer on Ag, picosecond Raman gain spectroscopy 80—25351
- CO adsorbed on Ni, energy depend. of vibr. excitation, electron energy loss spectra 79—28201

crystal surface and interface vibrations continued

- CO, adsorbed on Ni (100), freq. and amplitude of localised vibrs., cluster calc. 80—6616
- CO chemisorbed on Fe, low energy vibr. modes studied by tunnelling spectroscopy 80—78590
- CO, chemisorbed on Ni, vibr. spectra from electron energy loss spectra *(French)* 78—22951
- CO, chemisorbed on Ni(111), adsorption sites and long range order, vibr. spectra 79—46946
- $CaCl_2(Br_2)$, adsorption of NH_3 and ND_3, complex formation, IR and for IR spectra obs. 80—80063
- CaF_2, slab, surface modes of vibr. 78—71935
- CaF_2, slab with (110) free surfaces, lattice dynamics and thermodynamic functions 80—70519
- CaO:Mn phosphor, surface radical recomb. and cathodoluminesc. *(Russian)* 78—6787
- CdS 80—11398
- CdS, Brillouin scatt. of refl. light, surface ripple mechanism 77—73149
- CdS, bulk acoustic phonons, light scatt. from phonon-induced surface ripples 78—75924
- CdS, semicond. piezoelec. crysts., US interface waves rel. to acoustoelectric characts. 77—1456
- CdS-$NiCl_2$ interface, elec. props. using SAW techniques 79—56302
- $Co_{1-x}B_x$, polycrystalline and amorphous sputtered films, Brillouin spectra 80—2775
- $Co_{75-x}Fe_xSi_{15}B_{10}$, quenched ferromag. ribbon, Brillouin spectra 80—2776
- Cr (111) surface, acoustic phonons Brillouin scatt. data 78—95222
- CsCl, (110) free surfaces, shell model surface acoustic mode dispersion 77—15675
- Cu (001), inelastic scatt. of He atoms, 20K 79—8222
- Cu (001), surface relax. and thermal expansion calcs., equal-time vibr. correlation functions 79—23820
- Cu (100), adsorbed formate and acetate species, EELS study 80—76120
- Cu (100), chemisorption and decomp. of formic acid, EELS study 80—16729
- Cu (100), chemisorption of CO, vibr. excitations and struct., EELS and LEED study 80—39437
- Cu (100) reaction with ethanol and methanol, EELS study 80—16728
- Cu (100) surface, chemisorbed CO vibr. spectrum 79—69347
- Cu (110), adsorption of CO, electron energy loss vibr. spectra and LEED obs. 79—77902
- Cu, adsorbed mol. monolayers, UV-visible spectra 78—72619
- Cu, Ar^+ low energy refl., surface thermal vibrs. effect 77—16448
- Cu, low energy noble gas ion refl., surface thermal vibrs. effect 77—69955
- Cu, low energy noble gas ion refl., surface thermal vibrs. effect 77—73203
- Cu-epoxy-Cu sandwich, thermal boundary resist., 0.05-10K 78—14564
- α-Fe, (001), surface relax. and thermal expansion calcs., equal-time vibr. correlation functions 79—23820
- Fe film bounded by dielec. layers, surface polariton in ATR angular spectra 79—15545
- Fe, surface lattice dynamics 78—95224
- Fe, surface phonon spectra 78—71934
- $Fe_{1-x}B_x$, polycrystalline and amorphous sputtered films, Brillouin spectra 80—2775
- $Fe_{100-x}B_x$, quenched ferromag. ribbon, Brillouin spectra 80—2776
- $Fe(CN)_6$, adsorbed on Al_2O_3, tunnelling spectra, isotope shifts 80—29262
- $Fe_{76}Mo_4B_{20}$, quenched ferromag. ribbon, Brillouin spectra 80—2776
- $Fe_xNi_{80-x}B_{20}$, quenched ferromag. ribbon, Brillouin spectra 80—2776
- α-Fe_2O_3 microcrystals, surface phonon modes, IR study 80—55089
- $Ga_{1-x}Al_xAs$, surface phonon polaritons, frustrated total internal refl. expts. 78—47656
- $Ga_{1-x}Al_xSb$, surface oxidation, Raman spectra, residual Sb layers 80—71419
- GaAs (110), LEED intensities, dynamical calc. 79—77462
- GaAs (110) surface states, surface relax. models, tight-binding calcs. 79—4594
- GaAs, Al-coated, surface phonon Brillouin spectra 79—78694
- GaAs, Brillouin scatt. of refl. light, surface ripple mechanism 77—73149
- GaAs, Brillouin spectra, light scatt. cross section for surface ripples 80—71434
- GaAs, bulk acoustic phonons, light scatt. from phonon-induced surface ripples 78—75924
- n-GaAs, far IR propag. of surface EM waves 79—42615
- GaAs, intrinsic, on degenerate n-Ge, surface polaritons, hydrodynamical model 80—6752
- GaAs, phonon surface density, Brillouin elasto-optic cross section 78—72536
- GaAs, polaritons, surface nonlinear interactions, Green's function theory 78—42379
- GaAs, surface phonons, scatt. expts. 80—10772
- GaAs-AlGaAs superlattice, selective transmission of HF phonons 80—34154
- GaAs-native oxide interface, Raman scatt. expts. 77—85709
- GaAs-Pt-air system, far IR propag. distances of surface EM waves 79—42616
- $GaAs_xP_{1-x}$, surface phonon polaritons, total internal refl. *(Russian)* 79—38688
- GaP, Raman scatt. from surface polaritons, selection rules 77—52083
- GaP, Raman scattering selection rules for surface polaritons 78—72091
- GaP, surface polaritons, light scattering studies, effect of surface roughness 80—6753
- GaSe, lattice dynamics and elastic props., Born-von Karman model study 80—70337
- GaI, Brillouin spectra, light scatt. cross section for surface ripples 80—71434
- Ge, (111) surface, clean, double diffr. spots in RHEED patterns 79—90855
- Ge, optical surface modes calc. 77—59200
- H, adsorbed on Pt (111), vibr. modes, EELS study 80—15377
- H, chemisorbed on metal substrate, vibr., freq. shifts due to adatom interactions 80—39407
- ^{4}He liquid-solid interface, phonon transmission and Kapitza resist. 79—65271
- ^{4}He, quantum cryst., surface equilib. shape and vibrs. *(Russian)* 79—7732
- In, submonolayer superstructures on Si (111) isothermal desorption, RHEED meas., adatom vibr. periods 79—86992
- InAs, surface space charge investig., reson. enhanced Raman scatt. 77—20849

crystal surface and interface vibrations continued
InP, surface phonon polariton dispersion and damping, frustrated total internal refl. meas. 80—80792
InP, surface space charge layers and Schottky barrier form., Raman scatt. study 80—50319
n-InSb, rel. to damped surface magnetoplasmons, theory 79—7873
Ir (110) and (111) surfaces, Debye temps., LEED meas. 79—60619
K halides, surface lattice dynamics, by Green's function method 78—71936
KCl, (100) face, mol. dynamics computer simulation of surface props. 78—18880
KF(Cl)(Br)(I), surface lattice dynamics, Green function method 78—34693
LiF, 63 meV He atom scatt., single Rayleigh phonon interaction 78—80447
LiF (001), elastic and inelastic scatt. of He and Ne, selective adsorption 77—66564
LiF (001), He elastic scatt., hard corrugated surface model, GR Method 77—85863
LiF (001), surface phonon obs. in He atom inelastic scatt. 80—80927
LiF, (001) surface, He and Ne inelastic resonant scatt. assisted by phonons 77—73201
LiF, bulk and (001)-surface equal-time vibr. correlation function 78—47655
LiF film, surface phonons and thickness variation, EELS meas. 80—92774
LiF films, polycrystalline and single-cryst., comparative study of phonons by electron spectroscopy 80—25505
LiF surface, diffractive scatt. of H atoms, meas., Debye temp. and Morse pot. determ. 80—76124
LiF surface, He atom inelastic scatt., phonon coupling 80—71554
LiF, surface lattice dynamics, Green function approach 77—31865
methane-I plastic crystal, surface modes 78—71926
MgO, 15-layer unrelaxed slab, lattice dynamics using breathing-shell model 79—73389
MgO (001), surface relax. influence on surface vibr. modes, bulk shell model calcs. 78—71927
MgO, (001) surface, charge deform. and geometric relax., shell model 79—95255
MgO, bulk and (001)-surface equal-time vibr. correlation function 78—47655
MgO, cryst. surface strain and polarisation fields, breathing shell model calcs. 78—22946
MgO, reconstruction of the (001) surface 78—75922
MgO small cubes, surface vibr. modes, IR transmission obs. 78—22947
Mo (001) surface, electronic susceptibility and surface phase transition 79—33169
Mo, desorption of He, Mo-He and He-He interaction pot. 79—19459
N_2, monolayer adsorbed on graphite, lattice dynamics 78—75946
N_2 monolayer on graphite, phonon dispersion curves for postulated four sublattice struct. 78—47667
Na halides, surface rumpling at finite temps, Verwey model 79—51402
NaCl (001), surface relax. influence on surface vibr. modes, bulk shell model calcs. 78—71927
NaCl, adsorption of CO_2, zero point energy contrib. to adsorpt. energy 80—24738
NaCl, adsorption of methane, adsorpt. pot., localised and mobile phases, hopping adsorbates 80—24739
NaCl, bulk and (001)-surface equal-time vibr. correlation function 78—47655
NaCl, surface lattice dynamics, Green function approach 77—31865
NaF-^{4}He liquid interface, phonon propagation 78—14526
NaF-liquid ^{4}He interface, phonon ang. distrib. after refl. 79—55979
NaF-liquid He interface, freq. of emitted phonons 79—55978
NaI (001), surface relax. influence on surface vibr. modes, bulk shell model calcs. 78—71927
NaI, surface lattice dynamics, Green function approach 77—31865
Nb sputtered film, tunnelling characts. 79—4621
Nb_3Sn, softening of surface phonons in (100) plane 80—107627
Ni (100), adsorbed c(2×2) CO, photoemission orientation determ. 79—19974
Ni (100), O and S chemisorption, surface vibrs., electron energy loss spectra 79—33173
Ni (100) face, O-Ni system vibrs. rel. to struct. during oxidation 77—66089
Ni, (100)p(2×2)O and (100)c(2×2)O surfaces, struct. and vibrs. of adsorbed CO 78—2375
Ni (111), adsorbed H, angle-resolved and variable impact energy electron vibr. excitation spectroscopy 80—76119
Ni (111), coadsorption of CO and hydrocarbons $C\equiv O$ bond weakening 79—90863
Ni (111), with submonolayer of O, H or C_2H_2, surface phonons obs. by EELS 80—39403
Ni (111) and (100), chemisorption of benzene, vibr. EELS study 80—39436
Ni (1n0), surface phonons due to O_2 adsorption 78—2359
Ni, adsorption of ethylene at room temp., surface complex vibr. from electron energy loss spectroscopy 79—73404
Ni, Brillouin spectra, light scatt. cross section for surface ripples 80—71434
Ni catalyst, H_2+CO, adsorption, co-adsorption, reaction, neutron inelastic spectroscopy method 79—99408
Ni catalysts, chemisorption of $H_2(H_2O)$, dynamics, neutron spectrosc. obs. 80—59778
Ni, chemisorbed O influence 80—84361
Ni, chemisorption of H_2, Raman spectra, vibr. bands 79—61368
Ni film, phonon transport into SrF_2 substrate, diffusive scatt. at impurities 80—49487
Ni, lattice vibrations at (111) surfaces and stacking faults 79—86974
Ni(100), adsorbed CO vibr. EELS, large-ang. defl. 80—44405
Ni(111), adsorbed benzene, vibr. loss spectra 79—23838
O_2, monolayer, lattice dynamics 79—95095
OH adsorbed on Ni, energy depend. of vibr. excitation, electron energy loss spectra 79—28201
PbS, surface optical phonons, anal. of LEED results 79—69339
PbTe (111), lattice vibr. amplitude anisotropy, RHEED study 80—39408
Pd (100), adsorption of Xe and CO, lateral interactions, effect on work function, UPS, and IR spectra 79—77904
Pt (111), adsorption of NO, EELS, thermal desorption, LEED, and AES study 80—80086

crystal surface and interface vibrations continued
Pt (111), adsorption sites of CO, surface vibr. modes, electron energy loss meas. 77—43422
Pt (111), coadsorption of CO and hydrocarbons, $C\equiv O$ bond weakening 79—90863
Pt (111), relax. effects, and thermal vibrs., medium energy ion scatt. 79—28182
Pt (111), surface reaction with acetylene ethylene, and H_2, EELS 78—71947
Pt (111) adsorption state of acetylene on surface vibrs. meas. 77—76657
Pt (111) stepped surface, localised surface phonons obs. 78—95223
Pt, CO adsorption, electron energy loss spectra 77—69160
Pt, stepped surface, $6(111)\times(\bar{1}11)$, relax. and force const. 79—86973
Pt stepped surface, adsorbed H, adsorption sites study by EELS 80—49521
Pt(111), adsorbed benzene, vibr. loss spectra 79—23838
Pt(111), adsorption of NO, anal. of adsorption processes and surface reactions, vibration spectroscopy 78—87868
Pt(111) stepped surface, high freq. vibr. modes, cluster recursion method calcs. 80—6615
Pt(111) surface, identification of adsorbed OH species 80—49509
Pt(111) surface relaxation, temp. depend., He scatt. 79—19447
Rh (111), chemisorption of CO and CO_2, high resolution EELS, thermal desorption, and LEED study 80—44419
Rh, adsorption of CO, inelastic electron tunnelling spectra obs. 79—46962
Rh(111), surface geometry, vibrational props., Debye temp., LEED study 78—87852
Ru (001), CO adsorbed, temp. depend. ordering processes 80—80773
Ru(001), coadsorption of NO and CO, adsite symmetry determ. by EELS 79—99412
Ru(001) surface, adsorption of CO, IR spectra and LEED 79—37914
Sb_2S_3 layered biaxial cryst., surface phonon polaritons *(Russian)* 78—60021
Se, trigonal, surface lattice dynamics, mean square displacement spectra in long wavelength limit 80—54498
Si, (001), clean, double diffr. spots in RHEED patterns 79—90855
Si (001), surface Debye temp. meas. by HEED 77—89633
Si (100), reflection of high freq. phonons 79—65304
Si (111), chemisorption of H, localised model, ab initio HF-LCAO calc. 80—6930
Si (111), dynamic effective charge and surface reconstruction, soft-mode theory 79—4460
Si (111) surfaces, relax. and reconstruction using Si_4H_9 clusters, MINDO/3 calc. 79—42356
Si adsorbed on W(100) face, LEED, dynamic props. 77—89634
Si, adsorption of gases, electron energy loss spectra 77—69160
Si, Al-coated, surface phonon Brillouin spectra 79—78694
Si, amorphous, opaque, surface phonon attenuation, Brillouin scatt. 80—80808
Si, H chemisorbed, relation of Si-H vibr. freq. to surface bonding geometry 80—49502
Si, optical surface modes calc. 77—59200
Si, pure and with adsorbed Al(Au), thermal expansion and at. vibr. singularities 77—89635
Si:H, amorphous, Brillouin scattering from acoustic bulk and surface waves 80—11425
Si-^{3}He interface, phonon reflection 78—84043
Si-SiO_2, surface and interface phonons in bonded solids 78—71931
Si-SiO_2 interface, remote polar phonon scatt. in Si inversion layers 80—80095
Si-SiO_2 interface, thermal SiO_2 sputter induced roughness, Auger sputter profiling study 80—75424
SiO_2, amorphous, surface phonon theory 78—84044
SiO_2, amorphous and crystalline, surface polaritons and splitting of optical frequencies 78—72090
SiO_2, hydroxylated amorphous, small-particle dynamics, neutron scatt. 80—79899
SiO_2 powder, surface modes, IR spectra 78—92063
SiO_2, surface and interface phonons in bonded solids 78—71931
Sn film-quartz substrate interface, anomalous transmittance for thermally radiated phonons of thin metal films *(Russian)* 80—103664
α-Sn, optical surface modes calc. 77—59200
surface atoms, Debye temps. determ. during field evaporation and LEED 80—39406
Te, trigonal, surface lattice dynamics, mean square displacement spectra in long wavelength limit 80—54498
Th (111), struct., Debye temp., and oxidation, LEED and AES obs. 77—89625
TiO_2, electron energy loss spectra, 0.02-2 eV 78—39642
TiO_2-LiF film system, ATR, substrate surface polaritons reson. effect *(Russian)* 77—32384
W (001), atomic H adsorption, surface vibr., electron energy loss spectra 77—76664
W (001), chemisorption of H, surface phonons, lattice dynamical model 80—39405
W (001) surface, long-wavelength surface phonon spectrum 78—75921
W (100), adsorbed H, angle-resolved and variable impact energy electron vibr. excitation spectroscopy 80—76119
W (100), chemisorbed Ba, inelastic tunnelling spectra 78—47664
W (100), chemisorbed H, ν, vibrational mode IR study 80—60582
W (100), chemisorption of H, struct. determ. by surface vibr. modes anal., EELS obs. 80—39435
W (100), LEED intensities, temp. depend., surface struct. phases and surface Debye temp. 80—39395
W (100) and (110) surface, theoretical Debye-Waller factors 80—92773
W (100) surface, adsorbed H-induced lattice reconstruction, surface vibr. obs. 79—19445
W (100) with adsorbed CO, surface vibrs., EELS 77—62745
W, CO adsorption, electron energy loss spectra 77—69160
W, chemisorbed H_2, vibr. spectra characts., adsorption sites 80—70535
W surface, thermal accommodation of He, two-phonon contribs., DWBA calcs. 79—95893
W, surface phonon spectra 78—71934
W, vibr. states of H_2, D_2 and C_2H_2 adsorbates EELS 77—66090
WC, microcrystalline, mol. dynamics, motion of H_2O and H_2 mols. adsorbed on surface, catalytic activity 78—71941
W(100), adsorbed H, nondipole electron impact vibr. excitations obs. 78—63922
W(100), chemisorbed H, vibr. excitation of hydrogenic modes, angle dependent electron energy loss meas. 79—46914

crystal surface and interface vibrations continued
  W(100) surface, instability, distortion and dynamics 80—84360
  YIG, ferromag. film on nonmag. substrate, magnetoelastic wave propag. 79—99744
  YIG-LiF film system, ATR, substrate surface polaritons reson. effect *(Russian)* 77—32384
  ZnO, IR spectra, surface phonon modes 79—78668
  ZnO, microcryst., surface microscopic modes, IR detection 79—38527
  ZnO, optical surface phonon modes, far IR transmission 77—31863
  ZnO, small crystal, optical surface phonon modes 78—71940
  ZnO, small crystal, surface phonon modes, IR transmission spectra 80—11398
  ZnO, surface phonon-plasmon coupling (surface plasmarons) 80—54497
  ZnSe film, surface polaritons, thermostimulated emission *(Russian)* 78—10904
  $Zr(BH_4)_4$ catalytic reactions on Al_2O_3, inelastic electron tunnelling spectra 80—75425

crystal symmetry
  see also crystallography; group theory
  $\bar{4}3m$ symmetry geometric units, cryst. structs. 80—107087
  A15 compounds, high supercond., T_c, attributed to linear chains or cubic symmetry 79—38221
  A15 structure, O_h^3-Pm3n, group theory of phase transition 78—9992
  adamantane crystals, relative stability of ordered F$\bar{4}$3m and disordered Fm3m 79—73119
  algebraic definition of cryst. symmetry on n-dimens. space *(French)* 78—55824
  alkali chloride:Mn^{2+}, spin Hamiltonian parameters, binding energies for cation vacancy complexes 80—96461
  anisotropic constitutive equations and Schur's lemma 78—89337
  anisotropic materials, class D_{6h}, constitutive relations 80—59426
  anthracene, attachment energy as habit controlling factor 80—59421
  anthracene, metastable triclinic phase 80—59452
  asymmetrisation in the growth process, sectorial struct. and structural ordering 79—90581
  Belov's classes, and subclasses, distrib. of symmetry groups 79—14721
  benzil, structural transition model, cryst. symm. spontaneous strain components 80—2161
  $Bi_7Ni_4NbO_{21}$, crystal point group determ. by high resolution electron microscope image 79—51036
  bicrystals, symmetry and interfacial struct. 80—2274
  body-centred cubic cylinder packing, appl. to garnet 77—62497
  bond percolation in square, cubic, hypercubic lattice, probability renormalisation group method 80—31680
  Brillouin zone, special points, influence of symmetry and crystallographic class 77—7687
  broken translational symmetry *(Korean)* 78—22680
  cation-deficient close-packed structures, combinatorics 79—23558
  Cauchy symmetry, crystallographic point groups, elastic work functions 77—72644
  cellular automata and unified ways of describing structures 77—15333
  centrosymmetric molecules in centrosymm. space group statistical anal. *(German)* 78—42940
  centrosymmetry, statistical criteria for use of cumulative, semicumulative and distribution function tests 77—84688
  classification of crysts. by acoustic props. 78—79547
  coincidence site lattice rotations, permissible angles 79—32932
  colour symmetry groups, of coloured polyhedra and coloured simple forms 79—60294
  coloured lattices, rot. symmetry effect, appl. to mag. structs. 79—90587
  coloured lattices 79—90586
  conference, group theory and application to spectroscopy, Nova Scotia, Canada (Aug. 1978) 80—41947
  conference, International Crystallography Congress, Warsaw, Poland (Aug. 78) 79—23481
  conjugated elements, classes, of crystallographic groups *(French)* 79—7564
  continuous crystalline transitions, counterexample to maximal subgroup rule 80—59428
  coordination number, quantifying concept for irregular coordination polyhedra 78—95008
  corundum, attachment energy as habit controlling factor 80—59422
  cubic and non-cubic, distinguished by weak field galvanomagnetic meas. 80—60009
  cubic compounds of A15, C15 and B2 types, struct. phase transitions 77—4198
  cubic crystal system, symmetry restrictions, on 2nd order tensor components, error correction in International Tables for X-ray Crystallography 79—73120
  cubic crystals, local field factors, electric dipole approx. calcs. 80—54661
  cubic harmonics, $l \leq 17$ Cartesian coords. 77—51338
  cubic structures, symmetry of coincidence site lattices *(Russian)* 80—79807
  cubic-tetragonal transitions, symmetry anal. of deformable cryst. 80—10636
  3-cyanopyridine, NQR Zeeman obs., crystal packing 80—54978
  D_{2d} crystals, structural phase transitions, soft modes, group theory 80—92638
  decahedral particles, high symmetry orientations, HEED and TEM study 79—86732
  degenerate homogeneous linear structures, series 79—94941
  degenerate three dimensional local and quasi local vibration spectral distributions 80—29138
  Delaunay rotation stereohedra types for 3×432 group 80—38984
  diamond lattice, dynamic symmetry and plastic deform. 80—24527
  diatomic crystals, strain energy functions, crystal symmetry constraints 78—47467
  dicalcium strontium propionate, cryst. symmetry in low temp. phase 79—37693
  diffraction enhancement of symmetry, simple and double enhancement 77—51257
  diffraction symmetry enhancement rel. to Patterson function 79—73068
  dislocation core, symmetry of dynamical electron microdiffraction patterns 80—100140
  displacively modulated structures, symmetry operations 77—51337
  double point groups, Clebsch-Gordan products and extended integrity bases 79—69048
  double space groups O_h^6 (Fm3c) and O_h^8 (Fd3c), selection rules 80—10518

crystal symmetry continued
  dynamic symmetry, appl. for interpretation of X-ray diffr. patterns 78—47265
  dynamic symmetry 78—30572
  dynamical systems, new class of crystal models, symm. props. 77—19888
  elastic coefficients, independent 4th-order for all cryst. classes, numerical methods anal. 79—69219
  elastic media and crystal, groups of materials symmetry 80—70147
  elastic surface waves in crysts., special surfaces, directions 80—92604
  elastically bent single cryst., right-left asymmetry due to anisotropy on diffraction *(Russian)* 78—71699
  electron diffraction patterns, and optical transforms of atomic aggregates, symmetry aspects using computer simulation 79—7525
  electron microscope imaging 80—88006
  electronically degenerate states, asymmetric scattering tensors of normal modes, selection rules 77—12381
  EPR, low symmetry effects, review 80—71159
  EPR spectra, hyperfine structure, low symmetry effects, calc. 80—50165
  ethylene, isotopically mixed, crystal, dilute guest probe orientational energy, IR, Raman spectra 78—68496
  ferroelectrics, unit cell multiplication during phase transform., spontaneous polarisation 80—75983
  ferroic phase transitions, non-mag., unified classification 80—70387
  flavocytochrome b_2, rotation function study using X-ray data 79—51035
  four-dimensional space, crystallographic groups, book 79—27942
  fourth-order independent elastic coeffs. for trigonal and hexagonal symmetry classes 79—77665
  garnet structures, X-ray diffr. data 79—42024
  garnets, doped, site symm. exam., ang. variation of induced linear dichroism 78—95429
  geometric properties of cryst. lattices in spaces of arbitrary dimension 79—90588
  grain orientation, of neighbours, disorientation description 80—79725
  group theory, postgraduate textbook for physicists 77—41455
  group theory applications to physical and chemical systems in relation to struct. and substructs. 80—42921
  growth disorder models by symmetry imposition 77—31614
  growth models, attachment energy as habit controlling factor 80—59420
  growth-layering effect on optical symmetry in cubic crystals, rel. to cathodolum. data 80—88072
  holohedral varieties of simple forms of crystals 79—94940
  homogeneous linear structures, line symm. groups appl. 77—31624
  homogeneous linear structures, systemisation according to charact. numbers of position symbols 78—95009
  icosahedral multishell clusters, stability and formation modes *(French)* 80—79728
  implications in charge density studies 78—71694
  improper ferroelectric nonferroelastic transition, order parameter symm. 77—4608
  improper ferroelectrics, spontaneous polarisation, cryst. symm. in phase transitions 78—6645
  incommensurate crystal phases, symmetry, superspace-group approach, commensurate basic structs. 80—79726
  incommensurate crystal phases symmetry, incommensurate basic struct., superspace group approach 80—79727
  induced projective representations of finite group, cryst. symm. appl. 78—4461
  inner elastic constants, symm., depend. on symm. of interlattice tensors 79—28028
  interaction potential effect on cryst. nucleation and symmetry 80—34169
  internal dimensions in crystal space group symmetry 80—38983
  isocahedral particles, high symmetry orientations, HEED and TEM study 79—86732
  Jahn-Teller crysts., ferroelec. transitions, elastic and dielec. anomalies, microscopic model 80—71332
  lattice symmetry determination 80—49156
  Lifshitz's criterion for symmetry changes in second-order phase transitions 79—4392
  ligand field calculations for arbitrary point groups in strong field coupling, energy diagrams, plotter routines 77—76778
  linear chain model, symmetry-adapted, layer dynamics of high-symmetry crystals 80—34148
  low-symmetry crysts., propag. of quasivolume surface elastic waves 77—28070
  magnetic crystal symmetry 79—99100
  magnetic materials, symm. restrictions on constitutive eqns., group theoretical procedure 77—55255
  magnetic point groups, simplified calc. and tabulation of tensorial covariants belonging to same Laue class 79—19174
  magnetic structure, neutron diffr. study, symm. anal., polarisation effects 80—93083
  magnetic structure symm. anal. in neutron studies periodicity changes at mag. phase transitions 79—99680
  magnetic structures, symmetry anal. in neutron studies, phase transition concept 79—99679
  magnetic symmetry, improper symm. and Neumann's principle 78—38646
  magnetic symmetry groups, higher order elastic coeffs. calcs. 80—28939
  magnetostriction in terms of hexagonal and cubic harmonics up to degree 6 80—88856
  marcasite structure, space group selection rules 79—99099
  martensites, symmetry 77—62635
  metal oxide:U^{6+}, luminesc. sensitivity to vibrational fine structure 78—6772
  methane, phase II, nuclear spin-lattice relax. and site symm. 80—97155
  mixed metal chloride acousto-optical props. *(Russian)* 78—60419
  models, local symmetries 77—7685
  molecular crystal classes and subclasses prediction rel. to C_2 symmetry of mols. 77—7686
  molecular crystal structure classification 78—9985
  molecular crystal subclasses from intermol. interaction energy calcs. 77—4064
  molecular crystal symmetry props. from optical activity and gyrotropic birefringence calc. *(French)* 78—42941
  molecular crystals, dipolar coupling and phonon symm. *(Chinese)* 80—103437
  molecular crysts., symmetrised valence and relative motion coords. 80—84134
  molecular distortions, described in terms of symmetry coordinates 80—10517

crystal symmetry continued
- molecular low dimensional system, spontaneous symm. distortion 80—96456
- molecule struct., shapes symmetry 78—71697
- monoclinic space groups, use of Σ_1 relation 77—43165
- Mossbauer nuclei lattice with hyperfine interactions 78—67677
- multiply twinned particles, with decahedral and icosahedral pt. group symm., twin cryst. struct. 79—86801
- multivector analysis, comparison with tensor algebra 80—100195
- multivector analysis, comparison with vector anal. 80—100196
- naphthalene-d_8:naphthalene, symmetry reduction obs. of deformed crysts. by absorbt. spectrum method 79—15504
- non-rigid impurity centres, symmetry groups 79—77534
- noncentrosymmetric structures, antisymmetric atomic features, Bijvoet ratio 79—32925
- nonlinear optical polarisations, second and third order, general effects of cryst. symmetry and orientation 77—19358
- nontransition metal simple binary suboctet compounds, structural stability 77—58966
- normal mode calcs. of crystals and molecules, coordinates and force matrices generation, computer program 78—91393
- NQR spectra, crystal symmetry determ. and elec. effects 77—11450
- numerical integration over solid angle and vol. of Brillouin zone, any crystal symm. 77—27843
- octahedral molecule MX_6 with close-packed arrangement of X-atoms, possible cryst. struct. *(German)* 79—27940
- OD-groupoid families, complete list for OD-structures consisting of equivalent layers 78—59776
- optical material props., symmetries and tensorial relationships 80—108174
- optical SHG as crystal class detection method *(Chinese)* 79—81490
- order-disorder groupoid family, parameters, stacking 80—38982
- order-disorder structures, desymmetrisation 80—38986
- organic crystal, struct. and habit correspondence, mol. centre of gravity determ. *(German)* 79—32934
- organic crystals, macroscopic prop. observation forbidden by point group symm. *(Russian)* 80—88075
- organic homomolecular crystals, distrib. by chiral types and struct. classes 78—9986
- oxide systems, quasibinary and quasiternary, data base development for phase diagram calc. 79—96006
- Patterson function with translational pseudosymmetry, interpretation 80—33915
- Patterson synthesis, partial, derivation of 57 black-and-white symmetry groups, interpretation 79—60296
- periodic structure homometric set, search algorithm 80—75118
- periodically distorted crystals, symmetry 77—39553
- perovskite crystal, ABX_3, transition involving BX_6 octahedra rot., distorted phase symm. 77—4197
- perovskite-like structures, some remarks on the 'family tree' of Barnighausen 79—7565
- photogalvanic effect in crystal with polar axis *(Russian)* 77—80811
- piezoelectric crystals, of classes 422 and 622, transverse-transverse elastic polarisation waves 79—95077
- plastic crystal, orientational disorder, group theory method 80—107091
- plastic crystal, orientational dynamics, neutron scatt. data interpret. using functions derived from group theory 80—107092
- point group determ. by high resolution electron microscope image 79—51036
- point group symmetry, derivation and recognition schemes, computer assisted learning programmes 77—29973
- point groups, basis functions for irreducible representation, appl. to morphic effects on IR and Raman spectra *(Japanese)* 79—4265
- point groups, extended integrity basis 79—69047
- point groups, symmetry, teaching aid 78—77650
- point symmetries, struct. classification based on lattice 78—9983
- polyhedral cavity field tensors 80—100182
- polymeric series of coverings, symmetry, comparison with layers of real structs., Belov subclass development 80—84129
- polymers, structure classification, according to rel. between chain symmetry and space group *(French)* 79—51058
- polymers, symmetry props., classification using line groups 77—51327
- powder reflections, an error in several published tables of the multiplicities for Laue class $\bar{3}1m$ 79—14720
- powder reflections, computer program for determining multiplicities, correction for $\bar{3}1m$ Laue symmetry 79—10759
- primitive crystal forms, role of normaliser of crystal class 77—76346
- pseudo-centrosymmetry destruction by direct method 78—91286
- pseudo-groups applied to symmetry and defects ordered media 80—10541
- pseudosymmetric crystals, isovector struct. theory, Cochran struct. 80—88076
- quartz, habit variation of crystals of the $C3_12$-$C3_22$ space group 80—107090
- quasi-symmetry and double point groups C_4 and D_3 80—92472
- quintet, conditional probability distribution 77—43166
- Raman scattering, irreducible tensor operator for 32 cryst. point groups 77—8572
- reduction symmetry method in crystal field theory 80—70656
- revolution manifold isometric stereohedra 79—82170
- rhombohedral oxides, symmetry group *(French)* 80—84157
- rotational symmetry, and tensor props., 1-, 2- and 4-fold principal symmetry, trigonal, and hexagonal groups 80—100193
- rotational symmetry, and tensor props., method for group $3(3_z)$ 80—100192
- second-order phase transitions, changes in structural symmetry crysts. of D_4 and C_{4h} classes 77—89399
- selection rules, for crystals with imperfections, subgroup method *(German)* 80—38980
- Shubnikov antisymmetry groups, cryst. struct. examples 77—31625
- Shubnikov point groups, PUA representations 79—55690
- solid solutions, interstitial phase struct., reconstructive transition struct. symm. relationships 79—69246
- space group symmetry operations, program for deducing from symbolic notation 79—94942
- spectroscopic properties of crystals of C_{4h}, D_{2d} and D_4 symmetry at second-order structural transform. 78—22845
- squaric acid, second harmonic generation 79—46000
- star mayer graphs, ninth order, three-space lattice symmetry coeffs. *(Russian)* 78—29064
- stereographic projection model, construction, teaching appl. 78—86086
- stereographic projections, standard, computer generated 79—37579

crystal symmetry continued
- stereohedra, rotation, local transformations 79—94939
- Stoneley waves at (001) interface between cubic symm. cryst. 80—100388
- strontium acetate hemihydrate:Mn^{2+}(Cu^{2+}), EPR, spin Hamiltonian anal. and unit cell symmetry 80—29603
- structural diagram of compounds ABO_4 78—79548
- structural phase transformations, possible symmetry changes 78—2056
- structural phase transitions in crystals of $D_{2d}{}^3$ symm. 80—15986
- structure semi-invariants, representations method 80—79724
- structure type relationships, symmetry of plane homologous series, Belov classes and subclasses 78—26476
- symmetric Belov subclasses for homologous series of bases of structural minals 79—19176
- symmetry coordinate generation using multiplier representations of space groups 79—37646
- tensor components, unitary groups appl., and phase transition selection principles 79—46589
- tensorial covariants for the 32 crystal point groups 79—19173
- sym-tetrachlorobenzene, LF Raman bands and space symmetries 77—66504
- three phase struct. invariant, in $P2_1$, probabilistic theory 79—51033
- three-dimensional reciprocal lattice model 77—13551
- transition, cell-preserving, space group theory of translation, twin and translation-twin boundaries 77—19892
- transition metal complexes, octahedral substituted, ligand-fluid splittings, accidental degeneracy origin 80—10932
- transition metal dichalcogenide, stacking layer study, appl. of convergent beam electron diffr. 80—39116
- triclinic lattices, planewise summation method 80—107069
- TTF-TCNQ, symmetry changes and phase transitions 78—6299
- vector symmetry, in crystallography, basic theorems 79—23556
- vibration spectra and crystal symm., book 77—24365
- wave functions, symm. transformation, computer programs, symmetrisation procedure 78—10315
- wreath groups, symm. of crysts. with struct. distortions 80—75196
- X-ray intensites variation, effect of dispersion and higher symmetries 79—7520
- Zhdanov notation, resolution of ambiguities, homometric structs. 77—31619
- AgCl-AgBr mixed crysts., elastic consts. and cryst. symm. 80—70290
- $AgNO_3$, centre of symmetry and cryst. perfection *(French)* 80—107089
- $(AsO_4)_2H_2(UO_2)_2.8H_2O$, point group symmetry for ferroelec., antiferroelec. and paraelect. phases 78—42983
- Au, pentagonal symmetry, icosahedral struct. *(French)* 80—79729
- $BaCl_2$, Sn-activated, luminescence studies 80—108246
- BaF_2-NiF_2-CrF_3, X-ray crystallography study, phase identification at 700°C, cryst. symm. *(French)* 78—95733
- $(Ba_3Nb_6Si_4O_{26})_n.Ba_3Nb_4Ti_4O_{11}$, n=3/2 to 29/2, intergrowth series, electron microscope obs. *(French)* 78—83762
- $Ca_5(PO_4)_3F:Nd^{3+}$ site symmetries, EPR and spectral obs. 78—6571
- CdA_2X_4 (A=Ga,In; X=S,Se), Fourier IR and Raman spectra, cryst. struct. and symm. *(German)* 79—24313
- Cd_3As_2 type crystals, symmetry props. of energy bands 80—39500
- $CdF_2:R^{3+}$, cooperative luminescence influenced by symmetry of centres 78—6791
- $CsAlF_4$, single cryst., prep. and struct. *(French)* 80—79762
- $CsDy_2F_7$ and Cs_3DyF_6, cryst. symm. and cell parameters *(French)* 80—81040
- DyF_3-KF, phase diagram, cryst. symmetry and lattice constants of phases *(French)* 79—65171
- α-Fe-Cu, coordination fields of crystal struct., rigid-sphere model 78—47266
- Fe_3O_4, magnetite, magnetoelec. effect at 77K and cryst. symm. 80—29593
- Fe_3O_4, magnetite, magnetoelec. effect at 77K, elec. field depend. of mag. anisotropy 80—29594
- FePt lattice, symmetry, state of order, vibration, temp. effects *(German)* 77—4067
- Ga, orthorhombic asymmetry temp. depend. 77—51339
- $GeH_4:SiHD_3$, symmetries of GeH_4 cryst. phases, IR spectra meas. 79—19886
- HgA_2X_4 (A=Ga,In; X=S,Se), Fourier IR and Raman spectra, cryst. struct. and symm. *(German)* 79—24313
- HgS, habit variation of crystals of the $C3_12$-$C3_22$ space group 80—107090
- K_3AgO_2, determ. of cryst. struct. X-ray diffr. *(French)* 78—95029
- $KAlF_4$, single cryst., prep. and struct. *(French)* 80—79762
- K_2CO_3Sr-CO_3 phase diagrams, evidence of new compound *(French)* 78—95033
- $KDy(WO_4)_2$, phase transition mechanism, absorpt. spectra, symmetry props. *(Russian)* 80—55130
- $KMgF_3$, F-centre, superhyperfine interaction, g-factor, symmetry, ENDOR obs. 80—39893
- KNO_3, Raman spectroscopic study of $NO_3{}^-$ component with temp. 78—76458
- K_2SeO_4, symmetry determ. of commensurate and incommensurate phases by EPR of γ-irrad. crysts. 79—78525
- $LaBO_3$, single cryst., not cut parallel to principal axes, Raman spectra birefringence effect 79—69837
- LaF_3, zone centre optical phonon stress dependence, point group symm., Raman spectra meas. 79—78686
- $LaNbO_4$, room temp. form., symmetry determ. by convergent beam electron diffr. 80—79723
- $La_3S_4(Se_4)$, structural transitions, symm. anal. 80—92671
- $LiGaO_2:Fe$ IR emitting phosphor preparation and props. 78—6789
- $LiNO_3$, Raman spectroscopic study of $NO_3{}^-$ component with temp. 78—76458
- $LiYF_4$, elastic consts. and acoustic symm. 80—15182
- Mn_3GaC, mag. symmetry of ordered phases, mag. modes for point groups 78—71698
- NH_4AlF_4, single cryst., prep. and struct. *(French)* 80—79762
- $(NH_4)_2Cr_2O_7$ crystal hypomorphism and hypermorphism 80—59427
- $(NH_4)_2CuCl_4.2H_2O$, Raman sepctra, dynamics, struct., phase transition 79—47434
- NH_4LiSO_4, high press. phase, point group symmetry 79—51039
- NH_4LiSO_4, point group symm. at high press. phase 80—70150
- $(NH_4)_2PtI_6$, crystal symm., struct. phase transition, ^{127}I NQR freq. 80—34815
- $NaBrO_3$, cryst. chirality and optical rotation sense 78—10026
- $NaClO_3$, cryst. chirality and optical rotation sense 78—10026

crystal symmetry continued

- $NaIn(SeO_4)_2.6H_2O$, cryst. struct. by X-ray diffr., symm. 78−43004
- $NaNO_3$, Raman spectroscopic study of NO_3^- component with temp. 78−76458
- $Nb_{0.87}V_{0.13}Se_2$(4Hb), stacking layer study, appl. of convergent beam electron diffr. 80−39116
- $NdNbO_4$, room temp. form., symmetry determ. by convergent beam electron diffr. 80−79723
- $Pb_5I_2Br_8$, form., cryst. symmetry, X-ray diffr. obs. 79−23570
- $Pb_5I_4Br_6$, form., cryst. symmetry, X-ray diffr. obs. 79−23570
- $RbAlF_4$, single cryst., prep. and struct. *(French)* 80−79762
- $RbDy_3F_{10}$, $RbDy_2F_7$ and Rb_3DyF_6, cryst. symm. and cell parameters *(French)* 80−81040
- α-S, attachment energy as habit controlling factor 80−59421
- Se, habit variation of crystals of the $C3_12$-$C3_22$ space group 80−107090
- SiC (1 OH), phonon spectrum, dispersion curves energy discontinuity and vibr. modes, IR spectra obs. 80−44274
- SiO_2 system, spatial-symmetry laws of cryst. lattices 80−19784
- SiO_2, tridymite, non-integral phase from 150°-190° 79−99144
- SnI_4, attachment energy as habit controlling factor 80−59421
- $Sn_2P_2S_6$ ferroelectric semicond., polarisation Raman scatt. spectra, X-ray struct. study 79−95778
- Sn_2S_3, mixed valence semicond., long wavelength phonons, full space group theoretical anal. 79−65873
- $SrCl_2$, in-activated, luminescence studies at 77 and 300K 80−108247
- $Sr_2Nb_2O_7$, normal-incommensurate phase transition, electron microscopy and diffraction study 80−39277
- $Sr_2Ta_2O_7$, structural phase transition to superlattice, electron microscopy and diffraction study 80−39277
- $TaSe_2$, 1T and 2H superstruct., cryst. struct. using X-ray diffr. 80−39044
- $TaSe_2$ (2H), broken hexagonal symm., incommensurate charge-density wave struct. 80−96646
- $TaSe_2$(6R), stacking layer study, appl. of convergent beam electron diffr. 80−39116
- Te, breakdown of Friedel's law in Kikuchi patterns as obs. in TEM 79−69046
- Te, habit variation of crystals of the $C3_12$-$C3_22$ space group 80−107090
- α-$ThSi_2$-AlB_2 series, struct., symm. and rel. to other linear structs. 77−11525
- $TiSe_2$, lattice dynamics, charge density waves transverse phonon dispersion curves, model 80−49322
- $TlAlF_4$, single cryst., prep. and struct. *(French)* 80−79762
- $Tl_2Cd_2(SO_4)_3$, langbeinites, symmetry limitations on choice of hypothetical protophase 80−33916
- $TlGaTe_2$, multilayer cryst., lattice vibr. symm., IR absorpt. and Raman scatt. selection rules 80−39231
- $TlInSe_2(Te_2)$, multilayer cryst., lattice vibr. symm., IR absorpt. and Raman scatt. selection rules 80−39231
- TlSe type crystals, possible second-order phase transitions, group-theoretical anal. 80−92672
- V_2O_3, cryst. struct. charges due phase transition phenomena, EM obs. *(French)* 79−7688
- ZnA_2X_4 (A=Ga,In; X=S,Se), Fourier IR and Raman spectra, cryst. struct. and symm. *(German)* 79−24313
- $ZnSeO_4.6H_2O:Cu^{2+}$, crystal struct. orientational degeneracy removal scheme, space groups, ESR spectra 78−47267
- ZrS_3, Raman spectra and cryst. symm. 80−34922

crystal whiskers *see whiskers (crystal)*

crystallisation

see also crystal growth; dendrites; heat of crystallisation; nucleation

- activation energies of mass transfer at phase boundaries, quantum theoret. calcs. *(German)* 78−67671
- aligned composites, in-situ growth by disproportionation of amorphous metal systems 78−72755
- alkali metals, crystalline and alkaline, eqns. of state, zero compression isotherms *(Russian)* 80−103446
- α,ω-alkoxypolyethylene oxide, low mol. wt., crystallinity and fusion 78−51448
- alloy, binary, crystallisation kinetics, temperature dependence, kinetic phase diagrams 80−16294
- alloy, binary, crystallisation under parabolic stability *(Russian)* 79−70054
- alloy, binary, kinetic conditions for two phase zone form. *(Russian)* 77−66633
- alloy, liquid, crystallisation, fluidity resistance effects *(Russian)* 77−55957
- alloy, solid state reactions, effect on microstruct. 79−29015
- alloy crystallisation kinetic diagram appl. *(Russian)* 78−15384
- alloy melt, impurity conc. field model, growth by Czochralski method *(Russian)* 80−75191
- alloys, binary, kinetic crystallisation diagrams, given finite diffusion coeff. *(Russian)* 80−40341
- alloys, binary, nonequilib. dynamics, eqns. for supercooling, supersaturation of melt *(Russian)* 78−95736
- alloys, crystallisation, under conditions of temp.-conc. convective mixing of liq. nucleus, impurity distrib. *(Russian)* 80−40342
- alloys, crystallisation, variational approach to continuum theory 80−1951
- alloys, quasiequilibrium crystallisation in rotating systems *(Russian)* 80−16293
- aluminosilicate glasses, Cr_2O_3, TiO_2 and Nb_2O_5 containing, paramagnetic defect formation, ESR study during crystn. 79−65739
- amorphous alloy, and metastable phases, cryst. kinetics, review *(Japanese)* 80−38912
- amorphous alloys, thermal stability, crystn., DSC and elec. resist. study 80−107060
- amorphous ferromagnetic alloys, form. and stability 77−16515
- amorphous materials, laser irrad., electronic struct., one-electron approx. 80−70576
- amorphous metals, struct. imperfections, review of expt. evidence 79−37630
- amorphous semiconductor, elec. cond. obs. of crystn., expt. verification of model 77−20475
- amorphous semiconductors, decomposition 79−41959
- amorphous solid, rapid quenching, techniques for determ. very short room temp. lifetimes 80−84981
- anomalous eutectic, acicular, nonequilib. crystn. anal. *(Russian)* 80−25678
- anthraquinone, UV light effect on nucleation during crystallisation on anthracene surface 80−75478

crystallisation continued

- anthrone, UV light effect on nucleation during crystallisation on anthracene surface 80−75478
- aqueous solution, effect of surface condition on crystallisation in capillaries 79−56037
- p-azoxyanisole, directed crystn. in elec. and mag. fields 80−107052
- basalt rocks, crystallisation temp. determ. using Ni partitioning eqns. 79−88343
- batch agitated crystalliser, design 78−60558
- benzil cored fibres, void-free cryst. growth, X-ray diffr. and optical microscopy study 80−71586
- binary ferro alloys, crystallisation under forced mixing in ingot mould *(Russian)* 79−52192
- binary melt, analytic description with melt diffusion consideration 80−24390
- binary melt, crystallising, thermoconcentrational convection in liq., core 80−6043
- binary melt, solid-liq. zone during crystallisation 80−10131
- binary melt-crystal phase transformation kinetics, stat. modelling of cryst. growth mechanism 80−24389
- binary systems, crystallisation of solid particles due to concentration fluctuations 80−24391
- biophenol-A-polycarbonate, liquid induced crystallisation 80−30125
- biphenyl in low density polyethylene, oriented crystn. 78−9966
- bisphenol-A polycarbonate, crystallization, spherulitic growth of plasticized polymer 80−19726
- bisphenol-A polycarbonate, plasticized, melting and equilib. melting temp. 78−2234
- bisphenol-A-diglycidyl ether epoxies, struct., fracture and mech. response, cure and crystallisation conditions effects 79−15779
- borophosphate glasses, effect of F on props. 78−67657
- borosilicate glass, powder, sintering, foaming by chemical reactions 80−81017
- borosilicate glass containing simulated high level radioactive waste, characterization *(Japanese)* 79−93745
- bounded domain undergoing sequential crystallisation, stress and strain investigation 80−100183
- brine, $MgCl_2$, crystallising, direct contact cooling using kerosene drops 79−1053
- Bushveld Complex, diffusion-controlled crystn. model for Cr content vars. in magnetite 80−56421
- bytownite megacrysts., study of trapped basaltic melts, petrogenetic process study 78−95688
- calcite, crystal intergrowth condensation-crystallisation contact bridge, between dissimilar crystals 79−65332
- calcium oxalate hydrates, crystn. kinetics, comparison for mono-, di-, and trihydrates 80−81528
- capillary shaper, crystn. from melt, stability 78−2037
- caprolactam oligomers, low-mol. wt., crystallisation kinetics from melt, solid structs. *(Russian)* 79−69034
- Ω-caprolactam-ε-caprolactam polymers, vitrification, fusion, crystallisation *(Russian)* 77−47561
- carbide fusion cast ceramics, crystn., microstructures rel. to conditions 80−11638
- carbon tetrachloride, volume effect in metastability of crystalline phases on cooling 79−77716
- casting in space environment, dendrite remelting and macrosegregation in low-gravity 79−47669
- cellular phase separation rate, extremum condition 80−2137
- cellulose, fibres crystallised from hydrazine, texture by X-ray diffr. 79−69030
- cellulose, fibrous crystn., from flowing solns. 80−84106
- cellulose, shish kebab-like structures 77−62485
- ceramics acid-resistant, based on Artemov clay and obsidian 80−20852
- chalcogenide glass, elec. field influence on crystn. process, 60-240°C 77−76315
- chloroform, volume effect in metastability of crystalline phases on cooling 79−77716
- cholesteric mixtures, quasithermal crystn. 80−92652
- cholesteric nonanoate, isothermic crystallisation, microscopic exam. *(Polish)* 80−10651
- cholesterol liquid crystals, activation energy and growth rate of spherolites 79−94900
- cholesterol pelargonate, liq. cryst., crystallisation rate const. and Avrami index 78−94994
- cholesteryl caprinate spherulite growth rate and nucleation rate, optical method *(Polish)* 80−10652
- cholesteryl caproate, isothermal crystn., spherulites growth rate, optical microscopy obs. 79−32892
- cholesteryl caprylate solns. in decane, crystn., electrogravitational effect 77−62496
- cholesteryl laurate, crystallisation kinetics and phase transitions, differential scanning dilatometric obs. 79−69230
- chromites, from India, struct. and comp. 78−44807
- citric acid monohydrate, crystallisation and cryst. growth rate 78−87638
- composite, dispersion hardened, soln. method of synthesis and crystn. 78−3076
- composite material, matrix impurity distrib. in melt crystallisation *(Russian)* 80−100277
- conference, Lancaster, England, Sept. 1979 80−62369
- continuous multi-particle crystal growth in vertical cone 77−69978
- continuously cast billet with cubic cross-section *(Russian)* 78−19735
- controlled, from binary melt *(Polish)* 79−14708
- copoly(ethylene terephthalate/5-methoxyisophthalate), isothermal crystallisation, differential scanning calorimetry 78−30546
- copoly(ethylene terephthalate/isophthalate), isothermal crystallisation, differential scanning calorimetry 78−30546
- cordierite glass ceramics, effect of TiO_2 and ZrO_2 content on phase sequence during heat treatment 78−48381
- cordierite glass-ceramic, effect of crystn. on thermal diffusivity 79−33127
- corundum, Verneuil growth, directional depend. of crystallisation *(German)* 77−35496
- countercurrent melt crystallisation, ultra-pure substance prep. 80−100779
- counterflow crystal. process from melt, US method of monitoring 77−56175
- cryogens, porous solids, gradientless heat transfer, cryogenic liq. crystn. 79−59903
- crystal frequency distribution, simulation taking nuclei distrib. into account 80−100184

crystallisation continued
crystal growth, from liquids at high temps., review 79—15602
crystal growth, modified Czochralski method, variations of impurity distrib. 80—88193
crystal growth from melt, gas evolution and gas bubbles at crystallisation front 78—9980
crystal size distribution, from cascade of mixed tanks 78—39678
crystal size distribution prediction, modelling size dispersion 78—9971
crystal-size distribution, population models, review 80—49153
crystalline polymer, epitaxial crystallisation on surface of drawn polytetrafluoroethylene 78—14626
crystallisation, activation energies of mass transfer at phase boundaries, quantum theoret. calcs. *(German)* 78—67673
crystallisation, chain folding, statistical mechanical calc. 78—2020
cumulate nodules from Lesser Antilles island arc, crystallisation conditions 78—65267
cyclohexane, volume effect in metastability of crystalline phases on cooling 79—77716
deformation during combined sequential and bulk crystallisation *(Russian)* 77—59771
demonstration, teaching aids, convention of secondary school physics teachers *(Hungarian)* 80—67957
dendrite development and growth in very small crystals, Monte Carlo study 80—107683
diamond, high press. with catalyst and solvent *(Polish)* 79—87592
diamond, homogeneous formation in gas phase, laser beam effects *(Russian)* 80—104052
diamond, reactive pulse plasma crystallisation 79—95938
diamond, temperature field dynamics during synthesis 79—38755
diamond synthesis by graphitisation of carbon materials at high press. and temp., Ni influence 80—60795
dibenzyl-tolane, single cryst. growth from melt, influence of supercooling and impurity conc. on growth rate of faces 79—14714
p-dichlorobenzene, contact nucleation 77—52661
1,2-dichlorobenzene, volume effect in metastability of crystalline phases on cooling 79—77716
dielectric crystallisation kinetics, electric field effect, nucleation 80—19919
diffusion kinetics, crystallisation of salts from supersaturated solns. 79—23553
m-dinitrobenzene cored fibres, void-free cryst. growth, X-ray diffr. and optical microscopy study 80—71586
directed crystallisation, two-dimens. approx., numerical soln 80—15021
directional, techniques for calc. distrib. coeffs. from expt. data 78—75606
disjoining pressure repulsion of macroscopic particle ahead of crystn. front. 78—95005
dynamic isomers and spontaneous generation of optical activity, phase rule prediction 79—34421
EBBA, crystallisation and melting of metastable solid crystalline phases 78—2240
education, metallic glasses, phase transition and mech., elec. and mag. props. 78—36765
electric field effect on dielec. crystn. parameters *(Russian)* 77—55338
electrocrystallisation, chess board type computer simulation 80—54157
electrocrystallisation, galvanostatic transients, crystn. overvoltage 78—76867
electrocrystallisation, impedance frequency dependence, in the case of DC superposition 78—51844
electrocrystallisation, nucleation, phase form., symposium, Southampton, England (Dec. 1977) 80—51942
electrocrystallisation, nucleation and growth mechanism, ohmic overpotential effects, simulation 78—51842
electrocrystallisation, nucleation and growth mechanism, ohmic overpotential effects determ. 78—51843
electrocrystallisation, recent progress in electrochem. and physical methods *(French)* 80—7510
electrocrystallisation, twinning nucleation, mechanism 77—62495
electrocrystallisation noise, phenomenological model 78—51845
electrolytic crystal growth, role of screw dislocations 80—54540
enstatite-type glass-ceramic, crystn. kinetics and mechanism 77—55241
epitaxial growth from solution in melt, crystn. theory 80—16204
equilibrium properties of crystallising systems, theoret. interpret. of cryst. growth mechanism *(Rumanian)* 80—88073
ethanol-water system, metastable states, hydrates existence and props., low temp. 78—71835
α,ω-ethoxy-poly(ethylene oxide), crystallisation 77—51329
ethylene-vinyl alcohol copolymer, drawn samples, annealing effect around T_g temps. on shrinkage and mol. orientation 80—79712
Eu-Ag alloy, amorphous, formation and mag. props. 79—91216
eutectic colony growth, stability in presence of external perturbations *(Russian)* 80—16291
eutectic systems, condensed, course of crystallisation, computer calcs. 77—86018
face effect, with paraboloidal or ellipsoidal isotherm effect 80—107085
FCC crystal formation, soft-core model, geometrical anal. of crystallisation 78—42939
ferrite formation during calcining of sulphate mixture 77—63608
fibre reinforced composite prep. by crystallizing metallic and metal-ceramic eutectics *(Polish)* 79—20008
fibrous amphiboles, hydrothermal crystn. from talcs in NaOH soln. 80—20810
flexible chain polymer, topomorphism and phase dualism 78—14265
flow-induced, conf., Midland, Michigan, USA, Aug (1977) 79—82161
fluoramphibole fibres, synthesis by unidirectional crystn. 80—2941
fluorite, crystal intergrowth condensation-crystallisation contact bridge, between dissimilar crystals 79—65332
fluorophlogopite mica, glass-ceramic, thermal diffusivity, crystallisation effects 78—6190
fluorophosphate system glasses alkali free and crystn. products, struct. and IR spectra 79—94913
flux growth, crystn. conditions expt. method *(French)* 77—63552
fractional, in layered intrusions formation, computer simulation 77—33069
fractional crystallisation, applying very high pressure 80—100775
front interaction with turbulent alloy melt stream, heat exchange *(Russian)* 80—74708
front movement calc. in form of plate in melt *(Russian)* 77—21130
gas phase transport, definition of hydrodynamic regime acquired during crystn. 79—51029
gehlenite glass, crystallisation kinetics 79—4251
gelatin, aq., crystn. and melting 79—61914

crystallisation continued
glass, crystallisation and nucleation of reheating 80—84078
glass, crystallisation and opacity, exam. by high temp. viscometry and X-ray diffr. *(Polish)* 78—84875
glass, crystallisation-chemical composition relation, regressional analysis *(Polish)* 77—16535
glass, electrothermal props. in structural transform. zones *(French)* 80—88047
glass, phase separation and glass structure concept changes, review 77—65955
glass, struct. formation during crystallisation, Mossbauer obs. 77—48106
glass ceramic, bonding thermosprayed Si 78—23848
glass ceramic, form. characts. in slag glasses 77—8794
glass ceramic, nucleation and growth studies by small angle neutron scatt. 79—32913
glass ceramic mineralogy 80—60826
glass ceramic prep. by hot pressing and crystallisation of glass powder, mech. props. 78—15351
glass ceramics, transient heterogeneous nucleation 80—88042
glass chip, reducing agent effect 78—46736
glass fibres, aluminosilicate, crystn. during heat treatment 79—52258
glass forming liquids, nonisothermal crystallisation kinetics 79—51001
glass forming melts, crystn. kinetics processes 80—64905
glass forming systems, induced crystallisation, transient heterogeneous nucleation 80—64903
glass technology and applications, review of advances 77—66618
glass-ceramics and photosensitive glass, microstructure rel. to properties *(German)* 80—38926
glass-crystal transition energetics, Piloyan's method appl. 80—38916
glasses, refractory, obtained by hot pressing of gels, crystallisation *(French)* 78—11193
glasses and melts, nonisothermal, kinetics 79—94914
granitic magma of Bushveld Complex, crystallisation history as revealed by trace element abundances 80—109145
graphite, crystallisation from molten metal solns. *(Chinese)* 79—91634
graphite, from C melt, review 80—89165
growth affinity, a driving force for crystallisation 79—23554
growth curves, growth affinity presentation, for growth from soln. 79—27936
growth models, attachment energy as habit controlling factor 80—59420
growth rates, size depend., steady-state data, population balance calcs. 77—89394
guanyl ribonucleases of fungi, crystn. and X-ray diffr. 78—71718
gypsum, crystal intergrowth condensation-crystallisation contact bridge, between dissimilar crystals 79—65332
gypsum, crystallisation 80—100766
hardness, elastic moduli, density, cryst. temp., mech. props., for flywheel appl. *(Dutch)* 78—52878
heat resistant monocrystal growth apparatus, heat regimes, crystallisation *(Russian)* 80—107071
heat transfer during crystallisation on cooled wall with forced convection in melt 78—26022
heat transfer during crystallisation on vertical wall with thermal convection in melt 78—26021
Helmholtz free energy, crystn. of phase A from A+B melt 80—79911
hexachloroparaxylene, crystn. from heptane, optimising purification 80—100774
high moleculer weight, fibril structure induced by oriented crystallisation *(Japanese)* 79—90575
homogeneous, and heterogeneous nucleation processes for substance of different crystn. struct. 80—49144
homogeneous solid solution crystallisation crucible 80—45224
ice, crystallisation and melting rate in laminar stream of liquid 80—100770
ice, growth beneath water film, air bubble precipitation 78—83922
ice, heterogeneous crystallisation, of supercooled water, role of adsorption 79—95125
ice, on CuS aerosol prepared by burning pyrotechnic mixture, freezing temps. 78—96279
ice, water and gas bubble distrib. on crystallisation front movement 78—22830
ice crystal morphology, vapour growth, influence of vapour diffusion and heat diffusion 80—64933
icicles, examination between crossed polarizers, growth mode determination 79—41995
icicles, growth mechanism, structure and shape 80—59423
impurity role, in crystn. 80—49146
impurity trapping during dendritic crystal growth, computer simulation 78—38992
impurity trapping during dendritic crystal growth, expt. 78—38993
industrial, using geothermal power, feasibility assessment 79—48086
industrial crystallisation, conference, Warsaw, Poland (Sept. 1978) 80—46737
industrial crystallisation, progress in cryst. growth from soln. 80—49147
ingot, continually cast, optimum conditions for variable drawing rate *(Russian)* 79—70056
ingot, heat exchange between melt stream and crystn. *(Russian)* 79—69043
ingot, hollow cylindrical, temp. field and crystallisation front calc. *(Russian)* 78—63690
ingots in contact *(Russian)* 79—29039
instability zone rel. to new phase preformation and nucleation 78—10169
insulating films, on Si, struct. stability 80—54564
interface morphology during crystallisation, single filament unconstrained growth from pure melt 78—52787
interface morphology during crystallisation, single filament unconstrained growth from binary alloy melt 78—52788
Invar N36 melt, cast metal struct. depend. on heat treatment, subgrain struct. *(Russian)* 80—40343
IR emission spectra, during crystn., distinguishing features 80—1952
kinetic coefficients, of crystn. process 80—100188
kinetics, review, book contrib. 77—39550
kinetics, soln. pH effect 79—99095
Kolmogorov statistical model, monolayer, for cryst. vaporisation kinetics, pt.I 79—95151
Kolmogorov statistical model, monolayer, for cryst. vaporisation kinetics pt.II 79—95152
Landau theory, solidification and cryst. nucleation 78—83761
lead germanate glass crystallisation study by infrared spectrophotometry 80—6499

crystallisation continued
- Lennard-Jones 12-6 system, triple pt. props., mol. dynamics simulation 78—2231
- leucosapphire, supercooling and crystn. temp. determ. 79—51237
- Li_2O-Al_2O_3-SiO_2, effect of ZrO_2 on crystn. 77—16534
- linear hydrocarbons, cryst. nucleation and cryst.-melt interfacial tension 79—69024
- liquid, undercooled, Gibbs free energy change for crystallisation 80—25676
- liquid metal continuous casting, solidification process, convective heat transfer, anal. 78—84789
- lithium polyisoprene, struct. regularity and crystn. 80—103269
- lunar basalts, chemical differentiation by gravit. separation of quenching crysts. 77—60649
- lunar basalts, expt. crystallization at low press., Fe gain and loss problems 77—87293
- macroionic solution, plus counter ions, Kirkwood theory, mean field phase transition 78—38812
- macromolecular crystallisation, kinetic statistical theories *(Chinese)* 77—84683
- macromolecules, crystallisation thermodynamics, various degrees of coiling 78—51445
- macromolecules, epitaxial crystallisation, review 79—42409
- macromolecules, flexible, flow-induced crystallisation, nonhomogeneous shear rates effect 80—38952
- magmatic rocks, anchieutectic comp. 80—12381
- magnetic field effect *(Russian)* 79—37641
- melilith glass, crystn. temp. rel. to cryst. habit *(German)* 78—6017
- melt, heat convection *(Russian)* 78—15385
- melt crystallisation in self-excited vibr. regime 80—103275
- melt crystallizing with conc.-depend. convection, impurity distrib. 80—10642
- melt near solid-liquid interface, diffusion during crystallisation *(German)* 79—29046
- melting surface dynamics, phase boundary configuration calcs., moving heat source *(Russian)* 80—54342
- metal, FCC, modelling of growth from melt *(Russian)* 78—60664
- metal, FCC, with fibre texture, X-ray method of twin fault probability determ. 79—87817
- metal, freezing at mean heat exchange intensity in irregular mode stage *(Russian)* 79—52193
- metal, liquid crystallisation, fluidity resistance effects *(Russian)* 77—55957
- metal and alloy crystallisation, apparatus for decanting solid and liquid phases 78—56597
- metal refining by crystallisation and reflux, three component Raoultian behaviour 77—28799
- metal Taylor wires, texture and metastable phases 77—8812
- metal-metalloid amorphous systems, thermal instability, crystn. characts. 77—4044
- metallic alloy glasses, continuous cooling versus isothermal transformation diagrams, critical cooling rate 80—15012
- metallic glass, continuous-heating transform. diagram from isothermal time-temp. diagram 77—47558
- metallic glass, density and Young's modulus, struct. relax. effects 78—72804
- metallic glass, hardness, elastic moduli, density, cryst. temp., mech. props., for flywheel appl. *(Dutch)* 78—52878
- metallic glass crystallisation, appl. of Grange-Kiefer transform. method *(Hungarian)* 79—73105
- metallic glasses, annealing behaviour, thermal stability and crystn. 80—75167
- metallic glasses, crystn., thermosonimetric investigation 80—75180
- metallic glasses, mats. props. review 77—4043
- metals, crystal growth, electrochem. Czochralski method, growth rate limitations 78—88433
- metals, electrocrystallisation and passivation kinetics, multiple stationary states and dissipative structs. theory *(French)* 80—7804
- metals, glassy, structure, transport props., magnetic behaviour, review 80—70138
- metals, supercooling on homogeneous crystn. *(Russian)* 80—19914
- metals and alloys, crystn. process, X-ray fluoroscopic obs. 80—50620
- metastable crystal forms, crystallisation behaviour 79—86733
- Metglas 2826 ribbon, voids formation during crystallisation 80—108428
- Metglas 2826A, direct meas. of decomp. on crystn. by X-ray microanal. in STEM 79—48025
- migration of salts in a porous medium allowing for their crystallisation *(Russian)* 78—87388
- mineral crystallisation, barometric investigation autoclave 77—86241
- minerals, magnetic trends on alkali-Fe-Mg diagrams 78—85551
- Mullins-Sekerka instability, and pattern formation 80—35064
- mullite, crystallisation from SiO_2-Al_2O_3 melts 78—47243
- Na zirconogermanates hydrothermal crystn. 79—47604
- naphthalene-catechol eutectic struct., crystallisation behaviour 79—55868
- naphthalene-p. chloronitrobenzene system, eutectic, solidification 78—64530
- naphthalene-p-chloronitrobenzene eutectic system, phase diagrams and crystn. 77—47551
- natural mineral crystal growth characts. 78—32072
- nepheline concentrate, low Fe, phase composition 77—21110
- neutron activation anal., geochem. of genesis of ore deposits *(German)* 80—30301
- Nichrome based dispersion hardened material, Ti, Y, Zr addition effects on crystallisation *(Russian)* 79—74143
- n-nitroaniline, UV light effect on nucleation during crystallisation on anthracene surface 80—75478
- noncrystalline solids conf. Lyon, France (Dec. 1976) *(French)* 77—72560
- nonisothermal devitrification kinetics 80—92465
- nucleation of crystallization centres, low frequency vibration effects on rate *(Russian)* 78—15383
- Nylon 6, injection moulded, residual stresses 80—38950
- nylon 6, oriented glassy, mol. wt. influence on cryst. rate 80—44156
- Nylon 6, solution crystallization 79—86719
- nylon 6 fibre, melt spun crystallisation *(Chinese)* 79—14792
- nylon-11, folded-chain crystal, pressure-induced crystallisation from melt, annealing 77—84671
- nylon-12, folded-chain crystal, pressure-induced crystallisation from melt, annealing 77—84672
- nylon-6, chain extension mechanism during crystallisation under press. 77—56008

crystallisation continued
- nylon-6, pressure-crystallised, morphology and structure 77—84669
- Nylon-6, shish-kebab struct., obtained from quiescent soln. by self seeding 80—15017
- nylon-6 dilute soln., gelation and crystallisation, struct. determ. 79—37635
- nylon-6 pressure-crystallised, annealing under pressure 77—84670
- oligoethylene glycol, crystallisation kinetics in presence of tetrachloromethane, NMR investig. *(Russian)* 80—54153
- optical glass, melting, fining, surface tension, diffusion, nucleation in microgravity 80—81016
- partition coefficients, theoretical calc. of isovalent impurities with due regard for excess entropy of mixing in solid soln. and melt 79—65015
- percolation theory, Lindemann melting criterion and thermodynamic props. 79—28081
- periodic density patterns as uniform fluid crystallizes 80—107404
- periodic mass crystn., kinetics and max. supersaturation *(German)* 79—41997
- periodic structure homometric set, search algorithm 80—75118
- peritectic structure formation criteria *(Ukrainian)* 80—11636
- peritectic systems with separate crystallisation of phases, number of phase constituents, calc. *(Ukrainian)* 80—25702
- PET, crystallised by nonreactive liquids, exam. of mech. props. 79—43338
- PET, crystallised in liquid environment, exam. of crystallisation kinetics and X-ray scattering 79—41980
- PET, crystallization, lamellar growth kinetics and thickness 80—103266
- PET, densification, cryst. perfection, mechanism 79—66082
- PET, stress induced crystallisation, X-ray and light scattering obs. 79—99083
- PET film, crystallised by nonreactive liquids and vapours, exam. of diffusion of liquids and vapours 79—42314
- phenocrysts and megacrysts in basalts of Pinacate volcanic field, textures and genesis 77—81881
- piperidine solution of PbI_2, crystn. of intercalation cryst. 80—16170
- plane front stability in single component system 77—31616
- planetary system evolution from preplanetary gas disc, rel. to crystallisation and cryst. struct. *(German)* 78—93129
- polethylene-polypropylene blend, extruded, thermal swelling and mech. characterisation 80—81110
- poly(dimethyl siloxane), networks formed by gamma irradiation, crystallisation 77—51330
- poly(ethylene oxide), spherulite growth rate determ. method 77—62493
- poly(ethylene terephthalate), stress-induced crystn. from melt, optical studies 80—84113
- poly(ethylene-but-1-ene) copolymer, gelation and precipitation from solutions, NMR exam. 79—43641
- poly(ethylene-oxide), isothermal growth, thickening, melting, bilayer crysts. and chain end effects 80—38939
- poly(m-xylylene adipamide), crystallisation induced by water absorption *(Japanese)* 79—90573
- poly(m-xylylene adipamide), crystallised by water absorption, morphology *(Japanese)* 80—24378
- poly(m-xylylene adipamide), water induced crystallisation *(Japanese)* 79—90574
- poly(p-phenylene terephthalamide), quiescent and strain induced crystallization from H_2SO_4 soln. 79—90571
- poly(vinylcarbazole), stress-induced crystn. from melt, optical studies 80—84113
- poly(vinylidene fluoride), melting and crystn. temps., press. depend., DTA meas. 79—90568
- poly 2,6-dimethyl-1,4-phenylene ether, liquid-induced crystallisation 78—30551
- poly-1-butene, sheared melts, nucleation and crystal growth meas. 79—69027
- poly-ε-caprolactone, melt, crystallisation kinetics, shear effects 79—69021
- poly-ε-caprolactone-PVC blends, crystallisation kinetics 79—69020
- poly-bis-phenyl glutarate diacetylene, cryst., solid-state synthesis, struct. 79—15638
- poly-m-phenylene isophthalamide-ε-caprolactam, complex polymer cryst. 78—9967
- poly-tetramethyl-p-silphenylene-dimethylsiloxane block copolymers, crystn., morphology, kinetics 79—14695
- polyalkane imides, crystallisability, supermol. and crystalline structures 80—84100
- polyamides, preoriented, method for increasing elastic moduli 77—80425
- polyamidoimide film, thermomech. props. rel. to mol. struct. *(Russian)* 79—57029
- polybromoprene, crystn., morphology, kinetics *(Russian)* 79—4256
- high cis-,1,4-polybutadiene, orientation effects induced by shear rate in capillary extrusion 77—48389
- 1,4-polybutadiene, stress-induced crystn. from melt, optical studies 80—84113
- polybutene-1 glass, Raman spectra, low temp. crystallisation *(French)* 79—99875
- polybutylene terephthalate, melt crystallised, solvent crystallised films and moulded bars, morpholigical obs. 80—84101
- polycaprolactam, crystallisation effect on adhesion to Al 77—66742
- polycaprolactam, pure and TiO_3 filled, radiation effects *(Bulgarian)* 79—33015
- polycaprolactam film, subjected to 9 kV elec. discharge, X-ray obs. *(Russian)* 79—23536
- polycarbonate, struct. ordering changes after annealing 79—94921
- polycrystal, linear, E and G moduli, crystallisation effect *(German)* 80—59556
- polydiacetylene, extended-chain crysts., struct. and morphology 79—82165
- polydimethylcarbosiloxane net-type, crystallisation, NMR obs. *(Russian)* 77—20744
- polydioxolan, crystallisation, morphology and melting props. 78—14297
- polydioxolan, crystn. kinetics, dilatometric analysis and microscopy obs. 80—79706
- polydiphenylgermylene, crystn. from chem. transport reaction 80—104439
- polyester filaments, solvent-induced crystallisation 78—83754
- polyester-organic solvent mixtures, phase diagrams, eutectic props., devitrification, crystn. *(French)* 80—3015
- polyesters, epitaxial crystallisation, on organic and inorganic substrates 78—91565
- polyesters, thermotropic, quiescent crystn. 80—38937
- polyether sulphone, evidence for crystallinity 80—28928

crystallisation continued
polyether-polyester elastomers, differential scanning calorimetry, crit. points *(Japanese)* 80—75344
polyethylene, chain defects influence on crystn., reference to cryst. size and perfection 80—38942
polyethylene, comonomer unit partitioning, crystn. conditions effect 80—38943
polyethylene, crosslinked, super-oriented crystallisation under const. stress *(Japanese)* 78—34443
polyethylene, crosslinked networks, stress-induced crystallisation, theory 77—24277
polyethylene, crystallisation at high-pressure, obs. using new dilatometer *(Russian)* 77—17950
polyethylene, crystallisation kinetics, use of DSC, comparison with dilatometry 77—31601
polyethylene, crystallisation of thick film from glassy state by annealing 80—54151
polyethylene, crystn. at high press., small-angle neutron scatt. 77—55248
polyethylene, crystn. under high pressure 80—38946
polyethylene, electron microscopy with chlorosulphonation aid 77—89351
polyethylene, extended-chain cryst., high-press. crystallisation and melting obs. 77—27985
polyethylene, fibrillar, high mol. wt., oriented crystallisation, heat treatment effect *(Japanese)* 80—25738
polyethylene, from the melt, small-angle X-ray scatt. study of crystn. 79—14692
polyethylene, hexagonal, high press. crystn., review 79—23529
polyethylene, high density, crystallisation struct. revealed by solvent extraction 78—42922
polyethylene, high density, film, melt growth, cryst. superstruct., small angle light scatt. 77—31602
polyethylene, high density, inorganic filled, calendered sheet, crystallisation in capillary viscometer *(Japanese)* 77—70112
polyethylene, high density, oriented extended chain crystals, transparency *(Japanese)* 80—38955
polyethylene, high modulus filaments, form. from melt, cryst. nucleation effects 79—70034
polyethylene, hydrostatically compensated, SRO in precrystallisation phase 79—69033
polyethylene, lamellar structs. nucleated onto fibrous substrates for high modulus 78—75578
polyethylene, linear, ^{13}C spin-lattice relaxation 80—25235
polyethylene, linear, bulk-crystallised, morphology study 79—32918
polyethylene, linear, crystallised from melt, effect of crystallisation time on density, mech. props., X-ray scattering 80—25680
polyethylene, linear, melt-crystallised sharp fraction, lamellar morphology, electron microscopy obs. 80—84099
polyethylene, low density, melting and crystallisation, DSC characterisation 80—64927
polyethylene, low density, morphology and props. 80—64926
polyethylene, low-density, automated light-scattering apparatus 77—53969
polyethylene, mixed morphology and linear fractions, light scatt. obs. 78—2023
polyethylene, molecular clustering in mixtures with polyethylene-d_n, small-angle neutron scatt. 78—26451
polyethylene, MP, heat of fusion, degree of crystn. determ. by differential scanning calorimetry *(Russian)* 77—62489
polyethylene, oxidation rel. to spherulitic crystn. *(Russian)* 78—71689
polyethylene, pulsed NMR study of crystallization kinetics from melt and soln. 79—87624
polyethylene, quenched melt, factors controlling lamellar thickness 77—62484
polyethylene, radiation effects on EPR and differential thermal anal. *(Bulgarian)* 79—46698
polyethylene, rapid crystn. from melt rel. to struct. 80—44152
polyethylene, shish kebab structure, formation mechanism 78—14286
polyethylene, sp. ht. after annealing at low temps., cryst.-melting phenomenon interpret. 77—39679
polyethylene, spherulitic, nonexponential transformation equation 78—67662
polyethylene, stress crystallised, melting behaviour 77—47554
polyethylene, ultrahigh draw ratios, mol. wt. effects 79—74211
polyethylene crystal, longitudinal growth in flowing soln., melting of continuous fibrillar crystal 80—19917
polyethylene crystals, soln. formed, low mol. weight, swelling 79—94920
polyethylene films, hard elastic, deform. mechanism 77—32652
polyethylene flow crystallisation, in extensional flow developed by convergent capillaries, props. 80—84111
polyethylene fractions, quasi-binary systems, solidification and crystn. 80—84108
polyethylene melt, cryst. kinetics during cooling, nucleation density effect 80—100181
polyethylene melt, lightly crosslinked, crystn. under uniaxial compression, stretching 80—38957
polyethylene melt spinning, extensional flow induced crystallisation 78—55818
polyethylene oxide, block polymer, crystallisation 79—10817
polyethylene oxide, melt, crystallisation kinetics, shear effects 79—69021
polyethylene oxide trioxane mixtures, eutectic crystallisation 78—56626
polyethylene ribbons, flow-induced crystn. from melt, in dies fed by single screw extruder 80—84110
polyethylene spherulites, lamellar struct. obs. 78—30547
polyethylene surface-growth fibres, hot drawing 80—97517
polyethylene terephthalate, crystallisation kinetics from glassy state 78—75579
polyethylene terephthalate, differential scanning calorimetry of melting, mosaic block struct. of cryst. layers 78—26452
polyethylene terephthalate, effects of preliminary ht. treatment on crystallisation *(German)* 78—75593
polyethylene terephthalate, induced crystn. on metallic nucleating particles 79—15658
polyethylene terephthalate, nonisothermal crystallisation kinetics 79—32920
polyethylene terephthalate, oriented, amorphous, stress-induced crystn., shrinkage meas. 80—92466
polyethylene terephthalate, thermal diffusivity, conductivity meas., crystallisation rel. to glass transition 77—47632
polyethylene terephthalate, uni- and biaxially drawn films, preferred planar orientation 78—80590

crystallisation continued
polyethylene terephthalate sheeting, storage in aqueous media rel. to props. *(German)* 79—29250
polyethylene terephthalate-co-isophthalate, gelation and crystallization 80—24377
polyethylene-paraffin mixtures, crystallisation kinetics 79—41985
polyethylene-polystyrene blends, crystn. characts. 80—103261
polyethylene/polypropylene blends, surface growth of fibres and films 80—66470
polyethyleneterephthalate film, influence of crystallisation on adhesive and cohesive props. 79—56100
polyhexamethylene sebacate-poly 2-methyl-2-ethyl-1,3-propylene sebacate, cryst. multiblock copolymers, crystallisation 78—91269
polyhexamethylene terephthalate/polyoxytetramethylene block copolymers, melting and crystallisation 78—91260
polyisobutylene fibres, stretched, crystn. kinetic study using synchrotron radiation 80—33909
polyisoprene, from guayule rubber, TEM exam. of crystallisation 80—10508
trans-1,4-polyisoprene, kinetics of thin film growth from melt 80—10505
trans-1,4-polyisoprene crystals, press. effect on growth rate 80—88064
trans-1,4-polyisoprene crystals, press. effect on melting temp. and lamellar thickness, press. crystn. 80—88302
polymer, crystallisation, chain folding, statistical mechanical calc. 78—2020
polymer, crystallisation from melt at large undercoolings, kinetics 80—28925
polymer, crystallisation rates from melt, universal relation 79—10816
polymer, crystallising, defects and mech. relax. *(Russian)* 78—22789
polymer, crystn. at low supercooling 79—10823
polymer, crystn. rate eqn., effect of vol. relax. of amorphous material 77—62482
polymer, deformation effects 80—10504
polymer, fibrous crystallisation, chain extension and fibre form. 78—75573
polymer, high-modulus, behaviour in solid state, nonlinear irreversible thermodynamics approach 80—44154
polymer, mixed heterogeneous homogeneous nucleation and nonintegral exponents of time 78—55820
polymer, orientational ordering rel. to mech. props. *(Russian)* 78—59766
polymer, row nucleation, phenomenological model 78—14301
polymer, shear-induced crystallisation, optical study 78—14289
polymer, stressed, config. free energy change due to partial crystn. of chains, distrib. of cryst. orientations 79—94923
polymer blends, morphology and compatibility, X-ray and optical obs. 79—69026
polymer crystal growth, during annealing 78—14300
polymer crystallisation, growth rates, nucleation, annealing and random copolymer crystallisation 78—51435
polymer crystallisation, natural and artificial heterogeneous nucleation 78—51431
polymer crystallisation, review 78—51430
polymer crystallisation, review 80—64925
polymer crystallisation, thermodynamic analysis of nucleation *(Russian)* 77—19881
polymer crystallisation and fusion, conf., Louvain-la-Neuve, Belgium (1976) 78—51429
polymer crystals, topomorphism 77—43159
polymer fibres, ultra high modulus, prep. by soln. and melt spinning, review 79—11544
polymer fibrils, formation by flow-induced crystallisation 80—33908
polymer film, crystallisation induced by biaxial stretching during manufacture 79—82164
polymer lamella structure, crystallisation under high supercooling 79—69028
polymer melting, theoretical aspects 80—59633
polymer melts, crystallisation from melt 80—84107
polymer melts, crystallisation models, Avrami eqn. extension 80—19723
polymer microstructure morphogenesis, book contrib. 78—83757
polymer molecules crystallisation, surface area estimation and secondary nucleation theory 77—89396
polymer network, crystn. and form. through crystn., crystallinity influence on radiation induced form. 80—38964
polymer solution, dissolution rates and polymer-solvent system phenomena *(German)* 80—13167
polymer solution, short-range order and solvent crystallisation; spectroscopic and microcalorimetric, methods *(Russian)* 78—26416
polymer systems, crystallisation from solution 80—84105
polymer systems, crystallisation kinetic data, status of anal. 80—84104
polymer systems, flow-induced crystallisation, conference, Midland, MI, USA (Aug. 1977) 80—82576
polymer-metal adhesive bonds, shear resist., polymer crystn. effect 80—89462
polymers, amorphous, segmental distrib., crystallisation and viscoelastic relax. meas. 78—51443
polymers, crosslinked networks, stress-induced, crystallisation, theory 77—24277
polymers, crystalline, bulk, lamellar struct. and plasticity mechanisms 77—65957
polymers, crystallinity, characts., effect on props. 79—55673
polymers, crystallisation, morphology rel. to props., review 77—39546
polymers, crystn. under mol. orientation, formation of stacked lamellar structs. 80—84109
polymers, frictional props., crystn. effect 80—40551
polymers, linear, melt crystallisation, intrachain trans double bonds influence 79—14701
polymers, strain crystallised, electron microscope obs. of molecular struct. 78—26450
polymers, stressed, thermodynamically controlled cryst. orientation 80—84112
polymers, under extreme temp. and press. gradient 79—82163
polymers 79—82162
polyoxyethylene-glutaric acid eutectic, melting and crystn. 80—28924
polyoxymethylene, epitaxial crystn. during trioxane polymerisation 79—55676
polyoxymethylene, kinetics of epitaxy and over-growth on needle-like single crystals 78—14291
polyoxymethylene, rapid crystn. from melt rel. to struct. 80—44153
polyoxymethylene diacetate, bulk cryst. and melting, polyoxyethylene additive effects 79—32921

crystallisation continued
polyoxymethylenes, determ. of crystalline fraction from X-ray diffraction 80—44150
polypentenamer, thermodynamics *(Russian)* 77—21386
polypropylene, flow-induced crystn. from melt, in dies fed by single screw extruder 80—84110
polypropylene, impurities redistribution during crystn. 78—75577
polypropylene, isotactic, epitaxial crystn. on alkali halide surface 78—26787
polypropylene, isotactic, low temp. annealing, differential scanning calorimetry obs. 80—60895
polypropylene, isotactic, shear induced β-form crystallisation 78—18555
polypropylene, isothermal crystn., effect of contact with fibrous substrates 80—79708
polypropylene, shear effect on crystallisation *(German)* 78—75586
polypropylene oxide, isotactic, crystallisation, heterogeneous nucleation, interfacial energy effects 79—69023
polysilicic acid, IR spectra, struct., crystallisation effects *(Russian)* 78—72528
polystyrene, isotactic, morphology and growth of chain struct. *(German)* 78—75597
polystyrene, isotactic, orientation of remaining amorphous chains during crystallisation 80—10506
polystyrene, isotactic, spherulite radial growth retardation by SiO$_2$ nucleation 80—107066
polystyrene, soln. grown isotactic crystals, degree and distrib. of crystallinity, thermal stability 78—9964
polystyrene, solution grown isotactic crystal, thermal change kinetics study by X-ray diffr. 78—9965
polystyrene+poly(2,6,-dimethyl phenylene oxide), isotactic, crystallisation and melting 78—18554
polystyrene blends, isotactic and atactic, small-angle X-ray scattering 78—55817
polystyrene in tetrachloroxylene and tetrachlorobenzene, morphology of crystallized additives 79—99082
polystyrene-b-isoprene-b-styrene, struct. regularity and crystn. 80—103269
polystyrene-polyethylene oxide, cryst. multiblock copolymers, crystallisation 78—91269
polystyrene-tetrachloroxylene(tetrachlorobenzene) glassy solns., additive morphology rel. to mech. props. 79—65007
polyvinyl alcohol, crystallisation from dil. soln. by stirring *(Japanese)* 77—89388
polyvinylidene fluoride, crystallisation, α-polymorph equilib. melting point, heat of fusion determ. 77—4054
polyvinylidene fluoride, crystn. process and elec. cond., differential scanning calorimetry 79—24024
polyvinylidene fluoride, direct obs. of cryst. transform. process under high press. 78—38630
polyvinylidene fluoride, high-press. melting and crystallisation 78—91422
polyvinylidene fluoride, melt-solidified, crystn. and morphology 80—103461
polyvinylidene fluoride vinyl fluoride copolymer, epitaxial crystallization 79—65005
prefluorinated polymer, DuPont Krytox 143-AB, viscoelastic and dielectric props. 80—1503
proteins, effect of protein conc. and solubility on nucleation rate 78—87632
proteins, globular, cryst. growth kinetics 80—35823
PTFE, annealing effect on melting and crystallisation *(Japanese)* 80—20980
purification optimisation, by crystn. 80—100774
PVC, highly syndiotactic, X-ray diffr. and IR studies of annealed material, crystallinity 78—2022
PVC, influence of thermal history on physical props. 79—4984
quartz, crystal intergrowth condensation-crystallisation contact bridge, between dissimilar crystals 79—65332
quartz, cultured, prism faces growth and development, attached microcrystals role 77—31612
quartz, growth from soln., mechanism 78—83763
quartz, hydrothermal crystallization at 250°C and 15 kbar, mechanisms 78—49014
quartz, synthetic, Al centres conc. and anomalous pleochroism depend. on crystn. parameters 80—107311
quartz, synthetic, crystallisation and defects *(Chinese)* 79—69041
quartz glass, effect of fusion temp. and time 77—36441
quartz glass, effect of O vacancies and hydroxyl-group concs. on crystn. 77—16533
quartz glass, water vapour influence on crystn. stability 77—36440
quartz glasses, in different gaseous media 77—24269
quartz glasses, viscosity rel. to crystallisation 77—24386
rare earth chromite based electrode material development for MHD generators 80—84893
rare earth glasses, R$_2$O$_2$S-Ga$_2$S$_3$, (R=La to Nd), exam. of preparation and props. *(French)* 78—80504
rare earth metal oxide films, crystallisation, electron microscope obs. 79—15034
rare earth oxide (R$_2$O$_3$)-M$_x$O$_y$ glassy systems (M=Ti,Nb,Ta), rapid quenching by laser beam, exam. of composition and crystallization 78—52856
rare earth-3d transition metal amorphous alloys, crystallisation behaviour 80—49116
rare earth-gallium sulphide system glasses *(French)* 77—19877
rare earth-iron alloy amorphous film, crystn., TEM obs. 79—87019
regular eutectic composite, plane faced growth criterion *(Russian)* 79—56968
rotating container melt growth, crystallisation parameters calcs. 80—103285
rubber, natural, oriented, crystallisation kinetics and melting 78—75554
rubbers, cross linked, thermodynamic approach to stress induced crystallisation 79—41984
sapphire rod, crystn. from melt, capillary conditions 78—3020
saturated solution evaporation, crystallisation by epitaxial nucleation *(French)* 77—35831
secondary boundary formation during crystn. *(Russian)* 77—59767
semiconductor crystn. in constant electric field, thermoelectric parameters 77—44146
single crystal growth, techniques 80—108341
SiO$_2$-Al$_2$O$_3$-MgO(-K$_2$O-F) glass ceramic crystn., microstructures rel. to conditions 80—11638
size dependent crystal growth, new empirical kinetic equation 78—38637

crystallisation continued
size dependent crystal growth, two parameter kinetic equation 79—65016
sodalite single crystals, exam. of growth mech. in hydrothermal method, using SEM 79—52105
sodium aluminium tartrate, β-particle effects on crystallisation from aq. solns. 77—36387
Sodium ammonium tartrate, L- and D-mol. energy difference, parity violation 78—25744
soft-core model, geometrical anal. 79—42220
solid solution, single cryst. growth from melt, role of composition fluctuations 79—8239
soluble inorganic salts, crystal-solution interfacial tension, from crystn. meas. 79—69045
solute redistribution during crystallisation, interface field effects 80—84119
solution concentration, interconversion during crystn. 80—100773
solution crystallisation, US viscosities 80—100189
solvent crystn. in polymer-solvent systems, state diagrams *(Russian)* 79—52185
sorbitol, crystallisation, thermal investig. 78—47257
spherulite growth rate determ. method 77—62493
spherulitic, nonexponential transformation equation 78—67662
β-spodumene-mica glass ceramics, phase evolution and TiO$_2$, MgF$_2$ additive effects, exam. 78—44089
spontaneous, diffusion kinetics *(German)* 77—51334
stability during capillary shaping, general theory of capillary and thermal stability 80—107076
stability during capillary shaping for arbitrary small perturbations 80—107077
stability limit at low temp. 79—7539
statistic model 77—15332
steatite ceramic, sintering and crystn., depend. on original powder state 79—61527
steel, alloy, high C, amorphous, produced by rapid quenching from melt, hardness and strength 78—59764
steel, alloy, type Kh16N11M3, struct. changes during thermocyclic working, dislocation struct. *(Russian)* 80—54243
steel, austenitic, wire rod, austenite transform. kinetics accompanying interrupted cyclic cooling *(Russian)* 79—70064
steel, C-Cr(MO)(W), high-C, amorphous crystn. behaviour *(Japanese)* 79—94911
steel, C-Cr-Mo(Cr-W)(Mo-W)(Cr-Mo-W), high C, amorphous crystallisation behaviour *(Japanese)* 79—94911
steel, nonmetallic inclusion segregation during cooling *(Russian)* 80—100330
steel, W-Mo-Co, high-speed tool, struct. and props., cooling rate effect at primary crystn. temp. 80—76241
steel inclusions and plasticity, crystn. conditions influence *(Russian)* 80—20923
steels 45, 17G2AF, 55S2, 60S2, faceted Mn sulphide formation on crystn., dendrites *(Russian)* 80—50621
stress, and dislocations, creation during crystal growth *(Russian)* 80—103277
structure and crystallisation, review 78—2008
styrene-butadiene block polymers, multiphase systems, struct., props. 77—31600
succinonitrile, crystn. kinetics and shapes 77—31617
sucrose, crystn. rate in impure solns., influence of non-sugar and colouring substance quantity 80—100767
sucrose, mathematical model of crystn. rate in pure solns. 80—49151
sucrose crystal formation, and growth, effect of same metallic impurities 80—100768
supercooled fluid states, soft core system, mol. dynamics method 78—18565
supercooled fog, crystn. by means of powdered synthetic zeolite 77—37296
supercooled liquid in sound field, steady-state dynamics 80—15223
supercooling crystallisation, a false high-press. effect under nonequilib. conditions 79—77728
surface nucleation, method for determining kinetic parameters 79—46980
suspensions, crystallisation, aggregate stability and effect on purity of product 80—100769
systems, and their mathematical models 80—100186
TCNQ salts, crystallisation versus electrical conductivity 80—92885
technical crystallisation, modern trends, computer modelling 80—66406
tetrabenzo[a, cd, j, lm]perylene evaporated film, crystn., time depend. as function of purity 80—88449
tetraphenylsilane, crystn. from chem. transport reaction 80—104439
TGS, on Ag film, saturated soln. evaporation, crystallisation by epitaxial nucleation *(French)* 77—35831
thermal, heat transfer processes in the solidification of inorganic hydrates *(Japanese)* 80—6372
thermally induced structural changes, specimen surface influence 80—103559
thermodynamic driving force, for crystallisation, from solution 79—37643
thermodynamics of phase transition intensity in crystn. processes *(Russian)* 78—38636
topological modelling of crystal growth 80—59418
torbermorite study by X-ray line profile anal. *(Japanese)* 80—33984
transition metal amorphous alloys with metalloid elements, embrittlement/crystn. relationship *(Japanese)* 79—96134
transition metal complex, linear chain type, synthesis 78—6047
transition metal-boron alloy amorphous film, crystn., TEM obs. 79—87019
transition metal-Si-B ternary and quaternary amorphous alloys, effect of comp. on crystn. *(Japanese)* 79—94910
tristearin irreversible liq.-liq. phase transition, ^{13}C NMR meas. 78—26681
trivalent metal phosphates, condensed, synthesis in polyphosphoric acid melts, physicochem. equil. considerations 80—97419
tumour extracellular crystallisation, in controlled cryotumourectomy 77—25591
two-component system, master equations in theory of crystallisation *(Russian)* 78—47258
urea mixed and adsorption mixed crystals and epitaxial growth from solns., tracht and habit *(German)* 80—38973
urea monocrystals from aq. soln., growth kinetics 79—99092
vapour-liquid-solid growth mechanism *(Russian)* 80—107074
water, characteristic IR emission due to latent heat of transform. 77—31754
water, in magnetic field, crystal size reduction *(Russian)* 77—11670

crystallisation continued

- water, normal and heavy, glass-transition temp., crystn. temp., and dielec. const. 80—15229
- water, repulsion of macroscopic particles by gas layer at crystallisation front 78—18568
- water drops, kinetic parameters of AgI-type crystallising reagents *(Russian)* 77—81963
- water emulsions, dielec. props. obtained after crystallisation/melting cycle 77—86381
- wave mechanism of external fields effect on crystallisation 80—19733
- wear resistant material, US welding effect on struct. *(Slovak)* 79—74185
- whisker growth by vapour-liquid-solid mechanism, book contrib. 79—69383
- o-xylene, volume effect in metastability of crystalline phases on cooling 79—77716
- zeolite L-D, prep. and props., from crystn. of obsidian 79—100067
- zeolites, A-type, crystn. from Na-K silicaalumo gels, and characts. 79—52780
- zinc oxalate, crystallisation kinetics, specific surface energy at cryst.-soln. interface 78—26471
- zinc oxalate, effect of supersaturation on crystallisation kinetics, turbidimetry meas. 78—30569
- zinc oxalate, isothermal crystallisation from soln. 80—108336
- zone crystallisation, double-ellipsoid mirror furnace for expts. in Spacelab 79—78872
- zone melting crystn. parameters optimisation using temp. distrib. calcs. *(German)* 79—43140
- Ag, crystal (100) faces, polynuclear growth mechanism during electrocrystallisation *(German)* 78—18562
- Ag halide crystn. during double-jet emulsification *(Russian)* 79—58826
- Ag, oriented crystallisation on active amorphous C centres 79—7762
- Ag-Cd peritectic system, separate crystallisation of phases *(Russian)* 80—66497
- AgBr, thin layers, evaporation conditions, photoresponse *(Bulgarian)* 78—78017
- AgBr-AgI emulsion sensitivity improved by AgCl shell crystallisation *(German)* 80—104453
- AgBr(Cl) precipitates, phase boundary processes, quantum mech. law in mass transfer processes *(German)* 79—27937
- AgCl, surface crystallisation, due to colloid adsorption 80—54544
- AgCl-$AgNO_3$, eutectic mixture, estimation of impurity distrib. coeffs. 80—55290
- Ag_9GaSe_6, crystn. in Ag_2Se-$GaSe_3$ system, lattice parameters *(French)* 77—51472
- AgI film, crystallisation, exciton absorption spectra meas. 77—35483
- AgI-AgCl, eutectic mixture, estimation of impurity distrib. coeffs. 80—55290
- AgI-$AgNO_3$, eutectic mixture, estimation of impurity distrib. coeffs. 80—55290
- Al borates, synthesis, thermal anal. and micrography *(French)* 77—85967
- Al, crystallisation thermokinetics calc. of pure cylindrical specimen *(Czech)* 77—63654
- Al, molten, showering cryst. form. in mould cooled from top *(Japanese)* 80—66498
- Al, structure sensitive props., temp. hysteresis after melting and crystallisation *(Russian)* 79—29036
- Al-Cu, melt near solid-liquid interface, diffusion during crystallisation *(German)* 79—29046
- Al-Cu, molten, showering cryst. form. in mould cooled from top *(Japanese)* 80—66498
- Al-Cu alloy, nonstationary mass transfer in front of moving phase boundaries in mormal freezing *(German)* 77—44238
- Al-Cv (0.3 wt.%), moving solid-liq. interface, diffusion in liq. 80—107456
- Al-Mg, crystallization interface *(Slovak)* 79—78951
- Al-Mg alloy, crystallisation front form. props., casting in EM field *(Russian)* 80—55384
- Al-Mg-Ti-Zr alloy AL23-1, nucleating cellular dendritic crystallisation *(Russian)* 79—70055
- Al-Si hypereutectic alloy, dissolution and primary crystallization of Si *(French)* 77—59832
- Al-SiO_2, Al-SiO_2(SiO)-Si, solid-state reaction mechanism 77—52623
- Al-Ti, molten, showering cryst. form. in mould cooled from top *(Japanese)* 80—66498
- AlAs-GaAs heterostructure, fabrication by selective liq.-phase epitaxy 79—15618
- AlB_{12}, preparation of single crystal 78—43997
- Al_2O_3 fusion cast ceramics, crystn., microstructures rel. to conditions 80—11638
- Al_2O_3, thermal anal. using solar heating *(Ukrainian)* 79—77725
- Al_2O_3-B_2O_3-P_2O_5 glasses, formation and props. 78—83737
- Al_2O_3-SiO_2 glass powder, mullite crystallisation during hot pressing 78—60639
- Al_2O_3-SiO_2 powder, plasma-prepared, glass form. and phase transforms 77—44208
- Al_2O_3-SiO_2-P_2O_5, refractory glasses, exam. of liquid immiscibility and crystallisation 78—55814
- Al_2O_3-SiO_2-TiO_2-RO (where R=Ca, Sr, Ba) system glass-crystal material, elec. cond. 79—60876
- Al_2O_3-Y_2O_3, melting behaviour and metastability determ. by optical DTA 80—92648
- $Al_2(SO_4)_2$ $(NH_4)_2SO_4.24H_2O$, crystn. kinetics in an MSMPR crystalliser 80—100185
- AlSb, laser pulse annealing, induced nucleation, crystal growth 80—84966
- $Al_{23}Te_{77}$ glasses, crystallization 79—51000
- Al(111), oxide layer amorphous to cryst. surface transition, slow positron obs. 80—75417
- Ar, two-dimensional freezing, on differently graphitised carbon 79—77896
- As, amorphous, spontaneous crystallisation temp. determ. 77—27833
- As-Se system glasses, structural and electronic transitions 77—76890
- As-Se-Bi, semicond. chalcogenide glasses, crystallisation and electrophys. props. 78—9955
- As-Se-Te thin films, laser induced crystn. kinetics 77—76317
- As-Te-Ga system, glass-forming region and props. 80—25674
- As-Te-Ge chalcogenide films, thermally induced transformations, TEM obs. 79—94917
- As_2S_3, glassy, deep struct. changes, NQR obs., high-press. and temp. effects 80—54139

crystallisation continued

- As_2S_3-$AsBr_3$ and As_2Se_3-$AsBr_3$ systems, phase diagrams 77—8804
- As_2S_3-Tl_2S glass, phase relns. and crystallisation 78—23675
- As_2S_5, glassy, deep struct. changes, NQR obs., high-press. and temp. effects 80—54139
- $AsSe_{1.2}$:Fe, Fe effect on physiochem. props. of glass 80—24370
- As_2Se_3, film, influence of electric field on crystallisation kinetics 78—42914
- As_2Se_3 vitreous films, crystn. stimulated by org. subst. and electrophotographic parameters 77—76319
- As_2Se_3:B:, devitrification kinetics, Bi impurity effects 77—35675
- As_2Se_3:Bi, annealing kinetics, cond. activation energy and density 79—73503
- As_2Se_3-As_2Te_3 glasses 77—43156
- As_2Se_3-based glasses, crystallization, DTA investig. 78—22658
- $AsSe_{1.5}Sn_x$ glasses, crystallisation, Mossbauer obs. 77—47557
- $(AsSe)_{1-x}Te_x$ glasses, thermal props. and viscosity, temp. and conc. depend. 77—76324
- $AsSe_{1.1}Te_{0.2}$:Fe, Fe effect on physiochem. props. of glass 80—24370
- $As_{60}Se_xTe_{40-x}$ glasses, crystallisation 77—35488
- $AsTeS_x(Se_x)(Sb_x)(Bi_x)$, chalcogenide glass, thin film crystallisation 79—7758
- Au film, on Si or CaF_2, oriented crystn., formation of coincidence orientations on interphase boundary 79—90922
- $Au_{35}Si_{65}$, amorphous vacuum-deposited and liquid-quenched films, diffusion and crystn. 80—84094
- Au_xSi_{1-x} amorphous alloy, crystallisation, elec. cond. study 80—103246
- Au_xSi_{1-x} amorphous films, phys. studies 80—75476
- B, amorphous, crystn., α-rhombohedral B prep., book contrib. 78—48295
- β-B, electron beam zone melting growth, crystn. and defect form. 80—15020
- B-transition metal, amorphous thin film, crystallisation, TEM obs. 79—19483
- B-transition metal thin films, amorphous to cryst. transformation 80—7563
- BN, deposition of wurtzite type layers, by reactive pulse plasma crystallisation 79—28953
- B_2O_3-Li_2O-Fe_2O_3, prep. by quenching methods, exam. of microcrystalline precipitates of Li_2O-Fe_2O_3 *(French)* 79—20019
- $BaClO_3.H_2O \rightarrow BaClO_3$, dehydration process 78—59932
- $BaFe_2O_4$ amorphous film, prep. by RF sputtering, crystallisation 80—76183
- $Ba_2LiNb_5O_{15}$, Czochralski growth, crystn. 80—35081
- $BaM_2(PO_4)_2$, M=Ni, Co, Mg, melt growth, optimal crystn. conditions 77—59683
- $BaMoO_4$, single crystals, habit modification, growth kinetics in silica gel 80—20777
- BaO film on W surface, struct. of crit. nuclei in heterogeneous crystn., LEED and FEM 77—11817
- BaO-Al_2O_3-SiO_2-H_2O system, phase transitions during hydrothermal treatment 79—43216
- BaO-Fe_2O_3, splat quenching struct. and crystn. mechanism *(French)* 78—51426
- BaO-GeO_2-Na_2O-H_2O system, hydrothermal crystn., phase formation laws 79—46636
- BaO-La_2O_3-GeO_2, exam. of glass forming region, properties and crystallisation 78—88454
- BaO-SiO_2 glass ceramic, growth and nucleation kinetics 80—7528
- BaO-SiO_2 glass-ceramic, crystallisation mechanism 79—90559
- BaO-SiO_2-P_2O_5, effect of thermal history on crystallisation of glasses 77—80424
- BaO-SrO-Al_2O_3-TiO-SiO_2 glass ceramics, cryst. phases form., BaO/SrO ratio influence 80—19705
- $BaO.2SiO_2$, glass, spherulitic growth and recrystallisation 77—4046
- $Ba(PO_3)_2$-MgF_2, vitrification region 77—35676
- $BaPO_3F$-Al_2O_3-B_2O_3 glasses, viscosity in the softening region and crystn. range 80—29105
- $BaPO_3F$-Al_2O_3-B_2O_3 system, liq. phase separation, IR spectra, microstruct. 80—29940
- $BaSO_4$, crystal growth, effect of nitrilotri (methylenephosphonic acid) adsorption 78—88417
- $BaSO_4$, crystallisation, seeded growth kinetics, inhibitor effects 79—37644
- $BaTiO_3$, crystn. from melts, comparison of different prospective oxy-anion solvents 80—71583
- $BaTiO_3$-PbO-B_2O_3, liquid phase sintering, effect on props. *(German)* 79—33980
- $Ba_2Ti_9O_{20}$ single crysts., prep. and unit-cell parameters 80—103302
- $BaWO_4$, crystallization kinetics from saturated Na_2WO_4 solns. 79—99093
- Be metaphosphate glass, crystallization *(Japanese)* 77—72566
- BeO_2-Al_2O_3-SiO_2-MF_2 (MF) glasses, M=Mg, Ca, Sr, Ba, Li, Na, fluoride ion role during crystn. 79—65176
- Bi, amorphous metal films, crystallisation with and without mag. field 80—70570
- Bi-Sb, conditions for dendritic crystallisation, accompanying rapid cooling *(Russian)* 79—34020
- Bi-Sb, crystallisation temp., overcooling temp. *(Russian)* 80—97472
- Bi-Sb solid soln., crystallisation in capillaries *(Russian)* 78—44006
- Bi-Sb-Sn, Sn and Sb partition coeffs. during crystallisation 77—48394
- Bi-Sb-Te melt, Sb and Te distribution coeffs. during crystallisation *(Russian)* 80—93472
- Bi_2O_3-SiO_2(GeO_2), melt struct. model 80—33870
- Bi_2O_3-SiO_2(GeO_2), metastable phases form., crystn. conditions, melt viscosity and density effects 80—35167
- $6Bi_2O_3.SiO_2$, stable γ-phase cryst. form. from supercooled melt, metastable δ-phase precip., surface contamination role 79—91635
- BiTeI-SbTeI solid solns., form., crystn., elec., thermal props. 78—44003
- bonde fusion cast ceramics, crystn., microstructures rel. to conditions 80—11638
- C, amorphous film, struct. props., Raman scatt. study 80—11417
- C, diamond like, reactive pulse plasma crystallisation 79—95938
- Ca $(PO_3)_2$ glass, crystallisation below glass transition temp. *(Japanese)* 77—62480
- Ca, acoustic effect in crystallisation and melting *(Russian)* 79—51238
- Ca metasilicate glass, crystallisation kinetics 77—11486
- Ca-Al rich inclusion, rhonite bearing, in Allende meteorite, mineralogy rel. to crystallisation 79—2530
- $CaCO_3$ crystallisation from aqueous solutions, kinetic study 80—59419
- $CaCO_3$, crystallization inhibition by phosphate and glycerophosphate ions 78—23593

crystallisation continued

$CaCO_3$, nucleation mechanism accompanying Ostwald ripening 80—50641
$Ca_3Fe_{3.5}V_{1.5}O_{12}$, ferrogarnet, crystallisation field in $CaO-V_2O_5-Fe_2O_3-PbO$ 77—16548
$CaO-Al_2O_3-SiO_2$ based glasses, kinetic parameters of glass ceramic form. 77—24385
$CaO-Al_2O_3-SiO_2-ZnO$, continuous unidirectional crystn. of fibrous metasilicates from melt 78—95739
$CaO-MgO-Al_2O_3-SiO_2$, glass-ceramic prep. by hot pressing and crystallisation of powder 78—11192
$CaO-MgO-Al_2O_3-SiO_2$, glass ceramic, prep. by hot pressing and crystallisation, mech. props. 78—15351
$CaO-MgO-Al_2O_3-SiO_2$, shale glass, crystn. behaviour 78—22661
$CaO-MgO-Al_2O_3-SiO_2-ZnO$, continuous unidirectional crystn. of fibrous metasilicates from melt 78—95739
$CaO-MgO-Al_2O_3-SiO_2$, quartz sand-dolomite-magnesia-clay based glasses, crystn. 80—20915
$CaO-MgO-Al_2O_3-SiO_2$, glass formation, at molar ratio CaO: MgO=1 *(Russian)* 80—39269
$CaO-MnO-SiO_2$ system glasses, vitrification and crystallisability 77—7853
$CaO-SiO_2$ glass prep. by gel method 80—100824
$CaO-SiO_2-ZnO$ continuous unidirectional crystn. of fibrous metasilicates from melt 78—95739
$\beta-(CaO_2)-SiO_2-H_2O$, SEM and X-ray diffr. exam. of structure, crystallisation props. 78—73012
$12CaO.7Al_2O_3$, composition of gases released on heating, crystallisation *(Russian)* 80—93820
$Ca(PO_3)_2$, crystallisation below T_g 77—20056
$Ca(PO_3)_2$ glass, crystallisation below glass transition, stress effect 80—19709
$Ca(PO_3)_2$ glass, rate of crystallisation, SiO_2 additive effects *(Japanese)* 77—68927
$CaSO_4$, cryst. growth kinetics at heated metal surfaces, thermal cond. morphology and crystn. 80—29867
$CaSO_4$ crystallisation, from liq. solns. as heat-transfer surface 80—100772
$CaSO_4.2H_2O$, crystallisation 80—100766
$CaSO_4.2H_2O$, occlusion formation during dendritic crystal growth, expt. 78—38993
$\beta-CaSiO_3$ fibre, continuous unidirectional crystallisation from melt 78—95739
$CaSiO_3$, fibrous, controlled crystallisation and anisotropy 80—59425
$CaSiO_3$ fibrous crystal reinforced matrix, unidirectional crystallization, anisotropic properties 79—56969
$CaWO_4$, cryst. growth from solns. in melts, kinetics parameters and thermodynamic props. 80—59424
$CaWO_4$, crystn. from solns. in $NaWO_4$ melts, kinetics obs. by DTA 80—40246
$CaYAl_3O_7$, type of melting, crystallisation from melt 77—12515
Cd-Sb alloys, phase diagram and melts struct., crystn. depend. on heating conditions 79—52155
Cd_3As, film, amorphous, crystallisation effects 77—35482
Cd_3As_2, amorphous to crystalline transform. 79—77519
$CdCr_2Se_4$, crystn. from high temp. soln., $CdCr_2Se_4-CdCl_2$ phase diagram 78—3009
$Cd_{0.96}Ga_2Te_{4.1}$, amorphous film crystallisation and conductivity switching 77—4459
$CdGe_{1-x}M_xAs_2$ (M=Si,Sn,Pb), (x=0.0,0.1,0.2), amorphous struct. 78—22651
$Cd_xGe_yO_2$, hydrothermal crystallisation at 300°C 77—52241
$CdGe_{1-x}Sb_xAs_2$ system, amorphous and cryst. phases, DTA and microhardness obs. 78—22835
$Cd_xHg_{1-x}Te$, crystallisation from solution in Hg 77—19883
CdI_2 crystals, growth conditions effect on polytypism, X-ray diffr. study 80—28942
CdS, crystallisation and stability in high-temp. alkaline solns. 77—52240
CdS, electrocrystallisation of films on Cd 78—72014
CdSb-ZnSb, crystallisation characts., phase diagram 80—55383
CdTe films, structural imperfections depend. on crystn. temp. 79—90661
$Ce(CO_3)_5^{6-}$, in Na and guanidinium salts, struct./props. correlation *(French)* 78—95032
$Ce_2(MoO_4)_3$, crystn. from Na_2MoO_4 based melt 80—20920
$CeNH_4P_4O_{12}$ and $Ce(NH_4)_2(PO_3)_5$, synthesis by solid-phase reaction, characts. 80—60778
$Ce_2O_5-P_2O_5$ glass, crystallisation 77—51326
$(Co,Fe)_{0.75}B_{0.25}$ metallic glasses, annealed, equilib. crystalline phases 80—3019
Co-Fe-B, amorphous, crystn. and thermal stability 80—107057
Co-Fe-Si-B, amorphous alloys, substitution effect on mag. props. 79—69695
Co-Fe-Si-B, decomp. of amorphous state during annealing below recryst. temp., electron microscope study *(Russian)* 80—75164
Co-Mo-B metallic glass ribbons, tensile strength, crystn. temp. 80—89173
Co-Ni-Mo-C, amorphous alloys, med. props. and thermal stability *(Japanese)* 80—85049
Co-P metallic glasses, crystn. kinetics by differential scanning calorimetry 78—91257
Co-Si-B, embrittlement by crystallisation *(Japanese)* 78—48513
Co-Ti (22 at.%), amorphous eutectic phase 80—55360
Co-X-Co (X=Cr,Mo,W) systems, crystn. temp. and hardness 79—77529
Co-Zr, amorphous phase form. in Zr-poor region, hardness and fracture strength *(Japanese)* 80—84914
$(Co_{0.93}Fe_{0.07})_{75-x}Cr_xSi_{15}B_{10}$ amorphous alloy, thermal stability, Cr conc. effects, DTA expts. 80—59395
$Co_{70}Fe_5Si_{15}B_{10}$, amorphous, crystn. and thermal stability 80—107057
Co_5Ge_3 amorphous film, elec. resist., microstruct. and annealing 77—85188
$Co_{1-x}P_x$ glass, crystn., spin wave reson. 79—73104
$Co_{75}Si_{15}B_{10}$, amorphous, crystallisation study *(Japanese)* 78—9959
$Co_{75}Si_{15}B_{10}$, amorphous, crystn. and thermal stability 80—107057
$Co_{90}Zr_{10}$, ferromag. amorphous alloy, crystn. and domain struct. study 80—107056
Cr-X-C amorphous alloys, (X=Fe, Co, Ni, Nb, Mo and Ta), crystn. temp. and hardness 79—73133
Cr_2O_3, active, block growth in crystallisation 77—85972
Cs amsorphous film, catalytic crystallization by Ni particles 79—14683
$Cs(D_xH_{1-x})_2PO_4$, D distrib. during crystallisation from aq. soln. 77—11496

crystallisation continued

$CsNO_3$, anhydrous, kinetics of crystallisation 77—43164
$Cs_2O-MgO-SiO_2$ system, glasses, crystn. prods., composition, props. 79—41961
Cu electrocrystallisation on graphite electrodes, nucleation 80—93504
Cu melts, pure and alloyed, supercooled, influence of impurities on crystallisation 79—29042
Cu-Cr(Nb), formation of two phase microstructure, during volumetric, and directional crystallisation *(Russian)* 79—29040
Cu-Cu Zr eutectic composite, struct. and props., heat treatment and crystn. rate influence *(Russian)* 79—38813
$Cu-Cu_2O$ crystallisation from melt, influence of crystn. conditions on struct. *(Russian)* 79—38814
Cu-Ni, crystallisation temp., overcooling temp. *(Russian)* 80—97472
Cu-Ni, melt, accel. by shock wave treatment, crystallisation *(German)* 77—86022
Cu-Sb-S-I amorphous film formation and stimulated crystallisation, electrophysial props. *(Russian)* 78—30838
Cu-Zr (50 or 54 at.%), splat-quenched, glass transition and crystn. temps. determ. 78—22659
$CuGaS_2$, crystal growth by solid phase crystallisation 80—25556
$Cu(NO_3)_2$, frozen aq. soln., phase transitions, struct., ESR 77—16154
$CuO-CaO-P_2O_5$ glass devices, memory switching 78—56192
Cu_2S, molten, oxidation, exam. of product phase composition by X-ray anal. *(Russian)* 79—34166
$Cu_{60}Zr_{40}$, stability, crystallisation, ductility meas. 78—47246
$Dy_2(MoO_4)_3$, cryst. growth and props. 79—55727
ErO_x films, phase transforms. 77—62784
$EuS-Ga_2S_3-GeS_2$, chalcogenide glasses, conditions of form. of glassy prod. *(French)* 80—100325
$(Fe,Mo)_{80}B_{20}$, glassy alloy, Curie temp. and crystn. temp., Mo additions effect, Mossbauer spectra 78—68428
(Fe, Ni, Co)-Si-B, amorphous, compositional effect on struct. changes, after heating up to 700°C, exam. *(Japanese)* 78—48433
Fe, cast, eutectic cells microstruct., crystallisation kinetics *(Polish)* 79—52186
Fe, cast, grey eutectic transform. mechanism *(Russian)* 80—20924
Fe, cast, hypoeutectic, primary crystn. features by means of apparent viscosity meas. in early stages of solidification *(Japanese)* 79—43231
Fe, cast, with Mn, high S, exam. of sulphide phases, cocrystallisation during solidification 78—56646
Fe, cast, with spheroidal graphite, crystn. *(German, English)* 80—97473
Fe meteorites, crystallisation rel. to origin of magnetisation 78—65564
Fe, pure and alloyed, density and thermal expansion in liq. and solid states 80—96668
Fe-(Co)-B and Fe-Ni-B(P), amorphous, crystn. 80—79704
Fe-B, amorphous, crystn., metal or metalloid exchange influence 80—75172
Fe-B, amorphous metallic glasses, high-temp. mag. anal. 78—91258
Fe-B, eutectic, crystallisation *(Russian)* 79—70087
Fe-B, metallic glasses and vapour deposited films, amorphous to cryst. transition 80—88048
Fe-B amorphous, crystallisation, activation energy conc. depend., DTA calcs. 79—60284
Fe-B amorphous alloy, annealed, microstruct. and mag. domain changes 80—75790
Fe-B amorphous alloy, crystallisation kinetics 78—83736
Fe-B glass, crystallisation kinetics, elec. resist. meas. 78—83741
Fe-B glass, crystallisation kinetics, elec. resist. meas. 79—4254
Fe-B metallic glass, hardness, elastic moduli, density, cryst. temp., mech. props., for flywheel appl. *(Dutch)* 78—52878
Fe-B metallic glass, role of Fe_3B in crystn., mag. and Mossbauer expts. 78—94997
Fe-B metallic glass, struct. and crystallisation, Mossbauer spectra, calorimetry and magnetisation meas. 79—23528
Fe-B metallic glasses, crystn. kinetics by differential scanning calorimetry 78—91257
Fe-B metallic glasses, density, mech. and thermal props. 78—31432
Fe-B metallic glasses, diffusion coeffs. from primary crystn. data 80—100345
Fe-B metallic glasses, struct., stability and crystn. 80—75173
Fe-B-Cr(Mo), metallic glasses, mag., struct., and elec. props. 80—88751
Fe-B-Si amorphous alloys, crystallisation temp., Curie temps., saturation magnetisation 79—82820
Fe-B-Si-C amorphous alloys, prep. and props. 80—88748
Fe-B(-Co), two amorphous phases form. and crystallisation 79—27924
Fe-B(—Ni), chemical ordering, crystallisation and glass transition temp. 79—90563
Fe-based metallic glasses, effect of metalloidal elements on thermal stability, crystn. temp. *(Japanese)* 79—94909
Fe-C (4.3 wt.%), splat cooled, amorphous phase form. and crystn. 77—15323
Fe-C-Ti (0.2 to 1.8, 0.1 to 1.7 wt.%), crystallisation and microstruct. *(Russian)* 77—66632
Fe-Co-Mo-C, amorphous alloys, med. props. and thermal stability *(Japanese)* 80—85049
Fe-Cr, crystallisation temp., overcooling temp. *(Russian)* 80—97472
Fe-Cr-B amorphous alloys, corrosion resistance, Invar and Elinvar characts. *(Japanese)* 79—96213
Fe-Cu alloy, vapour-deposited, struct. and thermal stability 78—43265
Fe-Gd films, crystallisation, electron microscope obs. 79—15034
Fe-Mo-B metallic glass ribbons, tensile strength, crystn. temp. 80—89173
Fe-Ni, crystallisation temp., overcooling temp. *(Russian)* 80—97472
Fe-Ni, segregation of inhomogeneities during crystallisation *(Russian)* 78—27521
Fe-Ni base amorphous alloy, crystallisation 77—84660
Fe-Ni based metallic glasses, nonisothermal crystallisation kinetics, DSC anal. 79—27927
Fe-Ni film, amorphous, martensite form. time and struct. 80—104159
Fe-Ni metallic glasses, crystallisation 77—43157
Fe-Ni-B-Mo, crystn. temp. and elec. cond. correl., Mo effect 80—75179
Fe-Ni-B-Si, amorphous, mag. props., heat treatment effects 80—89370
Fe-Ni-C (0.15, 0.05 wt.%) pore formation kinetics during crystallisation, FORTRAN study *(Russian)* 80—54158
Fe-Ni-Mo-C, amorphous alloys, med. props. and thermal stability *(Japanese)* 80—85049
Fe-Ni-P-B, amorphous, crystn. and struct. 80—75175
Fe-Ni-P-B metallic glass, crystallisation temperature values from isothermal transformation times 80—59397
Fe-P-C, amorphous, crystn. and struct. 80—75175
Fe-P-C, amorphous, internal friction and shear modulus 77—25085

crystallisation continued
Fe-P-C, amorphous alloy, crystallisation 79—100112
Fe-P-C, embrittlement by crystallisation *(Japanese)* 78—48513
Fe-P-C amorphous alloy, small angle X-ray scattering study of struct. and crystallisation 79—50999
Fe-rare earth, amorphous thin film, crystallisation, TEM obs. 79—19483
Fe-Si, recrystallization, in situ studies, appl. of X-ray synchrotron topography 78—35610
Fe-Si (3 wt.%), tertiary products from deoxidation, electron emission microscope study *(Russian)* 78—11214
Fe-Si amorphous film, conversion electron Mossbauer effect 78—72440
Fe-Si amorphous film, crystallisation, Mossbauer studies 80—33900
Fe-Si amorphous film, struct. and crystallisation, Mossbauer study 80—11300
Fe-Si film, amorphous, conversion electron Mossbauer study, crystallisation obs. 78—84507
Fe-Si-B, embrittlement by crystallisation *(Japanese)* 78—48513
Fe-Si-B amorphous alloys, Mossbauer spectroscopy *(French)* 80—80653
Fe-Si-B glassy alloys, mag. props., comp. effects 80—88752
Fe-Si-B metallic glasses, mag. props. and crystallisation temp., depend. on metalloid content 77—85485
Fe-Si-B metallic glasses, crystn., differential scanning calorimetry obs. 79—82160
Fe-V-S-(C), sulphide nature exam. by X-ray spectral anal., solidification effects *(Russian)* 79—52191
Fe-Zr, amorphous phase form. in Zr-poor region, hardness and fracture strength *(Japanese)* 80—84914
$Fe_{1-x}B_x$ metallic glasses, struct. and cryst., Mossbauer spectra, DSC, and magnetisation meas. 79—94906
$Fe_{75}B_{25}$ metallic glass, nonisothermal meas. evaluation, non-existence of dynamic correction term 80—107406
$Fe_{80}B_{20}$, amorphous, crystallization 78—42917
$Fe_{80}B_{20}$, amorphous, crystn. temp. under press. 79—23523
$Fe_{80}B_{20}$, amorphous, crystn. 80—75187
$Fe_{80}B_{20}$ amorphous wire, crystn. by annealing at 780°C 80—100177
$Fe_{80}B_{20}$, binary amorphous ferromagnet, Mossbauer spectra 79—4749
$Fe_{80}B_{20}$, crystallisation of amorphous alloys, TEM and X-ray diffr. exam. of struct., growth characts. 78—79539
$Fe_{80}B_{20}$, elastic, magnetoelastic and thermal props. 79—19759
$Fe_{80}B_{20}$, metallic glass, elec. resist., 78 to 1000K, probe of crystn. process 77—76787
$Fe_{80}B_{20}$ metallic glass, crystn. and struct. relax., Mossbauer effect study 80—75182
$Fe_{80}B_{20}$ metallic glass, crystn. kinetics 80—84083
$Fe_{80}B_{20}$ metallic glasses, stability and transforms. 80—75174
$Fe_{83.4}B_{16.6}$, amorphous, mag. props. and microstruct., cooling rate and melt overheating effects 80—65965
$Fe_{83.4}B_{16.6}$ amorphous, mag. props., melt overheating and cooling rate effects 80—89371
$Fe_{84}B_{16-x}C_x$, amorphous alloys, short range order, Mossbauer and DSC study 80—39960
$Fe_{80}B_{20-x}M_x$ (X=Al, Si, Ge, C, P) and $(FeCo)_{80}B_{20}$ glass, magnetisation, Curie and crystn. temps. 79—87289
$Fe_{80}(B_{1-x}P_x)_{20}$ amorphous alloys, isothermal crystallisation kinetics 80—33895
$Fe_{80}B_{20-x}Si_x$, metallic glass, mech. and mag. props., depend. on metalloid content 79—91213
$Fe_{84}B_{13}Si_3$, metallic glass, electrical resistivity and crystallisation 80—88526
$Fe_{84}Bi_{16}$, metallic glass, electrical resistivity and crystallisation 80—88526
$Fe_{80}(C_{1-x}B_x)_{20}$ amorphous alloy, α-Fe crystn., morphology 80—70129
$Fe_5Co_{70}Si_{15}B_{10}$, amorphous, crystn. effect on mag. props. *(Russian)* 80—44858
$Fe_{85-x}Cr_xB_{15}$ metallic glass, Curie temp., crystn. temp. and room temp. elec. resist., Cr content effect 79—91229
Fe_5Ge_3, amorphous film, elec. resist., microstruct. and annealing 77—85188
$Fe_{83-x}M_xB_{17}$ and $Fe_{78-x}M_xSi_{10}B_{12}$ (M=refractory metal), glass form. and thermal stability 80—79703
$Fe_{78}Mo_2B_{20}$ glass, thermal expansion, glass transform. and crystn. temps. 80—2183
$Fe_{78}Mo_2B_{20}$, metallic glass, elec. resist., 78 to 1000K, probe of crystn. process 77—76787
$Fe_{80-x}Mo_xB_{20}$ metallic glasses, Curie temp., crystn. temp., elec. cond. as function of composition 79—60285
FeNi amorphous films, fast phase transition investigation by TEM method 80—107029
Fe_xNi_{1-x}, amorphous films, crystallisation, effect of codeposited O_2, N_2 or Kr gases 80—10807
$(Fe_{100-x}Ni_x)_{100-y}B_y$, metallic glass, embrittlement and crystn. 80—7685
$(Fe_{100-x}Ni_x)_{83}B_{17}$, amorphous, crystn. 80—75176
$(Fe_{100-x}Ni_x)_{83}B_{17}$ glassy alloys, Ni content influence on crystn., and bend ductility changes, during annealing 79—73103
$Fe_{40}Ni_{40}B_{20}$, amorphous, anomalous thermal dilatation 79—55668
$Fe_{40}Ni_{40}B_{20}$, amorphous, RF annealing effects 80—108037
$Fe_{40}Ni_{40}B_{20}$, metallic glass, embrittlement kinetics and crystn., quenching influence 78—68766
$Fe_{50}Ni_{30}B_{20}$, crystallisation of amorphous alloys, TEM and X-ray diffr. exam. of struct., growth characts. 78—79539
$(Fe_xNi_{100-x})_{80}B_{20}$, glassy, elec. resist. at elevated temp. 79—73484
$Fe_{32}Ni_{36}Cr_{14}P_{12}B_6$, elastic, magnetoelastic and thermal props. 79—19759
$Fe_{32}Ni_{36}Cr_{14}P_{12}B_6$, METGLAS 2826A, metastable crystallization phases, TEM obs. 79—55671
$Fe_{32}Ni_{36}Cr_{14}P_{12}B_6$, Metglas 2826A elec. resist. during crystn. 79—91014
$Fe_{32}Ni_{36}Cr_{14}P_{12}B_6$ glass, thermal expansion, glass transform. and crystn. temps. 80—2183
$Fe_{32}Ni_{36}Cr_{14}P_{12}B_6$ metallic glass, crystn. kinetics by TEM 80—75186
$Fe_{32}Ni_{36}Cr_{14}P_{12}B_6$ metallic glass, effect of pre-ageing on glass transition temp. 80—100326
$Fe_{40}Ni_{38}Mo_4B_{18}$, amorphous, crystallization, heat treatment and irradiation effects *(French)* 79—90558
$Fe_{40}Ni_{40}P_{14}B_6$, amorphous alloy, small angle X-ray scattering 77—65953
$Fe_{40}Ni_{40}P_{14}B_6$, amorphous, steady-state creep rate, cryst. effect 80—81102
$Fe_{40}Ni_{40}P_{14}B_6$, elastic, magnetoelastic and thermal props. 79—19759
$Fe_{40}Ni_{40}P_{14}B_6$ glass, crystn. kinetics, DSC expts. 78—26444
$Fe_{40}Ni_{40}P_{14}B_6$ glass, positron lifetimes in as-received, cold-rolled, embrittled and crystallized samples 79—74177
$Fe_{40}Ni_{40}P_{14}B_6$ glass, thermal expansion, glass transform. and crystn. temps. 80—2183

crystallisation continued
$Fe_{40}Ni_{40}P_{14}B_6$, glassy, mag. props., hyperfine interactions, and crystn. temp. 78—10812
$Fe_{40}Ni_{40}P_{14}B_6$, metallic glass, cryst., isothermal annealing behaviour 80—6367
$Fe_{40}Ni_{40}P_{14}B_6$ metallic glass, isothermal viscosity and crystn. 80—49395
$Fe_{40}Ni_{40}P_{14}B_6$ metallic glass, crystn. 80—70127
$Fe_{40}Ni_{40}P_{14}B_6$, Metglas 2826, acoustic emission during viscous flow 78—42915
$Fe_{40}Ni_{40}P_{14}B_6$, Metglas 2826, stability, crystallisation, ductility meas. 78—47246
$Fe_{40}Ni_{40}P_{14}B_6$, Metglas 2826, hot forming 80—84980
$Fe_{44}Ni_{40}P_{14}B_6$, homogeneous deformation effect on crystn. and Curie temp. 80—21045
$(Fe_{65}Ni_{35})_{75}P_{16}B_6Al_3$, amorphous, crystn. temp., press. and heating rate depend. 80—70132
$Fe_{29}Ni_{49}P_{14}B_6Si_2$ glass, crystn. kinetics, DSC expts. 78—26444
$(Fe_{1-x}Ni_x)_{80}PyB_{20-y}$, local struct. disorder and crystallisation, Mossbauer exam. 79—1728
α-Fe_2O_3 crystal flux growth, solubility and relative supersaturation in Fe_2O_3-PbO-V_2O_5 fluxed melt system 80—64934
$Fe_{80}P_{16}B_1C_3$, ferromag. metallic glass, Mossbauer spectra, crystn. 77—12276
$Fe_{80}P_{13}C_7$, metallic glass, crystallisation kinetics 77—66637
$Fe_{80}(P_{13}C_7)_{20-y}B_y(Si_y)$, density, microhardness, and crystn. temp., comp. depend. 80—84093
FeSb alloy films, vapour-deposited, formation of metastable phase 80—44437
$Fe_{78}Si_{10}B_{12}$, amorphous alloy crystallisation study *(Japanese)* 78—9959
$(Fe_{1-x}Si_x)_{1-y}$By, metallic glass, mag. props., crystallisation 80—65885
Fe_xSn_{1-x}, amorphous alloy stability, comp. and temp. depend. 79—19156
Ga, amorphous metal films, crystallisation with and without mag. field 80—70570
Ga selenites, binary, effect of nature of alkali metals on composition and props. of hydrothermal reaction products 77—24941
Ga-In (2 and 4 wt.%), binary, kinetic conditions for two phase zone form. *(Russian)* 77—66633
Ga-In-Sb system, phase diagram calcs. in Ga+In rich region 80—60842
$Ga_{1-x}Al_xP$ varigap structs., crystallation 80—80993
GaAs, anodic oxide for device application, crystallisation dynamics 79—66190
GaAs, implanted amorphous layer reordering 77—76435
GaAs, ion-implanted semiconductor, annealing, crystallisation, laser pulse energy depend. 78—34528
GaAs, laser reordering of implanted amorphous layers 78—43042
GaAs:Fe, LPE, phase diagram 77—16509
GaAs-Si eutectic alloy, effect of crystallisation rate on microhardness 79—96110
$GaH_2P_3O_{10}$, from Ga_2O_3 in H_3PO_4 79—52641
GaP films on Si, epitaxial crystallisation by nanosecond laser pulses 80—107674
GaP, vac. deposited film, structural, elec. and photoelectric props. 79—82698
$Ga(PO_3)_3$, crystn. from reaction of Ga_2O_3 with H_3PO_4 and K_2O 79—52642
$Ga(PO_3)_3$, from Ga_2O_3 in H_3PO_4 79—52641
GaSb film, gamma-irradiated, struct., TEM and SEM obs. 79—15033
GaSb-Ge eutectic alloy, effect of crystallisation rate on microhardness 79—96110
GaSe-InSe, heterostructure, optical crystallisation of amorphous films 79—73580
Gd-Co amorphous thin films, crystn. process and domain struct. *(Chinese)* 80—54533
Gd-Co(Ni)(Cu)(Rh)(Ru)(Pd)(Ga), amorphous, mag. props. and ferromag. reson. 80—75862
Gd-Fe amorphous alloys, mag. props. and crystn. 79—90557
$GdAl_3$ films, crystn. induced polytypism 79—99446
$Gd_3Al_5O_{12}$ phase obtained by crystallisation of amorphous $Gd_2O_3.5/3Al_2O_3$ by quenching 78—92224
$Gd_{0.27}Co_{0.64}Kr_{0.09}$, amorphous film, thermal release of Kr and H, meas. using UHV mass spectrometric technique 80—3439
Gd_2O_3-Al_2O_3 glasses, crystallization 79—50998
Gd_2O_3-Fe_2O_3-PbO-B_2O_3, primary crystallisation regions 77—12604
Ge alloys, amorphous film, crystn. transform. kinetics 78—22653
Ge, amorphous, 1 MeV electron irrad. influence on kinetics of crystallisation 77—89476
Ge, amorphous, deduction of crystalline fraction 80—33889
Ge, amorphous, elec. cond. obs. of crystn., expt. verification of model 77—20475
Ge, amorphous, growth rate of crystallisation, Raman spectroscopy study 80—44227
Ge, amorphous, ionisation enhanced crystallisation, elec. cond. meas. 77—35481
Ge amorphous film, crystn. front velocity during scanned laser crystn. 80—107662
Ge, amorphous film, DC sputter deposited, effect of trapped Ar on minimum temp. for impulse stimulated explosive crystallisation 80—100422
Ge, amorphous film, large aligned grain solid-phase growth during scanned laser crystallisation 80—49100
Ge, amorphous film, laser pulse annealing 80—15006
Ge amorphous films, structural relaxation and crystallisation 80—100170
Ge amorphous layer, crystallisation anal. by cond. meas. *(French)* 77—72599
Ge, amorphous thin films, fast crystn. and void precipitation in laser pulse annealing, TEM exam. 79—56086
Ge, evaporated film, lattice parameters and phase transition temp., surface influence of glass substrates 78—94996
Ge film, amorphous, crystn. kinetics, elec. cond. obs. 77—62767
Ge film, amorphous to crystalline transform. 77—20206
Ge, film, elec. resist. and struct., post-deposition heat treatment effects 79—78229
Ge film, electrical cond. during laser-induced crystallisation 79—47175
Ge, laser pulse annealing, induced nucleation, crystal growth 80—84966
Ge, non-cryst., high-press. expts., quenchable products 77—19874
Ge shaped single crystal, Stepanov method growth, temp. distri b. 78—2032
Ge single crystals, constitutional supercooling growth conditions, structural and chem. inhomogeneities 80—93473
Ge, solid-phase epitaxial growth through PdGe layers, channelling and backscatt. obs. 77—85936

crystallisation continued
- Ge:Sb, Czochralski growth, orientation depend. of impurity distrib. coeff. 79−69976
- Ge-Ga, segregation of Ga due to barometric mol. diffusion in gravitational, centrifugal fields 78−14472
- Ge-GaAs, crystallisation at superhigh cooling rates 80−54349
- Ge-GaSb, metastable continuous solid solutions 79−8284
- Ge-S glasses, Cu doped, thermal, structural and dielectric props. 79−60283
- Ge-Sb eutectic alloy, crystallisation in electric field *(Russian)* 77−52311
- Ge-Se-Te amorphous alloys, prep. and calorimetric obs. 77−11675
- Ge-Si:Sb, prepared in Universal Furnace expt. in Soyuz-Apollo programme, melting and crystn. 80−19737
- Ge-Si-S system, glass formation, transition temp., crystallisation and melting 80−100178
- Ge-Si-Sb, segregation of Si,Sb due to barometric mol. diffusion in gravitational, centrifugal fields 78−14472
- Ge-Sn solid solution, cooling rate effect on partition coeff. of Sn between liq. phase and crysts. 77−12510
- Ge-Sn-M, M=Cu, As, Sb, formation of Ge-based solid solns. during crystallisation 77−80625
- Ge-Te and Ge-Te-As system glasses, local struct., ^{119}Sn Mossbauer obs. 79−41968
- Ge-Te binary glass, eutectic, DSC obs., thermodynamic and thermokinetic characts. 80−39309
- $Ge_{15}As_4Te_8$, film, influence of electric field on crystallisation kinetics 78−42914
- GeO_2 glass, nonisothermal devitrification kinetics 80−92465
- GeO_2-$K_2O(Na_2O)(Li_2O)$, glass, Raman spectra, struct. and crystn. 80−92463
- GeS_x glass, $x=1.25$ to 1.5, softening and crystallization kinetics 79−32906
- $Ge_{2.33}SbSe_5$:Fe, Fe effect on physiochem. props. of glass 80−24370
- $GeSe_2$ amorphous semicond., DC conductivity, calorimetric, and X-ray diffr. meas. 79−78107
- Ge_xSe_{1-x}, $0<x<0.2$, crystallisation in amorphous bulk and thin films 78−55813
- Ge_xSe_{1-x} amorphous film, photocrystallisation, elec. cond. meas. 79−32911
- Ge_xSe_{1-x} amorphous film, photocrystn., elec. cond. and optical microscopy obs. 79−87024
- $Ge_{20}Se_{40}Te_{40}$ amorphous alloys, thermal crystn. study 78−26789
- Ge_xTe_{1-x} amorphous matrix with Te crystallites, effect of annealing 77−24274
- $Ge_{15}Te_{81}As_4$, influence of O_2 on phase separation of chalcogenide glasses 77−47354
- $HNO_3.H_2O$, devitrification crystallisation, fast Raman and wide-line NMR obs. *(French)* 79−73915
- He, liquid, surface liquid-crystal transition in two dimensional electronic system 80−88303
- ^{3}He-^{4}He mixture, near absolute zero, holographic interferometry exam. of phase changes 78−38905
- ^{4}He, crystallisation wave detection, solid-liquid boundary oscillation spectra *(Russian)* 79−90844
- ^{4}He crystals, nucleation and orientation 80−84339
- Hf-Mo-C, phase diagram, crystallisation patterns of partial system Mo-HfC-Hf 77−12598
- Hf-Mo-C, phase diagram and crystallisation of partial system Mo-HfC-C 77−12599
- Hf-Ni(Co), amorphous, formation, decomposition and elec. transport props. 80−20143
- $Hf_{1-x}Fe_x$ amorphous alloys, formation, crystallisation and electrical resistivity 80−96838
- HfO_2, thermal anal. using solar heating *(Ukrainian)* 79−77725
- Hg film, melting and crystallisation kinetics, electron microscopy 77−15725
- Hg-HgTe-CdTe system, equilib. phases comp. by dew point method 79−78941
- $Hg_{1-x}Cd_xTe$, mixed crystals, crystn. by chemical transport 80−20775
- α-HgI_2, single cryst. growth from iodomercurate complexes 80−35069
- α-HgI_2, single cryst. growth from dimethylsulfoxide complexes 80−35070
- α-HgS, crystn. in NaHs solutions 77−8740
- HgTe single crystals, crystn. from vapour phase, thermodynamical conditions 79−33908
- HgTe-CdTe, distrib. ratios of components during crystn. of melt 77−16485
- $Ho_{0.7}Er_{0.3}FeO_3$, crystn. on seeds, layer morphology 78−72041
- (In, Ga)Sb, sputter deposited amorphous film, impulse stimulated explosive crystallisation 78−84098
- In film, thermal hysteresis of phase transitions and mechanism of crystallisation 77−89679
- In island film, melting and crystn. kinetics, dark field electron microscopy 79−11026
- InAs:Cd,Te interaction between impurities, effect on elec. props., Hall effect. 80−19832
- $In_{1-x}Ga_xP$, compositional inhomogeneity 80−88444
- InI directional crystallisation, behaviour of Ag, Cu, Sn, Ni impurities, partition coeffs. 77−16491
- In_2O_3, lattice defects, optimum prep. conditions w.r.t. stoichiometry 79−27974
- In_2S_3, film struct. and props. 77−80706
- InSb film, gamma-irradiated, struct., TEM and SEM obs. 79−15033
- InSb thin layers, interface stability during crystn. 79−65326
- InSb-Ge eutectic alloy, effect of crystallisation rate on microhardness 79−96110
- In_2SnO_3 film, effect of ambient atmosphere during annealing, elec. props. 80−97510
- insular metal films, influence on crystn. of continuous films 80−88454
- $KAl(SO_4)_2.12H_2O$, occlusion formation during dendritic crystal growth, expt. 78−38993
- KBr bicrystal, grown from melt, interfacial substructure, impurity effects 77−4263
- KCl cryst., Sr and Na impurities radial distrib., influence of form of crystn. front 80−107312
- KCl, influence of collisions on cryst. growth and secondary nucleation under conditions of meas. crystn. 80−50544
- KCl-NaCl-$FeCl_3$ system, shape eutectics line calc. *(Russian)* 79−96016
- $KClO_4$ single crystals, gel growth, temp. effects etching 79−78862

crystallisation continued
- $K(D_xH_{1-x})_2PO_4$, D distrib. during crystallisation from aq. soln. 77−11496
- $K(D_xH_{1-x})_2PO_4$, monoclinic and tetragonal forms, existence in aq. soln. 78−47262
- $KEr(WO_4)_2$, crystallisation cond., stimulated emission in 2.8 μm band 80−53301
- $KGaHP_3O_{10}$, crystn. from reaction of Ga_2O_3 with H_3PO_4 and K_2O 79−52642
- $KGa(PO_3)_4$, crystn. from reaction of Ga_2O_3 with H_3PO_4 and K_2O 79−52642
- KH_2PO_4, kinetics of crystn. from soln., activities, interfacial energy and solubility 77−76340
- $KLa(MoO_4)_2$, solubility in aq. K_2MoO_4 solns., hydrothermal conditions 80−96651
- $K_5La(WO_4)_4$, formation possibility 77−36392
- $KMg_2(AlSi_3O_{10})F_2$-$KMg_{2.5}Si_4O_{10}F_2$, solid soln., melting and crystn., quenching and DTA study 80−39263
- $KMg_2LiSi_4O_{10}F_2$-$NaMg_2LiSi_4O_{10}F_2$, solid soln., solid solubility and swelling characts. 80−59660
- $KNbO_3$ crystals, bulk crystn. from melt 79−100041
- K_2O-Al_2O_3-SiO_2 system, crystallisation of glasses in primary phase field of leucite 78−67658
- K_2O-B_2O_3-SiO_2, glass, crystallisation range *(German)* 80−38934
- K_2O-MgO-SiO_2 glass, crystalline phase precipitation during crystallisation early stages, DTA *(Japanese)* 78−42919
- K_2O-SiO_2 glass, diffusion-controlled crystal growth 77−19876
- K_2SO_4, kinetics of crystn. from soln., activities, interfacial energy and solubility 77−76340
- K_2SO_4-Cs_2SO_4-MoO_3 system, fusibility diagram 79−87619
- K_2SO_4-$ZnSO_4$ system, glass formation and phase diagram study, physical props. 78−27500
- $La_2(MoO_4)_3$, crystn. from Na_2MoO_4 based melt 80−20920
- La_2O_3-GeO_2-$Ta_2O_3(HfO_2)(ZrO_2)$, vitrification, crystn. 77−15559
- La_2O_3-P_2O_5-H_2O, solubility, regions of crystallisation, 100-500°C 77−16483
- La_2O_3-SiO_2, gels, microstruct. and crystallisation, prep. method and thermal treatment effect 79−61913
- $La_2O_3GeO_2$-$Ga_2O_3(B_2O_3)$, vitrification and crystallisation 77−15558
- $La(PO_3)_3$, form. reaction from $La_2O_3+NH_4H_2PO_4$ 79−79235
- La_2Se_3-Ga_2Se_3-$GeSe_2$ ternary system, phase diags., glass formation *(French)* 78−3109
- $Li_2B_4O_7$, melt-crystal interface temp. meas. during crystallization of melts 79−44908
- LiCl:Na (K,Rb,Cs,Ag), theoretical and experimental study of partition coeffs. of isovalent impurities 79−65111
- $LiNO_3.3H_2O$, crystallisation kinetics 79−4264
- $LiNbO_3$, crystallisation from solution in borate, vanadate and tungstate melts 79−1820
- $LiNbO_3$:Cr^{3+} glass, roller quenched, crystn. kinetics 80−44143
- $LiNd(PO_3)_4$, crystallisation from $LiPO_3$ flux, exam. of optical props. *(German)* 79−11401
- LiO_2-$2SiO_2$, glass, devitrification with ageing 78−79536
- LiO_2-Al_2O_3-SiO_2, glass containing ZrO_2, cryst. process 80−103253
- LiO_2-Al_2O_3-SiO_2-TiO_2:Sn^{3+}, ESR and X-ray phase anal. 79−99752
- Li_2O-$2SiO_2$ glass, DTA study, Kissinger plot 80−84084
- Li_2O-$3SiO_2$ glass, crystallization 79−74141
- Li_2O-(Al_2O_3)-SiO_2 glass-ceramic, crystallisation mechanism 79−90559
- Li_2O-Al_2O_3-SiO_2, glass ceramic form. obs. using positron annihilation 77−7762
- Li_2O-Al_2O_3-SiO_2, kinetics of glass-ceramic formation, by modified broken total internal reflection method 77−36444
- Li_2O-Al_2O_3-SiO_2, phase separation of initial stages of sitallisation 80−88053
- Li_2O-Al_2O_3-SiO_2 glass, crystn. aggregation and migration of ion-implanted Ag 77−55240
- Li_2O-Al_2O_3-SiO_2-TiO_2 system glasses, Raman spectra obs. of glass-ceramics form. 80−60825
- Li_2O-$Al_2O_3(Ga_2O_3)(Bi_2O_3)$, quenched glasses, crystn. and ionic cond. 80−33899
- Li_2O-Fe_2O_3-siO_2 glass, struct. and crystallisation behaviour 78−83738
- Li_2O-MgO-Al_2O_3-SiO_2, effect of ZrO_2 on crystn. 77−16534
- Li_2O-SiO_2, effect of ZrO_2 on crystn. 77−16534
- Li_2O-SiO_2 glass, bulk crystn., SEM and optical microscope studies 80−44142
- Li_2O-SiO_2 glass, crystn. and phase separation, positron lifetime and annihilation lineshape meas. 78−23550
- Li_2O-SiO_2 glass, crystallisation and phase separation 79−10803
- Li_2O-SiO_2 glass, crystallisation study 79−90567
- Li_2O-SiO_2 glass, cryst. nucleation, test of classical nucleation theory 80−1939
- Li_2O-SiO_2 glass, water content effect on crystal nucleation and growth 79−55670
- Li_2O-SiO_2 glasses, crystn. kinetics from amorphous X-ray scattering study 80−38919
- Li_2O-SiO_2-P_2O_5 glass ceramic fibres, heat treatment, crystn., tensile strength 80−84995
- Li_2O-SiO_2(-TiO_2) glass, crystn., kinetic study using differential scanning calorimetry 80−44138
- (Li_2O-Al_2O_3-SiO_2):Fe_2O_3, glass, pyroceramic form., colour centres, magnetochem. investig. 77−16537
- $Li_2O.2SiO_2$ glass and glass ceramic, Auger electron signal decay, crystn. effects 80−25503
- $LiPO_3$, crystn. mechanism from melt 80−44139
- $Li_{x+2}P_xO_{3x+1}$, polyphosphate, melting and crystallisation 80−70376
- $Li_2Si_2O_5$ glass, steady state crystal nucleation rate 79−90564
- $Li_2Si_2O_5$ glass, steady state crystal nucleation rate 79−90565
- $Li_2Si_2O_5$-TiO_2 glasses, struct. and crystn. investigation using Raman spectra 80−38918
- $LiTaO_3$ glass-ceramics, transparent fabrication by crystn. of aluminosilicate glasses 77−59734
- Lu_2O_3-K_2O_3 (K=Ho, Er, Tm, Yb, Y), crystn. by Verneuil method 80−40254
- Mg-$MgNi_2$-Zn, diagram of state, Zn solubility, initial phase precipitation *(Russian)* 80−66478
- Mg-Zn metallic glass, hardness, elastic moduli, density, cryst. temp., mech. props., for flywheel appl. *(Dutch)* 78−52878
- MgO fusion cast ceramics, crystn., microstructures rel. to conditions 80−11638
- MgO-Al_2O_3-SiO_2, exam. of microstructure and crystallisation kinetics 78−80501

crystallisation continued
MgO-Al$_2$O$_3$-SiO$_2$, glass ceramic, structure and props. *(German)* 80–38927
MgO-Al$_2$O$_3$-SiO$_2$, melt and glass crystn. with ZrO$_2$-TiO$_2$ nucleants 77–31599
MgO-Al$_2$O$_3$-SiO$_2$ glass, features of crystallisation, in the presence of the thermal decomposition of tetrabutoxytitanium 78–87627
MgO-Al$_2$O$_3$-SiO$_2$ system glasses and glass ceramics, EPR obs. of transition elements, crystn. effects 78–23332
MgO-Al$_2$O$_3$-SiO$_2$: ZrO$_2$, TiO$_2$, glass, phase separation *(German)* 80–38932
MgO-CaO-Al$_2$O$_3$-SiO2(-TiO$_2$) systems, glass-ceramics, crystn. kinetics *(Russian)* 79–37626
MgO-FeO-P$_2$O$_5$ system, glass, ESR spectra, heat treatment conditions effect 79–65722
Mg(PO$_3$)$_2$ glass, rate of crystallisation, SiO$_2$ additive effects *(Japanese)* 77–68927
Mg$_{74}$Zn$_{26}$, glass, exam. of crystallisation 78–71681
Mn chalcogenides-II-VI compound solid solutions, cryst. growth and physicochem. props. 79–14711
Mn-Al alloy, vacuum codeposited, disorder of MnAl$_6$ phase in recovery process 78–51854
Mn-Bi film, amorphous, form. and crystn. 79–28923
MnAlGe film, mag. domains and amorphous to cryst. phase transition, electron microscopy obs. 80–71129
MnGaGe film, mag. domains and amorphous to cryst. phase transition, electron microscopy obs. 80–71129
Mo-Mo$_2$C(HfC)(TiC)(ZrC), eutectic formation of regular struct., crystn. *(Russian)* 80–66496
Mo-N, nonporous metal production accompanying arc plasma nitriding *(Russian)* 80–7712
Mo-W alloy type MW25N, crystallisation form, globular dendrites, grain boundaries *(Russian)* 80–66494
MoF$_5$, mol. and electronic struct., vitreous, liq., and tetrameric states, ^{19}F NMR obs., mol. mobility 80–34787
MoRh$_2$O$_6$, crystn. and cryst. struct., paramag. and elec. cond. props. *(French)* 77–80480
(Mo$_{1-x}$Ru$_x$)$_{80}$P$_{20}$, amorphous alloys, superconductivity, mag. susceptibility and electronic props., liq. quenching 78–88057
N$_2$, theory based on metallic cond. of porous network 79–59903
N$_2$, two-dimensional freezing, on differently graphitised carbon 79–77896
NH$_4$Cl-H$_2$O solidification model for showering cryst. form. in molten metal cooling *(Japanese)* 80–66498
NH$_4$H$_2$PO$_4$, crystal growth kinetics, in situ X-ray topography study 80–76167
Na polysilicates, IR spectra, struct., crystallisation effects *(Russian)* 78–72528
NaA and NaX zeolite crystals, crystn. study in presence of triethanolamine, Na$_2$O and SiO$_2$ content influence 79–65995
Na$_2$B$_4$O$_7$, melt-crystal interface temp. meas. during crystallization of melts 79–44908
NaBO$_2$.H$_2$O$_2$.3H$_2$O, crystallisation from aq. soln., nucleation rates with surfactant 78–91276
NaBO$_2$.2H$_2$O$_2$.3H$_2$O, crystallisation from aq. soln., growth kinetics with surfactant 78–91277
Na$_8$Ca$_3$SiO$_{1.5}$[Si$_2$O$_7$][PO$_4$]$_3$, synthesis conditions, cryst. struct. and IR spectra characts. 80–108335
NaCl, Czochralski growth, temp. distrib. near crystn. front 78–2036
NaCl, occlusion formation during dendritic crystal growth, expt. 78–38993
NaCl-KCl-CuCl system diagram investig. *(Russian)* 79–96015
NaCl-NH$_3$-CO$_2$-H$_2$O system, NaHCO$_3$ crystn. 80–100771
NaClO$_3$, composition of heat carrier heating aqueous solution system 77–12513
NaClO$_3$, growth from solution, effect of i.r. radiation on growth rate 77–1794
Na$_3$Cr$_2$(PO$_4$)$_3$, crystallographic data, ionic conductivity *(French)* 80–88077
NaF-SrF$_2$-CrF$_3$, glass transition, crystn. and melting temps., optical transmission *(French)* 80–64910
Na$_3$Fe$_2$(PO$_4$)$_3$, crystallographic data, ionic conductivity *(French)* 80–88077
Na$_2$Ge$_2$O$_5$, crystn., from Na$_2$O-GeO$_2$ glasses, lattice constants 79–77527
NaNO$_{3(2)}$, precipitation from mixed aq. solns. 80–100191
Na$_2$O-Al$_2$O$_3$-GeO$_2$-H$_2$O system, hydrothermal synthesis 77–36388
Na$_2$O-Al$_2$O$_3$-SiO$_2$, glass, nucleation, crystn., ceramic form. 80–84082
Na$_2$O-Al$_2$O$_3$-SiO$_2$-TiO, effect of Cr$_2$O$_3$, NiO, and MgO additions on crystallisation 78–87626
Na$_2$O-Al$_2$O$_3$-SiO$_2$-TiO$_2$-NiO glass, paramagnetic centres form. during crystn., ESR study 79–65710
Na$_2$O-B$_2$O$_3$ melt, crystallisation of Na$_2$B$_8$O$_{13}$ 78–59763
Na$_2$O-BaO-Al$_2$O$_3$-SiO$_2$, glass, nucleation, crystn., ceramic form. 80–84082
Na$_2$O-CaO-Al$_2$O$_3$-SiO$_2$-F-B$_2$O$_3$-ZrO$_2$ glaze, crystallisation, MgO, ZnO, BaO and SrO effects 79–60279
Na$_2$O-CaO-Al$_2$O$_3$-SiO$_2$ glass, crystn. for the purpose of obtaining vitroceramics *(French)* 80–75163
Na$_2$O-CaO-Bi$_2$O$_3$-SiO$_2$, electro-conducting glass-ceramic production by ion-exchange and reduction treatment 79–1616
Na$_2$O-CaO-SiO$_2$ glass, water content effect on crystal nucleation and growth 79–55670
2Na$_2$O-CaO-3SiO$_2$ glass, cryst. nucleation rate, viscosity, heat treatment 80–84081
Na$_2$O-Fe$_2$O$_3$-SiO$_2$, Mossbauer spectra, crystallisation study *(Russian)* 79–19816
Na$_2$O-P$_2$O$_5$-SiO$_2$ glass, substitution of Li$^+$, Mg^{2+}, Sr^{2+}, Ba^{2+}, Zn^{2+} for Na$^+$ 80–100332
Na$_2$O-PbO-SiO$_2$ glass-ceramic composite, directionally crystallised 80–107058
Na$_2$O-SiO$_2$, glass, devitrification with ageing 78–79536
5Na$_2$O.Fe$_2$O$_3$.8SiO$_2$, glass crystallisation study by Fe^{3+} EPR and Mossbauer spectra 80–64904
Na$_2$S$_2$O$_3$.5H$_2$O, solidification, heat transfer processes *(Japanese)* 80–6372
Na$_2$WO$_4$-CsWO$_4$-WO$_3$, system form., melting point 79–43222
Na$_2$WO$_4$-Pb$_2$WO$_4$-WO$_3$ system investigation, crystn. from melt, coordination compounds form. 79–52189
Nb-Ir(Rh) system glasses, form., crystn. and microhardness, resist. obs. 80–89178

crystallisation continued
Nb-Ni metallic glass, hardness, elastic moduli, density, cryst. temp., mech. props., for flywheel appl. *(Dutch)* 78–52878
Nb-Si(−V)(Zr)(Mo)(Ta)(W)(C)(B)(Ge), ductile amorphous, superconductivity 80–60131
Nb$_{40}$Fe$_{40}$P$_{14}$B$_6$, metallic glass, explosive compaction, mech. props. 80–89176
Nb$_3$Ge, RF and DC sputtered films comparison, O content effect 78–72022
Nb$_3$Ge, supercond. tape, growth technique via amorphous state 78–84708
Nb$_2$O$_5$-TiO$_2$, splat cooled, crystallization and ordering 77–68953
NdAl$_3$[BO$_3$]$_4$, single phase crystallisation region from solvent melt 80–38977
Ni $_{75}$Si$_8$B$_{17}$, amorphous alloy, crystallisation study *(Japanese)* 78–9959
Ni alloy powder, crystallised by supercooling methods, struct. props. *(Russian)* 80–54483
Ni, electrocrystallisation, reaction mechanism, appl. of impedance meas. *(French)* 80–103597
Ni film crystallisation on C fibres and sapphire crystals *(Russian)* 80–75455
Ni-B, film crystallisation on C fibres and sapphire crystals *(Russian)* 80–75455
Ni-B amorphous films, electronic transport and crystn. activation energies *(French)* 80–6807
Ni-base alloys, US vibration during crystallisation, effect on mech. props. *(Russian)* 78–19827
Ni-C-W-Cr(-Mo), Vickers hardness and crystallisation temp. 80–16361
Ni-Co-P, ferromag. film, amorphous to cryst. transition, diffr. and resistivity meas. 78–60587
Ni-Cr alloy, Kh20N80, inclusions and plasticity, crystn. conditions influence *(Russian)* 80–20923
Ni-Cr alloys, crystallisation anomalies *(Russian)* 78–19719
Ni-Cr film, struct. transforms. induced during annealing, resist. obs. 79–77965
Ni-Cr-P, amorphous, corrosion behaviour, immersion tests and electrochem. meas. *(Japanese)* 80–85085
Ni-Cr-Ti(Al), effect of ultrasound on crystallisation, dendritic structure, and plasticity *(Russian)* 80–11637
Ni-Mo-B metallic glass ribbons, tensile strength, crystn. temp. 80–89173
Ni-Mo-C(-Cr)(W), Vickers hardness and crystallisation temp. 80–16361
Ni-Nb amorphous alloy, transformation to crystalline state, ion emission microscope study *(Russian)* 79–82158
Ni-NbC eutectic, microstructure and strength depend. on composition and crystallisation conditions *(Russian)* 79–100128
Ni-P, electrodeposited films, amorphous and crystalline, electron microscopy, in-situ crystallisation 79–11043
Ni-P amorphous alloy, positron annihilation exam. of crystallisation 79–43061
Ni-P metallic glasses, crystn. kinetics by differential scanning calorimetry 78–91257
Ni-Ru peritectic alloys, rapidly cooled, crystn. peculiarities *(Russian)* 80–20922
Ni-Si-B, amorphous, thermal stability of ductility 80–76327
Ni-Si-B, embrittlement by crystallisation *(Japanese)* 78–48513
Ni-Ta (70, 30 wt.%) metallic glass, struct. and crystn. *(Russian)* 80–70136
Ni-Ti-P, amorphous, corrosion behaviour, immersion tests and electrochem. meas. *(Japanese)* 80–85085
Ni-Zn amorphous phase form. in Zr-poor region, hardness and fracture strength *(Japanese)* 80–84914
Ni-Zn-Mn-Fe spinel, crystn. from soln. in melt 80–2945
Ni$_{36}$Fe$_{32}$Cr$_{14}$P$_{12}$B$_6$, metallic glass 79–77520
Ni$_{36}$Fe$_{32}$Cr$_{14}$P$_{12}$B$_6$, amorphous, electrochem. corrosion in chloride solns. 80–50763
Ni$_{40}$Fe$_{40}$P$_{14}$B$_6$, amorphous alloy, microstruct. study of crystallisation 77–86062
Ni$_{0.625}$Ge$_{0.375}$, amorphous film, crystn. mechanism *(Russian)* 77–51623
Ni$_5$Ge$_3$, amorphous film, elec. resist., microstruct. and annealing 77–85188
Ni$_5$Ge$_3$, amorphous-crystalline transition, opt. and elec. characts. *(Russian)* 77–85191
Ni(H$_2$V)$_2$(H$_2$O)$_2$, synthesis and characterisation *(French)* 80–45225
Ni$_{78-x}$M$_x$Si$_{10}$B$_{12}$ (M=refractory metal), glass form. and thermal stability 80–79703
Ni$_{60}$Nb$_{40}$, stability, crystallisation, ductility meas. 78–47246
NiP$_4$O$_{11}$, formation in phosphoric acid melts 78–27394
(Ni$_{0.5}$Pd$_{0.5}$)$_{82}$P$_{18}$ amorphous alloy, liquid-quenched, crystn. kinetics, effect of thermal history 80–100175
(Ni$_{0.5}$Pd$_{0.5}$)$_{82}$P$_{18}$ amorphous alloy, liquid-quenched, crystn. kinetics, nucleation 80–100176
(Ni$_5$Pd$_5$)$_{82}$P$_{18}$, amorphous alloy, crystallisation 77–89382
(Ni$_5$Pd$_5$)$_{82}$P$_{18}$, phase separated, exam. of crystallisation by differential thermal analysis 78–87623
NiSi$_2$, amorphous, crystallisation by energy beam annealing 79–69012
Ni$_{100-x}$Zr$_x$, (x=34-40) metallic glass, cryst., isothermal annealing behaviour 80–6367
Ni$_x$Zr$_{1-x}$ metallic glass, crystallisation kinetics, elec. resist. and mag. susceptibility meas. 80–103659
P-Se, phase diag. and crystallisation of glasses at high press. 77–52297
POCl$_3$-SnCl$_4$:Nd^{3+}, liquid laser material, luminesc. centres conc., temp. depend. 79–50287
POCl$_3$-SnCl$_4$:Nd^{3+}, liquid laser material, luminesc. centres changes, crystn. process effects 79–50288
Pb glasses, Cu containing, crystallisation 78–47241
Pb, structure sensitive props., temp. hysteresis after melting and crystallisation *(Russian)* 79–29036
Pb-Bi, temp. regime of crystn. on rapid cooling *(Russian)* 80–66495
Pb-Sb eutectic alloys, solidification in space environment 79–47671
PbF$_2$-AlF$_3$ glass, optical props., crystn. and thermal expansion 80–48367
PbF$_2$-AlF$_3$ glass, prep. and props. 80–49120
Pb$_5$Ge$_3$O$_{11}$, ultrafine-grained crystallized from glass, ferroelectricity 78–39508
Pb$_5$Ge$_3$O$_{11}$, vitreous, crystn. via metastable phase 78–30543
PbO-B$_2$O$_3$-SiO$_2$-Al$_2$O$_3$-ZnO-CuO-Bi$_2$O$_3$ solder glass, crystallisation prevention by Cu addition 80–11654
PbO-B$_2$O$_3$-ZnO solder glass, with admixtures, crystallisation and thermal expansion 80–24364
2PbO-SiO$_2$-xSO$_3$ melts, crystn. 80–59400
PbO-ZnO-B$_2$O$_3$, Corning 7575 seal glass, devitrification 78–79532

crystallisation continued
PbO-ZnO-$\mathrm{B_2O_3}$, glass ceramic cements, crystallisation kinetics and character 77—85982
2PbO.$\mathrm{SiO_2}$, glassy, DTA obs. of crystn. kinetics 77—89381
2PbO.$\mathrm{SiO_2}$ melt, coding rate influence on constitution of silicate anions, crystn. kinetics 80—103248
12PbO.6$\mathrm{SiO_2}$.$\mathrm{PbSO_4}$, crystn. from 2PbO-$\mathrm{SiO_2}$-x$\mathrm{SO_3}$ melts, struct. and vibr. spectra 80—59400
PbS, crystallisation and stability in high-temp. alkaline solns. 77—52240
PbS(Se)(Te)-NiSb eutectic system, crystn. 79—52190
PbS(Te)-Sb eutectic system, crystn. 79—52190
PbSe-$\mathrm{PbCl_2}$, eutectic crystallisation, visual monitoring 77—44237
PbTe-SnTe solid solns., directional solidification 77—44149
$\mathrm{PbTiO_3}$, amorphous, crystallisation process, DTA and Raman spectroscopy meas. 80—75161
$\mathrm{PbTiO_3}$ glass-ceramics, transparent, fabrication method by crystn. 77—59733
Pd-Ag-Si alloys, amorphous, crystn. kinetics, DSC meas. 80—1933
Pd-Ni-Si amorphous alloys, crystn. process during isothermal ageing 80—89275
Pd-Si, amorphous, struct., crystn. and Hall effect meas. 80—75178
Pd-Si amorphous, internal friction and shear modulus 77—25085
Pd-Si amorphous alloy, heat treated, low temp. lattice sp. ht. 80—75368
Pd-Si amorphous alloy, positron annihilation exam. of crystallisation 79—43061
Pd-Si amorphous alloys, anal. of crystallisation kinetics 79—32912
Pd-Si-Sb, amorphous, phase separation and crystallisation 79—51002
$\mathrm{Pd_{78}Ag_4Si_{18}}$, amorphous, crystallisation kinetics 77—35487
$\mathrm{Pd_{77.6}Cu_6Si_{16.5}}$, metallic glass, viscosity meas. from rates of thermal transformations 78—26713
$\mathrm{Pd_{70}Fe_{10}Si_{20}}$ alloy, amorphous to cryst. transition, 350 to 450°C, Mossbauer spectra 78—59758
$\mathrm{Pd_{48}Ni_{32}P_{20}}$, metallic glass, viscosity meas. from rates of thermal transformations 78—26713
PdSi alloys, amorphous thermal behaviour and crystallisation kinetics 78—26446
PdSi, amorphous, crystn. kinetics 79—99078
$\mathrm{Pd_4Si}$ and $\mathrm{Pd_2Si}$, amorphous, crystallisation by energy beam annealing 79—69012
$\mathrm{Pd_{80}Si_{20}}$, amorphous alloy crystn., high press. effect 78—95001
$\mathrm{Pt_{45}Ni_{30}P_{25}}$, metallic glass, viscosity meas. from rates of thermal transformations 78—26713
$\mathrm{R_{1-x}Co_x}$, rare earth amorphous alloys, thermal stability, elec. cond. enthalpy 80—100172
$\mathrm{Rb(D_xH_{1-x})_2PO_4}$, D distrib. during crystallisation from aq. soln. 77—11496
$\mathrm{RbNO_3}$, anhydrous, kinetics of crystallisation 77—43164
S, glass, catalytic crystallization in organic media at room temp. 77—84657
S-Se amorphous alloys, crystn. kinetics, elec. cond. meas. 78—34441
$\mathrm{SSe_{20}}$, crystalline phase growth in amorphous solid and liquid samples 78—43107
$\mathrm{SSe_{22.5}}$, amorphous, photo-effect on crystn. kinetics, elec. cond. obs. 79—77522
$\mathrm{SSe_{22.5}}$, amorphous-cryst. transition, light effect, rel. to polymer crystallisation 79—99076
$\mathrm{SSe_{40}}$, amorphous alloy, crystn., elec. cond. meas. 78—34440
$\mathrm{SSe_x}$ (x=10, 15, 40), amorphous crystal transition, appl. of Kolmogorov-Avrami equation 78—67649
Sb, amorphous film on glass substrate, effect of substrate temp. on crystallisation 80—39468
Sb, critical thickness observations for crystallisation in amorphous thin films 79—69379
Sb electrodeposit, amorphous, explosive crystn., semicond-semimetal transition and IR absorpt. 78—51849
Sb evaporated film crystallisation rel. to substrate temp., −50° to 170°C 78—47680
Sb, thin layer, amorphous to crystalline phase transition *(German)* 77—69196
Sb:Te vapour saturation, diffusion zone struct. crystallisation orientation *(Russian)* 80—54438
Sb-Au amorphous films quench-condensed, resistivity and Hall effect meas. 79—99638
Sb-S-I glasses, activation energy of crystn. 80—64920
$\mathrm{Sb_2O_3}$-$\mathrm{SiO_2(GeO_2)}$-$\mathrm{Na_2CO_3}$-$\mathrm{H_2O}$, crystallisation 77—12605
$\mathrm{Sb_2S_3}$, vitreous, prep. elec., opt. and struct. props. 77—76889
$\mathrm{Sb_2S_5}$, deep struct. changes, NQR obs., high-press. and temp. effects 80—54139
$\mathrm{Sb_2S_2O}$, kermesite, synthesis, controlled precipitation and crystn. 77—48332
Se, amorphous, correl. between mol. struct. and props. 77—11484
Se, amorphous, elec. field effect 77—15318
Se, amorphous, influence of $\mathrm{O_2}$ on phase separation 77—47354
Se, amorphous, kinematic transform. study by DTA 79—27921
Se, amorphous and liquid state, Raman spectra, crystn. processes 80—60608
Se, amorphous film, crystn., thermal and photo-effects 77—47692
Se, amorphous film, photocond., dark cond., rel. to crystn. 80—88596
Se amorphous film, spherulite formation and role of stresses due to volume changes in crystallisation 77—1083
Se, amorphous films, evaporated, ageing and crystn., DTA 80—65413
Se, crystallisation kinetics correlation with molecular structure 78—94998
Se film, amorphous, block formation during crystn., electron microscope obs. 79—11030
Se film, amorphous, crystallisation induced by corotron charging 77—35832
Se film, amorphous, struct. and crystn., far IR transmission spectrum and DSC obs. 77—85106
Se film, amorphous, substrate effects on crystn. kinetics 77—1337
Se film, amorphous, thermo-crystn. obs. 77—11810
Se film, crystallisation using org. catalysts, struct. and elec. props. 77—51613
Se, film, effect of thermal history and substrates or crystn. by vac. condensation 77—15713
Se film, noncryst., ageing and crystn. obs., tentative struct. model 80—2295
Se film, noncryst., controlled vapour deposition, crystn., and optical props. 78—39696
Se, glass, catalytic crystallization in organic media at room temp. 77—84657

crystallisation continued
Se, hexagonal, resistivity depend. on applied elec. field freq. during crystn. 77—35938
Se layer crystallinity meas., combination microwave resonator method *(Russian)* 78—22652
Se, liquid-crystal phase transition, elec. cond. changes 79—33310
Se, vacuum evaporated film, photoinduced amorphous-crystalline transition obs. *(German)* 79—82156
Se, vitreous optical microscope obs. 77—84659
Se:As, continuous crystn. kinetics 77—24382
Se:Ge(Si)(Sn), vitreous, crystn. kinetics study by elec. cond. meas. 79—65526
Se:I, vitreous, crystn, kinetics determ. *(German)* 80—79936
Se:P, vitreous, crystn. kinetics study by elec. cond. meas. 79—64998
Se-Ge-Sb alloy glass, crystn. kinetics 77—20057
Se-S, glassy alloy, order-disorder transition kinetics 78—67650
Se-Te crystallised glasses, struct. transforms. and IR spectra 80—19712
$\mathrm{(Se)_x}$, crystn. and melting 80—40241
$\mathrm{Se_{0.09}Te_{0.05}}$, glass, effect of an alternating electric field 80—88054
$\mathrm{Se_{1-x}Te_x}$, amorphous film, photo-crystallisation 80—59839
$\mathrm{Se_xTe_{1-x}}$, amorphous, structural relaxation and crystallisation kinetics study by DTA 80—59394
Si, amorphous, CVD, retarding crystn. by alloying with C,N,B or Ge 80—44129
Si, amorphous, deduction of crystalline fraction 80—33890
Si, amorphous, implanted, struct. transition under laser irrad. 79—50992
Si amorphous film, crystn. on annealing at low temps. in contact with Al 80—24765
Si amorphous film, EPR rel. to elec. cond. 77—69692
Si amorphous film, vacuum deposited, microscopic voids, gas absorpt., crystn. study 80—49534
Si, amorphous films, crystallisation kinetics and morphology, TEM obs. 78—84093
Si, amorphous layer crystn., effect of ^{16}O, ^{12}C, ^{14}N and inert gases 78—14623
Si amorphous layers, glow-discharge, laser-annealed, elec. props. 80—75661
Si, amorphous layers, RF-sputtered on sapphire, crystallisation by CW ion laser annealing 80—80109
Si, crystallisation in Si-H-Cl system, adsorpt. layer comp. 77—15697
Si, crystn. front face effect on at displacements *(Russian)* 78—67781
Si, Czochralski growth, drop form. and crystn. rel. to dislocation struct. 78—2030
Si, epitaxial layer, growth mechanism from ion-molecular beams 80—2299
Si, epitaxy by solid phase crystn. of amorphous film 78—19663
Si film, amorphous, formed by CVD, crystallisation 77—39746
Si film, CVD or evaporated, covered with Al layer, solid-phase crystn. obs. 77—85100
Si film, crystallographic orientation using surface relief grating and laser crystn. 79—95277
Si film, elec. props., effect of amorphous to polycryst. transition 79—28425
Si, graphoepitaxy on fused $\mathrm{SiO_2}$ using surface micropatterns and laser crystn. 80—70554
Si implanted with ^{31}P, ^{75}As, ^{11}B, amorphous layer reordering 78—14622
Si, ion-implanted semiconductor, annealing, crystallisation, laser pulse energy depend. 78—34528
Si, laser annealing mechanisms, disordered overlayers, crystalln. 80—84967
Si, laser pulse induced amorphous to cryst. transition, thickness depend. 78—47678
Si, mol. beam and solid-phase epitaxies under ultrahigh vacuum 79—28945
Si, polycryst. with columnar struct., crystn. using casting technique and microstruct., book contrib. 79—43137
Si, RF sputtered amorphous film, high temp. metal induced crystn. 77—11825
Si ribbon parallel twinned structure development by shaped crystallisation 78—64465
Si, self-implanted, ⟨100⟩ and ⟨111⟩, crystallised layers by laser annealing, struct. 78—47644
Si, self-implanted layer, grain size, laser irrad. energy density depend. 78—72012
Si single crystal growth, Czochralski method, small-angle dislocation boundary form. anal. 80—89136
Si, solid-phase epitaxial growth stages in Si(crystal)-$\mathrm{Pd_2Si}$-Si(amorphous) system 77—85114
Si wafer, thin surface layers, amorphous to cryst. transform., obs. technique 80—107288
Si:P, implanted layers, ionisation-enhanced crystallisation 79—51151
Si-Al, silumin, crystn. of eutectic phases *(Russian)* 80—29942
β'-Si-Al-O-N, Mg-containing phases, crystn. 80—39297
Si-Al-O-N sintered ceramic, microstruct., phase composition and transformation mech., mech. props. 80—40309
Si-As-Te glasses, crystallisation kinetics under influence of water vapour 78—59762
Si-Ge amorphous films, effects of annealing and crystn., ESR microstruct. and elec. meas. 78—26790
Si-Ge-Te system glasses, structural and electronic transitions 77—76890
Si-Te system glasses, local struct., ^{119}Sn Mossbauer obs. 79—41968
SiC, epitaxial growth by sublimation sandwich method, effect of impurities 80—25568
$\mathrm{Si_2N_4}$ powders, synthesis, charact. 79—33977
$\mathrm{Si_3N_4}$ amorphous, crystallisation and sintering under pressure 79—87596
$\mathrm{Si_3N_4}$ amorphous films, struct., short-range order, and crystn. kinetics 79—28240
$\mathrm{Si_3N_4}$, dielectric film, on Si. crysts. from amorphous state 79—28225
$\mathrm{Si_3N_4}$ film, high temp. annealing effect on struct. and comp. 77—15714
$\mathrm{Si_3N_4}$, films, ion-beam synthesis, IR spectra, struct., crystallisation on annealing 77—16705
$\mathrm{Si_3N_4}$ films, struct. 80—54545
$\mathrm{Si_3N_4}$ with $\mathrm{Y_2O_3}$ and $\mathrm{Al_2O_3}$ additions, hot pressed, exam. of mech. props., grain boundary crystallization 79—20009
$\mathrm{Si_3N_4}$-$\mathrm{Al_2O_3}$-$\mathrm{Y_2O_3}$, sintered, observation of a noncrystalline phase 78—64536
$\mathrm{Si_3N_4}$.$\mathrm{Y_2O_3}$ prepared by hot press, cryst. struct., cryst. growth from glass phase 80—10534
$\mathrm{SiO_2}$, amorphous, induced crystallisation exam. 78—6016
$\mathrm{SiO_2}$, coesite, crystn. from soln. at high press. and temp. *(Japanese)* 77—72556

- **crystallisation** continued
  - SiO_2, dielectric film, on Si. crysts. from amorphous state 79–28225
  - SiO_2 film, amorphous, shock crystn. obs. 80–10828
  - SiO_2 films, stabilised by ion bombardment and heat treatment, crystn. and phase separation 79–77931
  - SiO_2, fused, surface crystn. by Li^+ ion implantation and annealing 80–89383
  - SiO_2 gel, steam treatment, struct. changes 80–35579
  - SiO_2 layers, crystallisation, structural props. rel. to annealing 78–34724
  - SiO_2-Al_2O_3, location of immiscibility gap 79–77724
  - SiO_2-Al_2O_3 (8 mol.%) glass, heat treated, devitrified phases 80–66469
  - SiO_2-Al_2O_3 system, location of metastable immiscibility gap 79–77521
  - SiO_2-Al_2O_3-CaO-MgO-TiO_2 system glasses, phase separation and crystn. 77–24384
  - SiO_2-Al_2O_3-CaO-MgO-NaO-K_2O-B_2O_3-ZrO_2, glaze, exam. of zircon crystallisation 79–19155
  - SiO_2-Al_2O_3-CaO-MgO, crystallized, prod. from inorganic waste *(Japanese)* 79–69017
  - SiO_2-Al_2O_3-CaO-MgO-Na_2O-K_2O effect of partial substitution of Na_2O by K_2O, on crystallisation 80–10499
  - SiO_2-Al_2O_3-CaO-MgO-Fe_2O_3 glass ceramic crystn., microstructures rel. to conditions 80–11638
  - SiO_2-Al_2O_3-CaO-MgO-FeO-Fe_2O_3 glasses, struct. transforms during heating 80–15014
  - SiO_2-Al_2O_3-Fe_2O_3-K_2O, form. of Al-Fe leucite, inversion temp. *(Japanese)* 77–62481
  - SiO_2-Al_2O_3-Fe_2O_3-CaO, basalt glass ceramics, crystallite form. due to heat treatment 80–38917
  - SiO_2-Al_2O_3-FeO-CaO-MgO pyroxene glasses, phase changes 80–15013
  - SiO_2-Al_2O_3-K_2O-Na_2O, exam. of leucite crystal growth 79–19496
  - SiO_2-Al_2O_3-Li_2O glass ceramic, crystn., microstructures rel. to conditions 80–11638
  - SiO_2-Al_2O_3-MgO-TiO_2 glasses, internal friction during crystn. 79–52285
  - SiO_2-Al_2O_3-MgO-TiO_2 devitrificates, microstruct. and props. *(Polish)* 80–70141
  - SiO_2-BPO_4, glasses and devitrificates prep., IR spectra *(Polish)* 80–71624
  - SiO_2-CaO-ZnO-B_2O_3-Na_2O-S, SrO effect on crystallisation 80–54135
  - SiO_2-Li_2O-K_2O-ZnO-P_2O_5, glass ceramic, phase changes and crystn. processes 80–7562
  - SiO_2-Li_2O-K_2O-ZnO glass ceramic, prep., phase transformations and physical props. 80–45299
  - SiO_2-RO-Na_2O-Li_2O (RO=MgO, CaO, SrO) glass-ceramic coating, optimisation of props. by selective oxide action 80–55552
  - SiO_2-TiO_2-Al_2O_3-SrO(BaO), glasses, ceramic form. rel. to Al_2O_3 content 77–25005
  - SiO_2-water system, inorg. polymer struct. form., globular crystn. 80–101042
  - SiO_2-ZnO-Na_2O-Li_2O, glass-ceramic coating, optimisation of props. by selective oxide action 80–55552
  - $SiO_2Al_2O_3$-CaO-K_2O system glass, phase separation and crystn., F catalytic effect 79–60280
  - Si_2ON_2, needle crystals, growth by nitriding process in powder compacts *(Japanese)* 78–76601
  - $Si_xO_yN_2$, dielectric film, on Si. crysts. from amorphous state 79–28225
  - Si_xO_yN, film, amorphous, shock crystn. obs. 80–10828
  - Sm-Co, amorphous, plasma-sprayed, role of Ar or H_2 atm. in mag. props. and crystn., rel. to H_2 storage 80–64898
  - $SmCo_5$, amorphous, supermag.-ferromag. transition and directional crystallisation 80–65891
  - Sm_2O_3-Ga_2O_3 system, garnet-perovskite transform., phase diagram relationships 80–97460
  - Sn film, melting and crystallisation kinetics, electron microscopy 77–15725
  - Sn film, thermal hysteresis of phase transitions and mechanism of crystallisation 77–89679
  - Sn, mechanism of influence of soluble impurities 78–71692
  - Sn-Bi, crystallisation temp., overcooling temp. *(Russian)* 80–97472
  - Sn-Bi(Pb)(Ga), temp. regime of crystn. on rapid cooling *(Russian)* 80–66495
  - SnO-SiO_2 glass, struct., X-ray density, IR obs. 79–46574
  - $Sr(NO_3)_2.4H_2O$, crystallisation kinetics 79–4264
  - SrO-Fe_2O_3, splat quenching struct. and crystn. mechanism *(French)* 78–51426
  - SrO_2-Al_2O_3-SiO_2 fusion cast ceramics, crystn., microstructures rel. to conditions 80–11638
  - $SrSO_4$, activation energies for mass transfer during crystallisation, surface active agent effects *(German)* 78–63689
  - $SrSO_4$, mass transfer in precip. from mixed solvents *(German)* 78–67674
  - $SrSO_4$, surface crystn., on $BaSO_4$, isotope exchange and electron microscopy study 80–34332
  - $SrWO_4$ cryst. growth, from Na_2WO_4 melts, thermodynamic props. 80–107084
  - SrW_20_4, kinetics of crystal growth from solns. in $Na_2W_20_4$ melts, by continuous cooling 80–11550
  - Ta-Ir(Rh) system glasses, form., crystn. and microhardness, resist. obs. 80–89178
  - Te, amorphous, obtained by splat cooling crystallisation 77–65949
  - Te, evaporated film epitaxial and amorphous-crystalline phase transition growth and struct. 79–51449
  - Te, Raman spectra, crystn. processes 80–60608
  - Te, single cryst. growth by hydrothermal method *(French)* 78–11096
  - Te-based eutectics, crystn. rate effect on electrophys. props. mutual solubility effect 80–60774
  - Te-Ge eutectic alloy, glassy, crystn. mechanism 78–22836
  - Te-Ge-Sn(Pb), Te rich, structural phase transformation concurrent with glass crystallisation, thermal evidence 79–4965
  - Te-Pb, amorphous, obtained by splat cooling, crystallisation, TEM obs. 77–66638
  - Te-Pb (20 at.%) alloy, amorphous, obtained by rapid cooling from liq. state, crystn. behaviour 78–26445
  - Te-Sn (20 at.%), amorphous, exam. of crystallisation by DTA, X-ray diffr. and TEM 78–47242
  - $Te_{80}Ge_{20-x}A_x$ glasses, rapid melt cooled, glass transition and stability range 80–75170
  - $Te_{80}Ge_{12.5}Pb_{7.5}$, phase-separated system, overlapping effects of glass transition and crystn., DSC results 78–83739
  - $Te_{80}Ge_{20-x}Sb_x(Bi_x)$, DSC studies of struct. phase transformation 80–66505
- **crystallisation** continued
  - TeO_2-V_2O_5-Fe_2O_3 system, phase equilib. and analysis, primary crystn. fields 77–66628
  - $TeSe_{12.5}$, amorphous alloy, thermal and elec. cond. during devitrification 78–26922
  - $TeSe_{19}$ glass, crystallisation kinetics 77–35484
  - $TeSe_{19}$, glasses, crystallisation kinetics, elec. cond. meas. 77–43155
  - $TeSe_{20}$, vitreous alloy, elec. and thermal cond. during crystallisation 79–7550
  - $TeSe_{50}$, amorphous to cryst. transition, kinetics 79–73099
  - $Te_{50-x}Se_{50}Sn_x$, thin films, elec. cond. and thermoelectric power meas. *(French)* 80–80335
  - Th-Fe (20 to 70 at.%), amorphous alloy, electrical resistivity and thermal stability 80–33901
  - $Th(CO_3)_5{}^{6-}$, in Na and guanidinium salts, struct./props. correlation *(French)* 78–95032
  - Ti alloys, ingots, produced by vacuum arc smelting, exam. of crystallisation process *(Russian)* 79–34019
  - Ti, crystallisation, effect of $SO_4{}^{2-}$ radical *(Chinese)* 79–51440
  - Ti-B-C system, complex carbide phase synthesis by crystallisation from gas phase 77–16526
  - Ti-Nb-Si, amorphous alloy, supercond. props. and crystn. behaviour, TEM and DTA study *(Japanese)* 80–84536
  - Ti-Si-C system, complex carbide phase synthesis by crystallisation from gas phase 77–16526
  - $Ti_{50}Be_{40}Zr_{10}$, amorphous, crystn. temp., press. and heating rate depend. 80–70132
  - $Ti_{50}Be_{40}Zr_{10}$, Metglas 2204, stability, crystallisation, ductility meas. 78–47246
  - $Ti_{70}Co_{20}B_{10}$, amorphous alloys, crystn. behaviour, TEM study *(Japanese)* 80–84087
  - $Ti_{70}Fe_{20}B_{10}$, amorphous alloys, crystn. behaviour, TEM study *(Japanese)* 80–84087
  - $Ti_{70}Ni_{20}B_{10}$, amorphous alloys, crystn. behaviour, TEM study *(Japanese)* 80–84087
  - TiO_2, amorphous film, vac. deposited, struct. and crystn., TEM obs. 80–2291
  - TiO_2, anatase, influence of Al_2O_3, Ga_2O_3 or In_2O_3 to polymorphic crysts. in vapour 79–78858
  - TiO_2 brookite synthesis from Ti in NaF or Ti compounds, form. mechanism *(Japanese)* 80–93529
  - TiO_2, obtained ions Ti_2OCl $(HCOO)_3(OH)_2$, by thermohydrolysis, exam. of crystallisation 80–2173
  - TiO_2, thermal anal. using solar heating *(Ukrainian)* 79–77725
  - $Ti(OH)_x$, amorphous, dehydration and crystallisation 77–43150
  - Tl-B-Se system, vitrification region, primary crystallisation fields 77–15321
  - Tl-Bi-Sb-Te system, peritectic reactions in $TlBiTe_2$-$TlSbTe_2$ cross section, crystn. character 80–108406
  - $TlAsS_2$, glass, effect of an alternating electric field 80–88054
  - $TlAsS_2(Se_2)(Te_2)$, vitreous, crystn. kinetics 80–64918
  - TlS_2, amorphous, struct. and origin of crystn. process 77–76322
  - TlS_x, struct. from radial electron density distrib. curves, entropies of melting and crystallisation 79–23527
  - Tl_2SO_4, elec. cond. rel. to thermodynamic props. in phase transitions 77–39690
  - Tm_2O_3 film, electron beam deposition, elec. props., and struct. 79–87580
  - USb_2, crystallisation from U-Sb, U-Sb-Sn liquid solutions 80–15024
  - V-Ni-Mo, structure in alloy crystallisation region, peritectic equilibria *(Russian)* 80–50622
  - V_2O_5 amorphous films, CVD prep., structural characts. 80–49114
  - V_2O_5, H_2O in noncryst. state, expulsion on crystallisation at 190°C *(French)* 78–42912
  - V_2O_5, splat-cooled, crystallisation, high-press. effects 78–9956
  - V_2O_5-based glasses, amorphous and crystallized electronic cond. and related props. 79–99547
  - V_2O_5-MoO_3, solid soln. thermogravimetric anal., ion formation on crystallisation 77–20076
  - V_2O_5-P_2O_5-MO system glasses, (M=Ba,Ca,Cu and Mg), phase separation, crystn. and EPR spectra 77–76321
  - V_2O_5-WO_5, solid soln. thermogravimetric anal., ion formation on crystallisation 77–20076
  - W, single crystal, crystallisation by containerless levitation 77–36394
  - W-Hf-C, phase equilib. 80–55348
  - WO_3, amorphous film, vac. deposited, struct. and crystn., TEM obs. 80–2291
  - WO_3 film, amorphous, struct. and crystallisation, high resolution electron microscopy 78–43268
  - WO_3 film, amorphous, struct. and crystn., TEM obs. 80–103606
  - WO_3, struct. transforms. during crystallisation from P_2O_5-WO_3-CaO 77–40343
  - WSi_2, amorphous, crystallisation by energy beam annealing 79–69012
  - YAG, crystallization kinetics and growth mechanism on oriented seeds in melt-solns. 79–14717
  - YAG, influence of facial growth effect on Yb ion incorporation 79–10822
  - YAG, single crysts., kinetic characts. of growth from melt-solns. on oriented seeds 79–14719
  - YAG, solubility in solvent $PbO_{-x}PbF_2$, phase form. in system Y_2O_3-Fe_2O_3-PbO-PbF_2-B_2O_3 78–95247
  - $YAl_3(BO_3)_4$, and $(Y,Er)Al_3(BO_3)_4$, crystallisation and growth characts., density and composition 80–35080
  - $YAl_3(BO_3)_4$, crystallisation from solution in a melt, solvent composition 80–38976
  - $Y_3Al_3O_{12}$ crystal growth from melt, gas bubble capture theory 80–64941
  - Y_2O_3-Fe_2O_3-Ga_2O_3-PbO-P_2O_3, primary crystallisation regions 77–44222
  - $Y_2Ti_2O_7$, precipitation from oxalates, carbonates, exam. 80–55641
  - Yb, amorphous metal films, crystallisation with and without mag. field 80–70570
  - Zn, electrocrystallisation, reaction mechanism, appl. of impedance meas. *(French)* 80–103597
  - Zn, structure sensitive props., temp. hysteresis after melting and crystallisation *(Russian)* 79–29036
  - Zn-Cd (1.4 at.%), crystallisation kinetic diagram appl. *(Russian)* 78–15384
  - Zn-Ga, temp. regime of crystn. on rapid cooling *(Russian)* 80–66495
  - $ZnC_2O_4.2H_2O$, crystn. kinetics by precipitation 80–50884
  - ZnO-Al_2O_3-SiO_2, transparent glass-ceramics, EPR obs. of glass crystallisation 78–80507

crystallisation continued
$ZnO-Al_2O_3-SiO_2$ glass, crystalline phase precipitation, crystallisation *(Japanese)* 79—32916
$ZnO-Al_2O_3SiO_2$, transparent glass-ceramic, microstruct., physical props., crystallisation ht. treatment depend. 78—80506
$ZnO-La_2O_3-GeO_2$, exam. of glass forming region, properties and crystallisation 78—88454
$ZnO-SnO_2-M_xO_y$, M_xO_y=glass-forming additive, I-V characts., heat treatment effects 77—43595
ZnS, with CdS or Cu_2S addition, phase transform. during crystn., 850 or 1150°C 77—48362
ZnS-CdS system, solid soln. form. mechanism 79—43177
$ZnSO_4.7H_2O$, meas. of water physically adsorbed rel. to water of crystallisation *(Japanese)* 80—6622
ZnSb, orientated crystn. conditions during reaction diffusion *(Russian)* 80—70558
Zr-Co(Ni) amorphous alloy, thermal stability and electronic props. 79—73487
Zr-Fe, amorphous alloy quenched by levitation method, crystallisation 79—55669
Zr-Nb-Fe (13 wt.%, 5 wt.%), struct. changes during decay of BCC β solid solution 79—15669
Zr-Nb-V-Fe (12 wt.%, 6 wt.%, 4 wt.%), struct. changer during decay of BCC β solid soln. 79—15669
Zr-ZrC, eutectic formation of regular struct., crystn. *(Russian)* 80—66496
ZrO_2, crystallisation from $Zr(OH)_4$, effect of water vapour, heat treatment and grain size *(Japanese)* 79—19170
ZrO_2, from $Zr(OH)_4$, influence of water vapour *(Japanese)* 79—78865
ZrO_2 gels, calcination 80—11964
ZrO_2 glass, melting depend. on minute components, surface crystallisation 80—84278
ZrO_2, glaze, liq. phase separation rel. to cryst. in glassy phase 80—103252
ZrO_2, thermal anal. using solar heating *(Ukrainian)* 79—77725
$ZrTiO_4$, form. mechanism from spray drying of solns., precip., of hydroxides and reactions of hydrates and solns. 79—43182

crystallite texture *see texture*

crystallites
see also crystal microstructure
anisotropic insulators, interaction of point charge and interface 79—69584
α-β brass, cold-rolled, energy dispersive X-ray diffr. studies 80—40379
α-brass, thin sheet, plastic anisotropy 77—63683
C, diffusely scatt., X-ray diffr. investig. of coherence strain, thermal vibr., preferred orientation 77—31595
carnauba wax, orientation prod., by mech. press. or US waves 78—64314
carnauba wax electrets, residual strain and crystal size of orienting crystallites and their effect on charge behaviour 80—11319
carnauba wax thermoelectret, charge behaviour 80—7276
carnauba wax thermoelectrets crystallite orientation, X-ray diffr. obs. 78—43774
catalyst, mag. characterisation, review 78—64881
cluster of curved crystallites with layer shift, X-ray diffr. intensities 80—39114
coatings, textured, crystallites faces determ. 80—64846
concentration variations, X-ray diffraction line profile anal. 78—75491
crystallites of supported catalysts, size distrib. from wide-angle X-ray meas. *(German)* 77—84566
cylindrical, with step displacement, particle sizes and distortion determ., by means of X-rays *(German)* 80—14960
cylindrical crystallite layer disorder, X-ray diffr. intensity effect 80—39113
Debye-Scherrer line profile intensity distribution *(German)* 77—55201
decahedral particles, high symmetry orientations, HEED and TEM study 79—86732
diamond, metastable crystallite overgrowths, in dissoln. medium in Ni presence at atm. pressure 79—51030
diamond, synthetic disorientation of crystallite subgrains *(German)* 77—68939
dimensions determ. using synchrotron radiation X-ray diffr. photographs 80—24313
diphenyl crystallites, changes in face growth rate from vapour phase 79—55686
direct ripening on substrate 79—42417
disordered cylindrical lattices, diffracted X-ray intensities 78—79493
dispersion, X-ray peaks width and mutual overlapping determ. 79—86649
distorted crystallites, aggregates, X-ray diffr. intensity, extinction effects 79—77452
electrophotographic KC film digital recording performance 78—78024
epitaxial small islands, one-dimens. model of mobility, parabolic substrate pot. 79—95299
fibrillas, crystallite shear deforms. rel. to small-angle X-ray scatt. pattern *(Russian)* 78—71690
finely divided solids, struct., thermal anal. methods *(French)* 78—14254
glass diode with electrothermal instability in switching channel 79—78238
graphite, neutron irrad., porosity changes, neutron small angle scatt. investig. 78—34544
graphite, nuclear, change in ratio of thermal expansion coeffs. at elevated temps., effect of crystallite size 79—42283
graphite, polycryst., EPR meas. rel. to temp., crystallite orientation, paramag. suscept. 78—35023
growth on curved metal surface, fragmentation *(Russian)* 78—22676
high resolution dark-field images 78—26398
high-melting metal multicrystal hollow ingot growth 79—69978
inert gas small clusters, three body interaction effects on thermodynamic props., comparison bulk props. 80—28128
ionic crystal spheroids, IR spectra, calc. using point matching method 77—32377
ionic crystallite, on substrate, IR active modes 77—1667
ionic rectangular crystallites, IR absorpt. calcs. 78—95583
island film growth, cluster size distrib. 80—107665
isocahedral particles, high symmetry orientations, HEED and TEM study 79—86732
Kevlar 49 fibre, poly p-phenylene terephthalate, Raman spectroscopy, heat, stress, radiation effects 79—65871
magnetic materials, anisotropy of magnetic and other props., crystallite orientation distrib. *(German)* 77—8307

crystallites continued
metal, BCC, fine particles formed by gas-evap. technique, cryst. struct. and habit 79—27935
metal, characterisation by selected-zone and weak-beam dark field TEM 80—79654
metal, orientation and shape determ. by TEM 80—1907
metal crystallites, polyhedral, growth in inactive gas, review 79—27934
metal supported crystallites, wetting in sintering and redispersion 80—24751
metals, electromechanical forces, theory *(Russian)* 77—81063
microcrystallites, LCAO-MO calcs, in HMO approx., influence of lattice distortion adsorption, absorpt. of gases *(German)* 78—30584
microcrystals on C foil, size distrib. from electron micrograph obs., UV absorpt. spectra obs. 80—55121
microparacrystallites, small angle X-ray scattering 79—10813
Mossbauer absorbers, deformation induced texture 79—8074
multiply twinned particles, with decahedral and icosahedral pt. group symm., twin cryst. struct. 79—86801
Nylon 6, fibre, crystallite dimensions, effect on struct., mech. and diffusive props. 78—11273
orientation distribution function, determ. from isolated axis density values 77—48612
PAN fibres, heat treatment, structural changes *(Polish)* 77—28835
particle size and distortion determination, crystallite with screw dislocation 80—15098
particle size meas. of crystallites in soln. by line-broadening meas. 78—18488
pentacene, evaporated on quartz, optical absorption, substrate temp. depend. 78—2932
perylene crystallite, photophoretic force, action spectrum determ. 79—50841
PET, fibre, crystallite dimensions, effect on struct., mech. and diffusive props. 78—11273
PET fibres, orientation distrib. of crystallites 79—86722
pigment crystalline soln., electrically induced fluorescence polarised component change meas. 80—32863
poly(2-vinylpyridine), isotactic, X-ray struct. determ. 77—84664
poly(chlorotrifluoroethylene) films, crystalline superstruct., mol. orientation, X-ray diffr., depolarised light scatt. 78—71685
poly-p-phenylene terephthalate, high modulus fibre, struct. obs. 78—75564
polycrystalline material, crystallite size distrib., X-ray diffr. determ. 77—27777
polycrystalline substances, use of Hall and Seebeck effects in phys. parameter determ. 77—12023
polyethylene, γ-irrad., asymmetric 002 X-ray line profiles, analysis 80—96567
polyethylene, γ-irradiated, luminesc. in warming and cooling 77—32450
polyethylene, crystalline, steric struct. modelling of end defects 80—6371
polyethylene, effects of mol. rot. and crosslink on specific draw ratios *(Japanese)* 79—96099
polyethylene, flow-induced fibril form. from soln. 80—59402
polyethylene, high density, effects of draw rate and temp. on necking stress *(Japanese)* 79—91757
polyethylene, hot-stretched, small angle X-ray scatt., computer anal. 79—14699
polyethylene, linear, γ-irradiated, crystallite size distrib. and lattice distortions 79—69157
polyethylene, linear, solution-crystallized, NMR anal. of phase struct. 78—71684
polyethylene, low-density, temp. changes in large period structure *(Russian)* 77—31603
polyethylene, oriented, partially crystalline, amorphous component obs., X-ray diffr. *(Russian)* 79—23534
polyethylene, oriented, shear strain, effect on stuct., props. *(Russian)* 80—7656
polyethylene, stress rel. to draw ratio during ultra draw *(Japanese)* 79—91759
polyethylene, struct. changes on hot-rolling 77—86051
polyethylene, structural changes on hot-rolling 77—86052
polyethylene, Young's modulus, crystallite thickness 78—76689
polyethylene film, elongated, TSC, 20 to 60°C 78—10826
polyethylene films, uniaxially and doubly oriented, crystallite size determ., microparacrystallite lamellar surface identification 78—48431
polyethylene terephthalate film, X-ray diffr. exam. of morphology 78—18558
polymer, oriented, amorphous-crystalline low ang. X-ray diagrams, supermol. struct. models, schematic representation *(Russian)* 78—87630
polymer, oriented, under load, crystallite stability, X-ray diffr. and IR spectra meas. 77—70126
polymer, semicryst., and filled, elastic modulus, strength, rel. to crystallite shape 80—45335
polymer matrix, amorphous, stressed, thermodynamics of embedded crystallite deform. *(Polish)* 77—52424
polymers, X-ray diffr., lateral grain boundaries 79—14700
polyoxymethylene, nascent, morphology, optical and electron microscopic obs. 80—59403
polypropylene-nylon 11 fibres, bimodal cryst. texture, X-ray diffr. and electron microscopy 78—75567
polytwin ferromagnetic cryst., crystallite thickness effects on mag. struct. *(Russian)* 77—80913
polyvinylidene fluoride, X-ray diffr. evidence for ferroelectricity 78—60399
polyvinylidene fluoride film, stretched, struct. and elec. props. 79—90572
PVC, highly syndiotactic, X-ray diffr. and IR studies of annealed material, crystallinity 78—2022
PVC, rheology, viscoelasticity, panel discussion 79—3984
PVC, rigid, microdomains, small angle X-ray scattering study 80—28930
PVC cpds., rigid, plasticised, capillary flow 79—4046
pyrocarbon coatings on HTGR fuel particles, Bacon anisotropy factors meas. technique 79—13418
quartz, crystallinity index 77—17080
Scherrer consts., review and variation with hkl, contour map representation 78—42854
semiconductor film, polycryst., Hall and drift mobilities 79—95531
size distributions, from X-ray line profile anal., smoothing and validity 78—34389
specific heat of microcrystallites 77—72696
steel, P, deep-drawing, spatial orientation distrib. of crystallites in cold-rolled and in annealed sheets 80—81079
surface decoration, localization of crystallites along steps 79—14992

crystallites continued
surface migration of small crystallites, Monte Carlo calc. with continuous time 78—26783
thin film growth due to crystallite surface migration, review 80—10810
three-dimensional epitaxial crystallite nucleation at substrate grain boundaries 77—76707
tight binding eigenvalues of finite SC and FCC crystallites with (100) surfaces 78—34745
tooth enamel crystallites, contrast effects in TEM 80—85572
topological modelling of crystal growth 80—59418
transition metal oxalate hydrates, powders, precipitation from aq. solns., cryst. numbers, sizes 77—44143
vacancy studies, model crystallites with two and three vacancies, topological approach 80—44202
weld pool, preferred growth direction of cellular-dendritic crystallites *(Russian)* 77—44236
X-ray diffracted intensities from curved crystallites with layer shifts 80—28879
X-ray diffraction by small crysts., intensity calc. method 79—27871
X-ray diffraction from small crysts., profiles calc. 79—27872
X-ray diffraction of elliptical crystallites 79—19122
X-ray powder reflection profiles calc., principles 80—100124
Ag thin films, deposited by cathodic sputtering using high-resolution electron microscopy, voids obs. 80—49557
Ag-Au, nucleation and growth on substrates 79—77956
Ag-Sn, splat-quenched, X-ray diffr. study 80—81094
AgBr, thin layers, struct. and photographic characts. 78—49919
Al, cryst. and polycryst., inhomogeneity effects on galvanomagnetic props. 78—60109
Al film, vacuum deposited, O_2 contamination effect on form. 79—82487
Al, wire, determ. of incomplete axial texture by X-ray diffr. 78—23720
Al-Cu-Zn (6, 0.3 wt.%), crystallite orientation distrib. function 79—83210
Al_2O_3, crystallite size and lattice distortion, determination using X-ray line broadening analysis, appl. to ceramic powders 79—8261
Al_2O_3, sintering behaviour, effect of calcination with mineralisers *(German)* 80—25622
β-$Al_2O_3.Na_2O$, ceramic tube fabrication, crystallite preferred orientation, ionic cond. 77—8781
$As_2S_3(Se_3)$ coating defects and impurities affecting damage threshold and absorptance 79—14065
Au, crystallite, surface decoration, depletion zone anal. along KCl slip step 79—90868
Au crystallites, vacuum deposited on MgO (111) surface, in-situ TEM obs. of mobility 77—76686
Au decoration technique, TEM and SEM study of localisation of decorating crystallites *(French)* 80—10470
Au film, on W substrate, chemisorbed N_2 effect on crystallite growth, FEM obs. 79—46976
Au films, condensation on alkali halides, growth, struct., stability *(French)* 78—38989
Au, formation in flowing Ar system, density, size distrib. and size dispersion 78—88415
Au particles, small single cryst., habit plane characterisation 80—79733
Au particles, small vapour deposited multiply twinned, struct. anal. using TEM 79—82488
Au, polycryst. film, RF bias-diode and triode sputtered, resist. and microstruct. 78—80072
Au, Volmer-Weber mode of epitaxy, deposition on KCl and MgO, post-nucleation phenomena 79—77955
BN prep. by water solvent, electron microscope charact. 78—47253
$BaCrO_4$, precipitation from aq. soln., cryst. growth kinetics 77—72574
$BaFe_{12}O_{19}$, powder, milled and annealed, phase composition, lattice conts. and crystallite size 80—71677
$BaTiO_3$ polymorph, hexagonal, low temp. and surface CO_3 adsorption and desorption 80—80713
$BaTiO_3$, powder compacts, sintered, physical and chem. inhomogeneities 79—87594
Be, growth on W, FEM obs. 78—26799
C, amorphous film, struct. props., Raman scatt. study 80—11417
C fibres, oxidation by NO_2, struct., props. modification 78—44237
C fibres, PAN-based type I, II and III, crystallite organisation, TEM study 79—77465
C, glassy, LMSC process prepared, exam. of props. by TEM and X-ray anal. 78—63675
C, glassy, struct. parameter var. with heat treatment temp. 77—11488
C, pregraphitic crystallites, appl. of theory of diamag. susceptibility of condensed ring systems 77—16039
Cd, film, freshly deposited, 77K, refl., annealing effect, thickness depend. 77—16413
$CdBr_2(I_2)$, vapour growth crystals, decomposition, electron microscope study 78—92268
CdI_2 polytypes, vapour growth mechanism 80—84124
CdO, formed by $Cd(OH)_2$ decomp., shape determ. *(French)* 78—10194
$Cd(OH)_2 \rightarrow CdO$, decomp. reaction, crystallite fragmentation, critical sizes and shapes 78—23635
$Cd(OH)_2$, decomposition into CdO, crystallite size and shape 79—57219
CdS film preferred orientation, internal stress, and interface characteristics 78—26795
CdS film solar cell yield rel. to crystallite column statistics 79—62005
CdS precipitates from acetate solns., crystal structure and photocond. obs. *(Japanese)* 78—10502
CdTe film formation on glass substrates, influence of sublayers of recrystn. stimulators 77—43455
Cl^-Ar_{N-1} small ionic clusters, thermodynamic behaviour 79—77769
$(Co,Fe)_{0.75}B_{0.25}$ metallic glasses, annealed, equilib. crystalline phases 80—3019
Co-P electroless film on Al base disc substrate, microstruct. rel. to mag. props. 78—68304
CrO_2 and CrO(OH), fine particle obs. of cryst. morphology and topotaxy 80—65969
Cr_2O_3 polycrystalline powder, crystallite sizes and surface areas 77—66086
Cr_2O_3 X-ray diffr. studies, crystallite size, phase transformation 77—21138
Cu, bright galvanic coatings, crystallite size determ. 79—66221
Cu, electrolytic epitaxial nucleation and growth, on (111) Ag 80—104081
Cu electrolytic form. by electrodeposition, structural defects 77—39749
Cu foil, polycrystalline struct. influence on transmitted 300 keV ion energy loss 79—95057

crystallites continued
Cu-Cd, structure, electrolytic deposition on monocrystalline Cu cathodes *(Polish)* 80—44435
Cu-Cd alloy electro deposits on Cu substrate, struct. *(Polish)* 79—51437
Cu-Cd alloys obtained by electrolysis, struct. 78—91552
Cu_2O, form. by Cu oxidation in CO_2, 800-1000°C 78—76784
Cu_2O on Cu, two stage metastable and stable surface nucleation, 800-1000°C 77—70214
D-T, solid, estimated heat capacity, enthalpy, thermal cond. and diffusivity 77—4228
Fe films, evaporated at oblique incidence, columnar struct. and texture 79—77967
Fe small particles, Mossbauer effect study of lattice vibr., Debye temp. of metallic core 80—44963
Fe, vacancy diffusion and vacancy lattices semi-empirical mol. orbital calcs. 77—1121
Fe-Pd(Pt), magnetic struct. changes assoc. with crystallite thickness increase *(Russian)* 77—80913
Fe_2O_3 crystallite formation in B_2O_3 and $Na_2O.B_2O_3$ glasses, Mossbauer obs. 78—68429
γ-Fe_2O_3 small particles, noncollinearity as crystallite-size effect, Mossbauer study 80—39939
Fe_2O_3, X-ray diffr. studies, crystallite size, phase transformation 77—21138
Fe_2O_3-Cr_2O_3, crystalline size and phase transform. study by X-ray diffr. 77—21138
Fe_3O_4, magnetite, oxidation kinetics, influence of cryst. size 78—79778
δ-FeO(OH) crystallites, TEM imaging investigation 80—39096
$Fe_{80}P_{13}C_7$, amorphous, mag. anisotropy, explained by fine crystallites 79—65670
Ga, electrode, crystallite interfacial impurities, electrochem. effects, microprobe anal. 77—44569
Ga, film, freshly deposited, 77K, refl., annealing effect, thickness depend. 77—16413
Ge amorphous layer, crystallisation anal. by cond. meas. *(French)* 77—72599
Ge particles, grown in Ar gas, cryst. struct. and habit, electron microscope study 79—74071
Ge_xTe_{1-x} amorphous matrix with Te crystallites, effect of annealing 77—24274
HfO_2 crystallite growth from oxide plasmas, growth morphology 80—59417
In, film, freshly deposited, 77K, refl., annealing effect, thickness depend. 77—16413
InSb, polycryst. film, Hall and drift mobilities 79—95531
α-In_2Se_3, X-ray diffr. line broadening 80—49047
KCl, agglomeration of crystals from aqu. soln. 79—90580
KCl crystallites, nucleation, oriented growth on amorphous SiO_2 using square-wave surface relief grating 78—47672
KCl, IR absorpt. calcs. in rectangular crystallites 78—95583
KH_2PO_4, dendritic growth in silica gel 80—35072
Li_2O-SiO_2 glass, cryst. nucleation, test of classical nucleation theory 80—1939
$MgCa(CO_3)_2$, dolomite, partial thermal decomp. into MgO and $CaCO_3$, product cryst. growth 80—108706
MgO, lattice defects., calcination temp. effect 80—15091
MgO, X-ray and electron diffr. crystallite size determ. *(Polish)* 79—100153
$Mg(OH)_2$, decomposition to MgO, mechanism, product crystallite size rel. to reaction rate 78—85152
Mo-low alloys, C enrichment mechanism of intercrystallite zones *(Russian)* 80—20963
NaCl, microcrystallites, sp. ht. calc. 77—72696
NaCl-$BaCl_2$ 1%, oriented growth of $BaCl_2$ phases, morphology 77—80627
Ni electrodeposit, crystallitemorphology *(French)* 77—32535
Ni electrodeposition, structure-internal stress relationship 80—70561
Ni foil, crystal struct. as function of substrate temp. during deposition 80—18742
Ni layer, vol. composition of sharp filamentary textures, elec. cond. meas. *(German)* 78—22978
Ni sputtered coating microstructure on mechanically activated cathode *(Russian)* 79—91586
Ni, vacancy diffusion and vacancy lattices semi-empirical mol. orbital calcs. 77—1121
NiZn ferrite, ZrO_2 additions influence on sintering and physicochem. props. 80—108369
Pb, cathodic deposition on Ag (111) and (100) surfaces, potentiostatic obs. *(German)* 79—15616
PbO layer vapour deposition, structure, and props. 80—65408
PbO-$2B_2O_3$-Fe_2O_3 glass, Mossbauer study, struct., crystallite formation, broadened quadrupole doublet 78—59761
PbS epitaxial film, struct., optical and elec. props. 78—19583
PbS film, soln. grown on Si, struct. and comp. of heterojunction 80—54530
PbTe, crystallite size in epitaxial layers by X-ray diffraction rocking curves 80—20052
Pd crystallite morphology, surface struct., electron microscopy obs. 80—29257
Pd-D, crystallite size effects, simultaneous sorption and X-ray study 80—65237
Pt, adsorption of H_2, electrolyte environment and crystallite size effects 78—27774
Pt, chemisorption of NO, effect of particle size of Pt supported on inorganic oxide carriers *(French)* 78—11552
Pt crystallite morphology, surface struct., electron microscopy obs. 80—29257
Pt foil, crystal struct. as function of substrate temp. during deposition 80—18742
Pt, on C electrode, surface area loss in H_3PO_4 80—101091
Pt, surface area loss, on graphite support, in H_3PO_4 78—73076
Sb, film, evaporated crystallite struct., texturisation 77—7991
Se film, amorphous, thermo-crystn. obs. 77—11810
Se film, vacuum deposited, struct. asymmetry, reflectivity elec. cond. 79—23855
Si films, polycryst., glow discharge deposited below 250°C, struct. and morphology 80—49535
Si particles, grown in Ar gas, cryst. struct. and habit, electron microscope study 79—74071
Si, polycryst, CVD, electron beam recrystn. 80—24759

crystallites continued
Si, RF sputtered amorphous film, high temp. metal induced crystn. 77−11825
SiC, synthesis by ion implantation of diamond and silicon, struct. characts. 77−76434
SiO_2 glass, electron microscopic determ. of struct. 79−90561
$SmCo_5$, sintered, high coercivity, microstruct. and mag. props. 77−69629
Sn polycrystalline films, elec. props. and crystallite size, 4.2K to room temp. *(Russian)* 80−93011
T-metal, thin film contact, time evolution of photovoltaic effect 80−65687
Te film, vacuum deposited, growth and morphology of crysts. 80−96766
Te textured thin films, prep., high solar absorptivity by multiples refl. 80−11568
Te, vacuum deposited on NaCl, crystallite growth and morphology, electron microscopy 80−65401
Te-Ag, thin film system, stress-relief appearance conditions 80−65416
Te-Bi thin film system, stress-relief appearance conditions 80−65416
ThO_2 crystallite growth from oxide plasmas, growth morphology 80−59417
ThO_2, particle size of crystallites in soln. by line-broadening meas. 78−18488
α-Ti, plastic deform., anharmonicity, and Gruneisen parameter 80−88246
TiB_2 thick film on low C steel substrate, CVD in US field, crystallite size 80−84854
TiO_x evaporated films, epitaxial growth on NaCl, electron microscopy obs. 80−10822
Tl, cathodic deposition on Ag (111) and (100) surfaces, potentiostatic obs. *(German)* 79−15616
UO_2 crystallite growth from oxide plasmas, growth morphology 80−59417
V_2O_4, struct. from electron microscopy of Tyep F-2 fibre 78−2087
WC, crystallite size distrib. of powder, SEM method *(German)* 78−47218
WO_3 film, amorphous, struct. and crystn., TEM obs. 80−103606
ZnO microcrystals, morphology, formed by Zn anodic electrocrystn. 77−80432
ZnO triode-sputtered film crystallite structure, X-ray evaluation 79−46987
ZrO_2 crystallite growth from oxide plasmas, growth morphology 80−59417
Zr_2O_3 microcrystals, tetragonal struct. stabilisation, crystallite size effect 78−51670

crystallographic shear
1 MHz crystal anharmonic AT modes, holographic displacement amplitude meas. 79−54097
Admiralty Metal, transgranular stress corrosion crack propag. 80−89402
BCC crystal, minimisation of shears for pencil glide 77−24319
BCC crystals in tension and compression, theoretical latent hardening 80−24459
α-brass, $(211)[\bar{1}11]$ single crystal, rolling deform. 77−21174
brass, orientation change in (211) $[\bar{1}11]$ single crystals during rolling *(Japanese)* 78−60712
brass, rolling texture development and deform. struct., shear bands effect *(Japanese)* 80−84952
brass, shear band development during rolling, twinning, metallographic obs. *(Japanese)* 78−39849
brass, simulation of rolling and shear texture, using an adapted Taylor theory 78−52835
brass α-β two-phase bicrystals, interface sliding studies 80−54248
composite piezoelectric medium, integral parameters at longit. shear *(Russian)* 78−30232
crack initiation notches, pure strain rate role, finite element computer program 77−70166
ductile single crystal, geometric effects in inhomogeneous deform. 79−46741
ductile single crystals, exam. of strain localisation 78−52912
etch figure rosettes, dislocation interaction in screw rays 78−47376
fracture, statistics in brittle materials with surface shear-sensitive cracks 79−41616
frictional slip progressing into contact zone of crack 80−16417
homogeneous material, 2D defects, interface problems 79−46674
isotropic crystal temp. shear coeff. determ. 78−2190
lithium ammonium tartrate monohydrate, spontaneous shear strain, X-ray obs. 78−56433
metal, BCC, polycrystalline aggregate, prediction of plastic props., deformation by $\langle 111\rangle$ pencil glide 80−11731
metal, slip-line analysis of scissors type shearing 78−23761
metallic shell, explosive expansion, deform. and rupture modes and mechanisms 80−85064
metals, dislocations and shock compression, thermodynamics 80−100235
minerals, dislocations and shock compression, thermodynamics 80−100235
modulated struct. phenomena, survey 79−95033
modulation operations and derived structs. 79−94930
PbO-Nb_2O_5 system, X-ray and electron microscopic phase and struct. determ. *(French)* 80−92508
planar defects, exptl. and calc. images at high resolution 77−35575
plastic deformation mechanism, meas. of microplasticity 78−60720
plate, simply supported, shear and bending moments by hydrodynamic analogy, results 79−64524
plate with line crack subject to antiplane shear 80−14618
polyethylene, crysts., subject to fold-surface tensile stress, elastic deform. 78−76712
polyethylene, oriented, shear strain, effect on stuct., props. *(Russian)* 80−7656
polyethylene, pyramidal crysts., soln.-grown, collapse mechanics 78−76713
polyethylene, roll oriented, superstructural change during uniaxial extension *(Japanese)* 77−52422
polyethylene terephthalate, shear compliances meas. of oriented sheet 80−104363
polymers, deformation under combined action of shear stress and hydrostatic pressure, testing equipment 77−56184
polypropylene, shear effect on crystallisation *(German)* 78−75586
polystyrene, intersections of coarse shear bands 79−100212
quartz, Brazil twins, twinning prod. by successive shears 79−19263
rare earth-Co phases, fault struct. and shear transform., stacking sequence notation 77−35571

crystallographic shear continued
serpentinites, Glenrock, New South Wales, microshear sets mimicking crenulation cleavage 80−21738
shear band effect 79−91675
shear band formation models, in rolling and extrusion 80−11666
simple shear generation *(German)* 77−44432
steel, Cr, lower bainite transform., significance of carbide precip. 80−97476
steel, Cr-Ni-Mn, adiabatic shear band determ. by surface obs. 80−97579
steel, high strength, low alloy, plate, impaired ductility in sheared edges 78−60727
steel, mild, plastic flow localisation under dynamic torsional loading, crit. variables 80−85015
steel, pearlite, deform. and fracture mechanisms, HV SEM obs. 80−104243
steel, stainless, single crystals, shear cracks, electron microscope study 80−40522
steel, type 4340, shear-band temp. meas. 80−48655
steel fracture mode, determ. from shear lip width 80−60968
transition metal oxide catalysts, reduction, cryst. defects influence, in-situ electron microscopy 80−81322
Ag, $(211)[\bar{1}11]$ single crysts., shear band effects on rolling deformation 80−50651
Al, scissors type shearing process, ductile sheet metal 78−19816
Al, type 2014-T6, shear-band temp. meas. 80−48655
Al-Zn-Mg, effect of microstruct. on localised shear failure 78−52996
α-Al_2O_3, sapphire lamellar crystal, growth twinning investig. 77−4113
Al_xVO_2, reduced, microstruct., crystallographic shear planes, electron microscope obs. 79−1443
BN, graphite-like, twinning and shear 77−4114
Cd, hardening resulting from pyramidal glide 77−48495
Cu, bicrystal, $\{110\}$ $\langle\bar{1}12\rangle$, deform. *(German)* 77−48513
Cu, deformation in ultramicrotomy 77−8874
Cu, void growth and localisation of shear in plane strain tension 78−64613
Cu-Al (15 at.%), rolled single crysts., metallographic study of deformation struct., orientational change, shear bonds *(Japanese)* 79−24582
Cu-Al (6.4 wt.%), rolled low stacking fault energy alloy, struct. and texture 78−52844
Cu-Co single cryst., precip. hardening *(German)* 80−84946
Cu_3Au-Co single cryst., precip. hardening *(German)* 80−84946
Fe, single crystals, work hardening and behaviour and dislocation struct. during simple shear tests 78−95762
Fe-Ni-Cr-P-B, Metglas 2826A, TEM of shear bands 78−48483
$Fe_{32}Ni_{36}Cr_{14}P_{12}B_6$ Metglas, bending deform., shear band form., high-speed cinematographic obs. 80−89322
Fe_2O_3-TiO_2 system, high temp. intergrowth struct., metal atom ordering in intergrowth boundaries 78−79573
Fe_xVO_2, reduced, microstruct., crystallographic shear planes, electron microscope obs. 79−1443
$GaNbO_4$, electron beam induced decomp., high resolution lattice imaging obs. 78−6161
Ga_xVO_2, reduced, microstruct., crystallographic shear planes, electron microscope obs. 79−1443
InP, plastic deform. and scratch microhardness meas. 78−27583
LiF, plastic strain accompanying local rise in surface temp., of natural shear *(Russian)* 80−6411
LiF, slip anisotropy under neutron irrad. and external stress, orientation of defects 77−31674
MoO_3, reduced crystals, planes of crystallographic shear, TEM study 79−46683
Nb, surface oxide softening, anisotropy 78−60716
Nb_2O_5-WO_3 system, TEM study of intergrowth of ReO_3 and tetragonal-type structs. 79−7580
$Nb_{28}O_{70-x}$, O diffusion, rel. to Nb_2O_5 nonstoichiometry *(French)* 78−47583
$Nb0_2F$, strain energy due to $\{001\}$ crystallographic shear planes 79−99223
$PbZrO_3$, ferroelec., crystallographic shear planes as nonstoichiometric defects 80−59484
$Pd_{80}Si_{20}$ metallic glass, tensile deform., shear band form., high-speed cinematographic obs. 80−89322
ReO_3 related oxides, elastic strain energy of matrix between shear planes, array microstruct. 78−43033
ReO_3 related oxides, formation energy of isolated crystallographic shear planes 78−43032
Si, ion implantation damage, annealing, role of stresses 78−75679
Tb, rel. to press. induced polymorphic transition mechanism 77−59113
Te, c-slip, asymmetry and orientation depend. 77−27888
Ti alloy, crack initiation on planar shear bands, H_2 assisted 80−71749
Ti, pure plate, silver band formation in ductile fracture process *(Japanese)* 80−16445
α-β Ti Widmanstatten alloy interfaces, elastic interact. stresses, effect on plastic flow onset 80−104218
Ti-11, unstable shear modes in fatigued β-annealed specimens 78−84984
Ti-alloy, IMI-685, unstable shear modes in fatigued β-annealed specimens 78−84984
TiO_2:Mg, high-resolution reflex images of crystal defects 78−6073
TiO_2-Fe_2O_3, comp. waves, Young's modulus minima rel. to crystallographic shear orientations 78−43034
TiO_2-Ga_2O_3, crystallographic shear planes and defect pair splitting, electron microscopy 77−76425
TiO_3:Cr_2O_3, dielec. consts., AC and DC resist. 80−20186
Ti_nO_{2n-1}, long-range strain and localised relax. energies of crystallographic shear structs. 79−94948
Ti_nO_{2n-1}, reduced rutile, elastic strain energy due to crystallographic shear plane arrays 78−55880
$TiO_{1.95}$iFe, quenched near melting point, transverse composition waves 79−99220
UO_2, lattice shear distortions 79−99221
VO_2, reduced, microstruct., crystallographic shear planes, electron microscope obs. 79−1443
V_2O_5 and lower oxides, defect structures and related props., review 80−59454
WO_3, reduced, elastic strain energy of crystallographic shear planes 77−69026
WO_3, reduced, elastic strain energy in cryst. shear planes 80−75239
WO_3, reduced, electrostatic interaction energy between crystallographic shear planes 77−47471
WO_3, reduction, defect role, in situ HVEM obs. 80−81323

crystallographic shear continued

WO_3, slightly reduced, interaction between non-parallel {102} crystallographic shear planes 77—80517

WO_3, strain energy, between parallel {001} shear planes 78—34523

WO_3-$N6_2O_5$ system, strain energy due to {001} crystallographic shear planes 79—99223

Zn, crystalline, wave formation during oblique collision *(Russian)* 77—89494

Zr-H alloy, precip. of γ-ZrH, shear mechanism 80—104170

Zr(Ca)O_{2-x}, internal, external distortion mechanisms, neutron diffr. study 78—83946

Zr(Ca)O_{2-x}, lattice shear distortions 79—99221

Zr(Y)O_{2-x}, internal, external distortion mechanisms, neutron diffr. study 78—83946

crystallography

see also crystal atomic structure; electron diffraction crystallography; gamma-ray diffraction; isomorphism; lattice constants; neutron diffraction crystallography; space groups; X-ray crystallography

algorithms, mol. fragment recognition in E maps and electron density maps 78—55772

anisotropy meas. by Twyman effect 78—31167

atom diffraction by cryst. surfaces, reson. effects 77—35447

atom packing projections, along real or reciprocal lattice directions, computer program 79—14707

atomic structure determination, experimental methods, review 79—68970

axiomatic construction, of geometrical principles of crystallography 80—38985

Bijvoet difference measurement, in crysts. with heavy atoms, stat. method for selecting reflections 79—50923

Bragg diffraction, errors in diffuse scattering meas. 79—50924

Bravais problem for n-dimensions (n>3) 77—15334

Cambridge crystallographic data centre: computer-based search, retrieval, analysis and display of information 80—1877

cavity location, computer program 78—18481

centrosymmetric crystal, probability distrib. of anomalous phase angles 77—31545

charge deform. models 78—71695

charge density mapping, limitations, appls. 78—71696

circular dichroism in presence of birefr. and linear dichroism, meas. method 78—27178

coincidence method, probabilistic theory for centrosymm. space groups 77—62433

coincidence method, probabilistic theory for noncentrosymm. space groups 77—62434

coincidence-site lattice interfaces 80—15381

compound nuclei as indicators in struct. anal., feasibility 77—35448

computer program for crystallographic data Cartesian translation 77—37196

computing correlation with artificial intelligence research 77—17960

conference, International Crystallography Congress, Warsaw, Poland (Aug. 78) 79—23481

constrained refinement, clarification on discussion 79—7507

coordinates calculation from distance information 78—38581

coordination number, proposed rigorous definition 79—99085

crystal, single, jig for precise orient. and grinding *(Czech)* 79—26047

crystal structure refinement with constraints, least squares refinement program 79—10744

crystallograms, cryst. struct. determ. method 80—103286

cumulative distributions, symmetry- and composition-dependent of normalized structure amplitude for use in intensity statistics 79—32847

cyanuric acid, X-N and X-X($1s^2$ core) maps 79—50922

cylindrical crystal turning in common lathe 78—18482

Debye-Waller factor, dynamic deformation effects 79—51207

density distribution of bonding electrons, simple refinement, method 78—18573

density distribution of bonding electrons, simple refinement, applic. to diborane 78—18574

derivative lattices, determ. of relationships 80—107012

determinantal inequalities, invariant joint probability distrib., heuristic derivation 79—32927

direct phase determ. of struct. factor 77—27774

disordered structures, two-dimensional, computer program for modelling *(French)* 80—59337

education, in crystallography, a survey in USA 79—9047

electron and magnetisation densities in molecules and crystals, Arles, France (Aug. 1978) 80—105428

electron charge density in crystal field theory, connections with molecular orbital theory 80—29514

electron density, minimising variance in integrals and derivatives 78—91195

electron density distrib. in crysts. and mols. from diffr. data 77—7632

electron density studies, appl. to diamond 78—38655

electron density studies, appl. to diamond 78—38656

electron density studies, appl. to melamine 78—38579

electron density studies, appl. to s-triazine 78—38578

electron density studies, appl. to Si 78—38657

electrostatic technique for crystal internal struct., appl. to diamond 80—10468

extinction theories, relation between incident point sources and homogeneous beams 77—65926

fast-rotation function representation in polar coordinate system 77—19813

Fejes problem: closest-packing of equal spheres on spherical surface 77—19809

Fourier map interpretation, formal aspects 77—1034

fragile lattice packings of spheres in 4D space 80—100194

gamma-ray diffraction applications 80—14972

gamma-ray scattering facility at MURR, accurate struct. factor determ., full-circle diffractometer 80—13192

generalized inverse matrices 78—9910

geology education, crystallography course 79—58459

goniometry, from photographs or angle-true sketches 79—55619

graph theoretical basis, trivalent graphs with 10 vertices 78—38644

Hamilton's R-factor ratio test, alternative with appl. to atom assignment problems 79—7506

hard-disc system, structures of close-packed thin layer 79—27941

hexagonal crystals, form factors, Fourier series representations, evaluation, special point formulae 78—22679

incommensurate crystal phases, symmetry, superspace-group approach, commensurate basic structs. 80—79726

crystallography continued

incommensurate crystal phases symmetry, incommensurate basic struct., superspace group approach 80—79727

infinite crystal, classical statistical mechanics 80—107067

inorganic cages, rel. to cubane and adamantane 80—19729

inorganic crystal, bond lengths prediction 77—47371

interatomic vectors construction, of crystal without calculating Fourier series 79—94840

interference fringes with projection hemisphere 79—94852

inverse structure, and generalised inverse matrix 77—19814

ionic crystal, arrangement of ions, eutactic 78—9982

isomorphous replacement data, new statistical model for describing errors, case of one derivative 79—50920

joint probability distribs. of struct. factors for space group P bar 1 from corresp. distribs. for space group P1 77—19811

lattice disorientations 80—28936

layered structure, spherical voids determ., APL program 77—27872

least-squares refinement, statistical bias 77—1039

living systems, molecular designing, essay 79—60214

macromolecule electron density map, low-resolution phase extension using matrix direct methods 77—66875

magic integer phase representation for complex structs., MULTAN program soln. 77—84571

martensite, shape memory, crystallographic similarities 79—66102

materials research for advanced energy technology, appl. of crystallography, review 79—96429

model, unit cell construction with polystyrene balls on rods 77—60882

molecular crystal structure classification 78—9985

molecular geometry, computer retrieval and anal., general principles and methods 78—83643

molecular geometry, computer retrieval and anal., geometry of β-1′-aminofuranoside fragment 78—83645

molecular geometry, computer retrieval and anal., variance and interpretation 78—83644

molecular packing arrangement drawings, plot of packing program POP1 79—94839

molecular packing plotter program 77—15272

molecular systems, electron density, spatial, rel. to conform. props., computer simulation 78—70763

multiple scattering from fixed scatt. centres, T matrix 77—15270

nomenclature recommendations of International Mineralogical Assoc. and International Union of Crystallography 77—65927

noncentrosymmetric structures, antisymmetric atomic features, Bijvoet ratio 79—32925

normalised structure factors, calc. of assoc. ε using rot. operators 77—1040

nuclear blocking patterns, crystallography demonstration, for teachers 79—40328

one-phase semiinvariants, practical aspects and appls. of probabilistic formulae 80—100119

one-phase structure semiinvariants, of first rank, estimation by generalised second representations 80—107013

one-phase structure seminvariants of first rank, estimation 78—79545

optical analogue of diffr. by dislocations and grain boundaries 78—38723

optical crystallography, book 80—12862

optical crystallography techniques, advances in spindle stage methods 78—85702

optimized conjugate gradient solution for least-squares equations 78—79495

order-disorder structures, desymmetrisation 80—38986

order-disorder structures, layer stacking 80—38981

organic homomolecular crystals, distrib. by chiral types and struct. classes 78—9986

orientational average, of $\exp[2\pi i(\mathbf{h}.\mathbf{x}+\mathbf{k}.\mathbf{y}+\mathbf{l}.\mathbf{z})]$ 79—7519

Patterson function for heavy atom struct., light atom position determ. 80—38866

Patterson function with translational pseudosymmetry, interpretation 80—33915

Patterson peak identification in presence of multiple peaks 77—35436

periodic bond chains, computer determ. *(French)* 78—26474

phase determination physical significance of triplets in direct methods 78—55776

phase probability of triple product, use of structural information 77—19810

phase relationships applic. to complex structures, MAGLIN, successor to MULTAN 77—19816

phase transformations, translational symmetry changes 77—62500

polycrystalline substances, fine structure characteristics, by integral method, appl. to C materials 77—43153

polymeric series of coverings, symmetry, comparison with layers of real structs., Belov subclass development 80—84129

polypeptide, packing anal. appl. to cyclic hexapeptide 77—2070

primitivity theorem *(French)* 77—80433

probabilistic procedure for phase determ., struct. factor algebra and quartet rels. 77—1037

protein structure, mol. replacement method for rennin and pepsin rel. mol. orient. 77—36866

protein structures, Fourier refinement 80—51037

proteins, model building procedure 80—51036

proton beams, low-energy, for cryst. material investigation, instrumentation aggregate 77—76266

protonography, appl. to grain boundaries in Cu *(Russian)* 78—38726

pseudo-extinctions, interpretation 78—55780

quartet theory, probabilistic approach 77—19808

quintets, joint probability distrib. of 15 struct. factors 77—62439

quintets, probabilistic theory of five-phase struct. invariant 77—62440

quintets, sequence of nested neighbourhoods of struct. factor 77—62438

radiation quanta, comparison of least-squares and maximum likelihood estimates for counts which follow a Poisson distrib. 79—23487

RE-1306 radiospectrometer improvement, use of LF modulation of magnetic field 80—57350

reciprocal lattice in crystallography, undergraduate demonstration 78—61989

recurrence relationship, for rapid relocation of misplaced molecules 79—99021

reduced cell for use in cryst. materials identification 77—15271

reflexion intensity, probability of meas. as negative 78—55781

Richard's box, low-cost, superimposing mol. models on 3D electron density maps 79—35495

rigid-body least-squares molecular fit routine 77—31546

rod packings 78—9981

crystallography continued

- rotational symmetry, and tensor props., 1-, 2- and 4-fold principal symmetry, trigonal, and hexagonal groups 80—100193
- rotational symmetry, and tensor props., method for group $3(3_7)$ 80—100192
- scattering experiments, small angle, interpretation of real-space information 79—50925
- Schmid equal factor, automatic curve plotting *(French)* 79—46507
- self-crystallising molecular models, mol. charge density contours 78—38645
- six-membered rings, conformation, nomenclature 80—78721
- spatial lattice distance, accurate and precise meas. *(German)* 80—19666
- sphere, largest possible inscribed between four spheres *(French)* 77—60906
- sphere tangent to four spheres, APL soln. 77—27773
- spheres, fragile lattice packings in 4D space 80—100194
- statistical system unknowns optimal evaluation *(French)* 79—9194
- stereodiagrams, 3D coordinates of mol. structs. 80—64824
- stereographic projections, standard, computer generated 79—37579
- stereoprojections for crystals of all syngonies computer program Mir-1 *(Ukrainian)* 80—24299
- structural types, coating genetics 77—31626
- structure analysis, separation of unknown parameters 80—28869
- structure factors and direct space information, algebraic and probabilistic relations 77—19812
- structure invariants $\phi_h+\phi_k+\phi_l+\phi_m$ in P1, probabilistic theory 77—62436
- structure invariants $\phi_h+\phi_k+\phi_l+\phi_m$ in P$\bar{1}$, probabilistic theory 77—62437
- structure invariants $\phi_h+\phi_k+\phi_l\phi_m$, sequence of nested neighbourhoods 77—62435
- structure model, photograph to digital convertor 79—60213
- structure semi-invariants, representations method 80—79724
- structure semiinvariants in P$\bar{1}$ space group, conditional probability distrib., higher-order terms 77—1036
- structure seminvariants in P$\bar{1}$ space group, first two neighbourhoods 77—1035
- superposition of similar structures, optimisation transformations 79—27865
- surface crystallography, ion beam, channelling and blocking effects, double alignment backscattering 80—65350
- $2F_0$-F_c synthesis, theoretical comparison with β and γ' synthesis 79—99018
- techniques and apparatus survey 77—4019
- texture, calc., library program, in FORTRAN IV 78—22598
- thermal-motion correction for bond angles, harmonic approx. 78—55777
- triplet relationship, probabilistic approach in P1 77—62432
- triplet relationship strengthening, new probabilistic approach in P$\bar{1}$ 77—1038
- two-phase semi-invariants, probabilistic theory of first rank via method of representations, practical appls. and aspects 79—50921
- two-phase seminvariants, of first rank, probabilistic theory via method of representations 79—32848
- validity of assuming symm. Laue diffr. conditions in diffr. contrast 79—50961
- vector symmetry, in crystallography, basic theorems 79—23556
- vector system interpretation by symmetrisation, Patterson function, Harker peaks 80—33914
- vectors, best proper rotation to relate two sets 78—91184
- Cd, metallic precipitates, crystallography dendritic origin of hexagonal prisms 79—66366
- Zn, metallic precipitates, crystallography dendritic origin of hexagonal prisms 79—66366
- $ZnSiP_2$, proton induced Kossel effect *(German)* 77—84601

crystals

- *see also bicrystals; crystal structure; crystallography; dendrites; epitaxial layers; liquid crystals; plastic crystals; whiskers (crystal)*
- No entries

Curie point *see Curie temperature*

Curie point writing *see thermomagnetic recording*

Curie temperature

- *see also ferroelectric Curie temperature*
- actinide elements and compounds, mag. props., book contrib. 80—75727
- alloys, amorphous, mag. props., review *(Japanese)* 78—52259
- alloys, binary, ferromagnetism and spatial long-range order 80—60159
- alumel, B versus H measurement from 25 to 180°C 78—23297
- amorphous alloys, at. order effects 77—73006
- amorphous alloys, Curie temp. comp. depend. 80—84597
- amorphous alloys, indirect exchange interaction and paramag. Curie temp. 80—75752
- amorphous ferromagnet, Ising model, Curie temp., exchange integral fluctuation effects 80—50121
- amorphous ferromagnet, Landau-Ginzburg theory, magnetisation and Curie temp. 80—75700
- amorphous ferromagnets, book contrib. 80—75743
- amorphous ferromagnets, Curie temp. depend. on nearest neighbour fluctuations 80—50120
- amorphous ferromagnets, mag. fundamentals, props. and appl. *(German)* 79—28557
- amorphous magnet, Bethe-Peierls-Weiss approx. 78—76263
- amorphous magnetism, Curie temperature and mag. excitation spectrum 78—10693
- amorphous systems, mag. props. effect of random anisotropy 79—4686
- anisotropic ferromagnet, magnon spectrum, FMR line intensity, Curie pt. behaviour *(Russian)* 77—69694
- anisotropic magnet mixture, Heisenberg spin system by Monte Carlo simulation 79—78408
- binary alloy, influence of chemical order on Curie temp. 79—87278
- binary alloys, strictly regular, quasi chemical model 78—39316
- binary magnetic alloys, Monte Carlo calc. beyond homogeneous mol. field approx., anomalous Kondo effect 77—8308
- biotite, thermal decomposition, stability of ferromag. products 78—57195
- bubble device materials, single-layer, ion-implantable small, design and development 79—82844
- $(CaO.6Fe_2O_3)_{97}(La_2O_3)_3$ compounds, effects of Nd_2O_3 substitution on magnetic props. *(Japanese)* 80—108010
- concentrated alloys, ferromag., spin fluctuations 78—64290
- copper formate anhydrate, cryst. struct. and mag. props. 80—79768
- cubic and tetragonal ferromagnets, crit. behaviour in mag. field 77—66329

Curie temperature continued

- cubic Ising ferromagnet, three spin interaction effect on mag. props. 80—54910
- degenerate ferromagnetic semiconductors, Curie temp. 78—6529
- di-(2,2,6,6-tetramethyl-4-piperidinyl-1-oxyl) suberate, nitroxide radical polarised neutron study in paramag. phase 79—47231
- dilute alloy, paramag. Curie temp., exchange field 77—47970
- dilute ferromagnet *(Japanese)* 79—33484
- dilute ferromagnets, with site and bond disorders, Curie temp. 77—59407
- diluted ferromagnetic systems, cluster theory, second-neighbour interaction 77—89965
- dilution effect in ferromagnet 79—47278
- dimethylammonium copper tetrachloride, crit. slowing down and anomalous relax. near Curie temp. 80—71053
- dimethylammonium copper tetrachloride, ferromag., quasi two-dimensional, ordering temp., press. depend. 80—84601
- dipolar uniaxial ferromagnet, equation of motion, nonlinear response near critical point 79—99717
- displacive ferroelectrics, Curie temp., microwave absorption, elec. field depend. 80—50280
- double exchange mechanism theory 77—24689
- electron-hole paired systems, ferromagnetic ordering phase diagram 80—97097
- Elinvar, Curie point, magnetisation and susceptibility, heat treatment effects *(Russian)* 78—47973
- extended defect system, phase transform., critical props. 80—103455
- FCC alloys, atomic ordering and antiferromagnetism 78—72330
- α-Fe, mag. ordering affecting homodiffusion coeff., 511-1200°C 79—73711
- α-Fe alloy, ferromagnetic, thermodynamic analysis of solubility and miscibility gap 79—60508
- ferrite, phase composition in magnetic field, use of DTA-TG-DTG *(Polish)* 78—31393
- ferrites, determination for toroidal samples as function of temp. 80—57346
- ferrites ball meas., by magnetic method *(Czech)* 79—93176
- ferrites of divalent metals, prep. by double decomp. reaction, mag. characts. *(French)* 79—33463
- ferroelectric crystal, displacive, effect of elec. field on thermal cond. 77—85002
- ferromagnet, critical dynamics above Curie pt. 79—87262
- ferromagnet, determ. using magnetic pendulum *(Japanese)* 80—82797
- ferromagnet, disordered, phase transitions, mol. field and Landau-Ginzburg theories 80—93118
- ferromagnet, dynamic slowing down of dislocations near Curie point *(Russian)* 79—8036
- ferromagnet, effects of biquadratic exchange and uniaxial anisotropy 80—60329
- ferromagnet, isotropic, dynamical spin-spin correl. function at Curie temp. in 6ϵ dimensions 77—4481
- ferromagnet, magnetic susceptibility, spin and charge density waves, Curie temp. *(Russian)* 80—100581
- ferromagnet, Mossbauer effect at temp. close to Curie temp. *(Russian)* 79—87339
- ferromagnet, $S=1$, variation of Curie-temp. with small uniaxial anisotropy 77—85448
- ferromagnet with random anisotropy, Curie temp., constant coupling approx. 78—76264
- ferromagnet with random anisotropy, spin-1 Ising model 77—28399
- ferromagnetic amorphous alloys, thermal expansion anomaly near Curie temp. *(Japanese)* 77—85542
- ferromagnetic anomaly of electron work function at Curie point, Vonsovsky-Sokolov model 77—12142
- ferromagnetic film, depend. of Curie temp. and spontaneous magnetisation on film thickness 77—32222
- ferromagnetic film, of cubic symmetry, depend. of Curie temp. on thickness and boundary conditions 78—19287
- ferromagnetic materials, Curie point determ. from saturation magnetisation-temp. charact. 78—60281
- ferromagnetic metal, itinerant electron model, for US propagation and structural instabilities 78—95508
- ferromagnetic metal, uniaxial, anisotropic spin fluctuations and anisotropic band struct. effects on resist. near T_c 80—65543
- ferromagnetic metals, spin fluctuation theory, Curie temp., mag. susceptibility 80—65937
- ferromagnetic metals, transport props., crit. behaviour 80—65522
- ferromagnetic plate, domain struct. near first-order phase transition resembling second-order transition 80—93139
- ferromagnetic semiconductor, optical transparency, photoferromag. effect, Curie temp. shift *(Russian)* 78—72387
- ferromagnetic semiconductors, s-f interaction on conduction band, red shift effect theory 80—59872
- ferromagnetic systems, inhomogeneous, Ginzburg-Landau theory, free energy and Curie temp. 79—51789
- ferromagnets, classical-spin model 79—33446
- ferromagnets, random, large exchange interaction, Green function theory 78—6537
- ferromagnets with double exchange, quantum theory 78—19204
- first-order magnetic transitions, intrinsic volume magnetostriction concept 80—29562
- garnet LPE film containing Lu, Curie temp. and flux spin-off, melt comp. effect 77—85515
- Green function theory, dipolar crit. temps. 77—89962
- group VIII and nearly related elements, cmpd. and superlattice form. 79—94955
- haemoilmenites, magnetic characts. of low-Curie point specimens 77—41022
- Heisenberg, ferromagnet, nearly two-dimensional and nearly one-dimensional thermodynamic props., Green's function investigation 79—15275
- Heisenberg amorphous ferromagnet, magnetisation and Curie temp., CPA calc. 80—75703
- Heisenberg and Ising dilute model, new cluster expansion, Curie temp. conc. depend. 77—89916
- Heisenberg ferromagnet, amorphisation, anisotropically distrib. exchange forces *(Russian)* 77—85408
- Heisenberg ferromagnet, anisotropic, with biquadratic exchange interaction and uniaxial anisotropy, Curie temp. 80—7118
- Heisenberg ferromagnet, biquadratic exchange, Green's function method, Hamiltonian and Curie temp. 80—15675

Curie temperature continued
Heisenberg ferromagnet, correlation functions in ferromagnetic and paramagnetic regions, RPA 80—71075
Heisenberg ferromagnet, Curie temp., decoupling of Green functions 77—12133
Heisenberg ferromagnet, dil., CPA theory, spin-wave stiffness and Curie temp. 78—31080
Heisenberg ferromagnet, low-dimens., crit. temp. *(Russian)* 78—23274
Heisenberg ferromagnet, magnon renormalisation 80—65849
Heisenberg ferromagnet, spin-one, with biquadratic and uniaxial anisotropy, Curie temp. 79—61123
Heisenberg ferromagnet, structural disorder effects on Curie temp. 79—78417
Heisenberg ferromagnet, structurally and chemically disordered, critical behaviour 77—43838
Heisenberg ferromagnet with s-d exchange interactions, Curie temp. 78—19255
Heisenberg magnet, dil., renormalisation group calcs. 79—56550
Heisenberg three-dimens. quantum models, ferromag. phase, conditions for T_c=0K 79—38345
Heisenberg-Ising magnets, random, critical temps., binary mixture, amorphous magnet and spin glasses 80—54911
Heusler alloy, Mn-containing hyperfine field and magnetic behaviour 79—78360
hexaferrites, M($BaFe_{12}O_{19}$), mag. characts. correlation with substituting ions at. nos. *(Russian)* 79—91218
hydrogen-bonded ferroelectric, Ising model in transverse tunnelling field and proton-lattice interaction 80—7307
induced moment systems, effect of spin fluctuations 80—2585
inhomogeneous ferromagnets, phase transitions, micromagnetic theory 80—65942
Invar, magnetic and thermal anomalies 80—34603
Invar, magnetisation curves in high mag. fields above Curie point 77—66386
Ising ferromagnet, one-dimens., with phase transition, thermodynamic props. calc. 80—80536
Ising ferromagnet, randomly dilute, with second neighbour expansion study 77—85452
Ising ferromagnet, two-dimensional, with second-neighbour interaction, computer simulation, series-expansion method 77—63052
Ising ferromagnets, correlation decay, zero-field susceptibility, mass gap 80—50116
Ising film, diluted, surface and bulk magnetic phases 79—82797
Ising mean cluster size near T_c, exponent interpretation 77—37820
Ising mixed ferromagnetic-antiferromagnetic systems with arbitrary spin, critical temp. 79—78407
Ising model, bond-dilute two-dimensional, crit. behaviour 79—8009
Ising model, Curie point in quenched bond model 78—56318
Ising model, effective field theory 80—7116
Ising paramagnet, impure, influence of spatial short range order 78—43542
Ising quadratic two-dimensional ferromagnet with three spin interactions 80—2542
Ising square lattice, phase transitions, next nearest neighbour interactions 80—50128
itinerant electron ferromagnet, magnon spectrum just below T_c, theory 80—65833
itinerant electron ferromagnetism, press. effects on mag. props. 77—66241
itinerant electron ferromagnetism, spin fluctuation theory 78—80151
itinerant electron ferromagnets, magneto-volume effects 80—60397
itinerant electron magnets, spin fluctuations and thermodynamic props. 79—65687
itinerant ferromagnetism with at. ordering 78—14920
lattice parameters, mag. and elec. props. 80—100578
liquid ferromagnet, model calculation 78—88088
magnetically dilute ferromagnets 79—11312
magnetically ordered metals, possible first order phase transformation 79—95589
measurement methods, using AC ccts. 77—49749
metal, amorphous ferromagnetic, paramagnetic Curie temp. determ. 78—76242
metal, freq. depend. elec. cond. near Curie point 77—66181
metal, indirect coupling between localised mag. moments by narrow band electrons 80—70942
metal particles, form. by evap., Curie temp. depend. 80—104053
metal-H systems at high H press., physicochemical props., book contrib. 80—24535
metallic glass, annealing, struct. relax. and crossover effect 79—86715
metallic glass, splat cooled, mag. props. 80—80491
metallic glasses, mag. props., struct., and prep., book contrib. 79—65665
metals, narrow-band, magnetism and mag. excitations 77—69478
metals and alloys, amorphous, exhibiting Mossbauer spectra, mean magnetic props. *(French)* 80—80489
Metglas 2826-A, anomalous magnetisation, critical effects, superparamagnetism 77—8328
minerals, constraints on Curie isotherms in deep crustal mag. anomalies 78—44805
minerals, HF meas. method *(Russian)* 79—39992
mischmetal-Co system, thermomagnetic analysis of intermediate phases 80—93115
$Mn_{1-x}Cu_xSb$ films, $0 \leq X \leq 0.3$, magneto-optical props. 79—51981
narrow-band s-d magnetic materials, ground state and thermodynamic parameters, cond. electron density depend. 78—47934
Ni single crystal near T_c, neutron transmission depolarisation 79—33479
one-dimensional diatomic chain, order-disorder transition, simple model 79—4394
order parameter spatial variation near Kondo impurity 80—103813
oxides, $RCu_3Mn_4O_{12}$, R=La to Lu, Y, synthesis and mag. props. 80—75717
pearlite in C steels (0.08 to 1.6 wt.%), exam. of temp. depend. of mag. coercivity 78—52304
phenyl alkyl ammonium copper chloride, quasi-two-dimens. Heisenberg ferromag., mag. props. 77—66273
planar Ising ferromagnet solvable model with roughening transitions 80—71069
pseudo one-dimensional kinetic Ising model, dynamic susceptibility 80—50025
random binary Ising system with transverse field, Curie temp., paramagnetic susceptibility 80—65938
random ferromagnets, Ginzburg criterion, critical fluctuations 80—71032

Curie temperature continued
random Ising model with transverse field term 79—56545
random mixture of ferro- and antiferromag. exchange interactions, high temp. expansion 78—23280
randomly diluted Heisenberg spin system with anisotropic exchange coupling, crit. temp. 79—99702
rare earth alloys, high pressure effects *(Japanese)* 80—20444
rare earth alloys, R_3Pt_4, R=Nd, Gd, Tb, Dy, Ho, Er, Tm, mag. props., 4.2 to 160K 79—78343
rare earth alloys, $R_{69}Ni_{31}$, amorphous, Curie temp., mag. susceptibility and coercive force, 4.2 to 300K 80—93092
rare earth alloys, $R(Fe_xRh_{1-x})_2$, mag. props., Mossbauer spectra 80—25108
rare earth alloys, R-3d alloys (3d=Mn,Fe,Co,Ni), magnetic properties 78—52231
rare earth alloys, RCu_x, mag. props., 4.2 to 200K 79—87233
rare earth alloys, RFe_4Al_8, mag. props., Mossbauer spectra, ordering effects 77—63179
rare earth Co Laves phase cmpds., elastic props. rel. to temp., mag. field 79—51834
rare earth compounds, pressure effect on mag. ordering temp. 80—100584
rare earth compounds, $R_2V_2O_7$, (R=Tm, Yb, Lu), physical props. 78—39320
rare earth garnet thin films, macroscopic magn. props., magneto-optical expts. 80—46764
rare earth heavy binary alloys, press. effect on mag. props. *(Japanese)* 77—43835
rare earth hydrides, props., book contrib. 80—45291
rare earth intermetallic, $R(Fe_{1-x}Mn_x)_2$, phase struct., mag. and Mossbauer meas. 77—20563
rare earth intermetallic compounds, ferromag. props., book contrib. 80—75726
rare earth intermetallic RCu_4Ag (R=Dy,Ho), mag. props. and cryst. struct. 77—20562
rare earth intermetallics, $RAu_{3.6}$, ordering temps. and effective moments 78—60283
rare earth intermetallics, RGa, mag. props., 4.2-350K 77—63230
rare earth intermetallics, RMg_2, cryst. and mag. props., ordering 78—68185
rare earth intermetallics, $RNiSi_3$, susceptibility, 80-1200K *(Russian)* 77—66281
rare earth iron alloy, amorphous film, cosputtered, struct. and mag. props. 78—60323
rare earth molybdates, mag. susceptibility meas. 79—69650
rare earth orthocobaltites, $R_{1-x}Sr_xCoO_3$ and $La_{1-x}M_xCoO_3$, itinerant electron ferromagnetism obs. 78—10660
rare earth palladinides, R_3Pd_4, mag. props. 77—47980
rare earth permanent magnets, physics and technology 80—20433
rare earth sesquioxides, 300 to 900K, mag. susceptibility and Curie temp. meas. 78—56288
rare earth ternary borides, RRh_4B_4, ferromag. Curie Temp., high supercond. transition temp. 77—89893
rare earth transition metal intermetallic permanent magnets, props. and technology, book contrib. 79—65696
rare earth tungstates, mag. susceptibility determ. 77—4495
rare earth-$(Co_{1-x}Ni_x)_5$, single cryst., mag. props., mag. reversal 77—85489
rare earth-Au(Cu), amorphous, mag. and transport props. 80—34605
rare earth-Co_2-Al, dil., nonmag. impurities effect on ordering temp. 78—84427
rare earth-Co, RCo_3 (R=Gd, Dy and Ho), effect of absorbed H_2 on mag. behaviour 79—33483
rare earth-Co alloy, Curie temp. determ. 79—65672
rare earth-Co alloys, ferromag., first and second order transitions 80—34631
rare earth-Co alloys, R_2Co_{17}, substituted 77—89947
rare earth-Co-Ni alloys, $Pr(CoNi)_5$ type, mag. props. and mag. reversal phenomena *(Russian)* 77—51924
rare earth-cobalt intermetallics, RCo_2, spontaneous vol. magnetostriction, first order phase transition obs. 77—12183
rare earth-copper intermetallic cpds., RCu_2, metamag., mag. props. 79—87242
rare earth-copper intermetallic cpds., RCu_2, metamag., mag. props. 79—87243
rare earth-Cu intermetallic compds. single crysts., mag. props. 80—54892
rare earth-Fe_2, mag. props. changes due to H_2 absorption, unit cell vol. 77—63178
rare earth-Fe_2 Laves phase intermetallics, mag. ordering temps. by DTA 79—47283
rare earth-Fe, intermetallic compounds, mag. props. *(Rumanian)* 78—92007
rare earth-transition metal alloys, amorphous, struct. and mag. props., book contrib. 80—39818
rare earth-transition metal amorphous alloy films with single mag. species 77—16121
rare earth-Ni alloy, RNi_2 (R=Gd, Tb, Dy, Ho or Er), Mossbauer effect of ^{57}Fe 77—69743
semiconductor, ferromag., red shift effect, optical absorpt. edge calc. 80—66140
semiconductors, ferromagnetic multivalley anisotropic, electron autolocalisation *(Russian)* 80—92848
semiconductors, magnetic, static magnetic properties, mean field approach 80—7090
semimetal, doped, interband transition, effect on Curie temp. of ferromagnetic phase transition 79—7994
simple ferromagnets, crit. behaviour 80—60331
singlet-doublet model of induced moment system, surface magnetism near Curie point 77—1530
singlet-triplet system in paramag. phase, low-freq. response 80—60172
spin glass, cluster mean-field model, static props. 79—4689
steel, austenitic, Ni-Ti, alloy N35T5, ageing, magnetisation and Curie temp. depend. on plastic deform., Mossbauer studies *(Russian)* 79—69669
steel, stainless, Fecralloy, creep-rupture props., 650-800°C 80—97535
steel, stainless, VNS-2USh, α to and from γ transformation investigation by thermomagnetic structural anal. *(Russian)* 79—83197
steel, transformations, influence of type of cold plastic strain *(Russian)* 79—52232
steel, VKS-210, α to and from γ transformation investigation by thermomagnetic structural anal. *(Russian)* 79—83197

Curie temperature continued
superconductivity-ferromagnetism coexistence, transition temp., magnon freq., indirect exchange 80−44757
superconductivity-ferromagnetism coexistence in two-band model *(Russian)* 80−84539
superconductor, ferromag., new phase, crit. temp. and wave number determ. 79−82705
superconductor with magnetic impurities, coexistence of superconductivity and ferromag., BCS and Zener models 80−88676
synthesis and characterisation 80−39039
temperature measurement, using magnetically controlled reed switches *(French)* 80−57291
TGS, gamma irrad. effects on heat capacity, Curie temp., permittivity 78−67737
TGS(Se), optical phonons near T_c, IR refl. and Raman spectra 77−48136
thin film alloys, surface magnetism props., Curie temp., Ising model 80−108039
three-dimens. quantum Heisenberg model, multi-neighbour interactions ferromagnetic Curie temp. 79−42786
titanomagnetites, Curie temps. rel. to domain struct. temp. var. 78−65272
titanomagnetites, temp. depend. cation distrib., mag. prop. obs. 80−85647
transition metal alloys, amorphous, mag. props., chem. short-range order 80−75739
transition metal alloys, amorphous, mag. props., structure and preparation 80−75737
transition metal alloys, high press. effects *(Japanese)* 80−20444
transition metal alloys, magnetovolume effects near crit. conc. for ferromag. 79−56591
transition metal amorphous alloys, mag. props. 80−29576
transition metal-H systems under high H pressure, phase diagrams., electrical cond., mag. props. 80−29923
transition metal-metalloid amorphous alloys, mag. props. review 78−52300
transition metal-metalloid glass, mag. props., charge transfer model 78−39324
transition metal-rare earth alloys, amorphous, mag. props., mean field anal. 79−4701
transition metals, 3d, ferromag. props., book contrib. 80−75724
transition metals, itinerant ferromagnetism theory 79−78301
transition metals and alloys, magnetisation in high mag. field, Arrott-Noakes plot 80−54919
triangular Ising lattice with anisotropic interactions 78−47926
TTF(MBDT) spin-Peierls transition, mag. exchange interactions, mag. props. 80−25138
uniaxial ferromagnet, domain struct. in mag. field 80−103853
X-Y ferromagnet, S=1, with uniaxial anisotropy, Curie temp. 79−78425
X-Y model, biquadratic, spin one, variation of Curie temp. 80−97102
^{6}, Heisenberg ferromagnet, spin dynamics, neutron scatt. expts. 77−20619
Al-Cu-Fe, liquid, mag. moment and transition from mag. to nonmag. state 79−24132
$AmFe_2$, high temp. mag. props., 300 to 1100K 79−51757
AuFe alloy films, mag. susceptibility, Fe concentration and annealing depend. 79−61119
$B_2O_3.Fe_2O_3.2CoO$, mag. props. up to 1200K transitions and magnetisation curves 77−36069
$B_2O_3.Fe_2O_3.2MgO$, mag. props. up to 1200K transitions and magnetisation curves 77−36069
$BaCo_2(AsO_4)_2$, planar X-Y model, mag. ordering 77−66256
$BaFe_{12-x}M_xO_{19}$ (M=Al, Ga, Sc, In) ferrites, mag. props. and struct. 80−15690
$BaFe_{12}O_{19}$, Ca^{2+} substitution effect on hexaferrite lattice and mag. props. 80−60243
$Ba_2NaNb_5O_{15}$, growth layer form., crystallization conditions effect, light diffr., Curie temp. 80−100778
$BaO-Fe_2O_3-B_2O_3$ glass, splat cooled, low temp. micromagnetism 80−34660
$BaTiO_3$:Dy ceramic, sintering, grain size, characterisation and props. 77−55923
Ba_2XRuO_6(X=La,Eu), ^{99}Ru Mossbauer spectra and other techniques 80−29659
$Ba_2Zn_{2-2(x+y)}Cu_{2x}Cd_{2y}Fe_{12}O_{22}$, mag. props. and Mossbauer spectrum 80−75765
$Ba_2Zn_{2-2x}Cu_{2x}Fe_{12}O_{22}$, hexagonal ferrites, prep. and mag. characterisation 79−1727
$BaZn_2Fe_{16-x}M_xO_{27}$ (M=Al, Ga, In, Sc), mag. props. and Mossbauer effect 80−75766
Bi-MnBi directionally solidified eutectic alloys, struct. and mag. props. 79−51815
$Bi_{3-2x}Ca_{2x}Fe_{5-x-y}In_yV_xO_{12}$, single crystal by flux method ferrimag. garnet *(Chinese)* 77−40056
$BiCoO_3$, paramagnetism, negative Curie temp. 79−64956
C chars, thermally activated paramagnetism, mag. susceptibility meas. 80−75709
$CH_3NH_3Ga(SeO_4)_2.12H_2O$, dielec. relax. near transition temp. 80−60493
Ca ferrite magnets, anisotropic, BaO substitution effect on mag. props. *(Japanese)* 79−99697
Ca, Ge-substituted garnet, LPE growth atm. effects on bubble props. 77−20655
$Ca(Cu_{0.78}Mn_{0.22})_3Mn_4O_{12}$, mag. structure, neutron diffr. powder data, 350K ferromag. T_c 77−69502
$Ca_xNi_{1-x}Fe_2O_4$, initial permeability and Curie temp. 80−25130
$(CaO.nFe_2O_3)_{100-x}(La_2O_3)_x$ ferrite, permanent mag. material, mag. props. and preparation 79−83148
Ca_2XRuO_6 (X=Y,La,Eu), ^{99}Ru Mossbauer spectra and other techniques 80−29659
$Cd_{1-x}Ag_xCr_2Se_4$, Ag acceptor states effect on exchange interaction 80−20397
$CdCr_2S_4$, EPR line profiles in paramag. and ferromag. phases 79−28602
$CdCr_2S_4$, single crystal ferromagnetic semiconductor, vapour-liquid transport growth method 77−21013
$CdCr_2S_4$, single crysts., EPR linewidth near Curie point, temp. and susceptibility depend. 77−63272
$CdCr_2S_4$, thermoreflectance near Curie point 79−78659
$CdCr_2S_4$:Cu, magnetic microregions caused by s-d exchange 77−77050
$CdCr_2S_4$:In(Ga), resist. and magnetoresist. meas., effect of donor impurities 79−19608

Curie temperature continued
$CdCr_2S_{4-\gamma}$, spinel, anomalies in paramag. susceptibility, Curie pt. *(Russian)* 77−80910
$CdCrSe_4$, ferromag. semiconductor, mag. props. near Curie pt., doping effects 79−1670
$CdCr_2Se_4$, deviation from Kittel's mag. resonance formula near T_c 79−87322
$CdCr_2Se_4$, Mott ferromagnetic semiconductor, optical absorption edge, critical behaviour 80−97226
$CdCr_2Se_4$, reactor radiation influence on ferromagnetic phase transform. *(Russian)* 80−75760
n-$CdCr_2Se_4$, single crystal, transport props. near Curie temp. *(Japanese)* 78−6406
$CdCr_2Se_4$:Ag(Gd), doping effects on exchange interaction 78−43579
$CdCr_2Se_4$:Cu(In), ferromag. semicond., mag. and elec. props. 77−20588
$CdCr_2Se_4$:Ga(In), photoconductivity, photomagnetoresistance near Curie point *(Russian)* 80−100485
$CdCr_2Se_4$:In, influence of Se-deficiency on props. 78−30921
$CdCr_2Se_4$:In(Ga)(Cu), magnetic microregions caused by s-d exchange 77−77050
$CdCr_2Se_4$:Ir(Cu), mag. props. near Curie temp. *(Russian)* 77−63234
$CdCr_2Se_4(S_4)$, ESR line intensity near Curie point 78−64269
$CdCr_2Si_4$:Ga, negative magnetoresist. effects near Curie temp. 79−11152
$Cd_{1-x}Cu_xCr_2S_4$, elec. resist., temp. depend., behaviour at Curie point 77−62929
$Cd_{1-x}Fe_xCr_2S_4$:Cu, effect of doping on elec. props. and Curie temp. 78−84214
$Cd_{1-x}Ga_xCr_2S_3$, spinel, anomalies in paramag. susceptibility, Curie pt. *(Russian)* 77−80910
$Cd_{1-x}In_xCr_2S_4$, ferromagnetic spinel, Cr^{3+} exchange interaction mechanism, Cr^{2+} relaxation, EPR line width depend. 79−69715
$Cd_{1-x}In_xCr_2S_{4-x}P_x$, ferromagnetic spinel, Cr^{3+} exchange interaction mechanism, Cr^{2+} relaxation, EPR line width depend. 79−69715
$Cd_{1-x}In_xCr_2Se_4$, electric, photoelectric and mag. props., metal-semicond. transition *(Russian)* 80−54738
$Cd_xMn_{1-x}Fe_2O_4$, substitution effect on mag. struct. and exchange interaction *(Russian)* 78−47949
$Cd_{1-x}Zn_xCr_2Se_4$, synthesis Curie pt., photomag. effect 77−51937
Ce-Co-Cu-Fe-Ti, sintered magnet, prep. and mag. props. 77−73043
CeAg, mag. and structural phase transition at hydrostatic press., elec. resist. meas. 79−61102
CeC_2, mag. props. 80−108008
Ce_2Co_7, and ternary hydride, mag. props. 80−108007
$Ce_xDy_{1-x}C_2$, solid solns., mag. props. 80−108008
$Ce_{0.73}Ho_{0.27}Ru_2$, spontaneous mag. order below superconducting transition temp., Mossbauer study 80−39701
$Ce_{3-x}S_4$, mag. ordering and elec. cond. 78−10681
$CeTiNbO_6$, electrophys. props. 78−23388
$Ce_2(WO_4)_3$, mag. susceptibility, paramag. Curie temp., 300-900K 79−82753
$(Ce_xY_{1-x})Fe_2$, mag. susceptibility and Mossbauer meas., lattice parameters 80−97068
Co alloys, amorphous, effects of metalloids on mag. props. 80−75738
Co, effect on oxidation kinetics 77−48592
Co, magneto-volume effects calc., rel. to itinerant electron model 78−43621
Co, sublimation rate near Curie temp. 80−49351
Co-B-Si, mag. props. different in amorphous and cryst. phases 77−69617
Co-Fe, soft mag. props. rel. to metallurgical aspects 80−88810
Co-Ga-Mn(Fe), small-angle mag. neutron scatt., states of mag. order study rel. to Mn and Fe substitution 79−11292
β-Co-Mn-Sn Heusler alloy, constitution and magnetic props. *(German)* 79−34009
Co-Ni (5 to 95 at.%), paramag. props., 800-1800°C *(Russian)* 77−55660
Co-V, Co rich, ferromag. behaviour, mag. moments, Curie temp., and NMR spectrum 80−70964
Co-V (12.4-18.7 at.%), ferromag. behaviour 79−24163
$Co_{100-x}B_x$ glassy alloys, mag. props. 79−73689
$Co_{1-x}Fe_xCr_2S_4$, ferrimag. spinel semicond., Curie temp. variation with composition and elec. props. 77−15849
$CoFe_2Se_4$, low-temp. thermal expansion anomalies and isothermal compressibility, mag. ordering and magnetorestriction 79−38363
$CoGa_{2-x}Fe_xO_4$, x=0.1−0.4, mag. susceptibility temp. depend. *(Russian)* 80−70957
Co(GaTiV) alloys, ferromag. onset, electron conc. depend. 80−60203
$(Co_{1-x}M_x)B$, M=Mn or Fe, ferromag., internal fields meas. by NMR spin echo 80−29646
$(Co_{1-x}Mn_x)_2B$, $0 \leq x \leq 1$, magnetisation, lattice consts., press. depend. of Curie temp. 80−7137
$Co_{50}Mn_xGa_{50-x}$, cryst. struct. transform. of B2 type *(German)* 79−91642
$Co_{50}Mn_xGa_{50-x}$, ordering and disordering phenomena, mag. study 80−70154
CoMnSi, $CoMnSi_{0.85}Ge_{0.15}$, mag. props. 79−42758
$CoMnSi_{1-x}Ge_x$, amg. props. 80−60270
$CoMoO_4$, mag. susceptibility and electrical transport props. 79−56511
CoNiP film, amorphous, electrolytic, prep. and props. *(Slovak)* 79−51823
Co_2P, Mossbauer obs. 77−40156
$Co_{80}P_{20}$ glass, mag. props. 77−63125
Co_2RhS_4, mag. semicond., mag. and elec. props. 80−93121
$Co_{75}Si_{25-x}B_x$ glass, metalloid comp. depend. 77−55665
Co_2(Ti,Mn)Sn, Heusler alloy, mag. meas. 79−47261
$Co_{1-x}Ti_x$, ferromag. props., Ti conc. effect 80−54872
$CoTi_{1-x}Al_x$, form. of mag. moment of Co atom, X-ray diffr., mag. meas. and NMR 77−43819
Cr-Co-Fe permanent magnet anisotropic alloys, plastic deform., ageing, particle alignment temp. 80−35254
Cr-Fe, superparamagnetism and mag. order charact. near critical conc., neutron scatt. study 79−11293
Cr-Fe (20 to 30 at.%), Mossbauer spectra temp. var. and ferromag. props. 77−81037
Cr-Fe-O, rutile type oxides, obtained from thermal decomp. of $Cr_{1-x}Fe_x$.OOH, Curie temp. and saturation magnetisation 79−24740
Cr-Ge system, phase anal. and physical props. 79−24160
$CrBr_3$ anisotropic ferromagnet. crit. mag. relax., field and temp. depend. 79−1717
$CrBr_3$, reflectance and thermoreflectance spectra in paramag. and ferromag. phases 79−56770

Curie temperature continued

- $Cr_2(CrO_4)_3$, ferromagnet, ESR spectra near Curie temp. 79−8042
- CrO_2 and tetravalent Cr oxide derivatives, metallic, chem. and phys. props. review 78−31069
- $Cr_{1-x}Rh_xO_2$, prep., Curie temp. evolution, SEM characterisation 79−43164
- $Cr_2Se_{3-x}Te_x$, mag. props. and lattice parameters, comp. depend. 77−66263
- $Cr_3Se_{4-x}Te_x$, mag. props. and lattice parameters, comp. depend. 77−66263
- CrTe, effect of high pressures on magnetic properties 78−52238
- Cr_5Te_6, high press. effects on magnetisation and mag. transitions, 77 to 360K 77−77057
- $CrTe_{1-x}Se_x$ (Sb_x), high press. and doping effects *(Russian)* 77−12125
- $CsMn_{1-x}Co_xF_3$, ferrimag., mag. props. and cryst. struct. 77−77056
- $CsMnF_3$, mag. phase boundaries, XY to Ising crossover, virtual bicritical point 80−50095
- $CsMnF_4$, planar ferromag., cryst. and mag. struct., Jahn-Teller effect 80−75715
- $CsMn_{1-x}Ni_xF_3$, ferrimag., mag. props. and cryst. struct. 77−77056
- Cu complex, halocuprates, ferromagnetic insulator, two-dimens. Heisenberg layers, mag. susceptibility 80−50068
- Cu, nuclear susceptibility thermometer rel. to ^{199}Sn Mossbauer effect thermometer, 6 mk to 1K 79−35737
- Cu, spin density wave fluctuations in nuclear spins, susceptibility, internal energy 80−50115
- Cu-Fe, supersaturated, spontaneous magnetisation region development, Mossbauer obs. *(German)* 78−64306
- Cu-Mg-FeO system spinel solid solns., synthesis, struct., and mag. props. 79−52142
- Cu-Ni alloy, critical conc. for ferromagnetism 78−14969
- Cu-Ni films, thickness depend. of Curie temp., resist. meas. 78−6545
- Cu-Ni-Fe, spinodal alloy, heat treatments for improved mech. props. 79−5024
- Cu-Ni-Fe alloys, quenched and aged, deformed, elec. resist. meas., shift of Curie point *(Russian)* 77−52514
- Cu-Ni-Fe alloys superparamag. early stages of decomp. *(Russian)* 78−6890
- $CuCr_2S_{4-\gamma}$, spinel, anomalies in paramag. susceptibility, Curie pt. *(Russian)* 77−80910
- $CuCr_2Se_4$, experimental obs. 78−76227
- $Cu_{1-x}Cr_2Se_4$, influence of excess Cu on physical props. 80−103836
- $Cu_{0.67}Cr_{1.78}Se_{2.67}Br_{1.34}$, polycrystalline mag. semicond., mag. and elec. props. 79−7846
- $Cu_yCr_2Se_{4-y}Br_x$, paramagnetic-ferromagnetic phase transition temp. depend. on element conc. 79−69672
- $CuCr_2Se_4(S_4)(Te_4)$, binary and ternary solid solns., mag. and elec. props. 80−2407
- $CuCr_2Se_{4-x}Y_x$, $(Y=Cl, Br)$, magnetisation, Curie const. 79−91225
- CuFe solid solns., quenched from vap. phase, mag. props. 80−60307
- $CuK_2Cl_4.2H_2O$, Heisenberg ferromag., press. effect on Curie temp. and susceptibility 77−28386
- $CuK_2Cl_4.2H_2O$, Heisenberg ferromag., mag. props. at high press. 77−69512
- CuMn, spin glass low DC field mag. susceptibility using SQUID 79−69684
- Cu_2MnAl, Heusler alloy, decomposition at 360°C 80−7536
- $Cu_2MnIn_{1-x}Sn_x$ alloy, compositional SRO, hyperfine interactions 80−71065
- $Cu(NH_4)_2Br_4.2H_2O$, Heisenberg ferromag. press. effect on Curie temp. and susceptibility 77−28386
- $Cu(NH_4)_2Br_4.2H_2O$, Heisenberg ferromag., corrections to scaling in sp. ht. 77−66328
- $Cu(NH_4)_2Br_4.2H_2O$, Heisenberg ferromag., mag. props. at high press. 77−69512
- $Cu(NH_4)_2Br_4.2H_2O$ Heisenberg ferromagnet, mag. props. in mag. field 80−34637
- $CuRb_2Br_1.2H_2O$, three-dimens. ferromag., crit. susceptibility exponents in Curie temp. region using relax. techniques 77−66304
- Dy, domain effects near order-disorder and order-order ferromagnetic transitions 80−65886
- Dy-Fe-O system, O-stabilised intermetallic $Dy_{12}Fe_{32}O_2$, prep. and characterisation 77−8956
- Dy-Th, single cryst., mag. susceptibility, transitions, anisotropy 80−54873
- Dy-Y, paramag. Curie temp. in basal plane and hexagonal axis 77−20548
- $DyAu_6$, mag. props. temp. depend. *(French)* 77−51879
- DyC_x, $0.28<x<0.53$, cryst. struct. and Curie temp. 79−86741
- $Dy_xCe_{1-x}Ru_2$, supercond., mag. props. 79−11267
- $Dy(Fe_xNi_{1-x})_2$, mag. behaviour, susceptibility and Mossbauer expts., 4.2-1300K 78−52235
- DyIG, mag. and magnetooptical props., temp. and field depends. 77−89927
- Dy_2O_3, 300 to 900K, mag. susceptibility and Curie temp. meas. 78−56288
- DySb, magnetisation study, intermediate metamagnetic phase transitions 79−99698
- $Dy_{1-x}Sm_x$, magnetoresist. of polycryst. specimens in fields up to 44 kOe *(Russian)* 80−92880
- $Dy_2(WO_4)_2$, mag. props., 300 to 900K 79−28510
- Er-Tb, elasticity modulus, ΔE-effect, internal friction, magnetic transformations *(Russian)* 79−91723
- $ErCo_3B_2$, ferromag. ordering and saturation moments 77−24711
- $(ErCo_2)_x(ErAl_2)_{1-x}$, mag. and struct. investigations of intermetallic systems 78−95440
- $Er_2Co_{17-x}Fe_x(Mn_x)(Ni_x)$, saturation magnetisation, Curie temp., easy direction, and anisotropy field 77−8304
- $Er_2Co_{17-x}M_x$, $M=Cr$, Ni, effect of substitution on mag. props. 79−78363
- $ErFe_2H_{3.9}$, mag. props. and lattice consts., effect of hydrogen absorpt. 77−20561
- $ErFe_2H_x$, mag. props. 80−25095
- $Er_3Fe_{5-x}In_xO_{12}$, lattice consts., T_c, mag. saturation, K-absorpt. and Mossbauer spectra, 80K *(Russian)* 77−20954
- $Er_6(Fe_{1-x}Mn_x)_{23}$, mag. props. and mol. field coeffs. 78−39319
- $Er_{1-x}Gd_xRh_4B_4$, supercond. and mag. transitions at press. up to 19 kbar 79−38236
- ErIG, magnetic props. of single cryst., 4.2-600K 79−78341
- Er_2O_3, 300 to 900K, mag. susceptibility and Curie temp. meas. 78−56288

Curie temperature continued

- $Er_2(WO_4)_3$, mag. props., 300 to 900K 79−28510
- EuB_6, ferromag., mag. props. 80−2561
- EuB_6, Hall effect and resistivity data, ferromagnetic ordering temp., pressure depend. 80−60010
- EuB_6, pure single crystals, magnetic and electric props. 80−11260
- $EuB_{6-x}C_x$, magnetic and elec. props. 78−91842
- $Eu_{0.5}Ba_{0.5}TiO_3$, ferromag., ferroelec., ceramic, Curie temps. determ. 78−68230
- $EuCu_5(Pt_2)(Pd_2)$, indirect exchange, spin echo NMR meas. 80−15822
- $Eu_{1-x}Gd_xO$, mag. props., transport meas. 80−97117
- $Eu_{1-x}Gd_xO_{1-x}N_x$, ferromag. semicond., prep., ferromag. props. *(French)* 77−69550
- $Eu_{1-x}Gd_xS$ films, mag. and elec. props. 80−15766
- $(EuLu)_3Fe_5O_{12}$, Ga, Al or (Ca,Ge) substituted, mag. props. and growth of 2 μm bubbles 78−91910
- $EuNi_xCu_{5-x}$, comp. depend., Mossbauer obs. of mixed valency of Eu 78−52407
- $EuNi_xZn_{5-x}$, comp. depend., Mossbauer obs. of mixed valency of Eu 78−52407
- EuO, Curie temp. raising by impurity addition *(Russian)* 77−47994
- EuO, Heisenberg ferromagnet, exchange interactions, neutron scatt. expts. 77−20579
- EuO, Heisenberg ferromagnet, static crit. props., neutron scatt. expts. 77−20618
- EuO, mag. struct. and transition temp., indirect exchange 78−91860
- EuO, nonstoichiometric film with excess EU, depend. on lattice parameter 79−8204
- EuO nonstoichiometric film, ESR spectra and exchange interaction 80−93176
- EuO, optical orientation of f-electrons, Curie temp. variation due to exchange interactions *(Russian)* 79−15431
- EuO, physical and physicochem. props., review 80−96875
- EuO, stoichiometric, crit. behaviour of piezotransmission at Curie temp. 77−85688
- EuO, transmission and resistivity, stress modulation effect near Curie temperature 80−96874
- EuO:Gd, critical specific heat depend. on doping, microwave cond. 79−95602
- EuO:Gd, elec. cond. under hydrostatic press., Curie temp. 80−96881
- EuO:La, photothreshold reduction by mag. induced space charge layer 78−72692
- $EuO_{1-x}N_x$, ferromag. semicond., elec. and mag. props. *(French)* 78−79993
- EuS, ferromag. semicond., optical spin orientation, Curie temp. increase 77−20627
- EuS, ferromagnetic film, optically induced magnetisation amplification, Curie temp. increase *(Russian)* 77−24719
- EuS films, mag. and elec. props. rel. to stoichiometry and defects 80−97122
- EuS, Heisenberg ferromagnet, exchange interactions, neutron scatt. expts. 77−20579
- EuS, Heisenberg ferromagnet, static crit. props., neutron scatt. expts. 77−20618
- EuS, mag. struct. and transition temp., indirect exchange 78−91860
- EuS, three dimens. Heisenberg ferromagnet, crit. relax. spectra mag. susceptibility 79−8000
- $EuS_{1-x}Se_x$, mag. phase diagram, from temp. depend. of magnetisation 80−7105
- $Eu_{1-x}Sm_xO$, ferromag. semiconductor with elevated Curie temp. 77−51903
- $Eu_{1-x}Sm_xO$, mag. semicond., thermodynamics of mag. quasimols. 78−19266
- $Eu_{1-x}Sm_xS$, electronic transition in Sm impurity ions, rel. to exchange interactions, L absorpt. spectra 77−59644
- $(Eu_{1-x}Sn_x)S$, high press. Mossbauer exam. of Curie temp. and transferred hyperfine field 79−56643
- $(Eu_{1-x}Sn_x)Se$, high press. Mossbauer exam. of Curie temp. and transferred hyperfine field 79−56643
- $Eu_xSr_{1-x}O$, ferromag. ordering and photoluminesc. 77−66313
- $Eu_xSr_{1-x}S$, ferromag. ordering and photoluminesc. 77−66313
- $Eu_2(WO_4)_3$, mag. susceptibility, paramag. Curie temp., 300-900K 79−82753
- (Fe,Co,Ni)-Si(B), amorphous mag. alloy, magnetostriction rel. to soft mag. props. 80−84633
- $(Fe,Mo)_{80}B_{20}$, glassy alloy, Curie temp. and crystn. temp., Mo additions effect, Mossbauer spectra 78−68428
- $(Fe,Ni)_{80}(P,B)_{20}$, quenched alloy ribbon, mag. moments, Curie temp. 77−40041
- Fe alloys, amorphous, effects of metalloids on mag. props. 80−75738
- Fe alloys, amorphous, mag. saturation, spin wave stiffness, temp. depend. 80−75741
- Fe alloys, amorphous, saturation magnetisation, Curie temp. and size effect 80−65815
- Fe alloys, magnetic sp. ht., Curie temp., alloying effects model 79−61116
- Fe and Fe-Ni Metglas alloys, ohmic and Hall resist. 100-700K, mag. behaviour 80−80254
- Fe base amorphous alloys, Invar and Elinvar characts. 80−29592
- Fe based metallic glasses, Curie temp., struct. relax. effects 77−8313
- Fe, calc. using model containing five bands 79−56536
- Fe, cold work stored energy effects on mag. moment vs. temp. curve 78−95419
- Fe, Curie point and A-γ transition to 53 kbar 79−56529
- γ-Fe epitaxial film, ferromagnetism, spontaneous magnetisation and Curie temp. determ. 78−2711
- Fe, ferromagnetic, cluster method, environmental effects 78−95405
- Fe, internal friction near Curie point 79−24567
- Fe, magnetisation curves in high mag. fields above Curie point 77−66386
- Fe, magneto-volume effects calc., rel. to itinerant electron model 78−43621
- Fe monocrystal, neutron crit. scatt. anisotropy 77−66327
- Fe, neutron magnetic critical phenomena, review of new effects 79−56534
- Fe, point contacts between ferromag. metals, singularities depend. in d^2V/dI^2, phonon spectra 79−60457
- Fe polycrystal, temp. shift of neutron crit. scatt. max., test of dynamic scaling theory 79−50953
- Fe, thermal cond., elec. resist., Lorenz number and magnetisation, crit. behaviour 77−4521

Curie temperature continued
- Fe, whisker, mag. crit. phenomena, size effects 78−68258
- Fe whisker, mag. memory function at crit. temp. 77−24714
- Fe whiskers, dynamics of mag. freq. response near Curie point 80−34648
- Fe whiskers, mag. anisotropy, magnetisation and temp. depend. near T_c 80−39766
- Fe-Al (25 at.%), anomalous magnetic behaviour *(Japanese)* 77−48011
- Fe-Al (25 at.%), double Curie point phenomena 77−73030
- Fe-Al(Si)(Ga)(Ge)(As)(Sn)(Sb) dil. alloys, mag. hyperfine fields, Curie temps. and Mossbauer meas. 77−63190
- Fe-B, amorphous alloy, mag. props. 80−84618
- Fe-B, amorphous ferromag., Invar type, magnetisation, elec. resist. and thermal expansion meas. 78−2663
- Fe-B, amorphous metallic glasses, high-temp. mag. anal. 78−91258
- Fe-B amorphous Invar alloy, elastic props., Elinvar characts. and ΔE effect 79−56595
- Fe-B-C, amorphous, effects of replacement of B by C on mag. props. 80−84621
- Fe-B-C amorphous alloy, formation, mag. props., thermal stability and density 80−75796
- Fe-B-C amorphous alloys, effect of Si addition on mag. props. 80−34694
- Fe-B-Cr(Mo), metallic glasses, mag., struct., and elec. props. 80−88751
- Fe-B-Si amorphous alloys, crystallisation temp., Curie temps., saturation magnetisation 79−82820
- Fe-B-Si-C amorphous alloys, prep. and props. 80−88748
- Fe-B(P) amorphous alloy, Invar effects, mag. props. meas. 79−56594
- α-Fe-Be(P)(Mo)(W)-Co, effect of Co on solubility anomaly due to mag. transition *(Japanese)* 79−42257
- Fe-C-Si alloy, lattice parameters of cementite after quenching 78−11198
- Fe-Cr (70-92 at.%), coexistence of ferro- and antiferromagnetism *(Russian)* 78−47955
- Fe-Cr alloys, crit. mag. props. near ferromag. Curie points 77−63216
- Fe-Cr-B, amorphous, Elinvar and Invar charact. *(Japanese)* 80−11832
- Fe-Cr-B amorphous alloys, corrosion resistance, Invar and Elinvar characts. *(Japanese)* 79−96213
- Fe-Cr-Co (31 wt.%, 23 wt.%), microstruct. and mag. props., ageing and thermomag. treatment effects 78−76769
- Fe-Cr-Co alloys, (5-9 wt.% Co), obtained by slow cooling under mag. field, permanent magnet props. 80−75797
- Fe-Cr-Co permanent magnets, phase diagram, miscibility gap 77−89984
- Fe-Cr-b amorphous Invar alloy, elastic props., Elinvar characts. and ΔE effect 79−56595
- Fe-N, hexagonal, ferromag. Mossbauer spectroscopy 77−63331
- Fe-Ni, Invar, Curie point, annealing effects and time depend. 80−80508
- Fe-Ni, thermal expansion, ferromagnetic-paramagnetic transition *(Russian)* 80−54412
- Fe-Ni alloy, cold work stored energy effect on mag. moment vs. temp. curve 78−95419
- Fe-Ni base amorphous alloys, effect of annealing on Curie temp. 80−34632
- Fe-Ni based metallic glasses, hydrostatic press. effect on mag. props. 78−19300
- Fe-Ni Invar, magnetisation and high field susceptibility 79−56518
- Fe-Ni Invar alloy, Curie temp. and elec. resist., effect of press. 77−85449
- Fe-Ni Invar alloys, splat quenched, mag. props. 80−75799
- Fe-Ni Invar alloys, thermodynamic props. 79−56560
- Fe-Ni Invar alloys of crit. conc., mag. props., flow theory methods *(Russian)* 80−65894
- Fe-Ni system, ferro-antiferromag. transition, γ phase mag. struct. 79−91231
- Fe-Ni-Al, Curie temp. depend. on ordering, antiferromag. ordering *(Russian)* 79−61101
- Fe-Ni-Al alloys, phase diagram, miscibility gap, mag. props. 78−92237
- Fe-Ni-Al-Co-Cu-Sn alloy YuNDK35T5, Sn addition effects on physicomechanical and magnetic props. and workability *(Russian)* 77−70101
- Fe-Ni-B-Si, amorphous, mag. props., heat treatment effects 80−89370
- Fe-Ni-Co-B-P soft magnetic metallic glasses, status report 78−64226
- Fe-Ni-Cr, Elinvar, struct. and mag. props., singularities during tempering *(Russian)* 80−50627
- Fe-Ni-P-B, metallic glasses, struct. relax., annealing effects on mag. props. 80−89261
- Fe-Ni-Te alloys, magnetisation 79−7975
- Fe-Ni(-Mn)(Cr)(V), concentration ferromag. antiferromag. phase transition and mag. state diagram. *(Russian)* 80−20401
- Fe-Ni(Co), solid and liq., paramag. susceptibility and electron struct., 800-1800°C *(Russian)* 80−25081
- Fe-Ni(Cr), Invar, exchange interactions between ferromag. and antiferromag. components 80−29545
- Fe-P-B, amorphous alloys, mag. props., conc. depend. 77−8314
- Fe-Pd, anomalous elec. cond. near mag. phase transition point, α to γ phase transition 80−15722
- Fe-Pd Invar alloy, Young's modulus, magnetostriction, Curie temp. 80−65988
- Fe-Pd Invar alloys, elec. and mag. props. and thermal expansion 80−75732
- Fe-Pt, Invar alloy, paramag. susceptibility 80−70940
- Fe-Pt Invar alloy, homogeneous strong ferromagnet, thermal expansion and mag. props 79−91278
- Fe-Si-Al (6,4 wt.%), Sendust alloy, effect of Ni content on mag. props. 78−72897
- Fe-Si-Al-Ni alloy, Super Sendust, Ni content and thermomag. treatment effects 77−4861
- Fe-Si-B amorphous alloys, metalloid content effects on Curie temp. and mag. moments 78−14956
- Fe-Si-B amorphous powder, production by spark erosion, and mag. props. 77−90290
- Fe-Si-B glassy alloys, mag. props., comp. effects 80−88752
- Fe-Si-B metallic glasses, mag. props., depend. on metalloid content 77−85485
- Fe-Si-B powders, prep. by atomisation technique 78−92213
- Fe-Si(Ge)(Al), solid and liq. paramag. props. *(Russian)* 77−66247
- Fe-V alloy, Curie temp. determ. using deviation from Mattheisen's rule 79−15306
- Fe-V alloy, elec. resist. between 78 and 1200K 77−8065
- Fe_2 magnetism, randomised exchange field theory 80−39733
- $(Fe\text{-}Co\text{-}Ni)_{78}Si_8B_{14}$, amorphous, low coercivity and zero magnetostriction 78−23299
- $Fe_{1-x}B_x$ amorphous films, mag. props. and thermal stability 79−78446

Curie temperature continued
- $Fe_{100-x}B_x$ ($11.5 \leq x \leq 22$), magneto-volume effect 78−91922
- $Fe_{100-x}B_x$, crystalline and glassy, low temp. magnetisation study 79−95608
- $Fe_{80}B_{20}$, binary amorphous ferromagnet, Curie temp. determ. by frequency counting 79−4749
- $Fe_{80}B_{20}$, metallic glass, ferromag. props. 77−16107
- $Fe_{80}B_{20}$ metallic glasses, stability and transforms. 80−75174
- $Fe_{84}B_{16-x}C_x$, amorphous, hyperfine interaction and Curie temps., Mossbauer meas. 79−73858
- $Fe_{80}B_{20-x}M_x$ (X=Al, Si, Ge, C, P) and $(FeCo)_{80}B_{20}$ glass, magnetisation, Curie and crystn. temps. 79−87289
- $FeBO_3$, crit. behaviour, Mossbauer and magnetisation meas. *(Russian)* 79−61106
- $FeBO_3$, displacement under press. up to 3 kbar 77−20603
- $Fe_{78}B_{12}Si_{10}$, amorphous, Mossbauer study of hyperfine interaction and mag. anisotropy 80−40027
- $Fe_{80}B_{20-x}Si_x$, metallic glass, mech. and mag. props., depend. on metalloid content 79−91213
- FeCo disordered alloys, Mossbauer spectra, hyperfine mag. field distrib., Curie temp. 80−7198
- $(FeCo)_{80}B_{20}$, metallic glass, saturation moments and Curie temp. 77−1542
- $(Fe_{1-x}Co_x)_yPBAl$ metallic glasses, influence of composition and ageing on Curie temps. 77−85445
- $Fe_xCo_{1-x}Si$ alloys, disordered, hydrostatic pressure effects on mag. props. 77−32175
- $Fe_xCo_{1-x}Si$, mag. props., effect of hydrostatic press. 77−12101
- $(Fe_{1-x}Co_x)_{77}Si_{10}B_{13}$, amorphous, mag. moments at 0K, Curie temp., mag. interactions 79−4670
- $(Fe_xCo_{1-x})_{100-y}(Si_{0.4}B_{0.6})_y$ amorphous alloy zero magnetostrictive, mag. props. 79−99743
- $(Fe_xCo_{100-x})_{100-(y+z)}Si_yB_z$ amorphous ribbon, mag. moment and Curie temp., comp. depend. 78−95421
- $Fe_xCo_{1-x}Si(Ti)$, magnetic props., sp. ht. and resist. meas. 79−61120
- $Fe_xCo_{1-x}Ti$, high press. mag. props. 78−23271
- $Fe_{85-x}Cr_xB_{15}$ metallic glass, Curie temp., crystn. temp. and room temp. elec. resist., Cr content effect 79−91229
- $FeCr_{2-x}In_xSe_4$, struct. and mag. props., comp. depend. 77−66262
- $Fe_{0.5}Cu_{0.5}Cr_2S_4$, ESR spectra, elec. and mag. props., Curie temp. 80−97137
- $Fe_{1-x}Cu_xCr_2S_4$, Hall effect and magnetoresist. 79−78119
- Fe_3Ge, mag. props. of cubic and hexagonal phases 77−8475
- Fe_2Hf, ferromagnetism in hexagonal and cubic compounds 77−36074
- FeI_2, first order mag. phase transition, neutron scatt. study 80−50090
- $Fe_{3-x}In_xO_4$, ferrospinels, cation distrib., Curie point and magnetisation meas. 79−42095
- $(Fe_{1-x}Mn_x)_3Si$, sp. ht. at low temps., mag. transitions *(Russian)* 77−32189
- $(Fe_{1-x}Mn_x)_2Y(B)$, Mn effect on Fe mag. moments, Mossbauer and mag. meas. 80−71016
- $Fe_{78}Mo_2B_{20}$, amorphous ferromag., mag. props. 79−38309
- $Fe_{78}Mo_2B_{20}$, exam. of mag. props. between 300 and 900K 78−85010
- $Fe_{80-x}Mo_xB_{20}$ metallic glasses, crystn. temp., elec. cond. as function of composition 79−60285
- $(Fe_{0.5}Ni_{0.5})$-Co, solid and liq., paramag. susceptibility and electron struct., 800-1800°C *(Russian)* 80−25081
- $(FeNi)_{80}B_{20}$, metallic glass, saturation moments and Curie temp. 77−1542
- $Fe_{40}Ni_{40}B_{20}$, amorphous, casting conditions effect on mag. props. *(Japanese)* 80−34698
- $(Fe_xNi_{1-x})_{80}B_{20}$, $(Fe_xNi_{1-x})_{80}P_{14}B_6$, new soft amorphous ferromagnetic glasses *(Croatian)* 79−11298
- $(Fe_xNi_{1-x})_{80}B_{20}$, amorphous, Mossbauer spectra, mag. props. 80−15843
- $(Fe_xNi_{100-x})_{80}B_{20}$, glassy, elec. resist. at elevated temp. 79−73484
- $FeNiBO_4$, mag. and Mossbauer studies 79−65661
- $FeNi_2BO_5$, mag. and Mossbauer studies 79−65661
- $(Fe_{0.5}Ni_{0.5})_{1-x}Co_x$, paramag. susceptibility, solid and liq. phases 1000-1800°C *(Russian)* 77−16040
- $Fe_{65}(Ni_{1-x}Cr_x)_{35}$, remanent magnetisation, temp. depend., anomalies near Curie temp. *(Russian)* 78−60310
- $Fe_{32}Ni_{36}Cr_{14}P_{12}B_6$, metallic glass, changes in Curie temp., physical dimensions and mag. anisotropy during annealing 77−85446
- $Fe_{32}Ni_{36}Cr_{14}P_{12}B_6$, Metglas 2826A, Hall resistivity, effect of thermal cycling and annealing 78−56125
- $Fe_{32}Ni_{36}Cr_{14}P_{12}B_6$, Metglass 2826A, mag. props. under high press., Mossbauer meas. 79−73860
- $Fe_{65}(Ni_{1-x}Mn_x)_{35}$, H solid solutions magnetisation behaviour in pulsed mag. fields 79−65674
- $(Fe_{1-x}Ni_x)_2P$, Curie temp., press. depend. meas. 80−97091
- $(Fe_{1-x}Ni_x)_2P$, mag. props. 78−23248
- $Fe_{27}Ni_{53}P_{14}B_6$, amorphous, Hall resist. and mag. props., short range order effects 80−34422
- $Fe_{27}Ni_{53}P_{14}B_6$, metallic glass, changes in Curie temp., physical dimensions and mag. anisotropy during annealing 77−85446
- $Fe_{40}Ni_{40}P_{14}B_6$, (Metglas 2826), ferromag. Curie temp. determ. 78−64206
- $Fe_{40}Ni_{40}P_{14}B_6$, glassy, mag. props. and hyperfine interactions, Mossbauer obs., 4.2-1000K 78−10812
- $Fe_{40}Ni_{40}P_{14}B_6$, metglas 2826, amorphous, Hall resistivity, thermal cycling and annealing effects 79−38050
- $Fe_{40}Ni_{40}P_yB_{20-y}$, amorphous, mag. props. effect of metalloid elements 79−28658
- $Fe_{44}Ni_{40}P_{14}B_6$, homogeneous deformation effect on crystn. and Curie temp. 80−21045
- $(Fe_xNi_{1-x})_{80}P_{14}B_6$, amorphous, Mossbauer determ. 78−6617
- $(Fe_{0.5}Ni_{0.5})_{75}P_{16}B_6Al_3$ glass, struct. relax. as origin of Curie temp. ageing 78−84418
- $Fe_{29}Ni_{49}P_{14}B_6Si_2$, metallic glass, changes in Curie temp., physical dimensions and mag. anisotropy during annealing 77−85446
- $(Fe_{1-x}Ni_x)_{77}Si_{10}B_{13}$ amorphous alloy system, saturation mag. moment, Curie temp., mag. susceptibility 80−39753
- $(Fe_{1-x}Ni_x)_{77}Si_{10}B_{13}$, amorphous, Landau-Ginzburg theory, magnetisation and Curie temp. 80−75700
- $(Fe_{0.2}Ni_{0.8})_{1-y}(SiO)_y$, Permalloy material, magnetisation, temp. and impurity atom conc. depend., band model calcs. *(Russian)* 80−93088
- $Fe_{1.985}Ni_{0.975-x}Zn_xCo_{0.04}O_{4+\gamma}$, elementary coupling energy of Co^{2+} to lattice 77−1549
- Fe_2O_3-PbO-B_2O_3 glass, X-ray and electron microscope studies, mag. and Mossbauer effect meas. 80−28919
- Fe_3O_4, crit. exponents meas. by polarized neutron scatt. 80−44828

Curie temperature continued
- Fe_3O_4, magnetite, oxidation rate anomaly at Curie temp. 79−96298
- $xFe_2O_3(1-x)[PbO.3B_2O_3]$ glasses, mag. props. 77−73012
- Fe_2P, magnetisation, susceptibility, thermal expansion and elec. resist. meas. 77−77037
- Fe_2P, magnetisation, susceptibility, thermal expsn. 79−11302
- Fe_2P, Mossbauer spectra and mag. props., Curie temp. dispersion 77−36162
- $Fe_{80}P_{20}$, binary amorphous ferromagnet, Mossbauer study 80−34829
- $Fe_{80}P_{20}$ glass, mag. props. 77−63125
- $Fe_{79}P_{13}B_8$ amorphous alloys, splat cooled, Mn, Cr and V substituted, mag. and transport props. 80−84593
- $Fe_{80}P_{13}B_1C_6$, ferromag. metallic glass, Mossbauer spectra, crystn. 77−12276
- $Fe_{77}P_{13}C_{10}$, glassy ferromag., crit. sp. ht. meas. 78−10716
- $Fe_{80}P_{20-x}C_x(Si_x)(Ge_x)$, amorphous, size effect of metalloids on mag. props. 80−84594
- $Fe_{80}P_{20-x}M_x$, M=B, C, Si, Ge, amorphous, effect of metalloids on mag. props. 79−11304
- $Fe_{25}Pd_{50}Au_{25}$, atomic ordering influence on mag. props. and elec. resistance *(Russian)* 80−7551
- Fe_3Pt, atomic thermal vibr. anisotropy, martensitic transform. model *(French)* 80−70355
- Fe_3Pt Invar alloy, anomalous Curie const., susceptibility meas. 80−75731
- Fe_3Pt Invar alloys, elec. resist. anomalous crit. behaviour 79−78067
- $FeRh_2S_4$, mag. semicond., mag. and elec. props. 80−93121
- $Fe_{1-x}Se$, phase relation 79−14926
- Fe_3Se_4, press. depend., determ. from thermal expansion and compressibility meas. 77−66318
- η-Fe_5Si_3, thermal and mag. props. 77−36080
- $Fe_{75}Si_{15}B_{10}$, mag. behaviour rel. to magnetostatic interactions 80−11224
- $(Fe_{1-x}Si_x)_{1-y}B_y$, metallic glass, mag. props., crystallisation 80−65885
- Fe_xSn_{1-x}, amorphous, mag. behaviour 78−95478
- $Fe_{1-x}Ti_x$, ferromag. props., Ti conc. effect 80−54872
- Fe_2TiO_4, ulvospinel, containing magnetized inclusions, mag. behaviour, cooling through Curie point 78−56314
- Fe_2TiO_4-Fe_3O_4, titanomagnetite, prepared at different oxidation conditions, hysteresis props. 78−56352
- $Fe_{80}b_{20-x}C_x(Si_x)(Ge_x)$, amorphous, size effect of metalloids on mag. props. 80−84594
- $Ga_{1-x}Mn_xSb$, elec. cond., mag. susceptibility, Hall const., and thermo-EMF, 80 to 1000K *(Russian)* 80−88549
- Gd, AC susceptibility, temp. modulation studies, domain property thermal relaxation 79−61072
- Gd alloys, amorphous, mag. props. and ferromag. reson. 80−54952
- Gd alloys, Curie temp. and saturated mag. moment, nonmag. solute effects 78−39301
- Gd, coil noise due to permeability fluctuations at phase transition temp. 80−84598
- Gd, domain effects near order-disorder and order-order ferromagnetic transitions 80−65886
- Gd, EPR linewidth and spin-spin relax. near T_c 78−68369
- Gd, ferromagnetic, crit. sp. ht. and thermal expansion 80−60343
- Gd, film, thermoreflectance dispersion curves at 315K and 97K 80−7332
- Gd, mag. domain struct., 230-293K 80−88783
- Gd, magnetisation and magnetocaloric effects *(Russian)* 78−34985
- Gd, magnetocrystalline anisotropy, temp. and press. depend. 77−20586
- Gd, sp. ht. near T_c, scaling behaviour 77−66333
- Gd, thermal conductivity critical behaviour near Curie point 80−75540
- ^{160}Gd, ferromagnetic, isotopically enriched single crystals short-range order 79−4653
- Gd-Ag, vap. quenched alloys, struct. and mag. props. 78−84461
- Gd-Ag(Cu) alloy film, amorphous, struct. and mag. props. 78−52318
- Gd-Al, amorphous film, microwave mag. reson. 78−91948
- Gd-Al, amorphous film, microwave mag. reson. 78−92060
- Gd-Al(C)(Cu)(Ga)(Ni)(Pd)(Rh) alloys, amorphous, mag. and elec. props. 80−80499
- Gd-Al(Cu)(Ga)(Rh)(Pd), amorphous alloys, mag. coupling of rare earth moments 78−88108
- Gd-Co, CPA calcs., moments and transition temps. 78−52252
- Gd-Co amorphous ribbons, mag. props. and Invar effects 80−2574
- Gd-Co(Ni)(Cu)(Rh)(Ru)(Pd)(Ga), amorphous, mag. props. and ferromag. reson. 80−75862
- Gd-Cu sputtered amorphous films, ferromag. props. 77−66393
- Gd-Fe, CPA calcs., moments and transition temps. 78−52252
- Gd-Mn(-Co) alloys, amorphous, ferrimag. props. and Hall effect 79−73692
- Gd-Ni, CPA calcs., moments and transition temps. 78−52252
- Gd-Ni, ferromag., elec. resist. temp. depend. 80−96843
- Gd-Tb, elasticity modulus, ΔE-effect, internal friction, magnetic transformations *(Russian)* 79−91723
- Gd-Y (40 wt.%) alloy, magnetic phase transitions, elastic consts. meas. 78−14957
- Gd-Y alloys, mag. crit. temp. gap 80−60260
- $GdAg_{1-x}In_x$, magnetic transition temp., effect of hydrostatic press. 78−76244
- $GdAl_2$, anomalous change of Curie temp. 78−47976
- $GdAl_2$, thermal expansion and heat capacity Curie temp. determ. 77−1559
- Gd_3Al, magnetic properties, 4.2 to 400K, metamagnetism 77−32193
- $Gd_{80}Au_{20}$, amorphous ferromag., critical phenomena and mag. props. 77−85469
- $Gd_{80}Au_{20}$, amorphous ferromag., mag. and transport meas. 77−89930
- $Gd_{1-x}Ca_xAl_2$, mag. props. and phase relations 80−107991
- $GdCo_2$, dilute ferromagnets, press. effect on Curie temp. 80−65873
- $Gd_{1-x}Co_x$ film, amorphous, effect of O or Ar impurity 77−40093
- Gd-Co, amorphous ferromag. obtained by splat cooling, local and bulk mag. props. 79−1685
- $Gd_{67}Co_{33}$, amorphous ferromag., mag. and transport meas. 77−89930
- $GdCo_2B_2$, ferromag. ordering and saturation moments 77−24711
- $Gd_{8.6}Co_{74.0}Mo_{12.8}Ar_{4.3}$, amorphous film, spin wave reson. 79−73823
- $Gd(Fe_{1-x}Al_x)_2$, magnetisation, Curie temps., and mean mag. moments 79−51817
- $(Gd_{1-x}Fe_x)_{1-y}Bi_y$ amorphous films, saturation magnetisation, Kerr and Faraday rotation 80−40093
- GdIG, thermoelec. power, elec. cond., 300-1200K, ferrimag. Curie temp. 79−99543
- $Gd_{1-x}M_x$, M=Co, Ni, Fe, temp. depend. of magnetisation 77−77043
- GdMg, sp. ht., magnetisation and stability of canted struct. 79−78412

Curie temperature continued
- $(GdMn_2)_x(GdAl_2)_{1-x}$, mag. and struct. investigations of intermetallic systems 78−95440
- $Gd_xNd_{1-x}Zn$, ferromag., mag. susceptibility and magnetisation, temp. depend. 80−70975
- $GdNi_2$, anomalous behaviour near Curie point 78−91880
- $Gd_{80}Ni_{20}$, amorphous ferromag., mag. and transport meas. 77−89930
- Gd_xNi_{1-x}, sputtered amorphous films, mag. props. and Hall meas. 78−95488
- $Gd_2Ni_{17-x}Al_x$, mag. behaviour in paramagnetic region 79−73675
- $GdNi_2H_4$, effect of absorbed H_2 on struct. and mag. behaviour 78−2682
- $GdNi_2H_4$, effect of H_2 absorption on struct. and mag. behaviour 78−10685
- $Gd_{3-x}S_4$, ferromag., elec. props. near Curie temp. 80−107788
- $Gd_{3-x}S_4$, mag. ordering and elec. cond. 78−10681
- GdTb, ferromag., magnetisation and microwave absorpt. 80−65816
- $Gd_{50}Tb_{50}$, magnetisation, AC susceptibility and microwave absorption meas. 80−60221
- $Gd_2(WO_4)_3$, mag. susceptibility, paramag. Curie temp., 300-900K 79−82753
- $(Gd_xY_{1-x})Al_2$, ferromag. and spin glass like behaviour, magnetisation meas. 80−75734
- $(Gd_xY_{1-x})_4Co_3$, Curie temp. and resist.-temp. curves, comp. depend. 80−71020
- $(Gd_xY_{1-x})Fe_2$, Fe mag. behaviour, FMR measurements, mag. props., Vangsness relation anal. 79−78336
- $Gd_xY_{1-x}Fe_3$, saturation magnetisation, magnetostriction, Curie temp., ferrimag. ordering, exchange field *(Russian)* 78−68343
- $Gd_xY_{1-x}Zn$, ferromag., mag. susceptibility and magnetisation, temp. depend. 80−70975
- $(Ge,Pb)_{1-x}Mn_xTe$, mag. and elec. props. meas. 80−29534
- $HgCr_2Sd_{4-x}Te_x$, ferromag. semicond., zero bandgap transition 80−96783
- $HgCr_2Se_4$, ESR line intensity near Curie point 78−64269
- $HgCr_2Se_4$, initial mag. permeability freq. depend. near Curie temp. 78−10729
- $HgCr_2Se_4$, n-type ferromag. semicond., galvanomagnetic props 80−70727
- $Hg_{1-x}Mn_xTe$, non-parabolic zero-gap semicond., indirect exchange interaction 80−80498
- $(Ho,Y)Co_2$, first order phase transitions 78−84426
- Ho particles, effect of size on paramag. Curie temp. 78−60317
- Ho_2Au, mag. props., 4.2-300K 79−7972
- $HoCo_2Si_2$, mag. props. 80−107988
- $HoFe_2H_{3.5}$, mag. props. and lattice consts., effect of hydrogen absorpt. 77−20561
- $HoFe_2H_x$, mag. props. 80−25095
- $Ho(Fe_xNi_{1-x})_2$, mag. behaviour, susceptibility and Mossbauer expts., 4.2-1300K 78−52235
- Ho_2O_3, 300 to 900K, mag. susceptibility and Curie temp. meas. 78−56288
- $Ho_xTb_{1-x}Co_2$ lave phase compounds, elastic props., temp. and magnetic field dependence 80−60393
- $Ho_2(WO_4)_3$, mag. props., 300 to 900K 79−28510
- $Ho_{1-x}Y_xNi$, ferromag. behaviour, struct., Curie temp. 79−99677
- InR_3 (R-Y, Nd, Sm, Gd, Tb, Dy, Ho, Er, Tm), mag. props., 4.2 to 270K 79−56512
- $InSb:Mn^{2+}$ nondegenerate semicond., mag. impurity indirect interaction *(Russian)* 80−34591
- $InMn_{1-x}Sb$ alloys, crysta. struct., and mag. props. 78−34466
- $K_2CuCl_4.2H_2O$ and isomorphous cpds., mag. interactions of H and D nuclei, NMR obs. 79−87251
- K_2CuF_4, 2-D ferromagnet, optical and magneto-optical props. 77−52062
- K_2CuF_4, Curie temp. XY-like anisotropy effect, inter-layer exchange 77−59406
- K_2CuF_4, quasi two-dimens. Heisenberg ferromag., spin wave spectrum lineshape, neutron scatt. obs. 77−66286
- $K_2Cu_{1-x}Mn_xF_4$ system, ($0\leq x\leq 0.2$), prep., cryst. chem., and ferromag. props., X-ray and neutron diffr. study 79−24162
- $K_2Cu_xZn_{1-x}F_4$, Cu conc. depend. 80−60255
- $KFeS_2$, magnetic reson. meas. 78−95524
- $KMnF_3$, mag. props. and struct. transitions, antiferromag. reson. meas. 79−8052
- $K_5V_3F_{14}$, ferrimagnetic props., ordering temp. and anisotropy *(French)* 77−47990
- La-Fe alloy, amorphous, sputtered at high rate, mag. props. 80−75753
- La-Fe bulk amorphous alloys, Fe depend. of Curie temp. *(Japanese)* 79−95588
- $(La_{0.8}Ca_{0.2})MnO_{3-x}$, mag. props., Faraday method meas. 80−103832
- $LaMnO_3$, orthorhombic lattice distortions, mag. props. rel. to prep. conditions 77−20592
- $LaNi_{1-x}Fe_xO_3$, mag. props., 7 to 300K 79−4648
- $LaNi_{1/2}Mn_{1/2}O_3$, Curie point rel. to Neel points of $Sr_{1-x}Ca_xMnO_3$, superexchange interactions 77−77055
- $La_{0.65}Pb_{0.35}MnO_3$, transport props. near Curie points 78−88100
- $La_{0.72}Pb_{0.28}MnO_3$, metal-semicond. transition at Curie point, transport props. obs. 79−73554
- $(La_{1-x}Pr_x)_3Tl$, mag. props., simple phenomenological model 77−16041
- $La_{3-x}S_4$, mag. ordering and elec. cond. 78−10681
- $La_{1-x}Sr_xCoO_3$ ($0.5\leq x\leq 1.0$), Curie and paramag. Curie temp. as function of composition 79−24154
- $La_{1-x}Sr_xCoO_3$, ($0.5\leq x\leq 0.9$), ferromag., elec. props., itinerant electron model 80−107785
- Li ferrite, fine particle, for arc plasma spraying mm-wave phase shifter 78−64469
- Li-Zn ferrite, magnetic props., effect of V_2O_5 addition *(Japanese)* 77−284[illegible]5
- $Li_2B_4O_7$-$LiFe_5O_8$, borate glass, mag. props. of Fe^{3+} cations 80−100599
- $Li_{0.5}Fe_{2.5}O_4$-$CuFe_2O_4$-$MnFe_2O_4$, structural characteristics and mag. props. of solid solutions 77−[illegible]
- Li-Gd, MoO_4, ferroelec. and paramag. props. 78−39517
- $LiHoF_4$, EPR studies, lowest levels of rare-earth ions, submillimetre freq. 80−39865
- $LiMnCrF_6$, ferrimagnetic, magnetic props. *(French)* 79−1668
- $Li_xMn_{1-x}Se$, anomalies obs. in mag. and elec. props. 77−69509
- LiMnZn ferrites, elementary coupling energy to lattice of Mn^{2+} ions, depend. on T_c 77−69534
- $LiNb_{1-x}Ta_xO_3$, Czochralski growth and basic props. 77−63556
- Li_2O-NiO-O_2, phase diagram and mag. props. of $Li_xNi_{1-x}O_{1\pm y}$ 78−48380
- $LiTbF_4$, EPR studies, lowest levels of rare-earth ions, submillimetre freq. 80−39865

Curie temperature continued
- LiTiZn ferrites, elec. resist., mag. props., effect of Bi addition 78-95474
- $Lu_2V_2O_7$, pyrochlore struct., mag. props. 78-72335
- MRh_4B_4 (M=trivalent transition metal, usually rare earth) supercond. and ferromagnetism, role of Sc 78-95438
- Mg ferrite, crystal lattice defectiveness and degree of inversion, effect of synthesis temp. 77-11501
- $MgGa_xFe_{2-x}0_4$, spinel struct., neutron diffr. exam. 77-12096
- MgO, mag. anisotropy, ionic distrib. and composition of magnesioferrite precipitates, ferrimag. reson. study 77-69699
- Mn-Bi eutectic alloy, mag. anisotropy 78-[illegible]
- Mn-Cu-Ni-Bi, magneto-optic film for storage appl. 77-[illegible]
- Mn-Zn ferrospinels, carrier transfer phenomena 80-54727
- $Mn_{1.11}Al_{0.89}$, crit. behaviour, neutron diffr. meas. 78-34982
- $Mn_{1.11}Al_{0.89}$, neutron diffr. investig. of mag. struct., degree of order 77-55662
- $Mn_{1.11}Al_{0.89}$, unit cell parameters, temp. depend. 79-55697
- MnAs, PTH phase diagram of mag. transitions, Curie point 80-44832
- Mn_2As-Mn_2Sb, structural and magnetic props. determ. 78-76248
- $MnAs_{1-x}P_x$ mixed crystals, metallic magnetically ordered, Hall effect 80-65536
- $Mn(CN)_3.(H_2O)_{0.57}$, mag. interactions, theory 80-97085
- $Mn_{1-x}Co_xSb$, press. effect on saturation magnetisation *(Russian)* 77-80919
- $(Mn_{1-x}Cr_x(Fe_x))B$, Invar charact. 77-15602
- $(Mn_{0.95}Cr_{0.05})_3Si$, sp. ht. at low temps., mag. transitions *(Russian)* 77-32189
- MnCuBi film, for mag. storage appl., prep. by RF sputtering, and props. 77-8369
- $Mn_{1-x}Fe_xAs$, magnetic transition under high press., exchange striction model calcs. *(Russian)* 80-50096
- $MnFe_2O_4$:Sn, hyperfine mag. fields at ^{119}Sn and ^{57}Fe nuclei, influence of press. 79-99811
- $MnNiSi_{1-x}Ge_x$, mag. props. 77-12118
- MnP, US vel. and crit. attenuation, longit. waves, external mag. field 78-27035
- MnSb, cryst. grown from nonstoichiometric melt 77-16488
- MnSb-Mn_2Sn alloy system, continuous series of solid solns., homogeneity and ferromagnetic props. 79-52159
- $MnSb_{1-x}Sn_x$ films, Faraday rotation, optical absorpt. coeffs. 80-97242
- $Mn_{1+x}Sb_{1-x}Sn_x$, magnetisation and Curie temp., prep. and comp. depends. 78-64200
- $Mn_5(Si_{1-x}Ge_x)_3$, magnetic and cryst. struct., ferromag. props. 77-59391
- MnZn ferrite, anomalous thermal change of permeability near Curie point 77-20638
- MnZn ferrite, polydispersive spin relax. near Curie temp., mag. susceptibility meas. 77-69513
- MnZn ferrite, prep. and magnetic props. 78-19254
- MnZn ferrites, cationic distrib. and Curie temp. *(Russian)* 79-91232
- $Mn_{1.18}Zn_{0.06}Co_{0.01}Fe_{1.75}O_4$, transport props. near Curie points 78-88100
- $(Mn_{0.7}Zn_{0.3})_xFe_yO_4$, electromag. props. rel. to Fe content 78-43613
- Mo, single crystal, thermal expansion in magnetically ordered phases 78-2269
- $(NH_4)_2Cd_5Fe_3Al(SO_4)_{12}.18H_2O$, determ. from EPR data 78-10762
- $Na_{1-x}Li_xNbO_3$, dielec. const. and X-ray diffr., for Curie temp. and phase diagrams 78-72768
- $NaMnCrF_6$, ferrimagnetic, magnetic props. *(French)* 79-1668
- $NaNH_4SeO_4.2H_2O$, ferroelectric crystal, effect of hydrostatic pressure on phase transition 78-52453
- $NbMn_2Si_2$, Mossbauer and magnetisation expts. 78-31138
- $Nd_xEu_{1-x}B_6$ solid solution, mag. susceptibility, lattice parameters, Weiss temp. 80-29535
- $NdFe_2$, Curie temp., elec. quadrupole couplings, Mossbauer study 80-39949
- Nd_2O_3, magnetisation and mag. susceptibility Curie-Weiss behaviour 77-4505
- $Nd_2(WO_4)_3$, mag. susceptibility, paramag. Curie temp., 300-900K 79-82753
- Ni, amorphous film, getter sputtered at 25K, resistivity, Curie temp. 78-52673
- Ni, anomalous resistivity near Curie temp., band theoretical calc. 78-56127
- Ni, calc. using model containing five bands 79-56536
- Ni, crossover phenomena, stress induced above Curie point, neutron scatt. study 79-61113
- Ni, effects of grain size on resist. anomaly near Curie point *(French)* 77-4318
- Ni, ferromag. props., teaching expt. 80-82608
- Ni, ferromagnetic, Hall effect, anomalous, rel. to scatt. processes 80-44572
- Ni film, effects of finite size on crit. phenomena, resistivity anomaly 79-38192
- Ni foil, critical exponent β determ. by microwave transmission 77-69575
- Ni, heat diffusivity and heat cond. near Curie point 77-24706
- Ni, high purity single cryst., sp. ht. near crit. temp. 78-64212
- Ni, hyperfine fields on ^{12}B, NMR obs., near T_c 77-28476
- Ni, internal friction near Curie temperature 78-44163
- Ni, magnetisation and relative vol. temp. depend. near Curie point *(Russian)* 78-14962
- Ni, magnetisation curves in high mag. fields above Curie point 77-66386
- Ni, magneto-volume effects calc., rel. to itinerant electron model 78-43621
- Ni, neutron depolarisation near Curie point *(German)* 78-14934
- Ni, optical spectrum, anomalous temp. depend. around T_c, band struct. 80-40128
- Ni, oxidation, electron beam influence, disappearance potential spectroscopy obs., near T_c 77-1766
- Ni, oxidation kinetics near Curie temperature 78-88578
- Ni, oxidation rate transition, at Curie temp. 78-27685
- Ni, photoelectric effect in paramag. and ferromag. states, Auger spectra 78-95649
- Ni, photoemission near Curie temp. 79-78841
- Ni, point contacts between ferromag. metals, singularities depend. in dV/dI, phonon spectra 79-60457
- Ni press. depend., using press. cell developed for meas. with cubic-anvil press 80-13109
- Ni, secondary electron emission under Ar^+ ion bombard. near Curie point 80-29838

Curie temperature continued
- Ni, spontaneous magnetostriction determ. method, molecular field theory study *(Russian)* 80-50157
- Ni, stress induced cross-over effect near Curie point *(German)* 80-103873
- Ni, stress induced crossover effect near Curie point *(German)* 80-103874
- Ni, temperature magnetic hysteresis near Curie temp. 79-56567
- Ni, thermal expansion anomaly 77-85474
- Ni:^{11}B, NMR, crit. slowing-down at Curie temp. 77-8418
- Ni:^{57}Fe, Mossbauer meas. near Curie temp. 78-10817
- Ni-Al-Ti ferromagnetic non-homogeneous alloy, composition determination by Curie temp. meas. 80-11196
- Ni-Au, local environment effects, magnetisation decrease 79-65664
- Ni-Co, solid and liq., paramag. susceptibility and electron struct., 800-1800°C *(Russian)* 80-25081
- Ni-Co (25 at.%), polycrystalline, mech. damping 77-28850
- Ni-Co-H, solid soln., Curie points and spontaneous magnetisation behaviour 80-50093
- Ni-Cu, ferromagnetic, Hall effect, anomalous, rel. to scatt. processes 80-44572
- Ni-Cu, hydrogenated, Curie point, cluster magnetism 78-14960
- Ni-Cu, local environment effects, magnetisation decrease 79-65664
- Ni-Cu, Ni rich alloys, magnetic phase transition, elec. resistivity meas. 300-700K 79-82781
- Ni-Cu, Ni-rich, temp. depend. resist. 80-10943
- Ni-Cu-H systems, Curie temp. during phase transitions under high press. H_2 80-71029
- Ni-Cu(Pd)(Pt)(Rh), ferromag., press. effect on Curie temp. 79-51781
- Ni-Fe, dil., temp. depend. of Mossbauer absorpt. near Curie point *(French)* 80-11305
- Ni-Fe, soft mag. props. rel. to metallurgical aspects 80-88810
- Ni-Fe based metallic glasses, Curie pt. anomalies 80-60256
- Ni-Fe-Cr, extraordinary Hall effect, elec. and mag. meas. at 77 and 300K 80-34421
- Ni-Fe-H, Curie points, mag. props. of H solutions FCC metal sublattice parameter behaviour 79-69671
- Ni-Fe-Nb-Mo-Al, head material for mag. recording, DC and AC mag. props. 80-88812
- Ni-Mn, ordered and disordered, press. effect on Curie temp. 80-71148
- Ni-Mn (up to 32 at.%), press. depend., using press. cell developed for meas. with cubic-anvil press 80-13109
- Ni-Mn disordered alloys, mag. moment and Curie point 78-76243
- Ni-Mn-Al-Si-Co, Alumel, Ettingshausen-Nernst coeff. and transport props. from 200 to 473K 80-44573
- Ni-Mn-H solid solutions, mag. props. 80-88753
- Ni-P, amorphous alloys, low temp. mag. props., comp. depend. 77-66387
- Ni-Pd, high mag. field effects, mag. isotherms near Curie point, exchange splitting energies 80-60272
- Ni-Pd-Mn, ternary FCC solid soln., saturation magnetisation and Curie temp., medical appl. *(Japanese)* 79-61114
- Ni-Pd-Mn ternary alloys, mag. characts., use for thermoseed 80-107995
- Ni-Pt alloys, mag. props. under hydrostatic press. 78-6556
- Ni-Rh alloys, thermal EMF, elec. resist., mag. susceptibility, mag. moment and Curie temps., 18-500°C *(Russian)* 77-20288
- Ni-Ti, Ni-rich, temp. depend. resist. 80-10943
- Ni-Ti (0-1.5 at.%), elec. cond., mag. phase transition, 300-750K 78-2678
- Ni-Ti (9.6 wt.%), mag. study on phase decomposition *(Japanese)* 80-15758
- Ni-Ti alloy, Curie temp. determ. using deviation from Matthiessen's rule 79-15306
- Ni-Zn ferrites, comp., lattice imperfections, sintering 78-3080
- Ni-Zn ferrites 600 NN and M450 NNI, Curie point radiative shift due to neutron irrad. *(Russian)* 80-39775
- Ni_3Al, elastic moduli changes at Curie point 77-66406
- $Ni(As_xS_{1-x})_2$, mag. elec. and structural props. meas. 77-85447
- $Ni_{1-x}Cd_xFe_2O_4$, mag. props. rel. to ionic struct. 80-75756
- $(Ni_{1-x}Co_x)_{0.78}P_{0.14}B_{0.08}$, amorphous, mag. props., local environment model 77-12119
- $Ni_{0.5-x}Co_xZn_{0.5}Fe_2O_4$ ferrospinal solid solutions, cryst. lattice defects and props. 80-19796
- $Ni_{1-x}Cu_x$+CO, $Ni(CO)_4$ form. activation energy, mag. phase depend. 80-3409
- $(Ni_xCu_{1-x})_2MnSn$, mag. props. and lattice parameter, composition depend. 77-80916
- $Ni_{0.7}$-$Cu_{0.3-x}Si_x$, magnetic props., 4.2 to 800K 77-8290
- Ni(Fe,Cr) and Ni_3(Fe,Cr), electron states density model and mag. characts. calcs. *(Russian)* 80-92804
- NiFe disordered alloys, Mossbauer spectra, hyperfine mag. field distrib., Curie temp. 80-7198
- $Ni_{36}Fe_{32}Cr_{14}P_{12}B_6$, metallic glass, mech. props. and thermal stability 80-76362
- $NiFe_2O_4$-Fe_2O_3, effects of excess Fe_2O_3 on mag. props. 77-85495
- $Ni_xFe_{3-x}O_4$, spinels, fine particles, magnetic properties obs. 80-71031
- $(Ni_xFe_{1-x})_{80}P_{10}B_{10}$, amorphous, Curie temp., press. effect 80-75833
- Ni_3Mn, magnetic phase exam. 77-20631
- Ni_3Mn, thermoremanent magnetisation and blocking temp. 80-34601
- $Ni_2Mn_xT_{1-x}Sn$, T=Ti(V)(Cr), ferromag., magnetisation, susceptibility 77-12102
- $Ni_{80}P_{20}$ glass, mag. props. 77-63125
- $Ni(Rh_{1-x}Cr_x)_2S_4$, ferromag. spinel system with metallic conduction 79-56513
- NiS_2, neutron diffr. anomaly at Curie temp., antiferromag. refl. 78-76260
- NiS_2, thermal expansion and cryst. distortion below antiferromag. Neel and weak ferromag. Curie temps. 77-15579
- $NiSiF_6.6H_2O$, ESR spectra at low temperatures and high pressures 78-52339
- Ni_2(Ti,Mn)Sn, Heusler alloy, mag. meas. 79-47261
- $Ni_{1-x}Ti_x$, ferromag. props., Ti conc. effect 80-54872
- NiZn ferrite, effect of reactor radiation on mag. props. 77-32215
- NiZn ferrite, ZrO_2 additions influence on sintering and physicochem. props. 80-108369
- $Ni_xZn_{1-x}Fe_2O_4$, crystals grown from BaO-B_2O_3-ZnO-NiO-Fe_2O_3 melt exam. of crystal props. 80-[illegible]
- $NpFe_2$, high temp. mag. props., 300 to [illegible]K [illegible]
- $NpOs_2$, band magnetism due to 5f-electrons, T_c [illegible]
- O_2 adsorbed over porous Vycor glass, props. characteristic of amorphous antiferromag. obs. [illegible]

Curie temperature continued
- $Pb_5Ge_3O_{11}$:Ba,O, impurities, static central peak 78−92079
- $PbSc_{2/3}Te_{1/3}O_3$-$PbSc_{2/3}W_{1/3}0_3(PbFe_{2/3}Te_{1/3}O_3)$ ferroelec. props. and lattice consts. 80−60520
- Pd, sd hybridisation, paramagnetic Curie temp. and susceptibility *(Russian)* 80−103808
- Pd-Co, pressure effect on Curie point, Debye temp. in ferromag. state *(Russian)* 77−32194
- Pd-Fe, magnetic anisotropy near Curie point, quasi domain struct. *(Russian)* 80−65867
- Pd-Fe, Mossbauer spectra, scatt. and transmission geometries, differences in crit. behaviour near T_c 78−76367
- Pd-Fe, scatt. and transmission Mossbauer spectra near Curie temp. 80−15864
- Pd-Fe disordered alloy, Landau model for mag. props. 77−66276
- Pd-Fe(Co)(Ni), dilute ferromagnets, press. effect on Curie temp. 80−65873
- Pd-Mn, Curie temp. and magnetisation, vol. depend. 80−34629
- Pd-Mn, ferromagnetism to spin glass behaviour transition 80−71062
- Pd-Ni, local susceptibilities, ^{61}Ni Mossbauer spectroscopy 78−95536
- Pd-Ni alloy, dil., ferromagnetism, local moments, susceptibility, magnetisation and Curie temp. *(Russian)* 78−88115
- Pd-Ni disordered alloy, Landau model for mag. props. 77−66276
- PdAgFe, ferromag., Curie temp. depend. on susceptibility, non-mean field theory 80−44829
- PdFeRh, ferromag., Curie temp. depend. on susceptibility, non-mean field theory 80−44829
- PdGdH, diagram of state elec. props., indirect exchange interaction, EPR study *(Russian)* 80−50179
- $Pd_{1+x}MnSb$ Heusler alloys, magnetic hyperfine fields on ^{111}Cd, TDPAC and magnetisation meas. 80−93219
- $Pd_{2-x}MnSb$, struct., appl. as improved neutron polariser 80−60199
- $(Pd_xPt_{1-x})_3Fe$ atomically ordered alloy, thermoelectric power, carrier energy spin shift, mag. props. 80−29394
- $(Pd_{95}Rh_5)Co$, exchange enhanced system, AC susceptibility meas. 77−16096
- $Pd_{80-x}Si_{20}Fe_x$, amorphous, low x, hyperfine interactions and mag. ordering temp. 79−15303
- $PrAg_x$, low temp. mag. meas. 80−107989
- PrB_4, mag. and elec. props. 80−20386
- $Pr_{1-x}Ca_xAl_2$, mag. props. and phase relations 80−107991
- $PrCo_2$, strongly exchange-enhanced paramagnetism, susceptibility 80−60179
- $PrCu_5$, nuclear induced ferromagnetism 79−61069
- $PrFe_2$, Curie temp., elec. quadrupole couplings, Mossbauer study 80−39949
- $Pr_{1-c}La_cAl_2$, mag. props. 79−65658
- Pr_3Tl, induced ferromag., mag. props. under hydrostatic press. 78−56315
- $Pr_2(WO_4)_3$, mag. susceptibility, paramag. Curie temp., 300-900K 79−82753
- Pt-Fe(Co), dilute ferromagnets, press. effect on Curie temp. 80−65873
- Pt-Ni disordered alloy, Landau model for mag. props. 77−66276
- $Pt_3Mn_xCr_{1-x}$ alloys, mag. props. 80−2562
- $PuFe_2$, high temp. mag. props., 300 to 1100K 79−51757
- R_2In, R_3In, R=Gd, Tb, Dy, Ho, Nd, mag. props. 80−108009
- $ROsB_4$, R=Y, Gd, Tb, Dy, Ho, Er, Tm, struct. and mag. props. 78−79584
- $RRuB_4$, R=Y, Cd, Tb, Dy, Ho, Er, Tm, struct. and mag. props. 78−79584
- Rb_2CrCl_4, two-dimens. easy-plane ferromag., cryst. and mag. struct., temp. variation of moment 77−66255
- $RbHSO_4$, isotope effect, dielec. const. and spin polarisation investigation 80−20574
- Rb_2ZnBr_4, incommensurate phase transition, neutron-scatt. obs. 79−4390
- Rh_2MnSn, and related cpds., with Heusler and Heusler-related struct., mag. props. 77−8311
- Rh_2MnX, (X=Al, Ga, In, Tl, Sn, Pb, Sb), Heusler and Heusler-related cpds., mag. and cryst. props. 77−20568
- $(Sc,M)Rh_4B_4$, M=Ca, Th or rare earth, supercond. and ferromagnetism 78−95438
- $ScFe_{2-2x}Al_{2x}$, mag. props., composition depend. 77−20593
- $(Sc_xLu_{1-x})_2V_2O_7$ 80−29547
- Si, ferromagnetism induced by ion irrad., e.p.r. investig. *(Russian)* 77−1595
- $SmAu_6$, mag. props. temp. depend. *(French)* 77−51879
- $SmCo_5$, specific heat and kinetic props. at elevated temp. *(Russian)* 79−28530
- Sm_xCo_y, mag. and struct. investigations of intermetallic systems 78−95440
- Sm_xCo_y, mag. props. 78−43568
- $SmCo_3B_2$, high coercive forces, ferromag. ordering and saturation moments 77−24711
- $Sm_2Co_{17-x}M_x$, M=Cr, Ni, effect of substitution on mag. props. 79−78363
- $Sm_xDy_{1-x}Co_5$, temp. compensated magnetic material, mag. and struct. characterisation 78−68177
- $Sm_xEr_{1-x}Co_5$, temp. compensated magnetic material, mag. and struct. characterisation 78−68177
- $SmMn_3C$ noncolinear mag. struct., mag. transition *(French)* 77−69494
- $Sm_6Mn_{23-x}Fe_x$, magnetic behaviour, temp. and comp. depend. 80−93090
- $Sm_xTb_{1-x}Co_5$, temp. compensated magnetic material, mag. and struct. characterisation 78−68177
- $Sm_2(WO_4)_3$, mag. susceptibility, paramag. Curie temp., 300-900K 79−82753
- $SrCoO_{2.70}$, growth and props. 78−48310
- $SrCoO_{3-\delta}$ $(0<\delta<0.5)$, ferromag., metallic elec. props. 80−70668
- $SrCoO_{3-\delta}$, crystal struct. and mag. props., O vacancy effect 79−95587
- $SrFe_{12-x}Cr_xO_{19}$, effects of substitution of Fe by Cr, Mossbauer spectra 80−2674
- $SrFe_{12}O_{19}$, Ca^{2+} additives effect on hexaferrite lattice and mag. props. 80−60243
- $SrFe_{12}O_{19}$, mag. props., effect of Sr dissolution by milling in water 77−25000
- $Sr_{0.3}La_{0.7}MnO_3$, neutron-irrad. induced phase transition 77−89952
- Sr_2YRuO_6, ^{99}Ru Mossbauer spectra and other techniques 80−29659
- Tb, magnetisation, AC susceptibility and microwave absorption meas. 80−60221
- Tb, small particles, disappearance of mag. order., mag. susceptibility and magnetisation meas. 77−16117
- Tb-Cu-Zn(Al), mag. props. *(Russian)* 77−51905
- Tb-Fe, amorphous magnetism in bulk samples 77−66278

Curie temperature continued
- Tb-Fe amorphous film, thermomag. contact printing 77−89986
- Tb-Fe film, undoped and O-doped, amorphous, microstruct. and mag. props. 79−91273
- Tb-Gd alloy, single cryst., mag., magnetoelastic and elec. props. *(Russian)* 78−2677
- Tb-Ho, thermal expansion in vicinity of Curie temp. 79−28524
- Tb-Sc(Y)(La)(Lu)(Yb)(Mg)(Th), mag. ordering temps., susceptibility meas. 80−25136
- Tb-Y-Zn, magnetic props. conc. and temp. depend. *(Russian)* 77−47989
- Tb-Y(Gd), mag. ordering temp. and indirect exchange integrals *(Russian)* 79−95590
- $Tb_{52}Ag_{48}$, amorphous, bulk magnetic props., evidence of strong local anisotropy 77−43830
- $TbAu_6$, mag. props. temp. depend. *(French)* 77−51879
- TbB_2, mag. props. and neutron diffr. 78−84401
- TbB_4, ferromag. ordering, neutron scatt. meas. 78−10655
- $TbCo_2Si_2$, mag. props. 80−107988
- $TbCrO_4$, mag. susceptibility and magnetis. meas., 1.7-1000K, Curie pt. positron 77−66266
- Tb_xGd_{1-x}, orientation phase transitions near Curie pt., magnetization and magnetocaloric effect meas. *(Russian)* 79−87261
- TbIG, magnetisation and mag. susceptibility meas. along (111) direction, 4.2-295K 77−80917
- Tb_2O_3, 300 to 900K, mag. susceptibility and Curie temp. meas. 78−56288
- $Tb_2(WO_4)_3$, mag. props., 300 to 900K 79−28510
- $(Tb_{1-x}Y_x)_3Co$, mag. props. and transitions, conc. depend. *(Russian)* 78−10671
- TbZn, ferromag., thermoelec. power, temp. depend. and crit. behaviour 80−96852
- $ThCo_{5-x}Mn_x$, struct. and magnetisation exam., temp. depend. 78−2662
- $ThCu_3Mn_4O_{12}$, mag. structure, neutron diffr. powder data, 430K ferrimag. T_c 77−69502
- Th_7Fe_3, H induced change from supercond. to mag. ordered state 79−28525
- $ThNi_{5-x}Mn_x$, struct. and magnetisation exam., temp. depend. 78−2662
- Ti-Cu alloys, mag. susceptibility meas., paramagnetic susceptibility meas. Curie temp. and mag. moments calc. *(Russian)* 78−34956
- $(Ti_{1-x} V_x)_2O_3$ spin glass, mag. props., metallic antiferromagnetism 79−82791
- $TiBe_{2-x}Cu_x$, C-15 lower phase, itinerant ferromagnetism 80−15723
- $TiBe_{2-x}Cu_x$, high press. study of Curie temp. and mag. susceptibility 80−84600
- $Ti(Fe,Co)H_y$, mag. and ^{57}Fe Mossbauer studies 80−71272
- $TiFe_{1-x}Co_x$, mag. props., under high press. and in high mag. fields 78−95423
- Ti_4O_7 and $(Ti_{1-x}V_x)_4O_7$, metal-insulator transitions, EPR, elec. and mag. props. 80−2336
- $Tl_2Cr_2O_7$, $Tl_2Mn_2O_7$, pyrochlore type, synthesis and physical props. 80−33963
- $TmFe_2H_{4.3}$, mag. props. and lattice consts., effect of hydrogen absorpt. 77−20561
- $TmFe_2H_x$, mag. props. 80−25095
- Tm_2O_3, 300 to 900K, mag. susceptibility and Curie temp. meas. 78−56288
- Tm_2O_3, susceptibility, 4.2-270K 77−12081
- $Tm_2V_2O_7$, pyrochlore struct., mag. props. 78−72335
- $Tm_2(WO_4)_3$, mag. props., 300 to 900K 79−28510
- U_3As_4, elec. resist. in vicinity of Curie point, influence of mag. field 77−69314
- $U(Co_{1-x}Fe_x)_2$, ferromag. onset, susceptibility and resist. meas. 80−70967
- UD_3, crystalline elec. field studies using neutron inelastic scatt. at NRCN 80−10931
- UFe_2, giant magnetoelastic deform. of cryst. struct. mag. props. *(Russian)* 80−93159
- UFe_2, magnetisation meas. 79−51756
- UFe_2, nonstoichiometry effects on Curie temp., susceptibility obs. 80−25131
- $UFe_3B_2(B_4)$, Mossbauer effect of ^{57}Fe nuclei, mag. props. 80−103907
- $U(Fe_{1-x}Mn_x)_2$, Curie temp. and saturation moment at 4.2K 80−70966
- UIG, Ga-substituted, computer simulation of temp. and field depend. of sublattice magnetisation and spin-flip transition 79−11300
- $U_2N_2Bi(Sb)(Te)$, mag. props. 78−72333
- U_3P_4, press. effects on elec. resist. and Curie temp. 80−75559
- US, elastic consts. temp. depend. in para- and ferromag. regions 79−77666
- US, ferromag., AC mag. susceptibility at high press. 80−7085
- UTe, crit. exponents, neutron and magnetisation meas. 80−88823
- $(U_xTh_{1-x})S$, mag. props. rel. to elec. struct., 1.5-300K 77−1557
- U_3X_4, (X=P, As, Sb, Bi), molecular field approx. study of mag. ordering, paramagnetic susceptibility 79−78410
- $U_xZr_{1-x}Fe_2$, Curie temp. and saturation moment at 4.2K 80−70966
- V, small particles, crystal structure, magnetic and superconducting props. 80−97121
- $V_xCr_{3-x}S_4$, elec. and mag. props. 79−28523
- VTe, mag. and elec. transport props. 80−92897
- $(Y,Gd,Yb)_{3-x}Bi_x(Fe,Al)_5O_{12}$, LPE, for magneto-optical appls. 78−48341
- $(Y,Sm,Lu,Ca)_3(Ga,Ge,Fe)_5O_{12}$, film growth and mag. props. for bubble-memory appl. 79−87297
- $(Y,Sm,Lu)_3(Fe,Ga)_5O_{12}$, LPE mag. film, suitability for 1 to 3 micron bubble devices 78−68323
- Y-Co, CPA calcs., moments and transition temps. 78−52252
- Y-Co, Curie temp. determ. 79−65672
- Y-Co, ferromagnet, first and second order transitions 80−34631
- Y-Ni amorphous alloy, spontaneous magnetisation, Curie temp. and paramag. susceptibility 78−68189
- YCo_2, density of states, mag. props. 79−90936
- $Y_{1-x}Co_x$, temp. depend. of magnetisation 77−77043
- $Y_{2+x}Co_{17-2x}$ single crystal, magnetocrystalline anisotropy 79−38320
- $Y_2(Co_{1-x}M_x)_{17}$, M=Al, Cu, single crystal, mag. props. 77−47993
- $Y_2Cr_2O_7$, $Y_2Mn_2O_7$, pyrochlore type, synthesis and physical props. 80−33963
- YFe_2, amorphous, mag. order, cluster phenomena, hyperfine struct. 77−16079
- $Y(Fe_cAl_{1-c})_2$, mag. props. 79−38308
- $Y(Fe_xAl_{1-x})_2$, mag. order in pseudobinary systems down to millikelvin temps. 78−19251
- $Y_6(Fe_{1-x}Al_x)_{23}$, cryst. struct. and mag. props. 79−82180
- $Y(Fe_{0.022}Co_{0.978})_2$, ferromag. relax. model, Mossbauer spectra 80−15853

Curie temperature continued
$Y(Fe_{0.022}Co_{0.978})_2$ mag. props., Mossbauer expts., 0.15-4.2K 78−43712
$Y(Fe_xCo_{1-x})_2$, $x \leq 0.2$, mag. props. and Mossbauer meas. 80−75798
$YFe_{1-x}Ga_xO_3$, zone refined, exam. of Curie point and magnetisation 79−4673
$Y_3Fe_{5-x}In_xO_{12}$, K absorpt. and Mossbauer spectra and other phys. props. *(Russian)* 77−32467
$Y(Fe_{1-x}Mn_x)_2$, mag. order onset 80−25135
$Y_6(Fe_{1-x}Mn_x)_{23}$, struct. and mag. props. 80−25083
$Y_6(Fe_xMn_{1-x})_{23}$, mag. order in pseudobinary systems down to millikelvin temps. 78−19251
$Y_2(Fe_{1-x}N_x)_{17}$, magnetic properties, Mossbauer spectra *(Chinese)* 78−95433
$YFeO_3$ orthoferrite, weak ferromagnet domain struct. near Neel temp. 79−99739
YIG, crit. behaviour, Mossbauer and magnetisation meas. *(Russian)* 79−61106
YIG, pure and Ga-substituted diffuse refl. and thermorefl. spectra near Curie point 80−40131
YIG, substituted, effect of electron bombardment on mag. and elec. props. 79−42103
YIG: Si single crysts., mag. props. 80−107981
$Y_{3-x}La_xFe_5O_{12}$, mag. props. rel. to ionic struct. 80−75756
$(Y_xLu_{1-x})_2V_2O_7$ semiconducting ferromag. pyrochlore, mag. props. 80−29547
$YMn_{2-x}Co_x$, mag. order in pseudobinary region 79−99689
$YMn_{2-x}Fe_xH_z$, mag. props., ordering temps. 80−71028
Y_xNi_{1-x}, amorphous, high press. magnetisation and Curie temp. 80−20442
$(YSmLuCa)_3(FeGe)_5O_{12}$, mag. props. and growth of 2 μm bubbles 78−91910
YbCuAl, mixed valence behaviour, mag. props. 78−68150
$YbFe_2$, Curie temp., elec. quadrupole couplings, Mossbauer study 80−39949
Yb_2O_3, 300 to 900K, mag. susceptibility and Curie temp. meas. 78−56288
Yb_xSy, synthesis and mag. props. 78−23242
$Yb_2V_2O_7$, pyrochlore struct., mag. props. 78−72335
$Yb_2(WO_4)_3$, mag. props., 300 to 900K 79−28510
$ZnGa_2O_4:Cr^{3+}$, weak exchange interaction determ., ESR study 80−93107
$Zn_xMn_{1-x}Fe_2O_4$, substitution effect on mag. struct. and exchange interaction *(Russian)* 78−47949
$Zn_xNi_{1-x}Fe_2O_4$, magnetic props. rel. to localised canting model 77−32161
Zr-Co-Ga alloy, mag. susceptibility in phases of structural type Th_6Mn_{23} *(Russian)* 79−24130
$Zr(Fe_{1-x}Al_x)_2$, Curie temp., magnetisation, and cryst. struct., conc. depend. 80−75730
$Zr(Fe_{1-x}Co_x)_2$, mag. props. and Mossbauer effects 79−91322
$Zr(Fe_{1-x}Co_x)_2$, press. effects on ferromag. to paramag. transition 77−66302
$Zr(Fe_xCo_{1-x})_2$, mag. order in pseudobinary systems down to millikelvin temps. 78−19251
$ZrZn_2$, high press. study of Curie temp. and mag. susceptibility 80−84600
$ZrZn_2$, high purity, mag. props., pulsed fields up to 17 T 78−64198

curium
see also nuclei with ......
antiferromag. state, paramag. suscept. meas., electronic struct. *(Czech)* 78−80133
atom, electron configurations, isotope shifts, visible and UV spectra 80−32641
atom, isotope shifts rel. to $|\psi(0)|^2$ 78−17580
atom, spectral classification, pattern recognition method 78−41983
build-up in Trino Vercellese PWR fuel rods 79−85754
determination in biological samples by solvent extraction and liquid scintillation counting 79−53260
electrical resistivity and mag. ordering 77−80760
isotope separation, chemical treatment of irrad. targets *(French)* 77−26883
magnetic structure, neutron diffr. meas., antiferomag. below 52K 77−63101
magnetic susceptibility meas., Faraday method 77−28369
marine ^{242}Cm conc. supported by ^{242m}Am 77−49091
movement through food chain 78−61264
oxalate precipitation for separation of Am, Cm, and trivalent lanthanides 80−83202
production by US irrad. in reactor, chem. separation, yield 77−63986
radioactive target preparation and characterisation 80−18734
radioactive wastes, leach behaviour of hydrofracture grout 77−10478
separation with phosphororganic extractants 77−26854
solar nebula, Th, U, Pu and Cm condensation and fractionation 79−35154
$^{241}Am(n,X)$, Japan Material Testing Reactor, separation of transuranium elements *(Japanese)* 80−52731
$BaF_2:Cm$, fluorite-struct., self-luminesc. 78−27309
$CaF_2:Cm$, fluorite-struct., self-luminesc. 78−27309
Cm+Pb, 1sσ excitation probability, scaling law, breakdown at very small internuclear distances 80−58365
^ACm, A=242, 244, in English Channel, transfer into S.North Sea 79−48519
^{242}Cm and ^{244}Cm in global fallout, lichen sample results 78−57263
^{242}Cm removal, Ca-DTPA vs. ZnDTPA as chelate, in rat 77−64141
^{244}Cm, biological availability, influence of DTPA at soil-plant and plant-animal interfaces 78−73264
^{244}Cm, emission spectrum, 2400-11200 Å, wavelengths, rel. intensities, Zeeman effect 77−46514
^{244}Cm, inhalation carcinogenesis of high-fired $^{244}CmO_2$ in rats 80−21502
^{244}Cm metal, mag. susceptibility meas. 77−28368
^{247}Cm in early Solar System, Allende $^{238}U/^{235}U$ ratio evidence 80−90347
^{247}Cm, K-shell fluorescence yields from Auger electrons and X-rays, precision meas. 79−31462
^{248}Cm, prep. and cryst. struct. 79−99115
$SrCl_2:Cm$, fluorite-struct., self-luminesc. 78−27309
$SrF_2:Cm$, fluorite-struct., self-luminesc. 78−27309

curium compounds
aqueous solution, electrochem. props., thermodynamic props., radiopolarography 77−29040
^{248}CmN, prep. and cryst. struct. 79−99115
$(Am,Cm)O_2$ solid soln., struct. changes under self- and reactor irrad. 77−27927
Cm-O system, phase obs. in $CmO_{1.50}$-$CmO_{1.71}$ region 77−36490
CmAs, lattice consts., X-ray diffr. study 80−33953
CmAs magnetic susceptibility meas., Faraday method 77−28369
$CmCl_3$, vapour phase hydrolysis and ht. of formation of CmOCl 78−20062
CmN, lattice consts., X-ray diffr. study 80−33953
CmN magnetic susceptibility meas., Faraday method 77−28369
CmO, and CmO_2, electronic struct. and chem. bonding and XPS line shape calcs. 79−33264
CmO_2, band struct., cryst. binding and ESCA spectra, X_α cluster calc. 78−64443
CmO_2, IR spectra, values of transverse vibr. frequencies 77−28585
CmO_2, lattice parameter, neutron diffr. meas. 77−63101
CmO_2, struct. changes under self- and reactor irrad. 77−27927
CmO_2, XPS meas. 77−48314
CmOCl, ht. of formation from vapour phase hydrolysis of $CmCl_3$ 78−20062
$^{244}Cm(OH_3)$, cryst., self-irrad. effects and lattice parameters 77−69013
CmP, lattice consts., X-ray diffr. study 80−33953
CmS, lattice consts., X-ray diffr. study 80−33953
CmSb, lattice consts., X-ray diffr. study 80−33953
CmSe, lattice consts., X-ray diffr. study 80−33953
CmTe, lattice consts., X-ray diffr. study 80−33953
$^{244}CmO_2$, mobility in bronchially intubated rat 80−30967

current (**electric**) *see electric current*

current algebra
see also elementary particle theory; hadron current; light cones; quantum field theory
$1/2^+$, baryons, vector mesonic decay, charm changing mode, SU(4) and SU(8) 80−47283
ΔI=1/2 dominated weak decays of strange hadrons, Weinberg-Salam scheme 80−27499
ΔS=1 nonleptonic weak decays, ΔI=1/2 rule, quark models and current algebra 80−47282
η′ meson as pseudoscalar gluon, current sum rule saturation in QCD *(Russian)* 79−71718
ρ-exchange isovector parity-violating potential 79−93525
σ-models, nonlinear, supersymmetric, nonlocal conserved currents and instanton-like solutions 80−86544
Adler sum rule subtractions and charge symmetry violation 77−18202
anomalies of quantum conserved currents in exactly solvable models 78−387
anomalous currents in curved space 78−62336
antiquark sea role in determ. of $\sin^2\theta_W$ from total neutron cross sections *(Russian)* 80−4910
axial anomalies and index theorems on open spaces 78−93821
axial current in dimensional regularization 80−13233
axial currents in nuclei, one-pion exchange diagram 78−46008
axial meson exchange currents and hard pions in nuclear physics 79−40854
axial vector anomaly, uniqueness 79−35965
axial vector anomaly and index theorem 78−29293
axial vector current anomaly in gauge field theory Green's function calc. *(Russian)* 80−27412
axial vector form factor from current algebra, π PCAC and covariant threshold electroprod. amps. 80−414
axial vector multiplets, mass spectrum, mixing angles, pseudoscalar mesons, decay consts. 77−13892
axial-vector current and dimensional regularization 80−42363
axial-vector currents, chiral and gauge invariant regularisation 80−4956
axial-vector neutral-current couplings from quark model anal. of Δ(1236) neutral-current neutrino prod. 77−61278
axial-vector-current divergences in constituent-quark basis 78−8557
baryon pionic transitions in MIT bag model using PCAC hypothesis 80−37228
beta decay, nuclear current matrix element 78−46031
Born-Infeld equation, two-dimensional system of conservation laws *(Russian)* 80−42365
bottom meson weak hadronic decays, Kobayashi-Maskawa weak current model 80−42456
box diagrams with nonvanishing external four-momenta in gauge theories 80−22525
Cabibbo current and CP violation in a six quark gauge model 78−70329
Callan-Gross relation, instanton violation, nonperturbation correction asymptotic behaviour 80−27409
causal logic of Minkowski space, states defined by conserved currents 79−54282
causality props. of form-factors of one particle matrix elements of current commutator 77−30385
charged current ν and ν̄ interactions, hadron prod. at high energy, quark parton model 79−36058
charged current Fermi four field point interaction, weak interaction theory, rescatt. graphs consequences 77−67555
charged current induced weak one pion prod., form factors from PCAC 80−18129
charged current neutrino physics with Gargamelle bubble chamber, book contrib. 79−30728
charged second class currents, model 77−213
charmed baryon decays, EM and weak, U- and V-spin generalisations 80−47284
charmed baryon decays, nonleptonic, parity-violating, single-quark and two-quark transitions 80−68453
charmed baryon decays, weak hadronic, SU(3) dynamical scheme 80−68454
charmed baryon nonleptonic decays, sum rules for ΔC=ΔS=1 S-wave decays 79−58957
charmed baryons, weak decays, quark model framework 80−62976
charmed current neutrino physics with Gargamelle bubble chamber, book contrib. 79−30728
charmed meson decay, SU(4) symm. breaking 77−26518
charmed mesons, nonleptonic decays, dual model current algebra relations and amplitudes 79−89132
charmed mesons, semileptonic decays, charged weak current struct. 80−102042

current algebra continued
- charmed weak current group struct., chiral $SU_4 \times SU_4$ breaking 77—65118
- chiral solutons and current algebra 79—40680
- chiral $SU(4) \times SU(4)$ representation mixing, algebraic struct. 77—34102
- coloured null flags and para-Fermi fields 77—5993
- conformal spinor current anomaly from symmetry arguments 78—4803
- conformal symmetry and the vector four-point function 79—49394
- conserved axial second class current, sum rule, commutation relations and axial formfactor 80—18090
- conserved axial second class current, sum rule, dispersion calc. 80—77986
- conserved currents and symmetries of the S-matrix 80—9110
- conserved opposite parity currents, coupling to single vector field 79—21990
- conserved vector current hypothesis, extension to gluons 77—71480
- conserved vector current hypothesis for gluons, hadroprod. of quark flavours 77—74617
- constituent quarks in SU(3) and SU(6), current algebra., hadron decays, review, book contrib. 80—47259
- correlation function finite temp. spectral function sum rules 77—67591
- Coulomb corrections, phase shift anal., S-matrix theory, below 300 MeV 79—85325
- CP^N σ-models, 2-dimens., local conserved currents, conservation laws 80—86579
- current conservation in perturbative sine-Gordon and massive Thirring models 79—9273
- current-current interaction, general props., book contrib. 78—78163
- CVC hypothesis and ^{12}N e^+ energy spectra, weak magnetism 77—54190
- deuterons, current conservation and off-shell effects with arbitrary interaction 79—45183
- dimensional reduction and axial anomalies 80—86561
- diquark contribs. to scaling violation and deep inelastic σ_L/σ_T, structure functions, QCD 80—22573
- double Wilson expansions of products of three-spinor operators 77—30232
- dual chiral pion model, partially conserved axial-vector current, S-matrix theory 78—58175
- dual current vertex, group theoretical struct. 78—74229
- dual string theory, local currents *(Russian)* 78—25024
- E based vector-like unified theory, group theoretical anal. of symm. breaking 77—87929
- effective lagrangian with no U(1) current problem for CP^{n-1} and QCD 79—89066
- eight quark model, modified left-handed currents, ν reactions and e^+e^- annihilations 78—16982
- Euclidean QFT, appl. of virial expansion derivation 78—37131
- exchange currents, meson fields and progenitor sum rules 78—17111
- extended meson fields as alternative to quark confinement, conserved current construction 77—22642
- extended partially conserved axial vector current hypothesis, Dashen mass formula, $\eta \rightarrow 3\pi$ 79—289
- extended PCAC+Veneziano type model, Goldberger Treiman relations, $\eta \rightarrow \gamma\gamma$or $\pi^+\pi^-\gamma$ 78—21354
- extended PCAC hypothesis, soft-meson chiral symm. breaking 78—21353
- fermions interacting via meson fields, heuristic Hamiltonian 77—6022
- field current relations, appl. in weak form to radial excited states *(Chinese)* 79—49420
- five-quark model with right handed current, weak interactions description 77—57485
- flavour-changing neutral-current process in gauge models and strong interactions 78—8541
- four flavour $SU(2)_L \times U(1)$, gauge model with unconfined colour, $\Delta I = 1/2$ rule, GIM currents 77—82708
- $g\phi^3$ model, supersymmetric, massive and massless, renormalised supercurrent and anomalies 79—6267
- Gamow-Teller matrix element, axial currents in nuclei, quenching mechanism 79—17859
- gauge fields, chiral fields on loop space, colour-electric flux rings 80—42327
- Gell-Mann-Nishijima formula for EM current operator generalised 78—78109
- generalised Federbush model, current definition, perturbation calcs., gauge transformations 79—6297
- generating functionals in current formulation of quantum meson field 78—16947
- geometrodynamics for quarks and hadrons, current definition and nonconservation 78—45809
- Goldstone boson, U(1) current, rel. to η' 79—89081
- Goldstone theorem, struct. of conserved currents and mass spectra 80—82920
- Goldstone theorem generalisation, scalar fields, conserved current and mass spectra struct. 80—68339
- gravitino, axial current anomaly, Faddeev-Popov ghosts 80—68120
- hadron bags, interactions under strict quark-line rule 78—41495
- hadron EM interactions, book 80—46749
- hadron-hadron weak interactions, right handed currents effects in QCD 79—13016
- hadronic charmed particle decays, quark and particle helicities, charm changing current chirality 80—37256
- hadronic EM current, short distance scaling, R(s) behaviour as $s \rightarrow \infty$ 79—22095
- hadronic EM interactions, review, book contrib. 80—47240
- hadronic structure using parton anal. of deep inelastic scattering and rel. processes 79—80803
- hadroproduction of quark flavours, extension of conserved vector current hypothesis to gluons 78—58159
- hierarchy in asymptotic reconstruction of spontaneously broken isotopic symmetry *(Russian)* 79—2968
- high energy charged current neutrino interactions, spherocity and thrust distribs., jets 79—85293
- high energy neutrino experiments, state of art 79—26322
- high energy neutrino interactions, quark parton model anal. 79—30730
- high energy neutrino physics, recent expt. results 80—4982
- high energy neutrino-hadron collisions, dilepton mass spectrum, V-A and Weinberg interaction calcs. 79—3010
- hyperon nonleptonic decay, implications for right handed current 77—67651
- hyperon nonleptonic decay, SU_3 symm., second class currents in effective Hamiltonian 77—41842

current algebra continued
- inclusive reactions, induced by EM or hadronic weak currents, single obs. π sum rules, PCAC 77—34161
- induced second-class currents from isospin and chiral-symmetry breaking 79—97538
- infinite nuclear matter, PCAC relations, πN vertices, π condensate instability *(Russian)* 80—13398
- instantons, generation of meson mass spectrum, current algebra, mixing angles 80—86567
- IR dynamics, classical current models 77—60947
- isoscalar axial-vector current in neutral-current phenomenology 79—93316
- isoscalar neutral current axial vector couplings and nucleon anomalous moments 80—27452
- isovector vector couplings from quark model anal. of $\Delta(1236)$ neutral-current neutrino prod. 77—61278
- jet cross sections and quark current-photon pointlike coupling, sum rules 80—32104
- left handed weak doublets with mixed quark states, appl. to $\nu N \rightarrow \mu^+ X$ 77—26514
- left-right symmetric gauge models, $SU(2)_L \times SU(2)_R \times U(1)_L \times U(1)_R$, weak currents, Z^0 prod. and mass 79—253
- left-right symmetric $SU(2)_L \times SU(2)_R \times U(1)$ theory, atomic parity, e^+e^- collisions asymm. at PETRA, PEP energies 78—12820
- light cone algebra approach to Glashow-Iliopoulos-Maiani model, charge symmetry violation 77—18194
- light Higgs boson, Weinberg-Salam model 78—45835
- light quark mass and low energy η meson interactions *(Russian)* 79—67513
- light-cone quantisation of scalar field, current nonconservation 80—47220
- local charge densities in quantum field theory, conserved local currents 77—2718
- locally conserved currents and energy-momentum tensor 77—60889
- low energy expansion of two current amplitudes, wavevector Compton scatt,., μ capture on p 78—16946
- magnetic moments of light nuclei, nucleonic currents 78—17100
- Markov representations, T-positivity 77—18199
- mass-sum rule, Veneziano-type amplitudes π and K mesons 78—74180
- massive Thirring model, conserved currents 77—198
- massive Thirring model, S-matrix calcs., required number of conserved currents 80—42329
- massless gauge theories, supersymmetric extension, supercurrent construction principle 79—40664
- Melosh transform., reln. to generalised $^3P_0$ model 78—12885
- meson decay, tensor, current algebra approach, symmetry-breaking Hamiltonian, chiral $SU(3) \times SU(3)$ or $SU(4) \times SU(4)$ 80—68450
- meson dipion cascade decays, current algebra techniques, pole plus remainder model, chiral symmetry breaking and QCD 80—62972
- meson exchange currents, conservation principles, symmetries, book contrib, 80—473
- meson exchange currents in electron scatt. from light nuclei 77—10390
- meson exchange currents in nuclei 78—12980
- meson theory of nuclear vector and axial vecotr exchange currents, review, book contrib. 80—474
- MIT bag model, PCAC effects, pion field exchange energy, η mass 79—93378
- mixing angle between ordinary and heavy leptons in a (V-A) model, constraints 78—4846
- muon capture, axial current role, possible solns. conserved isovector current hypothesis 79—26401
- muon capture, induced pseudoscalar form factor upper bound 77—82872
- muon-electron mass ratio in a semi-classical model 80—91072
- N=2 extended supersymmetry, Noether current multiplets, extended supergravity 79—40438
- N-flavour quark model, axial-vector current anomaly, decay constants and η-η'-η_c problem 79—13045
- neutrino as axial EM field source, symm. P-invariant broadened Maxwell eqns. *(Russian)* 78—58141
- neutrino charged current interactions at 3, 9 GeV, total cross section 79—71739
- neutrino interactions, experimental results for charged and neutral current interactions and multilepton prod. 79—49512
- neutrino oscillations, Majorana and Dirac mass mixing 80—101969
- neutrinos, gauge theories, EM props., forbidden processes and currents with anomalous Lorentz struct. 78—54599
- Noether map for equivalence classes of conserved currents, Lagrangian systems 80—371
- non abelian gauge fields, conserved axial vector currents 77—30264
- non-Abelian gauge theory in a nonlinear gauge, charged current description 79—12937
- non-Abelian group spontaneous violation, gauge models and external currents *(Russian)* 77—207
- nonAbelian gauge field, gauge-invariant conserved current *(Chinese)* 78—12806
- nonleptonic hyperon decays, final state interactions with inelastic effects, comments 80—99099
- nonleptonic interactions, enhancement and suppression factors for left handed current, K decay 79—385
- nonleptonic weak Hamiltonian, current×current theory, SU(4) representations 79—17666
- nonlocal currents for supersymmetric nonlinear models 80—52414
- nonrelativistic effective πN vertex, PCAC and σ-model 80—52591
- nuclear β-decay, weak magnetism and second-class currents 78—554
- nuclear currents, elementary particle description, microscopic anal., book contrib. 79—97664
- nuclear currents, microscopic anal. of elementary particle description 78—82304
- nuclear matter, S-wave πN interactions and PCAC 80—78185
- nuclear pionic field, isobaric excitation effects on weak axial coupling consts. 77—10328
- nuclei, exchange and renormalisation phenomena due to pion-nucleon couplings, PCAC 77—41893
- nucleon form factors and light front dynamics *(Russian)* 77—38172
- null plane current anticommutators, sum rules and appls. 80—52436
- null-plane charges and Fourier transforms, broken symm. 77—2771
- null-plane $U(6)_{W,\ currents}$ identification of hadronic states, necessity for Melosh-type transforms. 77—22667
- octet enhancement and Cabibbo angle in SU(3) breaking scheme 77—2785
- one-pion exchange current, conservation and form factors 77—38098
- oriented nuclei, β-γ ang. correl., G-parity nonconservation 78—54723

current algebra continued
  P-state particle, field current reln. and total width *(Chinese)* 78–82188
  parafield current algebra, Lagrangian quantum field theory *(Russian)* 77–13891
  parity violating currents in rotating thermal radiation 79–17633
  partial conservation of axial-vector current, dynamical theory, and dispersion relations 79–35966
  partially conserved axial vector currents, corrections, light-plane commutators, sum rules, meson decay 79–304
  partially conserved axial-vector current and model chiral field theories in nuclear physics 79–67698
  parton model interpretation of cut vertex formalism 80–86566
  PCAC, chiral anomalies and quark masses 78–8556
  PCAC, dimensional derivation of gravitational correction 78–21371
  PCAC, possible testing in ν-N interactions *(Russian)* 77–61280
  extended PCAC and chiral symmetry breaking 77–45986
  PCAC and dual resonance amplitudes, old and new mesons, charm 78–45885
  PCAC and quark model in $\pi \to e\nu\gamma$ 77–30366
  PCAC and weak nonleptonic strangeness changing Hamiltonian 77–71460
  perturbation theory of currents and continuous symmetry restoration in two dimens. 79–21910
  photoabsorption, σ_{-2} sum rule, gauge invariance and locality 77–34286
  photoproduction, vector-meson exchange 78–41557
  physical pion low energy electro- and photoprod., Ward identity, chiral symmetry breaking struct. 80–5003
  physical pion low energy photo- and electroprod., photoprod. phenomenology, quark mass 80–5004
  pion condensation in neutron matter: effects of pion-nucleon scattering 79–26388
  pion propagation and production in nuclear matter 79–80893
  pion-nucleus coupling constants, deduction using PCAC 79–40855
  pionic degrees of freedom in nuclei, axial currents 77–10326
  pions and isobars in nuclei—an overview, (π,π) and nuclear forces 79–85373
  pomeron current model for diffraction dissociation 78–4843
  potentially CP violating phase in QCD, alleged axion mass, PCAC quark masses 78–66080
  probability current and boundary conditions for wave functions of parity violating interactions 77–71459
  pseudoparticle fields, role of fermionic zero modes 78–74159
  pseudoscalar mesons, charge radii and PCAC without soft current limit 80–99070
  pseudoscalar mesons, $SU_4 \times SU_4$ chiral symm. 77–67583
  pure leptonic weak interaction with induced shadow states, renormalisable theory 78–37136
  QCD, gauge independence of IR cancellation, fermion-fermion scatt. 78–50006
  QCD, neutron electric dipole moment, chiral estimate, current algebra, CP violating reactions 80–27471
  QCD, spectral function sum rules in charged current sector 79–80796
  QCD and ψ parameters, charmed quark current in quark-gluon coupling *(Russian)* 80–13277
  QCD spectral function sum rules, EM current flavour components 80–99084
  QED, gauge invariant formulation using local currents 77–45997
  QED, supersymmetric, renormalised supercurrents and scale anomaly 80–105818
  QED, two-dimens. light cone formulation 77–57476
  QED, Ward identity, axial vector current divergence, chiral invariant regulator field 80–57526
  quantum chiral model, local polynomial current conservation in renormalised 1/N perturbation theory 80–13232
  quark charged current tests in neutrino expts. 77–22726
  quark geometrodynamics, baryon struct., current and meson couplings 79–6320
  quark light-cone model, current conservation 78–21386
  quark mass ratio from baryon mass splittings 80–42436
  quark models, axial vector mesons decoupling from local currents 77–87938
  quark models and unified field theories, review 79–80805
  quark-lepton correspondence, multigeneration $SU(2)_L \times U(2)$-based model 80–22584
  radiative corrections in gauge theories, QCD current algebra formulation, weak interaction universality 78–93883
  radiative muon capture, transition amplitude, PCAC test 80–83076
  relativistic confining potential model, current spectral functions, meson dominance calc. 79–71734
  relativistic corrections to weak exchange currents and μ-p capture 79–75756
  relativistic harmonic oscillator quark model, N and $\Delta(1236)$ form factors 78–93852
  relativistic many body theory, finite temp. and density., elementary particle symmetries 79–49403
  relativistic quantum fields, particles and currents, book 78–82117
  relativistic quantum mechanics, conserved four-vector currents for free particle 77–37778
  representation in ultralocal quantum field theory model 79–6288
  restored symmetries, quark system, Pomeron as Josephson current 77–61211
  right handed colour octet currents for charm and colour excitation in $\nu(\bar{\nu})$ reactions 78–93874
  right handed currents, $\Delta I = 1/2$ rules, nonleptonic decays, heavy-quark expansion, Zweig's rule 77–61217
  S- and P-wave hyperon decay amplitudes, $\Delta I = {}^1/_2$ rule deviations, weak current-current interactions 80–9166
  scalar meson decay width, meson-meson sigma terms and phenomenology 77–74680
  scale and conformal invariance, scalar currents, theory with continous mass spectrum 78–62335
  Schwinger model, Ward identity, fermion axial vector current divergence, chiral invariant regulator field 80–57524
  second class axial vector currents with mesonic effects, beta-decay 77–30520
  second class current problem in $A=8$ nuclear systems 77–41921
  second class current upper limit from β-decay data 80–47404
  second class currents, possible exist. in nuclei from $(ft)^+/(ft)^-$ Gamow-Teller data 77–26626
  second class currents and anomalies in neutrino reactions 77–57522
  second class currents in β-decay of polarised ^{12}B and ^{12}N 77–41920

current algebra continued
  second class currents in nuclear β-decay 77–41919
  second class currents on nuclei, effective two-body operator approach 78–54694
  second dip development in elastic pp scatt., Chou-Yang model current-current interaction 79–89192
  second-class currents and matrix elements in renormalisable field theory 77–10197
  second-class currents in field theory, general treatment 77–67590
  second-class currents in model of light quarks 77–10213
  second-class weak currents, experimental progress, few-body aspects 77–22665
  semi-leptonic weak interactions, book contrib. 78–78162
  semileptonic weak and EM interactions, nuclear current operators 79 6515
  short-distance and light-cone expansions for products of currents 79–17638
  sine-Gordon supersymmetric model, higher local quantum conserved currents 80–52435
  sine-Gordon supersymmetric theory, infinite set of bosonic conserved currents 78–62313
  single pion production in antineutrino induced charged current interactions 79–36063
  soft pion theorem, appl. to currents in nuclear forces and matter. 79 26377
  spectrum-generating SU(3) and local current algebra 80–9128
  spin-0 meson realisation, second class currents 77–30282
  spin-isospin polarizability of nuclear matter and renormalization of weak currents 79–67697
  spinor QED, current commutator anomaly, regularised dimensionally using hyperfunctions 78–12845
  spontaneously broken chiral SU_2 symm., equivalence to current algebra in field theoretic model 77–82688
  strangeness changing processes, gauge models with V+A currents, higher order effects 77–22677
  stratifying strong, weak, EM and gravit. interactions in five dimens., geometrical model 78–37166
  string in static field, conservation laws 79–21969
  strong interaction theory based on fibre bundle geom., currents 77 79204
  strong localised EM potential interactions with charged leptons or vac. state, critical pots., weak currents 78–54597
  strong PCAC appls., axial vector current 4-divergence, meson fields *(Chinese)* 80–42364
  structure function moment asymptotic behaviour and light cone singularities 78–4804
  SU_2 nonlocal conserved currents for two-dimensional chiral theories 80–52413
  $SU_L(4) \times U(1)$ as gauge symm. for quark, lepton quartets, weak and EM interactions, weak currents 78–74174
  $SU(2) \times U(1)$ gauge theory of weak, EM and dual EM interactions 80–52448
  SU(2n) principle models for integrable nonlinear systems, current constraints, conservation laws 80–86619
  SU(3), partial conservation of axial vector current in constituent quark basis 77–2773
  $SU(3) \times U(1)$ gauge models, exam. of weak currents and associated features 78–16975
  SU(3) rules for non- and semi-leptonic weak decays of charmed and strange mesons 78–45916
  $SU(4)_L \times SU(4)_R \times U(1)$ gauge, lepton weak interaction, right currents, effective Fermi interaction const. universality *(Russian)* 79–58921
  SU(4), broken Zweig rule and null plane 77–18225
  $SU(4) \times SU(4)$ chiral symmetry breaking, axial vector current divergences, kaon PCAC 79–45032
  $SU(4) \times SU(4)$ symmetry breaking, Cabibbo angle, nonlinear hadronic Lagrangian, PCAC *(Russian)* 80–42360
  SU(5) and E_7 unified gauge theories 78–54600
  SU(N) gauge theory, current synchrospherical symmetrical monopole in multisynchrospherical symmetrical case *(Chinese)* 80–22527
  subquark model of leptons and quarks, unification, currents and exotic states 80–86683
  supercurrent, existence and deduction from an arbitrary superfield Lagrangian *(Russian)* 78–89633
  supersymmetric nonAbelian gauge theory, supercurrent anomaly 78–24958
  supersymmetric nonlinear σ model, nonlocal charges and currents 80–27410
  supersymmetric QED, supercurrent gauge invariance, α-independ. 80–95233
  supersymmetric Yang-Mills field theory, point splitting regularisation, superformal anomaly 80–91014
  supersymmetric Yang-Mills theory in Wess-Zumino gauge, supersymmetric regulators and supercurrent anomalies 80–86614
  Thirring model, massive, with internal U(n) symmetry, zero mass limit 77–57466
  Thirring model with SU_n symmetry, scale invariance 79–9288
  topological setting for axial anomalies and index theorems on open spaces 79–303
  trace and axial vector anomalies, for spin 3/2 Majorana field, derivation using zeta function regularisation procedure 79–2700
  translationally noncovariant conserved local currents in Wightman's axiomatic field theory 78–32971
  two-current two-particle amplitude, narrow-reson. model, gauge invariance and scaling 77–74576
  two-photonic decays, weak, Hamiltonian derived in model with right-handed currents *(Russian)* 78–66119
  U(1) Goldstone boson, anal. of BRS invariance in nonAbelian gauge theories 79–80798
  unification of EM, weak and strong interactions, massless fermions coupling to vector mesons 80–73637
  unified gauge model with a nonlinear chiral hadron Lagrangian 80–42378
  unified gauge theories of weak currents of hadrons 79–80786
  unified quartet quark model extensions, weak interactions and right-handed currents 77–22678
  unified theory with right handed currents, SU(6) based vector-like gauge theory, proton stability 77–49890
  up-quark zero mass, critical anal. in current algebra framework 78–82144
  V+A current of charmed quarks for nonleptonic processes 77–30307

current algebra continued
$V+A$ currents coupling old quarks to new quarks 77−26486
V-A, evidence in $\bar{\nu}+N$ weak neutral current interactions 77−2815
vector current selection rules in new formal approach 77−30306
vector meson leptonic width, duality between vector mesons and perturbative QCD 80−57589
Ward identities and Bethe-Salpeter equations, meson and baryon EM current transition matrix *(Chinese)* 79−63375
weak $(V+A)$ interactions of leptons, possible existence *(Russian)* 77−74678
weak and EM interaction unification with strong interactions following τ and Υ, book contrib. 80−47235
weak and EM interactions at high energy [conf. Les Houches, France (July 1976)] 79−80785
weak axial coupling constants in nuclei, polarizability, pionic field, PCAC 77−6055
weak charged V-A current 78−74179
weak current colour-octet component, lepton-hadron correspondence 77−6077
weak interaction model with left-handed 8 quarks and 8 leptons 77−18218
weak interaction scheme, charmed hadrons expt. data, four flavour model explanation 78−45860
weak magnetism, review of evidence for its existence 79−49445
weak neutral current coupling const. from νN single pion prod. data anal. 77−13911
Wightman theory, all spontaneously broken symmetries for noncovariant currents 80−31975
Yang-Mills supersymmetric gauge theory, cancellation of supercurrent anomaly 78−8518
zero energy fermions in U(1) pointwise monopole field *(Chinese)* 80−42345
b quark prod., left-handed currents and lepton number nonconservation 77−67616
$D(1865)\to e\nu K^*(890)$, right handed current, eK^* ang. correl., energy spectra 78−74248
$D\to K\pi l\nu$, charm-changing weak hadronic current, models 80−57585
$D\to K\pi l\nu$, current algebra calcs., form factors and decay distribs. 80−42447
D mesons, decay const. using current algebra with Lagrangian model 78−58176
D-meson semi-leptonic decay, current algebra treatment, rel. to charmed current quark mass 79−97577
D^0 Cabibbo suppressed hadronic decays, Cabibbo universality fake violation, RH currents 80−73699
$D^0\to K^-\rho^+$ strong signal, $(\bar{c}s)_R$ current implications 79−36070
$D\bar{D}^*$ production and decay, VDM, dual amplitude anal., e^+e^- annihilation 77−49992
$\Delta(1232)$ decay width using little bag dynamics and axial vector current 79−75771
$\Delta(1236)$ production in νp reactions, multipole struct. of weak prod. by charged currents 78−29328
$\Delta(3,3)$ phase shift, current algebra model, πN decay channel 77−79232
e/μ charged current $\nu(\bar{\nu})$ interaction comparison in Ne-H_2 mixture, μ-e universality 79−9363
ed scatt., meson exchange currents for deuteron form factor 77−18290
e^+e^-, jet cross sections and quark current-photon pointlike coupling, sum rules 80−32104
e^+e^- annihilation, charge current asymmetry as QCD test, neutral gluons 80−57616
e^+e^- annihilation, superheavy flavour prod., weak current effects, Z^0 effects 80−57614
$e^+e^-\to\pi^+\pi^-\pi^+\pi^-$ cross section, current algebra calc., props. of hadronic axial vector current 79−17742
$e^+e^-\to\pi X$, soft π prod., PCAC hypothesis, current algebra commutator relations 78−33075
e^+e^- transversely polarised annihilation, heavy lepton prod. and decay 77−18261
$e^-\mu^-\tau$ asymmetry, conserved currents *(Chinese)* 79−58904
$eN\to e\pi_s+X$, test of soft-pion theorem in inclusive pion electroprod. 79−17739
eN inelasticcatt., low energy pion electroprod. and hadron form factors, book 79−85306
$\eta\to\pi^+\pi^-\pi^0$, on-mass-shell current algebra, $SU(3)\times SU(3)$ σ model 77−34151
$\eta'(958)\to\gamma\gamma$, decay rate, axial-vector current divergences 80−9172
$\eta'\to\eta\pi\pi$, current algebra calcs. with symmetry breaking, inconsistency with expt. 79−13114
F mesons, mass and decay const. using current algebra with Lagrangian model 78−58176
$F^+\to p\bar{n}$, decay mode meas. for PCAC test 80−91018
$F^+\to\pi^+e^+e^-$, enhancement due to π^+ EM form factor, generalised PCAC applicability 78−82164
$\gamma\gamma$, jet cross sections and quark current-photon pointlike coupling, sum rules 80−32104
$\gamma p\to W^+n$, current algebra and sum rules high energy W^+ prod. 80−102039
$K\to 2\pi$, comment of appl. of current algebra and bag model 79−97622
$K\to 3\pi$, CP violation, current algebra anal., six quark Weinberg-Salam model 80−47281
K electromag. form factor, current algebra used *(Japanese)* 78−17019
K nonleptonic decays, without dynamics enhancement *(Russian)* 79−30733
$K\to\pi^0\pi^0$, contrib. of 2nd. class currents to nonleptonic decay 79−13117
$K\to\pi^+\pi^-\mu\nu$ decay rate 77−6113
$K\to\pi l\nu_l$, form factor, parameter-free hard-meson prediction via current algebra sum rules 77−49954
$K\to\pi\pi$, $\Delta I=1/2$ rule using PCAC 80−4990
$K^+\to\pi^+e^+e^-$, decay amplitude using simple model with PCAC 80−9162
$K_L\to 2\gamma$ decay, contribution of Hamiltonian derived for weak two-photonic decays *(Russian)* 78−66119
$K_L\to 2\gamma$ or $\pi^+\pi^-\gamma$, Weinberg-Salam model, weak radiative decays, large dist. contribs. *(Russian)* 77−82740
K_{l4} decay in relativistic quark model, axial vector form factors and decay rate 78−66109
$K^+n\to K^{*0}p$, partial conservation of strangeness-changing vector current 77−22779
$K^-p\to K^{-*0}n$, partial conservation of strangeness-changing vector current 77−22779

current algebra continued
$K^-p\to K^-p\pi^0$, amplitude calc. for soft pion emission, using PCAC 79−13153
$\mu^-d\to nn\nu_\mu$, meson exchange currents effect on Λ_d and Λ_q transition rates 79−85256
μp charged current interactions, hadron production, quark-parton model comparison 79−40769
$\mu p\to\mu nW^+$, current algebra and sum rules high energy W^+ prod. 80−102039
N form factors, weak, asymptotic behaviour within QCD dipole and triplepole formulae 80−62987
n-p system, EM form factors in multipole parametrisation formalism 78−17022
$NN\pi$ amplitudes, weak, sum rules and theoretical description nonleptonic hyperon decays 79−17663
ν, $\bar{\nu}$ charged current induced one pion weak prod., $I=1/2$ resonant contrib. 80−47274
$\bar{\nu}$ anomalies and right-handed currents 78−8654
$\nu(\bar{\nu})$ charged current induced one π prod., model total cross sections 80−4979
$\nu(\bar{\nu})N$, 5-35 GeV, total cross sections via charged current channel, energy depend. *(Russian)* 80−4981
$\nu(\bar{\nu})N$ elastic scatt., symmetry relations, current matrix elements 78−54627
$\nu(\bar{\nu})N$ scattering, modified GIM model, scaling violations, naive parton model 78−21414
$\nu(\bar{\nu})N\to N'\gamma e(\bar{e})$, current algebras and high energy γ-prod., sum rules 80−102039
ν production processes, exclusive, neutral current props., Lorentz struct., internal symm. 77−18267
$\bar{\nu}$-nucleus charged current interactions 79−22275
$\nu_e(\bar{\nu}_e)e$, charged and neutral current interference, test of Weinberg-Salam model 80−42385
$\nu_\mu(\bar{\nu}_\mu)N$ charged current total cross sections, (V-A) interactions, nucleon struct. function scaling 78−25033
$\nu_\mu(\bar{\nu}_\mu)p$, 2 GeV elastic scatt., charged current/neutral current event ratio 80−57582
νN, charged and neutral current interactions, cross sections and scaling variable distribs. 80−57581
νN, inclusive charged current interactions, recent results 79−49506
νN, $\bar{\nu}N$, y-distributions, nonscaling and longitudinal struct. function effects 78−33053
$\bar{\nu}N$ deep inelastic scatt., net charge in current fragmentation region, quark fragmentation 80−62964
$\bar{\nu}N$ in Fe, μ^+ polarisation in high energy charged current interactions 79−93399
νN interactions, CVC and PCAC tests, book contrib. 78−78171
νN interactions, currents and symmetries, theoretical speculations following recent expt. results *(German)* 77−41837
$\nu n\to\mu^-n\pi^+$, weak current isospin struct. study 79−49507
$\nu n\to\mu^-p\pi^0$, weak current isospin struct. study 79−49507
$\bar{\nu}n\to\mu^+n\pi^-$, effects of second-class weak currents in $\Delta(1236)$ reson. region 78−8656
$\nu N\to\mu N\pi$, high energy behaviour, light cone commutators, PCAC calcs. 78−37199
$\nu N\to\mu\bar{N}\pi$, PCAC anal. in 1st reson. region 77−82730
$\nu N\to\nu N\pi\pi$, neutral-current cross sections for double-pion production by neutrinos 79−17712
$\nu_\mu N\to{}^-C_0{}^+$, $C_0{}^+\to\Lambda^0e^+\nu_e$ Λ polarisation, chiral props. of charmed current 77−61272
$\nu_\mu N\to\mu^-C_0{}^+$, $C_0{}^+\to\Lambda^0e^+\nu_e$, test of charmed current struct. 77−61271
$\nu_\mu N\to\mu^-N\pi$, cross sections and invariant mass distribs., inelastic charged current reactions 79−71742
$\bar{\nu}p$, 1.1 GeV, charged and neutral current events, strangeness changing currents, charm prod. 80−57583
νP, neutral to charged current cross section ratio, coupling constant 80−27497
$\bar{\nu}p$ charged current interaction, inclusive ρ^0 prod. 80−62963
$\nu p\to\mu^-D^+X$ or $\mu^-D^{*+}p$, cross sections estimation using $V+A$ form of charm current 77−41839
$\nu p\to\mu^-p\pi^+$, effects of second-class weak currents in $\Delta(1236)$ reson. region 78−8656
$\nu p\to\mu^-p\pi^+$, weak current isospin struct. study 79−49507
$\bar{\nu}_\mu p(n)$, charged current interactions in Ne, cross section ratio, scaling variables 79−75763
Ω^- decays and right-handed currents 78−17015
$\Omega^-\to\Lambda K^-$, current algebra calc. with phenomenological modification of nonleptonic decay amplitude 77−67650
$\Omega^-\to\Xi^*\pi(\Xi^0l^-\bar{\nu}_l)$, nonleptonic hyperon decays, QCD description, PCAC anal. 80−95269
$pn\to nK\Lambda$, field current relations *(Chinese)* 79−22126
pp elastic scatt., current-current interaction, spin depend. differential cross section 80−18147
pp reaction, exchange current corrections π and ρ exchange 80−26733
$\phi\to\pi\gamma$, $SU(3)\times SU(3)$ algebra, appl. to ground state mesons, coupling constraints and decay rate 78−58183
π electroprod., light cone dispersion sum rules, axial vector currents 78−41556
$\pi\to e\nu_e\gamma$, isospin-breaking, chiral limit, conserved-vector-current violation, σ model 80−62988
π photoproduction near threshold, interior dispersion relations appls. 78−93889
π photoproduction on nuclei, current algebra model with hard pions *(Russian)* 77−74890
π radiative catpure, current algebra model with hard pions *(Russian)* 77−74890
π radiative decay amplitude, low-energy expansion, currents, sum rules 80−52509
π-π interaction, lectures, theory and expt. results, analyticity, unitarity, phase-shifts, current algebra 77−50008
$\pi^+\to e^+\nu\gamma$ calculation using field-current identity *(Chinese)* 77−34149
$\pi C\to\pi C'$, constraints due to PCAC and charmed-baryon couplings 79−89082
$\pi^+d\to pp$, meson exchange currents, effects on pion absorption 79−85287
$\pi\,{}^3He\,{}^3He$ coupling on basic of PCAC 80−32196
πK scatt. and related processes *(German)* 79−30750
πK scattering amplitude, analytic continuation, chiral symmetry breaking 80−63027
πN elast. scatt., parity-violating scatt. amplitude calc. using soft-pion techniques 79−75787
πN elastic and photoprod. models, role of $\Delta(3,3)$ resonance 77−6146

current algebra continued
πN four invariant amplitudes at low energy, simultaneous analysis of effective resonance poles 79—67598
$\pi N\rightarrow\gamma\pi N$, recoil corrections to static model, interaction current 78—25072
πN interactions at low energy, theoretical anal. 79—85326
πN low energy scatt. amplitudes, constraints 77—38196
πN scatt., low-energy 77—18319
πN scattering, P-wave interaction, anal. based on PCAC and σ-commutator 79—85334
πN scattering, partial conservation of axial vector current limit, on shell corrections 77—18201
πN σ term in hybrid chiral bag model, PCAC and SU(3)×SU(3) symmetry violation 80—78096
πNN vertex function and off-mass-shell πN scatt. 80—73739
$\pi^-p\rightarrow e^+e^-n$, induced pseudoscalar nucleon form factor, current algebra appl. *(Russian)* 78—78212
$\pi^-p\rightarrow e^+e^-n$, induced pseudoscalar nucleon form factor, current algebra framework 79—22131
$\pi^+p\rightarrow\pi^+p\gamma$, 165 MeV, monotonically decreasing photon energy spectrum, no Δ^{++}(1232) bump 80—68476
ψ and ψ' hadronic decays and soft pion theorems in charmonium model 77—6117
ψ', ψ decay branching ratios, isospin and flavour symmetry breaking 80—95264
ρ chiral SU(3)×SU(3) representation, spontaneous symm. breaking, VDM, PCAC 77—57512
$\tau\rightarrow3\pi$ or 5π, decay rate using current algebra and PCAC 79—3062
$\tau\rightarrow3\pi\nu$ decay, current algebra calcs. 79—30764
τ decay, large timelike Q^2, conservation of vector current and current algebra 78—78155
τ decay and second-class currents 78—21352
$\tau\rightarrow\nu\pi\omega$, decay width and form factor calc. using vector dominance hypothesis *(Russian)* 80—47271
$\tau\rightarrow\nu\rho\pi$ decay parameters from PCAC and current algebra, A_1 characts. 80—37314
$\tau\rightarrow\rho\pi\nu_\tau$, quark model, current algebra model, divergence of axial vector current 80—57655
τ three particle semileptonic decays, leptonic weak current *(Russian)* 79—97643
$\tau^\pm\rightarrow\nu_\tau\rho^0\pi^\pm$, possibility of observing A_1 meson current algebra anal. 79—13176
6Li(p,n), 144 MeV, one pion exchange and PCAC expt. test 80—528
$^{35}Ar\rightarrow^{35}Cl$ β^+ decay and anomalous Cabbibo angle 77—74807
^{12}B, aligned, β-ang. distrib. and alignment correction coeffs., axial vector currents 80—5097
^{12}B, beta decay, PCAC and vector current conservation 79—93561
^{12}B, beta-ray spectra and conserved vector current 79—54409
$^{12}B\rightarrow B^-+^{12}C$, second-class current search, alignment correlation meas. by Zeeman technique 78—37313
$^{12}B\rightarrow\beta^-+^{12}C$, alignment correlation meas. by Zeeman technique, vector currents and form factors 78—37312
^{8}Be isovector radiative decay, conserved vector and second class current theory test 79—6488
Bi weak charge, SU(2)×U(1) model anal. 79—26281
$^{12}C(\mu^-,\nu_\mu)^{12}B$, data anal., second-class currents and CVC 77—82874
^{12}C(p,n), 144 MeV, one pion exchange and PCAC expt. test 80—528
^{20}F, β-γ directional correlation meas., search for second class currents 79—13245
^{20}F decay, β-γ ang. correlation, second class current contrib. 79—22236
$^{20}F\rightarrow^{20}Ne+e^-+\bar{\nu}_e$, CVC test in $2^+\rightarrow2^+$ transitions 79—6514
H parity violations, fundamental struct. of weak current, unified gauge theories 78—12849
$^{2}H(\mu^-,\nu)2n$, hard pions and axial meson exchange current effects 79—40906
^{3}H ν-decay, ρ exchange current, weak axial vector current low energy theorem 79—40886
$^{3}He(\mu,\gamma\nu)$, transition amplitude, PCAC tests 80—102152
$^{6}Li(\gamma,\pi^+)^{6}He$, analysis using current algebra model with rigid π-mesons *(Russian)* 77—14112
^{12}N, aligned, β-ang. distrib. and alignment correction coeffs., axial vector currents 80—5097
^{12}N, beta decay, PCAC and vector current conservation 79—93561
^{12}N, beta-ray spectra and conserved vector current 79—54409
$^{12}N\rightarrow^{12}C$(g.s.), second-class axial current, meas. alignment-positron-momentum correl. 78—82317
$^{12}N\rightarrow^{12}Ce^+\nu_e$, data anal., second-class currents and CVC 77—82874
^{14}N(p,n), 144 MeV, one pion exchange and PCAC expt. test 80—528
$^{16}N(0^-)\rightleftharpoons^{16}O(0^+)\beta$-decay and μ-capture, mesonic exchange correction 78—41673
^{20}Na, β-γ directional correlation meas., search for second class currents 79—13245

current collection, traction *see traction current collection*

current control, electric *see electric current control*

current density
see also critical current density (superconductivity); electron density
air-Earth current density latit. var., aircraft meas. 77—53141
arc-cathode emitting sites, effect of Cu-oxide thickness, obs. 77—55190
Bitter solenoid efficiency factor, allowance for cooling holes 79—30502
cathode spot of arc discharge, meas., expt. 78—9879
charged-particle beam, current density distrib. calcs. 77—27238
dense gas nanosecond discharge, cathode region field amplification 80—38855
displaced Maxwellian distribution, correction 78—10454
distribution in a band, integral Fredholm eqn. appl. *(Polish)* 77—23860
electric arc cathode spot, charact. parameters determ. *(French)* 78—14236
electrocrystallisation, galvanostatic transients, crystn. overvoltage 78—76867
electrolyte conductivity rel. to electrode current density *(Russian)* 78—64847
electrolytic capacitors effect of electrical parameters of Al foil capacitors *(Polish)* 80—30245
electromagnet windings with constant current density, maximum permissible mag. field 78—57990
electron beam from triode with explosive-emission cathode, variable current density 79—72475
electrosurgical dispersive electrode site temp. and current density distrib. model 79—92424

current density continued
EM scatterer surface current density, calc. using numerical technique 80—78747
field emission current density, max., rel. to cathode geometry and kinetic props. 78—72704
gain-guiding double-heterostructure laser transverse carrier diffusion effects 79—55139
glass diode with electrothermal instability in switching channel 79—78238
high-density current passage through electrolyte *(Russian)* 79—83461
hollow cathode arc, plasma column parameters *(French)* 78—9885
HV vac. diode, electron beams, numerical anal. 77—27748
ion beam, quasineutral, intense, focused, max. current density, Coulomb interaction 77—54666
ion selective membrane, polarisation at high current densities, Nernst model 79—91962
Joule heat concentrators, metal foil expts. max. heat release, cracks in conductors 80—92022
LED reference channel nonlinearities 79—78158
metallic thin film, refr. index for X-rays, elec. current density influence *(Spanish)* 79—78784
metals, cyclotron resonance in weak mag. fields surface impedance, current density asymptotic *(Russian)* 80—2641
MHD accelerator, thermodynamic props., mag. field strength, Hall currents in arc region 77—65917
MHD channel, anisotropically conducting plasma in inhomogeneous elec. and mag. fields, current calc. *(Russian)* 80—74995
MHD generator current density and elec. field dependence on plasma thermodynamic pulsation *(Polish)* 77—80268
microscopic charge and current densities in terms of polarisation and magnetisation fields 78—8251
MIM structures, zero bias anomaly due to elastic tunnelling, calc. 80—2483
mirror-antisymmetric two-dimensional compound region electrode current density *(Japanese)* 79—89842
moving arc, parametric study of current density distrib. at electrodes 77 24239
moving plamsa, high current ion beam extraction 79—68361
nonferromagnetic solid eddy currents, three-dimensional calc. *(French)* 79—41301
nonuniform band structure materials, Shockley like equations for current density and carrier density 80—60001
one-band approximation, current density under high elec. field 79—28352
optimal feedback control of plasma parameters in Tokamak 79—64891
p-n junctions, current density distribs. calc. 77—43703
photoconductive insulators, interdigital electrode method, current density and arrival time 79—33308
plasma, stability of stationary inhomogeneous electron temp. distrib. states and electrodynamic params. *(Russian)* 78—42749
plasma arc heating, equilib. in gas-melt system *(Russian)* 79—37512
plasma current multiplier, gas discharge device, current amplification 80—49018
prolate spheroid, induction by electromagnetic plane wave, missile guidance appl. 77—83782
pulsed electron accelerator current density distrib. multichannel recorder 78—58520
pulsed electron beams, measurement of current density distrib. 80—63426
radial electric fields from air polarisation due to Compton electrons excited by γ-quanta pulse 80—21805
relativistic electron beam, in conical diode, self-focusing 79—89840
resistive electrode current density distribution 80—21302
resistive films, AC and DC characteristics, algorithm anal. *(German)* 77—55618
semiconductor devices, definition 77—39835
semiconductor with energy-dependent relax. time, expression for total current density 79—56268
semiconductors with position-dependent band gap and electron affinity, current densities 77—85210
stabilisation of low-m kink modes in Tokamak 79—64890
Stark-Ladder current theory 78—68035
steel, mild, corrosion in complex aq. environment, linear polarisation investig. 78—76782
superconductor, radiation stimulated, current density Eliashberg theory 77—89895
superconductor, type II, with normal inclusions, current density distrib., theory 80—80461
surface current density calculation by mode-matching method with smoothing procedure, algorithm 80—9773
surface scattering from piecewise planar surfaces, algorithm 78—62983
temperature-field emission region, simplified current density formula 78—27384
thermionic convertor, long, cylindrical, current density distrib. 78—71552
TORTUR toroidal device, plasma confinement and skin currents 77—76180
two-dimensional compound regions with mirror antisymmetry 77—3508
ultracold neutron storage ring supercond. magnet design 79—31266
ultrathin-coil supercond. solenoids for high-energy accelerators and storage rings 79—31260
wave diffraction on circular cylinder with longitudinal slot *(Ukrainian)* 78—90345
wire-to-cylinder corona, current distrib. on cylinder surface 80—6302
Al alloy anodic dissolution in $NaClO_3$ and NaCl solutions compared *(Russian)* 80—21290
Al-Fe_2O_3-Al, space charge limited current, current density as function of elect. field and temp. 79—51688
AlGaAs-GaAs DH laser, carrier leakage, physical mechanisms 78—66824
$Al_xGa_{1-x}As$-GaAs, quantum-well heterostructure laser diode, temp. depend. of threshold current 80—87395
AlGaAsSb-GaSb heterojunction injection laser, radiative props. 1.4 to 1.8 μm range 80—91798
β''-Al_2O_3-Na_2O, solid electrolyte, behaviour at high current density, sodium heat engine mode 80—61330
Au film, threshold current density and incubation time to electromigration 78—14643
C cathode damage and vapour/thermionic arc transition obs. 78—71603
Cs fully-ionised plasma hollow-cathode arc discharge theory 78—67533
Cu cathode with oxide film, emitting site lifetimes and current densities, meas. 77—27761
Cu, dislocation increase by electron wind *(Russian)* 79—95024

current density continued

- Cu electrocrystallisation from $CuSO_4$ solns., current density under stationary surface diffusion *(Russian)* 79—8237
- Cu electrocrystallisation from $CuSO_4$ solns., current density/overvoltage curves *(Russian)* 79—8236
- Cu electrocrystallisation from $CuSO_4$ solns., expt. and slow surface diffusion theory *(Russian)* 79—11505
- Cu, electrodeposition from cyanide solns., interaction with 2-butynediol-1,4, obs. *(Russian)* 79—47936
- F_2, dissociative attachment of electrons, current density meas., in controlled discharge 77—23566
- Fe, H_2 charged, depend. of softening on specimen size, charging current density and strain rate 80—16455
- Fe-Ni-Co coating electrodeposition optimum conditions *(Russian)* 79 83292
- (GaAl)As DH laser, threshold current density, growth terraces effect 80—99723
- GaAs anodic oxide films, composition meas. by ion scatt. spectrometry, influence of current density 80—11802
- n-Ge, minority-carrier injection and extraction 80—49767
- Hg DC vacuum arc anchored cathode spot current density obs. 78—75467
- HgI_2, single cryst. elec. and thermal props. 79—11111
- InGaAsP DH lasers with etched reflectors, fabrication, current density 80—64050
- $In_{1-x}Ga_xAs_yP_{1-y}$ DH laser, low threshold current density, near equilibrium LPE growth 80—19040
- Li_xCoO_2, cathode material for batteries of high energy density 80—101089
- Na-S cells, factors affecting S electrode operation 79—29463
- Na_2O-Li_2O-Al_2O_3, local electrode current density and flow decoration 80—100935
- Ni-Fe-Cd, ternary alloy, electrodeposition from acetate bath 79—95950
- $Pb_{1-x}Sn_xTe$-PbTe heterojunctions, interface recombination velocity reduction with decreasing lattice parameter mismatch 79—98370
- PdH_2 internally-charged electrode stability rel. to charging current density 79—57251
- Si, high electronic current density in anodic oxidation 80—89386
- Si-on-ceramic solar cells, short-circuit current density meas. using light-beam-induced-current tech. 80—93887
- SiO_2 film, in MIS struct., current-field characts. 79—99623
- SnO_2, electrodes, effect of DC on corrosion in lead glass melt 80—85075
- Ti, anodic film structure, intensiostatically formed, pH and current density influence, TEM study *(French)* 79—66217
- Zn electrodeposit dendritic growth control using impedance meas. 78 84721

current distribution

see also current density

- 30 T pulsed solenoid construction and life tests 79—31297
- AC distribution in solid turns with skin effect, calc. *(German)* 80—69319
- antennas, horizontal, above infinite plane Earth, input impedance and current distrib. 80—90259
- arc moving in narrow insulating slot, magnetic blast-breaker, anal. 77 72515
- Bitter solenoid efficiency factor, allowance for cooling holes 79—30502
- circular loop induced eddy current distrib. and loss calc. 80—9771
- concentric spheres at pot. up to 15 MV, current flow 77—79726
- conducting plate with temp. depend. resistivity and surface heat loss, temp., current and elec. field distribs. 77—42696
- crystal with coplanar electrodes, potential and current distribution 79—33341
- current distribution cell for qualitatively predicting differences in barrel plating performance of electroplating solutions 80—71917
- diagonal-type nonequilibrium plasma MHD generator, electrode internal and external connection effects 78—91165
- ECG theory computer application programs *(Spanish)* 78—20165
- eddy current transient, in plate of finite thickness, due to coil of arbitrary shape *(German)* 79—27129
- education, Dirac delta function, appl. elec. current and mag. multipole distribs. 80—17740
- electrochemical electrodes, current distribution, network-type equivalent cct. investig. 78—35705
- electrochemical systems, current and potential distrib. calcs. 77—21394
- electrode, disc type, current distrib., analogue model investig. 79—34321
- electrodes in MHD generator channel current distribution 77—43084
- electromagnetic wave scattering, boundary conditions, described by Dirac's impulse first derivative 78—5402
- electron beam, fine-focused, current distrib. meas. method 77—83799
- electron beam cross section, current density distribution, calc. *(Russian)* 80—14276
- electrosurgical dispersive electrode site temp. and current density distrib. model 79—92424
- exploding foils, skin effect *(Russian)* 80—19628
- Faraday type MHD duct, lead wire position along resistive electrode, effect on current distrib. 77—76214
- Fredholm eqn. of the second kind for current distrib. in antenna theory *(Chinese)* 78—66708
- fuel cell, molten carbonate, scaled-up, performance and current distrib. model 80—55837
- hollow cathode, MPD arc config., 0.25-30 kA, current and pot. distribs. 78—9869
- infinite horizontal wire, current excitation by vertical electric dipole 77—14642
- injection stripe lasers, current carrier conc. distrib. *(Russian)* 78—13712
- ion beam, fine-focused, current distrib. meas. method 77—83799
- ion source with volume ionisation 80—23227
- Josephson junction, finite size, current distribution *(Russian)* 78—80103
- laser produced plasma, spatial correl. with irrad. distrib. 77—15217
- magnetic field calc. from current distrib., finite element techniques 78—94358
- MHD channel, with one pair of electrodes, current distrib. 77—39475
- MHD convertor channel and regions, eddy current losses due to magnetic field variations 80—40874
- MHD generator electrodes in arc regime of operation, math. model 79—86620
- multifilamentary composite superconductor transport current distrib. 79—30505
- multifilamentary superconductor, current distrib. close to input leads 78—84363

current distribution continued

- multipole expansion, concentrated current source representation 78—5390
- narrow stripe injection laser, voltage and current spatial var. 78—17936
- negative corona discharge in air, current distrib. 78—87539
- periodic metal surface, EM wave scattering 78—1128
- plasma, effective conductivity tensor, effect of spherical anisotropic inclusions 77—55546
- plasmatron, linear, 3-phase, current and voltage characts. *(Russian)* 77—84535
- Pocklington integral eqn. basis function continuity requirements 77—74208
- pulsed corona meas. in coaxial electrode structures 79—19114
- pulsed electron accelerator current density distrib. multichannel recorder 78—58520
- resistive films, AC and DC characteristics, algorithm anal. *(German)* 77—55618
- semimetal, by diffusion size effect 79—23987
- solenoid, semiinfinite, thin, mag. field and current density distribs. near edge Wiener-Hopf calc. 78—70999
- Space Shuttle lightning current distrib., circuit modelling and exptl. verification 78—49293
- Tokamak machine with iron cct., flux mapping and current distrib. 79—41866
- AgBr evaporated layer response in ionisation semiconductor photographic system *(German)* 80—101859
- Fe plating cathode current distrib. influences *(Russian)* 79—96197
- $MgF_2/In/MgF_2$ struct. surface plasma wave optical excitation in In 79—91516
- W electrochemical treatment, current distrib. and metal throughput *(Russian)* 79—15849

current fluctuations

see also noise

- 1/f current noise, random walk model 77—8162
- amorphous semiconductor, current fluctuations and switching 79—87133
- biomembranes, low noise amplification of voltage and current fluctuations 78—44741
- BWR in-core instrument tube vibration obs. by reactor noise techniques 78—94064
- chemically reactive arc-heated gas flow, ion saturation current fluctuation probe 78—63574
- electrochemical noise generated by anodic dissolution or diffusion 77—25277
- field emission electron source, current instability *(Japanese)* 78—43989
- gas discharges, electron swarm motion, computer simulation 77—89339
- n-hexane, impurity particle behaviour and cond. pulses 79—91059
- ion-selective membrane, flicker noise and turbulent convection in depleted layer 78—48692
- ionic fluid very long wave-length charge fluctuation spectra 77—59297
- isotropic media, current fluctuation anisotropy, electron diffusion, quasielastic scatt. *(Russian)* 80—107882
- Josephson junctions, natural fluctuations in tunnel current *(Russian)* 77—47937
- laser heterodyne signals from moving object, bandpass filtering by finite apertures 78—55306
- LF current fluctuations in stationary states, statistical mechanics *(Japanese)* 80—15658
- lightning stepped leader, electrodynamics, anal. *(French)* 78—28255
- metal film resistor, resistance fluctuations from spontaneous enthalpy fluctuations 78—72217
- MHD generator, arc switching near electrodes, elec. current oscills. 79—55569
- MHD generator, electric power fluctuations due to Hall and ion slip currents 77—68879
- MIM cathodes, LF noise sources and reduction 80—108328
- MIM tunnel junctions, roughened, photon emission, calc. 80—44738
- myotubes, human, cultured, acetylcholine-induced conductance fluctuations 78—61157
- nerve membrane permeability changes, fluctuation anal. 78—11636
- neurone Ca conduction units, Helix aspersa 78—77041
- noise in strong elec. field, interelectron collisions, drifted Maxwellian distribs. *(Russian)* 80—2436
- pacemaker intermittent runaway malfunction 77—81712
- photodetector, radiation detection in turbulent atm., current fluctuation statistics *(Russian)* 79—92591
- resistor, metallic, nonlinear current fluctuations, microscopic calc., heating, perturbation theory 79—69484
- semiconductor, current and voltage fluctuation determ. by noise spectral density meas. 80—15577
- semiconductor, electron quantum states, nonequilibrium current fluctuations in quantised mag. fields *(Russian)* 80—107704
- semiconductor, with transition to metallic state, low freq. current fluctuations 77—66189
- superconducting point contact, LF fluctuations, cond. and voltage *(Russian)* 77—20500
- vacuum diode, current fluctuations, elementary charge magnitude meas. *(Hungarian)* 77—49679
- Al thin conducting film, electromigration under superimposed DC and noise powers 80—107879
- CdSe, single crystal, low-frequency current noise, effect of temperature quenching of photoconductivity 78—34874
- GaAs, epitaxial layers, low freq. current noise between 4.4 and 300K 78—95388
- He, liquid, charged surface, current instability theory *(Russian)* 80—29243
- N gas discharges, electron swarm motion, computer simulation 77—89339
- Na channel fluctuations, phys. nature, microscopic model 80—35869
- VO_2, single crystal, fluctuations of current and switching time 79—38137
- W field emitter, current fluctuations from cryst. faces 78—35263
- ZnS, current oscills., 300K, 1-6 s period *(Russian)* 77—80819

current limiters *see limiters*

current measurement, electric *see electric current measurement*

current-mode logic *see emitter-coupled logic*

current transformers

see also electric current control; electric current measurement

- electric current measurement, AC, using magneto-optical methods, principles and advantages *(Polish)* 80—105676
- low leakage for Tokamak devices series coupled power crowbar system *(Japanese)* 78—55755

current transformers continued
- magnetisation curve, piece-wise linear, design method *(Russian)* 80—100598
- MV, constructional principles and production technology *(Hungarian)* 80—100118
- nonelectric variables meas., current transformer error level calc. 77—13743
- oil immersed transformers, dissolved gas causes and phenomena, anal. *(German)* 80—76570
- oil insulated, parameters influencing heating assessment using sensibility matrix *(Hungarian)* 80—87708
- rectified current supply modules, saturable transformer ferroresonance anal. using rectangular hysteresis-free approximation method *(Russian)* 77—55708
- toroidal core pulse current transformers, pulse permeability and loss in Ni-Fe cores 78—43615
- zero-flux, for AC/DC current meas. up to 25 kA 77—30177

current transients *see transients*

currents algebra *see current algebra*

curvature measurement
- aspherical surface measurement *(Hungarian)* 80—38087
- component profile inspection equipment 80—105608
- concentric round parts, profile determ., concentricity errors *(German)* 80—57249
- conic mirrors, caustic coordinates in Platzeck-Gaviola test 78—33799
- contact lens radii and thickness meas. by interferometry 80—8118
- corneal curvature meas., simple photokeratoscope 78—3624
- corneal lens, soft radius of curvature meas., using autostigmatic microscope 77—60198
- curved object shape description and recognition methodology 79—55077
- curved surface contouring, two-wavelength speckle imaging methods 79—85121
- cylindrical thread charact. meas. by interference fringe procedure *(German)* 78—4585
- double frequency grating shearing interferometer, slope and curvature meas. 80—13126
- error separation processes *(German)* 80—31701
- flexed plate, slope and curvature contours meas. using interferometer 77—87810
- gear tooth profile, portable meas. instrum. for large gears, interchangeable standard profiles 80—57259
- heteroepitaxial system, dislocation contrib. due to curvature 80—2017
- hip joint geometry, human, three-legged micrometer spherometric errors 79—83832
- inclined prism three-point meas. reliability *(German)* 80—28359
- interferometric profile scanning, automatic, contactless *(German)* 77—87729
- large curved surface coordinate determ. apparatus 78—77863
- lens sphericity non-contact testing method *(German)* 78—5534
- long-radius concave optical surface curvature meas., differential technique 80—74534
- lumbar spine curvature in sagittal plane, meas. and modelling 79—96607
- metal foil bulge-test samples, shape meas. by optical contouring 77—63843
- mirror surface curvature and local distortion meas. by holographic interferometry 79—76796
- Moire topographic method, anal., concave convex region discrimination 78—65901
- moire topography, real-time and time-resolved, in microseconds region 80—52154
- optical surfaces, concave and convex, radii of curvature meas. 80—83654
- pin bowing in AGR fuel elements, meas. by camera device 80—106146
- profile deviation from circular, invariant props. determ. 80—22326
- profile multiaxis meas. with vector drive 80—105609
- radiotelescope, surface meas. with two feeds 79—12403
- roundness, reference criteria 80—62628
- shape meas., space-time optics 79—6093
- speckle image for radius of curvature meas. of cylindrical surface *(French)* 77—34020
- spherical surface evaluation 80—36996
- spherical surfaces shape deviation determ., using sphero-interferometer *(Czech)* 80—58821
- steel component contours, using double image projector 77—88887
- stylus radius measurement, used in surface texture instruments 80—36986
- theoretical aspects of curved surface meas. 77—22524
- thin plates, plane reflecting, statically loaded, interferometric exam. of curvature and twist 78—45679
- three dimensional deformation measurement, Moire and light slicing methods 78—8382
- tooth-profile error of cylindrical gear wheels, using microscope 78—168
- Zygo interferometer system 80—73437

curvature of field *see aberrations*

curve fitting
- activation analysis, low-energy photon spectra, nonlinear least-squares fitting program 79—1987
- allyl ether, dielectric relaxation obs. at millimetric wavelengths 80—71311
- automatic reverberation time meas. 79—68518
- baseline recognition and baseline flattening algorithm 78—262
- biological data, nonlinear describing function 77—13045
- cerebral blood flow determination, computer assisted method for multi-exponential curve fitting 78—20246
- chemical kinetics meas. computational processing iterative optimisation techniques 77—32765
- chromosome density profiles, description and classification 79—43830
- composite exponential decay curve anal. 78—46241
- crack length determ., analysis of crack-opening-displacement meas. 78—5702
- creep data, 3- and 4-element response curve fitting, applic. to chipboard 77—90395
- curve information content, role of affinity and conservation of information *(French)* 78—24771
- deconvolution of exptl. curves. Fourier series 77—54493
- degree of fit, new criteria 78—57758
- empirical relationships for random self-avoiding walks on lattices 79—9190
- energy dispersive X-ray diffractometery, technique, apparatus, data processing, computer profile fitting 77—68892
- energy irradiance from pulsed source, curve fitting problems 77—71377

curve fitting continued
- experimental curves, information content, deconvolution using apparatus functions 79—40354
- experimental data expressed in closed mathematics form, approximation methods *(German)* 78—16632
- exponential clipped photon autocorrel. spectra, data anal. 79—2837
- Fermi surface calculation method *(French)* 80—2318
- flexible all purpose program 77—2531
- FM pressure transducer resonant diaphragm pressure-freq. characts. derivation 78—41295
- gamma spectra, accelerated fitting and nuclide identification by graphical and associative memory methods 79—9945
- gamma-ray spectral peaks, goodness of fit determ. using figure of merit 77—88360
- halftone or line printing, Yule-Nielsen curve fitting parameter 79—13906
- hard magnetic materials, demagnetisation curve, single function approx. using computer *(Hungarian)* 78—60307
- high-precision data, improved interpolation method 77—45838
- interactive curve-fitting program, for science students 77—60913
- ionosphere, analytic partial derivatives for incoherent scatter data least-squares fitting 78—73581
- least squares criterion, with reference to exponentials and Arrhenius plots 79—17200
- least squares regression analysis with confidence limits, calculator program 77—29060
- left ventricular boundary extraction from radioisotope angiocardiogram *(Japanese)* 77—81562
- linear regression, least-squares eqns. derivation, appl. to g determ., for teaching 78—45450
- logistic routine adapted to desk top computer, for radioimmunoassay and bioassay data processing 77—37059
- Lorentzian broadened K-series X-ray peaks of heavy elements, fitting algorithm 77—57799
- lung pressure-volume characts., curve-fitting anal. using programmable calculator 77—48821
- magnetisation and electrification curves, computer-aided *(German)* 77—8338
- malignant melanoma, relationship between total dose, fraction number, fraction size 79—5341
- medical computing, compartmental models short parameter-fitting routine 77—82378
- NMR, Voigt profile analysis, Fourier transform approach and least-squares curve fitting 77—20729
- noniterative method for fitting Gaussian to peaks from Ge(Li) and Si detectors 77—57840
- palaeomagnetic data smoothing, objective method 78—28159
- parabola fitting, filtering characts. of smoothing method *(Japanese)* 78—89084
- planetary orbits accuracy of Ptolemaic and Copernican theories using curve fitting techniques 78—32325
- potential energy surfaces, analytical expressions from constrained optimisation 77—6698
- program on KIM-1 using FOCAL 79—35693
- quadratic convergence curve fitting technique for evaluating complex permittivity of liquids at mm/cm wavelengths 80—13097
- radioactivity meas., low statistics data 80—9471
- radiocardiogram parameter identification *(Slovene)* 78—44586
- radiographic screen-film system, determination of charact. curve and its gradient 79—5362
- radioimmunoassay data processing, semiautomated polylinear system 79—70614
- random-variable probability density approximation by convex function *(Russian)* 77—9865
- rapid method of curve approximation using electron beam indicator 80—10166
- restricted range adaptive curve fitting 79—30214
- seismograms, interpolation of digitized curves 77—40999
- shape differences comparison, between two-dimensional irregular forms, computer program 77—87639
- single-mode obs. distributions, invalid data rejection algorithm *(Russian)* 79—21690
- spectral decomposition, generalised algorithm, appl. to UV, IR, at. emission spectrometry 77—12842
- surface profiles, reference line selection and fitting, based on random process analysis 78—45594
- TEM, quantitative elemental analysis 80—101060
- test apparatus based on curve-fitting method for thermal props. meas. at cryogenic temps., performance characts. 77—67441
- thin film meas. tool calibration by cubic spline fitting 77—18063
- toughness data, fitting curves 80—40511
- vapour pressure critical exponent optimal determ. 79—51271
- vibrating structure, modelling by freq. response data curve fitting 77—54922
- vision, Stiles Π-mechanisms candidacy for colour-matching fundamentals 78—56980
- width of Lorentzian convoluted with Gaussian 77—79528
- X-ray small angle scattering, curve anal., by triaxial body models using graphic display model 80—28873
- X-ray spectra, energy dispersive, peak separation from background 78—7310
- X-ray spectra, energy-dispersive detector, simplex method for fitting Gaussian profiles 79—722
- X-ray spectra analysis, with aid of computer 80—3433
- $CuCl_2.2H_2O$, X-band ESR magneto-microwave effects 77—28434
- $Cu(NH_4SO_4)_2.6H_2O$, X-band ESR magneto-microwave effects 77—28434

cutting
- *see also machine tools; machining*
- acoustic emission of cutting Al alloy on lathe 77—42675
- adhesion in metal cutting, direct SEM obs. of frictional sliding 80—104412
- arc plasma gun for metal cutting, transient performance, obs. 80—49017
- biological specimens, cryosectioning for X-ray microanal. 79—39626
- blood cells, red, human, frozen section prep. for electron probe anal., fracturing or cutting 79—39625
- cemented carbide ion plating, high-speed steel tools, cost and cutting performance 80—30174
- cemented carbide tools coated with HfN and TiC, machining evaluation 79—29253

cutting continued
  chip formation, frictional interactions between chip and rake face 79—52387
  cine-film slitting in the laboratory 78—93770
  compensating filters, as used in radiotherapy, semi-automatic machine 77—13001
  corneal mechanised trepan control 79—29659
  crystals, X-ray-aligned dielectric, using spark erosion machine 79—80592
  diamond, polycrystalline tool, wear in rock removal processes 78—64724
  diamond cutting traces, friction force 77—50781
  dividing machine type PTA, wire and strip specimens gripping attachment 80—40647
  electro-optic material cutting and polishing, book 79—81583
  fibre-optic waveguide, flat-surface ends preparation, using handheld tool 79—37062
  fluid, hydrolysed polyacrylonitrile based, operational characteristics 80—89359
  glass, with conc. energy sources *(Russian)* 79—38994
  glass fibre cutting device *(Italian)* 78—50951
  goniometer for cutting single crystals 80—86275
  guillotining materials, mechanics, fracture and burr formation 80—14619
  Inconel 718, superalloy, wear of superhard tool during cutting, SEM and metallographic obs. 78—64720
  instrumentation engineering, laser beam appls. in drilling, welding, cutting, definite abrasion and surface treatment *(German)* 80—108608
  irradiated stainless steel tube high-speed slitting machine 79—9210
  large-diameter radius surface generation with small cutters 79—94373
  laser application, CO_2 and Nd:YAG systems *(German)* 78—1294
  laser beam appl. in material-cutting, processing optimisation *(German)* 80—43384
  laser material processing, IR holographic elements appl. 80—37964
  machine tools, chip geometry and cutting forces 80—93629
  machine tools, diffusive wear, mag. field effect 80—60985
  mechanism during grinding, model 79—79124
  metal, appl. of Taylor eqn. for different cutting speeds *(German)* 78—72915
  metal, coated abrasive belt grinding, relation between wear of grain cutting edge and material removal 80—16507
  metal, cutting rel. to plasticity theory 80—16610
  metal, friction heating during cutting 79—39055
  metal cutting, chip forming mechanisms, deform. diagrams 77—28854
  metal cutting, with slowly varying system parameters, self vibrs. *(Ukrainian)* 77—68477
  metal cutting methods and machinery, noise reduction 80—53548
  metal powder, milling conditions effect on densification during pressing and sintering 78—11149
  metals, deformation structure during cutting, investigation by TEM *(Japanese)* 80—70086
  metals, submicroscopic surface relief after finishing 79—29276
  metals and alloys, ferrous and non-ferrous improved plasma torch design 79—8401
  microtome, automatic for cutting 400 μ fibre snippets 77—9999
  multispeed tool life tests with radioactive tools 78—44338
  oil performance, test machine 80—11848
  optical fibre cutting machine for rectangular and circular fibres 78—33932
  optical fibre cutting tool 80—1360
  optical fibre cutting tool 80—33255
  optical fibre cutting tool and automatic splicing machine 80—87575
  optical fibre cutting with hot metal wire 77—19462
  optical fibre ribbon cable cutting tool 80—19113
  plasma cutting at elevated press., underwater appl. 78—87507
  plasma cutting with additional heating of plasma-forming gas 80—24267
  plasma torch cutting-punch machine for steel panels 78—18466
  porous materials, effects of different methods of prep. on reproducing surface 80—60995
  porous strip, moving, transverse cutting criteria 77—55901
  reactor components and vessels, underwater plasma arc and explosive cutting 79—9922
  residual stresses rel. to grinding and cutting directions, X-ray diffr. obs. *(Japanese)* 78—23847
  rubber, cutting resistance measurement in absence of friction 79—5035
  shearing process, basal section profile effect 79—47754
  spherical optical component, cutting process for coarse grinding, optimisation 79—32103
  spring steel cutter for glass fibres 80—48468
  steel, C, machined, microdefects on surface 80—16607
  steel, Cr-W-Mo-Co, high-speed, from atomised powders, mech. and cutting props. 80—66556
  steel, grinding, effect of hardness, texture, and bond of grinding wheel, temp. effect *(German)* 79—43459
  steel, high speed, hardened, for drills, mech. and cutting props. 79—43407
  steel, high strength, use of metallic melts as lubricant-coolant, in drilling *(Russian)* 79—57201
  steel, high-speed, sintered, refractory carbide additions effect on hardness and cutting performance 77—66608
  steel, machining, adhesion mechanism of built-up edge and layer on rake face of cutting tool 79—47784
  steel, medium C, drilling in liq. Sn-Zn eutectic, cutting conditions rel. to tool parameters *(Russian)* 79—34187
  steel, sintered type M2 high speed, heat treatment response and cutting props. 78—15336
  steel, stainless, austenitic, CC Ni-Al, γ-phase, fracture mechanical aspects of abrasive friction, wear, chip formation 78—72865
  steel, stainless, smoothing for plastic pre-straining of material cut by turning *(Russian)* 80—60911
  steel, tool, cutting blades, heat treatment in fluidised bed, hardening 79—20087
  steel 1Kh18N9T, physico-mech. props. after boring in metallic melts *(Russian)* 78—56736
  steel 40Kh, surface working effects on crack resist. *(Russian)* 78—56734
  steel austenitic stainless, cold working type, heat treated, tool wear during cutting 79—47782
  steel cutting and grinding, surface adsorption effects 78—39938
  thin layer activation for testing cutting fluids 80—55619
  tool coating by cubic BN reactive vapour deposition 80—40545
  ultramicrotomy in corrosion and protection TEM 77—81358
  wood, vibratory cutting, behaviour of chip and effect on cutting force *(Japanese)* 77—77540
  wood cutting, stress distrib. and frictional coeff. at tool-chip interface, specific gravity effect *(Japanese)* 80—1492
  zircaloy-2 cladding tube, fission cutting *(Japanese)* 77—67808
  Ag-Cu, directionally solidified, obs. of cutting deform. zone *(Japanese)* 78—15422
  AgCl, surface layer stress distrib. after mech. treatment, polarisation-optical obs. 78—18887
  Al, cutting, temp. effect on built-up edge behaviour *(Japanese)* 78—7083
  Al, cutting mechanism, anisotropy effects 79—11760
  Al, cutting of bicrystal to compare mechanism for large crystals and polycrystals *(Japanese)* 78—60871
  Al, flow mechanism in cutting, crystal orientation effects in single crystal 79—100300
  Al, orthogonal cut surface, effect of cutting condition on residual stress *(Japanese)* 78—85035
  Al, orthogonal cut surface, relations between residual stress and moire strain, exam. *(Japanese)* 78—85036
  Al, polygon construction via diamond cutting 78—33919
  Al, reverse finish cutting, exam. *(Japanese)* 78—85034
  Al single crystals, crystal orientation effect on their cutting mechanism 79—34193
  Al, trial cuts at low speeds in relation with traction trials *(French)* 80—24448
  Al-Mg, type A5083P-0 effects of anisotropy in cutting mechanism *(Japanese)* 80—89232
  Al-Si, three dimensional dry cutting, with sintered diamond tool *(Japanese)* 80—25917
  Al_2O_3 cutting tool, performance relationships, porosity determ. 78—11169
  BN, cubic, sintering technology and cutting performance of tools 80—29919
  Cr, fracture during electrospark cutting *(Russian)* 79—87719
  Cr, powder comminution method effect on props. of TiC-steel+Cr composite 78—15341
  Cr-Fe (1 wt.%), fracture during electrospark cutting *(Russian)* 79—87719
  Cu, cutting of bicrystal to compare mechanism for large crystals and polycrystals *(Japanese)* 78—60871
  Fe, cast, gray, relationship between cutting conditions and reaming precision 79—61801
  Fe-Si (3.25 wt.%), single crystals and polycrystals, cutting surface texture 79—20291
  Fe-Si (3.5 wt.%), cutting of bicrystal to compare mechanism for large crystals and polycrystals *(Japanese)* 78—60871
  GeTe, machining effects on electrophys. props. 77—86199
  Nb_xC powders, plastic deform. characts. on vibratory milling 78—11183
  Pb-Sn superplastic alloy, cutting, stress distrib. *(German)* 79—24682
  Si, carrier lifetime degradation at room temp. 78—95301
  Ti-Ni alloy, effect on $[Cu(NH_3)_4.(H_2O)]^{2+}$ solns. on drilling *(Russian)* 78—53017
  WC base alloys, uncoated and TiC or Al_2O_3 coated, wear charact. 78—92365
  Zn, cutting mechanism of large crystals *(Japanese)* 77—48523
  Zn, cutting of bicrystal to compare mechanism for large crystals and polycrystals *(Japanese)* 78—60871

CVD *see chemical vapour deposition*

CVD coatings
  ball bearing surface CVD coating expts. 79—83366
  cptical fibres having surface compression, fatigue characts. 79—46064
  crack and pore imaging by electrographic printing 80—34333
  cutting tool coating by cubic BN reactive vapour deposition 80—40545
  dielectric films on semiconductor devices, review of deposition techniques 78—23611
  epitaxial films, model for autodoping lateral variation 80—103595
  glass film, SiO_2 rich, prepared by modified CVD, refr. index behaviour 78—60526
  graphite, CVD anisotropic thick hollow cylinder, residual stress due to uniform cooldown 79—42423
  III-V semiconductor thin film prep. by low temp. CVD 80—60789
  inorganic thin films, plasma-promoted deposition 79—78896
  insulating film for semicond. devices, props., rel. to deposition conditions 78—23612
  laser CVD, film physical props. and applications 80—93493
  materials for thermoelectric conversion of solar energy *(French)* 80—89660
  metallurgical coatings, conf., San Francisco, USA, April 1978 79—15052
  multilayer optical interference coatings via glow discharge polymerization techniques 78—87170
  optical fibre preform diagnostics, nondestructive noncontacting method 79—27376
  optical fibres and preforms, modified CVD, axial refr. index depression, interf. microscopy obs. 80—1319
  oxide, distributed fixed charge elimination using HCl 79—42661
  oxide film, As doped, roughening during As diffusion into Si, stress effect 78—2389
  oxide single and multi-layer optical coatings, light scattering reduction and meas. 80—48381
  passivation films, advances in deposition processes, review 78—23620
  phosphosilicate glass, bridge struct. across V-groove formed by etching in Si 80—104312
  phosphosilicate glass coatings, measurement of P content using SEM and energy-dispersive X-ray analyser 80—76588
  plastic resins, secondary coating of optical fibres, effect on transmission props. 80—58704
  pyrocarbon, microstructure of coatings on fuel particles, TEM study 78—25293
  pyrocarbon coating deposition by gaseous hydrocarbon pyrolysis, theoretical anal. 77—40459
  semiconductor thin films for solar energy conversion 77—32531
  silicate glass film, etching characts. in CF_4 plasma 77—90474
  solar convertor fabrication by CVD deposition of optical multilayer stacks 79—74519
  SOS early growth, island coalescence model 77—76704
  SOS early growth, transmission electron microscope obs. 77—76703
  spectrally selective surfaces for photothermal conversion of solar energy 80—101125
  spectrally selective surfaces in photothermal solar energy conversion, tandem stack fabrication by CVD 80—45753

CVD coatings continued
- steel, Cr-C and C, carbide coating by CVD, interlayer form. 80–11574
- steel, CVD coating temp. effect on hardness and dimens. stability 77–40470
- techniques and appls. 80–25573
- tribology appl. 78–64743
- VLSI multilayer metallisation interlayer dielectrics, CVD films 80–45235
- Ag, polycryst. boundary layer on seed cryst., role in hydrothermal growth mechanism of sodalite 78–30571
- Al on Ni base alloys, transport agent comparison 78–11429
- AlC_xN_y, refractory deposit, prep. by thermal decomp. of Al dialkylamides and characterisation 80–11572
- $Al_xGa_{1-x}As$, metalorganic-CVD, photopumped laser operation meas. GaAs quantum well 79–10303
- $Al_xGa_{1-x}As$-GaAs DH laser operation, phonon contrib. 80–102724
- $Al_xGa_{1-x}As$-GaAs laser, made by organometallic CVD, continuous room temp. operation 80–1201
- $Al_xGa_{1-x}As$-GaAs phonon-sideband metalorganic-CVD quantum-well heterostructure laser 79–64244
- $Al_xGa_{1-x}As$-GaAs quantum-well heterostructure laser, metalorganic CVD growth, CW operation 300 to 337K 79–10304
- AlN film, CVD, characterisation of film props. 78–43496
- AlN-Si_3N_4 CVD film preparation and props. 77–77408
- AlN-Si_3N_4 mixture film, CVD, characterisation of film props. 78–43496
- α-Al_2O_3, CVD-grown, cryst. perfection by transmission X-ray diffr. topography 79–65337
- Al_2O_3, facet coating for GaAs-$Ga_{1-x}Al_xAs$ laser, effect on degradation 78–13722
- Al_2O_3, film, CVD on Si, chem., phys. and elec. props. 77–12543
- Al_2O_3, film, form. in discharge, IR absorpt. spectra *(Russian)* 77–12461
- Al_2O_3 films obtained by pyrolysis of Al acetylacetonate, struct. and props. 77–85098
- Al_2O_3, form. and behaviour under particle bombard. 80–35029
- AlSb solar cell materials, epitaxy of metalorganic-CVD layers 80–61367
- AlSb, thin film growth on insulating substrates, by metal organics CVD 80–60786
- B, filament CVD technology, book contrib. 78–48352
- B, protective coatings for first wall, prep. by means of low press. plasma CVD 80–35103
- B, structure of deposits-process relations 78–27410
- B:H amorphous films, IR, visible, and near UV optical props. 80–50442
- B_4C, erosion rates under H^+ ion bombard., fusion reactor appls. 80–39179
- B_xCy, protective coatings for first wall, prep. by means of low press. plasma CVD 80–35103
- BN film, undoped and P-doped, effect of CVD parameters on props. 80–25571
- BN films, elastic stiffness and thermal expansion 80–49559
- BN films, humidity sensitive elec. props. and switching characts. 80–107938
- BN, pyrolytic, diffusion source for Si 78–91352
- B_2O_3-SiO_2 glass film, CVD, differential IR studies 80–55213
- BP coatings, on Mo by CVD and their composition and microhardness 79–28942
- C, amorphous, prepared by glow discharge method, elec. and optical props. 77–21036
- C, columnar and laminar forms, deposition on polycrystalline Ni foils 78–63943
- C fibre reinforced Al composite, CVD fibre coating, diffusion barrier and wetting agent 77–40458
- C film on substrates for STEM specimen support, prep. and observation 80–93496
- C, surface damage and erosion under energetic D^+ and $^4He^+$ irrad. 80–39174
- CdS:Li chemically deposited filter, elec. props. 80–11113
- CdS:Li film, optical props. 80–2886
- CdTe layers, on CdS substrate, cryst. perfection and defects, X-ray diffr. obs. 79–56081
- Cr, CVD protective coating on steel, struct. and carbide form. 77–40387
- Cr_7C_3 CVD coating on steel 79–83393
- Cr_2O_3/γ-Fe_2O_3/Pt electrode, two layer oxide surface film anal. by modulation spectroscopy *(Japanese)* 80–11491
- Fe_3O_4 film prep. and form. by Fe naphthenate thermal decomposition *(Japanese)* 77–32519
- GaAs, CVD on W coated graphite, characterisation, and Schottky barrier solar cell characts. 79–28930
- GaAs epitaxial layers, substrate prep. effect on surface morphology 78–26780
- GaAs MESFET layers, low-temp. halide epitaxial growth 77–77403
- GaAs shallow-homojunction solar cells on single crystal GaAs and Ge substrates, CVD fabrication and conversion efficiency 80–61364
- GaAs, VPE layer on Ge, antiphase domain structures 77–69193
- GaN CVD layer props. rel. to Ga-GaCl conversion efficiency and HN_3 decompositon 77–77404
- GaN, VPE growth rate influence on elec. and luminesc. props. 80–100702
- GaP, VPE layer on Si or Ge, antiphase domain structures 77–69193
- $GaP_{0.1}As_{0.9}$, gas-transport condensate with superlattice, structural and chemical inhomogeneity 77–85088
- GeC_x, amorphous, prepared by glow discharge method, elec. and optical props. 77–21035
- Ge_3N_4 CVD film prod. and Al-Ge-Ge_3N_4-Al structure V-I and V-C characteristics *(Russian)* 78–47893
- GeS, film on Ge, evaporation, thermogravimetric, electron microscopy investigs. 77–15715
- HfC, filaments on W-ThO_2 and SiC, coating effect on high temp. mech. props. 78–15347
- HfO_2, growth by thermal decomp. of β-diketonate complexes, characts. 79–100055
- In_2O_3, transparent conducting film, prep. by CVD, and characterisation 80–11571
- In_2O_3, transparent electrode deposition on PLZT ceramic, elec. and opt. props. 78–74848
- In_2O_3:Sn, electro-reflectance meas. 80–11496
- In_2O_3:Sn, transparent conducting films, prep. by $InCl_3$ thermal decomp., transmittance, resistivity 79–33944
- InP, epitaxial growth, thermodynamic conditions 77–89661
- p-InP film growth, by close space vapour transport 79–28944
- InP, on preferentially etched Mo, initial growth behaviour 78–51855

CVD coatings continued
- Mo, and oxide phase mixtures, optical props., solar absorber appl. 77–55844
- Mo, CVD films of high IR reflectance 79–52119
- Mo, deposited by low temp. carbonyl pyrolysis, struct. 78–72039
- Mo film, CVD, passivating against IR reflectance losses caused by oxidation 79–3758
- Mo on SiO_2 covered W-Re wire, for neurological electrode, elec. cond. and bending props. 78–11752
- Mo thin film fabrication for photothermal solar convertors 80–11573
- Mo thin films for solar photothermal conversion, CVD fabrication 80–7503
- Mo, with high IR refl. and large solar absorpt., prep. and props. 80–26163
- $MoSe_2$ lubricant, synthesis by Mo+Se vapour reaction, process kinetics 79–33942
- $MoSi_2$, diffusion grown layers, texture 79–74095
- Nb and Mo, evaporation, carburisation and diffusion behaviour 77–44410
- Nb on graphite, grain struct. depend. on temp. 80–25574
- Nb-Ge, A15 struct. superconductor, high field transport props. TEM study 80–34574
- Nb-Ge, supercond., two-phase tetragonal Nb_5Ge_3 phase identification by electron diffr. 77–89665
- Nb-Ge-Si, A15 struct. superconductor, high field transport props. TEM study 80–34574
- Nb-Ge-Si, struct., comp., stability and homogeneity 80–15421
- Nb-Ge-Sn A15 cpds., CVD, superconductivity 79–38222
- Nb-Si compounds, CVD, struct. and supercond. props. 79–24447
- NbC coating, vapour deposition, phys. and chem. props. 77–40456
- NbC coating on C steel and Armco Fe, deposition, struct. and props. 79–52462
- Nb_3(Ge,Si) A15 film, supercond. and structural props. 79–87177
- Nb_3(Ge, X), X=Si, Ga, CVD tapes, supercond. props. at high mag. fields 79–38279
- Nb_3Ge, CVD, impurity doping effect on supercond. crit. props. 78–52174
- Nb_3Ge CVD supercond. tape critical current anisotropy obs. 79–33372
- Nb_3Ge CVD tapes, supercond. props. at high mag. fields 79–38279
- Nb_3Ge, CVD-prepared, high field props. and scaling 79–56455
- Nb_3Ge film, CVD, thermal expansivity, X-ray diffr. meas. 78–6166
- Nb_3Ge film, nucleation of high-T_c phase in presence of impurities 78–88054
- Nb_3Ge films, correl. between crit. current density and microstruct. 79–38277
- Nb_3Ge, on inside of Cu tube, AC losses 77–28312
- Nb_3Ge, supercond. film, CVD, crit. temp., crit. current density 78–76204
- Nb_3Ge tape conductors, strain depend. of crit. current density 79–38278
- $Nb_3Ge_{1-x}Ga_x$ CVD films, supercond. transition temp. depend. on lattice parameter 79–38219
- $Nb_2Ge_{1-x}Ga_x(Sn_x)$ CVD films, supercond. props., 4.2 to 19K 79–42713
- Ni-P alloy, amorphous, NMR expts. and interpretation 79–8060
- Ni_2P, CVD on Mo plate, microhardness and resist. to chem. attack 79–66009
- P_2O_5-SiO_2 glass film, thickness and IR spectrum changes on heat treatment in H_2 80–70549
- PbS, chemically deposited film, photosensitivity, effect of morphological struct. 79–82647
- PbS, effect of morphological struct. on photosensitivity 80–70760
- Re, on cemented carbides, hardness *(German)* 78–64777
- $(SN)_x$ films, electrical properties 78–91782
- Si, amorphous, CVD, retarding crystn. by alloying with C,N,B or Ge 80–44129
- Si, amorphous, discharge produced, optical and photocond. props. 78–39147
- Si, amorphous and polycryst., solar thermal absorber, temp. variation of absorpt. edge 80–12028
- Si, amorphous and polycryst., microscopic surface roughness, effective-medium models, ellipsometric expts. 80–24756
- Si, amorphous CVD fabrication for solar photothermal conversion appl. 80–7504
- Si, amorphous CVD film photodetector for picosecond pulses 80–47101
- Si amorphous film, AC conduction 77–66213
- Si, amorphous film, IR and Raman spectra of Si-H bonds 78–19482
- Si, amorphous film prepared from glow discharge, quantitative H anal. 77–69188
- Si, amorphous film prepared by CVD, optical props. and struct., solar absorber appl. 79–52035
- Si, amorphous stabilised CVD films for high temp. solar photothermal conversion 80–26161
- Si, CVD amorphous films, effect of surface characts. on visible and UV optical props. 80–60698
- Si, CVD film, transport props. 79–24089
- Si CVD film on amorphous substrate, CW laser recryst. 79–90894
- Si, CVD films, polycryst., elec. and optical props., electronic density of states model 79–56332
- Si CVD grown polycrystal recrystallisation 78–64560
- Si, CVD layers, change of etch rate associated with amorphous to crystalline transition 78–7064
- Si, CVD mechanism, book contrib. 79–69991
- Si, CVD polycryst. solar cell, grain boundary effects rel. to dopant conc. 77–7744
- Si, covered with Al layer, solid-phase crystn. obs. 77–85100
- Si, epitaxial layers, cryst. quality improvement by ion implantation, backscatt. and TEM obs. 79–42397
- Si, film, CVD, low press., struct. and stability, X-ray diffr. and TEM obs. 78–91559
- Si, film, chemically deposited on amorphous SiO_2, influence of substrate temp. and SiH_4 to N ratio on struct. 79–65346
- Si film, low press. CVD prep., struct., elec. and optical props. 80–70548
- Si films, polycrystalline, elec. props., grain size and dopant conc. influence 80–29492
- Si heteroepitaxial growth using SiH_4 in He-H_2 atm. 77–77396
- Si horizontal epitaxial reactor transport expt. and model 77–77399
- Si on sapphire, laser annealing dynamics epitaxial regrowth, optical reflectivity 80–29285
- Si, on SiO_2 and Si_3N_4 substrates, nucleation in SiH_4-HCl-H_2 system at high temp. 80–49538
- Si plasma deposited amorphous hydrogenated film, optical props., annealing effect 79–56874

CVD coatings continued
Si, polycryst, CVD, electron beam recrystn. 80—24759
Si, polycryst., CVD, recrystn. on heating 80—80107
Si, polycryst., growth texture 77—7990
Si, polycryst., layer structure dependence on carrier gas moisture and O_2 content *(Bulgarian)* 80—59811
Si, polycryst., on oxide-covered single cryst. Si substrate, deform. 78—26778
Si, polycryst. CVD film electrical props. 78—6466
Si, polycrystalline, As segregation at grain boundaries, elec. props. meas. 80—75259
Si polycrystalline CVD film optical props. 77—77315
Si polycrystalline CVD film formation and props. 77—77401
Si polycrystalline CVD films, non-volatile memory switching 80—54814
Si, recrystallisation of CVD-grown polycryst. Si and influence of B, Al dopants on grain growth 80—54575
Si, semi-insulating polycrystalline, AES and XPS characterisation 80—16129
Si solar cell, fabrication using zone melting of CVD Si on graphite, and performance 77—85945
Si, solar cell, from film on foreign substrate 77—77390
Si solar cells, growth of large grain polycryst. layers on graphite substrates by CVD on liquid layers 80—55849
Si thin film, polycryst., CVD, elec. props. 80—107934
Si, underlying oxide layer thickness effect on in-process thickness monitoring 80—6679
Si whisker coated C fibres for composites, shear strength improvement 78—3093
Si, zone refined, prep. of solar cells 78—64475
Si:As, ion-implanted layers, ellipsometric anal. of laser annealing 79—73190
Si:As(P)(Sb), implanted, elec. cond., sheet resist. as function of ion dose and temp. 79—78235
Si:B, polycryst., effect of laser annealing on struct. and elec. props. 79—11243
Si:B, polycryst., N_2 heat treated, anomalous resist. change due to Bn form. 78—2591
Si:B amorphous film, EPR, elec. and optical props. 79—4558
Si:H, amorphous, prod. by high temp. thermal decomp. of SiH_4, and photocond. 79—87585
Si:H amorphous, elec. cond., effect of adsorbed gases and illumination 78—88048
Si:H amorphous semiconductors, prep. from SiH_4 and characts. 78—48326
Si:H(D), amorphous films, CVD, post-hydrogenation 80—54552
Si:O, CVD layer, RHEED study of surface crystallinity, annealing effect on structure 79—69371
Si:O film, near IR absorption, O impurity states 78—88333
Si:P, amorphous, CVD, defect compensation 80—54644
Si:P, amorphous, CVD, substitutional doping, electronic props. 79—23923
Si:p, film, polycrystalline, low press. CVD, resist. meas. 80—2494
Si:P, polycryst., CVD, elec. activation of impurities, EPR obs. 80—34774
Si:P amorphous films, doping and annealing effects on localized states, ESR meas. 79—38380
Si:P CVD films, ion-implanted, doping effect on elec. props. 80—2495
Si:P film, CVD polycrystalline, low press. and atmos. press., oxidation 80—3214
Si-B based CVD coating for gas turbine blading, props. 80—40615
Si-C amorphous wear-resistant coating 79—34165
Si-C films, plasma deposition with neutralisation 78—88429
Si-H:As alloy, amorphous film, coordination of impurities, EXAFS of data 77—84780
Si-N, passivation layer, density comp., and ref. index, Lorentz-Lorenz correl. 78—39697
Si-N films, reactive plasma deposited for MOS-LSI passivation 78—56584
Si_xB_{1-x} films, anal. of H ratios and profiling using nucl. techniques and Rutherford backscatt. 80—61202
SiC (6H), blue-emitting diodes by CVD 80—97439
SiC, CVD, polished, total integrated vac. UV scatt. 77—62029
SiC, CVD anisotropic thick hollow cylinder, residual stress due to uniform cooldown 79—42423
SiC coating on Mo, CVD and stability under thermal cycle conditions 80—7500
SiC coatings, CVD on microspheres in fluidised bed, parametric investig. 77—40457
SiC, diffusion behaviour of fission products, 1650 to 1850°C 78—79814
SiC pyrolytic coatings for HTGR fuel particles, props. rel. to deposition conditions 79—31088
SiC whisker coated C fibres for composites, shear strength improvement 78—3093
SiC-coated C fibre, compatibility with Al *(Japanese)* 80—71700
SiC_x, amorphous, prepared by glow discharge method, elec. and optical props. 77—21035
$SiCl_4$-$GeCl_4$-BCl_4 particulate layers consolidation, in fabrication of optical fibre preforms 80—60787
SiN_x film reactive plasma deposition enhancement 77—77405
SiN_x film reactive plasma deposition and characterisation 77—77406
Si_3N_4, amorphous, AES and EELS characterisation 79—90905
Si_3N_4, amorphous, core and valence electron excitations, low energy electron loss spectroscopy and AES 80—2365
Si_3N_4, CVD, chem. bond nature, Compton scatt. expts. 80—49539
Si_3N_4, CVD, chem. bound H, NH_3/SiH_4 ratio and annealing depend. 77—76680
Si_3N_4, CVD amorphous film, X-ray diffr. 79—87013
Si_3N_4, CVD film, elec. cond., film formation by pyrolysis of SiH_4-NH_3 79—91176
Si_3N_4 CVD film etching in acidic fluoride media 78—7071
Si_3N_4, CVD films, chemically trapped H reflection spectrometry 78—10081
Si_3N_4 CVD films, microstruct. and MNS struct. characts. 79—65339
Si_3N_4 CVD films on Si, dark currents 79—78240
Si_3N_4, encapsulant for annealing of GaAs, photolum. and AES evaluation 78—27657
Si_3N_4, encapsulant for annealing for implanted GaAs:Se 78—83834
Si_3N_4 film, CVD, etching in acidic fluoride media 78—39927
Si_3N_4 film, elastic stiffness and thermal expansion coeffs. 80—107451
Si_3N_4, film, H_2 concentration profile, chem. bonding 79—33205
Si_3N_4 film, in MNOS struct., mechanical stress and elec. props. as function of nitride deposition temp. 79—42651

CVD coatings continued
Si_3N_4 film on Si substrate, electrical properties *(Korean)* 80—55300
Si_3N_4 films, amorphous, CVD, IR spectra 77—21031
Si_3N_4 films, CVD in MNOS and MNS structs., elec. resist. 80—97019
Si_3N_4 films, plasma deposited over substrate steps, fast etching phenomenon 79—34168
Si_3N_4 films grown by pyrolytic reaction between silane and ammonia, DC cond. 79—15243
Si_3N_4, high-field dark currents 80—54791
Si_3N_4, ion implanted, compressive stress buildup 77—89456
Si_3N_4, low temp. deposition using microwave-excited active N_2 78—84718
Si_3N_4, non-stoichiometric films, struct. 79—42412
Si_3N_4, on Si, implantation effects on substrate hardening and film stress reduction 78—71748
Si_3N_4, on Si (111), EXAFS 79—95876
Si_3N_4, preparation, characterisation and appl. 80—40268
Si_3N_4, pyrolytic, prep. by CVD, bulk and coatings, exam. of electrical, optical and physical props. 79—95935
Si_3N_4, pyrolytically-deposited, engng. significance 79—38746
Si_3N_4, thermally grown films for high performance MNS devices 78—48322
Si_3N_4 thin film, multiple internal refl. IR spectroscopy 80—11499
Si_3N_4, with varying refr. index, AES and XPS 78—72029
Si_3N_4:H, amorphous, ion induced H transfer from N to Si, band passivation, elec. props. 78—47439
Si_3N_4:H, film, impurity profile determ. by 1.2 MeV proton-proton scatt. 80—49256
Si_xN_y, amorphous, prepared by glow discharge method, elec. and optical props. 77—21035
SiO_2, CVD film, hydration props., ellipsometry meas. 78—22986
SiO_2 CVD layer, high current injection from Si rich SiO_2 film 80—80430
SiO_2 coatings on SiO_2 substrate, cathodoluminescence spectra, electron irrad. 80—76085
SiO_2, encapsulant for annealing of GaAs, photolum. and AES evaluation 78—27657
SiO_2, film, formation from tetraalkoxysilanes in O_2 current, props. 77—44170
SiO_2 films, Si-rich, amorphous Si region obs. 80—84400
SiO_2, low temp. CVD on n-InSb, surface quality improvement and characterisation 80—49932
SiO_2 on Si producing near-ideal Si-SiO_2 interfaces, props. 80—80382
SiO_2 on W-Re wire, for neurological electrode, elec. cond. and bending props. 78—11752
SiO_2, pyrolytic, on Ge substrate, ellipsometry, TEM, electron diffr. studies of struct. 78—10297
SiO_2 pyrolytic film, conduction process determ. 77—20479
SiO_2 thin film, multiple internal refl. IR spectroscopy 80—11499
SiO_2 thin films, comparison of RI and IR spectra 80—11497
SiO_2, uniform film prep. by pyrolysis of tetraethoxysilane 77—40379
SiO_2/InP film/substrate system, interface formation during CVD, modelling 80—24764
SiO_2-P_2O_5 glass film, CVD, P conc. profile by etch rate technique 80—96450
SiO_2-TiO_2 films, obtained from $Si(OC_2H_5)_4$ and $TiCl_4$, exam. of props. 79—95934
SiO_x semi-insulating polycryst. films, AES and PES studies 80—107939
Si_xO_{1-x} films, anal. of H ratios and profiling using nucl. techniques and Rutherford backscatt. 80—61202
SiON/GaAs film/substrate system, interface formation during CVD, modelling 80—24764
SiO_xN_y, low temp. films, comp., chem. bonding and contamination 78—47676
SiO_xN_y thin film, multiple internal refl. IR spectroscopy 80—11499
$Si_lO_mN_p$, CVD from SiH_4-CO_2-NH_3-H_2 system, physicochem. props. 78—38978
$Si_xO_yN_2$ films, chemical struct. using AES 79—77945
$Si_xO_yN_z$, non-stoichiometric films, struct. 79—42412
$Si_xO_yN_z$, pyrolytic, on GaAs, evidence for growth-induced damage from photolum. expts. 78—75953
$SiO_{2-x}Nx$ thin CVD film processing and characteristaion 77—77413
$(SiO_2)_x(Si_3N_4)_{1-x}$ on GaAs, deposition method and props. 78—91796
Sn, CVD onto GaAs surface, anal. of conditions 79—87584
SnO_2 CVD coating on glass, elec. resist. rel. to cryst. microstruct. 80—84520
SnO_2 film, CVD using $SnCl_4$-H_2O and $SnCl_4$-H_2O_2 systems, elec. and optical props. 78—52686
SnO_2 film, pure and Sb doped, transparent cond., prop., characts., stability, struct. *(Japanese)* 78—47889
SnO_2, optical and elec. props., rel. to stoichiometric deviation and struct. 77—47701
SnO_2, semicond., surface and bulk cond., process parameters effect 77—1502
SnO_2, transparent conducting film, prep. by CVD, and characterisation 80—11571
SnO_2, transparent electrode deposition on PLZT ceramic, elec. and opt. props. 78—74848
SnO_2:As film, prep. and elec. cond. 80—2959
SnO_2:P, CVD films, elec. props., cryst. to amorphous transition effects 80—107933
SnO_2:P, CVD growth and etching characts., doping effects 80—107667
SnO_2:SB,X, X=Fe,Cu,S, CVD thin film, resist. temp. coeff. 79—38198
$(Ta,Ti)B_2$ on graphite, hardness meas., SEM study 80—24760
Ta, film, CVD on silica, struct. and mech. props. 77—24965
TaB_2, deposited on quartz substrate from $TaCl_5$-BCl_3-H_2-Ar gas mixture 80—29880
TaC, on filaments of W-ThO_2 and SiC, coating effect on high temp. mech. props. 78—15347
TaN, growth by CVD, microhardness and corrosion resist. 77—36404
$(Ti,Zr)B_2$ on graphite, hardness meas., SEM study 80—24760
Ti, CVD layers on Fe substrate *(Japanese)* 78—27415
Ti-B-N, CVD, lattice const. 79—74097
Ti-Zr-B system 78—60581
TiB_2 coatings, CVD, electron microprobe, SEM, X-ray diffr. characterisation *(French)* 78—43271
TiB_2, erosion rates under H^+ ion bombard., fusion reactor appls. 80—39179
TiB_2, prep. by CVD and interaction with substrate 79—24680
TiB_2, surface damage and erosion under energetic D^+ and $^4He^+$ irrad. 80—39174

CVD coatings continued
TiB$_2$ thick film on low C steel substrate, CVD in US field, crystallite size 80—84854
TiC abrasion-resistant coatings, glow discharge assisted CVD 79—83392
TiC, Au-dispersed, struct., hardness and wear rate 77—77493
TiC, CVD and activated reactive evaporation on WC-TiC-Ta(Nb)C-Co, substrate-layer interactions, AES obs. 79—24679
TiC, CVD coating on Co-bonded multicarbide substrate, SEM, RHEED, AES interface study 79—77927
TiC, CVD layers on Fe substrate *(Japanese)* 78—27415
TiC coated WC-Co cemented carbides, fracture toughness 80—85046
TiC coating on C fibre, by CVD TiC coated C fibre compatibility with Al *(Japanese)* 79—78898
TiC coatings, on cemented carbides, struct. and hardness 80—59771
TiC, erosion rates under H$^+$ ion bombard., fusion reactor appls. 80—39179
TiC film, CVD, on WC, diffusion processes, ion beam anal. 80—49424
TiC hard coating on Co, effect of martensitic transform. in substrate causing cracks 79—29060
TiC, laser CVD, coating characterisation 80—93494
TiC layers, on steel and cemented carbides, load-bearing capacities 80—40606
TiC, W$_6$Co$_6$C cemented carbide substrates, structure, composition and hardness exam. 78—11425
TiC$_x$ refractory layers on steel surfaces, ESCA obs. 80—39471
Ti(CN) coating for steel, abrasion resist., CVD parameter depend. 77—40471
TiC$_x$N$_y$ monolayer film, on C steel, CVD in US field, X-ray and SEM characterisation 79—65338
TiN, -Z *(Japanese)* 78—27415
TiN, CVD growth in US field, effect on adherence and hardness 77—59696
TiN, vapour deposited coating on cemented carbide tools, deposition parameter effects on wear 77—63563
TiN-Nb(Ta)N, microcomposite film prod. for radio resistors 78—3052
TiN-TiC$_x$ double layer coating, deposition on C steel, X-ray diffr. study 79—65338
TiO$_2$, anatase film, intermittent CVD conditions rel. to struct. 78—11119
TiO$_2$, rutile, thin film CVD 77—77409
UC$_2$ and (8Th, 1U)O$_2$ fuel kernel, experimental containing CVD ZrC coatings, irradiation behaviour 77—3103
VC$_x$ coating, C steel vanadisation by CVD 80—44454
VO$_2$, chemical transition layers at interface with substrate, AES and SEM obs. 79—95533
VO$_2$, V$_2$O$_3$ and V$_3$O$_5$, film prep. under equil. conditions, struct. and elec. props. 80—108352
V$_2$O$_5$ amorphous films, CVD prep., structural characts. 80—49114
W, CVD hardfacing of coal gasification unit components 77—40472
W, deposited by low temp. carbonyl pyrolysis, struct. 78—72039
W, dislocation struct., rel. to texture *(Russian)* 80—65394
W, on filaments of W-ThO$_2$ and SiC, coating effect on high temp. mech. props. 78—15347
W on Si, properties and kinetic parameters for deposition 78—91570
W, optical props., solar absorber appl. 77—55844
WSi$_2$, diffusion grown layers, texture 79—74095
YIG, on GdGaG, mag. excitations, diffusion layer effects 78—31112
YIG thin film, boundary effects, spin wave reson. meas. 79—78447
Zn$_x$Hg$_{1-x}$Se(Te,S) film preparation and props. *(Russian)* 78—11122
ZnO, amorphous and cryst. film prep. and elec. props. 77—76973
ZnO-CdSe thin film n-n heterojunctions, prep. elec. and optical props. *(Korean)* 77—28244
ZnS CVD IR material specifications 80—48364
ZnS CVD IR window, optical and physical characteristics 80—106620
ZnS, CVD sample, refractive index var. with temp., 22° and 34°C 79—14053
ZnS:Mn on SnO$_2$/glass transparent conductive base, surface morphology effects on electroluminesc. *(Russian)* 78—48238
ZnSe, CVD, delayed failure 79—99462
ZnSe CVD IR material specifications 80—48364
ZnSe, laser window material, impurity absorpt. meas. 78—25909
ZnSe, RF bias-sputtered CVD films on CaF$_2$ 79—14060
ZrC CVD coated fuel particles, diffusion of ^{137}Cs, ^{90}Sr and ^{144}Ce 80—13582
ZrC coating, vapour deposition, phys. and chem. props. 77—40456
ZrC-C composite system, negative magnetoresist. 80—60008
ZrO$_2$ film, CVD from organometallic cpds. and characterisation 78—23626
ZrO$_2$, growth by thermal decomp. of β-diketonate complexes, characts. 79—100055
CVD epitaxial growth *see vapour phase epitaxial growth*
CVD thin films *see CVD coatings*
cyanogen, C$_2$N$_2$ *see carbon compounds*
cybernetics
see also artificial intelligence; biocybernetics; economic cybernetics; information theory; man-machine systems; pattern recognition
catalysis significance by coordination complexes *(French)* 77—12797
crystallographic lattice, 3D, impulse automatic stochastic control 77—22499
education, pupil learning and teacher activity algorithms 78—49577
education, suggested uses of algorithms 78—49578
education appl., comparison with other methods *(Croatian)* 80—12866
entropy significance, thermodynamic approach *(French)* 77—5787
geophysical potential field data, interpretation methods 77—73861
learning in networks with minimal disruption 79—74628
cyclopentadienylides *see organometallic compounds*
cyclotron resonance
for ion cyclotron resonance spectroscopy see mass spectroscopy; for ion cyclotron resonance heating see plasma heating
see also diamagnetism; dopplerons
Alcator Tokamak submillimetric-wave emission obs. 79—32816
anthracene, cryst., cyclotron reson. and carrier scatt. 77—76746
anthracene, hole mobility mechanism interpretation of cyclotron reson. results 78—10438
Azbel-Kaner, surface impedance of a metal in magnetic field 78—87901
Bloch electrons in mag. field, transfer-matrix study 77—55472
charged particle acceleration in nonadiabatically varying uniform mag. field 77—27236
charged particle beam, instability normal to beam *(Russian)* 79—13883
charged particle motion in reson. conditions, asymptotic theory *(Russian)* 77—84397
cyclotron resonance continued
coherent radiation generation near cyclotron resonance 80—18979
cyclotron radiation transport in plasmas by neutron transport techniques 80—38660
degenerate electron liquid, skipping orbit cyclotron resonance, surface state transitions 80—103889
degenerate free electron metal, cyclotron wave propag., finite $\omega\tau$ effect 77—20228
Doppler effect, anomalous, amplification of slow waves in electron beam, obs. 80—78463
Doppler-shifted, anomalous propag. of US waves 79—73429
doppleron propagation in inclined mag. field spectrum, decay, polarisation study, Fermi surface model 80—44922
EBT heating, electron-cyclotron absorption and microwave propagation 80—64749
ECR lineshape, quantum theory, two-dimens. electron-impurity system 78—48045
electrical conduction in metals, neutral and charged impurity scattering, Matthiessen's rule 79—47081
electron beam, high-current, stability in mag. field in waveguide 78—66742
electron beams, relativistic intense solid, cyclotron maser instability 79—55494
electron cyclotron emission, meas. in hot plasmas, using microwave heterodyne radiometer 79—90463
electron cyclotron heating, superthermal electrons 80—64753
electron cyclotron maser, historical review 77—38843
electron cyclotron maser, instability, linear and self-consistent nonlinear theory 77—38844
electron cyclotron maser history 77—38845
electron cyclotron reson. ion source with permanent mags., plasma-wall interaction expts. 80—99378
electron cyclotron reson. lineshape analysis for cylindrical cavity field inhomogeneities 78—13560
electron cyclotron resonance plasma, metal surface cleaning *(Japanese)* 80—16572
electron effective mass localised above liq. ^{4}He surface, cyclotron reson. meas. *(Russian)* 77—11756
electron gas, two dimens., Coulomb interaction effects 78—60073
electron impurity system in two-dimens., cyclotron reson. width 77—35892
electron liquid, cyclotron reson. at skipping orbits *(Russian)* 78—72240
electron plasma in presence of EM wave, DC mag. field, Coulomb screening, dielec. const. 80—15464
electron-impurity system in two dimensions, theory of cyclotron reson. lineshape 78—19332
electron-phonon system, cyclotron reson. lineshape 80—97142
electron-phonon system, two-dimensional cyclotron resonance lineshape, quantum theory 79—47336
EM wave propagation near combined resonance 79—99772
Fermi-liquid parameter determ. from cyclotron reson. meas. 78—60069
ferrimagnetic semiconductor, cyclotron-magnon reson. 79—69725
ferrite-semiconductor film struct., cyclotron resonance in static elec. mag. fields 80—29624
ferromagnet, electron transport with arbitrarily oriented ellipsoidal Fermi surfaces, cyclotron wave excitation 78—23006
free electron gas, radiation shift of cyclotron freq. anal. *(Russian)* 77—8033
frequency dependence of relax. time, lattice heating 77—48054
frequency up-shift for cyclotron-wave instability on a relativistic electron beam 79—22883
gases, electron cyclotron resonance absorpt. signals 78—51278
glow discharge tube, EM MM-wave detection properties in mag. field 80—70059
graphite, far IR magnetospectroscopy of Landau level structure 79—73906
graphite intercalation cpds., C$_n$K, de Haas-van Alphen effect, cyclotron reson., and transport props. 80—44479
gyrotron efficiency, CW and pulsed power achievements 79—31849
halomethane mols., electron scavenging studied by electron cyclotron reson. 79—50143
heavily doped semiconductor, magnetoconductivity, effect of resonant phonon-plasmon coupling 80—24954
helical electron beams, extended and intense with space-charge forces, trajectory anal. *(Russian)* 79—918
Hercules X-1, struct. and higher harmonics of cyclotron lines in strong mag. field 78—20912
high magnetic field behaviour of solids and plasmas, conference, Cambridge, MA, USA (Sept. 1978) 79—60667
high power MM wave source—gyrotron *(Japanese)* 80—23654
III-V compounds, n-type, new meas. method for compensation and spatial fluctuations of impurities 78—6404
indirect exchange between local moments, cyclotron reson. effect 77—40051
inversion layers, carrier effective mass, contribs. of electron-electron and electron-phonon interactions 78—64087
inversion layers, mag. field depend. of reson. line width 78—56380
inversion-layer electrons, temp. depend. cyclotron reson. lineshape, theory 78—64086
ionic semiconductors, cyclotron resonance, elec. cond., electron-phonon interactions 80—93180
isolated 1 MeV electron, meas. of axial, magnetron, cyclotron and spin cyclotron beat frequencies 77—30300
Landau levels near mag. subband 80—39512
laser illumination, additional, effect on reson. effects in mag. field 78—72417
magnetic mirror, cyclotron and betatron oscills. in mag. mirror with RF field, cyclic accelerator theory 79—41051
magnetised semiconductor plasma, EM wave amplitude modulation and demodulation 80—84482
magneto plasma half space, reflected pulse, cyclotron and upper hybrid resonance freq. 78—63569
maser, multimode regimes *(Russian)* 77—31083
maser, synthesis of systems formation of screw electron beams *(Russian)* 78—17889
maser, theory of solid-state device 79—41361
maser amplifier with freq. conversion 78—55329
maser tube with transverse current, theory of oscillation 79—89877
maser with high current relativistic electron beam 79—13942
Matthiessen's rule and its variation for cyclotron reson. width in two and three dimensions 78—6578

cyclotron resonance continued
metal, anisotropy effects on US cyclotron resonance 79—73816
metal, cyclotron reson. and geometric oscills. of sound velocity 77—20230
metal, cyclotron reson. on open electron orbits *(Russian)* 80—88878
metal, dispersion relation for ordinary cyclotron waves, spherical Fermi surface 77—55474
metal, Doppler-shifted cyclotron reson., excitation of dopplerons and Gantmakher-Kaner waves *(Russian)* 77—32261
metal, EM props., general lecture 78—26901
metal, EM sound generation in cyclotron reson. regime *(Russian)* 77—69381
metal, EM waves near cyclotron reson. in inclined mag. field *(Russian)* 80—29625
metal, galvanomag. phenomena, quantum theory, cond. rel. to migration of cyclotron orbit centres *(Russian)* 77—66153
metal, isotropic Fermi surface, cond. tensor calc., cyclotron waves 79—42528
metal, line shape in inclined mag. field *(Russian)* 77—36136
metal, nonlinear cyclotron reson., anomalous skin effect *(Russian)* 77—28449
metal, surface impedance in mag. field, cyclotron waves 77—89787
metal, wave excitation, with mirror surface, near cyclotron resonance *(Russian)* 78—35040
metal spherical Fermi surface, cyclotron reson. line shape and cyclotron waves 78—95251
metal surface cleaning, by electron cyclotron resonance plasma of H 79—47821
metal with almost specular boundary *(Russian)* 78—10778
metallic thin film, EM wave transmission under resonance conditions *(Russian)* 80—54805
metals, attenuation length 77—90038
metals, compensated, Gantmakher-Kaner effect in strong mag. fields 78—91595
metals, cyclotron resonance depend. on surface, anomalous skin effect *(Russian)* 80—75860
metals, cyclotron resonance in weak mag. fields surface impedance, current density asymptotic *(Russian)* 80—2641
metals, cyclotron wave dispersion and obs. of many body effects 77—28097
metals, cyclotron wave excitation, diffuse boundary scatt. *(Russian)* 80—54729
metals, longitudinal weakly damped EM waves near cyclotron resonance 80—103890
metals, quantum oscillation effects in weak mag. field *(Russian)* 79—11105
metals, sound pulse spike like transport near acoustic cyclotron resonance *(Russian)* 80—100617
metals, surface impedance in mag. field, theory *(Russian)* 78—6427
metals and superconductors, quantum cyclotron reson. 79—61225
model interface in transverse mag. field 79—4726
MOS two-dimens. systems under strong mag. field, many-body effect on level broadening and cyclotron resonance 79—78195
narrow band gap semiconductors effects, review 79—95437
nonpiezoelectric dielectric, polarisation echo and polarisation avalanche signal form. *(Russian)* 79—61297
Phonon-cyclotron absorption in a transverse electric field 78—2741
plasma, electron beam space charge wave in mag. field, cyclotron damping 79—46459
plasma, ray tracing near electron cyclotron reson., finite temp. effect 80—53994
PLT Tokamak cyclotron radiation Fourier transform spectral analysis 79—32815
polar semiconductor, TO phonon-helicon coupling 79—73539
quadratic grouping of electrons directed by transversely inhomogeneous magnetostatic fields *(Russian)* 78—74822
retardation effects, microwave freqs., electron relaxation time 79—42839
retarded, effect of electron-phonon coupling *(Russian)* 79—8051
review of magnetic resonance, book contrib. 80—11242
semiconducting surface inversion layer, cyclotron reson. of interacting electrons 78—34885
semiconductor, anisotropic carrier energy spectrum, quantum cyclotron reson. line width 77—8008
semiconductor, combined resonance, basic mechanisms 79—61229
semiconductor, complex energy band under optical excitation, high-frequency negative cond. and population inversion 80—107858
semiconductor, far IR spectroscopy, appl. of far IR lasers 80—31914
semiconductor, galvanomag. phenomena, quantum theory, cond. rel. to migration of cyclotron orbit centres *(Russian)* 77—66153
semiconductor, impurity absorption in mag. field and resonant laser radiation 77—52145
semiconductor, intervalley cyclotron-phonon reson., IR absorption in mag. field 78—60448
semiconductor, IR expts., MG field production and appl. 79—71491
semiconductor, negative cyclotron resonance of hot carriers 78—2492
semiconductor, phonon-assisted cyclotron reson., single and two-phonon pinning, review 79—15356
semiconductor, piezoelec. and nonpiezoelec. cyclotron-phonon resonance due to polarisation scatt. from phonons 79—95649
semiconductor, pinning struct. of cyclotron reson. lines 78—72414
semiconductor, surface space charge layer spectroscopy 77—20386
semiconductor, theory 79—73817
semiconductor, transport and surface phenomena 78—6575
semiconductor, weak heating of electrons, cyclotron reson. conditions, quantising mag. field 78—39141
semiconductor, weakly polar, IR absorption by optical polaron in mag. field 77—66127
semiconductor, width due to electron-charged impurity interaction 77—55475
semiconductor, zinc blende struct., cond. band nonparabolicity and cyclotron reson. linewidth *(German)* 78—75993
semiconductor film, cyclotron-phonon absorption singularities 77—51955
semiconductor physics in high mag. fields, review *(Japanese)* 80—50192
semiconductor plasma, extraordinary electron cyclotron waves, transverse propag. in quantising mag. field 77—59298
semiconductor submillimetric-wave spectroscopy 79—33221
semiconductor surface, cyclotron reson., projection operator formalism 80—88524
semiconductor-insulator boundary, space charge layers, HF magnetoconductivity 78—60231
semiconductors, cyclotron reson. fine struct. *(Russian)* 79—4727

cyclotron resonance continued
semiconductors, cyclotron-phonon reson., review 79—56615
semiconductors, far IR cyclotron emission 79—61226
semiconductors, high frequency differential cond., needle shaped distribution model 79—65509
semiconductors, magneto-optical effect and cyclotron reson. in high mag. fields 80—27321
semiconductors, meas. using high mag. field installation *(Dutch)* 78—252
semiconductors, nondegenerate, free carrier absorpt. in quantising mag. fields 80—45044
semiconductors, quantum limit cyclotron resonance linewidth 80—7171
semiconductors electron-photon mechanism of cyclotron absorpt. hysteresis 79—69726
semiconductors with superlattices, Stark-cyclotron resonance, Larmour freq. *(Russian)* 80—60421
semimetAl, acoustic cyclotron reson., sound interaction with cyclotron waves *(Russian)* 77—35959
small-radius scatterers, cyclotron resonance harmonics 80—71183
solids and plasmas, cyclotron reson., review 79—61224
sound transmission by electrons in conditions of resonant interaction *(Russian)* 79—7774
spatially inhomogeneous system, galvanomagnetic effects *(Russian)* 78—72129
static conductivity change under quantum cyclotron reson. 78—39143
stimulated emission, gyrotron, review 77—34865
superdense stars, high mag. fields, cyclotron reson. emission 79—75207
surface electrons, reson. and cyclotron waves *(Russian)* 77—73081
surface impedance in mag. field 77—89786
surface impedance under nonresonant conditions, background signal in cyclotron resonance 79—38383
synchrotrons, accelerated particle resonances, perturbation treatment in classical dynamics 79—22506
Takamak plasma density profiles from electron cyclotron radiation spectra 80—103179
thermoelectromagnetic waves in conductors in a mag. field *(Russian)* 80—49695
thin conductors, SHG and size cyclotron reson. 78—72186
thin surface layer, interactions between nondegenerate electrons, effect on cyclotron resonance, mag. cond. *(Russian)* 80—15802
tilted magnetic field, reson. line shape, specular electron-surface refl. *(Russian)* 78—43286
Tokamak electron cyclotron emission spectrometry by plasma-scanned Michelson interferometer 79—32814
Tokamak plasmas, cyclotron radiation, diagnostic tool *(Dutch)* 78—30472
transverse dynamic magnetoresistance and cyclotron reson. damping 79—4576
trapped-ion cyclotron reson. spectra, intensity oscills. characterisation 78—48716
trichloroethylene, interaction with thermal-energy electrons, cyclotron reson. obs. 77—19097
turbulence effects in the cyclotron resonance of monochromatic whistlers 79—16759
two dimensional electron-impurity system, theory of transverse dynamic magneto-conductivity 79—38105
two dimensional electrons interacting with surface and volume phonon 78—80221
two-dimensional CDWs, pinning and cond. in mag. fields 79—42610
two-dimensional electron gas, electron-phonon interaction and cyclotron reson. 80—25014
two-dimensional electron gas, reson. excitations, using IR spectroscopy, review 79—60889
two-dimensional electron impurity system, quantum theory of cyclotron reson. lineshape 78—64083
two-dimensional electron-impurity system, theories of cyclotron resonance lineshape 77—85573
two-resonator CRM oscillator with external feedback 80—87362
VLF wave packet, cyclotron interaction with reson. electrons beam 79—53652
Warm nonuniform plasma, stress tensor for high freq. wave propag. 80—33764
weakly collisional inhomogeneous plasmas, cyclotron resonance destruction, cyclotron drift instabilities 79—77372
zinc blende structure semiconductors, cyclotron reson. *(German)* 78—10337
e^-p mass ratio, direct determ. using cyclotron resonance technique 78—70093
Ag, doppleron propagation, Fermi surface characts. 77—51642
AgBr, cyclotron reson. of polarons at high microwave fields 78—67958
AgBr, cyclotron reson. of polarons at high microwave fields 79—61228
AgBr, cyclotron reson. of polarons at high density excitation 80—75859
AgBr, streaming cyclotron motion of hot electrons, at intense microwave fields 80—6703
Al, EM excitation in metals with anisotropic Fermi surface 77—39768
Au, Fermi surface orbit integrals, tetrahedron method, cyclotron mass orientation depend. 80—44476
Bi, Azbel-Kaner type cyclotron reson. obs. 78—56379
Bi, electron band models, simultaneous meas. of giant quantum oscills. and diamag. reson. 78—14653
Bi, energy band model, resolution of theoretical discrepancy 77—11849
Bi hole pocket, far-IR magnetospectroscopy, electron-electron interaction effects 77—77211
Bi, hole relaxation time, temp. depend. 79—47108
Bi, magnetoplasma effects at 300 GHz in Voigt configuration 80—39619
Bi, magnetoresistance, high temp. oscills., props. *(Russian)* 80—65606
Bi, nonlinear resonance on EM wave irrad. *(Russian)* 79—73815
Bi, skipping electrons, electron-electron interaction parameter determ. 80—34351
Bi:Sb, semimetallic alloy, microwave spectroscopy 78—87908
Bi-Sb, semiconduct., e.m. wave propag. perpendicular to mag. field 79—82517
Bi-Sb, semimetallic, magnetoplasma effects at 300 GHz in Voigt configuration 80—39619
Bi-Sb, semimetallic alloy, cyclotron reson. and quantum oscillations 77—28096
Bi-Sb narrow gap semiconductor, EM wave propagation in direction parallel to mag. field 78—80014
BiSb, Azbel-Kaner type cyclotron reson. obs. 78—56379
n-BiSb, cyclotron mass meas., high hydrostatic press. 79—77991
n-$Bi_{1-x}Sb_x$, determ. carrier dispersion relation parameters 79—38107

cyclotron resonance continued
$Bi_{1-x}Sb_x$, EM wave propag. for rot. of mag. field from Faraday to Voigt config. 80—84419
$Bi_{1-x}Sb_x$, non-ellipsoidal Fermi surface, cyclotron reson. meas. at 35 and 70 GHz 77—62804
$Bi_{1-x}Sb_x$, semimetallic, plasma effects, submm. wave expts. 77—35881
CBr_x, graphite intercalated, de Haas-van Alphen effect and cyclotron reson. 80—44479
$C_{24}Rb$, graphite intercalated, de Haas-van Alphen effect, cyclotron reson., and transport props. 80—44479
Cd, Azbel'-Kaner high freq. reson., electron phonon interaction meas. 79—11056
Cd, Doppler-shifted cyclotron reson. of holes, nonlinear effects *(Russian)* 77—8010
Cd, inversion of cyclotron resonance data 78—91593
Cd, nonlinear cyclotron absorption of hole doppleron *(Russian)* 78—10779
Cd, surface impedance, in mag. field *(Russian)* 78—19079
Cd, surface impedance in mag. field, influence of nature of electron reflection 77—51803
Cd_x-$Hg_{1-x}Te$, cyclotron magneto-optical resons., photoconductivity meas. *(Russian)* 78—23133
CdS, IR cyclotron reson. in field up to 200 T 77—52059
n-CdS, new type photoconduction due to magneto-phonon reson. 77—55565
n-CdS, piezoelectric polaron and polaron pinning 77—35872
CdS, polaron cyclotron resonance freq. shifts, halfwidths, cumulant expansion method calcs. *(Russian)* 80—88880
CdS, polaron IR cyclotron reson. 80—25347
CdSe, polaron IR cyclotron reson. 80—25347
ClF_3, interaction with thermal-energy electrons, cyclotron reson. obs. 77—19097
Cs(Ar-Cs) plasmas, electron momentum transfer cross section, cyclotron reson., temp., cond., and vel. meas. 80—106930
Cu, cyclotron masses using tetrahedron method 79—90946
Cu, Fermi surface orbit integrals, tetrahedron method, cyclotron mass orientation depend. 80—44476
Cu, metal surface cleaning, by electron cyclotron resonance plasma of hydrogen 79—47822
Cu_20, pure and Fe doped, impurity scattering effects, polaron mass extrinsic origin assessment 79—56614
GE, microwave cyclotron resonance lineshape, magnetoplasma interference effect, reinterpretation of excitonic polaron 78—43287
Ga, spiral cyclstron waves excited by US in open Fermi surface metals *(Russian)* 79—99771
n-GaAs, Landau level lifetimes for electrons 79—87112
n-GaAs, mechanism of cyclotron reson. induced cond. 78—43396
GaAs, photoconductivity meas. of cyclotron resonance 79—82638
n-GaAs tunable far IR Landau emission with subnanosecond rise time 79—32015
GaAs:S^+ film, ion implanted carrier characterisation by cyclotron reson. 77—20472
GaAs-$Al_xGa_{1-x}As$ differentially doped heterojunction interface, two-dimens. electron gas obs. 80—49886
GaAs-AlGaAs:Si heterojunction interface, two-dimens. electron gas, Hall effect and cyclotron reson. meas. 79—65530
$Ga_xIn_{1-x}As_yP_{1-y}$, conduction band and phonons, Shubnikov-de Haas effect, magnetophonon resonance, Raman scattering 80—24795
$Ga_xIn_{1-x}As_yP_{1-x}$, epitaxial layers on InP, expt. determ. of effective masses 79—65370
$Ga_xIn_{1-x}As_yP_{1-y}$, electron effective mass, cyclotron reson. and magnetophonon effect meas. 80—103618
Ge, cyclotron reson. in strong elec. fields, classical theory 80—7172
n-Ge, cyclotron reson. line width in quantizing mag. field 78—10336
Ge, cyclotron resonance and radiative recomb. with laser excitation, book contrib. 80—11472
n-Ge cyclotron resonance line shape at 337 μm, obs. 77—39770
n-Ge, effect of non-parabolicity in quantum mechanical treatment of cyclotron reson. 77—31937
Ge, electron scatt. by charged impurities under cyclotron reson. conditions 77—63286
Ge, electron-hole droplet decay kinetics, microwave expts. 77—43517
Ge, electron-hole droplets, magnetoplasma reson. with submillimetre circularly polarised waves 77—89712
Ge, electron-hole liquid, strain-confined 78—10355
Ge, exciton and electron-hole drop diffusion coeffs. 77—48055
Ge, highly excited, electron-hole drops role 77—48056
n-Ge, IR cyclotron reson. in field up to 200 T 77—52059
Ge, irrad., electron scatt., 36 GHz, 1.8 to 4.2K 78—72416
Ge, irradiated and annealed, cyclotron reson. linewidth investig. of electron scatt. 77—55707
n-Ge, line shape cyclotron reson., 337 μm, 15-80K 78—6577
Ge, magnetoplasma reson. spectra, electron-hole drop shape effects 79—1712
Ge, pure, electron hole size distribution at pulse optical excitation 80—59883
Ge, quantum cyclotron reson. linewidth 77—15752
Ge slab in waveguide, microwave absorpt. due to geometric reson. of longitudinal-section elec. surface waves 80—39874
Ge, surface, high freq. cond. and cyclotron reson. 80—11273
Ge uniaxially deformed, cyclotron resonance of RF field heated hot holes, *(Russian)* 80—44925
Ge, uniformly deformed, free carrier cyclotron resonance, electron-hole drops *(Russian)* 80—71182
He, gas, laser-induced breakdown cyclotron reson. at low press. 79—60100
He, liq., electrons localised at surface, cyclotron freq. shift *(Russian)* 80—6582
He, liq., surface, two-dimensional electron gas, cyclotron reson. 79—60566
He liq. surface, cyclotron reson. of two-dimens. electrons *(Russian)* 80—88374
He, liquid, cyclotron reson. with surface electrons *(Russian)* 77—59319
He, liquid, cyclotron reson. freq. increase, electric field on surface dimple electrons 78—47624
He, liquid, nonlinear cyclotron resonance of localised surface electrons *(Russian)* 77—59318
^{3}He, liq., localised electron states, cyclotron reson. above surface *(Russian)* 80—6587
^{3}He, liquid cyclotron resonance of localised electrons above surface *(Russian)* 78—14533

cyclotron resonance continued
^{4}He, liq., cyclotron reson. of hot electrons 80—88377
^{4}He, liq., localised electron states, cyclotron reson. above surface *(Russian)* 80—6587
$Hg_{1-x}Cd_xTe$, cyclotron reson., 337 μm transmission expts., 77 to 150K 78—34750
$Hg_{1-x}Cd_xTe$, far IR cyclotron resonance in inversion layer 77—69396
$Hg_{1-x}Cd_xTe$, far IR cyclotron reson., band edge effective mass and relax. time 79—19781
$Hg_{1-x}Cd_xTe$, n-surface inversion layers study 80—25017
HgI_2, electrons and holes cyclotron reson. 78—72061
HgI_2, photoexcited, Hall effect, magnetocond., and cyclotron reson., carrier mobility and effective mass 77—59294
In, US wave polarisation plane and ellipticity rot. in mag. field, Doppler shifted acoustic cyclotron reson. *(Russian)* 79—15335
n-In-Sb, polar semicond., TO phonon-helicon coupling, Doppler shifted cyclotron reson. region 79—73539
InAs-GaSb superlattice, cyclotron resonance, energy level quantisation 79—73430
$InAs_{1-x}P_x$, electron effective mass cyclotron reson. and magnetophonon effect 80—24786
$InAs_{1-x}P_x$, evidence for reduction in momentum matrix element P^2 due to alloy disorder 79—65853
n-$In_{1-x}Ga_xAs_yP_{1-y}$, cyclotron reson., cond. band nonparabolicity 80—29311
n-InSb, anomalous three LO phonon assisted cyclotron resonance 80—108078
InSb, cyclotron harmonic transitions, warping and inversion asymm. effects 78—68383
p-InSb, cyclotron reson. of nonequilib. photoelectrons, distrib. function and line profile 78—60336
n-InSb, cyclotron reson. of conduction electrons, strong mag. field, hot electrons 80—2640
n-InSb, cyclotron reson. study of conduction electrons, strong mag. field 80—2639
InSb, cyclotron resonance lineshape 80—15801
n-InSb, directional temp. of hot electrons under elec. and mag. fields 78—84135
InSb film, threshold singularity on quantising mag. fields 78—87904
InSb film cyclotron-frequency submillimetric oscillation generation model 77—80801
n-InSb, frequency shift of combined resonance, influence of plasma oscills. of conduction electrons 79—7850
n-InSb, in MIS struct., accumulation layer submillimetric cyclotron resonance obs. 77—39912
InSb, laser beam self-focusing, effect of quantising mag. field 77—42578
InSb lattice, static dielec. const. and carrier conc. meas. via gyrotropic sphere reson. 80—97143
InSb, magneto-optical anomalies of impurity electrons, two-LO-phonon region 78—72415
n-InSb, magneto-photoconductivity, phonon assisted combined reson. magneto-optical absorpt. reson. 78—47831
p-InSb, magnetoconductivity and cyclotron reson. in inversion layers 80—49946
n-InSb, microwave helicon resonances, carrier density, mobility, dielectric const. 80—96930
n-InSb, nonlinear optical susceptibility, cyclotron reson. meas. *(Russian)* 79—50341
p-InSb, oscills. of microwave photocond. and cyclotron reson. of photoelectrons 79—28377
p-InSb, phonon assisted cyclotron harmonic transitions 78—48046
InSb, phonon assisted cyclotron resonance exact sol. of integral eqn. for Green's function 79—61227
n-InSb, phonon-assisted cyclotron reson. strongly depend. on surface condition 80—70755
InSb, pinning struct. of cyclotron-phonon reson., effect of nonequidistant Landau levels 77—11881
p-InSb, quantum resonances in valence band under uniaxial stress, far IR meas. 79—99481
n-InSb, surface accumulation layer, sub mm electron cyclotron reson. 78—6576
n-InSb tunable far IR Landau emission with subnanosecond rise time 79—32015
K, electron scatt. effect, excitation of cyclotron waves, calc. 78—6429
K, intermediate-wavelength cyclotron waves and Fermi-liq. effects 79—77986
K, microwave transmission modes at cryogenic temps. 79—42473
K-Na, dil., dynamical props. of quasiparticle excitations, de Haas-van Alphen effect meas. 78—84128
$LaAl_2$, magnetoresist. and de Haas-van Alphen effect, Fermi surface model 79—15069
Mg, Hall resistivity, 1.7-300K, up to 2 T, cyclotron motion breakdown 77—89751
Mo, cyclotron effective mass and identification of carriers on Fermi surface 79—65372
Mo, cyclotron resonance by microwave transmission and carrier identification on Fermi surface 79—60685
Mo, Doppler shifted cyclotron reson., doppleron-phonon reson. *(Russian)* 77—32262
Mo, effective mass meas. and electron velocities 80—96773
Mo, longwave dopplerons, nonlocal Hall effect, surface impedance, size effect *(Russian)* 80—80253
2H-MoS_2, far IR optical and magneto-optical absorpt., search for free carrier cyclotron reson. 77—52078
NO_2, electron attachment, ECR obs. *(German)* 79—10201
Na, microwave transmission modes at cryogenic temps. 79—42473
Nb, high frequency cyclotron resonance study 79—11057
Pb, cyclotron reson., anisotropy, line shape, relax. time and identification of orbits 77—35853
Pb, cyclotron reson., tipping effect of mag. field 77—35852
Pb, Fermi surface obs. *(Japanese)* 78—23009
Pb, neutron irrad. effect on cyclotron reson. *(Russian)* 77—69216
Pb, plastically bent, effect of dislocations on electron relax. time, cyclotron reson. 79—24217
p-$Pb_{1-x}Ge_xTe$ film, cyclotron reson. above and below struct. phase transition 80—88879
PbI_2 (2H), electronic transport and cyclotron reson. 79—28369
$Pb_{1-x}Sn_xTe$, basic electrons energy spectrum near mag. phase transition *(Russian)* 79—90955
$Pb_{1\ x}Sn_xTe$, diamag. reson. *(Russian)* 78—23347

cyclotron resonance continued
PbTe epitaxial film, many valley semicond., band population effects, intraband magneto-optical props. 79—78007
PbTe epitaxial layers, submillimetre spectroscopy 79—83048
PbTe, far IR magnetorefl., band struct. 80—76010
PbTe, far IR spin flip reson. 79—82979
p-PbTe film, for IR magneto-optics, 8-30K 78—23543
PbTe, ion implanted, magneto-optical expts. *(German)* 79—28848
p-PbTe, MIS struct. inversion layer sub-bands, IR magnetoreflectance obs. 80—44731
p-PbTe, magneto-optics of free and bound carriers 79—82985
PbTe, magnetoreflectance of surface space charge layers 78—52475
Rb, Landau Fermi-liquid-theory parameters, conduction-electron spin wave meas. 79—42472
Rb, microwave transmission modes at cryogenic temps. 79—42473
Rb-K, dil., dynamical props. of quasiparticle excitations, de Haas-van Alphen effect meas. 78—84128
Re, RF size effect, Fermi surface dimensions determ. 78—91598
Si (100) MOST, comparison of Shubnikov-de Haas effect and cyclotron reson. under uniaxial stress 80—20320
Si (100) surface, cyclotron reson. of electrons in surface space charge layers 77—8169
Si (100) surface, surface cyclotron resonance, freq. depend. 77—8170
Si, (100) surface space-charge layer, intersubband cyclotron combined resonances 79—69571
Si, accumulation layer, intersubband-cyclotron combined resonance, theory 80—20278
Si inversion layer, cyclotron resonance in extreme quantum limit, collective ground state 80—50191
Si, inversion layer, dynamic conductivity of electrons, temp. depend. 78—19115
Si, inversion layer, interacting electron system, cyclotron reson. 78—87902
Si, inversion layer, magnetoplasmon reson. lineshape theory 79—1615
p-Si, inversion layer, screening effect and quantum transport in strong mag. fields 78—19155
Si, inversion layer electrons, temp. depend. cyclotron reson. lineshape 78—10568
Si inversion layer surface cyclotron resonance, temp. and stress effects 78—60229
Si inversion layers, far IR reson. magnetotransmission, temp. and band gap light depend. 78—64363
Si inversion layers, stress effects on electronic props. 78—43476
Si, inversion layers, submillimeter cyclotron reson. at low electron density 79—60925
n-Si, inverted MOSFET surface, evidence for Lande factor g=2, finite valley splitting 80—6989
Si, laser annealed, EPR and cyclotron resonance 80—34773
Si, obs. of cyclotron reson. absorptions due to excitonic ion and excitonic mol. ion 77—73082
Si, quantum cyclotron reson. linewidth 77—15752
Si, stressed, at high mag. field, submillimeter cyclotron res. of electrons 77—81012
Si surface space charge layers, cyclotron reson. of holes 77—76932
n- Si, surface space-charge layer, intersubband-cyclotron combined reson. 78—68063
Si(III) inversion layers, CDW induced cyclotron reson. harmonics 78—64085
Si(100) inversion layers, effects of uniaxial stress on cyclotron reson. 80—20322
Te (11̄00) surface, electron-hole cyclotron resonance freq. depend. 79—69724
Te cyclotron resonance, transport and surface phenomena 77—40132
Te, dislocation density and config. effects on cyclotron reson. absorpt. 79—78526
Te, holes, with B⊥c 78—10777
Te, IR cyclotron reson. in field up to 200 T 77—52059
Te, in pulsed high mag. fields, cond. band struct. 80—59867
Te inversion layers in mag. fields 80—44690
Te, photo-excited carriers, far IR magneto-spectroscopy 80—50343
Te, surface cyclotron resonance, freq. depend. 78—64084
Te, uniaxially stressed, cyclotron resonance 79—87319
Te, uniaxially stressed, submm. cyclotron reson., deform. pots. and k.p coeffs. 80—54606
W, Doppler-shifted cyclotron reson. along nonprincipal cryst. directions *(Russian)* 79—4725
W, longwave dopplerons, nonlocal Hall effect, surface impedance, size effect *(Russian)* 80—80253
Zn, cyclotron mass and superconducting energy gap calc. as a function of Fermi surface position 79—69625
p-ZnTe, cyclotron resonance from photoexcited electrons 79—69723
ZnTe, spin flip scatt. of laser light 77—43976
ZnTe, spin flip scatt. of laser light 77—43977

cyclotrons
see also microtrons; synchrocyclotrons
4.2 GeV cyclotron kaon facility, parameters 77—54380
120-centimeter cyclotron, modernisation 80—99358
acceleration process and its influence on beam quality, theory 80—74051
accelerator complex for relativistic multicharged ions, Wideroe and cyclotron accelerator 79—54655
Alma Ata isochronous cyclotron, beam diagnostics, mag. field stabilising and resonator freq. control 79—54633
applications, radiation damage, radioisotope dating, and large-scale radioisotope prod. 79—54692
arc ion source, thyristor modulator 77—46438
Australian atmospheric contamination after 1974 French Pacific tests, cyclotron anal. by proton activation 79—57311
AVF, analytical theory of particle motion 79—54700
AVF cyclotron, central region, changes of puller shape, axial focusing 80—74050
AVF cyclotron, electromagnet 77—3198
AVF cyclotron, present and future *(Japanese)* 77—79487
AVF-cyclotron at Vrije Univ., timing expts., burst suppression 78—21793
axial cold cathode ion source, change time anal. 77—83392
beam automatic centring and matching 79—54708
beam bunch effects in the circular isochronous cyclotron 79—54716
beam buncher improvement at Univ. of Manitoba cyclotron 77—88308
beam diagnostic techniques, review 79—54731
beam emittance measurements with a dispersion-matched magnetic spectrograph 79—54732

cyclotrons continued
beam pulsing system for cyclotron beams 77—10514
beam transit phase automatic meas. 78—832
Berkeley, fast closing vac. valve for radioactive contamination protection 77—10501
Berkeley 88 inch cyclotron, systematics in the control settings, beam parameter prediction 78—78526
Bonn isochronous cyclotron, beam stabilisation and automatic energy variation 79—54705
Bonn isochronous cyclotron, external ion sources, inject lines, description 79—54675
booster accelerator for separated-sector cyclotron at Holifield heavy ion facility 77—83199
bunched beams, transport, second order aberrations 80—52801
Calcutta 224 cm variable energy cyclotron, initial operating experience and beam transport 79—54629
Calcutta variable energy cyclotron vacuum system design, testing.and commissioning 78—86707
cascade cyclotron magnet 77—83193
central position phase, definition and use 79—54714
Chalk River superconducting cyclotron 79—54657
Chalk River superconducting cyclotron project, injection system design 79—54615
Chalk River superconducting heavy-ion cyclotron RF struct. 77—88297
Chalk River supercondudting cyclotron, RF struct., commissioning status 79—54673
charge exchange losses during acceleration 79—54713
CNRS Orleans' isochronous cyclotron, beam lines, irradiation systems, current status 79—54637
collective ion acceleration by discrete cyclotron modes, computer simulation 77—83290
combined fixed freq. and freq. modulated cyclotron, mag. field design 79—54726
compact, applications *(Hungarian)* 78—74517
compact 103 cm and 60 cm cyclotrons, design models 79—54656
conference on cyclotrons and their appl., Bloomington, USA (Sept. 1978) 79—54626
coupling cct. for four resonators and one buncher 79—68052
cryopumps, selection criteria 79—54670
cyclotron corporation bus-oriented computer control system 79—54703
cyclotron magnet 1:6 model construction and operating experience 79—31261
Dee, bevelled, for beam centering in AVF cyclotron 80—63428
dee accelerating system, electric field calc., in presence of ion source and grounded frame 79—85844
dee voltage calibration using an intrinsic Ge X-ray detector 80—99359
Eastern Meson Facility, 580 MeV cyclotron, design concept and scientific justification 79—85839
economic aspects of appl., case study at Crocker Nuclear Lab. 79—54723
effective acceleration voltage calc. method using phase compression-expansion effect 79—54674
Eindhoven AVG cyclotron, on-line determ. of acceptances and emittances of beam guiding system 77—38515
electron acceleration in azimuthally varying electric field, isochronous uniform mag. field 77—50317
electron and positron depolarisation suppression in storage rings and cyclic accelerators 80—42882
electron beam intensity, synchrotron with cyclotron preaccel. 77—61642
electron cyclotron resonance ion source for CYCLONE, current status 79—54676
electrostatic inflector and extractor for cyclic accelerators, HV expts. 78—50421
energy boosters for electrostatic accelerators 78—33306
EUT (Eindhoven) cyclotron, multi-input phase measuring system 79—54689
extraction efficiency improvement through central region studies 79—54719
fast cyclotron beam emittance measuring device 79—54712
fast neutron facilities for radiobiological irrad. 80—109064
fast neutron prod. cross sections at Louvain la Neuve isochronous cyclotron 78—29682
fast neutron therapy history 79—20634
fast neutron therapy system using cyclotron beam, beam optics and shielding 79—57756
fast neutron therapy with medical cyclotron, clinical results 79—20643
fission fuel breeder target neutronics 79—81060
future needs of nuclear and meson physics 79—54722
GANIL, beam stripper interaction studies 79—54721
GANIL accelerator, construction, performance and capabilities in atomic physics *(French)* 80—14018
GANIL cyclotron resonator RF systems, main parameters 79—72118
GANIL heavy ion accelerator facility, status report on injector, magnets and RF system 79—54630
GANIL heavy ion beam tuning by secondary emission multiwire chamber 79—54733
GANIL separated sector cyclotron, injector design 79—54613
GANIL separated sector cyclotron, magnet description 79—54641
GANIL separated sector cyclotron, vacuum chamber description 79—54640
GANIL system, two separated sector cyclotrons, status report 78—55058
general orbit theory for accelerated particles in cyclotrons, appl. to synchrocyclotrons and omegatrons 80—74052
Grenoble separated sector booster cyclotron, SARA, current machine status 79—54634
Groningen 280 cm AVF cyclotron, radionuclide prod. for medical appl. 79—54696
Hamburg isochronous cyclotron, influence of phase or time struct. of internal beam on extraction conditions *(German)* 78—94155
Hamburg Isochronous Cyclotron, scatt. set-up for many particle correlation expts. 80—37711
harmonic beam interceptor, increased beam intensity 77—381
heavy element mass spectroscopy with the Berkeley 88-inch cyclotron 78—70217
heavy ion, current trends *(Hungarian)* 80—57786
heavy ion accelerator magnet configuration and construction technology 79—31264
heavy ion facility at Dubria 80—37662
heavy ion isochronous cyclotron, synergic focusing of football coil 77—83364

cyclotrons continued
heavy ion low and medium energy accelerators, recent design advances 79–67984
heavy ion national accelerator Ganil, principle and expected performances *(French)* 79–696
heavy ion research with cyclotrons, appl. to ^{208}Pb(^{16}O,^{15}N)^{209}Bi 79–54447
heavy-ion, collective accelerator as ion source and injector 79–54618
heavy-ion accelerators, book contrib., review 78–90003
heavy-ion beam intensity enhancement using support gas in ion source 77–34490
heavy-ion superconducting cyclotron at Chalk River, status 77–83192
HMI (Berlin) cyclotron, multi-input phase measuring system 79–54689
Holifield Heavy Ion Research Facility, new isochronous cyclotron 79–68015
Holifield heavy ion research facility, phase II cyclotron booster status 79–54660
Hungarian cyclotron investment project *(Hungarian)* 79–81104
Indiana Univ. Cyclotron Facility, status report 79–54644
INS 176 cm sector focusing cyclotron, present status, PIG ion source 79–54648
ion beam in IPCR cyclotron, turn separation and ν_z meas. *(Japanese)* 79–13566
ion source gas feed system 79–81112
IPCR proposed multipurpose separated sector cyclotron, LINAC booster 79–54662
IPCR separated sector cyclotron, injection 79–54614
irradiation facility of Stockholm 225 cm cyclotron 77–57781
isochronism studies at IUCF 79–54720
isochronous, 240 cm, at Kiev, development, design and construction 77–50318
isochronous, bunch phase behaviour, Monte Carlo simulation 77–54382
isochronous, future directions 79–54724
isochronous 150 cm cyclotron at I.V. Kurchatov Atomic Energy Institute, principal parameters 79–45488
isochronous cyclotron, energy variation, microcomputer control 79–13565
isochronous cyclotron mag. field automatic meas. system 78–82547
isochronous cyclotron sector magnet field calc., integral eqn. method 79–41053
isochronous meas. of phase angle variations of beam pulses by sampling technique *(German)* 78–74520
isochronous two stage ring cyclotron kaon factory 79–54728
IUCF, first year of operation, particle beams, energy resolution intensities, reliability 77–83273
IUCF 200 MeV cyclotron, isochronisation studies 79–72087
IUCF control system 79–54702
JINR U-400 isochronous heavy ion cyclotron, design features, parameters 77–83211
JULIC, beam phase detection with fixed intermediate frequency system 79–54711
JULIC beam quality improvement, beam phase optimisation 79–54653
Julich compact cyclotron, multi-purpose irradiation facility 77–57778
K=500 superconducting cyclotron, beam extraction system 79–54666
Karlsruhe cyclotron, computerised diagnostics, control and extended beam optimization 79–54709
Karlsruhe isochronous cyclotron, ECR type light ion source 79–68012
Karlsruhe isochronous cyclotron, routine prod. of ^{123}I 79–54694
Karlsruhe isochronous cyclotron, trim coil design 79–54654
Kiev 240 cm cyclotron facility, present status and accelerated beam characts. 79–54628
Kiev isochronous cyclotron, beam extraction and transportation 79–54717
Kiev isochronous cyclotron, diagnostics of beam phase characteristics 79–54718
Kurchatov Inst. cyclotron, heavy ion acceleration 79–54651
KVI cyclotron, dee voltage and beam RF phase stabilisation 79–54688
KVI cyclotron, status report 79–54650
LBL, MINUS3 general purpose data acquisition system 79–93901
LBL 88 inch cyclotron, high charge state heavy ion source, recent developments 79–54677
LBL 88 inch cyclotrons, cryogenic pumping system 79–54681
Leuven isotope separator on-line at CYCLONE cyclotron 78–70682
Louvain-la-Neuve ECR heavy source 79–72116
machine criteria for treatment of cancer patients 79–54691
magnetic analyser for compact cyclotron 78–66439
magnetic field calcs. for proposed supercond. machine at Milan 77–83200
magnetic fields, one parameter function representation 80–18725
Manitoba Univ. cyclotron, 20 to 50 MeV H^-, injection system, status report on upgrading 79–54646
Manitoba Univ. cyclotron, ^{123}I and ^{84}Rb prod. using ^{124}Te(p,2n) and ^{84}Kr(p,n) 79–54695
maser, high-current and plasma filled, theory 78–17890
mass analysis, high-energy, appl. to chem. anal., radioactive dating, and quark detection *(Czech)* 78–86375
medical, autmoatic radioisotope prod. devices 80–12260
medical accelerators, production of radionuclides and radiopharmaceuticals using proton and deuteron accelerators 79–53240
medical application of a compact cyclotron, isotope production *(Japanese)* 80–104757
medical cyclotron for radioisotope and labelled compound prod. 79–53245
medical cyclotrons for fast neutron radiotherapy and radioisotope prod. 79–53244
medical cyclotrons for radionuclide prod. 79–53238
medical ion accelerator, cyclotron and synchrotron design studies 79–54661
medical radioisotope yields 79–57776
Michigan State Univ. 500 MeV supercond. cyclotron, progress report 79–68011
Michigan State University superconducting cyclotron programme 79–54658
Milan superconducting 1:6 model magnet, mag. field meas. 79–54669
Milan superconducting cyclotron, RF cavity model study 79–54682
Milan superconducting cyclotron project, model studies and project status 79–54659
minicomputer data acquisition system for Princeton cyclotron facility 78–90048
Moscow University, 120 cm cyclotron modernisation 80–42881
MSU, 50 MeV cyclotron, computer control 79–54704

cyclotrons continued
MSU 500 MeV superconducting cyclotron, central region design 79–54667
MSU 500 MeV superconducting cyclotron, mag. field meas. 79–54668
MSU K=800 superconducting cyclotron, design characteristics 79–54664
MSU K=800 superconducting cyclotron, injection studies 79–54616
MSU superconducting cyclotron cryogenic system, operating experience 79–54672
multichannel nanosecond pulse generator for cyclotron stroboscopic system 79–68168
multipass beam breakup, depend. on accel. parameters 79–68017
MUSL-2, 6-pass microtron using superconducting linac, operating experience 79–72042
NAC, proposed transfer beamline preliminary design 79–72061
neutron beam production, energy spectra and dose distrib. spectra 77–70554
neutron detection and neutron reaction cross-sections, Van de Graaff generator and cyclotron facility 80–47805
neutron experiments, Braunschweig accelerator facility, data acquisition and anal. 80–47806
neutron radiation therapy, cyclotron biological intercomparisons 79–20589
neutron radiotherapeutic source developments at Cyclotron Corporation 79–20651
neutron shutter for cyclotron facility 78–21794
neutron spectra at 0° from 83.7 MeV deuterons and 100.2 MeV protons on Be 77–73593
neutron-neutron quasifree scatt. studies 77–34525
NIRS-CHIBA isochronous cyclotron facility, status report 79–54649
omegatron, characts. dependences *(Czech)* 79–41049
open sector injector cyclotron, for SIN 600 MeV ring accelerator, design of RF system 79–54685
orbit parameters in AVF cyclotrons with large field modulation, analytical expressions 77–6582
ORIC, heavy ion source support gas mixing expts. 77–83391
ORIC, Holifield Heavy Ion Research Facility, current status 79–45485
ORIC, radioactive nuclei acceleration 77–10502
ORIC, remapping of mag. field, meas. system 77–83221
ORIC mag. field meas. study implementation 79–68036
ORIC RF system, preparation by HHIRF 77–88300
Osaka RCNP 230 cm cyclotron, recent development and proposal for new ring accelerator 79–54632
Oslo, possible uses *(Norwegian)* 79–49881
Oslo University, 35 MeV, nuclear physics prospects *(Norwegian)* 79–31249
parametric resonance of betatron oscills., space charge influence 77–67923
particle generalised coordinate variations on crossing the gap *(French)* 80–37657
particle motion in cyclotron near reson., nonlinear behaviour *(Chinese)* 79–63828
pion radiotherapy facility at TRIUMF, dosimetry and radiobiology 77–70526
Polarised beam from the University of Manitoba spiral ridge cyclotron 78–70660
polarised proton 200 nA variable energy beam, TRIUMF 79–63848
power supplies, motor generator current control and stabilisation, semicond. device appl. 78–21790
preacceleration for 50 MeV electron synchrotron, VUV source 77–61641
precession injection cyclotron, high quality beams 79–54617
precession injection with new mag. config. in central region 77–10497
Princeton cyclotron data acquisition system 79–89528
Princeton Cyclotron data acquisition system 80–102415
proton beam burst width and phase drift at the Indiana University cyclotron facility 79–76216
proton beam heavy ion source, injector for cyclotrons, feasibility study 79–54730
proton cyclotron targets for prod. of e^+-emitting radionuclides for medical appl. 79–53241
PTB, emittance measuring instrumentation, program for phase ellipse area *(German)* 78–58512
pulse selection and shortening system for cyclotrons 79–54690
pulsed ion source, C, N, O and Ne ions, production and acceleration in cyclotron *(Japanese)* 78–5084
radial betatron oscillations, simulation of integral resonance motion *(Russian)* 77–10506
radioisotope dating using cyclotron as mass spectrometer 77–64489
radioisotope dating with cyclotrons 79–34990
radioisotope production for medical appl. 80–51256
radioisotope production for medical diagnostics 80–51255
radioisotope production in cyclotron for diagnostic medical research appls. *(French)* 78–48895
radionuclide production, UC-Davis program 80–51257
radiopharmaceuticals, cyclotron prod. for nuclear medicine appls. 77–44753
RCNP AVF cyclotron, outline of RF system and latest developments 79–54686
RCNP intermediate energy accelerator complex, design study 79–68013
relativistic isochronous cyclotron, possibility of betatron freq. confinement 79–85840
remotely controlled target transport system for cyclotron irradiations 80–69005
RF systems for cyclotrons, brief history 79–54671
S.African National Accelerator Centre, accessory design, current status 79–54631
secondary emission monitors at the Bevatron-BEVALAC 79–72186
sector focused cyclotron at neutron scatt. facility in 20-40 MeV range 77–26888
separated sector cyclotron, design of vacuum chamber for magnets 79–54639
separated sector cyclotrons, chromatic correlations at injection and ejection 79–72110
separated sector ring cyclotron intermediate energy particle accelerator, proposed design 79–54663
separated sector type, model magnet *(Japanese)* 80–874
separated-sector cyclotron, mag. field meas. processing methods 79–68037
separated-sector cyclotron multidisciplinary facility 77–83196
SIN, πE3 channel, cloud and surface muon studies 80–74055

cyclotrons continued
- SIN, pion beam line πE3 modifications 80−74054
- SIN 590 MeV ring cyclotron, recent and future developments 79−54642
- SIN 590 MeV ring cyclotron, RF system for flattop acceleration struct. 79−54683
- SIN 590 MeV ring cyclotron, setting up for single turn extraction 79−54707
- SIN 600 MeV cyclotron, therapy controllers for patient irradiation by pions 79−57754
- SIN πE3 channel, pion prod. meas. 80−74056
- SIN accelerator facility 79−85836
- SIN accelerator system, operation and new projects 80−74053
- SIN accelerators, operational experience and improvement programs 77−83284
- SIN high current injector cyclotron, Cockcroft Walton 860 keV preaccelerator 79−67975
- SIN injector cyclotron, design of central region including ion source 77−54379
- SIN injector cyclotron, RF system improvements 78−90005
- SIN meson factory, computer control strategies 79−54701
- SIN meson factory, facilities and expts. 78−13360
- SIN S90 MeV cyclotron, μsec pulsed beam system, high voltage trapezoidal wave form generation 79−54684
- single turn extraction for large phase width 79−54715
- small, applications *(Hungarian)* 78−70656
- split-pole isochronous cyclotron, SPC-120 78−17451
- SSC, energy spread without flat-topping 79−54698
- Stanford superconducting recyclotron, operation and performance of machine 79−72065
- superconducting, spiral electric gap effects on ion orbits, computer program calc. 80−52795
- superconducting, trim coil power requirement minimisation method 79−54665
- superconducting cyclotron in Milan, beam extraction studies 77−83361
- superconducting cyclotron in Milan, injection studies 77−83195
- superconducting cyclotron model magnet 77−83194
- superconducting cyclotron neutron source for radiotherapy 79−20655
- superconducting heavy ion cyclotron, Chalk River, movable steel trim rods, orbit dynamics 77−83267
- superconducting heavy ion cyclotron, proposed for Chalk River, mag. field related mech. tolerances 78−58511
- superconducting heavy-ion cyclotron at Chalk River, extraction system, design 77−83266
- superconducting recyclotron, operation and performance 80−23199
- superconducting recyclotron for 130 MeV electrons, proposed design 80−23198
- SUSE, supercond. sector cyclotron for Munich Tandem Lab. 79−68014
- synchrocyclotron, Orsay, experimental programs and results *(French)* 80−78464
- Texas A&M 88-inch cyclotron, heavy ion source 79−54680
- Texas A&M cyclotron, electron beam ion source, development report 79−54678
- Texas A&M polarised proton beam meas. 80−102360
- therapeutic proton and heavy ion source capabilities 79−20629
- Tohoku Univ. 680 model cyclotron facility, emittance meas. and energy resolution 79−54638
- TRIUMF, 500 MeV, 100 μA isotope production facility 80−68985
- TRIUMF, beam gap RF impedance calc. 79−68047
- TRIUMF, beam props. improvements 77−83397
- TRIUMF, improved beam quality 79−72060
- TRIUMF, variable energy polarised proton beam 79−72059
- TRIUMF 100 μA beam, achievement and control 79−54699
- TRIUMF biomedical negative pion beam line, tuning 78−96113
- TRIUMF Canadian cyclotron 78−13361
- TRIUMF cyclotron, meas. and corrections to beam props. 79−54710
- TRIUMF developments and projects, meson facilities 77−83291
- TRIUMF facilities and kaon factory designs 79−85837
- TRIUMF isochronous cyclotron, recent developments and thermal neutron facility 79−54643
- TRIUMF meson factory, basic and applied research 78−21792
- TRIUMF meson factory, preliminary research results on few body problems 77−18721
- ultra-compact AVF cyclotron, harmonic acceleration *(Japanese)* 77−61640
- vacuum chamber pumping system automatic control *(Japanese)* 79−85842
- variable energy, of Frederic Joliot Hospital Service, radioisotope production *(French)* 77−65361
- variable energy, shielding calcs., concrete and earth shield design 77−61622
- Variable Energy Cyclotron, Calcutta, design and operation 80−27841
- variable energy cyclotron at Calcutta 77−18720
- variable energy cyclotron at Calcutta 78−74518
- variable energy cyclotron at Chandigarh 77−23324
- VICKSI 6 MV Van de Graaff and split pole cyclotron, present status 79−67987
- VICKSI accelerator, computer aided control system 79−54697
- VICKSI beam line instrumentation and control system 77−83401
- VICKSI computer control system, operating experience 79−72215
- VICKSI cyclotron, automatic isochronisation and computer aided centering 79−54706
- VICKSI cyclotron, methods and results of RF system stability meas. 79−54687
- VICKSI cyclotron, RF system, design, operation 77−83300
- VICKSI facility, running in period and initial operating experience 79−54627
- π factories, multidisciplinary role 78−21791
- π production and properties, SIN and TRIUPF cyclotrons *(French)* 80−63417
- ^{14}C beam prod. from natural sample, radioactive dating 79−25352
- ^{14}C dating of CO_2 sample with accelerator, blind meas. 79−25362
- ^{14}C dating technique using cyclotrons, or Van de Graaff as mass spectrometer 80−5414
- D gas target with compact medical cyclotron, dosimetry of neutron field [illegible]73592
- ^{4}He liquid target with remote handling for TRIUMF cyclotron 78−25364
- Li(p,n) Be source of fast neutrons for small cyclotrons, neutron therapy appl. 79−57755
- Mo, activation in cyclotron by p, d, α, ^{3}He 79−30839

cyclotrons continued
- ^{13}N cpds., for environmental and biological research, cyclotron prod. 78−82551
- ^{13}N prod. by accelerators for nitrosourea-^{13}N prep. 79−53242
- W, activation in cyclotron by p, d, α, ^{3}He 79−30839

Czochralski method *see crystal growth from melt*

D-layer *see D-region*

D mesons
- $^1D_2$ level, charmonium model with relativistic corrections calcs. 79−13124
- anomalous Cabibbo suppressed decay ratios, simple model 80−42452
- asymptotic symm. for charmed mesons, new duality 78−21348
- axial vector mesons, three body decays, rel. between D(1285) and $A_1(J^P=1^{++})$ 78−78176
- beam dump neutrino experiments, promp neutrino meas. 79−63537
- Cabibbo angle universality and association with K, π and D meson mass 79−12974
- Cabibbo suppressed hadronic decays, Cabibbo universality fake violation, RH currents 80−73699
- Cabibbo-suppressed nonleptonic D decays, $\Delta I=1/2$ rule 80−52501
- charm meson mass spectra, electromagnetic interactions effect 80−47293
- charm particle nonleptonic weak decays, pole dominance model 79−63475
- charmed meson decay, simple symm. breaking 78−21418
- charmed meson prod. from ψ(4.0 to 4.5 GeV) decay 79−17719
- charmed meson spectra from effective quark-quark interaction, D^0 mass 79−36018
- charmonium narrow states, hadronic and EM decays 78−70343
- chromomagnetic and electromagnetic hyperfine interaction, charm meson spectrum 78−12879
- decay, charged Higgs boson couplings 80−62917
- decay, current algebra approach, symmetry-breaking Hamiltonian, chiral $SU(3)\times SU(3)$ or $SU(4)\times SU(4)$ 80−68450
- decay, hadronic, role of free-quark pairs 80−78059
- decay, hadronic, six-quark model, quark-mass dependence, final state interactions, mixing angle effects 80−62973
- decay, semileptonic and leptonic modes, electron momentum spectrum 78−8657
- decay, SU_4 20-plet dominance model, inclusive branching ratios 80−13299
- decay at ψ(3772), inclusive props. 78−93876
- decay constants from Weinberg type sum rules 79−54336
- decay CP violation effects, predictions of six-quark model *(Russian)* 79−93379
- discovery, review of exptl. results and theoretical advances *(German)* 78−66184
- EM mass difference using simple quark model, quark mass difference 77−71516
- EM mass differences, one gluon exchange contrib. 79−3024
- EM mass differences, quark behaviour 79−58941
- EM mass splittings, Born-term contribs. 78−78181
- EM properties of charmed hadrons, $SU_6\times U_c$ calcs., mag. moments, mass differences 78−70368
- e.m. props. of charmed mesons 78−8668
- exotic mesons and $p\text{-}\bar{p}(e^+\text{-}e^-)$ annihilation 78−21393
- hadron, fragmentation from heavy quark partons 78−8603
- hadron collisions, D-meson emission, two-gluon charm form. *(Russian)* 77−71489
- hadronic collisions, production of D- and ψ-mesons, QCD calc. *(Russian)* 79−9348
- hadronic decay, dD^0, D^+ branching ratios 78−45913
- hadronic decay and evidence for $(\bar{c}s)_R$ current 78−58167
- hadronic decays of charmed D meson, MIT bag model calcs. 78−82207
- heavy hadronic meson theory, gauge theoretic formulation of $SU_2\times U_1$ model, D-meson mass limit 78−70316
- heavy quark system prod. in QCD, duality predictions 79−13074
- intermultiplet mixing in nonperturbative approach to broken SU(4) 77−74653
- mass and mean life from high energy cosmic ray data *(Chinese)* 80−102045
- mass formulae and mixing in SU(8) and $SU_W(8)$ symmetries *(Russian)* 78−66097
- mass formulae in broken $SU(8)_w$ symmetry 78−37191
- mass spectrum, broken chiral $SU(4)\times SU(4)$ symmetry 79−93312
- masses, duality predictions 78−8619
- masses and leptonic decay consts. 78−66087
- masses of new mesons and effects of the fifth flavour 78−66098
- nonleptonic decay, matrix element computation and iteration 79−384
- nonleptonic decay rates and branching ratios, lifetimes 80−102047
- nonleptonic decays, uniformly populated Dalitz plot, soft π theorem appl. 80−52503
- nonleptonic decays of charmed mesons and chiral Lagrangians *(Russian)* 79−30732
- overlapping resonances with variable channel struct., ψ prod. 79−22118
- parity violating nonleptonic decays, vector meson dominance model 80−78058
- proton interactions, beam dump expt. at CERN SPS 78−45979
- quark fragmentation function for new particle ν-production 77−87968
- semi-leptonic decay, current algebra treatment, rel. to charmed current quark mass 79−97577
- semileptonic branching ratio and lifetime from $e^+e^-\to e^\pm X$ 80−4983
- semileptonic branching ratio at ψ''(3770) in $e^+e^-\to$hadrons 78−45934
- semileptonic decay, effective chiral Lagrangian method 78−74254
- semileptonic decay const., D and F decay const. ratio determ. 78−62392
- semileptonic decays, K-e correl. anal. 78−78179
- SPEAR data on narrow reson. at 1865 MeV/c^2 *(German)* 77−79294
- spin anal. in e^+e^- annihilation near 4.03 GeV 77−74697
- spin tests for charmed mesons produced in e^+e^- annihilation at $\sqrt{s}=4.028$ GeV 78−74269
- structure of hadrons containing heavy quark, MIT bag model 80−86672
- SU(3) rules for non- and semi-leptonic weak decays 78−45916
- two body nonleptonic decays, quark model predictions 80−9164
- two-body hadronic decays, six-quark model mixing angle constraints 79−97618
- two-step pot. model 77−74682
- valance quark distribs. in π, K, D, Regge trajectories, SU(3), SU(4) breaking 79−30703
- weak decay constant deduces from $D\to Kl\nu$ 79−93407
- weak selection rules in e^+e^- annihilation and ν scatt. 78−8679
- $B^-\to D^-X(F^-X)$, W-exchange dominance, decay rates 80−86706

D mesons continued
D, D*, Schwinger phenomenological and dyon description 78–82109
D(1285) from $\bar{p}p \to K\bar{K}\pi\pi\pi$, 700-760 MeV/c, spin-parity assignment, dominant decay mode 78–54646
D(1285)$\to\delta(975)\pi$ D meson spin parity determ. 79–3052
D(1865), charmed meson semileptonic decays 78–4854
D(1865) charmed meson hadronic prod., cross section limits from pN 79–89211
D(1865)$\to e\nu K^*(890)$, right handed current, eK* ang. correl., energy spectra 78–74248
D(1.87) isomultiplet, mass differences, effect of EM mixing on mass splitting *(Russian)* 78–89714
D(1.87) leptonic decay branching and $pp\to e^{\pm}\mu^{\mp}X$ upper limits 77–65186
D and D* production near 4 GeV in e^+e^- 77–82754
D charm decay, 20-dominance model validity from QCD 79–71747
$D\to e^-$ branching ratio from e^+e^- annihilation multiprong data 78–78200
$D\to e+X$, anomalous electron prod. from D meson decay at $\psi(3772)$ 78–37203
$D\to\eta\pi\pi$, D meson spin parity determ. by partial wave analysis 79–3052
$D\to K^-\pi\pi$, branching ratios, isospin anal. 78–70363
$D\to K\bar{K}\pi$, D meson spin parity determ. 79–3052
$D\to\bar{K}+l^++\nu$, semileptonic decay of charmed particles, formalism using helicity amplitudes 78–4852
$D\to K^*l\nu$, A(c,s) vector current 77–87976
$D\to K^*\mu\nu$, in e^+e^- annihilation, T-odd asymmetry in CP violation model *(Russian)* 80–105885
$D\to Kl\nu$, $K^*l\nu$, lepton spectrum anal. 78–4855
$D\to\bar{K}\pi$, branching ratios, charged and neutral D-meson lifetimes 78–62396
$D\to K\pi$, effective Hamiltonian in Kobayashi-Maskawa model 80–105887
$D\to K\pi$ and semileptonic decay in massive quark model 79–93376
$D\to\bar{K}\pi(\bar{K}\pi\pi)$, nonleptonic decay rates, quark diagrams and pole approx. 80–86707
$D\to K\pi(\pi)$, current algebra relations and dual model amplitudes 80–82969
$D\to K\pi l\nu$, charm-changing weak hadronic current, models 80–57585
$D\to K\pi l\nu$, current algebra calcs., form factors and decay distribs. 80–42447
D meson production in e^+e^- annihilation, c quark fragmentation function *(Russian)* 79–85312
$D\to\nu eK(K^*)$ at $\psi''(3770)$ from e^+e^- interaction 78–89693
$D\to\pi\pi\pi$, S_3 permutation group approach, charm model test 79–17723
$D^-\to\tau^-\bar{\nu}_\tau$, charmed mesons, heavy lepton decays, ν_τ neutrino mass depend. *(Russian)* 78–62394
D^0, $\bar{D}^0$, decays, charm changing neutral current limits, QCD depend., mass differences 80–32062
D^0, lifetime difference from D^+ 80–91084
D^0,D^+ decays, gluon enhancements in charmed-meson decays 80–95265
$D^0(1863)$, lifetime estimates, free quark model anal. 79–67544
$D^0(1865)$ prod. anal. *(Chinese)* 78–487
$D^0(1865)$ prod. from neutron interactions at 300 GeV/c 78–37244
$D^0(1.865)$ production in proton-nucleus collisions at 400 GeV/c 78–13099
D^0 and D^+, 3.772 GeV, mass and decay branching ratios 78–78199
$D^0(\bar{D}^0)$ high energy photoprod. in zero total visible strangeness events, cross section 79–80831
D^0 decay enhancement mechanism, quark diagram with gluon prod. 80–105891
D^0 hadronic decay modes, W boson exchange model clean test 80–57592
$D^0\to K^-K^+$, Cabibbo suppressed decay obs., partial decay widths 79–89149
$D^0\to K^-e^+\nu_e$ right handed currents 78–8662
$D^0\to K^-p^+$ signals, evidence for$(\bar{c}s)_R$ current 79–71745
$D^0\to K^-\pi^+$, Cabibbo suppressed decay compatibility with weak interaction mixing angles, branching ratios 79–97620
$D^0\to K^-\pi^+$, quark total number conservation, D^+ lifetime longer than D^0 80–57590
$D^0\to K^-\pi^+(K^-K^+)(\pi^-\pi^+)$, charmed meson nonleptonic decays and weak interaction mixing angles 79–85294
$D^0\to K^-\pi^+\pi^-$, obs. in 3.77 GeV e^+e^- annihilation 78–37206
$D^0\to K^-\pi^+\pi^0$, nonleptonic charm decay, branching ratio 78–70364
$D^0\to K^-\rho^+$ strong signal, $(\bar{c}s)_R$ current implications 79–36070
$D^0\to\bar{K}^0\pi^0$, branching ratio from final state soft gluon exchange 80–52498
$D^0\to\bar{K}^0\pi^0$, $\Delta T=1$ constraints and final state interactions 80–95267
$D^0\to\bar{K}^0\pi^0$, quark total number conservation, D^+ lifetime longer than D^0 80–57590
$D^0\to\bar{K}^0\pi^0(K^-\pi^+)$, weak interaction effects, $K\pi$ scatt. phase shifts 80–57591
$D^0\to\bar{K}^0\pi^0(\pi^+\pi^-)(K^+K^-)$, phenomenological model for inclusive and exclusive decays 80–99098
$D^0\to K^0\pi^+\pi^-$, prod. and decay from νN interaction 78–89700
$D^0\to K^+K^-$, Cabibbo suppressed decays, Penguin diagram contribution, mixing angles 80–22604
$D^0\to K^+K^-$, $\pi^+\pi^-$, branching ratio, $\Delta I={}^1/_2$ rule violation, colour radius interactions calc. 79–93412
$D^0\to K^{*-}\pi^+(K^-\pi^+)$, heavy quark weak isospin, constraints from nonleptonic transitions 79–85257
$D^0\to\bar{K}^*\pi^-$ signals, evidence for$(\bar{c}s)_R$ current 79–71745
D^0 lifetime from ν and $\bar{\nu}$ interactions 80–105890
D^0 nonleptonic decay, quark annihilation hypothesis test 80–102044
D^0 nonleptonic exclusive and semi-inclusive decays, pole model test 80–37258
$\bar{D}^0$ prod. and decay in high energy photon interaction, mass and decay time 80–42478
$D^0\to\pi^+\pi^-$, Cabibbo suppressed decay obs., partial decay widths 79–89149
$D^0\to\pi^+\pi^-$, Cabibbo suppressed decays, Penguin diagram contribution, mixing angles 80–22604
$D^0\to\pi^+\pi^-$ 79–97620
D^0-$\bar{D}^0$ mixing, flavour-changing Higgs bosons 80–62915
D^0-$\bar{D}^0$ mixing, neutral charm suppression 80–22553
D^+, D^0, weak nonleptonic decays, SU(3) symmetry and quark diagrams *(Russian)* 79–93411
D^+, D^0 nonleptonic decays, vectorial colour octet $q\bar{q}$ annihilation 80–52500
$D^+(1867)$, lifetime estimates, free quark model anal. 79–67544

D mesons continued
D^+ D^0 mass difference, quantitative meas. in chiral $SU(4)\times SU(4)$ model 79–93311
D^+ decay, Cabibbo suppression, strong 20-plet dominance and W exchange 80–42453
$D^+\to K_S\pi^+$ right handed currents 78–8662
$D^+\to\bar{K}^0\pi^+$, quark total number conservation, D^+ lifetime longer than D^0 80–57590
$D^+\to\pi^+\pi^+K^-$, contradiction in uniformly populated Dalitz plot 79–17724
D^+-D^0, Coulomb and tadpole contributions to EM mass differences 78–89713
D^+-D^0 mass difference, broken isospin symmetry in chiral $SU(4)\otimes SU(4)$ 78–89691
D^+-D^0 mass difference, form factors, SU(4) coupling, vector meson dominance model 79–391
D^+-D^0 mass differences, chiral $SU(4)\times SU(4)$ model, broken isospin symm. 77–87917
D^+-D^0 mass splitting and and forbidden decays $\psi'\to\eta\psi$, $\psi'\to\pi^0\psi$ 78–66114
$D^{\pm}$, weak decay constant from bag model extension 80–62967
$D^{\pm}(1870)\to\Lambda(K^0)+$hadrons, charm prod. cross section upper bounds *(Russian)* 78–89711
$D^{\pm}$ nonleptonic and semileptonic decays, isospin selection rule tests 80–73700
D^0,D^+, SU(3) predictions for decay using new weak mixing angles 79–97619
$D^0-D^{\pm}$ lifetime difference, possible mechanism $D^0\to s+\bar{d}+$gluon 80–37255
${}^3D_1$-charmonium decay into $e\bar{e}$ and relativistic effects of constituent quarks 79–3017
D*, pion and photon couplings, SU(4) violations, decay rates calc. 78–45914
D*(2.01) isomultiplet, mass differences, effect of EM mixing on mass splitting *(Russian)* 78–89714
D* widths, using finite energy sum rules for pion and photon couplings 77–67649
D*-D, F*-F, pseudoscalar-vector mass differences, QCD nonrelativistic quark model 79–6339
D^{*-} production in πN reactions at 10.5 GeV/c, near threshold 78–37249
D^{*+}, photoprod., D^0 mass difference 80–73720
D^{*+}-D^{*0}, QCD relation between EM mass differences 79–71750
D**, charmed tensor meson, strong and EM decay modes 80–68451
$D^*\bar{D}^*$ bound state, isospin mixing 78–41613
$\bar{D}^*D^*$ prod. in e^+e^- annihilation decoupling of higher vector mesons 77–87986
$D\bar{D}$, $D\bar{D}^*$, $D^*\bar{D}^*$, charm molecules, dynamical model, light meson exchange 80–57572
$D\bar{D}$ molecular charmonium from dual diagram and Schrodinger eqn. 80–86660
$D\bar{D}$ production in large p_T hadronic collisions, $e\mu$ and eK correlation study 79–40772
$D\bar{D}$ system, bound states near charm threshold 78–45857
D^+D^0 decays and lifetimes assuming sextet dominance and colour clustering 80–32094
d^+e^- annihilation, single inclusive lepton spectra 77–65161
D_tO^*, $D_t{}^{+*}$, weak decay modes, annihilation contribs. 79–93410
e^-e^+ annihilation, >2 GeV, production of charmed particles and charged τ lepton, review 78–17006
e^+e^- annihilation, 3.6-5.8 GeV, inclusive D and K meson prod. cross sections 79–93439
e^+e^- annihilation, CP violating effects, D^0, G^0 and H^0 meson decays 79–80769
e^+e^- annihilation, D and D* prod., form factors, and free quark model 78–37222
e^+e^- annihilation, quark model 78–8680
e^+e^- annihilation at 4.03, 4.41 c.m. energy, D-meson prod. and decay 77–87989
e^+e^- annihilation experiment review, ψ spectroscopy and charmed particles D and F 79–49533
$e^+e^-\to D^0$, SPEAR expt. results 79–93444
$e^+e^-\to D^+$, SPEAR expt. results 79–93444
$e^+e^-\to\bar{D}D$, above charm threshold at energy corresponding to $\psi''(3770)$ 80–73723
$e^+e^-\to D+$anything, 7 GeV, inclusive momentum and energy spectra 79–75780
e^+e^- inclusive hadron prod., polarisation and p nonconservation asymmetries, π, $K^{\pm}$, $D^{\pm}$ prod. 80–78084
$e^+e^-\to$quarkonium state, D,F, Υ mesons, importance as experimental tool in new particle searches 80–42425
γp, 40-70 GeV, inclusive $\bar{D}^0$ photoprod. cross sections, pair and associated prod. 80–91097
$K^-p\to\Lambda D$, 4.2 GeV/c, D(1285) prod. and decay props. 79–49517
μN deep inelastic scatt., D-meson muon progenitor 78–62407
ν production, prompt sources, and axion decays and interactions, pN beam-dump experiment 80–63028
ν production of charmed D mesons and $D^0\to K_S{}^0\pi^+\pi^-$ 78–70354
$\nu_\mu(\bar{\nu}_\mu)$N, multi muon events, associative charm generation mechanism, D, $\bar{D}$ mesons *(Russian)* 79–89145
νN, high energy, dilepton events, D meson semileptonic decay 80–42446
$\nu N\to\mu\mu X$, dimuon events, D prod., lifetime and fragmentation function 79–93397
$\nu p\to\mu^-pD^{*+}$, $D^0(1863)$ and inclusive D^{*+} (2009) prod., mass difference 79–93396
pN interactions, 400 GeV, D-prod., muon polarisation meas. 78–70413
pp, D, B, K prod., QCD model for heavy flavour prod., two gluon annihilation 80–86744
pp, ISR energies, p fragmentation, D^+ prod. from $\Lambda_c{}^*$ and Λ_b decay 80–102080
$\bar{p}p$ 12 GeV/c search for D, D* and λ_c charmed particles, charmed pair prod. 79–426
$pp\to$charm particles, 400 GeV, evidence for prompt single muon prod. 79–63536
$pp\to D\bar{D}$ cross sections, Monte Carlo anal., particle lifetime for detection in emulsion 78–82229
$pp\to D\bar{D}X$, 53, 63 GeV, inclusive prod. cross section anal. 79–54368
$pp\to D\bar{D}+X$, upper limit for $D\bar{D}$ prod. at 55 GeV 78–89758
pp interactions, charmed D^+ prod., total cross section, $D^+\to K^{*0}\pi^+$ observation 79–36102

D mesons continued

- $pp \to \mu^{\pm} e^{\mp} + X$, possible charmed meson pair prod., $D\bar{D}$ cross section 78−89751
- $pp \to \psi D\bar{D}X$, prod. suppression and OZI rule 77−65185
- π-Be, associative production of D^0 mesons, with muons 55 GeV/c *(Russian)* 79−3060
- $\pi^{\mp}U$ interaction at 55 GeV/c, search for long lived heavy mesons *(Russian)* 80−5029
- $\pi^- Be \to D^0\bar{D}^0X$, pair production at 55 GeV/c *(Russian)* 79−3059
- $\pi^- p$, 340 GeV, associated charm prod. evidence, $D^{\pm}$ prod. 80−86767
- $\pi^- p$, 70 GeV/c, directly produced electrons from charmed D particle decay, cross sections 80−73755
- $\pi^- p \to \eta\pi^+\pi^- n$, axial vector and pseudoscalar resonances near 1.275 GeV, D mesons 79−30747
- $\pi^- p \to K^- K^+ \pi^0 n$, D, E, and δ mesons, obs. at 12 and 15 GeV/c 79−9410
- $\pi^- p \to K^- K^+ \pi^0 n$, D, E, and δ mesons obs. at 12 and 15 GeV/c 79−3052
- $\pi^- p \to \pi^+\pi^+\pi^-\pi^- n$, D, E, and δ mesons obs. at 12 and 15 GeV/c 79−3052
- $\pi^+ p \to \bar{D}^0 C_1^{++}$, 4.5 GeV, prod. cross sections, decay branching ratios 78−41576
- $\psi(3772) \to D\bar{D}$, $D^{0,7}$ masses, branching fractions 78−17009
- $\psi(4.03) \to D\bar{D}(D^*\bar{D}, D\bar{D}^*, D^*\bar{D}^*)$, vector state strong decay 80−78057
- $\psi(4.414)$, width anal. in quark model 78−17010
- $\psi'''(4.42) \to D\bar{D}$, decay suppression, pseudo-dimension selection rule 80−9163
- $\psi''(4.028) \to D\bar{D}$, or $\bar{D}D^* + \bar{D}D^*$ or $D^*\bar{D}D^*$, strong decay theory, radial excitation of charmonium 78−12909
- Cu+p, 400 GeV, dimuon and trimuon prod., prompt ν source, $D\bar{D}$ prod., axions 78−89860
- $D \to K\pi l\nu$, hadronic current form factors, $(\check{c},s)$ weak current and symmetry props. 79−67545
- D^0, D^+ lifetimes, 6 dominance and W^+ exchange dominance 80−37254
- D^o, D^+ decay widths and branching ratios, quark recombination widths, free quark model 80−27500
- $D^0 \rightleftharpoons \bar{D}^0$, weak neutral current diagonality, mixing amplitude, multi-quark gauge model *(Russian)* 80−68414
- Fe+p, 400 GeV, missing energy associated with $\mu^+\mu^-$ prod. 80−22833
- pN, 350 GeV in Ne, $D^{\pm}$ prod. cross section and lifetime 80−68494
- $pp \to D^+X$, 53 GeV, $D^+ \to K^-\pi^+\pi^+$ *(Polish)* 80−9187

D-region

- absorption and forward-scatter radio-meteor data 79−75033
- auroral absorption event, lower ionosphere ion prod., density and comp. 80−36443
- auroral D-region, unusually strong partial refls. obs. during absorpt. event 78−36388
- baylike disturbance of mid-latit. D-region, energetic particles precip. 79−12333
- charged species relax. to photochem. equilib. within displaced air parcels 79−75030
- cluster ion formation, implications of laboratory determs. of NO^+ reaction rates 77−53308
- corpuscular radiation flux variations in daytime midlatit. mesosphere 77−29538
- D-region, negative ions effects on collision-dominated Thomson scattering 78−45118
- daytime D-region, characts. during polar cap absorpt. 77−37481
- daytime solar proton event-disturbed model 78−93038
- diffusion of weakly ionized multiconstituent plasma 78−57384
- diurnal tide meas., 80-100 km altitude, Arecibo radar obs. 77−2290
- drift velocity, by spaced fading obs. 80−41627
- electron conc. rocket meas., improved Faraday rotation expt. 77−9543
- electron concentration profiles, generalised exponential model 77−67005
- electron concentrations, diurnal vars. during storm after-effect 78−65451
- electron concs. above Arecibo 79−101014
- electron densities, diurnal, seasonal and solar cycle vars. 77−33267
- electron densities, low- and mid-latitude, derived from ground-based radio data, comparison 79−44302
- electron densities from inversion of differential absorpt. and phase integrals 77−45238
- electron density, intercomparison of groundbased techniques, wave interaction and partial reflection 77−45235
- electron density and composition, theoretical positive ion chemistry scheme 79−40007
- electron density and energy distrib., Langmuir probes appl. 77−82078
- electron density and recomb. coeff. profiles calc. rel. to absorpt. and rocket meas. 78−69559
- electron density at Saskatoon, Canada, time vars. compared with wind vars. 79−25389
- electron density distrib. at noon 77−53274
- electron density diurnal var. at midlatit., from VLF meas. 77−64520
- electron density during W.Europe 1975/6 winter anomaly 80−36440
- electron density during winter anomaly, temp. and NO density vars. effect 79−21087
- electron density in lower D-region, meas. via Faraday rot. and absorpt. 80−31162
- electron density in lower ionosphere, rocket meas. by VLF waves propag. characts. 78−49219
- electron density model distribs. over Delhi 79−88536
- electron density profiles, rocket meas., rel. to winter absorpt. anomaly 77−21990
- electron density profiles, statistical model 80−61964
- electron density profiles from gyrowave interaction expt., error anal. 79−5705
- electron density space-time vars. 77−17282
- electron density variation obs. *(Russian)* 78−61652
- electron density variations above Urbana, Illinois 77−60536
- electron density vars. in winter due to NO enhancements and electron precip. 77−60532
- electron density winter anomaly, recent advances 80−17437
- electron heating by EM emission of vertical lightning discharges 77−25818
- electron loss, steady state coeff., diurnal and seasonal var. 79−75023
- electron loss coefficient, review *(Russian)* 78−85756
- electron loss mechanism, normal and anomalous winter absorption 79−88537
- ELF propagation and midlatit. localized nighttime D-region disturbances 77−21989
- EM wave partial reflection, ang. variation obs. at 1.98 MHz 80−101487

D-region continued

- enhanced electron conc. at mid-latitude, positive-ion model 80−105115
- equatorial D-region, ionisation processes and ion comps. review 78−36362
- geomag. storm effects at low and mid latitudes, electron density vars. 80−101474
- ground diffraction pattern parameters assoc. with D-region partial reflections 77−60534
- gyrowave interaction expt., calc. of Fejer curves 80−36447
- HF wintertime absorption, O I airglow emission as precursor 79−58148
- HF/VHF absorption in disturbed D-region, meas. 77−53286
- horizontal drift obs., mean and periodic components at 35°S near Adelaide 77−9613
- ion bunching, model 78−73424
- ion chemistry, rel. to winter anomaly in ionospheric adsorpt. 78−20577
- ion chemistry during intense radiowave heating 80−61952
- ion composition, ionisation and profiles 77−49226
- ion composition at midlatitude in quiet conditions, model 80−109307
- ion composition models, unified reaction scheme 79−5704
- ion concentration, elec. cond. and vertical elec. field intensity meas., 0-85 km altitude 77−29359
- ion structure and winter anomaly 79−62660
- ionisation, by solar flares X-ray and EUV emission, models 77−5515
- ionisation, effects of solar flares Fe XXV 1.87 Å line emission 78−65588
- ionisation, geomag. control and possible coupling mechanism 77−9598
- ionisation 80−4167
- ionisation effects from cosmic X-ray sources 79−35048
- ionisation enhancements in lower D-region, rel. to radio waves winter absorpt. anomaly at middle latits. 80−67459
- ionisation measurements, rel. to mesosphere, NO conc. geomag. control 79−8651
- ionisation transient compressional response 77−53295
- ionization due to low level meteors, contrib. to LF propag., radio and optical obs. system 79−84514
- irregularities causing partial reflection of radiowaves 80−41629
- layer structures, density response to gravity waves 78−81290
- LF signals, var. over sunspot cycle 77−78560
- LF/VLF radiowave propag. characts. anal. 78−93049
- lightning location and ionospheric refl. heights from two-station mag. field meas. 79−70845
- mesoscale waves in D-region and F-region, temporal vars. 80−8483
- metallic species, chemistry, problems 79−35035
- MF pulsed transmissions, method for separating D- and E-region contribs. to toal absorpt. 78−69593
- MF wave absorpt. after HF wave heating 80−94646
- middle-latitude nocturnal D-region, maintenance by energetic electron precip. 77−25856
- midlatitude disturbances caused by high energy particles 77−60517
- modification studies, electron density determ. via complementary cross modulation technique 77−2275
- morphological scheme of post-storm event 79−88523
- mutual interaction between E- and D-regions during solar flare 77−45236
- negative ions, effect on Thomas scatt. in presence of electron heating 79−16739
- negative ions, Thomson scatt. detect. using Arecibo radar 79−62665
- nighttime ion conc., rocket meas. 77−29540
- NO height distribution from rocket ion comp. results 80−26674
- observations and chemistry, recent advances 79−8751
- partial reflection experiment, appl. of phase switched correlation polarimeter, 77−87169
- partial reflection experiment using FM-CW technique 77−29580
- partial reflection sounder, limited height resolution effect in differential phase meas. 77−21991
- partial reflections, filtering effect on drift parameters determined by full correl. anal. 78−65450
- partial reflections electron density profiles, sensitivity to irregularity comp. 78−81495
- payload B I, compact D-region expt. package for use on small sounding rockets 78−45190
- plasma and neutral gas composition and structure, anal. during winter anomaly 78−45191
- plasma density measurement, rocket borne expt. 78−45126
- polar D-region aeronomy 77−53311
- polar electron density profiles during solar proton event, from VLF refl. height vars. 79−8764
- positive ion concentration below 90 km altitude, rocket meas. 77−29539
- positive ions, effective recomb. coeff. vars. 77−13150
- quiet polar region characts. using partial refl. method 78−49215
- radio wave absorption, rel. to interplanetary mag. field polarity changes 77−33272
- radio wave absorption, riometer meas. 78−85763
- radio wave scattering from southern hemisphere D-region, obs. 78−36363
- radiowave absorption, effect on forward scatter radiometeor amplitude distrib. index 78−65552
- radiowave absorption, effects of solar X-ray and Lyman α radiation 78−40737
- radiowave absorption, winter anomaly 79−58176
- radiowave absorption at mid-latitude coupled to auroral activity 80−61945
- radiowave absorption diurnal var. at high latit., riometer data 77−53294
- radiowave absorption during solar minimum, 2.5-4.1 MHz 80−41628
- radiowave absorption freq. var., model 77−13169
- radiowave absorption meas. at Waltair, India, D- and E-region models 77−13173
- radiowave anomalous absorpt. during sudden disturbances, solar zenith angle depend., electron loss coeff. 78−69568
- radiowave partial reflections, ang. and temporal characts. 79−66858
- radiowave propagation, results during Western European Winter Anomaly Campaign (1975/76) 78−45123
- radiowaves, partially reflected, ang. distrib. meas. 78−49204
- radiowaves self-action effect *(Russian)* 77−41254
- recombination coeffs. for normal and winter anomalous days 79−35042
- relaxation after sudden cut-off of ionisation source 77−33254
- review 78−77392
- short-wave radio absorpt. vars., transient coupling with tropospheric planetary press. waves 77−33162
- solar X-ray control of ionisation 80−77198
- spectral analysis of wave perturbation 80−21873

- **D-region** continued
  - sunrise variations of negative ions and electron conc. 80—31157
  - thermal phenomena, investigation by cross modulation tech. *(Russian)* 78—24404
  - transport conditions var. and winter anomaly 79—66864
  - VLF guide over Atlantic Ocean, obs. of shadow of mesosphere O_3 on D-region 79—58161
  - VLF long-distance transmission at middle latit., lower ionospheric disturbances obs. 80—8485
  - VLF phase deviation, quantitative relationship to 1-8 Å solar X-ray fluxes during flares 77—87170
  - VLF phase disturbances and energetic electron precip. following 1971 Dec. 16 mag. storm 77—53284
  - VLF signal phase and amplitude vars. over transequatorial path, Australia-New Delhi 79—5703
  - VLF subionospheric propag., whistler-induced anomalies 80—26668
  - VLF sudden phase anomalies during 1972 Aug. 2-4 solar flares 78—40739
  - water cluster ions, mass spectrometer results analysis 78—61659
  - water cluster ions formation rel. to mesospheric temp. 77—21842
  - winds at Saskatoon, Canada, time vars. compared with electron density vars. 79—25389
  - winter anomalous D-region over Sardinia (40°N), simplified model 80—21871
  - winter anomaly, Western European study campaign (1975/76) 78—45122
  - winter anomaly absorption events and E_s-layer form. due to metallic ion drifts 77—9599
  - winter anomaly over W.Europe, 1975-6 obs. 80—36437
  - winter radiowave absorption, 1975/76, obs. at about 52°N, 9°E 78—45124
  - CO_3^-, thermally relaxed, photodetachment cross-section and solar detachment rate determ. 77—58094
  - Cl^- formation and destruction 78—12049
  - H_2O cluster positive ions prod. in quiet daytime D-region 77—45242
  - NO density enhancement on winter anomalous day at S. Uist 80—82130
  - NO^+ cluster ion formation, temp. control 80—61931
  - $NO^+ + 2N_2 \rightleftharpoons NO^+.N_2 + N_2$, rate const., enthalpy and bond strength 77—16809
  - NO_2^- ion chemistry 77—75236
  - NO_3^-, $NO_3^-.H_2O$, NO_2^-, $NO_2^-.H_2O$, and peroxy isomers, photodissoc. and photodetachment 3500-8250 Å 80—35554
- **D/A conversion** *see digital-analogue conversion*
- **dairying**
  - milk radioactive fallout monitoring in Britain 80—12283
- **damage, radiation** *see radiation effects*
- **damming** *see dams*
- **damping**
  - *see also dislocation damping; internal friction*
  - 3-layer plates, finite element analysis of harmonic response 80—53691
  - accelerometer, piezoelectric impact, effect of damping on dynamic error 79—30435
  - acoustic, by double walls, influence of cavity-volume damping on air layers stiffness *(German)* 77—80016
  - acoustic, impedance of closed front fibre masses 78—83144
  - acoustic by glass isolating panes, influence of gas filling on sound isolation *(German)* 77—80017
  - acoustic ducts, finite element simulation 78—38115
  - acoustic resonance absorbers, effects of additional damping *(German)* 77—14825
  - acoustic steady-state response of internally damped circular plates 80—106658
  - acoustic systems, finite element anal., reactive muffler performance evaluation 77—14844
  - acoustic waveguides, damping of normal and surface waves, depend. of vel. on losses 79—14135
  - acoustic waves in bubbly liq., damping rel. to bubble-size spectra determs. 78—9735
  - active damping of vibrations in elastic systems with distributed parameters, active stabilisation *(Russian)* 79—27577
  - active vibration-suppression systems, automation 78—18098
  - active vibration-suppression techniques for mechanical systems with many degrees of freedom 78—18101
  - aeroautoelasticity, active control and suppression of flutter in aircraft *(Russian)* 78—67079
  - air bubbles, production, pulsation and damping, in dil. polymer solns. 80—69879
  - air-water interface, surface waves damping rel. to adsorpt. and spreading films detect. 79—5690
  - airborne sound by laminated building components *(German)* 80—102877
  - aircraft vibration isolation for high-performance cameras 77—74543
  - Alfven wave damping in nonuniform plasma, continuous spectrum phase mixing 78—47112
  - Alfven waves collisionless damping in inhomogeneous plasma, initial value problem soln. 79—64864
  - amorphous polymer, super-glass transition processes, damping process 80—24573
  - analogue meters, ballistic performance specification 78—41293
  - anti-vibration systems, Fick boundary value problem soln. *(Russian)* 79—35540
  - artificial satellite, spin-stabilised, nutation damping *(Russian)* 77—64626
  - artificial satellites, dual-spin, nutational motion damping *(Russian)* 77—60570
  - atom, coherent transients, spherical tensor treatment 79—26940
  - attenuation of resilient mounts and dampers under actively vibrating machines 80—14514
  - austenite cladding layers, damping of ultrasound 80—104390
  - band (tape), endless, torsional vibrs. during const. axial vel., damping effects *(German)* 78—34065
  - bar, impact vibr., motion and dynamic stability analysis 78—26081
  - beams, large amplitude vibration damping by viscoelastic layers 78—63363
  - bending oscillations, damping props. investigation, new method 77—21340
  - boson field, damping superoperator eigenvalue problem, direct soln. 80—57180
  - brass, cold worked, or heat treated, or recrystallised wire specimen *(German)* 78—88489
  - α-brass, leaded and Pb-free mech. damping 77—63705
- **damping** continued
  - brass, mechanical damping in terms of Granato-Lucke theory, comparison with Cu_3Au and leaded brass 78—95772
  - Brownian motion, bistability effects in periodic potentials 80—68139
  - Brownian motion, nonlinear response to external field, in low-friction limit 80—4652
  - cantilever strips with inserts 80—38315
  - capacitive parametric transducer for displacements under dynamic damping 80—105626
  - capsules, neutrally buoyant, in Lake Tahoe, oscills. damping 80—12438
  - cello, wolf tone damping *(German)* 79—18633
  - cellulose film, meas. of shear modulus and damping in a torsion pendulum 79—4989
  - cetaceans, drag reduction and self regulation of skin damping while swimming *(Russian)* 77—32918
  - channel, straight (buckled), two-dimens. flow, stability anal. 78—59490
  - circular disk resonators in vicinity of thickness resonance, vibration mode anal. 80—48634
  - classical damped motion, role played by trajectory in Fokker-Planck solns. *(French)* 79—30347
  - close binary stars, tidal friction due to envelopes radiative damping 77—57013
  - coated beam method, error anal. in investig. complex modulus of viscoelastic materials 79—27565
  - complex cavities, reson. damping of violin-shaped and guitar-shaped cavities 77—50838
  - concrete, damping meas., expanded hysteresis loop method 77—12665
  - conducting cylinder motion in solenoid field, contactless elec. cond. meas. *(Russian)* 79—214
  - constrained viscoelastic, FEM of composite systems 80—83743
  - continuous systems, forced vibrations, Galerkin and Hamilton-Ritz methods 80—53684
  - cosmology, shock damping and entropy prod. in relativistic simple waves 77—17725
  - coupled flexural and longitudinal vibrations of finite structures, energy absorpt. estimation 78—1495
  - coupled large linear damped structures, eigenvalue anal. 78—1561
  - critical damping of simple-harmonic motion, for teachers 79—17
  - crossply glassfibre, cantilever beams, nonlinear damping for nonsinusoidal strain 79—47762
  - curved beam with viscous damping forced vibrations 79—50622
  - cushion dynamic props. by mech. impedance method 78—72953
  - cylinders heaving in water, added mass, damping coeff. 77—58828
  - cylindrical panel, motion stabilisation *(Russian)* 77—68498
  - cylindrical pipes, modal density and damping 78—13948
  - damped linear systems, freely vibrating, eigenvalue lower bounds 79—27569
  - damped linear systems, vibr. 79—18790
  - Debye relax. eqns. for stand. solid with high relax. strength 77—20011
  - dielectric waveguide hybrid and transverse mode dispersion calc. *(Russian)* 80—99857
  - discharge, pulsed, density perturbations, laser beam diagnostics 79—7498
  - discrete dynamic system with series structure, non-linearity of vibration 78—28935
  - dislocation pinning, no. of points per network length estimation from amplitude depend. damping peak anal. 77—27889
  - disordered systems, phonon-like excitations, dispersion and damping 80—49331
  - dissipative circulatory structural systems, dynamic behaviour 78—63364
  - double-cantilever beam, forced vibration technique for meas. of material damping 78—19964
  - double-pendulum vibration isolator with three-dimensional isolation 79—67295
  - drives, rotational, damping of torsional vibrations, experimental determ. *(Russian)* 80—74816
  - dye laser, N_2 laser-pumped, subns. relax. oscills. 78—82959
  - dye superradiance and damping characteristics obs. 77—83869
  - dynamic damping effect in small force measurement *(Russian)* 78—12687
  - dynamic problem of continua, reduction of stiffness, mass and damping matrices *(Polish)* 78—12565
  - dynamic vibration absorber, consisting of three permanent magnets 78—9614
  - E-glass epoxy beams, dynamic mech. behaviour, meas. and analysis 77—28844
  - effect on impact response, two degrees of freedom system 80—74587
  - elastic mechanical systems, vibr. damping by dampers with filled voids *(Russian)* 80—58954
  - elastic plate, stability via Lyapunov's Second Method 77—54914
  - elastic strips, flexural vibrations, active suppression 79—32354
  - elastic-viscoelastic-elastic beams, compressional damping in vibratory response 79—32323
  - elasticity, St. Venant planar theory, nonhomogeneous problem, logarithmic decrement *(French)* 78—49664
  - electric traction units, driving axle oscillations damping using seismic dampers *(German)* 80—62458
  - electrodynamic vibration test beds, feedback signals for correcting characteristics 80—53543
  - electrostatic noise damping by warm auroral electrons 80—41668
  - elementary excitations damping, theory of many-particle processes *(Russian)* 79—56522
  - epoxide resin cured with aliphatic dicarboxylic acids, fatigue behaviour *(Japanese)* 79—79092
  - fabricated unit structures, forced modes of vibration 77—65708
  - fibre reinforced silicone rubber composites, interfacial slip and damping 79—5010
  - flexible shafts on oil-film bearings, external damping 77—62199
  - flexural mode vibration damping by reinforcing beams 78—18097
  - floating body, oscillations damping by liq., inertial effects *(Russian)* 78—22295
  - floating rod with loaded end, damping during transverse vibr. 80—79205
  - floor vibrations, nature and effect on precision machinery, isolation methods 80—43522
  - flow, parallel, role of negative energy waves in some instabilities 79—59967
  - fluid and isotropic solid acoustic harmonic generation 77—27417
  - fluid induced, in refrigeration machinery manifolds 78—83164
  - fluids, acoustic wave propag., damping, flows in pipes *(French)* 77—19467
  - force and strain meas., spring-mass-damping system, dynamic errors *(German)* 79—12794

damping continued
- force transmissibility of resilient mounts supporting a vibration damped object 77—34992
- forced oscillations experiment for students 80—17780
- forced vibration of a damped linear system 79—18789
- forced vibration prevention by damped dynamic absorber 78—63355
- forced vibrations of continuous systems with damping Rayleigh-Ritz-Galerkin approx. 78—59332
- forced vibrations of systems with retardation and damping 78—83290
- forced vibrs. shell, viscoelastically damped, filled with pressurised liq., forced vibrs. 78—9584
- foundation dynamic interaction with viscoelastic half-space *(German)* 78—79228
- free damped mech. vibration logarithmic decrement, optoelectronic meas. 80—92095
- friction, stochastic quantisation, nonlinear Schrodinger equation 80—27164
- Friedel's theory of amplitude depend. damping 78—27552
- gas bubbles, oscillating, appl. of subharmonic threshold to damping meas. 77—31374
- gas bubbles, thermal effects and damping mechanisms in forced radial oscills. 77—31375
- general beam systems, optimal dynamic vibration absorbers 79—23255
- Gentalloy, in Fe-W system, damping capacity *(Japanese)* 79—20094
- geomagnetic pulsations, damping by ionosphere 78—49218
- glass fibre reinforced plastics, microstructure rel. to mech. props. 80—11685
- glass reinforced plastic, transverse flexural vibration, statistical charact. of logarithmic decrement 77—7334
- graphite particle-Al alloy composite, improved damping capacity and machinability 77—4786
- grid in viscous medium, basis for electrostatic viscometer 80—38308
- gyro in cardan mounting, resonant regimes calc. *(Russian)* 77—71312
- gyroscope, forced vibrations shock absorber selection parameters 80—43659
- gyroscope, stability of Staude's permanent rot. with damping 78—21126
- gyroscope, unsteady oscillations reduction using inner gimbal-base elastic damping coupling *(Ukrainian)* 77—30143
- gyroscopic system, linear, damped, modal anal., appl. to satellite 78—63275
- gyrostat motion time-optimal damping under random perturbations 77—68379
- hand-arm system, distributed-parameter dynamic model 78—92663
- hand-arm system, vibrational responses of hand 78—7380
- harmonic oscillator, canonical approach, for teaching 80—17757
- harmonic oscillator, quantization of inequivalent classical Hamiltonians, for teaching 79—35466
- harmonic oscillator, time-dependent 80—8826
- Hauger column critical load in presence of damping *(French)* 79—14291
- heavily damped waves, method for determ. wave number and damping coeff. 78—63557
- highly excited harmonic oscillator in crystal, damping 79—40408
- hydromagnetic waves in high β plasmas, propag. and damping 80—17482
- hysteresis damping, continuum description 78—67078
- impact absorber with linear spring and quadratic law damper 77—7332
- impact absorbers, optimum damping ratio 77—72225
- impact absorption with two-stage variable area orifice hydraulic damper 77—50953
- internal, in 2 and 3 dimens. continua 78—13970
- internal friction measurement by resonant specimen with a dumb-bell shape 80—48660
- intrinsic and modulus defect 77—75850
- ion acoustic waves in solar corona, Landau damping rel. to coronal heating 78—4181
- laminated composite panels, flutter instability, shear deformation and damping effects 79—72841
- Landau damping in regular wave interaction with noise 80—33284
- Landau damping of electrostatic wave in plasma 78—47111
- Langmuir waves, modulated, nonlinear Landau damping effect 78—81849
- layered cylindrical shells vibrating in axially symmetric modes, damping props. 77—14943
- leaded brass, mechanical damping in terms of Granato-Lucke theory, comparison with unleaded brass and Cu_3Au 78—95772
- linear mechanical systems, dynamic vibration absorbers for impulsive excitations 79—23271
- linear models of frequency-independent internal friction *(Russian)* 79—18834
- linear stable structure maximax response estimates compared 79—68626
- linear systems, damped free motion 79—64569
- linear systems, effect on vibration-stability reln. 77—19558
- linear systems, free vibrs., principal modes 77—68512
- liquid, in vessel, vibr. amplitude determ., structural damping and surface tension applied to stress anal. 80—19417
- liquid oscillations, hydraulic torsional vibration damper *(Russian)* 80—92164
- long-wave oscillation damping calc. *(Russian)* 78—75302
- Lorenz model, chaos and limit cycles 78—57787
- loudspeaker units, behaviour of damping materials *(Spanish)* 79—46146
- loudspeakers, acoustic damping effects, computer calcs. 80—14524
- machine vibrations anal. and obs. block deformability influence *(Italian)* 78—51108
- magnetosonic plasma waves, cyclotron resonance damping in plasma with admixed ions 77—24079
- materials, hinged-hinged beam, in terms of mode of vibration *(Japanese)* 80—91954
- Mathieu equation with damping, variational anal. 80—57079
- mesosphere, effect of Rayleigh frictional damping on mean meridional circulation 80—109219
- metal, damping capacity rel. to struct. defects *(Russian)* 77—44283
- metal, EM waves near cyclotron reson. in inclined mag. field *(Russian)* 80—29625
- metal ribbed strip filled with acoustically absorbent material, vibr. damping *(Russian)* 77—46864
- MHD turbulence in interstellar medium, damping and inertial range 77—45528
- Michelson interferometer, active noise compensation *(Russian)* 78—12751
- modal damping bounds by component modes method using Lagrange multipliers, natural freqs. 80—79213

damping continued
- model and full-scale cooling tower resonance tests 78—83291
- molecule above metal surface, damping of mechanism for excited state 78—92160
- non-linear dispersive wave, coupled modes approach, effect of dissipation on recurrence 78—49670
- nonconservative system resonance, modal analysis 78—42557
- nonlinear, parametrically excited oscill. of coupled second order systems 80—86078
- nonlinear dynamic damper, subharmonic oscillation extinction 79—25835
- nonlinear elastic systems, linear damping coefficients, experimental determ. 79—50680
- nonlinear mechanical systems with time optional condition 80—31492
- nonlinear oscillating system, delay effects *(German)* 77—53773
- nonlinear oscillations, damping decrement 77—58581
- nonlinear oscillatory systems with delay, stability props. of differential eqn. solns. *(Russian)* 77—41475
- nonlinear system with stops, viscous-Coulomb damping influence 80—36842
- nonlocal stochastic equation of motion with damping in electrodynamics 80—17872
- normal modes in irreversible thermodynamics 80—52148
- nuclear reactor building, soil-struct. interaction behaviour, damping effects, expt. anal. 77—38434
- nylon-1 polymers and copolymers, mech. props. rel. to glass transition 77—11625
- ocean internal waves, damping by rough bottom *(Russian)* 78—24293
- open dynamical system, equations with fluctuating parameters 80—62584
- optical equipment, precision, insulation against vibration using springs and viscoelastic substances *(German)* 80—17986
- optical structures, vibr. electronic damping using piezoelec. transducers 79—50372
- optimized speed-controlled suspension of a 2-DOF vehicle travelling on a randomly profiled road 79—72847
- oscillating system, light damping, influence of eigenvalues *(German)* 80—31490
- oscillation rods in viscous fluids, added mass and damping, finite element anal. 80—58967
- oscillations, free damped, differential eqn. soln., teaching appl. 79—62950
- oscillator, exact Green's function 79—80467
- oscillator motion, expansion in normal modes 80—67951
- oscillator with even non-linear damping 78—28938
- oscillators, with nonlinear damping, first passage failure time anal. 79—6053
- oscillators with nonlinear restoring forces, first passage failure probability calc. 78—42562
- oscillatory damped linear systems, eigenvalue bounds and subcritical damping 79—77005
- overhead crane, method 80—101711
- P-wave damping 77—2115
- paper, meas. of shear modulus and damping in a torsion pendulum 79—4989
- parametric amplifier, damping theory anal. 80—52118
- partition and glass windows, influence of vibration damping on acoustic transmission *(French)* 77—31176
- passive acoustic antivibrators for vibration absorpt. 79—23269
- passive vibr. isolation, shock absorber selection 78—55556
- pendulum, Foucault type, 10 m long, characts. *(Korean)* 79—21541
- pendulum oscillation optimal passive suppression *(Russian)* 79—10454
- pendulums characteristics meas., digital, using amplitude-time convertor *(Czech)* 77—71310
- piezoelectric radiators, field homogeneity enhancement 77—68358
- piezoelectric solids, shape-dependent damping 80—93242
- plasma, cold, bounded and cylindrical, viscous damping of magnetoacoustic oscillations 80—24151
- plasma, electron beam space charge wave in mag. field, cyclotron damping 79—46459
- plasma, electrostatic high frequency oscills., damping nonlinear Schrodinger eqn. calcs. 77—7530
- plasma filled waveguide, electron beam interaction, spatial evolution of complex EM modes, collision effects 79—14556
- plasma ion acoustic waves, damping and growth in plasma sheath 77—7531
- plastic material specimens, free oscillation attenuation constant meas. *(Czech)* 79—41634
- plastics, fatigue fracture props. correl. with viscoelastic damping 78—52993
- plate, in flowing water, loss factor rel. to fluid vel. *(German)* 77—820
- plate vibr. suppression by rate optimal response, numerical study 78—30229
- plates, active vibration suppression 79—23125
- plates, mechanical vibr. damping based on continuous system anal. 77—72214
- plates and shells, internal damping, influence of geometry 78—50996
- PMMA and PPMA, glassy state, cyclic loading effects on internal damping, shear modulus, heat capacity and density 77—43275
- pneumatic floor vibration isolators, with two-chamber damping systems, isolation of very sensitive meas. apparatus *(German)* 80—69590
- polyethylene, high-press. charact. by torsional vibration anal. *(German)* 77—59842
- polyethylene, low density, meas. of shear modulus and damping in a torsion pendulum 79—4989
- polymer, dynamic mech. anal. 78—60697
- polymer, viscoelastic, microrelax. model for moment effects interpret. 79—20098
- polymeric materials, engineering structures, design and meas. 78—87185
- polymers filled with agglomerated particles, dynamic mech. props. 80—66569
- power transmission lines, EHV, vibration reduction by damper, description 77—5660
- pressure-force transducer using 32.768 kHz X-Y flexure watch crystal 78—57934
- proportionally damped dynamic systems, eigenvalues *(German)* 79—21540
- proportionate Coulomb and viscously damped isolation system 78—42561
- proton (antiproton) beam in storage ring, stochastic cooling anal. 80—5420
- proton (antiproton) storage ring, incoherent motion damping by dissipative elements 80—5419
- proton beam radial damping, zero gradient synchrotron 77—83383

damping continued
- pseudoconservative systems, effect of damping on stability 78—81832
- quantum mechanical damping 80—46862
- radiation damping force, 1-D, new mechanics 80—82632
- radiation damping in general relativity 78—8310
- radiation damping in universe with topologically closed space sections 78—57828
- radioactive fallout damping coefficients 78—92961
- rectangular cavity, two-dimens., acoustic modes, damping 77—31149
- reinforced concrete structs., initial stress approach to nonlinear dynamic anal. 77—83036
- resonance-bar damping, automated meas. system 77—2649
- response calc. errors for nonclassically damped structures 78—9587
- rotary structural joints, energy dissipation 78—30245
- rotating body, stabilisation by passive dampers, asymptotic methods use *(Russian)* 78—20957
- rotating fluid dynamics expts. and problems *(French)* 78—9645
- rotor, flexible, on flexible bearing, viscous-damping, vibr. and balancing 78—63352
- rotor, passing through crit. speed, with gyroscopic effect, asymptotic calc. 78—63354
- rotors, elastic wave stability 78—87297
- rubber hydrochloride, meas. of shear modulus and damping in a torsion pendulum 79—4989
- sand, dynamic properties w.r.t. seismic risk prediction, stress condition effect *(Japanese)* 80—17235
- sandwich beam shear-damping reduction effects 78—42560
- sandwich beam subjected to moving forces, forced vibr. 78—13953
- sandwich beams, tapered symmetric, frequency and loss factors 78—38247
- satellite, spinning notion, optimal nutation damping by flywheel 77—53396
- satellite attitude control system, gyrodampers appl. 78—96379
- satellite rotation, exponential damping, magnetic field effects 78—69645
- satellite rotation, shielding effects on magnetic damping 78—69646
- sea surface waves, attenuation by energy transfer to sediment motion 78—73389
- semiautomated torsion pendulum for high temp. damping studies 77—11153
- semiconductors, heat pulse absorpt. in nonquantising mag. fields 80—60054
- shaft, symmetrical, nonlinear elastic and internal damping props., flexural vibrations 78—71290
- shape modes in damped systems 79—44715
- shell, thin cylindrical, stiffened with viscoelastic rings, vibr. damping characts. 80—28452
- shock absorber, elastic damping props. determ. unit 78—5703
- shock absorbers, telescopic, dynamical force measurement *(German)* 79—35732
- shock isolator for closed-cycle refrigerator of diode laser 78—50796
- short sandwich beams, vibr. freqs. and loss factors 77—75842
- short wave generation by cylinder oscillating at liquid interface 78—79331
- sliding condensed-matter system model, dynamical friction, elec. cond. 80—44258
- Snoek damping in sheet specimens, measurement using torsion pendulum of 3 components 79—63010
- solar atmosphere, radiative damping of acoustic waves 77—53496
- solar type III radio bursts, deconvolution and decay mechanism 77—45381
- solid friction damping of mech. vibrs., math. model approach 77—42764
- solid-gas flow, fluctuation damping 80—19478
- solitary waves, damping by weak dissipation 79—63053
- sound damping decrement in steam mixture with bubble struct. 79—55444
- sound generation and transmission in flow ducts with axial temperature gradients 78—90551
- sound pulsation noise damping from small air bubbles in water 80—64253
- sound transmission into heavily-damped cylindrical fuselage 78—83166
- space vehicle, disordered rotation damping by elastically suspended ballast *(Russian)* 77—45287
- speech, vocal tract losses, influence on damping of reson. freqs. 78—85325
- spin wave damping at low temp. *(Russian)* 77—36062
- spinning tops, mechanics *(German)* 78—87253
- spring-loaded mass system vibration analysis *(German)* 80—96224
- spring-mass system, optimum design of untuned viscous dynamic vibration absorber 79—86370
- standing waves in gas-liq. medium, effect of bubbles on acoustic damping 78—9474
- stars, neutrino damping of nonradial pulsations during gravit. collapse 77—56999
- steel, alloy 08kp, sheet material with laminar coating, damping capacity improvement 79—66098
- steel, austenitic, rod, coupled flexural and torsional vibrs., energy dissipation 80—89281
- steel, C, fatigue strength and damping capacity, short term cyclic overload effect 79—66157
- steel, ferritic, MA 956, oxide dispersion strengthened, mech. props. and damping behaviour 79—47702
- steel, ferromag., rod, coupled flexural and torsional vibrs., energy dissipation 80—89281
- steel, fully annealed tool, cantilever beams, nonlinear damping for nonsinusoidal strain 79—47762
- steel, low C, absolute dimensions effect on logarithmic decrement of torsional vibrs. 80—3150
- steel, low C, increased damping capacity, mathematical planning method *(Russian)* 80—45332
- steel, low C, microplasticity at high and low loading freq. *(Slovak)* 79—38910
- steel, low C fatigue, stability of energy dissipative charact. 77—21209
- steel, mild and HSLA, mech. behaviour, deform. rapidity influence *(French)* 79—57056
- steel, stainless, reinforced glass matrix, vibr. damping anal. rel. to internal friction 80—40413
- steel, stainless and ferritic, damping, logarithmic decrement meas. by torsion pendulum *(German)* 79—74195
- steel, structural, with elevated and high strength, damping capacity 77—21205
- steel, VNS-5, damping capacity 77—1849

damping continued
- steel 2Kh13, damping props., effect of plastic deform. by torsion 77—70095
- steel bar, effectiveness of rigid vibration-absorbing coating 78—18226
- steel base composite, sintering, mech. props. 77—21061
- steel Co-Ni three layer composite, high strength with increased damping capacity 77—1850
- steel sheet, damping induced during internal friction meas. 77—32752
- steel VNS-2, damping capacity, magnetomechanical, phase transform. effects 78—31445
- stochastic excitation systems, identification of damping and stiffness parameters *(Polish)* 78—69973
- structural, synthesis from substructure tests 77—31234
- structural damping constant evaluation by time series analysis 78—46902
- structural dynamics, unconditionally stable explicit algorithm 78—48
- structural fatigue life rel. to element uncertainty 79—27593
- structural vibration damping by rot. slip in joints 77—89059
- structure damping for noise control, evaluation of viscoelastic props. 80—43632
- structure vibrations, reduction by increase in damping factor *(French)* 77—19472
- tapered unconstrained beams, vibration damping 78—51106
- thermal instability of amplitude depend. internal friction 77—84838
- thermoelasticity models taking account of a finite heat propagation rate 79—94541
- thin infinite cylindrical shells, active vibration suppression 79—18797
- three layer vibration absorbing structures, temp. characts. of loss factors 79—64395
- three-layer elastic-viscoelastic beam damping characteristics *(Japanese)* 78—9575
- torsion pendulum, automatically driven, for continuous meas. of amplitude and amplitude-independent damping 77—35099
- torsion pendulum for damping capacity meas. and related phenomena 77—17687
- torsional damper using second order fluid *(German)* 79—68615
- torsional mass in gravimeter, vibration damping *(Russian)* 78—4015
- torsional pendulum oscillations, meas. system *(Polish)* 77—71314
- torsional vibrations, optimal damping *(Russian)* 77—57179
- torsional-vibration fluid damper design 77—71309
- transmission line aeolian vibrations, effect of 4R dampers 79—23259
- transmission line vibrations, effects of Stockbridge type dampers 79—14323
- turbomachine cascade wing profile oscills., aerodynamic damping, ang. of attack influence 79—37344
- U-tube manometers, Navier-Stokes equations solution and expt. verification *(Japanese)* 80—6142
- unsteady flow damping by compliant boundaries 77—31274
- urban railway vehicles with sound absorbing wheel systems, noise emission reductions *(German)* 79—50508
- US damping coeff. meas. 77—90575
- US transducer damping by multilayer front face 79—55301
- vestibular research, rotating room acceleration and damping 79—84048
- vibrating beam, optimum distrib. of additive damping 80—38310
- vibrating plates, unconstrained layer damping treated, response to random acoustic excitation 80—74798
- vibrating plates, unconstrained layer damping treated, response to random acoustic radiation 80—74799
- vibrating system modified by attached subsystem, by freq. and time domain responses 77—31250
- vibration, viscously damped dynamic absorbers of conventional and novel design 77—62096
- vibration absorbing coating, cut constraining layer effectiveness 79—32130
- vibration damping coatings for constructions, theory 80—10178
- vibration damping materials, review 78—13854
- vibration damping materials, testing and development 77—84059
- vibration excitation method in damping meas., equipment 79—1928
- vibration problems, Zienkiewicz four-time-level scheme for numerical integration 78—1594
- vibrations in one degree of freedom system *(German)* 79—32369
- viscoelastic body eigenfrequency determ., finite element method *(German)* 79—23270
- viscoelastic layer in two-layered beam, vibrational analysis *(Japanese)* 80—5968
- viscoelastic materials, design evaluation of damping treatments 79—18799
- viscosity, of water-fluidised bed, by oscills. damping meas. 78—59475
- viscous, effect on response of thick rectangular membrane to dynamic loading 78—46906
- viscous, optimum Lanchester damper for a single degree of freedom system, minimum force transmissibility criterion 80—52014
- water wave damping, effect of large grooves 77—11209
- wave-front method for dynamics of high damping bar 77—23895
- zero sound, in classical liq., excitation, damping, memory function approach 78—67771
- Al alloy, graphite dispersed casting, damping capacity *(Japanese)* 79—96059
- Al, cantilever beams, nonlinear damping for nonsinusoidal strain 79—47762
- Al, plastically prestrained, dynamic props. 79—15743
- Al, stiffness and damping in creep 78—23780
- Au-Ag, mech. damping 78—31444
- C fibre reinforced plastic damping capacities, cantilever beam tests *(Japanese)* 79—91869
- C-fibre reinforced epoxy resin, laminated structs. mech. props. 80—50672
- Co, US damping temp. and mag. field depend. *(Russian)* 78—23313
- Cr, anomalous US damping under hydrostatic press. 79—14890
- Cu alloy, graphite dispersed casting, damping capacity *(Japanese)* 79—96059
- Cu, fatigued, structural changes, damping and modulus 77—28906
- Cu-Ag (0.1 wt.%), cold-worked, internal friction peaks in kHz range 80—89276
- Cu-Zn-Al (19.5, 6.35 wt.%), martensitic, static stresses influences on damping behaviour 80—10594
- Cu_3Au, mechanical damping in terms of Granato-Lucke theory, comparison with leaded and unleaded brass 78—95772
- CuCl crystal resonant Raman scatt. and luminescence competition *(Japanese)* 80—80770
- Fe base composite, sintering, damping props. 77—21061
- Fe, cast, flaky graphite, damping capacity 77—8869
- Fe, damping during and after deformation 79—43344

damping continued
Fe, pure, magnetoelastic damping at low shear stress amplitudes *(French)* 77—59441
Fe-Co, damping capacity of Gentalloy, internal friction meas., mech. and mag. depend. *(Japanese)* 78—52875
Fe-Co (5 to 25 wt.%), exam. of damping capacity of Gentalloy 78—72800
Fe-Cr alloys, damping capacity 79—100206
Fe-Cr-Mo sintered, damping capacity and mech. props. 78—44161
Fe-Cr-Ti-Mo, sintered, mech. props. *(French)* 79—91726
Fe-Mo, damping capacity 77—86082
Fe-Mo, damping capacity *(Japanese)* 78—11259
Fe-V(Nb)-N, precipitation study, 550 to 600°C *(German)* 77—90350
Fe-W system, damping capacity of Gentalloy, internal friction, mech. and mag. props. 79—77679
He transfer line, oscillation damper 80—37041
^{4}He, superfluid, fourth sound attenuation 80—100370
KH_2PO_4, KD_2 PO_4 crystals used for laser control, acoustic vibr. suppression 78—1363
Mg-Al(Sn)(Ni)(Cu), damping capacity 77—48474
Mn-Cu, alloying addition and heat treatment effects on damping capacity 78—3165
Mn-Cu, alloying behaviour and high damping capacity 80—35160
Mn-Cu, fatigue, stability of energy dissipative charact. 77—21209
Mn-Cu (75, 25 wt.%), rod, coupled flexural and torsional vibrs., energy dissipation 80—89281
Mn-Cu structural alloys, physicomechanical props. 77—12652
Mn-Cu-Zn system, optimum heat-treatment routine for max. damping 79—87670
γ-Mn-Fe, Mn rich, damping capacity 79—83252
Mo, anomalous US damping under hydrostatic press. 79—14890
Nb, Friedel's theory of amplitude depend. damping 78—27552
Ni alloys, damping, logarithmic decrement meas. by torsion pendulum *(German)* 79—74195
Ni-Co (25 at.%), polycrystalline, mech. damping 77—28850
Ti alloy fatigue, stability of energy dissipative charact. 77—21209
ZN, anomalous US damping under hydrostatic press. 79—14890
Zn, dislocation damping on $\{\bar{1}2\bar{1}2\}\langle\bar{1}2\bar{1}\bar{3}\rangle$ slip system above Debye temp. 77—62538
Zn-Al eutectic alloy, uni-directionally solidified, damping capacity *(Japanese)* 80—16364
Zr, amplitude depend. damping 77—32617
Zr and Zircaloy-4, damping, amplitude dependent, at high temp. 77—52383

dams
see also civil engineering; hydroelectric power stations
Auburn Dam, case history for earthquake evaluation 79—88284
Campotosto reservoir, seismic recording network *(Italian)* 80—101446
concrete dam construction elements, appl. of fracture mechanics to thermal stress cracking 78—76766
damsites preliminary hydrologic assessment, streamflow generation 77—21817
Diyala catchment, Iraq, water balance between Derbendikhan and Himrin dams 80—12462
dynamic dam utilising ocean and river currents and tidal power 79—20865
earthquakes induced by reservoirs, tectonic and tectonophysical conditions for occurrence 77—81802
failure probability of finite reservoir with Markovian input 78—44887
flood forecasting in river, by unit hydrograph method 77—5254
ground loading causing geomagnetic variation, piezomag. effect during lake filling 80—8346
hydraulic conductivity clay mineral dispersion and swelling effects on earthen dams 78—53668
hydro-chemical analysis of water routes, flood gate of hydroelectric plant *(Croatian)* 80—12443
hydrodynamic press. on sloping dams during earthquake, momentum method 78—73412
hydrodynamic press. on sloping dams during earthquake exact theory 78—73413
Kama Reservoir, USSR, forecasting spring inflow 80—105008
Lake Jocassee, S.Carolina, seismicity rel. to Rn content of groundwater 80—94466
Lake Jocassee area, S.Carolina, seismicity, earthquake prediction algorithms 80—51345
Lake Keowee, S.Carolina, USA, 1978 earthquake swarm following filling 80—36255
Lake Oroville, California, weight-induced crustal stresses rel. to seismicity 77—9347
Lake Oroville, reservoir-induced pore pressure and seismic activity 79—2190
Maneri Bhali Hydel hydroelec. scheme, stage I, model, India 77—9452
photoelastic strain gauge, boundary stress meas. appl. *(Chinese)* 79—72867
porous media unsteady flow calc. by combined finite element/characteristics methods 78—91012
seepage, free water surface behaviour in porous media 80—8349
Spain, induced seismicity of dams and reservoirs 80—61776
Stefan and dam problems, free boundary convexity 78—83356
streamline water table shape through walled dam 77—78275
Suwannee River sill, effect on Okefenokee Swamp water level 80—8356
Tarbela reservoir, Pakistan Himalayas, seismicity during initial filling 80—56388
Tsengwen reservoir, Taiwan, seismicity due to fault and lake filling 80—81930
two-dimensional flow with singularities digital simulation by finite element method 78—90822
variable domain finite element model for dam unsteady compressible fluid flow digital simulation 78—90820
water breakthrough of Lake 2 at Tuyuksuy moraine *(Russian)* 77—53091

dark space *see discharges (electric)*

data acquisition
see also CAMAC; data handling; data processing; indicators; recorders
A/D data acquisition module for microprocessor systems, high-speed, multiple channel 77—57304
accelerator lab. system 79—89529
accuracy determ. based on risk for arbitrary volume of a priori data 80—95054

data acquisition continued
acoustic data buoy, microprocessor controlled, underwater signals processing 79—21024
acoustic emission signal processing and recording system, on-line 80—57266
acoustic noise, data accumulation equipment *(Japanese)* 78—42503
acoustic telescope appl. in architectural acoustics 80—5873
AES, digital acquisition and processing 79—43698
agrometeorological data, information flow organization and processing automation 77—78430
air pollution meas. network, nontelemetric, in Hungary *(Hungarian)* 77—64422
air pollution modelling 79—52984
air pollution source inventory for Tehran, methodology and approach 79—52996
airflow rate meas., with electrical indication and automatic data logging system 80—75014
altimetric data file acquisition automatic digital correlation method 78—61633
analogue memory charge-coupled devices, nucl. data acquisition 78—46250
analogue signals, fast, simultaneous recording using multichannel system 79—26045
analogue signals, multiple, collection and handling using system with Promin-2 computer 79—67267
analytical data acquisition, computer operational system *(German)* 78—27845
APODAS ocean profiling automatic data acquisition system *(Japanese)* 80—85769
application node system image manager subsystem within distributed function laboratory computer system 79—45606
artificial heart experiments with animals, data acquisition and monitoring system *(German)* 79—8582
astronomical data acquisition and processing, Rome Observatory *(Italian)* 80—8551
astronomical data compilation and acquisition techniques at telescope 77—78649
astronomy, data recording system for KSC 60 cm reflecting telescope *(Japanese)* 80—94717
asynchronous/synchronous FIFO data buffer *(German)* 77—9996
atmospheric, neutron activation anal. system appl. 77—81442
atmospheric energy budget over grasslands, eddy correl. sampling technique 77—78446
atomic absorption spectrometry, using a microcomputer 79—52794
auditory evoked potential data acquisition, dual-processor system 79—79712
Auger and line optical data acquisition, synchrotron radiation source 78—63019
Auger electron spectrometer, control using HP 9845 desktop computer 79—21726
autodensitometer, flatbed, for biophys. appl., error analysis 77—52937
autoguiders and acquisition systems for optical telescopes 80—82206
automated correlation spectrometer with two Ge(Li) detectors 78—82562
automated counting system, design philosophy 79—88923
automated multichannel data and meas. system type MIIS-1, for transducer data 79—2754
automated shipboard acquisition and processing of offshore geophys. data *(Russian)* 78—53750
automatic buoy systems, centre for data collection and processing *(Russian)* 77—78427
automatic data collection system for powder X-ray diffractometry 77—24244
automatic evaluation of isotope anal. of nuclear fuels, isotope dilution, mass and α spectrometry 78—55120
automatic system with SI 1.2 standard interface for calorimetric meas. *(German)* 77—37898
autoranging, in high speed systems 78—85233
BEBC, performance of external muon identifier, MWPC electronics and data handling 79—730
biological samples, multichannel analyser spectroscopy using XRF, minicomputer appls. 78—20106
biological STEM, low-dose, using digital data processing system 78—24203
biological STEM, on-line data processing system 78—24202
Biomation 8100 recorder interfaced to remote computer, photolysis expts. appl. 78—21107
biomedical engineering instruction, microprocessor-based instrumentation system 77—22361
biomedical instrumentation, microprocessor-based, present and future trends 80—26405
bit-slice microprocessor appl. 79—89566
body radioactivity measurement, SABRE 3 computer system 78—85425
body surface and epicardial activity, computer-aided meas. system 79—39551
body surface ECG potential mapping, data acquisition system 79—29653
body surface potential mapping, automated acquisition and processing system 78—81033
Bragg crystal spectrometer, on line, step scan control and data accumulation system *(Japanese)* 78—5088
brain autoradiographs, rapid quantification, data recording via microprocessor interface 80—41332
breath by breath anal. of ventilation and pulmonary gas exchange, minicomputer system 79—62393
Brilliant ADC, semi-autonomous controller for data acquisition 78—46245
bubble chamber picture digitisation system 79—63871
BWR neutron noise source identification, stochastic model data anal. 78—94106
C-CD transient data recorder, DC to 200 MHz 79—89540
calorimeter, AC, automatic data acquisition system *(Japanese)* 80—52215
calorimeter, adiabatic heat capacity small sample low temp., with automatic data acquisition system 78—12697
CAMAC based high-resolution repetitive waveform generator 79—76214
CAMAC based mobile automated high speed transient data recording and transmission system 77—54488
CAMAC high rate data acquisition system 80—23281
CAMAC I/O module, two-dimensional position sensitive detector system data 80—47835
CAMAC module for testing data acquisition systems 79—89568

data acquisition continued
- cardiac surgery, data acquisition and processing during operation by multiplexer *(German)* 78—92743
- cardiopulmonary stress test data acquisition and control systems 79—79673
- cerebral blood flow noninvasive regional meas. and computer analysis 78—35948
- cerebral regional blood flow meas., ^{133}Xe inhalation method with on-line computer 77—40734
- CERN 400 GeV proton synchrotron control consoles 77—38518
- chemical anal. by heavy-ion induced X-ray emission, automation 77—77863
- chemical identification of substances fixed on silica gel, using Raman spectroscopy *(French)* 78—88664
- clinical vascular laboratory instrum. management using computer 78—7460
- CODAS, Joint European Torus, control and acquisition system 78—36982
- code generator to identify time, date, and events in physiologic event recording 77—86674
- command language based data acquisition and anal. system for low energy nuclear physics 77—57846
- composite materials, thermographic technique, for examining damage extent 79—43540
- Computed Tomography radiological method for non-invasive examination 77—77979
- computer peripheral system for acquisition and processing of EEG data 80—41270
- computer system of automatic analysis of vectorcardiograms 78—20302
- computerised, for semiautomated X-ray gauging system 77—10156
- computerised pacemaker centre and follow-up network 77—81691
- computerised tomography, divergent beam reconstruction algorithms compared 79—83932
- computerised tomography, positron emission, data acquisition and processing electronics 80—61690
- conference on nuclear power systems, Washington, USA (1978) 79—41045
- controllable real-time data collection system for coastal oceanography 77—5329
- conversational data processing system for instrumental analysis *(Japanese)* 77—82496
- conversion from two to three functional modes of logical address space 78—36981
- COSMOS machine for automatic photographic plate image meas. 80—77293
- Coulter S blood analyser and IBM 1800 computer, minimum-interrupt digital interface 80—3849
- coupling apparatus for DVM and chart perforator to data compilation and registration system 79—93113
- cryogenic resistance and diode thermometer calibration 77—26311
- Crystal Ball data acquisition system 79—89531
- crystallography, electronic stationary picture method 78—38582
- Culham fusion expts., integrated data network for microcomputer based diagnostics 80—13910
- Culham fusion studies, appl. of microcomputer to data acquisition and control 80—13908
- cytological preparation evaluation, optical preliminary data reduction *(German)* 79—5392
- Daresbury Laboratory automated magnet field meas. facility 79—30509
- dead time correction for a counting rate measured with a system of buffer memories 78—86756
- deformation, cyclic, static, meas./recording, automatic system 79—15893
- digital, for computerized ultrasound imaging studies 79—39454
- digital data collection for ion scattering depth profiles 78—56942
- digital data recording, in instrumentation cameras, microprocessor technology 77—79189
- digital data store for radio monitoring of patients *(German)* 78—80998
- dilution refrigerator for low temperature nuclear orientation experiments on line to an isotope separator 79—752
- directional wave spectra meas. from fixed platforms 79—16724
- disc based distributed processing data acquisition and anal. system 77—65024
- discus buoy wave spectra, comparison of buoy-fixed and vertically stabilised accelerometers 79—5678
- distributed microcomputer control system for high-energy gas-laser facility 77—61975
- distributed processing data acquisition system at Brookhaven National Laboratory 79—89532
- diver-operable multiwavelength spectroradiometer 80—90251
- dosimetry, automated data acquisition and anal. system at LAMPF pion therapy facility 78—53506
- drift chamber and pulse height readout systems using analog multiplexing 77—54490
- drift chamber data acquisition, microprocessor based system 80—58066
- drift chambers, CAMAC/NIM for data acquisition and monitoring 77—88338
- Drifting Oceanographic Profile Buoy with minimum vertical motion 80—46306
- Dynasonde software, real-time data acquisition and display 80—36405
- Earth radiation budget data collection and interpretation model 77—37497
- Earth tides, tilts, parallel recording through digital print-out and photorecording channels *(Russian)* 78—88785
- ECG, low-power module for microprocessor systems 80—41292
- ECG body surface potential map estimation, limited lead selection 78—57111
- ECG body surface potential mapping data acquisition system 77—40861
- ECG computerised acquisition, compression, and retrieval 78—36019
- ECG digital recording by mobile cart with microprocessor and DC 300 cartridge recorder 78—85427
- ECG gated acquisition cardiac imaging, quantification of left ventricular function 79—70638
- ECG gated radionuclide cardiac imaging system 79—70639
- ECG signal quality assessment during acquisition 79—70666
- ECG surface mapping, gradient and potential data acquisition system 79—39555
- echocardiogram, M-mode, computer-assisted anal. 78—80942
- echocardiogram on-line computer anal. 78—80941
- echocardiography, real-time, using burst analogue sampling 77—9234
- echographic information related to left ventricle and mitral valve in diastole, anal. by small computer 78—80939

data acquisition continued
- EEG data, low cost microcomputer system 77—40881
- EEG digital recording system for epileptic event observation 78—3641
- EEG phasic event detection by microprocessor 78—57091
- EEG standardised classification, sequential epoch method 78—57101
- electrochemical fast processes, use of high speed electronic memory for data acquisition *(Italian)* 77—9088
- electromyography, computerised, software support in clinical dentistry 79—74780
- electron beam fusion accelerators, data acquisition and processing 78—37469
- electron beam treatment planning, patient specific data acquisition 79—100731
- electron beam treatment planning, symposium, Cincinnati, USA (July 1977) 79—100730
- electron diffraction pattern, digital scanning and recording system for TEM 77—13825
- electron energy-loss spectroscopy in context of TEM, review 80—31945
- electron microscope minicomputer combination and industrial research, method and experimental detail *(French)* 77—34056
- electron probe anal., energy dispersive/wavelength dispersive combined X-ray system, automated control 79—43705
- electron probe anal., X-ray energy dispersive spectrometer appl., data collection, review 77—56312
- electron test accelerator, Chalk River, control computer 78—90004
- electronic speckle pattern interferometry apparatus with multichannel data acquisition 79—80671
- electrophoresis, meas. system *(German)* 77—52692
- electrophysical information collection, recording and processing system 78—8388
- Electrophysiological Data Interface 79—79677
- ellipsometry with pulsed tunable laser sources 77—13796
- EMG, multichannel data acquisition system for the survey of intercostal muscle activity 80—81790
- EMG signal onset and termination establishment method 79—83761
- emission spectrophotometry, review of data processing systems *(Japanese)* 78—88685
- emission spectroscopy signal-to-noise ratio improvement and data processing *(Japanese)* 77—21448
- empirical relationships for random self-avoiding walks on lattices 79—9190
- environmental, Geostationary Operational Environmental Satellite 79—29977
- environmental data acquisition systems, SMART-I and CLEVER COUNTER 79—48196
- environmental information consequences in information systems 79—57500
- environmental obs. from space based systems, present and future 79—5657
- epicardial mapping, DC, during exptl. coronary occlusion, digital data acquisition system 80—85527
- EPR digital data acquisition using microprocessor 80—17975
- ERASMUS Tokamak data acquisition system, program struct. 80—49012
- error definition, for steady and unsteady states 80—95056
- ESCA 36 spectrometer, advanced data anal. 77—90684
- estuarine current meter data acquisition microcomputer system 80—46265
- ETA-BETA fusion expt., data acquisition and anal. programs 80—13914
- Euratom Data Acquisition Co-ordinating Committee activities 80—13904
- event handler, a fast, programmable, CAMAC-coupled data acquisition interface 79—45608
- evoked potential multi-channel data acquisition system, microprocessor controlled 78—11750
- evoked-response data acquisition system, specification and design 80—56165
- EXAFS and photo-electron spectroscopy expts., flexible data acquisition system 78—62676
- exponential decays analogue anal. using transient recorder 78—86244
- eye movement recorders, problems, use in laboratory 80—41331
- Fabry-Perot interferometer, piezoelectrically scanned, microcomputer-based data acquisition and stabilization system 80—62719
- fast event recorder utilizing a CCD analog shift register 79—45578
- fast signal averager based on sampling oscilloscope interfaced to minicomputer 77—57308
- FASTBUS, high speed nucl. data acquisition 78—46251
- FASTBUS, medium energy physics appls. 80—42912
- FASTBUS, molecular data bus system for high energy physics 80—42911
- FASTBUS, project evaluation 79—89555
- FASTBUS—details of addressing and bus mastership 79—89554
- Febry-Perot interferometer, with automated data acquisition and stabilisation system 78—70180
- Fermilab, multi-user control and data acquisition systems 77—54480
- ferroelectric material, dielectric aftereffect meas. with digital data acquisition 77—43952
- field ionisation kinetic data acquisition and processing, computer controlled 78—2999
- First GARP Global Experiment, data collection 79—58055
- flood prediction computer-operated telemetered gauge network 77—21818
- flow, combined visualisation-anemometry technique, appl. to turbulent boundary layer 78—91044
- flow at high Reynolds numbers, real-time statistical laser Doppler velocimeter system 77—3895
- flow microfluorometry instrumentation, rapid data collection, analysis and graphics 78—86348
- four-point sheet resist. meas., semicond. doping uniformity determ. 77—47475
- frequency modulated correlation chromatography, mulitple injection technique 80—40764
- fusion experimental facilities, computerised control and data acquisition 80—13890
- fusion experiments, microprocessor applications in data acquisition and control 80—13918
- fusion reactor, beam-profile fast scan monitor 78—54941
- fusion reactor, diagnostics of radial plasma transport rate, data acquisition and handling system 78—54937
- fusion reactor, mFTF plasma diagnostics Data Acquisition System 80—99319
- fusion reactor, TEXTOR, mag. diagnostics and monitoring systems data acquisition 80—99320

data acquisition continued
fusion reactor, Tokamak data acquisition, multichannel A/D subsystem 78—54936
fusion reactor Ingra injector, control and data acquisition system 80—13913
fusion reactors, PLT and PDX data acquisition systems, networking and distrib. processing improvements 80—99318
gamma camera image processing *(French)* 77—37038
gamma camera low loss data acquisition with subsequent computer anal. 79—49358
gas chromatography, data acquisition and use of microwave plasma detector as element analyser *(German)* 78—64895
gas chromatography-mass spectrometry data system, research-oriented, principles and applics. 80—40770
gel permeation chromatography anal., data acquisition, computer control 80—97746
general purpose automated meas. system based on synchronous waveform digitisation under computer control *(Portuguese)* 80—82753
general purpose laboratory microprocessor system, design and construction 80—82754
geophysical, Fourier series and Markov processes *(Italian)* 80—109254
geophysical balloon data storage, prior to transmission to ground via satellite 80—46263
geophysical ground surveying, portable data logger 80—26615
geophysics, digital signal processing appls. to seismology 79—29915
geophysics, empirical study of scanner system parameters 77—56743
Geostationary Operational Environmental Satellite data acquisition analysis and display 80—17382
geotechnical meas., interactive computerised system *(Italian)* 78—7771
Global Weather Experiment, communications and data management system 79—5620
Graphic Interactive System for Processing of Electrocardiographic Maps 79—39552
graphical information, precision two-coordinate one-mirror scanning device 77—26275
gravitational radiation obs. in 1973-74, data acquisition on Maryland-Argonne detector 77—22476
ground data, remotely sensed, developing countries appl. 79—34963
haemodynamic research, human, physiological signal acquisition and processing 77—44768
Hannover EKG system HES, description 78—7485
hardness testing, depth of impression meas., automated 79—15892
health care deliverty data processing course 79—80394
heat and mass transfer experimental data acquisition system operational analysis models *(Russian)* 79—80588
heavy ion-nuclear reacts., data from large area gas detectors 79—72202
high energy physics data acquisition packages 79—89535
high speed biological cell sorter, data acquisition and display 78—44622
high-performance data-acquisition and data-analysis computer system 79—93899
HISS computer facility 79—89559
hodoscope read-out, fast sparse-data-scan system using CAMAC compatible elements 79—45609
hodoscopic detector registration systems, data coding/reading block 78—78602
Holifield Heavy Ion Research Facility 79—93900
hybrid pulse pile-up rejection system, Rutherford backscatt. appl. 79—2884
hydrometeorological information, microprocessor appl. *(Italian)* 77—82067
Hydrometeorological monitoring in weather modification programs 78—69544
hydrophones, towed, location, data acquisition system 79—2401
IBM 3630 modular data acquisition and communication system for industrial production *(German)* 79—30438
imaging system fundamental limits and degrees of freedom 77—50630
incremental compiler for data acquisition 79—89550
infralow-frequency processes, probabilistic and statistical characts. meas. 79—71431
instrumentation tape recorders 78—49817
integrating vidicon systems at Cerro Tololo, data acquisition and reduction software 79—66924
intensified-Si intensity target vidicon application to IR astronomy 78—81544
interactive computer program for measurement of data obtained using the extra-stimulus technique during electrode-catheter studies 78—24156
interface, Event Handler II 79—89542
interferometer superposition fringe pattern, automated central achromatic fringe setting 78—24852
interplanetary charged particle flux meas. in space, digital onboard processor appl. 77—64610
intra-ocular pressure measurement using sonics and coherent optics 77—81548
intrinsic semiconductor IR detector array data acquisition system 78—77991
ion diffusion coefficients, meas., computer-assisted technique using Cottrell eqn. 80—3425
ionosonde, digital universal, operation modes 78—73577
ionosphere soundings using small spaced receiving system 80—36406
Ionospheric Sounding Satellite, telemetry receiving system *(Japanese)* 77—78610
Ionospheric Sounding Satellite control, data recording and anal. system *(Japanese)* 77—78611
Ionospheric Sounding Satellite control centre, automated telemetry data acquisition *(Japanese)* 77—78606
IPNS time of flight neutron scattering instruments system 79—89558
IR interference spectrometer data collection interface *(German)* 77—87854
IR spectrophotometer, digital data acquisition/analysis system 80—73482
JET, control and data acquisition system, CODAS 78—62619
JET, control and data acquisition system 80—13905
KEKNET, a high speed on-line network for high energy physics 79—36493
Knudsen cell quadrupole mass spectrometer, high temp., control and data acquisition, system 79—26171
Knudsen torsion-effusion pendulum data acquisition system, computer-automated, for meas. of vapour pressures at high temps. 79—49214
laboratory computer systems, minicomputers, microprocessors, uses 77—79072
laboratory data acquisition and control system based on Commodore PET microcomputer 80—204

data acquisition continued
LAMPF data analysis techniques 79—89562
LAMPF standard data-acquisition system 79—89534
land seismic reflection exploration data acquisition systems 77—29444
LANDSAT agricultural monitoring program to monitor corn in Iowa 77—78495
LANDSAT digital data for classifying vegetative cover 77—78543
LANDSAT sensing, territorial administration *(Italian)* 77—82057
large scale digitiser system for charge and time digitisation in high energy physics exptl. 77—54489
laser data acquisition/analysis system for Si vidicon optical detector 78—58041
laser Doppler anemometery digital data acquisition system 77—80253
Levitron experiment, Culham, plasma fluctuation and by microcomputer system 80—13911
lidar, data acquisition in DFVLR mobile system 77—53248
linked controllees and index-tabled techniques for data storage and rapid retrieval 79—9983
lip and jaw motion during speech, video-scanning system 77—56388
liquid, self-diffusion meas., automated technique, using NMR spin echo 78—27114
liquid chromatography, spectrometric detect., computer control of data acquisition, reduction and display 78—27850
liquid thermal conductivity meas., data storage in transient hot wire method 77—30144
Los Alamos P-9 accelerator facility, CAMAC data acquisition system 79—45607
low-temperature measurements of energy release and resistivity recovery in irradiated metals 80—31756
LSI-11 based auxiliary crate controller for beam line and experiment control 79—89565
lunar occultations observations, microprocessor-controlled data acquisition system 77—49311
Macsym One, automated measurement and control system based on 'real world' signals 79—17402
magnetic large aperture spectrometer for the study of multibody photoproduction in the incident energy range 1-5 GeV 79—715
magnetic spectrometers data acquisition and anal. 79—89530
magnetic susceptibility instrument, supercond., automatic, biological appl. 78—57153
magnetic tape station interface to CAMAC for on-line data acquisition and reduction system 77—34532
magnox fuel cladding, surface struct. data acquisition and processing system 80—898
marine deep seismic sounding system with digital data acquisition 77—87083
marine environment, air-sea interaction buoy, instrumentation and data acquisition 79—66813
marine environment test range semi-automatic data recording and monitoring (SADRAM) system 79—39993
marine profiling system for shallow water 78—36328
marine seismic data acquisition, minicomputer based system 77—82072
marine seismic exploration data acquisition systems 77—29445
marine waste disposal information reliability 79—12275
Martian gravity field spherical harmonic representation using short-arc technique 77—73999
mass spectra, automatic recording microphotometer modification 77—12845
mass spectrometer, double focusing type, automatic acquisition and shape anal. of metastable peaks 79—89036
mass spectrometer with computer controlled data collection 78—82071
mass spectrometry, computerised data acquisition and interpretation, review 78—321
mass spectroscopy computer acquisition and analysis of metastable transition data using electric sector voltage variation 78—70102
MDS-501 DMA channel controller, interface between Biomation 8100 and Intel MDS-800 microcomputer system 80—203
mechanics expts., model for computer based data acquisition and control 77—63844
medicine, nuclear, microprocessor systems for data acquisition, image processing, RIA anal., patient data retrieval 80—61670
meteorological, computerised data collection system *(German)* 80—37007
meteorological information flow system *(Japanese)* 77—56754
meteorological observation system using telephone switching network 79—80031
meteorological quantity mean value measuring system *(German)* 78—16220
meteorological real-time data acquisition and anal. 78—69466
meteorological satellite Earth-based receiving stations, minicomputer appl. 77—78431
meteorological systems for operators on continental shelf 79—70887
meteorology, boundary layer data acquisition and analysis system 77—60471
meteorology, system for airborne research 79—66808
Meteosat data collecting platform *(Danish)* 80—12637
Meteosat for weather data collection, single cabinet telecommunication equipment 78—36419
meterological radar data acquisition system at Spino d'Adda ground station 78—69468
micro-based, low cost, system, developed in Vienna 79—44905
microclimatology, process computer appl. thermal balance recording methods 80—82044
microcomputer based nuclear system 80—63500
microcomputer based ocean observation system 79—16677
microcomputer system, appl. to NMR experiments *(Japanese)* 79—75564
microcomputer system for automating analytical instrumentation 78—73127
microcomputer-based data acquisition and anal. system for CO_2 rebreathing studies 78—36005
microcomputer-based data acquisition and analysis system for CO_2 rebreathing studies 80—36161
microcomputer-based data acquisition system for NMR spectrometer interfacing 78—74042
microcomputer-based systems 80—27277
microcomputer-controlled, multifunctional seafloor instrumentation system development 79—53584
microcomputers in biomedical and clinical applications 78—73283
microprocessor—based unit data acquisition and reducing system 80—21598

data acquisition continued
microprocessor based data acquisition and exptl. control system 78—36086
microprocessor based timed reading and time plot CAMAC modules 77—54484
microprocessor controlled dual parameter ADC system with CAMAC interface 79—3337
microprocessor multiple arrays, operating systems for nuclear diagnostic system 79—49918
microprocessor-based, for wind study features 79—60087
microprocessor-based, programmable laboratory equipment controller and data acquisition system 79—6104
microprocessor-based data acquisition systems, data compression 79—12270
microprocessor-based for surveying data acquisition and processing 79—29913
microprogrammable system, MIDAS IIA, meteorological appl. 78—77374
microscope photometry, on-line data collection and processing for solids, fossils and organic matter *(German)* 79—26101
MIDAS, microprogrammable microprocessor-based integrated system 77—64496
minicomputer appls. in analytical laboratory 79—75508
minicomputer based, reflection spectra measurement 79—61402
minicomputer data acquisition system for Princeton cyclotron facility 78—90048
minicomputer driven microprobe *(French)* 78—74111
minicomputer general purpose system 79—89543
MINUS3—a general purpose data acquisition system at LBL's 88″-cyclotron and superHILAC 79—93901
Mississippi River computerized data bank 78—73520
mobile gamma camera with remote image processing computer system, for nuclear medicine 78—92700
modular minicomputer multiparameter data system, neutron spectrometer 77—23396
modular-programmed data acquisition/anal. in nucl. research 77—18766
moire fringe data handling system, industrial lab. appl. 79—30523
molecular biology, time resolved X-ray scatt. expts., rapid data collection systems 80—61740
Mossbauer CAMAC data acquisition system 79—30439
Mossbauer data acquisition system using minicomputer 78—90050
Mossbauer spectra, active data acquisition 80—9079
Mossbauer spectroscopy, data acquisition and processing system 80—18061
Mount Wilson solar magnetograph, computer-operated image scanning and data system 77—22073
multi-microprocessor auxiliary crate controller, data processing in CAMAC 78—46246
multi-parameter distributed processing data acquisition, display, and on-line analysis system 79—45612
multiaxis neutron diffractometer automation 80—102417
multiband radiometer for field research 80—90250
multichannel analogue transient acquisition system 78—4601
multichannel analyser to computer interface 79—93904
multichannel EKRAN installation for the treatment of random-process parameters 80—13047
multichannel electrometer data-acquisition system 79—89564
multichannel polarimeter, data acquisition and control system *(Japanese)* 80—77842
multichannel pulse height analyser adaptation for 4096×4096 two-parameter meas. 77—14316
multielement array underwater acoustic instrumentation 80—43571
multimicrocomputer system with dynamic variable hierarchy for real-time data acquisition 78—44654
multiparameter data acquisition and display program 79—89547
multiple data streams, dynamically configured software system 79—89548
multiple detector data acquisition system, microcomputer based 78—90049
multiple microprocessors for continuous patient monitoring 80—26389
multiplexing systems, microprocessor-based, remote- and central-type comparison, cost anal., appl. 78—89971
multiprocessor based data acquisition system, design 79—89556
multipurpose data acquisition and processing system based on Mir-2 computer 78—32799
multispectral aerial imagery capabilities for military geographic information acquisition 77—82054
multivariate discrete information analyser, particle recording appl. 78—78601
muscle contraction, time resolved studies using small angle X-ray diffr., design of data collection system 79—12052
MWPC, CAMAC readout system 78—46248
MWPC, correcting codes for information registration 78—94176
MWPC, flat area detector data acquisition system for X-ray crystallography 80—91381
MWPC, nondestructive readout system 79—3315
MWPC read out, fast clustering processor 79—76304
NDT, data processing and acquisition for product quality control 80—11862
Netherlands fusion expts., data acquisition and anal. systems 80—13915
neural spike trains rel. to physiology and behaviour 77—13035
neuromuscular miniature endplate potential online acquisition microcomputer system 78—36015
neuron and neuronal assembly 3D computer reconstruction 80—21596
neurophysiological experiments, fast data acquisition and processing system, minicomputer appl. *(Japanese)* 80—85536
neurophysiological spike unit data acquisition and reduction system 79—79713
neurophysiology, computer assisted unit data acquisition/reduction 78—61266
neutral beam injectors, spectroscopic diagnostics, on-line data acquisition, anal. 77—82643
neutrino channel monitoring system, acquisition of digital information 77—3199
neutron detector, expt. control and data acquisition system 79—45589
neutron experiments, Braunschweig accelerator facility, data acquisition and anal. 80—47806
neutron standard cross section expts., flux monitor, source, data acquisition and anal. 78—90039
Niels Bohr Institute on line data acquisition system 79—89557

data acquisition continued
NMR pulsed, automatic trigger pulse logic for pulse programmer 80—47084
NMR spectrometer-computer interface, demonstration expt., signal averaging influences on S/N ratio 80—36813
nonexponential nuclear relaxation data acquisition and processing system using Nairi-2 computer 78—32800
nonlinear optics, digital data acquisition and on-line processing at Moscow State University 78—46709
Northern Cross radiotelescope, data acquisition system *(Italian)* 77—5426
nuclear data acquisition real time flexible processing software 79—36495
nuclear detector data acquisition and processing equipment, evolution 79—72219
nuclear imaging 80—3801
nuclear instrumentation, computer-based data acquisition system for multi-station teaching laboratory 78—4446
nuclear instrumentation, standard microprocessor based 80—36822
nuclear instrumentation laboratory course, computer based data acquisition and anal. 80—36820
nuclear laboratory instruction with multichannel analyser/microcomputer system 80—31471
nuclear medicine, data evaluation system for use with gamma cameras 78—92732
nuclear medicine, digital data collection system, portable, cost-effective 80—41195
nuclear medicine, Janus III, computer system for acquisition, processing of diagnostic units data 78—80948
nuclear physics data acquisition with UNIX time-sharing system 79—41085
nuclear physics expts., versatile data handling system based on PDP 11/03 microcomputers 79—76319
nuclear physics GSI data acquisition system 79—89533
nuclear power stations, computer control systems for data acquisition and process control 79—22426
nuclear power stations, using fast analogue scanner 77—6656
nuclear power stations containment structures testing, for pressure tightness *(Spanish)* 80—13775
nuclear reaction on-line data acquisition system for monitoring high resolution multidimensional spectra 78—58567
nuclear research reactor program 78—86679
nuclear spectroscopy 14-channel linear multiplexer 78—33400
nuclear steam generator tubes testing and evaluation, using CIS/DASIO system *(Czech)* 80—63301
nuclear track emulsions, automatic plate scanning 79—72191
nuclear ventriculograms, processing and display 77—86627
numerical digital filter for on-line processing of wind tunnel data *(French)* 80—19537
obstetric computer-aided monitoring system *(German)* 80—41300
obstetrics, microprocessor based system for studying kinematics of labour 77—44769
obstetrics monitoring, microprocessor data acquisition and preprocessing with minicomputer signal processing 77—44775
ocean ambient noise, data acquisition system and statistical anal. 77—79996
ocean buoys, environmental data acquisition 78—36287
ocean data collection, drifting buoys appl. 79—5668
ocean dynamic data, acquisition and display by portable real-time minicomputer system 80—12552
ocean measurement remote data access systems 77—41172
ocean sediment geotechnical prop. determ. instrumentation problems 79—12304
ocean test structure for wave force meas., improved platform design [Ocean Test Structure] 79—12306
ocean wave directional spectra, from discus buoy, data processing 79—16723
ocean wave directional spectra, routine meas. system, from discus buoys 79—16722
ocean wave directional spectra monitoring horizontal-spar buoy, design 79—21083
ocean waves and currents on Norwegian continental shelf 79—12120
oceanic temperature-depth profiles, recording via solid-state memories 78—24383
oceanographic buoys, electronics and telemetry developments 79—5659
oceanographic data, US current meter applic. 77—41211
oceanographic data acquisition and processing system, microprocessor based, real-time 79—16676
oceanographic data buoys, environmental data quality estimates 77—5364
oceanographic data requirements for coastal and offshore structure study 79—12272
oceanographic information, automation of collection, processing and anal. on small-computer base 80—101439
oceanographic integrated research ship, with data acquisition and processing systems 79—34969
oceanographic measured data quantification 79—12274
oceanographic microprocessor applications *(Italian)* 77—82068
oceanographic monitoring stations in Arabian Gulf, computer control and data acquisition 79—8728
oceanography, information exchange between probe and computer during R/V 'Akademik Vernadsky' cruise *(Russian)* 78—77363
oceanography, Kiel multi-purpose sea probe microprocessor-based data acquisition system *(German)* 78—85701
oceanography, LANDSAT and SEASAT remote sensing 79—12309
ODMR spectrometer system, use of signal averager with minicomputer facilities for control, data recording and evaluation 80—31825
offshore environmental and platform data processing from Norwegian continental shelf 79—12273
Omo River project (Ethiopia) data management system appraisal 78—57326
on-line, for particle physics expts. using PDP-11 computers 80—27913
online analysis of large bubble chamber pictures, data acquisition system, CDC 1700 computer *(French)* 77—42223
online real-time data acquisition system design 78—35994
optical fibre data collection highway with piezoelectric phase modulators 77—39098
optical spectra, direct encoding using computer interfaced vidicon TV camera 77—10114
parallel preprocessing, nucl. data acquisition system 78—46247
Parkinson tremor, long-term recording and evaluation 77—21639

data acquisition continued
- partial discharge amplitude spectra, acquisition and automatic processing system *(Italian)* 79—93108
- partial discharge long-time tests, automatic data acquisition and computation *(German)* 79—71432
- partial discharges, on-line computerised system for meas. in insulation structures 77—5863
- particle and nuclear physics, conference, Santa Fe, NM, USA (1979) 79—88779
- particle beam phase space meas. at 2 MHz particle rate 77—54383
- particle counter, programmable command data acquisition equipment *(French)* 77—54464
- particle detectors, microprocessor-controlled data acquisition system for temporal/angular correl. between β- and γ-ray emission *(Spanish)* 80—106238
- particle track chamber, semi-automatic meas. instrum. register for camera photograph reduction 78—78575
- patient fluid management records system 79—25150
- patient-contouring, electronic device, for radiotherapy treatment planning 77—13029
- PDP 11 and MBD branch driver 79—89567
- PEP storage ring, high-speed data acquisition and analysis system 80—23194
- PETRA storage ring, serial data acquisition system 79—72085
- photoelasticity techniques, extension into IR region 79—30443
- photoelectric image acquisition system at Trieste Astronomical Observatory *(Italian)* 79—58256
- photoelectric spectrographic detection, direct reading attachment 80—275
- photoionisation mass spectrometer, balloon-borne for stratospheric gas meas. 78—85732
- photolysis and radiolysis, kinetic data acquisition, and anal., by computer based system 79—39180
- photometry, high speed digital compensation system 77—18112
- photometry for astronomical appl., data collection with aid of microcomputer *(Czech)* 80—67570
- photonuclear reactions, on-line acquisition of N-fold coincidences 77—79527
- physical activity determination, analogue/digital data output equipment appl. 77—70560
- physiological data recorder, microprocessor-based hybrid system 77—44872
- Pioneer Venus Differential Long Baseline Interferometry expt. 80—67578
- Pioneer Venus Multiprobe entry phase, telemetry recovery 80—67493
- PISCES submersible scientific equipment and data acquisition system 77—5381
- plasma diagnostics, Thomson scatt. system, analogue data processing circuits 78—87488
- plasma electron temp. and density meas., semiautomatic system for double probe anal. 78—87490
- plot system developed for nondestructive materials testing exam. 78—53067
- PLT, neutral beam test stand, data acquisition system 78—62622
- Plurimat 20 data acquisition system, phys. appls., automatic simultaneous data recording *(French)* 77—41579
- Portable Automated Mesonet, design, performance and operation, for meteorology 77—78426
- position sensitive detectors, pseudostructures in spectra caused by digital data acquisition 79—76320
- Princeton cyclotron data acquisition system 79—89528
- Princeton Cyclotron data acquisition system 80—102415
- proportional counter data acquisition system 80—42913
- prototype autoresonant, accelerator, computer system, data acquisition and processing 80—99433
- prototype CCD system for the time projection chamber 79—45575
- Pull-Up Shallow Water Seismometer, data acquisition system 78—45025
- pulmonary gas exchange data online acquisition system 78—28100
- pulse height analysers, CAMAC data acquisition interface 79—3336
- pulse height analysis programs for high event rates, organisation 77—407
- pulse-delay sampling system for nanosecond transient decay analysis of fluorescence 80—37004
- pulsed data A-D acquisition system 79—22572
- pulsed electrostatic probes as diagnostic for transient plasma 78—94937
- pulsed NMR data acquisition system, devel., appl. to polyisobutylene 80—34807
- PWR, thermohydraulic processes obs. in high press. water loop *(Hungarian)* 78—82432
- pyranometer for total hourly horizontal solar radiation data, USA 77—25765
- Q data acquisition system for PDP 11 79—89545
- Q system: an experiment in software standardization for data acquisition 79—89549
- QAL, data acquisition language 79—89551
- radar cross section meas. of cloud-to-ground lightning 77—2279
- radiation therapy simulator and linear accelerator meas. and control by microprocessor 77—40902
- radio astronomy, computer techniques for 8550 MHz sky survey 77—17708
- radioactivity meas., statistical distribs. accumulation in real time 78—94178
- radiographic imaging, digital video acquisition system for extraction of subvisual information 78—69208
- raingauges, tipping bucket type, digital recording system description and field testing 80—77161
- rapid CAMAC data handling in FORTRAN real time programs 79—45616
- real time data acquisition system for controlling and collecting data from laboratory instruments 78—54348
- recorders, rack-mounted and portable, state of art and appl. 79—40555
- remote platform data acquisition and control by minicomputer 77—5330
- remote sensing, data acquisition review 77—2286
- remote sensing, sensors and detectors in NASA's future mission 79—5656
- remote sensing by artificial satellites, geophysical applications *(Swedish)* 77—67001
- remote sensing image data processing/acquisition techniques 78—61627
- remote sensing of Earth from space, role of 'smart sensors', book 80—62402
- RF environmental field intensity automated meas. system 77—37947
- Rutherford Laboratory N5 expt. data acquisition system, program struct. and CAMAC hardware 78—90051
- SABRE computer system for assessment of body radioactivity 77—77998

data acquisition continued
- SAR: a fast computer for CAMAC data acquisition 79—89569
- SAR/LANDSAT data set assembly and anal. 77—78493
- satellite Anik 1 data collection development program, environmental data 79—39867
- satellite solar cells radiation damage obs., GaAs and Si 79—48134
- scanning wavelength kinetics experiments, statistically weighted principal component anal. 77—77826
- scattered light spectroscopy, data acquisition by add-subtract digital correlator 77—61053
- scintigraphic images, acquisition and processing system, simultaneous use of several radioisotopes *(French)* 77—70520
- seafloor earthquake meas. system, acoustic telemetry 79—5689
- seismic, Tasmania University seismic net, electronic development 80—82073
- seismic data, broadband, digital recording and anal. at Graefenberg array 79—25348
- Seismic Research Observatories, upgrading of worldwide seismic data network 77—5334
- seismological data collection and anal., detect. of possible violations of Nuclear Test Ban Treaty 79—39919
- seismological investigations, new instrumentation and recording techniques 77—53228
- serum samples, trace element anal., automatic data acquisition, on-line method 78—48726
- shipborne automatic data collection, GRAD system, for marine geophysics 77—78428
- Shiva laser beam diagnostics 78—59037
- Shiva laser computer control system 78—59034
- Shiva laser fusion facility, target diagnostic system, data acquisition and anal. 78—51366
- signature analysis systems with Fourier analyzer 78—87195
- SIMS, computerised system for energy spectra determ. 80—3423
- single-photon fluorimetry, time-correlated, data acquisition rate optimisation 79—20494
- solar collector-heat pump installations, meas. of efficiency under operational conditions *(German)* 80—101077
- solar data collection system using microprocessors 78—69542
- solar energy system control, 16 channel data logger and serial data link 80—50947
- solar furnace temp. meas. using digital pyrometry system 77—37896
- solar heating systems, instrumentation principles for performance meas. 80—35743
- Solar Radio Data Acquisition and Communication System (SORDACS) of Toyokawa Observatory 79—101074
- solar spectral distribution monitoring, broadband filter radiometry error anal. 77—53163
- solar-terrestrial environment monitoring and forecasting system, SELDADS, for radiocommunication appls. 79—58097
- SOLIS system 80—74030
- spececraft, manned, data acquisition and logging system incl. speech 80—61979
- spectral data, IR, microwave and Raman, simultaneous computer acquisition *(Japanese)* 80—4776
- spectrometer with high data rate, computer coupling system *(German)* 79—49212
- spectrophotometers, microprocessor based data acquisition and control system 80—22335
- spectroscopic observations of stars and planetary nebular, via multichannel analogue detector system 78—36461
- spectroscopy, compilation of computer-readable reference data libraries 78—64894
- speech analysis, computer-controlled method for articulatory activities meas. 77—56391
- SPEED 2, computer program for data reduction from automatic data acquisition systems in FORTRAN 80—27279
- stereo cassette tape recorder for recording analogue voltages by digital technique 77—61061
- stopped-flow spectrometry for acquisition of kinetic data *(French)* 77—12779
- stratified acreage estimates in Illinois crop-acreage expt. using LANDSAT data 77—78501
- striated muscle diffraction patterns, use of direct memory access microprocessor system 80—89918
- submersible data acquisition system SCRIBE 80—46266
- subnanosecond EM pulse data acquisition and processing system 78—32801
- Super-Phenix FBR, data processing and collection *(French)* 79—76107
- synchrotron radiation camera and data acquisition system for time resolved X-ray scattering studies 80—99023
- synchrotron radiation facility expts., distributed computing system for data acquisition and control 77—38513
- system assembly for pulsed fusion experiments 80—49011
- system designing for accelerator development facility 77—57307
- temperature measurement techniques, sensor/instrument interface optimisation 77—5835
- terrain classification using colour imagery, algorithms 77—78466
- terrain data production using distributed processing 77—37413
- Texas Experimental Torus, data acquisition and processing system 77—24217
- TFR Tokamak, microcomputer data acquisition system 80—13916
- thermal desorption mass spectroscopy, computer control, data acquisition, appls. 80—61181
- thermal plume measurement systems for Great Lakes coastal waters, data acquisition and handling 78—44891
- thermo-physical expts., information input unit for the 'Iskra-1122' electronic keyboard computer 80—201
- thermogravimetric data acquisition and reduction program 78—64901
- thermophysical process ambiguous data gathering and processing optimisation *(Russian)* 80—73335
- three-coordinate measuring machine, dynamic acquisition and automatic reduction of data 79—75507
- tide gauging network, automated, data acquisition and telemetry 79—5692
- time service, data acquisition and real time processing system *(Italian)* 80—8549
- time varying X-ray fields, digital acquisition system 77—57828
- time-freq. secondary standards, VLF radio station phase reception/processing convertor 77—87739
- time-freq. secondary standards automatic recording/processing system 77—87738

data acquisition continued
time-resolved X-ray diffraction counter and data acquisition system 78—45758
tissue parameter identification by digital processing of real-time US clinical cardiac data 80—51191
Tokamak far IR Fourier transform spectroscopic Michelson interferometer 80—59294
tomography, Donner 280-crystal positron tomograph, data acquisition, image reconstruct. and display 80—61671
transient data systems, state of the art and trends 79—89546
transient recorder for signal averaging, microcomputer-controlled 80—31723
TREAT fast-neutron hodoscope, time and mass resolution of fuel motion, data acquisition system 79—41003
TRIUMF biomedical pion beam automated dose mapping system 78—73254
TSC data handling by on-line use of computers 78—10832
turbulence structure around oscillating airfoils, digital processing of unsteady periodic signals 80—10340
two-channel data gathering and registration system for fast-action experiments 78—77877
two-probe synchronized sampling technique for measuring flows behind rotors, calibration 80—14865
unsteady aerodynamics research, data acquisition using minicomputer 80—10337
unsupervised data gathering, operation of receiving stations *(Italian)* 80—4692
urban hydrology, US National Weather Service programme 77—37267
US computerised tomography, improvements in data acquisition and pre-processing 80—26309
US computerised tomography 80—26310
US digital moving target indicator system for diagnostic use 78—11710
US imaging system appl. 80—99905
US National Earthquake Information Service seismic data acquisition 77—29446
USSR Hydrometeorological Service, automation of data collection and processing 79—34994
USSR State Time and Frequency System data collection and processing automation 77—79074
vapour pressure computer-automated meas. by simultaneous Knudsen torsion-effusion method 80—73334
vapour pressure measurement, torsion-effusion method, automatic data acquisition 80—52188
vascular interface system for automation of haemodynamic monitoring and therapy 78—81054
vectorcardiography, microcomputer system 79—70669
Venus Pioneer Orbiter, electron temp. probe data acquisition and handling 80—67500
very long base line radio interferometry, data recording and processing system *(Russian)* 77—5449
vidicon-camera parallel-detection system for angle-resolved electron spectroscopy 80—4817
voltammetry, cyclic, AC, on-line digital FFT faradaic admittance data acquisition 78—61118
vorticity measurement in unsteady flow, digital data acquisition 80—19525
wave data analyser system for buoys 77—5362
weight data, computerised acquisition and processing methods *(German)* 79—30437
wind pressure data acquisition system, microprocessor based 79—70888
wind tunnel system, for architectural and industrial testing, Oxford University 78—22443
wind tunnel testing, conference, Rhode-St-Genese (1976) 77—27634
wind velocity meas. system, computerised 77—56742
wind-tunnels appls., of digital filters for low freq. range 80—10336
Woodward polarcardiographic service for ECG diagnosis improvement 79—39583
X-ray diffraction, time-resolved, using position sensitive counter 77—13831
X-ray diffraction chem. anal., historical review 77—70383
X-ray diffraction data acquisition using position-sensitive counter *(Japanese)* 78—88774
X-ray diffraction diagrams time-resolved recording, muscle contraction kinetics obs. *(Japanese)* 80—56291
X-ray diffraction expts., SPADE software package 79—63195
X-ray image processing with SEM, automated data acquisition *(French)* 78—41379
X-ray photoelectron spectroscopy, quantitative, parameters, appls. 79—43697
X-ray survey instruments, automated calibration and recordkeeping system 77—37876
ZGS 500 MeV booster synchrotron, data acquisition and control, sequential logic and minicomputer 77—83304
Pr wire thermal cond. automatic meas. device 78—54362

data communication equipment
see also computer peripheral equipment; data transmission equipment
bidirectional fibre-optic data bus with T-couplers 77—19451
biomedical laboratory instrument to computer coupler 80—41271
coupling of fibre optic data links 80—43450
data bus system optical coupler with light conducting fibres *(German)* 80—43438
device coupler for interactive systems 78—24767
Earth satellite Meteosat for weather data collection 78—36419
facsimile features, ground receiving systems, Earth survey data 77—82012
fibre optic data bus systems 78—25949
fibre optic technology, advantages over elec. cable 77—7196
fibre optical digital data bus interconnect system techniques 78—13793
fibre-optic directional coupler developments and applications 79—94330
fibre-optic processor serial interconnect system 78—1426
fibre-optical, propagation principles *(German)* 79—81529
high concurrency data bus using arrays of optical emitters and detectors 79—76805
hybrid optoelectronic modules for OEM fibre-optic data systems 79—86259
IBM 3630 modular data acquisition and communication system for industrial production *(German)* 79—30438
medium-range data transmission optical cables 77—39096
mosaic liquid crystal controlled transparency for holographic store data input *(Russian)* 79—94182

data communication equipment continued
multimode fibre branch fabrication 77—88955
multimode fibre coupler for optical data bus systems 78—1414
optical data bus, glass fibre branch couplers, digital data transmission *(German)* 79—89999
optical data bus single mode fibre, with star couplers 80—64199
optical data highway junctions and systems 77—39097
optical fibre analogue data transmission *(German)* 80—23781
optical fibre angular scrambling star couplers 80—53465
optical fibre cable data highway and branch circuit 77—19453
optical fibre data bus, active fail-safe terminal 78—55438
optical planar coupler in data bus system with single multimode fibres 77—11024
optical waveguide data bus system configurations 79—18544
US switch appl., two-board design 78—46870
Ga$_{1-x}$Al$_x$As feedback-stabilised injection laser for fibre-optic data transmission 77—19343

data communication systems
see also computer peripheral equipment
1.6 km half-duplex optical data link 80—14470
5 km fibre-optic data transmission link 77—65622
10 Mb/s short-distance fibre-optic data bus 77—68276
16 and 32 Mb/s optical data links 77—68275
16 and 32 Mb/s short-haul high-performance optical data links 78—1421
aircraft satellite data link, for meteorological reconnaissance data transmission 78—96299
analogue fibre optics data communication system, high resolution 77—46810
astronomical balloon-borne equipment, data communications 79—16793
automated meteorological data transmission from commercial aircraft via satellite 78—57327
avionic multiterminal data link, fibre-optic interconnection system 78—46805
buoy for oceanographic and atmos. data acquisition, using Meteosat data transmission *(German)* 80—90224
decentralized instrumentation and control system with bus transmission in nuclear power plants 79—97847
digital data compositon for satellite and radar imagery 80—67413
ECG transmission, 3-lead, over Post Office telephone network, central computer analysis appl. 77—86698
Farley Nuclear Plant Data Link System 79—9797
Fermilab booster beam damping system, high-speed RF data transmitter 77—88296
fibre optic data distribution system using variable tap ratio couplers 77—83953
fibre optic systems 79—72676
fibre optics data link, radiation testing degradation, transient outage time performance 77—19405
fibre optics for computing system interfaces 77—68278
fibre optics tasks of NASA, review 78—42441
fibre-optic data bus design and circuit miniaturisation 79—90034
fibre-optic data bus system design and implementation 77—7017
fibre-optic data transmission, principle and methods 79—10393
fibre-optic data transmission links *(Danish)* 80—10009
fibre-optic data transmission systems for plasma diagnostics 80—79571
Finnish seismic array, data transmission, recording and handling 79—39917
Global Weather Experiment, communications and data management system 79—5620
Hermes, geostationary communications satellite, Canadian design 78—93068
interstellar probes, communications philosophy 79—21133
local distribution fibre-optic cable system 77—68277
low loss waveguide communicator, technological aspect *(Italian)* 79—50388
meteorological data communication system, Africa, SIRIO 2 satellite appl. 79—96806
meteorological data relay, aircraft-to-satellite 80—17380
military avionics interconnection fibre-optic data bus 78—46806
multimode fibre communications, electro-optic multiplexer system 79—18510
ocean bottom refraction seismograph, data telemetry to surface vessel 79—39892
oceanographic monitoring stations in Arabian Gulf, data telemetering and anal. 79—8728
oceanography, data exchange between probe and computer *(Russian)* 78—77363
offshore oceanographic buoy with new mooring design, antenna for satellite telemetry systems 79—5660
optical, effect of fibre wall thickness *(Spanish)* 79—18543
optical data bus system with planar access coupler, optimized layout 78—33823
optical data bus T-system, single multimode fibre, based on access coupler 78—46810
optical fibre, communication link between computer units, using LED-photodiode pair 78—71224
optical fibre bus systems, for electrical control TDM signals *(German)* 78—25968
optical fibre communication, cabling, light source and receiver technology, review 78—59125
optical fibre data and telemetry links 79—27390
optical fibre data transmission system, operational 18-channel 78—46823
optical fibre multiterminal data system for aircraft, based on time division multiplexing 78—46811
optical fibre system, data transmission performance study 78—38028
optical fibre waveguides, quasisingle-mode three-layer, data transmission 79—94360
optical fibres appl., in defence field 77—75670
optical fibres in Italy, short distance appl. 79—50369
optical link using wave division multiplexing 79—94365
paper tape data transmission, wavelength multiplexing, optical fibres 80—43454
parallel transmission system using high density optical fibres *(Japanese)* 80—87507
Pioneer Venus, Unified Abstract Data Library and Quick Look Data Delivery System 80—67494
Prestel, as an information service 79—48979
Prestel, Post Office viewdata system, Meteorological Office participation 79—16675
protocols, communication control and data nets 79—89576

data communication systems continued
- RESMAC, Mexican microwave seismic array 77−5355
- satellite transmission, distribution of sound, graphical pictures 80−31463
- seismic data teleprocessing global network 77−29255
- seismological data collection and anal., detect. of possible violations of Nuclear Test Ban Treaty 79−39919
- Seismological Service of Canada, instrumentation and data processing 79−39914
- Solar Radio Data Acquisition and Communication System (SORDACS) of Toyokawa Observatory 79−101074
- space information systems, real-time data management, economics 79−92600
- Spacelab, high rate data handling in space and on ground, multiplexing system 79−21138
- Spacelab, payload data path from user input (on-board) to user ouput (laboratory) 79−21137
- Spacelab data acquisition and communication system 79−84643
- teleconferencing, computer network appls. to geology 77−53202
- Vela seismological network, datacomputer communications protocols 78−81411
- waverider buoy GOES satellite relay system reporting 79−5663

data compression
- *see also information theory*
- aerosol pattern recognition using laser radar *(Japanese)* 80−51028
- astronomical plates meas. via automatic microdensitometer, data compression filters 79−80230
- biomedical signal and image processing, digital techniques *(Croatian)* 78−44623
- biomedical signal high efficiency freq. anal. and data compression through digital filtering 78−31939
- code delta-modulation for standard hydrophysical information compression *(Russian)* 78−65432
- data acquisition systems, microprocessor-based, processing technique 79−12270
- digital data compression device *(Russian)* 77−60484
- digital image processing applications, seminar, San Diego, CA, USA (Aug. 79) 80−105424
- display system for differential diagnosis hand tremors, artificial limb tracking appl. 77−86697
- Earth resource image processing techniques *(Italian)* 77−82063
- ECG compression by prediction or interpolation and entropy encoding 80−8199
- ECG computerised acquisition, compression, and retrieval 78−36019
- ECG data, quantisation studies 80−26396
- ECG data analysis for data compression 79−100766
- ECG numerical encoding and transmission, microprocessor appl. 77−44798
- ECG real time data compression, realisation techniques *(Italian)* 79−5389
- ECG signal processing appl. *(Italian)* 79−96670
- ECG/VCG storage and transmission technique 77−44796
- EEG data compression via computer-generated evoked response to sensory stimuli 78−36016
- EEG signals, reduced spline representations 77−44803
- EEG signals hierarchical modelling 80−109052
- geophysical data analysis, linear compression filter for random values separation *(Russian)* 79−74983
- LANDSAT multispectral sensor image adaptive coding techniques 78−45060
- medical US data compression 78−77093
- microprocessor-based ECG system 79−83989
- multispike signal detection and sorting hardware 79−79711
- Parkinson tremor, long-term recording and evaluation 77−21639
- partitioned Karhunen-Loeve expansion scheme for ECG/VCG data compression 79−79506
- remote sensing image data processing/acquisition techniques 78−61627
- rhythm analysis, long-term ECG data storage and multipass scanning 79−39578
- second-generation ECG monitoring system development 78−7480
- semiconductor memory system for biotelemetry radionuclide tracer data storage 77−90877
- spline approximation, input signal Fourier transform 79−35533
- television data, for cytology and chromosome anal. interface design 77−86683
- thin-film distributed optically excited laser, signal suppression by superluminescence radiation *(Russian)* 78−87091
- time-varying images, object displacement estimation adaptive algorithm 80−99668
- US pseudorandom signal-correlation system 80−43547

data conversion
- *see also analogue-digital conversion; digital-analogue conversion*
- EPR spectroscopy data handling and processing method *(German)* 77−53968
- methods, acquisition, analysis and display, from Geostationary Operational Environmental Satellite 80−17382
- multispectral scanner data principal-axis transformation to colour composite picture 79−29879

data description
- *see also computer software; data processing*
- uniform data description for a generalized real-time nuclear materials control system 80−63498

data dictionaries *see database management systems*

data handling
- air showers for 10^4 to 10^6 particles, lateral distrib. of EM component, detection 80−17459
- analogue signals, multiple, collection and handling using system with Promin-2 computer 79−67267
- background spectral radiance and contrast in the 1.5 to 13 micrometer region 79−8694
- curve fitting program on KIM-1 using FOCAL 79−35693
- data manipulation and handling, for teachers 80−4489
- digital data compositon for satellite and radar imagery 80−67413
- FASTBUS project, development status of high speed standard data bus 79−45605
- fusion reactor, diagnostics of radial plasma transport rate, data acquisition and handling system 78−54937
- fusion reactor, magnetic confinement, structural anal., combined interactive/batch computer environment 80−91255
- G-EXEC generalized data handling system, design philosophy 77−53210
- geodetic data base, basic entities definition 78−65392

data handling continued
- high speed biological cell sorter, data acquisition and display 78−44622
- high speed top mounted bus, prototype crate and module system 79−45611
- histogram manipulation program 79−54115
- instrument simulator, design and use 80−4490
- interferometer, data handling in high vibration environment 80−95132
- International Sun-Earth Explorers 1 and 2, fluxgate magnetometers command and data handling 78−85804
- Ionospheric Sounding Satellite control, data handling in automated system *(Japanese)* 77−78607
- marine profiling images, recording, signal amplitude preservation 78−36326
- modular data based codes, nuclear reactor simulation appl. *(German)* 78−17445
- multiband radiometer for field research 80−90250
- multielement array underwater acoustic instrumentation 80−43571
- neutron spectra analysis, informational-computer system *(Russian)* 79−89514
- nuclear reactor fuels, ceramographic data handling and storage 79−49811
- oceanographic information, automation of collection, processing and anal. on small-computer base 80−101439
- particle accelerators, future, LEP colliding beam machine, data handling and standard practices 80−58009
- particle detectors, high speed data processing, histogram and tape writing 80−58101
- photomultiplier assemblies and associated electronics for high energy physics large counter expts. 77−83469
- Pioneer Venus occultation experiment, radio science data generation 80−67492
- PIXE data handling, statistical techniques 77−52715
- pulse height anal. system, CAMAC based 77−87749
- real-time text processing for Italian text-to-speech synthesis system 79−64438
- satellite remote sensing system, CCD high speed data handling 77−91328
- seismic, Tasmania University seismic net, electronic development 80−82073
- sensory information processing, parallel and sequential *(French)* 77−12873
- spectrometers, off-line data anal., 168/E microprocessor 80−58102
- spectrophotometer (UR-20), data handling attachment 77−26409
- spectroscopy, multiplex and high-throughput 80−95145
- stellar magnitude, colour index and position meas. from astronomical photographs, automated technique 79−21194
- weight data, computerised acquisition and processing methods *(German)* 79−30437
- Woodward polarcardiographic service for ECG diagnosis improvement 79−39583
- XRF and emission spectrometry, equipment developments 79−20486

data loggers
- 3-channel, for precision meas. of resistance temperature detectors 79−88925
- automatic, airflow rate meas., with electrical indication 80−75014
- cassette data recorder *(Spanish)* 79−30441
- chart-recorder time markers, using digital clock module 79−30446
- data recording and reproduction using magnetic tape 79−88934
- digital, microprocessor-based, for radiation detectors 79−26848
- digital system, printer/paper tape punch format control 77−22538
- electron test accelerator, Chalk River, control computer 78−90004
- electrophysical information collection, recording and processing system 78−8388
- high speed photometer of Asiago Observatory, data logger and time base 79−25505
- interfacing and control of portable data loggers 78−93662
- laser pulse energy digital indicator *(Russian)* 79−22995
- mean square error minimisation by analogue computer *(Russian)* 77−9994
- minicomputerised pressure transducer data logging system *(Russian)* 79−6102
- multi-electron flame ionization detector for transient analysis of single aerosol particles 80−23246
- multichannel data logging minicomputer switching program synthesis *(Russian)* 77−9993
- multichannel digital temp. recorder, TR-2711, measuring 100 channels in 10 s 78−65931
- multichannel temperature recorder, Thermodac II with 24 channels using thermocouples 78−65930
- multichannel time-digit conversion modules of ‘Summa’ system for spark chambers 77−3236
- multiplexing data logger, resistance and voltage pulse measurement 80−42203
- noise level digital recording using programmable calculator 79−23130
- ocean digital survey fathometer, providing chart display and digital output 79−5665
- optical multichannel anal., data microprocessing of thermally stimulated luminescence 78−54347
- peak and trough voltage waveform measurement 77−22575
- portable, trends 78−41286
- punched-tape recording system, radioastronomy appl. *(Russian)* 78−65501
- review of developments and systems available 80−73337
- solar energy system control, 16 channel data logger and serial data link 80−50947
- solid-state instrum. for recording slow sea oscillations 80−36414
- spececraft, manned, data acquisition and logging system incl. speech 80−61979
- square root of time mark generator using TTL digital ccts. for chronocoulometry 80−35588
- status and prospects 79−93114
- system requirements for noise and vibr. monitoring 77−68351
- thermometer, multiple thermistor unit for use with data loggers 78−41303
- transient recorder, 1024-point, circuits, operation 77−53868
- versatile oceanographic data-logger 80−46264
- weighing, automatic, application in ceramics industry 80−95074
- YODAC-8, microprocessor controlled, for temp. data acquisition 78−49813

data preparation
see also word processing
radiolysis, pulse, composite optical spectra, synthesis, anal., computerised 77—12810

data preparation equipment
see also magnetic tape equipment; punched tape equipment
coupling apparatus for DVM and chart perforator to data compilation and registration system 79—93113

data processing
for computer applications see under relevant applications e.g. administrative data processing; computerised instrumentation; natural sciences computing
see also computer applications; data handling; data preparation; data reduction and analysis; management information systems
interferometer, data handling in high vibration environment 80—95132
NDT, equipment for production line inspection 79—29320
nuclear materials safeguards within Euratom framework, NUMSAS data processing system for statistical accountancy 80—73926

data processing (administrative) *see administrative data processing*

data reduction and analysis
see also data acquisition
absorption spectra quantitative analysis, appl. to N_2O 79—100461
absorption spectrum, press., temp., quantity and spectral resolution retrieval, appl. to N_2O 79—100462
acoustic emission data, digital registration and evaluation *(German)* 80—19178
acoustic intensity, Bruel and Kjaer acoustic level recorder type 2306, interfacing to a digital computer for a graphical output 80—53572
acoustic logging data averaging for seismic wave fields *(Russian)* 77—73673
acoustical data anal. using digital techniques 78—83193
acridine orange dye soln., dimerisation equilib., absorpt. spectra least squares anal. 79—50007
adsorption at soln.-electrode interface, AC polarographic data anal., computer program 80—3400
aerodynamic tube, nonsteady heat transfer method 79—37147
aeromagnetic anomaly from remanently magnetised Precambrian schist belt, Karnataka, India harmonic inversion 79—44094
aerosol electrical analyser, microcomputer-modified, for particle size anal. 80—40756
aerosols, size distrib. meas. by impactors, data inversion via nonlinear programming 77—2258
AES, anal. techniques 79—43691
AES, by computer *(French)* 80—7890
air monitoring, minicomputer data processing system 77—64439
air pollution, factor of safety calc. method 80—94140
air pollution data analysis using combined interactive graphic presentation and clustering technique 79—83656
air pollution data obtained near refineries, interpretation via pollution roses 78—81379
air pollution effects indicators, provisional map 78—81387
air pollution modelling 79—52984
air pollution remote sensing, use of computer-assisted correl. spectrometer 78—4002
airborne continuously recording ice nucleus counters, data anal. technique 77—78447
airborne gamma-ray spectrometry data processing using multivariable statistical analysis 79—35004
airborne spectroradiometric data, and LANDSAT data, hydrothermal alteration mapping appl. 79—34973
Alaska, earthquake, 1964, March 28, static displacement data inversion anal. 80—30998
ambiguous correlated measurements, regression problem 79—88903
amplitude distributions, appl. in practical data assessment problems 80—27107
analysis code for automated reduction of gamma ray data 78—23978
anodic oxidation, open-cct. transient method for overpotential anal. 78—27776
approximate realisation, new techniques 79—70898
aquatic sediment lipids, Recent and ancient 80—51583
astrometry, accuracy of average star positions obtained from overlapping plates 78—20622
astrometry, accuracy of star positions obtained by block adjustment 78—20623
astrometry, declinations differential determ. from obs. with vertical circle *(Russian)* 79—96888
astrometry, lateral refr. elimination from absolute declinations observed by micrometric method *(Russian)* 79—96890
astrometry using Palomar Schmidt plates, reduction procedures accuracy 78—57455
astronomical data acquisition and processing, Rome Observatory *(Italian)* 80—8551
astronomical data processing at Italian observatories *(Italian)* 79—62751
astronomical images, general anal. system 78—53834
astronomical laser ranging equipment, computer system *(Japanese)* 78—89080
astronomical observations errors, optimum linear estimation of mathematical expectation and standard deviation *(Russian)* 80—12673
astronomical photographs, reduction via intensity microphotometer with step-drives *(Russian)* 78—57457
astronomical plates, COSMOS measuring machine 77—64652
astronomical plates taken with photographic vertical circle, reduction using semi-automatic measuring machine *(Russian)* 79—96920
astronomical problem, pattern recognition appl. 80—8554
astronomy, least-squares adjustment with probabilistic constraints 78—32352
astronomy, least-squares polynomial fitting technique 80—12682
astronomy, meridian obs. of Ceres and Pallas, new reduction and collection 77—13277
astronomy, semi-automated blink comparator for large photographic plates *(Japanese)* 78—89081
atmosphere O_3 profile determ., outgoing thermal radiation meas. regression anal. 78—92945
atmosphere parameters, retrieval from scanning multichannel microwave radiometer obs. 80—90261
atmosphere radiances meas. from TIROS-N processing for temp. sounding 80—77133
atmosphere satellite picture anal. 79—8713

data reduction and analysis continued
atmosphere temperature field, spatial anal. from weather satellite meas. 78—20488
atmospheric mean temperatures, divisional and state, in Indiana, correction for non-climatic trends 80—51524
atmospheric precipitation, depth-area relations from digitised radar returns 77—91249
atmospheric radioactivity data, applicability of Weibull distrib. function 77—2230
atomic absorption spectrophotometer, microcomputer control and data reduction 78—35762
atomic elastic scattering, laboratory differential cross section data anal. via Monte Carlo averaging 78—21997
auto-correlations with irregular signals, time series anal., appl. to bubble chamber photographs 77—18767
automated microprobe *(French)* 79—6237
automated shipboard acquisition and processing of offshore geophys. data *(Russian)* 78—53750
automatic buoy systems, centre for data collection and processing *(Russian)* 77—78427
automatic contouring of faulted subsurfaces 77—45170
automatic curve slope meter for physical or chemical quantities 78—49812
automatic evaluation of isotope anal. of nuclear fuels, isotope dilution, mass and α spectrometry 78—55120
automatic structure analyser, EPIQUANT, quant. microscopic meas. 79—83409
Bayesian deconvolution, appl. and algorithm implementation 78—70103
beam-foil lifetime measurement, cascading problem, ANDC method use and error limits 80—14249
Bessel transforms, appl. in determ. of stellar rot. vels. 77—49369
binary stars, radial vel. curves anal. 80—90470
binary stars orbital solutions, derivation for unseen companions 78—93313
biological data, nonlinear describing function 77—13045
biological STEM, low-dose, using digital data processing system 78—24203
biomechanical data, mathematical function fitting 79—48278
biomechanics film data, cost effective method using PLATO system 79—35873
biomedical volume estimation, computer algorithm 80—98043
blood analysis in vivo, noninvasive spectroscopic method 77—60234
blood pressure ambulatory recordings, minicomputer processing 80—89887
blood pressure long-term recordings, fast data reduction, hybrid system 80—41278
body surface potential mapping, microcomputer processing system *(Japanese)* 80—72347
Bonner sphere spectrometer, least-squares technique for extracting neutron spectra 78—33366
Bouguer reduction of gravity anomalies using log data *(Russian)* 79—84082
breath by breath anal. of ventilation and pulmonary gas exchange, minicomputer system 79—62393
bremsstrahlung X-ray spectra stripping up to 300 kVp on desk type computer 79—83846
bubble chamber film, track rescue system 78—70728
bubble chamber film analysis, semiautomatic measuring system 80—58105
calorimetry, differential scanning, computer-interfaced, heat capacity meas. 78—65935
cardiac arrhythmia classification using R-R interval and difference histograms 77—40843
cardiac catheterisation data analysis via remotely located hybrid computer system 77—40869
cardiac catheterisation data on-line analysis by remote access computer system 77—40870
cardiac left ventricle blood flow field off-line computation from Doppler US velocimetry 79—62324
cardiocirculatory computer-aided monitoring after open-heart surgery, appl. to adrenaline effects meas. 78—81059
cardiopulmonary analysis 77—44814
cardiotopological data reduction 79—39392
CW Cassiopeiae, eclipsing, binary, anal. of V light curve 77—57009
cerebral regional blood flow meas., ^{133}Xe inhalation method with on-line computer 77—40734
CERN 2m HBC, automatic meas. of 12 GeV/c $\bar{p}p$ interactions 79—36471
CESSNA interactive spectrum anal. program on minicomputer 78—94177
chemical activation analysis, gamma-ray data automatic interpretation, computerised 77—44548
chemical analysis, energy dispersive electron probe X-ray, quantitative, compact procedure 80—40793
chemical data, factor analysis reliability improvement 77—36802
chiral molecules, detection, identification by Cahn-Ingold-Prelog rules, computer program, for teaching 79—58499
chromatograph, microcomputer controlled GC with data processor and printer-plotter *(Japanese)* 80—50921
chromatographic data processor, multistep calc. function *(Japanese)* 80—26091
chromatographic information processing by computer 80—71970
chromatography, microprocessor-based computing integrator 78—31737
chromatography, microprocessor-based data system 77—36826
cinematography, colour separation tests *(Russian)* 77—49796
cloud analysis via space-derived pictures, appl. of photographic equidensity curve method *(Russian)* 77—53155
clouds, anal. of satellite IR imagery 77—41122
clouds and atm. phenomena, integrated automatic processing of obs. data 79—29907
CODAS, Joint European Torus, control and acquisition system 78—36982
collocation method compared to traditional adjustment 80—77130
colloid size distrib., photon correl. spectroscopy, methods of cumulants, histogram and Laplace transform 79—58801
color map automatic digitisation, spectral classification scanner technique 80—17424
command language based data acquisition and anal. system for low energy nuclear physics 77—57846
common depth point seismic profiles, arc-shaped line-ups nature anals. *(Russian)* 79—44134

data reduction and analysis continued
compact radio sources, mapping from VLBI data 78—89266
compositional data Q-mode factor analysis 77—9503
computerised rapid-scan spectroscopy, at NAVWPNSUPPCEN Crane 78—41362
conversion from two to three functional modes of logical address space 78—36981
cosmic ray data selection and preprocessing in realistic error evaluation 77—53337
cosmological constant and data reduction 80—41923
crystal nucleation growth rates, on-line meas., data reduction technique 79—38730
crystal setting, and data reduction, on a PW 1100 diffractometer, program using simple method based on real space 80—59342
cubic spline interpolation of unequally spaced data points 79—30210
cup anemometer measurements, appl. to wind vel. spectra determ. *(Russian)* 77—13102
Cygnus X-1, data anal. for millisecond bursts, effects of shot noise 78—45429
cytological preparation evaluation, optical preliminary data reduction *(German)* 79—5392
data acquisition and processing system 80—18061
data management and analysis systems for hydrogeochemical reconnaissance 78—20520
data sets with jump discontinuities, interpolation method 79—30211
DC resistivity sounding method, appl. to evaluation of non-uniform water-bearing formation 78—40474
deconvolution, for detn. of linear system input from output data, thermokinetics appl. 78—12699
deconvolution of experimental outcomes, program DEO 78—70729
deep level transient spectroscopy, system effects and data anal. 79—99501
deep seismic profiling, Atlantic Ocean, automatic processing of bottom seismograph records 78—45030
dendrogram association analysis, FORTRAN IV program 77—5326
destructive examination of materials with data processing, microprocessor application *(German)* 80—93714
deterministic signals spectral anal., comparison of max. entropy method and nonrecursive technique 79—58112
digital data filtering, Lanczos filtering method 80—52176
digital data processing using integer arithmetic 80—27917
digital data spectral analysis, max. entropy method algorithm *(Japanese)* 77—17227
digital diurnal ionograms *(Italian)* 78—85699
digital radar data computer processing for High Plains Coop. Program (HIPLEX) 78—92989
digital seismic data processing, struct. anal. of graphs *(Russian)* 78—53749
directional data sets, axial asymmetry 80—21851
disc based distributed processing data acquisition and anal. system 77—65024
dosimetry, automated data acquisition and anal. system at LAMPF pion therapy facility 78—53506
drifter data analysis, sampling rate and random position error effects 80—26527
dynamic force measurement results, deformation expts. *(Hungarian)* 77—117
dynamic systems, elements of statistical energy anal. 77—75740
Earth conductivities mapping via multifreq. airborne EM system, data interpretation 79—5446
Earth conductivity, model for quantitative interpretation of towed-bird airborne EM system meas. 79—5447
Earth crust stress changes, data reduction formulae for in situ monitoring 79—29884
Earth dipole electrical soundings, perpendicular, numerical procedure for direct interpretation 79—34732
Earth free oscillation data inversion, asymptotic approach 79—92624
Earth free oscillations, interpretation of unresolved split normal mode multiplets spectra 79—74845
Earth induced polarisation soundings interpretation, freq.-effect transform function definition and appl. 80—56624
Earth resistivity sounding, buried electrode data interpretation using layered Earth model 79—29701
Earth tide observations processing, individual monthly sets weightings *(Russian)* 78—88789
Earth tides observations, monthly data set anal. *(Russian)* 78—88786
Earth vertical electric sounding curves, computer interpretation *(Russian)* 79—34741
EAS array, at Durham, data anal. 77—91392
ECG, Holter tape high speed digital anal. with full editing capability 80—89896
ECG, isopotential surface map data reduction 79—39557
ECG, microprocessor based ambulatory monitor 77—48918
ECG, precision requirements for computer anal. 77—81607
ECG data analysis for data compression 77—40862
ECG data analysis for data compression 79—100766
ECG waveform automatic processing using syntactic methods 79—44006
echelle spectrograms reduction, single procedure 80—56713
echocardiography, US, picture processing of 2-dimens. data 77—77958
echocardiography and pulsed Doppler, off-line data processing of left ventricle performance 79—62323
eclipsing binary light curves anal., linearised limb-darkening coefficients 78—49480
edge detection for meteorological data 79—100989
educational qualitative data analysis, networks anal. 80—31721
EEG, centro-occipital power and asymmetry, preprocessing by factor anal. 79—43996
EEG, digital computer period anal. for stroke prognosis 77—37096
EEG data, low cost microcomputer system 77—40881
EEG evoked frequency response polygons 77—40961
EEG from renal patients, compressed spectra array data matrix anal. 77—40882
EEG power spectra, parameter estimation using Gaussian functions 77—21635
EEG power spectral analysis to determine stage of anaesthesia in normal dogs and cats 77—37066
EEG signals, reduced spline representations 77—44803
effluent sampling programme data statistical evaluation 79—13547
electro-optical phenomena of disperse systems, computer calc. method 78—50699

data reduction and analysis continued
electrochemical impedance meas. method, automatic, computerised data anal. 77—70307
electrolytic soln. conductivities, conducting eqn. calcs., data anal., computer program *(German)* 77—32806
electron beam fusion accelerators, data acquisition and processing 78—37469
electron energy loss spectroscopy, anal. appl., processing requirements 79—43692
electron energy-loss spectroscopy in context of TEM, review 80—31945
electron image recording system, detection quantum efficiency 80—99009
electron linear accelerator, computer prediction and diagnosis of failures of systems 79—693
electron microprobe, automation using microcomputer system, anal. appl. 79—43703
electron probe anal., energy dispersive spectroscopy, quantitative, computer program 79—43689
electron spectroscopy, deconvolution methods, review 79—26188
electron test accelerator, Chalk River, control computer 78—90004
electrophysical information collection, recording and processing system 78—8388
EMG, rel. to skeletal joint torques, for prosthesis control 77—48953
emission spectrophotometry, review of data processing systems *(Japanese)* 78—88685
emission spectroscopy signal-to-noise ratio improvement and data processing *(Japanese)* 77—21448
energy dispersive X-ray diffractometery, technique, apparatus, data processing, computer profile fitting 77—68892
energy dispersive X-ray spectra, anal., computer techniques 79—43690
energy loss spectroscopy, quant. microanal. of thin foils *(French)* 80—50900
environmental samples anal. for U, Th, neutron activation anal. data resolution for high throughput system 79—11848
Eolian Islands, aeromagnetic and gravimetric data reduction rel. to basement structural trends 78—40519
Eotvos effect variations allowance in gravimetric studies, data processing 79—74969
epitaxial growth expt. data, of GaAs in $Ga-AsCl_3-He_2$ system *(Bulgarian)* 78—60580
EPR spectroscopy, absorption curve, spin concentration, numerical double integration, computer subtraction *(German)* 77—37954
evoked potential analysis, on-line signal optimisation using minicomputer 77—5112
Executive system for processing geological data 77—53212
experimental curves, information content, deconvolution using apparatus functions 79—40354
experimental data anal. using digital filter 79—17403
experimental data components isolation, Fourier transforms appl. 78—36434
exponential clipped photon autocorrel. spectra, data anal. 79—2837
exponential growth factors by Mangelsdorf's method, for teachers 79—71195
expt. data analysis, normal distribution verification algorithm *(Bulgarian)* 80—27261
fatigue data analysis, lifetime predictions for ceramic materials 78—95870
films electrophysical properties meas., using automatic recording and expt. data analysis 79—17446
fish stock discrimination, X-ray fluoresc. tissue anal., pattern recognition technique 77—60330
fitting data to dimensionless groups 79—40545
flow, gas-liq., hot-film anemometer signal anal. method 79—32639
flow, two-phase, nonequilib., spectral characts. 78—94854
flow, unsteady, transitional and turbulent boundary layers, expt. and calc. methods *(French)* 78—75125
flow angle and mass flow rate meas. in unknown flowfield 79—77306
flow around sphere, laminar, photographic-tracer film, vel. profile anal. 79—50698
flow correlations comparison, two-phase, through sharp edge metering orifices 78—26223
fluidised glass ballotini-packed fixed bed, at low/intermediate Reynolds nos. 79—1244
foetal breathing movement computer anal., from real-time US images 78—40375
foetal heart rate on-line data management during labour, prediction of one-minute Apgar scores 78—44655
Fourier spectroscopy in far IR 78—62240
Fourier transform NMR spectroscopy, clipped free induction decay signal anal. 77—63976
functional dependences, expt. determined, analysis method using osculating curves 79—93109
furnace at. absorpt. anal., computer-assisted, turnkey data system, natural water anal. appl. 77—77829
gait patterns, normalised, using computer anal. of EMG and fast-fall patterns 77—40819
galactic plane survey at 5 GHz, computer reduction of data 78—81686
galaxies angular diameter counts, determ. of selection criteria for deep Schmidt plates 77—91623
galaxies high-order clusters, detect. techniques 78—12386
galaxies photometry, reduction of magnitudes of Virgo area galaxies to standard B_T system 79—92852
galaxy redshifts survey, data reduction techniques 80—22074
gamma ray spectra anal., fast Fourier transform *(Chinese)* 80—77762
gamma-ray multiplicity meas., fast converging bootstrap method for data anal. 78—70730
gamma-ray spectra, rapid reduction via desk-top calculator 77—53870
gamma-ray spectrometry, data analysis, theoretical foundations 79—233
gas (mixture), compressibility, virial coeffs., Burnett data reduction, fast least-squares method 78—47082
gas chromatography-mass spectrometry integrated anal. systems, review 79—1972
gas phase electron diffraction analysis, use of spline functions, program description 79—89810
gas-phase electron diffraction analysis of molecules, computer generated backgrounds 79—97368
gel permeation chromatogram computer manipulation, substraction, appl. to polymeric materials 79—96387
geodesy, appl. of Very Long Baseline Interferometry (VLBI) *(German)* 78—45036
geodesy, foundation of collocation method *(German)* 77—86748

- **data reduction and analysis** continued
  - geodesy, systematic errors detect. by hypothesis tests using adjustment in sections *(German)* 79—44083
  - geodesy, uniformly distributed data harmonic anal. for global systems geocentric origins comparison 79—57839
  - geodetic data, anal. for Recent vertical crustal movements four-dimensional modelling 79—80055
  - geodetic data, vertical crustal movements interpretation in time-space domain 79—80056
  - geodetic measurements, parameters estimation models for crustal deformation anal. *(German)* 80—101319
  - geological compositional data Q-mode factor analysis, extended CABFAC and QMODEL programs 77—9504
  - geological records, coding method based on data transmission theory *(Russian)* 80—17383
  - geologo-geophysical research, efficiency improvement by computation nets 79—96835
  - geomagnetic and gravity anomaly data, curve-matching optimisation method *(Chinese)* 80—89935
  - geomagnetic anomalies, spectral anal. of step model total anomalies 79—5450
  - geomagnetic anomaly interpretation, bidimensional inhomogeneous problem soln. via Cauchy integrals *(Russian)* 79—35013
  - geomagnetic array data, empirical transfer functions for tectonomagnetic event detect. 79—16374
  - geomagnetic D_{st} variations analyses, comparison using distortion free filter 80—17419
  - geomagnetic data obtained from satellite magnetometer 80—77141
  - geomagnetic ground and airborne data, optical filtering 77—25797
  - geomagnetic measurements and data processing, new methods 79—39988
  - geomagnetic $V_{ZZ}(V_{\Delta}, Z_a)$ anomalies over stratified bodes, interpolation analytic method *(Russian)* 79—39968
  - geophysical acoustic logging, signals limited spectrum rel. to time interval and damping determ. accuracy *(Russian)* 79—39971
  - geophysical data, correlation functions for geometric models *(Rumanian)* 79—58124
  - geophysical data, real-time processing using DGU-2 curve plotter 80—36422
  - geophysical data, upward and downward continuation as inverse problems 79—44262
  - geophysical data analysis, random values separation *(Russian)* 79—74983
  - geophysical data processing by special purpose digital computers, accuracy *(Russian)* 79—62587
  - geophysical data reduction on arbitrary surface in regions of high topographic relief 78—61298
  - geophysical dipole soundings data obtained along crooked line, transform. 79—44259
  - geophysical fields, props. of linear transform. characts. *(Russian)* 79—35007
  - geophysical fields correl. anal., input conditions *(German)* 79—35014
  - geophysical linear inversion, non-uniqueness resolution via a priori appl. 79—44261
  - geophysical objects parameters, interval estimation via identification methods 77—82024
  - geophysical pot. field anomalies, statistical source models for geodynamic interpretation *(German)* 79—34782
  - geophysical potential field data, linear anal. theory *(Russian)* 79—35011
  - geophysical prospecting, induced polarisation decay curve, dynamic characts. *(Hungarian)* 80—21842
  - geophysical prospecting, instability of finite difference schemes due to boundary conditions 77—21912
  - geophysical prospecting, well logging, data transmission and processing *(Russian)* 79—62625
  - geophysical time series alignment, new statistical approach 79—92623
  - geophysical unit vectors, time series interpolation 79—92625
  - geophysics, analytic construction for two-dimensional gravimetric and magnetometric problem 80—21846
  - geophysics, combined interpretation of deep seismic sounding and gramimetry data 80—21845
  - geophysics, complex exponentiated data digital correl. *(German)* 79—44279
  - geophysics, equivalence of mag. and gravit. anomalies extrapolation *(Russian)* 79—39926
  - geophysics, interpretation of pulse neutron logging data in inhomogeneous beds *(Russian)* 79—44273
  - geophysics, meas. errors anal. in transient EM sounding records computer processing *(Russian)* 79—44269
  - geophysics, oil field data, fast processing *(Russian)* 79—84540
  - geophysics, regional background separation in gravity and mag. anomalies anal. *(Russian)* 78—40703
  - geophysics, solvability in finite form of inverse logarithmic-pot. problem for contact surfaces 77—82025
  - geophysics, two-dimensional resistivity and induced-polarisation data inversion 79—16695
  - Geos 3, altimetry data appl. to orbit determ. expt. 80—4226
  - Geos 3 altimeter data, appl. to geoid undulation and anomaly estimation 77—64178
  - Geos 3 altimeter data, processing for recovery of geoid undulations and gravity anomalies 80—3896
  - Geos 3 altimeter data in Tasman and Coral seas, anal. 80—3903
  - Geos 3 altimetry data, appl. to ocean geoid investigation 80—3906
  - geoscience, data graphical output, colour plotter system appl. 80—98467
  - giant H II regions, radio maps interpretation 78—85994
  - goniometer, electromech., for total motion knee goniometry 77—52902
  - gradiometer data integration in geomagnetic surveying 80—105064
  - gravimagnetic anomalies, interpretation on basis of pots. classes with inverse problem finite form 80—21847
  - gravimetry, direct and inverse problems soln. for hemispherical bodies *(Russian)* 79—35012
  - gravimetry inverse problem, assembling principle for constructing solns. *(Russian)* 77—44898
  - gravitational radiation, anal. of Maryland-Argonne detector 1973-74 data 77—22476
  - gravitational wave expt. at Rome Univ., data analysis 79—58614
  - gravitational wave expts., data analysis algorithms 79—67216
  - gravity, prospecting, accuracy, meas. spacings and contour intervals calc. techniques *(Russian)* 79—44272
  - gravity anomalies, geological reduction *(Russian)* 78—40467
  - gravity anomalies interpretation, computer modelling 79—34971
- **data reduction and analysis** continued
  - gravity anomalies measured in Krivoj Rog basin (Krivbas) underground workings, interpretation *(Russian)* 78—85466
  - gravity anomalies of two idealised bodies, theoretical transforms 79—5441
  - gravity anomaly from masses distributed over infinite regions, interpretation theory 80—82103
  - gravity complex fields interpretation via minimisation method, automated system appl. *(Russian)* 79—35006
  - gravity data reduction for geological interpretation *(Russian)* 79—84537
  - gravity prospecting, determ. of parameters of low-amplitude struct. with oil (gas) deposits *(Russian)* 79—44271
  - gravity $V_{zz}(V_{\Delta}, Z_a)$ anomalies over stratified bodies, interpretation analytic method *(Russian)* 79—39968
  - ground data, remotely sensed, developing countries appl. 79—34963
  - haemodynamic research, human, physiological signal acquisition and processing 77—44768
  - heart rate on-line statistical anal., using special-purpose computer 78—35984
  - heat exchanger fouling data analysis, for geothermal power plant appl., use of multivariate regression technique 79—52880
  - Helios zodiacal light expt., data processing and evaluation 79—80235
  - Hippuran plasma clearance meas. using gamma camera and cardiac background subtraction 77—52870
  - HISS computer facility 79—89559
  - histogram plotting, FORTRAN program 'HIST' 78—77876
  - holographic interferograms evaluation, of thermal boundary layers *(Czech)* 78—62220
  - holographic interferometry for study of wave propagation in rock 78—20536
  - homonuclear coupled spin system, inversion-recovery data anal. 79—33554
  - human disease study using mass spectrometry and metabolite profiling 80—51289
  - HVEM, image convertors 80—104839
  - hydrologic records analysis and comparison, statistical program suite 77—21819
  - hydrological forecasts, automatic processing of operational information 78—3842
  - hydrometeorological fields, probabilistic models for objective anal. *(Russian)* 77—56697
  - hydrometeorological information, optimum conversion to digital form 79—29903
  - hypersonic turbulent flow measurements, electron beam fluoresc. method 77—35282
  - image, meteorological interactive software system 80—36404
  - image reconstruction from incomplete and noisy data, examples and appls. 78—53837
  - implanted-ion range, computing moments of energy distrib. 77—4120
  - infrared intensity reference meas., spectrophotometric data reduction, modular computer programs appl. 80—3471
  - inland wetland photointerpretation evaluation, cell analytical method 79—29898
  - instrumental distortion correction 79—54116
  - integrating vidicon systems at Cerro Tololo, data acquisition and reduction software 79—66924
  - interactive verification of clinical trials data 77—48893
  - interferometry, multiwavelength testing using modified Twyman-Green interferometer 78—59169
  - internal friction curves, numerical anal., program in ALGOL-1900 *(Polish)* 79—95079
  - International Ultraviolet Explorer (IUE), ground data processing system performance 78—96383
  - interpolation methods for sparse data, appl. to atmosphere wind and conc. fields 80—51575
  - ion microprobe analyser, appl. to cast Fe nodule form. 79—43295
  - ionograms, minicomputer inversion procedure for electron density profiles calc. 77—41263
  - ionograms, true height calc. technique 80—8486
  - ionosphere incoherent scatter data, analytic partial derivatives for least-squares fitting 78—73581
  - ionosphere oblique sounding data, inversion method 77—41265
  - ionosphere sounding, filtering effect on drift parameters determined by full correl. anal. 78—65450
  - ionospheric data processing, improvement of convergence of least squares method *(Russian)* 78—85700
  - Ionospheric Sounding Satellite control, data recording and anal. system *(Japanese)* 77—78611
  - IR Astronomical Satellite (IRAS), ground operations and data processing 79—80193
  - IR scanning, three-component method of data analysis 77—48613
  - IR scanning radiometer data interpretation 79—30541
  - ischaemic episode, computerised continuous beat by beat anal. and rational plots 79—62394
  - isotachophoretic analysis, development of data processing system *(Japanese)* 79—24873
  - jet, free, turbulent flow, large scale struct., discrete values meas. 78—90840
  - kinetics computational processing, iterative optimisation techniques 77—32765
  - laboratory sample management using BASIC 78—24770
  - lake quality monitoring, multidate Landsat data extraction progrm 80—17299
  - LAMPF data analysis techniques 79—89562
  - land seismology, data anal. using mini-SOSIE 77—21917
  - LANDSAT computerised data anal. rel. to global development 78—36286
  - LANDSAT data per-field, classification, unsupervised clustering techniques 77—64437
  - LANDSAT imagery, appl. to hydrographic charts preparation 79—29894
  - Landsat imagery, planimetric restitution using Zeiss Stereotop 80—56648
  - laser anemometry, high Reynolds number flow, review, data anal. for photon correl. method, simulation 79—60082
  - laser Doppler velocimeter, output data anal., noise rejection 77—39378
  - laser emission spectrochem. anal., data reduction, KSR 4100 small process control computer 77—48707
  - laser-matter interactions, automatic treatment of data *(French)* 78—42830
  - latitude observations, technique for Earth daily free nutation, determ. 78—96126
  - least squares method, generalisation 80—62028

data reduction and analysis continued
- LEED beam intensity measurement by photographic method, use of Vidicon camera 77—7638
- LF atmospheric data anal. with PDP computer 77—82014
- light scattering, in macromolecular solutions in FORTRAN *(Rumanian)* 79—82990
- light scattering by solns., correction for effects of contaminating dust particles 77—37959
- line detection algorithm, for Landsat data 80—77150
- linear prediction in least-squares scheme, algorithms 80—98464
- linear prediction in least-squares scheme for max. entropy spectra, Fortran subroutines 80—98465
- linked controllees and index-tabled techniques for data storage and rapid retrieval 79—9983
- liquid chromatograph, microprocessor-based, reproducibility 77—9152
- liquid chromatography, spectrometric detect., computer control of data acquisition, reduction and display 78—27850
- liquid-vapour equilibrium data reduction by maximum likelihood 79—51244
- lunar occultations during 1943-74, anal., rel. to Brown's theory, FK4 right ascension system and Watt's charts corrections 79—48696
- lunar seismology, diffusion approach to seismic energy transmission in intensively scatt. environment 77—73685
- lung volume determination, interactive graphics 77—77985
- M 6000 display for spectrum reduction 80—42210
- machine processing of remotely sensed data, conference, West Lafayette, Indiana (1980 June 3 to 6) 80—82586
- macromolecular rotational diffusion, ^{13}C spin-lattice relax. data anal., computer program, appls. 79—95664
- macroseismic data processing and interpretation 78—61583
- magnetic anomalies interpretation, computer modelling 79—34971
- magnetic anomalies interpretation, estimation of cover thickness above magnetised mass *(Russian)* 80—105069
- magnetic field reduction to pole, fast Fourier series algorithm 77—5333
- magnetotelluric data, tensor anal. for two-dimensional geological structs 78—40471
- magnetotelluric data, two-dimensional inversion 77—73629
- magnetotelluric measurements, noise bias elimination using remote mag. reference 79—88245
- magnetotelluric resistivity and phase soundings interpretation, graphical procedure 78—40473
- magnetotelluric sounding, natural source obs. one-dimensional inversion 79—92479
- magnetotelluric study, S.Scotland, fieldwork, data anal. and results 79—29705
- magnetotelluric study, S.Scotland, Monte-Carlo data inversion 79—29706
- main program and overlay manager subsystem within distrib. function lab. computer system 78—36980
- marine gravity data reduction, considerations of indirect effect (geoid undulation effect) 80—3907
- mass spectra, continuous scan, time-sharing computer data system 77—18127
- mass spectra factor analysis 77—44534
- mass spectrometer, double focusing type, automatic acquisition and shape anal. of metastable peaks 79—89036
- mass spectrometry, computerised 80—57417
- mass spectrometry, computerised data acquisition and interpretation, review 78—321
- mass spectroscopic chem. anal. of mixtures, spectral target transform. factor anal. 77—52679
- mass spectroscopy, smoothing of experimental ion kinetic energy data by digital computer 79—93112
- mass spectroscopy computer acquisition and analysis of metastable transition data using electric sector voltage variation 78—70102
- mass spectroscopy data, thermal ionis., statistical data evaluation program 79—89037
- materials testing, nondestructive, radiometry methods, automatic data processing, development of models and algorithms 78—72991
- maximum likelihood test in estimation of exptl. inaccuracies, applic. to equilib. data 77—9867
- measurement data evaluation by probability calc., computer appl. *(Hungarian)* 78—8376
- mechanical impulse testing techniques, computer evaluation, high-speed film recording 78—44343
- mechanical testing of materials in complex stressed condition, automatic unit 79—15898
- medium energy physics, data analysis, array processor appl. 79—89560
- metal, positron annihilation, ang. correl. data analysis 78—52592
- metal fatigue test results *(Japanese)* 77—9013
- meteor radar system, Illinois University, data processing algorithm 77—41205
- meteorological real-time data acquisition and anal. 78—69466
- meteorological time-averaged data, variance by simple approx. 80—31139
- meteorology, boundary layer data acquisition and analysis system 77—60471
- meteorology, data processing of M-100 rocket soundings 77—53233
- meteorology, interpretation of asynchronous data 80—109271
- meteorology data acquisition and processing test for FGGE 79—16674
- meteorology inverse problems, estimation theory appls. 79—35018
- meterological radar data acquisition system at Spino d'Adda ground station 78—69468
- metrological, automation of meas. equipment state-inspection results, USSR Krasnodar territory 80—52152
- MHD convertor, U-25, diagnostics system data processing 78—26339
- microclimatology, process computer appl. thermal balance recording methods 80—82044
- microcomputer based system for automatic reduction of astronomical spectra 80—77296
- microcomputer system, appl. to NMR experiments *(Japanese)* 79—75564
- microcomputer-aided data-processor for mag. susceptibility *(Japanese)* 79—63283
- microcomputer-based data acquisition and anal. system for CO_2 rebreathing studies 78—36005
- microearthquake network data, automatic anal. 78—81412
- microearthquake research, methods and computer programs 79—39987
- microprocessor—based unit data acquisition and reducing system 80—21598
- microprocessor-based interferometric data reduction system versatility 80—73439

data reduction and analysis continued
- microscope photometry, on-line data collection and processing for solids, fossils and organic matter *(German)* 79—26101
- minerals electron microprobe data analysis, using FORTRAN IV programs 77—86878
- minerals modal analysis, from raw point-count data, using MODES (FORTRAN IV) program 77—86880
- minicomputer driven microprobe *(French)* 78—74111
- minicomputerised pressure transducer data logging system *(Russian)* 79—6102
- mitral valve replacement, prediction of postoperative systolic left ventricular wall stress 78—40427
- mixtures, anal. by retrospective computer subtraction of gas phase IR spectra 77—77824
- modular-programmed data acquisition/anal. in nucl. research 77—18766
- molecular spectra analysis, eval. of peak volume, position and width, computer program 80—18890
- motion analysis, human, 3D coordinate data processing 80—56260
- multi-faceted data gathering and analysing system 78—37530
- multi-parameter distributed processing data acquisition, display, and online analysis system 79—45612
- multicomponent spectra, numerical anal., least squares, optimisation methods 77—56264
- multicomponent systems, comput. techniques for thermodynamic data treatment and equil. calc. 78—10172
- multidimensional power spectral anal., new method, radioastron. appl. 77—17378
- multiple sclerosis diagnosis using cerebral evoked response and optokinetics 80—36183
- multiuser facility, experimental data processing 79—88922
- multivariate data set, directed canonical analysis 80—73333
- musical instrument timbre recognition, perceptive effects of data reduction *(French)* 80—28387
- myocardial infarct sizing using computer programming and 3-dimens. model 77—90888
- Nancay radioheliograph, Mark II, on-line data reduction methods 78—28517
- nerve impulse automatic identification and separation 79—16190
- nested variance power spectrum 80—8965
- neuron and neuronal assembly 3D computer reconstruction 80—21596
- neurophysiology, computer assisted unit data acquisition/reduction 78—61266
- neutron activation analysis, data reduction, computer language MULTELMT 78—85241
- neutron activation analysis, gamma-ray spectra prediction, detection limits, computational procedure 78—85242
- neutron activation and data reduction, flexibility, MULTELMT program 79—11856
- neutron elastic and inelastic scatt., 4 to 8.5 MeV, summary of ORNL programme 77—23090
- neutron experiments, Braunschweig accelerator facility, data acquisition and anal. 80—47806
- neutron spectra analysis, informational-computer system *(Russian)* 79—89514
- neutron spectrometer system, FORIST code 77—26930
- Nimbus 6 scanning microwave spectrometer data, parameterisation for atmospheric liq. water content determ. 79—58047
- NMR, Fourier transform, resolution enhancement using double exponential function 79—35804
- NMR Fourier transform spectroscopy, free induction decay, resolution enhancement function 79—80656
- NMR relaxation data processing *(Japanese)* 77—34008
- NMR relaxation detect. of tumours, spectrum anal. of multiple components data 78—48851
- NMR spectra, automatic system, for recording, processing and summation 80—27327
- NMR spectrometer, pulse, controlled by programmable digital unit *(Czech)* 78—77952
- noise pollution, factor of safety calc. method 80—94140
- nuclear, lognormal distribs. in least squares algorithm 79—93902
- nuclear cross section tabular file generation, utilisation techniques 77—23397
- nuclear engineering computer instrumentation, laboratory instructional programs 80—31472
- nuclear instrumentation computer network for on-line data processing 78—37529
- nuclear instrumentation laboratory course, computer based data acquisition and anal. 80—36820
- nuclear laboratory instruction with multichannel analyser/microcomputer system 80—31471
- nuclear materials accounting data analysis, dynamic 79—85684
- nuclear medicine, data evaluation system for use with gamma cameras 78—92732
- nuclear plant specific risk studies, data specialisation, Bayes' theorem 80—47601
- nuclear radiation detection lab., desk top calculators 80—36821
- nuclear reactor, HFIR, dimensionality reduction of noise signatures, improved automated noise anal. 77—6499
- nuclear steam generator tubes testing and evaluation, using CIS/DASIO system *(Czech)* 80—63301
- number oriented microprocessor appl. to real time data processing 79—49921
- numerical electronic technique, in physics education 80—46777
- nystagmus analysis system using microprocessor 77—48917
- obstetrics, microprocessor based system for studying kinematics of labour 77—44769
- obstetrics monitoring, microprocessor data acquisition and preprocessing with minicomputer signal processing 77—44775
- ocean ambient noise data, statistical anal. 77—79996
- ocean dynamic data, acquisition and display by portable real-time minicomputer system 80—12552
- ocean surface parameters, retrieval from scanning multichannel microwave radiometer obs. 80—90261
- ocean wave directional spectra, from discus buoy, data processing 79—16723
- ocean wave slope meter, fast response instrument, wind-wave moments meas. 78—45012
- oceanographic data, interpretation for design of ocean thermal energy conversion plant 78—44874
- oceanographic data acquisition and processing system, microprocessor based, real-time 79—16676

data reduction and analysis continued
oceanographic data objective anal. and classification 78—36318
oceanographic information, automation of collection, processing and anal. on small-computer base 80—101439
oceanographic multi-freq. microwave radiometer, data processing and performance evaluation 78—81417
oceanographic research, data processing and anal. 80—94605
oceanography, data anal. by Naval Coastal Systems Center (NCSC) environmental measuring system 80—12570
oceanography, Seasat-A, data processing and distrib. 78—45005
offshore environmental and platform data processing from Norwegian continental shelf 79—12273
Ohio Sky Survey, data reduction techniques 77—45325
optical crystallography computer anal. of spindle stage data 78—85702
optoelectronic analyzer for seismic data processing *(Russian)* 77—29516
oscillograms processing, in exploding wires expts., with aid of microcomputer and main-frame computer *(Russian)* 80—28854
palaeomagnetic data, angle in Fisher distrib. that will be exceeded by given probability 80—51325
palaeomagnetic data, Fisher's precision parameter 80—51326
palaeomagnetic data analysis, elimination of secular variation 80—61755
palaeomagnetic data analysis, modes of directional data 80—56352
palaeomagnetic data smoothing, objective method, comments 79—34975
palaeomagnetic directional data sets, shape 79—39881
palaeomagnetic inclination data analysis by statistical method 80—109101
palaeomagnetic records, running means calc. for Holocene short period secular geomag. vars. determ. 80—98221
parallel surface continuation, appl. to reduction of terrain induced aeromagnetic anomalies 78—61316
partial discharge amplitude spectra, acquisition and automatic processing system *(Italian)* 79—93108
particle size anal. using optical counting data 78—77842
particle track data in plastics, rapid anal. using interactive programming and graphic displays 78—66456
particle-particle correlation experiment, on-line four parameter anal. system *(Chinese)* 80—42910
pattern recognition methods, comparison 80—199
pattern recognition of ^{13}C NMR data 77—48059
PEP storage ring, high-speed data acquisition and analysis system 80—23194
phase vel. determ. of fundamental Love and Rayleigh waves 77—37148
photochromic tracer film, measurements using POLLY, film reading computer system 78—42696
photoelectric photometry at Trieste, real time data acquisition and processing *(Italian)* 79—62757
photographic images, quantitative anal. of autoradiographic image intensification using Thiourea-^{35}S 80—90343
photoluminescence data, deconvolution 78—5369
photolysis and radiolysis, kinetic data acquisition, and anal., by computer based system 79—39180
photon correl. laser anemometry, information extraction method 79—60081
photon correl. laser anemometry, on-line data reduction system 79—60080
physiological data recorder, microprocessor-based hybrid system 77—44872
physiological signals in time domain, techniques 77—44767
piping system anal. to nuclear standard regulations 77—6504
PIXE data handling, statistical techniques 77—52715
planetary astrometry, phase reduction formulae *(Russian)* 79—96891
planetary nebulae, isophote pictures rel. to spatial structure investigation by mathematical modelling *(Russian)* 79—101188
plasma, fluctuation diagnostics, digital time series anal. techniques 78—5951
plasma, submillimetre diagnostics, active, of Ar arc, data numerical anal. 80—48979
plethysmography, whole-body, automated real-time anal. system 78—28112
pneumodynamics, enforced smoothing techniques for recovering dV_A/dQ distribs. 79—43946
point to line data reduction, computer links and hardware processor test 79—45613
POL, data analysing interactive system 79—31347
polarising radiometer, data reduction technique 77—78472
pollution measurement, automated systems 77—21885
polymer, noncrystalline solid, preferred orientation from scatt. ang. distribs. 78—75560
polymer solns., phase diagrams, pulse-induced critical scatt. 79—1490
polystyrene solutions, light scatt., mol. parameters, computer anal. assessment 79—1766
positron annihilation, pulsed distrib. from expt. data, parameter reconstruction 78—41290
potential field data, constrained inversion, use of pseudohyperellipsoids 80—85752
potentiometric titrations, computer-calc. curves, linear learning machine training, testing 80—3426
powder X-ray diffraction data, cubic lattice parameter, Fortran program 77—11440
precision loss measurement of photoelectric pulse signals using microcomputer 80—13142
probe data reduction in axially symmetric expts. 78—89464
process gas chromatographs, microprocessor based, calibration and data reduction 80—81402
programs for high-school expts. 78—86094
prosthetic ventricle and valve evaluation, flow visualisation data anal. 78—40425
protein data measured on oscillation camera, collection and reduction method 79—29672
proton induced X-ray emission anal. of aerosols, spectral anal. computer program 77—60167
pulsars, vels. from anal. of interstellar scintillation 77—78811
pulsed neutron source on multiplying media, anal. and interpretation of experimental data *(Rumanian)* 78—46203
quasars, southern, optical monitoring, data reduction 79—58439
radio astronomy, computer data-processing techniques for 8550 MHz sky survey 77—17708
radio astronomy, direct transform hardware processing of rot. synthesis data 78—85856
radio astronomy, direct transform hardware processing of rot. synthesis data 78—85857

data reduction and analysis continued
radio astronomy, multidimensional power spectral anal. 79—12406
radio beacon position calc. from satellite Doppler data using microcomputer 79—12271
radio meteor wind data, anal. using finite element approximation 78—81475
radioassays, automated data processing 79—16299
radioastronomical data recording and processing, real-time, multichannel system *(Russian)* 78—65507
radioastronomical data reduction, via digital electronic integrator *(Russian)* 78—57465
radioastronomy, phaseless aperture synthesis technique 78—32353
radiographs processing 80—3259
radioimmunoassay anal. system 79—25100
radioimmunoassay and bioassay, logistic curve fitting routine adapted to desk top computer 77—37059
radiolysis, pulse, composite optical spectra, synthesis, anal., computerised 77—12810
radiometry of flat finite wave tank, three-dimensional vector modelling and restoration of meas. 77—22599
radiosources, two-dimensional max. entropy reconstruction of radio brightness 78—28534
rain cell radar monitoring, automatic detection and tracking algorithms 80—51544
random data, detrending and smoothing techniques 80—67425
random data, effects of detrending and smoothing 78—40685
real-time transfer function analysis, instrum., for rapid meas. of system kinetics 77—41578
recorders, transient, 1024-point, circuits, operation 77—53868
recovery from Utah tar sand deposit, by in situ combustion, use of on-site minicomputer 79—48046
reflection seismic recordings, minimum entropy deconvolution 78—81423
reflection seismograms signal anal., use of kepstrum 78—81425
reflection seismograph data, maximum likelihood filtering 79—5453
reflection seismology, time fields method for curved interfaces determ. *(Russian)* 79—35010
reflection seismology, wavefront sythesis for vel. estimation and downward continuation 79—16392
reflectivity meas., total, using specular-reflectance and diffuse reflectance references 80—73421
relaxation time data, bounded error anal. of expt. distribs. 79—88924
remote sensing, image processing and information extraction 77—64438
remote sensing data (multispectral), contextural classification 80—77149
remotely sensed data machine processing, symposium, West Lafayette, IN (1979 June 27 to 29) 79—88473
residual Bouguer anomalies, line masses depth estimation via Backus-Gilbert min. distance criterion 79—44257
respiratory response to exercise, on-line anal. 78—7458
reticulocyte blood count data analysis by maximum entropy spectral estimate 77—78017
retinal neurons studies, appl. of white noise anal. *(Japanese)* 79—66471
riverine and coastal effluents, remote sensing of thermal alterations and circulation patterns 79—57524
rocks, minerals, anal. of small samples using X-ray quantometer 78—61112
Rutherford Laboratory N5 expt. data acquisition system, program struct. and CAMAC hardware 78—90051
SABRE computer system for assessment of body radioactivity 77—77998
sarcomere dynamics in single skeletal muscle fibre, light diffr. spectra 78—15797
satellite altimeter data analysis, role of orbit determ. 78—77177
satellite image data acquisition system design 79—58098
satellite recorded data, ionospheric plasma obs. *(Spanish)* 78—16270
scanning microprobes, system for quantitative recording of elemental maps and spectra 80—42303
scintigraphic images, acquisition and processing system, simultaneous use of several radioisotopes *(French)* 77—70520
sea surface deviations from geoid, equal-area anal. rel. to geoid computation 77—64177
sea waves recording and analysis *(Italian)* 77—29458
SeaTrak Data Processor, surface data reduction system for current meter 78—45042
sediments, polymodal, of river-lake system, interpretation 79—25273
segment description, of unique set of reflections to data collection and data reduction 80—1881
seismic boundary images, reconstruction using numerical models *(Russian)* 79—39923
seismic common-depth-point stacking, appl. of multirate digital filtering approach to interpolation 79—29876
seismic cross sounding, data interpretation via reflected wave method *(Russian)* 78—92796
seismic data, appl. of PAL, highly tutorial interactive pattern recognition program 77—81833
seismic data, automatic earthquake recognition and timing from single traces 79—66822
seismic data, broadband, digital recording and anal. at Graefenberg array 79—25348
seismic data, common depth point ray modelling for three dimensional isovelocity layers 77—21914
seismic data, deconvolution with l_1 norm 79—88484
seismic data, noise-resistance of optically generated correlograms *(Russian)* 78—40699
seismic data, signatures of sedimentation models, appl. to hydrocarbon exploration 77—21913
seismic data, simultaneous inversion methods and resolving power 79—16699
seismic data, technique for dispersion continuous representation 80—51334
seismic data analysis, appl. of wavefront curvature expression in layered medium 79—29712
seismic data processing, Karhunen-Loeve transform. appl. *(French)* 79—44258
seismic data processing, predictive dynamic deconvolution *(Rumanian)* 80—8454
seismic data processing algorithms, sign coding appl. *(Russian)* 79—62616
seismic events visual correlation quantitative estimates based on min. average risk criteria *(Russian)* 79—44133
seismic exploration, iterative identification of non-invertible autoregressive moving-average systems 78—81422

data reduction and analysis continued
seismic instrumentation and data analysis, conf., Durham, England (Aug. 1977) 79−39905
seismic inverse problem for two-dimensional velocity variations 80−21833
seismic noise sources mapping in geothermal regions 77−81828
seismic observations digital processing, steady numerical solns. *(Russian)* 79−53317
seismic pattern recognition, fundamental problems 78−81428
seismic prospecting, inverse kinematic case soln. in layered Earth using reciprocal points *(Russian)* 79−44268
seismic recording network at Campotosto reservoir *(Italian)* 80−101446
seismic recordings, information quality and data processing techniques efficiency *(Russian)* 79−39666
seismic records, non-linear stochastic models with appls. in event identification 79−16396
seismic reflection data, inversion 77−21915
seismic reflection traveltime data, computerised method for effective vel. 80−21832
seismic refr. survey depth determination, program for pocket calculator 80−82088
seismic signals deconvolution, adaptive filter structs. 80−98451
seismic source depths, improved determ. using seismic coda 77−81829
seismic surface wave data inversion 77−37147
seismic surface waves, anal. using PDP-15 interactive graphics 78−81427
seismic surface waves, inversion of dispersion data with random errors 77−73681
seismic surface waves analysis, new techniques appl. to Adriatic subplate averaged model 79−44159
seismic surveys, residual static and crossdip corrections simultaneous estimation 79−92500
seismic surveys, source pulse processing rel. to zero time identification 77−21916
seismic travel times, anal. rel. to lithospheric slab penetration into lower mantle 77−73700
seismic wave path hodographs, imperfect knowledge appl. to seismic shocks location *(Russian)* 79−35009
seismic waveforms extrapolation, by Fourier methods 79−34978
seismic wavelet estimation, short-time homomorphic signal anal. appls. 78−81426
seismic waves, dynamic spectral ratios with variable freq. bands as seismic discriminants 77−81834
seismic wide angle refl. data from expendable sonobuoys, display and processing 79−39896
seismogram processing, for Rayleigh waves phase vel. investigations in middle Europe 79−44136
seismograms, algorithms for true Earth tremor vels. determ. 79−96743
seismograms, seismic field decomposition algorithm from spectral matrices 77−9370
seismological data collection and anal., detect. of possible violations of Nuclear Test Ban Treaty 79−39919
Seismological Service of Canada, instrumentation and data processing 79−39914
seismology, automatic vertical time-depth curve approximation via successive layer detect. *(Russian)* 78−40700
seismology, digital processing of CDP data for curvilinear reflecting boundaries *(Russian)* 79−84534
seismology, inverse problems interpretation *(Russian)* 79−34762
seismology, minimum data technique for earthquakes global location *(German)* 80−56627
seismology, multichannel subtracting filters for freq.-domain anal. *(Russian)* 78−49156
seismology, optimal vel. anal. in common depth point method *(Russian)* 78−40698
seismology, self-adaptive wave train subtraction in linear and three-dimensional surveying *(Russian)* 78−40695
seismology, synthetic sonic logs as process for stratigraphic interpretation 79−88483
seismology, transmission synthetic seismograms direct inversion 79−29877
seismology, wave refl. coeffs. identification from noisy data 79−29718
seismology common depth point data digital processing technique *(Russian)* 79−74875
self-consistent smoothing program 77−13596
semiconductors optical data, anal. rel. to optical props. determ. via Kramers-Kronig transform. 77−8537
sesimic data, detect. of waves and converted from P to SV in mantle 77−81810
Shiva laser fusion facility, target diagnostic system, data acquisition and anal. 78−51366
shortening operators used in gravity interp. data processing techniques 77−64179
SIMS, recording, optimisation 79−43683
SIMS ion images, multifeature mass analysis utilising digital image processing, Fe anal. appl. 79−43684
simulated underwater partial launch system, photogrammetric data reduction system 77−79075
single scattering particle laser Doppler measurements of turbulence, data reduction 77−39379
SIT vidicon detector system for Palomar 1.5 metre telescope, data reduction methods 79−92674
sleep EEG ambulatory monitoring and anal. 78−44650
smoothing of observational data 77−73969
soil bulk resistivity meas., digital data-processing techniques 78−24381
solar radio bursts, recording instrumentation and data reduction *(Italian)* 78−96458
solar spectrum, automatic processing by digital double-pass monochromator *(Russian)* 80−72777
solar type IV radio events, FFT anal. rel. to pulsating structs. 78−96455
solar wind protons cooling, evidence from Mariner 2 data 78−40789
solar X-ray images, quantitative interpretation by filter ratio anal. 79−40085
solar X-ray photographs, anal. and interpretation 78−4179
solar X-ray photographs anal. and interpretation, filter ratio method 79−40086
solid-state linear array appls. in remote sensing, user-oriented data processing 80−4151
sonar, testing for multivariate normality 79−59865
space domain filter method *(Chinese)* 80−89933
spacecraft data processing and analysis 77−78650

data reduction and analysis continued
Spacelab data processing system, 125 MS computer *(French)* 77−78594
spark chamber photographs, automatic and semiautomatic handling, comparison 77−23371
speckle interferometry, image restoration by least squares method 79−25514
spectra, photographically recorded, semi-automatic interpretation, mass, at. spectra appls. 77−48708
spectra of ^{60}Co gamma-ray source, for instrument calibration 77−6608
spectral anal. of randomly sampled records by direct transform 77−30134
spectral decomposition, generalised algorithm, appl. to UV, IR, at. emission spectrometry 77−12842
spectrochemical analysis in hydrocarbon flames, computer processed laser Raman spectra 79−43652
spectrograms, automatic precision wavelength comparator 78−82042
spectrophotometer (UR-20), data handling attachment 77−26409
speech analysis, computer-controlled method for articulatory activities meas. 77−56391
speech signals, data reduction, methods and results 79−81648
SPEED 2, computer program for data reduction from automatic data acquisition systems in FORTRAN 80−27279
spiral galaxies surface photometry, computerised data reduction system, (appl. to NGC 157) 79−40264
spirometric parameters, interactive on-line computerised computation 78−44656
statistical and computational methods, book 77−5655
steel, alloying element determ. by computer-controlled X-ray spectrometry 77−56318
stellar data in machine-readable catalogues, critical evaluation 77−78830
stellar photoelectric photometry at Hvar Observatory, instrumentation and reduction techniques 77−78643
stellar photographic photometry, PDS microdensitometer technique 79−88600
stellar photometric data, critical evaluation 77−78831
stellar photometry anal., vector space methods and appls. to O stars and interstellar reddening 78−49338
stellar polarisation meas., data reduction method 80−26748
stellar proper motions, maximum-likelihood method for open clusters membership determ. 78−16471
stellar right ascensions obs. with large transit instrument, accuracy of absolute chain method of equalisation *(Russian)* 79−96887
stellar speckle interferometry, transform for binary stars meas. 77−71011
stellar speckle interferometry data processing method 79−12409
stellar spectra, line profiles anal. using linear filtering theory *(Italian)* 80−90340
stellar spectral classification, errors detect. by cluster anal. 78−20819
stellar UBV photometry, influence of Balmer discontinuity on reductions 77−74046
stellar uvbyβ photometric data, appl. to MK spectral classification prediction 80−67700
STEM, computer driven, image registration 80−104838
stereo electron micrographs restitution, approximate soln. 79−26189
strain gauge meas. in cyclic elastoplastic tests, automatic processing on portable computer 77−5829
stratosphere sounding by multifrequency lidar, meas. inversion rel. to aerosol microstruct. *(Russian)* 77−64374
streak camera, direct readout devices 78−38037
stress/duress automated detect. system 80−76852
strong-motion accelerograph data management 78−36332
strong-motion accelerograph data processing 78−36330
strong-motion earthquake accelerograph records, data management 79−62629
surface profiles, reference line selection and fitting, based on random process analysis 78−45594
surveying, interpolation via groups of triangulation data points of different statistical characts. *(German)* 77−9321
systolic time interval, off-line processing of exercise data 77−40868
TEM, quantitative elemental analysis 80−101060
temperature meas., dynamic, data recovery by integral equation solution, computer-aided 77−5839
terrestrial electricity, DC resist. meas. interpretation 79−5449
thermal analysis data transfer to single recording instrument using multichannel commutator 79−52821
thermal analysis system, Du Pont 1090, microcomputer-controlled 80−16613
thermal storage unit, sensible-heat, solid, transient response 79−3892
thermo-physical expts., information input unit for the 'Iskra-1122' electronic keyboard computer 80−201
thermogravimetric data acquisition and reduction program 78−64901
thermometer, statistical, with temperature regimes evaluation *(Czech)* 79−63208
thermophysical experiment, automatic information-processing system 78−196
thin-layer fluorescence chromatograms, automatic meas. and data processing 79−29424
three-coordinate measuring machine, dynamic acquisition and automatic reduction of data 79−75507
thunderstorm radar information, automated acquisition and analysis 78−7772
tilt meter observations harmonic anal., influence of S$_1$ diurnal meteorological wave *(Russian)* 78−88788
time obs., data smoothing method *(Japanese)* 77−73973
time series analysis, by ARMA-modelling *(German)* 80−31129
time service, data acquisition and real time processing system *(Italian)* 80−8549
TLD data analysisusing a Texas Instruments programmable calculator 80−36136
tomography, high speed, special purpose digital processor architectures and numerical approx. methods 80−30878
toxicity experiments, processing of automatic analyser data using trace reader and computer 78−24195
toxicity studies, TOXIPAC-300 data processing system *(Japanese)* 79−25172
tracheal mucociliary transport, bronchoscopic evaluation 77−60270
transient astronomical phenomena, video detection and analysis techniques 79−80239
treatment planning in ^{60}Co radiotherapy using computerised tomography techniques 78−35964

data reduction and analysis continued
triangulation direction finding network for atmospherics sources fixing, data transmission and reduction 79—100981
truncated real sinusoids, frequency estimator methods 80—73161
turbulence breakdown coefficient determ., influence of data treatment technique *(Russian)* 78—7690
turbulent flow fields, evaluation of stereoscopic trace particle records 78—1648
two-dimensional data field, number of significant proper functions 80—27108
two-probe synchronized sampling technique for measuring flows behind rotors, calibration 80—14865
underground remains detection, acoustic meas. with computer data processing 79—76921
underwater camera data correl. and interpretation, systems approach 79—5688
upper atmosphere pitot meas. press. meas., data anal. for densities determ. between 50 and 120 km 78—45193
W Ursae Majoris binary stars, synthetic light curves calc., appl. to V566 Ophiuchi 77—74097
US evaluation, computer-assisted, review 79—43536
US flowmeter data processing, transfer function modelling of arteries 78—61225
US Geological Survey RASS-STATPAC system for mangement and statistical reduction of geochemical data 78—20522
US images corrected for refr. and attenuation, comparison of high resolution methods 80—30817
USSR Hydrometeorological Service, automation of data collection and processing 79—34994
van der Waerden's nonparametric X test in data processing 77—71304
vapour pressure, constrained fitting of limited data 78—34615
vapour pressure measurement, torsion-effusion method, automatic data acquisition 80—52188
vapour-liquid equilibrium, data reduction, extension of Barker's method 78—79735
vectorcardiography, computerised meas. and display system 77—40864
velocity measurement in rotating liquids, two-dimensional, using automatic analysis of trace particle motion 79—64810
ventilation inhomogeneity identification using minicomputer data processing 77—44816
ventricular ectopic activity, semiautomated data reduction 79—66573
virology laboratory minicomputer appls. 77—44856
voltammetry, linear sweep anodic stripping time, real time anal., recursive estimation 80—26067
Walsh transformation processing, matrix relationship with discrete Fourier transformation *(Russian)* 78—26
weather data, asynchronous, method for reduction to a common time 80—85735
weather data reduction for building and solar energy system optimisation 79—57397
weather forecasting processing of radar and satellite imagery data 80—109252
weighted entropy method for clinical data reduction 78—92742
well mud logging, online data processing *(Russian)* 78—40706
wind magnitude and persistence models, statistical analysis 79—5583
wind power site evaluation, data acquisition and processing 79—66400
wind remote measurements, individual particle scatt. and single-burst digital correl. 79—100980
wind-tunnel laser anemometer photon correlation techniques 77—80256
X-ray anal., conf., Denver, USA (Aug. 1976) 77—70382
X-ray and neutron small angle scattering, recent developments in instrumentation and data anal. 79—10750
X-ray astronomy, point-like sources lunar occultations data anal. 79—88567
X-ray diffr. powder phase identification, manual computer search techniques 77—70387
X-ray diffraction expts., SPADE software package 79—63195
X-ray fluoresc. anal., energy dispersive, least squares, Monte Carlo methods, mathematical anal. techniques 78—85243
X-ray fluoresc. anal. line intensities calc., computer program, appls. 78—61107
X-ray fluoresc. element anal. in pulps, conc. calcs., iterative method 78—61109
X-ray fluoresc. spectrograph, automatic computerised, for rock trace elemnt anal. 77—56320
X-ray fluorescence anal., matrix correction, computer program *(German)* 80—3427
X-ray fluorescence of rock samples, major-element data processing, SORT, REORD and MW programs in FORTRAN 77—86398
X-ray photoelectron spectra, surface chemical analysis through even derivatives 79—100463
X-ray powder diffractometer, APD3600, file searching techniques 80—24319
X-ray residual stress anal., computer controlled, software, precision 78—5712
X-ray small angle scattering, curve anal., by triaxial body models using graphic display model 80—28873
X-ray spectra, energy dispersive, peak separation from background 78—7310
X-ray spectra, energy-dispersive, nongaussian peak overlap problem 78—78050
X-ray spectrometer control, interactive program for data collection, manipulation chem. anal. appl. 78—7312
X-ray spectrometry, quantitative, comparison of mathematical models 79—17587
X-ray spectroscopy, air and water anal. 77—52689
X-ray survey instruments, automated calibration and recordkeeping system 77—37876
zodiacal light UV observation from D2B-Aura satellite, extraneous light evaluation 79—58299
ZPR, noise analyses, determination of kinetic parameters *(Rumanian)* 78—46139
$Cl^{4+}+Xe(Ar)(N_2)$, 20 MeV, electron loss cross sections, pot. model data anal. 79—27082
F III, IV, beam-foil spectra, mean lives, 2150-3200 angstrom 78—55224
H II regions radio emission analysis, consequences of improper analytic methods 78—54000
H(D)+Ar, differential collision cross sections, diffraction oscills., data anal. 79—22783
H_2O sources spectra, autocorrel. anal. 78—65713
Hg vapour-gas mixture, Hg diffusion, data correlation 78—79403

data reduction and analysis continued
$I^{5+}+Xe(Ar)(N_2)$, 20 MeV, electron loss cross sections, pot. model data anal. 79—27082
Mn nodule mining and processing with nuclear meas. 77—4975
NO, and isotopic forms, $X^2\Pi$ state, IR obs., mol. consts. 78—42045
Ni_3Mn, anal. of irrad. disordering data 79—1466
V, electrical resistivity, 200-2100K 79—33277

data security *see security of data*

data structures
array processing, algorithms and data structs. for conformational analysis of proteins 80—83530
data bank model, appl. to geological data 77—53199
data management systems in economic geology 77—53201
distributed data bases for structured data 77—53200
Fourier series in celestial mechanics, fast evaluation 80—56711
geographic information systems, topological data structs. conference, Dedham, Massachusetts (16 to 21 October 1977) 79—74826
multilevel syntax analysis for geological data compression 79—48569
pi systems representation, efficient computer manipulation 79—81148
Spar Buoy Oceanographic Telemetry System software engineering 80—46308

data tables *see collections of physical data*

data transmission equipment
see also data communication equipment; telemetering equipment
A/D convertor immunity noise abatement methods *(Russian)* 77—54838
duoPIGatron ion source, optical telemetry and data transfer system 78—66443
FASTBUS project, development status of high speed standard data bus 79—45605
fibre-optic integral data source/receiver package 78—63179
high speed top mounted bus, prototype crate and module system 79 45611
industrial fibre-optic data link integrated components 79—10392
laser beam deflector, electromechanical, for data transmission through free atmosphere *(German)* 80—38053
multichannel analog memory, using MOS transistors for data transmission to M6000 computer 79—26043
optical, 10.6 μm laser data relay link transmitter/receiver optical design 77—19442
optical data transmitter, laser and LED comparison *(German)* 80—14432
optical fibre eight-terminal data bus, using T-couplers 78—59129
optical fibre links, low cost, features 78—42413
photodetectors, highspeed, performance testing 79—26129
plasma diagnostics, Thomson scatt. system, analogue data processing circuits 78—87488
plastic fibre-optic assemblies 80—14433
proton storage ring, NAP-M, data transmission and supervisory system 77 65365
single fibre separate connectors, loss factors optical fibre 77—88939
telemetry, totally implantable, integrated power controllers and RF data transmitters 80—67295
triangulation direction finding network for atmospherics sources fixing, data transmission and reduction 79—100981
underwater data communication US standing-wave radiator 79—46104

data transmission systems *see data communication systems*

database management systems
acute lymphocytic leukaemia patient data analysis system CLINFO 77—66823
astronomical data base standards, management and security 77—82282
automated information retrieval system, data bank organisation *(Russian)* 77—1960
Canadian mineral occurrence index 77—53205
cardiovascular research database system 78—53549
chemical reaction sites automatic detection 78—92476
CLAIR data system overview 78—57325
continuous speech recognition system for data base consultation 80—91990
data bank model, appl. to geological data 77—53199
data management and analysis systems for hydrogeochemical reconnaissance 78—20520
distributed data bases for structured data 77—53200
Earth resources satellite data *(French)* 79—53526
economic geology management system 77—53201
electrode reaction kinetic parameters, programs for computer retrieval, in FORTRAN 78—31654
environmental information consequences in information systems 79—57500
fission reactor materials, experience at the International Atomic Energy Agency in processing safeguards information 80—63497
fusion reactor, MFTF, supervisory control and diagnostics system, database management system 80—99326
fusion reactor, MFTF, supervisory control and diagnostics system, database management system, data structs. 80—99327
G-EXEC generalized data handling system, design philosophy 77—53210
gas chromatography-mass spectrometry, computer-based library system 77—44523
general objective data base system for distributed cooperative researcher files 77—53213
geological and geochemical data management and processing 78—57324
geological computer design 77—53211
geological data management, conf., 1975, Nov., Paris, France 77—53198
geological surveys, Quaternary, automation 77—53209
hydrogeological, characts. *(Italian)* 80—109255
logical searching of the lunar data, FORTRAN program incorporating Boolean search capabilities 79—2491
mineral exploration, computer uses, limitations and requirements 77—53207
mineral resource data bases 77—53203
Mineral Resources Development Centre, developing countries computer aid 77—53215
MSDC/EPA/NIH mass spectral search system 78—65912
oceanographic data, retrieval-time data generation 77—5354
Omo River project (Ethiopia) data management system appraisal 78—57326
onshore borehole records, data bank system 77—53214
particle physics appl. 80—899
Pioneer Venus, Unified Abstract Data Library and Quick Look Data Delivery System 80—67494

database management systems continued
- river basin management system 79—25288
- SIGMI user-oriented file-processing system for geological data 77—9506
- space information systems, real time data management 79—92600
- Tennessee Valley Authority occupational radiation exposure data management system 79—9899
- Vela Seismological Network, use of Datacomputer 77—82013
- Vela seismological network, use of datacomputer 78—81411
- Mn nodule undersea mining data file, management and statistical anal. 77—53206

dating, Earth *see geochronology*

dating, radioactive *see radioactive dating*

Davydov splitting
- anthracene, Davydov splitting of lowest singlet exciton under high press. 77—72823
- anthracene, luminesc. spectra, exciton-phonon interaction, triplet exciton bands 79—65387
- anthracene, single cryst., piezomodulated reflection spectra 79—61392
- anthracene, singlet-triplet absorpt. spectra, 2-300K, photoexcitation spectra 78—43890
- anthracene, triplet exciton absorpt. lines 79—47475
- anthracene, triplet-exciton fine struct., high resolution optical meas. 80—45099
- carboxylic acid dimer, Fermi reson. 79—31501
- chain crystals, interchain correlations and energy spectrum, Davydov splitting 79—28309
- dicarboxylic acids, IR spectra Davydov splitting, methylene chain pendular vibrs. *(Russian)* 80—89008
- excitonic parameters, split absorption bands, organic molecule aggregates *(Spanish)* 79—59437
- excitons, in mol. cryst. with complex lattice 79—56132
- fluorene, lowest singlet state, exciton band struct. calc. 78—63983
- fluorene, near 6K, two-photon excitation spectrum, g-exciton states location 78—64393
- inorganic molecular crystals, metal complexes electronic spectra and intermolecular interactions 80—55137
- metallophthalocyanines, α-phase solid, absorpt. and MCD spectra 79—73964
- molecular crystal, kinematical interaction of excitons and Davydov splitting 79—82528
- perylene, cryst., fluoresc. spectra, time-resolved, excimer and excitons 79—78724
- phenanthrene, two-photon excitation spectra, exciton-phonon and intramol. vibronic coupling 80—84774
- polydiacetylene PTS crystal, Davydov splitting in spectra at 15000 to 19000 cm^{-1}, at low temp. 78—31212
- potassium formate, IR absorpt. spectra, sampling effects, Davydov splitting and struct. 78—52508
- pyrene, triplet exciton absorpt. lines 79—47475
- pyrene, triplet state, excitonic energy transfer, phosphoresc. and delayed fluoresc., 2 to 300K 80—84776
- rhodamine B, double Davydov's splitting of visible absorpt. band 78—82746
- scheelite crysts., Davydov splitting of vibr. levels, short range interaction 80—71418
- squaric acid thin films, Raman and IR spectra, Davydov splitting rel. to interlayer interaction 79—99878
- tetracene single crystals, Davydov splitting, press. depend., phase transition obs. 78—27250
- 1,2,4,5-tetrachlorobenzene, exciton states in crystals and dimers 80—70620
- Br_2, condensed phases, spontaneous and stimulated Raman scatt., weak and strong radiation fields 79—3450
- CdP_2, cryst., tetragonal, 2-phonon IR absorpt. 80—66176
- $FeCl_2.2D_2O$, metamagnetic, excitonic Davydov splitting in Raman spectrum 79—33704
- GaS, Davydov splitting of degenerate lattice modes 79—61382
- HCl, cryst., internal vibr. electrostatic interactions and IR bandshape 79—91417
- α-HIO_3, vibration level Davydov splitting, adiabatic potential role, dipole-dipole approx. *(Russian)* 80—29365
- KCN, ionic mol. cryst., exciton struct. 78—79935
- KHF_2, vibr. spectra, mol. interaction and Davydov splitting 79—8147
- $KReO_4$, vibr. spectrum, Raman and IR spectra obs. 80—55104
- PbI_2, polytype, lattice dynamics, influence of static dipole moments 79—28057
- ZnP_2, cryst., tetragonal, 2-phonon IR absorpt. 80—66176

Davydov states *see Davydov splitting*

dawn *see twilight*

dawn chorus *see atmospherics*

dayglow *see airglow*

d.c. amplifiers
- automatic range-changing amplifier, ionisation current pH and vacuum measurement appls. *(French)* 79—63262
- chemical analysis, for Beckman LB-1 CO_2 analyser 77—29215
- circuit design, to record heat pulse during material fracture 78—60921
- digital automatic thermodynamic enthalpy and specific heat determ. equipment 78—57951
- digital electrometer appl., cct. 78—77933
- electrometer, high-sensitivity, with modem amplifier 77—74447
- electrometer measuring unit and component requirements 77—74445
- electrometers, high-speed general-purpose, features 77—74448
- electronic sweep of magnet field in microwave spectrometer 78—12717
- high impedance IC amplifier, for thermoluminesc. signal meas. 79—99955
- for high impedance voltmeter, school expts. 78—12505
- IC four-channel EEG amplifier 79—39535
- linear pulse amplifier, fast DC coupled, gain and phase response design 80—58088
- low-level current amplifier for p-n junction radiation detectors 77—38573
- MOSFET electrometer amplifier, characts. 77—74446
- MOSFET electrometer amplifier type MDM 77—79106
- photoamplifier circuit, dynamic compensation of photodetector DC component temp. drift 80—73460
- temperature control of electrometer varactor-bridge amplifiers 79—9219
- thermistor thermostat for low-power semiconductor devices 79—71450
- two-laser frequency difference stabilisation electronic system 79—68401

d.c. generators
- *see also homopolar generators*
- disc dynamo, pseudo-stochastic behaviour in circuits with shunt, couple and series resistance 78—93608

d.c. machines
- *see also d.c. generators; d.c. motors; homopolar machines*
- MHD induction machines in DC breaking mode, operating anal. 80—48816

d.c. motors
- *see also homopolar motors*
- angular velocity meas., contactless method *(Russian)* 80—73329
- brushless, biventricular blood pump drive, development and in vivo evaluation 79—53285
- drive, gamma-ray transmission meas. instrument 77—9011
- micromotor controls feed rates in syringe pumps 78—48923
- PWM control, electric wheelchair appl. *(German)* 77—56491
- solar arrays and DC motors, direct coupling theory 80—3523
- solar electrical system comprising DC separately excited motor and mechanical load driven by solar cell array, performance analysis 80—16801
- traction, circuit fault detection by NDT method 79—39097

d.c. power transmission
- electrification of objects under DC transmission lines, charge simulation calcs. 78—78853

d.c. sputtering
- actinide target preparation by focused ion beam sputtering 80—23219
- amorphous alloys, prep. by high rate sputter deposition *(Japanese)* 79—95971
- cleaning, substrate surface contamination from dark-space shielding 77—8968
- compound films, prep. by magnetron sputtering, and special features 80—11565
- cylindrical magnetron sputtering sources, substrate heating 79—24435
- cylindrical magnetron sputtering system for coating solar selective surfaces onto batches of tubes 80—80967
- deposition by ion beam sputtering, composition and stress state 77—89674
- diffusion coefficient of sputtered atoms in Ar 79—87539
- film deposition with sputter gun 77—44162
- glow discharge techniques for surface treatment and coating 78—11374
- ion beam, thin film deposition and micromachining 77—55887
- ion beam sputtering, glow discharge source for nuclear thin film target prep. 78—55067
- isotopic target preparation by ion beam sputtering 80—23220
- Langmuir probe technique, plasma characts. in sputtering 80—80929
- low pressure plasma system, design and operating characteristics 79—64880
- magnetic alloys, bulk amorphous, prep. by high rate sputter deposition *(Japanese)* 80—29906
- magnetic bubble materials, props. and preparation models, review *(Rumanian)* 80—93149
- magnetically enhanced sputter sources, high-rate, basic physics and operational characts. 77—44159
- magnetron sputtering, basic physics appl. to cylindrical magnetrons 78—72664
- magnetron-plasmatron processing and instrumentation, review 80—35090
- metal film mirror prep. by ultraclean DC sputtering, optical props. 77—50748
- metallic films, deposited by cylindrical magnetron sputtering, internal stresses 80—24773
- negative ion sources, role of alkali metal 78—74526
- neutralised ion beam sputtering appl. to MIS and solar cell structures 78—3046
- Penning gas-discharge chamber for uniform thickness film manufacture 77—44153
- planar magnetron sputtering 78—72725
- planar magnetron sputtering developments and applications 77—77379
- planar-magnetron sputtering source, modified 78—95693
- plasmatron/magnetron systems, role in physical vapour deposition 79—24436
- polymer layer, glow deposition rate obs. in DC discharges 78—68633
- rare earth Fe garnet, difference in comp. between targets and sputtered films, expt. 78—6848
- Re-sputtering and implanting sputtered atoms during deposition 80—16137
- ring gap plasmatron for high rate sputtering 77—40368
- solar collector DC reactively sputtered metal carbide and silicide selective surface props. 79—62029
- sputter electrode preparation for multiply charged heavy ion sources 78—66009
- steel, stainless, amorphous film, sputtered, prep. and characterisation 78—43266
- steel, stainless, ground surface ion bombardment, in DC glow discharge 78—95098
- steel, stainless, vacuum components, sputtering and reactive effects during glow discharge treatment 78—70141
- system with in situ deposit thickness monitoring, nuclear science appl. 77—32520
- Al film, enhanced mirror, high-rate sputtering, reflectance and dispersion 77—42636
- Al, magnetron sputtering in Ar and Ar/O_2 mixtures, discharge characts. 80—89145
- Al, planar magnetron sputtering, H_2 effect on Ar discharge 80—80970
- Al:Si, film deposition by reactive sputtering 79—66005
- $Al_xIn_{1-x}Sb$, DC sputtering and struct. 78—52674
- AlN film, oriented c-axis, low temp. deposition by reactive magnetron sputtering 80—76180
- AlN films on glass substrate, prep. by reactive DC magnetron sputtering technique, c-axis orientation 80—89146
- Al_2O_3 films, DC reactive sputtering prep., IR spectra characterization 79—11513
- Au, DC reactive sputtering, glow discharge mass spectrometry and X-ray diffr. 79—38701
- $Bi_4Ti_3O_{12}$ stoichiometric thin film prep. by DC sputtering with powder target 77—90273
- C, colloidal layers, sputtering, chem. etching in DC glow discharge 78—27667
- CdO-SnO_2 DC reactively sputtered films, elec. and optical props. 80—103763

- **d.c. sputtering** continued
  - CdO-SnO$_2$ film, DC sputtering prep., visible and near IR transmission, resist. 78−88049
  - CdS sputtered film, photocond. props. 78−10586
  - Co, DC reactive sputtering, glow discharge mass spectrometry and X-ray diffr. 79−38701
  - Co films layered over Cr by DC sputtering for digital mag. recording 79−83118
  - Co-Mo-Cr-Si Laves phase, sputter deposited, struct. and wear props. 77−40477
  - Cr, sputtered wafer, internal stresses 77−39753
  - Cu, bias sputter parameters effect, hollow cathode 77−40369
  - Cu$_x$Mo$_6$S$_8$, Chevrel phase supercond. prep. and supercond. props. 79−28434
  - Cu$_x$O, film, thermoelec. power, activation energy variation with electrode spacing in DC sputtering 78−76099
  - ErRh$_4$B$_4$, film, sputter deposition and low temp. props. 80−2948
  - Fe film, high rate deposition by sputtering from two facing targets 77−85938
  - Fe-Cr-Si, heat resistive films prepared by sputtering, lifetime meas. 80−80132
  - Fe-Si-Al, Sendust, 12 μ thick film prep. by sputtering, mag. and other props. 77−55888
  - FeC$_x$-CrC$_y$-NiC$_z$, stainless steel carbide, solar selective surface, fabrication, magnetron sputtering system description 80−80967
  - FeC$_x$-CrC$_y$-NiC$_z$, stainless steel carbide, graded solar selective surface, magnetron sputtered 80−81485
  - FeC$_x$-CrC$_y$-NiC$_z$, stainless steel carbide, sputtered solar selective surface, grading profile 80−81486
  - Gd-Co amorphous film, DC or RF sputtered, mag. props., He$^+$-backscatt. investig. 77−20650
  - Ge, film, elec. props., prep. by DC sputtering *(Japanese)* 79−78237
  - In, reactive sputtering in DC triode config. 78−23618
  - In, reactive sputtering in Ar-N$_2$, N$_2$-O$_2$ discharges, mechanism, model 80−89109
  - InAs film, DC sputtering, struct. and elec. props. 77−66567
  - InN film growth by reactive sputtering in Ar-N$_2$ discharge, mechanism 80−89107
  - In$_2$O$_3$-InN film growth by reactive sputtering in N$_2$-O$_2$ discharge, mechanism 80−89108
  - In$_2$O$_3$-SnO$_2$ film, reactive DC diode sputtering, using large scale system 78−72723
  - InP cylindrical magnetron reactive sputtering, for solar cell appl. 78−39693
  - In$_{2-x}$Sn$_x$O$_{3-y}$ film, magnetron DC reactive sputtering, X-ray diffr. meas. 77−44160
  - Mn$_{46}$Co$_{54}$, amorphous alloy prep. by high-rate sputtering, struct. and prop. characteris. 79−24462
  - MnCo$_2$O$_4$ DC sputtered films, struct. and elec. props. 80−54812
  - Mo film, deposited by cylindrical magnetron sputtering, internal stresses, optical reflectance and elec. resist. 77−43449
  - Mo$_x$Si$_y$ films, magnetron DC reactive sputtering, struct. and props. 80−80966
  - Nb film magnetron-sputtered, intrinsic stresses and supercond. props. 80−24772
  - Nb film sputtered onto Cu substrate, microstruct. and supercond. props. 77−85370
  - Nb-Ta-N films and their anodic-oxides, elec. props. of resist. and dielec. films 80−11126
  - Nb$_3$Ge film, sputtered and evaporated, transition temp., critical field and current anisotropy 77−28328
  - Nb$_3$Ge films, form. of A15 phases by DC sputtering 79−38740
  - Nb$_3$Ge films, prep. by DC sputtering and solid state diffusion, supercond. props. and struct. 79−38212
  - Nb$_3$Ge, RF and DC sputtered films comparison, O content effect 78−72022
  - Nb$_3$Ge superconducting films, high critical temp., optimum sputtering conditions 80−15647
  - Nb$_3$Si films, form. of A15 phases by DC sputtering 79−38740
  - Nb$_3$Sn film, high T$_c$, high-rate magnetron sputtering, supercond. transition temp. meas. 77−43770
  - Ni film, deposited by cylindrical magnetron sputtering, internal stresses, optical reflectance and elec. resist. 77−43449
  - Ni$_x$O, film, thermoelec. power, activation energy variation with electrode spacing in DC sputtering 78−76099
  - Pb$_x$Mo$_6$S$_8$, Chevrel phase supercond. prep. and supercond. props. 79−28434
  - Pd-Si amorphous films, compositions and thermal behaviour 80−55292
  - Pt, DC reactive sputtering, glow discharge mass spectrometry and X-ray diffr. 79−38701
  - Si, amorphous, dark conductivity and photocond. obs. *(French)* 78−64155
  - Si p-n heterojunction, DC sputtering growth, photocond. and photovoltaic effects 79−33337
  - SiN$_x$, film by magnetron sputtering, composition, hardness and optical props. 78−3047
  - Si$_3$N$_4$ amorphous film deposition by high rate DC reactive sputtering, passivation appl. 80−100784
  - Sn, DC reactive sputtering, glow discharge mass spectrometry and X-ray diffr. 79−38701
  - Sn-Ni metastable equiatomic alloy, sputter deposition 78−3043
  - Sn$_x$Mo$_6$S$_8$ and (Sn-Al)$_x$Mo$_6$S$_8$, Chevrel phase supercond. prep. and supercond. props. 79−28434
  - SnO$_2$ film, growth by DC sputtering from compressed target, cond. and optical props. 77−59690
  - SnO$_2$, two-step deposition process using DC sputtering and oxidation, and characterisation 78−95691
  - SnO$_2$:Sb film, DC sputtered, substrate temp. effect on cond. 77−39971
  - SnO$_2$:Sb thin films DC sputtered, heat treatment effects, expt. 77−28719
  - SnO$_x$ films reactive DC sputtering prep., phase comp., X-ray diffr. and Mossbauer meas. 79−90914
  - Ta film, deposited by cylindrical magnetron sputtering, internal stresses, optical reflectance and elec. resist. 77−43449
  - Ta film sputtered onto Cu substrate, microstruct. and supercond. props. 77−85370
  - Ta-Cr-Si-Al, heat resistive films, prepared by sputtering, lifetime meas. 80−80132
  - TaB$_2$-Cr-Si-Al, heat resistive films prepared by sputtering, lifetime meas. 80−80132
- **d.c. sputtering** continued
  - Ti density, in DC sputtering discharge by atomic absorpt. spectroscopy 80−43973
  - Ti film, deposited by cylindrical magnetron sputtering, internal stresses, optical reflectance and elec. resist. 77−43449
  - Ti-W, bias-sputtered, resist. and comp. 80−25023
  - Ti-W magnetron sputtered films metallisation 80−45231
  - TiC coating, activated reactive evaporation and sputter deposition, wear characts. 77−44394
  - TiN film, magnetron DC reactive sputtering, X-ray diffr. and SEM 77−44160
  - TiO$_2$ and Dy$_2$O$_3$-TiO$_2$, high refractive index film growth by sputtering, waveguide appl. 77−48341
  - VO$_2$:Al(W), thin layer prep. by reactive DC sputtering doping effectiveness *(German)* 78−6847
  - WC, sputter deposited coatings, elec. resist., mag. susceptibility and adhesion meas. 77−44395
  - WC-Co coating, sputter deposition, friction and wear characts. 77−44394
  - WC-Co sputter deposited film, struct. and comp. 78−72023
  - W$_{50}$Fe$_{50}$ glassy alloy, refractory, triode sputtered 80−75185
  - YIG films, deposition by DC sputtering from two facing targets 78−31341
  - YIG target and DC glow discharge sputtered film compositions compared 77−55886
  - ZnO film, Zn target, fabrication, properties 78−3040
  - ZnO film on glass substrate, high-rate deposition using DC reactive magnetron sputtering 80−80978
  - ZnO low-loss optical waveguides on amorphous substrates 80−58793
  - ZnO piezoelec. film, fabrication and appl. *(Japanese)* 78−23616
  - ZnO piezoelectric film US transducers obtained by DC diode sputtering, dielec. breakdown props. 80−40066
- **d.c. to a.c. invertors** *see invertors*
- **d.c. transformers**
  - *see also magnetic amplifiers*
  - CERN SPS, zer flux DC current transformer 77−88306
  - ferromag. metals, domain wall motion, drag and inverse drag, appl. to DC transformer 80−34679
  - piezoelectric ceramic transformers, optimal transducer design *(Japanese)* 77−13770
- **DDA** *see digital differential analysers*
- **DDC** *see direct digital control*
- **de Haas-van Alphen effect**
  - *see also diamagnetic properties of substances; diamagnetism*
  - actinide intermetallic compounds, Fermi surface meas. 80−6698
  - actinide metals, Fermi surface meas. 80−6698
  - antiferromagnets, field depend. spin-splitting zero 80−84450
  - Bloch electrons in mag. field, transfer-matrix study 77−55472
  - bound state induced scattering reson. at dislocations, effect on de Haas-van Alphen freq. 78−76019
  - CDW system, nonlinear de Haas-van Alphen effect 77−43523
  - de Haas-van Alphen effect 79−99473
  - demagnetising fields and magnetic interaction 78−10332
  - diamagnetic metal, crit. point of diamag. transition of first kind, and NMR linewidth 77−59469
  - Dingle temperature and electron scatt. changes, accurate meas. method 77−51638
  - dislocation pot. rel. to de Haas-van Alphen effect, Dingle factor *(Russian)* 78−30885
  - electron fluid, adiabatic de Haas-van Alphen effect at low temp., Fermi fluid interaction and chem. pot. effects *(Russian)* 80−84442
  - electron gas, magnetised, confinement effects 79−28494
  - electron gas, sound velocity variation under de Haas-van Alphen conditions 79−60681
  - electron gas, two-dimensional, study in intermediate mag. field 79−60743
  - electron scatt., cut-off at small angles 77−59247
  - electron-phonon scatt. for de Haas-van Alphen effect, appl. to Hg 79−65360
  - electronic properties harmonic content of de Haas-van Alphen effect, appl. to dil. mag. alloys 78−84127
  - Fermi surface and pressure depend. determ. method 77−24511
  - Fermi surface volume depend. 79−65365
  - FFT spectral analysis of de Haas-van Alphen oscills. 79−42434
  - graphite, minority carriers and H-point magnetorefl. spectra 77−63398
  - graphite acceptor intercalation cpds., C$_n$Br and C$_n$NO$_3$H, electronic struct., quantum-magnetothermal oscills. 80−44478
  - graphite acceptor intercalation cpds., modulated electronic struct. 79−95310
  - graphite intercalated with AsF$_5$, quantum oscillatory phenomena 80−107823
  - graphite intercalation cpds., C$_n$K, de Haas-van Alphen effect, cyclotron reson., and transport props. 80−44479
  - graphite intercalation cpds., Fermi surface and transport props., LCAO model 80−80159
  - graphite-AsF$_5$ intercalation compounds, de Haas-van Alphen effect, charge transfer rate 80−54595
  - graphite-Br$_2$, intercalation process 78−63965
  - graphite-K intercalation compounds, electronic props., de Haas-van Alphen effects and Fermi surfaces 80−75498
  - graphite-K intercalation compounds, Fermi surface, transport and supercond. props. 79−65367
  - Hume-Rothery Phases, electronic struct., main features 79−23883
  - layered crystals, thermodynamic pot. in quantizing mag. field, conc. depend. *(Russian)* 79−15071
  - magnetic field dependent phase shifts present in the measurement of quantum oscillatory effects 79−77983
  - magnetic field sweeper and recorder drive for de Haas-van Alphen type phenomena 77−67474
  - magnetic interaction and phase smearing 77−11845
  - magnetic measurements, eddy currents 78−12730
  - magnetic oscillations, Fermi surfaces and high magnetic fields 79−73423
  - measurement using vibrating magnetometer *(Japanese)* 79−75559
  - metal, dislocated, Dingle temp. plots 77−59248
  - metal, dislocation scatt. and de Haas-van Alphen amplitudes 78−63967
  - metal, dislocation scattering and de Haas-van Alphen effect 79−77982
  - metal, influence of long-range dislocation pots. on de Haas-van Alphen effect 77−8009
  - metal films, mag. superlattice related to de Haas-van Alphen effect 79−61225

de Haas-van Alphen effect continued
metal whiskers, quantum oscills. of mag. moment 79—15280
metals and alloys, electrons at Fermi surface, book 80—105445
noble metals, thermopower calc. using dHvA data 79—65448
noble metals and their dil. alloys, de Haas-van Alphen studies, book 79—37966
noble metals and their dil. alloys, electronic struct., de Haas-van Alphen studies, book contrib. 79—37967
partially correlated phase smearing, effect on sum and difference de Haas-van Alphen frequencies 78—14655
quasilocal level role in electron energy spectrum 79—69398
quasiparticle approach 80—10897
quasiparticle picture 78—91592
semiconductor, influence of long-range dislocation pots. on de Haas-van Alphen effect 77—8009
semiconductor, with superlattice, magneto-oscillatory effects 77—85132
spin-splitting factor for Landau levels from de Haas-van Alphen effect first 3 harmonics 77—20226
transition metal, anal. by linearly recursive approx. 78—91603
transition metal, Fermi surface, stress depend., from quantum oscill. effects 78—91597
two-dimensional quantum plasma de Haas-van Alphen oscill. in correlation energy 79—60738
two-dimensional quantum plasma in mag. field, exchange energy 77—72904
A, magnetoresistance, field strength function, electrodeless methods 79—91026
Ag, conduction electron spin props., g-factor, de Haas-van Alphen oscill. amplitudes 77—35858
Ag, curvature factor, interpretation of de Haas-van Alphen oscillation amplitudes 79—47000
Ag, cyclotron mass and Fermi velocity meas. by de Haas-van Alphen effect 77—76734
Ag, Fermi surface and thermoelec. power, de Haas-van Alphen calc. 79—4503
Ag, spin props. of conduction electrons 79—46999
Ag, virtual bound states due to 4d- and 5d-transition metal impurities 80—70667
β'-AgMg, de Haas-van Alphen effect, LMTO band struct. and Fermi surface 78—75984
Al, Fermi surface, scattering anisotropy of conduction electrons on dislocations *(Russian)* 78—60051
Al, Fermi surface meas. 78—2412
Al, nonlinear helicon resonance *(Russian)* 77—28208
Al_2Cu, de Haas-van Alphen effect and LMTO band struct. 79—69396
Au alloys, dil., conduction electron-local moment interactions using dHvA waveshape anal. 79—77981
Au, conduction electron g-factor meas. 77—35859
Au, conduction electron spin props., g-factor, de Haas-van Alphen oscill. amplitudes 77—35858
Au, curvature factor, interpretation of de Haas-van Alphen oscillation amplitudes 79—47000
Au, cyclotron mass and Fermi velocity meas. by de Hass-van Alphen effect 77—76734
Au, Fermi surface and thermoelec. power, de Haas-van Alphen calc. 79—4503
Au, g-factor determ. 77—11847
Au, quenched and annealed, cond. electron scatt., de Haas-van Alphen Dingle temp. meas. 77—89688
Au, quenched and annealed, conduction electron scattering 78—47774
Au, spin props. of conduction electrons 79—46999
Au, virtual bound states due to 4d- and 5d-transition metal impurities 80—70667
Au-Co, dil. alloy, de Haas-van Alphen obs. of spin dependent scatt. by mag. pairs 77—32007
Au-Co, electron scatt. by mag. impurity pairs, de Haas-van Alphen obs. 77—66162
Au-Ga, dil. alloys, dHuA meas. and phase shift analysis of electronic scatt. anisotropy 77—35932
Au-Ga dil. alloys, electronic struct. 79—37974
β'-Au-Mg, de Haas-van Alphen effect, relativistic LMTO bandstructure, Fermi surface 79—37959
Be, magnetoacoustic quantum oscills. due to mag. breakdown orbits, and derivative of magnetisation meas. 77—43479
Bi alloy, mag. field depend. electron scatt. rates, de Haas-van Alphen meas. 78—10436
Bi, energy band model, resolution of theoretical discrepancy 77—11849
Bi, freq. mixing of de Haas-van Alphen oscills., quantum variations of Fermi energy 77—80721
Bi whiskers, de Haas van Alphen oscills. 4.2K, meas. using magnetometer 79—63284
Bi(:Si)(:Sb), mag. field dependent electron and hole scatt., quantum limit 77—15878
$BiIn_2$, Fermi surface determ., free-electron model 77—15744
Br-graphite, intercalation cpd., magnetothermal oscill. and charge-density waves 80—11199
CBr_x, graphite intercalated, de Haas-van Alphen effect and cyclotron reson. 80—44479
$C_{24}Rb$, graphite intercalated, de Haas-van Alphen effect, cyclotron reson., and transport props. 80—44479
$CaSn_3$, powdered, de Haas-van Alphen effect 80—59857
Cd and Cd-Mg, Fermi surface press. derivatives, de Haas-van Alphen effect meas. 77—43477
Cd, de Haas-van Alphen effect under press., Fermi surface and pseudopot. form factors 77—43475
Cd, de Haas-van Alphen effect and mag. breakdown *(Russian)* 77—80722
Cd, Fermi surface, strain depend., from US vel. oscills. 78—84133
Cd, Fermi surface changes under uniaxial compression 78—51876
Cd_3As_2, band struct. from Shubnikov-de Haas and de Haas-van Alphen effects 80—49597
Co, de Haas van Alphen oscill., effective mass 78—87900
Co, Fermi surface under press., de Haas-van Alphen effect meas. 80—75499
Co, ferromag., spin subband level position determ. by de Haas-van Alphen meas. under press. *(Russian)* 79—90947
Co, itinerant ferromag., Fermi surface and single particle excitations 80—34350
Cr, antiferromag., electron interference oscills. and spin-density-wave energy gaps at Fermi surface 80—49574

de Haas-van Alphen effect continued
Cr, antiferromag., stress depend. of Fermi surface, de Haas-van Alphen torque meas. 77—11846
Cr, antiferromag., stress depend. of spin density wave state de Haas-van Alphen torque meas. 77—63257
Cr, antiferromagnetic, pressure effect on Fermi surface by de Haas-van Alphen effect *(Russian)* 80—6701
Cr, Fermi surface under press., de Haas-van Alphen effect meas. 80—75499
Cs, Fermi surface, de Haas-van Alphen meas. 78—2411
Cu, conduction electron spin props., g-factor, de Haas-van Alphen oscill. amplitudes 77—35858
Cu, cyclotron mass and Fermi velocity meas. by de Haas-van Alphen effect 77—76734
Cu, Dingle temperature and electron scatt. changes, accurate meas. 77—51638
Cu, Fermi surface and thermoelec. power, de Haas-van Alphen calc. 79—4503
Cu, quenched, Hall coefficient, relaxation times, Fermi surface 80—84460
Cu, spin props. of conduction electrons 79—46999
Cu:Ni, Dingle temps. calcs., tetrahedron method 80—6699
Cu-H system, de Haas-van Alphen Dingle temps. for scatt. of cond. electrons determ. 77—76731
CuH dilute alloy, Hall coefficient, relaxation times, Fermi surface 80—84460
Fe, de Haas-van Alphen effect and exchange splitting, effect of pressure *(Russian)* 78—95252
Fe, Fermi surface under press., de Haas-van Alphen effect meas. 80—75499
Fe, ferromag., effect of pressure on electron struct. *(Russian)* 79—77987
Fe, itinerant ferromag., Fermi surface and single particle excitations 80—34350
$FeGe_2$, antiferromag., Fermi surface, stress effects, oscillatory magnetostriction and torque meas. 80—103616
$FeGe_2$, antiferromagnet, de Haas-van Alphen effect 79—4505
$FeGe_2$, Fermi surface press. depend., de Haas-van Alphen method 77—43478
Ga, expt. and interpretation 78—84132
Gd, de Haas-van Alphen effect, Fermi surface 80—15435
Gd, Fermi surface and de Haas-van Alphen effect frequencies meas. 77—69217
Gd, Fermi surface determ. 78—84138
Gd, ferromag., Fermi surface and band struct., press. effects 78—14656
Ge, electron-hole-liquid, de Haas-van Alphen-like oscills. in luminesc. lineshapes 79—60720
Hg, de Haas-van Alphen effect, influence of electron-phonon interaction 79—65361
Hg, de Hass-van Alphen effect, electron-phonon scatt. calc. 79—65360
Hg, single cryst., electron-phonon interactions, departure from LK theory 78—84130
$Hg_{3-\delta}AsF_6$, Fermi-surface of incommensurate Hg-chain compounds 79—56115
In_2Bi, de Haas-van Alphen effect 78—91594
K, de Haas-van Alphen freq., and Fermi surface anisotropy, press. depend. 80—59856
K, Dingle temperature and electron scatt. changes, accurate meas. 77—51638
K, pressure dependence of Fermi surface, de Haas-van Alphen meas. 78—26807
K-Na, dil., dynamical props. of quasiparticle excitations, de Haas-van Alphen effect meas. 78—84128
K-Rb(Na), dil., anisotropy of electron-impurity scatt. in K, de Haas-van Alphen effect meas. 78—18943
$LaAl_2$, de Haas-van Alphen effect, Fermi surface 80—15436
$LaAl_2$, magnetoresist. and de Haas-van Alphen effect, Fermi surface model 79—15069
LaB_6, de Haas-van Alphen effect and Fermi surface 77—15743
LaB_6, de Haas-van Alphen effect, low-field 80—75497
LaB_6, synthesis and props. *(Japanese)* 80—40255
LiC_6, band struct., density of states and Fermi surface props. 79—37982
Mg, Fermi surface, stress induced changes, kinetic, pot. energy contrib. 79—60683
Mg, Fermi surface changes under uniaxial compression 78—51876
Mg, pure and dil. alloys, electron lifetime anisotropy, Dingle temp. due to dislocation scatt. 79—78082
Mg-In dil. alloys, effect of alloying on Fermi surface, de Haas-van Alphen effect meas. 77—76732
Mg-In dil. alloys, effect of alloying on Fermi surface, pseudopot. model 77—76733
Mg-Li dil. alloys, effect of alloying on Fermi surface, de Haas-van Alphen effect meas. 77—76732
Mg-Li dil. alloys, effect of alloying on Fermi surface, pseudopot. model 77—76733
Mg-Mn, dil. alloy, de Haas-van Alphen effect, exchange interaction, Kondo effect 78—88093
$MgCu_2$, Fermi surface investig. by de Haas-van Alphen effect 77—35857
MgHg, de Haas-van Alphen effect obs. 77—24512
MgTl, fermi surface exam. by de Haas-van Alphen effect 78—34752
Mo, effective mass meas. and electron velocities 80—96773
Mo, vol. depend. of extremal cross sectional areas of Fermi surface from de Haas-van Alphen meas. 80—70589
MoO_2, effect of pressure on Fermi surface *(Russian)* 79—77988
Na, conduction electron spin props. 77—8036
Nb, de Haas-van Alphen study of Fermi surface, cyclotron effective masses, mag. breakdown effects, KKR calcs. 78—43288
Nb, high field de Haas van Alphen spectroscopy 79—73425
Nb_3Sb, de Haas-van Alphen effect and Fermi surface 78—6262
Nb_3Sn, A-15 superconductor, dHvA effect 78—75985
Nb_3Sn, de Haas van Alphen meas. of Fermi surface for $H \leq 40$ T 79—73424
Nb_3Sn, de Haas-van Alphen oscills. in normal state 79—56116
Nb_3Sn, normal state, Fermi surface, APW band calc. and de Haas-van Alphen oscills. 79—65369
Ni, absolute amplitude, Fermi surface neck 77—85134
Ni, anal. by linearly recursive approx. 78—91603
Ni, band structure, rel. to lattice const., spin polarised APW calc. de Haas-van Alphen effect meas. 80—20073
Ni, Fermi surface under press., de Haas-van Alphen effect meas. 80—75499

de Haas-van Alphen effect continued
- Ni, ferromag., de Haas-van Alphen effect, press. effects *(Russian)* 78—2413
- Ni, ferromag., effect of pressure on electron struct. *(Russian)* 79—77987
- Ni, itinerant ferromag., Fermi surface and single particle excitations 80—34350
- Ni, mag. excitations variation of de Haas-van Alphen frequency 79—8019
- Pb, de Haas-van Alphen γ oscill. for [011] symmetry direction 79—90944
- Pb, effective cyclotron masses of central and noncentral ζ orbits, de Haas-van Alphen effect 78—63968
- Pb, Fermi surface, uniaxial stress depend. 79—65362
- Pb, Fermi surface obs. *(Japanese)* 78—23010
- Pb, mag. induction oscillation 77—62806
- Pb, mag. interaction, de Haas-van Alphen effect 78—79921
- Pb, magnetic interaction effect and Dingle temperature of de Haas-van Alphen oscills. 79—69395
- Pb, phase smearing and mag. interaction, de Haas van Alphen effect 79—37961
- Pb, spin-splitting factor for Landau levels from first 3 harmonics 77—20226
- PbSb, meas. very high mag. field installation *(Dutch)* 78—252
- Pd, Fermi radii, Fermi velocities and many body enhancement 79—65363
- Pd, Fermi surface, extremal cross section, press. derivative, determ. by de Haas-van Alphen meas. 79—11055
- Pd, Fermi surface, stress depend., oscillatory magnetostriction and de Haas-van Alphen torque obs. 78—91602
- Pd, high field de Haas van Alphen spectroscopy 79—73425
- Pd-H, dil., electronic states, de Haas Haas-van Alphen effect meas. 77—47718
- Pd-H, electronic states from de Haas-van Alphen measurements 79—7777
- Pd-H dilute alloy, de Haas-van Alphen oscill. freq., absolute amplitude, Dingle temp. 80—49575
- α-PdH$_x$, electronic states and Fermi surface props. 80—29310
- PdSb, de Haas-van Alphen effect, Fermi surface 79—7773
- Pr, de Haas-van Alphen effect, Fermi surface 80—15435
- Pr, de Haas-van Alphen freq. determ. 79—11054
- Pt, Fermi surface obs. 78—91601
- Pt, high field de Haas van Alphen spectroscopy 79—73425
- Pt$_3$Sn, Fermi surface, de Haas-van Alphen effect meas. 77—24514
- Rb, Fermi surface, de Haas-van Alphen meas. 78—2411
- Rb-K, dil., dynamical props. of quasiparticle excitations, de Haas-van Alphen effect meas. 78—84128
- Re, Fermi surface, strain depend., from US vel. oscills. 78—84133
- Re, Fermi surface, stress depend., quantum oscills. obs. 78—91599
- Re, Fermi surface hydrostatic press. depend., de Haas-van Alphen phase shift meas. 80—54593
- ReO$_3$, anal. by linearly recursive approx. 78—91603
- ReO$_3$, Fermi surface, pressure induced anomaly 79—19505
- Rh, Fermi surface parameters 77—35851
- Rh-Fe, dil., anti-Kondo effect, de Haas-van Alphen obs. 79—73427
- Ru, Fermi surface energy spectrum, de Haas-van Alphen effect *(Russian)* 79—37964
- Sb, de Haas-van Alphen effect, effective mass, Fermi levels 78—75982
- Sb, spin splitting meas. from de Haas-van Alphen effect, g-factors 78—51881
- Sb:Te, de Haas-van Alphen effect, effective mass, Fermi levels 78—75982
- Sb-Sn, dil., de Haas-van Alphen effect, effective mass, Fermi levels 78—75982
- Sn, de Haas-van Alphen oscills., torque snap effect obs. 77—35850
- β-Sn, Fermi surface press. depend., de Haas-van Alphen meas. 79—73422
- Sn, white, Fermi surface, dilational strain depend., OPW calcs. 80—84418
- SrTiO$_3$:Nb, Fermi surface meas., oscillatory magnetothermal effect study 79—65357
- TaS$_2$ (2H), quantum oscillations and Fermi surface 79—37960
- TaSe$_2$, 2H, CDW, action on Fermi surface 77—76736
- TaSe$_2$ (2H), Fermi surface, de Haas van Alphen meas. 77—20229
- Tb, measurement and interpretation 77—15747
- Tc, Fermi surface, constant-energy-search KKR band theory calc., explanation for de Haas-van Alphen data 77—89689
- Te, optical activity, de Haas-van Alphen oscillations and cond. band parameters 80—54605
- Th, Fermi surface press. depend., de Haas van Alphen meas. 78—39006
- TiBe$_2$, de Haas-van Alphen effect, Fermi surface, theory 80—103614
- TiO, Fermi surface and de Haas-van Alphen effect *(Russian)* 80—49573
- Tl, mag. breakdown, electron energy spectrum 78—10335
- α-U, Fermi surface and effective masses, de Haas-van Alphen meas. 80—65426
- UGe$_3$, meas. comparison with band struct. calc. 78—72068
- UGe$_3$, spin fluctuation phenomena, band struct. calcs. and de Haas-van Alphen meas. 77—20225
- UIr$_3$(Rh$_3$), Fermi surface obs. 77—28099
- URh$_3$, magnetisation density 78—52203
- V$_3$Si, A-15 superconductor, dHvA effect 78—75985
- V$_3$Si, de Haas van Alphen meas. of Fermi surface for $H \leq 40$ T 79—73424
- V$_3$Si, de Haas-van Alphen oscills. in normal state 79—56116
- V$_3$Si, normal state, Fermi surface, de Haas-van Alphen oscills. 79—65369
- W, anal. by linearly recursive approx. 78—91603
- W, conduction electron g-factor, US vel. quantum oscills. 77—28100
- W, Fermi surface, uniaxial strain depend., quantum oscills. in magnetostriction, US vel., with torque 77—28094
- WO$_2$, effect of pressure on Fermi surface *(Russian)* 79—77988
- Y, de Haas-van Alphen effect, Fermi surface 80—15435
- Y, Fermi surface and de Haas-van Alphen effect 78—75983
- Y-Gd, de Haas-van Alphen effect, Fermi surface 80—15435
- YAl$_2$, de Haas-van Alphen effect 78—91590
- Yb, FCC, Fermi surface parameters, de Haas-van Alphen effect, press. depend. 77—28092
- YbSn$_3$, powdered, de Haas-van Alphen effect 80—59857
- Zn based Kondo alloys, with magnetic breakdown, anal. of de Haas-van Alphen effect 78—34751
- Zn, de Haas-van Alphen effect under press., Fermi surface and pseudopot. form factors 77—43475
- Zn, Fermi surface changes under uniaxial compression 78—51876
- Zn, oscill. freq., 1-140 bar *(Russian)* 79—19506
- Zn whiskers, quantum oscills. of mag. moment 79—15280
- Zr, high mag. field effects, fermi-surface model 80—6702
- ZrB$_2$, Fermi surface, de Haas-van Alphen effect meas. 78—84134
- ZrZn$_2$, de Haas-van Alphen effect, Fermi surface, theory 80—103614

Debye-Huckel theory
- alkali metal halides, solid phase free energies, Debye-Huckel theory 80—15263
- alkali metals, condensed phase, free energy, Debye-Huckel theory calcs. 80—79958
- Coulomb gas, classical, two-dimens., screening props. from sine-Gordon eqn. 79—4524
- crystal growth from solution, presentation of growth curves 79—27936
- double layer, aqueous, at charged plane interface, theories comparison 79—34317
- electric double layer, primitive models, pot. difference and charge density 80—76515
- electrolyte, Debye-Huckel ionic atmosphere, number density of ions 79—29369
- electrolytes, binary solns., nonideality, thermodynamics 79—39155
- glass, electrical relax., Debye-Falkenhagen theory 80—108155
- hot matter, conductive opacities and free-free Gaunt factors 80—3361
- ionic conductor, quasielastic scatt. of light, neutrons and electrons, Debye-Huckel eqn. *(Chinese)* 78—68521
- ionic solid volatilisation, surface charge effects 78—14457
- ionized gas, thermodynamic props., classical one-component Coulomb gas calcs. 77—5777
- macroparticles; charged spherical, dilute soln., Rayleigh scatt. 80—84748
- one dimensional fermion system, thermodynamics by cluster expansions 77—41535
- plasma, two-component, structure and thermodynamics, mean spherical approx. 80—64683
- point charge as electrically invisible object, nonlinear Poisson-Boltzmann theory Coulomb singularity 80—43228
- Poisson-Boltzmann theory, spherical, nonlinear, Debye-Huckel linearisation 80—35538
- polyelectrolytes, model 79—5162
- polyelectrolytes in soln., electrostatic persistence length rel. to unified theory 78—95932
- polymer, low conc., complex coacervation occurrence condition 80—79944
- polyvalent electrolyte apparent molal adiabatic compressibility and US vel. obs. 78—61028
- solvent struct. around ions as hard spheres, mean spherical approx. 79—70335
- strong electrolyte, Debye-Huckel theory, polar solvent struct. 77—21397
- H plasma, thermal emission and Debye shielding 80—64692
- α-LiIO$_3$ single crystals, electrical conduction and dielectric behaviour *(Chinese)* 78—30783
- NaCl-water-tetrahydrofuran system, heat. of soln. meas. using Calvet microcalorimeter *(French)* 77—44504

Debye-Scherrer cameras *see cameras; X-ray crystallography apparatus*

Debye temperature
- *see also specific heat*
- A15 compounds, linear muffin tin orbital band results by press. calc. 79—65356
- A15 type compounds, supercond. T_c in terms of Debye temp. and effective and reduced ionisation pots. 79—28435
- actinide metals, specific heat, Debye temp. 80—15258
- adamantane, Lennard-Jones (6-12) interaction pot., Debye temp. calc. 78—63828
- Al-Fe (0.02 at.%), rapidly quenched, ^{57}Fe Mossbauer spectrum associated with vacancy, Debye temp. determ. 78 -23378
- alkali halide, lattice dynamics calc., extended three body force shell model 78—47491
- alkali hydrides, crystal binding anal., interatomic force model, cohesive energy, compressibility 79—65030
- alkali hydrides, lattice props. from interacton pot. energy function 80—100199
- alkali hydrides, thermodynamic props. calc. using ionic pots. 78—10155
- alkali metals, elastic and thermal props. by pseudopotential method 80—19899
- alkali metals, equation of state and vol. depend. of thermodynamic props., pseudopot. theory 78—18738
- alkali metals, lattice sp. ht. and thermal vibrs. 78—30768
- alkali metals, rel. to elec. and thermal cond. in weak mag. fields 80—65535
- alkaline earth chalcogenides, crystal parameters calcs. using repulsive interaction pot. 79—37795
- alkaline earth oxides, cohesive and thermophysical props., role of three-body interactions 80—92477
- alloy, Debye temp., determ. from elec. resist. meas. *(French)* 77—4322
- anharmonic crystals, Debye-Waller factor, specific heat thermal behaviour 80—54335
- BBOA, smectic liq. cryst. glass-supercooled transition and Debye temp., ^{57}Fe Mossbauer effect 80—54999
- bicyclo [222] octane, Lennard-Jones (6-12) interaction pot., Debye temp. calc. 78—63828
- binary alloys, Debye temp., simple relation for additivity 80—10627
- bulk moduli, Wachtman's eqn., and temp. depend. 78—75799
- chalcogenide crystals with FCC structure, Moelwyn-Hughes parameter appl. to calcs. 77—80437
- chalcogenide spinels, thermal stability, thermochemical, thermodynamic and crystallochemical props. 77—51519
- Chevrel-phase superconductors, lattice dynamical calcs. 79—33056
- covalent crystals, lattice dynamics, unpaired forces effects 79—95096
- covalent semiconductors, displacement correlations, adiabatic bond charge model 80—70350
- crystals, quantum effects in plasticity 80—59561
- cubic solids, Debye temp., elastic consts. averaging 80—54332
- 1,1′-diacetylferrocene, MBBA soln. nematic glass-supercooled nematic transition, Mossbauer temp. obs. 79—95687
- dilute alloy, rel. to force const. changes due to substitutional impurities 77 - 24374
- DNA film *(Russian)* 77—51511

Debye temperature continued
- electron-proton interaction, two-body sum over states of static screened Coulomb pot. 78—55714
- elemental superconductors, review and table of props. 77—4460
- ferroelectric, tabulation of calorimetric values 78—51639
- fusion of metals, vacancy theory 80—44299
- glycerol, liq., effective Debye temp., temp. depend., quasi-cryst. model 77—4209
- graphite intercalation compounds with K and tetrahydrofuran *(French)* 78—26692
- HBPA, smectic liq. cryst. glass-supercooled transition and Debye temp., ^{57}Fe Mossbauer effect 80—54999
- high spin/low spin transition, model including lattice dynamics 77—63202
- high temperature variation *(French)* 78—63831
- insulator, thermal expansion, empirical determ. with no exptl. input 80—107450
- Invar, magnetic and thermal anomalies 80—34603
- ion system, internal energy, Debye temp. function, Monte Carlo method data 77—35314
- ionic crystals, vibrational surface modes, vibrational contributions to surface thermodynamic functions 77—47659
- LEED, high temp. limit Debye model 77—1207
- liquid, short-range order, theory 78—2264
- liquid metals, Debye temp. determ. from US vels. and thermodynamic data 79—99289
- liquid mixtures, US propag. parameters, effective Debye temp. 80—79882
- metal, BCC, calc. using modified noncentral force model 78—22807
- metal, BCC, lattice dynamical calc. 78—55925
- metal, cryst., Bloch-Gruneisen formula validity for elec. resistivity, temp. depend. 77—31991
- metal, cubic, relation between surface energy and Debye temp. 78—10271
- metal, Debye charact. temp. and fusion transitions 78—63864
- metal, Debye temp., determ. from elec. resist. meas. *(French)* 77—4322
- metal, deformed, microcrack effect on elec. resist. temp. depend. 77—51726
- metal, FCC, Debye-Waller factors, modified ang. force model 77—66013
- metals, BCC, phenomenological model for lattice dynamics 77—20017
- metals, elec. resist., intermediate temp., Bloch-Gruneisen formula, deviations 80—2375
- methane, solid, probing phase transition with Mossbauer effect in ^{57}Fe impurities 79—4751
- methane and methane-d$_4$, Lennard-Jones (6-12) interaction pot., Debye temp. calc. 78—63828
- migration and formation energies rel. to Debye temp. and melting point 78—22710
- mixed valence metals, elementary excitation damping, electron specific heat 79—95180
- Nb$_3$Ge, supercond., single phase, sp. ht. meas., 4-29K 78—72307
- Nb carbides, nonstoichiometric, elastic props., 20-2000°C 77—12661
- neopentane, Lennard-Jones (6-12) interaction pot., Debye temp. calc. 78—63828
- nitrides, surface energy for brittle fracture from phonon frequencies 78—67790
- ordered equiatomic, lattice specific heat meas., Debye temp. 80—54396
- parametrised model for obtaining effective Debye temperature from RF size-effect data 79—69541
- particle size effect on acoustic phonon spectrum 77—72666
- polyalkaneimide, mech. and thermophys. props. at liq. He temps. 80—3117
- rare earth Co Laves phase cmpds., elastic props. rel. to temp., mag. field 79—51834
- rare earth compounds, binary, regression eqns., for calc. props. from electron struct. 80—39498
- rare earth garnets, Debye charact. temp. and reciprocal lattice consts. 80—29144
- rare earth metals, elastic props., connection with electron struct. *(Russian)* 80—19895
- rare earth metals, thermodynamic props. determ. form US vel. meas. 78—55912
- rare gas crystals, lattice heat capacity, thermal vibrations, Lindeman parameter, lattice dynamic model *(Russian)* 80—29141
- resistivity strain coeff. calcs. 80—100449
- semiconductor, temp. depend. of energy gap 80—2321
- semiconductor single crysts, X-ray determ. 100-1000K *(German)* 78—30726
- semiconductors, isoelectronic series and trends in band struct. 77—89696
- sodium magnesium aluminium oxdate, elastic consts., Debye temp. 79—82275
- solid, thermal expansion at high temp. *(French)* 78—55960
- solid lattice thermodynamics, two-temp. Debye approx. *(Russian)* 80—77728
- solid-liquid transitions, freq. distrib. function 77—4183
- steel, Hadfield, Mossbauer spectra meas., 25-250°C *(Russian)* 77—51994
- superconducting high Debye temperature material, theoretical upper limit of crit. temp. 80—60129
- surface, rel. to He at. scatt. 77—63516
- TCNQ complexes, low temp. sp. ht. 77—51514
- TCNQ salt, acridinium (TCNQ)$_2$ low temp. heat capacity, Debye temp. 80—2180
- tetragonal crystal Debye temp. calc. from elastic consts. 80—29143
- tetragonal crystals with TII Laue symmetry, series expansion method 80—96615
- tight binding metal, vibr. freq. of atom normal to surface, Einstein model 79—51412
- tourmaline, elastic consts. by US phase-comparison method 80—2108
- transition metal binary alloy, amorphous and crystalline, superconducting transition temp. correlation with solute conc. 78—52139
- transition metal carbides and nitrides, surface energy for brittle fracture from phonon freqs. 79—86837
- transition metal silicides, group IV, thermal expansion, microhardness, Debye temp. meas. 77—35717
- transition metals, Y to Pd, comparison to X-ray charact. temps., temp. depend. 78—18731
- Ag (111) plane, specular refl. of He and H_2 beams, Debye-Waller factor and surface Debye temp. 79—47580
- Ag, Debye temp., X-ray diffr. determ., anharmonic parameters of pot. function 80—100320

Debye temperature continued
- Ag, Debye temperature correlations at high temp. 80—15210
- Ag fine particles, X-ray Debye temp. determ. using solid-state detector and continuous X-rays 79—50944
- Ag, modified CGW model calcs., phonon dispersion, sp. ht. and equiv. Debye temp. 78—10135
- Ag surface, scatt. of He, H_2, Debye-Waller factors, expt. 80—60736
- Ag, X-ray Debye temp. and isobaric Gruneisen coeff., anharmonicity effects 77—62654
- AgGaTe$_2$, Debye temp., standard entropies and enthalpies, sp. ht. meas. 78—30769
- AgInTe$_2$, Debye temp., standard entropies and enthalpies, sp. ht. meas. 78—30769
- Ag$_2$SnS$_3$(Se$_3$)(Te$_3$), Mossbauer effect, lattice dynamics obs. 77—43923
- Al, Debye temp., X-ray diffr. determ., anharmonic parameters of pot. function 80—100320
- Al, Debye temperature correlations at high temp. 80—15210
- Al, interaction between ^{57}Co atoms and quenched-in vacancies, Mossbauer meas. 80—7234
- Al, phonon density of states by neutron scatt., sp. ht. and Debye temp. 80—2132
- Al-Sn alloys, heat treatment effect on ^{119}Sn Mossbauer spectrum 80—7228
- Al$_2$Cu, single cryst. elastic consts., 4.2-300K 78—72803
- Al$_{10.4}$Ga$_{0.08}$V, low temp. thermal expansion 78—95167
- Al$_{10}$V, low temp. thermal expansion 78—95167
- Al$_{10}$V, well defined local modes, low temp. heat capacity meas. 78—26648
- Al$_{10}$V-Ga, dil., well defined local modes, low temp. heat capacity meas. 78—26648
- Am, Debye-Waller factor, temp. depend. 78—83902
- ^{241}Am metal, temperature depend. 15 to 300K 77—28019
- Ar, monolayer, compression on graphite, Debye temp. calc. 79—65316
- Ar monolayers, on graphite, condensation and compression, high resolution LEED obs. 79—77906
- As-Se-Te glasses, glass form., charact. temp., density, thermal expansion and dynamical viscosity, struct. model 78—26672
- Au, effect of press. on resistivity 78—79978
- Au, fine particles, gas evaporation technique of prep., X-ray diffr. study, charact. temp. 80—75328
- Au, modified CGW model calcs., phonon dispersion, sp. ht. and equiv. Debye temp. 78—10135
- Au thin films, electron diffr. investigation of Debye temp. 80—88420
- Au, var. at high temp. *(French)* 78—63831
- Au-Cd alloy, α and ζ phase, low temp. sp. ht. 78—18789
- B, liq., thermoelastic props. near melting point 80—19862
- BN, wurtzitic, temp. characts. of thermodynamic props., 5-320K 77—55361
- BP, sp. ht., Debye temp., compressibility and Gruneisen coeff. meas. 78—63865
- Ba, elastic properties, Debye temp., 20°C, 20 to 70 kbar, US wave velocity meas. 78—87735
- Ba(NO$_3$)$_2$, X-ray Debye temp. determ. 77—59088
- BaO, cubic NaCl-type cryst., Debye temp. 80—54333
- BaO, lattice dynamics, sp.ht., Debye temp. and Raman spectra calc. 77—1195
- BaO-P$_2$O$_5$, glass, US velocity rel. to elastic props. 80—103425
- BaTiO$_3$, soft mode dielec., anomalous low temp. sp. ht. 78—14423
- BaWO$_4$, slow neutron inelastic scatt. spectra, Debye temp. calcs. *(Russian)* 80—59347
- Be intermetallics, MBe$_{13}$, (M = Y, La, Ce, Lu, Th), lattice spacings and susceptibilities 80—65778
- Be, lattice dynamics, phonon dispersion relations and Debye temp. 79—42171
- Bi, phonon density of states by neutron scatt., sp. ht. and Debye temp. 80—2132
- Bi$_2$O$_3$, anharmonicity effect, Debye temp. determ. from Mossbauer spectra 77—63335
- Ca, lattice dynamics, phenomenological model 80—44265
- CaNi$_5$, Haucke compounds, low temp. heat capacity, Debye temp. 80—96663
- CaO-P$_2$O$_5$, glass, US velocity rel. to elastic props. 80—103425
- Ca$_5$(PO$_4$)$_3$F: Cr^{5+}, spin-lattice relax. time and Debye temp., EPR obs. 79—28601
- CaWO$_4$, slow neutron inelastic scatt. spectra, Debye temp. calcs. *(Russian)* 80—59347
- CaWO$_4$:Nd^{3+}, thermal behaviour of shape and width of 9145 Å laser line 78—6755
- Cd, Lindemann's rule and X-ray Debye temp., anisotropic single crysts. 79—28076
- Cd, phonon density of states calc. from neutron diffr. data 77—24369
- Cd$_3$As$_2$ and CdAs$_2$, molten, thermal expansion and atomic bond strength parameters 80—65257
- CdF$_2$, elastic constants. and Debye temp., 4.2-295K 78—38770
- CdF$_2$, low temp. heat capacity 78—47490
- CdNb$_2$O$_6$, sp. ht. and Debye temp. meas., 2-25K 79—73319
- Cd$_2$Nb$_2$O$_7$, ferroelec., sp. ht. and Debye temp. meas., 2-25K 79—73319
- CdO, X-ray determ., Debye-Waller factors, Debye temp. and vibration amplitudes 78—55928
- Cd$_{1.6}$Pd$_{0.4}$Nb$_2$O$_7$, ferroelec., sp. ht. and Debye temp. meas., 2-25K 79—73319
- Cd$_2$Re$_2$O$_7$, specific heats, electronic and lattice contrib. below 20K 80—34200
- Cd$_2$Ru$_2$O$_7$, specific heats, electronic and lattice contrib. below 20K 80—34200
- CdSb, thermodynamic props., effective Debye temp. 79—77767
- CdTe, temperature variation in bulk moduli in solids 79—73237
- CdTe(Se):Co, impurity luminescence no phonon line depend. on temp., Debye temp. 80—66273
- CdTl$_2$Te$_4$, single and polycryst. samples, linear expansion, heat capacity and thermodynamic props. 80—103489
- Ce, elastic properties up to 84 kbar, US vel. meas. *(Russian)* 79—60434
- Ce-Th, mag. suscept. and sp. ht. 79—78411
- Co$_{0.92}$Fe$_{0.08}$, phonon dispersion and Debye temp. temp. depend., neutron inelastic scatt. 79—33047
- CoO, cubic NaCl-type cryst., Debye temp. 80—54333
- CoSe$_2$, paramag. metal, sp. ht., Mossbauer effect, absence of ordering 77—16036
- Cr, Clark-Gazis-Wallis ang. force model, effective Debye temp. 78—22799
- Cr, cryst. equilib. lattice dynamical model 78—22811

Debye temperature continued
- Cr, lattice dynamics, improved Fielek model 80−59598
- Cr, lattice vibrations, Debye temp., freq. wave vector dispersion relations 78−63818
- Cr, phonon dispersion, Debye temp. and Debye-Waller factors, lattice dynamical model 78−55920
- Cr_3Si, specific heat at low temps., electron density of states, Debye temp. *(Russian)* 80−54398
- $CrVO_4$, temp. depend. of heat capacity, 60-1080K, Debye temp. 77−7869
- CsCl-type crystals, mean Debye-Waller factors, vib. amplitudes and Debye temp. 78−75792
- CsF, cubic NaCl-type cryst., Debye temp. 80−54333
- Cu (100), diatomic mol. scatt., energy transfer and dissociative adsorption 79−46961
- Cu (111), LEED crystallography and reliability indices 80−54081
- Cu, lattice specific heat, from two-parameter lattice dynamical model with dispersion 80−10678
- Cu, modified CGW model calcs., phonon dispersion, sp. ht. and equiv. Debye temp. 78−10135
- Cu, thermal displacement of surface atoms, elastic backscatt. of He atomic beam *(French)* 77−4709
- Cu-Al(Au), critical voltage effect *(Japanese)* 78−91206
- CuAu I, ordered equiatomic, lattice specific heat meas., Debye temp. 80−54396
- CuBr, Debye-Waller factors and Debye temp., powder neutron diffr., 295K 78−91407
- CuBr, specific heat and lattice dynamics 79−37798
- CuCl, phonon dispersion curves determined by neutron scatt. at 4.2K 78−6132
- CuCl, polycryst., sp. ht. at low temps. 77−55367
- CuCl(Br)(I), phonon dispersion, 9-parameter shell model, compared with expt., and Debye temp. evaluation 78−59891
- CuI, specific heat and lattice dynamics 79−37798
- $CuInSe_2(S_2)(Te_2)$, Debye temp., standard entropies and enthalpies, sp. ht. meas. 78−30769
- CuPt, specific heat, Debye temp. below 30K 78−55956
- $CuRhS_4(Se_4)$, press. depend. of supercond. transition temp. meas., rel. to Debye temp. 77−12050
- $Cu_2SnS_3(Se_3)(Te_3)$, Mossbauer effect, lattice dynamics obs. 77−43923
- D_2, solid, equation of state, at high pressure 79−46781
- D_2, solid, melting curve, meas. of P, V, T and longitudinal sound velocity 79−37814
- DX, X=Cl, Br, I, thermodynamic properties, phase transitions 78−47518
- $DyAsO_4$, phase transitions obs. 80−70412
- $DyVO_4$, phase transitions obs. 80−70412
- $Eu_3Fe_5O_{12}$, thermodyn. props. 77−84947
- $Eu_2Ir_2O_7$, pyrochlore, sp. ht. below 20K, Debye temp. 80−65241
- α-Fe, Clark-Gazis-Wallis ang. force model, effective Debye temp. 78−22799
- Fe complex, Fe^{2+} chelate of hydrazinecarboxylic acid, Mossbauer effect, cryst. field splitting 79−78591
- α-Fe, cryst. equilib. lattice dynamical model 78−22811
- Fe small particles, Mossbauer effect study of lattice vibr., Debye temp. of metallic core 80−44963
- Fe-Al(Cr)(Mn)(Pt)(V), X-ray exam. of dynamic characts. *(Russian)* 77−62608
- Fe-Ni, FCC and BCC lattices, X-ray characteristic temp. *(Russian)* 78−67797
- Fe-Ni Invar, low temp. struct. 79−55856
- Fe-Pd Invar, low temp. FCT phase obs. 80−93538
- $Fe_{0.2}Mg_{1.9}Ti_{0.9}O_4$, Mossbauer parameters temp. depend. 78−23381
- $Fe_{0.4}Mg_{1.8}Ti_{0.8}O_4$, Mossbauer parameters temp. depend. 78−23381
- $Fe_{0.49}Mn_{0.01}Ti_{0.5}H_x$, localised vibrs., sp. ht. obs., room temp. 80−65248
- $Fe_2(MoO_4)_3$, ^{57}Fe Mossbauer effect obs. 77−48108
- $FePS_3$, Goldanskii-Karyagin effect, Mossbauer spectra 79−99798
- Fe_3Pt:Sn Invar alloy, Mossbauer shift temp. depend. 80−100626
- $FeVO_4$, temp. depend. of heat capacity, 60-1080K, Debye temp 77−7869
- Ga II, superconducting high pressure phase, sp. ht. 80−70894
- GaAs, Debye temperature, atomic mean square displacement 78−87757
- GaAs, lattice dynamics, phonon freq., bond bending force model calcs. 80−70335
- $GaAs_xP_{1-x}$, elastic consts. and Debye temp. determ. 77−4142
- GaP, Debye temperature, atomic mean square displacement 78−87757
- GaS, anisotropic phonon dispersion 77−84864
- GaS, elastic prop. anisotropy, Debye temp. *(Russian)* 80−88244
- GaS, sp. ht., vibr. spectra and Debye temp. 78−87796
- GaS(Te)(Se), elastic characteristics, Debye temp., ultrasonic study *(Russian)* 80−79872
- GaSb, Debye temperature, atomic mean square displacement 78−87757
- GaSb, effect of n-doping on Debye temp. 80−2175
- GaSb, lattice dynamics, phonon freq., bond bending force model calcs. 80−70335
- GaSe, sp. ht., vibr. spectra and Debye temp. 78−87796
- GaTe, sp. ht., vibr. spectra and Debye temp. 78−87796
- Gd-Mg, X-ray determ. of Debye temp., mean amplitude of vibr. 78−38802
- Gd-Zn, X-ray determ. of Debye temp., mean amplitude of vibr. 78−38802
- Ge, lattice dynamics using Born-van Karman model 79−73271
- Ge, lattice thermal conductivity, effect of Debye temp. var. 78−18850
- Ge single crysts, X-ray determ. 100-1000K *(German)* 78−30726
- Ge:^{119m}Sn, impurity lattice dynamics, Mossbauer spectra, Debye temp. 80−84262
- GeP, thermodynamic characts. 10-300K, interatomic bond elasticity 80−59677
- p-H_2, solid, elastic consts., Brillouin scatt. obs. 79−8149
- H_2, solid, melting curve, meas. of P, V, T and longitudinal sound velocity 79−37814
- H_2, solid equation of state, at high pressure 79−46781
- HX, X=Cl, Br, I, thermodynamic properties, phase transitions 78−47518
- He, solid, vacancy tunnelling freq. calc. 77−80678
- ^{4}He, FCC quantum cryst., lattice dynamics 79−77859
- ^{4}He, solid-fluid, eqn. of state, melting props. under press. 80−96721
- Hg, temp. and press. depend. of Debye temp. 77−1202
- HgTe, 1.5 to 30K, thermal expansion and heat capacity meas. 80−59681
- In-Mg, ordered equiatomic, lattice specific heat meas., Debye temp., superconducting transition 80−54396
- InSb, Debye temperature, atomic mean square displacement 78−87757

Debye temperature continued
- InSe, elastic props. temp. depend. 78−10119
- Ir (110) and (111) surfaces, Debye temps., LEED meas. 79−60619
- Ir, phonon/wave vector dispersion relations, Debye temp., modified axial symmetric model 80−70339
- Ir-Y eutectic alloy, supercond. transition enhancement due to lattice softening 80−103775
- K, cryst., elec. cond., temp. depend. calcs. 77−59276
- K halide solids, lattice dynamics, three body force shell model studies 79−55841
- KCN, crystal props., log potential model calc. 78−63829
- KCN, cubic NaCl-type cryst., Debye temp. 80−54333
- KCl-KBr mixed system, Gruneisen coefficient evaluation 80−39240
- KCl(Br)(I), lattice dynamics, bond-bending force model 80−54322
- KCl(F)(Br)(I), elastic constants, temp. derivatives at constant volume 80−59549
- K_2CuF_4, Brillouin scatt. and US meas. of phonons, elastic moduli and Debye temp. calc. 79−87454
- K_2IrCl_6, sp. ht. meas. at low temp. 80−7119
- K_2OsCl_6, sp. ht. meas. at low temp. 80−7119
- K_2PtCl_6, diamag. sp. ht. meas. at low temp. 80−7119
- $K_xRb_{1-x}I$, Debye temp. conc. depend. 79−90746
- K_2ReCl_6, sp. ht. meas. at low temp. 80−7119
- Kr, solid, phonon freqs., lattice heat capacities, and Debye charact. temps. 79−10905
- La-Au liq.-quenched alloys, Mossbauer spectra, struct. 80−15841
- LaB_6, elastic consts. at room temp., US vel. meas., Debye temp. determ. 77−43268
- $(La_{0.8}Ca_{0.2})MnO_{3+y}$, mag. sp. ht. and Debye temp. 79−61124
- $LaNi_5$, Haucke compounds, low temp. heat capacity, Debye temp. 80−96663
- LiAl(In)(Zn), elastic moduli and Debye temp., US meas. 79−91724
- LiCl(F)(Br)(I), elastic constants, temp. derivatives at constant volume 80−59549
- LiF, (001) surface, diffractive scatt. of H atoms, 78K 80−76124
- LiH, cryst., specific heat at const. vol., isotopic modifications effects 80−103490
- ^{6,7}LiH(D), cryst., cohesive energy, force const., lattice freq., Debye temp., Gruneisen parameters, calc. 78−91293
- Li_3N, superionic conductor, cryst. growth and struct., phys. props., book contrib. 79−42308
- $LiNbO_3$, X-ray diffr. study of lattice dynamics parameters *(Russian)* 79−65156
- $LiTaO_3$, X-ray diffr. study of lattice dynamics parameters *(Russian)* 79−65156
- $LiTi_2O_4$, press. depend. of supercond. transition temp. meas., rel. to Debye temp. 77−12050
- $Li_{1-x}Ti_{2-x}O_4$, struct. phase transition and thermal expansion 78−14465
- Lu, specific heat from 1.6 to 18K, electronic coeff., Debye temp. at 0K 79−7700
- $Lu_2Ir_2O_7$, pyrochlore, sp. ht. below 20K, Debye temp. 80−65241
- Mg, lattice dynamics, phonon dispersion relations and Debye temp. 79−42171
- Mg, phonon density of states calc. from neutron diffr. data 77−24369
- Mg, phonon spectrum and thermodynamic functions, inelastic coherent cold neutron scatt. *(Russian)* 78−55917
- Mg, X-ray Debye charact. temp., powder specimens 77−84876
- MgO, critical voltage effect, effect of temp. *(French)* 80−10463
- MgO-P_2O_5, glass, US velocity rel. to elastic props. 80−103425
- Mg_2Si, charact. X-ray temp. and thermal expansion coeff. 77−15599
- MnO, cubic NaCl-type cryst., Debye temp. 80−54333
- MnO, multidomain single cryst. and monodomain cryst., crit. and elastic behaviour, T_N to 300K 77−66407
- MnS, cubic NaCl-type cryst., Debye temp. 80−54333
- MnS, X-ray determ., Debye-Waller factors, Debye temp. and vibration amplitudes 78−55928
- Mo (001) surface struct., LEED anal. 80−34282
- Mo, lattice dynamics, improved Fielek model 80−59598
- Mo, phonon dispersion, Debye temp. and Debye-Waller factors, lattice dynamical model 78−55920
- Mo_6NaS_8, specific heat and supercond. critical field *(Russian)* 77−77004
- MoS_2(2H), elastic consts., Debye temp. determ. 77−11618
- N_2, solid, exciton-phonon coupling in strong coupling limit, temp. depend. 80−92616
- NH_4I, cubic NaCl-type cryst., Debye temp. 80−54333
- Na (110) 77−72761
- Na, cryst., elec. cond., temp. depend. calcs. 77−59276
- Na, phonon dispersion curve, sp. ht. and Debye temp., ang. force model 77−15509
- NaBr, heat capacity, Gruneisen parameters, 2 to 20K 80−29180
- $NaBrO_3$, X-ray Debye temp. 80−103440
- NaCN, crystal props., log potential model calc. 78−63829
- NaCl, effective Debye temp., press. and temp. depend. 78−18728
- NaCl, elastic props. at press. up to 9 GPa, ultrasonic wave velocities 79−95073
- NaCl structure crystals, Debye characteristic temp. calcs. 79−37796
- NaCl(Br) (F) (I), lattice dynamics and statics, three-body-force shell model 80−49323
- NaCl(F)(Br)(I), elastic constants, temp. derivatives at constant volume 80−59549
- $NaClO_3$ temperature variation in bulk moduli in solids 79−73237
- NaF, He atom scatt., Debye Waller effects 79−8218
- NaF, heat capacity, Gruneisen parameters, 2 to 20K 80−29180
- NaIn(Tl), elastic moduli and Debye temp., US meas. 79−91724
- $Nb_3Al_{0.8}Ge_{0.2}$, supercond., sp. ht. meas. 77−28296
- $Nb_3Al_{0.83}Ge_{0.21}$, A-15 phase, sp. ht. meas., Debye temp., energy gap and crit. field 79−19689
- NbC, physicomechanical props. within the homogeneity range 77−1848
- NbC_x, static distortions and Debye temp. determ., neutron diffr. exam. *(Russian)* 77−80482
- NbC_xN_{1-x}, obs. of phonon anomalies, sp. ht. meas. and supercond. transition temp., 1.5-90K 77−39985
- $Nb_{0.75}Ga_{0.25}$, A 15 phase high transition temp., sp. ht. determ. 80−60140
- Nb_3Ga, Debye temp., determ. from elec. resist. meas. *(French)* 77−4322
- NbO_2, low temp. elastic consts. and Debye temp. 78−47463
- NbO_2, low temp. sp. ht. and Debye temp., role of phonon-like CDW excitations 77−80632
- NbO_2, semicond., thermal expansivity 80−34213

Debye temperature continued

- $NbSe_2$(2H), elastic consts., Debye temp. determ. 77−11618
- Nb_3Si, high T_c, supercond. props. from extrapolation of sp. ht. meas. on A-15 Nb-Si 80−25045
- Nb_3Sn, Debye temp., determ. from elec. resist. meas. *(French)* 77−4322
- Nb_3Sn, lattice microstrain induced metastable phase, low temp. struct. and props. 77−8482
- Ne, lattice vibrs., heat capacities 79−42169
- Ni-Al system, Mossbauer spectroscopy investigation *(Russian)* 80−20523
- Ni_3Al, at. displacements, characteristic temp. and lattice spacing, temp. depend. *(Russian)* 79−90598
- Ni_3Fe alloys, low-temperature specific heat, long and short range order effects 80−100339
- Ni_3Fe, Debye temp. determ. from elastic consts. and X-ray meas., effect of configurational order 78−30727
- NiO, cubic NaCl-type cryst., Debye temp. 80−54333
- $NiSiF_6.6H_2O$, single cryst., EPR, 77-300K, Debye temp. 77−85551
- $Ni_3(VO_4)_2$ temp. depend. of heat capacity, 60-1080K, Debye temp. 77−7869
- Np, ternary oxides, electronic and structural props., ^{237}Np Mossbauer spectroscopy 79−33570
- PLZT ceramics, sp. ht., 2-25K, field depend., phonon modes 77−47586
- Pb, X-ray Debye temp. calc. 79−19348
- PbF_2, inelastic neutron scatt. study of phonon dispersion relation, Debye temp. calc. 78−30712
- PbF_2, lattice dynamics 78−79697
- $Pb_5Ge_3O_{11}$, ferroelectric, anharmonic effects in low freq. symm. modes, Raman study 80−25365
- PbI_2, low temp. thermal props. 79−95178
- $PbMo_{5.1}S_6$, high supercond. T_c, soft mode behaviour 78−14855
- $PbNb_2O_6$, ferroelec., sp. ht. and Debye temp. meas., 2-25K 79−73319
- $PbNb_2O_6$, sp. ht. and Debye temp. meas., 2-25K 79−73319
- $Pb_2Nb_2O_7$, sp. ht. and Debye temp. meas., 2-25K 79−73319
- PbO, anharmonicity effect, Debye temp. determ. from Mossbauer spectra 77−63335
- PbS, X-ray determ., Debye-Waller factors, Debye temp. and vibration amplitudes 78−55928
- $PbTiO_3$, X-ray interference intensity temp. depend., lattice ion vibr. *(Russian)* 80−20601
- $PbZr_{0.95}Ti_{0.05}O_3$, soft mode dielec., anomalous low temp. sp. ht. 78−14423
- $PbZr0_3$, X-ray interference intensity temp. depend., lattice ion vibr. *(Russian)* 80−20601
- Pd, phonon dispersion curves, freq. spectrum, specific heat calc. 77−15516
- Pd, ultrafine particles, size effect on vibr. sp. ht. 78−10153
- Pd-Ag alloys, elec. resist. meas., density of states and Debye temp. 77−76715
- Pd-Co, pressure effect on Curie point, Debye temp. in ferromag. state *(Russian)* 77−32194
- Pd-D alloys, phonon dispersion relation meas., elastic constants and Debye temp. 78−26639
- Pd-Si amorphous alloy, heat treated, low temp. lattice sp. ht. 80−75368
- Pd-Si-Fe amorphous alloy, Mossbauer spectra, struct. and bonding 80−7224
- PdD_x, superconducting, molar sp. ht., γ-coeff. and Debye temp., 2 to 12K 77−1517
- β-$PdH_{0.66}$, elastic consts. 4 to 300K, Debye temp. 80−6455
- Pd_2Si film, on Si, resist. and Hall mobility meas., Debye temp. determ. 78−47886
- Pt, lattice dynamics, ang. forces and normal vibrs. 78−22810
- Pt, specific heat meas., 0.4 to 30K, Debye temp. 78−55955
- PuN, heat capacity, at low temps., Debye temp. determ. 79−24168
- Rb halides, role of quantum effects in lattice dynamics, Debye temp., shell model calcs. 80−70336
- RbCN, crystal props., log potential model calc. 78−63829
- RbCl, sp. ht. at low temps., Debye temp. determ. 80−2177
- RbCl(F)(Br)(I), elastic constants, temp. derivatives at constant volume 80−59549
- Re, plastic deform. rel. to low temp. sp. ht., supercond. *(Russian)* 78−31005
- ReO_3, elastic consts. determ. rel. to Debye temp. 77−11617
- Rh (111), LEED crystallography and reliability indices 80−54081
- Rh(111), surface geometry, vibrational props., Debye temp., LEED study 78−87852
- Sb, effective Debye scatt. temp., depend. on phonon drag. 79−73507
- Sc, sp. ht. data rel. to electronic props. 78−83971
- Sc-Fe alloy, electronic sp. ht. and Debye temp., 1-20K 77−7872
- Sc-Zr(Mg), low-temp. heat capacity 80−75370
- Se, Debye temp. calcs. using elastic consts. and Kopp-Neumann relations 78−2220
- Se, trigonal, low temp. sp. ht. and elastic consts., piezoelec. effect influence on phonons 80−54404
- Si (001), surface Debye temp. meas. by HEED 77−89633
- Si (111) surfaces, geometric struct., LEED obs. 80−49479
- n-Si, electronic effect 78−83901
- Si, influence of temp. and alloying on integral X-ray intensities *(German)* 77−69066
- Si, lattice dynamics using Born-van Karman model 79−73271
- Si, reconstructed surface physics, review 80−10766
- Si, temperature variation in bulk moduli in solids 79−73237
- Si:^{119m}Sn, impurity lattice dynamics, Mossbauer spectra, Debye temp. 80−84262
- Si:Sb, Mossbauer spectra of ^{119}Sn defect struct. 80−97174
- Si:Sn, Mossbauer study of defects due to ^{119}In implantation 80−80641
- Si:Te, Mossbauer spectra of ^{119}Sn defect struct. 80−97175
- SiP, thermodynamic characts. 10-300K, interatomic bond elasticity 80−59677
- SmS, Debye temps., vibr. amplitudes, X-ray diffr. determ. 78−2222
- SmSe, Debye temps., vibr. amplitudes, X-ray diffr. determ. 78−2222
- SmTe, Debye temps., vibr. amplitudes, X-ray diffr. determ. 78−2222
- Sn, binding state of atoms segregated at boundary of Fe and Fe alloys, Mossbauer study 80−7232
- α-Sn, ion implanted, defect struct., Mossbauer spectra 80−80214
- α-Sn, lattice dynamics 80−107389
- Sn, monocrystals with impurities, temp. depend. of Debye temp. 78−79975
- α-Sn:^{119m}Sn, impurity lattice dynamics, Mossbauer spectra, Debye temp. 80−84262

Debye temperature continued

- SnI_4 crysts., ^{119}Sn Mossbauer intensity, temp. depend., Debye temp. determ. 77−59495
- $SnMo_5S_6$, high supercond. T_c, soft mode behaviour 78−14855
- $SnMo_6S_8$, lattice softening, vibr. anisotropy 78−14428
- SnO_2, anharmonicity effect, Debye temp. determ. from Mossbauer spectra 77−63335
- SnTe, low-temp. sp. ht., thermal expansion and Gruneisen parameter 77−15601
- Sr, lattice dynamics, phenomenological model 80−44265
- $Sr(NO_3)_2$, X-ray Debye temp. determ. 77−59088
- SrO-P_2O_5, glass, US velocity rel. to elastic props. 80−103425
- $SrTb_2Fe_2O_7$, Mossbauer spectra, hyperfine parameters, ordering temp. 77−90079
- $SrWO_4$, slow neutron inelastic scatt. spectra, Debye temp. calcs. *(Russian)* 80−59347
- surface atoms, Debye temps. determ. during field evaporation and LEED 80−39406
- Ta, lattice vibrations, Debye temp., freq. wave vector dispersion relations 78−63818
- TaC_x, static distortions and Debye temp. determ., neutron diffr. exam. *(Russian)* 77−80482
- TaS_2.Sn, intercalated, Mossbauer effect, hyperfine interaction, lattice dynamics 77−8473
- Te, anisotropic thermal motion of atoms, X-ray exam. 78−18730
- Te, Debye temp. calcs. using elastic consts. and Kopp-Neumann relation 78−2220
- Te, galvano- and thermomagnetic effects 78−30939
- Te-Se, Debye temp. calcs. using elastic consts. and Kopp-Neumann relation 78−2220
- Th (111), struct., Debye temp., and oxidation, LEED and AES obs. 77−89625
- Th, crystal equilib., lattice dynamics 78−47479
- $ThC_{0.063}$ single crystal, elastic consts., Debye temp. and mag. susceptibility 77−90386
- $ThC_{0.75}$, specific heat, Fermi level density of states 80−10680
- $ThC_{0.6}N_{0.4}$, specific heat, Fermi level density of states 80−10680
- $Th_4H_{15}(D_{15})$ normal and supercond., low-temp. sp. ht., Debye temp. and supercond. props. 77−4466
- $ThNi_5$, Haucke compounds, low temp. heat capacity, Debye temp. 80−96663
- ThP, specific heat, Fermi level density of states 80−10680
- Ti, lattice specific heat and thermal expansion 79−73318
- α-Ti, X-ray Debye charact. temp., powder specimens 77−84876
- Ti-Mo, lattice parameter and Debye temp., comp. depend. *(Russian)* 78−47280
- TiC_x, static distortions and Debye temp. determ., neutron diffr. exam. *(Russian)* 77−80482
- TiC_xNy, elastic props., 290K 77−52379
- TiC_xO_y, elastic characts. 77−80568
- TiN, Raman scatt. supercond. transition temp., phonon density of states, Debye temp. 78−52499
- TiN_yO_y, cubic, thermal expansion coeffs., Ti-Ti bond screening 79−10970
- Tl, hexagonal lattice equilibrium, electron gas model with noncentral forces, lattice dynamics 78−95123
- TlBr, soft mode dielec., anomalous low temp. sp. ht. 78−14423
- TlCl, thermal vibr. amplitudes, 296-534K, X-ray obs. 77−35656
- TlSe, heat capacity, at low temp. and Debye temp. *(Russian)* 79−10962
- TmSe, Debye temps., vibr. amplitudes, X-ray diffr. determ. 78−2222
- UO_2, elastic props. at high press., US meas. 77−4141
- U_3O_{8-y}, depend. of therm. cond. on porosity, phonon mean free path calcs., Debye temps. 79−37886
- V, lattice dynamics, vibr. spectrum and sp. ht., CGW model 78−22793
- V, lattice dynamics and cryst. equilib. 78−75753
- V, pure and with O_2 additions, single cryst. elastic consts., 4.2 to 300K, and hardening 79−90712
- VC_x, static distortions and Debye temp. determ., neutron diffr. exam. *(Russian)* 77−80482
- V_3Ga, phonon densities of states and Debye temp. calcs. 79−51212
- V_3Ge, phonon densities of states and Debye temp. calcs. 79−51212
- V_2O_3, US vel. and elastic const. meas., 150-273K, Debye temp. determ. 77−15478
- V_3Si, phonon densities of states and Debye temp. calcs. 79−51212
- W (100), LEED intensities, temp. depend., surface struct. phases and surface Debye temp. 80−39395
- W, Clark-Gazis-Wallis ang. force model, effective Debye temp. 78−22799
- W, LEED and electron microscopic investigs., review *(Hungarian)* 77−47654
- W, phonon dispersion, Debye temp. and Debye-Waller factors, lattice dynamical model 78−55920
- W, rel. to Mossbauer effect *(Russian)* 78−23383
- WC, hexagonal, meas. of mean square shift of atoms in micron powders *(German)* 78−47313
- Xe, lattice vibrs., heat capacities 79−42169
- $Y_{0.7}Th_{0.3}C_{1.58}$, specific heat 78−91813
- YNi_5, Haucke compounds, low temp. heat capacity, Debye temp. 80−96663
- Zn, dislocation damping on $\{\bar{1}2\bar{1}2\}\langle\bar{1}2\bar{1}\bar{3}\rangle$ slip system above Debye temp. 77−62538
- Zn, hexagonal lattice equilib., electron gas model with noncentral forces, lattice dynamics 78−95123
- Zn, Lindemann's rule and X-ray Debye temp., anisotropic single crysts. 79−28076
- Zn, mean square displacement of atoms in cryst. lattice, rel. to sp. ht. *(German)* 80−79902
- Zn, phonon density of states calc. from neutron diffr. data 77−24369
- Zn, single cryst., mean square vibr. amplitudes X-ray diffr. 77−35640
- $ZnAs_2$, thermodynamic functions 79−10961
- Zn_3As_2 and $ZnAs_2$, molten, thermal expansion and atomic bond strength parameters 80−65257
- $ZnCr_xFe_{2-x}O_4$, Mossbauer spectra, quadrupole splitting, Debye temp. 80−93218
- $Zn_3(OH)_4(NO_3)_2$, sp. ht., 5-300K, thermodynamic props. 79−55900
- $Zn(OH)(NO)_3.H_2O$, sp. ht., 5-300K, thermodynamic props. 79−55900
- $Zn_5(OH)_8(NO_3)_2.2H_2O$, sp. ht., 5-300K, thermodynamic props. 79−55900
- ZnP_2, Brillouin scattering and optical props. meas. 80−76041

Debye temperature continued
ZnS, lattice dynamics, phonon freq., bond bending force model calcs. 80−70335
ZnS(Se)(Te):Co, impurity luminescence no phonon line depend. on temp., Debye temp. 80−66273
ZnSb, X-ray diffr., 78-300K, dynamical props. and thermal expansion *(Russian)* 77−7833
ZrC$_x$, static distortions and Debye temp. determ., neutron diffr. exam. *(Russian)* 77−80482
ZrN, physicomechanical props. with the homogeneity range 77−1848
ZrO$_2$:Y$_2$O$_3$, low-temp. specific heat, oxygen vacancy effects 80−49376

Debye-Waller factors
see also lattice dynamics
amorphous solids, Raman intensities, connection with EXAFS Debye-Waller factors 80−108214
analysis at high temp. 78−2465
anharmonic, temp. dependence 80−79903
anharmonic crystal, neutron scattering, effect of sublattice displacement 79−77458
anharmonic crystals, Debye-Waller factor, specific heat thermal behaviour 80−54335
anharmonic crystals, neutron scatt. cross-section, sublattice displacement effects 79−77460
anharmonic Debye-Waller factor, classical limit, calc. 80−54334
anharmonicity, low-temp. model, Debye-Waller factors of Mossbauer effect 78−55927
atom-surface scatt., lattice dynamics effects 80−2909
atom-surface scattering, quantum theory, Debye-Waller factor 80−7459
atom-surface scattering 78−92164
atom-surface scattering theory, use of Debye-Waller type factor 77−73204
tert-butanol, mol. dynamics, liq. and cryst. states, neutron inelastic scatt. obs. 78−75599
carnauba wax, electret states, role of crystallites 80−2686
cyclohexane, dynamic props. investig. by Rayleigh scatt. of Mossbauer radiation *(Russian)* 77−69760
cis-dekalin, dynamic props. investig. by Rayleigh scatt. of Mossbauer radiation *(Russian)* 77−69760
determination method using absolute areas 80−34161
diamond, electron density, neutron diffraction powder data 78−38655
diamond, electron density, X-ray powder diffraction data 78−38656
dynamic deformation effects, on Debye-Waller factor 79−51207
ethylene oxide clathrate, reorientation, residence times, Debye-Waller factors, activation energy, neutron scatt. study 79−41989
FCC metal, ^{119}Sn implantation by isotope separator method, Mossbauer spectra, Debye-Waller factors determ. 79−24240
FCC metal, Debye-Waller factor determ. from X-ray data 77−1205
finite one-dimensional lattice finite length effects, Debye-Waller factor and sp. ht., for teaching 77−33798
freezing, first principles order-parameter theory 79−77718
glissile dislocations, prod. by impurity atoms, Debye-Waller factor calcs. 78−2214
harmonic Debye solid, amorphous and disordered struct. factors 78−9954
impurity atom in solid, reson. fluoresc., transient spectrum, intensity, and intensity correl. 80−84777
incommensurate structure, Debye-Waller factors, modulation wave thermal fluctuations 80−84274
magnetic Debye crystal, with magnon-phonon coupling, crit. changes in vibr. modes 79−95094
metal, BCC, temp. depend. calc. 78−22807
metal, BCC, temp. variation, lattice dynamical calc. 78−55925
metal, FCC, Debye-Waller factors, modified ang. force model 77−66013
metal, FCC, phonon dispersion relations and Debye-Waller factor calcs. 78−51630
metal, FCC, vibr. anharmonicity and Debye-Waller factors, Willis approach 77−51467
metal, Mossbauer isomer shift, pseudopot.-Born-Oppenheimer theory development 78−2775
metal, struct. factor calc., n-phonon term 77−1206
metal, thermal vibration amplitude of atoms and fusion behaviour *(Korean)* 79−69218
metallic alloy, highly resistive, elec. resist. calc. including Debye-Waller factor 77−66150
metals, phonon limited resistivity, anharmonicity, Debye Waller factors, multiphonon terms 80−49691
metals electrical resistance at high temperature, T$^{3/2}$ depend. 77−43561
methane heavy cryst., temp. depend., Monte Carlo calc. 78−47492
molecules, internal modes contribution, to Debye-Waller factors 79−73263
monolayers of adsorbed atoms, props. 78−84057
Mossbauer radiation scatt. by condensed matter, review 79−78596
neutron diffraction absorption corrections 79−27876
n-octane-3,4,6,7-dibenzpyrene impurity, fluorescence impurity spectra, phonon free line broadening *(Russian)* 80−108279
piezoelectric crystal, X-ray refl., oscill. elec. field effects 79−78625
polycrystals containing defects with Coulomb displacement fields, X-ray scatt. *(Russian)* 78−38576
potassium iron tri(hydrazoformate), Debye-Waller factor, Mossbauer spectra obs. 79−56627
rare gas solids, Debye Waller factors from unpaired elastic force model 80−19896
recoilless fraction, integral evaluation 77−59090
semiconductor single crysts, X-ray determ. 100-1000K *(German)* 78−30726
solid phase chemical reactions, low temp. and fast, mol. motion effect 80−97681
statistical crystal model, small amplitude acoustic perturbations 78−55930
superconducting properties, effects of anharmonism *(Russian)* 78−39255
surface, rel. to He at. scatt. 77−63516
temperature dependence, empirical T$^{3/2}$ law 77−39652
o-terphenyl, liq. and glassy, dynamics of dissolved ferrocene, Mossbauer obs. 80−55000
tetrahydrofuran clathrate, reorientation, residence times, Debye-Waller factors, activation energy, neutron scatt. study 79−41989
transition metal surface (adsorbate), intermediate UPS/XPS synchrotron radiation study 78−52633
transition metals, Y to Pd, X-ray characteristic temps. 78−18731

Debye-Waller factors continued
urea, internal modes contrib. to Debye-Waller factors 79−73264
X-ray and neutron scatt. determ. methods 78−83974
X-ray diffraction and lattice dynamics, early work by I. Waller 80−62439
X-ray diffuse scattering data, role of Debye-Waller factors in analysis 79−23494
(K$^-$, π^-) on light nuclei, recoilless Λ prod. strength from DW factor 78−50116
^{159}Tb, 58 keV level, nuclear reson. fluorescence 78−33121
Ag (111) plane, specular refl. of He and H$_2$ beams, Debye-Waller factor and surface Debye temp. 79−47580
Ag, Debye temperature correlations at high temp. 80−15210
Ag, Debye Waller determ. from modified Cheveau model 78−59918
Ag, Debye-Waller factor temp. parameter 78−30725
Ag, modified Bhatia model, phonon dispersion, Debye-Waller factor temp. depend. 77−31729
Ag, phonon dispersion relations and Debye-Waller factor calcs. 78−51630
Ag surface, scatt. of He, H$_2$, Debye-Waller factors, expt. 80−60736
Ag, two-parameter dynamical model appl 80−10597
α-AgI, superionic compound struct., cation distrib., powder neutron diffr. 77−72595
Ag$_2$SnS$_3$(Se$_3$)(Te$_3$), Mossbauer effect, lattice dynamics obs. 77−43923
Al, Debye temperature correlations at high temp. 80−15210
Al, Debye Waller determ. from modified Cheveau model 78−59918
Al, Debye-Waller factor temp. parameter 78−30725
Al, modified Bhatia model, phonon dispersion, Debye-Waller factor temp. depend. 77−31729
Al, phonon dispersion relations and Debye-Waller factor calcs. 78−51630
Al, two-parameter dynamical model appl. 80−10597
Al-Fe, dil. solid soln., vacancy-trapped Mossbauer impurity Debye Waller factor 80−60468
Al-Fe alloy, dil., quenched secondary defects, Mossbauer spectroscopy 77−28491
Am, temp. depend., Mossbauer effect meas. 78−83902
^{243}AmO$_2$, neutron diffraction study, possible occurrence of antiferromagnetism 79−78332
^{241}Am, α-radiation self-damage effect on hyperfine interaction and Debye-Waller factor, Mossbauer meas. 80−7230
As, Debye-Waller factors and thermal expansion 78−43089
Au, Debye Waller determ. from modified Cheveau model 78−59918
Au, Debye-Waller factor temp. parameter 78−30725
Au, fine particles, gas evaporation technique for prep., X-ray diffr. study 80−75327
Au, fine particles, gas evaporation technique of prep., X-ray diffr. study, charact. temp. 80−75328
Au, modified Bhatia model, phonon dispersion, Debye-Waller factor temp. depend. 77−31729
Au, phonon dispersion relations and Debye-Waller factor calcs. 78−51630
Au, small particles, size-effect modifications of Debye-Waller factor 77−84877
Au-Fe solid soln., props. during preparation by diffusion heating 77−12260
BaTiO$_3$, struct. changes due to cubic-tetragonal phase transition 78−60407
BaTiO$_3$, transform. of cryst. struct., at cubic-to-tetragonal phase transitions 79−37827
Bi, Debye-Waller factors and thermal expansion 78−43089
CaF$_2$, lattice dynamics in ang. force model, Debye-Waller factors, sp. ht., dispersion relations 77−59081
CdO, X-ray determ., Debye-Waller factors, Debye temp. and vibration amplitudes 78−55928
Co, Debye-Waller factor and Lindemann parameter, temp. depend., lattice dynamical model calcs. 80−59610
Co-Ga alloys, transition metal partially substituted, elec. resist. anomalies 79−38044
Cr, Debye-Waller factors, extended de Launay model calcs. 80−70352
Cr, lattice dynamics, improved Fielek model 80−59598
Cr, phonon dispersion, Debye temp. and Debye-Waller factors, lattice dynamical model 78−55920
Cr, temp. depend. calc. 78−22807
Cs-graphite intercalated compounds, anisotropy of Debye-Waller factor, Mossbauer meas. 77−55738
CsCl-type crystals, mean Debye-Waller factors, vib. amplitudes and Debye temp. 78−75792
CsPbBr$_3$, struct., Debye-Waller factor, neutron diffr. study 79−90609
Cu, Debye Waller determ. from modified Cheveau model 78−59918
Cu, Debye-Waller factor temp. parameter 78−30725
Cu, EXAFS Debye-Waller factors 80−45168
Cu, modified Bhatia model, phonon dispersion, Debye-Waller factor temp. depend. 77−31729
Cu, phonon dispersion relations and Debye-Waller factor calcs. 78−51630
Cu, photoemission, temp. and photon-energy induced breakdown of direct transition model 78−95681
Cu surface, (100) coherent elastic scatt. of He, Ne, thermal attenuation 80−89105
Cu, thermal displacement of surface atoms, elastic backscatt. of He atomic beam *(French)* 77−4709
Cu-Fe, mixed cryst., Debye-Waller factors, Mossbauer spectra obs. *(German)* 78−52412
Cu$_3$Au, Debye-Waller factor measurement in anal. of diffuse scattering data 79−23494
Cu$_3$Au, heterophase fluctuations near order-disorder transform., X-ray and neutron diffr. 77−73272
CuBr, Debye-Waller factors and Debye temp., powder neutron diffr., 295K 78−91407
CuBr, neutron scatt. investig. of anharmonic effects on Debye-Waller factor 77−11658
CuCl, phonon dispersion curves determined by neutron scatt. at 4.2K 78−6132
CuSO$_4$.5H$_2$O, EXAFS, rel. between Debye-Waller factor and thermal parameters meas. by neutron diffr. 80−84803
Cu$_2$SnS$_3$(Se$_3$)(Te$_3$), Mossbauer effect, lattice dynamics obs. 77−43923
Er, Debye-Waller factor and Lindemann parameter, temp. depend., lattice dynamical model calcs. 80−59610
Eu$_{0.8}$Y$_{0.2}$S, Debye-Waller factor, X-ray diffr. meas. 77−11659
α-Fe, BCC, anharmonicity and Debye-Waller factors 77−47533

Debye-Waller factors continued
- Fe complex, dithiocyanato bis(4-methyl-1, 10-phenanthroline) iron, Mossbauer effect and magnetism down to 0.98K 77−28490
- Fe complex, Fe(papt)$_2$, high spin $^5T_2 \rightleftharpoons$ low spin $^1A_1$ transition, Debye-Waller factors and magnetism 78−80259
- α-Fe, Debye-Waller factors, extended de Launay model calcs. 80−70352
- Fe discontinuous film, Mossbauer effect exam. of magnetic state 77−24769
- Fe, EXAFS Debye-Waller factors 80−45168
- Fe, microcrystal, Mossbauer Debye-Waller factor size and temp. depend. 78−15065
- Fe, microcrystal, temp. dependent lowering of Debye-Waller factor 79−1736
- Fe powder, Debye-Waller factor by neutron diffraction 79−95113
- α-Fe, temp. depend. calc. 78−22807
- Fe-Mn, Mossbauer study near martensitic transform. temp. 78−3128
- Fe-Mn (18.6 wt.%), HCP-FCC martensitic transform., Mossbauer effect meas. 78−44121
- FeCl$_2$, adsorbed monolayers, gamma-ray reson. 77−8478
- Fe$_{1-x}$Ni$_x$ ($x<29$at.%), γ-phase dispersion, Mossbauer spectra 78−52399
- FeSiF$_6$, isotropy of Lamb-Mossbauer factor, Debye model 80−60465
- FeSiF$_6$.6H$_2$O, Lamb-Mossbauer factor isotropy in the Debye model *(French)* 80−44962
- GaAs, X-ray structure factors and Debye-Waller factor, from Bragg case diffr. curves 77−62509
- Ga$_x$In$_{1-x}$P, X-ray diffr. determ. *(German)* 77−27959
- Gd-Mg, X-ray determ. of Debye temp., mean amplitude of vibr. 78−38802
- Gd-Zn, X-ray determ. of Debye temp., mean amplitude of vibr. 78−38802
- GdS, Debye-Waller factor, X-ray diffr. meas. 77−11659
- Ge single crysts, X-ray determ. 100-1000K *(German)* 78−30726
- Ge, X-ray diffraction, effect of dislocations on temp. depend. of integrated intensities, Debye-Waller factor determ. 77−39513
- Ge:Li, dislocation free, anomalous transmission of X-rays *(Russian)* 77−15286
- He, liq. surface, electron solid, self-consistent Debye-Waller factors 80−84337
- ^{3}He, solid, valence band struct., zero-point motion effect 80−65333
- ^{4}He, HCP, Debye-Waller factor by inelastic neutron diffraction 78−43206
- KBr, Debye-Waller factors at 4.2 and 295K 79−7667
- KCl, powder diffr. using synchrotron radiation, energy-dispersive technique 77−24245
- LaNi$_5$H$_{\geq 3.0}$, H diffusion coeff., neutron scatt. obs. 80−24643
- Li, anharmonicity and low temp. phase struct., neutron diffr. study 80−107105
- LiF (001), He elastic scatt., hard corrugated surface model, GR Method 77−85863
- LiF (001), multiple Debye-Waller effects at selective adsorption in atom-surface scattering 80−76126
- metal, FCC, X-ray Debye-Waller factors, CGW vs. DAF models 79−37794
- Mg powder, temp. depend. of Debye-Waller factor, by energy dispersive X-ray method 79−51208
- MgO, electron diffr., dynamical effects for cryst. struct. determ. 78−83679
- MgO, room temp. Debye-Waller factors 77−62607
- Mg$_2$Si, charact. X-ray temp. and thermal expansion coeff. 77−15599
- Mg$_2$Sn, lattice dynamics, angular force model 77−4166
- Mn$_x$Cr$_{3-x}$O$_4$, cubic and tetragonal structs., neutron diffr. obs. 79−19369
- MnS, X-ray determ., Debye-Waller factors, Debye temp. and vibration amplitudes 78−55928
- Mo, lattice dynamics, improved Fielek model 80−59598
- Mo, modified ang. force model 77−76515
- Mo, phonon dispersion, Debye temp. and Debye-Waller factors, lattice dynamical model 78−55920
- ND$_4$NO$_3$, cubic, mol. orientation determ. by multipole anal. 79−73136
- (NH$_4$)$_2$BeF$_4$, incommensurate phase, Mossbauer spectrum 79−61276
- Na, BCC, anharmonicity and Debye-Waller factors 77−47533
- Na, Debye-Waller factors, extended de Launay model calcs. 80−70352
- Na, temp. depend. calc. 78−22807
- NaCl, powder diffr. using synchrotron radiation, energy-dispersive technique 77−24245
- NaF, He atom scatt., Debye Waller effects 79−8218
- Nb, Debye-Waller factor and H$_2$ diffusion, neutron spectroscopy study 79−37881
- NbH$_{0.02}$, diffusion of H, neutron scatt. study 79−60550
- Nb$_3$Sn, Debye-Waller factor temp. depend. 79−14907
- Nb$_3$Sn, proton and γ-irradiated, lattice dynamics from ^{119}Sn Mossbauer studies 78−39458
- Ni, Debye Waller determ. from modified Cheveau model 78−59918
- Ni, Debye Waller factor by mol. dynamics simulation 77−80598
- Ni, Debye-Waller factor temp. parameter 78−30725
- Ni, phonon dispersion relations and Debye-Waller factor calcs. 78−51630
- Ni powder, neutron diffr. study of Debye-Waller factor using reverse Fourier time-of-flight method 80−49050
- β-Ni$_{1\pm x}$Al$_{1\pm x}$, defect struct. and Debye Waller factors vs. composition 77−31658
- Ni$_3$B$_7$O$_{13}$I, phase transition, X-ray diffr. obs., 77-300K, rel. to mag. susceptibility anomaly 77−47573
- NiO (001), surface layers, sublattice magnetisation temp. depend., LEED exam. 78−27018
- Pb, Debye-Waller factor, temp. variation calcs. 80−34162
- Pb, Debye-Waller factor temperature parameters, vibr. depend. 79−99288
- PbF$_2$, anion disorder at high temps., neutron diffr. obs. 80−59614
- PbS, X-ray determ., Debye-Waller factors, Debye temp. and vibration amplitudes 78−55928
- PbTe (111), lattice vibr. amplitude anisotropy, RHEED study 80−39408
- PdD$_{0.63}$, phonon lineshapes Debye-Waller factors, 80K, inelastic neutron scatt. study 79−42187
- Pt, Debye-Waller factor temperature parameters, vibr. depend. 79 99288
- Pt, EXAFS Debye-Waller factors 80−45168
- Rb$_2$ZnBr$_4$, average struct. determ. from neutron diffr. diagrams, Debye-Waller factors 79−32955
- Ru, Debye-Waller factor and Lindemann parameter, temp. depend., lattice dynamical model calcs. 80−59610
- Sb, Debye-Waller factors and thermal expansion 78−43089

Debye-Waller factors continued
- Sb, Mossbauer radiation, Rayleigh scatt., Debye-Waller factor determ., annealing effect 80−39963
- Sb$_2$Te$_3$, Mossbauer radiation, Rayleigh scatt., Debye-Waller factor determ., annealing effect 80−39963
- Sc, Debye-Waller factor and Lindemann parameter, temp. depend., lattice dynamical model calcs. 80−59610
- Sc$_2$Pt, X-ray powder struct. anal., Debye-Waller factors 79−77553
- Si, multiphonon and one phonon X-ray scattering, and temp. depend. of Debye-Waller factors, shell model calcs. 79−99022
- Si:Sb, Mossbauer spectra of ^{119}Sn defect struct. 80−97174
- Si:Te, Mossbauer spectra of ^{119}Sn defect struct. 80−97175
- SmS, Debye temps., vibr. amplitudes, X-ray diffr. determ. 78−2222
- SmS, Debye-Waller factor, X-ray diffr. meas. 77−11659
- SmSe, Debye temps., vibr. amplitudes, X-ray diffr. determ. 78−2222
- SmTe, Debye temps., vibr. amplitudes, X-ray diffr. determ. 78−2222
- Sm$_{0.7}$Y$_{0.3}$S, Debye-Waller factor, X-ray diffr. meas., evidence of optic phonon softening 77−11659
- Sn, X-ray diffraction study of thermal motion of atoms in β-Sn 80−39243
- Sn$_{1-x}$Eu$_x$Mo$_6$S$_8$, supercond., Mossbauer effect, struct. phase transition 77−12290
- SnMo$_6$S$_8$, lattice softening, vibr. anisotropy 78−14428
- SnTe, phase transition obs. by Mossbauer spectroscopy 77−55740
- SrCl$_2$, anion disorder at high temps., neutron diffr. obs. 80−59614
- SrCl$_2$, specific heat anomaly and sublattice disorder, neutron diffr. meas. 79−42238
- Ta, Debye-Waller factor and H$_2$ diffusion, neutron spectroscopy study 79−37881
- Ta-H alloy, high conc., Huang diffuse X-ray scatt. from lattice strains 78−38746
- TaH$_{0.13}$, diffusion of H, neutron scatt. study 79−60550
- Th (111), struct., Debye temp., and oxidation, LEED and AES obs. 77−89625
- Th, crystal equilib., lattice dynamics 78−47479
- (Ti$_{0.9975}$V$_{0.0025}$)$_4$O$_7$, metal-insulator transition, struct. aspects 79−86752
- TlCl, Debye-Waller parameter by powder elastic neutron diffr. 80−29140
- TlCl, X-ray diffr., ion vibrs. 77−31742
- TmSe, Debye temps., vibr. amplitudes, X-ray diffr. determ. 78−2222
- UO$_{2\text{ and }2.11}$, temperature factor determ. by powder elastic neutron diffraction 78−10152
- V, Debye-Waller exponent, 4.2 to 296K, incoherent elastic neutron scatt. 79−4382
- V, Debye-Waller factor and H$_2$ diffusion, neutron spectroscopy study 79−37881
- V, lattice dynamics and cryst. equilib. 78−75753
- VH$_{0.07}$, diffusion of H, neutron scatt. study 79−60550
- V$_3$Si, powdered, Debye-Waller factors and lattice consts., 25-1000K, X-ray diffr. obs. *(German)* 79−33060
- W (100) and (110) surface, theoretical Debye-Waller factors 80−92773
- W, modified ang. force model 77−76515
- W, phonon dispersion, Debye temp. and Debye-Waller factors, lattice dynamical model 78−55920
- ZnSb, X-ray diffr., 78-300K, dynamical props. and thermal expansion *(Russian)* 77−7833

decay periods (radioactive) *see radioactive decay periods*

decay schemes (radioactive) *see radioactive decay schemes*

decay theory (nuclear) *see nuclear decay theory*

decision tables
- mass spectra, computer-aided classif., pattern recognition techniques, decision-tree approach 80−40774

decision theory *see decision theory and analysis*

decision theory and analysis
- *see also Bayes methods; dynamic programming*
- Bayes method appl. to nuclear fuel reprocessing analyses, USA policy 79 85737
- cervical cancer automatic cytoscreening, atypical cells classification 78−73289
- clinical diagnostic method effectiveness, decision probability calc. *(Hungarian)* 78−65146
- cloud classification techniques, comparative study 78−7809
- denumerable state infinite horizon contracted Markov decision processes, finite state approx. 80−46974
- digital seismic data processing, struct. anal. of graphs *(Russian)* 78−53749
- EEG automatic classification, decision rules comparison 80−109054
- EEG cluster separation by nonlinear decision boundaries and linear filtering 77−56509
- environmental assessment, graph-matrix method 79−57502
- fatigue crack detection and maintenance in pressure vessels, risk-sensitive Markovian policies 79−54534
- Markov decision process monotone optimal policies 77−53757
- Markov decision processes, infinite-horizon, denumerable-state, finite-state approx. 80−68130
- multiplicative Markov decision chain dynamic programming recursions 77−53758
- nuclear fuel cycle evaluation, decision anal. and probability assessments 80−47587
- nuclear fuel cycle facility safety evaluation physical security assessment results synthesis 79−85740
- nuclear material accounting, decision anal. 79−81049
- on-line surveillance of nuclear reactors based on decision theory 79 9775
- optical noise, Schade detail S/N ratio derived from decision theory 78−63022
- pattern recognition theory and application, book 78−64927
- plant information measures selection criteria nuclear reactor monitoring appl. 79−41006
- polarimetry of partially polarised waves, accuracy 77−46666
- quantum meas. theory Cramer-Rao inequality noncommutative analogues 77−26209
- radioactive waste, management alternatives for low-level waste 80−99259
- radioactive waste disposal, decision anal. 80−18488
- random field reconstruction using theory of statistical decisions 79 72509
- receiver operating characteristic analysis, derivation of curve, determination of diagnostic benefit 77−86563
- regenerative Markov decision models, iterative methods appl. 77−53756

decision theory and analysis continued
remote sensing, design and pot. of decision tree classifier 77—56745
solar thermal power systems, 0.1 to 10 MWe, comparative ranking anal. 80—30559
speaker recognition, multistage decision schemes 79—64435
synthetic fuel, alternative programmes, decision anal. 79—83548
visual perception, non-resolvable ambiguities model 79—34567
water pollution control, Rhine river study 77—66946
water resource problem with multiple objectives, interactive optimisation, Yodo River basin, Japan appl. 79—57516
weather modification, scientific and technological aspects 79—20934
SO_2 air pollution, decomposed model design for assessment of utility measure 79—66426

decoding
see also demodulation
1.5 Mb/s bipolar signal coding and decoding optical fibre link 77—27343
annular coded-aperture images, decoding techniques 78—37818
artifact-free region-of-interest reconstruction from coded-aperture recordings 79—89863
coarticulatory effect perception, maturational influences 79—94415
coded aperture imaging, review 80—101914
coded-aperture images, pre-folded Fourier filter reconstruction 80—53222
colour display technique for NMR imaging 77—57373
defect radiographs, method and apparatus for automatic decoding 78—40002
digital decoding technique, coded apertures, for gamma cameras 77—86620
Fourier holograms recorded and decoded in polychromatic light 80—37970
gammagraphy, 3-dimens. image processing appl. to coded aperture imaging *(French)* 78—57067
land seismology using mini-SOSIE, data decoding 77—21917
matched filters, using optical delay line provide encoding or decoding structures 78—74983
optical coding and decoding operations, parallel image transmission by single fibre 78—71216
optical decoders, based on controlled transparencies *(Russian)* 80—28321
optical decoding, Fresnel zone plate images feasibility analysis 77—86621
optical fibre network, for encoding and decoding 78—25963
optical processor, time- and space-integrating, for spread spectrum appl. 80—78777
paper tape data transmission, wavelength multiplexing, optical fibres 80—43454
particle track data in plastics, rapid anal. using interactive programming and graphic displays 78—66456
PCM encoding and decoding for optical memories 80—102658
picture direct transmission via single optical fibre 80—106628
radiography, flashing tomosynthesis 80—67243
radioisotope imaging, source dependent imaging system 77—77983
space-frequency conversions for image transmission and processing 78—71046
speech, continuous, experimental system for acoustic-phonetic decoding 79—59890
spread-spectrum signal optical processing 79—72518
synthetic aperture radar, satellite-borne, optical decoding 78—90384
universal product code symbol scanning, error modes and probabilities 77—621
US imaging techniques for medical diagnosis *(French)* 80—26304
virtual holography, method of source and channel encoding, decoding of information 79—94185
wavelength multiplexing for information transmission 79—22906

decomposition
microstructure features and processes only; for other aspects see dissociation and pyrolysis
see also spinodal decomposition
alkali borosilicate glasses, observation of phase separation using SEM-EDX technique 80—76224
alloy, cubic, computer simulation of formation of tweed and modulated structs. 79—96029
alloy, solid state reactions, effect on microstruct. 79—29015
alloy, ternary, transition of univariant form. equiliv. into decomposition equilib. *(German)* 79—43196
alloy decomposition kinetics, Johnson-Mehl-Avrami (JMA) formula appl. 80—16263
alloys, decomposing, internal friction peaks in grain boundary model *(Russian)* 78—35418
alloys, resistivity evolution during decomposition, theory *(French)* 80—75546
amorphous semiconductors, crystallisation 79—41959
austenite, Fe-C supersat. solid soln. decomp. and graphite surface energy determ. *(Russian)* 77—15677
austenite, quenched and tempered, effect of bainitic decomp. products on mech. props. 77—56007
austenite solid soln., decomposition, effect of struct. of initial state *(Russian)* 77—48442
austenitic steel, 17G1S struct. and austenite transformation kinetics variation on deform. *(Russian)* 79—70060
austenitic steel, solid solution decomposition at defects, TEM meas. 77—12656
binodal decomposition near crit. point, scaling hypothesis 80—79912
carbide solid solns. decomposition temp. expression 80—55398
composite growth by eutectoid or solid-state decomposition 78—44056
di(alkylammonium)$CdCl_2Br_2$, solid-solid phase transitions 80—84290
energy partitioning in ionic decomposition products 77—16819
ferrous alloys, phase transforms. and ordering, Mossbauer spectroscopy 77—12619
flip-flop decomp. 77—21095
formic acid on Ru (10$\bar{1}$), decomp. into H_2, CO_2, H_2O and CO 79—79245
graphite-DNO_3, intercalation cpd., mol. dynamics 79—28631
Guinier-Preston zones, X-ray small angle scattering, for extra-resist. calcs. 80—92873
Metglas 2826A, direct meas. of decomp. on crystn. by X-ray microanal. in STEM 79—48025
mischmetal-Co system, thermomagnetic analysis of intermediate phases 80—93115
ordered alloys with periodic struct., decomp. invest. *(Russian)* 80—93558

decomposition continued
oversaturated solid solution, directed decomposition *(Russian)* 80—97458
phase separation dynamics, renormalised time-depend. Ginzburg-Landau model 80—29175
polyhedrisation of quinary metallic systems with isomorphic intermediate phases *(Russian)* 80—45270
quasi binary eutectic systems, with inclusive phases, hardness, transform., decomposition *(Russian)* 80—97572
quenched binary alloy at low temps., time evolution, phase separation 78—68670
rare-earth intermetallics, R_2Co_7, polymorphism of Ce subgroup alloys, eutectic decomposition *(Russian)* 80—66504
semiconductor supersaturated solid solns., decomp., surface impurity content 78—51681
silicate glass decomp. in alkaline aq. soln. 77—48637
solid solution, supersatuated diffusive decomposition, universal distrib. function in dimension space for new-phase particles 78—48372
solid solution, supersaturated, cellular precip. features, review *(Russian)* 80—84937
solid solution, supersaturated, dissoc. kinetics determ. method 77—52317
solid solution, supersaturated, isomorphic decomp., elastic interaction of dilating particles *(Russian)* 79—47691
solid solutions, decomposition, two-phase. X-ray diffr. anal., exam. of method 79—52510
solid solutions, diffusion equation, during a decomp. process, role of non-linearised terms *(Japanese)* 80—92723
stainless steel, 36NKhTYu, highly deformed, discontinuous γ'-phase precipitates cell boundaries, formation during ageing 79—87641
steel, alloy, nonmartensitic decomposition of austenite, fracture strength of high tempered products *(Russian)* 78—11304
steel, alloy 36NKhTYu, deformation resistance, grain size effect *(Russian)* 78—11271
steel, austenite, abnormal decomposition kinetics and mechanism *(Russian)* 80—55344
steel, austenite decomposition, controlled rolling rel. to substruct., props. 79—29014
steel, austenitic, alloyed with N, decomposition of solid solution 78—23712
steel, austenitic, decomposition, exam. of phase transformation kinetics, using new method 79—52509
steel, austenitic, eutectoid decomposition, effect of liquation of alloying elements *(Russian)* 78—19708
steel, austenitic, high speed, supercooled, austenite decomposition kinetics 78—92233
steel, austenitic, metallography study of high temp. decomposition 79—61559
steel, austenitic, supercooled, decomposition by heat treatment, carbide particle morphology *(Russian)* 77—70076
steel, austenitic decomposition kinetics, crack sensitivity, H_2 effect *(Russian)* 80—20885
steel, austenitic heat-resisting, deformation and fracture rel. to grain-boundary reaction nodules 78—80591
steel, austenitic stainless, Mn-Cr, austenite decomposition by deform., rel. to mech. props. *(Russian)* 78—27515
steel, austenitic stainless B-containing, decomp. of solid solns., effect of cooling conditions 77—44256
steel, austenitic supercooled, transformation kinetics into spheroidised pearlite *(Russian)* 78—95742
steel, C, decomposition of supercooled austenite, exam. of carbide formation *(Russian)* 78—35388
steel, C, structural strength, increase by high temp. mech. treatment with austenite isothermal decomp. 79—24555
steel, C martensitic, tempering induced decomposition and segregation, atom probe study 80—3112
steel, carbide formation during tempering on martensite decomp. and ductility 78—23733
steel, cementite decomposition during plastic deform., alloying element effects 78—84768
steel, Co-W-Mo-V-Ti-C (25.3, 12.8, 6.2, 0.5, 0.5, 0.05 wt.%), martensitically aged, structural transformation, and strengthening mech. *(Russian)* 79—15676
steel, cold strained, defects interaction with carbide strengthening phases, carbide decomp. degree *(Russian)* 80—84955
steel, cold-worked, alloying elements effect on cementite decomp. during plastic deform., Mossbauer study 79—82900
steel, cold-worked, Mossbauer obs. of cementite decomp. and restitution 78—64558
steel, Cr, and Cr-Mo-Ni, austenite decomposition, deform. effects, ferrite reaction 79—1842
steel, Cr (0.5 wt.%), austenite-pearlite transformation 80—97480
steel, Cr (10 wt.%), precip. free ferrite form., STEM 80—84941
steel, Cr (2%), austenite decomp., phase diagrams and struct. form. kinetics 80—76223
steel, Cr (3 wt.%), $\gamma \rightarrow \alpha$ transformation singularities in intermediate transformation temp. interval *(Russian)* 79—91644
steel, Cr-Mn(Ni), Mn and Ni additions, effect on corrosion resistance and hardness 80—104342
steel, Cr-Mo-Mn-Si-W (3, 1.95, 1.55, 1.45, 0.95 wt.%), struct. and props. 80—104175
steel, Cr-MoV, isothermal decomp. of austenite and carbide precip. 79—38832
steel, high Cr, V additions effect on brittleness near 475°C *(Russian)* 78—19890
steel, high-C, type U12, U15, U17, cementite precipitation cryst. geometry singularities during decomposition of martensite *(Russian)* 80—7577
steel, high-speed cutting, struct. and props. Co addition effects *(Russian)* 77—21177
steel, maraging, Fe-Cr-Co-Mo, phase transforms. during high temp. austenitisation and solid soln. decomp. *(Russian)* 80—66524
steel, martensitic, Cr-Ni-Co-Mo-Ti, Kh12N8K5M3TYu, ageing of C free martensite *(Russian)* 79—1884
steel, martensitic, retained austenite study by X-ray diffr. *(Korean)* 78—44143
steel, martensitic stainless, type 05Kh13N4m, strength and embrittlement, early stages of martensite decomp. effect 80—35227
steel, medium-C, singularities in low temp. α-martensite decomp. *(Russian)* 77—8814
steel, Mn-Ni-Cr-C, supercooled austenite, influence of constant mag. field on diffusional decomp. *(Russian)* 79—4964
steel, Ni, martensite decomposition *(Russian)* 79—1841

decomposition continued
  steel, Ni-B, B effect on temperability and microstructure 79—15710
  steel, pearlitic, struct. variations under plastic strain and subsequent heating, cementite decomp. *(Russian)* 80—84954
  steel, semi-high speed, martensite degradation due to fatigue *(French)* 79—91615
  steel, sintered at various temps., isothermal decomposition of supercooled austenite 77—12617
  steel, stainless, δ-ferrite, isothermal decomposition and transform. of heating at 550 to 950°C *(Chinese)* 79—43239
  steel, stainless, ferrite to austenite decomp. 80—93554
  steel, structural, austenite decomposition, 500 to 450°C 77—16593
  steel, structural, supercooled austenite, structural characts. of decomposition 80—60870
  steel, thermally and thermomechanically treated, struct. and decomposition of martensite 78—19784
  steel, V, precip. and transform. kinetics, effect of N 80—97485
  steel, V-Nb and Cr-Mo-V-Nb, supercooled austenite isothermal decomp., struct., strength and fracture characts. 80—60966
  steel 80Kh5, thermomechanical treatment, high temp., effect of austenite deform. on martensite stability during low temp. tempering 79—57018
  structural steel, microstruct. and brittleness, rel. to austenizing and heat treatments 77—56091
  supersaturated multicomponent systems, theory of diffusive decomposition 77—76565
  supersaturated solid solution, diffusive decomposition 78—76653
  $\alpha+\beta$-Ti alloy, singularities of decomposition of β solid solutions, low temp. range *(Russian)* 79—1867
  two-phase multicomponent system, coalescence theory 77—81248
  YN, decomp. press.-temp. relations 78—52780
  YN-UN, solid soln., decomp. press.-temp. relations 78—52780
  Ag_7AsS_6, thermal, crystallographic and elec. props. *(French)* 80—40338
  Ag_7AsSe_6, thermal, crystallographic and elec. props. *(French)* 80—40338
  Al alloy, D16, extruded rod, substruct. anisotropy and decomp. at subboundaries *(Russian)* 77—25095
  Al alloy D16, supersaturated solid soln., decomp. process, electron microscope obs. and acoustic anal. *(Russian)* 79—15650
  Al-Ag, discontinuous decomposition *(Polish)* 78—52808
  Al-Ag-Zn, ring diffuse X-ray scatt. phenomena *(Russian)* 77—16538
  Al-Al_3Ni directionally solidified eutectic, microstructural degradation in temp. gradient 78—3145
  Al-Cd hypomonotectic alloy, rapid solidification and decomposition 80—50638
  Al-Cu, decomposition of Guinier-Preston zones *(German)* 80—30014
  Al-Ge alloy, effect of high press. on phase equilibrium *(Russian)* 79—1844
  Al-Li solid soln., decomposition exam. by secondary ion ion emission *(Russian)* 78—68696
  Al-Mg (1 to 11 wt.%), alloy A99, dissociation in solid soln., effect of treatment of liquid Al *(Russian)* 78—15353
  Al-Mg (33 at.%), liquisol quenched, decomposition 79—61622
  Al-Mg alloy, AL24M, decomp. kinetics and ageing mechanism *(Russian)* 80—45269
  Al-Mg solid solns., decomposition studied by ultrasonic meas. of elastic props. 80—35184
  Al-Mg-Be, solid soln. decomposition, metallographic study 77—16577
  Al-Mg-Zn, neutron small angle scatt. study 79—43255
  Al-Mn, direct chill-cast, struct. changes during heat treating *(German)* 80—40408
  Al-Mn alloys, study of solidification by rapid cooling *(Japanese)* 78—88459
  Al-Mn(Cr), quenched, thermal stability *(Russian)* 80—20976
  Al-Mn(0.6 wt.%), supersat. solid solns., isothermal decomp., Zr addition effects 77—63626
  Al-Pt (2 at.%), splat cooled, $AlPt_2$ phase, electron diffr. obs. 79—15657
  Al-Pt (2 wt.%), rapidly solidified alloy, metastable phase formation, decomposition during ageing 79—52194
  Al-Si, neutron small angle scatt. study 79—43255
  Al-Zn, ageing alloy, zonal decomposition stage, new effects in X-ray diffr. anal. *(Russian)* 79—4982
  Al-Zn, discontinuous decomposition *(Polish)* 78—52808
  Al-Zn, isothermal preprecipitation, small angle X-ray scatt. expts. 80—35186
  Al-Zn, neutron small angle scattering from above critical point 79—1840
  Al-Zn, neutron small angle scatt. study 79—43255
  Al-Zn (10 at.%), ring diffuse X-ray scatt. phenomena *(Russian)* 77—16538
  Al-Zn (10 wt.%), solid soln., decomposition meas. by resistivity meas. under isothermal conditions *(French)* 79—20025
  Al-Zn (15 at.%), supersaturated alloy, growth and decomposition kinetics 80—29965
  Al-Zn (60 or 71 wt.%), natural ageing *(Russian)* 78—48367
  Al-Zn (70, 30 wt.%), decomp. study, 25-160°C *(Czech)* 80—89225
  Al-Zn alloy, metastable phases formed at 200°C, room temp. stability 80—16315
  Al-Zn alloys, room temp. decomp. of metastable phases precipitated at 200°C 78—84814
  Al-Zn-Mg, decomp. kinetics and ageing mechanism *(Russian)* 80—45269
  Al-Zn-Mg, decomposition calorimetric study *(German)* 79—74165
  Al-Zn-Mg, plastic deform. influence on structural transform. and mechanical props. *(Russian)* 80—7623
  Al-Zn-Mg, polygonized struct. in extrusions, thermal stability and mech. props. 80—50659
  Al-Zn-Mg, solid soln. decomp., 20 to 200°C 79—38830
  Al-Zn-Mg (4.5, 2 to 3 at.%) solid state reactions by interrupted continuous heating 80—25737
  Al-Zn-Mg (4.5 at.%, 2 or 3 at.%), decomposition behaviour during continuous cooling, XSAS and TEM examination 80—16264
  Al-Zn-Mg (4.5 at.%, 2 to 3 at.%), decomp. behaviour during continuous heating 80—29922
  Al-Zn-Mg alloys, decomp. kinetics from Young's modulus obs., microprocesses *(German)* 78—64522
  Al-Zn-Mg alloys, decomposition kinetics, resistivity meas., extended jump model 78—84766
  Al-Zn-Mg alloys, precipitation behaviour *(German)* 78—39780
  Al-Zn(10 at.%), supersaturated solid soln., structural charact. of decomposition 77—70027
  Al_2O_3, fine powder, prep. by evaporative decomposition of solns. 78—39725

decomposition continued
  Al_2TiO_5, eutectoid decomposition, kinetic study *(Japanese)* 77—55941
  Al_2TiO_5 powders, decomposition kinetics using nucleation and growth-rate constants *(Japanese)* 80—35156
  Al_2TiO_5, sintering and annealing effect on decomposition *(Japanese)* 79—87606
  Au-Cu-Ag, phase transform. effect on mech. props. *(Russian)* 78—3122
  Au-Ge, liquid quenched, exam. of phase decomposition 78—48371
  Au-Ni (30 at.%), singularities of struct. state, diffuse electron and X-ray scatt. *(Russian)* 79—4945
  $BaFe^{2+}{}_2Fe^{3+}{}_{16}O_{27}$, metal deficient, hexagonal with W struct., chemical instability 78—27662
  Be-bronze BrB2, struct. and phase transform. during mechano-thermal treatment *(Russian)* 80—11667
  BiTeI crystals, eutectic decomp. in transmission electron microscope 79—20024
  CC Al-Zn-Mg (4.5,1(2)(3) at.%), decomposition during ageing, preageing and cooling rate influence 80—20938
  $CaAl_2O_4$, fine powder, prep. by evaporative decomposition of solns. 78—39725
  $CaCO_3$, decomposition, formation of Ca_3SiO_5 79—52651
  CaO, produced from $CaCO_3$ powder decomp. in vac. and in CO_2 80—45255
  Cd, low angle boundary decomp., dislocation struct. control *(Russian)* 78—3142
  $CdBr_2(I_2)$, vapour growth crystals, decomposition, electron microscope study 78—92268
  $CdCO_3$, three-fold transformation twin in topotactic decompositon 78—44078
  $Cd(OH)_2$, martensitic character of struct. transition, CdO crystallite shape determ. *(French)* 78—10194
  Ce-In, phase equilibrium and cryst. struct. 80—66483
  Ce-Ni, hydriding characts., applicability for H_2 storage material 78—83955
  Ce-Tl, phase equilibrium and cryst. struct. 80—66483
  Co-C supersat., solid soln. decomp. and graphite surface energy determ. *(Russian)* 77—15677
  Co-Cr-W-C, wear-resistant coating alloy, carbide form. and decomp. 77—32711
  Co-Ti (9 at.%), decomp. kinetics, elec. resist., hardness, and saturation magnetisation during ageing *(Russian)* 80—50587
  Co-W(25 wt.%), cellular decomposition, third element effects *(Russian)* 77—1837
  $(Co_{0.83}Cu_{0.17})_6Ce$, cryst. struct. and mag. props., decomp. during ageing *(Russian)* 79—37661
  Co_4CuCe, cryst. struct., mag. characts., ageing and decomposition *(Russian)* 79—4272
  Cr steel, austenite, abnormal decomposition kinetics and mechanism *(Russian)* 80—55344
  Cr-Ni steel, carburised, effect of atm. during heating to quenching temp. on austenite decomp. 77—56157
  CrC, plasma sprayed coating 78—68835
  $Cr_2(SO_4)_3$, stability in atmosphere containing O_2 and S, 880 to 1040K 79—57222
  Cu-Al-Fe-Mn, phase transform. during continuous cooling *(German, English)* 79—70044
  Cu-Al-Mn, partial decomp. of β_1 phase, effect on mag. props. and martensitic transform. *(Russian)* 80—45306
  Cu-Al-Mn(Ni)(Fe)(Co), hypereutectic, martensitic transform., effect of β_1-phase decomposition *(Russian)* 78—23705
  Cu-Be, quasiperiod struct. form. mechanism in eutectoid dissoc. 77—44257
  Cu-Be(30 at.%), eutectoid decomp., elastic interaction between precip. phase particles *(Russian)* 77—8833
  Cu-Cr alloys, isothermal decomp. diagrams 79—38791
  β-Cu-In eutectic, unidirectionally decomposed discontinuous coarsening reaction 78—27472
  Cu-In eutectoid, directional eutectoid decomposition growth, crystallography 80—29874
  Cu-Ni-Nb (30,1 wt.%), precipitation 77—86035
  Cu-Ni-Sn, thermal decomposition after prior cold work 78—15427
  Cu-Sb alloy, splat-quenched, energy dispersive X-ray diffr. 78—23728
  Cu-Ti, lattice parameter change during ageing *(Japanese)* 78—35411
  $CuFeO_2$-Fe_2O_3, decomposition kinetics and mechanism of spinel solid soln., composition and precipitation effects *(Japanese)* 77—77489
  $CuFe_5O_3$, cation substitution effect on eutectoid decomposition 78—68890
  $CuFe_5O_8$, sintered, eutectoid decomposition study by elec. resist. meas. *(Japanese)* 78—19711
  Cu_2MnAl, Heusler alloy, decomposition at 360°C 80—7536
  $CuSO_4$-$5H_2O$, decomposition anisotropy, reaction ellipsoid for transform. to trihydrate *(French)* 77—29003
  $CuSO_4.5H_2O$, anisotropy of decomposition, thermal gradient obs. by IR thermography *(French)* 78—40048
  CuSe film, phase transforms. and decomp., electron diffr. obs. 79—42418
  Fe alloy YuNDK35T5BA, thermomag. treatment, post-decomp. processes 79—87668
  Fe, cast, grey Al-Si, eutectoid decomp. of austenite 80—29951
  Fe, cast, Mg, high strength bainitic transform. in C-shape diagram *(Russian)* 79—1860
  Fe, rolled sheet, magnetic film form. at metal/calamine interface after ferrous products cooling *(French)* 79—43274
  Fe, sintered, austenitic nitriding and bainitic hardening 80—85084
  Fe-Al alloys, powdered composites, metastable gamma-phase decomp. *(Russian)* 77—59741
  Fe-B, rapidly quenched, metastable phases 80—76234
  Fe-C (0.8-4.2 wt.%), eutectoid transform., effect of heat treatment in H_2 *(Russian)* 79—4947
  Fe-C (4.3 wt.%), splat cooled, amorphous phase form. and crystn. 77—15323
  Fe-C solid solution, martensite, carbide decomposition, electron microscopy and X-ray diffr. obs., review *(Russian)* 79—33998
  Fe-C-Si-Mn (1.5-2.9, 2.4-3.4, 0.54-31.7 wt.%), discontinuous decomp. of supersaturated austenite *(Ukrainian)* 79—38788
  Fe-Co-Cr-Si, structural transform. and mag. props. following heat treatment *(Russian)* 77—81274
  Fe-Cr, decomposition Mossbauer study *(French)* 77—63678
  Fe-Cr, high purity binary alloy, isothermal decomp. of austenite 78—64525
  Fe-Cr-C (10,0.2 wt.%) isothermally transformed, carbide distrib., microstruct. development 80—3076

decomposition continued
Fe-Cr-Co, mag. alloys, Mossbauer spectra 78—19386
Fe-Cr-Co permanent magnets, phase diagram, miscibility gap 77—89984
Fe-Cr-(Co), decomposition of solid soln. in mag. field, neutron and X-ray diffr. study *(Russian)* 78—68694
Fe-Cu-Ni, Ni effect on austenite decomposition 80—3048
Fe-Mn (12% Mn), decomposition during plastic deform., Mossbauer parameters *(Russian)* 77—36166
Fe-Mn-Ni-V-C (0.5, 3.0, 1.0, 0.2 wt.%), austenite decomp., isothermal transform. characts. 80—97477
Fe-Mn-V-C (0.5, 1.0, 0.2 wt.%), austenite decomp., isothermal transform. characts. 80—97477
Fe-Mo(V), nitrided by const. activity ageing, X-ray studies 77—32720
Fe-N alloys, secondary ion emission, phase transforms. effect *(Russian)* 80—66347
Fe-Ni (23.1 wt.%), α to γ transformation, struct., conc, changes, heating rate, residual austenite influence *(Russian)* 79—83194
Fe-Ni (24 wt.%), isothermal decomp., mag. determ. of austenite content 80—20886
Fe-Ni (25 to 50%), FCC, meteorites and thermodynamic equilib., Mossbauer and X-ray diffr. study 80—88087
Fe-Ni alloy, α to γ slow transformation mechanism, Ni content influence *(Russian)* 80—7569
Fe-Ni-Al-Co-Cr-Ti, YuNDK35T5BA, exam. of hypodissociation process *(Russian)* 79—11547
Fe-Ni-Cr-Ti-Al Elinvar alloys, dispersion-hardened, structural transform. *(Russian)* 79—1872
Fe-Ni-Ti, undeformed metastable alloy, cellular decomposition of austenite during ageing *(Russian)* 79—100178
Fe-Si cast alloy with spheroidal graphite, transform. investigation during tempering *(Russian)* 80—97479
Fe-Zn, physical-chemical metallurgy *(German)* 80—108390
ε-FeAl, eutectoid, directional decomp. rate rel. to lamellar period 77—4773
ε-FeAl, eutectoid, directional decomp. rate, reply to comments 77—4775
ε-FeAl, eutectoid directional decomp. rate, comment 77—4774
$Fe_{1-x}O$, wustite decomposition, coherent magnetite precipitation, electron diffraction study *(Russian)* 80—16318
FeTi, surface and mag. props., heat treatment and hydrogenation effects 80—75447
n-GaAs, stabilisation against photodecomposition, surface damage influence 80—76390
GaAs:Cu, supersaturated solid solns., decomp., surface impurity content 78—51681
$GaNbO_4$, electron beam induced decomp., high resolution lattice imaging obs. 78—6161
Ga_2S_3-PbS system, phase diagram and crystallographic study *(French)* 80—29937
Ga_2Se_3MnSe system, peritectic decomp., crystallographic study, phase diagram, DTA and X-ray diffr. determ. *(French)* 79—24506
$Gd_3Ga_5O_{12}$, garnet-perovskite transform 80—15239
Ge:Al, solid solns. decomp. 80—15249
Ge:Li, supersaturated solid solns., decomp., surface impurity content 78—51681
Ge:Sb, solid solns. decomp. 80—15249
$Ge_{0.8}(GaAs)_{0.2}$, metastable solid solns., decomp. kinetics 79—38789
H_2O, decomp., H prod. by thermochemical and thermoelectrochemical cycles 80—26029
Hf-Co, phase diagram, X-ray diffr., thermal anal. and metallography obs. 78—60652
Hf-Nb (30 to 50 at.%) exam. of beta phase decomposition processes 78—76674
Hf-Ni(Co), amorphous, formation, decomposition and elec. transport props. 80—20143
$(Hf_xZr_{1-x})_{80}Nb_{20}$, influence of Hf additions to $Zr_{80}Nb_{20}$, beta decomposition anal. 79—8304
InP surface decomposition prevention in LPE growth 80—96749
β-In_3Sn, crystn., decomp. and superconductivity 79—91579
β-In_3Sn, decomposition, X-ray powder diffr. study 80—89196
KCl:Ba solid solution decomposition, elastic ordered structure formation 79—86896
KCl:Pb, solid solution, electron microscope exam. of decomposition, of naturally aged specimens 79—96030
La-Ni, hydriding characts., applicability for H_2 storage material 78—83955
$(La_{0.8}Ca_{0.2})MnO_{3+y}$, non-stoichiometry and lattice consts. 80—100212
$La_7Ni_3D_2$ storage material, neutron, X-ray diffr. study 78—83954
Li-LiH(D)(T), decomposition in $(\alpha+\beta)$ field 79—15652
Li-transition metal dioxide intercalation compounds, mag. props., decomposition effects 80—25075
$LiF:Co^{2+}$, solid soln. decomp., precip. of new phase, electron microscope expt. 79—11619
$LiF-Al(PO_3)_3$ glass, phase decomp., X-ray diffr. and IR spectra study 80—30003
$Li_{1+x}Ti_{2-x}O_4$, high temp. spinel-Ramsdellite transform. 80—70407
Mg-Al (9 wt.%), ageing via cellular reaction, microanal., cell boundary vel. meas. 78—11230
$Mg-Mg_2Ni$ eutectic alloy and Mg_2Ni, catalytic effect in hydrogenation, surface analysis 80—30283
MgO, produced by thermal decomposition of Mg cmpds. to periclase refractory, sinter adhesion 79—83164
γ-Mn-Cu, metastable, structural aspects of decomposition 79—1871
MnCu, neutron scatt. near crit. comp., effects of stress and ageing 79—19722
$NH_4Fe_3(SO_4)(OH)_5$, jarosite, decomposition 80—11624
NaCl:Eu, secondary Eu phase dissolution, EPR and optical absorpt. study 80—96655
$Na_2S_2O_4.2H_2O$ hydrogenase-catalysed decomposition for biologically-assisted H_2 prod. 80—61460
Ni-C, supersat. solid soln., decomposition and graphite surface energy determ. *(Russian)* 77—15677
Ni-Cu, hydrogenated, Curie point, cluster magnetism 78—14960
Ni-Cu-Si, Si effect on structural changes during ageing, TEM and X-ray obs. 78—15438
Ni-Mn-H, hydride phase form. and decomposition in hygh-press. gaseous H_2, magnetisation meas. 79—56953
Ni-Nb amorphous alloy, transformation to crystalline state, ion emission microscope study *(Russian)* 79—82158
Ni-Ti (12 wt.%), early stages of transformation 80—76251
NiH_x, formation and decomp. studies 80—71626

decomposition continued
Pb-As ($\sim$0.01 wt.%), enhanced precip. phenomena, invest. of mechanism by elec. resist. meas. 80—104162
Pb-Sb-As (1.1-1.8, $\sim$0.01 wt.%), enhanced precip. phenomena, invest. of mechanism by elec. resist. meas. 80—104162
$Pb_xMo_6S_{8-y}$, phase relns., stoichiometry, T_c 78—15378
PbTe-PbS, solid-phase solubility, use of diffusion couple 77—12602
$Pb(Zr_{1-x}Ti_x)O_3$ solid solution, piezoelectric ceramic, prop. improvement by multiple substitution 80—80702
Pd-Cu-Ga, cold work and annealing-induced hardening, X-ray diffr. anal. and metallographic exam. *(Russian)* 79—38844
Pd-H system, solvus hysteresis 80—71659
Sb_2O_5 hydrated, preseparation stage in dehydration, phase transformation 80—35524
Sc-H, p-T phase diagram and influence of H pressure, on decomposition temp., DTA exam. 80—29929
$Si:Fe^0$, solid soln. decomp., Fe deposition on dislocations 77—51943
β-SiC, polycryst., ^{30}Si self-diffusion 80—100350
Si_3N_4, porous, reaction sintered, organosilicon infiltrated, decomposition, strength, density 79—29000
Si_3N_4, sintering in powder bed with addition of MgO sintering aid 80—29910
Sm-Co-Cu-Fe-Zr alloy, reversible changes in coercive force and struct. state during heat treatment 400-800°C *(Russian)* 80—29574
$SmCo_5$ based solid soln., X-ray diffr. obs. of decomp. *(Russian)* 77—81264
$SmCo_5$, high coercivity isotropic plasma-sprayed magnet, eutectoid decomp. 80—80568
$SmCo_5$, isotropic plasma-sprayed high coercivity magnet, eutectoid decomp. 80—75810
$SmCo_5$ sintered magnets, eutectoid decomp. 80—89219
$Sm_3Ga_5O_{12}$, garnet-perovskite transform 80—15239
Sn-Bi alloy, splat-quenched, energy dispersive X-ray diffr. 78—23728
Sn-Pb alloys, dil., low-freq. phonon spectrum peculiarities 79—60463
Sn-Sb (10 wt.%), decomposition of supersaturated solid soln. 80—29960
steels, Cr-C-Mn(Ni), struct. prop. rel., design of struct. steels for high strength and toughness 80—97491
Te-In system, enthalpies of fusion, peritectic decomp. and allotropic transition, DTA *(French)* 80—76226
Te-Pb (20 at.%) alloy, amorphous, obtained by rapid cooling from liq. state, crystn. behaviour 78—26445
Ti alloy, VT16, decomp. of α'' martensite during continuous heating *(Russian)* 78—48370
Ti alloy, VT22, thermomechanical treatment, effects on struct. and props. *(Russian)* 78—19785
Ti alloy 679, thermal stability *(Chinese)* 77—73255
Ti alloy VT16, decomposition of metastable β-phase *(Russian)* 78—68710
Ti alloy VT23, quenched decomposition of metastable phases during heating *(Russian)* 78—15432
Ti-Al-Mo-Cr-Fe (6.4, 2.7, 1.6, 0.4 wt.%), quenched VT3-1, decomposition kinetics of α'' and β in annealing *(Russian)* 77—66662
Ti-Al-Mo-Zr alloy, VT9, decomp. kinetics of metastable β-phase, X-ray and mech. props. obs. *(Russian)* 78—48368
αTi-Al-(Zr), embrittlement due to ageing 78—56673
Ti-alloy, VTZ-1 and VT8, decomposition of metastable phases, effect of plastic deform. *(Russian)* 78—39770
Ti-Bi(Co)(Cr)(Cu)(Fe)(Mn)(Ni)(Pb)(Pd)(Pt), eutectoid decomposition 79—24491
Ti-Cr(Mo), alpha precipitation kinetics 78—68697
β-Ti-Fe, (7.1 wt.%) exam. of ω phase formation, by X-ray diffr. and Mossbauer spectroscopy 78—52800
Ti-Mo-V (8 wt.%, 8 wt.%), FCC phase, decay of β-solid soln., electron microdiffr. 79—15670
Ti-Mo-Zr(-Al) (15, 5 (3) wt.%), quenched and aged metastable β-phase, crystallography, morphology and decomposition 80—76262
Ti-Nb, phase transformation due to shock wave treatment *(Russian)* 79—91641
Ti-Nb-Al, decomposition during isothermal annealing 80—25653
Ti-Nb-Ge foils, β phase decomposition, electron microscopy struct. investigation *(Russian)* 79—83172
Ti-Nb-Ta-Ge (40,20,0.8 wt.%) foil, dispersion hardening, TEM and electron diffr. obs. *(Russian)* 79—1873
Ti-Ni, eutectoid decomposition, effect of interphase boundary struct. on mech. 79—4952
Ti-Si amorphous alloy, melt-quenched, transform. studies and mech. props. 80—100838
$TiC_{1-x}N_x$ formation in high temp. N flow, ultra disperse powder, thermodynamic anal. *(Russian)* 80—55325
TiCu intermetallic compounds, decomposition reaction by H_2 absorption *(Japanese)* 78—23668
TiD_2, film formed during simulated Tokamak gettering cycles, desorption 80—34296
Tl_3SnSe_3, peritectic decomposition *(French)* 79—83180
UO_2, sintered, production by gel calcination and drying, thermal anal. *(Czech)* 80—45260
WC, plasma sprayed coating 78—68835
Zn-Al, splat quenched and bulk specimens, eutectoid decomposition 77—63628
ZnS cubic single crystals, growth by double decomposition reaction in melt 78—60557
Zr base alloys, formation of phases precipitated from β solid solutions *(Russian)* 79—1869
β-Zr-Cr (1.9 wt.%), decomposition 79—87604
Zr-Cu (1.6 wt.%), near eutectoid, active eutectoid decomposition ageing and quenching effects 80—2993
Zr-Nb (2.5 wt.%), transforms. during annealing of welded joint, after thermal cycling *(Russian)* 80—29984
Zr-Nb alloy, isothermal decomposition at elevated temp. 78—27470
Zr-Nb-Fe (13 wt.%, 5 wt.%), struct. changes during decay of BCC β solid solution 79—15669
Zr-Nb-V-Al (Fe) alloys, decomp. of β solid soln., metastable and equilib. phases 79—11632
Zr-Nb-V-Fe (12 wt.%, 6 wt.%, 4 wt.%), struct. changer during decay of BCC β solid soln. 79—15669
Zr-Y (15 wt.%) solid solution, decomp., during heating and cooling cycles *(Russian)* 78—92267
Zr_3Al, ordered, oxidation, weight gain and metallography 80—89398

- **decomposition** continued
  - ZrO_2-CaO-Y_2O_3, formation, stability and elec. props. of fluorite-like solid solutions 77—16550
  - Zr_xWO_3, perovskite-type, stability in ZO_2-WO_2-WO_3 phase diagram 77—15582
- **decomposition, spinodal** *see spinodal decomposition*
- **decomposition, thermal** *see pyrolysis*
- **decorative coatings**
  - glaze-porcelain system, intermediate layer investig. by electron probe microanalysis 77—8965
  - glazes, opaque, with ZnO, microstruct. 79—60281
  - guanidinium aluminium sulphate hydrate, ferroelec., decoration patterns on cleavage surface, domain obs. 80—97218
  - guanidinium uranyl sulphate hydrate, ferroelec., decoration patterns on cleavage surface, domain obs. 80—97218
  - laminated papers, deform. and internal stresses 79—61671
  - metal coatings on steel for watch part finishing, ion plating *(French)* 78—23879
  - silicate thermoplastic pigments for glassware, chem. resist. 79—61755
  - steel products, colour coatings, thickness meas. by X-ray fluoresc. 77—54029
  - triglycine sulphate, ferroelec., decoration patterns on cleavage surface, domain obs. 80—97218
  - Al-Cu alloy, deposition from RF induction source, onto laminated polyimide substrates and characterisation 80—16535
  - Au decoration, of individual Ag crysts. by ion bombardment *(German)* 79—69164
  - Cu-decoration technique, lattice imperfection characterisation, of Si wafer *(Japanese)* 79—65069
  - NaCl cleavage step decoration, nucleation and growth of metallic thin films 77—69200
  - Ni-Cr coatings on steel, standardisation 79—57139
  - NiC, colour change on replacement of PbO in glaze *(German)* 79—91813
  - Pb glazes, Cu^{2+} doped, alkaline substitution, crystal field modifications, EPR study 79—95634
  - TiN coating on steel for watch part finishing, ion plating *(French)* 78—23879
  - TiN, on steel and Stellite, ion plating 78—11441
- **deep levels**
  - adsorbates deep level spectroscopy, many body effects 80—39441
  - amorphous solid, abnormal bonding and electronic states in forbidden energy gap 78—51942
  - Auger emission, photon-induced, deep-hole interferences 79—43098
  - Auger emission, photon-induced, deep-hole interferences 79—95900
  - Auger transition from excited Coulomb level of deep impurity centre to ground state 79—15116
  - 2-benzoylpyridine crystals, lowest triplet state, optically detected EPR 80—15827
  - bridge meas. system for assessment of deep levels in semiconductors 80—105674
  - bulk trapping processes and trap occupancy 77—39876
  - capacitance methods for minority and majority carrier trap characterisation 77—51692
  - capacitance spectrometer, appl. to p-n junctions and Schottky diodes deep level props. meas. *(German)* 80—15471
  - capture probabilities of two deep impurity levels, photoconductivity decay analysis 77—89808
  - chalcogenide glasses, electronic gap states, origin, structural relax., electronic transport and trapping 80—54648
  - crystal with narrow allowed band, elec. field ionisation of deep impurity level 79—15118
  - deep-level trap spectroscopy, signal analyser 77—87789
  - detection by admittance-freq. dispersion 77—43536
  - diamond:N, effect of displacement upon impurity levels, pseudopotential calc. 77—39803
  - diamond, cluster, electronic struct. of deep levels, LCAO, SCF method 79—82555
  - diamond Schottky barriers, photocapacity meas. 78—52057
  - DLTS, photo-excited, minority carrier trap meas. 80—96816
  - DLTS single temp. scanning, energy level and capture cross-section determ. 79—99506
  - electron capture, by deep centers, effect of vibration of adsorbed molecules 80—29458
  - electronic structure and lattice distortion, Green's function methods *(French)* 80—59917
  - elemental semiconductors, group IV, Mossbauer spectroscopy of defects, radiation damage and deep levels 80—59533
  - ferroelectric, photoinduced changes in refractive index and spontaneous polarisation 78—43804
  - n-GaAs:O, press. depend. of deep level associated with O, transient capacitance meas. 78—64000
  - Gunn diode, impact ionisation of deep levels, effect on time-averaged I-V characteristic *(Russian)* 77—62935
  - high field conduction in solids, effect of collision ionisation space charge 80—84469
  - high resistivity material, deep level spectroscopy 78—72165
  - II-VI semiconductor, two-photon and two-step absorption of light 80—7389
  - III-V compounds, deep centres exam., review 79—11086
  - III-V compounds and alloys, MBE process and problem areas, review 80—10815
  - III-V semiconductor, localised defects, one-electron pseudopot. 77—24533
  - III-V semiconductor deep impurity states and wave functions 78—10404
  - III-V semiconductors, deep centres, many-electron effects 79—15117
  - III-V semiconductors, deep level defects, review 80—24841
  - III-V semiconductors, electrolum. and related props., book contrib. 77—73173
  - III-V semiconductors, point defects and deep traps, thermodynamic history, model 80—59908
  - impurity centre conc. meas., junction capacitance technique, review *(Japanese)* 78—79958
  - impurity levels, spectroscopic determ. by compensation method 80—108229
  - inhomogeneous semiconductor, negative photocond. and IR quenching of residual cond. 77—24587
  - p-InSb:Cu, Ag, deep impurity centres, acceptor conc. effect on conduction type 80—44602
  - interface state energy determ. during capture of electrons and holes using DLTS 79—87107
- **deep levels** continued
  - large unit cell approach 78—23046
  - many-valley semiconductor, photoionisation of neutral deep impurity centres, photon drag of carriers 78—26828
  - many-valley semiconductor, two-photon transitions from deep neutral impurity centres, light absorpt. and drag effect 79—91478
  - many-valley semiconductors, donor impurity levels and excitons, shallow-deep instabilities 80—75520
  - metal, dynamic screening of core hole, semiclassical model 79—69445
  - minority carrier traps, detection using transient spectroscopy 79—65402
  - minority deep level investig. by new optical method 78—6331
  - MIS interface states and deep level impurities, DLTS, charge storage and charge release modes 80—49923
  - MIS structure, accidental deep centre investigation using capacitance method 80—39677
  - MIS structure, determ. of parameters in surface layer of semiconductor, admittance method 80—15612
  - MIS structure, interface states, deep level transient spectroscopy 79—78183
  - MOS capacitor, Au-doped, bulk and interfacial prop. determ. using quasiequilibrium and linear voltage ramp techniques 79—95501
  - MOS capacitor, interface state parameter determ. by DLTS 80—65642
  - MOS diodes interface trap states obs., due to electron beam lithography using DLTS *(Japanese)* 80—54787
  - MOS interface states density, photoemission obs. using photocurrent and photocapacitance meas. 80—92990
  - MOS structure, deep levels in semicond. surface layer, pulsed C-V study method 79—7905
  - MOS structure implanted with B ions, radiation defects and impurity activation 80—103757
  - MOS structures, ion implanted, spatial position of deep levels near Si-SiO_2 interface 77—12008
  - MOS surface states, DLTS spectra synthesis and anal. 80—11090
  - Multiphonon effects in the theory of electron tunelling between deep impurity levels and the conduction band in strong electric fields 78—2447
  - naphthalene, deep exponential distrib. of traps, long-time decay of surface pot. 79—47041
  - naphthalene, pure and doped, exciton-phonon luminesc. 80—84773
  - naphthalene, space charge transport 80—20209
  - nonradiative multiphonon carrier-capture cross-section, temp. depend. approx. 78—43415
  - ODMR, review *(French)* 80—60461
  - p^+-π-n^+ structure with low cond. region, double injection, IU characts. of single-level semicond. 79—56296
  - p^+-n diode under forward bias, effects of radiation-induced deep levels on admittance 78—23157
  - p-n junction, conc. profile of singly charged deep impurity, capacitance meas. 78—26945
  - p-n junction, diffused, conc. profile of deep-level impurity by capacitance method 77—55299
  - p-n junction, effect of overcharging of impurity ions on movement *(Russian)* 80—11079
  - p-n-n^+ structures containing deep traps, double injection currents 80—15592
  - Peierls-Frohlich state, electron excitation *(Russian)* 79—23909
  - perovskite oxides, single cryst., photocond. and TSC meas. 78—43436
  - photo-deep level transient spectroscopy, capacitance transient spectra with lock-in method *(German)* 79—65512
  - photoionisation, cross section calcs. allowing for Coulomb interaction between charged states 77—15793
  - poly(n-vinylcarbazole)-trinitrofluorenone films, charge carrier trapping 78—14846
  - poly-N-vinyl carbazole, trap-free lifetime, neutral traps, hopping systems 80—65566
  - polyacetylene films, AsF_5 doped, photocond. and junction props. 80—70770
  - polyethylene, elec. cond. of high and low density samples, oxidation effects 80—107784
  - polyethylene, high density, carrier transport 79—33288
  - polyethylene, high density corona charged, TSC, oxidation effect 78—26882
  - polyethylene, low density, γ-irrad., unixial elongation effect on elec. cond. 80—25812
  - radiationless Auger-recombination of electrons on three centres *(Russian)* 79—78114
  - radiative and nonradiative recomb. at metal ions, core struct. effects, review 79—4834
  - sapphire, Czochralski-grown, excess charge carriers, generation, transport and trapping 79—82646
  - Schottky diodes with deep acceptor impurities, inverse square capacitance curve, theory 80—2468
  - Schottky-barrier diodes, resonant tunnelling spectroscopy, deep centre detection 80—96968
  - semiconductor, acceptor binding energies 77—69270
  - semiconductor, acoustic studies progress *(Japanese)* 80—49310
  - semiconductor, Auger recombination cross sections associated with deep centres 78—47810
  - semiconductor, book contrib. 78—10403
  - semiconductor, capture probabilities of two deep impurity levels by photocond. decay 80—49799
  - semiconductor, compensated, influence of carrier heating on exclusion 77—8110
  - semiconductor, continuous energy spectrum, isothermal capacitance relaxation method 80—107741
  - semiconductor, deep bound states, temp. depend. of ionisation energies 77—31975
  - semiconductor, deep centres, nonradiative de-excitation 79—38644
  - semiconductor, deep impurities, exptl. techniques *(Japanese)* 80—15476
  - semiconductor, deep impurities, photoionisation 78—39061
  - semiconductor, deep impurity centre photoionisation cross-section, freq. depend. 77—55494
  - semiconductor, deep impurity centres, elastic light scattering 80—97315
  - semiconductor, deep impurity centres, two-electron model 79—65411
  - semiconductor, deep impurity state characterisation 80—6776
  - semiconductor, deep level parameters, TSC meas., rel. to photocurrent techniques 78—72249
  - semiconductor, deep level profile anal. by double deep level transient spectroscopy 77—20378
  - semiconductor, deep levels, review 80—103640

- **deep levels** continued
  - semiconductor, deep trap activation energy, effect of non-exponential transients, DLTs method 80—20115
  - semiconductor, deep-level centre discrimination from capacitance versus time transients 78—10395
  - semiconductor, deep-level impurities, insulating props. 78—39124
  - semiconductor, diamagnetism of deep impurities 79—23931
  - semiconductor, electronic struct. of deep levels, LCAO, SCF method 79—82555
  - semiconductor, excited state energies calc. 78—18997
  - semiconductor, Faraday rotation in presence of attractive traps 78—76081
  - semiconductor, Faraday rotation in the presence of deep repulsive traps 80—29724
  - semiconductor, impurity levels of transition metal ions in cryst. field 78—23059
  - semiconductor, impurity-level assisted two-photon interband absorption of laser radiation 78—23464
  - semiconductor, intense light absorption by deep impurity electrons 77—69871
  - semiconductor, ionisation energy of deep centres from absorpt. spectra, electron-phonon coupling 77—4663
  - semiconductor, ionisation of deep impurity centres by elec. field 77—8053
  - semiconductor, laser monopulse energy meas., time-resolved spectroscopic method *(Russian)* 79—94272
  - semiconductor, multiphonon recombination processes 79—38643
  - semiconductor, multiphonon thermal field ionisation *(Russian)* 78—14690
  - semiconductor, multiple-charge impurity states of transition and noble metal ions 79—33259
  - semiconductor, nonlinear light absorption, influence of transition via deep impurity centres 77—63446
  - semiconductor, overcompensated, p$^+$-n diode, capacitance method determ. of activation energy of deep centres 79—11215
  - semiconductor, photoelectric fatigue 78—10513
  - semiconductor, photoionisation of deep impurity centres, drag of electrons 78—51938
  - semiconductor, photoionisation of deep impurity centres in quantising mag. field 78—6330
  - semiconductor, photoionisation of deep impurity levels 80—34386
  - semiconductor, photoluminescence, deep level recombination temp. depend. 79—47497
  - semiconductor, recombination at deep traps, review 79—38100
  - semiconductor, remanent deep impurities, capacitative spectrosc. 79—82628
  - semiconductor, space charge region thickness, deep level props., determ. by γ-ray absorpt. 80—59995
  - semiconductor, spin relax. of deep impurity centres, exchange scatt. 77—43870
  - semiconductor, STEM spectroscopic techniques for simultaneous electronic and defect obs. 80—100145
  - semiconductor, strong electron-lattice interaction, review *(Japanese)* 80—49664
  - semiconductor, transient and alternating currents, influence of deep traps 79—73525
  - semiconductor, wave functions and optical cross sections associated with deep centres 78—34801
  - semiconductor deep transition metal impurity states, SCF CNDO cluster calcs. 80—100442
  - semiconductor devices, remanent deep impurities, capacitative spectrosc. 79—82628
  - semiconductor diode, with deep impurity levels, diffusion effect on negative resist. 78—56217
  - semiconductor diode, with overcompensated semicond., deep centres, isothermal relax. of current 78—52072
  - semiconductor diodes with large leakage currents, DLTS 80—34504
  - semiconductor impurities, photoionisation cross section calcs. 78—2450
  - semiconductor junction barrier depletion region, capture from free-carrier tails 80—70802
  - semiconductor junctions, electric field effect on thermal emission of traps 80—11073
  - semiconductor laser crystals, defect-forming resonance electron capture, theory 80—14341
  - semiconductor lasers, triggerable, light-coupled logic appl. 80—74360
  - semiconductor materials, shallow and deep level evaluation using Schottky contacts, conc. and distrib. 80—49669
  - semiconductor materials and devices, high power, detection of deep levels 79—28318
  - semiconductor wafers, deep level detect. using variable temp. apparatus 79—88951
  - semiconductor with deep traps, injection filament 77—76837
  - semiconductor with highly anisotropic bands, photoionisation cross section of deep impurity centres 78—56510
  - semiconductors, covalent, substitutional deep traps, theory 80—54651
  - semiconductors, deep defects, contrib. to binding energy 80—70634
  - semiconductors, deep impurity centres, photon drag effect in interband optical transitions 80—16069
  - semiconductors, deep level carrier trapping and emission, transient spectroscopy, book contribution 80—80216
  - semiconductors, deep level impurity photoionisation cross-section 80—65485
  - semiconductors, deep levels, self consistent LCAO MO calcs. 80—29353
  - semiconductors, defect-density profiles, constant-capacitance DLTS meas. 79—95361
  - semiconductors, electron scattering by deep level impurities 80—10968
  - semiconductors, evanescent states and complex bound structure 80—34387
  - semiconductors, II-VI and III-VI types, competition between two-photon absorption and two-stage absorption via deep traps 80—29764
  - semiconductors, impact ionisation, Auger recombination involving traps 80—80912
  - semiconductors, impact ionisation of deep impurity centres 79—73470
  - semiconductors, impurities and other point defects, electronic struct., review 79—7803
  - semiconductors, impurity electro- and magnetoabsorpt. coeffs., deep levels 79—24340
  - semiconductors, impurity photoionisation, quantum-defect, billiard-ball model comparison 80—65486
  - semiconductors, isothermal and non-isothermal C-V deep level meas. using Schottky contacts 80—88515

- **deep levels** continued
  - semiconductors, magnetic, static magnetic properties, mean field approach 80—7090
  - semiconductors, multiphonon capture rate 79—38022
  - semiconductors, nonradiative multiphonon carrier-capture cross section of deep traps, low temp. depend. 78—10469
  - semiconductors, optical transitions between deep impurity centre levels 79—61410
  - semiconductors, photoionisation cross-sections and phonon coupling 79—51518
  - semiconductors, recombination, conference, Southampton, England (Aug.-Sept. 1978) 79—38087
  - semiconductors, recombination processes, review 79—38088
  - semiconductors, recombination wave modes in case of several trap levels 80—39602
  - semiconductors, transient capacitance instrumentation for deep level impurities spectrometry 77—51816
  - semiconductors, zincblende struct., deep levels associated with 60° dislocations *(French)* 80—29352
  - semiconductors materials testing deep-level transient spectroscopy appl., using HP-IB instruments and desk-top computer 80—37091
  - semiconductors with deep impurities, double injection currents 77—55543
  - spectroscopic techniques, anal. with STEM for electronic anal. and obs. of defects in semiconductors 79—14812
  - $SrTiO_3$ (100) surface electronic structure, DV-Xα cluster method 80—39646
  - sucrose, single cryst., absorption spectrum of electron traps, pulse radiolysis obs. 80—93369
  - TCNQ solt, $CS_2(TCNQ)_3$, cond. and thermopower meas., deep level acceptor model 79—42529
  - transient spectroscopy, system effects and data anal. 79—99501
  - transient spectroscopy expts., high resolution anal. of exponentially decaying transients 80—10906
  - n-Si, deep levels in p-n junctions or Schottky barriers determ., hybrid method 79—24067
  - Ag_3AsS_3, proustite, nonequilibrium carrier exam. 77—15912
  - AgCl, luminescence, theory and measurement 79—19934
  - AgCl, luminescence fatigue, adsorbed Ag atoms 80—66281
  - $AgGaS_2$, deep level obs. by TSC meas. 80—65590
  - (Al,Ga)As double-heterostructure lasers degraded, deep-level changes during accelerated ageing at high temps. 80—74356
  - AlGaAs semiconductor lasers, single-mode stabilisation by traps 80—95893
  - AlGaAs-GaAs proton irradiated solar cells, deep-level defects, recombination mechanisms, performance characts. 80—81459
  - AlGaAs-GaAs proton irradiated solar cells, deep level defects and recombination parameters 80—94032
  - $Al_xGa_{1-x}As$ DH lasers, deep-level luminesc. 79—65913
  - $Al_xGa_{1-x}As$, DX photocond. centres, photocapacitance and DLTS meas. 80—11044
  - $Al_xGa_{1-x}As$, dependence of energy spectrum of levels introduced by electron irrad. on composition 79—60766
  - $Al_xGa_{1-x}As$, LPE layer, deep levels, photocapacitance obs. 77—15790
  - $Al_xGa_{1-x}As$, point defects, recomb. enhanced interactions with dislocation networks 79—60398
  - $Al_xGa_{1-x}As$:Cr, deep level props. 79—69465
  - $Al_xGa_{1-x}As$:O-n-GaAs heterojunction for MIS device, capacitance voltage meas. 79—87157
  - $Al_xGa_{1-x}Sb$-Pd contacts, band gap depend. of barrier height 80—65685
  - AlN:O, deep impurity states, orbital spectra, CNDO/2 calcs. 78—6319
  - AlN:O, energy spectrum of deep impurity 79—83035
  - As chalcogenides, deep levels, photoluminesc. and photocond. 80—70641
  - As_2Se_3, amorphous, hole emission defect states 80—49759
  - As_2Se_3:Al, glassy, energy spectrum of deep localized states, thermal dielectric relaxation 78—15088
  - $B_{14}Si$ elec. props., medium range disorder model 80—15522
  - $Bi_{12}GeO_{20}$, photoelectret state 80—11315
  - $CaCO_3$, calcite, X-ray irrad., luminesc. and dielec. loss decays 77—12431
  - CdF_2:In, evidence for strong impurity-lattice coupling 80—6775
  - CdF_2:In, shallow versus deep donors 77—85176
  - $CdGeAs_2$, elec. and optical props., acceptor levels and energy gap determ. 77—85218
  - $CdGeAs_2$, optical and elec. props. 79—19590
  - $CdIn_2S_4$, impurity centres, photoluminesc. and photocapacitance data on config.-coordinate diagrams 78—10938
  - CdS, deep level electron trap characts. 79—78036
  - CdS, deep level IR luminescence, origin 80—20704
  - CdS, deep level transient spectroscopy *(French)* 79—11079
  - CdS, electron traps, DLTS meas. 80—24949
  - CdS, hole-capture coeff. of deep charged centres, temp. depend., photocurrent meas. 79—7804
  - n-CdS, photocond. film, phase memory effect and deep levels 79—82556
  - CdS single crystals, Roentgenoluminescence, exciton interactions *(Russian)* 80—2853
  - CdS, up-conversion and optical storage, spatially modulated band struct. 78—64397
  - CdS:Cu, two-photon absorpt., impurity effects 77—16353
  - CdS:Cu film, dynamic quenching of photocapacitance, deep levels obs. 77—85175
  - CdS:Cu films IR quenching of photocapacitance, deep level detection 79—56258
  - CdS:Cu(In), two-photon and two-step absorption of light 80—7389
  - CdS:Li, anisotropy of the absorption by impurity centers in hexagonal crystals 78—88343
  - CdS:Li, pure and doped, green edge luminesc., complex nature of centres 80—60671
  - CdS_xSe_{1-x}, electron traps, DLTS meas. 80—24949
  - CdS(Se)(Te):Co^{2+}, IR luminesc. quenching, Co^{2+} level position, ionisation energy 80—16079
  - CdSe, deep dislocation levels, TSC and luminesc. obs. 77—8050
  - CdSe, optically pumped, dynamic polarisation of nucl. moments 78—68411
  - CdSe, photoionization cross-section temp. depend., deep local levels 79—65408
  - $CdSnP_2$:Cu, deep centres, emission transitions, polarisation *(Russian)* 78—84650
  - CdTe and CdTe:Cl, semi-insulating, electroabsorpt. by impurities and defects, dichroism 77—40270
  - n-CdTe layers, growth and characterisation, heterojunctions and Schottky barriers fabrication *(German)* 80—89151
  - CdTe, n- and p-type, elec. and galvanomag. props. 79—7830

deep levels continued

- CdTe, Schottky diode, capacitance behaviour in terms of deep level model 79—7899
- p-CdTe:Cl, deep level characterisation, gamma-ray detector parameters 77—39802
- CdTe:Cl, semi-insulating, Hall effect and cond. meas., carrier mobility 77—39849
- CdTe:Mn, photoionisation absorption spectrum 78—23502
- $CdTe_{1-x}Se_x$, multiband model of impurity complexes 80—65497
- $Cs_2UO_2Cl_4$, low-lying excited electronic levels, fluoresc. decay meas. 79—47491
- $CuGaS_2$, single cryst., photocond. spectra 78—84252
- Cu_2S-CdS heterojunctions, electron trap characterisation by capacitance transient meas. 79—78163
- Cu_2S-CdS heterojunctions, role of deep levels in controlling photovoltaic props. 80—92941
- Fe:Y, ion implanted, deep D traps due to Y-vacancy complex 80—103372
- Fe_xO_y thermal oxide film on Fe, capacitance, temp. and freq. depend., in aq. electrolyte soln. 80—54776
- GaAlAs DH laser diode, deep level associated with slow degradation 78—87050
- n-GaAlAs:Sn LED DH donor-level analysis, DLTS obs. 79—47040
- $Ga_{1-x}Al_xAs$, deep level-dislocation interactions, DLTS meas. 80—29357
- $Ga_{1-x}Al_xAs$, deep levels, pressure effects 80—49651
- $Ga_{1-x}Al_xAs$, epitaxial, radiative deep states 80—76061
- $Ga_{1-x}Al_xAs$, non-shallow levels and cond. band struct. from Hall carrier conc. meas. 80—39607
- $Ga_{1-x}Al_xAs$, photoluminescence, deep level trap emission capture 80—29805
- $Ga_{1-x}Al_xAs$, point defects and dislocation climb, interaction with deep level donor 79—82209
- $Ga_{1-x}Al_xAs$ structures, STEM and scanning deep level transient spectroscopy in defect centre anal, cathodoluminesc. techniques 80—103642
- $Ga_{1-x}Al_xAs$:Sn, layer Schottky barrier, deep level spectroscopy 80—49666
- $Ga_{1-x}Al_xAs$-GaAs solar cell, deep level obs. 77—89834
- $Ga_xAl_{1-x}As$:Cu epitaxial layers, spatial distrib. of nonradiative defects, STEM imaging spectroscopic technique 77—89438
- GaAs anodic MIS system, dynamic props. of interface state bands 80—49933
- GaAs, Auger de-excitation of metastable state 79—65410
- GaAs, boat-grown, deep levels *(Japanese)* 79—47043
- GaAs, compensated, photoabsorption, expt. 78—19521
- n-GaAs, conversion to p-type after 1 MeV electron irrad. 79—77636
- GaAs, deep centre free energy level determ. by transient capacitance technique 80—103641
- GaAs, deep centres, collective thermal emission of electrons 80—10918
- GaAs, deep centres, electron and hole capture cross sections 79—99510
- GaAs, deep impurity levels, activation energy 80—107742
- GaAs, deep level, strongly anisotropic field ionisation 79—28317
- GaAs, deep level impurities *(Japanese)* 77—89723
- GaAs, deep level photoionisation, absorpt. by derivative surface photovoltage spectroscopy 79—99575
- GaAs, deep level profile anal., double correlation technique 77—80830
- GaAs, deep level trap emission identification by indirect conduction minima technique 78—84163
- n-GaAs, deep level traps, transient and thermally stimulated capacitance meas. *(Chinese)* 79—91072
- GaAs, deep levels, optical and thermal spectroscopy, lattice relaxation *(French)* 80—66248
- GaAs, deep levels, photocapacitance meas. under hydrostatic press. 77—85259
- GaAs, deep levels investigation 77—76769
- GaAs, deep radiation centres from heat treatment, γ-irrad., deform., probability of nonradiative electronic transitions 80—50408
- GaAs, deep trap characts. by photocapacitance spectroscopy 78—6398
- GaAs, deep trap study by free exciton refl. spectra 79—60761
- GaAs, deep trapped impurities, photocond. spectra, interpretation 78—52030
- GaAs, deep traps exam. by capacitive method 77—11869
- n-GaAs, deform. produced deep levels, DLTS meas. 80—54634
- GaAs, effects of ion implantation, deep-level transient spectroscopy techniques 80—2046
- GaAs, electrical and optical props. at low temps. 80—39636
- GaAs, electron capture by multiphenon emission at B centre 80—24830
- GaAs, electron trap at E_c-0.75 eV, direct evidence for nonassignment to O 79—90988
- GaAs, electron-irrad., deep-level defect anal. using 2γ positron annihilation and IR absorption spectra 80—16120
- GaAs epitaxial film, deep centre reson. charging, photocapacitance meas. on Schottky barrier 78—26908
- GaAs epitaxial films, deep levels, impurity photocond. 80—20247
- n-GaAs, epitaxial layers, electrical parameter determ. by graphical method *(Russian)* 77—15975
- GaAs, epitaxial layers, elec. characterisation 78—91791
- GaAs, epitaxial layers, grain boundaries, deep level transient spectroscopy study 80—49234
- GaAs, epitaxial multilayer, electron irrad. defect study by transient capacitance 79—99241
- GaAs, epitaxy by metallorganic and chloride depositions, defect characterisation at growth interface 80—59817
- GaAs film, vapour-grown, effect of gas-phase stoichiometry on deep levels 78—10393
- GaAs, grain boundaries investigation using DLTS techniques, photovoltaic material appls. 80—92539
- GaAs grown by VPE using organometallic method, deep trap levels 80—10923
- GaAs, ideal vacancy, electronic struct., tight-binding calc. 79—4529
- GaAs, impurity centres ionis. by Auger electrons, carrier relax. *(Russian)* 79—51594
- GaAs, LPE, deep levels rel. to growth conditions 79—28314
- n-GaAs, LPE, deep trapping centre characterisation by Hall and photo-Hall meas. 80—88578
- GaAs, LPE, residual impurities and deep levels, FET fabrication 79—28964
- GaAs, LPE layer, deep levels, photocapacitance obs. 77—15790
- GaAs, LPE layers, ambient O_2 effect on defects and elec. props. 77—76683
- GaAs LPE layers, deep levels by photocapacitance and related techniques 78—6334

deep levels continued

- GaAs, laser irradiation effects, capacitance spectra 79—99987
- n-GaAs layer, VPE, influence of growth conditions on incorporation of deep levels 77—4310
- n-GaAs, low energy photolum., 77K, deep centre obs. 77—69877
- GaAs, luminesc. emitted by deep centres, illumination-induced change in internal quantum efficiency 79—91495
- GaAs, luminescence due to deep centres, annealing effect on quantum efficiency 77—55825
- n-GaAs, luminescence emitted from deep centres, γ-irrad. induced changes in internal quantum efficiency 80—20701
- GaAs, luminescence emitted from deep centres, plastic deform. effect on internal quantum efficiency 80—60672
- n-GaAs, MBE, correl. between electron traps and growth processes 80—65387
- GaAs MBE growth, deep levels effect on electron and hole trap densities 80—49652
- GaAs MESFET, deep trapping effects at GaAs-GaAs:Cr interface 78—72245
- GaAs MESFET struct., high-resolution deep level meas., photo-FET method 80—44531
- GaAs MOS diodes, interface states, deep-level transient spectroscopy 80—44727
- GaAs MOS system, surface and interface exam. by derivative surface spectroscopy 79—82674
- GaAs microcharacterisation for device appls. 80—10922
- GaAs, nonlinear light absorption, effect of deep impurity levels 77—77259
- GaAs, nonradiative capture and recomb. by multiphonon emission 77—43533
- GaAs, nonradiative multiphnon carrier-capture cross sections of deep traps, intermediate-temp. depend. 78—43414
- GaAs, optical cross sections associated with deep levels, O centre obs. 80—6777
- GaAs, organometallic VPE, with varying As/Ga ratios, deep states 80—65480
- GaAs, phonon assisted tunnel emission of electrons from deep levels 80—25532
- GaAs, photoionisation of impurities with deep levels 80—65484
- GaAs, photoluminescence, deep level trap emission capture 80—29805
- GaAs, proton irradiated, low energy, deep level defects and hole diffusion length meas. 80—60000
- GaAs, self-compensation due to shallow and deep levels 80—24837
- GaAs, semi-insulating, undoped and Cr-doped, compensation mechanisms, Hall effect and optical absorpt. meas. 80—84477
- GaAs solar cells, electron and proton radiation damage 80—94034
- n-GaAs surface barrier diodes for nuclear radiation detection, deep trapping centres 80—92849
- GaAs, transition element impurities, electron struct. of deep centres 78—39060
- GaAs, trapping levels obs. using deep level transient spectroscopy, laser irrad. effects 79—99499
- GaAs, VPE, hole diffusion lengths, effect of transition metal diffusional doping 80—15628
- GaAs, VPE, incorporation of deep levels, effects of growth conditions 80—20111
- GaAs, VPE film growth in Ga-$AlCl_3$-H_2 system, O_2 injection effect 79—100057
- GaAs VPE layers, elec. props., semi-insulating substrates effect 80—11123
- GaAs, VPE layers, growth conditions effect on deep levels 79—95360
- GaAs:0, effect of displacement upon impurity levels, psuedopotential calc. 77—39803
- GaAs:B, deep levels, optically stimulated transient current method *(French)* 80—59919
- GaAs:Be, deep levels 80—29358
- GaAs:Be(C)(Ge)(Sn), MBE layers, photoluminesc. 80—29803
- GaAs:Cr, current voltage characterisation, deep levels and Fermi level determ. 79—7823
- GaAs:Cr, deep acceptor level, DLTS and optical DLTS study 80—92852
- GaAs:Cr, deep levels, wavelength-modulated photocapacitance spectroscopy 80—76055
- GaAs:Cr, luminescence and absorption spectra, temp. depend. of fine structure 80—6779
- GaAs:Cr, semi-insulating, i.r. induced modulation of cathodoluminescence, and specimen current 77—1737
- GaAs:Cr, semi-insulating elec. compensation, Hall and resist. meas. 77—62855
- GaAs:Cr, semi-insulating, deep impurity level anal. 78—6332
- GaAs:Cr, semi-insulating, I-V characts. and photocond. spectra dependencies on Fermi level 79—99576
- GaAs:Cr, semiinsulating, I-V characts., photocond., Fermi level, and deep levels 78—39118
- GaAs:Cr, Si, deep centre photoluminescence spectra 78—95601
- GaAs:Cr, thermally grown, DLTS study of Cr trap density 80—96815
- GaAs:Cr diffusion profile meas. 80—6554
- GaAs:Cr photoconductivity, large scale fluctuations of impurity electostatic potential 77—8145
- GaAs:Cr^{2+}, dynamic Jahn-Teller effect, relaxation time for reorientation 80—6798
- GaAs:Cr(O), AC photocond. meas. 78—19082
- GaAs:Cr(O), mechanism of thermal quenching of luminesc. and photocurrent stimulation 77—55821
- GaAs:Cr(O), photocapacitance of deep levels obs. 79—38021
- n-GaAs:Cr(Si), deep-level extrinsic photocond. response, decay at 4.2K 80—2420
- GaAs:Cr(W), deep trapping centre exam. by thermally stimulated capacitor discharge method and luminesc. 77—55495
- n-GaAs:Cu, contaminated single cryst., deep level photoluminesc. model 78—68554
- n-GaAs:Cu, electron-phonon interaction in optical transitions between deep impurity level and allowed bands 79—42591
- GaAs:Cu, photoionisation spectrum of deep impurities in presence of weak electron-phonon interactions 79—51529
- p-GaAs:Fe, ESR line width, temp. depend., 4.2-330K 77—12195
- GaAs:Fe, photoionisation cross section meas. of deep levels 77—8042
- GaAs:Fe LPE layers, negative resist. effects and deep acceptor model 77—72929
- GaAs:Fe p^+-n junction minority carrier trap meas. by photo-excited DLTS 80—96816
- GaAs:Fe^{3+}, energy spectrum of deep centres, ESR spectrum 77—90023

deep levels continued
GaAs:Fe(Ni) O_2 effects on opt. props. 77—16350
GaAs:Ge, ion-implanted, photoluminesc., deep emission centres 80—34965
GaAs:Mn, photoluminesc., emission props. and radiative mechanism 79—56842
n-GaAs:Ni(Zn), VPE, deep-level transient spectroscopy 80—34383
GaAs:O, deep level, Franck-Condon shift, photocond. and Hall effect study 80—70642
GaAs:O, deep traps, photocapacitance meas., complementary transition energy threshold determ. 79—19550
GaAs:O, junction barrier depletion region, capture from free-carrier tails 80—70802
GaAs:O, optical characterisation of deep O implants 77—55294
GaAs:O, photocond., electron traps, level-broadening, 90 to 150K 78—60158
n-GaAs:O, photocond. associated with deep level at 0.4 eV 80—44640
GaAs:O, semi-insulating, excitation temp. effect on TSC 80—70717
GaAs:O p-ν-n structs., injection current and negative photocond., saturation mechanism 80—92967
GaAs:O(Cr), relax. semicond., Dember effects meas. 79—28372
GaAs:S, LPE, and doping characts. 79—33948
n-GaAs:S, Zn VPE film, LF current oscill., negative photocond. 77—80858
GaAs:Se, low dose Se^+ ions implanted, DLTS study of laser annealing 80—80204
GaAs:Si, Cr, carrier concs. from Hall effect, microscopy, localised vibrational modes absorption meas. 78—56104
GaAs:Si epitaxial films, elec. and photoelec. props., impurity distrib. 80—7006
n-GaAs:Sn, photoluminesc. spectra 79—43031
GaAs:Sn(Be) MBE films, elec. characterization 79—91168
GaAs:Te, ion implanted, laser annealing 79—73192
GaAs-(GaAl)As epitaxial layers and DH lasers, deep centre 1.02 eV luminesc. 78—80387
GaAs-$Al_{0.5}Ga_{0.5}As$-Cr/Au MIS capacitors, characts. meas. 78—95371
GaAs-$Al_xGa_{1-x}As$ LPE heterojunction, interface states 78—19128
GaAs-GaAlAs DH LED, transient current trap spectroscopy 78—80049
GaAs-GaAlAs LEDs, deep levels *(French)* 78—56218
GaAs-GaP, heterojunction, electronic processes *(Russian)* 79—56312
GaAs-InSe, heterojunction, electronic processes *(Russian)* 79—56312
n-GaAs-oxide, plasma-grown, surface states, modified DLTS meas. 80—11094
GaAs-Si heterojunction, IR quenching of photocapacitance 80—92968
$GaAs_{0.6}\ P_{0.4}$, deep level profile anal., double correlation technique 77—80830
GaAs(P), transition metal deep centres, model 79—78045
$GaAs_{0.6}P_{0.4}$ LED, deep level radiative defects detection during degradation 77—76770
$GaAs_{0.6}P_{0.4}$ LED, luminesc. investig. of degradation, deep-level form. at dislocations 77—40287
$GaAs_{0.6}P_{0.4}$, VPE, hole diffusion lengths, effect of transition metal diffusional doping 80—15628
$GaAs_{0.65}P_{0.35}$, gamma irradiated DLTS and photocapacitance methods *(Japanese)* 80—49665
$GaAs_{1-x}P_x$, $0 \le x \le 1$, evidence for common nature of certain deep-level radiative centres 78—6767
$GaAs_{1-x}P_x$, bound exciton, luminesc. reson. excitation 79—95840
$GaAs_{1-x}P_x$, dependence of energy spectrum of levels introduced by electron irrad. on composition 79—60766
$GaAs_{1-x}P_x$:S, deep level, photoconductivity, carrier nonradiative recombination 80—20112
GaN:Mg, epitaxial layer, characts from cathodoluminesc. 78—35208
GaN:Zn, VPE grown, optical cross sections, photoluminesc. and optical absorpt. meas. 80—55160
GaP, deep level impurities *(Japanese)* 77—89723
GaP, deep level profiles at substrate-epitaxial interfaces, photoionisation meas. 79—38025
GaP, deep levels investigation 77—76769
GaP, deep O^- state, model impurity calc. 80—6780
n-GaP, deep state controlled minority carrier lifetime 80—20211
GaP, donor-acceptor pair luminesc., excitation spectroscopy 80—25440
GaP, electrical and optical props. at low temps. 80—39636
GaP, electron traps around dislocations in p-n junction and metal-semicond. structs. 80—34388
n-GaP, epitaxial layers, electrical parameter determ. by graphical method *(Russian)* 77—15975
GaP, IR absorpt. spectra depend. on compensating defects and thermal treatment *(Russian)* 80—71465
GaP lamps, green emitting deep level photocapacitance spectra 77—69409
GaP, nonradiative capture and recomb. by multiphonon emission 77—43533
GaP p-n junction, capacitance-freq. dispersion and electroluminescence efficiency 78—64101
GaP, positron annihilation, deep acceptor level props. 79—11485
GaP, proton implanted, thermally stimulated current meas. 80—24943
GaP, spectral depend. of O photoneutralisation cross-section near threshold, and band gap 79—1788
GaP, VPE, background deep level defects, transient capacitance obs. 77—62854
GaP:0 effect of displacement upon impurity levels, pseudopotential calc. 77—39803
GaP:Bi(N), luminesc. decay kinetics 79—38646
GaP:Co, deep levels, IR photoluminesc., stress effects 80—55163
GaP:Cr, ESR of doubly ionised Cr acceptor and IR luminesc. 78—56374
GaP:Cr_2O_3, growth, dopant distribution, elec. resist. 78—34531
GaP:Cu, deep levels, photoluminesc. and optical cross sections 79—38653
GaP:Cu, thermally and optical excited cond., deep level centres 78—72190
GaP:Cu p^+-n junction, deep level parameters, TSC meas., rel. to photocurrent techniques 78—72249
GaP:Fe, current-voltage characteristics, p-i-n diodes, luminescence, absorpt. double injection methods 79—65407
GaP:Fe, optical absorption spectrum and Faraday effect 80—108245
GaP:Fe, photo-EPR study Fe($3d^6$) centres and deep electron traps 80—44910
GaP:$Fe^{2+}(Co^{2+})(Ni^{2+})$ d→d luminesc. spectra 80—7414
GaP:Fe^{3+}, deep impurity states investig. 77—15794
GaP:N LED, deep level studies, growth by time difference method at controlled vapour pressure 80—39522

deep levels continued
GaP:N VPE LED, deep level centres, DLTS studies 79—42493
GaP:N VPE layers, thermal emission energies, trapping, and carrier lifetimes, deep level capacitance spectroscopy 79—42487
GaP:Ni, deep traps, near IR luminesc., polarised spectra meas. 80—16077
GaP:Ni, electron-hole recombination via deep state 79—99560
GaP:Ni, Hall effect and absorpt. spectrum investig. of acceptor level 77—44033
GaP:O, EPR investig. of deep donor centre, delocalisation 77—28428
GaP:O, impurity concentration determ. by donor-acceptor luminescence 78—6090
GaP:O, optical transitions via deep levels, phonon interaction 78—87939
GaP:O, optical transitions via deep levels, cross section temp. depend. 78—87940
GaP:O, photoionisation of deep impurity levels 80—34386
GaP:O, wave functions and optical cross sections associated with deep centres 78—34801
GaP:O^-, two electron state, electron capture 78—39054
GaP:O^-, two-electron O^- state evidence, ODMR, IR emission, phonon replicas 80—15828
GaP:s, elec. props. following 1.7 MeV electron irradiation 78—80005
GaP:Ti(Co)(Ni), positron annihilation meas. rel. to deep levels study 80—60712
GaP:Zn,O, red LED, deep-level changes associated with degradation 77—1472
GaSe-InSe, heterojunction, electronic processes *(Russian)* 79—56312
Gap-Ge, compensated, photosensitivity 79—19624
Ge, compensated, impurity photocond. relax times 80—88592
Ge, deep and shallow levels of muonium, electronic struct. 78—39051
Ge, deep dislocation states 80—24836
Ge, deep donor character of muons and protons 80—10911
Ge, deep impurity levels, activation energy 80—107742
p-Ge, detector-grade single crysts., impurity background 79—11088
p-Ge, dislocations, grown-in defects, electrical props., deep level transient spect., Hall effect 80—39524
Ge, electrical and optical props. at low temps. 80—39636
n-Ge, electron irradiated, energy levels 79—28316
n-Ge, electron irradiated, threshold energy for atomic displacement, carrier traps 80—29351
Ge, ideal vacancy, electronic struct., tight-binding calc. 79—4529
Ge, impurity levels of H and muons 79—56162
p-Ge, Li-compensated, carrier capture 77—15792
Ge, slow surface, states, optical excitation investigation 78—76129
Ge surface, optical charging meas., 120-300K 80—49817
n-Ge:Au, negative photocond., field and temp. depend. 77—43660
n-Ge:Au piezoresistance in presence of deep levels, stress anisotropy 80—10979
Ge:B(Al)(Ga)(In)(Tl), binding energy, excited state spectra, photolum., semi-empirical short range pot. 80—44534
Ge:Be, P, absorption of radiation, 0.6-2.8 mm, 4.2 to 20K 80—66332
Ge:Cu, low frequency oscillations 77—15872
Ge:Cu, quenched, energy levels of thermal acceptors, annealing effect 78—34798
p-Ge:Ga, dislocation density effect on carrier lifetime and deep recomb. centres 79—51598
Ge:H, interstitial impurity levels, pseudopot. calc. 80—44533
Ge:Hg, S-type diode, elec. props. 80—20299
p-Ge:Hg(Cu)(Cd)(Zn), deep levels, optical-phonon-assisted capture of carriers 79—51597
n-Ge:Ni,Sb, transient response at 4K, nonequilib. carrier recomb. 77—43659
Ge:O, intrinsic γ detector, deep level defect connection with O content *(Russian)* 78—43331
n-Ge:Sb, deep levels obs., freq. depend. of capacitance of p-n junctions 77—4315
n-Ge:Sb, fast electron irrad. at 77K, radiation defect changes by annealing at 220K 79—37737
n-Ge:Sb, high-field Hall effect spectroscopy 80—65600
Ge:Sb, Ni(Mn), recombination wave spectrum, two-level traps 80—96906
Ge:transition metal, amorphous, impurity effects on hopping conductivity 79—65485
Ge-GaAs p-n junction, microparameters determ. 79—11216
In-GaAs:Cu-In S-type diode, role of deep trapping levels in form. of current-volt. characts. 77—76948
InAs:Cr, high-resist., energy positions of deep levels, elec. and optical props. 79—7807
$InAs_{1-x}P_x$, deep levels and semicond.-semimetal transition at high press. 80—11056
InGaAsP-InP, anomalous luminesc., near heterojunction interface 79—65932
$In_{0.85}Ga_{0.15}As_{0.39}P_{0.61}$, deep impurity levels 79—87058
InP, deep level electron traps, emission and capture props. 80—29806
InP, deep level trap interaction with lowest and upper cond. minima 80—49654
InP, deep trap characts. by photocapacitance spectroscopy 78—6398
InP, deep trap study by free exciton refl. spectra 79—60761
InP, deep-level traps and cond.-band struct. 79—19542
InP, electrical and optical props. at low temps. 80—39636
n-InP grown by synthesis solute-diffusion method, electron traps 79—90987
n-InP, hole traps by deep level transient spectroscopy and transient capacitance methods 79—51514
InP:Fe, deep acceptor levels, photocond. meas. 80—20116
InP:Fe, double injection, absorpt. and luminesc. study 79—56166
InP:Fe, influence of covalence on EPR spectra 78—26827
n-InP/SiO_2 capacitors, minority carrier generation 79—95496
InP-CdS p-n heterodiodes, junction props. study by using injection electrolum. 79—82667
n-InP-SiO_2 capacitor, carrier generation and trapping 80—49929
InSb film, degenerate, concs. and ionisation energies of defect levels, Hall effect meas. 79—91087
InSb films, melt-grown, point defect effect on elec. props., 77-300K 80—2502
p-InSb, high press. effect on elec. props., 50-300K 77—47807
n-InSb, magneto-optical transitions from deep levels, photocond. obs. 80—55069
InSb, reverse biased diode, negative resist. 78—19129
n-InSb:Cr, deep impurities, elec. cond. and Hall coeff. meas., 4.2 to 120K 80—107791
InSb:Cr, press. effects on transport props. 78—56146

deep levels continued

InSb:Cr, Zn impurity centre behaviour, impurity conc. and Hall coeff. meas. 80—65490
InSb:Cr,Zn, transport props. meas. 77—1424
InSb:Cr:Zn, magnetic freeze-out electrons at deep Cr level 79—15169
InSb:Cr(Zn)(Mn)(Ge), recombination of nonequilibrium carriers 79—65496
InSb:Ge annealing effect on electrical parameters, absorption spectra and photocond. 77—11939
InSb$_{1-x}$Bi$_x$ disordered solid solns, ionisation energy of fluctuation levels 78—72116
p-InsB, high-resist. compensated, elec. breakdown peculiarities 80—2398
KBr:Li^P(Na$^+$), electronic struct. of $(V_Ke)_A$ 78—95269
LiF, thermoluminescence intensity depend. on heating rate and deep trap 78—56527
LiNbO$_3$:Fe, thermally activated trapping caused by small polaron formation 77—20259
$(Mo_xV_{1-x})_2O_5$, mag. and spectroscopic investigation 80—25206
Pb$_9$As$_4$S$_{15}$, gratonite, single crystal, photoelectric props. 80—49822
3PbO.2GeO, TSC in thermoelectret state during ceramic synthesis, pyroelec. currents and energy struct. of capture centres 80—55014
Pb$_{0.78}$Sn$_{0.22}$Te:In epitaxial layers, dislocation density, Hall effect, conductivity, photoeffects 80—25024
Pb$_{1-x}$Sn$_x$Te, narrow gap solid solns., mag. susceptibility and energy band spectrum 79—28276
Pb$_{1-x}$Sn$_x$Te:Cd, deep energy level, temp. depend. of elec. cond. 78—18994
Pb$_{1-x}$Sn$_x$Te:In, with low carrier conc., transport phenomena 80—49783
PbTe epitaxial films, carrier recomb. and deep levels, photocond., Hall effect, and luminesc. meas. 79—38024
PbTe, resonant scattering, photocond. 80—6910
S:P, ion implanted, defect annealing 450-800°C, deep-level transient spectroscopy 79—47042
p-Se photocond. film, phase memory effect and deep levels 79—82556
Se, photoconductive film, field instability, Ar$^+$ ion irrad.-induced defects 78—87997
n-Si, A-centre ionisation energy change due to uniaxial deform. 78—71733
Si, amorphous, doped, density of states determ. from transport meas. 80—49720
Si, CVD films, polycryst., elec. and optical props., electronic density of states model 79—56332
Si, carrier capture at amphoteric deep level defects 80—88569
Si, deep and shallow levels of muonium, electronic struct. 78—39051
Si, deep centres, majority carrier thermal capture cross section, TSC meas. 78—10468
Si, deep centres associated with plastic deform. and quenching *(French)* 77—28145
Si, deep dislocation states 80—24836
Si, deep donor character of muons and protons 80—10911
Si, deep impurity levels, activation energy 80—107742
Si, deep level defects, struct. bonding, amphoteric centres 80—88506
Si deep level determ. using deep depletion MOSFET test structure 78—10571
Si, deep-level point defects, effective-mass nature 80—59922
Si, dislocation-free, deep centres formed after high temp. treatment 80—96824
Si doping by thermal neutron irrad., annealing characts. of bulk electron traps obs. 80—49244
Si, electron beam scan annealed, deep levels 80—65481
Si, electron emission coeffs. for electron and hole traps 79—91075
n-Si, electron-irrad., surface defect distrib., deep-level transient spectroscopy 79—1459
Si, electronic defect levels in self-implanted CW laser annealed samples 79—87053
Si, evaporated heteroepitaxial film, deep states obs. 78—72292
Si, float zone, meas. of deep levels by photovoltage spectroscopy 80—103723
p-Si, high ohmic material, deep level investigation, vacuum growth *(Russian)* 80—54654
p-Si, high-resistivity, TSC and photo-EMF in p-n junction, deep levels 77—72913
Si, ideal vacancy, electronic struct., tight-binding calc. 79—4529
Si, impurity levels of H and muons 79—56162
Si, ion implantation, TSC meas. of coupled levels 78—84165
Si, ion implanted, laser annealed, deep levels study 79—69457
Si, ion implanted, laser annealed, elec. props. and annealing kinetics 79—69508
Si ion implanted p-n junction, cryst. damage influence on elec. props. 78—56219
Si, ion-implanted, low-fluence, primary defects, transient capacitance spectroscopy 80—44238
Si junction diode, diffused, with deep level traps, negative capacitance 80—96976
Si, laser annealed, EPR and cyclotron resonance 80—34773
Si MOS diode, bulk traps and interface states determ., deep-level transient spectroscopy appl. *(Japanese)* 79—42645
Si MOS diodes, P$^+$ implanted, DLTS of bulk traps and interface states 79—33350
Si n$^+$-p junction solar cells, electron irrad., DLTS spectra and defect effects 80—93999
Si n$^+$-p solar cells, degradation mechanisms associated with Ti impurities 80—81465
Si n$^+$p solar cells, effect of elec. bus during 1 MeV electron irrad. and isochronal annealing, elec. characts. and deep level pop. 80—94086
Si, n-type and p-type, carrier removal rate by fission-fragment irradiation 77—51418
Si, neutral undistorted vacancy 78—91638
p-Si, neutron irrad. effects, admittance meas. of n$^+$-p diode 78—51587
Si, neutron transmutation doping, annealing, deep defect levels 80—20123
Si, neutron-produced defects, deep level transient spectroscopy 79—47047
Si, nuclear spin-lattice relax. in weak mag. fields *(Russian)* 79—51879
Si, polycryst., charges at laser recrystallised poly Si/insulator interface 80—54789
n-Si, Re-compensated, deep levels, electron traps, photocond. 77—15902
Si, resistivity and deep impurity levels at 300K anal. 77—43591
Si ribbon solar cell, EFG, rel. to diffusion length enhancement under illum. 78—14756
Si, self-implanted, defect-density profiles, constant-capacitance DLTS meas. 79—95361

deep levels continued

Si single crystal ingot growth from metallurgical grade Si, inhomogeneities 80—59416
Si solar cells, effect of Ti, Cu, and Fe 80—72064
Si solar cells, POCl$_3$ gettering of Ti, Mo and Fe-contaminated cells 80—94010
Si, transition metal deep centres, model 79—78045
Si, transmutation doped, deep trap level analysis 78—10471
Si, vacancies and interstitials 80—29015
n-Si wafer, trap centres of self-interstitials 80—75516
Si, with dislocations, noise spectrum 80—107881
Si:^{57}Co/^{57}Fe, Mossbauer spectra, deep level Co impurity study 80—29666
Si:0, electrical activity due to heat treatment, Hall effect meas. 80—15543
Si:Al, electron irrad. induced defects, transient capacitance study 80—59516
Si:Al, thermally induced deep levels, TSC meas. 77—31974
Si:Au, amphoteric centre, struct. bonding of deep level defects 80—88506
Si:Au, degeneracy factor of acceptor level 78—51927
Si:Au, influence of carrier heating on exclusion 77—8110
Si:Au, method of determining content of impurities with deep levels 80—2056
Si:Au, P-induced point defects influence on Au gettering mechanism 80—65030
Si:Au, thermally stimulated capacitance method fitting anal. 79—47107
Si:Au deep level parameter determ. by isothermal capacitance transient spectroscopy 80—88507
Si:Au n$^+$p diodes, deep level transient spectroscopy, system effects and data anal. 79—99501
Si:Au p$^+$-i-n$^+$ diode, I-V characts., recomb. centre influence 78—19134
Si:Au(Pt), electron and hole capture, DLTS obs. 80—49661
Si:Au(Pt), heavily doped, gradual p$^+$-n junctions, trap levels *(French)* 80—34392
Si:B, laser damage obs. by DLTS 78—76023
Si:B(Al)(Ga)(In)(Tl), binding energy, excited state spectra, photolum., semi-empirical short range pot. 80—44534
Si:Cd(Zn), n$^+$-n-n$^+$ structure, photocond. lifetimes, deep level occupancy in exclusion region 78—72253
Si:Co, minority carrier lifetime investigation 80—80292
Si:Cr, specific resistance, activation energy of deep levels, and carrier mobility *(Russian)* 78—72146
Si:Cr^0(Mn$^{)}$, spin-lattice relax. of Jahn-Teller centres, coexistence of minima with different symmetries 80—80602
n-Si:Fe 79—28312
Si:Fe group ion, energy spectrum of deep centres, ESR spectrum 77—90023
Si:Fe(Au)(Pt)(Ag)(Ti), photoionisation cross-sections and energy levels 79—87060
Si:Ga, electron irrad.-induced defects, DLTS meas. 80—24499
Si:Ga(Zn), impurity ground states 79—28313
Si:Ge, electron irrad.-induced defects, DLTS meas. 80—24499
n-Si:H, amorphous, bulk density of deep states, DLTS meas. 80—88518
Si:H, amorphous, discharge prod., optically induced cond. changes 80—96937
Si:H, amorphous, solar cells, trap spectroscopy using transient current techniques 80—104508
a-Si:H Schottky barrier diodes, capacitance studies 80—49908
a-Si:H/Pt, Schottky diode, influence of prep. conditions on forward bias currents 79—78171
Si:In, backward wave phonon spectroscopy 80—2357
Si:In, MOSFET device structure for characterising imperfection centres 79—73595
Si:N, laser-annealed, Jahn-Teller distorted donor, EPR meas. 80—84642
Si:Ni, capture probabilities of two deep impurity levels by photocond. decay 80—49799
Si:Ni,Co,Mn, γ-irrad., interaction of deep-level impurity atoms with radiation defects 77—76457
Si:Ni deep impurity levels, electron capture probabilities rel. to temp. 78—2523
Si:Os, photocapacitance meas. of impurity levels 77—55579
Si:P, defect annealing, ionisation effects, DLTS meas. 80—24483
Si:P, neutron transmutation doped, electron trap annealing, deep level transient spectra 78—14368
Si:P, neutron transmutation doped, radiation damage exam., elec. props. 78—95080
Si:Pd, deep levels, conc., activation energies, thermal emission rate 79—51524
Si:Pt, deep level, exam. by thermally stimulated current and capacitance techniques 79—1579
Si:Pt, elec. props., deep-level transient spectroscopy and thermal emission meas. 79—82542
Si:Rh(Pd), Schottky diode, capacitance characts., donor and acceptor levels 77—43697
Si:S, deep level characterisation, implantation predeposition technique 80—100444
Si:S, existence of isotope shift for S deep level, isothermal transient capacitance meas. 78—63999
Si:S diode, ionisation energies of S levels, photocapacitance meas. 77—4432
Si:S p$^+$-n junction, optical props., photocurrent meas. 77—4425
Si:Ti, deep level impurity, Hall meas. 80—6768
Si:Tl, energy level, deep level transient spectroscopy 79—19541
Si:transition metal, amorphous, impurity effects on hopping conductivity 79—65485
Si:V p-n junctions, thermal emission rates and capture cross sections of majority carriers at V centres 80—96980
Si:Y, photoelectric props. 80—107860
Si:Zn, minority carrier lifetime investigation 80—80292
Si:Zn, P$^+$-n-n$^+$ struct., deep doubly ionized centres, impedance calc. 79—11202
Si:Zn, photoionisation of deep impurity levels 80—34386
p-Si:Zn$^-$, deep levels, optical-phonon-assisted capture of carriers 79—51597
Si-SiO$_2$, intentionally contaminated interface, transient capacitance meas. 79—33349
Si-SiO$_2$, interface defect states obs. by constant capacitance DLTS 80—49924
Si-SiO$_2$, MOS interface states density, meas. techniques and model development 80—92988

deep levels continued
- $Si-SiO_2$ interface in MIS struct., B^+ ion implanted, elec. props. due to laser irrad. 78−72272
- $Si-SiO_2$ interface in MOS structs. low-energy electron beam irrad., charge accumulation process anal. 80−65701
- $Si-SiO_2$ MOS interface, surface-state density and minority carrier generation rate, meas. by DLTS, hot hole effect 80−100527
- $Si-SiO_2$ MOS interface states density, transient capacitance meas. eval. 80−92989
- Si(:Au), gamma-induced trapping levels 79−87059
- α-SiC, afterglow stimulated by IR radiation *(Russian)* 80−89066
- α-SiC, deep centre levels, IR photoluminescence 77−16387
- α-SiC(6H), two stage transitions, nonlinear absorpt., thermoluminesc. method 80−7425
- $Si_{1-x}H_x$, amorphous, gap states, DLTS 80−49656
- SiO_2, noncryst., MOS structure, ionic impurities motion, trapping layers 78−30999
- Si;O, effect of displacement upon impurity levels, pseudopotential calc. 77−39803
- $TlGaSe_2$, impurity conductivity and TSC 78−23128
- $Zn_{0.1}Cd_{0.9}S$, two-photon and two-step absorption of light 80−7389
- $Zn_{0.1}Cd_{0.9}S$:Cu, doping effect on two-photon absorpt. spectra, deep levels 77−69870
- p-$ZnGeP_2$, photoluminescence of crystals with varying comp. and dopants 77−32431
- ZnO, single crysts., photocond. lifetimes, Zn^+ hole traps 80−75581
- ZnP_2:In(Ga)(Ge)(S)(Se), doped and undoped, optical absorpt. spectra in range 0.5 to 2.2 eV 80−66250
- ZnS, green-blue luminesc. characts., model of luminesc. centres 79−73999
- ZnS, self-activated, trap distrib. and photoelectronic effect due to UV, IR and visible excitation 77−36282
- ZnS:Ag film, evaporated, IR quenching of photocapacitance, deep levels obs. 78−56180
- ZnS:Ag film, photocapacitance IR quenching, hole photoionisation energy and spectral distrib. 79−87127
- ZnS:Cl, single cryst., deep centre study by impurity electroabsorpt., photocond. meas. 77−12411
- ZnS:Cr^{2+}, photoionisation, lattice relaxation energy 80−6778
- ZnS:Ga(Cl), deep traps, impurity electroabsorpt. and photocond. meas. 78−6707
- ZnS:In, polarisation of deep centre electroabsorpt., effect of random electric fields 77−48148
- ZnS:Mn, electroluminescent film, stimulated emission *(Russian)* 77−19255
- ZnSSe:Cu, Br, SCL currents and electrolum. via rad. recomb. 77−44065
- ZnS_xSe_{1-x}, electron trap associated with anion vacancy, DLTS study 80−80210
- ZnS(Se)(Te):Co^{2+}, IR luminesc. quenching, Co^{2+} level position, ionisation energy 80−16079
- ZnSe, band-edge photoluminesc., far-below band-gap excitation 80−76063
- ZnSe, deep centres, photolum., photocapacitance and photocurrent expts. 78−39053
- ZnSe, donor-acceptor pair emissions characts. *(French)* 80−108249
- ZnSe, electron trap associated with anion vacancy, DLTS study 80−80210
- ZnSe, impurity effects on two-photon absorpt. spectrum 77−59597
- ZnSe, two-photon and two-step absorption of light 80−7389
- ZnSe:Cr^{2+}, photoionisation, lattice relaxation energy 80−6778
- ZnSe:Cu, deep energy levels 80−6774
- ZnSe:I/aqueous electrolyte junction, electrochem. behaviour in dark and under illum. 80−25003
- ZnSe:Mn^{2+} Schottky barrier diodes, spin depend. cond. and photovoltage, donor reson. deep centre studies 79−91141
- ZnSe:Ni, photocapacitance meas. of impurity level 77−69372
- ZnSe-Si heterojunctions, IR quenching of photocapacitance 80−92968
- n-$ZnSiP_2$, deep impurity levels, Schottky TSC meas. 79−95419
- p-$ZnSiP_2$, single cryst., recomb. processes, photoelec. props. *(Russian)* 78−68053
- ZnTe, edge luminesc. excited by electron bombard. 80−66308
- ZnTe, elec. field and impurity conc. effects on ionisation energy of impurities, appl. to acceptors 80−88514
- ZnTe single crystal electrodes, non-intentionally doped, electrochem. props. *(French)* 79−96326
- ZnTe:O, deep centres, photocapacitance detection 79−95362

defect electron energy states
- *see also colour centres; deep levels*
- acceptor-donor-acceptor complex, Frenkel excitons and ionic excited states 80−92824
- actinide carbides, lattice defects and rel. to phys. props., review 77−27874
- alkali halide, excitonic mechanism of defect form. 77−47737
- alkali halide, molecular model for F_A(II)-centre emission process 77−28616
- alkali halide, with oppositely charged defect centres, autoionisation-tunnel relax. of electron excitation 78−72112
- alkali halide crystals, deformation spectroscopy, dislocation interactions with electron and hole centres 78−10983
- alkali halides, intrinsic point defects, generalised Mott-Littleton approach 77−51698
- alkali halides, thermally stimulated depolarisation of NCO^- centres 80−80678
- alkali halides, U_2 centres, cluster-Bethe lattice calc. for electronic density of states 79−4531
- alkali halides, U-centre electronic struct. cluster-Bethe lattice calc. 80−107737
- alkali metal chloride crystal, F centre energy level shift and splitting in O^- field 80−70640
- amorphous, defect controlled electronic props. 80−49658
- amorphous group V semiconductors 79−87057
- amorphous semiconductor, cooperative charge disproportionations 80−54649
- amorphous semiconductor, defect chemistry and states in gap, models 79−38030
- amorphous semiconductor, tetrahedrally bonded, gap density of states 79−19545
- amorphous semiconductor, tetrahedrally coordinated, pnictide and chalcogenide, defect energies 80−54647

defect electron energy states continued
- amorphous semiconductor film, ion bombardment effect on electronic props. 79−65125
- amorphous semiconductors, group V, trends in defect controlled electronic props. 80−49658
- anthracene, monocryst., additional absorpt. spectrum at low temp. 78−92096
- anthracene, triplet exciton trapping by dislocations 78−30871
- BCC transition metals, screw dislocations, electronic theory, Peierls stress, core energy calc. 78−71737
- bound state induced scattering reson. at dislocations 78−76019
- burst noise, physical sources 79−24033
- capacitance transient spectroscopy, book contrib. 78−10548
- carrier densities, elec. cond. and Fermi level in defect semiconds. and insulators 77−43532
- chalcogenide glass, AC conduction, theory 78−23077
- chalcogenide glass, charged defect states, model 80−24847
- chalcogenide glass, charged defects, influence of ionicity 79−87063
- chalcogenide glass, mech. for electron-hole recomb. 78−72196
- chalcogenide glass-like semiconductors, defect model, neutral diamagnetic quasimolecules, excess orbital bonds *(Russian)* 80−70647
- chalcogenide glasses, defect pairing and effect on AC cond. 80−49725
- chalcogenide glasses, defect states 78−39066
- chalcogenide glasses, ionicity depend. of defect reactions and negative-U states 80−88511
- chalcogenide semiconductor, density of valence-alternation centres, influence of additives 78−47733
- charged defects, Holtsmark elec. field sitribs. and assoc. broadening effects 79−1584
- copper phthalocyanine, imperfect cryst. and film, elec. transport phenomena, trap. distrib. 77−1421
- covalent crystals., defect states, many-electron approach 78−67980
- covalent semiconductors, electronic interface states in intrinsic stacking-faults 80−75522
- covalent semiconductors, electronic struct. of localised defects, review 80−44535
- covalent semiconductors, vacancy screening, dielec. const., exchange correl. pot., Thomas-Fermi description 80−44528
- cubic crystals, Raman scatt. from tunnelling of substitutional molecules 80−40107
- D -centre electronic struct. in strong mag. field 78−51928
- D -state in semiconductors *(Japanese)* 77−85178
- degenerate semiconductors, heavy hole-phonon bound states for valence band with degeneracy point *(Russian)* 80−15461
- diamond, B doped, electron irradiated, defects at low temps., elec. resist. meas. 77−11593
- diamond, electron irradiated, photocurrent and Hall current, 290 and 4.2K 79−87129
- diamond, GR1 and UV band, fine struct. 80−20678
- diamond, Jahn-Teller coupling at ND1 and GR1 centres 78−56103
- diamond, low lying levels of GR 1 centre, satellite line struct. 77−20269
- diamond, natural, cathodoluminescence of defects *(French)* 80−34988
- diamond, natural, dislocation-N_2 impurity interaction, photoconductivity spectra, resistivity 79−91097
- diamond, neutral vacancy, generalised val. bond calc. 77−55493
- diamond, optical transitions between E and T electronic states each coupled to e-modes, GR1 band 80−20677
- diamond, radiation-induced optical absorption spectrum, 0.4-2.0 MeV electrons 77−84798
- diamond, relaxation about the vacancy 78−71722
- diamond, type Ia, electron irrad. effect on photocond., acceptor centre form. 77−47853
- diamond, vacancy, mol. orbital theory of transitions 77−85757
- diamond-type crystals, LCAO band structure, overlap and distant neighbour effects 80−49585
- dielectric, solid, energetic struct. of traps, from SCL currents 80−24941
- discrete spectrum of carrier states in defect-induced local deform. field 79−69470
- dislocated lattices, scattered wave functions 78−6326
- dislocation pot. rel. to de Haas-van Alphen effect, Dingle factor *(Russian)* 78−30885
- electron irrad., mobility increase due to defect prod. 80−24501
- electronic struct. determ. using LCAO method, appl. of cubic harmonic expansion 77−20268
- elemental semiconductors, hybridisation effect on dislocation electronic states 78−51936
- energetical trap distribs., first principles model, linear finite defect chain 80−59912
- EuSe, photocond. and photodiffusive voltage spectra 80−96940
- Frenkel exciton-charge transfer state mixing near charged defect model of photocond. 77−51663
- functional eqn., Tamm Dancoff procedure, canonical transformation *(German)* 80−84448
- gapless semiconductor, theory of resonance states in mag. field 80−6773
- Ge, heavily doped, dislocation vel., electronic effects 77−11547
- glasses, defect reactions, ionicity dependence, negative-U states 80−88510
- glasses, echoes and elec. dipole echoes at low temps. 79−69771
- glasses, electron physics, role of defects *(French)* 79−33225
- glow curve theory, temp. depend. of pre-exponential factor, activation energy calc. 80−2878
- grain boundaries, electronic structure, development of analytical electron microscope 80−86521
- graphite, electronic props., self consistent LCAO calc., point vacancy in 2-dimens. cryst. 78−51932
- graphite vacancy and substitutional impurities, moderately-large-embedded-cluster approach 80−49663
- halides, vacancy-interstitial pair prod. by electron-hole recomb. 79−4530
- homogeneous semiconductor, imperfections and photocond., electronic nonequilibrium behaviour 80−44667
- II-VI compounds, charged dislocations and plastic deform. 80−107264
- II-VI compounds, doubly ionisable centre binding energy 79−65405
- II-VI semiconducting phosphors, ODMR, defect excited states 78−80254
- II-VI semiconductors, impurity and defect centre energy states, luminesc. meas., review 80−55150
- III-V semiconductor, localised defects, one-electron pseudopot. 77−24533
- III-V semiconductor-oxide interface states, photoemission obs. of energy levels induced by adsorpt. 80−93000
- inert gas solid, delocalisation probability of interstitials 79−7801
- insulating crystals, conf., Gatlinburg, USA (Oct. 1977) 78−63755

defect electron energy states continued
interdislocation interaction on account of carriers bound with dislocations 78—75670
ionic crystal, intrinsic electronic excitations and defects, review *(Russian)* 80—10881
ionic crystals, dislocations, review 80—107236
ionic crystals, electronic and vibr. props. of point defects, book 80—5[illegible]62
ionic solids, lattice and defect props., modified electron gas approx. 79—42054
Ising model, two-dimens., ferromagnet-spin glass transition, Monte Carlo calc. 80—60287
light scattering by excitons localised at dislocations 78—60479
local formalism for very large bonded systems 77—4313
localised defects in solids, self-consistent approach to electronic struct., appl. to Si vacancy 79—78043
lone-pair semiconductor, defects, valence-alternation model and new directions 80—54646
metal, electron gas, local density functional for kinetic energy near defect, metal surface 80—20105
metal, electrons around vacancies, electron density calc. 78—64003
metal, nonlinear electron density distribution around point defects, formulation 79—19548
metal, nonlinear electron density distribution around point defects, applications 79—19549
metal, radiation defects, localized deformation of electronic state *(Russian)* 79—87061
metal, simple, vacancies and vacancy clusters, electronic struct. 79—11077
metal, thermodynamics of electrons, dislocation dipole and prismatic dislocation loop effects *(Russian)* 79—56161
metal, vacancies and interstitials, electronic struct. 78—47320
metal, X-ray excitation of surface plasmons on spherical voids 77—11974
metals, positron-defect interaction and annihilation characts., book contrib. 79—99978
metals, vacancies, corrected spherical model 78—34802
methylcyclohexane, trapped electron charge distribs., optical transitions 77—28139
3-methylpentane, trapped electron charge distribs., optical transitions 77—28139
molecular crystal, sensitised luminesc. calc. for trapping models using momentum-space theory of exciton transport 80—11447
monocarbides of subgroups IVa and Va, kinetic props., review 78—47613
MOS layer structure, UV illumination effect on elec. props. 79—82676
MOS structure, B ion implanted, form. and annealing of radiation damage 79—56321
MOS structure, quenched-in bulk defects and interface states, transient capacitance spectroscopy 79—24081
MOS structure, Si-SiO$_2$, specific memory effect, radiation effects 79—5[illegible]
naphthalene, electron excitation energy transfer efficiency, temp. depend. *(Russian)* 77—52182
narrow band gap semiconductors, conference, Warsaw, Poland (Sept. 1977) 79—82582
narrow band gap semiconductors, conference, Warsaw, Poland (Sept. 1977) 80—49703
non-metallic crystals, electric field influence on defect creation mechanism 80—70251
nontransition metal, density functional approach to electron and positron states 79—56107
one-dimensional crystals, matching conditions, Bloch functions, logarithmic derivatives 80—15475
one-dimensional periodic system, energy spectrum of defects, pseudopot. approach *(Russian)* 80—59909
one-electron approximation effect of correls. and defects 78—63960
optically unstable electronic defect-states, reson. Raman studies by double laser beam excitation 77—77220
orbit degenerate electron state localised at point defect, T-term multimode Jahn-Teller effect *(Russian)* 80—15490
p-n hot carrier functions, effect of space charge layer defects on characts. 80—25[illegible]
p-n tunnel junctions, photoinduced transitions, theory 80—65669
perovskite oxides, point defects, elec. cond., and electron energy spectra 80—70706
phosphate glasses, fading mechanisms 79—95851
photo-induced polarisation, model 79—56714
plastically deformed compound semiconductors, electronic transport and opt. props. of dislocations 80—80212
point defects, basis sets for study using Green's function methods 79—90994
point defects in crystals, book 77—47442
polyacetylene, intrinsic conformational defect states 80—65500
polydiacetylene, fully conjugated bond-alternation and orbital-flip defects 77—4311
polydiacetylene, intrinsic conformational defect states 80—65500
polymer, amorphous, excess charges, band gap levels and elec. props. 78—23053
polymers with defects, energy bands, ab initio SCF crystal orbital calcs. 78—30884
pressurised metal, containing dislocations, quantum oscillations of thermodynamic props. *(Russian)* 79—86899
quartz, smoky, γ-irrad., electric dipolar echoes 80—20604
renormalisation group calculation of defects in solids 79—7802
sapphire, F-type centre induction, 6.1 eV optical absorpt. band 78—44332
screw dislocations, interactions with Wannier-Mott excitons *(Russian)* 79—4513
self-consistent Green's function method, density matrix evaluation 80—293[illegible]
semiconductor, Balarin-Zetzsche evaluation method 77—43535
semiconductor, bound excitons, review, book contrib. 80—44519
semiconductor, Bourgoin mechanism, method for determ. 77—43534
semiconductor, cryst. field coeff. of point defect 77—43537
semiconductor, deep centre, electronic structure and lattice distortion, Green's function methods *(French)* 80—59917
semiconductor, defect electronic struct., SCF method 80—80208
semiconductor, defect electronic structure and lattice config., MO approaches 80—65495
semiconductor, detection by junction capacitance and current techniques [illegible]
semiconductor, dislocation cond. process at low temp. 79—99551
semiconductor, dislocation struct. and elec. props. 80—70201
semiconductor, electronic struct. of point defects, surfaces and interfaces, Green's function scatt. theoretic method 79—33258
semiconductor, extrinsic, defect level analysis, n(1/T) characts. 79—73464
semiconductor, ferromagnetic, localised states on imperfections and red shift of absorpt. edge 77—66527
semiconductor, ionic., ionisation of doubly charged centres 79—11085
semiconductor, localised states near displacive transition 80—70644
semiconductor, lone pair, defect chemistry 78—51935
semiconductor, quenching of luminesc. by charged defects 78—23531
semiconductor, recomb.-enhanced defect reactions 77—51377
semiconductor, recombination of nonequilib. carriers in presence of dislocations 79—82607
semiconductor, screened interaction of charged defects 78—39042
semiconductor, STEM spectroscopic techniques for simultaneous electronic and defect obs. 80—100145
semiconductor, strong electron-lattice interaction, review *(Japanese)* 80—49664
semiconductor, techniques for detecting electrons and holes trapped at bulk and interface imperfections 77—11934
semiconductor, tetrahedrally coordinated, dislocations, symposium, Hunfeld, Germany (Sept. 1978) 79—82214
semiconductor, tetrahedrally coordinated, effect of disorder and long range strain field on electron states 79—82545
semiconductor, tetrahedrally coordinated, effect of doping on dislocation mobility 79—82550
semiconductor, tetrahedrally coordinated electron states associated with dislocations 79—82544
semiconductor, with defects adsorbed mols. and metal overlayers, electronic structure 79—95466
semiconductor, with defects or impurities, local density of electron states 80—92857
semiconductor defects, electronic props. study by spectroscopic techniques 80—84446
semiconductor defects, entropy of ionisation and temp. variation of ionisation levels 77—11871
semiconductor neutral point defect electronic struct., self consistent method 78—91641
semiconductor thin quantised wire, with charged defects, interband light absorption *(Russian)* 77—59593
semiconductor with charged defects, elec. cond. and magnetoresist. 80—20225
semiconductors, amorphous, defects, band gap states 80—80215
semiconductors, cpd., large-lattice-relax. model for presistent impurity photocond. 77—85261
semiconductors, dangling-bond states theory 80—24840
semiconductors, defect-density profiles, constant-capacitance DLTS meas. 79—95361
semiconductors, defects and radiation effects, conf., Nice, France (Sept. 1978) 80—22140
semiconductors, electron states of point defects 80—39526
semiconductors, grain-boundary resist., DC voltage depend. 79—82597
semiconductors, impurities and other point defects, electronic struct., review 79—7803
semiconductors, multicharged defects, screening of electrostatic fields 78—79959
semiconductors, photoionisation cross-sections and phonon coupling 79—51518
semiconductors, recombination enhanced defect reactions 79—38094
semiconductors, thermally stimulated conductivity luminescence, defect levels, traps, book contribution 80—80296
semiconductors, thermally stimulated relaxation processes, book contribution 80—80295
semiconductors forward biased junctions, excess noise sources due to defects 79—38154
semicorductors, elemental and binary, under subthreshold irrad. conditions, defect formation ionisation mechanism possibility 80—6430
shell-model crystal, electron-phonon interactions effect of F-centre on shell screening 77—72825
shielded point defect potential well calcs. using Poole-Frenkel effect 80—20122
Si:B(p), dislocated crystals, microwave cond., localised electron energy spectrum 78—14694
silicate glass, dangling bond states 80—24846
single particle wave function random field calcs. *(Russian)* 80—34397
solar cells, polycryst., influence of grain boundaries electronic structure on diode characts. 80—94068
solid, one-carrier photoconductive process associated with broadened trap distributions 77—72881
solids, local defects, moderately-large-embedded-cluster approach 80—49663
Stark effect of localised electronic centres, point defects in ionic crystals. 77—66476
superconductor, defects in nucleation of superconducting phase *(Russian)* 77—36025
surface and interface defects, electronic struct., scatt. theory 80—84498
surface bands, lattice and symmetrical description 80—70785
ternary alloy semiconductors, disorder effects on electronic props. *(Japanese)* 80—49709
tetrahedrally coordinated covalent semiconductor point defects, multiple scatt. Xα model 80—54636
tetrahedrally coordinated semiconductors, electronic nature of vacancies 77—62863
theory of defects and defect processes 80—2009
thermal neutrons, inelastic scattering by one-dimens. defecton *(Russian)* 78—84169
transition metal alloy, dil., size effect 79—99508
transition metals, electronic structure of interstitials 79—1583
transition metals, ferromag., electronic struct. of interstitials 77—62867
trap depth, determ. from TSC, theory 80—70716
trap effects on exciton bands, masking by exciton-phonon coupling 80—80186
twin and stacking fault energies 79—38018
vacancy, Green's function calc. *(Russian)* 78—56101
vacancy, self-consistent electronic states 80—29354
vacancy formation energy, nonspherical contribution 78—83810
vacancy formation energy calc. within density functional and second order perturbation formalisms 78—67975

defect electron energy states continued
- voltage transients, defect centres emission rates and density profile 78–10467
- zero-gap semiconductors, reson. states, review 79–82558
- zinc blende type ionic semiconductors, vacancies, bound state energy level calcs., tight binding approx. 80–44694
- zinc blende-type semiconductors, interstitial PDs, electronegativity diff. and effective ionic charges 77–76766
- Ag halide, photographic image form., defect and impurity states, LCAO calc. 78–16876
- AgCl, colloid centres by heavy ion implantation 78–63780
- AgCl, irradiated, surface defect center, XPS study 79–28894
- Al, single vacancy formation energy calc., SCF-LCGO modified solid state scatt. theory 80–54637
- Al, vacancy electron density distrib. using Thomas-Fermi eqns. 77–15791
- Al, vacancy electron density, local electronic struct. theory 79–1580
- Al, vacancy electronic struct. LCGO calcs., solid state scattering theory 79–78044
- Al:H(He), interaction energy of two H(He) atoms, Hohenberg-Kohn-Sham density functional formalism 79–51519
- $Al_xGa_{1-x}As$ DH stripe-geometry lasers, degraded, capacitance spectroscopy 77–14715
- $Al_xGa_{1-x}As$, defect state identification associated with Ga vacancy 77–69269
- $Al_xGa_{1-x}As$, dependence of energy spectrum of levels introduced by electron irrad. on composition 79–60766
- n-$Al_xGa_{1-x}As$, nonradiative donor related defect centre obs. 78–23497
- Ar, vacancy, electronic structure, Green's function theory 80–39525
- As, amorphous, electronic struct. of defects using cluster-Bethe-lattice method 79–73471
- As, amorphous, theoretical calc. of defect states 80–49657
- As-Se chalcogenide glass, optical const. photoinduced changes mechanism 80–7321
- As_2S_3, amorphous, charged defect pair photolum. meas. 80–16078
- As_2S_3, glassy, photoinduced defects, EPR and absorpt. spectra 80–59398
- As_2S_3:B glass, impurity effect on photoluminesc. and optically induced EPR 79–65918
- As_xS_{100-x}, chalcogenide glass thin films, absorption in range of large optical densities *(Russian)* 80–11428
- As_2Se_3, amorphous, defect states, exptl. study. 80–54645
- As_2Se_3, amorphous, theoretical calc. of defect states 80–49657
- As_2Se_3 glasses, impurity effect on photoluminesc. and optically induced EPR 79–65918
- As_2Se_3, glassy defect electron states, tight binding calc. 80–96818
- As_2Te_3, amorphous, defect and impurity states, hopping cond. obs. 80–54650
- Au discontinuous film, electroluminescence obs. 80–103998
- Ba_2CaUO_6, luminescence and energy migration 79–4837
- BaF_2, influence of O_2 on elec. cond., 450-1150°C, anion Frenkel disorder model *(French)* 77–47619
- BaO-Al_2O_3-B_2O_3:Ag, X-ray irrad., atomic centre interactions, EPR spectra 80–25207
- BaS:Cu, thermoluminesc. and decay 78–80426
- $BaSO_4$, barytes, with large magnitude of emitted light, thermolum. curves 78–88368
- $BaTiO_3$, XPS and UPS from surface defects 80–76136
- $BaTiO_3$:La and undoped, defect chemistry elec. cond. at high temp. meas. 77–39858
- Be, twin and stacking fault energies 79–38018
- BeO, F-centre exam., pseudopotential calc. 78–43328
- Bi, neutral point defect electronic struct., self consistent method 78–91641
- C, glassy and fibrous, density of states, magnetoresistance theory appl. 80–44620
- C, vacancy, tight-binding calc. 80–24844
- Ca halophosphates, thermoluminesc., defects *(Russian)* 79–56869
- $CaCO_3$:Li, synthetic calcite, $(CO_3Li)^{2-}$-Li^+ defect after X-irrad., EPR study 80–75852
- CaF_2:Dy^{3+}, Mossbauer obs. 78–64303
- CaO, electron irradiated, photocond. and luminesc. meas., F-centre electronic struct. determ. 78–6409
- CaO:Ce,Gd phosphors, trap distrib., phosphoresc. decay characts. obs. 80–29773
- $CaWO_4$, type selfactivated luminophors, nature of optically active centres 77–69880
- $Cd_xHg_{1-x}Te$, solid solns., role of stoichiometry defects 77–47813
- $Cd_xHg_{1-x}Te$, vacancy electron states, acceptor behaviour, electron mobility 80–70193
- CdO-B_2O_3-SiO_2, glass, dielec.-relax. currents 78–52004
- CdS, characts. of interaction of light with dislocations 78–2137
- CdS, dislocation effects on radiative recombination processes 79–8186
- CdS, magnetic susceptibility, grinding-induced states 79–61040
- CdS, neutron irradiated, photoelectric props. 77–35962
- CdS, neutron irradiated, intrinsic defects 78–51599
- CdS, photocond. peaks due to exciton transition and S vacancies 77–8131
- CdS, plastically deformed, optical and electronic transport anisotropies 77–8611
- CdS, plastically deformed. electronic transport and optical props. 79–73508
- CdS, polycrystalline evaporated layers, donor and trap densities 80–20213
- CdS, single cryst., effects of annealing in Cd or S vapour on photoelectric props. 77–16370
- CdS, stress-induced photolum. bands, photocond., rel. to dislocation electron states 80–25447
- CdS:Cd(In), Cu- or defect-compensated, optical ageing rel. to storage cond. 78–84247
- CdS:$Li^+(N^+)(Ne^+)(P^+)$, ion-implanted, edge emissions 77–77274
- CdS-Cu_2S junctions, carrier trap density, deep level defects 80–107801
- CdS-Ge heterojunction, grown by chemical transport, props. 77–4422
- CdS(Se), with dislocations, optical props. 79–83001
- CdSe, electron irrad., edge emission 80–25461
- p-CdSe, Hall density and mobility, in Se vapour atm., 600-1100K 78–52014
- CdSe, heat treatment effect on carrier mobility, role of defect centres 77–72861
- CdSe, magnetic susceptibility, grinding-induced states 79–61040
- CdSe platelets, determ. of localised level energies by Fermi level statistics 77–31980

defect electron energy states continued
- CdTe, defect struct., review 77–39581
- n-CdTe, detector material, single crysts., activation energy anal. of defect levels 78–6321
- n-CdTe, photolum., plastic deform. effects 79–15509
- CdTe:Cl, electron irrad., defects 80–25460
- p-CdTe:Cl, influence of gamma-irradiation on elec. props. 77–62951
- CdTe:Cl, influence of lattice defects on electrical behaviour 78–2497
- Co-C, ferromag., prep. by splat-quenching, obs. of electronic struct. of interstitial C 77–62868
- $CoCr_2S_4$, ferrimag. semicond., magnetocrystalline anisotropy 80–71012
- CsCl, impurity and defect sites, elec. field gradient calc. 79–78034
- $Cs_2UO_2Cl_4$, low-lying excited electronic levels, fluoresc. decay meas. 79–47491
- Cu, screening charge density round $\Delta Z=-1$ impurities, vacancies, NQR study 80–103897
- Cu, surfaces and twin faults, electronic states calc. by surface Green's functions 80–39647
- CuCl, defect and impurity bands, lattice consts. 80–54638
- $CuInS_2$, optical and elec. phenomena 78–39605
- $CuInSe_2$, acceptor levels, elec. props. study 80–39578
- Cu_2O, defect levels, TSC 77–66138
- EuO, Eu-rich, IR absorpt. spectra, 4.2 to 300K, transitions assoc. with O vacancies 77–52142
- α-Fe, screw dislocation motion, orientation depend., tight-binding type electronic theory 79–51109
- Fe-C, electronic structure of interstitials 79–1583
- Fe-C, ferromag., prep. by splat-quenching, obs. of electronic struct. of interstitial C 77–62868
- $FeSb_xO_{4-y}$, defect struct. and mag. transition, elec. transport and Mossbauer expts. 78–59803
- Ga chalcogenides, energy spectrum of local levels *(Russian)* 79–51517
- n-GaAS, plastic deform. effect on elec. props., dislocation level 77–28178
- GaAlAs, surface vacancies, bound state energy levels calc. 80–80340
- $Ga_{1-x}Al_xAs$ epitaxial layers, spectroscopic technique for imaging spatial distrib. of nonradiative defects 78–23498
- $Ga_xAl_{1-x}As$:Cu epitaxial layers, spatial distrib. of nonradiative defects, STEM imaging spectroscopic technique 77–89438
- $Ga_{1-x}Al_xAs_{1-y}P_y$ epitaxial film, nonradiative recomb. at dislocations 80–44213
- GaAs (110), double-dangling-bond defects and band bending 79–69411
- GaAs (110), steps 80–49846
- GaAs, annealing rel. to stoichiometry deviation, Hall effect, electron microscope meas. 77–24410
- n-GaAs, conversion to p-type after 1 MeV electron irrad. 79–77636
- GaAs, defect state identification associated with Ga vacancy 77–69269
- GaAs, dislocation states 79–60762
- GaAs, elec. effects of dislocations 79–82586
- GaAs, elec. props. of dislocations review *(Japanese)* 78–6325
- GaAs, electron capture by multiphenon emission at B centre 80–24830
- n-GaAs, electron irrad. defects, carrier removal rate, annealing effects 80–75269
- GaAs, electron irrad. induced defect levels, hydrostatic press. effect 80–92858
- n-GaAs, electron irradiated, defect energy levels, influence of irrad. temp., photocond. meas. 78–2446
- GaAs, electronic states of neutral vacancies 77–11875
- GaAs, electronic states associated with 60° dislocations, tight-binding calc. 79–15114
- GaAs, epitaxial layers, electron irrad. deep level trap energy depend. 80–80205
- n-GaAs, heat treated, origin of 1.41 eV emission band, photolum. expt. 78–72579
- GaAs, highly deformed samples, absence of dislocation-induced luminescence 79–4835
- GaAs, ideal vacancy, electronic struct., tight-binding calc. 79–4529
- n-GaAs, intrinsic luminescence intensity, effect of 0.94, 1.0, 1.2 and 1.3 eV radiative centres 78–23517
- GaAs, ion implantation, disordered layer physical props. 79–77624
- GaAs, ion-bombarded, energy band struct., electrorefl. obs. 79–19517
- GaAs, melt grown, improve elec. and luminesc. props. after short time heat treatment 77–63452
- GaAs, point defects, multiple scatt. Xα model 80–54636
- GaAs, radiation defect obs. using Schottky diode characts. 78–76024
- GaAs Schottky barrier structure, defects from proton irradiation, thermal transients and optical capacity *(French)* 80–59534
- GaAs, semi-insulating substrate, characterisation and modification 77–81215
- GaAs, surface, electron struct. and Fermi level pinning by O_2 and metals 80–11066
- GaAs, surface, vacancies, bound state energy level calcs., tight binding approx. 80–44694
- n-GaAs, undoped, proton radiation defect detect. by transient capacitance spectroscopy 79–11089
- GaAs, vacancies Xalpha cluster model, electronic dangling bond effect elimination 79–99504
- GaAs:Cr, Cr^+ and Cr^{2+} centres, thermal treatment effects, EPR 80–65492
- GaAs:Cr, hole traps, ESR studies 80–75843
- GaAs:Cr, photoconductivity and photo Hall spectra 78–19091
- GaAs:Cr, photoionisation transition $Cr^{3+}\rightarrow Cr^{2+}$, EPR studies 80–60638
- GaAs:Cr (Cr-Te), and undoped, transverse-acoustoelec.-voltage spectroscopy 79–99586
- n-GaAs:Si(Te), radiative transitions induced by modest annealing, photoluminesc. spectra 80–55158
- n-GaAs:Te, electron-irrad., absorpt. spectra *(Russian)* 78–15200
- n-GaAs:Te, heavily doped, interband luminesc. intensity, heat treatment effect 78–72593
- $GaAs_{1-x}P_x$, dependence of energy spectrum of levels introduced by electron irrad. on composition 79–60766
- GaP diodes, TSCAP and admittance spectroscopy of gamma-ray induced defects 77–89472
- GaP, electronic props. of paramag. antisite P(Ga) defect 78–43327
- GaP, electronic states of neutral vacancies 77–11875
- GaP, electronic structure of neutral phosphorus vacancy, empirical pseudopotential 79–78042
- GaP, epitaxial layers, dislocation recomb., SEM cathodoluminescence studies 79–42558
- GaP, ion-bombarded, energy band struct., electrorefl. obs. 79–19517

defect electron energy states continued
- GaP, localised states in presence of P vacancy, pseudopot. calc. 78–18992
- p-GaP:Cr, hole traps, ESR studies 80–75843
- GaP:Fe, double Fe-thermal acceptor centre, energy states 80–96823
- GaP:Fe n-i-n epitaxial struct., photoconductivity, recombination scheme *(Russian)* 80–15569
- $GaS_xSe_{(1-x)}$ solid solns., electrical props. meas. 78–84216
- GaSb and alloys, struct. defect, photoluminesc. 80–25459
- GaSb, surface, electron struct. and Fermi level pinning by O_2 and metals 80–11066
- GaSb, undoped, intrinsic acceptors, parameters determ. 79–51515
- GaSb;Au overlayer, adatom interactions, photoemission obs. 79–33898
- GaSe, photolum. decay 79–15518
- GaSe, stacking disorder effect on Wannier excitons 77–62834
- Ge, amorphous, elec. and opt. props., review 78–23094
- Ge amorphous film, effects of alloying chalcogen atoms 80–49670
- Ge and Ge:O(Li), shallow defects, PTIS meas. 80–24971
- Ge, bound electron states close to conduction band due to 60° dislocations 77–28141
- Ge, compensated by thermal defects, Hall effect anomalies 79–69535
- n-Ge, deformed, 0.1 eV optical transition, interpretation using electronic states theory for Si 77–20261
- Ge, deformed at relatively low temps., Hall effect 79–82612
- Ge, dislocation electron states, from press. depend. of photocond. 80–96819
- Ge, dislocation energy band width, carrier lifetime anal. 77–11874
- Ge, dislocation energy levels, Hall effect meas. 78–6328
- Ge, dislocation-induced elec. pots., appl. 79–82551
- p-Ge, dislocations, grown-in defects, electrical props., deep level transient spect., Hall effect 80–39524
- Ge, edge-type dislocations, energy spectrum 80–24842
- p-Ge, electron bombard. at high temp., carrier lifetime and defect levels 77–55306
- n-Ge, electron occupancy of dislocation levels 77–15795
- Ge, electron states associated with core region of 60° dislocation 78–39057
- Ge, electron states below cond. band originating from dissociated 60°-dislocations, calc. using effective mass method 79–19546
- Ge, electronic states associated with 60° edge dislocation 77–89724
- Ge, electronic struct. of fast donor defect, stress effects, calc. 80–54641
- Ge, energy spectra of dislocations 80–70637
- Ge, entropy and enthalpy of vacancy form., comparison of theory with quenching expts. 77–11872
- Ge, fast and slow quenching defects 78–39052
- Ge, Hall effect, influence of dislocations 79–82611
- Ge, high-purity dislocation-free, divacancy-hydrogen complexes 78–2449
- Ge, ideal vacancy, electronic struct., tight-binding calc. 79–4529
- p-Ge, irradiation with fast electrons, defect distrib. with depth 80–19841
- Ge, LCAO band structure, overlap and distant neighbour effects 80–49585
- Ge, localised vacancy state 79–82543
- Ge, optical absorpt. in samples with 60° dislocations 78–39577
- Ge, optical excitation of dislocation states, photocond. meas. 77–69273
- Ge, optical excitation of dislocation states 77–85265
- Ge, p-type, and n-type converted to p-type by irradiation at 77K, defect form. mechanism 79–23651
- n-Ge, plastically deform., dislocation state spectrum, photocond., elec. cond., and Hall const. meas. *(Russian)* 80–2362
- Ge, plastically deformed, photocond. and absorpt. spectra, dislocation levels 77–28219
- Ge, plastically deformed, photocond. produced by polarised light 79–82641
- N-Ge, pressure influence on photoconductivity temp. dependence 78–76109
- Ge, quenched n- and p-type, intrinsic defects migrating near 100°C 77–62670
- Ge, recombination at dislocations 79–38023
- Ge, screw dislocations, effect of dislocation dissociation on localised electron and hole states 79–82546
- Ge, shallow acceptors produced by quenching 79–51523
- Ge, trapping defects, deep level transient spectroscopy 79–47045
- Ge, vacancy, tight-binding calc. 80–24844
- n-Ge:As(Sb)(Bi), irradiated with fast electrons at 77K, investigation of 300K annealing stage 79–51155
- Ge:Au, capacitance oscillations, trap recharging waves 77–43614
- Ge:Au, gamma-irradiated and electron irradiated, elec. props. meas. 77–62950
- p-Ge:Cd,Sb, electron irrad. at 300K, elec. props. 80–6435
- p-Ge:Ga, dislocation density effect on carrier lifetime and deep recomb. centres 79–51598
- p-Ge:Ga, lattice defects induced by γ-irrad. 80–29051
- n-Ge:Sb, fast neutron irrad. effects on donor conc., and annealing 78–56107
- Ge:Sb, γ-irrad., electron capture mechanism by radiation defects 78–26885
- n-Ge:Sb, γ-irrad. effects on donor conc. and compensation by acceptors 78–56106
- Ge:Sb, neutron irradiated, hopping cond. between shallow defect levels 77–4347
- Ge:Sb(As)(Ga), fast-neutron irradiated, shallow radiation defect levels, electronic props. 78–23049
- Ge:Sb(Ga), fast electron radiation defects, 0.52 eV absorpt. band, impurity photocond. and Hall effect meas. 78–27273
- Ge-S, Ge-S-Ag, amorphous prop. and origin of paramagnetic defects 79–10801
- Ge-S amorphous film, defect states, ESR 80–49670
- $Ge_{1-x}Se_x$, photolum. and optical props. meas. 77–20908
- Ge_xSe_{1-x} glasses, defect states, photoluminesc. and ESR obs. 79–61418
- Ge_4Se_5Te, amorphous layer, Poole-Frenkel controlled charge carrier transport, model of charged dangling bonds 80–49750
- HIO_3, polariton Fermi-resonance and dissociated phonon states *(Russian)* 80–20634
- $(Hg_{0.6}Cd_{0.4})_{1-x}Te_x$, defect anal., intrinsic material parameters 80–75519
- n-$Hg_{1-x}Cd_xTe$, far IR recomb. radiation in elec. field, acceptor states 77–16399
- $Hg_{1-x}Cd_xTe$, optical absorpt., quasilocal acceptor level effects, theory 80–92853
- HgTe, vacancy electron states, acceptor behaviour, electron mobility 80–70193

defect electron energy states continued
- InAs, radiation defect formation processes, effect on physical props. 78–2163
- n-InAs, undoped, electron irrad., Hall coeff., elec. resistivity, optical absorption 77–89479
- InP, electronic structure of neutral phosphorus vacancy, empirical pseudopotential 79–78042
- InP, radiation defect formation processes, effect on physical props. 78–2163
- n-InP, room temp. electron irrad., Hall coeff. meas. 77–89478
- InP, surface, electron struct. and Fermi level pinning by O_2 and metals 80–11066
- InP, surface vacancies, bound state energy levels calc. 80–80340
- InP_xAs_{1-x}, radiation defect formation processes, effect on physical props. 78–2163
- InSb film, degenerate, concs. and ionisation energies of defect levels, Hall effect meas. 79–91087
- n-InSb, proton irrad. defects energy level scheme, transport props. meas. 80–96576
- InSb:Cr, electron and hole lifetimes, recomb. at trapping and acceptor levels 77–51760
- p-InSb:Ge, proton irrad. defects energy level scheme, transport props. meas. 80–96576
- In_2Te_3 defect semicond., photoconductivity kinetics 80–11035
- KBr, spin-lattice relaxation time of relaxed excited state of F-centre, MCD meas. 79–61350
- KCl, F- and H-centre production by nonradiative decay of self-trapped exciton 78–23042
- KCl:$Br^-(I^-)$, interstitial atomic H centres, formation kinetics and struct. MO calc. and EPR studies 80–75854
- KCl:Ca(Yb), Z_2 and Z_2^+ centres, excited state, magnetooptical spectra 80–108233
- KCl:I^-, H, fluorescence of interstitial H-centres 79–73987
- KCl:Li,H optical and EPR exam. of H centre, $(LiH)^+$ absorpt. spectra 79–99920
- KCl:Na, F_B centre energy levels 80–107738
- KCl-Na, F_A, F_B and F_C-centres, wave functions and energy level of bound states 77–8049
- KCl(Br)(I), electronic struct. of self-trapped excitons calc. 77–39784
- KI, spin-lattice relaxation time of relaxed excited state of F-centre, MCD meas. 79–61350
- KN_3, ab initio calcs. of elec. props. of N_4^- 79–95363
- LiF, defect state model for localised excitations 77–43529
- LiF, F-centre electronic struct. determ. using LCAO method, appl. of cubic harmonic expansion 77–20268
- LiF, F-centres, defect electron struct., extended-ion model calcs. 80–59907
- LiF, TLD-100, trapping centres, optical absorpt. spectra defect and thermolum. mechanism models 80–50436
- LiF, V_k-centre generation, temp. depend. 78–18644
- LiF:Mg,Ti, defect states, ESR and ionic cond. study 80–108058
- LiF-Li_2O, F-aggregate centres *(Russian)* 78–64394
- LiH, cluster cryst., extended HMO calc. of defects 79–51521
- Li_3N, defect struct., quartet state paramag. centres, EPR meas. 79–42837
- $LiNbO_3$ surfaces, ion and electron bombard., photoelectron spectroscopy and electronic props. 80–71559
- $LiNbO_3$, XPS and UPS from surface defects 80–76136
- Mg, twin and stacking fault energies 79–38018
- Mg:H(He), interaction energy of two H(He) atoms, Hohenberg-Kohn-Sham density functional formalism 79–51519
- MgO, electron irradiated, luminescence, radiative recombination kinetics 80–7421
- $Mg_xZn_{1-x}Te$, temp. depend. of energy gap, near band gap reflectivity spectra 79–28786
- Mo, localised electronic states near dislocations 79–33257
- Mo, localized electronic states near ⟨100⟩ edge dislocation compared with perfect lattice 78–30888
- MoO_3, film and cryst., long range potential centres 78–30920
- N_2:N, dynamically induced electronic transitions of matrix isolated atom 78–63825
- Na, vacancy electron density distrib. using Thomas-Fermi eqns. 77–15791
- NaCl, electronic structure calculation, CNDO semi-empirical methods *(Russian)* 80–10909
- NaCl, pure, indoped, luminesc. obs. 77–32412
- NaCl-type crystals, donor levels due to dislocations, calc. 80–6771
- $NaClO_3$, reson. Raman scatt. from metastable O_2 produced by γ-irrad. 78–60432
- NbC, electronic struct. of vacancies, effect on supercond. transition temp. 80–29347
- NbC_x, stoichiometric and defective phases, electronic energy spectrum and physical props. *(Russian)* 77–35868
- Ne, vacancy, electronic structure, Green's function theory 80–39525
- Ni, defect electronic struct., strength characteristics relation by positron annihilation 79–91526
- Ni:He, defect props., quantum-chemical and lattice-defect hybrid approach 79–4528
- Ni-Ag, thin-film, effect on elec. cond. 79–7911
- Ni-C, ferromag., prep. by splat-quenching, obs. of electronic struct. of interstitial C 77–62868
- Ni-C interstitial alloys, electronic struct. 77–35886
- NiC, electronic structure of interstitials 79–1583
- PbI_2, defect levels, TSC meas., photoconductor models, trap level capture cross section 79–69463
- PbI_2 polytypes, elec. cond., band gap reduction due to stacking fault levels 77–32015
- PbI_2, single cryst., luminesc., photocond. and absorpt. after thermal treatment 79–56855
- PbI_2, TSC meas., localised levels in energy gap, depend. on purity and history 77–15856
- PbS:Tl, self-compensation of acceptors by vacancies, Hall coeff. meas. 80–92913
- PbSe:Tl, self-compensation of acceptors by vacancies, Hall coeff. meas. 80–92913
- p-PbTe, far IR obs. of shallow bound states in high mag. fields 78–23444
- PbTe film, ion-implantation-induced lattice defects 77–68985
- PbTe:As, hole conc. control, in LPE layers, plasma reflectivity and thermoelec. probe meas. 79–99640

defect electron energy states continued
RbBr, suprapure, thermolum. glow and emission studies at room temp. 80—7423
RbCl:Br$^-$(I$^-$), interstitial atomic H centres, formation kinetics and struct. MO calc. and EPR studies 80—75854
RbCl:I, H, fluorescence of interstitial H-centres 79—73987
ScN$_x$, region of homogeneity, physicochem. props. 78—52018
Se, amorphous, defect states, SCF pseudopot. and tight-binding calc. 79—65415
Se, amorphous, theoretical calc. of defect states 80—49657
Se, bonding coordination defects 80—59927
Se, glassy, structural excitation energies of defects, pseudopot. approach 80—107061
Se:As(Cl), trigonal, defect and impurity electron levels, surface photovoltage spectra 78—72108
Se-Ge, amorphous thin film, photocontraction rel. to surface struct. 80—49551
Si, amorphous, doping effects on cond. in hopping transport regime 79—28424
Si, amorphous, elec. and opt. props., review 78—23094
Si, amorphous, hydrogenation and density of defect states, hopping cond. 79—60757
Si, amorphous, photo-induced changes in elec. props., defect states 79—82553
Si, amorphous, spin-pairing at defect centres, mechanism in terms of chem. bonding 79—23928
Si, amorphous electron-hole recomb. mech. 78—72196
Si amorphous film, dangling bond ESR, light-induced quenching 80—50162
Si, annealed, ion-implanted, in MOSFET, defect spatial distrib. 77—11973
Si, bicrystals, grain boundary states and varistor characts. 80—24829
n-Si, carrier recomb. and photoionisation via E-centre resonance state 79—60847
Si, charge disturbance around neutral defect, simple new method, appl. to ideal vacancy 79—82554
n-Si, complex defect production rate introduced by high energy electron irradiation 77—72635
Si, core structure of glide-set 90° and 30° partial dislocations 80—96523
Si, deep-level point defects effective-mass nature 80—59922
Si, defects, divacancy and split 100 interstitial, electronic structure calc. 80—65494
Si, deformed, defect states associated with dislocations, capacitance transient spectroscopy 79—42483
Si, dislocation defect states, capacitance transient spectroscopy 79—82549
Si, dislocation electronic states, Schottky diode meas. 79—82548
Si, dislocation energy spectrum, appl. of EPR and elec. meas. 79—82547
Si, dislocation luminesc. obs. 78—15217
Si, dislocation-induced elec. pots., appl. 79—82551
Si, divacancy, hyperfine interactions from ENDOR meas. 79—42868
Si, divacancy, positive, EHT calcs. 79—99184
Si, divacancy charge states, photoconductivity spectra 77—15899
Si, edge-type dislocations, energy spectrum 80—24842
Si, elec. props., plastic deform. and annealing temp. depend., dislocation effects *(Russian)* 77—89765
Si, electrical props. affected by heat treatment *(Russian)* 78—11352
Si, electron bombarded, capacitance transient analysis of defect states 77—80545
n-Si, electron irrad., defect energy levels, energy depend. 79—33262
Si, electron irrad., limiting position of Fermi level, elec. cond. and optical absorpt. meas. 79—65484
Si, electron irrad. devices, dominant recomb. centres 77—72912
p-Si, electron irrad. induced defects, thermally stimulated capacitance 77—11933
Si, electron irradiated, EPR of C-O divacancy complex 77—69691
n-Si, electron irradiated, elec. props. 77—8041
n-Si, electron radiation defect annealing, negative stage, Hall coefficient, defect levels 79—90701
Si, electron states associated with core region of 60° dislocation 77—35887
Si, electron states associated with core region of 60° dislocation 78—39057
Si, electronic states associated with 60° edge dislocation 77—20261
Si, energy spectra of dislocations 80—70637
p-Si, energy spectrum and thermal stability of radiation defects, impurity photocond. spectra 77—4406
Si, entropy and enthalpy of vacancy form., comparison of theory with quenching expts. 77—11872
Si, extended Huckel theory calculations for positive divacancy 78—87938
p-Si, fast electron irrad., energy levels determ. by photocapacitance meas. 79—51531
p-Si, fast electron irrad., Hall mobility, temp. depend. 78—56165
Si film, amorphous and polycrystallised, localised states, elec. and optical props. 78—64008
Si, H-related interstitial defects, vibr. electronic struct., extended Huckel theory 77—62604
Si, Hall effect, influence of dislocations 79—82611
Si, heat-treated dislocation-free, elec. props. of stacking faults and precipitates 77—39796
Si, heavily disordered, fast neutron irrad., IR absorption following heat treatment 78—2448
Si, heavily doped, electronic effects on dislocation velocities 77—62531
Si, heavily doped, electronic effects on dislocation velocity 77—62532
Si, high-resistivity layer form. during electron irrad. 80—80352
Si, hydrogenated, amorphous, theoretical calc. of defect states 80—49657
Si, hyperfine interaction of divacancies, ENDOR meas. 77—4579
Si, ideal vacancy, electronic struct., tight-binding calc. 79—4529
Si, ideal vacancy, self consistent Green's function calc. 78—91640
Si, impurity interstitials, EHT calcs. 80—24845
Si, irradiated, nature of 0.97 eV A band luminesc. 77—44049
Si, isolated vacancy, electronic struct., SCF method 80—80208
Si, localised defect, self consistent Green's function calc. 80—10919
p-Si, low temp. defect prod., obs. by thermally stimulated capacitance technique 77—84801
Si, mag. props. of dislocations, spin polarons 79—82531
Si, neutral undistorted vacancy 78—91638
Si, neutral vacancy, generalised val. bond calc. 77—55493
Si, neutral vacancy electronic struct. 77—62865
p-Si, neutron irrad. effects, admittance meas. of n$^+$-p diode 78—51587
p-Si, neutron irradiated, elec. props. 78—51939

defect electron energy states continued
Si neutron-prod. defects, investigation by transcond. meas. of JFETs 77—15455
Si p$^+$-n junction diodes, flow fluence S implanted unequal defect densities, dynathermal obs. 80—20293
Si, partial dislocation electron states 79—60760
p-Si, photoabsorpt. associated with divacancies 79—15502
n-Si, photoionisation of doubly charged divacancies 79—51526
p-Si, piezo-spectroscopic study of defects *(Russian)* 77—28607
n-Si, plastically deformed, donor action of dislocations, elec. props. 79—11126
Si, point defects, H passivation 80—75515
Si, point defects, multiple scatt. Xα model 80—54636
Si, point defects, negative-U props. 80—49660
Si, poly crystalline, electronic behaviour of grain boundaries, solar cell appl. 80—92859
Si, polycryst., energy distrib. of trapping states, from impedance of MOSS struct. 80—65691
Si, polycrystalline, effect of H plasma on density of defect states 79—56158
Si, polycrystalline, neutron transmutation doped, grain boundary zero-bias resistance 79—15153
Si, polycrystalline barrier heights and passivation of grain boundaries 80—93890
Si, polycrystalline solar cell base material characterisation, defect states 80—50979
Si, radiation induced defects, IR absorpt. bands 80—25424
n-Si, recomb. parameters of heat treatment defects in diodes 79—56299
Si, recombination at dislocations 79—38023
Si, Schottky barrier structs., proton bombarded, defect states 80—29356
Si, self-consistent pseudopotential cal. of electronic states associated with reconstructed vacancy 79—73465
Si, self-implanted, defect-density profiles, constant-capacitance DLTS meas. 79—95361
Si solar cells, radiation damaged, origin of reverse annealing 80—76630
Si solar cells, radiation damage annealing mechanisms and low temp. annealing 80—94003
Si, spin dependent recomb. at dislocations, EPR and photocond. 79—38095
Si, spin effects in electron transitions via dislocation states 79—82642
Si, spin-depend. recomb. at exchange-coupled dislocation centres 77—89725
n-Si, sputtering-induced defects, elec. characts. 78—51941
Si, thermionic electron emission, from defect states at grain boundaries 79—91559
Si, two-step photoconductivity by dislocations 78—14761
p-Si, vacancy, charge states, Jahn-Teller stabilisation energy 80—80209
Si vacancy, defect electronic energy levels calc., optimisation 79—28315
Si vacancy, electron states, Anderson negative-U system 80—96820
Si, vacancy, local energy levels in Wannier approx. 77—20264
Si, vacancy, possible Anderson negative-U system 80—2358
Si, vacancy, self consistent Green's function method 80—24843
Si, vacancy, tight-binding calc. 80—24844
Si, vacancy electronic struct., self-consistent approach 79—78043
Si, vacancy electronic struct., self-consistent Koster-Slater method 80—10920
Si, vacancy screening, dielec. const., exchange correl. pot., Thomas-Fermi description 80—44528
Si with thermal defects, photocond., effect of annealing on elec. resist. 80—6837
Si:As, effects of recoil-implanted O on elec. activation of As 79—99227
Si:As, electron irrad. induced defect levels, annealing, deep level transient spectroscopy obs. 77—59044
Si:As, electron irradiated, majority carrier trap prod., effect of O_2 enhanced annealing 77—1151
p-Si:B, defect energy levels with 1 MeV electron irrad. and annealing, transient capacitance spectra 77—62860
Si:B, laser damage obs. by DLTS 78—76023
Si:B implanted wafers, ionis. assisted annealing and effects 80—100257
p-Si:B(Al), radiation defect form. and annealing study using Hall effect, cond. and carrier diffusion length 80—84214
Si:B(P), dislocated crysts., DC cond., Hall effect, and energy spectrum 78—10400
Si:Co, study of impurity states 78—76020
p-Si:Ga, neutron transmutation counterdoped, shallow defect levels, Hall effect and photocond. obs. 79—87055
n-Si:Ge, electron induced defects, room temp. instability 80—29052
Si:Ge,Sn, role of interelectronic correl. in paramag. props. of impurity-vacancy complex 77—62858
Si:H, amorphous, defect states, luminesc. and ESR obs. 80—76075
Si:H, amorphous, light-induced ESR and photoluminesc., dangling bonds with positive correl. energy 80—50161
Si:H, amorphous electronic struct. calc., rel. to UPS data 80—39527
Si:H, amorphous films, plasma-deposited, defect states, IR, ESR, and refractive index meas. 79—65944
Si:In, p-n junction, spin-dependent recomb. at dislocations, revealed at reverse current 79—24062
Si:Li, defect electronic struct. and config., semi-empirical calc. 80—107739
p-Si:Mn, defect levels, transient capacitance spectroscopy 78—6322
Si:Ni p$^+$n and n$^+$p diodes, thermally stimulated capacitance obs. of Ni acceptor levels 78—19137
Si:O, annealed, minority carrier lifetime 79—23985
Si:O, heat treated, excess carrier recomb. rate, defect levels 80—75579
Si:P, amorphous, CVD, defect compensation 80—54644
n-Si:P, edge dislocation energy level, differential capacitance meas. 79—23927
Si:P, polycryst. films, elec. props., EPR, defect states, doping effects 80—75660
Si:Sb, electron irrad. damage, electron trapping centres 77—39798
Si-H amorphous, defect model, light-induced ESR obs. 79—69721
Si-SiO$_2$, Al-implanted, low-temp. annealing effect on charge and surface state density 77—85337
Si-SiO$_2$, interface defect states obs. by constant capacitance DLTS 80—49924
Si-SiO$_2$ interface states, deposition of H containing layers and annealing 80—92991
Si-SiO$_2$ structures, B ions implanted, energy spectra of shallow traps at various implantation energies 80—80392
Si(:Au), gamma-induced trapping levels 79—87059
SiC (6H), IR absorpt., UV illumination effects, defect levels 80—66251

defect electron energy states continued

- β-SiC, cubic, electronic props. of vacancies and divacancies 77—76767
- SiO_2, amorphous, defect-controlled carrier transport 79—91049
- SiO_2, amorphous and crystalline, with O vacancy, cathodolum. meas. 77—24901
- SiO_2 clusters, CNDO/2 calc., appl. of cyclic boundary conditions 78—72110
- SiO_2 crystal and amorphous modifications, structural defect model 80—38915
- SiO_2, dangling bond states 80—24846
- SiO_2, fused, broken bond defect generation mechanisms 80—88044
- SiO_2 glass, optical props. of colour centres, intrinsic and modified defect states 79—60756
- SiO_2, vitreous, charged defect centres 80—107745
- SiO_2, vitreous, non-bridging O centre, optical props. and energetic struct. 80—34976
- SiO_2, vitreous, paramag. centres associated with bonding defects 80—80609
- SiO_2, vitreous, valence-attenuation pair defect, states, IR and Raman spectra 79—91442
- SiO_2-Si:A, effects of recoil-implanted O on elec. activation of As 79—99227
- SmS type semiconductors, electronic struct., influence of point defects 80—70650
- α-Sn, ion implanted, defect struct., Mossbauer spectra 80—80214
- SnSe, electronic props., region of existence *(French)* 77—35885
- SrF_2, neutron irrad., role of F-centres in thermoluminesc. 79—19941
- SrO, electronic struct. of F-centre 78—30887
- SrS:Hf, phosphor fluoresc. spectra, host lattice defect 77—12416
- $SrTiO_3$:B layers, ion implanted, conductive props. Hall mobility, defect energy levels 79—82693
- $SrTiO_3:Mn^{n+}$, reduced, EPR of Mn centres 78—35029
- Te, dislocations influence on galvanomag. props. 80—54722
- Te, induced acceptor levels and free-carrier mobility due to $\check{c}$-screw dislocations 77—89730
- Te, oriented films, semiconducting props., Hall coeff., band structure 80—70854
- Te, screw-dislocation-induced scatt. and acceptor states, galvanomag. and optical expts. 77—28142
- TiO_2, clusters, surface electron struct. and defect states, DV-Xα calc. 80—20268
- TiO_2, surface electronic struct. by discrete variational Xα cluster calc. 78—43449
- UO_2, point defects and electronic props., theoretical survey 77—31657
- VN, electronic struct. of vacancies, effect on supercond. transition temp. 80—29347
- W, screw dislocation motion, orientation depend., tight-binding type electronic theory 79—51109
- $W_xMo_{1-x}O_3$, reduction and temp. effect on electronic core levels, XPES 79—91564
- WO_3, reduction and temp. effect on electronic core levels, XPES 79—91564
- WO_5 film, amorphous, band structure and colour-centre band, fast electron energy loss spectrum 77—55478
- YAG, undoped and Ce^{3+}-doped, cathodolum. intensity and decay time, 10-480K 79—99952
- YAG-$Ce^{3+}(Eu^{3+})(Tb^{3+})(Gd^{3+})$, cathodolum. intensity, temp. depend., comparative study 79—99953
- $YAl_3[BO_3]_4$ crystals, capture centres, thermoluminesc. study 79—65935
- YIG, nonstoichiometry and electronic defects, thermogravimetric expts. and anal. of elec. data 78—6050
- $Zn_xHg_{1-x}Te$, vacancy electron states, acceptor behaviour, electron mobility 80—70193
- ZnO, defect struct. calc., doping effects 80—107218
- ZnO, F^+-centre exam., ground and first excited energy level 77—39800
- ZnO, F-centre exam., pseudopotential calc. 78—43328
- ZnO single crysts. with stoichiometry deviations, intrinsic defects, thermodynamic analysis 79—42485
- ZnO, surface phenomena, interpretation by compensation model 78—95323
- ZnO:Li, electron irrad., F^+ centre, photosensitivity of e.p.r. spectrum 77—1594
- ZnS, F-centre exam., pseudopotential calc. 78—43328
- ZnS_xSe_{1-x}, VPE, characterisation of defect centres by photoelectronic meas. 80—10914
- ZnSe, electronic struct. of charged Zn vacancy, cluster model 77—47764
- ZnSe, nature of large electric charges of moving dislocations *(Russian)* 78—39065
- p-$ZnSnP_2$, photolum. anisotropy, 77K 78—19557
- ZnTe, doping and intrinsic stoichiometric defects, self-compensation 80—59918
- ZnTe, edge luminesc. excited by electron bombard. 80—66308
- ZnTe, elec. active intrinsic defects, Hall meas. of carrier conc. 77—51700
- ZnTe, photoluminesc., donor and acceptor excited states 79—38622
- ZnTe, refined, undoped, Cu acceptor, optical absorption and photoluminesc. meas. 80—34970
- ZnTe:Ag, containing dislocation loops, optical absorption-edge fine struct. 78—43905
- ZnTe:Al,Cl, photolum., complex acceptor, ionization energy 80—20693
- ZnTe:In(Al), pure and doped, Zn vacancy energy levels, elec. and optical props. 79—4827
- $ZrSiO_4$, X-irrad., trapping and emission centres, OH^- ion contribution 80—80876

defects, crystal *see crystal defects*

defibrillators

- *see also patient treatment*
- 60 Hz half-cycle sinusoid for low-energy application 78—3664
- automatic, implantable, cardiac pumping detect., optimal electrode spacing 80—72373
- capacitor discharge, canine ventricular defibrillation thresholds 80—17182
- conference, Lafayette, USA, (Sept. 1977) 78—57047
- conference on cardiac defibrillation and cardiopulmonary resuscitation, Lafayette, USA (Sept. 1979) 80—67929
- damped sine wave, intact, evaluation of operating internal resist., inductance and capacitance 78—57120
- DC defibrillator discharge, contrib. of paddle electrode area and edge length to transthoracic impedance 80—3860

defibrillators continued

- delivered energy measurement methods, DC difibrillators appl. 78—61281
- digital cardiac defibrillator tester 80—41286
- electrode gel testing, meas. of impedance to transthoracic DC discharge 78—57056
- electrodes, recovery curves for different materials 80—67283
- electrodes for permanent implantable system, transvenous catheter and subcutaneous plate 79—39599
- emergency medical use, improvements and clinical studies needed 78—44678
- energy meters, traceable calibration methods 80—30928
- ground-loop current elec. skin burn computer simulation 77—78039
- implantable automatic device design, ventricular fibrillation/defibrillation threshold energy-time anal. 77—48924
- intensive care unit ECG protection against defibrillator pulse 77—25586
- miniaturised implantable, automatic, heart monitoring appl. 77—81645
- multiple-shock defibrillation, effect of shock separation time 78—57053
- myocardial damage from defibrillator discharges at various dosages 80—72368
- myocardial damage rel. to high-energy elec. current 78—57051
- performance characteristics of three commercial instruments in transthoracic ventricular defibrillation of animals 78—57048
- quality health care and cost containment, conf., Washington, USA (Mar.-Apr. 1978) 79—39333
- review of instruments and maintenance 78—69251
- staggered shock time interval, reduction of peak current and volt. requirements 77—40904
- thoracic impedance of humans, meas. using automatic recording device on defibrillator 78—61239
- transchest damped sine wave shocks producing cardiac damage 78—57052
- transchest defibrillation, strength-duration curves for trapezoidal waveforms of various tilts, dogs and ponies 78—57054
- transchest ventricular defibrillation, comparative efficacy of damped sine wave and square wave in dogs and ponies 78—57055
- transthoracic chest resist. of 100 kg calves defibrillated with rectangular pulses 78—36047
- transthoracic square-wave defibrillation experience in dog and calf 78—57050
- transthoracic ventricular defibrillation in adults, success rate rel. to energy used 78—57049
- trapezoidal waveform defibrillators, operating internal resistance and capacitance 80—72375
- trapezoidal waveforms, haemodynamic responses 80—72370
- ultrahigh energy, programming to deliver optimal quality rectangular wave shocks 77—37102
- ventricular defibrillation with myocardial electrodes in the dog, calf pony, and pig 80—72369

deformation

- *see also bending; cold working; creep; drawing (mechanical); elastic deformation; elongation; ferroelasticity; plastic deformation; shape memory effects; thermomechanical treatment*
- Adirondack anorthosite, deform. characts. 78—61399
- aggregate, polycrystalline, deform. 77—4816
- alkali halides, exchange charge shell model analysis of strain derivatives of static polarisability, effective charge parameter 78—91296
- alkali metal halides, ionic crysts., impulse compression temps. 80—100307
- alloy, two phase 77—8893
- N.American intra-plate crustal deformation, implications of VLBI meas. 80—51379
- amorphous metals, computer simulations of tensile deformation and radiation damage *(Japanese)* 79—42137
- anisotropic medium, deform. function construction 79—98633
- anisotropic plate finite element analysis 77—26174
- armour material, selection criterion 78—53063
- arterial vasa vasorum, hypertension effect *(Japanese)* 78—3544
- arterial wall, role of stress conc. in atherogenesis 80—16970
- astronomical mirror suspended on belt, deforms. during horizontal control 80—17494
- axisymmetric shells, two noded straight element including shear deformation effects 78—47
- basalt xenoliths in Massif central France, deform. rel. to mantle struct. and geodynamics *(French)* 79—48424
- beams, dynamic stability with shearing strains and rot. inertia 80—33498
- beams, end loaded cantilever, lateral buckling 79—50617
- beams, frames, arches, axisymmetric shells, finite element anal., Newton Raphson method, nonlinear equilib. eqns. 78—22282
- binary stars, very close, struct. eqns. including rot. and tidal distortions for ZAMS stars 80—22037
- bioconstructions, mech. deforms. at different stages of morphogenesis 80—51140
- biotite, deform. and recrystallisation in Woodroffe Thrust mylonite zone 80—21739
- biotite at Fleurieu Peninsula, South Australia, deform. rel. to slaty cleavage development 80—21735
- biotite deformation, comparison with muscovite from optical microstruct. 80—26507
- blood vessels, exam. of mech. props 80—12175
- bone, anelastic deform. and friction stress 78—19871
- bone, deformation capacity of compact tissue of human tibia subjected to torsion, age effect 77—52827
- bone, human, acoustic emission in restressing 80—3704
- bone, human, demineralized, deform. props. on stretching 80—3703
- bone mechanical model with appl. to human upper tibia, porous material, deform. *(Japanese)* 78—88724
- bone strains of canine radius and ulna, in vivo meas. and anal. 80—67130
- Bordoni relaxation models, internal friction and microdeformation rel. to dislocations *(French)* 79—37758
- brass, circular plate perforation and deformation by square section punch 79—34100
- brittle solids, shock deform., review of theory 80—72493
- butadiene-styrene block copolymer, viscoelastic props. 79—8336
- butadienepstyrene, surface phenomena in struct. rearrangement after deform. *(German)* 78—19913
- BWR containment vessels of prestressed concrete, pressure tests 80—81254
- calcite rocks, experimentally deformed, texture development 79—83230

deformation continued
- calcitic rocks deform., geological aspects of calcite microstructure 79—57933
- Cambrian slates of N Wales, mag. susceptibility anisotropy and correl. with strain 79—79832
- cantilever plate flexure, variational method *(Russian)* 79—7310
- cellular deformability, diffractometric method for meas. 80—98187
- cellulose film, moisture effect on phys. and mech. props. 80—40450
- CG method generalisation, linear and nonlinear problem appl. 79—30243
- chamotte glazed masses, deformation occurring during heat treatment 78—84747
- chiral smectic C, distortion under shear, optical study 77—39536
- coincidence site lattice rotations, permissible angles, effect of strain due to temp. or pressure changes 79—32932
- collagen, tendinous, highly ordered maromolecular composite, mech. props.-ultrastruct. relation 77—52826
- collagen fibril cross-striation, thermodeform., electron microscopy and X-ray diffr. 77—86438
- composite alloys, two-phase systems, deformation textures 79—83219
- composite materials, mech. props., theory, review 80—64392
- composites, multicomponent layered, time depend. of flexibilities 80—39205
- composites, stretching, zone of disturbed stress state calc. 80—39206
- composites transient hygrothermal stresses, coupled diffusion of heat and moisture 80—33451
- concrete, strain rate effect on strength and deform. during hardening process *(Japanese)* 80—93616
- contact structure, deformation of Lie algebra, of infinitesimal automorphisms *(French)* 80—62867
- continuous casting cylindrical ingot, development of elastic-plastic temp. stresses and deformations *(Russian)* 79—29151
- convex cylindrical surfaces, deformation anal. using moire fringes 80—14636
- β Coronae Borealis, Ap star, possible indication of mag. deform. 77—45454
- corrugated tubes, semi-circular, slender ring shell theory *(Chinese)* 80—19234
- creep deformation, effect of damage 78—79664
- crossply glassfibre, cantilever beams, nonlinear damping for nonsinusoidal strain 79—47762
- crystal, elastic moduli, calc. from interatomic forces 79—95071
- crystal potential formulation *(Russian)* 77—19894
- crystal rotations, under constrained deform. *(Japanese)* 80—92593
- crystalline materials, in situ deform. by high voltage electron microscopy 80—103352
- cubic crystals, tensile deform. induced transitions 80—59653
- curved crystal-monochromator, influence of elastic element area on reflecting surface relief *(Russian)* 80—64157
- curved surface, deform. meas. by dynamic moire method 80—14634
- cylinder, hollow thick-walled, having axial holes and varying section thickness, stress state anal. 80—100879
- cylindrical shell, dynamic response to concentrated impact load, radial displacement, stresses 78—67072
- cylindrical shell, nonaxisymmetric press., stability loss, deform. *(Russian)* 77—46951
- damping, internal, in 2 and 3 dimens. continua 78—13970
- deformable solids, singularities of dynamic processes, finite rate effect of heat propag. 80—19247
- deformed boundary determ. by method of caustics 77—89077
- deformed crystal, optical method for quantitative evaluation of electron channelling patterns *(German, English)* 77—7777
- dielectric, model of interactions 77—59521
- dilute suspension of spheres in power model fluid, apparent stress deform. behaviour 78—42578
- discrete structure solids, mathematical models for stress relaxation and deformation 77—14923
- discrete systems forming macroscopic body, probability theory 77—40
- displacement fields, strain state determ., using moire bands and deformed raster 78—63404
- dolomite, strain rate depend. inferred from impact and static compression studies 77—44977
- drawing, of continuous round ultrasonically perturbed profiles, stressed states at centre of deformation *(Russian)* 80—59557
- drop deformation and orientation in shear and extensional flow fields, dynamic interfacial props. 80—107611
- droplet, viscous, deform. due to deposition of surfactant 78—18876
- droplet deformation in extensional flow 80—19449
- dynamic force measurement results, data reduction and anal. *(Hungarian)* 77—117
- dynamic hot densification of porous blanks, degree of deformation 77—63585
- dynamics of shells of revolution under axisymmetric load involving shear deformation 78—79210
- Earth, strain-tide spectroscopy 78—73301
- Earth, three-dimensional geodesic mapping eqns. and best-known figure for non-rigid models *(German)* 78—73304
- Earth, tidal potential multiple expansion 79—12062
- Earth crust, anal. of thermoelastic strains and tilts 78—20346
- Earth crust, Central Alps structural zones and continental collisions 78—81124
- Earth crust, energy changes due to mining 77—64236
- Earth crust, foreland folding model 78—81141
- Earth crust, line length changes resolution by EM distance meas. ratio method 80—4143
- Earth crust, model for vertical displacements during rifting in Afar triangle 80—98295
- Earth crust, propagating deform. front in China rel. to Haicheng earthquake prediction 77—49028
- Earth crust, shear deform. zones along major transform faults and subducting slabs 78—73330
- Earth crust, static deform. of laterally inhomogeneous half-space by two-dimensional strike-slip fault 80—31012
- Earth crust, tectonic deform. characts. from seismological data in China *(Chinese)* 80—76951
- Earth crust, vertical movements in Tohoku district, Japan, 1900-1975, and tectonic implications 80—56453
- Earth crust, viscoelastic deform. by finite quasi-static sources 79—39686
- Earth crust anal. of Turgen' Geophysical Observatory data 80—76935
- Earth crust deformation analysis, models for estimation of parameters *(German)* 80—101319
- Earth deformation, mag. field effects 80—109085

deformation continued
- Earth strain measurements by bore-hole strainmeter at Matsushiro, seismic waves response *(Japanese)* 79—96745
- Earth strain tides in Great Britain, survey 79—44080
- Earth upper mantle, finite deformation during fluid flow 79—92519
- EBR-II, operating limits for subassembly deformation 78—21714
- elastic eqns. of uniform systems, general integral solns., appl. *(Russian)* 79—14272
- elastic plate, impact load impulse form determination by the displacements and strains of a circular plate *(Russian)* 80—74751
- elastic-plastic-creep-large strain analysis at elevated temperature by the finite element method 79—37185
- elastohydrodynamically loaded surfaces, interferometric deform. meas. 79—43532
- elastoplastic bodies, asymptotic behaviour under periodic loading 80—83740
- electrostatic forces effect on vacuum breakdown 79—56724
- epoxy-based crosslinked polymers, deform. and strength characts., temp. effects *(Russian)* 79—65139
- erythrocyte deformation in centrifugal field 78—27976
- ethylene propylene/polyolefin blends, radiation cross linking 80—66801
- extensible string motion in nonviscous fluid *(Russian)* 78—77718
- fcc crystals in tension, latent hardening, eqns. for tension and compression 79—77671
- FCC metals and alloys, deform. behaviour 77—8892
- fibre reinforced composite, fibre pull-out at high loading rate *(Japanese)* 80—45357
- fibre reinforced composite, response to hydrostatic states of stress 77—36602
- fibre reinforced composite bodies, structure optimisation in stability problems 80—58947
- fibre reinforced composites, mathematical theory 77—68453
- finite hollow cylinders, end problems, axisymmetric deformation *(Chinese)* 80—5930
- finitely deformed compressible materials, plane strain theory 79—72805
- fission reactor fuel rod geometry changes, mech. interactions calcs. 79—40993
- flanges, elastic-plastic deform., thermal stress effects calcs. *(German)* 78—34029
- flexible long cylindrical shell with variable parameters, deformation anal. *(Ukrainian)* 77—68388
- flexoelectricity of liquid crystals, microscopic interpretation 77—32339
- floating ice plate, time depend. deflections, linear viscoelasticity theory 77—17107
- fluid impregnated solids, elastic and dynamic response regimes 78—90713
- fluid interface, dynamic, and air entrainment prediction 78—2337
- Fohnsdorf tertiary basin, Styria, in situ tension measurements *(German)* 80—21665
- fusion reactor field coils, fabrication effects on structural behaviour 80—9406
- gauge blocks, contact deformation and corrections 79—26028
- generalised deformation minimum *(French)* 79—53977
- generalised thermorheologically simple porous materials, thermomechanical theory of viscoelasticity 80—33479
- geodesy, hypothesis tests for singular compensation problems *(German)* 78—44758
- geometric field theory of finite deformation in continuum mechanics *(Chinese)* 79—71248
- glass, flat, air cooled, duration of inelastic deformation 78—84908
- glass, photoelastic const. for chem. strenthening, circular plate compression method *(Japanese)* 80—93279
- glass fibre reinforced composite, semifinished product nonlinearity model, force anal. of winding 78—63325
- glass fibre reinforced plastics, under compressive load *(Japanese)* 78—92301
- granite, deformation and permeability of crushed samples 77—21763
- granite in W. Great Kabylia (Algeria), deform. by ductile shear *(French)* 79—39716
- granular materials, shear deform., microscopic and macroscopic exam., stress/strain characts. calc. *(Japanese)* 80—11691
- granular media, density measurement, plane strain conditions, acoustic method *(Polish)* 80—62635
- graphite, adsorption of CH_4, Kr, Xe, substrate deform. meas. 80—54520
- graphite, internal strain rel. to strain tensor, group theory anal. 79—86835
- graphite, nuclear, prestressing effects on nuclear graphites 78—14482
- graphite materials, isotropic, resist. to deformation and fracture under complex stress conditions 80—16479
- graphitic materials deformation, crack and fracture behaviour, SEM exam 80—11706
- Hamilton's principle for thermodynamic systems 79—88896
- Hamiltons principle appl. to large deformation problems 80—48600
- heterogeneous materials, cavities development *(Russian)* 79—55812
- HMTTF-TCNQ chain, three dimensional ordering, HMTTF chain deform. temp. var. 78—95152
- holed plates, stress and deformation, finite quadrilateral elements technique *(Rumanian)* 79—18707
- hologram real-time observation with photothermoplastic film *(German)* 78—1182
- holographic determination of in-plane and out-of-plane components 79—94193
- holographic interferometric deform. field meas. *(German)* 77—22594
- hydrostatic, meas., photoelasticimetry and holographic interferometry appl. 79—7353
- ice, experimental folding and resultant c-axis fabrics 79—57983
- ice, transverse flexure, refined Reissner anal. 80—88247
- ice domes, time dependent deformation 79—37152
- ideal crystals, principles of satbility analysis 77—45697
- ideal fibre reinforced composites, finite plane deformation and energy dissipation 78—79274
- inclusions behaviour, during processsing, effects on directionality 80—55345
- incremental deformations of initially stressed media with couple stresses 78—62077
- Indo-Australian plate, evidence for internal deform. 80—109134
- inelastic numerical analysis for quasistatic and dynamic problems 80—19233
- inhomogeneous viscoelastic bodies, deformation under quasistatic loading 80—14587
- internal stress, theoretical study of macroscopic meas. 80—25788

deformation continued
- internal stress field effect, on deformation rate, kinetic anal. 80−25787
- Jamaican blueschists, coaxial pure shear rel. to deform. assoc. with subduction 79−2236
- jointed granite in situ, elastic and transport props. 77−66909
- jointed rocks, strength and deformation characteristics in true triaxial compression 79−84235
- Jura fold limb rotation, geometrical adjustments 77−21747
- knee joint, appl. of anthropometric scaling method 77−52817
- laminated half space under influence of vibrations *(Russian)* 78−63370
- laminated plates subjected to transverse dynamic loading, transient response 77−31245
- Late Palaeozoic slate belt, structural succession and tectonic significance 78−81140
- lattice deformations, determ. by pendellosung X-ray fringes 80−54078
- layered composite containing a crack, impact response to shear deform. 77−50991
- liquid crystals, textures, deform. and struct. order, review 77−43135
- liquid gas interface, deform. in inhomogeneous elec. field *(Bulgarian)* 80−54474
- liquid surface, free, charged, isolated, exptl. study of deform. *(French)* 80−88240
- LMFBR, fuel pin deform. within wire-wrap fuel assembly, computer code anal. 79−71915
- loading surface deformation, analytical investigation *(Russian)* 79−80435
- localised function, integral eqn. 77−50932
- locally simple unsteady deformations 77−68506
- lung, finite element model for macroscopic deform. 80−108945
- lung, macroscopic deformation, finite element model 80−89781
- lung deflation, large-deform. anals. of strains in excised lobes, dog 80−3689
- machine vibrations anal. and obs. block deformability influence *(Italian)* 78−51108
- magnetic field, one-dimensional, force-free, adiabatically slow deform., singular lines *(Russian)* 79−48670
- material identification of soft tissue using membrane inflation 80−41345
- measurement, in-plane, by video-electronic hologram interferometry 80−106488
- measurement errors eval. for resistance strain gauges 79−75521
- media with internal structure, thermodynamics 79−88901
- Mersilene mesh, herniorrhaphic reinforcing prosthetic, mech. and struct. props., SEM study 79−74789
- metagabbronorite from DSDP hole 334, high-temp. deform. and recrysts. near Mid-Atlantic Ridge 77−91125
- metal, amorphous, deformation mechanisms *(Japanese)* 79−42136
- metal, BCC 77−4815
- metal, creep movement of dislocations, effect of stress distrib. at grain boundaries *(Russian)* 78−27564
- metal, deformed, transfer phenomena *(Russian)* 77−35906
- metal, thin sheet, crack growth, effect of strain rate 77−1869
- metal, US velocity, effects of deform. and high temps. 78−26626
- metal forging in closed dies, theory and expt. comparison *(German)* 80−25745
- metal plate high-gradient transverse deformation interferometry 78−82024
- metal strips, welded, aged, reduction of deformations *(Russian)* 80−97508
- metallic membrane, lifetime prediction and design 80−71752
- metals, ferrous and non ferrous, exam. of abnormal deformations and transformations *(French)* 78−60714
- metals, monovalent, mechanical ideal strength, pseudopot. model calcs. 79−77670
- metals, strain induced thermal signals, detection 79−1141
- metasedimentary sequence of N.Hill End Trough, NSW, metamorphism and deform. time relations 80−26510
- micromechanics of structured materials 77−67273
- microstructure with finite deformations, reciprocity theorem, stored energy function *(Italian)* 78−81836
- migmatite bodies, numerical expts. on ascent based on continuum dynamics 80−51381
- mild steel, circular plate perforation and deformation by square section punch 79−34100
- minerals of dyke walls, ang. relations as dyke injection direction criterion 79−79843
- mobile load on ideally packed material layer 80−99952
- Mohr-Coulomb material, axisymmetric compression around circular hole 79−57914
- moire fringe sensitivity in deformation meas. *(Rumanian)* 80−48654
- morphogenesis, growth, elastic and non-elastic deforms. 80−108928
- Morse model cubic crystals under hydrostatic pressure, stability 80−19870
- Mossbauer absorbers, deformation induced texture 79−8074
- multicomponent solid body undergoing allotropic transform., fundamental deform. eqns. *(Russian)* 78−16645
- multistage, simulation on torsion machine 77−40492
- muscovite deformation, comparison with biotite from optical microstruct. 80−26507
- naphthalene, spectra of directionally deformed crystals and phonon-exciton interaction constants 79−78703
- natural geometry of deformation processes *(German)* 79−86334
- nondeterministic thermal deformations of structures temp.-dependent material props. 77−65679
- nonextensible fibre reinforced material, plane deformation *(German)* 79−87702
- nonlinear deform. wave propagation in dissipative medium, interaction and reverse problems 78−53
- nonlinear interaction of deformable body with liquid pressure wave *(Ukrainian)* 78−65777
- nonlinear shell analysis via mixed isoparametric elements 78−1566
- nonlinear structural dynamics, Newmark's algorithm stability 77−26166
- nuclear fuel pin failure, pressure in duct due to gas discharge 78−675
- nuclear fuel rod anal. program CYGRO-4 78−41805
- nuclear reactor core mats., constitutive eqn. 78−80598
- one-dimensional crystal subjected to deform., static and dynamic equilib. 79−28037
- one-dimensional molecular chain, collective model for conformons 80−15456
- optical fibre refractive index change due to external forces 78−74971
- optical surfaces, measurement using real-time digital heterodyne broad-beam interferometry 79−85173

deformation continued
- osteosynthesis, internal, deform. of bone *(Croatian)* 80−108943
- out-of-plane, measurement using holographic interferometry and speckle photography, comparative accuracy 80−78804
- oxidation and corrosion induced deformation effects in nuclear reactors and mech. structures 80−3211
- particulate beds, sheared, mass transport kinetics, Markov chains appl. 79−60057
- periodically layered composites in plane strain, dispersion eqn. for waves 80−79212
- periodotite xenoliths of Massif Central, deform. rel. to upper mantle struct. and geodynamics 78−81120
- photogrammetric model deformation, interactive demonstration program 77−74183
- pigment dispersion rheology, kinetic model, expt. results 79−7361
- plane strain, spurious modes in two-dimensional isoparametric elements 80−52
- plane strain problem of hardening and softening plastic materials, theory 78−83869
- plastic, fibre-glass reinforced, flat stressed state, strength and deformation props. function of reinforcement struct. 80−19866
- plate, loaded cantilevered, exact eqns. for inextensional deformation 80−64399
- plate thick, circular hole under axisymm. radial load, stress anal., displacements 78−79201
- plate with periodic circular aperture system, elastoplasticity problem 78−9573
- plates, annular, of variable thickness, natural vibr. eigenfreq. Mindlin eqn. integration 80−38318
- plates, arbitrary, quadrilateral and triangular, inextensional deformation, alternate exact eqns. 80−69694
- plates, large deformation anal., variational formulations 80−92067
- plates, prestressed, edge deform. in transverse vibrs., numerical-perturbation anal. 77−27486
- plates, variable thickness annular, axisymmetric bending 79−46193
- plates laminated, shear deformations and correction factors, plate and elasticity theory 79−76963
- PMMA, kinetic theory of quasi-brittle fracture, crack tip inelastic deform. *(German)* 78−84991
- 1,2-polybutadiene, crosslinked in states of strain, entanglement networks, swelling anisotropy obs. 80−79666
- polycarbonate, anelastic component of strain *(Japanese)* 77−8870
- polydimethylsiloxane, end-linked chains, elastomeric properties, dilution effects 79−90570
- polyethylene terephthalate, oriented, amorphous, stress-induced crystn., shrinkage meas. 80−92466
- polyhedral sandwich domes, elastic behaviour, failure, practical investigation and numerical simulation 78−59309
- polymer, frost deform. 77−50624
- polymer, specimen size effect on mech. behaviour associated with crazing 77−73337
- polymer chain trapped in suddenly deformed gel, relaxation *(French)* 77−62483
- polymer crystallisation from solutions and melts 80−10504
- polymer melts, viscoelastic model of uniaxial and biaxial stretching 77−68547
- polymeric, liq., spike-strain test relevance for network connectivity destruction by deformation 80−6001
- polymers, damage accumulation problem *(Russian)* 80−21053
- polymers, fluid, harmonic distortions, under nonlinear periodic deform. 80−28482
- polypropylene, glass-fibre-reinforced, design stress data, w.r.t. time, temperature and composition effects 79−96098
- polypropylene, shear effect on crystallisation *(German)* 78−75586
- polystyrene, atactic, indentation recovery, defect struct. produced by deformation 79−43275
- polyurethaneurylenes, segmented, structural features *(Russian)* 77−47356
- porcine skin, herniorrhaphic reinforcing prosthetic, mech. and struct. props., SEM study 79−74789
- poroelastic cylinder, twisted pore effect on fluid flow, solid deformation and stress 80−64377
- powder, deforming, self-diffusion coeffs. in failure zones and percolation 80−76209
- practical constitutive equation covering a wide range of strain rates 79−80434
- precipitation hardening, effect on dynamic strain ageing and jerky flow 80−20945
- Pyrex glass, indentation recovery, defect struct. produced by deformation 79−43275
- quartz, synthetic, fading rel. to lattice deformation *(German)* 78−63760
- quartz, torsional vibration frequency temp. depend. 80−70294
- quartz c-axis orientation in Saxony Granulites, petrofabric anal. by optical and X-ray diffr. studies 80−21740
- quartz grains in Moine thrust zone, deformation-induced microstructs. rel. to differential stress 80−85652
- radiospectrometer resonator uniaxial crystal deformation unit 80−31822
- reactor fuel cladding strain, effect of fuel density and fuel relocation, in-reactor meas. 80−104408
- reactor fuel sheathing strain at high temp., steam oxidation effect 77−6525
- reactor graphite, stress and strain determ. depend. of mech. characts. on temp. and fluence 79−40998
- rectangular block, non-normality and bifurcation in plane strain tension and compression 80−19251
- rectangular plates, moderately thick, free flexural vibr., effect of geometric nonlinearity 79−3940
- red cell membrane, human, surface elasticity and viscosity 80−61608
- refractory ceramic, heterogeneous, significance of non-elastic deform. in fracture 79−47765
- refractory material, with phosphate binder base, filler content and temp. influence on strain and thermal expansion *(Russian)* 80−19964
- reinforced concrete containment model behaviour under thermal gradients and internal pressure 80−42837
- rib cage deformation during static inspiratory efforts 80−45933
- rock, diagnostic stress-relief curves in stress meas. by overcoring 79−29886
- rock, dry, quantitative model of dilatancy and appl. to Westerly granite 79−16445
- rock, strain estimation from deformed ellipsoidal objects, algebraic method 77−21766

deformation continued
rock, triaxial loading apparatus for time-depend. behaviour determ. 77—9538
rock elastic wave velocity, deformation of brittle rock at high-press. *(German)* 80—36296
rock failure precursors during anelastic deformation 78—61405
rock mass deformability determ., in situ tests 79—53341
rocks, anisotropic, irreversible deformation under hydrostatic pressure 77—73724
rocks, deform. expt. on granular material in transmitted light 77—86860
rocks, effect of stress cycling and inelastic volumetric strain on remanent magnetisation 78—88820
rocks, elliptical particles non-coaxial deform. 79—79829
rocks, finite and incremental deforms. recorded by planar subfabrics in S-tectonites 77—21767
rocks, metamorphic, thermomechanical expts. using shear machine *(French)* 79—5474
rocks, shape of single-layer folds at small but finite amplitude 80—56473
rocks, shortening/rot. relation for symmetrical folds straight limbs 79—79841
rocks, strained units stratigraphic thickness determ. 79—21034
rocks, struct.-forming props. of bedded forms. from modelling data *(Russian)* 79—8627
rocks anisotropy evolution under isotropic cyclic compression *(French)* 77—41021
rocks crenulation cleavage, mechanical significance investigations 80—21737
rocks experimental folding under confining press., drape folds partially scaled models 79—58127
rocks flow cleavage formation, significance of rocks mechanical heterogeneities 79—57934
rocks of crystalline basement, mechanical processes rel. to ductile deform zones and mylonites form. 79—53344
rocks rotational deformation, reversal of inclusion trails spiral direction in paratectonic porphyroblasts 79—39717
rocks single layer folds, arc lengths, comparison between theory and obs. 79—53345
rocks with foliation or faults, deform. due to plane strain 80—21720
rod, composite, stress deformation state calc. *(Russian)* 79—64527
rubber, natural, stretching effects on glass transition, sp. ht. obs. *(German)* 78—79753
Rzhanitsyn-Koltunov nucleus, anal. determ., relax. function for shear and stretching 80—58932
Sambagawa schist, Central Shikoku, Japan, deform. rel. to albite porphyroblasts growth 80—26509
sandstone, fault development, deformation bands and slip surfaces 79—20819
sandstone, small faults as deformation bands 79—25235
sandwich plates, simply supported in shear, critical stresses *(Polish)* 79—32247
sea ice field of Okhotsk Sea coast of Hokkaido, divergence and rot. meas. *(Japanese)* 78—96223
sheet metals, strain-induced changes in mech. props. and press formabilities 78—19781
shell, spherical, non-shallow, moderately thick, stresses and deform. 79—32241
shell design by finite element method, deformation and elasticity theory 80—74747
shell formed by truncated cones, stability and deformation 80—69691
shells, laminated composite circular cylindrical, prebuckling deformation effects on buckling 80—48609
shells, nonlinear Reissner-type theoretical relations *(Russian)* 79—55329
shells of arbitrary geometry, finite element anal. 78—34044
shells of revolution with inhomogeneous boundary conditions, deformation 80—33480
shock tube diaphragm opening process, model for inelastic diaphragm 79—7384
Signorini's problems, reciprocal variational inequalities soln. 79—41585
simple shear generation *(German)* 77—44432
single flat spring fulcrum, anal. *(Japanese)* 77—39214
skull, human, deformation, model of cupola with flat base 77—36966
sliding interfaces and impact, numerical treatment 79—41631
slope forms in Al(1) clay of Frankische Alb, statistical investigation of deform. *(German)* 78—57211
smectic cylinder, instabilities under mech. tension 77—19868
smectic liquid crystals, mech. instability under dilative or compressive stresses 77—31583
soil, water saturated-unsaturated flow in deformable porous medium, numerical model 77—91181
soils, non-linear seismic response and liquefaction 79—57862
solar wind cavity deformation by interstellar medium, effect on cosmic ray diffusion 79—53680
solid body, unbroken continuity conditions, role in description of deformed state *(Russian)* 77—84159
spherical indentation mechanics, appl. to reversible and irreversible contact between rough surfaces 78—13976
spherical pore in solid body, physiocomechanical processes 80—100364
stability study for three-dimens. deformable bodies 80—14596
steel, Cr-Ni-(Mo) (25, 28, 2 wt.%), lattice dilation by N_2 77—16592
steel, fully annealed tool, cantilever beams, nonlinear damping for nonsinusoidal strain 79—47762
steel, low C, low alloy, ferritic-pearlitic, high temp. mech. treatment, cooling effect 80—104193
steel, porous, permeability, deform. effects 79—100229
steel, sheet, effects of strain rate and deformation heating in tensile testing 78—85089
steel, stainless, beam, deformation rel. to H_2 diffusion 80—39360
steel, stainless, cladding dimensional changes in FBR $(U,Pu)O_2$ fuel pins due to swelling and inelastic strain 80—104296
steel, stainless, type 304, TEM study of dislocation emission from grain boundaries 79—66121
steel mesh, herniorrhaphic reinforcing prosthetic, mech. and struct. props., SEM study 79—74789
stellar models, tidally distorted, small oscills., Roche coordinates appl., second-order terms effect 79—44462
strain distribution near notch tip under mixed plane stress-plane strain condition *(Japanese)* 77—8891
strain driven thermoelastic instability toward brittle fracture 80—103415
strain-tensor components expressed in terms of lattice parameters 78—26618

deformation continued
structurally inhomogeneous solid bodies, mechanics *(Russian)* 79—30231
Sun, evidence for distortion rotating with period of 12.2 days 77—17502
surface and environmental effects 77—4145
surface forces power of medium with limited intensity of tangential stresses 79—14278
surface segregation, bond and strain energy effects, Monte Carlo method 79—74161
symmetry considerations for materials of second grade 79—37161
teeth and mandibles, deforms. due to occlusal forces, holographic interferometry 80—67205
telescope, altazimuth mounted, primary mirror deflection and stress anal. 80—58659
thermal, interference 80—78806
thermoplastic films, quasistatic theory of frost deform. 79—56052
thermoplastic recording material, latent image and surface deformation *(German)* 80—42284
thermoplastic recording media, electrocapillary effect, tangential extension influence on 'frost' deform. *(Russian)* 77—68249
thin bodies with cracks, deform. stability problem statement *(Russian)* 77—35081
three dimensional deformation measurement, Moire and light slicing methods 78—8382
αTi, work hardened in tension, developed of internal strain *(French)* 78—76716
transversely isotropic half space, indentation anal. 80—92090
triaxial stress condition, modelling *(Russian)* 79—27515
tube, porous, nonlinear viscoelastic materials, soln. using generalised correspondence principle 80—38288
underwater acoustical compliance tube for sound projectors, stress and deformation analysis 80—33310
urease shear inactivation, metal ion effect, rel. to shear deform. effects in enzyme catalysis 78—76982
viscida, buckling and stretching, surface tension effects 79—10512
viscoelastic, crack growth relations, for orthotropic, prestrained media 78—90772
viscoelastic bodies, deformation taking into account influence of accumulated defects 80—19252
viscoelastic deformation, apparent activation energy, creep T-jump expt. 79—37264
viscoelastic deformation of incompressible material, thermomechanical theory *(Russian)* 78—63327
viscoelastic multiple filament yarn, finite extension, slender curved rods theory 78—75076
viscoelastic rod, standard linear body, free torsional ascills. 80—99940
viscoelasticity, time reversal and symmetry relations 80—102970
wood, yield stress, strain-rate theory, moisture effects 77—16646
X-ray diffr. line profile analysis, on-line computer routine, microstrain determ. 78—79498
X-ray integration method, extension of $\sin^2\psi$ method *(German)* 80—92420
Zircaloy cladding, enhanced steam oxidation by deformation under LWR LOCA 80—73917
ZTL-180 zenith telescope, objective distortion determ. from visual obs. of star pairs *(Russian)* 78—89068
Ag, deformed, exoelectron emission and electron energy distrib. 80—7481
Ag, electron irrad., elastic moduli and internal function *(French)* 78—87703
Ag:Er(Dy), orbit-lattice coupling, nonuniform strain effects 78—88182
Al alloys, thermally activated deformation, exam. of hypothesis 78—72820
Al bronze, elastic limit after repeated transverse deformation *(Russian)* 77—66668
Al, cantilever beams, nonlinear damping for nonsinusoidal strain 79—47762
Al, circular plate perforation and deformation by square section punch 79—34100
Al, cold worked, effect of bias stress on US attenuation induced by geometrical kinks mobility *(French)* 77—31728
Al film, deform. under He ion bombardment 80—65073
Al, isoaxial bicrystal, Moire investigation of mechanical behaviour 77—16647
Al, polycrystalline, abrasion, deform., fatigue, study by exoelectron microscope *(Japanese)* 78—74108
Al, single crystal, deformation behaviour during cold rolling 79—47751
Al smelting cathodes, comp. and props. 77—28740
Al, surface strengthening of single crysts. on coating with evaporated films 77—8972
Al:Er(Dy), orbit-lattice coupling, nonuniform strain effects 78—88182
Al-alloys, precipitation hardening, effect on dynamic strain ageing and jerky flow 80—20945
Al-Zn-Mg, type 7075, strain rate effects on H embrittlement 80—3190
α-Al_2O_3:Co^{3+}, local deform. due to uniaxial stress 80—34140
α-Al_2O_3:Cr^{3+}, local deform. due to uniaxial stress 80—34140
α-Al_2O_3:V^{3+}, local deform. due to uniaxial stress 80—34140
Al_2O_3-Cr_2O_3, microstrain correction 78—59852
As, elastic moduli, calc. from interatomic forces 79—95071
$As_{50}Se_{50}$ and $As_{20}Se_{80}$ semicond. glasses, densified, photoluminesc., inelastic deform. effect 80—66293
Au, deformed, exoelectron emission and electron energy distrib. 80—7481
BN, wurtzite-type, lattice distortions 77—11636
Bi, elastic moduli, calc. from interatomic forces 79—95071
Bi_2O_3-Sm_2O_3 eutectoid system, isothermal deformation 77—63625
$Bi_{0.925}Sb_{0.075}$, semiconductor-semimetal transition under tensile strain, Shubnikov-de Haas oscills. obs. 80—44678
C adsorbent, granules and artifacts, strength, mech. characts. 78—23771
C, internal strain rel. to strain tensor, group theory anal. 79—86835
$CaCO_3$, with perfect struct., temp. depend. of rate of twinning 80—10561
CaF_2:Gd^{3+}, cubic, strain effects on EPR by UMER method 77—1592
Co, internal strain rel. to strain tensor, group theory anal. 79—86835
CsI:Tl single crystal gamma-optical converting screens, factors influencing relative afterglow intensity 79—8173
Cu, bidirectional twisting, effect on elongation and ductility changes 77—44315
Cu, circular plate perforation and deformation by square section punch 79—34100
Cu, deformation hardening by shock front, quasiisentropic compression, front width effects 79—100209
Cu, deformation in ultramicrotomy 77—8874

deformation continued
  Cu, pure, dynamic stress strain relations in combined tension and torsion, testing device 80—21197
  Cu-Mn (3 to 20 at.%), high temp. steady state tensile deform. *(Japanese)* 78—52917
  Cu-Ti (3.5 wt.%), aged by US strain, struct. and props. *(Russian)* 80—21003
  Fe, dynamic hot densification, degree of deformation 77—63585
  Fe, grey cast, deform. and fracture regions in microzones *(Russian)* 78—80585
  $Fe_{44}Ni_{40}P_{14}B_6$, homogeneous deformation effect on crystn. and Curie temp. 80—21045
  Ge, internal strain rel. to strain tensor, group theory anal. 79—86835
  Ge, stressed cryst., props. of strain-confined electron-hole liquid 79—7787
  H-bonded solid, bond failure theory 79—73246
  K arrested left ventricle finite deformation anal. in canine hearts *(Japanese)* 78—3543
  $LaAg_xIn_{1-x}$ alloys, structural instability 78—79562
  LiF, single crystal, dislocation generation, beneath static and rolling contact with sphere 78—87671
  $(Mg,Fe)_2SiO_4$, shock deform. expts., Hugoniot data implications 80—94497
  Mg-Si (5 wt.%), thermally induced strains, X-ray line broadening 77—4809
  $MgAl_2O_4$, internal strain rel. to strain tensor, group theory anal. 79—86835
  MgO, cryst., cumulative deform. by softer sliders 77—4154
  Mo crystals, joined by compression during heating, structural changes *(Russian)* 80—108513
  Mo, porous, permeability, deform. effects 79—100229
  Nb_3Sn, A-15 compounds, interlattice displacements, elastic consts. 78—55906
  Nb_3Sn, filaments in Cu matrix, thermal strain effects on superconducting critical temp. 80—93032
  Nd, internal strain rel. to strain tensor, group theory anal. 79—86835
  Ni, deformation hardening by shock front, quasiisentropic compression, front width effects 79—100209
  Ni, deformed by filing, fine struct. obs. *(Russian)* 77—21309
  Ni perfect crystal, stability under various stresses 80—104208
  Ni-Ti, Nitinol memory material heat engine, comment on efficiency 80—3529
  Ni-Ti, Nitinol memory material heat engine, reply to comments on efficiency 80—3530
  Ni-Ti, structural instability, deform. effects on electron energy spectrum 80—39284
  NiH, H impurity screening, lattice deformation, dipole force tensor component calcs. 79—77611
  Ni_3Mn, ordered at below Kurnakov temp. then deform., a/2⟨110⟩ dislocations and deform. antiphase boundaries *(French)* 77—51384
  $Pb_{0.94}Sr_{0.06}Ti_{0.47}Zr_{0.53}O_3$, piezoelectric ceramic, stress relax., time depend. deformation 80—60899
  $Pb(Zr,Ti)O_3$, fracture and deform. 80—79870
  $Pd_{77.5}Si_{16.5}Cu_6$ amorphous, indentation recovery, defect struct. produced by deformation 79—43275
  Re, Fermi surface, Landau quantum oscill. meas. in magnetostriction, stress and strain derivatives 80—107691
  Sb, elastic moduli, calc. from interatomic forces 79—95071
  Si, internal strain rel. to strain tensor, group theory anal. 79—86835
  Si, polycrystalline multilayer support struct., control of deform. in dielec. isolated substrates 80—107681
  Si surfaces, influencing microstruct. deform. process by impurity type *(German)* 79—65107
  Si wafer, deformation *(Japanese)* 78—43064
  Si whiskers, as basis for low-temp. sensors of temp. and deformation 79—5095
  Si:B(P)(Ge), strain distributions rel. to dopant conc., accurate determ. by X-ray Bragg reflection 77—19835
  Si:P, diffusivity, strain-induced band gap narrowing, E-centres 80—29228
  Sn plate rolling, cold, roll-force model 77—4788
  Sn, white, Fermi surface, dilational strain depend., OPW calcs. 80—84418
  Te, cryst., effect on Hall coeff. and conductivity 79—7847
  Te, elec. props. anisotropy, influence of deform. and annealing 77—15859
  α-Ti, strain driven thermoelastic instability toward brittle fracture 80—103415
  UO_2, lattice shear distortions 79—99221
  $V_3Si(Ge)$, A-15 compounds, interlattice displacements, elastic consts. 78—55906
  ZnSe:Cr, piezodichroism due to reorientation of Jahn-Teller centres 80—11363
  $Zr(Ca)O_{2-x}$, lattice shear distortions 79—99221
deformation lines *see Luder's bands*
degenerate semiconductor materials *see degenerate semiconductors*
degenerate semiconductors
  see also heavily doped semiconductors; superconducting semiconductors
  acoustodielectric effect, permittivity modulation by acoustic wave in resonance conditions 80—92944
  alignment and orientation of hot excitons, secondary radiation polarisation calcs. 79—65392
  antiferromagnetic degenerate semiconductor, thermal and mag. props. 78—19224
  antiferromagnetic-semiconductor, conduction electron spectrum, influence of nonlinear spin waves 79—28270
  Auger recombination, carrier density depend. 79—38089
  Auger recombination, phonon-assisted 77—59292
  band to band radiative recombination *(Russian)* 78—35200
  beat effect of sp. ht. due to impurities, in external mag. field 78—10401
  carrier densities and emitter efficiency in materials with position depend. band struct. 78—43378
  chalcogenide lone-pair semicond. charged impurities, effect on carrier concs., Street-Mott model 78—67984
  conduction current and generalised Einstein rels., from Boltzmann transport eqn. 77—15810
  conduction electron acoustic spin resonance, oscillations of absorbed power 80—108075
  conduction electrons, average energy in non-parabolic semiconds. 77—55521
  current instability, hydrodynamic modes, soft modes and fluctuation spectra 79—65491
degenerate semiconductors continued
  Debye screening length, non-parabolic bands, oscill. depend. on quantizing mag. field 78—2438
  diamagnetic excitons in semiconds. with degenerate valence band and oscillatory magnetoabsorpt. of GaSb 77—76754
  dielectric permeability sound wave induced nonlinear modulation *(Russian)* 80—16008
  diffusivity-mobility ratio under mag. quantisation, band non-parabolicity effects 77—20339
  education, Shubnikov-de Haas oscills., InSb degenerate semiconductor, third-year undergraduate expt. 79—9051
  Einstein relation, appl. of empirical approxs. 79—23970
  electric field influence on exciton states, Stark effect 80—54617
  electron density dependent ordering parameter and role in elec. prop. anomalies *(Russian)* 77—43582
  electron diffusion thermopower, oscillatory, mag. quantisation effects 79—91088
  electron g-factor determ. 80—20070
  electron traps, degeneracy factors, energy levels, solubility estimation 78—14691
  electron-hole drops, Auger recomb. 78—39600
  electron-hole plasma, coexisting phases 77—1374
  EM wave absorpt. due to electron-phonon collisions in quantising mag. field 79—7795
  EM wave absorpt. theory 79—33307
  EM wave absorption, depend. on external quantising mag. field 78—95308
  energy band structure effect on transverse magnetoresistance 80—88580
  entropy production and choice of heat flux 77—15778
  exciton dispersion 77—69248
  Fermi energies in semiconductors with nonparabolic energy bands, magnetic quantisation 78—30864
  ferroelectric transition, quantising mag. field effect 79—87403
  ferromagnetic, electric field response and electrofluctuation instability *(Russian)* 78—56083
  ferromagnetic, heavily-doped, surface magnetisation 77—8385
  ferromagnetic, mag. excitations, light scatt. 77—63161
  ferromagnetic degenerate semiconductor, magnon spectrum near instability of homogeneous state 79—28516
  ferromagnetic degenerate semiconductors, Curie temp. 78—6529
  ferromagnetic semiconductor, carrier-assisted radiation pumping of spin waves under strong mag. field 77—55667
  ferromagnetic semiconductor, homogeneous state, phase transition and stability 78—6528
  film, with different surfaces, transport effects in weak mag. fields 79—73607
  film, with unlike surfaces, theory of kinetic effects *(Russian)* 79—51694
  films, photogalvanic effect calcs., electron mean free path, size effect 80—34487
  galvanomagnetic phenomena, model, transport phenomena in presence of medium range disorder *(French)* 78—56162
  heavily doped, complex dielec. function 79—90982
  heavy hole-phonon bound states for valence band with degeneracy point *(Russian)* 80—15461
  helicons, LF, excitation and amplification by HF helicoidal wave 78—14755
  heterogeneous state, first-order phase transition, Ginzberg-Landau method analogue 80—70372
  hot electron transport in parabolic energy bands, kinetic theory, transport coeffs. 80—29412
  impact ionisation theory 80—49752
  impurity band struct. for dense donors and acceptors 80—29348
  intervalley phonon scatt., energy loss rate and momentum relax. time 79—15139
  ionic crystal/degenerate semiconductor interface, localised plasmon-optical phonon coupled modes 77—28071
  ionised impurity scattering cross-section, variational calc. 80—20180
  junction with position-dependent band struct., density-voltage relation 79—87150
  Kane semiconductor, nonlinear galvanomag. effects, quantum theory 77—55553
  longitudinal thermo-EMF in quantising mag. field, scatt. mechanism *(Russian)* 80—24960
  low-frequency polarisability of degenerate electron system, RPA calc. with temp. correction 79—95354
  magnetic semiconductor, magnon-acoustic phonon interaction 77—72893
  magnetites, cond mechanisms *(Russian)* 79—42539
  many-valley degenerate semiconds., supercond. transition temp. *(Russian)* 78—56254
  mobility due to point defect scatt. calc. 78—19029
  MOS, many-body effects in n-Si inversion layers, excitation to higher subbands 77—62997
  narrow gap semiconductors, ferroelec. phase transition, hybridization effect *(Russian)* 79—61319
  nonlinear current density, theory 78—56149
  nonparabolic, acoustic wave absorption/amplification coefficient 78—64069
  nonparabolic, acoustoelec. absorpt. theory 77—85269
  p-type, hot carrier distrib. function and cond. 77—28190
  Peierls instability in field of strong EM wave 79—15106
  permittivity of degenerate electrons interacting with optical phonons 77—24815
  photostimulated light absorption in Burnstein-Moss effect *(Russian)* 79—28706
  photostimulated odd magnetoresist. 77—15910
  piezoelectric, transverse magnetoresist. in strong field, quantum effect 80—80299
  plasma, Fermi energy determ., Coulomb collisions in quantising mag. field *(Russian)* 78—55715
  plasmon-plasmon interactions 78—30882
  polar, asymptotic soln. to Boltzmann transport equation 77—4332
  polar semiconductors, electron scattering interaction with coupled plasmon-polar-phonon modes 79—42536
  polaron gas, interacting, ground state energy 77—76758
  quantized film, screening of elec. field and Coulomb interaction in strong mag. fields 79—69611
  quasi-two-dimensional, warm electrons 78—60222
  quasione dimensional crystals, effect of band filling on features of struct. transition 78—2424
  Raman scattering, free carriers effect, complex band struct. 77—44001
  recombination-generation currents derivation 78—52007

degenerate semiconductors continued
- resonance Raman scatt., Green's function approach 80—80781
- Schottky barrier, low temp. capacitance 80—60075
- Schottky barrier with degenerate inversion layer, minority carrier injection 77—20434
- surface optical phonons 80—70520
- surface photo-EMF 79—69580
- surface photoelectric effects, influence of excitation rates 79—69547
- surface plasmon-optical phonon coupled modes at interface with ionic cryst. 78—38930
- surface polaritons, hydrodynamical model 80—6752
- tetrahedral, valence band degeneracy, polar electron-phonon interaction effect, exciton binding energy 79—56140
- transport properties, Sondheimer oscills., asymptotic behaviour 78—19059
- transverse magnetoresistance in strong mag. fields 79—99565
- US amplification by temp. gradient 77—20366
- valence band semiconductors, polariton effect 79—15102
- AlSb, indirect exciton dispersion, 'camel's back' 79—73447
- θ-$Al_{0.35}V_2O_5$, NMR of ^{51}V 80—71232
- Cd_3As_2, thermoreflectance spectra 78—6702
- Cd_3As_2, valence band struct., optical absorpt. meas. 80—50293
- $Cd_{1-x}Mn_xTe$, magnetic behaviour of Mn 78—14938
- Cd_3P_2, energy band struct. and electron mobility at low temp. 79—37984
- Cd_3P_2, g-factor of conduction electrons at low temp. 79—56118
- $Cu_yCr_2Se_{4-z}Br_x$, degenerate ferromag. semicond., resist. minimum 79—73517
- $CuInS_2$:Cd(Zn), elec. props. 77—62927
- $Cu_2S_{1-x}Te_x$, thermal conductivity 77—35765
- EuB_6, Hall effect and resistivity data, ferromagnetic ordering temp., pressure depend. 80—60010
- EuO, degenerate ferromag. semiconductor, mechanism of transition to insulating state *(Russian)* 77—8024
- EuO:La, photothreshold reduction by mag. induced space charge layer 78—72692
- θ-$Fe_{0.35}V_2O_5$, NMR of ^{51}V 80—71232
- GaAs epitaxial layer and Sn-doped bulk characterisation 79—82596
- GaAs, excitons, diamond like semiconductor, variational calculation of binding energies 78—79938
- GaAs, impurity band struct. for dense donors and acceptors 80—29348
- GaAs, nonequilib. electron distrib. functions 77—63394
- GaAs:Te, heavily doped degenerate semicond., Kondo effect 79—61053
- p-GaAs:Zn, Mn, degenerate, tunnel p-n junction and semicond.-metal struct., I-V characts. 78—72252
- GaP, indirect exciton dispersion, 'camel's back' 79—73447
- GaSb, degenerate valence band, diamag. excitons and oscillatory magnetoabsorpt. 77—76754
- n-GaSb, galvanomagnetic effects 78—72172
- n-Ge, Brillouin scatt. by phonon zero sound, in quantising mag. field 77—69847
- Ge, degenerate, doped with nonmag. impurities, Kondo effect 78—14746
- Ge, degenerate, scattering by light by phonon zero sound 79—56145
- Ge, highly degenerate multicomponent plasma thermodynamic props., electron hole drop transition 80—33739
- n-Ge, substrate for slab of GaAs, surface polaritons, hydrodynamical model 80—6752
- $Ge_{1-x}Mn_xTe$, magnetic behaviour of Mn 78—14938
- GeTe, degenerate semiconductor, EPR experiments on Mn^{2+} 79—11339
- GeTe:Mn, thermoelec. power, 2.5-25K, magnon drag effect 78—56169
- $Hg_{1-x}Mn_xTe$, magnetic behaviour of Mn 78—14938
- n-In Ar:Te(Sn), heavily doped, cathodoluminescence, doping effect on luminesc. band position and spectral profile 80—45153
- n-InAs, cathodoluminescence, radiative recomb. of hot carriers 77—8667
- n-InSb, acoustomagnetoelec. effect obs. 78—72207
- n-InSb film, degenerate, electron conc. and resist. temp. depend., band struct. 77—76971
- InSb film, degenerate, concs. and ionisation energies of defect levels, Hall effect meas. 79—91087
- n-InSb, highly doped, transverse magnetoresistance in strong mag. field 79—56246
- n-InSb, photoconductivity, 1.8K, hot-carrier and free-carrier absorption. effects 78—84254
- n-InSb, reson. excitation of Kondo effect and negative magnetoresist. *(Russian)* 78—56159
- InSb, surface photo-EMF depend. on bulk consts. 79—69580
- InSb:Te, heavily doped degenerate semicond., Kondo effect 79—61053
- Mo_6S_8 Chevrel phases with group IIIa metals, Nb, Hg, Pb and Cu, synthesis, stability and characts. 80—71608
- $Pb_{1-x}Ge_xTe$, degenerate semiconducting ferroelectric, structural phase transition temp., mag. field effects 80—45017
- PbSe, electron gas magnetisation, energy band parameters determ., use of Faraday effect 80—45047
- $Pb_xSn_{1-x}O_2$:Sb films, DC sputtered, elec. props. 80—80426
- $Pb_{1-x}Sn_xTe$, absorption edge shift, energy gap determ. 78—88308
- $Pb_{1-x}Sn_xTe$, displacive phase transition, effect of interband hybridisation 79—33233
- $Pb_{1-x}Sn_xTe$, electron-phonon interaction 78—71819
- $Pb_{1-x}Sn_xTe$, ferroelec. phase transition, hybridization effect *(Russian)* 79—61319
- $Pb_{1-x}Sn_xTe$, soft mode, ferroelec. phase transition crit. temp. and dielec. const. calcs. 77—8530
- PbTe, asymm. strip line wall, EM wave propag. in mag. field 77—76854
- Si, (111) surface, electron inversion layers, obs. of sixfold valley degeneracy 79—38176
- Si, Auger recombination 78—26883
- n-Si, degenerate, density of states from elastic consts. 80—6690
- p-Si, degenerate, Raman effect, interacting elementary excitations 78—43846
- n-Si:Mg, energy levels and degeneracy ratios determ. by Hall effect meas. 79—90993
- $Sn_{1-x}Mn_xTe$, degenerate mag. semicond., thermoelec. power meas. 80—29392
- $Sn_{1-x}Mn_xTe$, magnetic behaviour of Mn 78—14938
- SnO_2:Sb transparent conductive coatings for Cu_2S-CdS solar cells 79—61992
- SnTe, ferroelec. transition, quantising mag. field effect 79—87403
- SnTe, mag-props., effect of structure transition 78—6158
- SnTe:Mn, ferromag.-ordering, transverse magnetoresist. and Hall effect meas. 77—85240
- SnTe:Mn, NMR shift meas. 80—97154
- SnTe-MnTe, degenerate semicond., anomalous Hall effect 80—29420
- Te, optical activity rel. to band struct., 4 to 300K 77—77165

degenerate semiconductors continued
- TiS_2, carrier-lattice coupling 78—63822
- Tl_2O_3 single crystal, elec. cond., cryst. grown from vapour in air 77—85219
- Tl_2O_3, single crystal, elec. cond., annealing at 923K in O_2 effects 77—85220
- n-ZnO film, highly degenerate, IR absorption by free polarons 77—4697

dekatrons
- X-ray diffractometer scanning block modernisation by scaler adjustment 80—31958

delay circuits
- *see also delay lines; phase shifters*
- adjustable read delay device for sampling system Auto 200^{TM} for at. absorpt. spectroscopy 77—32846
- CRO time-mark circuit with controlled delay 79—35703
- digital trigger delay unit for automatic variable-path-length US meas. 77—11095
- high-speed rotational vacuum tap for discharge gas sampling 78—57969
- mass spectrometer electron multiplier three-state time delay switch 80—37116
- neural spike window discriminator confirmation by analogue delay cct. 77—21664
- oscilloscopes given dual delayed-sweep capability, low cost 77—18004
- paroxysmal supraventricular tachycardia management by scanning pacemaker system 77—81676
- second derivative of plasma probe charact. meas. by delay circuit 77—39461
- slave triggers for photographic flash 80—95168
- sonar time delay design using CCD 80—43570
- sound triggered electronic photo flash unit, using variable time delay 80—57407
- trigger, for N_2 pulsed laser interfacing with higher freq. electro-optic instrumentation 77—50698

delay-differential systems
- distributed parameter system control, conference, Coventry (1977) 79—3897
- second order, stable equilibrium state domain of attraction estimation 77—34374

delay elements (circuits) *see delay circuits*

delay lines
- *see also acoustic delay lines*
- amorphous ribbon, saturation magnetostriction, and electronically controllable delay line 79—1700
- bi-dimensional drift chambers with flexible PC balanced delay lines 79—3300
- bucket brigade, delayed auditory feedback unit for inhibition of stammering appl. 78—31825
- cable, controllable microsecond for logical nanosecond signals 77—18756
- capacitively coupled distributed parameter delay lines, development for use in a multiparameter focal plane detector 80—78491
- delay line readout for drift chambers 79—3317
- differentiator for meas. of electron energy distrib. function in plasma *(Japanese)* 80—84002
- digital, for sound recording and reproduction in cinematography *(Russian)* 79—27487
- drift chamber two-dimens., with thin printed-circuit tape delay line 77—54422
- electronic, dynamically variable, for real-time US imaging 79—46142
- electrostatic accelerator delay line voltage multiplier 78—33326
- EM delay lines readout in spark, proportional, and drift chamber appl. 78—74547
- EM line for position readout in wire chambers 80—18757
- fibre and integrated optical devices for signal processing 80—33233
- fibre optic, for pulse coding 77—83970
- fibre-optic delay line signal processing devices 80—48443
- flat helical, for position readout along anode wire of multiwire and drift chambers 77—54426
- frequency comparator for generator spectral line width measurements 79—6144
- garnet epitaxial film, elastic surface wave propag., magnetoelastic effect 77—20669
- helical delay line position sensitive proportional counters for mag. spectrometers 79—68160
- homogeneous RF field delay line probe for pulsed NMR, anal. 77—49758
- inductance-capacitance encoding live, in position sensitive X-ray detector 78—12800
- logic system, multichannel remotely programmable 77—10560
- matched filters, using optical delay line provide encoding or decoding structures 78—74983
- metal-magnetodielectric layered delay lines, dispersion eqn. *(Russian)* 80—88736
- MWPC, γ-image blurring reduction by delay line readout 78—37492
- MWPC, delay line readout of anode wires 77—38571
- MWPC, IC tapped delay line readout 80—5455
- MWPC, improvement of position resolution from delay line readout 78—74543
- MWPC, multi-delay line cathode readout 79—45573
- MWPC, position sensitive, fast delay line readout 78—37490
- MWPC using EM delay lines, read-out system *(French)* 77—88349
- optical, 3 μs delay, spherical mirrors, appl. to photography 77—764
- optical, freq. chirped pulse compression using phonon-polariton propag. modes 78—46689
- optical, multipath optical cavities in saturated absorpt. expts. 77—65610
- optical, OLZ-7 seven-frame, using multiple reflections in plane mirrors 79—23080
- optical, to control solid state laser output characts. 80—99758
- optical, using multiple refl. in spherical resonator 77—27368
- optical delay lines in laser cavity 77—720
- optical fibre delay line phase discriminator, operating principles 79—18507
- optical fibre network, for encoding and decoding 78—25963
- optical fibres, jacketed and unjacketed, pulse delay variations with stress and temp. 79—55232
- plasma waves, delay line simulation, wave propag. in dispersive and attenuating media 80—82606
- position sensitive proportional tube with helical delay line 79—3313
- programmable line using microstrip transmission line and temp. compensated ECL gates 79—26845

delay lines continued
proportional counters, position-sensitive, delay-line termination, timing-signals extraction 77—402
proportional delay line chambers for Fermilab external muon identifiers 78—37489
proportional wire devices with resistive cathodes, detection of induced pulses 78—70691
rods and clad rods, elastic waves anal., tutorial review 78—94608
ruby laser with optical delay line inside cavity resonator 77—42552
SAW delay line acousto-optic signal processing devices 79—94328
SAW device analogue signal processing appl. 77—27437
signal coupling of semiconductor detector to cold resistance preamplifier through cable or delay-line transformer 78—33401
signal processing fibre and integrated optical devices 79—76887
spiral, bubbles detection in insulating liquid flow 80—79415
tapped delay line focal plane detectors for mag. spectrometers 79—68161
US tracking focusing annular array transducer *(French)* 80—26301
wire readout system for spark chamber, transducer S/N ratio improvement 77—79518
Fe$_{100-x}$Be$_x$, amorphous ribbon, saturation magnetostriction, and electronically controllable delay line 79—1700
Na vapour, temporal compression of dye laser 5890 Å CW output 78—46688
Nd:YAG laser dispersive delay line, optical pulse compression of FM Nd:YAG laser 77—88815
(Tb,Dy)-Fe amorphous films prep. by cosputtering, magnetostrictive characts. 80—97429

delayed neutrons
A=135-143, odd A fission products, delayed n, decay studies and Q_β meas. 80—78227
A=79-145, β-delayed neutron emission probabilities, half-life 80—52634
A>70, review of beta-delayed particle emission 77—22972
beta strength function, half life and delays, nuclear- and astro-physics consequences 80—102149
beta strength function structures, nuclear- and astro-physics consequences 80—99152
conference on nuclear spectroscopy of fission products, Grenoble, France (May 1979) 80—77546
decay, appl. to comp. anal. of spent multicomponent reactor fuel 79—71899
delayed fission neutron technique, review 79—1979
EBR-II delayed neutron concentrations, computer modelling 80—27717
EBR-II delayed neutron monitor, response to tramp uranium and fission prod. test source 79—67919
emission probabilities of delayed fission neutrons, simple statistical model calcs. 77—50103
explosive r process cooling process 78—69791
far unstable nuclei, beta delayed two neutron emission, nuclear structure 80—68606
fast critical expts., effective delayed neutron fractions and central reactivity worths 78—62602
fast reactors, delayed neutron effective fraction sensitivity to basic data uncertainties 77—46207
FFTF, delayed-neutron parameters 79—80999
fissile material assay, cyclic method of neutron activation and delayed-neutron counting 77—34395
fissile materials, anal. by cyclic activation of delayed neutrons 78—53296
fission, yield calcs. from ENDF/B-VC 79—67798
fission product mass region, delayed neutrons and P_n values 80—78339
fission products, emission probabilities, semi-empirical formula 77—22976
fissionable isotopes in aq. soln., assay by pulsed neutron interrogation 78—68966
fissionable nuclei A=232 to 252, systemization of relative yields of retarded neutrons 79—40974
FTR, SNEAK, effective delayed neutron fractions, integral meas. on PuO$_2$/UO$_2$ 77—6497
Gamow Teller giant resonance struct., consequences for delayed neutron spectra and nucleosynthesis 77—2950
LASL Van de Graaff accelerator, nondestructive assay of fissile nuclear material 77—83182
LWBR delayed-neutron pellet assay gauge 79—54590
multigroup-multipoint diffusion operator spectrum with delayed n 78—74430
multigroup-multipoint diffusion operator with delayed neutrons, spectrum 77—54274
nuclear failed fuel element detection by delayed neutrons using solid state track-etch technique 80—5249
nuclear far from β-stability, delayed neutron energy spectra, structure effects 80—78226
nuclear reactor noise experiments with delayed neutrons, general theory 77—54316
parameters selection, for nuclear reactor calc. *(Slovak)* 78—21534
probe characts. for uranium exploration, field meas. 79—53568
pulse height spectra 78—78328
PWR, effect of measurement conditions on the design of delayed-neutron detector units *(French)* 79—97855
PWR primary circuit, delayed neutron meas., influence of photoneutrons *(Czech)* 80—5205
reactivity measurement by pulsed neutron technique, Sjostrand method foundations 78—17329
shell model approach, β-strength function 77—71595
single-particle approach, β-strengths to configs. in emitter nuclides 77—22975
spectra, gross props. 78—78327
spectra anal. using struct. of Gamow-Teller giant resonance 77—22974
spectroscopy with ^{3}He ionisation chamber 77—79501
subcritical cyclostationary nuclear reactor, neutron counting statistics, sinusoidally modulated neutron source 80—99203
time depend. neutron transport solns. in infinite media, multiple collision technique 77—82982
Z=37-43, neutron rich fission products, mass energy surface, decay props. 80—78228
β-delayed neutron decay, statistical model, Monte Carlo techniques, fictional pandemonium nucleus calcs. 78—89830
^{87}Br, delayed neutron carrier, sorption parameter determ., appl. to fuel element leak detection 79—97828
^{A}As, A=85-7, mass chain, half lives and n-emission probabilities of delayed-n precursors 78—70497

delayed neutrons continued
^{85}As, β-strength function energy struct., effect on delayed neutron emission prob. 79—75915
^{85}As, delayed neutron emission to excited states in ^{84}Se 77—14077
^{85}As, neutron and gamma-ray spectroscopy of delayed neutron emission 77—22973
Br isotopes, delayed neutron studies 77—22977
^{A}Br, A=85 to 89, total β-decay energies and atomic masses of neutron-rich isotopes 79—40889
^{A}Br, A=89-91, delayed neutron emission probabilities, β-decay half-lives 80—83078
^{87}Br, β-strength function energy struct., effect on delayed neutron emission prob. 79—75915
^{87}Br, neutron and gamma-ray spectroscopy of delayed neutron emission 77—22973
^{92}Br mass chain, half lives and n-emission probabilities of delayed-n precursors 78—70497
^{252}Cf spontaneous fission, search for low energy delayed neutrons *(Russian)* 77—34359
^{252}Cf spontaneous fission, symm. and asymm., fragment yields, β-decay chain lengths *(Russian)* 77—50181
Cs, fission fragment, delayed neutron branches from γ-spectroscopy 80—78230
Cs isotopes, delayed neutron studies 77—22977
Cs isotopes, delayed neutron Pn-values, beta+neutron+gamma decay modes 77—26639
^{143}Cs, delayed neutrons, energy spectra 80—99153
^{145}Cs, mass chain, half lives and n-emission probabilities of delayed-n precursors 78—70497
I isotopes, delayed neutron studies 77—22977
^{A}I, A=139-141, delayed neutron emission probabilities, β-decay half-lives 80—83078
^{137}I beta delayed neutrons, ^{137}Xe neutron unbound states, high energy X-rays 80—86856
^{137}I, neutron and gamma-ray spectroscopy of delayed neutron emission 77—22973
^{138}I, β-decay scheme, population of ^{137}Xe and ^{138}Xe levels, delayed neutron obs. 80—27600
^{A}In, A=120-129, total β-decay energies and masses of strongly neutron rich isotopes 78—86512
^{87}Kr energy levels from ^{87}Br β-decay, delayed neutrons, high energy γ spectra 78—25155
^{88}Kr level scheme and transitions, delayed neutrons from ^{88}Br β-decay 80—42600
^{11}Li beta decay, γ activity 80—106018
Na neutron rich isotopes, β-delayed emission of n, 2n, α, t 78—74343
^{A}Na, A=30,31,32, beta-delayed two-neutron emission 80—95316
^{239}Pu, anal. by cyclic activation of delayed neutrons 78—53296
^{239}Pu muonic atom, n emission, bound μ influence on fission barrier 78—89845
^{239}Pu(n,f), 35 to 1500 keV, near equilib. delayed neutron energy spectra 77—34354
^{239}Pu(n,f), absolute yields and group constants of delayed neutrons in fast fission 77—54261
^{239}Pu(n,f), sub MeV neutrons, equilib. delayed neutron energy spectra meas. 77—38308
Pu(n,f), delayed neutron spectra from thermal- and fast-neutron fission, reactor calcs. 77—34355
Rb, fission fragment, delayed neutron branches from γ-spectroscopy 80—78230
Rb isotopes, delayed neutron studies 77—22977
Rb isotopes, delayed neutron Pn-values, beta+neutron+gamma-ray decay modes 77—26639
^{A}Rb, A=93,94,95, delayed neutrons, energy spectra 80—99153
^{A}Rb, A=96 to 100, half-lives and neutron emission probabilities in neutron rich isotopes 79—17864
^{94}Rb β-delayed n decay, ^{93}Sr excited state depopulation γ-rays, n coincidence 80—52631
Sb, neutron rich isotopes, half-lives, fission yields, and neutron emission probabilities 77—67721
^{A}Sb, A=135-6, mass chain, half lives and n-emission probabilities of delayed-n precursors 78—70497
^{135}Sb, β-strength function energy struct., effect on delayed neutron emission prob. 79—75915
^{135}Sb, delayed neutron emission to excited states in ^{134}Te 77—14077
^{135}Sb, neutron and gamma-ray spectroscopy of delayed neutron emission 77—22973
^{93}Sr neutron binding energy from transitions and β-delayd neutron defined level correspondences 80—63070
^{232}Th, determ. of neutron multiplicities 80—32311
^{232}Th muonic atom, n emission, bound μ influence on fission barrier 78—89845
^{232}Th(n,f), 35 to 1500 keV, near equilib. delayed neutron energy spectra 77—34354
^{232}Th(n,f), fast neutrons, delayed neutron spectra, reactor calcs. 77—34355
U assay using continuous fast-neutron source 79—52849
U borehole logging system, delayed neutron activation anal. method using ^{252}Cf source 79—53569
U deposits, in situ assay logging system using delayed fission neutrons 77—37440
U exploration probes, meas. spatial depend. of delayed neutron signals 79—34989
U ore assaying by delayed fission neutron process 79—53536
^{A}U, A=235, 236, 238, determ. of neutron multiplicities 80—32311
^{A}U, A=236, 238, strength function of β-transitions, probability of delayed fission 80—22764
^{233}U-^{235}U fuel, nondestructive isotopic meas. using fission neutron counting 80—32385
^{235}U (n, f), thermal neutron fission, time-depend. delayed neutron group yields 79—54463
^{235}U, anal. by cyclic activation of delayed neutrons 78—53296
^{235}U, determ. of amount in urine by delayed-neutron counting 79—25118
^{235}U(n,f), absolute yields and group constants of delayed neutrons in fast fission 77—54261
^{235}U(n,f), thermal to 15 MeV, total delayed neutron yield calcs., energy depend. 77—34353
^{238}U(γ,f), delayed neutron energy spectrum 77—23155
^{238}U(n,f), absolute yields and group constants of delayed neutrons in fast fission 77—54261

delayed neutrons continued
U(n,f), A=233,235,238, 35 to 1500 keV, near equilib. delayed neutron energy spectrum 77—34354
U(n,f) A=235,238, sub MeV neutrons, equilib. delayed neutron energy spectra meas. 77—38308
U(n,f), delayed neutron spectra from thermal- and fast-neutron fission, reactor calcs. 77—34355

delayed protons
A>70, review of beta-delayed particle emission 77—22972
beta strength function, half life and delays, nuclear- and astro-physics consequences 80—102149
beta strength function structures, nuclear- and astro-physics consequences 80—99152
light nuclei, delayed proton precursors 77—22971
odd-odd neutron deficient nuclei, spectra of delayed protons and α-particles in β^+ decay *(Russian)* 78—46034
rare-earth isotopes, neutron deficient, β-decay and delayed protons 77—22953
^{35}Ar levels, transitions and β-delayed protons from ^{35}K decay 80—91156
Ba, A=117, 119, 121, delayed proton emitters, positron-proton coincidence meas. 78—78326
Ba isotopes, neutron deficient, β-decay and delayed protons 77—22953
Cd, A=97, 99, β delayed proton emission, spectra, branching ratio, half life 78—86517
Cs, A=114-118, neutron deficient isotopes, half lives, β^+,γ, delayed p and α meas. 78—70489
Cs, A=116-120, spectra of delayed protons and α-particles in β^+ decay *(Russian)* 78—46034
^{116}Cs, delayed particle emission in β^+ decay 78—8778
^{118}Cs, delayed particle emission in β^+ decay 78—8778
^{143}Gd^{m+g}, β^+ and EC decay 78—50130
^{65}Ge, proton spectra and $T_{1/2}$ meas. 77—38254
^{36}K, β-decay, delayed proton and alpha emission ^{36}Ar levels, J^π, transitions 80—52629
^{73}Kr, proton spectra and $T_{1/2}$ meas. 77—38254
^{85}Mo, proton spectra and $T_{1/2}$ meas. 77—38254
^{69}Se, decay, T=1/2 β-delayed proton precursor 77—88082
^{69}Se, delayed proton decay 77—22971
^{69}Se, proton spectra and $T_{1/2}$ meas. 77—38254
^{24}Si, isobaric multiplet mass eqn., test from decay 79—40890
^{77}Sr, proton spectra and $T_{1/2}$ meas. 77—38254
^{81}Zr, proton spectra and $T_{1/2}$ meas. 77—38254

delays
see also delay circuits; distributed parameter systems
acoustic Doppler effects, time delay statistics for randomly moving scatterers and platforms 77—62093
acoustics, echo time delay detection, effect of zero singularity smoothing 78—90605
acoustics, time delay estimation in presence of source or receiver motion 77—88977
acoustics, time delay meas. in noise identification problems 78—83193
adaptive delay element for seismic noise cancellation 79—74994
air breakdown formative time lag rel. to gap geometry, pressure, and overvoltage 79—18994
air gap corona pulse delay obs. and HV insulation design 79—19117
cabled fibre, temp. effect on transmission loss and pulse delay distortion 78—1407
dissector one-electron current pulse timing, delayed self-coincidence method 79—26846
Fourier spectroscopy, delay compensation, sampling error reduction 79—30566
gyroresonant electron-wave interaction without prespiralling *(Russian)* 77—31054
loudspeaker system group and phase delay requirements 80—92014
low-pass, nonrecursive filter based on analogue delay device, mass spectrometer appl. 78—92541
multidelay system coherence function meas. 79—68530
nonlinear oscillating system, delay effects *(German)* 77—53773
nonuniform helical delay system anal. *(Russian)* 79—18336
optical fibers, graded-index, wavelength dependence of differential group delay and appl. to fibre-link characterization 79—50440
optical fibre transmission loss and pulse delay distortion before and after cabling 78—1406
optical radar pulsed systems using photodetectors with lag, characts. 79—13918
parametric linear systems, time delays, optimality, control coordination and entropy *(French)* 77—9161
periodic dielectric rod array optical delay equalisation characteristics 78—5578
photon pulse delay estimation, nonregularity 78—29157
pushbroom CCD time-delay-and-integration mode image sensors 77—39087
round-the-world signal group delay, frequency dependence calc. *(Russian)* 78—61654
SAW delay calc. under uniform finite strain 77—39138
signal time delay estimation using parameter estimation of FIR filter 79—59867
sonar array paired element delay meas. with sequential state estimation 80—96128
speech intelligibility, time delay effect experiment 80—91996
transionospheric radio signal time delay spatial correlation 78—45117
troposphere communication channel, energy spectrum of delays 79—84442
underwater acoustic source location and motion estimation, joint reduction of bias and variance 80—96087
underwater acoustic time delay estimation, cross-correl. and smoothed coherence transform methods compared 80—96086
voltage delay in lithium non-aqueous battery systems 80—35662
X-ray diagnostic sets with automatic exposure relays, switching delays 77—48903
α-AlPO$_4$, berlinite, X-axis boule cut SAW props. 79—56061
LiTaO$_3$, rotated Y-cut, SH and Rayleigh surface waves 79—46910
N$_2$ breakdown formative time lag rel. to gap geometry, pressure, and overvoltage 79—18994
O$_2$ breakdown formative time lag rel. to gap geometry, pressure, and overvoltage 79—18994

delta modulation
adaptive, speech digitisation and bandwidth compression techniques *(Korean)* 79—59876

delta modulation continued
code delta-modulation for standard hydrophysical information compression *(Russian)* 78—65432
noise-tolerant continuously variable slope DM to linear predictive coding conversion 80—96141
speech digitization and bandwidth compression, ADPCM and ADM *(Korean)* 79—55273

demagnetisation
see also magnetisation
adiabatic demagnetisation, calc. of lowest temps. obtainable *(Dutch)* 77—61072
adiabatic demagnetisation using near nπ RF pulse strings 77—90050
adiabatic of nucl. spins, refrigeration 78—49844
automatic AF demagnetiser for igneous rock specimens 79—25347
automatic demagnetisation and measurement system for time decreasing permeability meas. 80—62696
chemical demagnetisation for red sandstones 80—26620
circular cylinder between infinite pole pieces, mag. field and demagnetising factor *(German)* 77—6972
curves, approximate graphic construction method for permanent mag. materials *(Chinese)* 78—80175
cylindrical demagnetisation matrix computation, FORTRAN IV program 78—76274
demagnetising field, calc. by FFT 79—38355
diamond-Co, sintered together, remanent magnetism 79—99731
domain boundaries, rigid, displacement theory including demagnetising field random perturbations *(Russian)* 77—8344
domain wall micromagnetic dynamics, numerical model 78—72381
eigenfunctions anal. of linear transverse magnetisation in long, thin stripes 80—34687
energy relations in hard and soft mag. materials 77—8353
γ-Fe$_2$O$_3$ acicular particles, remanent coercive force 80—44872
ferrites, partially magnetised, diagonal components of permeability tensor and resonance 79—47306
ferromagnetic bodies, dynamic demagnetisation 79—61184
ferromagnetic materials, demagnetisation level determination, after NDT 79—49261
ferromagnetic materials, grain-oriented demagnetisability 78—84449
ferromagnetic particles, mag. flocculation effects during mag. beneficiation 77—77809
ferromagnets, cyclically remagnetised, discrete spectra of induction calcs., demagnetising factor 80—103859
film, rel. to micromagnetic dynamics in domain walls, numerical model 78—72382
haematite, grain size and coercive force from high temp. AF demag. 77—37189
hard magnetic material, analogue perameameter appl. *(Polish)* 79—5099
hard magnetic materials, demagnetisation curve, single function approx. using computer *(Hungarian)* 78—60307
hard material demagnetisation curve evaluation 80—90869
high resolution beta spectrometer, BILL, optimal demagnetisation 77—23354
magnetic disaccommodation measurement, device, graphical or digital registration *(Polish)* 79—93180
magnetic refrigerator for operation near 2K 78—37012
magnetic tape, demagnetisation curve, hysteresis model represent. *(German)* 77—36096
mischmetal-based magnets, MM$_{1-x}$Sm$_x$Co$_5$, demagnetisation, temp. depend., 175 to 425K 79—78440
mountain rocks, directed demagnetisation rel. to palaeomag. prehistory determ. *(Russian)* 77—44917
multidomain grains, demagnetisation field 78—65273
multidomain magnetic disc, ferromagnetic reson. 78—68386
neodymium ethyl sulphate, cryst. c-axis demag. from 25000G, magnetohydrodynamic props. to 0.01K 77—20599
nonellipsoidal sample, demagnetising factor meas., magnetoelastic Rayleigh wave convolution 77—10072
nuclear demagnetisation refrigerator, microprocessor controller 80—37043
nuclear demagnetisation refrigerator, two stage *(Japanese)* 80—47063
one-dimensional system obeying third law of thermodynamics, exact theory of mag. cooling 77—66321
palaeointensity methods using AF demagnetisation and anhysteretic remanence, reliability 78—77352
Permalloy film, coercive force associated with domain boundary displacement *(Russian)* 80—50151
Permalloy film demagnetising field and magnetisation curve determ. 77—73059
permanent magnets review 79—42801
piezomagnetic rod, demagnetizing field effect, longitudinal-effect extensional vibration 78—95504
polycrystalline ferromagnets, demagnetisation and reptation (creep) anisotropy *(French)* 78—43616
rock samples, removal of rot. remanent mag. acquired during alternating field demag. 77—60474
sphere between pole pieces of electromagnet, demagnetizing factor 78—13643
steel, ferromagnetic, U8, magnetic method of martensite transform. study *(Russian)* 79—87631
steel, Mn-Si, mag. method of NDT of mech. props. 80—21211
steel, Si, permeability change due to stress variation after demagnetization in Rayleigh region 80—88854
superconductors with Ce impurities, sp. ht. jump, unified description of demagnetisation of Ce impurities 77—69450
temperature-dependent magnetic cleaning 77—41204
Ticonal, effect of rare earth metals on mag. props., struct., and phase transformations 79—99732
titanomagnetite in basalts, mag. coupling in partial self-reversal assoc. with increased mag. viscosity 77—73717
transformer steel magnetic loss variation due to nonuniform normal press. *(Russian)* 79—91250
type II superconductors, anisotropic, demagnetisation effects on lower critical field 80—97043
uniaxial crystal, with narrow domain boundaries, coercive force *(Russian)* 80—50140
Au$_{85}$Fe$_{15}$, and Au$_{82}$Fe$_{18}$, mag. props. 80—84592
Ba ferrite, FMR in uniaxial crystal plate with bubble domain lattice 80—93182
CeCo$_{5+x}$, Cu and Fe modified, coercive force *(Czech)* 79—42805

demagnetisation continued
$(Ce_xLa_{1-x})Be_{13}$, mag. intermediate valence behaviour 79—24131
Co-B-Si, mag. props. different in amorphous and cryst. phases 77—69617
Co-Cu-Fe-Ce, mag. characteristics of sintered permanent magnets 78—60312
Co-Cu-Fe-Ce alloys, sintered permanent magnets, mag. characts. 77—43855
Co-rare earth magnets testing method for mag. parameters 79—49260
$CsNiF_3$, demagnetising effects on antiferromag. reson. 80—15803
Cu, nucl. demagnetisation expts. 77—45851
$Cu(NO_3)_22.5H_2O$, spin-pair system, spin ordering, XY-model in external field 77—73033
$Cu(NO_3)_2.2.5H_2O$, adiabatic magnetisation cooling by pulsed mag. field 77—20600
Fe, high-purity, low-temp. mag. relax. after thermal ageing and demagnetisation 77—85502
Fe, Mossbauer spectra, demagnetising field effect on magnetic splitting 80—39932
Fe thin films, surface demagnetisation due to chemisorption, ferromagnetic reson. study 80—80616
Fe whisker, magnetic aftereffect in 180° mag. bowed Bloch walls 79—78432
Fe-Ni-Al-Co-Cu alloy, sintered single-crystal mag. prod., props. 77—66709
Fe-Si (3 wt.%), losses, demagnetisation freq. and grain orientation depend. 80—88796
Fe-Si (3 wt.%), nonoriented sheets, magnetisation, tensile stress effects 80—88845
$Fe_{80}B_{20}$ amorphous ribbon, initial susceptibility time lag 80—100579
γ-Fe_2O_3:Co, impact-induced demagnetisation, magnetostriction and coercive force, appl. in mag. recording 77—16111
Fe_3O_4:Co, impact-induced demagnetisation, magnetostriction and coercive force, appl. in mag. recording 77—16111
^3He, solid, production and obs. of ordered state, adiabatic demagnetisation *(French)* 77—59173
^3He, solid, strongly magnetised, low-temp. melting props. possible adiabatic demagnetisation 77—11765
In, two stage nuclear demagnetization experiments 79—65644
(La,Ce)B_6 dil. alloy, Kondo effect, impurity-impurity interaction, mag. susceptibility, mag. to non mag. transition 78—47948
$La_2Mg_3(NO_3)_{12}.24H_2O:Co^{2+}$, Ce^{3+}, relax. and ESR in magnetically cooled systems 78—88225
MgMn ferrite CVD epitaxial layers, bubble domains in remanence and demagnetised states 77—85516
MnBi particles, demagnetised, coercivity, remanence and magnetisation reversal 78—19281
Nb-Ti superconducting single layered multifilamentary coil, eddy current loss depend. on demagnetisation 80—97040
Ne solid, ultraslow diffusion of ^{21}Ne, adiabatic demagnetisation in rotating reference frame 77—73095
Ni (110) surface, positive spin polarisation in field emission and demagnetisation by H_2 adsorption 78—52646
Ni rod, polycryst., demagnetising factor 77—73046
Ni, thin films, surface demagnetisation due to chemisorption, ferromagnetic reson. study 80—80616
Ni_3Mn, mag. domains perpendicular to AC demagnetising field 77—20632
Ni_3Mn, magnetic phase exam. 77—20631
NiZn ferrite, magnetic props., porosity and grain size effects 77—36095
Pd-Fe alloys, hydrogenated and unhydrogenated, EPR and demagnetisation field 77—32250
$PrBe_{13}$, nuclear demagnetisation, prod. of μK temps. 77—17987
$PrIn_3$, two stage nuclear demagnetization experiments 79—65644
$PrNi_5$, two stage nuclear demagnetization experiments 79—65644
Sm-Co, alloy powders and sintered magnets, effect of chem. treatment on mag. props. 78—60311
Sm-Co alloy magnets, operational control of residual induction, maximum mag. energy 79—15324
Sm-Pr-Co, added Fe_2Sn, permanent magnets, demagnetisation curves, X-ray obs. 78—91900
$SmCO_5$ magnets, heating effects 79—38357
$SmCo_5$ magnets, ageing at high temp. 80—7129
$SmCo_5$, powder, exam. of protective preps. of organic media against oxidation 79—96220
$SmCo_{5+x}$, Cu and Fe modified, coercive force, demagnetization curves *(Czech)* 79—42805
Sm_2M_{17}, sintered magnet, hard mag. props. optimisation 77—8340
$TbFe_2$ monocrystalline (111), under elastic compressive stresses, domain structure *(Russian)* 79—91247
W, acoustic NMR line shape, effect of demagnetisation 79—95654
YIG, epitaxial, temp. stabilisation of ferrimag. reson. field by Ga, La substitution 77—77104

demagnetisation, adiabatic *see magnetic cooling*

Dember effect
anisotropic semiconductors, bulk photovoltaic effect and transverse Dember effect 77—55573
composites, interfacial polarisation and loading factor effects in dielec.-loss meas. 80—2693
1,1′-diethyl-2,2′-quinocyanine-[TCNQ]$_2$ anion radical salt single crystals, photovoltaic effect *(Japanese)* 78—2522
double injection into p^+-π-n^+ structures 79—42627
semiconductor, heterogeneous, Dember and photomagnetic effect, spectral characts. *(Russian)* 77—89809
semiconductor, inhomogeneous anisotropic, spectral characts. of transverse Dember effect 78—39161
semiconductor, superficially illuminated, space charge effect on Dember effect 77—8133
semiconductor, theory, allowance for long-range fields of charged impurities 79—24013
semiconductor film, photovoltaic and photodiffusion mechanisms responsible for anomalously high photovoltages 78—26910
semiconductor with anisotropic conductivity, elec. and photoelec. props., review 78—10447
semiconductors with deep impurities, double injection currents 77—55543
solar cell, absolute efficiency meas., influence of Dember effect 79 83597
Ag halide, Dember effect, photographic emulsion grain parameter depend. 78—16870
AgBr(I) microcrystals, photohole motion 78—26903

Dember effect continued
CdS-type semiconds., Dember effect, theory 78—72189
p-CdSb, photomagnetic and transverse Dember effects, 90 to 300K 77—4400
GaAs:O(Cr), relax. semicond., Dember effects meas. 79—28372
Ge, electronic subsystem heating by Dember field for ambipolar diffusion *(Russian)* 77—39898
InSb, photoresistor in mag. field, increased responsivity 78—39162
InSb-NiSb, photovolt. effects rel. to theory of semicond. with internal elec. short circuits 80—65620
LiH (D), single crystals, electronic excitations, review *(Russian)* 78—72574
ZnO, particulate, Dember effect, rel. to electrography 78—95314
Zn_3P_2, photocond. and Dember effect meas., 0.5 to 1.2 μm, possible detector appl. 78—91721

demodulation
see also demodulators; modulation
acousto-optic modulator for CO_2 laser rangefinder using heterodyne detect. 80—102825
coherent detection of partially coherent sources 80—47109
coincidence detection fo optical pulse streams, high resolution heterodyne system 77—690
complex demodulation for nonstationary data anal. *(French)* 79—70922
complex system characteristic derivative meas. by input deep modulation *(Russian)* 78—45588
differential absorption lidar system sensitivity with heterodyne reception 79—27310
differential heterodyne freq. conversion at 0.4 mm wavelength, Josephson-effect receiver 79—26125
FIR mixing with Josephson junctions 79—26121
flaw-detection apparatus, noise immunity, sounding signal freq. modulation 80—89441
Fourier transform spectrosc., new developments—passive heterodyne spectrosc. and diode laser absorpt. spectrosc. 80—95148
geomagnetic continuous pulsations, complex demodulation rel. to magnetosphere toroidal line resons. 80—21877
heterodyne coincidence spectroscopy for direct probe of three-body correlations in fluids 77—10118
heterodyne correlation radiometry 78—77980
heterodyne detection of random gaussian signals, pulse duration optimisation 79—12848
heterodyne lidar systems, signal-to noise ratio in presence of atmospheric turbulence 79—100949
heterodyne method of diffusive component meas. of laser mirrors 77—68217
heterodyne receivers of CO_2 laser emitters, antenna characts. meas. 77—67498
infrared heterodyne spectroscopy in astronomy 78—85859
interval modulation semiconductor laser communication system 78—9331
IR discretely tunable gas lasers and heterodyne detect. techniques for atm. monitoring 78—61605
IR heterodyne detect. of stars, atm. turbulence effects, corrections *(French)* 80—46409
IR heterodyne radiometer using tunable diode laser local oscillator 78—267
IR interferometer, 11 μm heterodyne system *(French)* 80—46397
IR laser heterodyne spectroscopy for trace gases remote detect. in planetary atms. 78—61606
IR scanning heterodyne interferometry for pulsed fusion reactors 77—84525
Josephson mixers for heterodyne reception at submillimetre wavelengths present expt. status, future developments 79—26120
laser heterodyne signals from moving object, bandpass filtering by finite apertures 78—55306
laser heterodyne spectroscopy for stratospheric trace constituents meas. 80—109257
laser heterodyne techniques, appl. to interstellar submillimetric lines detect. 79—44377
laser scanned acoustical imaging systems, demodulation scheme 79—59826
LF strong signal demodulation in subauroral ionosphere, geomag. oscill. freq. range *(Russian)* 77—41267
LF/MF radio transmissions, non-linear demodulation in auroral ionosphere rel. to ELF signals generation 80—94639
lidar, incoherent backscatter heterodyne, antenna parameters 79—72613
long wavelength IR heterodyne detection 77—45892
magnetised semiconductor plasma, EM wave amplitude modulation and demodulation 80—84482
marginal oscillator optimised for RF size effect meas., demodulation systems 77—26377
nerve trunk multifibre activity quantitation 80—76853
optical field distribution, heterodyne reception of information 78—87024
optical fields, heterodyne detection, optimum conditions 77—2694
optical folded spectrum processor, signal demodulation and radar processing appls. 78—5429
optical heterodyne array, joint signal probability distrib., clear air turbulent atm. 79—66804
optical heterodyne detectors, evaluation at 5145 Å 77—71370
optical heterodyne line-scan imagery, speckle noise model 79—50337
optical heterodyne receiver array for light propag. through turbulent atm. 79—64183
optical heterodyning, for light scatt. spectra 79—6186
optical heterodyning at single-photon level 79—26127
partially coherent radiation, optical heterodyne detection 80—77871
photodetector, heterodyne characts. meas. and modulation method 77—34029
plasma diagnostics, heterodyne detection of scatt. pulsed CO_2 laser 77—35389
RF SQUID magnetometer, synchronous demodulation, amplitude- and phase-sensitive detection 80—105679
Rydberg atom maser emission, heterodyne detection 80—78822
submillimeter wave heterodyne detection, with a laser LO 78—70183
thin film deposition control, thickness monitor using freq. demodulation technique 79—67249
underwater acoustic signals, freq. shift arrival time determ. 79—3875
n-$Hg_{0.8}Cd_{0.2}Te$, microwave bolometer heterodyne receiver based on magnetic field induced phase transition 80—13135

demodulators
see also demodulation; discriminators; modems
acousto-optic heterodyning image processor, OTF 80—5833

demodulators continued
- FM, stroboscopic, wide band-pass, for signal processing in laser Doppler velocity meas. *(Russian)* 78—36976
- FM AF PLL lock indicator and event alarm for multiplexed seismograph telemetry 79—62597
- heterodyne receivers for atmospheric optical communications 80—58663
- low-distortion FM demodulator using SAW delay device 78—51014
- microprocessor based telemetry demodulation system 79—20738
- optical heterodyne interferometer with improved two-channel crosstalk signal/noise ratio 77—10100
- PLL, ECG-telemetry apparatus appl. *(German)* 78—57097
- precision TV demodulator using high-performance SAW transversal filters 79—49258
- SAW transmitting hydrophone development and performance 79—53586
- PbSnTe detector and preamplifier modules for heterodyne detection of CO_2 laser radiation 78—32875

demography
- education, radioactive dating and population growth by dice game 80—57030
- effect on subjective road traffic noise investigations, a socioeconomic study 80—67022
- household fuel uses, ORNL model 79—79387
- nuclear power station, operation, socio-economic effects on demography, finance and local activities of region *(French)* 80—74038

demonstrations
- *includes student experiments*
- *see also student laboratory apparatus*
- α-particle in air, range, energy and range straggling, stopping power meas. 78—73815
- β-ray absorption, expt. using 1-ply toilet paper 77—22358
- Abbe's theory of imaging, lecture-room demonstration 78—41120
- AC rectification 80—77598
- AC repulsion, Elihu Thomson expt. 79—62980
- AC vector diagram, demonstration using CRO 77—37685
- acoustic combination tones 79—58507
- acoustic interference, refl. effects 77—22353
- acoustic resonance of violin cavity, reson. modified by He or CO_2 79—35484
- acoustical second-order Doppler effect, introductory expt. for special relativity 78—49584
- acoustics, demonstration cart 79—35481
- advanced student lab. course simulating research conditions, heuristic 77—87591
- air, buoyancy demonstration 80—67988
- air column resonance spectra, meas. using basic lab. apparatus 80—41998
- air pollution, undergraduate project using sulphation plates 77—49527
- alkali metal vapour, absorpt. spectra 79—21509
- alpha spectroscopy equipment and techniques *(Danish)* 77—49529
- apparent depth, viewing angle depend., ray tracing expts. 78—12475
- appearance pot. spectrometer design 80—105477
- Archibald rubber band heat engine, optimisation 79—5936
- arm, lower part, statics and equilib., for 1st yr. medics 79—35505
- astronomical distance measurement with a spectrometer 79—62969
- astronomy, Hubble's law as laboratory exercise 78—65740
- astronomy teaching, demonstrational appliances *(Hungarian)* 78—36772
- asymmetric rotators, singular motions, demonstration 77—13533
- atmospheric pressure meas. with syringe, student expt. 77—57122
- atmospheric refraction, using var. density sugar soln. 77—57134
- atomic flame emission anal., apparatus for teaching 77—29976
- atomic line spectra display, push-botton exhibit 77—57127
- atomic movements in solids, illustration model for univ. students 77—49531
- atomic spectra, quantum defects and ionis. pots., graphical procedure for students 80—7
- atomospheric pressure, using beer can 80—31460
- atoms in solids, focusing and defocusing collisions model 80—82618
- audio-visual presentatons for physicians, photography of medical X-ray plates 80—37103
- Aufbau, principle, low-cost classroom demonstration 80—42011
- ball, radius of gyration determ., using air track, undergrad. demonstration 78—49606
- ballistics, max. range at elevated launch height, expt. and BASIC program 79—97156
- balloon, hot-air, lectured sized 79—75308
- barometer, capillary tube type 80—73156
- beats, interference phenomenon demonstration 79—75307
- Bernoulli's eqn. and Hagen-Poiseuille's law, capillary bed representation 80—57039
- Bernoulli's principle, spin of balls and coins 80—77592
- Bernoulli force, coffee cup demonstration 79—35482
- binary heterogeneous vapour-liquid equilibrium, student experiment demonstrating miscibility effects 77—82352
- binary solid-liquid equilibria, student experiment, phase diagram computer program 78—89285
- biofeedback, student demonstration 79—44677
- bioinstrumentation teaching laboratory, efficient use of animal expts. 77—37700
- biomechanics using a crane boom 78—81759
- biomechanics velocity of sports activities meas., stroboscopic photography, teaching appl. 79—44679
- biomembranes, teaching demonstration using molecular membrane model 77—57117
- birefringence using calcite polished sphere as teaching aid 77—71172
- blackbody radiation and Planck function, derivative spectroscopy expt. 80—77563
- blackbody radiation constant, determ., teaching expt. 77—67160
- bouncing ball, student expt. 78—54122
- Brewster's angle measurement using ordinary lab. apparatus, for high-school students 78—86097
- Brownian motion of harmonically bound particle, simulation 80—17751
- buoyant bubble 79—30180
- capacitance meas. of parallel-plate capacitor, fringing field effect 77—87604
- capacitor, stored energy meas. 80—77585
- cardiovascular simulator for the undergraduate physics laboratory 79—84889
- cart wheels on inclined plane, theory and expt. 78—61977
- Cartesian diver, minimal buoyancy effects 80—67989

demonstrations continued
- castor oil dielectric fluid, microwave propag., permittivity effect 80—105468
- centre of gravity, clothespin-belt demonstration, anal. of forces 77—5612
- centre of percussion demonstration, using physical pendulums 80—46752
- centrifugal forces, simulation, on overhead projector, teaching appl. 77—41438
- Cepheid variable stars, simulated, for introductory astronomy course 79—44664
- change of state, of CO_2, syringe expt. 79—40325
- Charles' law, student expt. 78—36783
- chemical equilibrium, machine for teaching statistical basis 79—40337
- chemistry, lecture demonstrations with student participation 79—84911
- chemistry course for artists, art buffs 79—84880
- cholesteric liquid crystal, Bragg reflection of light, undergraduate expt. 77—60870
- classroom photometer with artificial star 77—74180
- close packed crystal struct. model, for handling and overhead projection 78—24625
- CO_2 laser construction as student project, design and building methods 79—97166
- coefficient of restitution, bouncing ball expt. 77—33738
- coefficient of restitution of bouncing ball expt. 78—86074
- coherence, simulation expt. 78—73810
- collision processes, kinetic theory, density effects expts. 78—12468
- colour mixing 79—58505
- colour physics demonstrations for polytech. students 77—49533
- compound pendulums, teaching appls. 78—12474
- Compton collision formula and Klein-Nishina formula ang. depend. verification, undergraduate expt. 78—62010
- concave mirror, real image demonstration device 77—41447
- contact potential difference, for physics course *(Russian)* 79—21508
- Coriolis effect, quantitative demonstration, apparatus design 77—49532
- Coriolis machine, inertial motion viewed from rot. reference frame, coordinate transformation 78—69934
- cornea, radius of curvature, quantitative geometric optics expt. 78—62004
- cosmic distance measurement using Cepheid variables 79—84920
- Coulomb's law, simple demonstration expt. 79—5940
- critical potentials measurement of He 80—12874
- crystal defects, two-dimens. model 77—78940
- crystal growth from solution, convection effects, holographic interferometic obs. 80—77565
- crystal model, unit cell construction with polystyrene balls on rods 77—60882
- crystal structure, nucl. blocking patterns, crystallography demonstration, for teachers 79—40328
- current balance, modified, for elementary physics laboratory 77—67163
- cylindrical cardboard model for a rotating system in special relativity 79—44661
- DC electricity, student expts. with batteries and bulbs 78—36777
- dielectric constant of liquids meas., student experiment appl. 77—37696
- dielectric consts. and capacitor dissipation meas., RLC ccts. 77—82339
- dielectric surface, reflectances, undergraduate exptl. meas. 78—73809
- diffraction, spatial filtering expts. 77—57120
- diffraction grating and interference effects, electronic cct. analogue 79—9052
- diffraction grating equation verification, student expt. 77—17741
- diffraction pattern classroom anal., image-space method 80—51983
- diffraction pattern display using photodiode array 78—86069
- diffraction pattern of hair 77—45648
- digital display for lecture hall use 78—86075
- dipole moment laboratory experiment 77—57116
- distance measurement, parallax method, undergraduate expt. 77—60871
- Doppler effect, ripple-tank demonstration 80—82621
- Doppler shift of laser beam 78—69939
- dye laser, tunable, undergraduate demonstration expts. 78—61988
- dye laser demonstration system, educational appl. *(German)* 80—51994
- Earth resistivity surveying, apparatus, interpretation, undergrad. fieldwork 78—49623
- Earth rotation, Foucault pendulum model 79—58472
- eddy current forces 79—62967
- eddy currents display with heat-sensitive liq. cryst. colour change 77—33804
- education, Shubnikov-de Haas oscills., InSb degenerate semiconductor, third-year undergraduate expt. 79—9051
- eductation, advanced undergraduate expts. in vacuum physics and mass spectrometry 80—73153
- electric resistance, temp. depend., qualitative anal. by audible demonstration 80—46775
- electrical circuit equivalent resistance and capacitance 78—69938
- electrochromism in WO_3, advanced lab. expt., colour centres, proton diffusion 80—17738
- electrolysis and recombination of water 77—9843
- electromagnetic wave propagation, dispersive effects 79—58486
- electromagnetic wave propagation in Al 80—73149
- electron interference using standard electron microscope and electron biprism as interferometer 78—62005
- electron microscopy, reproduction of micrographs and transparencies for publication and display 77—49817
- electron motion in elec. and mag. fields, student lab. and computing studies 80—27076
- electron rest energy, using X-ray photoelectron spectrometer, student expt. 79—25802
- electronic analogue of radioactive decay, demonstration apparatus circuit 78—41122
- electronic digital stopwatch for automatic time keeping, triggering ccts. 79—97158
- electrostatic dipole lines of force 77—78931
- electrostatic imaging problems with plane boundaries 80—90629
- electrostatics, attraction and repulsion of metallic particles over water 77—13559
- elliptically polarised light, quantitative anal., $^1/_4$-wave plate, student expt. 78—49608
- EM induction, emf, right hand rule etc., solenoid expts. 79—71204
- energy expts. for interdisciplinary general science course 78—65738
- energy source internal resistance meas. method 79—30176
- entropy change experiment, Pb block lowered into liq. nitrogen 79—71194
- environmental noise measurements, undergraduate research project 78—12472

demonstrations continued
- epithermal neutron radial flux distrib. in water, student expt. 79—97146
- EPR, introductory student expt. 78—41119
- equivalence principle, monkey and hunter demonstration 80—67984
- eye, intensity response of vision, simple expt. 79—71203
- falling domino chain, expt. and computer program 78—62009
- Faraday generator, one piece, paradoxical expt. from 1851 78—73813
- Fermat's principle, student expts. 79—30178
- ferrite spinels, normal and inverse, solid state chem. expts. for students 80—36815
- ferromagnetic material props., teaching expt. 80—82608
- fire extinguishing, experience in laboratory safety course 79—48995
- fluid properties, near critical point, student apparatus 77—60881
- fluorescence quenching rate constant, undergraduate expt. using Spectronic 20 77—57119
- fly wing mechanism, demonstration model 77—33799
- forbidden energy gap meas. in Si and Ge p-n junctions 80—57027
- force vectors, modified force table expt., load cells and hanging students 78—69947
- forced oscillations experiment for students 80—17780
- Foucault pendulum, continuously operating 80—73151
- Foucault prism for SHF radiation, phys. course demonstration *(Russian)* 77—13550
- Fourier transform interferometry, visible reflectivity spectra 77—33765
- Fourier transform IR spectrophotometer, underlying principles 80—36812
- Fourier transform spectroscopy for students 78—57722
- fovea, human, diameter meas. expt. 79—30
- Fraunhofer diffr. negative order pattern, He-Ne laser 77—78912
- Fraunhofer diffraction and polarisation 79—44666
- Fraunhofer diffraction patterns, phase reversal effect 80—101691
- free radical recombination, rate consts. meas., student expt. 79—48996
- freezing by boiling, using low capacity pump without acid 78—8192
- fresh river water-estuary halocline, expt. simulation, salt diffusion in tap water 78—61980
- fringe phenomena, demonstrations using float glass 78—41121
- fuel saving by thermostat setback 78—24626
- gas pressure gauge for student expt., mol. weight determ. by law of atm. 79—25795
- Gassiot's cascade, 19th century discharge tube demonstration 80—77586
- general relativity, expt. to demonstrate curved space 77—57130
- glass goblets, illusory effects of thickness and curvature 79—97154
- glass vessel shattering by sound waves, chamber for expt. 80—17752
- glasses, prescription meas. 80—67981
- gravitational acceleration, absolute determ. method 79—71187
- gravitational acceleration meas. using falling ball 78—28896
- gravitational acceleration meas. using phonograph turntable 79—44687
- gyroscope precession 80—73155
- gyroscopes, rolling and suspended, ang. momentum demonstration 79—9061
- Halley's comet, 1986 apparition, calcs. of orbit and spacecract interception 77—45652
- harmonic oscillation, normal modes, sinusoidal perturbation response, chart recorder 77—13539
- heat, boiling phenomena when red-hot balls enter water of different temps. 78—24627
- heat, enhancement using coolant sprays 80—8761
- heat of vaporisation of water, lab. meas. method 79—30175
- heliostat design teaching aids and demonstrations 79—62126
- Hero's engine, constructional details 78—69946
- hi-fi demonstration studio design *(German)* 79—94405
- hologram, single beam, 360°, recording and display expt. 77—60872
- holograms, 360° reflection, method of construction 77—26
- holograms, rainbow, demonstration of diffraction and interference of light *(Polish)* 80—68001
- holographic double exposure interferometry for small rot. meas. 78—36758
- holographic experiments on optical imaging 80—12872
- holographic plates, rear refl. elimination technique 80—73145
- holographic road show 79—58503
- holography, comparison of real and virtual lenses 78—16599
- holography, single beam, demonstrations 80—41983
- holography, using Hg vapour street light 78—24628
- homodyne microwave Doppler velocimetry, accel. meas. 77—78920
- Hubble law, laboratory exercise for students 79—35500
- human eye, artificial model, physics laboratory for medical students 78—62003
- human retina model for props. of vision 78—77655
- hypodermic syringe, disposable, plastic, physics expts. appls. 79—5935
- ice, ionic cond., elec. cond. temp. depend., dielec. props., undergraduate expts. 79—35503
- image light reflection, optical illusion 78—49604
- impact ball apparatus, teacher's demonstration 78—8195
- impulse recorder for small rocket engines 80—77595
- individualised laboratory system 78—36760
- inductor, establishing $V=L(dI/dt)$ directly 77—37688
- inert gases, self-diffusion coefficient, radioactive tracer meas. 77—13534
- inertia ball demonstration, theory 78—73811
- instantaneous axis of rotation, theory and demonstration apparatus 79—84903
- interactive computer terminal as 'lab. assistant' in introductory physics expt. 78—36761
- interference effects, multiple-beam, Edser-Butler plate, teaching, demonstration appls. 77—41439
- interference fringe intensity distribution, using vidicon *(Polish)* 79—40340
- interferometer, Doppler beats and interference fringes 79—62957
- intermolecular potential energy in gas, determ. from viscosity meas. 77—13556
- interstitial atoms in metals, struct., vibr., air table simulation 79—71186
- intra-aortic balloon pump simulator for dynamic demonstration and teaching 77—56537
- ion cyclotron resonance spectroscopy, interpretive expt. 80—36814
- IR detector, absolute detectivity determ. 77—13535
- IR image conversion tube, low-cost apparatus for teachers 79—71207
- isotope production, identification, by neutron activation 79—44675
- John Tyndall's demonstrations on sound (1854-82) 77—22362
- Josephson tunnel junction, Nb-PbSn, 3rd yr undergrad. expt. 78—54126
- Joule heat engine and pump 80—105480
- Joule heating, Peltier and Seebeck effects, Cu-Constantan thermocouple expt. 79—9056
- Kelvin, background, teaching motivation, demonstrations 80—42025

demonstrations continued
- Kelvin water dropper demonstration of electrostatic charges 78—28899
- kinetic analysis of rotation with air-cushion apparatus *(Hungarian)* 79—25811
- kinetic energy of rotating wheel, expt. using rocket accel. 79—17168
- kinetic molecular theory teaching, expt.-oriented approach 80—12868
- kinetic theory of gases, computer modelling of mol. vel. distribs. 79—30169
- Kuwaiti solar energy research, development and demonstration programme 79—57371
- laser beam UHF and audio freq. difference heats 80—73139
- laser source, He-Ne, using cold-cathode plasma tube, optical and communication expts. appl. 78—45448
- LED emission spectra temp. depend. 77—82348
- LED point source emitter 80—73150
- Leidenfrost effect, demonstrations 78—81744
- lens focal length meas. error 77—45653
- lens grinding, as student lab. project 77—5614
- LF oscillograph system for demonstrating mechanical vibrs. 77—64908
- light, turning through const. ang. by prism 79—25805
- light diffraction, demonstrations of Young's theory 77—78938
- light diffraction and interference, TV display 77—5613
- light diffraction kit 80—10
- light interference from two coherent sources 80—4496
- light polarisation classical model 80—77576
- light reflection, phase relations, phys. course demonstration *(Russian)* 77—13550
- light scattering, appl. to simulated microbes, suspension, size determ. 79—71178
- light scattering by surface tension waves 79—58469
- light sources, radiation superposition and the random flights problem 78—12467
- light transmission, through reflecting cylindrical tubes, demonstration 78—73812
- light velocity measurement, Foucault's method modification 79—40327
- light velocity measurement using TV ghost 77—13561
- light velocity measurement using two dollar rotators 80—77578
- linear motion, of glider on airtrack 78—12481
- liquid, possible excitations, ball bearing model 77—45642
- liquid crystal, order parameter measurement, phys. chem. lab. expt. 80—36818
- liquid rise in capillary tube, rate meas. demonstration 80—73147
- Lissajous figures, generation tech. 78—77656
- Lissajous figures, mechanical system 80—31459
- local inertial frame of reference 80—67982
- Lorentz transformation, model *(Danish)* 78—20923
- luminescence decay time evaluation, computer programs, student expts. 77—26115
- luminescence decay times and bimolecular quenching, ultrafast kinetics expt. for students 77—26116
- magnetic domains, dynamic behaviour, struct., rel. to ferromag., teaching appls. 78—86080
- magnetic domains, using Kerr magneto-optical effect 78—69949
- magnetic field lines, rot. mag.-Cu disc interaction 78—54131
- magnetic induction, large-scale demonstration 80—101699
- magnetic lines of force, casting to obtain permanent 3-dimens. patterns of Fe filings 78—8193
- magnetic stirrer, Lenz's law and induced current expts. 78—12485
- magnetic susceptibility, demonstration system for student laboratory 80—4491
- materials sci., undergraduate creative project 78—86082
- measurement errors, lecture demonstration for chem. course 80—17773
- mechanical laws, optoelectronic apparatus for classroom demonstrations 80—46773
- mechanical resonance, $J_0(x)$ obs. on reson. rot. vertical chain 80—42006
- metallic glasses, phase transition and mech., elec. and mag. props. 78—36765
- metals, heat capacities meas., undergraduate experiment 79—84915
- mirror preparation, electroless plating of Cu on treated glass 80—36817
- mode conversion, shear, Lamb and Rayleigh waves 80—101687
- molecular models based on Petri dishes stereochem. appls. 78—73817
- molecular size and Avogadro's number, determ., student expt. 78—81741
- molecule, diatomic, hyperfine struct. transitions, quantum theory, for undergraduate demonstration 80—17762
- monolayer, diameter of Styrofoam spheres determ., mol. monolayer experiment appl. 79—44678
- multiple lens experiment 80—82596
- multiple scatt., elastic and inelastic, two particle system with fixed wall, air track expt. 80—73135
- musical acoustics, octave synthesizer, teaching appl. 79—44680
- musical acoustics wave motion experiment, phase vel. meas. using spring 80—8762
- musical string vibrations 77—49536
- nail driven through 2 cm thick pine board using bare hands 80—42018
- nematic liquid crystals, demonstration expts. 77—60876
- neutron activation analysis, student experiment 78—77651
- neutron activation analysis course experiments with 14 MeV neutron generator 77—82353
- Newton's laws, simple demonstration 79—67129
- NMR in undergrad. instruction, general purpose microcomputers use for hypothetical spectra synthesis 80—42009
- NMR spectral lineshape analysis of two-site exchange kinetics, student expt. 77—26118
- NMR spectrometer-computer interface, demonstration expt., signal averaging influences on S/N ratio 80—36813
- NMR-ESR spectroscopy, miniature magnetic assembly 80—105467
- noise thermometry, elec. noise and Boltzmann's const. determ., absolute temp. scale noise thermometer 78—36767
- noise thermometry apparatus, solid-state 79—62959
- nonideality effects in kinetic theory, student experiment with surprise value 77—82351
- normal modes of vibr. between coupled bodies using stroboscope 77—87607
- nuclear chain reaction demonstration model 80—46774
- nuclear engineering, teaching laboratory for expansion of student knowledge horizons 78—4445
- nuclear engineering laboratory, computer modules for calculation of prompt-neutron generation time 78—4447
- nuclear engineering teaching laboratory, development at Ecole Polytechnique 78—4444

demonstrations continued
nuclear explosion, time distrib. and anal. fallout particles from 1977 Sept. 18 Chinese detonation 79—25796
nuclear fallout radioactivity γ-ray detection and anal., Chinese fission bomb anal. 78—49596
nuclear instrumentation, computer-based data acquisition system for multi-station teaching laboratory 78—4446
nuclear laboratory course at Purdue University 78—4443
nuclear physics experiments, teaching appls., using Van de Graaff generators 77—74178
nuclear spin-lattice relaxation times from CW spectroscopy, phys. chem. lab. expt. 80—17775
one beam transmission holography, practical hints 80—57046
ophthalmological instruments and eye models in teaching, training and education 80—51993
optical barrier penetration, teaching expt. 77—67159
optical directional alignment, meas. using bifocal lenses 80—46762
optical information processing experiment set for undergraduates 78—28885
optical laboratory experiments *(Spanish)* 79—21510
optical transforms of alphabet letters, Fraunhofer diffr. 77—57132
optics, focal length of thin lens under water, determ., teaching appl. 79—44676
optics, refr. index-matching soln. for Pyrex 78—12519
optics, the principal plane, its pedagogic role 79—97150
optics experiments, soln. to eliminate Pyrex glass-liq. interface effects 77—45655
optics experiments using He-Ne laser beams, book 77—27246
organic compounds, recrystallisation, solvent selection, student experiment 79—84917
oscillations, coupled, demonstration using permanent magnets 80—42015
oscillator, 0.25-2.5 Hz sine waves, for student lab. demonstrations 78—24624
parametric instability, demonstration and discussion 80—57032
parametric resonance, student expts. 79—58464
parametric spring pendulum, recurrence effects 79—5938
partially coherent light, lecture demonstrations 80—101700
particulate air contamination in Puerto Rico, student project 79—58504
pendulum, large amplitude expt. 77—45638
pendulum, string-coupled, normal mode anal. 79—21494
percolation clusters, as teaching aid for Monte Carlo simulation and crit. exponents 78—12477
phosphorescence, room temp., student demonstration 77—29
phosphorescence experiments using adsorbed dyes 77—26114
photoconductive recording film demonstrator/processor 79—17551
photoelasticity, colour image of stress pattern 77—13548
photoelectric effect, using electroscope 77—2505
photoelectric effect and electron diffusion in gases 78—81745
photogrammetric model deformation, interactive demonstration program 77—74183
photoresist, positive, formulation, photochem. props., chem. teaching appl. 78—89284
photovoltaic cell, operation using solar simulator lamp 80—42004
physical pendula, reconstructed 19th century expt. 80—82612
physical pendulum, computer-aided laboratory exercise 80—67985
physics, Stephen F. Austin travelling science show 78—36776
physics, undergraduate students teaching eighth grade classes 78—12446
physics demonstrations, resource letter 80—17754
physics experiments using photocells and oscilloscope 78—36778
physics field course, for school pupils 77—87612
physics teaching, recent advances, syllabus, apparatus, demonstration 77—22350
physics teaching aids, convention of secondary school physics teachers *(Hungarian)* 80—67957
planet diamter meas. by occultation obs., teaching expt. 78—12457
plasma diagnostics using commercial gas tubes 77—87597
plasma physics, low-cost advanced undergraduate lab. expt. 78—12456
plasma-laser beam self focusing using paint stripper flame 79—9066
plasmon surface polariton dispersion curve, optical obs. 80—101690
plastics identification by simple qualitative tests 79—5944
Poisson statistics demonstration using X-ray tube, electronic 'shot noise' 80—73129
polarised electronic absorption spectrum at 300 and 77K, phys. chem. lab. expt. 80—17774
polarised light methods 77—45657
potentiometric electrode, semi-auto titrator system, student constructed 79—84918
precessing spherical pendulum, nonreentrant orbits demonstration 79—5937
prism, min. ang. deviation, school corridor demonstration 78—81760
projectile acceleration meas. using stroboscopic picture 78—36779
psychoacoustical expts. with all pass networks 79—25787
pulsars, suggested expts. 78—61982
radiant energy measurement of small lamp, calorimetry 78—8191
radiation pressure effects, double exposure holographic interferometric demonstration 79—5943
radioactivity measurement, geometry factors, for teaching expts. 78—12471
random motion, roller device appls. 78—16600
ray decomposition into circularly polarised components, for physics course *(Russian)* 79—21508
RC exponential decay, two-component, apparatus using FET op-amps 79—62968
reaction kinetics, rate consts. rel. to equilib. consts., student demonstration 79—58501
reciprocal lattice in crystallography, undergraduate demonstration 78—61989
reduced eye, expts. in life science labs. 80—82617
reflectivity, quantitative meas., undergrad. lab. expt. 78—49624
refractive index, spatially varying, demonstration and theory 80—62425
refractive index meas., glass disc, laser beam path 80—46779
refractive index measurement by apparent thickness method 77—41445
refractive index measurement of perspex prism, crit. angle method 80—12873
refractive index measurements 80—77577
refractive index of beer, lecture room demonstration 78—54128
refractive index of liquids, meas. method., sensitivity, geom. optics 78—12480
refractive index of liquids, meas. method, sensitivity 78—12479
resistivity measurement 78—16612
resonance, shattering glass with sound 77—57129

demonstrations continued
resonance, using eddy currents from Fisher burner 78—28902
retinal internal circulation visualisation using Purkinje's methods 78—69043
rigid body dynamics, air table expt. 79—5941
r.m.s. values of AC, heating effect expt. 80—17753
Rochelle salt, ferroelec. props. 79—97162
rocket propulsion project for engineering students 77—9839
rolling object, frictional force, student lab. expt. 80—17764
rolling pendulum bob, conservation of energy and partitioning of kinetic energy 79—62956
rotating bodies, intermediate-axis theorem 78—61990
rotating objects, centre of mass rel. to centre of rotation 80—77579
rotational motion phenomena, turntable accessories 80—77571
Rubens flame tube demonstration of standing sound waves 80—8760
Rutherford scattering, analogous demonstration by mech. expt. using mag. disc *(German)* 78—81778
sand, moisture content, microwave optics determ. 77—37684
scientific investigation experiment, development of theoretical model 78—86066
second-order kinetics, student experiment 77—26117
seismic waves, P- and S-wave demonstration with student participation 79—30177
self-paced freshman physics laboratory and student assessment 80—51989
series RLC circuit, phase relationships demonstration 79—58466
simple harmonic motion demonstration on CRO 78—12518
simple pendulum, length definition 77—57131
skin effect apparatus 77—27
slide preparation techniques for audio visual aids 78—54139
Slinky as model for transverse waves in plasma 80—17741
slinky wave demonstrator, folding apparatus 79—44684
Snell's law, student expt. 78—36781
soap film in a wedge, expts. for teachers 79—17169
solar constant measurement, take-home expt. 77—49537
solar eclipse obs. *(Hungarian)* 78—36773
solar energy, student laboratory experiment 80—17776
solar energy collector, using black liq. 79—97140
solar energy meas., photometric and bolometric methods 78—12470
solar heating demonstration expt. 77—22355
solar system model 78—86095
some lecture demonstrations on the statistical properties of wave fields 79—67130
sound analyser, undergraduate lab. expts. 80—82600
sound-level meter, innovative high school teaching project 80—4495
spark chamber 80—77596
spectroscopy, chem. anal., mobile laboratory 78—93502
spectrum, continuous, optical filters, demonstration apparatus 77—45649
speed of light, meas., beat frequency method, using internal laser modes 80—41992
speed of sound, meas. by clapping technique 80—82620
speed of sound, meas. using beer bottle as Helmholtz resonator 79—71181
spring, energy changes, teaching expt. 80—46754
spring, oscill. and pendulum motion coupling 78—36768
statistical thermodynamics, teaching demonstration for 3rd form of secondary school *(Hungarian)* 77—49528
steel rods, longit. impact on plate, contact time meas., student expt. 79—5939
Stefan's law, W filament elec. lamp, student expt. 78—54125
Stephan's constant determ. 78—69948
stimulated Raman effect, electromagnetic-mechanical model experiment *(German)* 78—86077
Stokes' law, school lab. course 77—87613
straight-line kinematics demonstration 77—57124
stroboscopes appl. 78—55453
structural instability critical behaviour and broken symm. 80—105476
styrene derivatives, ^{13}C NMR spectra, Hammett eqn. appl., undergraduate experiment 79—84913
SUPERCHARGE game for student visualis. of equipot. surfaces 79—30179
superconductivity transition temp. determination, student expt. 77—24632
superfluidity and superconductivity phenomena demonstrated with He cryostat. *(Polish)* 80—86059
supersonic jet spectroscopy, appls., teaching approach 80—41996
surface tension measurement, student expt. 77—45651
technical meetings, visual and oral presentations, preparatory tech. for technicians 78—8215
Tel-X-Ometer apparatus for educational demonstrations 80—8763
television lecture demonstrations for general physics course 77—78939
thermal conductivity of gases 80—82614
thermionic emission expt. using phototube 77—24919
thermoelectric effects, low-temperature measurements, undergraduate lab. project 78—54119
three-dimensional reciprocal lattice model 77—13551
timing periodic events half-column method 78—12516
titration end-point, determ. using second derivative curves 79—84909
torque, use of modified beam-type torque wrench 77—41446
total reflection, of light and water waves, demonstration apparatus 77—67158
transient phenomena recording, microcomputer controlled, student experiment 79—84919
transistor identification, Si or Ge 77—17744
transverse pulse propagation along hanging chain 78—28898
triboluminescence spectra of common candies 80—17778
triple coupled pendulum, analogy with coupled stationary states 78—16598
tsunamis, simple demonstration apparatus 77—13531
TTL ICs, use of dry cells as power source 77—17745
TV, black and white, using photographs or slides 77—49538
uncertainty principle using single-slit diffraction pattern 78—69953
undergraduate experiments for applied physics laboratories *(Japanese)* 78—57724
undergraduate laboratory teaching philosophy 80—17758
uniform acceleration, student laboratory expt. 79—40326
US pulse-echo system, chopping circuit 77—67162
USA demonstration solar heating and cooling collector thermal performances 79—62059
variable star simulator 77—22357
velocity of light determ., undergraduate expt. 79—9060
vibrating plate reson. chracts., quality factor and nonlinearity 80—73133

demonstrations continued
- vibrating string, tuning guitar by television 80—73134
- vibration frequency of stretched wire, stiffness corrections for undergraduate expts. 78—12473
- vibrations, of bowed string, demonstration 77—13532
- video studio, in-lab, of modest cost and mobile 77—67165
- virtual image position determ., demonstration using TV camera 80—67992
- viscosity of liquids, capillarity method determ. 80—82619
- water, latent heat of vaporisation 80—27081
- wave passage through focus of lens, phys. course demonstration *(Russian)* 77—13550
- Western Canadian provincial and university solar energy activities 79—57381
- X-ray diffraction patterns, recording on photographic film 78—41130
- X-ray photography, using Polaroid film 77—67161
- Young's double slit experiment, modified 80—41994
- pp, elastic scatt., teaching expt. using Van de Graaff generator 77—74178
- Ag recovery from laboratory wastes, teaching appl. 79—84912
- ^{28}Al radioisotope source, activation expt. 79—31
- Cd, triplet states, hyperfine struct. obs., project expt. 77—33737
- ^{58}Co decay, student expt. 80—12875
- ^{19}F(p,$\alpha\gamma$)^{16}O, reson. reaction, teaching expt. using Van de Graaff generator 77—74178
- H_2, rot. energy, specific heat, temp. depend. determ., demonstration 78—12465
- H_2^+ molecule energy level splitting, lecture demonstration based on coupled elect. reson. ccts. 79—49949
- He-Ne laser demonstration of continuously varying refractive index *(German)* 80—8
- I_2, heat of sublimation, laser photometric meas. 79—5942
- N high pressure discharge and associated lasing phenomena 80—105475
- Na arc lamp, light-induced ignition method 80—77599
- NaI:Tl scintillator response, γ-ray, (X-ray) rel. $^1/_2$-width energy depend., undergrad. expt. 78—49600
- Pb complex, Pb$(C_2O_4)_2^{2-}$, stoichiometry, form. const. determ., teaching appl. 79—84916
- Si planar structures, Haynes-Shockley expt. for students 78—28888
- Si solar cells, undergraduate teaching expts. 77—74177

dendrites
- *see also crystal growth*
- Al-Si (2.4 wt.%), liq. fluidity, solid-liq. coexisting zone *(Japanese)* 80—15175
- alkali halides, growth shape stability, dendrite and prominences appearance *(Hungarian)* 80—7489
- Alnico 8 permanent magnet, magnetic props. rel. with crystallographic texture 78—95483
- anodic growth on W, during prebreakdown conditions in organic residual gas 78—44383
- brass, surface microstruct. changes on immersion in $CuSO_4+H_2SO_4+HI$ soln. 78—19945
- corundum, bladed crystals, morphology and struct. 77—84680
- dendrite development and growth in very small crystals, Monte Carlo study 80—107683
- deposition of aerosol particles on metal fibres 80—40755
- dilute binary alloy monocrystal, thermodynamics of growth, model *(French)* 78—87635
- electronic device dendritic growth mechanisms 78—56058
- graphite, single crystal, from Fe-C melt, morphology 78—42932
- growth, interfacial instabilities 79—82506
- growth, stability effects 78—26802
- growth models, steady state, exam. 78—72052
- growth on ion emitters for field desorption mass spectroscopy 79—2873
- growth theory, replacement of maximum velocity principle, by stability criteria 79—11049
- growth theory, surface tension effects 79—11051
- ice, dendritic growth in supercooled water, natural convection effect 77—7999
- ice, dendritic growth rates, evidence for a universal law 79—4496
- ice dendrite formation from vapour phase, morphology, sizes and growth rates 78—10313
- ice formation in flowing water pipes, blocking mechanism 77—47092
- impurity trapping during dendritic crystal growth, computer simulation 78—38992
- impurity trapping during dendritic crystal growth, expt. 78—38993
- instabilities and pattern formation, review 80—35064
- interface kinetics effect on growth rate 79—90927
- interface morphology during crystallisation, single filament unconstrained growth from pure melt 78—52787
- interface morphology during crystallisation, single filament unconstrained growth from binary alloy melt 78—52788
- Ivantsov needle crystal model, with zero capillarity and small Peclet number, stability analysis 79—11050
- lead tartrate, single cryst. growth in gel, dendrite form. and self-regulation 77—77352
- metal crystals, electrolytic growth, CCTV obs. 78—51863
- metal growth in space, theoretical models, comparison with ground expts. 78—84786
- metal transport reactions in molten salts, isothermal system *(German)* 77—63569
- Monte Carlo simulation of growth from melt 80—15427
- particle characterisation of automatic methods 80—25590
- phthalic anhydride, dendritic growth 78—18936
- snow, epitaxial relationship during three dimensional dendrite form. 79—23875
- solidification interface in reduced gravity, bubble interactions 78—84787
- spherical particle, growing from a binary alloy melt, morphological stability 80—29943
- steady state growth models 78—91576
- steady-state dendrite growth models, validity 78—34732
- steel, 10R6M5 and 10R6M5K5, atomised powders *(Russian)* 80—97446
- succinonitrile, dendritic growth rates, evidence for a universal law 79—4496
- succinonitrile, low entropy of fusion plastic crystal, dendritic growth, expt. test of theory 77—35842
- succinonitrile, undercooled, analysis of dendritic growth 78—75970
- surface-dynamics of growing crystals 80—44160
- web dendrites, dislocations, stacking faults, X-ray topographic study *(Chinese)* 80—88148

dendrites continued
- Ag electrodeposits, dendritic growth inhibition by tartaric acid and tartrates *(French)* 78—87894
- Ag, growth from supercooled melt 77—51628
- Al-Cu alloy, microsegregation *(Japanese)* 77—16589
- Al-Ni(Pt)(Zn), rapidly solidified, twinned dendrites 80—70572
- Al_3Ni dendrite facets, determ. cryst. direction by SEM *(French)* 78—87893
- As-Te-Ge chalcogenide films, thermally induced transformations, TEM obs. 79—94917
- BiSb, dendritic growth, transverse striations photomicrograph 77—4277
- C microneedles, grown on W wires under intense elec. fields, X-ray diffr. and AES 80—54580
- $CaSO_4.2H_2O$, occlusion formation during dendritic crystal growth, expt. 78—38993
- $CaSiO_3$, fibrous, controlled crystallisation and anisotropy 80—59425
- Cd chalcogenides, thin films, VPE, needle-like cryst. growth 80—80148
- Cd, electrocrystn. on Cu single cryst., snowflake dendritic growth, AC effect 78—10292
- Cr_xC, cathodic needle growth, at lower electric fields from $Cr(CO)_6$ vapour 80—76161
- Cu and α-Cu-Zn alloy, whisker growth in Zn reduction, morphological change to dendrites 79—28261
- Cu, electrodeposited, growth kinetics, cathode surface effects 79—70007
- Cu, growth from supercooled melt 77—51628
- Cu_2O, form. by Cu oxidation in CO_2, 800-1000°C 78—76784
- Cu_2O on Cu, two stage metastable and stable surface nucleation, 800-1000°C 77—70214
- Fe-Ni (30 wt.%), Ni segregation singularities during dendrito-cellular solidification *(Russian)* 80—7542
- Fe_2O_3, haematite, dendrite formation from high temp. soln. *(Japanese)* 80—107684
- $KAl(SO_4)_2.12H_2O$, occlusion formation during dendritic crystal growth, expt. 78—38993
- KH_2PO_4, dendritic growth in silica gel 80—35072
- $LiNiO_3$, surface dendrite occurrence, growth condition-depend. 80—2316
- Mo_xC, cathodic needle growth, at lower electric fields from $Mo(CO)_6$ vapour 80—76161
- NH_4Cl, growth at very low supersaturation 78—43277
- NH_4Cl-H_2O, binary dendritic system, exam. of solidification 79—11599
- NaCl, occlusion formation during dendritic crystal growth, expt. 78—38993
- NaCl:Mn^{2+} crysts., electrolysis, dendrite form., mechanism 77—1934
- NbN, Nb_4N_3-NbN, Nb_2N-Nb_4N_3, Nb_2N, cryst. growth parameters and morphology of chem. vapour deposition, X-ray diffr. and SEM study 79—23861
- Ni, on Al, CV, selective solar photothermal absorber 78—52683
- Ni-Al-Ta (7.5, 2.0 wt.%), dendritic monocrystal, microsegregation and nonhomogenisation 79—37940
- Ni-C, quenched, struct. of graphite precipitates, TEM obs. *(Russian)* 78—68695
- Pb-Sn(20 wt.%), partially remelted interdendritic fluid flow 77—4771
- $PbTiO_3$, optical birefringence in low temp. region 80—93276
- Si, dendritic film growth on alumina, solar cell appls. 77—77432
- Si dendritic web growth, correlation of solute and interface partition coeffs. 79—24427
- Si, dendritic web growth processes, computer modelling 79—11508
- Si materials, advanced, preliminary evaluation for space solar cells 80—94006
- Si ribbon, dendritic web growth, solar cell prod. and characterisation 77—77366
- Si ribbon, dendritic web growth from melt, solar cell module fabrication 80—93478
- Si ribbon, edge-defined film-fed growth, solar cell prod: and characterisation 77—77365
- SiO_2-Al_2O_3-K_2O-Na_2O, exam. of leucite crystal growth 79—19496
- TiN, gaseous phase, crystallisation, effect of temp., vapour-gas mixture conc., and deposition time 79—33910
- W needle crystal growth, discharge-induced decomp. of hexacarbonyltungsten mols. 80—84414
- W needles, mechanism of cathodic growth, decomp. of $W(CO)_6$ under high field conditions 80—76162
- W needles produced by $W(CO)_6$ decomp. 79—95302
- Zn aerosol condensation, prismatic and spherical particle form. 77—9135
- Zn chalcogenides, thin films, VPE, needle-like cryst. growth 80—80148
- Zn electrodeposit dendritic growth control using impedance meas. 78—84721
- Zn, on Cu single cryst. planes, electrocrystn. under influence of asymm. AC 77—28731
- ZnO, hollow crystals, growth by oxidation of ZnSe vapour, mechanism 78—34733

dendritic crystals *see dendrites*

dendritic structure
- Al-Si (2.4 wt.%), liq. fluidity, solid-liq. coexisting zone *(Japanese)* 80—15175
- alkali halide, CESR of dendritic metal phase precip. 77—24744
- alkali halide crystals, dendrite formation during electrolysis 78—95057
- alloy, laser surface melted, heat transfer props. and microstructs. 79—70085
- binary alloys, directional solidification, theory of dendritic growth 80—70145
- cast Fe, grey and ductile, subsurface defects, SEM and EDAX study 80—44400
- casting in space environment, dendrite remelting and macrosegregation in low-gravity 79—47669
- cellular and cellular dendritic growth, general microsegregation eqn. 80—84921
- Cunial MNA13-3, Mn addition effect on props. 80—21035
- dendrite development and growth in very small crystals, Monte Carlo study 80—107683
- directional solidification, dendrite growth *(German)* 79—34023
- eutectic alloy, dendrite growth—the coupled zone 80—97489
- glass-ceramics and photosensitive glass, microstructure rel. to properties *(German)* 80—38926
- Hastelloy X, mech. props. effect of solidification substruct. 77—25040
- Invar N36 melt, cast metal struct. depend. on heat treatment, subgrain struct. *(Russian)* 80—40343
- metal powder, method for TEM study 80—84038
- metallic sputtered powder, stuct. and phase composition, cooling rate effect *(Russian)* 79—56941

dendritic structure continued
- rare earth metal oxide films, crystallisation, electron microscope obs. 79—15034
- repeated precipitation on edge dislocations, micromechanisms 78—95752
- Silumin, AlSi10Mn, struct. and mech. props., Na modification effects 77—63786
- solidification, dendritic growth, fluid flow effect 78—11215
- solidification, gravity level effects, direct obs. 77—36494
- solidification during welding 79—87625
- steel, 34KhN1MAR structural heterogeneity of 70 ton ingots γ to α transform, in dendritic section 77—70047
- steel, alloy type, photoemission electron microscope obs. of high temp. precip. behaviour 80—108456
- steel, austenitic stainless, weld, ferritic-austenitic solidification mode 80—89214
- steel, cast, effect of non-uniform struct. on props. 78—84850
- steel, continuously cast, segregation at halfway cracks 80—60869
- steel, Cr-Ni-Al, intergranular crack investigation by etching *(Chinese)* 79—43457
- steel, low impurity, peritectic transformations, influence on initial struct., solidification, grain boundaries *(Russian)* 80—66621
- steel, martensitic, dendritic structure assessment with Elypovist electropolisher 77—52565
- steel, steady state unidirectionally solidified, dendrite morphology 77—16569
- steel, V, high C, faceted Mn sulphide formation on crystn., thermomech. treatment effect on dendritic struct. *(Russian)* 80—50621
- steel alloy, austenite transformation in hot rolled strips 80—55407
- steels 45, 17G2AF, 55S2, 60S2, faceted Mn sulphide formation on crystn., dendrites *(Russian)* 80—50621
- succinonitrile, crystn. kinetics and shapes 77—31617
- weld pool, preferred growth direction of cellular-dendritic crystallites *(Russian)* 77—44236
- Ag-Cu eutectic and off-eutectic alloys, thermal stability 77—25077
- Al alloy, forgings, unhealed porosities and crystalline steps *(Chinese)* 79—74178
- Al alloy, weld metal structure and hot cracking susceptibility 79—24595
- Al ingot, dendrite arm spacing through heat flow control 77—73267
- Al, molten, showering cryst. form. in mould cooled from top *(Japanese)* 80—66498
- Al-alloy ingots, crystallisation condition effects on fan-shaped zone struct. *(Russian)* 78—3114
- Al-Cd hypomonotectic alloy, rapid solidification and decomposition 80—50638
- Al-Cu, dendritic solidification, fluid flow effect 78—11215
- Al-Cu, molten, showering cryst. form. in mould cooled from top *(Japanese)* 80—66498
- Al-Cu (4.5 wt.%), growth structs. with dendrite growth directions differing from heat flow direction during solidification 79—43235
- Al-Cu (4.8 wt.%), secondary arms in dendritic growth, solidification effects *(Japanese)* 78—15387
- Al-Cu (5.7wt.%), unidirectionally solidified, dendritic morphology and dendrite arm spacing 79—29043
- Al-Cu alloy dendritic solidification kinetics 80—81041
- Al-Cu alloys, coarsening mechanisms of secondary dendrite arm, and organic analogue 80—81049
- Al-Cu alloys, hypo- and hyper-eutectic, dendrite coarsening during solidification 77—63651
- Al-Cu-Mg-Zn, Mg and Zn addition effects on dendrite struct. and mech. props. *(Korean)* 77—28796
- Al-Fe (0.5 wt.%)-Ti-Cr, Ti, Cr addition effects on toughness/microstruct. relationship *(Japanese)* 77—48525
- Al-Mg alloys, overheating effects on microstruct. and props. 77—63698
- Al-Mg-Fe-Mg-Si-Cr, alloys, dendritic segregation with Fe, Mg, Si and Cr additions *(Polish)* 79—56980
- Al-Mg-Si alloys, dendritic non-homogeneity 78—56641
- Al-Mg-Ti-Zr alloy AL23-1, nucleating cellular dendritic crystallisation *(Russian)* 79—70055
- Al-Pd, rapidly solidified, new ordered phase, electron microscope obs. 79—11645
- Al-Pt (2 wt.%), rapidly solidified alloy, metastable phase formation and decomposition 79—52194
- Al-Si (2.4 wt.%), liq. fluidity in solid-liq. zone 80—108429
- Al-Ti, molten, showering cryst. form. in mould cooled from top *(Japanese)* 80—66498
- Al-Ti alloys, growth crystallography and morphologies of Al$_3$Ti primary dendrites 79—43230
- Al-Zr (0.8 and 1.5 wt.%), hyperperitectic, non equilibrium solidification 78—3113
- Al-ζ(AlAg) eutectic and off-eutectic alloys, thermal stability 77—25077
- Al$_2$O$_3$-ZrO$_2$ cast refractories, nucleation processes reconstruction by SEM, TEM and STEM 78—35380
- AlZn, homogenization processes, dendritic struct. 79—15700
- Au-Co electrodeposit, struct. and hardness characts. 79—28245
- Au-Ge contacts on GaAs, SEM and TEM obs. of struct. 80—100522
- Au-Ni-Cu-Zn, white gold, metallographic struct., heat treatment and plastic working effect 80—40403
- Bi:Sb, solid soln. struct., growth rate effects 77—52246
- Bi-Sb, conditions for dendritic crystallisation, accompanying rapid cooling *(Russian)* 79—34020
- Bi-Sb, cryst., hopper growth 78—18564
- Cd-Ge broken lamellar eutectic composite, tensile and compressive props. 80—71694
- Cd-Zn eutectic and off-eutectic alloys, stability 77—25077
- Cd$_x$Hg$_{1-x}$Te, high-speed quenching of melt *(German)* 79—65997
- (Co,Cr,Ni)-TaC, eutectic alloy, directionally solidified, struct. defects, autoradiographic investig. *(Russian)* 77—25038
- (Co,Cr)-(Cr,Co)$_7$C$_3$, eutectic alloy, directionally solidified, struct. defects, autoradiographic investig. *(Russian)* 77—25038
- Co-Cr-W-C, hardfaced coating for high temp. liquid Na service, deposition and wear 77—32724
- Co-Ti(Hf)(Ta)(Mo)(Zr)(Al)(Fe)(Ni), dendritic segregation 80—76260
- 25Cr-20Ni stainless steel dendritic solidification, growth morphology and solute redistrib. *(Japanese)* 80—81045
- Cu, cementation, characterisation of nucleation and growth from aq. soln., TEM and SEM study 79—28972
- Cu-Al spherical crysts. grown from drop of melt, topography 80—84353
- Cu-Nb alloy, chill casting, consumable arc melting, ingot prep. techniques 80—84879
- Cu-Nb alloys for superconducting wire, casting of dendritic structure 80—2976

dendritic structure continued
- Cu-Si-Ni, undercooled, grain refinement 79—34079
- Cu-Sn (2 wt.%), effect of undercooling on crystal multiplication 78—84866
- Cu-Zn-Al alloys, dendritic struct. obs. 77—8810
- Fe, cast, hypoeutectic, primary crystn. features by means of apparent viscosity meas. in early stages of solidification *(Japanese)* 79—43231
- Fe, cast, with spheroidal graphite, crystn. *(German, English)* 80—97473
- Fe-Cu (30 wt.%) alloy, dendrite remelting during isothermal holding, microspin obs. *(Japanese)* 78—71836
- Fe-Mn, as cast, pseudo-composite struct. resulting from interdendritic segregation, cryogenic materials appl. *(French)* 80—93556
- Fe-Ni (31 wt.%) alloy, Bridgman grown, cellular to dendritic crystn. transition, morphology and microstruct. *(Russian)* 79—14709
- Fe-Ni alloy, cellular-dendrite struct., effect of temp. gradient and crystallisation rate on morphological singularities *(Russian)* 78—3115
- Fe-Ni film, amorphous, martensite form. time and struct. 80—104159
- Fe-Ni single crystal, pseudo-Kossel study of fibrous substruct. 77—1835
- Fe-Ni-Cr-Al-Ti-W-Mo (35, 15, 2.4, 2.3, 2.2 wt.%) wrought superalloy, freckles *(Chinese)* 80—104137
- GaP crystal, structure defect formation due to annealing and stress, dendrites, slip, dislocations 80—29026
- Ge, electron irrad., defect growth, struct. rel. to temp. 77—11591
- K$_2$O-SiO$_2$ glass, diffusion-controlled crystal growth 77—19876
- Mo-W alloy type MW25N, crystallisation form, globular dendrites, grain boundaries *(Russian)* 80—66494
- NH$_4$Cl-H$_2$O solidification model for showering cryst. form. in molten metal cooling *(Japanese)* 80—66498
- Nb fibre glass composites, new technique for producing fine metal fibres 80—108384
- Nb$_3$Sn superconducting wire, fabrication from Cu-Nb-Sn alloy using controlled high temp. gradient 80—25056
- Ni, pure, heavy ion irradiated, dendritic void growth 78—14386
- Ni-Al, ion irradiated, dendritic growth of voids 77—11605
- Ni-Al-Cr, IN-100, growth geometry of carbides in dendritic monocrystals, solidification effects 79—11597
- Ni-Al-Cr alloy IN 100 powder, rapidly solidified, effect of high melt superheat on microstructure 79—52195
- Ni-Al-Ta dendritic monocrysts., directionally solidified, coarsening kinetics 80—108425
- Ni-Cr-Mg alloy, KhN70VMTYu, Mg effect on grain boundary struct., props. 79—19261
- Ni-Cr-Ti(Al), effect of ultrasound on crystallisation, dendritic structure, and plasticity *(Russian)* 80—11637
- Pb, variations of energy of the ⟨111⟩ torsion joint as a function of the angle of torsion in metallic seeds [dendritic structure] *(French)* 80—25682
- Si, floating zone structural perfection changes by high temp. treatment, dendrites, dislocation interactions 80—29049
- Si, RTR ribbon, impact of defects on photovoltaic potential 79—11186
- Si, rapidly grown RTR sheet, props. and solar cell processing 79—100048
- Si, ribbons produced through capillary action shaping, elec. and struct. characts. 78—47804
- SiC, CVD, microstruct. obs., optical and TEM 79—7560
- Sm(Co$_{0.84}$Cu$_{0.16}$)$_{6.9}$, microstruct. and domain struct., mag. reversal *(Russian)* 80—20429
- Sn melt, highly supercooled, dendrite growth *(Russian)* 77—81253
- Sn, undercooled, dendrite growth rate 77—90339
- Sn-Bi (Pb) alloys, supercooled, dendritic growth rates *(Russian)* 78—80533
- Sn-Pb, dil., undercooled alloy, solidification 78—3120
- W dendritic surface anodisation for solar absorptance enhancement 79—34440
- W, dendritic surfaces, antireflection coated, reflectance geometrical study 79—91511
- Zn electrodeposition, inhibited, electrode kinetics and deposit morphology 79—56089
- Zn-Al-Cu casting alloys, mech. props. and dendritic morphology, Al content effect *(Korean)* 80—93612
- Zn-Ge, eutectic, form. of dendrites *(Russian)* 79—52187
- ZrO$_2$-SiO$_2$, liquid immiscibility, microstruct. of plasma dissociated ZrSiO$_4$ 80—107429

dense fluids, theory *see liquid theory*

densification
- *see also density; powders; sintering*
- agglomeration techniques in powder technology, review 78—39713
- alumina, role of $\alpha \rightarrow \gamma$ polymorphic transform. in hot pressing 77—63612
- aquifer, viscoelastic model appl. to subsidence and compaction due to pumping 77—91175
- atomised-Fe powder, friction of compaction process *(Japanese)* 77—59716
- borosilicate glasses, gamma irradiation effect on density, refractive index, thermal expansion 80—79838
- ceramic, compaction during liq. phase sintering 80—55335
- ceramic, compaction during pressing, green strength, effect of adsorbed layers *(German)* 78—6880
- ceramic, fine powder, compaction during pressing and green strength, absorbed layer effect *(German)* 77—77450
- ceramic compact, morphological investigations significance 79—33988
- ceramic powder pressing review 79—47652
- ceramic powder synthesis from laser-heated gas phase reactants 80—93525
- ceramics, self vitrifying, consisting of quartz, feldspar and kaolin, compaction press. during firing effects 80—29909
- chaoite, a new allotropic form of carbon, produced by shock compression 80—80997
- cladding and oxide fuel in LWR, FBR, irrad. behaviour, chemical process, densification, corrosion *(Japanese)* 77—83033
- clay, highly plastic, compaction and lime stabilization effect on pore size distrib. *(Japanese)* 78—31365
- compaction, by impact of projectiles launched by compressed air 80—2973
- compaction, of metal powders 80—40279
- corundum ceramic, high-temp. treatment, powder medium effect on microstruct., comp., strength and dielec. props. 79—33984
- diamond, shock synthesis *(Japanese)* 80—29918
- diamond powder, consolidation by thermal decomposition of methane and benzene 80—66448

densification continued
die filling and densification in hot extrusion forging of porous preforms 78—23645
dynamic hot densification of porous blanks, degree of deformation 77—63585
ferrite compacts, during hydrostatic pressing 80—25629
ferrite core, strength improvement method, SiO_2 and Bi_2O_3 additions, mag. characts. 79—24484
fibre reinforced composites densification in free forging, exam. of specific work and kinetics 80—16218
fibre reinforced composites with undeformable inclusions, sintering, densification kinetics prediction 77—63601
fibre reinforced porous matrix materials, densification kinetics in free hot pressing 80—25618
fibre reinforced powder, densification during hot pressing 77—12566
fission oxide fuels, in-pile densification of intergranular porosity, model 79—73345
glass, low density, sintering, expt. study 77—85980
glass, low density, sintering, pore size distrib. effect 77—85981
glass, polished surfaces, environment sensitive, ellipsometric obs. 77—48559
granular materials, density hardening, compacting 79—32283
granular materials, random packing, statistical mech. considerations 80—104088
graphite-BC body, hot pressing, props. *(Japanese)* 79—78923
hard-alloy powder mixtures, compressibility in hydrostatic working 78—68645
high-speed shaping of free-flowing materials, computer investigation 80—25591
hot pressing, reactive, identification of stages 79—11542
hot pressing review 79—74113
Incaloy IN 738, dispersion hardened superalloy 78—11156
isothermal densification, models for kinetics 79—78912
liquid phase sintering, expt. obs. of densification by sintering 80—11584
liquid phase sintering, role of grain and phase boundaries 78—72747
magnesite-chromite powder, exam. of rheological characts., compaction 78—60628
magnesium stearate-containing powder mixtures, bonding 78—84731
metal, plastic, work hardening, sintered, porous, irreversible deform. 78—19849
metal, porous, densification during volume plastic deform. without work hardening 77—40402
metal powder, milling conditions effect on densification during pressing and sintering 78—11149
metal powder, sintering, with intense energy release of interparticle contacts 78—60615
metal powder pressing-ejection unit, industrial, for long filter element prod. 77—63595
metal powders, on heating under high pressure, to 80 kbar 80—25602
metal powders, strip densification in forward slip zone in rolling 79—95972
metal powders, transverse pressing 79—100081
metal powders, vacuum treatment, method of calc. evacuation time and permeability 80—20827
metal power compaction equations, best description of expt. data 80—2974
metal shaving, densification, effect of intermolecular and electrostatic cohesive forces 77—77445
metal-glass material, relation between struct. and props., prod. by hot densification 78—11145
metallic oxide powders and mixtures, hydrostatic pressing, density and hardness variation 79—70029
mischmetal-Co-Cu-Fe-Mg, mag. props. 80—35353
mischmetal-Co-Cu-Mg, mag. props. 80—35353
mixed oxide reactor fuels. irradiation-induced densification characts. 79—49684
multi-layer soils, state vector approach to one dimens. consolidation 78—3757
Ni powder 2JJ, porous, effect of sintering conditions in struct. and strength 80—20823
nonisothermal sintering, densification of powder compacts 78—60596
nuclear reactor chop-leach fuel hulls, chemical decontamination and melt densification 77—65319
oxide fuels, in-pile densification by vacancy boil-off and vacancy knockout, model 79—8259
particle deformation during cold isostatic pressing 78—44052
Permalloy, pressing velocity effect on quality of compacts 80—20834
PET, densification, cryst. perfection, mechanism 79—66082
plasma sprayed coating consolidation by laser remelting 80—93697
PMMA, oriented, hypersound propag., elastic props. 78—75737
PMMA femoral cement compactor for total hip replacement 79—79688
polymer glasses, thermodynamics of densification process 78—95723
polynary complex powder mixture compaction, new equation 77—21045
polypropylene chloride co-polymer powder, cold compaction, product strength, heat treatment effects 80—11621
polypropylene powder, cold compaction, product strength, heat treatment effects 80—11621
porcelain, sintering charact. 79—83156
porous body during hot extrusion, theoretical analysis 77—44189
porous body in rigid sheath, energy expenditure in densification 80—16216
porous materials, densification kinetics in hot pressing, under quasi-isostatic conditions 80—11585
porous materials, densification kinetics in hot pressing under quasi-isostatic conditions 80—25592
porous materials, density variation during plastic shaping 80—84873
porous solid, densification during gasostatic hot pressing 77—12567
porous solid, mixture theory of thermomechanics 78—63315
porous solid, shear stress enhancement of void compaction 79—69182
porous solids, hot rolling, rheology, stressed state determ. 79—100194
porous solids in hot rolling 77—63583
powder, die compaction 79—61528
powder, dynamic compaction, review 78—3071
powder, two component mixture, compact growth in liquid phase sintering 80—20835
powder, under uniform directional loading 78—68644
powder compact densification characts., non-isothermal sintering 79—28976
powder compacts, effect of additional pressing at hydrostatic pressures on props. 78—56596
powder consolidation by pulsed magnetic fields *(German)* 77—8783

densification continued
powder consolidation process, exam. of quasimelt in pressing, sintering stages 80—20816
powder materials, densification laws 79—66021
powder metallurgy, electrohydraulic effect appl. 80—60798
powder metallurgy compact, elec. resistivity 78—64028
powder strip, rolled, effect of densification zone shape on density distrib. 79—95960
powdered compact, densification model with simultaneous grain growth 78—80486
powdered mixture, compaction, optimum porosity and particle sizes 77—85971
powders, during isostatic compression 80—66449
prefired substrate, acid treatment, improvement in as-fired surface finish 79—24636
preforming using high-voltage electrical discharge 80—84872
pressing, role in producing zero defect parts *(French)* 80—40380
pressing dies, dimensions of hard-alloy inserts calc. 78—60593
pressure sintering, inhomogeneous flow and effective press. 80—93512
PVC powder, cold compaction, product strength, heat treatment effects 80—11621
PVC-Cu composites, elec. resistivity rel. to compacting pressure 80—34495
quartz glass-ceramics, atm. influence on sintering rate 79—38784
refractory powders, wet decompaction and compaction 80—35150
SEM stereoscopic quantitative analysis 80—57433
snow containing liq. water, sintering and compaction 79—62536
soils, non-linear seismic response and liquefaction 79—57862
spherical powder sintering by surface diffusion, computer simulation 78—48344
stainless steel wire reinforced Al sheet, prod. by explosive compaction, and mech. props. 77—32542
steel, austenitic stainless, porous fibre, sintered and compacted, mech. props. 79—15623
steel, high speed, powder, cold isostatic compaction effect on thermophysical props. 78—52717
steel, high speed, W-Mo-Co-Cr-V, production from atomized powder 80—20837
steel, high-speed, sintered, refractory carbide additions effect on hardness and cutting performance 77—66608
steel, maraging, inert gas atomised, hot isostatic pressing temp. effect 79—24460
steel, Mn, sintered, production, effect of initial Fe powder struct. on mech. props. 80—104095
steel, powder, rotary forging, porosity and deform. 78—23646
steel, stainless, medium hardness, densification of particulate materials, general law 78—19692
steel fibre reinforced concrete, vibr. compaction, pressure compaction and curing *(Japanese)* 80—89179
superalloy, hot consolidation of rapidly solidified powders, review 79—33965
surface redistribution by grain boundary diffusion 80—84871
TCNQ salts, crystallisation versus electrical conductivity 80—92885
uniaxially reinforced powder, densification by dynamic hot pressing in rigid sheath 77—12568
vacuum techniques' contribution to powder metallurgy 78—84736
vibrational compaction, of bulk materials 78—52701
vibrovacuum compaction of fine powders and its influence on isostatic molding 79—83149
Zircaloy-2, hot-pressed, influence of diffused C on structure and oxidation 80—61016
ALN, O_2 effects on sintering 77—77451
Al, 78% dense porous, dynamic compaction 78—63315
Al powder, resist.-sintability *(Japanese)* 80—16228
Al, sintering, activated, under thermal cycling 77—21053
Al-C-silaceous sand mixture in N_2 atmos., weight loss during heating, compaction *(Japanese)* 80—35151
Al-Fe_3O_4 binary thermite powder mixture, compaction 79—74125
Al-powder based composite, hydrostatic pressing 77—63593
Al-Si-N-O system, comps. corresponding to β'-sialon phase reaction hot-pressing 80—84891
Al-steel mixture, wear resistant, produced by compaction by discrete shock waves 80—84882
AlN, hot pressed, effect of O_2 content on flexural strength and compact density 79—11668
AlN, powder shock wave compression prior to sintering 77—66615
AlN-Al_2O_3 powders, hot pressing, crystalline phase obs. 78—95720
Al_2O_3 ceramic, vacuum compacted using $MgCl_2$ soln. moistener and MgO additive 79—61546
Al_2O_3, ceramic compact, morphology 79—33988
Al_2O_3, crystallite size and lattice distortion, determination using X-ray line broadening analysis, appl. to ceramic powders 79—8261
β-Al_2O_3, effect of furnace atmosphere on sintering, and densification 79—20010
Al_2O_3, explosively compacted powder, struct. and annealing 77—55926
Al_2O_3, hot pressing, microstruct., texture 80—40299
β''-Al_2O_3, Li_2O-stabilised, hot-pressing 80—40298
Al_2O_3, sintered, MgO-enhanced densification, test of second phase and impurity segregation models 78—64511
Al_2O_3, sintering in reducing atmosphere, Na effect on density and strength 77—63613
Al_2O_3, spray dried agglomerates, compaction response, fracture, deform. 79—43172
Al_2O_3, surface smoothness and densification, effects of SiO_2 additives 78—27462
Al_2O_3, translucent, fabrication by high press. sintering 78—11167
Al_2O_3-MgO, MgO addition role in sintering 79—91608
β-Al_2O_3-Na_2O, vacuum hot pressed, densification kinetics 78—72758
Al_2O_3-$ZrSiO_4$ mixture, reaction sintering, correlation between densification and reaction 80—29911
As-Se system glasses, opt. absorpt. edge shift on densification 77—77250
As_2Se_3, vitreous, elec. and opt. prop. changes on densification 77—11958
$As_{50}Se_{50}$ and $As_{20}Se_{80}$ semicond. glasses, densified, photoluminesc., inelastic deform. effect 80—66293
BC, sintered, struct. and props. 80—104181
$B_{12}C_3$, sintering and subsequent high temp. annealing, struct. and props. 80—20858
B_4C, densification kinetics during hot pressing, 1800-2200°C 80—60817
BN powder, shock wave compression prior to sintering 77—66615
BN, shock synthesis *(Japanese)* 80—29918

densification continued
BaO.n Fe_2O_3, magnet, effect of SiO_2 on texture and densification behaviour *(German)* 79—24631
$BaTiO_3$, powder compacts, sintered, physical and chem. inhomogeneities 79—87594
$BaTiO_3$:La, Sb, second phase effect on elec. and mag. props. 80—60986
$BaTiO_3$-CuO(TiO_2)(ZrO_2) mixture, exam. of liquid phase sintering, densification 79—33979
Be-Si-Al-O-N ceramic, phase assemblages, relationships with props. 80—60848
Bi powder, sintering in air, glycerol or vacuum 79—91604
C, dense hard-type solids prep. from petroleum coke powder by grinding 79—20002
C powder, binary mixtures, bulk density, charact. curves interpret. 77—63574
$CaHPO_4$, powder and granules with starch mucilage binder, surface topography variation under compression 80—80998
CaO-CaF, hot pressed, effects of CaF_2 addition, sintering behaviours and microstructs. investig. *(Japanese)* 78—95721
CaO-SiO_2-Al_2O_3, wollastonite, low dielec. loss factors, fabrication *(Japanese)* 80—55032
CdO, effect of compacting pressure on consolidation and elec. cond. 79—29007
CdO, elec. cond. and IR refl. spectra after sintering and compaction 79—56945
CdO, influence of initial compacting press. on elec. resis. Hall coeff. 80—20872
Ce-Si-Al-O-N ceramic, phase assemblages, relationships with props. 80—60848
$3Ce_2O_3.2Si_3N_4$, ceramic, prep. by cold compaction and firing, struct. anal. 77—21070
Co, powder, hot pressing on steel substrate, densification kinetics 80—40290
Co powder, isostatic compression, elec. cond., densification models *(French)* 80—55321
Co-Ce Mischmetal powder, sintering 77—21055
Co-powder, isostatic compaction *(French)* 80—40285
CoO, pressure sintering densification model, computer program 78—44040
Cr_2O_3, effect of oxide additions on sintering in air and reducing atm. 77—59729
Cr_2O_3, influence of TiO_2 on sintering behaviour, densification as function of temp. 79—78919
Cu compact, exam. of anisotropic shrinkage as function of pressure 79—8257
Cu, densification of particulate materials, general law 78—19692
Cu, hot forged powder compact 77—24981
Cu PM parts, improving cond. by pretreatment of green compact 80—20824
Cu, powder, exam. of consolidation process based on electronic structure of solid 80—20842
Cu powder, flowability, apparent density and comp., effect of Na, Mg and Al additions 79—28986
Cu, powder, hot pressing on steel substrate, densification kinetics 80—40290
Cu powder, two layered medium dynamic compaction 80—35138
Cu, powder compact, elec. resistivity 78—64028
Cu-Ni-Fe, spinodally decomposable, densification using four different powder methods 80—40283
Fe compacts, porous, dynamic hot pressing, press. rel. to density, time 78—60599
Fe, dynamic hot densification, degree of deformation 77—63585
Fe, medium hardness, densification of particulate materials, general law 78—19692
Fe powder, density distrib. in rolling deformation region 80—40288
Fe, powder, exam. of consolidation process based on electronic structure of solid 80—20842
Fe, powder, hot pressing on steel substrate, densification kinetics 80—40290
Fe Powder, resist.-sintability *(Japanese)* 80—16228
Fe, powder, vibratory densification in vibratory press 77—12576
Fe, powder compaction, elect. cond. changes 79—66175
Fe powder compacts, pressed under static or vibr. load, shrinkage anisotropy during sintering 80—50574
Fe powder sintered compacts, mech. props. effect of powder type and processing conditions *(Czech)* 77—59830
Fe powders, cold-pressed, props., effect of air 80—100810
Fe, sintered parts, densification in burnishing process by rocking die method 78—35331
Fe, water atomized powder, compaction, bending strength *(French)* 80—40287
Fe/Fe-Cr composite powder, X-ray diffr. exam. of densification during rolling 80—40289
Fe/zinc stearate, compacts, admixing, effect on mech. props. 80—45402
Fe/Zn stearate powder compacts, admixing effect on apparent density, mixing, compaction 80—45403
Fe-C-Mn (0.5, 0.6 wt.%), powder forged, mech. props. 80—21096
Fe-Cr-SiC-B_4C powder mixture, compressibility and elec. cond. in cold pressing under low press. 78—60609
Fe-S-C (1,3 wt.%), sulphidised Fe-graphite bearing materials, sintering, struct. form. 78—60601
Fe-VC-WC(TiC), sintering, densification 80—25615
Fe-WC-VC(TiC), sintering, densification 80—25615
β-Fe_5Ge_3 formation in isothermal sintering, phase transition kinetics 80—89197
γ-Fe_2O_3, densified, rheological and mag. props. 80—44873
Fe_2O_3, powder, compression in moulds, meas. apparatus *(Dutch)* 77—44205
γ-Fe_2O_3 powders, influence of densification on mag. props. 78—95481
$Ge_{30}Si_{70}$, hot press sintering 80—50572
$LaCrO_3$-Cr cermet, effect of explosive compacting on props. 77—12557
$La_{1-x}Sr_xCrO_3$, densification 77—8780
$LiNbO_3$-CdO, CdO addition effect on sintering 79—83157
$Li_xNi_{1-x}O$ (x=0 to 0.03), solid soln. effect of Li on densification during sintering 80—25638
Mg-Si-Al-O-N ceramic, phase assemblages, relationships with props. 80—60848
MgF_2, hot pressing in vacuum, compaction kinetics, selective recryst. 77—16517
MgO (:CaO) powder compacts, sintering studies, SEM obs. 79—78918
MgO briquets, prep. by shock compaction and characteris. 79—43178

densification continued
MgO, effect of Cl^- and F^- ions on calcination and sintering *(Japanese)* 78—95719
MgO powders, hot pressing, mechanisms 80—40300
MgO, sintering, effect of Ca compound additions *(Japanese)* 80—55340
MgO-Al_2O_3 transparent spinel ceramic, fabrication by reactive hot pressing *(Japanese)* 77—77454
MgO-Cr_2O_3, reaction sintering *(German)* 78—11174
MgO-NaCl refractory clinkers, Cr containing, densification, thermal treatment and phase composition effect *(French)* 80—76219
MgO_2 powder exam. of packing behaviour *(Japanese)* 79—20016
(Mn,Zn)Fe_2O_4:Si, Ca, Ti, second phase effect on elec. and mag. props. 80—60986
Mn_2SiO_3, effect of vibration during sintering, on electrical resistivity 80—16258
MnZn ferrite, MoO_3 addition effect on grain growth kinetics and densification 79—61550
MnZn ferrite, spray dried agglomerates, compaction response, fracture, deform. 79—43172
MnZn ferrite powders, reactive, mag. materials obtained by compaction 80—89182
Mo, powder, cold isostatic compaction effect on thermophysical props. 78—52717
Mo powder, influence of powder reduction processes on props. 80—89175
Mo-Fe alloy powders, densification and alloy formation on sintering 77—63597
$MoSi_2$, ceramic additives effect on sintering, recrystallisation 80—40306
NaCl(:$CdCl_2$), sintering in air, densification kinetics and mechanism 77—4750
NaF, sintering, relation between densification and grain growth 77—12585
Na_2O-CaO glass phlogopite mica powders, composite fabrication, cellular struct. 80—84902
NbC_X powders, nonstoichiometric, sintering kinetics 79—100099
$Nb_{40}Fe_{40}P_{14}B_6$, metallic glass, explosive compaction, mech. props. 80—89176
Nd:YAG, solid-state formation 80—35121
Ni, ductile, electrolytic, densification of particulate materials, general law 78—19692
Ni, high temp. plasticity, oxide inclusion effect 80—50681
Ni, powder, hot pressing on steel substrate, densification kinetics 80—40290
Ni powder, porous, relationships between mech., physical, and microstructural characts. 80—20846
Ni powder, resist.-sintability *(Japanese)* 80—16228
Ni powders, stereological appl. in study of compacting process, elec. and mech. props. *(French)* 80—40286
Ni, volume strained, sintered, porous, physicomechanical props., electrical resistivity 77—12572
Ni-Zn-Co ferrites, synthesis from solid solns. of schoenite-type salts 80—93511
Ni-ZrB_2 powders, densification by hot pressing 80—25604
NiO-CaF_2 two-phase material, press. sintering, activation energy and compaction mechanism 79—47651
Pb, sintering, surface oxide layer effect 79—66024
$Pb_{0.94-x/2}Ba_{0.6}Nb_xZr_{1-x}O_3$, Nb dopant morphology effect on microstructure 80—81005
Pb(Ti,Zr)O_3, kinetics of initial stage of sintering 77—85973
Pb(Zr, Ti)O_3 cast tape, densification by pressing for piezoelec. devices 79—87595
Pb(Zr, Ti)O_3, piezoceramic, explosive synthesis 77—16525
Pb(Zr, Ti)O_3, Sc modified, sintering 77—44204
Re film, prep. by laser melting 80—84859
Si, nitridation kinetics, combined effect of Fe and H_2 78—95722
Si-SiO_2-Mg-Cu powder compact, nitridation to form Si_2ON_2 whiskers *(Japanese)* 80—93674
SiAlON, prepared from siliceous sand and Al powder, hot pressing, steatite contamination effects *(Japanese)* 80—93528
$Si_{6-z}Al_zO_zN_{8-z}$, β-Sialon, form. from Si_3N_4-SiO_2-AlN system *(Japanese)* 80—45261
β-SiC, sintering, B transport and lattice parameter change 80—108370
SiC, spray dried agglomerates, compaction response, fracture, deform. 79—43172
Si_3N_4, consolidation by hot isostatic pressing 80—11605
Si_3N_4, densification, role of $Ce_{4.67}(SiO_4)_3O$ 79—61549
Si_3N_4, hot pressing, starting powder requirements, review 79—33987
Si_3N_4, hot pressing with Mg-Si-N-O system additives *(Japanese)* 77—36437
Si_3N_4, hot pressing with Y_2O_3 and Li_2O additives 78—92220
β-Si_3N_4, hot-pressed, containing small amounts of Be and O in solid soln. 80—2985
Si_3N_4, hot-pressed with crystn. grain boundary phases, prep. 78—95715
α-Si_3N_4 powder, hot pressing, kinetics 77—55925
Si_3N_4, reaction bonded, post-sintering, injection moulding applications 80—60807
Si_3N_4, reaction-bonded, pore struct. variations 79—24480
Si_3N_4, reaction-bonded, theoretical model of manufacture, effect of ambient reaction temp. and compact size 80—108379
Si_3N_4, sintering in powder bed with addition of MgO sintering aid 80—29910
Si_3N_4 with Y_2O_3 and Al_2O_3 additions, hot pressed, exam. of mech. props., grain boundary crystallization 79—20009
Si_3N_4-Al_2O_3, hot-pressed with crystn. grain boundary phases, prep. 78—95715
Si_3N_4-Al_2O_3, Sialon, pressure sintering 77—55919
Si_3N_4-Al_2O_3-AlN, Sialon, fabrication and reaction sintering 77—44201
Si_3N_4-MgO, hot pressing and α-β phase transform. 78—27461
Si_3N_4-MgO (5 wt.%), microstructural changes during gas pressure sintering *(Japanese)* 77—12589
Si_3N_4-Si_2N_2O-Mg_2SiO_4, melting and eutectic studies 80—45285
SiO_2 glass, densified, enthalpy variation, heat of dissolution obs. *(French)* 79—34015
SiO_2, vitreous, compaction dependence on ionisation dose 78—67738
SiO_2, vitreous, electron irrad., vol., refr. index and stress changes 77—47482
SiO_2, vitreous, X-ray compaction efficiency 80—65044
$SmCo_5$ powder alloy, densification by cold working 77—4753
Sn bronze, air atomised, densification and pressure requirements during extrusion 77—59713
α-Sn, compact prep., from β-Sn containing 0.1 at.% Ge 80—55320
SnO_2, activated sintering 77—36415

densification continued
- $SrFe_{12}O_{19}$:Si, Sr, second phase effect on elec. and mag. props. 80–60986
- Ta, sintering with transition metal additions 78–15335
- TaC, ultrafine grain, high pressure hot pressing 79–70024
- ThO_2 base low burnup fuels, densification-related pellet diameter shrinkage 79–54510
- (Ti, Cr)B_2-based alloys, densification of powder mixtures by hot-pressing, elec. and mech. props. 80–20812
- Ti powder, resist.-sintability *(Japanese)* 80–16228
- Ti, powder, vibratory densification in vibratory press 77–12576
- Ti, strip prod. by powder rolling 78–80493
- Ti-Al system, compact growth in liquid phase sintering 80–20835
- TiC-Ni powder compact, wetting problems in sintering 80–11596
- TiC-Ni-Cr(Mo) hard alloy mixtures, pressing 77–63596
- TiC-steel alloy, struct. form. during sintering, strength, rel. to heat treatments 77–59717
- TiC_x, nonstoichiometric, densification during sintering 80–84895
- TiN, high dispersed superconductivity 78–43505
- TiN, highly dispersed, metallic thermo-EMF 78–43363
- TiN-Al_2O_3, exam. of sintering and densification kinetics, and physical props. 79–95986
- TiO_2, sintering, struct., pressing, atm., and doping effects 80–20873
- TlSe.As_2Se_3, $Tl_2Se.As_2Se_3$, γ-irrad. effects on mech. props. 77–80567
- (U,Pu)O_2, anal. of densification in BWR 79–49685
- (U,Pu)O_{2-x}, mixed oxide fuel, final stage densification 79–49681
- UO_2, in reactor densification 78–21648
- UO_2 irradiated fuel, densification algorithm 79–78913
- UO_2, irradiation induced vol. change 78–67740
- UO_2 pellet fuel, radiation induced densification 77–6519
- UO_2 pellets, thermal densification *(Korean)* 78–44065
- UO_2 powder, precompaction effect on compressibility 78–41846
- UO_2, powder, sintering effect of compaction 80–20874
- UO_2 powder compaction, force transmission and friction 80–71620
- UO_2, sintering, use of NH_3, grain size changes 77–55920
- UO_2, stoichiometric, sintering diagram *(Rumanian)* 79–87602
- UO_2, thermal and in-reactor densification 78–66364
- UO_2-20CeO_2 mixed powder, X-ray and microprobe exam. of homogenisation 80–25609
- W, brittle spiral fibre, densification of particulate materials, general law 78–19692
- W, enhanced low temp. sintering, temp. sensitivity causes 77–36418
- W, powder, cold isostatic compaction effect on thermophysical props. 78–52717
- W powder, hydrostatic pressing 78–11161
- W powder, pressing with dispersed strengthening phase additions using flexible bags 79–70016
- W powders, influence of geometrical props. on compaction *(Russian)* 80–20818
- W:Ni compacts, optimum conc. of Ni for activated sintering, optical microscopy obs. 79–38758
- W/Cu powders, liq. phase sintering, particle rearrangement 80–45253
- W-Cu, porous material, skeletal type, produced by liquid phase sintering, exam. of mech. strength, determ. resistance 80–16245
- W-Cu sintered alloy, produced from coreduced powders, densification 78–11154
- W-Ni system, grain growth and densification during liquid phase sintering 79–38760
- W_2B_5, sintering rel. to prod. by boron carbide process 78–11184
- WC, liquid phase sintering 77–4751
- WC-Co compacts and sintered alloy, fine struct. of carbide phases, preforms re-pressing under high press. effect 79–28987
- WC-Co powder, prep. by direct carburisation of WO_3 in presence of Co_3O_4 80–50573
- WC-Co-C based hard alloy VK6, densification kinetics in hot pressing 80–11600
- WSe_2, lubricant, prep. by self-propagating high-temp. synthesis, technological characts. 78–35338
- Y-Si-Al-O-N ceramic, phase assemblages, relationships with props. 80–60848
- Zn, die pressed powder, green strength 77–59876
- ZnO, segregation of Li_2O at grain boundaries 78–64513
- ZnO:Bi, Sb, Co, second phase effect on elec. and mag. props. 80–60986
- ZnSe cold pressing 77–52258
- ZrB_2, hot pressing, applied press. effect *(Japanese)* 79–38780
- ZrN-Al_2O_3, exam. of sintering and densification kinetics, and physical props. 79–95986
- ZrO_2 electrolyte cells, sintering 79–24476
- ZrO_2 shock wave treatment of powders *(Russian)* 77–44186
- ZrO_2, spray dried agglomerates, compaction response, fracture, deform. 79–43172
- $ZrSiO_4$-Al_2O_3 mixture, reaction hot pressing 79–38775
- $ZrSiO_4$-Al_2O_3 system, particle rearrangement kinetics due to densification 80–25626

densimeters *see densitometry*

densitometers *see densitometry*

densitometry
- *see also photometry*
- accuracy of optical density meas. by means of optical wedge 80–73416
- accurate fan-beam reconstruction 78–78931
- acetylene smoke particles, agglomerated, optical extinction meas. at 0.5145 and 10.6 μm 80–48155
- air/water mixture mass flow meas. by drag devices and γ densitometer 80–79385
- arc spectrography, applic. of equidensitometry *(German)* 77–1962
- arterial walls, human coronary, optical density determ. 80–12173
- astrometric techniques using PDS microdensitometer 78–16306
- autodensitometer, flatbed, for biophys. appl., error analysis 77–52937
- automated visual edge match system for image quality assessment 78–62218
- automatic flat-bed microdensitometer for X-ray crystallography use in molecular biology lab. 77–35438
- automatic microdensitometer, Electronika-100 computer interfacing 77–45908
- automatic system 79–26164
- autoradiography and soft laser scanning in radioisotope work, appl. to metabolic studies 78–3576
- biomedical transmission densitometry, modified method 80–36091
- bone mineral measurement using EMI scanner vs. densitometry 78–24119

densitometry continued
- bone strength determination, data on compressive strength rel. to density and strain rate 77–36976
- cancellous bone, Compton scatter densitometry meas. 79–39489
- chromatin structure of cell nuclei using scanning microphotometry and TV image anal. 79–34720
- chromatogram scanning spectrofluorimeter-densitometer 80–31901
- cine film colour duplication, Laboratory Aim Density control method 77–5953
- cine photomaterials sensitometric parameters automatic analysing instrument *(Russian)* 77–41720
- coherent optical image processing, halftone screen techniques 77–75434
- coherent-optical materials testing for vibration pattern and defect discrimination *(German)* 80–30181
- colour coded equidensities production using nonlinear filtering 77–75426
- colour densitometry on multi-emulsion imagery 79–53555
- colour film densitometer with Si photodetector 80–4791
- colour sensitometry characteristic curves corresponding to visual impression 80–82803
- colour sensitometry system based on spectral densitometer 80–82804
- colour sensitometry using densitometer with more than 3 channels, dye specific densities 80–82802
- combined scanning microdensitometer and diffractometer 80–73529
- compensation densitometer servosystem using integrated operational amplifiers 78–89525
- computerised tomographic scan edge position uncertainty reduction by density derivative processing 80–109017
- densitometer with resonating twin tube for ethane/propane design and tests 77–38052
- densitometers standardized density scale for photographic photometry *(Japanese)* 79–101075
- detection threshold and photometry, influence of granularity and light diffr. 79–21839
- differential capacitance sensor as position detector for magnetic suspension densimeter 80–196
- digital microdensitometer, for automatic astronomical photographic wavelength meas. 77–64655
- digital orthophoto production using scanning microdensitometers 80–41571
- dosimetry film exposure determ., comparison of X-ray fluoresc. and optical density 78–24137
- double exposure for controlled density eval., replacement of quarter wave plates 77–87859
- dyestuffs in fibres, distortion in microdensitometric determ. of conc. distribs. *(German)* 79–17464
- dyestuffs in polymers, conc. distrib., microdensitometric determ., stops effect *(German)* 78–11598
- electro-optical pyrometer single-pulse calibration flash tube 78–12702
- electron diffraction patterns of mols., photometry via IFO-451 microphotometer 77–27201
- electron microdensitometer system for use in TEM 80–95197
- electrophoretic waveform analysis for blood serum protein composition determ. 78–64928
- enzyme reactions in tissue sections, quantitative microscopy using microdensitometry 77–86728
- equidensitometric determ. of angular diameters of compact galaxies 78–16308
- equidensitometry, photographic, astronomical appl. 77–56833
- equidensitometry by coherent optical filtering 77–5936
- equidensity fringe pattern lines on special film, calibration 77–18118
- film-grain noise degraded images, nonlinear detection and estimation 77–50627
- finite-width line axial optical density prediction 79–27193
- flare light in microdensitometer, simple model 78–41341
- flare light in microdensitometer, simple model 78–58008
- flaw dimensions in direction of irradiation determ. from radiographs with aid of defectometer 80–71863
- flood-plain delineation by multispectral data analysis 77–73885
- fringe evaluation of equidensiometric technique (for photoelasticity) 77–27495
- fused xerographic images, optical density model 79–17550
- gamma beam densitometer calibration for mass flow rate meas. in two phase flow of PWR coolant 80–37552
- gamma densitometer meas., anal. of dynamic bias 80–27730
- gamma densitometry, static error evaluation 80–27729
- gamma multibeam nuclear hardened system for two phase flow meas. in PWR coolant 80–37550
- gamma ray, side-scatter, dynamic bias, nuclear react. appl. 80–27728
- gas mixtures, background gas penetration into underexpanded jets, densitometric obs. 79–94655
- glaucoma diagnosis by digital processing of optic nerve head images 78–81043
- granularity measuring system 78–21200
- granularity theory approximations 78–4721
- halftone noise characterisation, meas. technique using scanning microdensitometer 79–26151
- hardwired image analyser software control 78–57917
- heavy charged particle specific energy losses meas. using densitometric method *(Russian)* 80–63482
- high-speed automatic microdensitometer 80–101817
- image restoration, digital 77–23628
- image restoration, use of computerised microdensitometry 79–55066
- image weak modulation detection in film grain noise with partially coherent illumination 80–77897
- intensity microphotometer with step-drives, for negatives transparency conversion *(Russian)* 78–57457
- ion-sensitive photographic plate evaluation using optical wedge microdensitometer *(German)* 80–42298
- isolated atoms visualisation, by electron microscopy, evaluation using digitising microdensitometer *(French)* 78–24892
- Joyce-Loebl microdensitometer, principle, new appls. *(Czech)* 79–30524
- K-edge densitometer, appl. to Pu nuclear fuel reprocessing product soln. accounting 80–95352
- karyotyping automatic image processor *(French)* 77–40953
- large-spot laser damage meas., multibeam apparatus 77–19286
- laser beam metal-coated apodising apertures 77–19439
- laser light energy distribution analysis, film calibration method 77–79875
- laser microphotometry with laminar hydrodynamic focusing 77–37965
- laser scanner for anal. of radiographs 79–70619

densitometry continued

- liquid, extinction coefficient meas. using coaxial dual channel laser system 80—73425
- lung densitometer, 3-dimens., for oedema studies, using CdTe detectors 77—44749
- mammogram densitometric distinction between cancer and fibrocystic lesions 77—25551
- mass density evaluation in vivo from computerised tomographic scans 77—12992
- metrology appl. for microdensitometers 79—85195
- microcomputer contolled film densitometry for X-ray powder diffraction anal. 80—3454
- microdensitometer, platen effects 77—54000
- microdensitometer computer interface design and construction, for X-ray image anal. 77—44821
- microdensitometer flare, methodology for quantifying 80—52293
- microdensitometer optical performance, scalar theorx and expt. 77—61107
- microdensitometer performance, effective incoherence and flare tradeoff 80—77851
- microdensitometer precision focus control 79—58769
- microdensitometer temporal reponse, MTF determ. 78—32904
- microdensitometer with computer-controlled scanning table *(Russian)* 79—6197
- microdensitometer with He-Ne laser radiation source *(German)* 77—79174
- microdensitometer with minicomputer connecting facilities 78—21198
- microdensitometer with minicomputer for semiautomatic interpret. of spectral plates 78—21199
- microdensitometers, props. effect on photographic emulsion charact. curve 79—43673
- microdensitometers for highly accurate metrology, industrial use 80—9017
- microdensitometry, linear, sensor optics design 80—62710
- microphotometer, automated, SAMB, for morphometric and densitometric analysis *(French)* 77—10085
- microphotometry, compensation for fluctuations in illumination 80—73413
- microscopic image anal. system, cell cycle, cancerous blood and bone marrow cells appls. 79—88223
- microwave exposure, densitometry and dosimetry techniques in bioeffects research 77—78072
- monochrome photographic film densitometry errors and standards *(German)* 80—37102
- MTF evaluation with optical matched filters 77—27257
- myocardial contrast accumulation, densitometric evaluation 78—69216
- narrow-band densitometer with pulsed-xenon illumination 77—53994
- narrow-band densitometry with pulsed-xenon source 77—53993
- online shade monitor, strip materials 79—30526
- opacity measurement of smoke and suspensions under ambient lighting conditions 77—26382
- optical density difference measurement on X-ray film by analog measurer 79—39099
- optical fibre refractive index profile microdensitometry 80—106632
- Palomar Sky Survey plates, microdensitometer meas., photometric parameters and positions of images 78—24440
- personnel dosimetry, automatic film-badge reading system 78—40335
- photodensitometry of tracks of highly ionizing particles in the cosmic rays 79—22551
- photographic film spectral sensitivity meas., automated densitometer system 78—29190
- photographic materials, MTF automatic evaluation 80—95170
- photographic paper print residual thiosulphate, methylene-blue and Ag densitometric meas. correlation 79—74472
- photographic parameter estimation, colour and density table *(German)* 79—49309
- photographic pyrometry technique and external calibration 79—93144
- photographic sensitometry, black and white, photographic testing procedures, film evaluation 78—29191
- photographically recorded spectral lines, of nonuniform half-width, microphotometric errors 78—86337
- photography, densitometer measurement transformation into spectral density distrib. and colour coordinates *(Russian)* 80—77902
- photometric calibrator development and appl., inverse fourth power 80—73412
- polymer, dye conc. distrib. determ., microdensitometry *(German)* 77—37962
- print contrast measurement 77—34045
- processor control using preexposed control strips and visual comparative densitometry 78—69210
- pseudo colour equidensitometry, analogue optical method 78—32903
- pseudocolour density encoding of photographic materials, white light processing system 79—18360
- pulsed dye laser densitometry using optical delay 77—61104
- quantitative holographic interferometry in transonic flow *(French)* 77—65826
- reflection microdensitometry, optical principles and practical solutions 80—4790
- refractory products, apparent density determination, using surface γ densimeter 80—35464
- renal diagnosis by blood circulation angiocinedensitometry *(German)* 79—2127
- review of new approaches 78—307
- Roentgen cinefilms, circuit for densitometric evaluation *(German)* 79—53214
- roentgen densitometer for detect. of congenital heart defects, patient dose 77—9239
- scanning microscope stage for microdensitometry, computer-controlled 79—26117
- scattering media optical meas. for biomedical applications 79—83890
- secondary ion mass spectroscopy, image quantitation, by microphotodensitometry and digital processing 78—32914
- SEM, photographic densitometry, appl. to chromosomes 78—77168
- sensitometers, for radiographic processing quality assurance, performance evaluation 79—29617
- sensitometry, conference, Binghamton, N.Y., USA (Sep. 1976) 77—30214
- SIMS ion images, multifeature mass analysis utilising digital image processing, Fe anal. appl. 79—43684
- single beam microdensitometer, liquid electron diffraction pattern evaluation 80—86370

densitometry continued

- smoke plume concentration meas. by optical radar *(Chinese)* 78—58006
- solar corona and comet digital image enhancement 78—81556
- solid surface fluorescence analysis, calibration curves 78—31719
- spectrophotometer kinetic curve recording unit 78—86352
- steel, austenitic stainless, deformation induced cavitation, exam. 79—43363
- stenosis densitometric analysis from remote terminal 79—83900
- TEM, thin section uniform region quantitative meas. 78—58097
- thoracic X-ray image comparison automation *(Japanese)* 79—29615
- tonal reproduction via unscreened positive printing plates 79—17517
- turbid media, approx. linear relationship for optical response 78—90371
- US, two-phase flow density meas. in pressurised water reactor 80—77759
- vesicular film, contact printing density determ. by densitometer meas. 77—53995
- Vickers M85/M86 microdensitometer, film holder 79—21832
- videodensitometric camera and video disc system 77—40761
- videodensitometry and image analysis, minimum computer system 79—34664
- water penetration imagery, surface/depth data separation by multispectral scanning 78—69539
- wedges as flux modulators 77—27355
- X-ray focal spot, MTF, modified meas. method 80—37149
- X-ray microdensitometer for crystallographic investigations 79—54241
- X-ray microphotodensitometry in traumatology and orthopaedic surgery *(Croatian)* 80—109022
- X-ray photodensitometry determ. of compact bone mineral density 79—74739
- X-ray screen-film systems, H and D curves, factors affecting energy dependence 79—39484
- xerographic copy line profile meas. using microcomputer/microdensitometer system 78—74088
- ^{252}Cf wire neutron source distrib., meas. by autoradiography 77—61643
- $NaNbO_3$-$SrNb_2O_6$, phase diagram, props. meas. 79—11576
- Pu safeguards, product soln. gamma-ray NDA using K-absorption edge densitometer 80—83162
- U/Pu fuel reprocessing solutions, NDA using X-ray L-edge densitometer for materials safeguards 80—83167

density

see also atmospheric pressure and density; density control; density measurement; density of gases; density of liquids; density of solids

- alkali halide, melting mechanism, vol. and enthalpy changes 79—55866
- brain, experimental oedema, serial meas. of specific gravity and computerised tomography attenuation 80—98005
- S.China Sea, density interface rel. to internal waves refr. obs. 77—64298
- chromaffin granules, osmometer model for changes in buoyant density 77—90737
- clusters of galaxies, mean density and correl. function, theory and obs. 78—24559
- concrete, ultrasonic wave velocities and density, calc. and meas. 79—52545
- Coulomb systems, equilib. distrib. functions expansion in power of density 80—64681
- critical opalescence and density fluctuations in gravitational field 80—66137
- critical temperature determ. from expt. data on ρ_s(T) boundary curve 77—15539
- dilute gas, Boltzmann-Langevin eqn., light scatt. and density correlation function 77—11307
- dispersed medium freezing, origin of water aspiration 77—60130
- 30 Doradus nebula, density struct. and chemical comp. 80—62226
- early universe, adiabatic density perturbations evolution 79—25769
- early universe, density-temp. fluctuations present observability 80—82554
- early universe, nonlinear primordial fluctuations 79—25773
- early Universe initial density fluctuations implications of origin of baryons in Universe 79—62938
- Earth, density models appl. to geoid anomalies computation 80—3897
- Earth, gravity field anomalies sources depths determ. 79—16366
- Earth and crust, Bouguer formula rel. to gravity corrections 79—29692
- Earth crust, Michigan Basin deep borehole gravimeter survey 79—39634
- Earth interior, density distrib. from gravity logging data *(Russian)* 78—92999
- Earth mantle, density inhomogeneities, beneath oceanic trenches, island areas and marginal seas 80—21676
- Earth upper mantle, lateral anomalies 77—29261
- Earth upper mantle, possible density inversion 79—12099
- element, melting, vol. change, simple model 79—55865
- equatorial Indian Ocean, seasonal temp. and density fields caused by monsoons *(Russian)* 78—44839
- fibrosarcoma cells, buoyant density, effect of hypoxic growth conditions in vitro 80—104601
- fluid, rough sphere, kinetic theory, density fluctuations 78—131
- fluid monolayer at solid surface, density distrib. calcs. 80—49492
- galaxies, stars/gas density ratio rel. to local gravit. instability in double gaseous discs *(Chinese)* 79—17099
- Galaxy, local mass density rel. to force field normal to galactic plane 80—46669
- galaxy cluster halos, density distribs. as probe for expanding Universe primordial inhomogeneities 80—22122
- globular clusters, star space densities from multicolour strip photometry 78—89229
- gravimetric density formula for Earth of spherical shells 78—61303
- hard-sphere fluid, density profile near container wall, mean spherical approx. 77—15149
- hard-sphere fluid, eqns. of state, transport data, glass transaction 77—4182
- icy satellites, mass-radius relationships, density and temp. profiles 80—31222
- interstellar large globules, density radial distrib. rel. to dynamics 80—62246
- interstellar shocks, post-shock gas temp., density and vel. profiles, analytical results 80—56911
- Lennard-Jones 12-6 fluid, liq.-vap. interface, density and surface tension 79—90772
- liquid/vapour interface density profile, free-energy theory 80—10751
- mid-ocean ridge basalts, density var. rel. to magma mixing and primitive lavas scarcity 80—56460
- Moon, density model consistent with topographic, gravit., librational and seismic data 77—45332
- Moon, regolith density meas., review 78—16317

density continued
- muscle, human skeletal, mech. simulation 78−35878
- neopentane, critical, electron mobility, gravity effect 78−91738
- nonpolar binary mixture, partial molar vol. prediction from Lee-Kesler eqn. of state 80−10632
- ocean, buoyancy flux effects on density field and continental shelf circulation 80−72540
- ocean, two-layer, density stratification and locally generated internal waves *(Russian)* 79−16480
- ocean density gradient data, appl. to current flow vel. determ. 80−17415
- ocean large-scale density anomalies, non-linear evolution *(Russian)* 79−16479
- N Pacific Ocean waters, density 78−73391
- relativistic thermodynamics, density, momentum and energy laws 77−82424
- sea ice near Showa Station, Antarctica, density and salinity meas. *(Japanese)* 78−96226
- seawater, density field calc. in Kuroshio jet current region 78−92843
- sheet material, radioisotope method for measurement of average value, and dispersion in surface density 78−76811
- solar active region coronal loops, temp. and density struct. 79−8890
- solar coronal loops, temp. and density struct. 78−89155
- solar type III radio burst sources, density inhomogeneities rel. to plasma wave clumping 80−21959
- solar wind, noncompressive density enhancements 78−28479
- solar wind models, Alfven effects on density profile 79−16789
- spiral galaxies, surface mass density distribs. in galaxy form. model 80−90529
- stellar atmosphere in statistical equilib., effects of deviations from LTE on particle densities 80−31290
- Sun polar coronal hole, temp.-density model from EUV lines 79−5797
- supernova remnants, ambient density and energy 78−20868
- turbulent medium with density gradient, MHD effects, appl. solar convection *(Russian)* 78−47055
- universe, Friedmann model, with decoupled radiation field, density perturbations growth 80−109567
- Venus, density rel. to tectonics and comp. 80−72805
- water-air interface, overall heat transfer coeffs., humidity and density profiles, turbulent pulsations *(Russian)* 78−22349
- Al_2O_3, sintering behaviour and props. of 24 aluminas *(German)* 79−4932
- CaO-B_2O_3-GeO_2 glass system, physicochem. props., alkaline earth oxides effect 79−65827
- H II regions, influence of gas density on ionisation and temp. struct. 78−61911
- H II regions density fluctuatons, statistical approach 80−77468
- $(MgO)_x$-$(Al_2O_3)_y$ formation of nonstoichiometric spinel on heating hydrous $MgAl_2O_4$ 78−76672
- NH_4Cl, submicron particles, density, morphology 80−61166
- Ni-ZrO_2, thin layers, vapour deposited, dispersion strengthened, exam. of struct., mech. props. 78−80554
- ^{239}Pu, bone model for calc. of annual limits of intake in man 79−53252
- α-SiC, sintered, influence of B, C additives on microstructure, SEM exam. 79−8262
- SiO_2-Al_2O_3-CaO-BaO-SrO-ZnO-Na_2O-K_2O-B_2O_3, glaze effect of P_2O_5 additions 80−60824
- SrO-B_2O_3-GeO_2 glass system, physicochem. props., alkaline earth oxides effect 79−65827
- UO_2 microspheres, prep. from UO_3 $(NH_3)_2$, exam. of mech. and physical preps. 79−6758

density, atmospheric *see atmospheric pressure and density*

density, vapour *see density of gases*

density control
- electrophotographic dry powder toner concentration control *(Japanese)* 78−24878

density measurement
- *see also hydrometers*
- aerosols, atmospheric, mean bulk densities of dry samples 78−32204
- air, by weighing two bodies, for aerostatic-force correction calc. 77−9984
- air, ultrapure, molar density at 298.15K for mass transfer buoyancy corrections 79−88917
- air density direct determination in balance through artifacts characterised in evacuated weighing chamber 79−88916
- air density equation and mass unit transfer 79−88918
- alkali metals, equations of state and density meas. installation 77−43307
- alkaline glassy state, aq., density determ., radiation chem. 80−42197
- analogue device *(French)* 79−17399
- aspirating choked-nozzle probe for gas density meas., time response 77−84351
- atmospheric aerosol mass conc. meas. techniques, automatic 77−64459
- benzene, using flexible capillary 80−98886
- biological ultrathin section, electron probe microanalysis, local mass thickness meas. using STEM 79−62416
- bituminous paving mixtures 79−57188
- blood sedimentation rate free from gravity influence, rapid determ. from density meas. *(German)* 78−81085
- bone, osteoporosis early detection by Compton gamma-ray spectroscopy 78−11729
- bone density determination in vivo, computed tomography vs. mineral analyser 77−73567
- bone density measurement by ^{125}I photon absorptiometric anal., dialysis patients 80−36075
- bone mineral concentration estimation by beta-ray backscatt. *(German)* 78−69179
- bone mineral measurement using EMI scanner vs. densitometry 78−24119
- bone minerals, computerised radiography, healing process obs. appl. 78−15890
- ceramic density measurement, true and apparent, specimen liquid saturation cell 80−62636
- cigarette, density changes during burning as obs. by β-source attenuation 78−11792
- coal dust mass flow meas. methods *(German)* 80−92242
- coherent antiStokes Raman scatt. *(German)* 79−27321
- Compton scatter densitometry, geometrical considerations 80−30869
- concrete, density meas. by back-scattered gamma radiation 77−36699
- concrete, ultrasonic wave velocities and density, calc. and meas. 79−52545
- contactless, with radioactive isotopes *(Bulgarian)* 79−80578

density measurement continued
- corrosive-fluid density meter specification and dynamic characteristics *(Russian)* 77−9986
- cryogenic fluids, density reference system 78−54344
- cryogenic fluids, meas. via mag. suspension densimeter 77−10031
- cryogenic liquid, radio-isotopic method using γ-ray attenuation *(Russian)* 77−37847
- crystal, simple method 78−41278
- densimeter testing installation 79−80582
- diatomic gas, transient flow, temp. and conc. profiles, by rot. Raman scatt. 77−75995
- dilatometry with pressure transducing instrumentation, apparent molar vol. of NaOH in water 78−75702
- dynamic, by high energy photon scatt. 77−7485
- dynamic density measurement of body in a liquid, viscosity effects 79−6097
- Earth crust bulk densities, gravity borehole data accuracy 79−5632
- Earth crust density logging, influence of standard material comp. on readings *(Russian)* 79−74989
- elastic waveguide slow torsional wave sensors 79−46748
- electrolyte solutions in glycerol, investigation by US shear strains 80−88266
- ethyl methyl ketone+cyclohexane, measurements for determination of excess props. 80−37910
- ethyl methyl ketone+n-butanol, measurements for determination of excess props. 80−37910
- ethylene, liq., orthobaric density, 105 to 200K 79−35679
- ethylene, methods 77−37848
- ethylene, supercritical, mass-flow meter inaccuracy 79−68842
- ethylene gas-density meter, calibration method 77−84356
- floated density meter contactless electromagnetic transformer *(Russian)* 79−54099
- fluid, by freq. vibration method *(Russian)* 77−9985
- fluid, laser interferometry appl. 80−75018
- fluid, local density variations, capacitive system of meas. *(French)* 77−41574
- fluid, using gamma radiation, theory, practices and appl. 80−73325
- fluid density measurement techniques, biological macromolecules in solution appl. 78−92751
- fluid meas. in mechanical engineering, conf., Johannesburg, South Africa, (Feb. 1979) 80−75016
- fluids, simultaneous investigation of eqn. of state and elec. cond. 77−55337
- gas, by multibeam interferometry 78−58016
- gas, improved effusion method appl. *(Japanese)* 77−963
- gas, low density meas. by reson. fluoresc. 78−54341
- gas density measurement, high speed, using proton-induced X-rays 79−52805
- gas density transducer calibration method by National Measurement Laboratory 78−36971
- gas flow application of shearing interferometers 78−55706
- gas flowmeter, movable L-tube, with density meter *(Japanese)* 77−3900
- gas shock waves X-ray densitometer with high sensitivity and quantum flux 79−26031
- gas-liquid mixtures, flowing, gas conc. meas., acoustic method 78−59448
- gases, automatic measurement, buoyancy method *(German)* 80−36999
- geophysical prospecting, γ-γ well-logging for density, computerised instrumentation *(Hungarian)* 80−21843
- glass hollow spheres, hydrodynamical method *(Chinese)* 79−12773
- granular materials, particle density measurement by pycnometry 80−69903
- granular media, density measurement, plane strain conditions, acoustic method *(Polish)* 80−62635
- gravimetric measurement of sorption isotherms, errors 78−67905
- hot gas flows, X-ray diagnostics of density distrib. *(Russian)* 77−19647
- human body mass density distrib., in vivo meas. using ACTA scanner 77−29198
- human body mass density distrib., in vivo meas. using ACTA scanner 77−29199
- hydraulic fluids during flow using freq. methods *(Russian)* 77−26271
- hydrostatic density meter, temp. errors characterisation *(Russian)* 77−41573
- imaging space-time-density contours in gas, overlapping pulse technique 80−73320
- imaging system, real time Doppler, colour TV display of particle size or density 77−62038
- industrial gases, density meas. at melting, boiling points, survey of methods, apparatus *(German)* 79−30421
- inhomogeneous medium, density determ. by β-ray attenuation, calcs. and meas. 80−98182
- irradiated nuclear fuel reprocessing streams, remote anal. techniques 79−13510
- isotopic, of liquids, based on gamma radiation absorption, food industry appl. 79−44903
- laser Doppler velocimeter for particle size and density simultaneous determ. 80−98880
- liquefied natural gas, level, density and temperature measurement, prediction of roll-over 80−27269
- liquid, 25 to 100 C, up to 500 MPa, falling body instrument 80−103510
- liquid, complex apparatus for viscous and elastic prop. meas. at high press. 78−9734
- liquid, piezoelectric transducer appl. *(Russian)* 78−49799
- liquid, pneumatic diaphragm type instrument hydrostatic method *(Polish)* 77−74367
- liquid density transmitters, calibration 80−27265
- liquid media by dynamic method, description *(Russian)* 77−2637
- liquid metal, simultaneous meas. of density, elec. cond., abs. thermopower at high temp. and high press. 77−1402
- liquid metals, errors from pycnometers 80−73321
- liquid methane density meas. at cryogenic temp., commercial densimeters eval. 78−54343
- liquid streams, thermostating coil 78−8402
- liquid water, PVT props., density meas., 150-350°C, saturation to 1 kbar 78−34594
- liquids, acoustic method for determination as function of pressure 79−12771
- liquids, analytical one panned scales appl. based on solid body density standards *(Croatian)* 79−26033
- liquids, displacement sphere method *(German)* 80−52168
- liquids, hydrostatic lift method for wide temperature range *(Polish)* 79−97361

density measurement continued
- liquids, solid density standards, single-pan analytical balance *(German)* 80—52167
- liquids, using flexible capillary 80—98886
- LNG, automatic continuous level-gauging and temp. meas. system appl. 77—26272
- lung density, Compton scatt. meas., multiple photon interactions 80—67146
- magnetic float densimeter for measuring liquid density 78—49801
- magnetic supension densimeter, orthobaric liquid density, of Ar, 100 to 120K, and ethylene, 105 to 200K 79—35679
- magnetic suspension densimeter, differential capacitance sensor as position detector 80—196
- magnetic suspension densimeter, simplified, for absolute density meas. 77—30132
- magnetic suspension densitometer for cryogenic meas. 79—12805
- measurement methods in Yugoslavia *(Croatian)* 80—105616
- metal powder density meas. by US velocity 77—32760
- metallic liquids measurement technique using Archimedes' Principle 78—22784
- metals, 0-2000°C, automatic device using γ-ray transmission 79—87787
- metals, using X-ray total external reflect. and double crystal spectrometer 80—64831
- microparticles of cryst. sediment in bubbles in glass, density determ., flotation method 79—24692
- mineral microcrystals, mag. fluid technique for density determ. 80—85751
- molten salts, automated float method 78—12674
- non-metallic materials, flaw detection by tomodensitometry *(French)* 79—20295
- nuclear gauges 80—843
- ocean, density fields determ. 79—44195
- oscillating conductivity probe, density and density gradient meas., hysteresis effect 78—32796
- particles in dilute suspension in general flow, mass flow and density meas. 80—101784
- particulate materials, meas. by levitation in paramag. solns. 77—10070
- plasma, Thomson scatt. diagnostics using optical multichannel analyser 78—67432
- plasma wall sputtered metal density meas. by atomic fluorescence spectroscopy 78—67422
- polyester film 3-dimens. network, using chloroform sorption *(Russian)* 80—59405
- polymers, cryst. density, X-ray diffr. determ. 78—91273
- porous briquets, hydrostatic weighing method with preheating 79—49203
- present problems and future plans *(Hungarian)* 77—41570
- radio-isotope density meter calibration, temp. compensation method *(Russian)* 77—49713
- radio-isotopic concentration-density meter RKP-1, description *(Russian)* 77—33976
- radioactive waste density measuring meter, digital, remotely operated 80—68927
- radioisotope instrumentation, industrial appl. *(German)* 77—70245
- refractodensimetric analysis, liquor samples with low total solids 78—36972
- refractory products, apparent density determination, using surface γ densimeter 80—35464
- refrigerated hydrocarbon liquid, capacitance density meas. method 77—26273
- rocks, using pulsed gamma-ray method *(Russian)* 79—39956
- salts, molten, apparatus for meas. 77—53862
- seawater density determ. using gamma radiation *(Russian)* 77—82037
- seawater density meas., Mediterranean Sea samples 79—5486
- seawater salinity and density from gamma-ray attenuation *(Russian)* 79—39897
- sediment analysis using vibration-frequency method 79—49202
- serum of human, improved mech. oscillator technique *(German)* 78—28098
- sheet material surface density nonuniformity using beta radiation, effect on energy spectrum 77—77717
- shock wave density distrib. meas., at few torr, holographic technique 77—55038
- single energy electron backscattering method for solid density monitoring 79—97362
- snow, accuracy of water equivalent meas. with standard densitometer 79—29796
- solution density, in-tank based of differential press. meas. 80—78391
- standards, in solid density meas., hydrostatic weighing 80—77758
- stochastic models for density meter characteristics *(Russian)* 77—9987
- surface layer, thin, density meas. by total external X-ray reflection 78—14635
- surface layers, contactless, radioisotope appl. *(German)* 79—71414
- thermoplastic structural foams, charact. by equidensitometry and radiography 77—44417
- thick inhomogeneity effects on charged particle beams 79—25041
- two-phase flow system, local density measurements, side-scatter gamma technique 80—569
- ultrasonic system for online meas. 78—718
- US, impedance and velocity meas. methods comparison *(Russian)* 77—37846
- US densitometer for two-phase flow density meas. in pressurised water reactor 80—77759
- vapour density at elevated temperatures, simple apparatus 77—7491
- Venus, surface rock density meas. by Venera 10 lander 77—78690
- Venus rock density, method, equipment and results of Venera 10 meas. 78—28564
- water, pycnometer, precision hydrostatic, density comparison, influence of isotropic comp. and dissolved air 78—45597
- water, saline and pure max. density points meas. 78—57900
- water droplets in mists, clouds, size, density distrib. meas., laser remote sensing technique *(Japanese)* 78—49175
- Ar, meas. of orthobaric liquid density, 100 to 120K 79—35679
- B_4C absorber rods, nondestructive exam. with dual-energy gamma gauge and multigauge scanners 79—93721
- BN, degree of conversion from cubic to hexagonal, determ. method 79—15887
- $C_{12}Cl$ and $C_{16}Cl$ intercalation compounds, form. and struct. *(French)* 80—40674
- β-CoGa, Cu addition effects on defect struct. *(German)* 77—11546
- Cs-Au, liq., molar vol. meas. 80—59546
- Ge amorphous film, evaporated, non-destructive density meas. 80—6680

density measurement continued
- H_2, density meas. by resonance fluoresc. ($X^1\Sigma_g^+ \rightarrow B^1\Sigma_u^+$ transition) 80—5570
- H_2O, low density flow temp. and density meas. by submillimetre spectroscopy 80—43816
- HaO samples, meas. of small difference of density by elastic vibrator method *(Japanese)* 80—27272
- $LaS_{1.500}$-$LaS_{1.333}$, solid soln. region 80—95075
- N_2, density measurement up to 1800K and 8 kbar, procedure 78—81947

density of gases
- air, pressure as function of internal energy and density, algorithm *(Russian)* 77—58829
- air, ultrapure, molar density at 298.15K for mass transfer buoyancy corrections 79—88917
- air density direct determination in balance through artifacts characterised in evacuated weighing chamber 79—88916
- air density equation and mass unit transfer 79—88918
- air pollution density distrib., flow pattern in Tanabe area, Japan, numerical anal. *(Japanese)* 78—96289
- anthracene, optical determ. of vapour conc., vap. press. and heat of sublimation 78—22840
- automatic measurement, buoyancy method *(German)* 80—36999
- Bose-gas model, dil. hard sphere, calc. of low density atomic H gas props. 80—87194
- butene isomers, gaseous, density and temp. effects on electron mobilities 80—33725
- cis-butene-2, high density vapour thermal electron attachment density depend. 79—90369
- dense gas, logarithmic density dependence of viscosity and thermal cond. 77 51150
- dense gases, vel. autocorrelation function, memory function 80—59154
- diatomic gas, transient flow, temp. and conc. profiles, by rot. Raman scatt. 77—75995
- ethane, liq.-vap. coexistence curve, interferometric meas. 79—99303
- ethylene, high density behaviour, extrapolated PρT surfaces and critical density 80—87834
- flowmeter, movable L-tube, with density meter *(Japanese)* 77—3900
- fluid density bibliography, temp. range exceeding 40K 80—51980
- high-pressure gas equation-of-state meas. interferometry 80—77810
- improved effusion method appl. *(Japanese)* 77—963
- inert gas, at. polarisability variation with density 77—68131
- jet, propag. in deflecting airstream, trajectories, density influence 79—86480
- liquid-vapour critical region, empirical description from coexistence data 77 27973
- liquid-vapour interface structure near hard wall 80—14983
- methane, ν_1 line contour anomalous behaviour on pressure changes *(Russian)* 80—43052
- methane, gas density fluctuations, orthopositronium annihilation rate depend. 78—37773
- methane+Kr(Xe), ^{13}C-mag. shielding density depend. 78—9173
- molar volumes microscopic insight from macroscopic data, teaching appl. 78—69930
- pentane isomeric vapours, electon transport mechanisms, density induced transition 80—24122
- pentane isomers, vapour and liq., electron mobility 79—72984
- polar molecular gas, electron localisation, density fluctuation, mol. orient. 78—38446
- propylene, high density behaviour, extrapolated PρT surfaces and critical density 80—87834
- pulmonary airway constriction localisation using gases of varying density and viscosity 77—12949
- pulmonary gas exchange in man, effect of increased gas density 77—16947
- pulmonary resistance, lower, effect of gas phys. props. and flow 77—12945
- pulmonary resistance distribution, effects of gas density, viscosity and flow-rate 77—12948
- quasiparticle kinetic eqn. construction 80—53905
- respiration, density depend. of max. expiratory flow 78—27993
- shock wave, strong, piston struct. and gas distrib. 80—10265
- steam-air mixture, condensation, transport and thermodynamic props. *(Japanese)* 78—34251
- tetrachloromethane, fluid, collision induced light scatt. intensity 80—103955
- thermophysical props. tabulated for mixture composition certification 78—80818
- transport coefficients density expansion, 1st logarithmic term, moderately dense gas 78—94878
- Ar and Ar-NH_3 mixtures, viscosity under press., density depend. and mol. assoc. 80—1727
- Ar, gas, liquid, solid, refractive index, density and dielectric const. 80—66138
- As, crit. parameters determ. 77—47562
- BF_3-H_2O mixtures, vapour density and dissociation, 150-400°C 77—7491
- CO_2, high density behaviour, extrapolated PρT surfaces and critical density 80—87834
- CO_2 UV preionised laser discharge, large scale, aero-acoustic effects 79—36875
- CO_2+Kr(Xe), ^{13}C-mag. shielding density depend. 78—9173
- COS, density and refractive index, volumetric meas. by Burnett method 80—29707
- Cs, sat. vapour density from viscosity meas. up to 1620K 77—1254
- H beam, low temp., direct determ. of temp. and density 80—14875
- H, spin-polarised, density, magnetisation, compression and thermal leakage 80—44391
- He, electron mobility, anomalous density and temp. depend. at low temp. 78—75253
- ^{4}He vapour, thermal cond. as function of density 78—55712
- Kr, gas, liquid, solid, refractive index, density and dielectric const. 80—66138
- Kr, viscosity coeff., density expsn. 78—91054
- MoF_5, prep., melting temp., vapour density, press., enthalpy of fusion, meas., assoc. 78—38813
- N_2, density up to 2000K and 6 kbar by displacement method 78—51266
- N_2, gaseous, density behaviour of rototranslational spectrum, IR spectra obs. 80—28002
- N_2, high density behaviour, extrapolated PρT surfaces and critical density 80—87834
- N_2, molar volume measured by adiabatic compression 78—51267

density of gases continued

- NH_3, pure, Raman scatt., high press., high temp. 77−27077
- Na-He-N_2 dense vapour system, optical pumping, RF spectrum analyser appl. 79−76393
- Ne, molar volumes and thermodynamic props., 25 to 150C, up to 7 kbar 77−42957
- O_2, saturated, pressure-density temp. meas. 79−55802
- SF_6, coexisting densities, revised and extended scaling 78−34613
- (U,Pu)N, self-consistent normal fluid eqn. of state, press., density, and enthalpy of vaporisation calc. 78−8909
- UF_6, Raman scatt. cross section and density meas. 77−75160
- UF_6, temp. and density profiles in freely expanding gas for laser enrichment 78−74458
- UO_2 vapour bubble characts. determ. in LMFBR 79−22390
- Xe, gas, liquid, solid, refractive index, density and dielectric const. 80−66138
- Xe, high density behaviour, extrapolated PρT surfaces and critical density 80−87834

density of liquids

- *see also hydrometers*
- acetic acid-acetone mixture, physical parameters 80−2716
- acetonitrile-carbon tetrachloride-n-butanol, mixtures, compressibility, free length, molar and available vol., US meas. 78−2200
- acetonitrile-methanol, excess vol. and isentropic compressibility, from density and US vel. meas. 78−79776
- acetonitrile-toluene-n-butanol, mixtures, compressibility, free length, molar and available vol., US meas. 78−2200
- acoustic method for determination as function of pressure 79−12771
- adsorbed film, adsorbent effects on props., empirical relns. 78−6217
- alkali metals, density, enthalpy, up to 1500 bars 77−84821
- alkali metals, equations of state and density meas. installation 77−43307
- alkali nitrates, molten, pVT data, thermal press. coeffs., compressibilities 78−43097
- alkali-silicate glasses and melts, partial molar vols. 79−94915
- n-alkane-cyclohexane, liq. mixtures, density meas. for excess volume *(German)* 79−73324
- alkyl-cyano-biphenyls, nematic to isotropic phase transition, volumetric studies 79−86878
- N-alkylpyridium halides, molten, and mixtures with $AlCl_3$, density, elec. cond. and viscosity meas. 80−24630
- anisylidene-p-aminophenyl acetate, nematic liq. cryst., refractive index, density, orientational order 78−76419
- anisylidene-p-aminophenyl butyrate, nematic liq. cryst., refractive index, density, orientational order 78−76419
- anormal fluids, saturated liq. densities, four-parameter corresponding state theory 79−33066
- aqueous solns., max. density temp., structural interpretation 77−58933
- aqueous solns., max. density temp., structural interpretation 77−58934
- aqueous solution, shape of suspended oil droplet 79−77863
- benzene, density meas. using flexible capillary 80−98886
- benzene-ethanol, excess vol. and isentropic compressibility, from density and US vel. meas. 78−79776
- benzene-n-heptane, excess vol. and isentropic compressibility, from density and US vel. meas. 78−79776
- benzene-tetrahydrofuran, soln., excess thermodynamic props. and interactions, US vel. and density meas. 80−39288
- benzene-toluene and benzene-o-xylene mixtures, US vels., compressibility, expsn. coeff. 79−33038
- benzyl alcohol-n-butanol, excess vol. and isentropic compressibility, from density and US vel. meas. 78−79776
- binary acid + base mixtures, excess vol. and viscosity 77−21408
- binary mixtures, US props., excess density, interaction between components 78−63657
- binary mixtures near critical state, gravitational distrib. of thermodynamic props. *(Russian)* 80−88241
- 4,4′-bis(heptyloxy)azoxybenzene, nematic liq. cryst., refractive index, density, orientational order 78−76419
- 4,4′-bis(hexyloxy)azoxybenzene, nematic liq. cryst., refractive index, density, orientational order 78−76419
- Bose hard-sphere fluid model, density variation at fluid surface 77−20163
- bromides, and mixtures, molten, elec. cond., density, viscosity, surface tension, review 77−80638
- butanol-methylethyl ketone, soln., excess thermodynamic props. and interactions, US vel. and density meas. 80−39288
- N-(p-butoxybenzylidene)-p-pentylaniline, refr. index and density in nematic and isotropic phases 79−90538
- 1,3-butyleneglycol, density rel. to temp. and pressure *(Russian)* 79−10890
- caesium acetate, molten, elec. cond. and density 77−15613
- cavity model, refr. index and density, permittivity *(French)* 79−78642
- CBOOA, liq. cryst., temp. depend. of apparent viscosity and density 78−18542
- CBOOA, liq. cryst.-isotropic transition at high press., P-V-T eqn. of state 79−95135
- CBOOA, smectic A phase, specific volume and layer spacing, X-ray diffr. and dilatometry meas. 79−55659
- changes during melting by X-ray absorption 80−103462
- chloroform + acetone, isotropic light scattering, excess Gibbs function 79−8150
- o-chlorophenol-acetone (ethyl methyl ketone), thermodynamic and transport props. 80−92686
- cholesteryl myristate, density of smectic, cholesteric, blue, isotropic phases 78−42897
- cholesteryl nonanoate, liq. cryst.-isotropic transition at high press. 79−95135
- coolants and index matching media for Nd:glass laser systems 80−33015
- critical binary mixture, gravity induced gradients, optical meas. 77−4203
- cryogenic fluids, meas. via mag. suspension densimeter 77−10031
- cyano compounds, liq. cryst. phases, incommensurate coexistent density fluctuations 80−79691
- cyclohexane, liquid, density effect on transport properties 80−65264
- cyclohexane + benzene, excess volume 78−47527
- cyclopentane + isomeric octanes, excess volume 78−47527
- dense fluids, solvation forces between two solids, density profile calc. 80−64855
- p,p′-diheptylazobenzene, nematic, physical props. 78−79524
- dimethylsulphoxide, density up to 257°C, vap. press. up to 189°C, crit. density 79−90768

density of liquids continued

- dimethyltetraphenylmethylphenylsiloxanes, density, viscosity, surface tension and crit. temps. 79−86830
- dioxan-cyclohexane-chloroform, mixtures, compressibility, free length, molar and available vol., US meas. 78−2200
- EBBA, nematic liq. cryst., refr. indices, densities, polarisabilities and mol. order 77−28536
- elastohydrodynamic traction, granular behaviour 80−103008
- electrolyte solutions, light scatt., conc. depend. of compressibility and activity coeffs. *(Russian)* 77−1758
- ethane, excess electron localisation, density effects 77−31970
- ethane, liq.-vap. coexistence curve, interferometric meas. 79−99303
- ethanol$_{(l)}$, hydroxyl proton chem. shift, density and temp. effects 77−1607
- ethanol-water mixtures, specific volume, compressibility, viscosity, up to 3200 bar, 15, 25°C 78−10113
- p(p-ethoxyphenyazo)phenyl undecylenate, nematic liq. cryst., refractive index, density, orientational order 78−76419
- p(p-ethoxyphenylazo)phenyl heptanoate, nematic liq. cryst., refractive index, density, orientational order 78−76419
- p(p-ethoxyphenylazo)phenyl hexanoate, nematic liq. cryst., refractive index, density, orientational order 78−76419
- p(p-ethoxyphenylazo)phenyl valerate, nematic liq. cryst., refractive index, density, orientational order 78−76419
- ethylene, liq., orthobaric density, 105 to 200K 79−35679
- fatty acids in anhydrous solvents, partial molar volume from density meas. 79−43616
- film, mol. dynamics simulation of surface struct. 77−15666
- floated density meter contactless electromagnetic transformer *(Russian)* 79−54099
- fluctuation effect on Brownian particle freq.-depend. friction coeff., near crit. pt. 78−73929
- fluid, classical, density functional theory, direct correlation function-free energy relation 77−76285
- fluid density bibliography, temp. range exceeding 40K 80−51980
- halomethanes, liquid densities, data tables 78−75703
- hard spheres near hard wall, comparison of adsorption theories 78−38934
- hard-sphere fluid density, near ideal wall, Percus-Yevick rel. to superposition approx. 77−27802
- HDAB, liq. cryst., temp. depend. of apparent viscosity and density 78−18542
- heptanol isomers, static permittivity and density, press. and temp. depend. 78−35078
- p-p′-n-heptyl-cyanobiphenyl-isotropic solute systems, nematic-isotopic phase transformation, volumetric study 80−92653
- 4-4′-di-heptyloxyazoxybenzene, liq. cryst.-isotropic transition at high press. 79−95135
- hexafluorobenzene, liq., self-diffusion and denisty as functions of press. and temp. 80−92696
- n-hexane-cyclohexane mixture, 25 to 100 C, up to 500 MPa 80−103510
- N-p-hexyloxybenzylidene-p-toluidine, optical props., density, and order parameter in liq. cryst. phases 79−55657
- high pressure refractive index variation with density 79−28712
- Hildebrand's law, fluidity as a function of molar vol. *(French)* 78−63872
- hydraulic characts. of liqs. flowing through porous metal fibre mats., permeability laws 78−67848
- hydrocarbons, thermodynamic props. correls., third parameters 79−95184
- interfaces, liq.-cryst. and liq.-rigid wall, Monte Carlo simulation 79−27896
- iodides and mixtures, molten, elec. cond., density, viscosity, surface tension 77−80638
- isobutyric acid-H_2O, crit. mixture, partial molar vol., temp. depend. 78−18800
- laminar convection in vertical tube, thermophysical prop. temp. depend., effects 78−90895
- lecithin bilayers, density and mol. interactions 78−80837
- Lennard-Jones fluid, phase separation by spinodal decomposition, mol. dynamics computer simulation 79−10766
- liquid crystals, thermodynamic props. calc. 80−103464
- liquid mixing, volume changes, review 79−90782
- liquid-vapour critical region, empirical description from coexistence data 77−27973
- liquid-vapour interface nature, non uniform classical fluids statistical mechanics 79−77468
- liquid-vapour interface structure near hard wall 80−14983
- lubricants, viscosity and density determ. up to 150°C and 150000 psig 77−59940
- lysozyme aqueous solutions, viscosity and density 79−48208
- macromolecules in solution, density contrast, cross verification of X-ray scatt. and pycnometry expts. 79−10757
- MBBA, liq. cryst., temp. depend. of apparent viscosity and density 78−18542
- MBBA, liq. cryst.-isotropic transition at high press., P-V-T eqn. of state 79−95135
- MBBA, nematic-isotropic pretransition regions, ±15K, volumetric obs. 77−76535
- MBBA, volume meas. and phase transitions at high press. 79−90764
- meas., analytical one panned scales appl. based on solid body density standards *(Croatian)* 79−26033
- measureent, using flexible capillary 80−98886
- measurement by dynamic method, description *(Russian)* 77−2637
- measurement complex apparatus for viscous and elastic prop. meas. at high press. 78−9734
- measurement using hydrostatic lift method for wide temperature range *(Polish)* 79−97361
- measurement using piezoelectric transducer *(Russian)* 78−49799
- metal, density determ. by X-ray diffr. *(Russian)* 78−75529
- metal, measurement technique using Archimedes' Principle 78−22784
- methane, compressed, excess electron mobility, density depend. 77−11924
- methane, surface tension and density profile from expression for excess free energy 77−80681
- methane-propane(pentane)(n-heptane)(n-decane)(H_2S) mixtures, densities calc., van der Waals model 78−79740
- methanol, liq., compressed, self-diffusion, NMR spin-echo meas. 77−77122
- methyl cyanide (-d_3), vib. dephasing, Raman obs. 77−59566
- methylcyclohexane, dense liq., self-diffusion and viscosity 80−15278

density of liquids continued
- methylethyl ketone-butanol, soln., excess thermodynamic props. and interactions, US vel. and density meas. 80—39288
- 4-methylpentane-1, 302.55-450.80K and 0.098-68.6 MN/m^2 77—7780
- methylphenylsiloxanes, density, viscosity, surface tension and crit. temps. 79—86830
- microdrop, energy and mol. structure, mol. dynamics method 79—11004
- mixed halide melts, elec. cond., surface tension, density and viscosity, tables 79—60531
- mixed salt solutions, apparent and partial molal volumes, ternary systems 77—9114
- mixtures, perturbed hard chain theory, thermodynamic props., appls. in chem. technology 79—34343
- mixtures used in cryst. density determ. by flotation methods, rapid density determ. technique 78—41278
- molar volumes microscopic insight from macroscopic data, teaching appl. 78—69930
- molten salts, density and charge fluctuations 79—55645
- monatomic liquid, short wavelength collective density excitations 77—84610
- multicomponent liquid mixtures, empirical excess volume model, for estimating densities 79—1503
- natural gas, empirical excess volume model, for estimating densities 79—1503
- natural gas, liq., thermodynamic props. for mixed fluid densities 78—18775
- natural gas-related saturated liquid mixtures, molar vols. 79—1505
- nematic liquid crystal, diamagnetic susceptibility, refractive index, density and polarisability 77—15315
- nematic liquid crystals, refractive index, order parameter, density 79—38513
- nematic liquid crystals and mixtures, temp. dependence of density, obs. *(Russian)* 79—14681
- nonelectrolyte aqueous solutions, lattice model approach 79—32876
- nonelectrolyte aqueous solutions, temp. of max. density rel. to partial compressibility, struct. strengthening 80—30270
- nonuniform fluid state, Van der Waals theory, thermodynamics, struct. and phase stability 79—77475
- octafluorocyclobutane+n-butane mixtures, 233K, surface tension meas., excess vol. 79—19371
- N-p-octyloxybenzylidene-p-toluidine, optical props., density, and order parameter in liq. cryst. phases 79—55657
- oil, density change meas. at high pressure, using impact viscometer 79—14872
- one parameter family of equations of state 77—13722
- organic liquids, relation between density and refractive index *(Japanese)* 79—24279
- PAA, nematic-isotropic pretransition regions, ±15K, volumetric obs. 77—76535
- pentane isomers, vapour and liq., electron mobility 79—72984
- perfluorocyclobutane, dense fluid, self-diffusion, shear viscosity, density, and temp. depend., NMR 77—36152
- petroleum gas, liq., thermodynamic props. for mixed fluid densities 78—18775
- polar solvents, solvated electron absorpt. spectra, intrasolvent and intersolvent correls. 80—93840
- poly-(p-alkoxy-phenyl-p-acryloylbenzoates), nematic polymer, struct. determ. 79—99064
- poly-(phenyl-p-acryloyloxybenzoate), nematic polymer, struct. determ. 79—99064
- polybutene oil, rel. to elec. breakdown 79—91360
- polydimethylsiloxanes, linear, mol. wt. determ. from density and viscosity 79—81310
- polyesterimides, solns., ultrasonic vel. and Rao formulism 80—103422
- polyethylene glycols, aq. solns., volumetic props. 79—20460
- polyethylene imine, oligomers, solns., linear struct., props. *(Russian)* 79—50177
- polyethylene melt spinning, extensional flow induced crystallisation 78—55818
- polymer, Ising fluid equation of state 77—51469
- polymethylsiloxane-2, liq., thermodynamic props. at high press., US propag. meas. *(Russian)* 80—65157
- polystyrene in solns., unperturbed dimensions rel. to temp., solvent composition 79—64132
- potassium oxyacid salts, aq. electrolytes, apparent molar heat capacities and vols. 79—23744
- propane, excess electron localisation, density effects 77—31970
- n-propanol mixtures, US vel. depend. on association compounds 79—60436
- N-(p-propoxybenzylidene)-p-pentylaniline, refr. index and density in nematic and isotropic phases 79—90538
- PVC, density rel. to rheological, surface props. of PVC pastes *(Polish)* 78—85212
- pyridine, compressed liq., self-diffusion coeffs., viscosity, density, temp. press. depend., NMR spin-echo 79—37862
- reduced density metals, screening, struct. and elec. resist. 78—19016
- rubidium acetate, molten, elec. cond. and density 77—15613
- salts, molten, apparatus for meas. density 77—53862
- saturated densities of liqs. and mixtures, new correlation method 80—15174
- saturated liquid density correlation for normal fluids 79—51182
- Schiff's bases, nematic phys. props. 79—99057
- seawater, density, dependence on temp., salinity and press., math. expressions 80—94540
- seawater, standards, relative conductivity and density 77—64296
- seawater density determ. using gamma radiation *(Russian)* 77—82037
- seawater in Canaries Current, density-depth relation rel. to current tidal component *(Russian)* 78—77263
- simple liquid, rel. to self-diffusion and viscosity near MP, hard sphere model *(Russian)* 77—66035
- simple liquids, surface tension and density profile from expression for excess free energy 77—80681
- simple liquids, viscosity, density depend., theory 77—20105
- sodium oxyacid salts, aq. electrolytes, apparent molar heat capacities and vols. 79—23744
- sodium-caesium acetate, molten mixture, elec. cond. and density 77—15613
- sodium-rubidium acetate, molten mixture, elec. cond. and density 77—15613
- superfluid density in two-dimens., XY model 79—95242
- superheated liquid, spinodal, hole thoery 80—19232

density of liquids continued
- surface tension theory for liquid mixtures 80—88404
- ternary liquid mixtures, molecular interaction and thermodynamic props. 78—59861
- ternary liquid mixtures, physical props., determ. by density and US vol. meas. 79—37751
- tetrabutylammonium iodide, in aq. proline soln., elec. conductance investigation 80—10692
- tetrachloromethane, fluid, collision induced light scatt. intensity 80—103955
- tetraethoxysilane, −13.5 to +90°C 77—15637
- tetraethyl tin, −13.5 to +90°C 77—15637
- tetraglycine, aq. soln., density, viscosity and dielectric const., 0-60°C 78—47462
- tetrahedral mol. fluids, collision induced light scatt. intensity 80—103955
- tetrahydrofuran-benzene, soln., excess thermodynamic props. and interactions, US vel. and density meas. 80—39288
- tetramethoxysilane, −13.5 to +90°C 77—15637
- tetramethylammonium iodide, in aq. proline soln., elec. conductance investigation 80—10692
- 1,2,5-thiadiazole, liq., light scatt. from orientational and density fluctuations, hypersonic vel. 77—81110
- toluene, relationships between thermal cond., dynamic viscosity and density, high state parameters 78—83861
- transferrin, human anal. density gradient equilib. centrifugation for determ. of mol. wt., sp. vol., preferential hydration 77—64160
- transport properties, relationships between thermal cond., dynamic viscosity and density, high state parameters 78—83861
- triangular-potential fluid, Zwanzig's perturbation theory, appl. to thermodynamic props. 79—41920
- trifluoropropylmethylsiloxane fluids, viscoelastic props., mechanical impedance, viscosity and density meas. 80—79249
- triglycine, aq. soln., density, viscosity and dielectric const., 0-60°C 78—47462
- virial series divergence for hard discs and spheres at closest packing 79—94859
- water, compressed, thermodynamic props., evaluation by statistical error anal. 80—92685
- water, convective heat transfer, free, with density inversion, in confined rectangular vessel *(German)* 79—18671
- water, density, effects of isotopic comp., temp., press., and dissolved gases, review 78—26616
- water, density relation for pure and saline comp. 78—2185
- water, forced laminar convection in horizontal pipe, density inversion effects, numerical anal. 78—90900
- water, layer, semiinfinite, cooled (heated) from below, convection onset, density anomaly influence *(German)* 78—22350
- water, liq. props. representation, by modified Redlich-Kwong eqn. of state 78—34590
- water, non-Boussinesq convective struct. near 4°C, nonlinear density profile 79—18886
- water, on melting ice layer, heated, free convection onset criterion, density anomaly effect *(German)* 78—22351
- water, PVT props., density meas., 150-350°C, saturation to 1 kbar 78—34594
- water, relationships between thermal cond., dynamic viscosity and density, high state parameters 78—83861
- water, saline and pure max. density points meas. 78—57900
- water, thermal activity coeff., rel. to density, heat cond., sp. heat and viscosity meas. 77—7883
- water, transport and thermodynamic props. *(Japanese)* 78—34251
- water, vertical boundary layer convection, salinity and press. depends. 79—37316
- water(-d), high-press. supercooled, density max. 77—1162
- water-2-propanol, density, US vel. meas. 78—18529
- water-dioxane mixtures, compressibility, density, US vel. rel. to temp., conc., struct. *(German)* 77—43263
- zone stability, static or rot. 77—59182
- (Ag-M)Br, (M=Na, K, Rb, Cs) molten mixtures, molar vols. and molar conductivities *(French)* 79—77788
- Al, density fluctuations, neutron scatt. anal. 80—70349
- Al, density fluctuations 78—55806
- Al, melt density, temp. depend. *(Russian)* 79—69174
- Al-Cu, liq. alloys, surface tension meas. *(French)* 78—18875
- Al_2O_3-Cr_2O_3 melt, exam. of surface tension and density 79—1541
- Al_2O_3-SiO_2 melt, exam. of surface tension and density 79—1541
- Ar, gas, liquid, solid, refractive index, density and dielectric const. 80—66138
- Ar, meas. of orthobaric liquid density, 100 to 120K 79—35679
- Ar, rel. to mobility of excess electrons, deform. pot. theory 80—24982
- Ar, solid-liq. transition and mech. props., modified cell theory 79—23703
- Ar, surface properties of classical Lennard-Jones liquid *(Russian)* 79—77869
- Ar, surface tension and density profile from expression for excess free energy 77—80681
- Ar-H_2(Ne) liquid solution, dielectric props., intermolecular interactions *(Russian)* 80—88904
- Ar-He(Kr)(Ne), solubility in Ar, and related functions, three-body forces 79—10776
- As, crit. parameters determ. 77—47562
- As-S, melt struct., orientation birefr., viscosity, refr. index, and density 80—84713
- B, thermoelastic props. near melting point 80—19862
- Ba, density meas. at intermediate temps., method employs Archimedes' Principle 78—22784
- Ba, thermophysical properties, up to 1800K 78—30767
- Bi, liq., in fused alkali chloride binary mixtures, electrocapillary phenomena 77—40553
- Bi, molten, density, surface tension, temp. depend. 77—69147
- Bi-Pb-Hg, liquid, surface tension and density *(Russian)* 77—55418
- Bi_2O_3-Mo(W)O_3 melts, electrophys. props. 77—89817
- Bi_2O_3-SiO_2(GeO_2), metastable phases form., crystn. conditions, melt viscosity and density effects 80—35167
- Bi_2O_3-Si(Ge)O_2 melts, phys. props. 77—89566
- $3Bi_2O_3.5B_2O_3$, viscosity, molar volume of melt and enthalpy of fusion 79—10924
- C, near graphite-liquid-vapour triple point 77—62618
- COS, density and refractive index, volumetric meas. by Burnett method 80—29707
- Ca, density meas. at intermediate temps., method employs Archimedes' Principle 78—22784

density of liquids continued
- CaF_2, melts, elec. cond., surface tension, viscosity, density *(Russian)* 80-92758
- CaF_2-MgO-SiO_2, melts, elec. cond., surface tension, viscosity, density *(Russian)* 80-92758
- CaF_2-MgO(SiO_2), melts, elec. cond., surface tension, viscosity, density *(Russian)* 80-92758
- Ca(No_3)$_2$.3.91H_2O-$NiCl_2$ melts, glass forming, transport behaviour 78-59963
- CaO-Al_2O_3 melts, density, atm. comp. effect 78-22624
- CaO-SiO_2-MnO molten mixtures, struct. and phys. props. *(French)* 80-24635
- CaO-SiO_2-MnO system, melts, densities, molar vols., thermal expansivity *(French)* 79-51183
- Cd_3As_2 and $CdAs_2$, molten, thermal expansion and atomic bond strength parameters 80-65257
- $CdTl_2Se_4$(Te_4):Au, elec. cond., density, dielectric const., changes on fusion 80-88553
- Ce, surface and volume props., flow props., surface layer thickness *(Russian)* 80-59760
- Cs, liquid, meas. of density at high temp. and pressures 78-55903
- Cs, liquid, neutron diffr. struct. anal., density and viscosity temp. depend. 80-6352
- Cs-Au, liq., molar vol. meas. 80-59546
- CsCl, aq. soln., density, isothermal compressibility, 293.15K, up to 200 MPa 80-44243
- CsCl-UCl_3 melts, density, surface tension and viscosity 78-67764
- CsI-KI, binary molten mixture, surface tension meas. 79-65294
- Cu tripolyphosphate complexes, electrolyte development for direct deposition of Cu 80-45246
- $CuInSe_2$-$CuInS_2$, melts, viscosity, elec. cond., density composition prop. graphs 79-14948
- $CuSO_4$, aq. solns., densities, viscosities, elec. cond. meas., 20 to 70°C 80-59688
- $CuSO_4/H_2SO_4$ electrolytes, densities, elec. cond., viscosities 80-107455
- D_2O, effect of phase density on ionisation process and electron localisation 77-89731
- D_2O, liquid, volumetric and derived thermal characteristics at low temp. and high pressure 80-107352
- D_2O, temperature of maximum density in capillaries 78-51801
- Fe, cast, grey, density variation during slow crystallisation *(Russian)* 78-95737
- Fe, pure and alloyed, density and thermal expansion in liq. and solid states 80-96668
- Fe-As, liquid alloy, density and surface free energy *(Russian)* 78-11204
- Fe-As melts, influence of Sn, Si, Mn and Cr additions on surface tension and density *(Russian)* 80-15337
- Fe-As melts, surface tension, density, adsorption *(Russian)* 80-92757
- Fe-Co melt, volumetric characts., molar volume conc. depend. density *(Russian)* 80-33873
- FeO-SiO_2, molten, viscosity and density 78-59965
- Fr, properties from melting point to 7500K, prediction *(Russian)* 80-44296
- Ge-FeS, GeS-FeS, density of alloys, volume changes on melting 77-51473
- GeO_2 melts, density, viscosity, struct., at high and low press. 79-87431
- Ge_xSe_{1-x} melts, short-range order change with comp. and temp., anomalous density behaviour 77-11676
- H_2 and isotopes 77-72674
- HN(SO_2Cl)$_2$, physical props. meas. 79-51293
- H_2O-acetic acid-silver acetate, ternary liq., elec. cond. and density 78-91464
- HaO samples, meas. of small difference of density by elastic vibrator method *(Japanese)* 80-27272
- He, adsorbed film, density profile 78-10252
- He, equations of state, 3.3 to 14K *(Russian)* 78-83912
- He II, superfluid flow hydrodynamics, normal density component velocity depend. *(Russian)* 80-65326
- He liquid, plane surface layer, density profiles and pair correlation asymptotics *(Russian)* 80-88371
- ^3He, A and B-phases, viscosity and superfluid density meas. 77-66063
- ^3He, A-phase, props. near transition to A_1-phase *(Russian)* 79-7728
- ^3He, density tensor meas. for A and B phases 77-15652
- ^3He, equation of state and crit. exponents near liq.-vapour crit. point 80-24707
- ^3He, equations of state, 3.3 to 14K *(Russian)* 78-83912
- ^3He, liquid, surface tension and density profile at 0K 79-55997
- ^3He, normal phase, 2-29 bar 79-82408
- ^3He, significant structure theory, thermodynamic props. 78-51774
- ^3He, sound propag. at elevated densities, 0.35 to 1.4K *(Russian)* 80-92741
- ^3He, superfluid, Barnett effect 80-88388
- ^3He, superfluid, mag. reson., electron cloud distortion, viscosity and density meas. 79-65277
- ^3He, superfluid, size effect influence on fluid density and transition temp., fourth sound meas. 80-80022
- ^3He, superfluid B phase, gap distortion, depairing critical currents, all temperatures 80-92743
- ^3He, superfluid B-phase, press. depend. of superfluid density 79-51358
- ^3He, superfluid density and viscosity meas. 77-66061
- ^3He-^4He equimolar mixtures, excess vol., temp. and density depend. *(Russian)* 80-39380
- ^3He-^4He mixture, equation of state and crit. exponents near liq.-vapour crit. point 80-24707
- ^3He-^4He mixture, excess molar volume, temp. depend., 1.5 to 14K *(Russian)* 77-62700
- ^3He-^4He mixtures, superfluid normal density at elevated press. *(Russian)* 79-90841
- ^4He, dynamic structure factor near λ temp. 77-66049
- ^4He, in fine regular pores, superfluid density and superfluid onset temp. 79-51335
- ^4He, Lennard-Jones model at 0K, props. using Monte Carlo method 79-82401
- ^4He, liq., two-dimens., excitation spectrum and thermodynamic props. 79-86959
- ^4He monolayer, rel. to solidification 77-20158
- ^4He, phonon dispersion relation, thermal expansion meas. 77-7924
- ^4He, superfluid, density in submicrometer diameter channels, Helmholtz resonator meas. 79-77852

density of liquids continued
- ^4He, superfluid, density regions, λ transition and roton physical picture 79-82402
- ^4He, superfluid, density temp. depend. in restricted geometry, oscill. U-tube technique 77-35774
- ^4He, superfluid, roton-roton interactions and thermodynamic props. 79-60571
- ^4He, superfluid, thermodynamic versus neutron meas. at low temp. 79-51327
- ^4He, superfluid density depression by velocity 78-51760
- ^4He superfluid film, superfluid density and dissipation in transition region 79-51384
- ^4He, temp. depend., 0.1 to 0.82K, and entropy of solid ^4He 77-7925
- Hg, −20° to 300°C International Practical Temperature Scale of 1968 77-4139
- Hg, electrical and thermodynamic props. in metal-semicond. transition range 80-20144
- Hg expanded liquid, simultaneous investigation of eqn. of state and elec. cond. 77-55337
- Ir, thermophysical props. at temps. up to 7000K 80-103497
- K, density, at near critical temp. 80-103407
- K, density meas. up to 1800K and up to 100 atm. 77-43264
- K, isothermal compressibility calc. at 400 to 1800K from density data 78-2186
- K, liq., density, 1640-2030K, 36.1-100.2 atm 78-91369
- KCl, molten, vapour-liq. interface, mol. dynamics model 80-54362
- KCl, solution, apparent molar heat capacity and volume, at 298.15K 80-29179
- KCl-CuCl eutectic fused salt, potential as intermediate temp. solar heat transfer and storage medium 80-101135
- KCl-KNO_3-H_2O, apparent and partial molal volumes in mixed salt solns. 77-9114
- KNO_3, solution, apparent molar heat capacity and volume, at 298.15K 80-29179
- Kr, gas, liquid, solid, refractive index, density and dielectric const. 80-66138
- La, surface and volume props., flow props., surface layer thickness *(Russian)* 80-59760
- La_2O_5-$Na_2Si_2O_5$ molten glasses, surface tension and density, 900-1500°C 80-15334
- Li-Ag, liq. alloy, density, compressibility and diffr. data 77-47336
- LiCl, aq. soln., density, isothermal compressibility, 293.15K, up to 200 MPa 80-44243
- LiCl, aqueous solution at 298.15K, isentropic compressibility 78-22783
- LiCl-$LiNO_3$-H_2O, mixed salt solutions, apparent and partial molal volumes 77-9114
- LiCl-NaCl-$AlCl_3$ ternary melt, density as function of temp. and composition, meas. by macrometric method *(Japanese)* 79-42130
- LiCl+$NaNO_3$, apparent and partial molar volumes in aq. soln. 78-44396
- LiH, liq., density and surface tension, 982-1280K 80-59548
- $LiNO_3.3H_2O(D_2O)$, crysts. and melts, density, mol. vol., thermal coeff. of expansion, rel. to struct. 80-15270
- Mg-Sn melt, density and free surface energy *(Russian)* 77-66074
- $MnCl_2$-tetra-n-butylammonium halide melts, density, elec. cond., and viscosity 80-24631
- N_2, surface tension and density profile from expression for excess free energy 77-80681
- ND_3, effect of phase density on ionisation process and electron localisation 77-89731
- NH_3-metal, soln., thermophysical props., review 79-77758
- N_2O_4 liquid *(Russian)* 79-59863
- Na-Cs melt, density and molar volume *(Russian)* 78-15357
- NaCl, solution, apparent molar heat capacity and volume, at 298.15K 80-29179
- NaCl-CsCl-$MnCl_2$, molten salt system, molar volume and elec. cond. meas. 80-34218
- NaCl-CsCl-$MnCl_2$, ternary molten salt system 80-34217
- NaCl-$NaNO_3$-H_2O, apparent and partial molal volumes in mixed salt solns. 77-9114
- NaF-AlF_3 binary melt, density and elec. cond. *(Japanese)* 78-18814
- $Na_xH_2P_xO_{3x+1}$, conversion products in presence of orthophosphate effect on melt props. 77-25355
- NaI-KI(RbI) binary molten mixture, surface tension meas. 79-65294
- $NaNO_3$-KNO_3-Ca(NO_3)$_2$.4.09H_2O melt, mixed alkali effect 80-34219
- $NaNO_3$-$TlNO_3$-Ca(NO_3)$_2$.4.09H_2O melt, mixed alkali effect 80-34219
- NaO_2-B_2O_3 glass melts, fluctuations 79-94865
- NaOH, in water, apparent molar vel. determ., dilatometry with pressure transducing instrumentation 78-75702
- NaOH-KOH eutectic molten mixture, elec. cond. and sp. mass 79-82365
- Nd, surface and volume props., flow props., surface layer thickness *(Russian)* 80-59760
- Ni-Ge alloys, temp. depend., 1000-1700°C *(Russian)* 77-15662
- $NiCl_2$, aq. soln., viscosity meas., struct. props. 78-75863
- $NiCl_2$-tetra-n-butylammonium iodide melts, densities and kinematic viscosities 79-77793
- O_2, saturated, pressure-density temp. meas. 79-55802
- Pb, melt density, temp. depend. *(Russian)* 79-69174
- Pb, molten, density, surface tension, temp. depend. 77-69147
- Pb-Bi molten alloys, density, surface tension, temp. depend. 77-69147
- $PbO/PbF_2/B_2O_3$ solvent system, density, surface tension and expansivity data, effect of B_2O_3 conc. 79-19985
- PbO-SiO_2-(CaO)(SrO)(BaO)(NiO), melts, density *(Japanese)* 78-6908
- Pr, surface and volume props., flow props., surface layer thickness *(Russian)* 80-59760
- Pt-Pd (Co)(Su)(Al)(Si) melts, surface tension and density *(Russian)* 80-39388
- Rb, density functions, SCF method, coherent scatt. function 78-18527
- Rb, liquid, expanded, eqn. of state, transport up to 1700°C, 400 bar 80-2136
- Rb, simultaneous meas. of density, elec. cond., absolute thermopower up to 1400°C and 400 bar 77-1402
- RbBr, molten, density and charge fluctuations 79-55645
- RbCl-UCl_3 melts, density, surface tension and viscosity 78-67764
- Rn, calc. of critical density 80-59547
- SF_6, coexisting densities, revised and extended scaling 78-34613
- Se, electronic transport props., equation of state, to 1900K and 1800 bars 80-65574
- Se_xTe_{1-x} melt, densities and surface tensions 79-86831

density of liquids continued
Se_xTe_{1-x} system melts, bonding system change obs. using density meas. 77—11456
Si-B system, liq., surface tension, density, and oxidation kinetics, 1410-1700°C 80—20011
SiO_2-Al_2O_3 melts, densities 79—99259
SiO_2-Al_2O_3-CaO-MgO, liq. silicic and slag, struct, density, surface tension *(Polish)* 78—83711
Sn-Se, melt, density, kinematic viscosity, struct., 900-1400K 78—14395
Sr, density meas. at intermediate temps., method employs Archimedes' Principle 78—22784
Te, liquid, meas. of viscosity, density and surface tension *(French)* 78—91371
TiO_x melts, with differing valencies, density *(Russian)* 79—69173
$TlAsSe_2$, diamag., thermal expansion rel. to temp. at cryst.-melt transition 78—34954
Tl_2S-Tl_2Se systems, melts, ion transfer, diffusion coeffs., elec. cond., density meas. 77—1253
Tl_2Se, diamag., thermal expansion rel. to temp. at cryst.-melt transition 78—34954
Tl_2Se_3, diamag., thermal expansion rel. to temp. at cryst.-melt transition 78—34954
Tl_2Te_3, exam. of electrical props., density and viscosity, for solid or liquid states 79—95431
Tl_2Te_3:Ag(Sn), effect of dopant on electrical props., density and viscosity, for solid or liquid states 79—95432
UCl_4 molten mixtures with alkali metal chlorides, physicochemical props. 78—38915
UO_2, liquid, eqn. of state 79—14910
V, thermophysical props. at temps. up to 7000K 80—103497
W, density at onset of sharp fall in elec. cond. 79—33026
Xe, gas, liquid, solid, refractive index, density and dielectric const. 80—66138
Xe, sound propag. near critical pt. 79—82285
YAG solutions, in $PbO/PbF_2/B_2O_3$ solvent systems, density, surface tension and expansivity data, effect of B_2O_3 conc. 79—19985
Zn, melt density, temp. depend. *(Russian)* 79—69174
Zn_3As_2 and $ZnAs_2$, molten, thermal expansion and atomic bond strength parameters 80—65257
$ZnCl_2$-LiCl(NaCl)(KCl)(CsCl), molten, density meas. *(Japanese)* 79—19383
$Zn(NO_3)_2$-$Cu(NO_3)_2$ glass forming melts, density and viscosity 79—77794

density of solids
bis-(2-fluoro-2,2-dinitroethyl)nitramine, mol. density, depend. on ratio of intramolecular and intermolecular contacts 79—86781
ABA poly(styrene-b-butadiene) copolymer, physical props., casting solvent effects 77—55935
acoustic velocity, shock-compressed uniform solid, lateral discharge ang. semiempirical formula *(Russian)* 78—55910
alkali hydrides, structural transition from NaCl to CsCl type under high press. 80—96458
alkali-silicate glasses and melts, partial molar vols. 79—94915
alkaline earth silicate glasses, morphology effects on props. 80—49118
alkaline earth-silicate glasses, elastic props. and struct. 77—24273
alloy, binary, solidification, predicted volume change 77—28802
amorphous metals, struct. imperfections, review of expt. evidence 79—37630
baked C mixes, anthracite, petroleum, metallurgical and pitch cokes as fillers, chracteristics study 79—57052
balsa wood, cryogenic insulation, exam. of strength specifications, props. 80—25819
binary powders, inhomogeneous mixture, procedure for determining specific volume 78—48345
bone, compact, fracture mechs., effects of density and specimen thickness 78—3534
bone, elastic props. of cortical bone of female human femurs, noninvasive meas. 77—21552
bone, human vertebral, compressive strength and elastic mod. 77—36985
bone, mechanical properties rel. to density and mineral phase orientation and particle size 80—16989
bone, tensile strength rel. to strain rate, microstruct. and density 77—44703
bone china body, MgO effect on vitrification mech. props. *(Japanese)* 79—78922
bone compressive strength, rel. to density and strain rate 77—36976
bone strength, rel. to mineral supplemental diet in young rabbits 77—36986
borides, metallic, sintering, review, book contrib. 78—48359
boroaluminosilicate glasses, alkali free, density calc. *(Chinese)* 78—14396
borophosphate glasses, effect of F on props. 78—67657
borosilicate glass, phase-separated, refr. index. and density changes 77—66025
borosilicate glasses, gamma irradiation effect on density, refractive index, thermal expansion 80—79838
n-butanol, glassy and crystalline forms, trapped electrons, conc. of mol. vacancies determ. 77—65948
calcium alginate gels, Raleigh scatt., spectral broadening, density fluctuations 79—1776
catalase, from the fungus penicillium vitale pidopl. et bilai, preliminary crystallographic investigation and props. 79—66444
$Cd_xHg_{1-x}Te$, vertically grown crysts., effects of growth speed on comp. variations, density meas. 79—55684
ceramic, compaction during pressing, green strength, effect of adsorbed layers *(German)* 78—6880
ceramic, ferrimag. or ferroelec., microstructure and physical props. 78—72756
ceramic density measurement, true and apparent, specimen liquid saturation cell 80—62636
ceramics, granular, electrophysical props. depend. on porosity, temp., solid-phase props. 77—69764
chalcogenide glass, partial values and structure features 79—41969
chalcogenides of non-transition metals, at. vol. and semicond. props. 77—20089
changes during melting by X-ray absorption 80—103462
Chevrel type compounds, single crystals, growth, stoichiometry, elec. resist. 78—92187
concrete, porosity determ. from combined US and gamma absorption meas., mech. props. 79—29295

density of solids continued
creep damage and rupture criteria, cavity config., use of density meas. 78—60818
crystal thermodynamics in statistical theory, density Fourier coeffs., stress tenser, internal energy 80—13025
cubic crystals, theoretic props. at arbitrary press., density and bulk modulus 78—51606
diacetate-nitrocellulose, long period struct., 180-265°C, X-ray diffr. obs. *(Russian)* 79—24556
elastic waves in crystals, invariance relations 80—84250
femoral shaft, human, age and sex-related changes in struct. and strength 77—56401
femur, canine, in-depth mech. props. anal. 80—16979
filled samples, sp. ht., density 78—5645
floated density meter contactless electromagnetic transformer *(Russian)* 79—54099
floc, settling velocity, rel. to permeability 79—43636
fluorophlogopite mica, glass-ceramic, thermal diffusivity, crystallisation effects 78—6190
fluorophosphate glasses, rare-earth activated, luminesc., bonding 78—64415
glass, chalcogenide, ternary, correlation between specific volume and composition 77—9038
glass, flint, 4.23 to 8.0 gcm^3, acousto-optical props. and appl. *(Russian)* 80—2721
glass, optical grade, refractive index-density relationship changes assoc. with reannealing 78—27175
glass, structure, influence of thermal history *(German)* 80—38930
glass, tempered, density and refractive index variation 78—64564
glass-ceramics, transparent, microstruct. and props. 78—59960
gram atomic volume, density, atomic mass, packing factor, eqns. for calc. 79—95066
graphite, polygranular, flexural strength after heat treatment porosity correl. 80—84996
graphite, pyrolytic, structural factor effect on strength 79—66135
graphite, recompressed expanded, thermal conductivity, elastic moduli, density effects *(French)* 78—26744
gypsum, strength changes on setting *(Japanese)* 77—36619
ice, thermal conductivity of nine solid phases 78—30801
inertial confinement fusion target, density in fuel region by activation anal. 80—33807
isotactic polypropylene/butene-1 copolymers, soln. grown crystals, props. 77—55247
kaolin grog particles, shape and density 80—97450
Lexan, optical and phys. parameters 79—32004
metal powder explosive compaction 78—64501
metal powders, vacuum treatment, method of calc. evacuation time and permeability 80—20827
metal-metalloid amorphous systems, thermal instability, crystn. characts. 77—4044
metallic glass, hardness, elastic moduli, density, cryst. temp., mech. props., for flywheel appl. *(Dutch)* 78—52878
metallic glass, struct. relax. effects 78—72804
metallic glasses, mats. props. review 77—4043
metallic oxide powders and mixtures, hydrostatic pressing, density and hardness variation 79—70029
metals, polycrystn., creep damage and cavity growth, assessment using density meas. 80—104217
microparticles of cryst. sediment in bubbles in glass, density determ., flotation method 79—24692
mixed metal chloride acousto-optical props. *(Russian)* 78—60419
mixed-alkali borate-glasses with high-alkali content, densities *(Japanese)* 77—7794
molar volumes microscopic insight from macroscopic data, teaching appl. 78—69930
monitoring by back scattering of single energy electrons, coating thickness appl. 79—97362
Nafion, densities and expansion coeffs. as function of various parameters 80—79711
NASICON solid electrolyte, processing and phys. props. 80—60820
neutron radiometric inspection of materials on supply line 80—21205
non-stoichiometric phase, physico-chemical props. 80—29532
Nylon 6 film, prior high-press. treatment effects, weight swelling, density, IR crystallinity, X-ray and viscosity obs. 80—81025
organic, predictions from 'cryst. volume' 77—19815
PET, densification, cryst. perfection, mechanism 79—66082
photographic positive film density, depend. on conc. of stabilizers and antifoggants added to developer *(German)* 80—73497
plastics and reinforced plastics, tabulated data as design guide 77—21087
Plexiglas 55, optical and phys. parameters 79—32004
PMMA, constancy of composition obs., dosimetry appls. 79—60286
PMMA, dielec. relax. spectrum, thermodepolarisation and dilatometric meas. 77—32322
PMMA and PPMA, glassy state, cyclic loading effects on internal damping, shear modulus, heat capacity and density 77—43275
pnictides of non-transition metals, at. vol. and semicond. props. 77—20089
Polimal 109, polymer resin laminate, density porosity, water vapour diffusion sorption and permeation *(Polish)* 80—59665
poly-tetramethyl-p-silphenylene-dimethylsiloxane block copolymers, crystn., morphology, kinetics 79—14695
poly-vinylidene fluoride-co-tetrafluoroethylene, dipolar theory applications to piezoelectric props. 79—78627
polyamide single crysts., struct. *(Russian)* 77—43158
polybutyleneterephthalate, drawn annealed, struct. and props., X-ray scattering 79—7552
polycarbonate, glassy state, enthalpy relax., thermal density fluctuations 80—59678
polycarbonate fibre, highly-oriented, drawing behaviour and mech. props. 78—76708
polycarbonate film, struct. and mech. props. 79—19160
polyconjugate system, interrelation between physicochem. props. and microstruct. 78—55816
polyether-polyester elastomer, fine structure and mech. props. 77—59844
polyethylene, extended chain, prep. and study of separated single crystals 78—42924
polyethylene, high molecular weight, effect of density on properties 77—90403
polyethylene, high- and low-density, crystallinity degree, comparative obs. *(Polish)* 80—1943

density of solids continued
polyethylene, in toluene, pressure crystallised, swelling behaviour, rel. to densities 80—2167
polyethylene, irrad., thermophys. characts. of amorphous phase, effects on crystallinity 77—7870
polyethylene, linear, crystallised from melt, effect of crystallisation time on density, mech. props., X-ray scattering 80—25680
polyethylene, specific vol. under high press., appl. of novel dilatometer 77—37844
polyethylene fibres, high density, ultra oriented, physical, mech. props. 80—25649
polyethylene film, elec. props., effect of quenching 77—73114
polyethyleneterephthalate, film, props. of adhesive layer adsorbed on surface 79—56067
polyethyleneterephthalate film, influence of crystallisation on adhesive and cohesive props. 79—56100
polymer, amorphous, struct. determ. by small-angle X-ray and neutron scatt. 77—84668
polymers, hydrostatic extrusion effects on subsequent mechanical behaviour 77—90392
polyolefines, filled, struct.-mech. props. relation *(German)* 78—35451
polypropylene, cold-drawn isotactic bars and thin films, microstruct. and annealing 78—95760
polystyrene, constancy of composition obs., dosimetry appls. 79—60286
polystyrene, cryogenic foam insulators, low temp. props. 80—25818
polystyrene filament, melt spun, struct. and mech. props., effect of drawing, twisting, annealing, untwisting 80—45331
polystyroles, filled, struct.-mech. props. relation *(German)* 78—35451
polytetramethyl-p-silphenylenesiloxane, degree of crystallinity determ. by density method 78—26453
polytrivinyl benzene, thermal and mech. props. rel. to high-press. polymerisation conditions 79—70326
polyurethane, cryogenic foam insulators, low temp. props. 80—25818
powder particle motion and segregation by density difference in V-type mixer 80—45250
prefluorinated polymer, DuPont Krytox 143-AB, viscoelastic and dielectric props. 80—1503
n-propanol, glassy and crystalline forms, trapped electrons, conc. of mol. vacancies determ. 77—65948
PTFE fibres, US effects on structure *(Polish)* 78—68702
PVA carbonisation process and carbonised block props., high temp. resistant materials *(Russian)* 79—8268
PVC, filled, struct.-mech. props. relation *(German)* 78—35451
PVC, mech. comminution in fine struct. changes in porosity, density, specific surface area *(German)* 78—35345
pyrocarbon, low temp., isotropic, permeability study *(French)* 79—7549
quartz ceramic, physicomech. props., influence of surfactant incorporated during synthesis 80—20856
rare earth compounds, binary, regression eqns., for calc. props. from electron struct. 80—39498
rare earth germanates, R_2O_3-GeO_2 system cpds., physicochem. characts. 80—97469
rare earth oxyorthotitanates, crystallochem. classification 80—107142
rare earth RNb_3O_9, synthesis and physicochem. props. 77—90304
rare earth titanates, $R_2Ti_2O_7$, synthesis and phys. props. 79—43128
rare earth titanoniobates, $RTiNbO_6$, physicochem. investig. 77—47422
refractories, multichamotte, sintering additives effect on props. 80—35147
semiconductor, crystal-glass transition influence on local struct., cond. and density 77—36163
silicates, entropy estimates at 298K from molar vols. 77—1243
sintered material, relation between density and sound velocity 78—53173
sintered metal, cold forming with self aligning dies 78—11158
sintering, packing fraction effects *(German)* 78—64494
steel, austenitic stainless, porous fibre, sintered and compacted, mech. props. 79—15623
steel, cast structural, heat treatment and mech. working influence on mech. props. *(Russian)* 80—40392
steel, cavitation during superplastic flow, affecting factors 78—60728
steel, Cr-Mo-V, rupture ductility rel. to cavitation, density and SEM obs. 79—34142
steel, high heat resist., tool, density and extension coeff. *(Russian)* 79—51282
steel, high-strength, 30KhGSA and Kh12M, low cycle fatigue 79—87724
steel, plastic deform., density changes *(German)* 80—60908
steel, powder, rotary forging, porosity and deform. 78—23646
steel, solidification singularities in C and low-C steels *(Russian)* 78—80532
steel, stainless, atomised powder, effect of ultasonic refining on processing preps. 79—33972
steel, stainless, type 1.4970, density, thermal expansion 79—65223
steel, stainless 316, controlled-porosity, mech. props. 79—96083
steel fibre reinforced Al_2O_3-Al, production and mech. props. 80—11619
strontium calcium tartrate tetrahydrate, crystals grown by ion diffusion through silica gels, exam. of preps. 79—52102
technological strength and nondestructive methods of testing during heat treatment 78—85090
tellurite glasses, binary, struct. and props. *(Japanese)* 79—32917
tetramethyl-p-silphenylenesiloxane-dimethyl siloxane copolymers, degree of crystallinity determ. by density method 78—26453
thermal penetration property $\rho c k$ meas. instrum. 78—70120
thermoelectric materials, B_4C_x and $(B,Si)_4C_x$ P-type LaS_x N-type alloys, fabrication and thermoelectric props. 80—107771
thermoplastics, structural changes during deformation, rel. to impact resistance 80—25800
tissue-equivalent plastic A-150, density and composition uniformity 78—73252
titanomagnetite sand from New Zealand, density, elec. and mag. prop 80—98311
transition metal, 3d and 4d, local density theory, mech. and mag. props. evaluation 78—91630
transition metal carbonitrides, physicochem. props., comp. depend. 80—55370
transition metal-group IIIB alloys, relationship between struct. and thermodynamic props. *(German)* 78—91307
transition metal-metalloid glasses, struct., elec., supercond., and mech. props. 80—6365
transition metals, thermophysical data at high temps., submicrosecond-pulse-heating method 80—103459
triacetate-nitrocellulose, long period struct., 180-265°C, X-ray diffr. obs. *(Russian)* 79—24556

density of solids continued
TTT_2-$(I_3)_{1+x}$, physical props., elec., mag. and optical meas. 80—24908
viscose, long period struct., 180-265°C, X-ray diffr. obs. *(Russian)* 79—24556
water, normal and heavy, glass-transition temp., crystn. temp., and dielec. const. 80—15229
Zircaloy-2, irradiation growth, shape and volume changes 80—92562
Ag composite, SiC whisker-reinforced, prep. aboard Skylab. 78—84741
Ag specific volume meas., for ruby R_1 fluoresc. press. gauge calibration, 0.06-1 Mbar 78—70150
Ag-Sb-S, prep. and props. of glasses in the system 77—20053
$AgAsS_2$-$AgSbS_2$ system, thermal, microstructural X-ray phase anal. 77—32565
$AgPS_2$, single crystal, prep. and structure 77—35524
$Ag_4P_2S_7$, single crystal, prep. and structure 77—35524
$Ag_5Rb(PO_4)_2$, struct., density and elec. cond. 80—33952
Al alloys, effect of melt treatment with granules *(Russian)* 77—44190
Al, Gruneisen coeff. depend. on specific volume, phonon spectra calcs. 79—65165
Al-Cu, binary, solidification, predicted volume change 77—28802
Al-Cu alloy, deposition from RF induction source, onto laminated polyimide substrates and characterisation 80—16535
Al-rare earth alloys, granules, rolling to form foil, exam. 80—20825
Al-Si (8 wt.%), threshold H_2 for pore form. during solidification 78—52794
Al-Zn-Mg, cavitation during superplastic deform. *(Japanese)* 78—15464
AlN-Al_2O_3 composites, hot-pressed 77—52275
Al_2O_3 ceramics, elastic props. meas. in 100 to 300°C range 80—55445
Al_2O_3, plasmochemical synthesis, oxidised from metals, exam. of props. 80—2984
Al_2O_3, translucent, fabrication by high press. sintering 78—11167
Al_2O_3-B_2O_3-P_2O_5 glasses, formation and props. 78—83737
β-Al_2O_3-Na_2O, hot pressing and phys. props. 79—4940
β''-Al_2O_3-Na_2O solid electrolyte, processing and phys. props. 80—60820
β-Al_2O_3-Na_2O-SiO_2, solid electrolytes, exam. of microstruct. ionic resistivity 78—80566
$Al(PO_3)_3$-NaF-LiF glasses, mixed-alkali effect 80—19715
Ar, gas, liquid, solid, refractive index, density and dielectric const. 80—66138
Ar, solid, density at melting and isochoric equations of state 78—83915
Ar, solid-liq. transition and mech. props., modified cell theory 79—23703
Ar, X-ray determ. at melting 78—10174
As-S-Te, vitrification, density and elec. cond. measurements 79—7645
As-Sb-S-I system glasses, vitrification and volt-ampere characts. 77—31756
As-Se-Bi, semicond. chalcogenide glasses, crystallisation and electrophys. props. 78—9955
As-Se-Te glasses, glass form., charact. temp., density, thermal expansion and dynamical viscosity, struct. model 78—26672
As-Te-In, glass-forming, density and microhardness 80—103257
$AsSe_{1.2}$:Fe, Fe effect on physiochem. props. of glass 80—24370
As_2Se_3, glassy, influence of oxygen added in As_2O_3 and SeO_2 forms on phys. props. 77—76314
As_2Se_3:B:, devitrification kinetics, Bi impurity effects 77—35675
As_2Se_3:Bi, annealing kinetics, cond. activation energy and density 79—73503
As_2Se_3-$GeSe_x$-$SnSe_x$ (x=1,2), exam. of Sn valency and physical props. 79—4753
$AsSe_{1.1}Te_{0.2}$:Fe, Fe effect on physiochem. props. of glass 80—24370
$AsSe_{1.5-x}Te_x$ glasses, physical props. 78—68028
Au_xSi_{1-x} amorphous films, phys. studies 80—75476
Au_4Si.m, metastable phase, substruct. unit cell *(German)* 80—88091
B fibre reinforced Mg, exam. of fatigue props. and corrosion 80—11751
B films, prep. by H reduction of BCl_3, struct. and hardness 80—54543
B, tetragonal, X-ray diffr. and C doping obs. *(French)* 79—14731
B_4C fibres, yarn prep. from C fibres, mech., chem. props., struct., book contrib. 78—48365
B_4C, thermophysical props. and neutron absorpt. 80—103488
B_2H_6, cryst., mol. charge distrib. anal., using struct. factors from mol. densities 80—15068
B_2O_3-V_2O_5-P_2O_5, glass, mech. and elec. props 80—84228
$BaFe_{12}O_{19}$, effect of impurity concentrations, and sintering conditions on grain size *(German)* 79—23630
$BaGeO_3$-$(0.25MgF_2.0.75YF_3)$-Ga_2O_3 glass, synthesis and props. 80—25648
BaO-Al_2O_3-GeO_2-MF_2 ($M=0.45CaF_2+0.55MgF_2$), MgF_2 and CaF_2 effect on physicochem. props. 80—34876
BaO-B_2O_3-GeO_2, exam. of glass formation and physicochemical props. 79—4959
BaO-Fe_2O_3, chemically coprecipitated, mag. props., orientation 80—15763
BaO-La_2O_3-GeO_2, exam. of glass forming region, properties and crystallisation 78—88454
BaO-PbO-GeO_2-MF_2 ($M=0.45CaF_2+0.55MgF_2$), MgF_2 and CaF_2 effect on physicochem. props. 80—34876
$Ba(PO_3)_2$-AlF_3-BaF_2 (SrF_2), elec. cond., density, and IR spectra 79—95215
$Ba(PO_3)_2$-AlF_3-CaF_2, glass, elec. cond. and IR spectra 80—89005
$Ba(PO_3)_2$-AlF_3-MgF_2, glass, elec. cond. and IR spectra 80—89005
$BaPO_3F$-Al_2O_3-B_2O_3 glasses, phys. props. 78—63676
$Ba_3Pt_2O_7$, struct. model 77—72597
$BaSiO_3$-$BaGeO_3$, phase diag. 77—48404
$BaTiO_3$ ceramic, semiconductive sintering 77—36430
$BaTiO_3$:Al, 0.05-0.3 wt.%, ceramic dielectric, dielec. and mech. props. 79—8091
$BaTiO_3$-PbO-B_2O_3, liquid phase sintering, effect on props. *(German)* 79—33980
Bi-Sb, solidification, predicted vol. change 77—28802
$Bi_{12}GeO_{20}$, X-ray sensitive ceramic, sintering 80—25621
C, amorphous film, vac. evaporated, density meas., microcrystalline model of struct. 80—2313
C amorphous thin films prepared by vac. evaporation, density meas. 77—80714
C, anthracene char, density fluctuations effect on physical properties 78—51420
C, baked mix, optimum binder content estimation 77—73253
C, baked mixes, use of coal tar and petroleum pitches as binders 78—80483
C, dense hard-type solids prep. from petroleum coke powder by grinding 79—20002
C film, sputtered glassy, prep., mech. and struct. props. 77—66588

density of solids continued
C, glassy, graphitisation, density change 78—44142
C, polygranular, flexural strength after heat treatment porosity correl. 80—84996
C powder, binary mixtures, bulk density, charact. curves interpret. 77—63574
C reinforced plastic, degraded, study of strain, 20 to 1000°C 80—71680
C, vapour-deposited, transparent and hard insulating layer, struct. and props. 80—10830
C_8 crystalline diamond-like form, cryst. struct. *(Russian)* 79—99114
$CaCeAl_3O_7$, melilite struct., prep. and props. 80—93524
$CaEuAl_3O_7$, mechanism of solid-phase reactions of formation and physicochem. props. 77—52622
$CaEuGa_3O_7$, synthesis, mechanism and kinetics, cryst. props. 77—52268
CaO, density above 100 GPa rel. to high press. metallisation 80—84427
$CaO-Ga_2O_3-Bi_2O_3$, vitrification regions 77—15557
$Ca_{10}(PO_4)_6(OH)_2$, synthesis and characterisation in dense polycryst. form 77—4749
$Ca_5(PO_4)_3OH$ bioceramic, material props. 80—93523
$CaTaRO_6$, (R=La, Nd, Gd, Sm, Er, Lu), synthesis and physicochem. props. 79—52139
$CaTiO_3-TiO_2$, ceramic, phys. props. 78—43784
$CdCr_2S_{4-x}Se_x(O_x)$ X=0, 4, and solid solns., imperfect struct. model from cryst.-chem. investigs. 79—42053
$Cd_xHg_{1-x}Te$, single cryst. homogeneity and molar conc. determ. with electron microprobe *(German)* 78—2109
$CdLn(TiNb)O_7$, Ln=La-Lu, synthesis physicochem. props. 77—43186
$CdO-P_2O_5$ glasses, prep., density, elec. and optical props. 79—70033
$CdO-ZnO-P_2O_5$ glasses prep., density, elec. and optical props. 79—70033
$Cd_3(PS_4)_2$, synthesis by roasting, and exam. of props. 79—4926
$CdTl_2Se_4(Te_4)$:Au, elec. cond., density, dielectric const., changes on fusion 80—88553
CoGe, vacancy conc. in B2 phase exhibiting triple defects 79—42058
Co_5Ge_3, solid and liquid, physicochemical props. and structure 80—39548
Co_2Z ferroxplana form. process peculiarities 80—89368
Cr-SiO cermet thin films, thickness effect on density, resist., adhesion and annealing coeff. 77—69432
$CsMnCl_3.2H_2O$, diagonal elastic const., thermal expansion coeffs., ultrasonic velocity meas. 80—79853
Cu alloys, cavitation during superplastic flow, affecting factors 78—60728
Cu coating on Ni and Zr, thickness monitoring by back scattering of single energy electrons 79—97362
Cu, creep damage and cavity growth, assessment using density meas. 80—104217
Cu, powder, compression and stress relaxation *(Japanese)* 79—96060
Cu, powder, exam. of consolidation process based on electronic structure of solid 80—20842
Cu, specific volume meas., for ruby R_1 fluoresc. press. gauge calibration, 0.06-1 Mbar 78—70150
Cu-Cd-Se system, Cu-CdSe cross section and props. of cpds. formed 78—27491
Cu-Ni, sintered, props. and degree of nonhomogeneity 80—20848
Cu-P-Se system, glasses, semicond., density, microhardness, softening point rel. to conc. 77—7674
$CuAl_2$, constitutional defect struct., from X-ray and density meas. proposed substitutional-vacancy model 79—37696
$Cu_2{}^{I}B^{II}C^{IV}X_4$, ($B^{II}$=Zn, Mn, Fe, Co; C^{IV}=Si, Ge, Sn; X=S, Se), physical props. 79—65660
$Cu_xMo_6S_8$, constitution diagram, 11-2000K 80—108407
CuO, plasmochemical synthesis, oxidised from metals, exam. of props. 80—2984
$CuO-Nb_2O_5$, phase anal., density determ. 78—10015
$Cu_2O-Nb_2O_5$, phase anal., density determ. 78—10015
$Cu_{2-x}Te$, x=0 to 0.3, elec. cond., Hall const., carrier mobility, conc., thermoelec., density, lattice parameter 77—11915
$Dy_2(MoO_4)_3$, cryst. growth and props. 79—55727
Dy_2O_3-based ceramic, preparation, mech. props. 77—24998
$Er_2O_3-TiO_2-WO_3-PbO$, glass form., refr. indices and density meas. 77—90312
Eu_2O_3, mech. and physical props. rel. to reactor control rod appl. 78—21641
Eu_2O_3, sintering kinetics 78—52731
Eu_2O_3, thermophysical props. and neutron absorpt. 80—103488
Fe, Armco, dyuamic $\alpha \rightleftarrows \varepsilon$ transform., stress gauge meas. 80—96594
Fe compacts, porous, dynamic hot pressing, press. rel. to density, time 78—60599
Fe, porous, density, elec. cond., Young's modulus, toughness 78—64645
Fe, powder, atomised, processing props., particle size distrib. effect, with and without Zn stearate additions 79—100077
Fe, powder, exam. of consolidation process based on electronic structure of solid 80—20842
Fe powder sintered compacts, mech. props. effect of powder type and processing conditions *(Czech)* 77—59830
Fe, powder-forged, elastic consts., density depend. 80—84987
Fe, pure and alloyed, density and thermal expansion in liq. and solid states 80—96668
Fe/Zn stearate powder compacts, admixing effect on apparent density, mixing, compaction 80—45403
β-Fe-Al, struct. defect obs. 78—14337
Fe-B metallic glass, hardness, elastic moduli, density, cryst. temp., mech. props., for flywheel appl. *(Dutch)* 78—52878
Fe-B metallic glasses, density, mech. and thermal props. 78—31432
Fe-B_4C sintered material, mech. props. and struct. characts. 79—100084
Fe-B-C amorphous alloy, formation, mag. props., thermal stability and density 80—75796
Fe-B-Si-C amorphous alloys, prep. and props. 80—88748
Fe-C, binary, solidification, predicted volume change 77—28802
Fe-C (graphite, 0.3 wt.%), powder-forged, elastic consts., density depend. 80—84987
Fe-Co alloy, V addition effect on atomic order parameters, dislocation struct., mechanical props. 79—91762
Fe-Ni-Cr-P-B, Metglas 2826A, hardness, elastic moduli, density, cryst. temp., mech. props., for flywheel appl. *(Dutch)* 78—52878
Fe-Si (3 to 5 wt.%) sinters, mag. props., Si and Fe-Si additions effect 80—71104
Fe-Si-Al Sendust alloy ribbon form, rapid quench prepared, elec. cond., coercive field, permeability 79—83151
Fe-Si-B, surface tension, density, and oxidation kinetics 80—20028
Fe-Si(6.5 wt.%) steel, core mat. development *(Korean)* 78—60852
$(FeCo)_{80}B_{20}$, glass, elastic consts. 79—83249

density of solids continued
$(Fe_{1-x}Co_x)_{80}P_{13}C_7$ amorphous alloy, soft mag. material, props. 77—4533
$(Fe_{1-x}Co_x)_{75}Si_{15}B_{10}$ amorphous alloy, soft mag. material, props. 77—4533
FeF_2 (rutile), high press. phase transform. and zero-press. density increase 78—79761
$(Fe_{1-x}M_x)_{77}Si_{10}B_{13}$, M=Co, Ni, amorphous magnetic alloys, density meas. 80—1934
$(FeNi)_{80}B_{20}$, glass, elastic consts. 79—83249
$(Fe_{0.6}Ni_{0.4})_{100-x}B_x$ and $(Fe_{100-x}Ni_x)_{80}B_{20}$ amorphous alloys, X-ray diffr. struct. determ. 80—64906
γ-Fe_2O_3, densified, rheological and mag. props. 80—44873
Fe_2O_3, plasmochemical synthesis, oxidised from metals, exam. of props. 80—2984
Fe_2O_3, powder, preparation conditions rel. to morphology 77—8777
$Fe_{80}(P_{13}C_7)_{20-y}B_y(Si_y)$, density, microhardness, and crystn. temp., comp. depend. 80—84093
$Fe_{0.545}Sb$, temperature effect on lattice consts., Mossbauer spectra and density 80—88124
GaSb-GaAs-Ge system, props. and struct. 80—20232
$\alpha(\beta)$-Ga_2Se_3, cryst. growth, optical, X-ray diffr. and SEM study 80—71587
Gd-Co amorphous film, DC or RF sputtered, mag. props., He^+-backscatt. investig. 77—20650
Ge amorphous film, evaporated, non-destructive density meas. 80—6680
Ge, amorphous film, vac. evaporated, density meas., microcrystalline model of struct. 80—2313
Ge amorphous thin films prepared by vac. evaporation, density meas. 77—80714
Ge-FeS, GeS-FeS, density of alloys, volume changes on melting 77—51473
Ge-P-Se system, glasses, semicond., density, microhardness, softening point rel. to conc. 77—7674
Ge-Pb-Se-Te, glass form., DC cond., and mole volume 79—90560
Ge-S-In, chalcogenide glass, determ. of density using hydrostatic method 79—23526
Ge-S-Se system, glass-forming, struct. and props. 80—19713
Ge-Sb-Se glass, physical props., purification method for Sb, Se from surface oxides 78—46735
GeO_2, amorphous, obtained by hydrolysis of $GeCl_4$, exam. of props. 79—95956
$Ge_{2.33}SbSe_5$:Fe, Fe effect on physiochem. props. of glass 80—24370
$GeSe_2$, single crysts., 3 polymorphic forms, DTA, photolum., IR and Raman sepctroscopy 80—33923
$GeSe_2-As_2Se_3-Sb_2Se_3$ system glasses, vitrification and elec. cond. 79—50996
$GeSe_2-SnSe_2-As_2Se_3$, $GeSe-SnSe-As_2Se_3$, Mossbauer investigation 77—20052
$Ge_{30}Si_{70}$, hot press sintering 80—50572
$GeTe_x$ cermet specimens, 25 to 412°C, depend. on nonstoichiometry and annealing temp. 77—25004
H_2 and isotopes 77—72674
n-H_2, molar volume press. depend. at 77K *(Russian)* 79—86832
H_2, solid, high pressure phase, 57 kbar, 25°C, transparent crystalline mass 79—55870
^4He, Lennard-Jones model at 0K, props. using Monte Carlo method 79—82401
$HfF_4-BaF_2-LaF_3$ glass system, IR transmitting, synthesis and props. 80—71623
$HfF_4-BaF_2-ThF_4-(ZrF_4)$ glass system, IR transmitting, synthesis and props. 80—71623
Hg-S binary system, phase relations, bulk resist. meas. 79—66040
$HoAlO_3$, Czochralski growth and props. 77—48335
InAs, intrinsic point defects, nature and influence on electrophys. props. 78—79609
InAs, obtained by liquid-seal method, deviation from stoichiometry 77—40345
In_2Bi, cryst. struct. and density *(German)* 80—24407
$InVO_4.2H_2O$, $In_4(V_2O_7)_3.14H_2O$, physicochem. props. 77—85702
Ir, thermophysical props. at temps. up to 7000K 80—103497
KCl:Ca^{2+}(Sr^{2+}), impurity precip., flotation density obs. 78—51690
KCl:Pb^{2+} crystals, precipitation, density changes, nucleation mode, lattice relaxation, heat treatment 79—66066
KCl-CuCl eutectic fused salt, potential as intermediate temp. solar heat transfer and storage medium 80—101135
$K_2(F,O)-B_2O_3-SiO_2$, effect of replacing B_2O_3 by Al_2O_3 or Ga_2O_3 78—63677
$K_2O-BaO-SiO_2:Nd^{3+}$ glasses, absorption and fluoresc. spectra, density 80—25417
$K_2O-CaO-SiO_2$ glass, composition-density relationship 77—90326
$K_2SO_4-ZnSO_4$ system, glass formation and phase diagram study, physical props. 78—27500
Kr, gas, liquid, solid, refractive index, density and dielectric const. 80—66138
Kr, solid, density at melting and isochoric equations of state 78—83915
La, $(SO_4)_3.9D_2O$, soln. growth, struct., props. 77—77363
LaB_6 crystals, zone refined, chem. characterisation 80—93821
La_2Co_7, mag. saturation and anisotropy, density, lattice parameters 77—85426
$LaF_3-BaF_2-ZrF_4(-MF)$, M=Na, Li, glassy transition, refr. index, density and molar refr. 80—1937
$La_2O_3-Mn_2O_3-Cr_2O_3$, synthesis and properties of solid solutions 78—44038
$LaS_{1.500}-LaS_{1.333}$, solid soln. region, density meas. 80—95075
La_2Se_3, La_2Te_3, mutual solubility 77—21113
(Li,Na,Cu,Zn) ferrites, nonceramic synthesis, electrochem. investig. 78—35339
β-Li-Al, lattice parameters, density, defect struct. 80—24440
Li-B (0-60 at.%), density, elec. resist. and Hall coeff. 78—39089
Li-Na ferrite powders, props. rel. to Fe_2O_3 chem., thermal, mech. historical 79—11539
LiF, cohesion energy, compressibility and density, ab initio calc. 77—72648
LiF compact, particle size rel. to pore characts. 78—60631
LiF-NaF(KF)(CaF_2)(BaF_2), densities of binary molten salts *(Japanese)* 79—7644
LiF-$NaPO_3$-MeF_x (Me=Mg, Ca, Al) glasses, IR spectroscopy study 80—16042
$LiNO_3.3H_2O(D_2O)$, crysts. and melts, density, mol. vol., thermal coeff. of expansion, rel. to struct. 80—15270

density of solids continued
$LiNO_3.3H_2O(3D_2O)$, density, thermal apansion coeff., isotope effect 78–87733
$LiNbO_3$, growth from melt and characts. *(Chinese)* 80–54155
$LiNb_{1-y}Ta_yO_3$, Czochralski growth and basic props. 77–63556
Li_2O-Al_2O_3-SiO_2, glass, study of elastic props. 80–104205
Li_2O-B_2O_3-P_2O_5, glass, mech. and elec. props 80–84228
Li_2O-Na_2O-B_2O_3-Al_2O_3-SiO_2 glass, Young's modulus and density, ion exchange effects 80–84982
$LiRF_4$, R=rare earth, laser matrices prep. and characterisation 77–24945
M_2O-MnO-B_2O_3 glasses, M=Li, Na, K, glass-forming region and physicochem. props. 78–63678
Mg-Zn metallic glass, hardness, elastic moduli, density, cryst. temp., mech. props., for flywheel appl. *(Dutch)* 78–52878
$MgAl_2O_4$, composition rel. to ceramic microstruct. form., light transmission 79–43188
$MgFe_{2-y}Al_yO_4$, with added Co, effect of Na_2O admixture on props. 77–36423
$MgFeGe_2O_6$-$Ca(Mg_{0.5}Fe_{0.5})Ge_2O_6$, solid solns., phase equilibria, cryst. optical, X-ray struct. characts. 79–11577
$MgGeO_3$-$Ca_{0.5}Fe_{0.5}GeO_3$, solid solns., physicochem. props. 77–44223
Mg_2GeO_4-Mg_2SiO_4 system, struct. similar solid soln. obs. and characts. 80–108403
$MgIn_xFe_{2-x}O_4$ and $MgSc_xFe_{2-x}O_4$, Mossbauer spectra, elec. and mag. props. *(Russian)* 77–69737
MgO, plasmochemical synthesis, oxidised from metals, exam. of props. 80–2984
MgO polycrystals, hot-pressed, density changes on annealing 79–34073
MgO, single crystal, density rel. to elastic consts. and internal frictions 77–78165
Mn-Pt, Elinvar props., −150 to 500°C *(Japanese)* 77–52385
Mo form MoF_6 by H_2 reduction, 500 to 1200°C *(Russian)* 80–7516
Mo, monocrystalline, density change during plastic deformation *(Russian)* 79–87689
Mo, specific volume meas., for ruby R_1 fluoresc. press. gauge calibration, 0.06-1 Mbar 78–70150
$(Mo_{0.6}Ru_{0.4})_{82}B_{18}$, supercond. metallic glass, neutron irrad. effects 80–29060
$MoSi_2$-$CrSi_2$, phase equilib., struct. and props. 80–50608
$(NH_4)Cd_6[P_2O_7]_2[P_3O_{10}]$, with mixed anion radical, cryst. struct. by X-ray anal. 79–86771
$^{15}N_2$, solid struct., and thermodynamic props. *(Russian)* 80–88083
NaCl aerosols, density rel. to formation by condensation 78–7244
NaCl, elastic props. at press. up to 9 GPa, ultrasonic wave velocities 79–95073
NaCl with divalent impurities, lattice relax. from density meas. 80–70226
NaF, ab-initio calc. of cohesion energy, compressibility and density 78–71782
NaF, sintering, relation between densification and grain growth 77–12585
Na_2O-Al_2O_3-SiO_2 glass, formation from alkoxides, phys. and chem. evolution 78–80503
Na_2O-B_2O_3-P_2O_5, glass, mech. and elec. props 80–84228
Na_2O-BaO-SiO_2:Nd^{3+} glasses, absorption and fluoresc. spectra, density 80–25417
Na_2O-CaO glass phlogopite mica powders, composite fabrication, cellular struct. 80–84902
Na_2O-$CaO(Al_2O_3)$-SiO_2 glass, composition-density relationship 77–90326
Na_2O-$GeO_2(TiO_2)(SnO_2)(ZrO_2)(ThO_2)$-$SiO_2$ glass, density, refractive index, thermal expansion, hardness IR spectra, DTA *(Japanese)* 78–15535
Na_2O-SiO_2 glass, bridging to non-bridging ratio and correl. to glass density and refr. index, ESCA study 80–84832
Na_2O-SiO_2 glass, OH^- content effect on mech. and other props. 80–89337
Na_2O-SiO_2 glass drops, quenched from liq. state, thermally treated, density profile 80–81085
$Na_6W_7O_{24}.14H_2O$, crystal and molecular struct. X-ray determ. 79–82188
Nb, density, rel. to elastic const. calc. from US meas. 77–86079
Nb-Ni metallic glass, hardness, elastic moduli, density, cryst. temp., mech. props., for flywheel appl. *(Dutch)* 78–52878
NbC, elastic modulus, porosity factor 77–21207
$Nb_{40}Fe_{40}P_{14}B_6$, metallic glass, explosive compaction, mech. props. 80–89176
Nd_2Co_7, mag. saturation and anisotropy, density, lattice parameters 77–85426
Ni, powder charact. effects on sintering 77–1828
Ni-Co-Cr-Al-Ti-Mo superalloy IN738, casking porosity removal using hydrostatic press. sintering 80–55322
Ni-Cr-Mo-Mn alloy 02KhN40MB, corrosion-resist, heat-resist., phys. and mech. props. 80–35411
Ni-Fe alloy, FCC, density, lattice parameters, X-ray diffr. and hydrostatic weighing 78–55904
Ni-NiAl solid soln., high temp. transforms *(Russian)* 79–56973
Ni-P metal metalloid glass forming alloys, gram atomic volumes 78–38628
Ni-Zn ferrites, hot-pressed, key props. 78–15348
Ni-ZrO_2, dispersion-strengthened condensate, density and mech. props. 77–44196
$Ni_{0.5-x}Co_xZn_{0.5}Fe_2O_4$ ferrospinal solid solutions, cryst. lattice defects and props. 80–19796
NiGa, vacancy conc. in B2 phase exhibiting triple defects 79–42058
Ni_5Ge_3, solid and liquid, physicochemical props. and structure 80–39548
NiO, plasmochemical synthesis, oxidised from metals, exam. of props. 80–2984
β-Ni_3S_2, defect struct. 78–63754
β-Ni_3S_2, formed during sulphidation of Ni, defect struct. and chemical diffusion 78–2115
$Ni_{1\ 1}Sb$, temperature effect on lattice consts., Mossbauer spectra and density 80–88124
NiZn ferrite, ZrO_2 additions influence on sintering and physicochem. props. 80–108369
NiZn ferrites, density and mag. props., isostatic pressure effect 80–60816
O_2, density of solid in equilib. with vapour 78–93656
P-As-Se glasses, mag. susceptibility, dielec. const., opt. props. 78–64184
Pb bismuthate glass, IR transmission props., density 79–74127

density of solids continued
Pb-Bi, splat quenched, solubility limit, vacancy conc. and supercond. transition temp. 77–12046
Pb-Sn, solidification, predicted vol. change 77–28802
Pb-Sn eutectic, cavitation during superplastic flow, affecting factors 78–60728
Pb-Sn microduplex eutectic, cavitation during superplastic flow due to hard particles 77–36575
PbO-containing binary systems, acoustooptic props. from comp. and density 80–76000
PbO-MoO_3-P_2O_5, glass phase investigation, density determ. *(Polish)* 77–70039
PbS film, vac. deposited, optical and phys. props. 80–2315
$PbSe_xS_{1-x}$, comp. depend. of density, effect of defects 77–11538
$Pb_{1-x}Sn_xTe$ single crysts, energy gap determ. from density and lattice const. *(German)* 78–26812
$Pb_{1-x}Sn_xTe_{1-y}Se_y$, quarternary solid solns. with const. lattice parameter, cryst. growth and characts. 80–108332
$Pb(Zr, Ti)O_3$ cast tape, densification by pressing for piezoelec. devices 79–87595
$Pb(Zr, Ti)O_3$ ceramics, low temp. sintering, elec. and mech. props. 80–71616
$Pb(Zr_xTi_{1-x})O_3$, high density, sol-gel technique prep., piezoelec. props. 80–20596
Pd specific volume meas., for ruby R_1 fluoresc. press. gauge calibration, 0.06-1 Mbar 78–70150
Pd-Si, amorphous $Pd_{0.8}Si_{0.2}$, struct. anal. by dense random packing model 79–51003
$Pd_{1-x}M_xSe_2$ (M=Ru,Co,Ni), high pressure phase transformation studies, lattice constants and densities 79–65187
Pr_2Co_7, mag. saturation and anisotropy, density, lattice parameters 77–85426
$Pr(OH)_3$, low temp. heat capacity, thermophys. props. optical spectra, anal. of Schottky contributions, review 80–24611
Pt metals, lattice parameters, densities and atomic vols., tabulation 79–65033
S-based composite, engineering props. 77–86093
Sb_2S_3, vitreous, prep. elec., opt. and struct. props. 77–76889
ScN_x, region of homogeneity, physicochem. props. 78–52018
Sc_2O_3:MgO, defect struct., X-ray diffr. and pyrometric density 78–34524
Se, amorphous, elec. cond., activation energy, density, cryst. Se effect 80–65548
Se, amorphous film, vac. evaporated, density meas., microcrystalline model of struct. 80–2313
Se-As_2Se_3 system glasses, vibr. spectra and partial vols. of components 79–42973
Se-S, glassy alloy, order-disorder transition kinetics 78–67650
Si, porous, formation during anodic treatment in HF aq. soln., growth kinetics and density 80–20059
Si, steam oxidation, low temp., high press., oxide growth kinetics and props. 80–16523
Si, surface layer, thin, density meas. by total external X-ray reflection 78–14635
Si:H amorphous film, plasma-deposited, growth morphology and defects 80–44128
Si/SiC ceramic composite, room temp. props., effect of SiC content and orientation 78–27599
Si-N film, passivation layer, density comp., and ref. index, Lorentz-Lorenz correl. 78–39697
SiC coatings, CVD on microspheres in fluidised bed, parametric investig. 77–40457
SiC fibres obtained from polycarbosilane fibre 80–50582
β-SiC, powder, synthesis by chemical vapour phase reaction from methylsilane, exam. of props. *(German)* 79–4938
SiC, powder mixtures, composition vs. apparent density diagrams construction, model 78–60633
SiC, self-bonded, statistical distrib. of values of apparent density 78–68657
SiC:H amorphous reactively sputtered film, H content effect on film props. 80–75459
Si_2N_4 powders, synthesis, charact. 79–33977
Si_3N_4, porous, reaction sintered, organosilicon infiltrated, decomposition, strength, density 79–29000
Si_3N_4, rapid CVD, and struct. characts. 77–28767
Si_3N_4, reaction sintered, time depend. strength degradation 79–29235
β-Si_3N_4 solid soln. prod. by reaction sintering SiO_2-AlN mixture 80–25645
Si_3N_4-Mg_2SiO_4-Si_2N_2O, compressive creep, composition effect 80–50674
SiO, amorphous film, vac. evaporated, density meas., microcrystalline model of struct. 80–2313
SiO amorphous thin films prepared by vac. evaporation, density meas. 77–80714
SiO_2 (silicalite), hydrophobic crystalline mol. sieve, refr. index and density 78–30598
SiO_2 film, prep. using high press. O_2, residual stress, chemical etch rate, refr. index and density meas. 80–71768
SiO_2 glass, densified, enthalpy variation, heat of dissolution obs. *(French)* 79–34015
SiO_2 glass, formation by hydrolysis of $Si(OC_2H_5)_4$ with NH_4OH and HCl soln., and characterisation 80–71622
SiO_2, vacuum deposited, 7-10 μ, microhardness and structure 78–19669
SiO_2, vitreous, electron irrad., vol., refr. index and stress changes 77–47482
SiO_2, vitreous, H impregnated, γ radiation effects, hydride, hydroxyl formation 79–87874
SiO_2-Al_2O_3-B_2O_3-LiO_2 ($LiO_2.Na_2O$) (Na_2O) glass exam. of optical props. 78–88277
SiO_2-B_2O_3 glass system, gel hot pressing synthesis and characterisation *(French)* 80–66468
SiO_2-GeO_2 glass, refr. index and density, comp. depend. 78–23424
SiO_2-GeO_2-$Li_2O(Na_2O)(K_2O)$, refractive index and density 79–51926
SiO_2-K_2O-Na_2O-BaO-SrO-ZnO glass, props. optimisation 79–91611
SiO_2-Li_2O-K_2O-ZnO glass ceramic, prep., phase transformations and physical props. 80–45299
$SnSe_2$-$GeSe_2$-As_2Se_3 system glasses, vitrification and elec. cond. 79–50997
$SrAg(PO_3)_3$, physicochem. characts. 77–52302
Ta, density, rel. to elastic const. calc. from US meas. 77–86079
Ta, lattice parameter, X-ray meas., rel. to density and elastic moduli 77–89406

density of solids continued
  Ta, thermophysical props. and neutron absorpt. 80−103488
  Ta_2O_5, reactive DC sputtering deposited films with magnetron-plasmatron, mechanical elec., optical props. 80−25566
  $TaSi_2$-$CrSi_2$, phase equilib., struct. and props. 80−50608
  $Ta_{16}W_{18}O_{94}$, characterisation of thermally contracting tungstates 78−63869
  Ta_2WO_8, characterisation of thermally contracting tungstates 78−63869
  $Ta_{22}W_4O_{67}$, characterisation of thermally contracting tungstates 78−63869
  Tb-Sn-Se system, cross section Tb_2Se_3-$SnSe_2$ phase diagram, physicochem. anal. 79−87621
  TeO_2-MoO_3-V_2C_5, phase comp. determ. using X-ray diffr., electron microscopy and DTA *(German)* 80−88046
  $TeSe_{19}$ glass, crystallisation kinetics 77−35484
  $TeSe_{20}$, vitreous alloy, elec. and thermal cond. during crystallisation 79−7550
  $TeSe_{50}$, amorphous to cryst. transition, kinetics 79−73099
  ThO_2 ceramics, CaO and Y_2O_3 stabilised density, elec. cond., permittivity 78−47838
  α-Ti alloys VT1 and VT5, struct. and phys. props., H_2 effect 80−108576
  Ti base alloys, melt-extracted polycryst., mech. props. 80−76360
  Ti-Be-Si glass ribbons, physical and mech. props. 78−95767
  Ti-Cr-B system, self-propagating high temp. synthesis, crystallochemical and mech. props. 80−20861
  $Ti_{50}Be_{40}Zr_{10}$ glass, mech. props., X-ray diffr. exam. 78−11292
  TiC-TiN, physicochem. props., comp. depend. 80−55370
  $TiC_{0.93}$-$TiN_{0.818}$, structural parameters, and X-ray and pycnometric densities in homogeneity range 77−90311
  TiO_2, plasmochemical synthesis, oxidised from metals, exam. of props. 80−2984
  TiO_2, reactive DC sputtering deposited films with magnetron-plasmatron, mechanical elec., optical props. 80−25566
  TiO_2, sintering, hardness, density, elec. cond. and colour *(Japanese)* 78−68659
  TiO_2-Al_2O_3-SiO_2 system, ternary glass-forming region and phys. props. 80−84919
  TiO_x, anomalous difference between theoretical and expt. densities, nonvacancy character 79−90630
  $TiSi_2$-$CrSi_2$, phase equilib., struct. and props. 80−50608
  $Ti_{1-x}Ta_xO_2$, solid soln. formed in TiO_2-Ta_2O_5-Ta at 1100°C *(French)* 78−35375
  $TlAsSe_2$, diamag., thermal expansion rel. to temp. at cryst.-melt transition 78−34954
  TlBS, synthesis, struct., optical, spectral props. 79−15631
  $TlBi_2$, cryst. struct. and density *(German)* 80−24407
  $TlGaS_2$-$TlGaSe_2$, phase and composition-property diagrams 80−55366
  $TlInS_2$-$TlInSe_2$, phase and composition-property diagrams 80−55366
  Tl_2MoO_4, prep., characterisation 78−63731
  Tl_2Se, diamag., thermal expansion rel. to temp. at cryst.-melt transition 78−34954
  Tl_2Se_3, diamag., thermal expansion rel. to temp. at cryst.-melt transition 78−34954
  Tl_2Te_3, exam. of electrical props., density and viscosity, for solid or liquid states 79−95431
  Tl_2Te_3:Ag(Sn), effect of dopant on electrical props., density and viscosity, for solid or liquid states 79−95432
  Tl_2WO_4, solid-state prep., cryst. struct. and props. 78−38673
  UO_2 compact, density distrib. determ. using autoradioagraphy 77−25234
  UO_2 fuel, density, thermal conductivity, specific heat, thermal diffusivity, flash method 77−55362
  UO_2-$20CeO_2$ mixed powder, X-ray and microprobe exam. of homogenisation 80−25609
  V, density, rel. to elastic const. calc. from US meas. 77−86079
  V, thermophysical props. at temps. up to 7000K 80−103497
  VC, damage sustained during neutron irradiation 77−1841
  VO_x, struct. model accounting for low density 77−84707
  V_2O_5 film, amorphous, thickness, density and refr. index determ. from reflectance interference spectra 80−55206
  V_2O_5-P_2O_5 glass, density and O molar volume 78−59759
  $V_{1+x}P_{1-x}O_{5-c/2}$, density and struct. from X-ray scatt. meas. 77−89380
  W alloys, sintered relation between density and sound velocity 78−53173
  WC-Co hard alloys, hot pressed, mech. props. 79−100260
  WO_3, amorphous film, vac. evaporated, density meas., microcrystalline model of struct. 80−2313
  WSe_2, lubricant, prep. by self-propagating high-temp. synthesis, technological characts. 78−35338
  Xe, gas, liquid, solid, refractive index, density and dielectric const. 80−66138
  $YAl_3(BO_3)_4$, and $(Y,Er)Al_3(BO_3)_4$, crystallisation and growth characts., density and composition 80−35080
  YB_{68}, melt grown, props. meas. 77−11518
  Y_2O_3 ceramic, elec. resistance rel. to density 79−82594
  Y_2O_3, prep. of transparent ceramic, exam. of light transmission preps. 79−20013
  Yb_2O_3-based ceramic, preparation, mech. props. 77−24998
  $ZnAs_2$, homogeneity region and electrophys. props. 80−60833
  ZnB_2O_4-MF_2 (M=Mg, Ca, Sr, Ba) glass system, physicochem. props. 80−34877
  ZnO, plasmochemical synthesis, oxidised from metals, exam. of props. 80−2984
  ZnO-La_2O_3-GeO_2, exam. of glass forming region, properties and crystallisation 78−88454
  Zr-Al (8.6 wt.%), dimensional stability struct. and mech. props, effects of neutron irrad. 80−92563
  Zr-Cr-B system, self-propagating high temp. synthesis, crystallochemical and mech. props. 80−20861
  ZrC, elastic modulus, porosity factor 77−21207
  $ZrH_{1.8}$, radiation-induced defects in hydrogen sublattice 79−37739
  $ZrH_{1.9}$, neutron irrad. induced defects, nature and thermal stability 77−50246
  ZrO_2, cubic, anion vacancy form. during electrolysis, density change 77−80648
  ZrO_2, optimum sintering characts., density, X-ray diffr., IR spectrum, UV spectrum obs. 78−76617
  ZrO_2-$CaO(Y_2O_3)$ ceramics with grainy structure, props., effect of heating to 2000°C 80−104194
  ZrO_2-Y_2O_3, solid solns., density meas. rel. to O vacancy model 78−2113
  ZrO_2-Y_2O_3, stabilised, struct. of single crysts. 77−35527

density of solids continued
  $ZrO_2.SiO_2$-αAl_2O_3 mixed powders, solid state reactions 80−40337
  $ZrSiO_4$, natural zircon, nucl. radiation effect on elastic moduli 77−11616
density of states, electron *see electronic density of states*
deoxyribonucleic acids *see DNA*
deperming *see demagnetisation*
desalination
  25 kW solar photovoltaic flat panel power supply for electrodialysis water desalination unit 80−89643
  cellulose acetate membranes, modified, tensile props., desalination performance 79−11818
  chemical water treatment pH value calc. for district heating power station, computer-aided analysis *(Russian)* 79−43572
  desert pastures irrigation using solar desalination plants 80−89594
  deuterium distillation at desalination plants 77−67894
  direct contact cooling of crystallising $MgCl_2$ brine using kerosene drops 79−1053
  direct contact heat transfer, butane drop nucleation in flowing water 79−1099
  distillation using basin-type solar stills, use of wood charcoal beds 80−7924
  dual-purpose nuclear-electric reverse osmosis seawater conversion plant design and cost study 80−47683
  electrodialysis desalination plant, boundary layer thickness, effect on plant perform. and design 79−26725
  electrodialysis reversal process, with automatic self-cleaning facility 80−3357
  evaporator, falling-film, with vertically finned surface, hydrodynamics and heat transfer 80−58891
  evaporator-condenser tubes, grooved film-type, configuration effect on heat transfer 80−53604
  fission reactor for seawater desalination, evaluation of single purpose reactor 80−5319
  fluidised bed evaporator, liq.-solid wall to liq. heat transfer 79−1245
  gas turbine waste heat utilisation for elec. energy generation and desalination *(German)* 79−87936
  greenhouse solar distillation and cultivation materials 79−74496
  ion selective membrane, polarisation at high current densities, Nernst model 79−91962
  IPWR, appl. to district heating and desalination 78−41852
  LWR, heat supply for desalination, economics 78−41851
  multistage flash distillation process using nuclear power, design aspects 77−38390
  nuclear low temp. waste heat appl. 78−41850
  nuclear power station with desalination plant, steam-cycle and optimisation calc. 79−26724
  nuclear reactor near term feasibility 79−31172
  nuclear steam turbines for power prod., district heating, desalination 78−37438
  photoelectrochemical model energy conversion systems, evaluation 79−43777
  PWR appl. to multi-stage-flash desalination, small performance plants 78−37461
  reinforced cellulose acetate membrane water and salt permeability, complementary direct osmosis test 79−96359
  reverse osmosis, appl. of radiation grafted cellulose acetate-g-polyacrylamide membranes 80−45548
  reverse osmosis salt rejection, membrane pore size 77−9122
  reverse osmosis using solar and wind powered plant 80−61282
  sea water, nuclear reactor steam appl. 77−38385
  seawater, heavy water concentration, numerical model calc. 79−26514
  seawater desalination by wind power, anal. 80−108781
  seawater desalination plants using simplified nucl. reactor 78−13315
  seawater distillation, scale control, electrodeposition appl. 79−66302
  solar, combination with greenbouse installation *(French)* 80−55806
  solar and wind power utilisation, expt. installations based on reverse osmosis process *(French)* 80−55807
  solar collector systems appl., low-temperature multiple-effect plant supply technical and economic evaluation 80−55804
  solar desaliniation unit with evaporation chamber, test results 80−96178
  solar distillation plant, 5000 lit/day, drinking water production in India 80−61280
  solar energy appl., multistage flash evaporation process, demonstration project 80−61283
  solar energy powered plant, MSF, technical and economic evaluation 80−61281
  solar energy utilisation, India's 1978 development trends 79−74509
  solar energy utilisation, plant design w.r.t. efficiency 79−87973
  solar flate plate evacuated collector design 79−62099
  solar inclined-step distiller, test results 80−40901
  solar photoelectric electrodialysis desalination plant 79−39284
  solar powered electrodialysis appl. 80−55805
  solar-assisted reverse osmosis plant, design economic anal. 80−55891
  solar-MHD desalinator prototype, design and operation 79−74508
  thermal power plant, antiscale forming effectiveness of seeding crystals 80−89527
  THERMOS reactor energy source, operation *(French)* 80−47684
  THERMOS reactors, district heating and desalination appl. 78−41853
  ultrafiltration membranes appl., hybrid reverse osmosis 77−44507
  undersea resources and related topics, world-wide survey 80−35622
  water, electrodialysis and its applications 80−55702
  Al alloy welded, corrosion behaviour rel. to sea water desalination plant applics. *(Japanese)* 77−25192
desalting *see desalination*
describing functions
    see also control system analysis
  coupled biological oscillators, describing function techniques 77−25361
  visual evoked response of humans, nonlinear anal. 78−92622
design aids
    see also design engineering; nomograms
  capacitor banks, optimum design rules 78−74487
  fission reactor pressure vessels for high temp., computer appl. *(Japanese)* 78−673
  graphs for optical system design, multi-layer, using equivalent films *(Czech)* 78−90486
  medical equipment reliability requirement determ. and assessment method 77−5091
  optical fibre system design charts 79−7200
  strain gauge appl. 77−41591

design engineering
see also project engineering; systems engineering
1 GHz oscilloscopes for laboratory, design techniques 77−22540
60 m diameter wind turbine generator, design concept 80−61262
200 MW atmospheric fluidised-bed combustion steam generator, comparison of three designs 80−108776
475 MVA pulsed motor generators for TFTR 78−58498
600 kV repetitive stacked line transformer pulse generator 78−77935
600 MW pulsed energy convertors for toroidal field coil, design philosophy 78−58496
1000-2000 MVA turboalternators, for LWR power station, design *(French)* 77−3153
acoustic planning of plants, technical and economic advantages 80−3561
aerodynamic design, wind tunnel tests and numerical methods compared 77−27635
antifreezing circuit, Boolean algebra appl. *(German)* 77−64914
ASDEX circuit breaker system, design, calcs. and tests 78−55032
axial flow fan, control of tip-vortex noise 78−90593
biological form and engineering design mechanical aspects *(Japanese)* 78−24089
buried pipeline transient temp. distrib. estimation 78−75048
BWR, advanced reactor, design procedures *(French)* 77−74968
Calcutta variable energy cyclotron vacuum system design, testing and commissioning 78−86707
capacitor banks, optimum design rules 78−74487
coils for magnet airgap EM field uniformity correction *(Russian)* 77−53959
coils for RF powered implant telemetry 78−31926
cold water pipe designs for ocean thermal energy conversion plants 80−45725
compressors, high pressure, for low-density polyethylene process 77−13764
computer-aided ship structural design for diploma and undergraduate courses 79−35494
COS-B satellite, ESA extraterrestrial gamma radiation obs. project *(German)* 79−21151
crowbar transformer, low leakage and high current for ZT-40 toroidal pinch power supply 80−102322
cryopumps for fusion reactor high power neutral injectors, design and performance 78−74494
CTR, for power generation, design 77−3157
dielectric parts, stress patterns and deformation characts., computer anal. 80−17787
digital instruments design and technology 77−5821
digital multimeter, general-purpose, design practice 77−57348
direct coupled electrocardiograph *(Japanese)* 78−24166
double helix vacuum resistance heater element design and construction details 78−49839
dust meas. devices, radioisotope absorption type, cct. design *(Polish)* 78−29101
electric connectors, stress relax. estimation for Cu alloys and plastics, expts. 77−21206
electric machine air cooling using evaporative thermosiphon, nomogram 77−71194
electrical and electronic engineering undergraduate courses, engineering design importance 80−67972
electronic instrument design, modern circuit technologies impact 77−5861
electrostatic precipitator, free-fall, design and operating modes 78−71020
EM instruments for use in liquid sodium, theoretical anal. 78−54857
engineering education, importance of research and design for satisfying industrial needs 80−67974
epicyclic gears for wind power plants 80−61252
ferrofluid devices, magnetostatic and centrifugal, nonmagnetic body motion 80−33700
free vortices behind stationary wing as energy source, design parameters 80−40820
frontiers in education, conference, Urbana-Champaign (1977) 78−81779
fusion, toroidal field superconducting coil cryogenic stability and field anal., design parameter 80−106200
fusion reactor, ASDEX, neutral beam injection, beam line design 80−99395
fusion reactor, commercial Tokamak hybrid reactor, blanket and shield design 80−106179
fusion reactor, commercial Tokamak Hybrid Reactor, reference design 80−106171
fusion reactor, compact ignition test reactor, engineering design using Bitter type magnet 80−102310
fusion reactor, Doublet III, neutral beam test tank design 80−99301
fusion reactor, ETF, design considerations 80−95438
fusion reactor, experimental fusion reactor preliminary design 77−74981
fusion reactor, first wall blanket, cylindrical module, reference design 80−106181
fusion reactor, Heliotron E, helical coil design, mag. field perturbations 80−99300
fusion reactor, HFCTR, demonstration reactor conceptual design, high force density magnets and modularisation 80−95439
fusion reactor, ISX-B tokamak, design of bundle divertor expt. 80−102341
fusion reactor, JET, high voltage network to load AC/DC pulse power conversion 78−58497
fusion reactor, JXFR, superconducting mag. system conceptual design 80−99295
fusion reactor, Large Coil Program, low temp. stability, joints, design method 80−106195
fusion reactor, LARTS, extended burn operation, physics, engineering and economics 80−95440
fusion reactor, LINUS, imploding liq. liner system, engineering anal. 80−99315
fusion reactor, low power Tokamak experimental fusion power plant, scoping studies with empirical scaling, SISYFUS code 80−102309
fusion reactor, LPTT, engineering design 80−102308
fusion reactor, MFTF, intense neutron environment, test cell side wall design, shielding materials 80−102318
fusion reactor, MFTF, ion and neutral beams dumps, design 80−102317
fusion reactor, neutral beam ion source, core snubber network design, fabrication and testing 80−102378
fusion reactor, PDX, flexible work platform and balcony design 80−106161
fusion reactor, STARFIRE project, design parameters 80−106184

design engineering continued
fusion reactor, STARFIRE project, first wall and blanket design 80−106188
fusion reactor, STARFIRE project, superconducting poloidal coils design study 80−106185
fusion reactor, T-10M Tokamak, normal and supercond. inductive energy storage and switching 78−55018
fusion reactor, TEXT, assembly plan 80−99305
fusion reactor, TEXT, poloidal field power systems, design and anal. 80−102328
fusion reactor, TEXT, pulsed homopolar generator power supply, engineering and design 78−55016
fusion reactor, TFTR, blanket module expts., engineering test station design 80−102338
fusion reactor, TFTR, electrical power blanket module, conceptual design 80−102339
fusion reactor, TFTR, high energy heat sink, ion beam dump and calorimeter 80−99394
fusion reactor, TFTR, neutral beam injector prototype, construction and performance 80−99390
fusion reactor, TFTR, neutral beam source, arc current modulator design 80−102379
fusion reactor, TMX, injector system mech. design and installation 80−99393
fusion reactor, TMX, magnets, mech. design 78−58494
fusion reactor, TNS, electrical design costing 78−55014
fusion reactor, TNS, electron cyclotron heating startup system, design 80−99330
fusion reactor, Tokamak constant tension D-shaped coils, lateral support struct. 78−55013
fusion reactor, toroidal device with nonplanar mag. axis, magnet and coil engineering 78−55009
fusion reactor, toroidal field coil in-plane bending stress, struct. support design 80−106164
fusion reactor, torsatron, superconducting mag. engineering design 80−99297
fusion reactor, UWMAK-III, non-circular, Tokamak, power reactor design 77−74979
fusion reactor coil design, cost anal., for neutral beam magnets 78−55005
fusion reactor design and economics, confinement physics effects 78−50358
fusion reactor magnet coil, 125 kG, 1 m, design, fabrication 78−55008
fusion reactor neutral beam injection system cryopump, liq. He-cooled, for H_2 pumping 78−74495
fusion reactor RFC-XX, coil system, design, fabrication, testing 78−55007
fusion reactor solenoid, orthotropic, finite element stress anal. 78−55010
fusion reactor vacuum vessel, large, ultra high vacuum, design and manufacturing problems 80−99276
fusion reactors, Large Coil Program, superconducting mag. coil struct. design status 80−106189
fusion reactors, Tokamaks, maintenance design requirements and economics 80−99285
fusion reactors, ZT-40, reverse field pinch engineering prototype 80−102316
fusion-fission breeder reactor, supercond. poloidal field coil design 78−70640
gas turbine-HTGR system heat exchanger 78−739
glass fibre reinforced plastic panels, design for strength and stiffness 79−61601
head protective devices design, military 78−11793
heat exchanger design eqn., condensate film flow on finned surfaces 78−75038
heat-flux transducer, using artificially anisotropic thermoelec. materials 79−93136
high power industrial gas laser system design, 1 kW 77−19321
high temperature plant design methods, reference stresses and bounding theorems 80−58937
homopolar generator, fast discharge machine, design, fabrication, testing, for fusion reactor 78−54952
homopolar generator, radially stacked drum type, for Tokamak Ohmic heating coils 78−13337
homopolar machine, 10 MJ, fast-discharging, for fusion reactor 78−54950
implosion heating coil, radially fed, design, fabrication and appl. 78−55006
Incoloy 800, design codes and lifetime prediction aspects for nuclear and non nuclear appls. 79−47778
industrial machinery, noise reduction techniques appl. 79−18596
injector mixing chamber, steam-water flow 79−32635
instrumentation, innovation and business opportunity 80−98909
instrumentation design and development for space environment 78−4077
instrumentation systems, systematic design 78−24781
interdigital transducer design and component specification tradeoffs 77−27455
ion beam accelerator, multimegawatt, high-voltage power system, design philosophy, for fusion reactor 78−62613
jet, free, silencing, operational engineering principle *(French)* 79−32494
large flexible solar array design analysis and verification 79−96459
laser amplifier design using generalised experimental data 78−66836
maintenance-free water test stations, design aspects *(German)* 78−65403
materials science, life prediction and design, review 77−16475
mechanical ventilation systems noise control, design approach 78−42489
metals, engineering, multi-axial creep characts. 80−64398
MHD inductors with ring channels and DC exciting windings *(Russian)* 78−26347
mine concentrator X-ray on stream anal. system 78−35778
MW impulse generator system, for ion cyclotron heating, fusion reactor 78−70635
neutral beam, continuously operating, convectively cooled ion accelerator, mech. design and fabrication 80−102374
neutral beam, pulsed, arc (arc filament) power supplies, for fusion reactor 78−70637
neutral beam accelerator electrodes, spark discharge protection, for fusion reactor 78−62609
neutral beam injection vac. components, for fusion reactor 78−74493
neutral beam power supply, series switch/regulator system, 40 kV, 80 A, 10 ms, for fusion reactor 78−66366
nuclear power conf., Chicago, United States, July 1979 80−794

- **design engineering** continued
  - nuclear power plant design and operation, new security regulations in United States, impact 80—796
  - nuclear power plants, seismic design assessment 77—3179
  - nuclear power project, 480 V and 125/250 V auxiliary elec. unit design 77—3143
  - nuclear power stations, applications of multi-directional seismic inputs in the design of components 79—31238
  - nuclear power stations, turbogenerator overspeed protection, reliability study *(French)* 77—3156
  - nuclear powered artificial heart thermal oscillating pump 78—20317
  - nuclear reactor connector specification, performance, design and testing 77—23233
  - nuclear reactor containment structure design and service loads 80—106138
  - nuclear reactor containment structures, design and construction, ACI-ASME code of practice impact 80—798
  - nuclear reactor tank support ring *(German)* 77—42103
  - nuclear waste isolation plant design studies in USA 78—46151
  - numerical design of engineering structures and components, vital role of expt. stress anal. 79—32418
  - Ocean Thermal Energy Conversion platform environmental impact assessment 80—45726
  - open channel acoustic flowmeters, design, calibration and errors 78—55701
  - open channel acoustic flowmeters, design, meas. errors and operation 78—63516
  - optical fibre components selection for optical links in 1979 year of fibre optics *(French)* 79—37009
  - optical fibre system design charts 79—7200
  - pacemaker pulse generator design, manufacture and performance documentation for reliability 77—81715
  - particle accelerator, cathode plasma dispersion in transverse mag. field *(Russian)* 79—98997
  - photovoltaic systems, all component optimisation, theory and appls. 79—29475
  - poloidal field coil design and development of JT-60 Tokamak 79—31204
  - polymeric materials, vibration damping and control, design and meas. 78—87185
  - power plants noise control, objectives 77—75739
  - pulsed 20 tesla solenoid design for linear laser solenoid fusion reactor 77—35373
  - pulsed laser spectroscopic instrumentation 77—18105
  - pump design, gas-lift type, <8 mm riser dia. 80—10324
  - PWR, emergency core cooling system, fault-tree anal. and probabilistic evaluation methods 77—74976
  - PWR pressure vessel, novel design, advantages 77—79471
  - PWR pressure vessels *(German)* 77—42180
  - radiotelescope, for teaching, Jupiter bursts and quiet Sun obs. 80—17759
  - radome and backstructure design improvements 78—57449
  - reactor pressure vessel, advances 77—71640
  - reactor safety equipment, reliability in design 80—37555
  - refrigerator, closed-cycle, for supercond. electronic systems, design 78—93711
  - reversed field pinch, RFX constructional details 80—91277
  - ships, hull form evaluation by wake pattern analysis and compilation *(Japanese)* 79—27644
  - Shiva laser, 25 MJ energy storage and delivery system 78—55015
  - Shiva laser, 25 MJ energy storage and delivery system 78—59038
  - shrouded wind turbine, pilot plant design 80—66931
  - sI units in permanent magnet calculations 79—30406
  - solar collector, compound parabolic type, optical and thermal design 77—23735
  - solar collectors, parabolic cylindrical 77—23729
  - solar concentrators, paraboloid type with reduced wind drag 77—23731
  - solar domestic water heating systems, in Great Britain, design aspects 80—40835
  - solar electricity generating station design, Themis *(French)* 79—39290
  - solar energy closed loop systems, general design method 79—74542
  - solar heating systems for use in Britain, collector design aspects 80—35637
  - solar power satellite design and system engineering issues 79—96465
  - solar power satellite ground station rectifying antenna, basic design concepts 80—16782
  - solar radiation and wind power measuring instrument design 79—57404
  - solar stills, inclined-stage type, basic parameters determ. 80—89595
  - solar thermal collector, fixed, design optimisation 80—40905
  - solar thermal generating station design, engineering problems *(German)* 80—30381
  - solenoid windings, nonlinear eqn. for equal loading 79—55028
  - space antenna, self-deploying large parabolic antenna and array design 78—57450
  - spring, complex arch type, movable, snap-through action characts., appl. to microswitches 78—63339
  - spring, complex arch type, movable, snap-through action characts., microswitch appls. 78—63340
  - statically loaded structure design, limit load method *(German)* 79—50688
  - structural stress distrib. determ. by remote IR thermometry 80—87749
  - superconducting magnet cooling, optimal cryogenic gas flow 79—93149
  - systematic product related design procedures *(German)* 79—72649
  - thermal power station noise control, concepts 77—75738
  - thermal regenerator, with variable mass flow rate, computer model 78—75047
  - thermoelastic two-layer cylinder deform., rel. to microelectronic device manufacture 79—41561
  - thermoelectric coolers, heat load estimation curves 78—45613
  - toroidal field coil design and development for JT-60 Tokamak 79—31203
  - toroidal field coils, bending-free, for Tokamak reactor 78—55012
  - transducer, force measuring, EM, design and appl. *(Russian)* 78—16784
  - university engineering education courses economics 80—67973
  - US aperiodic piezoelectric sensor, fabrication and design problems 77—77713
  - US piezoelectric transducer for US imaging equipment 78—9525
  - vertical axis wind turbines 80—66929
  - vibration and pressure transducer design for nuclear reactor environment 78—823
  - Viking lander radar system mechanical design 78—57427
  - wave power convertor fully submerged model, design and experimental testing 79—92059
- **design engineering** continued
  - wind generator design, atmospheric turbulence structural influences 80—61247
  - CO_2 pulse laser discharge electric circuits parameters *(German)* 77—75473
  - $Cd_{0.2}Hg_{0.8}Te$ IR photoresistors/detectors, lateral geometry requirements *(German)* 79—93213
  - He-Ne, lasers, low-power low-cost design and manufacture 77—19329
  - N_2 high-power pulsed laser manufacture and reliability 77—19331
- **desk calculators** *see calculating apparatus; electronic calculators*
- **desk-top computers** *see minicomputers*
- **desorption**
  - adsorbed molecules, ratios between rates of thermal dissociation, desorption and diffusion 79—95265
  - adsorbed salt layers, field ion emission, field desorption and ionic cond. 77—16473
  - alkali halides, cluster ions and mol. ions in salt field desorption 80—40238
  - amino acid valine, heavy ion induced desorption, time-of-flight mass spectra anal. 80—54509
  - ATJ graphite, of H_2, H_2O, CO_2, CO and CH_4, ultrahigh vac. compatibility, outgassing characts. 79—81080
  - atom-surface one phonon scatt., 3-dimens., continuum model of thermal desorption 78—87860
  - atomic, classical theory of desorption rate vel. distrib., possibility of compensation effect 77—85068
  - atomically clean surface environment, confirmation using field electron emission 80—52250
  - biological membrane, egg yolk, freezing injuries, membrane destabilisation *(French)* 79—48221
  - breakthrough curves for adsorption-desorption, modelling using statistical moments 79—37916
  - Brownian particle, one-dimensional time-dependent escape problem 80—29278
  - charcoal, adsorbed fission gas release in spill accident 77—50262
  - chemical desorption theory, rates of reaction 80—71939
  - chemisorbed O_2 effects, CH formation 78—18902
  - chemisorbed species on solid surfaces, quantum-stochastic approach to desorption dynamics 80—66864
  - chlorophyll-a, hydration, field desorpt. mass spectral obs. 80—71936
  - cluster ions, field desorption, ion form. mechanism 79—15006
  - conference on solid-vacuum interface, Amsterdam, Netherlands (June 78) 79—42342
  - constructional materials, electron bombarded, gas evaluation obs. *(Russian)* 79—1460
  - cyclic hydrocarbons, chemisorpt. on W(100) surface, decomp., UPS and thermal desorpt. obs. 80—59782
  - damped oscillatory evaporation, of single crysts., empirical discussion 79—65327
  - desorption, electron stimulated, ion angular distributions, quantum scatt. theory 78—6221
  - diamond powders, of O_2, thermal desorpt. spectra 78—47661
  - dielectric solid surface breakdown in vac., desorption mechanism 78—67464
  - diffusion controlled processes, nonequilibrium decay effects 80—66764
  - diffusive release of gas from solid in presence of traps using linear tempering schedule 77—69187
  - dimethyl ether, condensed multilayers, electron bombard. effects, AES line-shape anal., XPS, and desorption meas. 80—7450
  - dissociatively chemisorbed molecules, desorption kinetics 79—86977
  - DNA, of water, thermal-stimulated press. and thermogravimetric anal. 80—8008
  - dynamic characts. of neutral particle desorption by surface ionisation voltage method 80—44426
  - EELS and concomitant surface anal. 80—7453
  - electrolyte aqueous soln. drops, ion emission due to laser heating 78—59063
  - electron and photon stimulated, from metal surfaces 80—75440
  - electron impact ionisation mass spectrometry using field desorption activated emitters as solid sample probes 77—90657
  - electron stimulated, ion angular distributions, quantum scatt. theory 78—6221
  - electron stimulated, LEED system 78—14567
  - electron stimulated, quantum theory 77—31892
  - electron stimulated, quantum theory 77—31893
  - electron stimulated, rel. to nondissociative chemisorption 77—85060
  - electron stimulated, reneutralisation 78—79894
  - electron stimulated, reneutralisation 78—84070
  - Electron stimulated desorption: a critical review 78—22958
  - electron stimulated desorption data, chemisorbed systems, reinterpretation in Auger decay model 79—42375
  - electron stimulated desorption ion ang. distrib. and three-dimens. model 78—26770
  - electron stimulated or photon stimulated, mechanisms 80—34301
  - electron-stimulated desorption ion imaging of adsorbate distrib. 80—103572
  - energy dependence and angle depend. desorption spectra, microscopic model 78—22954
  - enzyme reaction rate determ. by capacitance meas. 78—31997
  - epitaxial growth, vapour phase, growth mode characterisation 78—87885
  - epoxy, reinforced, outgassing rate in vacuum, control by pretreatment 79—40583
  - estuarine and continental shelf sediments, of ^{226}Ra, desorpt. flux 78—32061
  - fast ion induced desorption and collective electronic perturbation at the surface 80—10789
  - fast thermal desorption, adatom-adatom interactions 79—95256
  - ferrite, 350 NNI, for use in superhigh vacuum systems 80—108478
  - field desorption ion source for gas chromatograph-mass spectrometer *(Japanese)* 78—32920
  - field desorption mass spectrometry, analytical chem. uses 79—92015
  - field desorption mass spectrometry, appl. to biochemistry, medicine, and environmental science 80—35592
  - field desorption mass spectrometry of salts, emitter characts. and production 77—63980
  - field desorption mass spectroscopy, new sample supply technique 77—56279
  - field emission microscopy appls. 79—65982
  - field ion emission desorption, determ. of nanosecond high voltage pulse shape at emitter surface 77—12502

desorption continued
fission fragment induced desorption, method for correlated events in TOF mass spectrometry 78—58089
fission fragment induced mol. ions desorption, electrochemical surface pot. effect *(German)* 78—6228
fission-fragment induced mechanism, time of flight obs. 77—76674
flash desorption, phonon-mediated, quantum statistical theory 80—44410
flash desorption meas. from single cryst. surfaces, simple improvements 80—81360
flash desorption times, theory 80—15364
fusion reactor materials, D trapping, temp. depend. 80—37577
fusion technology, surface studies 80—23149
gas desorption from solid, two diffusion mechanisms 80—92784
gas-solid desorption, lattice motion effects, RRKM model 78—2367
general theory, surface-at. pot. determ. 77—62750
glass, gas content determ. by dynamic extraction method 80—61219
glow curves and desorption spectra anal. method 80—80053
graphite, CH_4 release, desorption study 79—51420
graphite, energetic ion sputtering, appl. of AES-SIMS (IMA)-FDS combined systems to physical and chemical processes 78—95636
graphite, of CO, CO_2, kinetics 78—60025
graphite, surface alteration by interaction with Ar^+ and Xe^+ beams, thermal desorpt. mass spectroscopy 78—91347
graphite, wall and limiter material for Tokamaks, induced desorption diffusion and gas production by 100 eV electrons and ions 79—675
graphite (0001), of Xe, kinetics using AES 77—72782
graphite (0001)/Xe system, isothermal desorption spectroscopy for 2-dimens. condensed phase obs. 77—69181
graphite fibre, Type-A, surface comp. and energetics 77—70024
graphite fibres, HM, surface comp. and energetics 80—54480
graphite monofluoride, surface alteration by interaction with Ar^+ and Xe^+ beams, thermal desorpt. mass spectroscopy 78—91347
heavy water production, by laser photodesorption 77—54365
heavy-ion induced desorption of organic cpds. from solid surfaces 80—100739
homogeneous surfaces, statistical mech. of collisions which lower desorption rate *(German)* 78—84072
hydrodynamic interfacial instability, mechanical, chem. and elec. constraints, review 80—34278
immiscible incompressible fluids, interfacial convective instability, diffusional exchanges, adsorption-desorption processes 80—70504
Inconel 600, fusion reactor vac. vessel, air, N, adsorpt., thermal desorpt., heat treatment effects 78—54880
Inconel 600, thermal outgassing after various surface preparations 79—67952
Inconel 675, wall and limiter material for Tokamaks, induced desorption diffusion and gas production by 100 eV electrons and ions 79—675
inert gas atoms, desorbing from solid surface apparatus for detection 78—32915
inert gas liberation in multiposition metallic reactor 78—59978
interstellar dust clouds heating due to molecules desorption from grains 77—9786
interstellar grains of molecules, max. temps. calcs. 77—49449
ion desorption by core hole Auger decay 78—48262
ion impact desorption 77—62758
ion trapping and gas release effects in cryst. lattices, thermal desorption spectrometry, review 77—43262
ions, photon stimulated desorption obs. 79—82459
IR (111) textured surface, O^+ desorption, electron stimulated, 300-1085K *(Russian)* 77—47672
isothermal desorption times, theory 80—15364
isotherms, and pore size distrib., adsorbate flow method meas. 77—80693
isotope effect in electron impact desorption of CO 77—55460
K-ramic^R, of H_2 and CO, ultrahigh vac. compatibility, outgassing characts. 79—81080
Kinetic theory description of electron stimulated desorption 78—14613
kinetics, heterogeneity effects *(German)* 79—51433
kinetics, Kramers-Langevin stochastic eqn., heavy-adatom limit, adatom-phonon coupling 78—84065
kinetics of two-dimens. phases on single cryst. substrate 78—14598
Kisliuk model for adsorption and desorption kinetics 79—73409
laser induced ionic desorption, Ge, Ni, KI substrates, mechanism 77—15686
laser stimulated desorption, quantum theory 78—79876
LEP, electron positron storage ring, vac. chamber, glow discharge surface cleaning 80—58010
lysozyme, sorption and desorption of water, thermal-stimulated press. and thermogravimetric anal. 80—8008
Macrotor Tokamak, laser-induced desorption of impurities from walls, spectral anal. 78—59681
membranes, linear laminated media, permeation, sorpt. 79—1966
metal, adsorbed O and CO layers, ion impact desorption, adsorption energy depend. 80—39442
metal, containing dislocations, thermal desorption of adsorbed atoms 78—47670
metal, fusion and evacuation after elec. contact treatment *(Russian)* 77—73365
metal, ion beam induced desorption of overlayers 80—59786
metal adsorbed layers on single crystal planes, kinetic investig. of structural changes and desorption, Au (111)/Bi^{3+} appl. 80—54500
metal oxides, thermodesorption of O_2, expt. technique *(French)* 78—64884
metal surface, atomic and mol. beam scatt., review 80—40203
metal surface, field desorption and field ionisation of Cs, H, and He 80—104047
metal surface, kinetics of adsorpt., desorpt. and migration, review 79—46921
metal surface, outgassing rate, upper bound 77—87773
metal tritide, ^{3}He detrapping and release after ^{3}H decay, strain model 77—60101
metal tritide, ^{3}He outgassing after ^{3}He decay, ^{3}H conc. effects 77—60100
metal-H_2 systems, determ. of absorption/desorption isotherms, high press. 78—51679
metal-H system, hydride formation in high press. range 80—65235
metal-metal contacts, use as prevention H escape from metals 80—24595
metallic surface, catalysed thermal desorption and dissoc. processes, microscopic theory 80—75439
metallic systems, rate equation for desorbing particles 79—46929
metals, chemisorption of gases, book 79—69370

desorption continued
metals, defect chemistry, He desorption spectrometry *(Dutch)* 80—96737
metals, of gas ions, ion collector for expt. investigation of absorpt. and reliberation 79—99254
metals and alloys, segregation studies by imaging atom probe microscopy 80—66911
methanol, condensed multilayers, electron bombard. effects, AES line-shape anal., XPS, and desorption meas. 80—7450
mica, of propylene from isomerisation of cyclopropane 79—74376
microscopic models of desorption spectra 78—71946
microsurfaces, obs. using thermal desorption spectroscopy combined with TEM and transmission electron diffr. 79—90888
mineral surfaces on Mars, photodesorption and effects on atmospheric stability 78—7903
Mischmetal-Ni alloy, H_2 adsorption and desorption *(Japanese)* 77—47668
mischmetal-Ni-Al alloys, H_2 absorpt.-desorpt. characts. 79—95168
Mischmetall-Co_5, absorpt.-desorpt. characts. for H_2 77—89640
mobile physically adsorbed layer, dynamics 79—95271
molecule desorption and surface diffusion from critical deposition rate 80—92786
monolayer, Brownian motion of particles near free surface 80—54503
monolayer desorption kinetics at air-water interface, humidity effects 79—52770
multicomponent systems, absorbent surfaces, Langmuir kinetic theory, laser rate equations 79—99407
multilayer insulation materials, ambient temp. outgassing rate 80—84370
multiphonon processes, quantum-statistical theory 80—107641
neutral molecule desorption in storage rings 79—76213
non-isothermal, approx. kinetic relation describing diffusion *(French)* 79—90864
one- and two-step mechanisms of desorption kinetics 79—46958
oxides, slow-electron-stimulated desorption 79—60623
peak width of a first or second order desorption transient for an arbitrary temperature sweep function 78—14614
phonon energy transfer model Hamiltonian in gas-solid interactions 80—34307
phosphatidylcholine hydration, adsorpt.-desorpt. isotherm and PMR 78—15781
phosphonium cations, quaternary, produced by field desorption, collisional activation spectra 78—56946
phosphosilicate glass, AES quantitative anal., electron irrad. induced surface comp. changes 77—48709
photochemistry and photodesorption, isotope separation aspects 78—64863
photodesorption, review 79—51424
phthalocyanine-dodecane interface, photostimulated charge transfer flash expt., trapping model 77—66182
plasma etching, mech., review 79—83348
PLT Tokamak vacuum vessel, residual gas and surface comp. changes with H_2 discharge cleaning 79—80631
polyacetylene:AsF_5, thermal decomp. kinetics, elec. cond., ESCA and mass spectra 80—50830
polyatomic ions, thermal desorption lifetime and kinetic characts. determ. 79—11018
polymer, volatile constituents anal. by thermal desorpt., gas chromatography and mass spectrometry 79—43664
porous material, outgassing, area/vol. config. influence 80—84371
positive ion photoemission, vacuum UV quantum yield limit 78—79896
precursor intermediates, desorption kinetics 78—87876
precursor intermediates in adsorption, desorption and reaction 80—108731
protein monolayer desorption 77—85053
proteins, on polymer surfaces, structural changes 80—89712
pulsed laser light stimulated desorption and local vaporization 77—16432
pulsed surface flashover mechanism involving electron-stimulated desorption 80—70055
pyrocarbon, desorption of D, activation energies 79—65330
rare earth-Cu double oxides, temp. programmed desorption experiment 79—66350
rare earth-transition metal intermetallic, H_2 desorption isotherms depend. on d-bandfilling 78—18912
refractory filament, temp. control method for thermal desorpt. expts. 79—9215
refractory materials, emission and adsorption props., rel. to electronic struct., review 77—76899
refractory metals, heat of desorption of alkali metals 80—75430
relaxation time approach limitations 80—93795
semiconductor, photodesorption, role of C 77—36787
short-lived large energy fluctuations, semiphenomenological collective treatment, Arrhenius approx. 78—43168
silica gel regeneration by adiabatic desorption mathematical model 79—1967
silicone rubber, RTV 560, diffusion of outgassing species, kinetics data 79—15010
single crystals, nonstationary evaporation phenomenological model 79—65328
solid surface, mol. dynamic processes interaction with laser radiation 80—71943
solid surface in localised physi-sorption, gas desorption times, local or nonlocal surface pot. calcs. 80—54499
solid surfaces, surface processes, and solid/gas interactions 80—73125
solute transport in soils, two-site adsorption-desorption model evaluation 77—41101
Spheron 6, surface group obs. using gaseous reagents, surface acidity evolution during heat treatments *(French)* 77—66767
sputtering, non-elemental solid surface, surface composition, yields, desorption effects, review 77—44111
stainless steel, gas desorption coeffs., electron- and ion-induced, bakeout temp. effect 79—65329
stainless steel sample, exposed to ISX and PLT plasmas, field desorption and field ion surface studies 80—34295
steel, stainless, 321 and 304, D implanted, thermal desorption and bombardment induced release 78—95072
steel, stainless, D implanted, thermal desorption 78—71750
steel, stainless, electron-bombardment surface prep. for Princeton Large Torus 77—59957
steel, stainless, gas liberation, 20°C, surface oxide effects *(Russian)* 80—3286

desorption continued
steel, stainless, gas liberation in vacuum, depend. on oxidation process *(Russian)* 80—25901
steel, stainless, ion and electron desorption of neutral molecules from type 304 79—83507
steel, stainless, ion induced release of trapped D 78—95095
steel, stainless, multilayer desorption meas. using heat of vaporisation spectrometer 79—82453
steel, stainless, O_2 desorpt. during laser irrad., etching, AES study 80—66338
steel, stainless, type 304, electron stimulated desorption rel. to CTR first wall appl. 78—51818
steel, stainless, type 316L, thermal outgassing properties 80—18649
steel, stainless, vacuum components, pre-vacuum surface finish influence on electron stimulated desorption in ultrahigh vacuum 80—57320
steel, stainless, wall and limiter material for Tokamaks, induced desorption diffusion and gas production by 100 eV electrons and ions 79—675
steel, stainless, X-ray induced desorption of gases from surface 77—35813
stochastic description of desorption rates 77—20184
sulphonium cations, tertiary, produced by field desorption, collisional activation spectra 78—56946
surface, adsorbed atoms thermal desorption, one dimens. microscopic model, weak binding case 80—96729
surface analysis, electron probe methods, AES, electron stimulated desorpt. 77—44098
surface analysis, scanning electron stimulated desorption 78—34700
surface bonding and kinetics, desorption methods 77—62746
surface charge state change during thermodesorpt. 77—80825
surface contamination, anal. using mass spectrometer system with laser heating 79—87903
surface interaction with adsorbed molecules, desorption 77—31874
surface layers, photon induced ion desorption, surface atom core ionisation, Auger decay 80—59809
surface processes, interatomic forces, theories 80—107632
Teflon, surface alteration by interaction with Ar^+ and Xe^+ beams, thermal desorpt. mass spectroscopy 78—91347
temperature programmed desorption with reaction 80—6621
thermal, generalised Langevin theory for surface dynamics 78—60024
thermal desorption, effect of temp. gradient along sample 77—62735
thermal desorption, theory 79—86976
thermal desorption and dissociation catalyzed by a solid surface 80—108734
thermal desorption kinetics, influence of weakly bound intermediate states 77—59214
thermal desorption mass spectra, activation energy, rate coeff., analytic expressions 78—60022
thermal desorption mass spectra, effect of heating rate and pumping speed, quantitative anal. 78—60023
thermal desorption mass spectrometry, effect of time delays 79—19466
thermal desorption mass spectroscopy, computer control, data acquisition, appls. 80—61181
thermal desorption model analysis *(German)* 78—63940
thermal desorption of gases from solid surfaces, quantum dynamical model 78—26762
thermal desorption spectra, effect of vacuum system time consts. 78—22960
thermal desorption spectroscopy, reaction order 77—31895
thermal desorption theory for catalyst surfaces 80—26052
thermal desorption with large variable friction constant 78—71974
thermal desorption with small friction constant 79—15012
thermal evolution spectra, difficulties of interpretation 80—34318
thermal-description kinetics, processing of experimental data with Promin-2 computer 79—67267
thermodesorption, temp. control device *(German)* 78—86251
time dependent escape rate from potential well 78—79888
transient ion desorption, work function, evap. rate, ion heat of adsorption 77—20198
transition metals, chemisorption of H, O and CO, interpretation of electron stimulated desorption spectra 78—2378
trapping and diffusion of particles near surface, attachment of mobile particles to non-saturable traps, theory 80—39417
two-dimensional condensed phases, isothermal desorption spectroscopy 77—69181
vacuum greases, vapour emission characts. 78—21147
vacuum system, press. due to adsorbed mols., upper bound 77—67446
vacuum system construction material selection and degassing 80—82783
valine surface, heavy-ion induced desorption of organic cpds. 80—100739
W, electron stimulated desorption of H^- from chemisorbed H_2 79—86999
W, oxidised polycryst. kinetics 78—75939
water, condensed multilayers, electron bombard. effects, AES line-shape anal., XPS, and desorption meas. 80—7450
WO_3, (100) and (111) layers, electron stimulated desorption of O^+, LEED obs. 79—23840
zeolite-water desorption, complex reaction interphase boundary kinetics 79—57203
Ag (110), adsorption, O_2-induced, and reaction of H_2, water, CO, and CO_2 80—55714
Ag (110) surface, adsorption of mol. O_2 species 80—103578
Ag (110) surface, clean and Na dosed, of NO, surface reactivity and chemisorption 77—31882
Ag (110) surface, of Na and Na+O_2, LEED and AES meas. 77—31883
Ag (111), adsorpt., coadsorpt., and reactivity of Na and NO 78—38948
Ag (111), adsorpt.-desorpt. props. and surface struct. chem. of Cl 77—89648
Ag (111), clean or Na-covered, adsorpt.-desorpt. props. of Br_2 78—38944
Ag (331), adsorpt.-desorpt. props., coadsorpt. and surface struct. chem. of O_2 and Cl_2 78—34711
Ag, adsorption and surface reaction of formic acid 80—40741
Ag, adsorption of pyridine, UPS, AES and flash desorption meas. 80—92776
Ag, field desorbed ions, appearance pots. 79—24417
Ag island films, on W, growth and desorption kinetics, mass spectra obs. *(German)* 79—46978
Ag, mass analysed thermal desorption spectra of O_2-CO coadsorbed complexes 77—60121
AgI, of H_2O, activation energy meas. 77—52212
Al, adsorption and decomp. of methanol, UPS, XPS and thermal desorption obs. 79—82441

desorption continued
Al alloy, 6061, vacuum material, desorpt. of neutral mols. by electron and ion bombardment 78—95229
Al alloy, gas desorption coeffs., electron- and ion-induced, bakeout temp. effect 79—65329
Al alloy 6061 79—675
Al, bulk and plasma-sprayed coating, D_3^+ trapping meas. 80—20754
Al foil, sputtering with ^{252}Cf fission products, desorbed secondary ions 78—68596
Al, propane adsorption SIMS and EID obs. 77—69167
Al sputtered film, effects of sputter etching and process technology on props. 79—83122
Al, thermal desorption of oxide film, influence of grain boundaries and recrystn. 80—61023
Al_2O_3 $(10\bar{1}2)$ surface, effect of multiple binding states on desorption and decomposition of Ga_2O 78—44406
η-Al_2O_3, chemisorption of propylene, desorption and D exchange obs. 78—51827
Al_2O_3 film pore size distribution meas., adsorpt.-desorpt. vs. TEM methods 77—74357
Al_2O_3, X-ray induced desorption of gases from surface 77—35813
β-Al_2O_3-Na_2O, thermal desorption of ions 77—7973
Ar, solid, desorption heat capacity of adsorbed ^3He 80—10735
Ar, solid, of He, appl. of simplified continuum model 78—87860
Ar surface, spin aligned condensed atomic H 78—63929
Au, energy and mass spectra of scattered 8 keV Ar^+ ions and desorbed species 77—32487
Au film, on W substrate, chemisorbed N_2 effect on crystallite growth, FEM obs. 79—46976
Au film growth on Mo (110) surface, AES, LEED, thermal desorption study 80—80130
Au, X-ray induced desorption of gases from surface 77—35813
B_xC_y, desorption of D, activation energies 79—65330
$B_xP_yO_4$, temperature programmed desorption, depend. on P/B ratio 79—23828
Ba, desorption from river-borne sediments in Hudson estuary 79—79877
$BaTiO_3$ polymorph, hexagonal, low temp. and surface CO_3 adsorption and desorption 80—80713
Be film, on W (110), growth mode, work function, thermal desorption, and struct. 80—75477
BeO, exoelectron emission from hydrated and dehydrated surfaces 80—11545
BeO, radiation induced detrapping of implanted D by ^3He and proton irradiation 80—32482
BeO, thermally stimulated exoelectron emission, influence of desorption processes 77—85906
Bi film, deposition props. on specially prepared substrate, desorption energy and surface diffusion 79—90917
Bi^{3+} monolayers on Ag(111), two-dimens. phase formation, desorption obs. 77—15680
C, activated, surface oxidised, of organic vapour, paramag. props. 77—32238
C, activated and impregnated, adsorption and desorption isotherms of phosgene and chloroform 77—70333
C, chemisorbed oxygen surface complexes, thermal desorpt. analysis 78—56032
C, of H, astrophysical system, appl. of simplified continuum model 78—87860
C, partially graphitised, K intercalation-desorpt. cycle rel. to stacking faults 78—47396
C/Pt-W (8 wt.%), desorption of K from C film surfaces 80—59784
CLi_3, desorption from graphite expt., ionis. pot. 79—34392
CO, adsorbed on Pd (210), inclined bonding config., electron stimulated desorption and LEED obs. 80—39430
$CaCl_2$, cluster ions and mol. ions in salt field desorption 80—40238
Cd film, deposition props. on specially prepared substrate, desorption energy and surface diffusion 79—90917
CdS, of chemisorbed species, influence of surface states on absorption edge 77—16344
CdS, of O_2, electron beam induced, AES meas. 79—77921
CdS, of O_2, photostimulated desorption temp. depend. 80—24737
CdS, thermal desorption of O_2, photopot. and surface pot. changes 77—11795
CdS-O_2, photoactivated O desorption 80—100391
CdSe, O_2 desorption by laser irradiation *(Russian)* 77—55462
CdSe, of O_2, photostimulated desorption temp. depend. 80—24737
CdSe-O_2, photoactivated O desorption 80—100391
Ce-Ni, hydriding characts., applicability for H_2 storage material 78—83955
$CeCo_5$, adsorption and desorption charact. of H_2 *(Japanese)* 77—47667
$CeNi_4Al$, mag. susceptibility, H adsorption-desorption cycle effects 80—107990
Co (0001), adsorption and reactivity of NO, LEED, AES, and thermal desorption study 80—80090
Co $(10\bar{1}2)$, struct. and CO chemisorption obs. 79—4474
Co, adsorption-desorption kinetics of CO, surface carbide form. effects 80—103574
Co film, evaporated, of H_2, surface pot. meas. 77—31890
Co film, texture and adsorption of CO *(German)* 77—24485
Co, pure surfaces, adsorpt. of water and decomp. *(German)* 80—26054
$Co_{56}Ga_{44}$, thermal release of injected He 77—31881
Cs desorption from graphite, release in nucl. reactor coolant 80—18431
Cu (110), O adsorption, low-energy ion bombardment investigation 80—34302
Cu (110) surface, oxidation of formaldehyde, temp. programmed desorption meas. 79—87878
Cu (111), adsorpt.-desorpt. props. and surface struct. chem. of Cl 77—89648
Cu (111), chemisorpt, of CO on differently prepared surfaces 78—6223
Cu (111) surface, negatively biased, positron impact, positronium form 80—35024
Cu, adsorption and desorption of water vapour, relative humidity effects 80—49505
Cu, adsorption and surface reaction of formic acid 80—40741
Cu film, partially oxidised, oxide removal and O_2 desorption on vac. annealing 77—12738
Cu films on Ru (0001), growth, struct. and electronic props. 79—77958
Cu foil, sputtering with ^{252}Cf fission products, desorbed secondary ions 78—68596
Cu, gas desorption coeffs., electron- and ion-induced, bakeout temp. effect 79—65329

desorption continued
Cu, of Ar, H_2, CO and methene, production and meas. of atomically clean surface environment 80−52250
Cu, of NO, species identification, struct., dissoc. chemisorption, desorption, UV photoelectron spectroscopy 78−52635
Cu surface, (110), methanol adsorption, XPS, UPS and thermal desorpt. study 80−84388
Cu, surface, electron stimulated desorption, glow discharge treatment 79−65964
Cu surface, fast D_2 desorpt. mechanism, time-of-flight spectra 80−84379
Cu-Ni (110), adsorption of CO and H_2, UPS, thermal desorption, AES,and LEED study 80−80087
Cu-Ni alloy, of CO and H_2, long and short range electronic effects in bonding 77−7974
Cu-Ni alloy surfaces, chemisorption of CO, LEED, AES, thermal desorption, and work function meas. 79−90879
Cu-Ni alloys, surface comp. and catalysis, AES and thermal desorption meas. 79−46898
CuO, desorpt. of ions by low power laser beam 80−80092
Cu_2O, adsorption and desorption of water vapour, relative humidity effects 80−49505
D, thermal desorption meas. of H-isotope retention in Alcator-A Tokamak 80−79588
$DyFe_3$ hydrides, desorption isotherms 80−103565
$DyFe_2H_x$, thermodynamic props., H_2 desorption isotherm meas. 80−89516
$ErFe_2H_x$, thermodynamic props., H_2 desorption isotherm meas. 80−89516
$ErT_{1.8}$, ^3He thermal desorption, comparison of aged and ^4He implanted samples 77−60102
Fe (100), adsorption of Br_2, AES, LEED, work function, and thermal desorption study 80−15375
Fe (100), adsorption of carbon tetrachloride, AES, LEED, work function, and thermal desorption study 80−15376
Fe (100), adsorption of Cl_2, AES, LEED, work function, and thermal desorption meas. 79−82465
Fe (100), adsorption of I_2, AES, LEED, thermal desorption, and work function study 80−15374
Fe (100), adsorption of tetrabromomethane, AES, LEED, work function, and thermal desorption meas. 80−39422
Fe (100) and (111) surfaces, chemisorption of CO, CO_2, acetylene, ethylene, H_2 and NH_3, LEED and thermal desorption 78−71996
Fe (110), adsorption and decomposition of ammonia, LEED, AES, UPS, work function and desorption meas. 79−69345
Fe (110), K promoted, adsorption of CO, UPS, XPS, AES, and flash desorption obs. 79−82463
Fe, adsorption and surface reaction of formic acid 80−40741
Fe desorption of H into ultrahigh vac. system, using permeation cell 80−86326
α-Fe, of He, computer simulation calc. of interaction with C impurities 79−99235
Fe, of $O_2(N_2)$, surface anal., XPS appl. 79−24875
Fe surface, (111) and (100), adsorpt. and decomp. of NH_3 78−40077
Fe surface, form. and decomp. of nitrides 79−24831
Fe surface, H_2 chemisorption LEED, UPS, thermal desorption spectroscopy, work function meas. 78−14566
Fe surface, N atom recomb., vibr. energy of desorbing N_2, electron beam induced fluoresc. 80−61149
Fe-Ti, D storage, desorption isotherm and struct. study by neutron diffr. 79−1549
$FeTiD_x$ $(0 \leq x \leq 1.9)$, structural phase transitions, absorpt. and desorpt. isotherms 80−19948
Fe(100), of CO and H_2, C, O, S and K adlayer effects 80−71573
GaAs (100), of Sb, AES obs. 80−80074
GaAs (110), of alkali halides, adsorpt.-desorpt. processes and phase transitions in adsorbed layers 78−2361
GaAs {100} surface, interaction kinetics of As_2 and Ga 77−60115
GaAs, adsorpt.-desorpt. of Zn, thermal desorpt., at. beam adsorpt., AES, SEM, RHEED 78−14591
GaAs, adsorption of O_2, adsorption states and Ga depletion, UPS, AES, and thermal desorption meas. 79−46952
GaAs, oxide film influence on adsorption and electrophys. props. 79−42369
GaAs, single cryst., adsorbed mol. lifetimes and desorption activation energy meas. 78−20072
GaAs(P), adsorption and field-desorption of O_2 and Au, FEM studies 80−34304
GaAs(111), O bonding, thermodesorption and ESCA meas. 77−86206
GaP (100), prep. of negative electron affinity surface by Cs adsorption 80−10768
GaP, (100) surface, thermal desorption props. of Cs and Cs-O adsorbed layers *(Japanese)* 80−15368
GaP, adsorption and desorption of Cs, LEED, AES, and photoemission meas. 80−70532
GaSb, adsorption and desorption of Cs, LEED, AES, and photoemission meas. 80−70532
Ge (111), adsorption of K and Cs, effect on surface elec. props. 79−90880
Ge (111), desorption kinetics of two-dimens. condensed phases of Ag 79−90882
Ge (111) of K and O_2, rel. to work function, K thermodesorpt. spectra 78−79874
Ge (111) surface, clean, O_2 adsorption rate and electron work function 80−59779
Ge, adsorption-desorption kinetics of H_2, O_2 and other gases, catalysis 77−47684
Ge film, elec. resist., long term stability rel. to ambient atmosphere changes 78−2597
a-Ge, Ge-O removal in pre-crystallisation annealing 78−9957
Ge, of reaction products with S vapour kinetics 78−35718
Ge:H, amorphous, H content determ. by IR absorpt., gas evolution and nuclear reaction methods 80−44130
H adsorption and desorption, self-consistent model calc. 79−46943
H from metal hydride beds, hydride conversion and storage system chemical heat pump 80−72077
H_2 absorption and desorption kinetics in $LaNi_5$-type ternary alloys 80−55932
H_2, effects of method of return to atm. press. for pressure vessel *(French)* 80−42233
H_2 sorption/desorption by ternary $LaNi_5$ type alloys, reaction kinetics 80−45813
desorption continued
H_2 surface, spin aligned condensed atomic H 78−63929
H_2O, effects of method of return to atm. press. for pressure vessel *(French)* 80−42233
H_2O, on Pt(111), identification of adsorbed OH species 80−49509
He desorption spectrometer, clustering of Kr in W (100) obs. 80−77908
He thermal desorption, attachment of mobile particles to non-saturable traps 80−39418
^3He, adsorbed monolayers on solid Ne, desorption heat capacity 79−51383
^3He, specific heat second layer adsorbed on Grafoil 78−87843
^4He films adsorbed on graphite, transition temp., entropies, internal energies and heats of desorption, vapour press. meas. 80−2238
Hf-H, diffusion in hydride phase, exam. 80−29204
In, epitaxial growth and desorption on W tips, high field microscopy obs. 79−69380
In film, $\sqrt{3}$ and $\sqrt{31}$ submonolayer superstructures on Si (111) isothermal desorption, RHEED meas. 79−86992
InSb, irrad. real and clean surfaces, work function 78−95336
Inconel 600 and 718, gas desorption coeffs., electron- and ion-induced, bakeout temp. effect 79−65329
Ir (100), of acetylene, benzene and ethylene, geometric and electronic effects 77−55457
Ir (110), adsorption of CO, O_2, H_2, N_2, ethylene and benzene 78−38961
Ir (110), adsorption of CO and reaction with O_2, transient study 80−30284
Ir (110), chemisorption of O_2, AES, LEED, thermal desorption mass spectra, and contact pot. difference meas. 79−77901
Ir (110), of CO, coverage dependence of kinetic parameters 79−19462
Ir (110), of H, thermal desorption mass spectrometry, order plots 80−44409
Ir (111), of Ba, conc. depend. of kinetic characts. of thermal desorption 78−2377
Ir (111) surface, chemisorption of O_2, dynamics, thermal desorption mass spectrometry meas. 77−59211
Ir, (111) surface, decomp. of hydrazone, N_2 emission, ang. depend. 80−97731
Ir (111) surface, electron beam induced desorption and dissociation of chemisorbed CO 78−56043
Ir, (111) surface, flash desorption spectra of NO, recombined mol. identification 79−86996
Ir, adsorbed gases, field desorption from field ion tips 80−59793
Ir, adsorption and condensation of Sm, thermal desorption mass spectra and thermionic emission meas. 79−69362
Ir, adsorption of H_2 and O_2, surface reaction, thermal desorption and FEM obs. 79−52774
Ir, chemisorption of H_2, adsorption and desorption kinetics, struct. of overlayer 80−84367
Ir covered with graphitic monolayer, Ba film growth, thermal desorption meas. 78−26791
Ir, of chemisorbed H_2 and hydrocarbons, LEED, AES meas. 77−1297
$KNbO_3$ catalysts, ferroelectric, for reactions involving CO and NO , and adsorption of NO 80−30282
Kr, on partially oxidised Gd-Co film 80−3439
Kr, solid, of He, appl. of simplified continuum model 78−87860
La-Ni, hydriding characts., applicability for H_2 storage material 78−83955
LaB_6, high temp. interaction with 0_2, AES and mass desorption expts. 80−7698
LaB_6, polycrystalline, negative surface ionisation of I atoms, negative ion desorption heat 79−78848
$La_{0.9}Eu_{0.1}Ni_{4.6}Mn_{0.4}$, absorption-desorption props. of H_2, degradation mechanism, Mossbauer study 80−88431
$LaNi_4$, absorption and desorption of H_2 77−81400
$LaNi_5$, adsorption and desorption charact. of H_2 *(Japanese)* 77−47667
$LaNi_5$ hydrides, of H_2, 4.2K paramag. susceptibility 80−70934
$LaNi_{5-x}Al_x$, H_2 absorpt.-desorpt. kinetics rel. to metal hydride appls. 77−86308
$La_7Ni_3D_2$ storage material, neutron, X-ray diffr. study 78−83954
$La_xNi_yH_z$, thermokinetics of H evolution 80−30593
LiF, of ^4He, comparison with quantum statistical theory of flash desorption 80−44410
Mg film, deposition props. on specially prepared substrate, desorption energy and surface diffusion 79−90917
MgO, catalytic behaviour, rel. to XPS obs. 79−24820
MgO, light emission during adsorpt. and desorpt. of O_2 78−38949
MgO powder, decomp. of chemisorbed ethanol, propanol and acetic acid 78−92502
MnO_2 coated Al_2O_3 and SiO_2 supports, N adsorption obs. of dispersion modes 80−81363
Mo (100), adsorption of O_2, AES, LEED, work function, and desorption meas. 80−6654
Mo (100), adsorption sites of CO, electron stimulated desorption and LEED meas. 80−49516
Mo (100), chemisorption of O, Cs submonolayers effect on electron stimulated desorption of O^- 79−86991
Mo (100), early stage condensation of Cu and Ag, comparison with W (100) 80−80072
Mo, (100) surface, O-covered, electron-stimulated desorption of O^+ and O^- ions 79−82444
Mo, chemisorption of CO, low energy SIMS and electron impact desorption expts. 78−38941
Mo, desorption kinetics of halogens, pulsed ion beam method 80−34300
Mo, electron stimulated desorption of negative ions from adsorbed gases 78−91549
Mo film, cc preparation by H_2 reactive sputtering, thermal desorption meas. of H content *(Japanese)* 79−95929
Mo, of He, during stage III annealing, vacancy model 77−1123
Mo, of He, Mo-He and He-He interaction pot. 79−19459
Mo, photodesorption of CO forming CO_2 79−52777
Mo surface, desorbed molecules, ang. distrib. using directional detector 79−80626
Mo, surface, electron-stimulated desorption of negative ions, work function 78−72654
Mo, thermal desorption of CO, effect of temp. gradient along sample 77−62735
Mo:C (110) surface, segregation, precip. and desorpt. of C, AES and LEED study *(French)* 80−103480
Mo:N single cryst., interaction of N with vacancies 79−82261
Mo-He and He-He Born-Mayer interaction potentials derived from He desorption expts. 79−99409

desorption continued
MoO_3, adsorption of water, temp. programmed desorption 79—77898
NI chemisorption of H_2, isothermal desorption near Curie temp., rate meas. 80—29268
Na (111) surface, epitaxial film, electron induced dissociation 80—6646
Na atoms, desorbed, ang. and velocity distrib. 80—75428
NaCl, deform. process, exoemission and desorption meas. *(Russian)* 78—75708
NaCl:Ca, single cryst., vaporisation kinetics meas. 78—18763
$(Na_2O)(Al_2O_3)x(SiO_2)$, zeolites, thermonic emission of alkali ions, desorption mechanism 79—4887
Na_xWO_3, x=0.6 and 0.8, surface characts. 80—39392
Nb, adsorbed H distrib., electron-stimulated desorption ion imaging 80—103572
Nb, desorption kinetics of halogens, pulsed ion beam method 80—34300
Nb, of O_2, electron-stimulated desorption study 79—11017
Nb-O solid solutions, of oxides *(French)* 78—14610
Ne, solid, adsorbed ^{3}He, desorption heat capacity 79—4452
Ne, solid, desorption heat capacity of adsorbed ^{4}He 80—10736
Ni (100), chemisorption of NO, LEED, AES, UPS, and thermal desorption study 80—39449
Ni (100), dissociative chemisorption and mol. adsorption of NO 80—65373
Ni (100), interaction of adsorbed H_2, CO, and methanol, temp. programmed desorption study 80—66876
Ni (100) and (110), reaction of acetylene, room temp., UPS expts. 80—61151
Ni (100) surface, adsorption of H_2, LEED, work function meas. and thermal desorpt. obs. 79—23843
Ni (100)-p(2×2)C surface, H_2, CO and $C0_2$ and decomp. of formic acid 79—91995
Ni (110), adsorption of CO and CO_2, electron bombard. effects, AES and electron stimulated ion desorption obs. 79—51430
Ni (110), chemisorption of N_2, mol. and dissociative mechanisms 80—39431
Ni (110), effect of surface O on catalytic and chemisorptive behaviour, flash desorption meas. 77—85066
Ni (110), NO chemisorption and dissoc. 77—15695
Ni (110) surface, ion impact desorption of O_2 by ion scatt. 77—35805
Ni (111), adsorption sites of CO using IR reflection-absorption spectroscopy and thermal desorption spectroscopy 79—69355
Ni (111), adsorption sites of CO, LEED, AES, thermal desorption, work function, and IR system meas. 79—77903
Ni (111), CO desorption preexponential factor 80—49515
Ni (111), chemisorption and reaction of NH_3, LEED, desorption and photoemission expts. 80—59799
Ni (111), chemisorption geometry of H, LEED, thermal desorption, and work function meas. 80—39433
Ni (111), dehydrogenated adsorption of ethylene, thermal desorption and AES study 80—29274
Ni (111), isothermal desorption of CO, UPS study, time-resolved approach 80—39440
Ni (111), of methanol. methanol, UPS and flash-desorption exam. 77—55455
Ni (111) surface, adsorption of Cl, LEED, AES, work function and flash desorption meas. 77—85069
Ni, (111) surface, S free and covered, D_2 desorption, ang. depend. of flux, mean energy and speed ratio 79—86993
Ni (111) surface, with O_2, Se, S and Te adsorbed layers, bonding geometry and electronic struct. 79—77909
Ni, associative desorption of NO 80—54512
Ni, chemisorption of O_2 and CO, ion bombard., particle ejection, SIMS obs. 79—78810
Ni, clean, chemisorpt. of S-containing alkanes, XPS and thermal desorpt. with mass spectrometric anal. 78—14595
Ni, deposited, on stress-annealed pyrolytic graphite, binding, thermal desorption spectroscopy 77—59210
Ni foil, sputtering with ^{252}Cf fission products, desorbed secondary ions 78—68596
Ni, H and CO adsorbates, ion impact desorption of atoms and molecules by low energy ion scattering 79—4883
Ni, of ^{3}He, low temp. release 80—34294
Ni, of CO, comparison of surface anal. methods 79—8213
Ni, of H_2, activation barrier with holes model 77—80697
Ni, of H_2, desorption kinetics, rate equations 79—82448
Ni, of H_2, HD and D_2, vel. distribs. 77—43431
Ni, of O, ion impact desorption 77—62758
Ni, polycryst., O_2 interaction obs. 78—76568
Ni, polycryst. and single cryst. surfaces, ang. distribs. of CsCl restituted to gas phase 80—6626
Ni, reaction of H_2 and O_2 on polycryst. surface, SIMS and thermal desorption meas. 80—40742
Ni surface, adsorbed CO and H_2 layers, laser induced desorption expt. 79—1548
Ni surface, adsorpt. and decomp. of formic acid, obs. using combined SIMS-FDS-AES system 78—40076
Ni surface, coverage and desorption of CO flash desorption spectrum 80—49493
Ni surface, polycryst., interaction with O_2, SIMS and flash filament meas. 79—47829
Ni surface, polycrystalline, adsorbed S, H_2^+ ion induced desorption 78—84069
Ni, trapping and release of inert gases, thermal evolution mass spectrometry 78—95077
Ni:Kr gas trapping and release, thermal evolution mass spectrometric study 80—34026
Ni/SiO_2, of NO, 200 to 400K *(German)* 78—30835
βNiH, decomposing, α-phase precipitate detection by Bitter powder pattern 79—28104
NiH_x, of H_2, effect of hydrogenation on fine struct. of polycryst. Ni 78—59950
Ni(100) and (111), of H, preexponential factors 79—46918
Ni(100)(2×1)C surface, of D_2, kinetics, LEED and AES meas. 77—47683
Ni(111), adsorption of acetylene, evolution of adsorber species, rel. to vibr. spectra 78—95952
O adsorbed layer on Cu (100), ejection by ion bombard 79—42373
O_2 adsorbed layer on Cu (100), ejection by ion bombard. 79—42373
O_2 desorption from Nb in a vacuum, thermodynamic props. calcs. *(Russian)* 80—54501

desorption continued
O_2 desorption from Ta in vacuum, thermodynamic props. calcs. *(Russian)* 80—54501
P, amorphous thin film, room temp. cond. after desorption of moisture on film surface 79—24011
P transport through sandy soils, nonlinear reversible adsorption-desorption model 77—66940
Pb film, deposition props. on specially prepared substrate, desorption energy and surface diffusion 79—90917
Pb monolayers on Cu stepped and low index surfaces, LEED, AES and desorption anal. 79—46942
PbS, of SO_2, optical excitation meas. of trap charging *(Russian)* 78—76180
$Pb_{0.8}Sn_{0.2}Te$ surfaces, oxidation in air and thermal desorption, XPS and LEED meas. 79—47830
PbTe surfaces, oxidation in air and thermal desorption, XPS and LEED meas. 79—47830
Pd (111), adsorpt. of NO, LEED, UPS, and thermal desorpt. expts. 77—69179
Pd (111), adsorpt. of O_2 and NO, LEED, photoelectron spectra and thermal desorpt. expts. 77—69180
Pd (111), adsorption of O_2, UPS and thermal desorption spectra meas. 79—78833
Pd (111), chemisorption of Cl_2, LEED, AES, thermal desorption, and work function meas. 80—75444
Pd (111) surface, adsorbed O_2, UPS and thermal desorpt. characts. 80—54754
Pd cluster, adsorption/desorption of CO, AES and thermal desorption meas. 80—75436
Pd ribbon, of H_2, thermal desorption and work function meas. 80—70538
Pd, surface, coverage and desorption of CO flash desorption spectrum 80—49493
Pd surface, fast D_2 desorpt. mechanism, time-of-flight spectra 80—84379
Pd-Fe-H, elec. resistivity, 4.2 to 300K, effect of H_2 desorption *(Russian)* 79—7814
Pd-Ni alloys, surface comp. and catalysis, AES and thermal desorption meas. 79—46898
PdH_x layer, galvanostatic desorption of hydrogen, quantitative theory 80—40694
Pd(110) surface, adsorption of Xe, flash desorption study 80—6633
Pd(111), of H, preexponential factors 79—46918
Pt (100), of cyanogen, flash desorption mass spectrometry 77—31884
Pt (100) (5×20) and (1×1) surfaces, stability and reactivity, adsorption of H 80—75434
Pt (110), acetylene adsorption, desorption and surface dissoc. 77—62749
Pt (111), adsorption of CO using XPS, UPS, TDS and dynamic meas. of work function 79—65322
Pt (111), adsorption of CO, XPS, UPS, thermal desorption, and work function meas. 79—77905
Pt (111), adsorption of NO, EELS, thermal desorption, LEED, and AES study 80—80086
Pt (111), chemisorption of Cl_2, LEED, AES, thermal desorption, and work function meas. 80—75444
Pt (111), clean and oxidised, binding states and sticking coeffs. of CO and H_2 77—72787
Pt (111), interaction with water, thermal desorption, UPS, and XPS study 80—80088
Pt (111), of H_2, obs. by dynamic meas. of work function 79—77915
Pt (111) and (100) superlattices formed by dissociative adsorption of HI, LEED, AES, and thermal desorption studies 80—55715
Pt (111) and Pt (S)-12(111)X(111)surfaces, adsorption of 0, thermal desorption, AES, XPS, and LEED study 80—70534
Pt (111) stepped surface, adsorption of O_2, CO, C_2N_2 and ethylene 78—71992
Pt (111) surface, of CO, LEED, desorption and work function meas. 77—72781
Pt, adsorbed O_2, isotopic exchange and thermal desorption *(French)* 78—43249
Pt, adsorption and desorption of O_2 on (110) surface, thermal desorpt., LEED/AES obs. 77—72788
Pt, adsorption of CO, O_2, NH_3, surface composition, AES and temp. programmed desorption meas. 80—34313
Pt, adsorption of water, H_2 and reaction between H_2 and adsorbed O 80—49514
Pt, associative desorption of NO 80—54512
Pt catalysts, supported, adsorbed CO, temp. programmed desorption 79—46915
Pt, of acetone, photoion emission, quantum yield limit 78—79896
Pt, of Ar, gas surface interactions, 3-D generalised Langevin model appl. 80—107637
Pt, of CO, binding states, desorption and adsorption kinetics 77—85065
Pt, of CO, O_2, H_2, thermal desorpt. spectra 78—14607
Pt, of H, (111) surface, role of at. steps. 77—15690
Pt, of H_2 and O_2, on surfaces with variable kink concs. 80—35576
Pt, of N_2, thermal desorption meas., α and β-status 77—15696
Pt, of Xe, gas surface interactions, 3-D generalised Langevin model appl. 80—107637
Pt, stepped surface, adsorpt. and decomp. of NO and NH_3, LEED, AES, and thermal desorption expts. 78—38943
Pt, surface, (111), O_2 interactions, UPS, EELS and thermal desorption study 80—100409
Pt surface, chemisorbed CO, IR refl.-absorpt. spectra, absorbate island struct. 80—84385
Pt surface, coverage and desorption of CO flash desorption spectrum 80—49493
Pt surface, mean residence time and ionisation efficiency meas. of K 77—85874
Pt surface, of water, D_2O+H, $D_2{}^{16}O+{}^{18}O$ exchange reacts. 77—80695
Pt surfaces, clean and S covered, desorption of CO, binding energy meas. 79—46950
Pt, surfaces (111) and 6(111)×(111), CO adsorption, EELS and thermal desorption spectroscopy 78—91547
Pt-Pd(Au) alloys, surface comp. and catalysis, AES and thermal desorption meas. 79—46898
Pt(S)-[9(111)×(111)] face, adsorption of O_2, flash desorption, LEED and AES obs. 77—69182
Pt(111), adsorption of Br, irreversible order-disorder transition, LEED AES, thermal description and work function meas. 79—69361
Pt(111), adsorption of NO, anal. of adsorption processes and surface reactions, vibration spectroscopy 78—87868
Pt(111), of H, preexponential factors 79—46918

desorption continued
- Pt(111), surface H-H interactions, heats of adsorption and desorption 78−18899
- Pt(111), Xe direct inelastic scatt. with trapping-desorption scatt., vel. and ang. distribs. 80−16140
- ^{226}Ra, desorption from river-borne sediments in Hudson estuary 79−79877
- ^{226}Ra desorption from sediments of Pee Dee River−Winyah Bay estuary, effects on dissolved ^{226}Ra 80−98360
- Re (0001), chemisorption of CO, role of d-orbitals, angular resolved UPS and thermal desorption meas. 80−40232
- Re, adsorption, oxidation, and hydrogenation of CO, XPS, UPS, and thermal desorption study 80−71571
- Re, coadsorption of ethylene and O_2, thermal desorption study *(French)* 78−85194
- Re, dissociative and mol. adsorption of NO and H_2O, XPS, AES and SIMS study temp. programmed desorption spectra *(French)* 79−69344
- Re, of Na, neutral and ionic desorpt. rates meas. via surface ionisation detector with field reversal 77−2710
- Re, of O_2, electron-induced desorption *(French)* 77−85853
- Re, photodesorption of CO forming CO_2 79−52777
- Re, polycryst. and (0001) single cryst., ethylene and acetylene adsorption 78−38947
- Re single crystal surface, thermal desorption of CO and NO *(French)* 78−22959
- Re surface, interaction with N_2^+ beam, reaction dynamics studied by XPS and thermal desorpt. spectrometry 80−93797
- Re, with adsorbed O_2, Na ionisation, field reversal and surface ionisation expts. 77−90232
- Re(0001), of O_2, CO, NO, and H_2O, XPS, UPS and temp. programmed desorption 80−71574
- Rh (110), chemisorption of CO and NO, LEED, AES, XPS, UPS, and desorption obs. 79−77899
- Rh (111), adsorption of O_2, AES, LEED, and thermal desorption mass spectra meas. 79−77900
- Rh (111), chemisorption of CO, thermal desorption mass spectrometry and LEED meas. 79−77917
- Rh (111), chemisorption of H_2, thermal desorption spectra and LEED obs. 79−86989
- Rh (111), chemisorption of CO and CO_2, high resolution EELS, thermal desorption, and LEED study 80−44419
- Rh (111), chemisorption of water, effect of adsorbed O, H, or CO, LEED and thermal desorption meas. 80−75435
- Rh (111), co-adsorption of H_2 and CO segregation of co-adsorbed species 80−65361
- Rh (111), coadsorption of O_2 and H_2 below 140K 80−29276
- Rh (111), dissociative chemisorption of CO_2, EELS and thermal desorption spectra meas. 80−6656
- Rh (111), interaction with O_2, thermal desorption spectra, AES and LEED obs. 79−51428
- Rh (111) and (100) surfaces, chemisorption of H_2, O_2, CO, CO_2, NO, C, ethylene, acetylene, LEED, AES and thermal desorption meas. 78−38951
- Rh, (111) surface, chemisorbed O_2, catalytic reaction between adsorbed O_2 and gaseous H_2 79−83503
- Rh, adsorption of CO_2+H_2 mixtures, reflection-absorption IR and thermal desorpt. obs. 78−6226
- Rh, coadsorbed CO and O, desorption spectra, Langmuir-Hinshelwood reaction between O and CO 79−47965
- Rh, coadsorption of CO and H_2, thermal desorption mass spectroscopy meas. 79−46948
- Rh, of CO, on (110) face 78−6225
- Ru (0001) surface, adsorption of H_2, N_2 and NH_3, AES, LEED and thermal flash desorption meas. 78−38954
- Ru (0001) surface, adsorption and desorption of NH_3, effects of electron beam 78−38955
- Ru (001), adsorption of CO, IR spectra, LEED, and thermal desorption meas. 80−70533
- Ru (001), adsorption of H_2S and S, LEED, UPS, AES, and thermal desorption meas. 79−99420
- Ru (001), chemisorption of CO, electron stimulated desorption ion ang. distribs. bonding geometry and bending vibrs. 79−33189
- Ru (001), coadsorption of O_2 and CO, uptake and flash desorption meas. 80−39450
- Ru (001), dissociation of adsorbed H_2S, chemisorption and electronic struct. of S layer 79−79292
- Ru (001), electron stimulated desorption of CO, correl. with other meas. 78−47658
- Ru (001) surface, adsorbed layer of CO, electron induced dissociation, thermal desorption meas. 77−59215
- Ru (001) surface, CO desorption 79−15001
- Ru $(10\bar{1}0)$ of NO and CO, dissoc. 77−72783
- Ru $(10\bar{1}0)$ surface, oxide form., thermal desorption and ESCA obs. 79−82442
- Ru (101), O_2 chemisorption, $CO+O_2$ interaction 77−73471
- Ru (110), methanol reaction, thermal desorpt. meas. 78−31685
- Ru, associative desorption of NO 80−54512
- Ru, clean and S covered, adsorption and desorption kinetics of CO 80−6643
- Ru, clean and S covered, adsorption and desorption kinetics of H_2 80−6644
- Ru, NO chemisorpt. and decomp. 78−18903
- Ru(001), chemisorpt. of H_2O, conformation, electron stimulated desorption ion ang. distribs. 77−89637
- Ru(101), of CO, surface structural chemistry and electron impact props. 77−1312
- S_2 polymerisation, kinetics obs. by pulsed field ionis. time-of-flight mass spectrometer 77−63890
- Si (100), oxides formed in Cs-O adsorbed films, ionisation loss spectra, Auger spectra 79−69365
- Si (111), adsorpt. of Cs, LEED, work function and thermal desorpt. 78−14590
- Si (111), of Au and Ag, kinetics of two-dimens. phases on single cryst. substrate 78−14598
- Si (111) 7×7 surface, desorption of H and O 80−10792
- Si (111)/Au deposit, isothermal desorption spectroscopy for 2-dimens. condensed phase obs. 77−69181
- Si, adsorption-desorption kinetics of H_2, O_2 and other gases, catalysis 77−47684
- Si, CF_3^+ ion bombarded, of F 79−70367

desorption continued
- Si, CVD from SiH_4-HCl-H_2 system, rate-determining reactions and surface species 80−84405
- Si, epitaxial growth, adsorbed layer model for autodoping mech. 80−7505
- Si, etching using XeF_2 vapour, adsorption/desorption process 79−43449
- Si film, amorphous, plasma-deposited, H_2 evolution, mass spectrometry and RHEED obs. 78−72050
- Si, whisker, amorphous, growth method for field desorption mass spectrometry 79−28262
- Si:As, segregation and desorption kinetics for evaporation of As 79−99410
- Si:H, amorphous, defect creation and H evolution 80−50392
- Si:H, amorphous, exodiffusion of H, EPR expts. 80−49102
- Si:H, amorphous, glow discharge deposited, thermal dehydrogenation, IR spectra 80−44442
- Si:H, amorphous, H content determ. by IR absorpt., gas evolution and nuclear reaction methods 80−44130
- Si:H amorphous film, sputtered IR vibr. spectra and photolum., effects of partial evolution of H 80−44413
- Si-H, amorphous, plasma-deposited, H evolution and defect creation 80−44914
- SiC, desorption of D, activation energies 79−65330
- SiC, energetic H and Ar ion sputtering, AES-SIMS-FDS combined obs. 78−80444
- SiC, energetic ion sputtering, appl. of AES-SIMS (IMA)-FDS combined systems to physical and chemical processes 78−95636
- SiO_2 films, desorption from Si single cryst., ellipsometric obs. 80−100410
- SiO_2 gel, meso-porous, of N_2, pore size distrib. calc. 77−4941
- SiO_2, growth and thermal evaporation kinetics of oxide film on Si surface 78−3246
- SiO_2-Si stratified system surface charges, adsorption and desorption effects *(Russian)* 80−49942
- Si(111), water vap. and O_2 interactions, EELS 78−14571
- $SmCo_5$, adsorption and desorption charact. of H_2 *(Japanese)* 77−47667
- SnO_2 surface, interactions with O_2, H_2O and H_2, desorpt., ESR and cond. meas 80−10790
- SnO_2:ThO_2, exposed to CO gas, self-oscill. phenomenon 78−68032
- SnTe surfaces, oxidation in air and thermal desorption, XPS and LEED meas. 79−47830
- $SrTiO_3$ surface, oxidation and reduction by D_2O, $H_2{}^{18}O$, D_2, isotope exchange study 80−104461
- Ta (110), electron-stimulated desorpt. of O 78−2363
- Ta, desorption kinetics of halogens, pulsed ion beam method 80−34300
- Ta, electron-stimulated desorption, Ta surface, electron-stimulated bound state obs., 300K 77−85082
- Ta, of CO(CO_2), FEM and flash filament method exam. 78−43245
- Ta, photodesorption of CO forming CO_2 79−52777
- Th-transition metal intermetallic, H_2 desorption isotherms depend. on d-bandfilling 78−18912
- ThO_2, temp. programmed desorpt. and photoluminesc. of surface states 79−73399
- Ti alloy, gas desorption coeffs., electron- and ion-induced, bakeout temp. effect 79−65329
- Ti, chemisorption of H_2 and CO, flash desorpt. mass spectrometry obs. 77−89646
- Ti, films, implanted inert gas desorption, reemission process 80−39453
- Ti thin films, H absorption and desorption, Tokamak gettering, Auger electron spectrosc. 80−75092
- Ti-H, diffusion in hydride phase, exam. 80−29204
- $TiCo_{1-x}Mn_x$, H absorption-desorption characteristics 80−96735
- TiD_2, film formed during simulated Tokamak gettering cycles 80−34296
- TiH_x film, anomalous H_2 desorption at room temp. 80−29261
- TiH_x film, kinetics of H_2 interaction 80−6620
- TiNi-H system, thermodynamic rels. and struct. transformations 80−49385
- TiO_2 (100), chemisorption of H_2, O_2, and H_2O, electron spectroscopy, evidence for Ti^{3+} photogeneration 78−38940
- TiO_2, H species characterisation by electron-stimulated desorption 80−34305
- TiO_2, photodesorption of H_2O, pulsed-laser-dynamic-mass-spectrometer study 80−35568
- TiO_2, photon-stimulated desorption of ions obs. 79−82459
- TiO_2 suspension, adsorption-desorption of IO_3^- 80−93804
- TiO_2:H photoanodes, diffusion and surface chemistry 80−35546
- V (100), sorption investig. using total current spectroscopy of slow electrons 77−8694
- V, dehydrogenation by annealing with Zr foils, internal friction meas. 80−96736
- V, oxidized, electron stimulated desorption of O^+ ions 79−99428
- V surface interaction with O_2, H_2, H_2+O_2 and H_2O, SIMS, EID 77−62753
- V-H, H on polycrystalline V, H detection by SIMS, flash-desorption obs. 79−24405
- $VH_{0.55}$, ultra-high vacuum cleavage, H_2 desorption 80−54514
- W (001) face, thermal desorption kinetics of Cs atoms and ions 79−28210
- W (001) surface, adsorption of CO, electron energy loss spectra and thermal desorption 78−71999
- W (011), field desorption of Ba atoms, conc. depend. 80−25533
- W (100), adsorpt. of acetylene, room temp., electron spectroscopy obs. 79−7749
- W (100), adsorption of CO, thermal desorption and work function meas. 80−29273
- W (100), adsorption of O_2, AES, desorption, LEED and work function obs. 77−1317
- W (100), adsorption of Zr, AES, LEED, thermal desorption, and work function meas. 80−39444
- W (100), CO/H_2 surface complex, flash desorption and AES obs. 78−73083
- W (100), chemisorption of Hg, AES, LEED, work function and thermal desorption expts. 78−34709
- W (100), coadsorption of CO and H_2, CO/H surface complex obs. 79−4478
- W (100), coadsorption of H and CO, photoemission and thermal desorpt. investig. 77−28079
- W (100), early stage condensation of Cu and Ag, comparison with Mo (100) 80−80072
- W (100), electron-stimulated desorpt. of O 78−2363
- W (100), formic acid decomp., flash desorption obs. 79−29402

desorption continued
W (100), laser induced desorption, mirror electron microscopy 78−84067
W (100), of Hg, fractional and zero order desorption kinetics 79−60634
W (100), of O, electron stimulated desorption ion energy distrib. and surface struct. 78−75940
W (100), of O_2, electron desorption cross sections 79−46944
W (100), of O^+ ion, electron stimulated, hysteresis and ion yield minimum 77−59218
W (100), reconstruction in presence of O half monolayer, struct. props. 80−44421
W, (100) and (110) faces, electron stimulated desorption of O_2, CO, and H_2, threshold behaviour 77−47678
W (100) and (111), O_2 electron stimulated desorption patterns, computer simulations 80−75443
W (100) stepped surface, adsorbed O, electron stimulated desorption ion ang. distribs. 80−20035
W, (100) surface, of CO, electron and photon-stimulated desorption 79−99414
W (110), adsorption of N_2, thermal desorpt. and work function meas. 77−1294
W (110), codeposition of Cs and O, Cs_2O form. 80−44425
W (110), electron impact desorption of CO and O_2, isotope effects 77−76658
W (110), of alkali atoms, trapping probabilities and desorption kinetics 77−62754
W (110), oxygenated and oxidised, Cs absorption 80−44424
W (110) and (100), adsorption of Xe and coadsorption with O, work function and thermal desorption meas. 80−39448
W (110) and (111) surfaces, KCl adsorption-desorption behaviour 80−75442
W (110) plane, of CO, electron impact desorption, thermal desorption and work function meas. 77−85064
W (110) stepped surface, electron stimulated desorption of O, atomic steps and defects influence 80−80091
W (110) surface, adsorbed Pd, growth, struct., stability, desorption 80−59794
W (110) surface, adsorption of O_2, LEED, AES and thermal desorption meas. 78−38957
W (111), 0_2 and CO adsorption, angle resolved electron stimulated desorption, LEED and AES 80−6645
W (111), adsorption of O_2, AES, LEED and electron stimulated desorption obs. 79−46935
W (111), angle-resolved photon-stimulated desorption of O^+ 80−88434
W (121), Ba atom desorption in strong elec. fields 80−29280
W {100}, electron stimulated desorpt. of CO, AES obs. 77−31897
W {110}, chemisorption of β-N_2, underlayer mechanism 80−39432
W, adsorbed gases, field desorption from field ion tips 80−59793
W, adsorbed Hg, thermal desorption kinetics, theory 80−59792
W, adsorpt. surface migration and thermal desorpt. of LaB_6, field emission microscopy 79−56075
W, adsorption and condensation of Fe, meas. by thermal desorption in time-of-flight mass spectra 79−15023
W, adsorption of benzene, isothermal ramped field desorption technique 79−82450
W, adsorption of N_2, effect of SIMS, sputtering induced recomb. anal. 80−55243
W, catalytic decomp. of NH_3 single pulses, mol. beam relax. spectrometry 80−21321
W, clean and oxidised, mol. binding states of SiO 79−7750
W, collective field evaporation from (110) face, field ion microscopy *(Russian)* 79−61504
W, desorption kinetics of halogens, pulsed ion beam method 80−34300
W, desorption of Cs, dynamic characts. of neutral particle desorption by surface ionisation voltage method 80−44426
W, desorption of D_2, meas. of fast desorption kinetics by laser heating technique 79−23837
W, direct inelastic and trapping-desorpt. scatt. of N_2, elementary steps in N_2 chemisorpt. 80−60737
W, electron stimulated desorption of F and Ba from polycryst. ribbon 77−11793
W, electron stimulated desorption of O from (100) and (110) surfaces, combined LEED and AES method 79−33181
W, electron stimulated desorption of O^+ and O^- from chemisorbed O_2 79−90875
W, electron stimulated desorption of O^- and O^+ ions from adsorbed CO 80−2270
W, H and CO adsorbates, ion impact desorption of atoms and molecules by low energy ion scattering 79−4883
W, hot emitter, surface struct. change during baking above 2000K 79−65971
W, K atom beam impact on gas-covered surface, K^+ ion current peculiar decay 79−74045
W, methane dissoc. by adsorption-desorption process 78−92511
W, O_2 adsorption on (110), electron impact and thermal desorption at high temp. 78−30821
W, of Ag, adsorption and desorption kinetics, mass spectra obs. *(German)* 79−46951
W, of CO, thermal desorption and conversion kinetics, AES study 78−71959
W, of Cl(Br)(I), field ion microscope exam. 78−35270
W, of Cs-O_2 80−103562
W, of H on (100), electron stimulated desorption, structural model 77−66091
W, of K, field desorption, from (001), (011) and (112) planes 78−34715
W, of Ni, effect on surface self-diffusion, FEM characts, desorption activation energy *(French)* 77−1296
W, of O^+ and O, electron stimulated, cross-section temp. depend. 77−31908
W, of Re, electron induced desorption *(French)* 77−85853
W, photodesorption of CO forming CO_2 79−52777
W, polycryst. surface, heat of desorption of Cs 80−75430
W, powder, gas adsorption and desorption *(Russian)* 80−75429
W ribbon, with adsorbed CO, CO_2, or methane electron beam induced C deposition, AES obs. 77−89651
W stepped surface, adsorption and desorption of O, LEED, AES and work function obs. 77−47675
W surface, (100), photon and electron stimulated desorpt. of O 80−100397
W surface, adsorbed CO, electron-stimulated desorption, photoemission, relax. energy 80−100401

desorption continued
W surface, adsorbed H_2, energy spectra for electron stimulated desorption of H^+ calc. 78−79892
W surface, electron-stimulated ion desorption of CO 80−59797
W, surface, isothermal ramped field-desorption of benzene 79−90870
W surface, of Cs ions, evap. isotherm from single cryst. faces 79−24829
W surface, polycryst., N_2 adsorption states 80−100404
W, surface (100) and polycryst., electron stimulated desorption of O^+ ions from adsorbed O 79−99428
W, trapping and desorption of alkali atoms on clean and O_2 covered (110) surface 77−11786
W(100), of O_2, H_2, N_2, CO, NO and water, adsorbate densities determ. 77−1320
W(110), Cs and O_2 coadsorption, surface anal. 77−89656
W(110) surface, of B monolayer, struct. transformation stages 77−47681
W(110) surface, of trapped K and Na, desorption energies determ., trajectory calcs. 77−48295
W{001}, photon and electron stimulated desorption energy and angular distributions for O^+ 80−96734
W{100} surface, co-adsorption of Cu and O_2, AES, thermal desorption, LEED and work function meas. 78−38950
Xe, solid, of He, appl. of simplified continuum model 78−87860
Zn film, deposition props. on specially prepared substrate, desorption energy and surface diffusion 79−90917
ZnO $10\bar{1}0$ surface, reaction of O_2, AES, LEED, EPR, desorpt., surface cond. and work function expts. 78−95950
ZnO $(000\bar{1})$ and $(10\bar{1}0)$ surfaces, clean and contaminated, reactivity to Cl_2 79−61904
ZnO $(10\bar{1}0)$ surface, of Zn, O_2, nonstationary sublimation *(German)* 78−60035
ZnO, electron beam induced decomposition and desorption, AES and contact pot. difference meas. 78−79893
ZnO, nonpolar surface, adsorption and desorption of CO and CO_2 79−65321
ZnO, of $H_2O(NH_3)(NO)$(acetone), photoion emission, quantum yield limit 78−79896
ZnO, of O_2, effect on conductivity of powder layers 78−43441
ZnO, photodesorption of CO_2, rel. to surface cond. and AES, band-bending model 77−47671
ZnO powder, CO_2 desorption during electron irrad. and interaction with atomic H 77−89638
ZnO, powder, surface cond., effects of O_2 chemisorption and CO_2 photodesorption 77−11980
ZnO powders, electron-beam-induced desorption, phase-sensitive detection 80−54502
ZnO, prismatic surface, O_2 interaction obs. 77−31899
Zr-H, diffusion in hydride phase, exam. 80−29204
ZrC and ZrC-Re alloys, desorption temp., flash temp. and initial sticking factor 79−19467
$Zr(Co_xM_{1-x})_2$ (M=V,Cr,Mn) H absorption and desorption props. 77−55448
$Zr(Fe_xM_{1-x})_2$, (M=V,Cr,Mn), H absorption and desorption props. 77−55448

detection (demodulation) *see demodulation*

detector circuits
see also demodulation; demodulators
autodyne, for low-temperature measurements up to 400 MHz 77−13755
autodyne spin detector, broadband, for NMR signal detection 77−74471
digital lock-in amplifier simulation 77−151
environmental effects on microphones and Type II sound level meters 77−62127
gamma-ray spectrometer self-stabilising peak detector *(Russian)* 79−26814
ion cyclotron resonance signal, broadband detection 80−62792
Josephson junction current-voltage charact., resonance detection cct. 78−54406
lock-in null detectors, phaser design 77−79122
mechanical respirator, ventilation failure detector cct. *(Spanish)* 77−52913
NMR receiver, description and design 78−21193
peak detector extremator, cct. 78−74096
peak-detecting window discriminator for neuronal spikes 77−60323
phase sensitive, for Auger electron spectroscopy, tailored waveform modulation calc. 77−32860
phase sensitive detector system for NMR/ESR wide-line spectroscopy 77−13791
phase-sensitive detector, programmable, for automatic bridge appl. 79−21773
polyphase envelope detection for physiological signals *(Korean)* 79−66565
pulsed NMR, extremely fast recovery time receiver 77−26376
quartz crystal impedance and admittance bridge development 77−37944
radiation detector lag correction network ccts. 78−288
semiconductor position detector analogue division cct. 77−54470
square law detector checking, for Hartshorn and Ward dielectric meas. 79−35777
submillimeter wave heterodyne detection, with a laser LO 78−70183
synchronous, for ESR spectrometer 79−35802
TIROS-N weather satellite, detection circuits and sync pulses for picture facsimile machine 79−53577
voltage peak amplitude detector for LF waveforms 77−2666
Hg drop fall detector, circuit, design appls. 77−63924

detectors
see also electric sensing devices; hydrophones; infrared detectors; microwave detectors; nonelectric sensing devices; particle detectors; photodetectors; ultraviolet detectors
averaging time measurement, methods *(Croatian)* 77−37849
Brillouin ring laser, fibre-optic, use for inertial sensing 80−87411
channelplate detector for SXAPS at primary electron currents $>10\ \mu A$ 79−49362
combustion sensor, Ca-Mg-Zr pipe-form ceramics appl. *(Japanese)* 80−55761
crime countermeasures, physical techniques for detection 79−12920
digital lock-in detection technique and appls. 79−49303
EM signals detection using MIM structures nonlinear properties *(Russian)* 78−34912
explosives materials detectors evaluation, for use in nuclear facilities 79−89451
fibre optic sensors appl. *(Norwegian)* 79−93121
flaw detection system, noise immunity 80−104385

detectors continued
- foreign-body detector for intraoperative localisation of stones in biliary tract 78—3657
- gas chromatograph element-specific detection systems *(German)* 80—93837
- gas permeability measurement in high polymers, techniques and detectors 80—14854
- history of sensing apparatus and techniques, source guide 78—4457
- inductive sonde, large bloodvessel movement, transcutaneous meas., design and realisation *(Italian)* 79—70602
- InSb subMM detector, fast response, for use in measuring electron cyclotron emission 80—27347
- liquid chromatography improvements 77—73492
- low-level gated oscillator, ion cyclotron resonance 80—86492
- magnetic field detector using second harmonic oscillation 79—54161
- magnetoelastic ribbon position sensor 79—80603
- magnetometer types, study and comparison *(Spanish)* 78—4008
- MM wavelength band radiometer, Josephson superconducting point contact as detector 80—21918
- multiple electrochemical analyser for flowing liquids and gases, features *(German)* 78—27846
- odour detection, instrumental techniques *(Dutch)* 79—16658
- optical radiation detector laboratory, graduate-level, expts. 80—62432
- periodic magnetic signal detection by magnetoresistance sensor *(Japanese)* 78—57997
- position-sensitive detector, appl. to high pressure X-ray diffr. using diamond-anvil cell 80—79632
- pyranometers for underwater total radiant energy flux meas. 77—9524
- quartz crystal gravitational radiation antenna, Q factor 78—16715
- resolution enhancement by deconvolution of detected signal 79—71440
- semiconductor diode sensors for low temp. thermometry *(German)* 79—35762
- semiconductor for testing SEM quality parameters 80—22484
- sensing techniques *(Japanese)* 80—73345
- shock wave, detonation wave propagation in shock tube, investigations on suitability of piezoelectric and magnetoelastic detectors *(Polish)* 80—79351
- snowfall detectors and automatic depth recorder *(Japanese)* 79—8700
- speed contactless meas., transit time determ. by pick-up *(German)* 80—14862
- strain gauge technique *(French)* 78—12686
- synchronised detection system, elimination of influence of low-freq. perturbations 78—45589
- US beam detector, two-dimensional 78—94495
- US boxcar detector using sample-and-hold circ., for student lab. 80—27083
- voltage waveform peak and trough precision detector, using operational amplifiers 77—87792
- wave profile measurement in shock-loaded solids 79—94564
- O_2 analysis, electrochemical sensors 80—93816
- Si diode radiation detector, stabilisation of radiation damage 80—91377
- SnO_2 thin films, solid state gas sensor 80—40790
- SnO_2:ThO_2, selective detection of CO, hydrophobic and hydrophilic silica effect 79—97372
- SnO_2-based gas sensors, resist. temp. depend. on exposure to CO, H_2, and propane 80—103694

determinants
- *see also matrix algebra*
- crystallography, determinantal inequalities, invariant joint probability distrib., heuristic derivation 79—32927
- elastic shear waves propagation in fibrous composites 80—58963
- fermion determinant in QED, asymptotic estimates 78—54593
- Fredholm, satisfying differential eqn., appl. to inversion formalism for parameter depend. potentials 77—22437
- Lanczos method, method of moments, tri-diagonalisation of a matrix 78—58240
- Lie groups, classical, reduced determinantal forms 80—22533
- multi-instanton determinants for covariant laplacian D^2, 't Hooft solution extension 80—13216
- quantum fluctuations of instantons 78—54530
- S-matrix theory, determinant and its relation to number of eigenvalues due to perturbation 78—58132
- secular equation of the 4th order, L-matrix approx. vs. HLFS methods, mol. force consts. appl. 79—36556
- Szego's theorem for Hankel determinants 79—49106
- Toeplitz, produced by substantially limited functions, generalised calc. *(German)* 80—26
- zeta-function regularization and multi-instanton determinants 80—13215

detonation
- *see also explosions; shock waves*
- acetylene+O_2 detonation products, enhancement of CO laser gain measurements 78—33729
- air, optical detonation threshold, press. depend. rel. to Ar 79—23438
- blast wave initiation and propagation of cylindrical heterogeneous detonation waves 80—74915
- blast waves with heat transfer 77—35166
- cell model, geometry, kinematics, mixture kinetics 79—66296
- Chapman-Jouget curved detonation wave, existence conditions *(Russian)* 77—51084
- Chapman-Jouget detonation wave near surface curvature rupture line *(Russian)* 78—46996
- Chapman-Jouguet wave, gas flow near line of discontinuity of surface wave curvature 79—86462
- concentric hyperdetonation on consideration of combustion kinetics 79—68748
- deposition of coatings, conducting powder temp. meas. 80—11559
- deposition of coatings, monitoring method 80—60780
- deposition of Cr_3C_2 (Cr_7C_3) based coatings, wear resist., 20-1000°C 80—11843
- deposition of hard alloy coatings from fine powder mixtures 79—100078
- ethylene-O_2-N_2-Al particle mixture, two-phase detonation and combustion *(French)* 80—61097
- fuel drops, liq., blast wave initiated detonation waves 79—64691
- fuel/air mixtures, conc. limits to initiation of unconfined detonation 80—38505
- gas detonation wave, calculation of equilibrium flow *(Russian)* 78—1690
- gas mixtures, detonating, symmetric piston motion 80—59073
- gas-ionising detonation wave, spatially-polarised struct., rel. to mag. viscosity *(Russian)* 77—39361

detonation continued
- gasdynamics of explosions, reactive systems, conf., Stockholm, Sweden (Aug. 1977) 79—64690
- heterogeneous solid explosives, spin detonation 79—14429
- homogeneous explosives, electrical polarisation with initiation of shock wave detonation 79—100378
- hydrodynamic thermal explosion in power-law fluid flow 79—77158
- laser supported detonation wave, Whitham's rule anal. 78—59423
- laser-supported detonation wave, jet flowfield 78—26171
- lattices, two-dimensional, detonation, shock propagation, computer simulation 79—64554
- LMFBR shock-induced fragmentation and detonating thermal explosions 79—13475
- mesh-initiated large area detonators 77—10001
- metal foils, electric detonation in vac., Xe, He, N_2 atoms., discharge rad. characts. *(Russian)* 77—11435
- methane-O_2 aquamechanical foam, propag. characts. of detonation waves 78—31713
- model optimization of detonation-wave description on consideration of combustion kinetics 79—91955
- momentum transfer by laser-supported detonation waves, optimisation 78—30307
- multicomponent media, cylindrical detonation wave propag. 79—86287
- nitromethane, DETA sensitized, steady state detonation vel., chemical inhomogeneity effect 80—89493
- nitromethane, detonation reaction time 77—4904
- nonconducting powder, temp. determ. in detonation deposition 80—226
- one-dimensional compressible flow, math. model rel. to detonation 80—41985
- oxyacetylene, critically-initiated detonation waves, quasi-steady regime 78—90930
- photodetonation and supersonic radiation wave propag. in Xe plasma *(Russian)* 80—10385
- plane hyperdetonation shock wave reflection from rigid wall 78—75167
- polymorphic detonation 79—42147
- products of condensed explosives elec. stability 79—86635
- propane-O_2 aquamechanical foam, propag. characts. of detonation waves 78—31713
- propane-O_2 mixture, combustion to detonation transition, stochastic aspects 79—100381
- propane-O_2 system with Ar, N_2 diluents, detonation wave instabilities 78—5762
- pulsation of cylindrical cavity in incompressible fluid, rel. to detonation *(Russian)* 77—24001
- pulsation struct., periodic instability *(Ukrainian)* 77—65751
- pulsed laser-generated impulse on a surface in supersonic flow 80—48917
- radiative MHD flow, detonation waves *(Russian)* 77—89207
- reflection of detonation waves from a wall 80—53885
- rotating shock and detonation wave anal. 80—53792
- segmented explosive charges, co-acting detonation and shock waves 77—927
- shock augmentation by bubble flow 77—3853
- shock wave front formation process, explosion due to inertial plate drive by pressure pulse 80—53811
- shock waves, starvation kinetics 78—64841
- slurry explosives, layered medium with liquid-polytropic gas structure, pressure pulse propagation 80—69872
- sound ranging in atmosphere, anal. problems 79—94393
- spherical detonation waves in media with volumetric viscosity 79—14332
- spin detonation, triple configurations, chemical equilib. 79—100379
- spinning detonation mechanism 78—22362
- spray deposition, powder introduction methods 79—70195
- spraying, pulse charact. 77—77607
- sputtering, exp. determ. of dynamic characts. of two-phase flow *(Russian)* 78—94852
- sputtering, gas flow parameters calc. *(Russian)* 80—16181
- sputtering, interaction between detonation waves and gas and powder flows *(Russian)* 80—16182
- steady-state detonation velocity effect of physical homogeneity 79—94641
- stochastic phenomena in detonation waves 79—77180
- superdetonation waves, in air, propag. towards laser beam, vel. meas. *(Russian)* 77—35159
- surface pressures from laser supported detonations 77—68836
- temperature meas., spectroscopic, theory and expt. results *(French)* 77—53917
- theory of detonation in wide tubes 80—53887
- transverse shocks in detonation waves, strength var. 78—26157
- triamino-trinitrobenzene, UV and shock-induced decomp. XPS obs. 79—31595
- two phase unmixed media, detonation development *(Russian)* 80—28556
- two-phase detonation, effect of secondary shock waves anal. *(Russian)* 77—931
- two-phase detonation front compression waves, solid particle oxidation reaction *(Russian)* 78—34207
- underwater charge, reflection of detonation wave from water surface 80—87628
- underwater explosion of detonating gas with high initial bulk energy density 80—5867
- unsteady flow fields with detonation, num. modelling 77—55107
- velocity transient meas. for Composition B-3 and PBX-9404 explosives 79—86450
- water, cavitation expts. using shock tube 80—87789
- wave magnification by pulsation energy 80—59075
- wave propag. with allowance for radn. and mag. field 79—64796
- wave propagation in channel in nonuniform EM field *(Russian)* 77—58798
- wave propagation investigations on suitability of piezoelectric and magnetoelastic detectors *(Polish)* 80—79351
- weak detonation waves 79—41710
- Al_2O_3 detonation deposited coatings, porosity and adhesion, processing parameters effects 79—70227
- Al_2O_3(-TiO_2) coatings, detonation deposited on steel, prep., wear resist., antifriction props. 78—60877
- Ar gas, supersonic radiation waves generated by CO_2 laser radiation 79—10593
- Ar liquid, shock compression temp., detonation front glow 80—43737
- Ar, optical detonation threshold, press. depend., rel. to air 79—23438
- CS_2-O_2 mixture, stimulated emission of CO behind overdriven detonation wave front *(Russian)* 77—23668
- H_2-O_2 system with N_2, O_2 diluents, detonation wave instabilities 78—5762

detonation continued
N liquid, shock compression temp., detonation front glow 80—43737
Ni coatings, detonation powder spray deposition 80—61028
$Pb(N_3)_2$-He system, high-velocity two-layer detonation 77—84278
$SF_6+SiH_4 \rightarrow S_2^*+SiF_4+HF+H_2$, laser augmented reaction, isotopic selectivity retention during detonation 78—48673

deuterium
absolute Raman cross sections determ. by indirect meas. of stimulated Raman gain, technique 78—66864
absorption and desorption isotherms in $FeTiD_x$, struct. phase transitions 80—19948
absorption by Ce binary alloys, T-getters for CTR evaluation 78—51683
absorption by La-Ni alloys, 500-700°C 79—23736
absorption features and interstellar D/H ratio towards δ, ε and ι Orionis 79—53865
absorption on rare earth metals 77—4257
abundance, Indian radioactive thermal spring water D content, mass spectrometric anal. 79—39765
abundance in Galaxy rel. to cosmology 78—69883
adsorbed on Re, interaction with CO 79—86987
adsorbed on W (111), vibr. states, EELS 77—66090
adsorption and absorpt. on Zr, dissoc. and diffusion 80—80085
adsorption by type 304 stainless steel container, surface treatment effects 77—59984
adsorption on graphite of p-D_2, NMR, orientational behaviour, weak crystal field 78—75935
adsorption on Pt, absolute coverage meas. using nucl. microanal. 80—54511
adsorption on rare earth metals 77—4257
adsorption on W (001) surface reconstruction and reordering 79—23835
alkali halide:D^-, local modes and colour centre absorpt. bands, analogy 80—60632
anharmonic spectral density of librons in o-H_2 and p-D_2 79—14899
areal distribution in California and Nevada precipitation, 1968-1969 period 79—100918
associative and Penning ionisation, autoionisation, calcs. 78—25674
atom, 1S Lamb shift and 1S-2S isotope shift 80—91464
atom, adsorption, on graphite (0001) surface, vibr. spectrum, at. beam scatt. obs. 80—92779
atom, detection by resonant three photon ionisation 78—74624
atom, electron impact, coherent excitation in longit. elec. field, Balmer-α flux 78—22035
atom, energy analysis, 200 eV-10 keV range 77—83763
atom, fluoresc., Balmer series, from mol. photodissoc. 77—27020
atom, ground state Lamb shift, isotope shift and relativistic nuclear recoil correction 78—82696
atom, handedness and parity non-conservation 78—29757
atom, hyperfine quadratic shift in electric field, pressure dependence 78—13442
atom, Lamb shift, from elec. field quenching radiation anisotropy 78—66502
atom, recombination, Morse oscillator model 78—20001
atom beam radiolysis of ethylene-butane matrix, ethyl radical proton exchange reaction indirect ESR obs. 80—16700
atomic, Fermi fluid, stabilisation 80—100374
atomic, stabilised in low. temp. frozen aqueous acidic solns., two-proton forbidden transitions 78—27804
atomic beam, superpermeability of Armco iron membrane 79—24830
atomic beam interaction with Pd membrane, permeability 77—51538
atomic X-ray absorption cross section enhancement by intense laser field 77—34582
atoms, ionisation by Nd laser radiation 80—70015
backscattering from solid surfaces, positive charge fractions 80—66375
chemisorbed on W (100), isotope effects obs. by SIMS 79—5234
chemisorption of $H_2(D_2)(HD)$ on Ni (100), vibr. excitation and struct., electron energy loss spectra 78—47660
chemisorption on Fe, equilibration and replacement reactions between H_2 and D_2, anisotropies 77—24482
chemisorption on $SrTiO_3$, oxidation and reduction, isotope exchange study 80—104461
compressed-D_2-filled glass microspheres for multibeam laser-target expts. 78—82509
compression to 44.7 kbar, apparatus and technique, diamond anvil cell 78—74017
cosmic abundance, prod. by high energy particles 77—33709
cosmic abundance rel. to density of matter in open, expanding Universe 79—12548
cosmological formation, inhomogeneity 79—21471
cryogenic data relevant to mag. fusion energy 80—8746
cryogenic gas target design for neutron therapy 77—75020
cryogenic pumping, large-capacity, for nucl. fusion 78—21151
CTR cryosorption vac. pumping of D, H and He at 4.2K 77—50298
o- and n-D_2, viscomag. effect, temp. depend. 78—9745
D_2 target fabrication for laser fusion *(Japanese)* 78—8971
D+He, low energy elastic scatt., pot. well depth determ. 77—6884
D-D cross sections for thermonuclear synthesis 80—18608
D-D nonideal systems, generalised feasibility criterion for controlled fusion 77—30658
D-T filled cryogenic spherical shell targets, laser implosion 77—74977
depth distrib. determ. in stainless steel, using $D(^3He,p)^4He$ 79—4326
depth profile in Ti film from gas emission during sputtering by Ar ions 77—35581
depth profiling of D by backward proton meas. from $D(^3He,p)$ 80—30309
depth profiling with $^2H(^3He,p)^4He$ react. 80—49262
desorption from Ni, H_2, HD and D_2 mol. vel. distribs. 77—43431
desorption from pyrocarbon, SiC and B_xC_y, activation energies 79—65330
desorption from S free and covered Ni(111), ang. depend. of flux, mean energy and speed ratio 79—86993
desorption of D_2 from W, meas. of fast desorption kinetics by laser heating technique 79—23837
deuterium-tritium thermonuclear ignition, high current density approach, expt. 78—54874
deuteron bombardment of pyrolytic C, methane form., energy depend. 78—95939
deuteron impact X-ray prod., 5 MeV/amu, projectile Z depend. 80—42982
diffusion and permeability in Fe at 49 to 506°C 78—59977
diffusion and permeation in stainless steel, ion beam meas. 80—59492

deuterium continued
diffusion and solubility in PTFE, activation enthalpy 78—79775
diffusion and solubility in vitreous SiO_2, 0-800°C, interaction with structural OH 77—89585
diffusion coefficients, Pd, Ni, and Cu, calc. *(Russian)* 78—91483
diffusion coefficients in austenitic stainless steel, ion beam meas. technique 80—75382
diffusion in BCC metals, phonon-assisted quantum-mechanical tunnelling of interstitials 80—59730
diffusion in Co_5Sm, mag. aftereffect meas. 79—56573
diffusion in glassy and rubbery polymer films, isotope effect 80—84327
diffusion in hydrogenated amorphous Si, SIMS anal. 78—75877
diffusion in ion implanted Fe:Y, deep D traps 80—103372
diffusion in Nb, Ta, low temp., from quenching and annealing study 80—6555
diffusion in Nb(V)(Pd), role of tunnelling, reson./nonreson. approaches 80—59718
diffusion in Nb and Mo, trapping at ion implantation induced defects 77—47622
diffusion in Ni, deuteron diffusion obs. by D(d, p)T reaction *(German)* 77—59150
diffusion in Ni, isotope effect, elec. resistivity meas. 79—86928
diffusion in niobium 78—6182
diffusion in No, Pd, Va, quantum rate theory for symmetric double well pot. 78—55970
diffusion in V, effect of impurities 78—47604
discharge, high current, pulsed, plasma composition, temp., electron density, press., spectral diagnostics 79—55459
discharge lamp in visible region *(German)* 79—59782
discharge lamps, influence of Ne and Ar on spectral parameters 80—86460
discharge plasma, resonant multiphoton optogalvanic spectroscopy, diagnostics appls. 79—23448
dissociation on Cu(100) and (110) surfaces, classical trajectory calcs. 77—60114
dissociative adsorption of H_2-D_2 mixture on stepped Pt surface, reactant ang. of incidence effects 77—47670
dissolution of interstitial atoms in metals, diffusion coeffs., reverse isotope effect *(Russian)* 80—88368
distillation of byproduct of desalination plants, feasibility study 77—67894
double quantum NMR in solids, magic angle spinning 80—108120
DT self-propelling pellets for fusion-reactor refueling 79—677
duopigatron gas discharge ion source, perform. characts. 78—54505
duoplasmatron gas discharge ion source, plasma expansion cup effects 78—58092
electric breakdown, Paschen's law violations 78—87570
electro fission on relativistic channelling in W *(Russian)* 80—54294
electrodisintegration neutron spectrum of Princeton Large Tokamak 77—84521
electromigration in Ti 80—34247
electromigration measured by resistance method in Nb and V 79—23783
electron impact dissoc., cross sections, isotope ratios and polarisation, B H_α and H_β emission 78—25729
electron surface barriers for dense phases 78—91754
enrichment, ultrahigh single step, by CO_2 laser photolysis of trifluoromethane 80—45527
enrichment by CW CO_2 laser induced reaction 79—18300
enrichment by CW vibr. photochem. of methane, economic aspects 80—11920
enrichment in Chainpur meteorite *(French)* 79—88628
exchange reaction between H_2 and water a hydrophobic catalyst supporting Pt 80—30208
flow, transient, temp. and conc. profiles, by rot. Raman scatt. 77—75995
fluid n-D_2, eqn. of state from P-V-T and US vel. meas. up to 20 kbar 78—63837
formation by nonequilib. processes 77—53423
fuel pellets, laser acceleration for injection into thermonuclear reactor *(Russian)* 80—52779
fusion reactor, cryosorption pumping, D_2-He (5 at.%), on mol. sieve, 5A, 4.2K 78—74499
fusion reactor, D-T to catalysed-D operation, trapped ion scaling law 78—66419
fusion reactor first wall, prod. of H, D and He by 15 MeV neutrons 79—93831
fusion reactor plasmas, pure deuterium and catalysed deuterium cycles, thermal stability 80—24207
fusion reactor with injection of deuterium and tritium ions, calc. of characts. 78—37447
fusion reactors, catalysed, power balance calc., plasma confinement 80—42847
fusion target, conical, laser irrad., neutron production 79—22467
fusion Tokamak experiments, H(D) recycling model, influence on discharge behaviour 80—10393
galactic distribution, radial gradient, from DCN/$H^{13}CN$ and $DCO^+/HC^{18}O^+$ ratios 79—40232
in galaxies, D abundances rel. to radio continuum radiation from discs 77—13460
gas, solubility in U BCC alloys 79—96302
gas, stimulated Raman scatt. of excimer laser wavelengths for new lines in UV 79—59755
gas, stopping power of alpha-particles 77—18758
gas, thermal cond. meas., 2-36 MPa 80—64668
gas mixture, reacting, atom conc. reson. absorb. meas., microwave discharge lamp calibration 79—92032
hailstone trajectories determ. from crystallography, D content and radar backscatt. 78—61614
hailstones, from storms in Transvaal, 1972 November 29, D content determ. 78—20483
heat of adsorption on polycryst. Fe film 78—91530
implantation of 5 keV D in BeO film 80—100268
implanted in pyrolytic graphite, depth profiles 78—95071
implanted into stainless steel, 321 and 304, thermal desorpt. and bombardment induced release 78—95072
implanted into Zr, temp. depend. depth profiles 78—95076
implanted stainless steel, TEM obs. of defect struct. 78—95073
impurity in V, trapping by O interstitials, channelling 79—4316
interstellar, enrichment in HCN and HNC 78—16500
interstellar absorption line at 327 MHz, search towards galactic centre 78—77599

deuterium continued
ion beams impurity production by gas discharge source, cathode material testing 79−86592
ion depth profile meas. by deuteron induced reactions 77−19978
ion dynamic profiling using low-energy D(d,p) 78−2153
ion implantation into solids, ranges of implanted 10-30 keV D^+ 78−83858
ion implanted in metal, interstitial positions and vibr. amplitudes, fast ion channelling study, review 80−79848
ion source, pressure regulation by regulating electrolyser 78−842
ion-ion hybrid damping in D_2-H_2 plasma 79−77361
ions, integral ang. distrib. in traversal of Au foil 79−93894
ions, polarised, form., charge exchange processes in Lamb-shift type ion source *(Rumanian)* 77−46445
isotope effect, corrosion stability in high temp. aqu. soln. 78−9091
isotope enrichment, laser methods for nuclear fuel reprocessing 77−38378
isotope enrichment by CW CO_2 laser-induced vibr. photochem. 79−36790
isotope enrichment in methane-H_2 mixture, by glow discharge exposure 78−13343
isotope separation, by tunable-laser predissoc. of formaldehyde 79−94095
isotope separation, laser method, depletion optimisation and photon efficiency 78−46175
isotope separation, laser multiphoton photodissoc. of fluoroform-d 79−94096
isotope separation by H_2-Pd system, effect of isotopic conc. on separation coeff. of H-T, H-D and D-T mixtures 79−71979
isotope separation by IR laser photolysis of trifluoromethane-d_1 79−79276
isotope separation single step enrichment by laser multiphoton dissoc. of dichlorotrifluoroethane 79−64112
isotopic exchange equilibrium with Li fusion blanket 79−49845
Jupiter, D-burning star hypothesis 77−13282
KBr(I):D, inelastic light scattering of localised vibration of interstitial H atom in alkali halides 80−88998
lamp, calibration, operating time variation of spectral radiance 77−10992
lamp, spectral irradiance standard for UV, calibration 78−42397
laser fusion microsphere targets, nondestructive anal. using rot. Raman spectroscopy 80−50896
laser isotope separation, large-scale, generalised concepts 80−68958
laser isotope separation, reaction chamber 78−55040
laser produced plasma in shell target, diagnostic methods 77−62408
liquid, self-diffusion 77−35746
liquid, US vel., 22-35K *(Russian)* 78−75731
liquid n-H_2, n-D_2, Ne mixtures, deviation from Rao-Wada rule 78−75729
liquid ortho-D_2, convertor for ultra cold neutrons 79−45520
local interstellar H and D densities, Copernicus obs. 78−16487
magnetic relaxation study in Fe 78−64228
Maxwellian ion plasma, neutron prod., ion temp. diagnostics appls. 80−49005
melting curve, meas. of P, V, T and longitudinal sound velocity 79−37814
metal:D, dynamic quadrupole nuclear spin relax., α or α' phases 77−48085
metallic, ground-state energies of liq. and solid phases, variational and Monte Carlo methods 80−70502
methane, deuterium substituted, in condensed inert gas, optical excitation of rotational transition, far IR absorption spectra 80−37808
migration and trapping in U and UO_2 during D^+ implantation 80−34243
molecular electron impact excitation, rot. transitions *(Russian)* 79−76524
molecular photodissoc., D(2p) dissoc. products detection 78−50605
molecular rotational levels and consts., nonadiabatic corrections 77−18906
molecular solid, eqn. of state, 4.2K isotherm, ortho-para depend. 79−7670
molecule, ${}^1\Sigma^+$ states, adiabatic calc. of vibronic states 78−5198
molecule, and H_2, dissociative electron attachment and vibr. excitation, low-energy 80−23565
molecule, c, I and i states, pot. energy curves and vibr. levels, Born-Oppenheimer approx. 78−931
molecule, Compton profile, impulse approx., electron correl., vibr. and rot. effects 78−17585
molecule, Compton profile determ. by high energy electron impact spectroscopy 77−68083
molecule, dissociative attachment of electrons *(Russian)* 78−13621
molecule, dissociative electron attachment, Faddeev calcs. of cross sections *(Russian)* 78−70945
molecule, effective vibr.-rot hamiltonian 77−27052
molecule, elec. field gradient, calc. of D quadrupole moment 79−93511
molecule, electron Compton profiles from energy loss spectra 79−7013
molecule, electron dissociative attachment rates, rot. (vibr.) excitation depend., in plasma 80−43848
molecule, electron impact, Balmer-α, β, γ radn. emission cross sections 78−1091
molecule, electron impact, Balmer-α emission Doppler profile energy depend. 77−42423
molecule, electron impact, H,D(2s,2p) prod. 78−42230
molecule, electron impact, H(2S) and D(2S) form., predissoc., time of flight obs. 79−86079
molecule, electron impact, threshold excitation and predissoc., electron-photon coincidence meas. 80−18941
molecule, electron impact dissoc., anticrossing signals, Doppler-profile technique 78−33619
molecule, electron impact dissoc. ionisation 80−83510
molecule, electron impact dissociation by vibrational excitation *(Russian)* 78−1096
molecule, electron impact dissociative ionisation near ${}^2\Sigma_g{}^+$ state, dissoc. threshold 80−43197
molecule, electron impact excitation, transfer of moment impulses, vibration-rotation states *(Russian)* 79−7024
molecule, electron impact spectroscopy, high energy, Compton defect 77−88578
molecule, electron scatt., isotope effects 77−58188
molecule, extremal scattering, from MgO (001) surface 79−95891
molecule, Fulcher band system, rot. struct. 79−98986

deuterium continued
molecule, G, K double-minimum excited state, vibr. eigenvalues 78−33442
molecule, high resolution CW CARS spectra of Q-branch 77−58023
molecule, in zeolitic matrix, IR active fundamentals obs. 77−71800
molecule, IR spectra, mol. rot. and vibr. const. determ. 80−78617
molecule, light scattering, intermol. collision process obs. 80−53001
molecule, Lyman bands, Morse Frank-Condon factors and R-centroids 77−58088
molecule, matrix rot. and vibr.-rot. spectra, free and hindered rot. 77−83607
molecule, ortho-para transistion, catalytic-, radiation-, and self-induced conversion, review 77−90633
molecule, photoabsorpt. spectra, rovibronic interactions 78−992
molecule, photoionisation, body-frame Hund's case b description 78−94295
molecule, predissoc. linewidths and shapes for $3p\pi D{}^1\Pi_u{}^+$ state 80−53066
molecule, Q(2) line, absolute Raman freq. meas. using CW CARS 78−29794
molecule, Raman spectra, vibr. freq. press. shifts 78−78703
molecule, rot. and vib. relax., semiclassical calcs. 77−34723
molecule, Rydberg state predissoc., Lyman and Balmer emission obs. 77−38702
molecule, Rydberg states, nonadiabatic effects, elec. field ionis. 80−9528
molecule, sticking and accommodation on low-temp. substrate, mol. beam expts. 80−84368
molecule, zeolite matrix isolated, induced IR spectra 78−46333
motion in Pd and $Pd_{0.9}Ag_{0.1}$ alloy, thermodynamic data 79−65254
muonic atom+Y, muon transfer mechanism from free muonic deuterium 80−69218
muonic D+He, μ^- transfer rate 77−42447
NMR spin echo responses in solids 80−25248
NQR, Robinson scheme, electronics appls. 80−63668
one dimensional motion, statistics 77−85050
origin, neutrino-induced nucleosynthesis 77−87582
origin, obs. and interpretations 77−71160
origin and abundance, cosmological appls. of pair prod. in intense mag. fields 77−13505
overbarrier states in metals, subsystem heat capacity, equilibrium props. *(Russian)* 80−79998
oxidation on Pt, matrix isolation and laser fluoresc. obs. of prods. 80−66865
paeonol and urinary metabolites labelled with ${}^{13}C$ and D, synthesis and physicochem. props. 80−67250
parity violation as consequences of isoscalar axial-vector current 79−93316
pectolite (hydrous silicate), lowest δD value 79−62513
pellet, ionisation by Nd laser irrad. 80−43949
pellet, plasma density distrib. prod. by ruby laser irradiation 77−3966
penetration, into Ni-Cu alloy, reversed kinetic isotope effects 77−43387
penetration through Armco iron, mass spectrometric obs. 78−47606
permeability, diffusivity and solubility in pure Fe at 10 to 60°C 78−75887
permeability, of Ni, anomalously high transmission, 20-520°C *(Russian)* 77−72752
permeation, in Pd, comparison to H_2 *(Russian)* 78−75881
permeation and diffusion in 310 stainless steel, 472 to 779K 79−55937
permeation eccentricities of He, Ne, and D-T, from SiO_2-CaO-Na_2O glass microbubbles 78−47598
permeation in Cu alloys, Cu-Au and Au, growth of permeation barriers 78−75883
permeation in stainless steel 80−34241
physisorbed monolayer on graphite, neutron scatt. studies 80−107655
plasma, beam-heated, in Princeton Large Tokamak, neutron emission profiles 78−63588
plasma, compression and heating by shell, thermonuclear neutron output *(Russian)* 77−371
plasma, dense focus, neutron production 77−74989
plasma, effect of Ar admixture on plasma temp. 79−37446
plasma, electrode discharge, nonhydrodynamic pinch compression, kinetics and D^+ focusing *(Russian)* 80−38689
plasma, high current pulse discharge investig. *(Russian)* 78−47171
plasma, in Alcator Tokamak high-density discharge, parameters for D_2, neutron emission 78−18438
plasma, in ring cusp type mag. bottle, width meas. 80−87927
plasma, inertial confinement, reaction gains, reheat calcs., collective model 78−59664
plasma, isolated energetic, prod. by CO_2 laser 79−14577
plasma, laser amplitude calibration from Raman spectra, for diagnostics *(Russian)* 80−38702
plasma, laser prod., interaction with mag. fields 77−76151
plasma, laser prod., multipulse heating 77−76152
plasma, neutral injection kinetics, Monte Carlo anal., local liberation to wall 77−42992
plasma, neutron generation by CO_2 laser implosion of polyethylene shell into conical region 78−87468
plasma, nonuniform Vlasov, linear normal modes of electrostatic perturbations, calc. method 77−42977
plasma, T-4 tokamak, ion cyclotron heating, obs. *(Russian)* 79−27796
plasma, TFR Tokamak current plateau, O_2 injection effect on Mo impurity 78−22565
plasma, theta-pinch, Pharos device with end stoppering, homogeneity, stability 78−34360
plasma diagnostic technique using self reversed deuterium D_α line 78−55746
plasma focus, Al ion acceleration *(Russian)* 79−77415
plasma focus heating by TEA CO_2 laser and anomalous absorpt. obs. *(Japanese)* 77−43013
plasma formation by ultrashort laser prepulse 77−72464
plasma in laser target, neutron meas. 77−7596
plasma production, Nd:glass laser irrad. of freely falling D_2 pellets 77−58874
plasmas, PLT Tokamak, ohmically heated plasmas, radiation, impurity effects, instability and particle transport 80−28833
polarised beam source, Crypol 2 79−63324
in powders, high speed rot., spin diffusion, NMR spin lattice relax. obs. of D 80−66056
pre-main-sequence stars, early evolution with D burning 80−51736
prep. by electrolysis of heavy water using self-controlled cell 78−80752

deuterium continued

- pressure effect on width and shift of atomic fluorescence of TlI 80—99475
- primordial black hole evaporation rel. to D origin *(Russian)* 77—74172
- probe for investigating ultraslow rot. in solids 80—88890
- production in advanced stellar evolution, reaction cross sections 80—56815
- production model limitations based on high-energy neutrino background 79—44328
- profiling of near-surface regions of materials during deuterium implantation 77—59037
- pumping by Ti film, pumping speed comparison between H_2 and D_2 78—51819
- pumping speed in Ti sublimation pump, deuteriding inhibition by surface contamination 77—57335
- pumping speed of overlaid Ti thin films 78—33286
- quadrupole resonance, double transitions, appls. 79—3465
- radiation induced detrapping of implanted D in BeO 80—32482
- radiation induced exchange reaction kinetics of H_2, D_2 and T_2, review 78—61005
- Raman spectra of molecules dissolved in vitreous SiO_2 79—33707
- reflection from amorphous Be, Fe, Mo, W, Monte Carlo study 80—40197
- release of hydrogen isotopes co-dissolved in Ti, Nb 80—37580
- scattering, adsorption, and absorpt. on Pd (111), mol. beam study 80—29277
- scattering from and selective adsorption on graphite (0001) surface 80—71553
- separation in NH_3+HD exchange 80—3310
- shell target compression on laser heating *(Russian)* 80—47718
- solar abundance determ. 79—66982
- solid, 0.5-3 keV electron penetration depth 78—56549
- solid, compressed, anomalons double peaked one-phonon for IR absorption 79—56788
- solid, elastic constants and anisotropic pair correls. 79—33042
- solid, electron emission under bombard. by keV electrons, H and D ion beams 77—73196
- solid, equation of state, at high pressure 79—46781
- solid, far IR absorption by phonons and librons in ordered state 78—80331
- solid, fundamental absorption spectra, 10 to 40 eV at 2K, using synchrotron radiation 79—73967
- solid, HCP, density depend. of elastic consts. 80—6589
- solid, HCP, effects of internal strains on elastic consts. 77—24343
- solid, interface with Cu, thermal boundary resist., 1-3K 77—20178
- solid, interface with Cu, thermal boundary resist. meas. above 1K 77—72769
- solid, intermolecular pair potential, from solid-state data 79—14727
- solid, libron spectra and conversion as function of ortho-para conc., Raman scatt. spectra 78—84570
- solid, ordered cubic phase, NMR spin echo responses 79—47356
- solid, para, roton dragging librons 78—67886
- solid, paraphase, orientationally ordered state, anomalous far IR absorption spectrum 78—10876
- solid, phonon absorption line shape as function of density 80—50329
- solid, phonons in linear chain with hard-core pot. 77—11644
- solid, press. depend. of phonon lineshape in ordered state, far IR spectra 79—56023
- solid, quadrupolar glass ordering NMR absorption line shapes 80—7178
- solid, Raman active optical phonon, density depend. 79—87432
- solid, Raman scatt. meas. of rotational spectrum under press. 77—69814
- solid, room temp. melting point, press. depend. calcs. 80—103463
- solid, secondary electron emission, electron and ion induced 79—1803
- solid, sp. ht. effect of Ne impurities 79—33099
- solid, thermal cond. *(Russian)* 78—38885
- solid adsorbed layer, porosity of solid gas layers, appl. to cryosorption pump *(Japanese)* 80—20031
- solid bombardment target, construction and operation 77—6590
- solid para-, bound libron state form., Raman scatt. data 77—80600
- solid target prep. for laser fusion research 78—17417
- solid-liquid coexistence curve anomaly *(Russian)* 78—75824
- solubilities in pyrolytic C 80—37443
- solubility, in nonstoichiometric Pd_3P_{1-x} 80—59662
- solubility in Nb-H(D) system, enthalpy and entropy, isotope effects 77—20069
- solubility in SiC, exam. 78—79816
- solubility of H_2 and D_2 in Y *(Japanese)* 78—18784
- solution in Pd, isotope effect model 77—66026
- solution in $TiCr_{1.8}$, enthalpy, solubility and mol. vibr. determ., comparison with soln. in metals and binary alloys 80—79951
- sorption at press. up to 1500 atm. on rare earth alloys, RM_x (M=Co, Ni) 80—97819
- source, magnetically insulated, pulsed, peak beam parameters 80—32548
- spatially correlated ions studies, cell survival obs. using diatomic deuterium 80—36026
- spin-aligned, ground-state energy and finite temp. props. 77—61014
- storage, in La_7Ni_3, neutron, X-ray diffr. study 78—83954
- supercooled, possible phase change to superfluid state 77—62707
- thermal desorption meas. of H-isotope retention in Alcator-A Tokamak 80—79588
- thermonuclear fusion plasmas, elem. processses and role of atomic, ionic and mol. data 80—14916
- Tokamak fusion reactor first walls, hydrogen profiles 80—37578
- tracing in Icelandic hydrothermal systems 78—69386
- transport in hot BH plasma, moment method calc. 78—22458
- transport through stainless steel membranes at low driving press. 78—34552
- trapped in stainless steel, ion induced release 78—95095
- trapping and replacement of 1 to 14 keV H and D in stainless steel 78—95070
- trapping in Fe alloys formed by ion implantation 80—15131
- trapping in fusion reactor materials, temp. dependence 80—37577
- trapping in ion-bombarded Be 79—19291
- trapping in irradiated stainless steel 316 78—95069
- trapping measurement in bulk and plasma-sprayed coatings 80—20754
- trapping of 6 to 15 keV in C, temp. depend. and depth profile 77—30664
- trapping of H isotopes, materials exposed to high power discharges in PLT 80—37576
- trapping up to 7 eV in austenitic stainless steel 316, depth profiles 78—71751

deuterium continued

- universal abundance 80—62356
- uptake kinetics and energetics by Mn vacuum evaporated films 80—88430
- UV lamp, microwave discharge in H_2-D_2-He, H and D Lyman-α line shapes 79—80698
- vapour pressures, 4 to 30K, isotope effects 77—72674
- VUV radiation, narrowband tunable, at Lyman-α wavelength 80—78907
- D-T pellet, ideal gas treatment, implosion and shock waves 78—55735
- DD reaction for neutron generation in thermonuclear reaction initiation *(Russian)* 80—42848
- ddμ mesic mol. form. in gas D_2, reson. depend. *(Russian)* 79—50171
- μd+d elastic scatt. cross section for muonic d 79—89811
- $\bar{p}$ radiative atomic recombination, antiprotonic atoms 80—83527
- $Ar^+(^2P_J)+D_2$, Ar^+ two spin orbit state, reaction cross section, direct determ. 80—93748
- $BF_3+BF_3(D_2)$ (inert gas), US dispersion meas. 78—17758
- $Ba^+ + D_2 \rightarrow D + BaD^+$, sequential impulse model, prod. bond dissoc. energy and cross section 80—81295
- $CH_2^+ + D_2$, reaction products translational energies 77—86298
- $CO+NO(O_2)(D_2)$, ($\nu=1$) relax., temp. depend., D_2 self-relax. 78—17760
- CO_2^+-D_2, DCO_2^+ and DCO^+ formation 77—60056
- CO_2+D_2, near reson. V-V exchange 77—27165
- $CO_2+H_2(D_2)$, ab initio LCAO-MO-SCF intermolecular pot. energy surface, V$\rightarrow$T transfer 77—50489
- $CO_2(00^01)+H_2(D_2)$, intramol. vibr.-vibr. transfer cross sections calc. 100-3000K 78—1053
- ^{13}C NMR, ^2H label quantitative meas. 77—50456
- $Cd(^3P_J)(^1P_1)+D_2$ reacts., CdH(CdD) yields, quenching cross sections 79—1948
- CdS:D^-, binding energy of D^- ion 80—92541
- $Cl+D_2 \rightarrow DCl+Cl$, LEPS pot. energy surface, rate consts., isotope effect, quasiclassical trajectory calc. 78—56887
- $Cl^+ + D_2$, inelastic and superelastic collisions, DCl^+ formation mechanisms 78—20011
- Cs-D_2, vap., oscill. production of particulates, by CW laser beam 77—77794
- D I Lyman α radiation scattering near Venus, Venera 9 and 10 obs. 77—78703
- D NMR, appls. for physics, chemistry and biology 77—87801
- D NMR, hydrocarbon chain ordering in model membrane, D quadrupole splitting 78—64947
- D^- ion source for high voltage neutral beams for fusion reactors 80—99379
- D^- ions, equil. charge state fractions of 3.3-39 keV D atoms and ions in Mg vapour 77—57788
- D^-, neutral beam production for plasma injection heating research 77—76118
- D^- polarised ion sources, recent advances 79—45498
- D^-, polarised prod. in ^1H+Cs atomic collision at 40 keV, 3.1 μA 78—55078
- D^-, prod. of 100 keV beam, transport, accel. and diagnostics 77—83440
- D^- source using surface ionis., continuous beam prod. 78—9021
- D^-, three-particle atomic system, binding energy, Faddeev method calcs. 77—57858
- D^+ beam production in relativistic electron beam oscill. diode 78—9861
- D^+, D_2^+, D_3^+, ion mass, energy, current density distribs. from duoplasmatron ion source 77—23339
- D^+, D_2^+ and D_3^+ fragments traversing thick foils, correls. in motions, integral ang. distribs. 80—16136
- D^+, mobility in He and Ne, 300K 77—11303
- D^+ source, performance improvement, appl. to fusion reactor neutral beam lines 79—22511
- D^+, sputtering yields 77—36343
- D/H for rocks in Tertiary igneous complex of Skye 77—33012
- D/H in Jupiter, ratio determ. using new spectroscopic method 79—84734
- D/H ratio, in Jupiter atmosphere 78—45265
- D/H ratio and cosmic ray ionization in interstellar clouds 79—17063
- D/H ratio in early Solar Systems, H and O isotope study in chondritic meteorites 80—36518
- D/H ratio in Uranus atmosphere, meas. 78—57497
- D/H ratio in waters from El Tatio geothermal field, N.Chile 79—16525
- D/H ratios in meteoric water over N.America (9500-22000 BP), climatic implications 77—60462
- D/H ratios of natural serpentines, rel. D/H fractionation factors between serpentine and water at 100-500°C 79—34803
- D-^{18}O relationship for atmospheric precip., global climatic interpretation 80—17331
- D-^3He, clean fusion reactor feasibility study 78—33288
- D-^3He fusion reactor advanced fuel development and confinement 79—13516
- D-^3He satellite fusion reactor, field-reversed mirror confinement 78—70643
- D-D fusion reactor advanced fuel development and confinement 79—13516
- D-D fusion reactor blanket, nucl. characts., summary 78—89973
- D-D nonideal system, generalised feasibility criterion for controlled fusion 77—46398
- D-H plasma, HF heating by magnetoacoustic waves *(Russian)* 77—3960
- D-plasma, interaction with Al_2O_3, surface effects 78—53010
- D-T, liq., dielectric constant and elec. cond. 80—84680
- D-T, solid, estimated heat capacity, enthalpy, thermal cond. and diffusivity 77—4228
- D-T, steady-state thermonuclear reaction in Tokamak *(Russian)* 77—18693
- D-T ball, compressive plasma fusion using CO_2 lasers 78—82507
- D-T ball, explosion compression of plasma up to critical values of thermonuclear microfusion 77—67873
- D-T ball, laser driven compression with profiled explosion induced precompression 77—68838
- D-T charges, explosion-induced compression for thermonuclear microfusion, power station paramèters 78—82508
- D-T compression, explosion-induced, thermonuclear avalanche reaction 78—47144
- D-T cylinder with plexiglass envelope, profiled cylindrical explosion-laser compression 77—68837
- D-T filled glass microshell, laser-irrad., plasma electron energy profile steepening, polarimetry obs. 78—34349
- D-T filled laser fusion microballoon targets, fuel content characterisation and press. retention meas. 79—54594
- D-T fusion fuel, liquid-vapour equilib., Raoult's law 79—67947

deuterium continued
D-T fusion plasma, parametric noise effect on temp. stability 77–39439
D-T fusion reactor, tritium recovery using Zr, Y *(Japanese)* 78–29646
D-T fusion reactor core plasma, α-particle heating, dynamic characts. 77–74985
D-T fusion sources, light water hybrid breeding reactors, source driven 79–13518
D-T laser fusion target, fabrication using cold-gas jets 79–49833
D-T layer implosion through nonhomogeneous transition layer 78–74465
D-T linear mag. fusion device, particle end loss reduction 78–33289
D-T magnetoplasma, fusion effects on diffusion and thermal cond. 77–67883
D-T microsphere, concentric cumulation of laser generated fast ions 78–30456
D-T miniball in heavy envelope, explosion compression of plasma up to critical values of thermonuclear microfusion 77–67872
D-T pellet neutron moderation on blanket neutronics of inertially-confined fusion reactors 80–836
D-T pellets surrounded by high density shells, implosion characts. 77–3969
D-T plasma, adiabatic heating and fusion energy production by compressible fast liner 79–31182
D-T plasma, EM field induced resultant drift inwards from boundary 80–38577
D-T plasma, fast-wave ion-cyclotron and 1st harmonic heating, in large Tokamak 77–51204
D-T plasma, hot, dense, alpha-particle transport calc., moment method 78–22458
D-T plasma, ion-cyclotron wave spectra dispersion eqn. numerical soln. *(Russian)* 78–59561
D-T plasma, kinetics of compression induced fusion chain reaction 78–50297
D-T plasma ball, critical continuously shaped concentric explosive compression, approx. estimate 78–87473
D-T shell, thin, hollow, laser-driven implosion, ignition problem 79–31183
D-T target, laser pulse compression, thermonucl. reaction initiation *(Russian)* 77–23249
D-T thermonuclear plasma, neutron collision diagnostics *(Russian)* 77–34471
D-Xe plasma, shock-wave struct., heavy doping effects *(Russian)* 77–11343
D+alkaline earth, D^- ion production, multiple charge-transfer collisions 79–89776
D+Ar, differential collision cross sections, diffraction oscills., data anal. 79–22783
D+Ar(Kr)(Xe), ion pair formation, curve crossing model 80–87216
D+atom, K_α/K_β ratio for at. X-ray transitions 80–27972
$D+Cl_2$, collinear reaction rate consts., quantum and semiclassical calcs. 77–12782
$D+Cl_2$, reaction probabilities, information theoretic anal. 77–16799
$D+Cl_2$, uni- and bimodal product energy distribs. 79–57207
$D+Cl_2$ 80–93734
D+Cs, ang. scatt., neutral beam form. via negative ions 77–46636
$D+D_2$, collinear reaction, transmission coeff. isotope depend., statistical theory, invariance 77–36748
$D+D_2^+(CO_2^+)(CO^+)(N_2^+)(HCN^+)$, reaction, ion cyclotron reson. mass spectrometric obs. 79–64098
$D+D_2(\nu)$, vibr. relax. in at. exchange reactions, classical trajectory calcs. 77–44467
$D+F_2$, DF initial vibr. energy distrib., IR chemiluminesc. obs. 80–45497
$D+F_2$, exothermic triatomic exchange reactions, dynamics, anal. theory 78–3322
$D+F_2$, impulsive triatomic reaction, vibr. state distrib., impulsive energy release model 78–92456
$D+F_2(Cl_2)$, exothermic triatomic exchange reactions, prod. energy distrib., statistical dynamic model 78–92455
$D+F_2\rightarrow DF+F$, exchange reaction, quasiclassical dynamics calcs. 79–91942
$D+F_2\rightarrow DF+F$, isotope effects, quantum mech. and information theoretic calcs. 78–44360
D+FD(FM), low barrier quantum model, vibr. deactivation on chemically reactive potential surfaces 80–69216
D+fluoromethane, reactions, selective vibr. excitation effects 78–35643
D+H, close coupling calc., resonant spin-flip process, Ramsauer-Townsend effects 80–99547
D+H, excitation transfer, thermal energy, dipole-dipole interaction 79–31666
$D+H_2$, pot. surface, isotropic part determ. 79–36729
$D+H_2$, vibr. excitation cross-sections, rot. averaging calcs. 78–9231
$D+H_2$ reaction, transition state theory calculations, kinetic isotope effect explanation 80–66784
$D+H_2$ reactions, accurate pot. energy surface, isotope effects, quasiclassical trajectory study 80–97698
$D+H_2$ rearrangement collision, vibr. excitation effects 80–71910
$D+H_2(HCl)$, relax. and chem. reaction, time resolved IR fluoresc. and mass spectrometry obs. 80–69177
$D+H^+\rightarrow H+D^+$ near threshold rel. to HD molecule formation in interstellar medium 78–89239
D+HBr, vibr. energy transfer, phase shift 79–64080
D+HCl(HBr), elastic scatt., van der Waals pot. meas. 77–58120
D+HCl(HBr)(HI), abstraction and exchange reactions 78–73025
$D+HCl\rightarrow DCl+H$, rate consts., EPR 77–9059
$D+HCl\rightarrow HD+Cl$ or $DCl+H$, branching ratios determ. 78–40046
D+HF, kinetic isotope effect and temp. depend. 78–53202
D+HF, vibr. threshold energies, reagent energy effects 78–85145
$D+HI\rightarrow H+DI$, Franck-Condon theory 78–60984
D+HX(H=Cl,I), HX dissociative ionisation, H^+ signal origin, mol. beam obs. 80–66778
D+He*, Penning and assoc. ionis. with metastable He, 0.01-10 eV beams 79–27074
$D+He(2^3S)$, Penning and assoc. ionis. cross sections, vel. depend. 79–22815
$D+M\rightarrow D^-+M^+$ (M=alkali metal atom), ion-pair form. 78–58779
$D+N_2$, fast collision, electron scatt. resons., ionisation, deexcitation 79–81268
D+Ne(Ar)(Kr)(Xe), free electron production, integral cross-sections determ. 79–89754
$D+O_3+CO_2$, mixing in supersonic streams to produce CO_2 chem. laser 77–676
$D+O_3+CO_2$ mixture supersonic jet, gain meas. for CO_2 laser 79–89902
D+PTFE, DF* prod., Fourier transform IR spectroscopy 80–87105
D+Sr, 2.7 to 31 keV, D^- equilib. charge-state fractions 78–17750
D+T, guiding centre distrib. spatial separation, reaction rate enhancement 80–33737
$D+T_2$, H-exchange studied by crossed molecular beam experiments 80–93747
D+toluene(1,3,5-trimethylbenzene), vibrational and rotational energy effect 80–76497
D^++Ar, electron capture to continuum states, forward ejected electron spectra 79–45831
D^++atoms (Z=27 to 34), K shell ionisation, nuclear Coulomb effect 80–91650
D^++Au(Pb)(Th)(U), L-subshell vacancy production, Coulomb deflection effects 80–9711
D^++CO_2, vibr. excitation, isotope and time effects 80–63773
D^++D, thermal energy collisions, quantum mech. calcs. 80–23507
D^++He, mobility and diffusion runaway effect 80–33727
D^++He, runaway mobility obs. 80–38517
$D^++Rb\rightarrow D^{-,0}+Rb$, equil. fraction of D^- ions, charge transfer cross section 77–65375
D^++Sr, 2.7 to 31 keV, D^- equilib. charge-state fractions 78–17750
D^++Xe double charge exchange, D^- prod. *(French)* 79–94080
D_2^+,(DT^+), IR transition freqs. calcs. 77–88452
D_2 (HD)+Ar, reson. energy transfer cross section, 1st Born approx. appraisal 77–65519
D_2, condensation in laser fusion targets 77–42190
D_2, elec. quadrupole vibr.-rot. spectrum, 2.8 to 3.9 μm 79–805
D_2, electric discharge, vibr. excitation spontaneous Raman scatt. obs. 78–5234
D_2, electron impact dissoc., excited atom kinetic energy distrib. *(Russian)* 78–22045
D_2, electron impact dissoc. to D^+ from autoionising states 79–54980
D_2, electron impact dissociative excitation 78–13618
D_2, electron scattering, total cross section meas. at very low energies 80–58398
p-D_2, far IR absorpt. in ordered state 79–91430
D_2, $G(3d)^1\Sigma_g^+$ and $g(3d)^3\Sigma_g^+$ singlet-triplet anticrossing 78–42138
D_2 gas discharge lamp as UV continuum source, space appls. 80–36505
D_2, HD, and H_2, nonadiabatic coupling of EF and GK $^1\Sigma_g^+$ states 79–59431
D_2, high press. discharge props. electrode influence, spectra obs. 80–38806
D_2 high pressure HF discharges and DC arcs, instability obs. 80–38807
D_2, intermolecular pair potential, from solid-state data 79–14727
D_2 matrix shift, CoM freq., in solid Ar, Kr and Xe 79–6969
D_2, mol. bands, electron impact excitation, rot. transitions, cross sections in plasma 80–37896
p-D_2, order parameter temp. depend. 79–42242
p-D_2, order-disorder phase transition 78–79726
p-D_2, orientational ordering, transition temp. and change of symm. 77–31609
D_2, photodissoc., fragment Balmer series fluoresc. 77–27020
D_2, quadrupole mass filter sensitivities and β-particle induced exchange kinetics 78–58090
p-D_2 quantum molecular crystal, quantum quadrupolar phase theory *(Russian)* 78–22929
D_2, rotational Raman intensities and polarisability anisotropy change meas. with internuclear distance 80–63641
D_2, semiempirical nonadiabatic pot. energy curves calcs. 78–17744
p-D_2, solid, libron spectrum calc. 78–79677
n-D_2, solid, nucl. spin-lattice relax. and evidence for low temp. phase transition 79–56022
o-D_2, solid, up to 150 kbar, 5K, Raman spectrum 80–50332
D_2, threshold photoelectron spectra, 15-20 eV 79–54912
n-D_2, triple point determ. 79–95124
D_2^-, collision induced dissoc., positive and negative ions form. 78–50612
D_2^+, 0.3-2 keV radiation damage of Mo, use of 300 eV D_2^+ as ion microprobe 77–43260
D_2^+, dissociative recombination, projection operator formalism 77–3479
D_2^+, dissociative recombination cross sections 79–59568
D_2^+, electron impact, dissoc. recomb., highly excited atom form. *(Russian)* 78–33621
D_2^+, expectation values, Born-Oppenheimer, adiabatic and non-adiabatic results 78–82624
D_2^+ implantation in Mo, radiation induced vacancies 80–65076
D_2^+ molecular ions, dissociation in migmacells II and III, advanced fusion fuel expts. 77–83088
D_2^+, muonic, three-body Coulomb interaction, adiabatic representation 79–31640
D_2^+, photodissoc. cross section, time of flight anal. of reaction products 77–83664
D_2^+, semiempirical nonadiabatic pot. energy curves calcs. 78–17744
D_2/CCl_4, inhomogeneous broadening of Morse oscillator, temp. depend. 77–61803
D_2-^{3}He, filled microspheres, implosion expts. 78–59672
D_2-^{3}He mixture plasma focus, ion temp. 78–5953
D_2-Ar, thermal dissoc. of dilute mols., vibr. bias mechanism 79–61854
D_2-CO_2, laser system, interaction between vibr. states, theory 77–23670
D_2-DT-T_2, three-phase region, temp.-press.-composition correlations 77–84889
D_2-DT-T_2 mixture, solid and liq., props. for fusion reactor applications 78–66415
D_2-filled cone, fusion neutron generation using explosive implosion of polyethylene shell 78–82510
D_2-H_2, liq. mixtures, self-diffusion 77–35746
D_2-HCl, vibr. relax. time meas., by coherent Raman-induced IR fluoresc. 79–7038
D_2-HCl electric discharge gasdynamic laser, turbulent mixing characts. 78–9366
D_2-HCl-Ar(He) gasdynamic lasers, gain 79–64217
D_2-inert gas, bound complex form., anisotropic intermol. pot., IR spectra anal. 78–37634
D_2-Ne capillary-arc lamp, optimum parameters 80–95971
D_2-T_2-H_2, fusion reactor fuel, isotopic exchanges, equilib. consts., 4.2-300K 77–70331
$D_2+^{38}Cl$, reactions, characterisation, effect of ethylene-I_2 scavenger 78–73071

deuterium continued

- $D_2+B^+(^3P_u)$, reactive scatt., 1-40 eV, ion products ang. and energy distrib. 79—98214
- D_2+Ba, radiation quenching of metastable Ba (5d ^1D) in gas 79—85932
- D_2+Br^-, total electron detachment cross sections for energies around threshold 80—99550
- $D_2+Br(4^2P_{1/2})$, electronic-vibr. energy transfer, fluoresc. meas. 79—72347
- D_2+C^+, $CH^+(D^+)$ $A^1\Pi$ rot.-vibr. population distribs. 80—23396
- $D_2+CH_n^+$, isotopic exchange, interstellar implications 80—61087
- D_2+CHF_3, vibr. relax. times at 298K 77—525
- $D_2+CO_2^+$, DCO_2^+ form., threshold form. energy 80—50844
- D_2+CO^+, state selected reaction cross-sections, coincidence technique obs. 80—66797
- $D_2+Cd(5^3P_{0,1})$, absolute quenching cross sections 80—5604
- D_2+chloroform, energy transfer laser 77—88701
- D_2+Cl, thermal rate constants, quasiclassical trajectory calcs., detailed balance 79—87822
- D_2+Cl^-, total electron detachment cross sections for energies around threshold 80—99550
- D_2+D, atom transfer reaction in gas phase, reaction rate computing, tunnelling corrections 79—79237
- D_2+D_2, ladder operators in vibr.-vibr. and vibr.-translational transitions at high collisional energies 80—106382
- D_2+D_2, rot. relax., close coupling calc. 77—58141
- D_2+D_2, total scatt. cross-section, below 10 meV 80—28087
- D_2+D_2, $V \rightarrow T$ rate constants, deconvolution 77—27152
- D_2+DF, vibr. relax., laser-induced fluoresc. obs. 79—64028
- D_2+F, absolute rate coeffs. at 295 to 765K 80—81303
- D_2+F, absolute reaction rate coeffs., time resolved IR emission meas. 79—68258
- D_2+F, rate consts., temp. depend. 80—81302
- D_2+F, reaction kinetics, pot. energy surface and Franck-Condon integrals 79—61855
- D_2+F, reaction rate constants, modified collision theory expression, comparison with exact expression 79—74370
- D_2+H, pot. curve, thermal energy absolute integral cross-sections meas. 80—53096
- D_2+H reaction, transition state theory calculations, kinetic isotope effect explanation 80—66784
- D_2+H reactions, accurate pot. energy surface, isotope effects, quasiclassical trajectory study 80—97698
- D_2+H_2, exchange reaction, gas phase, heterogeneous initiation *(French)* 78—85149
- D_2+H_2, reactive and inelastic scatt. using repulsive model pot. energy surface 78—66620
- D_2+H_2 exchange reaction, steady-state, surface reaction effects *(French)* 78—85148
- $D_2+H_2^+ \rightarrow D_2H^+ + H$, product angular and vel. vector distributions meas. by crossed beam expt. 80—101012
- D_2+H_2O, isotope exchange on Pt, CO poisoning effects 79—11824
- D_2+H_2O, isotope exchange on Pt over hydrophobic support 79—11823
- $D_2+H_2(N_2O)(O_2)$, Wassiljewa coeffs., thermal conds., 50 and 100°C 79—37437
- $D_2+H_2 \rightarrow 2HD$, transition state, study of Jahn-Teller instability of H_4 78—60995
- D_2+H^+, collisional complex form. 80—58339
- D_2+H^+, differential inelastic and reactive scatt., low energies 78—62911
- D_2+HCl, HCl ν_0-ν_1 band perturbations, linewidth and shifts calcs., IR spectra obs. *(French)* 80—58251
- D_2+HD, vibr. relax., 80 to 400K 80—5607
- $D_2+HD(Ne)(Ar)$, state-resolved $\Delta j=2$ rot. transitions 80—63772
- D_2+HF, vibr. relax. dye laser pumping effects 80—9703
- D_2+He, vibr. deexcitation, cross sections, rate consts., vibr. rot. model 78—62879
- D_2+He, vibr. relax., 400-80K 77—10736
- D_2+He, vibr. relax. times, 3D semiclassical theory 78—25667
- D_2+He, vibr.-rot. transitions, optical potential approach 78—62885
- D_2+He^+, dissociative ionisation, D^+ energy spectra 77—58154
- $D_2+He^+(Ar^+)$, small angle charge exchange, 0.5 to 1.0 keV, time of flight spectra 78—33604
- $D_2+He(2^3S$ and $2^1S)$, Penning, rearrangement and total ionis. cross sections, vel. depend. 79—22816
- $D_2+I(5^2P_{1/2})$, electronic to vibrational energy transfer 79—68259
- D_2+Li^+, vibr. excitation cross sections, 100-1200 eV 79—27077
- $D_2+Li^*(2^2P_J)$, collision induced quenching and transition rate coefficients meas. 80—74221
- D_2+N_2, vibr. relax. in liquid phase 79—847
- $D_2+NH(ND)$, $(b^1\Sigma^+)$ states quenching, kinetic isotope effects 77—63891
- D_2+NO^+, reaction rate consts. meas. 80—7782
- $D_2+Na^*(3^2P)$, electronic to vibr.-rot. energy transfer, differential cross sections 77—38715
- D_2+Ne, anisotropic potentials, direct inversion methods calcs. 80—69090
- D_2+Ne^+, elastic scatt. at small angles, 1.3-3.5 keV, scaling law 78—82812
- $D_2+Ne(Ne^+)$, energy-loss scaling in 0.5-3.5 keV 80—63768
- D_2+Ni^+, endothermic reactions, investig. 80—97692
- D_2+Y, high temp. equilib. meas. 80—66780
- $D_2^+ + D$, reaction, ion cyclotron reson. mass spectrometric obs. 79—64098
- $D_2^+ + N \rightarrow ND^+ + D$, product kinetic energy distrib. obs. 77—46619
- $D_2^+ + O(^3P) \rightarrow OD^+ + D$, reaction dynamics, cross-section at. quadrupole moment effects 78—3324
- $(D_2)_2$, and isotopic forms, Van der Waals complexes, mol. symmetry 80—42963
- D_3, emission spectra, rot. struct. obs. mol. const. determ., predissociation 80—106331
- D_3 Rydberg states, spectroscopic B_0 consts. 80—74109
- D_3^-, collision induced dissoc., positive and negative ions form. 78—50612
- D_3^- repulsive state, form. in $D_3^+ + Cs$ electron capture 79—59563
- D_3^0 repulsive state, form. in $D_3^+ + Cs$ electron capture 79—59563
- D_3^+ +inert gas, ion decay, 1-40 eV *(Russian)* 78—90286
- D_3^+, ab initio vibr. intervals and vibr. freq. refinement 80—47968
- D_3^+, IR spectrum, vibr.-rot. assignment 80—95627
- D_3^+, rot.-vibr. spectrum, ab initio calcs. 80—95595
- D_3^+, vibr. spectra, ab initio calcs. 77—83562
- $D_3^+ + Cs$, electron capture to D_3^- and D_3^0 repulsive states 79—59563
- D_δ line, Stark broadened, central struct., dense plasma 77—6722
- $D^0(D^+)+Cs$, D^- formation, ang. distrib., total cross sections 77—529

deuterium continued

- (DF) chain, D quadrupole coupling const. calcs. 79—49963
- $D_\alpha(H_\alpha)$ Stark broadening in Ar arc plasma 79—36582
- $D_2^+(HD^+)$, g-factors and related mag. props., calc. theory 79—41124
- $D(^6Li)$-T, inertially-confined, high thermonucl. gain with low T inventory 78—58403
- DT, condensation in laser fusion targets 77—42190
- DT fusion microballoon, Ne seeded, compression by CO_2 laser 79—22466
- DT fusion reactors, environmental aspects, review *(German)* 79—54599
- DT laser-driven plasma, thermonuclear burn wave with electron- and α-conductivities 77—18698
- DT, liquid and solid, collision induced infrared spectra 79—45717
- DT near critical explosion compression, neutron output 77—67867
- DT plasma in glass shell, laser-induced fusion, spectrum and absolute yield of α-particles 77—79482
- DT, solid and liq., fusion reactor applications 78—66415
- DT sphere compression, neutron yield, self-similar hydrodynamic model 77—18703
- DT thermonuclear miniexplosion produced by explosion compression, energy output minimisation 77—67896
- DT^+, adiabatic relativistic rot.-vibr. energy levels 77—57964
- $^nD_2$, compressed fluid, vibrational population relaxation time obs. 80—69219
- $D^{**}+N_2$ fast collisions, impulse approx. 80—106281
- D(2S), form. by electron impact from $D_2(HD)$, time of flight obs. 79—86079
- $D\alpha(H\alpha)$ plasma red shift meas. in Ar arc, ion dynamic depend. 80—10364
- $F+D_2$, electronic-to-rot. energy transfer cross sections 78—86935
- Fe, defect trapping of ion implanted D, depth profile, diffusion eqn. calcs. 80—2047
- n-GaAs:D, ion implanted, carrier removal, capacitance-voltage profiling 80—84195
- H containing mixture extraction from D compounds, ionis. radiation effects *(Russian)* 77—6961
- H/D, abundance ratio, mass spectrometric method 78—8462
- H/D isotope separation factors, and exchange efficiency at Pd electrodes 79—50149
- H/D ratio in planetary atmospheres, determ. from CH_3D 9613 Å band 78—86861
- H-D discharge, RF, meas. of excitation transfer rate by laser fluoresc. 80—9542
- H-D exchange, catalysis by α-$Cr_xAl_{2-x}O_3$ solid solutions 77—52631
- H-D mixture, selective chemisorption by KC_8 intercalation cpd. *(French)* 77—32830
- H-D plasma, fast magnetosonic wave mode conversion, in Tokamak 77—72436
- H-D plasma, He^+ local diagnostics after at. beam scatt. *(Russian)* 77—19774
- H+D, excitation transfer, spectral line broadening and shift 77—46531
- H+D, near-resonant excitation transfer cross sections 77—3446
- $H+D_2$, collinear motion, energy transfer and dissociation, collision dynamics 80—99563
- $H+H_2(HD)(D_2)$, exchange reaction rate consts. meas., vibr. effects 79—5134
- $H^+ + H(D)$, elastic scatt., rainbow struct. and g-u-interference effects 77—6886
- $H^+ + H(D)$, elastic scatt. and charge exchange, resonances 78—78777
- $H^+ + H(D)$, low energy elastic cross sections, impact parameter calc. 77—14526
- H_2/D_2 solubility ratios in Pd alloys, meas. 79—99325
- H_2-D_2, exchange on stepped Pt surface 77—1945
- H_2-D_2 gas, thermal cond. meas., 2-36 MPa 80—64668
- H_2-D_2 isotope separation by permeation through Pd membrane 80—68959
- H_2-D_2 vacuum deposited solid films, struct. study transmission electron diffr. obs. *(Russian)* 79—11035
- H_2-D_2-T_2 mixtures, mesic at. and mol. processes 80—23580
- H_2+D_2, exchange on Pt stepped surface mol. beam incidence angle depend. 78—31686
- H_2+D_2, exchange reaction, at. vs. mol. mechanism, at. absorpt. spectrometry 78—7190
- $H_2+D_2(N_2)(HCl)(CO_2)$, V-V transfer, pulsed fluoresc. obs. 77—14540
- $H_2+D_2 \rightarrow 2HD$ on stepped Pt surface, selective adsorption effect 78—20066
- $H_2+D \rightarrow HD+H$, three dimens. ab initio pot. energy surface 80—55646
- $H_2+H_2(D_2)$ potentials, isotropic part 78—5311
- HCl-D_2-He mixture, gasdynamic laser theory, gain depend. on parameters 78—50761
- $HCl(\nu=1)+H(D)(Cl)(Br)$ reactions, selective vibr. excitation effects, kinetics *(German)* 77—21364
- HD, Boltzmann-Langevin eqn., light scatt. and density correlation function 77—11307
- HD, detect. in Saturn and Uranus atms., D/H abundance ratio calc. 78—57495
- HD, nucl. spin-spin coupling, diamag. contrib. 79—36665
- $HD+D_2$, rot. inelastic differential cross sections, diffr. oscills. in elastic and inelastic scatt. 78—74743
- $H(D)+X_2$, (X=F,Cl,Br,I), exoergic collinear reactions, impulsive energy release model 77—90591
- $H_2(D_2)+Ag(111)$, energy transfer, quantum mech. theory 77—8699
- $H_2(D_2)+Ar^*$, de-excitation processes, pulse radiolysis, isotope effect 77—65529
- $HF+H_2(D_2)(N_2)$, 200K and 295K vibr. relax. rates 80—63766
- $H_2(HD)(D_2)$, ab initio pot. energy curves and vibr. levels, B'', $\bar{B}$, B' states 77—6754
- H_2S+D_2 homogeneous exchange reacts., kinetics 77—48633
- H_2-D_2, separation by Taylor diffusion 79—18303
- ^2H-^2H molten-salt-cooled fusion reactor blankets, nuclear heating and radiation leakage 78—78490
- ^2H-^3H fuel pellet electrostatic injection *(Japanese)* 80—78434
- ^2H-^3H ionised plasma, fast α particle energy deposition, transport eqn. 80—100071
- $^2H^3H\mu \rightarrow {}^4He+n+\mu$ +17.6 MeV, muonic catalysis in synthesis reactions *(Russian)* 80—52706
- $^2H(^2H, n)^3H$, fusion possibility in ^2H metallic state at low temp. 79—67806
- ^4He-D_2 mixture, binary diffusion coeff. near phase separation line *(Russian)* 80—6191
- $He^*+D_2(Ar)(Kr)$ interaction pots. 77—83674

deuterium continued
- KBr:Na,D, U-centres, HFS consts., g-factor, EPR spectra 80−39869
- KCl:D,Ag(Na), UV irrad., anionic D atoms, ESR and optical absorpt. expts. 79−99187
- $Kr^+.+H_2(D_2)$(HD) reactions, temp. depend., isotope effect 78−31630
- Li-D equation of state under extreme conditions, solid state to plasma region 80−69976
- MgO:D, electron irrad. induced diffusion of interstitial impurity 77−15452
- MgO:D, X-ray stimulated luminesc. 79−28802
- Mo:D, trapping of D and mutual replacement 80−59493
- $N_4^+ + D_2$, reaction rate determ. 78−60985
- Na-D photoneutron sources, construction, yield 77−23347
- NaCl:Li,D, U-centres, HFS consts., g-factor, EPR spectra 80−39869
- Nb:N,D, thermal cond., 0.07 to 1.5K, influence of N interstitials 79−65601
- $Ne+D_2$, anisotropic inversion pot., rot. inelastic cross sections 80−78696
- $Ne+H^-(D^-)$, electron detachment, dynamical phenomenon 80−106305
- Ni:D, diffusion study using D(d,p) reaction 79−5202
- $O^- + D_2 \rightarrow OD^- + D$, crossed beam studies product ang. and energy distrib. 78−53203
- $O_3 + He(D_2)(H_2)$, vibr. relax. rate consts. 80−74231
- p-oD_2, solid, slow neutron scatt. into external radiation field *(Russian)* 80−59348
- Pd-Au:D_2, thermodynamic props. at 555 and 700K, vibr. freqs. and excess entropies 80−29186
- Pd-D, vibr. modes, Raman study 77−85713
- $Pd_{0.9}Ag_{0.1}$:H(D), free energy, enthalpies of soln. 78−15692
- RbCl:Na,D, U-centres, HFS and g-factor, EPR spectra 80−39869
- SF_6+D_2, optically cascaded pulsed chem. laser 77−75497
- Si:D, amorphous, thermal stability, comparison with Si:F 80−49542
- Si:D, ion implanted, D depth distribs., SIMS meas. 80−54279
- Si:D, ion implanted, struct. of impurity centre 79−7623
- Si:H(D), amorphous films, CVD, post-hydrogenation 80−54552
- SiH_4-D_2, mixture, ion-mol. reactions, cross-sections 77−60061
- SiH_4+D_2, vibr. energy transfer 77−524
- SiO_2, D-impregnated, vitreous, radiation induced isotope exchange 79−99240
- SiO_2:H(D), γ-irrad., hydroxyls and hydrides form., detect. by Raman scatt. 77−32817
- SrO:D, γ-irrad., V_{OD} defects, EPR and ENDOR 78−27116
- $SrTiO_3$:H(D), controlled doping, IR spectra 79−28007
- β-Ti, dilute soln. of H and D 79−99322
- Ti:D, implanted, deuteride imaging using scanning Auger spectroscopy 80−89092
- Ti:D, implanted, nucleation and growth of TiD_2 80−97717
- Ti:D, ion implanted, depth profiles, temp. depend. 80−100270
- TiO_2:D, IR spectra, 300, 77 and 8K 78−35175
- $U^+ + N_2(D_2)(CD_4)$, endothermic reactions, heat of formation 77−73444
- V-$D_{0.01}$, enrichment of D during the ion bombardment 80−54288
- ZnO:Cu, D, and ZnO:Cu, H, D, IR absorpt. line spectra, OH and OD vibr., optical excitation 79−15498
- ZnO:Cu,D, OH and OD centres, IR-active absorpt. line spectra 79−15496
- Zr-He, implanted, superconductivity enhancement obs. 80−70884

deuterium compounds
- *see also heavy water*
- DF-CO_2 CW chemical transfer laser, comprehensive kinetics model 79−81422
- DSO, radical, electronic spectrum and struct. 77−75147
- graphite-DNO_3, intercalation cpd., mol. dynamics 79−28631
- halides, laser studies of relax. and reaction 80−11918
- halides, thermodynamic properties, phase transitions 78−47518
- halides$+I(5^2P_{1/2})$, collisional quenching, isotope effects 77−34583
- heavy ice, stopping power for low energy deuterons 77−35612
- hydrates, solid, electric field gradient tensors at deuterons, and vibr. motion 77−71792
- interstellar DNC detection, difficulties of chemical equilibrium hypothesis for D enrichment 77−82298
- β-Al_2O_3-D_2O, anhydrous, prep. and struct. of $DAl_{11}O_{17}$ 80−107187
- β-Al_2O_3-D_2O, neutron diffr. obs. of struct. 80−107512
- Ar.DBr, van der Waals complexes, rot. spectra and struct. 80−48055
- Br+DCl(ν'), reaction and relax. classical trajectory calcs. 77−48625
- Cu-Cs diluted deuterated Tutton salts, electron non-Zeeman system, nuclear relaxation study 80−44951
- D I, ionisation pot. photoionisation mass spectra 78−25632
- D_2+HF, vibr. relax. of HF (ν=3,4) 79−50117
- $DAl_{11}O_{17}$, anhydrous, cryst. struct. from powder neutron diffr. 80−1983
- DBF_2, harmonic force field and ground-state average struct. determ. 80−83342
- DBr, (1,0) fundamental IR band meas., isotope shifts 78−42052
- DBr, IR absorpt. in 5-0 band, high-resolution spectra 77−14431
- DBr, mol. consts., rel. to TBr mol. consts. *(French)* 77−57855
- DBr, orientational phase transitions, effective field approx. calcs. 77−24404
- DBr, spin-flip Raman laser double-beam spectrum, SFRL multiline output 79−7132
- DBr, vibr. energy transfer, laser selective isotope excitation 78−82790
- $D^{79}Br$, $D^{81}Br$, IR absorpt. spectra of 1-0, 2-0, 3-0, 4-0 bands 77−3360
- DBr-N_2O mixture, third harmonic generation obs. 79−23018
- DBr+DBr, vibr. energy transfer, dissimilar isotopic species 79−27067
- DBr+F, H abstraction reactions, temp. depend., laser photolysis IR fluoresc. obs. 80−93744
- DBr$+H_2$, vibr. relax. rate, stimulated Raman scatt. obs. 77−75269
- DBr$+I(5^2P_{1/2})$, collisional deactivation, rate consts. meas. 77−86300
- $DBr^+(A^2\Sigma^+)$, vibrational states, lifetimes, emission cross sections, prod. by electron impact 77−3419
- DBr(DCl), solid, ferroelec. and paraelec. phases, transitions, Raman scatt. 77−43980
- DCN, 250 mW continuous discharge laser at 195 μm 79−31949
- DCN, CW submm. waveguide laser, high volumetric efficiency 78−42351
- DCN, DNC, interstellar strongly deuterated mol. obs. and implications for interstellar chemistry 79−5891
- DCN dimer, microwave rot. spectrum, identification and struct. 77−50427
- DCN, dipole moment, relative sign w.r.t. normal coords. 78−46457
- DCN, electronic spectra, vibr. struct., ab initio calc. 78−9166
- DCN, in interstellar clouds, rot. excitation by electrons and H_2 77−22292

deuterium compounds continued
- DCN, integrated IR intensities of fundamental modes 79−98083
- DCN, $\nu_1+\nu_3$ combination bands, transition moments, integrated intensities 77−79610
- DCN, phonons meas. by neutron coherent inelastic scatt. 79−95097
- DCN, photodissoc., vibr. energy states population meas. 78−58751
- DCN, photodissoc. dynamics, rot. (vibr.) energy disposal 78−48672
- DCN, photofragmentation vibr. distribs. 77−18992
- DCN, predissociation, photofragment excitation spectra measurement 79−45777
- DCN, selected fragment vibr. energy distrib. in dissoc. processes 78−1036
- DCN, self-assoc. in matrices, IR vibr. spectra of multimers 78−86858
- DCN waveguide lasers, optimised 190/195 μm, amplifying medium characts. 80−99709
- $D(CN)_2^-$, IR spectra, rel. to mol. geom. 79−22702
- DCO^+, interstellar, radio detect. in NGC 2264, L134 and DR 21(OH) 77−2460
- DCO_2^+ threshold form. energy in $CO_2^+ + D_2$ reaction 80−50844
- DCl and $(DCl)_2$, matrix isolated Raman spectra 78−42063
- DCl dissociative-attachment cross sections, fine struct. 77−71884
- DCl, effect on CO_2 gasdynamic laser physical kinetics 78−5451
- DCl gas, tripling of CO_2 laser freq. 79−76751
- DCl, IR matrix isolation spectra, N_2 matrix effects 79−36634
- DCl, isotope exchange reactions, equilib. consts., adiabatic correction, electron correl. effects 78−88626
- DCl, liq., self-diffusion coeffs., NMR spin-echo meas. 80−50223
- DCl, liquid, on coexistence line, light scatt., orientational correlation function 80−20632
- DCl, matrix isolated, vibr. relax., IR fluoresc. obs. 79−45749
- DCl, orthorhombic, nucl. quadrupole double reson. obs. and interpret. 77−90070
- DCl, plastic cryst. phase, struct. and dynamics 80−92469
- DCl, polaris. anisotropy 77−83645
- DCl, two photon reson.-enhanced third harmonic generation 78−87094
- DCl, vib.-rot. spectra in hexadecane solvents of different mol. shapes 77−34623
- DCl, vibr. energy transfer, laser selective isotope excitation 78−82790
- $D^{35}Cl$, $D^{37}Cl$, IR absorpt. 3←0 band, dipole moment series expsn. 77−61747
- DCl-cycloalkane solns., CO IR vibr.-rot. spectra, solvent mol. struct. 77−83585
- DCl+Br, relax. rates, vibr. photochem. 79−66290
- DCl+CO, V-V energy transfer 80−78695
- DCl$+Cl_2$(DCl), vibr. relax., Monte Carlo quasiclassical trajectory calcs. 77−50502
- DCl+Cl(Br), vibr. relax. times, laser induced fluoresc. 77−27159
- DCl+DCl, vibr. energy transfer, dissimilar isotopic species 79−27067
- DCl+H, thermal rate constants, quasiclassical trajectory calcs., detailed balance 79−87822
- DCl$+H_2$, vibr. relax. rate, stimulated Raman scatt. obs. 77−75269
- DCl+He, slow collisions, rot. excitation cross- sections, quantum mech. calcs. 77−12795
- DCl(HCl)+Ar potential, asymmetric, isotope substitution effect, Legendre expansion coord. transformation 78−70894
- DD advanced fuel, fusion dynamics reactivity coeffs. 77−23296
- DF, CW chem. lasers, performance parameters and operating characts. 77−34885
- DF chemical laser, jet curtains for gas containment 78−63099
- DF, chemical laser, optical inhomogeneities in F_2-D_2-CO_2, interferometric meas. 77−674
- DF, chemical laser, small-scale CW, construction and performance 77−50682
- DF chemical laser, small-scale CW, operation 80−58528
- DF chemical laser, test of 1D flow model for press. recovery 77−71979
- DF, chemical laser kinetics, book contrib. 77−10903
- DF chemical lasers, high-performance dichroic beam splitters 80−95932
- DF, combustor-driven cold-reaction laser, book contrib. 77−10905
- DF, cryst., Raman spectra 80−55075
- DF, design of compact CW chemical laser using microwave discharge 79−72591
- DF, effect on CO_2 gasdynamic laser physical kinetics 78−5451
- DF, form., initial vibr. energy distrib., IR chemiluminescence. obs. 80−45497
- DF, IR chemiluminesc. quenching, (V-V) and (V-T, R) energy transfer rates 78−20018
- DF, IR chemiluminesc. quenching, (V-V) energy transfer rates 78−20019
- DF, IR laser spectra 79−45936
- DF laser, phase conjugation of 4 μm for single line and multiline radiation in Ge 80−83641
- DF laser, pulsed unstable resonator, mode control and performance studies 78−82995
- DF laser, refr. index changes during stimulated emission 78−17929
- DF, laser action by pulsed microwave discharge 78−58998
- DF optically cascaded pulsed chem. laser 77−75497
- DF, photoinitiated chain reaction laser, high elec. efficiency 77−3574
- DF pulsed chemical laser, flow technology 79−36934
- DF repetitively pulsed subsonic chem. laser, flameout using fluidic switching 78−29943
- DF repetitively pulsed chem. laser, scalable fuel/diluent feed system 79−36935
- DF TEA laser, He-free, with MW output 80−64060
- DF, threshold photoelectron spectra, photoionis. threshold, resonant autoionis. 77−499
- DF, vibr. relax., isotope effect, quantum model 80−91460
- DF-$^{35,37}ClF$, mol. beam elec. reson. spectra, config., bonding, spectroscopic consts. 77−30860
- DF-CO_2, CW and pulsed chem. transfer lasers, book contrib. 77−10907
- DF-CO_2, chem. amplifier of short light pulses, photolytic or fast electron initiation 78−13696
- DF-CO_2, chem. laser, vibr. energy transfer from DF to CO_2 mols. 77−23669
- DF-CO_2, chem. laser, high performance characts. 77−34881
- DF-CO_2, chem. laser utilising ClF_5, ClF_3, ClF and F_2, energy transfer characts. 79−94225
- DF-CO_2, chem. transfer laser, efficient performance 77−34886
- DF-CO_2, laser system, interaction between vibr. states, theory 77−23670
- DF-CO_2 CW chemical transfer laser, high pressure operating charact. 79−81449

deuterium compounds continued
DF-CO_2 chemical laser, possibility of increasing generation quantum yield and specific energy output 80−19025
DF-CO_2 chemical laser, photon branching in chain reactions, IR radiation initiation 80−91785
DF-CO_2 chemical laser, amplification of long and short pulses 80−95883
DF-CO_2 pulsed chemical transfer laser, analysis of calc. model 79−94226
DF-CO_2 pulsed photoinitiated chem. laser, characts. rel. to HF laser 79−64219
DF-CO-$_2$He CW optically reson. pumped transfer laser 77−75471
DF-HBr CW optical resonance transfer laser 80−64003
DF-HF CW lasers, performance, computer modelling 78−71094
DF+CO_2, vibr. relax. rate, chemiluminescence depletion method meas. 79−72399
DF+Ca(SR), beam reaction, vibr. excitation 78−68877
DF+$D_2(H_2)(N_2)$(HF)(CO_2), vibr. relax., laser-induced fluoresc. obs. 79−64028
DF+DF, vibr. energy transfer collisions, trajectory calc. 79−64079
DF+DF(HF), DF vibr. deactivation, semiclassical calcs. 80−48061
DF+H, reaction rate, DF fluoresc., shock tube obs. 77−12784
DF+He, slow collisions, rot. excitation cross-sections, quantum mech. calcs. 77−12795
DF* prod. from D+PTFE, Fourier transform IR spectroscopy 80−87105
DF($1 \leq n \leq 7$)+HF(0), vibr. deactivation calc., 300-3000K 79−31655
DF($\nu=1$)+DF($\nu=0$), deexcitation probability, low temp., hindered rot. and H-bond effects 77−88531
DF($\nu=1$)+F→DF($\nu=0$)+F, isotope effect 77−30959
DF($\nu=n$)+DF($\nu=0$)→DF($\nu=n-1$)+DF($\nu=1$)+ΔE, applic. of hydrogen-bond interac. model 77−30961
DI, crystalline, Raman and IR spectra, mol. vibr., libration and translation 80−2757
DI, dipole moment for $\nu=0$ vibr. level, calc. 77−75330
DI, IR absorption bands 4←0 and 5←0 79−98091
DI, photolytically-driven hot-atom reactions, appl. of kinetic theory 79−74408
DI, solid and liquid, thermodynamic properties 78−47517
DI+Cl→DCl+I, thermal rate const., 220-400K, H/D isotope effect 79−47906
DIO_3, cryst., NQR coupling const. and field gradient tensors 79−73828
DN_3, and HN_3, pure rot. Raman spectra, rot. consts., K-depend. parameters 78−29791
DN_3, IR multiphoton dissoc., form. and reaction of electronically excited ND 78−80771
DN_3, microwave spectra, 8-340 GHz, spectrosc. consts. for ^{13}N isotope 79−85958
DN_3+ND*→ND_2*+N_3, chemiluminesc. reaction of electronically excited species, rate const. 78−80771
DNC, anharmonic force field, equilib. struct., rot. consts. and bond lengths 78−90147
DNC in HNC interstellar clouds, temp. effects and D fractionation 79−44578
DNC, interstellar, detect. at 152.6 GHz in NGC 1333, 2264, Orion A and L134 dark cloud 78−4334
DNC, vibronic coupling and linear to bent transitions 79−45694
DNCS, ground state spectroscopic constants and elec. dipole moment, from microwave and millimetre wave spectra 79−804
DNF_2, photoelectron spectra, vibr. struct. obs, ionisation pot. determ., ab initio calcs. of ionic geometry 80−83418
DNO, fundamental vibr. bands, laser Stark spectra 77−38692
DNSO, IR spectra obs., mole. vibr., anharmonicity constant determ. 80−83357
D_2Ne, mol. interactions, differential scatt. cross-sections meas. 79−89732
DO_2, IR spectra, config. of $^2A'$ and $^2A''$ states 79−36636
DO_2, ν_2 fundamental band, 9.8 micron, laser mag. reson. spectroscopy 79−85961
DO_2+NO, reaction kinetics, near IR chemiluminesc. determ. 80−21261
D_2O dissolved CO_2 Raman spectra 77−65467
D_2O, far IR superradiant laser, 114, 66 μm emission, time-resolved pulse and wavelength meas. 77−88715
D_2O ice, thermal cond., H and D order effects 78−67871
D_2O, in lyotropic phase, spin-lattice relax. time meas., density matrix formalism 77−18944
D_2O laser, 66 μm, with unstable reststrahlen resonator 80−83619
D_2O laser, high power, narrow linewidth, at 384.6 μm 77−10894
D_2O laser, optically pumped, superradiant line obs., 235, 280, 97 and 98 μm 78−1215
D_2O, models of bond distribution functions, anharmonicity effects on electron diffr. pattern 80−69234
D_2O, reaction with W at high temps. and low press. 77−86379
D_2O, saturated and superheated steam, eqn. of state up to 500°C 78−79401
D_2O, single-mode optical pumping, superradiant far IR emission 78−42329
D_2O, vapour, mol. association entropy and enthalpy, thermal cond. meas. 80−7777
D_2O, vibr. relax. rates 80−95717
D_2O-H_2O ice, thermal cond., H and D order effects 78−67871
$D_2O+H_3O^+(H_2O)_n$, binary reactions, rate coeffs. and product ion distributions determ. 80−81305
D_2O+He(Ne), metastable, chemi-ionisation and secondary ion reactions 77−40531
$D_2O+U^+(UO^+)$, reaction cross-sections, ion beam apparatus study 80−97691
D_2O_2, equilib. geometry, O-D bond length and angle 77−75326
D_2O_2, lattice dynamics, neutron scatt. study 79−42176
D_2O_2, lattice phonons by neutron scatt., covalent force model 78−67782
D_2O_2, vibr. consts., rot. struct. doubling, Raman spectra assignment 77−54563
$D_5O_2{}^+$, in 5-sulphosalicylic acid dideuterate, neutron diffr. 77−35543
$D_5O_2{}^+$, isotope effects, easily polarisable H and D bonds 78−94231
DOD, vibr. intensities, ab initio and empirical calcs. 80−78592
DOD, vibr. intensities, ab initio and empirical calcs., band strengths 80−78593
$D_3O^+(D_2O)_n+H_2O(NH_3)$, binary reactions, rate coeffs. and product ion distributions determ. 80−81305
$D_3O^+(H_2O)_{0,1,2}+H_2O$ reactions, SIFT studies, review 80−58435
$D_3O.ClO_4$, solid, neutron powder diffr. study 80−107176
$D_3O.ClO_4$, specific heat anomalies, investig. of solid phases 77−47591

deuterium compounds continued
D_2S, CO_2 laser pumped, high power far IR superfluorescent emission 79−27243
D_2S, energy levels and mol. vibr., internal coord. model 79−799
D_2S, photodissoc., SH internal energy distribution 80−95697
D_2S, separated product rules for high and low vibr. freqs. in isotopic mols. 77−34611
D_2S, solid, low-temp. phase, IR, far IR and Raman spectra 78−27218
D_2S+K, collisional ionisation, positive and negative ion energy spectra obs. 80−63775
$D_2S+O_2(^3P)$, reaction rate, flash photolysis-reson. fluoresc. obs. 77−4918
D_2SO_4, pure, IR and Raman spectra in liq. state, assignments and cryst. spectra comparison *(French)* 79−33699
D_2Se, inertia defects and dipole moments by kinetic consts. method 80−928
DSiCl, $^1A''$ states, geometry, bending pot. and vibr. freqs. 79−59593
$DSiCl_3$, Raman and IR spectra, mol. motion 78−64353
D_3SiNCO, low freq. bending mode, pot. function 78−82728
DT, vibr. rot. Raman anal. 80−87126
D_xTaS_2, struct., form. by cathodic reduction, neutron diffr. obs. 79−73150
DX+F, (X=I, Br, Cl), H abstraction, absolute reaction rate, H/D isotope effect 78−80721
F+HCl(DCl)→HF(DF)+Cl, dynamical props., pot. energy hypersurface computer anal. 77−77735
H+DCl→HD+Cl or HCl+D, branching ratios determ. 78−40046
HCN, photofragmentation, initial excitation effects calcs. 78−17734
HCl-DBr, absorpt. spectra near 3.5 μm, equilib. config. of complexes *(French)* 78−42046
HCl-DCl, absorpt. spectra near 3.5 μm, equilib. config. of complexes *(French)* 78−42046
HCl-DCl mixed crystal, IR spectra, freqs., bandwidths and ν_{01} simultaneous transition 77−28564
HCl-DCl mixed crysts., ferroelec. transition, ^{35}Cl NQR study 80−71233
HD, adsorbed on Re, interaction with CO 79−86987
HD, quadrupole mass filter sensitivities 78−58090
H(D)I+Cl, exothermic triatomic exchange reactions, prod. energy distrib., statistical dynamic model 78−92455
HF, low-impedance Blumlein discharge initiated laser, efficient operation 79−36919
HF-DF, CW chem. laser, freq. stability and stabilisation 78−22141
HF-DF, pulsed chem. laser, efficient excimer flashlamp initiation 77−88754
HF-DF laser, 10 W repetitively pulsed closed cycle system, elec. excitation 77−88753
HF-DF simultaneous laser excited by ferroelec. ceramic capacitatively coupled discharge 80−69413
H_2O:D_2O, ice Ic, vibr, decoupling, IR spectrum 79−13706
H_2O-HCl(HBr)(DBr) complexes, IR matrix isolation spectra, struct. 78−29781
$^2HN_3$ IR multiphonon dissociation with electronic excitation 80−11934
I*+$H_2O(D_2O)$(HDO), $5^2P_{1/2}$ electronic to vibr. energy transfer, quenching and time resolved IR fluoresc. 79−3537
LiCl-D_2O glass, trapped and quasifree electrons optical transitions, bound-continuum character 78−6660
$N^+ + H_2$(DH), >6 eV reaction dynamics 77−32779
$Na_2CO_3.1.5D_2O_2$, neutron profile refinement and deuterium positions 79−90602
TlD_2PO_4, antiferroelectricity, permittivity, electric field double hysteresis loops 80−60512

deuteron effects
anthracene, scintillation response to deuteron bombardment, energy, temp., and deuteron direction depend. *(German)* 78−6779
benzophenone, aqueous system, LET depend. of transient yields in deuteron and alpha pulse radiolysis 77−63940
t-butanol, aqueous system, LET depend. of transient yields in deuteron and alpha pulse radiolysis 77−63940
Nimonic PE-16, damage in high energy fluence D plasma 77−34427
quartz, ion bombardment, extrusion, evidence for radiation-induced stress relax. of silica network 77−24335
refractories, swelling on proton, deuteron and He ion bombardment 78−67750
silicate glasses, swelling on proton, deuteron and He ion bombardment 78−67750
stainless steel, type 316, deuteron and proton bombarded, irrad. creep under stress 80−39209
steel, austenitic stainless, type 316, irrad. induced creep 80−93606
steel, stainless, deuteron trapping model, of gas sputtering 80−49398
steel, stainless, retention and re-emission of 0.125-1 keV D^+ ions 80−66349
TTF-TCNQ, controlled defects effect on microwave cond. and dielec. function 80−24885
TTF-TCNQ, irradiated, IR reflectance, optical and low-freq. transport comparison 79−51961
Al-Ag (0.10 at.%), channelling meas. of trapping efficiencies of solute atoms for self-interstitials 79−86829
Cd, quadrupole hyperfine interaction of ^{111}Cd, effect of radiation defect annealing 78−43741
$CdCr_2Se_4$:Ag, magneto-optical effects in impurity spectral region 80−97313
$CdSiP_2$, PAC examination of deuteron irrad. damage, annealing effects 78−47446
Cu, annealing elec. resist. changes freq. factors, activation energy distrib. 79−77648
Cu, deuteron irradiated, dynamics of radiation blistering and near-surface deuterium retention 77−84807
Cu, low temp. D^+ irradiated, radiation blistering onset 80−2081
Cu-Be (0.25 at.%), channelling meas. of trapping efficiencies of solute atoms for self-interstitials 79−86829
D(d,p)T spectroscopy for studying dynamic deuteron implant effects 79−51160
GaAs device isolation with deuteron bombardment 80−75248
Hg, thick target, proton and deuteron irradiation, Tl yield determ. 78−2174
LiF, high-energy particle bombard., F-centre creation, optical meas. and model 77−47497
Mg-Ag (0.18 at.%), channelling meas. of trapping efficiencies of solute atoms for self-interstitials 79−86829

deuteron effects continued
NaOH, aqueous system, LET depend. of transient yields in deuteron and alpha pulse radiolysis 77−63940
NbO, ion channelling, 1 MeV deuterons 79−60416
NbO, ion channelling, neutron and deuteron radiation damage 79−65131
Nb$_3$Sn superconductor, low temp. deuteron irradiation 78−52182
Ni, creep, irrad. induced with 17 MeV deuterons 80−93607
Ni, deuteron irrad. induced creep mechanisms 80−39171
Ni, deuteron range profiles in 100 to 400 keV region, expt. and computer simulation 77−51422
Ni, irrad. induced creep, defect investigation 78−80597
Ni-In, dil., uncorrelated radiation damage, TDPAC meas. 78−43343
Pb, radiation damage and recovery processes 77−69002
Pb-Cu, damage and recovery processes 77−69002
Pt, deuteron irrad., close Frenkel pair recomb. during annealing 78−87716
Pt, deuteron irrad., energy release and resist. recovery, self-interstitial-atom interaction energies 79−95002
Si, high fluence deuteron bombard. and implantation 77−59033
TTF-TCNQ , elec. props. in high temp. regime, effect of controlled disorder 78−30912
Zr, 10 keV deuteron irradiated, retention and precipitation 80−34099

deuteron interactions *see deuteron-nucleus reactions; hadron-deuteron interactions; lepton-deuteron interactions; meson-deuteron interactions; photon-deuteron interactions; proton-deuteron interactions*

deuteron-nucleus reactions
for inelastic deuteron-nucleus scattering, see 'deuteron-nucleus scattering' see also nuclear fusion
0.7-8 GeV, scaling and nonscaling of inclusive π prod. 79−22296
^{56}Co particle-hole states, T=1, zero DWBA anal. 80−78308
A=21 to 44, spectroscopic factors for single-nucleon transfer, review 77−71563
A=3, d+n clustering, D-state effects in (d,t) and (d,^{3}He) 79−22302
A(d,π)X, relativistic energies, Glauber theory 77−30540
A(d,p)X, stripping at relativistic energies, Glauber theory 77−30540
charged particle cross sections, exotic fusion fuels 77−23293
coupled channels approach, deuteron breakup in field of nucleus 78−33195
cumulative effects, phenomenological model for pion prod. and elastic scattering involving deuterons 78−58267
(d,3nγ), A=159-181, delayed feeding $T_{1/2}$, rot. band transitions 77−34211
(d,τ) reactions, 52 MeV, analyzing powers, spins of proton hole states 78−25111
(d,n) on Be, C, Al, Ni, Cu, Mo, Ta and Pb, secondary neutron emission characts. 79−30843
(d,p) off-shell effects 78−62545
deformed tensor interactions, folding model 80−57783
differential cross sections meas. by SPES I 79−75983
disintegration reactions on zero-isospin nuclei, strong nonconservation of isospin 78−13106
emulsion nuclei, g-proton energy and ang. characteristics *(Russian)* 79−40937
emulsion nucleus+deuteron, 9.38 GeV/c, nucleon stripping probability and charged particle multiplicity 80−78306
folding model potentials, mass no. systematics 77−2964
heavy nuclei, direct reaction with many particle final states, DWBA theory 78−21539
high-energy, at Saturne I, five years of expts. *(French)* 79−3262
light ion direct reactions, polarisation expts., tensor polarised deuteron beams 78−54732
light relativistic ion-target interactions, particle emission 80−102193
meson prod., inelastic rescatt. contrib. to cumulative prod. *(Russian)* 77−61334
multi-nucleon transfer and direct reactions, nuclear struct., review 78−50060
nucleus-nucleus total cross section energy depend. 80−106071
one-nucleon transfer reactions, high energy, reaction kinetics and struct. determ. *(French)* 79−535
optical model calcs., tensor spin-orbit interaction 78−13112
polarisation meas. with low energy proton and deuteron beams 77−2970
polarised deuteron beam uses in nuclear structure studies 77−71612
rare earth nuclei (d,t) reactions, band heads, two-step process 78−62551
spallation in d+nucleus reactions distrib. of spectator neutrons, theory and expt. comparison *(Russian)* 78−58290
stripping and breakup, adiabatic theory 77−18512
three-body model of deuteron breakup and stripping 79−515
(d,α) reactions, ang. momentum transfers, determ. using polarized beams 78−37354
(d,d′X), 4.5 GeV/c/N, secondary charged particles azimuthal correlations *(Russian)* 80−27651
(d,^{3}He) on ^{12}C, ^{16}O, ^{24}Mg, ^{40}Ca, 29 MeV, polarised d, low lying analogue states, DWBA anal. 78−82285
(d,^{3}He) reactions, normalisation and finite-range effects in DWBA calcs. 77−10416
(d, ^{6}Li), 54.25 MeV, α-cluster spectroscopic factors, DWBA anal. 80−52571
(d,^{6}Li), A=144-238, alpha-cluster transfer from alpha-decaying nuclei 80−91166
(d,^{6}Li), A~60,116, L=0 transitions, cross sections, microscopic anal. 80−78189
(d,^{6}Li), α-clustering and spectroscopic factors, shell effects and deformation correlations 79−6436
(d,^{6}Li) reaction, 80 MeV, on ^{14}N, ^{16}O, ^{20}Ne, ^{24,25,26}Mg, ^{40}Ca targets, resonance-like phenomena 79−13308
(d,n) diagnostic neutron spectra from deuterons 2.5, 3.0, 3.5 MeV on ^{12}C, ^{27}Al, ^{19}F, CH$_2$, CD$_2$, Teflon 79−40933
(d,p), 12.08 MeV, ^{154}Sm, ^{166}Er, ^{170}Yb, ^{176}Yb, final nucleus level struct., DWBA anal. of ang. distribs. 79−30788
(d,p), 1.7-15 MeV, rearrangement collisions three body model, bound state approx., DWBA calcs. 79−93595
(d,p), appl. of three-body K-operators and unitary approx. to model processes 77−18499
(d,p), composite particle scatt. breakup mechanism 80−83105
(d,p), effects of d deformation and D-state influence, wave functions 79−13201
(d,p), multistage processes and methods 77−41974
(d,p), O and N profiles determ. in steel surfaces 79−5216
(d,p), reduced normalisations 78−86522

deuteron-nucleus reactions continued
(d,p), role of ΔN=2 interaction, differential cross sections, DWBA anal. 80−91189
(d,p) and (d,t) reactions producing ^{105}Pd, level scheme 77−82849
(d,p) cross-section, effect of nuclear vertex form factor in peripheral model *(Russian)* 77−82889
(d,p) low energy direct processes new model, ^{12}C(d,p)^{13}C appl. 77−88097
(d,p) on ^{124}Sn, ^{130}Te, ^{138}Ba, ^{140}Ce, ^{142}Nd, ^{208}Pb below and near Coulomb barrier 78−29483
(d,p) reactions, δ-shell method for approx. finite range DWBA calcs. 79−555
(d,p) reactions, stripping of relativistic deuterons, Glauber theory 78−94014
(d,p) reactions on ^{16}O and ^{90}Zr, finite-range coupled-channel calcs. 77−10377
(d,p) reacts. at intermediate energies, triangle graph model 80−27616
(d,p) stripping reaction test from (p,π^+) 79−85436
(d,p) stripping reactions, approx. DWBA methods 77−14137
(d,p) stripping reactions, energies below Coulomb barrier, theory 77−6394
(d,π), 350 MeV, backward π^+ prod., momentum depend., scaling, Monte Carlo calcs. 79−13305
(d,π), 4.2, 4.5 GeV/N, pion multiplicities and theoretical models, review 80−42657
(d,π) reactions, prod. cross sections near threshold, non-nucleon model 77−41976
(d,t), 12-50 MeV 80−42670
(d,t), 12.08 MeV, ^{154}Sm, ^{166}Er, final nucleus, level struct., DWBA anal. of ang. distribs. 79−30788
(d,t), DWBA anal., form factors and d-t overlap integral S- and D-state components 80−18320
(d,t), deep hole states observed in particle transfer reactions 80−68511
(d,t), role of ΔN=2 interaction, differential cross sections, DWBA anal. 80−91189
(d,t) anomalous transitions in rare earths, inadequacy of CCBA 78−70543
(d,t) on ^{12}C, ^{16}O, ^{24}Mg, ^{40}C, 29 MeV, polarised d, low lying analogue states, DWBA anal. 78−82285
(d,t) reactions, normalisation and finite-range effects in DWBA calcs. 77−10416
(d,X), 70, 80 MeV, charged light particle spectra and ang distribs. excition model anal. 79−40935
(d,X) on light nuclei, 1.55, 2.89 GeV/c, total and inelastic cross sections 79−6610
d breakup effect on spin orbit and tensor pots. 80−32286
d-d neutral beam facility neutron yield meas., shielding and diagnostics 79−9878
d+A, 6.3 GeV/c, A=H, D, C, Al and Bi, inclusive spectra of fast p and d *(Russian)* 78−46075
dA$\rightarrow\pi^-$+X, scaling invariance of interactions of relativistic nuclei, the cumulative effect *(Russian)* 79−93611
(dp) stripping, two-body rearrangement collision, effect of continuum contribution 79−13262
(dx) breakup on nucleus, adiabatic treatment stripping and forbidden transition cross section 80−9299
n-p potential form, influence on differential cross-section of d break-up *(Russian)* 80−78173
π, super-fast prod. in relativistic deuteron-proton and nucleus collisions 77−18362
^{A} Si(d,X), A=112, 124, 7.6 GeV/C, isotopic cross section ratios, He, Li fragments isotopic effects *(Russian)* 80−63154
^{27}Al(d, ^{3}He)^{26}Mg, 12.4 MeV, tensor analysing power, D-state component in ^{3}He wave function 78−54769
^{27}Al(d,^{3}He)^{26}Mg, 12.4 MeV polarised beam, $d_{5/2}$-$d_{3/2}$ admixing in pickup strength 77−6399
^{27}Al(d,^{3}He)^{26}Mg, 12.4 MeV, tensor analysing power, ^{3}He D-state effects 78−4948
^{27}Al(d,α)^{25}Mg, 1.5-2.5 MeV, intermediate resonance widths 77−88151
^{27}Al(d,α)^{25}Mg, analysing power calc., distorted wave method 77−6404
^{27}Al(d,α)^{25}Mg, nuclear microanalysis of Al impurities in Si epitaxial layers 80−61193
^{27}Al(d,p$_0$)^{28}Al, coherence energies in pre-equilibrium emission 79−63652
^{27}Al(d,pX), 25.5 MeV, inclusive p spectra and cross sections from d breakup 79−13303
^{27}Al(d,pX) 80 MeV, inclusive proton spectra, d break-up, DWBA anal. 80−91190
^{27}Al(d,p)^{28}Al, 1.5 to 3.0 MeV, excitation functions 79−40932
^{27}Al(d,p)^{28}Al, 1.5-2.5 MeV, intermediate resonance widths 77−88151
^{27}Al(d,p)^{28}Al, 1.58 to 3.03 MeV, calc. of differential cross sections, spectroscopic factors 77−6394
^{27}Al(d,p)^{28}Al, 3.1 MeV, high spin states of ^{28}Al anal. 77−74856
^{27}Al(d,pγ) 2.4 MeV, ^{28}Al levels, $T_{1/2}$, J^π below 5.45 MeV 77−57623
Al(d,p), 6.3 GeV/c, p momentum spectra from d breakup 78−89887
^{241}Am(d,p)^{242}Am, 12.1 MeV, energy level determ. 77−26578
^{241}Am(d,t)^{240}Am, 12.1 MeV, energy level determ. 77−26578
^{243}Am(d,t)^{242}Am, 12.1 MeV, energy level determ. 77−26578
^{36}Ar(d,p), Tabakin pot. calcs., differential cross sections, ang. distribs. 78−611
^{38}Ar(d,pγ), 4.4 MeV, ^{39}Ar, energy level spin and parity assignments, level spectroscopy 78−93943
^{40}Ar(d, p)^{41}Ar, 1.354 MeV, spectroscopic factor comparison with isobaric analogue reson. 79−30787
^{40}Ar(d,p) and ^{40}Ar(d,n), lifetime meas. of ^{41}Ar, ^{41}K, by DSA method 78−78308
^{75}As(d,^{3}He), 26 MeV, spectra of ^{74}Ge 78−25112
^{75}As(d,p) 11 MeV populating ^{76}As low-lying states 77−10319
^{73,74}As, yields in α, d and p interactions on Ge, Ga and As 77−54223
^{197}Au(d, f), 2.1 GeV, binary and ternary fission kinetics *(French)* 78−70577
^{197}Au(d,f), 80 MeV, post neutron emission fission products 80−83136
^{197}Au(d,γ), 5-26 MeV, experimental and calc. compound nucleus cross sections 79−76002
^{197}Au(d,pX), 80 MeV, inclusive proton spectra, d break-up, DWBA anal. 80−91190
^{197}Au(d,pn), E_d=13.6 MeV, disintegration reactions, isotopic effects 78−13108
^{197}Au(d,pn) 13.6 MeV disintegration, neutron elastic scatt. effect *(Russian)* 77−34322
Au(d,np), 23 to 26 MeV, diffraction theory calcs. 79−6537

deuteron-nucleus reactions continued
^{10}B(d,^{2}He), 55 MeV, cross sections, ^{2}He energy spectra and ang. distribs. 80−18321
^{10}B(d,3α), 360 keV, sequential decay, absolute three-particle cross section meas. 78−17220
^{10}B(d,3α), 4.4 to 5.6 MeV, ^{12}C excited states 77−18576
^{10}B(d,α), cross-section contrib. from ^{8}Be 3^{+} states, isospin mixing model 78−89789
^{10}B(d,α)^{8}Be(g.s.), excitation functions struct., isoscalar giant resonances in ^{12}C 78−46073
^{10}B(d,$\alpha\alpha$)^{4}He, $E_d<3.4$ MeV, reaction mechanism 77−6362
^{10}B(d,$\alpha\alpha$)^{4}He, $Q=17.88$ MeV, quasi-free effect search 78−4947
^{10}B(d,$\alpha\alpha$)α, ^{12}C excited states between 29 and 34 MeV 78−21494
^{10}B(d,p)^{11}B, 1 to 2 MeV, ang. distribs., reduction factor, spectroscopic factors 77−41977
^{10}B(d,p)^{11}B, 2.5 to 21.0 MeV, angular distrib., DWBA analysis 80−68675
^{10}B(d,p)^{11}B, appl. to B predeposited Si wafer anal. by combined ion beam techniques and X-ray microanal. 79−5238
^{10}B(d,p)^{11}B, $E_d=0.8$ to 2.4 MeV, reaction mechanism 79−17910
^{11}B+d→3αn, 3.75 MeV, sequential decay reaction mechanism from ang. distrib. anal. 79−6631
^{11}B(d,α_0)^{9}Be, Hauser-Feshbach statistical theory *(Spanish)* 77−67753
^{11}B(d,α)^{9}Be, non-relativistic, analytic S-matrix theory *(Spanish)* 77−67754
^{11}B(d,p)^{12}B reactions, 1.3 to 3.0 MeV, DWBA analysis of magnetic substate populations of residual nucleus 78−29480
^{138}Ba(d,^{6}Li), 35 MeV, ang. distrib. meas., deduced α-particle spectroscopic factors, reduced widths, decay lifetimes 77−18571
^{138}Ba(d,γ), 5-26 MeV, experimental and calc. compound nucleus cross sections 79−76002
Be+d, 40 MeV, target system neutron spectra 79−9595
Be+d neutron source, material damage study, He prod. and neutron fluence per neutron obs. in irrad. material 78−86710
^{9}Be (d,t), cross-section contrib. from ^{8}Be 3^{+} states, isospin mixing model 78−89789
^{9}Be(d,^{3}He)^{8}Li, isospin mixing of states in ^{8}Be near 17 MeV 77−65198
^{9}Be(d,α_0)^{7}Li, 0.9 to 2.5 MeV, ang. distribs. 77−18573
^{9}Be(d,α_1)^{7}Li*, 0.9 to 2.5 MeV, ang. distribs. 77−18573
^{9}Be(d,α)^{7}Li 12.17 to 14.43 MeV, α ang. distribs., excitation functions 78−54770
^{9}Be(d,α)^{7}Li to g.s. and 1st excited state, $E_d=2.25$-3.1 MeV, DWBA anal. 77−30610
^{9}Be(d,n), 14-23 MeV, thick target neutron yields 77−57791
^{9}Be(d,n), 14.8-23 MeV, thick target neutron yields 77−26752
^{9}Be(d,n), 40 MeV deuterons from ORIC, intense neutron source 77−83425
^{9}Be(d,n) 83.7 MeV, 0° neutron spectra, comparison with Serber model calcs. 77−6400
^{9}Be(d,n)^{10}B, polarised 4.5 MeV neutron source 77−57790
^{9}Be(d,n)^{10}B use of neutrons for meas. of full cross sections *(Russian)* 80−69008
^{9}Be(d,n)^{10}Be, neutron distrib. from bombardment of thick Be target 77−83408
^{9}Be(d,p)^{10}Be, appl. to Be determ. in metals using nuclear microprobe anal. 79−5204
^{9}Be(d,p)(d,α), appl. to obs. of interstitial atom trapping in Cu-Be cryst. 78−14384
^{9}Be(d,pγ)^{10}Be, 1.5 MeV, angular correlation meas. 78−94015
^{9}Be(d,t), 12 MeV polarised deuterons, analysing powers, j-mixing ratio 77−82937
^{9}Be(d,t)^{8}Be, isospin mixing of states in ^{8}Be near 17 MeV 77−65198
^{9}Be(d,t)^{8}Be 12.17 to 14.43 MeV, t ang. distribs., excitation functions, spectroscopic factor 78−54770
^{10}Be(d,p), 25 MeV, ^{11}Be single neutron strength, levels, spin assignments, spectroscopic factors 79−36156
Be(d,n), 16 and 28 MeV, neutron spectra 80−524
Be(d,n), activation cross-section, integral tests, dosimeter appl. 80−32553
Be(d,n), stripping-theory anal. of thick-target neutron prod. 77−6600
Bi (d,p), 6.3 GeV/c, p momentum spectra from d breakup 78−89887
^{208}Bi(d,f), 2.1 GeV, binary and ternary fission kinetics *(French)* 78−70577
^{210}Bi^{m}(d,p), 20 MeV, ^{211}Bi levels, spin assignments and spectroscopic strengths 79−6418
^{210}Bi^{m}(d,t), 17 MeV, ^{209}Bi levels and spectroscopic factors, ^{210}Bi(9^{-}) parentage 80−78158
^{79}Br(d,pxn), excitation functions for neutron deficient isotope form. via high-energy d-Br reactions 78−44609
^{79}Br(d,xn), excitation functions for neutron deficient isotope form. via high-energy d-Br reactions 78−44609
^{81}Br(d,pxn), excitation functions for neutron deficient isotope form. via high-energy d-Br reactions 78−44609
^{81}Br(d,xn), excitation functions for neutron deficient isotope form. via high-energy d-Br reactions 78−44609
C, 180° prod. of protons in high-energy reacts. 78−8816
^{12}C+d, 1.1-4.6 GeV/nucleon, nuclear fragmentation meas. *(Russian)* 78−54773
^{12}C+p(d)(α), transparency in composite particle reactions 80−9273
^{12}C(d,^{2}He), 55 MeV, cross sections, ^{2}He energy spectra and ang. distribs. 80−18321
^{12}C(d,^{6}Li)^{8}Be, 54.25 MeV, residual nuclei excited states angular distribs. 79−6624
^{12}C(d,X), 4.2 GeV/c, multitudes of secondary negative particles, momentum distrib. ratios *(Russian)* 80−63178
^{12}C(d,α)^{10}B, 20.7 and 29 MeV, polarised deuterons 77−82938
^{12}C(d,α)^{10}B(1.74 MeV, T=1), coupled channel anal. of energy depend. isospin violation 78−70541
^{12}C(d,n), 6-10 MeV polarised deuterons, differential cross-section, vector analysing power 77−6398
^{12}C(d,n), spectral line shape anal. 78−25203
^{12}C(d,np), n-p rescattering and d break-up in FSI 77−10417
^{12}C(d,p$_0$)^{13}C, proton polarisation in stripping reaction, obs. and DWBA calc. 79−30816
^{12}C(d,p)^{12}C*, reaction mech., relation to ^{12}C(d,d), S-matrix theory, 1.63 to 2.05 MeV *(Chinese)* 78−78393
^{12}C(d,p)^{13}C, 0.5 to 2.5 MeV, excitation functions and angular distribs., possible doorway state *(Chinese)* 80−68679
^{12}C(d,p)^{13}C, 1.5 to 3.0 MeV, excitation functions 79−40932
^{12}C(d,p)^{13}C, 1.58 to 3.03 MeV, calc. of differential cross sections, spectroscopic factors 77−6394

deuteron-nucleus reactions continued
^{12}C(d,p)^{13}C, 2.64-2.82 MeV, new model calcs. for p ang. distribs. 77−88097
^{12}C(d,p)^{13}C, C depth profiling in solids 79−5212
^{12}C(d,p)^{13}C, differential cross sections at 9.0 MeV deuteron energy, two-step processes 77−74857
^{12}C(d,p)^{13}C, light element profiling of tapered corrosion sections 79−92036
^{12}C(d,p)^{13}C* leading to unbound states, neutron form factors, coupled channel DWBA anal. 77−26775
^{13}C(d, ^{3}He), isospin violating direct reaction, Coulomb interaction role 80−102170
^{13}C(d, t), isospin violating direct reaction, Coulomb interaction role 80−102170
^{13}C(d,^{3}He), polarised d, 29 MeV, ^{12}B J-transfer determ. 79−49579
^{13}C(d,X), 13 MeV, cross section, vector and power, optical model parameters, DWBA anal. 79−22301
^{13}C(d,γ_0)^{15}N, $E_{exc}=17.7$ MeV, 95° differential cross section resonance struct. 78−37351
^{13}C(d,γ)^{15}N, polarised d, ^{15}N giant resonance and cross sections 79−93587
^{13}C(d,p), 2.7 MeV, ^{14}C first excited 0^{+} state, lifetime and E^{0} decay 80−102145
^{13}C(d,t) polarised d, 29 MeV, ^{12}C J-transfer determ. and isospin mixing 79−49579
^{17}C(d,p)^{13}C, high resolution depth profiling of C by spectral deconvolution 77−1966
^{23}C(d,γ)^{15}N, 2.90-9.95 MeV, cross sections, ang. distrib. meas. 77−6395
^{40}Ca+p(d)(α), transparency in composite particle reactions 80−9273
^{40}Ca(d,^{6}Li), 80 MeV, ground state α-spectroscopic factors, ^{36}Ar relative spectroscopic factors 79−93509
^{40}Ca(d,^{6}Li), DWBA anal., angular distrib., spectroscopic factors 79−6625
^{40}Ca(d,α)^{38}K, 7.5, 7.75, 8.0 MeV, polarised d, J$^{\pi}$ assignment 77−6401
^{40}Ca(d,np), n-p rescattering and d break-up in FSI 77−10417
^{40}Ca(d,p), 4.5-5.4 MeV, ^{41}Ca excited states, excitation functions and ang. distribs., statistical anal. 80−57686
^{40}Ca(d,p), 7 MeV, cross-sections calcs. from pseudopotentials, spectroscopic factors 78−572
^{40}Ca(d,p)^{41}Ca(J^{+}) 11.0 MeV, analysing powers, CCBA and DWBA anal. 77−6402
^{40}Ca(d,pγ), 2.01 MeV, ^{41}Ca parity doublet gamma lifetimes, 3/2 levels, parity mixing 80−78209
^{41}Ca(d,^{3}He), 20 MeV, ^{40}K energy levels and spectroscopic strengths 79−89238
^{41}Ca(d,α), 22 MeV, ^{39}K high spin states, J$^{\pi}$ assignments, DWBA anal. 79−40851
^{41}Ca(d,p), wave functions of O^{+} states in ^{42}Ca 78−74308
^{41}Ca(d,p)^{42}Ca, 11 MeV, cross section, vector analysing power, spectroscopic strengths 78−74374
^{41}Ca(d,p)^{42}Ca, two-body matrix elements in fp shell 78−21574
^{44}Ca(d,α)^{42}K, 11 MeV, particle-hole states in ^{42}K 78−8723
^{48}Ca(d,α), pol.d, 7.5-9.0 MeV, ^{46}K levels, J$^{\pi}$ and tensor anal. powers 80−102113
^{48}Ca(d,n), 20 MeV, ^{49}Sc proton single particle states, spectroscopic factors, DWBA anal. 80−99118
^{48}Ca(d,p), 11.9 MeV, analysing power, cross section, ^{49}Ca levels, spins, parities, spectroscopic factors 78−78391
^{48}Ca(d,t$_0$) and (^{3}He,d), comparison with ^{40}Ca data, isotope shifts of 1f$_{7/2}$ radii 77−34222
^{48}Ca(d,t)^{47}Ca, 13.5 MeV, polarised deuterons, low-lying levels in ^{47}Ca 78−13114
Ca(d,p), A=40, 48, Tabakin pot. calcs., differential cross sections, ang. distribs. 78−611
Ca(d,p)Ca, A=40, 42, 44, 48, at 2.5 MeV, spectroscopic factors *(German)* 77−18567
C(d,X), 4.2 GeV/N, multiple π^{-} prod., mean multiplicity *(Russian)* 80−27647
^{110,112}Cd(d,^{3}He) 50 MeV, populating Ag proton hole states 77−18369
C(d,p), 6.3 GeV/c, p momentum spectra from d breakup 78−89887
^{40}Cd(d,p)^{41}Ca, 11 MeV, effect of Skyrme type density depend. effective pots. 78−46069
^{116}Cd(d,n)^{117m,g}In, excitation functions 78−13105
Cd(d,xn), $E_d\leq27.5$ MeV, cross sections for form. of ^{114m}In and ^{116m}In 80−13482
^{140}Ce(d,p)^{141}Ce, 17 MeV, spectra and ang. distrib. obs., DWBA anal. 77−38283
^{142}Ce(d,p), ^{143}Ce quasi-f$_{7/2}$ low lying states spectroscopic factors, cluster-vibr. model 80−47391
^{142}Ce(d,t), 17 MeV, ^{141}Ce levels, single neutron holes, spectroscopic factors, DWBA anal. 79−85353
Ce(d,^{6}Li), (A=140, 142), 35 MeV, ang. distrib. meas., deduced α-particle spectroscopic factors, reduced widths, decay lifetimes 77−18571
^{37}Cl(d,t)^{36}Cl, 12.0 MeV, polarised deuterons, vector analysing power 77−14094
^{59}Co(d,p), ^{60}Co low lying states, DWBA anal. 78−29478
^{59}Co(d,p), 14 MeV, ^{60}Co, level struct., spectroscopic factors, DWBA anal. 78−86478
Cr (d,p), A=50, 52, 54, Tabakin pot. calcs., differential cross sections, ang. distribs. 78−611
^{50}Cr(d,p), 12.3 MeV polarised deuterons, analysing powers, ^{51}Cr spin assignments 77−30608
^{52}Cr(d,n)^{53}Mn, cyclotron preparation of ^{53}Mn, extraction, anal. 77−61441
^{52}Cr(d,p), 7-11 MeV, coupled-channel anal. 77−18579
^{52}Cr(d,p), cross section, stripping channel effect, coupled channel model, DWBA anal. 77−57676
^{52}Cr(d,p), polarised d, obs. of D-state and compound nucleus effects 77−34319
^{52}Cr(d,p)^{53}Cr, 10 MeV polarised beam, structure of ^{53}Cr low-lying levels 77−18395
^{52}Cr(d,p)^{53}Cr, Coulomb stripping, 2.12-2.48 MeV, DWBA anal., spectroscopic strengths 80−516
^{52}Cr(d,p)^{53}Cr, deuteron break-up model anal. of cross-section, vector analysing power and angular correlation 80−27648
^{52}Cr(d,pγ), 8.0 MeV, particle-gamma correlation meas. 77−61437
^{54}Cr(d$_{pol}$,p), cross section and vector analysing power, ^{55}Cr deduced levels and spins 80−52684
^{133}Cs(d,2n)^{133m}Ba, thick-target yield for ^{133m}Ba prod. for medical use 77−60251

deuteron-nucleus reactions continued
^{63}Cu(d,^{3}He), 9 MeV, polarised d, tensor anal. power and D-state effects 79−85446
^{63}Cu(d,X), 247 MeV, ^{66}Zn* composite particle emission, ang.-distribs., exciton-coalescence model 80−78265
^{63}Cu(d,X), X=p, d, t, ^{3}He, α, 24.7 MeV continuous spectra and ang. distribs. meas. 77−3016
^{63}Cu(d,p2n), 5.8-49.6 MeV, absolute cross sections for ^{61}Cu prod. 79−36249
^{63}Cu(d,p), 5.8-49.6 MeV, absolute cross sections for ^{64}Cu prod. 79−36249
(d,X), neutron excess isotope prod. in fragmentation, ^{6,8}He, ^{7,8,9,11}Li *(Russian)* 80−86888
D+d reaction, 6.8 to 11.1 MeV, beam dosimetry 78−53509
DY(d,t), ^{A}Dy, A=161, 163, Nilsson state ΔN=2 mixing, rot. bands 80−95295
D(d,n)^{3}He, 1.1 to 2.5 GeV/c, energy depend., cross sections, reaction mech. 78−54643
D(d,n)^{3}He, fusion cross sections and thermonuclear reaction rates 80−533
D(d,p), 6.3 GeV, proton momentum spectra 79−6621
D(d,p), dynamic profiling of D impurities 78−2153
D(d,p)T, channelling studies on the trapping of deuterium in vanadium by O-interstitials 79−4316
D(d,p)T, fusion cross sections and thermonuclear reaction rates 80−533
D(d,p)T, light ion diffusion in solids obs., using nuclear reaction depth profiling 79−5202
^{A}Dy(d,t), A=162, 164, coupled-channels Born approx. anal. 80−83104
Dy(d,p), ^{A}Dy, A=161, 163, Nilsson state ΔN=2 mixing, rot. bands 80−95295
^{A}Er(d,t), A=166, 168, coupled-channels Born approx. anal. 80−83104
^{166}Er(d,^{6}Li), 35 MeV, ang. distrib. meas., deduced α-particle spectroscopic factors, reduced widths, decay lifetimes 77−18571
^{167}Er(d,t)^{166}Er, 2-quasiparticle states obs. 80−18198
^{168}Er(d,t), 9-15 MeV, ^{167}Er levels and transitions, spectroscopic factor bombarding energy depend. 79−495
^{168}Er(d,t)^{167}Er, 17 MeV, DWBA anal. of ang. distribs. 78−17222
^{168}Er(d,t)^{167}Er, 17 MeV, band heads, two-step process 78−62551
^{254}Es fission coincidence data from d, t, and ^{3}He induced reactions 80−42720
^{152}Eu(d,p), 20 MeV, ^{153}Eu $5/2^{+}$ ground state rot. band, J$^{\pi}$, shape coexistence 80−86799
^{152}Eu(d,t), 20 MeV, ^{151}Eu narrow band and pickup strength shape coexistence 80−86799
^{19}F(d,^{3}He)^{18}O*, meas. of ^{6}He mass 78−41628
^{19}F(d,X), X=^{7}Li, ^{7}Be, 13.6 MeV, diff. cross sections, ^{5}He cluster direct transfer *(Russian)* 80−52650
^{19}F(d,α)^{17}O, 1.8 to 3.0 MeV, vector analysing ability using polarised deuterons *(Russian)* 80−32288
^{19}F(d,d)^{19}F, 1.8 to 3.0 MeV, vector analysing ability using polarised deuterons *(Russian)* 80−32288
^{19}F(d,p), 12.0 MeV, obs. of ^{20}F 4 to 6 MeV levels 78−25118
^{A}Fe(d$_{pol}$,p), A=54,58, cross section and vector analysing power, ^{55,59}Fe deduced levels 80−52684
^{56}Fe(d,α), pol.d, 7.5-9.0 MeV, ^{54}Mn low lying 2p-4h states, J$^{\pi}$ from tensor anal. powers 80−99124
^{69,71}Ga(d,^{3}He), 26 MeV, spectra of ^{68,70}Zn 78−25112
^{160}Gd(d,t) ^{159}Gd, coupled-channels Born approx. anal. 80−83104
Ge, 250 MeV deuterons, diode detector telescope for particle spectroscopy, design and performance 78−13384
^{A}Ge(d,^{3}He) 26 MeV, A=70, 72, ^{A}Ga, A=69, 71, spectroscopic factors, occupation number anomalies 78−82279
^{A}Ge(d,^{3}He) 26 MeV A=74, 76, ^{A}Ga, A=73, 75, deduced levels, occupation number anomalies, spectroscopic factors 78−82279
^{70}Ge(d,t),(d,p), differential cross sections and vector analysing powers 78−17221
Ge(d,^{3}He), ^{73,75}Ga Q-values and mass excess 80−9222
^{1}H(D,2p)n, 26.5 MeV, 4 dimens. comparison with local S-wave interaction Faddeev calcs. 79−17866
^{1}H(d,X), 3.3 GeV/c, two-nucleon mass enhancement assoc. with spectator high momentum tail in breakup 77−18569
^{1}H(d,pn), 45.4 MeV, tensor anal. powers 79−85447
(^{2}H,^{3}H), form factors and normalisation consts. using cluster wavefunctions 77−54168
(^{2}H,^{3}He), form factors and normalisation consts. using cluster wavefunctions 77−54168
^{2}H deformation effects in nuclear interaction, DWBA anal. *(Japanese)* 78−21575
^{2}H(^{2}H,n)^{3}He, fusion through metallic D 80−13517
^{2}H(d,^{3}He), differential cross sections at 13.2 MeV, DWBA anal. 79−45276
^{2}H(d,^{3}He)n, 2-20 MeV collimated monoenergetic neutron beam prod. using associated particle technique 77−83418
^{2}H(d,N), 50-85 MeV, ang. distribs., PWBA anal. 79−76005
^{2}H(d,X), x=p,n, ^{4}He continuum microscopic calcs. cross sections and levels 80−57702
^{2}H(d,2n)2p, proposed expt. to determ. nn effective range 77−18585
^{2}H(d,2p2n), 80 MeV, PWBA, double spectator process 78−41731
^{2}H(d,dp)n, 50-85 MeV, p-n coincidence spectra 77−18568
^{2}H(d,n), 13.6, 24.3 MeV, 0° absolute differential cross section 80−27649
^{2}H(d,n), 18-26 MeV, differential cross sections, ang. distribs., ^{4}He broad level search 80−102117
^{2}H(d,n), 290, 460 keV, neutron polarisation, ang. depend. 80−42632
^{2}H(d,n), 50-85 MeV, ang. distribs., PWBA anal., two body final states 79−6636
^{2}H(d,n), anal. power, comparison with mirror reaction (d,p) 79−75964
^{2}H(d,n), intense fast neutron beam prod. in high-press gas target 77−3201
^{2}H(d,n), pol.d, anal. power and polarisations in R-matrix methodology, comparison with (d,p) 80−78273
^{2}H(d,n), polarised d, <5.5 MeV, comparison of analysing power with ^{2}H(d,p) 79−17911
^{2}H(d,n), signal to background ratio for 10 to 14 MeV neutron prod. 77−30683
^{2}H(d,n)^{3}He, 1.5-15.5 MeV, tensor anal. power, charge symmetry violation in mirror reaction 80−13368
^{2}H(d,n)^{3}He, 35-275 keV, neutron polarisation determ. 77−41942
^{2}H(d,n)^{3}He, 6 to 17 MeV, n prod. absolute differential cross sections 78−74373
^{2}H(d,n)^{3}He, four-body model of the four-nucleon system 79−63643

deuteron-nucleus reactions continued
^{2}H(d,n)^{3}He, neutron polarisation meas. with Mott-Schwinger scatt. polarimeter 79−22571
^{2}H(d,n)^{3}He, struct. and form factor models in mass-3 system 79−45274
^{2}H(d,n)^{3}He, total cross-section energy depend. 78−29477
^{2}H(d,n)^{3}He source spectra, TUNL fast neutron cross section facility 77−26931
^{2}H(d,p), (d,n), 50-85 MeV cross-section meas. 79−13307
^{2}H(d,p), anal. power, comparison with mirror reaction (d,n) 79−75964
^{2}H(d,p), pol.d, anal. power and polarisations in R-matrix methodology, comparison with (d,n) 80−78273
^{2}H(d,p), polarised d, <5.5 MeV, comparison of analysing power with ^{2}H(d,n) 79−17911
^{2}H(d,p)^{3}H, ^{2}H(d,n)^{3}H, analysing power meas. 78−25204
^{2}H(d,p)^{3}H, 13.4, 17 MeV, pol. d, anal. power direct reaction and isospin symmetries 80−515
^{2}H(d,p)^{3}H, 1.5-15.5 MeV, tensor anal. power, charge symmetry violation in mirror reaction 80−13368
^{2}H(d,p)^{3}H, cross-section anal. using four-body integral eqns. 77−18577
^{2}H(d,p)^{3}H, four-body calc. solns. 79−71855
^{2}H(d,p)^{3}H, four-nucleon integral eqn. solns. using effective UPA 79−71794
^{2}H(d,p)^{3}H, struct. and form factor models in mass-3 system 79−45274
^{2}H(d,p)^{3}H and ^{2}H(d,n)^{3}He, comparison of analysing powers 2.5 to 11.5 MeV 79−6628
^{2}H(d,p)T, differential cross sections at 13.2 MeV, DWBA anal. 79−45276
^{2}H(d,pd)n, 12.2 MeV, collinearity condition repeat experiment 79−76004
^{2}H(d,pnd), 52 MeV, break-up mechanism 78−74375
^{2}H(d,t)^{1}H, differential cross sections calc. using DWBA, distortions 78−54772
^{3}H(^{2}H,n)^{4}He, chain carriers in fusion reaction kinetics 80−86969
^{3}H(d, n)^{4}He, meas. of mean d interaction energy in tritiated Ti layer 79−31281
^{3}H(d,n), pol. d, below 6.75 MeV, tensor anal. power 80−42633
^{3}H(d,n)^{4}He, 150 keV, vector polarised detuerons, n-p analysing power 78−62544
^{3}H(d,n)^{4}He, 6 to 17 MeV, n prod. absolute differential cross sections 78−74373
^{3}H(d,n)^{4}He, 7-17 MeV, absolute differential cross section meas. 77−26780
^{3}H(d,n)^{4}He, 700 keV, n polarisation meas., scintillation + TOF technique 78−86538
^{3}H(d,n)^{4}He, associated particle methods for neutron flux monitoring 79−9977
^{3}H(d,n)^{4}He, neutron energy meas. with Si detector 80−32566
^{3}H(d,n)^{4}He, neutron fluence and energy transfer standard 80−102194
H(d,2p)n, 26.5 MeV, Faddeev cross section and scatt. symmetries over 50% of total phase space 79−76003
H(d,n)^{3,4}He reactions, NA-2 neutron generator, fast neutron spectrum, stilbene scintillation spectrometer meas. *(Czech)* 77−71710
H(d,p), A=1,2, 6.3 GeV/c, p momentum spectra from d breakup 78−89887
H(d,pp)n, polarised d, polarisation effects in 3-body system 79−80946
^{3}He+d breakup, quasifree processes 77−18575
^{3}He(d, α)H, replacement of implanted ^{3}He by subsequent ^{4}He bombardment in Nb, and vice versa 79−4325
^{3}He(d,α)^{1}H, use in depth resolution by ^{3}He profiling 78−58557
^{3}He(d,α)H, depth profile meas. of He in Ni and Nb 79−14839
^{3}He(d,d)^{3}He, 0.3-8 MeV, single-level reson. and ^{5}Li parameters 77−30606
^{3}He(d,n)^{4}He, 14 MeV polarised neutron facility 79−85851
^{3}He(d,p), 6.44 MeV polarised d, absolute standard of d vector analysing powers 77−34281
^{3}He(d,p), pol. d, below 6.75 MeV, tensor anal. power 80−42633
^{3}He(d,p), polarised d, 10-17 MeV, cross sections, vector and tensor anal. powers 79−75966
^{3}He(d,p)^{4}He, 8.5-10.5 MeV polarised deuterons, max. tensor analysing power 77−6397
^{3}He(d,p)^{4}He, fusion cross sections and thermonuclear reaction rates 80−533
^{3}He(d,p)^{4}He, polarimeter for deuteron beams 80−47834
^{3}He(d,p)^{4}He, use in deuteron tensor polarimeter 77−3242
^{4}He(d, n), 50 MeV, neutron polarisation meas. 78−70726
^{4}He(d,n)αp, 50 MeV, differential cross-section and polarisation meas. 77−88157
^{4}He(d,p), 6.8 , 7.8 MeV, continuous proton spectra obs. 78−37352
^{4}He(d,p)^{4}He n, 15 MeV polarised deuterons, differential cross sections, vector analysing powers 78−89884
^{4}He(d,pα)n, at E$_{d}$=8.9 MeV, absolute cross-section meas. 77−34317
^{4}He(d,pn), break-up process, NN interaction, numerical calc. of cross section 77−74858
^{4}He(d,pn)^{4}He, differential cross section and polarisation, three body model 80−47460
^{4}He(d,pn)^{4}He, Faddeev eqns., separable pots., total cross sections 78−21571
^{4}He(d,t)^{3}He, charge asymmetry effects, cluster model calc. 77−14136
^{178}Hf(d, 2n), 13.5 MeV, ^{178}Ta level properties, rot. bands, transitions and level lifetimes 79−36158
^{127}I(d,2n)^{127}Xe production of di-iodomethane target 79−79651
^{115}In(d,^{3}He), 50 MeV, proton hole states in ^{114}Cd, DWBA anal. 78−8829
^{191}Ir(d,2n), 13 MeV, ^{191}Pt level scheme, γ, conversion electron spectra, spins, parities 78−25149
^{39}K(d,α)^{37}Ar, 1.83-2.53 MeV, fluctuations analysis and spin values deduced 77−23095
^{41}K(d,p), 10 MeV, cc ^{42}K levels and ang. distribs., spectroscopic factors, DWBA anal. 79−17806
^{78}Kr(d,t), polarised d, 15.95 MeV, ^{77}Kr, low lying state J$^{\pi}$ assignments, anal. powers 79−45153
^{82}Kr(d,3n)^{81}Rb, non-linear behaviour of gas targets for isotope prod. 78−25361
^{84}Kr(d,p), polarised and unpolarised d, ^{85}Kr level struct. and spectroscopic factors 79−471
^{86}Kr(d,p), polarised and unpolarised d, ^{87}Kr ground state spin assignment 79−471
^{16}L(d,^{6}Li)^{12}C, 50 to 80 MeV, spectroscopic factors energy depend. 79−6622
^{16}L(d,α_{3})^{14}N, 6.7-12.5 MeV, differential cross sections and anal. power, ^{18}F unnatural parity states 79−3160

deuteron-nucleus reactions continued
^{6}Li, 180° prod. of protons in high-energy reacts. 78−8816
^{6}Li+d, 0.1-1.0 MeV, DWBA and R-matrix cross section anal., direct contribution 79−67758
^{6}Li+d, extrapolation of low-energy reaction cross-sections 77−2955
^{6}Li+d, thermonuclear reaction rate parameters calc. 77−61436
^{6}Li+d, three body reactions, low energy, reaction mechanisms 78−13111
^{6}Li+d reactions, low-energy, CTR appl. 77−83097
^{6}Li+d$\rightarrow\alpha\alpha^{*}\rightarrow\alpha$tp, 1.2-8 MeV, ^{8}Be, highly excited $\alpha\alpha^{*}$ states 78−78262
^{6}Li(d, α), polarised d, 5-10 MeV, $A_{y}=1$ and $A_{yy}=1$ points search 79−36223
^{6}Li(d,^{2}He), 55 MeV, cross sections, ^{2}He energy spectra and ang. distribs. 80−18321
^{6}Li(d,X) system, resonating group method, single channel approx., cluster states 80−57782
^{6}Li(d,α), 100-180 keV, low energy cross sections, astrophysical region extrapolation 80−22843
^{6}Li(d,α), 21-28 MeV, ^{8}Be resonant state, $\alpha\alpha^{*}$ cluster and sympletic model anal. 79−9537
^{6}Li(d,α), 2.25-6 MeV, absolute cross sections 77−23297
^{6}Li(d,α), (d,p), simultaneous determ. of p and α particle ang. distribs., cellulose nitrate detector 79−737
^{6}Li(d,α), cross sections, low energy extrapolation, 3 keV-1 MeV, thermonuclear reaction rate parameter 79−6635
^{6}Li(d,α), extreme values of analysing power 77−3018
^{6}Li(d,α)^{4}He, 1.5-11.5 MeV, resonance behaviour, analysing powers 77−82935
^{6}Li(d,α)^{4}He, below 12 MeV, analysing powers, *8*Be reson. levels 77−82936
^{6}Li(d,α)^{4}He, light ion diffusion in solids obs., using nuclear reaction depth profiling 79−5202
^{6}Li(d,α)^{4}He*, 13.6 MeV, α spectra, excited state of ^{4}He, spin, parity 78−54771
^{6}Li(d,α)α, 0.1 to 1.0 MeV, absolute cross sections 78−25205
^{6}Li(d,αt), 1.2-8 MeV, ^{8}Be high spatial symmetry excited states, resonances, rot. band 80−86780
^{6}Li(d,γ)^{8}Be, first T=2 state radiative width 77−14130
^{6}Li(d,n$_{1}$)^{7}Be*, 0.6-1.0 MeV polarised deuterons, vector and tensor analysing powers 78−4925
^{6}Li(d,n^{3}He)^{4}He, absolute and total cross sections 79−40936
^{6}Li(d,n)^{7}Be, 0.2 to 0.9 MeV, absolute cross sections 78−25205
^{6}Li(d,n)^{7}Be, 0.2-0.9 MeV, differential and total cross sections for neutrons 77−23096
^{6}Li(d,n)^{7}Be, 0.4-1.0 MeV cross-section meas. 79−76017
^{6}Li(d,n)^{7}Be, low energy cross section, 100-180 keV 78−4949
^{6}Li(d,p$_{0}$)^{7}Li, 0.6-1.0 MeV polarised deuterons, vector and tensor analyzing powers 78−4925
^{6}Li(d,p$_{1}$)^{7}Li*, 0.6-1.0 MeV polarised deuterons, vector and tensor analyzing powers 78−4925
^{6}Li(d,p^{3}H)^{4}He, absolute and total cross sections 79−40936
^{6}Li(d,p), 100-180 keV, low energy cross sections, astrophysical region extrapolation 80−22843
^{6}Li(d,p), 2.25-6 MeV, absolute cross sections 77−23297
^{6}Li(d,p)^{7}Li, 0.1 to 1.0 MeV, absolute cross sections 78−25205
^{6}Li(d,tp)^{4}He, 0.465 MeV, quasi-free contribs. 78−614
^{7}Li(d, t), 12 MeV, nuclear vertex constant in peripheral model for virtual decay ^{7}Li$\rightarrow\alpha$+t 80−18295
^{7}Li(d,^{3}He)^{6}He, meas. of ^{6}He mass 78−41628
^{7}Li(d,α_{1})^{5}He, $E_{d}=250$ to 750 keV, cross section determ. in absolute current meas. reaction chamber *(French)* 78−78388
^{7}Li(d,α), 1.5-11.5 MeV, meas. of differential cross section and analysing powers 77−3017
^{7}Li(d,$\alpha\alpha$)n, 2 MeV, quasi free reaction, ^{7}Li struct. 78−41727
^{7}Li(d,$\alpha\alpha$)n, excitation energy and width of ^{5}He first excited state 77−276
^{7}Li(d,$\alpha\alpha$n), 7.0 MeV, prevalence of ^{8}Be formation 78−82357
^{7}Li(d,n), 14-23MeV, thick target neutron yields, spectral distribs. 77−57791
^{7}Li(d,n), 14.8-23 MeV, thick target neutron yields 77−26752
^{7}Li(d,n), neutron spectra and yields from thick targets 77−30602
^{7}Li(d,p), 0.7-3.4 MeV, absolute total cross section, ^{8}Li β-decay half life 80−13483
^{7}Li(d,t), 12 MeV, ^{7}Li$\rightarrow\alpha$t virtual decay vertex constant 80−78231
Li(d,n), neutron spectra from thick target bombardment for therapy 78−28049
^{A}Mg(d,^{6}Li), 80 MeV, A=24, 26, ground state α-spectroscopic factors 79−93509
^{A}Mg(d,^{6}Li), 80 MeV, A=24,26, α-spectroscopic factors and ang. distribs., DWBA anal. 80−99126
^{24}Mg(d, pγ)^{25}Mg, differential and double differential cross sections, Hauser Feshbach anal., compound nucleus 79−89282
^{24}Mg(d,^{6}Li)^{20}Ne, 28 MeV, α pick up, angular distribs. and spectroscopic factors 78−78352
^{24}Mg(d,$\alpha\gamma$)^{22}Na, 7.75 MeV, ang. correl. meas. using tensor polarised deuterons 77−22934
^{24}Mg(d,d$_{1}$), vector analysing power, d$_{1}$-γ ang. correl., DWBA and CCBA anals. 77−30605
^{24}Mg(d,n)^{25}Al, stripping reactions to unbound states from p-n correlations, spin, parity and widths 78−62547
^{24}Mg(d,p), 1.5-2.5 MeV, fluctuation anal., ^{25}Mg highly excited states 78−46071
^{24}Mg(d,p)^{25}Mg, 8-13 MeV, vector polarised deuterons, excitations function of cross sections 78−8826
^{24}Mg(d,p)^{25}Mg, stripping reactions to unbound states from p-n correlations, spin, parity and widths 78−62547
^{24}Mg(d,pγ)^{25}Mg, particle-gamma and gamma-gamma coincidence, energies and branching ratios 77−22892
^{25}Mg(d,α), 12.07 to 11.57 MeV, angle-integrated cross section, ^{23}Na, spin, parity, energy levels 78−50179
^{26}Mg(d,p), 3.1, 3.5 MeV ^{27}Mg energy levels, spectroscopic factors, DWBA, Hauser-Feshbach anals. 80−52581
^{26}Mg(d,pγ)^{27}Mg, study of ^{27}Mg excited states up to $E_{x}=7976$ keV 77−41981
Mo, activation in cyclotron by p, d, α, ^{3}He 79−30839
Mo bombardment, yields of Tc isotopes, energy depend. 77−23098
^{A}Mo(d, ^{6}Li)$^{A-4}$Zr, 45 MeV, A=94,96,98,100, unusually strong excitation of 1.59 MeV O^{+} state in ^{100}Mo(d, ^{6}Li) 79−49584
^{92}Mo(d,n)^{93m,g}Tc, excitation functions and yields 77−41975
^{94}Mo(d,2n)^{94m,g}Tc, excitation functions and yields 77−41975
^{98}Mo(d,n)^{99m}Tc, excitation functions and yields 77−41975

deuteron-nucleus reactions continued
^{98}Mo(d,p), 10 MeV, ^{99}Mo first excited state g factor 79−17801
^{98}Mo(d,p), (d,n), (d,α), activation analysis, excitation functions 80−22842
^{98}Mo(d,p)^{99}Mo, excitation functions and yields, <13 MeV 78−37353
^{100}Mo,(d,p)^{101}Mo excitation functions and yields, <13 MeV 78−37353
^{100}Mo(d,n)^{100}Mo(d,n)^{101}Tc, excitation functions and yields 77−41975
Mo(d,α)Nb, on natural Mo, A=92,94,97,98, up to 13 MeV, excitation functions and yields 77−82933
^{14}N(d, α), pol. d., vector anal. capacity energy and ang. depend. 80−18281
^{14}N(d, α), pol.d, 1.5-3 MeV, vector anal. capacity for two α-particle groups 80−78266
^{14}N(d, p$_{5}$)^{15}N, cross sections determ., 0.32-1.45 MeV 80−42671
^{14}N(d, p)^{15}N, 12 to 52 MeV, stripping reaction anal., distorted wave method 79−80948
^{14}N(d,^{6}Li), 80 MeV, DWBA calcs. spectroscopic factors 79−6623
^{14}N(d,^{6}Li)^{10}B, 80 MeV, four-nucleon pickup from ^{14}N, spectroscopic factor determ. for ^{10}B 79−63679
^{14}N(d,α)^{12}C, search for quartet excited states in ^{16}O 77−57600
^{14}N(d,n)^{15}O, non-linear behaviour of gas targets for isotope prod. 78−25361
^{14}N(d,p$_{0}$)^{15}N, 52 MeV, DWBA and impulse approx. anal. 77−34318
^{14}N(d,p), pol. d, 10 MeV, ^{15}N low lying states, cross sections and anal. power, transitions, spectroscopic factors 80−32183
^{14}N(d,p)^{13}N, search for quartet excited states in ^{16}O 77−57600
^{14}N(d,p)^{15}N, 0.309-0.638 MeV, differential cross-section, ang. distrib. meas. 77−6396
^{14}N(d,p)^{15}N*, Q-value, test of differential hysteresis in Enge split-pole spectrograph 78−55082
^{15}N(d,α), $E_{d}<3$ MeV, intermediate structure 77−10412
^{15}N(d,p), 1.4-2.7 MeV, excitation functions 77−23094
^{15}N(d,p), 5.048 MeV, ^{16}N $J^{\pi}=1^{-}$ assignment 79−30786
^{15}N(d,p)^{16}N off-shell effects 78−62545
^{23}Na(d,^{3}He)^{22}Ne, 12.4 MeV polarised beam, $d_{5/2}$-$d_{3/2}$ admixing in pickup strength 77−6399
^{23}Na(d,p)^{24}Na, 1.5 to 3.0 MeV, excitation functions 79−40932
^{23}Na(d,p)^{24}Na, 1.58 to 3.03 MeV, calc. of differential cross sections, spectroscopic factors 77−6394
^{93}Nb(d,pX), 25.5 MeV, inclusive p spectra and cross sections from d breakup 79−13303
^{93}Nb(d,pX), 80 MeV, inclusive proton spectra, d break-up, DWBA anal. 80−91190
^{142}Nd(d,t), 17 MeV, levels in ^{141}Nd anal., DWBA calc. 77−41979
^{143}Nd(d,2N), 13.5 MeV, ^{143}Pm high spin states, J^{π}, transitions, isomer g-factors 80−32154
^{143}Nd(d,p), 25 MeV, obs. of ^{144}Nd levels 77−6241
^{144}Nd(d,p), 12.1 MeV, ^{145}Nd energy levels, DWBA calcs. 80−68533
^{144}Nd(d,t)^{143}Nd, 12.1 MeV, ^{143}Nd nucleus levels, intermediate coupling unified model calcs. 78−89791
^{146}Nd(d,pγ), 10 MeV, ^{147}Nd low spin states ns lifetimes, particle rotor model interpretation 80−78207
^{146}Nd(d,t), 12.1 MeV, ^{145}Nd energy levels, DWBA calcs. 80−68533
^{148}Nd(d,2n), 6.5-52 MeV, ^{148}Pm^{m,g} isomeric pair prod. 77−88144
^{148}Nd(d,t)^{147}Nd, energy levels of ^{147}Nd 78−507
^{148}Nd(d,t)^{147}Nd, vector analysing powers, spin determ. of ^{147}Nd 78−609
Nd(d,^{6}Li) (A=142, 144, 146), 35 MeV, ang. distrib. meas., deduced α-particle spectroscopic factors, reduced widths, decay lifetimes 77−18571
Nd(d,t), 17 MeV, ^{A}Nd, A=145, 147, 149, single neutron hole states spectroscopic factors, DWBA anal. 80−78109
^{20}Ne(d,^{6}Li), 80 MeV, ground state α-spectroscopic factors 79−93509
^{20}Ne(d,^{6}Li)^{16}O, Goldfarb-Buttle method *(Chinese)* 78−8834
^{20}Ne(d,α), 10.5 to 12.0 MeV, tensor analysing power meas., ^{18}F level spin, isospin and parity assignments 78−74305
^{20}Ne(d,p$_{0}$)^{21}Ne, 0.5-0.662 MeV, resonance obs., ^{22}Na levels 78−46072
^{20}Ne(d,p), 10-12 MeV, pol. d, ^{21}Ne states cross section, anal. power, coupled channel and fluctuations anal. 80−27617
^{20}Ne(d,p)^{21}Ne, 0.5-0.66 MeV, proton ang. distrib., excitation function, DWBA calc. 78−29475
^{20}Ne(d$_{pol}$,p), 10 MeV, ^{21}Ne deduced spectroscopic factors, levels and anal. powers 80−83087
^{22}Ne(d,α)^{20}F, 10 MeV, study of ^{20}F states up to 7 MeV excitation 77−10414
^{A}Ni(d,X), A=58, 64, 7.6 GeV/c, isotopic cross section ratios, He, Li fragments isotopic effects *(Russian)* 80−63154
^{58}Ni(d,$\alpha\gamma$), 7 MeV, mean lifetimes of ^{56}Co levels 78−4950
^{58}Ni(d,p)^{59}Ni, deuteron break-up model anal. of cross-section, vector analysing power and angular correlation 80−27648
^{58}Ni(d$_{pol}$,p), cross section and vector analysing power, ^{59}Ni deduced levels 80−52684
^{61}Ni(d,^{3}He), ^{60}Co low lying states, DWBA anal. 78−29478
^{61}Ni(d,p), low lying ^{61}Ni collective states, spectroscopic factors 77−61433
^{62}Ni(d,pX), 25.5 MeV, inclusive p spectra and cross sections from d breakup 79−13303
^{64}Ni(d,^{3}He)^{63}Co, proton pickup strength determ. in ^{63}Co 79−22163
Ni(d,p)Ni, A=58, 60, 62, 64, at 2.8 MeV, cross-sections and spectroscopic factors *(German)* 77−18566
^{237}Np(d,p) 12 MeV, ^{238}Np energy level scheme determ. by Nilsson model 79−26370
^{16}O+p(d)(α), transparency in composite particle-nucleus reactions 80−9273
^{16}O(d, ^{6}Li)^{12}C, 50 to 80 MeV, ^{12}C, α-transfer spectroscopic factors for O^{+}, 2^{+} and 4^{+} states, transitions 80−13370
^{16}O(d,^{3}He)^{15}N, 82 MeV, finite-range DWBA calcs. 77−10416
^{16}O(d,^{6}Li), 80 MeV, ^{12}C deduced levels and spectroscopic factors, ang. distribs., DWBA anal. 78−94013
^{16}O(d,^{6}Li)^{12}C, 35 MeV, finite range CCBA calcs. 77−6403
^{16}O(d,^{6}Li)^{12}C, 50, 65, 80 MeV, energy depend., spectroscopic factors 78−74372
^{16}O(d,^{7}Be)^{11}B, angular distribs., direct five nucleon transfer $E_{d}=80$ MeV 79−6627
^{16}O(d,X), X=d or N, elastic scatt. and stripping, three body calc. 80−91165
^{16}O(d,α_{3}), 6.84 MeV polarised d, absolute standard for d vector analysing powers 77−34281
^{16}O(d,α)^{14}N, ^{16}O conc. profiles anal. with high resolution mag. spectrom. 79−5215
^{16}O(d,α)^{14}N, 0.66 to 1.10 MeV cross section determ. for O_{2} profiling 79−45275

deuteron-nucleus reactions continued

^{16}O(d,α)^{14}N, low conc. ^{16}O depth profiling by α-particle energy anal. 79—5214

^{16}O(d,n), ^{17}F half life meas. 77—88085

^{16}O(d,p), 12 MeV, ^{17}O, cross sections to ground, 0.87 and 5.09 MeV states, neutron strength 80—5066

^{16}O(d,p), 12 MeV, stripping reaction differential cross section, d distortion effect *(Japanese)* 80—22796

^{16}O(d,p), <4 MeV, vector analysing power, level characts. of ^{18}F compound nucleus 77—61434

^{16}O(d,p)^{17}O, ^{16}O conc. profiles anal. with high resolution mag. spectrom. 79—5215

^{16}O(d,p)^{17}O, anal. using deuteron deform. effects *(Japanese)* 78—37355

^{16}O(d,p)^{17}O, appl. to B predeposited Si wafer anal. by combined ion beam techniques and X-ray microanal. 79—5238

^{16}O(d,p)^{17}O, channel coupling array and coupled reaction channel methods 78—8831

^{16}O(d,p)^{17}O, coupled channel variational method for multi-step direct nuclear reactions. II. Test on a (d,p) reaction 78—66259

^{16}O(d,p)^{17}O, O depth profiling in solids 79—5212

^{16}O(d,p)^{17}O*, channelling studies on the trapping of deuterium in vanadium by O-interstitials 79—4316

^{16}O(d,p)O*, decaying states, DWBA 77—57677

^{17}O(d,^{3}He), (d,t), 52 MeV, isospin mixing in ^{16}O determ 78—8832

^{17}O(d,t) and (d,τ) pick-up reactions, particle-hole spectra of ^{16}O, ^{16}N, spectroscopic strengths 78—58288

^{18}O(d,α), 8.5 to 11.3 MeV polarised deuterons, ^{16}N levels, spin parity assignments 78—89886

^{18}O(d,p), pol. d, 8-12 MeV, ^{20}F cross sections and anal. power, compound nucleus contrib. Ericson fluctuations 80—22803

^{18}O(d,p)^{19}O, ^{19}O level p-γ correl. meas. 77—10353

^{18}O(d,t), 17 MeV, ^{18}O ground state wave function 78—66287

^{18}O(d,t)^{17}O, ^{18}O(d,τ)^{17}N, 52 MeV, ^{17}O, ^{17}N levels anal., 1p spin-orbit splitting 77—41980

^{188}Os(d,p)^{189}Os, 12 MeV, ^{189}Os spectroscopy, Nilsson model, triaxiality 77—14035

^{190}Os(d,p), ^{192}Os(d,t), energy levels and spectra of ^{191}Os determ. 77—41917

^{190}Os(d,t)^{189}Os, 12 MeV, ^{189}Os spectroscopy, Nilsson model, triaxiality 77—14035

^{192}Os(d,3nγ) 19 to 28 MeV, ^{191}Ir levels, Coriolis coupling model and asymmetric rigid rotor model 79—22164

^{192}Os(d,p)^{193}Os, ^{193}Os energy levels, neutron separation energy 78—41642

^{31}P(d,α)^{29}Si, 1.5-2.5 MeV, intermediate resonance widths 77—88151

^{31}P(d,α)^{29}Si, 2-3 MeV, excitation functions and ang. distribs. 77—79386

^{31}P(d,p), 1.5-2.5 MeV, ^{32}P spectroscopic factors and level transition excitation function anal. 78—74371

^{31}P(d,p), (d,α), cross-section fluctuations at 150° 78—29476

^{31}P(d,p)^{32}P, 1.5-2.5 MeV, intermediate resonance widths 77—88151

^{A}Pb(d,X), A=207,208, E$_d$=13.6 MeV, isotopic effect in differential cross section 79—9540

^{204}Pb(d,p), 13.0-20.0 MeV, populating ^{205}Pb hole states below MeV 2.56 77—30478

^{204}Pb(d,p) 13.0 MeV, populating ^{205}Pb particle states 77—34216

^{207}Pb(d,f), 2.1 GeV, binary and ternary fission kinetics *(French)* 78—70577

^{207}Pb(d,p), 26.2 MeV, ^{208}Pb 7064 keV level negative parity, EM deexcitation pattern 79—36148

^{207}Pb(d,pn), E$_d$=13.6 MeV, disintegration reactions, isotopic effects 78—13108

^{207}Pb(d,pn) 13.6 MeV disintegration neutron elastic scatt. effect *(Russian)* 77—34323

^{208}Pb(d,^{6}Li) ^{204}Mg, SS MeV, levels and spectroscopic factors, α clustering, DWBA anal. 79—67694

^{208}Pb(d,3n), 25 MeV, ^{207}Bi high spin states, level decays, three particle interactions 79—49567

^{208}Pb(d,3n)^{207}Bi, spin and parity assignment of ^{207}Bi levels 78—89788

^{208}Pb(d,nγ), half life of ^{209}Bi 2442.8 keV lowest 2p 1h state 78—74331

^{208}Pb(d,p), polarised d, tensor anal. powers, sub-Coulomb stripping calc. corrections 79—80918

^{208}Pb(d,p), tensor analyzing power, deuteron wave functions 80—99137

^{208}Pb(d,p)^{209}Pb, 12.3 MeV, tensor analysing powers 78—29479

^{208}Pb(d,p)^{209}Pb, 9.0 MeV, effects of d D state determ. 77—67752

^{208}Pb(d,pn), E$_d$=13.6 MeV, disintegration reactions, isotopic effects 78—13108

^{208}Pb(d,pn) 13.6 MeV disintegration, neutron elastic scatt. effect *(Russian)* 77—34322

^{208}Pb(d,pn) 13.6 MeV disintegration, neutron elastic scatt. effect *(Russian)* 77—34323

^{208}Pb(d,t), 10 MeV, polarised d, tensor anal. power and D-state effects 79—85446

Pb(d,α)Tl, A=208,206,204 at 80 MeV, high-spin states, α-spectra 78—504

Pd+d, 3.6 GeV, emitted proton vel. spectra max. *(Russian)* 79—9571

^{210}Po(d,p), 17 MeV, ^{211}Po deduced levels, J$^{\pi}$ assignments, spectroscopic factors 79—22197

^{210}Po(d,t), 17 MeV, ^{209}Po deduced levels, J$^{\pi}$ assignments, spectroscopic factors 79—22197

^{141}Pr(d,3n), simple formula for excitation functions 78—93978

^{A}Pt(d,t), A=192-198, even, 26 MeV, levels obs. 78—50089

^{196}Pt(d,p) 13.5 MeV, ^{197}Pt states from ang. distribs. and spectroscopic factors 78—78267

^{198}Pt(d,t) 13.5 MeV, ^{197}Pt states from ang. distribs. and spectroscopic factors 78—78267

^{239}Pu(d,p), 4.0-6.2 MeV, reson. in fission probabilities of ^{240}Pu 78—78429

^{239}Pu(d,pf), 11-17 MeV, ^{240}Pu, subbarrier resonances and fission probabilities 79—13266

^{242}Pu(d,p)^{243}Pu, populating Nilsson and rot. levels 77—6202

^{242}Pu(d,t)^{243}Pu, populating Nilsson and rot. levels 77—6202

^{96}Ru(d,p), 16 MeV, spectra and ang. distribs. meas., ^{97}Ru levels anal. 77—38284

^{96}Ru(d,p)^{97}Ru, 11.5 MeV, study of states in ^{97}Ru 77—18570

^{100}Ru(d,p)^{101}Ru, 11.5 MeV, study of states in ^{97}Ru 77—18570

^{32}S(d,α)^{30}P, 2 to 2.5 MeV, fluctuation anal., ^{24}Cl compound nucleus 78—46070

^{32}S(d,α)^{30}P, statistical fluctuations at 135°, 2.0-2.5 MeV 78—89882

^{32}S(d,p), DWBA anal. converging overlap integrals, stripping to decaying states 79—6530

^{32}S(d,p)^{33}S, excited states, ang. correl. meas. 77—38239

deuteron-nucleus reactions continued

^{32}S(d,p)^{33}S, statistical fluctuations, at 135°, 2.0-2.5 MeV 78—89882

^{32}S(d,p)^{33}S*, 12 MeV, ratio to (n,n) cross section, DWBA anal. 77—57677

^{32}S(d,t) and (d,^{3}He), ^{31}S, ^{31}P analogue spectroscopic factors, charge asymm., DWBA anal., optimum Q-value 77—54229

^{34}S(d,α)^{32}P, 8.25-9.50 MeV, tensor-polarised deuterons, spin-parity assignments to ^{32}P levels 78—17219

^{34}S(d,p)^{35}S, 11.8 MeV vector polarised deuterons, optical pot. 77—88149

^{36}S(d,α) 3.05-3.26 MeV, α-spectrum, ^{34}P mass and energy levels 79—6632

^{36}S(d,p), 3.2 MeV, proton spectra meas., ^{37}S energy level scheme *(Russian)* 78—41733

^{36}S(d,p), 3.55 MeV, ^{37}S level scheme and excitation energies *(Russian)* 79—30790

^{121}Sb(d,Zn), 12 MeV, ^{121}Te isomeric state, spin, lifetime and mag. moment 80—47387

^{121}Sb(d,2n)^{121m,g}Te, 4-24 MeV, yield meas. 78—37349

^{123}Sb(d,2n)^{123m}Te, 4-24 MeV, yield meas. 78—37349

Sb(d,2n), 13.5 MeV, ^{A}Te, A=117, 119, 121, collective excitations, high spin states and transitions 80—13346

^{45}Sc(d,p), (d,t), reanalysed data, sum rule anal. and spectroscopic factors 78—8828

S(d,p), A=32, 34, Tabakin pot. calcs., differential cross sections, ang. distribs. 78—611

Se (d,p), 12.5 MeV, ^{77,79,81,83}Se level struct., spins, parities, cross section, vector analysing power 78—89885

^{74}Se(d,p), 6 MeV, ^{75}Se energy levels, DWBA, sum rule anals., spectroscopic factors 78—66285

^{80}Se(d,α)^{78}As, 16.0 MeV, levels of ^{78}As 78—8827

Se(d,^{3}He), ^{79,81}As Q-values and mass excess 80—9222

^{28}Si(d, p), ^{29}Si rot.-vibr. coupling effects, excitation spectrum and ang. distribs. 80—57661

^{28}Si(d, p)^{29}Si$_{g.s.}$, 12.1 MeV, vector polarization transfer coeff., deuteron D-state effect 77—14135

^{28}Si(d,^{3}He)^{27}Al, multistep processes, CCBA anal., SU(3) model 77—30609

^{28}Si(d,p$_8$)^{29}Si, Si-row channelling effect studies in V$_3$Si single crystal 79—4362

^{28}Si(d,p), ^{29}Si 3/2$^+$ and 5/2$^+$ states population, (p,π^+) comparison 80—95307

^{28}Si(d,p), 18 MeV, cross-sections calcs. from pseudopotentials, spectroscopic factors 78—572

^{28}Si(d,p), 6 to 10.46 MeV polarised d, study of Ericson fluctuations 78—54735

^{28}Si(d,p), 8.05 MeV, stripping reaction differential cross section, d distortion effect *(Japanese)* 80—22796

^{28}Si(d,p), Tabakin pot. calcs., differential cross sections, ang. distribs. 78—611

^{28}Si(d,p)^{29}Si, 12.3 MeV, tensor analysing powers 78—29479

^{28}Si(d,p)^{29}Si, 1.0 to 2.5 MeV, excitation functions and angular distribs., DWBA anal. 78—62543

^{28}Si(d,p)^{29}Si, 1.8 to 3 MeV, energy behaviour of vector analysing power, intermediate resonances *(Russian)* 79—49617

^{28}Si(d,pn), ^{29}P and ^{29}Si nucleon unbound states, spin, parity, partial width 80—102118

^{28}Si(d,pn) 10-11.8 MeV, p-n ang. correl., unbound states, DWBA anal. 77—6236

^{28}Si(d,t) and (d,^{3}He), ^{27}Si, ^{27}Al analogue spectroscopic factors, charge asymm., DWBA anal., optimum Q-value 77—54229

^{28}Si(d$_{pol}$,pγ), ^{29}Si, low lying energy level structure, multi-step reaction calcs. 80—68537

^{29}Si(d,p), 1.1-2.1 MeV, excitation functions, statistical fluctuations anal. 80—95322

^{30}Si(d,α)^{28}Al, 18 MeV, cross-section and vector analysing power ang. distribs. 78—41728

^{30}Si(d,α)^{28}Al, 8-12 MeV, polarised d, spin-parity assignments in Al 77—6222

^{30}Si(d,p), pol.d, 1.9-2.5 MeV, anal. power excitation function anomaly 80—5118

^{A}Sm(d,^{3}He)$^{A-1}$Pm, A=144,148,152,52 MeV, strong exhaustion of 1g$_{9/2}$ strength by deeply-bound proton-hole states in Pm isotopes 79—45142

^{144}Sm(d,p), ^{145}Sm neutron separation and level exciton (n,γ) and (d,p) correlations 80—22756

^{144}Sm(d,p), ^{145}Sm primary γ-rays, direct capture and neutron separation energy, (n,γ) correlation 80—57738

Sm(d,^{6}Li) (A=144, 148, 150, 154), 35 MeV, ang. distrib. meas., deduced α-particle spectroscopic factors, reduced widths, decay lifetimes 77—18571

Sm(d,3nγ)Eu, 18-25 MeV, band struct. in ^{149,151}Eu determ. 77—41913

^{A}Sn(d,^{6}Li)^{108}Cd, even A=112 to 124 spectra for E$_d$=33 MeV 79—6626

^{116}Sn(d,p), pol. d, 8.22 MeV, vector anal. power, p and d spin depend. effects 80—5114

^{116}Sn(d,t), fine struct. in deeply bound hole states in ^{115}Sn 77—41874

^{116}Sn(d,t)^{115}Sn, 23 MeV, populating ^{115}Sn levels to 4 MeV excit. 78—612

^{119}Sn(d,pX), 25.5 MeV, inclusive p spectra and cross sections from d breakup 79—13303

^{119}Sn(d,t), 6 MeV, polarised d, tensor anal. power and D-state effects 79—85446

^{122}Sn(d,2n)^{122}Sb, ^{122}Sb 5$^+$ state mag. moment and g-factor 77—71567

^{122}Sn(d,2n)^{122}Sb, ^{122}Sb 5$^+$ isomeric state mag. moment determ. 78—21493

Sn(d,^{6}Li), Cd 2$_1^+$ excitation, α-spectroscopic factors in IBA model 80—105967

Sn(d, ^{6}Li)Cd, alpha-cluster pickup reactions, spectroscopic factors and reduced widths 80—534

Sn(d,^{6}Li)Cd, microscopic description of alpha-transfer reactions 79—6615

Sn(d,t)Sn, even A=112 to 124, deeply bound hole states of odd A Sn 78—8725

^{86}Sr(d,α)^{84}Rb, nuclear structure determ. 77—46118

^{86}Sr(d,p)^{87}Sr, transfer reactions, nucl. struct. obs. 77—46118

^{88}Sr(d,α)^{86}Rb, transfer reactions, nucl. struct. obs. 77—46118

^{88}Sr(d,p), two step processes, excitation of core coupled states, in ^{87}Sr 77—88150

^{88}Sr(d,p)^{89}Sr, 12 MeV polarised d, ^{89}Sr level transitions and spin assignments 78—66286

Ta, 180° prod. of protons in high-energy reacts. 78—8816

^{181}Ta(d,X), 4.2 GeV/c, multitudes of secondary negative particles, momentum distrib. ratios *(Russian)* 80—63178

deuteron-nucleus reactions continued
^{181}Ta(d,pX) 25.5 MeV, inclusive p spectra and cross sections from d breakup 79—13303
Ta(d,X), 4.2 GeV/N, multiple π^- prod., mean multiplicity *(Russian)* 80—27647
Ta(d,X), 4.2 GeV.c^{-1}, inelastic cross section meas. and multiplicities obs. *(Russian)* 79—9580
Ta(d,X), 8 GeV, β-active superdense nuclei search *(Russian)* 80—42535
^{99}Tc(d,t), 15,19 MeV, ^{98}Tc excit. in 0.43-1.32 MeV range 77—18370
T(d,n)^{4}He, fusion cross sections and thermonuclear reaction rates 80—533
T(d,n)^{4}He, time correlated associated particle method for measuring neutron induced fission cross section of ^{235}U 80—52702
^{120}Te(d,p)^{121}Te, energy levels spectroscopy of ^{121}Te 77—41973
^{123}Te(d,p)^{124}Te, energy levels spectroscopy of ^{124}Te 77—41973
^{126}Te(d,t), 17 MeV, ^{125}Te low lying negative parity high spin states multistep induced population 80—57657
Te(d,^{6}Li), Sn $2_1{}^+$ excitation, α-spectroscopic factors in IBA model 80—105967
Te(d, ^{6}Li)Sn, alpha-cluster pickup reactions, spectroscopic factors and reduced widths 80—534
^{230}Th(d,p), 17 MeV, form-factor and multistep effects 77—79388
^{232}Th(d,2n)^{232}Pa, 10-26 MeV, excitation function meas. 77—79391
^{232}Th(d,f), 2.1 GeV, binary and ternary fission kinetics *(French)* 78—70577
^{232}Th(d,t)^{231}Th, 17 MeV, form-factor and multistep effects 77—79388
^{A}Ti(d,^{3}He)$^{A-1}$Sc, A=46, 48, 50, 52 MeV, Sc positive parity states, spectroscopic factors, ang. distrib. 79—97656
^{46}Ti(d,p), polarised d, obs. of D-state and compound nucleus effects 77—34319
^{46}Ti(d,p) 7,10 MeV, ^{47}Ti levels, DWBA and Hauser Feshbach anal., compound nucleus cross sections 80—47377
^{48}Ti(d,^{6}Li), 55 MeV, ^{44}Ca 3.59 MeV 0^+ state config. 79—9472
Ti(d,p)Ti, A=47, 49, 13.6 MeV differential cross-sections 77—18574
^{A}Tl(d,xn) A=203, 205, ^{201}Tl, production in neutron therapy cyclotron idle beam using Tl(d,xn) 79—20669
^{A}U(d,f), A=235, 238, 2.1 GeV, binary and ternary fission kinetics *(French)* 78—70577
^{233}U(d,pf), 11-17 MeV, ^{234}U subbarrier resonances and fission probabilities 79—13266
^{233}U(d,pf), fission fragment energy-velocity correlation meas. 79—45309
^{234}U(d,t), 14 MeV, states in ^{233}U 78—66208
^{235}U(d,f), ^{235}Np fission lifetime meas. 80—63216
^{235}U(d,p), 11 MeV, ^{236}U shape isomer, γ branch upper limit, γ-yields 80—99145
^{235}U(d,pf), ^{236}U fission total kinetic energy release 80—27682
^{235}U(d,pf), ^{236}U isomeric and prompt fission, nuclear superfluidity evidence 80—68711
^{235}U(d,pf), 11-17 MeV, ^{236}U, subbarrier resonances and fission probabilities 79—13266
^{235}U(d,pf), 17-25 MeV, ^{236}U^{m} isomeric to prompt fission ratios; fission fragments 80—86940
^{235}U(d,pf), 23 MeV, total KE release 78—78426
^{238}U, deuteron and proton bombardment, excitation function determ. 78—41709
^{238}U(d,p), 12 MeV, ^{239}U level assignments 78—66209
^{238}U(d,p), induced fission, subthreshold cross section meas., 2-centre shell model calc. 79—6719
^{238}U(d,pn), quadrupole moment of 200 ns isomer in ^{238}U 79—71856
U(d,pnf), 17-25 MeV, ^{236,238}U^{m} isomeric to prompt fission ratios; fission fragments 80—86940
^{51}V(d,^{3}He)^{50}Ti, 30-80 MeV, finite range DWBA calcs. 77—10416
^{51}V(d,^{3}He)^{50}Ti, normalisation const. from J-depend. sum rule anal. 77—34321
^{51}V(d,t)^{50}V, 80 MeV, finite-range DWBA calcs. 77—10416
W, activation in cyclotron by p, d, α, ^{3}He 79—30839
W(d,X), 8 GeV, β-active superdense nuclei search *(Russian)* 80—42535
^{172}Yb(d,p)^{173}Yb, 14 MeV, proton spectra and ang. distrib. meas. level struct. determ. 78—29482
^{174}Yb(d,p), 14 MeV, ^{175}Yb level structure, band structure and J^{π} assignments 79—40850
^{174}Yb(d,t)^{173}Yb, 14 MeV, proton spectra and ang. distrib. meas. level struct. determ. 78—29482
^{176}Yb(d,p), 14 MeV, ^{177}Yb level structure, band structure and J^{π} assignments 79—40850
^{176}Yb(d,t), 14 MeV, ^{175}Yb level structure, band structure and J^{π} assignments 79—40850
^{176}Yb(d,xnγ), 14 MeV, gamma-ray spectra *(Russian)* 78—54720
Zn+d production of ^{64}Cu, ^{64}Cu and ^{67}Ga and bleomycin labelling with ^{67}Cu or ^{64}Cu 78—28066
^{A}Zn(d,^{3}He), 23.3 MeV, A=64-70, p pickup spectroscopic factors, ang. distribs. 79—6422
^{64}Zn (d,^{3}He), polarised d, 13 MeV, vector analysing power, ^{63}Cu levels deduced 77—88100
^{64}Zn(d,^{3}He)^{63}Cu, 13 MeV, polarised d, tensor analysing powers 77—88101
^{64}Zn(d,^{3}He)^{63}Cu, proton pickup strength determ. in ^{63}Cu 79—22163
^{64}Zn(d,^{6}Li), 55 MeV, cluster model DWBA anal. 78—21573
^{64}Zn(d,t), polarised d, 13 MeV, vector analysing power, ^{63}Zn levels deduced 77—88100
^{64}Zn(d,t)^{63}Zn, 13 MeV, polarised d, tensor analysing powers 77—88101
^{66}Zn(d,p)^{67}Zn, 12 MeV, levels, ang. distribs., spectroscopic factors meas. 77—22891
^{67}Zn(d,p), low lying ^{68}Zn collective states, spectroscopic factors 77—61433
^{67}Zn(d,p)^{68}Zn, 12.3 MeV, tensor analysing powers 78—29479
^{70}Zn(d,^{3}He), ^{69}Cu Q-values and mass excess 80—9222
Zr, isotopes, neutron separation energies, (d,t) reactions *(German)* 77—57592
Zr neutron separation energies from (d,t) and (d,p) reactions 80—47489
Zr+d, excitation functions and thick target yields 78—50182
^{90}Zr(d,p), improved coupled-channel treatment of (d,$\bar{n}$) threshold effect 77—74859
^{90}Zr(d,p)^{91}Zr, 12.3 MeV, tensor analysing powers 78—29479
^{90}Zr(d,p)^{91}Zr, 5.5 MeV, effects of d D state determ. 77—67752
^{91}Zr(d,^{3}He), 24.3 MeV, ^{90}Y low lying multiplets, DWBA anal. for spectroscopic factors 80—57685
^{91}Zr(d,p), 12 MeV, ^{92}Zr level struct. and reduced spectroscopic factors 80—32192

deuteron-nucleus reactions continued
^{91}Zr(d,p), pol. d, 12 MeV, ^{92}Zr levels, J^{π}, cross sections, vector anal. power, optical parameters 80—78268
^{91}Zr(d,t), 6 MeV, polarised d, tensor anal. power and D-state effects 79—85446

deuteron-nucleus scattering
^{116}Sn(d,d), polarised d, 8.22 MeV, anal. power 80—5114
antisymmetrisation effects on d-heavy nucleus scattering, nuclear matter model 78—70545
coupled channels approach, deuteron breakup in field of nucleus 78—33195
(d,d) scatt., discretized three-body problem 78—33194
deformed tensor interactions, folding model 80—57783
differential cross sections meas. by SPES I 79—75983
eikonal approx. and distortions in heavy particle stripping mechanism *(Russian)* 78—78337
elastic deuteron-nucleus scattering, breakup corrections to spin depend. 78—58289
elastic scattering folded potential, Pauli correction *(Portuguese)* 77—46175
few-nucleon system investigation using polarised deuterons 77—18578
folding model potentials, mass no. systematics 77—2964
high-energy elastic and inelastic scatt. by light nuclei, mechanism and struct. determ. *(French)* 79—534
inelastic reactions at 3.6 GeV/nucleon 78—82358
light ion scatt., optical pot. and proximity pot. comparison 79—3121
light nuclei, backward scatt. and heavy-particle stripping 78—13107
optical model analyses *(German)* 80—68676
optical model calcs., tensor spin-orbit interaction 78—13112
optical pot. uniqueness of (d, d) and (^{3}He, ^{3}He) 79—97685
optical potential, imaginary L.S interaction 78—41729
partial wave expansions for arbitrary spin, non-central forces 78—21535
polarisation transfer in elastic scatt., tensor interaction 77—57647
polarised deuteron elastic scatt. from ^{12}C, ^{28}Si, ^{40}Ca, ^{56}Fe, ^{58}Ni, ^{64}Zn, ^{90}Zr, ^{118,120}Sn, ^{208}Pb at 30 MeV 77—54228
three-body d+nucleus scatt. model, effects of imaginary pots. 79—9532
(d,d), A=27-238, 12-90 MeV, global optical model pot. 80—78305
(d,d), appl. of three-body K-operators and unitary approx. to model processes 77—18499
(d,d), folding model modification due to strong Pauli distortion 79—6620
(d,d), pol. d, 12 MeV, A=46-82, cross sections, anal. powers, global optical model anal. 80—47459
(d,d), pol. d, 56 MeV, A=16-208, cross sections, optical parameters, anal. powers 80—78270
(d,d), pol.d, 52 MeV, A=12-197, vector anal. power and optical parameters 80—57764
(d,d) 12 MeV, tensor polarised, differential cross section, vector and tensor analysing power 78—78357
(d,d) breakup channel contrib. to optical pot. in 3-particle approx. 79—6630
(d,d) elastic and inelastic, diffraction scatt. theory, d dissociation and stripping reactions 79—6633
(d,d) medium heavy nuclei, optical model anal., cross sections, anal. powers 80—73839
(d,d) scatt. on ^{16}O and ^{90}Zr, finite-range coupled-channel calcs. 77—10377
(d,d'), A=40 to 208, 108 MeV, giant monopole resonance excitation and ang. distribs. 80—102164
d-α elastic scatt., three body calcs., Pade technique 78—46074
d-α elastic scattering, ^{6}Li energy levels, three body calcs. 77—54158
d+A, 6.3 GeV/c, A=H, D, C, Al and Bi, inclusive spectra of fast p and d *(Russian)* 78—46075
^{1}H(d,d), 5-45 MeV deuteron wave function asymptotic D- to S-state normalisation, anal. power 80—78304
^{27}Al(d,d), energy depend. of vector analyzing capacity, 1.8 to 3.0 MeV, 120 to 150° scatt. 79—9592
Al(d,d), 4.3, 6.3, 8.9 GeV/c, secondary momentum spectra, multiple scatt. model anal. *(Russian)* 80—27650
^{40}Ar(d,d), optical model parameter investigation using 9-12 MeV polarised d 78—94016
^{10}B(d, d'), energy depend. isospin violation in 10 MeV region 77—14134
^{9}Be(d,d'), 12.8 MeV, two stage mechanism described by square Feynman diagrams *(Russian)* 79—22299
^{9}Be(d,d), 12.17 to 14.43 MeV, elastic and inelastic scatt., optical model anal. 78—89883
Bi(d,d), 4.3, 6.3, 8.9 GeV/c, secondary momentum spectra, multiple scatt. model anal. *(Russian)* 80—27650
^{12}C α-decay, (d,d') excited, 4π ang. pattern meas., DWBA anal. 79—67720
^{12}C(d, d'), isospin violating direct reaction, Coulomb interaction role 80—102170
^{12}C(d,d'), spin-flip transitions, microscopic α-spectator model 77—79400
^{12}C(d,d')^{12}C, 24-29 MeV, ratio of isospin forbidden/allowed yield 77—18385
^{12}C(d,d), 1.69 GeV/c, Coulomb interference region, Glauber theory anal. 80—99178
^{12}C(d,d), 650 MeV, Glauber theory approx. anal. using realistic deuteron wave functions 77—46176
^{12}C(d,d), 650 MeV, Glauber model calcs. for cross sections 79—13306
^{12}C(d,d), incident ion binding energy effects on scatt., qualitative anal. 79—9600
^{12}C(d,d)^{12}C, reaction mech., relation to ^{12}C(d,p), S-matrix theory, 1.63 to 2.05 MeV *(Chinese)* 78—78393
^{13}C(d,d'), 12.8 MeV, two stage mechanism described by square Feynman diagrams *(Russian)* 79—22299
^{40}Ca(d,d), 4.5-5.4 MeV, excited states, excitation functions and ang. distribs., statistical anal. 80—57686
C(d,d), 4.3, 6.3, 8.9 GeV/c, secondary momentum spectra, multiple scatt. model anal. *(Russian)* 80—27650
^{250}Cf(d,d'), 15 MeV, vibr. states, J^{π} and reduced transition probabilities 80—47351
^{37}Cl(d,d), 12.0 MeV, polarised deuterons, vector analysing power 77—14094
^{50}Cr(d,d), 12.3 MeV polarised deuterons, precision tensor analysing power meas. 77—3019
^{52}Cr(d,d), 10 MeV, polarised d elastic scatt., optical model anal. 79—36248
^{52}Cr(d,d), 7-11 MeV, coupled-channel anal. 77—18579
^{52}Cr(d,d), 7-11 MeV, stripping channel effect, coupled channel model, DWBA anal. 77—57676

deuteron-nucleus scattering continued
(d,d), A=24-54, pol.d, 20 MeV, quadrupole transition amplitudes 80−99148
^{167}Er(d,d′), 12.1 MeV, excitation of Nilsson states, Coriolis coupling 78−33190
^{19}F(d,d), elastic scatt., 1.2-2.5 MeV, excitation functions, ang. depend., optical model anal. 79−9594
^{54}Fe(d,d), 10 and 13 MeV, polarised d elastic scatt., optical model anal. 79−36248
Gd(d,d'), A=155, 157, 12.1 MeV, excitation of Nilsson states, Coriolis coupling 78−33190
^{A}Ge(d,d) 16 MeV, A=70-74, polarised d, elastic and inelastic, levels and deformation 79−554
^{1}H+d, polarised projectile, parity nonconservation in low energy scatt. 78−66271
^{1}H(d,d), 2 GeV, polarised d, tensor and vector asymmetries 80−9285
^{1}H(d,d), 20 MeV, measurement on T_{21}, three nucleon Faddeev calc. comparison 79−71857
^{1}H(d,d), 35, 45 MeV, d wave function D- to S-state ratio from anal. power and cross section 79−89314
^{1}H(d,d), 45.4 MeV, tensor anal. powers 79−85447
^{1}H(d,d), anal. power ang. distrib., d D-state asymptotic normalisation 79−36247
^{1}H(d,d), deuteron D-state asymptotic normalisation 79−71858
^{1}H(d,d), elastic backward scatt., GeV energies, tensor anal. power 79−80916
^{1}H(d,d), polarised d, 5-13 MeV, analysing powers 79−71833
^{1}H(d,d), polarised p and d, analysing power data 79−71830
^{1}H(d,d) 10, 20 MeV, 79−13304
^{1}H(d,dγ) 6.3-7.1 MeV, bremsstrahlung anomaly near breakup threshold 78−89888
^{2}H propagation in nucl. matter, spin depend. of optical pot. 79−93635
^{2}H(d,d), ^{4}He continuum microscopic calcs. cross sections and levels 80−57702
^{2}H(d,d), 4.3, 6.3 and 8.9 GeV.c, struct. of secondary d spectra high momentum parts *(Russian)* 78−78394
^{2}H(d,d), 4.3 to 8.9 GeV, momentum spectra at 103 mrad lab. angle 79−6641
^{2}H(d,d), 50-85 MeV, ang. distribs., PWBA anal., two body final states 79−6636
^{2}H(d,d), 50-85 MeV cross-section meas. 79−13307
^{2}H(d,d), 53, 63 GeV, inelastic intermediate state effects, Glauber multiple scatt. theory 79−36104
^{2}H(d,d), medium energy, total cross section, optical model calcs. 79−9593
^{2}H(d,d)^{2}H, four-body model of the four-nucleon system 79−63643
^{2}H(d,d)^{2}H, up to 14 MeV elastic and inelastic cross sections, phase shift anal. 77−22996
^{2}H(d,d)D, differential cross sections at 13.2 MeV, DWBA anal. 79−45276
^{3}H(d,d), elastic scatt. $\sqrt{s}=53$ GeV, narrow min, and inelastic shadow effects, Glauber theory 78−89740
^{3}H(d,d)^{3}H, up to 14 MeV, elastic and inelastic cross sections, phase shift anal. 77−22996
H(d, d), 800 to 1430 keV, differential cross section meas. 79−80947
H(d,d), A=1, 2, E=52 MeV, polarised deuterons, vector analysing power 78−584
H(d,pp)n, 12.9 MeV, differential cross-sections meas. 78−13113
^{3}He(d,d), 0.32 MeV, continuum ambiguity in phase shift anal. 79−76006
^{3}He(d,d), 0.32-5.0 MeV, anal. power, scatt. amps., ^{5}Li states, phase shift anal. 80−47382
^{3}He(d,d), polarised d, 10-17 MeV, cross sections, vector and tensor anal. powers 79−75966
^{3}He(d,d), polarised d, 1.5-11.5 MeV, differential cross sections and anal. powers 79−85443
^{4}He (d,d), 17-45 MeV, differential cross section and tensor and power ang. distribs. 80−42631
^{4}He (d,d), pol. d, 20 MeV, optical pot. strong tensor term, anal. powers 80−37364
^{4}He (d,d) pol. d, 17-43 MeV, vector anal. power, highly excited six nucleon system 80−47458
^{4}He(d,d), 4.8-6.8 MeV, ^{6}Li resonances, phase shift analysis 79−75953
^{4}He(d,d), 870-1430 keV, differential cross sections and resonance parameters *(Russian)* 79−59075
^{4}He(d,d), cross sections and polarisation parameters, three-body NNα model *(French)* 77−71598
^{4}He(d,d), distortion effects, orthogonality condition model 80−63190
^{4}He(d,d), Faddeev Lovelace eqn. soln. 78−54767
^{4}He(d,d), Glauber theory at high energy *(Russian)* 78−41732
^{4}He(d,d), noncentral forces, Pauli principle effects on d polarisation, orthogonality condition model 79−6614
^{4}He(d,d), pol. d, 12-17 MeV, differential cross sections, anal. powers, phast shift anal. 80−13449
^{4}He(d,d), polarised d, 20.2 MeV, elastic scatt. tensor anal. power 79−85450
^{4}He(d,d)^{4}He, 6-7 MeV, polarised d, ^{6}Li 1^{+} reson., analysing powers 77−88095
He(d, d), 9.0, 19.8 GeV/c, small angle, total and differential cross section, scatt. amplitude *(Russian)* 79−97711
Li(d,d), 3-10 MeV, A=6,7, differential cross section, optical model anal. 77−61435
^{24}Mg+d, 10 MeV vector polarised deuterons scatt., nuclear shape effects, optical pot., analysing power 78−54768
^{A}Mo(d,d), A=92-100, 21.5 MeV, elastic and inelastic cross sections, coupled channel anal., deformation 79−553
Mo(d,d), A=92, 94, 96, 98, 100, elastic, inelastic scatt., coupled channel, optical model anal., deformation parameters 78−94017
^{14}N(d, d′), energy depend. isospin violation in 10 MeV region 77−14134
^{14}N(d,d′), 10-17 MeV, isospin non-conservation, direct DWBA and Hauser Feshbach anal. 79−67757
^{15}N(d,d), 1.4-2.7 MeV, excitation functions 77−23094
^{20}Ne(d,d), pol. d, 10-12 MeV, cross section, coupled channel and fluctuations anal. 80−27617
^{58}Ni(d,d′), 10 MeV, diff. cross sections and d-γ ang. correlations, multishell coupled channel calcs. 80−83064
^{58}Ni(d,d), 10 MeV, multishell form factors 79−93636
^{58}Ni(d,d), three-body model with adiabatic approx. 79−40934
^{60}Ni(d, d), 9, 12 MeV, polarised d, excitation functions, optical model parameters and spin-orbit pot. 79−67756

deuteron-nucleus scattering continued
Ni(d,d), 13-80 MeV, second order breakup corrections in DWBA 80−86910
^{16}O, treatment as three-body problem 79−6618
^{16}O+light ion scatt., exchange Coulomb kernel in resonating group formulation 79−6531
^{16}O(d,X), X=d or N, elastic scatt. and stripping, three body calc. 80−91165
^{16}O(d,d), <4 MeV, d polarisation, vector analysing power, level characts. of ^{18}F compound nucleus 77−61434
^{16}O(d,d)^{16}O, resonating group method with generator-coordinate technique 77−10415
^{192}Os(d,d′), 23.2 MeV, γ-ray spectra, energy level scheme 77−34243
^{205}Pb(d,d′), 14, 17 MeV, direct population of collective states, multiplets, deform. parameters 78−74376
^{208}Pb(d,d′), 24 MeV, mag. dipole states, spin, parity, transition strengths 77−14129
^{208}Pb(d,d′), 86 MeV, giant monopole and quadrupole resonances, multipole excitations 80−106031
^{208}Pb(d,d′), RPA calcs., existence of breathing mode 78−25163
^{102,104}Ru(d,d′) 12 MeV, collective excit., J, B(E2), B(E3) 77−26557
^{32}S+d, 10 MeV vector polarised deuterons scatt., nuclear shape effects, optical pot., analysing power 78−54768
^{34}S(d,d), elast. and inelast. scatt. of 11.8 MeV polarised deuterons 78−33191
^{A}Se(d$_{pol}$,d), A=76,78,80,82, 12 MeV, two-step scatt. process via $J^{\pi}=2_1^{+}$ excited states 80−57781
Se(d,d), 12 MeV polarised deuterons, shell closure effects 77−38281
Se(d,d), polarised deuterons, vector analysing power, optical model calcs. 78−62550
^{28}Si+d, 10 MeV vector polarised deuterons scatt., nuclear shape effects, optical pot., analysing power 78−54768
^{28}Si(d,d′), 6 to 10.46 MeV polarised d, study of emission fluctuations 78−54735
^{28}Si(d,d), 6-8 MeV, compound nuclear polarisation effects 77−3020
^{28}Si(d,di), 20 MeV, vector polarised deuteron scatt. from deformed nuclei 79−6629
^{122}Sn(d,d), 15 MeV, optical model calc. 78−41729
^{99}Tc(d,d′), 17.2 MeV, level struct., spin-parity assignments 78−8743
^{46}Ti(d,d), 10 and 13 MeV, polarised d elastic scatt., optical model anal. 79−36248
^{46}Ti(d,d), 10 MeV, optical model calc. 78−41729
^{46}Ti(d,d), 7,10 MeV, ang. distribs., DWBA and Hauser Feshbach anal. 80−47377
^{233}U, excited octupole states in odd U isotopes, vibr. states, deuteron scatt., 13.1 MeV 77−46099
^{233}U(d,d′), multipolarities and reduced transition probabilities 78−17215
^{235}U, excited octupole states in odd U isotopes, vibr. states, deuteron scatt., 13.1 MeV 77−46099
^{235}U(d,d′), 13.1 MeV multipolarities and reduced transition probabilities 78−17215
^{238}U(d,d)^{238}U, 17 MeV elastic and inelastic scatt., nuclear-Coulomb interf., optical pot. 77−79389
^{64}Zn(d,d), polarised d, 13 MeV, optical model parameters, vector analysing power 77−88100
^{68}Zn(d,d), 10 and 12 MeV, polarised d elastic scatt., optical model anal. 79−36248
Zn(d,d), A=66, 67, 12.3 MeV polarised deuterons, precision tensor analysing power meas. 77−3019
^{90}Zr(d, d), 10, 11, 12 MeV, polarised d, excitation functions, optical model parameters and spin-orbit pot. 79−67756
^{90}Zr(d,d), 10 and 12 MeV, polarised d elastic scatt., optical model anal. 79−36248
^{90}Zr(d,d), 10 and 15 MeV, optical model calc. 78−41729
^{91}Zr(d,d), pol. d, 12 MeV, ^{92}Zr levels, J^{π}, cross sections, vector anal. power, optical parameters 80−78268

deuteron photodisintegration
amplitudes with arbitrary number of EM multipoles 79−93437
cross section calcs., local static pots. 77−22997
differential cross section of photodisintegration at 0° for outgoing protons 77−88109
differential cross-sections from 74 to 241 MeV 77−30552
forward proton cross-section, D state depend. 77−67735
fragmentation of nucleus caused by decay of bound muon *(Russian)* 79−68333
meson exchange current and isobar config. effects 79−71840
nuclear forces, energy levels, nonlocal separable interactions and odd-mass nuclei studies 77−2917
proton polarisation anomalous struct. in photon energy range 325-725 MeV 77−30551
quadrupole contribution to cross-section, isospin sum rules 77−30550
recent experiment review, future experiment suggestions 80−37382
relativistic effects 77−18519
soft-core potentials calculations 77−57648
tensor force and d(γ,p)n forward p prod. 77−57649
$\gamma d \rightarrow nn\pi^{+}$, threshold form factors 79−85453
$\gamma d \rightarrow np$, 300 MeV, dibaryon resonance manifestation, pseudoindependent amplitude elimination *(Russian)* 80−57612
$\gamma d \rightarrow np$, 400-650 MeV, proton polarisation and possible dibaryon resonances 80−105908
$\gamma d \rightarrow pn$, 350-700 MeV, p polarisation meas. 78−82215
$\gamma d \rightarrow pn$, proton polarisation energy depend., 400-700 MeV *(Russian)* 80−63000
$\gamma d \rightarrow pp\pi^{-}$, cross section, double pion photoprod. on one nucleon 78−70378
NN potential depend. of characts., 10 to 180 MeV *(Russian)* 77−6350
^{2}H photodisintegration and electrodisintegration, weak interaction and P nonconservation 78−89849
^{2}H(e, e)pn, polarised e, neutral weak currents, right-left asymmetry 79−80787
^{2}H(γ, NNπ), threshold to $\Delta(1236)$ region, EM props. of NNπ system 78−41694
^{2}H(γ, pp)π^{-}, high momenta of emitted nucleons 78−70512
^{2}H(γ, π^{+})nn, excitation function, cross-section, threshold π^{+} prod. 77−26670
^{2}H(γ,n), 20.3 MeV, linearly pol. γ, neutron yield and cross section 80−91171
^{2}H(γ,n), forward angle cross section and sum rule from Siegert's theorem 79−80925
^{2}H(γ,n)^{1}H, 400-700 MeV, p polarisation *(Russian)* 80−106046

- **deuteron photodisintegration** continued
  - ^{2}H(γ,n)p, 375-650 MeV, proton polarisation energy depend. at CMS angle 90° *(Russian)* 80—63159
  - ^{2}H(γ,n)p, cross section and polarisation with arbitrary number of EM multipoles 79—80923
  - ^{2}H(γ,n)p, cross section asymmetry polarised photons 400 to 600 MeV, resonances *(Russian)* 79—89294
  - ^{2}H(γ,n)p, differential cross section and proton polarisation using supersoft core pot. 79—89287
  - ^{2}H(γ,n)p, parity violation expts. review, weak NN interaction 80—73792
  - ^{2}H(γ,np), <800 MeV, proton polarisation in $\gamma n \rightarrow \pi^{-} p$ *(Russian)* 78—41700
  - ^{2}H(γ,p)n, EM properties of πNN system, virtual π reabsorption 79—22109
  - ^{2}H(γ,p)n, forward proton prod., low energy theorems 78—70510
  - ^{2}H(γ,π^{-}p)^{1}H, 250-500 MeV, Δ(1236) region, cross section 78—41693
  - ^{2}H(γ,π^{0})^{2}H, threshold and Δ(1236) region, EM props. of πNN system 78—41695
  - ^{2}H(γ,π^{+})nn, threshold cross-section, impulse approx. 77—38256

- **deuteron polarisation**
  - depolarisation during acceleration and storage of polarised protons and deuterons 78—58519
  - deuterated polarised target, calibration of deuteron polarisation 77—3200
  - display and calibration using automatically tuned NMR spectrometer 80—37669
  - ionisation of polarised deuteron beam in Penning discharge, beam intensity, tensor polarisation 77—3203
  - polarimeter designs for high energy p and d beams, polarised beam spin anal. 78—58516
  - tensor polarimeter using ^{3}He(d,p)^{4}He at keV 77—3242
  - vector polarised deuterons in ^{3}H(d,n)^{4}He at 150 keV, n-p analysing power 78—62544
  - ed, elast. scatt., polarisation meas. and percentage D state of deuteron 80—420
  - ed elastic scattering, neutral weak currents *(Russian)* 78—21434
  - $\gamma d \rightarrow \pi^{0} d$, recoil deuteron polarisation statistical tensors anal. 78—74348
  - πd scatt., 142 MeV, polarisation observables 78—78210
  - ^{40}Ca(d,α)^{38}K, 7.5, 7.75, 8.0 MeV, polarised d, J^{π} assignment 77—6401
  - ^{3}He(d,p)^{4}He, polarimeter for deuteron beams 80—47834

- **deuteron scattering** *see deuteron-nucleus scattering; hadron-deuteron scattering; lepton-deuteron scattering; meson-deuteron scattering; photon-deuteron scattering; proton-deuteron scattering*

- **deuterons**
  - *see also cosmic ray deuterons*
  - 6 quark system, wave function, elastic form factor, NN forces, spectroscopy *(Russian)* 78—50015
  - bag model, hadronic deformation energy, two-nucleon interaction 78—45852
  - beam, energy spectra in plasma focus discharges 80—24262
  - beam production, by localised source in focused discharge 78—58093
  - break-up effect in two-step process 78—62534
  - charge form factor accompanying high imparted momentums *(Russian)* 78—58189
  - charge form factor falloff at large q^{2} in dispersion approach *(Russian)* 79—3027
  - D-state, determ. in $\pi^{+} d \rightarrow pp$ at 40-60 MeV 77—2864
  - D-state about 4%, appl. to reaction data anal. 78—70461
  - D-state probability, review of spin, binding energy, magnetic and quadrupole moment 78—62488
  - D-state probability, three lower bounds 80—102129
  - D-state wave function calc. 78—8740
  - deuteron, EM form factors relation to wave functions 78—37210
  - dibaryonic six-quark states as possible model for deuteron 78—21378
  - eight quark model, ang. momentum group anal. 79—89098
  - elastic form factor calcs. with Bethe-Salpeter eqn. 79—67554
  - EM form factor, data anal. and asymptotic behaviour 79—89155
  - EM form factor, relativistic description 79—54340
  - EM form factor determ., relativistic impulse approx. 77—65158
  - EM form factor determ. 77—61287
  - EM form factors, D-wave admixture in the dispersion approach *(Russian)* 79—30737
  - EM form factors at large transferred momentum, six-quark state *(Russian)* 78—89715
  - EM form factors of n-p system in multipole parametrisation formalism 78—17022
  - EM inelastic form factors, exchange current effects in electrodisintegration 79—93418
  - EM props. in relativistic one boson exchange model 79—67678
  - EM quadrupole form factor peak value, determination of percentage D-state 78—93950
  - exchange effects, trace of energy-momentum tensor, in weakly bound states 78—37293
  - fast stable particles from light emulsions nuclei following 1.5 GeV/c K^{-} interactions 78—17245
  - few-body break-up reactions, three body vertices, singlet or triplet deuteron interpretations 77—82901
  - few-body problem, deuteron, EM effects, three body bound state, break-up reactions 79—85384
  - form factors and spectroscopic factors in heavy spherical nuclei, shell model *(Russian)* 80—63078
  - form factors relation to wave functions 78—70462
  - generation of 1 to 5 MeV beam by plasma focusing *(Russian)* 77—38537
  - giant dipole state, teaching example 77—22902
  - gluon distribution from elastic dd scatt. 80—82939
  - hidden colour and the isobar content of the deuteron 80—102024
  - inclusive quasielastic d prod. in heavy ion collisions, quasiclassical description 79—6695
  - laser deuteron source for pulsed neutron generator 80—27844
  - micrononcausal Euclidean wave functions for hadrons. virtual mesons in deuterons 78—41408
  - migma, localised MeV d^{+} trapping observation, density and confinement time meas. 79—14596
  - propagation in nuclear matter, spin depend. of d optical pot. and binding energy 78—70545
  - quadrupole moment, calc. from elec. field gradient of D_2 79—93511
  - quadrupole moment and percentage D state lower bounds 78—37286
  - relativistic description, elastic and inelastic form factors 79—30752
  - relativistic deuteron wave function *(Chinese)* 80—47411

- **deuterons** continued
  - relativistic deuteron wave functions, π-NN coupling, numerical integration 80—22595
  - relativistic heavy ion collisions, d prod. mechanism, three models, fireball rate eqns. 80—63198
  - relativistic nuclear collisions, p, d, and t inclusive energy spectra 80—63199
  - relativistic space-time description and short distance effects 77—2795
  - six-quark state and EM struct., two nucleon bound state model *(Russian)* 79—13031
  - stripping cross sections to a resonance, exact and DWBA anal. comparison 78—93985
  - structure function, determ. from strongly inelastic ed-scatt. in region forbidden to single nucleon scatt. *(Russian)* 77—6130
  - structure function parametrisation 77—22734
  - transversely polarised deuteron target for kaon-nucleon interaction studies 80—37669
  - wave equation, relativistic, in EM fields *(Russian)* 79—89248
  - wave function at short range 77—50065
  - wave functions from ^{208}Pb(d,p) tensor analyzing powers 80—99137
  - d and $\bar{d}$ prod. by 200 GeV protons 79—9563
  - d breakup into Δ resonances, probability, isobar model, static NN-$\Delta\Delta$ mixing pot. 78—29438
  - $\Delta\Delta$ component from pd 19 GeV/c interactions 80—42500
  - (p,X) emulsion, 400 GeV/c slow deuteron and proton prod. 80—52666
  - pp inclusive collisions at CERN ISR, d and $\bar{d}$ prod. 78—33099
  - 'H(d,d), 5-45 MeV deuteron wave function asymptotic D- to S-state normalisation, anal. power 80—78304
  - ^{2}H D-state probability lower bound, binding energy, quadrupole moment 80—91137
  - ^{2}H quadrupole moment, energy depend. of NN interaction anal. 77—74775
  - ^{2}H(d,d), 4.3 to 8.9 GeV, momentum spectra at 103 mrad lab. angle 79—6641
  - ^{2}H(p,2p)n, 22.7 MeV, proton analysing power 80—78302

- **developers (photographic)** *see photographic materials*

- **development, photographic** *see photographic process*

- **development management** *see research and development management*

- **diagnosis, patient** *see patient diagnosis*

- **diagnostics, particle beam** *see particle beam diagnostics*

- **diagnostics, plasma** *see plasma diagnostics*

- **diagrams**
  - *see also Bode diagrams; circuit diagrams; Feynman diagrams; flowcharting; nomograms; Nyquist diagrams; phase diagrams*
  - BFM diagram, hydraulic geometry, graphical analysis 77—33097
  - EM wave strong scatt. in random media, operator and diagram techniques for intensity moment eqns. 79—64154
  - high cycle fatigue diagram based on dynamic severity criterion 78—60759
  - Hubbard model, Green's function determ. using group theoretical diagram method 77—62791
  - metrological defectoscopy, US materials testing refinements *(German)* 78—15638
  - multicomponent impedance diagrams for electrochem. cells, resolution technique 80—66959
  - nonresonant Argand loops, pseudoresonances 77—61264
  - relativistic energy and momentum triangles, modified versions applicable to accelerated motions 79—88803
  - triangle diagrams for physical determ. of garnets 77—70839
  - wind obs., freq. isopleth diagram 77—73892

- **dialogue programming** *see interactive programming*

- **dialogue systems** *see interactive systems*

- **diamagnetic properties of substances**
  - *see also de Haas-van Alphen effect; diamagnetism*
  - p-alcoxybenzilidene butylaniline, liq. cryst., mag. anisotropy and polymorphism *(French)* 77—76532
  - alkali halide, ionicity trends in diamagnetism and its temp. depend. 79—19717
  - alkali metal azides, diamag. susceptibility, rel. to cryst. struct. 79—24127
  - alkaline earth transition metal ternary and quaternary oxides, ATO_3, $ATi_{1-x}T_xO_3$, and $AZr_{1-x}T_xO_3$, prep., mag. props. and struct. 79—15277
  - alkanes, diamag. susceptibility, graph theoretical anal. 78—33449
  - alkenes, diamag. susceptibility, graph theoretical anal. 78—33449
  - p-alkoxybenzylidene-p-n-butylanilines, optical and mag. anisotropies in liq. cryst. phase, thermal variations of order parameter *(French)* 79—82149
  - alkyl β-ketoacetals, cyclic, diamag. susceptibility, O at. contribution rel. to ring closure 77—14606
  - p-alkyl-p′-cyanocyclohexylcyclohexanes, thermotropic nematics with positive dielectric and negative diamag. anisotropy 78—34435
  - anthracene, mag. susceptibility anisotropies, high field ^{2}H NMR quadrupolar effects obs. 80—25225
  - aromatic compounds, diamag. susceptibility 78—80123
  - azoxybenzenes, nematic, mag. susceptibility, orientational order parameter 78—34426
  - α-B, rhombohedral, magnetic props. and ESR spectra 80—20452
  - bicyclohexanes, nematic liq. crysts. with negative diamag. anisotropy, high resolution NMR spectrometry 79—40596
  - biphenyl, diamagnetism and thermal motion 80—25076
  - carboxylic acids, diamag. susceptibility of carbonyl group 77—75329
  - carnauba wax thermoelectret, mag. anisotropy evidence for dipolar orientation 77—16240
  - chrysene, mag. susceptibility anisotropies, high field ^{2}H NMR quadrupolar effects obs. 80—25225
  - coronene, mag. susceptibility anisotropies, high field ^{2}H NMR quadrupolar effects obs. 80—25225
  - cyano-biphenyl cpds., nematic, mag. susceptibility and order parameters 79—86709
  - 4-cyanobenzoyloxy-4′-pentylstilbene, nematic, smectic A, and orthogonal smectic B phases 80—64890
  - cyanobiphenyls, nematic, diaelec. consots. and diamag. anisotropies 80—7253
  - cyanocyclohexylcyclohexanes, nematic, diaelec. consots. and diamag. anisotropies 80—7253
  - cyanophenylcyclohexanes, nematic, diaelec. consots. and diamag. anisotropies 80—7253
  - diamagnetism with quasilinear dispersion law, orbital susceptibility, valence bands *(Russian)* 80—80475

diamagnetic properties of substances continued
- dicarboxylic acid, solid, binary mixtures of long chain mol. systems, diamag. susceptibility 77—32154
- 1,5-dinitronaphthalene, diamag. cryst., mag. axis, struct. interpretation 80—50039
- electron gas, paramag. and diamag. susceptibilities, density depend., ring diagram contrib. 79—95571
- esters, diamag. susceptibility of carbonyl group 77—75329
- glass, small ang. optical beam polaris., by Faraday rot. *(Korean)* 78—50918
- graphite, 4.2K magnetisation meas. in mag. fields up to 150 kG, diamag. props. 77—32156
- graphite, low temp. magnetisation in strong mag. fields, filled band contrib. 77—32157
- graphite intercalation compounds with alkali metals and halogens, physical props. 78—31050
- graphite intercalation cpds., mag. susceptibility, tight-binding model 80—44796
- graphite ribbon, interlayer interaction effects on diamagnetism London theory 78—52201
- halomethanes, ^{13}C chemical shifts, diamag. susceptibility, effect of non-bonded interactions 78—78726
- III-V semiconductors, calc. using MOLCAO approx. 79—42732
- IV-VI semiconductors, mag. susceptibility near ferroelec. transition pt. *(Russian)* 79—95568
- lymphocytes, living and dead, mag. props. and mag. sedimentation 80—35925
- lyotropic liquid crystals, orientation in mag. field, glass interface effects 79—1390
- lysozyme, anomalous diamag. susceptibility and elec. cond. 79—29498
- lysozyme, mag. suscept. 77—43807
- magnetic susceptibility behaviour *(Russian)* 77—80912
- marble, mag. susceptibility anisotropy development through cryst. preferred orientation of calcite 78—56286
- MBBA, nematic, mag. susceptibility and order parameters 79—86709
- Merck nematic phases, ZLI 1052 and ZLI 389, mag. susceptibility anisotropy and order parameter 79—86704
- mesomorphic mixtures, binary phase diagrams, thermodynamic props., diamag. anisotropy 78—95139
- mesophase pitch, magnetically-oriented, phys. props., mol. struct. 80—64885
- metal, diamag. domain, helicon attenuation *(Russian)* 78—10721
- metal whiskers, quantum oscills. of mag. moment 79—15280
- metallo-proteins and model systems, susceptibility and struct., SQUID magnetometer uses 79—53036
- metals, mag. susceptibility, determ. from average internal pot. 77—28367
- nematic layer, magnetic threshold field 79—86710
- nematic liquid crystal, diamagnetic susceptibility, refractive index, density and polarisability 77—15315
- nematic liquid crystal, susceptibility from EPR study 78—38615
- 4-octyloxy-4′-heptyl-α-cyanstilbene liquid cryst., mag. props. 78—87615
- organic compounds, diamagnetic susceptibility calcs., extended London theory 79—47228
- organic liquids, diamagnetism, mass mag. suscept. meas., temp. depend. 80—97054
- organo-silicon compounds, diamagnetic susceptibility, semiempirical calcs. 78—17820
- PAA, nematic liq. cryst., thermomagnetic behaviour *(French)* 78—87612
- PAP, nematic liq. cryst., thermomagnetic behaviour *(French)* 78—87612
- paraffins, solid, binary mixtures of long chain mol. systems, diamag. susceptibility 77—32154
- paraffins, solid and liquid, diamagnetic susceptibility 78—14923
- p-pentoxybenzilidene alkylaniline, liq. cryst., mag. anisotropy and polymorphism *(French)* 77—76532
- phenyl benzoate and thiobenzoate, 4,4′-disubstituted, mag. susceptibility anisotropy and order parameter 79—86704
- phenylcyclohexanes, p-disubstituted, elastic consts. and diamag. anisotropy 79—65639
- poly-γ-benzyl-L-glutamate, lyotropic liq. cryst., trifluoroacetic acid effect on viscoelasticity, susceptibility 77—84644
- poly-γ-benzyl-L-glutamate, soln., liq. film, diamagnetic susceptibility 78—74794
- polycyclic aromatic hydrocarbons, diamagnetic susceptibility NCHF (SCF-PPP) calcs. 77—6686
- polyribonucleotide complexes, mag. field orientation of nematic liq. cryst. solns., light scatt. and birefr. meas. 79—82152
- proteins, diagmagnetic anisotropy, struct. origins 79—92136
- pyrocarbon, diamagnetic susceptibility increase, mag. field intensity depend. *(Russian)* 79—82752
- p-quinquephenyl, nematic, mag. susceptibility and order parameters 79—86709
- rare earth metasilicates, $R_2(SiO_3)_3$, mag. susceptibility, temp. depend., 77-800K 80—20372
- Schiff's bases, nematic phys. props. 79—99057
- semiconductor, amorphous, diamagnetic susceptibility enhancement 79—65640
- semiconductor, diamagnetic susceptibility of excitonic molecules *(Russian)* 80—7074
- semiconductor, tetrahedrally coordinated, temp. depend. of diamagnetic susceptibility *(Rumanian)* 80—88717
- semiconductors, glassy, diamag., photostructural changes, mechanism 80—92557
- solids crystallised from melt, mag. field effect on props. 79—37815
- solution, rel. to magnetochem. separation 77—20628
- TCNQ salt, TMTSF-DMTCNQ, mag. susceptibility meas. under press. 80—29521
- ternary chalcopyrite, diamag. susceptibility, bond orbital theories 77—55761
- tetramethylammonium cadmium trichloride:Mn^{2+}, EPR spectrum temp. depend. 78—19314
- thermoelectret and magnetoelectret states, diamag. anisotropy 80—97053
- $(TMTSF)_2PF_6$, quasi-dimens. cond., diamagnetic AC susceptibility 80—103781
- transition metal chalcogenides, struct. and mag. props., book contrib. 77—43808
- Ag, mag. susceptibility, Animalu model pot. calc. 80—75711
- Ag-Cu composite wires, size effect and interface contribution to diamagnetism 77—69490
- Ag-S(Se)(Te), liq., mag. susceptibility meas., electron localisation and chem. bonding 80—60178
- $Ag_{1-x}Sn_{1+x}Se_{2-y}$, supercond. and normal state props. 77—36008

diamagnetic properties of substances continued
- Al alloys, non-transition metal effect on Landau diamag. susceptibility 77—63075
- Al, dynamic susceptibility, model pot. theory 80—75710
- Al, supercond. film, precursor diamagnetism, magnetisation meas. 77—32115
- Al, with diamag. domains, helicon attenuation below 1K *(Russian)* 77—85254
- As-Se(Te) systems, mag. susceptibility comp. depend. 77—80908
- Au, mag. susceptibility, Animalu model pot. calc. 80—75711
- Ba_xI_y cyclodextrin, quasi-one-dimens. cpd., synthesis, elec. and mag. props. 80—2380
- $BaTiO_3$ and $BaTi_{1-x}Fe_xO_{3-x}F_x$, electrical, optical and mag. props., photoelectrolysis 77—47856
- $BaTiO_3$, magnetochemical exam. of phase transition, mag. suscept. meas. 78—88265
- $BaVSe_3$, one-dimensional, struct. and mag. props. 80—28993
- Be, magnetic suscept. anomalous temp. depend. *(Russian)* 79—4650
- Be, orbital magnetism, effect of energy spectrum features *(Russian)* 77—85414
- Bi-Sb, magnetic susceptibility, 4.2 to 270K, field and band parameter depend. 77—36051
- Bi-Se, fused, mag. susceptibility, temp. and conc. depend. 77—36052
- Bi-Sn, maximum diamagnetism rel. to electron density 80—54865
- Bi-Te, fused, mag. susceptibility, temp. and conc. depend. 77—36052
- Bi-Te(Se), liq., diamag. susceptibility, semicond./metal behaviour 78—14927
- C, evaporated, paramag. and diamag. susceptibility meas., 77 to 1400K 77—28362
- C fibre, as-processed, diamag. studies 77—25165
- C fibre reinforced epoxy resin, diamag. susceptibility as fibre alignment characterisation method 78—84381
- C, pregraphitic, diamag. suscept. rel. to temp., energy level calcs. *(French)* 78—34951
- C, pregraphitic crystallites, appl. of theory of diamag. susceptibility of condensed ring systems 77—16039
- C-C composites, existence diagram and properties *(French)* 78—64517
- C-fibres, from pitch mesophase, ptich and PAN, diamag. susceptibility meas. 79—69649
- CS_2, liq., diamagnetism, mass mag. suscept. meas., temp. depend. 80—97054
- $CaCO_3$, calcite, cryst. preferred orientation in marble, mag. susceptibility anisotropy development 78—56286
- $CaS_2O_3.6H_2O$, cryst. data and mag. susceptibility 77—76368
- Cd alloys, spin and spin-orbit contribs. to mag. susceptibility *(Russian)* 79—11287
- Cd, spin-orbit interac. contrib. to mag. susceptibility of interacting electrons 77—63084
- $CdGe_{1-x}M_xAs_2$ (M=Si,Sn,Pb), amorphous struct., mag. susceptibility 78—22651
- $Cd_{1-x}Mg_x$, magnetic susceptibility anisotropy, press. effects, electronic phase transitions *(Russian)* 80—54869
- $CdPS_3$, layered, organometallic intercalates, X-ray diffr., optical absorpt. and mag. props. 80—45103
- CdS, flux exclusion, superconductivity at high temp. 80—97058
- CdS, powder, mechanically induced localised states in energy gap 80—2354
- CdS, press. quenched, mag. moment, semicond.-conducting transition 80—15683
- CdTe, mag. susceptibility at 20-1400°C 77—12085
- CdTe:Ge, mag. props. 78—56289
- $CoAs_3$, prep. and characterisation 77—77356
- CoP_3, prep. and characterisation 77—77356
- $CoSb_3$, prep. and characterisation 77—77356
- Cs, fluid, metal-nonmetal transition and mag. interactions 80—49602
- Cu, dynamic susceptibility, model pot. theory 80—75710
- Cu, mag. susceptibility, Animalu model pot. calc. 80—75711
- Cu, with diamag. domains, helicon attenuation below 1K *(Russian)* 77—85254
- Cu-Cd, exam. of diamagnetic susceptibilities *(Russian)* 79—28504
- Cu-Ga(Ge), liq., mag. susceptibility 78—72326
- CuCl, anomalous diamagnetism, high temp. Meissner effect *(Russian)* 78—34955
- CuCl, behaviour under press., possibility of superconductivity 79—38239
- CuCl, disordered, diamag. transition 80—34636
- CuCl, electronic struct., self consistent all electron approach 80—2333
- CuCl, high press. phases and anomalous props. 79—7689
- CuCl, interface superconductivity? 80—39696
- CuCl, interface supercond., piezoelec. hypothesis 80—60128
- CuCl, possibility of high temp. superconductivity 79—38238
- n-$CuInS_2$, mag. props., obs. 80—70939
- $(Cu_3Pt)_{1-c}Mn_c$, mag. suscept. and effect of atomic order and disorder 77—24669
- $Cu_{2-x}Se$, nonstoichiometric, diamag. and paramag. props., susceptibility meas. 80—70936
- $Cu_xV_2O_5$, nonmetallic bronze, low field sp. ht. and mag. suscept. 78—72357
- α-FeP_4, diamag., semicond., Mossbauer study 80—50243
- FeS_2, Mossbauer effect in mag. field, absence of mag. moment 77—12288
- FeS_2, natural single cryst., mag. susceptibility, 4.2-620K 77—40031
- $Fe(Sb_{1-x}Te_x)_3$ system cpds., prep., cryst. struct., elec. and mag. characteris. 80—108349
- GaAs:C(Sn), diamagnetism quenching 80—6782
- GaP:S(Se)(Te), pot.-depend. g-values and quenched diamag., props. of donor states 77—62861
- GaP:S(Se)(Te), pot.-depend. g-values and quenched diamag., pseudoacceptors D^0, X 77—62862
- $GdCoO_3$, spin state of Co^{3+} ion, X-ray photoemission line broadening 79—82751
- Ge powder, diamag., strong mag. particle form., mag. props., EPR *(Russian)* 80—54863
- Ge-As-Te system, glasses, magnetochemical exam. 78—88092
- $HoCoO_3$, spin state of Co^{3+} ion, X-ray photoemission line broadening 79—82751
- In powders, uncoated and Cu-coated, fluctuation diamag. susceptibility above T_c 79—78309
- In-Se(Te), liq., mag. susceptibility meas., electron localisation and chem. bonding 80—60178
- InAs, fine struct. of diamag. excitons, oscillatory magnetoabsorpt. obs. 78—18971

diamagnetic properties of substances continued
- InP:Te, mag. props. of conduction electrons 78−6510
- $In_{1-x}Pb_xTe$, single crystals, mag. susceptibility 79−51738
- $IrGe_{1.5}S_{1.5}(Se_{1.5})$, new skutterudite relation compounds, prep. and charact. 78−52700
- IrP_2, prep. and characterisation 78−39679
- $IrSn_{1.5}S_{1.5}$, new skutterudite relation compounds, prep. and charact. 78−52700
- KH_2PO_4, low impurity content, magnetic anisotropy *(Russian)* 78−6506
- $K_2Pt(CN)_4Br_{0.3}.xH_2O$, one-dimensional cond., effects of dehydration on mag. props. 77−85549
- K_2PtCl_6, diamag. sp. ht. meas. at low temp. 80−7119
- LiH, solid, mag. susceptibility calc. 77−85412
- $Li_{2.33}Si$, cryst. struct. and electrochem. anal. *(German)* 80−88132
- Mo, Knight shift and mag. suscept. temp. depend. 78−15043
- Mo_2B_5 and MoB_4, thermal, elec., and mag. props. 80−20187
- $Mo_6Cl_{10}S$, struct., dielec. and diamag. props. *(French)* 78−67691
- $Mo_6Cl_{10}Se$, struct., dielec. and diamag. props. *(French)* 78−67691
- $Mo_6Cl_{10}Te$, struct., dielec. and diamag. props. *(French)* 78−67691
- NH_4N_3, diamag. susceptibility, rel. to cryst. struct. 79−24127
- Na-Cd, liq., mag. susceptibility 78−72326
- Na-Tl, liq., mag. susceptibility 78−72326
- $NaBrO_3$, dispersion of Faraday effect 80−2731
- $NaClO_3$, dispersion of Faraday effect 80−2731
- $Na_2(Fe(CN)_5.NO).2H_2O$, powder, Mossbauer absorption in mag. field 78−68418
- $Na_xV_2O_5$, nonmetallic bronze, low field sp. ht. and mag. suscept. 78−72357
- $NbS_{1.6}Se_{0.4}$, layered supercond., fluctuation induced diamag. and dimensionality 77−77006
- $NbSe_2$, layered supercond., fluctuation induced diamag. and dimensionality 77−77006
- $NbSe_3$, phase transitions, phys. props. meas. 77−8005
- $NbSe_3$, superconducting transitions and diamagnetism 80−84526
- P-As-Se glasses, mag. susceptibility, dielec. const., opt. props. 78−64184
- P-Se system glasses, magnetochem. investig. 77−51325
- PbS, mol. diamag. susceptibility, bonding types 78−31046
- p-$Pb_{0.82}Sn_{0.18}Te$; mag. susceptibility, inversion layers effect *(Russian)* 77−72996
- $Pb_{1-x}Sn_xTe$, mag. and kinetic props. near ferroelec. transition 80−11160
- PbTe:In, mag. susceptibility, temp. depend., 4.2 to 200K 80−65773
- Pd-Si(−Cu), glassy, liq. and cryst., mag. and elec. props. 77−66249
- $Pd_{68.5}Cu_{15}Si_{16.5}$ glass, elec. resist., struct. and mag. props. 79−65423
- $RhGe_{1.5}S_{1.5}$, new skutterudite relation compounds, prep. and charact. 78−52700
- $Ru_2Ge_{3-x}Sn_x$, and $Ru_2Ge_{3-y}Si_y$, diffusionless phase transitions, elec. and mag. props. 80−96871
- RuP_2, prep. and characterisation 78−39679
- RuS_2 amorphous, preparation at ambient temp., magnetic susceptibility meas. 80−35119
- $(SN)_x$, magnetization meas. in supercond. regime 79−56375
- $(SNBr_{0.4})_x$, magnetization meas. in supercond. regime 79−56375
- Sb-Te, fused, mag. susceptibility, temp. and conc. dependence 77−36052
- Sb-Te(Se), liq., diamag. susceptibility, semicond./metal behaviour 78−14927
- Sb_2Te_3, free charge carrier mag. susceptibility, 300-600K 78−10644
- Sb_2Te_3, mag. and elec. props., carrier excitation 78−43395
- ScN_x, region of homogeneity, physicochem. props. 78−52018
- Si, amorphous, diamagnetism temp. depend. 78−47940
- Si, diamag. and dielec. susceptibility, temp. depend. 78−10646
- Si, diamagnetism of excitons and biexcitons, recomb. spectra *(Russian)* 80−7412
- Si, liq., mag. susceptibility and diamag.-paramag. transition at melting pt. 78−95415
- Si, muon depolarisation, diamag. and paramag. states obs. *(Russian)* 79−87370
- Si:Gd, magnetic props. and interaction of impurities 79−11286
- SiTe-ATe, A=Ga, In, Tl, solid solns., mag. suscept. meas., defects 78−43552
- SmS, press. effect on lattice parameter, mag. susceptibility, and reflectivity 79−56272
- Sn, diamag. moment meas., dislocation supercond. above crit. temp. *(Russian)* 79−4619
- Sn-Se(Te), liq., mag. susceptibility meas., electron localisation and chem. bonding 80−60178
- SnSe, and $SnSe_2$, mag. susceptibility components 78−43551
- $Sr_2(SbCo)O_6$, spin state of Co^{3+} ion, X-ray photoemission line broadening 79−82751
- $TaSe_3$, superconducting transitions and diamagnetism 80−84526
- Te, hole susceptibility anisotropy, spin contrib. and total 77−85413
- Te, liq., mag. susceptibility, temp. depend. 78−47943
- TiC, mag. suscept. rel. to temp. in homogeneity region 78−34953
- $TlAsSe_2$, diamag., thermal expansion rel. to temp. at cryst.-melt transition 78−34954
- TlN_3, diamag. susceptibility, rel. to cryst. struct. 79−24127
- Tl_2Se, diamag., thermal expansion rel. to temp. at cryst.-melt transition 78−34954
- Tl_2Se_3, diamag., thermal expansion rel. to temp. at cryst.-melt transition 78−34954
- Tl_xSe_{1-x}, liquid semiconductor, diamagnetism and paramagnetism, dangling bond paramag. centres, mag. susceptibility obs. 80−44797
- Tl_xTe_{1-x}, liq. semicond. alloy, mag. susceptibility rel. to diffusive transport 77−20541
- $Tl_2Te(Se)(S)$, liq., mag. susceptibility 79−24128
- Tl_2WO_4, solid-state prep., cryst. struct. and props. 78−38673
- W_2B_5 and WB_4, thermal, elec., and mag. props. 80−20187
- $YCoO_3$, spin state of Co^{3+} ion, X-ray photoemission line broadening 79−82751
- YFe_2Si_2, mag. props. 4.2 to 950K, diamag. Fe atoms 77−20544
- Yb intermetallic compounds, mag. susceptibility, 1.4 to 1060K, investig. of Yb valency 77−20543
- YbB_6, mag. and transport props. 80−54689
- $YbCl_2$, mag. props., 77-292K 78−52197
- Zn, magnetic susceptibility behaviour, dislocation and elastic deform. effects *(Russian)* 77−80912
- Zn, spin-orbit contrib. to mag. susceptibility of interacting electrons 77−63084
- Zn whiskers, quantum oscills. of mag. moment 79−15280
- $ZnF_2:Co^{2+}$, Raman tensor calcs. of isolated impurity in diamagnetic matrix 80−76025

diamagnetic properties of substances continued
- $Zn(NH_3)_4(ClO_4)_2$:Mn, EPR study of Mn^{2+} detection of structural transition 79−87308
- ZnS(Se), ionicity trends in diamagnetism and its temp. depend. 79−19717

diamagnetic resonance *see cyclotron resonance*

diamagnetism
- *see also cyclotron resonance; de Haas-van Alphen effect; diamagnetic properties of substances*
- atomic, Kirkwood relation in at. diamag., satisfaction by Thomas-Fermi model 78−9266
- atomic scattering factors of first row atoms and ions, diamagnetic susceptibilities 77−68133
- band structure diamag., first principles calc. 80−88470
- band structure in mag. field, second order calc. using Landau functions 80−24784
- Bloch electrons, nonlinear orbital magnetisation in weak mag. fields *(Russian)* 80−70931
- complex molecules, π-electron pair correl. of supercond. type, appl. to optical and mag. props. 79−54778
- condensed ring systems, diamag. susceptibility, appl. to pregraphitic C 77−16039
- conjugated hydrocarbon, graph theoretical formulation of London diamag. 80−27919
- conjugated molecule diamagnetic anisotropy, graphical anal. 79−76360
- disordered system, diamag. susceptibility, variational calcs. 77−8265
- domains, diamag., study by positive muon method 80−60174
- electron gas, classical diamagnetism, Gibbs method *(Russian)* 78−73918
- electron gas, diamagnetism and surface currents 80−88496
- electron gas, Hubbard model at low temp., mag. props. *(Russian)* 78−43550
- electron gas, magnetised, confinement effects 79−28494
- electron gas in ultraquantum limit of strong mag. field, mag. moment *(Russian)* 77−28361
- electrons in rectangular box, orbital mag. suscept. 77−85166
- EPR of V^{4+} in diamagnetic lattice, cryst. field effects 78−64263
- exciton, Bose condensation and superdiamag. current prod. possibility 80−65456
- free partical in classical electron theory with zero point radiation, diamagnetism 80−42082
- graphite, diamagnetism with quasilinear dispersion law, orbital susceptibility, valence bands *(Russian)* 80−80475
- hydrogenic atom in weak mag. field, polarisability, ground-state energy 79−3594
- impurity effects on anomalous diamag. of system with electron-hole pairing *(Russian)* 77−69318
- insulating solid, nonmagnetic, anisotropic mag. effect 78−6509
- ionic cubic lattice in homogeneous mag. field, oscillations 78−91868
- itinerant system of coupled diamagnetic pairs of electrons, electronic and magnetic correlations 79−61033
- magnetisation thermal fluctuations, diamagnetic contrib. 78−23240
- magnetosphere, plasma injection and diamagnetism 79−80085
- metal, crit. point of diamag. transition of first kind, and NMR linewidth 77−59469
- metal film, size effect in Landau diamagnetism, surface pot. effect *(Russian)* 80−93012
- metals, magnetic suscept., optical data determ. of individual contributions 77−12088
- molecular, Kirkwood equation applicability charged anisotropic harmonic oscill. 78−5365
- molecular diamagnetic susceptibility, interatomic charge transfer in diatoms, mol. second moments, additivity formulas 78−70961
- polarisation and magnetisation of electronic matter 80−75929
- quantum theory, non-coupled Hartree-Fock-Roothaan method satisfying gauge invariance *(French)* 77−67984
- radially resolving diamagnetic loop, appl. to flux conservation test 78−12734
- rigid-body molecules, diamagnetism and thermal motion 80−25076
- semiconductor, diamagnetism of deep impurities 79−23931
- semiconductor, diamagnetism rel. to chem. bonds 77−59380
- semiconductor with nonparabolic bands, diamag. excitons, optical absorpt. in mag. field 77−55487
- semimetal, mixed superconducting-excitonic insulator phase, diamagnetism, virtual intraband transitions 80−2520
- simple metals, solid and liq., electronic struct., mag. susceptibilities calc. 78−52204
- sphere, strongly magnetised, interaction with weakly magnetised particles carried by fluid flow 80−69320
- superconducting film, resistive transition 80−7049
- superconducting magnets, tape-wound cylindrical, trapped fields, diamag. effects 77−26355
- superconductivity and magnetism *(Hungarian)* 79−47226
- superconductor, critical temperature mag. field depend., strong diamagnetism *(Russian)* 80−7022
- superdiamagnetism, spontaneous current model *(Russian)* 78−43628
- susceptibility calculation using Pascal's consts., BASIC program 80−37717
- two-phase conducting diamagnetic system, coeff. of EM ejection of particles *(Russian)* 78−94364
- type II superconductor, giant-vortex state, temp. depend. 80−7051
- type II superconductors, fluctuation induced diamagnetism above H_{c2} 78−80097
- Ba, diamag. quasi-Landau spectrum near ionis. threshold, two-photon ionis. spectra obs. 78−58642
- Ba, quadratic Zeeman effect, diamagnetic shift, Rydberg series, strong field mixing 78−946
- LiHLiH array, Mott transition mag. analog, Hamiltonian for paramagnetic-diamagnetic transition 79−95565
- Na, Rydberg states, diamag. struct. 78−50484
- Rb Rydberg levels in intense mag. field, diamag. struct. 79−26958
- ^{85}Rb, ground state dipole HFS diamagnetic shift, high field optical pumping expt. 78−90129
- ^{85}Rb, hyperfine struct., diamag. shift obs. 77−61717
- Sr, diamag. quasi-Landau spectrum near ionis. threshold, two-photon ionis. spectra obs. 78−58642
- Sr, quadratic Zeeman effect, diamagnetic shift, Rydberg series, strong field mixing 78−946
- $TaS_2(pyridine)_{1/2}$ intercalated layered supercond., fluctuation induced diamag. and dimensionality 77−77006

diameter measurement
aperture diameter inductive meas. device 77—26268
artery, using US transit-time micrometer 78—7410
astronomy, size limit for uniformly pulsating EM radiation sources 79—84656
bubbles, acoustical meas. of gas bubble volumes and gas flow rates 80—62633
caliper gauges for meas. outside dia. 79—12766
capacitive bore gauge 78—21097
cell membrane particle diameters meas. by computer from electron micrographs 80—101307
contact lens, soft, in-office meas. 78—7339
cortical bone diameter meas., manual and computer-aided methods comparison 78—85376
cylindrical products, interfering factors elimination 80—77755
cylindrical surface two-wavelength speckle pattern intensity distrib. at optical transform plane 80—106487
diameter meas., high speed noncontact light scatt. technique 77—83956
dimensional gauging using scanning laser beam 78—57898
droplet, transparent, diameter meas. by side reflection 78—59518
electrically conductive filaments, fine and superfine, instrument for contact free measurement 78—93655
electro-optical gauging system, microcomputer-controlled 79—86271
electro-optical instrument for hole-diameter meas. 80—98882
erythrocytes of human blood, diameter meas. by specific elec. cond. 78—53353
extended part diameter meas. contactless instrument *(Russian)* 80—27270
Fabry-Perot interference ring diameter meas. using CCD linear sensors 79—93210
feedback monitoring, normal conditions for linear and angular measurements 79—75492
FFTF element measuring system 79—9729
fibre diam. meas. with He-Ne laser 79—97352
fibre diameter checking, laser interference method 78—18080
fibre-optic cable manufacture, testing, and installation *(German)* 78—33863
foetal diameter, assessment of gestational age 78—7415
glass micropipettes, comparative calibration by optical microscopy and SEM *(German)* 80—98201
glass tubing dia. and wall thickness meas., P-329M instrum. 80—86262
hole diameter meas. with universal microscope and electronic contact indicator 77—79055
horizontal optical meas. machine adjustable-tip internal horseshoe gauges 77—74360
human lung endothelial cell nuclei, estimation of mean caliper diameter using serial section reconstruction models 79—29679
impressions in alloys, portable microscope for parameter meas. with 1 μ accuracy 77—53856
inorganic fibre, diameter measurement by microscopy *(French)* 79—93095
instrument for large internal diameter mass. *(Japanese)* 77—22522
internal, 4 to 80 mm, miniature instrument with spring-loaded head 77—9982
internal, reference standard 78—29090
internal gauge, microinterferometer IZK-61 78—89438
isolated surface circular defect diameter determ. based on Fraunhofer diffr. 80—73307
laser bar gauge for diameter measurement of hot or cold objects 80—105605
laser beam diameter meas. using a grating 80—102745
laser beam diffraction appl., using moire fringes *(Czech)* 79—40530
laser scanned gauge *(Chinese)* 80—77756
laser-beam noncontact gauging systems, advantages and appl. 79—2745
long hole, inductive rod gauge operational principles *(Polish)* 78—29086
magnetic bubble diameter, collapse field and runout field intensity meas. 79—78490
microbores meas. for use as standards *(German)* 80—31710
nuclear methods, glass tubing production appl. *(Czech)* 77—5803
openings, using mechanical, pneumatic and optical-mechanical methods *(Slovak)* 79—71407
optical fibre, 50-150 μm, characterisation system 77—88920
optical fibre, computerised forward scattered light system appl. 78—62176
optical fibre, graded index, diameter determ. from backward scattered pattern 80—5820
optical fibre, mech. deform. meas. by light scatt. method 80—14452
optical fibre diameter measurement using fast Fourier transform 80—91894
optical fibre drawing, semi-automatic machine development 79—27449
optical fibre preform core diameter and Ge doping profile meas., X-ray nondestructive method 80—64231
optical fibre waveguide and cable parameter meas. techniques *(German)* 78—33860
optical fibres, single-mode and multimode, automatic geometric meas. 79—36988
optical fibres, using microprocessor based system 78—1443
photo-optic measuring systems using bifurcated fibre-optic probe 79—81569
photoelectric laser meas. equipment, semi-automatic 78—36966
Pioneer images of Galilean satellites, edge-finding technique for dias. determ. 78—85893
pore size distribution measurement, Al_2O_3 films, adsorpt.-desorpt. vs. TEM methods 77—74357
pore size measurement, comparison of methods 80—62622
primary meas. transducer error twin-circuit correction *(Russian)* 79—71404
profilometer, EBR-II subassembly, at HFEF 77—54299
projected inertial confinement fusion reactor target evaluation by buoyancy analysis 80—78442
radii of cylindrical and spherical segments, linear scale instrum. accuracy anal. 77—87732
radio sources, ang. dias. meas. errors 79—12534
rat lung cell nuclei, estimation of mean caliper diameter using serial section models 79—25165
reactor fuel pin diameter meas., sectioning cutoff saw adaptation 79—9748
reactor fuel pin imagery, computer enhancement and mensuration 78—37395
red blood cell diameter meas. from He-Ne laser beam diffr. pattern 77—86582

diameter measurement continued
reference ring gauge, precision improvement in meas. internal dia. 79—17388
right atrium, dynamic/static, using US sonomicrometer technique *(Japanese)* 78—3568
ring inner diameter, using optical microscope and electronic contact indicator, Soviet (Ukrainian) developments 80—52162
slide calipers, bench for production testing of wear resistance 80—8959
small holes, opticomechanical instrum. 80—77750
specimen cross section during low temp. compression, apparatus design 78—57940
sphere population overall mean caliper diameter estimation 79—70719
Styrofoam spheres, diameter determ., mol. monolayer experiment, teaching appl. 79—44678
tape-controlled remote automatic diameter meas. machine, report 78—86241
threads, meas. by three wire method, influence of shape deviation of taut measuring wires *(German)* 78—77845
vibrational contact means of measuring small, complicated and inaccessible shapes 79—97353
water drops, size meas., evaluation of direct methods 77—22527
wires, circular cylindrical, interferometric and diffraction methods using He-Ne laser 79—21703
wool fibre, diameter meas. for grade determ., truncated sequential sampling 79—87802
SiC filamentary crystals, dia. determ. by X-ray extinction method 79—97343
SiO_2 fused fibres, radii determ. by multiwavelength laser light scatt. 80—22321

diamond
ab initio calcs. of struct. using FSGO method 77—80753
ab-initio HF and PCILO calc., C-C bond lengths, force consts., cluster construction 78—42951
abrasive grains, single, wear on steel, exam. *(Japanese)* 78—44230
accelerator irradiation, heavy ion irradiation damage 80—100291
acoustic phonon geometric propag., anisotropic continuum acoustics 77—4170
adamantine ceramic, structural, thermophysical and electrophysical props. 80—6918
air bearing and diamond machine design for optics 80—1365
amorphisation during ^{133}Xe implantation, Mossbauer effect study 80—40010
amorphization process, ^{133}Cs Mossbauer spectra 79—99809
anivls, megabar pressure meas. to determ. depend. of strength on nitrogen platelet conc. 79—91888
anomalous muonium in diamond-struct. crysts., μ^+ meson probe appl. *(Russian)* 79—28665
anvil, oscillating device for high press. X-ray diffr. 79—4209
anvil cell for high pressure measurement, with uniform internal stresses at 200 kbar 79—67334
anvil high-pressure cell as sampling device in IR expts. 79—93157
anvils in high-press. devices for IR and Raman spectroscopy 77—57413
artificially coloured diamonds, spectroscopic diagnostic technique 78—65281
aspherical surface diamond turning machine development 80—1372
band structure, cluster type effect 77—28109
band structure of diamond like crystals, cluster-Bethe lattice model calc. 80—6713
binding energy, Wigner-Seitz effective quasiparticle pot. 79—50160
bolometer, Ge-diamond, operated at 4.2, 2.0, 1.2, 0.3, 0.1K, design and construction 80—77868
bonding, struct. stability, SCF perturbation theory appl. 79—37658
bremsstrahlung spectrum of 800 MeV electrons, low-energy γ ray anomalous yield, collimation effect 79—91521
brilliance, sparkliness and fire of diamond simulants 78—90363
Brillouin spectra, meas. using Fabry-Perot interferometers with 20 cm^{-1} free spectral range *(Japanese)* 77—87847
Burgers vestor of grain boundary dislocations *(Russian)* 79—73176
cathodoluminescence, polarised in near IR, from platelet defects 77—48253
cathodoluminescence, topographically identifiable sources 77—55836
cathodoluminescence at discolations 79—47524
ceramic, elec. cond., temp., freq. depend. 80—54687
ceramic, elec. cond., thermal cond. rel. to temp. 79—15140
ceramic containing diamond, impact hardening 79—15828
channelled 800 MeV electrons, radiation of 79—61274
channelled electrons, gamma emission 80—54293
channelling of 4.7 GeV electrons, γ-quanta yield *(Russian)* 79—69170
cluster, electronic struct. of deep levels, LCAO, SCF method 79—82555
coatings, diamond-based, fabrication and wear resist. 80—40576
coatings, for increased wear resist. 80—76371
coincidence-site lattice interfaces, crystallographic description 80—15381
colloidal particles in water, elec. polarisability anisotropy 79—39208
colloidal suspension in water, dichroism in homogeneous elec. field 79—8122
composite with Cu-Ti matrix, microstresses, X-ray diffr. exam. 78—56679
compressibility, appl. of Murnaghan eqn. of state, Morse pot. 80—79861
compressive strength for [111] loading 79—79036
Compton profiles, directional, X-ray scattering factors and 1-electron density matrix 80—10458
Compton profiles, X-ray struct. factors, band struct., LCAO calc. 78—51889
computer-controlled machine tool for diamond-turned surface accuracy improvement 80—1367
core electron expansion, kinetic energy in Compton profiles 78—72628
Cosserat continuum model, elastic props., lattice dynamics 80—59552
cracking and fatigue under repeated indentations 77—59905
crystal maximum temperature measuring system using irradiated diamond powder, engineering applications 77—33991
crystallisation, high press. with catalyst and solvent *(Polish)* 79—87592
crystallisation in C-metal system, kinetic peculiarities of transport processes 77—15331
cubic structure, kink formation and migration, rel. to Fermi level 79—82218
cutting traces of single diamond, friction force 77—50781
defect electronic struct. and lattice config., MO approaches 80—65495
defects and impurities 80—29017
diamond:^{111}In, ion implanted, intrinsic limitations of doping 80—34019

diamond continued
diamond:^{129}Xe, implanted, elec. quadrupole interaction, integral perturbed ang. correlation study 79−11364
diamond: Li, ion implantation doped, IR photocond. 80−20249
diamond: Sb, ion implanted, defect study using optical absorpt. and EPR 80−24480
diamond:B, B conc. and impurity-to-band activation energy 79−56165
diamond:B, synthetic, current-voltage characteristics, temp. depend. *(Russian)* 79−7825
diamond:B, synthetic semicond., thermostimulated conductivity *(Russian)* 79−7834
diamond:B, thermoluminesc., TSC, correlation meas. 78−88369
diamond:B, variable-range hopping cond., effect of electron irrad. induced compensating centres 77−43599
diamond:B hopping conductivity in range 12 to 1300K 78−51994
diamond:Ge(B)(B$_4$C), doping by diffusion at high temp. and press. 79−19273
diamond:Li, electron transport character 80−92917
diamond:N, dissociation of N aggregates by high-press.-high temp. treatment 78−43904
diamond:N, effect of displacement upon impurity levels, pseudopotential calc. 77−39803
diamond:N, photocond. in N2 absorpt. band 79−91102
diamond:N, spin-lattice relax. of Jahn-Teller N centre 77−66412
diamond:Ni, synthetic, X-ray absorpt. fine structure study of impurities 80−55133
diamond:Sb, implanted, radiation damage and annealing study 80−100263
diamond:Sb, ion implanted under channelling conditions, depth profile, distribution tail 80−2057
diamond:Xe, quadrupole interaction of implanted Xe 79−61279
diamond, electric quadrupole sum rules rel. to optical consts. 79−38036
diamond, electron density, neutron diffraction powder data 78−38655
diamond, energy band calcs. using intersecting spheres model 77−66110
diamond, metastable overgrowths in dissoln. medium in Ni presence at atm. pressure 79−51030
diamond, pseudopotential method of band struct. anal. 78−51886
diamond, radiation detector for light and charged particles 78−49900
diamond, synthetic, topographic structures and origin *(German)* 77−85036
diamond, vacancy enhanced N aggregation, electron irradiation effects IR spectra 80−70245
diamond Ge(B)(B$_4$C), doping by diffusion at high temp. and press. 79−19273
diamond-anvil press. cell for photoluminescence meas. 80−108256
diamond-graphite equilib. line, from synthesis and graphitisation of diamond 78−24811
diamond-Si heterostructure, Auger spectra electron microscopy study 80−34340
dielectric band structure calc. 79−47034
dielectric breakdown, two-photon absorpt. and other optical damage mechanisms 78−84684
dielectric constant calc. and local-field correction 80−11312
dielectric function, optical frequency model calcs. 78−51921
dielectric polarisation calcs., microscopic local fields 80−20582
dielectric properties, mean point value calc. 78−87930
diffuse reflectance Fourier transform IR spectroscopy using diamond anvil cell 80−101855
dislocation growth degree of supersaturation determ. 80−88145
disordered lattice, numerical simulation of cond. in Anderson's model 79−78092
dynamic Jahn-Teller distortions at trigonal optical centres 79−87069
effective ion interaction and force consts., model of Si point defect 80−65185
effective supersystem cryst. simulation method, geometrical parameters, bulk moduli, impurity levels calcs. *(French)* 80−15430
elasto-optical constants, determ. from piezobirefringence 79−73899
electroless Ni coating containing diamond, fabrication and props. 79−47795
electroluminescence, thermoluminesc., photocurrents 79−38675
electroluminescence at high temp. 80−45145
electrolytic grinding, magnetic field effect 80−11790
electron and neutron irradiated, paramag. centres with S=5/2 at room temperature 79−47334
electron channelling, γ-ray spectra *(Russian)* ·79−61280
electron channelling gamma-ray spectra 80−40023
electron channelling radiation comparison with coherent stopping radiation *(Russian)* 80−103403
electron density, bulk and surface atoms, from ab initio model calcs. 79−4590
electron density, X-ray powder diffraction data 78−38656
electron irrad. at 77K, annealing, EPR 77−59045
electron irradiated, B doped, defects at low temps., elec. resist. meas. 77−11593
electron irradiated, B-doped, threshold energy for atomic displacement, elec. cond. meas. 77−11594
electron irradiated, photochromism 80−71454
electron irradiated, photocurrent and Hall current, 290 and 4.2K 79−87129
electron irradiated, type Ib, migration of N, optical absorption meas. 78−56505
electron irradiated Ib type, 2.367 eV vibronic absorpt. system, optical study 79−73975
electronic energy bands of diamond-type crysts., appl. of EHT method 78−87907
electronic properties, ground-state, in local-density formalism 77−69223
electronic structure, self consistent local description 80−20067
electroplated diamond-composite abrasion-resistant coatings 79−61737
elemental concs. and Pb and Sr isotopes in S.African diamonds 79−34775
elementary excitations in crystals, dielectric theory 78−60076
energy loss of protons, alpha particles and ^{7}Li 80−42905
enthalpy of solution at 1320K, heat of transformation to graphite 78−59945
epitaxial films of diamond-graphite, deposition on diamond substrate 77−4271
epitaxial layer form., SiC layers on diamond (111), (100) 77−15720
epitaxial synthesis by C-ion deposition at low energy, and struct. 79−1559
EPR, of electron irrad. type IIa diamond at liquid N$_2$ temp. 78−76310
EPR of defect centres in powders 77−66423

diamond continued
EPR spectra of diamonds synthesised in metal-carbon medium by static and dynamic methods 77−90015
erosion impact of annealed 310 stainless steel, SEM and TEM study 78−64725
ESR studies, review 78−95521
etch-pit formation on cube faces, electron microscopy obs. 80−75232
etching, by high press. water 77−55285
etching, HF ion-plasma, cryst. surface layers treatment and study *(Russian)* 80−16517
exchange interaction of N paramag. centres, spin density delocalisation 80−39847
film, diamond-like C, produced by RF glow discharge of hydrocarbon gases, props. and coating rates 80−21146
film, plasma stream condensation with RF pot., props. 79−15612
formation by shock compression of graphite, cryst., surface struct. 78−44060
four-wave mixing spectroscopy in crysts., nonlinear spectroscopy developments 80−91861
Fresnel diffraction at platelets, defect struct. anal. by 3 Å phase-contrast microscopy 78−87701
friction in contact with W, temp. depend. *(Russian)* 77−73350
frictional anisotropy, cathodoluminesc. study 80−35340
gamma radiation angular distribution of channelled 900 MeV electrons *(Russian)* 80−19858
gas-solid interface, electronic struct. HFR calc. 80−54745
Gaussian model in three dimensions, differential real-space renormalisation 80−17896
GR1 and UV band, fine struct. 80−20678
GR1 band, anal. of satellite lines by quadratic Jahn-Teller coupling 80−97295
GR defect, high resolution optical spectra after electron irrad. 78−56515
graphite$\rightleftarrows$diamond equilib. transition press. 78−34617
graphite-diamond, shock induced transform. anal., post shock graphitisation 80−79933
graphitisation, elec. resist. meas., 30-550°C *(Russian)* 77−39676
grinding tool, wear during optical glass grinding 77−7225
growth of diamond with rhombic dodecahedral faces 77−48339
Gruneisen spectroscopic mode parameters via Raman spectra 77−7876
half wavelength and stopping power of planar channelled protons 80−65087
hard conducting C ion implanted layer, resistivity 77−15974
Hartree-Fock calculations, unrestricted, for five atom clusters 77−11866
Hartree-Fock energy band struct. determ. using LCAO basis 77−35848
high press. appl. by spherical diamond indentor, plastic deform. obs. method 78−35619
high pressure cell used in automatic diffractomter up to 90-kilobars 78−54387
high pressure cell using miniature diamond anvil 80−237
high temp. ion implantation 79−23623
high-pressure appl. of diamond indentor-anvil·system, resist.-vs-press. relations 79−77681
homogeneous formation in gas phase, laser beam effects *(Russian)* 80−104052
hydrocarbon dissociation formation, Hugoniot data, high temp. and press. 79−47927
identification by electron refl. *(German)* 80−54080
identification from reflection pattern photographs 78−54481
implanted ^{129m}Xe, lattice location, combined Mossbauer and IPAC meas. 78−43733
impurity centres, vibronic spectra, Van Hove singularities, quasilocal vibrs. 77−85782
indentor against diamond flat, high press. generation, thin film effect 79−55821
industrial, anal. cathodoluminesc. studies in SEM 80−81410
internal structure by electrostatic charging technique 80−10468
ion beam analyses in relation to the physical properties of diamond 79−5219
ion channelling and dechannelling meas. 80−65090
ion implantation, investigation of Li$^+$distrib. 79−77630
ion implantation, review 78−87698
ion implanted, p-i-n structure, double injection of carriers 79−11214
ion polishing for diamond-turned mirror dielectric coating adhesion 80−1370
IR internal reflection spectroscopy, appl. of diamonds 78−24871
irradiated, Hall current meas. by split electrode method 77−1435
irradiated, MCD spectrum of GR1 line, neutral vacancy model 77−69850
irradiated, optical spectrum 78−6719
irradiated, optical study of TR12 and 3H defects 77−85772
irradiated stainless steel tube high-speed slitting machine 79−9210
isomer shift values of implanted ^{133}Xe/^{133}Cs, Mossbauer spectra 80−7240
isotopically light C, in diamonds from Lesotho kimberlite pipes 79−48487
Jahn-Teller coupling at ND1 and GR1 centres 78−56103
Jahn-Teller coupling at neutral vacancy 80−71453
Jahn-Teller effect, GR1 band, E to T state transitions coupled to e vibrs. 77−12430
large unit cell semiempirical mol. orbital approach to props. of solids 79−87036
laser beam drilling of diamond, process mech., thermal stresses, elec. surface forces *(Dutch)* 77−7759
laser beam use for processing, quality improvement and monitoring *(Russian)* 78−31595
lattice dynamical calc. using extended Born-von Karman scheme 78−59889
lattice dynamics, pseudopot. calc. 77−43295
lattice dynamics, valence force field, rel. to tensor force consts. 80−79888
lattice dynamics, X-ray characts. *(Russian)* 77−80593
lattice energy, strong orthogonality, requirement in calcs. dealing with crysts. by geminal method 78−14307
lattice potential, high energy electron diffr. and refr. study 80−54165
lattice vibrational spectrum 79−90741
light coupling prism, Raman spectra for thin film props. study 80−88978
light ion damage, channelling investigation 80−65068
linewidth of GR2-8 transition 78−60488
local field, microscopic electronic polarisation 80−25283

diamond continued
- lonsdalite→graphite phase transform. mechanism, electron diffr. expts. 79−28099
- low lying levels of GR 1 centre, satellite line struct. 77−20269
- machine tool computerised control for diamond-turned surface finish 79−98517
- machined optical surface specification 80−48472
- magnetic field and stress splitting of GR1 line 78−60095
- mechanical strength, depend. on thermal working parameters, microcracks *(Russian)* 80−55501
- 'melting' to solid metallic C phase above graphite triple point 80−15236
- metal-diamond interface, Schottky barrier theory, ionicity depend. 78−52086
- metal-diamond strip, strength props. 79−61678
- metastable metallic form, possibility, summary of research 79−42146
- micromechanical characteristics 79−20190
- momentum density, Compton profile 77−20235
- monocrystals, coherent electron bremsstrahlung *(Russian)* 77−6603
- Mossbauer spectroscopy of defects, radiation damage and deep levels 80−59533
- N9 and ND1 energy levels, electron irrad. photocond. obs., thermolum. 78−6324
- natural, (110) and (210) defects, X-ray diffr. pattern weak extra reflections 79−82257
- natural, anisotropy and saturation of hot carrier drift velocity 80−6867
- natural, defect struct., recent obs. by new methods 78−30628
- natural, dislocation-N_2 impurity interaction, photoconductivity spectra, resistivity 79−91097
- natural, elec. cond. and thermoelec. power 78−39115
- natural, electron effective mass and lattice scatt., Monte Carlo anal. 80−44484
- natural, free exciton luminesc. line shape 80−40165
- natural, high conc. of implanted Si ions, He backscatt. and IR absorption 77−89466
- natural, impurity complexes, shape and dimens., diffuse X-ray scatt. obs. 78−47398
- natural, lattice scattering and effective mass of holes 79−60842
- natural, microhardness 78−35504
- natural, N3 centre, EPR obs. 79−51842
- natural, N3 luminesc. decay time 78−76520
- natural, $N_{S(111)}$ impurity segregation on diffuse X-ray scatt. 79−95046
- natural, polycryst., distinctive features of struct. 79−92530
- natural, rate of donor defect introduction by 2 MeV electrons, 0.348 eV absorption band 77−89477
- natural, thermal cond. with absorpt. at 3.22 μm 79−73353
- natural, thermoluminescence, phosphorescence, defects, low temp. 78−11000
- natural, topography of impurity distrib. and neutron-induced colouring 77−39613
- natural, trace element anal., genetic significance 80−55759
- natural, type IIa, thermal cond., 0.5 to 20K, anisotropic heat cond. in boundary scatt. regime 79−65267
- natural gem, H impurity conc., ion beam spectrochemical anal. 78−14374
- natural octahedron, etching at high temp. and pressure 80−39097
- natural semicond. motor photocond. and internal photoemission 79−69546
- natural semiconducting diamond, sub PPM determ. of B, identification of acceptor centre 77−59035
- natural type Ia, dechannelling and nature of defect structures 80−49282
- natural type IB, thermal conductivity anomaly, defects obs. 77−85003
- NC diamond turning system evolution 80−1369
- neutral vacancy, generalised valence band. calc. 77−55493
- neutron activation analysis, sub-surface contamination by hot-atom recoil 77−60144
- NMR spectra 79−51862
- nonlinear optical susceptibility, tight binding bonding orbital model 80−5784
- nuclear particle detector, transport props 85 to 700K 79−45542
- nuclear target preparation for tandem expts. 80−23222
- nucleation and growth, 55 kbar and 1450K 79−99087
- obs. and interpretation of spirals for spiral growth 80−15027
- olivine inclusion epitaxy, Brazilian diamonds 77−78173
- optical absorption and luminesc. spectra, review 80−2848
- optical absorption lines, GR4 and GR8, effect of uniaxial stress 80−34956
- optical characterisation for IR diamond-turned aspherical elements 80−1373
- optical component fabrication by diamond turning 79−76899
- optical diamond turning air-bearing spindle and eddy-current motor 80−5851
- optical diamond turning and precision engineering 80−1364
- optical fabrication diamond turning, Honeywell Corporation facilities 80−5852
- optical spectra, role of electron-hole interaction, review 80−45113
- optical surface modes calc. 77−59200
- optical surfaces, diamond turning, on electroless Ni 80−1375
- optical transitions between E and T electronic states each coupled to e-modes, GR1 band 80−20677
- optically active centre effect on strength props. 80−40462
- optically active defects, anomalous X-ray scatt. 77−89434
- origin, role of C in Earth upper mantle 80−81845
- p-type, electroluminescence 78−15229
- p-type, synthetic semiconducting, photoconductivity spectra 79−69550
- paramagnetic centres, ESR spectra 77−36132
- paramagnetic N centres spatial distrib., EPR imaging method 79−65732
- particles, finely dispersed, in active C shock wave produced powder, electron diffr. identification 80−1903
- phase equilibrium, with graphite, thermodynamic stability, effect of particle size 79−65184
- phase transition from graphite under shock wave loading *(Chinese)* 79−82337
- phonon dispersion relation, adiabatic bond charge model 77−69057
- phonon dispersion relations, Born-von Karman study 79−86855
- phonon frequencies, model calc. using tight binding Hamiltonian 78−59894
- phonon spectra calc. using dielectric matrix approach 79−4381
- phonon transmission from incoherent radiator into cryst., anisotropic continuum acoustics 77−47521
- photoconductivity in electron-irrad. type Ia cryst., acceptor centre form. 77−47853

diamond continued
- photoionisation cross-sections of valence s- and p-electrons *(Ukrainian)* 77−73211
- planar defects, in {100} planes, electron microscopy 77−11569
- planishing treatment of Al alloy effect of struct. and comp. 79−43237
- plastic deformation at room temperature 78−52927
- plastically deformed, EPR of two N atom centre 78−72408
- platelet structure, N-decorated stacking fault model, from phonon scatt. freq. depend., type I_a 77−4173
- platelets, giant, on cube planes, electron microscopy 77−84765
- point defect grasshopper effect 79−90830
- polarisation charge density and microscopic local field induced in external elec. field 80−49645
- polycrystal, sintered under ultra high press., binary inclusion content effect on thermal stability *(Chinese)* 80−66453
- polycrystal, sintering *(Chinese)* 77−59706
- polycrystal growth, phenomenon of catalyst movement *(Chinese)* 77−77806
- polycrystal growth under ultra high pressure *(Chinese)* 79−78863
- polycrystalline, growth at high temp. and press., morphology 77−11495
- polycrystalline film growth from gas phase 78−48332
- positron implantation profile and mobility, elec. field effects 77−48273
- powder, consolidation by thermal decomposition of methane and benzene 80−66448
- powder, explosion synthesized, impurity distrib. and thermal stability 80−15147
- powder, rapid oxidation development, kinetic model *(French)* 78−68917
- powder, sintering with Co binder 78−27450
- powders, C metastable phases prod. during sintering 77−89404
- powders, Mo coated, X-ray diffr. study 80−100936
- powders, oxidised surfaces, thermal desorpt. spectra 78−47661
- pressure calibration by resistance-jump transitions up to 500 kilobars 78−54388
- production by C shock compression 80−11613
- proton channelling, transverse energy evolution in planar channels, computer simulation 80−79849
- pseudo-Jahn-Teller effects in H3 vibronic spectrum 77−90182
- quasiparticle states, quantitative calc. 80−88499
- radiation damage processes, 0.4-2.2 MeV electrons 77−84798
- radiation damage tetragonal R2 centre, optical and EPR spectra 78−2888
- radiation dosimeters, evaluation 80−78456
- Raman spectra, coherent nonlinear two-phonon 79−19878
- Raman spectrum, two-phonon cut-off, harmonic pot. and bond polarisability model 77−77213
- Raman spectrum, two-phonon peak linewidth, bond polarisability model 77−77212
- rare gas isotopic compositions, rel. to atm. comp. 78−24270
- reactive pulse plasma crystallisation 79−95938
- refractive index, temp. and press. var. 78−27174
- refractive index dispersion 79−24280
- resonant Raman scatt., first and second order 78−60471
- resonant Raman scattering 78−48176
- Rockwell diamond indenters, meas. method rel. to standards 79−66251
- roughening transition on solid-fluid interface, Monte Carlo simulation 79−99088
- round brilliant cut diamond, statistical assessment of brilliance and fire 78−90361
- round brilliant cut diamond style modifications, brilliance, sparkliness and fire 78−90362
- Schottky barrier, electronic struct., pseudopot. calc. 78−95364
- Schottky barrier, electronic struct., pseudopotential method, jellium model 79−38162
- Schottky barriers, photocapacity meas. 78−52057
- section topograph technique, high resolution, applicable to synchrotron radiation sources 80−57449
- segmental wheel, wear resistance 78−48539
- self-interstitial, struct. and motion 79−37700
- semiconducting, (111) surface, quantum photoyield and secondary-electron distribs., stable negative-affinity emitter 79−100023
- semiconducting, applications in electronics *(Czech)* 77−1414
- semiconducting, band gap temp. depend, dilation and vibr. contribs. determ. 80−10868
- semiconducting, cathodoluminescence of defects *(French)* 80−34988
- semiconducting, depend. of energy gap on short-range order 78−84142
- semiconducting, electron irrad., charge carrier mobility 77−11921
- semiconducting, electron-hole liquid formation conditions and parameters 79−78013
- semiconducting, GR1 cathodoluminescence, fine struct. 78−68566
- semiconducting, Li ion implantation, Hall effect and elec. cond. meas. 80−15526
- semiconducting, natural, isothermal annealing of electron radiation damage 77−7764
- semiconducting energy band struct., elec. and optical props., review 77−35862
- semiconducting epitaxial layer, B doped, charge transfer and acceptor state 78−19169
- semiconductor, B-doped, photocond. and electroabsorpt. spectra 77−4647
- semiconductor properties and use for making devices, review 78−60131
- shock synthesis *(Japanese)* 80−29918
- sintered compact, fracture and fatigue 79−52352
- sintered compact, stress-strain curves using ultrahigh-pressure apparatus 79−43322
- sintered with Co, remanent magnetism 79−99731
- sintering of a polycryst. diamond with Ni additives under ultrahigh pressures 80−84870
- sintering under high press., binary inclusion-diamond interaction *(Chinese)* 78−80484
- sintering under quasi-hydrostatic high press. *(Chinese)* 78−11141
- solid thermal cond. and interface resistance meas. by radiation thermometry 80−86289
- sound excitation orientational effect due to channelled electrons 80−84254
- specific heat at constant volume, leading anharmonic contribs. 77−89549
- spin-spin interaction of N_2 and Ni centres, temp. effects 78−88177
- stacking faults in natural crystals 78−26582
- static dielectric function, local field correction, tight-binding model 79−95355
- stress effects on GR 2-3 absorption lines 78−72563
- structural changes induced by Ar ion bombardment, depth profiles, using XPS 78−34554

diamond continued
- structure transformation from graphite probability under high temp. and press. *(Chinese)* 80–65220
- stylus sliding on rubber, orientation effects, expt. test of theory 77–86188
- substitutional impurities 79–87056
- subsurface damage exam. using cathodoluminescent mode of SEM 77–80398
- subthreshold defect formation due to electron irrad., cathodoluminescence study *(Russian)* 80–45152
- surface, (100), electron states, SCF extended tight-binding method 77–47881
- surface, electron inelastic scatt. differential cross-sections 77–76652
- surface, polished, RHEED pattern 80–65345
- surface, secondary electron emission spectrum 77–72759
- surface (110), ion implantation, heteroatom size and reactivity effect 80–44226
- surface (111), relax. and reconstruction using C_4H_9 clusters, MINDO/3 calc. 79–42356
- surface (111), surface states and relax., modelling using mol. SCF calcs. 78–39186
- surface (113), scattering factor, Bragg reflection Pendellosung interference study 80–1885
- surface electronic struct., self consistent pseudopotential calc. 78–47842
- surface soldered to metal film, contact strength determ. device 78–60910
- surface structure and interaction with gases and metals 77–72758
- suspension, particle size distrib. function, electrooptical diffusion method for determ. 80–8956
- synchrotron electron beam damage, study by optical, cathodoluminesc. and X-ray topography 80–39155
- synthesis, shock loading from graphite-metal mixtures *(Russian)* 77–90298
- synthesis *(Japanese)* 80–80994
- synthesis and characterisation 80–50580
- synthesis by graphitisation of carbon materials at high press. and temp., Ni influences 80–60795
- synthesis from graphite, nucleation rate 79–16032
- synthesis on nondiamond substrate, electron diffr. and luminesc. exam. 77–76344
- synthesis using Ni catalyst, intermed. phases of Ni-C system, satellite structures *(German)* 77–32538
- synthesis with Ni catalyst, growth mech. *(Japanese)* 77–60122
- synthetic, γ-Mn cluster existence, neutron diffr. obs. 77–89464
- synthetic, carbonado type, struct. and microhardness 78–84994
- synthetic, Co-C satellite phase, C content determ. *(German)* 77–72690
- synthetic, cryst. growth, review *(German)* 79–33926
- synthetic, disorientation of crystallite subgrains *(German)* 77–68939
- synthetic, doped electroluminescence exam. 78–6783
- synthetic, elec. cond. 78–56144
- synthetic, electroluminescence excitation mechanism, role of defects 78–52581
- synthetic, history and present status 79–33906
- synthetic, N impurity effect on strength characts. and thermal stability 80–11726
- synthetic, oxidized in fused salts, etch features 80–97604
- synthetic, polarised IR cathodolum. 80–89073
- synthetic, transition metal impurity effect on IR absorpt. 79–82980
- synthetic, X-ray exam. of inclusion 77–84788
- synthetic and natural, neutron irrad., optical and elec. props. *(Russian)* 78–59841
- synthetic diamond drills, improved durability 80–87573
- synthetic diamond external crystal morphology, SEM obs. 79–73078
- synthetic grains, dynamic calibration thermoelectrodes, grinding temp. measurement appl. 77–55985
- synthetic grits, crystal morphology of cyclic twins 80–2037
- synthetic high strength material structures, mechanical strength, microstress levels *(Russian)* 80–76334
- synthetic micropowder, degree of charging of polished Ti and Fe surfaces 78–60880
- synthetic monocrystals, inclusions phase comp., radiographic method 80–100978
- synthetic powder, thermal cond. 80–96702
- synthetic semiconductor, IR spectroscopy and cathodoluminesc. *(Ukrainian)* 79–78758
- synthetic semiconductor, p-n junction prod. and doping, I-V characts. 77–15943
- temperature field dynamics during synthesis 79–38755
- thermal conductivity, 320-450K *(French)* 78–43189
- thermal conductivity, high temp., electron irrad. effects 80–65318
- thermal conductivity at low temperature, correl. with IR absorpt. features 80–49435
- thermal conductivity measurement using thermal comparator 79–80613
- thermal conductivity of single cryst. 78–65921
- three-body abrasive wear with small size diamond abrasives 80–76373
- tool, metallic binder, microstruct. charact. by electron probe anal., SEM obs. *(Rumanian)* 79–74114
- tool, polycrystalline, wear in rock removal processes 78–64724
- tool bit machining, comparison with conventional optical process 80–69569
- trace elements in diamonds of different types 79–14838
- transformation of type IB dispersed N into type IA aggregate N 78–6089
- turned surface production, interferometric test repeatability 80–74538
- turning machine characteristics and turned surface microtopography 80–33263
- turning precision machine tool system 80–69568
- twin boundaries in synthetic crystal, obs. by optical microscopy 77–39596
- two-phonon bound state, Raman freq. 80–65179
- type I, cryst. defects of platelet nature, TEM study 79–37719
- Type I from Arkansas, Ar isotopic composition 80–94493
- type Ia, max. lattice freq., IR absorpt. spectra 80–16026
- type Ia, secondary absorpt. edge, optical study 79–19912
- type IIa, electron irradiated, annealed to high temps., EPR spectrum 77–90034
- type IIb, soft X-ray source for high resolution X-ray lithography 79–97481
- type-I, electron irrad., annealing at 800-1500°C 80–24500
- type-IIa, electron irrad., EPR spectrum 80–25210

diamond continued
- type-IIa, electron irradiated; thermal cond. reduction at low temps. 77–47631
- ultradisperse, ESR, particle size and lattice microdistortions 80–97140
- ultradisperse, obtained by high temp. synthesis in explosion, struct. 79–29003
- ultrarelativistic electron beam self acceleration probability 79–86819
- uniaxial stress splitting of E to E transitions at trigonal centres in cubic crystals 80–97312
- UV absorpt. produced by substitutional N_2 pairs 80–29770
- vacancy, mol. orbital theory of transitions 77–85757
- vacancy charge states, visible absorpt. spectrum after electron irradiation 77–90177
- valence band calculation using many-electron theory 80–15434
- valence electrons, energy-depend. photoionisation probability calc. 77–16462
- valence electrons XPS spectrum, OPW calc. 77–4715
- van Hove singularities, absorpt. and luminesc. electronic-vibr. spectra 80–70639
- vibrating suspension, defective surface layer formation on transparent materials *(Russian)* 78–53007
- vibronic bands at 2.498 eV (H4), 2.417 eV and 2.536 eV, absorpt. and luminesc. under stress 77–85758
- vibronic spectra of deep centres, changes in Van Hove singularities 77–8645
- VPE, deposition on powder from methane 77–11805
- wear during hard rock drilling, effect of chemomechanically active fluids 79–15802
- wear during hard rock drilling, effect of chemomechanically active fluids 79–15803
- wear on steel, effects of clean surface reactions 78–85008
- X-ray diffraction, three and four wave, comparison of diamond type crysts. 78–67608
- X-ray diffraction patterns, extra-reflections obs. 77–59042
- X-ray photoelectron spectra and density of states, strong-coupling method 77–28679
- X-ray source for high-resolution lithography 79–21884
- XPS anal. of Ar and ^{57}Fe ion-bombarded 77–11769
- yield stress from Hugoniot elastic limit and elastic consts. 79–83261
- zone-centre optical phonon, effect of uniaxial stress, elastic consts. determ. 78–91399
- Be-diamond support, for high-pressure X-ray diamond-anvil cell 78–30515
- C, noncrystalline conversion to diamond, diffusion conversion enhanced rate due to shock compression 80–39221
- C-C bonding, Compton profile calcs. 77–75232
- DN_3, microwave spectra, 8-340 GHz, spectrosc. consts. for ^{13}N isotope 79–85958
- Fe/Mg partitioning between coexisting olivines and orthopyroxenes *(Portuguese)* 78–65284
- Fe-C (synthetic diamond) role of diffusion of graphitisation in phase interaction 77–36449
- N_2^+ + Group IV elements and oxides, XPS and UPS prod. determ. 78–73084
- S^+ ion implantation, SiC synthesis and struct. characterisation 77–76434

diaphragms
- *see also valves*
- artificial heart, system for continuously monitoring pumping diaphragms 77–44844
- blinds with internal diaphragms, light-blocking effectiveness 79–50405
- blood pressure transistor device, high sensitivity, quasi-digital 79–79675
- contactless electropneumatic transducer parameter determ. *(Bulgarian)* 80–47045
- corrosive atm. pressure or vacuum meas. isolation chamber 77–30174
- double layer, electro-osmosis of different arrangements of layers, rel. to poles of current source 79–70373
- electrolysis cells, current yields of alkali 79–100402
- electron-optics, two-lens projection systems, reduction of third-order distortion 80–48134
- ferrite pot core pressure transducer development and compensation 79–75519
- flow meas. appl. *(Bulgarian)* 78–47077
- fluid volume evaluation in spherical vat with deformable metal diaphragm 77–57310
- gapped pot core and Permalloy foil pressure transducer 79–75520
- hydraulic characts., measurement precision 79–82004
- iris, for variable optical attenuator *(Japanese)* 79–98378
- laser cavity diffraction experiment with 1-D diaphragm 80–95920
- left ventricular assist device design and performance 79–96708
- loudspeaker's, composite, B-Ti, preparation by physical vapour deposition *(Japanese)* 80–58883
- loudspeakers, using carbon reinforced olefin polymer, with high specific modulus, flexural rigidity and loss factor *(Japanese)* 80–53596
- physiological miniature strain-gauge pressure transducers 79–100778
- pressure meas. at solid-lubricant interface, strain and deform. meas. techniques with diaphragms, comparison *(French)* 79–30453
- pressure sensors using wire strain gauges *(German)* 79–80569
- pressure-force transducer using 32.768 kHz X-Y flexure watch crystal 78–57934
- programmed camera exposure setting accuracy 79–75639
- shock tubes, use of fast-acting valves instead of diaphragm-breaking 80–24052
- unity-magnification projection system characteristics 79–27367
- variable pressure drop flowmeters, drainage coefficient reliability 77–58824
- Si diaphragm pressure sensor, integrated signal conditioning 80–76859

dichroism
- *see also magnetic circular dichroism; pleochroism*
- absorbing anisotropic and gyrotropic slab between crossed polarisers, transmitted intensity patterns 80–78762
- absorbing crystal, appearance of optical activity and circular dichroism, theory 77–63390
- acetaldehyde, dichroic effects, computational expts. 80–83424
- acridine C-radical, polarised absorpt. and ESR spectra, dichroism and HF-CI calc. 78–50563
- actinomycin-DNA bindings, first-neighbour specificities, circular dichroism 78–3442
- activated crystals, Jahn-Teller effect in optical bands of impurity centres 78–6706

dichroism continued
adipic acid, monoclinic crystals, IR absorption and dichroism 78−88293
adrenocorticotropic hormone polypeptide chain left helical conform., aqueous soln. 77−70414
alanine-d_3, vibr. circ. dichroism, mechanism 78−33505
alcohols, chiral, circular dichroism, RPA calc. 79−36672
alkali halide phosphors, Tl^+ doped, uniaxial stress effects 78−48202
alkali halide photodichroic crystals use for coherent opt. data processing 77−68248
alkali halides, linear dichroism spectra, stress-induced, reorientation of O_2^- and NO_2^- impurity ions *(Russian)* 80−45127
alkali halides, photodichroic, as optical processing elements 78−83056
alkali metal atom, heavy, polarised, circ. dichroism of ang. distrib. of photoelectrons 80−37789
alkali silicate:Nd_2O_3 glasses, coloured, dichroism *(Polish)* 79−99919
p-alkoxybenzylidene-p,n-butylanilines, IR absorpt. spectra, elec. field effects, orientational order parameter determ. by IR dichroism 80−80778
p-alkoxybenzylidene-p-aminocyanoanilines, IR absorpt. spectra, elec. field effect, orientational order parameter determ. by IR dichroism 80−80777
amino acid photoresolution, rel. to origin of optical activity in life 77−40634
anthracene, 340-310 nm absorption spectrum dichroism, masked ^1L_b-$^1A_1$ transition 78−17685
anthracene, dispersed in stretched PVC, dichroic meas. of orientation 77−30867
anthracene, orientated in nematic liq. cryst., UV-visible dichroism meas. *(German)* 77−34668
anthracene, orientation in polyethylene film, linear dichroism 78−29864
anthracene in PVC film, photodichroism at 257 and 383 nm 79−31539
anthracene-β-sulphonic acid, 340-310 nm absorption spectrum dichroism, masked ^1L_b-$^1A_1$ transition 78−17685
atomic degenerate system, Doppler-free laser-induced dichroism and birefringence 78−82711
atomic resonant lines, ang. momentum depend. of laser-induced birefr. and dichroism 79−10367
ATPase, Ca^{2+}-activated, of sarcoplasmic reticulum, rot. motion and evidence for oligomeric structs. 80−72124
p-azoxyanisole, orientated in nematic liq. crysts., UV-visible dichroism meas. *(German)* 77−34668
azulene, induced circular dichroism of π-π^* bands in presence of (+)-nopinone 80−53058
bacteriochlorophyll electronic transition moment directions 79−100572
bacteriorhodopsin phototransients, circular dichroism meas., comment 78−21954
bacteriorhodopsin reorientation due to elec. field 77−66789
benzene, excited state props., by electrochromism in polymer matrix 79−22737
benzil, optical activity and circular dichroism 79−61328
1,1′-bianthryl derivatives, dimer optical activity, vibronic circ. dichroism, theoretical anal. 78−62821
1,1′-bianthryl derivatives, theoretical analysis of UV, circular dichroism and optical rotating dispersion vibronic spectra 77−34652
bianthryls, vibronic anal. of circular dichroism and absorption spectra 77−38683
biaryls, dimer optical activity, vibronic circ. dichroism, theoretical anal. 78−62821
biaryls, model, mol. vibronic circular dichroism 78−37665
1,1′-binaphthyl, conformational changes, picosec. dynamics 78−25625
biopolymers, circular dichroism, optical rotatory dispersion, conformational anal., review 77−3497
biopolymers, studied by circular dichroism and optical rot., review 78−44457
birefringence modulator devices for sensitive polarisation determ. 78−8437
Born-Oppenheimer approx., IR absorption, circ. dichroism using vibronic gauge function 78−967
Bowman-Birk soybean proteinase inhibitor, gamma irrad. 78−53343
butadiene chromophores, cis- and trans- (α- and β-phellandrene) absorpt. and CD spectra 78−62834
caesium tartrate, optical rot. dispersion, dichroism and spectra, in soln. and cryst. *(Russian)* 77−90124
calibration apparatus for dichrograph 185 to 600 nm 77−5886
(X)-D-camphor, circularly dichroic band at 3000 Å, RPA calc. 78−94267
d-10-camphorsulphonic acid ammonium salts, characts. rel. to spectropolarimetry 77−24816
β-carotene, orientated in nematic liq. crysts., UV-visible dichroism meas. *(German)* 77−34668
β-carotene, solubilised in lecithin liposomes, linear dichroism, absorption statistics 78−1014
cellulose hydrated film, orientational heterogeneity, IR spectra and dichroism obs. *(Russian)* 78−38990
cellulose macromolecule, conform. states and IR dichroism calcs. 80−55986
cetyltrimethylammonium bromide, micellar soln., internal elec. fields, linear dichroism obs. 77−86325
chalcogenide vitreous semicond. films, photoinduced optical anisotropy, spectral responses 79−65948
chiral biomolecules, temp.-jump relaxation studies, transient CD meas. 78−5372
chiral compound, circular dichroism, polarisation modulated photoacoustic spectroscopy 80−18018
chiral molecule, interference effects, natural dichroism line shape 78−82758
trans-1,4-chlorobromocyclohexane, liquid, crystalline and amorphous state, conformation and vibr. spectra, IR obs. 80−60568
trans-1,4-chloroiodocyclohexane, liquid, crystalline and amorphous state, conformation and vibr. spectra, IR obs. 80−60568
chlorophyll a and protochlorophyll a, optical transitions anisotropy 79−43825
chlorophyll pigments, aggregated forms in soln., spectral-luminesc. characts. *(Russian)* 78−23529
chloroplasts and subchloroplast fractions, linear dichroism 77−90744
cholesteric films, absorpt. and contrast in dichroic liq. cryst. displays 80−75155
cholesteric liquid crystal, gyrotropy, depend. on thickness of layer 77−40204
cholesteric liquid crystal, struct. charact. from opt. circ. dichroism 77−62476

dichroism continued
cholesteric liquid crystals, gyrotropy, region of electron absorption bands 78−10866
cholesteryl alkanoates, orientational order, spectral depend. of circular dichroism 78−26437
cholesteryl nonanoate, polymorphism of blue phase, circular dichroism at high-press. 79−37821
cholesterylalkanoates, liq. cryst., optical anisotropy and struct. ordering *(Russian)* 78−87616
chromophone aggregates in Frenkel exciton model, dynamic perturbation effects on circular dichroism intensity 80−93273
chromophore aggregates, circular dichroism spectra, calc. involving band shape 78−46478
chromophore aggregates, optical absorpt. and circular dichroism spectra, degenerate ground state model 79−70523
chromophore orientation in micellar, liposome solns., liq. cryst. phases, dichroism, NMR 79−53059
chromophores, circular dichroism, dipole approx. 77−71795
circular, for scattering objects, examination using double-beam spectrophotometer 79−35853
circular dichroism in presence of birefr. and linear dichroism, meas. method 78−27178
circular dichroism instrum. for use with standard rapid reaction techniques, conversion from Cary 60 spectropolarimeter 80−52296
circular dichroism meas. in vacuum UV 78−49913
circular dichroism of phototransients, meas. apparatus using modulation excitation 77−46656
circular dichroism spectrophotometer, near IR, microprocessor controlled 80−22454
circular differential photoacoustic spectroscopy 80−47114
classical coupled dipole oscillators, optical props., normal mode treatment 79−36611
collagen, enzyme- and alkaline-soluble, optical rot. dispersion and circular dichroism 77−70411
colloid, dichroism in homogeneous elec. field 79−8122
colloidal particles, intrinsic optical anisotropy, anomalous diffr. approx. 80−53213
complex, (E+A)*e systems, Jahn-Teller, pseudo Jahn-Teller coupling and circular dichroism 79−68247
composite thermal/visual display superposition technique 78−77992
condensed phases, picosec. relax. polarisation spectrosc. meas. 78−68530
conjugated molecules, linear and mag. cir. dichroism interpretation 78−62835
cyanine dye sensitisers, J-aggregates, circular dichroism and induced Cotton effect 77−70319
cyanine dye sensitisers, J-aggregates, meso substituents effect on mol. assoc. 77−70320
cyanine dyes, J-aggregates, swirl-induced optical activity 78−72482
cyclic ketones, electrochromism and electric dichroism for studying transitions to second excited singlet 80−63692
β-cyclodextrin-azulene complex, circular dichroism spectra 78−58713
cylinder, optically active, EM wave scatt. 78−82912
decyloxybenzoic acid, vibr. bands., IR dichroism, phase change effects *(Russian)* 78−15174
dichrograph, control unit construction 78−21122
dichroic colloidal particles, size distrib. determ. by electro-optical method 79−6087
differential absorption at high modulation frequencies using a Fourier transform infrared spectrometer 80−95160
L-β-3,4-dihydroxyphenyl-α-alanine with L-glutamic acid, polymers and copolymers, synthesis and conform. 79−33996
dimethylammonium cadmium tetrachloride, far IR refractive index, extinction coeff. and dichroism obs. 80−66144
3,6-diphenyl-pyridazine, valence electronic structure 79−72360
3,6-diphenyl-s-tetrazine, valence electronic structure 79−72360
disperse system, dilute, orientationally induced conservative dichroism 80−102623
disperse systems, electro-optical phenomena, induced dichroism rel. to elec. field calc. 78−50699
dispersion induced circular dichroism, determ, of mag. dipole allowed transitions 80−14163
dispersion induced circular dichroism, spectroscopic appls. 77−27101
dispersion-induced, new theory of olfaction 77−56393
DNA, dye labelled elec. dichroism and birefringence, comparison with mol. props. from polarised fluoresc. 80−84785
DNA, Hg (II) and Ag (I) complexes in soln., theoret. interpret. of elec. dichroism obs. 80−85347
DNA, linear dichroism in pulsed elec. field, meas. apparatus 80−90875
DNA, monodisperse, rod-like mols,, transient elec. dichroism 78−94344
DNA-adduct systems, binding geometry, determ. by induced circ. dichroism 80−55988
Doppler-free intracavity polarization spectroscopy using elliptically polarized light 80−5537
dye solution, induced birefringence as result of illumination dichroism 79−28709
dyes, rot. diffusion of prolate, oblate mols. from absorpt. relax. 80−1008
EBBA, IR absorpt. spectra, elec. field effects, orientational order parameter determ. by IR dichroism, bend elastic consts. 80−80778
EBBA, orientational order in glassy and nematic phases, IR dichroism meas. 80−64891
electric circular dichroism in optically active fluid 79−19862
electric dichroism measurement instrument with digital processing 80−82800
electric dichroism spectroscopy 78−1013
electronic spectra of molecules, pure elec. quadrupole transition polaris. 80−63691
erythrosine B, dye soln., transient dichroism, rot. diffusion anomalies 79−87414
ethylenediamine sulfate, cryst., induced gyrotropy of CrO_4^{2-} ion 80−108175
ferricytochrome c structure, effect of different phospholipids 78−68981
ferrites, EM wave effects on mag. and optical props., lecture 78−27031
ferroelectric, large-gap type, vibronic theory and opt. props., anomalous bulk photovoltaic effect 80−103939
fluorescence detected circular dichroism, direction dependent opt. activity of photoselection 77−36279
fluorescence detected circular dichroism, theory 77−30914
form dichroism, theoretical treatment, determ. of macromol. shape 78−60417
Fourier transform IR vibrational circular dichroism 79−99845

dichroism continued
- Fourier transform spectroscopy-differential interferometery meas. 79—71514
- free particle on helix, light circular dichroism and optical rotation, theoretical anal. 80—66146
- garnets, doped, site symm. exam., ang. variation of induced linear dichroism 78—95429
- garnets, photoinduced phenomena 79—99718
- gas, anisotropy in strong EM field 79—98434
- gas, nonlinearly absorbing medium, light-induced optical activity 79—72615
- gas, reson. optical activity induced by right-left nonsymm. mol. collisions 78—75254
- gelatin-Pd II complex formation, circular dichroism and absorpt. spectra meas. 79—61881
- graphite, suspensions, particle shape influence on light absorpt. in mag. field 80—60549
- helical wormlike chain, dipole moment, elec. birefringence, elec. dichroism, statistical mech. calcs. 80—14262
- n-heptyl cyanobiphenyl, near IR dichroic spectrum, using unpolarised radiation 78—27201
- 4-n-heptyl-4′-cyanobiphenyl, linear dichroism spectra in nematic and isotropic phases 80—25336
- histone H4 N-terminal oligopeptide struct., circular dichroism and IR spectroscopy 78—24025
- histones, conform. state in water, circular dichroism 77—56335
- HOAB-DOBAMBC nonchiral-chiral smectic C mixture, spontaneous polarization and induced circular dichroism 79—27910
- 2-hydroxytropone, in β-cyclodextrin complex, UV circ. dichroism spectrum assignments, complex struct. 78—46358
- III-V semiconductors, linear circular dichroism near the two-photon absorpt. edge 79—61334
- image difference detection using the Weigert effect 79—81376
- indole, oriented in polyethylene film, dichroism spectrum 79—54864
- insulin and analogue, side-chain mobility and tyrosyl circular dichroism 78—15770
- isotropic medium, moments of optical rotary power and circular dichroism 80—88956
- Jahn-Teller centre optical band polarisation dichroism, forbidden transitions 80—55062
- Jahn-Teller impurity centre, electroabsorption moments 77—48205
- KI, linear dichroism spectra, stress-induced, reorientation of O_2^- and NO_2^- impurity ions *(Russian)* 80—45127
- lactams, optical rot. strength, sector rules 78—17737
- lactones, optical rot. strength, sector rules 78—17737
- laser-induced amplitude and phase gratings, transient dichroism signal 79—94302
- laser-induced circ. dichroism, quantum electrodynamical anal. 77—75193
- laser-induced optical activity, QED theory of multiphoton processes 79—31794
- linear dichroic polarisers, spectral props. and appls. 77—46809
- linear dichroism in pulsed elec. field, meas. apparatus 80—90875
- linear dichroism meas. over large wavelength ranges 80—98962
- linear dichroism measurement, appl. of polarisation scrambling using photoelastic modulator 78—4683
- linear dichroism spectroscopy, and its applications 78—1011
- linear dichroism spectroscopy for mol. orientation in model membrane systems 78—29864
- lipid lamellar liquid crystalline systems, orientation studies of probe molecules by linear dichroism 77—90718
- liquid, symmetric mols., anisotropic light scatt., correlation function calc. 77—12356
- liquid crystal, dichroic dyes for guest-host interactions 77—59554
- liquid crystal display, with dichroic dye guest, field-induced colour switching 80—1327
- liquid crystal matrix, orientational distrib. coeffs. from UV and circular dichroism meas. 80—92452
- liquid crystals, cholesteric, Bragg diffraction, light Pendellosung fringes, theory 77—27830
- liquid crystals, guest-host interaction, optical shutter appl. 78—74988
- macromolecular, solutions, mol. orientation, time-depend. torque, rot. diffusion eqn. 78—68471
- macromolecular rapid circular dichroism meas. with small gas lasers 77—37968
- macromolecule, circular dichroism, exciton dimer and helix-free particle absorption 79—94116
- magnetic colloids, birefringence and dichroism, magnetically-induced, sign inversion 80—60548
- magnetic fluids, optical birefr. and dichroism in mag. field 80—60547
- magnetic materials, transparent, optical studies of phase transitions 77—66481
- magnetically induced linear optical birefringence and dichroism in colloidal dispersions 78—8431
- MBBA, electronic spectra 78—52530
- MBBA, IR absorpt. spectra, elec. field effects, orientational order parameter determ. by IR dichroism, bend elastic consts. 80—80778
- MBBA, orientational order in glassy and nematic phases, IR dichroism meas. 80—64891
- β-melanocyte stimulating hormone and β-lipotropic hormone fraction, spectral study 77—36863
- 1-methylindan, circular dichroism, rot. strengths, CNDO/S calc. 79—3452
- molecular dimers, circ. dichroism spectra, quadratic vibronic coupling effect 79—76402
- molecular orientation, extensional effects, IR obs. 77—23591
- molecular vibrational circular dichroism, anharmonic effects 78—29769
- molecule, electric circ. dichroism, QED 78—37666
- molecule, electric circular dichroism, QED 79—22738
- molecule, moment summation method 77—27102
- Mossbauer rays, polarised 80—7201
- multi-sample wheel for far-infrared dichroism measurements 80—47086
- β-naphthol, IR dichroic ratio, oriented gas and effective charge models calcs. 78—60437
- nematic liquid crystal appl. as anisotropic solvents in optical absorpt. spectroscopy, band polarisation determ. 77—42344
- p-nitrotoluene, in nematic mixture of octyl cyanobiphenyl, octyloxy cyanobiphenyl, dichroic exam. 78—27201
- nucleic acid optical measurements in presence of phenol and protein impurities 77—56546
- optical linear dichroism meas., single-beam microspectrophotometer 80—37097

dichroism continued
- optical waveguides, slab-type, mode coupling via dichroic absorpt. of M centres 80—33178
- optically active crystal, modulated polaris. spectra 78—23429
- organic molecules, electronic transitions polaris. determ. by dichroism in nematic solvents 77—42344
- Orientational optic effects from above Rayleigh particles 80—106453
- oriented circular dichroism DNA [-] dichroism [DNA, oriented circular dichroism meas.] meas. 80—55060
- oxazine dyes, orientation of $S_1 \rightarrow S_n$ transition moments, continuous ps photometry 79—10152
- oxy- and deoxyhaemoglobin, optical spectra, dichroism 79—20514
- 2-oxyphenylbenzoxazol, proton intramolecular transfer, light absorpt. and emission, dichroism, polarised fluoresc. 80—87166
- parametric transformation of light polarisation in crystals 78—1153
- partially oriented molecules, uniaxial, two-photon processes, polarised spectrosc. 80—74209
- PCP, oriented swollen soln., IR dichroism, short-range orient. order *(Russian)* 79—51941
- peptides, optical rot strength, sector rules 78—17737
- phase modulation spectrophotometer, for polarisation spectroscopy, optical calculi 78—45715
- (+)-(S)-2-phenyl-3,3-dimethylbutane, optical activity, circular dichroism, polarisability model 80—43082
- phenylalanine, and derivatives, circ. dichroism and mag. circ. dichroism 79—87418
- photoacoustic spectroscopy, dichroism meas. 78—62227
- photoanisotropic materials for polarisational holographic recording 77—75443
- photodichroic materials, computer polarisation holography appl. 78—42299
- photodichroic materials as coherent optical computing elements 77—71962
- photodichroic spatial light modulator for joint Fourier transform correlation 80—106617
- photoreceptor form dichroism in vertebrates 78—56969
- photosynthetic bacterium Chromatium minutissimum, linear dichroism of oriented chromatophores and pigment-protein complexes 80—35841
- photosynthetic membrane, optical and electrochromic props., chloroplast chlorophyll orientation 77—48763
- pigment associations, conc. effects, luminesc., absorpt. spectra and dichroism obs. 80—1007
- pigment molecule organisation and interaction in reaction centres of Rhodopseudomonas viridis 80—35843
- planar molecule, oriented in transparent polymer films, dichroism of absorpt. bands *(Russian)* 79—31506
- planar molecules in stretched polymer films, solute orientation, transition moment direction, dichroic spectra 78—58742
- plasma protein interaction with polyion complex studied by circular dichroism and UV spectroscopy *(Japanese)* 80—12316
- polarimeter for reflected or transmitted light 77—74487
- polarisation 80—9573
- polarisation spectroscopy, Doppler free intracavity 80—52335
- polarised light in chemistry, linear, circular and vibr. circular dichroism 77—45896
- Polaroid, X-ray optical props. determ. using novel X-ray polarimeter 79—6251
- polaroids for sub-mm. range based on dichroic crystals 78—5555
- poly(vinylidene fluoride) orientation, solid state deformation by coextrusion 80—40394
- poly O-carbobenzoxyl-L-tyrosine, in soln., conformation, helix-coil transition, circular dichroism, NMR spectra 77—31037
- poly-β-benzyl-L-aspartate films, circular dichroism, IR spectra, α, β, ω conforms. 77—48197
- polycarbonate, glassy, IR dichroism at small strains 78—56475
- polydisperse system, rotatory diffusion const., electro- optic decay curve, size distrib. 78—20079
- polyethylene, polarised Raman studies of crystalline and amorphous orientation 78—67660
- polyethylene, stretched, linear dichroism of aromatic molecules 77—88480
- polyethylene film, drawn, dielec. breakdown and morphological struct., dichroic ratio 80—25813
- polyethylene stretched, film, effects of vapour phase application of compounds 77—90276
- polymer, infinite helical, classical theory of circ. dichroism 77—65550
- polymer, magneto-optical props., MCD, Frenkel exciton model 78—10873
- polymer film, proton intramolecular transfer, light absorpt. and emission, dichroism, polarised fluoresc. 80—87166
- polymer film, stretched, interpretation of polarised absorption and emission spectra of molecules 78—1012
- polymer film, stretched, mol. distrib. determ. by polarised spectra 78—27298
- polymer films stretched, orientation and transition moment directions of small planar molecules 78—1015
- polymer orientation measurement, in solid, by spectroscopic techniques, mech. anisotropy 78—75558
- polymer solution, short-range solvent orientational order, IR dichroism and photoelasticity obs. *(Russian)* 78—26415
- polymers, synthetic, chiral, with aromatic side chains, conform. from circ. dichroism 79—55014
- polynucleotide, double-stranded, conform. inhomogeneity of sugar-phosphate chain rel. to compact particle optical activity 80—35839
- polynucleotide solution, elec. field induced orientation and effects 80—85348
- polypeptide monolayers, circ. dichroism 79—74598
- polypeptides, 3_1 helix-coil transition, circular dichroism obs. 78—35795
- polypeptides, α-helical, π-π^* absorpt. and circular dichroism spectra 80—23398
- polypeptides, poly-L-lysine based, comb-like, struct., physicochem. props. *(Russian)* 79—55644
- polypeptides, unordered, circular dichroism, Green operator method 77—14467
- polyproline, optical activity rel. to ordered aggregation 79—11899
- polypropylene, mag. polarisation, optical studies 80—55013
- polypropylene monofilaments, tensile props., orientation degree depend., IR dichroism obs. 78—3163
- polystyrene, atactic, uniaxially oriented, Fourier transform IR spectroscopic exam. 80—25360

dichroism continued
polytetramethylene oxide-polytetramethylene terephthalate, block copolymer, props. 78—51438
polyvinylidene fluoride films, stretched and rolled, electrostriction and piezoelectric effects *(Japanese)* 80—55041
poly[(R)-oxypropylene], opt. rot. dispersion and vac. UV circular dichroism 80—40084
prealbumin, human, struct., X-ray diffr., amino acid sequence, circular dichroism meas., comparison 77—42450
prealbumin, human plasma, secondary struct. refinement from circular dichroism data 78—27888
pressure jump method for fast kinetics using optical rotation and circular dichroism 78—77175
N-p-propoxybenzylidene-p-pentylaniline, orientational order in glassy and nematic phases, IR dichroism meas. 80—64891
propyleneimine, circular dichroism, optically active Rydberg transitions 77—18952
pseudoisocyanine bound by sulphated polysaccharides, dil. aq. soln., visible and circular dichroism spectra 80—45107
purple membrane fragment suspensions, elec. dichroism obs., trimer model interpret. 80—89728
purple membrane structure, effects of bleaching and regeneration, H-halobium 77—86532
PVC, stretched at various elongation degrees, dichroic meas. of anthracene orientation 77—30867
pyrazine, dispersion induced circular dichroism, determ, of mag. dipole allowed transitions 80—14163
pyrene, orientated in nematic liq. crysts., UV-visible dichroism meas. *(German)* 77—34668
pyridine, dispersion induced circular dichroism, determ, of mag. dipole allowed transitions 80—14163
pyrylium dye J-aggregate species, circular dichroism spectropolarimetric characts. 79—3456
rare earth orthoferrite, linear dichroism influence on Faraday effect 80—2737
resonance medium, induced dichroism and gyrotropy 80—9971
rhodamine, dye soln., photoinduced dichroism and vibronic relax. 77—14465
rhodopsin, bovine, conform. in situ and solubilised with detergent 77—44587
riboflavin, transition moments in 300 nm region 79—53042
ribosomal protein S4 from Escherichia coli, circular dichroism obs. of conformation 78—96003
ring laser, emission spectrum control by mag. field induced phase anisotropy of active medium 79—94264
rod external segment surface membrane, lateral diffusion of rhodopsin 78—15828
rubidium tartrate, optical rot. dispersion, dichroism and spectra, in soln. and cryst. *(Russian)* 77—90124
ruby, optically-pumped, excited-state Raman processes 79—4798
SHG, consecutively disposed crysts. optimisation *(Russian)* 77—7158
silicate glass surface, photodichroic for laser recording 80—102785
silicate glasses, radiation coloured, photoinduced dichroism 79—69808
sodium uranyl acetate, absorpt. spectra, MCD and natural dichroism, UV and visible 79—69853
sodium uranyl acetate, fluoresc., circ. dichroism 79—38598
solid-state circular dichroism spectra, phase modulation spectrosc. obs. 80—93271
solute orientation in stretched polymer matrix, dichroism anal. 80—75998
solutes in stretched polymers, linear dichroism methods for analysis 80—63693
spectral shared aperture beam splitter for high-energy laser systems 80—14477
spectroscopy, circular dichroism sum rules, SCF mol. orbital theory 78—58059
Stokes parameters, of light beam, polarisation modulation meas. 79—21803
suspension of absorbing particles, simultaneous meas. of dichroism and birefringence in elec. field., photocurrent signal obs. 80—82801
p-terphenyl, valence electronic structure 79—72360
tetraphenylporphyrin, dispersion induced circular dichroism, determ, of mag. dipole allowed transitions 80—14163
time-dependent birefringence, linear dichroism, and optical rotation resulting from rigid-body rotational diffusion 79—47411
transition metal complexes, mol. dissymmetry, book 80—27057
2,4,6-trimethyl pyridine-N-oxide, linear dichroism in liq. cryst. matrix, out-of-plane components 78—17701
twisted anisotropic media, light propag., appl. to photoreceptors 78—63004
two-level atom gas, optically induced optical activity 79—18490
uranyl acetates, cubic crysts., optical spectra fine struct. 77—1693
uranyl propionates, cubic crysts., optical spectra fine struct. 77—1693
UV microscope for polarised light, determ. of birefringence, linear dichroism and optical rotary dispersion *(German)* 78—29152
vacuum UV circular dichroism instrument improvement 77—49786
vacuum UV circular dicroism spectroscopy using synchrotron radiation 80—91575
vanadyl bisacetylacetonate, polarised X-ray absorption and double refraction 80—50459
vibrational circular dichroism, vibronic interaction theory 78—46380
vibrational circular dichroism in the mid-infrared 80—87157
vibrational circular dichroism spectrometer, using CaF_2 photoelastic modulator and Xe lamp 78—54476
vibrational circular dichroism theory, localised mol. orbital model 77—75192
visual excitation, mol. mechanism for initial process, optical activity in rhodopsin and bathorhodopsin 77—52783
vitamin B_{12}, circular dichroism and birefringence, polarisation modulation meas. 79—21803
volume amplitude holograms in photodichroic materials 78—17871
X-irrad., optical absorpt. spectra and dichroism meas. 80—108239
xanthrene, dye soln., transient dichroism, rot. diffusion anomalies 79—87414
Ag halide emulsions, induced sensitized photodichroism 80—9061
Ag halide photochromic glasses, optical absorp. of Ag, optically induced dichroism 80—108177
Ag halide thin-film optical recording medium 80—102786
Ag-AgCl emulsion, anisotropy induced by two coherent perpendicular light vibrs. 79—55196
Ag-AgCl films, photoinduced dichroism *(Russian)* 79—56878

dichroism continued
Ag-AgI film, photoinduced dichroism *(Russian)* 77—1743
Ag-AgI island granular film, Weigert effect, anomalous dichroism 77—12455
Ag-AgX films, (X=Br,Cl,I), Weigert effect 79—64298
Ag-containing glasses, colour adaptation, photoinduced optical anisotropy 79—61331
AgCl emulsion, anisotropy induced by two incoherent and perpendicular light vibrs. 79—41428
AgCl emulsion, spatial differentiation, of intensity distrib., using Weigert effect 79—81377
AlN epitaxial films, optical props. in vac. UV region 79—56872
α-Al_2O_3:Co^{3+}, local deform. due to uniaxial stress 80—34140
α-Al_2O_3:Cr^{3+}, local deform. due to uniaxial stress 80—34140
α-Al_2O_3:Cr^{3+}, stress-induced linear dichroism in $^3A_2(^3T_1)\rightarrow{}^3T_2$ transition, Jahn-Teller effect 80—34884
α-Al_2O_3:V^{3+}, local deform. due to uniaxial stress 80—34140
α-Al_2O_3:V^{3+}, stress-induced linear dichroism in $^3A_2(^3T_1)\rightarrow{}^3T_2$ transition, Jahn-Teller effect 80—34884
As_2S_3, electron beam deposited film, photoinduced birefringence and dichroism *(Russian)* 78—2934
As_2S_3 suspension dispersed in gelatin, photoinduced dichroism 79—98453
$AsSeI_{0.3}$, chalcogenide vitreous semiconductors, reversible photoinduced changes in optical, physicochem. and contact props. 79—24378
$BaMnF_4$, struct. phase transition, optical parameters obs. 80—100328
$BaTiO_3$, vibronic theory and opt. props. 80—103939
CS_2, excited state props., by electrochromism in polymer matrix 79—22737
CaF_2, additively coloured, new type of F_3-centre, absorption bands obs. 78—35172
CaF_2:Co, X-irrad., F-centre form., optical absorpt. spectra and dichroism obs. 79—42998
CaF_2:Ni, X-irrad., optical absorpt. spectra and dichroism meas. 80—108239
CaF_2:R^{3+}, dichroism, elec. field effects *(Russian)* 77—24823
CaF_2:Sm^{2+}(Eu^{2+}), cubic crysts., vibronic spectra, induced dichroism method 77—81131
CaO, ODMR and spin coherences in phosphorescent state of exchange-coupled F^+-centre pairs 79—87336
$CdCr_2Se_4$ film, mag. linear and circular dichroism and Faraday rot. 79—99966
CdS, linear-circular three-photon dichroism 79—51930
CdTe and CdTe:Cl, semi-insulating, electroabsorpt. by impurities and defects, dichroism 77—40270
Co complex, $C0(l\text{-spartein})Cl_2$, IR circular dichroism spectra, vibr.-electronic interaction 80—55074
Co complex, circ, dichroism of Co(III) complex d-d transitions *(Japanese)* 78—13555
Co complex, $\Lambda(+)[Co(en)_3]^{3+}$, quadrupole transition circ. dichroism, production mechanism 79—3428
$CoCO_3$, weak ferromagnet, light absorpt. dichroism and mag. config. *(Russian)* 79—87457
$CoCO_3$, weakly ferromag., light absorpt. dichroism and mag. config. 80—66223
Cr complex, $(-)_D$-tris(ethylenediamine) chromium (III), solid-state circular dichroism spectra, phase modulation spectrosc. obs. 80—93271
Cr complexes, circ. dichroism of Cr(III) complex d-d transitions *(Japanese)* 78—13555
$Cr(CO)_6$, linear dichroism, distortion and local field contribs. 79—87415
CrO_2 acicular particle suspensions, mag. props., optical meas. 80—44874
Cs, forbidden M1 transitions, parity nonconserving effects 78—21844
CsBr, linear dichroism spectra, stress-induced, reorientation of O_2^- and NO_2^- impurity ions *(Russian)* 80—45127
CsBr:Cu^-, excitation and absorpt. spectra 80—108255
$CsFeCl_3$, linear chain ferromag., optical absorpt. and dichroism in mag. field 77—77237
CsI, linear dichroism spectra, stress-induced, reorientation of O_2^- and NO_2^- impurity ions *(Russian)* 80—45127
CsI:Na, tunnelling recomb. of electron-hole pair, optical detection of ESR and circ. dichroism 79—47360
CsI:Na, X-ray irradiated, optical and ESR studies in IR absorption band 80—80828
CsI(Br)(Cl):Tl, $[X_2^-]$ centre dynamic props. 79—65730
$CsNiF_3$, field depend. mag. behaviour, mag. linear dichroism 79—73903
$CsUO_2(NO_3)_3$, absorpt. spectra, MCD and natural dichroism, UV and visible 79—69853
Cu complex, bis-L-tyrosinato copper(II) complex, electronic spectra and dichroism 79—41183
Cu complexes, electronic transitions polaris. determ. by dichroism in nematic solvents 77—42344
Cu-Cd-Cl stretched photochromic glass, polorisation effects 79—95729
Cu(II) complexes, electronic transitions, dispersion induced circular dichroism spectra 77—27101
Cu_2O, energy band interactions under uniaxial compression 80—25412
DNA, linear dichroism, strand separation determ. 79—62188
$DyFeO_3$; linear dichroism influence on Faraday effect 80—2737
Eu chalcogenides, paramagnetic, optical orientation of 4f electrons 77—69799
EuS, ferromag. semicond. film, Hanle effect, optical orientation time consts. meas. 77—40214
Fe film, evaporated at oblique incidence, optical and mag. anisotropies 80—7134
$FeBO_3$, mag. linear dichroism and absorpt. spectra, Jahn-Teller effect 80—54662
$FeBO_3$, mag. linear dichroism and absorpt. spectra, exciton-magnon absorpt. mechanism 80—66160
Fe_3BO_6, Faraday rotation and birefringence 80—100650
$Fe(ClO_4)_2.6H_2O$, single cryst. polarised opt. spectra 77—48188
γ-Fe_2O_3:Cr, pure and doped, acicular particle suspensions, mag. props., optical meas. 80—44874
GaSe, anisotropy effects on electroreflectance spectra at oblique incidence 77—52042
GaSe, optical orientation and free exciton alignment on reson. excitation *(Russian)* 77—69812
Hg_2Cl_2, cryst., birefringence and dichroism, 200-500 nm and far IR 78—27257
I polariser, for liquid crystal display 77—46807
I_2, high-dispersion polarisation-labelled spectrum 80—990
InAs, three-photon absorption, transition effects *(Russian)* 78—35147
KBr, cation defects creation mechanism 80—75224

- **dichroism** continued
  - KBr, colour centre form. under polarised UV irrad., dichroism in absorption spectra 80—107232
  - KBr, F_2 centres triplet state, radiative and nonradiative decay 79—11438
  - KBr, linear dichroism spectra, stress-induced, reorientation of O_2^- and NO_2^- impurity ions *(Russian)* 80—45127
  - $KBr:H^-$, U-centre absorpt. band shape, piezodichroism dispersion curve and electron-phonon interaction 77—24873
  - KCl and $KCl:NO_2$, X-irrad. crysts., Cl_3^- centres photodissoc., optical anisotropy and creation mechanisms *(Russian)* 80—66235
  - KCl, diffr. by M-centres, thick plane wave hologram recording 77—7021
  - KCl, hologram recording by photodichroic F_A centres at room temp. 77—34846
  - KCl, linear dichroism spectra, stress-induced, reorientation of O_2^- and NO_2^- impurity ions *(Russian)* 80—45127
  - $KCl:Cu^-$ excitation and absorpt. spectra 80—108255
  - KCl:H, dichroic H- and U-centres by polarised bleaching of interstitial H 80—29766
  - KCl:I crystals, V-band development using X-rays 78—88337
  - KCl:Li, $(F_2^+)_A$ centres, optical props. 80—89026
  - KCl:LiCl photodichroic crystals as adaptive spatial filters 79—72713
  - KCl:Na, absorption from relaxed excited state by F_A and F_B centres 77—44031
  - KCl:Na, photodichroic holographic recording, polarisation sensitivity 78—29911
  - KCl:Na, photoinduced reorientation of A-centres near room temp. 78—64344
  - K_2CuF_4, 2-D ferromagnet, optical and magneto-optical props. 77—52062
  - K_2CuF_4, two-dimens. ferromag., magneto-optical props., absorpt., MCD and MLD 79—87419
  - KF:LiF, photodichroic, real time recording medium, for optical spectrum analyzer 78—71174
  - KF:LiF photodichroic crystals as adaptive spatial filters 79—72713
  - $KFeCl_3$, linear chain ferromag., optical absorpt. and dichroism in mag. field 77—77237
  - KH_2PO_4 crystal, optical activity 80—71373
  - KI crystals, containing excess of halogen, V-centres *(Japanese)* 77—59596
  - $KI:Tl^+$, phosphor, anomalous stress-induced dichroism 79—4828
  - $KI\text{-}KCl:Cu^+$ mixed cryst., off-centre Cu^+ 79—65112
  - $KLiSO_4:(Cr)$, uniaxial crysts., circular dichroism and optical activity 80—45029
  - $KMgF_3:Co^{2+}$, MCD and linear dichroism, 3d→4s transitions 79—56768
  - $KMgF_3:Mn^{2+}$, MCD and linear dichroism, 3d→4s transitions 79—56768
  - $KMgF_3:V^{2+}$, MCD and linear dichroism, 3d→4s transitions 79—56768
  - $LaNbO_4:Eu^{3+}$, single cryst., photoluminesc. obs., vibronic transition dichroism 77—69890
  - LiF:Mg,Ti, optically induced dichroism of Z_2-centres 79—28710
  - $LiNbO_3$, pure and Fe doped, photorefraction kinetics under irradiation and heating 79—42934
  - $LiNbO_3:Co$, optical props. 78—64383
  - $MgF_2:Co^{2+}$, MCD and linear dichroism, 3d→4s transitions 79—56768
  - $MgF_2:Mn^{2+}$, MCD and linear dichroism, 3d→4s transitions 79—56768
  - $MgF_2:V^{2+}$, MCD and linear dichroism, 3d→4s transitions 79—56768
  - MgO, electron irrad., V^--centres, stress-induced optical dichroism, absorpt. spectra 79—61406
  - $MgO:Cr^{3+}(V^{2+})$, ${}^4A_{2g}\rightarrow{}^4T_{2g}$ spectra, new expt. results 80—11441
  - MgO:Li, $[Li]^0$ defect, stress induced optical dichroism 78—35179
  - $MnCl_2$, $MnBr_2$, mag. phase diagram, optical absorption meas. 77—4514
  - MnO, linear optical anisotropy meas. at antiferromag. transition 77—36205
  - $Mo(CO)_6$, in nematic matrix, linear dichroism, distortion and local field contribs. 79—87415
  - $Mo(CO)_6$, polarised absorption, field effects in condensed media 78—997
  - $MoS_2(Se_2)$, effect of uniaxial stress on excitonic optical spectra 78—84606
  - Na vapour, Zeeman coherence, transient and stationary, polarisation spectroscopy 80—58212
  - NaCl, gamma irradiation, optical and thermal bleaching of colour centres, trapped electron centre form. 79—95814
  - $NaCl:H^-$, U-centre absorpt. band shape, piezodichroism dispersion curve and electron-phonon interaction 77—24873
  - NaCl(Br), X-ray or UV irradiated, cation defects creation mechanism 80—75224
  - NaF, computer generated polarisation hologram 77—61923
  - NaF, M-centres, dichroim absorpt., appl. to optical waveguide polariser 79—995
  - NaF, photodichroic, direct-writing M-centre, Hurter-Driffield curves 77—4662
  - NaF photodichroic crystals, hologram synthesis in in-line scheme 77—88670
  - NaF:Li, combined suppressive and extinction writing, using $M(M_A)$ centres 77—7164
  - $Na_3Pr(C_4H_4O_5)_3.2NaClO_4.6H_2O$, absorpt., circular dichroism, and mag. circular dichroism spectra 80—97243
  - $NdMoO_4$, photoacoustic spectroscopy, dichroism meas. 78—62227
  - Ne, two and three level systems, laser induced dichroism and birefr. 78—79065
  - Ni complex, Ni(l-spartein)Cl_2, IR circular dichroism spectra, vibr.-electronic interaction 80—55074
  - $NiSO_4.6H_2O$, uniaxial crysts., circular dichroism and optical activity 80—45029
  - PbF_2-ZnSe multilayer 16 μm dichroic mirror, 16 μm region, mech. stress compensation 80—74465
  - $PbMoO_4$, near-edge absorpt. band, fluoresc. and photocond. 77—44017
  - Pr tinted glasses, transparency, dichroism and colour effects *(Polish)* 80—71371
  - RbCN, ferroelasticity and F- and M-centres absorpt. 79—87475
  - RbCl(Br), cation defects creation mechanism 80—75224
  - $RbFeCl_3$, linear chain ferromag., optical absorpt. and dichroism in mag. field 77—77237
  - Se formed in chiral polymer matrix, circular dichroism 77—85685
  - n-Si, nonlinear birefr. and dichroism at microwave freqs. and intervalley scatt. 79—19602
  - Si:B, irrad. with fast neutrons true profiles of impurity photocond. bands from piezodichroisms 79—91103
  - $SmFeO_3$, orthoferrite, anisotropy of Faraday rotation 79—61341
  - SmI, Zeeman coherence, transient and stationary, polarisation spectroscopy 80—58212
  - $Sm_{0.55}Tb_{0.45}FeO_3$ orthoferrite, optical and magneto-optical props. 79—61396
  - $SrF_2:Nd^{3+}$, linear dichroism induced by electric field orientation kinetics of Nd^{3+} centres 79—69868
  - Te, optical activity rel. to band struct., 4 to 300K 77—77165
  - Tl, $6^2P_{1/2}\text{-}7^2P_{1/2}$ M1 transition, parity violation detection in neutral weak interaction 77—30819
  - $W(CO)_6$ dissolved in oriented compensated nematic mixture, distortion of cubic mol., linear dichroism obs. 79—95797
  - $W(CO)_6$, in nematic matrix, linear dichroism, distortion and local field contribs. 79—87415
  - $WS_2(Se_2)$, effect of uniaxial stress on excitonic optical spectra 78—84606
  - $YFe_{1-x}Co_{x/2}Ti_{x/2}O_3$, orthoferrite, anisotropy of Faraday rotation 79—61341
  - $YFeO_3$, Faraday rotation anisotropy 77—20837
  - Zn complex, Zn(l-spartein)Cl_2, IR circular dichroism spectra, vibr.-electronic interaction 80—55074
  - ZnP_2, birefringence, circ. dichroism, temp. depend. *(Russian)* 79—1748
  - ZnSe:Cr, piezodichroism due to reorientation of Jahn-Teller centres 80—11363
  - $ZnSe:Cr^{2+}$, stress-induced alignment of Jahn-Teller centres 79—78651
  - $ZnSiP_2$, photocond. and photolum. spectra, optical anisotropy 78—72200
- **dictionaries** *see glossaries*
- **dielectric breakdown** *see electric breakdown*
- **dielectric constant** *see permittivity*
- **dielectric depolarisation**
  - alkali halide:Me^{2+}, nearest-neighbour theory of dipole polarisation and depolarisation, cation vacancies 77—16243
  - alkyl halides, depolarisation thermocurrent obs. of main relax. around glass transition 78—27158
  - apatites, dipolar reorientations, TSD study 80—107068
  - composite media, dielec. and optical props. 78—84546
  - dielectric-photosemiconductor two component systems, photoelectret state 80—25287
  - electret discharge model, injection relaxation mechanism, space-charge cond. 78—80279
  - electrets and dielectrics, conf., Sao Carlos, Brazil, Sept. (1975) 80—7251
  - ferroelectrics, photoelectretic states in real time spatial light modulators, photorefractive effect 80—80676
  - field induced thermally stimulated polarisation-depolarisation currents, relaxation, book contribution 80—80687
  - glasses, high-resistivity, uniform and space charge polarisation, thermally stimulated depolarisation anal. 78—15085
  - 4-n- heptyloxyphenyl 4-n-hexydexybenzoate, liquid crystal, freezing polarisation, electret effect *(Polish)* 80—10496
  - nonDebye dielectric solid, thermally stimulated depolarisation 78—10830
  - PET, pyroelectric effects and depolarisation currents, illumination effects 80—34859
  - photo-induced polarisation, model 79—56714
  - piezo-stimulated current spectra 77—69767
  - piezoelectric rod, depolarising-field effect, longitudinal effect extensional vibration 78—95551
  - PMMA, dielec. relax. spectrum, thermodepolarisation and dilatometric meas. 77—32322
  - poly-α-naphthol, semicond., isothermal depolarisation currents, electron trap parameters 80—60492
  - polycarbonate films, high temp. relaxations 80—97187
  - polychlorotrifluoroethylene, electret, TSC 80—7266
  - polyethylene, anomalous photodepolarisation, trapping 78—10838
  - polyethylene, high and low density, depolarisation thermocurrent study, relax. modes 80—7263
  - polyethylene terephthalate, anomalous photodepolarisation, trapping 78—10838
  - polymer dielectrics, electrical conduction and polarisation phenomena at low fields 78—48113
  - polymers, thermodepolarisation 77—66453
  - polyvinylacetate film, effect of electrode metals on depolarisation current characts. 78—76387
  - polyvinylidene fluoride, dielectric relax. mechanism 80—55023
  - polyvinylidene fluoride film, polarisation and depolarisation processes 80—11318
  - polyvinylidene fluoride films, field depend. depolarisation behaviour 80—20580
  - PVC, plasticised, thermomechanical and dielec. relax. props. rel. to degree of processing 79—70124
  - PVC, rigid, physical ageing effect on elec. props. 78—10836
  - PVF_2 pyroelectric coeff., depolarisation current meas. 79—56737
  - pyroelectric substance, adiabatic depolarization under cryogenic conditions 80—55045
  - TGS, Brillouin scatt. spectra, depolarisation field effect 78—15177
  - TGS, internal field prod. in layer periodical domain struct. by X-ray irrad. 80—71359
  - TGS, vacuum-cleaved cryst., charge compensation, ferroelec. field effect obs. 78—95556
  - TGSe, Brillouin scatt. spectra, depolarisation field effect 78—15177
  - thermally stimulated processes 78—10829
  - uniaxial ferroelectrics, domain formation during second order phase transition 79—38505
  - urethanic polyester elastomers, dielectric relax., spatial network density *(Russian)* 80—71310
  - vinylidene fluoride trifluoroethylene copolymer, ferroelec. behaviour 80—50284
  - $BaF_2:K^+$, cryst., thermal depolarisation 79—82912
  - $BaF_2:La^{3+}$, thermal depolarisation of $La^{3+}\text{-}F_i^-$ defect dipoles 80—75926
  - $CaF_2:La^{3+}$, thermal depolarisation of $La^{3+}\text{-}F_i^-$ defect dipoles 80—75926
  - $CaF_2:Na^+$, cryst., thermal depolarisation 79—82912
  - $CaWO_4:Gd$, thermally stimulated depolarisation current, 100 to 300K 80—7280
  - $GeS_{1.5}:Cu$, interpretation of dielectric behaviour 79—33595
  - H_2SO_4, solns., static permittivity, kinetic depolarisation, time-domain spectroscopy 78—68440
  - $KI:S^{2-}$, vacancy dipoles, photo-induced polarisation and depolarisation 80—2690
  - $Li_2B_4O_7$, ferroelectric glass, phase transition, permittivity, electrochromism, photochromism 80—80719
  - α-$LiIO_3$, depolarisation current, dielectric const. relaxation behaviour *(Chinese)* 80—88905
  - 3PbO.2GeO, TSC in thermoelectret state during ceramic synthesis, pyroelec. currents and energy struct. of capture centres 80—55014
  - $Pb(Zr, Ti)O_3$, ferroelectric ceramic discs, axial-current-mode shock depoling 79—78631

dielectric depolarisation continued
- $Pb(Zr,Ti)O_3$, porosity-permittivity relations, depolarising factors determ. and pore effects *(Japanese)* 80—97189
- $Pb(Zr,Ti)O_3$, shock wave compressed, dielec. props. 77—48139
- $PbZr_{0.95}Ti_{0.05}O_3$, impact loading, mech. and elec. response, elec. state effect 78—64317
- $Pr(NbO_3)_3$ form. mechanism, struct., dielec. props. 77—16235
- $RbBr:Ba^{2+},Sn^{2+}$, thermal depolarisation meas., relax. processes 78—23389
- S, polycryst., photoelectret state following X-irrad. 80—60485
- SbSI, adsorption polarisation and depolarisation currents 77—43942
- Si powder semicond., microwave propagation, Rayleigh limit 79—78126
- $SrF_2:La^{3+}$, thermal depolarisation of La^{3+}-F_i^- defect dipoles 80—75926
- $SrF_2:Na^+$, cryst., thermal depolarisation 79—82912
- $SrTiO_3$ ceramic, electrocaloric effects for refrigeration at cryogenic temp. 80—77789
- TeO_2, ferroelectric glass, phase transition, permittivity, electrochromism, photochromism 80—80719
- TiO_2, porosity-permittivity relations, depolarising factors determ. and pore effects *(Japanese)* 80—97189

dielectric devices
- *see also capacitors; ferroelectric devices; insulators; piezoelectric devices; pyroelectric devices; space-charge limited devices*
- capacitative transducer, appl. to elimination of transducer bond corrections in US wave vel. meas. 77—46873
- electret dosimeter and its principles of operation *(Japanese)* 79—81092
- electroradiographic image laser readout 80—41225
- laser triggered solid dielectric switches with low jitter and inductance 80—54066
- laser triggered switching of solid insulated spark gap 80—54065
- particle track detector, for neutron dosimetry *(Czech)* 78—66425
- pickup for shock wave meas. 78—5707
- semiconductor-dielec. superlattice, high freq. electromagnetic response 78—19073
- solid state heat engine, experimental demonstration of heat-to-electricity conversion within a dielectric 80—35707
- three-layer dielectric reflectivity standard error analysis 77—79727
- PZT paraelectric ceramic one-dimensional spatial light modulator 79—55240

dielectric function
- alkali fluoantimonates, dielectric props. and structural phase transitions *(German)* 80—25274
- alkali halide, static and dynamic props., appl. to KCl 77—7798
- alkali halide elastic dielectrics, Gruneisen parameter, effective ionic charge volume derivative 80—84273
- alkali halides, dielectric constant, first and second order strain derivatives 78—47719
- alkali halides, three-body interactions, effect on electronic polarisabilities and photoelastic behaviour 79—47382
- alkali halides, vol. depend. of dielec. consts. and effective charge parameter, under hydrostatic press. 78—14689
- alkali metal, electron-electron scatt. in terms of dielec. and vertex functions 79—95351
- alkali metal, thermal expansion and Gruneisen parameters 78—38857
- alkali metal-ammonia solns., metal-insulator transition, h.f. and u.s. props. 77—1369
- alkali metals, cohesive energy, dielectric function calcs. 78—2060
- alkali tungsten bronzes, struct. and supercond. 79—82703
- alloy, dil., wave-vector-nonconserving optical transitions 78—72100
- amino acid, cryst., mol. dielec. function 79—7043
- anisotropic continuum, with anisotropic surface layer, coeff. of attenuated total reflection 80—60535
- anisotropic dielectric crystal, EM fluctuations 79—19857
- anisotropic saddle point, electro-optical signal *(Japanese)* 77—43968
- anthracene-pyrometallitic dianhydride cryst., refl. and absorpt. spectra of singlet charge transfer excitons 80—71442
- aqueous media, ion-pairing, hard sphere model 80—96428
- arbitrary surfaces, and size-quantised metals, electrostatic response problems 77—31968
- band structure, dielec., of solids 79—47034
- binary alloys, random, dielec. matrix and related props. 78—51916
- binary composites, percolation effects and sum rules in optical props. 79—69801
- Bloch electron system, exchange correction to dielec. function, local exchange approx. 77—1384
- Bose gas, charged, in uniform mag. field, zero-temp. dielec. response 77—5758
- Bose gas, two-dimens., charged, in zero mag. field, dielec. response, RPA 80—142
- Brillouin scattering, resonant, analogy to modulation spectroscopy *(Japanese)* 78—68526
- n-butanol, dielectric response function, by lumped capacitance method 78—95539
- CDW, one-dimensional, commensurability pinning versus impurity pinning 79—11075
- CDW distorted solid, quasi-one-dimens., charge density fluctuations and dielec. matrix 80—107726
- cermet film granular media, dielectric function theory, permittivity, percolation transport props. 80—88498
- charged fluids near freezing point, static dielectric behaviour 78—56417
- chlorobenzene submillimetric permittivity obs. and Debye eqn. extrapolation 77—40173
- Clausius-Mosotti relations in dielec. matrix calcs. 80—59898
- complex reflection amplitudes of photons, sum rules 78—63006
- composite material, theory 79—56753
- composite materials, small particle, optical props. 78—56445
- composite media, dielec. and optical props. 78—84546
- composite media, dielec. and optical props. electrostatic polarisability calc. 79—51507
- convalent crystals, fundamental absorption band struct. in quasimolecular model 77—24868
- Coulomb gas, classical, two-dimens., screening props. from sine-Gordon eqn. 79—4524
- Coulomb gas, correlation functions, dielectric function 79—85071
- Coulomb gas, two-dimensional, dielec. function, and mag. susceptibility of one-dimensional Fermi system 78—10387
- Coulomb screening in presence of two EM waves 79—15107
- Coulomb system, two-dimensional, props. 77—62337
- covalent semiconductors, vacancy screening, dielec. const., exchange correl. pot., Thomas-Fermi description 80—44528

dielectric function continued
- cubic crystals, local field factors, electric dipole approx. calcs. 80—54661
- cubic symmetry cryst., quadrupole exciton theory 80—103632
- p-$CuInTe_2$, single cryst., IR study of lattice and free carrier effects 80—45074
- cupric formate tetrahydrate, dielec. props. under hydrostatic press. 77—12343
- data presentation and interpretation 78—76376
- degenerate electron gas at metallic densities, nonlocal interactions, compressibility and dispersion 80—107730
- degenerate semiconductor, permittivity of electrons interacting with optical phonons 77—24815
- deuterated Rochelle salt, complex dielec. const., 5 MHz-24GHz, −45 to +45°, relax. mechanism 80—15983
- diamond, dielectric function, optical frequency model calcs. 78—51921
- diamond, dielectric properties, mean point value calc. 78—87930
- diamond, electric quadrupole sum rules rel. to optical consts. 79—38036
- diamond, polarisation charge density and microscopic local field induced in external elec. field 80—49645
- diamond, static dielectric function, local field correction, tight-binding model 79—95355
- diamond with local-field correction, dielec. const. calc. 80—11312
- dielectric, complex reflection, spectra, dispersional anal. 77—36239
- dipolar liquid, dielectric function rel. to microscopic correlation function 80—7290
- discrete states, interaction with many continua 77—47707
- disordered conduction, dielectric function, phenomenological derivation 80—77692
- disordered semiconductor, single site theory of Wannier excitons 79—99486
- dispersion of dielectric axes in monoclinic and triclinic crystals related to lattice dynamics 78—87920
- dispersion self-energy of an electron in a dielectric 79—42461
- dye monolayer coating Ag film, anomalous dispersion of surface plasma oscills. 79—8203
- dynamical local field corrections 80—88500
- electron correlation at low densities 78—23038
- electron dielectric function, second-order RPA 78—49753
- electron fluid, two-dimensional, collective modes 77—80661
- electron gas, dense, response at any degeneracy 77—71269
- electron gas, dielectric function, freq. depend. non-RPA contribs. 77—51686
- electron gas, dielectric response and Kohn effect in strong mag. field 77—4279
- electron gas, dynamical exchange decoupling, plasmon dispersion, SDW and CDW 80—59900
- electron gas, dynamical exchange effects 80—54629
- electron gas, freq. dependent exchange correction 77—35880
- electron gas, generator coordinate method 78—60077
- electron gas, homogeneous, dielectric response, pair correl. function 77—72832
- electron gas, interacting, quadratic electronic polarizability 78—6310
- electron gas, jellium model, dynamic correlations, first-order perturbation theory 80—44527
- electron gas, mean free path of low energy electrons, influence of damping 78—10385
- electron gas, metallic densities, dynamical dielectric function and paramagnetic spin susceptibility 80—39514
- electron gas, optical props. in generalised HF approx. 80—24825
- electron gas, pair correlation function, consistency relations 80—49640
- electron gas, quasi-one-dimensional, pair correl. function and plasmon dispersion curve 77—62851
- electron gas, two-dimens. longit. and transverse dielec. function including exchange correls 77—66133
- electron gas of arbitrary degeneracy charge screening 77—76763
- electron liquid, calc. of dielec. function 77—80749
- electron liquid, density response function 78—67961
- electron liquid, local field factor, freq. depend., absence of logarithmic singularity 80—29343
- electron liquid, local field factor, freq. depend., dynamical exchange effects 80—29342
- electron liquid, local field factor freq. depend. 79—38009
- electron liquid, pair correlation function and correlation energy using Tripathy-Mandal dielec. function 79—19536
- electron liquid with any spin polarisation, correlation energy, local exchange-correlation pot. 79—65399
- electron plasma in presence of EM wave, DC mag. field, Coulomb screening, dielec. const. 80—15464
- electron scattering, inelastic, dynamical diffraction and generalised dielec. response function 80—75120
- electron-hole plasma, two particle state influence on dielectric function 79—56154
- electron-ion system, effective ion interaction and force consts. 80—65185
- elemental semiconductor, electric susceptibility from chemical-bond approach 78—51922
- elemental semiconductor, local field effects in static response 78—76010
- elementary excitations in crystals, dielectric theory 78—60076
- ellipsometric function, Kramers-Kronig relations and sum rules, Lorentz oscillator model 80—102617
- ellipsometry, metallic films and surfaces, nonlocal effects, theory 80—104006
- EM wave propag., self-consistent approach 78—51920
- exciton resonances, interacting, dielec. theory 78—14673
- fast charged particle traversing ferromag., dynamic mag. field, RPA 79—73230
- fast ion in solid, oscillatory wake, trapped electron binding energy, RPA calc. 80—96575
- fast moving ions traversing solid, wake-bound states, dispersive and surface effects 79—73231
- Fermi gas, correlation functions, dielectric function 79—85071
- ferroelectric, relaxation processes in Ising model, cluster approx., complex dielectric const. *(Russian)* 80—11352
- ferromagnet, harmonic rotator, Coulomb plasma and related model, two dimens. case 78—88137
- ferromagnetic semiconductors, dielectric function depend. on magnetisation, light absorpt. coeff. *(Russian)* 80—15467
- ferromangetic conductor, electric field response and electrofluctuation instability *(Russian)* 78—56083
- formamide, liq., vac. UV optical and dielec. meas. 80—25329
- frequency dependent dielectric constant, rel. to dielec. polarisation 78—56425

dielectric function continued
- frequency dependent dielectric function of gapless semiconductors in a magnetic field 78—63994
- glass, undergoing phase separation and homogenisation, light scatt., kinematic theory 79—24326
- glycerol, liq., reflectivity, in VUV region, for optical and dielec. functions 79—15475
- granular metal, Maxwell-Garnet and effective medium theories 77—47760
- graphite, electronic props., self-consistent LCAO calc. 78—51887
- graphite, IR optical properties, refl. data and complex dielec. function 78—10889
- graphite, model of collective modes in layer cpds., appl. to electron energy loss data 77—47754
- graphite, pyrolytic, IR reflectance meas. 15 to 500 meV 77—55781
- graphite, reflectivity in near IR under hydrostatic press., lineshape anal. 79—91424
- graphite, wave-vector depend. of electron energy losses 77—51688
- graphite film, relativistic excitations by inelastic electron scatt. 77—1463
- graphite intercalation compounds, band struct. model, dynamical dielec. function, reflectivity 80—34348
- graphite surface, asymptotic interaction with He, H, and H_2 79—99429
- graphite surface interaction with He atom 80—34316
- graphite-$FeCl_3$ intercalation cpd., electronic excitation spectrum, high resolution EELS meas. 80—45182
- graphite-K intercalation compound, dielec. function, EELS study 80—45183
- H_2, metallic, stable phase at high press. 77—72740
- HCP metals, lattice dynamics, local pseudopotential approach, dielectric functions 80—34151
- HCP metals, phonon dispersion relations, effect of different dielec. functions on model pseudopot. calc. 79—33055
- heavily doped degenerate semiconductor, complex dielec. function 79—90982
- heavily doped semiconductor, n-type, Mott transition, dielec. enhancement and conduction electron screening, unified treatment 78—72073
- hemicylinder-air-quartz system, semi-infinite crystal, dispersion of surface phonon polaritons 78—71939
- highly conducting material, electroreflectance by deep field penetration 79—19864
- Hubbard model, 1-dimens. 79—60740
- Hubbard model, electrical conductivity calculation, dielectric function and plasma oscillations 78—64020
- Hubbard model, strong correlation limit 78—87929
- III-V, tetrahedrally bonded, electronic density of states and optical spectrum 77—62797
- III-V semiconductor, electronic dielectric const. 79—65398
- III-V semiconductor, energy gap and static dielectric const. 79—11062
- III-V semiconductors, ionic tetrahedral, electrical susceptibility, chemical bond approach 78—87931
- inert gas solids, collective excitations and EELS, calc. 80—92842
- inhomogeneous material, complex permittivity in freq. range 10^2 to 10^7 Hz *(Russian)* 79—8088
- inhomogeneous media, elec. transport, optical props., exact theory 78—56119
- inhomogeneous media, surface plasmon dispersion 77—24602
- inhomogeneous media, surface plasmon dispersion 77—28229
- insulator, semiinfinite, spatial dispersion influence on EM props. 77—24814
- interacting electron system, dielectric permeability theory *(Russian)* 80—6762
- inverse dielectric matrix calc. via recursion method 80—88495
- inverse RPA calcs. at metal-vacuum interface 78—14789
- ionic conductor, frequency-dependent dielec. response 79—60538
- ionic conductor, inductive contrib. to real part of dielec. const. 79—55918
- ionic crystal, electronic dielec. const. strain derivative, photoelasticity 77—4620
- ionic crystal plate, line widths in spectrum of surface vibr. 79—33174
- ionic crystals, vol. depend. of electronic dielec. const. 77—40170
- ionised impurity scatt. limited mobility in semiconductors with spatially variable dielec. function 78—51986
- isotropic media, phase shift sum rules 79—69802
- IV-VI semiconductors, cubic dielectric constant from band struct. calc. 80—15463
- jellium, static dielectric function exam., Wigner distrib. function 77—66132
- jellium, two- and three-dimens., CDW, appl. to liq. He surface and semiconductors 80—65476
- Josephson junctions, collective excitations in superconductors below T_c, tunnel current fluctuations 79—33403
- Kohn singularities near gapless state 80—59904
- Kramers-Kronig relations, validity for dielec. permittivity 77—32346
- layered compounds, optical props., book contrib. 77—44023
- Lindhard dielectric function for degenerate electron gas, exchange contrib. 77—51685
- Lindhard dielectric tensor, branch cuts in complex-wavenumber plane 80—34377
- Lyddane-Sachs-Teller relation, cryst. with Debye polarisation 77—20256
- many-electron system, antiparallel spin correls. 77—4307
- many-valley semiconductors with anisotropic masses, screened donor impurities 78—10399
- margaric acid film, HF dielectric const. 77—36175
- Maxwell-Garnet theory for optical props. of heterogeneous grains 77—79750
- metal, electron gas, correlation effects on polarisation 80—54628
- metal, highly reflecting, determ. of IR optical constants by surface plasmon excitation 78—76418
- metal, interacting metal half spaces, effect of retarded-surface-plasmon dispersion and Van der Waals interaction 79—69452
- metal, local potential screening at finite temp. *(Russian)* 77—51684
- metal, memory function for response of conduction electrons 78—56096
- metal, non-simple, dielectric matrix, analytic model 80—75512
- metal, normal and magnetic, temp. depend. of plasma freq. 78—56100
- metal, optical functions, effect of surface roughness 78—56447
- metal, plasmon dispersion, effect of band struct., dielec. function calc. 78—26825
- metal, static dielectric permittivity sign *(Russian)* 78—76012
- metal, work function, pseudopot. calc. 80—96970
- metal fibre, micron sized, light scatt. 77—65571
- metal optics 79—19858

dielectric function continued
- metal particles, small, dielectric function and IR absorption 80—60607
- metal surface, enhanced Raman scatt. from adsorbed mols., effect of dielec. function 79—99882
- metal surface, force on moving charge, spatial dispersion effects 80—65646
- metal surface, van der Waals, interaction with mol., effect of spatial dispersion 78—10534
- metal surface electronic struct., linear response theory, appl. to Na 78—56197
- metal-dielectric interface, static point charge in dielec., pot. distrib. *(Russian)* 80—60088
- metal-insulator transition, dielec. function calc., interfacial roughening transition, renormalisation group theory 79—2734
- metallic aggregated system, optical props., interband transitions and optical cond. reson. 77—44016
- metallic particles, ultrafine, far IR absorpt. calc. 78—60454
- metallic thin films, density response function and dynamic struct. factor, nonlocal effects 79—69447
- metals, classical plasma frequency in long-wavelength limit, quantum correction 80—107728
- metals, electronic transport eqns., optical cond., number conserving relaxation time approx. calcs. 80—49681
- metals, ground state energy, structural expansion, HF approx. 80—65420
- metals, simple, electron-electron interaction, self-consistent perturbation theory based on Hartree-Fock theory 79—95357
- methylammonium aluminium selenate dodecahydrate, dielec. dispersion and relax. 77—28515
- MIM tunnel junction, surface plasmon excitation 78—10578
- molecular crystals, dielectric susceptibility tensor of composite lattice 77—12355
- molecular crystals, microscopic dielec. theory 80—97186
- molecular relaxation, statistical treatment, review 77—51284
- moment sum-rule approach, comparative view of dielec. functions 78—47722
- multiple-band systems, dielec. function in generalised relax.-time approx. 80—103637
- narrow band gap semiconductor, cubic, electronic contrib. to dielec. permittivity, calc. 77—59265
- noble metal, rel. to proton diffusion, config. and activation energies 79—37878
- noble metals, pseudopot. exam. of electronic props. 78—51960
- non-linear transport theory, field depend. of carrier screening 80—29415
- non-local electrostatics, appl. to cylindrical interface 80—18955
- non-specular conducting surfaces, classical electrodynamics 77—85280
- non-specular dielectric surfaces, classical electrodynamics 77—85279
- octupole modifications of Clausius-Mossotti relation 80—49179
- olivine, heavy ion irradiated, dielectric function and interstellar extinction 79—53873
- one-dimensional electron-phonon system, dynamics, Frohlich model 77—15781
- one-dimensional systems, exchange effects in plasmon dispersion 79—60741
- optical absorption by excitons 77—80734
- optical coating, highly dispersive artificial dielectric utilising metal spheres 80—5690
- organic charge transfer complexes, refl. spectra, excitons 79—47477
- p-n junctions, Thomas-Fermi calcs. of analytic charge distrib. 79—78161
- palmitic acid film, HF dielectric const. 77—36175
- paramagnetic semiconductor, heavily doped, linear response functions and magnetoresist. 77—51770
- perovskites, matrix element effects in freq. dependent dielectric function 80—70632
- phenanthrene, cryst., refl. spectra of first singlet transition 78—88323
- phonon-magnon interactions, dielectric function, theoretical anal. 78—80275
- piezoelectric cubic crystals, stimulated Raman effect 79—73927
- plane-parallel absorbing layer, nonlinear optical props. 80—58631
- plasma, complex dielectric function long wave limit, Coulomb systems with bound states, elec. cond. 80—33738
- plasma, one dimens. screening 80—65478
- plasmon dispersion beyond k_c, dynamic struct. factor, calcs. 79—56157
- PMMA, electron energy loss spectra, optical props. 79—10887
- Poisson's equation for impurity ion in medium with strongly variable dielec. constant, variational principle 77—69271
- polar dielectric interface, phonon-polariton modes 77—24474
- polar dielectrics interface, phonon-polariton damping 77—51587
- polar semiconductors, highly excited, optical dielec. function of electron-hole plasma 80—92847
- polariton frequency shift, cryst. surface and dielec. function depend. 80—44522
- polariton modes at interface between two conducting or dielec. media, review 78—87922
- polaritons, LT mixed mode, dispersion relation 80—65470
- Poley absorption magnitude 77—24813
- poly-2-hydroxyethyl methacrylate, dielectric γ relaxation 80—34850
- poly-2-vinylpyridine, electron energy loss spectra, for optical and dielec. props. 79—15569
- polyethylene oxide, aq. soln., dielec. relax., interferometric transmission obs. 78—52437
- polymer, complex dielectric const. determ. from polarisation current 77—66451
- polystyrene, electron energy loss spectra, for optical and dielec. props. 79—15569
- polystyrene, film, optical props. from near IR to X-ray, sum rules 77—48195
- polystyrene, mean excitation energy from dielec. function 79—78031
- polyvinyl methyl ether, aq. soln., dielec. relax., interferometric transmission obs. 78—52437
- power law frequency dependent dielectric function and nonanalyticity properties 78—60387
- pseudo one-dimensional metal, modified Coulomb interaction 77—1387
- PVA, aq. soln., dielec. relax., interferometric transmission obs. 78—52437
- quasi one dimensional crystals, Frohlich collective mode and dielectric permittivity *(Russian)* 77—89722
- quasi-one-dimensional solid, CDW distorted, macroscopic dielec. function 80—39515
- quasi-two-dimensional electrons, electrodynamics 77—89829
- quasistatic approximation, comment on optical props. of small particles 79—51927

dielectric function continued
β-quinol clathrate, CH_3OH mol. reorientation investig. by IR and dielec. meas. 77–12369
reflection spectra, Kramers-Kronig anal. with preliminary dispersion anal. 78–49915
reflectivity extrapolations in Kramers-Kronig anal. 78–19438
relativistic degenerate electron plasma, dielec. response function 78–71529
resonant Brillouin scatt. as form of modulation spectroscopy 79–91456
sea ice, complex dielec. const., 0.1-40 GHz 78–61430
semi-infinite spatially dispersive absorbing dielectric, energy flow 77–4611
semiconductor, carrier scattering by impurity potentials with spatially variable dielec. functions 79–69507
semiconductor, core level spectra, electronic polaris. effects 79–90985
semiconductor, deformation potential, possibility of screening by free carriers 77–72826
semiconductor, dielec. response function, local field effects 79–51505
semiconductor, dielectric response, local field effects in phonon-induced density change 79–51510
semiconductor, dielectric screening, Thomas-Fermi model 80–49648
semiconductor, disordered, absorption edges, temp. depend. 77–77160
semiconductor, doped, static dielec. response using simple homogeneous and isotropic model 79–73460
semiconductor, dynamical effective charges, pseudopotential calc. 78–30881
semiconductor, electron scattering interaction with coupled plasmon-polar-phonon modes 79–42536
semiconductor, electronic polarizability as function of Penn gap 80–49638
semiconductor, EM properties, general lecture 78–27173
semiconductor, exchange and correlation energies, local field effects 78–39044
semiconductor, ferromagnetic, longitudinal response function 77–72831
semiconductor, freq.- and wave-vector-depend. dielec. function 79–33253
semiconductor, heavily doped, degenerate, electroreflectance and complex interband dielec. function 80–40088
semiconductor, impurity ion pot., approx. equivalence of Csavinszky and Resta models 80–59901
semiconductor, local fields, nonuniform charge distrib. 80–24826
semiconductor, Moss formula, refr. index rel. to energy gap 80–108173
semiconductor, optical properties, equivalence of local field corrections and dynamical screeening 79–33250
semiconductor, Penn gap, energy gap, and dielec. function 79–82520
semiconductor, reson. in fundamental absorpt. region, quasi-mol. model interpretation 78–76490
semiconductor, saturated, dielectric response 78–10384
semiconductor, shielding by electron gas in magnetic field 80–107727
semiconductor, Thomas-Fermi dielectric screening eqn. 78–10388
semiconductor, zero-gap props. correlated to Γ_8 symmetry, review 80–6717
semiconductor carrier scattering by ionized impurity potentials incorporating spatially variable dielectric functions 79–42535
semiconductor electron-hole plasma, spherical model, dielec. function calc. 80–49613
semiconductor surface plasmon dispersion, appl. to InSb 77–1464
semiconductor with spatially variable dielec. const., impurity ion pot. 77–47769
semiconductors, dielec. function, modulation spectroscopy and elec. field effects book contrib. 80–80201
semiconductors, free electron scattering and dynamical cond. 78–2476
semiconductors, optical props. above band edge, book contrib. 80–84425
semiconductors, spatially variable dielectric functions, ionized impurity limited mobility 79–42534
Si inversion layers, prep. domain studies of intersubband optical transitions 80–20637
simple metals, model pseudopot. appl. to various props. 80–59845
simple metals, optical properties, equivalence of local field corrections and dynamical screeening 79–33250
simple metals, plasmon dispersion anal. from electron gas dielectric response 80–6761
smectic liquid crystal, chiral, optics and electro-optics, kinematical diffr. theory 80–92461
solid electrolyte, dielec. response 80–10899
solid insulator, effective screening function 78–10383
solid with thermal or static disorder, optical props. 79–42936
solids, approxs. for treatment of local field effects 79–47033
solitons, correlation functions, dielectric function 79–85071
spinach chloroplasts, laser photoinduced changes in high freq. dielectric constant 80–85449
static electron gas dielectric function, simple useful anal. form 78–79953
static macroscopic dielectric function, tight binding calcs., density response and local field effect 80–49644
stimulated acoustooptical effects due to nonlinear photoelasticity 80–103941
superconducting transition temp., local field effects, theory 78–14848
superconductor, two-particle correlation functions below transition temp. 77–24640
superconductors, charged, collective excitations and longitudinal US spectrum 79–56389
surface, lattice force constant determination 78–71933
surface dielectric response in local representation, microscopic theory 77–85289
surface plasmon dispersion relation at short wavelengths 80–96962
surface plasmon dispersion relation in presence of spatial dispersion 79–42612
surface roughness effect on image potential electron energy loss, plasmon electron scatt. 80–54748
TCNQ, metallic reflection band, vibronic struct. 78–19502
TCNQ salt, K-TCNQ, energy gap, electron-phonon interaction, IR spectrum 78–15167
TCNQ salt, MTPA $(TCNQ)_2$, IR refl., dielec. function and cond. 80–34924
TCNQ salts with asymmetric donors, transport props. 79–23953
TCNQ-HMTSeF, polarised single cryst. reflectance obs. and one-dimens. behaviour interpret. 78–6690
TCNQ-K, dielectric function of 1-dimens. Hubbard model 79–60740
TCNQ-TSef, Drude optical edge, press. depend. 79–19882
TEA $(TCNQ)_2$, mixed electronic-vibr. states in far IR spectra, dielec. const. *(Russian)* 77–36249
TGS, deuterated, dielectric props., ageing 77–16257

dielectric function continued
TGSe, deuterated, dielectric props., ageing 77–16257
thermally stimulated depolarisation, many-body model of universal dielec. response 80–75927
thin film, optical characterisation *(French)* 79–11402
thiourea, IR reflectivity study of ferroelec. and antiferroelec. phases, dielec. function model 79–33686
thiourea, Raman spectra of external frequencies 77–24840
thiourea, soft mode and Debye relaxations 78–80347
time-correlation functions of permanent dipole moments and induced polarisation 80–11316
time-dependent Hartree-Fock dielec. function 79–69448
transition metal, 3d, charact. losses from expression for permittivity 79–69455
transition metal compounds, phonon anomalies rel. to superconductivity 77–12055
transition metal oxides, dielec. behaviour 78–71703
transition metals, BCC, thin films, optical props. 79–78781
TTF-TCNQ, and related 1D conductors, temp. depend. microwave dielec. const. 77–31967
TTF-TCNQ, conductivity and dielec. permeability, freq. depend. 78–79984
TTF-TCNQ, controlled defects effect on microwave cond. and dielec. function 80–24885
TTF-TCNQ, Drude optical edge, press. depend. 79–19882
uniaxial crystals, Faraday effect at ε-isotropic point 77–12367
universal dielectric response in condensed matter 79–28674
valence electrons, finite energy, f-sum rules 78–88276
van der Waals force in cond. media, fluctuating electrodynamics, nonlocal dielec. constant 78–30876
wake potential of swift ions in solids 77–20257
water optical constant submillimetric wave meas. 79–33656
water-in-hexadecane, microemulsion, dielectric behaviour, Cole-Cole type relax., temp. depend. 78–56426
Wigner instability, Mott's $T^{1/4}$ law as evidence 77–80751
zero gap semiconductor, thin layer, dielec. response 80–103635
zero-gap semiconductors, dynamic dielec. function in mag. field, appl. to magnetoreflection spectra 79–15108
zinc blende semiconductors, small-gap, electron scatt. and transport props. 78–95294
zinc blende semiconductors, small-gap, electron scatt. and transport props. 78–95295
Ag, aggregated film, optical props., 0.35-1 μm 77–66548
Ag, discontinuous film, light absorpt. spectra, dielec. function calcs. 79–51507
Ag film, optical props. in intermediate region between pure Drude and interband absorption 77–81170
Ag, film, plasma reson. radiation exam. *(German)* 79–69453
Ag foil-electrolyte boundary reactively formed oxide layers, differential reflectance 79–69856
Ag halides, dielectric behaviour and optic mode Gruneisen parameters 79–10907
Ag, intraband optical conductivity, electron-electron scatt. 78–35166
Ag particles, lattice defect influence on size effect 78–88329
Ag surface, inert gases adsorption, physisorption energies 78–71944
Ag, thin layer on Al surface, surface plasmon ATR spectroscopy 79–78770
Ag-Cd dilute α-phase alloys, optical gaps, thermoreflectance meas. 77–66520
Ag-Zr(Nb)(Mo) film, dielec. const., optical props., DC resist. and thermoelec. power 77–85824
Ag_3AsS_3, proustite, cryst., vibr. spectra 78–48172
Al, dielectric function, wave-vector and freq. dependence, energy loss spectra 77–1385
Al, dielectric function pseudopot. theory, vol. plasmon dispersion 79–23917
Al film, optical dielec. const. in visible region, 300 to 1.5K 77–90211
Al, interband damping of long-wavelength plasmons 77–85165
Al, plasmon dispersion, dynamical exchange effects 79–51509
Al, plasmon dispersion, effect of band struct., dielec. function calc. 78–26825
Al, vacancy electronic struct. LCGO calcs., solid state scattering theory 79–78044
AlF_3 film, RF sputtered, dielec. props. meas. 77–36173
Al_2O_2-SiO_2, mullite 2:1 cryst., dielectric tensor components 77–48142
anthracene, polycrystalline, optical props., 3.2-9.3 eV 80–76097
As, interband, magnetorefl. for circularly polarised radiation 78–2840
As, rhombohedral, electronic struct. and optical props. var. with internal displacement parameter 79–60702
$As_{1-x}S_x(Se_x)$, bulk-quenched glasses, opt. freq. dielec. const., chem. ordering effects 78–23472
$As_2S_3(Se_3)(Te_3)$ glass, electronic struct. calc. by extended Huckel theory 78–23012
Au, aggregated film, optical props., 0.35-1 μm 77–66548
Au film, optical dielec. const. in visible region, 300 and 2.5K 77–90211
Au film, polycrystalline, temp. depend. of Drude absorption 79–78779
Au, intraband optical conductivity, electron-electron scatt. 78–35166
Au, ion implanted, ellipsometry, 1.8-5.5 eV 78–6697
Au, local pseudopotential, phonon frequencies, binding energy and liq. metal resist. calc. 77–20216
Au, optical props., dielec. function, void model, sample effects 80–76048
Au solar black, optical props., microstruct. influence 79–42937
$Au_{1-x}Si$ amorphous metallic films, optical props. as function of composition 79–95865
AuSn, optical props., 0.5-5 eV 78–39522
Ay, discontinuous film, light absorpt. spectra, dielec. function calcs. 79–51507
BN, electronic energy band struct., X-ray spectra, pseudopotential calcs. 79–78008
BN, from electron energy loss meas. 77–51688
$BaMnF_4$, low temp. dielec. props. and phase transitions 77–20790
BaO-B_2O_3, glass, refraction, refractive index from 0.365 to 2.50 μm 80–88953
BaO-La_2O_3-B_2O_3, glass, refraction, refractive index from 0.365 to 2.50 μm 80–88953
$BaTiO_3$ crystals, mechanically compressed, dielec. const. 79–56711
$BaTiO_3$, ferroelec. cryst., IR and Raman spectra, mode coupling 80–66194
$BaTiO_3$, soft mode spectroscopy IR refl. meas. 80–88982
Be, dielectric function from APW calcs. 79–65817
Be, longitudinal dielec. function calc. 77–1358

dielectric function continued
- BeF_2, vitreous, Raman and IR spectra 78—39549
- BeO film, amorphous or polycryst., dielec. function, refl., from electron energy loss meas. 78—43947
- BeO, free film and Au substrate, transmission spectra and photoemission characts. 77—24925
- BeO, small crystal, surface phonon modes, IR transmission spectra 80—11398
- Bi, superconducting transition temp., two-band model 80—25034
- Bi-Sb, semiconducting, lattice dielec. const., comp. depend. 80—39516
- $Bi_{1-x}Sb_x$, lattice dielec. const. from helicon wave propag. 77—47756
- $Bi_{100-x}Sb_x$, lattice dielec. const. meas. 78—10490
- BiTeI, melt and vapour grown, optical props. 80—84746
- $Bi_8Te_7S_5$, anisotropic dielec. const., oblique incidence reflectivity data 77—73124
- Ca film, imaginary part of permittivity determ., 2-5.6 eV *(French)* 77—4694
- Ca film, optical absorption and plasma reson. 77—40296
- Ca, optical props., 2-11 eV 78—15191
- CaO-B_2O_3-Fe_2O_3 glass, dielec. relax., AC and DC cond., dielec. const. and loss 78—23393
- $CaSO_4$, anhydrite and gypsum, phonon spectroscopy, lattice dynamical calc. 80—19889
- Cd_3As_2, elec. resist. and HF dielec. const. calcs. *(French)* 77—59284
- $CdCr_2S_4$, ferromag. semicond., IR refl. spectra, phonon props. and dielec. function 80—66191
- $CdCr_2Se_4$, magnetic red shift origin, specular reflectivity, band struct. 80—40127
- $Cd_xHg_{1-x}Se$ mixed cryst., electron mobility and electron scatt. 78—95296
- $Cd_xHg_{1-x}Te$, disorder scatt. 78—39137
- $CdI_2(Br_2)(Cl_2)$, dielec. function and band struct., EELS meas. 80—40195
- CdS 80—11398
- CdS, theory of photoelastic effect 77—55769
- CdS(Se)-Al function formation, coupled interface plasmons, low energy electron energy loss spectra 77—24621
- CdSe, undoped and Cr doped, far IR transmission and reflectance spectra 80—71429
- $CdSiP_2$, reflectance spectra at 300K 80—25407
- CdTe, energy bands and optical props. calc., tight-binding model with spin-orbit interaction 80—65448
- $Cd_{1-x}Zn_xS$ 10 μm film optical and electrical characterisation *(French)* 78—64153
- CeN, optical props. and valence mixture 78—56450
- $CoFe_{2-x}Ga_xO_4$, IR reflection spectra, permittivity spectra and effective ionic charges 79—69841
- $Co_{1-x}Ni_xSi$, IR refl. spectra in plasma refl. region 78—27233
- CoSi, IR refl. spectra in plasma refl. region 78—27233
- CrO_2, optical conductivities and dielec. functions in 0.2-6 eV range, rel. to band struct. 79—42938
- CsBr, temp. depend. of Cs colloids absorption bands 80—40145
- CsI, temp. depend. of Cs colloids absorption bands 80—40145
- Cu, aggregated film, optical props., 0.35-1 μm 77—66548
- Cu, discontinuous film, light absorpt. spectra, dielec. function calcs. 79—51507
- Cu, electron energy loss spectrum, complex dielec. function calc. 77—11862
- Cu film, electron energy loss spectra meas., optical functions calc. 78—19618
- Cu film, optical props. in intermediate region between pure Drude and interband absorption 77—81170
- Cu, inelastic electron scatt. data anal. 77—73199
- Cu, intraband optical conductivity, electron-electron scatt. 78—35166
- Cu, photoemission spectra and band struct., extensions of combined interpolation scheme 79—78844
- Cu-Al, optical composition modulation spectra, dielec. const. var., Fermi surface and electronic level shifts 80—6707
- Cu-Al film, electron energy loss spectra meas., optical functions calc. 78—19618
- Cu-Zn, optical composition modulation spectra, dielec. const. var., Fermi surface and electronic level shifts 80—6707
- CuBr, exciton absorpt. band shape, dielectric const. real part derivatives *(Russian)* 80—25413
- CuCl, dielectric function for semiconductors with high exciton conc. 80—84443
- CuCl, electrooptic props. below absorpt. edge 77—28548
- CuCl-Ag system, photosensitivity spectrum in region of CuCl exciton absorpt. *(Russian)* 79—78707
- CuO film, electron energy loss spectra meas., optical functions calc. 78—19618
- Cu_2O, exciton spectra, extended effective mass theory 79—69423
- Cu_2O film, electron energy loss spectra meas., optical functions calc. 78—19618
- Dy_2S_3, optical props. and electronic struct. in fund. absorpt. region 80—80817
- EuSe, dynamical conductivity in high mag. fields 79—78118
- Fe-Co alloys, optical and spectrosc. props. *(Russian)* 78—72529
- $FeCl_3$ intercalated with graphite, stage 1, dielec. response and intraband plasmon dispersion 80—59902
- $FeCl_3$-graphite intercalation compound, dielec. function, band struct. EELS study 80—49643
- α-Fe_2O_3, IR lattice vibr. and dielectric dispersion 78—6679
- α-Fe_2O_3 microcrystals, surface phonon modes, IR study 80—55089
- Fe_2O_3-B2O_3-PbO glasses, visible and UV optical props. *(Rumanian)* 78—48196
- Fe_3O_4, dielec. function and polar Kerr rotation, 0.5-3.6 eV 80—66221
- Fe_3O_4, magnetite, charge carriers, optical props. 80—34874
- Fe_3O_4, optical props. in spectral range 0.03 to 12 eV 79—51977
- Fe_3O_4, polar Kerr effect invisible and near IR spectral regions 80—108187
- GE, microscopic inverse dielec. matrix, local field correction and acoustic sum rule 77—84863
- Ga film, optical props., 2-15 eV 77—77308
- Ga, optical properties in 0.3 to 5 eV range 78—31196
- Ga, optical props. in 0.5-60 eV range, dielectric const. and loss functions *(French)* 77—12353
- Ga, thermoreflectance, in near IR, down to 0.3 eV 77—85722
- $Ga_{1-x}Al_xAs$:Te, plasmon-LO-phonon coupling, IR refl. obs. 80—50335
- GaAs amorphous film, EXAFS, optical and elec. props. 80—49547

dielectric function continued
- n-GaAs, coupled plasmon-LO phonon modes and Lindhard-Mermin dielec. function 79—82540
- GaAs, effective dielectric function calc., exchange interaction effects 79—99494
- GaAs oxide, anodic, optical props., 1.5-6.0 eV 77—90209
- GaAs, plasma-grown oxides, in situ anal. using spectroscopic ellipsometer 79—79138
- n-GaAs, Raman scatt. by wavevector depend. coupled plasmon-LO phonons 77—40232
- GaAs, Schottky barrier ellipsometric electroreflectance spectra, energy band parameters 79—99853
- GaAs:Te, amorphous, ion implanted layers, optical refl., 1.5-7.0 eV 79—8152
- GaAs-AlAs and related monolayer heterostructures, pseudopot. calc. 78—60198
- GaAs-$Ga_{1-x}Al_xAs$ repeated monolayer heterostructure, electronic struct. 77—66197
- $Ga_{1-x}In_xSe$ solid solution, IR spectra of static reflectivity 79—69849
- GaP amorphous film, EXAFS, optical and elec. props. 80—49547
- GaP, dispersion of refr. index and permittivity 77—55765
- GaP, oxide, anodic optical props., 1.5-6.0 eV 77—90209
- GaP, polariton linewidth in k-space, anharmonicity and permittivity 77—85155
- GaP, refr. index, 100 to 420K, permittivity calcs. *(Russian)* 77—90156
- GaP, surface polaritons, light scattering studies, effect of surface roughness 80—6753
- GaP, Thomas-Fermi theory, dielectric functions, screening, dielectric constants 79—99497
- GaP, upper polariton branch obs. by ATR 78—68510
- GaS layer semiconductor, IR derivative absorpt. spectra 78—6666
- GaSb oxide, anodic, optical props., 1.5-6.0 eV 77—90209
- GaSe layer semiconductor, IR derivative absorpt. spectra 78—6666
- GaTe layer semiconductor, UV-visible wavelength derivative and thermorefl. spectra 78—6666
- GaTe, reflectivity, 1-35 eV, electron props. determ. 77—20872
- Ge, dielectric const. associated with direct interband transitions 77—20817
- Ge, dielectric properties, mean point value calc. 78—87930
- Ge, effective dielectric function calc., exchange interaction effects 79—99494
- Ge, effective screening function 78—10383
- Ge, electric quadrupole sum rules rel. to optical consts. 79—38036
- Ge, electron mobility is semiconductors based on dielectric function modification of Dingle pot. 79—60836
- Ge, IR absorption and scatt. by electron-hole drops 78—51903
- Ge, impurity-ion potential, electron-conductivity mobility, spatially variable dielectric function calcs. 79—78105
- Ge, ionised impurity scatt. limited mobility in semiconductors with spatially variable dielec. function 78—51986
- Ge, localised states due to isocoric donor impurities 77—76768
- Ge, microscopic screening of ion-ion interaction and phonon dispersion, tight-binding calc. 77—24528
- Ge, static dielectric function, local field correction, tight-binding model 79—95355
- Ge surface, (111), ion-bombarded and annealed, spectroscopic ellipsometry study 80—103543
- GeS, far IR reflectivity spectra, lattice vibr. and dielec. const. 77—52068
- GeS_2, energy gap and optical props. in IR region 79—51948
- GeS(Se), dielec. function, optical and electron energy loss spectroscopy 78—15189
- $Ge_{1-x}S_x(Se_x)$, bulk-quenched glasses, opt. freq. dielec. const., chem. ordering effects 78—23472
- $GeSe_2$, far IR reflectivity spectrum, dielec. const. and lattice vibrs. 77—52069
- $GeSe_2$, IR and Raman spectra 78—95585
- GeTe, electron-phonon interactin induced phase transition 79—82338
- ^4He, liq., HF cond. of electrons trapped at surface 78—10238
- $Hg_{0.75}Cd_{0.25}Te$, single crystal, reflection spectra 80—40140
- $Hg_{0.75}Cd_{0.25}Te$, thermorefl. spectra, effect of excitons on E_1 and $E_1+\Delta_1$ structs. 80—16057
- $Hg_{1-x}Mn_xTe$, far IR studies of lattice and free carrier effects 78—39544
- $Hg_{2.91}SbF_6$, anisotropic visible and IR refl. rel. to metallic cond. 77—8602
- HgSe, dielec. function at 2, 95, and 300K, reflectivity spectra meas. 79—15458
- HgSe, two-phonon resonant effect, far-infrared reflectivity 80—108203
- HgSe(Te), dynamic dielectric function, IR absorpt. meas. 78—68508
- p-HgTe, dynamic dielectric function, experimental and theoretical study 78—92069
- HgTe, energy bands and optical props. calcs., tight-bonding model with spin-orbit interaction 80—65448
- n-InSb, elec. cond., press. dependence 80—6830
- InSb inversion layer, electromagnetic mode 78—60080
- InSb-type semiconductor, spatial dispersion of permittivity 78—67967
- InSe, band structure, pseudopotential calc. 80—24799
- Ir, electronic struct. determ. from optical refl. meas. 77—62812
- K, surface electron states and optical props. in IR spectral range *(French)* 80—54757
- K-intercalated graphite (stage-1), electron energy loss expts. and band struct. theory 79—100001
- K-Rb, internal energy, heat of mixing, entropy, dielectric function 80—88340
- KCl, transverse optic mode self energy, freq. and temp. depend. 77—80589
- KCl:Li^+, press. tuning of motional behaviour in shallow off-centre pots. 79—78718
- KD_2AsO_4, LF dielectric dispersion near phase transition 77—59530
- KH_2AsO_4, LF dielectric dispersion near phase transition 77—59530
- KH_2PO_4, dielec. functions above and below ferroelec. transition 79—33588
- KH_2PO_4, dielectric const. at ultra low freq., domain wall relax. effects 77—12348
- KH_2PO_4, soft mode behaviour, dispersive Fourier transform spectroscopy 77—7823
- $KMgF_3$, extreme UV spectra, 9-30 eV 78—23486
- $K_{1.6}Mg_{0.8}Ti_{7.2}O_{16}$, solid electrolyte, dielec. response, 5.2-77K 79—56709
- KNO_3, far IR study of dielec. function by asymmetric Fourier spectroscopy 79—51947
- $KNbO_3$, complex electronic dielectric const. from tight binding energy bands 78—60054

dielectric function continued
$KNbO_3$, ferroelec. cryst., IR and Raman spectra, mode coupling 80—66194
K_2O-CaO-BaO-B_2O_3, glass, refraction, refractive index from 0.365 to 2.50 μm 80—88953
$K_2Pt(CN)_4Br_{0.3}2.6H_2O$ crystal, quasi-one-dimensional, optical consts. and dielec. permittivity dispersion 77—1695
K_3Sb, optical and dielectric props., energy spectra, density of states calcs. 80—20083
K_2SeO_4, incommensurate and ferroelec., far IR and mm dielectric response 79—73955
$KTaO_3$, complex electronic dielectric const. from tight binding energy bands 78—60054
$KTaO_3$, freq. depend. of soft mode self-energy, for IR dielec. response meas. 79—33632
$KTaO_3$ pseudodisplacive ferroelec., temp.-dependent dielectric response obs. 77—40247
La, soft phonons, f-band induced instability 78—83907
La_2S_3, optical props. and electronic struct. in fund. absorpt. region 80—80817
Li deposits, optical consts., Kramers-Kronig anal., 0.5-10.7 eV 77—40201
Li, elec. resist., effects of core and correl. corrections 78—64026
Li film, optical absorpt. spectra, rel. to phase struct. 77—4651
LiF, imaginary part of dielec. const., freq. depend. 79—55843
$Li_{0.5}Fe_{2.5}O_4$, magnetooptical spectra, polar Kerr rotation, dielectric tensor elements spectra 80—40091
$Li_{1-x}H_xIO_3$, dielec. behaviour, Raman and IR spectra 77—32357
Li_3N, IR and Raman spectra and lattice dynamics 78—48177
$LiNbO_3$, IR reflectivity temp. depend. 78—27202
LuH_2, electronic struct., optical studies, 0.2-5 eV, 4.2-340K 79—78005
Mg, dielectric function from APW calcs. 79—65817
Mg, longitudinal dielec. function calc. 77—1383
$MgAl_2O_4$, IR spectrum exam. 78—76454
MgO, dielectric properties, mean point value calc. 78—87930
MgO, free film and on Au, transmission spectra and photoemission 77—24925
MgO microcrystals, IR absorpt. 79—42963
Mn ferrites, Fe-excess, charge carriers, optical props. 80—34874
MnAs, optical props., 0.3-14 eV 77—52122
$MnAs_{0.85}P_{0.15}$, optical props., 0.3-14 eV 77—52122
$Mn_xFe_{3-x}O_4$, dielec. function and polar Kerr rotation, 0.5-3.6 eV 80—66221
$Mn_xFe_{3-x}O_4$, optical props. 80—20606
$MnSe_2$, IR lattice vibrs., dielectric dispersion 79—28735
Mo, dielec. function and energy loss function, APW band struct. calc. 77—62850
Mo film, polycryst., energy loss function, Kramers-Kronig anal., reflectivity, optical props., EELS 80—40194
MoO_2, optical conductivities and dielec. functions in 0.2-6 eV range, rel. to band struct. 79—42938
$MoS_2(Se_2)(Te_2)(2H)$ polytypes, Kramers-Kronig anal. of reflectivity spectra, 0-30 eV, band model 79—51976
NH_4SbF_5, dielectric props. and structural phase transitions *(German)* 80—25274
Na (001) surface electronic struct., linear response theory 78—56197
Na, IR and optical props., surface-plasmon-mediated absorpt. mechanism 80—93308
Na, liquid, optical conductivity 77—63425
Na-Cs, internal energy, heat of mixing, entropy, dielectric function 80—88340
Na-K, internal energy, heat of mixing, entropy, dielectric function 80—88340
$NaBr:Cu^+$, press. tuning of motional behaviour in shallow off-centre pots. 79—78718
NaCl, dielectric properties, mean point value calc. 78—87930
NaCl, imaginary part of dielec. const., freq. depend. 79—55843
NaCl transverse optic mode anharmonic self-energy meas. by dispersive Fourier transform spectroscopy 77—39642
NaCl, transverse optical mode anharmonic self energy, far IR spectrum 78—6131
$NaCl_{1-x}Br_x$, mixed crysi., vibr. and optical props. 80—29133
$Na_2KSb(Cs)$, photocathode, optical props. 79—78827
$NaMgF_3$, extreme UV spectra, 9-30 eV 78—23486
Na^ANO_3, (A=14,15), dielec. const. in terms of frequency-dependent damping factor 79—56796
Na_2S, dielectric const., transverse and longitudinal optical mode, static dielectric const., effective charge 79—73892
Na_xWO_3 bronzes, electroreflectance vs. bulk dielectric behaviour, classical model 77—66479
Na_xWO_3, intra- and interband plasmons, inelastic electron scatt. exam. 78—72098
Na_xWO_3, metallic, optical and electronic props. 80—24398
Na_xWO_3, optical props., analysis of free- and bound-electron contribs. 77—77248
Na_xWO_3, optical props. 79—38515
Nb alloys, optical props., 0.1-25 eV, band models 78—10892
Nb, dielec. function and energy loss function, APW band struct. calc. 77—62850
Nb, superconducting, optical props. and electron-phonon interactions 80—2510
NbC, supercond., phonon anomalies, microscopic theory 78—14867
$Nb_3Ge(Sn)$, superconducting, optical props. and electron-phonon interactions 80—2510
Nd_2S_3, optical props. and electronic struct. in fund. absorpt. region 80—80817
Ni, dielectric matrix, analytic model 80—75512
Ni, electronic structure and optical consts. by inelastic electron scatt. 80—7451
β′-NiAl, electronic struct. and optical props. 80—97228
Pb, liq., elec. resist. calcs., pseudopot. depend. 80—96840
$Pb_{1-x}Cd_xS$ epitaxial layer, metastable, optical props. and electronic struct. 79—15543
$Pb_5Ge_3O_{11}$, dielec. functions above and below ferroelec. transition 79—33588
$Pb_5(Ge_{1-x}Si_x)_3O_{11}$, dielec. spectra, ferroelec. behaviour 78—60406
$Pb_{1-x}Ge_xTe$, Raman scatt. from soft TO-phonon modes 79—95773
PbI_2, 2H polytype, anisotropy of lattice vibrs. 77—7807
PbI_2, complex dielectric and optical consts., ellipsometric determ. 78—23425
PbI_2, exciton absorpt. band shape, dielectric const. real part derivatives *(Russian)* 80—25413

dielectric function continued
PbO layers on Pb films, optical props. 79—83042
$Pb_3(PO_4)_2$, IR dispersion at room temp. 79—15460
$Pb_3(P_xV_{1-x}O_4)_2$, ferroelastic phase transitions, lattice dynamics, dielec. and optical props. meas. 77—55334
PbS, wave-vector depend. of electron energy losses 78—11041
PbSe, wave-vector depend. of electron energy losses 78—11041
PbSnTe, optical dielectric const. variation with carrier conc. 80—84709
$Pb_{1-x}Sn_xTe$, lattice and electronic props. and g-value 80—80161
$Pb_xSn_{1-x}Te$, RF-sputtered epitaxial single-cryst. films, thermorefl. spectra 77—63476
PbTe, electron-phonon interactin induced phase transition 79—82338
PbTe epitaxial film, many valley semicond., band population effects, intraband magneto-optical props. 79—78007
PbTe epitaxial layers, submillimetre spectroscopy 79—83048
PbTe, far IR magnetorefl., band struct. 80—76010
n-PbTe, far IR magnetotransmission and refl., dielec. function 77—52091
PbTe, index matching far i.r. method for static dielectric const. meas. 77—1678
PbTe, microwave magnetoplasma exam. of lattice and electronic props. 77—69364
PbTe, wave-vector depend. of electron energy losses 78—11041
$PbWO_4$, reflectivity, dispersion parameters and optical const. temp. depend. 77—28575
Pd, electronic struct. determ. by relativistic APW method, rel. to UV spectroscopy 77—4289
Pd, optical properties, 0.1 to 6 eV 78—92092
$Pd_{0.775}Cu_{0.06}Si_{0.165}$ glass, optical props. in energy range 0.67 to 5.6 eV 80—34872
PdO, optical props., 0.5-5.4 eV 79—56813
$Pd_{81}S_{19}$ and $Pd_{84}Si_{16}$, metallic glasses, optical refl. spectra and optical consts. 79—87464
PdSb, optical props., 0.5-5 eV 78—39522
$RbBr:Ag^+$, press. tuning of motional behaviour in shallow off-centre pots. 79—78718
$RbCl:Ag^+$, press. tuning of motional behaviour in shallow off-centre pots. 79—78718
$RbHSO_4$, dielec. dispersion near ferroelec. phase transition 80—2684
ReO_3, intra- and interband plasmons, inelastic electron scatt. exam. 78—72098
Rh, electronic struct. determ. from optical refl. meas. 77—62812
$(SN)_x$, electronic struct. and opt. props. 78—6256
$(SN)_x$, X-ray and optical props. 78—39632
Sb_2S_3 film, amorphous and crystalline, optical props. 79—95867
SbSBr glass, IR reflectivity spectra 80—71403
Sc, HCP, optical examination of electronic struct. 77—89694
ScH_2, electronic struct., optical studies, 0.2-5 eV, 4.2-340K 79—78005
ScH_2, optical interband struct. and low energy plasmons 78—31200
Se, amorphous, bulk, reson. Raman scatt. 80—60597
Se, amorphous, electronic struct. and optical props., pseudopot. calc. 80—65428
Se, dielectric function in trigonal phase, model calc., local-field corrections 78—39045
Se, electronic struct. of cryst. phases and hydrostatic press. effects 80—59865
Se, trigonal, dielec. matrix calcs. 80—54630
Se, trigonal, inverse dielec. tensor in static limit local field corrections 77—51690
Si, amorphous, electronic struct. and optical dielec. function, LCAO calc. 79—42478
Si amorphous film, film, glow discharge deposited, refl. spectra and dielec. function 80—50360
Si, dielectric function spectra, ellipsometric determ., many-particle effects at E_1-transition 80—93363
Si, dielectric properties, mean point value calc. 78—87930
Si, dielectric screening and zone-centre phonons 78—67785
Si, effective dielectric function calc., exchange interaction effects 79—99494
Si, electron mobility is semiconductors based on dielectric function modification of Dingle pot. 79—60836
Si, electroreflectance, dielec. function, ellipsometric meas. 79—4790
Si films, CVD, amorphous and polycryst., microscopic surface roughness, effective-medium models, ellipsometric expts. 80—24756
Si, glow discharge deposited, optical spectra, reflectance, dielectric function and oscillator strength 80—11492
Si, impurity-ion potential, electron-conductivity mobility, spatially variable dielectric function calcs. 79—78105
Si, ionised impurity scatt. limited mobility in semiconductors with spatially variable dielec. function 78—51986
Si, laser induced dense plasma, dynamics 80—65612
Si, local pseudopotential, Gaussian band charge model 80—88477
Si, localised states due to isocoric donor impurities 77—76768
Si, microscopic inverse dielec. matrix, local field correction and acoustic sum rule 77—84863
Si, optical properties of monocrystal by electron energy loss meas. *(German)* 79—24283
Si, optical spectrum, many particle effects, band struct. 80—89024
Si, plasmon dispersion relation, local microscopic field effects 80—20103
Si polymorphs, optical props., orthogonalized LCAO calc. 78—10345
Si, pseudopotentials for band struct. and cryst. energy calcs. 79—82514
Si, static dielectric function, local field correction, tight-binding model 79—95355
Si, vacancy screening, dielec. const., exchange correl. pot., Thomas-Fermi description 80—44528
Si-Si_3N_3, dielec. function calc. 79—95862
Si-SiO_2, dielec. function calc. 79—95862
SiC, refractive index dispersion, 0.4-50 μm, 105-297K 78—84548
Si_3N_4, electronic struct., LCAO calc. 80—96776
SiO_2, freq. and wavenumber depend. dielec. function, bond-charge approx. 79—56155
SiO_x, dielec. and optical props., chemical disorder effects 80—80815
SiO_x, electronic struct., mixed-crystal and random-bonding models 79—65029
SiO_x, freq. and wavenumber depend. dielec. function, bond-charge approx. 79—56155
Sm monochalcogenides, electronic struct., optical props. 0.03 to 12 eV 77—28594
α-Sn, dielectric properties, mean point value calc. 78—87930
$SnCl_2.2H_2O$, dielectric dispersion and absorpt. and proton spin-lattice relax. at phase transition 77—8437

dielectric function continued

- $Sn_{1-x}Mn_xTe$, IR reflectivity, elec. susceptibility mag. order effects 79—47433
- SnS, far IR optical props. 77—12375
- SnS_2, refl. using Kramers-Kronig anal., optical functions 79—95798
- SnS(Se), dielec. function, optical and electron energy loss spectroscopy 78—15189
- SnS(Se), IR reflectivity and Raman spectra, phonon frequencies and dielec. const. 77—48166
- SnSe, far IR reflectivity spectra, lattice vibr. and dielec. const. 77—52068
- $SnSe_2$, refl. using Kramers-Kronig anal., optical functions 79—95798
- SnTe, bond gap, phase transform., optical dielec. const. meas. 80—10630
- SnTe, electron-phonon interactin induced phase transition 79—82338
- SnTe, Raman scatt. from soft TO-phonon modes 79—95773
- $SrTiO_3$, calc. of matrix element effects in freq. dependent dielectric function 80—70632
- $SrTiO_3$, freq. depend. of soft mode self-energy, for IR dielec. response meas. 79—33632
- $SrTiO_3$ pseudodisplacive ferroelec., temp.-dependent dielectric response obs. 77—40247
- $SrTiO_3$, surface EM wave propag., IR refl. expts. 78—39553
- TGS, ferroelec. cryst., complex permittivity at microwave freq. and high press. 80—2685
- TGSe, ferroelec. cryst., complex permittivity at microwave freq. and high press. 80—2685
- Ta-W optical props., temp. depend., 4.2-1100K 78—2874
- TaS_2 mixed coordination polytypes, optical props. 0.5-6.0 eV range, dielec. function calcs. 79—15476
- $TaSe_2$(2H), plasmon behaviour at charge density wave onset 80—10900
- Te, amorphous, electronic struct. and optical props., pseudopot. calc. 80—65428
- Te, dielectric function in trigonal phase, model calc., local-field corrections 78—39045
- Te, electronic struct. of cryst. phases and hydrostatic press. effects 80—59865
- Te, trigonal, dielec. matrix calcs. 80—54630
- Th, interband structure and role of 5f electronic states, optical reflectivity meas. 77—76744
- TiN, optical props. at 300K 78—19466
- TiO_2, non-stoichiometric rutile, LO phonon-plasmon coupling, IR refl. spectrum 77—32376
- TiO_2, rutile, optoelectronic props., band struct., theory 80—80175
- TiO_2 single cryst., refl. and electrorefl. spectra 78—2870
- TiO_2 single cryst., refl. and electrorefl., energy levels 78—2871
- TiO_{2-x}, plasmon and polar optical phonons 77—39794
- TiS_2, electron energy loss spectra, reflectivity absorption coeff. 79—69937
- TlBr, electromodulation spectroscopy of excitons 79—73444
- TlBr pseudodisplacive ferroelec., temp.-dependent dielectric response obs. 77—40247
- TlCl, band structure and optical spectra, local field and exchange effects 80—24798
- TlCl, electromodulation spectroscopy of excitons 79—73444
- $TlGaS_{2x}Se_{2(1-x)}$ layer solid soln., long wave lattice vibrs., IR reflection spectra 80—11388
- TlI:Cs, dielectric const. temp. and freq. depend. 77—32315
- $TlInS_{2x}Se_{2(1-x)}$ layer solid soln., long wave lattice vibrs., IR reflection spectra 80—11388
- TlSe, vibrational spectrum, IR spectra meas. 78—35146
- UO_2 and U_4O_9 single crysts., optical props. rel. to chem. bonding 77—28598
- UO_2, localised versus itinerant 5f electrons exam., reflectivity meas. 79—19905
- UO_2, optical props. and electronic struct. 78—68527
- USb, localised versus itinerant 5f electrons exam., reflectivity meas. 79—19905
- VO_2 film, optical and elec. props., 0.8 to 4.2 mm, near metal-semicond. transition 77—32473
- V_2O_3, effect of metal-insulator transition on V K-absorption spectrum 79—19950
- V_2O_5 energy band struct. rel. to expt. studies 80—70603
- V_3Si, superconducting, optical props. and electron-phonon interactions 80—2510
- W (110) surface, adsorption of H, band struct. and adsorbate geometry, surface-reflectance-spectroscopy 80—44416
- W surface, (110), chemisorpt. effects on dielec. function, refl. spectra 80—75616
- W-Fe spin glass, optical props. and electronic states 80—20412
- W-Re, optical props., temp. depend., 4.2-300K 78—2874
- WO_2, optical conductivities and dielec. functions in 0.2-6 eV range, rel. to band struct. 79—42938
- WO_3 film, intra- and interband plasmons, inelastic electron scatt. exam. 78—72098
- WO_3, optical props. 79—38515
- Y film prepared in ultrahigh vac., optical meas. 6 to 14 eV 79—78767
- YH_2, electronic struct., optical studies, 0.2-5 eV, 4.2-340K 79—78005
- YIG, magnetooptical spectra, polar Kerr rotation, dielectric tensor elements spectra 80—40091
- $ZnIn_2S_4$, layered semicond., reflectivity spectra 79—8155
- ZnO film, high-resist., band and hopping cond., AC cond. and capacitance meas. 77—72928
- ZnO, small crystal, surface phonon modes, IR transmission spectra 80—11398
- ZnO, theory of photoelastic effect 77—55769
- ZnO-B_2O_3, glass, refraction, refractive index from 0.365 to 2.50 μm 80—88953
- ZnO-La_2O_3-B_2O_3, glass, refraction, refractive index from 0.365 to 2.50 μm 80—88953
- ZnS, theory of photoelastic effect 77—55769
- $ZnSiP_2$, reflectance spectra at 300K 80—25407
- ZnTe, excitonic effects on E_0 and E_1 gaps, Kramers-Kronig analysis of measured spectrum 79—61400
- ZnTe, wavelength-modulated reflectance spectrum, electron-phonon and exciton-phonon interactions 79—11434
- ZrN, optical props. at 300K 78—19466

dielectric heaters *see dielectric heating*

dielectric heating

- ZnS film, Joule heating, I-V characts. 78—2599

dielectric hysteresis

- L-p-alkoxybenzylidene p′-amino 2 methylbutyl cinnamate chiral smectic liq. cryst., dielec. and ferroelec. props. 79—91394
- ceramics, transparent ferroelectric, composition selection for appl. in light modulators *(Russian)* 80—91869
- cholesteric liquid crystals, mixtures, hysteresis, bistability effects under elec. fields 78—42907
- copper formate tetrahydrate, dielec. props. under hydrostatic press. 77—20789
- cupric formate tetrahydrate, dielec. props. under hydrostatic press. 77—12343
- curves, computer-aided approximation *(German)* 77—8338
- dicalcium barium propionate, ferroelec. in press. induced phase VI 79—91393
- dicalcium barium propionate, press. induced ferroelectricity, dielectric meas. 79—51920
- dicalcium lead propionate, ferroelec., annealed, crit. exponents, dielec. const. temp. depend. 80—55050
- diglycine nitrate, cryst. growth, dielec. and electromech. props. 80—2701
- DNA, dielectric hysteresis loop 79—83691
- DOBAMBC, ferroelec. liq. crysts., elec. and optical props., appls. *(Japanese)* 80—88943
- L-DOBAMBC, smectic liq. cryst., ferroelec. behaviour 77—43949
- ferroelctric crystals, parameter meas. *(Polish)* 78—88272
- ferroelectric hysteresis cycle computing from a statistical model *(French)* 79—11393
- ferroelectric liquid crystals, temp. depend. of elec. susceptibility and spontaneous polarisation *(Japanese)* 78—68467
- ferroelectric material properties study, LF HV generator applic. *(French)* 77—41647
- ferroelectric materials, high press. studies, rel. to Earth and planetary interiors 78—69334
- ferroelectric materials for dielectric power conversion, dielectric prop. anal. 80—80712
- ferroelectric phase transitions in electric field, double hysteresis loop criteria 79—65806
- ferroelectric thin film hysteresis, electronic system for display on CRO 78—89496
- ferroelectricity, hysteresis loops and butterfly loops, macroscopic theory 80—66132
- ferroelectrics hysteresis loop sensing *(Czech)* 80—82792
- guanidine aluminium sulphate hexahydrate, ferroelec. cryst., growth, domain struct., dielec., switching props. 77—43950
- MIS structure, on thermal SiO_2, polarisation hysteresis, ion motion *(Russian)* 80—54793
- piezoelectric ceramic, nonlinear charge release under uniaxial press. 80—80706
- PLZT ceramics, ferroelec., special props. 79—42916
- PLZT coarse-grained solid solutions, electro-optical processes induced by longitudinal electric field *(Russian)* 80—80750
- polyvinylidene fluoride, hysteresis phenomena under high elec. field 80—66134
- polyvinylidene fluoride film, cryst. dipole orientation in elec. field 78—80286
- polyvinylidene fluoride film, hysteresis and dipolar orientation 80—97217
- pyroelectric high power density heat engine, dielectric losses, polarisation 80—80689
- rare earth arsenates, $RAsO_4$, ferroelectricity, dielec. meas. 80—60515
- reversible nonlinearity in dielectric films 78—92024
- RNA, solid hydrated samples, hysteresis loops, nonlinear dielectric properties 80—71294
- sodium acetylacetonate, anomalous dielec. behaviour, evidence for ferroelectricity 79—91390
- tetramethylammonium cobalt tetrachloride, ferrielectricity, triple 60 Hz D-E hysteresis loops 80—71365
- tetramethylammonium tetrachloroferrate, press. induced ferroelectricity, dielec. and DTA meas. 80—80722
- tetramethylammonium zinc tetrachloride, ferrielectricity, triple 60 Hz D-E hysteresis loops 80—71365
- TGS:Cr^{3+}, EPR and spontaneous polarisation stabilisation during annealing 77—4610
- TGS:$Cr^{3+}(VO^{2+})$, polarization reversal, static hysteresis loops, switching processes, EPR 78—43633
- TGS:$Fe^{3+}(Cu^{2+})(Mn^{2+})(Ni^{2+})$, dynamical props. using slowly varying elec. fields, hysteresis *(Spanish)* 77—69785
- TGS, ferroelectric hysteresis, dielectric and pyroelectric props. *(Chinese)* 80—88938
- TGS, internal bias field, hysteresis loops *(Chinese)* 80—84705
- TGS, L-α-alanine disordered regions, dielec. prop. changes in transition region 80—108159
- TGSe, deuterised, elec. field induced Merz double hysteresis loop obs. 78—31164
- thiourea monocrystals, γ-irrad. effects on dielec. props. 79—91391
- trisarcosine calcium chloride crystals, ferroelec., electrooptic and ferroelastic props. 80—34865
- TSCC ferroelastic monodomain crysts., dielec. behaviour 79—42888
- vinylidene fluoride trifluoroethylene copolymer, ferroelec. behaviour 80—50284
- wheat, pyroelectric props. 77—12322
- $Ba_{0.92}Ca_{0.08}TiO_3$ ceramic, uniaxial stress effects, US dilatometric and dielec. meas. 78—52454
- $Ba_2NaNb_5O_{15}$ crystal domains, amplitude modulation of light by diffr. 79—59832
- BaT:O_3:Mn, ferroelec. domain stabilisation by bulk ordering of defects 79—42925
- $BaTiO_3$ ceramic dielectric capacitor, processing prop. relations, hysteresis, permittivity 80—80730
- $BaTiO_3$, controlled surface layers 78—48120
- $BaTiO_3$, doped, loss mechanism and domain stabilisation 78—84542
- $BaTiO_3$, ferroelec., reduction of hysteresis losses 79—42926
- $BaTiO_3$, ferroelec. thin films, r.f. sputtering, X-ray and microprobe obs. 79—47627
- $BaTiO_3$ film, sputtered, elec. props. 79—42676
- $BaTiO_3$, molecular field statistical model, ferroelectric materials, props. *(French)* 79—69793
- $BaTiO_3$, nonstoichiometry of vac. condensates, effect on dielectric props. 77—16260
- $BaTiO_3$ on Si substrate, prep. and elec. props., expt. 77—20460
- $BaTiO_3$ RF sputtered ferroelectic film on Si substrate, ferroelectric props. 80—80697

dielectric hysteresis continued
- $Ba(Ti_xSn_{1-x})O_3$ thick film, ferroelec., phase transitions and dielec. props. 80−97215
- Bi_3GeVO_9, dielec. props. and twin struct. 77−12350
- Bi_2MoO_6 ceramic, permittivity, ferroelec. T_c and hysteresis 79−82932
- $Bi_4Ti_3O_{12}$ ceramics, ferroelectric, hot-forged, grain orientation and dielectric props. 80−40076
- $Bi_4Ti_3O_{12}$, elec. characts., phase transition obs. 80−60517
- $Bi_4Ti_3O_{12}$, ferroelec. film, on Si substrate, polarisation reversal and film struct. 79−91392
- $Cd_2Nb_2O_6S$, pyrochlore struct., ferroelec., dielec. and structural study 79−38488
- $CdTiO_3$, single cryst. growth and props. 79−100046
- $Cd_2Ti_2O_5F_2$, single cryst. growth and props. 79−100046
- CsD_2PO_4 80−25317
- CsH_2PO_4, dielec. props., press. and temp. depend. 80−25317
- CsH_2PO_4, ferroelec., press. induced antiferroelectricity 79−4774
- CsH_2PO_4, press.-induced antiferroelectricity *(Japanese)* 80−15992
- CsH_2PO_4-d, antiferroelec. under hydrostatic press. 79−91384
- $GaAs_{0.6}P_{0.4}$ anodic oxide hysteresis effect on C-V meas. 79−61771
- $GaAs_{1-x}P_x$, thermal oxide, dielec. leakage current and C-V hysteresis effects, effect of annealing 79−61772
- KCN-KCl mixed system, order-disorder transition, dielec. props. meas. 78−15112
- KD_2PO_4, X-irradiated, hysteresis effects obs. by ESR 80−103928
- KH_2PO_4, and isomorphs, dielec. props. and birefr., simultaneous obs. 78−15130
- KH_2PO_4, X-irradiated, hysteresis effects obs. by ESR 80−103928
- K_2SeO_4, ferrielectricity, triple 60 Hz D-E hysteresis loops 80−71364
- $KTa_{1-x}Nb_xO_3$ film, RF sputtering, structural and electrical properties obs. 78−88426
- $KTaO_3$, crit. dielec. and optical props. and storage, 4K 77−24805
- $KTaO_3$, polarisation, dielectric. const., relax. effects, electret state 77−12302
- K_2ZnCl_4, ferrielectricity, triple 60 Hz D-E hysteresis loops 80−71365
- $LiN_2H_5BeF_4$, hysteresis loop, protonic cond. model *(French)* 77−32320
- $(NH_4)_2,SO_4$, ferrielectricity, triple 60 Hz D-E hysteresis loops 80−71364
- $(NH_4)_2BeF_4$, effect of surface layer on spontaneous polarisation 79−38445
- $(NH_4)_2BeF_4$, ferrielectricity, triple 60 Hz D-E hysteresis loops 80−71364
- NH_4HSeO_4, cryst. struct., dielec. and ferroelec. props. 80−60528
- NH_4HSeO_4, para- to ferroelectric transition obs. by permittivity meas. 79−51916
- $Na_{0.5}Bi_{0.5}TiO_3$, dielectric const. thermal hysteresis, ferroelectric-antiferroelectric transitions 80−50281
- $Na_{0.5}Bi_{0.5}TiO_3$, phase transition, hysteretic behaviour 80−71330
- $NaH_3(SeO_3)_2$, dielec. props. 78−43764
- $NaNbO_3$, hydrostatic press. effect on permittivity, phase transition, hysteresis 80−80670
- PLZT ceramic, ageing, dielec. props. 80−88940
- PLZT ceramic, optical gate, dielec., optical props., electro-optical effect meas. 78−42418
- PLZT ceramic;, visible light scatt. depend. on photoferroelectric space charge fields 80−80806
- PLZT film, growth by RF sputtering, struct. and ferroelec. props. 77−48340
- PLZT, reduced, exam. of ageing phenomena, using dielectric hysteresis *(German)* 79−33647
- PLZT, thin film prep. by RF sputtering, struct. and ferroelec. props. *(Japanese)* 77−69992
- PLZT, transparent ferroelec., RF sputtering and film characterisation 78−72727
- PLZT type ceramics, calorimetric meas. of energy of electrical polarisation 79−2770
- $PbBi_2Nb_2O_9$ ceramic, grain oriented, dielectric and piezoelectric props. 79−42896
- $Pb_5Ge_3O_{11}$ single crystals, switching behaviour and hysteresis 80−40077
- $Pb_5(Ge_{1-x}Si_x)_3O_{11}$, electrogyration, phase transition and dielectric props. 80−93269
- $PbIn_{0.5}Nb_{0.5}O_3$, ferroelectric, dielectric props. 80−103923
- $PbNb_{0.5}Sc_{0.5}O_3$, ceramic, dielec. props. 79−11392
- $Pb(Ti,Zr,[Fe_{1/2}Ta_{1/2}])O_3$, pyroelec. props. at transition between ferroelec. phases 78−52447
- $Pb(Ti,Zr)O_3$:Fe(Mn)(Al), internal bias field and hysteresis relaxation 78−43823
- $PbTiO_3$ ferroelec. thin film, prep. by RF sputtering and dielec. props. 79−100052
- $PbTiO_3$ ferroelectric thin films, fabrication by RF sputtering, characts. 80−40261
- $Pb(Zr,Ti)O_2$ ceramic, surface barrier electroreflectance, hysteresis, ageing 80−80752
- $Pb(Zr,Ti)O_3$ film, prep. by electron beam evaporation technique 77−1809
- $Pb(Zr,Ti)O_3$ films, ion beam sputtering, dielec. and ferroelec. props. 79−78881
- $Pb(Zr,Ti)O_3$, piezoelectric bimorph, quasistatic response exam. 78−43794
- $Pb(Zr,Ti)O_3$ thin films, fabrication and characterisation electron-beam deposition 80−16188
- $Pb(Zr,Ti)O_3$:Mn ceramics, anomalous dielec. losses 79−42892
- $Pb(Zr,Ti)O_3$:Nb ceramic, stress effects on ferroelec. hysteresis, macroscopic strain, US vel. 79−4778
- $Pb(Zr_xTi_{1-x})O_3$ films, ion beam deposition, struct., dielec. and ferroelec. props. 80−20788
- RbH_2AsO_4, phase transition, dielec. pyroelec. and internal friction meas. 77−16261
- RbH_2PO_4, X-irradiated, hysteresis effects obs. by ESR 80−103928
- $RbH_3(SeO_3)_2$, repolarisation in region of improper ferroelec. phase transition 77−8497
- $RbLiSO_4$, thermal and dielectric props., ferrielectricity 79−28688
- Rb_2ZnBr_4, dielectric const. and ferroelectric hysteresis 78−84535
- Rb_2ZnBr_4, ferrielectricity, triple 60 Hz D-E hysteresis loops 80−71365
- Rb_2ZnBr_4, ferroelectricity, hysteresis loops and dielec. const. meas. 78−23416
- Rb_2ZnCl_4, ferrielectricity, triple 60 Hz D-E hysteresis loops 80−71365
- Rb_2ZnCl_4, ferroelectricity, hysteresis loops and dielec. const. meas. 78−23415
- $SbNbO_4$, ferroelec. film characts. 77−48127
- SbSI, domain struct. relaxation 78−48135
- $Sr_{0.25}Ba_{0.75}Nb_2O_6$ film, growth and electrophys. props. 79−42928

dielectric hysteresis continued
- $Sr_{0.75}Ba_{0.25}Nb_2O_6$, ceramic ageing dielec. props. 80−88940
- $Sr_6Ti_2Nb_4O_{20}$, new class of layer ferroelectrics. X-ray anal. and permittivity meas. 77−16266
- $SrTiO_3$, crit. dielec. and optical props. and storage, 4K 77−24805
- $TlNbO_3$, ceramics, hysteresis loops and dielec. props. 79−42885
- $TlTaO_3$, ceramics, hysteresis loops and dielec. props. 79−42885
- Tl_2TaO_6, Tl I lone pair stereochem. activity rel. to ferroelectricity 78−15131
- $Tl_2Ti_4O_9$ ceramics, hysteresis loops and dielec. props. 79−42885
- V_2O_5, ferroelec. semicond., dielec. and elec. meas. 80−60516

dielectric-loaded antennas
- far IR antennas for 0.1 to 3.0 mm range, review 80−69553
- IR and submillimetric-wave antenna design and simulation 79−30552
- microstrip slot radiator for medical appls. 80−108994
- microwave dielectric spherical radiator, horn-fed, near field characteristics 77−56543
- microwave Gaussian beam launcher, for selective partial body exposure of biological substances 79−29578
- scattering by dielectric-loaded trough, in conducting plane 77−54655
- Schottky-barrier diode monolithic detector dielectric plate antenna 79−30548
- semiconductor plasma containing system, cylindrical, with ring source of magnetic current, radiation pattern calc. 77−3951

dielectric-loaded waveguides
- anisotropic dielectrics parameter meas. using resonance of waveguide-dielectric system 80−27274
- arbitrarily shaped dielectric body inside waveguide, three-dimensional anal. 78−71005
- asymmetric gas-dielectric optical waveguide with wall resonances 79−7216
- coherent microwave Cherenkov radiation generation, relativistic electron beam-dielectric loaded waveguide 77−58246
- coherent submillimetric Cherenkov radiation generated by relativistic electron beam 77−38793
- complex dielectric constant of semiconductors as SHF, measurement techniques 78−95542
- dielectric complex permittivity meas., two coupler method 78−21167
- EM field calc., produced by transverse electric waves *(Russian)* 78−82884
- EM wave propag. along rotating dielectric column in circular waveguide 78−1133
- inhomogeneous dielectric filled uniform waveguides, EM wave propag. 80−83666
- laser pulse display and shaping, subnanosecond electro-optic technique 77−19270
- light polarisation in twisted tape lightguides and braided cylindrical liquid-filled lightguides *(Russian)* 80−19107
- lossy waveguide attenuation and phase meas. 77−26343
- Maxwell eqns. for six-component fields, discretisation method *(German)* 77−53790
- metal-dielectric waveguide, third harmonic generation enhancement, comment 79−94283
- multilayer lossless transient field distribution 80−23604
- propagation in coaxial cylinders separated by dielectrics *(Russian)* 78−17845
- relativistic electron beam driven, coherent submillimetre Cherenkov radiation generation 77−38788
- strip lines meas., small standing wave ratio and losses meas. 80−77811
- symmetrical rib optical waveguide fundamental modes 77−23744
- VHF waveguide dielectric scatt. model for pulse-probe data interpretation *(Russian)* 80−62682
- Ge slab in waveguide, microwave absorpt. due to geometric reson. of longitudinal-section elec. surface waves 80−39874

dielectric loss angle *see dielectric losses*

dielectric loss-angle measurement *see dielectric loss measurement*

dielectric loss measurement
- *see also dielectric losses*
- anisotropic dielectrics parameter meas. using resonance of waveguide-dielectric system 80−27274
- automatic, high resolution, at 100 MHz to 300 MHz and 2°C to 40°C 80−68219
- automatic equipment, for solid and liquid dielectrics meas., temp. dependence *(Polish)* 78−32836
- calorimetric determ. of dielectric loss factors at 1 kHz and 4.2K 80−98921
- cell design for small loss tangents meas. at low temp. 80−42237
- ceramic low-loss foils, microwave meas. method *(Polish)* 78−37028
- coaxial line resonator used for complex dielectric data measurement 78−8419
- coaxial lumped capacitance resonators design for dielec. material investigs. 77−67460
- combined total reflection-transmission method, appl. to dielec. spectroscopy 78−86295
- cyclohexane loss meas. at 35, 72 and 144 GHz 77−82560
- extended standing wave method, for low dielec. loss meas., permittivity, loss angle calc. *(Japanese)* 77−45869
- glass-plastic, engineering, nondestructive structural identification 78−92422
- high pressure apparatus for dielectric meas. at high freqs. 79−67346
- high sensitivity meas. using supercond. microwave resonators in oscillator loop 77−10043
- integrator for low freq. current meas., appl. to dielec. polarisation *(French)* 77−71348
- liquid, determ. of very low losses at 9 and 29 GHz via waveguide interferometer 77−8503
- liquid, dielec. spectroscopy at microwave freqs. 77−41646
- liquid solidification press. meas., dielectric loss method 77−45868
- loss angle/permittivity meas. as function of temp. at 9-10 GHz 77−82559
- loss-angle meas. at 100 GHz range, precision, Fabry-Perot resonator 78−70163
- low dielectric loss meas. apparatus for 0.1 to 200 MHz 80−15958
- low loss liquids, loss angle temp. var. meas. at microwave freqs. 78−48114
- low temperature method, expts. on polymers, 0.1-10 GHz, 2.2-4.2K 77−24786
- low-loss material, for supercond. cable fabrication, meas. using supercond. reson. cavity 77−8501

dielectric loss measurement continued
low-loss solid dielectric meas., automated resonance substitution systems 80—15957
material testing, nonuniformity of dielec. props., at mm wavelengths, method of determining 78—40001
micrometer electrode for improved meas. in 1-200 MHz range 78—49864
microwave, von Hippel's method, appl. to Eccosorb HF-2050, 500-2000 MHz 77—32314
microwave cavity resonator bridge method 77—37914
microwave freq., rectangular waveguides *(Russian)* 79—2788
microwave resonator bridge method 78—54391
on-line calculator-based meas. system 78—54397
PMMA, electret, dielectric meas. at ultralow freq. by reheating 80—4741
polar dielectrics, in wide frequency interval 77—12310
polar liqs. using a lumped-capacitance method for coaxial lines 78—77936
polyethylene, loss tangent variation obs., under long term irradiation by ^{60}Co rays *(German)* 80—75266
polyethylene used in submarine telecommunication cables, measurements at high pressure and freq. 80—27316
polymeric solids, measurement using superconducting microwave resonators, 2.2 to 15K 79—67316
procedure for measurement, using Q meter in freq. range 50 to 35 MHz 78—54394
radiation losses meas., through connecting-coupling hole in microwave cavities 77—79105
Schering bridge appl., principles *(Portuguese)* 77—67461
smoky quartz, thermal props. at very low temp. 80—24610
solid dielec., high sensitivity, using supercond. high-Q resonator 78—93733
strip lines, dielectric, use of tuned reflectometer 80—77811
three-terminal test cell for rapid dielectric loss and resistivity meas. of oil samples 77—67465
time domain spectroscopy for low loss dielectric meas. 80—98983
tissue dielectric loss and permittivity spectrometer 79—57743
tissue LF dielectric dispersion calc. and meas. *(Russian)* 80—21512
transformation method for low-loss measurement in 300 to 1000 MHz range 79—93165
tubular dielectric, complex permittivity and loss angle meas. in X-band using H_{011} cavity resonator method *(German)* 80—62690
UHF meas. using waveguide-dielectric resonances 77—55760
variable frequency method 79—93169
InSb, MIS struct., background radiation effect on photoelec. processes 80—25015

dielectric losses
see also loss angle
acetylacetone, H bonding, dielec. dispersion obs. 77—63356
adsorbed layers, Maxwell Wagner and Debye processes, differentiation using temp. depend. of dielec. loss 79—28195
albumin, bovine serum, hydrated, dielectric props. at 9.9 GHz 78—15758
alcohols, dil. solns., dielec. loss and relax., microwave and sub-mm. wave absorpt. obs. *(German)* 78—23396
aliphatic ethers, dil. solns., dielec. loss meas. for dielec. relax. 78—68451
alkali halides, off to on centre defect transitions under hydrostatic press 78—15199
alkyl trichloroacetates, solns., intramol. rot., permittivity and dielectric loss, microwave meas. 78—31145
4′-n-alkyl-4-cyanobiphenyls, dielec. dispersion 78—2798
aminobenzotrifluoride, benzene soln., permittivity and dielec. loss 78—64320
aminopyridines, in 1,4-dioxane soln., dielec. consts., losses and relax. 78—64319
anilines, substituted, in nonpolar solvent, dielec. relax. obs. 80—55022
anisotropic artificial dielectrics, dispersion props, investigation, electrodynamic method 80—88903
apatites, dipolar reorientations, TSD study 80—107068
barium margarate film, thickness influence on dielec. loss meas. 77—81051
barium palmitate film, thickness influence on dielec. loss meas. 77—81051
benzene sulphonyl hydrazine, in nonpolar solvent, thermodynamics of dipolar relax. 79—91347
benzothiazole, dielec. loss, relax. and const. in liq. and soln. 79—91346
benzoylacetone, dil. soln. in benzene, dielectric behaviour 79—42886
benzoylacetone, H bonding, dielec. dispersion obs. 77—63356
benzoylacetones, p-substituted, dil. soln. in benzene, dielectric behaviour 79—42886
biological substances, tabulation for freq. range 10 kHz to 10 GHz 80—108143
bis[catena-poly(methylarsenic)], LF dielec. response 79—56719
bone, bovine cortical, dielec. relax. 77—40964
bromal, in benzene soln., dielec. relax., loss, and dipole moment 80—2692
bromoform, solid, phase transform., dielec. dispersion and differential scanning calorimetric obs. 80—24582
butane diol, asymm. dielectric dispersion, 1-25000 MHz 78—15092
1,4-butanediol, dielectric behaviour, LF dispersion 77—48126
2,3-butanediol, dielectric dispersion 78—72455
calcium behenate monomolecular layers between Al electrodes, nonlinear dielec. props. 80—80405
cellulose electrets, TSC and dielec. losses and relax. 80—25284
cellulose esters, plasticiser effects on mech. and dielec. relax. 80—40047
cellulose fibre, moist, dielec. props. 78—76380
ceramics, ferroelec., dielec. losses due to domain wall oscill. 78—84541
ceramics, granular, electrophysical props. depend. on porosity, temp., solid-phase props. 77—69764
charge carrier contrib. 79—56718
chloral, dielec. consts. and dielec. losses meas. 77—20795
chloral, in benzene, permittivity, dielectric loss, 36 GHz 77—32323
chloral, liq., permittivity, dielec. loss, up to 60 GHz 78—60384
chloranil pellets, thermally stimulated discharge current and dielectric studies 80—93236
4-chloro-3-nitrobenzotrifluoride-benzene (carbon tetrachloride) dilute soln., dielec. relax. time, dipole moment, microwave obs. 78—35084
4-chloro-3-nitrotoluene-benzene (carbon tetrachloride) dilute soln., dielec. relax. time, dipole moment, microwave obs. 78—35084
chlorobenzene-cis-decalin, mixtures, dielec. const. and loss tangent in liq. and solid phases 80—100628

dielectric losses continued
chlorobenzene-cis-decalin mixtures, phase transitions and dielec. behaviour study in 77-330K 80—29680
chlorobenzotrifluoride, benzene soln., permittivity and dielec. loss 78—64320
o-chloronitrobenzene-benzene (carbon tetrachloride) dilute soln., dielec. relax. time, dipole moment, microwave obs. 78—35084
cholesterin ethers, dielec. absorption, heating/cooling and oxidation depth effects *(Russian)* 79—50984
cholesterol, dielectric props. under UV excitation 80—6912
cholic acid, dielectric props. under UV excitation 80—6912
coal dispersions, solvent refined, elec. props., surface characts. 80—80333
complex dielectric, humidity, temp., density, freq. and granulometric composition effects on elec. characts. *(Russian)* 79—42881
composites, interfacial polarisation and loading factor effects in dielec.-loss meas. 80—2693
cooperative model of dielec. behaviour, susceptibility amplitude, rel. to freq. of max. loss 80—2694
corundum ceramic, high-temp. treatment, powder medium effect on microstruct., comp., strength and dielec. props. 79—33984
cryogenic gases and liquids, dielectric breakdown 80—40051
crystals, dipole-impurities, one-band isotropic effective-mass and Born approxs. 77—63363
cyanobiphenyls, physical props., appl. to Kerr cells 79—19142
cyclohexanol, polymorphism, Raman spectroscopy 77—73138
cytochrome-c, hydrated, dielectric props. at 9.9 GHz 78—15758
defect-free crystals, dielec. losses due to phonon system perturb. in elec. field 80—80693
defective dielectrics, EM heating with time depend. param., WKB calcs. 80—71367
diamagnetic glassy semiconductors, at. tunnelling states, dielec. and elastic losses 79—87385
dibenzoyl methane, H bonding, dielec. dispersion obs. 77—63356
1,1-dichloro-1-nitroethane, dil. soln. in benzene, dielec. relax. study 80—29679
1,2-dichloroethane, enclathrated, conform., reorientation, PMR line shape anal., dielec. absorpt. meas. 79—91300
dichloromethane-decalin glass, mol. dynamics, from dielec. loss meas., 107-148K, 293K 78—76379
dicyanoalkanes, in benzene soln., microwave absorption, internal rot. 78—60385
dielectric film, AC props., model 79—91352
dielectric relaxation and LF anomalous dispersion obs. *(Japanese)* 78—49056
dielectric surface, charge accumulation, losses, electron-beam treatment *(Russian)* 80—75931
diethylene glycol, asymm. dielectric. dispersion, 1-25000 MHz 78—15092
diffusion traps for divalent ions, dielectric loss and ionic thermocurrent techniques 80—6566
diglycine nitrate, dielec. relax. in paraelec. and ferroelec. regions 78—31149
1,3-dihalopropane, dielectric permittivity and loss, dipole moment 78—60383
dihydroxy benzenes in ethyl alcohol, dielec. dispersion charact. 80—75932
dihydroxy toluene in ethyl alcohol, dielec. dispersion charact. 80—75932
dimethyl propane diol, dioxane soln., asymm. dielec. dispersion, 1-25000 MHz 78—15092
diphenyl ether, dil. solns., dielec. loss and relax., microwave and sub-mm. wave absorpt. obs. *(German)* 78—23396
dipolar material, derivation of dielec. loss formula, appl. to relax. in glassy systems 80—50262
dipolar materials, temp. depend. of loss peak freq. 80—88922
disperse system, high conc., interfacial polarisation, dielec. consts. and relax. freqs., numerical estimation 77—32833
dye, dielec. const. and loss meas., 10^2 to 10^5 Hz 78—6622
EBBA, in benzene soln., dielec. relax. meas., 4.0, 9.4 and 30.4 GHz 77—40176
EBBA, nematic liq. cryst., RF dielec. props. 79—4238
EBBA, solid and liquid states, temp. and freq. depend. *(Russian)* 78—72450
EBBA, stable and metastable solid phases, dielec. dispersion meas. 78—60390
Eccosorb HF-2050, low temp., 500-2000 MHz 77—32314
elastin, hydrated, dielectric relax. 79—5247
electrets and dielectrics, conf., Sao Carlos, Brazil, Sept. (1975) 80—7251
energy basis of dielec. relax. loss 78—31150
epoxy resin, hardening, mechanical and dielectric losses 78—48115
epoxy resin systems, synthesis review, phys. and mech. props. at low temps. 80—25650
epoxy resin-ferroelectric Pb(Zr,Ti)O$_3$ composite, dielec., elastic and piezoelec. consts. 77—8515
epoxy resins, mech. and elec. low temp. props. 80—25814
ester-imide varnishes, electroinsulating, thermal resist. *(Polish)* 78—84014
ethanol solution in benzene, dielec. relax. time by RF cond. meas. 80—71302
p-p-ethoxyphenylazophenyl hexanoate, dielec. relax. in stable and metastable solid phases 80—34851
ethyl trichloroacetate, in benzene, permittivity, dielectric loss, 36 GHz 77—32323
ethyl trichloroacetate, in non-polar solvents (cyclohexane, p-xylene and p-dioxane) 78—2796
ethyl trichloroacetate, soln., dielectric props. and relax. mechanisms at microwave freqs. 78—15089
4-ethylaminobenzil, dil. soln. in benzene, cyclohexane and dioxane, dielectric behaviour 78—52421
ethyltrichloroacetate, dielec. consts. and dielec. losses meas. 77—20795
ethyltrichloroacetate, liq., permittivity, dielec. loss, up to 60 GHz 78—60384
explosive mixtures, dielec. consts. and losses below 100 kHz 78—56422
fatty acids, dielectric meas. at microwave freqs. 79—19827
ferrites, microwave, dielectric constants and permeability *(Chinese)* 80—66096
ferroelectric, polarisation switching influence of mobile point defects 78—31165
ferroelectric, textured layered prep. by HF sputtering 77—85947
ferroelectric ceramic, mech. and elec. losses, correl., theory and expt. 80—66133
ferroelectric ceramics, materials and dielec. props., review 80—75957

dielectric losses continued
- ferroelectric domain wall shift, mobile point defect interaction effects 77—32338
- ferroelectric film, appl. and props. at microwave frequencies 77—1632
- ferroelectrics, centrally-symm. displacement type, dielec. losses, weak elec. field effect *(Russian)* 80—29683
- fibreglass/epoxy laminate curing by microwave heating 77—77457
- gelatin film, dielectric losses and breakdown, struct. effects *(Russian)* 77—52017
- glass, dielectric relax. loss, two level Anderson Halperin Varma model 80—66106
- glass, liquid-phase separated, struct., use of elec. methods 79—66249
- glass, peak frequency, rel. to DC cond. 79—78621
- glass, relaxation phenomena and Raman spectroscopy, review of developments 78—22665
- glass fibre reinforced non woven epoxy laminates comparison with paper phenolic and woven glass epoxy, dielec. props. 78—35635
- glycine silver nitrate, dielec. relax. in paraelec. and ferroelec. phases 80—29678
- haemoglobin, dielectric props. under UV excitation 80—6912
- halide-insulator interface, interfacial polarisation, dielec. loss meas. 77—2705
- n-heptyl-4-cyanobiphenyl, nematic phase, diffusion equation 80—71305
- heterogeneous dielectric system, Maxwell-Wagner losses, theory, crit. anal. 78—43781
- heterogeneous matrix system, generalised conductivity and loss, tangent 80—7289
- hexafluoropropylene-tetrafluoroethylene copolymer, surface component of vac. absorpt. and resorpt. currents, source of dielec. loss 80—70792
- N-(p-hexyloxybenzylidene)-p-toluidine, dil. soln. in benzene, dielectric behaviour 79—42893
- inhomogeneous insulating materials, AC dielectric props., effect of superimposed DC voltage 78—31144
- insulators, prebreakdown phenomena, freq. dependent dielectric losses 80—45006
- inverse scatt. problem of lossy dielectrics, exact soln. 77—79732
- ionic crystals, dielectric loss and relaxation theory and kinetics 80—11335
- kaolinite rare-earth complexes, relax., molar free energy of activation for dipole relax. 80—88919
- Langmuir molecule films, thickness influence, evidence 77—81051
- laser induced microwave damage, space simulation 77—81050
- lead phthalocyanine:O_2(I), Schottky barrier effect on AC current response 80—75623
- liquid and solid complex permittivity meas., rectangular waveguide method 80—15941
- liquid crystals with nematic and smectic modifications, dielec. relax. and losses 77—69769
- liquid dielectric gassing rate and discharge energy loss meas. 80—15965
- liquids, freq. depend. of dielec. losses, empirical eqn. 80—55025
- low frequency dielec. characts. from complex impedance and complex elec. modulus 79—82922
- lysozyme, hydrated, dielectric props. at 9.9 GHz 78—15758
- marble, LF dielectric props. 80—34843
- MBBA, dielec. permittivity and loss meas., −196 to 0°C 77—59511
- MBBA, dielec. relax. in metastable modification of solid phase 80—84689
- MBBA, in benzene soln., dielec. relax. meas., 4.0, 9.4 and 30.4 GHz 77—40176
- medical imaging, ceramic and PVF_2 transducers compared 79—57734
- methanol solution in benzene, dielec. relax. time by RF cond. meas. 80—71302
- methyl trichloroacetate, soln., dielectric props. and relax. mechanisms at microwave freqs. 78—15089
- microstrip, analysis of losses, Schelkunoff method *(Spanish)* 80—45005
- microwave absorbing ferrite-dielectric composite 77—7880
- microwave freqs., two coupler method modification 80—100632
- molecular solid, dielectric loss, multimultiple relaxations, comparison with polymers 78—19409
- natural clay permafrost, elec. props. *(7-44967)* 77—44967
- nematic liquid crystals, molecular mechanisms of dielec. polarisation and relaxation 80—34846
- nitrobenzotrifluoride, benzene soln., permittivity and dielec. loss 78—64320
- n-p-octyloxybenzylidene-p-toluidine, dielectric behaviour in nematic mesophase at RF 80—34842
- organic rigid molecules solns. and mixtures, dielectric relax., const. and loss factor, microwave region 77—55747
- oxide glasses, elec. cond. and dielec. relax., correl. 78—79801
- paper capacitors, effect of simultaneous application of AC and DC voltages, freq. and temp. depend. 78—15091
- parylene polymers, synthesis, elec., phys., corrosion props. *(German)* 78—64521
- phenolic Mannich bases, dielec. relax. study 80—97196
- phenols, dil. solns., dielec. loss and relax., microwave and sub-mm. wave absorpt. obs. *(German)* 78—23396
- photographic composite film with high loading factor, extension of Maxwell-Garnett dielectric loss theory 79—19835
- photographic emulsion layers 79—19836
- piezoelectric ceramic resonators, eigencoupling state space vector representation 80—2697
- piezoelectric solids, shape-dependent damping 80—93242
- plastics and reinforced plastics, tabulated data as design guide 77—21087
- PMMA, electret, dielectric meas. at ultralow freq. by reheating 80—4741
- PMMA-PVC mixtures, dielec. relax. and struct. rel. to formation *(Russian)* 77—20073
- polar liquids in double layer capacitors, RF conduction, ion diffusion effect 80—107883
- polar molecules, in nonpolar solvent, dipole moments and relax. times 78—43782
- poly(γ-methyl L-glutamate), electric conduction mechanism *(Japanese)* 80—54696
- poly-2-hydroxyethyl methacrylate, dielectric γ relaxation 80—34850
- poly-γ-benzyl-L-glutamate, synthetic polypeptide, nonlinear dielectric effect in nonpolar medium 80—84682
- poly-ε-caprolactone in dioxane soln., low freq. dielec. response 77—40177
- poly-N-vinylsuccinimide, dielec. and pulsed NMR relax. glass-rubber transition, mol. motions 77—48125
- poly-p-xylylene films, carrier traps, X-ray induced TSC, thermolum. and dielec. loss study 80—88570

dielectric losses continued
- polyacrylate solutions, dielec. relaxation 80—40045
- polybenzoxazole, dielectric β relaxation, role of water molecules 77—90100
- polycarbonate, γ-irradiated, dielec. behaviour and glass transition 80—97182
- polycarbonate, plastic insulation for cryogenic power cable, exam. of dielectric, tensile props. 80—25823
- polycarbonate, sorption of water and its effect on dielec. behaviour 79—11383
- polychlorotrifluoroethylene, crystalline and amorphous peaks, dielectric props. 80—93237
- polydimethylsiloxane fluid permittivity and dielectric loss 78—6621
- polyester, linear aliphatic, mol. motions determ. by dielec. relax. and loss meas. 77—63364
- polyester (Mylar), plastic insulation for cryogenic power cable, exam. of dielectric, tensile props. 80—25823
- polyester varnishes, electroinsulating, thermal resist. *(Polish)* 78—84014
- polyesters, linear, H_2O absorption and electrio loss factor *(German)* 80—34849
- polyethersulphone, dielectric γ losses 78—68449
- polyethylene, γ-ray polymerised, dielectric loss reduction 77—24783
- polyethylene, alcohol infused, loss peaks due to secondary groups 80—84688
- polyethylene, at very low temperatures *(Japanese)* 80—11331
- polyethylene, contributory factors, 4.2K 77—24787
- polyethylene, dielec., cryogenic tunnelling losses at microwave frequencies 77—52016
- polyethylene, dielec. loss below 4.2K arising from proton tunnelling 77—52015
- polyethylene, dielec. loss meas. using supercond. microwave resonators in oscillator loop 77—10043
- polyethylene, dielec. props. rel. to mol. struct. 80—29681
- polyethylene, dielec. relax. mechanism, 1-80K *(German)* 78—76384
- polyethylene, gamma radiation effects on dielect. parameters, expt. *(Hungarian)* 78—59836
- polyethylene, high-density, dielec. loss, below 4.2K, antioxidant, annealing and drawing effects 78—84518
- polyethylene, low density, dielec. behaviour, struct. props. influence *(German)* 78—92017
- polyethylene, low temp. dielec. loss due to antioxidants 79—99822
- polyethylene, low-density natural, at elevated temps. 80—97185
- polyethylene, mech. and elec. low temp. props. 80—25814
- polyethylene, microwave dielec. losses variation rel. to different sample treatments 80—25881
- polyethylene, oxidised, low-temp. dielectric spectrum 79—61304
- polyethylene, plastic insulation for cryogenic power cable, exam. of dielectric, tensile props. 80—25823
- polyethylene electrets, charge trapping mechanism, TSC, DTA and optical meas. 80—11322
- polyethylene terephthalate, β relax., dynamic mech. and dielectric loss data 79—15399
- polyethylene terephthalate, oriented, directional anisotropy, of dielec. β-relaxation 77—16247
- polyethylene terephthalate, TSC and thermolum. due to electron detrapping by local mol. motions 80—96898
- polyethylenes, dielec. losses, for use in AC superconducting power transmission lines 80—25302
- polyethylenes, dielectric γ-dispersion, crystallinity effect *(Japanese)* 79—87384
- polyferrocene film, plasma polymerised, dielec. props., 40 kHz to 50 MHz, 30-400°C 78—52439
- polyhydroxyl alcohols, H-bonded solns., microwave dielec. relax. 79—33599
- polyimide film, dielec. props. 100 Hz to 100 kHz, expt. 78—43783
- polymer, 0.1-10 GHz, 2.2-4.2K 77—24786
- polymer, complex dielectric const. determ. from polarisation current 77—66451
- polymer, glass transition under high-press., dielec. loss method obs. *(Russian)* 78—71841
- polymer electret, charge dissipation, transport mechanisms 80—7268
- polymer glass transition, dynamic props., mol. model *(Russian)* 78—87777
- polymer-TiO_2 composite, dielec. props. *(Japanese)* 78—95540
- polymers, effect of stretching *(German)* 79—43446
- polymers, elec. props. and morphology, correl. review 78—43786
- polyphenyl chinoxalines, dielectric relaxation *(German)* 77—59513
- polyphenylisobutylsilsesquioxane, dielectric investigation of molecular mobility 77—58960
- polyphenylsilsesquioxane, dielectric investigation of molecular mobility 77—58960
- polypropylene, contributory factors, 4.2K 77—24787
- polypropylene, effect of corona treatment on dielectric props. for capacitor appl. 79—33607
- polypropylene, plastic insulation for cryogenic power cable, exam. of dielectric, tensile props. 80—25823
- polypropylene films, dielec. props., impurity effects 80—71304
- polypropylene films, meas. of dielectric losses at cryogenic temps. 80—25301
- polypropylene glycol melt, mol. motion, dielectric and Kerr effect relax. obs. 80—60498
- polypropylene-polyurethane laminates, meas. of dielectric losses at cryogenic temps. 80—25301
- polypyromellitimide, low temperature relax., NMR, dielec. and mech. losses 78—71686
- polystyrene particle colloidal suspension in KCl(LiCl) aq. solns., dielectric loss 78—35728
- polystyrenes, anionic, TSC obs. of T_g and T_{ll} transitions 80—84686
- polysulphone, dielectric γ losses 78—68449
- polysulphone, elec. appl., dielec. props. meas. 77—55750
- polysulphone, plastic insulation for cryogenic power cable, exam. of dielectric, tensile props. 80—25823
- polytetrahydrofuran film, electrochemically prepared between Pt and Au electrodes, AC elec. props. 80—40062
- polytrifluoroethylene, dielectric relax. processes above and below glass trans. *(Japanese)* 80—55028
- polyvinyl acetate, struct. relax., enthalpy and elec. polarisation obs. 79—41978
- polyvinyl cinnamate, and photocrosslinked form, low freq. dielec. loss evaluation 79—82919

dielectric losses continued
polyvinylidene fluoride, γ-phase containing films, thermocurrent spectra 79—42555
polyvinylidene fluoride, correlated mol. motion in dielec. props. 77—55749
polyvinylidene fluoride, dielec. props. and phase transitions *(French)* 80—55008
polyvinylidene fluoride, US transducers, dielec. and acoustic losses 80—48541
polyvinylidene fluoride fan, electromech. conversion efficency and high field dielec. loss 79—82926
power law frequency dependent dielectric function and nonanalyticity properties 78—60387
propane, gaseous, dielectric losses, absorpt. of 8 and 12 mm radiation under pressure *(French)* 79—93991
1,2-propane diol-dipropylene glycol, dielec. dispersion charact. 80—75932
propanes, substituted, liq., microwave absorpt., dielectric relax., loss, permittivity, moments and reorientation 77—63362
propyl acetate-propyl alcohol, dielec. dispersion charact. 80—75932
n-propyl trichloroacetate, soln., dielectric props. and relax. mechanisms at microwave freqs. 78—15089
propylene glycols, dielec. props., chain length effect 80—44995
PTFE, spacer material for supercond. cable, meas. using supercond. reson. cavity 77—8501
PVC, dielectric props. in ultra-low freq. range *(French)* 78—23395
PVC, gamma radiation effects on dielect. parameters, expt. *(Hungarian)* 78—59836
PVC, reduced, dielec. props. rel. to mol. struct. 80—29681
PVC film, soln.-grown, between Al electrodes, AC elec. props. 80—15619
PVC loss factor at 10-90 kHz range 77—86235
PVC-polyvinylidene chloride copolymer, dielectric loss at low-temp 78—95543
pyridines, substituted and N-oxides, dielectric relax. in solns. 78—6627
pyroelectric detector, temperature noise and dielec. loss 77—17975
pyroelectric high power density heat engine, dielectric losses, polarisation 80—80689
quartz, effect of neutrons on electr. characts. *(Russian)* 77—48119
quartz, electron irradiation effects on optical, dielec., elastic props. 80—59521
rare earth aluminate, scandate and zironate film coatings, electrophys. props. w.r.t. prep. technology 80—60781
rare earth oxides, dielec. const. and loss at low temp. 80—93229
relaxation intensity evaluation from dielectric loss data, empirical formulae 80—25292
rigid polar molecules in dil. solns., dielectric loss in far IR region *(German)* 77—16248
Rochelle salt, dielectric props. near upper Curie pt. under hydrostatic press. 79—82935
rubber, natural, with furnace soot or acetylene black, natural ageing and dielectric props. *(German)* 78—19795
rubber, styrene butadiene, dielectric const. and loss, lignin content depend. 80—29670
rubber mixtures, synthetic, natural ageing effects on dielec. props. 77—24778
rubber-channel black mixtures, natural ageing effects on dielec. props. 77—24777
sapphire, HF dielectric losses, loss angle upper limit *(Russian)* 77—24785
scattering by lossy dielectric wedge, numerical soln. 77—19144
silicone, film deposition, glow discharge polymerisation, elec. and thermal characts. 78—6467
sodium acetylacetonate, anomalous dielec. behaviour, evidence for ferroelectricity 79—91390
sodium benzoylacetonate, dielec. props. and cryst. struct. 79—8099
solid dielectric loss peak, many-body interpretation 80—15953
solid universal dielectric response law, many-body interpretation 80—15952
solids and liquids, dielectric loss characterisation 78—88252
solvent, ion migration and frequency-dependent dielectric loss 79—19832
space charge effect 77—63366
squaric acid-d_0,-d_2, 2-dimens. antiferroelec., dielec. props. and phase transitions, press. effects 79—95700
stearic acid film, in MIM struct., AC cond. and dielec. props., freq. depend. 80—55030
stearic acid films, evaporated, vac. effects 80—97435
stearic acid multilayer films, dark and photo-generated dielec. response 77—72882
steatite, dielectric ceramic 77—32546
stibiotantalite type structure ferro- and antiferroelectrics, props. and crit. points 79—38460
styrene-butadiene-styrene triblock copolymers, dielec. props. 78—95545
styrene-butyl vinylpyridinium-TCNQ copolymer, dielectric const. *(Japanese)* 78—60375
styrene/n-butyl-2-vinylpyridinium-TCNQ copolymer, dielec. permittivity *(Japanese)* 78—56416
testosteron, dielectric props. under UV excitation 80—6912
1,1,2,2-tetrabromoethane, dil. soln. in benzene, dielec. relax. study 80—29679
tetraglycine, aq. soln., static dielec. const. and microwave dielec. loss 78—47462
TGS, complex dielec. permitt. near Curie temp., ferroelec. polarisation mechanism interpretation 78—43808
TGS, deuterated, undoped and alanine-doped, growth by rotating disc method and elec. props. 79—47611
TGS, pyroelec. IR detectors, permanent polarisation due to X-rays, optimum non-ferroelec. behaviour 77—41684
TGS, tan δ depend. upon sample thickness 77—59510
thermal charge carrier movement in lossy dielecs. 80—88920
transient excitation, energy flow analysis 78—80282
transient species, detection by dielectric loss meas., microwave method 79—74467
transition metal oxide films, dielec. dispersion and polarization 78—2803
tremolite asbestos, fibrous. elec. anisotropy 78—80273
trifluoroacetates, methyl and ethyl, intramol. relax. at microwave freqs. 80—55020
triglycine, aq. soln., static dielec. const. and microwave dielec. loss 78—47462
TSC technique for nonexponential dielec. response materials 79—47383
TSCC ferroelastic monodomain crysts., dielec. behaviour 79—42888
universal dielectric response in condensed matter 79—28674
universal dielectric response in condensed matter 80—11333

dielectric losses continued
DL-α-valine in aq. soln., dielectric dispersion 78—20141
viscous liquid, glassy state, effect of fictive temp. on dielec. relax. 79—24256
vitreous systems, local motions, dielec. losses and relax. phenomena 80—108154
vitrified conc. aq. solns., ionic hydration and secondary dielec. relax. and loss 79—24882
Ag-halide microcryst., space charge characts. 78—15097
AgBr (100) microcryst., dielectric loss meas., ionic conductivity 77—43931
AgBr and AgBr:$PbBr_2$, emulsion grains, dielec. loss, ionic cond. and surface space charge 77—28038
AgBr, ionic cond., dielec. loss meas. 79—23768
AgBr microcrystals, measurements on photographic emulsions to determine ionic conductivity 79—23778
AgBr(I) microcrystal dispersed in gelatin, effect of I^- on interstitial Ag ions 78—26726
AgCl:OH^-, dielec. meas., defect reorientation 77—19947
AgCl:Pb^{2+}, ionic cond. and dielec. loss relax. vacancy-impurity complex. form. 77—1259
Ag_2HgI_4, order-disorder transform. at 51°C, sound vels. and dielec. losses 78—10129
β-AgI, ionic cond. and Frenkel pair form., dielec. loss meas. 79—33112
Ag_5SbS_4, dielec. and acoustic props. *(German)* 78—64335
Al, ultrafine particles, far IR absorpt. 77—52084
Al-Al_2O_3-Al, thin film capacitors, dielec. losses 78—76382
Al-CdTe-Al thin film VLF dielectric props. *(Slovak)* 79—7907
Al-rare earth metal oxide dielectric-Al, characts. and design considerations *(Russian)* 77—1638
Al-stearic acid-Al, low-loss thin film capacitor 80—71317
AlF_3 film, dielec. characts. 77—85650
AlF_3 film, RF sputtered, dielec. props. meas. 77—36173
AlF_3 in Al-AlF_3-Al MIM thin film structures, dielec. and elec. props. *(Slovak)* 80—100536
β-Al_2O_3, conduction and dielec. loss mechanisms, paired interstitialcy model 80—107468
Al_2O_3 film, dielec. props., AC and DC elec. characts. 78—68445
β-Al_2O_3-Na_2O, AC ionic cond., dielec. and NMR relax. 80—59713
β-Al_2O_3-Na_2O $(Li_2O)(K_2O)(Ag_2O)(H_3O)$, with mobile ion species, dielec. relax. 79—91351
As amorphous solid dielectric loss meas. by submillimetric waveguide laser 79—33603
As-Ge-Te glass, dielectric meas. 79—87382
As_2Se_3 glass, rel. to microwave elec. cond. 80—49793
As_2Se_3:Ag, amorphous, doping effect of gap states and elec. cond., dielec. relax. and DC cond. meas. 79—47098
β-B, rhombohedral, dielec. loss temp. depend., −196 to 350°C 80—20585
B_2O_3-CaO-Fe_2O_3 glasses, semicond., cond. models, electronic props., 77-800K 80—54688
B_2O_3-NaKO glass, dielectric relaxation at low temp. 79—11384
BaBrF, reacted flux growth, dislocation density, dielec. const. and loss, IR spectra 77—36214
$BaFe_{12}O_{19}$, ferrite, DC cond., dielec. props., lattice consts. 80—80272
$Ba_3Fe_2ReO_9$, siegnette magnets with hexagonal barium titanate structure 78—76397
$Ba_3Fe_2TeO_9$, siegnette magnets with hexagonal barium titanate structure 78—76397
$BaMnF_4$, low temp. dielec. props. and phase transitions 77—20790
BaO-Nd_2O_3-TiO_2-Bi_2O_3 system ceramics, high stability low loss dielectric preparation 80—81008
BaO-TiO_2-Nd_2O_3, exam. of compositional and dielectric props. 79—33601
$Ba(PO_3)_2$-alkaline earth fluoride and $Ba(PO_3)_2$-YF_3 glasses, pseudobinary, elec. cond. and dielec. losses 77—7890
$(Ba_xSb_{1-x})TiO_3$ 80—60514
$Ba_{0\,54}Sr_{0.46}Nb_2O_6$:Y(La)(Tm), dielectric and electrooptic props. 78—68466
$Ba_xSr_{1-x}Nb_2O_6$, struct. and dielec. props., isomorphic substitution effect 78—27165
$(BaSr)TiO_3$ film, ferroelec., dielec. props. in strong elec. fields 78—27163
$Ba_{0.4}Sr_{0.6}TiO_3$, ferroelec. thin film, fabrication, props. 77—28521
$BaTiO_3$, c-domain cryst., HF dispersion of permittivity 78—60379
$BaTiO_3$, ceramic, effect of grain size on nonlinear dielec. props. 77—8522
$BaTiO_3$, doped, loss mechanism and domain stabilisation 78—84542
$BaTiO_3$ film, dielectric props. depend. on sinusoidal elec. field 80—71318
$BaTiO_3$ film, struct. and dielec. props. 80—60514
$BaTiO_3$ films, ferroelec., effect of elec. field on dielec. props. 79—33642
$BaTiO_3$, monocrystalline, superposition of unidirectional electric field effect, time depend. *(Slovak)* 78—52435
$BaTiO_3$ type perovskite ferroelectric, neutron irradiated, amplification of freq. dispersion of permittivity *(Russian)* 78—52419
$BaTiO_3$, X-ray irrad. effect on dielec. props. 78—15082
$BaTiO_3$:$BaTi_3O_7$, dielec. props. and microstruct. 80—60481
$BaTiO_3$:Nb, ferroelec. and paraelec. phases, props. 79—42919
$BaTiO_3$:ZrO_2, dielec. loss tangent and const. 79—4769
$BaTiO_3$-$BaNbO_3$ system, solid solns., thermal ionic relaxation, vacancy form. 77—8499
$BaTi_4O_9$ effect of chemical treatment on loss quality, at microwave wavelengths 79—34159
$Ba_2Ti_9O_{20}$, effect of chemical treatment on loss quality, at microwave wavelengths 79—34159
$Ba(Ti_xSn_{1-x})O_3$ film, struct. and dielec. props. 80—60514
$BaZrO_3$-$LaAlO_3$ systems, sintering conditions, elec. props. 79—43184
Bi complex oxides, antiferroelec. and ferroelec., pyrochlore struct., dielec. and structural study 79—38488
Bi_2O_3, anodic film, dielec. props. 77—20794
Bi_2O_3 film, dielec. meas. 80—2696
Bi_2O_3, thin film, struct. and dielec. meas. 79—78622
Bi_2O_3 vacuum deposited films, dielec. props., 90 to 298K, freq. range 0.1 to 10 kHz, ageing effect 80—55036
$Bi_4Ti_3O_{12}$ ceramics, ferroelectric, hot-forged, grain orientation and dielectric props. 80—40076
Bi_2WO_6, ferroelectric, dielectric props., elec. cond. and relaxation phenomena obs. 80—80692
Bi_2WO_6, ionic cond. and relaxation polarisation, capacitance, losses 80—24657
$CH_3NH_3Ga(SeO_4)_2.12H_2O$, dielec. relax. near transition temp. 80—60493

dielectric losses continued
$CaCO_3$, calcite, X-ray irrad., luminesc. and dielec. loss decays 77−12431
CaF_2, hot pressed, dielectric, optical props. 79−56720
$CaF_{2-x}H_x$, ionic cond. determ. from admittance and dielec. loss meas. *(French)* 80−107479
CaO-B_2O_3-Fe_2O_3 glass, electronic and dielec. props. meas. 77−24574
CaO-B_2O_3-Fe_2O_3 glasses, effect of heat treatment on electronic props. 78−2480
CaO-B_2O_3-Fe_2O_3 glass, dielec. relax., AC and DC cond., dielec. const. and loss 78−23393
CaO-MgO-Al_2O_3-SiO_2, shale glass, glass forming and dielec. props. 78−22660
CaO-SiO_2-Al_2O_3, wollastonite, low dielec. loss factors, fabrication *(Japanese)* 80−55032
Ca_2SiO_5, hydraulic reaction observed by microwave dielectric meas. 78−80745
$CaTiO_3$-$CaTiSiO_5$, sintering and dielectric props. 80−40307
$CaTiO_3$-TiO_2, ceramic, phys. props. 78−43784
CdI_2, dielec. props. rel. to polytypically modulated structs. 79−94971
CdI_2 polytypic crystals, dielectric loss behaviour 80−66108
CdS:Cu binder layer, photoactive, AC impedance meas. 80−25299
CdTe, dielec. const. and loss tangent, temp. depend., 15.95 GHz 77−69763
CeO_2, elec. cond. and dielectric props. at low temp. 78−72447
$Co_xZn_{1-x}Fe_2O_4$, ferrite, DC cond., dielec. props., lattice consts. 80−80272
Cr_2O_3, dielectric const. and loss, cond., 10^2-10^7 Hz, 30-450°C 77−59504
CsBr, crystal, short range interaction polarization, dielectric const. loss, and elec. cond. 10^2 to 10^7 Hz 79−99814
CsH_2AsO_4 crystals, dielectric radiation effects, γ-radiation 80−93234
CsH_2AsO_4, ferroelec., RF dielec. relax., loss mech. 79−38448
CsH_2AsO_4, influence of γ-radiation on dielec. props. 79−46703
CsH_2AsO_4, RF dielec. response close to transition temp. 77−90099
EuO, ferromag. reson. and nonlinear phenomena 79−28627
EuO, ferromagnetic resonance and dielectric losses 78−2748
Eu_xO_y film, dielec. props. rel. to annealing 79−99636
FeO-P_2O_5 glasses, electrical and mechanical losses 78−80283
Fe_3O_4, mag. relax., permeability and loss tangent determ. at 4.2 to 300K 77−32263
Ga, optical props. in 0.5-60 eV range, dielectric const. and loss functions *(French)* 77−12353
GaAs:Cr, semi-insulating, complex permittivity, 2.5-36 GHz, 300-400K 77−69763
GaP LED, negative differential resistance and conductance associated with dielectric losses 77−63468
GdGa garnet, microwave losses 77−4531
Ge amorphous solid dielectric loss meas. by submillimetric waveguide laser 79−33603
GeO_2-Na_2O, DC cond. rel. to dielectric loss peak freq. 79−78621
H_2O, adsorbed on kaolinite clays, dielec. props. 78−76381
H_2O reorientation in H-bonding free solvents, IR absorpt., dielectric loss 77−36233
HgI_2:CdS, photodielectric effect 77−11955
$K_xAl_xTi_{8-x}O_{16}$, $1.6 \leq x \leq 2.0$, dielec. response in freq. range 10^{-3} to 10^6 Hz 79−65785
$KBr:Cl^-$, diffusion traps for divalent ions, dielectric loss and ionic thermocurrent techniques 80−6566
KCN-KCl mixed system, order-disorder transition, dielec. props. meas. 78−15112
KCl, colloidal suspension, radiowave dielec. dispersion 80−11311
KCl:Li, ⟨111⟩ off centre Li^+ under biaxial stress, bistable tunnelling 78−15090
$KCl:Sr^{2+}$, X-irradiated, thermolum. decay, effect of impurity aggregation 77−85814
KCl-KBr, mechanism of aggregation of divalent impurities, dielectric loss meas. *(Japanese)* 79−60394
$KCl_xBr_{1-x}:Sr^{2+}$, dielec. loss 77−85646
$KClO_4:CrO_4^{2-}(SO_4^{2-})$, AC electrical conductivity meas. between temp. range 25-325°C, automated technique 80−59699
KD_2PO_4, attenuation const. meas. by SHF dielec. resonance 79−47406
$K_4Fe(CN)_6.3H_2O$, ferroelec. and paraelec. phases, dielec. props. meas. 80−60494
KH_2AsO_4, ferroelec., RF dielec. relax., loss mech. 79−38448
KH_2PO_4, amplitude depend. of permittivity and losses 79−99842
KH_2PO_4, attenuation const. meas. by SHF dielec. resonance 79−47406
KH_2PO_4, ferroelec., RF dielec. relax., loss mech. 79−38448
$K_xMg_{x/2}Ti_{8-x/2}O_{16}$, $1.6 \leq x \leq 2.0$, dielec. response in freq. range 10^{-3} to 10^6 Hz 79−65785
$KNbW_2O_9$, crystallography, polymorphism and phys. props. 78−79599
$K_2SbNb_5O_{15}$, dielec. and pyroelec. props. 79−99841
LaF_3 films, electron beam evaporated, dielec. props. 79−91375
$(Li, Na)NbO_3$ ceramic, dielectric and electromechanical props. 77−40183
Li ferrites, MW dielectric losses, causes and reduction *(Chinese)* 80−75930
LiCd ferrite, dielec. const. and loss meas., 50-10^6 Hz 77−77135
LiCl, colloidal suspension, radiowave dielec. dispersion 80−11311
$LiD:Mg^{2+}$, X-irrad., dielec. loss 80−55024
LiF, plastic deform. and dielec. losses 78−19410
$Li_{1-x}H_xIO_3$, dielec. behaviour, Raman and IR spectra 77−32357
Li_3N, superionic conductor, far IR absorption, temp. and isotope effects 79−51969
$LiNbO_3$, single crystal, dielectric const., dispersion, loss tangent and susceptibility 77−16245
$LiNbO_3$:$3Li_2O.Nb_2O_5$ eutectic, dielectric props. 79−1743
Li_2O-B_2O_3 glass, conductivity, permittivity, and dielectric loss obs., mixed isotope effect 78−95182
LiZn ferrite, dielec. const. and loss meas., 50-10^6 Hz 77−77135
Mg-Cu-Mn-Ni-Fe-O, UHF ferrites, synthesis, physicochem. state, mag. and dielec. parameters 79−11536
$MgO:Li^+$, quenched, elec. polarisation, thermal depolarisation and dielectric loss meas. 79−1738
5 wt.% MgO-Si_3N_4, hot-pressed, dielec. props. 78−10822
$Mg_{0.25}Zn_{0.75}Fe_2O_4$, ferrite, DC cond., dielec. props., lattice consts. 80−80272
MnZn ferrite, mag. relax., permeability and loss tangent determ. at 4.2 to 300K 77−32263
NH_3, liq., relax. time and activation energy 79−91335
$NH_4Al(SO_4)_2.12H_2O$, dielectric losses, proton spin lattice relaxation by NH_4^+ hopping 79−56721
$NH_4Cl:[MoOCl_5]^{2-}$, single cryst., struct. investigations 77−66524

dielectric losses continued
NH_4HSO_4, dielectric relax. in ferroelectric and paraelectric phases 77−16246
NH_4HSO_4, ferroelec., critical slowing down of dielec. relax. *(Japanese)* 77−90109
$(NH_4)_2SO_4$, 210-250K, 1 MHz-25 GHz, ferroelec. transition obs. 77−59541
$(NH_4)_2SiF_6$, low-temp. dielec. loss maxima in cubic and trigonal crysts. 79−19831
NaCl, interfaced polarisation and losses, superimposed AC and DC voltage study 80−25276
NaCl, plastic deform. and dielec. losses 78−19410
NaCl:Ca, aggregation and precip. hardening in impurity vacancy, dipole decay 80−16322
$NaCl:Ca^{2+}$, dipole concs. determ. considering aggregation, expt. and theoretical comparison 80−59512
$NaCl:Ca^{2+}$, highly doped, aggregation of point defects, NMR and dielec. loss meas. 79−10847
$NaCl:CaCl_2$, quenched, aggregation process of Ca^{2+} ion-vacancy dipole, elec. cond. and dielec. loss meas. 77−80535
$NaCl:Cd^{2+}$, dielectric loss following plastic deform. 80−84690
NaCl:Mn, impurity-vacancy dipole aggregation, role of dimers and trimers, reanal. of dielec. and cond. data 79−1458
$NaCl:NaOH(NaNO_3)$, absorpt. spectra and dielectric losses 78−19524
NaCl:Sr, dimer and trimer aggregate formation by NMR, ionic cond. and dielectric losses 80−15094
NaCl:X (X=Ca, Sr, Ba, Mg, K, Li, Tl, Ag), impurity conc. effect on mech. and elec. props. 78−47469
$NaH_3(SeO_3)_2$, dielec. props. 78−43764
$NaNO_3$, dielec. loss anal., Debye type loss peaks 80−50260
$NaNbO_3$-$SrNb_2O_6$, phase diagram, props. meas. 79−11576
Na_2O-SiO_2 glass, conduction and dielec. loss mechanisms, paired interstitialcy model 80−107468
Na_2SO_4, high temp. phase, DTA and dielec. meas. 79−82333
$Na_3Sc_2(PO_4)_3$, ferroelectric props., X-ray diffr. study 79−69789
$Na_3Sc_2P_3O_{12}$, fast-ion conductor, struct. phase transition 80−88362
Nb-Nb_2O_5-Nb structure, Schottky barrier effects on capacitance and loss tangent 77−8203
$NdAlO_3$ films, preparation, electrophys. props. in MIM structs. 77−24956
$Nd_{1/3}NbO_3$, $NdNbO_4$, structural characteristics and residual polarisation 77−15361
$NiSiF_6.6H_2O$, dielec. loss and relax., 100-270K, reorient. mech. 78−35088
PLZT ceramic, ageing, dielec. props. 80−88940
PLZT ceramics, ferroelectric and struct. transitions, crystallographic, thermal, and dielec. anal. 80−29693
PLZT, effect of ageing on temp. depend. of permittivity, for ferroelectric and antiferroelectric compositions 78−48121
PLZT, fine grained 90° electric domain wall movement, interpretation of dielectric losses *(German)* 79−33646
PLZT, mech. and elec. losses, correl., theory and expt. 80−66133
PLZT modified high voltage dielectric, permittivity, Curie temp., loss meas. 80−80720
P_2O_5-MO-Al_2O_3, (M=MgO, CaO, SrO, BaO) (45, 5 wt.%) glass, electron irradiation effect on dielec. props. 80−29056
$(Pb, Sr)_5Ge_3O_{11}$, single crysts., growth and X-ray and dielec. investigations 80−88127
Pb_z-$Sr_{1-z}(Zr_x$-$Ti_{1-x})O_3:Cr_2O_3$, ferroelec. ceramic, reversible characts. and dielectric losses *(Russian)* 78−84517
$PbBi_4Ti_4O_{15}$ ceramic, dielec. props., temp. depend. 78−95561
Pb_2CrO_5, thermal X-ray and dielec. investigations 79−47403
$Pb_3Fe_2WO_9$, perovskite ferroelec., dielec. permittivity and loss meas. 77−8496
$Pb_3Ge_2O_7$, dielectric thin film, obtained by sedimentation, exam. of dielectric props. and structure 80−2282
$Pb_5(Ge_{1-x}Si_x)_3O_{11}$, dielec. spectra, ferroelec. behaviour 78−60406
PbI_2, dielectric props., elec. cond., space charge polarisation 80−100631
PbI_2 single crysts., photo-induced AC impedance meas., photodielec. effect 78−52034
$PbLaZrNbO_7$, dielectric with zero temp. coeff. of dielect. consts., electrophys. props. 77−52010
$PbMg_{1/3}Nb_{2/3}O_3$, dielec. props. under high hydrostatic pressure near phase transition point 80−44997
$Pb(Mn_{1/2}Ta_{1/2})O_3$, ceramic, for thermal and dielectric isolation at low temp. 80−39365
$PbNb_{0.5}Sc_{0.5}O_3$, ceramic, dielec. props. 79−11392
PbO, disordered photoconductor, dielec. props., temp. depend. anomalies 78−43765
$15PbO.3B_2O_3.2WO_3$, struct. and electrophys. characts. 77−84716
$Pb_{0.94}Sr_{0.06}(Ti_{0.47}Zr_{0.53})O_3$-NiO, modified, dielec. and piezoelec. props. 80−11342
$Pb_{0.95}Sr_{0.05}(Zr_{0.53}.Ti_{0.47})O_3$, low temp. internal friction in ferroelectric ceramic 77−21200
Pb_2TaMnO_6, reaction of form. from oxides, ferroder. props. 80−55326
$PbTiO_3$, anomalies in elec., photoelectric and mechanical props. 80−55051
$PbTiO_3$ ferroelec. thin film, prep. by RF sputtering and dielec. props. 79−100052
$PbTiO_3$ ferroelectric thin films, fabrication by RF sputtering, characts. 80−40261
$PbTiO_3$-$La_2O_3.3TiO_2$, struct. and dielec. props. 80−54200
$PbTiO_3$-$PbZrO_3$-$PbNb_{2/2}Zn_{1/3}O_3$(-$PbNb_{2/3}Co(Mg)_{1/3}O_3$) solid solutions, dielec. and piezoelec. props. 79−87393
$Pb(Zr, Ti)O_3$ ceramics, low temp. sintering, elec. and mech. props. 80−71616
$Pb(Zr,Ti)O_3$ thin films, fabrication and characterisation electron-beam deposition 80−16188
$Pb(Zr,Ti)O_3$ thin film, ferroelec., fabrication by RF sputtering *(Japanese)* 80−25560
$Pb(Zr,Ti)O_3$ thin layers, tan δ temp. dependence obs. *(Bulgarian)* 78−88259
$Pb(Zr,Ti)O_3$:Mn ceramics, anomalous dielec. losses 79−42892
$Pb(Zr,Ti)O_3$-$Pb_3Ge_5O_{11}$ ceramic, sintering conditions rel. to piezoelec., dielec. props., microstruct. 77−16252
$PbZrO_3$ based ferroelec. ceramic, pressure-temp. phase diagrams 79−24273
$PbZrO_3$ pyroelectric detector, low temp. behaviour, expt. 80−31869
$Pb(Zr_{0.47}Ti_{0.43}Sn_{0.10})O_3:Cr_2O_3$, ferroelec. ceramic, reversible characts. and dielectric losses *(Russian)* 78−84517
$RTiNbO_6$, R=rare earth, electrophys. props. 78−23388

dielectric losses continued

- RbCN, molecular motion and ordering from dielec. and Raman techniques 79—73932
- RbCl:Co^{2+}, dielectric loss, impurity sites 79—91348
- RbCl:Li^{+}, new off-centre defect system, studied with dielec. techniques under hydrostatic press. 79—19834
- RbH$_2$AsO$_4$, attenuation const. meas. by SHF dielec. resonance 79—47406
- RbH$_2$AsO$_4$, phase transition, dielec. pyroelec. and internal friction meas. 77—16261
- RbH$_2$PO$_4$, attenuation const. meas. by SHF dielec. resonance 79—47406
- RbHSeO$_4$, ferroelec. props. and domain struct. 79—78637
- RbNO$_3$, single cryst., DC cond., dielec. and thermophys. props., temp. depend., transitions interpret. 78—26682
- rubber, gamma radiation effects on dielect. parameters, expt. *(Hungarian)* 78—59836
- SbNbO$_4$, ferroelec. film characts. 77—48127
- SbNbO$_4$ single crystals, pure and doped, growth and pyroelec. and ferroelec. props 80—40248
- Sb$_2$S$_3$, thin film, dielectric props. 79—15392
- SbSI single crysts., nonlinear dielec. effects and microelectronic applics. 77—43944
- SbSI, single- and poly-domain, complex permitt. and dielec. relax. losses 79—28699
- Se, amorphous film, dielec. activity obs. near glass transition temp. 80—75933
- Se amorphous solid dielectric loss meas. by submillimetric waveguide laser 79—33603
- Se film, amorphous, empirical formula for temp. depend. of dielec. loss peak 80—97197
- Se:As, amorphous film, dielec. activity obs. near glass transition temp. 80—75933
- Se:Tl, and undoped material, dielec. losses and permittivity meas. 77—28518
- Se-Ge-Te glass, dielectric meas. 79—87382
- Si$_{(6-z)}$Al$_z$O$_z$N$_{(8-z)}$, sialons, hot-pressed, dielec. props. 78—10822
- Si$_3$N$_4$, hot-pressed, dielec. props. 78—10822
- SiO-B$_2$O$_3$ composite dielec. films, EPR, dangling bonds and dielec. loss 80—11246
- SiO$_2$, hydrated vitreous, spectrum of low-energy dipolar states, dielec. const., dielec. losses and relax. 77—90098
- SiO$_2$, vitreous, dielec. absorpt. saturation, 0.4-8K 78—23394
- SnO$_2$-rare earth metal oxide dielectric-Al, characts. and design considerations *(Russian)* 77—1638
- Sr$_{0.75}$Ba$_{0.25}$Nb$_2$O$_6$, ceramic ageing dielec. props. 80—88940
- SrClF, SrBrF, reacted flux growth, dislocation density, dielec. consts. and losses IR spectra 77—36214
- SrGa$_2$Si$_2$O$_8$-SrGa$_2$Ge$_2$O$_8$, solid solution, exam. of elastic and electrical props. 79—96057
- SrTeO$_3$, ferroelec. vacuum condensates 77—40180
- SrTiO$_3$, central peak in spectrum of ferroelec. mode fluctuations and dielec. losses, 4.2K 78—19432
- SrTiO$_3$, dielectric loss at microwave frequencies *(Russian)* 78—52440
- SrTiO$_3$ film, behaviour of ferroelecs. in strong elec. microwave field 79—42884
- SrTiO$_3$ film, polycrystn., dielec. props. and struct. 77—81057
- SrTiO$_3$ film, polycryst. dielec. losses, influence of amplitude of measuring microwave field 79—99829
- SrTiO$_3$-Bi$_2$Ti$_2$O$_7$-CaTiO$_3$ system, solid solns., elec., optical props. 79—11375
- Ta-Ti-O, reactive sputtered film, elec. props. 78—84336
- Ta$_2$O$_5$, anodic, on sputtered Ta$_2$N dielec. props., 20-10^5 Hz, 150-500K 79—87386
- Ta$_2$O$_5$ film, reactively sputtered on SI, dielectric and optical props. obs *(Bulgarian)* 80—89144
- TeO$_2$ thin films, dielec. props. rel. to fabrication conditions 80—97199
- TiO$_2$ based ceramic dielec. materials, medium permittivity, elect. charact. 78—35086
- TiO$_2$ film, RF sputtering, dielec. props. and X-ray phase analysis 78—80288
- TiO$_2$, nonstoichiometric rutile, dielec. props. 10 Hz to 30 kHz 77—28507
- TiO$_2$-Fe$_2$O$_3$-CaO-V$_2$O$_5$ system ferrites, TiO$_2$ content and thermomag. effects on dielec. props. 77—43927
- Tl$_x$NbO$_{2+x}$F$_{1-x}$, pyrochlore phase, Tl^{+} mobility 79—95209
- VO$_2$, elec. cond. and dielec. props. 79—11379
- V$_2$O$_5$-In(Tl)$_2$O$_3$, ceramic, elec. resist., dielec. props., porosity 77—8093
- WO$_3$-P$_2$O$_5$ glass, AC cond. and dielec. props. 80—92717
- YIG, elec. props. 79—99552
- YIG, MW dielectric losses, causes and reduction *(Chinese)* 80—75930
- Y$_2$O$_3$-AlN-SiO$_2$ oxynitride glasses, elec. props. 80—80267
- Y$_2$O5d3 films, preparation, electrophys. props. in metal-oxide-metal structs. 77—24956
- Yb$_2$O$_3$ film, amorphous, electron beam deposited, dielec. props. 79—91339
- ZnO, doped, dielec. losses 77—81049
- ZnO non-ohmic ceramic, degradation props. under AC and DC bias 80—80262
- ZnO pellets, and ZnO:Li single crysts., photo-induced AC impedance meas., photodielec. effect 78—52034
- ZnO, varistor, low temp. AC props. 79—38434
- ZnO-based nonohmic ceramic, dielec. dispersion and equiv. circuit 77—73110
- ZnTe, photoinduced dielec. loss and capacitance changes, rel. to space charge polarisation 80—2417

dielectric materials

see also antiferroelectric materials; dielectric thin films; electrets; ferroelectric materials; glass; insulating materials; insulation; piezoelectric materials

- acoustic wave propagation, phonon relax. time 80—44263
- ageing anal., equiv.-circuit appl. *(Bulgarian)* 77—66467
- capacitive stress transducer optimum dielectric selection 77—73428
- capacitor dielectric fluid test and anal., quality assurance 78—80272
- capacitors, power, dielectric liquids flammability and degradation 80—88944
- Casimir effect in dielectrics using source theory, surface tension and latent heat 79—8109
- ceramics, granular, electrophysical props. depend. on porosity, temp., solid-phase props. 77—69764
- coherent light pulse, steady propagation in dielectric medium, spatial dispersion effects 79—72480

dielectric materials continued

- conference, Electrochem. Society fall meeting, Las Vegas, USA (Oct. 1976) 77—16831
- conference, electrochem. society fall meeting, Las Vegas, USA (Oct. 1976) 77—77787
- conformal transformation, allowing for spatial dispersion *(Russian)* 80—53183
- deep fast trapping dielectric, SCL current injection 80—6862
- dielectric discs in rectangular waveguides, permittivity measurements, EM wave scattering *(Russian)* 77—18050
- dielectric flows, EM method for flowrate and velocity meas. 80—53893
- elastic, containing 2 rigid spherical conductors, electrostrictive stress conc. 77—23883
- electric, optical and acoustic interactions from Lagrangian representation, book 80—2715
- electric phenomena, space charge studies 80—24939
- electro-optical inspection of internal defects 78—56869
- electromagnetic parameter measurement using HF cavity resonator method 79—80642
- electron beams as virtual electrodes, review 80—6861
- electron penetration, 20-50 keV, sandwich method meas. 80—6436
- emulsion, magnetic and dielectric, prep. *(German)* 78—3376
- energy loss of electrons 80—24522
- EPR *(Japanese)* 77—85550
- high-loss dielectrics, applic. of cavity perturbation method to complex permittivity meas. 78—24815
- infinite elastic dielectric with Griffith crack, EM wave propag., Voigt-Toupin model 80—1469
- inhomogeneous coating, produced by high temp. sputtering, spectrophotometric props. *(Russian)* 78—39613
- ion implantation, space charge elec. field effect 79—82250
- laser induced microwave damage, space simulation 77—81050
- lossy dielectric materials containing short randomly distributed metal fibres, elec. props. 80—20584
- Maxwell-Hopkinson dielectric theory electric displacement fields, growth estimates 79—24278
- measurements and applications, conference, Birmingham (1979) 80—12854
- moistening diffusion kinetics, forecasting *(Hungarian)* 80—96692
- molded parts, stress patterns and deformation characts., computer anal. 80—17787
- NDT using Kirlian effect, high freq. technique 80—66749
- nonlinear, linearly polarised plane EM pulse propagation 77—75365
- nonlinear elastic dielectrics, thermodynamics and entropy flux 79—67164
- nonlinear refractive index n$_2$ of transparent dielectric crystals *(Chinese)* 80—45028
- nonuniformity of dielec. props., at mm wavelengths, method of determining 78—40001
- optical nonuniformity, spatial distrib. determ. 80—13116
- phase transition, optical studies, use of diamond anvil devices *(Japanese)* 80—49362
- phonon thermal conductivity, Umklapp process, comparison with LiF data 80—39367
- plastic dielectrics with general work-hardening, phenomenological theory 79—8113
- Plexiglass, spark press. field in solid dielectric 77—24233
- polar dielectrics, triplet two electron states 80—24810
- polarized, props. and appls. *(French)* 79—51902
- positron annihilation, phase composition determ. *(Russian)* 79—91527
- pre-breakdown luminescence in dielectrics, intensification of underexposed photographs 77—24793
- radiation method for electric potential distrib. meas. 77—41640
- radio detection of local defects, strongly absorbing dielec. medium 80—35481
- raw material acceptance testing for dielectric applications 80—97646
- solid, elec. and mech. props. at increased temps., meas. equipment 77—71342
- solid dielectrics, treeing 78—80285
- solid transparent dielectric, absorpt. of laser radiation by defects in surface layer *(Russian)* 80—25497
- steatite, dielectric ceramic 77—32546
- surface, exposed to electron beam, effect of bulk and surface cond. on pot. 80—2446
- thermal explosion theory in strong elec. field 79—91954
- thermal method of investigating hidden nonuniformities in flat dielectric materials 78—56868
- thermally stimulated depolarisation as method of studying charge trapping 80—11325
- thermorigid, nonlinear thermodynamic theory 80—10149
- transfer processes, theoretical model review 80—15529
- transparent, solid, ionisation threshold development in field at single powerful focused laser pulse *(Russian)* 77—69771
- Bi$_{12}$GeO$_{20}$ monocrystal optical homogeneity requirement for light beam control 79—82952
- Bi$_{12}$SiO$_{20}$ monocrystal optical homogeneity requirement for light beam control 79—82952
- CaO, optimum composition of dielectric materials for AC-operated plasma display panels 80—14945
- Gd$_3$Ga$_5$O$_{12}$ monocrystal optical homogeneity requirement for light beam control 79—82952
- Gd$_2$(MoO$_4$)$_3$, piezoelectric and electrostriction coeffs. near ferroelastic transition *(French)* 77—40182
- HF(Cl)(Br)(I), ferroelec. and paraelec. phases, elec. multipole interactions 77—59522
- KCl:OH^{-} type paraelec. systems, phonon superradiant phase transition *(Russian)* 79—69206
- La$_4$(TiO$_4$)$_3$, electrical props., effect of initially used La$_2$O$_3$ *(Polish)* 77—59508
- NaCl, damage caused by CO$_2$ laser radiation 77—90222
- SF$_6$ under pressure, partial discharge overvoltage dependence 77—76243
- SiO$_2$ quartz glass sputtering by high frequency plasma, deposition products study *(Russian)* 77—21023
- SrO, optimum composition of dielectric materials for AC-operated plasma display panels 80—14945

dielectric measurement

see also dielectric loss measurement; permittivity measurement

- 10-150 GHz frequency range, precise 79—30491
- aggressive liquids, cell for meas. of dielec. props. 78—21170
- automatic, microwave, using resonance substitution techniques 77—82573

dielectric measurement continued
biological liquids, reflection meas. of complex dielectric const. 80—101309
biological substances, dielectric props. meas. at RF and microwave freq. by coaxial line reflection methods 80—109065
breakdown, using discharge figures 80—11338
1-butanol, permitt., dielec. time domain spectroscopy, total transmission method study 80—27323
1-butanol, time domain spectroscopy, superposition integral approximation 77—1630
cavity resonator, containing dielec. sample, num. soln. of charact. eqn. *(French)* 78—13649
cell for electromechanical props. meas. of solid dielectrics 79—93163
complex dielec. and mag. props., modified von Hippel least square fit determ. 78—21179
complex permittivity of low-to-medium loss standard liqs., meas. at 285 GHz 78—15083
conducting solutions, bridge method for meas. dielectric relaxation 80—82793
conductive liquid Kerr constant meas. 78—88279
corn, shelled, 1 MHz-2.45 GHz, freq. and moisture dependence props. 77—77142
cylindrical cavities in E_{010} mode relations for dielec. parameter eval. 79—35783
cylindrical resonator, E_{010} perturbation theory, error estimation *(Russian)* 77—18051
data sampling process for dielec. dispersion meas. in freq. range $<10^{-1}$ Hz *(French)* 79—49257
dielectric constant, laser photoinduced changes, of chloroplasts and dyes 80—85449
dielectrometry, applic. to alkaline earth carbonate thermal decomp. in vac. 77—16802
dielectrophoretic effect techniques 77—22570
dynamic dielectric anal. of solids, automated technique 79—63271
electric strength determination, equipment and test results for liq. N_2 79—38451
electrospark inspection unit for tube defect obs. 78—92431
evaluation, transformation method *(German)* 77—90089
ferroelectric material, dielectric aftereffect meas. with digital data acquisition 77—43952
film, spatial charge distrib. meas. technique 77—32327
film and slab-like materials, open transmission line UHF CW phase technique 79—35778
fluids and dispersions, dielec. meas. using cell 78—93725
Hartshorn and Ward, square law detector checking 79—35777
HF time-domain spectroscopy, at high permittivity *(German)* 78—16816
hydration kinetics, microwave obs. 79—34255
ice containing ionic impurities, relax. meas. by blocking layer method 80—103914
in vivo probe measurement technique for determining dielectric properties at VHF through microwave frequencies 80—85542
insulating gases and gas mixtures, maximum electric strength and vapour pressure relationships 80—92249
insulator parameters meas., freq. and mode variation in cavity 80—13102
ionization density distrib. meas. during pulsed electron beam irradiation 77—20810
LF measurements using time-domain technique, 20 Hz to 10 kHz 80—57329
liquid, new method for charge density meas. 80—4743
liquid crystal, dielectric anisotropy over wide freq. range 79—33594
liquids, coaxial transmission line terminated by shielded open circuit 80—82789
liquids, meas. methods comparison in freq. range 1 GHz to 4 THz 80—100639
long-time-constant polarisation spectrum selective meas., DC methods 80—15944
low-loss dielectric meas. at millimetric and submillimetric wavelengths 77—37943
materials, measurements and applications, conference, Birmingham (1979) 80—12854
micro-organism electrical characteristics meas., elec. cond. and dielec. props. *(Italian)* 78—3684
microwave absorption by water in heterogeneous organic materials 80—15998
microwave Q-factor meas. system 78—54396
millimetre wave frequencies, using inverted strip dielec. waveguides 79—26081
monopole immersed in lossy medium, elec. props. of in vivo tissues 80—12205
murine malignant tumours, in vivo probe dielectric meas. 78—11761
nonlinear dielectric measurement by detection of third order harmonics *(French)* 77—67459
nonperturbing dielectric microthermometer probes 78—11743
parameters meas. at microwave freq. by cavity-perturbation technique 80—9002
permeability of dielectrics with one sided access to part 78—89500
piezoelectric ceramic, meas. using autocorrel. anal., stress characts. 77—1639
2-propanol, dielec. time domain spectroscopy, total transmission method study 80—27323
1-propanol, time domain spectroscopy, superposition integral approximations 77—1630
pseudo-random noise dielec. spectrometer, evaluation using PBLG solns. 78—15084
Q-meter measurement range expansion method 78—74023
rapid low-temp. dielectric meas. method 79—12818
refractive index meas. in sub-mm. wavelength for solid dielectrics 77—18074
relaxation spectroscopy, liquids, frequency and time domain expt. methods 80—40044
response function relaxational frequency spectra, simultaneous meas. by digital signal processing 80—15959
Schering bridge appl., principles *(Portuguese)* 77—67461
solid dielectric complex and power reflectivity determ., 100 GHz to 3 THz 80—15999
solid dielectric props. meas. with superconducting resonators 78—21180
solid dielectrics, elec. and mech. props. at increased temps., meas. equipment 77—71342
solid electrolyte, polycryst., impedance and modulus spectroscopy 77—12309

dielectric measurement continued
solid insulating materials, dielectric properties at cryogenic temps. 80—90867
solids and liquids, dielec. characts., temp. depend., laboratory installation for meas. 80—37051
space charge meas. in thin film by Maxwell stress method 80—22389
spectrometer for 20 Hz-80 kHz range, automatic 77—13768
structuring dispersions, dynamic dielectric behaviour, meas. device 79—12816
structuring dispersions, dynamic dielectric behaviour, reply to comments 79—35785
structuring dispersions, meas. device for dynamic dielectric behaviour 78—31710
thin film properties, student expt. 79—40323
time domain dielectric spectroscopy, discrete Fourier transform appl. errors *(French)* 80—13105
time domain meas., multicomponent exponential decay curves, analysis method *(French)* 77—52007
time domain spectroscopy, superposition integral approximations 77—1630
time domain spectroscopy, survey 80—68212
time-domain spectroscopy, comparison of methods 80—52310
two layer medium with metallic base, dielectric charact. determ. using reflected electromagnetic wave 79—35688
VHF waveguide dielectric scatt. model for pulse-probe data interpretation *(Russian)* 80—62682
water pollution, dielectric props. and determ. of microwave emissivity 80—101142
CCl_2F_2-CO_2 gas mixture, field breakdown gradients calc. method 80—92248
CCl_2F_2-N_2 gas mixture, field breakdown gradients calc. method 80—92248

dielectric phenomena
see also dielectric hysteresis; dielectric losses; dielectric properties of substances; dielectric relaxation; dielectric resonance; electric strength; ferroelectricity; photodielectric effect; piezoelectricity; solvated electrons
adiabatic and isothermal order-parameter susceptibilities and the thermal diffusion mode 80—36962
anisotropic moving media, polarisation relations and dispersion eqns. to EM waves 80—9779
apolar viscoelastic dielectrics, thermodynamic theory, linear effects 78—67059
charge carrier drift simulation using stochastic graphs 80—15539
dielectrophoretic force, theory expt. 80—72403
elastic dielectric, EM wave effect on displacement field of crack 78—30231
electric fields, stability and growth estimates 79—71262
electrode systems, nonequilib. polaris. states props. overvoltage theory, in book, for teachers 78—8205
electrostatic drop formation characteristics using dielectric liquid 80—37926
electrostatic problems with simple dielectric boundary, solution method 78—12458
EM radiation, from line sources interacting with moving uniaxial dielectric or plasma half-space 79—92661
EM wave, evanescent, quantisation, near dielectric surface, field momentum 80—43231
EM wave, nonlinear excitation in dielectric cylinder by relativistic magnetised electron beam 77—19129
EM wave propagation, in inhomogeneous dielec. perturbation theory approach 78—17847
flexoelectricity of liquid crystals, microscopic interpretation 77—32339
fluid-fluid interface, stability in elec. and gravit. fields *(Russian)* 77—27617
fluid-fluid interface, stability in elec. field *(Russian)* 77—27616
geminate recombination, time depend. Onsager problem anal. soln., critical elec. field 78—72446
holohedral isotropic dielectric concavity arguments and growth estimates for damped linear integrodifferential eqns. 79—28703
liquid crystal electro-optical props. and applications 77—77174
MBBA, HF electrohydrodynamic instability in NLC *(Russian)* 80—54130
metal-semiconductor junction photoelec. phenomena, effect of dielectric gap and surface states *(Russian)* 78—84299
microwave irradiation of dielectric, near-field theory 79—41288
naphthalene, charge separation during cryst. growth, Costa Ribeiro effect 80—7316
naphthalene, single crystal, anomaly in permittivity, Costa Ribeiro effect 80—7258
neutral periodic assembly of charged particles, electrostatic lattice sums 79—71376
plane wave scatt. from dielectric cylinders 79—55057
plasma, harmonic oscillator, and rigid dipole dielectrics, dielec. friction 80—53928
plasma (fluid), hydrogenic, transverse dielec. function, excitation spectrum 78—67311
polar solvent molecule interactions in the adsorbed state 80—21299
polymeric capacitors, injection charging 77—76902
radiative transfer in plane stratified dielectric 78—51050
randomly inhomogeneous medium, mean EM field *(Russian)* 80—32882
relativistic effects, ponderomative laws of electrodynamics 77—41519
rotational swings of colliding dipoles, contrib. to nonlinear dielectric constant 78—27171
space charge distrib., carrier mobility and interface injection mechanism identification 80—15974
sphere, dielectric, motion in travelling elec. field 78—50685
stress determ. by EM waves *(Ukrainian)* 79—32254
surface with accumulated air positive ions, vacuum breakdown obs. 78—75464
thermodielectric electret, Costa Ribeiro effect 80—7272
thermoelastic dielectric, linear, wave propag., singular surfaces 77—72216
transition radiation and transition scatt., review 79—27143
wedge, review of theory of EM field behaviour 78—66712

dielectric polarisation
see also Barkhausen effect
acetic acid, dil. soln., dielectric polaris., linear correlation factor 78—6624
acetic acid-aniline (pyridine) complex, in CCl_4, dielec. polarisation 80—29675

dielectric polarisation continued
- air-dielectric interface, EM wave reflection and transmission in terms of polarisation, education 80—105458
- alcohol, thermal electret, persistency of surface change *(Japanese)* 77—81048
- alcohols, monohydric, dielec. polarisation 79—99818
- alkali halide:Me^{2+}, nearest-neighbour theory of dipole polarisation and depolarisation, cation vacancies 77—16243
- alkali halide, dielec. const., press. depend. from ionic polarisability and bulk modulus 79—19828
- alkali halide, exchange charge polarisation, dielectric const., Dick and Overhauser model 78—55832
- alkali halide, polarisation energy for core states 80—10903
- alkali halide, transverse optic mode Gruneisen parameter and dielectric props. 77—31747
- alkali halide crystal, permittivity and polarisation behind shock wave front 77—52013
- alkali halide crystals, high freq. dielectric const. press. derivative model calcs., electronic polarisation 80—7255
- alkali halides, polarization, photoinduced, rel. to exchange between vacancy and impurity 80—59914
- alkali halides, static dielectric behaviour, vol. depend., many-body interactions effects 78—2786
- alkali halides, three-body interactions, effect on electronic polarisabilities and photoelastic behaviour 79—47382
- alkaline earth glasses, $45RO.5Al_2O_3.50P_2O_5$, ($R=Mg,Ca,Sr,Ba$), electron beam irrad., temporal change in electric field produced 79—4760
- n-alkanes, dielec. permittivity and pvT data 80—44996
- n-alkanes, solid, core electron relax. energies and valence band form., XPS exam. 77—36372
- L-p-alkoxybenzylidene p′-amino 2 methylbutyl cinnamate chiral smectic liq. cryst., dielec. and ferroelec. props. 79—91394
- alkyl halide, amorphous, depolarisation thermocurrents and dielectric relaxation time distrib. *(French)* 80—60490
- ammonium Rochelle salt, thermodynamics of ferroelec. transition 80—84702
- amorphous solid, constitutive relation derivation 80—84684
- anisotropic moving media, polarisation relations and dispersion eqns. to EM waves 80—9779
- anodic oxide film, photodepolarisation *(Russian)* 77—32316
- asymmetric top rotational Brownian motion and electric polarisation calc. 80—15949
- bilayer lipid membranes, flexoelectric polarisation at blocked flip-flop 79—100582
- biomolecules, dielectric transient response following UV-irradiation 80—51166
- bipolymer, charge carriers origin and mobility, adsorbed water effects 79—92461
- bone, human cortical, local piezoelec. polarisation as function of stress freq. 77—32933
- boracites, trigonal, spontaneous polarisation behaviour 77—43945
- m-bromaniline delayed depolarisation obs. *(Russian)* 79—95703
- bromoform delayed depolarisation obs. *(Russian)* 79—95703
- butanediol terephthalate-polytetramethylene oxide terephthalate copolymers, dielec. props. 78—95546
- 1-butanol, time domain spectroscopy, superposition integral approximation 77—1630
- t-butanol and -d_1, deuteration effect on self-assoc., dielectric polaris meas. 79—28672
- calcium behenate monomolecular layers between Al electrodes, nonlinear dielec. props. 80—80405
- capacitors, decay voltage and recovery voltage curves 79—61295
- carnauba wax, polarised, simultaneous variation of dielec. const. and discharge current, room temp. to beyond melting point 80—11314
- carnauba wax, thermal electret, persistency of surface charge *(Japanese)* 77—81048
- carnauba wax electret, effective charge rel. to polarisation tmep. 78—15086
- carnauba wax thermoelectret, mag. anisotropy evidence for dipolar orientation 77—16240
- cellophane membrane, polarised, electret transport props., permeability coeff. 80—7860
- charge build-up on air/dielectric separation surfaces 80—25288
- chiral smectic C, ferroelec. props., dielec. meas. 78—52463
- chiral smectic liquid cryst., ferroelectric, flexoelectric effects, dielectric const. 80—33877
- chloranil pellets, thermally stimulated discharge current and dielectric studies 80—93236
- chloroform delayed depolarisation obs. *(Russian)* 79—95703
- chloroform HV polarisation and space charge obs. *(Russian)* 80—25277
- coal dispersions, solvent refined, elec. props., surface characts. 80—80333
- complex polarisability, transform. of complex permittivity, determ. of LF dispersions in solids *(German)* 77—90089
- composite media, dielec. and optical props. 78—84546
- composites, interfacial polarisation and loading factor effects in dielec.-loss meas. 80—2693
- conductivity measurement, difference between electrification and resorption currents 77—62932
- copper formate tetrahydrate, ice rule ferroelectric, polarisation correlations 80—97190
- crystalline dielectric, local electric fields near surface 80—80733
- crystalline slab of point molecules, dielec. theory 80—97222
- cubic lattice of polarisable spheres, dielectric constant 80—60483
- cubic lattices, dipole moments of point polarisable atoms, uniform applied electric field, SCF equations 80—50257
- decay functions, cole-cole and Davidson-Cole plots, constant temperature *(Spanish)* 79—61294
- diamond, dielectric polarisation calcs., microscopic local fields 80—20582
- diamond, local field, microscopic electronic polarisation 80—25283
- diatomic crystal, photoelasticity, exchange charge polaris. effect 77—81046
- dicalcium lead propionate, ferroelec., annealed, crit. exponents, dielec. const. temp. depend. 80—55050
- dicalcium strontium propionate, Landau theory breakdown in ferroelec. transition 77—12344
- dielectric constant and polarisability strain derivatives 77—90088
- dielectric relaxation and LF anomalous dispersion obs. *(Japanese)* 78—49056
- dielectric-vacuum interface, spatial dispersion in optical props. 77—4613
- dielectrics, partial polarisation fluctuations, macroscopic phenomenological eqn. and thermodynamic fluctuation theory study 79—78615

dielectric polarisation continued
- dielectrics, radiation induced charging and discharging, analytic solution 79—78612
- dipolar liquid time-variation of dispersion and absorption of third-order electric polarisation, mol. relax. times 80—60487
- dipolar molecular lattice, dielec. absorpt. of disordered mol. solids, electrodynamic influences 80—40040
- dipolar point defects, studied by ITC 80—6405
- dipolar relaxation study using thermally stimulated polarisation currents 80—7278
- dipole in polarizable fluid, effective field 77—76280
- dipole-dipole coupling, inertial effect 80—40049
- disperse system, elec. relax. in external fields, contrib. to elec. susceptibility 80—55720
- disperse system, high conc., interfacial polarisation, dielec. consts. and relax. freqs., numerical estimation 77—32833
- DOBAMBC, chiral smectic, flexoelectric effect and polarisation props. *(Russian)* 80—15002
- DOBAMBC, chiral smectic C-phase ferroelectric liq. crystal film, classical X-Y system, props. 80—44123
- DOBAMBC, chiral smectic phases, pyroelectric and dielec. props. 79—91380
- DOBAMBC, ferroelec. props. 79—32884
- echoes and avalanches, possibility in non-piezoelec. materials 79—69767
- education, homogeneous ellipsoidal inclusions, general theorems, Poisson theorem, dielectric polarisation, conduction and elasticity 78—61979
- elastic dielectrics, nonlinear compatibility equations and Bianchi-type identities 79—41574
- elastic dielectrics, stress tensor, polarisation vector, electric tensor 80—55018
- elastic half space with point charge, stress and polarisation anal. 77—83776
- electret, spatial distrib. of charges and dipoles, transient heating technique 77—12303
- electrets, prepolarised, meas. microphones appl. 80—74649
- electrets, radiation-induced charge storage and polarisation effects 80—80684
- electrets and dielectrics, conf., Sao Carlos, Brazil, Sept. (1975) 80—7251
- electric dielectric, hyper-, with saturated polarisation, variational and invariance principles 80—74730
- electrical response of relaxing dielectrics compressed by shock waves, axial mode problem 78—80280
- electron-hole pairing systems, current states and domains 80—54614
- electronic matter, polarisation and magnetisation 80—75929
- electrophoresis, nonlinear, of dielectric and conducting ideally polarisable particles 77—25270
- EMF production by shock compression of solids 77—31719
- epoxy-resin, Nomex-filled, space charge polarisation, thermal depolarisation current study 80—7282
- ester, smectic C phase liq. cryst., ferroelectricity and spontaneous polarisation *(Russian)* 79—8102
- esters, SLC, ferroelectric behaviour, specific heat, spontaneous polarisation 80—75958
- esters, thermal electret, persistency of surface charge *(Japanese)* 77—81048
- extrinsic ferroelectrics, transition, polarisation, dielectric divergence 80—80718
- fatty acids, thermal electret, persistency of surface charge *(Japanese)* 77—81048
- ferroelctric crystals, parameter meas. *(Polish)* 78—88272
- ferroelec. crystal, Barkhausen effect study 79—38507
- ferroelectric, Barkhausen effect, contrib. to repolarisation process *(Russian)* 77—32330
- ferroelectric, eight-site order-disorder model, influence of tunnelling 80—2709
- ferroelectric, local potential approach *(Japanese)* 77—43939
- ferroelectric, photoinduced changes in refractive index and spontaneous polarisation 78—43804
- ferroelectric, uniaxial, Urbach rule and polarisation fluctuations, optical absorpt. edge 80—88910
- ferroelectric ceramic, acoustic vel. anisotropy 79—55835
- ferroelectric ceramic, rel. to mech. and elec. losses, correl., theory and expt. 80—66133
- ferroelectric ceramic, shock induced polarisation 77—48133
- ferroelectric crystal, fluctuons, calc. by method of parametric potential *(Russian)* 79—69784
- ferroelectric crystals, finite, with surface energy 79—56741
- ferroelectric dipole waves, low temp. sp.ht. and spontaneous polarisation calc. 79—33614
- ferroelectric domain walls motion in strong fields and polarisation wave spectrum *(Russian)* 79—87409
- ferroelectric film switching transition meas. instrument, operating principle 79—17443
- ferroelectric films, surface effects on phase transitions, local spontaneous polarisation 80—2708
- ferroelectric liquid crystals, kinetics of spontaneous polarisation *(Russian)* 79—8101
- ferroelectric liquid crystals, temp. depend. of elec. susceptibility and spontaneous polarisation *(Japanese)* 78—68467
- ferroelectric liquid crysts., chiral smectic C phase, phys. props., review 80—75150
- ferroelectric material properties study, LF HV generator applic. *(French)* 77—41647
- ferroelectric materials, refractive index variation, fluctuative mechanism *(Russian)* 79—56755
- ferroelectric materials, repolarisation in SEM 79—15424
- ferroelectric materials for dielectric power conversion, dielectric prop. anal. 80—80712
- ferroelectric models, existence of phase transition near displacive limit, onset of spontaneous polarisation 79—8104
- ferroelectric phase transitions, crystals with noncentral ions, rel. to spontaneous polarisation 80—15991
- ferroelectric plate, polarisation distribution, permittivity, domain structure 80—29704
- ferroelectric powders, origin of memory in echo-phenomena 79—38440
- ferroelectric semiconductor, band bending in surface layer 80—60061
- ferroelectric semiconductor, solid solution, phys. characts. nonlinearity near phase transition 78—43812
- ferroelectric semiconductors, props., book 80—82590
- ferroelectric thin film, thermodynamics in vicinity of first order phase transition *(Russian)* 80—45014

dielectric polarisation continued
- ferroelectricity, nonclassical, nonclassical ferroelectricity, phase transitions 80−25320
- ferroelectrics, automated meas. system 79−67268
- ferroelectrics, unit cell multiplication during phase transform., spontaneous polarisation 80−75983
- ferroelectrics hysteresis loop sensing *(Czech)* 80−82792
- field induced thermally stimulated polarisation-depolarisation currents, relaxation, book contribution 80−80687
- film, spatial charge distrib. meas. technique 77−32327
- fluctuation theorems 79−47381
- fluctuations in dielectric mag. media 77−81047
- fluctuations in regions bounded by semi-potentials 79−82917
- frequency dependent dielectric constant, rel. to dielec. polarisation 78−56425
- glass, dielectric instabilities in high permittivity glass 78−52433
- glasses, echoes and elec. dipole echoes at low temps. 79−69771
- glasses, high-resistivity, uniform and space charge polarisation, thermally stimulated depolarisation anal. 78−15085
- guanidine aluminium sulphate hexahydrate, ferroelec. cryst., growth, domain struct., dielec., switching props. 77−43950
- harmonic generation in piezoelectric crystals under the action of homogeneous external fields 79−32121
- helicoidal ferroelectric smectic A-smectic C phase transition, low freq. polarisation fluctuation spectrum 79−95714
- 4-n-heptyl-4′-β-cyanovinylbiphenyl, liq. cryst., isotropic mechanism of mol. rot., dielec. permitt. meas. 80−10491
- 4-n- heptyloxyphenyl 4-n-hexydexybenzoate, liquid crystal, freezing polarisation, electret effect *(Polish)* 80−10496
- heterogeneous matrix system, generalised conductivity and loss, tangent 80−7289
- 4-n-hexyl-4-cyanobiphenyl, liq. cryst., isotropic mechanism of mol. rot., dielec. permitt. meas. 80−10491
- p-hexyloxyphenyl-p-pentoxybenzoate, nematic liq. cryst., elec. discharge meas. of persistent internal polarisation 80−10488
- HOAB-DOBAMBC nonchiral-chiral smectic C mixture, spontaneous polarization and induced circular dichroism 79−27910
- ice, polarisation processes, in lattice, Kirkwood's theory rel. to thermodynamics of irreversible processes 79−38447
- ice, polarisation processes, in lattice, thermodynamics of irreversible processes, universal relation 79−38446
- II-VI semiconductors, correlation between electronic dielec. constant and ionic separation 79−4758
- III-V compounds, piezoelec. coupling and dislocations 79−91377
- III-V semiconductors, correlation between electronic dielec. constant and ionic separation 79−4758
- III-V semiconductors, piezoelectric induced polarization charge distribs. around point defects 79−56725
- improper ferroelectrics, spontaneous polarisation, cryst. symm. in phase transitions 78−6645
- induced (galvanic) polarisation in solids with electrolytic pore filling, theory *(German)* 79−88344
- inhomogeneous semiconductor, acoustoelectric interaction, elec. cond. 79−95453
- insulating thin film, polarisation dispersion characts. meas. under high DC elec. fields *(Japanese)* 77−63013
- interfacial polarisation effect on dielectric props., sandwich capacitor model 80−15614
- ionic conductor, interfacial polarisation effects 79−60538
- ionic crystal, space charge polarisation involving electrode reaction with surface adsorption 77−12019
- ionic crystals, effect of Lundqvist's many body potential on phototelastic behaviour 77−63391
- ionic polarisability in crystal lattice, quantum mech. model 79−47384
- ionic solid, deformation dipole model 78−72454
- isoquinoline, solns., dielec. polarisation, π-electron system effects 77−90096
- IV-VI compounds, dielec. props., elec. meas. 78−15119
- leaves of palmlike plant Encephalartos villosus, induced pyroelec. polarisation 77−77876
- $^6LiH_3(SeO_3)_2$, absolute atomic arrangement rel. to spontaneous polarisation, neutron diffr. study 80−15067
- linear gyrotropic media, E2, M1 moment contribs. to linear polarisation *(Russian)* 77−8540
- liquid, electric polaris. theory, approxs. 78−10839
- liquid, microdielectric interaction with EM and thermomechanical fields 78−39518
- liquid crystal, ferroelectric, review of props. 77−85667
- liquid dielectrics, local field, two-parameter mean field approach 80−93232
- liquid nonlinear third-order polarisation, transient effects elucidating molecular props. 80−15955
- liquid-vapour interface, non-polar fluid, variation of local field 80−80734
- long-time-constant polarisation spectrum selective meas., DC methods 80−15944
- lossy dielectric material containing short randomly distributed metal fibres 80−20584
- lossy dielectrics, thermal charge carriers movement 80−88920
- Lyddane-Sachs-Teller relation, cryst. with Debye polarisation 77−20256
- lysozyme bound water, thermally-stimulated press. and current 78−15757
- macromolecular, electrically induced fluorescence depolarisation 77−27210
- Maxwell-Wagner dielectric dispersions, vol. ion polarisations 80−97188
- mean internal stress potential of polarisable dielectric crystals, subject to a constant magnetic field and in vibratory motion *(Italian)* 79−65797
- methyl bromide delayed depolarisation obs. *(Russian)* 79−95703
- methyl iodide delayed depolarisation obs. *(Russian)* 79−95703
- methylammonium chromium selenate, lattice consts. and ferroelec. props. 79−33641
- methylammonium gallium selenate, lattice consts. and ferroelec. props. 79−33641
- methylammonium-$Ga(SO_4)_2.12H_2O$, ferroelec. alum single crysts., dielec. dispersion and characts. 79−15408
- methylene chloride HV polarisation and space charge obs. *(Russian)* 80−25277
- 3-methylpentane glass, electron-ion pair polarisation, γ-irrad. induced current and IR photocurrent 77−69768
- micro-organism electroretention effectiveness rel. to electrode type *(Russian)* 80−26419

dielectric polarisation continued
- MIS structure, on thermal SiO_2, polarisation hysteresis, ion motion *(Russian)* 80−54793
- MIS structures, dielectric polarisation effects on instability 77−69418
- molecular crystals, microscopic dielec. theory 80−97186
- molecular liquid, of polarisable and deformable mols., theory 79−99043
- molecular solid, electronic polaris. energy, quantum dynamic rel. to classical microelectrostatic approach 78−52427
- Mott transition in Hubbard long range model, isostructural instability, thermodynamic props. *(Russian)* 80−65454
- negative currents caused by injection-controlled polarization 79−28675
- nematic liquid crystal, threshold flexoelectric effect 79−94878
- nematic liquid crystals, molecular mechanisms of dielec. polarisation and relaxation 80−34846
- nematic liquid crysts., dielec. polarisation and relax., mol. mechanisms 80−29673
- nematic liquid crysts. of mols. containing nitrile groups, dipole moments determ. 77−19872
- niobates, Lorentz elec. field, and short-range Nb-O interactions 77−43941
- nitrobenzene, polarised, simultaneous variation of dielec. const. and discharge current, room temp. to beyond melting point 80−11314
- nitromethane, shock-induced elec. polarisation *(French)* 79−11381
- NOBAMBC, chiral smectic phases, pyroelectric and dielec. props. 79−91380
- non polar fluid dielectrics, mechanical forces 80−60529
- nonlinear dielectric relaxation 78−60389
- nonlinear dielectrics potential distribution 77−66452
- nonoptically active media, susceptibilities, elec. and mag. polarisation fluctuation 77−77140
- nonpiezoelectric dielectric, polarisation echo and polarisation avalanche signal form. *(Russian)* 79−61297
- nonpolar crystal, struct. transition, macroscopic quadrupole moment meas. *(Russian)* 77−62642
- nonpolar crystal, temp.-depend. polarisability, anharmonic oscillator anal. 79−8087
- nonpolar molecule substituting polar mol. in mol. dipole lattice, dielectric alignment 77−89359
- nonstoichiometry and dielectric props. 78−43135
- n-octadecane, surface charge decay 78−43463
- octupole modifications of Clausius-Mossotti relation 80−49179
- 4-n-octyloxy-4'-cyanobiphenyl, liquid cryst., dielect. polarisation and its dispersion 79−1397
- p-octyloxyphenyl-p-pentoxybenzoate, nematic liq. cryst., elec. discharge meas. of persistent internal polarisation 80−10488
- orientation transitions, stabilising effect of high freq. fields *(Russian)* 77−89972
- orthovanadates, centrosymmetric exhibiting cooperative Jahn-Teller effect, dielec. props. 79−28694
- osteon system piezoelec. polarisation model 78−3540
- oxide ceramic, ferroelectric, with perovskite struct., cond. and polarisation 77−12325
- oxyfluoride ferroelectrics, chemical bonding, Curie temp., spontaneous polarisation 80−75981
- p-alkoxybenzylidene-p′-amino-2-chloropropyl-cinnamate, chiral smectic, dielec. props. 80−96441
- PAN, spectroscopic analysis of electrically polarised films 78−68443
- paraelectric-ferroelectric-antiferroelectric phase transitions, electrostrictive effects 80−97209
- perovskite oxides, single cryst., photocond. and TSC meas. 78−43436
- phenol I and II, permittivity and molar polarisation at pressures between 140-2000 bar 77−77136
- phosphate glass, electron-irradiated, charge accumulation, comp. depend. 78−2159
- photo-induced polarisation, model 79−56714
- piezoceramic, polarisation method effect on mech. strength 78−39879
- piezoceramic planar Poisson ratio variation with poling conditions 79−11391
- piezoelectric and photoelastic interactions elec. polaris. effects *(German)* 78−35091
- piezoelectric ceramics, photovoltaic effect application to information storage 80−80316
- piezoelectric crystals, polarisation echo 77−90104
- piezoelectric powder, memory echo, dipolar field contrib. 80−84700
- piezoelectric powder, polarisation echo, long memory times 77−8516
- piezoelectric powder, polarisation echo and surface props. theory *(Russian)* 77−48122
- piezoelectric powder, polarisation echo for system of anharmonic oscillators *(Russian)* 77−81062
- piezoelectric semiconductor, US absorption 80−44670
- piezoelectric semiconductors, polarisation echo *(Russian)* 78−15099
- piezoelectricity, mechano-electric coupled fields, polarisation gradient 80−75940
- piezoelectricity theory of dielectrics, polarisation gradient elasticity theory, coupled mechano-electric fields 80−55037
- plastics, radio and light polarisation stress analysis 78−68857
- PLZT ceramics, ferroelec., special props. 79−42916
- PMMA, and related cpds., ionic charge carriers, dielec. studies 80−25291
- PMMA, shock induced polarisation, dielec. const., dipole lifetime rel. to particle velocity *(French)* 77−69776
- PMMA moist surface mech. strength reduced by electric charge *(Russian)* 80−60486
- PMMA thermo-electrets, temp. and field effects 78−31148
- polar gas, polarisation by external and internal elec. fields 78−12459
- polar liquids, dielectric behaviour in far IR spectral range, theory 77−28509
- polar liquids, elec. polarisation theory 77−4596
- polar molecules, spontaneous surface polarisation during adsorption 79−42381
- polar polymer, piezoelectricity and pyroelectricity 80−7267
- polarisation echo, physical nature 77−1635
- polarization echo and induction signals excited by pulses of various duration *(Russian)* 79−61298
- poly(2-vinyl pyridine), electronic struct., molecular-ion states and dielectric props. 79−37969
- poly(pyromellitimide), shock-induced electrical activity, mechanically induced bond scission model 80−50256
- poly vinylidene fluoride, injection process nature during poling, rel. to pyroelectricity 78−19422

dielectric polarisation continued
- poly-γ-benzyl-L-glutamate, synthetic polypeptide, nonlinear dielectric effect in nonpolar medium 80—84682
- polyacene quinone radical copolymer, reversal of usual electric field effect and nomadic polarisation 77—12304
- polyacenequinones, dielec. polarisation, role of conducting mol. chains *(Russian)* 79—65794
- polyacetylene:I, dc microwave cond., permittivity 80—107843
- polyacrylonitrile, elec. polarisation 80—7275
- polyacrylonitrile, film, dielectric polarisation 78—52431
- polyacrylonitrile, film, IR attenuated spectra determ. of chem. origin of TSC 77—55746
- polycarbonate thin films, solution-grown, dielectric relaxations 80—55029
- polychloroprene, polar dielectric, mech. polarisation *(Russian)* 77—40174
- polydomain ferroelectrics, spontaneous polaris. screening *(Russian)* 79—91395
- polyelectrolyte membranes, persistent polarisation in aq. environment, neural model 78—48763
- polyester foil, static polarisation depend. on heat ageing 78—60688
- polyethylene electret, internal pot. topography, Raman and IR spectra 80—7362
- polyethylene film electrets, polarisation obs. and influence of wax impurities, TSC obs. and analysis *(French)* 80—44999
- polyethylene oxide, elec. polarisation in suspension, Kerr effect 77—63359
- polymer, conductive, freq. depend. of elec. cond. and polarisation 77—11918
- polymer coatings for corrosion protection, electrochem. techniques for performance monitoring 80—3234
- polymer dielectrics, electrical conduction and polarisation phenomena at low fields 78—48113
- polymer electret, charge dissipation, transport mechanisms 80—7268
- polymer film transducer, piezoelec. and pyroelec. response rel. to dipole polarisation 80—7267
- polymer gels, comb-like, dielec. polarisation *(Russian)* 77—48698
- polymeric solids, shock-induced electrical activity, mechanically induced bond scission model 80—50256
- polymers, elec. props. and morphology, correl. review 78—43786
- polypeptides, helical, dielectric polarisability, side chain motions 78—76378
- polypropylene film and diarylalkane, Maxwell-Wagner dielectric polarisation 80—29676
- polypyromellitimide, thermal depolarisation current 78—52429
- polystyrene:I films, thermally stimulated discharge, I conc. and polarisation temp. depend. 80—107937
- polystyrene, pure and doped, metal contact effect on persistent internal polarisation 79—78617
- polystyrene composite with mica flakes, TDC meas., interfacial polarisation 78—64316
- polystyrene film, thermally stimulated discharge currents 80—71300
- polystyrene thin films, TSC and surface charge meas. 80—103769
- polystyrene-polyethylene oxide copolymer, elec. polarisation in suspension, Kerr effect 77—63359
- polyvinyl acetate, struct. relax., enthalpy and elec. polarisation obs. 79—41978
- polyvinyl alcohol, bulk polarisation, thermally stimulated discharge current meas. 80—40039
- polyvinyl alcohol, ionic charge carriers, dielec. studies 80—25291
- polyvinylidene fluoride, corona-charged, surface effects 80—66102
- polyvinylidene fluoride, electro-optic and elasto- optic effects 80—80754
- polyvinylidene fluoride, film, piezoelec. relax. 79—87394
- polyvinylidene fluoride, hysteresis phenomena under high elec. field 80—66134
- polyvinylidene fluoride, piezoelec., pyroelec., and improper ferroelec. 80—7301
- polyvinylidene fluoride, piezoelec. and pyroelec., rigid dipolar model *(French)* 79—8090
- polyvinylidene fluoride, piezoelec. props., polarisation and appls. 80—75947
- polyvinylidene fluoride, piezoelectric effect formation due to injection process, TSC *(French)* 80—34856
- polyvinylidene fluoride, plasma poling, piezoelec. and pyroelec. responses 80—71296
- polyvinylidene fluoride, poled, dielec. relax. spectra 80—80690
- polyvinylidene fluoride, poling by corona charging, pyroelec. effect 78—19423
- polyvinylidene fluoride, poling process, kink propag. model 80—80679
- polyvinylidene fluoride, poling process, solitary wave propagation model 79—87398
- polyvinylidene fluoride, poling process effect on fine struct. 80—7285
- polyvinylidene fluoride, struct. study, piezoelec. and pyroelec. props. 80—7300
- polyvinylidene fluoride, uniaxially stretched, piezoelec. and pyroelec. 77—40181
- polyvinylidene fluoride film, cryst. dipole orientation in elec. field 78—80286
- polyvinylidene fluoride film, hysteresis and dipolar orientation 80—97217
- polyvinylidene fluoride film, polarisation and depolarisation processes 80—11318
- polyvinylidene fluoride film poling rates, 20 to 100°C 77—77138
- powder, three pulse echo, mechanism contribs. 78—68444
- 1-propanol, time domain spectroscopy, superposition integral approximations 77—1630
- PVC, rigid, physical ageing effect on elec. props. 78—10836
- PVC films, soln. grown, DC cond. mechanisms, field and temp. depend. 80—97021
- PVF_2 charge injection from metallic electrode, obs. 80—15947
- PVFD, electret, polarisation process 80—7273
- pyridine, solns., dielec. polarisation, π-electron system effects 77—90096
- pyroelectric, uniaxial, spontaneous polarisation, calc. from results of optical meas. 78—27162
- pyroelectric high power density heat engine, dielectric losses, polarisation 80—80689
- quartz, natural, virgin (γ-irradiated), polarisation effect on thermolum. sensitivity 80—11483
- α-quartz, obs. of reversible elastic Dauphine twinning 78—87684
- α-quartz plate frequency changes rel. to electroelastic tensor and second-order phenomena 78—60398
- quasi-one-dimensional solids, nomadic polarisation 77—63357
- quinoline, solns., dielec. polarisation, π-electron system effects 77—90096

dielectric polarisation continued
- reflection in terms of polarisation 79—82916
- relaxational polarisation, theory development and applicability 80—11334
- resonance media, dielec. props., resonance pumping effect 80—55054
- RNA, solid hydrated samples, hysteresis loops, nonlinear dielectric properties 80—71294
- Rochelle salt, dielectric props. near upper Curie pt. under hydrostatic press. 79—82935
- Rochelle salt, polarisation echo, near ferroelec. transition 78—88266
- Rochelle salt, polarisation echo in ferroelec. phase transition region 79—42920
- Rochelle salt, polarisation relaxation, US vel. and attenuation meas. 77—28512
- Rochelle salt, thermal expansion and spontaneous strain meas., −40 to 40°C, electrostrictive consts. 77—16262
- salicelidenanilines, SLC, ferroelectric behaviour, specific heat, spontaneous polarisation 80—75958
- schultenites, ferroelectric, sp. ht. 79—19853
- semi-infinite cubic lattice, response to static point charge 80—75928
- shock compression of solids, review 80—24534
- silica gel, struct., dielec. polarisation, IR spectral investigs. *(French)* 77—81427
- silicate glass, space charge distrib. after 2.1 MeV electron irrad. *(Russian)* 77—69772
- sisal wax, electronic conduction and persistent internal polarisation 78—80277
- sisal wax thermoelectrets, thermally stimulated discharge and internal polarisation 80—55016
- SLC, chiral structure in electric field, dielectric permeability, spontaneous polarisation *(Russian)* 80—75159
- smectic C liq. crystal with induced helical struct., ferroelectric props. and spontaneous polarisation, C→A transition 80—54123
- smectic helixing crystal, dielec. props., temp. and freq. depends. *(Russian)* 78—60380
- smectic liquid crystal, C-phase, optical props. *(French)* 77—43959
- smectic liquid crystal, ferroelec. props., temp. depend. *(Russian)* 77—32332
- smectic liquid crystals, spontaneous polarisation meas. *(French)* 77—69765
- sodium ammonium tartrate, polarisation, improper ferroelec. transition 78—72477
- solid, many body model 78—10840
- solid, many body model 78—15087
- solid dielectrics, molecular optics model, macroscopic theory 80—84683
- solute-solute-solvent interaction, dielec. behaviour problems, review 80—25298
- solvent effects on chemical reactions, semiempirical model 80—25986
- space-charge behaviour, effect of relax. processes 80—40057
- spatially dispersive dielectric, boundary conditions for polarisation waves 79—61296
- stearic acid multilayer films, lattice and carrier contribs. to dielec. polarisation 77—69775
- Stockmayer fluids, static dielec. props. 80—93231
- styrene-acrylonitrile copolymer film, multiple relax. obs. using TSC 80—45000
- styrene-butadiene-styrene triblock copolymers, dielec. props. 78—95545
- surface charge density determ., rel. to measurable parameters 77—48120
- surface polarisation from sessile drop contact angle meas. 77—85365
- suspension, of ideally polarisable spherical particles, low-frequency dielectric dispersion 79—61912
- suspensions, concentrated, of shell-spheres, dielectric theory, interfacial polarisation, anal. of biological cell suspensions 80—45563
- suspensions of ellipsoidal particles covered with shell, dielec. behaviour, rel. to biological cells 80—51057
- tapered piezoelectric bar transducer with transverse polarisation of piezoceramic, acoustic props. 78—1537
- Teflon foils, cryst. struct. and texture changes due to polarisation process *(Polish)* 80—35209
- terylene film, electret state prod. using electrochem. injection, adsorbed states, frozen field 79—91344
- tetrachloroethylene-benzene(toluene)(p-xylene)(carbon tetrachloride) binary mixtures, dielec. polarisations 79—56713
- tetramethylammonium tetrachlorocobaltate, ferroelec., pressure-temp. phase diagrams 80—97205
- tetramethylammonium tetrachlorozincate, ferroelec., pressure-temp. phase diagrams 80—97205
- tetramethyldiaminodiphenyl ketone, binder layer, photoinduced polarisation and voltage 80—75923
- TGFB:Cr^{3+}, polarisation reversal and ageing mechanisms, EPR meas. 79—8044
- TGS:α-alanine, single crysts., dielec. spectrum in RF range *(Russian)* 80—66097
- TGS:α-alanine, single crysts., pyro- and dielectric props. *(Russian)* 77—59520
- TGS: nitroaniline, dielec. and pyroelec. props. 80—75916
- TGS:Cr^{3+}, EPR and spontaneous polarisation stabilisation during annealing 77—4610
- TGS, complex dielec. permitt. near Curie temp., ferroelec. polarisation mechanism interpretation 78—43808
- TGS, correlation between domain struct. and dielec. props. 79—42927
- TGS, deuterated, dielectric props., ageing 77—16257
- TGS, elastic vs. polarisation energy near transition 78—15118
- TGS, exponential switching by sidewise domain wall motion 80—29703
- TGS, ferroelec., spontaneous polarisation, 2.2-20K 79—19849
- TGS, ferroelec. crystal, Barkhausen effect study 79—38507
- TGS, ferroelec. domain struct., polarisation obs. *(Chinese)* 80—20603
- TGS, L-α-alanine disordered regions, dielec. prop. changes in transition region 80—108159
- TGS, polarisation reversal, cryst. defects effect 78—27156
- TGS, pyroelec. IR detectors, permanent polarisation due to X-rays, optimum non-ferroelec. behaviour 77—41684
- TGS, spontaneous polarisation, low temp. meas. 80—75921
- TGS, spontaneous polarisation and coercive field from 30 to 1000 Hz 77—66464
- TGS, surface alignment of nematic liq. cryst. controlled by domain struct. 79—99068
- TGS, switching induced electrolum. 79—38669
- TGS, temp. depend. of spontaneous polarisation, microscopic mechanism, NMR expts. 77—81070
- TGS, temp. depend. of spontaneous polarization near ferroelec. transition 79—33597

dielectric polarisation continued
TGS crysts., effects of radiation induced defects on internal bias field 80–88941
TGS substrate, ferroelec. field effect in Te films 79–42675
TGS-TGSe solid soln., phase transitions under hydrostatic press. 79–99840
TGSe, deuterated, dielectric props., ageing 77–16257
TGSe, dielectric const. near ferroelec. transition temp., effect of surface capacitance 78–56438
TGSe, surface layers effect on coercive field, spontaneous polarisation, and dielec. const. 79–61321
thermodynamic vectorial internal degrees of freedom, dielec. and mag. relax. phenomena 77–77145
thiourea monocrystals, γ-irrad. effects on dielec. props. 79–91391
time domain spectroscopy, superposition integral approximations 77–1630
time-correlation functions of permanent dipole moments and induced polarisation 80–11316
time-dependence determ. using time-domain spectroscopy 80–52310
titanates, Lorentz elec. field, and short-range TiO interactions 77–43941
transition metal oxide, electronic polarisability of ions 77–40175
transition metal oxide films 78–2803
transition metal oxides, dielec. and thermophys. props. 77–52009
transition metal oxides, electronic polarisability of ions 77–19901
triglycine fluoroberyllate, thermodynamic props. 78–15123
trisarcosine calcium chloride crystals, ferroelec., electrooptic and ferroelastic props. 80–34865
TSC technique for nonexponential dielec. response materials 79–47383
TTF-TCNQ, antiferroelectric ordering of TCNQ ion elec. polarisation 80–20598
TTF-TCNQ crystal, antiferroelec. ordering of electronic polarisation, simple model anal. 78–92028
two-layer dielectric interface polarisation charge expt. 80–15946
uniaxial dielectric crystals, wave propag., polarisation relations and dispersion eqns. 80–64723
uniaxial ferroelectrics, microscopic theory, crit. behaviour and anomalous elastic consts. 79–38463
universal dielectric response in condensed matter 79–28674
universal dielectric response in condensed matter 80–11333
vibronic ferroelectric semiconductor, tunnel effect 78–10853
vibronic theory of ferroelectricity 79–19854
vinylidene fluoride copolymer electret, charge and polarisation distribs. meas. 78–35081
vinylidene fluoride trifluoroethylene copolymer, ferroelec. behaviour 80–50284
vinylidene-fluoride-trifluoroethylene copolymer, piezoelectricity 80–88930
vinylidenefluoride/tetrafluoroethylene copolymer, piezoelect. and pyroelect. response rel. to dipole polarisation 80–7267
water, amorphous solid, spontaneous electric polarisation rel. to solid struct., 20 to 100K 79–65791
water, polarisation fluctuations, effective freq. calcs. 77–90093
X- and γ-ray region dielectric permittivity, review 80–44998
Ag halides, correlation between electronic dielec. constant and ionic separation 79–4758
Ag_3AsS_3, proustite, cryst., temp. depend. of macroscopic polarisation 79–61317
Ag_3AsS_3, proustite crystals, stoichiometric composition derivation influence on phase transition 79–95715
AgBr, exchange charge polarisation 78–92016
AgCl, exchange charge polarisation 78–92016
$AgNa(NO_2)_2$, ferroelec. transition, ^{23}Na elec. field gradient tensor, NMR meas. 79–4777
$AgNa(NO_2)_2$, ferroelectric phase transition, theory 79–24272
$AgNa(NO_2)_2$, order-disorder ferroelec., influence of hydrostatic press. on polarisation dynamics 80–103913
Ag_3SbS_3, pyrargyrite, order-disorder phase transition and elec. polarisation 79–38468
β''-Al_2O_3-Na_2O, Li_2O stabilised, electrolyte polarisation anal. by complex admittance method 80–2689
Ar:Xe^+, 0.1-1.4 gm cm^{-3}, adiabatic electrostatic polarisation energy, calc. 77–85640
Ar-O_2 liquid mixture, dielectric polarisation and permittivity *(Russian)* 77–90095
$As_xSb_{1-x}SI$, solid solns., ferroelec. props. 78–23409
Au, dielectric const. by multiangle reflection meas., optical props. 79–95723
Au-Cu, dielectric const. by multiangle reflection meas., optical props. 79–95723
$(Ba,Sr)TiO_3$, ferroelec. solid solution, dielec. nonlinearity in nonpolar phase *(Russian)* 77–32317
$(Ba,Sr)TiO_3$, ferroelec. props., press. depend., anharmonic oscillator model 80–80716
$BaCoF_4$, low temp. magnon effects on polarisation 79–42905
$Ba(H_2PO_4)_2$, dielectric const. and polarisation, antiferroelectricity 77–59526
$BaMgF_4$, low temp. phonon effects on polarisation 79–42905
$BaMnF_4$, low temp. phonon, and exciton effects on polarisation 79–42905
$Ba_{2.09}Na_{0.72}Nb_{5.02}O_{15}$, cryst. growth, monodomenisation, detwinning, optical homogeneity, composition, dielec., spectral props. 77–44151
$BaNiF_4$, low temp. magnon effects on polarisation 79–42905
$BaNiF_4$, obs. of anomalous pyroelec. behaviour due to cooperative mag. singularity 77–59517
BaO, dielectric behaviour 79–91343
BaO-K_2O-VO_2-SiO_2, glass, elec. cond. rel. to ion polarisability, polarons 80–49729
BaO-$La_{0.6}O$-VO_2-SiO_2, glass, elec. cond. rel. to ion polarisability, polarons 80–49729
BaS, dielectric behaviour 79–91343
$Ba_xSr_{1-x}TiO_3$, disordered ferroelec., dielec. const. and spontaneous polarisation meas. 78–48130
$BaTiO_3$, adsorption of $O_2(H_2)$, effect on work function and spontaneous polarisation *(Russian)* 78–6211
$BaTiO_3$, ceramic, effect of grain size on nonlinear dielec. props. 77 8522
$BaTiO_3$, Co substituted, ferroelec., diffuse behaviour 79–38475
$BaTiO_3$, controlled surface layers 78–48120
$BaTiO_3$, dielectric const. and polarisation, fluctuations, catastrophes 77–8491
$BaTiO_3$, doped, loss mechanism and domain stabilisation 78–84542

dielectric polarisation continued
$BaTiO_3$, ferroelec., X-ray diffr. topographic study of polarisation reversal 79–38442
$BaTiO_3$, ferroelec. inhomogeneous impurity distrib., distrib. of spontaneous induction 77–28530
$BaTiO_3$ film, dielectric props. depend. on sinusoidal elec. field 80–71318
$BaTiO_3$ films, ferroelec., effect of elec. field on dielec. props. 79–33642
$BaTiO_3$, LF relaxational polarisation 78–68460
$BaTiO_3$, light emission during repolarisation 77–36299
$BaTiO_3$, polarisation reversal and surface neutralisation 78–27169
$BaTiO_3$ RF sputtered ferroelectic film on Si substrate, ferroelectric props. 80–80697
$BaTiO_3$, spontaneous polarisation, low temp. meas. 80–75921
$BaTiO_3$:Al, 0.05-0.3 wt.%, ceramic dielectric, dielec. and mech. props. 79–8091
$BaTiO_3$:Co, charact. behaviour of spontaneous polarisation and dielec. const. 78–60382
$BaTiO_3$:Fe, short circuit photocurrent, depend. on polarization 79–38121
$BaTiO_3$:Nb, ferroelec. and paraelec. phases, props. 79–42919
$Ba(Ti_xSn_{1-x})O_3$ thick film, ferroelec., phase transitions and dielec. props. 80–97215
$BaZnF_4$, low temp. phonon effects on polarisation 79–42905
BeO, thermoelectret props. 80–7269
BeO, thermoelectret state, effect of gamma radiation 80–7270
$(Bi_{2/3},Sr)TiO_3$, ferroelec. solid solution, dielec. nonlinearity in nonpolar phase *(Russian)* 77–32317
$Bi_{12}FeO_{20}$, longitudinally vibrated bars, reson. freq., DC elec. field effects, elastic coupling polarising correction terms 80–60503
$Bi_4Ti_3O_{12}$, ferroelec. film, on Si substrate, polarisation reversal and film struct. 79–91392
Bi_2WO_6, ionic cond. and relaxation polarisation, capacitance, losses 80–24657
CaF_2:alkali metal cation, thermal depolarisation study 80–108147
CaF_2:Er, near-Debye dielectric responses 80–71291
CaF_2:rare earth ion, elec. dipole-dipole interaction, ionic thermocurrent and EPR study 80–108060
$Ca(NbO_3)_2$, thermally stimulated currents exam. 77–69766
CaO, dielectric behaviour 79–91343
$CdBr_2$ and $CdI_2(4H)$, electric field effect on NQR, elec. polarisation mechanism 77–20746
CdF_2 crystals, electrode polarisation 78–76377
CdF_2, electrical transport limitation by electrodes, polarisation effects 80–96689
CdF_2:Eu, role of solution and precipitation phenomena on ITC spectra 80–7265
CdS crystal growth with strong long-lived polarisation echoes 79–43113
CdTe film, photopolarisation 80–25286
CdTe-Cl, compensated, Schottky diode, longtime polarisation 79–7899
CoO, dielec. behaviour, Dick and Overhauser shell model calcs. 80–45001
CsBr, crystal, short range interaction polarization, dielectric const. loss, and elec. cond. 10^2 to 10^7 Hz 79–99814
CsD_2PO_4 80–25317
$Cs(H_{1-x}D_x)_2PO_4$, dielec. props., temp. meas. 80–71335
CsH_2PO_4, dielec. props., press. and temp. depend. 80–25317
CsH_2PO_4, ferroelec., X-ray and dielec. studies on phase transition 79–38477
CsH_2PO_4-d, antiferroelec. under hydrostatic press. 79–91384
Cs_2SO_4-$(NH_4)_2SO_4$ mixed cryst., ferroelec. transition, structural and dielec. props., proton spin-lattice relax. 78–39512
Cu, dielectric const. by multiangle reflection meas., optical props. 79–95723
Cu halides, correlation between electronic dielec. constant and ionic separation 79–4758
$Cu_3B_7O_{13}Cl$, dielec. const. and elec. resist. 77–69783
donor polarisability, enhanced, below insulator-metal-transition, self-consistent calc. 80–7262
$Fe_3B_7O_{13}I$, spontaneous polarisation, dielec. const., d.c. resist., sp. ht. 77–1643
FeF_3 thin film, polarisation mechanism, AC and TSC study 80–66104
FeO_x-P_2O_5 glass, semicond., dielec. props., thermally stimulated depolarisation meas. 79–95704
GaAs, piezoelec. coupling and dislocations 79–91377
GaAs powder, RF field depend. of memory echoes 79–8095
GaAs, thermally stimulated relax. under internal field conditions 80–7279
Gd_2O_3, B-type monoclinic, DC(AC) elec. cond., thermoelectric power; dielectric const., temp. depends. 80–59980
Ge, dielectric polarisation calcs., microscopic local fields 80–20582
Ge, local field, microscopic electronic polarisation 80–25283
Ge:Sb, shock polarisation anisotropy in elastoplastic compression range 77–16244
GeSe amorphous films in Al-GeSe-Al structs., AC cond. and capacity, thickness depend. 79–65566
$K_xAl_xTi_{8-x}O_{16}$, $1.6 \leq x \leq 2.0$, dielec. response in freq. range 10^{-3} to 10^6 Hz 79–65785
KCl, low temp. space charge polarisation 78–43789
KCl, soln., elec. cond., dielec. relax., kinetic characts. 78–34641
KCl:Pb, light induced ionic polarisation 80–7264
KCl:Sr^{2+}, polarisation-plastic effect 78–2794
KD_2, PO_4, polarisation echo, near ferroelec. transition 78–88266
KDP-type crystals, polarisation, dielec. const. thermodyn. props. 77–59527
KD_2PO_4 monocrystal, electrooptical props. in paraelectric phase *(Polish)* 80 11368
KD_2PO_4, polarisation fluctuations, wavevector depend. 80–71295
$K_4Fe(CN)_6.3H_2O$, ferroelec., sp.ht. and spontaneous polarisation, −65 to 0 degrees C, mol. field model 78–64333
$K_4Fe(CN)_6.3H_2O$, nature of phase transition 79–38470
K_2FeF_4, charge transport and polarisation 80–80681
$K(H_{1-n}D_n)_2PO_4$, degree of deuteration, depend. of Landau kinetic coeff. 77 85670
$K(H_{1-x}D_x)_2PO_4$, ferroelec., spontaneous polarisation, pseudo-spin model calc. 77–52024
$K(H_{1-x}D_x)_2PO_4$, static dielec. props., and Curie temp., press. depend. 79 87405
KH_2PO_4, central components in ferroelec. phase 78–56436
KH_2PO_4, dielectric const. and polarisation, fluctuations, catastrophes 77–8491
KH_2PO_4, dynamic central peak in ferroelectric phase 78–84538
KH_2PO_4, ferroelec., change of sign in pyroelec. coeff. 79–82929

dielectric polarisation continued

- KH_2PO_4, ferroelectric transition, order-disorder character of hydrogen bond 80—93251
- KH_2PO_4, Landau-Devonshire coeffs. 78—15116
- KH_2PO_4, polarisation echo in ferroelec. phase transition region 79—42920
- KH_2PO_4 powder, dynamic polarisation echoes 79—4773
- KH_2PO_4, press. and deuteration effects on static ferroelec. props., four-particle cluster approx. 80—34861
- KH_2PO_4, spontaneous electrooptic effect in far IR 79—95734
- KH_2PO_4, spontaneous polarisation, low temp. meas. 80—75921
- KH_2PO_4-KD_2PO_4 mixed cryst., dielec. polarisation, Green's function anal. 77—52011
- KH_2PO_4-type ferroelectrics, dielec. props., four-cluster approx. 80—97202
- $KI{:}S^{2-}$, impurity-vacancy dipole UV absorpt. and ionic thermocurrent, F-centre form. 77—36271
- $KI{:}S^{2-}$, vacancy dipoles, photo-induced polarisation and depolarisation 80—2690
- $K_xMg_{x/2}Ti_{8-x/2}O_{16}$, $1.6 \leq x \leq 2.0$, dielec. response in freq. range 10^{-3} to 10^6 Hz 79—65785
- $K_{1-x}Na_xTaO_3$, quantum ferroelec., elastic compliance, impurity effects 79—99835
- $KNbO_3$, dielec. spectrum rel. to polarisation effects 80—15984
- $KNbO_3$, spontaneous polarisation and pyroelec. effect meas. 77—90107
- $KTa_{1-y}Nb_yO_3$, quantum ferroelec., elastic compliance, impurity effects 79—99835
- $KTaO_3$, electromech. props. and electron tunnelling 78—23403
- $KTaO_3$, relax. effects, electret state 77—12302
- $KTaO_3{:}Li$, polarised cluster stabilisation by Li defects, polar glass form. 79—91342
- K_2ZnCl_4, ferroelec. props. 79—4772
- K_2ZnF_4, charge transport and polarisation 80—80681
- LiH, ionic polarisability in cryst. lattice, quantum mech. model 79—47384
- $LiH_3(SeO_3)_2$, ferroelec., absolute atomic arrangement and spontaneous polarisation, neutron diffr. study 80—59442
- $LiNH_4SO_4$, ferroelectric phase transition, lattice parameters and thermal expansion coeffs. 80—40074
- $LiNH_4SO_4$, phase transitions, temp. depend. of NMR, spontaneous polarisation, birefringence and SHG 78—10191
- $LiNbO_3$, band struct. and spontaneous polarisation calcs. 78—95261
- $LiNbO_3$ crystals, activated by $3d^n$ ions, enhancement of polarisation echo 79—38439
- $LiNbO_3$ crystals, low temp. polarisation reversal 79—61322
- $LiNbO_3$, influence of spontaneous polarisation on photoelec. emission 79—28898
- $LiNbO_3$, powder, polarisation echo, repetitive read out effect 79—82913
- $LiNbO_3$, spontaneous polarisation, low temp. meas. 80—75921
- $LiNbO_3{:}Fe$, polarization echo signals amplification *(Russian)* 78—43780
- $LiNbO_3{:}Fe$, spontaneous polarisation reversal and photorefractive effect 78—31163
- $Li_2SO_4.H_2O$, linear pyroelectric, temp. depend. of polarisation 79—99821
- α-Sn, local field, microscopic electronic polarisation 80—25283
- $MNbO_3$, orthorhombic, electronic struct., SCF-MS-Xα calc. 80—70600
- $MNbO_3$, tetragonal, electronic struct., optical anisotropy 80—70599
- $Mg_3B_7O_{13}Cl$, pyroelec. effect, spontaneous polarisation, domain struct. 77—8520
- MgO, dielectric behaviour 79—91343
- MgO, dielectric polarisation calcs., microscopic local fields 80—20582
- MgO, local field, microscopic electronic polarisation 80—25283
- $MgO{:}Li^+$, quenched, elec. polarisation, thermal depolarisation and dielectric loss meas. 79—1738
- MnO, dielec. behaviour, Dick and Overhauser shell model calcs. 80—45001
- $(ND_4)_3D(SO_4)_2$, ferroelectricity and isotope effect on ferroelec. activity 77—85660
- $(ND_4)_3D(SeO_4)_2$, phase transitions, isotope effect, dielectric and dilatometric meas. 79—38500
- (NH_4BeF_4) crystal, spatial polarisation modulation, macroscopic quadrupole moment anomalies *(Russian)* 79—65808
- $(NH_4)_2BeF_4$, effect of surface layer on spontaneous polarisation 79—38445
- NH_4Br, cubic-tetragonal transition, macroscopic quadrupole moment meas. *(Russian)* 77—62642
- NH_4Br, self-polarisation at order-disorder transition 78—52432
- $(NH_4)_2Cd_2(SO_4)_3$, dielec. and spontaneous polarisation, −195 to −180°C, particle size depend. 80—97200
- NH_4Cl, doped and undoped, spontaneous polarisation at order-disorder phase transition 80—25281
- NH_4Cl, pure and NH_3 and $NiCl_3$ doped, TSC obs. of polarisation 79—78618
- NH_4Cl, self-polarisation at order-disorder transition 78—52432
- $NH_4H_2PO_4$ crystal, ferroelectricity, spontaneous polarisation obs. 79—28687
- NH_4HSeO_4, cryst. struct., dielec. and ferroelec. props. 80—60528
- NH_4HSeO_4, ferroelec. phase transition, pyroelec. props. 80—60513
- NH_4HSeO_4, ferroelec. props. rel. to struct. 80—71345
- NH_4HSeO_4, para- to ferroelectric transition obs. by permittivity meas. 79—51916
- $(NH_4)_3H(SeO_4)$, ferroelec. transition, press. and temp. effects on dielec. props. 78—23413
- $(NH_4)_3H(SeO_4)_2$, ferroelec. phase transition, dielec. meas. 77—63376
- NH_4IO_3, ferroelec., structural phase transition 80—7308
- NH_4NBeF_4, successive phase transitions, dielec. and optical props. obs. 80—50275
- $((NH_4)_{1-x}Rb_x)_2SO_4$, isomorphic impurity effect on dielec. and nonlinear optical props. 80—88911
- $(NH_4)_2SO_4$, ferrielec., dielec. behaviour and nature of phase transition 78—88262
- $(NH_4)_2SO_4$, phase transition theory 79—24275
- $Na_9(Al_6Si_6O_{24})(OH)_2.6H_2O$, hydrosodalite, ferroelec. transition, pyro- and piezoelec. activity 79—15421
- NaCl, dielectric polarisation calcs., microscopic local fields 80—20582
- NaCl, dipole polarisation, depend. on AC and DC voltage superposition 80—20577
- NaCl, interfaced polarisation and losses, superimposed AC and DC voltage study 80—25276
- NaCl, local field, microscopic electronic polarisation 80—25283
- NaCl, low temp. space charge polarisation 78—43789

dielectric polarisation continued

- NaCl, polarisation mechanism and lattice mechanics, microscopic approach 78—59888
- $NaD_3(SeO_3)_2$, ^{23}Na resonance line temp. depend., of first order quadrupole shift and spontaneous polarisation 79—8069
- NaF, reversible optical storage element using M-centre polarisation 78—94416
- $Na_8(Ge_6Al_6O_{24}).CO_3.nH_2O$, linear pyroelectric, temp. depend. of polarisation 79—99821
- $NaH_3(SeO_3)_2$, ferroelec. crystal, Barkhausen effect study 79—38507
- $NaNO_2$, ^{23}Na elec. field gradient tensor from NMR satellite lines near phase transition 80—71191
- $NaNO_2$, band struct., polarisation and piezoelec. consts. calc. 78—52448
- $NaNO_2$, ferroelec., dielec. and thermal behaviour 80—80680
- $NaNO_2$, ferroelec., X-ray diffr. topographic study of polarisation reversal 79—38441
- $NaNO_2$, ferroelec., X-ray obs. during polarisation reversal 79—51921
- $NaNO_2$, ferroelec. nuclear quadrupole coupling const. and spontaneous polarisation 80—71229
- $NaNO_2$, polarisation reversal by time-resolved X-ray diffr., NO_2 radical rot. 77—63382
- $NaNO_2$, second order phase transition prod. by strain 79—15420
- $NaNbO_3$, hydrostatic press. effect on permittivity, phase transition, hysteresis 80—80670
- $Nd_{1/3}NbO_3$, $NdNbO_4$, structural characteristics and residual polarisation 77—15361
- Ni-I single crystals, mag. and dielectric props. 80—93095
- NiO, dielec. behaviour, Dick and Overhauser shell model calcs. 80—45001
- NiZn ferrite, dielec. props., Jahn-Teller ion effects 80—97181
- PLZT ceramic;, visible light scatt. depend. on photoferroelectric space charge fields 80—80806
- PLZT ceramics, electro-optical props. *(Korean)* 79—11406
- PLZT ceramics, pulse charging of nanofarad capacitors from shock depoling 79—42913
- PLZT ceramics, short circuit photocurrent, depend. on polarization 79—38121
- PLZT, reduced, exam. of ageing phenomena, using dielectric hysteresis *(German)* 79—33647
- $(Pb,Ba)Nb_2O_6$, polycryst., orientational polarisation and phase comp. in strong field 78—27157
- $(Pb,La)(Zr,Ti)O_3$, ferroelec. ceramic, polarisation distrib. obs. using electro-optic effect 80—25278
- $(Pb,Sr)TiO_3$, ferroelec. solid solution, dielec. nonlinearity in nonpolar phase *(Russian)* 77—32317
- $(Pb,Sr)TiO_3$, ferroelec. props., press. depend., anharmonic oscillator model 80—80716
- Pb_z-$Sr_{1-z}(Zr_x$-$Ti_{1-x})O_3{:}Cr_2O_3$, ferroelec. ceramic, reversible characts. and dielectric losses *(Russian)* 78—84517
- $(Pb_xBa_{1-x})_5Ge_3O_{11}$, electrogyration, and dielectric props. 78—19444
- $Pb_{0.94-x/2}Ba_{0.6}Nb_xZr_{1-x}O_3$, Nb dopant morphology effect on microstructure 80—81005
- $(Pb_{0.8}Ba_{0.2})(Zr_{0.8}Ti_{0.2})O_3$, ferroelec. ceramic, pulse-like voltage generation using polarisation reversal 78—2809
- $PbCo_{0.33}Nb_{0.66}O_3$, ferroelectric, exam. of permittivity and dielectric props. 79—1742
- $Pb_3Fe_2WO_9$, perovskite ferroelec., characts. of dielec. polarisation 77—8496
- $Pb_5(Ge,Si)_3O_{11}$, dielec. and elec. props., 20 to 250°C 80—29697
- $Pb_5Ge_3O_{11}$ bonded $Pb(Zr,Ti)O_3$ composites, piezoelec. props. 79—78629
- $Pb_5Ge_3O_{11}$, photodielectric effects, Curie temp., permittivity and polarisation 80—40034
- $Pb_5Ge_3O_{11}$, pulsed polarisation switching process depend. on illumination 80—93253
- $Pb_5Ge_3O_{11}$, ultrafine-grained crystallized from glass, ferroelectricity 78—39508
- $Pb_5Ge_3O_{11}$, uniaxial displacive ferroelectrics, domain wall dynamics 79—73890
- $Pb_5Ge_3O_{11}{:}Gd^{3+}$, ferroelec. transition, temp. depend., EPR study 80—66127
- $Pb_5(Ge_{1-x}Si_x)_3O_{11}$ solid solutions, dielec. props., ferroelec. phase transitions 80—15988
- $Pb_5Ge_{3-x}Si_xO_{11}$, ferroelec., switching vel. and spontaneous polarisation 78—84543
- $PbH(D)PO_4$, $PbH(D)AsO_4$, ferroelectric, sp. ht. 79—19853
- $PbHPO_4$, single cryst., dielec. props. 79—38426
- $PbHf_{1-x}Ti_xO_3$, phase diagram, influence of poling treatment, ferroelec. antiferroelec. transition *(French)* 77—63374
- PbI_2, dielectric props., elec. cond., space charge polarisation 80—100631
- PbI_2(2H and 4H), layer cryst., elec. field effect on NQR, elec. polarisation mechanism 77—20746
- $Pb_2KNb_{5-x}Ta_xO_{15}$, ferroelastic-ferroelectric coupling, dielec. props. 79—38433
- $Pb(Mg_{1/3}Nb_{2/3})O_3$, electrostrictive effect 80—66113
- $Pb(Mg_{1/3}Nb_{2/3})O_3{:}PbTiO_3$, ceramic dielectric, electrostriction, relaxation, polarisation 80—80700
- $PbMg_{1/3}Nb_{2/3}O_3$-$BiMg_{2/3}Nb_{1/3}O_3$, dielectric polarisation of solid solutions 78—43776
- $PbMg_{0.33}Ta_{0.66}O_3$, ferroelectric, exam. of permittivity and dielectric props. 79—1742
- $PbNb_2O_6$, ferroelectric strain polarisation interaction, domain wall formation 79—56750
- $PbNb_{0.5}Sc_{0.5}O_3$, ceramic, dielec. props. 79—11392
- PbO-SiO_2 glasses, elec. cond. and dielec. behaviour 80—44361
- $Pb_3(PO_4)_2$, ferroelastic, dielectric anomalies, phase transitions, permittivity, relaxation *(Russian)* 80—71293
- $Pb(Sb_{1/3}Mn_{2/3})O_3$-$PbTiO_3$-$PbZrO_3$, remanent dielec. polarisation of poled ceramic, heat treatment 79—87390
- $Pb(Ti, Zr)O_3$, piezoelectric-ferroelectric ceramic, polarisation processes, X-ray obs. 80—34847
- $Pb(Ti,Zr)O_3$, polycryst., orientational polarisation and phase comp. in strong field 78—27157
- $PbTiO_3$, anomalies in elec., photoelectric and mechanical props. 80—55051
- $PbTiO_3$, cryst., polarisation and resistivity, elec. field effects 78—64313
- $PbTiO_3$, mechanical twinning, spontaneous polarisation shielding 79—42930
- $PbTiO_3$ single crystal, channelling of He^+ ions, polarisation effects 79—99258
- $PbTiO_3$, spontaneous polaris. shielding destruction by polishing and scribing 79—15427

dielectric polarisation continued
- $PbTiO_3$, switching, domain structure reorganisation and polarisation change 77—1645
- $PbTiO_3$, tetragonal deform. of TiO_6 octahedron 77—55759
- $xPbTiO_3+(1-x)PbCd_{1/3}Nb_{2/3}O_3$, phase transition spread, polarisation relaxation, dielectric susceptibility *(Russian)* 80—75922
- $Pb(Zn_{1/3}Nb_{2/3})O_3$, diffuse phase transition, electro-optical and dielec. obs. 79—82933
- $Pb(Zr,Ti)O_2$ ceramic, surface barrier electroreflectance, hysteresis, ageing 80—80752
- $Pb(Zr,Ti)O_3$ ceramics, low field depoling charact. 77—8492
- $Pb(Zr,Ti)O_3$ ceramic, permittivity and resonant frequency ageing, space charge field effects 77—85657
- $Pb(Zr,Ti)O_3$, ceramic vibrator, resonant freq. temp. stability *(Chinese)* 79—47386
- $Pb(Zr,Ti)O_3$ ceramics, modified, automated system for electrical field-polarisation studies 79—67268
- $Pb(Zr,Ti)O_3$ ceramics, space charge field meas. by ferroelec. domain switching current, piezoelec. reson. freq. ageing characts. 80—7296
- $Pb(Zr,Ti)O_3$ film, ferroelec. and optical props. 77—85674
- $Pb(Zr,Ti)O_3$, polarisation effect on deform. and strength, Curie pt. region 79—42902
- $Pb(Zr,Ti)O_3$ thin film, ferroelec., fabrication by RF sputtering *(Japanese)* 80—25560
- $Pb(Zr,Ti)O_3$:$PbTiO_3$ (up to 5%), dielec. props. and ferroelec. transitions 77—20806
- $PbZr_{1-x}Ti_xO_3$, paraelec. phase, first-order phase transition 77—89540
- $PbZrO_3$, electric field induced phase transitions, 20 to 160°C 77—43947
- $PbZrO_3$-monocryst., elec. cond., permittivity, polarisation, para- and ferro- to antiferroelec. phase transistions 78—60402
- $PbZr_{1-x}Ti_xO_3$:Nb_2O_5 ceramic, ferroelec. transitions, polarisation meas. *(French)* 80—66124
- $PbZr_xTi_{1-x}O_3$ solid solutions, tricritical behaviour 78—80296
- $Pb(Zr_{0.47}Ti_{0.43}Sn_{0.10})O_3$:$Cr_2O_3$, ferroelec. ceramic, reversible characts. and dielectric losses *(Russian)* 78—84517
- $Pn_2Nb_2O_7$, relax. phenomena, meas. of dielec. const., polarisation and sp. ht. 77—4597
- $RTiNbO_6$, R=rare earth, electrophys. props. 78—23388
- $RbBr$:Cu^+, off-centre ion position, ionic thermocurrent study 80—7271
- $Rb_2Cd_2(SO_4)_3$, pyroelectric and dielectric props., ferroelectric transitions 79—38458
- $RbCl$:Cu^+, off-centre ion position, ionic thermocurrent study 80—7271
- $RbD_3(SeO_3)_2$, spontaneous polarisation meas. below T_c 77—24801
- RbH_2PO_4, static dielec. props., and Curie temp., press. depend. 79—87405
- $RbHSO_4$, ferroelec., dielec. crit. phenomena, spontaneous polarisation meas. 77—85641
- $RbHSO_4$, ferroelec. with small Curie-Weiss const., dielec. props. 78—39496
- $RbHSO_4$, isotope effect, dielec. const. and spin polarisation investigation 80—20574
- $RbHSeO_4$, ferroelec. props. and domain struct. 79—78637
- $RbHSeO_4$, ferroelec. props. rel. to struct. 80—71345
- $RbH_3(SeO_3)_2$ crystal, incommensurable phase, quadrupole moment study 80—97213
- $RbH_3(SeO_3)_2$, piezoelectric effect, near nonintrinsic ferroelectric phase transition 78—2815
- $RbH_3(SeO_3)_2$, repolarisation in region of improper ferroelec. phase transition 77—8497
- Rb_2SO_4-$(NH_4)_2SO_4$ mixed cryst., ferroelec. transition, structural and dielec. props., proton spin-lattice relax. 78—39512
- Rb_2ZnBr_4, ferroelec., photovoltaic and photorefractive phenomena 80—75598
- Rb_2ZnBr_4, incommensurate and commensurate phases, neutron scatt. meas. 79—82936
- SbSI, abrupt polarisation changes under influence of external forces 78—68459
- SbSI, absorption edge, elec. field effect rel. to ferroelec. props. 80—97240
- SbSI, adsorption of $O_2(H_2)$, effect on work function and spontaneous polarisation *(Russian)* 78—6211
- SbSI, adsorption polarisation and depolarisation currents 77—43942
- SbSI, aggregates of needle-like crystals, nonstoichiometric, ferroelectric properties *(Japanese)* 78—43821
- SbSI, Barkhausen effect, contrib. to repolarisation process *(Russian)* 77—32330
- SbSI, dynamic dielectric nonlinearity, in microwave band 78—35109
- SbSI, ferroelec. semicond., influence of internal fields on polarisation reversal process 79—38443
- SbSI, ferroelectric, dark current and spontaneous polarisation, ferro-paraelectric transitions obs. 80—60521
- SbSI, ferroelectric semiconductor, polarisation switching processes, effect of surface electron states 77—90115
- SbSI, max. vel. of domain boundaries in polarisation reversal, Barkhausen effect meas. 78—60411
- SbSI, paraelectric phase, jump-like switching processes, ferroelec. surface layer 78—92038
- SbSI, surface layer exam. 78—48119
- SbSI, uniaxial displacive ferroelectrics, domain wall dynamics 79—73890
- $SbSI_xBr_{1-x}$, T-p-x phase diagram *(Russian)* 77—16241
- Si, dielectric polarisation calcs., microscopic local fields 80—20582
- Si, dielectric screening, microscopic theory, phonon dispersion, moment expansion calcs. 79—55839
- Si, local field, microscopic electronic polarisation 80—25283
- Si:P, dielec. susceptibility meas., polarisation catastrophe at metal-insulator transition 80—59873
- SiO_2 glass, relax. times of mol. OH^- ions at very low temps., elec. dipolar echoes 79—78616
- SiO_2:OH^-, vitreous, elec. dipolar echoes 78—52430
- SiO_x thin film dielec., in MIM struct., interfacial props. rel. to non-stoichiometry 80—80399
- Sm_2O_3, B-type monoclinic, DC(AC) elec. cond., thermoelectric power, dielectric const., temp. depends. 80—59980
- α-Sn, dielectric polarisation calcs., microscopic local fields 80—20582
- $Sr_{1-x}Ba_xNb_2O_6$, photorefraction in space charge field, phase transitions 80—97229
- SrF_2:Ce^{3+}, dipole reorientation, Ce^{3+} conc. effect 78—10841
- SrF_2:rare earth ion, elec. dipole-dipole interaction, ionic thermocurrent and EPR study 80—108060
- $Sr_4NaLiNb_{10}O_{30}$, electro-optic, pyroelec., dielec. and piezoelec. props. *(Chinese)* 79—69810

dielectric polarisation continued
- SrO, dielectric behaviour 79—91343
- SrO:Ni^{2+}, ionic thermocurrent meas. 80—108148
- SrS, dielectric behaviour 79—91343
- $SrTiO_3$ glass ceramics, polarisation and dielec. const., 4-77K 77—32319
- $SrTiO_3$, impure, low temp. polarisation, thermoelectret state 77—12301
- Tb_2O_3, B-type monoclinic, DC(AC) elec. cond., thermoelectric power, dielectric const., temp. depends. 80—59980
- TiO_2 single cryst., refl. and electrorefl., energy levels 78—2871
- TlD_2PO_4, antiferroelectricity, permittivity, electric field double hysteresis loops 80—60512
- V_2O_5, rel. to permittivity, 50-200K *(Russian)* 78—39498
- ZnO, piezoelec. powder, dynamic polarisation echoes 78—52443
- ZnS:Cu powder exam. of dielectric constant anomaly, in terms of polarisation catastrophe phenomena 79—51897

dielectric power factor *see power factor*

dielectric properties of gases
- bromomethane, dielectric susceptibility at radio frequencies 78—14123
- chloromethane, dielectric susceptibility at radio frequencies 78—14123
- complex permittivity meas. at microwave, two coupler method 78—21167
- cryogenic gas, dielectric breakdown 80—40051
- cyanomethane, dielectric susceptibility at radio frequencies 78—14123
- electric strength molecular property correlation, general conclusions 77—76025
- ethyl chloride, second dielec. virial coeffs. *(German)* 79—32729
- fluorocarbon vapours, sparking potential meas. 77—65922
- fluoromethane, dielectric susceptibility at radio frequencies 78—14123
- halomethanes, second dielectric virial coeff. of polar gas, temp. depend. *(German)* 78—26234
- impurity particle field-enhanced motion, computer-aided modelling 77—43932
- iodomethane, dielectric susceptibility at radio frequencies 78—14123
- methyl halides, second dielec. virial coeffs. *(German)* 79—32729
- nonlinear effects in polarised gases, complex dielectric constant evaluation 78—1787
- orientational correlation functions, for mol. reorientation 79—36798
- pentane isomeric vapours, electon transport mechanisms, density induced transition 80—24122
- polar gas, dielec. permeability, spherical approx. *(French)* 77—45786
- polar gas, polarisation by external and internal elec. fields 78—12459
- polar mol. rot. relax., dielectric friction, Onsager cavity model 80—64664
- resonant dielectric susceptibility, collective excitation transfer effect 77—76024
- resonant dielectric susceptibility, high density gas, many body theory 77—76023
- He, dielec. const. gas thermometry, 4-27K, and eqn. of state 79—63222
- SF_6, dielectric strength, breakdown tests *(Czech)* 78—30498
- SF_6, pure and mixtures, dielec. props., ionisation and attachment coeffs. 80—33726
- SF_6 with gaseous contaminants, arc decomposition kinetics investigation by combined gas chromatograph-mass spectrometry methods 80—92250

dielectric properties of liquids and solutions
- acetamides, N-methyl-, N,N-dimethyl-, in organic solns., dielec. const., dipole moments, monomer-dimer equilib. 80—40031
- acetic acid, dil. soln., dielectric polaris., linear correlation factor 78—6624
- acetic acid-aniline (pyridine) complex, in CCl_4, dielec. polarisation 80—29675
- acetylacetone, H bonding, dielec. dispersion obs. 77—63356
- β-alanine, aq. soln., dielectric relax. spectrum, Debye domains 77—8498
- albumin, bovine serum, hydrated, dielectric props. at 9.9 GHz 78—15758
- albumin, bovine serum, in soln., five-component dielec. dispersion 78—15759
- alcohol, dielec. const., hindered mol. rot. influence 78—43767
- alcohol binary mixtures, nonlinear dielec. effects, shift in assoc. equilib. 77—73108
- alcohols, aliphatic, permitt., dielec. relax., time-domain multiple refl. meas. 77—57350
- alcohols, dil. solns., dielec. loss and relax., microwave and sub-mm. wave absorpt. obs. *(German)* 78—23396
- alcohols, monohydric, dielec. polarisation 79—99818
- alcohols in solution, dielectric relax. depend. on conc. 77—1636
- aliphatic, in dil. solns., dielectric relax. dipole reorientation, rot., microwave obs. 77—28516
- aliphatic esters, mol. dielec. relax. in soln. 79—82918
- aliphatic ethers, dil. solns., dielec. loss meas. for dielec. relax. 78—68451
- alkali metal-ammonia solns., metal-insulator transition, h.f. and u.s. props. 77—1369
- trans-p-n-alkoxy-α-methyl-p′-cyanophenyl cinnamates, nematic liq. cryst., static dielec. props. 78—60376
- p-alkoxybenzal-p′-ethoxyaniline, even-odd effect and chain config. 79—50989
- L-p-alkoxybenzylidene p′-amino 2 methylbutyl cinnamate chiral smectic liq. cryst., dielec. and ferroelec. props. 79—91394
- p-alkoxyphenylazo-p’ phenyl esters, nematic liq. cryst., dielec. anisotropy *(French)* 77—80414
- p-alkoxyphenylazoxy-p’ phenyl esters, nematic liq. cryst., dielec. anisotropy *(French)* 77—80414
- alkyl trichloroacetates, solns., intramol. rot., permittivity and dielectric loss, microwave meas. 78—31145
- 4′-n-alkyl-4-cyanobiphenyls, dielec. dispersion 78—2798
- 4-n-alkyl-4-cyanobiphenyls, liq. cryst. of strong positive dielec. anisotropy, static dielec. consts. meas. 78—2790
- p-alkyl-p′-cyanocyclohexylcyclohexanes, thermotropic nematics with positive dielectric and negative diamag. anisotropy 78—34435
- allyl ether, dielectric relaxation obs. at millimetric wavelengths 80—71311
- amides, in carbon tetrachloride, dielec. relax., time-domain reflectometric obs. 79—4762
- aminobenzotrifluoride, benzene soln., permittivity and dielec. loss 78—64320
- 4-aminophthalimide soln., fluoresc. nanosec. kinetics, dielec. relax. 79—78737
- aminopyridines, in 1,4-dioxane soln., dielec. consts., losses and relax. 78—64319
- aniline, in benzene, polar dielectric system, RF cond. and dipole moment 78—2788
- anilines, substituted, in benzene soln., dielectric relax. time, dipole moment 80—50259
- anilines, substituted, in nonpolar solvent, dielec. relax. obs. 80—55022

dielectric properties of liquids and solutions continued
anisotropic molecular fluids, local elec. fields 77—59545
aryl esters, cyano-substituted, liq. cryst. props. 77—27822
associated solutions, H bonding and anomalous saturation 78—52426
azoxybenzenes, nematic, refr. index, birefringence, internal field 78—34427
benzene sulphonyl hydrazine, in nonpolar solvent, thermodynamics of dipolar relax. 79—91347
benzene-hexafluorobenzene, mixtures, dielectric relax. and US absorpt. 77—12307
benzenes, substituted, dielectric absorpt. and NMR 78—88251
benzol, monohalide-substituted, electrical model of conductivity *(Russian)* 77—8101
benzonitrile, hexane and CCL_4 solns., nonlinear dielec. effect 79—78602
benzonitrile-isooctane mixture, dielec. const. near consolute point, temp. and freq. depend. meas. 80—71292
benzophenone, in o-terphenyl soln., dielectric absorp. studies, molecular relax. 78—95544
benzothiazole, dielec. loss, relax. and const. in liq. and soln. 79—91346
benzoylacetone, dil. soln. in benzene, dielectric behaviour 79—42886
benzoylacetone, H bonding, dielec. dispersion obs. 77—63356
benzoylacetones, p-substituted, dil. soln. in benzene, dielectric behaviour 79—42886
benzyl cyanides, α-substituted, in dil. soln., dielec. absorpt. obs., enthalpy of activation 80—55019
binary liquid mixture, critical conc. determ. from dielectric const.. meas. 77—20788
binary liquid mixtures near crit. pt., nonlinear dielectric effect 78—23384
biomolecular aqueous solution, attractive and repulsive dispersion forces 78—44447
biphenyl-4-p-n-alkoxybenzoates, nematic liq. cryst., static dielec. props. 78—60376
bis-heptyloxy-azoxybenzene, tilt angle in C-phase, dielectric measurements 78—63673
breakdown influence of US excitation 80—15964
bromal, in benzene soln., dielec. relax., loss, and dipole moment 80—2692
m-bromaniline delayed depolarisation obs. *(Russian)* 79—95703
4-bromo-m-thiocresol, liq., dielectric relax. mechanisms 79—42891
bromobenzene, nonlinear dielectric effect temp. depend. 79—82908
bromobenzene solutions, influence of strong elec. field on dielec. permeability 77—90086
bromoform delayed depolarisation obs. *(Russian)* 79—95703
m-bromophenylbenzoyloxybenzoate, nematic phase, freq. depend. of dielec. props. *(French)* 79—91337
bubble creation in high elec. field, explained in terms of struct. 79—91370
butane diol, asymm. dielectric dispersion, 1-25000 MHz 78—15092
2,3-butanediol, dielectric dispersion 78—72455
n-butanol, dielectric response function, by lumped capacitance method 78—95539
1-butanol, permitt., dielec. time domain spectroscopy, total transmission method study 80—27323
t-butanol and -d_1, deuteration effect on self-assoc., dielectric polaris meas. 79—28672
t-butyl acetate, rot. isomerism, dielect. and Raman spectra 80—106328
t-butyl alcohol, self-assoc., linear and nonlinear dielec. effects obs. 80—60484
tert-butyl alcohol in nonpolar solvents, liq. struct. from dielectric studies 80—38894
t-butyl derivatives, liq., reorientational correlation times, Hubbard model 79—61353
t-butyl formate, rot. isomerism, dielect. and Raman spectra 80—106328
capacitance cell, guarded cylindrical 80—86268
capacitor dielectric fluid test and anal., quality assurance 78—80272
carnauba wax, polarised, simultaneous variation of dielec. const. and discharge current, room temp. to beyond melting point 80—11314
castor oil dielectric fluid, microwave propag., permittivity effect, demonstration 80—105468
cavity model, refr. index and density, permittivity *(French)* 79—78642
CBOOA, liq. cryst. of strong positive dielec. anisotropy, static dielec. consts. meas. 78—2790
charge generation and transport from contacting surface, Mach-Zehnder and Schlieren obs. 80—20589
charged fluids near freezing point, static dielectric behaviour 78—56417
chloral, dielec. consts. and dielec. losses meas. 77—20795
chloral, in benzene, permittivity, dielectric loss, 36 GHz 77—32323
chloral, liq., permittivity, dielec. loss, up to 60 GHz 78—60384
4-chloro-3-nitrobenzotrifluoride-benzene (carbon tetrachloride) dilute soln., dielec. relax. time, dipole moment, microwave obs. 78—35084
4-chloro-3-nitrotoluene-benzene (carbon tetrachloride) dilute soln., dielec. relax. time, dipole moment, microwave obs. 78—35084
4-chloro-α-toluothiol, liq., dielectric relax. mechanisms 79—42891
2-chloro-p-nitroaniline, in benzene soln., dipole moment from solute relax. time-solvent viscosity relation 80—37905
chlorobenzene, HF dielec. relax. test for extended Nee-Zwanzig formula 79—33602
chlorobenzene, in CCl_4 soln., quadratic changes in elec. permittivity, intermol. interactions 77—73107
chlorobenzene, liquid, submillimetre wave dispersive Fourier transform spectroscopy obs. 77—37915
chlorobenzene, nonlinear dielectric effect temp. depend. 79—87372
chlorobenzene submillimetric permittivity obs. and Debye eqn. extrapolation 77—40173
chlorobenzotrifluoride, benzene soln., permittivity and dielec. loss 78—64320
chlorofluoromethanes, liq., NMR spin-lattice and dielec. relax. 79—33604
chloroform delayed depolarisation obs. *(Russian)* 79—95703
o-chloronitrobenzene-benzene (carbon tetrachloride) dilute soln., dielec. relax. time, dipole moment, microwave obs. 78—35084
o-chlorotoluene(-benzene), liq. and dilute soln., microwave absorption and relax. processes 79—82920
cholesteric liquid crystal with anisotropic dielec. permeab., transient electrodynamic instability *(Russian)* 78—51418
cholesteric liquid crystals, mixtures, hysteresis, bistability effects under elec. fields 78—42907
cholesteric positive dielectric anisotropy mixture, helix pitch increase below 20 kHz 80—15997
cholesteryl laurate-cholesteryl caprylate (75 wt.%), polymorphic behaviour, optical, elec. and dielec. meas. 80—65208

dielectric properties of liquids and solutions continued
cholesteryl linoleate, dielec. props., phase transitions rel. to temp. 79—33592
complex permittivity meas., rectangular waveguide method 80—15941
complex permittivity measurement by node displacement method *(Russian)* 78—27155
conducting solutions, bridge method for meas. dielectric relaxation 80—82793
conduction and breakdown in dielec. liqs., conf., Mont-Saint-Aignan, France (July 1978) 79—91354
continuum dielectric approx. relax., Poisson-Boltzmann thermodynamics 77—36762
critical binary mixtures, dielec. props., droplet model 79—69762
critical phenomena isomorphism 79—33649
critical point and eqn. of state investig. by optothermodynamic method *(Russian)* 79—33068
cryogenic liquid, dielectric breakdown 80—40051
cryogenic liquids, elec. breakdown characts. 79—91364
4-cyano-4′-octylbiphenyl, dielec. props., 1 Hz-1 GHz, in smectic, nematic and liq. phases *(French)* 77—40168
4-cyano-4′-octylbiphenyl, dielectric relax. anal. in nematic and smectic phases 80—108153
p-cyano-p′-pentylbiphenyl/p-pentylbenzoic acid, mixture, induced smectic phase, dielec. props. 80—6498
cyanobiphenyl nematic homologous series, Kerr consts., relax. times, refr. index, dielectric const. 79—19863
2-p-cyanophenylazo-S-akloxypyridines, synthesis, phase transition temps., and dielec. props. 79—86876
m-cyanophenylbenzoyloxybenzoates, nematic phase, freq. depend. of dielec. props. *(French)* 79—91337
cyclic carbonates, supercooled liqs., dielec., acoustic, NMR, viscoelastic relax. props. 77—1609
cytochrome-c, hydrated, dielectric props. at 9.9 GHz 78—15758
Debye absorption at crit. liq.-vapour transition in dielec. fluid 80—100322
Debye generalised fluid model, dielectric relax., depolarised dynamic light scatt. 80—108156
p-n-decyloxybenzoic acid p-n-hexyloxyphenyl ester, dielec. permittivity in nematic and smectic phases 79—32899
dextran aqueous solutions, microwave dielec. behaviour 78—92018
Dextrane in aqueous solution permittivity meas., dielec. relaxation study 77—77143
DHAB, nematic, ordering change due to external DC elec. field, permittivity obs. 78—94990
di-(4-n-alkyloxy) benzoic esters, of hydroquinone series, effect of polar substituents on electro optical props. 79—46569
dialkyl carbonates, liq., US, microwave dielect. relaxation 79—56717
dibenzoyl methane, H bonding, dielec. dispersion obs. 77—63356
dicarbonyl compounds in soln., internal motion, dielectric relax., ^{13}C NMR relax., far IR spectra 77—28517
1,1-dichloro-1-nitroethane, dil. soln. in benzene, dielec. relax. study 80—29679
o-dichlorobenzene(-benzene), liq. and dilute soln., microwave absorption and relax. processes 79—82920
dichlorophenol isomers, elec. dipole moments determ. *(Spanish)* 77—69762
dicyano compounds, liq. crysts., synthesis and dielec. props. 79—86685
dicyanoalkanes, in benzene soln., microwave absorption, internal rot. 78—60385
dielectric constant meas., student experiment appl. 77—37696
dielectric kernel, functional differential equn. 79—32871
N,N-diethyl formamide, dipole moment, dielectric relax., internal rot., microwave absorpt. 79—56716
N,N′-diethyl-p-nitroso aniline, dil. benzene soln., dielec. props., microwave region, mechanisms 78—35085
diethylene glycol, asymm. dielectric. dispersion, 1-25000 MHz 78—15092
1,3-dihalopropane, dielectric permittivity and loss, dipole moment 78—60383
dihydroxy benzenes in ethyl alcohol, dielec. dispersion charact. 80—75932
dihydroxy toluene in ethyl alcohol, dielec. dispersion charact. 80—75932
dil. soln., dielectric relax., solid rotator phase 79—42890
dimethyl propane diol, dioxane soln., asymm. dielec. dispersion, 1-25000 MHz 78—15092
dimethyl silicone oil, laser-induced breakdown mechanism *(Japanese)* 77—43935
N,N′-dimethyl-p-methyl aniline, dil. benzene soln., dielec. props., microwave region, mechanisms 78—35085
N,N′-dimethyl-p-nitroso aniline, dil. benzene soln., dielec. props., microwave region, mechanisms 78—35085
N,N-dimethylacetamide in tetrachloromethane, dielectric relax. and complex permittivity 80—108149
dimuristoyl-1-3-lecithin aqueous soln., pulse relaxation method for dielec. const. determ. *(German)* 80—71308
diphenyl ether, dielec. relax. pseudorot. diffusion 79—33600
diphenyl ether, dil. solns., dielec. loss and relax., microwave and sub-mm. wave absorpt. obs. *(German)* 78—23396
dipolar fluid mixtures, dielec. const. calcs. 79—64969
dipolar fluids, equilib. statistical mechanics, struct., dielec. and thermodynamic props. 80—6345
dipolar liquid, dielectric relaxation 80—7290
dipolar liquid time-variation of dispersion and absorption of third-order electric polarisation, mol. relax. times 80—60487
dipolar molecules, zero-THz liq. phase dielec. absorpt. and rot. Langevin eqn. 80—40032
dipolar molecules in dil. soln., nonlinear dielec. relax., effective relax. time 80—97195
dipole, spherical, steadily rot., dielec. friction 78—87600
dipole moment laboratory experiment 77—57116
divinyl benzene suspension, dielectrophoresis 80—3362
DNA, calf-thymus Na-DNA aq. solns., dielec. behaviour in 5 kHz to 100 MHz range 80—85330
DOBAMBC, and DOBAMBCC, chiral smectic C liq. cryst., dielec. consts., electroclinic effect 78—94980
DOBAMBC, chiral smectic, flexoelectric effect and polarisation props. *(Russian)* 80—15002
DOBAMBC, chiral smectic phases, pyroelectric and dielec. props. 79—91380
DOBAMBC, dielec. dispersion at ferroelec. smectic A-smectic C transition 79—91385

dielectric properties of liquids and solutions continued
DOBAMBC, dielec. props. near ferroelec. smectic A to C transition 80−45015
dye, dielec. const. and loss meas., 10^2 to 10^5 Hz 78−6622
EBBA, in benzene soln., dielec. relax. meas., 4.0, 9.4 and 30.4 GHz 77−40176
EBBA, nematic, dielec. permittivity and transmitted light intensity, in DC field 77−12296
EBBA, nematic, mol. alignment, elec. and mag. field effects, dielec. const. obs. 77−11472
EBBA, nematic and isotropic phases, dielec. props. 79−87383
EBBA, nematic liq. cryst., RF dielec. props. 79−4238
EBBA, solid and liquid states, temp. and freq. depend. *(Russian)* 78−72450
electric breakdown mechanism, high speed photography expts. 79−91367
electric polarisation, third-order, in liqs., appl. of theory of nonlinear rot. relax. 77−90097
electric polarisation theory, approxs. 78−10839
electrical conductivity and breakdown, liquid impurity effects 80−11340
electrical field intensity and space charge in liquid dielectrics 80−11339
electrolyte, dielectric dispersion and friction, viscous momentum transport and relax., ion mobility 78−27775
electrolyte solutions, dielec. dispersion and dielec. friction 78−52436
electromagnetic parameter measurement using HF cavity resonator method 79−80642
electrostatic drop formation characteristics using dielectric liquid 80−37926
electroviscous effect, AC characteristics, pressure-drop fluctuations 80−107457
emulsion, permittivity of nonpolar dielectrics *(French)* 78−39497
erythrocytes, human, haemoglobin's suspending medium, dielec. props. obs. 80−76716
ethanediol, 10 MHz-70 GHz, 10-40°C, Debye dispersion 78−43769
ethanes, substituted, dielec. relax. by intramol. motion 78−23391
ethanol, alcoholic electrolytic solutions, Dielectric constants 79−99813
ethanol, assoc. in dil. soln., dielec. obs., dipole moment meas. 78−83714
ethanol, dielectric const. in mag. field 79−78606
ethyl cellulose in benzene, shear-rate depend. of relative permitt. 77−8489
ethyl trichloroacetate, in benzene, permittivity, dielectric loss, 36 GHz 77−32323
ethyl trichloroacetate, in non-polar solvents, dielectric const., dielec. loss meas. 78−2796
ethyl trichloroacetate, soln., dielectric props. and relax. mechanisms at microwave freqs. 78−15089
ethyl-3-chloropropionate, liq., microwave absorption and relax. 78−60386
ethyl-(methoxybenzylidene-amino)cinnamate, low freq. dielec. constant meas. in cryst. and liq. cryst. phase 78−91226
4-ethylaminobenzil, dil. soln. in benzene, cyclohexane and dioxane, dielectric behaviour 78−52421
ethylene-maleic acid copolymer 78−84515
ethyltrichloroacetate, dielec. consts. and dielec. losses meas. 77−20795
ethyltrichloroacetate, liq., permittivity, dielec. loss, up to 60 GHz 78−60384
eutectic mixture, glassy nematic phase, complex permittivity tensor 79−91336
fatty acids, dielectric meas. at microwave freqs. 79−19827
ferroelectric liquid crystal, soft modes 79−55653
ferroelectric liquid crysts., chiral smectic C phase, phys. props., review 80−75150
film condensation, heat transfer enhancement in elec. field 78−55551
fluid mixtures, dil., spherical mols., struct. and permittivity 80−92433
fluids and dispersions, dielec. meas. using cell 78−93725
9-fluorenone, in o-terphenyl soln., dielectric absorp. studies, molecular relax. 78−95544
fluorobenzene, nonlinear dielectric effect temp. depend. 79−87372
fluorobenzene(-benzene), liq. and dilute soln., microwave absorption and relax. processes 79−82920
fluorobenzene solutions, influence of strong elec. field on dielec. permeability 77−90086
fluorocarbon, breakdown characts., comparison with hydrocarbon liqs. 79−91361
fluorocarbon liquid prebreakdown light emission obs. 80−15963
formamide, 10 MHz-70 GHz, 10-40°C, Debye dispersion 78−43769
gassing rate and discharge energy loss meas. 80−15965
glycerol, highly viscous state, static and dynamic Kerr effect obs. 80−60545
Graphon, in butan-1-ol, colloidal particles, dispersion force interactions calcs. 79−24842
HAB, dielectric and calorimetric investig. in solid, liq. cryst. and liq. phases 77−84639
2-halopropionates, liq., dielec. relax. and permittivity 80−15948
hard sphere fluid, dielectric const., Monte Carlo simulations, mol. dynamics calcs. 80−28897
hard-sphere fluid with dipoles and quadrupoles, integral eqns. approx. 80−24334
HBBOP and HBH-HBBOP nematic mixtures, relax. freqs. and dielec. anisotropy, binary system behaviour *(German)* 79−33606
heat transfer in liquids by dielectrophoresis 78−94874
heavy water dielectric constant meas. over temp. range 473K to 643K 80−103912
heptanol isomers, static permittivity and density, press. and temp. depend. 78−35078
4-n-heptyl-4′-β-cyanovinylbiphenyl, liq. cryst., isotropic mechanism of mol. rot., dielec. permitt. meas. 80−10491
4-heptyl-4′-cyanobiphenyl, liq. cryst., dielec. props. *(French)* 78−10820
n-heptyl-4-cyanobiphenyl, nematic phase, dielec. loss, diffusion equations 80−71305
n-heptyl-cyanobiphenyl, dielec. relax. in nematic and isotropic phases 79−82151
n-heptyloxy-cyanobiphenyl, dielec. relax. in nematic and isotropic phases 79−82151
heterocyclic compounds in dilute solutions, dielectric relax., microwave technique 78−84520
n-hexane, prebreakdown events, divergent field study 79−91371
hexanetriol 1,2,6, liq., light scatt. study of struct. relax., viscosity and dielec. relax. 79−86672
4-n-hexyl-4-cyanobiphenyl, liq. cryst., isotropic mechanism of mol. rot., dielec. permitt. meas. 80−10491
N-(p-hexyloxybenzylidene)-p-toluidine, dil. soln. in benzene, dielectric behaviour 79−42893

dielectric properties of liquids and solutions continued
high-field electron transport *(Japanese)* 78−2495
HOBACPC, chiral smectic C liq. cryst., dielec. consts., electroclinic effect 78−94980
hydrocarbon, breakdown characts., comparison with fluorocarbon liqs. 79−91361
hydrocarbons, high-field carrier transport at pre-breakdown and breakdown regions 80−25305
hydroxy compound dilute solutions, dielec. relax. at 20 to 40°C *(German)* 79−33605
hydroxylic solvents, dielec. consts., effect of non H-bonding solutes 77−48673
ice microcrystals, emulsion, complex dielec. permittivity meas. *(French)* 78−10821
impurity particle field-enhanced motion, computer-aided modelling 77−43932
inelastic electron interactions in liq. dielec. obs. using FEM and energy analyser 79−91369
insulating oil, breakdown in long gaps, impurity effects 79−91359
integrated absorption due to superimposed resonances 78−39500
iodobenzene, nonlinear dielectric effect temp. depend. 79−82908
iodobenzene, soln., non-linear dielec. effect, comparison with fluoro, chloro and bromobenzene 80−60478
ion-selective electrodes, liq. membrane, free and supported, ion transport, bulk elec. props. 79−83534
isopropyl alcohol-carbon tetrachloride, mixture, dielec. const., two-sided estimate 79−42262
isoquinoline, dil. soln., dielec. absorpt., relax. and thermodynamic parameters meas. 80−50258
isoquinoline, solns., dielec. polarisation, π-electron system effects 77−90096
laser-induced breakdown, expt. results for various liqs. 79−91363
liquid crystal, ferroelec., helicoidal, smectic-C, dynamics 79−1396
liquid crystal, ferroelectric, review of props. 77−85667
liquid crystal, internal field, dipole correlation factor 78−34428
liquid crystal, isotropic and nematic, with positive dielec. anisotropy, EHD instability *(Russian)* 77−31594
liquid crystal with negative dielectric anisotropy, cholesteric planar texture EHD distortion 78−42894
liquid crystals, prep. and phys. props., book 80−105444
liquid crystals with nematic and smectic modifications, dielec. relax. and losses 77−69769
liquid dielec. permittivity meas., sub-mm wave, using laser- and Fourier transform-spectrometry 78−95568
liquid dielectric, with free boundary, equilib. between 2 charged spheres *(Russian)* 78−46482
liquid dielectrics, magnetic field effect on breakdown voltage 79−42894
liquids, meas. methods comparison in freq. range 1 GHz to 4 THz 80−100639
local field, two-parameter mean field approach 80−93232
losses in simple liquids, freq. depend., empirical eqn. 80−55025
losses in solids and liquids, characterisation 78−88252
low loss liquids, loss angle temp. var. meas. at microwave freqs. 78−48114
lysozyme, hydrated, dielectric props. at 9.9 GHz 78−15758
macromolecules and colloids, conf., Uxbridge, England (Apr. 1978) 80−82577
Maxwell-Wagner dielectric dispersions, vol. ion polarisations 80−97188
MBBA, dielec. relax. in nematic phase 79−82153
MBBA, dielectric and calorimetric investig. in solid, liq. cryst. and liq. phases 77−84639
MBBA, dielectric permitt. rel. to molecular props., effect of anisotropy of medium and local field 80−25270
MBBA, in benzene soln., dielec. relax. meas., 4.0, 9.4 and 30.4 GHz 77−40176
MBBA, nematic, dielec. permittivity and transmitted light intensity, in DC field 77−12296
MBBA, nematic and isotropic phases, dielec. props. 79−87383
MBBA, nematic liq. cryst., dielec. relax. under shear 79−10794
MBBA, nematic liq. cryst., flexoelectric and dielec. relax. behaviour 78−94979
MBBA, nematic liq. cryst., temp. depend. of EHD instability 78−1998
MBBA, nematic liquid cryst., omeotropically aligned thin slice, dielectric permeability *(Italian)* 80−6354
MBBA, pretransitional effects above phase transition temp., nonlinear dielectric meas. 79−15390
MBBA binary mixtures with a nematogenic or nonmesogenic cpd., dielec. relax. 78−72457
MBBA-based binary nematic mixtures, dielec. L-relax. 77−40178
MBBA-CPB nematic complex, dielec., elastic and electro-optical props. 77−32350
MBBA/non-mesogenic cpd., binary nematic mixtures, dielec. relax. and intermolecular interaction 79−91350
mechanical perturbation effects on breakdown, theory and expt. 79−91366
merocyanine dye, solvent-depend. hyperpolarisability, polar (nonpolar) solvents 78−70962
methane+N_2(Ar), compressed-liquid dielectric const., derived excess vol. 79−11377
methanol, 10 MHz-70 GHz, 10-40°C, Debye dispersion 78−43769
methanol, alcoholic electrolytic solutions, Dielectric constants 79−99813
methanol, dielectric const. in mag. field 79−78606
methanol, in carbon tetrachloride, permitt. meas. by time-domain spectroscopy 77−43926
methanol aqueous soln., temp. depend. of dielec. relax. time *(French)* 77−59509
methanol-ethanol mixture, dielectric const. composition depend. rel. to struct. effects 79−11378
methyl alcohol, dielec. relaxation spectroscopy in microwave region, double-beam interferometry *(German)* 80−71309
methyl bromide delayed depolarisation obs. *(Russian)* 79−95703
methyl chloride, liq., NMR spin-lattice and dielec. relax. 79−33604
methyl cyanide, liq., NMR spin-lattice and dielec. relax. 79−33604
methyl iodide, liq., mol. reorientation, dielec. and viscosity meas. 80−100157
methyl iodide delayed depolarisation obs. *(Russian)* 79−95703
methyl isothiocyanate, in benzene (tetrachloromethane), nonlinear dielectric solvent effect 79−28702
methyl methacrylate, oligomers, dielectric relax., end-group effects 78−92019

dielectric properties of liquids and solutions continued
- methyl trichloroacetate, soln., dielectric props. and relax. mechanisms at microwave freqs. 78—15089
- methyl-3-bromopropionate, liq., microwave absorption and relax. 78—60386
- methyl-4-chlorobutyrate, liq., microwave absorption and relax. 78—60386
- methylene chloride, liq., NMR spin-lattice and dielec. relax. 79—33604
- 3-methylthiomethylpropionate, liq., dielec. relax. and permittivity 80—15948
- micro-dielectrics, electro-thermo-mechanics 78—39518
- microwave frequency dielec. spectroscopy 77—41646
- microwave props. using modified cavity perturbation technique 80—42239
- mineral oil in large gaps, electric strength study 79—38452
- mixed salt solution approximating seawater composition, dielec. and radiation characts. 80—97184
- mixture of dipolar hard spheres, dielec. props. 80—24335
- molecular fluid, dielec. const. and equilib. props., interaction site cluster theory 77—84614
- molecular liquid, of polarisable and deformable mols., theory 79—99043
- molecular reorientation, dielec. friction theory 78—87599
- naphthalenes, substituted, dielec. relax. and permittivity in pure liqs. 78—64318
- naphthalenes, substituted, dielectric relax. in solns. 78—2795
- nematic liquid crystal, dielectric properties and dielectric relax. *(Russian)* 79—61301
- nematic liquid crystal, material consts., solute effects 77—1072
- nematic liquid crystal, temp. depend. of EHD instability 78—1998
- nematic liquid crystal mixtures, dielec. permittivity dispersion 80—88921
- nematic liquid crystal mixtures with low-freq. dielec. relax., phase behaviour 78—91246
- nematic liquid crystals, dielectric characteristics obs. *(Russian)* 79—15400
- nematic liquid crystals, LF dielec. relax., Freedericksz transition technique meas. 78—1987
- nematic liquid crystals, molecular mechanisms of dielec. polarisation and relaxation 80—34846
- nematic liquid crystals, relaxation process characts. *(Russian)* 78—48116
- nematic liquid crystals, temp. dependent props., twisted nematic displays 79—32901
- nematic liquid crysts., dielec. polarisation and relax., mol. mechanisms 80—29673
- nematic liquid crysts. of mols. containing nitrile groups, dipole moments determ. 77—19872
- nematic liquid-crystal mixtures, switching dynamics, with low freq. dispersion of the dielectric anisotropy 79—56708
- nematic-isotropic mixture, dielec. props., phase diagram 78—52424
- nematic-positive liq. crysts., deform. by elec. field between two co-axial cylindrical electrodes 79—50986
- 3-nitro-o-anisidine, in benzene soln., dipole moment from solute relax. time-solvent viscosity relation 80—37905
- nitrobenzene, dielectric const. in mag. field 79—78606
- nitrobenzene, polarised, simultaneous variation of dielec. const. and discharge current, room temp. to beyond melting point 80—11314
- nitrobenzene, solns., elec. permittivity near crit. point 78—76372
- nitrobenzene-hexane, soln., dielec. permitt. in two phase region 80—2682
- nitrobenzene-hexane critical solutions, crit. exponent determ. by nonlinear dielec. method 79—87373
- nitrobenzene-hexane mixtures, nonlinear dielec. effect beyond critical pt. 79—99816
- nitrobenzotrifluoride, benzene soln., permittivity and dielec. loss 78—64320
- nitroethane, crit. soln. in cyclohexane, nonlinear dielectric effect 78—27152
- nitroethane, cyclohexane and benzene solns., nonlinear dielec. effect 79—78602
- nitroethane-cyclohexane, pretransitional effects above phase transition temp., nonlinear dielectric meas. 79—15390
- nitromethane, shock-induced elec. polarisation *(French)* 79—11381
- 4-nitrophenyl-4-octyloxybenzoate, nematic and smectic-A phase, dielec. meas. 78—60392
- nitrotoluene-pentane, pretransitional effects above phase transition temp., nonlinear dielectric meas. 79—15390
- o-nitrotoluene-saturated hydrocarbon soln., critical exponent, permittivity meas. 78—22858
- nitroxyl radical rotation in liquids, ESR, dielec. relax. 77—28447
- NOBAMBC, chiral smectic phases, pyroelectric and dielec. props. 79—91380
- non polar fluid dielectrics, mechanical forces 80—60529
- non-exponential decay in dielectrics, and correlated systems dynamics 79—73882
- nondipolar liquid, determ. of very low losses at 9 and 29 GHz via waveguide interferometer 77—8503
- nonlinear dielectric measurement by detection of third order harmonics *(French)* 77—67459
- nonlinear rigid polar molecular fluid, dielec. const. 78—72451
- nonlinear third-order polarisation, transient effects elucidating molecular props. 80—15955
- nonpolar fluid dielectric constant, comparison of formulae 77—20787
- 1-octanol, dielec. consts., solvent struct., effect of H bonding solutes, chain length 77—48674
- 1-octanol-H-bonding solute system, chain assoc., dipole correl. theory, dielec. const. anal 77—48675
- 1-octanol-nonhydroxylic solvent complexes, H bonding, assoc. consts., elec. dipole moments, dielec. consts. 77—48672
- 4-octyl-4′-cyanobiphenyl, liq. cryst. phases, dielec. relax. meas., short range interactions 78—94976
- octyl-cyano-biphenyl, nematic and smectic-A phase, dielec. meas. 78—60392
- 4-n-octyloxy-4'-cyanobiphenyl, liquid cryst., dielect. polarisation and its dispersion 79—1397
- n-p-octyloxybenzylidene-p-toluidine, dielectric behaviour in nematic mesophase at RF 80—34842
- organic binary liq. mixture, relax. times and dipole moments, RF and microwave obs. 77—12308
- organic liquid systems, dielectric and dynamic Kerr-effect studies 80—60496
- organic liquids, complex permittivity in UHF region *(Japanese)* 79—8085

dielectric properties of liquids and solutions continued
- organic liquids in freq. range 400 MHz to 285 GHz, internat. comparison of meas. methods *(German)* 80—68168
- organic rigid molecules solns. and mixtures, dielectric relax., const. and loss factor, microwave region 77—55747
- organo tin dichlorides, tetrahedral, dilute soln., dielec. and thermodynamic behaviour, microwave region 77—36170
- p-alkoxybenzylidene-p′-amino-2-chloropropyl-cinnamate, chiral smectic, dielec. props. 80—96441
- PBLG in dioxan, freq. and shear-rate depend. of relative permitt. 77—8489
- PBLG solns., dielec. meas., using pseudorandom noise dielectric spectrometer 78—15084
- PCB, nematic, smectic phases, dielec. and optical props. 78—60377
- p-pentoxy-benzylidene-alkylaniline series, smectic phases, dielec. anisotropy 80—55010
- 4-n-pentyl phenyl-4(4-pentyl benzoyloxy)3-chlorobenzoate, liq. cryst., flexoelectric and dielec. relax. behaviour 78—94979
- pentylcyanobiphenyl, nematic, elastic and dielec. props. from capacitance-voltage curve 79—32894
- 4-n-pentyloxy-phenyl-4′-n-octyloxybenzoate, nematic, dielec. relax. and freq. depend. of threshold voltage 80—60497
- perfluorinated polymer, Krytox 143-AB, viscous, viscoelastic and dielectric properties 80—70440
- permittivity, by microwave freq. meas., student expt. 79—40320
- permittivity, dipolar hard sphere fluid, interaction-graph theory 79—51898
- permittivity, polar solute dipole moment determ. 77—6956
- permittivity meas., of liquids with high dielectric losses, 300 MHz to 6 GHz *(German)* 80—13106
- permittivity meas. of lossy liquids at 70 GHz using precision waveguide cells 78—37032
- p-phenitidine, in benzene soln., dipole moment from solute relax. time-solvent viscosity relation 80—37905
- phenols, dil. solns., dielec. loss and relax., microwave and sub-mm. wave absorpt. obs. *(German)* 78—23396
- phenyl 4(4-alkylphenyl)cyclohexanecarboxylates, mesomorphism and dielec. props. 77—27810
- phenyl 4-alkylbiphenyl-4′-carboxylates, mesomorphism and dielec. props. 77—27810
- phenyl 5-alkoxypicolinates, synthesis, phase transition temps., and dielec. props. 79—86876
- phenyl 6-alkoxynicotinates, synthesis, phase transition temps., and dielec. props. 79—86876
- phenyl isothiocyanate, in benzene (tetrachloromethane), nonlinear dielectric solvent effect 79—28702
- phenylcyclohexanes, nematic, low melting liq. crysts. with positive dielec. anisotropy, phys. props. 77—43148
- 3-phenylpropanol-hexane, nonlinear dielectric effect, critical exponent 80—93227
- phenylpyrimidines, liq. crysts., synthesis and phys. props. 78—1995
- polar fluid, molecular pair effects, Onsager dielec. theory breakdown 80—75917
- polar fluid of heteronuclear molecules, dielectric const. 78—84514
- polar fluids in elec. fields, statistical mechanics 80—54085
- polar liq. in nonpolar solvent, dipole moment extrapolation procedure 79—33650
- polar liqs. permittivity, computer simulation with hard sphere point dipole pot. 80—103911
- polar liquid, complex permittivity meas., lumped capacitance method 78—77936
- polar liquid, integrated absorpt., microstruct. effect *(French)* 78—10823
- polar liquid, nonlinear effects, permittivity, dipolar pot. 78—39493
- polar liquid, relative permittivity, dielectric and Kerr effect relaxation in alternating elec. fields 78—80284
- polar liquid, theory of dielec. relax. 77—8502
- polar liquid solns., H bonding, dielec. theory, apparent dipole moment, chem. model 77—48671
- polar liquids, binary mixtures, Sarma and Rao's rel. for dielectric relax. time 80—88914
- polar liquids, dielectric behaviour in far IR spectral range, theory 77—28509
- polar liquids, elec. polarisation theory 77—4596
- polar liquids in double layer capacitors, RF conduction, ion diffusion effect 80—107883
- polar liquids soln., mol. electric dipole moments, extrapolation formula 79—38437
- polar molecular solution, local order and vibr. coupling, Raman bands, dielec. const. 79—99868
- polar molecule, dielec. friction effect on reorientation in liq. 80—40048
- polar molecule/nonpolar solvent, dielec. relax. computation from viscosity data 80—11330
- polar molecules, in nonpolar solvent, dipole moments and relax. times 78—43782
- polar molecules, viscosity activation energy and relax. time, RF cond. meas. 80—96677
- polar molecules in liq. state, dielec. relax. time, dielec. const. 78—19408
- polar molecules in nonpolar solvent, dielec. props. in far IR range 77—85639
- polar molecules in nonpolar solvent, far IR spectra and dielec. relax. 80—71312
- polar solutes, in o-terphenyl soln., dielec. relax. 79—33598
- polar solvents, solvated electron absorpt. spectra, intrasolvent and intersolvent correls. 80—93840
- polar-polar liquid mixture, significant structure model applic. to dielec. const. correl. 77—8487
- polarity effect on breakdown voltage in inhomogeneous field 77—52018
- poly-4-chlorostyrene, undiluted, dielec. relax. spectrum above Tg 80—97194
- poly-ε-caprolactone in dioxane soln., low freq. dielec. response 77—40177
- polyacrylate solutions, dielec. relaxation 80—40045
- polybutene oil, direct voltage elec. strength 79—91360
- polydiethylsiloxane chains, dipole moments 78—78844
- polydimethylsiloxane film, non-pure, dielec. behaviour 80—29672
- polydimethylsiloxane fluid permittivity and dielectric loss 78—6621
- polyethylene, alcohol infused, loss peaks due to secondary groups 80—84688
- polyethylene oxide, aq. soln., dielec. relax., interferometric transmission obs. 78—52437
- polyethylene oxide, dil. soln., chain dipole moment, dielec. const. meas. 77—40169

dielectric properties of liquids and solutions continued
polyhexamethylene oxide, dil. soln., chain dipole moment, dielec. const. meas. 77—40169
polyhydroxyl alcohols, H-bonded solns., microwave dielec. relax 79—33599
polymer chains with rigid bonds, local relax. times, mol. dynamics study *(Russian)* 80—59373
polymer solution, flexible chain, entanglement effects in segmental motion, dielec. obs. 80—40050
polymer solutions, dielectric relaxation time, diluent effects 78—10843
polymers, electric phenomena, book 80—46746
polymers, electrical phenomena, nature and appl., book contrib. 80—50254
polymers, flexible, solns., shear flow, dielec. anisotropy, appls. 79—15393
polypeptides, helical, dielectric polarisability, side chain motions 78—76378
polypropylene glycol, low freq., multiple relaxation behaviour, dielectric and dynamic Kerr-effect techniques 80—29682
polypropylene glycol melt, mol. motion, dielectric and Kerr effect relax. obs. 80—60498
polypropylene oxide, solns., mol. relax., dielectric relax. and Brillouin scatt. obs. 77—23590
polypropylene sulphide, atactic chains, dipole moments, dielec. const. meas 80—23584
polystyrene, bridge method for meas. dielectric relaxation 80—82793
polystyrene, in butan-1-ol, colloidal particles, dispersion force interactions calcs 79—24842
polystyrene particle colloidal suspension in KCl(LiCl) aq. solns., dielectric loss 78—35728
polytrimethylene oxide, soln., chain dipole moment, dielec. const. meas. 77—81043
polyvinyl methyl ether, aq. soln., dielec. relax., interferometric transmission obs. 78—52437
1,2-propane diol-dipropylene glycol, dielec. dispersion charact. 80—75932
propanes, substituted, dielec. relax. in liquid state 77—8500
propanes, substituted, liq., microwave absorpt., dielectric relax., loss, permittivity, moments and reorientation 77—63362
p-propoxybenzylidene-p-butylaniline, nematic and isotropic phases, dielec props. 79—87383
propyl acetate propyl alcohol, dielec. dispersion charact. 80—75932
n-propyl trichloroacetate, soln., dielectric props. and relax. mechanisms at microwave freqs. 78—15089
propylene glycols, dielec. props., chain length effect 80—44995
proteins, dimensions, shape, conformational transitions, use of dielectric relaxation method 79—11888
PTFE, in butan-1-ol, colloidal particles, dispersion force interactions calcs 79—24842
PVA, aq. soln., dielec. relax., interferometric transmission obs. 78—52437
PVA, liq., mobilities at const. temp., vol. 78—95174
pyridine, solns., dielec. polarisation, π-electron system effects 77—90096
pyridines, substituted and N-oxides, dielectric relax. in solns. 78—6627
quinoline, dil. soln., dielec. absorpt., relax. and thermodynamic parameters meas. 80—50258
quinoline, solns., dielec. polarisation, π-electron system effects 77—90096
refractive index transients, laser-induced, low-temp. solns., excited triplet state polarisabilities role 79—87411
relaxation parameters, mol. and intramol. relax. 79—56715
relaxation spectroscopy, liquids, frequency and time domain expt. methods 80—40044
relaxation time rel. to single particle correl. time 80—97193
trans-retinal, ground and excited state dipole moments, permittivity, solvent effects, spectrophotometry 78—27883
trans-retylidene-n-butylamine, ground and excited state dipole moments, permittivity, solvent effects, spectrophotometry 78—27883
rigid polar molecules in dil. solns., dielectric loss in far IR region *(German)* 77—16248
rotational swings of colliding dipoles, contrib. to nonlinear dielectric constant 78—27171
salt solutions in porous media, dielectric meas. *(French)* 79—52677
sea water, dielectric permeability calc. *(Russian)* 78—77261
silicon oil, behaviour under HV stress 79—91368
silicone fluid, discharge propag. 79—91362
small liquid biological sample microwave complex permittivity meas. 80—17222
smectic A mesophase exhibiting positive and negative dielec. anisotropy 79—10793
smectic helixing crystal, dielec. props., temp. and freq. depends. *(Russian)* 78—60380
smectic liquid crystal, A phase, dielec. permittivity 78—71673
smectic liquid crystals, spontaneous polarisation meas. *(French)* 77—69765
smectic phases, dielectric constant theory 79—78604
smectic phases, long mol. axis reorientation, LF dielec. dispersion 80—70124
solute-solute-solvent interaction, dielec. behaviour problems, review 80—25298
solvation, classical mean space charge model 78—76841
solvent, ion migration and frequency-dependent dielectric loss 79—19832
solvent, polar, spherical ion radius and limiting elec. cond. Brownian motion 78—95168
solvent dielectric attenuation of substituent effects, field transmission in partially occluded cavities 78—2789
solvent effects, virtual charge model representation of solvent polaris. 78—74593
spheroids, in streaming suspension, dynamics, dielectric consts. 78—76374
stationary EHD instability, charge carrier mobility temp. induced variations effects 79—77269
trans-stilbene, soln., lifetime and anisotropic fluoresc., viscosity effects *(German)* 80—106352
Stockmayer fluids, static dielec. props. 80—93231
Stockmayer fluids with dipoles and quadrupoles, spherical harmonic coeffs., dielec. const. and Kerr factor calcs. 80—84678
Stockmayer molecular fluid, 2-dimens., permittivity and dynamic props. 80—103910
Stockmayer molecules, two dimens. fluid, static props., dielec. const. mol. dynamics calcs. 80—54094
submillimetre region, Poley absorption interpetation 77—36167
Sumoto effect under transient conditions 80—97198

dielectric properties of liquids and solutions continued
suspension, dielectric, convective heat transfer, rheodynamics, in horizontal coaxial cylindrical channel 78—59494
suspensions, dielectric separation of solid particles 80—16213
suspensions of ellipsoidal particles covered with shell, dielec. behaviour, rel. to biological cells 80—51057
TDOBAMBCC, chiral smectic C liq. cryst., dielec. consts., electroclinic effect 78—94980
temperature dependence, laboratory installation for meas. 80—37051
1,1,2,2-tetrabromoethane, dil. soln. in benzene, dielec. relax. study 80—29679
tetrabutylammonium iodide, in aq. proline soln., elec. conductance investigation 80—10692
tetrachloroethylene-benzene(toluene)(p-xylene)(carbon tetrachloride) binary mixtures, dielec. polarisations 79—56713
tetraethylene glycol dodecyl ether-H_2O, binary micellar solns. and emulsions, dielec. behaviour 80—44994
tetraethylene glycol dodecyl ether-H_2O-heptane, binary micellar solns. and emulsions, dielec. behaviour 80—44994
tetraglycine, aq. soln., static dielec. const. and microwave dielec. loss 78—47462
tetramethylammonium iodide, in aq. proline soln., elec. conductance investigation 80—10692
tetraphenylboron sodium aqueous soln., dielec. relaxation spectroscopy in microwave region, double-beam interferometry *(German)* 80—71309
tolualdehyde, dil. soln., dielectric relax., solid rotator phase 79—42890
toluene, liq., NMR spin-lattice and dielec. relax. 79—33604
trans-p-n-alkoxy-α-methyl p′-cyanophenyl cinnamates, liq. cryst. of strong positive dielec. anisotropy, static dielec. consts. meas. 78—2790
transient species, detection by dielectric loss meas., microwave method 79—74467
trichloracetonitrile, IR dispersion, complex refractive index and permittivity, time correl. function 80—45057
1,1,1-trichloroethane, in nonpolar solvents, permanent dipole moment determ. 77—43125
triethylenediamine aq. soln., dielectric relaxation rate 79—78619
trifluoroacetates, methyl and ethyl, intramol. relax. at microwave freqs. 80—55020
1,3,5- trifluorobenzene, liq., NMR spin-lattice and dielec. relax. 79—33604
triglycine, aq. soln., static dielec. const. and microwave dielec. loss 78—47462
DL-α-valine in aq. soln., dielectric dispersion 78—20141
vinyl acetate, oligomers, dielectric relax., end-group effects 78—92019
viscous liquid, glassy state, effect of fictive temp. on dielec. relax. 79—24256
water, complex permittivity meas. and microwave heating for specific purities and salt soln. 80—60480
water, dielec. relaxation of compressed liquid at 17.613 GHz using microwave refl. meas. method *(German)* 80—71306
water, dielec. relaxation spectroscopy in microwave region, double-beam interferometry *(German)* 80—71309
water, dielectric constant of bonded lattice model 78—23386
water, dielectric relaxation rate 79—78619
water, heavy water, and ionic solns., high-field nonlinear effect, Piekara factor meas. 78—68441
water, liquid, zeroth order random network model, dielec. const. calc. 79—68993
water, permittivity at mm wavelengths 80—66098
water, polarisation fluctuations, effective freq. calcs. 77—90093
water, simulation, Monte-Carlo method, 1 g cm^{-3}, 300K, using Rahman Stillinger ST2 pot. 77—51290
water, supercooled emulsified droplets, relative permitt. and cond., Maxwell-Wagner interfacial polarisation 78—52423
water emulsions, dielec. props. obtained after crystallisation/melting cycle 77—86381
water film, between muscovite sheets, permittivity change meas. method, 20-70°C 80—55009
water pollution, dielectric props. and determ. of microwave emissivity 80—101142
water-in-dodecane microemulsions, dielec. study of phase transition 79—28668
water-in-dodecane microemulsions, struct. transitions in liq. cryst. phase, dielec. props. 79—28669
water-oil microemulsions, optical matching 80—61157
Ar, fluid, light scatt., collision-induced, line-shape theory and mol. dynamics 79—41921
Ar, high-field carrier transport at pre-breakdown and breakdown regions 80—25305
Ar, liq., dielec. const. meas. by reson. method *(Russian)* 77—28511
Ar:Xe$^+$, 0.1-1.4 gm cm^{-3}, adiabatic electrostatic polarisation energy, calc. 77—85640
Ar-O_2 liquid mixture, dielectric polarisation and permittivity *(Russian)* 77—90095
Bi_2O_3-ZnO(CdO), elec. cond., dielec. const., mag. susceptibility meas., effect of melting transition 77—7849
CO group, NMR chem. shift, solvent's dielectric const. effect, mag. anisotropy 79—42847
CS_2, emulsion theory, appl. to the permittivity of nonpolar dielectrics *(French)* 78—39497
Cu complex, bis-ethylene diamine copper(II) sulphate, dielectric relaxation studies 78—84519
$CuSO_4$, dielectric relaxation studies 78—84519
D-T, liq., dielectric constant and elec. cond. 80—84680
ethanol-water system, complex dielec. permitt. in UHF region and NMR spectra *(Japanese)* 80—100620
$FeCl_3$, nonaq. solns., solvent-solute interactions, Mossbauer investig. of equilib. consts. 79—1729
H-bonded complexes, in polystyrene matrix, mol. relax. processes 79—24259
H_2, liq., normal and para-, dielectric props. *(Russian)* 79—87374
H_3BO_3, aq. soln., dielec. props. and struct. 77—89369
H_2O reorientation in H-bonding free solvents, IR absorpt., dielectric loss 77—36233
H_2O_2 aq. solns., struct. and dielec. props. 78—63659
H_2SO_4, solns., static permittivity, kinetic depolarisation, time-domain spectroscopy 78—68440
He, high-field carrier transport at pre-breakdown and breakdown regions 80—25305
He, liquid, electrical strength, breakdown voltage depend. on electrode configuration 80—7293

dielectric properties of liquids and solutions continued
- ^{3}He, superfluid A-phase texture, elec. orientation 80—6585
- ^{4}He, liq. and solid, dielec. const. meas. 77—20143
- ^{4}He, superfluid, quantized vortices and dielec. const. splashes in crossed fields *(Russian)* 79—19410
- KCl aqueous solution emulsions, complex permittivity meas., dielec. relax. 78—72459
- KCl, soln., elec. cond., dielec. relax., kinetic characts. 78—34641
- K_2SO_4, dielectric relaxation studies 78—84519
- $LiClO_4$, organic solns., complex permittivity meas., dielec. relax. spectrum *(French)* 78—27154
- N_2, breakdown by field induced microbubbles 79—91365
- N_2, breakdown strength, in mm gap range, press. effects 79—91357
- N_2, dielectric strength, bubble-phase equilib., high press., low temp. *(Russian)* 77—20798
- N_2, discharge development in nonuniform elec. field 79—91358
- N_2, electric strength determination 79—38451
- N_2, high-field carrier transport at pre-breakdown and breakdown regions 80—25305
- N_2-Ar(methane)(ethane) binary and ternary mixtures, dielec. const., excess vol. 80—7254
- NH_3, liq., relax. time and activation energy 79—91335
- NaCl, monoelectrolyte, highly mineralised salt soln., dielec. and radiation characts. 80—97184
- $Ni(ClO_4)$, dielectric relaxation studies 78—84519
- $Ni(NH_3)_6SO_4$ solution, dielectric relaxation studies 78—84519
- $NiSO_4$, dielectric relaxation studies 78—84519
- SF_6, critical isochore, dielectric const. critical anomaly upper bound 80—84679
- $Sc_2(SO_4)_3$ aqueous soln., dielec. relaxation spectroscopy in microwave region, double-beam interferometry *(German)* 80—71309
- Se, liq., dielectric relax. and elec. cond. 80—108150
- Se-Tl-S alloys, liq., dielectric relax. and elec. cond. 80—108150

dielectric properties of solids
- α-quartz, constitutive eqns. by group theoretic methods 80—1954
- abietic acid glass, determ. from TSC curves 77—55744
- absorption band struct. resolution by using complex dielectric const. 78—72546
- AC response, influence of states in gap and generation-recomb. effects 77—4362
- alcohol, thermal electret, persistency of surface change *(Japanese)* 77—81048
- alkali borate and phosphate glasses, mech. and dielec. relaxs. and interpet. 78—27159
- alkali halide:Me^{2+}, nearest-neighbour theory of dipole polarisation and depolarisation, cation vacancies 77—16243
- alkali halide:NH_2^-, paraelectric alignment, UV electroabsorpt. and Kerr effect 77—12413
- alkali halide, dielec. const., press. depend. from ionic polarisability and bulk modulus 79—19828
- alkali halide, divalent metal doped, dipolar relax. induced by AC field in various crystallographic directions 79—19833
- alkali halide, exchange charge polarisation, dielectric const., Dick and Overhauser model 78—55832
- alkali halide, polarisability analysis using Narayan-Ramaseshan repulsive pot. 77—76353
- alkali halide crystals, high freq. dielectric const. press. derivative model calcs., electronic polarisation 80—7255
- alkali halide crystals, Szigeti effective charge parameter, strain derivative 79—7571
- alkali halides, dielectric constant, Clausius-Mossotti and Mott-Littleton theories 79—82910
- alkali halides, electronic and static dielec. consts., strain derivative theory 79—95701
- alkali halides, electronic dielec. const., evaluation of second order strain derivatives 78—2792
- alkali halides, Mott-Littleton dielectric theory 78—80274
- alkali halides, optic mode Gruneisen parameters 78—43088
- alkali halides, props. under hydrostatic press. 79—38436
- alkali halides, static dielectric behaviour, vol. depend., many-body interactions effects 78—2786
- alkali halides, static polarisability, vol. depend. 78—52428
- alkali metal compounds, $ASbO_3.1/6AF$, dielec. spectroscopy study, 100 Hz to 10 MHz, 238 to 417K *(German)* 80—108144
- alkali metal halides, Born repulsive parameters and dielectric behaviour 77—72579
- alkali metal metaphosphate glass, dielec. relax. at medium temp. 79—24257
- alkaline earth fluoride, doped with trivalent rare earths, migration entropy for bound fluorine motion 80—71303
- alkaline earth glasses, $45RO.5Al_2O_3.50P_2O_5$, (R = Mg,Ca,Sr,Ba), electron beam irrad., temporal change in electric field produced 79—4760
- alkaline-earth fluorides, electronic and static dielec. consts., strain derivative theory 79—95701
- alklai halide, optic mode Gruneisen parameters and strain derivatives, Born-Mayer and Sziegti model 78—55929
- alkyl halides, depolarisation thermocurrent obs. of main relax. around glass transition 78—27158
- alums, dielec. behaviour and ferroelectricity 79—38431
- ammonium hydrogen oxalate hemihydrate, low temp. dielec. and thermal props. 77—28510
- amorphous dielectrics, dielectric anomalies at very low temps., acoustic anomalies analogy 78—31146
- amorphous dielectrics, universal relaxation time at low temp. 80—55026
- amorphous high dielectric materials *(Japanese)* 79—73876
- amorphous insulators, anomalous props. from EM/acoustic cross-expts. *(French)* 77—72658
- amorphous materials, dielec. and US dispersion at low temps. freq. and temp. depend. 79—95092
- amorphous solid, constitutive relation derivation 80—84684
- amorphous solid, very far IR props. 78—80344
- anisotropic artificial dielectrics, dispersion props, investigation, electrodynamic method 80—88903
- anisotropic bodies properties interpretation, using inverse tensor property *(Rumanian)* 77—55743
- aromatic aldehydes, in polystyrene matrix, group relax., weight factor effects determ. 78—68446
- band structure, dielectric 79—47034
- barium ternary fluorides, $BaXF_4$, (X = Mg, Zn, Co, Ni, Mn), polarisation and pyroelec. response 79—42905

dielectric properties of solids continued
- benzaldehyde, in polymer matrix, dielec. absorption, Eyring parameters 79—4761
- benzenes, substituted, cryst., reorientation motion, site models with nonequivalent sites, dielec. relax. 79—11382
- binary crystals, press. depend. and theories of electronic dielec. const. 77—24780
- binary solids, $A^{N}B^{8-N}$, average energy gap, quantum-dielectric-ion-depend. model 80—49571
- bis[catena-poly(methylarsenic)], LF dielec. response 79—56719
- bone, piezoelectric, dielectric and elastic constants, rel. to temp. and hydration 77—16946
- borosilicate glass, new dielec. props. at 5 mK 77—63354
- brain tissue, dog, dielectric props. between 0.01 and 10 GHz 80—16915
- 4-bromobiphenyl, dielectric const., mol. reorientation in solid 78—72448
- bromoform, solid, phase transform., dielec. dispersion and differential scanning calorimetric obs. 80—24582
- 1,4-butanediol, dielectric behaviour, LF dispersion 77—48126
- 1,4-butanediol, low freq. dielectric dispersion, charge carrier hopping anal. 78—43772
- butanediol terephthalate-polytetramethylene oxide terephthalate copolymers, dielec. props. 78—95546
- n-butyl-4,5,7-trinitrofluorenone-2-carboxylate/Lexan polycarbonate, dielectric. relax. 77—4598
- calcium behenate monomolecular layers between Al electrodes, nonlinear dielec. props. 80—80405
- calcium strontium propionate, compressed powder, dielectric props., particle size effects 77—59503
- carnauba wax, polarised, simultaneous variation of dielec. const. and discharge current, room temp. to beyond melting point 80—11314
- carnauba wax, thermal electret, persistency of surface chargo *(Japanese)* 77—81048
- carnauba wax thermoelectret, mag. anisotropy evidence for dipolar orientation 77—16240
- β-carotene, hole mobility, photocond. and dielec. const. meas. 77—11957
- cellulose esters, plasticiser effects on mech. and dielec. relax. 80—40047
- cellulose fibres, elec. anisotropy 80—97220
- cellulose hydrate, nondestructive control of mech. props. anisotropy, appl. of capacitance method 77—86277
- celsian, with CaF_2 and ZnO additives, props. obs. *(Bulgarian)* 80—50579
- cetyliodide, cryst. phase transitions, mol. dynamics, spectroscopic and dielectric meas *(Russian)* 79—51965
- chloranil pellets, thermally stimulated discharge current and dielectric studies 80—93236
- coal, dielectric relaxation and conductive impurities 79—82921
- complex and power reflectivity determ., 100 GHz to 3 THz 80—15999
- complex permittivity meas., rectangular waveguide method 80—15941
- composite material, two-component, complex dielectric constant, exactly solvable microscopic geometries and rigorous bounds 80—75918
- composite materials, phys. props. review 77—4720
- composite media, dielec. and optical props. electrostatic polarisability calc. 79—51507
- composite medium, with regular struct., dielec. props. 80—20576
- composites, interfacial polarisation and loading factor effects in dielec.-loss meas. 80—2693
- copper formate tetrahydrate, antiferroelec., dielec. anisotropy 78—43768
- copper formate tetrahydrate, dielec. anisotropy and dimer theory 79—38427
- copper formate tetrahydrate, dielec. props. under hydrostatic press. 77—20789
- Corning 7070 glass, relative permittivity at 3 GHz 79—33591
- corundum ceramic, high-temp. treatment, powder medium effect on microstruct., comp., strength and dielec. props. 79—33984
- crystalline dielectric, local electric fields near surface 80—80733
- crystals, dipole-impurities, HF elec. cond., dielec. losses and light absorption 77—63363
- cupric formate tetrahydrate, pressure effect on dielectric props. *(Japanese)* 79—65787
- cupric formate tetrahydrate, uniaxial stress effect on dielec. props 78—48125
- current limitation in injected beam of fast electrons, stationary MFP *(Russian)* 77—4349
- 9-cyanoanthracene, cryst., polarised refl. spectra at 2K, 360-460 nm, dielec. function 79—91461
- data presentation and interpretation 78—76376
- decalin, liq. and glass mol. motion, kinematic and electrodynamic solns. 80—25293
- defect-free crystals, dielec. losses due to phonon system perturb. in elec. field 80—80693
- degenerate electron system, low-freq. polarisability, RPA calc. with temp correction 79—95354
- diamagnetic glassy semiconductors, at. tunnelling states, dielec. and elastic losses 79—87385
- diamond, dielectric polarisation calcs., microscopic local fields 80—20582
- diamond, dielectric properties, mean point value calc. 78—87930
- diatomic crystal, photoelasticity, exchange charge polaris. effect 77—81046
- 4,4′-dibromobiphenyl, dielectric const., mol. reorientation in solid 78—72448
- dicalcium barium propionate, press. induced ferroelectricity, dielectric meas. 79—51920
- dicalcium lead propionate, effect of particle size on dielec. behaviour 79—38429
- dicalcium lead propionate, ferroelec., annealed, crit. exponents, dielec. const. temp. depend. 80—55050
- dicalcium lead strontium propionate, mixed cryst., phase diagram, dielec. and dilatometric anomalies 77—11689
- dicalcium strontium propionate, effect of particle size on dielec. behaviour 79—38429
- 1,2-dichloroethane, enclathrated, conform., reorientation, PMR line shape anal. 79—91300
- dichloromethane-decalin glass, mol. dynamics, from dielec. loss meas., 107-148K, 293K 78—76379
- dielectric loss, charge carrier contrib. 79—56718
- dielectric matrix with spherical metallic inclusions, permittivity, conductivity 78—48108
- dielectric permeability sound wave induced nonlinear modulation *(Russian)* 80—16008
- dimensional effects in ultrasonic wave absorpt. coeff. *(Russian)* 80—70321

dielectric properties of solids continued
- dimethylammonium manganese chloride, perovskite-type layer structure submillimetric-wave spectroscopy 79—33540
- dipolar molecular lattice, dielec. absorpt. of disordered mol. solids, electrodynamic influences 80—40040
- discharge breakdown, mechanism determ. in solid dielectrics using scanning electron microscope 77—85649
- DNA, dielectric hysteresis loop 79—83691
- dynamic dielectric anal. of solids, automated technique 79—63271
- EBBA, stable and metastable solid phases, dielec. dispersion meas. 78—60390
- Eccosorb HF-2050, AC resistivity meas., 100-320K, 500-2000 MHz, von Hippel's method 77—32314
- elastic, constitutive eqns. 77—8512
- elastic dielectric, crack tip stresses, EM field distrib. 79—68641
- elastic dielectric, crack tip stresses generated by EM field 79—68642
- elastic dielectric, crack tip stresses in EM field, Williams method 79—68640
- elastic dielectrics, group theoretic methods 80—1954
- electret effect, homo and heterocharge charge distribution 80—11317
- electric breakdown in dielectric solids 80—66111
- electric breakdown mechanism, discharge development, electron impact ionisation 80—15961
- electrical conductivity investigation, current injection method appl. *(Portuguese)* 80—20179
- EM field effect on crack propagation in elastic dielectric 79—68576
- epoxy resin-ferroelectric $Pb(Zr,Ti)O_3$ composite, dielec., elastic and piezoelec. consts. 77—8515
- epoxy resins, mech. and elec. low temp. props. 80—25814
- esters, thermal electret, persistency of surface charge *(Japanese)* 77 81048
- Estrodur 31s, polyester moulding material *(Polish)* 80—66523
- ethers, and alkane solid solns., dielec. props. and IR spectra *(French)* 79—4378
- p-p-ethoxyphenylazophenyl hexanoate, dielec. relax. in stable and metastable solid phases 80—34851
- ethylammonium tetrachloromanganate, dielec. props. in phase transition region 80—55011
- ethylene-methacrylic acid copolymer, dielectric relax. and IR obs. 79—69772
- eukaryotic cell cycle, long-range dielec. aspects 80—94182
- exciton dielectric, current state *(Russian)* 79—60726
- fatty acids, thermal electret, persistency of surface charge *(Japanese)* 77—81048
- ferrite spinels, dielec. permeability tensor and transmittance, transition to single lattice struct. *(Russian)* 79—87465
- ferrites, microwave, dielectric constants and permeability *(Chinese)* 80—66096
- ferroelectric, textured layered prep. by HF sputtering 77—85947
- ferroelectric crystal with defects, permittivity, nonlinearity 78—27170
- ferroelectricity, conference, Leningrad, USSR (1977) 79—15406
- ferroelectrics, temp. depend. of soft mode freq. and its damping 79—38484
- field eqns. for dielectric comprising several molecular species 77—5668
- fluctuation theorems for dielectrics with periodic boundary conditions 80—80735
- food, semi-solid, at low, intermediate and high moisture contents 80—101157
- frequency and time responses, universality, review 77—63352
- frozen meat dielectric properties, expt. 80—56332
- glass, dielectric instabilities in high permittivity glass 78—52433
- glass, electrical relax., Debye-Falkenhagen theory 80—108155
- glass, fracture, electrical energy losses and causes, atm. humidity effect 80—55498
- glass, relaxation phenomena and Raman spectroscopy, review of developments 78—22665
- glass, simple molecule, dielec. relax., 4-77K 77—73109
- glass, tunnelling systems, intrinsic elec. dipole moment, coherent elec. echo obs. 80—29705
- glass characteristics, electromagnetic, mechanical and thermal props. 80—106587
- glass fibre reinforced non woven epoxy laminates comparison with paper phenolic and woven glass epoxy, dielec. props. 78—35635
- glasses, acoustic and dielec. props. at low temps., review 78—6128
- glasses, echoes and elec. dipole echoes at low temps. 79—69771
- glasses, thermal, acoustic, and dielec. props. at low temps. 79—65164
- glycine silver nitrate, dielec. relax. in paraelec. and ferroelec. phases 80—29678
- HAB, dielectric and calorimetric investig. in solid, liq. cryst. and liq. phases 77—84639
- heavily doped degenerate semiconductor, complex dielec. function 79—90982
- heterocyclics, in polystyrene matrices, energy barriers, dielec. absorpt. meas. 78—70958
- heterogeneous dielectric, bounds on energy and mean square fields 77—31042
- 2,4-hexadiyne-1,6-diol bis-(p-toluene sulphonate), dielec. const. during solid state polymerisation 79—51899
- p-n hexyloxy benzylidine-p-toludine, liquid crystal, elec. cond. and dielectric constant, in solid phase 79—61293
- high polymer physics, conf., Washington, USA (March 1978) 79—11633
- ice, anisotropic props. in 50-150 MHz range 80—17274
- ice, Arctic drift, microwave dielec. const. and absorpt. coeff. anisotropy 78—49037
- ice, dielectric const., Onsager-Slater theory and unit model, Bjerrum defects 80—11310
- ice, dielectric relaxation in presence of ionic impurities, block layer meas. tech. 80—103914
- ice, Ih phase, dielec. anisotropy 78—64310
- ice, permittivity at mm wavelengths 80—66098
- ice, polarisation processes, in lattice, Kirkwood's theory rel. to thermodynamics of irreversible processes 79—38447
- ice I_h, hexagonal, ferroelec. transition 79—91386
- ice Ih, Curie-Weiss behaviour of static dielectric constant of Debye component 77—81044
- ice microcrystals, NH_4Cl doped, activation energy of Debye's dipolar relax., influence of salt content *(French)* 78—56424
- ice VI, polymorphic transition at high-press., 123.1K, HF permittivity study 79—55883
- incommensurate lattice, energy gap in phonon spectrum. role of Coulomb forces, dielec. props. 80—44269

dielectric properties of solids continued
- interstellar grains, exact Debye theory for max. temps. 77—49449
- ionic crystals, dielectric loss and relaxation theory and kinetics 80—11335
- ionic crystals, lattice defects, conference, Canterbury, England (Sept. 1979) 80—105420
- ionic polarisability in crystal lattice, quantum mech. model 79—47384
- langbeinite-type crystals, phase transitions, dielec. props. obs. 78—6643
- laser-induced evaporation of nonlinearly absorbing dielectric surface 78—80438
- lead phthalocyanine:O_2(I), Schottky barrier effect on AC current response 80—75623
- lithium formate monohydrate, elec. props. 79—87371
- loss peak, many-body interpretation 80—15953
- losses in solids and liquids, characterisation 78—88252
- lossy dielectrics, thermal charge carriers movement 80—88920
- low-frequency dispersion, in carrier-dominated dielectrics 79—47380
- low-loss solid dielectric meas., automated resonance substitution systems 80—15957
- lunar and planetary surfaces 77—60678
- marble, LF dielectric props. 80—34843
- MBBA, dielec. relax. in metastable modification of solid phase 80—84689
- MBBA, dielectric and calorimetric investig. in solid, liq. cryst. and liq. phases 77—84639
- metal film, complex permittivity, microwave meas. 79—24253
- metal-dielectric interface, static point charge in dielec., pot. distrib. *(Russian)* 80—60088
- methanol-β-quinol clathrate, orientation and reorientation dynamics, dielec. and NMR obs. 79—99783
- methyl methacrylate-methacrylic acid copolymer, hydrogen bonding effect on dielec. relax., T_g region 77—59512
- methyl methacrylate-p-chlorostyrene copolymer, side-group rot. and dielec. relax. 79—61303
- methyl methacrylate-styrene copolymer, dielec. characts. change rel. to composition 80—25296
- methyl methacrylate-styrene copolymer, side-group rot. and dielec. relax. 79—61303
- methylammonium aluminium selenate dodecahydrate, dielec. dispersion and relax. 77—28515
- methylammonium aluminium sulphate dodecahydrate, ferro to paraelectric transition, low freq. dielectric behaviour 79—4770
- methylammonium alums, dielec. relax. near transition point 80—71301
- methylammonium gallium sulphate dodecahydrate, dielec. relax. meas. 79—28677
- methylammonium-$Ga(SO_4)_2.12H_2O$, ferroelec. alum single crysts., dielec. dispersion and characts. 79—15408
- 3-methylpentane glass, electron-ion pair polarisation, γ-irrad. induced current and IR photocurrent 77—69768
- mica, pulse electric breakdown under pressure, lamination effects 80—66110
- molecular crystal, band structure, excitonic processes, trap distrib. 80—6720
- molecular crystal, dielec. singularity causing phase transition, anomaly and soft modes 79—60470
- molecular optics model, electrodynamic eqns. derivation 78—27151
- molecular optics model, macroscopic theory 80—84683
- molecular solid, dielectric loss, multimultiple relaxations, comparison with polymers 78—19409
- multiphase material, average bulk props. calc., bounds 77—16237
- nitrobenzene, polarised, simultaneous variation of dielec. const. and discharge current, room temp. to beyond melting point 80—11314
- p-nitrophenyl p-n octyloxy benzoate, liquid crystal, elec. cond. and dielectric constant, in solid phase 79—61293
- non-exponential decay in dielectrics, and correlated systems dynamics 79—73882
- non-stoichiometric solids, correl. between dielectric const. and defect struct. 77—85638
- noncrystalline model systems, local elec. field, embedding-field method 80—108169
- nonlinear electroacoustics of dielec. cryst., fundamentals and appl. 80—34489
- nonstoichiometry and dielectric props. 78—43135
- Nylon 7-7 and 11, dielectric const. and dielectric relax. 80—25294
- p-n octyloxy benzylidine-p-toludine, liquid crystal, elec. cond. and dielectric constant, in solid phase 79—61293
- OHMBBA, solid phase dielectric relax. times and strength, mol. rot. 78—72456
- one-dimensional conductor, microwave permittivity measurement techniques 78—10825
- one-dimensional semiconductor, delocalisation and superalternation effects in nonlinear susceptibilities 77—11840
- oxide glasses, elec. cond. and dielec. relax., correl. 78—79801
- PA6, loss factor rel. to fatigue strength *(Polish)* 77—28904
- pentachloronitrobenzene crystal, anomalous microwave permittivity, IR absorption and Raman spectra *(Japanese)* 78—15169
- Perspex, dielec. breakdown and space charge, treeing 78—27160
- perspex, electric conduction and isothermal dielectric relax. 80—80285
- PET, pyroelectric effects and depolarisation currents, illumination effects 80—34859
- photoconductivity in dielectrics, transient, trap-controlled, numerical study 80—50285
- photodielectric effect in photocond., improved model including effect of traps 77—1445
- piezoelectric powder, polarisation echo for system of anharmonic oscillators *(Russian)* 77—81062
- plastic crystal, with steric hindrance, dielectric const. 77—24779
- PLZT ceramics, ferroelec., special props. 79—42916
- PMMA, and related cpds., ionic charge carriers, dielec. studies 80—25291
- PMMA, dielec. relax. spectrum, thermodepolarisation and dilatometric meas. 77—32322
- PMMA, electron energy loss spectra, optical props. 79—10887
- PMMA, shock induced polarisation, dielec. const., dipole lifetime rel. to particle velocity *(French)* 77—69776
- PMMA glass, electron bombard. induced elec. discharge, electromech. effects *(Russian)* 77—32324
- PMMA-PVC mixtures, dielec. relax. and struct. rel. to formation *(Russian)* 77—20073
- PMMA-wood polymer composite, dielec. prop. at low temp. *(Japanese)* 78—31545

dielectric properties of solids continued
polar molecule, in polymer matrix, dielec. absorption 79—4761
polarisation echoes and avalanches, possibility in non-piezoelec. materials 79—69767
poly(4-chlorostyrene, 4-methylstyrene) copolymer, time-depend. ang. correls. 79—73881
poly(L-histidine), molecular motions in solid state, NMR and dielec. meas. 80—11332
poly(vinylidene fluoride) films, poled, piezoelec. activity and field-induced cryst. struct. transitions 80—20592
poly (4-chlorosytrene, styrene), linear copolymers ang. correls., dipole moments and dielec. consts. 77—61884
poly vinylidene fluoride, injection process nature during poling, rel. to pyroelectricity 78—19422
poly-2-hydroxyethyl methacrylate, dielectric γ relaxation 80—34850
poly-α-naphthol, semicond., isothermal depolarisation currents, electron trap parameters 80—60492
poly-L-proline, TSC and dielec. study of multiple relaxations 77—55748
poly-N-vinylsuccinimide, dielec. and pulsed NMR relax. glass-rubber transition, mol. motions 77—48125
polyacenequinones, dielec. polarisation, role of conducting mol. chains *(Russian)* 79—65794
polyacetylene:I, electric props. in semicond. and metallic regions 80—29432
polyacetylene film, anisotropy of dielec. const. 80—108146
polyacrylonitrile, film, dielectric polarisation 78—52431
polyacrylonitrile, film, IR attenuated spectra determ. of chem. origin of TSC 77—55746
6-polyamide, dielec. relax. time, thermally stimulated current neas. 79—87381
polyamide-12 plasticized with sulphonamides, relaxation props. *(Russian)* 80—55031
polycarbonate, γ-irradiated, dielec. behaviour and glass transition 80—97182
polycarbonate, sorption of water and its effect on dielec. behaviour 79—11383
polycarbonate thin films, solution-grown, dielectric relaxations 80—55029
polychlorotrifluoroethylene, crystalline and amorphous peaks, dielectric props. 80—93237
polydiethylene glycol terephthalate, relaxation, dielectric prop. 78—68447
polydimethylsiloxane, crystalline and amorphous, characterised by DTA, polarised light microscopy, dielectric relax. 80—25295
polyester, linear aliphatic, mol. motions determ. by dielec. relax. and loss meas. 77—63364
polyesters, linear, H_2O absorption and electric loss factor *(German)* 80—34849
polyethylene:NaCl, internal field strength, Raman spectra obs. 80—40061
polyethylene, γ-ray polymerised, dielectric loss reduction 77—24783
polyethylene, crystal, dielectric α-relax., soliton as crystal defect 80—45004
polyethylene, dielec., cryogenic tunnelling losses at microwave frequencies 77—52016
polyethylene, dielec. loss, 4.2K 77—24787
polyethylene, dielec. loss below 4.2K arising from proton tunnelling 77—52015
polyethylene, dielec. loss meas. using supercond. microwave resonators in oscillator loop 77—10043
polyethylene, elec. empulse breakdown strength, rel. to rate of drawing 80—15960
polyethylene, gamma radiation effects on dielect. parameters, expt. *(Hungarian)* 78—59836
polyethylene, linear, effect of pressure on vol. and dielec. relax. 79—61302
polyethylene, loss tangent variation obs., under long term irradiation by ^{60}Co rays *(German)* 80—75266
polyethylene, low density, dielec. behaviour, struct. props. influence *(German)* 78—92017
polyethylene, low temp. dielec. loss due to antioxidants 79—99822
polyethylene, low-density natural, at elevated temps. 80—97185
polyethylene, mech. and elec. low temp. props. 80—25814
polyethylene, microwave dielec. losses variation rel. to different sample treatments 80—25881
polyethylene, mol. motions, α relax, chain transport 79—15398
polyethylene, oxidised, low-temp. dielectric spectrum 79—61304
polyethylene, oxidised, paraelectricity, dielec. relax. obs. 77—48123
polyethylene, oxidised and chlorinated, dielec. ops. of mol. relax. 77—40179
polyethylene, polymer life eqn. appl. to dielec. strength 80—25304
polyethylene, thermally oxidised, low-temp. dielec. relax., dipolar tunnel states 78—2797
polyethylene film, drawn, dielec. breakdown and morphological struct., dichroic ratio 80—25813
polyethylene film, partial discharge degradation, effect of discharge products in air *(Japanese)* 77—69774
polyethylene film electrets, polarisation obs. and influence of wax impurities, TSC obs. and analysis *(French)* 80—44999
polyethylene terephthalate, β relax., dynamic mech. and dielectric loss data 79—15399
polyethylene terephthalate, oriented, directional anisotropy, of dielec. β-relaxation 77—16247
polyethylene terephthalate, polymer life eqn. appl. to dielec. strength 80—25304
polyethylene terephthalate film, space charge quantity meas. by Maxwell stress method 80—22389
polyethylene terephthalate sheeting, storage in aqueous media rel. to props. *(German)* 79—29250
polyethylene-terephthalate, field-controlled photogeneration and carrier trapping 80—25285
polyethylenes, dielec. losses, for use in AC superconducting power transmission lines 80—25302
polyethylenes, dielectric γ-dispersion, crystallinity effect *(Japanese)* 79—87384
polyferrocene film, plasma polymerised, dielec. props., 40 kHz to 50 MHz, 30-400°C 78—52439
polyimide film, dielec. AC props., expt. 78—43783
polymer, amorphous, excess charges, band gap levels and elec. props. 78—23053
polymer, amorphous, segmental distrib., light-, neutron- and X-ray scatt., piezooptical and dielec. meas., review 78—51444

dielectric properties of solids continued
polymer, complex dielectric const. determ. from polarisation current 77—66451
polymer, conductive, freq. depend. of elec. cond. and polarisation 77—11918
polymer, glass transition temp., dilatometric and dielectric relaxation data 80—6497
polymer, glass transition under high-press., dielec. loss method obs. *(Russian)* 78—71841
polymer, loss tangent, 0.1-10 GHz, 2.2-4.2K 77—24786
polymer, relaxation investigation *(German)* 78—31152
polymer, relaxation spectra determ. from electric discharge meas. with increasing temp. *(German)* 78—31151
polymer, TSD and dielec. loss, comparison of activation energies 78—10834
polymer films, dielectric constant meas. parallel to film surface 80—97183
polymer gels, comb-like, dielec. polarisation *(Russian)* 77—48698
polymer materials, NDT, rigidity and hardness from acoustic, thermal, optical and dielectric props. *(Russian)* 77—48601
polymer network formation, relaxational props. variation 80—38961
polymers, activation energy, dielectric relax. meas. method 77—24784
polymers, conversion of dielectric to viscoelastic data 78—48109
polymers, elec. capacity calc. strip electrodes system for dielec. props. study 80—25327
polymers, electric phenomena, book 80—46746
polymers, electrical phenomena, nature and appl., book contrib. 80—50254
polymers, morphology and elec. props., correl., review 78—43786
polymers, multiple dielectric relax. processes, mol. aspects, book contrib. 80—50264
polymers, relaxation and heating rate 77—66453
polyoxymethylene, dielec. relax., 90-300K, 400-10^4 Hz *(Russian)* 77—69770
polypentenamers, phosphonylated, hydrogenated derivatives, dynamic mech. and dielectric props. 78—68448
polyphenyl chinoxalines, dielectric relaxation *(German)* 77—59513
polypropylene, dielec. loss 4.2K 77—24787
polypropylene, film, isotactic, ion injection, space-charge-limited currents 79—69775
polypropylene films, meas. of dielectric losses at cryogenic temps. 80—25301
polypropylene-polyurethane laminates, meas. of dielectric losses at cryogenic temps. 80—25301
polysiloxane dizwitterionomers, mech., dielec. relax., effect of H_2O sorpt., thermal history 80—50261
polystyrene, momentum-depend. dielectric response 79—69160
polystyrene, thin film, TSC and dielectric props. *(Japanese)* 80—15632
polystyrene atactic carrier transport and photogeneration 80—80318
polystyrene-wood, polymer composite, dielec. props. at low temperature range *(Japanese)* 78—95541
polystyrenes, comparison of head-to-head, head-to-tail, by thermally stimulated discharge 79—15396
polysulphone, elec. appl., dielec. props. meas. 77—55750
polytrifluoroethylene, dielectric relax. processes above and below glass trans. *(Japanese)* 80—55028
polyvinyl acetate, struct. relax., enthalpy and elec. polarisation obs. 79—41978
polyvinyl alcohol, bulk polarisation, thermally stimulated discharge current meas. 80—40039
polyvinyl alcohol, ionic charge carriers, dielec. studies 80—25291
polyvinyl butyral film, charge storage mechanism, TSC expts. 80—25280
polyvinyl chloride, dielec. props. at ULF, superimposed direct voltage *(French)* 78—15138
polyvinyl cinnamate, and photocrosslinked form, low freq. dielec. loss evaluation 79—82919
polyvinyl fluoride, dielectric support for glass transition 78—2239
polyvinylcarbazole, Coloumb trap controlled hopping mobility model tests, mobility and permittivity meas. 79—56226
polyvinylidene fluoride, correlated mol. motion in dielec. props. 77—55749
polyvinylidene fluoride, cryst. form II, anisotropy of dielec. relax. 80—103915
polyvinylidene fluoride, dielec. props. and phase transitions *(French)* 80—55008
polyvinylidene fluoride, piezoelectric and dielectric consts. rel. to suitability for underwater transducers 78—1531
polyvinylidene fluoride, poled, dielec. relax. spectra 80—80690
polyvinylidene fluoride, poling by corona charging, pyroelec. effect 78—19423
polyvinylidene fluoride film, biaxially oriented, charact. for transducer appl. 80—88931
polyvinylidene fluoride film, polarisation and depolarisation processes 80—11318
polyvinylidene fluoride films, field depend. depolarisation behaviour 80—20580
polyvinylidene fluoride-PTFE, thermoelectret, IR spectra, struct. modifications and dielec. props. 77—55785
potential distrib. determ., non-destructive method *(French)* 80—40060
prefired substrate, acid treatment, improvement in as-fired surface finish 79—24636
prefluorinated polymer, DuPont Krytox 143-AB, viscoelastic and dielectric props. 80—1503
protein-methylglyoxal complex, electronic props., energy band cond. 79—24936
PTFE, spacer material for supercond. cable, dielec. loss meas. using supercond. reson. cavity 77—8501
pulsed RF radiation produced by scratching dielectrics *(Russian)* 78—19607
PVC:Cu films, electron transport and dielec. props. 79—82700
PVC, dielectric props. in ultra-low freq. range *(French)* 78—23395
PVC, gamma radiation effects on dielect. parameters, expt. *(Hungarian)* 78—59836
PVC, magnetoelectret form., RF thermomagnetic treatment, dielectric aftereffects 78—6625
PVC, plasticised, thermomechanical and dielec. relax. props. rel. to degree of processing 79—70124
PVC, rigid, physical ageing effect on elec. props. 78—10836
PVC film, soln.-grown, between Al electrodes, AC elec. props. 80—15619
PVC-polyvinylidene chloride copolymer, dielectric loss at low-temp 78—95543

dielectric properties of solids continued
PVDF dielectric, piezoelec. and pyroelectric props. rel. to crystalline forms 80−15982
pyrene, band structure, excitonic processes, trap distrib. 80−6720
α-quartz, complex dielec. const. at audio freqs., 5.5 to 380K 80−25272
quartz, effect of neutrons on electr. characts. *(Russian)* 77−48119
quartz, fused, dielec. const. meas. at 40-1500 MHz *(Japanese)* 77−87780
quasi one-dimensional charge transfer salts, soliton model for dielec. permeability 79−91338
quasi one-dimensional conductors, conference, Dubrovnik, Yugoslavia, (Sep. 1978) 80−12853
quasi-one-dimensional solids, nomadic polarisation 77−63357
β-quinol clathrate, CH_3OH mol. reorientation investig. by IR and dielec. meas. 77−12369
radiation induced charging and discharging, analytic solution 79−78612
rare earth aluminate, scandate and zironate film coatings, electrophys. props. w.r.t. prep. technology 80−60781
rare earth aluminates, effects of roasting in reducing and oxidizing media on elec. props. 78−52736
rare earth arsenates, $RAsO_4$, ferroelectricity, dielec. meas. 80−60515
rare earth oxide thin films, in MOS struct., elec. props. and band struct. 80−7013
rare earth oxides, dielec. const. and loss at low temp. 80−93229
$(\text{rare-earth})_2\ Ti_2O_7$, ($RE = La\text{-}Nd$, Sm, Gd, Y), ferroelec., layer type struct., cryst. growth 80−108348
relaxation processes, simulation using network model 80−40046
resorption current calc., boundary conditions using method of joint characts. 80−40055
resorption current due to space charges 80−40053
resorption current for steplike charge distribs. 80−40054
RNA, solid hydrated samples, hysteresis loops, nonlinear dielectric properties 80−71294
Rochelle salt, dielectric props. near upper Curie pt. under hydrostatic press. 79−82935
Rochelle salt, polarisation echo in ferroelec. phase transition region 79−42920
rubber, styrene butadiene, dielectric const. and loss, lignin content depend. 80−29670
rubber mixtures, synthetic, natural ageing effects on dielec. props. 77−24778
rubber-channel black mixtures, natural ageing effects on dielec. props. 77−24777
sapphire, complex dielec. const. at audio freqs., 5.5 to 380K 80−25272
semiconducting film, exciton oscillator strength, EM wave-polaritan propagation, reflective power *(Russian)* 79−99491
semiconductor, amorphous, dielec. relax. current meas. method and uses 77−77141
semiconductor, photodielectric effect associated with impurity excitation 79−82630
semiconductor, polydispersed, surface elec. cond. of particles influence on dielec. characts. *(Russian)* 77−16270
serum albumin, bovine, hydrated, dielec. and elec. props. 80−97854
solid dielectrics, surface resistivity meas. and calc. 79−1617
space charge, conference, Karpacz, Poland (Sept. 1977) 80−36766
space charge density distrib. and I-V characts. from current injection coeff. 80−39589
space charge distribs., indeterminability limits 80−40056
space charge phenomena, decay function and resorption current 80−40052
space charge problems by analogue modelling on field analyser 80−40058
space charge static states and evolution dynamics *(French)* 79−69774
space-charge behaviour, effect of relax. processes 80−40057
space-charge distrib., investigative method 80−40059
spacecraft dielectrics, charging and discharging 80−71315
spacecraft materials, surface discharge arc propag. and damage 80−71314
specimen holder for transmission dispersive far IR Fourier transform spectrometry 80−86468
spherical shells, dielectric body between two concentric spherical surfaces, stresses 80−45011
squaric acid, dielec. const. and PMR near struct. phase transition 79−10946
squaric acid, dielec. props., press. and temp. depend. 79−99815
squaric acid, hydrostatic press. effect on phase transition, dielec. and dilatometric meas. 78−55941
statistical test of solid dielectrics in pulse irradiation regime 78−95548
stearic acid film, in MIM struct., AC cond. and dielec. props., freq. depend. 80−55030
stearic acid film, permittivity meas. using varying gap immersion method 78−6620
stearic acid multilayer films, dark and photo-generated dielec. response 77−72882
stearic acid multilayer films, lattice and carrier contribs. to dielec. polarisation 77−69775
stearic acid multilayers, dielec. props. 80−80404
stibiotantalite type structure ferro- and antiferroelectrics, props. and crit. points 79−38460
styrene-acrylonitrile copolymer film, multiple relax. obs. using TSC 80−45000
styrene-butadiene-styrene triblock copolymers, dielec. props. 78−95545
styrene-butyl vinylpyridinium-TCNQ copolymer, dielectric const. *(Japanese)* 78−60375
styrene/n-butyl-2-vinylpyridinium-TCNQ copolymer, dielec. permittivity *(Japanese)* 78−56416
succinonitrile, plastic cryst. with steric hindrance, dielectric const. 77−24779
TCNQ salt, K-TCNQ, high and low temp. phases, dielec. const. 80−34844
TCNQ salt, $MEM(TCNQ)_2$, dielec. const. obs., DC and microwave cond. obs. 80−59963
TCNQ salt, NMP-TCNQ, realisation of disordered Hubbard model, dielec. props. 78−79917
TCNQ salt, $Qn(TCNQ)_2$, decrease of electronic coherence length by impurities 79−69501
TCNQ salt, $Qn(TCNQ)_2$, defect depend. of dielec. permeability and cond. 79−78608
TCNQ salt, $Qn(TCNQ)_2$, defect depend. of dielec. permeability and conductivity 79−91340

dielectric properties of solids continued
TCNQ salts, $Qn(TCNQ)_2$ and $NMeAd(TCNQ)_2$, dielec. const. and elec. cond. 78−60116
TCNQ salts with asymmetric donors, transport props. 78−60115
temperature dependence, laboratory installation for meas. 80−37051
o-terphenyl, dipolar solutes, reorientational motions, dielectric relax. below glass transition 80−19706
terylene film, electret state prod. using electrochem. injection, adsorbed states, frozen field 79−91344
tetramethylammonium tetrachloroferrate, press. induced ferroelectricity, dielec. and DTA meas. 80−80722
TGFB, deuterated, single cryst. growth from soln., dielec. and pyroelec. props. 79−24422
TGS:α-alanine, single crysts., dielec. spectrum in RF range *(Russian)* 80−66097
TGS:α-alanine, single crysts., pyro- and dielectric props. *(Russian)* 77−59520
TGS: nitroaniline, dielec. and pyroelec. props. 80−75916
TGS:Cr single cryst., lattice defect influence on critical behaviour 80−25315
TGS:nitroanilines, permittivity, elec. cond. and Curie temp. 80−25273
TGS, correlation between domain struct. and dielec. props. 79−42927
TGS, critical behaviour in thermal expsn. coeff. and dielectric const. 79−91334
TGS, deuterated, ferroelec., dielec. nonlinearity 80−75959
TGS, effect of Fe^{3+} admixture on phys. props. 80−76052
TGS, electrostrictive and dielec. coeffs., neutron diffr. study 80−75943
TGS, ferroelec. domain struct., polarisation obs. *(Chinese)* 80−20603
TGS, growth from solution containing aniline, dielec. and pyroelec. props. 78−6639
TGS, L-α-alanine disordered regions, dielec. prop. changes in transition region 80−108159
TGS, monocrystalline, ferroelectric, domain boundary dynamics contrib. to permittivity near Curie point *(Russian)* 79−73875
TGS, spontaneous polarisation, low temp. meas. 80−75921
TGS, with radiation defects, dielec. dispersion 79−42882
TGS powder, complex dielectric const. temp. depend. 79−47379
TGS powders, dielec. dispersion 80−97180
TGSe, deuterated, thermal and dielectric props. at high hydrostatic press. 80−34864
TGSe, ferroelec., dielec. nonlinearity 80−75959
TGSe, ferroelec., effect of gamma irradiation on dielec., piezoelec. and elastic props. 77−43943
TGSe, surface layers effect on coercive field, spontaneous polarisation, and dielec. const. 79−61321
thermal breakdown, theory 80−75938
thermally stimulated characts., dipolar relaxation time, trap levels and ionic space charge polarisation 80−84685
thin ferroelectric layers, permittivity tensor at microwaves 79−42883
thiourea formaldehyde polymer, pyroelectricity and dielec. props. 79−91379
tracking phenomena in solid dielectric materials under moist conditions, expt. 77−43934
transition metal oxide films, dielec. dispersion and polarization 78−2803
transition metal oxides, dielec. and thermophys. props. 77−52009
transition metal oxides, dielec. behaviour 78−71703
transition metal phosphate glasses, ohmic contact and dielectric. relax. 79−65795
tremolite asbestos, fibrous. elec. anisotropy 78−80273
triethylene, in polystyrene matrix, energy barriers, dielec. absorpt. meas. 78−70958
TSC technique for nonexponential dielec. response materials 79−47383
TSC with two trapping levels, calc. 80−60489
tungstates, hexagonal bronze type struct., cryst. struct. and props. 77−39574
universal dielectric response in condensed matter 79−28674
universal dielectric response law, many-body interpretation 80−15952
urethanic polyester elastomers, dielectric relax., spatial network density *(Russian)* 80−71310
US Gruneisen parameter for nonconducting cubic crystals 78−87744
vibronic ferroelectric carriers, dependence of plasma frequency on spontaneous lattice distortion *(Russian)* 79−15410
vinyl aromatic polymer series, dielec. relaxs. at 220°C, −50°C and ~120°C interpret. 77−43929
vinyl chloride-vinyl acetate copolymer film, dielec. relax. and thermally stimulated depolarisation current meas. 80−11336
vitreous systems, local motions, dielec. losses and relax. phenomena 80−108154
wax-graphite composite, specific capacitance, temp. and grain size depend. 80−50286
Wigner crystal, lattice quantum oscills. in mag. field, specific heat, mag. moments *(Russian)* 80−49636
zeolite-S layers, high-temp. activated dipole moments in S clusters *(Russian)* 80−20575
X-zeolites, dielectric relax. anal. 80−108153
ALF_3 film, amorphous, AC elec. props. 78−2804
Ag halides, static dielec. constant, strain derivatives 80−100629
Ag halides, static dielectric const. strain derivatives, using extended many body lattice theory 79−56710
Ag, halides, strain derivatives of elastic and dielectric consts. 79−60421
AgBr and $AgBr{:}PbBr_2$, emulsion grains, dielec. loss, ionic cond. and surface space charge 77−28038
AgBr, dielectric behaviour under hydrostatic press. 78−52420
AgBr, exchange charge polarisation 78−92016
AgBr(I) microcrystal dispersed in gelatin, effect of I^- on interstitial Ag ions 78−26726
AgCl, dielectric behaviour under hydrostatic press. 78−52420
AgCl, exchange charge polarisation 78−92016
$AgCl{:}OH^-$, dielec. meas., defect reorientation 77−19947
$AgCl{:}Pb^{2+}$, ionic cond. and dielec. loss relax. vacancy-impurity complex. form. 77−1259
AgCl(Br), electronic dielec. const., vol. depend., Clausius-Mossotti model 80−100630
AgCl(Br)(I), static polaris. and effective charge parameters, Born-Mayer pot. 77−31628
$Ag_{26}I_{18}W_4O_{16}$, struct. phase transition, dielectric, cond. and Raman obs. 79−19368
$AgNO_2$, single crystal, dielec. const., low temp. meas. 80−71290
$AgNa(NO_2)_2$, crit. dynamics, hydrostatic press. effect, dielec. props. meas. 80−71328

dielectric properties of solids continued
$AgNa(NO_2)_2$, order-disorder ferroelec., influence of hydrostatic press. on polarisation dynamics 80—103913
Ag_2O-P_2O_5 system, electrical conductivity and dielectric relaxation *(Japanese)* 77—66455
Ag_3SbS_3, pyrargyrite, order-disorder phase transition and elec. polarisation 79—38468
Ag_5SbS_4, dielec. and acoustic props. *(German)* 78—64335
$Al/Al_2O_3/Al$, dielec. props. 80—80404
Al-SiO_x-Al evaporated film anomalous dielectric dispersion under high DC field 80—15620
AlF_3 film, dielec. characts. 77—85650
AlF_3 film, RF sputtered, dielec. props. meas. 77—36173
$Al_2In_{12}S_{21}$, dielec. const., temp. depend. 79—82909
β-Al_2O_3, conduction and dielec. loss mechanisms, paired interstitialcy model 80—107468
α-Al_2O_3, dielectric constant, effect of degree of purity and perfection 77—48117
Al_2O_3 film, dielec. props., AC and DC elec. characts. 78—68445
Al_2O_3 film, RF sputtered by planar magnetron, phys. props. 77—43448
β-Al_2O_3-Na_2O, AC ionic cond., dielec. and NMR relax. 80—59713
β-Al_2O_3-Na_2O, electrolytes, electric modulus spectroscopy 77—84974
β-Al_2O_3-Na_2O, microwave absorpt., low-temp. dielectric props. anomalies, ion tunnelling states 78—92013
β-Al_2O_3-Na_2O $(Li_2O)(K_2O)(Ag_2O)(H_3O)$, with mobile ion species, dielec. relax. 79—91351
Al_2O_3-P_2O_5 glass, electron bombard. induced elec. discharge, electromech. effects *(Russian)* 77—32324
As-Ge-Te glass, dielectric meas. 79—87382
As-Se-Te system glasses, AC cond. and permittivity, freq. and temp. depend. 77—76857
$As_{25}Ge_{10}Te_{65}$, chalcogenide glasses, dielectric relaxation 80—55027
$As_xGe_{10}Te_{90-x}$ glass, cond. and dielec. const. from 77 to 383K and from DC freq. to 5 MHz 79—23964
$As_{10}Ge_{15}Te_{75}Ag_x$ glass, elec. and dielec. props., Ag additions effect 80—65558
$AsSe_{10}$, stable thermoelectret, effects of anisotropic external perturbation *(Russian)* 77—63361
As_2Se_3 glass, rel. to microwave elec. cond. 80—49793
As_2Se_3, glassy, dielectric const. determ. 78—72449
As_2Se_3, glassy, influence of oxygen added in As_2O_3 and SeO_2 forms on phys. props. 77—76314
Au small particles in glass, transition cluster-solid state 79—33593
Au-MgO cermet film, dielectric const. and selective solar absorption 78—2937
B and borides, conference, Varna, Bulgaria (Oct. 1978) 80—12842
β-B, rhombohedral, dielec. loss temp. depend., −196 to 350°C 80—20585
B_2O_3-CaO-Fe_2O_3 glasses, semicond., cond. models, electronic props., 77-800K 80—54688
B_2O_3-SiO_2 (95.5 wt.%) glass, dielec. relaxation 79—78620
BaBrF, reacted flux growth, dislocation density, dielec. const. and loss, IR spectra 77—36214
BaF_2, dielec. const., 5.5 to 400K 80—50249
BaF_2, electronic polarizability and dielectric const., strain derivatives 78—19406
$BaF_2:K^+$, cryst., thermal depolarisation 79—82912
$BaFe_{12}O_{19}$, ferrite, DC cond., dielec. props., lattice consts. 80—80272
$BaM_2(PO_4)_2$, $M=Co$, Ni, Mg, Zn, dielec. permittivity and elec. resist., temp. depend. 77—59502
Ba_2MgTeO_6, ferroelec. behaviour, microwave dielec. props. meas. 77—43948
$BaMnF_4$, antiferromag., dielec. anomalies at low temp. obs. 77—20791
$BaMnF_4$, phase transitions, review 79—78378
$Ba(NO_3)_2$, low temp. struct. changes, elec. props. 79—87377
$Ba_2NaNb_5O_{15}$, cryst. comp. effect on low temp. phase transition 80—71346
$Ba_3Nb_{10}O_{28}$, diffuse ferroelec. phase transition, dielec. const. and X-ray diffr. meas. 78—23419
BaO, dielectric behaviour 79—91343
BaO-TiO_2-Nd_2O_3, exam. of compositional and dielectric props. 79—33601
$Ba(PO_3)_2$-alkaline earth fluoride and $Ba(PO_3)_2$-YF_3 glasses, pseudobinary, elec. cond. and dielec. losses 77—7890
BaS, dielectric behaviour 79—91343
$(Ba_xSb_{1-x})TiO_3$ 80—60514
$Ba_{0.725}Sr_{1.775}Li_xNb_{5-x}Ti_xO_{15}$, solid soln., prep., struct., dielec. props. *(French)* 77—69782
$Ba_{1.35}Sr_{0.65}NaNb_5O_{15}$ crystals, struct., dielec. and pyroelectric characts. 79—51913
$Ba_xSr_{1-x}Nb_2O_6$ crystals, struct., dielec. and pyroelectric characts. 79—51913
$Ba_xSr_{1-x}Nb_2O_6$, struct. and dielec. props., isomorphic substitution effect 78—27165
$(BaSr)TiO_3$ film, ferroelec., dielec. props. in strong elec. fields 78—27163
$Ba_xSr_{1-x}TiO_3$, disordered ferroelec., dielec. const. and spontaneous polarisation meas. 78—48130
$BaTiO_3$, ceramic, effect of grain size on nonlinear dielec. props. 77—8522
$BaTiO_3$, Co substituted, ferroelec., diffuse behaviour 79—38475
$BaTiO_3$, ferroelec., reduction of hysteresis losses 79—42926
$BaTiO_3$, ferroelec., susceptibility of eight site order-disorder model calcs. 77—8523
$BaTiO_3$, ferroelec., X-ray diffr. topographic study of polarisation reversal 79—38442
$BaTiO_3$, ferroelectric ceramic, dielec., piezoelec. and elastic props., orientational contrib. 78—68468
$BaTiO_3$ film, sputtered, elec. props. 79—42676
$BaTiO_3$ film, struct. and dielec. props. 80—60514
$BaTiO_3$ films, ferroelec., effect of elec. field on dielec. props. 79—33642
$BaTiO_3$, nonstoichiometry of vac. condensates, effect on dielectric props. 77—16260
$BaTiO_3$, paraelectric crystal, nonlinear props. 80—84699
$BaTiO_3$, polycrystalline, dielec. nonlinearity coeffs. difference in free and clamped specimens *(Russian)* 80—25314
$BaTiO_3$, pure, dielec. behaviour at ultralow freq. 79—38425
$BaTiO_3$, single cryst., dielec. const., var. with applied AC field and temp. 78—2787
$BaTiO_3$, single cryst., dielec. breakdown and electroluminesc. 78—2917
$BaTiO_3$, single crysts., dielec. spectrum 80—25275
$BaTiO_3$, spontaneous polarisation, low temp. meas. 80—75921

dielectric properties of solids continued
$BaTiO_3$ thin film microwave complex permittivity meas. 79—73879
$BaTiO_3$, transform. of cryst. struct., at cubic-to-tetragonal phase transitions 79—37827
$BaTiO_3$ type perovskite ferroelectric, neutron irradiated, amplification of freq. dispersion of permittivity *(Russian)* 78—52419
$BaTiO_3:BaTi_3O_7$, dielec. props. and microstruct. 80—60481
$BaTiO_3$:Co, charact. behaviour of spontaneous polarisation and dielec. const. 78—60382
$BaTiO_3$:Nb, ferroelec. and paraelec. phases, props. 79—42919
$BaTiO_3$-$BaNbO_3$ system, solid solns., thermal ionic relaxation, vacancy form. 77—8499
$BaTiO_3$-PbO-B_2O_3, liquid phase sintering, effect on props. *(German)* 79—33980
$BaTi_4O_9$ effect of chemical treatment on loss quality, at microwave wavelengths 79—34159
$Ba_2Ti_9O_{20}$, effect of chemical treatment on loss quality, at microwave wavelengths 79—34159
$Ba(Ti_xSn_{1-x})O_3$ film, struct. and dielec. props. 80—60514
$Ba(Ti_xSn_{1-x})O_3$ thick film, ferroelec., phase transitions and dielec. props. 80—97215
$BaZrO_3$-$LaAlO_3$ systems, sintering conditions, elec. props. 79—43184
BeF_3, water free vitreous, preparation and props. 79—66033
BeO, thermoelectret state, effect of gamma radiation 80—7270
Bi complex oxides, antiferroelec. and ferroelec., pyrochlore struct., dielec. and structural study 79—38488
Bi mixed-layer type cpds., $Bi_4A_{2m-1}B_{2m+1}O_{6m+9}$, cryst. struct. and dielec. const. 77—47428
Bi-NbO_2-Bi system, Schottky barrier effects in transport and dielec. props. 80—29486
$Bi_{12}GeO_{20}$, electrophys., props. determ. *(Russian)* 78—51987
Bi_2O_3, anodic film, dielec. props. 77—20794
Bi_2O_3 film, dielec. meas. 80—2696
Bi_2O_3 layer thermally grown on Bi film, thickness meas. by capacitance method 79—1554
Bi_2O_3, thin film, struct. and dielec. meas. 79—78622
Bi_2O_3-ZnO(CdO), elec. cond., dielec. const., mag. susceptibility meas., effect of melting transition 77—7849
Bi_2S_3-$CuPbBi_5S_9$, solid solution, semiconductor and dielectric props. 79—69511
$Bi_xSb_{1-x}SI$, atomic substitution and ferroelec. phase transition 78—68464
$Bi_4Ti_3O_{12}$, elec. characts., phase transition obs. 80—60517
$Bi_2TiO_4F_2$, one-layer perovskite-like ferroelec., dielec. study 79—38486
Bi_2WO_6, ferroelectric, dielectric props., elec. cond. and relaxation phenomena obs. 80—80692
$Bi_2W_2O_9$, struct., dielec. props., melting character and thermal stability 79—23572
β-AgI, ionic cond. and dielec. meas., Frenkel defect formation energy 78—87814
$CH_3NH_3Ga(SeO_4)_2.12H_2O$, dielec. relax. near transition temp. 80—60493
$Ca_{12}Al_{14}O_{33}$, piezoelectric material, cryst. growth and characterisation 79—99825
$CaCO_3$, calcite, complex dielec. const. at audio freqs., 5.5 to 380K 80—25272
$CaCO_3$, calcite, X-ray irrad., luminesc. and dielec. loss decays 77—12431
$CaCo_2(PO_4)_2$, dielectric permittivity and elec. resist., temp. depend. 77—59502
CaF_2, cryst., dielec. props. in ULF range 80—7288
CaF_2, dielec. const., 5.5 to 400K 80—50249
CaF_2, doubly doped, dielec. relax. 80—50263
CaF_2, electronic polarizability and dielectric const., strain derivatives 78—19406
CaF_2, hot pressed, dielectric, optical props. 79—56720
CaF_2, rare-earth-doped, cluster-associated relax., 5.5-400K 78—31153
CaF_2:Er, defect structure, quenching effect, dielec. relax. and optical absorption 80—65031
CaF_2:Er, near-Debye dielectric responses 80—71291
$CaF_2:Eu^{3+}$, dielec. spectrum 77—36171
CaF_2:Li(Na)(K)(Rb), dielec. relax., activation energy, rel. to vacancy pair reorientation 80—88917
$CaF_2:Na^+$, cryst., thermal depolarisation 79—82912
$CaF_{2-x}H_x$, ionic cond. determ. from admittance and dielec. loss meas. *(French)* 80—107479
CaO, dielectric behaviour 79—91343
CaO-B_2O_3-Fe_2O_3 glass, electronic and dielec. props. meas. 77—24574
CaO-B_2O_3-Fe_2O_3 glass, dielec. relax., AC and DC cond., dielec. const. and loss 78—23393
CaO-MgO-Al_2O_3-SiO_2, shale glass, glass forming and dielec. props. 78—22660
CaS, dielectric props., effective ionic change 79—65783
Ca_2SiO_5, hydraulic reaction observed by microwave dielectric meas. 78—80745
$CaTiO_3$-$CaTiSiO_5$, sintering and dielectric props. 80—40307
$CaTiO_3$-TiO_2, ceramic, phys. props. 78—43784
$CdAs_2$ based glasses, cond. and permittivity, freq. depend. 77—76859
$CdBr_2$ and CdI_2(4H), electric field effect on NQR, elec. polarisation mechanism 77—20746
CdF_2:Eu, role of solution and precipitation phenomena on ITC spectra 80—7265
CdI_2, dielec. props. rel. to polytypically modulated structs. 79—94971
CdI_2, polytypes, dielec. const., periodicity and disorder depend. 77—28506
CdI_2 polytypic crystals, dielectric loss behaviour 80—66108
$Cd(NO_3)_2$, phase transition, SHG, optical and dielec. meas. 80—71334
CdS, elastic, piezoelec. and dielec. props. 80—108157
CdS, elastic, piezoelectric, and dielec. props., 4.2 to 300K 80—60508
CdS:Cu binder layer, photoactive, AC impedance meas. 80—25299
CdS:Li film, optical props. 80—2886
CdTe, dielec. const. and loss tangent, temp. depend., 15.95 GHz 77—69763
$CdTiO_3$, single cryst. growth and props. 79—100046
$Cd_2Ti_2O_5F_2$, single cryst. growth and props. 79—100046
CeO_2, elec. cond. and dielectric props. at low temp. 78—72447
CoO, dielec. behaviour, Dick and Overhauser shell model calcs. 80—45001
$Co_xZn_{1-x}Fe_2O_4$, ferrite, DC cond., dielec. props., lattice consts. 80—80272
Cr_2O_3, dielectric const. and loss, cond., 10^2-10^7 Hz, 30-450°C 77—59504
Cs halides, dielectric const. meas. at 1 MHz 77—16238

dielectric properties of solids continued

- $Cs(B_xW_{3-x})O_9$ (B=Na, Ca, Co, Ni, Cd, Ga, Bi, Nb, Ta) cryst. struct., temp. dielec. anomalies 80−1998
- CsBr, crystal, short range interaction polarization, dielectric const. loss, and elec. cond. 10^2 to 10^7 Hz 79−99814
- CsCl(Br)(I), dielectric const. meas. at 1 MHz by immersion method *(Japanese)* 77−90087
- $CsCuCl_3$, piezoelectricity, Jahn-Teller type phase transform. 80−40065
- $CsFeF_4$, two dimensional structural phase transitions, sp. ht., optical, dielec., X-ray diffr. meas. 79−69240
- CsH_2AsO_4, ferroelec., RF dielec. relax., loss mech. 79−38448
- CsH_2AsO_4, influence of γ-radiation on dielec. props. 79−46703
- CsH_2AsO_4, RF dielec. response close to transition temp. 77−90099
- $Cs(H_{1-x}D_x)_2PO_4$, dielec. props., temp. meas. 80−71335
- CsH_2PO_4, ferroelec., X-ray and dielec. studies on phase transition 79−38477
- CsH_2PO_4-d, antiferroelec. under hydrostatic press. 79−91384
- CsI, far-IR optical props., shell-model calcs. 77−28557
- $Cs_8Nb_{22}O_{59}$, melt growth and struct., dielec. and optical characterisation 78−35294
- Cs_2SO_4-$(NH_4)_2SO_4$ mixed cryst., ferroelec. transition, structural and dielec. props., proton spin-lattice relax. 78−39512
- CuCl(Br), electronic dielec. const., vol. depend., Clausius-Mossotti model 80−100630
- CuCl(Br)(I), static polaris. and effect charge parameters, Born-Mayer pot. 77−31628
- CuPbBiS, ferroelec. semicond., elec. cond., photocond. permittivity, phase transitions 77−47822
- donor polarisability, enhanced, below insulator-metal-transition, self-consistent calc. 80−7262
- $DyAsO_4$, cooperative Jahn-Teller phase transitions, dielec. anomalies 78−64312
- $DyVO_4$, cooperative Jahn-Teller phase transitions, dielec. anomalies 78−64312
- EuO, mag. semicond., dielec. and optical props. 78−10824
- EuO, microwave and DC cond., dielec. const., 1.7 to 300K 77−20347
- Eu_2O_3, elec. cond., thermoelec. power, dielectric const. 79−69763
- Eu_xO_y film, dielec. props. rel. to annealing 79−99636
- EuSe, mag. semicond., dielec. and optical props. 78−10824
- EuSe, microwave and DC cond., dielec. const., 1.7 to 300K 77−20347
- EuSe, polarisability of shallow donors, permittivity meas. 80−24833
- $Eu_2(WO_4)_3$, mag. susceptibility, elec. cond. and dielec. const. meas. 77−11916
- Fe-Ge, characteristic energy losses and optical props. 80−29834
- FeI boracite single crystals, dielectric, pyroelectric props., vapour phase transport growth 80−80673
- FeO_x-P_2O_5 glass, semicond., dielec. props., thermally stimulated depolarisation meas. 79−95704
- Fe_3O_4, dielec. props. of low temp. phase, at microwave freq. 78−64309
- Fe_3O_4, mag. relax., permeability and loss tangent determ. at 4.2 to 300K 77−32263
- $FePb_4Sb_6S_{14}$, photosensitive semiconductor, with high permittivity, elec. props. 79−65518
- FeS_2, dielec. constant meas. 79−15395
- $FeSO_4.7H_2O$, single cryst., elec. and dielec. props., temp. depend. 79−19826
- $FeSb_2S_4$, berthierite cryst., anomalies in elec. and dielec. props. 77−47821
- Ga, optical props. in 0.5-60 eV range, dielectric const. and loss functions *(French)* 77−12353
- Ga ultrathin metallic filaments, appearance of dielec. instability, coexistence with supercond. 80−103784
- GaAs, permittivity at laser transitions freq., excess carriers effect 77−14719
- GaAs, semi-insulating, microwave permitt. meas. 80−60479
- GaAs:Cr, semi-insulating, complex permittivity, 2.5-36 GHz, 300-400K 77−69763
- GaN, preparation variables rel. to dielectric data, GaAs conversion 78−60591
- $Gd_3Ga_5O_{12}$, dielectric constant, effect of degree of purity and perfection 77−48117
- Gd_2O_3, elec. cond., thermoelec. power, dielectric const. 79−69763
- c-Gd_2O_3, electrical cond., dielectric const. mag. susceptibility, polymorphic transition 77−59505
- Ge, dielectric polarisation calcs., microscopic local fields 80−20582
- Ge, dielectric properties, mean point value calc. 78−87930
- Ge:Sb, low-freq., low temp. dielec. behaviour below metal-insulator transition 80−50250
- Ge-S glasses, Cu doped, thermal, structural and dielectric props. 79−60283
- GeH_4, heat capacity, dielectric const., thermodynamic props. 78−83967
- GeS amorphous layers between Al electrodes, dielec. relax. currents, pot. distrib. 77−16250
- GeS, far IR reflectivity spectra, lattice vibr. and dielec. const. 77−52068
- $GeS_{1.5}$:Cu, interpretation of dielectric behaviour 79−33595
- H_2, dielec, const., 4.2-15K 77−8488
- He, dielec. const., 0.8-4.3K 77−8488
- ^4He, liq. and solid, dielec. const. meas. 77−20143
- Hg ultrathin metallic filaments, appearance of dielec. instability, coexistence with supercond. 80−103784
- $Hg_{1-x}Cd_xTe$, anodic oxide films, formation and props. 80−3212
- Hg_2Cl_2, elec., dielec., and thermophysical props. 79−10989
- HgI_2, dielectric const., up to 500 bar, press. depend. 78−27153
- HgI_2, IR lattice vibr. and dielec. dispersion 80−76018
- $HgSb_4S_8$, photosensitive semiconductors with high permittivity, elec. props. 79−65518
- In ultrathin metallic filaments, appearance of dielec. instability, coexistence with supercond. 80−103784
- In-O film, AC behaviour, dielec. relax. 77−52019
- In_2O_3 film, AC behaviour and dielec. relax. 77−52019
- $(K,Na)NbO_3$ ceramic, hot pressed, dielec. props. 79−87375
- $K_xAl_xTi_{8-x}O_{16}$, $1.6 \leq x \leq 2.0$, dielec. response in freq. range 10^{-3} to 10^6 Hz 79−65785
- $K(B_xW_{3-x})O_9$ (B=Na, Ca, Co, Ni, Cd, Ga, Bi, Nb, Ta) cryst. struct., temp. dielec. anomalies 80−1998
- KBr:Se^{2-} single cryst., dielec. relax. of impurity-vacancy dipoles, ITC meas. 79−91349
- $K_2Cd_2(SO_4)_3$, langbeinite type cryst., search for ferroelec. phase transition 77−59535
- KCl far IR complex permittivity meas. by dispersive Fourier transform spectroscopy, 7 to 300K 80−15940

dielectric properties of solids continued

- KCl, γ-irradiation effect on dielectric const. *(Japanese)* 79−51896
- KCl, low temp. space charge polarisation 78−43789
- KCl:Li, $\langle 111 \rangle$ off centre Li^+ under biaxial stress, bistable tunnelling 78−15090
- KCl-KBr, mechanism of aggregation of divalent impurities, dielectric loss meas. *(Japanese)* 79−60394
- KCl_xBr_{1-x}, dielectric const. determ. 80−108145
- KD_2PO_4, order-disorder type ferroelec., HF dynamics 77−39657
- $KDy(WO_4)_2$, Jahn-Teller transition, permittivity behaviour 80−55012
- $K_4Fe(CN)_6.3H_2O$, ferroelec. and paraelec. phases, dielec. props. meas. 80−60494
- $K_4Fe(CN)_6.3H_2O$, Raman spectrum and dielec. relax. 78−19476
- $KFeF_4$, struct. phase transitions obs. by dielec. const. and X-ray diffr. studies 79−95161
- KH_2AsO_4, ferroelec., RF dielec. relax., loss mech. 79−38448
- $K(H_{1-x}D_x)_2PO_4$, ferroelec., complex dielec. const., mm wave meas. 77−1633
- $K(H_{1-x}D_x)_2PO_4$, ferroelec., dielec. susceptibility, pseudo-spin model 77−52024
- KH_2PO_4, critical and tricritical phenomena, susceptibility, exponents 80−75976
- KH_2PO_4 family of crystals, proton modes, dielec. spectroscopy 80−75915
- KH_2PO_4, ferroelec., RF dielec. relax., loss mech. 79−38448
- KH_2PO_4, polarisation echo in ferroelec. phase transition region 79−42920
- KH_2PO_4, RF dielec. response close to transition temp. 77−90099
- KH_2PO_4, spontaneous polarisation, low temp. meas. 80−75921
- KH_2PO_4-KD_2PO_4 mixed cryst., dielec. polarisation, Green's function anal. 77−52011
- KH_2PO_4-type ferroelectrics, dielec. props., four-cluster approx. 80−97202
- $K_3H(SO_4)_2$, and $K_3D(SO_{42})_2$, dielec. props. and phase transitions 80−60482
- $K_2Mg_2(SO_4)_3$, langbeinite type cryst., search for ferroelec. phase transition 77−59535
- $K_{1.6}Mg_{0.8}Ti_{7.2}O_{16}$, solid electrolyte, dielec. response, 5.2-77K 79−56709
- $K_xMg_{x/2}Ti_{8-x/2}O_{16}$, $1.6 \leq x \leq 2.0$, dielec. response in freq. range 10^{-3} to 10^6 Hz 79−65785
- $K_2Mn_2(SO_4)_3$, langbeinite type cryst., ferroelec., phase transitions, dielec., elastic and pyroelec. meas. 77−59535
- $K_2Mn_2(SO_4)_3$, phase transition press. effect, dielectric const. meas. 79−37834
- $K_{1-x}Na_xTaO_3$, quantum ferroelectric, dielec. susceptibility 80−103922
- $KNbO_3$, single cryst., dielec. breakdown and electroluminesc. 78−2917
- $K_5Nd(MoO_4)_4$, dielec. and optical props. 79−33590
- K_2OsCl_6, single cryst. with H^+ interstitials, protonic cond. from dielec. meas. 80−107515
- K_2SO_4, phase transform., mech. of thermal hysteresis, DTA, dilatometry and dielec. meas. 80−75353
- K_3Sb, optical and dielectric props., energy spectra, density of states calcs. 80−20083
- K_2SnCl_6, phase-transition-induced dipolar relax. 80−66107
- $KTa_{1-x}Nb_xO_3$, quantum ferroelectric, dielec. susceptibility 80−103922
- $KTaO_3$, crit. dielec. and optical props. and storage, 4K 77−24805
- $KTaO_3$, dielec. nonlinearity and parametric interactions at low temps. 79−38430
- $KTaO_3$, electromech. props. and electron tunnelling 78−23403
- $KTaO_3$, polarisation, dielectric. const., relax. effects, electret state 77−12302
- $KTaO_3$:Li, polarised cluster stabilisation by Li defects, polar glass form. 79−91342
- $KTaO_3$:Li, susceptibility extrinsic peak, dielectric const. meas. 79−11394
- $KTiF_4$, struct. phase transitions obs. by dielec. const. and X-ray diffr. studies 79−95161
- KVF_4, struct. phase transitions obs. by dielec. const. and X-ray diffr. studies 79−95161
- $K_2Zn_2(SO_4)_3$, langbeinite type cryst., ferroelec., phase transitions, dielec., elastic and pyroelec. meas. 77−59535
- La, $(SO_4)_3.9D_2O$, soln. growth, struct., props. 77−77363
- La_2O_3, elec. cond. and dielec. const., 400-1180K, phase transition 79−56224
- LiD:Mg^{2+}, X-irrad., dielec. loss 80−55024
- LiF films, polycrystalline and single-cryst., comparative study of phonons by electron spectroscopy 80−25505
- LiF, plastic deform. and dielec. losses 78−19410
- Li_2Gd_4 $(MoO_4)_7$, ferroelec. and paramag. props. 78−39517
- Li_2GeO_3, components of elastic, piezoelec. and permittivity tensors meas. 77−8518
- LiH, ionic polarisability in cryst. lattice, quantum mech. model 79−47384
- $Li_{1-x}H_xIO_3$, dielec. behaviour, Raman and IR spectra 77−32357
- α-$LiIO_3$ single crystals, electrical conduction and dielectric behaviour *(Chinese)* 78−30783
- Li_3N, superionic conductor, local ionic motion, anisotropic dielec. behaviour 78−87817
- Li_3N, superionic conductor, cryst. growth and struct., phys. props., book contrib. 79−42308
- Li_3N, superionic conductor, far IR absorption, temp. and isotope effects 79−51969
- $LiNH_4SO_4$ and $LiND_4SO_4$, dielec. pyroelec., and thermal props. 80−60509
- $LiNbO_3$ crystals, activated by $3d^n$ ions, enhancement of polarisation echo 79−38439
- $LiNbO_3$ piezoelectric coeff. and permittivity meas., small-sample method 80−15981
- $LiNbO_3$, polydomain, nonstoichiometric crysts., elastic, piezoelec., dielec. constants. 77−8513
- $LiNbO_3$, powder, polarisation echo, repetitive read out effect 79−82913
- $LiNbO_3$, single crystal, dielectric const., dispersion, loss tangent and susceptibility 77−16245
- $LiNbO_3$, spontaneous polarisation, low temp. meas. 80−75921
- $LiNbO_3:3Li_2O.Nb_2O_5$ eutectic, dielectric props. 79−1743
- Li_2O-B_2O_3 glass, conductivity, permittivity, and dielectric loss obs., mixed isotope effect 78−95182
- $LiTaO_3$-$CaZrO_3$, struct. and dielec. props. 78−80298
- Lu_2O_3, elec. cond. and dielec. const., 400-1180K 79−56224
- Mg-Cu-Mn-Ni-Fe-O, UHF ferrites, synthesis, physicochem. state, mag. and dielec. parameters 79−11536
- MgF_2, complex dielec. const. at audio freqs., 5.5 to 380K 80−25272

dielectric properties of solids continued
MgF_2 film, crystn., AC glec. props. 78−2804
MgF_2:LiF crystal, defect struct., anelastic and dielec. relax. meas. 77−27938
MgO, dielec. const., 5.5 to 400K 80−50249
MgO, dielectric behaviour 79−91343
MgO, dielectric polarisation calcs., microscopic local fields 80−20582
MgO, dielectric properties, mean point value calc. 78−87930
MgO:Li^+, quenched, elec. polarisation, thermal depolarisation and dielectric loss meas. 79−1738
5 wt.% MgO-Si_3N_4, hot-pressed, dielec. props. 78−10822
Mg_2SiO_2:SiO_2, elec. and dielec. props. 400-900°C 80−104953
$Mg_{0.25}Zn_{0.75}Fe_2O_4$, ferrite, DC cond., dielec. props., lattice consts. 80−80272
MnO, dielec. behaviour, Dick and Overhauser shell model calcs. 80−45001
MnZn ferrite, mag. relax., permeability and loss tangent determ. at 4.2 to 300K 77−32263
$Mo_6Cl_{10}S$, struct., dielec. and diamag. props. *(French)* 78−67691
$Mo_6Cl_{10}Se$, struct., dielec. and diamag. props. *(French)* 78−67691
$Mo_6Cl_{10}Te$, struct., dielec. and diamag. props. *(French)* 78−67691
$ND_4D_2PO_4$, cryst., transverse and longit. elec. susceptibilities, modified Ising model calcs. 80−97203
$(ND_4)_3D(SeO_4)_2$, phase transitions, isotope effect, dielectric and dilatometric meas. 79−38500
NH_4 halides dielectric const. meas. at 1 MHz 77−16238
$NH_4Al(SO_4)_2.12H_2O$, dielectric losses, proton spin lattice relaxation by NH_4^+ hopping 79−56721
$(NH_4)_2BeF_4$, effect of surface layer on spontaneous polarisation 79−38445
$(NH_4)_2BeF_4$, far-infrared and submillimetre dielectric response 80−80782
$(NH_4)_2BeF_4$, incommensurate phase superstructure, linear and nonlinear cryst. optics *(Russian)* 80−14387
$(NH_4)_2BeF_4$, polycrystalline, surface layer effects on dielec. behaviour 78−39494
$(NH_4)_2Cd_2(SO_4)_3$, dielec. and spontaneous polarisation, −195 to −180°C, particle size depend. 80−97200
NH_4Cl, doped and undoped, spontaneous polarisation at order-disorder phase transition 80−25281
NH_4Cl, pure and NH_3 and $NiCl_3$ doped, TSC obs. of polarisation 79−78618
NH_4Cl:$[MoOCl_5]^{2-}$, single cryst., struct. investigations 77−66524
$NH_4Cl_{1-x}Br_x$, dielectric const. meas. at 1 MHz by immersion method *(Japanese)* 77−90087
$NH_4Cl(Br)(I)$, dielectric const. meas. at 1 MHz by immersion method *(Japanese)* 77−90087
$NH_4H_2PO_4$, cryst., transverse and longit. elec. susceptibilities, modified Ising model calcs. 80−97203
NH_4HSO_4, dielectric relax. in ferroelectric and paraelectric phases 77−16246
NH_4HSO_4, ferroelec., critical slowing down of dielec. relax. *(Japanese)* 77−90109
$(NH_4)_3H(SO_4)_2$, press.-induced ferroelectricity, dielec. const. meas. 77−12328
NH_4HSeO_4, cryst. struct., dielec. and ferroelec. props. 80−60528
NH_4HSeO_4, ferroelec., phase transitions, permittivity and pyroelectricity meas. 80−71350
$(NH_4)_3H(SeO_4)_2$, ferroelec. phase transition, dielec. meas. 77−63376
$NH_4IO_3.2HIO_3$, dielec. constant, elec. cond. phase transition and cryst. struct. 80−1999
$(NH_4)_{2(1-x)}Rb_{2x}SO_4$, mixed crystal, dielectric and US meas. of ferroelec. phase transition *(Japanese)* 80−7305
$(NH_4)_2SO_4$, ferrielec., dielec. behaviour and nature of phase transition 78−88262
$(NH_4)_2SO_4$, static and dynamic dielec. behaviour 80−71337
$(NH_4)_6Sb_4(SO_4)_3F_{12}$, dielec. props. and phase transitions 79−69765
$(NH_4)_2SiF_6$, low-temp. dielec. loss maxima in cubic and trigonal crysts. 79−19831
NH_4X, X=halogen, phonon dispersion, cohesive and dielec. props. in three body force shell model 80−79892
NaA zeolite, dielectric polaris., cation distrib. *(French)* 79−51903
$NaBi(MoO_4)_2$, low-temp. paraelectric, permittivity meas., 4.2-400K 79−95702
NaCl, dielectric polarisation calcs., microscopic local fields 80−20582
NaCl, dielectric properties, mean point value calc. 78−87930
NaCl, dipole polarisation, depend. on AC and DC voltage superposition 80−20577
NaCl, interfaced polarisation and losses, superimposed AC and DC voltage study 80−25276
NaCl, low temp. space charge polarisation 78−43789
NaCl, plastic deform. and dielec. losses 78−19410
NaCl:Ca, aggregation and precip. hardening in impurity vacancy, dipole decay 80−16322
NaCl:Ca^{2+}, dipole concs. determ. considering aggregation, expt. and theoretical comparison 80−59512
NaCl:$CaCl_2$, quenched, aggregation process of Ca^{2+} ion-vacancy dipole, elec. cond. and dielec. loss meas. 77−80535
NaCl:Cd^{2+}, dielectric loss following plastic deform. 80−84690
NaCl:Mn, impurity-vacancy dipole aggregation, role of dimers and trimers, reanal. of dielec. and cond. data 79−1458
NaCl-type crystals, ionic polarisabilities, pseudopot. calc. 80−88913
Na_2CoGeO_4, single cryst. growth and study of their piezoelec. and elastic props. 79−4906
NaF:Ca, migration enthalpy and entropy, TSC obs. 80−54716
Na_2HAsO_4, hydrogen bonded, ^{75}As NQR study 79−38399
$Na(H_{1-x}D_x)_3(SeO_3)_2$, ferroelectric, dielectric behaviour at RF and microwave freq. 79−33640
$Na_{1-x}Li_xNbO_3$ mixture, ferroelec.-paraelec. transitions, dielec. props. meas. 80−66125
$NaNO_2$, complex dielectric constant, sinusoidal phase in ferroelectric material 79−11376
$NaNO_2$, ferroelec., dielec. and thermal behaviour 80−80680
$NaNO_2$, ferroelec., X-ray diffr. topographic study of polarisation reversal 79−38441
$NaNO_2$, nonlinear dielec. anomaly in paraelec. phase 78−39495
$NaNO_2$ powder, surface layer effects on dielec. props. 77−1631
$NaNO_3$, dielec. loss anal., Debye type loss peaks 80−50260
$NaNO_3$, low temp. struct. changes, elec. props. 79−87377
Na_2O-SiO_2 glass, conduction and dielec. loss mechanisms, paired interstitialcy model 80−107468

dielectric properties of solids continued
Na_2O-TiO_2-SiO_2 glass, elec. props. and energy gap 78−26921
Na_2SO_4, high temp. phase, DTA and dielec. meas. 79−82333
$Na_3Sc_2P_3O_{12}$, fast-ion conductor, struct. phase transition 80−88362
$Na_{0.33}V_2O_5$, dielec. const. and microwave cond. 78−60378
$Na_5W_3O_9F_5$, phase transitions obs. *(French)* 80−6516
$Na_5W_3O_9F_5$, single cryst., prep., optical and dielec. studies *(French)* 80−15994
Nb, anodic oxidation, open circuit transient anal., dielec. and elec. props. of oxide film 80−3245
$NbSe_3$, freq. depend. conductivity 80−107838
$NdAlO_3$ films, preparation, electrophys. props. in MIM structs. 77−24956
Nd_2O_3, elec. cond., thermoelec. power, dielectric const. 79−69763
$Nd_2(WO_4)_3$, elec. transport and mag. props. meas. 77−24668
Ne, dielec. const., 4.2-15K 77−8488
Ni-Zn ferrites, hot-pressed, key props. 78−15348
NiBr boracite single crystals, dielectric, pyroelectric props., vapour phase transport growth 80−80673
NiO, dielec. behaviour, Dick and Overhauser shell model calcs. 80−45001
NiZn ferrite, dielec. props., Jahn-Teller ion effects 80−97181
PLZT ceramic, ageing, dielec. props. 80−88940
PLZT ceramic, optical gate, dielec., optical props., electro-optical effect meas. 78−42418
PLZT ceramics, modified by $Ca^{2+}(Sr^{2+})(Nd^{3+})(Y^{3+})$, dielec. behaviour 80−60519
PLZT, diffuse phase transitions, Curie temp., dielectric props. 80−75979
PLZT, reduced, exam. of ageing phenomena, using dielectric hysteresis *(German)* 79−33647
PLZT, with broad phase transition, birefr., electro-optic and dielec. props. 77−16280
P_2O_5-MO-Al_2O_3, (M=MgO, CaO, SrO, BaO) (45, 5 wt.%) glass, electron irradiation effect on dielec. props. 80−29056
$(Pb,Ba)_5Ge_3O_{11}$ ferroelectric crystals, influence of Pb replacement by Ba on props. 79−87402
$(Pb,Ba)(Zr,Ti)O_3$, diffuse phase transitions, Curie temp., dielectric props. 80−75979
$(Pb,La)TiO_3$, paraelec. phase, anomalous dielec. behaviour 78−23387
$(Pb_{1-x}Ba_x)_5Ge_3O_{11}$, ferroelec. transition blurring, US relax., dielec. and opt. props. 78−95559
$(Pb_{1-x}Ba_x)_5Ge_3O_{11}$, ferroelec. phase transition, dielec. const. and quasi-elastic light scatt. 80−71289
Pb_2CrO_5, thermal X-ray and dielec. investigations 79−47403
$Pb(Fe_{1/2}Nb_{1/2})O_3$-$La_2O_3(CeO_2)$ ferroelec. ceramics, electrophysical props. 78−35099
$PbFe_{2/3}W_{1/3}O_3$-$BaTiO_3$ system ferroelec., antiferromag., ESR and dielec. props. meas. 77−40172
$Pb_3Fe_2WO_9$, perovskite ferroelec., characts. of dielec. polarisation 77−8496
$Pb_3(Ge,Si)_2O$, growth from melt, struct. and dielec. props. 77−44148
$Pb_5(Ge,Si)_3O_{11}$, dielec. and elec. props., 20 to 250°C 80−29697
$PbGeO_3$, single cryst. films growth, temp. depend. of dielec. constant 79−100066
$Pb_3Ge_3O_{11}$, uniaxial ferroelec., thermal expansion and dielec. permittivity in vicinity of transition points 77−66459
$Pb_5Ge_3O_{11}$, ferroelec., surface capacitance effect on dielec. props., DC cond. and dielec. const. meas. 79−91333
$Pb_5Ge_3O_{11}$, photodielectric effects, Curie temp., permittivity and polarisation 80−40034
$PbHAsO_4$, ferroelec., far IR and microwave dielec. props. 80−55108
$PbHPO_4$, crystals, ferroelec. phase transition, hydrostatic press. influence, dielec. meas. 80−88936
$PbHPO_4$, microwave permitt. and far IR refl. spectra in paraelec. and ferroelec. phases 80−40033
$PbHPO_4$, single cryst., dielec. props. 79−38426
PbI_2, complex dielectric and optical consts., ellipsometric determ. 78−23425
PbI_2(2H and 4H), layer cryst., elec. field effect on NQR, elec. polarisation mechanism 77−20746
$PbLaZrNbO_7$, dielectric with zero temp. coeff. of dielect. consts., electrophys. props. 77−52010
Pb_2MTeO_6, (M=Ca,Cd,Mg), ferroelec. behaviour, microwave dielec. props. meas. 77−43948
$Pb(Mg_{1/3}Nb_{2/3})O_3$:$PbTiO_3$, ceramic dielectric, electrostriction, relaxation, polarisation 80−80700
$Pb(Mg_{1/3}Nb_{2/3})O_3$-$Pb(W_{1/2}Mg_{1/2})O_3$, struct. and dielec. props. 80−25312
$Pb(Mg_{0.5}W_{0.5})O_3$-$BiFeO_3$, dielec. props., cryst. struct. 78−84534
$Pb(Mn_{1/2}Ta_{1/2})O_3$, ceramic, for thermal and dielectric isolation at low temp. 80−39365
PbN_x, pressed, lag time of breakdown and dielec. strength 77−36174
$Pb(NO_3)_2$, low temp. struct. changes, elec. props. 79−87377
$PbNbO_3$ thin film microwave complex permittivity meas. 79−73879
$PbNb_2O_6$, ferroelectric strain polarisation interaction, domain wall formation 79−56750
$PbNb_2O_6$, O defects and elec. props. anomalies 79−42898
$Pb_2Nb_2O_7$, electric cond. and dielect. props. of cathodic-sputtered films *(French)* 79−33371
$PbNb_{0.5}Sc_{0.5}O_3$, ceramic, dielec. props. 79−11392
PbO layers on Pb films, optical props. 79−83042
PbO-SiO_2 glasses, elec. cond. and dielec. behaviour 80−44361
3PbO.2GeO, TSC in thermoelectret state during ceramic synthesis, pyroelec. currents and energy struct. of capture centres 80−55014
$15PbO.3B_2O_3.2WO_3$, struct. and electrophys. characts. 77−84716
$Pb_3(PO_4)_2$ ferroelastic, dielec. consts. and birefringence meas. 78−2793
$Pb_{1-\alpha x}R_xTiO_{3+x(1.5-\alpha)}$, R=La or Sm exam. of permittivity as function of temp. 79−33586
PbS(Se)(Te), energy gap and dielec. props., 77 to 373K 80−66100
$Pb_6Sb_{14}S_{27}$, zinkenite, electrophysical properties 78−34834
$PbSc_{0.5}Nb_{0.5}O_3$, single cryst., dielec. props. 80−66126
$Pb_{1-x}Sn_xTe$, soft mode, ferroelec. phase transition crit. temp. and dielec. const. calcs. 77−8530
$Pb_{0.94}Sr_{0.06}(Ti_{0.47}Zr_{0.53})O_3$-NiO, modified, dielec. and piezoelec. props. 80−11342
$Pb_{0.95}Sr_{0.05}(Ti_xZr_{1-x})O_3$, solid solns., parameters of Curie Weiss law, permittivity meas. 78−15129
$(Pb_{0.97}Sr_{0.03})Zr_{0.51}Ti_{0.49}O_3$, ferroelec. phase transition under high press. 77−36188
$Pb_2Ta_{2-x}M_{2x}O_{7-x}$, (M=Ti, Sn Zr), oxygen deficient, form., IR spectra, dielec. const. *(Japanese)* 77−48171

dielectric properties of solids continued
Pb_2TaMnO_6, reaction of form. from oxides, ferroder. props. 80—55326
p-PbTe, lattice dielectric const. in far IR region, magnetotransmission meas. 79—78605
$PbTiO_3$, cryst., polarisation and resistivity, elec. field effects 78—64313
$PbTiO_3$, ferroelectric ceramic, dielec., piezoelec. and elastic props., orientational contrib. 78—68468
$PbTiO_3$ ferroelectric thin films, fabrication by RF sputtering, characts. 80—40261
$PbTiO_3$, mechanical twinning, spontaneous polarisation shielding 79—42930
$PbTiO_3$-$PbZrO_3$-$PbNb_{2/2}Zn_{1/3}O_3$(-$PbNb_{2/3}Co(Mg)_{1/3}O_3$) solid solutions, dielec. and piezoelec. props. 79—87393
$Pb_3(VO_4)_2$-$Pb_3(PO_4)_3$ solid solutions, ferroelastic, dielec. consts. and birefringence meas. 78—2793
$Pb_3(VO_4)_3$, ferroelastic, dielec. consts. and birefringence meas. 78—2793
$Pb_{1.8}Zn_{0.15}Na_{0.05}Nb_2O_{6.95}F_{0.05}$, electric cond. and dielect. props. of cathodic-sputtered films *(French)* 79—33371
$Pb(Zr,Ti,Sn)O_3$ ceramics, ferroelec., doped with tri- and pentavalent oxides, piezoelectric props. 78—19413
$Pb(Zr,Ti)O_3$ ceramic-polyvinylidene fluoride composite film, complex piezoelec. props. 78—64323
$Pb(Zr,Ti)O_3$ ceramic, interconnected porous, props. 80—43579
$Pb(Zr,Ti)O_3$ ceramics with ladder type struct., prep. and props. 80—75945
$Pb(Zr,Ti)O_3$, dielectric thin film, geometry effect on props. *(Russian)* 77—90102
$Pb(Zr, Ti)O_3$, ferroelectric ceramics in solid matrix, temp. and quasi-hydrostatic pressure effects 77—16259
$Pb(Zr,Ti)O_3$, porosity-permittivity relations, depolarising factors determ. and pore effects *(Japanese)* 80—97189
$Pb(Zr,Ti)O_3$ pyroelectric ceramics 79—47649
$Pb(Zr,Ti)O_3$ thin film, ferroelec., fabrication by RF sputtering *(Japanese)* 80—25560
$Pb(Zr,Ti)O_3$:Cr_2O_3 ceramic, electrical cond. and dielectric const. meas. 80—2389
$Pb(Zr,Ti)O_3$:Mn ceramics, anomalous dielec. losses 79—42892
$Pb(Zr,Ti)O_3$-$Pb_3Ge_5O_{11}$ ceramic, sintering conditions rel. to piezoelec., dielec. props., microstruct. 77—16252
$PbZrO_3$ based ferroelec. ceramic, pressure-temp. phase diagrams 79—24273
$Pb(Zr_xTi_{1-x})O_3$ films, ion beam deposition, struct., dielec. and ferroelec. props. 80—20788
Pd, dielec. screening and phonon frequencies using isotropic noninteracting s-d-band model 79—19343
$Pn_2Nb_2O_7$, relax. phenomena, meas. of dielec. const., polarisation and sp. ht. 77—4597
$Pr(NbO_3)_3$ form. mechanism, struct., dielec. props. 77—16235
Pr_6O_{11}, mag. and transport props., multiphonon hopping conduction 78—19211
Pt, dielec. screening and phonon frequencies using isotropic noninteracting s-d-band model 79—19343
$RbAg_4I_5$, single cryst., dielectric relax. *(German)* 79—4764
$Rb(B_xW_{3-x})O_9$ (B=Na, Ca, Co, Ni, Cd, Ga, Bi, Nb, Ta) cryst. struct., temp. dielec. anomalies 80—1998
RbBr:Ba^{2+},Sn^{2+}, thermal depolarisation meas., relax. processes 78—23389
$Rb_2Cd_2(SO_4)_3$, pyroelectric and dielectric props., ferroelectric transitions 79—38458
RbCl:Co^{2+}, dielectric loss, impurity sites 79—91348
RbCl:Li^+, new off-centre defect system, studied with dielec. techniques under hydrostatic press. 79—19834
$RbFeF_4$, two dimensional structural phase transitions, sp. ht., optical, dielec., X-ray diffr. meas. 79—69240
RbH_2AsO_4, phase transition, dielec. pyroelec. and internal friction meas. 77—16261
RbH_2PO_4, critical and tricritical phenomena, susceptibility, exponents 80—75976
$RbHSO_4$, ferroelec. with small Curie-Weiss const., dielec. props. 78—39496
$Rb_3H(SO_4)_2$, and $Rb_3D(SO_4)_2$, dielec. props. and phase transitions 80—60482
$RbHSeO_4$, ferroelec. props. and domain struct. 79—78637
$Rb_3H(SeO_4)_2$, phase transitions, dielec. behaviour 79—90777
$RbLiSO_4$, thermal and dielectric props., ferrielectricity 79—28688
$Rb_2Mg_2(SO_4)_3$, langbeinite type cryst., search for ferroelec. phase transition 77—59535
$RbNO_3$, single cryst., DC cond., dielec. and thermophys. props., temp. depend., transitions interpret. 78—26682
Rb_2SO_4-$(NH_4)_2SO_4$ mixed cryst., ferroelec. transition, structural and dielec. props., proton spin-lattice relax. 78—39512
$Rb_6Sb_4(SO_4)_3F_{12}$, dielec. props. and phase transitions 79—69765
rubber, gamma radiation effects on dielect. parameters, expt. *(Hungarian)* 78—59836
SSe_9, stable thermoelectret, effects of anisotropic external perturbation *(Russian)* 77—63361
$Sb_{1-x}Bi_xSI$, mixed cryst., ferroelec. phase transition 79—33629
Sb_2S_3, thin film, dielectric props. 79—15392
SbSI, aggregates of needle-like crystals, nonstoichiometric, ferroelectric properties *(Japanese)* 78—43821
SbSI, central mode, microwave freqs. 79—19852
SbSI, ferroelec., dielec. props. 79—38428
SbSI, ferroelec. semicond., influence of internal fields on polarisation reversal process 79—38443
Sb_2Se_3 single crysts., phys. prop. anomalies, 400-450K *(German)* 79—38072
Se, amorphous, TSC, dielec. relax. modes 77—90090
Se amorphous layers, dielectric relax. in glass transition range, ageing 79—82923
Se and Se-As, amorphous, dipolar activity at glass transition temp., AC method 77—66454
Se film, amorphous, empirical formula for temp. depend. of dielec. loss peak 80—97197
Se:Tl, and undoped material, dielec. losses and permittivity meas. 77—28518
Se-Ge-Te glass, dielectric meas. 79—87382
Si, amorphous film, electron beam evaporated, freq.-depend. dielec. behaviour 79—99549
Si, complex permittivity and cond., microwave meas. 79—65784
Si, dielectric polarisation calcs., microscopic local fields 80—20582
Si, dielectric properties, mean point value calc. 78—87930

dielectric properties of solids continued
Si oxide film, porous Si layer oxidation, dielec. props. 80—55556
Si-CaF_2 film, dielectric const. and selective solar absorption 78—2937
Si-MgO film, dielectric const. and selective solar absorption 78—2937
Si-SiO_2-polySi thin film structures, dielectric props. *(Slovak)* 80—75934
$Si_{(6-z)}Al_zO_zN_{(8-z)}$, sialons, hot-pressed, dielec. props. 78—10822
$Si_{6-x}Al_xO_xN_{8-x}$, x=1.5, 3, 4, Sialon ceramics, elec., thermal cond. 79—33124
$Si_{100-x}Au_x$, amorphous, dielec. anomaly, rel. to nonmetal-metal transition 78—2791
Si_3N_4, hot-pressed, dielec. props. 78—10822
SiO-B_2O_3 composite dielec. films, EPR, dangling bonds and dielec. loss 80—11246
SiO_2 film, thermally grown, pore size influence of punch-through voltage 78—6632
SiO_2 films, thickness and dielectric const., elec. cond. mech. *(Japanese)* 79—8084
SiO_2, fused, as-received and irrad., dielectric props. 79—65786
SiO_2, hydrated vitreous, spectrum of low-energy dipolar states, dielec. const., dielec. losses and relax. 77—90098
SiO_2 layers, dielectric strength, dislocation effect 78—31154
SiO_2, stoichiometric condensate form. during electron beam evaporation of quartz, electrophysical props. 77—16496
SiO_2, thin film, prep. from low-temp. oxidation of tetraisopropoxysilane, dielec. props. 77—8759
SiO_2, vitreous, dielec. absorpt. saturation, 0.4-8K 78—23394
SiO_2, vitreous, effect of neutron irrad. on low temp. dielec. susceptibility 79—73878
SiO_2:OH^-, vitreous, elec. dipolar echoes 78—52430
SiO_x, dielec. and optical props., chemical disorder effects 80—80815
SiO_x film, MIM struct., DC bias dependent dielectric dispersion props. 78—76178
Sm_2O_3, elec. cond., thermoelec. power, dielectric const. 79—69763
α-Sn, dielectric polarisation calcs., microscopic local fields 80—20582
α-Sn, dielectric properties, mean point value calc. 78—87930
Sn ultrathin metallic filaments, appearance of dielec. instability, coexistence with supercond. 80—103784
$SnCl_2.2H_2O$, layered, dielectric anomaly calc. using Ising model, possibility of antiferroelectricity 77—12341
SnS(Se), IR reflectivity and Raman spectra, phonon frequencies and dielec. const. 77—48166
SnSe, far IR reflectivity spectra, lattice vibr. and dielec. const. 77—52068
$Sr_{0.5}Ba_{0.5}Nb_2O_6$ crystals, ferroelec., dislocation free, pyroelec. props. 79—42907
$Sr_{0.75}Ba_{0.25}Nb_2O_6$, ceramic ageing dielec. props. 80—88940
SrClF, SrBrF, reacted flux growth, dislocation density, dielec. consts. and losses IR spectra 77—36214
SrF_2, dielec. const., 5.5 to 400K 80—50249
SrF_2, electronic polarizability and dielectric const., strain derivatives 78—19406
SrF_2:La, type-I dipole reorientation, activation vol. determ. from dielec. const. 80—88916
SrF_2:Na^+, cryst., thermal depolarisation 79—82912
$Sr(NO_3)_2$, low temp. struct. changes, elec. props. 79—87377
$Sr_4NaLiNb_{10}O_{30}$, electro-optic, pyroelec., dielec. and piezoelec. props. *(Chinese)* 79—69810
$Sr_2Nb_2O_7$, phase transition at 215°C, physical props. obs. 79—56744
SrO, dielectric behaviour 79—91343
SrS, dielectric behaviour 79—91343
$SrTiO_3$, crit. dielec. and optical props. and storage, 4K 77—24805
$SrTiO_3$, dielec. nonlinearity and parametric interactions at low temps. 79—38430
$SrTiO_3$, dielec. props. in microwave region, 4.2-78K 77—16239
$SrTiO_3$ film, behaviour of ferroelecs. in strong elec. microwave field 79—42884
$SrTiO_3$ glass ceramics, polarisation and dielec. const., 4-77K 77—32319
$SrTiO_3$, impure, low temp. polarisation, thermoelectret state 77—12301
$SrTiO_3$, intrinsic quantum paraelec. below 4K, dielec. const. meas. 79—73877
$SrTiO_3$-$Bi_2Ti_2O_7$-$CaTiO_3$ system, solid solns., elec., optical props. 79—11375
$SrTiO_{3-x}$-In contacts, differential capacitance, elec. field depend. permittivity effect 80—54779
TGSe:D,L-α-alanine crysts. with large unipolarity, dielec., piezoelec., elastic props. and internal friction 79—33615
Ta_2O_5, anodic, on sputtered Ta_2N, dielec. props., 20-10^5 Hz, 150-500K 79—87386
Ta_2O_5, elec. props. as dielec. in Ta solid dielectric capacitor *(Spanish)* 78—19405
Ta_2O_5, film, dielec. props. meas., two layer Maxwell-Wagner model 78—76373
Ta_2O_5 film, temp. and time characts. of breakdown *(Russian)* 77—55751
TeO_2-WO_2 glass, dipole correlations, capacitances and TSC meas. 79—28670
Ti-Al_2O_3 system mixed films, prep., phase comp., struct. and elec. props. 79—37930
TiO_2 based ceramic dielec. materials, medium permittivity, elect. charact. 78—35086
TiO_2, nonstoichiometric rutile, dielec. props. 10 Hz to 30 kHz 77—28507
TiO_2, porosity-permittivity relations, depolarising factors determ. and pore effects *(Japanese)* 80—97189
TiO_2 rutile, dielec. const., 10^2-10^7 Hz, DC bias effect 79—78603
TiO_2, rutile, ferroelectric ceramic, dielec., piezoelec. and elastic props., orientational contrib. 78—68468
TiO_2, sintered ceramic, props. rel. to additives, impurities 78—35329
TiO_2-Fe_2O_3-CaO-V_2O_5 system ferrites, TiO_2 content and thermomag. effects on dielec. props. 77—43927
Tl halides, static dielec. constant, strain derivatives 80—100629
Tl halides, strain derivatives of elastic and dielectric consts. 79—60421
TlBr, dielectric behaviour under hydrostatic press. 78—52420
TlCl, dielectric behaviour under hydrostatic press. 78—52420
TlCl-TlBr, single cryst., composition determ. by reflection spectrophotometry 77—1961
TlCl(Br)(I), static polaris. and effective charge parameters, Born-Mayer pot. 77—31628
TlH_2PO_4 and TlD_2PO_4, press. effect on dielec. props. 79—99832
TlH_2PO_4 and TlD_2PO_4, dielec. props. under hydrostatic press. up to 7 kbar 80—29696
TlI:Cs, dielectric const. temp. and freq. depend. 77—32315

dielectric properties of solids continued
- $TlNbO_3$, ceramics, hysteresis loops and dielec. props. 79—42885
- $Tl_xNbO_{2+x}F_{1-x}$, pyrochlore phase, Tl^+ mobility 79—95209
- $TlTaO_3$, ceramics, hysteresis loops and dielec. props. 79—42885
- $Tl_2Ti_4O_9$ ceramics, hysteresis loops and dielec. props. 79—42885
- V, dielec. screening and phonon frequencies using isotropic noninteracting s-d-band model 79—19343
- VO_2, elec. cond. and dielec. props. 79—11379
- VO_2 film, optical and elec. props., 0.8 to 4.2 mm, near metal-semicond. transition 77—32473
- V_2O_5, dielec. polarisation, permittivity meas., 50-200K *(Russian)* 78—39498
- V_2O_5, ferroelec. semicond., dielec. and elec. meas. 80—60516
- V_2O_5-$In(Tl)_2O_3$, ceramic, elec. resist., dielec. props., porosity 77—8093
- V_2O_5-MoO_3-P_2O_5 glass, semicond., DC cond., dielec. props 79—91044
- V_2O_5-P_2O_5 glass, dielec. relax. mechanism, SDRC investigation, Schottky barrier formation in metal-glass-metal systems 78—60388
- V_2O_5-P_2O_5 glass, in metal-semicond.-metal struct., TSC of dielec. relax. *(Russian)* 77—35998
- W, anodic oxidation, open circuit transient anal., dielec. and elec. props. of oxide film 80—3245
- W-MgO cermet film, dielectric const. and selective solar absorption 78—2937
- WO_3-P_2O_5 glass, AC cond. and dielec. props. 80—92717
- Y, reflectivity spectrum, 3.5 to 30 eV dielectric function and plasmons 77—44014
- YIG, elec. props. 79—99552
- Y_2O_3-AlN-SiO_2 oxynitride glasses, elec. props. 80—80267
- Y_2O5d3 films, preparation, electrophys. props. in metal-oxide-metal structs. 77—24956
- Yb_2O_3 film, amorphous, electron beam deposited, dielec. props. 79—91339
- $Zn_{1-x}Cd_xS$ films, polycryst., reactively sputtered, MSM struct. obs. of dielec. props. and cond. mechanism *(French)* 78—14841
- ZnO ceramic varistors, trapping by localized states, effect on dielec. and elec. props. *(Russian)* 79—28671
- ZnO, doped, dielec. losses 77—81049
- ZnO, elastic, piezoelec. and dielec. props. 80—108157
- ZnO non-ohmic ceramic, degradation props. under AC and DC bias 80—80262
- ZnO particles, average dielectric const. generalised theory, appl. to IR spectra 79—28667
- ZnO-based nonohmic ceramic, dielec. dispersion and equiv. circuit 77—73110
- ZnO-Bi_2O_3-CoO-MnO-Sb_2O_3 (97.5, 0.5, 0.5, 1.0 mole%), exam. of elec. props. at different annealing temps. 80—3099
- ZnS:Cu powder exam. of dielectric constant anomaly, in terms of polarisation catastrophe phenomena 79—51897
- ZrF_4 based glass, elec. and dielec. props. in freq. and temp. ranges 5-500 kHz and 130-280°C *(French)* 79—23772
- ZrO_2 film, CVD from organometallic cpds. and characterisation 78—23626

dielectric properties of substances
- *see also antiferroelectricity; dielectric depolarisation; dielectric function; dielectric materials; dielectric measurement; dielectric phenomena; dielectric polarisation; dielectric properties of gases; dielectric properties of liquids and solutions; dielectric properties of solids; electric strength; optical susceptibility; permittivity; piezoelectricity; pyroelectricity*
- adsorbed layers near λ-transition, thermodynamic relns. of Pippards type for dielectric and mag. props. 78—79881
- biological, dielectric constant meas. 80—94417
- biological substances, tabulation for freq. range 10 kHz to 10 GHz 80—108143
- E.coli suspensions, dielec. anal., interfacial polarisation theory appl. 80—97876
- electrostatic props., theoretical 77—63365
- flexoelectricity of liquid crystals, microscopic interpretation 77—32339
- inhomogeneous dielectric, EM wave scatt. and propag., Born approx. 79—41308
- polyvinyl alcohol, hydrocarbon suspension, temp. depend. of electroviscous effect and dielectric parameters 79—79299
- relativistic quantum electron gas, dielec. permeability rel. to thermonuclear reactions *(Russian)* 77—17350
- starch, hydrocarbon suspension, temp. depend. of electroviscous effect and dielectric parameters 79—79299
- tissue, in vivo meas. 10 MHz to 6 GHz 77—78071
- SiO_2 gel, hydrocarbon suspension, temp. depend. of electroviscous effect and dielectric parameters 79—79299

dielectric relaxation
- *see also dielectric resonance*
- acrylic ester polymer networks, low temp. dielectric relaxation 77—36172
- adsorbed layers, Maxwell Wagner and Debye processes, differentiation using temp. depend. of dielec. loss 79—28195
- adsorbed water, detection of OH groups for adsorption centres in plant tissues, dielectric relaxation *(Japanese)* 80—7999
- β-alanine, aq. soln., dielectric relax. spectrum, Debye domains 77—8498
- albumin, bovine serum, in soln., five-component dielec. dispersion 78—15759
- alcohols, aliphatic, permitt., dielec. relax., time-domain multiple refl. meas. 77—57350
- alcohols, dil. solns., dielec. loss and relax., microwave and sub-mm. wave absorpt. obs. *(German)* 78—23396
- alcohols in solution, dielectric relax. depend. on conc. 77—1636
- aliphatic, in dil. solns., dielectric relax. dipole reorientation, rot., microwave obs. 77—28516
- aliphatic esters, mol. dielec. relax. in soln. 79—82918
- aliphatic ethers, dil. solns., dielec. loss meas. for dielec. relax. 78—68451
- alkali borate and phosphate glasses, mech. and dielec. relaxs. and interpet. 78—27159
- alkali halide:Me^{2+}, nearest-neighbour theory of dipole polarisation and depolarisation, cation vacancies 77—16243
- alkali halide, cation motion energy parameters, dielectric relax. meas. 78—30784
- alkali halide, divalent metal doped, dipolar relax. induced by AC field in various crystallographic directions 79—19833
- alkali halides, doped, AC field induced impurity-vacancy dipole relax. 79—11385
- alkali halides, impurity-vacancy dipoles, activation energy 79—33013
- alkali halides, thermally stimulated depolarisation of NCO^- centres 80—80678

dielectric relaxation continued
- alkali metal metaphosphate glass, dielec. relax. at medium temp. 79—24257
- alkali metal-ammonia solns., metal-insulator transition, h.f. and u.s. props. 77—1369
- alkaline earth fluoride, doped with trivalent rare earths, migration entropy for bound fluorine motion 80—71303
- alkyl halide, amorphous, depolarisation thermocurrents and dielectric relaxation time distrib. *(French)* 80—60490
- alkyl halides, depolarisation thermocurrent obs. of main relax. around glass transition 78—27158
- 4′-n-alkyl-4-cyanobiphenyls, dielec. dispersion 78—2798
- allyl ether, dielectric relaxation obs. at millimetric wavelengths 80—71311
- aminobenzotrifluoride, benzene soln., permittivity and dielec. loss 78—64320
- 4-aminophthalimide soln., fluoresc. nanosec. kinetics, dielec. relax. 79—78737
- aminopyridines, in 1,4-dioxane soln., dielec. consts., losses and relax. 78—64319
- amorphous dielectrics, universal relaxation time at low temp. 80—55026
- amorphous polymer multiple dielectric relaxation, time-correlation function representation 80—15951
- aniline, in benzene, polar dielectric system, RF cond. and dipole moment 78—2788
- anilines, substituted, in benzene, dielectric relax. and mutual viscosity, obs. 79—38449
- anilines, substituted, in benzene soln., dielectric relax. time, dipole moment 80—50259
- apatites, dipolar reorientations, TSD study 80—107068
- aromatic aldehydes, in polystyrene matrix, group relax., weight factor effects determ. 78—68446
- aromatic butadienes, dipole moment and dielectric relax. meas. 80—83516
- aromatic ethylenes, dipole moment and dielectric relax. meas. 80—83516
- associated liquids, correl. between dielec. and acoustic relax. times 78—9925
- asymmetric top rotational Brownian motion and electric polarisation calc. 80—15949
- benzaldehyde, in polymer matrix, dielec. absorption, Eyring parameters 79—4761
- benzene sulphonyl hydrazine, in nonpolar solvent, thermodynamics of dipolar relax. 79—91347
- benzene-hexafluorobenzene, mixtures, dielectric relax. and US absorpt. 77—12307
- benzenes, nitrohalide substituted, microwave absorpt., mol. struct. 78—75522
- benzenes, substituted, cryst., reorientation motion, site models with nonequivalent sites, dielec. relax. 79—11382
- benzenes, substituted, dielectric absorpt. and NMR 78—88251
- benzophenone, in o-terphenyl soln., dielectric absorp. studies, molecular relax. 78—95544
- benzothiazole, dielec. loss, relax. and const. in liq. and soln. 79—91346
- benzoylacetone, dil. soln. in benzene, dielectric behaviour 79—42886
- benzoylacetones, p-substituted, dil. soln. in benzene, dielectric behaviour 79—42886
- benzyl cyanides, α-substituted, in dil. soln., dielec. absorpt. obs., enthalpy of activation 80—55019
- bone, bovine cortical, dielec. relax. 77—40964
- bone, fluid-saturated, dielec. props. obs. 80—51316
- borosilicate glass, new dielec. props. at 5 mK 77—63354
- bromal, in benzene soln., dielec. relax., loss, and dipole moment 80—2692
- 4-bromo-m-thiocresol, liq., dielectric relax. mechanisms 79—42891
- m-bromophenylbenzoyloxybenzoate, nematic phase, freq. depend. of dielec. props. *(French)* 79—91337
- 1,4-butanediol, dielectric behaviour, LF dispersion 77—48126
- butanediol terephthalate-polytetramethylene oxide terephthalate copolymers, dielec. props. 78—95546
- t-butyl derivatives, liq., reorientational correlation times, Hubbard model 79—61353
- n-butyl-4,5,7-trinitrofluorenone-2-carboxylate/Lexan polycarbonate 77—4598
- N-t-butylformamide, in carbon tetrachloride, dielec. relax., time-domain reflectometric obs. 79—4762
- capacitors, decay voltage and recovery voltage curves 79—61295
- cellulose, dielec. relax. studies, TSD meas. 80—88907
- cellulose, thermally stimulated discharge studies 80—11329
- cellulose electrets, TSC and dielec. losses and relax. 80—25284
- cellulose esters, plasticiser effects on mech. and dielec. relax. 80—40047
- chalcogenide glasses, dielectric relaxation 80—55027
- chiral smectic C, ferroelec. props., dielec. meas. 78—52463
- chloral, dielec. consts. and dielec. losses meas. 77—20795
- 4-chloro-3-nitrobenzotrifluoride-benzene (carbon tetrachloride) dilute soln., dielec. relax. time, dipole moment, microwave obs. 78—35084
- 4-chloro-3-nitrotoluene-benzene (carbon tetrachloride) dilute soln., dielec. relax. time, dipole moment, microwave obs. 78—35084
- 4-chloro-α-toluothiol, liq., dielectric relax. mechanisms 79—42891
- 2-chloro-p-nitroaniline, in benzene soln., dipole moment from solute relax. time-solvent viscosity relation 80—37905
- chlorobenzene, HF dielec. relax. test for extended Nee-Zwanzig formula 79—33602
- chlorobenzene-cis-decalin mixtures, phase transitions and dielec. behaviour study in 77-330K 80—29680
- chlorobenzotrifluoride, benzene soln., permittivity and dielec. loss 78—64320
- chlorofluoromethanes, liq., NMR spin-lattice and dielec. relax. 79—33604
- o-chloronitrobenzene-benzene (carbon tetrachloride) dilute soln., dielec. relax. time, dipole moment, microwave obs. 78—35084
- o-chlorotoluene(-benzene), liq. and dilute soln., microwave absorption and relax. processes 79—82920
- cholesterol, dielectric props. under UV excitation 80—6912
- cholic acid, dielectric props. under UV excitation 80—6912
- coal, and conductive impurities 79—82921
- Cole-Cole dielectric relaxation distrib. function, circuit model 80—7291
- Cole-Cole dispersion function isomorphism 79—47385
- conducting solns., highly, measurement using transformer ratio arm bridge, 10^2 to 10^6 Hz 79—80641
- conducting solutions, bridge method for meas. dielectric relaxation 80—82793

dielectric relaxation continued
corona charged PVF$_2$ α_c relaxation obs. 80–15956
4-cyano-4′-octylbiphenyl, dielec. props., 1 Hz-1 GHz, in smectic, nematic and liq. phases *(French)* 77–40168
4-cyano-4′-octylbiphenyl, dielectric relax. anal. in nematic and smectic phases 80–108153
cyanobiphenyl liq. cryst. mixtures, mol. mechanism producing dielec. relax. 78–84521
t-cyanobutane, dielectric relaxation study, complex permittivity 80–80688
m-cyanophenylbenzoyloxybenzoates, nematic phase, freq. depend. of dielec. props. *(French)* 79–91337
cyclic carbonates, supercooled liqs., dielec., acoustic, NMR, viscoelastic relax. props. 77–1609
data representation by Havriliak-Negami formalism 80–15950
data sampling process for dielec. dispersion meas. in freq. range $<10^{-1}$ Hz *(French)* 79–49257
Debye generalised fluid model, dielectric relax., depolarised dynamic light scatt. 80–108156
decalin, liq. and glass mol. motion, kinematic and electrodynamic solns. 80–25293
deuterated Rochelle salt, complex dielec. const., 5 MHz-24GHz, −45 to +45°, relax. mechanism 80–15983
dextran aqueous solutions, microwave dielec. behaviour 78–92018
Dextrane in aqueous solution permittivity meas., dielec. relaxation study 77–77143
dialkyl carbonates, liq., US, microwave dielect. relaxation 79–56717
dicarbonyl compounds in soln., internal motion, dielectric relax., ^{13}C NMR relax., far IR spectra 77–28517
1,1-dichloro-1-nitroethane, dil. soln. in benzene, dielec. relax. study 80–29679
o-dichlorobenzene(-benzene), liq. and dilute soln., microwave absorption and relax. processes 79–82920
dielectric anomalies at very low temps., acoustic anomalies analogy 78–31146
N,N-diethyl formamide, dipole moment, dielectric relax., internal rot., microwave absorpt. 79–56716
N,N′-diethyl-p-nitroso aniline, dil. benzene soln., dielec. props., microwave region, mechanisms 78–35085
diglycine nitrate, dielec. relax. in paraelec. and ferroelec. regions 78–31149
1,3-dihalopropane, dielectric permittivity and loss, dipole moment 78–60383
dil. soln., dielectric relax., solid rotator phase 79–42890
N,N′-dimethyl-p-methyl aniline, dil. benzene soln., dielec. props., microwave region, mechanisms 78–35085
N,N′-dimethyl-p-nitroso aniline, dil. benzene soln., dielec. props., microwave region, mechanisms 78–35085
N,N-dimethylacetamide in tetrachloromethane, dielectric relax. and complex permittivity 80–108149
dimuristoyl-1-3-lecithin aqueous soln., pulse relaxation method for dielec. const. determ. *(German)* 80–71308
p-dioxane-H$_2$O at 11 and 25°C, US absorption 80–65171
diphenyl ether, dielec. relax. pseudorot. diffusion 79–33600
diphenyl ether, dil. solns., dielec. loss and relax., microwave and sub-mm. wave absorpt. obs. *(German)* 78–23396
dipolar fluid dielectric relaxation, far IR absorption spectrum models 80–15954
dipolar liquid, dielectric function rel. to microscopic correlation function 80–7290
dipolar liquid time-variation of dispersion and absorption of third-order electric polarisation, mol. relax. times 80–60487
dipolar material, derivation of dielec. loss formula, appl. to relax. in glassy systems 80–50262
dipolar molecules in dil. soln., nonlinear dielec. relax., effective relax. time 80–97195
dipole-dipole coupling, inertial effect 80–40049
dipole-orientation relaxation times, meas., temp. depend. 78–84512
dipoles in asymmetric potentials 80–88915
disperse system, diphasic struct., systematic anal. to determ. permittivity and elec. cond. from dielec. relax. 78–56423
disperse system, elec. relax. in external fields, contrib. to elec. susceptibility 80–55720
disperse system, high conc., interfacial polarisation, dielec. consts. and relax. freqs., numerical estimation 77–32833
distribution function of relax. times, first order moments from permittivity data *(French)* 80–88918
distribution functions for relax. times using deconvolution technique 78–6628
DOBAMBC, chiral smectic phases, pyroelectric and dielec. props. 79–91380
DOBAMBC, dielec. dispersion at ferroelec. smectic A-smectic C transition 79–91385
DOBAMBC, dielec. props. near ferroelec. smectic A to C transition 80–45015
DOBAMBC, ferroelec. props. 79–32884
EBBA, in benzene soln., dielec. consts. and loss meas., 4.0, 9.4 and 30.4 GHz 77–40176
EBBA, nematic and isotropic phases, dielec. props. 79–87383
EBBA, nematic liq. cryst., RF dielec. props. 79–4238
elastin, hydrated, dielectric relax. 79–5247
electret discharge model, injection relaxation mechanism, space-charge cond. 78–80279
electret effect, homo and heterocharge charge distribution 80–11317
electrets and dielectrics, conf., Sao Carlos, Brazil, Sept. (1975) 80–7251
electrical response of relaxing dielectrics compressed by shock waves, axial mode problem 78–80280
electrolyte, dielectric dispersion and friction, viscous momentum transport and relax., ion mobility 78–27775
electrolyte solutions, dielec. dispersion and dielec. friction 78–52436
electrolytic solutions, dielectric relaxation studies 78–84519
energy basis of dielec. relax. loss 78–31150
enzyme activity rate reduction by EM fields *(Russian)* 78–61142
epoxides, dielectric relax. and deform props., cross-link density effect *(Russian)* 80–60942
epoxy resin, curing investigation by polarisation current method 80–3345
ethanes, substituted, dielec. relax. by intramol. motion 78–23391
ethanol, electron solvation, ps laser study 80–101032
ethanol solution in benzene, dielec. relax. time by RF cond. meas. 80–71302

dielectric relaxation continued
p-p-ethoxyphenylazophenyl hexanoate, dielec. relax. in stable and metastable solid phases 80–34851
ethyl trichloroacetate, in non-polar solvents (cyclohexane, p-xylene and p-dioxane) 78–2796
ethyl trichloroacetate, soln., dielectric props. and relax. mechanisms at microwave freqs. 78–15089
ethyl-3-chloropropionate, liq., microwave absorption and relax. 78–60386
N-ethylacetamide, in carbon tetrachloride, dielec. relax., time-domain reflectometric obs. 79–4762
4-ethylaminobenzil, dil. soln. in benzene, cyclohexane and dioxane, dielectric behaviour 78–52421
ethylene-CO copolymer, dielec. absorpt. meas., permittivity *(French)* 80–103916
ethylene-CO copolymer, highly alternating, melting and internal motion 77–51474
ethylene-methacrylic acid copolymer, dielectric relax. and IR obs. 79–69772
ethyltrichloroacetate, dielec. consts. and dielec. losses meas. 77–20795
experimental data of relaxation times, bounded error anal. of expt. distribs. 79–88924
ferroelectric, relaxation processes in Ising model, cluster approx., complex dielectric const. *(Russian)* 80–11352
ferroelectric bodies, deformable, coupled electroacoustic eqns. 80–96092
ferroelectric domain wall shift, mobile point defect interaction effects 77–32338
field induced thermally stimulated polarisation-depolarisation currents, relaxation, book contribution 80–80687
9-fluorenone, in o-terphenyl soln., dielectric absorp. studies, molecular relax. 78–95544
fluorobenzene(-benzene), liq. and dilute soln., microwave absorption and relax. processes 79–82920
frequency dependent dielectric constant, rel. to dielec. polarisation 78–56425
Gaussian distrib. of relax. times, evaluation of charact. parameters *(French)* 80–34848
Gaussian relaxation time distrib., new permittivity formula *(French)* 79–42880
glass, dielectric relax. loss, two level Anderson Halperin Varma model 80–66106
glass, electrical relax., Debye-Falkenhagen theory 80–108155
glass, high-field ionic and polaronic cond., dielec. relax., Poole-Frenkel theory 80–100351
glass, loss peak frequency, rel. to DC cond. 79–78621
glass, relaxation phenomena and Raman spectroscopy, review of developments 78–22665
glass, simple molecule, dielec. relax., 4-77K 77–73109
glasses, dielectric relax., order parameter model appl. 80–108151
glasses, high-resistivity, uniform and space charge polarisation, thermally stimulated depolarisation anal. 78–15085
glycerol, highly viscous state, static and dynamic Kerr effect obs. 80–60545
glycine silver nitrate, dielec. relax. in paraelec. and ferroelec. phases 80–29678
HAB, dielectric and calorimetric investig. in solid, liq. cryst. and liq. phases 77–84639
haemoglobin, dielectric props. under UV excitation 80–6912
2-halopropionates, liq., dielec. relax. and permittivity 80–15948
HBBOP and HBH-HBBOP nematic mixtures, relax. freqs. and dielec. anisotropy, binary system behaviour *(German)* 79–33606
n-heptyl-cyanobiphenyl, dielec. relax. in nematic and isotropic phases 79–82151
n-heptyloxy-cyanobiphenyl, dielec. relax. in nematic and isotropic phases 79–82151
heterocyclic compounds in dilute solutions, dielectric relax., microwave technique 78–84520
N-(p-hexyloxybenzylidene)-p-toluidine, dil. soln. in benzene, dielectric behaviour 79–42893
HOAB, effect of smectic C struct., on dielectric relax. 79–19140
hydrate, struct. I clathrate hydrate, H$_2$O mol. reorientation and diffusion, PMR and dielectric relax. 77–36142
hydroxy compound dilute solutions, dielec. relax. at 20 to 40°C *(German)* 79–33605
hydroxyapatites, dipolar reorientations, TSC study 80–60491
ice, dielectric relaxation in presence of ionic impurities, block layer meas. tech. 80–103914
ice Ih, Curie-Weiss behaviour of static dielectric constant of Debye component 77–81044
ice microcrystals, NH$_4$Cl doped, activation energy of Debye's dipolar relax., influence of salt content *(French)* 78–56424
inhomogeneous isotropic dielectric, anal. 78–68450
inhomogeneous material, complex permittivity in freq. range 10^2 to 10^7 Hz *(Russian)* 79–8088
ionic conductive crystal, statistical theory of relaxation current and low-freq. dielectric dispersion 78–60391
ionic crystals, dielectric loss and relaxation theory and kinetics 80–11335
ionic defect pairs, electric-field-modulated EPR of paramagnetic ion probe 78–23392
isoquinoline, dil. soln., dielec. absorpt., relax. and thermodynamic parameters meas. 80–50258
itinerant oscillator model, anal. for dielectric relax. and incoherent neutron scatt. 79–90509
kaolinite rare-earth complexes, relax., molar free energy of activation for dipole relax. 80–88919
ketone-paraffin solid soln., dielec. relax., temp. and lattice const. depend. *(German)* 78–76383
Langmuir film, dark and photo-stimulated relaxation similarity 78–92021
lanoline emulsion of KCl aqueous solutions, 1 MHz to 70 GHz 77–77144
LF fluctuation, dissipation and relaxation properties, universality 80–84687
liquid, dielectric relax. time rel. to single particle correl. time 80–97193
liquid, mol. and intramol. relax. parameters 79–56715
liquid crystal, positive, dielec., Kerr effect and orientational relax. 77–77171
liquid crystal, rotary motion about short axis, dielectric and splay viscosity meas. 77–43145
liquid crystals, dielectric relaxation at phase transitions 79–28090

dielectric relaxation continued
liquid crystals, nematic and smectic mol. dynamical investigation 78—91252
liquid crystals with nematic and smectic modifications, dielec. relax. and losses 77—69769
liquid nonlinear third-order polarisation, transient effects elucidating molecular props. 80—15955
liquids, associated, mechanism of structural dielectric relaxation 80—107034
liquids, dielectric relax., order parameter model appl. 80—108151
liquids, third-order elec. polarisation, appl. of theory of nonlinear rot. relax. 77—90097
loss data, evaluation of relax. intensity 80—25292
low frequency dielec. characts. from complex impedance and complex elec. modulus 79—82922
low-frequency fluctuation, dissipation and relaxation properties 80—39661
lysozyme bound water, thermally-stimulated press. and current 78—15757
macromolecular chain dynamics model interpret. of dielec. relax. data 77—52014
materials, measurements and applications, conference, Birmingham (1979) 80—12854
MBBA, dielec. relax. in metastable modification of solid phase 80—84689
MBBA, dielec. relax. in nematic phase 79—82153
MBBA, dielectric and calorimetric investig. in solid, liq. cryst. and liq. phases 77—84639
MBBA, in benzene soln., dielec. consts. and loss meas., 4.0, 9.4 and 30.4 GHz 77—40176
MBBA, nematic and isotropic phases, dielec. props. 79—87383
MBBA, nematic liq. cryst., dielec. relax. under shear 79—10794
MBBA, nematic liq. cryst., flexoelectric and dielec. relax. behaviour 78—94979
MBBA binary mixtures with a nematogenic or nonmesogenic cpd., dielec. relax. 78—72457
MBBA-based binary nematic mixtures, dielec. L-relax. 77—40178
MBBA/non-mesogenic cpd., binary nematic mixtures, dielec. relax. and intermolecular interaction 79—91350
methacrylic polymers, multiple dielectric relaxations, investigation by thermally stimulated current and creep methods 80—93238
methanol, electron solvation, ps laser study 80—101032
methanol aqueous soln., temp. depend. of dielec. relax. time *(French)* 77—59509
methanol molecule enxlosed in β-quinol clathrate, mol. reorientation, diele meas. 78—2026
methanol solution in benzene, dielec. relax. time by RF cond. meas. 80—71302
methanol-β-quinol clathrate, orientation and reorientation dynamics, dielec. and NMR obs. 79—99783
methyl alcohol, adsorbed on silica, low temp. thermally stimulated depolarisation spectra fine struct. 79—78611
methyl chloride, liq., NMR spin-lattice and dielec. relax. 79—33604
methyl cyanide, liq., NMR spin-lattice and dielec. relax. 79—33604
methyl iodide, liq., mol. reorientation, dielec. and viscosity meas. 80—100157
methyl methacrylate, oligomers, dielectric relax., end-group effects 78—92019
methyl methacrylate copolymers in solution 77—85644
methyl methacrylate-methacrylic acid copolymer, hydrogen bonding effect on dielec. relax., T_g region 77—59512
methyl methacrylate-p-chlorostyrene copolymer, side-group rot. and dielec. relax. 79—61303
methyl methacrylate-styrene copolymer, dielec. characts. change rel. to composition 80—25296
methyl methacrylate-styrene copolymer, side-group rot. and dielec. relax. 79—61303
methyl trichloroacetate, soln., dielectric props. and relax. mechanisms at microwave freqs. 78—15089
methyl-3-bromopropionate, liq., microwave absorption and relax. 78—60386
methyl-4-chlorobutyrate, liq., microwave absorption and relax. 78—60386
methylammonium aluminium selenate dodecahydrate, dielec. dispersion and relax. 77—28515
methylammonium alums, dielec. relax. near transition point 80—71301
methylammonium chromium selenate dodecahydrate crystals, complex electric permittivity meas. 80—40043
methylammonium gallium sulphate dodecahydrate, dielec. relax. meas. 79—28677
methylammonium-$Ga(SO_4)_2.12H_2O$, ferroelec. alum single crysts., dielec. dispersion and characts. 79—15408
methylene chloride, liq., NMR spin-lattice and dielec. relax. 79—33604
N-methylformamide, in carbon tetrachloride, dielec. relax., time-domain reflectometric obs. 79—4762
3-methylthiomethylpropionate, liq., dielec. relax. and permittivity 80—15948
microemulsions, struct. aspects, using dielec. relax. and spin label techniques 80—26199
microwave relaxation in muscle 80—51146
MIM structure, rel. to isothermal current-time characts. and trap parameters determ. 77—89879
MIM structure, thermal dielec. relax. 77—76941
MIM structures, thermal dielec. relax. 79—11237
molecular orientational motions, time-dependent distribution functions, pictorial representation, correlation functions 80—55021
molecular reorientation, orientational autocorrelation functions, appl. to rot. Brownian motion 78—18520
molecular reorientational motions rel. to dielec., Kerr effect relaxations 77—4599
molecular solid, dielectric loss, multimultiple relaxations, comparison with polymers 78—19409
molecule, short-chain, coupled rot. diffusion-conform. change 79—95706
N-methylpropionamide, in carbon tetrachloride, dielec. relax., time-domain reflectometric obs. 79—4762
naphthalenes, substituted, dielec. relax. and permittivity in pure liqs. 78—64318
naphthalenes, substituted, dielectric relax. in solns. 78—2795
nematic liquid crystal, dielectric properties and dielectric relax. *(Russian)* 79—61301
nematic liquid crystal mixtures, dielec. permittivity dispersion 80—88921

dielectric relaxation continued
nematic liquid crystal mixtures with low-freq. dielec. relax., phase behaviour 78—91246
nematic liquid crystals, dielectric characteristics obs. *(Russian)* 79—15400
nematic liquid crystals, LF dielec. relax., Freedericksz transition technique meas. 78—1987
nematic liquid crystals, molecular mechanisms of dielec. polarisation and relaxation 80—34846
nematic liquid crystals, multicomponnet mixtures, dielec. props. 80—38909
nematic liquid crystals, relaxation process characts. *(Russian)* 78—48116
nematic liquid crysts., dielec. polarisation and relax., mol. mechanisms 80—29673
nematic-isotropic mixture, dielec. props., phase diagram 78—52424
3-nitro-o-anisidine, in benzene soln., dipole moment from solute relax. time-solvent viscosity relation 80—37905
nitrobenzotrifluoride, benzene soln., permittivity and dielec. loss 78—64320
nitromethane, shock-induced elec. polarisation *(French)* 79—11381
4-nitrophenyl 4-octyloxybenzoate, smectic-A and nematic phases, dielectric meas. 79—23516
4-nitrophenyl-4-octyloxybenzoate, nematic and smectic-A phase, dielec. meas. 78—60392
nitroxyl radical rotation in liquids, ESR, dielec. relax. 77—28447
NMR and dielectric relaxation, defect diffusion models 79—15375
NOBAMBC, chiral smectic phases, pyroelectric and dielec. props. 79—91380
non-exponential decay in dielectrics, and correlated systems dynamics 79—73882
non-Markovian effects 78—52434
nonlinear, rotational Brownian motion of symmetrical top 78—60389
nonlinear, theory, using rot. Smoluchowski eqn. 80—25300
nonspherical top, rotational Brownian motion, and its appl. to dielec. relax. theory 78—21071
Nylon 7-7 and 11, dielectric const. and dielectric relax. 80—25294
4-octyl-4′-cyanobiphenyl, liq. cryst. phases, dielec. relax. meas., short range interactions 78—94976
octyl-cyano-biphenyl, nematic and smectic-A phase, dielec. meas. 78—60392
octyl-cyano-biphenyl, smectic-A and nematic phases, dielectric meas. 79—23516
4-n-octyloxyphenyl 4-n-pentyloxybenzoate, permittivity, microwave dielectric relaxation 80—80671
OHMBBA, nematic, dielectric behaviour at RF 79—7548
OHMBBA, solid phase dielectric relax. times and strength, mol. rot. 78—72456
oil film transient heat exchange in transverse electric field *(Russian)* 79—94607
organic binary liq. mixture, relax. times and dipole moments, RF and microwave obs. 77—12308
organic compounds, structural energy characteristics, rotational isomerism, mol. motion *(Russian)* 79—56602
organic liquid systems, dielectric and dynamic Kerr-effect studies 80—60496
organic rigid molecules solns. and mixtures, dielectric relax., const. and loss factor, microwave region 77—55747
organo tin dichlorides, tetrahedral, dilute soln., dielec. and thermodynamic behaviour, microwave region 77—36170
oxide glasses, elec. cond. and dielec. relax., correl. 78—79801
oxide glasses with Bi or Se granules, elec. props. and microstructure 78—2490
oxide semiconducting glass, structural energy characteristics, rotational isomerism, mol. motion *(Russian)* 79—56602
p-n junction, majority carrier flow model, diffusion effects in equilib. field distrib. 77—51808
PAA, methoxy deuterated, reorientational correl. times, comparison of neutron scatt. and dielec. relax. data 79—7545
paraelectric defect relaxation process, quantum interference and multilevel aspects 79—95109
4-n-pentyl phenyl-4(4-pentyl benzoyloxy)3-chlorobenzoate, liq. cryst., flexoelectric and dielec. relax. behaviour 78—94979
4-n-pentyloxy-phenyl-4′-n-octyloxybenzoate, nematic, dielec. relax. and freq. depend. of threshold voltage 80—60497
perfluorinated polymer, Krytox 143-AB, viscous, viscoelastic and dielectric properties 80—70440
perspex, electric conduction and isothermal dielectric relax. 80—80285
Perspex pyramid electret, thermally stimulated discharge currents 80—2688
PET fibre, anisotropy of dielectric relaxation 80—25297
p-phenitidine, in benzene soln., dipole moment from solute relax. time-solvent viscosity relation 80—37905
phenolic Mannich bases, dielec. relax. study 80—97196
phenols, dil. solns., dielec. loss and relax., microwave and sub-mm. wave absorpt. obs. *(German)* 78—23396
piezo-stimulated current spectra 77—69767
piezoelectric and dielectric relax., difference between 78—72458
piezoelectric powder, polarisation echo and surface props. theory *(Russian)* 77—48122
piezoelectric solids, shape-dependent damping 80—93242
piezostimulated current curves, theoretical and exptl. anal. methods, for dielec. relax. time determ. 78—92020
piezostimulated currents, new method for exam. of dielec. relax. 78—10847
PMMA, dielec. relax. spectrum, thermodepolarisation and dilatometric meas. 77—32322
PMMA, effect of fillers on molecular motions, dielectric relax. meas. 80—80691
PMMA, shock-wave compressed, dielectric props. 78—80281
PMMA, thermorheologically simple material, thermostimulated depolarisation currents 77—90092
PMMA-PVC mixtures, dielec. relax. and struct. rel. to formation *(Russian)* 77—20073
polar fluids, dielec. relaxation spectroscopy in microwave region, double-beam interferometry *(German)* 80—71309
polar fluids, rigid, dielectric relaxation theory 80—60495
polar liquid, dielec. props. in far IR range 77—85639
polar liquid, relative permittivity, dielectric and Kerr effect relaxation in alternating elec. fields 78—80284
polar liquid, theory independ. of continuum hypothesis 77—8502

dielectric relaxation continued
polar liquids, binary mixtures, Sarma and Rao's rel. for dielectric relax. time 80—88914
polar liquids, HF conductivity and relaxation time 80—96929
polar liquids in double layer capacitors, RF conduction, ion diffusion effect 80—107883
polar molecule, dielec. friction effect on reorientation in liq. 80—40048
polar molecule/nonpolar solvent, dielec. relax. computation from viscosity data 80—11330
polar molecules, in nonpolar solvent, dipole moments and relax. times 78—43782
polar molecules, viscosity activation energy and relax. time, RF cond. meas. 80—96677
polar molecules in liq. state, dielec. relax. time, dielec. const. 78—19408
polar molecules in nonpolar solvent, far IR spectra and dielec. relax. 80—71312
polar solutes, in o-terphenyl soln., dielec. relax. 79—33598
poly(4-chlorostyrene, 4-methylstyrene) copolymer, time-depend. ang. correls. 79—73881
poly(L-histidine), molecular motions in solid state, NMR and dielec. meas. 80—11332
poly-2-hydroxyethyl methacrylate, dielectric γ relaxation 80—34850
poly-4-chlorostyrene, undiluted, dielec. relax. spectrum above Tg 80—97194
poly-ε-caprolactone in dioxane soln., low freq. dielec. response 77—40177
poly-gamma-benzylglutamate, oriented films, piezoelectric relax. 77—24798
poly-L-proline, TSC and dielec. study of multiple relaxations 77—55748
poly-N-vinylsuccinimide, dielec. and pulsed NMR relax. glass-rubber transition, mol. motions 77—48125
polyacrylate solutions, dielec. relaxation 80—40045
6-polyamide, dielec. relax. time, thermally stimulated current neas. 79—87381
polyamide-12 plasticized with sulphonamides, relaxation props. *(Russian)* 80—55031
polybenzoxazole, dielectric β relaxation, role of water molecules 77—90100
polycarbonate, dielec. relax. and ductile brittle transition 78—52438
polycarbonate, effect of thermal treatment on strength, TSC meas. 77—52368
polycarbonate, TSC anal. by activation energy spectra 80—20579
polycarbonate films, high temp. relaxations 80—97187
polycarbonate thin films, solution-grown, dielectric relaxations 80—55029
polydiethylene glycol terephthalate, relaxation, dielectric prop. 78—68447
polydimethylsiloxane, crystalline and amorphous, characterised by DTA, polarised light microscopy, dielectric relax. 80—25295
polyelectrolyte, plasticised, effect of ion placement and struct. on props. 79—7679
polyester, linear aliphatic, mol. motions determ. by dielec. relax. and loss meas. 77—63364
polyethylene, alcohol infused, loss peaks due to secondary groups 80—84688
polyethylene, crystal, dielectric α-relax., soliton as crystal defect 80—45004
polyethylene, dielec. props. rel. to mol. struct. 80—29681
polyethylene, dielec. relax. mechanism, 1-80K *(German)* 78—76384
polyethylene, linear, effect of pressure on vol. and dielec. relax. 79—61302
polyethylene, low density, absorption currents exam. 78—43785
polyethylene, mol. motions, α relax, chain transport 79—15398
polyethylene, oxidised, low-temp. dielectric spectrum 79—61304
polyethylene, oxidised, paraelectricity, dielec. relax. obs. 77—48123
polyethylene, oxidised and chlorinated, dielec. ops. of mol. relax. 77—40179
polyethylene, thermally oxidised, low-temp. dielec. relax., dipolar tunnel states 78—2797
polyethylene oxide, aq. soln., dielec. relax., interferometric transmission obs. 78—52437
polyethylene oxide, elec. polarisation in suspension, Kerr effect 77—63359
polyethylene terephthalate, β relax., dynamic mech. and dielectric loss data 79—15399
polyethylene terephthalate, Mylar C film, high field relaxation currents 79—11259
polyethylene terephthalate, oriented, directional anisotropy, of dielec. β-relaxation 77—16247
polyethylene terephthalate, TSC and thermally stimulated creep, dielec. and mech. retardation modes 79—78613
polyethylene terephthalate electrets, formed by electron injection, TSC meas., space charge drift 80—11321
polyethylene-terephthalate, field-controlled photogeneration and carrier trapping 80—25285
polyhydroxyl alcohols, H-bonded solns., microwave dielec. relax. 79—33599
polyimide films, transient current in time range 10^{-4} to 10 s at temps. 180 to 280°C 80—65729
polymer, amorphous, excess charges, band gap levels and elec. props. 78—23053
polymer, dielectric relaxation time distrib. function determ. 77—73111
polymer, glass transition temp., dilatometric and dielectric relaxation data 80—6497
polymer, relaxation investigation *(German)* 78—31152
polymer, relaxation spectra determ. from electric discharge meas. with increasing temp. *(German)* 78—31151
polymer, secondary relaxation, TSC meas. 77—85643
polymer, structural energy characteristics, rotational isomerism, mol. motion *(Russian)* 79—56602
polymer, thermally stimulated discharge, thermal sampling technique 77—85645
polymer, TSD and dielec. loss, comparison of activation energies 78—10834
polymer chains with rigid bonds, local relax. times, mol. dynamics study *(Russian)* 80—59373
polymer coatings for corrosion protection, electrochem. techniques for performance monitoring 80—3234
polymer dynamics simulation, relax. rates and dynamic viscosity 78—91211
polymer electret, thermally stimulated discharge, compatibility and impurity effects 77—4595
polymer film, relax. mechanism of electret charge at high humidity *(Russian)* 77—63360

dielectric relaxation continued
polymer glass temp., correl. to dilute soln. dielec. relax. rates 78—10175
polymer network formation, relaxational props. variation 80—38961
polymer relaxation phenomena, conference, San Francisco, CA, USA (Aug. 1976) 79—4257
polymer solution, flexible chain, entanglement effects in segmental motion, dielec. obs. 80—40050
polymer solutions, dielectric relaxation time, diluent effects 78—10843
polymeric matrix, dielec. relax. processes of introduced polar mols. *(Russian)* 79—87387
polymers, activation energy, dielectric relax. meas. method 77—24784
polymers, electric phenomena, book 80—46746
polymers, heating rate and relaxation behaviour 77—66453
polymers, meas. using automatic dielcometer 77—45864
polymers, multiple dielectric relax. processes, mol. aspects, book contrib. 80—50264
polyoxymethylene, 90-300K, 400-10^4 Hz *(Russian)* 77—69770
polyoxymethylenes, dielec. relax. and IR spectra, 90 to 300K *(Russian)* 79—28678
polyoxymethylenes, dielectric property relaxation, unidentical relaxator system activation model *(Russian)* 80—80694
polyoxymethylenes, dielectric relaxation, molecular mechanism *(Russian)* 80—88923
polypentenamers, phosphonylated, hydrogenated derivatives, dynamic mech. and dielectric props. 78—68448
polyphenyl chinoxalines, dielectric relaxation *(German)* 77—59513
polypropylene, TSC meas. of relax. modes, apparent double glass transition 80—11323
polypropylene film, dielectric relaxation, β-mode investigation 80—93239
polypropylene glycol, low freq., multiple relaxation behaviour, dielectric and dynamic Kerr-effect techniques 80—29682
polypropylene glycol melt, mol. motion, dielectric and Kerr effect relax. obs. 80—60498
polypropylene oxide, solns., mol. relax., dielectric relax. and Brillouin scatt. obs. 77—23590
polysiloxane dizwitterionomers, mech., dielec. relax., effect of H_2O sorpt., thermal history 80—50261
polystyrene, measurement of dielectric relaxation using transformer ratio arm bridge, 10^2 to 10^6 Hz 79—80641
polystyrene, particles in dil. soln., bridge method for meas. dielectric relaxation 80—82793
polystyrene-chloranil molecular complex, glass-rubber and liquid-liquid transitions 80—45002
polystyrene-polyethylene oxide copolymer, elec. polarisation in suspension, Kerr effect 77—63359
polytrifluoroethylene, dielectric relax. processes above and below glass trans. *(Japanese)* 80—55028
polyurethane, TSD rel. to glass transition dipole relax. activation *(Russian)* 77—20793
polyvinyl butyral film, charge storage mechanism, TSC expts. 80—25280
polyvinyl carbazole, and ring chlorinated derivatives, dielectric and NMR relaxation 79—73883
polyvinyl cinnamate, and photocrosslinked form, low freq. dielec. loss evaluation 79—82919
polyvinyl difluoride, γ-irrad., low-temp. TSD obs. 77—63358
polyvinyl methyl ether, aq. soln., dielec. relax., interferometric transmission obs. 78—52437
polyvinylacetate film, effect of electrode metals on depolarisation current characts. 78—76387
polyvinylidene fluoride, correlated mol. motion in dielec. props. 77—55749
polyvinylidene fluoride, cryst. form II, anisotropy of dielec. relax. 80—103915
polyvinylidene fluoride, dielectric relax. mechanism 80—55023
polyvinylidene fluoride, poled, dielec. relax. spectra 80—80690
population distributions of dielec. relax. times 79—24258
power law frequency dependent dielectric function and nonanalyticity properties 78—60387
prefluorinated polymer, DuPont Krytox 143-AB, viscoelastic and dielectric props. 80—1503
propanes, substituted, dielec. relax. in liquid state 77—8500
propanes, substituted, liq., microwave absorpt., dielectric relax., loss, permittivity, moments and reorientation 77—63362
1-propanol, low temp. pulse radiolysis, solvated electrons, absorpt. spectral changes 77—12813
p-propoxybenzylidene-p-butylaniline, nematic and isotropic phases, dielec. props. 79—87383
n-propyl trichloroacetate, soln., dielectric props. and relax. mechanisms at microwave freqs. 78—15089
proteins, dimensions, shape, conformational transitions, use of dielectric relaxation method 79—11888
PVA, aq. soln., dielec. relax., interferometric transmission obs. 78—52437
PVA, liq., mobilities at const. temp., vol. 78—95174
PVC:Cu films, electron transport and dielec. props. 79—82700
PVC, reduced, dielec. props. rel. to mol. struct. 80—29681
PVC film, soln.-grown, between Al electrodes, AC elec. props. 80—15619
pyridines, substituted and N-oxides, dielectric relax. in solns. 78—6627
β-quinol clathrate, CH_3OH mol. reorientation investig. by IR and dielec. meas. 77—12369
quinoline, dil. soln., dielec. absorpt., relax. and thermodynamic parameters meas. 80—50258
relaxational polarisation, theory development and applicability 80—11334
response function relaxational frequency spectra, simultaneous meas. by digital signal processing 80—15959
restricted rotational diffusion, dipolar autocorrel. function calcs. 79—4763
Rochelle salt, freq. and temp. depend., 10 kHz-1 MHz, 16-28°C 79—82930
Rochelle salt, polarisation relaxation, US vel. and attenuation meas. 77—28512
rotational Brownian motion of spherical polar mol., diffusion eqn. study, complex polarisability 77—67381
semiconducting ferroelectric glass-ceramics, dielectric dispersion *(Russian)* 79—8097
semiconductor, amorphous, dielec. relax. current meas. method and uses 77—77141
serum albumin, bovine, hydrated, dielec. and elec. props. 80—97854
silicate glass, space charge distrib. after 2.1 MeV electron irrad. *(Russian)* 77—69772
simulation using network model 80—40046

dielectric relaxation continued
smectic phases, long mol. axis reorientation, LF dielec. dispersion 80—70124
snow, dielectric breakdown characteristics *(Japanese)* 78—40669
snow, dielectric relaxation and LF anomalous dispersion obs. *(Japanese)* 78—49056
soil, moist, dielectric relaxation model suitable at microwave frequencies 77—43930
solid electrolyte, polycryst., impedance and modulus spectroscopy 77—12309
solute-solute-solvent interaction, dielec. behaviour problems, review 80—25298
space charge effects, model of relax. phenomena 77—63366
space-charge behaviour, effect of relax. processes 80—40057
spectroscopy, liquids, frequency and time domain expt. methods 80—40044
stiff polymer chain dynamics, local and global mode interaction, dil. soln. viscosity, dielectric relax. 78—37776
trans-stilbene, soln., lifetime and anisotropic fluoresc., viscosity effects *(German)* 80—106352
styrene-acrylonitrile copolymer film, multiple relax. obs. using TSC 80—45000
styrene-butadiene-styrene triblock copolymers, dielec. props. 78—95545
styrene-sodium methacrylate (9 mol.%) copolymer cond. relax. 78—38874
tartrate, $Na[K_{1-x}(NH_4)_x].C_4H_4O_6.4H_2O$, dielec. relaxation 80—108152
o-terphenyl, dipolar solutes, reorientational motions, dielectric relax. below glass transition 80—19706
testosteron, dielectric props. under UV excitation 80—6912
1,1,2,2-tetrabromoethane, dil. soln. in benzene, dielec. relax. study 80—29679
TGS, γ-irrad., lattice defect effects on ferroelec. dispersion 79—51904
TGS, elastic and dielec. consts. from Brillouin scatt. 77—48180
TGS powders, dielec. dispersion 80—97180
TGSe, low freq. dielec. dispersion near Curie point 79—38432
thermally stimulated depolarisation, many-body model of universal dielec. response 80—75927
thermally stimulated polarisation currents method for dipolar relax. study 80—7278
thermally stimulated processes 78—10829
thermodynamic vectorial internal degrees of freedom, dielec. and mag. relax. phenomena 77—77145
thin film capacitor, time const. of ion current 78—23390
thiourea, ferroelec., soft mode and Debye relax., IR reflection spectra 77—90111
time range spectroscopy with real-time evaluation for nanosecond range *(German)* 80—71307
tissue LF dielectric dispersion calc. and meas. *(Russian)* 80—21512
tolualdehyde, dil. soln., dielectric relax., solid rotator phase 79—42890
toluene, liq., NMR spin-lattice and dielec. relax. 79—33604
transition metal oxide films, dielec. dispersion and polarization 78—2803
transition metal phosphate glasses, ohmic contact and dielectric. relax. 79—65795
triethylenediamine aq. soln., dielectric relaxation rate 79—78619
1,3,5- trifluorobenzene, liq., NMR spin-lattice and dielec. relax. 79—33604
urethanic polyester elastomers, dielectric relax., spatial network density *(Russian)* 80—71310
DL-α-valine in aq. soln., dielectric dispersion 78—20141
vinyl acetate, oligomers, dielectric relax., end-group effects 78—92019
vinyl aromatic polymer series, dielec. relaxs. at 220°C, −50°C and ~120°C interpret. 77—43929
vinyl chloride:vinyl acetate copolymer film dipole continuous relax. spectrum 78—91700
vinyl chloride-vinyl acetate copolymer film, dielec. relax. and thermally stimulated depolarisation current meas. 80—11336
viscoelastic materials, thermally stimulated processes 78—10829
viscous liquid, glassy state, effect of fictive temp. on dielec. relax. 79—24256
vitreous systems, local motions, dielec. losses and relax. phenomena 80—108154
vitrified conc. aq. solns., ionic hydration and secondary dielec. relax. 79—24882
water, adsorbed on silica, low temp. thermally stimulated depolarisation spectra fine struct. 79—78611
water, dielec. relaxation of compressed liquid at 17.613 GHz using microwave refl. meas. method *(German)* 80—71306
water, dielectric relaxation rate 79—78619
water-in-hexadecane, microemulsion, dielectric behaviour, Cole-Cole type relax., temp. depend. 78—56426
Williams-Watts type, normalised complex permittivity, num. table 80—7287
X-zeolites, dielectric relax. anal. 80—108153
$AgCl:Pb^{2+}$, ionic cond. and dielec. loss relax. vacancy-impurity complex. form. 77—1259
$AgNa(NO_2)_2$, crit. dynamics, hydrostatic press. effect, dielec. props. meas. 80—71328
$Ag_2O-B_2O_3$ glasses, electrical props. and dielectric relaxation *(Japanese)* 80—20199
$Ag_2O-P_2O_5$ system, electrical conductivity and dielectric relaxation *(Japanese)* 77—66455
$Al-Al_2O_3-M$, thin film sandwich, leakage current and dielec. relax., 80-500K 78—76158
$Al-Si_3N_4-SiO_2-Si$ capacitors with optical data writing 78—76154
Al_2O_3, anodic film, trapped O_2 and effect on dielec. stability 80—100634
Al_2O_3-loaded epoxy, shock-wave compressed, dielectric props. 78—80281
β-$Al_2O_3-Na_2O$, AC ionic cond., dielec. and NMR relax. 80—59713
β-$Al_2O_3-Na_2O$ $(Li_2O)(K_2O)(Ag_2O)(H_3O)$, with mobile ion species, dielec. relax. 79—91351
As-Ge-Te glass, dielectric meas. 79—87382
$As_{25}Ge_{10}Te_{65}$, chalcogenide glasses, dielectric relaxation 80—55027
$As_{10}Ge_{15}Te_{75}Ag_x$ glass, elec. and dielec. props., Ag additions effect 80—65558
As_2Se_3, localised gap states estimated by dielec. relax. 78—35087
$As_2Se_3:Ag$, amorphous, doping effect of gap states and elec. cond., dielec. relax. and DC cond. meas. 79—47098
$As_2Se_3:Al$, glassy, energy spectrum of deep localized states, thermal dielectric relaxation 78—15088
Au/n-TiO_2 Schottky diodes, I-V and C-V characts. 80—96988
B_2O_3-NaKO glass, dielectric relaxation at low temp. 79—11384
$B_2O_3-SiO_2$ (95.5 wt.%) glass, dielec. relaxation 79—78620

dielectric relaxation continued
$BaF_2:Gd^{3+}$, dielectric relax. and EPR line broadening 79—56608
$BaF_2:La^{3+}$, thermal depolarisation of La^{3+}-F_i^- defect dipoles 80—75926
$BaTiO_3$, c-domain cryst., HF dispersion of permittivity 78—60379
$BaTiO_3$, LF relaxational polarisation 78—68460
$BaTiO_3:Nb$, ferroelec. and paraelec. phases, props. 79—42919
$BaTiO_3-BaNbO_3$ system, solid solns., thermal ionic relaxation, vacancy form. 77—8499
Bi_2O_3, anodic film, dielec. props. 77—20794
Bi_2WO_6, ferroelectric, dielectric props., elec. cond. and relaxation phenomena obs. 80—80692
Bi_2WO_6, ionic cond. and relaxation polarisation, capacitance, losses 80—24657
$CH_3NH_3Ga(SeO_4)_2.12H_2O$, dielec. relax. near transition temp. 80—60493
CaF_2, cryst., dielec. props. in ULF range 80—7288
CaF_2, doubly doped, dielec. relax. 80—50263
CaF_2, mixed cluster, doubly-doped with rare earths, elec. dipole relax. 79—82924
CaF_2, rare-earth-doped, cluster-associated relax., 5.5-400K 78—31153
CaF_2:alkali metal cation, thermal depolarisation study 80—108147
$CaF_2:Er$, defect structure, quenching effect, dielec. relax. and optical absorption 80—65031
$CaF_2:Eu^{3+}$, dielec. spectrum 77—36171
$CaF_2:La^{3+}$, thermal depolarisation of La^{3+}-F_i^- defect dipoles 80—75926
$CaF_2:Li(Na)(K)(Rb)$, dielec. relax., activation energy, rel. to vacancy pair reorientation 80—88917
$CaF_2:O^{2-}$, $CaF_2:Na^+$, O^{2-} and $CaF_2:Y^{3+}$,O^{2-}, thermal depolarisation obs. of defect clusters 80—71299
$CaF_2:R^{3+}$, R=rare earth, dipole reorientation of charge compensation centres, ionic thermocurrents meas. 79—73880
$CaF_2:Y^{3+}$, ionic cond. and thermal depolarisation obs. of defect clustering 80—71298
$CaF_2:Y(La)$, dielec. relax. spectrum, ion size trends 78—72460
$CaO-B_2O_3-Fe_2O_3$ glasses, effect of heat treatment on electronic props. 78—2480
$CaO-B_2O_3-Fe_2O_3$ glass, dielec. relax., AC and DC cond., dielec. const. and loss 78—23393
$CaWO_4:Gd$, thermally stimulated depolarisation current, 100 to 300K 80—7280
$CdO-B_2O_3-SiO_2$, glass, dielec.-relax. currents 78—52004
CdTe negative dielectric relax. of hot electrons 78—52001
CsH_2AsO_4, ferroelec., RF dielec. relax., loss mech. 79—38448
CsH_2AsO_4, RF dielec. response close to transition temp. 77—90099
Cu-Ni, dil. alloy, optical reflectivity meas. virtual bound state model analysis 78—2873
$Fe(CO)_5$, microwave dielec. relax., fluxional mechanism 78—94235
$FeO_x-P_2O_5$ glass, semicond., dielec. props., thermally stimulated depolarisation meas. 79—95704
GeO_2-Na_2O, DC cond. rel. to dielectric loss peak freq. 79—78621
GeS amorphous layers between Al electrodes, dielec. relax. currents, pot. distrib. 77—16250
H-bonded complexes, in polystyrene matrix, mol. relax. processes 79—24259
H_2O, adsorbed on kaolinite clays, dielec. props. 78—76381
H_2O, dielectric relaxation in plant tissues 78—88692
H_2O_2 aq. solns., struct. and dielec. props. 78—63659
In-O film, AC behaviour, dielec. relax. 77—52019
In_2O_3 film, AC behaviour, dielec. relax. 77—52019
$KBr:Se^{2-}$ single cryst., dielec. relax. of impurity-vacancy dipoles, ITC meas. 79—91349
KCl aqueous solution emulsions, absorption band determination 78—72459
KCl, soln., elec. cond., dielec. relax., kinetic characts. 78—34641
KCl:Li, ⟨111⟩ off centre Li^+ under biaxial stress, bistable tunnelling 78—15090
$KCl:Li^+$, press. tuning of motional behaviour in shallow off-centre pots. 79—78718
$KCl:SrCl_2$, Z_1-centres, dipolar relax., ITC meas. 78—75660
$KCl-KF:Pb^{2+}$, point defects, ionic thermal currents and optical meas. 80—6403
$KClO_4:CrO_4^{2-}(SO_4^{2-})$, AC electrical conductivity meas. between temp. range 25-325°C, automated technique 80—59699
KD_2PO_4-type crysts., relax. processes in order-disorder transitions under short range correl. conditions 79—73889
$K_4Fe(CN)_6.3H_2O$, ferroelec. and paraelec. phases, dielec. props. meas. 80—60494
$K_4Fe(CN)_6.3H_2O$, Raman spectrum and dielec. relax. 78—19476
KH_2AsO_4, ferroelec., RF dielec. relax., loss mech. 79—38448
KH_2PO_4, dielec. functions above and below ferroelec. transition 79—33588
KH_2PO_4, ferroelec., RF dielec. relax., loss mech. 79—38448
KH_2PO_4, RF dielec. response close to transition temp. 77—90099
KI:Cl, dielec. relax. of impurity-vacancy complexes, ionic thermal current meas. 77—48124
$KI:S^{2-}$, vacancy dipoles, photo-induced polarisation and depolarisation 80—2690
K_2SeO_4, dielec. dispersion, 5-900 MHz, near incommensurate-commensurate transition 80—60522
K_2SnCl_6, phase-transition-induced dipolar relax. 80—66107
$KTaO_3$, crit. dielec. and optical props. and storage, 4K 77—24805
$KTaO_3$, polarisation, dielectric. const., relax. effects, electret state 77—12302
$KTaO_3:Li$, polarised cluster stabilisation by Li defects, polar glass form. 79—91342
LaF_3 films, electron beam evaporated, dielec. props. 79—91375
$LiClO_4$, organic solns., complex permittivity meas., dielec. relax. spectrum *(French)* 78—27154
LiF:Be(Mg), Maxwell-Wagner relax. induced by impurity clouds around dislocations, ionic thermocond. meas. 80—7281
$Li_{1-x}H_xIO_3$, piezoelectric props., space charge effects 78—6637
α-$LiIO_3$, depolarisation current, dielectric const. relaxation behaviour *(Chinese)* 80—88905
α-$LiIO_3$, dielectric constant and elec. cond. of single crystals *(Chinese)* 77—77134
α-$LiIO_3$, statistical theory of relaxation current and low-freq. dielectric dispersion 78—60391
Li_3N, superionic conductor, local ionic motion, anisotropic dielec. behaviour 78—87817
$MgF_2:LiF$ crystal, defect struct., anelastic and dielec. relax. meas. 77—27938

dielectric relaxation continued
$MgO:Li$, internal friction, mech. and dielec. relax. *(German)* 80—34135
NH_3, liq., relax. time and activation energy 79—91335
NH_4HSO_4, dielectric relax. in ferroelectric and paraelectric phases 77—16246
NH_4HSO_4, ferroelec., critical slowing down of dielec. relax. *(Japanese)* 77—90109
$(NH_4)_2SO_4$, ferroelec. dispersion in microwave region, transition to ferrielectric structure 80—45016
$(NH_4)_2SO_4$, static and dynamic dielec. behaviour 80—71337
NaA zeolite, dielectric polaris., cation distrib. *(French)* 79—51903
$NaBr:Cu^+$, press. tuning of motional behaviour in shallow off-centre pots. 79—78718
$NaCl:Mn^{2+}$, dimer detection, EPR and ITC expts. 78—59833
$NaCl\text{-}NaF:Pb^{2+}(Eu^{2+})(Zn^{2+})(Mn^{2+})(Sn^{2+})$, point defect ionic thermal current and optical meas. 80—6403
$Na(D_xH_{1-x})_3(Se_3)_2$, ferroelec. dispersion 80—40069
$Na_2O\text{-}B_2O_3$ glasses, electrical props. and dielectric relaxation *(Japanese)* 80—20199
$Na_2O\text{-}GeO_2$, electric cond. and dielec. relaxation *(Japanese)* 78—19905
$NiSiF_6.6H_2O$, dielec. loss and relax., 100-270K, reorient. mech. 78—35088
PLZT ceramic, ageing, dielec. props. 80—88940
$P_2O_5\text{-}MO\text{-}Al_2O_3$, (M=MgO, CaO, SrO, BaO) (45, 5 wt.%) glass, electron irradiation effect on dielec. props. 80—29056
$Pb_3Fe_2WO_9$, perovskite ferroelec., dielec. permittivity and loss meas. 77—8496
$Pb_5(Ge,Si)_3O_{11}$, dielec. and elec. props., 20 to 250°C 80—29697
$Pb_5Ge_3O_{11}$, dielec. functions above and below ferroelec. transition 79—33588
$PbHAsO_4$, ferroelec., far IR and submillimetre dielec. dispersion 79—38528
$PbHPO_4$, ferroelec., far IR and submillimetre dielec. dispersion 79—38528
$Pb(Mg_{1/3}Nb_{2/3})O_3:PbTiO_3$, ceramic dielectric, electrostriction, relaxation, polarisation 80—80700
$Pb_3(PO_4)_2$, ferroelastic, dielectric anomalies, phase transitions, permittivity, relaxation *(Russian)* 80—71293
$Pb_6Sb_{14}S_{27}$, zinkenite, electrophysical properties 78—34834
$xPbTiO_3+(1-x)PbCd_{1/3}Nb_{2/3}O_3$, phase transition spread, polarisation relaxation, dielectric susceptibility *(Russian)* 80—75922
$Pb(Zr,Ti)O_3$ ceramic-polyvinylidene fluoride composite film, complex piezoelec. props. 78—64323
$Pb(Zr,Ti)O_3$ thin layers, tan δ temp. dependence obs. *(Bulgarian)* 78—88259
$Pn_2Nb_2O_7$, relax. phenomena, meas. of dielec. const., polarisation and sp. ht. 77—4597
$RbAg_4I_5$, single cryst., dielectric relax. *(German)* 79—4764
$RbBr:Ag^+$, press. tuning of motional behaviour in shallow off-centre pots. 79—78718
$RbBr:Ba^{2+},Sn^{2+}$, thermal depolarisation meas., relax. processes 78—23389
$RbBr:Cu^+$, off-centre ion position, ionic thermocurrent study 80—7271
$RbCl:Ag^+$, press. tuning of motional behaviour in shallow off-centre pots. 79—78718
$RbCl:Cu^+$, off-centre ion position, ionic thermocurrent study 80—7271
$RbHSO_4$, ferroelec., dielec. dispersion 80—97179
$RbH_3(SeO_3)_2$, dielec. relax. near ferroelec. Curie temp. 80—97207
Rb_2ZnCl_4, dielec. dispersion, 5-900 MHz, near incommensurate-commensurate transition 80—60522
SbSI, cryst., low temp. dielec. anomalies and domain struct. 80—40035
SbSI, single- and poly-domain, complex permitt. and dielec. relax. losses 79—28699
Se, amorphous, TSC, dielec. relax. modes 77—90090
Se, amorphous film, dielec. activity obs. near glass transition temp. 80—75933
Se amorphous layers, dielectric relax. in glass transition range, ageing 79—82923
Se amorphous layers, substrate range depend. on dielec. relax. in glass transition temp. 79—69773
Se and Se-As, amorphous, dipolar activity at glass transition temp., AC method 77—66454
Se, liq., dielectric relax. and elec. cond. 80—108150
Se:As, amorphous, pure and doped, photoelectronic preps. in glass transition region 79—4583
Se:As, amorphous film, dielec. activity obs. near glass transition temp. 80—75933
Se:Tl, and undoped material, dielec. losses and permittivity meas. 77—28518
Se-Ge-Te glass, dielectric meas. 79—87382
Se-Tl-S alloys, liq., dielectric relax. and elec. cond. 80—108150
Si, optical constants, heavily doped crystals, Kramers-Kronig analysis 77—85676
Si, uncompensated, influence of carrier transit time on small-signal admittance of SCLC diode 77—85305
$Si\text{-}SiO_2$ interface traps energy distribution meas., in MOS devices, under non-steady-state *(Korean)* 78—64119
$Si\text{-}SiO_2$-polySi thin film structures, dielectric props. *(Slovak)* 80—75934
SiO_2, evaporated film, Debye-type dielec. dispersion props. 78—56421
SiO_2, fused, as-received and irrad., dielectric props. 79—65786
SiO_2, hydrated vitreous, spectrum of low-energy dipolar states, dielec. const., dielec. losses and relax. 77—90098
SiO_2 pyrolytic film, conduction process determ. 77—20479
SiO_x film, MIM struct., DC bias dependent dielectric dispersion props. 78—76178
$Sr_{0.75}Ba_{0.25}Nb_2O_6$, ceramic ageing dielec. props. 80—88940
$SrF_2:Gd^{3+}$, dielectric relax. and EPR line broadening 79—56608
$SrF_2:La$, type-I dipole reorientation, activation vol. determ. from dielec. const. 80—88916
$SrF_2:La^{3+}$, thermal depolarisation of $La^{3+}\text{-}F_i^-$ defect dipoles 80—75926
SrF_2:rare earth, electric dipoles, relaxation parameters and dipole-dipole interaction 79—24255
$SrTiO_3$, crit. elec. and optical props. and storage, 4K 77—24805
Te_xSe_{1-x}, localised gap states estimated by dielec. relax. 78—35087
$Tl_xNbO_{2+x}F_{1-x}$, pyrochlore phase, Tl^+ mobility 79—95209
VO_2, elec. cond. and dielec. props. 79—11379
$V_2O_5\text{-}P_2O_5$ glass, dielec. relax. mechanism, SDRC investigation, Schottky barrier formation in metal-glass-metal systems 78—60388
$V_2O_5\text{-}P_2O_5$ glass, in metal-semicond.-metal struct., TSC of dielec. relax. *(Russian)* 77—35998

dielectric relaxation continued
$V_2O_5\text{-}P_2O_5\text{-}CaO$ glass with metal electrodes, elec. characts., thermal conditions effect *(Russian)* 78—47884
$WO_3\text{-}P_2O_5$ glass, AC cond. and dielec. props. 80—92717
Xe hydrate, reorientation and diffusion of H_2O, PMR and dielectric relax. 77—36142
YIG, elec. props. 79—99552

dielectric resonance
see also dielectric relaxation; paraelectric resonance
alkali metal-ammonia solns., metal-insulator transition, h.f. and u.s. props. 77—1369
ferroelectric, H-bonded, parametric reson., influence of lattice vibr. by parallel electric microwave pumping 77—48140
one-dimensional conductor, microwave permittivity measurement techniques 78—10825
quartz, smoky, γ-irrad., electric dipolar echoes 80—20604
resonance media, dielec. props., resonance pumping effect 80—55054
Schottky-barrier diode monolithic detector dielectric plate antenna 79—30548
strip waveguide type gratings, resonance props. *(Ukrainian)* 80—33157
TGS, piezoelectric resonance spectra in 17 to 60 MHz range 77—16269
thermal conductivity at low concentration of phonon scattering centre, freq. crossing signals 80—2224
waveguide-dielectric resonances for UHF meas. of dielectric parameters 77—55760
Ar, liq., dielec. const. meas. by reson. method *(Russian)* 77—28511
$(Ba,Sr)TiO_3$ polycrystalline solid soln., electrostriction constants, reson.-antireson. meas. *(Russian)* 78—10849
Ge, electron-hole drop magnetoplasmas, radius-independent elec. and mag. reson. 79—73446
KD_2PO_4, attenuation const. meas. by SHF dielec. resonance 79—47406
KH_2PO_4, attenuation const. meas. by SHF dielec. resonance 79—47406
$PbTi_xZr_{1-x}O_3$, ferroelec., electric field depend. of contour mode reson. 77—12351
$Pb(Zr,Ti)O_3$ ceramic, permittivity and resonant frequency ageing, space charge field effects 77—85657
RbH_2AsO_4, attenuation const. meas. by SHF dielec. resonance 79—47406
RbH_2PO_4, attenuation const. meas. by SHF dielec. resonance 79—47406
SbSI, paraelec. phase, microwave reson. dielec. dispersion, near T_c 79—99839
$Sr_{0.61}Ba_{0.39}Nb_2O_6$, electromechanical props., permittivity, elastic compliance, piezoelectric moduli 80—29691

dielectric strength *see electric strength*

dielectric susceptibility *see optical susceptibility*

dielectric thin films
see also ferroelectric thin films; insulating thin films; optical films; piezoelectric thin films
AC properties, model 79—91352
alkali halide:Ag film, EPR and optical exam. of Ag impurity centres 77—85562
amorphous, covalent, disruption of stationary state and electrical breakdown 77—20332
amorphous, ionic, disruption of stationary state and electrical breakdown 77—20333
anodic oxide film, photodepolarisation *(Russian)* 77—32316
anodic oxide films, space charge, TSC obs. 77—32326
barium stearate, thickness measurement using Talbot effect 78—9321
biomedical electrode with SiO_2 film *(Japanese)* 80—3848
borosilicate glass, vapour-deposited, structural model, IR spectra meas. 77—1084
breakdown strength, statistical analysis 78—2603
breakdown voltage and self-healing effects mag. method 79—87388
capacitive stress transducer optimum dielectric selection 77—73428
cathodic sputtering deposition of oxides and oxyfluorides *(French)* 78—80468
complex dielectric constant meas. in mm-wave region, method *(German)* 79—58755
deposition methods, electrical properties 78—2802
elastic constants and SAW velocity and attenuation meas. 79—56101
electron bombardment deposited, anomalous optical absorpt. 77—20947
electron microscopy, dielectric support film screening effects 80—86504
ellipsometry for semiconductor process control, dielec. layers meas. 78—49887
epitaxial growth, low temp., by laser sputtering 80—34335
etching, optical monitoring technique 79—52412
evaporated dielectrics, ion drift and diffusion numerical calc. 77—4215
excitation of conductive body, covered with thin dielectric layer, integral equation solution *(Russian)* 79—18322
Fabry-Perot resonator cavity, dielectric film effect on characts. 79—94134
field emission through semiconductor and dielectric layers on metal 77—12501
gelatin film, dielectric losses and breakdown, struct. effects *(Russian)* 77—52017
glow polymerised, struct. and props. *(German)* 77—20799
hexamethyldisiloxane plasma polymerised thin film, charge trapping characts. 80—96895
integrated optics, waveguides, new wave phenomena, review 77—54817
interfacial polarisation effect on dielectric props., sandwich capacitor model 80—15614
interferometric meas. of refractive index, thickness and phase shift 78—276
laser deposited, optical and struct. props. 80—7506
margaric acid film, HF dielectric const. 77—36175
measurement technique, for dielectric props., student expt. 79—40323
MIS structures, elec. strength *(Slovak)* 78—56231
multilayer dielectric microwave reflectance and transmittance, characteristic matrix formalism 80—239
multilayer thin films, spin wave resonance, model 78—76316
optical coating, highly dispersive artificial dielectric utilising metal spheres 80—5690
optical thin-film waveguides fabrication, review *(Polish)* 79—3775
organic films, electronics and communications engineering appls. *(German)* 78—44011
palmitic acid film, HF dielectric const. 77—36175
particle track detector and particle discrimination 78—17511
permittivity and thickness determ. using differential-gap varying method *(Japanese)* 80—4739
permittivity calc. in partly-filled resonator cavity 78—45652

dielectric thin films continued
permittivity meas., of stearic acid film, using varying gap immersion method 78—6620
permittivity standard certification 77—74444
phosphosilicate glass, vapour-deposited, structural model, IR spectra meas. 77—1084
planar magnetron sputtering 78—72725
plasma anodisation of metals and semiconductors, model 79—28952
polariton standing wave struct. as test of boundary conditions for spatial dispersion theories 79—4865
polychlorotrifluoroethylene, electret, TSC 80—7266
polyethylene, drawn, dielec. breakdown and morphological struct., dichroic ratio 80—25813
polyethylene, electrets, polarisation obs. and influence of wax impurities, TSC obs. and analysis *(French)* 80—44999
polyethylene, low density, absorption currents exam. 78—43785
polyethylene, partial discharge degradation, effect of discharge products in air *(Japanese)* 77—69774
polyethylene terephthalate, electret, TSC, due to injected charge 77—16242
polyethylene terephthalate, space charge quantity meas. by Maxwell stress method 80—22389
polyferrocene film, plasma polymerised, dielec. props., 40 kHz to 50 MHz, 30-400°C 78—52439
polymer, dielectric film on cond., sliding spark development in air 79—86634
polymer, relax. mechanism of electret charge at high humidity *(Russian)* 77—63360
polymer films, dielectric constant meas. parallel to film surface 80—97183
polymerisation on carrier foils, film production *(German)* 77—16508
polymerized dielectric thin films deposited by glow discharge, time-dependent props. 77—63564
polyphenylene oxide thin films, electrochem. prep., impurity effects on cond., electroforming 80—88655
polypropylene, effect of corona treatment on dielectric props. for capacitor appl. 79—33607
polypropylene film, corona-charged, TSC and space charges 80—40041
polypropylene film and diarylalkane, Maxwell-Wagner dielectric polarisation 80—29676
polypropylene films, dielec. props., impurity effects 80—71304
polystyrene, formed by RF electrodeless excitation, dielec. props. 77—24795
polystyrene film, thermally stimulated discharge currents 80—71300
polystyrene films, soln. grown, elec. cond. meas. 80—97020
polytetrahydrofuran, electrochemically prepared between Pt and Au electrodes, AC elec. props. 80—40062
pore formation in electron beam produced films, statistical model *(Russian)* 80—6667
PVC films, soln. grown, DC cond. mechanisms, field and temp. depend. 80—97021
PVF_2 film pyroelectric radiation detector sensitivity *(Japanese)* 79—93222
rare earth compound vaporisation by cathode ray and HF ion-plasma methods 77—77380
rare earth metal oxide dielectrics using electron beam, capacitor, characts. and design considerations *(Russian)* 77—1638
refractive index and structure, deposition temp. depend. 79—4857
refractive index and thickness, spectrophotometric determ. 78—29144
refractive index meas., synchronous angle integrated optical method 80—15976
reversible nonlinearity analysis 78—92024
silicate: Yb_2O_3 glassy film, Yb laser spectral microanalysis 80—76585
silicone, film deposition, glow discharge polymerisation, elec. and thermal characts. 78—6467
space charge quantity meas. by Maxwell stress method 80—22389
spatial charge distrib. meas. technique 77—32327
spatially dispersive, transmissivity and reflectivity 77—8672
stearic acid, vacuum evaporated film, for low-loss capacitors 80—71317
stearic acid films, evaporated, vac. effects 80—97435
stearic acid multilayer films, dark and photo-generated dielec. response 77—72882
stearic acid multilayer films, lattice and carrier contribs. to dielec. polarisation 77—69775
surface charge density determ. on ultra-thin dielectric layer on semicond. *(Polish)* 79—51675
Teflon FEP, thermoelectret, TSC spectra 77—52012
thickness and refractive index, accurate meas. by symmetric prism wave couplers *(Chinese)* 80—2885
thickness and refractive index meas. by photoelectric scanning 80—105606
thin island films, statistical theory for dielectric props. 80—80699
transition layer vibrs., resonance region auxiliary surface polaritons *(Russian)* 80—2347
transition metal oxides, dielectric dispersion, dielectric polarisation 78—2803
two-wave laser coatings for 0.63 and 3.39 μ line prod. *(Russian)* 77—83895
vacuum deposited, formation during ion implantation, electric field effects 78—2801
ALF_3, evaporated layers DC props. and α-particle scatt. 78—14845
ALF_3 film, amorphous, AC elec. props. 78—2804
AgCl, on complementary cleavage planes of TGS, morphology, electron microscope obs. 79—15031
AgI, crystallisation, exciton absorption spectra meas. 77—35483
AgI-RbI films, vacuum deposited, cond. determ. 77—39689
$Al-Ta_2O_5-Al$, healing of defects in dielec. film by anodisation 80—65406
AlF_3 film, dielec. characts. 77—85650
AlF_3 films, electronic transitions near optical absorpt. edge, depend. on prep. conditions *(French)* 77—63429
AlF_3 in $Al-AlF_3-Al$ MIM thin film structures, dielec. and elec. props. *(Slovak)* 80—100536
AlF_3, optical absorption meas. rel. to prep. conditions *(French)* 77—44078
AlN films, RF reactive ion-plating, struct. and morphology 80—104074
Al_2O_3, dielec. const. and resist., thickness depend. 78—39502
Al_2O_3, film deposition from pyrolysis of Al acetylacetonate 77—85943
BN films, optical and electrophysical props. *(Russian)* 77—20941
$BaF_2:Gd^{3+}$ film, Gd^{3+} luminesc. spectrum and kinetics 78—6763
BaO-CaO, amorphous, Cu-electrodes, electrical props. 77—35997
$BaTiO_3$ ceramic films, dielec. strength, statistical anal. 80—75935

dielectric thin films continued
$BaTiO_3$ film, dielectric props. depend. on sinusoidal elec. field 80—71318
$BaTiO_3$, RF sputtered amorphous films, phys. and elec. characterisation 79—83119
Bi_2O_3, dielectric meas. 80—2696
Bi_2O_3, thermally grown on Bi film, thickness meas. by capacitance method 79—1554
Bi_2O_3, thin film, struct. and dielec. meas. 79—78622
Bi_2O_3 vacuum deposited films, dielec. props., 90 to 298K, freq. range 0.1 to 10 kHz, ageing effect 80—55036
$CaF_2:Gd^{3+}$ film, Gd^{3+} luminesc. spectrum and kinetics 78—6763
CeF_3 film, in MIM struct., dielec. props. *(Czech)* 80—25309
$Er_2M_3(BO_3)_4$, M=Ba,Cu, thin-film capacitor mats., synthesis and props. 77—48128
FeF_3 thin film, polarisation mechanism, AC and TSC study 80—66104
GaAs oxide film form., ion implantation effects 80—100266
GeO:Cr, dielectric thin film, transmission and EPR spectra 77—69676
GeS amorphous layers between Al electrodes, dielec. relax. currents, pot. distrib. 77—16250
In-O film, AC behaviour, dielec. relax. 77—52019
In_2O_3 film, AC behaviour, dielec. relax. 77—52019
LaF_3 films, electron beam evaporated, dielec. props. 79—91375
$La_xM_3(BO_3)_4$, M=Ba,Ca, thin-film capacitor mat. synthesis and props. 77—48128
LiF, boundary influence on IR spectrum 77—40243
LiF, characteristic energy loss and secondary electron spectra *(Japanese)* 78—15266
LiF, electronic excitations, inelastic electron scatt. spectra 77—32479
LiF film, ATR spectrum, reson. between longit. phonons and substrate surface polaritons *(Russian)* 77—32384
MgF_2 deposited quartz resonator, restricted mass range due to film stress 78—11116
MgF_2 film, crystn., AC glec. props. 78—2804
MgF_2 films, electronic transitions near optical absorpt. edge, depend. on prep. conditions *(French)* 77—63429
MgF_2, optical absorption meas. rel. to prep. conditions *(French)* 77—44078
MgO, intrinsic surface states at (100) and (110) surfaces 78—91740
$MoSi_2$ oxide film, dielec. props. and growth kinetics 80—81215
$NdAlO_3$, dielectric films, phase composition and structure 80—39464
$NiFeF_5$, form. on Fe-Ni alloys by fluorination 80—101035
$Pb_3Ge_2O_7$, dielectric thin film, obtained by sedimentation, exam. of dielectric props. and structure 80—2282
$PbNbO_3$ thin film microwave complex permittivity meas. 79—73879
$Pb(Zr,Ti)O_3$, dielectric thin film, geometry effect on props. *(Russian)* 77—90102
Sb_2S_3, thin film, dielectric props. 79—15392
$Si-SiO_2$ interface, barrier height in MOS tunnelling structures 80—88644
Si_3N_4, amorphous, optical props., band gap and surface roughness 77—32396
Si_3N_4 film, ion beam effects on opt. props. *(Russian)* 77—48265
Si_3N_4 film, laser coupling, new technique for refr. index and thickness meas. 77—88965
Si_3N_4, growth by reactive sputtering, influence of electron-ion bombard. *(Russian)* 77—28717
Si_3N_4, high temp. annealing effect on struct. and comp. 77—15714
Si_3N_4 thin film, reactively sputtered, struct. and elec. props. 80—88656
SiO deposition using solar furnace 80—89148
$SiO-B_2O_3$, composite, EPR, dangling bonds and dielec. loss 80—11246
SiO_2, elec. strength in $Al-SiO_2-Si$ MOS structures meas. *(Slovak)* 78—56231
SiO_2 film, dielectric breakdown and I-V characteristics 77—63368
SiO_2 film, ion beam effects on opt. props. *(Russian)* 77—48265
SiO_2 film, laser coupling, new technique for refr. index and thickness meas. 77—88965
SiO_2 film formed by ion implantation, dielectric props. 78—35090
SiO_x, evaporated film, influence of electronic leakage current on meas. of ion polarisation 77—63014
SiO_x, on $YZ-LiNbO_3$, SAW props. 80—84356
SiO_x thin film dielec., in MIM struct., interfacial props. rel. to non-stoichiometry 80—80399
SiO_xN_y film, ion beam effects on opt. props. *(Russian)* 77—48265
SnO_2, sputtered thermal ageing, thickness dependent effects 78—6462
$SrF_2:Gd^{3+}$ film, Gd^{3+} luminesc. spectrum and kinetics 78—6763
$Sr_2Nb_2O_7$, sputtered films, amorphous, dielec. props. 80—54573
$SrTiO_3$ film, polycrystn., dielec. props. and struct. 77—81057
Ta-Ti-O, reactive sputtered film, elec. props. 78—84336
Ta_2O_3, form. on GaAs after oxidation of Ta 79—61769
Ta_2O_5 film capacitative humidity sensor Panahume *(Japanese)* 80—105658
Ta_2O_5, reactively sputtered on Si, dielectric and optical props. obs. *(Bulgarian)* 80—89144
$Ta_2O_5-TiO_2$, anodic film, Rutherford backscatt., capacitance 77—16734
TeO_2 thin films, dielec. props. rel. to fabrication conditions 80—97199
TiO_2 film, ion plated, DC cond. study 80—100457
TiO_2 film, RF sputtering, dielec. props. and X-ray phase analysis 78—80288
TiO_2, formation by pyrolysis of tetrabutoxytitanium 80—55311
TiO_2, rutile, film, CVD in $TiCl_4-H_2O$ system 77—12541
TiO_2, rutile, thin film CVD 77—77409
TiO_2-SiO_2 mirror, dielectric, Rayleigh scatt. at 441.6 nm 80—97367
$(Y,Gd,Yb)_{3-x}Bi_x(Fe,Al)_5O_{12}$ film growth on $Gd_3Ga_5O_{12}$ substrates 79—78623
$Y-Y_2O_3-Au$, self-healing dielec. breakdown 80—11104
$Y_2M_3(BO_3)_4$, M=Ba,Ca, thin-film capacitor mat. synthesis and props. 77—48128
$ZnS-MgF_2$ mirror, dielectric, Rayleigh scatt. at 441.6 nm 80—97367

dielectric triodes *see space-charge limited devices*

dielectric waveguides
see also optical waveguides
asymmetrical gas dielectric waveguides, with resonances in walls 77—65639
circular screened three-layer waveguide, cut-off characteristics and modal inversion 80—1303
collective ion acceleration, dielectric guide controlled rel. electron beam propag. 80—14001
collective ion acceleration and intense electron beam propagation within an evacuated dielectric guide 80—14002
collective ion acceleration and intense electron beam propag. in vacuum dielectric channels 80—14003

dielectric waveguides continued
- complex waves in a circular dielectric waveguide 79—81337
- coupled thin-film dielectric waveguides with tapered edges, EM surface waves 79—3792
- cylindrical inhomogeneity in homogeneous medium of infinite extent, guided EM field numerical computation 80—14274
- dielectric/piezoelectric layered waveguide, surface acoustic wave amplification *(Russian)* 78—23138
- elliptical dielectric waveguides, higher-mode cutoff conditions 79—98479
- far IR antenna appls., reviews 80—69553
- flow detection using UHF EM field pattern display 80—104378
- hollow cylindrical anisotropic dielectric guide, propagation 79—32047
- inhomogeneous dielectric waveguide propagation, generalised WKB solns. 77—75385
- inverted strip guide, for dielec. prop. meas. at millimetre wave freqs. 79—26081
- jet with plane laminar flow, waveguide effect stability, anal. *(Russian)* 77—7546
- low-loss dielectric tube leaky waveguide, transmission characts. 80—95999
- microwave gas spectrometer using dielectric image waveguide 79—93229
- multilayer, electronic phase shifter for submillimetre waves, theory 77—34003
- nonlinear slab, surface wave propagation characts. 77—42609
- nonparallel dielectric waveguides, degenerate mode coupling 79—37006
- nonuniform dielectric regions, remote probing wave impedances 77—13781
- optical rib waveguide, propag. and radiation characts. 77—79933
- planar, interacting discontinuities, anal. 79—27445
- planar waveguide with interacting step discontinuities, field and network anal. 79—55214
- reflection from moving boundary between two dielectrics in waveguide 77—584
- rib guides, field expansion analysis, measurements at mm-wavelengths, approx. solutions 77—54778
- rod waveguide in magnetoplasma, TM mode propag. 78—51314
- scattering from arbitrarily located inhomogeneity 78—87161
- scattering matrix and radiation characts. of junction between monomode waveguides 77—34946
- step discontinuity, radiation loss 77—42588
- strip waveguide type gratings, resonance props. *(Ukrainian)* 80—33157
- weakly anisotropic rectangular dielec. optical waveguides, wave propag. anal. using coupled modes 80—64154
- $LiNbO_3$ $\Delta V/V$ waveguide SAW propagation obs. and modal analysis 78—38128

dielectrics *see dielectric materials*

diesel-electric power stations
- hybrid solar-diesel power stations for optimum energy utilisation 80—89598
- present net value anal., cost reduction factor 80—94027

diesel engines *see internal combustion engines*

diesel power stations *see diesel-electric power stations*

difference amplifiers *see differential amplifiers*

difference equations
- ablation, multidimens., embedding in inverse heat cond. problem, finite difference method 78—94508
- acoustic streaming, multidimens., numerical anal. 77—962
- acoustic wave refl. from general surface, geometric props. 77—84026
- ADI difference of schemes, high order, wave eqn. soln. 79—66
- advection-diffusion equation, weighted-mean schemes for finite-difference approx. 78—34103
- aerodynamics, high Reynolds number, global approach and coupling approach 80—48742
- aerodynamics, implicit difference schemes 77—35160
- aerofoil in unsteady viscous flow, numerical soln. procedures 78—75165
- air flow over irregular surface, three dimens. finite difference model, terrain following coord. transform 77—60452
- airfoil, conformal mapping, including multiply connected regions 77—23981
- algorithm for high order polynomial extrapolation 79—88798
- annular turbulent flows with heat transfer 78—94718
- antenna radiation field, soln. as initial value problem *(Chinese)* 78—9294
- approximate viscosity matrix, differential-difference representation 80—31518
- atmosphere potential vorticity, conservation by finite difference eqns. in generalised vertical coordinates 80—26576
- atoms and ions, valence region energies, electronegativity, Politzer-Parr partitioning, finite difference approx. 78—78612
- axial hyperchannelling theory, momentum approx., difference eqns. 77—20001
- axisymmetric confined flame, aerodynamic and heat transfer, finite difference scheme, program 78—94689
- axisymmetric duct design for incompressible flow 77—47090
- axisymmetric nonstationary flow around an obstacle in a cylindrical tube 79—77169
- axisymmetric streaming flow past torus, Stokes eqn. soln. method 78—14026
- beam in transverse vibr., optimisation of higher order eigenfrequencies 77—78971
- biharmonic function difference eqn., improved, appl. for elasticity 77—68411
- binary mixture vapour condensation, forced-free convection, finite difference treatment 78—5741
- biocybernetic model of influence of hypnosis on motor response of hemiparetic patients *(Slovenian)* 79—2037
- blast waves, spherical, time-depend. energy deposition 78—9655
- blunt body in supersonic flow, Navier-Stokes eqns. numerical computation 80—10263
- boundary layer, calc. on spinning and curved surfaces 77—65737
- boundary layer and freestream with separated flow, simultaneous soln. 78—38271
- boundary layer flow, three-dimensional, in orthogonal curvilinear coordinates 77—23940
- boundary layer flows, finite difference method 78—51155
- boundary layer flows in tilted square cavity, finite difference method 77—7385
- boundary layer theory, Mises' equation, first order perturbation by finite differences method 77—39271

difference equations continued
- boundary layer turbulence, differential methods and finite-difference methods comparison 78—18279
- boundary layer with blowing, numerical exponential box scheme 79—1240
- boundary layers beneath pot. vortex, finite-difference schemes 77—14982
- bridge, appl. of finite difference method to numerical study of dynamic effects *(French)* 78—36826
- bubble growth in superheated water at reduced pressures, finite difference anal. *(Japanese)* 80—92150
- calculus teaching, discrete approach using computer 79—80398
- Caldirola equations, generalised, for classically radiating electron 77—82401
- cascade flow, transonic anal., by conformal mapping and relax. techniques 77—75934
- cascade with slender profiles, transonic flow, numerical soln. 80—38436
- central difference approximations to the heat transport equation 79—3885
- centred finite difference scheme for 3-D eqns. of elastodynamics, stability 78—63294
- Chandrasekhar's X-function, reln. to eigenvalues of integral operators with difference kernels 77—71280
- channel, curved, of rectangular cross section, 3-dimens. MHD, numerical investigation 79—94734
- chaotic behaviour of physical and biological systems 78—62158
- chemically reacting flows, turbulent, steady and unsteady, computation in axi-symmetrical domains 80—1697
- chemically reactive flow, stiff boundary valued problems in kinetics and diffusion, numerical methods 79—86525
- CIDNP, numerical methods, model depend. 78—13530
- Clairaut eqn., connection to satellite geodesy and Jupiter 78—11795
- clamped skewed plates, elastic deformations by dynamic relaxation 78—34049
- classical theory of electron, finite difference eqns. basis 78—24925
- cloud droplets, stochastic collection eqn., computational instability in numerical soln. 77—2211
- coastal aquifer water flow analysis 80—26654
- column, nonuniform, lower bound buckling load, finite difference scheme 78—18200
- combined convective laminar boundary flow, vertical cylinder in horizontal flow, finite difference approx. 78—90893
- compact finite-difference methods and boundary conditions 77—49582
- compartmental models with delays, phys. realisability 78—53313
- complete conservative difference schemes for Landau equations *(Russian)* 79—77343
- complex submerged structures, vibr. anal. by discrete element techniques 77—68520
- composites transient hygrothermal stresses, coupled diffusion of heat and moisture 80—33451
- compressible flow, steady, thermodynamic consistency, finite difference scheme 80—48732
- compressible flow, upstream-centred finite-difference scheme 77—27547
- compressional impulse interaction with slot normal to surface of elastic half space 79—50626
- computational methods, book 78—81820
- conducting slab response to source fields, EM analogue model and finite difference calcs. 78—61329
- conduction-convection problems, error growth for explicit difference schemes 80—92017
- conference, computing methods in applied sciences, Le Chesnay, France (Dec. 1975) 77—33846
- conformal mappings for curved boundary finite-difference problems 79—3912
- conical diffuser, with suction, compressible boundary layer swirling flow 78—38360
- conservation equation, numerical soln. by variational approach, mass transfer problem appl. *(French)* 80—19317
- constrained material continua, eqn. formation 79—40360
- container subjected to forced pitching oscillation, liquid motion, nonlinear anal. 80—96270
- continued fraction solutions to systems of linear eqns. 77—2506
- convection, forced, from hot-film probe in reversing flow, finite-difference soln. 80—12177
- convection, forced, turbulent, in square cavity, shear effect 79—1180
- convection, laminar mixed forced/free, about sphere, buoyancy effects 77—75907
- convection, mixed, about sphere with uniform surface heat flux 79—32519
- convection, natural, in confined region between two concentric square ducts 79—23320
- convection, natural, in confined region between two horizontal ducts for variable fluid properties 79—23321
- convection, natural, transient and steady-state numerical solns. 80—10119
- convection, nonsteady, finite difference scheme numerical anal. 78—46884
- convection, upstream-centred finite-difference schemes 77—27548
- convective difference schemes and Hermite interpolation 77—68368
- convective difference schemes and Hermite interpolation 78—63268
- convective losses in 2-D, differentially heated, inclined cavities *(French)* 79—24906
- convective transport eqns., modified upwind scheme and conjugate gradient method 79—77107
- convergence rate estimation *(German)* 80—36
- counter current extraction column, efficiency, using nonlinear PD model *(Russian)* 79—64808
- coupled finite element-finite difference anal. of hydrodynamic and elastoplastic problems 77—71200
- Cowell's difference formula, modification for two-body problem *(Russian)* 78—32329
- crack propag. simulation, using moving grid based finite difference scheme 78—83334
- cracks dynamic propagation in anti-plane shear, anal. by finite differences 80—84240
- crystal surface vibration modes, effective-modulus approx. 79—19446
- curved beam with viscous damping forced vibrations 79—50622
- cylindrical heat cond. eqn., implicit difference methods 79—41551
- Czochralski bulk flow in the growth of garnet crystals 80—38979
- Darcy flow, chilled pipe freezing zone, finite difference method 78—94734

difference equations continued
- dielectric, inhomogeneous, electrostatic pot., numerical soln., finite difference method *(Spanish)* 79—89824
- dielectric gratings, arbitrary profiles, scatt. and guiding of EM waves 80—96005
- dielectric surface grazing discharge, elec. field config. 80—44069
- difference analogues to nonlinear partial differential eqns., reducible to linear eqns. 79—25831
- differential approximation method analysis of difference scheme props. 77—57172
- diffusion coefficient time depend. from single (de)sorption expt., step-by-step calc. method 78—87859
- diffusion solution for point defects in stress field, steady state and transient 78—30780
- diffusion-convection const. coeff. eqn., centred differencing, box scheme, mesh size, errors 77—7386
- diffusion-convection eqn. anal. with explicit difference methods 78—62165
- diffusion-convection equations, finite difference scheme 78—42596
- discrete inverse scatt. theory, Schrodinger eqn., difference approxs. 78—32724
- discrete special relativity, bases 77—71208
- dispersive wave equation, spatial discretisation effect on steady state and transient solns. 77—30014
- drop, impact dynamics on solid surface 79—86488
- duct, annular, turbulent flow and heat transfer over backward facing step, finite difference soln. 79—1175
- duct flow, laminar, finite element methods compared to Doppler meas. 79—1253
- duct flow with oscill. plate, numerical soln. 79—50794
- duct rotating around perpendicular axis, flow and heat transfer, finite difference method 78—94752
- DuFort-Frankel difference scheme, inertial oscills. in rot. fluid 77—51035
- dynamic problem of continua, reduction of stiffness, mass and damping matrices *(Polish)* 78—12565
- dynamic response of elastic shell of revolution in acoustic medium 77—19566
- dynamic stresses induced by moving cracks, numerical soln. 77—11146
- dynamical grid method for time-dependent simulations of axisymmetric instabilities in tokamaks 79—10702
- dynamical systems, determ. of global regions of asymptotic stability 77—67225
- education, conservative discrete models, difference eqn. formulation, nonlinear solid, fluid phenomena, computer calc. 77—78924
- education, stochastic model, radioactive decay, difference-differential eqns. 80—51992
- elastic collisions of three spheres in a line, eigenvalue and difference eqns. solns., for teaching 77—33786
- elastic cylinder surface impact, numerical soln. 80—38274
- elastic solid, difference and finite-element method for dynamical thermodiffusion problem 77—62154
- elastic/viscoplastic plate, combined longitudinal/torsional stress wave propag. *(Japanese)* 78—38227
- electric fields, intensity, numerical calculation methods *(French)* 80—106413
- electrochemical mechanisms, simplex fitting and finite difference simulation anal. 78—44381
- electrostatic field equation, general orthogonal curvilinear coords., finite difference approx. 77—38770
- elementary length and time interval *(French)* 78—77743
- elliptic PDE with discontinuous coeff., finite difference soln. 78—89347
- e.m. induction in Earth, two-dimens., finite difference soln. 77—2101
- energy dependent transport theory, exact solns. 80—32319
- equilibrium equations soln. for rapidly rot. stars 78—65601
- estuary, tidal and thermal propag., numerical model 79—12133
- Euler's finite difference scheme and chaos 79—80523
- Euler-Maclaurin summation rule, anal. of unsteady thermal stress problems 80—48580
- evolution equations in fluid dynamics, soln. by second order backward difference method 79—92950
- explicit finite difference method, anal. of dynamic crack and fracture 77—75860
- F_2-layer, plasma continuity eqn., comparative anal. of numerical soln. methods 78—69578
- fast fracture and crack arrest, finite difference anal., appl. to steel, epoxy resin 78—1607
- FBR sphere-pac fuel, prediction of thermal conductivity 79—59174
- ferromagnetic cylinders, sinusoidally varying end fields, eddy current phenomena numerical calcs. *(German)* 79—94131
- ferromagnetic object inspection, method of higher harmonics, difference schemes 80—89444
- fibreglass composite, oriented, model, conditions of monolithicity, exam. 78—67044
- finite, anal. of vibrs. of rectangular isotropic plate with two opposite edges simply supported 79—18782
- finite difference approx. of boundary conditions along irregular boundaries 78—36804
- finite difference calc., campylotropic coords. for boundary value problems 78—65757
- finite difference equations, appl. of group representations 77—13580
- finite difference equations, generalized vertical coordinate, total energy conservation 79—84363
- finite difference evaluation of heat transfer in nucl. fuel pins 78—82419
- finite difference method, appl. to bodies in non-planar stream *(Russian)* 78—75116
- finite difference method, appl. to thermal stress anal. with phase changes 78—79218
- finite difference method appl. to advection processes, balanced expansion technique 78—77719
- finite difference method appl. to oscillations of liquid in complex cavity *(Russian)* 77—72227
- finite difference methods for nonlinear two point boundary value problems 77—33849
- finite difference modelling, P-pulse propag. in elastic media 77—73868
- finite difference scheme, appl. of second and third degree methods 77—5651
- finite difference scheme solution of physical instability and weather prediction problems 77—53763
- finite difference schemes for heat eqns. 79—37109
- finite difference solns. to nonlinear bending of elastic rods 77—46953
- finite difference stencils from isoparametric elements 78—4472

difference equations continued
- finite difference technique, involving discontinuous derivatives, for flow problems 79—32435
- finite-difference scheme, elastic wave in vertically inhomogeneous media 77—73675
- finite-difference/Galerkin finite element soln. for turbulent boundary layer 78—26104
- flame, laminar mixed-mode forced-free diffusion type, on vert. burning fuel slab 78—91033
- flexible plate, stress distrib. through crack 77—89074
- flow, annulus entrance, heat transfer 79—4013
- flow, confined, numerical simulation, anal. of higher order methods 80—19316
- flow, fully-developed, in non-circ. passages, prediction method 79—1254
- flow, highly accelerating flow near smooth wall, prediction method 80—1550
- flow, in channel, turbulent vel., press., and temp. fields, direct numerical simulation 80—19361
- flow, in channel array with interconnections, finite-difference scheme 79—4012
- flow, in square duct, turbulence development computation 80—1554
- flow, multiply connected flow fields, numerically mapped macro-elements 79—1252
- flow, recirculating, numerical prediction 79—1152
- flow, rod cluster with blockage causing recirculation, finite difference method for temp. 79—3200
- flow, separated, internal, computation using coupled boundary layer-inviscid core, elliptic representation 80—1549
- flow, separated incompressible boundary layer prediction, including viscous-inviscid interaction 80—1548
- flow, supersonic, parabolic Navier-Stokes equations, implicit finite-difference method using fractional steps technique 80—69866
- flow, transient boiling in duct, dynamics 78—94528
- flow, transonic, steady and unsteady, implicit finite difference simulation 80—19429
- flow, turbulent, complex geometry, finite difference techniques accuracy 80—19357
- flow, turbulent, incompressible, numerical prediction 79—1171
- flow, turbulent wake of axial flow turbomachinery rotor blades, numerical anal. 80—1596
- flow about arbitrary 2-dimens. boundary, implicit finite difference simulation 78—94628
- flow and boundary layer development, finite difference and marching integration in straight core annular diffusers 80—53760
- flow between concentric rot. spheres, nonlinear, axisymmetric 80—19412
- flow calc., unsteady, in tubes with variable cross-section *(German)* 80—6155
- flow depend. expansion process, initial value problem, two step difference method *(German)* 78—57877
- flow field, multiply connected, curvilinear coords. and macro-elements 80—19318
- flow in ducts, quasi-one-dimensional fluid, time depend. computations 77—84324
- flow of compressible, viscous, heat-conducting gas, numerical simulation methods 80—38449
- flow of recirculating type, numerical methods in Navier-Stokes eqns. 79—1202
- flow problems in highly irregular domains, by finite-difference method 80—6166
- fluid dynamics, duct flow, 2-D viscous and compressible, momentum and energy transport, streamwise computation 80—53858
- fluid flow, finite difference methods 79—9117
- fluid flow, finite-difference schemes, comparative criteria 78—5720
- fluid flow, marker and cell technique 79—9121
- fluid flow, numerical methods comparison 79—9123
- fluid mechanics, num. methods and associated problems, book contrib. 77—89087
- fluid mechanics integral theorems, difference schemes 78—14032
- fluid simulation of plasmas, MHD particle code 79—68948
- fluidised bed, numerical soln. to 20 unsteady diffusion eqn. for vortex flow 77—84320
- Fourier analysis of difference schemes for Laplace eqn. in rot. symm. system 78—77677
- fourth order systems near bifurcation, numerical anal. 78—24653
- frequency anal. of unsupported structures 79—32333
- frictionless tidal channel behaviour 78—92876
- frustum of cone, laminar natural convection flow 80—53768
- fuel pin rupture in FBR, implicit compact difference method for solving linearized fuel sweepout equations 79—89355
- furnaces, walking-beam, numerical soln. of two-dimens. temp. field, boundary condition modification *(Polish)* 80—87706
- Galerkin method, fluid flow appl. 79—9118
- gas body, low-density, entry motion in exponential atmosphere *(Russian)* 78—77376
- gas dynamics, partial ionis. computation method 78—38447
- gas particulate flow on flat plate, laminar boundary layer, finite difference method 80—43688
- gas-dynamics, non-stationary, one-dimens., computational methods *(Russian)* 77—19618
- gas-particle flow in shock tube, finite difference calc. *(Japanese)* 80—79390
- gas-solid reaction, transient anal., sigmoidal conversion-time behaviour 77—66768
- general nonlinear differential difference eqns., solvable by inverse method, complete integrability 79—62999
- general nonlinear differential-difference equations, integrability by inverse scattering method 79—12575
- generalised random walks, transform. of recursion relations 80—101757
- geothermal reservoir exploitation, finite difference modelling 80—55798
- gravity waves, one-dimens., finite-element and finite-difference techniques comparison 79—18902
- gravity waves, two-dimens., finite-element and finite-difference techniques comparison 79—18903
- grid generation, automatic mesh-point clustering elliptic partial differential eqns, grid generation, automatic mesh-point clustering 80—31487
- group velocity, W.R. Hamilton's investigation 80—17815
- gulfs, tides and currents, math. models, finite difference techniques 79—12130
- Haar series use in constructing difference schemes for meteorological appl. 79—58125

difference equations continued
hard rods and spheres, radial distrib. function, differential difference eqns. in Percus-Yevick approx. 79—18701
Hartmann-Sprenger tube, thermal effects, finite difference method for analysis 80—14771
heat and mass transfer differential eqns., chessboard difference soln. method 77—82471
heat cond. eqn., synthesis of optimum boundary control *(Ukrainian)* 78—55544
heat conduction, diff. approx. *(Russian)* 77—7280
heat conduction analogue simulation *(Japanese)* 78—1664
heat conduction conjugate problems, finite difference solns. 80—19213
heat conduction eqn., variational-difference schemes for nonregular grids 80—38219
heat conduction equation with radiation boundary condition, implicit iterative soln. 78—5635
heat conduction inverse boundary-value problems, finite difference method 78—63263
heat flow eqn., different schemes 78—90627
heat flow in ring-shaped thin conductor, difference eqn. soln. for periodic problems 79—94460
heat pipe, evaporator section, evap. and vap. flow between parallel planes 80—10115
heat transfer, nonlinear, iterative-variational method 78—94511
heat transfer finite difference computer programs 79—14221
heat transfer simultaneous eqns. soln., matrix iterative substructuring 79—10564
helical springs, numerical soln. of dynamic response 78—67026
heterogeneous reactor, homogenization, finite difference eqns. of neutron distrib. 79—40992
heterogeneous reactor eqns., difference eqn. approach to soln. 77—61485
heterogeneous-reactor eqns., difference-scheme soln. 78—37404
higher-order monotonic convective difference schemes 77—13597
HTR cores, comparison of energy group models for Xe transients determ. 77—67803
hydrodynamics models, nonstationary gas flow, two dimens., variational approach to finite difference scheme 78—51147
hydroelastic shell opening in fluid flow numerical soln. *(Ukrainian)* 79—50592
hydromagnetic thermal instability of rotating fluid layer, Hall current effects 79—27699
hyperbolic eqns. in one space dimens., finite-difference approx., method of lines 77—2525
hyperbolic eqns. soln. by method of lines 77—5648
hyperbolic partial differential equations linear system, numerical soln., boundary methods accuracy 77—67245
hypersonic gas flow past thin triangular wings, difference method anal. *(Ukrainian)* 78—1686
hypersonic viscous shock layer equations, num. soln. scheme 79—90280
ideal gas in ejector nozzles, theory of combined flow of high/low pressure streams 80—6123
immiscible liquid-liquid system, laminar jet, vel. profiles and form 79—64752
implicit finite difference method, Romb, for numerical solution of hydrodynamic flow and heat conduction *(Russian)* 80—14725
implicit nonstationary iteration, appl. to 3D neutron diffusion 79—63712
incompressible flow, Navier-Stokes eqn. soln. by integro-differential method 77—72266
incompressible flows in three dimensions, finite-difference methods 80—33554
incompressible temp. boundary layer, von Mises variables, explicit finite difference method 79—80448
inelastic power-law fluid, unsteady flow in circular tube; implicit finite difference anal. 80—83821
inhomogeneous partial difference eqns., nuclear masses calc. 77—6268
intense laser beam diffraction by long US wave in liquid column 78—60421
interblock hydraulic conductivity values for transient unsaturated flow problems, finite difference soln. 80—12460
inverse heat conduction problem, finite difference soln., appl. ablation 77—46886
inverse method for solving differential-difference and difference-difference eqns. 80—105513
inviscid fluid conservation law eqns., coeff. matrices for implicit finite difference soln. 78—42580
ion beam source, optical props., convergent iterative numerical procedure 79—3620
Ising, quenched dil. random-bond model, CPA difference eqn. and crit. curves 80—2584
iterative solution of eqns. of radiative heat transfer *(Russian)* 77—58540
jet, buoyant, turbulent in cross flow, finite difference method 78—90907
jet, turbulent, deflected, 3-dimens. vel. field, finite-difference soln. 78—47009
jet, turbulent, free, three-dimens., k-ε model calc. using finite difference procedure 80—19468
jet flow, numerical modelling of boundary layer 78—22397
jet pump, finite-difference performance anal. 77—31348
jets, turbulent two-dimens., parallel, mixing 78—51209
jets discharging into quiescent ambient, finite difference anal., turbulence modelling 78—30332
lakes, wind effect eqns., finite difference schemes 79—12163
laminar boundary layer flow, direct finite difference calc. of through separated regions 77—35115
laminar duct entrance flow, 2nd order numerical method 78—38407
laminar flow in circular tubes, forced and combined convection, finite difference anal. 80—48711
laminar jet in liq.-liq. system, vel. profile, numerical method 80—28545
laminar unsteady flow past flat plate, finite difference method 79—18864
large defection anal., hybrid finite element and finite difference approach 77—72201
large deflection analysis of plates and shells by discrete energy method 79—3918
laser beam propagation eqn., finite difference approx. *(French)* 77—72017
lasing, in glow discharge, excitation freq. calc., electron upflux, book contrib. 77—50648
Lax-Wendroff difference scheme, appl. in fluid dynamics 78—65758
Leap Frog scheme, anal. for any number of space variables 79—2616
linear difference equation, optimal estimates for soln. on circle 77—25920

difference equations continued
linear differential eqns., fourth order, finite difference formulae for boundary value problems 78—73856
linear finite-difference eqns., first and second order eqn. solns. 78—8221
linear n-term recurrences, appl. in applied math. and theoretic physics, review *(French)* 79—97183
linear Navier-Stokes equations. numerical solution error anal. 78—38268
linear plate bending, finite difference energy techniques 79—55330
lossy corrugated structures, plane wave scatt., quantitative results 80—96005
MacCormack finite-difference scheme, over-relax. procedure 77—26161
magnetic fields, boundary-value problems, finite element and finite difference anal. 78—94353
magnetic problems, grid and metric optimisation, finite difference and finite element methods 78—94352
magnetostatic field, rotational-symmetrical, modelling, variational method, difference equations *(Polish)* 79—81319
mechanics, mountain massif, pre-face zone, stressed state, finite difference method *(Ukrainian)* 80—74735
metal, axisymmetric drawing simulation, numerical method development 78—30206
meteorology, optimum difference schemes, synthesis on sphere 78—93011
MHD, discrete mathematical model construction from principle of least action 80—38502
MHD, nonsimilar incompressible laminar boundary layers, finite-difference scheme 78—79386
MHD, transient phenomena, simultaneous solns. to coupled gasdynamic-EM equations of motion 80—6157
MHD axial flow in triangular pipe, finite difference method 78—59498
MHD between coaxial cylinders, difference eqn. soln., Dean's problem 79—94731
MHD conversion channel plasma flow computation 78—22470
MHD flows in the presence of a transverse magnetic field 79—55425
MHD stability of laminar boundary layer flow along flat plate with transverse mag. field 79—27709
micropolar continuum, 2-D model 77—74227
micropolar fluid, nonsimilar incompressible laminar boundary-layer flow 77—35184
micropolar fluids, stability of laminar flows between parallel walls 79—1160
minicomputerized automatic radiocardiogram analysis *(Japanese)* 79—29614
mixed 2-D flows of supersaturated and two-phase medium with nonequilib. phase transitions 79—77224
mixed finite difference and differential eqns., generating function, electron theory appl. 77—82371
monotone difference schemes for diffusion-convection problems 80—8801
movable net difference scheme for the solution of viscous gas equation *(Russian)* 79—50838
multi-dimensional two-phase flow 80—18564
multicomponent time depend. diffusion with radioactive decay, HTGR appl. 79—85588
multidimensional compressible Navier-Stokes eqn., generalised implicit method 77—68557
multiparameter splitting schemes for solution of spatially three-dimensional nonstationary problems 80—68047
Navier-Stokes eqn., steady, numerical soln. by highly accurate finite-difference method *(French)* 78—86163
Navier-Stokes eqns., central difference algorithm for high mesh Reynolds nos. 78—46920
Navier-Stokes eqns., finite difference methods, recent advances 77—80136
Navier-Stokes eqns., finite difference scheme 78—71306
Navier-Stokes eqns., finite difference schemes, stability anal. 78—89346
Navier-Stokes eqns., general finite difference formulation, appl. to vorticity eqns. 77—39269
Navier-Stokes eqns., numerical soln., vector and scalar pot. method 77—68558
Navier-Stokes eqns. for viscous and potential flow about arbitrary 2-D bodies 77—65730
Navier-Stokes equations, finite difference soln. errors 80—17807
Navier-Stokes equations, finite element and finite difference methods, efficiency comparison 79—1148
Navier-Stokes equations, finite-difference methods 79—1145
Navier-Stokes equations, Hermitian finite-difference method 79—1144
Navier-Stokes equations, laminar flow through cylinder array, finite difference method 78—42585
Navier-Stokes equations, theory and numerical analysis, book 78—77721
Navier-Stokes equations, two dimensional, numerical soln. methods *(Russian)* 80—101718
Navier-Stokes equations solution, two-dimensional, by multi-point finite differences 77—89083
Navier-Stokes solvers, efficiency, vorticity-stream function form 77—58632
neutron diffusion, mixed-lattice multidimensional reactor calcs., coarse mesh finite difference method 77—34375
neutron diffusion calcs., appl. to reactor design and anal. 77—79427
neutron diffusion coefficient adjustment using transport theory results 79—22359
neutron diffusion eqn., multichannel synthesis approximation, basis functions 80—47528
neutron diffusion eqns., finite difference method approx. by coarse mesh method 77—88185
neutron diffusion equation, three dimens., MULTIPOL code for coarse mesh approx. *(German)* 77—88186
neutron diffusion synthetic acceleration methods for diamond differenced discrete ordinates eqns. 77—82983
neutron transport, 2D time depend. P_1 eqn., numerical soln. 79—40980
neutron transport codes, linear continuous triangular-mesh difference scheme 79—59134
neutron transport discrete-ordinate transport eqn., variational difference schemes 77—65250
neutron transport eqn. cylindrical and spherical geometrics, characteristics formulation in CHART program 80—5197
neutron transport equations, discrete-ordinates, in slab geometry, convergence rates of spatial difference equations 80—27688
Newton's method, appl. to renal network flows 77—16945
non-equilibrium laminar boundary-layer, of dissociating air 77—952
non-Newtonian flow in pipe, finite difference methods 78—94770
non-Newtonian flow with moving boundaries 79—23343
non-Newtonian fluid duct flow, heat transfer 79—1219

difference equations continued
- nonlinear, difference analogue of Korteweg-de Vries eqn. 78—55
- nonlinear, difference analogue of sine-Gordon eqn. 78—20976
- nonlinear, difference analogue of Toda eqn. 78—20975
- nonlinear, heat conduction problems solution, finite difference methods appl. time spacing selection *(German)* 80—33418
- nonlinear, partial difference eqn., Backlund transformation, discrete-time Toda eqn. 78—73829
- nonlinear difference eqn. and soln. by inverse scatt. 77—9861
- nonlinear difference-difference equations, derivation of infinite number of conservation laws 78—89324
- nonlinear differential difference eqns. with N-depend. coeff. 79—71274
- nonlinear differential eqns. with N-depend. coeff. 79—71275
- nonlinear differential equation solution, computational accuracy 79—3997
- nonlinear differential-difference and difference-difference eqn. generation, exactly soluble 77—49564
- nonlinear elastic stability problems using a finite difference perturbation method 78—83273
- nonlinear heat transfer on boundary, difference method of solving conjugate nonstationary convection problem 80—92020
- nonlinear hyperbolic conservation laws, finite difference methods 78—49649
- nonlinear mathematical model of the propagation of tides in interlacing channels 79—39720
- nonlinear modified difference eqns., ALTRAN computer programs 79—9092
- nonlinear oscills. of round plate, difference eqn. approx., Lyapunov methods *(Russian)* 77—39259
- nonsimilar laminar free convection flow along a nonisothermal vertical plate, finite difference method 78—75119
- nonsteady flow of dropping compressible liquid in pipes, effect of friction laws 77—55091
- nonthermally conducting gas, monotonic difference scheme of open calculation *(Russian)* 80—103039
- nonuniform grids in finite difference approximations, application to fluid flow problems 80—105507
- nozzle, heat transfer of transonic air flow 79—1230
- nuclear containment vessel response to impact using PISCES finite difference codes 77—3097
- nuclear mass relations and eqns. 78—66194
- nuclear reactor, LMFBR, struct. response to HCDA, coupled Euler Lagrange computer program 77—71671
- nuclear reactor transient heat conduction, soln. by hybrid method 78—681
- numerical method, fast, iterative, implicit, for solving multidimensional partial differential eqns. 78—93519
- numerical prediction of recirculation flows with free convection encountered in gas-agitated reactors 79—10602
- numerical simulation of fluid motion, conf., Melbourne, Australia (1976) 79—9116
- optical waveguide calc., finite difference methods *(Russian)* 80—64189
- ordinary differential eqn. extended difference soln. *(German)* 79—21538
- orthogonal decomposition of 2-D periodic discrete vector fields 77—67196
- otolith membrane, variable gravity model 80—85573
- parabolic eqn. boundary value problems, differential, difference method *(Russian)* 79—58534
- parabolic marching problems, edge-corrected linearisation technique 77—89081
- parabolic nonlinear partial differential equation, numerical soln. using asymm. finite difference eqns. 77—33845
- parabolic partial differential eqns., finite difference methods, comparison of accuracy 79—72796
- parabolic partial differential equations, operator compact implicit soln. methods 78—89348
- parallel flow stability, numerical calc. 79—32460
- partial cell marker and cell method for vertical water entry into cone 77—42801
- partial differential eqns. reduction by Galerkin, collocation, and method of lines 78—77693
- partial differential equations, time depend., Method of Lines compared to finite difference scheme 78—79291
- partial differential equations extrapolation appl. 78—36810
- particle, spherical, convective heat and mass exchange, $\mathrm{Pe} \leq 1000$ 78—55683
- particle behaviour in a turbulent field, dispersive approach *(French)* 79—72882
- particle transport theory, integro-differential eqn. soln. 80—36955
- penetrative convection in rotating fluid, finite difference method 79—81902
- periodic solns. to eqns. with damping term 77—86489
- peristaltic flow, Navier-Stokes eqns., implicit finite difference method using orthogonal curvilinear coords. 77—39346
- peristaltic flow, nonlinear, calc. and expt. 78—9718
- pipe, curved, in creep, flexibility 78—34039
- pipe, straight, fracture under large deflection, pipe pressures, finite difference code 77—58616
- pipeline gas non-steady state flow linearisation coeffs. calc. 77—72395
- pitch angle diffusion eqn. of trapped particles in presence of loss. cone, finite difference integration 79—70931
- plane strain shear cracks, rupture vel., rel. to earthquakes 77—17043
- plane wave diffraction by circular transmission grating: finite-difference approach 79—68352
- plasma, current-driven drift-wave eigenmodes, stability criteria 79—32769
- plasma MHD, numerical simulation, variational approach 80—28625
- plate, optimal design under dead weight and surface loading 79—3915
- plate bending, curvilinear finite difference method for biharmonic equation 79—64539
- plates, thin rectangular elastic, bending, finite difference anal. 79—46181
- Plexiglas, spark energy balance 79—23474
- point-defect clustering during irradiation 80—92521
- Poisson's eqn., finite-difference soln. in rectangular of arbitrary proportions 77—64939
- Poisson's equation, finite difference form, numerical soln., unconditionally stable scheme 79—50
- Poisson eqn. on surface of sphere, shooting method for finite-difference soln. 77—2527
- Poisson equation over complex domain, finite difference method, Neumann boundary conditions 78—79189
- polymer dynamics simulation, general theory 78—91210

difference equations continued
- polymer extrusion flow and heat transfer relationships, numerical anal. 79—77188
- polytropic star, equilib. poloidal mag. field, finite difference-finite expansion method, Fortran program 77—13322
- population dynamics equation, as simulacrum of astronomical X-ray burster phenomenon 77—87570
- porous moist body, contact heating moulding, temp. distrib. heat/mass transfer 77—75784
- pulsating turbulent flow onto elastic surface, finite difference method *(Russian)* 78—75153
- pulsating turbulent pipe flow, vel. distrib. 79—32666
- PWR core, large, appl. of coarse-mesh finite difference eqns. for k_{eff} and peak power factors 78—17305
- quantum dissipative systems, time evolution of state vector 80—12935
- quench front in 2-D, difference method 77—79419
- radiative transfer in closely packed media, difference eqn. 78—12654
- rainfall-runoff process identification, Semois river appl. 79—5537
- reactor, core power and flux distribs., BITNOD large-mesh code appl. 78—17304
- reactor neutron field analogue simulation *(Russian)* 78—74416
- reactor pressure vessel, bimetallic, composite geometry, subjected to thermal shock, temp. decay, 2-D soln. 77—88209
- recirculating flow of incompressible fluid in square 2-D cavity, large Re, convergence of numerical solutions 80—33611
- recirculating flows, review of computing methods 79—10565
- reflector surface design by numerical method, bivariate beamshaping in elliptic case 77—27225
- reinforced organic composite, graphite, or C-C, ablation, mathematical modelling 79—41564
- renal counterflow system transient soln. computation 77—40699
- resistive MHD instabilities, diffuse pinch configs., numerical study 77—58853
- RF cavities with cylindrical symm., evaluation by computer program SUPERFISH 77—18714
- rod, thermal conduction, dynamic behaviour of distributed systems *(Dutch)* 80—28407
- rotating cylinder, source-sink flows, numerical anal. 79—4018
- Schrodinger eqn., time depend., two-dimens., finite difference schemes 80—97
- Schrodinger eqn. explicit method stabilisation difference eqn. *(Italian)* 77—71225
- Schrodinger equation, finite-difference, with time dependent operator, soln. 77—5692
- Schrodinger equation, math. props. of finite difference eqn., appl. to free electron *(Italian)* 77—78993
- Schrodinger equation, nonlinear time-depend., one dimens. wave packet soln., Fortran prog. 77—9897
- second-order, inverse scattering theory *(Russian)* 77—29990
- seismic depth migration after stack, finite-difference method 80—98254
- seismic depth migration before stack, finite-difference method 80—98255
- shaft, circular, with surface traction, perturbation of shear stresses 79—41577
- shell of revolution in acoustic medium, steady state motion 79—18728
- shell wall anal., circular tanks under axisymmetrical pressure 79—46202
- shells, truncated conical, thermal buckling, axisymmetric initial deflections 78—79240
- shells of resolution, transient dynamic and inelastic anal., survey of programs 77—3767
- shells of resolution under asymmetrical loading, creep deformation anal. 77—3751
- shock structure, numerical, nonlinear corrections for difference schemes in conservation form 80—36878
- shock tube flows, unsteady non-equilibrium, discretisation of boundary layer terms 80—14742
- shock wave ionisation in transverse magnetic field, finite-difference methods 78—51249
- shock wave propagation in inhomogeneous medium using finite differences 77—7414
- shock wave reflection from concave surface, numerical simulation 79—18913
- shock wave-obstacle three-dimensional interaction 80—53814
- shock waves, differential analysers, theory 77—15059
- simple unsteady flow, of viscous fluid, implicit divergent difference formulation *(Russian)* 77—51022
- singular perturbation problems 77—33850
- slab with temp. depend. thermal cond., convective boundary, transient cond., finite difference method 78—75031
- sliding interfaces and impact, numerical treatment 79—41631
- soil, unsaturated, coupled heat and water movement prediction, math. model 78—61446
- soil water flow modelling, finite difference and Galerkin techniques 78—81249
- solid-state convection in planetary interiors, numerical methods 79—84693
- solitary wave interactions, finite difference soln. of Boussinesq eqn. *(Russian)* 79—77141
- spatial differencing schemes for slab transport eqns., linear characteristic and quadratic methods 80—47524
- spectral transform, nonlinear discrete evolution equations 80—4553
- spectral transform method extension for solving nonlinear differential difference eqns. 78—81804
- stability of difference schemes for multidimensional equations of acoustics 80—105512
- stability theory *(Chinese)* 78—81803
- steady flow about blunt bodies, finite difference methods 80—96280
- steady-state recirculating flows, finite difference schemes, practical evaluation 80—106776
- steady-state response of difference eqns., digital computation schemes 78—57718
- stenosed tube, numerical solns. of Navier Stokes problems 80—16975
- stiffened cylinder, geometrically imperfect, buckling anal. under axial compression 77—62179
- stiffened layered structs., dynamic large-deflection inelastic and thermal stress anal. 77—3752
- Stirling cycle numerical analysis, computerised, accuracy evaluation 79—48170
- Stokes flow, free convection effects, finite difference anal. 80—14695
- Stokes problem, second-order difference scheme 80—90678
- subcritical steady flow past swept semi-infinite elliptic cylinder 77—62275

difference equations continued
subsonic and slightly supercritical aerodynamic flow, rapid finite-difference computation 77–23979
supercritical boiler, algorithm for numerical determ. of transient heat transfer processes 77–23944
supersonic cone flow at high angle of attack, numerical simulation, laminar and turbulent flow 79–77178
supersonic flow, finite difference method calcs. *(French)* 78–34157
supersonic flow, inviscid, over external axial corner, shock wave and vortical singularities 77–42866
supersonic flow, wake of axisymmetric body, ideal gas, numerical anal. 78–59420
supersonic flow past flat faced cylinders, second order shock capturing finite difference method *(Japanese)* 79–4038
supersonic laminar flow over backward facing step, numerical soln. at high Reynolds number 77–47040
supersonic thermal boundary layer, effect of wall hollow-induced separated bubble *(French)* 78–5784
supersonic three-dimens. flow, finite difference method 78–51190
surface waves, long period, explicit-implicit method 79–4026
surface waves, over submerged obstacle, finite-difference method 79–4027
Taylor vortex flow, finite difference transient implicit method, stability 79–14404
Taylor vortices, finite difference numerical computation 77–62259
terrestrial atmosphere, low-density gaseous body motion, rel. to Tunguska catastrophe 79–84554
thermal buckling of truncated conical shells with various axisymmetric initial deflections, finite-difference anal. 79–90162
thermal characteristics of finite element and finite difference calcs. for transient problems, comments 80–69633
thermal conductivity, three-dimensional solution for arbitrary shape bodies 77–75774
thermal regenerator, with variable mass flow rate, computer model 78–75047
thermogravitational convection asymmetry, finite difference method 78–59267
thermoviscoelasticity, bound dynamical problems, approx. calc. methods for crit. thermal states *(Russian)* 78–28949
thick spherical shell under thermal loading, numerical anal. 77–68445
third-order difference schemes, stability and boundary conditions, smoothing of discontinuities use 77–53762
three dimensional laminar flow in curved pipes, Navier-Stokes eqn. numerical soln. technique 79–10611
three-dimensional laminar incompressible internal flow, general computation method 77–42803
tidal flow, interlacing channels, nonlinear computer model 79–34828
tidal flow, shallow water eqns., semi-implicit approach 79–34829
tidal model of Corio Bay, Victoria, finite difference approach 79–12131
tidal propag. equations, finite difference and analytical methods 79–12134
Toda lattice, poles, soliton solns. 79–75368
transient 1-D two-phase flow eqns., finite difference approx. 78–51229
transient combined heat cond. and convection problem 79–81869
transient thermal problems, finite difference and finite element calcs., suddenly cooled boundary 80–14554
transonic axisymmetric pot. flow around inlets, Cartesian mesh soln. 77–72323
transonic flow, finite element and finite difference calcs., book contrib. 79–32558
transonic flow, three-dimens., flow analysis using STAR-100 computer 79–94644
transonic flow around airfoil, finite-difference calc., computer code 78–26147
transonic flow past swept wing, solutn. by finite volume method 80–19431
transonic flows, exact shock-jump conditions, numerical solns. 79–41704
transonic nacelle flow fields, accelerated iterative calc. 78–26145
transonic small-disturbance eqns., shock-fitting appl. to relax. solns. 77–84275
transonic streamline shape, influence of nonconservative differencing 77–23983
transport eqn. soln., dispersion corrected numerical schemes 78–36946
triangular finite difference scheme for large deflection problems 79–32233
triangular gratings, surface wave guiding, quantitative results 80–96005
tropical cyclone surge model, finite difference method 79–12132
truncated conical shells, thermal buckling 77–68467
tsunami, generation and propag., simulation using shallow water eqns. 80–41407
tube banks in turbulent flow, heat transfer prediction 79–1080
tubes flow with periodic step changes in diameter, numerical soln. 78–22423
turbulence, large eddy simulation 80–19333
turbulent air flow in round tube, high-temp., friction resistance, cooling *(Russian)* 78–75135
turbulent boundary layer, Hassid-Poreh energy model anal., inc. accel. and surface heat transfer step change 78–51158
turbulent boundary layer with separated flow, integral method 80–1547
turbulent channel flow, secondary current numerical simulation 78–94828
twisted gas flow in pipe, numerical soln. 77–84261
two dimensional, nonlinear partial difference eqns., two point function 80–101762
two dimensional recirculating flow, finite difference grid for non-rectangular flow fields 79–14374
two dimensional vorticity eqn., soln. using difference methods *(Chinese)* 79–72895
two dimensional vorticity equation soln., difference method *(Chinese)* 79–50729
two or three electrons, interacting with localised mag. moment, wave function determ., Sommerfeld's method, second and modular difference eqn. solns. *(French)* 79–12636
two-phase flow equation systems, characteristics, stability and short wavelength phenomena 78–38395
two-phase fluid dynamics, semi-implicit differencing method calcs. 78–42649
two-point boundary value problems, accurate method 79–88795
uncertainty analysis of P input into a lake 78–81262
unsteady pipe flows, finite difference scheme 80–6146

difference equations continued
unsteady supersonic flow around wings with detached shock wave, numerical soln. 79–94647
upper atmosphere neutral gas expansion differential eqns. soln. 79–12325
upwind second-order difference schemes for aerodynamic flow 77–23975
velocity distribution, in abruptly expanding circular duct 77–65798
vertical tube with laminar combined convection, water, finite difference anal. 78–90894
vibrating thin rectangular plates, influence of thermal grad. on natural freq. 79–32353
viscoelastic fluid, stability of laminar boundary layers *(German)* 77–72335
viscoelastic fluid flow, eqns. of state and motion, direct numerical soln. 79–60021
viscoelastic fluid flow between rotating coaxial disks, numerical anal. 79–77041
viscous flow, 2nd order upwind scheme critique 78–94744
viscous flow, 3D, finite difference method 79–32447
viscous flow, downstream boundary layers finite-difference and Chebyshev approx. 80–33555
viscous flow, time-dependent two-dimensional, moving boundary walls 78–14059
vortex sheet, unsteady, self-similar, rolled-up, large scale struct. 79–32531
vortex wakes, implicit finite-difference procedure 78–14018
wall with one-way heat flow, vertical inclined cavity stack 79–3899
water subcooled films on horizontal tubes, heat transfer correlation 79–77114
water wave propag., long-period, finite difference-element integration scheme 78–75157
wave diffraction by thin phase grating, difference eqn. solns. 78–54198
wave equation in domain with moving boundaries, difference schemes on non-uniform grid *(Russian)* 77–22380
wave equation with extended stability range, explicit difference method 80–4538
wave propagation inverse problem soln. using J-fraction expansion 78–11819
wave propagations in orthogonally reinforced fibre composites 78–41168
waves in shallow water, improved finite difference scheme 79–4028
weather prediction by finite difference scheme *(Chinese)* 80–46234
Wendroff type discrete inequalities and their applications 80–17786
wing, supersonic gas flow, numerical method and routine 80–38440
wing, swept, 3-dimens. turbulent boundary layer, numerical anal. 80–1621
ψ^{2N} field theory, asymptotic graphs counting techniques 79–17608
Al, quenched, diffusion solution for point defects in stress field, steady state and transient 78–30780
Cu, continuum representation of computer simulated dislocations 78–30623
H atom, energy level calcs. in superstrong mag. field 80–37737
LiNbO$_3$, SAW propagation and scatt., finite difference anal. 80–20595
N_2O_4, dissoc. flow in tube, heat transfer and drag 78–71402
Na, liq., in fast nucl. reactor outlet plenum, transient flow and heat transfer 79–26472
Th-PuO$_2$ kernels, effect of fuel particle size on power excursions, Doppler feedback mechanism 79–30911

differential amplifiers
analogue differential preamplifier for mechanical recording 78–40447
balanced bias differential current amplifier cct. for detection of laser-induced multiphoton ionisation 80–37909
biomedical IC differential amplifiers 77–48891
direct-reading phase meter with Schmitt trigger *(Spanish)* 77–37935
electron beam parameter meas. collector plate amplifier 79–75653
EMG biofeedback device 79–96706
modern electrometer techniques, review 80–37052
photoelectric colorimeter reconditioning methods 79–39618
plasma turbulence meas. with spectrum analyzer and differential amplifier 77–43081
transresistance instrumentation amplifier, dosimeter appl. 79–22561
voltmeter anxiliary equipment appl., for low voltage meas. in high ohmic circuits *(Czech)* 78–4664
wideband isolated for biological signals, cct. 78–57089

differential analysers
see also digital differential analysers
DIA analogue processing system *(Russian)* 77–12849
eye movement detect., on-line analogue analyser 79–79699

differential calculus *see differentiation*

differential equations
see also boundary-value problems; difference equations; Green's function methods; integro-differential equations; linear differential equations; Navier-Stokes equations; nonlinear differential equations; partial differential equations
^{3}He-^{4}He dilution refrigerator process anal. 79–93150
abstract evolution eqns., almost automorphic solns. 78–65754
aerodynamics and aeroacoustics, discontinuous solns. of differential eqns. using generalized differentiation 78–33940
aerosol, radioactive charging, transient mean particle charge 78–23973
air-water bubbly mixtures, press. wave propag. *(French)* 78–22402
Aitken δ^2 transformation, geometric approx. 77–10595
Alfven ion cyclotron waves, in finite length plasma, differential eqn. 78–91097
analysis, manifolds, calculus and other fundamental maths. book 78–28918
annular elastic membranes, large deflections, theoretical and expt. exam. 78–30186
arbitrarily defined differential equations, automated soln. using FORSIM VI program package 79–63007
asymptotic behaviour of differential systems rel. to competition of species *(French)* 77–67197
asymptotic method using projection iteration, linear and nonlinear differential eqn. systems, errors, convergence *(Russian)* 77–57169
asymptotic solution of a class of singularly perturbed nonlinear boundary value problems via differential inequalities 79–5970
atmospheric temperature, vertical profile, from satellite data, information retrieval 78–3959
atom+molecule, rotational rainbow maxima: a time dependent study 80–58353
atomic collisions, quasiclassical theory, transition between spatially degenerate levels 80–43150

differential equations continued
atomic collisions, rotationally induced transitions in two-state model 80—47945
atomic system, N-level, reson. excitation 79—68374
atoms, general adiabatic-diabatic transformation matrix, electronic non-adiabatic transitions 80—93751
autonomous differential system, equilib. positions bifuration conditions, closed orbits *(Russian)* 77—57157
autonomous system of ordinary differential equations, normal forms calculation *(Russian)* 77—57158
Backlund transformations, group struct. 80—13219
Bateman equations of radioactive decay, soln. using transition matrix approach 77—57632
beam eqn. integration for randomly curved cylinder with variable refractive index *(Russian)* 77—31139
bifurcating periodic solutions at LF 78—16657
bifurcation and transition toward stochasticity for dissipative dynamical systems 80—57201
bifurcation of higher dimensional tori 79—67143
biochemical multiple-loop negative feedback control networks, oscills., periodic metabolic systems 78—85285
Bochner curvature tensors, Kahler manifolds *(Japanese)* 79—12663
boundary layer, intermittent laminar/turbulent transition, local skin friction 78—30260
boundary layer problems, singular perturbations, stability and convergence 78—90827
boundary layer turbulence, differential methods and finite-difference methods comparison 78—18279
boundary layer turbulence, velocity profile calc. by Du Fort Frankel scheme 79—94600
boundary-value problems, three-point, solutions existence and uniqueness 78—32655
Brillouin theorem, proof 80—91415
bubble motion under gravity in rotating fluid, differential equations of motion *(German)* 78—90918
Bubnov-Halyorkin method, stability for one-order differential equations *(Russian)* 79—9081
Burgers equation, relationship to differential stochastic eqn. 80—36869
canonical systems of differential eqns. in resonant case, periodic solns. 79—44345
Carson-Cambi, periodic, second-order, perturbation solutions 77—67207
cellular control of gene expression by positive feedback, differential eqns. 79—66460
Chebyshev polynomial method for computing analytic solns. to eigenvalue problems, appl. to anharmonic oscillator 78—62058
chemical kinetics models, partial and differential eqn. parameters, estimation using Galerkin's method 79—66258
chemically reactive flow, kinetics, stiff ordinary differential eqns. numerical soln. 78—48631
classical Lagrangian theory with radiative reaction, Rohrlich two field formalism extension to include monopoles 78—45488
collocation and finite element methods 77—71198
comparison and existence theorems 77—9857
completely integrable systems and symplectic actions 79—44712
composite media with complex geometry, pot. field problems 78—16663
condensate film flow on finned surfaces, heat transfer, heat exchanger design 78—75038
conference, numerical treatment of differential equations, Oberwolfach, Germany (Dec. 1977) 79—92930
convection, natural, in confined region between two concentric square ducts 79—23320
correctness of equations with nondifferentiable operators *(Russian)* 79—58529
coupled second-order differential equations, Weyl's theory appls. 79—30375
covariant σ models, first order system of differential eqns. 80—31978
Curtis' (11,8) explicit Runge-Kutta method 77—17796
damped Mathieu oscill., parametric random excit., moment stability 77—9869
dangling spider problem for elastic-perfectly plastic material, ordinary differential eqn. 79—94502
decomposable differential operators in cosmological context 78—57825
delta wing equations, high freq. solns. 79—46337
determination from experimental curves 80—77604
detonations, sound ranging in atmosphere, anal. problems 79—94393
dielectric kernel, functional differential equn. 79—32871
diffusion, multi-group, FBR neutron-physical calc. *(Czech)* 78—66332
diffusion approximations to neuronal activity and to the time dependent threshold problem 79—74639
diffusion equation for a bounded source, propagation compound *(French)* 77—78958
diffusion solution for point defects in stress field, steady state and transient 78—30780
diffusion-reaction equations systems, existence, stability 79—20365
diffusion-type problems, mixed explicit implicit iterative finite element scheme, theory 77—22399
diffusion-type problems, mixed explicit-implicit iterative finite element scheme, soln. and examples 77—26155
Dirichlet problem response function method solution 80—27106
discharge lamps, high pressure, simulation of dynamic behaviour, differential eqn. 77—31532
discrete random walk, differential equations for transport in two or more dimensions 79—85073
distributed parameter nuclear reactor three-point model, neutron and delayed-neutron emitter behaviour, describing differential equations *(Spanish)* 80—22889
Duffing's eqn. forced by periodic impulses, harmonic solns. 78—89325
dusty gas, two fluid model field eqn., time interval for soln., iteration method *(German)* 78—63489
dusty gas, unsteady flow in cylinders, numerical soln. 78—51231
dynamic systems, equations of motion canonical transform 80—36843
dynamical equations, symmetries and first integrals 80—22221
dynamical system, limit cycles and symmetries 80—62462
dynamical systems, iteration scheme 77—57167
education, energy conservation and human body weight, diet, exercise and differential eqn. 77—87598
education, stochastic model, radioactive decay, difference-differential eqns. 80—51992
education, Sturm-Liouville problem, eigenfunctions normalization 77—78910

differential equations continued
effective pair potentials, first order derivation of differential equations 80—1041
eigenvalue systems of second order differential eqns., numerical soln., matching method 78—8232
eigenvalues, coupled second-order differential eqns., numerical soln. method 80—94976
elastic continuum dynamic response determ. using modal anal. 78—8242
elastic cylinder under stress, biharmonic problem solution 80—4532
elastic lateral torsional buckling of unbraced and braced planar frames 79—46236
elastodynamics, linear, stability theorems for abstract eqn. in Hilbert space 78—36832
electric field automatic computation, three methods, comparative study *(French)* 79—68346
electron beam, relativistic, radially inhomogeneous, unneutralised, linear theory 79—50201
electron micrograph, computer simulation for crystal defect identification 78—30525
electrostatic precipitator, free-fall, motion of charged particles, determ. 78—71020
Elenbaas Heller equation, soln. method 80—14952
elliptical, harmonic functions generalisation *(Ukrainian)* 77—49560
ELMO bumpy torus, macroscopic MHD stability and beta limit 79—31186
EM field calculation by successive overrelaxation (SOR) method 79—92964
EM induction, one-dimens. problem, Frechet derivative 77—48996
EM wave propagation in ionosphere, generalised differential eqn. 78—53770
energy conversion, intuitive thermodynamics *(German)* 79—14225
energy-absorbent media, wave theory generalisation *(Russian)* 78—77725
enzymatic open reaction, mathematical model 79—53024
epidemic models for malaria progress 77—22397
Euler's method, computer programs for high-school expts. 78—86094
evolution eqns. freq. domain conditions, reactor dynamic model appl. *(French)* 77—67201
evolution equations, connection to P-type differential eqns. 80—57078
excitable membrane phenomena, mathematical analysis 79—74635
fatigue crack growth, model prediction, two coupled differential equations 78—67103
ferrite rod phase shifter, azimuthally magnetised, soln. of differential eqns. in terms of Bessel and Neumann functions 79—55025
ferromagnetic cylinders, sinusoidally varying end fields, eddy current phenomena numerical calcs. *(German)* 79—94131
Feynman Lagrangian for short diffusion processes 80—31551
fibre optics, uniform asymptotic theory 80—28323
finite element analysis of cylindrical shell, with end plate subjected to centrifugal force *(Japanese)* 79—1104
first order matrix differential eqn., soln. 78—32653
first-order, infinitesimal operators of Lie group symm., algebra *(Russian)* 77—30034
first-order differential eqns., common derviation of averaging method and two-timescale method 78—85835
first-order hyperbolic differential equations, with split boundary conditions, numerical soln. 77—87634
first-order random functional differential eqn., soln. 78—32656
fission reactor digital simulator software development, kinetic equations integration, numerical solution method 80—68901
Fitzhugh nerve conduction equations, appl. of higher order Hopf bifurcation formula 77—86483
flow, in annulus, axial, numerical stability anal. 78—83363
flow, plane parallel, finite amplitude stability, perturbative and iterative methods 78—38293
flow, stratified, environmental, finite element analysis, book contrib. 79—34875
flow on flat plate with chem. surface reaction, mass transfer *(German)* 79—72961
fluid, cold, displacement by hot fluid in porous medium, stability 79—27691
fluid flow, boundary elements method soln. 78—90821
fluid flow, model eqn. of Lagerstrom 79—12612
Fokker-Planck-Vlasov eqn., weak solns., uniqueness and stability 79—92951
forced vibrations of freely supported continuous beam *(Rumanian)* 78—75085
fourth-order ordinary eqn., numerical soln., convergence 77—87636
Fredholm determinant satisfied, appl. to inversion formalism for parameter depend. potentials 77—22437
Friedrich extension for differential operators with strongly singular potentials 80—27150
gas and solid particles energy balance anal. 77—77812
gas core reactors, temp. profile and power calcs., uniform density diffusion model 80—37553
gas flow regime choice in pipes with max. temp. at outlet 80—19396
gas turbines, temperature gradient along cooling channel surface, heat transfer in initial hydrodynamic section, effects 79—18892
gauge field operator quantisation rules 78—41405
geometry, differential, appl. to geophysical fields configurations analytical description *(Russian)* 79—74986
Gibbs-Duhem eqn. solns. 79—85106
global element method, appl. in discontinuous nuclear pot. calc. 79—3089
global first integral for dynamical systems, importance of div. 77—82374
graphite arc, in Ar flow, meas. of anode voltage drop 80—84022
gravity waves, long-period, on fluid of rapidly varying depth 78—9647
group analysis, generalization to transformation groups *(Russian)* 79—92991
Gurney's ballistics calc. 80—67946
gyroscopic system, linear, damped, modal anal., appl. to satellite 78—63275
Hamilton equations, n distinct periodic solns. on each energy level *(French)* 79—44710
Hamilton-Jacobi equation, symmetry and separation of variables, normal parabolic equation *(Russian)* 79—6292
Hamilton-Jacobi equation, symmetry and separation of variables, nonparabolic equation *(Russian)* 79—6291
Hamiltonian autonomous system with 2 degrees of freedom, stability in 1st order reson. *(Russian)* 77—53776
Hamiltonian eqns., infinite-dimens., integrable 78—57744

differential equations continued
- harmonic oscillator, time-depend., invariants 77—64942
- heat and mass transfer in domains with variable and fixed boundaries 78—33995
- heat and mass transfer with condensation from turbulent nonuniform boundary layer, appl. 77—89124
- heat conduction in cylinders of an anisotropic medium 79—94458
- heat conduction solution, generalised differential operator appl. *(Hungarian)* 79—14202
- heat exchange in dense layer at large Biot no. *(Russian)* 78—83400
- heat flow in ring-shaped thin conductor, difference eqn. soln. for periodic problems 79—94460
- heavy liquid flow, existence and uniqueness 80—1511
- Helmholtz, scalar, eigenvalues calc., simplified integral equation method 77—78964
- high-current electron-optical systems, asymptotic synthesis 79—7067
- higher monotonicity properties of certain Sturm-Liouville functions 78—57750
- highly-ionised free-fall positive column, differential eqn. system 78—67489
- holographic gratings, 4-port Bragg device anal. 80—83564
- hydrology, modified Richards' eqn., oscill. of numerical soln. 78—81243
- hyperbolic differential equations, difference and finite element anal. methods 79—49059
- hyperbolic orbits, differential eqns. *(Russian)* 77—78622
- hypergeometric, five-parameter second order eqns., solns. 77—64926
- ideal gas in ejector nozzles, theory of combined flow of high/low pressure streams 80—6123
- initial value equations soln. in dynamical astronomy, new Runge-Kutta algorithms 79—12387
- integrable evolution equations, general struct. 79—30201
- integrable in generalised hypergeometric functions *(Russian)* 79—12572
- integral transform groups for differential operators from Lie algebras 80—4887
- intensity distribution inside absorbing-isotropically scatt. semiinfinite medium 78—32335
- interactive buckling analysis of box sections using dynamic relaxation 79—7304
- inverse problem for general first order differential eqn. systems 78—74181
- irrotational shearfree motion of perfect fluid in general relativity 79—27715
- iterative Newton-Raphson method, stability anal. of nonlinear dynamical systems 77—72150
- Kepler problem, non-compact Anosov flows and hyperbolic motion *(Russian)* 77—7360
- Kepler problem, time transformation stabilisation *(German)* 78—89333
- Lagrange diffusion in planetary boundary layer 77—56667
- Lagrange eqn. symmetries and equivalent Lagrangians 80—86071
- Landeu model, critical multiple correlations 79—75440
- Lane-Emden eqn., new solns. 79—96994
- Lane-Emden equation for index 5, non-elliptic soln. 77—41377
- left-heart haemodynamics, mathematical model 78—65074
- light ellipticity, azimuth and system parameters linking eqns., 3-dimens. model propag. 78—50695
- linear induction motor, fluid flow induced in liquid metals, investigation 80—43800
- linear physical systems analysis, with periodic inputs, with aid of computer 79—51
- linear stochastic differential equations in Hilbert spaces 79—63148
- Lippman-Schwinger equation, soln. for n delta-shell pots. 78—41112
- local heat transfer in tubes with heat flux constant over length and variable over perimeter 78—30163
- Lorentz Dirac equation, further constraints for unique physical solution 78—41172
- Lorentz-Dirac eqn. for classical charged particle, mass renormalisation 78—62007
- Lorentz-Dirac equation 80—12921
- lossy integrator, response for time variable counting rate *(Rumanian)* 78—90045
- lunar orbit evolution, differential eqns. for semi-major axis and inclination var. 80—8565
- Lyapunov functions construction by iterative process, almost diagonal systems of differential eqn. *(Russian)* 77—57168
- M-matrices; numerical solution methods *(German)* 77—82377
- magnetic resonance, single differential eqn. soln. *(Russian)* 77—28424
- magnetic-bubble material, struct. of 180° ferromag. domain wall 79—24205
- mass degeneracy at fixed particle number, differential eqn. for bootstrap degeneracy 78—24732
- material particles movement, numerical solution *(Croatian)* 79—25983
- mathematical modelling of highly parametrised integral or differential equations 79—35492
- Mathieu eqns., generalised, stability criteria 77—26137
- Mathieu equation with damping, variational anal. 80—57079
- Maxwell's time depend. eqns., solns. by successive overrelaxation (SOR) method 79—92963
- Maxwell eqn. finite difference soln., perfect conductor simulation 77—74236
- membrane, weak ion exchange, nonequilib. props., steady flow in const. elec. field 78—23966
- metal, dissolved species in cracks, linear differential eqn. problem 79—51316
- metal cutting appl. of Taylor eqn. for different cutting speeds *(German)* 78—72915
- MHD, discrete mathematical model construction from principle of least action 80—38502
- MHD Stokes approx., eqns. with homogeneous operators *(Russian)* 79—60071
- Michaelis-Menten mechanism for quasi-steady state and quasi-equilibrium, approx. soln. 79—70511
- micropolar fluid boundary layer flow past circular cylinder 79—41658
- mixed finite difference and differential eqns., generating function, electron theory appl. 77—82371
- mixed type, with three independent variables, solution with aid of integral operators *(German)* 80—27
- model, with distributed parameters, inverse problem 79—75322
- modified, finite difference soln. 79—9092
- modulated normal wave interaction 79—21563
- molecular collisions, turning point region, approx. method 79—72373
- molecular electron density calc., approx. differential eqn. 80—47864

differential equations continued
- MOS transmission line models, differential eqn. solns. generalised to lossy cases 79—38182
- multilayered cylinders, nonstationary temp. fields with rotational symmetry *(German)* 78—79190
- N-body problem, variation eqns. and eleventh integral *(French)* 77—25921
- nilpotent Lie groups, book 77—26133
- non-Newtonian fluid, effective diffusion of impurity in laminar flow of liquid 78—67228
- non-Newtonian liquid, heat flux from nonisothermal surfaces to gradient flows *(Russian)* 79—68767
- nonhomogeneous elastic rods, similarity soln. of wave propagation 78—59323
- nonLie method for mathematical physics eqns. group props. investigation 80—36832
- nonlinear elastic rods, shear and necking instabilities 77—65682
- nonlinear elasticity, boundary value problems, numerical anal. 79—92945
- nonlinear field eqn. and differential Schrodinger eqn. correction *(French)* 80—77637
- nonlinear functional analysis in Banach space, book 77—2516
- nonlinear optical amplifier, coherent radiation statistical props.• 80—99691
- nonlinear sonic wave, excitation by quasi-monochromatic Alfven pumping 80—106649
- nonlinear transformation-operators, appl. in explicitly solving differential eqns. 79—12568
- nonmonotone stochastic integrals and stochastic differential calculus *(French)* 80—90779
- nonparametric identification for diffusion processes 79—30374
- nuclear reactor safety analysis, void fraction prediction, depressurization of diabatic systems 77—23222
- numerical integration methods, conservation props. 78—45464
- numerical solution, free boundary conditions *(German)* 80—35
- numerical solution, generalised splines and linear multistage formulae *(German)* 80—34
- oil-bearing layer with input parameter correction, discrete dynamic model 80—83778
- one-component plasma in two and three dimens., static props., semi-analytic theory 80—87853
- one-dimensonal heat equation with nonlinear time-dependent boundary conditions, global attraction 78—16754
- operational second-order with feature, self-conjugate extensions *(Russian)* 77—22381
- operational-differential equations of arbitrary order, regularisation of improperly posed initial-value problem *(Russian)* 77—67206
- operator with highly oscill. pot., spectrum *(French)* 77—71180
- optical Bloch equation, stochastic incoherences 79—68373
- optical fibres, uniform theory of inhomogeneous waveguide modes near cut-off 80—28324
- optically thin phase grating, comparison of optical path and differential eqn. methods 80—102823
- optimal control, differential eqn., canonical, functional relation expressed by Volterra series *(French)* 80—73159
- ordinary, numerical integration error estimation 77—9874
- ordinary, suppression of inherent instabilities in initial value methods 79—9090
- ordinary, with numerous discontinuities, numerical anal. 79—21535
- ordinary differential eqn. extended difference soln. *(German)* 79—21538
- ordinary differential eqns., invariant imbedding, Riccati transformations and eigenvalue poblems 77—37
- Orr-Sommerfeld eqn. eigenvalues, series representation 78—38280
- oscillatory theorems for eqns. with functional arguments 77—67209
- Painleve eqn. of third kind, one-parameter bounded solns. 77—57155
- Painleve second transcendent, numerical and asymptotic approx. 78—49675
- Painleve transcendents, geometric struct. and inverse scatt. problems 80—31600
- parabolic free boundary problems, 1-D 77—23856
- parameter sensitivity analysis method for differential eqn. models 78—81453
- Paris differential eqn. for fatigue cracks, numerical calc. of eqn. parameters 78—63384
- particle density in linear harmonic oscillator potential 79—92966
- pendulum, simple, large-amplitude, Fourier anal., for teaching 80—17767
- perturbed boundary conditions, for differential equations in theory of atoms 78—33432
- perturbed motion rel. to KS transformation osculating variables 80—109344
- photographic process, reaction tensor analytical treatment *(German)* 79—83481
- physical growth laws, equations for the growth of a distribution of small physical objects 80—4630
- physical parameter reduction and similarity anal., mathematical theory 80—98785
- piecewise homogeneous body, heat cond. eqn., construction method *(Ukrainian)* 80—33414
- plasma, current-driven drift-wave eigenmodes, stability criteria 79—32769
- plasma, inhomogeneous, Alfven and ion-Bernstein waves, mode conversion and tunnelling 78—34300
- plasma, rapidly changing, numerical integration of ionisation rate eqns. 78—55734
- plasma centrifuges, fluid flow analysis, third-order differential equation solution *(Japanese)* 80—53949
- plasma probe, spherical, slightly ionised continuum, current-pot. curves 77—72494
- plastic hardening medium, equations of steady-state motion 79—12597
- plate, circular, with annular circle constraints, vibrs. and buckling 79—98652
- plate, infinite, with doubly periodic elliptical hole array, two-dimens. stress anal. 78—46892
- Plexiglas, spark energy balance 79—23474
- Poincare-Chetaev's equations, integration *(Russian)* 79—35547
- pointlike and nonpointlike transforms of differential eqns. in cartesian coords., geometrical treatment 78—54159
- Poisson's eqn. in 3-d, direct solns. using algorithms 78—20954
- polymer diffusion equation with hydrodynamic interaction, equiv. normal coord. 80—79966
- polymer dynamics simulation, general theory 78—91210

differential equations continued
polymerisation, multicomponent, differential and integral rate eqn. 78 23944
polynomial approx. for gravity wave diffraction *(Russian)* 79—77143
potential operators and the inverse problem of classical mechanics, differential eqns. 79—2618
preturbulence in Lorenz fluid flow model 79—72883
product integration with applications to differential eqns., book 80—41967
pseudo-differential eqns., Fourier integral distribs. and Denjoy-Carleman classes *(French)* 77—67198
pulmonary gas transport models, boundary conditions and geometry 80—85426
quantum scattering theory, variable interval variable step method for soln. of linear second order coupled differential eqn. 80—105527
quantum three particle system, action-angle variables 80—95708
quasi-one-dimensional flow equations, exterior differential form represent. *(Japanese)* 78—8243
radiative heat transfer problem solvability, radiation, scatt., absorpt. 80 33436
radiative plus conductive heat transfer, differential anal. method 80—74699
randomly transitional phenomena in the system governed by Duffing's equation 79—54055
rapid reaction of two chemical species in the presence of weak random advection and molecular diffusion 79—66261
reaction-diffusion systems with explicit traveling wave and transient solutions 80—22207
real ray tracing when ray direction is complex 79—9126
real-space renormalisation giving differential renormalisation-group eqns., two-dimens. triangular Ising lattice 78—65881
rectangular plates, semi-analytic solution for free vibr. 79—18778
reduced model theory, hydrodynamical approach for vel. autocorrelation functions 80—27135
relay systems, bifurcation and stability from third order differential equation *(Russian)* 79—46247
renal counterflow systems, numerical soln. using sparse matrix. techniques 77—21545
Ricatti eqns. depending on parameter, soln. of Fredholm integral first kind eqn. *(Russian)* 78—54153
Riccati equation, matrix differential, steady-state soln. calc., iterative algorithm *(Russian)* 77—49585
right-hand part determ., inverse problems, uniqueness theorems *(Russian)* 77—22376
rigid body motion about fixed pt., order reduction of differential eqns. *(Russian)* 77—49590
rod, thermal conduction, dynamic behaviour of distributed systems *(Dutch)* 80—28407
rotational Brownian motion of an asymmetric body 79—54062
rotationally inelastic scatt., coupled eqns. for single initial state, variation-iteration method 79—68301
Runge-Kutta-Nystrom condition equations, resolution through eighth order 77—22398
satellite motion, numerical integration of eqns. of motion 77—33327
saturated steam parameters in reactor containments with escape of coolant, equations of state 80—68764
scattering, inelastic, of ats. and mols., coupled eqns. soln. method in adiabatic approx. 79—3524
Schrodinger, roundoff error anal. by Numerov method 79—2643
Schrodinger one-dimens. operator, bound state in one-dimens. 78—62
Schwarzschild black hole, master differential eqn. for perturbations 77—26214
SCL current charge distribution discharge, with shorted and open electrodes 80—6863
second order, for lagrangian system 80—52015
second order, without first derivatives, fourth-order numerical method 80—86107
second order differential equations, symmetries and invariants 80—82915
second order equation invariants, auxiliary, eqn. struct. 80—68021
second order hyperbolic differential equations, initial value problems *(German)* 78—20952
second order linear systems with periodic coeffs., approx. method for stability anal. 80—12892
second-order, degenerative, boundary-value problem solution, asymptotic expansion *(German)* 80—32
second-order, hysteresis model *(Russian)* 77—33840
self-adjointness of Schrodinger-type operator powers 78—81877
self-oscillating system analysis, accuracy of first approx. *(Russian)* 77—26134
semiconductor, math. simulation of zone melting process *(German)* 79—28913
series analysis methods, integral approx. methods, appl. to Ising model susceptibility 79—71392
sharp boundary Vlasov-fluid screw pinch, free and forced m=0 oscillations 80—38636
shear stress distribution caused by transverse force, rails of DIN 15087E *(German)* 79—61647
shell, spherical, non-shallow, moderately thick, stresses and deform. 79—32241
shell wall anal., circular tanks under axisymmetrical pressure 79—46202
shells, cylindrical, thermoelastic problem 80—38273
shells, thin conic, with asymmetric edge loading, Newton polygon soln. *(German)* 77—57199
shells of variable thickness, eqns. of motion *(Russian)* 77—39226
single sphere, mathematical model of melting *(German)* 77—89521
single-rotor corrected gyrocompass motion subject to random parametric disturbance *(Russian)* 79—10456
singular perturbed system of semiconductor theory, asymptotic soln. *(Russian)* 77—57160
singularly perturbed boundary value problem with turning point 79—5972
smooth profile in perfect incompressible fluid in irrotational motion, periodic solns. to eqns. of motion *(French)* 79—41703
soil model, viscoplastic, eqns. and expt. determ. *(Russian)* 78—7619
solar, water heater, low-temp., tubular heat receiver, temp. distribution, heat-balance differential equation solution 79—94464
solar wind two fluid model, numerical soln. using shooting-splitting integration 77—73919
solution righthand part in form of second order homogeneous multinomial *(Russian)* 78—54157
solution using imbedding techniques 79—21536

differential equations continued
sound wave diffraction by hollow elastic cylinder in partial annular layer of finite thickness 80—14506
spin-weighted angular spheroidal functions 78—8222
stability of motion on a ring *(Russian)* 80—42052
state depend. delay difference eqns., jump discontinuities 77—41456
stationary system, diffusion mixing model, approx. soln. 80—79410
steel, deform. resist., softening effects, analytical depend. calcs. *(Russian)* 80—49293
steel, stainless 304, cyclic plasticity, exponential stress-strain law 77—25157
step operators, Lie algebraic props. 78—62052
stiff, soln. method 79—15960
stiffness matrix for sandwich beams with thick anisotropic laminated faces 79—46182
stochastic, and differential inequalities 77—5641
stochastic, with non-Markov processes 79—25989
stochastic and ordinary, connections *(French)* 77—37734
stochastic constraints on iterative maximisation of system of differential eqns. 78—57757
stochastic differential eqns., Green's function soln. by hierarchy method, closure approx. error 80—149
stochastic differential eqns., stability anal. *(Russian)* 77—71188
stochastic differential eqns., stability and boundedness rel. to generalised norm 80—12993
stochastic differential equations, diffusion approx. corrections 79—40466
stochastic differential equations, solns., splitting correls. 78—49770
stochastic eqns. in nonlinear filtering *(French)* 77—17787
stochastic evolution eqns. with general white noise disturbance 78—16734
stochastic functional differential eqns. and systems of differential inequalities 78—77801
Stokes phenomenon associated with differential eqns., numerical investigation 77—41464
stress analysis of cylindircal shell with rigid circular inclusion 79—14267
string response to accelerating mass 77—50875
Sturm Liouville eqns., numerical anal. and eigenvalue problems 80—90655
supernovae, type II, light curves analytic solns. 80—77427
supersonic wave drag of planar singularity distributions 78—83430
swirling viscous flow with applied mag. field, differential eqns. for boundary layer 78—22428
symmetric gyroscope motion, differential eqns. stabilisation procedure including perturbing torques 80—4244
symmetries, first integrals, splittability of dynamical systems 78—36795
symmetries, method of obtaining, relation to separable coord. systems 77—17781
symmetries and differential equations 80—105807
symmetry, algebraic classification *(Russian)* 77—74193
symmetry, group props. *(Russian)* 77—74192
symmetry, non-pointlike transformations 80—98786
symmetry of systems of differential eqns. 78—4465
system of differential eqns., review of Einstein's strength concept 78—16706
teaching with interdisciplinary models and computer 78—77640
temperature pulsation balance in turbulent streams 79—14385
tension determination in elastic element on motionless sheave, hybrid calculator appl. *(Bulgarian)* 80—23894
ternary system isothermal Gibbs-Duhem eqn., direct numerical soln. 79—1511
thinwall framed beam, numerical integration of differential eqns. 77—19520
third order, conditions for asymptotic stability of trivial soln. 79—2599
time depend. diffusion eqn. for neutronic calcs., use of exterior differential forms 78—54871
Toda chain, integrability of two dimensional generalisation *(Russian)* 80—17889
Toda lattice Darboux transformation, differential difference evolution eqns. 80—156
translational motion of nonlinear oscillating gas bubble in compressible liquid in an inhomogeneous sound field *(German)* 80—53495
transonic flow, steady three-dimensional, finite vol. soln. of Euler eqns. 77—55028
transport-relaxation equations, time-depend. variational principle and reciprocity theorem 78—12655
turbulence, two-dimensional free shear flow, modified one-equation model 80—6034
two parallel elastic plates with ribs, deformation, stationary problems, differential eqns. 80—33465
two-dimensional radiative transfer in planar geometry, differential eqn. methods 78—40810
two-electron systems, pair function calcs. 80—32590
two-fluid stratified layers in trapezoidal channel, nonuniform steady flow *(Rumanian)* 79—14452
two-level spin system, mag. moment dynamics in mutually perpendicular mag. fields, of arbitrary freq. 79—3415
two-phase flow in a nozzle, max. mass flow rate determ. 78—71384
underground railway tunnel microclimate, calc. method *(Russian)* 79—68548
upper atmosphere neutral gas expansion, numerical soln. 79—12325
variational inequality related to elasticity operator, soln., dual problem 79—9109
ventilation, human, twin exponential model fitting process development 79—48284
vibrating system solution, linear, damped, of finite degrees of freedom, transformation to quadratic algebraic equation 78—24656
virtual photon spectra calc. by matrix differential eqn. 77—88115
viscoelastic body, forced, geometrically nonlinear vibrations 77—3762
viscoelastic body containing cracks, durability calcs. 80—79227
viscoelasticity, stability problems in mathematical theory 80—27133
viscoplastic medium, optimum control of transient process under press. *(Russian)* 79—72821
viscous incompressible liquid, heat conductivity problem *(Russian)* 80—69897
Volterra eqns., generalised, stability theorem 78—86116
Volterra soliton, collapse into weak monotone shock wave 78—49673
volume holograms with elec. polarisation in grating plane, 2D theory 79—72532
volume phase gratings at higher Bragg angle incidence, coupled wave differential eqns. 80—102666
volume phase holograms, 3-D vectorial theory 79—81385
volume phase holography, vector differential equations solns. 79—81386

differential equations continued
- water drops deformational breakup in wet-steam stream, particular solutions 79−14462
- water transport through unsaturated soil, conservation laws derived from statistical mechanical methods 79−16540
- wave equation with extended stability range, explicit difference method 80−4538
- wave field statistical moments in medium with large-scale inhomogeneities 80−37953
- wave hierarchy interpretation of multiple trapping model 80−6894
- wave motions in continua calc., one-dimensional, non-propagative modes *(Japanese)* 80−4539
- wave processes description *(Russian)* 78−81850
- wave propagation in nonhomogeneous media, Fuchsian differential equation aspects 78−9302
- waveguide theory, cylindrical inhomogeneity in homogeneous medium of infinite extent, guided EM field computation 80−14274
- Weyl's m-coefficient in a B*-algebra 79−63374
- Weyl's theory, singular second order differential eqns., HgH resons. and eigenvalues 77−18997
- Weyl's theory, singular second order differential eqns., predissoc. in mols. 77−18996
- WKB method improvement 79−75383
- WKBJ method, deductions from artificial RI profiles, based on elementary functions 77−38778
- Al, quenched, diffusion solution for point defects in stress field, steady state and transient 78−30780
- H$_2$, diffusion in interstitials, master equation equivalence 78−79794
- He, afterglow, intermediate press., plasma discharge parameter time depend. calc. 79−19102
- He, supercritical, laminar free convection heat transfer, analytical study 79−23311
- ^{3}He-^{4}He dilution refrigeration system, choice of tube lengths and diameters 80−57308

differential scanning calorimetry *see thermal analysis*

differential thermal analysis *see thermal analysis*

differentiating circuits
- ECG R-wave identification by derivative amplitude meas. *(Bulgarian)* 79−96536
- electron beam parameter meas. collector plate amplifier 79−75653
- LF signals, applications to biological expts. 79−12044
- neutron radiography edge enhancer 79−24706
- voltage-time derivative, determ. from slowly varying voltages 77−82546

differentiation
- *see also differential equations*
- backward differentiation method, extrapolant formulation, appls. to chem. kinetics eqns. 78−48628
- differential operators, direct derivation in curvilinear coords. 78−12478
- education, exterior algebra and exterior differential forms for electromagnetic problems 80−57037
- elasticity equations transformation 79−2630
- error estimates 80−29
- first derivatives, construction of approximations of high order of accuracy *(Russian)* 77−9873
- full-field numerical differentiation 79−59922
- generalized calculus and its applications, review 79−35527
- global numerical differentiation by compact polynomial splines, accurate space derivative method 77−13597
- interfacial tension, electrochem. data numerical differentiation by Fourier transformation 78−41139
- IR spectra differentiation using Fourier transforms 79−67397
- molecular mechanics computer program MOLMEC, design and performance 78−13410
- numerical differentiator for atom orbital calcs. 79−81147
- objective and regular differentiation and integration, constitutive law and transport *(French)* 80−57090
- parabolic partial differential eqns., finite element methods 79−72797
- partial derivatives, teaching, appls. to environmental problems 77−13523
- spectra, filtering props. of polynomial methods 80−66900

diffraction
- *see also acoustic wave diffraction; diffraction gratings; diffractometers; electromagnetic wave diffraction; electron diffraction; neutron diffraction*
- acoustic-gravity waves in upper atmosphere, diffr. around spherical Earth 78−4016
- atom diffraction by cryst. surfaces, reson. effects 77−35447
- atomic scattering theory, diffraction and angular momentum effects 79−89734
- atoms, diffr. by crystal surface, quantum theory approach 80−42104
- boundary diffracted wave calculation, potential vector singular over closed curves in surface *(Spanish)* 80−12911
- caustics anal. in two dimens. diffraction catastrophe patterns 77−17827
- corner diffraction, Albertsen's coeff. testing via spectral domain approach 80−87304
- cylindrical longitudinal pulse, diffracted by crack 80−92082
- diffractals (wave interaction with fractals) 79−58549
- diffraction of plane shock wave at angle in ideal compacting medium *(Russian)* 78−63357
- dipole, electric, on system of two concentric spherical segments *(Ukrainian)* 80−23603
- direct method in diffraction problems at smooth unbounded wavy surfaces in inhomogeneous medium *(Russian)* 79−75363
- elastic longitudinal waves, diffr. at elastic circular inclusions (fibres) *(Russian)* 78−63368
- elastic spherical wave at wedge *(Russian)* 77−35073
- elastic wave, diffr. at segment, exact solns. 77−84189
- elastic wave, two-dimensional, for semi-infinite plane screen *(Russian)* 78−28955
- elastic wave front excitation and diffr., by point source with semi-infinite shield 80−79202
- elastic wave sH wave diffraction by spherical stratified medium *(French)* 80−53674
- elastic waves diffraction by small cylindrical cavities 79−68636
- elliptical cavity, wave diffraction 80−38320
- EM field of infinitely long cable, diffr. over wedge-shaped conducting media *(Russian)* 78−40484
- forward diffraction of Stokes waves by a thin wedge 80−92167
- Fraunhofer diffraction pattern, angular meas. appl. *(Japanese)* 80−52159
- Fresnel integrals, computer evaluation, for teaching 77−33795

diffraction continued
- harmonic wave diffraction at axisymmetric inhomogeneity, polynomial approx. *(Russian)* 77−50968
- Helmholtz equations, accurate approx. to solns. *(Russian)* 77−57171
- homogenised medium, with periodic structure, wave diffraction *(French)* 79−49057
- hydrodynamic surface gravity waves diffraction at vertical obstacles *(Russian)* 77−55012
- integral transform, associated table 79−97185
- integral transform, sampling theorem 77−45678
- integral transform associated with Helmoltz eqn. in diffr. theory 77−67300
- invariant properties *(Russian)* 77−82470
- Kelvin wave diffraction from rotating channel with infinite and semi-infinite barrier 79−46331
- kinematic polarisation of large-mass final states, helicity violation 77−82723
- linear viscoelastic waves, theory of diffraction *(Russian)* 78−65787
- Love waves in infinite strip with surface step, transmission, reflection and diffraction 79−88260
- NMR determination of phys. and biological struct. *(Rumanian)* 78−49874
- non-homogeneous media, non-stationary problem 80−22211
- pattern diameter from theory of extremal functions *(French)* 80−46835
- phase-space projection identities for diffraction catastrophes 80−27162
- plane elastic wave diffraction by wedge, three dimensional nonstationary problem 80−69723
- plane pulse diffracted by plane screen 80−82652
- plane wave, by circular disc 79−53984
- plane wave, on periodic array, reduction of infinite eqn. systems *(Ukrainian)* 77−67205
- plane wave diffraction by smooth cylindrical surfaces *(Russian)* 78−12577
- plane wave field diffraction on terminated wedge, uniform asymptotic *(Russian)* 77−74234
- quantum diffraction, formulation, representations, relativistic and high energy, mixed systems 78−36885
- scalar wave diffraction by two parallel slits in plane 78−49671
- scalar wave diffraction problem for slit, soln. using Fourier orthogonal functions transform. 77−13599
- sea surface waves, structures loading calc., using finite and infinite elements 77−81910
- seismic long-period P-waves diffraction, obs. at Matsushiro *(Japanese)* 79−96744
- seismic wave diffraction at coal seams, approx. diffr. theory for transparent half-planes 80−89974
- seismic waves, diffr. wave features on seismograms in faults prospecting by diffr. method *(Chinese)* 79−12286
- seismic waves, refl. refr. and diffr. in media with elliptical vel. depend. 79−5454
- semishadow field diffraction, boundary wave uniform asymptotics *(Ukrainian)* 78−89350
- shear waves, diffr. at row of round elastic fibres 78−67083
- shear waves, horizontally polarised, finite crack in linear elastic media 79−68652
- shock wave diffraction at small angles in ideal compacting medium *(Russian)* 78−67082
- shock wave diffraction on plane with semicircular cylindrical roughness, numerical integration *(Ukrainian)* 80−22201
- shock waves, von Neumann paradox, Mach reflection 80−28535
- shock waves diffraction and reflection from shock tube, numerical computation *(Chinese)* 80−43735
- simple harmonic waves in infinite nonhomogeneous elastic medium, diffr. by Griffith crack, rigid strips 77−54913
- solitary wave, diffraction by circular island in ocean, shallow-water theory *(French)* 80−83803
- solitary wave diffraction in water, amplitude and direction determ. 78−22361
- Sommerfeld's diffraction problem 80−12916
- spherical wave diffracted by plane screen 80−82652
- stationary problem in non-homogeneous media 80−68
- surface gravity wave diffraction at underwater axisymmetric obstacle, polynomial approx. *(Russian)* 79−77143
- surface gravity wave diffraction by cylinders *(Russian)* 77−68605
- vertical body of revolution beneath surface, waves, scatt. wave field 78−38347
- water-wave diffr. by semi-infinite vertical barrier on rotating Earth 78−83417
- wave diffraction theory, infinite systems of eqns. *(Ukrainian)* 79−49060
- Li$^+$+K, rot. coupling, Fraunhofer diffraction effects 77−65526
- NiO (001), diffr. of monoenergetic He atoms 79−61487
- WC$_x$, (3×5) struct. on W (110) surface, at. beam diffr. and scatt., surface characteris. 79−78819
- ZnSiP$_2$, proton induced Kossel effect *(German)* 77−84601

diffraction gratings
- *see also holographic gratings*
- a spherical, elimination of aberrations 80−33181
- aberration balancing for grating mountings with large aberrations 78−66906
- aberration theory, geometrical 79−55068
- absolute calibration of grating spectrograph for laser wavelength meas. 78−90528
- absolute efficiency meas. device 80−87540
- achromatic interferometer, image form. 78−16838
- alignment monitoring by diffr. from superimposed dual gratings 79−41447
- amorphous semiconductors 77−10989
- amplitude grating plus ultrasound beam, thick-screen diffr. theory for light temporal modulation 77−50755
- anastigmatic mounting for ellipsoidal concave grating 80−106634
- angle measurement between edges of distant objects using diffr. grating 80−86259
- anthracene vapour, optically induced dynamic gratings 80−28289
- aspheric grating for EUV astronomy 78−57451
- aspherical diffraction gratings produced by dioptric elasticity method 77−73962
- astigmatism compensation for concave grating, comparative characts. 79−32067
- astronomical grating spectrographs, physical principles *(German)* 77−56830

diffraction gratings continued
astronomical grating spectrometer, transmission efficiencies of EUV and soft X-rays 77−60621
astronomical universal stellar photometer, using diffr. grating *(German)* 77−17379
asymmetric grating formation on glass waveguide surface, ion etching method 79−10418
autocollimation, resonance light scatt. by echelon *(Russian)* 77−88640
beam sampling mirror gratings, optimal design 77−14791
beam splitter using diffr. grating combination, for Michelson interferometer 78−70205
bi-metallic diffraction grating study 80−87525
binary phase gratings for fibre-optic communications 80−64201
blaze properties, first, second and third order 77−79945
blaze wavelength change of concave gratings 77−58448
blazed, diffr. efficiency theory 78−13790
blazed dielectric gratings, Bragg-reflection approach 79−1013
blazed dielectric gratings, surface wave scattering 80−48136
blazed dielectric gratings for integrated-optics applications, microwave models 80−87564
blazed dielectric gratings with high beam coupling efficiencies 80−64211
blazed grating efficiency and selection criteria 78−25966
blazed grating optical multiplexer, 1.1 to 1.5 μm, for WDM transmission system 80−38100
blazed gratings in extreme off-plane mountings, X-ray efficiencies 77−82656
blazed replica grating coupler for optical waveguides, design and fabrication 77−88972
Bragg and Raman-Nath diffr. regimes rel. to grating thickness 78−71028
Bragg diffraction grating, guided light refl., deflector appl. *(French)* 77−65621
Brewster affect analogues 79−13901
broad band grating filters for thin film waveguides 77−83962
buried metal grating coated with polished dielec. layer and dielec. multilayer, phenomenological theory 79−50374
causality and classical interference and diffraction phenomena 79−55049
CdS, single crystals, laser emission from surface diffraction grating 80−95900
chalcogenide amorphous film, grating direct writing using SEM 78−83121
chirp-grating lens for guided-wave optics 79−7232
chirped gratings for integrated optics 77−34963
chirped gratings in broad band filters, theory 78−25994
chirped-grating multiplexers in dielectric waveguides 77−58445
circular scale calibration by reflection grating polygon *(German)* 80−86250
coded grating method for measuring three dimensional objects 78−86240
coherent optical system, resolving power enhancement by aperture synthesis 78−25987
coherent synthesized aperture system, image form., resolution improved by diffr. grating 78−50715
colour filtering, zero diffr. order microimage system 79−18503
concave, defocusing compensation in const.-deviation monochromator 78−46792
concave, efficiency changes across the ruled area 80−91896
concave, for tunable linearly polarised TEM$_{00}$ operation of CO$_2$ laser 77−19344
concave, meridional focal curves of Seya-Namioka mounting *(Russian)* 77−64658
concave, stigmatic, numerical control ruling engine development *(Japanese)* 77−19464
concave, with curvilinear lines, ray path calcs. *(Russian)* 77−88958
concave grating, polarisation anomalies 80−69519
concave grating efficiency in VUV region, diffusion pump oil contamination effect 80−14429
concave grating efficiency meas. at grazing incidence 78−33825
concave grating grazing incidence mounting, use of curved slits 79−58858
concave grating mirror stable resonator, approx. anal. *(Chinese)* 79−50324
concave grating mounting, for visible spectroscopy 78−50913
concave grating optical demultiplexer, 0.7 to 0.9 μm, expt. results 80−38099
concave spherical gratings with compensated astigmatism in Rowland mountings 78−30081
concave stigmatic grating mech. prod. on spherical surface 80−38109
conducting rectangular bar transmission gratings 78−62993
conical and classical diffraction mountings, for XUV gratings 79−3780
corrugated dielectric waveguide, radiation loss calcs. 79−41461
corrugated waveguide boundary, TM-polarized light diffraction, zero diffraction effect 79−64339
corrugated waveguide leaky modes, anomalies of dielec. coated gratings *(French)* 77−79969
corrugated waveguides and lasers, improved coupled mode analysis 78−46842
cosmic X-ray spectroscopy, transmission grating behind grazing incidence telescope 77−64654
coupler, chirped and curved, for focusing beam 80−78979
couplers, anal. and design 78−1320
cross-hatched grating replica for calibration of electron microscope 79−2893
crossed (doubly-periodic) gratings, finite-difference method 79−1002
crossed Gaussian volume grating, Bragg diffr. of Gaussian beam 77−65569
crossed gratings, EM theory of diffraction and absorption 79−18337
crossed gratings, finely conducting, appl. to solar absorpt. of metallic mirror 79−23057
crossed lamellar transmission grating, exam. of diffr. props. 78−59139
crossed-beam diffraction gratings theory 79−23071
crossed-beam volume gratings, three dimens., diffr. characts. 80−78975
curved, coupled mode theory 80−83668
curved-line grating form., use as reflectors and laser resonators 77−88971
Czerny-Turner grating monochromator, Cary principle dynamic dispersion determ. 80−58666
deep dielectric gratings, light diffr., transform. props. 80−99835
demultiplexer, low-loss optical, for wavelength division multiplexing systems, 0.8 μm region 79−98463
demultiplexer for wavelength division multiplexing system 79−64309

diffraction gratings continued
DFB resonators, dielectric waveguide with periodic surface inhomogeneity 77−7146
dielectric, plane wave scatt., numerical anal. 79−886
dielectric coated gratings, complete absorpt. of P-polarised specific wavelength light 78−25957
dielectric coated gratings, general integral theory 78−66909
dielectric gratings, arbitrary profiles, scatt. and guiding of EM waves 80−96005
dielectric gratings for beam couplers, network methods for integrated optics 78−38070
dielectric waveguide, energy diffraction input induced power depend. on impact parameter 80−64170
differentiation by spatial filtering 78−1171
diffractive logic elements for optical computers 80−78993
β-dinaphthylene oxide vapour, optically induced dynamic gratings 80−28289
dispersive delay line, optical pulse squaring effects 77−88808
displacement angle monitoring using diffr. gratings 77−33973
double grating diffraction shearing, for MTF meas. 79−64366
double grating P-polarised plane wave diffr., Fabry-Perot interferometer appl. 79−81544
double monochromator, GDM 1000, spectral anal. of low intensity emissions 79−80701
double monochromator with nonclassical concave diffraction gratings 80−38110
double-grating monochromator, theory 80−58708
dual-grating direct-reading spectrograph mirror system design and performance 80−81397
dye DFB laser with integrated Si and polyurethane channel waveguide 80−74373
dye laser, double wavelength operation using gratings at grazing incidence 80−53317
dye laser, tunable DFB, with fan-shaped grating 77−88739
dye laser, two-wavelength single mode operation, using grazing incidence grating 80−53329
dye laser cavity, pulsed, concave grating for beam expansion and spectral dispersion 79−59721
dye laser systems with dynamic DFB, freq. tunable over whole gain profile 79−50317
echelle efficiencies, theory and expt. 80−102802
echelle grating monochromator, spectral efficiency 79−98461
echelle spectrograph for high-resolution stellar spectra 78−96396
echelle spectroscopy, astronomical applications 77−25951
echelle-type grating spectrograph, advantages *(Polish)* 80−26745
edge-type reflection gratings, anal. algorithms 78−86998
education, diffraction grating and interference effects, electronic cct. analogue 79−9052
efficiency, and scattered light, groove shape effects 77−39044
electrically controllable refl. type, for intracavity laser modulation 77−58357
electrically controllable reflection type, effects of electrode config. on voltage depend. diffr. pattern *(Japanese)* 79−94347
electro-optical, polarisation refl. 77−3660
electro-optical Bragg deflection modulators in corrugated waveguides 79−59844
electron-beam and photolithographic fabrication of guided-wave optical components 78−13818
electronic, moire topography appl. *(Japanese)* 79−75577
electronic analog 80−46753
electrooptic deflector of blazed grating type, multistage system 80−106625
electrooptic diffraction modulator, large-aperature 80−33179
EM theoretical developments 80−106633
EM wave props., theoretical model 80−91732
EM wave reflection from boundary of medium with sinusoidally modulated permittivity 78−25778
EM wave scatt. by plane grating in homogeneous medium, point matching method 78−1132
embedded, optical imaging, for meas. by moire fringes *(German)* 80−23805
embossable surface relief structures for black and white, colour reproduction, ZOD images 78−65990
energy absorption and anomalies, rel. to surface waves, general theory 78−94447
etching monitoring using grating test pattern, appl. to SiO$_2$ and Si$_3$N$_4$ 78−76775
evanescent wave holography using Gaussian beam, recording geometry and colour sensitivity 80−58473
fabrication, photochemical replication for space astronomy 80−14490
fabrication and performance testing 77−27361
far IR polarising metallic cloth with periodic slits 79−14112
far IR research, grating era (1925-60) 78−4455
far UV transmission grating monochromator for use with reson. radiation lamps 77−27364
film waveguide, diffr. optical coupling 77−11045
filter with surface corrugated diffr. grating, characts. for oblique incidence 78−50949
finitely conducting cross grating theory 80−106635
finitely conducting crossed grating applications 80−106636
first order waveguide grating filters, random fluctuations 79−94369
fixed groove depth lamellar grating Fourier transform spectrometer 80−77885
formation on optical waveguide surface, ion-beam etching through photoresist mask 80−14492
four-layer waveguide diffractive injection efficiency optimisation *(Russian)* 80−64206
four-wave diffraction of thick transmission gratings, analytical solutions 80−23617
Fourier hologram recording in optical system with synthetic aperture 80−95852
Fourier multiple-imaging system, compensation of distortion 79−76640
Fraunhofer diffraction pattern by ultrasonic phase grating with laser point source 77−79747
Fredholm integral eqn. formalism 78−63192
frequency shift laser meas. of water and wind velocities 77−39385
Gaussian beam diameter measurement, Ronchi ruling method 79−55169
Gaussian beams, waveguided, coupled by misaligned or curved grating effect 80−33228
generation by microcomputer, appls. to human visual system 79−2172
geometric optical theory 80−32904

diffraction gratings continued
- grating equation, Hilbert's independence integral 79—899
- grating mirrors, periodic mode losses and optimal geom. characts. *(Russian)* 79—27434
- grating profile optimization, inverse scattering methods 80—48142
- grazing incidence diffraction gratings, efficiency in soft X-ray region 78—63187
- grazing incidence grating efficiencies, rel. to dye laser tuning 79—36990
- grazing incidence grating techniques to tune flash lamp pumped dye lasers 80—95914
- Hadamard spectrometer, curved slits used to increase throughput 80—95149
- harmonic phase grating with inclined layers, Bragg peak angular widths 80—58712
- p-n-heptyloxybenzoic acid, smectic C liq. cryst., two dimensional diffr. grating due to AC electric field, pulsating diffr. 78—15148
- high-energy, IR laser component optical characterisation techniques 80—14347
- high-energy laser diffraction grating evaluation approach 80—14474
- holographic, diffr. efficiency with modulation depth var. 77—3553
- holographic platform, optical path stabilisation with magnetooptic periodic grating 80—99678
- human visual system, adaptation to coloured gratings, aftereffects *(Japanese)* 79—79547
- illuminator using laser light source, geometrical optical anal. *(Russian)* 78—79094
- image, dissector tubes, echelle spectrographs, design considerations 80—91918
- image deblurring using Ronchi rulings 80—43274
- image transmission through monomode fibres, restoration using grating 80—69512
- imaging anal., displacement transducer design appl. 79—86258
- inductive grids for solar appl., theory 77—75666
- infinite multilayered grating, near-field pattern 79—86256
- integrated grating circuit for guided-beam multiple division fabricated by electron-beam direct writing 80—91934
- integrated optical grating circuit fabrication by electron beam direct writing 80—64214
- integrated optical mixer in waveguide based on phase diffr. gratings, for multichannel optical communication lines 79—18554
- integrated optics, crossed gratings appls. *(French)* 79—50441
- integrated optics, determ. of ray directions coupled out of waveguides through prisms and gratings 79—59841
- integrated optics, double diffraction grating coupler with high efficiency 79—3812
- integrated optics demultiplexer with matrix of Si waveguide photodetectors 79—32095
- integrated programmable planar waveguide components formed by optically writing Bragg diffraction gratings into photochromic structs. 80—79011
- integrated-optics elements with distributed coupling, surface waves, review 79—64361
- integrating rod as grating detector 79—94334
- interference diffraction gratings, holographic hallmarkings 79—911
- interference generation method for integrated optics using Fresnel mirror 80—48460
- interferometer-grating spectrograph for high resolution spectroscopy in middle UV 78—77490
- interferometers, grating, used in ballistic experiments 79—97426
- interferometric gratings, three beam interf. images, sinusoidal complex object with phase modulation 80—53208
- interferometric piecewise generation 77—42590
- interferometric spectrometer, moving grating, analysis of spectral imaging capabilities 79—58799
- ion beam erosion, grating profile evolution 79—94374
- IR material and lens evaluation interferometer 77—39121
- IR multidetector spectrometer for atm. temp. sounding 79—25365
- IR planar waveguide with chalcogenide glass-BaF$_2$ emitting grating, mech. fabrication 79—50443
- IR polariser grid prod. process *(Russian)* 78—46795
- IR spectrophotometers using double blazed grating *(Japanese)* 79—40633
- Josephson optical modulator with weak-link diffraction grating 79—98486
- jump in grating period, anomalous wave scatt. 79—18548
- lamellar grating, reson. anomalies, analytical and numerical study using modal expansion technique 79—31791
- lamellar grating Fourier spectrometer for sub-mm and mm spectroscopy *(Japanese)* 77—67504
- lamellar grating interferometer, for optical props. meas. of solids in far IR 79—58774
- lamellar grating resonance anomalies, properties 79—50393
- lamellar gratings, power losses 80—38091
- lamellar reflection grating, theory 78—74982
- laser beam diameter meas. using a grating 80—102745
- laser beam modulator using rotary diffraction grating 78—87080
- laser beam multiplication, interferometric method *(Ukrainian)* 78—90442
- laser beam steering device, magneto-optic stripe domain approach 78—13816
- laser damage resistances compared 77—19283
- laser Doppler anemometers, rot. diffr. gratings for use as beam splitting freq. shifters 77—68721
- laser grating method appl., strain distrib. meas. in plane, opaque surface 79—32407
- laser heterodyne apparatus for measuring small angle scattering from particles 80—1261
- laser mode selector in form of diffr. struct. 79—89951
- laser passive pulse shaping by delayed superposition using grating 77—75580
- laser produced gratings, review *(Rumanian)* 80—87542
- laser pulse shaping with grating pair and filters 79—89940
- laser resonators folded by diffr. grating 78—33755
- laser velocity meter with rotating radial diffr. grating, for vibr. meas. 79—98675
- laser wavelength tuners 79—86183
- laser-induced amplitude and phase gratings, theory 79—94302
- laser-induced grating phenomena, review 77—46752
- laser-induced gratings, method for study of optically excited solids, forced light scatt. 79—41408
- Lau effect, explanation based on coherence theory 80—23619

diffraction gratings continued
- light-induced grating, possible energy transfer control by acoustic vibrs. 80—28267
- liquid crystalline, light diffraction phenomenon *(Polish)* 77—68272
- long-wavelength IR optical filter development status 79—27423
- lossy corrugated structures, plane wave scatt., quantitative results 80—96005
- lossy structures, Brewster phenomena 78—5419
- low-absorption grating beam sampler design, fabrication and testing 80—14475
- magnetic diffraction gratings with alterable magnetic domains for optoelectronics 78—63197
- magnetic domain gratings, and appl. 80—88970
- masters, manufacture using radial metrological pattern generating engine 80—57282
- mechanically ruled and holographic concave diffr. grating parameter relationships 80—87543
- metal shallow grating diffr. efficiency, Rayleigh type and surface plasmon reson. type anomalies 79—55050
- microgratings for guided-beam deflection, electron-beam direct-writing fabrication 80—102856
- modelling of planar transmission-type diffraction gratings compatible with synchrotron radiation sources 80—90964
- modulation-interference spectrum analyser 77—79161
- Moire contouring using virtual moving gratings simulated on computer 78—73968
- moire fringe properties and appls. with regular interval spiral gratings *(Japanese)* 80—53434
- Moire fringe self images of two gratings without contact, partially coherent illum. *(French)* 77—83806
- moire fringes, profile prediction method, fringe sharpening 78—87009
- moire gratings strain meas., long time high temperature appl. 80—38361
- moire interferometry with white light using auxiliary compensator grating 80—31847
- moire pattern calculations, geometrical approach 77—19164
- moire pattern detection by solid-state dynamic self-scanned photocell array 79—32084
- Moire photography, appls. of slotted apertures 77—65053
- moire technique for image alignment, focus and scaling 77—27362
- monochromator, real instrumental function 80—43452
- monochromator for UV-visible spectrophotometer, stray light 78—94445
- monochromator interdependent parameters and performance tradeoffs 79—90006
- monochromator mounting with ruled diffr. grating at 45° off-plane 80—87479
- monochromators of concave grating mounting for space telescopes, VUV region 78—73629
- moving blazed grating, freq. shifting of laser radiation 77—88822
- multichannel apparatus for material analysis using atomic spectra 80—76586
- multicolour image storage on black and white film, using crossed grating 79—31813
- multifunction integrated optic device with mag. alterable phase grating 77—11048
- multiple beam gratings produced by PWM and PPM, high efficiency, beam splitter appl. 79—81515
- multiple beam spectral analyser with thin film waveguide feed, prism radiation tap 77—34944
- multiple imaging with thin phase filters, signal processing approach 78—66772
- multiplexer, microoptic grating, fibre-optic communication applications 80—48408
- multiplexer design for optical wavelength-division multiplexing transmission via single fibre 80—33222
- multiprofile buried gratings, dielec. coated metallic, use as beam sampling mirrors, theory 78—79120
- multisectional linear metrological gratings, prod. technique 77—3686
- nematic liquid crystals, mixtures with optically active substances, stable inhomogeneities and diffr. gratings 78—1988
- non-optical surface topography, by oblique fringe projection from diffr. gratings 78—89437
- null Ronchi grating from spot diagrams 78—5548
- optical demultiplexer, using diffraction grating, for FDM fibre transmission system 80—5845
- optical demultiplexer using Si echelette grating 80—53422
- optical dispersive resonators with system of reflective gratings *(Russian)* 80—96029
- optical filters, diffractive, prepared by reactive sputter etching, microfabrication and evaluation 79—90008
- optical integrated circuits, SEM written gratings in chalcogenide films 79—32087
- optical processor, incoherent, for making 'spectrogram' of 1-D function 80—87528
- optical ray operator method for anal. of diffraction by periodic structs. 80—43257
- optical waveguide photoresist., grating coupler fabrication *(Czech)* 80—28354
- optically etched, transient diffr. light signals 77—19263
- parallel plane, periodic structure, diffr. of plane wave 80—102620
- parallel plate grating, freq. modulation non-redundant scanning of light beam 78—78907
- parametric oscillator, grating-coupled CdSe, tunable 15.5 to 16.5 μm 77—58376
- perfectly conducting gratings, inverse diffr. study 79—94149
- perforated screen, hologram on layers of photoresist 80—28178
- periodic amplitude grating, diffr. of wave with spatial phase modulation 79—98274
- periodic grating, mixed diffraction problem *(Ukrainian)* 80—69323
- periodic grating of cylinders, plane EM wave diffr., orthogonalisation method 77—10821
- periodic grating reflector array for thin film Fabry-Perot laser 78—55471
- periodic media diffr., equiv. of multiwave coupled-wave and modal theories 79—41331
- periodic object single sideband Fresnel diffr. pattern studies 80—106440
- periodic structure generation by coherent beam interference 80—69570
- periodic surface characterisation by US diffraction spectroscopy 78—60974
- phase diffraction grating as laser beam coupler, radiation parameters monitoring 80—10033
- phase distribution controlled correction, thin-film optical waveguide with diffr. grating 79—76850

diffraction gratings continued
- phase grating, 3-dimens., electrodynamic perturbation theory for light diffr. 80—28327
- phase grating, optically thin, comparison of optical path and differential eqn. methods 80—102823
- phase grating testing and meas., visual demonstration of non-uniformities 77—34966
- phase gratings, Bragg regime diffraction criteria 80—48143
- phase gratings, coherently illuminated, defocused diffr. images 78—46523
- phase gratings, Raman-Nath regime diffraction criteria 80—48144
- phase imaging systems, chromaticity, luminous efficiency 78—33824
- phase profiles, waveguides and gratings by optical methods 78—38071
- phase reflection gratings, theory 79—27417
- phase shifts and resonances 78—94446
- phase-anisotropic, diffraction orders state of polarisation *(Russian)* 77—34818
- phase-frequency response of diffraction coupling between two optical waveguides *(Russian)* 79—3778
- phase-inverting grating construction, use in deblurring filters 80—48398
- photoelectric stellar radial velocity spectrometry, use of echelle grating *(French)* 77—91438
- photoelectric transducer for linear displacement meas. 79—50404
- photomixer with spatially periodic photodetectors, characts., appls. 79—12852
- photoreproduction grating with non-regular element struct., freq.-contrast characts. *(Russian)* 79—58825
- photoresist, Shipley AZ-1350B, linearity and enhanced sensitivity 77—72090
- photoresist and GaAs, exposure and etching time optimalisation 80—23816
- photoresist grating structures with variable period, fabrication 77—19460
- picosecond laser pulse length meas. using fast optical shutter and echelette grating 79—64266
- planar, beam scattering at multilayered dielectric structures 77—42630
- planar optical waveguide concentric-arc grating for thin-film spectrograph 80—58778
- planar waveguide, isotropic, polarisation conversion by Bragg deflection coupled mode theory 80—48461
- planar waveguide, isotropic, polarisation conversion by Bragg deflection, expt. results 80—48462
- planar waveguide blazed dielectric diffraction gratings, anal. and design 80—58779
- plane absorption grating, light diffr., effect of total internal refl. 79—64330
- plane four-layer waveguide with diffr. grating, surface light waves 79—55250
- plane grating as polar heliostat for solar chromosphere and prominence obs. during eclipse 79—84674
- plane grating monochromators, fourth-order aberrations 77—62056
- plane gratings, in series, angular amplification 79—90014
- plane metallic gratings, EM wave diffr. 79—10245
- plane transmission diffraction grating in convergent beam 79—72693
- plane wave diffraction by circular transmission grating: finite-difference approach 79—68352
- plasmon anomalies, energy absorpt. theory *(French)* 77—65628
- PMMA, optical waveguide, direct writing of gratings by electron beam 79—46091
- polarisation characteristics, concave gratings mounted in Seya-Namioka monochromator 79—18526
- polarisation properties, phase difference and efficiency quotient 77—768
- polariser for IR spectral region 79—55221
- POPOP vapour, optically induced dynamic gratings 80—28289
- position monitoring technique using double diffraction phenomenon 79—17389
- predisperser for large plane-grating spectrograph 80—73477
- premonochromator for stray light rejection in Raman spectroscopy 77—58438
- prism-grating, prism-prism and grating-grating compounds for deflection angle compensation 80—95990
- production, photographic method 79—71191
- projected, use in direct determ. of bending strain in plates 79—32420
- projection, shape testing appl. *(German)* 79—29322
- pulse shaping and compression using electrooptic deflector with Fourier optical elements 80—53421
- radial grating lateral shear heterodyne interferometer, adaptive optics appl. 80—77843
- radiation generators, echelette use, electron flow *(Russian)* 80—69314
- Raman laser, CW fibre, bandwidth reduction using prisms, gratings and etalons 80—53366
- Raman spectrum of dielec. film, excitation using diffr. grating *(French)* 77—41694
- reciprocity theorem for corrugated surfaces used in conical diffraction mountings 80—1333
- rectangular groove grating as IR polariser 77—3674
- rectangular groove grating efficiency optimisation for visible, IR regions 79—81525
- reflecting polygonal obstacles of approx. 1 wavelength, apparent size 79—89844
- reflection from ideal grating, reson. phenomena 79—3787
- reflection grating polariser for IR 79—1001
- reflection grating with perfect blazing at $n=-1$, design dimensions 77—65555
- reflection gratings, perfectly blazed with rectangular grooves, EM reflection characts. 79—10246
- reflection theory, Rayleigh hypothesis validity conditions 79—50195
- reflective, high efficiency, scattering types 80—99619
- reflective rectangular grating with finite cond. *(Russian)* 77—75414
- relief grating, diffr. anomalies near crit. angle for total internal refl. 80—10035
- replication process 78—66962
- residual ruling errors, magnetostrictive correction method 79—50454
- review of Japanese research 80—10018
- rhomb laser beam sampler, two-grating, inherent aberration correction, inverse filter description 80—37954
- rotating radial diffraction grating, in two-component laser Doppler anemometer 77—3898
- rotating radial diffraction grating as beam splitting freq. shifter in laser Doppler velocimetry 77—39382
- Rowland circle, corrected, least-squares method derivation 80—64161
- ruby:Cr, lifetimes of laser-induced population density gratings, comparison with fluoresc. lifetimes 79—64276

diffraction gratings continued
- ruled, lamellar and holographic, equivalence in const. deviation mountings 80—87474
- ruled blazed plane gratings, efficiency, synchrotron radiation monochromisation 78—63189
- ruled steel grating system for length meas. 80—13039
- ruling engine with piezoelec. control 78—83128
- SAW acousto-optical light diffraction grating, gas laser tuning *(Russian)* 78—33759
- saw-tooth wave target, modulation by optical system with triang. and assoc. filters 80—9817
- scalar domain, asymptotic theory 78—66910
- scattered light, specification and meas. from diffr. gratings 78—78905
- Schlieren apparatus with multiple slit graging, optical inhomogeneity study *(Hungarian)* 80—69515
- second order coherence meas. using microscope and grating 77—41672
- second- and higher-order waveguide grating filters, refl., transmission and loss coeffs. meas. 80—19110
- second- and higher-order waveguide grating filters, spectral response calcs. 80—19109
- self-calibrating grating spectrograph, for light wavelength meas. 78—24869
- self-imaging process, partially coherent light effects *(French)* 77—23621
- SEM written diffraction gratings for integrated optics, characts. 79—68450
- semi-infinite solid-state phase grating, optical props. 78—87155
- semiconductor, ambipolar diffusion meas. using nonlinear transient gratings 78—80000
- semiconductor thin film waveguides, radiation modulation by stationary phase gratings *(Russian)* 78—22209
- servosystem, opto-electronic, correction of nonrectilinearity of ruling engine 78—87174
- shadow-moire fringes, interpretation, grating rot., translation effects, surface topography appls. 79—20304
- SHF two-layer asymmetrical characts. *(Russian)* 77—54649
- sieve screens, two-dimens. array, diffr.-interf. patterns, Kirchhoff approx. 78—83088
- silicate Fe activated glass, diffraction trating recording by UV laser 80—5842
- sine wave grating, linearly variable freq., production method by interferometry 80—10028
- sine-wave grating, average-luminance surround effect 80—51092
- sinusoidal amplitude grating, with apodisation filter, coherent imagery 79—55067
- sinusoidal groove depth determ. using laser 77—83949
- sinusoidal groove gratings, first and second order spectrograph mount efficiencies 78—32889
- sinusoidal interface light diffraction 79—13900
- sinusoidal surface grating, surface plasmons effect on diffr. orders 77—42618
- SISAM, diffracted light from grating affecting modulation 79—6187
- soft X-ray performance of toric gratings fabricated with plane waves 80—90967
- soft X-ray spectra, meas. by photoelectron anal. 80—73557
- Solar Maximum Mission UV polarimeter design, operation and calibration 79—80225
- spatial gratings, transient light-induced, by successive optical coherent pulses 80—64115
- spectrograph, astronomical, with holographic and ruled diffr. gratings 78—40831
- spectrographs, anamorphic magnification and appl. 79—66927
- spectrometer with diffraction grating for X-ray microanalyzer 78—4746
- spectrophotometer, cutoff system for filtering out higher spectral orders in 400 to 200 cm^{-1} region 80—28334
- spectrophotometer, stray light sources 77—41701
- spectrophotometer for measuring small sharp absorption bands in solids at low temps. 80—86456
- spectroscopic resolution increased with separated gratings and prisms 80—43271
- spherical concave gratings, off-plane stigmatic imaging 77—38808
- spherical grating stigmatic grazing incidence spectrometer, using toroidal mirrors 79—71539
- spherical lamellar grating interferometer for airborne far IR astronomy 77—25942
- square wave grating with μm dimensions, reactive sputter etching 78—33921
- stepped-phase grating spectral charact. 79—76846
- strip waveguide type gratings, resonance props. *(Ukrainian)* 80—33157
- strongly dispersive grating pair, compression of freq. chirped optical pulses 79—50373
- student experiment and gratings made from photographic negatives 77—17741
- surface grating, epitaxial waveguide laser *(Russian)* 78—29973
- surface grating relief pattern profile altering, oblique shadow deposition technique 79—68451
- surface impedance behaviour in vicinity of gratings, EM theory 77—65557
- surface plasmons rel. to diffr. order intensity profile, higher harmonics influence 78—25981
- surface polariton generation through grating couplers 77—85153
- surface polariton interaction with periodic surface struct. 77—47879
- surface relief, for colour image storage and display 77—84004
- surface relief gratings with linewidths below 2000 Å, fabrication 78—42478
- surface-relief phase gratings for image recording and display 77—19429
- symmetry properties of lossless diffraction gratings, time reversibility 80—48422
- tandem Wadsworth mount for high resolution UV spectrography appl. 79—25520
- Tandem Wadsworth spectrographs, horizontal foci calcs. 79—49298
- tapered highly reflective surface-wave grating, refl. spectrum, distortion 78—13867
- TE-wave scatt. from blazed dielectric gratings 77—11005
- telescope-spectrometer combination, optical props. 80—87455
- theoretical model and numerical appls. 80—95786
- thermally induced index gratings Bragg refl., IR optical image conversion, thermal index changes 79—59753
- thick dielectric grating on asymmetric slab waveguide, scattering losses approximate theory 77—68257
- thick planar grating, Bragg diffr. of finite beams, coupled-wave theory 80—63917

diffraction gratings continued
thin absorption and transmittance gratings, diffr. efficiencies 79—27166
thin film electrooptic deflector using induced grating with variable blaze angle 80—99862
thin film optical waveguide, with emitting diffr. grating, inhomogeneity in thickness 80—48425
thin phase grating diffr. eqn. solns. 78—54198
thin phase gratings with arbitrary grating shape, diffr. efficiency 78—66911
thin-film chirped gratings, mode coupling 80—23808
thin-film laser with a two-dimensional diffraction grating 80—9906
thin-film waveguide, with plane diffr. grating, radiation fields and spectrosc. characts. 79—3790
three-dimensional diffraction grating, for integrated optics, Al diffusion into glass 78—42480
tissue characterisation by US diffraction 77—21585
toroidal, monochromatic image of entrance slit, form., theory *(Russian)* 78—12770
toroidal diffraction grating, spectral image at point at spectrometer entrance slit *(Russian)* 78—57452
toroidal grating for EUV spectrograph, stigmatic performance 80—36498
total light absorption, shallow grooves 77—14805
transmission grating, facet-type, aberrations for cosmic X-ray and XUV spectroscopy 78—85851
transmission grating diffraction regimes 78—66912
transmission grating efficiencies for wavelengths between 5.4 Å and 44.8 Å 79—40077
transmission grating efficiencies in 50 to 250 Å range 79—98466
transmission grating for X-ray diffr. into orders, efficiency 80—47157
transmission gratings for meas. of optical constants of An, 100 to 1000 eV 80—93258
transmission lamellar grating theory, diffracted light intensity anal. 78—74981
transmission phase with deep rectangular grooves, light diffr. theory 79—10257
triangular gratings, surface wave guiding, quantitative results 80—96005
triangular groove gratings, first and second order spectrograph mount efficiencies 78—32889
triangular groove gratings, simultaneous blazing 78—38004
triple grating polychromator for Thomson scatt. 77—43059
tunable moire grating for optical mapping 80—5832
tunable narrow-band thin-film waveguide grating filters, performance 80—38124
two-dimensional waveguide analysis with misaligned or curved gratings 79—23092
ultramicrometer technique using composite diffr. grating 78—4589
unpolarised monochromatic light, total absorption by crossed grating 80—106448
UV region, 300 to 2000 Å, simple selection rules 78—55435
UV space instrumentation, comprehensive analysis of gratings 79—8839
vacuum UV efficiency, conference on synchrotron radiation instrumentation, Orsay, France (Sept. 1977) 78—62999
vacuum UV region, use of diffr. gratings, review 79—46029
vapour dispersive delay line, pulse squaring effects 77—72035
volume diffraction gratings as filter, for image restoration 78—94378
volume diffraction gratings with inclined layers in thin-film optical waveguides, coupling efficiency 79—90028
volume reflecting grating parameters determ. for freq. selective optical elements *(Russian)* 80—74492
VUV concave gratings, holographic and conventionally ruled, efficiency meas. 80—91910
waveguide grating, diffraction efficiency, Brewster's law 80—91935
waveguide lenses, Bragg and Luneburg type 80—10050
waveguide single beam coupler with large grating periodicity 77—39114
wavelength multiplexing devices for multimode optical fibres 77—79926
wavelength tuning of SISAMs 79—26143
white light processing using diffr. grating method 80—106470
wire, potential use in meas. of IR laser beam parameter 77—730
Woods anomaly angular alignment gratings 80—69503
X-ray, concave grating in Apollo Telescope Mount EUV spectroheliograph expt. S082A 77—60597
X-ray blazed gratings, photofabrication 77—5966
X-ray grating, astronomical spectroscopy appl. 77—10155
X-ray grating optimal blazing configuration calc. 80—105762
X-ray gratings, diffraction efficiency and radiation resistant substrate materials 80—90960
X-ray gratings for wavelength 0.05 to 20 nm 77—54030
X-ray gratings in GMS mount 79—75664
X-ray grazing incidence spectrometer, crossed optics principle 80—314
X-ray lithography, spatial period division, submicrometre linewidth grating prod. 80—69556
X-ray spectrometer-telescope system for solar corona studies 80—105168
X-ray spectroscopy, ultrasoft, electron microprobe local anal. of light elements 80—99027
X-ray transmission gratings, aberrations, testing, astronomical appl. 79—25508
X-ray transmission gratings, expt. and theoretical props., astronomical appl. 79—25509
X-ray transmission gratings for 7-304 Å operation, efficiency and resolution 80—82195
XUV gratings, classical and ionical mountings, EM diffraction 78—63188
XUV spectroscopy, grazing incidence spectrograph-monochromator, 5-900 Å region 79—17506
zero order diffraction microimage reproduction from surface relief gratings 79—17518
Ag weakly modulated surface, light diffr. 77—31132
Ag, with LiF coating, p-polarised reflected light intensity, reson. anomalies 77—3665
Al, Au coatings, UV light polarisation at grazing incidence 78—87129
Al blazed grating, MgF_2 coated complete absorpt. of P-polarised specific wavelength light 78—25957
AlGaAs DH laser with external grating oscillation properties 80—48247
AlGaAs heterostructures in integrated optics 77—75713
As_2S_3 amorphous film waveguide and grating coupler 80—53448
As_2S_3 film, diffr. efficiency of continuously etched gratings 78—38019
As_2S_3, film waveguide, acoustooptic deflection and modulation of light by stationary phase grating struct. 80—5841
As_2S_3 thin film, diffr. grating production, using laser photolithographic process, image evaluation 78—42479

diffraction gratings continued
As_2S_3 thin films for integrated optics, photodetector elements, relief-type diffraction gratings 79—32094
$Ba_2NaNb_5O_{15}$ crystal domains, amplitude modulation of light by diffr. 79—59832
CdS, obs. of acoustically induced space charge gratings 77—7203
GaAS, (110) oriented, preferential chemical etching of blazed gratings 79—37067
GaAs, diffraction gratings prod. by interference photoetching 77—46805
n-GaAs, surface recomb. vel. meas., diffr. from transient optical grating 79—1604
GaAs:Zn waveguide, light coupling at fundamental absorption edge 79—23082
GaAs-GaAlAs grating coupled lasers, output power efficiency 77—79858
GaInPAs/InP heterostructure DFB laser under optical pumping, lasing characts. 80—87396
Ge reflectivity changes due to illumination by beams of unequal frequency 79—76749
Ge surface reflectivity changes and moving diffr. grating efficiency 80—58662
InAs, temporary diffr. grating form. on surface 79—59801
InP, n- and p-type, surface recomb. vel. meas., diffr. from transient optical grating 79—1604
$LiNbO_3$, acousto-optic interaction, phase grating production 79—41454
$LiNbO_3$, acoustooptic interaction, unguided light deflection via SAW 77—8543
$LiNbO_3$ blazed grating electro-optic deflector development 77—42627
$LiNbO_3$ diffused waveguide, induced diffr. grating, integrated optics applications 79—98511
$LiNbO_3$ grating-tuned picosecond IR source with CdSe down-conversion 80—74435
$LiNbO_3$ waveguide, corrugated, electro-optic scanning of light diffr. from grating output coupler 78—63172
$LiNbO_3$:Ti optical waveguide, SiO_2 thin film grating, surface wave mode conversion, static strain-optic effect 80—87561
MgF_2 layered Al, coating effects on diffraction grating efficiency 77—39064
Nd:YAG laser, coherence time meas. of picosecond pulser by light-induced grating method 80—53347
(Pb,Sn)Te diode laser, grating coupled emission 77—79860
Pb(Zn,Ti)O_3 piezoelectric electrically deformable diffraction grating 80—78963
SiO_2 thin film grating for $LiNbO_3$:Ti waveguide mode convertor and reflector 80—64216
YIG magnetic bubble domain grating, light diffr. *(German)* 79—95737

diffraction instruments *see diffractometers*

diffraction model
$\pi N \to \pi(N\pi)$ diffr. process, $N\pi$ absorbed two-component model 77—18254
absorptive diffraction cross section zeros 78—29322
associated prod. Mueller-Regge theory, average multiplicities determ. 78—45893
atmospheric secondary nucleon spectra, 10^2-10^4 GeV, 2-component model *(Russian)* 78—41612
Ball-Zachariasen model of diffractive scattering, numerical soln. near singularity of Frechet derivative 80—9158
Chou-Yang model and s-channel helicity conservation 79—63449
coherent production on nuclei and measurements of total cross sections for unstable particles 80—102034
convergent polynomial expansion, lines of zeros, slopes of diffr. scatt. 78—45892
current-current model for diffractive processes, pomeron-photon analogies 77—87984
Deck model, rescattering effects for diffr. dissociation of hadrons 78—4844
Deck model of diffraction dissociation, rescattering effects, analytic treatment 79—22080
diffraction peak slope inequality in elastic collisions of particles of arbitrary spin 77—41832
diffractive bumps, gluonic excitation Regge trajectories from bag and dual models 79—2978
diffractive dissociation in high-energy collisions, information about pomerons 77—71533
diffractive dissociation of 200 GeV/c protons, 4 and 5 particle final states *(Russian)* 77—34188
diffractive dissociation processes and quark-antiquark jets 80—95246
diffractive hadronic reactions, statistical description of multipion prod. 80—95260
diffractive production amplitudes for $\alpha_P > 1$ 77—38151
diffractive production and hadron structure 79—71732
diffractive resonance prod. and pomeron f-dominance 77—41830
diffractive scatt., field theoretic model with quark field operators 79—26318
diffractive states, large mass, forward prod., multichannel eikonal model 78—82181
dissociation, duality and mass-slope correl. 77—82725
double pomeron exchange characteristics, inclusive hadron-hadron reactions, cross section 78—17003
Drell-Hiida-Deck model and diffractive dissociation, review *(Russian)* 79—3007
dual Deck model, three component, factorisation and double diffraction dissociation 78—8621
dual unitarization scheme with several trajectories, diffractive scatt. predictions 79—89133
eigenchannel versus physical channel approaches in D-many channel problem 79—54328
eikonal model of hadronic matter distribution of particles and nuclei 79—26317
eikonal Regge model, opacity and diffr.-dissociation cross section of grey disks 78—4845
elastic absorptive amplitudes, unitarity bounds involving total cross section, forward slope and curvature 79—75750
elastic hadron-hadron diffraction scatt. processes, scaling, conformal mapping without spurious cut 80—82992
elastic scattering, small and large momentum transfer relations *(Russian)* 80—86698
elastic scattering of diffractive states, shadow approach 77—67638
exclusive ν production processes, neutral current props., Lorentz struct., internal symm. 77—18267

diffraction model continued
exotic baryon interpretation of narrow mass enhancement at 1360 MeV, diffr. dissociation 78−12888
factorisation props. in direct and crossed channels 78−45894
fine structure of inclusive and semi-inclusive spectra, fragmentation, cluster, Chew-Pignotti models *(Chinese)* 79−58984
hadron diffractive dissociation in the quark model *(Russian)* 79−2994
hadron dissociation, diffractive dissociation model, quark states 79−75752
hadron interactions, neutral heavy lepton detection probability 78−8612
hadron parton struct. and diffraction scatt. for soft processes 79−344
hadron photoproduction, diffractive high energy processes, review, book contrib. 80−47309
hadron-hadron diffraction scatt., convergent polynomial expansion, scaling 79−45096
hadron-hadron diffractive phenomena, review 77−57552
hadron-nucleon forward amplitudes, Reggeon exchange absorptive corrections 79−40765
hadronic diffraction, elastic scatt. as tunnelling phenomenon, dual model relation 80−57575
hadronic diffraction mechanism, geometrical space-time formulation 78−443
high energy diffraction scatt., model with shielded pomeron, pp, πp, Kp investigation 78−17004
high-energy diffractive production mechanisms, review 79−36052
high-mass diffraction in the supercritical region 79−22081
hopping model of diffractive and elastic prod. processes 77−22711
impact param. anal. of pp, p$\bar{p}$, Kp, and πp elastic scatt. 77−22799
inelastic diffraction, compatibility of D peripherality with nondiffractive two component struct. 79−13092
inelastic diffraction, unitarity bounds, evaluation including real parts 77−82724
inelastic diffraction cross section, quark model and three reggeon limit 80−102035
inelastic diffraction dissociation cross section, const. fraction of unitary bound 77−10286
inelastic processes, possible extraction of one-photon exchange, $\pi p\rightarrow A_2p$ anal. *(Russian)* 78−444
jet-enhancement coeffs., diffr. scatt. *(Russian)* 78−29316
KNO scaling and multicomponent cluster models 77−49918
low mass diffractive dissociation in a simple t-depend. dual bootstrap model 79−13089
low mass diffractive dissociation in a simple t-dependent dual bootstrap model 79−36042
low multiplicity diffractive dissociation, 1/N dual unitarisation scheme 79−75753
massless non-abelian gluon confinement and rising total cross sections 80−13264
meson diffraction dissociation and helicity conservation, Deck model description 77−38153
meson prod. by neutrinos 78−21416
mixed two-ion component model, charge transfer 77−22701
multiparticle final states and shadow scatt., coherent state representation 77−18255
multiple diffraction exact and approx. calcs. 77−41831
Neveu-Schwarz dual model for $\rho\pi$ system 78−82175
nucleon diffraction dissociation, Deck model with absorption 77−26548
nucleon diffraction fragmentation in NN collisions around 10 TeV, rel. to γ-quantum prod. 79−80174
P+f diffraction model, two component duality and flavouring, Regge fits and pomerons 80−95261
pion multiplicity distribs. in impact parameter space, multi-Regge model 77−14001
polarisation theorem for diffractive excitation at large momentum transfer, favoured helicities 77−71497
pomeron and f exchange in elastic and inelastic scattering 79−36049
pomeron current model for diffraction dissociation 78−4843
pomerons and reggeons *(Swedish)* 77−65146
pp inelastic scatt. diffractive many-channel problem, absorptive s-channel unitarisation 79−17700
proton-hadron high energy collisions, hadron struct. 79−67614
quantum diffraction, formulation, representations, relativistic and high energy, mixed systems 78−36885
quark-gluon interpretation of enhancements in diffractive dissociation processes 78−45839
recoil nuclei registration in particle coherent diffractive prod. *(Russian)* 79−30810
ring hopping model, multichannel eikonal model, nucleon diffractive excitations, falling total cross section 78−21404
scaling of diffraction peak in collisions of arbitrary spin particles 77−18252
scattering amplitudes satisfying geometrical scaling, low and high-energy props. 78−86447
secondary particle multiplicity distribution in nuclei, 200 and 800 GeV *(Russian)* 78−89879
slope of forward diffraction peaks in K^-p, and π^-p elastic scatt. 79−36103
space-time description of hadronic diffraction 77−87960
t-channel diffractive scatt., elastic peak and hadron size 79−45083
three particle systems, diffractive prod. and relativistic rescatt. 79−12988
total cross section rise, parton mechanism *(Russian)* 78−41505
uncorrelated cluster emission model, diffr. dissoc. and multiplicity distrib. 77−13949
uncorrelated jet model, diffractive dissociation 77−6099
unitarity and crossing in high energy scatt., differential cross section in diffraction region *(Russian)* 79−80764
unitarity restrictions on meson-nucleon helicity-flip amplitudes and slope of the diffraction peak 79−54348
unitary bounds on elastic absorptive amplitudes involving total cross section, forward slope, curvature 77−49881
unstable particle+nucleon, total cross section, from diffractive prod. on nuclei, multiple scatt. approach 78−41441
vector gluon exchange model of pomeron, diffraction scatt. 77−30345
VMD model, vector meson diffr. neutrino prod. 77−61277
d inelastic screening, form factor at $t\neq0$ 80−91070
$ep\rightarrow ep\rho^0$ or eX, polarised beam and target, cross section asymm., vector-meson dominance model 77−6135
$\gamma N\rightarrow\phi\pi^0N$, diffractive photoprod., OZI rule violation and cryptoexotic mesons 79−71760

diffraction model continued
$\gamma NN\rightarrow\gamma NN$ forward scatt. amplitude and generalised optical theorem, dispersion relations 79−93446
$\gamma p\rightarrow\pi^+\pi^-\pi^+\pi^-\pi^+\pi^-p$, diffractive production, jet-like structure 80−57606
$\gamma p\rightarrow q\bar{q}p$, quark-antiquark jet diffractive photoprod. in perturbative QCD 80−73714
$K^{\pm}n$, inelastic charge exchange scatt., diffraction approach, convergent polynomial expansion, scaling 80−78095
$Kp\rightarrow K^*p(K^{**}p)$, diffractive prod. and Reggeon-photon coupling analogy 78−45890
Kp meson diffr. dissociation, Deck model and helicity conservation 77−30344
$Kp\rightarrow Qp$, diffractive production, unitary analytic coupled channel model 79−36051
K^-p, 10 and 16 GeV/c, diffractive dissociation, multiplicity structure 79−89197
K^-p, 14.3 GeV/c, momentum transfer distribs. of some diffractive enhancements 77−65179
K^-p, 32 GeV/c, exclusive reactions, diffractive dissociation processes, $\pi^+\pi^-$ and K^+K^- prod. 80−86760
K^-p interactions, 14.3 GeV/c, two body diffraction dissociations, cross sections, mass spectra 78−62464
$K^-p\rightarrow K^-X$, 32 GeV, single and double diffractive dissociation 79−58982
$K^-p\rightarrow N\bar{K}3\pi$, 10 and 16 GeV/c, diffractive dissociation of $K^-\rightarrow\bar{K}3\pi$, $p\rightarrow N3\pi$ 77−46085
$K^+p\rightarrow K^+p\pi^+\pi^-$, 2.7 to 32 GeV/c, impact parameter bounds, energy and effective mass dependence 80−57640
$K^{\pm}p$, elastic scatt. and diffractive dissociation, Regge model with $\alpha_P(0)>1$ *(Russian)* 80−57630
$K^{\pm}p$, inelastic charge exchange scatt., diffraction approach, convergent polynomial expansion, scaling 80−78095
$l+N\rightarrow l'+V+N$, diffr. prod. cross-section calc. 77−34167
μN, 209 GeV, ψ diffractive prod. cross section, $\psi\rightarrow\mu^+\mu^-$ decays 80−102054
$\mu N\rightarrow(x\mu)X$, dimuon and trimuon prod., heavy quark and 4 diffractive prod. 79−93429
$\mu N\rightarrow\mu\psi X$, diffractive and non-diffractive ψ leptoprod. in QCD 80−424
$(n,p\pi^-)$, 100 to 300 GeV, coherent neutron dissociation on nuclei 78−29465
N diffr. dissoc., slope-mass correl. pion-exchange amplitude anal. 77−87959
N diffractive dissociation into Nπ system, near threshold calcs., appl. to $pn\rightarrow pp\pi$ *(Russian)* 78−54623
$n\rightarrow p\pi^-\pi^0$, diffractive dissociation induced by 12 GeV K^- 79−40805
$N\rightarrow\pi N$, diffraction dissociation, two-component model 79−3037
$n+C\rightarrow(n^*\rightarrow\Lambda k\pi)X$, 45 GeV, production cross section 77−82795
$n+N\rightarrow(n^*\rightarrow\Lambda k\pi)X$, 45 GeV, decay prob. 77−82795
$n+p\rightarrow(p\pi\ )+p$, 35-65 GeV/c, diffr. dissoc. 77−13988
$Nd\rightarrow(N\pi)d$, ISR energies, single and coherent nucleon diffraction dissociation 80−22640
$nd\rightarrow(p\pi^-)d$, 26.6 GeV/c coherent interaction, peripherality of nucleon diffr. dissoc. 79−45108
$nd\rightarrow p\pi d$, interference phenomena in coherent production, nucleon diffractive amps., helicity-flip 80−47329
$NK\rightarrow NK^*$, diffractive process, Pomeron current model 77−87958
$NN\rightarrow(N\pi)N$, Deck-model baryon-exchange contribs. 77−49933
$NN\rightarrow(N\pi)N$, mass-slope correl. in Reggeised Deck model 77−22712
$NN\rightarrow(N\pi)N$, nucleon exchange, decay ang. depend., high energy nucleon diffr. dissoc. 77−79284
$nn\rightarrow(p\pi^-)(p\pi^-)$, double diffraction dissociation process in deuteron colliding beams 77−13994
NN inelastic processes, SU(3) breaking, N(1688), Λ(1815) and Σ(1915) states 77−71526
$NN\rightarrow N(N\pi)$ diffractive dissociation process, one pion Regge-pole exchange amplitude *(Russian)* 80−42491
$Np\rightarrow(N\pi)p$, diffraction dissociation, absorptive effects 80−5009
$Np\rightarrow(N\pi)p$, double peripheral description in diffraction model 78−58204
np high-energy scattering, review 77−79283
$np\rightarrow p\pi^-+p$, neutron dissociation reaction, 50 to 300 GeV/c 79−17765
$N\pi\rightarrow N^*\pi$, Gribov-Morrison rule as kinematic effect 77−49999
$N\pi\rightarrow N\pi^*$, diffractive process, Pomeron current model 77−87958
$\nu p\rightarrow\nu+$vector meson + X, neutral currents, generalised VDM, Regge pole anal. 78−41532
p elastic scattering on ^{3}He, ^{3}H, 156 MeV, differential cross section, diffr. theory of multiple scatt. 77−61404
$p\rightarrow p\pi^+\pi^-$, coherent difractive excitation at 20.8 GeV/c *(Russian)* 77−34187
$p+A\rightarrow p\pi^+\pi^++A$, 2.25 and 15.3 GeV, coherent diffr. reaction, Glauber model fits 77−22809
p+emulsion nuclei diffractive coherent prod., inclusive and exclusive channels 78−62530
p+n nucleon diffractive 19.2 GeV/c excit., 2- and 3-particle decays *(Russian)* 78−473
$pd\rightarrow d+X$, high energy, screening effect in diffr. dissoc. anal. 77−71541
$pd\rightarrow p\pi^+\pi^-d$, interference phenomena in coherent production, nucleon diffractive amps., helicity-flip 80−47329
pn, 37 GeV, diffr. dissoc. of neutrons 77−2873
$pn\rightarrow pp\pi$, 19 GeV/c, neutron dissociation 79−36106
$pn\rightarrow p\pi^+\pi^-n$, isobar prod. in proton diffractive dissociation *(Russian)* 79−80836
$\bar{p}p$, 22.4 GeV/c, multiplicities and forward-backward correls. 78−17061
pp, 63 GeV, Λ_c^+ diffractive prod. at CERN ISR, $\Lambda_c^+\rightarrow K^-p\pi^+$ decay mode 79−89204
pp, diffraction dissociation, dip and kink structs., differential cross sections 80−95284
$\bar{p}p$, pp, elastic scatt. and diffractive dissociation, Regge model with $\alpha_P(0)>1$ *(Russian)* 80−57630
pp 4-prong interactions, 25 and 200 GeV, anal. using parameter invariant quantity *(Russian)* 79−49559
$pp\rightarrow(p\pi^+\pi^-)(p\pi^+\pi^-)$, 24 GeV/c, double diffraction dissociation reaction, cross sections, mass spectra 78−93908
pp and pn polarisation expts. description 77−57564
$\bar{p}p$ annihilation cross sections, corrected differences, fireball model, diffraction cross sections 80−91108
pp diffraction dissociation, 25 and 200 GeV/c, parameter invariant quantities *(Russian)* 78−54655
pp diffraction elastic scatt., Lorentz-contracted geometrical model 77−74722

diffraction model continued
pp diffraction elastic scatt., 200-2000 GeV/c total cross section, energy depend. 79—30753
pp diffraction scattering, convergent polynomial expansion and scaling 79—40797
pp diffractive inelastic scatt. at 42.5 and 52.2 GeV/c *(Russian)* 77—82777
$pp\to\Delta^{++}n$, polarised proton, spin effects in SU(3) and quark model 77—30399
$pp\to\Delta^{++}\pi^{-}p$, polarised proton, spin effects in SU(3) and quark model 77—30399
pp elastic amplitude, geometrical scaling real part effects 78—37232
pp elastic multichannel eikonal model, diffractive dissociation 77—10229
pp elastic scatt., high energy, large momentum transfer, diffraction model with nucleon core 78—74281
pp elastic scatt. cross section structureless behaviour, 53 GeV, disagreement with diffraction models 77—22798
pp large inelastic diffraction in the quark-glue model, gluon distrib. in parton model 79—89138
$pp\to p\Lambda K^{+}$, 12, 24 GeV/c, diffr. dissoc. 77—82779
$pp\to pX$, 50-400 GeV, differential cross sections, P diffractive dissociation *(Russian)* 80—5030
$pp\to pX$, triple-Regge fits, duality struct. of inclusive diffr. dissoc. 78—8715
$pp\to pn\pi^{+}$, 19 GeV/c, nucleon dissociation and spectator concept 77—30447
$\bar{p}p\to\bar{p}p2\pi^{+}2\pi^{-}$, 100 GeV/c, diffraction and ρ^{0} prod. in exclusive interactions 78—93909
$\bar{p}p\to\bar{p}p\pi^{+}\pi^{-}$, 100 GeV/c diffraction and Δ^{++} prod. in exclusive interactions 78—93909
$\bar{p}p\to\bar{p}p\pi\pi$, 12 GeV/c, final state diffraction dissociation, cross section 80—99109
pp scatt., absence of multiple-dip struct. in differential cross section 78—82246
pp scatt. at higher energies, differential cross section ratio scaling 80—73741
pp six-prong interaction, 205 GeV/c, diffractive cross-section determ. 78—33097
pp total cross section and small angle elastic scatt. 23.5-62.5 GeV, diffraction peak 79—424
$\phi\pi$ prod. in $e^{+}e^{-}$ annihilation and diffractive photoprod., 4 quark state signature 79—6324
π diffr. dissoc. into 5π at 16 GeV/c 78—82252
π scattering by few-nucleon nuclei, diffractional approx., nuclear structure *(Russian)* 78—650
π^{-}+nucleus$\to(3\pi)^{-}$+nucleus, 15 GeV/c, diffractive dissociation *(Russian)* 78—25250
πN collisions, $N\to N\pi^{-}$ diffractional dissociation, Deck mechanism *(Russian)* 80—86699
πN in nucleus, diffraction dissociation, dip and kink structs., differential cross sections 80—95284
$\pi N\to\pi(N\pi)$ diffraction dissociation, role of nucleon exchange 77—38192
$\pi N\to\pi\pi N$, 16 GeV/c, model for diffractive scatt. 77—50014
πN single and double diffractive prod., monopole transitions and slope-mass relation 77—38152
$\pi^{-}n\to\pi^{-}\pi^{-}p$, 15 GeV/c diffr. dissociation and N* prod. by pomeron exchange 77—41865
$\pi^{\pm}n\to(p\pi^{-})\pi^{\pm}$, 5.1, 9 GeV/c, neutron diffr. dissoc. 77—74714
πp, 16 GeV/c, diffr. dissoc. into $\bar{K}K^{*}$, $\bar{K}^{*}K$ 78—41594
πp, inelastic charge exchange scatt., diffraction approach, convergent polynomial expansion, scaling 80—78095
$\pi p\to 2\pi^{+}\pi^{-}\pi^{0}p$, diffractive dissociation at 16 GeV *(Russian)* 80—22639
$\pi p\to(\pi\rho)p$, A_1 reson. diffr. prod., unitary coupled-channel anal. 78—8687
$\pi p\to(\rho\pi)p$, A_2 diffractive prod., Deck model and Pomerons 79—71733
$\pi p\to(\rho\pi)p$, diffr. dissociation, Deck model and helicity conservation 77—30344
$\pi p\to A_2p$, diffractive prod. and Reggeon-photon coupling analogy 78—45890
πp interaction characteristics at 40 and 10^{4} GeV, comparison 77—61335
$\pi^{-}p$, 150 GeV/c, leading particles and diffraction dissociation, 2-, 4- and 6-prong events 80—68486
$\pi^{-}p$, 200 GeV/c, inelastic diffractive-dissociation cross section 79—22151
$\pi^{-}p$, diffraction scatt. slope parameter oscillation, lines of zeros, convergent polynomial expansion 79—93455
$\pi^{-}p$ differential cross section, diffraction peak compatibility with unitary bounds 79—97610
$\pi^{-}p\to\eta n$, Reggeon field theory, behaviour of A_2 trajectory 80—22594
$\pi^{-}p\to\pi^{-}\pi^{-}\pi^{+}p$, 147 GeV/c, diffraction dissociation 77—2869
$\pi^{-}p\to\rho^{0}\pi^{-}X$, diffractive contrib. in multi-Regge factorisation 80—73753
$\pi^{+}p$, 16 GeV/c, narrow mass enhancement at 1.36 GeV in diffractive (πN) systems 79—45109
$\pi^{+}p\to 3\pi^{+}\pi^{-}n$, diffractive dissociation at 16 GeV *(Russian)* 80—22639
$\pi^{+}p\to(\pi^{+}p\bar{p})p$ 50 GeV/c, narrow baryonium states, diffractive prod. cross sections 80—442
$\pi^{+}p$ inelastic diffr. scatt. at 42.5 and 52.2 GeV/c *(Russian)* 77—82777
$\pi^{+}p\to\pi^{+}(\pi^{+}n)$, 16 GeV/c, prod. and decay processes, Drell-Hiida-Deck model predictions 77—41864
$\pi^{+}p\to\pi^{+}(\pi^{+}n)$, partial-wave struct. of Drell-Hiida-Deck amplitude in diffractive πN system 77—41863
$\pi^{+}p\to\pi^{+}(\pi N)$ 16 GeV/c diffr. process, Drell-Hiida-Deck model anal. 77—61326
$\pi^{\pm}p$, 14 GeV/c, N diffr. dissoc., bubble-chamber anal. 78—66175
$\pi^{\pm}p$, elastic scatt. and diffractive dissociation, Regge model with $\alpha_{P}(0)>1$ *(Russian)* 80—57630
$\pi^{\pm}p\to p\pi^{+}\pi^{\pm}\pi^{-}$, 16 GeV/c, clustering, multidimens. study using Yang variables 80—5020
$\pi^{\pm}p\to\pi^{\pm}(N\pi)^{+}$, 16 GeV/c, spin-parity anal. of diffractively prod. low-mass $N\pi$ 78—17055

diffractometers
see also X-ray diffractometers
θ-θ diffractometer with monochromator *(French)* 79—32058
Astacus, a time focussing neutron diffractometer based on the reverse Fourier principle 79—77457
combined scanning microdensitometer and diffractometer 80—73529
crystallography, modern techniques and apparatus survey 77—4019
electron, electronometric method of meas. intensities, efficiency 79—27881
electron, high-temperature techniques and apparatus, review 80—52237
electron microscope image correction and anal. 78—21275

diffractometers continued
full-circle diffractometer, additional differential ω-motion and linear drive system, γ-ray scatt. for cryst. struct. meas. 80—13192
gamma-ray, using ^{198}Au source at FRM reactor 78—54514
gamma-ray diffractometer, study of electron densities in solids, Compton scattering, Bragg diffraction 80—18059
gamma-ray diffractometry, phase transitions, domain structures, twinned texture studies 80—19678
Harwell, neutron diffractometers, spectrometers and ancillary equipment 79—45527
high-speed scanning laser diffractometer 79—68437
laser diffractometer for rapid anal. of microparticles and biological cells 79—66589
LEED, high-resolution 77—4025
light, on-line electron-optical correlation computing, in CTEM 80—99008
light optical, for electron microscope images operating on line 80—101900
Mossbauer diffractometer using microcomputer 80—7210
multiaxis neutron diffractometer automation 80—102417
neutron, construction, appl. to cation distrib. determ. in nonstoichiometric MnZn ferrite *(Bulgarian)* 78—83656
neutron, flat-cone, utilising linear position-sensitive detector 78—67624
neutron, Multidetector LMT LC 400 CP *(French)* 78—42866
neutron, SIMON, FORTRAN Monte Carlo program for time-of-flight neutron diffractometer simulation 79—50955
neutron, temp. block for 79—94849
neutron, transit-time, for structural investigations of monocrystals 80—64840
neutron diffractometer, converging beam small-angle, calculated resolution 79—10761
neutron diffractometer, time of flight small-angle, for a pulsed neutron source, design study 79—10762
neutron diffractometers using position sensitive BF_3 counters 77—35444
neutron diffractometry, automatic, development, review 79—27879
neutron four-circle, intensities meas. method and computer program for use with twinned and clustered crysts. 78—14247
neutron four-circle diffractometer, cooling down to 3.9K 77—27789
neutron powder diffractometer, KSN-2 diffractometer using nucl. reactor 79—86655
neutron powder high-resolution diffractometer, D1A, mylar collimators 77—4024
neutron time of flight single crystal diffractometer using a position sensitive detector 80—99404
on-line ECIL TDC-312 computer-controlled four-circle neutron diffractometer 78—55787
optical, attachment to electron microscope for immediate image analysis 79—6225
optical, indexing of spiral biological objects on microphotographs 78—96121
optical diffractometer, for anal. scanning electron micrographs, review 79—21864
optical diffractometer analogue of electron microscope 80—69494
photolithographic mask linewidth meas. by diffraction pattern analysis 77—37960
structurometer, diffraction, annular method of recording scatt. indicatrix 79—54165
two crystal diffractometer, neutron spectrometer component, luminosity 78—21807
Si bent crystal gamma diffractometer, X-ray topographic study of large crystals 77—57805

diffusion
see also biodiffusion; diffusion in gases; diffusion in liquids; diffusion in solids; electromigration; membranes; osmosis; permeability; self-diffusion; surface diffusion; thermal diffusion; turbulent diffusion
absorptive medium, signal form distortion *(Russian)* 78—46856
admixtures, convective-diffusive transfer in cylindrical channel, soln. 77—7391
adsorbates, surface diffusion calcs. 80—107633
advective diffusion in branching channels 80—92223
Aerosil, diffusion coeffs. and characterisation by photon correl. spectrosc. *(German)* 79—29418
aerosol, large particle, diffusional phoresis theory 79—55408
aerosol, polydispersity, unipolar charging, charging mobility analysis 78—61059
aerosol, unipolar diffusion charging, particle dielectric constant and ion mobility effects 78—61058
aerosol particle deposition in channel due to diffusion and electric charge 78—90978
aerosol particle settling in flow in parallel plate channel, diffusion effect 79—66371
aerosol particles, volatile, diffusion-phoretic motion 77—56259
aerosol particles diffusion and gravitational settling in tube 78—90976
aerosol ultrafine particle size meas., diffusion battery anal. 79—92010
air pollutants long distant transport, analytical diffusion model 80—94125
air pollution transport, air quality models development for limited wind fetch 80—104533
Allende meteorite, tracer elements high-temp. diffusion rel. to primitive meteorites thermal metamorphism 80—109401
Am-type stars, He downward diffusion effect on envelope circulation 80—4370
ambipolar diffusion eqn. in gravit. field, analytical solns. appl. to F-region 77—78562
anharmonic oscillators, two-component system, diffusion description of vibr. relax. 80—23528
anisotropic porous media, degrees of anisotropy of fluid flow and diffusion (elec. conduction) 77—51109
approximate solutions using Galerkin method 80—166
approximate viscosity matrix, differential-difference representation 80—31518
artificial diffusion parameter, χ, improved form 79—64649
atmosphere, advection diffusion model for real-time forecasting of air pollution episodes in Venetian region 80—77096
atmosphere, eddy diffusion models for mesosphere and lower thermosphere 80—109198
atmosphere, Lagrangian similarity modelling of vertical diffusion from ground-level source 80—51480
atmosphere lowest layers, diffusive character rel. to solar modulation of lunar tide 80—94593

diffusion continued
  - atmosphere pollutants diffusion, field meas. of benefits of increased stack height 80—76676
  - atmospheric aerosol, produced by α-particles, evolution of <0.02 micron particles *(French)* 79—43640
  - atmospheric diffusion, pseudospectral soln. 78—32172
  - Backward stochastic partial differential eqns. and diffusion processes with noisy observations *(French)* 79—54052
  - Baltic Sea horizontal mixing, Lagrangian and Eulerian meas. 80—17290
  - bidisperse pore catalysts effectiveness factors 80—16719
  - binary mixtures, diffusion processes master eqns., kinetic eqns. 79—75446
  - binary solution, advance of interphase boundary 77—9968
  - binary system cluster dynamics, critical diffusion and phase separation kinetics 77—61042
  - bistable nonlinear diffusion eqns., long time behaviour of solns. 79—94759
  - bistable potential, systematic WKB treatment 80—46975
  - bistable potential field, model for diffusion 79—75458
  - bistable potential field, solvable diffusion model 78—8362
  - blood oxygenator, stationary membrane type, O_2 and CO_2 diffusion process 77—78046
  - boundary layer with blowing, numerical exponential box scheme 79—1240
  - boundary value problems, approx. analytical soln. by finite zone continuity method 78—36947
  - boundary-value problem for regions with moving boundaries and particle conservation 77—49696
  - branching diffusion and Markov processes *(Russian)* 79—26009
  - Brownian motion in Bogolyubov's method of abbreviated description 79—21669
  - Brownian motion in periodic potential, correlation functions, Fokker-Planck eqn. method 79—165
  - Brownian moving particle, hyperbolic diffusion eqn., effect of finite correlation time 80—86214
  - Brownian oscillators, non markovian diffusion and Fokker Planck eqn. 77—57285
  - Brownian particle mobility in periodic pot. 79—35632
  - Brownian particles, diffusion of interacting spherical particles suspended in fluid 78—54304
  - Brownian particles, k-dependence of long-time diffusion 80—5645
  - Brownian particles, treated as many boson problem 79—164
  - Brownian particles solutions, diffusion effects, light scatt. theory 77—4939
  - Brownian rotation in external fields, Fokker-Planck eqn. 79—30372
  - Brownian rotational diffusion in n-fold periodic pot., time correlation functions 79—21668
  - Brusselator, two-box model, multiple stable steady states, chem. hysteresis 79—100428
  - bundle divertor, Tokamak plasma, scrape off layer density decrease, model 80—28851
  - Bushveld Complex, diffusion-controlled crystn. model for Cr content vars. in magnetite 80—56421
  - butane, flexible chain molecules, momentum space diffusion eqns. 80—75142
  - capillary-porous bodies, internal mass transfer, influence of inhomogeneous elec. and mag. fields 80—6138
  - catalyst, diffusion in pores, gas chromatography obs. 79—70372
  - catalyst pellet, transient diffusion-react. eqns., approximation using Galerkin technique 79—96357
  - Cauchy problem, classical mechanics of diffusion and Schrodinger eqn. 78—28985
  - ceramic body growth, diffusion theory *(Czech)* 79—69269
  - charged particle transport in turbulent magnetic fields, perpendicular diffusion coeff. 77—42920
  - chemical and biochemical nonlinear processes, oscillations 77—73440
  - chemical diffusion-reaction equations, semilinear parabolic systems, soln. existence and stability 79—47889
  - chemical instabilities model, role of diffusion 79—16027
  - chemical reaction, conc. fluctuations, use of master and Langevin eqns., diffusion effect 78—3313
  - chemical reaction, diffusion equation, nearly degenerate bifurcations, mode interactions 80—85149
  - chemical reaction, diffusion-controlled, encounter-result probabilities, Onsager Monchick methods unification 79—87823
  - with chemical reaction, probabilistic interpretation 78—35645
  - chemical reaction diffusion systems, Chapman-Enskog development of multivariable master eqn. 80—81283
  - chemical reaction diffusion systems, quantum statistical theory, multichannel reactive scatt. 80—81284
  - chemical reaction nonlinear eqns., secondary bifurcation 77—9860
  - chemical reaction-diffusion system, bistable, stationary solns. bifurcation 79—79224
  - chemical reaction-diffusion system, nonlinear, multiscale propag. phenomena 79—91910
  - chemical reactions, diffusion-controlled, continuous-time random walk modelling 80—3297
  - chemical reactions, diffusion-controlled, freq. depend. rate coeff. theory 77—66746
  - chemical reactions, lattice model, coupling of translational and reactive dynamics 78—55696
  - chemical reactions, macroscopic equivalence of fluctuation descriptions 77—77734
  - chemical reactor, diffusion-coupled system, bifurcation diagram and nonhomogeneous steady states 80—16647
  - chemical system, two chemical species reacting at boundary 80—93733
  - chemically induced dynamic spin polarisation, orientation depend. 80—63656
  - chemically reacting multicomponent systems, Langevin forces and noise correls. 77—16823
  - chemically reacting system, coupled heat and mass transfer, finite element soln. 80—68153
  - chemically reactive flow, stiff boundary valued problems in kinetics and diffusion, numerical methods 79—86525
  - coefficient meas., optimal conditions and measuring functionals 77—20106
  - Cole-Hopf transformation for nonlinear parabolic and hyperbolic equations, diffusion and turbulence 79—41680
  - colloid coagulation, 1st-order diffusion effects 79—39213
  - comet belt beyond Neptune, orbital diffusion rel. to short-period comets origin 80—94759

diffusion continued
  - complex diffusion processes and nonrelativistic quantum mechanics 80—90707
  - composite laminates, transient moisture sorption induced stress field 78—34021
  - concentration dependence of diffusion coeff. from single (de)sorption expt., step-by-step calc. method 78—87859
  - conformational dynamics and the rotational isomeric state model 78—90315
  - constrained systems, Hamiltonian construction and diffusion eqns. derivation 80—73258
  - controlled processes, nonequilibrium decay effects 80—66764
  - controlled reactions, passage time approach 80—71903
  - convecting fluid, renormalisation of diffusion coefficient 78—5747
  - convection-diffusion eqn. soln 78—90888
  - convection-diffusion equation, stability of finite difference approximations 80—82730
  - convection-diffusion partial differential eqns., finite element method soln. 78—90889
  - convectional diffusion in parallelogram cross-section pipe with plug flow *(German)* 80—100000
  - convective diffusion to a particle in a fluid with linear kinetics 80—69943
  - convective transport eqns., modified upwind scheme and conjugate gradient method 79—77107
  - cooperative diffusion in temporary network 78—77820
  - cosmic ray diffusion coefficients, calcs. from diurnal intensity var. 79—29952
  - cosmic ray diffusion theory, vel. correl. function 77—73913
  - cosmic ray electrons, galactic confinement and radio emission 77—73910
  - cosmic ray interstellar diffusion in galactic models with halo appl. to proton nucleon component 80—61971
  - cosmic rays, diffusion in solar wind deformed by interstellar medium 79—53680
  - cosmic rays, field-aligned inward diffusion rel. to large amplitude wavetrains of neutron intensity 80—94660
  - cosmic rays, low-rigidity, weak turbulence diffusion theory rel. to mean free paths 80—98524
  - cosmic rays, scatt. in simulated interplanetary mag. field fluctuations 80—51626
  - cosmic rays electron component, diffusion model of propag. 79—53679
  - cosmic rays from 1972, August 7 solar flare, interplanetary diffusion coeffs. 79—12360
  - cosmic rays interplanetary anisotropic diffusion, solar daily vars. vector computation 80—4209
  - cosmic rays interplanetary diffusion, fluctuations and noise rel. to neutron monitor diurnal anisotropy 77—45264
  - cosmic rays nuclear component, diffusion model of propag. 79—53678
  - cosmic rays of highest energy, diffusion from Virgo cluster 80—4208
  - cosmic rays propagation, diffusion model and galactic electrons source spectrum 79—53677
  - cosmic rays propagation, non-field-aligned diffusion effects on neutral monitor diurnal anisotropy 78—32304
  - cosmic rays spatial diffusion coeffs., computation using nonlinear particle trajectories 77—45262
  - cosmological fluid, lepton era, transport coeffs., Weinberg-Salam model 78—32623
  - critical fluctuations, description by means of most probable path 79—49166
  - critical region, appl. of E.V. Tolubinskii's integral method *(Russian)* 77—24378
  - curved shock waves in ideal fluid mixtures with multiple temps., theory of singular surfaces 80—28533
  - cylinder array, convective mass transfer with surface reaction 78—79369
  - dechannelling theory, axial and planar conditions, anal. methods for dechannelled fraction calc. 79—4359
  - dielectric relaxation, by restricted rot. diffusion, dipolar autocorrel. function calcs. 79—4763
  - diffusion process with critical point, eigenvalues discretisation technique 80—172
  - diffusion-controlled processes among partially absorbing stationary sinks 79—54074
  - diffusion-convection const. coeff. eqn., centred differencing, box scheme, mesh size, errors 77—7386
  - diffusion-convection eqn. anal. with explicit difference methods 78—62165
  - diffusion-reaction equations systems, existence, stability 79—20365
  - diffusive motion in periodic potentials, low friction nonlinear mobility 79—35645
  - dioctyl phthalate, polydisperse, spectronephelometer studies 79—21797
  - disordered system, donor-acceptor energy transfer, diffusion modulated 80—71888
  - dissipative structures, nonlinear reaction-diffusion model, stability of secondary multiple steady states 80—76485
  - dissociation, diffusion-controlled reaction, theory 78—64820
  - dissolved species, advection-diffusion eqn. in pulsating crack 80—96312
  - double-diffuse convection, diffuse interface model, high Rayleigh nos. 78—90963
  - droplets, kinetics of processes controlled by diffusion 79—11828
  - early universe, photon and neutrino diffusion rel. to nonlinear primordial fluctuations 79—25773
  - education, random walk approx., theory of generating function and method of steepest descent 78—36744
  - Einstein relation, VHF extension for diffusion noise 80—17901
  - elastic waves propagation in highly scattering medium, diffusion approach 77—86804
  - electric analogies *(Hungarian)* 79—17361
  - electrical circuit analogue, for teachers 78—86089
  - electrochemical cell, convective diffusion eqn., computer soln., numerical methods 77—16830
  - electrochemical diffusion, boundary value problems, orthogonal collocation calcs. 78—40053
  - electrodes, sheet, mass transfer to continuous moving surface 80—69821
  - enzyme particle, encapsulated, reactor systems, effects of mass transfer resistances 79—96522
  - equation, linear, separation of variables *(Russian)* 77—13712
  - equation, numerical integration using time level schemes 79—2609
  - equation, soln. by mixed finite elements *(French)* 77—71283
  - equation, sols. by Picard's method 79—7273
  - equations, Galilean invariance, rel. to Lorentz invariance of wave eqns. 79—17276

diffusion continued
- escape probability calc. for diffusion controlled reactions 79—1934
- evolution systems and convection-diffusion, stiffness and stability, Gershgorin theory 80—77626
- excitable medium diffusion discrete models and spatial patterns 78—93629
- extinction time for fast diffusion 79—75477
- Feynman Lagrangian for short diffusion processes 80—31551
- Fick's second law, rapid numerical soln. where difusion coeff. is conc. dependent 77—7887
- Fick's second law, soln. for non-isothermal conditions with external forces *(German)* 79—46826
- fine particle deposition, on rotating disc surface, convective diffusion under elec. double layer forces 78—61060
- fission reactor, spatial mesh effect in 3-D burnup calcs. *(Japanese)* 80—47544
- flame, laminar mixed-mode forced-free diffusion type, on vert. burning fuel slab 78—91033
- flame, premixed, propag. in large-scale turbulence 79—50813
- flameless atomisers, diffusion process anal. 79—87925
- flexible molecules, chain end diffusion 80—23569
- flow depend. expansion process, initial value problem, two step difference method *(German)* 78—57877
- fluid, crit. fluctuations, Stokes-Einstein diffusion coeff. determ. 80—90783
- fluid saturated porous solid, fundamental solns., deformation, pore-fluid diffusion, soil mechs. 77—84160
- fluidised bed, chaotic motion of particles, statistical characteristics determ. 77—51140
- fluids, atomic and molecular, collision induced light scatt. *(German)* 79—27057
- Fokker Planck eqn., non-linear, with nonconstant diffusion, non-Gaussian time dependent 80—31686
- Fokker-Planck eqn. expansion, weak diffusion, critical point 80—57228
- Fokker-Planck eqn. soln. by path integral method 77—2628
- Fokker-Planck equation, formal soln. using operator approach 79—35647
- Fokker-Planck equation, manifolds of equivalent path integral solns. 80—4687
- fractured medium, transient 2-D diffusion 80—106841
- function space entropy density, diffusion induced, Onsager-Machlup function 79—17375
- galactic cosmic rays, effect of directional medium-scale interplanetary vars. on diffusion 77—29605
- galactic cosmic rays, semiannual flux var. origin and mag. field perpendicular diffusion coeff. 79—16777
- Galerkin finite element and finite difference anal. *(Japanese)* 79—30391
- gas core reactors, temp. profile and power calcs., uniform density diffusion model 80—37553
- gas mixture, flowing, separation by thermal diffusion 79—68755
- gas transport, in synthetic polymer membranes, history 78—76912
- generalised diffusion eqn., solns. qualitative props. 80—170
- generalised diffusion equations, derivation 77—87705
- geometric approach to diffusion eqns., equivalent set of differential forms 78—54321
- globular cluster stars, He settling and effect on inferred ages 80—73013
- Green's function and scatt. length 77—13629
- growth and patterns of spatial organisation 80—81287
- hard-rod clusters, one-dimens. diffusion, stochastic calcs. 77—9948
- harmonic oscillators, randomly disordered linear chain, normal frequencies 78—36818
- heat and mass transfer, at turbulent boundary layer, diffusion model 78—94544
- heat transfer, nonstationary, finite element calcs. 80—83795
- heating surfaces, furring, mass transfer, convective heat transfer, mathematical model *(German)* 77—23854
- heterogeneous system with chaotic structure, generalized conductivity coefficients, review 77—87708
- homogeneous mixtures, general theory 79—90360
- homogenisation of a class of nonlinear problems *(French)* 79—71250
- hydrocarbon gas, sorption and transport in ethyl cellulose membrane 78—76913
- hydrodynamic diffusion tensors, translation-rot. coupling effects 78—29038
- impact parameter for given diffusion angle *(French)* 80—68155
- inhomogeneous Boltzmann gas, lumped phase space, non-linear diffusion approx., stochastic hydrodynamic theory 80—64666
- inhomogeneous films and membranes, diffusion, theory 78—76914
- interferometrically recorded sedimentation, diffusion and thermal diffusion expts., reference marks arrangement 77—87813
- intermicellar kinetics theory, stochastic approach, master equation for, irreversible reactions 80—76561
- internal diffusivity, meas. by pulse gas chromatography in packed bed 79—48002
- interplanetary recurrent proton streams, 1.3 to 2.3 MeV protons radial diffusion coeff. 79—16774
- inverse problem, approx. soln., linear programming, regularisation 78—32775
- ion exchange membranes, ion diffusion studied by autoradiography 77—90637
- ion flow through membrane, effect of chem. reaction on time depend., binding of mobile ion 78—95954
- ion recombination, partially diffusion-controlled, appl. to irradiated-liq. NH_3 solvated electron yeild 79—100409
- ionic exchanges at water-sediment interface in Norwegian Sea and Intertropical Atlantic *(French)* 79—62523
- ionosphere, diffusion and heat flow eqns. with large temp. differences between interacting species 79—66857
- ionosphere plasma, positive ions interdiffusion rel. to cond. 79—53609
- irreversible thermodynamic treatment of particle diffusion among immovable particle system *(Russian)* 77—5778
- isolated pairs in condensed media, partially diffusion controlled reaction 78—92441
- itinerant oscillator model, Mori formalism calcs. 77—58634
- Jovian electron propagation close to Sun, three-dimensional diffusion-convection model 79—101034
- Jupiter magnetosphere, diffusion coefficients determ. from Io observed effects 78—32388
- Kawasaki inequality genralisation for diffusion consts. 78—70076
- kinetic fluctuations of Brownian motion 79—25984
- kinetics of reacting solns., diffusional barrier crossing processes, trajectory simulation 80—81280

diffusion continued
- laminar flow mass transfer with axial diffusion in pipe with chem. reaction 77—55101
- Landau-Zener problem, random nature of motion role in intersecting terms problem 80—8937
- layered porous medium transient 2-D diffusion 80—106841
- leaching from model porous bodies by reflection spectroscopy 80—100031
- Lennard-Jones (100) crystal-liquid interface, structure 78—91284
- light scattering in dynamical props. study, principles spectra derivation and applics. 80—53218
- linear Boltzmann system, appl. of parabolic diffusion equation 77—82468
- linear equation, separation of variables, covariant and symm. props. *(Russian)* 77—26135
- linear non-stationary diffusion models, non-parametric estimation by Grenander's method of sieves *(French)* 80—57219
- linear one-dimens. diffusion eqn. improved method for soln. 80—13008
- linear stochastic diffusion equations, two-dimens. system, asymptotic behaviour of functional for distribs. from argument of soln. *(Russian)* 78—21083
- linear sweep voltammetry, charge transfer, diffusion control 80—45583
- liquid-gas interface, Stefan flow of binary mixture, with evap. or condensation 79—37381
- local fluctuations in chemical reactions, nonlinear master eqn., dimensionality expansions, augmented mean field theory 78—73019
- localized patterns in reaction-diffusion systems 80—59130
- macromolecule rotational diffusion props., validity of general ellipsoid model 80—95751
- magnetic diffusion in interstellar clouds, rel. to OB associations subgroups sequential form 80—4408
- magnetodiffusion of charged particle in unpolarised electromag. beam 78—57858
- magnetosphere, electron pitch angle diffusion instabilities rel. to pulsating aurora 3 Hz modulation 79—25391
- magnetosphere, particles pitch angle diffusion by bounce reson. 78—36408
- magnetosphere trapped particles, self-consistent diffusion on bounce-drift reson. with geomag. pulsations 79—58188
- many-particle system, generalised diffusion processes 78—73942
- marine sediments diffusion coefficients determ., resistivity techniques validity 79—92601
- Markov processes, extremal paths 78—73944
- Markovian diffusion, dynamical theory 79—80515
- mass or heat transfer across plane membrane in the way of a flowing stream *(German)* 79—41557
- mass transfer coefficients, concentration dependent diffusivities effect 80—98864
- melting/diffusion, linear correlation 77—20108
- membranes, carrier-mediated photodiffusion 78—23965
- membranes, diffusive flow, frictional coeff. formalism and mech. equilib., mol. scale 77—90638
- memory function approach to the dynamics of interacting Brownian particles 79—25979
- mesosphere, turbulent diffusion coeff. seasonal vars. 79—53424
- metals, phase formalism in diffusion layers between solid and liquid metals *(Russian)* 79—69257
- meteor plasma diffusion, geomagnetic field effect expt. *(Russian)* 78—61814
- meteor trails, atmospheric ambipolar diffusion coeff. meas. errors 78—88952
- meteor trial, diffusion of weakly ionised plasma filament forming angle with mag. field 79—53610
- methane in marine sediments, diffusion rel. to conc. profiles meas. 80—12373
- micelle-confined molecules reaction, diffusion-controlled, luminesc. quenching, excimer form. 80—50890
- middle atmosphere (mesosphere), eddy diffusion coeff. determ. from energetics and thermal struct. 80—98412
- mixed explicit-implicit iterative finite element scheme, soln. and examples 77—26155
- mixed explicit-implicit iterative finite element scheme, theory 77—22399
- mixtures, motion of, generalized diffusion theory 79—17233
- model, statistical distribution of particles over given volume 77—82467
- modelling, equivalence of different methods 78—57818
- monotone difference schemes for diffusion-convection problems 80—8801
- most probable path for diffusion processes, path integral technique 79—9196
- multicomponent fluid systems, symmetry of transport matrix for diffusion and heat flow 80—99997
- multicomponent inhomogeneous system, diffusion with moving boundaries and swelling at const. volume 80—44353
- multicomponent system, heat transfer rates effect on diffusion 77—7393
- multidimensional bistable potential, diffusion, WKB calc. 80—101770
- multidimensional diffusion equation, class of general boundary conditions 80—90796
- multiperforate laminae, mass transfer of chem. species by diffusion, plate and associated boundary layer case 80—40736
- multiple dimensional parabolic free surface problems, alternating direction method 77—37826
- multiple scatt. of particle beams, axial mag. field effect 78—70712
- multiplicative functionals on diffusion processes 80—73286
- multivariate master eqn. diffusion operator, reaction diffusion system eigenfunctions 78—29077
- multivariate master equation for reaction-diffusion system 80—95045
- neuronal activity and the time dependent threshold problem, diffusion approximations 79—74639
- neutrino systems, relativistic kinetic theory of transport processes 80—73283
- non-Newtonian fluids, flow method for measuring diffusion coeffs. 77—55045
- non-stationary one-dimensional, psi-functions 78—54322
- nonequilibrium and Wiener processes, functional integral 77—26253
- nonequilibrium effects, Fokker-Planck eqn., rel. to path sums, Feynman proof 77—2629
- nonequilibrium processes in open systems, fluctuation dissipation relations, p-n junction appl. *(Russian)* 79—58668
- nonideal fluid mixtures, generalised film model for mass transfer across interfaces 77—67387
- nonlinear, entropy change 77—49700
- nonlinear, stability 78—8366

diffusion continued
nonlinear convective diffusion problem, application of stable explicit finite difference scheme 78—151
nonlinear diffusion eqns., evolution of stable profile 79—17363
nonlinear diffusion equation, general class of similar solns., laser interactions, thermal cond. 77—37827
nonlinear diffusion equation, invariance props., Lie-Backlund groups 80—62596
nonlinear diffusion equation, similarity solns. 80—27239
nonlinear diffusion equation, stable profile evolution 80—82731
nonlinear diffusion problem, dual extremum principles 77—67218
nonlinear diffusion problem, soln. with const. flux boundary conditions 77—75782
nonlinear diffusion process, path integral evaluation, by Fourier series 78—70075
nonlinear diffusion-process, appl. of Onsager-Machlup function 79—44888
nonlinear diffusion-reaction with autocatalysis and saturation law, single perturbation approach 80—35502
nonlinear eqn., analogue and numerical simulation using variable-element networks *(French)* 77—5653
nonlinear eqns., numerical finite difference methods *(French)* 77—5654
nonlinear equation, asymptotic behaviour of solns. 78—24744
nonlinear equation, perturbation, iterative and optimal techniques for arbitrary diffusivity 77—66943
nonlinear equations, approach of solns. to travelling front solns. 78—24743
nonlinear filtering, conditional laws, smoothness, stochastic calculus of variations *(French)* 80—68128
nonlinear Markov processes, curved phase spaces, path integral soln. Lagrangian, appl. to general relativity 77—26216
nonlinear problem, integral soln. 78—36945
nonlinear processes, slowly modulated oscillations 78—16758
nonlinear reaction-diffusion eqns., large time behaviour of solns. 79—12741
nonlinear reaction-diffusion equations, pattern selection at the bifurcation point 80—50827
nonlinear reaction-diffusion models for interacting populations 78—65886
nonlinear singular diffusion eqn., perturbation soln. 79—71387
nonlinear systems, dynamics, heavy damping limit 80—86199
nonlinear waveshapes generated by possibly finite initial disturbances 78—36948
nonparametric identification for diffusion processes 79—30374
nonspherical molecules, rot. diffusion tensors determ. from rot. friction tensor calcs. 80—63861
nonstationary one-dimensional diffusion under forced convection, Omega functions as auxiliary functions 78—93631
nonuniform multicomponent system with multidimensional regions *(Russian)* 79—12743
nuclear reactor structures, two dimens. diffusion problems, singularities in finite element approx. 77—6496
numerical solution of problems in unbounded regions, use of coord. transforms 78—8219
ocean, multiple components transport through thermohaline diffusive interfaces 80—12396
one dimensional diffusion system, boundary control problem, exact soln. *(German)* 79—85101
one group, integral transport eqn. for homogeneous sphere, neutron scatt., classical diffusion, anal. 78—62589
one-dimensional diffusion, soluble model potentials 79—35649
one-dimensional diffusion process, and Onsager-Machlup function, functionals of paths 77—17932
one-dimensional diffusion with absorption, exact results 80—10689
Onsager Machlup formula for 1-D nonlinear diffusion processes 78—77816
Onsager-Machlup function, Lagrangian for diffusion process most probable path 78—73940
Onsager-Machlup Lagrangian for general diffusion processes, Fourier series anal. 79—6060
Onsager-Machlup Lagrangian in theory of stationary diffusion processes 80—128
optically thick horizontal fluid layer heated below, heat transfer 80—99993
optimal stopping rules for diffusion processes with small diffusion *(Russian)* 77—87710
orientational time correlation functions for J and M diffusion models 78—73939
pair configuration space diffusion eqn., thermal fluctuations, kinetic theory 79—17362
particle, in fluctuating medium, memory effects on quantum diffusion 79—49180
particle deposition, onto rot. disc, convective diffusion, external force field 78—40081
particle diffusion across mag. fields, stable profile for nonlinear diffusion eqns. 78—22456
particle diffusion in electrostatic precipitators 77—3526
particle diffusion in nonuniform medium, thermal fluctuations 77—87709
particle growth, mathematical modelling, continuity eqns. for particle distribs. 78—65863
particle motion delocalisation in non-uniform HF field with finite correl. time 80—58450
particle transport to rotating disc surface under external force field 78—15718
particulate materials, cohesionless, mixing and segregation, microscopic mechanisms 79—37848
passive scalar, effective long-time diffusivity in Gaussian model fluid flow 79—32439
path integral formulation of general diffusion processes 77—33844
path integrals for diffusion processes in Riemannian space 79—17370
percolation system, square network diffusion, numerical expts. *(French)* 77—41550
periodic wind-tree model 80—86230
permeable barrier transient diffusion, applied to NMR with pulsed field grad. 78—91986
phenomenological theory 78—93626
phospholipid lateral diffusion in membranes, photochem. method 79—100583
photographic emulsion production, effect of mixing on diffusion rate *(Russian)* 80—3388
plasma diffusion rates, automatic computation, stellar interiors appl. 78—57434

diffusion continued
plasma transport, anomalous, electron temp. gradient instability 80—75034
pollutent, Gaussian plume model parameters for ground-level and elevated sources 80—82010
polystyrene in cyclohexane photon-correlation spectroscopy obs. 79—41255
porous carbonaceous materials, transient diffusion coeff. meas. 78—38400
porous catalyst, simultaneous forced convection, diffusion and reaction 77—35254
porous medium, transient diffusion, Fick's law validity 80—13003
probabilistic anal. of Lagrangian of diffusion process 78—62170
probability process, product of two diffusions *(French)* 80—8909
processes satisfying Ventcel's boundary conditions, existence *(French)* 77—71182
programmable calculators appls. in scientific calcs. 77—64940
protons of inner radiation belt, radial diffusion rel. to energy and pitch angle distrib. 80—67471
quantum mechanics, intrinsic diffusion quantum coefficient 80—22222
quasideterministic Fokker-Planck dynamics 78—93627
quasilinear parabolic system, chemical reaction study 80—7759
radiation belts, particles radial diffusion from geomagnetic field fluctuations at synchronous orbit 78—96359
radiatively driven diffusion in upper main-sequence peculiar stars, rel. to chemical and physical props. 80—82374
radioactive pollution, atmospheric, concentration time integral *(German)* 80—26378
radioactive waste migration, groundwater environment, hydrodynamic dispersion in transport models 80—17146
radiowaves in ionosphere, limited beam diffusion due to scatt. on random inhomogeneities 77—91349
random chain, low-energy density of states and long-time behaviour, scaling approach 79—25994
random heat eqn. soln. by iterative scheme 79—9195
random media, anisotropic, Fourier transformation of space-time transport equation 80—62595
random networks near percolation threshold, ant in labyrinth problem 80—77732
reacting-diffusing system, turbulent spatio-temporal dynamics 78—56880
reaction rates, diffusion theory, rate consts. and transmission coeffs. calcs. 80—89464
reaction-diffusion eqns., axi-symmetric time periodic solns. 78—81930
reaction-diffusion eqns., stability of solns. 78—16759
reaction-diffusion equation solutions, Lotka scheme 79—34280
reaction-diffusion problem, nonlinear, dissipative structures, stability anal. 79—1938
reaction-diffusion system with one degree of freedom, stability anal. of dissipative structs. 79—87826
reaction-diffusion systems, bifurcation theory, classification 80—108713
reaction-diffusion systems, periodic solns. and multiple steady states 79—54082
reactive-diffuse systems with Arrhenius kinetics, multiple solns., ignition and extinction 79—66260
recombination probability, reactivity depend., scavenger effects 80—76494
relativistic kinetic gas theory, electron-neutrino system 77—5756
resonance transfer rate of electron excitation, model of convergent terms, effect of diffusional motion of particles 80—8936
rolled vortex sheets, viscous diffusion 79—46325
Rossby wave critical layer, evolution, vorticity outward diffusion 78—79329
rotational Brownian motion of spherical polar mol., diffusion eqn. study, complex polarisability 77—67381
scavenging, in-cloud, rel. to aerosol particle size, mechanisms 78—16108
Schwinger-DeWitt expansion, boundary terms, flat space results 78—77815
seismic energy transmission in intensively scatt. environment, diffusion eqn. 77—73685
semiclassical bosons and fermions 79—40446
sensitivity anal. of partial differential eqns. 79—49178
separation method, flow field-flow fractionation 77—960
series solution method for linear diffusion eqn. 80—8939
sine-Gordon chain, mass diffusion, soliton solns. 79—85102
slip boundary condition for rough sphere rotation 77—31335
Smoluchowski equation, derivation from Fokker Planck equation using perturbation methods 78—54117
Smoluchowski process, number fluctuation anal. of random locomotion 78—54318
solar atmosphere, influence of diffusion on O abundance 80—4318
solar cosmic ray propagation, anisotropic diffusion-convection eqn., dimensional soln. 80—17453
solar cosmic rays propag., diffusion in mag. fields, convection in solar wind, dimens. method soln. *(Chinese)* 78—81511
solar quiescent prominences, neutral atoms diffusion rel. to downward motions 78—20779
solid particle systems, high Reynolds numbers, mass transfer, Karman-Pohlhausen method 80—79378
solid-liquid extraction, diffusion processes, general soln. 78—20136
solid-state diffusion in elec. field, Monte Carlo demonstration 80—27072
solutes in aqueous fissures in porous rocks, effects of diffusion into rock on transport 80—94553
Soret driven convective instability, mass diffusion and boundary effects 80—53776
spectral anal. of time-depend. particle diffusion, integral approach 78—45582
spherical particle in free-fall, time-to-complete-dissolution prediction 80—15245
spin echo expts. for diffusion in bounded heterogeneous media, stochastic Liouville eqn. 80—54992
stars in main sequence, diffusion and turbulence rel. to abundance anomalies 78—89198
stationary diffusion through composite medium, appl. to Laplace eqn. systems 79—80550
stationary system, diffusion mixing model, approx. soln. 80—79410
statistical system unknowns optimal evaluation *(French)* 79—9194
steady nonionic countergradient transport through membranes by coupled diffusion [dialysis application] 80—16718
steady-state recirculating flows, finite difference schemes, practical evaluation 80—106776
steel-V interface, diffusion above 500°C *(German)* 79—28156

diffusion continued
  Stefan multi-phase problems, similarity solns. 79—12742
  stellar interiors, astrophysical context of diffusion 80—77381
  stochastic description, diffusion processes 78—41253
  stochastic theory, Markov and non-Markov forms of diffusion eqns. 77—13715
  stratosphere, vertical eddy diffusion profile from N_2O profiles and instantaneous global photochemical reaction rates 80—17335
  stratosphere transport, one-dimensional parametrisation using ^{95}Zr data from Chinese thermonuclear explosions 79—2342
  subsea permafrost heat and mass transport processes, mol. diffusion and consequences anal. 79—2302
  Sun, He diffusion theory 77—56888
  superradiant emission, diffusion equations invariant solns. 77—75458
  ternary, two moving boundaries 77—35760
  test particle diffusion, in conservative field, integral Boltzmann eqn. solns. 79—97324
  test particle diffusion under conservative field, integral Boltzmann eqn. soln. 79—97325
  thermal-ignition analysis in boundary-layer flows 79—64800
  thermophoretic and diffusiophoretic particle deposition estimation 77—90644
  thermosphere, lower, one-dimensional diffusion-photochemical model for O and O_2 distrib. simulation 80—4159
  thermosphere, lower, turbulent diffusion coeff. seasonal vars. 79—53424
  thin-layer cell, fast reaction, kinetic consts., diffusion and conc. impedance 78—73053
  tidal propagation in shallow rivers, diffusive model 79—2303
  time-dependent birefringence, linear dichroism, and optical rotation resulting from rigid-body rotational diffusion 79—47411
  Tokamak, DITE, impurity ion concentrations and diffusion, spectroscopic measurement 80—28771
  Tokamak fusion reactor first walls, hydrogen profiles 80—37578
  Tokamaks, transport losses, computer modelling and scaling 80—28612
  transient diffusion with n-order irreversible chem. reaction, finite element method 78—85122
  transient heat conduction and moisture migration problems, finite element approach 78—12653
  transient nonlinear diffusion method of differential quadrature 78—16755
  transmission line modelling of diffusion 79—26011
  travelling waves for a model non-linear reaction-diffusion system 80—89476
  tubular reactor with non-Newtonian laminar flow, diffusion and raction analysis 77—68703
  two-level system, kinetics at diffusion modulated local interactions *(Russian)* 79—2716
  two-way diffusion equations, separation of variables, decaying and growing eigenfunctions 80—62594
  variables separation in diffusion eqn. 80—73285
  in viscoelastic layer, mathematical analysis *(Russian)* 77—51539
  viscoelastic media, deform. theory with account of thermodiffusion *(Ukrainian)* 78—67052
  wave fronts, definition of diffusion *(French)* 77—67386
  white dwarfs, diffusion time scales 79—92761
  Al, of Cu(Zn), isotope effect 78—84006
  BaO, in upper atmosphere, flow rel. to striation struct. in Ba^+ clouds 77—25833
  C membrane, graphitised, adsorption meas. in situ using steady state flows and time lags 79—33183
  Cu-In solid/liquid interface, laws governing diffusive interaction *(Russian)* 78—95156
  H release from fusion reactor wall materials 80—37579
  H_2 diffusion flame, Rayleigh temp. profiles meas. 80—16692
  H_2, through Pd membrane, diffusion-cell for separation H_2 containing mixtures, solar furnace appl. 80—92245
  He in stellar envelopes, radiative forces rel. to He abundance anomalies 80—31291
  He-proton diffusion coeff. in stars 79—16811
  Hg discharge, high-pressure, NaI and TlI additives, line broadening and radiative transport 80—74199
  HgMn stars, diffusion and line asymmetries 78—40948
  HgMn stars, diffusion model rel. to obs. of Hg in thin atmospheric layer 80—105243
  O diffusion with absorption, cubic spline appl. to moving boundary problem 79—75475
  Rn diffusion, effectiveness of U mill tailing covers 79—93838
  ^{222}Rn, diffusion and exhalation meas. from U mill tailings pile 79—92109
  SiO_2 hydrosols, diffusion coeffs. and characterisation by photon correl. spectrosc. *(German)* 79—29418
  V-Ni(Fe) interface, diffusion above 500°C *(German)* 79—28156

diffusion coefficient *see diffusion*

diffusion creep
  atomic diffusion mechanisms *(Hungarian)* 78—38868
  bicrystals, diffusion growth of pores under creep conditions 77—15404
  bound theorems and large strain diffusion flow 78—84895
  cavity growth, creep mechanisms, independent and sequential 80—55480
  ceramic, polycrystalline, diffusion creep activation energy 78—11274
  creep crack growth, appl. of fracture mechanics 78—18237
  crystal, diffusional motion and distortion of macroscopic inclusions under influence of elastic stresses *(Russian)* 77—66676
  deformation, and diffusion controlled creep crack growth 80—79867
  dislocation and diffusion creep transition 80—88253
  forsterite, ^{18}O self-diffusion expts., high-temp. creep implications 80—81870
  gas, binary mixture, moderate density diffusive creep along flat surface 80—43822
  grain boundaries, as point defect sources or sinks 79—37757
  grain boundaries, interfacial structure effects on high temp. mechanical behaviour 80—59480
  grain boundary, stress induced drift diffusion, appl. to creep and growth of grain boundary voids 78—72811
  grain boundary drift diffusion under influence of stress fields 79—77835
  grain boundary sliding, containing particles, during diffusional creep, dislocation bowing 79—37712
  grain boundary sliding, stresses and deform. 78—68739
  grain rearrangement, solids wth hexagonal grain struct. 78—84896
  high temperature mechanical behaviour of crystalline solids 80—59568
  metal, radiation stimulated diffusional flow, neutron irrad. *(Russian)* 79—29132

diffusion creep continued
  metal, small-angle boundary migration in steady creep state 77—39624
  Nabarro-Herring creep, stress irradiation induced mass transport, anal. soln. 79—60401
  olivine and ultrabasic rocks, diffusion and diffusion creep, rel. to upper mantle deform. 77—9409
  oxides, nonstoichiometry influence on plasticity *(German)* 79—24592
  polycrystals, models for constrained cavity growth 80—44251
  power law creep, exam. of whether creep is diffusion controlled 78—52890
  radiation creep rate as function of point defect formation rate and temp. 79—69187
  sapphire, white, three-point bending test, dislocation climb *(Japanese)* 79—96104
  silicates, nonstoichiometry influence on plasticity *(German)* 79—24592
  slip band theory, model for creep based on dislocation climb at grain boundaries 79—37756
  solid solutions and interstitial phases, theory *(Russian)* 80—40437
  steel, austenitic stainless, interaction of grain boundary dislocations with precipitates during high temperature creep 80—16384
  steel, stainless 77—77529
  threshold stress in particle inhibited diffusive creep 79—38922
  viscoelasticity, stress/strain relationships, fluctuations 80—17802
  voids, review of diffusional growth of creep voids 78—71720
  Zircaloy fuel sheathing, NIRVANA high temp. creep model 79—87704
  Ag film, sputtered, hillock growth and agglomeration by annealing, SEM obs. 80—2309
  Ag films, hillock form. hole growth and agglomeration 80—44455
  Ag, thin film, hillock growth due to thermal stress relax. of diffusion creep and surface diffusion 79—65345
  Al, creep behaviour, at high temp., influence of oxidation 80—97538
  Al, grain boundary migration, TEM obs. on mechanism 80—79812
  Al, pure, polycryst., steady-state flow, stress and temp. depend. 80—45341
  Al_2O_3, ambipolar diffusion in deformation mechanism maps 78—48454
  Al_2O_3, fine grained, interface-controlled diffusional creep 80—60915
  Al_2O_3, polycrystalline, diffusion creep activation energy 78—11274
  Al_2O_3:MgO, diffusion creep examined under three-point bending *(Japanese)* 79—96104
  Cu annealed and cold rolled, with bamboo structure, exam. of grain boundaries as vacancy sources in diffusional creep 78—88508
  Cu, grain boundary migration, TEM obs. on mechanism 80—79812
  Cu, nucleation and growth of oxidation zones during diffusional creep *(Russian)* 79—52431
  Cu-Al_2O_3 (1 vol.%), effect of second phase particles on diffusional creep 78—31472
  Cu-Ni, nucleation and growth of oxidation zones during diffusional creep *(Russian)* 79—52431
  Fe_2SiO_4, nonstoichiometry influence on plasticity *(German)* 79—24592
  GeTe based thermoelec. materials, creep mechanisms 77—16643
  KBr, single cryst., high-temp. creep, rel. to pipe diffusion, dislocation climb 77—11626
  LiF, small-angle boundary migration in steady creep state 77—39624
  Mg, grain boundary diffusion creep 78—11291
  Mg-Mn-Ce (1.5, 0.3 wt%), superplasticity role of diffusional creep *(Russian)* 80—97528
  Mg-Zr alloy, cavitation during diffusion creep 77—44296
  MgO, polycrystalline, diffusion creep activation energy 78—11274
  MgO polycrystals, ultrafine-grained, creep microstruct. 80—35246
  Mg_2SiO_4, ^{18}O self-diffusion expts., high-temp. creep implications 80—81870
  Mo filament, coated with thin Ni film, creep and recrystn. *(Russian)* 78—19822
  NaCl polycryst. containing Al_2O_3 dispersion, diffusive creep 80—97531
  Ni, creep rate at low stresses, effect of grain size 80—71707
  Ni, oxide dispersion strengthened materials, effect of prior creep at 1365K on room temp. tensile props. 78—39857
  Ni-Cr-(Al), oxide dispersion strengthened materials, effect of prior creep at 1365K on room temp. tensile props. 78—39857
  NiO, stress appl. high temp. creep and point defects, creep rate obs. 80—49297
  $Ni_{0.5}Zn_{0.5}Fe_2O_4$ coarse grain polycryst. ferrite, diffusional creep *(Japanese)* 80—104238
  Pb and Pb-Tl (2.5 wt.%), grain boundary sliding, grain size and stress effects 78—27571
  Pb film, thermal strain, strain relax. mech. 79—42427
  Pb, film, thermal strain, strain relax. above room temp. 80—59841
  PbTe based thermoelec. materials, creep mechanisms 77—16643
  Si-Al-O-N ceramic, grain boundary desegregation and intergranular cohesion 80—100872
  Si_3N_4-MgO, compressive creep, source of viscoelastic effect 80—50675
  UO_2, fine grained, low-stress creep study, metallographic obs. 79—43312
  UO_2, grain boundary diffusion, sintering and creep correlation, reinterpretation of creep mechanism 79—66111
  W filament, coated with thin Ni film, creep and recrystn. *(Russian)* 78—19822
  W, filament, incandescent lamps, creep, failure, life prediction 78—84927
  Zn-Al (22 wt.%) superplastic alloy, grain growth texture 80—81075

diffusion in gases
  see also self-diffusion in gases; thermal diffusion in gases
  aerosol, ambient, sulphate particles diffusion sampling for size discrimination and chemical comp. 78—69528
  aerosol, diffusion and sedimentation in Poiseuille tube flow 78—59463
  aerosol, spherical particle phoresis in multicomponent gas mixtures 78—22446
  aerosol diffusion and sedimentation in horiz. cylinder 78—3385
  aerosol dry deposition, filtration model rel. to trace metal deposition from atmosphere 78—73441
  aerosol particle settling and diffusion from stationary gas in tube or duct 77—52678
  aerosol unipolar diffusion charging in continuum regime 77—25319
  air, electron radial diff. coeff. to mobility ratio 77—19666
  air pollution density distrib., flow pattern in Tanabe area, Japan, numerical anal. *(Japanese)* 78—96289
  alkali metal vapour-He(Ar)(N_2), alkali condensation in flow, heat and mass transfer 78—75192
  aluminisation in Al packs, for protective coating form., kinetic diffusion theory 77—32727
  atmosphere, comment on one-dimensional models and appl. to CO 77—45086

diffusion in gases continued
- atmosphere, convection-diffusion coupling near flames 77—7481
- atmosphere, pollutants diffusion-deposition-resuspension problem, formulation and soln. 77—2229
- atmosphere, stratified surface layer, turbulence and diffusion, basic Lagrange characts. 78—81270
- atmosphere, turbopause eddy diffusion coeff. semi-theoretical global models 79—21086
- atmosphere, vertical diffusion study using airborne gas-chromatography and numerical modelling 78—69435
- atmosphere plumes, diffusion rel. to dry deposition and concs. prediction 78—28307
- atmospheric diffusion, tracking elec. charged air by ground level elec. field meas. 77—78450
- atmospheric diffusion in canyon with rough mountainous terrain, comments 77—45096
- atmospheric stratified surface boundary layer, turbulent diffusion from stationary linear source 77—56668
- atmospheric transport problems, contaminant movement, Galerkin finite element method 80—74902
- atmospheric wave propag., viscous diffusion, heat loss damping mechanism 80—56516
- atom diffusivity meas., independence of wall reactivity 77—3909
- atom distribution, in flame spectrometry, moving point source model 78—61084
- atomic diffusion in diatomic gases, dominant coupling limit 78—63524
- atoms in resonance cell, coeff. meas. using self-oscillating quantooptical magnetometer 77—76018
- axial diffusion in gas blanketed vapor condensers *(German)* 80—38516
- benzene-H_2N_2 gas ternary diffusion coefficient obs. *(Japanese)* 79—10626
- binary gas mixture, free expansion through channel, composition change 79—64709
- binary isotopic gas mixture, convection-diffusion eqn. soln. for centrifuge axisymm. vel. field 78—17434
- binary mixtures, diffusion coeffs. lists 78—34254
- binary mixtures, nonreacting, nonlocal continuum 78—51268
- binary mixtures, use of diffusion and second virial coeffs. to predict viscosities 79—14506
- binary systems, precise diffusion coeffs., appl. to two-bulb cells calibration 77—76019
- boundary conditions to diffusion eqn., recoil/sticking probabilities at wall 77—51149
- bubble size distribution, changes due to interbubble gas diffusion 78—85204
- cell design for diffusion coeff. meas. in gas phase 78—55709
- chlorofluoromethanes, $CHFCl_2$ and CHF_2Cl, diffusion and chem. reaction 77—70804
- chlorofluoromethanes, laser photolysis, product vibr. relax. rates and diffusion coeffs. 80—55680
- circular positive column with one and two step ionisation, charact. eqn., diffusion controlled 80—44033
- coefficient determination, using Stefan cell 77—51136
- coefficient determination using lamella pulsation diffusion apparatus 79—99340
- combustion and non-combustion flow fields with swirl, numerical anal. 79—98821
- CVD, RF plasma activated, kinetic model 78—27416
- dense gases, mutual diffusion coeff., spin-echo meas. 78—67303
- dibutylphthalate, supersaturated vapour, aerosol form. by mixing of flows 79—39212
- diffusophoresis of nonspherical aerosol particles in a free molecular flow 80—43765
- dilute gas mixtures, transport props., calc. prog. 80—10342
- dilute gas of nearly spherical rot. mols., diffusion of rot. energy 77—964
- dimers, dissociating, in nonisothermal ideal gas phase, stationary state anal. 78—76848
- droplet evaporation, diff. coeffs., vap. press. and Lennard-Jones pot. function determ. 77—80262
- dust diffusion through gas in force field, theory 78—18366
- electric discharge, positive column, characts. rel. to diffusion and ionisation coeffs. 80—33833
- electron diffusion in gas, Maier-Leibnitz expt. reexamined 78—83516
- electron diffusion in high electric fields 77—51757
- electron drift velocity in counter gas mixtures 80—28590
- electron swarms in electrostatic fields in gases, inelastic collisions effect on diffusion coeffs. 77—76022
- electron transport, diffusion theory and Monte Carlo calcs., depend. on initial ang. distrib. of injected electrons 80—53136
- electrons, Monte Carlo simulation 77—84392
- ellipsoidal aerosol particles in binar binary gas mixture, diffusophoresis under hydrodynamic conditions 80—66888
- fast diffusion meas., nondestructive, using positron emitter as tracer 78—54519
- Fick's diffusion coefficients, of pseudobinary gas-steam mixtures rel. to mag. tapes prod. *(German)* 79—27735
- Fick's law modification 80—96333
- Ficks law for gas diffusion samplers, comparison with Ohm's law 80—43819
- flame, laminar jet diffusion flame size prediction, Burke-Schumann theory extension 78—14096
- flame, laminar jet diffusion flame size prediction from diffusion coeff. 78—14097
- fluid, reacting spheres, kinetic theory 78—35668
- fluoromethanes in air 77—15154
- foam, interbubble gas diffusion, effect of initial bubble size distribution 79—79304
- freons in nitrogen, interdiffusion coefficient, calc. and obs. *(Russian)* 77—76017
- gas, dilute, reacting, mass and momentum transport, DIPR model extension 78—35666
- gas phase transport, definition of hydrodynamic regime acquired during crystn. 79—51029
- gas-porous electrode, mass exchange in transport zones 77—32801
- gaseous mixture separation, with asymmetric dense polymeric membranes 78—9696
- hard sphere gas, binary mixture, diffusion coeffs., relativistic kinetic theory 77—3908
- heat pipe, gas-loaded, near ideal, analytical model 80—53615
- hydrocarbon diffusional combustion in air, finite activation energy anal. 78—95930

diffusion in gases continued
- ice crystal morphology, vapour growth, influence of vapour diffusion and heat diffusion 80—64933
- inert gas, transport and equilib. props., using LJ (12-7) pot. 79—98849
- inert gases, metastable atom diffusion, state decay, VUV obs. from discharge afterglow 80—44061
- inferferometric method for binary gas mass diffusivities determ. 77—62326
- inhomogeneous diffusion equations, analytic solutions, and diffusion coeffs. 78—34267
- intermolecular pair pot. energy function from gaseous transport coeffs., unlike monatomic interactions 78—62871
- ion mobility and diffusion in elec. fields of arbitrary strength 78—30398
- ion transport, three-temp. theory generalisation, appl. to $Cs^+ + Ar$ 80—6202
- ionic transport, data transport 80—12857
- ionosphere modification by release of highly reactive molecules, diffusion aspects 77—21988
- kinetic theory of vaporisation and condensation, physical-mathematical problems *(Italian)* 79—40505
- laser irradiated, anisotropy of inelastic scatt. and selective diffusion 80—53907
- laser separation 79—77331
- light induced atomic ground state transition absorpt. of monochromatic wave *(Russian)* 79—77335
- light induced diffusion of gases, isomer, isotope separation *(Russian)* 80—79430
- mass spectrometer sample line diffusion processes 78—64907
- Maxwell and Wien processes, special case of generalised Feller eqn. 77—26251
- membrane, porous, hydrophobic, anomalous gas mixture flow into liqs. 80—40744
- metal vapour diffusion coefficients, data correl. 79—77330
- meteors, luminous gas diffusion rate from television spectra 77—67076
- methane, diffusion in Kr, isotope effects at various densities 77—68732
- methane, electron radial diff. coeff. to mobility ratio 77—19666
- methane, gas, Rayleigh-Brillouin scatt., hydrodynamic effects calcs. 77—470
- methane diffusion in He, coeff. determ., gas chromatography method 77—11298
- methane-ethane-propane-butane, binary and multicomponent mixtures, viscosity, diffusion coeffs. 78—94883
- molecular dynamics studies of the role of diffusion in chemical models with absorbing boundary states 79—8424
- molecular gas, diffusion coeff. and mean free path, higher order approx. calcs. 79—27734
- multicomponent gas diffusion *(German)* 79—98845
- multicomponent gaseous diffusion coeffs., mean free path theory 78—18365
- multicomponent mixtures, diffusion eqn., approx. mass transfer description 77—47609
- multicomponent viscous gas flow, diffusion, boundary layer eqn. soln. *(Russian)* 77—7493
- multireaction chem. transport of solids, theoretical anal. 77—52236
- naphthalene sublimation, radial diffusion rate, mothball lifetime, for teaching 78—54124
- neutral gas diffusion in nonuniform chemically reactive atmosphere, three-dimensional time depend. modelling 79—66846
- non-equimolar mathematical study 79—94761
- nonlocal constitutive relations and continued fraction expansion, for wave vector depend. coeff. 77—76016
- nonuniform vapour, nucleation model, cluster diffusion effects 77—4206
- particle in gas stream, convective, diffusion with nonlinear kinetics of heterogeneous chem. reaction 78—83499
- planetary boundary layer, similarity theory appl. to Lagrange diffusion characteristics 77—56667
- pollutant transport eqn., 3-D, numerical algorithm 80—106811
- polyatomic gas, Dufour effect, mag. field influence, Onsager relation 78—18369
- polyatomic gas-inert gas mixture, viscomag. diffusion flux 78—47087
- premixed burning in diffusion flames, Libby Economos flame zone model 79—60093
- quantum state diffusion, in nonequilib. polyatomic gas, kinetic theory 77—62325
- radioactive gas diffusion, adsorpt. in porous media *(Russian)* 77—27591
- reaction-diffusion eqns., slowly varying waves and shock structures 77—66747
- reactive atom diffusion, by reson. ionis. spectrosc. 79—18984
- relativistic Lorentz gas of hard spheres, diffusion coeff. 77—5743
- RF breakdown in longit. mag. field, diffusion theory validity 77—39491
- slip flow in porous medium, effective diffusion coeff., variational method 79—90325
- solar nebula, diffusion and physiocochemical mechanism of planetary system form. 79—8857
- solutes at infinite dilution predicting diffusion coeffs. for liq.-liq. and liq.-gas systems 80—15272
- steam-air mixture, condensation, transport and thermodynamic props. *(Japanese)* 78—34251
- supersonic jet, diffusion of gas 79—32604
- teaching, relax. approx. to Boltzmann eqn. approach 78—73804
- ternary gas diffusion, heat transfer rates effect 77—7393
- test particle slowing down, rarefied gas added to host, with external conservative force 79—97326
- thermosphere, wind-induced diffusion rel. to diurnal vars. in temp. and comp. 77—87141
- true diffusion coeff. by Chapman method 77—51152
- two component Boltzmann gas, fluctuating kinetic eqn. 80—171
- upper atmosphere, ambipolar diffusion wavenumber regions rel. to meteor trails electron density fluctuations 78—73687
- upper atmosphere enhanced diffusion, study via $O_2(^1\Sigma)$ airglow, theory 79—29918
- vapour dynamic diffusion batcher with porous partition 78—79404
- vapours and gases, high-temp. characterisation, conf., Gaithersburg, USA (Sept. 1978) 79—40579
- vertical mass diffusion coeff. in atm., Rn tracer determ. *(Spanish)* 77—70717
- water droplet, laser induced evaporation, diffusion coeff. temp. depend. 77—20062
- water vapour, anal. of skin evaporimeter performance 80—56256
- Ar, electron drift and diffusion, Monte Carlo simulation 79—7441
- Ar, electron mobility and lateral diffusion coeff. 77—35307

diffusion in gases continued
- Ar, electron radial diff. coeff. to mobility ratio 77–19666
- Ar, metastable Hg atoms diffusion coeffs., temp. depend. 77–68731
- Ar, sputtered atoms, diffusion coeff. 79–87539
- Ar-CO_2(He), natural diffusion coeffs., press. effects 78–26229
- Ar-Cu, Cu diffusion coeff. determ. volatile salt dissoc. in pulsed discharge 80–33721
- Ar-ether(acetone)(benzene)(ethanol), conc. profile and interdiffusion coeffs. meas. 79–94763
- Ar-Hg, gas mixture, diffusion coeffs. and electron temps. 77–62327
- Ar-Kr, pair pot. energy functions, gas phase bulk property reproduction 77–27642
- Ar-Ne(Kr) systems, pot. parameters from binary diffusion coeffs. 78–37700
- Ar-O_2, diffusion, search for Senftleben-Beenakker effect 77–15155
- Ar+Ar($^3P_2$)($^3P_0$), flowing afterglow metastable decay rates, diffusion, two- and three-body rate consts. 78–73027
- Ar+Kr($^3P_2$), flowing afterglow metastable decay rates, diffusion, two- and three-body rate consts. 78–73027
- Ar+Xe($^3P_2$), flowing afterglow metastable decay rates, diffusion, two- and three-body rate consts. 78–73027
- BO_2, laser saturation spatial spectroscopy of diffusion coeff., interaction pot. 77–75341
- Br, diffusion coeff. in laminar flames 78–51272
- Br, diffusion in Ar at 298K, time resolved mass spectrometric determ. 79–90365
- Br^-, in He, ion reduced zero field mobility and free diffusion coeff. 77–47139
- Br_2, diffusion in NO at 298K, time-resolved mass spectrometric determ. 79–90365
- C particle combustion, diffusion and reaction in stagnant boundary layer 77–68705
- CF_4-He(Ne)(Ar)(N_2)(CO_2)(CH_4) mixtures, viscosity and diffusion coeffs. 77–89225
- CO, diffusion coeff. in laminar flames 78–51272
- CO diffusion through cigarette papers 80–43824
- CO, ratio of lateral diffusion coeff. to mobility for electrons 79–50840
- CO_2, ratio of lateral diffusion coeff. to mobility for electrons 79–50840
- CO_2-Ar(He), natural diffusion coeffs., press. effects 78–26229
- CO^+.CO, lateral diffusion in CO, mass spectra meas. 78–91055
- CS_2 gas binary diffusion coeff. obs. in H_2, He, N_2, air and Ar *(Japanese)* 79–10627
- CS_2+He(Ar)(N_2), perturbed rot. diffusion of CS_2, IR spectra 78–75245
- Cl in Ar and He gas, diffusion const. of atom 78–71417
- Cl^-, in He, ion reduced zero field mobilities and free diffusion coeffs. 77–47139
- Cl^--Ne(Ar)(Kr)(Xe), longitudinal diffusion coeff., generalised Einstein relation 79–86552
- Cs atoms, optically pumped, spin relax. in presence of N_2 79–59420
- Cs diffusion in Ar, time-resolved meas. 77–90588
- Cs, diffusion in Kr(Xe), determ. of diffusion coeffs. using π-pulse optical pumping method 79–68895
- Cs in Ar-methane, by reson. ionis. spectrosc. 79–18984
- Cs vapour, optically pumped, transverse relax. times and diffusion coeff., spin echo meas. 79–10062
- Cs^+ in He and Ne gas, ion mobility and longit. diffusion coeff. 78–67308
- Cs^+, in mol. gases, generalised Einstein relation, exptl. test 77–89224
- Cs^+, ion mobility in Ar, Kr, Xe, diffusion, generalised Einstein relation 78–67298
- F^-, in He, ion reduced zero field mobilities and free diffusion coeffs. 77–47139
- F^- ions in Kr and Xe; mobilities and diffusion coeffs. determ. 80–100048
- H, diffusion coeff., in H_2, luminesc. intensity meas. 80–103098
- H-air, laminar diffusion flames, chem. nonequilib. effects model 78–48654
- H_2 in fused quartz tube, meas. using mass spectrometer *(Japanese)* 77–58832
- H_2, lateral diffusion to electron mobility ratio 79–1284
- H_2-H, low-density gas, H-atom diffusion, 4.2-77K 79–50053
- H_2O^+, mobility in He, flow drift tube obs. 78–34257
- $H_2{}^{16}O$, $HD^{16}O$, $H_2{}^{18}O$, mol. diffusivities in N_2, isotope effects 79–1282
- $H_3O^+.H_2O$, mobility in He, flow drift tube obs. 78–34257
- $H_2(^3\Sigma_u{}^+)$-He(2^3S), discharge ionisation growth, diffusion coeffs. 78–83636
- H_2-D_2, separation by Taylor diffusion 79–18303
- He, coeff. from thermal conductivity, 400-2500K 77–54586
- He, electron radial diff. coeff. to mobility ratio 77–19666
- He gas, ion mobility and longit. diffusion of Ar^+ and $CH_x{}^+$ *(French)* 79–94766
- He, positive column, with diffusion loss to wall, axial elec. field effects *(Japanese)* 78–47196
- He, positron diffusion, annihilation and scatt. 77–19074
- He-Ar, diffusion coeff., two-bulb meas. 77–11299
- He-Ar(CO_2), natural diffusion coeffs., press. effects 78–26229
- He-Ar(N_2)(O_2)(CO_2), binary diffusion coeffs., press. depend., 300 and 323K, Thorne's eqn. 80–1724
- He-H, low-density gas, H-atom diffusion, 4.2-77K 79–50053
- He-Kr mixture, diffusion coeff. meas. by diffusion in flowing gas 80–83876
- He-Kr mixture, diffusion coeff. meas. by diffusion in flowing gas 80–83877
- He-M, M=CH_4, C_2H_6, C_3H_8, C_4H_{10}, O_2, CF_4, C_2F_6, C_3F_8, SF_6, N_2O binary gas mixture, mutual diffusion press. depend. 77–24047
- He-N_2, mutual diffusion coeff. meas. depend. on cell geometry 77–3911
- He-Ne(Ar)(N_2)(CO_2), thermal diffusion factors, (m,6,8) pot. calcs. 79–50835
- He-O_2, diffusion, search for Senftleben-Beenakker effect 77–15155
- He-O_2 diffusion coeff., two-bulb meas. 77–11299
- He+(H^+)(D^+), mobility and diffusion, runaway effect 80–33727
- He+Ar, interatomic pot. well depth, SPFD pot., diffusion, viscosity and second virial coeff. 80–5599
- He+Cs(Rb), interatomic pots., hyperfine shifts, diffusion coeffs., perturbation exchange theory 79–41220
- ^{4}He-D_2 mixture, binary diffusion coeff. near phase separation line *(Russian)* 80–6191
- Hg vapour-gas mixture, Hg diffusion, data correlation 78–79403
- Hg($6^3P_{2,0}$)+inert gas, diffusion in low-current discharge 78–63618
- I, diffusion coeff. in laminar flames 78–51272

diffusion in gases continued
- I^-, in He, ion reduced zero field mobility and free diffusion coeff. 77–47139
- I_2, laser saturation spatial spectroscopy of diffusion coeff., interaction pot. 77–75341
- $^{131}I_2$, $CH_3{}^{131}I$, radioactive, airborne, diffusion coeffs. 79–2142
- Kr in Xe, diffusion coeff. density expansion, search for log. term 79–82024
- Kr-He(Ne)(Ar)(Xe), gas, diffusion coeffs. meas., 350-1200K 80–14869
- Li/He heat pipe, start-up power, heat transport, thermal regulation 80–53615
- N_2, lateral diffusion to electron mobility ratio 79–1284
- N_2, vibr. energy diffusion coeff., 900-2000K 78–26227
- N_2-Ar corona dishcharge, convection and mixing, atm. press., mass spectra obs. 80–1853
- N_2-chloromethane mixture, binary diffusivities, 25-110°c 79–23391
- N_2-He-CO_2, discharge ionisation growth, diffusion coeffs. 78–83636
- N_2-methane mixture, binary diffusivities, 25-110°c 79–23391
- N_2-NO(He), discharge ionisation growth, diffusion coeffs. 78–83636
- $N_3{}^+$, $N_4{}^+$, lateral diffusion in N_2, mass spectra meas. 78–91055
- NH_3, diffusion rate appl. to atmospheric NH_3 determ. method 80–56614
- NO, electron radial diff. coeff. to mobility ratio 77–19666
- N_2O_4, turbulent dissoc. flow, along heated tubes, heat transfer 80–63225
- Na gas diffusion induced by resonance light field 80–53918
- Na vapour, diffusion coeff. of oriented atoms in buffer gases 80–53908
- Na vapour, in Ar(He), diffusion coeffs. meas. by Stefan method 79–41785
- Na vapour, laser induced diffusion *(Russian)* 80–6195
- Na^+, mobility and longit. diffusion coeffs. in Kr and Xe 80–106866
- Ne discharge in high press. narrow tube, Kadomtsev-Nedospasov instability 80–107004
- Ne isotope separation by gaseous diffusion transport in regular geometries 79–94099
- Ne, metastable Hg atoms diffusion coeffs., temp. depend. 77–68731
- Ne, positive column, with diffusion loss to wall, axial elec. field effects *(Japanese)* 78–47196
- Ne-Ar(He), thermal diffusion factors, (m,6,8) pot. calcs. 79–50835
- O_2, rotational collision number, diffusion coeffs. 79–1281
- $O_2{}^+$, lateral diffusion in O_2, mass spectra meas. 78–91055
- O_2-He(Ne)(CO_2)(CF_4)(SF_6) mixtures, viscosity and diffusion coeffs. 77–89225
- Pb vapour, diffusion-limited condensation meas. rel. to vacuum processing of metallurgical melts 77–8775
- RPO_4+3PBr_3, exam. of diffusion coefficients of gas mixture resulting, using chemical transport theory 79–1945
- Rb^+ in Kr(Xe), longit. diffusion and generalised Einstein relation 79–10625
- Rb^+, longit. diffusion coeffs. in elec. field, mass spectrometric determ. 77–7502
- Rn decay products, influence of elec. charge and humidity on diffusion coeff. 80–6192
- ^{220}Rn and ^{222}Rn, decay products, diffusion coeffs. in air and Ar 79–90366
- ^{220}Rn unattached decay products, diffusion coeff. depend. on ventilation and rel. humidity 77–9279
- ^{222}Rn content in air, diffusion in lower atm., U deposits prospecting appl. *(Spanish)* 77–78303
- SF_6-He(Ne)(Ar)(N_2)(CO_2)(CH_4)(CF_4) mixtures, viscosity and diffusion coeffs. 77–89225
- Si, CVD, gas phase diffusion and surface reactions 79–15614
- $SiBr_x$, x=1,2,4, diffusive mass transfer of Si, calc. for closed system 77–44169
- Tl, diffusion coeff. in laminar flames 78–51272
- Tl, metastable atoms quenching, diffusion and decay in buffer gases 79–54953
- ^{235}U enrichment by pulse gas diffusion 79–36380
- ^{235}U, large scale enrichment using separation nozzle 79–94654
- Xe+He(Ne)(Ar)(Kr), binary mixture viscosity and diffusion coeffs. 78–38443
- Xe_2, time and energy resolved fluorescence, radiative lifetime, collisional mixing, pulsed synchrotron radiation obs. 79–98136
- Zn vapour, diffusion-limited condensation meas. rel. to vacuum processing of metallurgical melts 77–8775
- Zn-H_2(He)(Ar) mixtures, binary diffusion coefficients, 1 atm., 720-1120K 80–1725

diffusion in liquids
- *see also electromigration; self-diffusion in liquids; thermal diffusion in liquids*
- 1:2 electrolytes, conc. solns., vel. correls. calcs., diffusion, cond. and transference props. 78–85166
- acetonitrile-d_2, liq., intermol. ^{1}H spin-lattice relax. and pair-diffusion 79–99781
- air bubble, in hydraulic oil, effect of diffusion on diameter change 78–90966
- albumin, bovine serum, charged macromol. translational diffusion coeff. 79–70510
- albumin, bovine serum, diffusion, hydration and soln. environment effects 77–19116
- albumin, bovine serum, diffusion, hydration effects, finite conc. 77–19115
- albumin, bovine serum, diffusion, hydration effects 77–19114
- albumin, bovine serum, macroion soln. viscosity and diffusion, quasielastic light scatt., electrostatic interaction 79–70508
- alkali chloride, molten, interdiffusion of Ag^+ *(Japanese)* 79–60530
- alkali chlorides, molten, Ag^+ impurity diffusion 80–59685
- alkali nitrates, molten, Rb^+ and Cs^+ ion tracer diffusion coeffs. meas. 80–70437
- alkane chains in liquids, rot. and torsional dynamics, Riemann tensor theory 80–54084
- n-alkanes, translational diffusion coeff. calc. 77–14626
- S-alkyl-isothiouronium iodides in methanol-water mixtures, conductance at 25°C, solute-solvent interaction 79–95194
- allene, rot. diffusion in CS_2 soln., IR spectral profiles 79–87426
- alloy, chem. diff. coeff. meas. 77–1249
- alloy, complex melt, processes taking place during vaporisation *(Russian)* 79–73298
- 4-aminomethylphthalimide-decalin-n-propanol, electronic spectra of 3-component solns., temp. depend. 79–4822

diffusion in liquids continued

- aniline+cyclohexane critical mixture, gravity-induced concentration gradients 77—28004
- anisotropic fluid, diffusion, EPR spin exchange and nuclear spin relax., theory 80—34753
- anisotropic liq. ang. correl. functions, memory function approach, Mori theory and extended diffusion eqn. 80—10489
- annulus with non-Newtonian fluids, mass transfer to inner wall, Leveque soln. adaptation 80—10267
- anthracene dianions in dimethyl ether, rotational diffusion meas. 80—65262
- bead solutions, quasielastic light scatt. in small wave vector limit 80—45088
- bimolecular autocatalytic reaction-diffusion system with Michaelis-Menten saturation law, multiple steady states 78—40045
- bimolecular reaction, partly diffusion-controlled, physical and chem. kinetics competition 79—43567
- bimolecular reaction, partly diffusion-controlled, physical and chem. kinetics competition 79—43566
- binary fluid mixture, in centrifugal field, crit. dynamics 80—44310
- binary hard-sphere mixture, mutual isothermal diffusion Onsager reciprocity relations effect 78—30773
- binary homogeneous mixtures, motion in infinite rot. cylinder, generalised diffusion theory 80—79328
- binary liquid mixture, diffusivity from simple kinetic model 79—23752
- binary liquid mixtures, spinodal decomposition, review 80—96657
- binary melt crystallisation, analytic description with melt diffusion consideration 80—24390
- binary mixture, conc., diffusion coeffs. at any temp., graphical correl. method 77—39683
- binary mixtures, film boiling, theory 77—84912
- binary system forming simple association complexes, liq. diffusivities prediction 80—34216
- binary systems, diffusion coeffs., stochastic theory of nonideal behaviour 80—44346
- biological material, prep. for X-ray microanal. of diffusible elements, methods of drying ultrathin cryosections 78—77166
- biological material prep. for X-ray microanal. of diffusible elements, rapid freezing and ultrathin section prep. 78—77165
- blood flowing in channels, diffusion of O_2 and CO_2 77—60303
- blood plasma, constituents rel. to O_2 diffusivity 79—92460
- Brownian motion and NMR spin relax., book 78—15054
- bubble growth, inertia and diffusion controlled, implosion, pure and binary systems 78—1552
- carbon tetrachloride-benzene-cyclohexane system, quaternary diffusion, capillary-cell method using ^{14}C labelling 78—87800
- carbowax in benzene, evaporation, vapour press. determ. from gaseous diffusion coeff. 80—10654
- carboxymethyl cellulose, aqueous soln., diffusion and mass transfer from rotating disc 80—83827
- cathodic diffusion boundary layer, free convective flow obs. with shadow Schlieren method 78—68894
- cavity flows, two and three dimens., multistep technique with implicit difference schemes 79—37398
- cellodextrin alditols, alkali solns., hydrodynamic props., frictional envelope form. 77—28031
- chain molecule dynamics, intramolecular diffusion controlled reaction for pr. terminal reactive groups 78—9289
- chemical reaction, diffusion controlled, kinetic studies by light scattering, one-step reaction case 78—35659
- chemical reaction bimol., diffusion-controlled, reversible, detailed equilib. principle 80—7770
- chemical reaction rate constants, in solution, short-range caging effects 79—96286
- chemical reactions in solution, formulation for effect of diffusion 78—40031
- chemical reactions rate constants, in solution, escape probability and time-depend. reactivity 79—96287
- chemical surface reaction with orientational selectivity, diffusion controlled effective reaction rate 79—16040
- chemiluminescence, step expts., analytical treatment of diffusion and electron transfer 78—27763
- classical liquids, microdynamics, book contrib. 79—60248
- classical liquids, vel. correl. and relative diffusion 78—14262
- cluster diffusion in non-ideal liquids 80—65260
- coefficient determination, using Stefan cell 77—51136
- coefficient determination in bubble column by method of stationary dissolving sample 77—51529
- coefficient determination using lamella pulsation diffusion apparatus 79—99340
- coefficient meas. and refractive index depend. on concentration at different wavelengths 80—88346
- colloidal dispersion dynamics, review 80—71956
- compressible inviscid fluid, profile of isogradient vaneless diffusor with swirl flow 79—86445
- concentration profile during zone melting, radiometric determ., slot method *(Czech)* 80—55289
- convection-diffusion equation, 1-D, finite elements method, weighted residuals 80—53775
- convective diffusion to drop, large Peclet no., finite Reynolds no., asymptotic soln. 79—41742
- crystal growth by travelling solvent method, heat flow, diffusion and convection 77—39549
- crystal growth from solution, diffusion controlled 77—72571
- crystallisation, spontaneous, diffusion kinetics *(German)* 77—51334
- cyclodextrins, diffusion in aq. polymer solns., complex form. 78—91460
- dendritic growth, diffusion in semi-solid region 80—15281
- dielectric, charge transport by solid particles 77—4329
- diffusive mass transfer in crystal growth, exam. 78—67669
- diphenyl ether, dielec. relax. pseudorot. diffusion 79—33600
- dispersion of contaminant mol. in laminar flow 77—39347
- dissolved substance diffusion to drop (bubble) chain at large Peclet nos. 79—86489
- DNA, calf-thymus, diffusion coeff. meas. using quasielastic light scatt. apparatus *(German)* 80—12314
- p-dodecanoylbenzylidene-p′-aminoazobenzene, smectic A mesophase, diffusion of trichlorotrifluoroethane, NMR spin echo obs. 78—94975
- drops, diffusophoresis in viscous media 78—35731
- drops in liquid, diffusional interaction 79—81947
- dye in Baltic Sea, expt. 79—2276
- dye solutions, high power UV irrad., bleaching and diffusion 77—42533

diffusion in liquids continued

- dye solutions, in micellar media, rot. diffusion, transient absorpt. meas. 79—92005
- dyes in organic solvents of high viscosity, diffusion coeffs. 78—10203
- electrical double layer, ionic mass transport, discreteness-of-charge effect 77—32800
- electrochemical cell, AC component effect on convective diff. processes, characts. 77—63929
- electrochemical convertors, conc. type, for elec. signals, diffusion theory of conc. networks 78—61026
- electrochemical diffusion, to spherical and cylindrical electrodes, Cottrell eqn. corrections calcs. 78—48658
- electrochemical flux equations, solns. with variable diffusion coeff. and transference number 78—48666
- electrochemical noise generated by diffusion of reacting species 77—25277
- electrochemical pit growth, convective diffusion in pits, ionic components conc. calc. 80—45409
- electrochemical solutions, diffusion coeff. determ. using pipe wall electrode 79—14947
- electrochemical system, diffusion layer theory, exptl. test 78—35701
- electrodiffusion problem solution for arbitrary system of singly charged ions 80—21300
- electrolyte, correlation between experimental and theoretical diffusion coeffs. 77—24421
- electrolyte, diffusion interactions between electrodes spaced on oscillating cylinder *(French)* 78—64849
- electrolyte, thermodynamic coefficients in presence of mag. induction *(French)* 77—51533
- electrolyte solution, tracer and mutual diffusion, open-end capillary method 79—28119
- electrolytes, aq. soln., molecular dynamics simulation 80—54097
- Erdogan-Chatwin nonlinear diffusion eqn., asymptotic solns., pipe flow solute dispersion 79—32673
- erythrosine B, dye soln., transient dichroism, rot. diffusion anomalies 79—87414
- estuary halocline, expt. simulation, salt diffusion in tap water, educational aspects 78—61980
- ethane-propane, binary mixture near crit. point, conc. fluctuation decay rate, spectrosc. obs. 77—81108
- eutectic colony growth, stability in presence of external perturbations rel. to diffusive exchange *(Russian)* 80—16291
- exponential diffusion eqn. *(Japanese)* 79—65230
- falling drops, optical technique for convective diffusion study 78—42690
- fast diffusion meas., nondestructive, using positron emitter as tracer 78—54519
- ferrofluid, mag. birefringence pulsed field meas. 79—82943
- ferrofluid, suspension, magnetodiffusion, interferometric obs. *(Russian)* 77—4946
- Fick's law, applications, theory *(French)* 78—18813
- Fick's law modification 80—96333
- flow in porous media, diphasic incompressible, diffusion-convection eqn., mixed finite element method, water flooding 80—74969
- flow on interacting surfaces, laminar and turbulent, in Newtonian or non-Newtonian fluids *(French)* 77—27516
- fluid, dense, chem. reacting, Enskog theory 78—35667
- fluid, reacting spheres, kinetic theory 78—35668
- fluorescence, long-range energy transfer combined with isotropic or anisotropic diffusion 79—11461
- fluorescence energy transfer in the rapid-diffusion limit 79—92151
- fractional uptake technique for determining diffusion coefficients 80—2184
- free volume theory, Macedo-Litovitz eqn. 77—51530
- furfural-water interface, anomalous mass transfer, coupling of heat and mass transfer 77—80626
- gas bubble growth in over-saturated liquid-gas soln. 78—1733
- gas cavitation nuclei stabilization using skins of varying permeability 79—81611
- gas diffusion, quantum effects, predictive formula 78—30771
- gas diffusion through surfactant films, interfacial resistance 80—39385
- gas-liquid diffusivities prediction 78—2270
- gas-liquid interface, absorption rate, diffusion coeff., stat. thermodynamics anal. 77—76644
- gas-liquid metal reactions, mixed transport control 77—72709
- gas-liquid moving interface diffusion 78—22404
- gas-porous electrode, mass exchange in transport zones 77—32801
- gels, dynamic light scattering in poor solvent 78—88318
- glass, melt, bubble behaviour during refining, math. model 80—81277
- glass melt, diffusion, review 78—2017
- glass phase separating, interpretation of temp. dependence of transport process 78—87806
- glycerol solutions, diffusion coeffs., viscosity 78—51711
- glycol solutions, diffusion coeffs., viscosity 78—51711
- gravity wave, liquid with superficial film and diffusion effect *(French)* 78—75156
- haemoglobin, in salt soln., diffusion rel. to intermol. interactions, light scatt. investig. 77—44585
- hard sphere fluid, impurity self-diffusion coeff., ring approx. 78—6167
- hard sphere fluid near hard wall, diffusion coefficient, mol. dynamics simulation 80—64858
- hard sphere liq., dil. impurity diffusion coeff., quasihydrodynamic approx. and simulation 80—49066
- n-heptyl-4-cyanobiphenyl, nematic phase, dielec. loss, diffusion equations 80—71305
- heterogeneous liquid stream, stress diffusion effect, molar diffusion coeff. 78—79338
- p-hexanoylbenzylidene-p′-aminoazobenzene, smectic A mesophase, diffusion of trichlorotrifluorethane, NMR spin echo obs. 78—94975
- hinged rods, exception to Einstein relation 79—2736
- histone lysine-rich, diffusion coeff. from laser scattering spectra 77—29095
- holographic interferometric meas. 79—37861
- hydrocarbons, fluoresc. quenching by TMPD cations, diffusion effects 77—6823
- impurity diffusion coeff. in convecting fluid 78—5747
- inert gas liquids, of H_2, diffusion and NMR 79—61249
- inhomogeneous diffusion equations, analytic solutions, and diffusion coeffs. 78—34267
- inhomogeneous flows of non-Newtonian fluids: generation of spatial concentration gradients, stress and diffusion effects 79—60032

diffusion in liquids continued
- inhomogeneous liquid, diffusion model, correctness of boundary value problems 78—30774
- ionic diffusion in naturally-occurring aqueous solns., use of activity coeffs. in transition-state models 78—57224
- isotope transport in reversibly reacting species systems, isotopically labelled solvent and friction coeffs. 80—54420
- isotopic mass effects in diffusion of small light solutes in solvent of larger heavier mols. 78—34639
- Kramer's chemical reaction model, barrier mediated diffusion, generalisation to include viscosity term 80—71890
- Kuroshio jet current region, nonlinear density diffusion rel. to density field calc. 78—92843
- lamellar eutectic diffusion problem, numerical solns. determ. using elec. analogue 78—3116
- laminal flowing liquids, concurrent, in horizontal cylindrical channel 80—79397
- laminar dispersion in circular tubes, approx. anal. 77—46986
- laminar liquid flow around plate, boundary-value problem soln. for generalised diffusion eqn. 77—7366
- latex, sol, diffusion coeff. meas. by photon correl. spectroscopy 77—10117
- latex particles in ionic solution, in aq. soln., hindered diffusion through small pores 79—43622
- Liesegang rings demonstration of transient state pot. flow 78—63408
- liquid, symmetric top molecule, angular velocity correlation function, from angular position correlation functions 79—86661
- liquid alloys, determ. of diffusion coeff. from meas. of resist. 77—55375
- liquid metals, diffusion mechanisms, and coeff. determ. *(Russian)* 80—34215
- liquid-liquid mixing analysis, lamellar model 80—15246
- LMFBR, yield characts. of short-lived fission products in Na heat-transfer agent 78—66338
- low-conductivity fluids, dark currents, forced diffusion model 79—15182
- macromolecular diffusion, direct and hydrodynamic forces effect 79—50172
- macromolecular flexibility, detect. by time-depend. diffusion coeffs. obs. 80—23585
- macromolecular fluid, stress-induced diffusion 78—10205
- macromolecular hard-sphere system, diffusion, hydration and soln. environment effects 77—19116
- macromolecular hard-sphere system, diffusion, hydration effects 77—19114
- macromolecular hard-sphere system, diffusion, hydration effects, finite conc. 77—19115
- macromolecular solns., self-diffusion coeff. 78—6168
- macromolecular solutes, finite conc., isothermal diffusion and quasielastic light scatt. 79—82367
- macromolecular solution, gel conc. and diffusivity at gelling determ. by ultrafiltration 80—21325
- macromolecular solution, rot. diffusion coeff. calc. method w.r.t. mol. struct., elec. birefringence relax. time data interpret. 80—85331
- macromolecular solution, semidilute, scaling law describing conc. depend. 79—70377
- macromolecular solutions, kinetic theory and rheology 77—7424
- macromolecular solutions, review 80—15273
- macromolecule, rigid, in soln., depolarised Rayleigh spectroscopy 79—94119
- macromolecules, coiled linear, effective diffusion tensor of chain mol. in shear flow 77—50579
- macromolecules, interacting, spherical, light scatt., conc. fluctuations, transport eqn. 79—1775
- macromolecules in soln., sedimentation, expt. determ., errors due to diffusion *(Russian)* 78—76934
- macroparticle diffusion, role of inertial effects 80—29196
- macroparticles; charged spherical, dilute soln., Rayleigh scatt. 80—84748
- mass transfer inside drops in continuous fluid, effect of pulsation *(French)* 78—55686
- MBBA, liq. cryst., mass diffusion meas., tracer dye-laser method 78—59738
- MBBA, nematic, diffusion coeff. determ. *(German)* 79—51291
- measurement, apparatus and appl. to ^{85}Kr in fluid Kr 78—54520
- measurement, bubble evolution method using crit. size concept 80—4828
- measurement method for diffusivities of gases 77—15608
- melts, impurity distrib. ratios, kinetic depend., cryst. growth appl. 78—43044
- membrane transport, chemical reaction augmented, facilitation factors, prediction, appl. 79—91992
- metal, electron probe microanalysis for high-temp. applic. *(French)* 77—29074
- metal, entropy of fusion and activation energy for self-diffusion 79—28121
- metal, of oxygen, electrochem. obs. using solid oxide electrolytes 80—59669
- metal, phys. chem., conf., Konigstein, Germany (Mar. 1976) 77—1059
- metal refining by crystallisation and reflux, three component Raoultian behaviour 77—28799
- metals, diffusion, electrotransport and thermotransport 77—55371
- metals, isotope effect determ. using radioisotopes 79—95191
- metals and alloys, book 78—51406
- 9-methylanthracene, solubilisation in water by hypercoiled polymethacrylic acid 80—91591
- MHD, steady, diffusive instability, rel. to geomagnetism 79—50807
- micellar diffusion-controlled reaction kinetics 80—30213
- microemulsions, aerosol OT, inhomogeneous interior, fluoresc. and polarisation decay probes 80—50891
- microemulsions, quasi-elastic light scatt. 80—108755
- migration mechanism of approaching particles, energy transfer, luminesc. quenching study 80—100343
- mixed ion-dipole systems, rot. diffusion, statistical theory *(Russian)* 77—80403
- mixed strong electrolytes, relax. effects in limiting law region, integral representation 77—86322
- mode-mode coupling theory of chemical reaction in a dense fluid 79—57218
- molecular reorientational motions rel. to dielec., Kerr effect relaxations 77—4599
- molecule, fluorescent, rot. diffusion coeff. from polaris. anisotropy meas., photon counting technique 77—18072
- molecules, spheroid-cylindrical, dynamics in dilute soln. 80—44090

diffusion in liquids continued
- molecules with internal rot., forced diffusion, correlation function 77—80402
- molten metals, impurity atom diffusion, hard sphere fluid model calcs. *(Russian)* 80—49089
- molten salt, mol. dynamics simulation, of liquids with ionic interaction 80—54097
- molten salt transport reactions, isothermal system *(German)* 77—63568
- molten salt transport reactions, isothermal system *(German)* 77—63569
- molten salts, transport coeffs., integral representations 78—67842
- moving semipermeable boundary, diffusion transport in liquid solution 77—80639
- multicomponent mixtures, diffusion eqn., approx. mass transfer description 77—47609
- multicomponent mixtures, mass transfer, penetration depths 79—42286
- multicomponent systems, rel. to electroepitaxy, theoretical model 80—65396
- NaCl, of Li^+ ion *(Japanese)* 78—14489
- NMR diffusion and flow meas., spin phase graphing 78—47074
- non-Newtonian falling film, Taylor diffusion of solute 77—39317
- non-Newtonian fluid, effective diffusion of impurity in laminar flow of liquid 78—67228
- nonelectrolytes in dil. soln., diffusion coeff., Hammond-Stokes plot 79—42287
- nonlinear diffusion-reaction problems with time-dependent diffusion coefficient 79—98823
- nonlinear thermosolutal convection 79—10557
- Norwegian Sea pycnocline, apparent vertical eddy diffusion rates from T vertical distrib. 78—81185
- nucleation, diffusion-controlled, time lag 78—47497
- Nylon 12, short-time adhesion, rel. to diffusion properties *(Japanese)* 79—70294
- Nylon 12 melt, diffusion *(Japanese)* 79—95192
- ocean, admixture diffusion in vortex flow 79—2277
- ocean, relative diffusion meas. at small scales 78—88838
- ocean benthic boundary layer, diffusion-controlled model for deep-sea Mn nodules growth 79—2212
- ocean layered fine-structure form. and destruction by double-diffusive processes 77—29303
- ocean microstructure, double-diffusive intrusions into density gradient 78—85569
- ocean water diffusion diagrams, scale-dependent diffusion modeling 77—56640
- ocean-dumped sewage sludge tracking, using 200 kHz echo sounder 77—2182
- oceanic fronts cabbeling and double diffusion rel. to frontal circulation 79—2263
- oceanic internal waves, induced diffusion reson. interaction 77—45010
- oil in water microemulsion, added NaCl, light beating spectroscopy of micelles mutual diffusion coefficient 78—80793
- one dimensional isothermal diffusion in two layer medium *(Russian)* 79—28117
- optical method for mutual diffusion coeff. determ. from refractive index gradient profile 77—30198
- organic molecules, long-chain, diffusion through polymer matrix, hydrostatic press. effect on diffusion coeff. 80—92697
- particle in hard sphere liquid, translational theory, mol. theory 79—42288
- pentacene dianions in dimethyl ether, rotational diffusion meas. 80—65262
- pentyl-cyano-biphenyl, nematic phase, transport props. of dissolved ionic species, electrochem. meas. *(French)* 79—90811
- phase fluorometry as a probe of diffusion-controlled molecular encounters in dense fluids 80—32799
- photographic, film development kinetics of viscous solutions *(German)* 79—83482
- plant protein diffusion coeff. meas. using quasielastic light scatt. apparatus *(German)* 80—12314
- plumes, vertical, round, diffusion, flow props. 80—43755
- PMMA soln. in toluene, diffusion, viscosity rel. to temp. *(German)* 79—42289
- PMMA solution, diffusion coeffs. and thermodynamic props., conc. depend. 80—15274
- polar liquids in double layer capacitors, RF conduction, ion diffusion effect 80—107883
- polar solvent mixtures, solvated electron diffusion, 2-absorber model 80—85206
- polarography, pulse, chronoamperometric, chronocoulometric techniques, kinetic, mass transport effects 77—25334
- polarography, pulse time scanning, limiting current diagnostic differentiation technique 77—25339
- pollutant dispersion from point source with and without chem. reaction in semi-bounded waters 77—64329
- poly(2-vinyl pyridine), dil. solns., translational diffusion, chain conformation influence 80—103508
- poly-γ-benzyle-L-glutamate in dioxane solution, relax. mechanisms, light scatt. spectra 80—20659
- poly-p-phenyleneterephthalamide, diffusion in conc. H_2SO_4 *(Russian)* 79—65232
- polyacrylamide, aq. solns., conform. changes, intermol. interactions, optical mixing spectroscopy 79—10770
- polyacrylamide-water gel, translational and collective diffusion 79—52787
- polyelectrolyte solution, polyion-polyion interaction effects, computer simulation 80—35817
- polyelectrolytes, translating, electrolyte friction theory 80—29194
- polyethylene, diffusion of long chain molecules 79—23784
- polyethylene, liq. diffusion coeffs. determ., G-L chromatography, modified Deemter eqn. 78—2277
- polyethylene oxide, dil. soln., neutron scatt. mol. motion obs. 77—23593
- polymer, entangled, phenomenological consequences of Doi-Edwards viscoelasticity theory 80—79250
- polymer blends, interdiffusion, meas. method 79—69271
- polymer diffusion equation with hydrodynamic interaction, equiv. normal coord. 80—79966
- polymer film, swollen, diffusion-relax. cojpling, two-stage sorption correl. 79—94864
- polymer solns., dynamic scaling theories at nonzero concs., tagged chain translational diffusion coeffs. 80—75143
- polymer solution, diffusion, viscosity and dynamic struct. factor, dynamic scaling theory 79—64977
- polymer solution, diffusion of a chain, conc. effects 80—70103

diffusion in liquids continued
polymer solution, dilute, chain mol. dynamics and transport processes 80—14989
polymer solution, dissolution rates and polymer-solvent system phenomena *(German)* 80—13167
polymer solutions, aqueous, diffusion and mass transfer from rotating disc 80—83827
polymer solutions, diffusion of ionic species, meas. by diffusion controlled electrolysys 80—74920
polymer solutions, diffusion of tagged interacting spherically symmetric polymers 79—81314
polymer solutions, dil., dynamical props. 78—38608
polymer solutions, dil., dynamics, model 79—73086
polymer solutions, mol. diffusion coeff. meas. using impedance meas. technique 79—23328
polymer solutions, transport coeffs. and scaling laws in dil. regime *(French)* 79—82372
polymer solutions and gels, dynamic behaviour obs. using light scatt. 80—55727
polymer solutions and networks at equilib. swollen state, inelastic light scatt. by gel modes 78—1972
polymers in dilute solutions, diffusion and relaxation time 78—55964
polyphenyl ether in benzene, evaporation, vapour press. determ. from gaseous diffusion coeff. 80—10654
polyphenylquinoxaline, soln., conform., equilib. rigidity *(Russian)* 79—55643
polystyrene, conc. solns., diffusion and sedimentation, frictional coeff., crit. soln. temp. 79—95195
polystyrene, in mixed theta solvent, intramol. motion, photon-correlation spectra obs. 79—77480
polystyrene, melt, bulk diffusion, local diffusion *(Japanese)* 78—95170
polystyrene, moderately conc. solns. in cyclohexane, polymer diffusion and dimensions 77—62462
polystyrene, sulphonated, polyelectrolyte solution, correlations and dynamics 80—104446
polystyrene in cyclohexane, dil. theta soln., translational diffusion coeffs., conc. depend., Rayleigh scatt. meas. 79—90812
polystyrene latex, colloidal crystal, grain boundary struct. and boundary diffusion obs. *(Japanese)* 78—15721
polystyrene solns. at theta conditions, Rayleigh scatt. determ. of conc. depend. of diffusion coeff. 79—77790
polystyrene solutions, dilute, diffusion coeff., solvent effect 80—19971
polystyrene-co-divinylbenzene microgels in dimethylformamide, diffusion coeff., viscosity and mol. wt. meas. 80—30286
polystyrene-fluorescent conjugates in melt, local diffusion *(Japanese)* 79—23757
polystyrene-PMMA-benzene, soln., polystyrene diffusion, photon correl. spectroscopy 80—34220
polystyrenes, in toluene 79—1773
polystyrenes, toluene soln., diffusion through cellulose membrane, friction coeffs. 78—73085
porous electrode diffusion controlled operation, mass transport with memory 80—21298
porous media, thermomigration, capillary diffusion coeffs. *(French)* 77—89006
protein, high conc. soln., quasielastic light scatt. line breadth meas., diffusion coeffs. 77—1976
protein solutions, quasielastic light scatt. in small wave vector limit 80—45088
PVC solution, diffusion coeffs. and thermodynamic props., conc. depend. 80—15274
PVC-poly-ε-caprolactone, interdiffusion, meas. method 79—69271
pyrene dodecanoic acid, lateral diffusion at air-water interface, monomer excimer dynamics 80—92693
quiescent two-phase systems, interfacial resistance to interphase mass transfer 78—67828
radical pair generation, diffusion, spin motion, recombination in soln. nanosecond scale 77—77798
rate constant of reaction, determ. from overall crystal growth coeff. 78—59773
rate processes, effect of intermol. force field 77—35733
reacting particle in fluid, convective diffusion, nonlinear surface reaction kinetics 80—106854
reacting substances counterdiffusion, conditions for stationary boundary 79—1933
relaxation processes and spectra in liqs. and dense gases 77—58935
resonant bubbles in standing wave acoustic field, diffusion in stable arrays 77—79988
rhodamine 6G, in water, fluorescence intensity correlation, photon counting using clip-correlator *(Russian)* 80—42271
rhodamine 6G, micellar soln., aq., fluoresc. decay for rot. diffusion const. 79—11826
t-RNA, rot. relax. time, 10^{-9}s range Fabry-Perot and photoelectron time of arrival method 80—21437
rod-shaped molecules, restricted rot. diffusion, time correl. functions 80—79655
rotational diffusion in solvents with large characteristic lengths 79—73329
rotational tunnelling and diffusion in condensed mol. systems, neutron scatt. 78—63658
Savart plate interferometry for isothermal diffusion meas. 78—45678
seawater, vertical diffusion of radioactive admixture *(Russian)* 77—60417
silicophosphate melts, diffusion 79—46824
sintering, liquid phase, computer simulation of chemically driven grain growth 80—55427
smectic liquid crystal, A-phase, impurity diffusion, appl. to TMS in BBOA 77—43140
sodium dodecyl sulphate NaCl aq. soln., micellar props., laser light scatt. exam. 78—92513
soil water absorption with exponential diffusivity, infiltration and perturbation methods 77—66944
sol crystals, grain boundary struct. and boundary diffusion obs. *(Japanese)* 78—15721
solid spheres, reacting, in periodic array, convective mass transfer in liq. laminar flow 80—96176
soluble fluids in laminar, turbulent flows, stretch model appls. to mixing, diffusion, react. 79—94736
solute diffusion in laminar pipe flow 77—39345
solute layering, in low aspect enclosure, effect on lateral heat transfer 77—75776

diffusion in liquids continued
solutes, high molecular weight, limiting diffusion coeff. estimation 80—24626
solutes at infinite dilution predicting diffusion coeffs. for liq.-liq. and liq.-gas systems 80—15272
solution, diffusion coeff. meas. by conc. gradient method and light scatt. 79—99339
solution of diffusion eqn. for capillary method with no external stirring 78—54518
solutions, dynamic orientational correlation functions, coupled translational-rot. diffusion model 77—84604
solutions with large conc. gradient, in capillary, diffusion near crit. point *(Russian)* 77—84958
solvated electron+phenanthrene, diffusion controlled reactions in polar solvents, reaction parameters 80—97687
solvated electrons, diffusion controlled reactions in polar solvents, reaction parameters 80—97687
space environment, transport processes in fluids 79—46825
spherical gas bubble, in nonNewtonian liquids, growth by solute diffusion 78—34677
steel, alloy, Fe-C-Si-S, liquid, desulphurisation with CaO, exam. of reaction mechanisms 78—80742
steel, diffusion melting in Fe-C melts, heat transfer correl. 80—54348
steel, disintegrated stream, simplified model of oxidation 77—73373
steel, graphite dissolution, segregation and diffusion *(Russian)* 78—11201
Stefanian cell diffusion coefficients, effect of heat of vaporisation *(Japanese)* 79—86882
Stokes problem for suspension of spheres, effective medium theory 79—81836
styrene-acrylonitrile copolymer solutions, dilute, diffusion coeff., solvent effect 80—19971
styrene-butadiene-styrene copolymer, struct. investigation by diffusion anal. 78—42884
surface diffusion flux in Newtonian or nonNewtonian fluid, laminar flow, double pulse meas. *(French)* 78—40055
suspension of rod-like molecular particles, rot. diffusion coeff. from decay rate of birefr. 79—38520
suspensions, deposition in channel entrance, combined influence of diffusion, electricity and gravity 80—1674
symmetric top mol. with internal rot., extended diffusion and reorientation in fluids 77—20101
ternary polymer systems, diffusion controlled formation of porous structures 80—7539
ternary systems, diffusion coeffs., stochastic theory of nonideal behaviour 80—44346
tetracene dianions in dimethyl ether, rotational diffusion meas. 80—65262
tetrachloromethane-cyclohexane system, interdiffusion, ternary diffusion eqn., radioactive tracer obs. 78—79792
tetrafluoromethane, Kr diffusion, 243.15K, density depend., size effect 78—75859
thin-layer cell, concentration impedance, unequal diffusion coeffs. and 2nd-order reactions effects *(French)* 78—53214
thin-layer cell, concentration impedance reactive and nonreactive diffusion effects *(French)* 78—53213
three-component liquids, analysis of measured values of coeffs. *(Japanese)* 78—91463
trace element separations in igneous rocks, possible diffusional effects 77—41008
tracer diffusion coefficients, capillary method determ. calcs. 78—91462
tracer diffusion coefficients, open-eded continuous capillary method determ. 78—75861
tracer dispersion in annular climbing film flow 79—64751
tribromomethane-propyl alcohol conc. fluctuation kinetics, holographic study *(Russian)* 78—19508
unsaturated porous media, moisture transfer due to small temp. gradients *(French)* 78—150
unsteady MDH convective diffusion, exact anal. 79—72953
uramine, in water, fluorescence intensity correlation, photon counting using clip-correlator *(Russian)* 80—42271
US waves, standing, directional independence of freezing-in-effect, diffusion gradient *(German)* 77—50786
viscoelastic cylinder, optimal management of diffusion treatment rel. to conc. depend stresses 79—94510
viscosity measurement method at high press. 80—69955
viscous liquid, three-dimensional flow and convective diffusion toward particle, nonlinear kinetics 80—19397
water, diffusion of O_2, N_2, H_2 and Ar, laser interferometric study 77—76584
water, of air, experimental determ. of mol. diffusion coeff. 77—28029
water, of H, review of neutron radiography results 78—59961
water-toluene-sodium dodecyl sulphate-butanol 1 mixture, interface light scatt., interface tension meas. 80—76039
water/air surface tension, effect of air diffusion and interface struct. 77—4246
Widom-Rowlinson hard-sphere mixture model, transport props. 80—14981
xanthrene, dye soln., transient dichroism, rot. diffusion anomalies 79—87414
Ag-In melt system, conc. depend. of component and impurity diffusion coeffs., radioactive isotope method *(Russian)* 80—107454
AgBr, crystal growth behaviour, influence of Gibbs-Thomson effect 78—24883
Ag_2S and Ag_2Se melts, electrotransfer, ionic component of elec. cond., Ag ion diffusion 79—51640
Al melts, metallic materials diffusion rate, meas. apparatus 79—86913
Al, molten, dissoln. kinetics and diffusion coeffs. of Fe, Co and Ni 80—59666
Al, molten, impurity diffusion of fourth period solutes and homovalent solutes *(Japanese)* 80—70436
Al, of Co and Fe, coeff., 700-900°C *(Russian)* 77—59119
Al, of W, under low gravity *(Russian)* 78—22875
Al, phase form. and diffusion interaction with W-Re alloy, under weightlessness *(Russian)* 78—22876
Al-Cu, liq. diffusion coeff. meas. using temp. gradient zone melting 78—26710
Al-Cv (0.3 wt.%), moving solid-liq. interface, diffusion in liq. 80—107456
Al-Mg alloys, distrib. of liquid Mg at liquid-solid interface *(Slovak)* 79—91637
Al-Ni solid, liquid mixture, diffusion processes *(Russian)* 80—107563

diffusion in liquids continued
- Al-Si, liq. alloy, chem. diff. coeff. determ. 77—1249
- Al-Si(Mn)(Ti)(Cr)(Ni)(Cu)(Fe), liq., dissoln. and diffusion of alloying components, 700-1000°C *(Russian)* 80—15275
- Al-Sn, liq. alloy, chem. diff. coeff. determ. 77—1249
- Al-Sn(Ag), of Ge, mech. *(Russian)* 80—15276
- Al-Sn(Ag)(Cu)(Au), liquid alloys, exam. of Si diffusion *(Russian)* 79—28118
- $Al_xGa_{1-x}As$, epitaxial layer crystn. from soln. in melt, diffusion limited 78—35321
- Ar, liq., electron mobility/diffusion coeff. 80—44593
- B_2O_3, molten, growth and dissolution of air, N_2, O_2 gas bubbles 77—20070
- Bi, of Sb, 713-853K *(Russian)* 77—15611
- Bi-Sb, melts, interdiffusion, long capillary method and electron probe obs. 77—89563
- Bi_2Te_3-Bi_2Se_3 thermoelectric alloys, diffusion and evaporation of volatile component during prep. 80—35118
- CO, liq., ^{13}C NMR for mol. diffusion and spin-rot. interaction, 0-1.73 kbar 79—99777
- CO_2 diffusivities in aq. mixed electrolyte solns. 79—95190
- $CaCl_2$, correlation between experimental and theoretical diffusion coeffs. 77—24421
- CaO-SiO_2 melt, tracer diffusivity of Ca^{45} and elec. cond. 79—60532
- Co^{3+} complex ions, diffusion coeffs. meas., computer-assisted technique using Cottrell eqn. 80—3425
- CoO, high temperature physico-chemical interactions with oxygen under pressure *(French)* 78—31549
- Cr^{3+} complex ions, diffusion coeffs. meas., computer-assisted technique using Cottrell eqn. 80—3425
- CsCl of Li^+, Na^+, Rb^+ and Cs^+ ions *(Japanese)* 78—14489
- CsCl-$BaCl_2$:U^{3+}, melt, diffusion coeffs. and mechanisms 79—73330
- Cu and Cu-S, liquid, oxidation kinetics, by CO_2 77—28986
- Cu, diffusion coeffs. of ^{124}Sb, ^{113}Sn, ^{110m}Ag and ^{195}Au 79—95196
- Cu diffusion layer cathodic deposition and anodic dissolution rates 80—93503
- Cu, impurity diffusion of Ru, In, Sn, Sb *(Japanese)* 78—10204
- Cu, liquid, impurity diffusion, shear cell assembly meas *(French)* 80—75375
- Cu, molten, diffusion of H_2, stationary method determ. *(German)* 79—10974
- Cu, of Tl, Ir, Rb and Bi *(Japanese)* 78—59962
- Cu-Ag film preparation with const. comp., by diffusion-limited evaporation from liquid 77—21038
- Cu-Pb liquid alloys, exam. of O diffusivity at 1430K using electrochemical cell 78—51713
- ^{19}F, spin-rot. tensors, in trichlorofluoromethane and ClO_3F, appl. to liq.-phase rot. diffusion 80—43068
- Fe alloy, molten, N_2 diffusion, effect of Si, P, Al and B *(German)* 77—20099
- Fe alloys, complex, diffusivity and solubility of N_2 at 1600°C 77—39684
- Fe, diffusion melting in Fe-C melts, heat transfer correl. 80—54348
- Fe, diffusion of O_2, Ar, H_2 *(Russian)* 77—55369
- Fe, liquid, alloying element effect on H_2 diffusion *(Russian)* 79—69270
- Fe, molten, diffusion of V, Co, Mb *(Japanese)* 77—51531
- Fe, O_2 diffusivity, meas. by EMF method 78—14494
- Fe, of alloying elements *(Russian)* 78—79791
- Fe, of H_2 *(German)* 78—14487
- solid Fe/liquid Zn, interdiffusion reaction 79—77845
- Fe-based solns., liq., diffusion of N 78—75862
- Fe-C, levitated drops, carburisation and decarburisation in CO-CO_2 gas mixture, exam. of reaction kinetics 78—85053
- Fe-Cr (Mn)(Ni)(Si), liquid diffusion of H_2 *(German)* 78—14487
- Fe-Ni liquid alloy, physical and chemical props. deviations from Raoult's law *(Russian)* 78—95729
- Ga, diffusion coeff. of As at 720°C during LPE growth 80—54419
- Ga-GaAs melt, mutual diffusion from soln. kinetics, self-diffusion coeffs. 77—47608
- Ga-In, liq., O diffusion coeff., thermodynamic activity and solubility 78—38860
- GaAs, LPE growth from supercooled soln., thickness uniformity 80—54547
- GaAs:Sn, dopant segregation during liq. phase electroepitaxy 80—54384
- Ge:B, single crystals, grown by Czochralski method, exam. of B distribution ratio and diffusion coeff. 79—95042
- H_2O in biological samples, PMR, fast-exchange model interpretation via differential kinetics clarified 80—67033
- He II-^3He, ^3He diffusion coeff., order parameter relax., second sound 78—30808
- He, impurity ion mobility 77—7921
- ^3He-^3He normal solution, size effect influence on capillary mass transport *(Russian)* 80—70497
- ^3He-^4He mixture, dilute, diffusion const. and thermal cond. along λ line 77—47644
- ^3He-^4He solutions, mass diffusion coeff. meas. 78—47630
- Hg, of Al, diffusion coeff. meas. 80—24627
- Hg-In, liq. alloy, chem. diff. coeff. determ. 77—1249
- I, activation enthalpy of diffusion in mixed solvents 78—14492
- In, diffusion coeff. determ. of P, mathematical model, numerical method 79—23754
- In-P melt, diffusion coeff. of Ga 77—85927
- KCl, melt, mol. dynamics simulation 80—54097
- KCl of Li^+ *(Japanese)* 78—14489
- KF, correlation between experimental and theoretical diffusion coeffs. 77—24421
- KF-H_2O, diffusion coeffs., diaphragm cell expts. *(German)* 78—83986
- KNO_3, of Tl^+, high dilution diffusion, interferometry 78—47546
- K_2SO_4 aqueous solutions, differential diffusion coeffs. determ. diaphragm cell method 79—95193
- Li aluminosilicate glasses, variation of refractive index during ion-exchange diffusion from molten salts *(Russian)* 77—28539
- Li, in fusion reactor, estimate of diffusion coeff. of Pb 79—93828
- (Li-K)NO_3, molten, K^+(Rb^+)(Cs^+)(Tl^+) diffusion, wavefront shearing interferometric obs. 79—60535
- LiCl-KCl:Cu^+, fused eutectic, diffusion and surface effects, chronopotentiometry *(French)* 78—11524
- LiF-NaF-KF molten mixture, diffusivity and solubility of H_2 78—34640
- Li_2O-Al_2O_3-SiO_2 glass melts, alkali ions interdiffusion coeffs., conc. depend. 79—65231
- Mg, diffusion and thermal diffusion of Fe, Si and Al, obs. using unidirectional solidification 78—30772

diffusion in liquids continued
- $MgCl_2$-NaCl-H_2O, ionic diffusion theory, use of activity coeffs. in transition-state models 78—57224
- $Mg(NO_3)_2$, correlation between experimental and theoretical diffusion coeffs. 77—24421
- $MgSO_4$ soln., thermal and Fickian diffusion 78—2272
- Mo, impurities, interaction mechanism and saturation limit *(Russian)* 77—55358
- NaCl, mass transfer from sedimentary deposit layer to stationary water region *(Japanese)* 77—25700
- NaCl, water-HMPT soln., ionic diffusion coeffs. meas. *(French)* 80—65265
- NaCl-KCl-H_2O, ionic diffusion theory, use of activity coeffs. in transition-state models 78—57224
- $NaClO_3$, growth and dissolution kinetics, diffusion and convection regimes 78—63684
- $NaNO_2$ aqueous solutions, differential diffusion coeffs. determ. diaphragm cell method 79—95193
- $NaNO_3$, of Tl^+, high dilution diffusion, interferometry 78—47546
- $NaNo_2$, correlation between experimental and theoretical diffusion coeffs. 77—24421
- Na_2O-Al_2O_3-SiO_2 glass melts, alkali ions interdiffusion coeffs., conc. depend. 79—65231
- Na_2O-CaO-SiO_2, multicomponent liq. state diffusion 78—55962
- Na_2O-K_2O-SiO_2 melts, Na^+ and K^+ diffusion and interdiffusion processes 80—34221
- Na_2O-SiO_2 melt, diffusion coeffs., electron microanal. meas. of Na and Si concs. 77—31790
- Na_2O-SiO_2(-CaO) glass, molten, metal ion diffusion and redox behaviour, electrochemical studies 80—81332
- Na_2SO_4 in aqueous soln., diffusion coeffs. and Onsager-Fuoss theory disagreement 80—40729
- Ni, diffusion of O_2, Ar, H_2 *(Russian)* 77—55369
- Ni, O_2 diffusivity, meas. by EMF method 78—14494
- Ni, of N_2 *(Russian)* 78—18812
- Ni superalloy, transient liq. phase diffusion bonding and mechanism *(Japanese)* 78—2279
- Ni-Cr (Mo)(W) melts, N_2 diffusion *(Russian)* 78—18812
- O_2, diffusion coeff. in liqs. determ. by ESR line widths 78—91929
- Pb, $^{113,117m,125}Sn$ diffusion coeff. meas. *(Ukrainian)* 80—10690
- PbO-SiO_2 melts, ionic transport, tracer diffusion and chem. interdiffusion 79—77785
- Pu, hard-sphere model, phys. prop. meas. interpret., adjacent solid phase implications 77—19866
- $RbNO_3$, of Tl^+, high dilution diffusion, interferometry 78—47546
- Sb, liquid, diffusion of O_2, activity coeff. 80—65267
- Se, estimate of self-diffusion coeffs. from viscosity data 77—55370
- Si, molten, dissolution of SiC, Fick's law calc. 79—99319
- Si:As, melting by high power ns laser pulsing, As diffusion 78—79789
- SiO_2, fused, He solubility and diffusion above transform. range 80—79965
- SiO_2-NaO-K_2O-CaO-MgO-Al_2O_3 melt, anodic dissolution of Co and Ni in melt 78—88582
- Sn, diffusion and electrotransport of impurities meas. 77—51535
- Sn, diffusion coeff. of ^{113}Sn, ^{124}Sb, ^{110}Ag, and ^{195}Au 80—96676
- Sn, liquid, impurity diffusion, shear cell assembly meas *(French)* 80—75375
- Te, estimate of self-diffusion coeffs. from viscosity data 77—55370
- Te, of Hg and Cd 77—84955
- Tl_2S-Tl_2Se systems, melts, ion transfer, diffusion coeffs., elec. cond., density meas. 77—1253
- TlSe, Tl_2Se, Tl_2Se_3, of Sn, Ag, and Tl *(Russian)* 77—28030
- Tl_2Se, fused, diffusion of ^{204}Tl, ^{110}Ag, ^{112}Sn impurities 80—54415
- U, hard-sphere model, phys. prop. meas. interpret., adjacent solid phase implications 77—19866
- U, in alkali, chloride eutectic melts, interdiffusion, chronopotentiometric meas. 77—80637

diffusion in plasma *see plasma transport processes*

diffusion in solids
  see also electromigration; ionic conduction in solids; self-diffusion in solids; surface diffusion
- A15 compound formation by diffusion from ternary bronzes, thermodynamics 78—84740
- A15 compounds, disordered, reordering kinetics 80—96678
- A-15 compounds, models for growth kinetics, solid state diffusion 79—46847
- abietic acid in polymer matrix, photosensitised oxidation, singlet O_2 diffusion *(Russian)* 79—52655
- activation energy for thermochemical treatment process *(Russian)* 79—77800
- activation enthalpy and entropy and defect form., basic thermodynamic relation, validity limit 78—47557
- adsorbed molecules, ratios between rates of thermal dissociation, desorption and diffusion 79—95265
- alkali boroaluminosilicate system, self-focusing fibres with aperture of 0.18 80—87548
- alkali chlorides, positron-trapping colour centre dynamics, positron annihilation study 80—108294
- alkali germanate glasses, He permeability, diffusivity and solubility 79—51308
- alkali halide:alkaline-earth cations, defect structs. examined by methods based on Mott-Littleton techniques 80—59487
- alkali halide crystals, inhomogeneous transport at low temp. 77—43382
- alkali halide crystals, kinetic shape stability loss in faced cavities in diffusion zone 79—55916
- alkali halides, diffusion of H and H_2 activation energy calcs. 77—51546
- alkali halides, divalent impurity diffusion, penetration plot deformation 80—24666
- alkali halides, doped, F-centre accumulation efficiency temp. depend. 77—76394
- alkali metal chloride: F^-(Br^-)(I^-), anion impurities substitution, energies of soln., association and migration 78—83831
- alkaline earth fluorides, thermodynamics and kinetics of O incorporation 77—84778
- alkaline earth oxides, point defect props., band struct., lattice simulation calc. 80—19797
- alloy, atomic diffusion when exposed to liquid Na 77—7899
- alloy, binary, conc., with short and long range order, computer simulation of diffusion 78—30778

diffusion in solids continued
alloy, binary, interdiffusion coeff. and Matano interfaces *(Japanese)* 78—14516
alloy, binary, intrinsic diffusion coeffs. meas. method *(German)* 77—28036
alloy, binary, single phase, empirical relationship for homogenization 79—55892
alloy, coarsening by temp. cycling 79—29111
alloy, production process strength *(Russian)* 77—21152
alloy, role of phase boundaries in phase transformations 78—72772
alloy, single phase, annealing of diffusion layer 78—14518
alloy, solid soln., grain boundary mobility 79—46676
alloy, three component, conditions for mass transfer, diffusion processes 80—54445
alloy powder, two component, sintering 80—20847
alloy powders, production using electrodeposition and heating in reducing atm. 79—100079
alloy random, binary, diffusion correlation factors calc., comparison of matrix inversion, Monte Carlo and diffusion of probability techniques 78—30779
alloys, anisotropic binary, HCP struct., influence of spatial nonuniformity of short-range order on interdiffusion *(Russian)* 78—6187
alloys, binary, marker displacements as result of diffusion 80—92724
alloys, free energy calc. for any conc. of implanted atoms, diffusion current in chem. pot. gradient *(Russian)* 78—34657
alloys, impurity diffusion and distrib. 79—33118
alloys, irradiated, segregation, inverse Kirkendall effect, effect of constitution on void swelling 78—91472
alloys, spinodal decomposition, review 80—96657
alloys, ternary, interdiffusion coeffs., expt. determ. 79—95221
β''-alumina, K^+ ion nonuniformity, in contact with $NaNO_3$ and Na_xS_y melts 78—10215
aluminisation in Al packs, for protective coating form., kinetic diffusion theory 77—32727
aluminosilicate glass, diffusion of Sn(IV) 80—49417
amethyst, Fe^{3+} diffusion, associated phenomena 77—36269
amorphous, vac. evaporated, doping, transport and optical props. 80—49715
amorphous solids, diffusion of nonspherical particles, correl. effects 80—39337
anis otropic, limits bimol. exciton recombinations kinetics 77—4295
anisotropic diffusion in stress fields 78—55973
annealing, struct. and grain boundary mobility 79—47728
antiphase boundary motion, microscopic diffusional theory, appl. to domain boundary coarsening 79—61563
a-As_2Se_3, diffusion of Ag and Au 77—51549
atom jumping correlation, new calculation method *(French)* 77—39691
atomic diffusion mechanisms *(Hungarian)* 78—38868
atoms diffusing in periodic lattices, quasi-elastic neutron scatt., use of Monte Carlo calcs. 79—60557
Au film, diffusion of Ag along grain boundaries, scanning Auger microscopy obs. 78—22897
austenitic stainless steel, recrystallisation transformation energies, α' to γ, effect of Si content and deformation by rolling *(French)* 77—48433
barrier layers, against diffusion 80—66444
batch adsorption for pore diffusion with film resistance and an irreversible isotherm 78—84047
bbok 77—24422
BCC metal, of H isotopes, self-capture effect and activation energy *(Russian)* 78—75879
BCC metals, of H_2 and its isotopes, phonon-assisted quantum-mechanical tunnelling of interstitials 80—59730
bimetallic diffusion couple, interdiffusion coefficients and phase width calc. 77—62685
bimetallic epitaxial film, modification of interfaces during interdiffusion 78—71890
binary alloy, solidification chemical inhomogeneity *(Russian)* 80—75335
binary alloys, generalised coarsening theory 78—39778
binary and multicomponent solids, chem. diffusion coeff., Darken's expressions modification 80—59738
binary metal alloys, surface segregation correlation with bulk diffusion 80—54388
binary metallic solid solns., thermodynamic quantities rel. to vacancy and diffusion characts. 79—95204
binary multiphase system, interdiffusion coeffs. determ. 80—70477
binary solids, preferential sputtering, diffusion enhancement effects on comp. changes 79—47574
binary substitutional solid solution, diffusion, correl. effects and jump freq. ratios 79—99350
binary systems, calculating interdiffusion coefficient in case of cylindrical symmetry *(Russian)* 79—69297
binary-multiple phase systems, phase growth kinetics accompanying interdiffusion *(Russian)* 80—19992
boride coating of metals, diffusion soaking effect on struct. 78—18846
boride diffusion coatings on steel, fractographic exam. of struct. 78—44270
brass, morphological stability of α/β phase interface, interface moving direction effect 77—15700
α-brass, of H_2 77—62675
brass, plastic flow, rate controlling mech. at high temps. 77—81308
brass, sliding contact in magnetic field, model for cross diffusion 79—79121
α/β-brass bicrystals, two-phase, with nearly uniform and thermodynamic equilib. concs. 80—65383
brass bicrystals, two-phase (α/β), interphase boundary sliding at high temperature 80—88164
brass multiphase binary diffusion couple, layer growth rate of intermediate phase, numerical calc. *(Japanese)* 78—14513
brittle materials, intergranular creep crack growth, diffusion controlled theory 78—84950
bronze-steel, phase composition and struct. of diffusional interlayer in fusion zone, X-ray analysis 78—56821
Brownian particle motion in periodic field of force, diffusion coeff. in large friction limit 78—38869
butadiene copolymers, diffusion and solubility of S and 2,2′-dioxy-3,3′-di(α-methylcyclohexyl)-5,5′-dimethyldiphenylmethane *(Russian)* 79—33092
butyl rubber ethylene propylene ternary copolymer mixture, permeability, diffusion of gases and solvents 79—95217
calcium alginate gels, dextran fractions, globular protein diffusion coeffs., heterodyne beat spectrum 79—1776

diffusion in solids continued
camera speed diffusion transfer offset master on filmbase 80—37108
camera speed negative working diffusion transfer material 80—37107
camera speed overlay colour system, negative and positive working, diffusion transfer based 80—37109
d-camphor, NO diffusion, ELDOR, self-diffusion 77—1618
capillary mass transfer of porous solids based on pore distrib. curves 77—7443
carbons, active, micropore filling and adsorption of simple gases, Dubinin theory 77—47661
carburized single crystal sheets, lattice strain during interstitial diffusion *(Japanese)* 78—10220
carburizing in glow discharge methane plasma 79—11724
Caskey-Pillinger finite difference method, solns. to McNabb Foster diffusion and trapping eqns. 80—29201
cation exchange membrane, counterion interdiffusion 80—26044
cavity growth, by surface diffusion in polycrystn. metals 80—104217
cavity growth, creep mechanisms, independent and sequential 80—55480
cellophane membrane, transient diffusion of unstirred polystyrene solns. 78—92508
cellulose acetate film, diffusion and permeation of gases 79—55934
cement, water adsorption, NMR relax. exam. 78—48354
ceramic fission reactor fuels, high temperature chemistry, nonstoichiometry, review 77—14238
ceramic nuclear fuels, irrad. induced rare gas diffusion 80—59524
ceramics, chemical reactions, high temp., diffusion controlled 79—91935
ceramics, lattice and grain boundary diffusion consts., correls. 80—96679
chabazite type zeolite, cation substituted, IR spectra, cation migration 78—10933
chalcogenide glass film, drift and thermal diffusion of Au electrodes, α-particle backscatt. meas. 79—4434
chalcogenide glass film, thermal diffusion of Au electrode layer, backscatt. anal. 78—10228
charcoal, adsorbed fission gas release in spill accident 77—50262
cheese cloth filled cellulose acetate film, diffusion and permeation of gases 79—55934
chemical potential of impurity-vacancy pairs 77—11587
chemical reaction 79—33120
chemoepitaxial nucleation during reaction diffusion, thermodynamic anal. *(Russian)* 80—15394
chondrite Kirin H, inert gas content interpretation *(German)* 80—46505
clad material, of C *(German)* 77—50230
Clausius-Mossotti problem for cubic arrays of spheres 78—52422
clusters of diffusing substances, formation on matrix defects *(Russian)* 79—1519
coal, permeability to methane, influence of temp., geostatic and stratal press. *(Russian)* 79—66695
coalescence of gas-filled pores *(Russian)* 78—18679
coarsening, time depend. of average particle size 80—79994
coated particle fuel, ^{110}Ag release 77—88228
coating, charact. of conc. distrib. during form. 78—18839
coating, diffusion solution, relaxation of residual stresses *(Russian)* 77—70195
coating, two phase, resulting from constant surface flux of solute, solvent-fixed coordinate system appl. 78—26718
coating of plate, residual stresses, with allowance for phase transform. *(Russian)* 78—11357
coefficient meas. using ion beam sputtering as microsectioning technique 78—47551
coefficients evaluation, numerical algorithm for using α spectrometry 80—34223
coherent quantum diffusion in a single band, theory 80—107463
coke, chamber and formed, binary diffusion of CO_2 with CO and CO with N_2 *(German)* 80—100356
composite, diffusion theory of medium theory 78—22884
composite layered slab, solute diffusion, conc. depend., with/without chem. reactions 80—54427
composite material, cubic arrangements of spherical particles in isotropic matrix, effective conductivities 78—55547
composite material, two phase diffusion model 79—55936
composite resin, Langmuir type model for anomalous moisture diffusion 78—67867
composites, planar, dissolution of precipitate plates, one-phase diffusion controlled 80—15244
composites transient hygrothermal stresses, coupled diffusion of heat and moisture 80—33451
compound semiconductor-metal reactions, book contrib. 79—1622
concentration depend. diffusion coeff. in semi-infinite media 77—31798
concentration variations, diffr. strudies 79—42322
concentration-dependent diffusion in a finite slab with and without chemical reaction 79—30389
concrete and containment uptake of fission product I, sorption and diffusion 79—67898
condensed media, low-temp. particle transport theory, impurity electron transfer 80—19974
constant coefficients model, appl. to diffusion in solids *(Russian)* 79—4424
contact film absorption on plastic deform. of contacting bodies *(Russian)* 80—93596
continuum model for diffusion in region with multiple diffusivity 79—77801
controlled pore glass, pore struct., determ. by electron microscopy and Hg penetration 78—43165
copper phthalocyanine-iodine, amorphous cpd. prep. by I_2 diffusion in polycrysts., triplet EPR signals obs. *(Russian)* 80—66016
correlated particle migration in cryst. struct. *(Russian)* 80—96683
correlation factor, Monte Carlo calc. 79—82375
correlation function, two point, distinguishable particle hopping on uniform one dimens. chain 78—43169
couple, diffusion, low order correction for subsurface contribs. 77—62661
creep, steady state, climb controlled, at high and intermediate temps., theoretical description 79—95074
crowdions, prop. anal. using Frenkel-Kontorova model 79—42056
crystal, diffusional motion and distortion of macroscopic inclusions under influence of elastic stresses *(Russian)* 77—66676
crystal growth by solid state techniques review 77—85935
crystal lattice sites, many-particle random motion 80—92703
crystalline solid, particle jumps, diffusion correlation factor 79—99351
cyclohexane, NO diffusion, ELDOR, self-diffusion 77—1618
dechannelling theory, γ-factor and diffusion processes 77—7775
defect annealing, diffusion controlled, generalised theory 80—92520

diffusion in solids continued
  defect diffusion coeffs., site blocking, correlated defect motion 80—84315
  defect recombination, diffusion-controlled, incorporating Coulomb interaction and annihilation 78—23044
  defect theory and processes, review 80—2009
  defective crystals, diffusion processes and multistate diffusion 79—19389
  defective solids, Haven ratio in athermal lattice gas;, Monte Carlo method 80—84313
  defects, description of diffusion-limited reactions 77—1147
  defects, influence on solid-state props., review 77—7709
  defects, radiation effects 78—87827
  dekryptonation thermal anal. using flow type GM detector 77—66786
  dekryptonisation thermal analysis, apparatus *(German)* 77—90699
  delayed cracking by H_2 gathering simulations at plastically deformed notch, finite element anal. 78—31539
  depth profiling techniques for thin film interdiffusion and interfacial reactions, book contrib. 79—1564
  diamond, structure and motion of self-interstitials 79—37700
  diamond, transformation of type IB dispersed N into type IA aggregate N 78—6089
  diamond and HCP lattices, random walks 78—71876
  diamond Ge(B)(B_4C), doping by diffusion at high temp. and press. 79—19273
  dielectric moistening diffusion kinetics, forecasting *(Hungarian)* 80—96692
  diffusion coefficient measurement in solid materials, geometry factor from variational principles 79—42290
  diffusion in Ni, ion radiation effect on redistrib. 78—34551
  diffusion into Si, in open tube, high vacuum system 78—91349
  diffusion of radical-ion pairs, spatial distrib., electron spin echo obs. 80—29622
  diffusion potential, concept. rel. to Maxwell's eqns. and irreversible thermodynamics 79—63171
  diffusion solution for point defects in stress field, steady state and transient 78—30780
  diffusion traps for divalent ions, dielectric loss and ionic thermocurrent techniques 80—6566
  dilute alloys, solute diffusion 78—47589
  discontinuous swelling, type II diffusion as particular soln. of conventional eqn. 78—91471
  discrete lattice model, Frenkel pair annihilation 77—59009
  dislocation creep, diffusion controlled 79—46745
  dislocation creep, diffusion controlled 79—46744
  dislocation mobility, description using diffusion eqns. 78—38697
  dislocation pipe diffusion, calc. 79—82374
  disordered lattice long-time behaviour of classical diffusion 80—29200
  disordered one-dimensional lattice systems, diffusion and hopping conductivity 80—59991
  disordered system, exact solution for diffusion const. 78—22885
  disordered system, particle diffusion in Anderson model 79—33273
  dispersion hardened alloy, calc. of back stress decrease, due to Orowan dislocation loop climb 78—83812
  distorted crystal structure, random migration *(Russian)* 78—47554
  double diffusion, gettering of impurities 80—75383
  double diffusivity media, discrete random walk model 80—92702
  double oscillatory tunnelling, soln. by effective Hamiltonian method 77—20109
  drift-diffusion problem with special boundary conditions, numerical soln. by integral eqns. 77—76591
  dye-polymer system, diffusion based direct marking process, laser induced, spectral thermal characteristics 79—76779
  edge effects in diffusion and cond. meas. 78—32810
  education, electrochromism in WO_3, advanced lab. expt., colour centres, proton diffusion 80—17738
  education, solid state diffusion, atomistic model, pedagogical use of Monte Carlo method 79—25797
  elastic amorphous medium, relax. by defect diffusion 80—58925
  elastic fluid diffusion in elastic solid, mechanical theory 77—59136
  elastic medium, diffusion *(Rumanian)* 78—47558
  electroluminescent films, activating impurity diffusion coeff. *(Russian)* 77—84995
  enamel-metal interface, diffusion phenomena, spectroscopic investig. *(Russian)* 77—90508
  energy spike development and quenching depend. on thermal diffusion 80—88367
  enhanced diffusion mechanisms, review 78—67847
  epoxy meas. of H_2O diffusion by radionuclides, corrosion effects *(Czech)* 77—48566
  epoxy resin, destruction by diffused water 78—48511
  eutectic alloys, surface energy considerations 78—44152
  exit problem, diffusion across pot. barriers, chemical reactions and crystal diffusion 79—80527
  exotic atoms, conf., Erice, Sicily, (1979) 80—67939
  fast volume diffusion during cryst. growth 79—99352
  ζ-Fe-Zn layer formed during hot dip galvanizing, texture 79—29287
  ferrite, polycrystalline, ionic diffusion and dislocation movement during creep deform. *(Japanese)* 77—28039
  ferrite spinel films, LPE growth and props., SIMS, X-ray diffr., and spin wave reson. obs. 80—34323
  ferromagnets, sintering theory and diffusion flow 79—28977
  fibre, high modulus, diffusion barrier appl. 77—77449
  Fick's equations solutions for impurity diffusion, dislocations, interstitials, vacancies 80—70469
  Fick's second law, anal. soln. for diffusion coeff. as linear function of conc. 78—34644
  Fick equation, validity limits, atomic struct. effect on diffusion *(French)* 77—84965
  film, effect of partial sink in binary diffusion 78—43166
  film, effect of surface condition at low temps. 78—91469
  film, grain-boundary diffusion, analytic and numerical solns. 77—4274
  film, interdiffusion and reactions, book 79—1561
  film, interdiffusion and reactions, book contrib. 79—1562
  film, isolated grain boundary diffusion, analytical model 77—4275
  film, multiple grain boundaries and surface diffusion 77—4276
  film systems, grain boundary diffusion, book contrib. 79—1526
  finite single- and two-phase systems, atomic diffusion, iterative solns. 77—4224
  first order reaction in catalyst particle, conc. depend. diffusion coeff., effectiveness factors 78—48693
  first wall of thermonuclear reactor, diffusive action of radiation *(Russian)* 78—29639

diffusion in solids continued
  fission fuel grain boundary loss terms, use in fission gas release and swelling models 80—63257
  fission oxide fuels, intergranular densification model due to the diffusion of pt. defects and pore destruction 79—73345
  fission product release, enhanced by grain boundary diffusion 78—4986
  fission reactor materials, radiational growth due to diffusional anisotropy 79—71897
  fission reactor materials, UO_2 high temp. reaction with Zr-Nb 78—66344
  float glass, Sn penetration depth meas. 77—76614
  float glass, Sn penetration in bottom surface, synthesis 80—79993
  flow of solute atoms near crack tip, time dependent, exam. 78—75722
  formation kinetics of solid layer on surface in reaction diffusion 78—63938
  Fourier expression, of diffusion equation and its appl. *(Japanese)* 80—49400
  Fourier transform, of diffusion eqn. with non-linear terms 80—103514
  Frenkel defects, form. and collapse, defect migration, electron irrad. effects, computer simulation 80—92523
  fuel element, Cs, fission product, release and diffusion *(German)* 78—25298
  p-GaAs:Zn, diffusional doping, photoluminesc. in mag. field 77—16384
  gas, thermal evolution from solid following detrapping and diffusion during linear tempering schedule 78—75889
  gas behaviour in closed porosity body, exam. 80—24642
  gas bubble diffusion mobility in solids, radius depend. 80—39357
  gas diffusion in linear elastic solid, stress-assisted 80—65294
  gas diffusion study by press. oscillation method 78—47597
  gas in porous medium, continuity of soln. in n space dimensions 78—95130
  gas-liquid inclusions, in crysts., movement in temp. field gradient 79—55942
  gas-solid catalysed reactions effect of nonuniform activity distrib. 79—96362
  gases in metals, detection by vacuum spark technique, appl. to Al wire 78—61094
  Ge:P, radiation-accelerated diffusion 80—6559
  gelatin layers, permeation of photographic developer, potentiometric exam. *(Russian)* 80—73500
  generalised atomic hopping problem, occupancy correlation functions 77—66038
  generalised atomic hopping problem, particle correlation functions 77—66039
  glass, Ag^+ migration for planar waveguide form. 77—27352
  glass, chemically strengthened, ion exchange temp. and time influence on stress profiles and strengths 78—31417
  glass, coloured layers containing Pb and Cu 77—36677
  glass, conc. distrib. in surface layer after contact with $AgNO_3$ melt, $AgNO_3/NaNO_3$ mixture 80—44372
  glass, diffusion coefficient equation 80—103521
  glass, diffusion profiles analysis, grinding and etching techniques comparison 78—26732
  glass, diffusion strengthening technique 78—31418
  glass, float, low-Fe, weathered, surface, characterisation 80—93666
  glass, He gas diffusivity effects on blister formation by 150 keV He^+ irrad. 77—35604
  glass, nonequilib. thermodynamics *(German)* 78—83746
  glass, of K^+, plane optical waveguide form. 79—90043
  glass, of Na, model, single alkali silicate glass 77—84990
  glass, partially devitrified, grain boundary diffusion, new percolation problems 78—18844
  glass, permeability of He *(Japanese)* 79—7715
  glass, refractive index gradients, form. using ion exchange diffusion 80—64227
  glass, review 78—2017
  glass, surface layer, structure and processes *(German)* 80—38928
  glass, Tl ion thermal migration formed optical waveguide, props. 79—46031
  glass bead sintered pellets, pore struct. and diffusibility *(Japanese)* 78—14509
  glass cation ion exchange interdiffusion, nonidealness degree 80—39362
  glass fibre reinforced epoxy resin, destruction by diffused water 78—48511
  glass fibre reinforced epoxy resin, destruction by freezing or boiling of phase separated water 78—48512
  glass membranes, transient diffusion of sucrose, mannitol, pentaerythritol stirred aq. solns., thermodynamics 78—92507
  glass microsphere laser targets, He and H_2 permeation 77—83078
  glass microsphere laser targets, He and H_2 permeation 77—83079
  glass of optical fibre, chem. incompatibility 77—75694
  glass surfaces, interdiffusion of H^+ and alkali ions, extended Boksay-Doremus theory 80—34254
  glasses, spinodal decomposition, review 80—96657
  glasses, thermal cond. rel. to diffusion process due to phonon-defect interaction 80—34259
  glassy polymer multi-phase Stefan problem describing swelling and dissolution 78—2263
  glassy polymers, powders, transport props., vapour sorption expts. 78—76919
  glaze/glass-ceramic, interface reactions, electron microprobe anal. 80—84398
  Gorsky effect for low interstitial conc., theory 79—10896
  graded index materials, optical props. meas., ion diffusion effect on refr. index 79—9237
  grain boundaries during superplastic deform., dislocation density and diffusion parameters 79—65099
  grain boundary diffusion coeff. determ. using surface anal. 77—11742
  grain boundary diffusion with radioactive decay 78—59967
  grain boundary drift diffusion under influence of stress fields 79—77835
  grain boundary interaction with disperse inclusions of soluble phase, theory *(Russian)* 77—80513
  grain boundary migration, diffusion induced 79—77833
  grain boundary migration, effect of solute atoms 79—28124
  grain boundary migration, group mechanism *(Russian)* 77—80514
  grain boundary migration kinetics, atom diffusion across boundary, theory 80—79809
  grain boundary migration vacancy generation, and drag force 80—15090
  grain boundary permeation in solids, appl. to Au and Cr in Pt 79—65253

diffusion in solids continued
grain boundary sliding and intercrystalline fracture in high temp. creep *(Czechoslovakian)* 77—32642
grain rearrangement, solids wth hexagonal grain struct. 78—84896
grain-boundary diffusion at low temperature, anal. of surface accumulation method for film systems 79—77838
graphite, Br_2 intercalation, oxidation and residual Br effects 79—43565
graphite, of ^{90}Sr in HTGR fuel elements 79—67869
graphite, of Br_2, HNO_3 and $PdCl_2$ 79—42310
graphite, of Cs 77—7901
graphite, of Sr, lab. determ. 77—7900
graphite, of T *(German)* 77—24442
graphite, pyrolytic, of Nb, 1450 to 1950°C 77—39693
graphite fibre reinforced composites, damage by moisture, diffusion anal. 80—81227
graphite intercalation cpds., effect of graphite struct. on intercalation rate 78—31356
graphite powder compacts, of H_2 and N_2, time-lag analysis 78—2301
growing phase diffusivity determ. 80—24641
growth kinetics of plate-like precipitates, vol. diffusion controlled growth 78—6935
Gunn planar elements, stationary domains 79—56238
H_2 diffusivity and solubility, in He, H_2 and heavy ion bombardment, to simulate microstruct. damage from fission or fusion neutrons 79—46723
hard spheres permeation through hard disc monolayers, interfacial mass transfer 80—107460
Hastelloy, C-276, H transport rel. to ageing treatment 80—75384
Hastelloy X, H permeability using permeation method *(Japanese)* 78—51740
heat conduction and diffusion localisation in const. property media 80—58888
heat of transport in cryst. solids 77—55383
heteronuclear system, spin diffusion, NMR 78—88213
hexamethyldisilane, plastic deform., and diffusion of hexamethylethane-^{14}C 78—14510
high diffusivity paths, new interpretation of diffusion, continuum approach 79—42291
high strength steels HT80, HY130, quenching and tempering effect on H_2 diffusion *(Japanese)* 78—64565
homogeneous doped semiconductor, influence of internal elec. field on diffusion of ionised impurity 79—55940
hopping among inequivalent octahedral sites in body-centred tetragonal lattice 79—1520
hopping of a pair of distinguishable particles on uniform one dimensional chain, time-dependent correlations 78—88212
HTGR fission product diffusion through core materials during LOFC, exact analytical soln. 80—47554
hydrate, struct. I clathrate hydrate, H_2O mol. reorientation and diffusion, PMR and dielectric relax. 77—36142
hydride forming materials, H_2 induced delayed cracking 78—27623
hydrogen permeation characts. 79—67948
III-V semiconductor, of Zn, by isoconc. technique, anal. of 'up-hill' region 77—35755
III-V semiconductor heterostructures, growth and dissolution kinetics by LPE 80—49543
III-V semiconductors, diffusion theory for impurities 79—82246
III-V semiconductors, point defects and deep traps, thermodynamic history, model 80—59908
implant ion collection with radn. enhanced diffusion and sputtering of implant 80—2055
impurities, interaction and diffusion, near structural phase transition of matrix 79—42083
impurities, Kramer's rate formula 78—83992
impurity, light, interstitial, quasi-optical model, solvent nuclei vibr. anharmonicity effects *(Russian)* 77—24433
impurity atoms diffusion and impurity-vacancy interactions *(Russian)* 80—19985
impurity diffusion, and distrib. in films 79—69146
impurity diffusion, correl. factor, computer simulation 79—19404
impurity diffusion coeffs., determ. from optical absorpt. 79—69294
impurity diffusion profile computation *(Russian)* 77—47621
impurity diffusion profiles, influence of limited solubility 78—55989
impurity diffusion with complex form. 77—76616
impurity distribution, calc. for cryst. solid with inhomogeneous layers *(Russian)* 78—14500
impurity precipitation on dislocations, and competitive diffusion sinks 77—76455
impurity profiles calc. for two-step diffusion 78—30662
impurity transport by dynamic crowdions, computer simulation 78—18843
inclusions, equations of motion 80—75387
inclusions, macroscopic, diffusion motions in nonuniform compressive stress fields *(Russian)* 80—88351
Incoloy 800, clean and steam oxidised, T_2 permeation 80—88364
Incoloy 800, mechanisms of corrosion in He, solid state diffusion 79—47843
Incoloy 903, H_2 permeation and diffusion 78—26730
Incoloy-800, meas. of H and D permeation for reactor safety anal. 79—77822
Inconel 600, atomic S diffusion *(French)* 79—74307
Inconel 600, S penetration leading to sulphide form. *(French)* 79—74306
Inconel 617, creep, morphological changes of carbides, affect on creep props. 80—108509
Inconel 625, creep rupture behaviour in Ag environment 80—25853
Inconel 718, H_2 permeation and diffusion 78—26730
Inconel-625, hydrogen permeation characts. 79—69295
inert gas crystals with imbedded impurities, struct. and diffusion props., review 80—10563
inhomogeneous solid solutions with conc. expansion, thermodynamics, energy defect diffusion calcs. 80—24618
insulating film, detection of self-drifting of ionic charges by surface potential decay method 78—72295
interacting particle diffusion in periodic pots., two particle model, random motion 79—46828
intercalation and substitution-intercalation cpds. in dichalcogenide hosts, factors affecting ion mobility 80—59707
intercalation compound electrodes, thermodynamic and transport props. 80—66963
interdiffusion coefficient determ. by modified Holl method *(Russian)* 77—51553

diffusion in solids continued
interdiffusion coefficients, determ. in growing multiphase layer 80—70477
interdiffusion in specimens of closed form, singularities of pore formation *(Russian)* 77—59151
interface-controlled to diffusion-controlled coarsening kinetics, particle size distrib. 80—7579
interfacial diffusion effect on nucleation kinetics at grain and interface boundaries 77—35761
interfacial geometry and D-variation effects in two-phase systems 80—2219
intergranular cavity growth in uniform stress field ahead of crack-like stress concentrator 80—107366
interparticle percolation, lateral and axial diffusion coeffs., shear cell appl. 79—61666
interparticle percolation, statistical mech. anal. 79—96281
interstitial, influence of impurities 78—38879
interstitial alloys, interstitial atomic arrangement and mobility at high degrees of interstice filling *(Russian)* 80—107223
interstitial defects, migration kinetics and thermodynamics 80—107461
interstitial diffusion, nonadiabatic quantum theory 78—79818
interstitial diffusion, retardation by point defects *(Russian)* 77—59143
interstitial diffusion in crystal with random impurities, incoherent scatt. law 77—1266
interstitial phases, thermodynamic relationship between chemical diffusion coeff., true diffusion coeff. 80—49397
interstitial solid solution, growth rate of layer of new phase containing impurity atom traps 77—76620
interstitialcy diffusion, correl. factor estimation 78—43167
intrinsic point defect-impurity atom mobile complex form., influence on defect diffusive fluxes 80—2063
ion beam induced atomic transport and conc. profiles 80—59723
ion implantation, radiation enhanced outdiffusion 79—73200
ion plating, interface broadening 80—65405
ion trapping and gas release effects in cryst. lattices, thermal desorption spectrometry, review 77—43262
ion-bombardment induced atomic mixing, diffusion model 77—90228
ion-exchanged glass, diffusion coeffs. of Tl^+ ions 77—89583
ionic, in natural materials, cathodolum. and AES obs. 80—71497
ionic crystal pair, AB-AC, mutual diffusion, vacancy supersaturation 77—59153
ionic crystals, thermodynamics and kinetics of lattice defects 77—84738
ionic impurity, drift mobility in electric field, computer simulation 79—82388
ionic materials, grain boundary diffusion, space-charge contrib. 77—55386
ionic solids, diffusion routes and thermal vibrs., calc. method 80—107462
ionised impurity, diffusion, in semi-infinite semiconductor 78—75886
irradiation effects, void nucleation, swelling, creep, rate eqns. 80—49274
irradiation enhanced diffusional mass transport 79—14844
island film growth, cluster size distrib. 80—107665
isotropic media, current fluctuation anisotropy, electron diffusion, quasielastic scatt. *(Russian)* 80—107882
kinetic model for solid diffusion with competing surface reaction 78—51719
kinetic theory of correlation effects in diffusion in substitutional solid solutions 79—69278
kinetics, diffusion-controlled particles accumulation, in two dimensions *(Russian)* 80—39339
kinetics of diffusion limited reactions *(Dutch)* 80—96682
lamellar intercalation compounds, NMR studies 80—39882
lamellar systems, mol. diffusion, incoherent neutron scatt. function 79—23501
laminate, fibre reinforced composites, moisture diffusion, 3-D Fick's law 78—10218
laser stimulation of light interstitial diffusion in semiconds. and insulators, theory 77—15630
lattice atom displacements near end of implanted μ^+ tracks 78—55890
lattice defect information from diffusion studies *(Dutch)* 80—96681
lattice defects and diffusion processes in solids, book 80—107207
lattice diffusion, Heisenberg ferromagnet 78—88090
lattice gas, isothermal transport 80—8927
lattice gas, phys. correl. factor in Nernst-Einstein relation 80—105591
layer growth kinetics, effect of heat release during diffusion reaction *(Russian)* 77—55397
lifetime, log normal distrib. theory 79—99348
light interstitial diffusion, quantum theory *(Russian)* 77—15632
linear elastic solid, gas diffusion 79—14967
liquid inclusion migration, nonequilib. morphology 78—38882
liquid inclusion migration in temp. gradient field 78—18842
liquid inclusions, thermal migration, dislocation drag 77—7911
liquid metal wire, thermomigration through a solid in thermal gradient, force model 78—67870
long-range, anelasticity, review 80—60904
luminescence, diffusion-drift problem with plane symm. 77—8652
lunar fires, rare gas diffusion as bubbles 79—48695
macroscopic inclusion motion due to field of struct. inhomogeneity 77—89569
magnetic materials, sintering, structure and props., external mag. and elec. field influence 80—50570
marine sediments, of Cl^-, hydrostatic press. effect, in situ expt. 78—44878
mass spectrometry, molecular beam, appl. to coupled diffusion and chem. reaction 77—73497
measurement in presence of background mag. field gradients, pulsed-gradient multiple-spin-echo NMR technique 79—30517
media with double diffusivity, diffusion theory, boundary value problems 80—75378
media with double diffusivity, diffusion theory, mathematical results 80—75377
melt-grown crystals, striated impurity distrib. calc. 80—24488
membrane, diffusion of $^{241}Am^{3+}$ ions, autoradiographic method 78—35721
membrane, parchment-supported $AgPO_3$, determ. of thermodynamics of ionic diffusion processes 78—20068
membranes, linear laminated media, permeation, sorpt. 79—1966
metal:D, dynamic quadrupole nuclear spin relax., α or α' phases 77—48085
metal, μ^+ diffusion, μSR linewidths anal. 79—56691
metal, μ^+ SR, localisation and diffusion, rel. to H 80—50248
metal, BCC, diffusion of heavy interstitial atoms 79—90829

diffusion in solids continued
metal, BCC, low activation energy classical interstitial H diffusion mechanism 79—55852
metal, BCC, quantum diffusion model of light interstitial atoms 80—2212
metal, BCC, small-polaronic diffusion of light interstitials 79—42315
metal, clean surface, H release rate 78—95187
metal, coated, heat resistance assessment at varying temps. *(Russian)* 77—25189
metal, creep, point defects 78—48462
metal, diffusion, radiation effects 78—47555
metal, diffusion bonding 77—62687
metal, diffusion of H_2, quenching method appl. *(Japanese)* 80—7604
metal, diffusion welding, migration of oriented intergranular boundary with pores *(Russian)* 80—84943
metal, dissolved species in cracks, linear differential eqn. problem 79—51316
metal, FCC, H isotope diffusion coeffs. calc. *(Russian)* 78—91483
metal, FCC, muon diffusion, theory 78—22883
metal, grain boundary diffusion, temp. depend. and activation energy 78—95191
metal, H_2-diffusion-rate-limited hydriding and dehydriding kinetics 80—35764
metal, H(D) diffusion, role of tunnelling, reson./nonreson. approaches 80—59718
metal, He migration and defect interactions, role in radiation damage processes 77—28041
metal, impurity atoms, diffusion in region of dislocations *(Russian)* 80—24670
metal, interstitial diffusion, cooperative nature 78—47556
metal, microanalysis of migration processes 77—36706
metal, muon macroscopic diffusion 79—56698
metal, O_2 diffusion and dissolution effects on optical props. in radiative heating, appl. to Ti 79—65884
metal, of H_2, neutron radiography meas. 77—24438
metal, of H, correlated jump diffusion model, nonlinear eqns. 79—82386
metal, of H(D), slow neutron scatt. obs., review 80—34248
metal, of interstitial solute 77—62672
metal, oxidation of high temp. material, lattice vacancy effect 77—70203
metal, oxide film growing by cation diffusion, stress generation 78—60865
metal, positive muon diffusion 79—19388
metal, proton movement in FCC, BCC and HCP metals 79—69293
metal, quantum theory of light interstitial diffusion 79—56690
metal, self- and impurity diffusion, connection between preexponential factor and activation enthalpy 77—69111
metal couple, porous homogeneous vacancy migration and void form. 77—55401
metal extraction kinetics, from deep-sea Mn nodules, pore diffusion controlling case 77—28984
metal extraction kinetics, from deep-sea Mn nodules, pore diffusion with chemical reaction 77—28985
metal film, nucleation controlled interaction with Si substrate, silicide form. 80—10711
metal film interdiffusion and reactions, effect on Si device technology, book contrib. 79—1620
metal junctions, diffusion of interstitial H, interface pot. 80—44368
metal oxide film, optical and diffusion consts. meas., dynamic method *(Russian)* 78—43950
metal oxides, diffusion activation process, interatomic bonding energy *(Russian)* 80—54428
metal powder mixture with decomposing oxide, growth kinetics of surface film during annealing 79—96216
metal refining by crystallisation and reflux, three component Raoultian behaviour 77—28799
metal silicide formation, induced by scanning CW laser, reaction rates, analytical model 80—66334
metal silicide growth on Si 78—10230
metal tritide, ^{3}He detrapping and release after ^{3}H decay, strain model 77—60101
metal-H system, basic props., book 79—82349
metal-H system, hydride formation in high press. range 80—65235
metal-H system, solubility, mobility, and phase transitions, book contrib. 79—82350
metal-H system, thermal neutron scatt., general multisublattice jump diffusion model 77—66045
metal-H system, thermal neutron scatt., general multisublattice jump diffusion model 77—66046
metal-H system study by neutron scattering, review *(French)* 80—34226
metal-metal contacts, use as prevention H escape from metals 80—24595
metal-metal system, interdiffusion, book contrib. 79—1529
metal-nonmetal system, reaction diffusion analysis 77—28049
metal-semiconductor interfacial reaction, AES study *(Japanese)* 80—96701
metal-Si system, ion implanted, inert-gas-bubble form., TEM and Rutherford backscatt. anal. 79—90682
metal-slag interface, interaction under diffusion conditions, impurity oxidation *(Russian)* 80—35390
metallic membrane, of H isotopes, apparatus for meas. *(Russian)* 77—70248
metallic solid soln., diffusion by press. *(Russian)* 78—18833
metallic thin films, surface and grain boundary diffusion, charact. temp/melting point ratio 79—90919
metallographic determ. between coated metal carbide and steel *(German)* 78—15623
metals, μ^+ diffusion, LAMPF results 80—71285
metals, atomic binding energy and surface energy rel. to prediction of physical props. 80—59434
metals, BCC and FCC, H-diffusion and trapping 80—70447
metals, carburising in fluidised bed of C-graphite materials 79—20276
metals, coeff. determ. in system of one-dimens. eqns. 77—28035
metals, diffusion of H, complex jump diffusion model rel. to quasi-elastic neutron scatt. by H 80—24638
metals, dissolution of interstitial H_2 and D_2, diffusion coeffs., reverse isotope effect *(Russian)* 80—88368
metals, FCC, H_2 diffusion, isotope depend. 80—59727
metals, FCC, of H_2, anomalous isotope effect 77—24444
metals, FCC, pair potentials calc., appl. to point defect props. 80—19798
metals, H^+ diffusion studies 79—55933
metals, H permeability, general transport eqn. 80—54426

diffusion in solids continued
metals, irradiated, validity of rate theory, point defect diffusion eqns. 79—55777
metals, lattice and grain boundary diffusion consts., correls. 80—96679
metals, light interstitials, self-trapped, quantum diffusion 79—19405
metals, muon spin rot. diffusion expts. 79—56680
metals, of H_2, at low temps. 79—55941
metals, of H_2, neutron scatt. studies 79—42316
metals, of H, theory, book contrib. 79—82389
metals, of O, new EMF method 77—84994
metals, overbarrier states of H and D, subsystem heat capacity, equilibrium props. *(Russian)* 80—79998
metals, point defect diffusion controlled reaction theory, book contrib. 80—103318
metals, point defect dynamic props. and diffusion controlled reactions, book 80—101674
metals, polycrystn., creep damage and cavity growth, assessment using density meas. 80—104217
metals, thermochemical treatment *(German)* 78—15598
metals and alloys, chemicothermal treatment, process kinetics 80—35415
metals and alloys, diffusion layers, effect of chemicothermal treatment on struct., surface energy, and bulk props. 79—96207
metals and alloys, FCC, interstitial diffusion, theory *(Russian)* 80—65296
metals and alloys, meas. of conc. profile by changes in polarisation current density 77—89584
metals and alloys, sulphidation mechanism, review *(Polish)* 80—45413
metals diffusion thermodynamics, kinetics and mechanism 78—95179
metals in gaseous oxidative medium, reaction diffusion theory 79—20463
metals irradiated, heavily, exam. of percolative mass transfer 78—79639
metastable state, quantum kinetics of phase transitions *(Russian)* 79—51235
methane and N_2 counter diffusion through porous solids 77—80649
mica, Pb diffusion rel. to Po haloes 79—44186
microporous graphite compact, anomalous diffusion of N_2, time-lag and transient-state kinetic analysis 78—34655
microstructural phenomena, physical chemistry 79—11550
MIS solar cells, interface problems, AES, SIMS and XPS study 80—89627
mixed-gas reduction, diffusion 79—61902
mixtures with diffusion, axiomatic theory of mech. behaviour 77—858
MNOS structures, high temp. H anneal, effects of fast surface states 79—38178
molecular crystals, diffusion and point defect struct., review 79—82373
molecular crystals long-range energy transfer combined with isotropic or anisotropic diffusion 79—11461
molecular sieve, gas diffusion coeff., problems in appl. of process identification methods *(French)* 77—31800
Mossbauer line broadening, influence of diffusion *(German)* 78—84510
Mossbauer spectroscopy applics. 77—12749
multicomponent diffusional impregnation, role of phase transformations 77—62686
multicomponent system, determ. of diffusion coeff. 77—55381
multicomponent system experiencing mutual drag, symm. of kinetic coeffs. *(Russian)* 77—31801
multilayer thin film system, scaling law for interdiffusion 79—65262
multiphase binary diffusion theory 77—7885
multiphase ternary diffusion couples 78—10227
multistate diffusion in perfect and defective system, stochastic theory 79—93066
multistate diffusion in perfect and defective systems, stochastic theory 79—93067
muon, diffusion in presence of traps, spin depolarisation, stochastic theory 79—28666
muon diffusion and trapping in solids 80—71283
muon motion in solids 79—56681
muons diffusing in presence of traps, spin depolaris. 79—56682
Nb-O, effect of O_2 on penetration of Li at 400°C 79—11719
nitridation of steel, ionic, in glow discharge *(Russian)* 77—11412
nitriding in glow discharges, influence on phase comp. and plasticity of diffusion layer *(Russian)* 80—76400
NMR and dielectric relaxation, defect diffusion models 79—15375
NMR technique for slow diffusion in multispin system exam. 77—51970
noble metal alloy, dil., solute segregation and subsequent film growth in corrosive environment, model 79—24649
noble metal contact, substrate material diffusion and corrosion film formation, model 80—2312
noble metals, divacancy contrib. to impurity diffusion 78—79812
noble metals, impurity diffusion, electrostatic interaction theory, impurity-vacancy pair 78—43181
non-IPS geometric surface relief effects rel. to diffusional phase transform. 77—15667
non-metals, low-temperature strong enhancement of diffusion and defect generation 79—28149
non-perfect solvent crystals, thermodynamics and diffusion of interstitial solute atoms 79—90825
nonclassical processes 78—47591
noncrystalline solids, mass transport phenomena and interpret. 78—26720
noninteracting particle diffusion between semipermeable cell walls 80—70442
nonlinear equations, identification of thermal cond. and sp. ht. *(French)* 77—47614
nonlinear jump diffusion model appl. to incoherent thermal neutron scatt. 77—28034
nonmetals, V_K-centre dynamic model, fluctuation production of barriers, diffusion *(Russian)* 78—47372
nonuniformly stressed crystal, statics and kinetics of vacancies *(Russian)* 78—55863
nonvinyl polymers, diffusion of simple penetrants, statistical mechanical model 80—6556
NQR caused by vacancy diffusion of impurities, spectral density 78—68408
nuclear fuel particles, coated, metallic fission product migration 77—50231
nuclear fuels, radiation enhanced kinetics in the fuel lattice 80—59522
nuclear magnetic relax. time, influence of correlation in diffusion of nuclei *(Russian)* 77—51977
nuclear reactor fuel transient heating conditions, mobility of fission gas bubbles 79—59189
nuclear reactors, fission gas behaviour, calc. fo diffusive flow to spherical boundary 80—47574

diffusion in solids continued

- nuclear spin relaxation by translational diffusion 77—16195
- Nucleopore membrane, pore struct., determ. by electron microscopy and Hg penetration 78—43165
- Nylon 6, fibre, crystallite dimensions, effect on struct., mech. and diffusive props. 78—11273
- Nylon 6 film, prior high-press. treatment effects, weight swelling, density, IR crystallinity, X-ray and viscosity obs. 80—81025
- olivine and ultrabasic rocks, diffusion and diffusion creep, rel. to upper mantle deform. 77—9409
- one dimensional diffusion, iterative solns. with time varying surface comp. and comp. depend. diffusion coeff. 80—84314
- one-dimensional hopping, moment expansions and occupancy (site) correlation functions 78—55972
- optical fibres, diffusion of OH in core and H_2O in cladding, transmission props. 78—42420
- optical fibres, water diffusion, measured changes with time in OH absorpt. 79—46082
- ordering alloys, BCC lattice, diffusion of insterstitial atoms *(Russian)* 79—19400
- oxide, tracer diffusion obs., RF sputtering as microsectioning technique 78—14499
- oxide films, passivating, transient growth kinetics 80—93672
- oxide fuel, of fission produce Ba 79—19373
- oxides, impurity diffusion and self-diffusion, review and bibliography 80—59719
- oxides, point defects diffusion coeffs. calc. *(Japanese)* 80—15302
- oxides at high temperatures, crystalline and non-crystalline, surface mass transport mechanisms obs. *(Japanese)* 80—54479
- parallel plates, one-dimens. diffusion-controlled growth 80—55410
- particle dispersion coarsening, computer simulations 80—30289
- particle drag retardation of surface smoothing and sintering 77—12561
- particle escape over dynamic barrier, impurity diffusion in solid 80—107569
- particle/matrix interface, coarsening of disperse particles, diffusion control 80—30288
- path independent integral for symmetric stress-diffusion fields surrounding line cracks 78—67130
- pentacene, in p-terphenyl, electronic excitation transport, acousto-optical effects 78—72079
- with periodic potentials, dynamic correlation functions 77—59138
- perlite, low temp., processes occurring during firing 80—11607
- Permalloy-Cu(Al) two-layer films, mag. anisotropy, grain boundary diffusion *(Russian)* 80—71122
- permeation of gases, nondissoc. and dissoc. 78—34645
- permeation through Incoloy-800 reactor material 79—77822
- permeation time-lag analysis of anomalous diffusion, exptl. results 78—2301
- PET, fibre, crystallite dimensions, effect on struct., mech. and diffusive props. 78—11273
- PET, penetrant diffusion, statistical mech. model 80—44352
- PET film, crystallised by nonreactive liquids and vapours, exam. of diffusion of liquids and vapours 79—42314
- phase transitions, kinetic theory, master equations *(Russian)* 78—47498
- phenomenological laws 80—39341
- phlogopite mica, press. depend. of Ar diffusion 77—86861
- phosphate glasses, fading mechanisms 79—95851
- phosphors, physicochemical choice of optimum conditions for production and examination 78—10940
- phosphosilicate films, deposited, P conc. meas. 79—69014
- photographic development, penetration of developing agents into gelatine films, approx. modelling using diffusion theory *(Russian)* 79—67411
- photographic layer, homogeneous solid, diffusion, one-dimensional case *(German)* 80—73495
- photographic treatment processes, diffusion kinetics 79—20447
- photovoltaics and absorber/reflectors, diffusion, chemical reactions, contamination, AES and SIMS 80—72066
- plane steady solutions for stress-assisted diffusion 79—90136
- PMMA, diffusion-controlled penetration by monohydric normal alcohols 78—76918
- PMMA, reactor irrad., growth of macroscopic radiolytic gas bubbles, diffusion model 80—65058
- point defect diffusion in stress field of edge dislocation of irrad. solid 78—51720
- point defect diffusion-controlled reactions, theory, rate equations 78—18677
- point defect distrib. in bounded media under irradiation 77—7712
- point defect migration in crystals, anharmonic model description 77—65976
- point defect trapping and migration, calcs., in presence of rare gases and dislocations 79—77834
- point defects, steady-state diffusion, to dislocation loops 77—62529
- point traps, effect on diffusion and diffusing element distrib. function in crysts. *(Russian)* 80—59692
- Polimal 109, polymer resin laminate, density porosity, water vapour diffusion sorption and permeation *(Polish)* 80—59665
- poly(dimethyl siloxane) diffusion of dichlorodifluoromethane, conc. and pressure dependence 77—55392
- poly(m-xylylene adipamide), water induced crystallisation *(Japanese)* 79—90574
- polyalkyl methacrylates, oriented stretched membrane, gas diffusion, entropy correl. theory 79—69291
- polycarbonate, amorphous morphology, from NMR obs. of swelling penetrant mol. motion 79—27929
- polycarbonate membrane, porous, gas permeability *(Japanese)* 78—31698
- polycrystalline film couples, diffusion during recrystn., numerical simulation 79—77844
- polycrystalline materials, diffusion controlled stress rupture 77—32681
- polycrystalline materials, diffusion-controlled stress rupture 80—3186
- polycrystals, containing stationary or migrating grain boundaries, diffusional across transport 79—77832
- polycrystals, intergranular void stability during diffusion growth *(Russian)* 80—10540
- polydimethylsiloxane membrane, permeability of triethylamine vapour *(Japanese)* 78—31697
- polyester, ion mobility from ionic injection current at strong diffusion 80—2210
- polyester resin, water diff. meas. by radionuclides, corrosion effects *(Czech)* 77—48566

diffusion in solids continued

- polyester-E glass composites, types SMC-25, SMC-65 and SMC-30EA, moisture absorpt. 80—93799
- polyethylacrylate, benzene penetrant diffusion, statistical mech. model 80—44352
- polyethylene, diffusion of long chain molecules 79—23784
- polyethylene, diffusion of long molecules, meas. and results 78—55987
- polyethylene, diffusion of long molecules, topological constraints 78—55986
- polyethylene, diffusion of long molecules 77—27213
- polyethylene, drawn low-density, sorption and diffusion of methylene chloride 79—74210
- polyethylene, impurity gas diffusion expts., test of two-phase cond. theory 79—69288
- polyethylene, migration and solubility of antioxidants *(French)* 79—46839
- polyethylene, solid, nucl. spin-lattice relax. time, freq. depend. defect diffusion, 77-373K 78—72428
- polyethylene matrix, trapped free radicals, decay in single crystal and diffusion 77—52657
- polyethylene terephthalate CO_2 permeability above and below glass transition 79—73340
- polymer, amorphous, diffusion of large penetrant molecules 80—15305
- polymer, diffusion of simple penetrants, statistical mechanical model 80—10704
- polymer, Fickian diffusion of a solvent, and organic penetrant in a polymer 79—42292
- polymer, glassy, gas sorption and transport, review 80—15360
- polymer, glassy, sheets and spheres, gel diffusion with discontinuous swelling 80—44354
- polymer, penetrant diffusion, statistical mech. model 80—44351
- polymer blends, interdiffusion, meas. method 79—69271
- polymer coated glass, current leakage path form. by water diffusion 78—10535
- polymer film, diffusion of Au electrode 79—77821
- polymer film, glassy and rubbery, isotope effect in H_2 and D_2 diffusion, T_g region behaviour 80—84327
- polymer films, diffusion coefficients of organic vapours calc. from sorption data 79—77831
- polymer films, instrument for studying sorption and diffusion of low-molecular liqs. 79—100305
- polymer films, permeation, diffusional time lags determ. 80—65272
- polymer membrane, laser stimulated active diffusion, appl. to isotope separation *(Russian)* 78—2302
- polymer membranes, use of McInnes glass electrode for determ. of CO_2 diffusion coeffs. 78—20067
- polymer networks and semi-crystalline polymers, diffusion mechanism and model, local conform. change 80—15288
- polymers, diffusion coeffs. of gases, sorption, permeation investigs., review 78—67868
- polymers, glassy, sorption of solvents, sample-dimension effects 79—52766
- polymethacrylic acid, benzene penetrant diffusion, statistical mech. model 80—44352
- polypropylene, impurity gas diffusion expts., test of two-phase cond. theory 79—69288
- polypropylene, isotactic, diffusion const., increased hydrostatic press. effect 78—22898
- polystyrene, unmodified and rubber modified, craze initiation in n-alcohols, kinetics 80—25894
- polytrifluoroethylene and copolymer, γ-irrad., Ar diffusion and solubility *(Russian)* 79—51315
- polyurethane foams, elastic, stability against organic solvents *(German)* 80—85074
- polyurethanes, rigid foamed, cellular struct. effect on water absorpt. 80—39416
- polyvinyl fluoride, glass transitions, Ar permeability and diffusion obs. 79—32919
- polyvinylidene fluoride, glass transitions, Ar permeability and diffusion obs. 79—32919
- polyvinyltrimethylsilane, diffusion, sorption, solubility, permeation of hydrocarbons, Xe *(Russian)* 80—6564
- polyvinyltrimethylsilane, sorption, diffusion, solubility of hydrocarbons, Xe rel. to temp. *(Russian)* 80—6565
- pore shrinkage 79—28131
- porous body, gas diffusion estimate 77—62662
- porous material, gas diffusion technique for pore struct. investigation 80—30185
- porous materials, gas diffusion through pore during sintering 80—40281
- porous materials, melt infiltration, math. model 79—100089
- porous media, laminar flow, velocity and longitudinal dispersion, deterministic model 80—83842
- porous solid, reaction with mixed gases 78—44404
- porous solid, sintering, diffusion of O 77—90286
- porous solid sintering, role of gas in healing of isolated pore by volume vacancy diffusion 78—15330
- porous solids, diffusion of gases, Monte Carlo simulation 80—65299
- positive muons as light isotopes of H, book contrib. 79—82907
- powder mixture, effect of granulometric distrib. on importance of Kirkendall effect during calcination *(French)* 77—11721
- power law frequency dependent dielectric function and nonanalyticity properties 78—60387
- precipitate, disc-shaped, kinetic approach to equilib. shape 77—90357
- precipitate migration in applied field by vol. diffusion 78—64545
- PTFE, $H_2(D_2)$ solubility and diffusion, activation enthalpy 78—79775
- PTFE, Ne, Ar, Xe and He diffusion and solubility 80—6561
- PTFE grafted membranes, struct.-properties relationships for poly-N-vinylpyrrolidone-containing membranes *(French)* 80—61138
- PVC, rigid plate, simultaneous diffusion and dechlorination in H_2SO_4 *(Japanese)* 77—52521
- PVC powder, quinoline diffusion, microdiffusion technique 79—7713
- PVC-poly-ε-caprolactone blends, gas permeation and compatibility 79—4433
- Pyrex glass, cation exchange and interdiffusion 80—80002
- pyrocarbon, diffusion coeff. of Cs and Ag by post irradiation annealing of coated 78—13247
- pyrocarbon, diffusion of Pu in HTGR 78—29578
- pyrocarbon, of Ag 77—24441
- pyrocarbon coated particles, influence of fast neutrons on transport behaviour of solid fission products *(German)* 79—13427
- pyrocarbon coatings, neutron induced fission gas permeation 77—79435

diffusion in solids continued
pyrocarbon coatings for Biso fuel, permeability 77—79433
quantum, features of thermomigration 77—55384
quantum diffusion, Hall effect 78—18820
quantum diffusion in crystals, radiation enhancement conditions 78—47607
quantum rate theory for symmetric double well pot. 78—55970
quantum solid behaviour, defect and impurity diffusion, review 77—7945
quartz, of Ag, radiation stimulated diffusion *(Russian)* 77—39694
quartz, synthetic, deuterisation, EPR and IR absorpt. characterisation 80—92721
quartz, synthetic, electron beam irrad., defect form., annealing and migration effects, ESR obs. 80—50180
quasi-elastic neutron scatt. laws at finite concs. of elements diffusing in cryst. 79—77829
quinolinium $(TCNQ)_2$, charge transport, proton spin-lattice relaxation 80—88545
radiation effects, distrib. functions of point defects and moving gas filled holes 77—55302
radiation enhanced diffusion, approx. solns. of chem. rate eqns. and appl. to expts. 79—73344
radiation-induced, unstable Frenkel pair mechanism 80—34050
radiation-stimulated dissociative diffusion, model 79—23785
radioactive gas distrib. in porous medium, diffusion and sorption effects 79—81964
radiotracer diffusion rates in ionic solid, influence of transmutation products 77—89568
random capillary networks, interdiffusion of gases, struct. factor calc. 78—14080
random primitive cubic alloys, diffusion correlation 77—80640
random walk model, for diffusion in presence of high diffusivity paths, random walk model 80—24640
random walk model with correlated jumps, appl. to H in metals 80—24639
rare earth-Fe_2, mag. props. changes due to H_2 absorption, unit cell vol. 77—63178
rare earth-Se film couple, formation and crystallographic charact. of thin film phase 78—91574
rate equations, transport theory formulation for fusion reactor materials 79—95050
rate processes in condensed media, anharmonicity effects 79—19349
reactive diffusion in silicides with small homogeneity region, kinetics and mechanisms 77—35751
recrystallisation nucleation, model for strain induced grain boundary migration 79—46675
refractory compound fibre reinforced cpd. materials, diffusional reaction, effect of alloying calc. 80—20851
refractory materials, contrib. of segregation and diffusion to heat cond. 80—20001
refractory metal, generalised model for prediction of periodic trends in sintering activation 78—64498
refractory metals, enhanced diffusion model for activated sintering 80—25612
refractory metals, group V, diffusions of O and N, statistical calculations on Arrhenius lines 80—59722
rotational tunnelling and diffusion in condensed mol. systems, neutron scatt. 78—63658
rubber, blooming by waxes 80—104109
rubber, penetrant diffusion, statistical mech. model 80—44352
Sanicro 31, T_2 permeation 80—88364
sapphire filaments in Al_2O_3:MgO matrix, single cryst. boundary migration 80—44369
second phase particle, diffusional relaxation 80—60898
sectioning diffusion specimens in liquid N 79—67276
semi-infinite medium containing one or more phases of different solubility, model calc. *(German)* 79—28126
semi-infinite solid, tempering induced diffusive release of gas in presence of traps 77—28045
semiconductor, amorphous, diffusion phenomena, mechanisms and meas. 77—76608
semiconductor, anomalous diffusion from doped oxides due to dopant depletion effects 77—89461
semiconductor, apparent ageing, caused by defect migration, dark and photocond. 79—11169
semiconductor, charged impurity diffusion 80—6563
semiconductor, elastic stresses effect on diffusion processes 78—10226
semiconductor, ionization and subthreshold effects in defect creation and annihilation 77—84811
semiconductor, laser-assisted diffusion of dopants 80—55431
semiconductor, polycrystalline, grain boundary effects, doping tech. for study and control 80—79815
semiconductor, predeposition diffusion profiles, errors in iterative numerical calcs. 78—26591
semiconductor, recoil- and field-enhanced mechanisms, theory 77—89567
semiconductor doping, impurity distribution, calc., using multicomponent diffusion theory 79—1456
semiconductor doping, thermomigration method, using molten wires, nonequilib. morphology of migrating liq. inclusions 78—38882
semiconductor doping diffusion process, built-in elect. field diffusion enhancement factor, anal. 78—55985
semiconductor epitaxial structures, atomic diffusion 77—85110
semiconductor-metal system, photochemical transformations rate rel. to light-stimulated diffusion coeff. 77—76626
semiconductors, atomic diffusion, review 79—4423
semiconductors, charge neutrality produced by impurity diffusion 80—59724
semiconductors, doped and amorphous, ionised centre diffusion accel. by electrostatic fields 80—70473
semiconductors, Gaussian diffusion determ., alternative method to angle lap and strain anal. 79—86925
semiconductors, Watkins-type radiation defects, low temp. form. mechanism 80—15153
Si, diffusion coeff. of Se, by sheet Hall coeff. meas. 79—46843
Si, of P, excess vacancy generation by E-centre dissociation 77—72720
Si, X-ray step scanning section topography, lattice imperfection characterisation, automatic Bragg angle control 79—60221
silicate glass, hydration thermodynamics 80—81313
silicate glaze, diffusion of Sn(IV) 80—49417
silicone rubber, RTV 560, diffusion of outgassing species, kinetics data 79—15010
Silumin, CsSi phase form. due to Cs diffusion 79—38798

diffusion in solids continued
simple crystal with random distrib. of traps, atomic diffusion 78—34646
sintered mats., complex diffusion alloying 78—68650
sintering, cold, under high pressures, correlation to plastic props. and diffusion 79—38757
sintering, final stage, steady state diffusion models, testing of models by numerical simulation 79—4428
sintering, initial phase kinetics, model with diffusion *(French)* 78—35328
sintering, ohmic, temp. distrib. influence 80—92704
sintering by diffusion mechanisms, kinetics of contact form. 77—85956
size variation technique for diffusion coeff. determ. 78—83991
Sn coated Cu, fine struct. in diffusion zone and mech. props. 77—11739
soda-lime and reactor waste glasses, reaction with water, determ. of diffusion controlled hydration and surface etching 79—54519
solar cells, polycryst., influence of grain boundaries electronic structure on diode characts. 80—94068
solid electrolytes and mixed conductors, materials stability and chem. diffusion 80—65292
solid solution, diffusion, influence of conc.-induced stresses *(Russian)* 78—55969
solid solution, diffusion in force field 78—10211
solid solution, interstitial, chem. diffusion in presence of solute atom gradient 77—76612
solid solution cathodes for electrochem. power sources, dynamic aspects 80—3508
solid solutions, diffusion equation, during a decomp. process, role of non-linearised terms *(Japanese)* 80—92723
solid solutions, Fourier transform, of diffusion eqn. with non-linear terms 80—103514
solid solutions, multicomponent, diffusion processes *(Russian)* 78—47552
solid solutions and interstitial phases, diffusive creep, theory *(Russian)* 80—40437
solid-solid interface, chemistry and physics, book contrib. 79—1551
solid-solid pellet systems, diffusion and reaction 78—85139
solid-solid reactions, analysis and reaction development, review 80—16648
solid-state diffusion from a limited source 80—70444
solute-induced jump correlations during diffusive processes 79—51297
sorbent, biporous, internal diffusion 80—44414
sorbent solid, moisture diffusion, diffusion cell and pore diffusion 78—10210
space charge limited current with diffusion theory, for exponential trap distribution 80—10992
spherical particles with moving interfaces, single-component diffusion 80—15290
spherical pore in solid body, physiocomechanical processes 80—100364
spherical precipitate isotropic diffusion controlled growth 80—100344
spheroidal precipitate motion in temp. gradient by vol. diffusion 78—64544
steel:Si alloy formation kinetics at solid cathodes, metal electrodeposition from molten salt electrolytes 80—26028
steel, alloy, diffusion modelling of carburization 79—24657
steel, alloy, forgings, H precipitation kinetics, diffusion to voids, effect on shattercrack formation 80—16344
steel, alloy, structure and properties after nitriding in molten salts, steel 08kp with Al diffusion coating 80—35418
steel, aluminising, thermodynamic anal. of phase transforms. 80—76413
steel, austenite stabilisation during $\alpha\rightleftarrows\alpha'$ transition *(Russian)* 78—44117
steel, austenitic, containing Ti, nitriding and nitride composition 79—20278
steel, austenitic, diffusion saturation with Cr in closed reaction space, kinetics and mechanism 79—52458
steel, austenitic, dislocation struct. formed by interstitial diffusion of C 77—4223
steel, austenitic, high-temp., carbonitriding, saturation kinetics *(Russian)* 79—52450
steel, austenitic, wire rod, austenite transform. kinetics accompanying interrupted cyclic cooling *(Russian)* 79—70064
steel, austenitic 18KhGT, carburising in vac., rate, austenite grain size, C distrib. 79—20277
steel, austenitic stainless, Cr-Ni (25, 25 wt.%) grain size, temp. and stress influence on creep 80—30021
steel, austenitic stainless, creep dependence on electron irrad., in type SS316 steel, dislocation motion *(Russian)* 80—108495
steel, austenitic stainless, D diffusion coeffs., ion beam meas. technique 80—75382
steel, austenitic stainless, grain growth kinetics, effects of C content and rolling *(French)* 77—81269
steel, austenitic stainless, high temp. oxidation, high temp., in low O_2 press., surface anal., impurity diffusion effects 77—56142
steel, austenitic stainless, internal friction due to H_2 gas molecules 80—71682
steel, austenitic stainless, N diffusion 77—62677
steel, austenitic stainless, powder, sintering behaviour 78—44051
steel, boriding in powdered mixture with high activity 80—30164
steel, C, carbide deposition on surface, exam. *(Russian)* 79—34200
steel, C, diffusion of H_2, effect of quenching and tempering 77—7908
steel, C, diffusion of H_2, SCC via martensite form. cooling rate changes on Mn and Ni addition *(Russian)* 78—56813
steel, C, dissolution of Cr_7C_3 in austenite *(Russian)* 80—103479
steel, C, hydrogen embrittlement, elastic interaction of H_2 with precipitates 78—92340
steel, C, pore formation in surface layers, during As diffusion redistrib. 80—49421
steel, C, sintered, diffusional boronizing, exam. of process 79—96219
steel, carbonisation, cementation process testing, foil samples method 79—70238
steel, carburisation, calc. of mass transfer in diffusional saturation 80—24676
steel, carburizing, vacuum, case depth 80—100956
steel, chemicothermal treatment, diffusional basis 80—104343
steel, chromoaluminosiliconising with electroheating, for oxidation resistant coatings 79—52457
steel, Cr (13 wt.%), abnormal behaviour of H_2 at low temps. *(Russian)* 77—24434
steel, Cr-C and C, carbide coating by CVD, interlayer form. 80—11574
steel, Cr-Mn, high temp. oxidation, sub-cinder layer formation, protective coating role *(Russian)* 80—93686

diffusion in solids continued

- steel, Cr-Mo (2.25, 1 wt.%), quenched and tempered, diffusion and solubility of H_2 *(Japanese)* 79−65255
- steel, CrMoV, low alloy, coarsening rate and activation energy of M_4C_3 and M_7C_3 carbides *(Czech)* 80−108480
- steel, diffusion coatings, carbide and boride, props. *(Russian)* 79−52443
- steel, distribution of H_2 in 12Kh18N10 and 12Kh18N10T after 12 days in H_2-T_2 mixture *(Russian)* 77−7752
- steel, fatigue fracture after Fe and Ce diffusion coating, microstruct. investigation *(Russian)* 79−52446
- steel, high speed tool, diffusion wear model 79−29230
- steel, high speed tool, sliding contact in magnetic field, model for cross diffusion 79−79121
- steel, high-strength, H distrib. and delayed brittle fracture 80−108577
- steel, high-strength low alloy, H_2 attack, 350-510°C 80−97636
- steel, HSLA type 4340, hydrogen diffusivity and solubility, correl. with embrittlement and SCC phenomena 79−83323
- steel, hydrogenation and cracking in H_2 S, cathodic polarization and surface layer effects *(Russian)* 77−52528
- steel, low alloy, crack branching in delayed fracture 79−79067
- steel, low C, kinetic aspects of diffusion zone and compound layer formed during ion-softnitriding *(Japanese)* 79−15866
- steel, low C, Ti inclusion nucleation, effect on crack formation *(Czech)* 79−91782
- steel, low-alloy Si-Mn, uphill diffusion of C, at brazed joint with pig Fe 78−44280
- steel, martensitic, quenched, strength variation rel. to H behaviour 77−59924
- steel, mild, and cold-rolled, diffusion, permeation, and accumulation of H_2 *(Japanese)* 77−39692
- steel, mild, sliding contact in magnetic field, model for cross diffusion 79−79121
- steel, mixed alloy, sintering, reaction kinetics of Fe and graphite powders 77−55907
- steel, Mn, diffusion of C, Si, V, W, electron probe microanalysis *(Czech)* 77−59149
- steel, Mn-Ni-Cr, diffusion of Fe, Mn, Si, V and W *(Czech)* 77−59148
- steel, neutron irradiated, liberation of He in uniform heating 77−50248
- steel, Ni, maraging, H_2 diffusion, diffusivity and solubility *(Japanese)* 79−42311
- steel, Ni-Cr-Mo-V, corrosion fatigue crack growth in NaOH soln., cathodic pot. effect 80−89403
- steel, nitriding in molten nitrates 80−35417
- steel, of B, boride coating formation, pack cementation process, microstruct. and mech. props. 78−15592
- steel, phase boundary decarburization of pouring jets and droplets *(German)* 77−90318
- steel, plain C eutectoid, schematic isothermal transform. diagram 78−48393
- steel, quenched, tempered, intergranular failure during fatigue crack growth 79−8357
- steel, rolled products, H flaking 80−50719
- steel, SAE 1045, permeation meas. of H trapping, rel. to cryst. microstruct. 80−84328
- steel, saturation with Sb and As under glass fusion treatment *(Russian)* 78−35585
- steel, Si, commercial, O_2 diffusion coeff. determ. *(Slovak)* 79−39040
- steel, St3 and 12Kh18N9, of S 78−2306
- steel, stainless, 304L, T grainboundary diffusion and trapping, autoradiographic exam. 78−51738
- steel, stainless, beam, H_2 induced tip deflection 80−39360
- steel, stainless, D_2^+ diffusion and permeation, ion beam meas. 80−59492
- steel, stainless, D transport through membranes at low driving press. and 15 keV D bombardment 78−34552
- steel, stainless, deuteron trapping model, of gas sputtering 80−49398
- steel, stainless, diffusion of Cs study using ion beams 77−20125
- steel, stainless, diffusive crack growth under plastic deform. 79−20182
- steel, stainless, equivalence, coeff. determ., generalised method, by diffusion couples *(French)* 77−62676
- steel, stainless, Fecralloy, creep-rupture props., 650-800°C 80−97535
- steel, stainless, martensitic 403, heat treated struct. effect on H_2 diffusion 77−63703
- steel, stainless, N-implanted, type 304, surface hardness and abrasive wear resist. 80−50746
- steel, stainless, retention and re-emission of 0.125-1 keV D^+ ions 80−66349
- steel, stainless, type 1Kh18N9T, Cu surface barrier influence on C diffusion *(Russian)* 80−54434
- steel, stainless, type 1Kh18N9T, W-Ni alloy surface barrier influence on C diffusion *(Russian)* 80−54434
- steel, stainless, type 4301, radiation enhanced permeation of H_2 80−59732
- steel, stainless, void swelling, Si point defect trapping, interstitial loop growth rate temp. depend. obs. 80−49270
- steel, stainless, with Pd coating, interdiffusion at reactor wall temps., Rutherford backscatt. obs. 80−39361
- steel, stainless 310, permeation and diffusion of H and D, 472 to 779K 79−55937
- steel, stainless 430, diffusion of H_2, effect of heat treatment 77−47627
- steel, stainless types 321-SS and 430-SS, alumina coated, H_2 permeation 80−34244
- steel, stainless/Nb interaction in vacuum percussion welding, Ni interlayer effect 79−29061
- steel, steady diffusion-migration eqns., representing mass conc. of dissolved species in cracks 80−30108
- steel, surface deposit of ZrC, exam. of composition *(Russian)* 79−34201
- steel, type 304, twinning and martensitic phases on hydrogen-charging, TEM 77−21222
- steel, Zn coated, cold rolling influence on struct. and deform. of diffusional layer *(Russian)* 80−55465
- steel 20, diffusion coating for protection against H_2 effect on mech. props. 78−31589
- steel cold plastically deformed, exam. of structure of diffusion layers after borating *(Russian)* 79−34054
- steel Cr-Mo, Ni-Cr, Ni-Cr-Mo, Cr, quenched and tempered struct. effect on H diffusion coeff. and solubility *(Japanese)* 78−52857
- steel high strength, Cr, Cr-Mo, Ni-Cr, and Ni-Cr-Mo, diffusion of H_2, effect of quenching and tempering 77−90384
- steel welds, bead-on-plate, H_2 diffusion and trapping 80−96697

diffusion in solids continued

- steel-bronze bimetal mech. props., diffusional interlayer effects 79−29169
- steels, austenitic 361-SS, 321-SS, hydrogen permeation characts. 79−69295
- steels, ferritic and martensitic, C and N migration at low temps., monograph 80−22149
- stressed solid, of H_2, towards crack, eigensoln. 77−24446
- strong drift effects 78−87808
- submarine basalt, K diffusion model rel. to sea water weathering effect on K-Ar ages 77−86830
- substituent impurities in diamond-structure crystals, diffusion equation, complex formation, theory 80−24677
- superconducting composites, Kirkendall void elimination by solution anneals 80−7520
- superconductors, multifilamentary, bronze process fabrication, voids growth obs., via hot stage SEM 80−70089
- superionic conductor, scattering of light and neutrons in diffusion model 78−26719
- superionic conductors, book 80−22156
- superionic fluorites, structure and transport 80−84318
- superlattice thin films, sputtered, ion-bombardment-enhanced diffusion during growth 78−87882
- superplastic flow in two-phase mats., role of interphase-boundary dislocations, ledges and diffusion 78−11295
- superplasticity, region I characteristics 80−107357
- supersaturated solid solution, diffusive decomposition 78−76653
- supersaturation, of H, produced by dislocation motion 77−36640
- through surface film, into half-space, theory *(Russian)* 78−47553
- surface-moving grain boundary interaction, anal. *(Russian)* 78−67721
- surfaces and interfaces, elastic energy of point defects and inclusions 80−73272
- Ta, of O, new EMF method 77−84994
- technical superconductor requirements and main properties 79−30511
- ternary, two moving boundaries 77−35760
- ternary semiconductor device applications, review 78−39207
- TFTR vacuum vessel, T permeation and wall loading 79−45412
- theory, connection between D_o and Q for self- and impurity diffusion 78−30777
- thermoelastic stressed solid, gaseous diffusion, thermodynamic struct., transport theory 78−51065
- thermoelastic stressed solid, gaseous diffusion, thermomech. formulation 78−51064
- thick film diffusion experiment, introduction of weights to least squares anal. 80−49399
- thick film solution, least-squares anal. to the diffusion eqn. 79−33107
- thin film, influence of grain boundary migration on diffusion behaviour 80−88460
- thin polycrystalline films, rate of mixing depend. on grain boundary struct. 80−107578
- three-dimensional lattices, random walks, probability of eventual return calc. by matrix method 78−6172
- three-dimensional lattices with coord. number 4, random walk calcs., tracer diffusion 80−13001
- tracer diffusion, Hart-Mortlock equation interpretation 78−43184
- tracer diffusion activation energy determ. without depth meas. 78−47592
- tracer diffusion via vacancy mechanism, correlation factor, modified derivation 78−87809
- transition metal, BCC, neutron spectroscopy of fast H diffusion 80−59731
- transition metal, of C, electronic state effect *(Russian)* 77−1264
- transition metal, penetration of interstitial elements during surface treatment 77−12737
- transition metal hydrides, synthesis and physicochemical props., conf., Moscow, USSR (Jan. 1978) 80−27032
- transition metals, group IV, diffusion mech. based on geometric configuration, analogous to chemical compound omega phase *(Russian)* 79−14956
- transition metals, H diffusion 80−29219
- transition metals, of H 78−47596
- transition metals, positive muons as light isotopes of H, book contrib. 79−82907
- trioctadecanoate solution in toluene, diffusion through cellulose membrane nonstationary 79−52767
- two-layer medium, 1-D isothermal conjugate problem *(Russian)* 77−53838
- two-phase diffusion controlled dissolution in planar finite multilayer couples 79−42293
- two-phase dispersion by volume diffusion 79−100146
- two-phase multicomponent system, coalescence theory 77−81248
- two-phase system, field-induced vol. diffusion 79−77802
- two-spin system in FCC cryst. and third-nearest-neighbour jumps on a SC lattice 79−15127
- unsaturated medium, diffusion of water, nonlinear equation solution, using finite element method *(French)* 77−78965
- vacancies, formation volume, anal. of diffusion expts. under press. 78−55971
- vacancies in crystal in temp. gradient, conc. rel. to enthalpy 80−49217
- vacancy hopping, appl. of dynamic quadrupole spin relax. 77−8436
- vacancy-impurity complexes effect, appl. to nonequilib. segregation near grain boundaries *(Russian)* 80−44350
- VC-EVAC graft copolymer, mech. props., effect of heat treatment *(German)* 77−63702
- vinyl and related polymers, diffusion of simple penetrants, statistical mechanical model 80−10705
- void sink strength depend. on mutual recombination, point defect loss to fixed sinks 80−33995
- void size distribution during irradiation and annealing, time depend. computation 78−30674
- void-point defect reactions, conc. depend. of rate const. for diffusion or reaction controlled reactions 79−7625
- voids, lenticular, thermal gradient migration 80−2216
- waveguide fabrication in glass, optical, by low-temperature diffusion process 80−102867
- weld metal, Type 316, transformation of δ-ferrites, diffusion model 80−40347
- weldability, diffusion, surface treatment by glow discharge effect 78−7089
- X-ray diffraction line broadening from small subgrains containing gradients of spacing 78−67612
- β-Zircalloy, creep charact. 79−8317

diffusion in solids continued
zircaloy, H diffusion, effect of reactor irradiation 77—14231
Zircaloy, hydriding reaction kinetics, oxidised specimens 78—26728
β-Zircaloy, O_2 diffusion 78—6181
Zircaloy, O diffusion during UO_2-Zircaloy interaction 79—10986
Zircaloy, of H, neutron scatt. and absorpt. study 79—60556
Zircaloy, steam oxidised, partitioning behaviour of O_2 78—68839
Zircaloy-2, tritium diffusion 80—32341
Zircaloy-4, ^{51}Cr bulk diffusion 79—73347
Zircaloy-4, diffusion bonding with 304 stainless steel 78—34658
Zircaloy-4, interdiffusion with Ni 79—42320
α-Zircaloy-4, O stabilized, O diffusion using ^{18}O tracer 78—51737
Zircaloy-4, oxidation in steam, 900-1500°C, O diffusion in oxide and α-phases 79—100288
Zircaloy-4/stainless steel, diffusion bonding in presence of Fe intermediate layer 79—10987
Zircaloy-Z, thermal diffusion of H, numerical soln. with computer *(Korean)* 80—19989
Ag, compact, on H_2 permeated backing, precipitation *(Russian)* 78—27520
Ag, diffusion of Zn 79—77825
Ag diffusion transfer systems, graphic arts appl. 80—37106
Ag, electrostatic model for impurity diffusion 78—2300
Ag film, Ge coated, electrical resistance and ageing *(Russian)* 80—103759
Ag film growth on Pd substrate, interface cpd. form., AES study *(French)* 80—80131
Ag halides, impurity ion migration 79—19406
Ag, of Cu, SIMS investigations 80—59717
Ag, of Fe 78—10225
Ag, of H, using membrane permeability method 79—37879
Ag, of Ni, resistometric technique 78—38880
Ag, of S 78—47599
Ag, of Ti, V, Cr and Mn, characts. 80—15308
Ag, proton diffusion, config. and activation energies 79—37878
Ag/Al thin film couples, diffusional alloying, Kiessig X-ray interf. obs. 80—10713
Ag/Au thin film couple, interdiffusion mechanism 77—20132
Ag-Al polycryst. thin-film couples, interaction process 79—51443
Ag-As chalcogenide glass systems, reaction and diffusion 79—77826
Ag-As_2S_3 sandwich structure, holographic characts., recording kinetics 78—29913
Ag-Au, pseudoalloy behaviour at interfaces, grain boundary diffusion 80—6567
Ag-Au thin film couples, polycrystalline, low temp. diffusion, resist. obs. 79—4435
Ag-Au thin films, interdiffusion, pore formation, stress effects, adhesive effects *(Russian)* 79—82502
α-Ag-Cd, chemical interdiffusion and Kirkendall shifts 78—87829
Ag-Cd(-Ni), internally oxidised, oxide particle size control *(Japanese)* 80—89480
Ag-Cu couple, grain boundary diffusion of Ag through Cu film, Rutherford backscattering obs. 80—34252
Ag-In-Sn, internal oxidation, solute element and O_2 behaviour *(Japanese)* 80—89479
Ag-InP interface, AgP_2 formation during sintering 80—65309
Ag-metals thin film couples, room temp. interactions 80—2220
Ag-S solid solution, grain boundary segregation and S diffusion in Ag 80—25700
Ag-Zn, interdiffusion coeff. in ε phase *(Japanese)* 79—14969
Ag-Zn (30 at.%), electron irrad., mobilities of self-interstitials and vacancies 77—84795
Ag-Zn-Te(-Sn)(-In), internally oxidised, oxide particle size control *(Japanese)* 80—89480
AgBr, migration entropy of Na^+ diffusion 79—14965
AgBr, Na^+, NQR caused by vacancy diffusion of impurities, spectral density 78—68408
AgBr, of Fe^{2+}, vacancy migration evidence 78—47603
AgBr:Cl, impurity diffusion, vacancy pair and single vacancy contribs. 79—77830
AgBr:$Na^+(Li^+)$, correlated diffusion of impurities, nuclear spin relax. meas. 80—108094
$Ag(CN)_2$, adsorption on activated charcoal, kinetics and thermodynamics 79—82456
AgCl:Na^+, Frenkel defect formation energy, impurity diffusion and migration 79—99179
AgCl:Sr, effect of impurity doping on Sr^{2+} diffusion 78—84002
AgI/RbI quasibinary system, solid state reactions and transport props. 80—96700
AgMg two phase bicrystal, growth by solid state diffusion couple method 80—60773
Ag_2S film reduction, effect of Ag interdiffusion on the catalytic activity of Pt and Pd films 78—14519
α-Ag_2Se, growth of single crysts. in solid/vapour system 77—85907
AgX, X=halide, form. and migration of catalytic nuclei *(Russian)* 79—70378
(Al,Ga)As:Zn planar stripe lasers with deep Zn diffusion, guiding mechanisms controlled by impurity concs. 80—78853
Al, ⟨111⟩ tilt boundaries kinetic properties 78—34522
Al, AES study of Sn diffusion and surface segregation in limit of small conc. 79—82384
Al alloy-Cu alloy evaporated couples interdiffusion *(Russian)* 77—43389
Al and Al/Nb superimposed layer, anodic oxidation, ^{18}O and MeV ion beam obs. of ion movement 78—15604
Al, and Al-Zn-Mg (5, 2 wt.%), of ^{65}Zn, 165 to 645°C and 165 to 560°C respectively 77—11743
Al bimetal film with Cu, Ti(V,Ni) and alloy MLT(RS-3710), struct. and macroscopic defects *(Russian)* 79—1555
Al, diffusion coeffs. of Zn, Co, and Ni, resistometric determ. 79—51313
Al, diffusion of ^{85}Kr *(Russian)* 79—65258
Al, dissolution rate of amorphous Si 78—95188
Al film, of Cu, lattice and grain boundary diffusivities 78—2303
Al film, struct. and props., effect of ion implantation 79—77936
Al films on Si substrates, electromigration and diffusion of Cu 79—77820
Al, grain boundary diffusion of Zn, nonvacancy mechanism *(Russian)* 80—24669
Al, grain boundary migration, TEM obs. on mechanism 80—79812
Al, muon diffusion, μSR 79—56696
Al, muon diffusion at low temp., effect of nuclear elec. field gradients 77—52005

diffusion in solids continued
Al, μ^+SR diffusion, temp. depend. 78—39490
Al, of ^{28}Mg 77—20127
Al, of Ag, in polycryst. sample in temp. gradient 77—76619
Al, of H_2, desorption meas. 78—30797
Al, of H_2 *(Japanese)* 79—99370
Al, of Hg, Tl, Pb *(Japanese)* 79—19403
Al, of impurities 78—47595
Al, of Zn along grain boundaries, effect of grain boundary struct. *(Japanese)* 77—15628
Al, pipe diffusion along segment of faulted dislocation loops during annealing 80—107256
Al, plastically deformed by pulsed mag. field, mobility of Fe atoms, radiotracer profiles 79—28584
Al, secondary H porosity, development and pore growth *(Russian)* 80—19946
Al whisker, of Zn, temp. depend. 77—85122
Al, Zn diffusivity along grain boundaries, grain boundary struct. effects 77—20128
Al:^{12}B, relax. mechanism for polarised implant 78—87693
Al:^{24}Na, diffusion of Na, determ. of diffusion coeff. and activation energy 78—51746
Al/brass/Al bimetal, three layers, formed by cold rolling, exam. of formation of intermetallic phases at interface 78—56658
Al/Cr thin films, interdiffusion meas. 79—82391
Al/Cu thin film couples, interfacial reactions, low temp. contact resist. meas. 80—44709
Al/Cu thin film couples, TEM study of intermetallic nucleation at interface 80—65305
Al/Ge/Al sandwich structs., interdiffusion effect on Ge film conductivity 79—23788
Al/Ge(Si) thin film couples, accel. ageing 80—44726
Al-Ag(Ge)(Mg)(Zn) alloy, dil., electron-irradiated, impurity-interstitial interaction 77—15449
Al-Al_3Ni, electrolytic prep. of Al_3Ni fibres, SEM and anodic polarisation 80—100817
Al-Al_3Ni eutectic, thermal stability in temp. gradient 79—61611
Al-Au, interdiffusion *(Czech)* 77—62684
Al-Au bimetal thin film interdiffusion zone, intermetallic phase form kinetics, 70-160°C 78—75891
Al-Au(Cu), growth kinetics of plate-like precipitates, vol. diffusion controlled growth 78—6935
Al-Cu (4.8 wt.%), homogenization, temp. gradient driver process 77—52362
Al-Cu alloys, positive muons diffusion and trapping 79—11372
Al-Cu thin film couple, interdiffusion, AES obs. 80—6569
Al-Cu-Mg (2.0, 1.1 wt.%), Ostwald ripening of S′ precipitates *(Korean)* 79—38831
Al-Cu-Zr (6, 0.4 wt.%), superplastic flow activation energy rel. to bulk and grain boundary diffusion 80—11701
Al-$CuAl_2$ eutectic, thermal instability in temp. gradient 78—52851
Al-$CuAl_2$ lamellar eutectic, computer simulation of two dimensional Zn diffusion 78—30799
Al-Fe bimetal, O_2 effect on diffusion inhibition 77—89597
Al-GaAs interdiffusion, 250-450°C, AES meas. 77—1263
Al-Li, diffusion coeff. determ. during hydriding *(German)* 79—29288
Al-Mg, dil. alloy, ^{65}Zn diffusion 77—51540
Al-Mg (7 wt.%), β-phase soln. behaviour and mech. props. *(Korean)* 78—11277
Al-Mg-Zn, interdiffusion 78—51751
Al-Ni, interdiffusion and intrinsic diffusion in NiAl δ phase 79—10988
Al-Ni multiphase system, simultaneous diffusion in cylindrical symm. *(Russian)* 80—100357
Al-Ni solid, liquid mixture, diffusion processes *(Russian)* 80—107563
Al-Pt film sandwich, interdiffusion and intermetallic form. 77—24448
Al-Sb, laser induced surface alloy formation and Sb diffusion 80—54439
Al-SiO_2, surface reactions and interdiffusion, photoemission study 80—49532
Al-SiO_2-Si struct., mobile ion neutralisation in SiO_2 layer, TSC and C-V characts. meas. 79—95503
Al-SiO_2-Si structure, positive interface charge, exciton and H diffusion models 80—2471
Al-silicide-Si systems with $CoSi_2$, $Pt_xNi_{1-x}Si$, and $MoSi_2$ as silicide, diffusion, compound form., and microstructure 80—34253
Al-Sio_2, reactions and wetting behaviour 77—15664
Al-Ta-poly-Si interdiffusion, Ta barrier effect, Auger anal. 78—71888
Al-Ti system, interdiffusion coeffs. determ. 80—70477
Al-Xe film, ion implanted radiation enchanced Xe outdiffusion, Rutherford backscatt. 77—76609
Al-Zn, dil., grain boundary diffusion 78—91475
Al-Zn, interdiffusion meas. by elec. resist. 80—49433
$Al_{0.7}Ga_{0.3}As$, of Zn, comparison with GaAs 78—26589
p-$Al_xGa_{1-x}As$:Be layer, MBE growth, Be doping and diffusion 77—51397
$Al_xGa_{1-x}As$-GaAs, epitaxial heterostructure, influence of defects on diffusive distrib. of group I impurities 78—43045
$Al_xGa_{1-x}P$, Zn diffusion behaviour, device appls. 77—11741
$Al_xGa_{1-x}Sb$:Zn, impurity diffusion, p-n junction depth 80—24678
$AlMg_2Mn$, H impurity detection by $^1H(^{15}N,\alpha\gamma)$ reaction 80—55767
$AlMn_x$, muon diffusion, μSR 79—56696
Al_2O_3, activated, moisture diffusion 78—10219
Al_2O_3, composite base ceramic coating, hot pressed, H_2 permeability 77—56164
Al_2O_3, initial sintering, method for obtaining surface diffusion coeffs., appl. to shrinkage data 78—95713
β-Al_2O_3, internal friction and Na transport 80—59578
Al_2O_3, metal layer interdiffusion, Rutherford backscatt. 77—85000
Al_2O_3, of T 77—55391
Al_2O_3, permeability and solubility of H_2, 1200-1450°C 80—39351
Al_2O_3, pure and Fe or Cr doped, polycryst., creep, diffusion mechanisms 78—11272
Al_2O_3:Ti^{3+}, corundum, point defect diffusion and interaction with impurity, Ti^{3+} to Ti^{4+} reaction 79—10985
Al_2O_3-BaO-SiO_2 glass coatings in fission and fusion reactors, permeation, elec. cond. and dielectric breakdown 80—18439
Al_2O_3-glass seals, diffusion of Al, electron microprobe study 80—107577
β-Al_2O_3-NH_4^+, NH_4^+ jump diffusion and rotational tunnelling, proton NMR, spin isomerism theory 79—99778
β-Al_2O_3-Na_2O, H_2O effect on Na^+ diffusivity 77—31806
Al_2O_3-P_2O_5-Mg(Ca)(Sr)O glasses, Na^+, Sr^{2+} diffusion coeffs. rel. to temp. 78—30787

diffusion in solids continued
- Al_2SiO_5, solid state reaction with $Ca_2P_2O_4$ *(Japanese)* 78—19702
- As_2S_3 film, on Ag, light activated reactive diffusion of metal into chalcogenide 77—55393
- As_2S_3, glassy, diffusion, elec. transport and first group impurities effect on elec. and opt. props. 77—76623
- As_2S_3, glassy, photoreactive diffusion of Ag 80—19991
- As_2S_3-Ag system, photosensitivity depend. on As_2S_3 thickness *(Russian)* 80—54784
- $As_2S_3(Se_3)$:Ag glassy films, doped by photodiffusion and thermodiffusion, photocond. 80—29441
- As_2Se_3:Cu, amorphous, diffusion, electrodiffusion profile determ., Fickian diffusion behaviour 78—6185
- Au (111)/Ag (111) thin film system, diffusion processes 79—77843
- Au, Cr diffusion along grain boundaries, analytic and numerical solns. 77—4274
- Au diffusion, and elastic strain, influence on O_2 state in Si *(Russian)* 79—69181
- Au, diffusion/oxidation of underlying Cu, rate-controlling step 80—34240
- Au film, Cr and Si low temp. diffusion, CO effect 80—100361
- Au film, interface reaction with n-type $Ga_{0.7}Al_{0.3}As$ and GaAs 80—39482
- Au film on Si, use of sputtering for layer removal 79—78813
- Au film sandwiches, recovery kinetics and early stages of diffusion, DC resist. expts. 79—77971
- Au films on Si substrate, solid-solid reactions 78—95369
- Au, of Co, temp. depend. of isotope effect 78—47563
- Au, of Co and Fe, 700-1050°C *(Russian)* 77—80651
- Au, of Cu, 75-150°C, AES, device appls. 77—1262
- Au, of Ni and Cu, relative diffusion rates 77—80652
- Au, of Pd and Pt, 700-1000°C *(Russian)* 78—91484
- Au, proton diffusion, config. and activation energies 79—37878
- Au, proton irrad. at 0.3K, resistivity annealing 77—76475
- Au, serration and dissociation of edge dislocations in low-angle tilt boundaries 77—72621
- Au substrate, for vacuum deposited Fe, interaction layer formation mechanism 80—54559
- Au thin layers, diffusion rate of H_2, N_2, Ar, CO_2, air, and O_2 80—100359
- Au/Ag couple, diffusion induced stresses and plastic deform. 78—26736
- Au/Al thin film, Al diffusion studied by attenuated total reflection method 80—92722
- Au/$AuPb_2$ interface, Pb and Au diffusion, LEED, AES study 78—71988
- Au/Cu, bilayers, interdiffusion phenomena, lattice dislocations, TEM obs. 80—59736
- Au/Fe/Au superimposed layers, influence of O_2 on interdiffusion, controlled-atmosphere electron microscopy 77—51552
- Au/In film structure, interdiffusion at room temp. 77—39703
- Au/Ni(Ni-P), interdiffusion, backscatt. study 80—79991
- Au/Pb thin film couple, room temp. interdiffusion study 79—28154
- Au/Pt/Cr films, of Si, depth anal., optical and Rutherford backscatt. meas. 79—10981
- Au/Si films, laser-irrad., phase transform. study 80—49536
- Au/Sn evaporated film, interdiffusion, X-ray diffr. and ion backscatt. obs. 79—33121
- Au/Sn films, evaporated, microstructure and texture, TEM obs. 80—39481
- Au/Ti thin film, temp. and humidity effect on interdiffusion 79—51317
- Au-Ag bilayers, conc. profile by AES, interdiffusion coefficient determ. *(French)* 78—84077
- Au-Ag film system grain-boundary diffusion at low temp., meas. by surface accumulation method 79—77839
- Au-Al system, influence of current on phase form. in diffusion layer *(Russian)* 78—52826
- Au-Al thermocompressional contacts, diffusional zones, phase growth during annealing *(Russian)* 80—75389
- Au-Al/GaAs interfaces, atomic interdiffusion, soft XPS studies 80—65302
- Au-As, system interactions due to heat treatment, As outdiffusion, backscattering anal. 79—91719
- Au-Cr bifilm, resistivity and struct. changes under heat treatment, diffusion effects 77—1497
- Au-Fe solid soln., props. during preparation by diffusion heating 77—12260
- Au-GaAs interface, atomic modulation of interdiffusion, effect of reactive Al monolayers 80—49432
- Au-Ge thin film couples, activation energy for interdiffusion, accelerated ageing studies 79—82671
- Au-InP, Schottky diode, heat treatment in N_2 and O_2, distrib. profiles of elemental species 79—78172
- Au-refractory thin film systems, interdiffusion obs. by combination of scattering techniques 80—65308
- Au-Sb, system interactions due to heat treatment, backscattering anal. 79—91719
- Au-Sb thin film interdiffusion 77—59152
- Au-Si contacts, of O, determ. by SIMS, nuclear reaction and Rutherford backscatt. anal. 79—4482
- Au-Si interface, critical Au-film thickness obs. for room temp. interfacial reaction 80—75390
- Au-Si interface, valence band and core levels, Si diffusion, alloy form., photoelectron spectra obs. 80—45205
- Au-Si thin film double layer, silicide form., electron diffr. study 80—80005
- Au-Sn evaporated films, comp. and annealing behaviour, 20-400°C 77—76695
- Au-Sn film, evaporated, interdiffusion and phase formation, in situ He ion backscattering meas. 78—22901
- Au-Sn layer system, on glass, thin film interdiffusion 77—20134
- Au-Ti/n-GaAs contacts, interdiffusion and Schottky barrier height variations 77—89849
- Au-W/n-GaAs contacts, interdiffusion and Schottky barrier height variations 77—89849
- (Au-Ge)-Ni film, for contacts to n-GaAs, metallurgical investigation using inert substrate 77—85313
- (Au-Ge)-Pt film, for contacts to n-GaAs, metallurgical investigation using inert substrate 77—85313
- AuAl formation by thin film interactions, identification by X-ray diffraction 79—99442
- $Au(CN)_2$, adsorption on activated charcoal, kinetics 79—82457
- AuGe/n-GaAs, SIMS study Au behaviour during annealing 78—75947

diffusion in solids continued
- $Au_{35}Si_{65}$, amorphous vacuum-deposited and liquid-quenched films, diffusion and crystn. 80—84094
- Au(111)/Ag(111) thin film system, diffusion processes, diffused Ag composition profile 79—90832
- B fibre reinforced Al, interaction between fibre and matrix 80—10712
- B, semicond., of Au, Ag and W, temp. depend. of coeffs., mechanism 77—7898
- BN glass transfer process 80—107459
- BaF_2:Y^{3+}, diffusion of bound and free $F_{(i)}^-$ interstitials, NMR meas. 79—78542
- BaO, CO_2 transport kinetics following $BaCO_3$ decomp. 79—23780
- BaO crown and flint glasses, Ag and Cu diffusion for optical waveguide fabrication 78—59166
- $BaTiO_3$, chemically precipitated, exam. of sintering behaviour by isothermal shrinkage *(German)* 79—4935
- $BaTiO_3$, doped, defect chemistry and elec. cond. kinetics of equilib. restoration 77—39700
- $BaTiO_3$-$BaNbO_3$ system, solid solns., thermal ionic relaxation, vacancy form. 77—8499
- Be, muon location and diffusion, μSR 79—56693
- Be, of Al, diffusion mobility and solubility 77—35758
- Be, of Co, 1250 to 1493K, radioactive tracer method *(Russian)* 80—24668
- Be, of differing purities, C diffusion *(Russian)* 80—19984
- Be, of V, Nb, Ce, diffusion coeffs. and solubility 77—35757
- Be:Li, ion-implanted, interstitial props. 79—37876
- Be-Al-Fe, phase equilibria and diffusion using high energy ion beams 77—16542
- BeO, of T 77—55391
- Bi, impurity diffusion, of Rb, Sr, Ba, Cs 79—77819
- Bi, thin film, oxidation process rel. to X-ray diffraction *(Japanese)* 79—29273
- Bi_2O_3-CdO system, solid-state reaction, kinetics and mechanism 77—90303
- Bi_2Te_3-Sb_2Te_3 solid solns., plastically deformed by hot extrusion, diffusion meas. using micro-X-ray spectrum anal. 79—14954
- C, columnar and laminar forms, deposition on polycrystalline Ni foils 78—63943
- C diffusion from graphite to W coating prevention, in metal-graphite layer structure of X-ray tube *(German)* 80—105759
- C fibre, of Ni, ZrN (TiC) diffusion barrier effectiveness 78—60624
- C fibre reinforced, C oxidation behaviour, rate-controlling steps 80—55550
- C fibre reinforced Al composite, CVD fibre coating, diffusion barrier and wetting agent 77—40458
- C, glassy, migration into steel during shock compression 80—24679
- C, noncrystalline conversion to diamond, diffusion conversion enhanced rate due to shock compression 80—39221
- C, pyrolytic, tritium diffusion coeffs. and deuterium solubilities 80—37443
- C/epoxy laminates, moisture diffusion 79—65252
- CC PbTe-PbSnTe heterjunction, misfit dislocations, etch pit and electron probe study, Sn self diffusion 79—77926
- $CaAl_2O_5$, form by interdiffusion of CaO and Al_2O_3 79—28998
- $CaAl_2O_5$, form. by solid state reaction of CaO and Al_2O_3, electric field effects 79—28997
- CaF_2:Na, vacancy motion activation vol., complex dielec. const. meas. 80—39356
- CaF_2:Y^{3+}, diffusion of bound and free $F_{(i)}^-$ interstitials, NMR meas. 79—78542
- CaF_2-CaO, elec. cond. meas., CaO solubility, O^{2-} diffusion const. 78—30760
- CaO, CO_2 transport kinetics following $CaCO_3$ decomp. 79—23780
- CaO-Al_2O_3-SiO_2 diffusion triangular diagram, diffusion between lime and sintered kaolinite *(French)* 79—69296
- $(CaO)_3.SiO_2$, adsorption of H_2O, NMR exam. 78—48354
- CaS, solid, tracer diffusion coefficient of S by ion microanalyser *(Japanese)* 80—34233
- Cd-Sb diffusion couple, layer growth of CdSb phase at high press. 80—2217
- Cd-Sb diffusion couple, layer growth of CdSb phase at high press., elec. meas. 80—2218
- $Cd_xHg_{1-x}Te$, diffusion and struct. of defects 77—84775
- $Cd_xHg_{1-x}Te$(:Ag), impurity diffusion, gamma-ray effects 80—54441
- CdO, point defect props., band struct., lattice simulation calc. 80—19797
- CdS, diffusion of In, 729-1411K 78—22895
- CdS, photosensitivity degradation mechanism due to photocurrent, phtot-carrier lifetime 80—6903
- CdS, thin film, diffusion of Cu, 20 to 200°C *(French)* 80—15424
- CdS:In(Ga)(Al), cathodolum. on diffusion front 77—32447
- CdS:Li, subjected to elec. fields, drift of defects 80—6558
- CdS:Mn, vacuum deposited film, Mn migration, EPR and X-ray study 80—65411
- CdS-Al(Au) interfaces, bonding and interdiffusion, XPS obs. 80—80000
- CdS-Cu_2S, rel. to widening of space-charge in CdS due to heat treatment 79—56294
- CdSe film polycryst., thermal diffusion of Cr, 240-400°C 80—80001
- CdSe, of Cu, effect of laser radiation on diffusion 79—10983
- CdTe, diffusion of Cu at 250 to 500°C, interstitial process 77—11737
- CdTe, diffusion of Sn and intrinsic defects role 79—33116
- CdTe, growth on Te substrate by solid-state reaction 79—95287
- CdTe, of Ge, 630-800°C, prep. conditions depend. 80—103519
- CdTe, of Li, 300°C 77—43383
- CdTe:As(P), ion implanted, elec. props. 80—65021
- CdTe:In precipitation and out-diffusion of solute during cooling 80—100840
- $CeCo_{5-x}Cu_x$, $0 \leq x \leq$ internal oxidation kinetics, oxide struct., X-ray study 80—104329
- $CeO_2La_2O_3$, ceramic, thermal stability, sintering, deform., effect of La_2O_3 79—11532
- Co base alloys, of B, boride coating formation, microstruct. and mech. props. 78—11427
- Co, compact, on H_2 permeated backing, precipitation *(Russian)* 78—27520
- Co film, on Si substrate, laser irrad., cellular struct. and silicide form. 80—10710
- Co, magnetic aftereffects of H isotopes, book contrib. 79—82835
- β-Co, of C, high temp. vacuum metallography investigation *(Russian)* 77—72718
- Co, of Mn, 860-1246°C, mag. transform. effects 77—24427

diffusion in solids continued
Co, positive muons as light isotopes of H, book contrib. 79—82907
Co-Cr-Al, protective coating, exam. of interdiffusion kinetics, development of analysing procedure 79—5085
Co-Cr-Al, ternary system, interdiffusion, electron probe anal. 80—34256
Co-Fe(Ni) system, interdiffusion zone growths *(Czech)* 78—84009
Co-Mn, interdiffusion 77—89595
Co-Ni, interdiffusion coeffs. and conc. penetration curves, electron microprobe meas. 77—66047
Co-Ni interface, intrinsic interdiffusion coeffs. and activation enthalpies 77—84998
Co-Ni sandwich system, interdiffusion, Kirkendall effect 77—69121
Co-Si film system, diffusion marker expts. 78—79824
Co-Si film system, interaction kinetics 78—79823
Co-Ti, dilute, internal oxidation 77—31810
CoAl, compositional depend. of oxidation rates 79—8393
$Co_{56}Ga_{44}$, thermal release of injected He 77—31881
Cr, antiferromagnetic, positive muons as light isotopes of H, book contrib. 79—82907
Cr, CVD on Ni, reaction mechanism, growth rate and struct. obs. 80—39476
Cr, diffusion coating strengthening by plastic deformation, controlling physical factors *(Russian)* 77—25187
Cr substrate for CdSe, thin film transistor, cryst. struct., substrate defect effects 80—70563
Cr/Au layered films, microstruct. and interdiffusion during ageing, 423 to 573K 79—46965
Cr-Au film structure, on Si interdiffusion 77—39698
Cr-Mo (2.25, 1 wt.%) steel, T permeation rate at 400 to 500°C, rel. to LMFBR conditions 78—17319
Cr-Ni, H_2 penetration from N_2-H_2 mixtures *(Russian)* 77—69117
Cr-Pt thin film couple, diffusion, new Cr-Pt phases obs. 79—42319
Cs, diffusion in high temp. alloys, AES, SIMS depth profile study *(German)* 78—84008
$CsCl+NaI \rightarrow CsI+NaCl$, solid-state displacement reaction due to diffusion of I^- and Na^+ 77—52635
$Cs_2GeF_6.4HF$, HF molecule activation energy and spatial symmetry of arrangement 79—42313
CsI:Tl, precipitation of Tl solid solns. 80—70419
$Cs_2SnF_6.4HF$, HF molecule, activation energy, and spatial symmetry of arrangement 79—42313
^{137}Cs, diffusion in bitumen block coating, radioactive waste treatment *(Russian)* 80—52771
Cu, activation energy of proton diffusion 77—62678
Cu, Ag impurity diffusion coeff., 759 to 1081°C 79—10982
Cu alloy-Al alloy evaporated couples, interdiffusion *(Russian)* 77—43389
Cu alloys, H and D permeation, in situ growth of oxide barriers 78—75883
Cu and Cu alloys, diffusion in systems involving group VA elements, review 77—39697
Cu, atom size effect in tracer diffusion 78—84005
Cu, compact, on H_2 permeated backing, precipitation *(Russian)* 78—27520
Cu crystal-Ni crystal contact, diffusion coeff. using method of nets 78—22903
Cu, diffusion coeffs. calc. for H and D *(Russian)* 78—91483
Cu, diffusion of ^{32}P in single- and polycrystals, 548 to 1046°C 77—1265
Cu, diffusion of interstitial O_2, sink/barrier phenomena 79—60553
Cu, diffusion of muons and protons 79—56689
Cu, diffusion of Ni, resistometric meas. 80—29222
Cu, diffusion of stable Ge isotopes, isotope effect 79—60552
Cu, diffusion of Zn 79—77825
Cu, electron-irradiated, monovacancy migration during stage III annealing, NQR study 80—107576
Cu, electrostatic model for impurity diffusion 78—2300
Cu, fatigue behaviour effect of Zn, Au diffused coatings 78—72850
Cu film, on Au substrate, oxidation and interfacial behaviour, ion scatt. spectroscopy study 80—66691
Cu film, on Ni, recrystallisation and interdiffusion, electron microscope obs., 450-600°C 80—39363
Cu, film, on Ni single cryst., diffusion coeff., using method of nets 78—22903
Cu film, partially oxidised, oxide removal and O_2 desorption on vac. annealing 77—12738
Cu, grain boundary migration, TEM obs. on mechanism 80—79812
Cu, H_2 diffusion, isotope depend. 80—59727
Cu, He defect complexes and depth distribution, production theory 77—31686
Cu, impurity diffusion, mass depend. of energy factor of isotope effect 78—30795
Cu, impurity diffusion of ^{113}Sn and ^{124}Sb 79—77828
Cu, impurity diffusion of V^{th} period elements and self-diffusion 80—65301
Cu in Au electrodeposited coating, under high temperature, influence on contacts performance obs. *(Czech)* 78—91486
Cu, initial sintering, method for obtaining surface diffusion coeffs., appl. to shrinkage data 78—95713
Cu, interdiffusion with sintered Al powder, struct. effect at high press. 78—60606
Cu, isotope effect for diffusion of Ge 78—2285
Cu, lattice and grain boundary diffusion of P, exam. of diffusion rates by tracer sectioning technique 78—79817
Cu, liq. and solid Pb, diffusion, melting curve, high press. effect 80—49337
Cu membrane, kinetics of permeation of H_2 79—99371
Cu, muon diffusion at low temp., effect of nuclear elec. field gradients 77—52005
Cu, μ^+SR diffusion, temp. depend. 78—39490
Cu, of ^{110}Ag, activation energy, form. enthalpy of vacancies 78—51736
Cu, of Au(Pb)(Bi), diffusion coefficient temp. depend. *(Russian)* 77—84987
Cu, of Be, 800 to 1016°C, Be determ. using $^9Be(d,p)$ and $^9Be(d,n)$ 79—5204
Cu, of Fe, resistometric technique 78—38880
Cu, of Fe, study at high temp. using molten salt electrochemistry 77—84997
Cu, of O_2, temp. depend., 650-1020°C *(Russian)* 77—84996
Cu, of S 78—47599
Cu, of Sn, via surface segregation 77—7905
Cu, of V, Cr, Mn 77—62674

diffusion in solids continued
Cu, of Zr, microstruct. and microanal. study of coating formed *(Rumanian)* 78—19917
Cu, oxidation kinetics, influence of intermediate annealing treatment 80—89412
Cu, positive muons as light isotopes of H, book contrib. 79—82907
Cu, positron annihilation, source interaction effects 78—31272
Cu, proton diffusion, config. and activation energies 79—37878
Cu, solid, solubility and diffusivity of F, electrochem. meas. 79—46808
Cu substrate, ion induced intermixing of Au or Ag surface film 80—15420
Cu, vacancies, formation entropy, diffusion const. by determinant and Green's function methods 79—77595
Cu:Be, alloy formation kinetics at solid cathodes, metal electrodeposition from molten salt electrolytes 80—26028
Cu/Al film system, interdiffusion and phase growth kinetics 77—69122
Cu/Au planar interface, formation of ordered phases CuAu and Cu_3Au 79—82392
Cu/Ni film counter, surface counting method for diffusion study 79—42321
Cu/Ni multilayer films, electron beam induced diffusion during AES depth profiling 80—19993
Cu/Sn-Ni/Au tricouples, electrodeposited, interdiffusion obs. 80—84331
Cu-Ag, surface segregation of S, Auger spectral study diffusion 80—76549
Cu-Ag interface, interdiffusion, X-ray and electron microprobe data 77—4225
Cu-Al (14.3 wt.%), ^{110}Ag diffusion in β/γ_2 interphase boundary 80—79989
Cu-Au film, aged, strength failure due to Kirkendall porosity 79—77969
Cu-Au film, short wavelength composition modulation, interdiffusion exam. 77—72723
Cu-Au interdiffusion, Cu contact tarnishing 78—7098
Cu-Au solid soln., Cu rich, meas. of interdiffusion, intrinsic and tracer diffusion coeff. 78—47608
Cu-Au thin film system, interdiffusion coeff. from cond. and Auger anal., 25 to 250°C 77—59154
Cu-Au thin films after accelerated ageing, failure by Kirkendall porosity 80—6675
Cu-CdS, Schottky barrier, Cu diffusion and photovolt. mechanism 80—6980
Cu-Cr eutectic, thermal stability in temp. gradient 79—61611
Cu-Fe phase diagram, 650 to 1050°C *(German)* 78—60658
Cu-Ge alloy clad V wire, V_3Ge multifilamentary supercond. form. by composite diffusion process 77—85959
Cu-In dilute, In^{114} impurity diffusion 79—65256
Cu-M alloys (M=Zn,Al,Sn,Mn,Pb), diffusive redistrib. during friction *(Russian)* 78—52999
Cu-metal thin film couples, room temperature interactions 80—96699
Cu-Mn, interdiffusion 78—18848
Cu-Mn alloys, γ-phase interdiffusion obs., chem. comp. depend. *(Japanese)* 78—2307
Cu-Mn alloys, interdiffusion *(Japanese)* 77—51554
Cu-Nb-Sn(Ge), phase relations and diffusion layer form. 77—36458
Cu-Ni, bimetallic film, exam. of diffusion by electrical resistivity meas. *(Russian)* 79—14970
Cu-Ni, diffusional homogenisation in compacted powder blends, X-ray diffr. line profile analysis 78—80491
Cu-Ni, evaporation limited segregation 80—70513
Cu-Ni, sintering, Kirkendall effect 80—93518
Cu-Ni (0.1 to 51 wt.%), oxidation, diffusion kinetics in porous inner layers 80—16546
Cu-Ni (20 and 50 wt.%), sulphidation, exam. of scale growth kinetics 78—88560
Cu-Ni (40 at.%) alloy, grain boundary migration, intergrain liq. layer effects *(Russian)* 77—15633
Cu-Ni alloys, chemical interdiffusion under uniaxial stress 80—65307
Cu-Ni bicrystal, misfit dislocation config., moire patterns, interdiffusion effects 78—84110
Cu-Ni bicrystals, epitaxial growth, chemical interdiffusion, X-ray diffr. line profile anal. 79—1527
Cu-Ni bimetallic film, Moire patterns, interdiffusion effects 77—51621
Cu-Ni bimetallic films, dislocation wall form. during interdiffusion, TEM obs. 78—51856
Cu-Ni bimetallic thin film, effect of microstructre on interdiffusion 79—77840
Cu-Ni diffusion couple, diffusion bonding process, fracture surface exam. *(German)* 77—35762
Cu-Ni evaporated thin film couple interdiffusion obs. 78—43187
Cu-Ni film system, time depend. diffusion coeffs., grain boundary and dislocation effects 77—80656
Cu-Ni thin film couples, interfacial reactions, contact resistance meas. 78—63882
Cu-Ni thin thin film couples, polycryst., interdiffusion singularities, Frenkel and Kirkendall effects *(Russian)* 77—24447
Cu-Ni-Zn, Cu rich, penetration tendency model for diffusion 77—39701
Cu-Ni-Zn, diffusion couples, zero-flux planes and flux reversals 80—15313
Cu-Ni(Ag)(Al), diffusion bonding 77—62687
Cu-Pb thin film couple, interdiffusion and recrystallisation, grain size effects 77—76625
Cu-Sn industrial bronzes, Sn diffusion in deform. zone influence on wear resistance, friction *(Russian)* 80—108582
Cu-Ti system, diffusion obs. *(German)* 78—63881
Cu-Zn, phase boundary motion kinetic during interdiffusion *(Russian)* 79—60559
Cu-Zn multilayer condensate, diffusion process, brass formation 78—43186
$Cu_{(s)}+Zn_{(l)}$, chemical reaction and diffusion 77—9127
$CuGaS_2$, crystal growth by solid phase crystallisation 80—25556
$CuGaS_2$, ESR assessment of S diffusion behaviour on annealing 78—35036
$CuInS_2$, p-n junction photovoltaic props. and detectors 79—99574
$CuInSe_2$, photovoltaic props. and p-n junction form. 77—69371
$CuInTe_2$:Zn, donor impurity in diffusion, elec. and optical props. 78—68504
$Cu_xMo_6S_6I_2$, x=0 to 1.2, synthesis by Cu diffusion into $Mo_6S_6I_2$ 79—69618
Cu_2O, epitaxial, on Cu(111), misfit dislocation annealing, TEM obs. 79—82228

diffusion in solids continued

- Cu_2S-CdS solar cells, prep. and stoichiometric control of Cu_2S film 78—2560
- Cu_3Sb, formed by saturation of Cu grains with Sb, electron diffraction exam. of diffusion layer *(Russian)* 79—33119
- ε-(Cu_3Sn)-Cu diffusion couples, growth of intermediate phase layers *(Japanese)* 80—49431
- $CuWO_{4-x}$ prod. from $CuO+WO_3$ solid state reaction 80—66796
- Er, diffusion of ^{198}Au anisotropy, interstitial solute diffusion mechanism 80—29223
- Er_2O_3, of Hf, vol. and grain boundary diffusion coeffs., tracer sectioning technique 79—7712
- Er_2O_3-Ta, oxide grain growth at interface 77—81245
- Fe alloy, crevice corrosion by water vapour, CO, methane in HTR coolants, model 77—25202
- Fe alloys, H_2 trapping, electrical analogue model 79—46841
- Fe and alloys, diffusion impregnation of enhancement by Fe powder addition to impregnant mixtures 77—28044
- Fe, annealed, Hz permeation, 230 to 300K *(Japanese)* 78—84004
- Fe, annealed and cold-rolled, diffusion, permeation and accumulation of H_2 *(Japanese)* 77—39692
- Fe, Armco, D penetration, mass spectrometric obs. 78—47606
- α-Fe, Armco, determ. of H solubility 80—54390
- Fe, Armco, H_2 diffusion 0 to 300°C, effect on elongation tension *(Russian)* 77—66044
- Fe, BCC, of C and N 77—4222
- Fe base ternary soln., containing interstitials and substitutional solutes, thermodynamic and kinetic props. 78—2297
- Fe, cast, diffusion saturation and form. of FeB and Fe_2B coatings 78—53032
- Fe, cast, grey, carbide-free Cr diffusion coating 79—96205
- Fe, chem. diffusion coeffs. and solubility limits for Cu, 690-1050°C 77—59146
- Fe, chemically induced grain boundary motion, in Zn atmos. 78—38724
- Fe, commercial, diffusion with Cr in closed reaction space, kinetics and mechanism 79—52458
- Fe, compact, on H_2 permeated backing, precipitation *(Russian)* 78—27520
- Fe, defect trapping of ion implanted D, depth profile, diffusion eqn. calcs. 80—2047
- Fe desorption of H into ultrahigh vac. system, using permeation cell 80—86326
- Fe, diffusion and solid solubility of Sb, 773-873K, ion backscatt. anal., rel. to intergranular embrittlement 78—71880
- Fe, diffusion process acceleration, accompanying US treatment *(Russian)* 80—19976
- Fe, Fe-C, diffusion coating by Cr and Pb melt bath, kinetics *(Korean)* 78—60873
- Fe film, coated, interface magnetism by Mossbauer spectroscopy 80—75890
- γ-Fe, grain boundary diffusion of Ni 79—23787
- Fe, H diffusion coeff. meas. at low temps. by electrochem. alternating method *(Japanese)* 80—39354
- Fe, H martensite production *(Ukrainian)* 77—52321
- Fe, high-purity, H_2 charged, resist. recovery at low temps. 78—26729
- Fe, in Mo, rel. to transforms. 77—4214
- Fe, irradiated with electrons then annealed, magnetoresistance at 20K *(French)* 80—103677
- Fe, lattice distortions due to H, X-ray diffr. exam. 78—79629
- Fe, motion of H and D, mag. relax. meas. 78—64228
- Fe multilayer films stability, Mossbauer spectra 80—29651
- Fe, muon diffusion, spin relax. 79—78599
- Fe, muon diffusion and relaxation studies 80—75913
- Fe, muon quantum diffusion 79—78598
- Fe, muon$^+$ diffusion, spin rotation, effect of impurities 80—7249
- α-Fe, μ^+ diffusion 79—56687
- Fe, μ^+SR, theory of spin depolarisation rate 78—80271
- Fe, of C, diffusion coeff. meas. by mag. aftereffect 78—29129
- γ-Fe, of C, high temp. vacuum metallography investigation *(Russian)* 77—72718
- Fe, of C, under US vibrs., initial struct. effect *(Russian)* 78—38876
- Fe, of C and Cr, US effects *(Russian)* 77—59144
- γ-Fe, of Cu, lattice diffusion and grain boundary diffusion *(Japanese)* 78—18836
- Fe, of H, 230 to 300K 79—95220
- Fe, of H, book contrib. 79—82390
- Fe, of H_2 and D_2 at 49 to 506°C 78—59977
- γ-Fe, of Ni, grain boundary mechanism *(Japanese)* 78—18837
- α-Fe, of Zn, multiphase diffusion 78—79822
- Fe, penetration of H_2, influence of microstruct. changes induced by cold working *(Russian)* 77—20182
- Fe, permeability, solubility and diffusion of H and D, 9 to 73°C 77—76560
- Fe, plastically deformed by pulsed mag. field, mobility of Fe atoms, radiotracer profiles 79—28584
- Fe, positive muon diffusion 79—56688
- Fe powder based sintered porous permeable materials, diffusion chromising 80—100958
- Fe, pure, of H and D at 10 to 60°C 78—75887
- Fe, pure, Sn and Cr diffusion, effect of boundary struct., autoradiography study *(Japanese)* 80—49419
- Fe, quantum diffusion of positive muons, 3 to 300K 80—75909
- α-Fe, S and C diffusion, AES obs. 77—51543
- γ-Fe, S diffusion, grain size effect 79—86930
- α-Fe, single crystal, Sb diffusion induced dislocations 78—30798
- Fe, softening vs. hardening effects produced by high fugacity H charging 79—74172
- Fe, surface segregation of Sn, AES obs. 77—20172
- Fe through surface corrosion prod., grooving mech. at Fe-liquid Li interface 77—6522
- Fe, trapping of H, average trapping depth and trapping sites density 80—84297
- α-Fe vacancies, formation entropy, diffusion const., determinant and Green's function methods 79—77595
- Fe, white cast, migration of C to the surface, solubility *(Russian)* 80—92720
- Fe, zone melted, H_2 diffusion, reversible lattice dilation 77—11732
- Fe:Y, ion implanted diffusion of D, deep traps 80—103372
- Fe:Yb,^{18}O, interaction between implants 77—27921
- Fe:Yb(Au), radiation-damage evolution, influence on lattice-location meas. 80—6426

diffusion in solids continued

- solid Fe/liquid Zn, interdiffusion reaction 79—77845
- Fe/ZrB_2, metal-like cpd. form. in diffusion layer during solid phase saturation 80—19994
- Fe-Al, antiphase boundary motion, microscopic diffusional theory, appl. to domain boundary coarsening 79—61563
- Fe-Al, diffusion bonding 77—62687
- Fe-Al, rate of form. and thickness of diffusion layer, 200 to 600°C 80—15315
- Fe-Al (1 to 4 wt.%), effect of nitriding on surface structure and props., and on diffusion layer *(Russian)* 79—34197
- Fe-Al (40 at.%) B_2 type ordered alloy, C migration, resistivity meas. *(French)* 78—52868
- Fe-Al α phase solid solution, interdiffusion coeff. depend. on ordering *(Russian)* 79—99373
- Fe-Al-C alloys, C migration and mag. aftereffect, mag. permeab. disaccommodation and long-range order meas. 79—8020
- α-Fe-Al(Zn), $\langle 111 \rangle$ fibre texture development through diffusion process without α-γ transform 79—100170
- Fe-based powder PZh2K, diffusion chromising with sintering, effect of porous struct. 79—66219
- Fe-C, interstitial diffusion in presence of chem. conc. gradient 77—76612
- Fe-C, of Sn, microprobe anal. of intermediate phases *(French)* 80—50596
- Fe-C (1.0 wt.%), mixed powder compact, sintering, C diffusion meas. 77—90293
- Fe-C (synthetic diamond) role of diffusion of graphitisation in phase interaction 77—36449
- Fe-C-N, annealing in dry H_2, below 1180K, to purify to low C and N concs. 78—3072
- Fe-C-Si, spheroidization 77—66665
- Fe-Co alloy, electrodeposited, comp. and struct. effects on H_2 diffusion and evolution overpot. 77—43377
- Fe-Co alloy, of H_2, diffusion coefficient and permeability *(Russian)* 78—79819
- Fe-Co-Ni-Al-Cu alloy, polycryst. hard mag., C diffusion 79—77827
- Fe-Cr, of C 77—7907
- Fe-Cr, role of C in transform. by heating in $(\alpha+\gamma)$ phase *(French)* 78—52798
- Fe-Cr diffusion couple, tracer diffusion meas. using tracer anal. 79—7716
- Fe-Cr-Al, scales, α-Al_2O_3, early stages development at high temp. 80—89413
- Fe-Cr-Al-Y, high temp. corrosion depend. on Y, oxidation, stress growth *(Russian)* 80—40588
- Fe-Cr-Al-Y, scales, α-Al_2O_3, early stages development at high temp. 80—89413
- Fe-Cr-Ni system, diffusion coeff. consts. calcs. for multi-component systems *(Russian)* 79—90815
- Fe-Cr-Ni system, isothermal diffusion *(Russian)* 79—69300
- Fe-Cr-O system, phase relations at 1200°C using diffusion couple technique 80—89205
- α-Fe-Cr(V)(Ti)(Mo)(W), morphology and growth kinetics of δ-eutectoid produced by carburisation 77—16618
- Fe-graphite, sintered, diffusion layer form. 79—100299
- Fe-H, deformed, internal friction 79—57041
- Fe-H, of H, during recovery of hydrogenated and quenched alloy 77—77510
- Fe-Mn (3 wt.%), Sn diffusion along grain boundaries, micro-Auger spectroscopy 77—11740
- Fe-Mn diffusion pair, mutual diffusion coeffs. calc. by computer 79—69299
- Fe-Mn(Ni) systems, struct. defects effect on interdiffusion 80—15314
- Fe-N system, Fe_4N growth kinetics *(Korean)* 80—93540
- Fe-Ni, ferro-nickel oxidation, appl. of mag., thermomag. methods *(French)* 79—20318
- Fe-Ni, magnetic ordering, effect on diffusibility, penetrability and solubility of H_2 *(Russian)* 77—24435
- Fe-Ni (20 to 100 wt.%), exam. of C diffusion coeff., in temp. range 950 to 1100°C 78—51747
- Fe-Ni alloy, $\alpha \rightarrow \gamma$ transform., role of grain boundary diffusion, Mossbauer obs., homogenisation effect *(Russian)* 79—52197
- Fe-Ni alloys, diffusivity of N_2 79—46845
- Fe-Ni mixed powders, effect of Ni particle size and unequal interdiffusion, on sintering process *(Japanese)* 78—84728
- Fe-Ni system, interdiffusion zone growths *(Czech)* 78—84009
- Fe-Ni_3S_2 reaction couple solid-state displacement reactions 79—77841
- β_2-Fe-Ni-Al, diffusion 77—24449
- Fe-Ni-Al system, multiphase diffusion at 1000°C, diffusion structs. and props. 80—19995
- Fe-Ni-Al system, multiphase diffusion at 1000°C, interdiffusion coeffs. for β and γ alloys 80—24684
- Fe-Ni-Cr (30.6, 21.3 wt.%), Alloy 800, high temp. oxidation at low O_2 press., SEM, AES and electron probe microanal. study 80—93688
- Fe-Ni-Cr alloy, carbide form. by C diffusion, precip. distrib. and morphology 80—104164
- Fe-Ni-Cr-C, ferritic, P segregation to free surface, 723 to 823K, AES 78—48411
- Fe-Ni-Cr-Y, Y addition effect on selective oxidation/diffusion phenomena relationship *(French)* 80—108623
- Fe-Ni-Mn-steel 48, struct. defects effect on interdiffusion 80—15314
- Fe-Ni(Co), powder mixture, effect of granulometric distrib. on importance of Kirkendall effect during calcination *(French)* 77—11721
- Fe-Sb system, α-phase, interdiffusion 79—73349
- Fe-Si (3 wt.%), temp. depend. of migration rate of secondary recrystallisation grain boundaries *(Russian)* 79—1436
- Fe-Ti, multiphase binary diffusion couple, layer growth rate of intermediate phase, numerical calc. *(Japanese)* 78—14513
- Fe-Ti, solubility and diffusivity of H and D in mixed crystal phase, elec. cond. meas. *(German)* 80—107575
- Fe-Ti multiphase, binary diffusion couple, layer growth rate of intermediate phase *(Japanese)* 78—14514
- Fe-Ti-Si-Ni-P-C-S, H_2 segregation kinetics *(Russian)* 78—18832
- Fe-Zn, chemically induced grain boundary motion 78—38724
- Fe-Zn, diffusion coefficients in δ_1 phase *(Japanese)* 78—14512
- Fe-Zn, layer formed in diffusion couple, effect of small alloying element addition *(French)* 77—43388
- Fe-Zn compound form. after hot galvanising Fe with liquid Zn and by diffusion *(French)* 79—20275
- Fe-Zn couple, Zn electrodeposited on polished Fe, reaction rate in solid state *(Japanese)* 78—15322

diffusion in solids continued
Fe_3O_4, magnetite, diffusion of Cr, as function of O partial press. 78—43183
Fe_3O_4, substituted magnetite, oxidation kinetics 77—1889
Fe_3O_4-$Fe_{2.8}Ti_{0.2}O_4$, interdiffusion expts. 78—55991
Fe_3O_4-$FeAl_2O_4$ spinels, Fe^{59} diffusion 80—59721
FeOCl-pyridine intercalate, mechanism, nucleation and diffusion 80—49420
$Fe_{1-x}Pd_x$ film, vac. deposited, oxidation and corrosion, AES, XPS and STEM obs. 79—100286
FeTi ferrite, H trapping study by high resolution autoradiography and degassing *(French)* 77—81368
GaAlAs DH laser, In solder deterioration, Au diffusion in In 80—33019
GaAlAs, heterostruct. formed by LPE, growth and dissolution kinetics 79—99439
(GaAl)As, Zn diffused DH laser with twin transverse junctions, low threshold current 79—98393
(GaAl)As, Zn diffused proton bombarded stripe laser 79—98392
GaAlAs-GaAs heteroepitaxial devices, interstitial impurities and degradation, Auger obs. 80—99730
GaAlAs-GaAs heterostruc. lasers, interstitial impurities and degradation, Auger obs. 80—99730
$Ga_{1-x}Al_xAs$, of Zn, depend. on Al content 78—59981
GaAs, anomalous diffusion of Sn from doped oxides due to dopant depletion effects 77—89461
GaAs, carrier diffusion in transient response regime 80—103688
GaAs, diffusion of Cr and Ag, radiotracer profiles 80—24680
GaAs, gamma and electron irrad. defect formation depend. on interface, luminescence study 80—34057
GaAs, heavy metal migration, ESCA study *(French)* 78—75885
GaAs, influence of radiation damage on diffusion of implanted P and Kr atoms 78—6082
GaAs, ion implanted, capless annealed and dielectrically annealed, comparison of doping profiles 80—100278
GaAs, ion implanted, diffusion of Zn and Ag, profiles 80—24681
GaAs, LPE layers, outdiffusion of recomb. centres from substrate during growth 80—39466
GaAs layers, Cu diffusion along grain boundaries, spectroscopy study 80—49234
GaAs, low temp. selective Zn diffusion process using anodic oxides 78—47399
GaAs, minority carrier diffusion lengths, contact metal effects 78—72260
GaAs, modification of Zn diffusion profiles by proton irrad. 78—43043
GaAs, of Be, SIMS and electrical profiling 78—47605
GaAs, of Cr and Zn, interimpurity interaction effect on distrib. profiles of impurities diffusing simultaneously 77—76451
GaAs, of Se 77—51547
GaAs, of Sn, effect of ambient As vapour press. on surface stability 80—2208
GaAs, open tube diffusion of Zn 80—84326
GaAs, Pd/Ge interdiffusion below 350°C on substrate, Auger spectra, Schottky barrier energy 79—69581
GaAs, planar diffusion of Sn from doped SiO_2 films, for planar junction fabrication 79—69289
GaAs substrates, out-diffusion of Cr 80—10708
GaAs thin film polycrystalline solar cells, grain boundary edge passivated 80—94069
GaAs thin Schottky barrier metallisation, thermal reactions 79—78176
GaAs, VPE, hole diffusion lengths, effect of transition metal diffusional doping 80—15628
GaAs VPE layers, back surface gettering, Cr out diffusion 80—10802
GaAs:Ag, diffusion of Ag at 1000°C, profiles, Schottky barrier and Hall effect meas. 80—54435
GaAs:B(Ge)(Mg), impurity distrib. and diffusion by glow-discharge optical spectroscopy 80—49258
GaAs:Be, annealing effect during MBE 78—79898
p-GaAs:Be layer, MBE growth, Be doping and diffusion 77—51397
GaAs:Cd, time depend. of Cd diffusion from gaseous phase 79—46844
GaAs:Co, effect of complex formation on impurity diffusion 77—11736
GaAs:Co, epitaxial layers and bulk, diffusion and elec. activity of Co 79—56333
GaAs:Cr, bulk and epitaxial, ion implanted, Cr conc., depth distrib. and diffusion coeff. 80—49243
GaAs:Cr, Cr distrib. and heat-treatment migration studies by SIMS 80—107305
GaAs:Cr, semi-insulating, damage gettering of Cr during annealing of Cr and S implants 80—107304
GaAs:Cr diffusion profile meas. 80—6554
GaAs:Cr substrates and LPE layers, Au film deposition and annealing, Cr redistrib. 80—15312
n—GaAs:Fe, diffusion doped compensated layers 80—15125
GaAs:Li diffused, lattice imperfections, TEM 77—80521
GaAs:Mn, photoluminesc., emission props. and radiative mechanism 79—56842
GaAs:Na, impurity solubility and diffusion 79—55930
GaAs:Se, fast diffusion of elevated temp. ion implantation, SIMS meas. 78—34527
GaAs:Si, ion implanted effect of anneal ambient and occurrence of compensated regions in Si implants 77—51394
GaAs:Si, Li, IR absorpt., microstruct., charge compensation 80—107565
GaAs:Si,Cr, under layer of SiO_2, effect of annealing, on electron concentration and mobility, and impurity distrib. 79—4323
GaAs:Sn thermal diffusion from spin-on SnO_2/SiO_2 source 80—96691
n-GaAs:Sn(Te), pure and doped, diffusion of Sn, radiotracer profiles 79—23782
GaAs:$Te^+(Se^+)(Sn^+)(Ge^+)$, ion implanted, laser annealing effect on elec. characts. 79—73195
GaAs:Zn, diffusion during LPE, impurity gradients and annealing effects 80—29882
GaAs:Zn, diffusion of Zn by two-temp. method, LED fabrication 80—49416
GaAs:Zn, high surface conc. Zn diffusion for good ohmic contact 77—11575
GaAs:Zn, surface conc. control 79—55758
GaAs:Zn ion implanted ionic alloy, electrophysical props., annealing 80—39133
GaAs/Au-Ge/Ni, Schottky barrier energy var. with interdiffusion 77—20435
p-GaAs-Al interface, produced by diffusion method using heavily doped GaAs, rectifying props. 79—28409

diffusion in solids continued
GaAs-$Al_xGa_{1-x}As$ heterojunction, MBE, diffusion across interface, optical annealing expts. 78—2305
GaAs-AlGaAs half-ring laser, fabrication by deep Zn diffusion 78—17960
GaAs-Al(Ga)(Ge), surface reactions and interdiffusion, photoemission study 80—49532
GaAs-Au, Schottky barrier energy var. with interdiffusion 77—20435
GaAs-Au(Ag) Schottky barrier solar cells, interface problems, AES, SIMS and XPS study 80—89627
GaAs-Cu:Tl, cathode luminescence spectra, Hall effect, cryst. defects 80—76087
GaAs-$Ga_{2.2}Al_{0.8}As$:Be, LPE, diffusion of Be into GaAs substrate 80—103517
n-GaAs-n-GaN, diffusion growth kinetics, morphology and electrical properties 80—20294
GaAs-Pd junction, contact reactions 79—56308
$(GaAs)_n(AlAs)_m$ multilayers, MBE, interdiffusion, X-ray diffr. study 80—70474
$GaAs_{0.1}P_{0.9}$:Zn, shallow Zn diffusion profile determ. using anodic oxidation and double radioactive tracer method 77—43239
$GaAs_{0.6}P_{0.4}$, VPE, hole diffusion lengths, effect of transition metal diffusional doping 80—15628
$GaAs_{0.6}P_{0.4}$:Zn, control of Zn diffusivity by multiple implantation 78—38877
$GaAs_{1-x}P_x$, diffusion of implanted Zn ions, ion microbe analysis 78—95190
$GaAs_{1-x}P_x$, solid state diffused, conc. distrib. obs., electroreflectance and tracer sectioning obs. 80—54389
$GaAs_{1-x}P_x$:Zn implanted, Zn diffusion 77—84993
GaInAsP-InP planar stripe lasers, Zn diffusion, sputtered SiO_2 film as mask 80—48249
GaInAsP-InP Zn diffused stripe geometry DH diode laser fabrication 79—98386
$Ga_xIn_{1-x}P$, epitaxial film, diffusion of Cu(Au)(Zn), intrinsic impurity effects 78—87825
$Ga_xIn_{1-x}Sb$ diode, with Au metallisation, interdiffusion effect of heat treatment 78—14820
Ga_2O_3-Fe_2O_3 system, anomalous Mossbauer line shapes, incomplete annealing 78—92006
GaP, diffusivity and solubility of Cu 78—51743
GaP, dislocations induced by diffusion of Zn with or without P 77—19955
GaP, LEC, SSD and CVD samples, Zn tracer diffusion profiles in solids 78—95189
GaP, low temp. selective Zn diffusion process using anodic oxides 78—47399
GaP, n-type, Zn diffusion, p-n junction depth 77—89841
GaP, of Cr and Zn, interimpurity interaction effect on distrib. profiles of impurities diffusing simultaneously 77—76451
GaP:Au, diffusion, solubility, and electrotransport of Au 78—91489
GaP:Cr, diffusion parameters and solubility and influence on elec. and optical props. 79—73343
GaP:Fe, diffusion, solubility, elec. activity and energy levels 77—55395
GaP:Zn, dopant diffusion profiles at 900°C, radiotracer meas. 77—59147
GaP:Zn, shallow Zn diffusion profile determ. using anodic oxidation and double radioactive tracer method 77—43239
GaSb, diffusion of In, 520 to 712°C 80—79995
GaSe, ^{110}Ag diffusion, temp. depend. and solution *(Russian)* 80—70467
GaSe:Sn, ^{113}Sn diffusion, temp. depend. and Sn solubility *(Russian)* 80—70466
GaTe, ^{110}Ag diffusion, temp. depend. and solution *(Russian)* 80—70467
Gd, AC susceptibility, freq. depend., impurity diffusion mag. after effect 79—61072
Gd, positive muons as light isotopes of H, book contrib. 79—82907
Gd-Fe amorphous film, atomic diffusion of deposited Co 79—73346
Ge, defect form. under radiation-accelerated diffusion conditions 80—19854
Ge, diffusion of Ga along dislocations 79—82385
Ge, effect of Au on film props. 78—76161
Ge, film, epitaxial growth on Si, interdiffusion, plasmon energy loss anal. 77—31916
Ge, heavily-doped single cryst., macroinclusions, annealing in elec. field 77—47474
Ge, heterodiffusion due to H atom surface recombination stimulation, Cu, Zn, In coated *(Russian)* 80—59726
Ge, n- and p-type, solubility and diffusion of Na, vacancy mechanism 77—89592
Ge, of ^{6}Li, diffusion coeff. calc. from depth profile meas. using $^6Li(p,\alpha)$ 79—5202
Ge, of H, effective diffusion coeff. at 430°C 78—39052
Ge, of In, Al, Ga and Li, effects of ultrasound 77—69119
Ge, p-i-n struct., Li ion drift thermal profile 77—51813
Ge, self- and impurity diffusion 80—29213
Ge, single cryst., ^{18}F penetration, charged particle activation anal. 80—93828
Ge:Cu, anelastic relax., internal friction temp. depend. meas. 79—65143
Ge:Li, determ. of drift parameters of Li 78—17509
Ge:Mg, diffusion and p-type cond. 80—6419
Ge:P, conc. depend. of diffusion coeff. at P diffusion 78—95185
Ge:Sb(As)(P), implantation doping, annealing and doping profile determ. 77—19972
Ge-Au-Ni(Pd)(Pt) trilayer film, interdiffusion obs., on annealing 78—2308
Ge-Au-Ni(Pt)(Pd) trilayered films, annealing, interdiffusion 78—22902
Ge-GaAs (110), heterojunction chemistry, photoemission expts., interdiffusion obs. 78—95244
Ge-Na interfaces, interdiffusion, electron states, EELS study 80—50484
Ge-Sb, chemical diffusion *(Japanese)* 78—14515
Ge-Si alloy p-n junction, Sb-diffused, TSC 80—20289
Ge_2S_3, photoenhanced diffusion of Ag 79—65257
Ge_2S_3-Ag contact, photoinduced diffusion of Ag in amorphous semicond. film 80—49418
H depth profiles in solids, using neutron time of flight meas. in H(t, n) 79—5198
H diffusion, and solubility in solid metals 80—49422
H diffusion in electrolytic Ni, coeff. determ. *(Russian)* 79—8441
H embrittlement, trap theory 80—89325
H embrittlement cracking at notches, model, based on stress induced diffusion of H atoms 78—39897
H embrittlement cracking at notches 78—84985

diffusion in solids continued
H storage materials, H diffusion in $Ti_2NiH_2(FeTiH)(LaNi_5H_6)$, neutron diffr. obs. 80−51013
H thermal diffusion, apparatus 80−100358
H trapping mechanisms, by permeation techniques 79−37880
H_2 embrittlement cracking and impurity atom migration *(Chinese)* 80−104247
H_2 permeation through HTGR heat exchanger tubes, reduction using calorising method *(Japanese)* 80−100360
H_2, random walk models, generalisation to correlations over two jumps 78−79794
H_2, single crystals, NMR, dynamic effects 80−107608
O-H_2, solid, quantum diffusion of p-H_2 impurities 80−88398
H_2, solid, quantum diffusion 80−107607
H_2 transport by dislocations 77−21263
He, energy absorpt. and size effect, point defect diffusion *(Russian)* 77−4243
He, solid, coherent diffusion of isotropic impurities 80−54468
He, solid, theory and thermodynamic props., book contrib. 77−47646
^{3}He, phase separation of dil. ^{4}He impurities 80−88393
^{3}He, quantum diffusion in solid ^{4}He, tunnelling jumping approx. *(Russian)* 78−87844
^{3}He-^{4}He solid mixture, dil. ^{3}He conc., diffusion coeff. obs. by NMR, impurity-phonon scatt. *(Russian)* 77−62701
^{4}He, diffusion coeff. of ^{3}He 79−56026
^{4}He, of ^{3}He, quantum diffusion, pulsed NMR exam. *(Russian)* 78−71902
^{4}He, quantum diffusion of ^{3}He, tunnelling jumping approx. *(Russian)* 78−87844
^{4}He, solid, diffusion coeff. of ^{3}He, detection and study of impuriton-phonon scatt. mech. 79−56029
^{4}He, solid, impurity interaction anisotropy and quantum diffusion of ^{3}He 79−56028
^{4}He:^{3}He, quantum diffusion of ^{3}He, impurity interaction anisotropy *(Russian)* 78−30810
β-Hf, electrotransport and diffusion of Ta impurities *(German)* 78−87826
Hf, thermotransport and thermopower of O_2 78−76055
Hf-H, diffusion in hydride phase, exam. 80−29204
$Hg_{1-x}Cd_xTe$, doping props. of selected impurities, diffusion behaviour 77−72632
$Hg_{1-x}Cd_xTe$, grown from melt, Kirkendall and Frenkel effects 80−100365
$Hg_{1-x}Cd_xTe$-In contact, diffusion of In 80−103520
$HgCl_2+AgI \rightarrow AgHgClI_2(AgHgCl_2I)$, solid state diffusion controlled reaction at 100°C 78−34659
HgSe, epitaxial growth on CdSe, struct., Cd distrib. and electrophysical props. 77−12540
HgTe, single crystal, diffusion of transition metals 79−77818
HgTe-CdTe, epitaxy by evap. and interdiffusion under isothermal conditions book contrib. 77−12549
HgTe(:Ag), impurity diffusion, gamma-ray effects 80−54441
p-Hz, quantum diffusion of O-H_2 impurities 80−96719
In, of Pb, diffusion coeff. determ., RF size effect meas. *(Russian)* 78−91717
$In_xGa_{1-x}As$, Zn diffusion coeff. and surface conc. 80−39122
InGaAsP-InP, Zn diffused DH structures, oxide defined transverse junction stripe lasers 79−98389
InP, diffusion of Cd acceptors 79−82246
InP, of Ag, low temp. 78−75884
InP, planar Zn diffusion process for p-n junction formation 78−43040
InP, Schottky diode, barrier height control by S diffusion 77−85309
InP, Zn diffused single-crystal, substitutional dopant and hole conc. meas. 80−75260
InP:Cd, p^+-p^--n^- junction form. by diffusion doping 80−84504
InP:Cd(Zn), avalanche photodiode characts., impurity diffusion effects 80−70709
InP:Co(Fe), diffusion solubility and elec. activity of Co and Fe 77−43240
InP:Zn, isoconcentration diffusion of Zn at 800°C 78−6186
InP-metal Schottky barriers, effects of heat treatment characterised by SIMS 78−6446
InSb:Cd, diffusion props. of Cd, modified C-V technique meas. 79−19401
InSb:F, acceptor props. and diffusion coeff. of F 80−70643
n-InSb:Zn, Zn diffusion out of implanted layers 79−10984
InSb:Zn p-n junctions, ion implantation and diffusion spreading, elec. and photoelec. props. 79−73573
InSb/GaSb superlattice thin films, sputtered, ion-bombardment-enhanced diffusion during growth 78−87882
InSb-GaSb, compositionally modulated sputtered superlattice, growth and interlayer diffusion 79−56930
InSb-GaSb superlattice, interlayer diffusion 77−85086
InSe, ^{110}Ag diffusion, temp. depend. and solution *(Russian)* 80−70467
Ir, diffusion of C from surface into bulk, theory 80−6562
Ir-Fe, spin fluctuation alloy, thermopower peak diffusion origin 80−88542
$IrSi_x$, formation, Ir films on Si, He ion backscatt. X-ray diffr. study 79−82471
KBr, electrolytically coloured single cryst., ionic SCL current, F-centre diffusion 77−62937
KBr in contact with KCl, mutual diffusion, development of relief on contact surfaces 78−22964
KBr, of Br_2, 375 to 600°C, obs. using OH^- centre decomp. 77−43378
KBr:Cl^-, diffusion traps for divalent ions, dielectric loss and ionic thermocurrent techniques 80−6566
KCl, annealed in KBr vapour, crack and pore formation, diffusionally induced stress relaxation *(Russian)* 80−40388
KCl bicrystals, grain boundary migration kinetics, effect of solutes 78−43185
KCl, Born-Mayer parameters of He and Ar, interstitial interaction with neighbouring ions 80−100228
KCl, doped, grain boundary diffusion, space-charge contrib. 77−55386
KCl, electrolytically coloured single cryst., ionic SCL current, F-centre diffusion 77−62937
KCl, ion processes in $F \rightarrow Z_1$ transition, photocond. meas. 77−15412
KCl, migration of brine inclusion, nonequilib. morphology 78−38882
KCl, of ^{54}Mn(^{85}Sr), isothermal diffusion 77−47625
KCl, of Ba^{2+}, light scatt. meas., dipole mechanism *(Russian)* 78−22900
KCl, of radioactive and stable Tl^+, transmutation effect 77−89589

diffusion in solids continued
KCl, of Sr and Ca, simultaneous diffusion coeffs. 78−79813
KCl single crysts., thermal stability of neutron induced damage 78−79634
KCl:Ba^{2+}, localised stress relaxation in excess vacancy system, prismatic loops *(Russian)* 80−88160
KCl:Ba^{2+}, precipitation kinetics, supersaturation effects, geometry of formed heterophase struct. *(Russian)* 78−84824
KCl:Ca^{2+}, Cl^-(Br^-), diffusion traps for divalent ions, dielectric loss and ionic thermocurrent techniques 80−6566
KCl:H, migration and stabilisation of H atoms, ESR and thermolum. study 79−1430
KI, electrolytically coloured single cryst., ionic SCL current, F-centre diffusion 77−62937
K_2OsCl_6, single cryst. with H^+ interstitials, protonic cond. from dielec. meas. 80−107515
$K_2SnF_6.4HF$, HF molecule, activation and spatial symmetry of arrangement 79−42313
$LaNi_5$, absorption of H_2, kinetics, diffusion consts. 78−14508
$LaNi_5$, H_2 absorpt. kinetics *(Chinese)* 80−103561
$LaNi_5H_x$ hydrogen storage system, $(0 \leq x \leq 6)$, neutron scatt. obs. of static and dynamic props. 78−14323
La_2O_3, fast ionic O_2 diffusion, neutron scatt. evidence 79−99357
Li-Al system, Li solubility and chem. diffusion in Al, electrochem. study 80−107432
β-Li_5AlO_4, microcryst., neutron irrad., ^{3}H diffusion studies, fusion blanket appl. 80−18627
LiF, alkali ion implantation, migration, segregation, effect on optical props. 80−100269
LiF, deformed in liquid He, penetration of He, dislocation effects 77−20131
LiF, of O_2, high-temp. 77−84988
LiF:Mg^{2+} deformed in ^{3}He and ^{4}He, screw dislocation density reduction due to He diffusion 79−69112
LiF:Ni, dislocation behaviour in diffusion zone, Cottrell clouds *(Russian)* 80−70212
Li_3N thin film, vacuum evaporation on WO_3, retarded deposition 80−108351
$LiNbO_3$, diffusion of Co, Ni, Zn and Cu and its effect on acoustic velocity 77−84847
$LiNbO_3$, diffusion of alkali metals and self-diffusion 77−84989
$LiNbO_3$ layers, Li out-diffused, SHG phase matching temp. variation 80−69455
$LiNbO_3$, OH^- ion incorporation, mobility and optical absorpt. 77−35583
$LiNbO_3$, of Ti, exam. by electron probe anal. and X-ray diffr. 78−47588
$LiNbO_3$, of Ti, optical waveguide, +4 valence state, XPS 77−11014
$LiNbO_3$, of Ti, optical waveguide construction *(Czech)* 79−41452
$LiNbO_3$, of Ti, surface acoustic waveguide formation 77−79998
$LiNbO_3$ optical waveguides, elimination of Li_2O out-diffusion waveguide 77−65641
$LiNbO_3$ planar waveguide, refractive index rel. to Ti diffusion *(Russian)* 78−59120
$LiNbO_3$, Ti diffused optical waveguide, ferrolectric domain inversion 79−94338
$LiNbO_3$, Ti diffused slab waveguide, mode control by doping 77−88903
$LiNbO_3$, Ti diffusion and characts. of graded-index lightguide 79−27433
$LiNbO_3$, Y-cut, waveguide form. by Ti diffusion, refr. index and electrooptic coeffs. 79−14114
$LiNbO_3$:Fe, ferroelectric, treated in Li_2CO_3, formation of Fe^{2+} state, Mossbauer effect 78−92003
$LiNbO_3$:Ti, planar and channel optical waveguides, anisotropic diffusion expts. 80−64200
$LiNbO_3$:Ti diffused, optical waveguide, fabrication problems *(Japanese)* 80−33256
$LiNbO_3$:Ti diffused optical waveguide, guided light scatt. sources 80−78966
$LiNbO_3$:Ti in-diffused optical waveguide fabrication 79−76892
$LiNbO_3$:Ti optical waveguide, technique for suppressing Li_2O out-diffusion 78−18040
$LiNbO_3$:Ti planar and channel optical waveguides, Ti diffusion coeff. meas. 80−19096
$LiNbO_3$:Ti waveguide, diffused, Mg diffusion effects on characts. 78−66905
$LiNbO_3$:Ti Z-cut crystals, Ti diffusion process parameters 80−102849
Li_2O-Al_2O_3-GeO_3, glass, interdiffusion coeffs. of Li and Na 80−88369
Li_2O-Al_2O_3-SiO_2, glassy and polycryst., interdiffusion coeffs. for ion exchange 78−26738
Li_2O-Al_2O_3-SiO_2 glass, crystn. aggregation and migration of ion-implanted Ag 77−55240
Li_2O-Al_2O_3-SiO_2 glass, He migration, struct. effects 77−55389
Li_2O-B_2O_3-SiO_2 glass systems, phase separation effect on the diffusion processes 78−26734
$LiTaO_3$, Czochralski growth technique, light guide prod. by Nb diffusion *(German)* 80−20783
$LiTaO_3$:Ti, diffused waveguide prep., parameters determ. 80−14465
Li_xTaS_2 and Li_xTiS_2, chem. diffusivity of Li at 30°C 80−59737
$LifaO_3$, optical waveguides, elimination of Li_2O out-diffusion waveguide 77−65641
Lu, diffusion of H, hopping process 80−24673
Mg hydriding, Kirkendall marker movement 80−75385
Mg, of H_2 77−28042
Mg/Mg_2Cu eutectic, hydriding and dehydriding kinetics obs. by press. sweep method 80−35765
Mg-Ce, diffusion coeff. determ. during hydriding *(German)* 79−29288
$MgCr_2O_4$ spinel, exam. of expansion during synthesis 79−20012
MgF_2, optical absorption following pulsed electron irrad., 100-500K 79−8164
MgF_2:Li^+, atom transport, diffusion and ionic cond. meas. 80−107492
$MgFe_2O_4+ZnO$, powders, cation mutual diffusion coeffs. calc. 77−15635
MgO crystal, of ^{51}Cr 77−35754
MgO, EPR of Mn^{2+} diffusion 78−91477
MgO, electron irradiation induced mobility of substitution H 77−55390
MgO, technical powder purity, of technical purity powders 77−63586
MgO:Fe, Fe^{2+} oxidation and Fe^{3+} reduction kinetics, EPR obs. 79−70399
MgO:H(D), electron irrad. induced diffusion of interstitial impurity 77−15452

diffusion in solids continued

- $MgO-Al_2O_3-SiO_2$: ZrO_2, TiO_2, glass, phase separation *(German)* 80–38932
- Mn-H, hydride formation in high press. range 80–65235
- Mn-Sb two layer film, cpd. formation kinetics, ion backscatt., X-ray diffr. and mag. meas. 77–72801
- MnZn ferrite, gas phase fluorination for improved props. 78–52306
- MnZn ferrites, impurity induced exaggerated grain growth 78–92222
- Mo, adsorption of N_2, surface coverage and diffusion in bulk 78–60036
- Mo and Mo alloy TZM, solid-state bonding, tensile strength of bond *(German)* 79–47756
- Mo, chromizing, formation of ordered solid soln. *(Russian)* 78–11402
- Mo, compact, on H_2 permeated backing, precipitation *(Russian)* 78–27520
- Mo, diffusion and solubility of C *(French)* 79–55932
- Mo, diffusion anomalies, vacancy model *(French)* 77–43366
- Mo, diffusion of Li, Cs, vacancy and divacancy mechanisms *(Russian)* 80–70472
- Mo electrodes, in glow discharge, H penetration and diffusion 77–7629
- Mo, fatigue charact., effect of Ni and Re surface doping on mech. props. *(Russian)* 80–7660
- Mo film, electron beam deposition on Si, X-ray obs. of silicide form., diffusion processes *(German)* 77–1341
- Mo film, on Si substrates, laser irrad., cellular struct. and silicide form. 80–10710
- Mo film on Si surface, $MoSi_2$ form. conditions *(French)* 78–43270
- Mo, gas permeability (H, He, Ar) through monocrystalline and polycrystalline specimens *(Russian)* 79–60554
- Mo, H_2 diffusion enhanced by self-interstitial atoms, surface reaction const. determ. 80–75386
- Mo, impurities, interaction mechanism and saturation limit *(Russian)* 77–55358
- Mo, ion bombardment by Ni^{2+}, TEM study of damage depth distrib. 78–10101
- Mo, ionic siliciding, diffusion layer prod. 78–23855
- Mo, nitriding kinetics 80–35415
- Mo, of C 77–43384
- Mo, of H, penetration of Mo cathode in glow discharge, point defect depend. 79–41903
- Mo, of H_2, 900-1100°C *(Russian)* 78–79811
- Mo, of H(D), trapping at ion implantation induced defects 77–47622
- Mo, of Li, mechanism 78–84007
- Mo, of volatile fission products ^{140}Ba and ^{132}Te, 1400-2000K *(Russian)* 78–91485
- Mo, RF sputtered, diffusion barrier props. 78–71887
- Mo, vacancy mutation to divacancies by He trapping, percolation onset 78–51601
- Mo:C (110) surface, segregation, precip. and desorpt. of C, AES and LEED study *(French)* 80–103480
- Mo:N, ion implanted proton-irradiated, annealing behaviour 78–91362
- Mo-Al, thin film system, phase growth kinetics *(Russian)* 77–43390
- $Mo-Mo_2C-La_2O_3-Pt$ cathode, Pt effect on work function *(German)* 79–74048
- Mo-Nb, dil., impurity diffusion and vacancy-impurity binding energy of Nb and Mo impurities 80–15307
- Mo-Ni film system, diffusion reaction, phase form. 77–84999
- Mo-Si film-substrate interface, reaction on heat treatment, silicide formation 80–79999
- Mo-Ti-Zr, diffusion and solubility of C *(French)* 79–55932
- Mo-Zr, interaction with $MoSi_2$ diffusion coating, at elevated temps. *(Russian)* 79–28150
- $MoGe_2-Mo$ diffusion couple, nucleation of $Mo_{13}Ge_{23}$ *(French)* 77–55398
- MoO_3, diffusion of H_2, $H_{1.6}MoO_6$ bronze form. *(French)* 80–45247
- MoO_3, of C 77–11734
- $MoSi_2$, diffusion grown layers, texture 79–74095
- $MoSi_2$, diffusion marker for backscatt. studies of W+Mo bilayer film 78–87828
- $MoSi_2$, reactive diffusion of Si, kinetics and mechanism 77–35751
- NaCl, Born-Mayer parameters of He and Ar, interstitial interaction with neighbouring ions 80–100228
- NaCl, energy of migration of Cl^-, Br^-, I^- and F^- ions 77–43380
- NaCl, impurity precipitation and grain boundary diffusion 80–107567
- NaCl, mass transfer from sedimentary deposit layer to stationary water region *(Japanese)* 77–25700
- NaCl, of ^{54}Mn, isothermal diffusion 77–47625
- NaCl, of Pb^{2+}, activation energy for clustering of Pb^{2+} vacancy pairs 77–72610
- NaCl polycryst. containing Al_2O_3 dispersion, diffusive creep 80–97531
- NaCl:H (Cl) interstitials repulsive parameters from electronic charge density overlap, diffusion 77–59006
- $NaCl:OH^-$, additively coloured, form. and decay of defect clusters and elec. double layers, Au decoration obs. 79–10850
- NaCl-KCl, interdiffusion and demixing, electron microprobe anal. *(French)* 80–54444
- NaCl-KCl system, interdiffusion, miscibility, Kirkendall effect 80–107568
- $NaCl(:CdCl_2)$, sintering in air, densification kinetics and mechanism 77–4750
- NaMgA zeolites, diffusion anomaly of n-alkanes *(German)* 79–77817
- $Na_2O-Al_2O_3-SiO_2$ glass, He migration 77–7902
- $Na_2O-Al_2O_3-SiO_2$ glass, of Ca and Mg, SIMS study 79–82387
- $Na_2O-Al_2O_3-SiO_2(-K_2)$ glasses, ion exchange kinetics and interdiffusion mechanisms 80–80003
- $Na_2O-B_2O_3$ glass, covered with PbO film, deep penetration of Pb^{2+} ions 78–79535
- $Na_2O-B_2O_3$ glass, Na and Ag diffusion, elec. cond. 79–51300
- $Na_2O-CaO-SiO_2$ glass, effect of phase on liquids and gas diffusion *(German)* 80–38931
- $Na_2O-CaO-SiO_2$ glass, leaching studies by sputter-induced photon spectrometry 80–80004
- $2Na_2O-CaO-XSiO_2$ glass, He mobility, interconnectivity, miscibility limits, effect of morphology 78–67864
- Na_2O-SiO_2 glasses, water reactions at elevated temps. and press. 80–81312
- $Na_2O.2SiO_2$ glass, diffusion of Ag into surface layer from $AgNO_3$ melt 80–44371
- Na_2WO_4, solid electrolyte, diffusion, electromigration of Ag^+ ions in $Ag/Na_2WO_4/Ag$ cell 77–1255
- Nb alloy, oxidation protection from $MoSi_2$ coating, diffusion-slip casting appl. method 80–21187

diffusion in solids continued

- Nb alloys, diffusion and trapping of O_2 79–77816
- Nb coated Mo, Ti, evaporation, carburisation and diffusion behaviour 77–44410
- Nb, Debye-Waller factor and H_2 diffusion, neutron spectroscopy study 79–37881
- Nb, diffusion and trapping of O_2 79–77816
- Nb, diffusion anomalies, vacancy model *(French)* 77–43366
- Nb, diffusion coeff. of O meas. 77–90390
- Nb, diffusion constant of H, anomalous temp. depend., quasielastic neutron scatt. 77–43381
- Nb, diffusion of H, influence of H-H pairing, jump model 78–75878
- Nb, diffusion of H, neutron radiography meas. 77–39696
- Nb, diffusion of interstitial O_2, sink/barrier phenomena 79–60553
- Nb, diffusion of N, alloying additions and struct. defects effect 79–55938
- Nb, diffusivity of O, N, exam. 78–51741
- Nb, electron irradiated, muon diffusion 80–80668
- Nb film on Si, Ar ion bombard., $NbSi_2$ form. 80–10709
- Nb foils, coated with H-permeable Pd film, AES and SIMS 79–52467
- Nb foils, polycryst., proton irrad., diffusion of nuclear react. products *(German)* 77–35756
- Nb, H_2 diffusion, low temp. recovery 79–73342
- Nb, incoherent struct. factor of H, neutron scatt. exam., quasielastic energy spectrum 79–99186
- Nb, isotope effect for H diffusion 78–6182
- Nb, isotope effects for H_2 diffusion, crystal field stabilisation 80–59728
- Nb, low temp., diffusion of H and D from quenching and annealing study 80–6555
- Nb, muon diffusion, μ^+SR meas. 78–39487
- Nb, muon diffusion at low temp., effect of nuclear elec. field gradients 77–52005
- Nb, muon diffusion in presence of traps 79–56684
- Nb, muon location and diffusion, μSR 79–56693
- Nb, muon spin depolarisation, trap effects 79–56683
- Nb, $muon^+$ depolarisation rate, anomalous temp. depend. 78–48104
- Nb, NMR study up to 1700K, Knight shift and spin-lattice relax. time impurity diffusion activation energy 80–2653
- Nb nitriding, high-temp., kinetics and mechanism *(Russian)* 79–74300
- Nb, nitriding kinetics 80–35415
- Nb, of ^{95}Zr, diffusion coeff., effect on Nb self diffusion isotope effect 78–47602
- Nb, of Fe, Co and Ni, radiotracer and electron microprobe meas. 77–76615
- Nb, of Fe, effect on self diffusion 77–84992
- Nb, of Fe, mechanism 78–47590
- Nb, of H, book contrib. 79–82390
- Nb, of H, D, electromigration measured by resistance method 79–23783
- Nb, of H, lattice distortion and migration energy of H impurities 78–30796
- Nb, of H and D, diffusion coeff. at high concs., Gorsky effect meas. 78–26731
- Nb, of H_2 *(Japanese)* 78–10221
- Nb, of H(D), trapping at ion implantation induced defects 77–47622
- Nb, of O, interstitial diffusion coeff., effective charge *(German)* 77–35759
- Nb, of O and N from internal friction meas. 77–89586
- Nb, of O_2, 550-1100°C 78–2298
- Nb, proton diffusion, NMR obs., 120-480K 80–34812
- Nb, pure and O doped, muon diffusion and trapping 79–56685
- Nb, resistivity studies of interstitial He mobility 79–14800
- Nb, review of neutron radiography results 78–59961
- Nb, spin polarised μ^+ meas., localisation and thermal diffusion 78–39489
- Nb, spreading kinetics of Sn-Cu film and reactive diffusion *(Russian)* 77–80680
- Nb thin foils, surface segregation during sputtering at elevated temps., Auger study 80–54386
- Nb:N, H, atomic tunnelling of interstitial pair, specific heat meas. 78–47600
- Nb-Fe, formed on laser irradiation of Nb-Fe interface, Mossbauer spectra *(Russian)* 79–60560
- Nb-Ge system, reaction diffusion, electron probe anal. 79–28152
- α-Nb-H, thermal neutron scatt., general multisublattice jump diffusion model 77–66046
- Nb-H system, local frequency spectrum, mean thermal displacement of H 80–59604
- Nb-Mo(Ti)(Zr), nitriding, diffusive saturation, lattice spacing and activation coeffs. *(Russian)* 80–21168
- Nb-N, of H, incoherent neutron scatt., interstitial effects 79–60558
- Nb-O, Snoek mechanism and long distance diffusion under strain ageing *(French)* 77–81279
- Nb-Ru(Pd), dil., impurity diffusion and vacancy-impurity binding energy of Ru and Pd impurities 80–15307
- Nb-Sn, reactive diffusion *(Russian)* 77–20133
- Nb-Ta alloys, H diffusion at 296K 80–84329
- Nb-W-Mo-Zr (5, 2, 1 wt.%), surface-layer struct. and mech. props., effect of O_2 diffusion saturation 79–5087
- Nb-Zr, of O_2, 550-1100°C 78–2298
- Nb-Zr (1 wt.%), D_2 diffusion coeffs., 923-1148K 77–84991
- Nb-Zr (1 wt.%), internal oxidation state of O_2, dispersion hardening by diffusion alloying, X-ray diffr. and internal friction *(Russian)* 79–70102
- Nb_3Au, supercond. diffusion layer prep. 79–1834
- $NbBe_{12}$, by diffusion saturation in vacuum, resistance to heat 78–44259
- NbC, and NbC-ZrC solid soln., prep. by impregnation, strength, surface submicrocracks 77–16661
- NbC coating on C steel and Armco Fe, deposition, struct. and props. 79–52462
- NbC single cryst., Vickers microhardness, slip mechanism 80–71732
- $NbC_{0.89}$, implantation or diffusion of C rel. to supercond. transition temp. 77–69442
- $NbFe_2$ layers form. by diffusion during Nb wire drawing 79–28153
- Nb_3Ge films, prep. by DC sputtering and solid state diffusion, supercond. props. and struct. 79–38212
- Nb_3Sn, effect of diffusion couple Sn content on superconductivity 79–61009
- Nb_3Sn, monofilaments, radiation-enhanced diffusion growth, crit. current density 80–65758
- Nb_3Sn, stabilized multifilamentary superconductor, internal Sn diffusion process 79–61749

diffusion in solids continued

- Nb_3Sn supercond. tape substrate structural changes 79—33373
- Nb_3Sn, superconducting formed from Cu-Sn alloy, Sn diffusion in Cu 79—42709
- Nb_3Sn superconductors, Kirkendall voids, effects on mech. and supercond. props. 79—33429
- Nb_3Sn superconductors, mech. behaviour, diffusion *(German)* 78—39880
- Ni alloy, crevice corrosion by water vapour, CO, methane in HTR coolants, model 77—25202
- Ni alloy, of aluminide coating, spontaneous form. of diffusion barrier *(German)* 78—71886
- Ni alloy, ZhS6K, diffusion layer form. on Nb addition, struct., comp. *(Russian)* 78—56814
- Ni alloy 718, creep crack growth 77—63776
- Ni alloys, aluminising, thermodynamic anal. of phase transforms. 80—76413
- Ni aluminisation, soln. of binary multiphase diffusion problem allowing for variable diffusivity 77—16744
- Ni, B-containing diffusion layer formation *(Russian)* 77—48570
- Ni, B-containing multicomponent diffusion layer formation *(Russian)* 77—44400
- Ni base superalloy, single crystal, apparent and effective creep parameters, incubation period 77—63715
- Ni, compact, on H_2 permeated backing, precipitation *(Russian)* 78—27520
- Ni, deuteron diffusion obs. by D(d,p)T reaction *(German)* 77—59150
- Ni, diffusion and solubility of S *(Russian)* 80—70465
- Ni, diffusion coeffs. calc. for H and D *(Russian)* 78—91483
- Ni, diffusion of D, isotope effect, elec. resistivity meas. 79—86928
- Ni, diffusion welding, migration of oriented intergranular boundary with pores *(Russian)* 80—84943
- Ni, dislocation struct formed by C diffusion in single crystals, electron microscope obs. *(Japanese)* 78—10053
- Ni, dynamic rearrangement of atomics in large cluster using Frohlich-Raimes method 78—30586
- Ni, effect of plastic deform. and martensite transformation on Fe atom mobility *(Ukrainian)* 78—55974
- Ni ferrite, gas phase fluorination for improved props. 78—52306
- Ni foil, of H_2, surface states and thermo EMF 78—91674
- Ni, H diffusion in H_2 quenched sample, elec. resist. recovery 78—2299
- Ni, H diffusion in imperfect lattice, annealing and cold rolling effect 80—49425
- Ni, H permeability using permeation method *(Japanese)* 78—51740
- Ni, H-charged cold-worked, internal friction peak 80—107368
- Ni, internal friction near Curie temperature 78—44163
- Ni, interstitial diffusion of C in single crystals, stress distrib. changes 77—47626
- Ni, magnetic aftereffects of H isotopes, book contrib. 79—82835
- Ni, of Ag, In, Sn and Sn, activation energies, expt. and by Le Claire method *(Russian)* 79—99369
- Ni, of Ag, volume and grain-boundary, diffusion parameter temp. depend. meas. *(Russian)* 78—67863
- α-Ni, of C, high temp. vacuum metallography investigation *(Russian)* 77—72718
- Ni, of D, diffusion coeff. calc. from depth profile meas., using D(d,p) 79—5202
- Ni, of H, book contrib. 79—82390
- Ni, of H, D and T 79—77823
- Ni, of H, permeability and diffusivity *(Japanese)* 78—66345
- Ni, of H, recovery of quenched-in solute H 77—62673
- Ni, of H *(Japanese)* 78—51739
- Ni, of H_2 in single- and polycrystals at 60°C grain boundary effects *(German)* 80—2211
- Ni, of In, temp. depend. *(Russian)* 78—75880
- Ni, oxidation kinetics, influence of intermediate annealing treatment 80—89412
- Ni, positive muon diffusion 79—56688
- Ni, positive muons as light isotopes of H, book contrib. 79—82907
- Ni, self-diffusion and vol. diffusion coeffs. of Co and W, 1050 to 1400°C *(Russian)* 79—28147
- Ni, transport of H, effect of plastic deformation 80—21044
- Ni, vol. diffusion of As, 970-1360°C *(Russian)* 80—29218
- Ni whiskers, diffusion parameters of Zn, 750 to 950°C 77—66101
- Ni:C, H(D), isotope effects of C-H and C-D complexes 77—20129
- Ni:Cr, He^+ radiation-enhanced diffusion and segregation effects of point-defect trapping 79—77824
- Ni:Mn, radiation-enhanced diffusion, effect of point defect fluxes 77—89588
- Ni/Fe layers, interdiffusion, Auger sputter profiling obs. 79—46848
- Ni/Pt double layers on Si substrate, silicide formation 78—84010
- Ni-Al, (2 and 6 wt.%), oxidation, α-Al_2O_3 growth, microstruct., precip. 80—108626
- Ni-Al, diffusion coeff. differences, rotating-disc determ. 80—39330
- Ni-Al (0.5 wt.%), microstruct. formation during internal oxidation, effect of additional microalloying *(Russian)* 77—80650
- ζ Ni-Al system, solid soln., interdiffusion *(Japanese)* 80—70476
- Ni-Cr, Ni rich, discontinuous precipitation *(German)* 79—91653
- Ni-Cr (20 wt.%), oxidation, 800 to 1300°C, effect of volume and intergranular diffusion *(French)* 77—86228
- Ni-Cr (25 to 40 wt.%), transport numbers of alloy components determ. 77—62667
- Ni-Cr/Au films, interdiffusion processes and oxidation phenomena 80—59735
- Ni-Cr-Al, protective coating, exam. of interdiffusion kinetics, development of analysing procedure 79—5085
- Ni-Cr-TaC eutectic-like composite, obs. of interfacial diffusion by high resolution TEM 79—4432
- Ni-Cr-W, oxidation behaviour in air at 1000-1250°C 80—89407
- Ni-Cr(Fe)(Cu) alloy, matrix effect in SIMS anal. using ${O_2}^+$ primary beam 80—76576
- Ni-Cu, high temp. compatibility with pyrolytic C 79—65261
- Ni-Cu (30 at.%), H(D) penetration, reversed kinetic isotope effects 77—43387
- Ni-Dy, annealing behaviour of implantation damage, Dy outdiffusion, TEM obs. 77—77505
- Ni-Fe, magnetic aftereffects of H isotopes, book contrib. 79—82835
- Ni-Fe_3O_4 system, interdiffusion 79—69301
- Ni-Fe-H and Ni-Co-H, hydride formation in high press. range 80—65235
- Ni-In, ion-implanted, impurity defect interaction and diffusion, Rutherford backscatter and TDPAC expts. 80—34039

diffusion in solids continued

- Ni-MO, phase boundary motion kinetic during interdiffusion *(Russian)* 79—60559
- Ni-Mn, permeability, diffusion and solubility of H 80—107573
- Ni-Mn (10~40 wt.%), γ solid soln., interdiffusion 80—100366
- γ-Ni-Mn solid soln., interdiffusion 1073 to 1323K *(Japanese)* 79—99374
- Ni-Mn-Cu, interdiffusion at 1173K *(Japanese)* 79—99375
- Ni-Nb_2O_5, fibrous composite, aligned in situ growth by preferential internal oxidation 78—6879
- Ni-Se interface, reactive diffusion, electronic struct., UPS study 78—51748
- Ni-Si film system, silicide first phase form., reaction kinetics 78—79821
- Ni-Si film-wafer interface, marker motion in Ni_2Si formation 77—89593
- Ni-Si interface, NiSi formation from Ni_2Si, Pt marker study 78—87830
- Ni-Si:Cr, He^+ radiation-enhanced diffusion and segregation effects of point-defect trapping 79—77824
- Ni-SiC coating adhesion to Al alloy, metal interdiffusion *(Russian)* 80—66697
- Ni-steel U8 system, struct. defects effect on interdiffusion 80—15314
- Ni-thoria dispersed (2 vol.%), meas. and eval. of H_2 trapping by permeation technique 79—60555
- Ni-Ti thin film, phase growth kinetics due to diffusive processes *(Russian)* 77—72722
- Ni-V, interdiffusion coeffs. in phase transform. range, 810-1175°C *(Russian)* 78—91490
- Ni-V, solid soln., diffusion and thermodynamic props. 80—65278
- Ni-V system, interdiffusion, kinetics of phase growth *(Russian)* 80—29230
- Ni-W (2%), Mg diffusion meas., 970-1330K, appl. of vapour collect and AES method 78—75876
- α-Ni-Zn, solid soln. diffusion annealing effect *(Japanese)* 80—34255
- Ni-Zn diffusion couple, annealing and reaction diffusion *(Japanese)* 78—51749
- β-NiAl, oxidation, α-Al_2O_3 growth and microstruct. 80—108627
- Ni_2Al_3/Ni(NiAl) substrates, interface diffusion *(French)* 80—35127
- Ni_3Fe, change of H_2 diffusivity with order-disorder transformation 80—59729
- $NiFe_2O_4$+ZnO, powders, cation mutual diffusion coeffs. calc. 77—15635
- $Ni_{98}M_2$, M=impurity metal, formation of MH(D)-complexes 80—65236
- Ni_3Mn, change of H_2 diffusivity with order-disorder transformation 80—59729
- NiO, diffusion of ^{35}S by two different modes 80—59720
- NiO, of ^{35}S 77—15629
- NiO, of Cr_2O_3, calc. of kinetic parameters for spinal formation via solid state reaction 78—34644
- NiO, of Ga^{3+}, influence on reaction rate of $NiGa_2O_4$ spinel form. *(German)* 78—22894
- NiO, single cryst., of S 78—95186
- NiO-Al_2O_3 reaction at film-substrate interface, Rutherford backscatt. obs. 80—59733
- NiO-Al_2O_3 system, concurrent meas. of vol., grain boundary and surface diffusion coeff. 77—55399
- NiO-ZnO, solid solution, exam. of mechanism and kinetics of reaction with Fe_2O_3 ferrite formation 80—3309
- Ni_3Pt, change of H_2 diffusivity with order-disorder transformation 80—59729
- No, $H_2(D_2)$ diffusion model, quantum rate theory for symmetric double well pot. 78—55970
- ^{16}O, diffusion profile determ. in natural feldspars by ion analyser *(French)* 77—55400
- ^{18}O, diffusion profile determ. in natural feldspars by ion analyser *(French)* 77—55400
- P_2O_5-glass, of Cu^+ ion, fluoresc. meas. 78—59980
- Pb and Pb alloys, interstitial substitutional model for anomalous diffusion 80—84330
- Pb, atom size effect in tracer diffusion 78—84005
- Pb, diffusion and saturation solubility of Pt, melting curve, conc. profiles 80—88365
- Pb, impurity diffusion and self-diffusion activation volumes 80—2209
- Pb, ion implanted, diffusion of Co, exam. by activation analysis 78—91488
- Pb, of ^{64}Cu, electromigration, thermomigration, and solubility 78—71882
- Pb, of Au, ultra-centrifuge study 78—47593
- Pb, of Hg and Cd diffusion at high press. 77—72721
- Pb, of Sn, press. effect up to 30 kbar 78—10224
- Pb, of Zn, pressure effect on diffusion and solubility 77—43385
- Pb-Ag(Pd), diffusion of Au, de-enhancement by impurities 80—19990
- Pb-Au (0-0.0918 at.%), lattice parameter changes due to Au dissolution 79—77558
- Pb-Au (2.5 wt.%) film, In diffusion, alloy form. 78—22899
- Pb-Cd dilute alloys, conc. depend. of Cd diffusivity enhancement 79—73348
- Pb-In/Pb couple, FCC, Kirkendall interdiffusion, conc. depend. 77—39702
- Pb-Tl, sliding and its accommodation during creep and superplasticity 77—40436
- PbF_2:Mn, mag. tagging of ion diffusion, ^{19}F NMR meas. 80—108106
- PbO film, on vitreous SiO_2, interdiffusion reactions, UV spectroscopy obs. 78—51750
- PbO film on Na_2O-B_2O_3 glass, interdiffusion layer 79—51318
- PbO thin layers on PbO-SiO_2 glass, reaction behaviour 78—34660
- PbO:Ag film, X-ray stimulated diffusion, current-voltage characts. 77—80653
- PbO-SiO_2 interdiffusion layer optical waveguide, prep. and props. 80—43489
- PbS, hot-pressed compact, elec. behaviour, adsorbed atmos. gas effects 77—66601
- $PbS_{1-x}Se_x$ diode laser, contact degradation due to diffusion 80—102734
- n-PbSe, heterodiffusion of Sn 80—34245
- $Pb_xSn_{1-x}Se(Te)$ film, Bi and Tl impurity dopant incorporation and diffusion during MBE growth 79—66012
- $Pb_{1-x}Sn_xTe$, Cd-In diffusion, changes in elec. props. 78—91348
- $Pb_{1-x}Sn_xTe$, diffusion of Cd, Hall effect, cond. and solubility meas. 79—69292
- $Pb_{1-x}Sn_xTe$ diode laser, contact degradation due to diffusion 80—102734
- $Pb_{1-x}Sn_xTe$:Cd, Cd diffusion obs. using Hall mobility and Cd solubility expts. 78—26584
- $Pb_{1-x}Sn_xTe$-PbTe heterojunction, Sn diffusion and elec. effects of dislocations, elec. and metallurgical expts. 77—89839

diffusion in solids continued
$Pb_{1-x}Sn_xTe$-PbTe heterojunction, Sn diffusion profile, X-ray diffr. data interpretation 78—51832
PbTe, diffusion of Ag, effect of gamma irradiation 80—59515
PbTe, diffusion of Cd, Hall effect, cond. and solubility meas. 79—69292
PbTe film, Bi and Tl impurity dopant incorporation and diffusion during MBE growth 79—66012
PbTe:Cd, Cd diffusion obs. using Hall mobility and Cd solubility expts. 78—26584
Pd alloys, effect of alloying on activation energy of H_2 diffusion 80—107571
Pd, diffusion coeffs. calc. for H and D *(Russian)* 78—91483
Pd, film, electrical resist., influence of hydrogenation 77—85348
Pd film, high dose Si^+ ion implantation, silicide phases, backscatter spectra 80—19820
Pd film, on Si substrate, laser irrad., cellular struct. and silicide form. 80—10710
Pd film on Si, Xe ion beam induced form. of PdSi 80—10800
α-Pd, H_2 diffusion by galvanostatic charging 78—84001
Pd, $H_2(D_2)$ diffusion model, quantum rate theory for symmetric double well pot. 78—55970
Pd, H(D) interstitial interactions rel. to diffusion and ordering transition 80—34249
Pd, motion of H and D, thermodynamic data 79—65254
α-Pd, next-neighbour jumps of H in quasi-elastic neutron scattering 78—91487
Pd, of H, book contrib. 79—82390
Pd, of H, effect on mechanical props. 79—65138
Pd, of H, model 79—73338
Pd, of H_2, 496 to 946°C 79—77815
Pd, of H_2, elastic energy dissipation peak 80—60905
Pd, of H_2, induced elec. pot. meas. *(French)* 77—43379
Pd/Si interface, chem. and struct. props. during silicide form., AES and TEM obs. 80—49430
Pd-Ag, of H_2, elastic energy dissipation peak 80—60905
Pd-Ag (25 at.%) H_2 permeability and solubility, comparison with other Pd solid soln. alloys 79—23738
Pd-Ag(V), H mobility and solubility, appearance pot. spectra obs. 80—55231
Pd-Ce (5.75 at.%), H_2 permeability and solubility, comparison with other Pd solid soln. alloys 79—23738
Pd-Fe (1 wt.%), alloy component surface conc. changes kinetics under vac. sputtering and volatilisation *(Russian)* 79—60608
Pd-H, of H_2, Mossbauer study of local environment of substitutional Co and Fe impurities 80—60475
Pd-H, solid soln., excess entropies, variation of H solubility with pressure 79—46846
Pd-H and Pd alloy-H systems, review of props., book contrib. 80—24605
Pd-H system, local frequency spectrum, mean thermal displacement of H 80—59604
Pd-Ni, spin fluctuation alloy, thermopower peak diffusion origin 80—88542
Pd-Ni-H, hydride formation in high press. range 80—65235
Pd-Pt, of H_2, elastic energy dissipation peak 80—60905
Pd-Pt, of T, effect on freq. factor and activation energy 78—63880
Pd-Rh-H and Pd-Ni-H, hydride formation in high press. range 80—65235
Pd-Si (111) interface, microscopic Pd_2Si form., UPS obs. 80—24743
Pd-Si layers, form. by laser irrad. of Pd film on Si substrate 79—99438
Pd-W (20 wt.%), permeability, diffusion, and solubility of H_2, elec. resist., heat treatment effects *(Russian)* 79—51307
Pd-Y (8 at.%), H_2 permeability and solubility, comparison with other Pd solid soln. alloys 79—23738
$Pd_{0.7}$, D spin-lattice relaxation time, D quadrupole coupling, D atom diffusion 79—73844
$Pd_{0.9}Ag_{0.1}$, motion of H and D, thermodynamic data 79—65254
$(Pd_{80}Au_7Si_{13})/Fe_{30}$, compositionally modulated amorphous film, diffusion, struct. relax. 80—103518
$Pd_{77.5}Cu_6Si_{16.5}$ metallic glass, diffusion of Au 78—55983
β-PdH_x, diffusion-induced reduction of ^{57}Fe Mossbauer fraction 80—108131
α-PdH_x, impurity motion, neutron scatt. obs. 80—24682
PdH_x:Co(Fe), diffusion and interstitial site occupancy, Mossbauer spectra 80—20555
Pd_2Si, form. by laser irrad. of Pd film on Si substrate, Rutherford backscatt. obs. 79—42317
$(Pd_{85}Si_{15})_{61}/(Fe_{85}B_{15})_{39}$, compositionally modulated amorphous film, diffusion, struct. relax. 80—103518
Pt, diffusivity permeability and solubility of H_2 79—95170
Pt electroplated film, Schottky barrier metallisation, Au diffusion, AES obs. 79—14968
Pt membranes, of H_2, diffusion at high press. and temps. 78—55984
Pt, of ^{199}Au, diffusion at low temp. 78—30789
Pt, of H, diffusivity and diffusion-elastic phenomenon 79—51310
Pt-(Re-Mo) bimetal sheet specimens, interdiffusion, 1500°C *(Russian)* 77—62683
Pt-Al (22 wt.%), elec. props. of growing alumina scales 79—20282
Pt-Au film couple, diffusion of Au, depend. on annealing ambient, AES exam. 77—1261
Pt-Cr(Si) interface, low-temp. diffusion, ambient effects 80—100355
Pt-GaAs contacts, sintered, eval. of W, Ti, Mo and Hf barrier metals 77—8193
Pt-Mo bimetal sheet specimens, interdiffusion, 1500°C *(Russian)* 77—62683
Pt-Ni vacuum condensates on Si and SiO_2, thermally treated, X-ray anal. *(Russian)* 80—70559
Pt-Re bimetal sheet specimens, interdiffusion, 1500°C *(Russian)* 77—62683
Pt-Si film system, silicide first phase form., reaction kinetics 78—79821
Pt-Si layers, form. by laser irrad. of Pt film on Si substrate 79—99438
$Pt_{90}Rh_{10}$/Pt thermocouple, Inconel sheathed, MgO-insulated, decalibrations during 1200°C use, ion microprobe obs. 78—57957
PtSi film, form. problems, diffusion coeff. of Si 80—100782
PtSi, growth under protective layers on Pt covered Si substrates, X-ray diffr. and Rutherford backscattering anal. 78—22965
Pt_2Si, and PtSi, growth rate for form. by Pt film deposition under ultrahigh vac. and controlled impurity atm. 80—65388
Pu, of Co in FCC and BCC phases, diffusion coeff. and mechanism 77—28046
Pu-Cu, of T, effect on freq. factor and activation energy 78—63880

diffusion in solids continued
PuO_{2-x}, O_2 chem. diff., dilatometry and thermogravimetry study *(French)* 79—73339
RbCl, of $^{20}Ne(^{22}Ne)$, isotope effects 78—18841
RbCl, of $^{3}He(^{4}He)$ isotope effects 78—18841
RbCl-KCl powder blends, diffusional homogenisation, X-ray diffr. exam. 78—18847
Re, polycryst., of adsorbed C *(French)* 77—28075
Re-Mo bimetal sheet specimens, interdiffusion, 1500°C *(Russian)* 77—62683
Rh-Si thin film interaction, interdiffusion, temp. depend. 80—54443
Rn diffusion through inactive rock sections 77—5194
^{222}Rn diffusion through U mill tailings covers, coeff. meas., lab. techniques 80—95387
RuO_2 porous powder electrodes, proton diffusion meas. 80—54436
Sb:Te vapour saturation, diffusion zone struct. crystallisation orientation *(Russian)* 80—54438
Sb-Sn (8 at.%) alloy, grain boundary migration, intergrain liq. layer effects *(Russian)* 77—15633
Se film, metal ion diffusion during memory switching 78—26976
Se films, Ag diffusion, effect on interferometric thickness meas. 80—96695
Se, of Ag, role of Ag in switching effect in amorphous Se 78—19163
Si (111)-Au interface, chemically driven intermixing, UPS study 80—50533
Si, amorphous, film, hydrogenation by H diffusion, effect on elec. cond., band gap *(Korean)* 80—45326
Si, amorphous, hydrogenated, of D_2, SIMS anal. 78—75877
Si, amorphous, hydrogenation using DC and HF plasma treatment 80—59497
Si, amorphous, thin film reaction with Pd, metal-rich silicide formation 80—2284
Si, amorphous layer prod. by ion implantation, diffusion broadening, ESR study 80—92552
Si, Au diffusion enhancement by photo- and electron irrad. 77—27901
Si, B impurity diffusion, separation factor estimation 79—86926
Si, comparison of interactions between sequential Ga-P and Ga-As diffusions 77—80655
Si, Czochralski grown, oxide precipitates, diffusion-limited growth 80—97484
Si, Czochralski-grown cryst., swirl defect formation and defect migration 77—76405
Si, deep diffusion of B and P, expt. results 80—54437
Si, deep planar Ga and Al diffusion 79—69290
Si, defect form. under radiation-accelerated diffusion conditions 80—19854
Si device metallisation, TiN and TaN as diffusion barriers 80—65304
Si, diffusion coefficient determ. from carrier conc. depth profile 80—107566
Si, diffusion layers, B distrib. 77—7753
Si, diffusion of B,P and Sb, implantation damage effects 78—55988
Si, diffusion of B and P, influence of dislocations 78—18840
Si, diffusion of Ga in closed capsule, surface damage elimination 78—87691
Si, diffusion of Ga through SiO_2 layer, junction depth 78—51574
Si, diffusion of impurities accelerated by γ rays 77—55394
Si, diffusion of P, dislocations, creation conditions 79—95039
Si, diffusion of P, oxidation effects 79—51309
Si, diffusion of P from spin-on SiO_2:P film 80—2050
Si, diffusion of self-interstitials and As, B and P, radn.-enhanced 80—29216
Si, diffusion of transition elements, anomalous behaviour 80—29044
Si, diffusion profiles, P and B diffusion determ. *(Rumanian)* 79—77615
Si, diffusion-induced lattice strain and dislocation obs. by X-ray diffraction *(Japanese)* 77—84753
Si, dislocation free, C and O impurity clouds, heat treatment influence on light scatt. 80—6427
Si, doping, low temp. radiation induced impurity diffusion 77—15439
p-Si, doping by Ti diffusion 78—18670
Si, doping impurity distrib., during cryst. growth by Czochralski method *(Russian)* 80—100276
Si, doping process, effect of disloc. density *(Hungarian)* 77—62553
Si, epitaxial film on sapphire, optical absorption and interface comp. profiles 77—12459
Si epitaxial layers, vacuum deposited, conditions for impurity migration from B, P, Sb doped sources *(Russian)* 80—107570
Si, etching by CF_4, plasma deposition reactor gas phase characts., mass spectra 80—70566
Si, feeding-in and blocking of 2 MeV protons, simple diffusion model 78—22782
Si, gettering effects *(Japanese)* 79—83356
Si, He impurity props. investigation by EHT calcs. 79—99183
Si, implanted crystal, laser induced annealing and diffusion behaviour 80—88202
Si impurity diffusion through SiO_2 layer, physicochemical processes *(German)* 78—2149
Si, interactions between sequential dopant diffusions, review 77—27900
Si, ion implanted Kr migration during anneal 78—18834
Si, ion-implantation damage, annealing using pulsed-electron-beam 79—55768
p-Si, low temp. defect prod., obs. by thermally stimulated capacitance technique 77—84801
Si, masking effects of Sb diffusion, from doped oxide source 77—15437
Si, migration of Au, electron bombardment effects 80—100362
Si minority carrier lifetime degradation effect of $POCl_3$ emitter diffusion 77—76917
Si, minority carrier lifetime degradation by $POCl_3$ emitter diffusion 78—2496
Si, mobility of segments of dislocation loops, model of nonconservative dislocation motion 78—18647
Si, models for irradiation effects on impurity diffusion 77—80654
p-Si, monocryst., diffusion of As, Henry const., temp. depend., 1448 to 1523K 79—42399
Si, monocryst. plates, purification by thermal diffusion, impurity migration anal. 80—25553
p-Si, Na impurity diffusion, ion irrad., defect form. effects *(Russian)* 77—43386
Si, of ^{71}Ge and ^{32}P, effect of dislocation struct. on migration rate 77—51551
Si, of AS, TEM obs. 77—63674
Si, of Al, open-tube high-vacuum method 78—6084

diffusion in solids continued
  Si, of As, from As-doped oxide source 77—47477
  Si, of As, from doped polycryst., conc. depend. 78—34656
  Si, of As, laser induced diffusion and annealing processes 77—69943
  Si, of B, from CVD BN covered with Si_3N_4, appl. to master slice p-MOS IC 80—107564
  Si, of B, in oxidised atmosphere, minicomputer model *(Rumanian)* 79—82247
  Si, of B, rel. to B autodoping during epitaxy from SiH_4 77—47476
  Si, of Li, photostimulated using concentrated solar rays 77—51544
  Si, of Na, retarding action of radiation defects on diffusion 77—1140
  Si, of Ni below 475°C, role of defects 79—51319
  Si, of nitrogen during annealing, effects on ion implanted layers 77—24436
  Si, of O, coeff. from optical absorpt. 79—69294
  Si, of Os, diffusion parameters using photocapacitance and four-probe methods 79—51314
  Si, of P, 900-1150°C, controlled surface conc. condition 77—7746
  Si, of P, elastic deform. relax. and dislocation generation 80—79997
  Si, of P, mechanism, migration channels along vacancies and interstices 80—79996
  Si, of P(B)(As), proton enhanced diffusion and vacancy migration 78—67747
  Si, of Sb, along dislocations, 1165-1320°C 77—15631
  Si open tube system, diffusion of Ga 80—19822
  Si, open-tube P diffusion kinetics 79—33117
  Si, oxidation, oxidation-induced lattice defects, review *(Japanese)* 78—39931
  Si, oxide scale microstruct. of oxidised single cryst. 80—108613
  Si, P diffused sample, stacking faults and dislocations formation from interstitials 78—95059
  Si, polycryst., lateral diffusion of B, influence on submicron MOST fabrication 78—26588
  Si, polycryst. film doping during deposition and with diffusion 78—6088
  Si, polycryst. rods, p-n junction appls. and transport props. 79—99612
  Si, polycrystalline, solar cells, grain-boundary hydrogenation technique for improvement 80—85273
  Si, precipitation of Au, supersaturated soln., Hall effect meas. 77—89465
  Si, radiation-stimulated dissociative diffusion of Au, model 79—23785
  Si, radiation-stimulated vacancy diffusion, mechanisms 77—55396
  Si, rel. to oxidation stacking faults and microdefects, growth behaviour during high temp. annealing 78—72901
  Si, Schottky diode ageing, influence of metal electrode O diffusion coeffs. 79—99620
  Si, self- and impurity diffusion 80—29213
  p-Si, self-interstitials, influence of white light on annealing process *(German)* 79—19245
  Si, SiO_2 diffusion sources under oxidising ambient conditions, solar cell fabrication 78—2148
  Si single crystal, Ni pseudodiffusion, AES obs. 78—2396
  Si solar cells, diffusion fabrication process, low cost, highly automated 80—30487
  Si solar cells, realisation by laser induced diffusion of deposited Sb 80—93998
  Si solar cells, solid source diffusion process for fabrication 80—93994
  Si solubility and transport behaviour of water, dissolution 80—93801
  Si, sputtered, cluster formation, influence of HF plasma interaction 78—64441
  Si, stacking fault annihilation by impurity diffusion 77—19968
  Si, stress enhanced diffusion of B, using SiO_2 diffusion masks, photodiode fabrication 78—67865
  Si substitutional diffusion model 78—71884
  Si substrate, ion induced intermixing of Pd or Pt film 80—15420
  Si, subthreshold irrad., migration of Sn, Mossbauer obs. 77—15462
  p-Si, surface elec. behaviour after chem. treatment 80—20185
  Si surface electron beam deposited silicide formation using scanning CW laser beam 80—66862
  Si thermomigrqation of molten Ga 77—69118
  Si, thin sheet, Sb impurity profile eval. in p-n diffusion junction by anodisation and resist. meas. 79—46695
  Si, tracer diffusion of ^{71}Ge and ^{31}Si in intrinsic and doped samples 80—29214
  Si two-step impurity diffusion, effect of internal elec. field 77—76624
  Si, vacuum deposition, combined with Sb ion implantation *(Japanese)* 78—88428
  Si wafer, stresses generated by thermomigration of liquid inclusions 79—37875
  Si wafer stacking faults, preoxidation gettering by reverse side P diffusion-induced misfit dislocations 80—60988
  Si wafers, Au contamination during plasma etching 80—19831
  Si wafers, planar source diffusion system props. 77—7751
  Si: (B, P, Ge), impurity-pair diffusion, influence of elastic stresses 78—87824
  Si:Ag (Zn,Fe), diffusion mechanism of fast impurities, distrib. in surface layers 77—11735
  p-Si:Al, diffusion and incorporation of dopant in closed system, elec. props. 77—59026
  Si:Al, polycryst. film, grain boundary diffusion, Auger sputter profiling 80—75388
  Si:Al film, low-temp. diffusion of Al 78—38878
  Si:Al p-n lamellar structures, processing by molten Al rich wire thermomigration 78—10068
  Si:Al(Ga), O_2 diffusion, conc. profile meas. 80—79990
  Si:As, diffusion model, degeneracy and partial ionisation effects 80—96693
  Si:As, diffusion of implanted As induced by laser annealing 77—89590
  p-Si:As, electrochem. doping, depth profile analysis 77—72630
  Si:As, heavily As-diffused, Hall mobility and resist. rel. to carrier conc. 80—107815
  Si:As, high conc. diffusion from double-layer sources 78—10075
  Si:As, implantation into polycryst. Si and diffusion into Si substrate 77—59025
  Si:As, implanted, thermal diffusion of As 80—39352
  Si:As, ion implanted, anomalous diffusion of As 79—14842
  Si:As, relation between total and electrically active As conc. produced by diffusion 79—55773
  Si:As, shallow junctions by high-dose implants 80—96694
  Si:As ion implanted, laser induced diffusion modelling 80—24672
  Si:As laser annealing, heat and mass transport model 80—92546
  Si:As(P), oxidation-enhanced diffusion of impurities 79—46840

diffusion in solids continued
  Si:As(Sb), implanted, pulsed ruby-laser annealing, Rutherford backscatt., TEM and ion channelling study 79—86805
  Si:Au, diffusion of Au anal. 79—23786
  Si:Au, effect of C concentration 78—10076
  Si:Au, impurity capture cross section and generation lifetime determ., MOS expts. 78—91772
  Si:Au, impurity diffusion and distribution obs. by neutron activation analysis *(Japanese)* 77—84787
  Si:Au, neutron irradiated, penetration of Au into Si 78—59984
  Si:B, annealing mechanism of radiation change and dopants in pulsed laser irrad. ion implanted layers 79—46691
  Si:B, conc. depend. of B diffusion coeff. 80—39353
  Si:B, diffusion for very shallow defect free p$^+$-n junc. for solar cells 79—15218
  Si:B, diffusion from BN source with H_2 injection, AES study 80—19986
  Si:B, diffusion of As atoms from ion implanted layers, conc. profiles 77—43376
  Si:B, diffusion of B atoms and growth kinetics of oxidation induced stacking faults, correlation 79—37720
  Si:B, diffusion of B from B_2H_6-CO_2 system, lower temp. limit of 775°C 77—43232
  Si:B, diffusional impurity redistrib., elastic stress field effect *(Russian)* 77—72719
  Si:B, He$^+$ irradiation-induced diffuiion, effect on impurity distrib. 80—70470
  Si:B, heavily doped, annealing characteristics obs. *(Japanese)* 78—18666
  Si:B, high conc. effects in ion implantation 80—75245
  Si:B, implanted, effectiveness of charged vacancies in diffusion 80—34239
  Si:B, influence of proton beam irrad. on concentration profiles *(French)* 77—51402
  Si:B, ion implanted, SOS device struct., nonlinear impurity redistrib. 79—1625
  Si:B, ion implanted, structure defects formation and behaviour under annealing in various ambients 80—65033
  Si:B, ion-implantation doped, influence of radiation dose on diffusion processes 77—1141
  Si:B, lateral effect of oxidation on B diffusion 80—29217
  Si:B, low conc. B diffusion using doped-oxide film 77—76431
  Si:B, near intrinsic ⟨100⟩ and ⟨111⟩ samples, inert and oxidising ambients, diffusion, segregation 78—75882
  Si:B, P, high temp. diffusion, effects of laser irrad. on diffused layer 79—14834
  Si:B, P, long range enhancement of B diffusivity by P diffusion 80—103386
  Si:B, p-n junction form. by B deposition and laser-induced diffusion 78—87690
  Si:B, proton-irrad.-enhanced diffusion 80—29227
  Si:B, randomly implanted ion diffusion during high temp. processing 77—24439
  Si:B, with insulating coating, mechanical stress influence on B diffusion, strained surface layers 80—29224
  Si:B,P, anomalous diffusion 80—29229
  Si:B,P, diffusion patterns obs., for SiO_2 deposited by means of centrifuge *(Bulgarian)* 77—76429
  Si:B,P, high conc. diffusion without disloc. generation 78—10072
  Si:B,P, simultaneous diffusion, radioactivation techniques 77—76622
  Si:B diffusion at Si-SiO_2 interface, Auger spectra, Rutherford backscattering 80—70471
  Si:B epitaxial layer, B diffusion coeff. 79—99372
  Si:B redistribution after oxidation, integro-differential eqn. 77—76453
  Si:BF_2^+, anomalous migration of F and electrical activity of B 78—34654
  Si:BF_2^+, recrystallisation of implanted amorphous layers, F migration 79—55763
  Si:B(P), diffusion induced imperfections, laser annealing, rel. to junction characts. 78—75678
  Si:B(P), heavily diffusion-doped layers, Co diffusion 78—59982
  Si:B(P), impurity-peak form. during proton-enhanced diffusion 79—55772
  Si:B(P), proton enhanced diffusion, vacancies diffusion length 80—29226
  Si:B(P), proton-irrad., impurity uphill diffusion, vacancy mechanism 80—92719
  Si:B(P)(As), impurity diffusion from implanted layer, influence of radiation damage 77—76621
  Si:B(P)(As)(Cu)(Fe), thermal and mass diffusion calcs. 79—69148
  Si:B(Sb), deform. coeff. due to impurity diffusion 78—18671
  Si:Bi, ion-implanted, solid phase epitaxial growth during annealing, supersaturated solid soln. form. 80—103384
  Si:C(O)(Sb), striated impurity distrib. calc. in melt-grown crystals 80—24488
  Si:Co, diffused, and annealed, localisation of Co atoms, Mossbauer obs. 80—39140
  Si:Co, diffused distrib. and state of Co atoms 77—1146
  Si:Co, diffusion coeff. of Co meas. 77—20126
  Si:Co, diode minority carrier lifetime, Lax method meas., effect of Co diffusion 79—69525
  Si:Co, substitutional Co and Co precipitates, identification by Mossbauer spectroscopy 79—11631
  Si:Cr, ion implanted, Cr conc., depth distrib. and diffusion coeff. 80—49243
  p-Si:Cu, influence of Cu on diffusion of Au 77—62679
  Si:Fe, B thermally activated Fe interstitial, elec. and kinetics props. *(German)* 80—34035
  Si:Fe, EPR and neutron activation anal. of thermal defects 78—91355
  Si:Fe, solubility study by EPR and neutron activation anal. 80—75361
  Si:Ga, As, sequential diffusion, radiotracer obs. 78—10073
  Si:Ga, diffusion of impurity into cryst., doping profile 79—77621
  Si:Ga, gettering of Au and Cu during Ga diffusion 78—91350
  Si:Ga, heavily damaged, channelling investigation of diffusion behaviour 79—37877
  Si:Ga, sealed tube diffusion, Au and Cu gettering behaviour 77—76445
  Si:Ge B, strain compensation, X-ray Bragg reflexion 80—39137
  Si:H, amorphous, defect creation and H evolution 80—50392
  Si:H, amorphous, geminate recombination model for photoluminescence decay 80—71481
  a-Si:H sputtered films, ohmic contacts by H depletion, H diffusion 80—34511
  Si:H(D), amorphous films, CVD, post-hydrogenation 80—54552

diffusion in solids continued
Si:In(Sb), incorporation of implanted impurities during amorphous layer regrowth 79—55761
Si:Ir, Ir diffusion and solubility 77—15448
Si:Li, amorphous, interstitial doping by in-diffusion and implantation and elec. characterisation 78—26585
p-Si:Li, dislocation free, minority carrier lifetime, effects of heat treatment *(Japanese)* 79—65492
p-Si:Li, electrolytical doping, depth-profile anal. 79—77623
Si:Li, evaporated amorphous film, doping by in-diffusion 79—51127
Si:O, impurity solubility and diffusion props. 78—6093
Si:P, and of P diffused layers 78—38736
Si:P, anomalous doping profiles, numerical anal. 79—73206
Si:P, B diffusivity, versus Si oxidation rate 77—15436
Si:P, BF_2^+ ion implantation, anomalous carrier profiles 80—2048
p-Si:P, Cu, influence of Cu on diffusion of P meas. 77—1267
Si:P, diffusion eqn. numerical soln. 79—51311
Si:P, diffusion from ethylene glycol grown anodic oxide 77—76440
Si:P, diffusion of P, 900-1100°C, distrib. of excess vacancies 77—72631
Si:P, diffusion of P impurities stimulated by gas discharge Ar plasma, low temp. 80—6560
Si:P, diffusion-doped laser irradiation effects, electrical reactivation of P 80—39124
Si:P, diffusional doping, diffusion-induced strain and dislocation effects 79—42084
Si:P, diffusivity, strain-induced band gap narrowing, E-centres 80—29228
Si:P, doping by diffusion from phosphosilicate glass sheets *(German)* 77—39604
Si:P, electrostatic field on impurity atoms, heavy doping effects 78—51570
Si:P, emitter-misfit dislocation formation during P diffusion 78—91338
Si:P, excess vacancy generation by P diffusion *(Japanese)* 77—89460
Si:P, Ge, simultaneous diffusion processes, elastic stress influence 77—89591
Si:P, heavily doped, diffusion of Au 77—51550
Si:P, heavily doped wafer, anomalous bending obs. 78—10074
Si:P, mechanism of diffusion of P 77—7906
Si:P, quantitative model for diffusion of P and emitter dip effect 77—76611
Si:P, secondary defect generation suppression and diffusivity restraint by HCl oxidation 79—70191
Si:P, strain-induced band-gap narrowing effect on P diffusion 79—55935
Si:P,B, wafer, long range enhancement of B diffusivity induced by high surface conc. P diffusion 79—46687
Si:P bipolar transistors, interstitial supersaturation and misfit dislocation climb, TEM study 80—70203
Si:P non-Fickian diffusion, parameter depend. on doping level and impurity gradient *(German)* 80—54440
p-Si:P p-n junctions, dislocations investig. rel. to P diffusion, SEM, X-ray topography techniques 77—76433
Si:P^+, misfit dislocation net propagation due to osmotic forces 79—65108
Si:P(B), high temp. impurity diffusion via vacancies and self-interstitials 80—24667
Si:Pb, diffusion behaviour of Pb in high dose implanted Si layers during isothermal annealing 79—1525
Si:Pb, implanted and annealed, impurity redistrib. 78—75689
Si:Sb, diffusional doping by doped oxide method 80—15127
Si:Sb, high dose implanted, orientation dependent annealing effects 78—18665
Si:Sb, ion implanted, Sb diffusion during oxidation, snow-plough effect 80—88366
Si:Sb, laser doping, evaporation loss and diffusion of Sb, under pulsed laser irrad. 80—59508
Si:Sb, redistribution of thin impurity layers after laser annealing, theoretical model and expt. results 79—69147
Si:Sb,As, autodoping effect of Sb-As simultaneous diffusion 77—80522
Si:Sb vacuum deposited coating, p-n junction, pulsed electron beam annealing doping, diffusion 80—75480
Si:Se, diffusion coeff., solubility and energy level determ. 79—35825
Si:Se,B(Ga)(Al)(In), diffusion of Se, solubility and ionization levels, Hall effect and photocond. meas. 79—42486
Si:Zn, implanted atom diffusion during laser annealing 79—37725
Si/Al and Si/Al-Si(Cu), Si regrowth minimisation through overlying Al or Al alloy film 80—70569
Si/metal system, silicide form. by thin film interactions, review 80—49429
Si/Pd-W, contact reactions, backscattering, X-ray diffr. meas. 80—20040
Si/refractory metal-Ni(Pd)(Pt) interactions, phase separation 80—65303
Si/surface porous oxide film, impurity distrib. during P diffusion 77—39944
Si-Al system, Si regrowth minimisation methods in Al films 80—15384
Si-Au substrate-film system, relax. effects, internal friction meas., temp. range 20 to 900°C 78—18886
Si-Au(Rh)(In), Schottky diode, X-ray effects on elec. props., irrad. induced diffusion 77—4439
Si-B, exam. of two stage diffusion of B, under a gas phase oxide film 79—95044
Si-B, P diffusion and activity after Ar ion bombardment 78—95192
Si-B, using BN, expt. *(Bulgarian)* 78—59824
Si-borosilicate glass, B diffusion from sputtered glass film into Si 80—29040
Si-In(Rh)(Au) Schottky diodes, X-ray irradiated, radiation-accelerated diffusion of impurities in Si 78—26952
Si-Li(Au)(Cu), diffusion-induced defects, X-ray triple cryst. diffractometry 80—2213
Si-metal contacts, low temp. reactions 78—2567
Si-metal interface, silicide formation, interface marker technique obs. 80—59734
Si-Mo diffusion couples, $MoSi_2$ or Mo_3Si/Mo_5Si_3 form. 79—77836
Si-Pd-Ti, silicide form. in evaporated films 80—80006
Si-refractory metal structs., interface modification by ion implantation 80—70475
Si-Rh interface, RhSi form. by lattice diffusion 78—71891
Si-SiO_2, thermally oxidised, origin of fixed charge, Si diffusion in transition region 77—20381
Si-SiO_2 interface, Au surface state energy levels and Au diffusion 79—51652
Si-SiO_2 interface, model for doped-oxide-source diffusion with chemical reaction 77—39954

diffusion in solids continued
Si-SiO_2 interface in MOS capacitors, lateral diffusion of Na^+, neutralisation 80—92986
Si-SiO_2 structure, alkali metal ion migration and accumulation, interface struct. 80—107574
Si-transition metal interface, silicide formation, book contrib. 79—1530
SiAlON, prepared from siliceous sand and Al powder, hot pressing, steatite contamination effects *(Japanese)* 80—93528
SiC, diffusion behaviour of fission products, 1650 to 1850°C 78—79814
SiC, diffusion coeff. of Cs and Ag by post irradiation annealing of coated 78—13247
SiC, diffusion of B, elec. cond. meas. 80—96696
SiC, diffusion tracer deposition, using travelling solvent zone 78—51742
SiC, exam. of T_2 diffusion coeffs. and D_2 solubility 78—79816
SiC, of B, polytype struct. effect 78—59983
SiC, oxide scale microstruct. of oxidised single cryst. 80—108613
SiC, permeability and solubility of H_2, 1200-1450°C 80—39351
β-SiC, sintering, B transport and lattice parameter change 80—108370
SiC:B(Be), dislocation induced deceleration of impurity diffusion 77—28043
SiC:Be, film donor impurity, diffusion influence on elec. and optical props. 78—87942
Si_3N_4 film, diffusion of Al, AES and depth profiling 78—51744
Si_3N_4, film, H_2 concentration profile, chem. bonding 79—33205
Si_3N_4, reaction-bonded, internal oxidation processes role in high-temp. mech. props. 79—38915
Si_3N_4, solid-solid reactions with Fe, Ni and Mo alloys 79—28151
SiO_2 based optical fibre waveguides, water impurity 77—68270
SiO_2, CVD film, hydration props., ellipsometry meas. 78—22986
SiO_2, D-impregnated, vitreous, radiation induced isotope exchange 79—99240
SiO_2, diffusion of As, diffusivity and masking oxide thickness 80—39350
SiO_2 film, migration parameters of alkali ions, elec. meas. 80—39359
SiO_2 film, on n-GaAs, Ga content after annealing at 730-940°C neutron activation anal. 78—43255
SiO_2 films, spin-on diffusion sources, debris-induced effects 80—39465
SiO_2, MOS gate insulator, mobile K ions 77—47623
SiO_2, mobility and trapping of ions, Si-SiO_2 interface states 80—92985
SiO_2, mobility of K^+ ions, triangular voltage sweep technique 79—95206
SiO_2, of As, O_2 effects 78—43180
SiO_2, vitreous, D_2 diffusion and solubility, 0-800°C, interaction with structural OH 77—89585
SiO_2, vitreous, hydroxyl free, reaction with H, diffusion, absorpt. spectra 80—85210
SiO_2:P, diffusion from spin-on source 80—44367
SiO_2-B_2O_3-Al_2O_3-$Na_2O(K_2O)$ glasses, Ag interdiffusion, optical and NMR studies 80—24683
SiO_2-borosilicate glass, B diffusion from sputtered glass film into SiO_2 80—29040
β-SiO_2-MgO reaction, diffusion controlled 78—6882
SiO_2+H_2 reactions, rate controlling processes for H_2 transport in vitreous silica 78—26733
SiO_x, metal layer interdiffusion Rutherford backscatt. 77—85000
^{31}Si, radioactive marker in thin film silicide form. 77—62681
Si(111):Pb ion implanted amorphous layers, recrystallisation, impurity out-diffusion model *(Chinese)* 80—88363
$SmCo_5$, magnetic aftereffect of H and D 79—56573
$SmCo_5$ spheres, exam. of sintering in vacuum and Ar atmospheres 78—84738
Sn coating on Cu wire, growth of diffusion layer due to ageing effect *(Polish)* 80—34227
β-Sn, dissociative diffusion of ^{57}Fe, Mossbauer expts., 90-462K 79—7714
Sn/Au thin film diffusion couples, Kirkendall void form. 80—96698
Sn/CU electroplated bimetallic films, interfacial reaction 80—96765
SnO_2, film, diffusion of impurities *(Japanese)* 79—95218
SnO_2/n^+-pSi heterojunction solar cells, fabrication by paint-on-diffusant method 80—94048
$SrF_2:Y^{3+}$, diffusion of bound and free $F_{(i)}^-$ interstitials, NMR meas. 79—78542
SrF_2-BaF_2, interdiffusion 77—7912
$SrTiO_3$, sintering kinetics rel. to added SrF_2, ZrO_2 78—44037
^{90}Sr, diffusion in bitumen block coating, radioactive waste treatment *(Russian)* 80—52771
T permeation through steam generator alloys 80—34250
$TABe_{12}$, by diffusion saturation in vacuum, resistance to heat 78—44259
Ta, adsorption of LaB_6, work function, activation energy for diffusion 80—20039
Ta base alloy, thermotransport of O 79—95216
Ta, Debye-Waller factor and H_2 diffusion, neutron spectroscopy study 79—37881
Ta, diffusion and surface distrib. of N, probed by (p,γ) resonance broadening method 78—38918
Ta, diffusion anomalies, vacancy model *(French)* 77—43366
Ta, diffusion of H, neutron radiography meas. 77—39696
Ta, diffusion of interstitial O_2, sink/barrier phenomena 79—60553
Ta foils, coated with H-permeable Pd film, AES and SIMS 79—52467
Ta, internal friction meas. of O, N diffusion 78—75888
Ta, low temp., diffusion of H and D from quenching and annealing study 80—6555
Ta, muon diffusion, μ^+SR meas. 78—39487
Ta, muon location and diffusion, μSR 79—56693
Ta, μ^+SR diffusion, temp. depend. 78—39490
Ta, of H, book contrib. 79—82390
Ta, of H, electromigration temp. depend. *(Russian)* 77—84986
Ta, of H, lattice distortion and migration energy of H impurities 78—30796
Ta, of H and D, diffusion coeff. at high concs., Gorsky effect meas. 78—26731
Ta, of H_2 *(Japanese)* 78—10221
Ta, of U, high temp., determ. from neutron fission tracks meas. 77—89587
Ta, polycrystalline, trace diffusion of nuclear reaction products, lanthanides 78—22896
Ta, review of neutron radiography results 78—59961
Ta, single cryst., positive muon diffusion 78—80267
Ta, static and dynamic props. of O and H impurities, Mossbauer meas. 80—7246
Ta, thermo EMF, effect of H diffusion 79—23950
Ta, thermoelectron emission, S impurity atom effects, electron spectra *(Russian)* 77—8712

diffusion in solids continued
Ta-H system, local frequency spectrum, mean thermal displacement of H 80—59604
Ta-H(D), anelasticity due to long-range diffusion 80—60904
Ta-Nb(Re)(W) (50,20,0 at.%), with N_2, spectral emissivity, N_2 absorption rate, N_2 solubility, thermodynamic data *(German)* 77—25026
Ta-T(D), diffusion and resistivity at low temps. 78—14511
TaC, of W, correl. with self-diffusion 77—24437
TaC_x, solubility of H, X-ray diffr. exam. 80—44318
Ta_2C_x, solubility of H, X-ray diffr. exam. 80—44318
$Ta_2C_xO_y$, solubility of H, X-ray diffr. exam. 80—44318
$TaD_{0.06}$, D diffusion, 6.2 keV Mossbauer reson. of ^{181}Ta 78—39472
TaS_2:NH_3, mol. motion, neutron quasielastic scatt. obs. 79—90827
$TaS_2(NH_3)$ intercalation complex wideline NMR obs., translational and reorientational effects 77—1602
Te/Ag double films, interdiffusion and struct. modifications *(French)* 77—62682
Te-Au thin film interface, evolution, switching effects *(French)* 80—6660
Th, diffusion and electrotransport of Fe, Co and Ni, 965-1625°C 79—90828
Th metal, diffusion and electrotransport of Th metal 78—86611
Th, of fission products 77—4220
Th, of Ni, Fe, Fe-Ni-Cr, at 500 to 800 °C *(German)* 79—28157
Th-U-Pu-C-O-N, kernel migration for HTGR fuel 77—38335
ThO_2-based ceramic impurity diffusion, electrotransport method 78—67869
Ti alloy, H_2 embrittlement, directional diffusion of H_2 *(Russian)* 79—15763
Ti alloy in Al alloy melt, raction zone formation, component interaction *(Russian)* 80—54377
Ti alloys, H_2 diffusion at room temp. 79—51312
β-Ti, diffusion of H, neutron radiography meas. 77—39696
Ti fibres, high-temp. nitriding kinetics *(Russian)* 80—21166
Ti film, solid state reaction with Si or SiO_2 substrates, backscatt. anal. 80—34257
β-Ti, isotope effect for diffusion of Sn 77—76617
Ti, nitriding kinetics at 1230 to 1500°C, diffusion and struct. investig. *(French)* 77—36683
α-Ti, O_2 diffusion from oxide surface layer, chem. anal. by nucl. reaction *(French)* 79—7710
Ti, of Be, temp. depend., radioactive tracer method *(Russian)* 80—10703
Ti, of Fe, under plastic deformation *(Russian)* 79—28146
Ti of H_2, nonisothermal, in temp. field of instantaneous plane heat source *(Russian)* 77—20123
β-Ti, of H_2 *(Korean)* 78—18838
Ti, of N_2, at elevated temp., kinetics and mechanism of reaction 77—12741
α-Ti, of O, atomic jumping model 80—44366
α-Ti, of O_2, 700 to 950°C, lattice parameter and microhardness meas. *(French)* 79—86929
Ti, overlaid thin films, D pumping speed 78—33286
Ti, oxidation, linear, O diffusion coeff. depend. on rutile layer struct. *(French)* 80—104328
Ti, oxidation behaviour under pure O_2 atmos., temp. range 600-800°C 80—89415
α-Ti, oxidation in O_2 atmosphere, role of oxide layer and mechanism of oxidation *(French)* 78—23859
Ti, review of neutron radiography results 78—59961
α-Ti, S, C and Cl diffusion, AES meas. 78—51735
Ti, thermo EMF, effect of H diffusion 79—23950
Ti, uphill diffusion of H and progressive H embrittlement 77—90454
Ti:D, ion implanted, depth profiles, temp. depend. 80—100270
α-Ti-Al, H_2 diffusion *(Korean)* 78—30794
Ti-Al alloy, H_2 diffusion at room temp. *(Japanese)* 80—19987
Ti-Al diffusion coatings on C steel, struct. and props. 79—57156
Ti-Al-Nb-Ta-Mo (6, 2, 1, 0.8 wt.%), elevated temp. flow strength, creep resist., diffusion welding characts. 80—30033
Ti-Al-V (6,4 wt.%), microstruct. effect of base metals on diffusion welding *(Japanese)* 80—89296
Ti-Al(Cr), of N_2, at elevated temp., nitridation behaviour 77—12742
Ti-C system, reaction diffusion analysis 77—28049
Ti-Cr alloy, H_2 diffusion at room temp. *(Japanese)* 80—19987
Ti-Cu interdiffusion 77—89596
Ti-Fe, diffusion of stored H, Mossbauer study 80—34838
β-Ti-Fe, of H_2 *(Korean)* 78—18838
β Ti-Fe (1 to 6 wt.%) alloys, H diffusion *(Korean)* 79—42312
Ti-H, H diffusion and phase consistution, V influence, proton spin-lattice relax. meas. 78—27484
Ti-Mn (0.4 and 12 wt.%), bonding between α-β interfaces, subsequent deform. 78—14517
Ti-Nb (4.32 wt%), high temp. oxidation kinetics under 1 bar pressure, 1255-1471K 80—89410
Ti-Ni alloy, H_2 diffusion at room temp. *(Japanese)* 80—19987
Ti-Permalloy films, interdiffusion, Auger anal. and X-ray diffr. obs., degradation of mag. props. 80—34251
Ti-Permalloy thin film diffusion couples, low temp. interdiffusion interdiffusion 78—71889
Ti-Si film thin film interaction, metallisation, X-ray diffr. and sheet resist. 80—54442
Ti-Ta (4.37 wt%), oxidation kinetics, 1258-1473K, and at pressure of 0.013, 0.133 and 1.0 bar 80—89411
Ti-TiN phase system, diffusion of N_2 77—39699
Ti-W/Au, metallisation on Al, temp. stability, barrier props., barrier props. 79—23868
TiC film, CVD, on WC, diffusion processes, ion beam anal. 80—49424
TiC, high temp. thermal cond., ambipolar diffusion contrib. 78—26742
TiC, sintering and grain growth, metallographic anal. 80—25642
TiCuH, H-atom diffusion, PMR obs. 78—91978
β-$TiFeH_{1.03}$, H diffusion, NMR meas. 80—10707
TiO_2, diffusivity of T and Raman scatt. meas. 79—86927
TiO_2, of Na and H from Na amalgam, room temp. coloration technique 78—84611
TiO_2, rutile, mechanisms for H diffusion 79—73341
TiO_2:H photoanodes, diffusion and surface chemistry 80—35546
TiO_2-M_2O_3 (M is Al, Sc, Y or Er) system, dislocation mechanism of diffusion processes 79—77837
TiO_2-SiO_2, submicron dispersion of impurity, chem. diffusivity and elec. cond. 79—1528

diffusion in solids continued
Ti_nO_{2n-1}, ^{18}O tracer diffusion coeff. determ. by continuous mass spectrometry 77—20124
$TiS_2(NH_3)$, intercalation complex, wideline NMR obs., translational and reorientational effects 77—1602
TlCl+KI, solid state displacement reaction, kinetics and mechanism 79—11788
$(U,Pu)O_{2-x}$, mixed oxide fuel, final stage densification 79—49681
U, D migration and trapping during D^+ implantation 80—34243
UC, nuclear fuels, irrad. induced kinetics, diffusion and fission gas resoln. 80—59523
$UC_{1\pm x}$, C diffusion 80—49428
UO_2, D migration and trapping during D^+ implantation 80—34243
UO_2, diffusion of Kr and Xe fission gas atoms 79—6746
UO_2, high burnup nuclear fuels, relation between fission product release and fuel microstruct. 80—57845
UO_2 irradiated, grain edge porosity growth 79—19285
UO_2, irradiated, spacing of intergranular fission gas bubbles 78—66340
UO_2, mobility of intergranular gas bubbles 80—15310
UO_2, mobility of intragranular bubbles during irradiation 77—6520
UO_2, monocrystalline, fission gas release charact. during irradiation 78—4985
UO_2, neutron irradiated, diffusion of fission product T 78—67866
UO_2 nuclear fuels, irrad. induced kinetics, diffusion and fission gas resoln. 80—59523
UO_2, of Ar, solubility and diffusion, 400-600°C, polycrystalline 77—20130
UO_2, of P 79—7711
UO_2, review of diffusion coeff. of fission product rare gases 78—33248
UO_2, transfer of fission gas between grain faces and edges 78—79815
UO_2-PuO_2 fuel, O_2 diffusion at low temps. 78—8899
UO_2-PuO_2 powder compacts, homogenization kinetics using modified Barrer's model to diffusion 79—37883
UO_2-SiO_2, 1000-1400°C, Ar solubility and diffusion 77—20130
UO_{2+x}, sintering mechanism 77—21071
$(U_1Pu)O_2+x$, O_2 chem. diffusion *(French)* 80—49427
U_3Si-ZI_4 interface, 700 to 800°C, exam. using metallographic and local X-ray spectral anal. 79—90831
V, 80 keV ^{4}He irrad., depth profiles, migration, release, surface effects, blistering 77—35606
V, Debye-Waller factor and H_2 diffusion, neutron spectroscopy study 79—37881
V, diffusion and trapping of O_2 79—77816
V, diffusion of H, neutron radiography meas. 77—39696
V, diffusion of H and D, effect of impurities on coeff. 78—47604
V, diffusion of positive muons 78—47601
V, electro- and thermotransport of O and N 77—28040
V foils, coated with H-permeable Pd film, AES and SIMS 79—52467
V, H solubility and diffusivity around room temp. 80—29225
V, H_2 permeability, surface impurity layer effect 77—24440
V, isotope effects for H_2 diffusion, crystal field stabilisation 80—59728
V, muon diffusion, μ^+SR meas. 78—39487
V, muon diffusion and trapping 79—56686
V, μ^+SR diffusion, temp. depend. 78—39490
V of H, book contrib. 79—82390
V, of H, D, electromigration measured by resistance method 79—23783
V, of H, lattice distortion and migration energy of H impurities 78—30796
V, of H_2 *(Japanese)* 78—10221
V, of O, lattice distortion and migration energy of O impurities 78—30796
V, of O and N, least squares computer technique 78—38881
V, of TA, 1100 to 1800°C 77—24443
V, review of neutron radiography results 78—59961
V thin film-amorphous Si interface, V silicide formation, backscattering diffraction meas. 80—2285
V-Be diffusion couple, ion backscatt. anal. 77—35752
V-Cr(Fe)(Nb)(Ti), of H_2 *(Japanese)* 78—10221
V-H system, local frequency spectrum, mean thermal displacement of H 80—59604
V-H(D), anelasticity due to long-range diffusion 80—60904
V-Nb(Ti)(Zr)(Cr)(Mo)(Fe)(Cu), H solubility and diffusivity around room temp. 80—29225
V-SiO_2 interface reaction, identification of diffusion species 78—75890
VC single cryst., Vickers microhardness, slip mechanism 80—71732
V_3Ga layer on bronze, diffusion of Ga *(Russian)* 80—65297
V_2Hf base Laves phase compound tapes, supercond. props., prep. 77—40011
Va, $H_2(D_2)$ diffusion model, quantum rate theory for symmetric double well pot. 78—55970
W, activated sintering, diffusion mech. *(Korean)* 77—73248
W, diffusion anomalies, vacancy model *(French)* 77—43366
W, diffusion barrier between Ni-Cr-Al coatings and Ni eutectic alloys in gas turbines 79—24673
W, diffusion of Li, Cs, vacancy and divacancy mechanisms *(Russian)* 80—70472
W fibre, KSiAl doped, recrystallisation, Li diffusion effects, hardness, strength, microstructure meas. *(German)* 78—64644
W film, electron beam deposition on Si, X-ray obs. of silicide form., diffusion processes *(German)* 77—1341
W, incoherent twin boundary microfaceting on annealing, field ion microscope determ. 79—77608
W, ion implantation, $^4He^+$ range profile and ^{4}He diffusivity meas. 79—33022
W, of liquid Al *(Russian)* 78—26735
W, of P, 1880-2180°C *(Russian)* 78—43182
W of U, high temp., determ. from neutron fission tracks meas. 77—89587
W, porous, chromising 80—100959
W siliciding, in vacuum, diffusion saturation, effect of NaCl, kinetics 79—15859
W, sintering, Ni activated, grain boundary diffusion mechanism 79—91606
W:Re, polygonisation in diffusion process, glide dislocation interactions 80—38998
W-Cr solid solution, precipitation behaviour, reaction front motion, lattice parameters *(German)* 80—55401
W-Cr-Pd, Pd effects on diffusion 77—24445
W-Cu pseudoalloy, porous, chromising 80—100959
W-Ni system, liq. phase sintering, 1640°C, solubility and vol. diffusion of Ni in W 79—86895

diffusion in solids continued
W-ThO_2-B, thermocathodes diffusion mobility, based on deboronation kinetics 80−39349
W-Zr system, kinetics of interdiffusion process *(Russian)* 79−69298
WC-Co, phase comp. and oxidation resist. of coatings deposited by thermal diffusion using TiB_2 80−21173
WC-Co, sintered hard alloy, mechanism of penetration of liquid metals 78−60619
WC-Co-Cu, interdiffusion up to 1120°C 78−11492
WC-Ni hard alloys, sintered, with uneven binder metal distrib., molten Ni migration 78−35336
WO_3 thin film, Li diffusion, appl. of AC techniques 80−70468
WSi_2, diffusion grown layers, texture 79−74095
WSi_2, diffusion marker for backscatt. studies of W+Mo bilayer film 78−87828
WSi_2, steam-oxidized, Auger sputter profiling studies 80−107663
Xe hydrate, reorientation and diffusion of H_2O, PMR and dielectric relax. 77−36142
^{133}Xe in a plastic catheter, diffusion dynamics obs. 80−79973
Y, of C, radiographic meas. *(Russian)* 77−31809
Y, of Fe, rapidly diffusing, Mossbauer exam. 78−27138
Y, of H, neutron scatt. and absorpt. study 79−60556
YBe_{13}-Mo, solid state reaction, 1000 to 1400°C *(Russian)* 78−18845
YIG film, on GdGaG, mag. excitations, diffusion layer effects 78−31112
Y_2O_3-Nb_2O_5, solid state reactions, 1275 to 1350°C, electron microscopy, EPMA, X-ray diffr., dilometry *(Japanese)* 78−63883
Yb-Al mixed valent film form., XPS study 80−80943
Zn, 6.1 MeV α-particle irrad., stage III and IV recovery kinetics, defect diffusion 77−76474
Zn grain boundaries, activationless motion, group co-operative transition mechanism 80−2039
Zn, of C, radiographic meas. *(Russian)* 77−31809
Zn, phosphidation in P vapour, kinetics and associated diffusion coeffs. 80−3405
Zn:Al, ion implantation of Al, defect flow induced outdiffusion 78−63779
Zn/Cu film system, UPS during atomic diffusion 79−43097
Zn-Ag-Cu alloy powder, brazing solder, production using electrodeposition and heating in reducing atm. 79−100079
Zn-Sb diffusion couple, layer growth of ZnSb phase at high press., elec. meas. 80−2218
Zn-Sb diffusion couple, ZnSb phase layer growth kinetics, 240-320°C, up to 30 kbar 78−10229
$ZnFe_2O_4$+NiO_2(MgO) powders, cation mutual diffusion coeffs. calc. 77−15635
ZnO, dislocation loop nucleation on prismatic faults in high voltage electron microscope 77−72620
ZnO-based ceramic microstructure and nonlinear props., B diffusion effects *(Russian)* 80−49423
ZnS, electrolum. phosphors, surface phenomena occurring during ageing *(Russian)* 79−33842
ZnS:Mn, electrolum. films, activating impurity diffusion coeff. *(Russian)* 77−84995
ZnS-CdS, equimolar solid soln. formation kinetics 80−39289
ZnS_xSe_{1-x} layer on ZnS, ZnSe, growth by solid-state diffusion technique 78−56578
ZnSb, orientated crystn. conditions during reaction diffusion *(Russian)* 80−70558
ZnSe, charged dislocation motion mechanism *(Russian)* 78−79820
ZnSe, of Cu, luminescence and diffusion behaviour of Cu impurities 78−35188
ZnTe, low voltage green LED, struct. double diffusion procedure 80−100697
ZnTe:Ag, doped during frowth and by diffusion, defect form. 80−15129
ZnTe:Li, diffusion investigation by SEM and TEM 80−10706
ZnTe:Li, Li in Te precipitates, diffusion during thermal anneal 80−39358
Zr alloys, H_2 diffusion at room temp. 79−51312
Zr alloys, of O, 675-1800°C, α and β alloys 77−62680
Zr and its alloys, H diffusion, NMR study 80−108088
α-Zr, anelastic relaxation and O_2 diffusion 77−4219
α-Zr, atom size effect in tracer diffusion 78−84005
β-Zr, Cr diffusion rates in temp. range 914 to 1240°C 80−15304
β-Zr, diffusion and solubility of H, above 1000°C and below 1×10^{-4} mm Hg *(Russian)* 80−24671
α-Zr, diffusion of C, 620 to 830°C *(Russian)* 79−46842
Zr fibres, high-temp. nitriding kinetics *(Russian)* 80−21166
Zr, interaction kinetics with graphite, reactive diffusion 79−42318
α-Zr, internal friction and O_2 pair diffusion 77−16634
α-Zr, O stabilized, O diffusion using ^{18}O tracer 78−51737
α-Zr, of O, 290 to 1500°C 77−76613
Zr, of T, method for determ. of diffusion coeff. 80−15306
α-Zr, point defect props., effect on irradiation behaviour of Zr alloys 78−30609
Zr, thermo EMF, effect of H diffusion 79−23950
Zr:He, diffusion of He studied by thermal evolution spectrometry 77−69120
Zr-Al_2O_3 couple, diffusion welding, 1000 to 1300°C *(German)* 79−28155
Zr-Al-O system, diffusion welding, 1000 to 1300°C, Al_2O_3-(Zr-Al) alloy, ZrO_2-(Zr-Al) alloy, Al_2O_3-ZrO_2 couples *(German)* 79−33122
Zr-H, diffusion in hydride phase, exam. 80−29204
Zr-H, inhomogeneous system, time changes of Hall voltage 79−87080
Zr-Mn alloys, impurity and self-diffusion 79−60540
Zr-Nb (2.5 wt.%), hydride forming materials, H_2 induced delayed cracking 78−27623
Zr-Ni, of H_2, 900 to 1080°C *(Korean)* 80−19988
Zr-Zr_2Al_3, diffusion weldings between 1000 and 1300°C, electron microprobe anal. *(German)* 78−84011
ZrC, and ZrC-NbC solid soln., prep. by impregnation, strength, surface submicrocracks 77−16661
ZrC CVD coated fuel particles, diffusion of ^{137}Cs, ^{90}Sr and ^{144}Ce 80−13582
ZrC coating on refractory metal fibre, diffusion barrier, deposition 77−4759
ZrC, of W, correl. with self-diffusion 77−24437
ZrC, solubility, diffusion and permeation of Cs 78−51684
ZrO_2:CaO, polycrystalline, grain boundary enhanced interdiffusion, flux density eqn. 80−29220
ZrO_2:Cu, point defects, electrochem. characterisation 80−35599

diffusion pumps
back-streaming, review 78−21155
cold traps, liq. N_2, automatic level controller, transfer system 78−24805
counter-flow mass spectrometer leak detector 79−63248
fluid, vacuum use of perfluoro polyether 80−52251
heater problems and solns. 77−41629
hydrocarbon contamination, of vacuum dependent scientific instruments 79−63259
integrated, with backing/roughing valve, features 79−26063
jet assembly and vaporiser design optimisation 78−81999
leak detection, trapless, use of reversed diffusion pump 77−2662
mass spectrometer leak detector, increasing sensitivity by selective gas accumulation 79−6215
oil backstreaming in turbomolecular and oil diffusion pumps 79−80636
operation and maintenance, contamination minimization 79−44913
operation and specifications *(Hungarian)* 77−71334
power consumption problems 79−49242
review, advantages over other types, newest devices 80−57321
ultrahigh vacuum pumps 78−89488
vacuum production, past, present and future 80−31775
vapour, vacuum behaviour of perfluoro polyether 79−63254
vapour pump, recent developments 79−63250
Hg use and abuse for vacuum production and meas. 78−81998

diffusivity *see diffusion*

diffusivity, thermal *see thermal diffusivity*

digital-analogue conversion
see also analogue-digital conversion
4-bit digitally driven integrated optical amplitude modulator for data processing 80−53476
analog signal processing, book 80−86047
audio signal processing, spurious signals and their suppression *(Czech)* 79−98555
charged particle track anal. in multiplane hodoscope 77−14325
CRO storage, Gould Advance OS4000 using A/D and D/A convertors 78−93673
CRO with digital storage, OS4000, features *(Spanish)* 79−6116
data manipulation and handling, for teachers 80−4489
digital colour recording system for digital-analogue hybrid image processing 78−16880
direct time to digital convertor with multi-stop facility, appl. to neutron TOF meas. 77−14317
experimental heat transfer data processing, automatic unit 79−93110
Fabry-Perot interferometer digital electronic system 78−12748
four fold coincidence system, simultaneous counting of true and random events 79−81140
frequency-voltage, frequency meas. using NC 170 convertor *(Czech)* 80−13043
highly stable, resettable const. current supply, SQUID appl. 79−67289
laser Doppler microscope period meas. signal analyser *(Japanese)* 79−88998
logarithmic frequency-voltage convertor design 77−13775
mark:space ratio highly linear D/A convertor 77−82495
modules of 'Summa' system for information output to oscilloscope, digital display and digital printing 77−3244
multichannel time-digit conversion modules of 'Summa' system for spark chambers 77−3236
PQR line shape, digital-analogue interface for data processing 79−45615
proton storage ring, NAP-M conversion equipment in supervisory system 77−65365
semiconductor device C-V and G-V measurements using automatic technique, 50 Hz to 300 KHz 80−31800
stereophotogrammetry, digital profile to contour convertor, display 77−9501
transducer, pulsed frequency, continuous random signals errors evaluation, by means of computer simulation 77−74386
transducer response linearisation using programmable multifunction module 78−45604

digital arithmetic
see also roundoff errors
decimal/residue/decimal optical converters 79−22905
holographic, image digital reconstruction with limited-length arithmetic register *(Russian)* 79−22910
linear eqns. integral soln. using integer arithmetic 78−69960
mechanics conservation law derivation using digital computers 78−12552
modular arithmetic inner product processor optical implementation 80−48170
numerical optical data processor, representation and implementation 78−78947
numerical optical processor combining prime residue arithmetic representation and spatial light modulator 79−76871
optical computation using residue arithmetic 79−31808
optical residue arithmetic, correlation approach 79−31809
residue arithmetic computation, integrated-optical methods 79−76886
residue arithmetic computer, optical 79−98296
residue number optical processor design concepts 80−48168
residue-based optical processor 80−48169

digital circuits
see also adders; digital integrated circuits; pulse circuits; switching circuits
astronomical laser ranging equipment, telescope drive *(Japanese)* 78−89078
automatic digital circuit for selecting information bearing components of output voltage of electromagnetic transducer 79−2760
calibration cct. for deep level transient spectrometer 80−37067
capacitance meter, linear direct reading, cct. *(French)* 78−237
clock synchronisation circuit, digital clocks, using transmitted time code 79−67257
correlator with blinker facility for photon correlation spectroscopy 80−37092
decade counter for measuring thickness of multilayer electrodeposits *(Czech)* 80−95071
digital frequency-to-temp. convertor for use in radio telemetry systems 80−8119
display adaptor for Victoreen 440 survey meter 79−70644
dual integrated gate generator 78−55112
electron microscope spherical aberration effects, digital circuit corrector, spiral scanning attachment 79−2889
far IR laser stabilisation servo electronics 77−38928
gray tone display processor for CRT, US materials testing appl. 78−44284

digital circuits continued
heart beat frequency monitoring circuit *(Bulgarian)* 77—78006
integrator, automatically triggered, for flame AAS with discrete nebulization 80—35610
integrator, for flameless at. absorpt. 77—38014
integrator, for pulsed NMR spectrometer 77—26372
integrator, for radioastronomical obs. processing *(Russian)* 78—57465
laser frequency-offset lock system, for use with stabilised lasers 78—29960
liquid N_2 two-level controller 80—52241
lock-in for photon counting systems, fast low cost design 77—62036
magnetic stirrer with no external moving parts appl. 78—93666
oscilloscope eight channel store accessory cct. *(German)* 78—45607
phase measurement of digital signals, using PLL method for low S/N ratio 78—16810
pulse programmer, auto-increment cct. 77—79134
pulse programmer circuit, for NMR spectroscopy 77—74474
small capacitances measurement by comparison, cct. 80—57327
square root of time mark generator using TTL digital ccts. for chronocoulometry 80—35588
syneuristor discrete digital component design 79—96727
teaching apparatus, evaluation of PASCO scientific digital mini-modules 77—57126
three-chip digital scale zeroes tare weight, cct. 80—27282
timer with memory, appl. to dynamics experiments, principles of electronic circuitry 80—67994
X-ray tube anode voltage compensation under dropping power condition, digital compensation system *(Bulgarian)* 79—35902

digital communication systems
1 Gb/s laser space communication system 77—7213
2 km 20 Mb/s optical fibre transmission system 78—42437
6.3 Mb/s optical fibre communication for power system protection and control 78—1423
8.448 Mb/s optical cable feasibility trial *(German)* 78—33888
16 and 32 Mb/s short-haul high-performance optical data links 78—1421
31st Annual Frequency Control Symposium, Atlantic City (1977) 78—57905
32 km optical fibre transmission with data-rate-transparent repeaters 79—76875
32Mb/s optical fibre transmission system planning and expt. 78—1418
35 Mb/s optical fibre cable transmission using IR LED optocouplers 80—33156
44.7 Mb/s fibre optic transmission system expts. 78—1420
45 Mb/s fibre-optic transmission system performance 77—27376
140 Mb/s fibre-optic field demonstration system *(German)* 78—33889
400 Mb/s optical fibre communications, integrating and transimpedance front end performance comparison *(German)* 78—33879
400Mb/s SELFOC fibre transmission system expt. 78—1419
565 Mbit/s signal transmission on optical waveguides and coax cables 80—43483
800 Mbit/s optical transmission experiments with dispersion-free fibres at 1.5 μm 80—58680
800 Mbit/s optical transmission expt. *(Japanese)* 80—33164
binary optical communication system, atm. scintillation effects 77—71943
decentralized instrumentation and control system with bus transmission in nuclear power plants 79—97847
ECG analogue and digital transmission 79—39564
ECG numerical encoding and transmission, microprocessor appl. 77—44798
electro-optical channel waveguide switch for computer communication bus 80—9987
fibre, multilevel signals theory 79—22900
fibre optic link, commercial components survey *(French)* 79—90007
fibre optic undersea cables, small, recent experiences 80—14488
fibre optics developments in West Germany, 1978 survey *(Swedish)* 79—55209
fibre-optic digital transmission, shot noise probability distribution function 78—50717
fibre-optic transmission expts. at 1.3 μm wavelength *(Japanese)* 80—28318
fibre-optic transmission system, UK Post Office feasibility trial 78—1417
fibre-optic transmission system average error probability 77—27380
Gaussian signals in Gaussian noise transmitted over digital channel, degradation of S/N ratio 80—64298
gigabit laser communication 78—66860
HF pulse transmission, distortion due to reflection by the ionosphere 79—84568
high-speed optical systems at 0.85 μm, modal noise and optical feedback 80—87323
hybrid digital optical fibre transmission system, terminal equipment and reshaping/regenerative repeaters *(German)* 78—33880
hybrid p-i-n photodiode-FET preamplifier design for digital optical receivers *(German)* 78—33878
interoffice trunk fibre-optic experimental transmission system 77—54795
Italian local digital network applicability of optical cables *(German)* 78—33886
laser digital communication system, 100 Mb/s, optical receiver and pulse generator *(Russian)* 79—94170
laser level-control circuit for high-bit-rate system using slope detector 79—18430
laser systems, acousto-optical multiplexing and demultiplexing techniques for multigigabits/sec transmission 79—86132
lightwave communications, Bell system evaluation in Chicago 78—46821
matched electromagnetic pulse transmission, for good conducting media 79—36823
medium and long distance digital optical fibre communication systems 78—50941
microwave link, cross-polarisation on terrestrial path, wind, raindrop size and canting angle effects 79—66736
multilevel pulsed phase modulation, channel capacity in optical links 78—78934
multimode digital system wavelength multiplexing constraints in 850 nm region 80—63942
noise-tolerant continuously variable slope DM to linear predictive coding conversion 80—96141
optical, CO_2 laser 300 Mb/s communications terminal 77—19441
optical, development problems 79—3806
optical, GaAlAs laser transmitter 78—90423
optical, interoffice trunking exptl. optical fibre communication system 77—19454

digital communication systems continued
optical, LED optical fibre system, source-drive optimisation 77—11007
optical, Nd:YAG laser 1 Gb/s satellite communication system 77—19440
optical, optimum index profile for dispersive multimode fibre 77—7192
optical cabling technology, recent trends 79—3781
optical data bus, glass fibre branch couplers, digital data transmission *(German)* 79—89999
optical fibre, 137 Mb/s data links using LEDs, material dispersion limited operation 77—88908
optical fibre, 5 Gbit/s multiplexer 78—18044
optical fibre, Australian development 77—65630
optical fibre, dispersion-free single-mode fibre transmission experiments up to 1.6 Gbit/s 79—59812
optical fibre, expt. 78—66943
optical fibre, intermode phase scanning for recovering phase-modulated signals on multimode optical fibres 80—58682
optical fibre, systems analysis 77—65631
optical fibre 32 Mbit/s non-repeatered 50 km transmission expt. 78—79108
optical fibre analogue/digital communication system with 5 MHz bandwidth *(German)* 78—30062
optical fibre cable, technological advances, thermoplastic materials reinforcement, cabling *(French)* 77—11020
optical fibre cable links installed in operational ducts, transmission meas. 78—50928
optical fibre cables, graded-index, transmission expts., 1.2-1.6 μm wavelength range 80—102813
optical fibre communication, A-7 ALOFT economic analysis, EM interf. and pulse tests 78—42448
optical fibre communication lines, use of semicond. lasers and avalanche photodiodes 78—46793
optical fibre communication link for 1 Gbit/s *(German)* 79—81565
optical fibre communication system, average error probability calc. 80—53228
optical fibre communication system, cost model 78—42447
optical fibre communication system operating at 44.7 Mb/s, devices and perform. 77—27382
optical fibre communication systems in Japan 78—46815
optical fibre communications, PAM-PPM signalling format 79—27190
optical fibre data link, high bit rate, using InGaAsP 1.3 μm LED 78—46825
optical fibre data link, integrated industrial, circuit and system considerations 78—46817
optical fibre digital data transmission, design criteria and experimental results *(Rumanian)* 78—46791
optical fibre digital transmission system, 2 km, for field use at 20 Mb/s 78—38064
optical fibre link for Command and Control System 280 78—42445
optical fibre link systems, UK expts. 78—42462
optical fibre system, 4-level digital, using LED, meas. at 68 Mbit/s 80—1313
optical fibre telephone carrier systems 78—42463
optical fibre transmission capability expansion 78—66914
optical fibre transmission experiment, 800 Mbit/sec at 1.05 μm 78—83075
optical fibre transmission expts. at 34 Mb/s with HDB3 line code 80—64198
optical fibres, multimode, structural design and determination of repeater spacing in digital transmission systems *(Japanese)* 79—59820
optical fibres, single- and multimode, fundamental mode signal transmission 78—42442
optical fibres in Italy, short distance appl. 79—50369
optical long-span single-mode fibre transmission characts. in long wavelength regions 80—99850
optical PCM with envelope modulation, pulse detection characteristics 77—11010
optical pulse high-speed transmission at 1.29μm, using low-loss single mode fibres 79—23067
optical repeater section lengths rel. to transmitter power and fibre dispersion *(German)* 78—38012
optical space communications with Nd:YAG laser 78—66859
optical systems characts., and state of development *(German)* 79—999
optical waveguides using silica fibre for wavelengths beyond 1 μm 78—50907
PARCOR analysis-synthesis telephony, improvement of speech quality 79—50534
PCM 480 system for Deutsche Bundespost using fibre-optic link 80—38120
perceptual coding in the cosing transform domain 80—102635
plastic fibre-optic assemblies 80—14433
radiation monitoring system, communication techniques 79—49866
satellite links, PSK modems, high rate data communication, 77—49268
SAW compensated filter used in wide spread MSK waveform generator 80—74670
Shiva laser fibre-optic digital links 79—85804
Spacelab, high rate data handling in space and on ground, multiplexing system 79—21138
speech interpolation system called adaptive DPCM with time assignment speech interpolation 80—99903
speech transmission, forward and backward prediction in adaptive differential PCM over nonideal channels 80—99902
transmission system design, influence of optical component baseband frequency response 78—1415
UK Post Office junction and trunk network applications for optical fibre systems *(German)* 78—38016
voice multiplex systems, acquisition performance of frame synchronisation system 80—99901
wavelength division two-way fibre optic transmission expt. using micro-optic duplexers 78—22194
X-ray picture digital transmission over voice-grade telephone channels, laser scanning system 78—80953
(GaAl)As-GaAs narrow stripe laser, improved optical communication system performance 80—102733

digital computers
for computer applications see under relevant applications e.g. administrative data processing; computerised control; natural sciences computing see also digital systems; electronic calculators; microcomputers; minicomputers; satellite computers; special purpose computers
125 MS, Spacelab data processing system *(French)* 77—78594
development, historical review 80—4503

digital computers continued
- Netherlands fusion expts., data acquisition and anal. systems 80—13915
- signal detection, optical vs digital Fourier transform computers 79—27181
- technology developments in relation to nuclear research 77—13566

digital control
- *see also numerical control*
- AGC of multichannel radiometers *(Russian)* 77—26399
- anaesthesia level system by EEG analysis 79—83974
- Auger SEM incorporating concentric hemispherical energy analyser 77—79199
- BWR nuclear plant nonlinear digital simulator, optimal digital control methods appl. 79—9826
- camera, Canon A-1, digital logic principles 78—70206
- CANDU, digital computer control 77—54324
- cardiac assist devices, in-series, digital afterload phase angle controller 77—44843
- co-evaporation prep. of two component alloys, control system 79—24457
- digital computer control in Canadian nuclear plants, past performance and future outlook 78—58383
- electrostatic generator terminal voltage on-line feedback stabilisation using digital computer 78—82004
- EMG digital processor design and performance 79—96712
- far IR laser stabilisation servo electronics 77—38928
- filter, programmable, characts., hearing equipment appl. *(Swedish)* 78—36055
- HWR dynamics modelling for digital control system design 79—9829
- injection diode modulated laser pulse generator and digital control cct. *(Russian)* 80—14372
- Large Azimuthal Telescope program control system 79—16829
- light chopper with digital control circuit *(Japanese)* 79—3784
- liquid chromatograph, microprocessor-based, reproducibility 77—9152
- mechanical actuator, stepper motor, appl. to control of scientific apparatus 78—62683
- microprocessor controlled digital spectrum stabiliser for scintillation counter 77—38572
- microprocessor speech synthesiser terminal 79—81660
- monochromator drive, using high-speed digital servo 78—36992
- multichannel wide-range oceanographic sonar 80—46295
- neutral beam filament supply, 15 V 10^3 A, programmable, regulated, for fusion reactor 78—70630
- nuclear reactor control using optimal control and state estimation 80—37554
- optical aspheric rotationally symm. surface generation, computer control 77—27395
- optical surface, computer controlled polishing, optimisation 77—23787
- particle size meas. by laser beam expt. 78—70098
- particle track chamber, semi-automatic meas. instrum. register for camera photograph reduction 78—78575
- photogrammetry using digitally controlled differential rectifiers *(German)* 77—60495
- programmable for Fresnel lenses manufacture *(Russian)* 78—50884
- pulsed ion cyclotron resonance spectrometer, integrated control system 79—71560
- PWR control, computer program *(German)* 79—59249
- radiographs optical and digital image processing 77—70241
- Raman spectrometer, digital control system, appl. to soft mode spectroscopy 78—86345
- scanning Auger electron microscopy, synchronous modulation technique 79—17570
- seismometer digital automatic amplitude controller with preliminary smoothing, parameter selection *(Russian)* 79—74985
- shutter system, digitally controlled, for spectroscopic appls. 77—82609
- signal amplitude digital auotmatic control system, instrumental realisation algorithm *(Russian)* 79—39924
- spectral slit, digitally controlled 77—34035
- stepping motor control system for repetitive scanning of a monochromator 78—54355
- stepping motor presettable digital control for neurophysiological microelectrode drive 78—36079
- Tokamak Fusion Test Reactor, conceptual digital computer control systems 77—23281
- ventilator, for respiratory therapy, digital electronic control 77—40897
- visually evoked response test goggle system using liquid crystal shutters 79—79676
- H_2O vapour under point corona discharge, microprocessor control for vapour generator and EHD phenomena 80—106852

digital differential analysers
- blood cell differential counter, ADC 500, pattern recognition based image processing system 78—73282
- photogrammetry using digitally controlled differential rectifiers *(German)* 77—60495

digital filters
- *see also multidimensional digital filters; signal processing; wave digital filters*
- 2-D recursive phase filters for solution of two-dimensional wave eqns. 79—86295
- $|\omega|$ filter, generalised, 3-D reconstruction, for tomographic machines 78—4741
- acoustics, speech and signal processing, IEEE international conf., Washington, DC, USA, 1979 Apr. 79—55275
- aerospace systems and electronics, IEEE conference, Washington D.C., USA, 26-29 Sept (1976) 77—5420
- Anger camera image digital filtering 77—9256
- astronomical plate processing, two-dimensional digital filtering techniques 79—16835
- auditory evoked potential data acquisition, dual-processor system 79—79712
- basilar membrane model for voice features extraction 78—77069
- biomedical signal and image processing, digital techniques *(Croatian)* 78—44623
- biomedical signal high efficiency freq. anal. and data compression 78—31939
- biomedical signal processing and telemetry, digital bandpass analysis 78—57107
- Butterworth low-pass filter, oceanographic data appl. 79—16704
- catheter pressure meas., transducer smearing correction using microprocessor based discrete deconvolution 80—67275
- coal seam acoustic imaging 79—53585

digital filters continued
- composite filter in spectral analyser, frequency overlap requirements and detectability 79—1032
- computer contouring method using digital filter, bathymetry appl. 79—39894
- correlation TOF spectroscopy 79—49894
- data manipulation and handling, for teachers 80—4489
- distorted image convolution deblurring by Fourier-Bessel transform holograms *(Russian)* 79—22897
- ECG, implemented on microprocessor 78—85428
- ECG signal processing appl. *(Italian)* 79—96670
- edge detection, numerical, optical and hybrid methods compared 80—102662
- EEG, filtering of muscle artifact 79—100764
- electron micrograph optical and digital spatial freq. filtering 78—70231
- EPR spectrum analysis, polynomial regression and nonderivative search technique 77—14461
- experimental data anal. appl. 79—17403
- external gravity field calc., signal processing approach 78—24708
- fast convolution by finite ring arithmetics 80—36837
- FFT filter, appl. to biomech. impact data 77—78070
- fluctuation anal. of signals from nuclear reactor ex-core ion-chamber 77—54312
- foetal heart rate variability monitoring by digital filtering 79—48353
- frequency instability meas. *(Russian)* 80—57264
- Hankel transforms, related, of orders 0 and 1, numerical integration by adaptive digital filtering, FORTRAN IV algorithms 79—92599
- hydrophysical nonstationary processes, real time digital filtration *(Russian)* 78—65425
- image processing, local filtering methods *(French)* 80—46406
- instrument simulator, design and use 80—4490
- inverse filtering of visual evoked responses 79—53098
- ionospheric electron content data processing methods 80—56629
- Kalman, phasemeter appl., synthesis with a priori uncertainty of data 80—98934
- Lanczos filtering method, in one and two-dimens. 80—52176
- linear filters for dipole to Schlumberger curve transformation in resistivity soundings 78—45015
- linear filters for transformation of apparent electrical resistivities 78—96304
- linear sonar array processor finite impulse response digital filter design 80—43549
- lung compliance loop recovery eliminating cardiac interference 79—20570
- medicine, nuclear, digital filtering and edge detection 80—58065
- microcomputer based digital filter for electroencephalogram processing 78—73278
- microprocessor speech synthesiser terminal 79—81660
- mosaic IR image differencing for track assembly 80—86420
- multimicroprocessor implementation of all-digital speech synthesizer 80—96143
- musical appls., digital phase shifter using Bell Labs digital filter module 80—5884
- NMR, resolution enhancement by digital filtering with sinusoidal window function 77—18060
- noise-reduction filter for resolution enhancement in Fourier transform NMR 80—73403
- nonlinear, medical radioisotope imaging appl. *(Japanese)* 78—35930
- numerical digital filter for on-line processing of wind tunnel data *(French)* 80—19537
- optical fibre nonlinear equalisation by shaping filter *(German)* 78—33882
- photogram optimal filtering technique *(Italian)* 79—58268
- polynomial filter, appl. to biomech. impact data 77—78070
- quadrature sampled digital bandpass filters 77—23816
- quasi-staring IR sensor clutter rejection processor design 80—86417
- R-C filter, appl. to biomech. impact data 77—78070
- radiograph digital tomogrpahic restoration 78—40322
- radioisotope imaging, digital low-pass filtering, random noise removal 77—5065
- random pulse train inputs *(Japanese)* 78—53547
- recursive filter, generation of 1/3 octive data 78—87211
- SAW digital filter design using optimum pulse response techniques 77—46872
- scintigraphy, multichannel, collimated, Compton effect on spatial resolution, digital spatial filtering 78—69182
- seismic data, broadband, digital recording and anal. at Graefenberg array 79—25348
- seismic data, optimum mixed delay spiking filters appls. 78—77346
- seismic surface wave dispersion, digital processing *(Chinese)* 78—24374
- seismology, bandpass filter type and operator parameters selection for instrumental realisation *(Russian)* 79—74984
- signal processing technology assessment seminar, Aviemore (1976) 77—39166
- sinusoidal window filtering for resolution enhancement in Fourier transform NMR 79—93195
- sleep EEG, digital filtering for estimation of alpha-delta 78—44652
- Spar Buoy Oceanographic Telemetry System software engineering 80—46308
- speckle image digital processing 78—71053
- speech extraction from noise by adaptive digital filtering *(Japanese)* 78—13863
- speech production model, with digital filters 79—81661
- speech signal pitch determ. using nonlinear digital filter *(German)* 80—91972
- surface profile filtering using digital filters 80—36994
- Three Array Processor beamforming system 80—43550
- time-domain finite length filter, exact wave-shaping, geophys. appl. 77—2266
- tomographic machines, back projection speed improvement for 3-D reconstruction 78—4742
- two-dimensional, image enhancment appl. *(Italian)* 78—53539
- US medical image digital processing methods *(Chinese)* 80—30805
- vectorcardiogram parameter sensitivity to digital filtering 79—39576
- whistlers, spectral-temporal anal. using Gaussian filters 80—4175
- Wiener filter, appl. to vessel edge detection in angiograms, book contrib. 79—92357
- wind tunnels appl., for low freq. range 80—10336
- He speech unscrambling by nonlinear power spectrum conversion 79—46134

digital instrumentation
see also digital readout; digital voltmeters
5 MHz digital frequency meter *(German)* 78—62206
5120-channel digital cross-correlator for Westerbork radiotelescope 77—64650
A/D convertor with special appl. to medium precision Pt resist. thermometry 80—86297
AC panel meters, self-powering, COUNTERBALANCE A/D conversion technique 77—37909
AC voltmeter type F4850 and wattmeters type F4860, operational principles *(Russian)* 78—70158
acoustic excitation impulse generator 78—90618
acoustic frequency meter for meas. of tonal error in musical sounds *(German)* 77—830
AD2037 voltmeter and AD2038 thermometer, features 79—58684
add-subtract digital correlator, design and performance 77—61053
aerosol classification pulse amplitude analyser 78—61587
analogue digital double integration joulemeter, AC loss meas. in superconducting magnets 80—57325
anemograph, for wind direction and average speed meas. *(Czech)* 80—77174
angular and longitudinal displacement meas., magnetic scale recording system 77—2635
audiometer, automatic, for mass hearing examinations 80—33379
Auger SEM using digital integrator 80—37131
automatic blood pressure recorder *(Japanese)* 78—24168
automatic digital magnetic recording system in Tihany Observatory 79—39989
auxiliary information recording with B3-15 digital printers 79—26044
averaging meter for nonelectric periodic quantities, dual slope principle *(German)* 78—73983
balances, precision, electronic methods *(French)* 80—62660
Barkhausen computer interface for thin mag. film props. anal. 78—82008
barometer, Hg, precision, automatic, 710 to 770 torr 80—47046
barometer description and applics. 77—41208
beamformer with programmable time delay and sum 80—53592
bellow-type transducer for pressure meas. *(Polish)* 78—93719
biofeedback thermometer, low-cost research-oriented, with digital readout 79—29673
biomedical thermometer, simple, inexpensive design 80—36178
block, for electronic sweep of mag. field for microwave EPR spectrometer 77—26371
blood clotting characterisation by US digital fixed path interferometer 78—44670
blood coagulation parameter selection for automatic digital recording 77—21543
blood pressure meas. using sphygmomanometer *(Spanish)* 77—40846
blood pressure transistor device, high sensitivity, quasi-digital 79—79675
blood pulse wave velocity meter *(Japanese)* 79—39546
bubble chamber film, track rescue system 78—70728
calibration requirements digital instrumentation, requirements 77—37907
calorimetric system for measurement of average heat capacity of materials 79—71453
Calvet-type twin calorimeter using digital calculating integrator 80—77786
capacitance meas. dynamic method *(Czech)* 79—63272
capacitance meter, design and construction 80—57275
capacitance meter, using 555 oscillator 77—53926
capacitance meter, utilising CR discharge 79—12819
capacitance meter *(Spanish)* 80—13062
capacitance meter with automatic range selector *(German)* 78—45648
capacitance-based surface texture meas. systems 78—4593
cardiac defibrillator tester 80—41286
cardiotachometer, digital device using sliding averages 77—56503
Cary 14 spectrophotometer, remote control via digital interface 77—2697
chronometer 'Heathkit', operating instructions *(French)* 78—24765
chronometer with seven-function selector *(French)* 78—12677
clock CADM for extension of standard freq. line 79—67288
clock synchronisation circuit, digital clocks, using transmitted time code 79—67257
clocks, standard-freq. controlled, for high precision time meas. *(German)* 78—77871
Coanda fluidic gas flowmeter 80—59138
code generator to identify time, date, and events in physiologic event recording 77—86674
colour integrator 78—29138
combined instruments provide several test functions DMM, oscilloscopes, frequency counters, signal generators 77—34000
construction, component element design improvements, electric variable measurement appl. *(Rumania)* 77—74451
contactless for production process linear dimensions meas. *(Polish)* 78—93652
convertor, stroboscopic, soft-magnetic materials properties meas. appl., during pulse remagnetisation 77—5876
correlator, for signal preprocessing on spacecraft 77—64609
counters and timers, accurate meas. techniques 78—45605
crystalline sample fusion temp. meas. automatic instrument 78—57945
current and voltage monitoring instrument for biological ion transport studies 79—74815
DC picoammeter, digital *(Spanish)* 79—88980
defibrillator energy meters, traceable calibration methods 80—30928
design and technology 77—5821
device for determination of the ratio of two numbers mass spectrometer appl. *(Bulgarian)* 79—85199
differential pressure and flow meas., technique 78—38424
differential pulse rate meter, nuclear plant radiation monitoring appl. 78—37451
digital dynamic method for precise meas. of static characteristics 78—54389
digital freq. counter in probe, 0 to 750 kHz, using CMOS ICs 79—49209
digital lineariser for nonlinear transducers 78—57931
digital lock-in amplifier simulation 77—151
digital thermometer types and technical data *(Russian)* 77—53911
digitiser, compact, for bubble chamber pictures 77—83452
Digitron fast multichannel time recorder 77—67949
display of neuronal average firing freqs. 77—5117
display technological varieties 79—80587
dosimeter, neutron, portable battery-operated, design details 79—18052
double insulation reduces measuring problems, safety aspects 78—32802
drive system displacement meas., features *(Polish)* 80—86260

digital instrumentation continued
drop timer for precise determ. of drop times at dropping Hg electrodes 78—3394
DVMs, DMMs and counter-timers, review 77—37913
dynamometer DE 1, mass diagnosis locomotor and nervous system disorder appl. 77—40854
ECG systems testing 80—81756
EEG electronic recording and display systems *(French)* 77—13025
electrical quantities, discontinuous and quanstationary, time measurement application *(Rumanian)* 77—79120
electrical resistivity expts. in He II environment using computerised facility 80—31799
electron microscope image enhancement, digital processing method *(German)* 78—89599
electronic digital thermometer *(German)* 78—54368
electronic microbalance and precision balance design *(German)* 78—57935
electronic scales and precision instrum. *(German)* 78—70100
energy dispersive X-ray particle analysis system using beam blanking and digital scan-stop 78—24004
event timer, liquid crystal display 77—5811
events analyser of low-cost construction 80—57267
expendable bathythermograph digital recording and display system 80—46318
F-30 digital avometer, MUF-30 control module in CAMAC standard 79—88942
Fabry-Perot interferometer digital electronic system 78—12748
filter for frequency instability meas. *(Russian)* 80—57264
Fizeau wavelength meter, laser and other monochromatic sources, digital display 78—89450
FM detector, multichannel, EEG appl. *(Danish)* 78—35980
frequency counter, 100 MHz microprocessor controlled, Hewlett Packard (5315A) *(French)* 79—88938
frequency counter, LSI design, for microwave band 80—213
frequency counter design, 1 GHz, use of custom LSI 80—8973
frequency counter design technology 80—8974
frequency counter/timers, avoiding compromises in accuracy 80—8970
frequency counters and timers, var. in counting cct., techniques 80—8971
frequency meter, 250 MHz precision, eight digit devices reading portable instrument 77—71339
frequency meter, accuracy and noise rejection increase, weighting method *(Russian)* 80—27281
frequency meter, CMOS seven digit 200 MHz range 77—74427
frequency meter, for burst-like laser Doppler signals 77—72376
frequency meter, for LF meas., using TTL ICs 78—86296
frequency meter, Heathkit IM-4100 multi-function, circuit diagrams and performance data *(French)* 80—73348
frequency meter, LF and infra-LF, with digital positive feedback, metrological characteristics improvements with aid of computer simulation *(Russian)* 78—4656
frequency meter, up to 50 MHz, with seven-digit display *(Czech)* 80—8979
frequency meter, using variable measuring times and automatic scale conversion *(Spanish)* 78—49862
frequency meter for use with freq. convertor *(Russian)* 77—71346
frequency meter impulse noise effect on accuracy *(Russian)* 77—41575
frequency meter with high noise immunity 78—8412
frequency meters, series TF 2430, LSI 77—53936
frequency synthesizer, 10-29.999 MHz range 77—45860
frequency synthesizers, low-freq. signals, performance data for LEA GSN 20 and GSN 80 series *(French)* 80—73393
gas chromatography/mass spectroscopy system for cancer research 80—22469
heart beat counter, versatile digital SAMI 80—85510
heart-rate meter, instantaneous, precision 77—86681
heterodyne interferometer, real-time digital broad-beam, for measurements of deforming surfaces 79—85173
high pressure piston flowmeter with digital readout *(Polish)* 80—64661
histogram output 77—41652
hyperthermia generator digital readout device 79—70697
IC capacitance meter *(German)* 79—67339
illuminance at reflex-reflector, photometer for performance meas. 78—45668
impulse meter, 5 to 500 N range 78—191
inductance meter, low-cost instrum. 78—32832
integrating microphotometer 77—71360
interferometer for measurement of wavelength of gas laser lines 80—37079
ionosonde, universal, for multi-parameter ionograms 78—73577
IR, digital thermometer improvement *(Japanese)* 78—41306
isotope ratio meas. system, using programmable calculator with double collector mass spectrometer 80—63845
Jodrell Bank 1024 channel digital autocorrelation spectrometer 77—73970
klirr-factor unit dimension meas., errors evaluation 80—98873
laboratory automated systems and digital techniques 78—57922
laser pulse energy digital indicator *(Russian)* 79—22995
latency meter for evoked potentials 77—60322
least or greatest interval timer 78—62183
light rangefinder principle, construction and test results 79—27427
lightning counter, multichannel 80—51570
linear digicon detector, for astronomical speckle interferometry 77—78648
linear dimension meas. using freq. differences between two quartz oscillators 79—93097
linearised NTC circuits with A/D convertor for temp. meas. *(German)* 79—80619
liquid level meter, using conversion in binary-decimal refl. code *(Polish)* 77—17949
lock-in detection technique and appls. 79—49303
low frequency short duration pulse meas. equipment *(German)* 77—87735
magnet tester, automatic, with incompletely closed mag. system 79—9226
magnetic iron concentration monitoring in flowing ore suspension *(Russian)* 77—53879
magnetic tape linear velocity meas. scanistor 79—71425
magneto-optical stroboscope with pulse height analyser for rapid magnetisation variations 79—67356
manufacture in Rumania, frequency meters, voltmeters *(Rumanian)* 77—74452

digital instrumentation continued

- mass spectra registration system for digital recording 79—93252
- mass spectrometer recording system for automated isotropic anal. 78—12783
- mass spectrometrer, double collecting, device for automatic digital measurement of isotopic ratios 80—31932
- mass spectroscopy, smoothing of experimental ion kinetic energy data by digital computer 79—93112
- mass-measuring device, automatic, 0 to 9.99 g 79—71417
- mean time value signal generator, plug-in module printer controller appl. *(German)* 77—67414
- meteorology and oceanology *(German)* 78—53745
- meter for inductance coil parameters meas. 78—12718
- meters, analogue or digital differences and basis for rational choice 80—52184
- microdensitometer, for automatic astronomical photographic wavelength meas. 77—64655
- microdensitometer with computer-controlled scanning table *(Russian)* 79—6197
- microhmmeter, Sefelec RCNF-1, characts. *(French)* 77—53953
- micromanometer, conversion to large range digital readout 77—2716
- micrometer, development and appl. 78—65902
- micrometer/counter accuracy assessment *(Polish)* 78—45654
- microphotometer, multipurpose integrated digital, type TsIMF-2 80—4753
- microprocessor based digital scan generator, interface to image processing computer 79—12902
- microprocessor-controlled digital integrator for quantitative NMR measurements 80—11971
- microwave counters, modern techniques 78—32831
- midline echoencephalography, automatic histogram prod. system 77—64102
- million channel 300 MHz bandwidth digital spectrum analyser for Deep Space Network and SETI 78—73642
- millisecond timer and event counter 79—67256
- mitral valve velocity meas. by digital echocardiographic tracking system 77—21579
- modulator and synchronous demodulator system, alternative to analogue phase detector 78—70107
- modules of 'Summa' system for information output to oscilloscope, digital display and digital printing 77—3244
- Mossbauer systems, synchronous digital triangle generator and servo loop pre-amp 77—88351
- mulitmeters, Gould Alpha III, features *(French)* 78—77943
- multichannel digital correlator for optical mixing spectroscopy 79—93234
- multichannel digital temp. recorder, TR-2711, measuring 100 channels in 10 s 78—65931
- multichannel temperature recorder, Thermodac II with 24 channels using thermocouples 78—65930
- multidiscriminator for use in γ-γ coincidence expts. 78—70707
- multifunctional, for school use 78—12504
- multimeter, automatic PM 2517 80—22347
- multimeter, Avo DA117, overview of field servicing appls. 80—68210
- multimeter, control functions performed using 4 bit, microprocessor chip *(Slovenian)* 79—181
- multimeter, cost effective design using LSI 77—45858
- multimeter, D 3012, high accuracy *(German)* 80—22343
- multimeter, design based on Intersil ICL IC series 80—206
- multimeter, Fluke 8500 A microprocessor-based instrum., characts. *(French)* 77—53954
- multimeter, general-purpose, design practice 77—57348
- multimeter, hand-held instrument with liquid-crystal displays, includes A/D convertor chip 77—74423
- multimeter, LCD based on Intersil ICL ICs *(German)* 79—6138
- multimeter, LD 130 IC 78—16817
- multimeter, Matsushita VP-2500 A 80—212
- multimeter, MOS/LSI, mains/battery operated, construction and performance *(French)* 77—61090
- multimeter, using advanced LSI technique, Philips (PM 2517) 79—80640
- multimeter, with LED or LCD display *(French)* 78—57986
- multimeter conductance function introduction 79—93167
- multimeter for RMS meas., 30 Hz to 100 kHz *(German)* 77—5860
- multimeter innovation *(French)* 77—10045
- multimeter Quadriovameter MX 737A *(German)* 78—57988
- multimeter technology and future development 77—57345
- multimeters, automatic range selection, HV meas., general discussion 77—41639
- multimeters, comparison of analogue and digital instruments *(German)* 79—44917
- multimeters, microprocessor controlled 78—93721
- multimeters, selection criteria 77—45859
- multimeters, Weston model 6000, review 77—37908
- multiple digital differential thermal analysis instrumentation, synthetic chemicals production appl. 78—77902
- NCAR digital barometer 77—29453
- NMR freq. to magnetic field convertor, digital circuit 77—61097
- NMR gaussmeter using hybrid IC 79—71501
- noise and vibration measurement, Bruel & Kjaer products review 78—94493
- noise immunity control and meas., methods *(Russian)* 77—42663
- NQR spectrometer, digital freq. modulation 78—21189
- nuclear gauge, with digital response, statistical method for stability testing *(Rumanian)* 80—9459
- nuclear medicine, digital data collection system, portable, cost-effective 80—41195
- nuclear reactor instrumentation, microprocessor controlled, digital period meter, hardware and software 80—63473
- ocean bottom seismograph using digital telemetry and floating-point conversion 77—41197
- ocean digital survey fathometer, providing chart display and digital output 79—5665
- open channel acoustic flowmeters, design, calibration and errors 78—55701
- optical fibre transmission characteristic meas. by digital processing oscilloscope 79—12787
- oscillographic ferrometer 77—71353
- oscilloscope, operation and transients *(Danish)* 78—8392
- oscilloscope generation of moving grating patterns 77—40957
- oscilloscopes, multimeters, function generators and frequency counters, technology trends *(German)* 79—71437

digital instrumentation continued

- pacemaker impulse and pulse rate self-monitor 77—81719
- panel meter requirements, future trends, planar gaseous discharge display, LSI, microprocessing techniques 77—37867
- panel meters, characts. and appls. 80—68190
- pH meter, manual, automatic temp. compensation, laboratory appl. *(Rumania)* 77—74453
- phase meter, 2 Hz to 200 kHz, without freq. tuning *(German)* 78—54409
- phase meter, Dranetz model 314, comparison with analogue techniques and significant advantages *(Italian)* 80—68211
- phase meter, using delayed pulse train 77—49742
- phasemeter, tracking, quantisation error reduction *(Russian)* 77—61079
- phasemeter with indicator using seven-segment luminescent vacuum lamps, counter scheme 78—4648
- Philips digital multimeter, PM 2517, test report *(German)* 79—49220
- photoelectric condensation nucleus counter with digital recording 80—8448
- photoelectric digital energy meter for laser pulse meas. 77—71375
- photoelectric microscope, digital localisation of objects *(Slovak)* 77—18089
- photometer, laser Raman and spectrofluorometer systems appl. 77—5881
- photometric meas., digital meter, cct. and operation *(Polish)* 78—65943
- planimeter, used with trinocular microscope and TV receiver for TV photomicrography 79—71523
- polarimeter, digital lock-in technique using electro-optic cryst. 78—273
- positive displacement measurement system for diesel pump and injector performance testing, microcomputer-controlled 80—24112
- power and energy meas., errors sources and suppression *(Rumanian)* 80—47078
- pressure indicator construction and application 78—21112
- programmable, for liquid level and weight meas. *(Hungarian)* 78—32795
- psychrometer, ventilated, for direct reading of relative humidity 79—35763
- psychrometer, ventilated direct reading relative humidity meter using thermistors 79—2777
- pulse continuous RF signal amplitude and phase difference measuring device 78—12719
- pulse counter for cardiovascular monitoring 78—35978
- punched register for astronomical elec. photometer *(Russian)* 78—93117
- PWR, digital rod position indicator system for control rod drive line dynamic characts. study 78—33265
- PWR control rod digital position indicating system *(Japanese)* 80—63314
- pyrometry in solar furnace *(Japanese)* 78—32821
- Q-meter, automatic, design procedure 78—70155
- quartz crystal thermometer principle and technical parameters *(Polish)* 78—24791
- quartz thermometer *(Russian)* 79—49229
- radar reflection factor data, cartesian interpolation and display 80—31136
- radioactive waste density measuring meter, digital, remotely operated 80—68927
- radiometer/photometer (Tektronix) optical transmission characts. meas. *(French)* 79—89000
- raingauge recording system 77—70862
- raingauges, tipping bucket type, digital recording system description and field testing 80—77161
- recorder for astronomical meas. *(Polish)* 79—88598
- recorders, transient, 1024-point, circuits, operation 77—53868
- refractometer for atmospheric radiowave refractive index meas. 78—86321
- resistance bridge type thermometer, operational principles *(Polish)* 78—49834
- respiratory rate and ventilation digital recorder 78—81005
- reverberation time digital meas. instrum. for auditoria and studios *(Japanese)* 80—64321
- reversible counter for oscillograph logging, geophysical meas. appl. *(Russian)* 77—41209
- RMS error calc. *(Russian)* 79—97336
- SAW spectrum analyser, digital signals processing 78—26007
- scan convertor for use in medical US scanning 80—30816
- scanning and recording system for spot electron diffr. patterns 77—13825
- scanning electron diffractometer, appl. to radiation sensitive materials 78—87596
- seismic digital signal detect. system *(Russian)* 77—29515
- seismograph system, digital-recording, for Seismic Research Observatories project 77—5334
- SEM image processing systems, summary of useful techniques and anal. 79—12901
- semiautomatic digital coercimeter, exam. of design 78—76817
- semiconductor device C-V and G-V measurements using automatic technique, 50 Hz to 300 KHz 80—31800
- sidereal digital clock 78—36464
- SIMS, depth profiling, automatic sequential mass analysis 80—108764
- sinewave generator, for wattmeter calibration at zero power factor 77—18039
- single-sweep waveform recorder with automatic range selection 78—77889
- six-channel scanning thermometer type AD2036 operational principles 78—86269
- solar double-pass monochromator, with digital device for obs. and spectrum processing automation *(Russian)* 80—72777
- sonic digitiser method for biomechanical spatial data collection 79—39441
- sound vel. meas. instrum. using pulse-echo overlap method 79—37097
- sound velocity measuring instrument, comments on errors 80—14528
- spectrometer with high data rate, computer coupling system *(German)* 79—49212
- spectrophasemeter, rheological, for polymer systems meas., dynamic elastic moduli determ. 80—33547
- spectrophotometer, double-pass, with digital registration, spectrum registration precision *(Russian)* 79—96917
- spectrophotometer accessory for digital absorption and transmission meas. *(German)* 77—57408
- sphygmanometer, Omron's 77 model, accurate meas. 79—74773
- stack release radioactivity monitoring with digital processing 79—3253
- STEM image accumulation, storage and display system 80—37132
- stopwatch for automatic time keeping in undergraduate lab. 79—97158

digital instrumentation continued
- storage instrum. and function generator electronic modelling appls. 78—77937
- storage oscilloscopes, Gould Advance OS4000, using A/D and D/A convertors 78—93673
- stretch meter, ribbons in industrial processes, stretch measurement *(Polish)* 80—42194
- submarine quantum irradiance and photoperiod meter, with digital recording 80—98474
- sulfur dioxide concentration automatic digital recording system 77—25776
- synchronous reversing decade counter, readout, and memory 77—71728
- tachometer, for heart rate measurement 80—17162
- tachometer, for meas. steady-state shaft speed 79—6101
- tachometers, error analysis 80—90832
- temperature determ. of molten metal *(Russian)* 80—90846
- temperature meas., portable IR pyrometer principles *(German)* 80—42229
- temperature meas. by compensated thermocouples *(German)* 78—41304
- temperature meter, 4 to 300K, with Ge pickups 80—31747
- temperature meter, with Wien-Robinson oscillator, and digital frequency divider *(German)* 78—29110
- temperature recorders, advantages over analogue instruments 80—210
- temperature transducer, solid-state, using automatically balanced Wheatstone bridge *(Rumanian)* 80—57287
- Tesla-ammeter (F4354/1), improvement for investigation of const. mag. fields 77—26364
- teslameter, circuitry and calibration 79—63287
- test instrument survey *(German)* 78—8394
- theodolite microprocessor selection, development, and programming 78—24218
- thermal meas. using data logger and computer 78—81966
- thermocouples, cold junction compensation methods *(Italian)* 78—37002
- thermodynamic enthalpy and specific heat determ. equipment 78—57951
- thermometer, biomedical precision for 35 to 40°C, operation *(German)* 77—56499
- thermometer, electronic, with two sensors, in kit form *(French)* 80—4712
- thermometer, for 4 to 300K range 80—4709
- thermometer, linear, 0 to 99.9°C range *(German)* 78—93684
- thermometer, portable, with liquid crystal display *(German)* 78—29112
- thermometer, process meas. control appl. 78—49833
- thermometer, type 2572, with temp. range 4K to 1760°C with 0.1°C resolution 78—65929
- thermometer, type DTM 1, with LED display *(German)* 80—27302
- thermometer, using a thermistor bead 79—21741
- thermometer, with crystal resonator temp. sensor 77—82514
- thermometer LSI, remote sensing, cct. construction 80—27301
- thermometer using LSI ADC 79—44907
- thermometer with seven-segment display 79—21746
- thermometers, 300°C-1800°C range, features *(Russian)* 78—65926
- thermometers using quartz crystal oscillator high accuracy achieved 78—65932
- thin film thickness measurements, instrumentation system 78—89436
- time interval extensometer using voltage-pulse technique and reversing binary circuit *(Russian)* 77—53888
- time interval meas. instrument with 2 nsec accuracy 78—77867
- time interval meter, broadband 80—31729
- time interval synthesiser, computer-controlled 78—8386
- time pulse thermometer, technical description and error anal. *(Russian)* 79—49228
- time-domain reflectometer for dynamic shock position measurements 80—79248
- time-interval digital extensometer appl. *(Russian)* 77—53888
- time-interval meter for CRO 79—35702
- time-interval meter test rack 77—74373
- timer, IC, high accuracy and repeatability, photographic appl. 79—35683
- timer for electroadsorption studies 77—90670
- timer with memory, appl. to dynamics experiments, principles of electronic circuitry 80—67994
- tomography, focal-plane, image reconstruction using digital computer 80—61674
- total exposure error meas. instrument for cameras with or without built in exposure meter 79—6208
- transient recorders, enhancement of signal averaging using microcomputer 78—57930
- transient recorders, multichannel *(German)* 78—235
- treatment voltage and current, fast technique *(Polish)* 80—86340
- TV camera system for digitising single shot oscillograms at sweep rate 0.1 ns/cm 77—406
- TV detector, for stellar radial vels. determ. using cross-correl. techniques 78—16305
- two-channel data gathering and registration system for fast-action experiments 78—77877
- UNIPAN 545 thickness gauge, US 80—47019
- universal bridge, digital meter used to measure L, R, and C 78—12715
- universal timer-counter, design aspects 80—8972
- unsteady pressure coefficients digital measuring unit for wind tunnel tests *(French)* 80—68169
- US distance measuring device with decremental acquisition of the measuring results *(German)* 80—19199
- US echo-pulsed digital thickness gauge 77—74359
- US propagation velocity, and attenuation factor in solid materials, instrument for direct meas. 79—14179
- US pulsed thickness meter 77—45823
- US thickness gauge, portable 78—92427
- US transmission time meter, with digital readout 77—40485
- US vel. meter using freq. counter 80—38202
- UV radiometer, Spectroline DM series 80—77854
- V-delta-P digital flowmeter 77—84363
- velocity meas. device, error calc. *(Russian)* 80—86266
- Victoreen 555 integral and rate exposuremeter, digital display plug-in module 77—405
- video-electronic hologram interferometry for in-plane displacement measurement 80—106488
- viscometer, absolute oscillating cylinder, with digital data acquisition system 79—82003
- volt-ohm meter, 2.5 digit LED display 78—21162
- Watford Electronics 0-050 MHz digital frequency meter measures frequency and time intervals 80—68191
- wattmeter, for compact electronic equipment 80—209

digital instrumentation continued
- waveform recorder functions and appls. 80—57278
- wavemeter for CW lasers 78—89447
- wind gust recorder 77—56762
- wind meter, with speed and direction indication 80—207
- Si digital Sun sensor electrical and optical props. *(Japanese)* 78—32313
- $ZnSO_4.7H_2O$ electrolytic solution impurity meas. appl. *(Polish)* 78—31653

digital instruments *see digital instrumentation*

digital integrated circuits
- *see also integrated logic circuits; integrated memory circuits; microprocessor chips*
- asynchronous/synchronous FIFO data buffer *(German)* 77—9996
- automatic blood pressure recorder *(Japanese)* 78—24168
- chronometer with seven-function selector *(French)* 78—12677
- clock using MM5315 IC and CMOS ICs *(Spanish)* 79—8841
- digital phase shift for meter calibration 79—44898
- high speed decade counter, binary-decimal convertor digital readout 77—75028
- home-made IC digital voltmeter *(German)* 77—10062
- laboratory automated systems and digital techniques 78—57922
- miniature pressure-frequency convertor with pulse output 78—57926
- phasemeter with indicator using seven-segment luminescent vacuum lamps, counter scheme 78—4648
- precision thermometer, using 3 ICs *(French)* 79—80616
- printing scalar, single channel, for photon counting 77—5919
- pulse programmer, microprocessor-based, for NMR appls. 80—52289
- tank water flow control and meas. appl. 77—41569
- x-t chart recorder, frequency marking 77—53947

digital readout
- *see also digital instrumentation*
- astronomical images, interactive program for digital display *(Italian)* 80—98559
- automatic linear expansion coefficient meter with digital readout 80—106713
- automatic thermal conductivity meter with digital readout 80—106714
- blood clotting time measurement system, four-digit display *(Danish)* 77—90826
- bubble chamber picture digitisation system 79—63871
- CAMAC hodoscopic recording system, coding and reading data unit 78—13397
- CAMAC standard 160-MHz decade counter with digital readout 78—9041
- camera character-forming display, based on LEDs and internal or external timing circuits 79—9251
- capacitance meter, utilising CR discharge 79—12819
- Cherenkov light photograms, automatic scanning by TV digitiser 80—52822
- continuous radiogauges with digital meas. system, dynamic characts. 79—59311
- darkroom exposure control circuit *(German)* 79—6198
- DC voltmeter, hand held design 80—17931
- delay line for position readout in wire chambers 80—18757
- digital data processing using integer arithmetic 80—27917
- direct-reading displacement digitiser construction and coding *(Russian)* 77—9983
- display for lecture hall use 78—86075
- display format, new arrangement reduces observational error 77—5822
- display stabilising circuit, for systolic-diastolic blood-pressure monitors 78—40364
- drift chamber and pulse height readout systems using analog multiplexing 77—54490
- Earth tides, tilts, parallel recording through digital print-out and photorecording channels *(Russian)* 78—88785
- electric dichroism measurement instrument with digital processing 80—82800
- electrophotographic KC film digital recording performance 78—78024
- electrophotographic spectrographs with electronic pulse readout 79—26147
- event timer, liquid crystal display 77—5811
- exposure meter, enlarging, digital, using photodiode, for black-and-white photography 79—85190
- flash chambers of polypropylene sheets 79—26833
- flash tube discharge mechanism determ. from digitisation pulse output 78—17504
- general-purpose meas. microscope with photoelectric readout 79—71524
- high speed decade counter, binary-decimal convertor, integrated circuitry 77—75028
- holographic memory photodiode matrix readout system *(Russian)* 77—58266
- in-core movable neutron flux mapping computerised console development 78—13308
- inductance meas., automatic, 1 μH to 100 H *(French)* 79—85152
- intelligent oscilloscopes used for production testing, dynamic analysis 77—37929
- LaCoste-Romberg gravimeters, digital voltmeter reading evaluation 79—96830
- liquid level meter, using conversion in binary-decimal refl. code *(Polish)* 77—17949
- magnetic disaccommodation measurement, device, graphical or digital registration *(Polish)* 79—93180
- mass read-out system for magnetic sector mass spectrometers 79—67422
- micrometers with transmission and counter type display *(German)* 77—26278
- modular 125 ps resolution time interval digitizer for 10 MHz stop burst rates and 33 ms range 79—45591
- modules of 'Summa' system for information output to oscilloscope, digital display and digital printing 77—3244
- MWPC, γ-image blurring reduction by delay line readout 78—37492
- MWPC, CAMAC readout system 78—46248
- MWPC, delay line readout of anode wires 77—38571
- MWPC, high-flux fast readout system based on new monolithic integrated ccts. 78—37491
- MWPC, interwoven grid wires for second coordinate readout 80—27897
- MWPC, large cylindrical dual coordinate 80—18759
- MWPC, multi-delay line cathode readout 79—45573
- MWPC, position sensitive, fast delay line readout 78—37490
- MWPC, position sensitive system with digital read-out for Munich Q3D-spectrograph 77—10549

digital readout continued
- MWPC compact chambers and electronics for crystal ball detector 79—45534
- MWPC focal plane detector system with digital readout 79—68158
- MWPC read out, fast clustering processor 79—76304
- MWPC readout system 78—17505
- MWPC using EM delay lines, read-out system *(French)* 77—88349
- nuclear track sensitive target expts., automatic film meas. 78—55105
- panel meters, characts. and appls. 80—68190
- phasemeter testing, automatic modulation method 77—53939
- phasemeter with indicator using seven-segment luminescent vacuum lamps, counter scheme 78—4648
- photomultiplier HV readout system 77—54492
- position sensitive detectors, for X-rays and γ-rays *(Japanese)* 78—33397
- precision thermometer, using 3 ICs *(French)* 79—80616
- proportional counter data acquisition providing max. spatial resolution at high rates 79—45572
- proportional delay line chambers for Fermilab external muon identifiers 78—37489
- proton spectrometer/polarimeter for photoreactions below 1 GeV 80—18751
- prototype CCD system for the time projection chamber 79—45575
- radiotherapy Clinac-18, satellite digital display 78—3599
- recording system, for automatic US flaw detection system 78—76815
- refractometer, laser, automatic systems appl. 77—67492
- resistive unidimensional detectors employing rise time readout method, position resolution and linearity 80—14048
- spectrophotometer (UR-20), digital output of experimental data 77—26409
- synchronous reversing decade counter, instrument appl. 77—71728
- temperature monitoring, deep body, cardiac surgery appl. 77—29223
- thermocouples, noise study 77—22544
- thermogravimetric apparatus, automatic device with digital output 78—7281
- thermometers, high precision using MPUs 79—54130
- thermometers, using LED display 77—37884
- time projection chamber multichannel ADC and readout system 79—45590
- time shared display, for two simultaneous inputs 77—74424
- time-interval meter for digital display pulse echo thickness gauges 78—48594
- torquemeter, capacitive with digital display *(German)* 77—34006
- weighing system, electronic, digital transducer instruments 80—95076
- weighing system, microprocessor based electronic scale 77—74421
- X-ray powder diffractometer proportional counter detector system, digital read-out 78—4751
- X-ray tube kVp indirect determ. using digital readout device 78—53486

digital signals
- 1.5 Mb/s bipolar signal coding and decoding optical fibre link 77—27343
- atmosphere radar signal processing, for SOUSY-VHF-radar, using preprocessor 80—85774
- binary image analysis, distance and region association algorithms 79—72523
- CRO used for accurate time measurement *(German)* 79—30423
- Doppler sonar, digital processing of signals 77—46856
- EMG processor and three-state myoelectric control design 79—53283
- generator for rapid scan differential pulse voltammetry 80—61182
- image enhancement by median masking technique 80—106483
- image improvement, thermal imager pictures delining 80—106466
- image processing, book 79—910
- image processing applications, seminar, San Diego, CA, USA (Aug. 79) 80—105424
- image processing developments 80—14287
- NMR spectroscopy, Fourier, S/N ratio optimisation, influence of receiver circuit and digital processing *(Czech)* 79—17461
- optical fibres, digital techniques for evaluation 79—94346
- plasma probe, digitised random signal analysis method, power spectrum, phase vel. 77—84509
- processing techniques, meteorological satellite NOAA appl. *(Japanese)* 78—24424
- radio antenna arrays, incoherent optical 1-bit cross-correlators, radioastron. appls. 80—98555
- reflection seismograms signal anal., use of kepstrum 78—81425
- speech signals, data reduction, methods and results 79—81648
- time-integrating acousto-optical correlator design and performance 80—106618
- wandering in turbulent atm., error probability in binary signal reception 79—10337

digital simulation
- acid mine drainage in impoundments 77—37260
- acoustic real-time and frequency-domain processor simulation 79—81643
- acoustic transmission system with radiation, finite element simulation 79—3862
- adaptive optical system, performance with extended dynamic targets 77—46798
- adsorbed chain structure, Monte-Carlo simulation *(Russian)* 77—19122
- adsorption, computer simulation 79—65308
- adsorption, density functional theory, computer simulation 80—24735
- advection-diffusion simulations, finite-element and finite-difference methods comparison 77—22424
- ageing metals, new particle phase spatial distributions, computer calcs. *(Russian)* 79—83202
- agglomeration, computer simulation *(Japanese)* 78—95706
- agglomeration, Monte Carlo simulation *(Japanese)* 78—95707
- aggregation simplifying simulation, neural net appl. 79—8497
- air pollution density distrib., flow pattern in Tanabe area, Japan, numerical anal. *(Japanese)* 78—96289
- alkali chlorides, thin film, crystal-vacuum (100) surface, mol. dynamics computer simulation 80—34288
- alkali halides, thin films, crystal-vacuum (110) interfaces, mol. dynamics computer simulation 80—34289
- alkali metal, bulk properties, computer simulation 78—30729
- alkali metal halide, laser damage morphology simulation 80—35015
- alloy, binary, conc., with short and long range order, computer simulation of diffusion 78—30778
- alloy, binary, order-disorder transition kinetics, computer simulation 80—92643
- alloy, binary, quenched, computer simulation of cluster dynamics of two dimensional model systems 78—31434

digital simulation continued
- alloy, cubic, computer simulation of formation of tweed and modulated structs. 79—96029
- alloy, FCC, binary, on Ising system, sublattice magnetisation, tricrit. point, simulation 79—33491
- alloy, FCC, Monte Carlo simulation of surface segregation 78—31413
- alloy, quenched, binary, time evolution, computer simulation of three-dimensional model system 78—31433
- alloy design by automatic modelling, CAD system *(Japanese)* 77—52607
- alloy melt, temperature distribution during cryst. growth by Czochralski method *(Russian)* 80—75192
- alloy random, binary, diffusion correlation factors calc., comparison of matrix inversion, Monte Carlo and diffusion of probability techniques 78—30779
- alloys, binary substitutional, determ. of local atomic configurations 79—86739
- ambulatory neuromuscular activation control model 79—57638
- amorphous Lennard-Jones solid, edge and screw dislocation, stability, elasticity, simulation 80—15099
- amorphous metals, computer simulations of tensile deformation and radiation damage *(Japanese)* 79—42137
- amorphous solid, structural defects, computer simulation study 80—88040
- amorphous structure, computer simulation 78—30541
- amorphous surface, energy profile and binding energy, computer simulation 80—100381
- amorphous thin film on crystalline substrate, computer simulation 79—15045
- amygdaloid kindling phenomenon extended first approx. model 78—53378
- ang. and energy relationships, 1-3 keV *(Russian)* 79—78802
- angiography, comparison of convolution and ray tracing computations of small blood vessel images 77—48863
- angiography, effects of asymm. focal spots 77—21617
- angiography, validity of computer simulation of blood vessel imaging 78—3594
- anharmonic atomic chain breakup, molecular dynamics calcs., deformation dynamics 80—29117
- anisotropic solid fluid flow with free or artesian surface analysis, finite element method appl. 78—92872
- anisotropic system, computer simulation, energy and specific heat temp. depend. 78—9947
- anthracene, single cryst., fluoresc. decay, Monte-Carlo simulation *(German)* 79—61440
- architectural acoustics, image method for simulating impulse response between two points in small room, using digital computer 79—68487
- arterial segment loading-unloading simulation and analysis 79—83844
- artificial heart test system, simulation of artificial ventricle and mock circulatory system 77—52933
- astronomical optics, computer modelling 79—8836
- astronomical spectra obtained with low-dispersion Fehrenbach prism, computer simulation 78—57468
- atmosphere models, advection in flux formulations for variable grid models 77—29380
- atmospheric boundary layer turbulence, multi-component linear digital simulation 78—61513
- atmospheric showers, γ-ray initiated, computer simulations, Cherenkov radiation, geomag. field effects 77—49254
- atmospheric transparency meas., computer prediction *(Italian)* 77—91333
- atom ejection studies by classical trajectory simulation 80—108311
- atom-atom collision cascades localisation, impurity and thermal vibr. influence, computer simulation method 80—88227
- atomic dislocation modelling, flexible boundary conditions and nonlinear geometric effects 78—75667
- atomic scale computer simulation of lattice defects, stress tensor determ. 78—30602
- atomistic computer experiments of point and extended defects 78—30610
- auditory neural network modelling by computer simulation, spatial firing patterns 79—74686
- auditory neuron, characts. of digital model 78—3516
- austenite, computer simulation of C diffusivity 79—77803
- automated simulation of direct school/society interaction 79—35487
- axial channelling, in monatomic and diatomic cryst., multistring model computer simulation, foreign atom location appl. 79—42128
- axial-flow compressor cascade flows computer simulation 78—79333
- axisymmetric field problem soln. by Gaussian surface charge simulation 80—95758
- backscattering of low energy noble gas ions from single cryst. surface, computer simulation of ang. depend. 79—19961
- ball screw type wave power generator, continuous system simulation language 80—35632
- barrier island migration simulation 78—20384
- BCC crystal, electron microscope image contrast, theoretical predictions for non-edge dislocation loops 80—24326
- benzil triplet-anisole, reversible exciplex form., phosphorescence, photostationary and transient obs., simulation 78—9182
- binary alloy, model quenched computer simulation of time evolution in nucleation region 79—82344
- binary collision model for plasma simulations, Monte Carlo method particle code 78—9824
- binary crystal growth, computer simulation 78—9979
- binocular stereopsis Julesz stereogram simulation 77—44671
- biochemical pathway enzymes kinetics *(German)* 77—5102
- biological differentiation and morphogenesis, computer simulation 80—30691
- biological evoked potentials, single trial, S/N ratio and response variability 78—61159
- biological intraluminal conc. flow-reaction-absorption systems *(Japanese)* 77—86525
- biological macromolecules, computer simulation of solvent struct. 78—40113
- biological research, math. modelling, role of computers *(Chinese)* 79—1996
- biomolecular systems, topographic analysis in FORTRAN IV 79—88050
- biomolecular systems 79—88049
- biostereochemical modelling, interactive computer graphics, appl. to DNA-protein interaction 78—88693
- biped locomotion control 78—80904

digital simulation continued
- bladder smooth muscle impulse propag., math. anal. *(Japanese)* 78—53359
- blast loading on three-dimensional structures, transient 77—68624
- block iterative finite element preprocessed scheme, large nonlinear problem simulation 79—53
- blood pulsative flow, finite element method appl. 78—92670
- borides, lightweight ceramic armour appls., ballistic tests, computer simulation, book contrib. 78—48556
- Bouguer gravity model, interactive CRT display, for geology CAI 77—22
- brain, math. models of parallel and sequential processes 77—48785
- brain cortices large-scale simulation via BOSS system 79—2039
- brain function comparison with associative storage system capabilities *(German)* 77—29123
- brain rhythmic activity generation models *(Dutch)* 78—73150
- brass, stress corrosion cracking constitution of Pourbaix diagrams for ternary systems by digital computer 78—35595
- brittle material, fast crack propagation, computer simulation 80—38331
- bronze 905, partially solid, die thermal behaviour in machine casting 78—6917
- building solar-climate control systems, control options evaluation by simulation 80—40844
- bulk trap energetic distribution props., space charge limited current meas. use 80—80293
- BWR nuclear plant nonlinear digital simulator, optimal digital control methods appl. 79—9826
- CAI in physics, student response to comput. phys. teaching lab. project at Surrey Univ. 77—53724
- cancer problem cell kinetic study based on automatic control theory 77—40639
- cardiac and torso models for ECG forward and inverse problems 77—40837
- cardiac assistance, in-series, by intra-aortic balloon pumping, haemodynamic responses, computer model 79—96711
- cardiac potential distribution, human body surface 77—29221
- cardiac stroke volume meas. from impedance, rel. to aortic flow waveform 77—86522
- cardiac US data, moving heart surfaces extraction 80—8114
- cardiovascular computerised modelling, pressure regulation in hypertension 79—88098
- cardiovascular modelling to study effects of pressure regulation: hypertension 79—25027
- casting, continuous, heat transfer anal. by finite element anal. 78—30167
- casting solidification simulation, use of general purpose software 77—52312
- cavitation bubble collapse, num. simulation 77—58747
- Cebysev mixing transformations, use in random process digital simulation 79—80510
- celestial mechanics, computer simulations of self focusing particle streams 79—53704
- cell clone growth computer model 77—40643
- cell membrane particles, max. density of random placing 79—44862
- cell population survival kinetic parameters derived by computer simulation of radiobiological data 77—56433
- central pairwise potential alternative in computer simulation in materials science 78—30585
- cerebellar Golgi-granular system simulation *(Japanese)* 79—29522
- cerebral blood flow, linear computer model 79—92288
- cerebral blood flow dynamics, computer model 79—83837
- cermet film, as solar selective absorbers, production, struct. and optical props. 79—29485
- chain molecules in soln., thermodynamic props. related to chem. pot. 80—3394
- chaotic branched macromolecules, struct. simulation, parameters calcs. *(Russian)* 80—69283
- Charpy V-notch toughness test, computer simulation 79—70138
- chemical kinetics, discrete simulation methods, appl. 78—48627
- chemical potential, computer simulation 78—31683
- chemical processes, many-body, classical trajectory simulation 80—35504
- chemical reactions 78—48646
- chemical system, equilibrium fluctuations, deviations from Poisson behaviour, molecular dynamics 80—86211
- chemical system dynamics, Markov chains 77—60035
- chemiluminescence, electron transfer reaction zone, simulation techniques 79—8200
- chloromethane, IR spectrum, evidence for $2\nu_3$ overtone 79—68226
- chlorotrifluoremethane, IR rovibr. spectrum *(German)* 80—47998
- chromatography, nonlinear, nonideal, computer simulation models 80—62639
- circadian rhythm related to human body temp. 79—70525
- circulatory clinical model matching techniques 79—53176
- cloud seeding, num. simulation technique 79—84519
- cochlear hydrodynamics model 78—31821
- collective modes in solids 80—54325
- colliding particles in gravitational field, numerical simulations 79—16802
- collimated electron trajectory in nonuniform transverse mag. field 80—53201
- combustion and non-combustion flow fields with swirl, numerical anal. 79—98821
- comets, computer generated pictures 80—17549
- complex chemical systems, chemical process and rate models, computer simulation appls. 78—48620
- composite electrostrictive resonators, finite element simulation 78—59237
- composite ion implantation profiles, computer simulation 77—80528
- composite ion implantation profiles, computer simulation 77—84786
- composite piezoelectric US transducer, finite element simulation *(Japanese)* 79—68537
- composite superconductors, stability anal. by thermal analyser digital computer program 78—54995
- computed electron micrographs, use in defect identification 79—69101
- computed tomography image discrepancies due to object-time depend. in several geometries 80—46044
- computer applications to process control, conference, The Hague (1977) 78—49808
- computer modelling of matter, conf., Anaheim, USA (March 1978) 80—51954
- computer simulated laboratory exercises, validity of graphic approach 78—81780
- computer simulated patients for teaching students of speech and hearing 79—17162
- computer-generated 80—9841

digital simulation continued
- computerised tomography, iterative three dimensional reconstruct. from twin cone beam projections, simulation study 78—80949
- computerised tomography, reconstruction simulation, no. of rays versus no. of views 78—69214
- computers, appls. in University research 79—54114
- concrete, unreinforced pavement slabs, environmentally induced stresses, computer experiments 78—35435
- condenser efficiency and performance enhancement, evaporative cooling *(German)* 79—72781
- contact angle for liquid-solid-vapour 78—2340
- continental margin sedimentation, computer simulation 78—15998
- cooled epoxy resin vacuum mould computational simulation of design *(German)* 80—81020
- coral growth form, light control 77—2076
- core operating limit supervisory system stochastic simulation 79—630
- corner, three-dimens., Navier-Stokes eqn. soln., numerical code 78—30314
- cosmic ray anisotropy, COS approx. appl. to expt. data, computer simulation 77—5457
- counterpulsation dynamics simulation, rel. to heart assist. blood pump 80—16996
- coupled biological oscillators, interactive modules 78—35792
- coupled chemical reactions, exact stochastic simulation, using digital computer algorithm 78—48625
- coupled chemical reactions, stochastic time evolution, Monte Carlo simulation procedure 77—9047
- crack growth in concrete, computer simulation using Monte Carlo method 78—76764
- crack propag. simulation, using moving grid based finite difference scheme 78—83334
- crack propagation, computer simulation 80—59573
- crack propagation under compression, finite element anal. *(Japanese)* 78—42567
- crack simulation computer program for plate structures *(Japanese)* 80—79218
- cryogenerators, thermally activated closed-cycle regenerative 79—58742
- crystal defects, simulation of high resolution images 80—107208
- crystal defects and disorders, computer simulation of electron dynamical diffuse scattering 79—23505
- crystal growth, from soln., implication for industrial crystn. 80—49147
- crystal growth, Monte Carlo calc. 78—26463
- crystal growth from vapour 78—31312
- crystal surface, ion bombardment, equilib. at. struct. 79—56051
- crystal surface structures, Monte Carlo simulations, appl. of statistical tests, cryst. growth 77—4060
- crystalline solutions, binary isostructural, thermodynamic mixing parameters computation, FORTRAN IV subroutines 77—86344
- crystallisation in layered intrusions formation 77—33069
- crystallography, modelling of FCC solid solutions 78—26475
- cyclic voltammograms at spherical electrodes, switching pot., drop size effects, digital simulation technique 80—40766
- Czochralski crystal-pulling process, digital simulation of flow patterns 78—15304
- Darrieus wind turbine system, parametric performance analysis by digital simulation 80—40817
- defect images produced by piezobirefringence, simulation 78—30521
- defect superlattices, hardening influence, computer simulation *(Russian)* 79—83206
- dendritic crystal growth computer simulation, impurity trapping 78—38992
- dendritic membranes, active vs. passive effects on simulated neuron transfer properties 79—24976
- dendritic particle characterisation of automatic methods 80—25590
- dense gases and liqs., three-body nonadditive interactions, thermodynamics props., mol. dynamics simulation 79—7435
- dense liquids and their mixtures, mol. dynamics, numerical algorithm 80—28890
- diatomic molecules, homonuclear, molecular dynamics, time-dependent statistical props. 80—44093
- diatomic molecules, homonuclear, molecular dynamics, translation-rotation coupling 80—44094
- 1,2-dichloroethane, enclathrated, conform., reorientation, PMR line shape anal. 79—91300
- dielectric liquid, DC cond. due to impurity particles, computer simulation and comparison with expt. 79—91060
- diesel-driven chiller system, with multi-tank thermal storage system, for large commercial buildings appl. 79—48187
- differential chromatogram simulation and analytical feasibility *(Russian)* 78—35758
- differential pulse polarography of irreversible reactions, anal. appl. 79—79325
- diffuse light scattering, mathematical modelling 80—106450
- digestive tract electrical rhythms simulation 78—64970
- digital lock-in amplifier simulation 77—151
- dipolar liquid, far IR absorpt. rel. to Mori continued fraction for autocorrel. function 78—2875
- direct radiator loudspeaker model, finite element approach 80—69622
- direction sensitivity in visual cortex, neural net model 79—48248
- direction-sensitive displacement analysis by multiple freq. holographic interferometry 78—54338
- dislocation, straight line, motion in conc. solid soln. computer simulation 77—81268
- dislocation array, equilibrium configuration by computer simulation 78—30616
- dislocation configurations, jog and dipole, computer simulation of electron microscopic diffr. contrast 77—84750
- dislocation glide through fields of point obstacles 78—34521
- dislocation groups, of opposite sign emitted from a stressed source, computer simulation of dynamic behaviour 80—6406
- dislocation image in X-ray plane wave topography 80—54234
- dislocation motion, lattice resist., effect of impurity interstitials 80—84170
- dislocation motion, straight line, in concentrated solid soln., computer simulation 77—15413
- dislocation motion through random array of point obstacles, thermally activated, computer simulation 78—30636
- dislocation motion through random array of short range barriers 78—30634
- dislocation motion through random array of weak obstacles of finite width, digital computer simulation 78—30633

digital simulation continued
dislocation percolation through absolute obstacles in impurity crystals *(Russian)* 80—70196
dislocation segment oscillations, internal props., point obstacle collisions, glide plane motion *(Russian)* 80—39088
disordered crysts., optical transforms 80—78783
dispersion strengthening, dislocation interaction treatment, digital simulation models 78—31419
displactive structural transition anal., mol. dynamics calc. 79—86865
distortive phase transitions, order-disorder and displacive regimes, mol. dynamics study 80—75324
disturbed cell renewal control system modelling and simulation 79—29510
disturbed cell renewal systems simulation via microprocessor system 79—48227
DNA, hydrodynamic shearing simulation 80—16895
DNA hydrodynamic shearing model 79—39337
domestic wind power system including storage, simulation analysis 79—92058
ductile fracture, computer model based on plastic strain, fracture toughness prediction, comparison with steel data 79—32383
ductile fracture in random distrib. of voids, computer simulation 79—90723
ductile-brittle transition, atomistic simulation by computer, exam. of thermal activation of crack tip plasticity 78—60801
dye laser, energy transfer, computer simulation 79—13964
dynamic emission computed tomography, quantitative pots. 78—77105
dynamic stability of dislocation sub-boundaries during straining, computer simulation 78—30635
Earth electrical conductivity modelling using finite element numerical technique 78—20357
earthquakes computer simulation 78—48987
EAS data relation to high-energy particle prod. models, simulation 77—70962
ECG, surface potential distributions, equiv. dipole recovery in presence of noise 79—70671
ECG activity models for computer simulation *(Spanish)* 78—11758
ECG digital simulator, for test appl. *(Spanish)* 78—40359
ECG signals, diagnostical functions, effect of random noise *(Croatian)* 80—98169
ECG simulation using a microprocessor 80—61726
ECG theory computer application programs *(Spanish)* 78—20165
echosonde antennas performance, simulation rel. to influence of echo carrier freq. and antenna dimensions 78—1474
eddy current through type transducer, operating condition simulation when inspecting ferromagnetic rods 78—53077
edge dislocation motion, glide and climb resist. due to dragging a Cottrell atm. 79—99194
edge dislocation thermally activated motion, appl. to KCl-KBr solid soln., computer simulation 79—19249
education, variable star, digitally synthesized, diagram 79—9067
elasto-plastic flow in computer simulated, A533 steel 78—56720
electric field computation by charge simulation and finite element methods 80—95759
electrochemical mechanisms, simplex fitting and finite difference simulation anal. 78—44381
electrochemical processes with free convection, numerical simulation 79—52681
electrochemical surface processes, kinetics simulation 79—16004
electrochemical surface reacts. driven by linear pot. sweep, kinetics 77—25275
electrochemical surface reacts. driven by linear pot. sweep, sequential reactions, kinetics 77—25276
electrochemical treatment cathode with honeycomb arrangement of drain apertures *(Russian)* 79—96164
electrocrystallisation, chess board type computer simulation 80—54157
electromagnetic wave propagation, discrete random medium, statistical approach, computer simulation 77—75391
electron density, bulk and surface atoms, from ab initio model calcs. 79—4590
electron diffraction patterns, and optical transforms of atomic aggregates, symmetry aspects using computer simulation 79—7525
electron liquids, two-dimensional, self-diffusion constant, molecular dynamics 80—34372
electron micrograph, computer simulation for crystal defect identification 78—30525
electron microscope imaging of isolated individual sheets of graphitic carbon 79—2890
electron microscopy, phase contrast of support films, simulation 80—4812
electron microscopy, simulation of digital image restoration 77—57431
electron microscopy, structure image high-speed calc. methods 79—55622
electron microscopy of biological objects, 3-dimens. image, computer simulation 77—13046
electron motion in elec. and mag. fields, student lab and computing studies 80—27076
electron solid, two-dimens., shear modulus and melting, temp. depends. 80—158
electron trajectory simulation, in material media *(Rumanian)* 80—24520
electrosurgical dispersive electrode site temp. and current density distrib. model 79—92424
ellipsometer, polarisation-modulation, Fortran simulation program ELLIPS 78—271
EMG, slow motor nerve cond. meas. by blocking technique 78—36027
EMG, surface, digital simulation, spectral anal. 78—80863
EMG, surface, model for digital simulation 78—80862
EMG, surface pots. rel. to force transients in muscle 77—44642
energy planning in Arab world 80—26122
entropy calculation with computer simulation 77—22504
environmental release prediction, time split finite element algorithm 78—92880
enzyme kinetics simulation 79—15961
enzyme-substrate reactions in differential scanning calorimeter, digital simulation 79—74794
epileptic activity modelled as chain reaction within system of interconnecting cells 77—48787
epitaxial films, condensed from vapour or molecular ion beams, impurity distrib. 80—65032
EPR, rat liver and hepatoma mitochondrial lipids, stochastic anal. 78—76984
EPR and saturation transfer EPR, fast computation, perturbation approx. extension for overmodulation 78—82754

digital simulation continued
EPR and ST-EPR spectra of nitroxide spin labels in rigid-lattice limit, rapid computer simulation 79—93189
EPR of free radicals, simulated spectra, compensation for integerisation errors 79—33537
EPR of $S={}^1/_2$, $I={}^3/_2$ system, quadrupole effects 79—42827
EPR powder spectral simulation, paramagnetic ions 78—80194
ESR spectra, simulation by FFT 79—19763
estuarine dynamics, mass balance eqn., longitudinal dispersion function estimation 77—37262
excitons, diffusive and percolative lattice migration 80—59879
explosive forming, computer numerical simulation 80—59560
external disturbance transformation into boundary layer waves 80—28523
eye, direction-selective cells formation modelling in developing retina 80—30721
eye movements, vergence and version, reciprocal innervation model 77—48798
fatigue behaviour of fibre reinforced plastics, under random loadings *(Japanese)* 80—85032
fatigue crack, computer simulation of propag., model based on Elber's eqn. *(Japanese)* 78—7030
fatigue crack, dynamic treatment of growth *(Japanese)* 78—34084
fatigue crack closure, computer model, based on surface roughness and residual strain 77—73347
fatigue crack growth rate data, effect of meas. precision and data processing procedures on variability 79—61817
fatigue crack path prediction by finite element method *(Japanese)* 78—42568
fatigue crack propag., computer simulation based on crack closure concept 78—68793
fatigue cracks, computer simulation of propag. based on BCS model *(Japanese)* 78—7029
fatigue testing, computer controlled system, simulated service loading 79—15885
fatigue testing, digital simulation of environmental processes 77—40499
FCC crystal-melt interfaces, mol. dynamics simulation 80—79913
FCC lattice, computer simulation of low energy displacement cascade 78—47367
FCC metal, polycrystalline, computer simulation of rolling texture *(Japanese)* 77—63686
FCC metals and alloys texture transitions, computer simulation 79—90666
FCC/BCC partial coherent, boundaries, computer modelling 79—46669
femur, human, with implanted Charnley prosthesis, stress anal. 78—20314
Fermilab booster, simulation of injection dynamics, linac bunch struct. reappearance 77—83261
ferromagnetic alloys, disordered cryst. and amorphous, mag. dipolar field distrib., computer simulation 80—65790
ferromagnetic alloys, disordered crystalline and amorphous, dipole field distribution 80—25101
ferromagnetic crystal, domain wall pinning effect and intrinsic coercivity, computer simulation 78—64217
fibrous material failure kinetics, internal stresses, computer simulation *(Russian)* 80—40479
field effect transistors, computer simulation, student lab expt. 79—44673
field evaporation of W in FIM, computer simulation 77—69973
film, amorphous, of hard spheres, computer simulation 78—22984
film growth modelling, condensation coeff. influence evaluation *(Czech)* 79—77935
finite element determ., operational stress-state of field ion microscope specimen 78—32933
fission reactor digital simulator software development, kinetic equations integration, numerical solution method 80—68901
fission research reactor computing, three-dimensional SNAP diffusion theory, including up-scattering 80—5208
flagella bend propagation, derivation of eqns. of motion and simulation 78—77074
flame, mutual ion neutralisation 80—35537
flames, unsteady, propagation, numerical modelling 79—64794
flexible structures, dynamic simulation by substructure synthesis 80—87733
flood flows routeing in rivers, parameter optimisation 77—37263
flow, boundary-layer, laminar to turbulent transitions, numerical simulation 78—38286
flow, confined, numerical simulation, anal. of higher order methods 80—19316
flow, in channel, turbulent vel., press., and temp. fields, direct numerical simulation 80—19361
flow, new viscous-inviscid interaction method 79—1154
flow, transonic, steady and unsteady, implicit finite difference simulation 80—19429
flow, turbulent, numerical simulation with three-dimens. vortex in cell method 80—19330
flow, viscous, time-dependent, integral representation approach to simulation 80—38375
flow about arbitrary 2-dimens. boundary, implicit finite difference simulation 78—94628
flow of compressible, viscous, heat-conducting gas, numerical simulation methods 80—38449
FLUCOMP numerical river flow model 80—26653
fluence limit analysis of nuclear reactor component, damage function methods 77—18668
fluid, cavity-biased (T,V,μ) Monte Carlo method, computer simulation 80—92434
fluid, classical, transport coeffs. computation by cell hydrodynamics 78—38600
fluid, of hard prolate spherocylinders, pair distrib. function expansion validity 80—24336
fluid dynamics 80—17805
fluid structure, ionic, boundary conditions distorting effects in simulation 79—50968
fluid velocity vector and temp. fields reconstruction, three-dimens., from acoustic transmission meas. 78—51261
formic acid, cryst., H bonded, IR spectrum computer simulation 80—97253
Fourier transform holography system, lensless, at 14 and 34 kHz *(Japanese)* 78—30133
fracture processes and fibre strength, in brittle fibre reinforced alloys, anal. by Monte Carlo computer simulation *(Japanese)* 78—80634

digital simulation continued
fracture toughness testing, elastoplastic range, computer simulation 80—21217
free electron lasers, energy transfer, computer simulation 80—83578
free surface flow, finite element method appl. 78—90819
frequency meter, LF and infra-LF, with digital positive feedback, metrological characteristics improvements *(Russian)* 78—4656
frequency swept holography, computer simulation 77—75446
frequency swept holography, computer simulation 77—75447
Fresnel zone plate aperture for γ-ray imaging system, digital modelling 78—7442
frictionless tidal channel behaviour, finite element and finite difference methods appl. 78—92876
fusion reactor, low power Tokamak experimental fusion power plant, scoping studies with empirical scaling, SISYFUS code 80—102309
fusion reactor, MFTF, power supply system, digital simulation using EMTP code 80—91286
fusion reactor, TFTR energy conversion system simulation 80—99303
fusion reactor design and performance requirements, cost and systems anal. 78—50357
fusion reactors, JT-60, poloidal field power supply system, AC voltage behaviour, simulation 80—91287
gamma camera oscilloscope display, performance meas. 78—7425
gamma camera scintigrams, influence of digital representation on image quality *(German)* 78—88738
gamma spectrometry, low-level, in vivo, optimum detector size and position 78—28075
gamma-ray spectral anal. using FFT *(Japanese)* 78—90047
gammagraphy, 3-dimens. image processing appl. to coded aperture imaging *(French)* 78—57067
gas bubbles, on liq. surface, bursting, jet and droplet form., math. model *(German)* 77—24012
gas stripping column, periodically cycled, feedback control, simulations 79—1231
gas-filled microballoons, radiation effects MEDUSA code calcs. 80—83220
gas-fired heat pump systems, energy performance anal. by computer 80—35728
gas-liquid surface 78—2341
gas-liquid surface of mol. fluids, mol. dynamics computer simulations 80—39387
gas/solid surface collisions, vel. depend. of ang. distribs., interaction pot. effect 79—11491
general heat transfer, CSMP package 78—75145
generalised routine for defect image simulation in TEM obs. 78—29220
geologic processes, for teaching 77—17
geologic strata, for teaching 77—18
geothermal binary cycle calc., hydrocarbon working fluid selection 79—48091
Gifting propeller operation characts. by computer aided numerical anal. 80—6068
global climate and changes, computer modelling 80—46250
grain boundaries, molecular dynamics studies, use of coincidence lattice theoretical model 78—30645
grain boundaries computer simulation, effects of rigid body translations 79—60386
grain boundary entropy computation in computer simulation 78—30647
grain boundary migration, effect on thin film diffusion behaviour 80—88460
grain density, determ. in space filling geometries from measurable 2D parameters, computer simulated model verification 79—38838
grain growth, chem. driven, during liq. phase sintering, computer simulation 80—55427
grain growth, steady-state and dynamic, computer simulation 79—38836
graphite, interaction with Cs, study of surface diffusion, computer simulation 78—30837
gravitating, 3-dimens. system of colliding masses 77—9654
ground surface profile, crest and trough height distrib., Monte Carlo simulation *(Japanese)* 79—34180
ground surface profile power spectrum, Monte Carlo simulations *(Japanese)* 79—34179
groundwater discrete kernel generator, finite element method appl. 78—92873
groundwater flow model using finite element method 78—92874
groundwater singly dispersive convection, finite-difference simulation 77—37265
groundwater two-dimensional flow, finite element method appl. 78—93018
Guinier-type focusing cameras, powder diffr. line profiles, simulation 79—58856
Gunn diode, anode domain disappearance dynamics, computer simulation calcs. 80—6859
hand prosthesis development, electromyograph controlled aid *(Spanish)* 78—15924
hard rod system, initially ordered, one-dimens., mol. dynamics computer simulations 78—71658
hard sphere fluid near hard wall, diffusion coefficient, mol. dynamics simulation 80—64858
hard sphere liq., dil. impurity diffusion coeff., quasihydrodynamic approx. and simulation 80—49066
heart, cross-sectional shape change during beats, simulation 77—44714
heart valve prosthesis, tilting disc type, computer prediction of thrombogenic sites 77—44834
heat conduction, inverse nonlinear problems, simulation methods 78—94513
heat exchanger, dynamic analysis, digital algorithm for initial value problem 77—42727
heat pump, solar-boosted 79—57414
heat treatment, prediction of large component response 78—31435
Heisenberg dilute systems, computer simulation, mag. conc. of clusters, linearised eqns. of motion 79—78409
Heisenberg spin glass, spin wave stiffness 79—78405
helicopter rotor, nonlinear mathematical simulation of unsteady flow past rotor 79—86442
HF radiometer random process dynamic simulation models 79—80686
high-power low-freq. klystron as drive for LAMPF, design, simulation 77—83174
holographic, image digital reconstruction with limited-length arithmetic register *(Russian)* 79—22910
homogeneous nucleation and growth processes, computer simulation 78—30764

digital simulation continued
hopping conduction, random one-dimens. system, Monte Carlo computer simulation 80—80278
house energy conservation measures obs. and evaluation, using minicomputer, Philips expt. house (West German project) 79—61951
HTGR steam power plant, nonlinear dynamic model 78—78437
human movements, computer modelling 77—21544
human respiratory system, role of the Van der Pol oscillator 78—65073
hybrid river models software support 80—56499
hydration, hydrophobic, of nonpolar mols. in dilute aq. soln., Monte Carlo simulation 80—3314
hydraulic fracturing operations, material and structural simulations 78—31540
hydrodynamic numerical modelling of tidal basins, Lagoon of Venice appl. 79—34832
hydrodynamic stability problems with time-depend. boundary conditions, numerical simulation methods, review 80—19411
hydrogen-bonded liquids, HF, H_2O, NH_3, computer simulation, intermolecular potentials 80—38890
hydrologic records analysis and comparison, statistical program suite 77—21819
hydrological processes, using super-kurtic probability density function 80—26558
hydrological system tracer, finite element method appl. 78—92881
ice, dislocation form. kinetics, computer simulation 78—30622
III-V compound crystal growth from solution, computer simulation 77—51332
image formation, partially coherent, two dimens., computer simulation 80—106434
image formation by inversion of scatt. field data, expts. and computer simulation 79—89852
image from inline hologram, interfering output suppression using digital processing technique 79—50248
image reconstruction, Fourier techniques evaluation in relation to number of X-ray sums 78—77112
image restoration and synthesis, Japanese activities 77—58273
image restoration by Gauss LU decomposition 79—76600
image restoration by Wiener filtering, signal dependent noise 77—88645
immiscible liquids, separation kinetics in low gravity environment, computer simulation study 78—34629
impression creep, digital simulation by finite element method 78—7142
incoherent image processing by multiple aperture scanning 79—76627
inelastic material behaviour in struct. anal. 78—34041
information display using the methods of digital holography 79—72529
ingot, temp. field calc. approx. by equiv. cylinder *(German)* 78—84788
inter/cross modulation levels for GaAlAs diode laser 78—55455
interfaces, liq.-cryst. and liq.-rigid wall, Monte Carlo simulation 79—27896
intestinal myoelectrical activity model 79—70537
intracranial pressure dynamics modelling 79—25026
ion+neutral neutron, ion speed effects in flow-drift tubes, Monte Carlo simulation 77—56221
ion beam trajectory focusing effects on toral reflection coeff., computer studies 80—89102
ion bombardment collision cascades, computer simulation, Monte Carlo code 78—67756
ion implantation, in crystals of diamond struct., computer modelling 77—43235
ion scattering by atomic chains on solid surface 79—52065
ion scattering by crystalline solids, techniques 78—15270
ion scattering by single cryst., orientational effects in charge state 79—52064
ion scattering from single crystals, computer simulation 80—2911
ion-lattice interactions, modelling displacement correls. in computer simulations 78—2179
ion-solid interactions ion motion computer simulation 79—43088
ion-surface impact, interatomic pot. screening function correction factor for computer simulation 78—23574
ionic crystal, stacking fault computer simulation 78—30652
ionic impurity, drift mobility in electric field, computer simulation 79—82388
ionosphere radio drift meas. simulation and analysis of correlation methods 78—45033
ischaemic and infarctive ECG simulation during ventricular activation and recovery 78—36018
Ising model, nonequilib. intensive parameters and detailed balance, computer simulation calcs. 78—76208
Ising model, quenched two-dimensional single spin-flip kinetic, Monte Carlo simulation 78—34943
Ising two-dimens. random bond model, evidence against spin-glass order 80—15747
island films, statistical model 80—92795
JET, synchronous generator, bridge convertor and ohmic heating systems, digital simulation 78—54960
Johnson-Mehl and cellular microstructure, comparative analysis, computer simulation 80—54392
Josephson interferometer resonance amplitude theory, SFQ memory cells 80—27317
lakes or bay landslide wave generation, Galerkin finite element appl. 78—92879
laminar separated flow between periodically varied walls, num. simulation using perturbated primitive variables method 77—54971
laminate, time and temp. effects, mech. response, computer simulation 78—35466
land surfaces, erosional potentials generation from topographic information, LEAP programs 77—33075
landform erosion simulation program 80—85650
LANDSAT data correction for haze, Sun angle and background reflectance effects 77—78491
large amplitude water wave, finite element method appl. 78—92851
large cosmic ray showers, computer simulation using models of hadronic collisions 78—57415
large molecules, multiphoton excitation models, numerical simulation 80—53078
large network models using the brain organisation simulation system 79—8496
large-scale hydrodynamic system simulation programs 77—21799
laser anemometry, high Reynolds number flow, review, data anal. for photon correl. method, simulation 79—60082
laser fusion, parameter study of exploding pusher target *(Japanese)* 80—96376

digital simulation continued
laser fusion simulation, hydrodynamical behaviour *(Chinese)* 80—1823
laser fusion system beam quality, Laser Optical Train Simulation code 80—78886
laser plasma compression, computer simulation of implosion struct. *(Japanese)* 79—14587
laser tracker, target induced pointing noise 78—5519
lattice dislocation calcs., classical elastic line force solution 78—22718
lattice drag force on moving dislocation, zero temp. 79—95006
lattice model chain dynamics, simulation *(Russian)* 79—22876
lattices, two-dimensional, detonation, shock propagation, computer simulation 79—64554
left ventricle stress and power 77—56406
left-heart haemodynamics, mathematical model 78—65074
Lennard-Jones 12-6 system, triple pt. props., mol. dynamics simulation 78—2231
Lennard-Jones fluid, nonequilibrium molecular dynamics, $t^{-3/2}$ long-time tail for stress-stress time correlation 80—70100
Lennard-Jones fluid, phase separation by spinodal decomposition, mol. dynamics computer simulation 79—10766
leucine aminopeptidase crystalline aggregates, interpretation of electron microscope images 78—68988
light pulse excited decay curve simulation, finite breadth *(Hungarian)* 80—11473
lightly doped semiconductors, impurity band struct. 79—69461
linear accelerator simulation, code PARMILA, longitudinal tuning of LAMPF 77—83159
liquid, associated, radial correlations, comparison of Monte Carlo and Ewald mol. dynamics calc. methods 80—14984
liquid, polar, computer simulation, thermodynamic props., diffusion coeffs. 79—90507
liquid, simulated two-dimensional, cooperative atomic motions 79—90513
liquid crystal, microscopic model of structural organisation, mol. dynamics method 80—10492
liquid metal MHD loop dynamic analysis 77—39479
liquid structure, S-D periodic particle-particle/particle-mesh program P3M3DP 80—84041
liquid-vapour interface, fluid phase coexistence, Monte Carlo computer simulation 80—49349
liquids, monoatomic, quasi-crystalline structure, role of vacancies in dynamics 80—92438
LMFBR, SNR-300, HCDA anal. by failure incoherence modelling, HOPE computer code 77—88237
Lorentz gas, two-dimens., collision-induced absorption, simulation 78—46424
Lorentz microscopy, mag. domain images resolution, computer calcs. 78—35004
Louisiana canals hydrologic model 80—31080
low-temperature plasma production by electron beam ionisation of gas mixture 80—87908
lung, nonlinear mathematical model, parameter tracking adaptive algorithm 77—60227
macromolecule. branched, particle scatt. factor, light, computer simulation 79—64128
macromolecule, simulation of Brownian motion of chains, chain dynamics 79—86099
macromolecule, simulation of Brownian motion of chains, local motions and chain conformations 79—86098
macromolecules in solution, US degradation simulation program 79—14148
magnetic alloys, binary, spinodal decomp., computer simulation study of interface behaviour 80—84913
magnetic binary alloy, computer simulation, time evolution 79—56488
magnetic bubble motion, computer simulation 77—85526
magnetic domain wall pinning simulation, coercive force, susceptibility, defect depend. 77—16103
magnetic hysteresis 77—85500
magnetic hysteresis model, of dipole element, use of cubic spline functions *(German)* 79—4706
magnetic MG field generation by EM flux-compression, computer simulation 79—50189
magnetic moment spatial distribution in single ground state systems with impurities 80—97074
magnetisation transient and steady-state characts. with hysteresis 77—66385
magnetocardiogram study appl. 78—3528
mass spectrometer, quadrupole mass filter with flat electrodes, computer simulation 78—54492
materials appl. conf., Gaithersburg, USA (April 1976) 78—27387
materials normal grain growth 79—11546
matrix exponential method, dynamic response via digital simulation 77—72149
Maxwell eqn. finite difference soln., perfect conductor simulation 77—74236
McCollough effect, synaptic modification associative learning model 77—21531
measurement errors, random, simulation (Monte Carlo) method, teaching appl. 78—86062
mechanical heart 79—70709
medical X-ray diagnostics, NDT impetus, novel techniques *(German)* 78—7146
melt flow during Czochralski growth, computational simulation 78—48306
melting, Lennard-Jones two-dimensional systems, Monte Carlo study 80—49338
melting and freezing, computer simulation of simple systems using array processor 80—54353
melting curve maximum phenomenon, computer simulation using two species soft core model 78—6146
mesenteric artery Na kinetics, digital simulation of 3 compartment model 77—44616
metal, BCC, computer simulation of stacking faults 78—30653
metal, BCC, computer simulation of twin boundary and twinning dislocation struct. 78—30644
metal, BCC, struct. of twinning dislocations, computer simulation 78—2140
metal, FCC, structure and dynamics of multiple interstitials 78—47330
metal, plastic flow, during extrusion, computer simulation 78—31491
metal BCC, divacancy binding energy, appl. stress effect, computer simulation 77—15408
metal crystal, lattice defects, relax. studies 78—79604

digital simulation continued
metal hydride, computer simulation of H reflection and scattering 79—1806
metal surface, self consistent electronic struct. effect on atomic positions, computer simulation 78—30969
metal working by pressure, full scale adaptive simulation applied to computer aided management 79—79055
metallic glass, composition, mech. props., simulation 80—49117
metals, constitutive model at high strain-rate, shear modulus, yield strength 80—75292
metals, FCC, twist boundaries, high-angle (001) CSL, struct. by computer simulation 79—46677
metals, FCC, twist boundaries, struct. invest. using computer simulation technique 80—84185
metals, FCC and BCC, grain boundary struct., and segregated impurity sites, computer simulation 79—73173
metals, grain struct. form. during two-dimensional recrystallisation, simulation on electronic calc. machine *(Russian)* 79—87666
metals, HCP, vacancy and interstitial config. 79—65071
metals, point defect relaxation volumes, dipole tensors and Kanzaki forces 80—54222
methane, freq.-depend. shear viscosity 79—77798
methane, liq., mol. dynamics simulation using singularity-free algorithm 80—54116
methanol, liq., simulation using modified intermol. dimer pot. function 80—32629
MHD converter, supersonic flow of combustion products, nonequilibrium physicochemical processes, open-cycle MHD generator 80—103196
MHD/steam combined-cycle plant, combustion air temperature variations reduction 79—52943
MHSS, material handling system simulator 77—38337
micellar diffusion-controlled reaction kinetics 80—30213
microcirculation autoregulation mechanistic theories 78—27995
microphysics to macrochemistry, discrete simulations, review 80—54102
microstructure alterations and texture form. in normal grain growth, computer simulation 79—90679
microstructures micrographs, based on optical, electron and field-ion microscopy 80—19679
microtron, electron injection and capture processes, digital simulation 77—18717
microwave holography, computer simulation and image reconstruct. *(German)* 78—46540
microwave irradiated breast tumour thermal pattern calc. *(French)* 80—3759
middle ear systems simulation from physiological data 78—44514
MIM system, electron emission modelling *(Czech)* 80—2479
MIS solar cells, optimal interface design using computer simulation and expt. meas. 80—16805
mixing of multicomponent solids, mixing index and contact number estimation by spot sampling 80—16214
MO200 model for evaluating safeguards in mixed-oxide fuel-rod fabrication plant 77—38372
Moire contouring using virtual moving gratings simulated on computer 78—73968
molasse basin formation 77—9428
molecular dissociation, collision-induced, high-efficiency, in RF-only quadrupole 79—67419
molecular dynamic simulation, event scheduling 80—49069
molecular dynamics, dilute gas simulation, pattern recognition algorithm for mol. formation 77—75249
molecular dynamics method in statistical physics, review 80—18895
molecular dynamics of diatomic liqs. 77—50493
molecular dynamics of liqs., neutron scatt. and computer simulation 78—63650
molecular dynamics simulation of a small drop 78—15719
molecular dynamics studies of the role of diffusion in chemical models with absorbing boundary states 79—8424
molecular fluid, computer simulation of liquid-vapour surface 80—54478
molecular fluid, hard-core triatomic, Monte Carlo simulations 80—38880
molecular fluids, free energy, computer simulation and quantum corrections 80—28905
molecular fluids, translational motion, Mori three variable theory and mol. dynamics simulation 78—63651
molecular modelling, design of computing systems 77—18814
molecular spectroscopic laboratory strategies, queueing theory and digital simulation use 80—30299
molecular systems, electron density, spatial, rel. to conform. props., computer simulation 78—70763
molecule images, simulation by point models and kinematical struct. amplitudes 80—103223
monatomic liquids, short wavelength collective density excitations, computer simulation 79—46540
monopole mass spectrometer, simulation, rel. to determining operating parameter tolerances 78—21260
monsoon, digital simulation of evaporation phase, development of moisture eqn. 77—56712
monsoon circulations 80—21812
Monte Carlo simulation diffusion and evaporation on (100) surface of FCC crystal 78—30836
Monte Carlo simulation of finite fluctuations, master eqn. description 77—87693
Monte Carlo simulation of quantum spin systems, two dimens. X-Y model 78—27011
Mori theory evaluation, molecular dynamics simulation 80—92443
MOS inversion layer, 2-dimens. disordered electron systems in strong mag. fields 77—76930
MOS transmission line, resistive, free charge transport, simulation, distrib. model 78—68092
MOSFET, n-type inverted Si (100) surfaces, quantitative determ. of valley splitting 79—51678
motor unit action potential study using computer simulation 79—11914
moving dislocations, low-temperature statistical characts. *(Russian)* 79—90654
multibody system equations of motion, computer-aided formulation *(German)* 78—39
multicomponent percolation, conduction 80—92871
multidither adaptive optics system, speckle interactive effects 77—46797
multilayer part, discontinuity type defect revealability, comparison of thermal inspection methods, computer simulation 79—79207
multiplane tomographic scintillation camera image quality improvement 79—92338

digital simulation continued
- multiple Markov sequences of interpoint intervals, inverse density modulation, rel. to removal spike trains 79—20529
- multiply charge of beams in linear accelerator with variable-phase focusing, general soln. 80—13992
- multislit spectrometer for the night airglow observation 78—73542
- multispectral scanning sensor system, Fourier transform method 79—29997
- multitarget association problem, image reconstruction approach 79—72522
- myocardial regional blood flow from dynamic anal. of ^{201}Tl 79—70627
- n-type semiconductor anode, illum., charge transfer modes, digital simulation 80—2464
- nanosecond beam dynamics in linear electron accelerator 80—86996
- nematic liquid crystal, Maier-Saupe lattice model, stochastic model method simulation 77—43129
- nematic liquid crystals, Marangoni effect 78—6009
- neural nets, frequency response characteristics analysis, interactive model implementation 78—44487
- neural nets *(Polish)* 79—16189
- neuromuscular response to ankle rotation, human, simulation with segmental reflex model 79—8500
- neuromuscular system deterministic neuron models 79—29523
- neuromuscular system output response, effect of correlated adjacent interspike interval sequences of input 78—80858
- neuron model *(Russian)* 78—27924
- neuronal populations, diffusely-connected, computer simulation 78—53384
- neutron diffraction, multiple scatt. correction, Monte Carlo simulation 78—9913
- neutron diffraction, pulsed source expts., optimized Monte Carlo simulation 78—9914
- noise, environmental, urban, computer aided evaluation and control *(Japanese)* 79—88033
- non-ferrous, recycling, system study, computer simulation 78—35278
- nonlinear coupled dynamic physiological systems, network thermodynamic simulation 79—96504
- nonlinear diffusion eqns., finite difference methods *(French)* 77—5654
- nonlinear free surface flow, boundary integral eqn. method appl. 78—92850
- nonlinear systems, mode-locking, computer simulation 77—12872
- nuclear accidents, loss-of-coolant, data analysis using computer-aided models *(Czech)* 80—73949
- nuclear fuel cycle, GASP IV simulation model 78—41847
- nuclear fuel cycle material shipment 79—85743
- nuclear fuel design, LMFBR oxide fuel analysis system 77—46227
- nuclear fuel element performance modelling using LIFE-III, UNCLE-I and LIFE-LWR codes 77—46229
- nuclear fuel pin inelastic modelling and stress analysis using FULMOD code 77—46233
- nuclear fuel pin modelling principles and developments 77—46232
- nuclear fuel pin performance modelling codes for overpower performance analysis 77—46230
- nuclear fuel restructuring and relocation under irrad., COMETHE code calcs. 77—46235
- nuclear fuel rod behaviour modelling using LIFE-III code 77—46234
- nuclear fuel rod modelling complexities 77—46231
- nuclear fuel rod ramp tests analysis using SAFE-2D program 77—46228
- nuclear fuel rod thermal characteristics, on-line simulation by elec. heated rod 77—46209
- nuclear fuel sheath deform. following fuel power transients, simulation 78—33258
- nuclear fusion plasma simulation with parallel pipeline programming 79—68947
- nuclear material control system simulator 79—85685
- nuclear material monitoring, VACOSS electronic sealing system appl. 79—85687
- nuclear plant risks assessment, of accidents and normal operation 78—50281
- nuclear power station installation policies analysis using TOTEM-3 code 77—65323
- nuclear power station radioactive releases, tolerable level assessment, appl. 78—46145
- nuclear reactor, BWR, vent clearing transients calc., press. suppression system, digital computer simulation 77—3132
- nuclear reactor anal., LEAHS and ARMP languages 77—67866
- nuclear reactor core simulation, few group coarse mesh diffusion scheme, expt. verification 77—23223
- nuclear reactor fuel reprocessing, in-process inventory dynamic measurement 77—38371
- nuclear reactor kinetics eqns. 77—88216
- nuclear reactor LOCA reflood phase, hydrodynamics, moving control vol. method 78—704
- nuclear reactor NSSS, computerised simulator 80—22914
- nuclear reactor spatial kinetics approx. techniques 77—38334
- nuclear reactor subassembly response to simulated accident conditions, finite element anal. 77—3123
- nuclear reactors, computer modules appl. *(German)* 79—49788
- nuclear reactors, initial fissile U requirements for fuel cycle, computer simulation 78—17320
- nuclear safeguard systems effectiveness, SNAP network analysis technique 79—26658
- nucleation models, 2D, computer simulation of cryst. growth 79—73116
- nucleation processes, computer simulation, single spin flip kinetic Ising model 77—62613
- nucleic acids, bases and base pairs, water struct. in soln., Monte Carlo simultion 80—76709
- numerical solutions of three dimensional dynamic crack problems and simulation of dynamic fracture phenomena by a 'non-standard' finite difference method 79—41613
- ocean depth, analogue/hybrid solution 80—36336
- ocean mapping, bottom return signal model and signal processor simulation 77—2272
- ocean receivers for acoustic signals from moving radiating sources 79—59859
- ocean tides mapping with satellites, computer simulation 79—39880
- ocean waves generation, propagation and dissipation spectral simulation model 80—31060
- oceanography, coastal current flows, Po delta application *(Italian)* 77—70667
- oceanography, turbidity current flow, computer simulation 78—15997

digital simulation continued
- n-octane fluid, gauche-trans. relax. 79—69002
- oil spill simulation in Florida Gulf outer continental shelf 78—73406
- one-dimensional chain, thermal fluctuation induced rupture, computer simulation 78—91378
- one-dimensional crystal subjected to deform., static and dynamic equilib. 79—28037
- one-dimensional polycrystalline structure, computer simulation *(German)* 77—68935
- optical communication, light scatt. by clouds 77—88651
- optical communication channel and photodetector array, computer simulation 77—71944
- optical computing for image bandwidth compression, analysis and simulation 78—94373
- optical cross correlation by complex exponentiation of input data 77—71942
- optical data transmission systems 77—54675
- optical multilayer filters, non normal incidence, optical monitoring, allowable tolerances *(French)* 80—87526
- optical sensor system simulation elements and techniques 79—76851
- optical signal receivers, optimal and nonoptimal, logical structs. efficiency comparison, simulation *(Russian)* 78—71041
- optical system simulation for luminescence spectroscopy 77—34036
- optimal numerical filters fitted for noise damping, atm. circulation simulation appl. 78—92997
- opto-acoustic transducer, for biomed. diagnostic imaging, equiv. cct. and simulation 77—60283
- organic crystal growth from soln. 78—30558
- organic synthesis, computer simulation *(French)* 79—52653
- oxyhaemoglobin dissociation curve direct obs. in man in vivo, computer investigation 78—85433
- papillary muscle Na kinetics, diffusional and compartmental models 77—44617
- particle dispersion coarsening, computer simulations 80—30289
- particle physics, relativistic discrete unified field theories, computer field interaction simulation system 80—68412
- PASOLE, thermal network simulation for microeconomic anal. of passive solar heating systems design 80—35744
- pericardial potential simulation and mapping in dog 79—39399
- permittivity meas. through ponderomotive forces determ., computer-aided field analysis 79—215
- petrochemical process plant expansions, noise levels control 79—68480
- phase contrast of W support film in electron microscopy 78—334
- phase diagrams and synthesis of soln. thermodynamics, computer anal. 78—30739
- phenoformaldehyde thermosetting resin, computer stimulation of form *(Japanese)* 77—66619
- phosphor, rare earth activators, sensitized luminesc., computer simulation 78—6723
- photochemical air pollution formation simulation 80—81504
- photochemical smog, transferred contaminant air pollution model *(Japanese)* 78—32217
- photochemical smog dynamics and control strategies *(Japanese)* 78—32220
- photographic process, Syntha Vision computer animation process 77—183
- photoproduction of lepton pairs in thick target, Monte Carlo simulation 78—21432
- photoreceptor models, vertebrate, response waveforms 79—43894
- photovoltaic generator operation and cost simulation 79—61975
- physics computer-aided teaching, hinted finding scheme, appls. *(French)* 80—98777
- physics laboratory experiments, graphic computer simulations 80—105470
- physiological excitation spread equation boundary conditions for undistorted impulse movement pattern 77—56365
- physiological stimulator, programmable, real-time numerical simulation appl. to laboratory instrumentation 77—44873
- physiological system biochemical activity modelling 77—40629
- piezoelectric thickness vibrator, digital computer simulation 77—88998
- pipeline systems, nonstationary flow distrib. modes simulation, computer-aided methods 79—94717
- planar channelling effects for relativistic protons and π^- mesons, deflection effects 79—77656
- plane coalescence, at grain boundaries 80—70221
- planetary and satellite systems evolution 80—77308
- plasma, laser produced, ionisation process computer simulation code, atomic transition processes 80—28764
- plasma, one-dimensional, electrostatic simulation code 77—58888
- plasma, pressure, virial kinetic definition, spherical geometry calcs. *(French)* 80—69973
- plasma confinement mag. field, computer simulation of finite linear multipole with closed ends 77—35382
- plasma sheaths of satellite and spherical probe, static and dynamic behaviour, simulation 77—25907
- plastic zone ahead of crack, development under creep conditions, computer simulation 78—34091
- point defects short term annealing, in α-Fe 80—54282
- polar liquid surface tension calcs. 77—31841
- polar systems, structure, effect of boundary conditions, Onsager models 80—44095
- polarography, differential pulse type, digital simulation with incremental time change 77—90662
- polarography, pulse, chronoamperometric, chronocoulometric techniques, kinetic, mass transport effects 77—25334
- pole pieces with cavities, correction effect modelling *(Czech)* 79—45879
- pollutant dispersion in shallow sea, model 77—29324
- pollution patches evolution modelling for southern North Sea 77—45018
- polyethylene crystal, computer simulation of {110} twin boundary 78—30646
- polymer, amorphous, conform. from simulation of filling diamond lattice with chains *(German)* 78—75595
- polymer, amorphous, conform. from simulation of thermal motion *(German)* 78—75594
- polymer, conformational transitions, Brownian dynamics, simulation 79—45873
- polymer chain, linked rigid body, Brownian dynamics 80—74267
- polymer chain, of bistable oscillators, Brownian dynamics of transitions 78—86983
- polymer chain dynamics, in soln., computer simulation 78—83718
- polymer chain in restricted environment, Monte Carlo simulation 77—46663

digital simulation continued
- polymer chains in cubic lattice solvent, thermodynamic props., Monte Carlo method, computer simulation *(Russian)* 77—31787
- polymer dynamics simulation, general theory 78—91210
- polymer dynamics simulation, relax. rates and dynamic viscosity 78—91211
- polymer films, vertical development, from gas phase, computer simulation *(German)* 77—27839
- polymer foil, electron irradiated, charge dynamics, computer simulation 79—82915
- polymer impregnated concrete, computer simulation 78—31375
- polymer network formation, struct. and mech. props., computer simulation 80—38965
- polymer solution, concentrated, computer-aided simulation of individual chain conforms. *(Russian)* 77—42454
- polymer solution, simulation of macromol. dynamics, Monte-Carlo method, conc. depend. *(Polish)* 78—51404
- polymer solutions, coil dimensions, Monte Carlo calc., computer simulation *(Polish)* 79—3606
- polymeric macromolecule containing mesogroups, phase diagrams *(Russian)* 80—58433
- polymerisation, radiation-induced, solid state, computer modelling 79—66294
- polymethylene coils in solution, dimension and shape, computer simulation *(Russian)* 80—54111
- polymorphic transformations kinetics model, computer modelling *(Russian)* 80—97478
- polytypes, computer simulation 80—79734
- porous media one-dimensional unsteady drainage, finite element method appl. 78—91011
- positive and negative ion beams nonlinear interaction, math. simulation and expt. 77—595
- positive photoresist., computer simulation of exposure and development 79—54208
- positron lifetime spectra, of metals, lifetimes and intensities 79—33858
- potential landslide sites mapping 77—37204
- prosthetic coupled arm for feeding, kinematic anal. 78—3682
- protein molecule, simulation of single mol. images combining computer and electron micrograph analysis 78—37781
- proton dynamics in linear accelerator with variable phase focusing, space charge effect, simulation 79—13561
- pulmonary gas exchange function model *(Russian)* 79—2092
- pulsatile flow in arteries simulation, utilitarian approach 80—3669
- pulsating overpotential Cu electrodeposition, appl. 77—81410
- pulsed laser Doppler velocimeter signal processing, FFT and pulse-pair estimation 79—77322
- pulverised coal combustion, in combustion chambers of steam generators *(German)* 78—27758
- pupil, human, normal and diseased, model for computer simulation 77—77895
- PWR, operational dynamics, digital simulation model 80—27751
- PWR plant, dynamics, digital simulation 78—8882
- PWR power plant, transient state 77—14263
- pyrene, laser-induced two-photon photoionisation, simulation, double pulse investig. 78—37690
- quadrupole distorted NMR powder patterns, simulation, Fortran program 77—77105
- quantum mechanical measurements, simulation using programmable pocket calculator 80—41982
- quartz, surface structural modification by high temp. gases, computer simulation of RHEED patterns *(German)* 79—95251
- radar, digital sensor simulation 77—33213
- radar image simulation, point scatt. model, remote sensing appl. 79—12296
- radiation counting rate meter output at threshold, fluctuation and arrival shift by computer simulation 80—106240
- radiation damage computer simulation system, WINERY 78—30675
- radiation damage in crystals, computer modelling methods 77—7760
- radiation damage produced by energetic heavy particles, computer simulation *(Japanese)* 80—29094
- radiation induced low-energy collision cascades in Cu, computer simulation 78—87705
- radioastronomical systems and radioastronomical information processing methods *(Russian)* 77—22097
- radiocardiogram parameter identification *(Slovene)* 78—44586
- radiographic image formation, perceptual eval. of phys. parameters, computer-simulated images 80—41222
- radiography, photon path visualisation by Monte Carlo simulation 77—66848
- radioisotope thermoelectric generator, selenide, power degradation predictions 79—48148
- radionuclide accumulation in marine organisms, computer kinetic modelling 79—53261
- radionuclide angiocardiography determ. of ventricular ejection fraction, correction of noisy data 77—48868
- radionuclide mean clearance time transverse section imaging 78—73222
- rain impact damage to supersonic missile radomes simulation 77—40500
- rain parameters, meas. by optical scintillation, correl. method simulation 78—36290
- rainfall runoff from multiple watersheds system 79—29805
- random acoustic field model 79—50495
- random lattice, with purely off-diagonal disorder, electron localisation 80—49672
- random packing of spheres modelling 80—77705
- range distributions of energetic protons in Si, Monte Carlo computer simulation 78—22777
- REACT program for computer-assisted simulation of chemical reaction sequences, structure elucidation applications 78—92477
- reaction mechanisms, models, computer method appls., conf., New Orleans, USA (1977) 78—48645
- reactor neutron flux regulation dynamic simulation algorithm 80—27738
- real time phaseless filter with delay circuit, ECG appl. *(Japanese)* 80—56253
- Regional Activities Model for economic and environmental impact evaluation 77—37376
- regional wastewater treatment system 77—41064
- reinforced organic composite, graphite, or C-C, ablation, mathematical modelling 79—41564
- relativistic electron beams simulation 79—26789
- remote sensing system specification using computer image simulation 80—48439

digital simulation continued
- renal countercurrent mechanism, transient and steady state simulation 77—36967
- renal dialysis, improved patient management by computer simulation 79—70703
- repetitive firing computer models nonlinear systems anal. 78—80854
- respiratory tracer gas nonlinear computer anal., non-invasive meas. method 79—62395
- retinal model, layered visual processing 80—16925
- retinal models, experimentation, program framework 79—53108
- rheological electrokinetic phenomena in rectangular capillary 80—26023
- river basin, Monongahela, acid mine drainage problems treatment via QUAL II simulation 79—29806
- river basin study model 80—31079
- river stages model 80—31078
- rivers, ungauged, distributed numerical model development for estimating runoff and sediment discharge 77—91178
- rivers, ungauged, distributed numerical model for estimating runoff and sediment discharge 77—91177
- rivers, ungauged, runoff and sediment discharge estimation, distributed numerical method comparison 77—91179
- road traffic acoustic behaviour near traffic lights, computer simulation 78—90597
- road traffic noise, traffic passing through road intersections controlled by roundabouts, model 80—64280
- rocket attitude measurement using laser system 79—12763
- rolling texture formation, computer simulation in HCP and orthorhombic metals 80—3095
- room acoustics and subjective sound perception *(Polish)* 79—7258
- rotating disc electrode, with optically transparent ring, digital simulation 78—53210
- rotating fluid, trapped oscillations, viscous effects, num. simulation 77—55015
- rotating two-ring electrode, constant current effects, digital simulation *(French)* 78—7212
- rough sphere fluid, computer simulations 79—99041
- rough surfaces computer simulation of contact 79—19470
- round notch tension test, computer simulation 79—24705
- Rutherford 180° backscatt. anomaly in solid, Monte Carlo simulation 80—45189
- sapphire, dislocation obs. by weak-beam TEM 77—47461
- satellite plasma sheaths, streaming instabilities, elec. equilib., one-dimens. particle simulation 77—22036
- saturable transformer magnetisation characts. using rectangular hysteresis-free approximation method *(Russian)* 77—55708
- SAW resonator, distributed-feedback *(Flemish)* 80—5899
- sedimentology, ellipsoidal grain thin sections, Monte Carlo simulation 77—5332
- sedimentology, Rayleigh-Ritz method appl. 78—92878
- seismic structure yielding rate approx. 77—2522
- self-diffusion, flux of vacancies and atoms, computer simulation 79—73332
- SEM voltage state prediction 79—40644
- semiconductor, amorphous, field effect and capacitance-voltage meas. anal., localised density of states 80—103686
- semiconductor, bulk, negative-cond., transverse spreading of high-field domain, two-dimens. simulation and equivalent cct. model 79—1602
- semiconductor, ion implanted, pulsed laser and electron beam annealing comparison 80—92547
- semiconductor, SEM electron beam induced current images of dislocations and stacking faults, computer simulation 80—70198
- semiconductor crystal growth, Czochralski bulk flow 78—31320
- semiconductor CW lasers, intensity self-pulsation simulation 79—94232
- semiconductor electrode, charge injection, space charge region 77—15949
- semiconductor electrode, open-circuit photopotential 77—15950
- semiconductor electrode, photogenerated free carriers and photocurrent relax., simulation 77—15951
- semiconductors, disordered, carrier mobility and transient pulse dispersion for hopping mechanisms 80—44586
- semiconductors, doped, variable range hopping, computer simulation 80—24929
- sensory neuron, second order, summation of excitation and inhibition 80—76769
- separated flows, three-dimens., with vortex filaments, num. simulation 77—58706
- shallow water with moving boundaries, finite element method appl. 78—92847
- shear elasticity in liqs., oscillat cup expt. 77—72190
- shells, plastic, explosive forming, computer numerical simulation 80—59560
- shock wave reflection, regular to Mach transition, Monte Carlo simulation 77—75936
- shock wave reflection from concave surface, numerical simulation 79—18913
- signal analysis and simulation program 79—79678
- simulated and optically produced holograms compared 77—75456
- simulation of the infrared astronomical satellite (IRAS) telescope system 79—29976
- single channel two freq. ^{14}N NQR pulse spectrometer, multiplet spectra 80—17968
- single crystals, growth simulation 80—88069
- sintering process 79—61526
- skeletal muscle dynamics, isometric and isotonic contraction model 78—31807
- skeletal muscle mechanical props. and model, contractile force depend. *(Japanese)* 80—56091
- skin burns, elec., due to defibrillator ground-loop current 77—78039
- Skylab, anticipated attitude motion for revisit mission, digital computer simulation 79—16794
- soft-sphere mixture viscosity, nonequilib. mol. dynamics 80—19680
- solar air conditioning system, using evacuated tubular collectors, comparison with actual performance 79—61949
- solar collector-heat storage systems, thermal simulation 80—45758
- solar domestic space heating in Ireland, computer simulation model of thermal performance 80—45732
- solar energy simulations, typical weather determination 79—16614
- solar energy space and water heating systems, Markov model 79—74501
- solar energy system simulation, diffuse and total solar radiation relationship 79—57398
- solar energy systems, Conf., San Francisco, CA, USA, (Dec. 1978) 79—83635

digital simulation continued
- solar energy thermal processes 79−24890
- solar flat plate collector anticonvective-antiradiative system model 79−62082
- solar heated house, Trombe-Michel wall system design and performance 79−62143
- solar heating, of dwelling independent of servicing networks 79−62149
- solar heating systems performance over range of storage capacities, prediction 80−45642
- solar power systems, correlation equation for hourly diffuse radiation 77−81981
- solar powered Rankine cycle system 79−52911
- solar radiative heating, in presence of aerosols 79−16665
- solar space heating system analysis, based on Markov chain models 79−61950
- Solar Thermal Test Facility, 5 MW, heliostat focus and alignment system 78−50894
- solar water heating models comparison 80−30387
- solid, mol. dynamic simulation of shock wave propagation, kinetic energy and temp. profile 79−14882
- solid laser, CW, actively mode locked, picosecond pulse form., computer model 79−36939
- solid soln. strengthening, conc. 78−31420
- solid solution hardening, statistical behaviour analysis *(Japanese)* 80−11658
- SOLMET 80−35640
- solvation of large dipoles, mol. dynamics study 79−77470
- sonar signal processor, 36-channel, programmable 78−66976
- sound amplifying systems in halls, model *(French)* 79−37090
- sound-absorbing wedge design, reflection characts., materials and dimens. *(Japanese)* 80−64322
- southern Iranian solar pond performance simulation 79−62096
- spacecraft solar cell arrays, power system perform. anal. using computer modelling 80−30497
- speckle image digital processing 78−71053
- speckle interferometry of binary stars, computer simulations in photon-counting mode 78−53836
- spherical powder sintering by surface diffusion, computer simulation 78−48344
- spin wave parametric excitation, stochastic auto-oscills., Kolmogorov entropy *(Russian)* 80−75749
- sputtering mechanism for light ions, computer simulation 79−56901
- square-well fluid, viscosity below critical density, molecular dynamical calcs. 80−79661
- staircase voltammograms, synthesis, anal., convolution, devolution 77−25336
- steel, alloy, tension test, computer simulation of deform. to fracture 79−11667
- steel, stainless, hot rolling resist., multistage mode of deform. effects *(Russian)* 78−80583
- steel, stainless, stress distribution effect on chipping of blanking punch *(Japanese)* 78−31543
- steel, type SAE 1008, finite fatigue life distribs., various load-time histories 80−97589
- Stirling cycle, numerical methods accuracy evaluation 79−48170
- Stirling cycle machines optimisation, free piston design 79−48172
- Stirling engine, research, JPL laboratory 79−48171
- stochastic processes computer simulation in science teaching 77−17739
- storm water and sediment hydrographs from small watersheds 77−37264
- stratified turbulent flow, finite element method appl. 78−90964
- stray light phenomena, GUERAP III Monte Carlo simulation 78−58907
- stray light simulation with advanced Monte Carlo techniques 78−58906
- stress meas., absolute retardation patterns, laser diametrically compressed photoelastic disc 77−27496
- stress wave propagation, nonlinear, in perfectly flexible string 78−5670
- stretch reflex system in human forearm, adaptive control characts. 79−83758
- strip telescope, image synthesis, computer simulation 77−29660
- strong ground motion representation and simulation 79−16388
- structural network and continua, finite element method 77−50882
- submillimetric magnetoresonant scatt. from relativistic electron beams 77−38792
- superionic conductors, theoretical models, review 80−107465
- surface diffusion, influence on surface anal., model calc. 79−15016
- surface roughness meas., effect of stylus radius meas., digital simulation 77−67413
- suspension, random behaviour simulation, interval of quiescence method 78−31708
- Tahoe-Truckee system water-quality simulation 77−37261
- teaching, Newtonian motion anal. using micro-computer simulations *(Japanese)* 80−31462
- teaching, two-dimens. Brownian motion simulation on micro-computer *(Japanese)* 80−31461
- TEM crystal atomic structure imaging technique and applications 80−105752
- TEM imaging of W(111) split crowdion interstitial, computer simulation 78−71723
- TEM micrograph image restoration, of weak-phase object using computer *(Japanese)* 79−71571
- temperature and EM fields simulation, inductively heated semiconductor 78−55961
- tension test, computer simulation, effect of testing conditions 80−7729
- texture development in grain growth, computer simulation 79−96036
- texture transformations, 'brass to copper' in FCC metals 80−76246
- textures, deformation, eulerian simulation 80−3096
- thalamic ventrobasal neurone discharges during sleep and wakefulness 79−20533
- thermal conduction of solids, temperature stochastic field in cylinder computing *(Polish)* 79−71370
- thermal conduction of solids, temperature stochastic field in cylinder computing *(Polish)* 80−17879
- thermal conductivity prediction of heterogeneous mixture, digital simulation technique 78−87247
- thermal drag force on moving dislocation, non zero temp. 79−95007
- thermal pressure in solid and eqn. of state, computer simulation 78−34593
- thermal regenerator, numerical accel. 77−23855
- thermal regenerator, with variable mass flow rate, computer model 78−75047
- thermal stress simulation in continuous casting, finite element method 78−30170

digital simulation continued
- thermodynamic activity of C in austenite, computer simulation 79−37852
- thermodynamic functions of gases, liquids by computer simulation 79−86866
- thermodynamic properties, of interacting particle ensemble, by simulation of stochastic disordering 77−87697
- thermoregulatory system simulation, rat 80−3594
- thin film condensates coalescence, influence on morphological changes, modelling 80−107676
- thin film deposition process, line-edge profile simulation appl. 80−104068
- three-dimensional thin pyroelectric IR detector simulation 80−57375
- thylakoid membrane of green plants, simulation of electron transport in primary photosynthesis reaction, in PL/1 *(German)* 77−86468
- thyroid function assay 77−44778
- thyroid radiation protection during radioiodine-labelled pharmaceutical administration 78−44616
- tidal estuary two-dimensional hydrodynamic model using finite element method 78−92846
- time series analysis on R-R intervals of electrocardiogram using autoregressive model 79−83972
- TiO, single cryst., short range ordering of vacancies, X-ray anal., computer simulation 79−73163
- Tokamak ohmic heating pulsed power supply 78−8991
- tomographic image correction, with simulation 80−85470
- tornado-like boundary layer flow, two-eqn. simulation 77−35151
- torus with three coil arrangements, simulation 78−18434
- total artificial heart haemodynamic study 79−84018
- traffic flows, car following theory, intersections having traffic lights 80−72109
- trajectory estimation, real time, of lowest flying Earth satellite by square root filter *(Japanese)* 80−4235
- transaxial X-ray tomography reconstruction using convolution methods *(Japanese)* 78−35931
- transcapillary water movement resulting from non-oncotic osmotic forces 78−44548
- transducers errors evaluation, continuous random-signals reproduction from pulse-frequency sequence 77−74386
- transition metal, amorphous and liq. state, simulated model 79−14733
- transmitter kinetics model computer simulation results 78−92617
- transonic flow, num. simulation by finite element method using optimal control theory 77−55025
- transonic flow, unsteady, implicit shock-fitting computational scheme 78−94763
- transonic flow simulation by finite element method via optimal control, book contrib. 79−32557
- tsunami, generation and propag., simulation using shallow water eqns. 80−41407
- tsunami long wave propagation analysis, finite element method appl. 78−92849
- tsunami wave propagation, finite element method appl. 78−92848
- tumour growth, in vitro 77−86464
- turbine cascade flow, surface-oriented coords. in num. simulation 77−55018
- turbulence, helical isotropic, Lagrangian vel. covariance 77−62240
- turbulence, inhomogeneous, simulation, clipping approx. 80−19331
- turbulence, large eddy simulation 80−19333
- turbulence-degraded image compensation, computer simulation techniques 77−60625
- turbulent mixing layer, numerical simulation via vortex dynamics 80−19362
- turbulent shear flow, large eddy simulation 80−38390
- two-dimensional flow with singularities, finite element method appl. 78−90822
- two-dimensional hydrodynamics and water quality by finite element method 78−92877
- two-dimensional MHD turbulence, small-scale struct., singularities form. 79−46396
- two-phase flow through porous media, simulation by finite elements 79−41752
- type II superconductor, elastic vortex lattice, pinning by lattice defects, computer simulation 79−56465
- ultrasonic sound field, in air, quantitative visualisation *(French)* 78−87212
- undersea acoustic signal coherence fluctuations 80−46191
- underwater acoustic holographic image reconstruction for moving objects 78−75019
- upper atmosphere neutral gas expansion, numerical soln. 79−12325
- urbanisation effect on floods, predictive model 77−37276
- US attenuation measurement of soft tissues, signal processing of broadband pulsed US 78−77094
- US visualisation for NDT of solids 80−22424
- UV radiation sources modelling, upper atmosphere appl. 80−1288
- vacuum system transient simulator, appl. to Princeton TFTR 78−74496
- variable domain finite element model for dam unsteady compressible fluid flow 78−90820
- ventilation-perfusion ratio intraregional maldistribution simulation 78−31834
- ventilator-patient coupling, effects of positive press. ventilation on cardiac output and pulmonary arterial flow 78−31852
- ventricle, artificial, sac-type, in mock circulation 78−11780
- ventricle excitation spread *(Japanese)* 80−3847
- ventricular arrhythmia model 80−89893
- ventricular excitation, digital simulation, computer model evaluation 78−85302
- ventricular function computer simulation, development of model and parameter estimation 78−53439
- vestibulo-ocular reflex, horizontal, linear system anal. appl. to alert rhesus monkey 79−100600
- vibration modal anal. *(French)* 80−42216
- Viking Orbiter uplink command generation and validation simulation 77−22040
- visual and nervous systems, straight line recognition algorithm 79−34562
- visual cortex neural circuitry model for orientation sensitivity 79−11927
- visual foveation system, afferent part, computer model 77−25437
- VLBI, simulation of beam patterns *(Japanese)* 80−26754
- vocal cords vibratory behaviour in tension and mass imbalance 79−83803
- void sink strength depend. on mutual recombination, point defect loss to fixed sinks 80−33995

digital simulation continued
Volta Lake, hydrological models, data bases and computerised control 80—4057
vortices, in mixing layer, numerical simulation 78—90853
waiting time calc. of dislocation motion 78—30638
water, cooperative effects importance in computer simulation calcs. 80—28906
water, liq., Monte Carlo studies of struct., review 80—54101
water, Monte Carlo simulation of struct. and thermodynamic props. 80—88017
water excretion control by antidiuretic hormone, modelling 78—31830
water quality modelling of high mountain stream of Bishop Creek, California 78—53666
water quality monitoring system CAD 77—41100
water resource finite element anal., conf. at London, England 1978 78—92867
water resource management, gaming-simulation appl. in Hunter River Valley, New South Wales 79—57517
wavelength modulation spectrometry, computer modelling 77—63974
weather, matrix generalised eigenproblem developments 77—25760
weather, severe convective event numerical simulation and prediction, Navier-Stokes eqns. initialisation 80—31111
weather prediction, using multimicroprocessor system SMS 201 79—53500
weldbonded joint deform., finite element simulation 78—35636
welding, thermal stresses and metal movement, computer simulation 78—34002
well flow analysis, finite element method appl. 78—92870
wind energy conversion system control, on-line, performance in turbulent wind environment 79—48069
wind energy storage systems, SIMWEST program package 79—52872
wind turbine generator dynamic stability 79—96415
wind-wave interaction, two-layer flow, numerical simulation 78—92823
windmill arrays, wake interaction, theory and preliminary results 80—61246
writing aid for motor handicapped, microprocessor-based device, LOGOS 78—81077
X-ray crystallography computer simulation of back reflection Laue patterns 77—55199
X-ray fluoresc. anal. of atmospheric particulates, Monte Carlo simulation of self-absorpt. effects 77—60165
X-ray topographs of stacking faults 78—30513
X-ray topography, computer simulation methods 79—23484
X-ray traverse topographs, computer simulation on basis of Green function method 80—49044
zone plate camera longit. tomogram digital processing, computer simulation 78—40311
π^-p inelastic interactions at 205 GeV/c, three-fireball model, computer simulation 78—474
AgBr, molten, Monte Carlo computer simulation 78—26426
Al alloy die casting, heat transfer coeff. 79—81685
Al alloys, fatigue crack initiation, computer simulation 80—100893
Al, computer simulation of tilt grain boundaries 78—30642
Al, ion-induced Auger electron emission, depend. on ion energy 79—78814
Al, periodic grain boundaries struct., computer simulation 77—89448
Al, plane stress calc. with two dimensional elastic-plastic computer program 78—35465
Al, step coverage optimisation by computer simulation and SEM 78—51838
Al, symmetrical high angle boundaries computer simulation 77—51389
Al, tilt boundaries ⟨110⟩, computer simulation, struct. and symmetry 79—37713
Al-$CuAl_2$ lamellar eutectic, computer simulation of two dimensional Zn diffusion 78—30799
AlF, hyperfine structure simulated by computer programme 78—50538
α-Al_2O_3, axial-to-planar channelling transition computer simulation 79—4367
Al_2O_3, Czochralski bulk flow, in microgravity, digital simulation 80—28934
Al_2O_3, sintering of single phase and multiphase components *(German)* 78—80494
Ar, fluid, light scatt., collision-induced, line-shape theory and mol. dynamics 79—41921
Ar liquid, quasi-crystalline structure, role of vacancies in dynamics 80—92438
As_2S_3 structure simulation of some tellurite and chalcogenide glasses quasi-crystalline structural diffusion method *(Russian)* 80—54147
Au (110) surface, proton reflection, influence of channelling 80—54295
Au, atomic struct. of large angle {001} twist boundary, determ. by computer modelling and X-ray diffr. study 80—70162
Au, curved cryst., planar and axial channelling of protons, numerical simulation 79—65132
Au, polycrystn., deformed, computer simulation of vacancy annihilation to dislocations *(Japanese)* 80—88205
Au, surface proton and electron channelling on reflection 80—39193
B diffusion in oxidised atmosphere, minicomputer model *(Rumanian)* 79—82247
BaO-P_2O_5:Mo^{5+} glass, EPR spectra, computer simulation 80—88872
Be, twin boundaries, computer simulation 80—39109
Br_2, liq., struct., theory and computer simulation 78—59734
C graphitic, imperfectly ordered, high resolution electron microscopy imaging, computer simulation calcs. 79—77463
CO_2, electron swarm parameters for high E/N, Monte Carlo simulation 80—19548
CO_2 laser, efficiency at 14 and 16 μm 79—59670
CO_2 laser Antares fusion system optical diffraction computation 80—74424
CO_2 laser pulse, nonlinear propagation, computer simulation *(Japanese)* 80—95963
CS_2, liq. struct., mol. dynamics simulation 79—77488
^{13}CH fragment, selective population transfer expts., density matrix formalism appl. to NMR spectroscopy 78—15059
Ca^{2+} concentration in extracellular fluids in body, digital simulation of short term regulation 79—83725
CaF_2, fast ion transport, computer simulation 80—107485
Cd, twin boundaries, computer simulation 80—39109
n-CdS/n-InP/p-InP heteroface solar cell with ultrathin window layer, computer anal. 80—97788
Cl-HBr chemical laser, pulsed, computer simulation, effects of rot. nonequilib. 77—40547

digital simulation continued
Cl_2-H_2 mixture, detonation initiation, nonequilib. physicochem. process simulation 80—38431
$Co_{1-p}Mg_pCl_2$, magnetic excitations, antiferromagnetic resonance spectra response simulation 79—99775
^{60}Co irradiation sterilisation processing, nonstandard double carton simulation 79—26760
CsCl-type lattice, (111) superlattice screw dislocation motion, computer simulation 80—79793
CsCl(Br)(I), molten, structural props., computer simulation 77—84616
Cu, amorphous, sputtering, computer simulation in binary collision approx. 79—56900
Cu complexes, spin-labelled, EPR, electron-electron coupling 79—51858
Cu, continuum representation of computer simulated dislocations 78—30623
Cu, electron radiated, formation of Frenkel pairs 79—23598
Cu, neutron irrad., replacement sequences, calcs. using ADDES and COMENT codes 79—46714
Cu, polycryst., back sputtering of 100 to 500 eV Ne ions, computer simulation 78—60537
Cu-Ni, quantitative AES anal. of M_1 VV transition, computer simulation 79—91542
$CuCl_2.2H_2O$, X-band ESR magneto-microwave effects 77—28434
Cu_3Mn, atomic short-range order, TOF neutron diffraction 79—10831
$Cu(NH_4SO_4)_2.6H_2O$, X-band ESR magneto-microwave effects 77—28434
$Cu_{57}Zr_{43}$, amorphous alloy, computer simulation of atomic structure 80—70125
α-Fe, a/2 ⟨111⟩ {110} edge dislocation, at. simulation 77—89435
Fe, amorphous, realistic structural model, search for Bernal holes 78—83734
Fe, BCC, computer simulation of entropy of $^1/_2$⟨111⟩{110} edge dislocation 78—67716
α-Fe, BCC, migration of vacancies near twin boundaries 78—51535
Fe, BCC, vib. entropy of $^1/_2$ ⟨111⟩ {110} edge dislocations 78—63768
Fe, BCC surface ledge simulation, dislocation-like relaxation 78—30620
Fe, cast, quantitative metallography, study by image anal. 78—31492
Fe-N single crystals, solid soln. stress assisted nucleation of α'' precipitates 78—52810
Fe-Si(4 wt.%), (110) and (100)[001] oriented, simulation of domain wall bowing 80—44854
Fe_3Al, computer simulation of energy dissipation from near threshold knock-ons 78—30666
$Fe_{1-p}Mg_pCl_2$, magnetic excitations 78—91852
Fe_3Pt Invar alloy, thermal expansion and spontaneous magnetisation, Invar anomalies, low spin model 80—71001
GaP-Si heterojunction solar cell, computer simulation 79—74529
H^+ beam, 0.5 TW pulses, production with spherically focusing mag. insulated diode 79—31288
H_2, vibr. relax. in H_2-Ar mixtures, mechanism, computer simulation 78—46434
H_2+Ar, 4500K shock wave expt. simulation, vibr. state changes and dissoc. 79—61850
HC-NO_x photochemical smog, smog chamber simulation model *(Japanese)* 77—29087
HCL, fluid states, mol. dynamics simulation 80—79671
HCl laser, V=3 to V=2 band process, computer simulation 78—71095
H_2O, liq. struct. and dynamics, simulation using central force pots. 78—38607
H_2O, vap., depolarised Rayleigh scatt. and Raman spectra 78—33513
$(H_2O)_2$ dimer intermolecular pot., liq. struct. mol. dynamics simulation 78—71657
^3H kinetics in freshwater marsh, simulation model 78—24318
$Hg_{0.8}Cd_{0.2}Te$-ZnS MIS struct., nonparabolic bond semicond., surface state studies, capacitance measurements 79—78190
I, recombination in inert gas buffer, computer simulation, rate const., press. depend. 77—25261
K, liquid, shear waves, molecular dynamics 80—44096
KCl microcrystal, computer simulation of melting and glass form. 79—65173
KCl, molten, vapour-liq. interface, mol. dynamics model 80—54362
KCl-KBr solid soln., highly conc., computer simulation of dislocation motion *(Japanese)* 77—68972
KH_2PO_4, liquid inclusion form., hydrodynamics and supersaturation role 78—30559
Kr, molecular dynamics simulations, three effective interactions 79—69224
Kr submonolayer films on graphite, mol. dynamics simulation 80—88425
Kr VII, beam-foil excitation, 4s4p $^1P_1{}^0$ level decay simulation 80—78578
Li, twin boundaries, computer simulation 80—39109
Li-I_2 power cell accelerated discharge test for battery longevity model 80—30938
Mg, HCP, vacancy clusters and interstitials, computer simulation study 80—64992
Mg, ion-induced Auger electron emission, depend. on ion energy 79—78814
Mg SiO_3 melt, instantaneous struct. simulated by mol. dynamics 80—84049
Mg, twin boundaries, computer simulation 80—39109
Mo, localised electronic states near dislocations 79—33257
N_2, dense molecular gas, breakdown due to laser radiation, numerical simulation 80—38686
N_2, electron swarm parameters for high E/N, Monte Carlo simulation 80—19548
α-N_2 simulation of dynamical props. of molecular solids 78—30710
NH_4Cl, aq. soln., struct. props., mol. dynamics simulation 79—82142
$(NH_4)H_2PO_4$, single cryst., X-ray diffr. contrast at twin boundaries, computer simulation 79—33000
Na exchange in tissue, incorporating diffusion effects into multicompartment models using digital simulation 80—3611
Na, liquid, shear waves, molecular dynamics 80—44096
Na medullary depletion during diuresis 77—60226
Na-K alloy, liq., collective excitations, mol. dynamics calc. 80—28895
NaAr, ground and excited state pot. curves, dispersed fluoresc. spectrum 79—98140
NaCl, edge dislocation dissoc., computer simulation of core struct. 79—37703
Nb-Zr (1.5 wt.%) alloy, field ion microscopy investigation, surface struct. 80—45220
Nb_3Sn fatigue effects in unidirectional composites, computer simulated model 80—35289

digital simulation continued
Nd complex, Nd^{3+}:ATP, electron spin echo decay envelope anal. 79—54871
Nd:glass mode locked ring laser, unidirectional travelling wave operation 77—88812
$Ne^{+}+Co_2$, three dimens. quadrupole ion storage, ion mobility, effect of charge exchange reactions, Monte Carlo calcs. 80—55738
Ni (110) surface, Ar^{+} refl. at grazing angles, computer simulation 79—87549
Ni porphin, reson. Raman excitation profiles, simulation, vibronic coupling consts. 77—65471
Ni-Cd spacecraft batteries, power system perform. anal. using computer modelling 80—30497
Ni-Fe Invar, thermal expansion and spontaneous magnetisation, Invar anomalies, low spin model 80—71001
Ni_4Mo, statistically homogeneous ordering, computer-simulated field ion images 78—9991
O_2-CO_2 transport real-time and interactive control in mechanically ventilated patients in ICU 79—62404
$Pd_{77.5}Cu_6Si_{16.5}$, ternary miscibility gap, simulation, dispersed phase composite form. 80—54379
Rb, simulated fluid, atom pairs, dynamic behaviour 80—44098
Rh, catalytic oxidation of CO on polycrystalline sample 79—79294
Si, ion-implanted, laser annealing at 1.06 μm, computer simulation 79—47556
Si, ion-induced Auger electron emission, depend. on ion energy 79—78814
Si, oxide growth, ambient water vapour trace effects 77—77618
Si, perfect cryst., X-ray acoustic reson. 79—27873
Si wafer, ion implanted, electron beam annealing, computer simulation 80—96569
Si:As ion implanted, laser induced diffusion modelling 80—24672
Si:Au deep level parameter determ. by isothermal capacitance transient spectroscopy 80—88507
SiO_2-layers, charge transport induced by electron beam, simulation *(German)* 79—51702
Ta BCC lattice, strain ordering in interstitial solutions 80—107420
TeO_2, structure simulation of some tellurite and chalcogenide glasses quasi-crystalline structural diffusion method *(Russian)* 80—54147
$Ti_{1+x}S_2$, polytypic struct., Ti ordering, two-dimensional model, X-ray diffuse scatt. intensity, computer simulation 79—14776
VB, nuclear quadrupole parameters 80—103896
VCl_4, liq., struct. factor, mol. dynamics calc. 80—38898
V_3Si, grown-in dislocations, diffr. contrast behaviour 79—86794
V_3Si, single cryst., computer simulation of channelling meas. 79—51180
W support film for high resoln. electron microscopy, phase contrast, computer modelling 78—1144
W/Cu powders, liq. phase sintering, particle rearrangement 80—45253
WO_3 electrodes, electrochromic processes, digital simulation model 80—76518
Xe anode-directed streamer propagation simulation 78—67591
Xe, solid, elastic consts., thermodynamic props., Monte Carlo simulation 77—62575
XeCl* spectra, for $Xe(6s,{}^3P_2)+RCl$ vibr. energy disposal assignment 79—100345
YAG, high-resolution many beam lattice image anal. 80—14979
YIG, amorphous, ionic glass, hard-sphere random-packing model 80—24369
Zn, twin boundaries, computer simulation 80—39109
$Zr(Ca,Y)O_{2-x}$, local ionic arrangement, X-ray diffr. study 80—100203

digital storage
see also cellular arrays; content-addressable storage; cryoelectric stores; cryotrons; magnetic storage systems; optical stores; random-access storage; read-only storage; self-organising storage; semiconductor storage systems
acoustic emission, digital memory storage and source isolation 78—27712
array processor for seismology, advantages 79—70899
capillary and clad acoustic fibre delay line storage 78—9504
computerised tomography, picture documentation and filing 79—66554
CRO storage, Gould Advance OS4000 using A/D and D/A convertors 78—93673
CRO with digital storage, OS4000, features *(Spanish)* 79—6116
ECG, analogue distortion 78—44674
electron image recording system, detection quantum efficiency 80—99009
EM image accumulation, digital storage and processing system 80—101901
flaw detector with automatic mechanical scanning, TV signal form. on basis of digital memory 80—71864
frame, telecine FDL 60 appl. 80—278
Harris data memory, operation and educational uses 80—17779
heart-rate store, PLL circuit, portable *(German)* 78—65139
holographic storage of TV signals 80—87353
liquid crystal devices, electro-optical props. of cholesteric liquid crystal mixtures *(Rumanian)* 79—78657
magneto-optic memory, Mn-Bi system 77—85511
METEOSAT synchronisation and image channel system *(Italian)* 77—82110
musical tones synthesis from impulse response stored in digital memory 80—48525
oscilloscope principles and applications *(Danish)* 80—62647
recorders, transient, 1024-point, circuits, operation 77—53868
reliability physics, conference, Las Vegas (1977) 77—79086
sample/long term hold digital circuit, for physiological signal monitoring 77—40803
sapphire torsional wave delay line, dispersion rel. to information storage 77—84053
satellite universal telemetering system for magnetospheric and ionospheric research *(German)* 77—73924
telecine scanning appl. *(German)* 80—4786

digital systems
see also computer networks; digital computers; fast-response computer systems; multiprocessing systems; real-time systems; sampled data systems; time-sharing systems
biological STEM, low-dose, using digital data processing system 78—24203
biological STEM, on-line data processing system 78—24202
cinematography, sound recording and reproduction systems *(Russian)* 79—27487
Doppler sonar, digital processing of signals 77—46856
frontiers in education, conference, Urbana-Champaign (1977) 78—81779

digital systems continued
gait recording technique 79—70725
holography appl. to borehole EM wave exploration *(Chinese)* 80—82080
IEEE International Microwave Symposium, Orlando (1979) 79—68356
image digitising system for computer input of crystallographic structure models 79—50939
image processing applications, conference, San Diego (1977) 78—81528
ionsophere sounding techniques improved by digitization 80—36427
marine deep seismic sounding system with digital data acquisition 77—87083
ocean bottom seismometer with digital recording system 77—64472
plot system developed for nondestructive materials testing exam. 78—53067
SEM image processing systems, summary of useful techniques and anal. 79—12901
spectrometer with high data rate, computer coupling system *(German)* 79—49212
structure model, photograph to digital convertor 79—60213
US moving target indicator system for diagnostic use 78—11710

digital voltmeters
$3^1/_2$-digit voltmeters using new A/D convertors *(French)* 78—21114
9 V range, successive LED indication, variable voltage power supply appl. 77—53950
AC measurement, using digital instruments 78—93726
AC portable voltmeter and calibrator 78—74019
AC type F4850, operational principles *(Russian)* 78—70158
AC with double integration, speed increase method *(Russian)* 77—2642
amateur construction project *(German)* 77—82542
amplitude digital voltmeter for periodic or pulsed signals 79—26073
analogue calculating type used for true effective voltage meas. *(French)* 80—42213
automatic test method for pulse-counting digital voltmeters 80—57240
automatic testing, error determination algorithm 77—53938
autoranging, for soil bulk resistivity meas. 78—24381
calibration, simplified method 79—49248
calibration approaches and limitations 79—93126
calibration using potentiometer, errors analysis 77—10059
capability expansion for 8 channel DVM 78—45645
capacitance meter, using DVM and diode pump cct. 80—62656
capacitance/loss tangent of capacitor meas., three voltmeter method *(Russian)* 78—70159
characteristics of Shch1312, Shch1413, and Shch1513 models 78—8413
coupling apparatus for DVM and chart perforator to data compilation and registration system 79—93113
cryostat temperature controller appl. *(Czech)* 78—29120
DC, general purpose, description *(Russian)* 77—65047
DC, high-impedance, parity circuit design 77—142
DC, high-speed, precision 78—8420
DC and AC, analogue voltmeter and ammeter calibration appl. *(Polish)* 78—45655
digital readout format, new arrangement reduces observational error 77—5822
dual scale, using MOS IC, description *(Italian)* 79—6150
ECG digital voltmeter with output to punched tape 77—21646
effective value, with intermediate freq.-pulse conversion *(Russian)* 77—71347
errors evaluation, causes and prevention *(Czech)* 77—57361
errors sources and reduction, test using linearly rising voltage *(German)* 77—5791
hand held DC design 80—17931
high-performance multimeters and voltmeters with microprocessors *(French)* 79—67349
home-made IC digital voltmeter *(German)* 77—10062
IEC-bus coupler for digital voltmeters *(German)* 79—93118
IEEE-488 bus compatible DVM variations and advanced features 80—86279
instrument selection tables, recent developments 80—13055
instrumental error estimation 80—57239
integrating, for low-level DC bipolar voltage 77—37922
Intersil ICL 7106 LSI chip DVM evaluation kit 79—80599
LaCoste-Romberg gravimeter appl. 79—96830
liquid crystal display appl. *(German)* 78—21165
manufacture in Rumania *(Rumanian)* 77—74452
measurement errors reduced by user-controllable filtering 78—77931
microprocessor controlled, calibration and averaging 79—40550
microprocessor controlled, with automatic calibration and meas. uncertainty readout 79—35787
microprocessor-based millivoltmeter use in ion-selective electrode appls. 80—16752
miniature, for battery and mains supply *(German)* 78—86289
miniature, mains/battery, construction and calibration *(German)* 78—93723
miniature battery-operated digital voltmeter with liquid crystal display *(German)* 79—80601
multifunction, performance comparison 77—30176
multimeter accuracy, resolution and sensing accuracy 77—74428
multimeters, accuracy specifications, sources of error 77—116
for noise and vibration meas. 78—55538
panel meters, noise resist and CMRR improvement, power source interference elimination 80—211
pH meas. appl. use of double ramp method *(Spanish)* 78—20133
with plug-in convertor, type Shch68002, 1 microvolt-1 kV range 77—74436
pocket automatic, construction *(German)* 77—10046
portable digital multimeter 79—71427
precision DC and AC digital voltmeter tester *(Russian)* 79—26080
precision thermometer, using 3 ICs *(French)* 79—80616
principles, operation A/D convertors, table currently available multimeters *(German)* 77—34007
programmable, microprocessor controlled, features 78—93720
RMS digital voltmeter, description and application *(German)* 77—18048
RMS digital voltmeter calibrator for VLF 78—86293
RMS voltmeter with analogue input processing *(Russian)* 77—10049
Rubin-I linear voltmeter, improved version using FET 79—21781
selective, electronic control of tuning frequency 77—10052
self-calibrating high-resolution digital voltmeter 77—57346
sound level meter output level measurement 80—79077
speech voltmeter using microprocessor 79—72768
thermometer sensor nonlinearity correction *(Russian)* 79—26054
time shared display, for two simultaneous inputs 77—74424

digital voltmeters continued
- time-interval meter, reads digitally to 99.9 ms on a DVM IC 77—74429
- transfer standard, portable, SM 215, A/D conversion techniques 78—41325
- true RMS, technology *(French)* 77—53952
- universal, type Shch68001, features 77—74435
- universal counter, HP 5328A 78—29125

digitisers *see analogue-digital conversion*

digraphs *see directed graphs*

dilatometers *see extensometers*

dilute alloys
- *see also impurity electron states; Kondo effect; magnetic properties of dilute systems*
- Al-Mn(Fe)(Co)(Ni)(Cu), alloy, dil., electronic states, XPS meas. 77—44117
- alkali alloy, dil. solid solution, atomic displacement near solute atom and in asymptotic range 79—65162
- alkali metal alloys, dil., binary, equilib. at. vol. and compressibility 80—70295
- alkali-alkali dilute alloys, lattice relax., energy of mixing 77—84936
- Anderson model, mag. field and impurity interaction effects on resist. 79—51554
- atomic displacements around impurity and three body interaction 78—91406
- binary alloy, unidirectional growth, morphological stability of planar interface 80—84920
- binary alloy monocrystal, thermodynamics of growth, model *(French)* 78—87635
- binary liquid, calc. of triplet correlation functions on basis of thermodynamic quantities for solute atoms 80—49087
- Cu-Co, dil., rotational hysteresis of Co fine particles 78—23301
- Cu-Ni, dil. alloy, optical reflectivity meas. virtual bound state model analysis 78—2873
- de Haas-van Alphen effect 79—99473
- diffusion, book 77—24422
- dissociative equilibrium, solute and solvent diffusion 77—76593
- elec. resist. for non-orthogonal Anderson model 80—59947
- electrical resistivity, Kondo effect vs. spin glass behaviour 78—68269
- electrical resistivity, low temps., Matthiessen's rule deviations *(Croatian)* 79—11099
- electrical transport and deviations from Matthiessen's rule 80—65524
- electron scattering by tetrahedral impurity cluster, lattice distortion and backscatt. effects 77—20306
- electron self-energy, Fermi surface changes and generalized golden rule 80—10858
- electron sound absorpt., disordered mag. impurities, spin glasses *(Russian)* 80—80503
- electronic configuration and vol. of formation 79—90991
- equilibrium distrib. coeff. relationship *(Russian)* 79—83186
- ferromagnetic and antiferromagnetic, linear spin-wave theory, effective medium approach 80—20393
- fission reactor materials, defect trapping and solute segregation in irradiated alloys 80—13603
- force constant changes due to substitutional impurities 77—24374
- formation energy, lattice relax. and zero-point vibrations 78—83771
- formation energy, lattice relax. and zero-point vibrations 78—87646
- impurity electron states, method of orthogonal operators 79—33254
- interstitial index, definition and variation with temp. *(French)* 80—2011
- interstitial solute in multicomponent substitutional solvent, quasi-chemical approach to thermodynamics 77—28784
- Knight shift for ions with Z>83 77—12275
- Kondo alloy, dil., thermoelec. power in asymmetric single-orbital Anderson model, perturbation calc. 79—99534
- Kondo alloys, calc. of host nucl. spin-lattice relax. 78—88215
- Kondo alloys, DC Josephson effect 80—88690
- Kondo system, magnetoresist calc. 77—62918
- Kondo system, nuclear orientation and magnetisation expt. comparison 77—63297
- Kondo temperature, lattice vibr. effect 78—19025
- Linde law, validity in normal metal based alloys *(Russian)* 77—80759
- liquid, binary, partial interference functions, short range chem. order effects 79—7541
- liquid, partial interference functions of solutes 79—19139
- liquid, ternary, heteroatomic solute, thermodynamic partial pair struct. factor, sticky hard sphere 79—32867
- liquid binary alloys, dilute, conduction electron scatt. cross section and component effective charges *(Russian)* 77—8082
- local moment formation, nonequivalent orbitals model 80—11164
- localised magnon mode in extended Wolff-Clogston 79—61097
- low temp. props. 80—2569
- low temperature nuclear orientation investigation 80—15825
- magnetic, configuration fluctuations 79—33449
- magnetic, in finite mag. field, Suhl's dispersion eqns. 77—24673
- magnetic, transport props. from Suhl's dispersion relations 77—62891
- magnetic 3d impurity in non-magnetic metal, effective ion Hamiltonian 78—64016
- magnetic alloy, thermopower, interconfig. fluctuations 79—65412
- magnetic alloys, dil., transition metal hosts, props. review 78—84417
- magnetic alloys, dilute, thermopower 79—65455
- magnetic crystal fields for mag. ions from itinerant electrons 80—39537
- magnetic impurities and Kondo effect, theoretical model 79—33455
- magnetic ordering of localised spins 77—1541
- magnetic oscillations, Fermi surfaces and high magnetic fields 79—73423
- magnetism of dilute and conc. alloys *(Rumanian)* 78—91843
- matrix effects quantitative Auger analysis 79—69927
- metals, noble, dilute alloys, solute vacancy binding energy, Dingle temp. 80—49177
- metastable alloy formation by ion implantation 80—15130
- noble metal, solute segregation and subsequent film growth in corrosive environment, model 79—24649
- noble metal based, disordered, virtual bound states, reson. model pot. theory 79—23934
- noble metal based, residual resist. calc. 77—28156
- noble metal electronic struct., de Haas-van Alphen studies, book contrib. 79—37967
- noble metal-rare earth alloy, dil., magnetotransport props., theory 78—39097
- noble metals, monovalent, magnetic susceptibility, impurities effect, Fermi surface effects 79—91207

dilute alloys continued
- noble metals containing rare earth impurities, magneto-transport props. 78—68015
- with off-diagonal disorder, density of states 78—34741
- perturbation expansion for the asymmetric Anderson Hamiltonian 80—80202
- point defect electric field gradient, anisotropic screening effect 79—56177
- radiation induced solute segregation and precipitation study by means of Johnson-Lam kinetic model 79—43252
- rare earth alloys, dil., ESR linewidth of rare-earth ions 78—68373
- rare earth alloys, line width of cryst. field excitations 77—85183
- rare earth dil. alloy, nucl. spin-lattice relax. of ^{165}Ho 78—48069
- rare earth-Au, dil., Mossbauer exam. of mag. hyperfine field at ^{197}Au impurity 78—88244
- residual resistivities, relax. energies and charge transfer 77—85177
- residual resistivity, nearly free electron metal 77—1406
- Seebeck coefficient, electron-phonon enhancement 80—70685
- solid solution, dilute, residual resistance, pseudopotential calc. *(Russian)* 79—33276
- solidification, numerical soln. model 79—69228
- solubility of H, isotope effect 78—14470
- solute diffusion, review 78—47589
- specific heat, electronic, mass renormalisation and band density of states influences 78—43137
- spin glasses, mean field theory, replica method 80—34658
- substitutional, volume change calc. using Morse pot. function 77—15342
- superconducting dilute alloys, eqn. for crit. temp. 78—72300
- surface segregation, bond and strain energy effects, atomic calc. 79—69256
- surface segregation, time of flight atom-probe FIM exam. 79—19437
- ternary, substitutional solute element effect on diffusivity of interstitial solute element 78—59969
- ternary alloy, combined inner adsorption *(Russian)* 77—76568
- thermoelectric coeff., vertex and other electron-phonon corrections to impurity scatt. 79—95390
- thermoelectric effects, near cancellation of electron-phonon corrections 79—33283
- thermoelectric effects 79—38054
- thermopower and resistivities, validity of Nordheim-Gorter relation 78—91671
- transition and noble metal dilute alloys, Einstein's temp. and vibrational entropy, rel. to electronic struct. 78—83900
- transition metal, dilute alloys, component segregation to interfaces 79—51398
- transition metal, size effect 79—99508
- transition metal impurities in transition and noble metal hosts, electronic struct. 78—75990
- transition metal magnetic alloys, dilute, props., review of theory 79—15282
- transition metal-rare earth alloy, dilute limit model of mixed-valence effect 77—47768
- transition metal-simple metal, electronic states, reson. model pot. method 79—77995
- transition metals, ferromag., interstitial or substitutional sp impurity doped, electronic struct. 80—34384
- transitional and noble metal impurities in simple metals, electronic struct. 77—43528
- transport properties in magnetic field, impurity-electron scatt. 80—65541
- vacancy type point defects, calc. of migration energies in pure metals and dilute alloys 78—47572
- wave-vector-nonconserving optical transitions 78—72100
- A-Mn, dil., mag. susceptibility and single impurity effects 78—64186
- Ag, cryst. growth from melt, distrib. of growth directions 79—33924
- Ag, metal and dil. alloys, electrical resistivity at low temp., ultra high resolution meas. 79—60795
- Ag-Al(Ga) electric field gradient temp. depend., nearest neighbour impurity mass effect, TDPAC meas. 78—6612
- Ag-Au, dil., low temp. elec. resist. 78—51964
- Ag-Cd, dil., DPAD meas. on ^{107}Cd and ^{109}Cd, nucl. Larmor precession meas., role of hyperfine interactions 79—47363
- α-Ag-Cd, dil., electronic struct. determ. from thermoreflectance and XPS 78—39011
- Ag-Cd dilute alloy, isotope effect and correlation factor for Cd diffusion 78—14501
- Ag-Co, dil., binding and caging of impurities and trapped interstitials 78—39462
- Ag-Cr, dil., elec. cond. meas., 1.5 to 30K 77—62914
- Ag-Cr, dil., negative magnetoresist. in pulsed fields up to 35T 77—62899
- Ag-Cu(Au)(Zn)(In)(Sn)(Bi), dil., elec. quadrupole interactions on ^{111}Cd probe nuclei, time differential PAC meas. 78—15066
- Ag-Cu(Sn), dil. alloys, EFGs at impurities, ^{111}Cd TDPAC 77—16213
- Ag-Dy, dil., Schottky effect, sp. ht. meas. 78—34633
- Ag-Dy, dil., thin films, ESR spectra, stress effects 80—39866
- Ag-Dy, EPR linewidth anisotropy and mag. field depend., internal stress effects 79—33532
- Ag-Dy(Tb) alloy, dil., magnetoresistance meas., contrib. from quadrupole and exchange scatt. 79—78078
- Ag-Er, dil., reflection EPR residual linewidth 77—81004
- Ag-Er film, stress-induced g-anisotropy, EPR of Er 77—85566
- Ag-Fe, dil., estimate of Kondo temp. from static mag. susceptibility meas. 78—19214
- Ag-Fe, ion implanted, phase comp., Mossbauer study 80—7244
- Ag-In, dil., interaction between recoil implanted impurities and lattice defects, TDPAC meas. 78—39467
- Ag-Mn, dil. alloy, transverse magnetoresist. in spin glass regime 80—34417
- Ag-Mn, dilute spin glass, AC susceptibility and ESR meas. 79—7968
- Ag-Mn, magnetoresistance and Hall effect, field-depend. electron scatt. 77—43581
- Ag-Mn alloys, dilute, low temp. elec. resist. *(Russian)* 78—68024
- Ag-Pd(Pt), dil., electric field gradient temp. depend., TDPAC meas. 78—39451
- Ag-Pd(Pt), dil., electric field gradient meas. by TDPAC method 78—39452
- Ag-Pd(Pt), dil., TDPAC exam. of radiation damage 78—39464
- Ag-Sn, dil. alloys EFG at impurity, ^{111}Cd TDPAC 77—16213
- Ag-Sn, high perfection single cryst. growth, strain-anneal technique 78—44010
- Ag-Sn (In)(Sb), dil. alloys, single crystals, dynamic dislocation behaviour 77—4108
- Ag-Zn(Cd), production and annealing of radiation defects 78—47362

dilute alloys continued
- $Ag_{0.6}Au_{0.4}Mn$, dil., effect of mean free path on strength of RKKY interaction 78−39291
- AgNi, dil., mag. susceptibility of isolated Ni atoms 80−65777
- AgPd, dil. alloys, electronic states, virtual bound states model test *(French)* 77−62809
- Al alloy, dil., recrystallisation during hot rolling 79−47732
- Al alloy, dilute, Matthiessen's rule deviations in strong mag. field 80−44571
- Al alloy, neutron irradiation 78−22766
- Al alloys, depend. of electron scatt. rate on lattice relax. 77−69311
- Al alloys, dil., diffusion thermopower, inelastic electron-phonon interaction 80−96851
- Al alloys, dil., quenched, foreign element effects on dislocation loop form. 80−54239
- Al alloys, dil., size effect of impurity atoms rel. to trapping radii for migrating self-interstitials 78−75690
- Al alloys, dil., size effect, valency factor and point defect interactions 79−51143
- Al alloys, screening charge anisotropy around impurities, nucl. quadrupole couplings meas. 77−32286
- Al, cold worked, internal friction peaks 80−97520
- Al, metal and dil. alloys, electronic thermal cond. calc. 78−47764
- Al-3d transition metal, dil. alloy, preasymptotic charge oscillations around 3d impurities 77−36055
- Al-3d transition metal, dil., localisation of additional screening charge 79−47051
- Al-3d transition metal, dil., pre-asymptotic charge oscills. 80−20099
- Al-3d transition metal, electronic states, reson. model pot. method 79−77995
- Al-3d transition metal, transport props., sp. ht. and supercond. crit. temp. calc. 77−1393
- Al-3d transition metal alloy, dil., electronic charge density around impurities 78−34799
- Al-(Mg)(Fe), pure (dilute), large wire drawing plastic deform. 80−108508
- Al-Ag, dil., deviation from Matthiessen's rule at high temps. 77−69294
- Al-Ag, dil., radiation damage by channelled and random He^+ ion beams 79−46719
- Al-Ag (0.10 at.%), channelling meas. of trapping efficiencies of solute atoms for self-interstitials 79−86829
- Al-Ag(Cu), alloying effect on phonon spectrum and lattice heat cond. 77−62695
- Al-Ag(Cu)(Mg)(Si)(Zn), dil., μ^+ depolarisation 79−56697
- Al-Ag(Ga)(Ge) dil. alloys, Hall coeff., residual resist., and relax. times 79−11107
- Al-Ag(Ge)(Mg)(Zn), electron-irradiated, impurity-interstitial interaction 77−15449
- Al-Ag(Mg)(Zn)(Ga)(Ge), dil., deviations from Matthiessens's rule, 4-OPW approx. calc. 79−19574
- Al-B, dil., diffusion of ^{12}B 79−60541
- Al-based, Hall coeff., calc. by 4-OPW approx. 78−76052
- Al-based, with 3d or 4f elements, XPS, virtual bound state 78−15285
- Al-Ce, very dil., low temp. sp. ht. 79−51745
- Al-Co, dil., binding and caging of impurities and trapped interstitials 78−39462
- Al-Co, dil., electron and neutron irradiation, interstitital atom clustering at ^{57}Co impurity, Mossbauer meas. 78−30607
- Al-Co dil., fast neutron irradiation, Mossbauer spectra, interstitial atom trapping 77−27914
- Al-Cr, Al-Mn, Al-Cr-Mn, dil. alloys, Hall coeff. and elec. resist. 77−11898
- Al-Cr, dilute, morphological stabilities of planar solid-liquid interfaces during unidirectional solidification 79−4960
- Al-Cr(Mn), anisotropic electron scattering, Hall coefficient, path integral calc. 79−91027
- Al-Cr(Ti), electron irradiated, interstitial trapping and detrapping at undersized impurity atoms 78−47424
- Al-Cr(V)(Ti), dil., electron irradiated, interaction of self interstitials with undersized solute atoms 78−63789
- Al-Cr(Zr), vacancy-impurity interaction investig. by tempering method *(French)* 77−68995
- Al-Cu, dil., anisotropic scattering of conduction electrons on dilute Cu impurities 79−47082
- Al-Cu, dil., virtual bound states 77−43528
- Al-Cu, dil. alloy, quench condensed thin films, supercond. and struct. from electron diffr. patterns 78−47901
- Al-Cu, implanted metal system, Cu redistrib. after laser irrad. 79−69163
- Al-Cu, pulsed ruby laser irrad., noncryst. phase form 80−35012
- Al-Cu (0.5 wt.%), evaporated layers, electromigration, linewidth depend. 80−65277
- Al-Cu alloys, dil., EXAFS spectra 80−2898
- Al-Cu dil. alloys, elec. resist. temp. depend. 77−8068
- Al-Cu dilute alloys, vein closing mechanism in fluidity tests 80−84924
- Al-Cu-Mg, dil. alloys, ageing response *(Korean)* 77−28832
- Al-Cu-Mg (2.6, 0.4 wt.%), Fe, Si, Mn and Ti addition effects on age-precipitation *(Japanese)* 80−20937
- Al-Cu(Ag)(Ge), dil., deviation from Matthiessen's rule at high temps. 78−64025
- Al-Cu(Mg), dil. binary alloy, planar interface stability during solidification *(Slovak)* 80−108424
- Al-Dy, dil., ion implanted, crystal hyperfine field interaction, Mossbauer spectroscopy study 80−44968
- Al-Er, dil., lattice location of ^{169}Er ions after implantation, Mossbauer effect of ^{169}Tm 78−39460
- Al-Er, dil., supercond., order parameter dynamics and collective modes, pair tunnelling meas. 79−56409
- Al-Fe, annealing after cold working, impurity-vacancy interactions, Mossbauer meas. 80−7236
- Al-Fe, dil., defects and phases, Mossbauer studies 80−40004
- Al-Fe, dil., phase analysis by Mossbauer spectra 80−15922
- Al-Fe, dil., quenched secondary defects, Mossbauer spectroscopy 77−28491
- Al-Fe, electron irradiated, interstitial-solute complexes, internal friction spectra 78−92289
- Al-Fe, Mossbauer spectra of implanted ^{57}Fe, ageing behaviour 80−7233
- Al-Fe (1 wt.%), depth resolved ^{57}Fe conversion electron Mossbauer spectra 79−38413
- Al-Fe dil., magnetisation, 2-0.01K 79−4652

dilute alloys continued
- Al-Fe dil. alloy, bamboo struct., grain boundary internal friction peak 79−43306
- Al-Ga, dil., low-temp. electron-diffusion magnetothermopower meas. 77−15833
- Al-Ga, dil., neutron irrad., 4.2K, defect prod., recovery 77−1155
- Al-Ga(Ag), Hall coeff. by OPW Fermi surface model 80−6816
- Al-Ga(Ge)(Mg)(Si)(Zn)(Ag), dil., Dingle temp. calc. 78−39005
- Al-Ge, galvanomag. transport coeffs., Hall effect 79−91029
- Al-Ge, magnetoresist., temp. depend. 80−70682
- Al-Ge(Mg)(Zn)(Ga), dil., electronic transport coeffs. for point defect scatt., 4-OPW calc. 79−42531
- Al-In, dil., vacancy trapping and detrapping at ^{111}In, PAC spectra 78−39461
- Al-In alloy, dilute, electron irradiation, interstitial dislocation loop obs. 78−18681
- Al-Li, dil. alloy, cold-worked, annealing spectrum 78−39801
- Al-Li, dilute substitutional alloy, impurity Knight shift and electric field gradient 80−44940
- Al-Li, Fermi surface impurity scatt. 79−56114
- Al-Li, quenched and irrad., recovery, resist. and internal friction obs. 78−52848
- Al-M, dil. alloy, electronic states of 3d-transition metal (M) impurities 78−64005
- Al-Mg, determ. of distortion field, induced by substitutional defect 80−44536
- Al-Mg, dil., ang. correlation of annihilation radiation from impurity trapped positrons 80−104010
- Al-Mg, dil., form of distortion field produced by Mg substitution, elastic neutron scatt. meas. *(German)* 79−42092
- Al-Mg, dil., long-range solute-host interactions 78−95062
- Al-Mg, dil., neutron irrad., 4.2K, defect prod., recovery 77−1155
- Al-Mg, dil. alloy, ^{65}Zn diffusion 77−51540
- Al-Mg, dil. alloy, residual resistivity, model pseudopot. form factors 77−8062
- Al-Mg, dilute, dislocation loops, interstitial, size distrib. for metal irradiated in high voltage electron microscope *(Russian)* 80−103335
- Al-Mg, foil, oxidation in O_2 atm., TEM study 80−104356
- Al-Mg, thermal generation of vacancies involving dislocation climb 77−59808
- Al-Mg-Si, dil. alloy, Mn additions and heat treatment effect on $\beta \rightarrow \alpha$ transformation 80−7566
- Al-Mn, dil., ^{54}Mn Knight shift meas. using nucl. orientation 78−68396
- Al-Mn, dil., coherent propag. and strain-induced localisation of muons 78−95537
- Al-Mn, dil., magnetisation, 2-0.01K 79−4652
- Al-Mn, dil., superconducting and normal state, ^{27}Al spin-lattice relax. rates 79−60977
- Al-Mn alloys, dil., magnetoresist. meas. 77−62900
- Al-Pb, pulsed ruby laser irrad., noncryst. phase form 80−35012
- Al-Sc, dil., thermomigration of Sc 79−69280
- Al-Si, dil., mechanism of dissolution of Si 79−19375
- Al-Si alloy, dilute, electron irradiation, interstitial dislocation loop obs. 78−18681
- Al-Si-Zn alloy, creep rates, pre-torsional deformation effect 79−96096
- Al-Sn, dil. alloy, vacancy-impurity interaction, exam. by electrical resistivity meas. at 77K *(German)* 78−83846
- Al-Sn dil. alloy, cube orientation texture development 79−96040
- Al-Ti, dilute, morphological stabilities of planar solid-liquid interfaces during unidirectional solidification 79−4960
- Al-Ti dilute alloys, solute distribs. during unidirectional solidification 79−4961
- Al-transition metal, dil., residual resist. of 4d and 5d impurities 77−28155
- Al-transition metal, residual resistivity, effect of 4d and 5d transition metal impurities 79−60791
- Al-V, dil., superconducting and normal state, ^{27}Al spin-lattice relax. rates 79−60977
- Al-V(Ti)(Fe), dil., screening charge around 3d impurities, NQR meas. 77−32287
- Al-Y, hyperfine interactions, $^{87}Y^m$ nuclear orientation meas. 78−43715
- Al-Zn, dil. alloy, ^{65}Zn diffusion 77−51540
- Al-Zn, dil. alloy, ageing and reversion, annealing curves, X-ray obs. 78−88485
- Al-Zn, magnetoresist., temp. depend. 80−70682
- Al-Zn (0.041 to 4.4 at.%), clusters, electrical resistivity meas. *(Japanese)* 77−21168
- Al-Zn (0.14 at.%), nuclear acoustic reson., 20-80K 79−8058
- Al-Zn-Mg (Fe), dil. alloy, ^{65}Zn diff. 77−51540
- $Al_{0.965}Ag_{0.035}$, reson. splitting of phonons 77−59086
- $Al_{10}V$-Ga, well defined local modes 78−26648
- Au-^{171}Yb, nuclear induced resistivity drop 78−10431
- Au-^{174}Yb, nuclear induced resistivity drop 78−10431
- Au-Ag-Cd, γ-ray PAC of ^{111}Cd, nearest neighbour contrib. to elec. field gradient 77−36161
- Au-Ag(Cu), dilute, low temp. thermoelec. power, electron diffusion and phonon drag 77−20301
- Au-Co, dil, local moments, third harmonic de Haas-van Alphen wave shape anal. 78−84127
- Au-Co, dil. alloy, crystalline electric field and spin-orbit splitting, NMR results 77−32274
- Au-Co, liquid alloys, ^{59}Co NMR studies 79−95660
- Au-Cr, dil., elec. resist., generalised phase shift anal. of Kondo effect 80−75556
- Au-Cr, dil. alloys., elec. resist., deviations fro Matthiessen's rule 80−75541
- Au-Cr, dil. spin glass elec. resist., press. and conc. depend. 80−24864
- Au-Cr Kondo alloy, effect of press. on resistivity 78−79978
- Au-Cu, dil., electron irradiated, interstitials and their clusters, diffuse X-ray scatt. study 80−33997
- Au-Cu(Ag)(Pt), cold worked, impurity conc. rel. to internal friction Bordoni peak, solid soln. hardening mech. 80−16363
- Au-Dy, dil., hyperfine interaction, Mossbauer study, Kramers quartets 80−66083
- Au-Dy, hyperfine interaction of Γ_8 quartet, Mossbauer expt. 78−43718
- Au-Er film, stress-induced g-shift, ESR meas. on Er 77−51951
- Au-Fe, anomalous Hall effect, asymm. scatt. of itinerant electrons 77−43569
- Au-Fe, dil., approach to saturation of magnetisation 78−56293
- Au-Fe, dil., contact charge density, internal conversion meas. 79−56630
- Au-Fe, dil., local mag. moments, neutron scatt. study 79−61058

dilute alloys continued
Au-Fe, dil., local moments, third harmonic de Haas-van Alphen wave shape anal. 78−84127
Au-Fe, dil. alloy, transverse magnetoresist. in spin glass regime 80−34417
Au-Fe, dil. alloys, spin glasses, modified bond model calcs. 79−33489
Au-Fe, ion implanted, phase comp., Mossbauer study 80−7244
Au-Fe, thermopower, interconfig. fluctuations 79−65412
Au-Fe, very dil. alloy, Kondo temp. 78−91688
Au-Fe (1-7 at.%), extraordinary Hall effect, near ferromag. percolation limit 79−19575
Au-Fe (4.4 and 4.8 at.%), isotropic spin glass behaviour and transverse magnetoresist. 77−15830
Au-Fe alloy, dil., Mossbauer exam. in spin glass regime 79−61289
Au-Fe(Mn) dil. spin glass alloy, impurity-impurity interaction press. depend., resistivity meas. 77−20308
Au-Ga, dil. alloys, dHuA meas. and phase shift analysis of electronic scatt. anisotropy 77−35932
Au-Ga dil. alloys, electronic struct. 79−37974
Au-Gd, dil., crystal-field splitting of localised Gd^{3+} moments, ESR obs. 79−82869
Au-Ni, surface segregation, strain effects 80−80042
Au-Pd dil. alloys, electronic states, virtual bound states model *(French)* 77−62809
Au-rare earth, magnetoresist., quadrupole scatt. effects 78−39096
Au-Rh(Y)(Zr)(Nb)(Pd), dil., Friedel d-reson. scatt. and elec. resists. 80−44566
Au-Sn (100 ppm), quenched and aged, small vacancy clusters, electron microscope obs. 78−76671
Au-Sn(Cu), quenched vacancy cluster form. 77−62546
Au-Ti, dil., virtual bound states, optical absorption meas. 78−2891
Au-transition metal, residual resistivity, effect of 4d and 5d transition metal impurities 79−60791
Au-Y, hyperfine interactions, $^{87}Y^{m}$ nuclear orientation meas. 78−43715
Au-Yb alloy, high field nuclear relax. of ^{173}Yb, anisotropic cond.-electron exchange 77−8434
Be, metastable alloy form. by ion implantation 79−82252
Be-based, metastable, produced by ion implantation, lattice location of impurities 79−51132
Be-Ru, dil., quadrupole interactions at ^{99}Ru, TDPAC meas. 78−91996
BeNi, dil., electronic struct., NMR study 80−108085
Bi-Cu, liquid, interstitial index, definition and variation with temp. *(French)* 80−2011
Bi-Mn, dil. liq. alloy, static and dynamic props. of localised Mn moments 79−82755
Bi-Sb, dil., magnetothermal oscillation and spin splitting of electrons 78−43362
Bi-Sb alloys, magnetoacoustic attenuation, tilt effect 79−91106
Bi-Sn(Pb), electrical cond. and thermal EMF at press. up to 12 kbar 77−47806
Bi-Te, dil. alloy, elec. cond. depend. on Te conc. *(Russian)* 78−76042
Bi-Zn, liquid, interstitial index, definition and variation with temp. *(French)* 80−2011
C-Mo, dil., brute-force nucl. orientation meas. 77−59466
Cd-Ag (0.015 to 0.25 at.%), critical resolved shear stress at low temp. 77−69035
Cd-Cr, dil., estimates of s-d interaction from supercond. transition temp. and mag. susceptibility 78−43561
Cd-Mg, dil. alloy, single cryst., electrical resistivity and deviations from Matthiessen's rule 79−23943
Cd-Mg, elec. resist., phonon local mode effect 78−6347
Cd-Mn, dil., lattice state effects on pair breaking 77−8219
Cd-Mn, single cryst., low temp. mag. anisotropy 77−59386
Cd-Sb, dil., loss of nucl. alignment of ^{115}Sb by radiation induced defects 78−43344
Cd-Sn(-Pb) liquid (0.03 to 0.10 at.% Cd), Cd activity coeffs., interaction parameters, EMF depend. on temp. 80−49383
Ce-alloys, dil., elec. resist. in presence of external mag. field 78−19022
$Ce_{1-x}La_x$, dil., $\gamma-\alpha$ transition temp. and press., elec. resist. meas. up to 10 kbar 80−59643
$Ce_{1-x}La_xAl_2$, extraordinary Hall effects, 4.2-300K, cryst. field interaction 78−79980
$CePd_3$, dil., local mag. moments, neutron scatt. study 79−61058
Co alloy, dil., liquid, thermodynamics 77−20086
Co alloys, factors affecting high-temp. oxidation behaviour 77−77638
Co-Cd, dil. alloy, impurity hyperfine interactions 78−84416
Co-Fe-Mn, dil. ferromag. alloy, mag. moment, saturation magnetisation meas. 78−64195
Co-Mn, dil., hexagonal hyperfine field at ^{54}Mn, nucl. orientation meas. 79−8057
Co-Ru, dil., mag. hyperfine fields, TDPAC meas. 78−43702
Co-Sn, dil., ferromag., temp. anomalies of Sn mag. hyperfine field and thermal expansion 79−33270
Co-Sn, dil., hyperfine field, press. depend., Mossbauer spectra meas. 79−95375
Co-Ti, dilute, internal oxidation 77−31810
Co-Zr, dil., mag. annealing effect, depend. of uniaxial mag. anisotropy on Zr conc. 80−39772
Cr-Co alloys, with local mag. moments, Neel temps. 79−73713
Cr-Fe, dil., latent heat exam. of magnetic transitions 79−61156
Cr-Fe_x ($x=0.5$, 1.5 and 3.5 at.%), antiferromag., Kondo anomaly 80−11163
Cr-Fe-Co dilute alloys, Neel temp., thermal expansion rel. to Co content 79−47281
Cr-Fe(Cu), dil., exchange interactions 77−47986
Cr-Ge, phase diagram of spin density wave states 79−24158
Cr-Pd dilute alloys, itinerant antiferromag., neutron diffr. meas. 77−77032
Cr-Pt, dil., effect of Pt on itinerant antiferromagnetism 78−64191
Cr-rare earth, dil., oxidation of Cr, effect of rare earth impurities 79−79160
Cr-Re, dil. alloy, mag. susceptibility temp. depend., thermal expansion coeff. *(Russian)* 78−76225
Cr-Rh, dil., hyperfine fields meas. 79−47056
Cr-Ru, dil. absence of mag. hyperfine field, TDPAC meas. 80−50237
Cr-Si, dil., latent heat exam. of magnetic transitions 79−61156
Cs-Ag, dil., electronic struct., density functional approach 80−44492
Cu alloys, dil., size effect of impurity atoms rel. to trapping radii for migrating self-interstitials 78−75690
Cu alloys, dil., size effect, valency factor and point defect interactions 79−51143

dilute alloys continued
Cu alloys, thermopower and resistivity, Nordheim-Gorter relation 79−65438
Cu based 3d-transition metal dil. alloys, residual resist., Dingle temp. 77−1409
Cu based dilute alloys, enthalpy of formation and excess entropy 80−55347
Cu dilute binary solid solutions, enthalpies of mixing and excess free enthalpies *(French)* 80−107427
Cu, dislocation inertial effects in plastic deform., internal friction meas. 77−36609
Cu, localised phonons due to substitutional impurities 79−77711
Cu, metastable alloy form. by ion implantation 79−82252
Cu-3d transition metal alloy, dil., electronic charge density around impurities 78−34799
Cu-Ag, dil. molten alloy, Ag activity determ. by two-component evap. *(Japanese)* 77−48395
Cu-Ag-O alloys, dil., O-metal interactions, activity coeff. meas. at 1423K 80−93792
Cu-Al, change in force constant due to volume effects 78−75778
Cu-Al, dil., thermal expansion *(French)* 79−95185
Cu-Al, impurity concentration effects 78−75777
Cu-Al alloy, dil., lattice expansion and localised vibr. mode 79−37789
Cu-Al dil. alloy crystal, dislocation etch pits on {111} surfaces *(Japanese)* 77−62536
Cu-Al dil. alloys, dislocation etch pit obs. on {111} surfaces 79−10861
Cu-Al spherical crysts. grown from drop of melt, topography 80−84353
Cu-Al-Fe, dil. liq. alloy, localised mag. state interactions *(German)* 77−1539
α-Cu-Al(Fe) dil. alloys, Al ion charge screening, elec. resist. obs. 77−4500
Cu-alloys, dil., optical props. and electronic struct. 78−35164
Cu-Au, dil., enhanced lattice sp.ht. 78−51699
Cu-Au, dil., O_2 solubility, thermodynamic and residual resist. study 78−59952
Cu-Au, dil., thermal neutron irradiated, isochronal resist. recovery, 30-400K 79−19287
Cu-Au, magnetoresist., temp. depend. 80−70682
Cu-Au-O alloys, dil., O-metal interactions, activity coeff. meas. at 1423K 80−93792
Cu-Au(Be)(Sb), dil., electron high dosage source for residual resistance specimens and irradiation expts. *(German)* 78−21274
Cu-Au(Ga)(Ge)(Zn), Matthiessen's rule deviations above room temp. 79−91023
Cu-based, compositional changes in oxide thin films, Auger electron microanalysis *(Japanese)* 77−21319
Cu-based dilute alloys, nonmagnetic, electric field gradient tensor 77−72843
Cu-Be, impurity concentration effects 78−75777
Cu-Be (0.25 at.%), channelling meas. of trapping efficiencies of solute atoms for self-interstitials 79−86829
Cu-Bi (0.02 wt.%), intergranular fracture, Kossel X-ray diffr. in SEM obs. 80−108579
Cu-Cd (0.03 at.%), single cryst., deformed, dislocation arrangement 79−10856
Cu-Cd (1.0 wt.%), yield stress and flow stress 80−97524
Cu-Co, dil., binding and caging of impurities and trapped interstitials 78−39462
Cu-Co-Fe, dil. alloy, low temp. resistivity maxima *(Russian)* 79−87091
Cu-Co(Fe)(Ni), dil. mag. alloy, NMR of ^{63}Cu around impurities 77−16187
Cu-Cr, dil., elec. cond. meas., 1.5 to 30K 77−62914
Cu-Cr, dil., negative magnetoresist. in pulsed fields up to 35T 77−62899
Cu-Cr, dil., thermal and elec. cond., deviations from Wiedemann-Franz law 77−66151
Cu-Cr, dil. alloy, Knight shift temp. depend., electronic struct. 78−84488
Cu-Cr, dil. alloy, Kondo resist. at 35 GHz 79−60814
Cu-Cr, dil. alloys, Frenkel defects, effects on anomalous resistivity and thermopower 77−8084
Cu-Cr(Mn)(Fe), NMR data, ionic model and Kondo temp. 78−68399
Cu-Cr(Mn)(Fe), NMR satellite data, rel. to electronic struct. 78−68398
Cu-Fe, diffusion and ageing processes, Mossbauer study 80−7245
Cu-Fe, dil., local mag. moments, neutron scatt. study 79−61058
Cu-Fe, dil., local susceptibility, Mossbauer meas. 78−19400
Cu-Fe, dil., powder, transferred orbital hyperfine field on near neighbours, NMR meas. 78−27098
Cu-Fe, dil., transmission ESR meas. 2 to 40K 78−68364
Cu-Fe, dil. alloy, quench-condensed thin film, annealing effect on resistivity 78−43488
Cu-Fe, dil. alloy, spin relaxation rates, neutron scatt. study 79−47235
Cu-Fe, dil. alloy solubility and diffusion of Fe 78−43170
Cu-Fe, dynamic susceptibility around T_k, satellite nucl. spin-lattice relax. time meas. 77−4573
Cu-Fe, internally oxidised, mag. and electrical props. 77−12100
Cu-Fe, ion implanted, phase comp., Mossbauer study 80−7244
Cu-Fe, thermopower, interconfig. fluctuations 79−65412
Cu-Fe (0.04 to 0.9 at.%), film, resistivity temp. depend., 1.5 to 17K, impurity interactions 77−63007
Cu-Fe (0.2 at.%), clustering, precipitation, and oxidation, 298 to 919K, Mossbauer study 80−7242
Cu-Fe (0.2 at.%), quenched, Fe dimers and defects 80−40007
Cu-Fe dilute alloy, host NMR spin lattice relaxation 79−51873
Cu-Fe group, dil., NMR satellite data calc., struct. of mag. impurities 80−103894
Cu-Ge, dil., point defect props., density functional approach 80−29013
Cu-Hg, dil., pool electrodes, passivation in alkaline soln. 79−70214
Cu-In, dil., point defect trapping after ion implantation, DPAC meas. 78−43728
Cu-Ir, dil., impurity diffusion, temp. depend. *(Russian)* 78−67851
Cu-Mn, dil., anomalous thermal expansion below 50K 78−51710
Cu-Mn, dil., local mag. moments, neutron scatt. study 79−61058
Cu-Mn, dil., mag. heat capacity, conc. and temp. depend. 79−61164
Cu-Mn, dil., spin density magnetisation near magnetic atoms 79−33545
Cu-Mn, dil., spin-glass dynamics, NMR meas. 78−31120
Cu-Mn, dil. alloys, conc. depend. of resist. maximum 77−62893
Cu-Mn, magnetoresistance and Hall effect, field-depend. electron scatt. 77−43581
Cu-Mn dil. spin glass alloy, impurity-impurity interaction press. depend., resistivity meas. 77−20308

dilute alloys continued
- Cu-Mn spin glass, magnetisation reversal and macroscopic mag. domain obs. 79−61168
- Cu-Mn(Fe)(Co), Kondo system, host NMR exam. 78−80246
- Cu-Mn(Ti)(Sn)(Si), dil., oxide film form. in ammoniacal Cu(II) solns., AES obs. 80−45415
- Cu-Nb-Sn dil. alloys containing Nb_3Sn precipitates, superconductivity 78−43507
- Cu-Ni, dil., electronic struct., virtual bound state due to s-d hybridisation 78−75990
- Cu-Ni, dislocation damping, 95-297K, at high strain amplitudes 78−39824
- Cu-Ni, far IR absorpt. appl. of multirefl. cell 77−18075
- Cu-Ni dil. paramagnetic alloys, sp. elec. resist., effect of Ni clusters *(German)* 78−95293
- Cu-Ni(Pd)(Pt), dil., screening charge density round $\Delta Z=-1$ impurities, vacancies, NQR study 80−103897
- Cu-Ni(Zn)(Ga)(Ge), dil. impurity electron struct., self-consistent Korringa-Kohn-Rostoker Green's function calc. 79−78040
- Cu-O-Zn dilute liquid alloy, Zn-O interaction parameter 80−55694
- Cu-Pb-O, liquid, dil. alloy, O_2 activity, 1100 to 1200°C 80−25662
- Cu-Pd, dil, perturbed angular correlation exam. of Pd impurity, ^{111}Cd probe 79−78588
- Cu-Pd dil. alloys, electronic states, virtual bound states model test *(French)* 77−62809
- Cu-Pt-O alloys. dil., O-metal interactions, activity coeff. meas. at 1423K 80−93792
- Cu-Rh (0.5 at.%), nucl. quad. relax. 79−82898
- Cu-Sb, grain growth rate, 520-970°C *(Russian)* 80−29972
- Cu-Sb solid solution, dil., FCC, intergranular solid shortness mechanism *(Russian)* 79−5032
- Cu-Sc, impurity effects on annealing and resist., vacancy-Sc interaction 79−51142
- Cu-Si, change in force constant due to volume effects 78−75778
- Cu-Si, impurity concentration effects 78−75777
- Cu-Si(Sb), dil,, chemical etching and X-ray topography obs. of cellular struct. *(French)* 79−96249
- Cu-Ti, dil. alloy, cellular precipitates, nucleation, TEM study 80−3069
- β-Cu-Ti, dil. alloy, growth phenomena associated with precipitation, TEM study 80−3070
- Cu-Ti (5.7 at.%), dil., β-phase struct. 79−55700
- Cu-transition metal, residual resistivity, effect of 4d and 5d transition metal impurities 79−60791
- Cu-transition metal dil. alloy, virtual bound states 79−37975
- Cu-Zn-Sn (24-34, 1.0 wt.%), cold-worked microstruct., X-ray diffr. obs. 80−3088
- Cu+3d alloying impurities, solid soln., exam. of thermoelectricity *(Russian)* 79−28339
- Cu_3Au-Co, dil., LRO 78−18584
- Dy-Ta, elec. field gradient at ^{181}Ta, temp. depend., TDPAC meas. 79−95689
- Er-Ta, dil., mag. hyperfine field determ., TOPAC meas. 79−91330
- Er-Ta, elec. field gradient at ^{181}Ta, temp. depend., TDPAC meas. 79−95689
- $Eu_xLa_{1-x}Al_2$, dil. EPR, cryst. fields and effective exchange interaction 80−66029
- Fe alloys, charge transfer and alloy binding Thomas-Fermi-Dirac approx. 77−76775
- Fe implanted alloys, residence sites of Fe, Mossbauer data 80−39299
- α-Fe, interstitial or substitutional sp impurity doped, electronic struct. 80−34384
- Fe, metastable alloy form. by ion implantation 79−82252
- Fe-Al, dil. alloy, temp. depend. of ^{27}Al hyperfine field 78−47972
- Fe-Al, film, NMR spin echo, rel. to struct. inhomogeneities *(Russian)* 80−29644
- Fe-Al, residual elec. resist., contrib. from static lattice distortions and short-range parameters *(Russian)* 79−51548
- Fe-Al(Si)(Ga)(Ge)(As)(Sn)(Sb) dil., mag. hyperfine fields, Curie temps. and Mossbauer meas. 77−63190
- Fe-Al(Si)(Ga)(Ge)(As)(Sn)(Sb), dil., XPS meas. 77−63538
- Fe-based, hyperfine field at positive muon 80−40029
- α-Fe-based dil. solid solutions, electronic struct., hyperfine interactions 78−79968
- Fe-C, ageing late stages, diffusional coalescence of precip. along dislocation lines *(Russian)* 77−25060
- Fe-C, dil. alloys, softening, conventional and in situ expt. 79−47744
- Fe-C, dilute alloys, softening, conventional and in situ expt., HVEM obs. 79−47743
- Fe-C, Hall-field electrotransport of C, effective valence numbers 79−28148
- Fe-Co, dil., Mossbauer source, self-absorption effects *(French)* 79−24246
- Fe-Co, film, NMR spin echo, rel. to struct. inhomogeneities *(Russian)* 80−29644
- Fe-Co-Mn, dil. alloys, NMR freq. temp. depend., spin echo meas. 78−64296
- Fe-Cr, mag. props. of Fe, local coupling with spin modulation of matrix 79−15299
- Fe-Cu (75 ppm), internal oxidation, local struct. determ. by EXAFS 80−25916
- Fe-In, hyperfine field of In, clustering effect, nucl. orientation obs. 77−16188
- Fe-In, superconducting Kondo alloys and alloys with strong electron-magnetic impurity interaction, EM absorpt. of light 80−39711
- Fe-M, M=transition metal, impurity electronic struct., multiple scatt. approach 80−92856
- Fe-Mn, dil. alloy, mag. moment distrib., temp. depend., diffuse polarised neutron scatt. study 79−47250
- Fe-Mn, short-range ordering and segregation, ascending diffusion *(Russian)* 77−24406
- Fe-N alloy, dil., galvanomag. effects, 4.2-250K 78−87964
- Fe-Ni, impurity electronic struct., multiple scatt. approach 80−92856
- Fe-Ni-Mn, dil. alloys, NMR freq. temp. depend., spin echo meas. 78−64296
- Fe-Ni-Si, double spontaneous reversible deformation during thermal cycling 78−84942
- Fe-Sb-Ti(V)(Cr)(Mn)(Co)(Ni), dil., interactions and precip., Mossbauer study 80−39997
- Fe-Sb(Sn), dil., spontaneous magnetoresistance anisotropy and deviations from Mattheissen's rule 79−51553

dilute alloys continued
- Fe-Sn, dil., ferromag., temp. anomalies of Sn mag. hyperfine field and thermal expansion 79−33270
- Fe-Tb, amorphous, small angle mag. scatt. 78−27021
- Fe-Ti (V)(W), dil., thermophysical props. and elec. cond., temp. depend. 80−96842
- Fe-Ti (0.15 wt.%), Ti distrib., segregation, FIM anal. 80−84200
- α-Fe-V, dilute alloy, Mossbauer diffusion line broadening, exponential fitting evaluation 78−52379
- Fe-X-Sn dilute alloy, Mossbauer meas. of Sn interaction with solute atoms 80−15856
- Fe-Y, hyperfine interactions, $^{87}Y^m$ nuclear orientation meas. 78−43715
- Fe-Zr, dilute solid solution, surface segregation, AES exam. 77−43413
- $Fe_{70}Cr_{30}$, disordered X-ray spectra study of electronic struct., dil. alloy model interpretation 77−77324
- $Fe_{1-x}P_x$, electronic struct., mag., elec. and struct. props. 79−37971
- Fe_3Si-based dil. alloys, conduction electron polarisation, moment perturbations 78−68225
- Ga-Fe dilute alloy, Mossbauer spectrum 77−90080
- Ga-In, dil., elec. resist., temp. and impurity depend., deviation from Matthiessen's b-axis crystals 78−51970
- Ga-Sn, dil., elec. resist., temp. and impurity depend., deviation from Matthiessen's b-axis crystals 78−51970
- Ga-Zn, dil., elec. resist., temp. and impurity depend., deviation from Matthiessen's b-axis crystals 78−51970
- Gd-Dy, impurity component of elec. resist., meas. 1.5 to 390K 77−39831
- Gd-Ta, dil., mag. hyperfine field and elec. field gradient at ^{181}Ta impurities, TDPAC meas. 79−47361
- Gd-Ta, elec. field gradient at ^{181}Ta, temp. depend., TDPAC meas. 79−95689
- Gd-Yb(Ir), dil., ferromag., mag. hyperfine fields of ^{170}Yb and ^{193}Ir, Mossbauer effect meas. 79−24242
- $Gd_{0.99}Ho_{0.01}(Rh_{1-x}Fe_x)_2$, spin echo meas. on ^{165}Ho, quenching effect of Fe substitution 78−48079
- $Gd(Rh_{1-x}Fe_x)_2$, $x\leq0.15$, magnetisation and EPR studies 80−34767
- Ge-Si, dil. alloy, IR absorpt. and first-order Raman scatt. due to single and paired impurity atoms 79−82976
- Ge-Si, impurity concentration effects 78−75777
- Hf-Ir, dil., elec. field gradient at ^{193}Ir, Mossbauer meas. 80−66090
- Hf-Ta, dil., hydrostatic and uniaxial compression, elec. field gradient at Ta, time differential PAC meas. 77−69739
- Hg liquid amalgams, dil., elec. and thermoelec. power 77−55511
- Hg-Au(Tl)(Bi), liquid dilute amalgams, elec. cond. and thermoelec. power 78−51976
- Hg-Zn(In)(Pb), dil. liq. amalgams, expanded, cond. at high temps. and press. 77−20287
- Ho-Sn, dil. alloy, hyperfine interaction of ^{119}Sn, Mossbauer meas. 78−91998
- Ho-Ta, dil., mag. hyperfine field determ., TOPAC meas. 79−91330
- Ho-Ta, elec. field gradient at ^{181}Ta, temp. depend., TDPAC meas. 79−95689
- $Ho_{0.01}Gd_{1-x}Y_xNi_2$, spin echo meas. on ^{165}Ho, limited quenching of Ho moment by cryst. field 79−73851
- ^{181}Ho-^{181}Ta, dil., elec. field gradient at impurity, anomalous temp. depend., host 4f levels, γ-γ correls. 78−95272
- In, Nielsen-Taylor effect in thermopower meas. 77−66157
- In-Ag, dil., TDPAC technique appl. to diffusion model 79−78589
- In-Bi, supercond., ideal superheating and supercooling limits 77−4465
- In-Bi, supercond. penetration depth field depend. meas. 77−4464
- In-Cd, dil., elec. field gradient at Cd impurities, press. depend., TDPAC meas. 78−64302
- In-Fe film, dil., supercond., Raman scatt. of light 79−73634
- In-Mn, dil., supercond. film, H_{c2} meas., mag. impurity effects, pair breaking theory 79−42708
- In-Mn, dilute alloy, local excited states, electron tunnelling observation 80−34565
- In−Gd film, dil., fluctuation induced cond. above supercond. transition temp. 79−47196
- K-Na, dil., dynamical props. of quasiparticle excitations, de Haas-van Alphen effect meas. 78−84128
- K-Rb, dil., calc. of press. depend. of low-temp. transport props. 78−30905
- K-Rb(Na), dil., anisotropy of electron-impurity scatt. in K, de Haas-van Alphen effect meas. 78−18943
- K-Rb(Na), dil., anisotropic scatt. of conduction electrons by impurities 78−18944
- $(La,Ce)B_6$ dil. alloy, Kondo effect, impurity-impurity interaction, mag. susceptibility, mag. to non mag. transition 78−47948
- $(La, Ce)Sn_3$, dil. alloys, supercond. and normal state props. 78−76184
- $(La,Gd)Al_2$, dil. alloy, magnetoresistivity determ. 79−73495
- $(La,Gd)Al_2$, reverse Kondo alloy, transport props. at finite mag. field 80−6812
- $(La,Gd)Al_2$, very dil., resist. 79−23958
- $(La,Gd)B_6$, dil. alloy, spin glass behaviour, 4.2 to 200K AC mag. susceptibility, RKKY calcs. 78−47994
- (La,Na)Sn alloys, supercond. transition temp. 79−78254
- La-Eu, DHCP, impurity effects on supercond. T_c, electron pair breaking 77−36013
- La-Gd, DHCP, impurity effects on supercond. T_c, electron pair breaking 77−36013
- La-Sm-Sn, dil. alloy, Kondo effect obs., supercond. transition temp. meas. 77−51837
- $(La_{1-x}Gd_x)Al_2$, dil., reverse resistance anomaly 78−76054
- $LaSn_3$, containing light rare earth impurities, press. depend. of supercond. transition temp. 79−47184
- Li, metal and dil. alloys, electronic thermal cond. calc. 78−47764
- Li-M, impurity and conduction electron scatt. at 4.2K *(Russian)* 77−35931
- Lu-Ir, dil., elec. field gradient at ^{193}Ir, Mossbauer meas. 80−66090
- Lu-rare earth, dil., cryst. fields 78−80127
- Lu-rare earth, dil. alloy cryst. field determ. 78−10651
- Lu-rare earth metal alloys, dil., elec. resist. 79−82578
- Lu-rare field, dil. alloy, cryst. field parameter determ. 78−10650
- $LuRh_2$-Nd^{3+}, dil., ESR, hyperfine crysts. of $^{143,145}Nd$, g-factor, crystalline field splitting 78−52349
- Mg, dynamic recrystn. during creep, dislocation substruct., quartz comparison 80−109142
- Mg-Ag (0.18 at.%), channelling meas. of trapping efficiencies of solute atoms for self-interstitials 79−86829

dilute alloys continued
Mg-Al, dil. alloy, residual resistivity, model pseudopot. form factors 77—8062
Mg-Eu, mag. suscept. meas. 77—89925
Mg-Fe, dil. alloy, single impurity Kondo behaviour in elec. resist. *(French)* 79—60815
Mg-Fe alloy film, quench-condensed, resistance meas. 79—15235
Mg-Gd(Ho), magnetoresist., anomalous Hall effect 80—15502
Mg-In dil. alloys, effect of alloying on Fermi surface, de Haas-van Alphen effect meas. 77—76732
Mg-In dil. alloys, effect of alloying on Fermi surface, pseudopot. model 77—76733
Mg-Li dil. alloys, effect of alloying on Fermi surface, de Haas-van Alphen effect meas. 77—76732
Mg-Li dil. alloys, effect of alloying on Fermi surface, pseudopot. model 77—76733
Mg-Mn, dil. alloy, de Haas-van Alphen effect, exchange interaction, Kondo effect 78—88093
Mg-Mn, dil. alloy, single impurity Kondo behaviour in elec. resist. *(French)* 79—60815
Mg-Nd-Zn dilute alloy, metallography and precip. kinetics 80—71655
Mg-rare earth metal dil. alloys, anisotropic magnetoresist. 77—62905
Mg-Tb(Dy)(Ho)(Tm), dil., macroscopic shape effect due to quadrupole orientation, magnetostriction and thermal expansion meas. 80—60396
Mg-Yb, dil., Kondo scatt. from Yb, low temp. elec. resist. meas. 80—44578
MgEu, dil. alloy, cold worked, valence transform. of Eu due to defect association, mag. suscept. and Mossbauer meas. 77—51404
Mn-Tb, dil., hyperfine interactions, nuclear orientation 80—15929
Mo, HVEM bombarded, neutron damage simulation, defect cluster and dislocation obs. 80—107330
Mo-C dilute alloy defect cluster nucleation and growth under 1250 keV electron microscope *(Japanese)* 78—87663
Mo-C-Zr-B (0.004, 0.12, 0.002 wt.%) effect of grain size, cellular dislocation structure, on mech. props. *(Russian)* 79—34105
Mo-Nb, dil., impurity diffusion and vacancy-impurity binding energy of Nb and Mo impurities 80—15307
Mo-Zr-B-C, dil. alloy, struct. changes under prolonged high temp. annealing *(Russian)* 78—6944
Mo-Zr-C-B, dilute, electron microscope obs. of planar defect diffr. contrast patterns 77—43227
Na alloys, very dilute, sp. ht. meas. close to melting point 78—47501
Na-Se system, liq., thermodynamic props. 80—21319
Nb alloys, diffusion and trapping of O_2 79—77816
Nb-Pu(Pd), dil., impurity diffusion and vacancy-impurity binding energy 80—15307
Nb-Ru(Re)(Os), dil., impurities effect on elec. resist. at 0.4 and 77.3K *(Russian)* 79—91196
Nb-Zr(Nf)(Mo)(W)(Rh), dil., neutron irradiation at 4.6K, influence of impurities on defect prod. 79—55790
$NbSe_2$-Fe, dil. alloy, magnetotransport and superconductivity 77—55516
Ni alloys, anomalous Hall effect meas., two current model 77—62906
Ni alloys, dil., hyperfine field distribs., DPAC meas. 80—93222
Ni alloys, dilute, near surface composition, effect of irradiation and sputtering 79—33168
Ni alloys, factors affecting high-temp. oxidation behaviour, alloying effects 77—77638
Ni dilute alloys, implant profiles modification by radiation enhanced diffusion and segregation 80—88217
Ni, metastable alloy form. by ion implantation 79—82252
Ni-Al, dil., oxidation mech. at 800 to 1200°C 77—90483
Ni-As, dil., temp. depend. of hyperfine field, TDPAD meas. 78—43700
Ni-Au, dil., orientation depend. of surface segregation, AES and SEM obs. 78—71908
Ni-based, hyperfine field at positive muon 80—40029
Ni-based, impurity effects on grain boundary mobility *(Polish)* 79—96073
Ni-Co-Mn, dil. alloys, NMR freq. temp. depend., spin echo meas. 78—64296
Ni-Co-Mn, dil. ferromag. alloy, mag. moment, saturation magnetisation meas. 78—64195
Ni-Co(Fe)(V)(Ti), dil., optical absorpt., electronic struct. 80—108227
Ni-Cu-Mn, dil. alloys, NMR freq. temp. depend., spin echo meas. 78—64296
Ni-Cu(Zn)(Ga)(Ge)(As)(Se)(Br)(Kr), dil., ferromagnetic, hyperfine field and relax. time obs. of impurity heavy nuclei 80—75533
Ni-Pd (1 at.%), surface comp. and surface segregation, AES obs. 79—51404
Ni-S, AES of grain boundaries *(French)* 80—50477
Ni-Sb, dil., vacancy-impurity binding enthalpy, positron annihilation 79—91525
Ni-Sn(Sb), dilute ferromagnetic alloy, resistivity and magnetoresist. anisotropy 79—11106
Ni-Ta, dil., crit. behaviour of local magnetization, PAC and magnetisation meas. 78—48098
Ni-Ti (12 wt.%), dil. alloys, transform. early stages 78—3096
Ni-V, oxidation behaviour at 1200°C 77—77636
Ni-V(Nb)(Ta)(Si)(Ge), dil., mag. props. at elevated temps. 77—63089
$Ni_{0.97}Cu_{0.03}$, photoemission study, surface, bulk electronic struct. 78—48281
$Ni_{98}M_2$, M=impurity metal, formation of MH(D)-complexes 80—65236
$Ni_{0.98}Pd_{0.02}$, dil. ferromag., nucl. mag. relax. meas. 77—16198
$Ni_{0.97}Ru_{0.03}$, mag. moment distrib. polarised neutron study 79—42738
NiSb, dilute alloy, impurity-induced vacancy clustering 79—99972
P+Nb, dil. alloy, NMR obs. of ^{93}Nb 80—71203
Pb alloys, dil., diffusion thermopower, inelastic electron-phonon interaction 80—96851
Pb, dislocation inertial effects in plastic deform., internal friction meas. 77—36609
Pb-Ag(Pd), diffusion of Au, de-enhancement by impurities 80—19990
Pb-Mg, dil., resistivity, multiple plane wave calc., Fermi surface, vel. and band struct. 77—51723
Pb-Mn, dil., supercond. film, H_{c2} meas., mag. impurity effects, pair breaking theory 79—42708
Pb-Sn, dil., dislocation inertial effects, internal-friction meas. on normal and superconducting states 79—38883
Pb-Sn(Ag), dil. alloys, dislocation motion and electron-dislocation interactions 77—7728
Pb-Sn(Bi) alloys, dil., impurity effects on softening at T_c *(Russian)* 78—23220
Pd based 3d metal alloys, mag. phase diagram calc. 78—80144

dilute alloys continued
Pd Ni, effect of hydrogenation on thermopower 80—39562
Pd-Co, dil., Mossbauer emission spectra, fast relaxation regime, ^{57}Co hyperfine field 78—60362
Pd-Co, dilute alloy, ferromag. ordering, depend. on Co impurity at low temp. 79—61055
Pd-Co, extraordinary Hall effect meas., 2-250K 80—34420
Pd-Co, giant moment and Kondo-like coupling, nuclear orientation meas. 77—32160
Pd-Co, relax. of oriented ^{57}Co nuclei, Mossbauer meas. using ^{3}He-^{4}He refrigerator 78—24909
Pd-Co, very dil., Mossbauer emission spectra of ^{57}Co, relax. effects 80—29656
Pd-Co (0.1-45.7 at.%), thermo EMF at 4.2-300K *(Russian)* 80—92881
Pd-Co(Ni), dil. local orbital moment evidence 77—20299
Pd-Cr, dil., temp. dependent scatt. 80—59973
Pd-Cr, elec. resist., 7.4 to 300K, anomalous temp. depend. associated with cond. electron scatt. 79—73491
Pd-Cu-H(D) dilute alloy soln., thermodynamic props. at high-temp. 79—99334
Pd-Er, dilute alloy, EPR spectrum, effect of fine and hyperfine interactions 78—19323
Pd-Fe, dil., anisotropy of neutron polarisation near ferromag. phase transition 77—32234
Pd-Fe, dil., anomalous lattice parameters and H_2 solubilities 79—33091
Pd-Fe, ferromag. and spin-glass states, cond. electron polarisation studied by positive muons 77—28397
Pd-Fe, magnetoresist., rel. to dil. ferromag. model 78—30907
Pd-Fe, muon$^+$ Knight shift, cond. electron polarisation 77—66450
Pd-Fe, very dil., Mossbauer emission spectra, relax. effects 80—66084
Pd-Fe (0.54-8.0 at.%), thermo EMF at 4.2-300K *(Russian)* 80—92881
Pd-Fe-Mn, dil. alloy, high press. study 80—34600
Pd-Fe(Co)(Ni) dilute alloys, ferromag., magnetoresist. 78—91665
Pd-Gd, EPR, 35 and 9 GHz, very dil. limit 78—15019
Pd-Gd (1 at.%), lattice distortion around impurities determ. by polarised neutron method 79—1372
Pd-H, dil., electronic states, de Haas Haas-van Alphen effect meas. 77—47718
Pd-H dilute alloy, de Haas-van Alphen oscill. freq., absolute amplitude, Dingle temp. 80—49575
Pd-H dilute alloy, impurity elec. struct. 80—103643
Pd-H-Fe, Mossbauer effect, hyperfine field, effect of changing spin susceptibility 77—20494
Pd-Mn, dil., mag. moment distrib., polarised neutron diffuse scatt. meas. 77—80914
Pd-Mn, dil., mag. ordering, sp. ht. calc. by Monte Carlo method 77—77030
Pd-Ni, Zeeman splitting of cond. electrons 77—11884
Pd-Ni (15-90 at.%), thermo EMF at 4.2-300K *(Russian)* 80—92881
Pd-Ni alloy, dil., magnetothermopower meas. 79—78079
Pd-Rh, dil., hyperfine anomaly between bound negative muon and Rh nucleus 79—56707
Pd-transition metal, dil., itinerant versus localised magnetism 78—64188
PdCo, effect of hydrogenation on thermopower 80—39562
$Pd_{0.98}Fe_{0.01}Gd_{0.01}$, ferromag., Pd-Gd exchange const. and Pd polarisation, neutron scatt. meas. 80—25122
PdHg-Rh, dil., quadrupole interaction of ^{100}Rh 79—99520
$PdPb_2$-Rh, dil., quadrupole interaction of ^{100}Rh 79—99520
$Pd_{1-x}Pr_x$ (x=0.02 and 0.03), dil. alloy, min. resist. around 20K 79—19583
PdSb-Rh, dil., quadrupole interaction of ^{100}Rh 79—99520
$Pd_{0.97}Sm_{0.03}$ dil. alloy, assist. meas. 79—19583
Pd_xSn_y (x=0.95, y=0.05; x=3, y=1), Mossbauer spectra, high press. effects, force consts. 80—84669
PdTe-Rh, dil, quadrupole interaction of ^{100}Rh 79—99520
$Pd_{0.97}Tm_{0.03}$, dil. alloy, elec. resist. meas. 79—19583
Pr-rare earth dilute alloy, low field magnetic props. 78—84443
Pt-Au, recovery spectrum after thermal neutron irrad., Au effect and defect conc. depend. 80—65057
Pt-Co, dil, magnetopower, magnetoresistivity 78—68016
Pt-Co, thermopower and magnetothermopower 79—65456
Pt-Cr, elec. resist., 7.4 to 300K, anomalous temp. depend. associated with cond. electron scatt. 79—73491
Pt-Cr (0.3 and 0.5 at.%) anomalous resist. associated with conduction-electron scatt. from Cr impurities 79—99530
Pt-Cr alloy, (13-18 at.% Cr) resistivity and AC susceptibility, temp. 1.4—300K 78—2461
Pt-Cr(Fe)(Ni), dil., surface segregation, equilib. surface compositon, AES meas. 77—85039
Pt-Cr(Nb)(Re)(Rh)(V), dil. alloy, 0.5 at.%, ^{195}Pt NMR for local mag. susceptibility 78—84484
Pt-Fe, very dil., Mossbauer emission spectra, relax. effects 80—66084
Pt-In, dil., damage induced quadrupole interactions, DPAC exam. 78—39465
Pt-Mn, dil., nuclear orientation exam. 79—61171
Pt-transition metal, dil., mag. susceptibility and NMR meas. 78—39290
PtV, dil. alloys, NMR obs. of ^{51}V 80—71203
Rb-K, dil., dynamical props. of quasiparticle excitations, de Haas-van Alphen effect meas. 78—84128
Rh-Fe, dil., anti-Kondo effect, de Haas-van Alphen obs. 79—73427
Ru-Fe, dil., localised spin fluctuation system, supercond. transition temp., conc. depend. 78—56253
Sb-Ge (1.2 to 2.2 at.%), carrier transport, magnetoresistivity, field-dependent tensor study 80—39609
Sb-Sn, dil., de Haas-van Alphen effect, effective mass, Fermi levels 78—75982
Sb-Sn (0.5 to 1.0 at.%), carrier transport, magnetoresistivity, field-dependent tensor study 80—39609
Sc-Dy(Er)(Tb), dil. alloy, high field magnetisation 78—56292
Sc-Ir, dil., elec. field gradient at ^{193}Ir, Mossbauer meas. 80—66090
Sc-rare earth, dil. alloy, cryst. field parameter determ. 78—10650
Sc-rare earth, dil. alloy, cryst. field determ. 78—10651
Se-Na, and Se, liqs., elec. resistivity and phase separation 79—82573
Si-Fe-W, dil. alloy, compositional changes on sputtering, projectile energy depend. 80—66362
Sn-In, dil., amplitude depend. US attenuation in normal and supercond. state 77—28299
Sn-In, dil., intermediate state, US attenuation 79—42694
Sn-In dil. liq. alloy, electrodiffusion and electroconvection, effective diffusion coeff., apparent effective valence 78—87802
Sn-Pb, dil., undercooled alloy, solidification 78—3120

- **dilute alloys** continued
  - Sn-Pb, lattice dynamics, sp. ht., resist., thermal expansion and nuclear γ reson. expts. *(Russian)* 78—87749
  - Sn-Pb alloys, dil., low-freq. phonon spectrum peculiarities 79—60463
  - Sn-rare earth , dil. liq., elec. resist. and mag. susceptibility 78—43350
  - Sn-Sb dil. liq. alloy, electrodiffusion and electroconvection, effective diffusion coeff., apparent effective valence 78—87802
  - Sn-Zn(Hg)(Tl)(Bi) dilute alloys, thermo EMF *(Russian)* 79—33285
  - TaS$_2$-Fe, dil. alloy, magnetotransport and superconductivity 77—55516
  - TaSe$_2$-Fe, dil. alloy, magnetotransport and superconductivity 77—55516
  - Tb-Ta(Cd), elec. quadrupole interaction, temp., and press. depend., TDPAC meas. 80—60469
  - Tc-Fe, dil., effect of Fe impurities on superconductivity 79—61007
  - Tc-Fe alloy, Mossbauer spectra, hyperfine field 80—20526
  - Tc-Fe dilute alloys, supercond. and mag. props. 80—29494
  - Te-Co(Cr)(Au)(Ag), dil. liq. alloy, elec. cond. at high temp. and press. 78—87959
  - Te-transition metal, liquid, dil., elec. resist., cond. electron conc. 77—15814
  - Th-Gd(Tb)(Dy)(Ho)(Er)(Tm)(Lu) (1 at.%), Heisenberg exchange, residual resist. meas. 80—75558
  - Ti-Al(Sn) alloys, thermal and athermal solid solution strengthening 77—4787
  - Ti-Fe, diffusion of stored H, Mossbauer study 80—34838
  - Ti-Fe, dil., phase analysis by Mossbauer spectra 80—15922
  - Ti-Fe-C-N, ion irradiated, microstruct. study using TEM 80—96572
  - Ti-Ir, dil., elec. field gradient at ^{193}Ir, Mossbauer meas. 80—66090
  - Ti-Mo-Fe (3, 0.13 at.%), metastable phases, Mossbauer study 80—7243
  - Ti-O, dil. HCP solid soln., O interstitial distrib. effect on lattice parameters 78—30588
  - Ti-Pd, ion implanted, corrosion rate and electrochemical props. 79—43467
  - Ti-U(Cr)(Mo)(W), dilute, superconducting transition temp. and mag. suscept. 78—47899
  - TiD$_x$, α- and β-phases, D-site occupancy, neutron diffr. study 79—42014
  - Tl-Cd, dil., quadrupole interaction, γ-γ ang. correl. meas. 79—56629
  - V-Pd, dil. alloys, surface segreg. 78—18883
  - V-Pt, inelastic neutron scatt. and quasilocal vibrs. *(Russian)* 77—80595
  - V$_2$Hf$_{1-x}$Ta$_x$, C15 supercond., electronic and lattice props. 78—68110
  - V$_{0.97}$U$_{0.03}$, phonon spectrum, quasi-local vibrs., inelastic incoherent neutron scatt. 77—15519
  - W-Co, dil., excess resistivity, temp. depend., Kondo effect 78—68011
  - W-Fe, dil., excess resistivity, temp. depend. 78—68011
  - W-Fe, dil., spin glass props., DC mag. susceptibility meas. 78—68283
  - W-Re, dil., excess resistivity, temp. depend. 78—68011
  - W-Re (3%), W adatom-substitutional Re atom interaction, FIM obs. 77—89626
  - Y-Cd, dil., electric field gradient, γ-ray ang. correl. meas. 79—56632
  - Y-Ir, dil., elec. field gradient at ^{193}Ir, Mossbauer meas. 80—66090
  - Y-rare earth, dil., cryst. fields 78—80127
  - Y-rare earth, dil. alloy, cryst. field parameter determ. 78—10650
  - Y-rare earth, dil. alloy, cryst. field determ. 78—10651
  - YAl$_2$-Er, dil., EPR, Er^{3+} Γ_8 ground state 80—15798
  - Zn-Ag, polycryst., amplitude-depend. internal friction *(Polish)* 79—96079
  - Zn-Al, isotherm of internal adsorption at dislocations 79—37733
  - Zn-Al dilute alloy, Kondo effect anisotropy 77—43578
  - Zn-Al(Cu), dil. alloy, creep ductility 79—38899
  - Zn-Fe, dil., ^{57}Fe Mossbauer effect meas. 78—95534
  - Zn-Fe alloys, dil., positron-electron annihilation spectra, Doppler broadened 79—65953
  - Zn-Mn, dil., Kondo effect and impurity interactions in resist., 0.05-14K 78—14721
  - Zn-Mn dilute alloy, Kondo effect anisotropy 77—43578
  - Zn-transition metal, residual resistivity, effect of 4d and 5d transition metal impurities 79—60791
  - ZnMn, dil., magnetoresist. meas., temp. depend. anisotropy 80—65532
  - Zr-Cu, dil. martensites, struct. and strength 79—29077
  - Zr-Dy dil. alloys, plastically deformed, mech. props. and microstruct. *(Russian)* 79—20112
  - Zr-Ir, dil., elec. field gradient at ^{193}Ir, Mossbauer meas. 80—66090
  - Zr-Mn (up to 0.3%), high-magnetic field magnetisation and magnetoresistance 78—10652
- **dimensions**
  - analysis, modification and generalisation in physics teaching 80—105481
  - automatic dimensional analysis using symbolic maths. 77—57173
  - dimensional analysis 80—27263
  - Dirac's large-number hypothesis, dimensionless coincidence between physical and astronomical quantities 80—18091
  - electromagnetism, dimensions and symmetry considerations, duality transformations 80—28139
  - flow, gas, measurement techniques, rel. to significance and treatment of phys. quantities *(German)* 78—1775
  - geometric objects with fractional dimension, seacoasts, galaxy clusters, turbulence and soap, book contrib. 77—87640
  - klirr-factor unit dimension meas., digital, errors evaluation 80—98873
  - linear and angular dimensions, classification and symbols for means of meas. 79—6081
  - measurement units, historical review and current systems in use *(German)* 80—68166
  - physical quantities, use in metrology 80—77740
  - wet steam, high speed flows, drop dimensions meas. method 80—90817
- **dimers** *see molecules*
- **dineutrons** *see neutrons*
- **Dingle temperature**
  - de Haas-van Alphen effect, accurate meas. of Dingle temp. changes 77—51638
  - de Haas-van Alphen effect, electron-phonon scatt. calc., appl. to Hg 79—65360
  - de Haas-van Alphen effect, FFT anal. 79—42434
  - de Haas-van Alphen effect in metals, intermetallic compounds and dilute alloys 79—99473
  - dislocated metals, perpendicular to orbit, Dingle temp. plot calc. 77—59248
  - dislocation pot. rel. to de Haas-van Alphen effect, Dingle factor *(Russian)* 78—30885
  - graphite, neutron irradiated, effect on quantum limit Shubnikov-de Haas oscills. 78—95304
  - graphite acceptor intercalation cpds., C$_n$Br and C$_n$NO$_3$H, electronic struct., quantum-magnetothermal oscills. 80—44478
- **Dingle temperature** continued
  - metal, dislocation scatt. and de Haas-van Alphen amplitudes 78—63967
  - metal, dislocation scattering and de Haas-van Alphen effect 79—77982
  - metals, effect of alloying on Fermi surface and Dingle temp. 77—47719
  - metals, noble, dilute alloys, solute vacancy binding energy, Dingle temp. 80—49177
  - noble metals and their dil. alloys, electronic struct., de Haas-van Alphen studies, book contrib. 79—37967
  - transition metal hydrides, electronic struct., heat of formation, single particle lifetimes, Dingle temp. meas. 78—51923
  - Al-3d transition metal, dil., transport props., sp. ht. and supercond. ant. temp. calcs. 77—1393
  - Al-Ga(Ge)(Mg)(Si)(Zn)(Ag), dil., Dingle temp. calc. 78—39005
  - Al-Li, Fermi surface impurity scatt. 79—56114
  - Au, conduction electron scatt. from vacancies 77—76735
  - Au, quenched and annealed, cond. electron scatt., de Haas-van Alphen Dingle temp. meas. 77—89688
  - Au, quenched and annealed, conduction electron scattering 78—47774
  - Au-Ga dil. alloys, electronic struct. 79—37974
  - Bi alloy, mag. field depend. electron scatt. rates, de Haas-van Alphen meas. 78—10436
  - Bi(:Si)(:Sb), mag. field dependent electron and hole scatt., quantum limit 77—15878
  - Cd, de Haas-van Alphen effect and mag. breakdown *(Russian)* 77—80722
  - Cu based 3d-transition metal dil. alloys, residual resist., Dingle temp. 77—1409
  - Cu, de Haas-van Alphen effect, accurate meas. of Dingle temp. changes 77—51638
  - Cu, Fermi surface orbit integrals, tetrahedron method, Dingle temps. for 3d transition metal impurities 80—44477
  - Cu:Ni, Dingle temps. calcs., tetrahedron method 80—6699
  - Cu-H system, de Haas-van Alphen Dingle temps. for scatt. of cond. electrons determ. 77—76731
  - CuH, electronic struct., heat of formation, single particle lifetimes, Dingle temp. meas. 78—51923
  - n-GaSb, Shubnikov-de Haas effect, effective mass, Dingle temp., and g-factor 79—51602
  - Hg, de Hass-van Alphen effect, electron-phonon scatt. calc. 79—65360
  - HgSe, Dingle temp. exam. 79—65358
  - HgSe, Shubnikov-de Haas oscills., electron conc., g-factor and Dingle temp. 77—69354
  - n-InAs, Shubnikov-de Haas effect, effective mass, Dingle temp., and g-factor 79—51602
  - In$_x$Ga$_{1-x}$P$_y$As$_{1-y}$, electron effective mass and Dingle temp., Shubnikov-de Haas oscills. 80—59859
  - n-InSb, Shubnikov-de Haas effect 80—11015
  - K, de Haas-van Alphen effect, accurate meas. of Dingle temp. changes 77—51638
  - K-Rb, dil., calc. of press. depend. of low-temp. transport props. 78—30905
  - K-Rb(Na), dil., anisotropy of electron-impurity scatt. in K, de Haas-van Alphen effect meas. 78—18943
  - Mg, pure and dil. alloys, electron lifetime anisotropy, Dingle temp. due to dislocation scatt. 79—78082
  - Mg-Mn, dil. alloy, de Haas-van Alphen effect, exchange interaction, Kondo effect 78—88093
  - MgCu$_2$, Fermi surface investig. by de Haas-van Alphen effect 77—35857
  - NbSe$_3$, oscillatory magnetotransport, Fermi surface anisotropy, Hall effect, g-factor, Dingle temp. 78—51975
  - Pb, magnetic interaction effect and Dingle temperature of de Haas-van Alphen oscills. 79—69395
  - n-Pb$_{0.82}$Sn$_{0.18}$Te, conduction band struct., determ. by Shubnikov-de Haas meas. 78—2504
  - Pb$_{0.82}$Sn$_{0.18}$Te, narrow band gap, relax. time for Shubnikov-de Haas effect 78—80006
  - Pb$_{1-x}$Sn$_x$Te narrow gap solid alloys, hole Fermi surface, galvanomag. and oscill. effect obs. *(Russian)* 77—69345
  - Pd-H, electronic states from de Haas-van Alphen measurements 79—7777
  - Pd-H dilute alloy, de Haas-van Alphen oscill. freq., absolute amplitude, Dingle temp. 80—49575
  - PdH, electronic struct., heat of formation, single particle lifetimes, Dingle temp. meas. 78—51923
  - Rh-Fe, dil., anti-Kondo effect, de Haas-van Alphen obs. 79—73427
  - Sb$_{1-x}$Bi$_x$ alloys, Shubnikov-de Haas *(Russian)* 78—23007
  - TaSe$_3$, oscillatory magnetotransport, Fermi surface anisotropy, Hall effect, g-factor, Dingle temp. 78—51975
  - Yb, FCC, Fermi surface parameters, de Haas-van Alphen effect, press. depend. 77—28092
  - Zn$_x$Hg$_{1-x}$Se, galvanomagnetic effects, Shubnikov-de Haas oscill. determ. of band struct. 80—6884
- **diode lasers** *see semiconductor junction lasers*
- **diode sputtering**
  - amorphous films of rare earth transition metal system, preparation by co-sputtering 79—56928
  - asymmetric diode system design for RF sputtering device, vac. system *(German)* 77—12527
  - closed anode bias sputtering method for film deposition *(Japanese)* 80—93484
  - coating techniques, for SEM and X-ray microanalysis 79—12783
  - cool diode sputter coater for heat-sensitive SEM specimens 78—24204
  - cylindrical magnetron sputtering sources, substrate heating 79—24435
  - deposition by ion beam sputtering, composition and stress state 77—89674
  - deposition rates calc., at. scatt. in system 78—52670
  - euglenoid flagellates, sputter and vacuum evap. coating, comparative effects on delicate features 78—24205
  - fusion reactor first wall, reduction of effective sputtering yield by honeycomb structures 79—23440
  - getter pumping for economical sputtering with Xe 77—40371
  - high rate deposition using ring gap plasmatron discharge 77—44175
  - ion sputtering pumps, power supply, press. control *(Spanish)* 77—37902
  - magnetron ion-sputtering system, operating principles and appls. 79—100050
  - magnetron sputtering equipment and application status 79—83124
  - modular system, production of thin films by cathode sputtering 77—81219
  - negative ion MFP in diode sputtering 78—95641

diode sputtering continued

- plasmatron/magnetron systems, role in physical vapour deposition 79—24436
- ring gap plasmatron for high rate sputtering 77—40368
- surface damage induced by RF-diode sputtering 77—90274
- Al metallization of semiconductor devices by high rate magnetron/plasmatron sputtering 79—28919
- Al, planar magnetron sputtering, H_2 effect on Ar discharge 80—80970
- Au, polycryst., RF bias-diode and triode sputtered, resist. and microstruct. 78—80072
- Cr-Si, amorphous sputtered film, material for kilo-ohm sheet resistances, prep. and props 79—78227
- Fe-Cr-Si, heat resistive films prepared by sputtering, lifetime meas. 80—80132
- Gd-Co film, amorphous, selective resputtering-induced anisotropy 78—72376
- In_2O_3-SnO_2 film, reactive DC diode sputtering, using large scale system 78—72723
- NiFe, film deposition, sputter gun system, bubble device appls. 77—12532
- Si, amorphous hydrogenated, manufacture of Schottky-barrier and MIS tunnel solar cells *(French)* 79—24897
- Si, minority carrier lifetime, effect of SiO_2 coating deposited by RF diode sputtering 80—11003
- SmAu, negative ion MFP 78—95641
- Ta-Cr-Si-Al, heat resistive films, prepared by sputtering, lifetime meas. 80—80132
- TaB_2-Cr-Si-Al, heat resistive films prepared by sputtering, lifetime meas. 80—80132
- Ta_2N, thin film deposition by closed anode bias sputtering *(Japanese)* 80—93484
- Ti, in Ar-O plasma, effect of oxidation on reactive sputtering rate 77—24955
- Ti-W, bias-sputtered, resist. and comp. 80—25023
- Ti-W RF sputtered films, comparison with magnetron sputtered films 80—45231
- TiO_x, reactive sputtering, film prep. conditions rel. to stoichiometry 77—40370
- ZnO film, Zn target, fabrication, properties 78—3040
- ZnO piezoelectric film US transducers obtained by DC diode sputtering, dielec. breakdown props. 80—40066

diode tubes *see diodes*

diodes

- *see also plasma diodes; rectifier tubes; rectifiers; semiconductor diodes*
- beam stability and current loss in magnetic insulation 79—94141
- cathodic protection using lightning conductors connected with diodes, for metals and concrete reinforcements 79—52418
- coaxial, with mag. insulation, ion acceleration *(Russian)* 80—10402
- coaxial field emission diode, comparison of Ar_2, Kr_2, and Xe_2 laser action 80—28201
- cylindrical relativistic diode, space charge limited, voltage distrib. and current calc. 80—63437
- cylindrical vacuum diode, convergence conditions for particle beam motion *(Russian)* 79—76567
- electric field distribution, in diode with sharp point cathode 80—5657
- electron and ion beam generation at high power, review 80—13988
- electron beam production, μs, high-current, device design and characts. 77—82642
- energy fluctuations power conversion, in diode circuit, thermodynamics 80—17911
- explosive emission diode, plasma pot. oscills., probe diagnostics 80—6284
- explosive emission of electrons, minimal current *(Russian)* 77—15256
- field emission diode, electron beam prod. using Tesla transformer accelerator 78—326
- flashover of insulator surface in vacuum mag. inhibition 77—11411
- foil-less diodes, relativistic electron beam generation 78—89593
- gas-filled diode, rarefied gas breakdown time delay statistics 78—87571
- high current vacuum diode, breakdown, electron beam prod. 77—82641
- high power field emission diode, space charge limited current flow 77—39477
- intense relativistic electron beam generation by foilless diodes, simulation 80—63438
- Knudsen discharge in gas diodes, initial transient kinetics calcs. 77—35430
- low impedance relativistic electron diode, behaviour in converging mag. gradient 77—370
- magnetically insulated diode, characts. of hollow electron beam 80—5398
- magnetically insulated diode, for 20 GW proton beam focusing 77—67533
- magnetically insulated vacuum diode, μs pulse insulation, ion beam generation 77—26431
- magnetoresistive, for contactless noncircuit-breaking large current meas. 78—8410
- Marx generator, μs-pulsed ion beam extraction 79—49886
- metal whisker point contact junctions, tunnelling and rectification characts. 80—6955
- noncylindrical symmetric space-charge flow, Coriolis and centripetal accel. 78—91182
- noncylindrical symmetric space-charge flow, momentum eqns. 78—91181
- nonlinear electron transport in vac. diode 77—13718
- optical diode to enforce one-direction travelling wave operation 80—69427
- particle accelerator, cathode plasma dispersion in transverse mag. field *(Russian)* 79—98997
- proton accelerating mechanisms in vacuum diodes, induced radioactivity 79—97470
- pulsed, HV, acceleration of filamentary macroparticles 78—47200
- radial-electron-beam diode for gas-laser excitation 79—94239
- SCL current in diode with local ionisation, critical conditions *(Russian)* 77—15255
- self-scanning linear diode array, appl. to laser bandwidth and wavelength stability meas. 78—86343
- space-charge limited, rigorous Poisson eqn. integration, three halves law derivation 77—50605
- spherical diode with plasma anode, use in electron gun 77—591
- thermionic, planar low press. gas discharges, space charge regime, volt-ampere characts. 79—77434
- thermionic diode, nonlinear electron and ion transport 77—13717
- thermionic planar low pressure gas discharges, plasma regime, plasma characteristics 79—77435

diodes continued

- thermionic uniformly heated, non-Boltzmann distrib. of free electrons, high space charge conditions 77—84390
- vacuum beam diodes, repetitively pulsed, lifetime and stability 80—63386
- vacuum diode, current fluctuations, elementary charge magnitude meas. *(Hungarian)* 77—49679
- vacuum diode, plasma expansion study by spectroscopic method 79—55551
- vacuum type, with sharp tip cathode, collective ion accel., by 180 kV pulses 78—37104
- Si diode radiation detector, stabilisation of radiation damage 80—91377
- W-Ge whisker diode, 337 μm IR detector *(French)* 78—8445
- W-Ni, MBM diode, resist. depend. of detected signals 80—2482

dipole antennas

- boundary-value problem, dipole in warm isotropic plasma, multiple water bag model 78—91115
- electromagnetic field of antenna buried in stratified anisotropic media 79—94128
- in electron plasma, isotropic, dipole radiation of longitudinal waves in infinite plasma 79—4153
- EM field of dipole above layered anisotropic medium 77—10812
- EM near field power density meas. *(Polish)* 79—21721
- EM wave propagation in composite media, air and three-layered earth 78—22076
- excitation of ion waves 77—3950
- horizontal magnetic dipole in geophysical subsurface probing with e.m. fringes method 77—5336
- LF noise induced in dipole antenna in ionospheric plasma 79—80072
- magnetic coated small dipole antenna, basic parameters *(Chinese)* 79—50193
- magnetoactive plasma surrounding dipole antenna, radiation pattern 80—100079
- in metal cased borehole, EM fields 77—46672
- modulated backscatter from reed switch loaded dipole 77—75386
- moving collisional plasma and moving plasma with intrinsic spatial dispersion, emission of longit. waves 80—87848
- non-planar dipole antenna in weakly ionised plasma, radiation pattern 77—3944
- plasma microfield cross spectrum meas. with two dipole antennas, theory 77—51227
- radiation patterns, two layered medium, geophysical subsurface probing 78—7788
- random linear electrostatic waves, cross spectrum measurement in isotropic Maxwellian plasma 79—46450
- Schottky-barrier diode monolithic detector dielectric plate antenna 79—30548
- thin wire antenna coupling with human body 77—21563
- transponder dipole antennas in and near three-layered body 80—98181
- vertical magnetic dipole on two-layer Earth 80—76906

dipole moment, electric *see electric moments*

dipole moments, magnetic *see magnetic moments*

Dirac electron theory *see Dirac equation; electron theory*

Dirac equation

- *see also electron theory*
- γ^5-invariant eqns. for massive particle 78—29262
- accurate solutions, for charge moving in crossed homogeneous fields *(Russian)* 77—30289
- action-at-a-distance theory of electrodynamics with Dirac's monopoles 79—63059
- additional symmetry 78—89
- algebraic struct., rel. of Pauli and Dirac eqns., from geometric interp. of Heisenberg's commutation rule 78—93549
- angular momentum of scalar isodoublet in magnetic monopole field 78—41428
- antimatter, defn. in quantum theory of perception 78—24674
- APW method, linearised relativistic using approx. pure spin basis functions 80—70581
- associative algebra of tensor fields, duality and Dirac identities 79—71618
- atomic, transitions induced by gravitational radiation *(French)* 78—29026
- atomic shells, internal conversion coefficients, numerical solution of Dirac equation 80—47434
- atoms, analytical relativistic SCF calcs. 80—83248
- axial anomalies and index theorems on open spaces 78—93821
- axial anomaly and Atigah-Singer theorem 78—377
- axial vector anomaly and index theorem 78—29293
- Backlund transform. derivation in inverse scatt. formalism 80—8810
- band structure, relativistic spin polarised calc., technique and its appl. to Gd 77—85128
- baryon field equation for arbitrary spin 79—63389
- baryon model based on Dirac eqn. with confining pots., independent quark model 78—425
- baryons, gluon exchange corrections in model with confining potentials 78—21379
- baryons with arbitrary spin, generalisation of Dirac eqn., group scheme 80—73615
- black holes, small, absorpt. cross section for Dirac and scalar particles 77—26023
- bound system of Dirac particle+fixed mag. monopole, elec. and mag. dipole moments 78—24966
- Bunge-Kalnay position operator 78—36864
- canonical formalism for Dirac field, Lagrangian formalism basis 78—49989
- canonical formalism on lightlike hyperplane, neutral scalar field, Dirac's theory 77—79214
- causal independence in local relativistic free quantum fields 79—21894
- channelling particles, relativistic, quantum theory of spontaneous γ-radiation 77—19997
- charge quantisation condition with N strings, charge monopole systems 77—65121
- charge Ze particle scatt. by mag. monopole, helicity amplitudes 77—65123
- charged particle scattering by mag. monopoles, SO(3), gauge theory 77—13907
- charged particles in external fields, classical Dirac, Klein-Gordon eqns. 77—49829
- charmonium spectrum, relativistic potential model, linear potential 79—58922

Dirac equation continued
- classical Lagrangian theory with radiative reaction, monopoles and positrons in Rohrlich formalism 79−72
- classification of Dirac operator terms 77−82672
- coherent states of relativistic particle in external EM field 77−2721
- Compton bound electron state scatt., binding and off-mass shell effects, relativistic anal. 78−17637
- conformal invariant 2- and 3-point functions for tensor fields with arbitrary spin 78−49977
- conformal spinors, $O_{2,4}$ transformations in $E_{2,4}$, components obeying Dirac eqn. 78−45504
- conformally covariant spinor field equations 79−22004
- conformally covariant structure 78−41417
- conservation laws for the classical Maxwell-Dirac and Klein-Gordon-Dirac equations 79−49066
- Coulomb multicentre pot., distinguished self-adjoint extension for Dirac operator 77−18156
- Coulomb pot. exact bound w.r.t. Dirac operator 79−21988
- covariant Dirac equation as basis for unified treatment of electromagnetic and gravitational theory 78−8314
- covariant method for soln. *(Russian)* 78−33007
- covariant quantisation of quark binding string 78−4829
- curved space of const. curvature, Dirac eqn. 77−87898
- De Sitter gauge transformation, gravit. field interaction 77−67563
- De Sitter symm. space, gravit. interaction and spinning electron eqn. 78−103
- derivation, inhomogeneous media electrodynamics refraction *(German)* 79−13005
- derivation of iterated second-order eqn., electrodynamics of inhomogeneous medial *(German)* 79−81349
- diagonal form for free electron and anomalous mag. moment in mag. field 77−22650
- diagonalisation of Dirac and Sakata eqns. with const. mag. field 77−34081
- diffusion model for the Dirac equation 79−30277
- Dirac's extended electron model 79−26269
- Dirac's monopoles and action-at-a-distance theory: classical dynamics 80−95210
- Dirac electrons, moving in periodic mag. fields, one-photon emission 78−12844
- Dirac essentially self adjoint operator, resolvent estimator near infinity 78−49992
- Dirac fields in a curved space-time 80−18070
- Dirac fields in Riemannian space time, geom. props. 79−75430
- Dirac fields in Riemannian space-time, geom. props. 79−75431
- Dirac Hamiltonian in presence of instanton and meron fields, fermion zero modes and level crossing 79−21927
- Dirac massless field theory, pot. method anal. 77−82668
- Dirac particle in mag. field, symmetry breaking by monopole singularities 78−16977
- Dirac particle propagator, supersymmetric methods 80−342
- Dirac particles, massless bound state, Coulomb potential 80−37189
- Dirac S-matrix in k-plane 78−54577
- Dirac singletons, equivalence with massless particle 79−21903
- Dirac spinor amplitudes, calc. by complex Lorentz transforms. and trace calculus 80−42322
- Dirac strings, theory 77−22634
- Dirac-Coulomb functions, asymptotic expansions of radial integrals 79−308
- Dirac-Coulomb waves in electron theory, involutional transforms 80−99037
- Dirac-Fock relativistic free-electron gas, relativistic exchange pots. 77−13628
- dual charged solution in curved space time, Dirac quantisation, SU(2)×U(1) gauge theory 78−12827
- education, Dirac γ matrices 77−45637
- education, Dirac monopole, calc. of strength 77−33764
- effective range approx., bound states near limit of lower continuum 77−49638
- Einstein's field theory with teleparallelism and Dirac's electrodynamics *(German)* 79−40418
- Einstein unitary field theory with tele-parallelism, Dirac's classical theory of electrons 79−12685
- Einstein-Dirac eqns., ν radiation in general relativity *(Russian)* 78−49727
- Einstein-Dirac equation, soln., neutrino representation 79−58596
- electron elastic scatt., by spatially bounded mag. field 77−13834
- electron gas, thermodynamic properties, weak field expansions, in uniform mag. field at $T=0K$ 79−85066
- electron in coherent EM field, null-plane formulation, Volkov soln. expansion 77−13898
- electron inertial mass, asymptotic soln. of Dirac eqn. 79−2961
- electron mean motion in gravit. field 77−22478
- electron motion in standing wave fields 80−22539
- electron pair photoproduction, in field of bichromatic plane EM wave *(Russian)* 77−30291
- electron spin, Dirac equation, mechanical sphere, magnetic momentum and lines of force *(Hungarian)* 80−68344
- electron with anomalous moments, motion in parallel elec. and mag. fields *(Russian)* 78−37161
- electron with anomalous moments in EM field 80−37197
- electrons, runaway solutions and finite size 77−45710
- electrons in logarithmic pots., Dirac eqn. soln. 78−41448
- elementary derivation, rel. to electrodynamics *(German)* 80−356
- EM field, minimal coupling, relativistic wave equations for particles of unique mass, constraints 80−22526
- EM vector and scalar pot., soln. 79−63398
- equivalence principle test for spin-$^1/_2$ particles 79−12707
- Euclidean operator zero-eigenvalue solns. in presence of pseudo-particle field 77−67569
- Euclidean Yukawa_2 quantum field theory, FKG correlation inequality 80−68357
- exact scatt. soln. of eqn. with short range pot. 79−17268
- exact solutions for charge in mag. field *(Russian)* 78−45775
- exact solutions of Dirac, Klein-Gordon and Lorentz eqns. *(Russian)* 77−79205
- exact solutions of eqns. of motion of charge *(Russian)* 78−49954
- expanding universe effect on quantum mechanics of electromag. bounded spin 1/2 particles 78−54271
- extended electron model, quantum and classical theory elaboration 78−82134

Dirac equation continued
- extended model of Dirac electron 77−22436
- Fermi-Bose and internal symmetries with universal Clifford algebras 78−24970
- fermion pair with instantaneous interactions, relativistic bound-state equations 80−13200
- fermion-meron interactions in Minkowski space-time, classical Yang Mills fields 79−2913
- fermions, massless, isospin 3/2, coupled to N-particle field 79−6298
- fermions and vortex solutions in Abelian and non-Abelian gauge theories 79−12959
- fibre bundles, internal affine symm. of Dirac fields 78−24697
- fibre bundles, Poincare group canonical representation, Lagrangian formalism 79−30678
- fibre bundles $P(M_4,G)$, invariant eqns. 77−17864
- Foldy-Wouthuysen representations, Dirac and Dirac-Pauli eqns. 77−65090
- Foldy-Wouthuysen time-depend. transformations, gauge invariance and Pauli Hamiltonian 77−41762
- fractional winding numbers and surface effects 78−8579
- free Dirac field, algebraic struct. of set of local observables 79−58883
- free electron laser, quantum theory 80−23656
- free EM field quantisation, gauge invariant fields 80−105817
- free massive anticommuting spin 3/2 field, quantisation using Dirac's Hamiltonian method 78−58113
- free-particle wave function generalisation, quark theory with internal coords. 77−65135
- general relativistic Dirac-Pauli particle, underlying classical model 77−45743
- general relativity, the Dirac equation, and higher symmetries 79−25931
- generalised Hamiltonian dynamics, appl. to nonlinear field theory 79−75678
- generalized phase factors and the interaction of Dirac particles 80−27168
- generalized total ang. momentum operator in curved space time 79−49128
- geometrodynamical superHamiltonian and supermomentum, Dirac field in curved spacetime 78−45518
- $GL_{4,R}$, nonlinear two valued realizations, Dirac eqn. nonlinear form 79−80748
- Gordon decomposition and tidal interaction 78−8324
- Grassmann variant of classical mechanics, particle spin dynamics 77−41495
- gravitation quanitsation theory, Dirac's constraints, geometric approach *(Italian)* 78−21044
- gravitational field and arbitrary gauge field, equations of motion, Heisenberg and classical, force term, spin-curvature coupling 80−57158
- gravitational interaction of spin-1/2 particles, Lorentz invariant theory 80−22257
- graviton-matter interaction, Zitterbewegung interpretation 80−122
- hadronic atoms in momentum space, Dirac, Schrodinger and Klein-Gordon eqn. eigenvalues 79−872
- hidden-parameter theory of extended Dirac electron 77−57212
- holonomic quantum fields, deformation model 79−25907
- Huyghens' principle, validity for spinor field eqns. *(French)* 77−41487
- hydrogenic atom, Dirac eqn. approx. soln., Moore's method appl. 80−42926
- identical motion in relativistic quantum and classical mechanics 77−61177
- index theorem, axial-vector anomalies, in Schwarzschild and Taub-NUT spaces 78−93832
- infinitesimal symplectic relations and generalized Hamiltonian dynamics 79−25878
- instanton Green functions and tensor products 79−54252
- instanton soln. 78−82100
- instantons, local supersymmetry transf. and fermion solns. 78−74177
- internal $GL_{2,c}\times GL_{2,c}^*$ symmetry of Dirac equation with external electromagnetic field 79−93324
- intrinsic SO(2,1)×GL(1,R) invariance of Dirac eqn. 78−93826
- invariance algebras of Schrodinger and Dirac eqns. *(Russian)* 80−68081
- invariance groups for class of countable systems of first-order partial differential eqns. 78−49635
- invariance groups of Dirac and Kammer-Duffin-Petiau eqns. 77−67320
- inverse scattering method, massive Dirac system soln. using connection with matrix Schrodinger eqn. 79−2655
- ion, highly-stripped, quantum defects 79−41147
- ion+atom collision, electron spin coupling in rot. frame, X-ray emission 79−36724
- isofermion Dirac particles, energy spectra in 't Hooft Polyakov monopole field 78−24965
- K-shell atomic ionisation by heavy particle, electronic relativistic effects, Dirac wavefunctions, semiclassical effects 78−78792
- Kaluza-Klein bundle, unified theory 80−37153
- Kerr Newman black hole, electron eqn. separation 77−2583
- Kerr space-time, anomalous Zeeman splitting of energy level 77−74081
- Kerr-Newman black hole, massive spin-1/2 wave, non-allowed superradiant scatt. 77−61002
- in Kerr-Newman space of black hole, class of solns. 77−49828
- Klein paradox and the mass spectra of the neutral vector mesons 79−26299
- Klein paradox as many-particle problem 77−2717
- Kramers-Heisenberg dispersion formula, Dirac transformation generalisation 78−16960
- Lagrangian field theory, vector bundles, rth order Noether invariants and canonical symmetries 78−86409
- large-complex-charge behaviour of the Dirac determinant 79−93328
- lattice Dirac eqn., spectral degeneracy as function of lattice shape 78−376
- lattice fermions, Dirac fields and Thirring fields, spontaneous breaking of chiral symm. 78−24962
- lattice field theory Dirac eqn. 78−24924
- lepton bound in Coulomb field of nucleus 79−94115
- lepton wave packets produced by strong short-range potentials 78−45828
- Levinson's formula, inverse problem of scattering theory *(Russian)* 79−9315
- Levinson theorem and its generalization in relativistic quantum mechanics *(Chinese)* 79−92988
- linear potential, QCD appl. 80−27392
- Lorentz's equations, relativistic and nonrelativistic, maximally extensive local group of invariance 80−77946

Dirac equation continued
- Lorentz basis of quantum fields 80—86565
- Lorentz space relativistic path integrals, Dirac electron perturbation expansion 79—85000
- Lorentz transform as space-time reflection 77—57187
- Lorentz-Dirac eqn. constraints 78—77736
- Lorentz-Dirac equation 80—12921
- M_4 factorisation, spinor algebra, Dirac equation geometrical, interpretation 80—62838
- magnetic monopole, gauge independ. formulation 78—41427
- magnetic monopole, relativistic theory, canonical quantisation 78—45517
- magnetic monopoles, PT-invariant theory of massive dually charged particles, Dirac-like eqn. 80—52429
- magnetic poles, singularity lines, kinematic origin *(Russian)* 77—74606
- magnetic resonances between massive and massless spin-$^{1}/_{2}$ particles with magnetic moments 80—62895
- massive Dirac system, nonlinear evolution eqns., inverse scatt. method soln. 79—2654
- massless particles, new invariance algebras 79—58909
- massless particles, number of quanta in neutrino field 78—4765
- maximum principle appl. to essential self adjointness of Dirac operator 80—18794
- ME-EM field model of free electron state 78—49988
- Melosh transformation, group theoretical anal. 77—2749
- Melosh transformation determ. 77—13919
- meson theory with internal coords., Dirac eqn., Bethe Salpeter eqn., quark model 77—13937
- Minkowski covariance in Kerr-Schild metric 77—64977
- monopole + electron, scatt. through small angles, Dirac-Schwinger monopole 80—68398
- monopoles and Hopf map $S^3 \to S^2$ 80—32042
- motion of charged particle in uniform magnetic field motion of charged particle 80—90690
- muon mass 78—33011
- muonic atom energy levels, computer calc. codes 79—31743
- muonic atom energy levels 79—76533
- neutrino wave equations in conformal space, Dirac theory 78—21364
- Newtonian interaction between particles satisfying Dirac eqn., Einstein-Sciama force 78—32745
- nongrassman quantisation, path integral approach in phase space 79—97496
- nonlinear, interpretation of Backlund transformations 78—49965
- nonlinear, soliton solns. 79—71591
- nonlinear classical fields, stationary localised solns. 77—74572
- nonlinear Dirac equation, spinor solitons or bags 78—12817
- nonlinear Dirac equation with SU(3) colour symmetry, vanishing soliton solns. 79—71693
- nonlinear Dirac field free soln., classical electrodynamics 79—80752
- nonlinear fermion system of self-interacting particles, field patterns 78—16909
- nonlinear spinor eqns. with localised solns. 78—49964
- nonlinear spinor field, charged Coulomb-like potential, localised solns. 80—68351
- nonliner eqn. in four dimens., asymptotic solns. 77—6016
- nonlocal properties of fermionic matter in strong gravitational fields 79—26210
- nonrelativistic limit of Dirac theory, scatt. theory 77—67319
- nonrelativistic limits for Klein-Gordon and Dirac eqn. 80—330
- nonzero mass quantum field theory, Lorentz (Poincare) transformation laws 78—37123
- normalisable solutions in the presence of magnetic monopole 79—67488
- nuclear deep lying level props. in strong electrostatic field *(Russian)* 77—2910
- one-body effective eqn. from Bethe Salpeter eqn. 77—54040
- one-dimensional with external pot., T-ordered exponentials 77—17832
- one-electron atom in curved space-time, energy shifts 80—78509
- one-electron polynuclear systems, Dirac eqn., variational soln. 80—83242
- operators, distinguished self adjoint extensions 79—25880
- particle bound by short-range forces in electric field 79—2963
- particle in const. elec. field with plane EM wave 77—30297
- particles, creation in general relativity with torsion and constant electric field 79—88857
- particles, creation in general relativity with torsion and electromagnetism, general formalism 79—88856
- particles in stationary spherically symmetric gravit. field 77—41293
- partitioning technique for approx. soln., appl. to H(1s, 2s, 2p) 80—23284
- Pauli matrix algebra formulation, 1-by-4 Dirac field as 2-by-2 matrix 78—74185
- perturbed boundary conditions, for differential equations in theory of atoms 78—33432
- phase equations solns. for Dirac particles, method of formal series 77—45993
- photon, Dirac-like eqn., transform. props. 79—58914
- plane waves in Dirac electron theory, involutional transforms 80—99036
- polarisation in external EM field 78—58116
- polarised light beams in gravitational fields, Dirac-spinor form of Maxwell's eqns. 78—50696
- potential interaction using a metric space 80—82879
- potential model, Dirac eqn. with linear confining pot., symmetric model 79—364
- potential model based on Dirac eqn. with linear confining pot., asymmetric model 79—363
- pseudoparticle fields with massless excitations, Dirac eqn. equivalence for spinor with chirality 78—4788
- QED tests of electron propagator, vacuum polarisation 80—77994
- quantisation of massive spin 3/2 particle coupled with magnetic field 79—75703
- quantum defect method, rel. to phase shifts for Klein-Gordon and Dirac eqns. *(Russian)* 77—79207
- quantum Dirac field, scatt. automorphisms, external field perturbations 78—58112
- quantum gravity, positive action conjecture and asymptotically Euclidean metrics 79—58611
- quantum numbers for Dirac spinor fields on a curved space-time 79—97277
- quantum processes in strong EM field *(Russian)* 77—13902
- quark confinement, Dirac equation with quadratic scalar potential 80—27459
- quark confinement, Dirac equation with relativistic linear potential, baryon properties, SU_6 representations 80—47261

Dirac equation continued
- quark field quantum fluctuation computation in arbitrary Yang-Mills instanton background 80—13268
- quark theory with internal coords., Dirac eqn., Bethe-Salpeter eqn. 77—18224
- quarks, dynamic models with confinement and linear trajectories without parity doubling 77—2797
- quasi-light-cone frame and approx. Galilean symmetries 77—13844
- quasistationary levels in lower continuum of Dirac eqn. solns. *(Russian)* 78—45826
- quaternion limitations on higher dimension spacetimes for unified field theories 78—45545
- radiating particles of finite size, Dirac's subtraction formalism *(German)* 80—91740
- reduction to Pauli-type equation, metric and EM field theory *(German)* 77—9894
- reduction to Pauli-type equation *(German)* 77—57
- Regge pole calc. by formal series 77—6056
- relativistic, classical interacting fields, virial theorem and stability of localised solns. 78—21342
- relativistic charged particle in arbitrary EM field, radiation, accel. 78—42269
- relativistic electron scatt. from 2-centre pot., approx. soln. 77—18187
- relativistic electron scattering from a two-centre potential 78—66058
- relativistic electron wave diffraction by cylindrical capacitor 80—5671
- relativistic electron wave equation 80—101702
- relativistic electrons, radiation in periodic mag. array, wavelength and polarisation 78—58149
- relativistic field equations with 2(2j+1) components derived from Bargmann-Wigner wavefunction 78—58105
- relativistic free-electron in uniform mag. field, Green's function of Dirac eqn. 80—18098
- relativistic H atom, Dirac eqn., operator structs. for consts. of motion 78—37124
- relativistic localisation and operator density current 78—32709
- relativistic moving charge in EM field, exact solns. *(Russian)* 77—71468
- relativistic phase shift in Dirac scatt. 77—67596
- relativistic scattered wave theory, normalisation and symmetrisation 78—62694
- relativistic theory, quantum defect phase shift relationship 79—771
- relativistic two body problem, critical mass, bound state spectrum 77—26457
- relativistic wave eqn. of electron *(Hungarian)* 79—12928
- relativistic wave packets, 3D, arbitrary sharpness with positive solns. 77—61186
- relativistic Wigner superoperator and its distribution 77—33897
- retarded self-interaction of classical point electron, divergences anal. 77—13620
- Rutherford scattering with radiation reaction, Lorentz-Dirac eqn. soln. for opposite point charges 78—55289
- S wave kinks of Dirac-Weyl eqn. 78—29292
- scalar potential inter-relation between non-relativistic and relativistic wave eqns. 78—58110
- scalar relativistic approximation 79—26899
- scattering problem for eqn. with oscillating pot. *(Russian)* 77—79225
- scattering theory with one-dimens. step potentials 77—49642
- Schrodinger equation for Dirac bubble potential 79—80456
- Schwinger model, pseudoparticle configs., Dirac eqn., dynamical mass generation 78—32982
- second-quantised Dirac and Klein-Gordon eqns., external fields 77—26472
- self-adjointness of Dirac operators, maximum principle 80—68352
- semiclassical approx. for Dirac eqn. in strong fields *(Russian)* 78—89645
- semiconductor or semimetal, screened and localised impurity states in 'optical' and exciton insulators *(Russian)* 77—62870
- single particle state obeying Dirac eqn., new bound state to continuum formulation 78—78335
- Sl(2,R) non-compact group for Dirac eqn. 80—22503
- soliton solns. in three space dimensions for scalar field interacting with Dirac field 77—26453
- soliton solns. of self-interacting Dirac field in three-dimens., quark confinement 77—26461
- soliton trajectories from nonlinear field eqns. of Dirac field, Lorentz and gauge invariant 78—4791
- solution of the Dirac equation with anomalous magnetic moment 78—82133
- solutions using a quadratic scalar potential 80—86564
- space-time symmetries on square lattice, (2+1) dimens. eqn. 78—4799
- spin 1/2 massive and massless particles, invariance algebra, Maxwell eqn. extension 80—82923
- spin 1/2 tachyons, nonexistence of conserved probability, Dirac eqn. general soln. 77—67554
- spin 1/2 wave equations irreducible under Poincare group, degenerate to Dirac eqn. 78—21332
- spin 3/2 wave eqn. 77—71231
- spin half field theory in Rindler space, Green's functions 78—12826
- spin motion eqn. in external field, Dirac particle quasiclassical theory 80—18099
- spin projection operators for fields of any spin *(Japanese)* 78—32733
- spin-1/2 charged particle with extra mag. moment in mag. monopole field, bound states 77—67604
- spin-3/2 field, Hamiltonian formulation and quantisation 78—8325
- spin-$^{1}/_{2}$ quantised Dirac theory, field representation 80—4845
- spinning electron, quantum mech. rotor, dynamics, invariance requirements 78—70250
- spinning particle, Lagrangian formulation of classical and quantum dynamics 77—18173
- spinning particles interacting with external fields, invariance groups of relativistic eqns., SU_3 symm. 78—49962
- spinor analysis of Yang-Mills theory 78—8532
- spinor and scalar fields in 4-D non-Euclidean momentum space, eqns. of motion, vacuum momentum 80—68379
- spinor electrodynamics, conformed invariance 80—99074
- spinor electrodynamics, quasiclassical approx. *(Russian)* 78—49996
- spinor field coupling to Klein-Gordon field, invariance prop. 78—4763
- spinor field eqn. conformal covariance 80—52442
- spinor field quantisation 78—45777
- spinor function, covariant derivative in Minkowski space with torsion 78—57824

Dirac equation continued
- stress-energy tensors 77—87672
- strong external fields, fermion and boson interactions 78—49987
- strong field QED in atomic phys., Dirac eqn., autoionisation model, QFT 77—54495
- strong gravity and Dirac numbers 78—21372
- strong localised EM potential interactions with charged leptons or vac. state, critical pots., weak currents 78—54597
- SU$_2$ monopole harmonics 79—17646
- SU(2) harmonic analysis as basis for quantisation 80—9116
- SU(3) theory of Yang-Mills-Higgs fermion-monopole system, topologically stable soln. 77—13888
- superheavy atoms from heavy ion collisions, electronic binding energy, wave functions 78—46252
- superheavy elements, $118<Z<138$, electronic spectra, anomalous levels 77—14331
- superradiance absence in Kerr metric 77—67578
- supersymmetric quantum theory construction around supertranslated soliton soln., Dirac's method 78—45783
- supersymmetries and pseudoclassical relativistic electron 77—13845
- supersymmetry and position operators 79—6305
- tetrad formalism for Einstein-Dirac eqns. and spinor Lagrangian 78—102
- Thomas-Fermi-Dirac eqn. nonlinear problem 77—22483
- time depend. scatt. theory, for Dirac particle with highly singular potential 78—21359
- Tomonaga fermions and three-dimens. Dirac eqn. 79—58633
- topological methods for gauge theories, winding numbers, euclidean Dirac eqn. 79—26206
- topological setting for axial anomalies and index theorems on open spaces 79—303
- translations as gauge transformations using fibre bundles formalism 78—12808
- two component form *(Russian)* 77—45934
- two-centre problem for Dirac eqn. 77—67328
- two-component first-order equations for the quantum-relativistic electron 79—17649
- two-dimensional Dirac eqn. on spatial lattice 79—93325
- two-photon synchrotron radiation of ultrarelativistic electron, Dirac eqn. anal. *(Russian)* 77—2719
- type D vacuum space-time, soln. of Dirac eqn. 77—74578
- ultrarelativistic particle in homogeneous mag. field, trajectory, radiation damping 80—18104
- unification of Maxwell, Dirac and Yang-Mills eqns., octave algebra 79—2967
- unification with electromagnetism, Einstein-Maxwell, field theory with teleparallelism and Dirac electron *(German)* 79—9168
- vacuum with spin in the ECSK-theory of gravitation 79—44830
- weak gravitational field, connection between Dirac and Dixon eqns. 78—124
- Wigner rotations and associated matrices for Dirac particles 77—2761
- WKB approximation at $Z>137$ 79—17650
- WKBJ approx. for classical particles with spin in external field 78—32692
- zero-energy eigenstates for the Dirac boundary problem 80—101961
- zero-energy solutions in N-pseudoparticle field 77—49845
- Zitterbewegung of Dirac particle in time-asymmetrical gravit. field 77—54067
- e gyromagnetic ratio in Coulomb field 80—82870
- p-$\bar{p}$ symmetry, mass difference, Dirac and CPT theory test 78—82125
- πN, pseudoscalar and pseudovector coupling to bound Dirac nucleon 78—25073
- Bi, at. polarisability, oscillator strength and radial integral 79—22620
- Ca(e,e′), A=40, 4, at 250 MeV, coupled-channel partial wave anal. 77—74837
- H atom, Dirac and Klein-Gordon relativistic eqns., energy level splitting 80—77938
- H atom in superstrong magnetic field, relativistic theory 80—23320
- H atom theory, Schrodinger-Dirac spaces of entire functions 77—54494
- H, atomic struct., relativistic Dirac eqn., for teachers 78—62019
- H, Dirac equation calcs. 80—46760
- H, Lamb shift, anomalous mag. moment relativistic Dirac eqn. 80—42954
- H, relativistic, in strong mag. field 80—9518
- H-like ion, elec. multipole polarisability, relativistic corrections, shielding factors, Dirac eqn. 78—13441
- Pb at. polarisability, oscillator strength and radial integral 79—22620
- SU$_2$ exact symmetry 77—65077
- Tl, at. polarisability, oscillator strength and radial integral 79—22620

direct analogues
- *see also electrolytic tanks*
- Wien bridge oscillator, critical phenomena simulation, threshold instabilities 77—1211

direct coupled amplifiers *see d.c. amplifiers*

direct current amplifiers *see d.c. amplifiers*

direct current generators *see d.c. generators*

direct current machines *see d.c. machines*

direct current motors *see d.c. motors*

direct current power transmission *see d.c. power transmission*

direct digital control
- *see also control systems*
- gas flow control, automated, transducer 78—59508
- gas stripping column, periodically cycled, feedback control, simulations 79—1231
- LMFBR, computer control system for Na test loops 79—26550
- Lucke texture goniometer with computer control X-ray pole figure plotting appl. 78—18500
- nuclear power plant, CANDU, DDC, dual redundant minicomputer system max. utilisation 79—36375
- resistance furnaces, aperiodic transfer functions determ. *(German)* 77—3709
- WWR-SM research reactor computerised control system, on-line alarm anal. 79—76104
- X-ray spectrometer, computer controlled, for steel alloying element determs. 77—56318

direct energy conversion
- *see also cells (electric); magnetohydrodynamic conversion; photothermal conversion; plasma diodes; solar energy conversion; thermionic conversion; thermoelectric conversion*
- bimorph vibrator pump characts., using ferroelectric crystals 79—48182

direct energy conversion continued
- Canadian R and D program for energy storage and conversion, review 79—29457
- catalysed-D Tokamak reactors, direct energy converter attachment 77—88277
- chemical energy conversion to mechanical and electrical energy *(French)* 79—52954
- chemical energy to elec. energy at p-n junction 78—39201
- chemical to electrical conversion using semiconductors 80—66984
- conf., 14th Intersociety energy conversion eng. conf. [Boston, MA, USA (Aug. 1979)] 80—31424
- digester gas cogeneration facilities Los Angeles 80—30514
- duplex chemical system for storage and transport of heat from LWR, district heating 78—37460
- efficiency increase, 1978 state and development trends 79—52917
- EHD power generator, performance characts. 80—40877
- Electrochemical Society Meeting, Boston, USA, (May, 1979) 79—91959
- energy conversion engineering, alternative energy sources *(Japanese)* 80—26105
- fission electric cells, synergetics using catastrophe theory 80—45761
- fossil fuelled advanced energy conversion systems, review 80—16772
- fusion mirror reactor, direct energy conversion 78—5018
- fusion reactor, beam and plasma direct converters 80—42861
- fusion reactor, TFTR, high power direct energy convertors for beams and plasma 80—99334
- fusion reactors, light nuclei fusion of charged particles 79—18032
- fusion reactors, open system, AC direct energy convertor 79—4197
- fusion switch vacuum arc development 78—13341
- heat transformer for energy cascading using metal hydrider, book contrib. 80—26151
- immersed parallel-plate duct, wave tank expts. 79—52873
- ion beam deceleration across mag. fields, expt. 80—99384
- ion-exchange membrane, electroosmotic energy conversion efficiency 80—61430
- large-scale elec. energy storage, review 80—89676
- laser to HV elec. energy conversion 77—88834
- magnetically stored energy, fast switching into external load, for pellet fusion 78—13339
- marine structures for energy conversion 79—43712
- mechanical-chemical conversion in artificial muscle polymers *(Russian)* 77—64167
- metal hydride chemical heat pumps, materials and performance characts. 80—40927
- NASA space power technology program, chemical energy conversion and storage 80—30494
- ocean thermal energy conversion concept 79—83577
- ocean thermal energy conversion programme, review 79—92066
- Osmo-Hydro power systems, technical feasibility and economics of salinity power 80—40893
- photoelectrochemical conversion, p-GaP electrode appl. 80—55673
- piezoceramics, electromechanical energy conversion in nonuniformly deformed bodies *(Russian)* 78—19418
- plasma spraying utilisation in research work 79—83117
- pulsed power conversion with inductive storage, for particle accel. in fusion device 78—13340
- pyroferroelectric energy convertor under thermocycling 78—15102
- radio wave action on rod, current, voltage generation EM to ampere energy conversion *(Russian)* 79—76548
- seawater thermal energy conversion expt. OTEC, Hawaii 80—40896
- shock wave mechanical energy conv. to electrical energy using ferroelectrics 80—61429
- solar electricity production, photovoltaic, photoemissive, photogalvanic, and photomagnetic, review 80—50981
- solar energy conversion and alternative working fluids, book 79—42428
- space charge based convertor, numerical simulator 77—35406
- steam power plants, energy conversion by alternative working fluids, book contrib. 79—43783
- Stirling free-piston engine/linear alternator system, 1978 development status 79—48178
- Stirling isotope power system, 1 kWe 79—48176
- synthetic and fissile fuel prod. by Cat-D fueled SAFFIRE reactors 80—99280
- thermal plasma energy, direct conversion to electrical energy *(Russian)* 78—87502
- thermodynamic energy conversion efficiencies 80—101081
- thermoelectric coolers with high current pulse and finite cold junction, fast transient behaviour 80—27290
- thermomagnetic motor, dynamic characts. and stable operation *(Japanese)* 80—16840
- water-nitrobenzene interface, mechanoelectrical energy conversion using interfacial tension changes 79—14982
- wave power absorption, by two independently oscillating bodies 79—52874
- wind characteristics for energy conversion systems, variance anal. 78—49100
- X-rays to electricity conversion scheme for advanced fusion reactors 78—70641
- Bi$_2$Se$_3$, mechano-caloric energy conversion 80—10962
- Bi$_2$Te$_3$, mechano-caloric energy conversion 80—10962
- CO$_2$ laser energy to HV electrical energy using laser-produced plasma 78—18427
- Cu$_{2-x}$S-CdS p-n heterojunction, optical energy convertor, struct. and recomb. props. 80—72065
- Sb$_2$Te$_3$, mechano-caloric energy conversion 80—10962

direct nuclear reactions and scattering
- *see also pick-up reactions; stripping reactions*
- ^{2}H, isobar knock-out theory 77—18510
- A(p,p′)X, inclusive reaction cluster emission models 79—6441
- antisymmetrisation effects in nuclear collisions, projection operator techniques 78—46036
- break up process as three body problem, Faddeev eqns. 78—89842
- capture reactions with n,p,α, direct-semidirect model 80—37385
- cluster spectroscopic factors for p-shell nuclear in shell-model 77—30486
- clustering studies, ang. correl. anal. 79—6547
- clusters of nuclei, quasielastic knocking on by hadrons, Young-Trayman angle *(Russian)* 78—33159
- collision expts. with final state partial resolution, maximal entropy procedure and surprisal anal. 80—18279
- compound particle knock out reactions, account of residual interaction *(Russian)* 77—14090

direct nuclear reactions and scattering continued
cool compound nucleus formation with oriented heavy ions, $^{258}104$ and $^{260}106$ prod. 80−99179
coupled channel Born approximation code, OUKID, finite range heavy ion direct reactions, appls. 78−89832
coupled channel variational method for multi-step direct nuclear reactions. I. Formalism and numerical test 78−66258
deep inelastic processes as multi-step direct reactions, (p,p′) appl. 77−26652
deformed nuclei, single nucleon form factor for knockout and pick-up reactions, (p,2p) calcs. 78−93999
deuteron breakup and stripping, three-body model 79−515
distorted waves method, finite radius of interaction, reaction mechanisms *(Russian)* 80−52647
DWBA computer program for heavy-ion transfer reactions 78−50145
DWBA integrals, evaluating strategies for computation 80−86863
E1-E2 direct-semidirect model for fast nucleon radiative capture, γ ang.-distribs. 78−62536
effective form factor pot. due to unbound core after direct process, asymptotic behaviour 80−27560
elastic and transfer processes, channel coupling and nonorthogonality 77−10377
elastic two fragment collisions, Pauli principle and optical pot. 80−63153
electroproduction of light fragments on nuclei, quasielastic knockout by electrons, general theory *(Russian)* 79−13276
emulsion nuclei, He nuclei emission in 7.5 to 200 GeV hadron interactions *(Russian)* 80−9325
exchange effects in direct reactions, antisymmetrisation and three body models 80−13446
few-body approaches 77−18511
few-body problem, deuteron, EM effects, three body bound state, break-up reactions 79−85384
first order optical pot., knockout cross section approx. to total cross section 79−22254
fragmentation, clustering and absorption mechanisms in p and π induced reactions 79−6546
fragmentation, phenomenological model and experimental proofs, cross sections 79−97694
fragmentation cross sections, dependence on cascade process and target and fragment characts. *(Russian)* 80−13447
fragmented analogue states produced in proton-nucleus reactions, fine struct. anal. 77−6391
fusion, power prod. in reactors, and astrophys. appl. *(Norwegian)* 79−30872
generalised Low eqn. approach to reaction matrix 79−85491
giant dipole resonance region radiative nucleon capture, expt. ang. distrib. coeffs., direct-semidirect theory 78−74354
hadron-nucleus collisions, mean effective mass number for big hadron model, knock-out proton and pion contamination 79−63704
hadron-nucleus reactions, quasi-elastic cluster knock-out, multiplicities 78−46042
heavy ion collisions, composite particle formation, direct, classical thermodynamic and quantum statistical theories 80−32297
heavy ion deep inelastic and high energy reactions, fragmentation cross section 80−78259
heavy ion direct transfer reactions, DWBA approach review 79−49614
heavy ion dynamical props. from coupled channels calcs. total, direct and fusion cross sections 79−67772
heavy ion fusion and transfer reactions, resonance effects 80−9283
heavy ion induced direct reactions and scatt., multi-step processes 78−50190
heavy ion induced two nucleon transfer, exact finite range microscopic DWBA, FORTRAN program SATTNT 77−61449
heavy ion inelastic scatt., coupled channels calcs. for direct reactions, long range Coulomb coupling 80−83117
heavy ion inelastic scatt., direct reactions, coupled channel calcs., coupled radial eqns. 80−83118
heavy ion projectile fragmentation in nuclear emulsions at 2.1 GeV/nucleon 78−70561
heavy ion reactions, energy depend. struct., review, book contrib. 80−27671
heavy ion transfer reactions, single and multi-step direct reaction anals. 80−5166
heavy-ion peripheral fragmentation, direct reaction model 78−8847
heavy-ion two-nucleon transfer cross sections 77−14155
high energy heavy ion collisions, single nucleon knockout, DWIA formalism 80−99165
knock-on reactions, absorpt. and polarisation effects *(Russian)* 77−79354
knock-out reactions, energy depend. correction to plane wave impulse approx. 77−22981
knock-out reactions, polarisation phenomena in the presence of strong absorption *(Russian)* 80−37360
level densities, thermodynamic temps., spin cutoff factors, nuclei with $23 \leq A \leq 40$, expt. calcs. 77−30492
light ion direct reactions, polarisation expts., tensor polarised deuteron beams 78−54732
light ion reactions, two step processes, effective interaction, CC and DWBA 78−54733
light nuclei, α transfer and knockout reactions, α clustering 78−41687
many particle final states, DWBA theory 78−21539
many-body scatt. theory, orthogonalised distorted waves and optical potentials 79−75940
multichannel direct resonance and heavy ion reactions, exactly solvable model *(Russian)* 79−67732
multichannel nuclear reactions, connected kernel formalism 78−46038
multiple scattering with rearrangement 79−504
nuclear continuum spectrum from disintegration by high energy particles, direct and resonant mechanisms *(Russian)* 79−30803
nucleon transfer reactions, centre-of-mass corrections to overlap factors 77−308
nucleus-nucleus pot., folding model, single nucleon knock-out exchange contrib. 77−305
one-nucleon transfer, sum rule anal., shell model validity 77−67730
orbital rearrangement and energy sum rule, ^{40}Ca anal. 77−79353
(p,α) direct reactions on light nuclei, alpha cluster breakup effects 79−6550
particle transfer spectroscopy with radioactive targets for study of nuclei far from stability 77−22990
plane wave description, DWBA 78−54734

direct nuclear reactions and scattering continued
precompound nuclear emission models, Feshbach theory, multistep direct and compound emission 79−71829
preequilibrium Griffin model, complex particles and direct nuclear reactions 77−88098
quasi-elastic direct transfer reaction to continuum states, DWBA and diffraction model 80−18277
quasifree cluster knockout reactions, cluster spectroscopic factors, medium and high energies, review 79−6440
radiative nucleon capture, pure resonance model, direct-semidirect model, pure semidirect model 80−78257
rearrangement reactions description by coupled channel eqns. 79−89271
relativistic heavy ion collisions, fragmentation cross sections, abrasion-ablation model, factorisation 80−78261
relativistic heavy ion collisions, projectile fragmentation, two step abrasion-ablation model 79−97724
relativistic heavy ion fragmentation reactions, abrasion-ablation model 79−97695
relativistic nuclear collisions, inclusive ρ spectra, knock-out mech. 77−82950
relativistic nuclei disintegration, spectator fragments distrib. 79−22261
semiclassical theory, complex paths and uniform approximations 77−71244
semiclassical theory, time-independ. formulation in three-dimens with complex trajectories 80−27605
spectral function deduced from knock-out reactions 78−582
Sturm-Liouville expansion method, one- and two-particle transfer form *(Russian)* 78−89844
three body sequential decay processes, α-transfer reaction studies 79−6526
three-hadron physics, book 77−45980
transfer reactions, 3-body with sequential decay, spectroscopic information 77−54203
two-nucleon transfer form factors, Taylor-series method 77−10382
two-step direct reactions through doorways, fluctuation effects 80−13445
(α,2α), A=9, 12, 16, 20, 22 80−68629
(α, 2α) 700 MeV, cross section, effective cluster number from PWIA, momentum distrib. 79−40940
(α,2α) comparison with (p,pα) reactions, antisymmetrisation effects 79−6575
(α, ^{3}HeX), 1 GeV/N, momentum distribs. after high energy fragmentation, spectator peak 80−99164
(α, N), DWBA finite range calc. 79−9541
(α,X), relativistic collisions, slow and fast fragment correlations, multiplicity association 80−86886
(d,p), multistage processes and methods 77−41974
(d,p) low energy direct processes new model, ^{12}C(d,p)^{13}C appl. 77−88097
d and t quasifree knockout at 62 mrad, differential cross sections *(Russian)* 79−30819
(e,α), Z=29-79, direct and statistical effects, cross sections and ang. distribs. 79−530
(e, e′p), eN interaction in quasifree scatt., nonrelativistic Hamiltonian through 2nd order 80−52663
(γ,n), 45-160 MeV, cross sections in quasi-deuteron model for direct reactions 80−63170
(γ,N), ang. distribs. from direct-semidirect model 79−71852
(γ,N), intermediate energies, nucleon current interactions, direct knock out mechanism 80−27624
(γ,p) 60-100 MeV, single particle knock-out using shell model wavefunctions, mass depend. 79−13273
(N,α) knock on reactions, final nucleus polarisation, polarised N capture 78−74352
(N,γ), ang. distribs. from direct-semidirect model 79−71852
(n,γ) total 14 MeV cross sections, meas. and anal. with statistical and direct reaction models 77−54226
(n,n′), 14 MeV, continuous spectra, multi-step direct reaction anal. 80−78258
(n,n′), 9-14 MeV, anal. of twice differential cross-sections 77−30590
(N,N′) microscopic description of direct processes, effective interaction 78−12979
(p,2p), distorted momentum distrib., and pp collisions, geometry choice for independent study 79−6597
(p,2p), off shell effects using optimum geometrical conditions 79−6598
(p,2p) high-energy knockout reactions, factorisation corrections 79−17885
(p,2p) knockout, DWIA and PWA mechanisms 77−88120
(p,2p) knockout experiments at Maryland, DWIA anal. 77−88118
(p,2p) knockout expts. at E>100 MeV 77−88119
(p,α), polarised p, anal. power, direct 3-nucleon transfer reactions, microscopic approach review 79−6545
(p, α) reaction, statistical direct reaction model 79−80913
(p, n), 22.2 MeV, A=27-197, neutron spectra, direct and equilib. processes *(Russian)* 80−52648
(p,p′), 800 MeV, cross sections, quasifree knockout mechanisms, PWIA calcs. 80−78294
(p,t), pol. p, strong ground state transitions, anomalous anal. power, direct and sequential processes 80−5115
(p,t) reactions, two stage processes in direct reactions, (p,d)(d,t) *(Dutch)* 78−29439
(p,X), 5-9 GeV/c, total inelasic and knock-out cross sections, nuclear RMS radius *(Russian)* 80−32175
(p,X), neutron excess isotope prod. in fragmentation reactions ^{6,8}He, ^{7,8,9,11}Li *(Russian)* 80−86888
(p,X), relativistic collisions, slow and fast fragment correlations, multiplicity association 80−86886
p+nucleus reactions, 400 MeV, multi-nucleon removal, p-γ coincidence spectra 79−6549
(π^-,2n) struct. and reaction information, two hole states, direct mechanism 79−85496
(π^-,γ), unified description of direct and resonance processes 78−86551
(π,πd) 115 MeV, light emulsion nuclei, integral reaction and differential cross sections *(Russian)* 79−13351
(π,πHe) 115 MeV, light emulsion nuclei, integral reaction and differential cross sections *(Russian)* 79−13351
(π,πN), quasi-elastic scatt., N knockout, coincidence measurement optimum conditions 79−76027
(π,πN) knockout reaction, nonanalogue nucleon charge exchange transitions 79−22336
(π, πp), emulsion light nuclei, 112 MeV, cross sections and mechanisms *(Russian)* 79−97733

direct nuclear reactions and scattering continued
- (π,πp) 60 MeV, light photoemulsion nuclei, direct knock-out model anal. *(Russian)* 79−54461
- (π^+,π^+p), strong absorpt. model for π induced knockout reactions 78−74404
- (π^-,X), 1.75-6.5 GeV/c, total inelasic and knock-out cross sections, nuclear RMS radius *(Russian)* 80−32175
- (π^-,X), n and charged particle emission following π^- capture 80−73867
- (τ,t) reactions, two stage processes in direct reactions, (τ,α)(α,t) *(Dutch)* 78−29439
- ^{A} Si(d,X), A=112, 124, 7.6 GeV/C, isotopic cross section ratios, He, Li fragments isotopic effects *(Russian)* 80−63154
- ^{208}(N,γ), pol. N, anal. power and giant multipole resonances, direct-semidirect model 80−18265
- A(a,ax)B, optimum kinematic conditions for quasi-free knock-out reactions 79−6548
- Ag(p,α)X, direct knockout model for fragmentation, (p,pα) predictions 80−18275
- Al(Ne,X), 400 MeV/N, direct vs. thermal particle emission, inclusive cross sections 80−52688
- Al(Ne,X), proton inclusive spectra, direct plus thermal model 80−57799
- ^{27}Al(^{20}Ne,^{12}C), 120 MeV, anal. of continuous spectra by multi-step direct reaction theory 79−45287
- ^{27}Al(^{20}Ne,^{16}O), 120 MeV, anal. of continuous spectra by multi-step direct reaction theory 79−45287
- ^{27}Al(α,X), 20, 40 MeV/N, α breakup yield, fragment yield ratios 80−9300
- ^{27}Al(p,α)X, direct knockout model for fragmentation, (p,pα) predictions 80−18275
- ^{27}Al(p,pα), 600 MeV, α-cluster quasielastic knockout, expt. methods, separation energy spectra 79−13275
- ^{27}Al(p,pα), 600 MeV, quasi-electric knockout reaction, PWIA calcs. 79−6581
- ^{27}Al(π,π'p), 255 MeV, quasielastic knockout, proton yield, $\sigma(\pi^+)/\sigma(\pi^-)$ cross section ratio 80−32305
- ^{27}Al(π,xγ), gamma ray coincidence spectra, nuclear surface clustering evidence 79−6707
- ^{27}Al(π^-, pxγ), 300 MeV, proton-gamma ray coincidence spectra 79−6704
- ^{27}Al(π^-,π^-n) and (π^-, π^-p+π^0n), knockout reactions, cross sections, nucleon charge exchange model 78−25246
- ^{27}Al($\pi^\pm$,$\pi^\pm$xγ), 300 MeV, pion-gamma coincidence spectra 79−6705
- ^{27}Al($\pi^\pm$,xγ), 300 MeV, gamma-ray coincidence spectra, clustering evidence 79−6706
- ^{28}Al ground state doublet ang. distrib., direct charge exchange model anal. from ^{28}Si(^{18}O,^{18}F) 80−9307
- Au+^{12}C, 25 GeV, momentum transfer to target fragmentation products 79−6691
- ^{197}Au(^{19}F,^{12}B), 186 MeV, deeply inelastic, direct processes and continuum cross sections 79−80951
- ^{197}Au(p,X)^{149}Tb, target fragmentation momentum transfer, collective tube model, collectivity effects 80−37359
- ^{197}Au(p,x), 197-800 MeV, ^{24}Na fragment emission excitation functions cascade-evaporation anal. 79−6553
- ^{11}B(n,α)^{8}Li, 14.4 MeV, ang. distrib., total cross sections 79−89303
- ^{11}B(p,^{6}Li)^{6}Li, 51.9 MeV, five nucleon transfer mechanisms, DWBA calcs. 80−73845
- ^{11}B(p,γ) 40,60,80 MeV, photon spectra direct reaction calc. 79−89281
- Be(^{48}Ca,X), 212 MeV/amu, neutron rich nuclide yields from ^{48}Ca fragmentation 80−27660
- ^{7}Be(p,γ), low energy cross section from direct, capture potential model 80−102184
- ^{8}Be cross sections and ang. distribs., direct knockout model anal. of ^{12}C(π^+,$\pi^+\alpha$) *(Russian)* 80−27620
- ^{9}Be(d,α)^{7}Li to g.s. and 1st excited state, E_d=2.25-3.1 MeV, DWBA anal. 77−30610
- ^{9}Be(e,e'p), single hole state momentum and energy distribs. 80−22674
- ^{9}Be(p,α)X, direct knockout model for fragmentation, (p,pα) predictions 80−18275
- ^{9}Be(p,pn)^{8}Be, 10-24 MeV, cross section, reaction mechanism, ^{9}Be level excitation 79−22284
- ^{9}Be(π^-,πN), 1 GeV/c, heavy fragment knockout process, ^{8}Li ang. distribs. 80−106036
- Be(p,X), 200, 300 GeV/c direct photon prod., η/π^0 and γ/π^0 prod. ratios 80−27618
- ^{209}Bi(^{136}Xe,X), 940 MeV bombarding energy depend., fragment deformation, sequential fision 80−86938
- ^{209}Bi(α,X), 20, 40 MeV/N, α breakup yield, fragment yield ratios 80−9300
- ^{209}Bi(n,n), direct scatt., polarised thermal neutrons, empirical parity-violating potentials and neutron optical activity 79−59074
- ^{12}C, π^+ induced two nucleon removal 78−25242
- ^{12}C+n, 18.2 MeV, multiparticle breakup, three-α correl. spectra 77−6364
- ^{12}C+p, 4.3 GeV/c, search for d knockout 79−6580
- ^{12}C(^{16}O,^{20}Ne), 10-15.5 MeV, cross sections and ang. distribs., resonances, direct and stat. anal. 79−67730
- ^{12}C(^{40}Ar,X), 213 MeV/N, relativistic fragmentation, microscope and macroscopic calcs., np correlation 80−13495
- ^{12}C(^{6}Li,α)^{14}N, E(^{6}Li)=20 MeV, using polarised ^{6}Li source, exact finite range DWBA anal. 78−58293
- ^{12}C(^{6}Li,d), ^{16}O level configuration mixing anal., α-spectroscopic strengths 79−6683
- ^{12}C(^{6}Li,d)^{16}O$\rightarrow$^{12}C+α, reaction mechanism from ang. correlations, direct transfer 80−78319
- ^{12}C(^{9}Be,^{9}Be), ang. distrib. from pick-up model anal. *(Russian)* 80−37396
- ^{12}C(^{9}Be,α)^{17}O, ang. distrib. from pick-up model anal. of cluster transfer *(Russian)* 80−37396
- ^{12}C(d, d'), isospin violating direct reaction, Coulomb interaction role 80−102170
- ^{12}C(d,p)^{13}C, 2.64-2.82 MeV, new model calcs. for p ang. distribs. 77−88097
- ^{12}C(e, e'p), eN interaction in quasifree scatt., nonrelativistic Hamiltonian through 4th order 80−47469
- ^{12}C(e, e'p), quasifree scatt., spin-orbit distortion of emerging nucleon 80−52664
- ^{12}C(e,e'd), deuteron knock-out yield, contrib. to inelastic scatt. cross section *(Russian)* 80−27621
- ^{12}C(ee'd), electroproduction cross section, Born approx. *(Russian)* 79−26427

direct nuclear reactions and scattering continued
- ^{12}C(γ,π^-), (γ,π^-p), knockout p interaction, optical model and quasifree π photoprod. mechanism *(Russian)* 80−42638
- ^{12}C(μ^-,ν)^{12}B*, average polarisation of recoil ^{12}B in direct capture 79−93602
- ^{12}C(p, 2p), 400 MeV, quasifree knockout cross sections 79−93614
- ^{12}C(p, pn), 400 MeV, quasifree knockout cross sections 79−93614
- ^{12}C(p,^{6}Li)^{7}Be, 36 to 56.8 MeV, differential cross section meas., reaction anal. 79−85467
- ^{12}C(p,X), reaction and scatt. dynamics, optical and coupled channel anal. 80−78297
- ^{12}C(p,α)^{9}B, knockout mechanism 78−29474
- ^{12}C(p,α)^{9}B$_{gs}$, 45.2 MeV comparison to ^{12}C(p,α*)^{9}B$_{gs}$ 79−6586
- ^{12}C(p,d), 4.3 GeV, deuteron knockout search *(Russian)* 79−3158
- ^{12}C(p,p'), 64 MeV, direct reaction, model t-matrix test, cross section and anal. power 79−93594
- ^{12}C(p,pα), 600 MeV, α-cluster quasielastic knockout, expt. methods, separation energy spectra 79−13275
- ^{12}C(π, πp)^{11}B, knockout reaction, cross section ratio $\sigma(\pi^+,\pi^+\text{p})/\sigma(\pi^-,\pi^-\text{p})$ meas. 80−32254
- ^{12}C(π^+, π^+p), 100, 180 MeV, knock out reaction, cross section and pion distortion in DWIA 80−91167
- ^{12}C(π^+,$\alpha\pi^+$)^{8}Be, 112 MeV, pole approx. anal., knock out reaction mechanism *(Russian)* 78−86553
- Ca+α, 100 MeV, fireball and coalescence model anal. 79−93642
- Ca(^{12}C, ^{8}Be), 45 MeV, even isotopes A=40-48 77−88172
- ^{40}Ca+$\pi^\pm$, multinucleon removal, prompt de-excitation γ-spectra obs. 79−6708
- ^{40}Ca(^{13}C,^{9}Be), 149 MeV, α-transfer cross sections, direct reaction theory anal. 79−67767
- ^{40}Ca(^{14}N,^{10}B), 153 MeV, α-transfer cross sections, direct reaction theory anal. 79−67767
- ^{40}Ca(^{16}O, ^{16}O'), 60 MeV, direct reaction calcs., ang. distribs. 78−58298
- ^{40}Ca(^{20}Ne,^{16}O), 262 MeV, α-transfer cross sections, direct reaction theory anal. 79−67767
- ^{40}Ca(^{40}Ca,X), 400 MeV, fragment energy spectra struct., giant resonances, direct process 80−47452
- ^{40}Ca(K$^+$,Kp$^+$), DWIA calc. of proton knockout as probe of deep hole states 78−13163
- ^{40}Ca(e,e'), quasi-elastic scatt., scaling law test, knockout process contribution 79−22274
- ^{40}Ca(n,γ_0)^{41}Ca, 6 to 13 MeV quadrupole radiation, direct-semidirect model calcs. 79−545
- ^{40}Ca(n,γ), direct-semidirect and compound nucleus contribs. to cross sections 80−68662
- ^{40}Ca(p,2p), 200 MeV, cross section and asymmetry meas. 79−6583
- ^{40}Ca(p,pα), 600 MeV, α-cluster quasielastic knockout, expt. methods, separation energy spectra 79−13275
- ^{41}Ca giant dipole resonance, isospin struct., direct-semidirect anal. from ^{40}K(p,γ) 80−47449
- ^{48}Ca+^{16}O 56 MeV, transitions to resolved levels, optical model parameter 78−41758
- ^{141}Ce collective M1 excitation effects on γ-ang. distribs., direct semidirect model of ^{140}Ce(n,γ) 80−57733
- Cl(Ar,X), 800 MeV/N, single particle spectra from high multiplicity events 80−99184
- Cl(Ar,X), proton inclusive spectra, direct plus thermal model 80−57799
- ^{37}Cl(n,γ), spectroscopic factors calc. using potential capture model 77−30583
- ^{59}Co(n,2n) direct process contrib., cross section and secondary n spectrum *(Russian)* 78−78386
- ^{59}Co(p,2p)^{58}Fe, 17 MeV, search for double-direct reaction 77−30576
- ^{59}Co(π^-, xn), single and correlated n spectroscopy, nuclear temp. 79−6713
- C(p,X) *(Russian)* 80−52649
- C(p,3p), 640 MeV, proton pair quasifree knock-out 80−22795
- C($\pi^\pm$, $\pi^\pm$X), X=He or d, 170 MeV, cross sections and ang. distribs., direct knockout mechanism *(Russian)* 80−86887
- C(π,πp), 170 MeV, two stage and knock out contribs., π^+,π^- spallation differences *(Russian)* 80−68632
- C(π^+,π^+p)C, 170 MeV, direct-knock-out dominant mechanism *(Russian)* 77−61460
- Cr+^{14}N(^{12}C), single- and multi-nucleon transfer reactions at 60, 70 and 90 MeV 77−14146
- ^{50}Cr(τ,α), 16 MeV ^{49}Cr energy levels, spins, parities, spectroscopic factors 78−33199
- ^{52}Cr+^{13}C, 105 MeV, ^{51}V, ^{51}Cr, ^{53}Mn, level scheme, DWBA and optical model anal. 79−36159
- ^{65}Cu analogue resonance direct n decay, stat. anal. from ^{64}Ni(p,nγ) *(Russian)* 80−5104
- ^{65}Cu(p,2p)^{64}Ni, 17 MeV, search for double-direct reaction 77−30576
- (d,X), neutron excess isotope prod. in fragmentation, ^{6,8}He, ^{7,8,9,11}Li *(Russian)* 80−86888
- ^{162}Dy(p, α), statistical direct reaction model calc. 79−80913
- ^{A}Er(p, α), A=166,168, statistical direct reaction model calc. 79−80913
- ^{19}F(d,X), X=^{7}Li, ^{7}Be, 13.6 MeV, diff. cross sections, ^{5}He cluster direct transfer *(Russian)* 80−52650
- ^{19}F(π^-, π^-n) and (π^-, π^-p+π^0n) knockout reactions, cross sections, nucleon charge exchange model 78−25246
- Fe(^{6}Li,d)Ni, A=54,56,58, at 34 MeV, comparison with (t,p) and (^{3}He,n) reactions 77−30631
- ^{A}Fe(p,γ_0)Co, A=54,56, giant dipole resonance splitting, direct-semidirect capture model anal. 80−106055
- ^{54}Fe+^{14}N(^{12}C), single- and multi-nucleon transfer reactions at 60, 70 and 90 MeV 77−14146
- ^{54}Fe(^{6}Li,t)^{57}Ni, t-energy spectra and reaction mechanism 78−41756
- ^{54}Fe(α,γ)^{58}Ni, 7.6 to 12.8 MeV, giant electric resonances in ^{58}Ni 78−41739
- ^{54}Fe(n,2n) direct process contrib., cross section, DWTA and DWBA anal. *(Russian)* 78−78386
- ^{54}Fe(p,p'), 39, 62 MeV, DWBA anal., collective spectra, direct process contrib. *(Russian)* 80−13408
- (^{56}Fe,X), 2 GeV/N, anomalous nuclei among relativistic projectile fragments 80−106034
- ^{56}Fe(^{6}Li,t)^{59}Ni, t-energy spectra and reaction mechanism 78−41756
- ^{56}Fe(e,e'α), 60 and 120 MeV, evidence for α-clusters 79−6569
- ^{56}Fe(n,2n), direct process contrib., cross section, DWTA and DWBA anal. *(Russian)* 78−78386
- ^{160}Gd(^{12}C, αxn)$^{168-x}$Er, particle fragmentation accompanied by incomplete fusion, two step model 80−86947

direct nuclear reactions and scattering continued
- ^{2}H breakup into Δ resonances, probability, isobar model, static NN-$\Delta\Delta$ mixing pot. 78—29438
- ^{2}H-N breakup calcs., separable interactions with P-waves and tensor forces, polarisation 77—50101
- ^{2}H(N,N′), three and four nucleon low energy scatt. expts., review 79—80945
- ^{2}H(α,α)np, 20-28 MeV, total reaction cross section 79—89317
- ^{2}H(α,αn), quasi-elastic scatt., direct reaction unitarised impulse approx. 80—42674
- ^{2}H(α,αn)^{1}H, 27.2 MeV, absolute differential cross sections 79—9599
- ^{2}H(d,p)^{3}H, 13.4, 17 MeV, pol. d, anal. power direct reaction and isospin symmetries 80—515
- ^{2}H(e, ep)n, spectator momentum distrib., quasielastic knockout mechanism *(Russian)* 79—30817
- ^{2}H(e,e′p), single hole state momentum distrib. 80—22674
- ^{2}H(n,n′), 14.8 MeV neutrons, d break-up cross section meas. 79—80932
- ^{2}H(p, 2p), 400 MeV, quasifree knockout cross sections 79—93614
- ^{2}H(p, pn), 400 MeV, quasifree knockout cross sections 79—93614
- ^{2}H(p,pp)n, polarised p, polarisation effects in 3-body system 79—80946
- ^{2}H(π,nπ), total cross sections 79—85510
- ^{2}H($\pi^{\pm}$,p$\pi^{\pm}$)n, 350 MeV break-up, differential cross sections 79—85509
- H(d,pp)n, polarised d, polarisation effects in 3-body system 79—80946
- ^{3}He(γ,2p)n, 80-120 MeV, proton energy distribs., diffr. cross sections, direct breakup 80—86897
- ^{3}He(p,dp)p, 156 MeV, p-d scatt. at small rel. energy in FSI region 79—85441
- ^{3}He(τ,τp)d, 120 MeV, coincident energy spectra, quasi-free scatt. 79—22303
- (^{4}He,^{8}He), direct four neutron cluster transfer from consideration of angular distrib. of ^{64}Ni(^{4}He,^{8}He)^{60}Ni 78—29488
- ^{4}He+α break-up reactions, 130 MeV, continuous energy spectra of emitted particles 79—76013
- ^{4}He+π^{+}, 110, 160 MeV, cross section ratio of (π^{+},π^{+}p) to (π^{+},π^{+}n)+(π^{+},π^{0}p) reactions 78—74403
- ^{4}He(^{3}He,^{3}He), 60.2, 113.1 MeV, ang. distrib., optical and coupled channel anal., cross sections 80—47492
- ^{4}He(p,X)^{3}He, 6.85 GeV/c, Glauber multiple model 79—63664
- ^{4}He(p,d)^{3}He, direct-reaction mechanisms 78—581
- ^{4}He(π^{+},π^{0}p), 120-165 MeV, 3 nucleon exchange in knock-out reactions, cross sections 79—85437
- ^{4}He(π^{+},π^{+}n), 120-165 MeV, 3 nucleon exchange in knock-out reactions, cross sections 79—85437
- ^{4}He(π^{+},$\pi^{\pm}$p), 120-165 MeV, 3 nucleon exchange in knock-out reactions, cross sections 79—85437
- ^{A}Hf(p, α), A=176,178,180, statistical direct reaction model calc. 79—80913
- H(p,x), direct and charge transfer scattering processes, second quantisation 80—78289
- K(Ar,X), 800 MeV/N, single particle spectra from high multiplicity events 80—99184
- K(Ar,X), proton inclusive spectra, direct plus thermal model 80—57799
- Kr(p,X), fragment prod. by two body breakup 79—85440
- (^{6}Li,X), 156 MeV, projectile break up in continuous particle spectra, cross section, fragmentation 80—86889
- ^{6}Li+d, 0.1-1.0 MeV, DWBA and R-matrix cross section anal., direct contribution 79—67758
- ^{6}Li(^{3}He, ^{3}He^{3}He)^{3}H, 132 MeV, quasifree scatt., ^{3}He-^{3}He two body cross sections 79—76011
- ^{6}Li(^{3}He,$\alpha\alpha$p), 2.5 MeV, ^{5}Li or ^{8}Be formation, direct or compound nucleus mechanism 77—57678
- ^{6}Li(^{6}Li, 3α), 2 MeV, DWBA anal. of direct prod. of 3 α final states 77—74882
- ^{6}Li(^{6}Li,$\alpha\alpha$)α, 36 to 46 MeV, reaction mechanism 80—83113
- ^{6}Li(d,n^{3}He)^{4}He, absolute and total cross sections 79—40936
- ^{6}Li(d,p^{3}H)^{4}He, absolute and total cross sections 79—40936
- ^{6}Li(n, p)^{6}He, 6.77-4.71 MeV, ang. distrib. excitation function, DWBA, optical model, anal. 77—18539
- ^{6}Li(n,γ), cross section and spectroscopic factors from direct capture pot. model 80—99171
- ^{6}Li(p,γ), cross section and spectroscopic factors from direct capture pot. model 80—99171
- ^{6}Li(p,pt)^{3}He, 1 GeV, knock-out of clusters, distorting factors, microscopic approach *(Russian)* 78—58285
- ^{6}Li$\rightarrow$^{3}He+^{2}H+n (^{3}H+^{2}H+p), zero degree fragmentation of relativistic ^{6}Li 79—85438
- ^{A}Li(p,pα), A=6,7, 600 MeV, α-cluster quasielastic knockout, expt. methods, separation energy spectra 79—13275
- ^{24}Mg ground and γ-bands, direct and multistep processes from (α,^{6}He), (p,t), (^{16}O, ^{16}O) 80—102094
- ^{24}Mg(^{18}O, ^{14}C)^{28}Si, ground-state excitation function structure 79—63694
- ^{24}Mg(^{6}Li,t)^{27}Si, t-energy spectra and reaction mechanism 78—41756
- ^{24}Mg(p,pα), 600 MeV, α-cluster quasielastic knockout, expt. methods, separation energy spectra 79—13275
- ^{94}Mo, analogue resonances, direct neutron decay, anal. of ^{93}Nb(p,n)^{93}Mo data *(Russian)* 79—3128
- ^{13}N, quadrupole strength, from ^{12}C(p,γ)^{13}N, semi-direct capture model calcs. 80—47370
- ^{14}N+^{12}C, 34.1-178.1 MeV, fusion and peripheral reaction cross sections, direct yield 79—67771
- ^{14}N(d,d′), 10-17 MeV, isospin non-conservation, direct DWBA and Hauser Feshbach anal. 79—67757
- Na(Ne,X), 800 MeV/N, direct vs. thermal particle emission, inclusive cross sections 80--52688
- ^{23}Na level α-spectroscopic strengths assuming direct cluster transfer from ^{19}F(^{6}Li,d) 80—27552
- ^{A}Nb, A=90,91,94 neutron spectra, level density, direct processes from Zr(p,n) *(Russian)* 79—67666
- (^{20}Ne,X), relativistic collisions, slow and fast fragment correlations, multiplicity association 80—86886
- ^{20}Ne breakup cross section, direct mechanism, DWBA anal. of ^{40}Ca(^{20}Ne,^{16}O) 80—18276
- ^{20}Ne(p,p′), differential cross-sections, analysing powers in direct reaction theory 77—65223
- ^{21}Ne(^{3}He,α)^{20}Ne, large angle excitation function fluctuations, DWBA and opt. model calcs. 79—89318
- Ni mass region, α transfer reactions, pairing vibr. model anal. 79—13272
- Ni+α, 100 MeV, fireball and coalescence model anal. 79—93642
- ^{A}Ni, A=64, 58, level ang. momentum and spin values, DWBA anal. from (t,d) polarised t 79—36163

direct nuclear reactions and scattering continued
- ^{A}Ni(d,X), A=58, 64, 7.6 GeV/c, isotopic cross section ratios, He, Li fragments isotopic effects *(Russian)* 80—63154
- ^{A}Ni(p,X), A=58, 64, 7.6 10 GeV/C, isotopic cross section ratios, He, Li fragments isotopic effects *(Russian)* 80—63154
- ^{A}Ni(p_{pol}, α), A=58, 60, 62, 22 MeV, analysing power and cross sections, Co proton-hole states 80—68663
- ^{58}Ni(^{18}O,^{18}O$_{2}$*)^{58}Ni, 79—6676
- ^{58}Ni(^{3}He,α)^{57}Ni, 15-205 MeV, zero-range DWBA normalisation, energy depend. 77—34280
- ^{58}Ni(^{6}Li,t)^{61}Zn, ^{61}Zn mass, t-energy spectra and reaction mechanism 78—41756
- ^{58}Ni(α,X), 20, 40 MeV/N, α breakup yield, fragment yield ratios 80—9300
- ^{58}Ni(α,tp), double differential cross section, t-p ang. correlation function, direct breakup 80—22797
- ^{60}Ni(e,α)e′X, alpha particle spectra, statistical model calc., direct reaction component 78—41704
- N(p,X), 340, 660 MeV, ang. distribs., proton quasi-elastic knockout *(Russian)* 80—52649
- N(π,πp), 170 MeV, two stage and knock out contribs., π^{+},π^{-} spallation differences *(Russian)* 80—68632
- N(π±, $\pi^{\pm}$ X), X=He or d, 170 MeV, cross sections and ang. distribs., direct knockout mechanism *(Russian)* 80—86887
- (^{16}O,X), 2 GeV/N, anomalous nuclei among relativistic projectile fragments 80—106034
- (^{16}O,X), A=54-208, direct transfer to discrete and continuum states, DWBA diffraction model 80—78262
- ^{16}O α-cluster states, widths and resonances, optical model, direct transfer in ^{12}C(^{6}Li,d) 80—105975
- ^{16}O fragmentation at intermediate energies, statistical fluctuation, fragment momentum distribs. 80—78263
- ^{16}O, π^{+} induced four nucleon removal 78—25242
- ^{16}O+p fragmentation reaction, 2 GeV, three-stage model anal. 79—6551
- ^{16}O(d,p)^{17}O, coupled channel variational method for multi-step direct nuclear reactions. II. Test on a (d,p) reaction 78—66259
- ^{16}O(e,e′p), single hole state momentum and energy distribs. 80—22674
- ^{16}O(p,^{6}Li)^{11}C, 51.9 Mev, five nucleon transfer mechanisms, DWBA calcs. 80—73845
- ^{16}O(p,2p), 320 MeV polarised protons, quasifree scatt., spin orbit coupling 78—66272
- ^{16}O(π,γn), direct and resonance reaction unified shell model, n, γ spectra 80—52696
- O(p,X), 340, 660 MeV, ang. distribs., proton quasi-elastic knockout *(Russian)* 80—52649
- O($\pi^{\pm}$, $\pi^{\pm}$X), X=He or d, 170 MeV, cross sections and ang. distribs., direct knockout mechanism *(Russian)* 80—86887
- O(π,πp), 170 MeV, two stage and knock out contribs., π^{+},π^{-} spallation differences *(Russian)* 80—68632
- O(π^{+},π^{+}p)O, 170 MeV, direct-knock-out dominant mechanism *(Russian)* 77—61460
- Pb(Ar,X), 800 MeV/N, single particle spectra from high multiplicity events 80—99184
- ^{206}Pb(n,γ), direct-semidirect and compound nucleus contribs. to cross sections 80—68662
- ^{208}Pb (n,Zn) direct process contrib. n angular correlations *(Russian)* 78—78386
- ^{208}Pb, fast neutron quadrupole radiative capture, direct-semidirect model 77—26711
- ^{208}Pb(^{12}C,^{11}B), 77 MeV, bound and continuum state excitation, direct and two step processes 80—63205
- ^{208}Pb(^{16}O,^{15}N), 104-312 MeV, fragment emission at high energies, Q value effects 79—6653
- ^{208}Pb(^{16}O,X), 140-315 MeV, projectile fragmentation, ^{15}N, ^{12}C transfer spectra, direct contrib. 80—63155
- ^{208}Pb(N, γ_{0}), γ-ray ang. distribs., giant E3 resonances, direct-semidirect model 79—67727
- ^{208}Pb(N,γ), 6 to 40 MeV, dipole/quadrupole interference, direct-semidirect model, γ ang. distrib. 78—93994
- ^{208}Pb(n,γ), fast, direct-semidirect and pure resonance model calcs. 80—47486
- ^{208}Pb(p, γ), γ ang. distrib., isovector giant quadrupole resonance, direct-semidirect model 79—63647
- ^{208}Pb(p,d), two stage processes in direct reactions *(Dutch)* 78—29439
- ^{208}Pb(p,γ), γ-ray ang. distribs. asymmetry effects through IAR, direct-semidirect model 80—42581
- ^{208}Pb(p,γ) fast capture, direct-semidirect model excitation function calcs. 78—94004
- ^{208}Pb(p,p′), 39, 62 MeV, DWBA anal., collective spectra, direct process contrib. *(Russian)* 80—13408
- ^{208}Pb(π,π′p), 255 MeV, quasielastic knockout, proton yield, $\sigma(\pi^{+})/\sigma(\pi^{-})$ cross section ratio 80—32305
- ^{A}Pd(p,X), 6 MeV, A=102,104,106,108,110, quadrupole deformation, cross sections, direct processes, optical parameters *(Russian)* 79—67753
- Pd(p,t)Pd, A=104, 108, 110, at 52 MeV, direct and indirect interf. 77—54220
- ^{119}Sb intrinsic high spin state population, cluster DWBA anal. of ^{116}Sn(α,p) 79—67630
- ^{28}Si+^{9}Be, localisation of direct reaction processes, fusion and total cross sections 78—78353
- ^{28}Si(^{32}S,X), 135 MeV, multi-particle prod., two fragment reactions, kinematical anal. 80—83111
- ^{28}Si(^{6}Li,t)^{31}S, t-energy spectra and reaction mechanism 78—41756
- ^{28}Si(n,n′γ), 13.9 MeV, spin flip probability from 1.78 MeV state, direct theory 80—9234
- ^{28}Si(p,γ), 1.3-2.3 MeV, resonant and direct capture, ^{29}P excitation functions and spectroscopic factors 79—80912
- ^{28,30}Si(^{19}F,^{16}O)^{31,33}P 60 MeV, j depend., spin-orbit effects, optical pot. 77—41993
- ^{145}Sm primary γ-rays, direct capture and neutron separation energy, (d,p),(n,γ) correlation 80—57738
- ^{148}Sm(^{18}O,^{16}O), interference effects, coupled channels calc. with BCS+RPA wavefunctions 77—26787
- ^{150}Sm(^{16}O,^{18}O), interference effects, coupled channels calc. with BCS+RPA wavefunctions 77—26787
- ^{152}Sm ground and γ-bands, direct and multistep processes from (α,^{6}He), (p,t), (^{16}O,^{18}O) 80—102094
- Sn mass region, α transfer reactions, pairing vibr. model anal. 79—13272
- ^{A}Sn(p,X), A=112, 124, 7.6, 10 GeV/C, isotopic cross section ratios, He, Li fragments isotopic effects *(Russian)* 80—63154

direct nuclear reactions and scattering continued
- ^{118}Sn(^{18}O,^{16}O)^{120}Sn, 53 to 62 MeV, optimum Q value at the Coulomb barrier 78—78413
- ^{120}Sn(p,n), statistical multistep direct emission, p-h and DWBA calcs. 80—106035
- ^{181}Ta(p,n)^{181}W, multi-step compound and direct reactions, statistical theory 80—57761
- ^{50}Ti+^{14}N(^{12}C), single- and multi-nucleon transfer reaction at 60, 70 and 90 MeV 77—14146
- U(Ne,X), 250, 400 MeV/N direct vs. thermal particle emission, inclusive cross sections 80—52688
- U(Ne,X), proton inclusive spectra, direct plus thermal model 80—57799
- ^{238}U(^{84}Kr,X), mass fragmentation, dynamical theory, two centre shell model, binary decay process 80—68628
- ^{238}U(n,γ), 5-20 MeV, direct and collective capture, excitation curve, γ-spectra 78—94001
- ^{238}U(p,X), 0.8-400 GeV 80—83099
- ^{238}U(p,X), 400 GeV, ^{A}Sc, A=44m,46,47,48, fragment emission, two-step model applicability 80—99177
- ^{51}V(p,2p)^{50}Ti, 17 MeV, search for double-direct reaction 77—30576
- ^{181}W level density, n spectra and ang. correls., direct and nonequilib. processes from ^{181}Ta(p,n) *(Russian)* 80—68631
- ^{136}Xe(n,γ), thermal, Lane-Lynn theory of direct neutron capture verification 79—36218
- Xe(p,X), fragment prod. by two body breakup 79—85440
- ^{89}Y(n,γ), direct-semidirect and compound nucleus contribs. to cross sections 80—68662
- ^{90}Zr(α,X), 20, 40 MeV/N, α breakup yield, fragment yield ratios 80—9300
- ^{90}Zr(p,n), IAS transition, 18.5 to 45 MeV, microscopic model anal. 77—82927

directed graphs
- multirooted directed graphs, percolation theory 79—44701
- neural network, dynamic characteristics 79—74630
- nuclear facility safety assessment, material control and accounting system 79—85673
- percolation theory 77—37718
- polymer chains, statistics, dynamics and graph theory 77—14627
- undirected multigraph conversion for tree-finding *(Russian)* 77—57150

direction finders, radio *see radio direction-finding*

directional antennas *see directive antennas*

directional couplers
- adjustable single-fibre connector and output monitor *(German)* 78—38011
- compact optical directional coupler design and test results 78—1410
- curved dielectric waveguides, coupling characteristics, coupled-mode equations 80—48455
- electro-optical directional coupler switch, used as amplitude modulator, exam. 78—42467
- fibre or integrated optics appls., accuracy of directional coupler theory 79—3810
- fibre-optic directional coupler developments and applications 79—94330
- fused biconical tapered couplers, full duplex optical transmission 78—1341
- GaAs homojunction rib waveguide directional coupler switch 80—69554
- glass fibre branch couplers for optical data bus *(German)* 79—89999
- integrated directional coupler switches, modulators and filters using $\Delta\beta$ reversal techniques, review 80—38132
- integrated optical directional coupler modulator, 1 Gbit/s 80—38125
- integrated optical switch, optically controlled two channel, based on directional coupler 78—83116
- integrated optics sub-ps gate 80—58809
- interference filter all-fibre for wavelength division multiplexing 80—91900
- light coupling from Lambertian source into optical fibre, coupling efficiency calc. *(Japanese)* 78—42407
- micro-optic directional coupler, aberration losses 80—48395
- microwave reflection coefficients measurement *(French)* 79—67350
- modulator switch, balanced bridge, using Ti-diffused LiNbO$_3$ strip waveguides 78—63201
- multimode coupling structure of two parallel parabolic index waveguides, exact analysis 79—90013
- multimode fibre coupler for optical data bus systems 78—1414
- multimode fibre directional coupler 79—37002
- narrowband optical wave filter with stacked directional coupler 79—7226
- optical, coupling length adjustment by loading a metal film 79—23055
- optical, distributed capacitance of planar electrodes 77—27387
- optical, elec. controlled, fluoresc. visualisation 78—38049
- optical, fabricated in TiO$_2$ diffused LiNbO$_3$, phase tuning 77—75680
- optical, for multimode fibres 77—3649
- optical, integrated, operation and manufacture *(German)* 77—75673
- optical, phase tuning by photostructural effect of chalcogenide glass film 77—83963
- optical, phase tuning using bias voltage 77—10999
- optical, with variable spacing, closed form solns. 78—46759
- optical bidirectional central couplers, for links with fibre bundles 78—46809
- optical channel waveguides and directional couplers with graded-index profile, analysis 79—81542
- optical coupler, made from plane gyroscopic, anisotropic light guides 79—18547
- optical coupler as 2×2 switch, coupling length adjustment 79—94370
- optical coupler filter, composed of coupled nonidentical LiNbO$_3$ strip waveguides, description 78—38083
- optical coupler switch, polarisation independ., using weighted coupling 80—28352
- optical couplers with weighted coupling 80—9992
- optical dielectric multilayered filters, wave division multiplex system appl. 79—94365
- optical directional coupler phase tuning by chalcogenide glass film loading 78—1373
- optical directional couplers with graded index profile, variational analysis 80—96037
- optical directional coupling device of two glass prisms, geometrical optics *(German)* 79—18524
- optical fact directional coupler switch/modulators, novel ps optical pulse sampling method 80—58784
- optical fibre 10 dB directional coupler 77—19452
- optical fibre communication devices, directional couplers, atennuators, switches development 79—3782

directional couplers continued
- optical for guided-wave signal transformers, synthesis 80—1358
- optical slab-type directional coupler with activated rhodamine 6G top layer, amplified oscill. 80—99718
- optical strip waveguide directional coupler, leaky-wave 78—38058
- optical subpicosecond gate, velocity-matched directional coupler 80—74512
- optical tunable switched directional couplers of two thin film waveguides using SAW 78—75003
- optical waveguide, 1-D confined planar anal. 78—38027
- optical waveguide directional couplers, parameter meas. using radiation patterns 79—3771
- optical waveguide tap with infinitesimal insertion loss 80—99883
- optical waveguides, codirectionally coupled, with weighted coupling, filter characts. 79—23068
- polarisation-independent optical switch using weighted directional coupler 80—58798
- rib waveguide switches with MOS electrooptic control, monolithic integrated optics in GaAs-Al$_x$Ga$_{1-x}$As 78—87168
- rotation-splice tapered fibre star coupler directivity and mode dependence 80—58748
- single mode grating coupling between thin-film and fibre optical waveguides 79—1012
- single multimode optical fibre communication directional couplers *(German)* 78—33873
- single-mode fibre multiterminal star directional coupler 79—98473
- single-mode fibre optic directional coupler 80—58683
- stepped switched optical directional couplers with unequal section lengths 80—33235
- travelling wave optical modulator using a directional coupler LiNbO$_3$ waveguide 80—96035
- As-Se-S-Ge chalcogenide glass films, appls. to passive optical waveguide components 79—37048
- Ga$_{1-x}$Al$_x$As Schottky directional coupler switch, construction and operation 78—25960
- Ga$_{1-x}$Al$_x$As-GaAs injection laser, branching waveguide coupler fabrication by LPE 78—63202
- GaAs directional couplers and electrooptic switches, wavelength depend. 78—79143
- GaAs, directional-coupler switch with stepped $\Delta\beta$ reversal 77—79968
- GaAs directional-coupler switch with stepped $\Delta\beta$ reversal 77—88962
- GaAs electro-optic rib waveguide directional-coupler switch with stepped $\Delta\beta$ Schottky electrodes 79—98507
- GaAs layer grown by MBE, direction coupler switch 79—76878
- GaAs, p$^+$-n$^-$-n$^+$ electro-optical directional-coupler switch 77—7217
- GaAs rib-waveguide directional-coupler switch with Schottky barriers 78—63204
- LiNbO$_3$, modulator/switch, switched directional coupler principle 77—7191
- LiNbO$_3$, Ti diffused, optical directional couplers, characts. 80—33145
- LiNbO$_3$ waveguide modulators and switches, Ti-diffused, fabrication on directional coupler principle 80—83678
- LiNbO$_3$:Ti optical waveguide directional coupler type modulator 78—66951
- LiNbO$_3$:Ti optical waveguide electrooptic devices, polarisation independ. directional coupler switch 80—58783
- LiNbO$_3$:Ti waveguide directional coupler switches, optically-induced crosstalk 80—48417

directional patterns *see antenna radiation patterns*

directive antennas
- *see also loop antennas*
- electron, excitation by three-ring antenna, radiation characts. 78—91107
- large adjustable parabolic antennas, vibr. behaviour anal. using dynamic equivalent models *(German)* 77—2342
- meteor recording freq., influence of form and orientation of antenna directivity diagram *(Russian)* 80—67665
- miniature, design, for geophys. probing from boreholes 79—12297
- parabolic aerial with monopulse exciter for meteorological satellite S-band reception *(German)* 79—92628
- short-wave plasma diagnostics, EM diffr. on cylindrical column 77—80376
- troposphere communication channel, energy spectrum of delays 79—84442

directors (programs) *see supervisory and executive programs*

dirty superconductors
- A-15 superconductors with defects, transition temp. 78—14857
- boundary resistance from microscopic theory calc. 79—60993
- CESR due to exchange and spin-orbit scatt. 77—28300
- collective excitations and electron-phonon scatt. *(Russian)* 77—85380
- correlation functions, two-particle, below transition temp. 77—24640
- dirty superconductors, anisotropic, fluctuation magnetoconductivity 79—56393
- dynamical electrical conductivity below transition temp. 78—2623
- dynamics in supercond. below T$_c$ 80—44760
- electromagnetic properties in strong HF fields, dissipative part of cond. *(Russian)* 77—63028
- electron-hole coupling, dynamic behaviour *(Russian)* 78—76187
- EPR relaxation time, thermal behaviour, slightly dirty superconds. 79—47195
- ferromagnetic superconductor, paramagnetic fluctuations, influence on superconductivity 80—70900
- filaments, phase-slip state theory 79—56371
- film, resistive transition 80—7049
- film, topological excitations in two-dimensional superconductors 79—56458
- fluctuation diamagnetism *(Russian)* 79—51721
- fluctuation sound attenuation, depend. on critical temp. *(Russian)* 80—34553
- Ginzburg-Landau equations, time-depend., near supercond. transition temp. 80—70886
- Ginzburg-Landau theory, time depend., dissipative current carrying states in supercond. filaments 78—47906
- Hartree-Bogolubov method for pairing in gapless supercond. 77—55636
- intercalated dirty layered superconductor, fluctuation cond. 80—49994
- Josephson current in superconductors with nonmagnetic impurities 78—39269
- junction, superconductor-normal metal-supercond., impurities in normal metal layer, pair penetration depth determ. 80—29508
- local electronic spin susceptibility, effect of superconducting fluctuations 77—72943

dirty superconductors continued
localised state near dislocation, influence of impurities 80—10917
magnetic impurities, Shiba theory consequences beyond s-wave scatt. 80—2516
magnetic ordering in superconductors, susceptibility calcs. 79—99656
magnetoconductivity induced by supercond. fluctuations in anisotropic bulk and fibrous samples 79—95545
microbridges, with paramag. impurities, Josephson steady-state effect *(Russian)* 80—93042
microjunction phonon spectroscopy in dirty limit *(Russian)* 79—11272
mixed state, thermal cond. anisotropy 80—7036
mixed state, transverse thermal conductivity 77—32117
mixed state, vortices, transport entropy theory 78—43534
mode propagation in superconductors near T_c 79—19682
multiphoton absorption, electron-impurity scatt. *(Russian)* 77—36022
nonequilibrium superconductor, normal component drag by condensate, tunnelling *(Russian)* 80—93051
normal-superconducting interface, microscopic theory of current-voltage relationship 79—73637
normal-superconductor interface, boundary conditions, theory 80—39708
paraconductivity in supercond. containing mag. impurities, effect of perpendicular mag. field 77—85389
periodic structures, crit. fields *(Russian)* 80—88700
proximity systems, DC Josephson effect 79—56425
quasi-two-dimensional dirty superconductor, nonstationary Josephson effect *(Russian)* 80—100556
rare earth rhodium boride system, ternary, supercond., phase diagrams at upper crit. fields 80—2531
rare earth superconductors, upper crit. fields in the dirty limit, depend. on intra- and interaction exchange interactions 79—56461
rare earth ternary compounds, supercond. and antiferromag. coexistence 80—25030
resistance from superconductor in supercond.-normal metal interface 78—43525
S-N-S sandwiches, boundary conditions for Usadel eqns. and props. 79—60990
sandwich system, near transition temp., proximity effect and Josephson current 80—7039
sandwich system, theoretical investigation of transition temp. 79—73638
spin susceptibility of conductivity electrons, spatial dispersion *(Russian)* 79—51719
supercond. cylinder, order parameter enhancement by microwave irrad. 80—70896
superconductor-normal metal interface, boundary conditions, pot. barriers effects 80—34554
supercurrent-thermal gradient interaction, branch imbalance generation 79—99657
third harmonic response to weak EM field near transition temp. 79—38249
type II, fluctuation induced elec. cond. 79—38251
type II superconductors, fluctuation induced diamagnetism above H_{c2} 78—80097
US attenuation in mixed state 77—8231
zero-gap dirty, cond. electron spin resonance theory 80—103888
Al film, granular, crit. field anisotropy and fluctuation cond. 78—26994
Al film with Er impurity, spin-flip scatt. and supercond. order parameter dynamics 79—78267
Al-Formvar-Sn tunnel junctions, mode propagation, well below crit. temp. 80—15662
$Cu_2Mo_6S_8$, normal state and superconducting property measurements 78—91660
$Cu_xMo_6S_8$, sintered and sputtered, supercond. upper crit. field 78—23215
In film with dirty type II supercond. props., flux flow resistivity 77—51859
Nb, effect of changes in $\alpha^2(\Omega)F(\Omega)$ on the zero-temp. energy gap 80—97025
$Nb_{\sim 3}Au$, upper crit. field 79—82729
Nb_3Ge, CVD-prepared, high field props. and scaling 79—56455
Nb_3Sn, effect of changes in $\alpha^2(\Omega)F(\Omega)$ on the zero-temp. energy gap 80—97025
Pb, crit. mag. field, functional derivatives 78—91798
Pb, effect of changes in $\alpha^2(\Omega)F(\Omega)$ on the zero-temp. energy gap 80—97025
Pb-In, viscous drag on mobile dislocations, plastic deformation, critical temp. magnetic data 78—43514
Pb-In (21 at.%), mixed state, anisotropic thermal cond. 79—56385
Pb-Sn(Bi), dirty strong-coupling supercond., Ginzburg-Landau parameters, type II behaviour deviations 77—8249
$PbMo_6S_8$, normal state and superconducting property measurements 78—91660
Ta, effect of changes in $\alpha^2(\Omega)F(\Omega)$ on the zero-temp. energy gap 80—97025

discharge lamps
see also arc lamps; flash lamps; fluorescent lamps; metal vapour lamps
cold-cathode lamp, current-regulated power supply design 77—57409
collimator, differentially pumped isolating, for windowless lamps 80—13156
continuous light source, applic. in UV and visible *(Japanese)* 79—80702
current pulse formation from pulse-gas-discharge lamp using thyristor keys *(Bulgarian)* 78—33795
electrodeless discharge lamps, for elements forming gaseous covalent hydrides, spectrosc. appls. 77—67500
electrodeless discharge lamps, pulsed RF excited, for at. absorpt. and at. fluoresc. spectrosc. 79—21816
electron-atom-bremsstrahlung standard radiometric source improvement 78—67484
EM shock tube for obtaining short pulses of visible radiation, plasma flow anal. 78—1909
film lighting intensity ripple caused by metal halide with alternating supply 79—75641
flow lamp light source for ionised and neutral metal spectra 79—27355
Fresnel zone plate support UV window as lens and monochromator 80—1326
gas mixture, reacting, atom conc. reson. absorb. meas., microwave discharge lamp calibration 79—92032
gas-whirl stabilized discharge, theory and calc. results *(Russian)* 80—33843
glow, alternative scanned light sources 80—69477
glow discharge plasma lamp detector design, for real-time microwave holography 78—37859

discharge lamps continued
grazing incidence far UV monochromator for differentially pumped discharge lamps 77—3677
Grimm lamp, glow discharge, for emission spectrographic anal. of binary alloys *(Japanese)* 79—99015
halogen lamps, KIM 9-75, relative spectral distrib. determ. 79—7189
HF, with hollow electrode, for atomic spectroscopy 80—26090
high pressure, simulation of dynamic behaviour 77—31532
hollow cathode lamp, spectral lines width and intensity, high freq. field effects 78—16856
hollow cathode type, discharge excitation characts. obs. 80—42260
holographic displays, conventional light sources 79—50261
inert gas high-current discharges, Z-pinch dynamic and radiative characts. 80—19631
laboratory discharge lamp source for O_2 atmospheric bands and 0 I 5577 Å and 6300 Å lines 80—4148
low and high pressure discharges, analysis *(French)* 78—14240
LV deuterium lamp. stabilised, as secondary radiation standard in 220-360 nm 78—77998
microwave, VUV resonance radiation source for photochemical work 80—59330
microwave discharge lamp for atomic resonance absorption/fluorescence spectrometry 78—89586
microwave power source for electrodeless discharge lamps 79—36969
microwave-excited electrodeless discharge lamps. fabrication and operating conditions effects 78—29179
NDT method development using discharge current harmonics 80—44029
Penning source, continuous discharge, with 50 Å to 300 Å emission lines 79—50363
photoreceiver time resolution meas. using gas-discharge lamps 80—73461
pulsed hollow cathode lamp, transient emission characts. in microsecond region for atomic absorption spectrophotometry *(Japanese)* 77—70365
pulsed hollow cathode lamp characteristics 78—67530
radio-frequency excited pulsed hollow-cathode lamp, absorpt. and emission characteristics 80—89550
spectral irradiance scale comparison 77—106
spherical integrating photometers, luminous flux meas. accuracy, expt. anal. of group discharge lamps *(Polish)* 80—73407
sunlight simulation, review of various light sources 80—87454
total luminous energy transfer, scatt. medium effect 77—65577
UV, high intensity, for angle resolved photoemission spectroscopy 79—12870
UV, rotating triple-reflection polariser 78—94443
UV electrodeless lamp for curing coatings 77—70199
UV inert gas monochromated discharge lamp, addition to XPS spectrometer 78—89601
UV light source, pulsed high-power 79—18496
vacuum UV pulsed controlled source 78—87115
VUV He reson. line radiation source, for UHV photoelectron spectroscopy 78—89602
VUV high intensity low-voltage lamp, tubular design 79—64300
waveguide mount for 60 to 90 GHz range, rectangular to circular waveguide transition 79—26074
windowless AR discharge VUV lamp, for matrix isolation spectroscopy, spectrosc. evaluation 78—45730
Ar lamp, pulse-operated, for VUV irrad. *(Russian)* 78—75453
D, atomic light source *(German)* 79—59782
D, transfer standards for UV spectral emission scales determination 78—78001
D_2 gas discharge lamp as UV continuum source, space appls. 80—36505
D_2 lamps, influence of Ne and Ar on spectral parameters 80—86460
D_2, magnesium fluoride windowed, radiance transfer standards from 115 nm to 370 nm 80—87451
D_2, vac. UV radiation scales 78—1309
DyI_3/CsI/Hg arc, oscillations induced by external mag. field, arc constriction 79—60205
H, atomic light source *(German)* 79—59782
H discharge lamp, integration with vacuum monochromator into vacuum UV source 77—42582
H lamp, organic film form. on windows 77—58412
H lamp using hollow lightguides, optical and operational characts. 80—53395
H_2 lamp window, radiation coloration removal methods 79—72698
H_2-D_2-He, microwave discharge lamp, H and D Lyman-α line shapes 79—80698
He atomic light source *(German)* 79—59782
He I polarised radiation source for surface studies 78—74959
He II resonance discharge lamp, for UV photoelectron spectroscopy 79—58847
He II resonance lamp for UV photoelectron spectroscopy 79—93232
He, pulsed microwave discharge, vac. UV emission characts. 77—35408
He, unbacked Al windows as part of Cu seal between UHV flanges 79—97397
He, with Be film optical filter, for photoelectron spectroscopy 78—79115
Hg discharge, high-pressure, NaI and TlI additives, line broadening and radiative transport 80—74199
Kr, resonance lamp in vac. UV, new developments 79—32017
N6d2-Ne discharge lamp, meas. method for partial H_2 press., selective gettering action 77—87775
Na, high press., laser action of Na_2 mols. obs. 77—31091
Ne-filled discharge lamp, for AAS isotope anal. of B 78—20097
U vapour production using pulsed hollow cathode lamp *(French)* 79—82107
^{238}U vapour, hollow-cathode generator, energetic yield 80—47724
W-O-F system, gas phase, comp. and chem. transport reactions in discharge lamp *(German)* 77—32826
Xe, discharge lamps, 147 nm resonance line production 77—39497
Xe, electronic ignition for cine projector *(Russian)* 77—41719
Xe lamp, pulsed, effect of gas heat capacity on characts. 78—42838
Xe, large, electrode temp. meas. by photographic method *(Russian)* 80—47057
Xe motion picture switching projection lamp, transfer processes from thyristor rectifiers *(Russian)* 78—94421
Xe optical discharge radiation source 78—87116
Xe, resonance lamp in vac. UV, new developments 79—32017
Xe, tubular, with short discharge, characts. *(Russian)* 79—32019
Xe-Kr-Ar mixtures, VUV continuous spectrum prod. in low volt. lamp *(Russian)* 78—75451

discharge lasers *see gas lasers*

discharge tubes *see gas discharge tubes*

discharges (electric)
see also arcs (electric); electric breakdown; exploding wires and foils; flashover; glow discharges; high-frequency discharges; lightning; partial discharges; positive column; sparks; surface discharges; Townsend discharge
absorption coeff. spatial distrib., laser scanning method *(Russian)* 78—22551
AC discharges between isolated electrodes, gas temp. depend. 80—38800
AC display discharge, charge modes, between insulated glass electrodes *(German)* 77—43087
AC electrodeless narrow gap discharge, anal. and plasma display design 80—70063
aerosol, elec. breakdown, due to pulsed, RF, and static fields 77—76242
air, dry, electron lateral diffusion to mobility ratio 80—6203
air, dry, HV diffuse discharge, gas stream temp. inlfuence 79—32842
air, electrode free discharge, appl. to plasma deposition of films *(Russian)* 80—16197
air, emission from excited metal atoms in cathode region 78—1939
air, high current discharge temp. and density 77—62427
air, high-current discharge, current-carrying zone investig., induction method *(Russian)* 78—26355
air, long distance discharge probability calc., for switching surges *(French)* 77—39493
air, non-self-sustaining discharge, ionisation instabilities *(Russian)* 78—26268
air, predischarge-stabilised breakdown voltage *(German)* 78—63608
air, pulsed, high-current, channel temp. profile 77—27768
air, streamer to spark transition *(French)* 79—73053
air diffuse discharge, gasdynamic effects 78—81294
air discharge, sputtered cathode metal atoms, time-resolved light emission 78—71601
air discharge, turbulent flow stabilisation effect *(Russian)* 79—99010
air discharge plasma column, CO_2 laser beam attenuation 80—19062
air gaps, pre-breakdown phenomena under impulse voltage, streamers obs. *(Japanese)* 78—5972
air high-current discharge cond. zone, HF mag. field probe 78—71589
air high-current pulse discharge, near-electrode process dynamics 78—71602
air plasma, gas-discharge, meas. of electron energy loss distrib. 77—35418
air-H_2 (methane) mixtures, ignition energy by capacitive discharge *(French)* 80—10446
air-SF_6 mixture, breakdown voltage and discharge extension of long gaps 77—84550
aircraft skin, lightning damage simulation 78—87575
Alcator Tokamak, energy balance, MHD activity 80—28838
alkali metal seeded plasma, calc. of thermal nonequilib. near-electrode region 77—55186
anodal spots form. on hot electrodes in plasma stream 78—42842
anode potential drop, calorimetric meas. 77—35433
anode sheath in a strong transverse magnetic field 80—6310
anode-directed streamer maximum velocity estimation 78—67593
Ar, plasma rotating, weakly ionised, diagnostics 79—82122
arc hollow cathode, diagnostics 80—44043
atmosphere, point discharge currents during solar eclipses 78—16094
atmospheric arc initiation from erosion discharge 79—90490
atmospheric negative ions, electron detachment rates, time lags to breakdown 78—87564
atomic emission spectroscopy, discharge localisation with oxidised electrodes *(Russian)* 77—52728
atomic O, form. and recomb. in U-tube downstream from DC discharge 78—67333
atoms, absorpt. spectra, flame and discharge laser irrad., opto-galvanic spectroscopy 80—42272
avalanche discharge model, unstable boundary layer in crossed fields 78—83641
back discharge in electrostatic precipitator, light meas. technique 77—76232
bakeable hollow cathode, ion-molecule reaction study in discharge gas mixtures 80—37117
ball lightning, elec. discharge into sand layer expts., erosion-discharge model 78—81322
beam plasma discharge, electron beam energy distrib., in E-region approximated plasma 80—103163
beam-plasma discharge, characts. in crossed elec. and mag. fields *(Russian)* 80—10396
beam-plasma discharge, in supersonic gas jet flowing into high vacuum *(Russian)* 79—55583
beam-plasma discharge, near Zarnitsa-2 rocket, parameter estimation *(Russian)* 78—26357
beam-plasma discharge for plasmochemical reactions *(Russian)* 79—37508
beam-plasma interaction fast processes in gas and Penning discharges 79—64879
biological objects, elec. discharge study, charge image method 80—8238
biological objects, elec. discharges, electrographic investigation methods 80—46118
book, gaseous electronics and gas lasers 80—73120
book, principles of laser plasmas, for graduate students and researchers 77—50647
breakdown condition, atm. press., photoionis. process 77—27770
breakdown conditions, inhomogeneous transverse mag. field effects 79—64947
breakdown phenomena in short point-plane electrode systems, critical survey 79—4206
breakdown wave propagation in ionised gas in nanosecond discharges 80—87890
capacitor discharge, current increments, using arc channel hydrodynamic model *(Russian)* 79—82109
capacitor discharge temperature jump apparatus, nanosec. resolution 77—79159
capillary, ohmic superheating in dense plasma 77—35362
capillary, with evap. walls, phase transitions 78—42839
capillary, with evaporable wall, plasma parameters axial distrib. *(Russian)* 78—75280
capillary discharge, dense plasma, phase transitions, doubly-charged ions effects *(Russian)* 77—35429
capillary discharge, high-current, magnetogasdynamic regime 79—86628

discharges continued
capillary discharge with vaporising walls, one-dimens. theory 78—42840
cathode directed streamer propagation, charge sheath model 78—67459
cathode discharge, hollow, Al spectral line, pulse feeding 80—64797
cathode elementary discharge theories *(Polish)* 80—19661
cathode fall in electron beam controlled stationary non-self-sustained discharges 78—71613
cathode sheath, ion field effect on field emission characts. 77—66582
cathode sheath, weakly ionised impurities effect *(Russian)* 78—22582
cathode spot shape and kinetics, cathode photoeffect from discharge UV irradiation 80—38836
cathodic potential drop in discharge controlled by electron beam *(Russian)* 78—22581
charged microparticles productions under high electric field intensity in ultra high vacuum, measurement *(Japanese)* 80—96411
charged particle beam production, in variable density gas discharge 78—51381
charged particle trajectories in radial electric and uniform axial magnetic fields 79—77336
chemical transformation, diagnostic techniques 78—3338
circuit related instability of a plasma discharge 79—73056
classification of discharge types with oscillating electrons *(Russian)* 78—1929
CO_2 lasers, CW, high-power appl. of photoinitiated impulse-enhanced electrically excited discharge 78—50785
coaxial cold cathode discharge, props. of medium press. diffusion plasma column 77—51237
coaxial cylindrical discharge tube, diffusion plasma column density and pot. distribs. 79—41797
coaxial high current discharge, exploding cylindrical foils in air, compression and expansion 80—38841
coaxial plasma source, in axisymm. mag. field, plasma flow diagnostic meas. 77—35419
cold-cathode controlled gas discharge switch 78—86300
cold-cathode ion gun for sputter-etching, discharge characts. and improvements 80—105748
collective interactions, effects in high current discharge 79—55603
columns, electron density distribs. for electron prod. and loss rates linear and quadratic in electron density 80—96400
combined discharge in average press. gas using two HV pulse sources, gas laser development 80—44027
combined pulse and DC discharge to pump fast-flow CO_2 laser 78—71117
combustion product plasma, discharge on cooled Cu electrodes, rel. to erosion damage in MHD channels 78—1925
combustion product plasma, near-electrode contraction conditions 78—94946
composite discharge plasma, rate of heating of dry air as function of voltage and density *(Russian)* 79—37513
concentric discharge, in controllable ion gun with high brightness 77—87871
condensed media, electrodynamics problems, theoretical investigation *(Russian)* 80—75116
conference, general congress, Societe Francaise de Physique, Toulouse, France (June 1979) 80—77536
conference, Liverpool, England, Sep. 1978 78—87521
conference on phenomena in ionised gases, Grenoble, France (July 1979) 80—36767
constricted, plasma parameters meas. *(Russian)* 77—7598
contaminated cathodes in UHV discharge 79—41889
continuous optical discharge convective flow, thermogasdynamic instability 78—75397
contracted discharge, in crossed fields, struct. 77—84560
contraction in electronegative gases *(Russian)* 77—43096
contraction in inert gas discharge, electron distrib. *(Russian)* 78—91176
corona, discharge pulses, field strength and electron density calcs. 80—38814
corona discharge, decomposition of CO, qualitative chemical anal. of reaction products 78—60992
corona discharge over insulating surfaces, interaction study *(French)* 77—4016
corona positive discharges, in atmospheric air, positive ions distribution determ. *(French)* 77—4015
counterrotating electrical discharges in uniaxial mag. field, boundary value problem 78—42844
cross-sectional shock shape meas. using columnar and plane discharges 79—27666
crossed field plasma discharges characts. 80—100116
cumulative plasmadynamic discharge, dynamics and radiation, UV source appls. *(Russian)* 79—55578
current carrying double layer production in focus device 80—83953
current density in ionised gas in macroscopic field, direct meas. by Stark broadening of H lines *(French)* 78—9839
current fluctuations, discharge contractions, in combustion products plasma 80—14953
current wave, EM field nonlinear diffusion 77—51254
cyclotron self-absorption in two-temp. plasma, temp. and density meas. 80—48987
cylindrical, rotation by elec. and mag. fields, isotope separation appl. 77—39486
cylindrical discharge plasma, radial electron density gradient in electronegative gas 78—87433
DC and UHF electrodeless discharges, charact. comparison 80—38762
DC corona discharges in coaxial cylinder electrode 80—33837
DC discharge, isotope enrichment by reson. trapping and cataphoresist. 77—27752
DC gas discharges, photoionisation of excited atoms by low intensity light 79—50904
decaying HV discharge, for nanosec. X-ray impulse generation *(Russian)* 77—34061
deionisation, caused by internal surfaces, dispersion model anal. *(Russian)* 78—5961
deionisation of low press. plasma in gas discharge gap, elec. strength *(Russian)* 78—1921
dense gas nanosecond discharge, cathode region field amplification 80—38855
detonation products in discharge gap, electric breakdown 79—10736
device with ionizing beam regeneration for semi-self-maintained discharge 78—22586
diatomic species nonequilibrium dissoc., numerical and analytical results compared 78—71428

discharges continued
- dielectric liquids, cond. and breakdown, conf., Mont-Saint-Aignan, France (July 1978) 79−91354
- dielectric liquids, prebreakdown phenomena in sphere-sphere electrode configurations 77−85647
- dielectric materials, spacecraft, charging and discharging 80−71315
- dielectric spark discharge, conditions for building up compression rings 78−38493
- differential pumping, of gas discharge columns, ionisation enhancement 79−67330
- diffuse discharge, current constriction near anode in combustion product plasma 80−103201
- diffuse discharge, HV, anodic region anal. at 10 to 400 mm Hg 77−43094
- diocotron-instability pulses, discharge current and electron loss effects 77−62423
- diode, nonlinear electron transport 77−13718
- diode, with local ionisation, critical conditions for SCL current *(Russian)* 77−15255
- disc cathode in He flow, spectrosc. investig. 80−64809
- discharge cleaning in JFT-2 Tokamak, AES 78−51316
- discharge current magnetude, influence of interval between discharges *(Russian)* 80−49020
- discharge plasma, diffusion regime, elec. sheath theory 80−1810
- discharge-flow systems, noise reduction in EPR studies 79−39256
- distributed spark discharge for volume photoionization laser appls. 79−14634
- DITE, low Q discharges 80−92374
- drift tube, parallel-plate, Monte Carlo simulation 77−58914
- drift-dissipative waves, weakly ionised plasma, column steady state 80−38613
- dust clouds, industrial, existence of lightning-like dicharges 78−14235
- dye gas laser, excitation by elec. discharge, electron beams, optical stimulation *(Czech)* 78−79016
- dye vapour lasers, molecular excitation and relaxation, discharge excitation 77−10916
- dynamic atmospheric pressure discharge, electron beam excitation 77−27764
- education, capacitor complete discharge time, thermal noise 80−17727
- electric breakdown mechanism, discharge development, electron impact ionisation 80−15961
- electric strength and elec. cond. 78−91180
- electrode, deterioration by conc. heat fluxes in pulse discharge 77−51251
- electrode erosion, pulse discharge on various materials *(Russian)* 77−51255
- electrodeless discharge, medium press., in rapidly pulsed high freq. field *(Russian)* 79−55581
- electrodes, screening, discharge phenomena with UHV positive and negative lightning and switching pulses for dimensioning *(German)* 80−87963
- electroionised discharges, theory 80−38816
- electrolyte, pulsed discharge, gasdynamic model 79−10732
- electrolyte pulsed discharge, radiation and equilib. composition 78−5975
- electron beam, low current passage through gases, peculiarities 80−38812
- electron beam controlled discharge, cathode density waves 80−38798
- electron beam excited gas discharge, space charge and inhomogeneous ionisation *(Russian)* 77−47281
- electron beam extraction from pulsed plasma of hollow cathode discharge 78−12790
- electron beam ignition of plasma discharge in high density gas *(Russian)* 78−1853
- electron beam plasma discharge, in crossed elec. and mag. field *(Russian)* 78−87458
- electron beam prod. by cold cathode, effects of discharge gases *(Korean)* 79−27848
- electron beam stabilised discharge in flowing medium, numerical calc. 78−94943
- electron cloud in equilib., mag. field effect, pot. and space charge distrib. 80−92410
- electron current component meas. method for hollow cold cathode 80−54043
- electron cyclotron resonance plasma, for metal surface cleaning 79−47821
- electron density in hollow cathode discharge, laser heterodyne meas. 78−30483
- electron diffusion to absorbing electrodes, Monte Carlo and Boltzmann calc. comparison 80−6204
- electron diffusion to anode, Monte Carlo and Boltzmann calcs. comparison 80−38519
- electron drift tube, photon emission investig. 78−87566
- electron energy balance calc. *(Russian)* 77−76223
- electron energy distrib. for high press. discharge sustained by electron beam 77−65923
- electron energy distribution in positive column 78−67465
- electron energy distributions in a sputtering discharge *(French)* 79−55557
- electron energy spectrum, for PIG and arc type discharge plasmas, comparison *(Russian)* 77−15263
- electron neutral inverse bremsstrahlung in electron beam sustained discharge 78−63604
- electron vel. distrib. in reflex discharge, Thomson scatt. meas. 78−34368
- electron-beam controlled, evidence for $^1\Delta_g$ singlet O at 200 mbar *(French)* 77−30880
- electron-ion oscillating discharge, excitation of EM oscill. in plasma zone 77−55188
- electronegative gas plasma, negative ion ambipolar diffusion coeffs. 80−44046
- electrophotoionised discharge, inert gases-halide mols. laser mixtures, current voltage characts. 80−38821
- electrostatic, on Meteosat spacecraft 80−17463
- electrostatically deposited films obs., using image intensifier and laser Doppler anemometer 80−71593
- electrovortic flow, in discharge between hyperboloidal electrodes *(Russian)* 78−75217
- element mass separation mechanism in plasma discharge in intersecting fields *(Russian)* 80−14943
- excimer laser, nonself-sustained discharge, ionisation instability buildup 80−9858
- excitation, by HF oscillatory circuit, operation anal. 77−39494

discharges continued
- explosive electron emission, cathode plasma emission surface processes 78−71569
- extended high-current discharge, initiation by long laser spark *(Russian)* 80−10404
- externally maintained discharge with gasdynamic window for low energy electron beam 79−32843
- Faraday rotation anomalies in an Ne discharge in a weak magnetic field 80−38659
- fast electron beam, transition from non-selfmaintained volume discharge to spark discharge *(Russian)* 79−23466
- fast RCL discharge circuit, exploding Ni wire resistivity determ. 77−31995
- field emitter vacuum breakdown, external mag. field effects, transition period 80−38824
- field emitting micro-points, location, nanosecond UHV discharges 78−332
- fission reactor, gas-discharge, fuel element component conc., plasma temp. profile instabilities 80−63253
- flare discharge, dielectric coated anode, surface and excess vol. charge meas. 77−11426
- flash lamp, discharge-channel development, effect of reflected shock waves, photographic obs. 77−43093
- flash lamp, unconfined discharge channel, spatial instability 78−38571
- flow patterns, rot. forces, numerical anal. 78−34380
- fluid, radio band pulse radiation due to spark initiated cavity dynamics, sonoluminescence *(Russian)* 80−66313
- fluid dynamic considerations, nonlinear electron acoustic waves, book 77−78906
- fluid dynamical properties, nonlinear electron acoustic waves, book contrib. 77−80395
- focused discharges, electron beam and deuteron beam prod. 78−58093
- foil explosion caused by electric discharge, cylindrical foil, obs. 79−55597
- formaldehyde+O, absolute rate consts., discharge flow and flash photolysis reson. fluoresc. meas. 80−55648
- FT-1 Tokamak, discharges in low density plasma *(Russian)* 80−106958
- galvanic detection of optical absorpt. in gas discharge 77−15251
- gamma source, unsteady, EM field amplitude 77−88619
- gas, distribution function of carriers in electron avalanches 77−47287
- gas, homogeneous discharge, development, effect of initial conditions 78−63613
- gas, low density, space charge limited current flow 80−79605
- gas discharge, mass spectrometry, corrections 79−82100
- gas discharge, tubular source, emission props. *(Russian)* 80−28860
- gas discharge between coaxial electrodes with dielectric layer 78−75476
- gas discharge in crossed fields, obs. 78−75471
- gas discharge instability near electrode 80−70064
- gas discharge plasma, holographic time-differential cine interferometry 80−38716
- gas discharge positive column plasma, absolute and convective instabilities of helical waves *(Russian)* 79−37478
- gas discharge with travelling mag. field, isotope separation by mass diffusion 80−44050
- gas discharges, electron swarm motion, computer simulation 77−89339
- gas lasers, use of surface discharge for gas preionisation 79−46504
- gas mixtures, ignition energy by capacitive discharge and through discharge of person charged with static elec. *(French)* 80−10446
- gas space discharge, non-self-maintained, asymptotic analysis of structure *(Russian)* 79−14635
- gas waveguide lasers, props. and current-voltage characts. of discharges 78−1208
- gas-discharge plasma, laser, Faraday rot. diagnostics 80−43981
- gas-dynamic pulsation effects on turbulent gas flow discharges *(Russian)* 79−7500
- gas-filled gap, electric breakdown *(Russian)* 78−22580
- gaseous dielectric, discharge development, relative motion between gas and electrode, theory 78−63616
- gaseous electronics, conference, Pittsburgh, PA, USA (Oct. 1979) 80−22142
- gases as electrical insulators, nature and practice 78−83632
- Gassiot's cascade, 19th century discharge tube demonstration 80−77586
- geometrically extended electrode, charged particle and energy fluxes 78−79442
- grazing, incomplete, gas temp. and electron density diagnostics 79−55600
- guiding effect, laser produced plasma channels 78−71568
- H_2 (He_2) obs. 80−44053
- H-pinched discharge, low-current, optical, elec. and erosion studies 77−35417
- halide counters, photon-induced discharges propag. 77−26942
- halide vapour, discharge, potential fusion laser systems 78−63074
- Hamilton-Jacobi eqn. soln. for discharge in quadrupole EM field *(Russian)* 77−11433
- helicopters, electrostatic discharger *(French)* 80−28863
- heterogeneous medium discharge 80−38858
- heterogeneous plasma discharge, spatial information modelling and processing algorithms 78−14229
- HF discharge, in low press. gas, multipacting breakdown mechanism 79−97144
- HF discharge, ionisation overheat instability in EM wave field *(Russian)* 80−106990
- high current, high press. discharges, conductivity meas. 80−38793
- high current, shock wave parameters, radn. effects *(Russian)* 77−7620
- high current diffuse discharge with explosive cathode process 80−38785
- high current discharge, in thyratron, nanosec. grid extinction time *(Russian)* 80−54057
- high current discharge from cold LaB_6 cathode 80−107011
- high current discharge in dense plasma source 78−9888
- high press. gas discharge prebreakdown processes, electrode surface inhomogeneity effects 79−14628
- high pressure, discharge, in H_2 (D_2)(inert gas), props., electrode influence, spectroscopic obs. 80−38806
- high voltage opening switch using spoiled electrostatic confinement 80−103205
- high voltage Penning discharge reflex system, confinement in mag. mirror field 79−86600
- high voltage unipolar spark discharge, spectrochem. anal. *(Russian)* 78−15750
- high-current, gas superluminesc. polarisation due to Zeeman level splitting 80−100060

discharges continued
high-current evaporating wall discharge, pulsed press. 79—27838
high-current pulsed discharge, plasma props., spectral meas. 78—87535
high-current vacuum discharge, cathode region mag. field effects, elec. and thermal characts. 77—62412
high-density electrode discharge stability in very strong mag. field 78—75478
high-power non-self-sustained discharge with ionisation by repetitive electrodeless pulses in closed-cycle laser 78—71514
high-pressure discharge, Hg line profile and shift at 546.1 nm *(French)* 79—785
high-repetition-rate short-pulse gas discharge for discharge pumping gas lasers 80—1233
high-speed rotational vacuum tap for discharge gas sampling 78—57969
high-vacuum gap breakdown, effect of transverse mag. field and geometry 78—38567
HIP-1 hot ion plasma, effect of anode-cathode geometry on performance characts. 77—24112
hollow cathode, electrical characts. 77—68890
hollow cathode, use in determ. of natural spectral line width *(Russian)* 77—46529
hollow cathode discharge, as spectroscopic light source, LTE and non-LTE conditions effects *(German)* 78—32891
hollow cathode discharge, for spectrochem. anal. of microimpurities in amorphous B 80—85247
hollow cathode discharge, laser induced impedance change, U cathode 79—46500
hollow cathode discharge, particle diagnostics with mass spectrometer 79—46476
hollow cathode discharge, slow electron energy distrib., density and temp. 77—55197
hollow cathode discharge as electron beam generator 80—44039
hollow cathode discharge as negative ion source 78—82072
hollow cathode discharge ion source, with drift tube, for reaction rate consts. meas. 78—64834
hollow cathode discharge plasma, entry of Co, Ni, Ti, V, Cr, Fe and Mn 79—41891
hollow cathode discharge process, mass and energy anal. for incident ions on substrate 78—23630
hollow cathode discharge with variable voltage 80—59336
hollow cathode inert gas discharge, excitation and ionis. mechanisms, spectra obs. 77—15261
hollow cathode spectroscopic light source, characts. using Ar(He) carrier gases, Al(graphite) cathodes 78—82047
hollow-cathode, holographic meas. of radn. coherence props. 79—76784
hollow-cathode discharge alignment, electron collisions 79—64944
hollow-cathode discharge plasma, mol. beam sampling and fast neutral prod. 77—68865
hollow-cathode type, cathode fall width determ. with fixed shadow probe 80—24292
homopolar corona, plane parallel field, outer region electrical characts. calc. *(Russian)* 78—67447
hot cathode Penning discharge plasma, HF oscills. and electron beam relax. 80—38614
hot cathode reflex discharge in cusp and uniform mag. fields 78—67456
hot-cathode, electrostatic double layer obs. 78—34337
HV AC Penning discharge, vacuum pumping characts. 78—93713
HV electrode, Fe microsphere impact, charge reversal, oxidation effect 77—12042
HV nanosecond discharges in air at atm. press. *(Russian)* 77—72512
HV nonosecond transient meas. from pulsed low inductance gas discharge, Kerr effect 78—51380
HV vacuum gap, inter-electrode bouncing of Fe microspheres 77—11124
hydrocarbons, liquid, high-speed schlieren studies of elec. breakdown 77—89332
hydrodynamic processes in pulsed discharge 77—47290
hypersonic plasma jet discharge, highly effective radiation sources prod. using freq. doubled pulses 79—93235
hypersonic plasma jet discharge, pulsed radiation source *(Russian)* 78—74073
impulse discharge cathode streamer, emitted photons estimation *(Japanese)* 79—32845
impulse high voltage discharge, effect of mag. field *(Russian)* 79—19099
impulsive corona discharge around conductors, phys. aspects consideration *(French)* 80—92406
impurity concentrations on wall during Tokamak discharges, laser probing technique 80—49013
in transverse magnetic field, anode sheath, theory 77—35432
inert gas, electroionisation discharge, negative cathode pot. drop 80—79615
inert gas, formation of fast radiating Z-pinches at medium press. *(Russian)* 79—37526
inert gas, hollow-cathode, partially ionised plasma diagnostics by electron beam scatt. 80—28824
inert gas, reson. radiation imprisonment model 80—38756
inert gas DC discharge, ionis. wave wavelength, electron gas state depend. 78—1918
inert gas discharge, electrophoresis anal. using plasma kinetic eqns. 77—43100
inert gas discharge, moderate press., visible and UV radiation spectrum 77—31533
inert gas discharge, spatial mass division in crossed elec.-mag. field *(Russian)* 78—5960
inert gas halide laser, discharge excited, gas composition and lifetime studies 80—53268
inert gas ion laser, high voltage-low press. discharges, stationary props. 80—92400
inert gas mixture, electrophotoionization discharge, laser pumping 80—91781
inert gas mixtures for particle detection, high-pressure discharges in nonuniform elec. fields. 78—74545
inert gas molecule in high press. short discharges population inversion 77—71974
inert gas-halogen bearing molecule three-component mixture, self-sustained electric photoionization discharge 80—54073
inert gas-halogen mixtures, UV laser output from elec. discharge after X-ray preionisation 79—64205
inert gases, atomic alignment in positive column *(Russian)* 80—87981
inert gases, metastable atom diffusion, state decay, VUV obs. from discharge afterglow 80—44061

discharges continued
inert gases, self-sustained discharge possibility with bulk photoionisation impurities 80—75113
insulating liquid, electronic processes in elec. breakdown, streamer growth 77—89333
insulating oil, breakdown in long gaps, impurity effects 79—91359
insulator surface, in liq. He, elec. discharges 77—84558
insulators, HV, influence of air pollution on dielectric rigidity *(Slovenian)* 80—64801
intense electron current and secondary plasma formation in H plasma discharge 79—64929
ion beams impurity production by gas discharge source, cathode material testing 79—86592
ion composition of plasma of pulsed discharge in He, H_2^+ current time evolution 80—54046
ion composition of pulsed discharge plasma, optical, probe, mass spectroscopic anal. 80—33840
ion emission, mass spectrometric obs. *(French)* 78—1919
ion exchange currents (microdischarges), in vacuum accelerator tube 78—55057
ion magnetron scaling law 79—27855
ion noise instability propag., weakly ionised plasma, dispersion eqn. *(German)* 77—31439
ion pressure discharge theory in the strong ionisation regime 80—38734
ion source, high energy characts. 78—42772
ion source discharge, stable, theory 79—31278
ion source discharge chamber with volume ionisation, current distrib. 80—23227
ion sources, elementary discharge theory, discharge equilibrium problem, single-valued soln. 79—26801
ion sources, fundamental and special physical processes 80—32559
ion transport 78—87435
ion-acoustic dissemination in moving plasma jet 80—38707
ion-acoustic instability supression by microwave field 78—71466
ionisation instability of semi-self-maintained discharge caused by stepwise ionisation 77—15262
ionisation waves in gas discharge, kinetic theory 78—22454
ionised gases, conf., Berlin, E.Germany (Sept. 1977) 78—63615
ionising wave propag., appl. to air discharges 77—58918
ions energy distribution function, in homogenous medium *(French)* 77—19796
JAERI Tokamak, Ti coating for improved plasma characts. 80—24232
Jupiter Voyager electrostatic discharge protection 78—89042
Knudsen discharge in gas diodes, initial transient kinetics calcs. 77—35430
laser, elec. discharge-pumped excimer type, model 80—58516
laser, high-press. ioniser-sustainer, far IR absorpt. determ. of electron densities 77—14695
laser discharge, high-power, stabilisation with mag. field 80—99739
laser pumping using self-sustained electron-photoionization discharge 80—33013
laser triggered fast-response sealed dischargers 78—51391
laser wavelength calibration using optogalvanic effect, atlas 80—62727
laser-triggered discharge gap characts., influence of discharge medium, electrooptic switch control appls. 80—64818
lasers, high-power, model for stable high-density discharges 79—13943
LF waves, plasma ionisation instability, dispersion rel. *(Russian)* 78—83519
Lichtenberg figures 79—44693
Lichtenberg figures at cryogenic temperatures *(German)* 77—82536
light source, electrodeless, slab-line cavity design 80—83652
light sources, reproducibility for emission spectroscopy 78—3429
limiting current in steady state diffusion-recombination discharge 78—67466
liquid, coordinate detection system 78—24824
liquid cavity collapse, accompanied by RF emission 80—87790
liquid dielectrics, electrical conductivity and breakdown, liquid impurity effects 80—11340
liquid metal cathodes, nanosec. discharge form. in H_2 atmosphere 78—87578
low and high pressure discharges, analysis *(French)* 78—14240
low press. gas discharge, emitted photon probe for electron swarm parameters 80—43839
low pressure gas, electron energy distribution meas. 80—96412
low pressure plasma arc, energy parameters experimental study 80—75117
low-frequency instability, crossed E and H fields 78—18475
low-pressure, shape and width of ion line, use on diagnostic 77—35386
low-pressure discharge, in crossed axisymmetric elec. and mag. fields 79—55602
low-pressure discharge, restriction of current with hollow cathode *(Russian)* 78—94944
low-pressure discharge anode sheath in crossed fields, electron density distrib. 78—75424
low-pressure discharge electron kinetics 78—75483
low-pressure discharge striking in axisymmetric elec. and mag. fields 78—75472
low-pressure gas discharge, mean free path and viscosity, mag. field effects 80—24282
low-pressure gas discharges, model 79—37560
low-pressure gas gap, two breakdown voltages, breakdown prevention method 80—6207
low-pressure pulsed Hg discharge, props. 79—64916
low-voltage pulse discharge plasma, radial temp. distrib. and chem. comp. determ. *(Russian)* 78—71544
lower hybrid waves in toroidal discharge, parametric decay 80—38596
luminescence discharge, appl. in spectrochem. anal. of metallic corrosion *(Spanish)* 79—92029
luminescence lamp, external and internal probe meas. 80—43978
luminescent, in He, electrons energy distribution function evaluation, by Monte-Carlo type simulation *(French)* 77—19795
macroscopic particles in high voltage diode, filamentary shape to explain high accel. 78—47200
magnetic dipole transitions in TiXIV, TiXV, TiXVII ground state terms in Tokamak discharge 80—63575
magnetised DC discharge plasma, pot. difference meas., anomalous resist. 78—87434
magnetoplasma compressor, radial limitation of focal zone, dynamic, energy, spectral characts. 79—55477
mains voltage generators, constructional theory and problems *(Slovenian)* 80—10451

discharges continued
maser dissociator, H beam production performance characts. 78—87034
mass identified ions in O, N, CO and CO_2, transport properties, obs. and calc. 79—50837
maximum constriction phase of a weakly ionized discharge in helium 79—90486
metal foils, electric detonation in vac., Xe, He, N_2 atoms., discharge rad. characts. *(Russian)* 77—11435
metal halide AC discharge, TlI, NaI and InI impurities, atomic plasma characts., a priori method 80—44034
metal oxide reduction by electron cyclotron reson. plasma of H, model study on discharge cleaning 80—76548
metal surface, electrical pulsed discharge action under air environment *(Russian)* 77—43091
metal vapour laser, hollow cathode, review *(Rumanian)* 80—87409
metal vapour laser discharges, stability criteria 78—66802
metal-vapour recombination lasers using segmented plasma excitation 80—74370
metallic vapour, low press. discharges in inert gases, models *(Dutch)* 80—33839
methane, triboelectric discharge of Hg rolling on glass, chem. effect *(French)* 79—77438
MHD accelerators, electrodynamic characts. 80—64788
MHD flow due to an electric discharge from a finite size electrode 78—79388
MHD generator, discharge struct. 78—91166
microsecond stratified pulsed discharge 80—87975
microwave plasma production at atm. press., surface wave propag. method 80—10408
migration control by laser beam *(Russian)* 77—55198
molecular dissociation on bombardment by low energy electrons 80—43845
molecular gas, discharge compression, thermal balance *(Russian)* 77—7615
molecular gas, vol. discharge with UV preionisation by capillary discharge, ionis. pots. depend. 80—44065
molecular gas heating in electron beam maintained discharge 79—27804
molecular gas ionisation instability, suppressed by varying elec. field 79—23476
molecular mixture, strongly excited, vibr. relax. 80—102555
molecular noble gas ions in hot cathode ion source 80—306
molecule, absorpt. spectra, flame and discharge laser irrad., opto-galvanic spectroscopy 80—42272
moving striations, conditions for self-excitation 80—69358
multicharge heavy ion emission from strong-current low induction discharge plasma *(Russian)* 80—14033
multicharged ion heating in Z-pinch, column compression, temp. and density *(Russian)* 80—64754
multiplier-assisted, new type of cold cathode 79—55591
nanosecond discharge in vac., cathode polishing effect 80—79599
nanosecond gas discharge, explosive emission 78—9889
nanosecond pulsed space discharge, spark channel and cathode spot *(Russian)* 77—76222
negative corona, effects over surfaces, investigation by spectrophotometry and granulometry methods *(French)* 77—4014
negative ion production, in surface plasma source with unclosed electron drift discharge 80—38846
non self maintained discharge, three-body electron attachment to O *(Russian)* 80—14881
non self sustained repetitively pulsed discharge in N_2-CO_2 and N_2, instability obs. 80—38820
non-self sustained discharge current, gas purity effects 80—38845
non-self-maintained, three-body electron attachment to O_2, plasma decay obs. 80—43844
non-self-maintained, with regeneration of ionising beam *(Russian)* 77—11428
non-self-maintained discharge, plasma probe currents 78—63631
non-self-maintained discharge in N flux, arc in near cathode region *(Russian)* 80—54056
non-self-maintaining gas discharge, oscill. of space charge in cathode layer 79—86641
non-self-sustained discharge due to electron beam, chem. reactions 79—7502
non-self-sustained discharge plasma, thermal instability development, laser appls. 78—71611
nonequilibrium discharge at atm. press., self-consistent model 78—5969
nonideal plasma, measured props. and nonideality influence 80—43869
nonideal plasma generation, by electrolyte impulse diaphragmic discharge 78—71506
nonpolar electrolyte, on anode, ion attachment and ion emission 78—65998
nonselfmaintained discharge, current voltage characts. 80—44045
optical discharge, continuous, in focused laser beam numerical study 79—14632
optoelectronics, appl. in measuring gas discharge phenomena 80—107007
optogalvanic effect, theory based on multiplication of electron within plasma 80—38741
optogalvanic effect characts. in discharge plasmas 78—63583
organic xerographic photoconductors, bimolecular recomb., reciprocity failure 80—49798
ORMAK Tokamak, runaway-electron-dominated discharges 80—87971
oscillatory discharges in magnetron-type cold cathode ion gun for sputter etching apparatus 79—34170
overheating instability, HF EM field effect 78—9771
pacemakers, implanted, galvanic coupled interference effects 77—81753
parallel discharge growth during impulse breakdown in air, mechanism *(German)* 78—63607
Penning, hot plasma devices, ion heating mechanism *(Rumanian)* 78—59710
Penning, study of hot plasma obtained *(Rumanian)* 79—7504
Penning cold-cathode discharge, m=0 mode instability investigation 79—98894
Penning discharge, Hall crit. mag. fields 79—27146
Penning discharge, in mag. mirror field, characts. 77—72520
Penning discharge, ion heating and collisional energy loss 77—72519
Penning discharge as photoelec. UV spectroscopy source 120-300 Å 77—75637
Penning discharge for polarised deuteron beam ionisation, beam intensity, tensor polarisation 77—3203
Penning discharge ion source, ion current depend. on mag. field and anode diameter 80—54072

discharges continued
Penning discharge ion source with hollow cathode, HF instabilities 80—43997
Penning discharge plasma source, form. mechanism 78—18423
Penning discharges, high-pressure, low-frequency instabilities, role of temp. gradient 79—37567
Penning gas-discharge chamber for uniform thickness film manufacture 77—44153
Penning magnetised discharge, stabilisation, use as ion source 78—9895
Penning mixture, voltage breakdown curve 78—19616
Penning pulsed high voltage discharge, column plasma parameter determ. *(Russian)* 79—7485
Penning-type HV, ionis. average freq. in anode sheath 80—44012
perturbation by longitudinal turbulence 80—24271
photoionisation, at low intensity illumination, nonlinearities, effective cross section 78—87517
photopreionisation-stabilised nanosecond discharges at high temps. and pressures, apparatus for production 79—98982
pinched discharges, runaway electron model for X-ray emission 79—46497
plane parallel electrodes, axial and radial development, computation 77—19794
plasma, pulse discharge, in H_2 and/or N_2, electron conc. *(Russian)* 77—27753
plasma, synchronisation of optical discharge image with electrical parameters 80—31919
plasma, temperate, microwave propag. const. determ. method 80—53992
plasma, weakly ionised, excitation rate in strong external field 77—62333
plasma accelerator, closed Hall current discharge, anode sheath struct. 77—76215
plasma accelerator, pulsed, nonstationary 2-dimensional MHD soln. in coax. channel *(Russian)* 77—27745
plasma beam discharge, electron kinetics, charge particle finite lifetime effect 80—92404
plasma beam discharge, electron kinetics, deexcitation processes effect 80—92405
plasma compression between parallel plates, recomb. press., phase transition 80—64799
plasma current multiplier, gas discharge device, current amplification 80—49018
plasma decay under constant voltage *(Russian)* 80—106988
plasma discharge, light emission efficiency, electrostatic confinement effects 80—33752
plasma discharge, second harmonic generation by surface waves 79—1306
plasma expansion in vacuum diode, study of spectroscopic method 79—55551
plasma impurity deposition, in ISX-Tokamak, time resolved measurements 80—38694
plasma motion H-constricted discharge, mag. field effects and cross-currents *(Russian)* 77—68761
plasma optical diagnostic multichannel apparatus 79—50896
plasma return current discharge, prod. and heating of large-volume plasmas 78—94920
plasma shell, cylindrical, apparatus for production 80—106948
plasma source, pulsed high-intensity elec. discharge between parallel plates in air 80—1857
plasma source characteristics for chem. reactors *(French)* 78—11605
plasma spatially-resolved spectrometry, radial emission line profiles, Abel inversion 77—12841
plasma stream, supersonic dense, shock braking processes, radiation-gasdynamic obs. 80—19635
plasmo-chemical reaction in electrical discharge, metal vapour prod. *(Russian)* 77—63913
point discharge current for fog forecasting 77—70748
poloidal rotation velocity determ. in FT-1 Tokamak *(Russian)* 80—19565
polyatomic compounds, fluoresc. in discharge 79—54891
positive, propag. in transformer oil and silicone fluids, variations 80—88926
positive column, characts. rel. to diffusion and ionisation coeffs. 80—33833
positive column constriction, cryogenic discharge, ambipolar wall diffusion 78—18468
positive corona, conditions for flare discharge on direct voltage appl. *(Russian)* 80—14948
positive corona electrode, negative ion counterflow, elec. field strength meas. 80—38817
positive corona onset in atmospheric air—A multiple avalanche process 80—38786
positive discharges in long air gaps, anode geometry effects *(French, English)* 77—89334
positive gas-discharge column with allowance for metastable atom effect, excitation of strata 80—96410
positive leader, in long nonuniform air gap, growth 78—75444
positive leader propagation mechanism 78—79483
positive streamer velocities meas. in quasi-uniform electric fields 80—72625
powerful pulse discharge, form. and stability of fibrous struct. of current shell 77—31535
prebreakdown ionisation current spatial growth expts., initial photoelec. current changes 78—67566
preforming using high-voltage electrical discharge 80—84872
preionised discharge in a narrow gap, one-dimensional model 79—64948
prepulse discharges in high current accelerator diodes with double shaping line 80—5399
pressure wave generation and propagation by spark discharges in liquids *(Japanese)* 80—70060
primary electron-gas ionization sustained discharges in incompletely ionised plasma 79—50910
probe cct. used in pulsed plasma diagnostics 80—87947
propane, triboelectric discharge of Hg rolling on glass, chem. effect *(French)* 79—77438
n-propanol, sparking pot. and ionis. coeffs. 80—1864
pulse, characts. w.r.t. IR spectra *(Russian)* 79—32826
pulse, low voltage, radial temp. distrib., chem. composition determ. 79—50845
pulse blended discharge, spectral chronographic and equidensitometric investig. 80—44055
pulse character in strongly heterogeneous field formed by electrodes point-plate arrangement *(Czech)* 80—70048

discharges continued
pulse discharges in gases under conditions of strong ionization by electrons, review 80—44064
pulse hollow cathode discharge, time resolved high resolution spectroscopy 80—38759
pulsed, approx. soln. for damage to metal electrode 77—39500
pulsed, displacement currents compensation *(Russian)* 78—9870
pulsed, inhomogeneous gas heating, acoustic wave temp. determ. 77—55175
pulsed, initiation by 2-channel instrument *(Russian)* 78—1946
pulsed, quasistationary stage, plasma parameters calc. method 78—38560
pulsed avalanche discharge at high gas press., homogeneous form. conditions 80—49027
pulsed discharge, in long tube, discharge struct. 79—10734
pulsed discharge of inductive storage element into fluid gap, electrohydraulic effect *(Russian)* 80—100117
pulsed discharges in gases, theoretical and expt. study 80—92416
pulsed erosion jet, energy characts., heat flow distribution *(Russian)* 80—33825
pulsed high-current discharges, fast particle emission 77—19707
pulsed induction discharge, Hall effect 79—64833
pulsed ionisation initiated, non-self-maintained, instability 79—86572
pulsed limiter discharge, multicomponent nonideal plasma, chem. composition 80—19657
pulsed micro-discharges, optical interferometry obs. 80—38804
pulsed non self maintained, ionisation, high electron beam current effects *(Russian)* 80—14951
pulsed non self sustained discharges, peculiarities 80—38811
pulsed ns discharge in dense gas, high energy electrons, particle diagnostics 79—60210
pulsed transversally excited discharge, appl. to N$_2$ laser *(French)* 80—107009
radial structures in He and Ar discharges 77—31541
radiation temp. of weakly ionised gas discharge *(Russian)* 78—59697
rare earth elements, spectral determination using hollow cathode discharge in mag. field *(Russian)* 79—52859
real gas discharge, thermodynamic stability 80—38852
recovery electric strength, effect of plasma parameters 80—6294
reflex discharge, plasma quiescence 80—64806
relativistic electron beam discharges, thin targets, spatially resolved VUV emission 77—89323
reliability physics, conference, Las Vegas (1977) 77—79086
resonance scattering in an argon high current low pressure discharge 80—38735
retrograde cataphoresis process 78—15680
retrograde current motion, in discharge in transverse electric mag. field 78—9887
RF discharge, electrode voltage drop 78—9875
RF discharge, inert gas isotope separation in travelling magnetic field 80—78719
RF discharge plasma conditions, plasma processing apparatus 77—72521
RF electrodeless discharge sputtering system *(Japanese)* 80—16183
RF plasma etching, ion energy *(French)* 79—46495
RF plasma etching, ion energy 79—73049
RF sputtering systems, discharge suppression within piezoelectric gas admission valves 80—100110
ring discharge, 1st to 2nd stage transition obs., press. and freq. depends. 78—83635
ring gap discharges for high rate vac. coating 77—69991
rod-to-plane air gap impulse-voltage delayed streamer and leader formation 78—67570
rod-to-plane air gap impulse-voltage primary and secondary streamer obs. 78—67569
saddle-field ion sources, props. and appl. 79—76239
seeded combustion gas near cold electrodes, MHD boundary layer 80—48865
self-contained discharge, mechanism of short form. time at high press. 78—1922
self-sustained gas discharge, mol. vibr. relax. effect on thermal stability 80—10358
semi-self-maintained gas discharge, ionisation instability theory 78—67511
semi-selfmaintained discharge, elec. field distrib. near anode *(Russian)* 77—47284
SF$_6$ discharge inception voltage affected by avalanche growth space charge *(German)* 80—75109
sheet discharge, MHD flow analysis *(Chinese)* 79—72997
shock wave visualisation, by elec. discharge radiation 77—72371
short-gap atmospheric discharge, using needle-sphere electrodes 77—4008
silent discharge, excited species reactions, discharge channel characts., numerical simulation 80—38813
silicone fluid, discharge propag. 79—91362
simulated combustion gases, mode and sparking characts. of back discharges, NO conc. effects 80—6301
simulation, interactive programme, adaptation to disc supported microcomputer 80—24269
simulation of axially symmetric narrow discharge at high overvoltage 79—19101
simulation of the growth of axially symmetric discharges between plane parallel electrodes 78—91173
single pulse, prediction of conditions for prod. 77—31539
sintering, metal powder+punch electrode reactions 78—11148
sintering of binary powder mixtures 77—63594
sintering of metal powder, with intense energy release of interparticle contacts 78—60615
skimming discharges for pulsed gas-discharge laser preionisation, spectral characts. 80—99740
Skynet system-generated EM pulse response, spontaneous discharges, electron charging effect 79—25432
sound effects of positive corona discharge 80—28858
space charge filled gap, discharge current induced by charged particle motion 80—24283
spacecraft charging by magnetospheric plasmas, effects, counter measures 77—22035
spark, appl. to multielement spectrochem. anal. 78—40103
spark, streamer-induced form. model based on neutral dynamics 79—55588
spark discharge plasma electron temperature, time development 77—11394
spark gaps, HV switching surges, influencing factors *(German)* 80—87958
spark gaps, long air, disruptive voltage calc. with positive switch voltages *(German)* 80—87964
spark tracing, high frequency, application in engineering and aerodynamics 78—38434
sparking potential dependence on nature of the wall 78—67552
spectrographic characteristics, electrolyte filled narrow channel *(Russian)* 77—52726
spectroscopic electron density meas., hot point low induction vacuum spark gas *(Russian)* 80—92390
stability conditions of discharge in gas stream 78—18480
Stark broadening of spectral lines, electron density, determ. in stages of spark discharge *(Russian)* 80—28859
stationary, ionisation, high electron beam current effects *(Russian)* 80—14951
stationary RF discharges of stellarator configuration, meas. with ion sensitive probe 79—60194
stratified gas discharge, binary charge layer creation recombination depend. *(Russian)* 78—22591
stratified pulsed discharge, struct. and emission 79—64946
stratified pulsed discharge with limited surface area 80—87974
streamer propagation mechanism based on plasma vibrs. *(Russian)* 77—84546
striation, running excitation, metastable atom lifetime effect 80—38760
striking in highly inhomogeneous axisymmetric mag. field 78—75473
strong current discharge with reverse current in optically opaque plasma *(Russian)* 77—31544
superluminescence polarisation obs. of high-current pulsed discharge in gas with anisotropic gain 79—14515
supersonic boundary layer, density distrib., cathode emanation perturbation, gas laser appl. 77—84544
supersonic gas flow, transversally combined discharges, low temp. *(Russian)* 78—22590
sustained by uniform ionisation source, props. 78—71605
sustained optical discharges in molecular gases 80—100085
TEA laser discharges, inhomogeneities 77—14687
temperature measurement of heavy particles in gas discharges by contact methods 79—30476
Tesla transformer accelerator, high-voltage head discharge rel. to electron beam prod. 78—326
testing, Voyager spacecraft, JPL, Pasadena, USA 80—92415
tetrafluoromethane, plasma oxidation in presence and absence of Si in tubular-alumina fast-flow reactor 79—96297
theory of the main discharge of lightning *(French)* 78—92887
thermal instability, in self-sustaining gas discharge *(Russian)* 79—55582
thermionic diodes, planar low press. gas discharges, plasma regime, plasma characts. 79—77435
thermionic diodes, planar low press. gas discharges, space charge regime, volt-ampere characts. 79—77434
thermionic triode, oscills. in low press. inert gas discharge 80—79590
thermoautoelectronic emission into plasma, individual ionic field effects 79—69949
thin film, Kirlian-type images and transport in high-voltage corona discharges 79—55590
threshold voltage prediction in presence of conducting particle 77—11422
through sheet of paper, printed letters transcription onto plate 79—75634
thyratrons, nanosecond discharge of the H_2 plasma deionisation, spectroscopic study *(Slovak)* 77—47279
Tokamak, Alcator, high-density D_2 discharge parameters obs. 78—18438
Tokamak discharge gas breakdown time model 78—67555
Tokamak plasma, very-low-q discharges in DIVA 80—64765
Tokamak Thor, discharge, electron distribution function, laser Thomson scatt. 80—59327
toroidal discharge, dynamic stabilisation in weak longit. mag. field *(Russian)* 78—87476
toroidal discharge, Hall effect investig. 80—38701
toroidal discharge, minimum energy state 80—44058
transient electric discharge power and energy meas. using wideband ICs 78—87520
transverse convection conditions 80—24272
turbulent current discharge, high energy ion form., electrostatic analyser 77—19785
turbulent skinned discharge, thermalisation of directed motion of plasma fluxes *(Russian)* 77—11373
two-temperature discharge, transport eqns., transient phenomena 80—96402
ultrahigh vacuum discharge cathode erosion minimum conditions 78—75461
underwater, compression wave calc. and obs. *(Russian)* 79—1354
underwater discharge, gas bubble energy 77—19804
underwater electric discharge, acoustic, hydraulic and total efficiency 78—51388
uniform source of ionisation, props. 78—38564
unipolar pulsed LCD discharge, spectrum, time scanning 80—64774
UV radiometric standards, gas discharges, plasma diagnostics appls. 80—47088
vacuum, cathode processes, surface contamination effects 78—34375
vacuum breakdown, thermal anode instability in prebreakdown stage 79—77445
vacuum breakdown, Trump-Van de Graaff condition anal. 80—79613
vacuum breakdown mechanisms, electron-beam bombarded anode 78—18476
vacuum conductivity in high voltage gaps, emission mechs. 79—41905
vacuum far-ultraviolet light source, strong-current plasma dynamic discharge *(Russian)* 77—49789
vacuum gap, breakdown initiation, microparticles electrical charge 77—76231
vacuum gap, effect of conditioned metal electrodes on elec. strength 79—90489
vacuum gap, electrically stressed, microparticles obs. 78—30500
vacuum gap electrode surface sorption, mass spectroscopic obs. 78—75466
vacuum insulated gap, HV, microparticle trigger discharges and impact damage 77—24227
vacuum to gas breakdown transition, discharge phenomena 80—38825
velocity meas. using photomultipliers 79—19086
Venus, Pioneer Orbiter obs. of lightning 79—70979
vibrationally excited gas, in elec. discharge, sound propag. 78—18370
volume discharge, instability with electron beam at front of accelerating pulse 79—10739

discharges continued
volume discharge excited by electron beam, mag. field influence 79—27241
volume forces in weakly ionized plasmas 79—73055
volume high-pressure discharge with photoionization for laser pumping 80—54058
volumetric discharge, semi-self-maintaining, excited by electron beam, current maintenance in cathode layer 80—59322
water vapour, electron energy distrib. function, electron sink and plasma resist. effect *(Russian)* 80—106987
weakly inductive vacuum discharge, multiply ionised Fe ion spectra *(Russian)* 77—76224
weakly ionised gas, relaxing, negative cond., kinetic eqn. anal. *(Russian)* 79—4101
weakly-ionised, drift-dissipative instability, review 77—7536
windowless discharge, for vac. UV matrix photolysis 77—71798
wire explosion plasma production, diagnostics by Bartels method 79—10686
wire/plane electrode air discharges in strong nonuniform field *(Rumanian)* 79—68964
X-ray preionisation for elec. discharge lasers 79—64205
Z discharge between electrodes, relax., toroidal config. possibility 80—28802
Ag, population mechanism, highly-excited states, hollow cathode discharge *(Russian)* 78—63610
Al, cylindrical foil, elec. explosion, current distrib. in high current shunting discharge 79—41855
Al discharge, hollow cathode with pulse feeding, spectroscopic study 78—34377
Al ion laser, CW, in HV hollow cathode discharge 78—9371
Al, spectral anal. in HV impulse discharge sensitivity limit 79—29420
Ar, $3p^5 5p$ config. aligned in discharge, interf. signals, lifetimes and collision cross sections 78—70796
Ar, afterglow, pulsed discharge, acoustic oscills. in emitted radiation 77—89309
Ar, CW optical discharge in laser plasmatron mode 80—75078
Ar constricted discharge, electron density and temp. and gas temp., iterative method *(German)* 78—83627
Ar, continuous optical discharge, mag. field effect 78—18479
Ar continuous optical discharge maintenance in applied mag. field 78—75396
Ar DC discharge plasma parametric instabilities near lower hybrid frequency *(Japanese)* 79—7450
Ar decaying pulsed discharge plasma, acoustic waves density modulation 80—103143
Ar discharge, ion density profile, reson. laser light meas. 80—92401
Ar, discharge, pulsed, neutron species spatial distrib., laser beam diagnostics 78—38543
Ar discharge, pulsed, weakly ionised, neutrals effect, interferometric obs. 79—27854
Ar discharge rotating plasma column LF oscillations 78—71481
Ar, discharge sudden contraction, effect of gas heating 79—27859
Ar electrical discharge, electron-collisional excited-state kinetics 77—24226
Ar, electrode free discharge, appl. to plasma deposition of films *(Russian)* 80—16197
Ar, electron energy distrib. function, Boltzmann eqn. 79—50911
Ar, electron swarm characts. 79—77441
Ar, excitation by pulsed electric discharge, luminescence obs., time resolved spectra meas. 80—102482
Ar, gas discharge, ionisation waves, kinetic theory 78—22454
Ar, high press. gas discharge form. 78—87567
Ar highly ionised low press. plasma produced in pulsed discharge, characts. *(French)* 77—58901
Ar, inhomogeneous plasma laser diagnostics 77—19770
Ar, laser discharge, spontaneous emission, at. line shapes, interferometric obs. 77—30816
Ar, laser-initiated plasma, gasdynamic instabilities and convective flow parameters 78—22525
Ar low pressure gas, Z-discharge, formation of current layer *(Japanese)* 79—37570
Ar, low-pressure, energy balance and Coulomb relax. 77—43098
Ar, luminous channel form. meas. 79—64945
Ar, nonequilib., atm. press., self-consistent model 78—5969
Ar, nonequilibrium discharge radial characts., two-temp. model 79—94833
Ar plasma, 14000K, continuum emission coeff., laser spark temp. meas. 77—31527
Ar, plasma, electron-ion recombination, 300 to 500K, in discharge tube 78—59714
Ar plasma interaction with flat anode 78—71497
Ar, positive column, 4S and 4P levels populations, rel. theory with recomb. 77—10766
Ar, pulsed highly ionised low press. discharge 77—62398
Ar, sputtered atoms, diffusion coeff. 79—87539
Ar, time-depend. of radiation in pulse discharge regime *(Russian)* 77—84548
Ar, twin-hollow-cathode interferometer-spectrometer, discharge characts. *(German)* 78—67461
Ar, W multicavity cathode, power and V-I characts. 78—26360
Ar, weakly ionised, energy transfer at high press. 78—58845
Ar-air, transformer plasmatron, LF discharge, electrical and energy props. 80—103200
Ar-Cu, Cu diffusion coeff. determ. volatile salt dissoc. in pulsed discharge 80—33721
Ar-Hg-Cl_2, elec. discharge, electron inelastic collision props. 80—79617
Ar-N_2(CO), non-self-sustained discharge instability, negative differentiated cond. *(Russian)* 80—38740
Ar-Ne, mixture, cataphoretic segregation, spectroscopic meas. 79—79261
Ar-SF_6, volume discharge excited by electron beam, stable region *(Russian)* 78—22589
Ar-SF_6 mixture, space discharge excited by electron beam *(Russian)* 78—83629
Ar-SF_6 mixture, space discharge excited by electron beam *(Russian)* 78—83630
ArF, excimers, power superluminescence, in elec. discharge *(Russian)* 77—7621
Ba discharge, dipole-dipole pair absorpt. obs. using optogalvanic detect. 80—54064
CO discharge, $C_2(A^3\Pi_g$-$X'\ ^3\Pi_u)$ band system obs. 77—42332
CO discharge, low-pressure laser striation obs. 78—66814

discharges continued
CO electric discharge lasers, vibr. kinetics, modelling and expts. 80—69374
CO electrical discharge laser, vibr. excitation rate levels and energy balance 79—81413
CO, electron energy distrib. and kinetic coeffs., ground-state mols. 80—43867
CO laser, externally sustained discharge, energy characts. 80—28207
CO low-press. laser discharge, effects of O_2 78—17914
CO, nonequilib. dissoc. induced by electron-vibr. and IR laser pumping 79—86016
CO supersonic lasers, CW double elec. discharge performance 80—69416
CO, vibr. excitation calc. 79—77442
CO-Ar mixture non-self-sustained discharge instability obs. 78—71612
CO-He, plasma-injection-stabilised discharges at low temp. 78—17959
CO-He-O_2-H_2O laser discharge, stability, influence of recombination and ion chem. 78—17915
CO-N_2, energy balance, influence of N_2 rot. level reson. excitation 78—17903
CO-N_2 discharge, plasma characts. and vibr. kinetics anal. 80—59331
CO_2, CO_2-CCl_2F_2, under pressure in elec. fields, breakdown voltage data *(Rumanian)* 77—19782
CO_2, closed cycle CW electrodeless pulse ionisation discharge *(Russian)* 77—75474
CO_2, decaying discharge plasma, contraction in const. elec. field *(Russian)* 79—37447
CO_2, dissoc. in nonequilib. plasma of stationary plasma-beam discharge *(Russian)* 79—99006
CO_2 dissociation in a nonequilibrium plasma 80—87851
CO_2, electrodeless discharge closed cycle laser theory *(Russian)* 77—75475
CO_2, electron drift vels., time-of-flight meas. 80—28855
CO_2 fast-flow CW laser characts., DC self-sustained excitation 80—53259
CO_2, formative time lags, expt. 77—1025
CO_2 gas transport laser, discharge and power extraction characts. *(Rumanian)* 80—95869
CO_2 high-press. laser with cascade discharge 79—68407
CO_2 laser, double transverse pulsed discharge characteristics 78—71617
CO_2 laser, high press. stabilised discharge 78—17904
CO_2 laser, high-press., homogeneous self-sustained discharge 80—9852
CO_2 laser, pulsed, elec. field distrib. in vol. discharge controlled by electron beam 80—58505
CO_2, laser, semi-self-sustained discharge, optical homogeneity, mol. gas heating 80—37990
CO_2 laser excitation using double pulse discharge excitation scheme 77—19319
CO_2 laser self-sutained discharge, effect of low-ionisation-potential additives 78—71616
CO_2 laser stationary discharge positive column, electron density distribution *(Russian)* 80—54031
CO_2 lasers, CO_2-CO-N_2-He, ionisation wave, slow changes, dispersion curves 80—38822
CO_2, negative ions and volt.-current characts. 78—71574
CO_2 TEA laser, UV preionised, characts. 80—69414
CO_2, time-depend. of radiation in pulse discharge regime *(Russian)* 77—84548
CO_2, vibr. excitation calc. 79—77442
CO_2 waveguide laser, multibeam, excited by AC discharge 80—99754
CO_2 waveguide laser with pulsed high-freq. discharge 80—99755
CO_2-Cs-He discharge, CO_2+Cs reaction rate meas. by IR absorption, press. depend. 78—44367
CO_2-N_2 mixture, strongly excited, vibr. relax. 80—102555
CO_2-N_2-H, laser discharge circuit parameters, effect on energy imput mode 77—75476
CO_2-N_2-He, energy balance, influence of N_2 rot. level reson. excitation 78—17903
CO_2-N_2-He, pulse-periodic operation of electron-beam-controlled discharges, energy characts. changes 80—102695
CO_2-N_2-He, vol. discharge, negative ions effect 80—14956
CO_2-N_2-He discharge, voltage drop, impedance 77—47291
CO_2-N_2-He discharge, electron distrib. relax., numerical study 80—54070
CO_2-N_2-He pulsed transverse discharge, investigation of gain 80—9855
CO_2-N_2-He volume discharge, self-sustained, with UV preionis. 79—60211
CO_2-N_2-He-O_2 discharge mixture, three body electron attachment to O_2 80—64779
Ca plasma, Knudsen discharge, longitudinal mag. field, emission polaris. 77—76211
Cd, low-press., high current, intensity in middle UV 78—50878
Cd, Paschen pot. and light emission 80—1863
$CdGa_2$, excimer visible emission spectra in RF discharge, vibr. struct. 79—18201
CdHg*, metal vapour exciplex laser, stability criteria 78—66802
Ce, gas discharge, two-photon ionis. by laser light 78—87534
Cl_2, electron-attachment rate const., room temp. and 250°C, in Ar(N_2) discharges 79—45841
Cn, vapour laser excited by single elec. pulse, lasing characts. 80—87386
Cr III, spectra obs. in low-voltage sliding-spark discharge 77—6710
Cs, 1st reson. level, effective electron-ionis. cross sections, plasma discharge method 78—13603
Cs, assoc. inoisation, in low press. discharge, 6P and 5D states effects 77—75284
Cs, assoc. ionisation, in low press. discharge, upper and intermediate states effects 77—75283
Cs discharge, high-press., pulsed, in capillary energy balance diagnostics 77—65920
Cs, discharge, hot cathode diode, low-press., initial stage transient processes 78—51382
Cs discharge plasma, optogalvanic effect characts. 78—63583
Cs hollow cathode discharge, volt-ampere characts. 78—71563
Cs-Ar, low-pressure discharge, energy balance and Coulomb relax. 77—43098
Cs-N_2 discharge, $Cs_2{}^+$ form. rate, mass spectra obs., N_2 press. depend. 79—27853
CsI-Hg-Ar discharge, high-press., temp. and plasma comp. determ. 79—10709
Cu, acoustic emission under action of single elec. pulse discharge *(Russian)* 77—59071
Cu discharge, hollow cathode in pulse mode, spectral lines and intensities 78—34376

discharges continued
- Cu electrodes, breakdown voltage, prebreakdown current in vacuum, crossed elec. mag. fields depend. 80—79604
- Cu, excited states population in high-current hollow-cathode discharge *(Russian)* 77—35421
- Cu II, laser construction and performance, novel hollow cathode discharge structs. 80—38000
- Cu, population mechanism, highly-excited states, hollow cathode discharge *(Russian)* 78—63610
- Cu vapour, conc. determ. in hollow-cathode discharge from autoionised line intensity *(Russian)* 77—84547
- Cu vapour impulsive production after discharge current pulses through halide vapour *(Russian)* 79—90492
- Cu-Ne mixture, 3-20 kHz pulse discharge obs. 78—71092
- CuCl/Ne discharge, extrema of electron density and output pulse energy 79—10283
- D_2 discharge, high current, pulsed, plasma composition, temp., electron density, press., spectral diagnostics 79—55459
- D_2, electric discharge, vibr. excitation spontaneous Raman scatt. obs. 78—5234
- Eu^+ metastable states in discharge plasma, anomalously high speed deexcitation, modulation of induced radiation obs. 80—44014
- F_2, dissociative attachment of electrons, current density meas., in controlled discharge 77—23566
- F_2, electron dissociative attachment rate consts. at 300 and 500K 80—43849
- F_2, stationary vol. discharge, reduced power meas. 80—75115
- Fe discharge, hollow cathode in pulse mode, spectral lines and intensities 78—34376
- Fe microspheres, impact on mech. polished electrodes, contact pot. influence on charge transfer *(French)* 78—47198
- Fe spherical microparticles impact on polished electrodes, mech. effects *(French)* 78—22595
- GaAs, luminescence during streamer discharge *(Russian)* 77—55835
- H , Rydberg consts., saturated absorpt., spectroscopy meas. 80—105604
- H, determs. in fast flow discharge systems, titration methods 79—34393
- H isotope trapping, materials exposed to high power discharges in PLT 80—37576
- H, light source, Doppler effects *(German)* 79—44946
- H plasma, dense, produced by conic electrode source, mag. field effect on flow 77—58873
- H-He, light source, Doppler effects *(German)* 79—44946
- H_2 beam discharge, electron kinetics in collisionless non-equilibrium plasma 80—92402
- H_2 discharge cleaning of PLT vac. vessel, residual gas and surface comp. changes 79—80631
- H_2 dissociation, in discharge, as atomic H source for maser 79—86637
- H_2, dissociation rates in elec. discharge, calc. 77—46616
- H_2, electric discharge, vibr. excitation, spontaneous Raman scatt. obs. 78—5234
- H_2 hot-iron plasma, ion temp. and electron density depend. studied by laser light scatt. and emission spectroscopy 80—96342
- H_2, non-equilib. ionisation rate calcs. 80—59319
- H_2, ohmic heating, ionization meas., axial discharge 78—38511
- H_2, optogalvanic spectroscopy in discharge, 570 to 620 nm 79—54862
- H_2, time-depend. of radiation in pulse discharge regime *(Russian)* 77—84548
- H_2+Ar, H_2 dissoc. rates, nonequilib. vibr. populations, elec. discharge conditions 77—88535
- H_2+He, N_2, Ne, Ar, Kr, Xe admixtures for increased proton yield in HF ion source 80—57422
- H_3, discrete Rydberg spectrum in hollow cathode discharge 79—68239
- HCN CW laser, auxiliary DC discharge effects 79—31925
- HCl, vibr. excitation in electric discharge 80—87978
- HF chemical laser, stable discharges, with large electrode separation 78—55371
- HF, nonequilibrium dissociation in electric discharge, vibrational excitation 78—94306
- HF-DF simultaneous laser excited by ferroelec. ceramic capacitatively coupled discharge 80—69413
- H_2O, liq., pulsed elec. field applied to sharp point, prebreakdown field 80—6308
- H_2O vapour under point corona discharge, microprocessor control for vapour generator and EHD phenomena 80—106852
- $H_2(^3\Sigma_u{}^+)$-He(2^3S), discharge ionisation growth, diffusion coeffs. 78—83636
- He, 504.7 nm line profile 77—18848
- He at low temp., discharge voltage anal. 77—89341
- He Blumlein-type transverse fast, voltage meas discharges (electric) 80—19642
- He condensed spark discharge, integrated luminosity, pulsed longit. mag. field 77—76233
- He cryogenic discharge, current oscills. 78—67463
- He DC discharge electron free streaming wave propagation obs 78—75314
- He discharge, atmospheric press., for microwave plasma spectrometry 79—16052
- He discharge, EM fields near antenna, probe diagnostics .77—24095
- He, discharge, level populations, time resolved spectra 77—80391
- He discharge, three-body electron attachment to O_2 80—24245
- He discharge, time-resolved population meas. using N_2-laser-pumped dye lasers 77—80362
- He discharge, VUV continuum kinetics 79—94827
- He, Doppler-free two-photon optogalvanic spectroscopy 80—52960
- He, gas discharge, high voltage, low current, anal. of cathode fall 78—51375
- He, gas discharge flow, contracted strata rel. to turbulence 78—1923
- He high-current pulse discharge plasma kinetic and dynamic processes 78—67601
- He, hollow-cathode type, spectroscopic obs., laser light source appl. 80—59335
- He I 4^3D, ^3F-2^3P line struct., in low-press. linear discharge 79—14523
- He II resonance radiation intensity, He gas press. depend. 77—84553
- He, liq., elec. discharges at low temps., appl. to elec. insulation for supercond. cables 77—27757
- He, low press. discharge, electron free streaming waves expansion 80—79595
- He, low pressure, line spectrum, mol. transisions effects 79—60212
- He, multi-channel, in inhomogeneous field, at 1 to 5 atm *(Russian)* 77—89335

discharges continued
- He non-equilib. plasma diagnostics, PLTE model and steady state attainment 80—38715
- He plasma, ion state and electron temperature in high-current pulsed discharge *(Russian)* 79—27844
- He, plasma, non-equilib., of strong current pulse discharge, diagnostics *(Russian)* 78—75271
- He, positive column plasmas, metastable atom density meas. by improved self absorpt. method 80—87968
- He, probe meas. of plasma props. 77—47292
- He pulsed discharge, He_2 mol. formation in early afterglow, time-resolved spectra 78—63585
- He, pulsed elec. discharge, high-current, diagnostics and nonequilib. state 79—64942
- He, radiation from hollow-cathode discharge in weak mag. field 78—70789
- He, self-oscillating props. of discharge in mag. field 80—64814
- He, synchrotron and laboratory discharge light sources comparison 79—10371
- He, twin-hollow-cathode interferometer-spectrometer, discharge characts. *(German)* 78—67461
- He, twin-hollow-cathode of interferometer-spectrometer, radial electron temp. *(German)* 78—67462
- He, vibr. excitation calc. 79—77442
- He-Ar hollow cathode discharge, CW laser oscill. obs. 78—5454
- He-Ba discharge, dipole-dipole pair absorpt. obs. using optogalvanic detect. 80—54064
- He-Cd DC discharge, excited at. densities, I-V characts. 78—14230
- He-Cd discharge, principal Cd ionis. mechanism, radial profiles meas. 77—27758
- He-Cd positive-column laser discharge, excitation mechanisms from radial profiles 77—68205
- He-Cd^+ positive column laser discharge, ion density 77—68885
- He-Co_2-Xe plasma discharge electron conc. and temp., optical diagnostics method 79—41871
- He-Cs, turbulent plasma, characts., electron energy balance *(Russian)* 79—27779
- He-Cs discharge plasma, high freq. oscills. in crossed elec. and mag. fields *(Russian)* 77—15189
- He-Cu discharge, Cu ion laser, at. emission obs. of plasma props. 80—19021
- He-H_2 DC discharge, H Balmer-α fine struct. lines, anomalous shifts 79—45677
- He-Kr hollow cathode CW laser, Kr II 4584 Å generation 80—58510
- He-N_2 plasma, N_2 $B^3\Pi_g$ state excitation, role of long lived states, luminesc. 80—37829
- He-N_2-CO_2 mixture, IR laser output from elec. discharge after X-ray preionisation 79—64205
- He-Ne, gas discharge laser, stimulated emission, vel. to striation 80—37994
- He-Ne discharge, striation oscills., spectral width variations 77—62429
- He-Ne discharge, striation parameters, discharge current modulation effect 77—84555
- He-Ne discharges, striations in narrow discharges 80—38736
- He-Ne gas discharge, positive column striations characts. 80—49032
- He-Ne laser, 6328 Å power fluctuations due to striation noise 80—78834
- He-Ne laser, compact, transverse microwave discharge, energy characts. 80—64064
- He-Ne ring laser, Ne isotopic composition changes during prolonged discharge *(Russian)* 78—22110
- He-Ne waveguide lasers, props. and current-voltage characts. of discharges 78—1208
- He-O_2 DC discharge, electron distrib. function 80—92407
- He-Xe optical amplifier, striation form. for DC discharge plasma, noise anal. 80—43366
- He-Xe-F_2 mixture, pulsed avalanche discharge at high gas press., homogeneous form. conditions 80—49027
- Hg electrical discharge, electron-collisional excited-state kinetics 77—24226
- Hg, high-pressure discharge, temp. and electron density meas. *(French)* 78—59705
- Hg, radial distrib. of low-freq. oscills. *(Russian)* 78—1928
- Hg vapour line splitting on Tonks-Dattner reson. 80—59317
- Hg-A positive column, scaling towards display cells 77—84565
- Hg-Ar, low-pressure discharge, energy balance and Coulomb relax. 77—43098
- Hg-Ar(Kr)(Xe) mixtures, prebreakdown discharges, discharge current depend. on electron mobility 79—77433
- Hg-He(Ar), modulated discharge, elec. and optical props. 77—7627
- Hg-Tl-I discharges, 50 H_z, Tl atoms axial segregation 80—38781
- Hg-Tl-I discharges, 50 Hz, axial segregation effect on elec. field strength 80—59320
- $HgBr_2$ dissociation laser, elec. excited, kinetic processes 80—48231
- $HgBr_2$/HgBr dissociation laser, oscillator and oscillator-amplifier expts. 80—48232
- $HgCl^*$, metal vapour excimer laser, stability criteria 78—66802
- Hg(6^3P_1) resonance level population, in vap. and inert gas modulated discharges 77—83532
- I nanosecond single pulse laser, open electric discharge pumping 80—5763
- I^- beam, duoplasmatron ion source for SIMS, Ar-I_2 medium 77—18123
- In normal atom conc. determ. by resonance line broadening with Hg press. 80—43883
- K, 1st reson. level, effective electron-ionis. cross sections, plasma discharge method 78—13603
- K discharge plasma, K_2 excited mols. form. by K(4P) collisions 80—44013
- K-H plasma, low temp. discharge, ion constitution mass spectra *(Russian)* 77—4000
- K_2, in discharge plasma, anomalous 5725 Å band, photorecomb. mechanism 79—50088
- $K_2{}^+$ ion formation in low press. K discharge plasma 80—43862
- $K_n{}^+$, ion formation in elec. discharge, n=2-6, 10^{-3}—1 torr. *(Russian)* 79—77448
- KCL, spark channel in solid, plasma light absorpt. coeffs. 79—7501
- Kr, discharge, non-self-maintained, ionis. instability of excited ats. and excimers *(Russian)* 77—84557
- Kr discharge, secondary ionisation processes 78—59711
- ^{86}Kr, discharge, metastability-exchange cross section 80—99464
- Kr-F_2 mixture, preionised electric discharge stability 79—64865
- ^{86}Kr-^{78}Kr, discharge, metastability-exchange cross section 80—99464

discharges continued
$KrCl^*+Xe$, substitution efficiency during excitation in transverse AC electric discharge 80—50850
KrF, excimers, power superluminesc. in elec. discharge *(Russian)* 77—7621
KrF^*, waveguide laser excited by capacitively coupled discharge 78—94391
^{85}Kr aerosol discharge devices, fabrication and use 79—1969
Li plasma, electrode pot. layer characts., surface ionisation and Schottky effects 77—15260
Li plasma, low-temp nonequilib. plasma flux, ionis. rate const. 77—47143
Mg, hollow cathode discharge, excitation mechanisms of triplet state atoms and decay obs. 80—44015
Mg-Xe discharge and MgXe excimer band, emission intensities and excited-state densities meas. 80—92413
MgO-Ag porous layer, secondary electron emission from ion impact, gas discharge device appl. 78—68586
Mn vapour impulsive production after discharge current pulses through halide vapours *(Russian)* 79—90491
Mo, dislocation structure evolution near electro-eroded crater *(Russian)* 80—100237
$MoCl_5$, dissoc, in pulsed discharge, interference method obs. 77—58186
$MoCl_5$, pulsed discharge dissoc., for Mo I oscill. strengths meas. 78—25479
N discharge, externally maintained, instability growth time, associative ionisation 80—6254
N gas discharges, electron swarm motion, computer simulation 77—89339
N_2, a.c. discharge, stability *(Russian)* 78—26358
N_2, diffusion approx. of Boltzmann eq. for slow electrons 79—82044
N_2 discharge, anomalous heating *(Russian)* 80—1866
N_2 discharge, effect of Cs additive on I-V characts. 79—32813
N_2, discharge, elec. and optical props. calcs. *(Russian)* 79—10741
N_2 discharge, electron shock wave formation, numerical simulation 80—38777
N_2 discharge, flowing, electron-beam maintained, cathode shape effects 79—27850
N_2 discharge, high-current, with inductive storage bank, exploding wire-initiated 80—10450
N_2, electric breakdown, vol. discharge with external photoionisation, plasma focus spark channel *(Russian)* 80—38738
N_2, electrical and optical discharge parameters at moderate press. 80—6300
N_2, electrical discharge excitation, vibr. level population distrib., electron beam fluoresc. obs. 80—48031
N_2, electron beam sustained high press. discharge, time behaviour of recomb. coeff. 80—10447
N_2, electron drift vels., time-of-flight meas. 80—28855
N_2 electron-beam-sustained discharge stability model 78—71608
N_2, excitation efficiency of rot. and vibr. levels, heating due to elastic collisions and relax. 80—38751
N_2, gas discharge, external ionisation, cathode fall and I-V characts. 77—55193
N_2 gas filled chamber, passage of low current electron beam 80—38523
N_2 glow discharge, non-self-sustained, cathode spots annular structure investig. 80—24281
N_2, HV diffuse discharge, gas stream temp. inlfuence 79—32842
N_2, heating in combined discharge 77—84387
N_2, high-pressure vol. discharge, quasi-stationary stage characts. *(Russian)* 77—27756
N_2, high-speed Raman spectroscopy, condensed discharge vibr. excitation, vibr. temp. 78—82740
N_2, homogeneous overvolted discharge, electron density evolution 79—1359
N_2, inductively coupled plasma discharge, temp. and vel. profiles 77—4004
N_2, internal discharge initiation, expt. 77—24220
N_2, ionisation current increase, metastable mol. induced cathode secondary electron emission 80—38830
N_2 laser discharge, SF_6 addition, negative ion prod., altered discharge parameters 80—38818
N_2 laser discharge emission model and meas. 78—71093
N_2, liq., discharge development in nonuniform elec. field 79—91358
N_2, low pressure discharge, gas temp., laser interferometric meas. *(German)* 79—68951
N_2, non-Boltzmann vibr. level populations, CARS determ. 78—5968
N_2 non-LTE, pulsed discharge, I-V characteristic obs. 78—71618
N_2, non-self-maintained discharge, high press., ionisation instability, pulse discharge train *(Russian)* 77—47282
N_2, nonequilibrium dissociation rates in electrical discharges, temp. depend. 78—33447
N_2, optogalvanic spectroscopy in discharge, 570 to 620 nm 79—54862
N_2, plane overvoltage discharge 77—19780
N_2 plasma, 18000-45000K, continuum emission coeff., laser spark temp. meas. 77—31527
N_2 plasma, electron temp. and conc. meas., complete LTE 77—65908
N_2 plasma, non-equilib., excited species, vibr.-rot. anal. fluoresc. obs. 80—54034
N_2 plasma, radial distrib. profile of atom conc., Lewis-Rayleigh afterglow radiation 77—89312
N_2 plasma discharge stream, rarefied, diagnostics using sounding and UHF interferometry 79—41872
N_2, stationary beam discharge plasma, electron kinetics 80—38775
N_2, time-depend. of radiation in pulse discharge regime *(Russian)* 77—84548
N_2, vibr. excitation calc. 79—77442
N_2-Ar mixture non-self-sustained discharge instability obs. 78—71612
N_2-CO, electrical discharge excitation, vibr. level population distrib., electron beam fluoresc. obs. 80—48031
N_2-CO_2, N_2 non-self-maintained discharge, high press., ionisation instability, pulse discharge train *(Russian)* 77—47282
N_2-CO_2 laser mixture, electron drift vels., time-of-flight meas. 80—28855
N_2-CO_2(-He) volume discharge, N_2 vibr. levels, stepwise excitation, effect on electron energy balance 80—54071
N_2-F_2 mixture, fast Blumlein discharge excited, intense 3371 Å laser emission 79—41365
N_2-He, barrier discharge, struct., spectral anal. *(Russian)* 77—21463
N_2-He-CO_2, discharge ionisation growth, diffusion coeffs. 78—83636
N_2-methane, rapidly developing discharge, streak camera records interpretation 80—59280
N_2-NO(He), discharge ionisation growth, diffusion coeffs. 78—83636

discharges continued
N_2-SF_6 mixture, breakdown voltage and discharge extension of long gaps 77—84550
N_2+H_2, N_2 dissoc. rates, nonequilib. vibr. populations, elec. discharge conditions 77—88535
NF_3, electron dissociative attachment rate consts. at 300 and 500K 80—43849
NH_2, optogalvanic spectroscopy in discharge, 570 to 620 nm 79—54862
N_2H_4 production from NH_3 in atmospheric press. electron-beam controlled discharge 80—38799
NO+N ^{4}(S) state reaction rate, discharge flow and photolysis reson. fluoresc. method 79—5142
NO_2, optogalvanic spectroscopy in discharge, 570 to 620 nm 79—54862
N_2O, triboelectric discharge of Hg rolling on glass, chem. effect *(French)* 79—77438
Na, low press. depleted discharge, recomb. struct. 79—94837
Na normal atom conc. determ. by resonance line broadening with Hg press. 80—43883
Na-Hg high-press. discharge, Na reson. radiation, self-reversed maxima shifts 80—92411
Na-Ne-Ar, low-pressure discharge, AC operated, time-resolved afterglow 77—43099
Na-Ne-Ar AC discharge, positive column 77—39487
Na-Ne-Ar discharge low-press., instability 78—9868
Na-Xe, high-pressure discharge, electron density, interferometric meas. 78—75415
Na-Xe vapour, high power discharge, potential excimer laser 78—82957
Na_2CO_3 electrolyte, silent discharges elec. characts., expt. *(Korean)* 78—40057
NaCl-oil boundary, formation of discharge in system of electrodes *(Russian)* 79—8089
α-Nb_2O_5, reduction in H_2 discharge, AES and SEM anal. 77—59708
Ne absorber discharge, 3 nsec laser pulse propag., self-induced transparency 77—10986
Ne discharge, Boltzmann eqn., numerical study 77—35424
Ne discharge, ionis. waves coherent nonlinear coupling 79—55497
Ne discharge, spectral line intensity radial distrib. 78—5930
Ne discharge, time-resolved population meas. with N_2-laser-pumped dye lasers 77—80362
Ne discharge, wavenumber spectra of turbulent ionisation waves 78—71541
Ne discharge in high press. narrow tube, Kadomtsev-Nedospasov instability 80—107004
Ne, discharge streamer propagation mechanism based on plasma vibrs. *(Russian)* 77—84546
Ne, discharge transition, diffuse to contracted state, ionis. waves *(Russian)* 78—30511
Ne, electron energy distrib. meas. in moving striations 77—55191
Ne, electron energy distrib. function, Boltzmann eqn. 79—50911
Ne, excitation mechanisms investig. using radial distrib. of excited atoms 80—38744
Ne flash tube, investigation of forms. and decay mech. of internal fields 78—58552
Ne, high current discharge, short light pulse form. *(Russian)* 79—27846
Ne hot cathode discharge plasma, second order harmonic surface wave generation 80—38849
Ne, isotope separation by cataphoresis in DC gas discharge 80—103213
Ne, laser irrad. and voltage changes 78—63606
Ne, low press. discharge, electron free streaming waves expansion 80—79595
Ne, low press. discharge, kinetics and column impedance *(German)* 77—58845
Ne, metastable level deactivation by electron collision in low press. discharge 78—83520
Ne, numerical study 79—32838
Ne, plasma column dynamic behaviour, equivalent circuit *(German)* 77—76217
Ne positive column, 3S and 3P level populations, rel. theory with recomb. 77—10766
Ne positive column plasmas, metastable atom density meas. by improved self absorpt. method 80—87968
Ne, pulsed discharge, spectral characts. *(Russian)* 78—47201
Ne pulsed transverse discharge, spectrosc. absorpt. investig with nanosec. time resolution *(Russian)* 80—64782
Ne, radial distrib. of line intensities, level population 78—18473
Ne, radiation from hollow-cathode discharge in weak mag. field 78—70789
Ne, spectral line relative intensity, radial depend. in low press. discharge 80—37764
Ne, streamer plasma characts., cond., plasma density and field strength calcs. *(Russian)* 77—47262
Ne, thermalisation of level populations, occurrence in elec. discharge 78—66649
Ne, weakly ionised, energy transfer at high press. 78—58845
Ne-Ar, high press. mixture, AC discharges, one-dimensional numerical simulation 78—67451
Ne-Ar mixture, transient cataphoresis, time depend. 80—38753
Ne-Ar Penning mixture, pulsating discharge, emission spectra, Ne state population 79—55594
Ne-Cu laser, discharge processes, cathode sputtering 78—5463
Ne-Cu pulsed discharge, electron energy distrib., ionis. rate 78—51387
Ne-HCl(CH_4) mixture breakdown obs. 78—67553
Ne-He mixture discharges, origin of dark spaces in plasma 78—9881
Ne-N_2 AC discharge, pulse to continuous mode transition, Ne metastable effects *(German)* 80—84011
Ne-N_2 mixture, cataphoretic segregation in DC discharge, mass spectral anal. 77—32799
Ne-Xe, LF oscillations, modulation by gravitation and inertia forces 77—11429
$Ne+H_2O$, hollow-cathode discharge, Ne spectral intensity 79—4202
Ni-Cd batteries, button and cylinder types, self discharge behaviour during storage *(German)* 80—66960
Nz, electron beam sustained discharge, performance 78—75365
Nz, formative time lags, expt. 77—1025
O plasma electron energy distribution obs. 78—63595
O^- electron detachment, discharge in air 79—54961
O_2, $A'^3\Delta_u$ state, inversion, presence in nightglow and discharges 80—63616
O_2, conditions, self-consistent electron energy distrib. functions calc. 80—38746

discharges continued
O_2, discharge, nonequilib. vibr. population, dissoc. rate, role of ats. and dissoc. 79—64933
O_2 discharge, O_3 production 80—38780
O_2, discharge development, relative motion between gas and electrode, theory 78—63616
O_2 discharge plasma, metastable states role, two step ionisation, electron densities and transition pts. 80—44019
O_2, dissociation rates, nonequilib., vibr. populations in elec. discharges 78—46427
O_2, electron energy distrib. function, electron sink and plasma resist. effect *(Russian)* 80—106987
O_2, electron gas, transport coeff. and energy distrib. function calcs. 77—68742
O_2, electron impact vibr. excitation, direct and stepwise, rate coeffs. 80—5630
O_2, electron lateral diffusion to mobility ratio 80—6203
O_3 generation in air-fed ozonisers 80—3323
O_3 yield, rel. to discharge field strength and gas pressure 79—19116
O_x metastable and O_3 production in electron-beam-controlled high-pressure discharge 78—71607
$OH+HO_2 \rightarrow H_2O+O_2$ gas flow reaction, upper bound and probable value of rate const. 79—24730
$OH(^2\Pi)$, rot and translational temps. in gas discharge 78—5243
Pb-He discharge, excitation process, Pb^+ emission lines 78—66803
PtAl, form. in hollow cathode discharge, emission spectrum obs. 78—27819
PtD, form. in hollow cathode discharge, emission spectrum obs. 78—27819
PtH, form. in hollow cathode discharge, emission spectrum obs. 78—27819
PtO, form. in hollow cathode discharge, emission spectrum obs. 78—27819
Rb, 1st reson. level, effective electron-ionis. cross sections, plasma discharge method 78—13603
$Rb_2{}^+$, form. by electron impact in elec. discharge, low-press. vap. 79—10738
S (S-He) discharges, stability, emission spectra 80—107003
SF_6, compressed, negative ion drift in applied field 78—87565
SF_6, discharge development, relative motion between gas and electrode, theory 78—63616
SF_6, electric strength, electrode surface roughness effects, model *(German)* 78—63609
SF_6, expt. *(German)* 79—10726
SF_6, high-current discharge plasma column, radiation charact. and struct. *(Russian)* 80—106989
SF_6 insulation, under impulse voltage stress, effects of pressure and vol. on firing delay *(German)* 80—87959
SF_6, predischarge-stabilised breakdown voltage *(German)* 78—63608
SF_6-inert gas mixture, high power cylindrical spark discharge, dynamic and visible charact. 80—64816
SF_6-N_2-Ar mixture high-current multispark discharge switching characteristic 78—67444
SiO_2 surface, Ar plasma-treated, O_2 adsorption reactivity, EPR obs. 79—51418
SrII, near IR laser transitions in hollow cathode discharge 80—1194
Ti density, in DC sputtering discharge by atomic absorpt. spectroscopy 80—43973
Ti plasma impurity, atom-electron collisions in inner discharge column *(Russian)* 80—38529
Tl, in gas discharge, optical self pumping, hyperfine struct., microwave-optical spectroscopy 80—32680
Tl, normal atom conc. determ. by resonance line broadening with Hg press. 80—43883
Tl vapour impulsive production after discharge current pulses through halide vapours *(Russian)* 79—90491
Tl-Xe, electric discharge excitation of Tl in high-press. Xe 80—49025
U, vapour prod. by sputtering, Ne, Ar, Kr, carrier agents, density meas. *(French)* 78—86967
W, acoustic emission under action of single elec. pulse discharge *(Russian)* 77—59071
W filaments, operated as cathodes in gas discharge characts. 79—50913
W, high-current hollow cathode, energy balance *(Russian)* 77—58910
Xe, Blumlein-type transverse fast, voltage meas discharges (electric) 80—19642
Xe discharge plasma spectral and integral characteristics calc. 78—71583
Xe, gas discharge, laser beam polarisation plane rot. near reson. 77—1024
Xe, in gas discharge, collisional excitation, radiation lifetimes, macroscopic alignment obs. 80—33734
Xe, ns. discharge, energy balance, optical meas. 78—1935
Xe, pulse gas discharge, high-intensity, energy storage and temp. in channel 78—1926
Xe, pulsed discharge, superheating instability, effect of secondary ionisation 77—55189
Xe, time-depend. of radiation in pulse discharge regime *(Russian)* 77—84548
Xe-Br_2 discharge, atomic state density determ. 79—36573
Xe-F two module discharge laser, gain and temporal characts. 80—87385
XeCl laser, discharge stabilisation with 50 nsec electron beam 80—23716
$XeCl^*+Kr$, substitution efficiency during excitation in transverse AC electric discharge 80—50850
XeF, excimers, power superluminesc. in elec. discharge *(Russian)* 77—7621
XeF laser using Ar-Xe-NF_3 mixture, discharge stabilised by short-pulse electron beam 80—14358
XeF^* gas-discharge excimer laser, kinetics 80—48226
XeF^*, waveguide laser excited by capacitively coupled discharge 78—94391
^{136}Xe $7p[3/2]_1$ level, cascade alignment in discharge 80—44057
Y_2O_3 capillary discharge plasma, temp., radiation screening elimination 80—64682
Zn afterglow diffusion coeff. for metastable Zn atoms 77—23542
Zn, pulsed supply, hollow cathode, optimisation of spectral lines 78—33471
$ZnGa_2$, excimer visible emission spectra in RF discharge, vibr. struct. 79—18201

discharges (partial) *see partial discharges*

disclinations
Ag-Cu fibre composites, highly deformed, lattice defects, X-ray interference lines anal. 80—10559
amorphous magnets, disclinations and solitons 80—75786
amorphous solids, crystallography tentative description 80—6360
antiferromagnet, dislocations producing domains and disclinations *(Russian)* 77—32213
broken twist boundary, model 78—47394
carbonaceous mesophase, twist disclinations 79—95010
CBOOA, nematic-smectic transition, singularities, elastic const. var. 77—39537
cholesteric, Grandjean lines, optical study *(French)* 79—46560
cholesteric, liquid crystals, disinclinations, rotation defects, topology *(French)* 80—79679
cholesteric liquid crystal, investig. by homotopic topology methods *(Russian)* 77—69140
cholesteric liquid crystals, topological classification of distortions 78—79523
cholesteric liquid crystals dispersed in polyurethane elastomers, optical props. 78—1986
cholesteric planar texture, planar-finger print texture transform. around Cano disclinations 80—14999
cholesteric screw sense, form of spiral disclination lines calc. 78—67643
cholesteric wedge layers, planar alignment, paired disclinations and disclinations of strength O 79—86696
cholesteryl oleate, thin film, disclination morphology *(Russian)* 77—62474
Cosserat's medium, linear and surface defects, stresses 78—83813
Cosserat continuum, analogy between disclination rank and vortex line invariant *(French)* 78—1977
Cosserat theory of crystal plasticity, appl. to anal. of lattice rotations under constrained deform. *(Japanese)* 78—2189
dipole, elastic interaction with dilatation centres 77—68994
dipole, of infinitesimal width and straight dislocations 79—51104
dislocation-straight disclination, elastic interaction 79—55740
dislocations, vel. to disclinations 78—22717
dislocations and melting in two and three dimensions 80—103454
dynamics, field equations, four dimensional space-time setting 80—96521
elastic energy of disclination segments and quadrupoles 77—39585
elastic field interaction 80—54233
elastic interaction between disclination loops and straight disclinations 80—2015
elastic interaction with dislocations and dispiration elastic energy 79—19248
ferromagnet, local variation in mag. anisotropy due to linear defects *(Russian)* 78—68214
finite solid, dislocations, disclinations and grain boundaries 80—2019
force-free disclination motion, dynamic field theory *(German)* 77—1127
fragmented structures, dislocation and disclination kinetics *(Russian)* 80—79788
Frank disclinations in isotropic elastic micropolar continuum, stress and couple-stress fields 77—72245
gauge transformations admitted by the equations of defect dynamics 79—27981
geometrical theory, four-dimensional 79—84954
glass, disclination lines, topological stability 80—33902
hexagonal liquid crystals, developable domains 80—92453
kinematics, continuous distrib. of disclinations and dislocations 78—63764
linear elastic body, disclination dynamics 78—34510
liquid crystal, cholesteric defect struct. near smectic A transition 79—46559
liquid crystal, lyotropic, parabolic focal conic struct., disclination/dislocation relation 79—27909
liquid crystal, smectic A and C phases, classification of defects 78—26433
liquid crystal, twisted nematic display, control and elimination 77—68912
liquid crystal carbonaceous mesophase, disclinations 77—43147
liquid crystals, defects, struct., optical, electron microscopy *(French)* 79—46567
magnetostrictive displacement at surface due to mag. domain wall junctions 78—48014
MBBA, annihilation of disclinations with Frank index $m=+2$ 77—58955
MBBA, light scatt. by disclinations, spatial coherence props. 77—8544
melting, two-dimens., dislocation-mediated theory predictions, light scatt. use as probe 80—92651
mesomorphic phases, disclinations *(French)* 79—41947
metallic glasses, structures based on disclination-dislocation model 79—82159
microcrack formation, disclination mech. 79—23674
micropolar continuum, isotropic, elastic fields of dislocations and disclinations 77—68971
micropolar Cosserat media, theory of disclinations 78—38698
nematic and cholesteric liquid crystals, disclinations, generation process, matrix representation 78—59743
nematic and smectic liq. cryst., viscous and plastic behaviours 79—86686
nematic liquid cryst. soln., thermodynamic treatment 79—32903
nematic liquid crystal, acoustic emission due to release of elastic energy in defect dynamics 79—55654
nematic liquid crystal, cavity interaction with singularity 77—84635
nematic liquid crystal, circumferential surface orientation, in capillary, optical studies 77—47349
nematic liquid crystal, critical radius for homeotropic domain 79—19148
nematic liquid crystal, homeotropic cylindrical boundary, in capillary, cols and noeuds 77—47350
nematic liquid crystal, parallel and cross-like domains due to DC and LF electric fields 79—46557
nematic liquid crystal, rel. to cryst. screw dislocations 77—11477
nematic liquid crystals, AC Josephson effect, phase slippage 79—46565
nematic liquid crystals, acoustic emission, appl. to defect dynamics study 78—91232
nematic liquid crystals, biaxial, defect props. *(French)* 77—31587
nematic liquid crystals, interaction between surface and bulk disclinations, continuum theory 79—86694
nematic liquid crystals, radial and circular disclinations *(Russian)* 77—11762
nematic mesophase, surface disclination lines rel. to surface-induced homogeneously tilted alignment 77—58950

disclinations continued
nematics, topological instability of singularities at small distances *(Russian)* 78—79531
orientational bistability, nematic storage effects 80—70112
planar magnetic media, defect hydrodynamics *(Russian)* 80—49445
plastic deformation, macroscopic theory, dislocation and disclination kinetics *(Russian)* 80—49225
plastic deformation, partial disclination dipole motion 79—73165
plasticity, Cosserat continuum, non-Reimannian geometrical theory of imperfections 80—53639
Poisson brackets, nonlinear hydrodynamics eqns. in condensed matter physics 80—54296
polyethylene, crystalline, twist disclination formation and longitudinal motion of defects 80—19810
random anisotropy and random field models, textural singularities and frustration 79—24182
rare earth metal based compounds, spin glasses 80—50132
rectangular twist disclination loops, elastic energy and stresses 79—27987
review 78—38704
smectic C liquid crystal, striped patterns in thin droplet 78—26430
smectic C liquid crystals, chiral, defects induced by planar anchoring *(French)* 78—94978
smectic C liquid crystals, elasticity and defects 78—91233
smectic phases, cofocal conics 79—1395
stationary lattice defects as sources of elastic singularities 78—59800
straight wedge disclination near a free surface 80—96511
surface dislocations, universal concept, rel. to disclinations and grain boundaries 80—100231
theory, rel. to X-ray topography data 78—64254
topological theory of defects in ordered media 79—93072
twist disclinations, differential geom. 79—14805
two-dimensional triangular lattice, melting theory 78—71833
two-face dislocation boundary, energy and induced stresses *(Russian)* 80—103331
n-undecyl-p-azoxy-α-methylcinnamate, smectic C phase, domains, walls, and disclinations 79—86687
wedge, differential geometry, simple cubic crystals 77—59011
wedge disclinations in cellular struct. 77—62533
wedge disclinations in continuum mechanics model, geometry and forces *(German)* 78—34511
wedge disclinations near surface of semi-infinite cryst. *(Russian)* 80—49224
Fe, stress fields and strains energies associated with closure domains 77—1563
$Gd_2(MoO_4)_3$, ferroelec. and ferroelastic, electron microscopic study 77—85675
Si-Fe, ferromagnetic domains and their junctions, simulation of X-ray topographs 79—78434

discontinuous control systems *see sampled data systems*

discontinuous metallic thin films
AC equivalent circuit anal. 79—51690
alkali metal, multipole oscillations in small hemispherical particles 79—78774
conductivity, appl. of percolation theory 80—65712
dielectric constant, Maxwell-Garnet and effective medium theories 77—47760
dynamic coalescence origin *(French)* 77—51612
electric and magnetic field distrib., TEM obs. 79—95518
electric conductivity temp. depend. 77—47903
electric field distrib. and emission currents of island condensates 78—88047
electrical conduction, review 78—19167
electrical conduction and current noise mechanism, theory 78—56244
electrical noise, high temp. behaviour 80—54807
electrical properties, effect of distrib. of particle size 77—66209
electroluminescence, comparison with MIM struct. 78—23533
electroluminescence mechanism *(Russian)* 79—47523
electron transmission between two neutral islands, necessary energy determ. 77—80852
epitaxial small islands, one-dimens. model of mobility, parabolic substrate pot. 79—95299
field effect of elec. cond. series-connected island model 79—78219
field effect of electrical conductance, series-connected islands model *(Japanese)* 80—11107
field effect of electrical conductance 77—39964
film island coalescence of real cryst. surface, unattenuated sputtered atom source 80—6672
granular, superconductivity quenching when charging energy exceeds Josephson coupling energy 77—47943
granular, thermally activated hopping, carrier-carrier interaction 77—15972
granular films, optical and microwave props. of microscopically inhomogeneous materials 77—77161
granular two-dimensional film subjected to elec. field, metallic grain polarisability 79—4859
growth due to crystallite surface migration, review 80—10810
high temperature elec. cond., model 79—78220
island film, two-dimens. distrib. system, optical refl. and transmission calcs. 79—4862
island films, coalescence kinetics, ageing rate, Kahlweit approx. *(Russian)* 80—59838
island films, diffusive mass transfer, review 80—20054
island type metal condensates on insulator, elec. cond., statistical theory 78—10582
islands, rotation and translation on substrate 80—10811
islet film, cond. currents and electron emission, electron heating effect 78—10581
luminescence, electron beam excited *(Russian)* 79—47526
maximum metallic resistivity, approx. expressions 78—14773
metal particle composite, physical and optical props. 78—56528
microcrystals on C foil, size distrib. from electron micrograph obs., UV absorpt. spectra obs. 80—55121
millimetric and IR discontinuous-metal-film detector 78—289
millimetric-wave and IR detectors *(Japanese)* 77—49771
noble metal aggregated film, absorpt. peaks, collective oscills. of electrons 78—80428
noble metal aggregated film, light scatt. 78—64423
nucleation, oriented island growth on point defects 78—87889
nucleation on alkali halide crystals, effect of ionisation of condensing flux 80—107675

discontinuous metallic thin films continued
optical properties of rough surfaces, discontinuous films, heterogeneous materials, review 80—103935
optical props. rel. to multipole oscills. in hemispherical particles in granular metal thin films 80—7431
refractory metal films, evaporated, optical props., rel. to struct. 80—55211
resistance and strain gauge factors expressions, quantitative formulation 79—95521
resistive layer microstructure on superconducting Al surface *(Russian)* 80—34567
review of struct., optical and electrophys. props. 77—76698
structure, review 77—89671
supported crystallites, wetting in sintering and redispersion 80—24751
surface disperse system, distrib. function calc. *(Russian)* 77—35840
thickness measurement, electron mode microanalyser 79—2744
tunnel conduction, temp. depend. 77—20467
Ag, adsorption of alkali halide mols., effect on elec. cond. 80—2487
Ag, aggregated film, optical props., 0.35-1 μm 77—66548
Ag, electron beam plasma sputtered coatings on KCl substrate, islet struct. *(Russian)* 80—39460
Ag film, 1/f noise and its temp. depend. 79—60939
Ag film, elongated epitaxial (111) island growth on Cu(001), interface misfit, dislocations 79—82493
Ag, film growth on C, conductance meas. 79—82495
Ag film growth on Si (111), nucleation and growth modes, SEM study 80—100423
Ag, granular, adhesion measurement 80—50807
Ag, granular film, anomalous light absorpt., oblique incidence 79—6205
Ag, granular films, optical props., depend. on refractive index of surrounding medium 78—84672
Ag granules and colloidal particles on Cs_2O film in Ag-O-Cs photocathode *(Chinese)* 80—2279
Ag, initial stages of growth on Si (111) 7×7, LEED, AES and UPS expts. 78—38988
Ag, island film on Ni foil substrate, elec. props. 77—43745
Ag island films, on W, growth and desorption kinetics, mass spectra obs. *(German)* 79—46978
Ag islands, on Al_2O_3 substrate, adsorption of ethanol, inelastic electron tunnelling spectra and TEM obs. 79—90884
Ag, light absorpt. spectra, dielec. function calcs. 79—51507
Ag, on (001) MgO, low energy electron spectrum 77—48288
Ag, on mica, microstruct. changes 78—72013
Ag particles on graphite, particle motion rel. to heating in gaseous environments 78—34695
Ag ultrafine particles evaporated on glass, optical transmittance meas. 79—78772
Ag-AgI island granular film, Weigert effect, anomalous dichroism 77—12455
Al, electron beam plasma sputtered coating, islet struct. *(Russian)* 80—39460
Al, epitaxial growth on MgO, liquid-like coalescence of three-dimens. islands 77—1325
Al film, condensation from partially ionised vapour flow, peculiarities of form. and struct. 79—28252
Al film, influence of predeposited island film on crystallisation of continuous film 78—18930
Al, granular, hopping cond., supercond., magnetoresist., Zeeman splitting 78—60243
Al, granular, transition to localisation, elec. resist. 80—70877
Al granular films, inhomogeneous supercond. transitions, microwave meas. 80—103789
Al, quench-condensed ultrathin film, two-dimensional elec. cond. 78—39233
Al, RF impedance temp. and freq. depend. 77—4453
Au, aggregated film, optical props., 0.35-1 μm 77—66548
Au, condensation kinetics on KCl substrate, evolution of size distrib. function 79—28243
Au, degradation under MeV heavy ion bombard., Rutherford scatt. and TEM obs. 79—24397
Au, diffusion on atomically clean Si (111) surface 78—72037
Au discontinuous film, electroluminescence obs. 80—103998
Au, discontinuous film, optical absorption 77—69927
Au, discontinuous film, optical transmittance 78—56529
Au, elec. cond. and current noise, temp. depend. meas. 78—56245
Au film, discontinuous, centre-to-centre particle distrib. determ. 80—96761
Au film, electron emission and electroluminesc. 77—90257
Au film, influence of predeposited island film on crystallisation of continuous film 78—18930
Au film, multiple attenuated total reflection spectroscopy, initial growth process 79—19490
Au, film growth on mica substrate, surface defects and heterogeneous nucleation 78—47684
Au film on Al, reflectance and absorpt. obs. 80—7426
Au films, condensation on alkali halides, growth, struct., stability *(French)* 78—38989
Au films, on sapphire substrates, electrical noise, high temp. behaviour 80—54807
Au films, optical transmittance, effect of island morphology 78—84673
Au, high temp. elec. cond., model 79—78220
Au island condensate, on LiF or NaCl, nucleation kinetics, influence of ionised atoms 77—11816
Au island film, on NaCl cleaved surface, growth, effect of perp. elec. field *(German)* 77—76697
Au island film, on SiO_x, growth and struct., effect of perp. elec. field *(German)* 77—76696
Au island film real structure and electrical conductivity obs. 79—77948
Au island films, forming process, I-V characts., and switching 79—11242
Au island films on CaF_2 in acidic medium, morphological changes, C replica method 77—1286
Au islands, role in oriented crystallisation of Ag on active a-C 79—7762
Au, light absorpt. spectra, dielec. function calcs. 79—51507
Au, mobility of small crystallites on KBr cleavage planes 79—23857
Au, morphology and size distribs. of islands, electron microscope obs. 77—62766
Au, nuclei interaction on KCl (100) surface 77—89670
Au, nuclei on KCl, collective behaviour, monatomic step influence 77—15719
Au, on CaF_2, oriented crystn., formation of coincidence orientations on interphase boundary 79—90922

discontinuous metallic thin films continued
- Au, on GaAs, effect on photoelec. memory effect 77—55570
- Au, on KCl, nucleus growth mechanism and kinetics, electron microscope obs. 77—62780
- Au oriented islands as nucleation centres of evaporated Te films, Te grain growth 78—2388
- Au particles condensed on NaCl surface, electron diffr. pattern interpretation, computer simulation *(French)* 77—76700
- Au, quench-condensed ultrathin film, two-dimensional elec. cond. 78—39233
- Au, structural props., electrical props. 78—6246
- Au, substrate radiation damage effect on resist. and strain gauge stability 79—95520
- Au, thin film, discontinuous, high resist., Hall effect meas. 80—65716
- Au, ultrathin island films, band struct. formation 77—85893
- Au, vac. deposited films, surface pot. and work function rel. to thickness 79—42672
- Au vacuum deposition on dielectric substrates, ellipsometric and electron microscopic meas. 79—74011
- Au, vacuum evaporated on C and SiO, struct. and elec. cond. 80—39686
- Ba, growth on (111) face of Ir covered with graphite monolayer 78—26791
- Ba islands on Ir (111), growth of 2-dimens. islands in presence of activation barriers at island boundaries 78—43274
- Bi, granular enhancement of laser machining and ageing characts., using $Mg_{0.25}In_{0.75}$ sensitising layer 77—62020
- Cr, atoms, vapour deposited on polystyrene, core-level spectra 79—56911
- Cr film, AC equivalent circuit anal. 79—51690
- Cr island film nonlinear I-V characteristics, 20 Hz to 15 GHz 79—7910
- Cr island film photoconductivity obs. 78—95392
- Cr island film real structure and electrical conductivity obs. 79—77948
- Cr particles, on reflecting substrate, selective absorpt. of solar energy, model calcs. 79—79405
- Cu, ageing effect on elec. cond. 79—24084
- Cu, aggregated film, optical props., 0.35-1 μm 77—66548
- Cu, diffusion-induced redistribution of atoms between islands during thin film growth 77—89672
- Cu film, 1/f noise and its temp. depend. 79—60939
- Cu film growth on amorphous C, energy characts., in situ electron microscope determ. 79—11027
- Cu, film growth on graphite and amorphous C, electronic struct. by photoemission and Auger obs. 79—77947
- Cu, light absorpt. spectra, dielec. function calcs. 79—51507
- Cu, quench-condensed ultrathin film, two-dimensional elec. cond. 78—39233
- Cu, RF impedance temp. and freq. depend. 77—4453
- Cu, vapour deposited, on polystyrene, surface complex, XPS obs. 78—72026
- Dy, electronic conduction mechanism 79—87169
- Fe discontinuous film, Mossbauer effect exam. of magnetic state 77—24769
- Fe granular deposits, plasma reson., rel. to interstellar dust extinction curve 79—21387
- Fe, granular film, microstructure using X-ray, electron diffr. and TEM 79—65344
- Hg, melting and crystallisation kinetics, electron microscopy 77—15725
- In, discontinuous film, DC resist. in normal and supercond. states 79—56357
- In, film growth on C, conductance meas. 79—82495
- In, island film, melting and crystn. kinetics, dark field electron microscopy 79—11026
- In particles, grown in ultra-high vac. on KCl substrates, struct. and orientation 80—10814
- In submonolayer growth on Si(111)7 surface, superstruct. 79—77930
- In thermal hysteresis of phase transitions and mechanism of crystallisation 77—89679
- Li aggregated deposits, optical props., 1-6 eV 77—66549
- Mo islet films, effect of external elec. field on electron emission 80—80952
- Mo, RF impedance temp. and freq. depend. 77—4453
- Mo, room temp. oxidation rate consts., resist. meas. 77—32723
- Ni film on leucosapphire, island growth as annealing in Ag vapour *(Russian)* 78—51830
- Ni film on W (110), field ion microscope exam. 78—34731
- Ni, granular, tunnelling of spin-polarised electrons and magnetoresist., exchange effects 77—12024
- Ni island film, cond. of two-layer metal systems *(Russian)* 79—51693
- Ni, on pyrolytic graphite, binding 77—59210
- Ni, vapour deposited on polystyrene, core-level spectra 79—56911
- Ni-SiO_2, granular film, hopping cond., magnetoresist. 78—56240
- Pb granular film, Josephson coupled, resistive transition 80—88683
- Pb, quench-condensed ultrathin film, two-dimensional elec. cond. 78—39233
- Pd, chemisorpt. of CO, ultra high vacuum technique 78—71960
- Pd film on W (110), field ion microscope exam. 78—34731
- Pd, on Melinex, resistance-strain behaviour, island struct. effects 77—55621
- Pd, on rocksalt, H_2 absorpt. effects on elec. cond. 77—47905
- Pd particle array, on amorphous SIO_2 substrate, model catalyst, electron microscopy and UPS expts. 79—4899
- Pt, adsorption of alkali halide mols., effect on elec. cond. 80—2487
- Pt, elec. cond. and current noise 78—72286
- Pt film on W (110), field ion microscope exam. 78—34731
- Pt island film photoconductivity obs. 78—95392
- Pt particles supported on SiO_2 gel, reaction between adsorbed H_2 and O_2, low press. 77—52668
- Pt, RF impedance temp. and freq. depend. 77—4453
- Pt small particles deposited on NaCl and mica substrates, struct. and orientation *(French)* 77—43458
- Pt, ultrathin film, elec. cond., amorphous Ge overlayer thickness depend. 78—72284
- Pt-SiO_2 granular sputtered film, size effects in electronic sp. ht. 77—43346
- $(SN)_x$, discontinuous film, DC resist. in normal and supercond. states 79—56357
- Sb, discontinuous thin films, cluster shape models 80—100419
- Sn, aggregate film, resist., temp. depend. 78—39230
- Sn, globular film, interf. and diffr., solar selective props. 79—4860
- Sn globular film, solar selective props., effect of dielec. layer addition 79—4861
- Sn, melting and crystallisation kinetics, electron microscopy 77—15725

discontinuous metallic thin films continued
- Sn, quench-condensed ultrathin film, two-dimensional elec. cond. 78—39233
- Sn, thermal hysteresis of phase transitions and mechanism of crystallisation 77—89679
- Sn thin film, kinetics of agglomeration effects 77—15708
- Sr submonolayers adsorbed on Mo crystal, LEED and contact pot. study 80—2271
- Ti, chemisorption of O_2 and CO, quartz cryst. microbalance obs. of O/Ti and CO/Ti atom ratios 79—4475
- W epitaxy on W(110) substrate, work function meas., LEED investigation 80—80103
- W-Al_2O_3 granular film, percolation conductivity 78—84319
- Zn island films, effect of surface press. on lattice spacings 79—11045

discrete symmetries
- *see also C invariance; CP invariance; CPT invariance; P invariance; parity; T invariance*
- baryons, SU(1,4) dynamical group, anal. of discrete representations, mass formulae 77—45982
- charmed baryons, $\Delta C=\Delta S=1$ nonleptonic decays, amplitude relations 79—54339
- conserved currents and symmetries of the S-matrix 80—9110
- disconnected gauge groups and the global violation of charge conservation 78—78086
- discrete symmetries, natural flavor conservation and weak mixing angles 79—49438
- EM systems, parity and time inversion symmetries 79—67169
- G-parity nonconservation in β-decay of polarised ^{12}B and ^{12}N 77—41920
- gauge model with six quarks, discrete symmetries, Cabibbo universality, flavour mixing angles 78—62346
- Green's function formalism of quantum field theory with broken discrete symm. 77—57436
- integrable system concealed symm. *(Russian)* 80—91016
- quantum field theory, relativistic, discrete symmetries 80—68387
- quaternion model, quark mass matrix, CP violation and Cabbibo angle *(Russian)* 79—40751
- scale symmetry and virial theorem 79—58894
- $Sp(4)\times U(1)$ theory of weak and EM interactions, little groups and discrete symmetry 79—26283
- $SU(2)\times U(1)$ model, quark mass matrix and discrete symmetries 78—54607
- $SU(2)\times U(1)$ six quark model, uniquely determined discrete symmetry 79—93360
- $U_A(1)$ symmetry and flavor mixing, Cabibbo angle and quark mass ratio relation 79—93355
- e/μ mass ratio, extended Weinberg model with heavy leptons, discrete symm. appls. 77—57482
- t-quark mass from discrete symmetries 79—63462

discrete systems
- *see also discrete time systems; sampled data systems*
- conservative discrete-continuous system, free vibration *(Russian)* 80—23950
- discrete-continuous system, vibrations 80—23951
- Markov system, nonstationary, profit accumulation process *(Ukrainian)* 78—89308
- molecular structure models, discrete optimal control 77—61694
- multi-degree-of-freedom systems, discrete, maximax response 79—81712
- periodic systems, optimisation by analytic construction of control 79—21543
- quantum systems control, pure states and mean values 80—22210
- sekeletal muscle dynamics, isometric and isotonic contraction model 78—31807

discrete time systems
- *see also sampled data systems*
- blood pressure automated control in dogs using microprocessor 80—81797
- cancer cell cycle kinetics, flow microfluorometric DNA distribution representation 77—21669
- Doppler frequency meter for blood flow imaging 79—57704
- Fourier transform systems, discrete-time windows, optimum low-order 77—5631
- neural net discrete-time model and applications *(Russian)* 79—2020
- nonlinear field eqns., time discretisation and mixed finite element methods 79—40384
- pollution control, air, optimal timings and number of observations determ., w.r.t. cost 79—88026
- satellite onboard feature classification by CCD analogue signal processing 77—70980
- three dimensional rotation system, probability density function representation 77—17782
- ^{133}Xe washout curve discriminant analysis for lower extremity vascular impairment 78—35949

discriminators
- *see also demodulators*
- acoustic emission, automatic threshold discrimator *(French)* 80—23851
- amplifier-discriminator for magnetostriction spark chambers 78—868
- avalanche transistor discriminator for low energy radiations 80—5450
- brain unit and slow-wave field activity, telemetry with FM pulse subcarrier 77—25625
- composite amplifier-discriminator cct., RMS noise meas. 77—54473
- constant fraction 100 MHz discriminator using hybrid microcircuit technology 78—33402
- DC coupled discriminator with continuously variable width, fast switching characts. 77—6643
- digital frequency-offset lock system designed for use with stabilised lasers 78—29960
- direct meas. of β absorbed dose rate by discriminator and filter *(Japanese)* 78—74511
- double sample-and-hold circuit for deep-level trap spectroscopy 77—87789
- edge reflection SAW absorber, FM discriminator appls. 78—1517
- gamma-ray spectra reduction via desk-top calculator, insignificant peak rejection 77—53870
- gated constant-fraction discriminator for use with fast-focused photomultiplier tubes 78—58063
- high-speed broadband amplitude discriminator that does not change pulse duration 79—26842
- high-speed preamplifier discriminator for high accuracy pulse counting 77—401

discriminators continued
high-speed pulse shaper/discriminator for scintillation and Cherenkov counters 78—86748
integrated window discriminator TCA965 used to control LED temp. display 77—128
lightning ground-flash multiple-stroke discriminator cct. 78—81446
microprocessor based telemetry demodulation system 79—20738
mixed n-γ field portable scintillation spectrometer with pulse shape discrimination 77—77992
multimode optical fibre phase modulators and discriminators, theory 78—55446
multimode optical fibre phase modulators and discriminators, expts. 78—55449
multiunit spike train sampling control by peak discriminator 79—34717
neural spike window discriminator confirmation by analogue delay cct. 77—21664
neuronal spike activity discriminator 77—48966
optical Doppler frequency discriminator applic. in laser velocimeter 78—26220
optical fibre delay line phase discriminator, operating principles 79—18507
optical interference discriminator, for laser freq. stabilisation, optimisation 79—31962
peak-detecting window discriminator for neuronal spikes 77—60323
phase-locked loop, five channels, automatic meas. of whistler dispersion *(Japanese)* 80—31143
photon count cct. using high-speed comparator 78—77979
photon counting appl., system components evaluation 78—21215
PLL, appl. to meas. of occurrence rate of whistlers during geomagnetic magnetospheric storms 80—12621
PLL for automatic observation of whistlers 78—89014
precision integral linearity measurement instruments for nuclear spectroscopy 77—67951
pulse counter, high-speed DC coupled, sensitivity and performance 79—89524
pulse counting measurement systems, optimum parameters determ. 79—89523
pulse-width discriminator for multilayer scintillators 80—27883
reflecting interferometer design with predetermined characteristics *(Russian)* 79—93206
stabilized differential discriminator with automatic threshold control 79—26841
ten-channel differential discriminator for radiation detection spectra 78—78593
time clamping to nuclear particle detector signals, discriminator employing ICs 79—3323
time-amplitude window discriminator, multi-unit neuronal spike train separation appl. 77—86726
US, automatic noise-blanking, pulse-timing discriminator for production inspection of parts 80—76472
X-ray astronomy, risetime discrimination appl. to pressurised Xe gas proportional counter for hard X-ray detect. *(Japanese)* 79—80219
X-ray proportional counter background reduction by leading-edge discriminator 78—78561
zero crossing discrimination technique for constant fraction timing 79—76308
^{10}B-loaded liquid scintillator with pulse-shape discrimination 79—59309
^{6}Li-loaded liquid scintillators with pulse-shaped discrimination 79—59310

disinclinations *see disclinations*

disintegration (radioactive) *see radioactivity*

disintegration energies *see radioactivity*

dislocation anchoring *see dislocation pinning*

dislocation arrays
anisotropic media, stress fields of dislocation arrays *(German)* 79—23615
bicrystal, dislocation arrays at interfaces, stress fields 79—99432
α-brass, fatigue crack propag., role of dislocation substruct. 80—60963
coherent motion, lattice dynamics 78—71738
computer study 78—30617
continuum model of dislocation core 77—76399
crack dislocation model 80—69741
cracks, discrete dislocation analysis 80—84236
creep, ratio of cell diameter to dislocation spacing 77—24348
edge dislocation interactions in infinite array, elastic energy 78—55871
elastic energy of slightly incoherent twins 77—72616
elastic field of dislocation networks and grain boundaries 79—60362
electron dynamical diffraction from periodic arrays of dislocations 78—83669
equilibrium configuration by computer simulation 78—30616
finite solid, dislocations, disclinations and grain boundaries 80—2019
finite-two phase bodies, response to internal and external stresses, numerical considerations 80—24742
grain boundary dislocations, effects on grain boundary processes of the steps in boundary plane 80—79785
III-V heterojunctions, misfit dislocation banding, stress-induced birefr. 77—28542
impurity crystal, microstructural plastic instability *(Russian)* 79—99190
Incoloy 901, foil prep. for TEM exam. 80—88001
non-hardening material, under plane strain, rel. to stress distrib. around crack tip 80—10189
plate, elastic, under uniform twisting, periodic collinear cracks *(Japanese)* 78—67097
point defects, stress induced absorpt. and emission by grain boundaries 80—39081
polycrystalline solids, radiographic determ. of dispersion of disordered and ordered dislocation distribs. 77—51373
polyethylene, crysts., subject to fold-surface tensile stress, elastic deform. 78—76712
α-quartz, synthetic, growth, defects induced by seed orientation 80—96454
sapphire ribbon crysts., grown by edge-defined film-fed growth technique, X-ray topography study of dislocations 79—4305
smei-infinite solid, edge dislocation behaviour with surface energy effects 79—55743
solid, finite stressed, surface dislocation model 79—73247
steel, austenite/ferrite interface, struct. and diffr. effects, TEM exam. 80—16308
steel, low alloy, 10KhN1M, heat treated, effect of holding temp. on characts. of dislocation arrays 79—15788

dislocation arrays continued
steel, Ni, struct. change of hot-worked austenite during post-deform. holding 80—35228
stress field computation method, appl. to X-ray diffr. anal. 78—30624
stress-free motion of dislocation arrays 79—65083
surface dislocation model, Z-phase interface boundary problem 80—39085
Al, compressed, nucleation and recrystallisation study by electron microscopy and Kikuchi diffr. 79—52236
Al, surface deformation and wear track obs. using analytical electron microscope 80—108687
Al-Mg, grain boundary dislocation identification, TEM obs. 77—62534
Au film bicrystal, grain boundary dislocations in plane matching boundaries 80—39110
Au, serration and dissociation of edge dislocations in low-angle tilt boundaries 77—72621
Cd, Cottrell-Stokes law, 4.2 to 300K, forest dislocations and other obstacles 77—43269
Cu, epitaxial, on (111) Au, periodic arrays of misfit dislocations, electron diffr. 78—51857
Cu, fatigue crack propag., role of dislocation substruct. 80—60963
Cu, HVEM determ. of true segment length and interforest spacings of recovered dislocation arrays 78—30631
Cu, shock loaded, work hardening and press. depend. of dislocation arrangement and density 78—48429
Cu, single crystals, neutron irradiated, stresses and secondary slip between overlapping and dislocation arrays 80—88162
Cu-Al (10.5 at.%), dislocation generation and displacement in single crystal in bending 79—60368
Cu-Al-Ni (14.5, 3 wt.%), fatigued, polycrystn., pseudoelastic, dislocation and martensite substructs. 79—82223
Cu-Ni bimetallic films, dislocation wall form. during interdiffusion, TEM obs. 78—51856
Cu-Ni-Al (5, 2.5 at.%), precip. hardening *(Japanese)* 80—71663
Cu-Si alloy, rel. to correl. of periodicities in diffr. patterns and images from grain boundary 78—14362
Fe, epitaxial growth on Au platelets, dislocations 80—96760
Fe, FCC, grain boundary struct. and energy, computer expt. 78—30643
Fe whisker crystals, domain walls, interaction with dislocation bundle, X-ray topography obs. 79—87282
Fe-Au (111) bicrystal films, misfit dislocations obs., for 500°C substrate temp. 77—51624
Fe-C-Si (0.62, 2.0 wt.%), interfacial struct. of broad faces of ferrite plates 79—46660
Ga$_{1-x}$Al$_x$As DH catastrophically degraded laser, TEM obs. of defects 80—32989
GaAs, (100) surface, etch pit density meas. using automatic struct. analyser EPIQUANT *(German)* 77—62619
GaAs-GaAlAs, DH laser material, rapid optical degradation 77—7083
GaAs-GaAlAs LPE layers, DH material, TEM obs. of crystal defects 78—6241
GaAsP epitaxial film, TEM obs. of misfit dislocation arrays, nucleation and multiplication 77—39742
GaAs$_x$Sb$_{1-x}$, epitaxial layer, struct. defects rel. to luminesc. 78—72040
Ge, amorphous, struct., dislocation model 78—42911
Ge single crystals, constitutional supercooling growth conditions, structural and chem. inhomogeneities 80—93473
InP/In$_{1-x}$Ga$_x$As$_y$P$_{1-y}$ heterostruct., optically induced degradation 79—86791
Mg, pure and dil. alloys, electron lifetime anisotropy, Dingle temp. due to dislocation scatt. 79—78082
MgO, etchant for revealing dislocations in (100) surface 79—19252
MgO, tensile creep of single crystals, substruct. effect 79—66113
Mo, block boundary dislocation struct. singularities under high temp. steady state creep conditions *(Russian)* 79—90670
Mo, ion bombardment by Ni^{2+}, TEM study of damage depth distrib. 78—10101
NaCl, plastically deformed [001] orientated single crystal, glide props. and X-ray topography 77—21228
Nb, dislocation substruct. in deformed and recovered single crystal 77—8897
Nb single crystals, growth by pulling from a melt on a pedestal, charact. arrangement of dislocations 79—4911
Ni, shock loaded, work hardening and press. depend. of dislocation arrangement and density 78—48429
NiAl-Cr, eutectic, directionally solidified, temp. behaviour of misfit dislocations *(German)* 78—3119
NiO, single crysts., annealed, dislocation arrays in low angle tilt boundaries, TEM study 79—37707
PbFe$_{12}$O$_{19}$, dislocation etch pit morphology study *(Chinese)* 80—88150
Pd, epitaxial, on (111) Au, periodic arrays of misfit dislocations, electron diffr. 78—51857
Si, dislocation motion from indentation rosette 80—79798
n-Si films on sapphire, crystalline defects effect on elec. props. 77—20470
Si:P, emitter-misfit dislocation formation during P diffusion 78—91338
Si:P, thermally annealed, high dose, ion-implanted, dislocation array prevention by prior laser annealing 79—73187
Sn, single crystal, dislocation walls consisting of double arrays 79—46664
Sn, white, elastic stiffness consts. calc. 78—39825
Ta, rolled single crystal, recovery and recrystallization 80—3093
Ta-N, domain configurations of new phase *(French)* 78—56648
W, block boundary dislocation struct. singularities under high temp. steady state creep conditions *(Russian)* 79—90670
WC grain, with grown-in stacking fault, contrast effects in electron micrographs 77—19959
Zn, Cottrell-Stokes law, 4.2 to 300K, forest dislocations and other obstacles 77—43269

dislocation breakaway, pinned *see dislocation damping*

dislocation climb
anelastic creep, contrib. of climb rate of dislocation links and config. 77—52431
carburized single crystal sheets, lattice strain during interstitial diffusion *(Japanese)* 78—10220
ceramic, creep, porosity depend. 80—97530
ceramic oxide, TEM study of deform., review 79—87686
coherency loss in modulated structures, approx. criterion 77—48391
creep, irrad. induced in transient irrad. environments 80—92598
creep, irradiation induced, dislocation glide enabled by preferred absorption of point defects 80—88250

dislocation climb continued
- creep, steady state, climb controlled, at high and intermediate temps., theoretical description 79—95074
- creep, swelling and growth, radiation induced, bias factors estimated from self-consistent model 80—88249
- creep, transition between dislocation and diffusion 80—88253
- creep and growth, radiation induced, fundamental mechanisms 80—92596
- dispersion hardened alloy, calc. of back stress decrease, due to Orowan dislocation loop climb 78—83812
- dispersion-hardened single crystals, theory of high-temp. strength 77—48445
- dispersion-strengthened alloys, threshold stress for creep 80—93626
- double jog side-motion, elastic theory 80—84171
- driving force and climbing force on dislocations 78—43017
- edge dislocation, climb rate and core diffusion 80—10553
- edge dislocation climb, numerical anal. 78—71736
- edge dislocation climb processes in high temp. recovery-creep 77—19965
- edge dislocation motion, glide and climb resist. due to dragging a Cottrell atm. 79—99194
- elasto-diffusive solids, singularity movement, appl. to fracture propag. 78—30235
- faulted dislocation loops induced by elastic interaction, climbing motion 80—75227
- FCC material, irradiation induced creep, climb induced glide model 80—89292
- grain boundaries, absorption of dislocations 77—80538
- grain boundary dislocation model, relative rotation of unconstrained polycrystals 77—27896
- grain boundary dislocations, effects on grain boundary processes of the steps in boundary plane 80—79785
- grain boundary sliding, containing particles, during diffusional creep, dislocation bowing 79—37712
- high temp. cracks, discrete dislocation anal. 78—48514
- III-V crystals, thermally enhanced diffusion of point defects near dislocations during device operation 79—90820
- III-V semiconductor, point defects and dislocation climb 79—82209
- incubation period following stress reduction during creep 79—7603
- intrinsic point defect-impurity atom mobile complex form., influence on defect diffusive fluxes 80—2063
- irradiation creep, climb-enabled glide of dislocations resulting from preferred absorpt. of point defects 79—82280
- irradiation creep due to dislocation and glide 77—69009
- irradiation creep due to stress induced preferred absorption of point defects, anisotropic dislocation struct. effects 79—42140
- irradiation creep mechanisms, theoretical assessment 79—55817
- metal, creep, point defects 78—48462
- metal, FCC, climb model of extended dislocations 78—6059
- metal, recovered dislocation substructure, prod. and utility, review 77—84749
- metals, submicroscopic defects, influence on HVEM in-situ expts. 80—103392
- misfit dislocations, Volterra-type model and relax. of nonequilibrium arrangements 80—2020
- modulated structures, dislocation climb under irradiation conditions 80—70195
- neutron damage simulation, using HVEM, state-of-the-art 77—51417
- neutron irradiation, precipitation of point defects near grown-in dislocations 78—26600
- Nimonic 90, dispersion hardened, friction stress rel. to initial and secondary creep 80—11711
- olivine, hardness var. with temp., rel. to polycryst. yield stress 80—26500
- olivine, plastic flow of oriented single crystals, mech. data 78—36155
- oxides, dislocation climb model 80—100230
- oxides, plastic deform., TEM obs. *(French)* 77—44304
- Peierls-Nabarro model, screw dislocation with nonplanar core 77—1126
- point defects, stress induced absorpt. and emission by grain boundaries 80—39081
- quartzite, deformation in Earth crust, dislocation climb mechanism 79—60425
- recovery-creep, steady state, in pure materials, model 77—75815
- recrystallisation nucleation, model for strain induced grain boundary migration 79—46675
- repeated precipitation on edge dislocations, micromechanisms 78—95752
- sapphire, white, three-point bending test, dislocation climb *(Japanese)* 79—96104
- semiconductor, recomb.-enhanced defect reactions 77—51377
- semiconductor, tetrahedrally coordinated, dislocation struct. 79—82206
- semiconductor, zincblende struct., dislocation climb model, appl. to degradation of lasers and LED's 77—1125
- slip band theory, model for creep based on dislocation climb at grain boundaries 79—37756
- spinels, mass transport by dislocation climb 79—32996
- steady state dislocation motion via mol. dynamics 78—10049
- steel, austenitic stainless, interaction of grain boundary dislocations with precipitates during high temperature creep 80—16384
- steel, austenitic stainless, V alloyed, creep mechanism 77—36591
- steel, austenitic stainless, V alloyed, creep mechanism 77—48514
- steel, cold-rolled, recovery of lattice defects in cementite 77—90370
- steel, low C, tempered, lath martensite, Ni (5 wt.%), microstruct./yield strength relationship 77—21234
- steel, stainless 316, creep under high stress 78—52892
- steel austenitic stainless, Cr-Ni 316 type, electron irradiated, void swelling 79—42104
- stress induced dislocation climb, stress and irradiation induced mass transport, anal. soln. 79—60401
- superplastic flow in two-phase mats., role of interphase-boundary dislocations, ledges and diffusion 78—11295
- two phase polycrystals, grain size stability and switching, dislocation climb and glide, computer model 78—75715
- Zircaloy-2, electron irradiation damage, direct obs. 80—84212
- Zircaloy-4 cladding, steady-state creep, 940 to 1873K 79—15759
- Ag, polygonisation, impurity effects rel. to stacking fault energy 77—63685
- Ag, surfaces, dislocation climbing, etch pit investig. 79—19260
- Al and Al-Mg alloys, thermal generation of vacancies involving dislocation climb 77—59808
- Al, creep behaviour, at high temp., influence of oxidation 80—97538
- Al, internal friction, dislocation glide and jog climbing *(French)* 78—11261

dislocation climb continued
- Al-Cu (96.5, 3.5 wt.%), characts. of disappearance of excess vacancies on dislocations 80—33991
- Al-Mg, creep behaviour in broad stress interval at 623K 80—30044
- Al-Mg (2 wt.%) subgrain formation at low stresses 78—84928
- Al-Si crystals, work hardened, softening and creep rates on annealing 80—11663
- Al-Zn solid soln., controlling creep mechanisms, role of diffusion 78—31469
- Al-Zn solid soln., controlling creep mechanisms role of diffusion 78—31470
- $Al_xGa_{1-x}As$, point defects, recomb. enhanced interactions with dislocation networks 79—60398
- Al_2O_3:MgO, diffusion creep examined under three-point bending *(Japanese)* 79—96104
- $(Al_2O_3)_nMgO$, n=1.1, high temp. creep, dislocation behaviour 78—80593
- $(Al_2O_3)_nMgO$, spinel composition, dislocation climb, mass transport 79—32996
- CoO, polycrystalline, high temp. deform. 78—3174
- CoO, single crystal and polycryst., subgrain boundary form. and creep mechanism 77—39594
- Cu alloys, FCC, climb of extended dislocations due to irradiation in HVEM 80—103343
- Cu, polygonisation, impurity effects, rel. to stacking fault energy 77—63685
- Cu single crystals, climb rate of Orowan loop anal. by dislocation pipe diffusion 79—83211
- Cu-Al, dislocations, dissociated, climb mechanism, nucleated loops, Burgers vectors 80—65002
- Cu-Al (10, 16 at.%), influence of jogs on extension of dislocation nodes 80—84176
- Cu-Al alloy, irrad. in HVEM, climb of dissociated dislocations and point defect absorpt. 80—107257
- Cu-Ni alloys, chemical interdiffusion under uniaxial stress 80—65307
- Cu-Ni alloys, dislocation climb sources activated by 1 MeV electron irradiation 77—89443
- Cu-Si (7 at.%), influence of jogs on extension of dislocation nodes 80—84176
- GaAlAs-GaAs DH lasers, degradation caused by growth of dislocation networks 80—53289
- $Ga_{1-x}Al_xAs$, point defects and dislocation climb, interaction with deep level donor 79—82209
- $Ga_{1-x}Al_xAs$-GaAs laser, degradation, appl. of dislocation climb model 77—1125
- GaAs degraded lasers, climb asymmetry, TEM obs. 80—79802
- GaAs heterojunction laser, origin of dislocation climb during laser operation 77—51380
- GaAs laser material, secondary dislocation climb during optical excitation 78—75672
- GaAs, point defect generation by electron-hole recombination at dislocations 79—37699
- GaAs-$Al_xGa_{1-x}As$ double heterojunctions, dark-line defects and recomb. centres, scanning photocurrent microscopy 79—35822
- GaAs-GaAlAs DH laser material, secondary dislocation climb in optical degradation 78—17935
- GaAs-GaAlAs DH lasers, optical studies of defects and degradation 78—18654
- GaAs-GaAlAs DH material, dislocation glide and climb, electron diffr. 78—83824
- GaAs(-GaP) single cryst., defect distrib. near abraded surface 80—92533
- GaP, green LED, degradation, appl. of dislocation climb model 77—1125
- GaP single cryst., defect distrib. near abraded surface 80—92533
- $Gd_3Ga_5O_{12}$, decorated dislocations, large interstitial climb loops round precip. particles 77—19960
- $Gd_3Ga_5O_{12}$, precipitates assoc. with dislocation climb trails *(German)* 77—35567
- $Gd_3Ga_5O_{12}$, single cryst., helical dislocation obs. by etching 77—11558
- Ge, dissociated dislocations, constriction correlation with jogs 80—79801
- ^3He, BCC, plastic flow 79—46880
- KBr, single cryst., high-temp. creep, rel. to pipe diffusion, dislocation climb 77—11626
- Mg-Al spinel, non-stoichiometric, climb dissociation of network dislocations 80—2031
- $MgAl_2O_4$, dislocations, sessile dissoc. 79—46663
- MgO, climb of $a\langle100\rangle$ dislocations, TEM obs. 78—71741
- MgO, compressive stress-strain behaviour at high temps. 80—25774
- MgO, single cryst., tensile creep, stress induced dislocation structs. 80—96539
- MgO.1.1 Al_2O_3 spinel, high temp. deform., cryst. orientation effect 80—107263
- NaCl, plastic deformation influence on shape recovery effects 80—6684
- NbC single cryst., Vickers microhardness, slip mechanism 80—71732
- Ni and Ni-Co, recovery of single crystal after varying amounts of cold work 79—100162
- Ni base superalloy, single crystal, apparent and effective creep parameters, incubation period 77—63715
- Ni, creep, irrad. induced with 17 MeV deuterons 80—93607
- Ni, thermal softening, influence of alternating mag. field *(Russian)* 78—23312
- Ni, transient irrad.-induced creep under D bombardment, mechanism 78—80597
- Ni-Al, solid soln. and solid soln. hardened, stead state creep 78—27578
- Ni-Al (6.2 wt.%), high temp. creep *(Czech)* 77—63727
- Ni-Cr-ThO_2 (20, 2 wt.%), dispersion hardened, model for high temp. deform. based on struct. obs. 78—19809
- β'-NiAl, dislocation climb, hot stage TEM 77—24318
- γ'-Ni_3Al-Fe (10 at.%) alloy, steady-state creep 78—15460
- NiO, polycrystalline, high temp. deform. 78—3174
- NiO, single crysts., annealed, dislocation arrays in low angle tilt boundaries, TEM study 79—37707
- $Ni_{0.5}Zn_{0.5}Fe_2O_4$ coarse grain polycryst. ferrite, diffusional creep *(Japanese)* 80—104238
- Pb, film, hillock formation by grain boundary sliding 80—107673
- Sb, electron microscope irradiation effects, agglomeration of point defects, dislocation climb and loops *(French)* 80—59518
- Si, diffusion of ^{71}Ge and ^{32}P, effect of dislocation struct. on migration rate 77—51551
- Si, dislocation free, O_2 precipitation, stacking fault form. 78—38731
- Si, epitaxial wafer, saucer pit microdefects reduction by intrinsic gettering 80—75450
- Si, single crystals, dynamical recovery and self-diffusion 78—87816

dislocation climb continued
Si:As, ion implanted, laser annealed, lattice defects, epitaxial regrowth 80—103334
Si:B, implanted, shrinkage of rod shaped defects 78—6061
Si:B, ion-implanted, dislocation climb, TEM obs. 78—6062
Si:Cu, interaction between vacancy emitting absorbing precipitates and dislocations, TEM obs. 78—71755
Si:P bipolar transistors, interstitial supersaturation and misfit dislocation climb, TEM study 80—70203
Si:P(B), high temp. impurity diffusion via vacancies and self-interstitials 80—24667
(U,Pu)O_2, thermal creep in 40 to 100 N/mm^2 stress range 77—28881
UO_2, config. and climb rate of dislocation links, contrib. to anelastic creep 77—52431
UO_2, thermal creep in 40 to 100 N/mm^2 stress range 77—28881
V, substrct. changes during creep dislocation density *(Russian)* 78—23782
VC single cryst., Vickers microhardness, slip mechanism 80—71732
V_3Si single cryst., creep deform. 80—71695
YIG, deformed at high temp., subgrain boundaries and dissociations of dislocations, TEM obs. 79—90658
Y_2O_3, dislocation and plasticity dissociation 80—107247
Y_2O_3, electron irrad., dislocations *(French)* 80—2076
Zn bicrystals, ⟨10$\bar{1}$0⟩ tilt, misorientation depend. of grain boundary sliding 80—15119
Zn, creep in temp. range of dynamic recovery *(Russian)* 77—81294
Zn, vacancy conc., lattice parameters meas. 78—10040
ZnSe, electron irrad., dislocation climb, TEM obs. 79—1461
Zr alloys, creep and growth, irradiation induced, microstruct. depend. 80—93602
Zr, electron irradiation damage, direct obs. 80—84212
Zr-Nb (2.5 wt.%), annealed, irradiation growth at 353K 79—46710
Zr-Sn(Fe)(Ni) (0.15 wt.%), electron irradiation damage, direct obs. 80—84212

dislocation damping
see also Bordoni effect
amorphous film-crystalline substrate, relaxation process dislocation misfit theory *(Russian)* 80—39461
crystal with impurities, dislocation internal friction *(Russian)* 77—73297
diffusion along dislocations, effect on linear stress, internal friction *(Russian)* 77—80505
dislocation damping during electron irradiation, new model for peaking effect 78—87683
ferromagnet, pinned domain wall motion, magnetic damping studies 80—65956
ferromagnetic crystal, magnetic damping due to pinned domain wall motion 79—56598
Granato-Lucke model, fitting of expt. data 77—43213
Kolsky bar technique, use for dislocation damping evaluation 80—54251
loop-length distribution and frequency-dependent damping form for small impurity concs. 80—49232
metals, Snoek-Koster relaxation, theory 80—16369
misfit dislocations, Volterra-type model and relax. of nonequilibrium arrangements 80—2020
quartz, dislocations rel. to strain amplitude depend. of internal friction 77—27939
steel, austenitic, creep, low-temp., during dynamic relaxation, effect of dislocation struct. *(Russian)* 77—25103
steel, maraging, Cr-Ni-Ti, effect of Ti addition on hardness and energy scatt. 79—15687
stress wave dislocation damping, strain-amplitude depend., KGL String model 77—4101
Ta, single crystals, microyielding, high amplitude damping 77—52396
unified theory, point defect dragging 80—88144
Al, creep, low-temp., during dynamic relaxation, effect of dislocation *(Russian)* 77—25103
Al, internal friction, strain amplitude dependent damping at 8.3×10^{-3} Hz 77—1172
Al, internal friction, strain amplitude dependent, hydrostatic press. effect 77—77520
Al, strain-amplitude-depend. damping at very low freq. 77—1172
Al-Mg, plastic deform., separation of internal friction components *(Russian)* 79—52282
Au, work hardened, Hasiguti peaks, spectrum and recovery, impurity effects *(French)* 77—66670
Be, internal friction, temperature spectrum and dislocation damping, anelastic relaxation *(Russian)* 80—2118
C, heat-treatment and neutron irrad. effects on US atten. and Young's modulus 79—11644
Cd, internal friction, cryst. orientation depend. *(Russian)* 77—7730
Cu, creep, low-temp., during dynamic relaxation, effect of dislocation struct. *(Russian)* 77—25103
Cu, dil. alloy, dislocation inertial effects in plastic deform., internal friction meas. 77—36609
Cu, dislocation damping during electron irrad. 77—76462
Cu, dislocation damping strain amplitude depend. on 1 MeV electron irrad. and quenching 79—95023
Cu, electron-irradiation internal friction behaviour, shear modulus and damping meas. 80—55444
Cu, HF ultrasound, viscous and relax. components of dislocation attenuation 80—15196
Cu, low temp., internal friction and microplastic strain 77—84839
Cu-Au, (0.02-5 at.%), cold worked, internal friction peaks 79—11652
Fe, internal friction near Curie point 79—24567
Fe, magnetic disaccommodation, low temp. in neutron-irrad. sample, Bordoni relax. 77—4542
α-Fe, plastically deformed and/or irrad., high purity, internal friction peaks due to dislocation relax. 77—86075
Fe, pure, deformed, internal friction, dislocation relax. and dislocation-defect interactions 79—29125
Fe-Al(Ti), O containing, mag. aftereffect and disaccommodation meas., time depend., activation energy, and ageing props. 80—88836
Fe-Ti (0.056 at.%), stress relaxation curves, anal. interpretation 77—59847
Ge single crysts., US absorption investigation *(Russian)* 77—62589
Ge, US absorpt., correl. between orientational factors and damping coeffs. 79—69197
^{4}He, HCP, dislocation damping, MHz sound freq. depend. attenuation 77—72739
^{4}He HCP crystals, US attenuation, dislocation damping 80—24711

dislocation damping continued
^{4}He, solid, pure and with ^{3}He admixtures, effect of plastic deform. and impurities on internal friction *(Russian)* 79—77860
KCL, US attenuation, dislocation damping 77—1181
KCl, strained single crysts., dislocation damping of ultrasound 77—1181
(La,Gd)Al_2, normal and supercond. state, US attenuation, freq. depend. and mechanisms 80—49992
LiF, shock wave, precursor decay, stress threshold 77—4156
LiF, US attenuation, 4.2 to 300K 77—47513
Mg, internal friction, cryst. orientation depend. *(Russian)* 77—7730
NaCl, changes in internal friction and discharge following plastic deform. 79—99191
NaCl, interrupted neutron irrad. expts. involving dislocations 79—99208
NaCl, reduction of dislocation density during isothermal annealing *(Russian)* 79—4303
NaCl, spiral dislocation mobility depend. on elec. field, relaxation time 80—39105
Nb, cold-worked, Snoek-Koster relaxation transient period, comparison with Schoeck's theory 79—34086
Nb, dislocation damping, amplitude depend. 80—59469
Nb, high purity, dislocation relaxation by internal friction meas. over wide freq. range 79—38876
Nb, plastically deformed, hydrostatic pressure effect on dislocation relaxation, US exam. 78—76696
Ni, cold-worked, rel. between dislocation and ferromag. damping 80—107369
Pb, dil. alloy, dislocation inertial effects in plastic deform., internal friction meas. 77—36609
Pb, superconducting and normal, electronic damping of dislocation, US meas. 79—27997
Sb, dislocation internal friction changes due to high-amplitude US oscills. *(Russian)* 80—10556
Sn crystal, white, time-dependent internal friction 80—7610
Sn, US attenuation and dislocation damping 79—95086
YIG, phonon viscosity effect on dislocation motion 80—24450
Zn, pyramidal edge and screw dislocation mobility, obs. by compressional stress pulse technique 77—19957

dislocation density
adamantane, rel. to variability of cryst. growth from vapour under const. conditions 78—34452
alkali halide, deformed single cryst., dislocation struct. formation *(Russian)* 77—7733
alkali halide crystals, defect state change during electrolysis 78—95057
alkyl ammonium copper chloride, dislocation density from low temp. lattice cond. 77—4227
anthracene, dislocations effect on elec. props. 77—35947
austenite formation, dislocation density effects, α→γ transform. temp. *(Russian)* 77—8813
brittle crack, plane, crit. size *(Russian)* 77—44329
brittle crystal grown from melt residual stress rel. to dislocation density 78—2042
brittle-plastic phase transform. 77—11630
collective behaviour, velocity of slip band and mobile dislocation densities, HVEM study *(French)* 80—65006
continuous distributed dislocations, transport eqns. *(Russian)* 79—32997
β-copper phthalocyanine, dislocation detection *(German)* 78—63773
corundum, growth of large crystals of high opt. quality 77—34916
corundum, shaped crystal, grown from melt, struct. perfection 78—3021
corundum single crystals, stress relax., cracking during growth 78—47263
crack tips, blunting during conc. plastic flow *(Russian)* 78—7013
crystal growth, physical vapour transport method for low dislocation density crysts. 78—43992
crystal growth from melt, stress form., dislocation density estimation *(German)* 80—15022
crystals with dislocations, phase transitions of the second kind, dislocation superparamagnetism *(Russian)* 80—1957
defect dynamics, closure of governing eqns., plastic state theory 79—37702
deformation conditions and initial defect struct. effects on dislocation multiplication 78—30614
delayed cracking by H_2 gathering simulations at plastically deformed notch, finite element anal. 78—31539
diamond, ultradisperse, obtained by high temp. synthesis in explosion, struct. 79—29003
dielectric, thermal mechanism of plastic deformation and fracture by laser beam 77—11553
discrete obstacle model, dislocation and stress field distrib. 80—79794
dislocation wall form. in contact with surface active melt, stacking fault energy *(Russian)* 77—72626
dynamic recrystallisation model *(German)* 77—4792
elastic-viscoplastic materials, dislocation densities as hardening parameters 78—46895
elastoplastic body, tensor dislocation density near crack vertex 78—26090
eutectic alloy, yield point analysis 77—8875
film/substrate, two-layer structs., relaxation of internal stresses 80—34341
film/substrate interface, misfit dislocation obs. using electron microscopy 80—103605
fracture, appl. of continuum theory of dislocations fracture mechanics 78—67767
fusion reactor first wall material, mobile He inclusion in void swelling rate theory model 80—34069
gauge transformations admitted by the equations of defect dynamics 79—27981
grain boundaries during superplastic deform., dislocation density and diffusion parameters 79—65099
grain boundary sliding model 80—75237
grain boundary structure, differential geometry 80—54253
graphite, fast neutron irrad. damage theory and modifications 77—67805
Hastelloy C-4, loaded at high temp., useful life 80—40523
heteroepitaxial structures, misfit, strain and dislocations, book contrib. 79—82499
heterojunction devices, double and triple layer, density of misfit dislocations 78—51850
ice, Antarctic deep core, X-ray diffr. topographic studies 78—63803
III-V epitaxial layers, minority carrier lifetime, correl. with defect props. 77—89835
III-V semiconductor, epitaxial layers, dislocations nature, origin and effects 79—28232

dislocation density continued

- n-InSb, acceptor effect of plastic bending 80—6885
- Invar N36 melt, cast metal struct. depend. on heat treatment, subgrain struct. *(Russian)* 80—40343
- irradiation effects, low dose, void incubation, rate theory approach 79—77635
- isotropic polycrystalline plasticity, dislocation theory 79—14875
- Kapitza conductance, dislocation depend. near acoustic mismatch 79—33172
- limiting value, theory 77—27882
- low-angle grain boundary dislocations, periodic clustering, TEM 79—46681
- macroscopic inclusion motion due to field of struct. inhomogeneity 77—89569
- magnetic 90° domain wall-dislocation tangle interaction, magnetomechanical damping expts. 79—78496
- martensite, rel. to struct. transforms. during deform. *(Russian)* 77—16606
- melting, dislocation model, appl. to FCC cryst. 78—26658
- melting, dislocation model 78—26657
- metal, cold worked, grain size depend. of dislocation density 79—7614
- metal, damping capacity rel. to struct. defects *(Russian)* 77—44283
- metal, dislocation density, positron annihilation method 77—85834
- metal, dislocation dynamics study by current noise measurements 79—14813
- metal, FCC, dislocation behaviour at high strain rates, US detection method, data analysis basis 80—85136
- metal, FCC or BCC, dislocation annihilation during tensile and cyclic deform. and limits of dislocation densities 80—34007
- metal, near surface microstructure effect, on wear 78—64730
- metal, plastic deformation under pulse action 77—76486
- metal, volume changes under plastic deform. *(Czech)* 77—63729
- metal film bonded to rigid substrate, yield stress 79—99463
- metals, BCC and FCC, dislocation dynamics method appl. to plastic flow 79—47745
- metals, dislocations and shock compression, thermodynamics 80—100235
- metals, point defect and microstruct. behaviour during irrad., appl. to fusion reactors 79—23638
- metals, work-hardening, dislocation multiplication model 79—61608
- metals irradiated general rate theory model of void swelling 79—23655
- $(Mg_{0.88}Fe_{0.12})_2SiO_4$, natural peridot, shock-prod. olivine glass, TEM 78—10178
- minerals, dislocations and shock compression, thermodynamics 80—100235
- mobile dislocation density determ. from sound velocity 79—19258
- mobile dislocations, dynamics during strain rate changes *(German)* 78—18655
- mobile dislocations, theory 79—7604
- monocrystal surface layer damage depend. on abrasive working parameters *(Russian)* 80—76368
- MOS structure, surface charge, effect of process induced defects in Si 78—72274
- Nimonic alloy PE-16, irradiated, numerical simulation of void nucleation, dislocation densities, pt. defect conc. 79—73208
- nonstationary temperature field, dislocation struct. dynamics *(Russian)* 77—27884
- nuclear reactor fuel transient heating conditions, mobility of fission gas bubbles 79—59189
- nucleation, criterion for dynamic recrystallisation during hot working 78—52852
- obstacle strength determ. in solid soln. 78—68704
- olivine, naturally deformed, recovery process, rel. to Earth upper mantle mech. state 78—96202
- oxide single crystals, Czochralski grown, thermoelastic stresses 78—55822
- phthalic anhydride, single crystals growth and perfection 79—78869
- plastic deformation, partial disclination dipole motion 79—73165
- plastic deformation and grain size, rel. to dislocation density *(Russian)* 78—22715
- plastic deformation instability, effects of physical parameters 79—47758
- plastic deformation theory, thermally activated dislocation transforms. 77—20008
- plastic zone, direct meas. in side grooved fracture toughness specimens 78—68864
- plastically deformed crystal, lattice defects influence on axial shadow figure *(Russian)* 80—25508
- plastically deformed metal, positron annihilation examination of recrystallisation *(German)* 77—70252
- plasticity, polycrystalline, probabilistic approach 78—26621
- plasticity spread from stacked stress concentrations, dislocation distrib. 77—31259
- plate, elastic, under uniform twisting, periodic collinear cracks *(Japanese)* 78—67097
- polycrystalline aggregate, continuous distrib. of dislocations, stress fields, movements in elastic-plastic deform. 78—75709
- polycrystals, problems of X-ray determ. of dislocation density from one diffraction line *(German)* 78—2129
- polyethylene, lamellar stacks, screw dislocations 80—19728
- polystyrene, lamellar stacks, screw dislocations 80—19728
- pore healing under press., initial stage of dislocation config. form. *(Russian)* 78—10050
- quartz, etching technique for deformed grains 77—39590
- quartz, synthetic, characterisation by IR adsorption 79—56824
- quartz, twinned crystals, after Japan Law, investigation of regrowth 80—54162
- quartz, US absorption, influence of plastic deform. and electrostatic field *(Russian)* 80—39226
- reactor materials, radiation creep due to stress-induced preferential absorpt., theoretical model 79—89379
- Rene 80, dislocation behaviour during plastic deform. *(Japanese)* 80—108504
- resonant bending fatigue apparatus for approx. determ. of dislocation density 77—86279
- rocking curve half-width obtained by double X-ray crystal spectroscopy in single crystal 78—2131
- ruby, single crystal surface disruption after polishing investigation by chemical etching *(Russian)* 79—38995
- ruby, structural defects due to laser irrad. *(Russian)* 80—100303
- sapphire, shaped single crystals, porosity, microstruct. 78—2125
- sapphire ribbon crystals, EFG growth and charact., voids, grain boundaries and dislocations 80—103283

dislocation density continued

- sapphire substrates, prep. for GaN epitaxy 78—39929
- SEM selected area channelling patterns determ. 78—34407
- semiconductor, dislocation density determ. with Kontrast automatic mineralogical analyser 79—51111
- semiconductor, plastic deformation under pulse action 77—76486
- semiconductor, rel. to degradation of LEDs, high-radiance lamps and lasers, review 77—28630
- semiconductor devices, effects of dislocations 79—82221
- semiconductor dislocation Burgers vector exam., birefringence method 78—30626
- slip band steady-state expansion, dislocation vel. theory 77—24320
- slip lines, average length, rel. to rate of dislocation pile-up *(Russian)* 77—76416
- Sn coated Cu, fine struct. in diffusion zone and mech. props. 77—11739
- steel, 0Kh12G14N4Yu2, struct. after deformation under conditions of superplasticity 80—21031
- steel, 12Kh1MF, influence of preferred dislocation orientation on high-temp. strength *(Russian)* 79—4999
- steel, austenitic, gas implantation effects, fusion reactor first wall damage simulation 80—29079
- steel, austenitic, nitrided, creep, effect of N_2 and Ti and prior deform. 78—23789
- steel, C, U8A, struct. after low-temp. thermomech. treatment 79—79008
- steel, C, wear, struct. changes in centres of galling 79—38985
- steel, Cr-Mo(-V), ductility and heat resistant prop. prediction rel. to fine struct. and solid soln. state 79—15751
- steel, Cr-Ni (1.47, 1.48 wt.%), lath martensite microstruct. and props., cold rolling effect 80—55422
- steel, Cr-Ni-Nb, containing controlled particle dispersions, creep strength 77—52425
- steel, heat-resistant, 12Kh1MF, yield point rel. to dislocation density and cryst. lattice spacing *(Russian)* 77—44291
- steel, high speed, plasticity depend. on plastic strain gradient *(Russian)* 79—57048
- steel, high-strength, strain relax., model *(Spanish)* 77—73296
- steel, hypoeutectoid Widmanstatten struct. form., contrib. to the laws *(Slovenian)* 78—84817
- steel, low alloy, toughness, effect of packet size and lath width 77—16677
- steel, low C, tempered, lath martensite, Ni (5 wt.%), microstruct./yield strength relationship 77—21234
- steel, low-C, ferritic, deform. microstruct., electron microscopy *(German)* 78—64589
- steel, maraging Ni-Co-Mo, strengthening by repeated strain ageing *(Japanese)* 79—100157
- steel, medium C 80—11752
- steel, mild, cold-deformed, struct. changes during annealing, electron microscope obs. *(Russian)* 78—23722
- steel, mild, with different grain sizes, surface strengthening by high frequency loading *(Czechoslovakian)* 77—28934
- steel, Mn (13.5 wt.%) hardening mechanism during friction 79—96152
- steel, Mn-Cr-B (1.46, 1.03, 0.003 wt.%) 80—55422
- steel, Mn-Mo-Nb-C, transform. charact. and struct. during continuous cooling 79—29057
- steel, Mn-Sn(-Nb), extra low C, shear transformation struct. *(German)* 80—60873
- steel, Ni-Co-Mo (17.55, 8.02, 4.92 wt.%) maraging, lath martensite microstruct. and props., cold rolling effect 80—55422
- steel, problems of X-ray determ. of dislocation density from one diffraction line *(German)* 78—2129
- steel, quenched-tempered, relationship between half value breadth and hardness *(Japanese)* 77—52366
- steel, shock transition rise-time meas., limiting viscosity coeffs. 79—77680
- steel, stainless, austenitic, deform. substruct. and annealing, stacking fault tetrahedra form 80—107282
- steel, stainless, electrohydraulic effect and struct. changes *(Russian)* 78—23783
- steel, stainless, electron irradiated, dislocation assisted vacancy diffusion 78—55891
- steel, stainless, fracture and crack tip plastic zones, in situ obs. 80—108686
- steel, stainless, in-pile irrad. effect simulation by Ni ion bombardment, dislocation density, swelling 77—347
- steel, stainless, martensite nucleation mechanisms, HVEM obs. 80—104157
- steel, stainless, radiation damage by 1 MeV electrons, dislocation struct., brittleness *(Russian)* 80—75226
- steel, stainless, shock loading parameter effect on substruct. and mech. props. 79—52360
- steel, stainless, steady state creep, microstructural parameters 78—39870
- steel, stainless, type 304, TEM study of dislocation emission from grain boundaries 79—66121
- steel, stainless, type 316, irradiated, numerical simulation of void nucleation, dislocation densities, point defect conc. 79—73208
- steel, stainless SUS 316, creep fracture at elevated temps. vacuum environment effect *(Japanese)* 77—8942
- steel, stainless type 316, effect of damage rate on void growth, point defect conc., microstruct. development 79—73209
- steel cylindrical bar loaded by longitudinal impact, dislocation struct. and plastic deform. *(Czech)* 78—60713
- steels, 110G13 and 40Kh10G10, hardening and structural transformations during friction *(Russian)* 77—52527
- steels, low alloy, particle coarsening reactions, effect of cold deform. 80—71664
- steels, tool, type U10A and R6M5, phase comp. and phys. props. after hydrostatic extrusion 79—96053
- strain rate, dislocation density, dislocation motion and dislocation constitutive eqns. 80—103329
- straining experiments, in situ, strong frictional force, quantitative anal. 80—100244
- stress relaxation in crystals, review 79—73248
- stress-intensity factors calculated by dislocation theory *(Chinese)* 79—42063
- strontium calcium tartrate tetrahydrate, crystals grown by ion diffusion through silica gels, exam. of preps. 79—52102
- strontium calcium tartrate tetrahydrate, gel grown mixed single crystals, defect characterisation 80—2027
- TEM, distances between parallel dislocations determ. 78—34514
- tensile strength, dislocation density depend. *(Russian)* 78—19820

dislocation density continued
4-m-toluylene diamine, single crysts., conditions of growth and heat treatment influence in dislocation struct. 79−95020
twisting, differential geometry 77−84834
ultrasonic absorption in high dislocation density crystals dislocation internal friction *(Russian)* 80−34146
X-ray diffraction, line broadening of crysts. containing dislocation distrib. 79−37578
Zircaloy tubes, grain struct., texture, dislocation density effect on irradiation creep, X-ray diffr. and optical microscopy anal. 79−74208
Zircaloy-2, pressure tubes, irrad. creep and growth, anisotropy factors 80−97536
Ag and Ag-Sn(In)(Sb) dil. alloy, single crystals, dynamic dislocation behaviour 77−4108
Ag, dislocation recovery *(Russian)* 77−65980
Ag, FCC, polycrystalline, deformation-strain curve description using substruct. parameters *(Russian)* 79−87690
Ag single crystal, dislocation density decrease during reverse deform., obs. by etch-pit method 77−7725
Ag, vapour-deposited on rotating substrate at oblique angle, X-ray struct. anal. 77−62775
Ag-Cu, composite, fibre and layer structs., anomalous props. caused by internal phase boundaries 78−72754
Ag-Cu, highly deformed eutectic composite wire, anomalous props., fibre diameter and foreign atom effects *(German)* 77−36566
α-Ag-Ge, cold-worked, lattice imperfections, X-ray diffr. study 78−38732
Ag-Ge (4.5 at.%), FCC, vapour-deposited, lattice imperfections, X-ray diffr. 78−72032
Ag-Ni, composite, fibre and layer structs., anomalous props. caused by internal phase boundaries 78−72754
Al 2024 alloy, Young's modulus, dislocation densities with shock loading 77−32611
Al, defect structure after plastic deformation, X-ray investigation 78−31467
Al, dislocation density, prep. of high-purity cryst. by strain-anneal method 78−48314
Al, FCC, polycrystalline, deformation-strain curve description using substruct. parameters *(Russian)* 79−87690
Al, fatigue crack propag., grain size effect *(Japanese)* 78−39889
Al, fatigue damage, test temp. effects *(Japanese)* 77−52475
Al films, plastic deformation, appl. of current noise technique for dislocation processes 80−35442
Al, fracture mechanism, plastic strain role 79−38977
Al, ion-implanted, dechannelling by dislocations, backscatt. expts. 79−7642
Al, mobile dislocation density determ. from sound velocity 79−19258
Al, perfect single crystal growth from melt, different orientations of crystallisation front *(Russian)* 77−55881
Al, plastically deformed, spreading of extrinsic grain boundary dislocations 78−43023
Al, polycrystalline, movement of 3-fold nodes of boundaries in high temp. creep 80−89317
Al sheets, dislocation obs. at high temp., annealing effect *(Japanese)* 80−34003
Al, shock transition rise-time meas., limiting viscosity coeffs. 79−77680
Al single cryst., latent hardening in tension 80−60878
Al, struct. changes during cyclic deform. *(Russian)* 77−25127
Al, struct. changes in single cryst. under influence of static and dynamic stresses *(Russian)* 78−92300
Al, surface strengthening of single crysts. on coating with evaporated films 77−8972
Al, thin foil, adhesion and friction, rel. to observed dislocation density 78−64706
Al, transient creep, effect of pre-torsional deform., dislocation glide and density 77−4147
Al, vacuum condensate, struct. and mech. props. depend. on deposition conditons 80−15417
Al wire, grain boundary internal friction after recrystn. annealing *(Russian)* 80−66561
Al wire, hot and cold deformation drawing strengthened, thermal EMF study *(Russian)* 80−54674
Al, zone refined, vacancy annihilation to dislocations, annealing profiles 77−80536
Al-Al$_2$O$_3$ alloys, dilatometric method for studying relaxation of conc. of defects 77−55288
Al-Al$_6$Fe, fibre reinforced eutectic, deformation behaviour by rolling, TEM and SEM study 79−29129
Al-alloy, type 2024, fatigue life prediction, X-ray diffr. method 80−25837
Al-Cu (4 wt.%), supersaturated and aged conditions, high strain deform. 80−60907
Al-Mg (5.5 at.%), stress change expt. on creep 79−24584
Al-Mg-Si, effect of quenching on recrystn. after hot working, dislocation density as function of time 79−43289
Al-Zn (30 wt.%), precipitation ageing plastic deform. effects 77−66645
AlCu-NiCo (5 at.%), θ' hardened, creep mechanism 80−85013
Al$_x$Ga$_{1-x}$As-GaAs, epitaxial heterostructure, influence of defects on diffusive distrib. of group I impurities 78−43045
Al$_2$O$_3$:Cr$_2$O$_3$(Ti$_2$O$_3$), dopant influence on struct. and mech. props. 80−24471
Au, deformed, annealing kinetics of vacancies *(Japanese)* 80−88139
Au/Cu, bilayers, interdiffusion phenomena, lattice dislocations, TEM obs. 80−59736
Au/Cu, initial epitaxial growth at room temp. 80−59829
BN, cubic single crysts., dislocations and other defects, X-ray topography study 79−99207
BN, dislocation tilt boundaries, Laue photograph exam. 77−11562
BaBrF, reacted flux growth, dislocation density, dielec. const. and loss, IR spectra 77−36214
Ba$_x$Sr$_{1-x}$Nb$_2$O$_6$ crystals, optical defects and edge dislocation distributions 80−19806
BaWO$_4$, flux- and gel-grown, comparative microtopography 77−31852
Be, polycryst., plasticity and cleavage, yield and flow stresses 80−44249
Bi, (111) plane, chem. and thermal etch pit orientation, reactivity depend. 77−35559
Bi, US propagation anomalies, under hydrostatic press. *(Russian)* 78−83884
Bi:Sb, solid soln. struct., growth rate effects 77−52246
C, heat-treatment and neutron irrad. effects on US atten. and Young's modulus 79−11644

dislocation density continued
CC Si:P, secondary defect generation suppression and diffusivity restraint by HCl oxidation 79−70191
CaCO$_3$, growth dislocations obs. using Lang X-ray topography 78−2133
CaF$_2$, plastic deform, work hardening regions, TEM obs. 80−3140
Cd films, vacuum deposited, microstruct. exam., X-ray diffr. profile anal. 79−46973
Cd, hardening resulting from pyramidal glide 77−48495
Cd$_3$As$_2$, vapour phase single cryst. growth, X-ray topographic obs. of perfection 78−9976
CdS, cryst. grown from melt under press., microstruct. 77−59019
CdS, exciton optical and luminescence spectra characts. near dislocation slip bands 80−45111
CdS-based phosphor, microstruct. and luminesc. efficiency 78−10959
CdS-Cu$_2$S solar cells, microstructural study of heterojunction materials 80−93978
CdTe, grown by chem. transport, morphology, struct. and microhardness *(Russian)* 78−22729
CdTe, single cryst. sublimation growth, X-ray topographic characterisation 80−29866
Co-Ga β' quenched single crystals, annealing-out of point defects 80−55426
Cr-GaAs, metal-nn$^+$ Schottky diode, I-V characts., inverse branch, effect of dislocation defects *(Russian)* 79−15217
Cr-Si, metal-nn$^+$ Schottky diode, I-V characts., inverse branch, effect of dislocation defects *(Russian)* 79−15217
Cu, activation vol. and dislocation density determ. from relaxation tests 78−3264
Cu, amplitude depend. modulus effect 78−64573
Cu, annealing twins density, photoemission microscopy 80−35208
Cu, commercial pure, creep-rupture props., vacuum,, dislocation density increase *(Japanese)* 78−72843
Cu, cracks in fatigue early stages, direct obs. of substruct. by electron microscope *(Japanese)* 78−7028
Cu, deformed by hydrostatic extrusion, drawing or drawing under press., dislocation struct. obs. *(Russian)* 77−21213
Cu, dislocation content at large plastic strains 79−74224
Cu, dislocation density in fatigue, approx. determ. by resonant bending fatigue apparatus 77−86279
Cu, dislocation form. during sintering *(German)* 78−31361
Cu, dispersion hardened, mobile dislocation density and length of slip lines 77−51387
Cu electrocrystallisation from CuSO$_4$ solns., exptl. methods *(Russian)* 79−8235
Cu electrodeposit, US agitation effect on hardness, porosity and grain size, work-hardening 77−60075
Cu, FCC, polycrystalline, deformation-strain curve description using substruct. parameters *(Russian)* 79−87690
Cu, fatigued, structural changes, damping and modulus 77−28906
Cu film, electron transport props., struct. defects role 77−40117
Cu, high-purity, grain size and strain rate influence on mech. behaviour, precursors existence 80−85016
Cu, limiting value, theory 77−27882
Cu, plastically deformed, containing dislocation distribs., X-ray diffr. line broadening 77−43218
Cu, polycryst., low temp., plastic deform., structural defects, elec. resist. meas. *(Russian)* 78−39844
Cu, polycryst., surface layer hardening by multiple impact 80−108469
Cu, polycrystn., cold worked, calc. of dislocation density as function of plastic strain 79−38924
Cu, shock loaded, work hardening and press. depend. of dislocation arrangement and density 78−48429
Cu, shock transition rise-time meas., limiting viscosity coeffs. 79−77680
Cu, single cryst., deform. process, effect of surface layer 79−8315
Cu single cryst., latent hardening in tension 80−60878
Cu single crystals, [100]- and [111], dislocation density meas. using TEM 80−79803
Cu, soft crystal, US irrad. induced dislocation distrib. 77−32584
Cu, struct. changes in single cryst. under influence of static and dynamic stresses *(Russian)* 78−92300
Cu superfluid ^{4}He interface, Kaptiza conductance, depend. on dislocation density near interface 79−33170
Cu, vacuum condensate, struct. and mech. props. depend. on deposition conditons 80−15417
Cu/Cu system, explosive cladding, TEM obs. and thermomech. model 79−96041
Cu-Ag, deformed, recrystallization nucleation at second phase particles, electron microscope obs. 79−34059
Cu-Al, vacuum condensate, struct. and mech. props. depend. on deposition conditons 80−15417
α-Cu-Al (0.5 to 10 at.%), latent hardening and dislocation density 78−19853
Cu-Al (15 wt.%) single crystal, steady state deform. at high temps. *(Japanese)* 78−19833
Cu-Al (3 wt.%), annealing twins density, photoemission microscopy 80−35208
Cu-Al (4.5 at.%), alloy, dislocation recovery anomalies *(Russian)* 77−21163
Cu-Al (9.3 wt.%), in torsion, deformation temp. depend., superplasticity due to grain size, dislocation density *(Russian)* 79−74200
Cu-Al-Ni alloys, deformed, fine struct. of martensite *(Russian)* 78−6923
Cu-Al(Si), single crysts., latent hardening study by meas. of flow stress on secondary systems *(Japanese)* 79−24538
Cu-Fe, composite, fibre and layer structs., anomalous props. caused by internal phase boundaries 78−72754
Cu-Fe (1.5 wt.%), precipitation-effect on void formation during electron irradiation 80−84211
Cu-Ga, high dislocation density alloys and oxide precipitated struct., NMR, spin echo 80−39892
Cu-Nb multifilamentary composite, dislocation resistivity 80−70671
Cu-Ni (10 at.%), creep, substruct. and internal stresses *(Russian)* 80−97527
Cu-Ni (10 at.%), hardening, recovery, and struct. changes during high temp. creep *(Russian)* 80−89288
Cu-Ni (10 at.%) alloy, creep, dislocation density variation *(Russian)* 79−96101
Cu-Ni alloy, dislocation density during deform., comparison of electron microscopy and X-ray diffr. *(Russian)* 79−5002
Cu-Ni bimetallic thin film, effect of microstructre on interdiffusion 79−77840

dislocation density continued
  - Cu-Ni-Zn alloy, FCC, cold-worked, X-ray diffr. obs. 78-3143
  - Cu-Ni(Al), strength and substruct., strain point influence *(Russian)* 79-52233
  - Cu-Si, high dislocation density alloys and oxide precipitated struct., NMR, spin echo 80-39892
  - Cu-Sn, deformed, martensitic transformation *(Russian)* 79-15668
  - $CuFeS_2$, explosive-shock deform. 78-95108
  - Cu_2O, epitaxial, on Cu(111), misfit dislocation annealing, TEM obs. 79-82228
  - Cu_2O, radiation damage 77-84809
  - γ-Fe alloy, supersat. solid soln., recrystn. inhibition by cold rolling 77-73286
  - Fe and Fe-Cr, flow stress, effect of cathodic, H_2 charging *(Japanese)* 79-52313
  - α-Fe, deformed, changes in dislocation density, mech. props., dependence on deformation temp. *(Russian)* 79-20130
  - Fe, deformed, dislocation structure determ. from magnetic props. 78-55874
  - Fe, deformed single crystal, dislocation distrib. 77-59880
  - α-Fe, dislocation density determ. after quenching, internal friction meas. 78-18658
  - α-Fe, exam. of structural defects due to shock waves, and induced hardness 78-48427
  - Fe, high purity, dislocation-magnetic domain wall interaction, magnetomechanical damping expts. 78-39360
  - Fe, high purity single crystals, dislocation density rel. to work hardening *(German)* 77-32590
  - Fe, microcracks formed by H_2 precipitation, SEM and TEM obs. *(Japanese)* 79-70071
  - Fe, penetration of H_2, influence of microstruct. changes induced by cold working *(Russian)* 77-20182
  - Fe, strengthening in H_2S04, H_2 hardening rel. to struct., anodic behaviour *(Russian)* 79-15855
  - Fe, zone refined, strained, substructural changes during annealing *(Slovenian)* 78-84845
  - Fe/Fe-Cr composite powder, X-ray diffr. exam. of densification during rolling 80-40289
  - Fe-Al (25 at.%), long-range ordered, compression induced mag. anisotropy 77-69546
  - Fe-Cr (1.20, 3.63, 7.98 wt.%), Mossbauer spectra shape depend. on deformations 79-61272
  - α-Fe-Cr alloys, recrystallised, C segreg. effects, TEM *(French)* 77-28828
  - Fe-Mo (4.1 wt.%), substructs. developed during steady state creep at 1100-1200K, TEM obs. *(Japanese)* 79-38900
  - Fe-Mo(4.1 wt.%), steady state creep at high temps. 80-89316
  - Fe-Ni (32 wt.%), electrohydraulic effect and struct. changes *(Russian)* 78-23783
  - Fe-Ni-C, HVEM study of strain induced martensite 79-20047
  - Fe-Ni-C, intercrystalline embrittlement in tempered martensite, elimination by reaustenitization *(Slovak)* 80-108548
  - Fe-Ni-Cr (25, 15 wt.%), mobile dislocation density in steady state creep, strain transient dip test, TEM exam. 80-7650
  - Fe-Ni-V-C alloy, reverse α to γ transformation, previous deformation influence on struct. and props. *(Russian)* 79-100139
  - Fe-Si, dislocation wall form. in contact with surface active melt, stacking fault energy *(Russian)* 77-72626
  - Fe-Ti (0.056 at.%), stress relaxation curves, anal. interpretation 77-59847
  - $FeGe_2$, single cryst. perfection depend. on growth rate and direction 80-55284
  - FeNi-Cu, composite fibre and layer structs., anomalous props. caused by internal phase boundaries 78-72754
  - (GaAl)As-GaAs, double heterostructure laser, TEM study of dark line defect growth from dislocation clusters 79-33206
  - $Ga_{0.9}Al_{0.1}As$:Ge(Si) epitaxial layers, defect obs. by TEM 77-51618
  - $Ga_xAl_{1-x}As$:Cu epitaxial layers, spatial distrib. of nonradiative defects, STEM imaging spectroscopic technique 77-89438
  - GaAs, ⟨100⟩ cryst., quantitative light microscopy 77-31661
  - GaAs crystal growth, thermal and elastic const. evaluation 80-92586
  - n-GaAs, crystal growth by Czochralski method kinetics, total emittance determ. 80-75193
  - GaAs, Czochralski growth, melting and regrowth, inclusion density and dislocation generation 77-21016
  - GaAs, dislocation density effect on polarisation and intensity of reflected $CuK_{\alpha 1}$ radiation 77-1131
  - GaAs electron-pumped uncooled laser, degradation rel. to dislocation density 80-14344
  - GaAs epitaxial growth, in $GaAs-AsCl_3-H_2$ system, elec. field effect 80-2306
  - GaAs epitaxial layers, structural defect and conc. inhomogeneities influence on barrier diode I-V characts. 80-15602
  - GaAs epitaxial multilayer photocathode structures, TEM obs. of dislocations generated 80-100241
  - GaAs, grown-in dislocation density, impurity effect 78-51543
  - GaAs, impurity effect on grown-in dislocation density *(Japanese)* 78-6063
  - GaAs, luminescence emitted from deep centres, plastic deform. effect on internal quantum efficiency 80-60672
  - GaAs, pulled, dislocation generation, thermoelastic anal. 80-79787
  - GaAs, travelling heater method growth, dislocation elimination 77-7684
  - GaAs VPE layers, role of diffused Ga vacancy in degradation 78-95050
  - GaAs:Si defect density before and after Zn diffusion, SEM and TEM obs. 80-96529
  - $GaAs-Ga_{1-x}Al_xAs$ LPE wafer stress-free dislocation generation 77-75527
  - $GaAs-GaAs_{0.5}P_{0.5}$ almost perfect epitaxial multilayers, TEM obs. 77-89668
  - GaAs(-GaP) single cryst., defect distrib. near abraded surface 80-92533
  - $GaAs_{1-x}P_x$ film, VPE grown, photolum. spectra, vel. to dislocation density 79-73997
  - $GaAs_{1-x}Sb_x$ layer on GaAs, dislocation density reduction by improved LPE growth method 80-76202
  - $GaAs_xSb_{1-x}$ solid solution epitaxial layer, morphology and defect structure 77-1330
  - $GaAs_{2-x-z}Sb_xP_z$, LPE growth, continuous comp. grading, use as secondary substrate 77-31913
  - $Ga_xIn_{1-x}P_yAs_{1-y}$, 111-A and 111-B faces, defect struct., etching and X-ray diffr. obs. 80-2026

dislocation density continued
  - $Ga_xIn_{4-x}PyAs_{1-y}$, In rich bulk single crysts. growth from melt via gradient freeze method, and characterisation 78-68618
  - GaP, crystal, growth conditions rel. to dislocation struct. 80-88151
  - GaP, dislocation obs., SEM EBIC vs SEM CL micrographs 77-80511
  - GaP, dislocations induced by diffusion of Zn with or without P 77-19955
  - GaP, electron traps around dislocations in p-n junction and metal-semicond. structs. 80-34388
  - GaP epitaxial layer, crystal defects influence on luminesc. obs. 79-87511
  - GaP, growth of dislocation free crysts. from stoichoometric melt. 77-81212
  - GaP, LEC, SSD and CVD samples, Zn tracer diffusion profiles in solids 78-95189
  - GaP, preferential etching of dislocations and stacking faults 77-39589
  - GaP single cryst., defect distrib. near abraded surface 80-92533
  - GaP, VPE layer structures for LED's, SEM, and TEM obs. of dislocation density reduction expt. 80-100425
  - n-GaP:In, LPE from In solvent, dislocation density reduction by doping 78-18919
  - GaP:S, defect struct. and tetrahedral precipitates, TEM study 80-107246
  - GaP-ZnS, solid solns., microstruct. investig. 78-2128
  - $GaP_{0.1}As_{0.9}$, gas-transport condensate with superlattice, structural and chemical inhomogeneity 77-85088
  - GaTe, hexagonal, vacuum deposited, physical parameters and substruct. 78-2393
  - Gd, electron irradiated, relation of defect densities to Rayleigh parameters 77-62517
  - $Gd_3Ga_5O_{12}$ dislocation anal. at inclusions by repeated etching technique 80-29024
  - Ge, amorphous, struct., dislocation model 78-42911
  - n-Ge, current carrier-dislocation interactions, resistance in UHF range *(Russian)* 80-54732
  - Ge, deformation, annealing characts., X-ray study 78-75713
  - Ge, dislocation energy levels, Hall effect meas. 78-6328
  - p-Ge, dislocation microwave cond. and Hall effect meas. *(Russian)* 77-47848
  - Ge, dislocation-induced elec. pots., appl. 79-82551
  - Ge epitaxial films, structural perfection rel. to deposition conditions 78-43258
  - Ge, epitaxial growth from monogermane at 685°C 78-51833
  - Ge, influence of dislocations on free-exciton lifetime 78-60064
  - Ge, melt grown single crystals, preferred growth directions and perfection 79-77537
  - Ge monocrystal, dynamic interaction of screw dislocations with flat clusters of dislocations on other slip planes *(Russian)* 79-86800
  - Ge, phonon scattering and dislocation effect on low temp. phonon cond. 78-51754
  - Ge ribbon single crysts. grown from melt, dislocation struct. form. under thermal stress 80-107082
  - Ge single crystals, constitutional supercooling growth conditions, structural and chem. inhomogeneities 80-93473
  - Ge, X-ray diffraction, effect of dislocations on temp. depend. of integrated intensities 77-39513
  - p-Ge:Au, interaction of primary radiation defects with Au atoms, after irrad. and annealing 79-51145
  - p-Ge:Ga, dislocation density effect on carrier lifetime and deep recomb. centres 79-51598
  - Ge:P(Sb), growth atm. effect on struct. microdefect form. 80-20779
  - Ge-GaAs, $p-nn^+$ junction, I-V characts., inverse branch, effect of dislocation defects *(Russian)* 79-15217
  - HIO_3:Cr(Ni)(Fe)(Mn), growth and struct. perfection, effect of impurity ions 77-12514
  - ^4He, HCP, dislocation damping, MHz sound freq. depend. attenuation 77-72739
  - ^4He, solid, thermal cond., 0.4 to 1.8K *(Russian)* 80-103535
  - HfO_2 single crystals, Y_2O_3 stabilised, optical props., impurities and annealing conditions influence 79-52399
  - HgSe, CVD crysts., electrophys. characts. 77-85910
  - InAs films, MBE grown on GaAs, electron mobilities, lattice mismatch effect 80-80419
  - $In_{1-x}Ga_xAs$, LPE layer on InP substrate, phys., elec. and optical props. 78-39235
  - $In_xGa_{1-x}As$ (x=0.03 and 0.05), grown as GaAs substrate, with InGaAsP buffer layer, exam. of dislocation density 80-44447
  - InGaAsP, epitaxial layer, defect evaluation by cathodoluminescence 80-2866
  - InGaAsP, LPE growth on InP, influence of lattice mismatch on surface morphology 79-1553
  - $In_{1-x}Ga_xP$, epitaxial growth on GaAs substrate, formation of intermediate layers 80-2304
  - InP, and InP_xAs_{1-x}, 111-A and 111-B faces, defect struct., etching and X-ray diffr. obs. 80-2026
  - InP, grown-in dislocation density, impurity effect 78-51543
  - InP, impurity effect on grown-in dislocation density *(Japanese)* 78-6063
  - InP substrate, LEC-grown, defect evaluation by cathodoluminescence 80-2866
  - InP, VPE, etch pit density, dislocation density 79-87569
  - InP:S, SSD growth of low dislocation density crystals 80-89135
  - InP:Te(S), heavily doped, dislocation imaging using transmission cathodoluminesc. 80-29023
  - InSb, dislocations due to thermal stress, single and composite crysts. 78-2124
  - InSb, galvanomagnetic props. of annealed single crystals 80-96909
  - p-InSb, influence of plastic deform. on elec. props. 80-103711
  - InSb, plastically bent single crysts., dislocation struct. obs. 78-59816
  - InSb-GaSb superlattice, density of microtwins and dislocation boundaries, depend. on composition modulation 79-56930
  - KBr, electrolytic coloration effect on dislocation density 77-4106
  - KBr, quench hardening related to dislocation density and slip 78-52855
  - KCl, additively coloured, colloid nucleation and growth, TEM 77-62526
  - KCl, crystals, grown by Czochralski method, effect of growth rate on defect generation 79-51032
  - KCl, electrolytic coloration effect on dislocation density 77-4106
  - $KCl:Br^{2+}$, solid solution periodic precipitation in inhomogeneous conc. field 80-103485
  - KCl:Ca(Ba), effect of doping on dislocation distrib., in melt grown cryst. 80-6410

dislocation density continued
KCl:Pb^{2+}, γ-irrad., rel. to props. 78—31262
KCl:Sr, mechanical props. as function of dopant conc., dislocations 77—69027
KCl:TlCl, lattice defects, X-ray line profile obs. 80—24455
KCl-BaCl$_2$ supersaturated solid soln., deformed, BaCl$_2$ precipitation kinetics, metastable region *(Russian)* 78—60673
KCl-KBr, mixed cryst., radiation hardening 79—99238
KCl-KBr single crysts., mobile dislocation density at yielding, solid soln. hardening model 77—72649
KClO$_4$, cryst. growth from gelatin gels, exam. of growth and morphology 80—7488
KClO$_4$ single crystals, gel growth, temp. effects etching 79—78862
KCoF$_3$, KFeF$_3$ and KNiF$_3$, crystal growth from flux, degree of perfection and dislocation density 77—77359
LiF, dislocation structure, influence of variable deform. temp. 80—70211
LiF, γ-irradiated crysts., dislocation retardation centre 79—95051
LiF, rel. to cryst. orientation effects on dynamic strength 78—39846
LiF single crystals, dislocation motion and generation on plate impact 79—95011
LiF single crystals, stepwise creep, 300K, in dislocation depletion conditions, thermal cycling effects *(Russian)* 77—15484
LiF, viscous drag of dislocations exam., using mobility of individual dislocations 79—14814
LiF, X-ray integrated intensities in Bragg and Laue geometries 77—31553
LiF:Be(Mg), Maxwell-Wagner relax. induced by impurity clouds around dislocations, ionic thermocond. meas. 80—7281
LiF:Ni, dislocation behaviour in diffusion zone, Cottrell clouds *(Russian)* 80—70212
α-LiIO$_3$, dislocation struct. 77—1132
α-LiIO$_3$, surface defect layer struct. due to mechanical working *(Russian)* 80—100238
Mg, pure and dil. alloys, electron lifetime anisotropy, Dingle temp. due to dislocation scatt. 79—78082
MgO, fracture and crack tip plastic zones, in situ obs. 80—108686
MgO single cryst., internal stresses and dislocation mobility, stress relaxation method 80—6413
MgO, single cryst., tensile creep, stress induced dislocation structs. 80—96539
MgO, slip line struct. using replica electron microscope technique 79—7605
MgO, substructure, X-ray diffraction study, rel. to preparation by thermal decomposition 77—12581
MgO:Li, mech. deformed crysts., imprinting of slip bands using Li impurities 80—59473
MgO:Li$^+$(Na$^+$), precipitation rel. to dislocations *(French)* 79—51163
MgO.1.1 Al$_2$O$_3$ spinel, high temp. deform., cryst. orientation effect 80—107263
MgZn$_2$, solid soln. softening in homogeneity range, dislocation density and velocity *(German)* 77—44264
Mo alloy:Re, effect of Re on mechanical props. 80—35196
Mo alloys, dil., HVEM bombarded, neutron damage simulation, defect cluster and dislocation obs. 80—107330
Mo, defect struct. in plane strain deformed single crystal 77—63751
Mo deformed single crysts., struct. state and dislocation splitting *(Russian)* 80—29029
Mo, dislocation ⟨100⟩ density variation, deformation effects, dislocation stability *(Russian)* 80—15108
Mo dislocation a ⟨100⟩ stability, plastic deform. at high-press. 78—43030
Mo, fracture and crack tip plastic zones, in situ obs. 80—108686
Mo, irrad.-induced voids and dislocations, annealing, theory *(Russian)* 78—47418
Mo, plastic deform. by rolling at 293K, dislocation struct. *(Russian)* 77—48481
Mo, plastically deformed single cryst., mag. susceptibility *(Russian)* 80—93074
Mo polycrystn., cyclically deformed, dislocation arrangements 80—108506
NH$_4$ClO$_4$:Cu^{2+}, dislocation etch pits exam., rel. to thermal decomp. 77—11555
NH$_4$H$_2$PO$_4$, dislocation obs. using electron microscopy and replica method 77—59013
NaCl, deform. process, exoemission and desorption meas. *(Russian)* 78—75708
NaCl, deformed, dislocation densities, TEM 77—43219
NaCl, dislocation density, laser beam effect, electron microscopy of etch pits 77—11553
NaCl, dislocation density in monocrystal deformed under high hydrostatic press. 80—70216
NaCl, dislocation ordering influence on integrated X-ray coeff. 80—103357
NaCl, effect of dislocation density on viscous drag dislocation coeff. *(Russian)* 77—80512
NaCl, high density of dislocations meas., new etchant 78—43019
NaCl, high resolution TEM and radiation sensitivity, dislocation obs. on deformed crysts. 80—107260
NaCl, hydrostatically compressed crysts. in easy glide stage, plastic deformation 80—7630
NaCl, interrupted neutron irrad. expts. involving dislocations 79—99208
NaCl, monocrystalline, defect struct. and intrinsic ionic cond. relationship 79—95211
NaCl, plastically deformed, containing dislocation distribs., X-ray diffr. broadening 77—43218
NaCl, polishing of single crystals, kinetics of defect formation *(Russian)* 78—95819
NaCl, quench hardening related to dislocation density and slip 78—52855
NaCl, reduction of dislocation density during isothermal annealing *(Russian)* 79—4303
NaCl single crystal, stained by abrasion, struct. defects *(Russian)* 79—74262
NaCl, spiral dislocation mobility depend. on elec. field, relaxation time 80—39105
NaCl:Sr, mechanical props. as function of dopant conc., dislocations 77—69027
Nb, influence on degree of perfection of rate of cryst. growth *(Russian)* 77—43162
Nb, plastic deformation effects on superconducting specific heat transition 80—20352

dislocation density continued
Nb$_3$Al superconductors, sputter deposited, BCC to A15 transition, microstruct. investig. 78—27512
Ne, solid, lattice thermal cond. 0.5 to 10K, dislocation densities, average grain sizes 78—79830
Ni, (99 wt.%), annealing twins density, photoemission microscopy 80—35208
Ni alloy, recryst. after hot deform. *(German)* 80—25716
Ni and Ni-Cr(Mo), wear tracks, TEM obs., tested in simulated face seal 77—52508
Ni, carbonyl powder, dislocation density sintering 80—108372
Ni, creep, substruct. and internal stresses *(Russian)* 80—97527
Ni, decrease due to D bombardment, 22 MeV 78—80597
Ni, deformed by hydrostatic extrusion, drawing or drawing under press., dislocation struct. obs. *(Russian)* 77—21213
Ni, dislocation structure evolution after hydroextrusion *(Russian)* 80—96530
Ni, dislocation structure parameter determ. due to plastic deformation *(Russian)* 80—54242
Ni electrodeposits, struct., electrolyte anions influence 80—20056
Ni, FCC, polycrystalline, deformation-strain curve description using substruct. parameters *(Russian)* 79—87690
Ni, ion irrad. with 20 and 500 keV ^{4}He$^+$, depth distrib. of cavities and dislocation damage 80—107346
Ni, irradiated, numerical simulation of void nucleation, dislocation densities, pt. defect conc. 79—73208
Ni, mass transfer parameters, lattice defect effects under laser pulse action *(Ukrainian)* 80—6537
Ni monocrystals, struct., effect of stress applied during electrodeposition 78—26777
Ni, polycryst., hydrogenation rel. to fine struct. 78—59950
Ni, polycrystalline, strain hardening, dislocation link length model 80—84953
Ni precipitates, isothermal annealing influence on structural state, X-ray diffr. anal. *(Russian)* 80—100849
Ni, push-pull fatigued polycrystals, point defects, elec. excess resist. meas. 80—100910
Ni, self-ion irradiated, defect clusters, annealing 78—18687
Ni, shock loaded, work hardening and press. depend. of dislocation arrangement and density 78—48429
Ni, shock loading parameter effect on substruct. and mech. props. 79—52360
Ni sputtered coating microstructure on mechanically activated cathode *(Russian)* 79—91586
Ni, structural changes, creep mechanism, multiple dislocation cross slip *(Russian)* 80—59476
Ni, transformed into hydride and decomposed, dislocation density and dislocation profile depth, positron annihilation and X-ray estimation 78—38711
Ni, variation in dislocation density during creep, determ. by X-ray diffr. analysis *(Russian)* 80—76302
Ni-Al(Cr)(Ti), ion irradiation induced void swelling and defect microstructs., TEM obs. 79—51164
Ni-Fe, 79 NM alloy, gamma and neutron influence on mag. susceptibility comparative study *(Russian)* 80—39751
Ni-Fe, film, magnetisation induced uniaxial anisotropy, substrate temp. depend. 77—8367
Ni$_3$Al-Ni$_3$Nb eutectic alloy, ^{63}Ni diffusion rate rel. to struct. defects *(Russian)* 78—2288
Ni$_3$Fe, dislocations, rate of piling up, rel. to average length of slip lines *(Russian)* 77—76416
Ni$_3$Fe, superlattice dislocations, compression induced mag. anisotropy 77—85442
Ni$_3$Fe, superlattice dislocations, compression induced mag. anisotropy 77—85443
NiO, single crysts., TEM of dislocations 79—4306
Pb films, vapour deposited FCC, normal and oblique incidences, microstructure, X-ray diffr. study 80—20048
Pb, plastically bent, effect of dislocations on electron relax. time, cyclotron reson. 79—24217
Pb single crystal, normal-superconducting transition and plastic flow 78—3166
Pb thin films, thermal strain, multiple cycling to 4.2K effects 79—90918
Pb-In (5%), supercond. mobile dislocation density, instantaneous flux change meas. 80—15670
PbS, epitaxial film, struct. perfection, two cryst. X-ray spectrometry 78—26792
PbS, epitaxial layer, structural nonuniformities and dislocation struct. 79—23852
Pb$_{0.78}$Sn$_{0.22}$Te:In epitaxial layers, dislocation density, Hall effect, conductivity, photoeffects 80—25024
Pb$_{1-x}$Sn$_x$Te ($x=0.15$ to 0.20), SEM study, dislocation density, and carrier density and mobility 79—69107
Pb$_{1-x}$Sn$_x$Te LPE grown heterostructures, dislocation etch pitch, interfaces 80—2023
Pb$_{1-x}$Sn$_x$Te, large non-seeded single cryst. growth by sublimation method, and characterisation 79—78860
Pb$_x$Sn$_{1-x}$Te, grown by vap. transport in closed system, quality improvement 77—40341
PbTe-PbSnTe heterjunction, misfit dislocations, etch pit and electron probe study 79—77926
Pd-H system, solvus hysteresis 80—71659
Se, undeformed rhombohedral, dislocations, electron microscope obs. *(French)* 78—51548
Se$_{90}$Te$_{10}$ whiskers, chem. and thermal etching 77—15417
Si, ⟨100⟩, defect etch for evaluation 79—90657
Si, Bragg diffraction from crysts., Mo K$_\alpha$ radiation polarisation 80—1893
Si, controlled dislocation formation, struct. density *(Russian)* 80—107244
Si, cryst., impurities rel. to lattice parameters, dislocation density, stresses *(German)* 77—51403
Si, cryst. growth, temp. field, stresses rel. to dislocation density *(German)* 77—51335
Si, crystal, dislocation multiplication *(German)* 78—38721
Si crystal limited topogram technique for investigation of dislocation distrib. 79—23496
Si crystals, photoelectret state investigation 80—97191
n-Si, current carrier-dislocation interactions, resistance in UHF range *(Russian)* 80—54732
Si, damage in electron bombardment, threshold voltage 77—27910

dislocation density continued
Si, deformation, annealing characts., X-ray study 78—75713
Si, deformed, faulted dipole, TEM obs. 78—38712
Si, deformed crystal, faulted dipoles 78—59814
Si, diffusion of ^{71}Ge and ^{32}P, effect of dislocation struct. on migration rate 77—51551
Si, diffusion of P, elastic deform. relax. and dislocation generation 80—79997
Si, diode, high dislocation density effect on charact. *(German)* 79—33336
Si, dislocation dynamics during plastic deform., stress-strain characts. 79—27996
n-Si, dislocation free, process induced cryst. defects 80—24392
Si, dislocation mobility and mech. behaviour 79—82208
Si, dislocation structure, effect of induction heating *(Russian)* 77—21180
Si, dislocation-induced elec. pots., appl. 79—82551
Si, dislocations, depth distrib. planar channelling anal. with 2 MeV He backscattering 79—7640
Si, dislocations, luminesc. spectra *(Russian)* 77—90197
Si, effect on C-V characts. of MOS struct. *(Russian)* 78—6447
Si, effect on doping process *(Hungarian)* 77—62553
Si, elec. props., plastic deform. and annealing temp. depend., dislocation effects *(Russian)* 77—89765
Si epitaxial layer, on Si ribbon substrate, X-ray obs. 77—85102
Si epitaxial layers, X-ray topographic study using Berg-Barrett techniques 79—28221
Si film, high electron mobility, grown on sapphire at high growth rate 77—81225
Si film, MBE, cryst. defect props., substrate treatment effects 80—70551
Si, growth mechanisms of single crysts. with and without dislocations 77—89395
Si, high O conc., electrical and mechanical props., influence of heat treatment 77—35934
Si, influence of temp. and alloying on integral X-ray intensities *(German)* 77—69066
Si, low dislocation density, plastically deformed, electron mobility anisotropy anomaly *(Russian)* 77—80777
Si, MBE, on n$^+$ Si, with wide range doping control 78—27402
Si monocrystalline rod growth from gas phase 78—64453
Si, plastic deformation, dislocation density in yield point area *(German)* 78—38720
Si, rel. to diffusion of Sb, along dislocations, 1165-1320°C 77—15631
Si slices meas., using ellipsometer *(Hungarian)* 79—99198
Si, with various dislocation densities, ang. depend. of X-ray polarisation of curve of 111 Bragg reflection 79—46509
Si:B, ion implanted, laser annealed, thermal annealing effect 79—73191
Si:B, ion implanted, structure defects formation and behaviour under annealing in various ambients 80—65033
Si:B, with insulating coating, mechanical stress influence on B diffusion, strained surface layers 80—29224
p-Si:P p-n junctions, dislocations investig. rel. to P diffusion, SEM, X-ray topography techniques 77—76433
n-Si:P(B), elec. cond. oscills., electron instability effects due to dislocations 80—103704
Si-Fe, ferromagnetic domains and their junctions, simulation of X-ray topographs 79—78434
$Si_{0.92}Ge_{0.08}$ film on Si, elastic strain, misfit dislocation density 77—85119
Si_xGe_{1-x}-GaAs, p-nn$^+$ junction, I-V characts., inverse branch, effect of dislocation defects *(Russian)* 79—15217
Sn, white, single crystal, dislocation movement in pre-yield region, etch hillock technique 79—60371
Sn white crystals grown by Bridgman method, dislocation density, cryst. width 79—100045
$Sr_{0.75}Ba_{0.25}Nb_2O_6$, large cryst. growth, control of opt. defects 78—76595
$Sr_{1-x}Ba_xNb_2O_6$, and Nd doped growth of low dislocation density cryst., dislocation struct. 77—40348
SrClF, SrBrF, reacted flux growth, dislocation density, dielec. consts. and losses IR spectra 77—36214
$SrTiO_3$, defects grown by Verneuil method 77—51390
$SrTiO_3$, flame fusion growth, dislocation density, lattice const. and EPR spectra 78—11099
$SrWO_4$, flux- and gel-grown, comparative microtopography 77—31852
Ta, single crystal, microyielding microflow parameters 77—52395
Te, deformed and annealed crystal, dislocation multiplication, effect on Hall coeff. and conductivity 79—7847
Te, dislocation density and config. effects on cyclotron reson. absorpt. 79—78526
Te, elec. props. anisotropy, influence of deform. and annealing 77—15859
Te, hexagonal film vac.-evaporated at normal incidence, X-ray Fourier line shape anal. 79—99454
α-Ti, plastic deform., anharmonicity, and Gruneisen parameter 80—88246
Ti-Al-Mo-Sn alloy, elastically and plastically deformed, positron annihilation meas. of deformation 80—21038
Ti-Al-V (6,4 wt.%), to H effect on fracture props. and microstruct. 80—40512
Ti-Mo-Zr-Sn (11.5, 6.0, 4.5 wt.%) alloy, struct. as affected by processing history 80—84972
V, dynamic deformation, influence of previous static loading *(Russian)* 78—6972
V_2O_5, low dislocation density cryst. growth, opt. props. 77—63551
W fibres, dependence of fine struct., on processing parameters 79—34082
W, high purity, zone-refining growth, radial distrib. of structural defects *(Russian)* 79—19250
W, plastically deformed single cryst., mag. susceptibility *(Russian)* 80—93074
W single crystal, creep, excess edge and screw dislocation density calc. *(Russian)* 78—34519
W, vapour deposited, dislocation struct., rel. to texture *(Russian)* 80—65394
WC-Co and WC-Co-TaC-TiC-NbC cemented carbides, microstructure, high temp. deformation, uniaxial plastic compression 80—40451
WC-Co compacts and sintered alloy, fine struct. of carbide phases, preforms re-pressing under high press. effect 79—28987
YAG:Nd, laser cryst., dislocations density and propag., rel. to Czochralski growth *(Chinese)* 77—11552
YIG, Ga and Al substituted, single cryst. growth by the travelling solvent float zone technique, dislocation density meas. 79—43138
YIG, plastic deform. and mag. props 77—40087

dislocation density continued
Y_2O_3, cooling rate in melt-growth effect on struct. perfection 77—85925
Y_2O_3, dislocation density depend. on crystal pulling rate 77—81210
Y_2O_3 fused single crystals, struct. 80—19804
Y_2O_3(:Nd) single crystal growth, floating zone method with Xe arc lamp imaging furnace 80—60777
Zn, basal slip, early stages in single crystal 77—72623
Zn crystal, $\{11\bar{2}2\}\langle 11\bar{2}3\rangle$ slip system, deform. stress, dislocation density depend. *(Russian)* 80—103353
Zn, deforming stress under basal slip, contrib. of forest and primary dislocations 78—3186
Zn, density of basal dislocations, rel. to deforming stress, 1.5-300K *(Russian)* 80—29028
Zn film, vac. deposited, X-ray diffr. study of microstruct. 78—26796
Zn, film, vac. deposited, X-ray diffr. study of microstruct. 78—75966
Zn, glide dislocations, second order pyramidal band, etch pit obs. of pure single cryst. *(Japanese)* 78—38716
Zn, highly perfect crysts., Bridgman growth, dislocation density rel. to annealing *(Japanese)* 80—40252
Zn, isothermal annealing effect at 400-410°C, on dislocation struct. in monocrystals *(Russian)* 79—20082
Zn, plastic deform., effect of hydrostatic press. stress relax. meas. *(Russian)* 79—96102
Zn, single cryst., contribution of basal dislocations to residual elec. resist. *(Russian)* 80—75539
Zn, US attenuation under high hydrostatic press., dislocation mechanism 77—43284
Zn, vacancy concentration meas., lattice parameter and length changes, form. parameters 79—37697
Zn_3As_2-ZnSe(ZnTe) solid solutions, single cryst., phase equilib. and props. 80—16283
ZnS, cryst. grown from melt under press., microstruct. 77—59019
ZnS, single cryst. vap. growth by sublimation and chem. transport 78—27390
ZnS-based phosphor, microstruct. and luminesc. efficiency 78—10959
ZnSe, single cryst. vap. growth by sublimation and chem. transport 78—27390
ZnTe, real structure effect on luminescence and absorption spectra, dislocations 80—16085
ZnTe, single cryst. vap. growth by sublimation and chem. transport 78—27390
ZnTe:Ag, real structure effect on luminescence and absorption spectra, dislocations 80—16085
Zr alloy, neutron irradiated, in-pile dimensional changes 77—24331
Zr alloys, creep and growth, irradiation induced, microstruct. depend. 80—93602
Zr-Nb (2.5 wt.%), pressure tubes, irrad. creep and growth, anisotropy factors 80—97536
ZrO_2 single crystals, Y_2O_3 stabilised, optical props., impurities and annealing conditions influence 79—52399

dislocation dipoles
alkali halides, charged dislocations for case of saturated region 79—46657
amorphous ferromagnet, micromagnetic theory 78—10661
amorphous ferromagnetic alloys, domain struct. and mag. microstruct., review 80—15751
amorphous ferromagnetic alloys, micromagnetic eqns. for case of dipolar and magnetocryst. fluctuations 80—11171
anisotropic elastic medium, elastic field prod. by straight dislocation dipole 79—99195
computer simulation of electron microscopic diffr. contrast 77—84750
Cu-Al, FCC, study of dipoles using weak-beam electron microscopy 78—22724
electron microscopy, calc. of weak-beam images 80—75231
EM field due to dipole-equivalent defect in conducting half-space *(Russian)* 77—71904
faulted dipoles, formation and props. 77—72615
FCC materials, dissociated dislocation dipoles, weak-beam electron microscopy technique 78—34516
FCC materials, jogs on extended defects, weak-beam electron microscopy technique 78—38713
ferromagnetic resonance line, uniform, at finite temps., dislocation broadening 78—19334
Ge, heavily doped, dislocation vel., electronic effects 77—11547
ice, edge dislocation dipole form. by heat treatment, X-ray diffr. topography 79—99203
II-VI compounds, charged dislocations and plastic deform. 80—107264
III-V crystals, piezoelectric effect due to dislocations 77—81059
interaction between dipole and dislocation, theory *(Russian)* 77—80504
ionic crystal, point defect-dislocation interactions 78—63787
ionic single crystals, elec.-mech. coupling of dislocations 78—75676
melting, cooperativity in dislocation theory 78—59934
melting and dislocations in two and three dimensions 80—103454
metal, thermodynamics of electrons, dislocation dipole and prismatic dislocation loop effects *(Russian)* 79—56161
metals under load, plastic deform. local instability *(Russian)* 77—76415
narrow dipoles, high density, electron diffr. numerical eval. 78—71645
ordered alloy, noncoaxial dislocation loop behaviour 77—11549
semiconductor, charged dislocation, hole capture cross section *(Russian)* 78—23108
semiconductor, electron multiphonon capture by edge dislocation *(Russian)* 79—86861
semiconductor, recomb.-enhanced defect reactions 77—51377
steel, austenitic stainless, US fatigue meas. 80—40489
steel, pearlitic, deform. microstruct. and cementite fracture, −196 to 700°C 78—27576
steel, stainless, austenitic, deform. substruct. and annealing, stacking fault tetrahedra form 80—107282
steel, stainless, austenitic Ni-Cr type, creep deformed, dislocation multipole obs. 80—107258
two dimensional crystal, rel. to melting transition 78—51645
Ag, fatigued single crystal, annealing of deform. struct. 78—3204
Bi, deformed cryst., phonon scatt. by lattice defects, thermal cond. calc. 78—22802
CdI_2 polytypic crystals, dielectric loss behaviour 80—66108
Co, single crysts., $\{11\bar{2}1\}$ twins, accommodation and form. 80—96540
Cu-Al, faulted dipoles, geometry and form. 78—59809
Cu-Al, linear dislocation multipoles, weak-beam TEM 80—75233
Cu-Al (5.8 at.%) dislocation multipoles, weak-beam electron microscope obs. 79—73171

dislocation dipoles continued
Cu-Cr (0.55 wt.%), crystallography of precipitates, strain field study 80—25699
Cu-Cr-SiO_2 system, age and dispersion strengthened, dislocation struct. around SiO_2 particles 80—108468
Cu-Si (6.5 at.%) alloy, easy glide deform., obs. and mechanism 77—8887
(GaAl)As-GaAs, double heterostructure laser, TEM study of dark line defect growth from dislocation clusters 79—33206
GaAlAs-GaAs DH lasers, degradation caused by growth of dislocation networks 80—53289
$Ga_{1-x}Al_xAs$ DH catastrophically degraded laser, TEM obs. of defects 80—32989
$Ga_{1-x}Al_xAs$, degraded DH LED, defect struct. by electrolum. topography and TEM obs. 79—60369
$Ga_{1-x}Al_xAs$, rapidly degraded LED, defect struct. of ⟨100⟩ dark lines 78—10052
$Ga_xAl_{1-x}As$-GaAs DH laser, degraded, nature of ⟨110⟩ dark-line defects, TEM 77—89439
GaAs heterojunction laser, origin of dislocation climb during laser operation 77—51380
GaAs, point defect generation by electron-hole recombination at dislocations 79—37699
GaAs-GaAlAs LPE layers, DH material, TEM obs. of crystal defects 78—6241
GaP, dislocation loops and bipolar obs. by chemical etching 78—55873
GaP, LPE layer perfection, effect of dislocation loops in GaP substrate 78—30843
KCl (100), elec.-mech. coupling of dislocations 78—75676
KCl, dislocation motion in micro-plastic region, direct obs. via charged dislocation p.d. 78—91341
KCl, elec. field effect on flow stress, charged-dislocation model 77—27935
LiF (100), elec.-mech. coupling of dislocations 78—75676
LiF, dislocation structure, influence of variable deform. temp. 80—70211
NaCl (100), elec.-mech. coupling of dislocations 78—75676
NaCl, dislocation motion in micro-plastic region, direct obs. via charged dislocation p.d. 78—91341
NaCl, γ-irrad., F-stimulated inversion of sign of dislocation charge 80—59475
NaCl, high resolution TEM and radiation sensitivity, dislocation obs. on deformed crysts. 80—107260
NaCl, plastically deformed, integrated X-ray reflection coeff. determ. 77—65981
NaCl, X-irrad. dose depend. of dislocation charge 77—47464
NaCl(:Mn^{2+}), influence of elec. field on flow stress 79—51193
Ni, stacking fault energy, by electron microscope obs. of dissoc. edge dislocations and faulted dipoles 77—72627
Si, Czochralski grown crystals, swirl-type defect obs. 80—100236
Si, deformed, faulted dipole, TEM obs. 78—38712
Si, deformed crystal, faulted dipoles 78—59814
Si, dislocation dipole lattice image, stacking fault energy 79—60375
Si, floating zone structural perfection changes by high temp. treatment, dendrites, dislocation interactions 80—29049
Si, thermally induced microdefects, effect of C, TEM obs. *(Japanese)* 80—54244
Si:B, implanted, shrinkage of rod shaped defects 78—6061
Si:B, ion-implanted, dislocation climb, TEM obs. 78—6062
Si:B, ion-implanted, rod-like defects, TEM obs. 77—68975
Si:Cu, interaction between vacancy emitting absorbing precipitates and dislocations, TEM obs. 78—71755
V_3Si, lattice defect, high voltage electron microscopy *(French)* 79—27993
Y_2O_3, plastically deformed monocryst., HV electron microscopy obs. of dislocation config. *(French)* 79—55747
ZnS crystals, structural change under plastic deform., partial dislocation movement 80—79736
ZnS, glide plane of dislocations 79—46667
ZnS, interaction between charged dislocations and luminesc. centres *(Russian)* 79—56860
ZnS, plastic deform. induced luminesc., dislocations role *(Russian)* 78—10985
ZnSe, nature of large electric charges of moving dislocations *(Russian)* 78—39065

dislocation drag
alloy, substitutional solid soln., irradiated creep rate enhancement theory 77—63739
α-brass, single crystal, deform. and ductility at elev. temps. *(Japanese)* 79—5012
edge dislocation motion, glide and climb resist. due to dragging a Cottrell atm. 79—99194
ferromagnet, flow stress, effect of magnon mechanism of dislocation drag 77—69662
ferromagnetic metals, dislocation drag by conduction electrons 80—24451
internal friction peaks, dislocation-defect elastic force in dragging model 80—39104
lattice drag force on moving dislocation, zero temp. 79—95006
liquid inclusions, thermal migration, dislocation drag 77—7911
magnetically ordered cryst., dislocation drag, magnetoelastic waves 80—103332
metal, electron drag od dislocations 80—10961
phonon wind as a nonlinear mechanism of dislocation dragging 79—69215
point defect dragging, unified theory of dislocation damping 80—88144
point-defect dragging effect on dislocation motion, extended model 78—10083
segments, pinned, effects of viscosity on quantum motion *(Russian)* 80—44207
steel, low-alloy, plastic deform. mechanisms under dynamic loading 80—100883
thermal drag force on moving dislocation, non zero temp. 79—95007
viscoplastic flow, coupling of dissipative mechanisms 78—38206
Al, creep and rupture, in torsion, mech. *(Russian)* 79—5030
Al, electron drag on mobile dislocations at low temps., strain rate, temp., and field depend. 80—19808
Al-Cu (4 wt.%) alloy, coherency loss of θ'-phase due to deform. 77—15424
Al-Mg (0.3 wt.%) single cryst., dislocations obs. by high voltage electron microsc. 80—79796
CsI, yield point, obstacles to dislocation motion 77—43270
Cu, dislocation damping during electron irrad. 77—76462

dislocation drag continued
Cu, electron drag on mobile dislocations at low temps., strain rate, temp., and field depend. 80—19808
Cu-Al (10 at.%) alloy, work hardening at high temp. 77—32589
LiF single crystals, dislocation motion and generation on plate impact 79—95011
LiF, viscous drag of dislocations, internal friction, 4.2-300K 77—11566
LiF, viscous drag of dislocations exam., using mobility of individual dislocations 79—14814
NaCl, effect of dislocation density on viscous drag dislocation coeff. *(Russian)* 77—80512
NaCl, viscous drag of dislocations, internal friction, 4.2-300K 77—11566
NaCl:Co^{2+}, dynamic braking of dislocations *(Russian)* 78—6068
Nb, electron drag on mobile dislocations, flow stress meas. 79—91197
Ni cryst., 80 and 298K, dislocation drag coeffs. and US wave attenuation 77—76491
Pb, dislocation electron drag coeff. temp. depend., internal friction method, superconducting state 80—29031
Pb-2n, work hardening in mixed state *(Russian)* 79—42707
Pb-In, viscous drag on mobile dislocations, plastic deformation, critical temp. magnetic data 78—43514
Pb-Sn(Ag), dil. alloys, dislocation motion and electron-dislocation interactions 77—7728
Sb, temp. depend. of dislocation drag const. 77—11565
Si:Cu, interaction between vacancy emitting absorbing precipitates and dislocations, TEM obs. 78—71755
Si:Sb(P)(B)(Ga), low angle boundary formation, in single crysts., effect of impurities on cryst. growth conditions 80—11555
Ta, flow stress, temp. and strain rate depend. 77—77534
Ti, cold worked, annealed, internal friction meas. of H degassing *(French)* 79—43304
Ti, high purity, flow stress relaxation *(French)* 77—86117
Zn, twinning, influence of dislocation drag. mag. field effects 80—59472

dislocation energy
alkali halide, deformed single cryst., dislocation struct. formation *(Russian)* 77—7733
anthracene, slip systems in deformed crysts., dislocation elastic energy 79—42138
anthracene crysts., mol. orientational disorder calc. vacancies, dislocations, photodimerisation 77—4915
composite dislocations, asymm. equilib. positions and line tensions 79—51108
creep, minimisation of free energy due to viscoelastic strain and dislocations 77—24348
crystal elastic and plastic anisotropy and dislocations *(Japanese)* 79—95069
displacement energy determ. by electron beam induced conductivity 80—70097
dissociation, effect on dislocation energy and line tension 79—27985
epitaxial interface, energy of dislocation 77—43457
film/substrate, two-layer structs., relaxation of internal stresses 80—34341
foils, interaction of finite co-planar dislocation pieces 77—51375
grain boundary energy-misorientation relationship use in modelling grain boundary defects and props. 80—84188
HCP crystals, dislocation-point defect interactions in slip systems 78—47417
heterojunction, compositionally graded, misfit dislocation energy calc. 77—59237
III-V compounds, dislocation half-loops, nucleation and generation 79—95009
melting, dislocation theory, Clausius-Clapeyron eqn. and cross press. depend. 78—18744
metal, BCC, screw and 71° dislocations, energies of kinks and contrictions *(German)* 77—19950
metallic thin film, polycryst., plastic flow, dislocation slip 79—82505
metals, BCC, dislocations, anisotropic elasticity theory *(Japanese)* 79—10853
metals, stacking fault energy meas. by electron microscopy *(French)* 79—42079
metals and alloys, relative cavitation strength 77—12672
muscovite, exam. of dislocations and props. using elasticity theory *(German)* 79—10854
Peierls model, dislocation core energies 79—27984
plastic shear crack, discrete dislocation anal. 79—50659
polyethylene, theory of adhesion to alkali halide crystals, allowance for boundary dislocations 77—70280
quartz, dislocations, elastic energy *(French)* 79—14807
self-energy of straight line dislocation segments, pseudo-continuum theory 78—30613
semiconductor, dislocation pot., free carrier absorpt. spatial orientation and freq. depend. obs. 80—39546
stacking fault, antiphase boundary energies, investig. methods, review, appls. to FCC metals *(French)* 79—42080
straight edge dislocation in nonlocal elasticity, stress field, elastic energy 77—35555
straight edge dislocations, nonlinear computation of anisotropic elastic fields 77—7718
superconductor, electrostatic interaction of dislocations *(Russian)* 78—23198
two-dimensional Lennard-Jones model, computer calc. 77—11550
two-face dislocation boundary, energy and induced stresses *(Russian)* 80—103331
two-phase anisotropic medium, interfacial dislocation, stresses, displacements and energy calc. 80—79786
Ag, dislocation core energy, core tension, Peierls model 79—27984
AgMg, B2 intermediate phase, slip system, ordering energy and atomic size ratio depend. 80—59471
AgZn, B2 intermediate phase, slip system, ordering energy and atomic size ratio depend. 80—59471
$Al_2Be_3(Si_6O_{18})$, beryl single crysts., dislocations obs., X-ray topography *(French)* 79—37709
As, rhombohedral crystals, slip dislocations and slip systems 79—23617
AuMg, B2 intermediate phase, slip system, ordering energy and atomic size ratio depend. 80—59471
Bi, rhombohedral crystals, slip dislocations and slip systems 79—23617
Cu, dislocation core energy, core tension, Peierls model 79—27984
Cu, meas. of stored energy by work hardening and dislocations *(French)* 77—44273
Cu-Al, dislocation core energy, core tension, Peierls model 79—27984

dislocation energy continued
Fe-Co, film, magnetisation induced uniaxial anisotropy, dislocations effects 78—43618
Ge, plastically deformed, photocond. and absorpt. spectra, dislocation levels 77—28219
Hg, rhombohedral crystals, slip dislocations and slip systems 79—23617
Kr monolayer, on graphite, misfit dislocations and lattice parameters, model 78—34708
MgO, core struct. and energy of dislocations, breathing shell model calc. 77—39586
MgO crystals, dislocation core energy from etching data 80—39100
NaCl, edge dislocation, core struct. and props., theory 80—70194
NaCl, edge dislocation dissoc. energy, atomistic calc. 77—27883
NaCl, edge dislocation dissoc., computer simulation of core struct. 79—37703
Ni 200, C interstitial effect of yield point develop. during static strain ageing, model 78—88498
Ni, dislocation core energy, core tension, Peierls model 79—27984
Ni-Co, film, magnetisation induced uniaxial anisotropy, dislocations effects 78—43618
Nr-Cr-ThO_2 (20, 2 vol.%), Orowan stress/creep threshold stress comparison 77—8901
Sb, rhombohedral crystals, slip dislocations and slip systems 79—23617
Si, Frank hexagonal interstitial loop, dissoc. energy 77—35556
TiO_2, crystal dislocations, elastic parameters, elastic energy, stress field, anisotropic elasticity theory 79—95008
Xe monolayer, on graphite, misfit dislocations and lattice parameters, model 78—34708

dislocation etching
alkali halides, exposed to US waves, dislocation multiplication in original stage 78—47383
alumina, prismatic slip dislocations in single crystals, obs. *(French)* 77—59016
amethyst crystals, dislocations, selective etch method 78—75674
anthracene, dislocations effect on elec. props. 77—35947
anthracene crystals, basal dislocations, fluoresc. spectra and etching obs. 77—84755
β-brass, dislocation etchant, $(NH_4)_2S_2O_8$-HCl-H_2O 80—65004
C GaP on GaAs substrate, heteroepitaxial layers, stuct. defects *(German)* 79—23865
β-copper phthalocyanine, dislocation detection *(German)* 78—63773
β-copper phthalocyanine, dislocation etching kinetics *(German)* 78—67719
β-succinic acid, cryst., slip system and dislocation detect. by etching 77—59015
diamond octahedrons, by high press. water 77—55285
dielectric, thermal mechanism of plastic deformation and fracture by laser beam 77—11553
dislocation density, rocking curve half-width obtained by double X-ray crystal spectroscopy in single crystal 78—2131
etch figure rosettes, dislocation interaction in screw rays 78—47376
ferrites, etch pitting of single crystals *(German)* 78—26568
graphite, single crystal, from Fe-C melt, morphology 78—42932
ice, dislocations revealed by etching 78—22725
III-V semiconductors, structural etching, characterizing $A^{III}B^{V}$ compounds, misfit dislocations 80—39099
light figures, math. description based on simplified morphological model 77—4104
lithium formate monohydrate, thermal dehydration, dislocation effects 80—3331
monostearine crystals, spiral growth from organic soln. 80—93467
phthalic anhydride, single crystals growth and perfection 79—78869
quartz, dislocation struct. in deformed grains 77—39590
quartz, hydrothermally grown single crystals, real struct. investig. of rhombohedral faces *(German)* 78—2348
quartz, synthetic, inclined dislocations 79—99200
α-quartz dislocation free and low dislocation, prep. by hydrothermal crystallisation 78—72712
ruby, single crystal surface disruption after polishing investigation by chemical etching *(Russian)* 79—38995
sapphire substrate, Czochralski grown, etch pits and dislocations 79—37708
semiconductor, dislocation density determ. with Kontrast automatic mineralogical analyser 79—51111
sodium tartrate tetrahydrate, gel-grown single crysts., charact. 77—90261
starting stresses of dislocations obtained from etch figure rosettes 77—68979
statistical approach to dislocation multiplication 80—49230
stearic acid, etch pit obs. of dislocations 78—87676
stearic acid, etching on large single crysts. 77—89442
stearic acid crystals grown from solution, spatial correlation between growth spirals and inclusions 80—96527
steel, mild, fractography study of shear mode fatigue crack growth by etch pits *(Japanese)* 80—108545
surface dislocation, depth localization definition by HF gas-discharge plasma *(Russian)* 77—31664
m-toluenediamine, single crysts., revealing dislocations by selective etch pit technique 77—11560
velocity, thermal activation exam. of applied stress and temp. depend., expt. methods *(French)* 80—59474
Ag and Ag-Sn(In)(Sb) dil. alloy, single crystals, dynamic dislocation behaviour 77—4108
Ag single crystal, dislocation density decrease during reverse deform., obs. by etch-pit method 77—7725
Ag, surfaces, dislocation climbing, etch pit investig. 79—19260
Al, high purity single cryst., etch pit morphology and their correl. with microstruct. *(French)* 79—69106
$Al_xGa_{1-x}As$, epitaxial layer struct., dislocation etching obs. 77—85095
AlGaAsP(Sb), compositional grading by LPE 80—10844
Al_2O_3, substrate material requirements for GaN VPE *(Polish)* 77—43440
As, (111) surface, freshly cleaved, vaporisation, surface morphology changes obs. 77—80612
BaBrF, reacted flux growth, dislocation density, dielec. const. and loss, IR spectra 77—36214
BaF_2, synthetic single crystals alkali compounds etching 79—95018
BaFBr, single cryst. growth by flux method, dislocation etch pits on dissoln. 79—56925
$BaT{:}O_3$, surface microrelief revealed by ion irradiation 80—54485

dislocation etching continued
Be_2SiO_4, phenakite, flux grown single crysts., twinning study by hydrothermal etching and X-ray diffr. 80—107271
Bi, (111) plane, chem. and thermal etch pit orientation, reactivity depend. 77—35559
Bi-Sb, single cryst., role of complexing agents on etching characts. 80—54238
$Bi_{12}GeO_{20}$, selective dislocation etching in nonaq. Br_2 solns. 79—77601
Bi_2Te_3 single crystals, melt grown, structural perfection 80—15101
CaF, etched in H_2SO_4, dissolution kinetics of $CaSO_4$ on {111} faces 80—2028
CaF_2, adsorption mechanism in selective etching 77—7727
CaF_2, cryst., (111) faces, selective etch rate and etch pit morphology, acid conc. and temp. effect 80—96524
CaF_2, crysts., adsorption processes in selective etching 80—39098
CaF_2, etching behaviour in HCl vapour 78—59812
CaF_2, etching in H_2SO_4, etch pit morphology and $CaSO_4$ growth 80—6408
CaF_2, fluorite crystals, surface struct., growth mechanism 79—99096
CaF_2, single cryst., dislocation etch pit shapes, dislocation line inclination effects 77—7722
$Cd_xHg_{1-x}Te$, crystallisation from solution in Hg 77—19883
$Cd_xHg_{1-x}Te$, determ. of slip planes by dislocation etching 79—82220
CdS, cryst. grown from melt under press., microstruct. 77—59019
n-CdTe, cathodoluminescence microscopy obs. of dislocations, compared with etch pit pattern 79—69105
CsI, {100} faces, form. of etch pits of different size and morphology, segregation influence 78—2130
CsI cryst., dissolution, selective etching rel. to $CuCl_2.2H_2O$ additive in ethanol 77—72618
CsI, selective etching, growth and dissolution in alcohols 78—71739
Cu, dislocation motion in highly perfect crystals *(Japanese)* 79—60373
Cu, electron irrad. at 100K, dislocation vel. meas. etch pit technique 80—49271
Cu, etch pit formation on single cryst. planes by dil. H_2SO_4 78—14348
Cu, highly perfect crystal, dislocation motion obs. *(Japanese)* 79—60372
Cu, ion bombarded, cone form. and associated surface features 77—59054
Cu, neutron irradiation at 200 to 400°C, decoration of dislocations damage clusters 77—24332
Cu plastically deformed crystals, SEM exam. of light and dark etch pits, dislocation arrangements 78—87679
Cu, prismatic dislocation loops revealed by X-ray topography and etching 77—11563
Cu, single crystals, dislocation breakaway, etch pit study 78—6064
Cu, soft crystal, US irrad. induced dislocation distrib. 77—32584
Cu, well annealed crystal, etch pit technique refinement, dislocation config. study *(Japanese)* 79—4307
Cu-Al, single crystal, dislocation velocity meas. 78—3171
α-Cu-Al (0.5 to 10 at.%), latent hardening and dislocation density 78—19853
Cu-Al (10.5 at.%), dislocation generation and displacement in single crystal in bending 79—60368
Cu-Al (15 at.%), single crystal, steady state deform. with ⟨001⟩ axis at high temp. *(Japanese)* 78—6980
Cu-Al (15 wt.%) single crystal, steady state deform. at high temps. *(Japanese)* 78—19833
Cu-Al (2.5 at.%), single crystal, steady state deform. at high temps. *(Japanese)* 77—52415
Cu-Al (7.5 at.%), single crystal, etched under load, slip bands 77—89446
Cu-Al (<3 at.%), new type of discontinuous slip at low temps. 77—12676
Cu-Al dil. alloy crystal, dislocation etch pits on {111} surfaces *(Japanese)* 77—62536
Cu-Al dil. alloys, dislocation etch pit obs. on {111} surfaces 79—10861
EuS, defect struct., etch pitting and electron microscopic obs. 79—27989
Fe, microhardness of single crysts. effect of temp. on dislocation structure *(German)* 79—52357
Fe-Si as grown crystal, dislocation study by etching and X-ray topography 78—47377
$FeGe_2$, single cryst. perfection depend. on growth rate and direction 80—55284
FeS_2, adsorption mechanism in selective etching 77—7727
FeS_2, etching of dislocations 77—7726
Fe_3Si, etching of slip produced antiphase domain boundaries 78—63769
$Ga_{1-x}Al_xAs$-GaAs, grown by LPE, direct obs. of dislocations 79—65087
$Ga_{1-x}Al_xAs$-GaAs heterojunctions grown by metallorganic CVD 80—15599
GaAs, (100) surface, etch pit density meas. using automatic struct. analyser EPIQUANT *(German)* 77—72619
GaAs {001} layer, LPE, dislocation etch pits revealed by molten KOH 78—63772
GaAs, AB etch reappraisal 78—6065
GaAs, anodically oxidised, etch pits, defect characterisation 77—56122
GaAs cryst., creep and dislocation vel. at different doping and temps. 78—95783
n-GaAs, current-voltage characts., dislocation etch pits and perfect cryst. 80—70695
GaAs, defect revealing etchant, electrochem. process in $NH_4OH{:}H_2O$ 78—6060
GaAs, dislocation etching of {100} and {111} planes of As 77—43215
GaAs, doped with Group IV elements, etching, electron spectra, cathodoluminesc. study of inhomogeneities 77—11556
GaAs, epitaxial layer, nondislocation etch pits 80—92535
GaAs, etched, saucer-pit defect identification 78—43021
GaAs, LPE, dislocations obs. by etching 79—95284
GaAs LPE (001) layer, etching by molten KOH 78—34515
GaAs, LPE layers, ambient O_2 effect on defects and elec. props. 77—76683
GaAs, n- and p-type, velocities of α- and β-dislocations, double-etch method 77—51382
GaAs, polishing dislocation etch 78—6066
GaAs, structural defects, detection by electrochemical etching 78—55872
GaAs surface morphology during etching with H_2O vapour 80—39094
GaAs, travelling heater method growth, dislocation elimination 77—7684
GaAs-AlGaAs DH laser, improved lifetime by defects reduction during LPE 77—75547
Ga(AsP), dislocation etching of (001) faces with H_3PO_4 etchant 80—15103
(GaIn)P, dislocation etching of (001) faces with H_3PO_4 etchant 80—15103

dislocation etching continued
- $Ga_xIn_{1-x}P_yAs_{1-y}$, 111-A and 111-B faces, defect struct., etching and X-ray diffr. obs. 80−2026
- GaN:Zn LED, electrolum. centres, rel. to growth morphology, Zn conc. and etch patterns 77−1733
- GaP (001), dislocation etch pits 78−14351
- GaP, dislocation etching of (001) faces with H_3PO_4 etchant 80−15103
- GaP, dislocation loops and bipolar obs. by chemical etching 78−55873
- GaP, electron traps around dislocations in p-n junction and metal-semicond. structs. 80−34388
- GaP epitaxial layers grown in Ga-PCl_3-H_2 system, surface defects 77−7993
- GaP, LEC crystal, cathodolum. and photolum. around dislocations 78−84663
- GaP LPE layers and LEC substrates, correlation between dislocation pits 78−38706
- GaP, mech. props. and photomechanical effect 77−84833
- GaP, polishing dislocation etch 78−6066
- GaP, preferential etching of dislocations and stacking faults 77−39589
- GaP, structural etching, characterizing $A^{III}B^{V}$ compounds, misfit dislocations 80−39099
- GaP, thermal etch-pits, morphology 80−34002
- GaP:S LEC grown crystals, HVEM investig. of defects 79−60376
- GaP-ZnS, solid solns., microstruct. investig. 78−2128
- GaSb, dislocation velocities, double etch technique exam. 78−30629
- $Gd_3Ga_5O_{12}$, decorated dislocations, large interstitial climb loops round precip. particles 77−19960
- $Gd_3Ga_5O_{12}$ dislocation anal. at inclusions by repeated etching technique 80−29024
- $Gd_3Ga_5O_{12}$, single cryst., helical dislocation obs. by etching 77−11558
- Ge, dislocation motion near surface 79−82219
- Ge, microdefect distrib. due to dislocation injection, selective etching 78−2122
- Ge, screw dislocation loops, shrinkage vel. and cross slip freq., activation energies *(German)* 78−43028
- InAs, dislocation velocities, double etch technique exam. 78−30629
- InAs, undoped n-type single crystals, dislocation velocity 77−11559
- InBi, single cryst. zone melting growth and etching 79−34189
- $In_{1-x}Ga_xAs$, LPE layer on InP substrate, phys., elec. and optical props. 78−39235
- InP, and InP_xAs_{1-x}, 111-A and 111-B faces, defect struct., etching and X-ray diffr. obs. 80−2026
- InP, Czochralski grown, etch pit obs., produced by new etchants HBr/HF or HBr/CH_3COOH 79−60370
- InP, dislocation etching of (001) faces with H_3PO_4 etchant 80−15103
- InP, synthesis solute diffusion grown, elec. props., photoluminesc., etch pit profiles 79−4914
- InP:Te(S), heavily doped, dislocation imaging using transmission cathodoluminesc. 80−29023
- InP/InGaAsP/InP double heterostructure, grown on InP(111)B substrate, threading dislocation multiplication 80−54237
- InSb, plastically bent single crysts., dislocation struct. obs. 78−59816
- KBr, quench hardening related to dislocation density and slip 78−52855
- KBr, rot. of vacuum thermal etch pits 78−87674
- KCl, crystals, grown by Czochralski method, effect of growth rate on defect generation 79−51032
- KCl, dislocation etchant 77−4103
- KCl, etching, double poison role 80−54240
- KCl-KBr, mixed cryst., radiation hardening 79−99238
- KCl-KBr mixed crystals, microhardness studies, nonlinear depend. on composition 78−83872
- KH_2PO_4 single crystal evidence for spiral growth on pyramidal faces 80−84120
- K_2O-SrO-Nb_2O_5 system, selective delineation of dislocations by etching 77−72617
- LiF, (100) face, surface layer and dislocation etch pits 77−19962
- LiF crystal, dislocation movement study with new chem. polish 78−15614
- LiF, deformed, influence of surface on density of edge components of dislocations 77−31670
- LiF, dislocation distrib. on surface parallel to Burgers vector 79−65090
- LiF, dislocation structure, influence of variable deform. temp. 80−70211
- LiF, single cryst., impression creep 78−6986
- LiF single crystals, dislocation motion and generation on plate impact 79−95011
- α-$LiIO_3$, dislocation etching 78−18653
- α-$LiIO_3$, dislocation struct. 77−1132
- Mg, etch pits at dislocations in single crystal 77−72622
- MgO, adsorption mechanism in selective etching 77−7727
- MgO crystal, chemical etchant for old and fresh dislocations 79−65088
- MgO crystals, dislocation core energy from etching data 80−39100
- MgO, crysts., adsorption processes in selective etching 80−39098
- MgO, dissolution mechanism in acids 80−39296
- MgO, etchant for revealing dislocations in (100) surface 79−19252
- MgO, in acids, surface micromorphology 77−15419
- MgO, precipitation on dislocations, ultramicroscopy and chem. etching 78−67720
- MgO, single crystals, compressed, SEM exam. of cathodoluminescence 78−56525
- MgO, spherical particle impact damage, effect of crystallographic orientation 79−79135
- $MgSiO_2$, kinetics of dislocation etching 80−6409
- Mg_2SiO_4 crystals, morphology and dislocation etch pits, (010) surface 80−24457
- Mg_2SiO_4 crysts., dislocations configuration and cleavage steps dissoln. 80−107250
- Mg_2SiO_4, dislocations revealed by etching 79−99199
- Mg_2SiO_4, single cryst., (010) cleavages, etch patterns and dislocations, interferometric obs. 78−2127
- Mg_2SiO_4, single cryst., preferential dissolution in molten KOH (NaOH), etching obs. 78−34513
- Mg_2SiO_4, etch pits in cleaved faces, revealing low angle boundaries 79−14818
- NH_4ClO_4:Cu^{2+}, dislocation etch pits exam., rel. to thermal decomp. 77−11555
- $NH_4H_2PO_4$ single crystal evidence for spiral growth on pyramidal faces 80−84120
- $(NH_4)_2S_2O_8$-HCl-H_2O dislocation etchant for β-brass crysts. 80−65004
- $Na_2Al_2Si_3O_{10}.2H_2O$, natrolite, cleavage etching in acidic and neutral media 80−6407

dislocation etching continued
- NaCl, and NaCl-NaBr, Ca-doped, dislocation struct., etch pit obs. 78−43020
- NaCl, deformed, influence of surface on density of edge components of dislocations 77−31670
- NaCl, dislocation density, laser beam effect, electron microscopy of etch pits 77−11553
- NaCl, dislocation distrib. on surface parallel to Burgers vector 79−65090
- NaCl, dislocation rosettes around Vickers diamond pyramid indents, quenching effect 80−11740
- NaCl, effect of annealing and neutron irrad. on block struct. 80−29061
- NaCl, effect of dislocation density on viscous drag dislocation coeff. *(Russian)* 77−80512
- NaCl, high density of dislocations meas., new etchant 78−43019
- NaCl, motion of individual surface dislocation semi loops *(Russian)* 78−51542
- NaCl, quench hardening related to dislocation density and slip 78−52855
- NaCl, strained in one glide system at 450°C, dislocation struct. 78−22728
- NaCl type crystal, dislocations due to high temp. stress relax. 78−2126
- $NaClO_3$, cryst. growth from soln., selective etching technique for observation of dislocations 79−19251
- NaF, deformed, influence of surface on density of edge components of dislocations 77−31670
- Nb, dislocation etching of single crystal 78−14352
- Nb, single crystal, surface oxide softening, TEM obs. 77−40462
- Nb, surface oxide softening, anisotropy 78−60716
- $NdGa_5O_{12}$ wafer, dislocations, etch pits and birefr. obs. 78−83818
- $Nd_xY_{1-x}P_5O_{14}$, NdP_5O_{14}, laser materials, flux evaporation growth, dislocation etch tunnels 77−35560
- Ni-Cr alloys, method of etching in Br-methanol reagent 77−90516
- $PbFe_{12}O_{19}$, dislocation etch pit morphology study *(Chinese)* 80−88150
- $PbNb_2O_6$, surface (001), microstruct. obs. by optical, etching, and interferometric techniques 79−11399
- PbS, adsorption mechanism in selective etching 77−7727
- PbS, epitaxial layer, structural nonuniformities and dislocation struct. 79−23852
- $Pb_{1-x}Sn_xTe$ LPE grown heterostructures, dislocation etch pitch, interfaces 80−2023
- $Pb_{1-x}Sn_xTe$-PbTe heterojunction, Sn diffusion and elec. effects of dislocations, elec. and metallurgical expts. 77−89839
- Se-Te single crystals, chem. etching 80−96526
- $Se_{90}Te_{10}$ whiskers, chem. and thermal etching 77−15417
- Si, ⟨100⟩, defect etch for evaluation 79−90657
- Si, crystal defects and impurities interaction obs. by electron microscopic methods 80−65003
- Si, Czochralski cryst., hillock etching of microdefects, TEM obs. 78−87678
- Si, Czochralski grown, intrinsic gettering by oxide precipitate induced dislocations 77−27903
- Si, Czochralski grown crystals, swirl-type defect obs. 80−100236
- Si, Czochralski growth, drop form. and crystn. rel. to dislocation struct. 78−2030
- Si Czochralski wafer oxide precipitate-dislocation complex characterisation 78−14357
- Si, dislocation dynamics during plastic deform., stress-strain characts. 79−27996
- Si, dislocation etch pits on various cryst. planes 77−24317
- Si, dislocation formation, under high stress, low temp. 78−47386
- n-Si, dislocation free, memory effect associated with appearance of prismatic dislocation loops 77−1130
- Si, dislocation generation in local oxidation 80−107245
- Si, dislocation motion near surface 79−82219
- Si, dislocation-free single crystals, growth microdefects, etching and X-ray expts. 78−47385
- Si epitaxial stacking fault nucleation site identification, annihilation, and suppression 77−76705
- Si, filamentary crystals, branching and bending obs. 77−7954
- Si film, high electron mobility, grown on sapphire at high growth rate 77−81225
- Si film, on sapphire, etching method 78−7070
- Si, integrational etching composition and method 78−10055
- Si, isolated dislocation motion, velocity determ. *(Chinese)* 80−107243
- Si, lattice damage, influence of laser annealing 79−23608
- Si, MBE, on n^+ Si, with wide range doping control 78−27402
- Si, microdefect distrib. due to dislocation injection, selective etching 78−2122
- Si, new preferential etch for defects in (100) and (111) oriented n- and p-type cryst. 77−59954
- Si, nucleation of stacking faults at oxide precipi tate-dislocation complexes, TEM 77−19967
- Si, polycryst. film on Si, disloc. config. obs. 78−10312
- Si single-crystal grown-in structural defects 79−10860
- Si substrate, stress field, induced by Si_3N_4 film edge, indentation-injected dislocation half-loops obs. 78−30839
- Si, swirl type defects in float-zone and Czochralski single crysts. 79−27992
- Si thin films, selective etchant 79−86793
- Si, zone melting, swirl defects A-type as source of dislocation generation on macroscopic scale 80−25554
- Si:As, ion-implanted, dislocation loops and etch pits, X-ray diffr. and TEM obs. 79−42068
- Si:B(Sb)(P), microdefect formation depend on doping, Cu decoration, X-ray transmission topography, preferential etching 79−69120
- 6H-SiC, dislocation etching 78−22721
- Si_3N_4 film on Si substrate, dislocation generation at film edge, suppression effect of SiO_2 80−2025
- Sn, edge dislocation walls with Burgers vector 1/2⟨111⟩ 79−99202
- Sn, single crystal, dislocation walls consisting of double arrays 79−46664
- Sn, white, configurations, formation and Burgers vector of coupled dislocations stradlling polygon wall 78−26569
- Sn, white, single crystal, dislocation movement in pre-yield region, etch hillock technique 79−60371
- SnS, single cryst. growth and struct. props. 79−52109
- $Sr_{1-x}Ba_xNb_2O_6$, and Nd doped growth of low dislocation density cryst., dislocation struct. 77−40348
- SrClF, SrBrF, reacted flux growth, dislocation density, dielec. consts. and losses IR spectra 77−36214
- $SrTiO_3$, surface microrelief revealed by ion irradiation 80−54485

dislocation etching continued
Te, a-edge dislocated crystals, mobility anisotropy 80—107781
Te crysts., thermal etch pits shape on cleavage faces 80—107251
W, vapour deposited, dislocation struct., rel. to texture *(Russian)* 80—65394
W wire reinforced Cu, microfield, flow stress 78—27575
$(YBi)_3.(FeGa)_5O_{12}$ film, interaction between Bloch walls and dislocations *(Russian)* 79—61196
YIG, single cryst., high temp. dislocation mobility 79—19255
Y_2O_3 fused single crystals, struct. 80—19804
Zn, basal slip, early stages in single crystal 77—72623
Zn, dislocation etch on (0001) surface of single crystal 79—65091
Zn, dislocation etch pits on (0001) surface of single crystal *(Japanese)* 78—59811
Zn, dislocation mobility under action of current pulses, selective etching meas. 79—19259
Zn, glide dislocations, second order pyramidal band, etch pit obs. of pure single cryst. *(Japanese)* 78—38716
Zn, highly perfect crysts., Bridgman growth, dislocation density rel. to annealing *(Japanese)* 80—40252
Zn, vacancy concentration meas., lattice parameter and length changes, form. parameters 79—37697
ZnS, (111) face, flux-grown cryst. dissolution characts. 77—59014
ZnS, cryst. grown from melt under press., microstruct. 77—59019
ZnSe, growth centres, crystallographic parameters and etching patterns study *(French)* 79—41998

dislocation glide *see slip*

dislocation interactions
see also impurity-dislocation interactions; vacancy-dislocation interactions
alkali halide, doped single crystals, plastic anisotropy 78—26575
alkali halide, low temp. radiation hardening mechanism, dislocation-interstitial elastic interaction 79—23636
alkali halide conc. solid solns., hardening theory, dislocations, stress effects 79—32994
alkali halide crystals, deformation spectroscopy, dislocation interactions with electron and hole centres 78—10983
alkali halides, microcryst. powders, colour centres, refl. spectra 78—23493
alloy, two phase, deform. 77—8893
alloy with dispersion precipitate of ordered phase, yield limit theory surmountable pair mech. *(Russian)* 77—1855
alloys, $L1_2$, superstructure, dislocation link strength and strain hardening at high degrees of deform. *(Russian)* 78—39792
amorphous Lennard-Jones solid, edge and screw dislocation, stability, elasticity, simulation 80—15099
anthracene, triplet exciton trapping by dislocations 78—30871
antiferromagnet, moving dislocations, interaction with spin waves *(Russian)* 78—56303
BCC metal, discrete-continuum hybrid method for dislocation-point defects interaction 77—89467
bias and point defect relaxation volumes 79—99248
Bordoni relaxation models, internal friction and microdeformation rel. to dislocations *(French)* 79—37758
with coherent, stress-free, ordered particles 79—27988
collective behaviour, velocity of slip band and mobile dislocation densities, HVEM study *(French)* 80—65006
collective dislocation motion, dynamic effects 78—79632
computer simulation of straight dislocation line motion in concentrated solid soln. 77—15413
Coulomb vector gas in two-dimens., melting 79—69449
crack propagation effect of 2- or 3-dimensional macrodefect *(Japanese)* 80—104261
creep, swelling and growth, radiation induced, bias factors estimated from self-consistent model 80—88249
critical resolved shear stress, from misfitting particles 78—79613
cross slip dislocation self-interaciton, Orowan loops 80—24453
crystal elastic and plastic anisotropy and dislocations *(Japanese)* 79—95069
crystalline body, dislocation interaction between pores while being healed by external pressure *(Russian)* 77—19963
cubic crystal edge and screw dislocation—point defect elastic interactions 80—15151
cylindrical inclusion, motion in dislocation strain field, diffusion theory *(Russian)* 78—18676
cylindrical surface crystals, dislocation interactions 78—95055
dechannelling mechanism due to dislocations, anal. 80—59538
diamond, optically active centre effect on strength props. 80—40462
dilatation centre or disclination, elastic interaction with dislocation 79—55740
dipole-dislocation interactions, theory *(Russian)* 77—80504
discrete obstacle model, dislocation pile-up kinetics dislocation mobility activation parameters 80—29022
dislocation motion, extended model of effects of point defect dragging 78—10083
dislocation movement, in volume dispersion of obstacles, stochastic model, low temp. anomalies rel. to yield stress 79—60367
edge dislocation interactions in infinite array, elastic energy 78—55871
elastic field interaction 80—54233
elastically nonlinear medium, dislocation interactions *(Russian)* 79—42064
electron irradiation, dislocation damping 77—35632
etch figure rosettes, dislocation interaction in screw rays 78—47376
F-centre, dislocation influence on optical props. 80—108234
ferroelastic, dislocation-phonon interactions, phase transition effects 80—59600
ferromagnet, dynamic dislocation deceleration by spin waves *(Russian)* 77—28379
flexible repulsive dislocations, interaction in intersecting slip planes 80—39087
glide, interacting dislocation motion, resisted by point-like barriers, computer simulation 78—71742
gliding, by-passing of hardened particles, coplanar Orowan loops form., stress-strain curves 80—49226
grain boundaries, absorption of dislocations 77—80538
grain boundaries during superplastic deform., dislocation density and diffusion parameters 79—65099
grain boundary dislocation interactions, electron microscopic obs. 78—34517

dislocation interactions continued
grain boundary sliding, containing particles, during diffusional creep, dislocation bowing 79—37712
HCP crystal, dislocation-point defect interactions, anisotropic elasticity theory, appl. to Zr 77—11588
HCP lattice, dislocation nodes equilibrium config. *(Russian)* 78—38699
ice, plastic deformation, ultrasonic wave attenuation by dislocations *(French)* 80—59564
III-V semiconductor, epitaxial layers, dislocations nature, origin and effects 79—28232
III-V semiconductors, piezoelectric induced polarization charge distribs. around point defects 79—56725
Inconel 600, mechanisms of dynamic strain ageing and jerky flow 79—79024
inelastic interaction of crystal lattice defects, estimate of interaction energy 79—69154
interaction force between dislocation, and misfitting ordered particle, calc. 78—83815
interdislocation interaction on account of carriers bound with dislocations 78—75670
internal friction peaks, dislocation-defect elastic force in dragging model 80—39104
ionic crystal, point defect-dislocation interactions 78—63787
ionic crystals, dislocations, review 80—107236
irradiation creep and stress-induced interaction between point defects and dislocations 79—19313
jog-kink interaction, nonlocal continuum theory 77—59043
loops, elastic fields near stress-free surface, loop-point defect interaction 79—4301
magnetic domain boundary, interacting with localised defects, unidimensional flow of configs. *(Russian)* 80—65954
magnetic domain wall, flexibility, rel. to hysteresis 77—4525
mass flux, irradiation enhanced, dislocation interactions 80—88206
metal, electron irrad., elastic point defect-dislocation interactions, defect dragging model extension 80—65050
metal, electroplastic effect 79—24589
metal, FCC or BCC, dislocation annihilation during tensile and cyclic deform. and limits of dislocation densities 80—34007
metal, irradiated, ordered arrangement of micropores on dislocations 77—19943
metal, stress-induced EM effect, phys. model 78—55909
metal, superconducting transition, effect of change of electrostatic interaction of defects 78—10610
metal systems, high voltage electron microscopy of dislocation dynamics *(Japanese)* 77—47458
metallic ferromagnetics, two-magnon scatt. on dislocations, resonance linewidth broadening 77—20708
metallic glasses, structures based on disclination-dislocation model 79—82159
metals, BCC, dislocations, anisotropic elasticity theory *(Japanese)* 79—10853
metals, FCC, dislocation barriers at coherent twin boundaries, anisotropic elasticity solns. 80—96522
metals, FCC, misfit defect and extended screw dislocation anisotropic elastic interaction 80—96563
metals, irradiation induced swelling, bias factor 80—2062
metals, point defect diffusion controlled reaction theory, book contrib. 80—103318
metals, positron trapping at dislocations 78—10091
Mossbauer line broadening, drift-induced, in elastic field of dislocation *(Russian)* 78—19382
motion through random array of point obstacles, vel. load depend. 77—7732
moving dislocations, low-temperature statistical characts. *(Russian)* 79—90654
ordered alloys, effect on mechanical strength *(Czech)* 77—1854
oxides, interaction between point defects and dislocations, cryst. plasticity 80—15149
parelastic force on homogeneous cryst. inclusion, theory 80—79777
periodic grain boundary struct., interaction with lattice dislocations 79—51117
phonon-dislocation interactions, drag of phonon gas by moving dislocations 80—70218
plastic deformation, phenomenological theory, with mobile and immobile dislocations 78—75714
point defect electrons and vibrations, dislocation field effect, dislocation photoconduction spectrum *(Hungarian)* 80—51977
point defect sink strength in irradiated materials 77—51368
point defect-dislocation interaction, radiation-induced creep, rate expression 78—87706
point defect-edge dislocation interaction near solid surface 80—79834
point defects, in non-uniform stress field, localised force approx. 80—15150
point defects, stress induced absorpt. and emission by grain boundaries 80—39081
quantum motion of dislocations through local barriers *(Russian)* 79—60363
radiation creep, contrib. of stress induced preferential attraction of interstitials to dislocations 80—2064
radiation creep rate as function of point defect formation rate and temp. 79—69187
reactor materials, radiation creep due to stress-induced preferential absorpt., theoretical model 79—89379
screw dislocation, deformation potential operator, electron-dislocation interaction *(Russian)* 80—2021
screw dislocation interaction with Wannier-Mott exciton 78—10361
screw dislocation interactions with Wannier-Mott excitons *(Russian)* 79—4513
screw dislocation-phonon interaction in cryst. with anisotropic slip system 80—29137
segment oscillations, internal props., point obstacle collisions, glide plane motion *(Russian)* 80—39088
smectic A-nematic transition, smectic dislocations, elastic interaction 79—14916
solid, finite stressed, surface dislocation model 79—73247
solid solution hardening, dynamic simulation 79—11635
spin wave resonance line broadening by dislocations 78—64275
spring constant between edge dislocation and loop *(French)* 80—54280
steel, austenitic, ageing and plastic deform. effect on struct. and mech. props. of N15Kh5G3T3 *(Russian)* 80—71691

dislocation interactions continued
steel, austenitic stainless, extrinsic grain boundary dislocation spreading 79—57004
steel, austenitic stainless, interaction of grain boundary dislocations with precipitates during high temperature creep 80—16384
steel, Cr maraging, internal friction, 120 to 700K *(Polish)* 79—96075
steel, high-speed, low temp. mag. cycling effects, dislocation interactions with mag. domain walls. 80—100928
steel, low C, hysteresis loop initiation mechanism under repeated load *(Japanese)* 78—39851
steel, medium and high C, deformation ageing, entropy, free energy, dislocations *(Russian)* 80—66581
steel, pearlitic, struct. variations under plastic strain and subsequent heating, cementite decomp. *(Russian)* 80—84954
steel, plastic deform. resist. during continuous hot rolling *(Russian)* 80—55462
steel, plastic working of wires, high-density current appl. 79—57002
steel, stainless, in-situ obs. of deform. in HVEM 80—103338
steel, stainless, irradiation creep and swelling, microstructural modelling 77—52407
steel, stainless, radiation damage by 1 MeV electrons, dislocation struct., brittleness *(Russian)* 80—75226
strain ageing, dynamic, and serrated yielding, mechanism 80—88245
stressed crystal, dislocation superradiance collapse *(Russian)* 78—79706
stressed crystal, point defect interaction with dislocation 77—80537
structural defects, interaction effects, review *(Russian)* 79—42098
superconductor, dislocation-point defect interaction, rel. to internal friction *(Russian)* 77—36018
superconductor, electrostatic interaction of dislocations *(Russian)* 78—23198
surface dislocation model, Z-phase interface boundary problem 80—39085
thin film bicrystal, grain boundary interaction, electron microscopy technique 80—54281
tilt grain boundaries, stress-induced migration in cubic crysts. 80—44252
transition metals, BCC, interaction energy between self-interstitial and screw dislocation, calc. 80—70248
two-dimensional triangular lattice, melting theory 78—71833
type II superconductor, cylindrical, flux-density profile, pinning force *(German)* 77—24653
type II superconductor, dielastic, interaction of flux line lattice with internal stresses of cryst. imperfections 78—14906
type II superconductor, flow stress of flux-line lattice *(German)* 77—24652
void coalescence kinetics in cryst. with dislocations and volumetric generation of point defects 77—68996
void swelling, rate theory, effect of recombination on sink strengths 78—87712
wedge disclinations near surface of semi-infinite cryst. *(Russian)* 80—49224
Zircaloy-4, quenched, strain ageing behaviour, ageing time and temp. effects 78—56657
Zircaloy-4, quenched and annealed, strain ageing 77—25071
Ag, electron irradiated, thermal variation of dislocation pinning by point defects 79—51150
Ag, neutron irradiation, low temp. recovery, effect of plastic deform. 78—51588
Ag, positron annihilation radiation, ang. correl. shape, deform. effects 77—85831
Ag-Al, dislocation interactions with migrating interphase boundary electron microscope obs. 77—55963
Al alloys, age-hardening, resistivity charge by low temp. deform., GP zone cutting *(Japanese)* 78—84831
Al, dislocation and point defect interactions, US study under quasistatic stress *(French)* 80—2061
Al, high purity, cyclic torsional deform., factors influencing ductility 77—56031
Al, high-temp. internal friction peaks, deformation and annealing effects 77—32615
Al, internal friction due to dislocation-loop interaction *(French)* 79—79017
Al, plasmon-dislocation interactions, electron microscope investig. 77—15421
Al, polycryst. in annealed and creep conds., dislocation interactions with grain boundaries 79—42067
Al, polycrystn., HVEM in-situ investigation of creep mechanism 80—104214
Al, positron annihilation radiation, ang. correl. shape, deform. effects 77—85831
Al, recovery annealing, exam. using in situ high voltage electron microscopy 80—7596
Al, superconducting, yield stress increase by destruction of Cooper pairs by dislocations 79—43313
Al-Cu, age hardened, coherency stresses, composition and dislocation interactions for θ'' precipitates 77—36525
Al-Cu (1 wt.%) alloy, plasmon dislocation interactions, electron microscope investig. 77—15421
Al-Cu full coherent precipitation hardened alloy, high temp. cyclic deform. 80—25711
Al-Cu single cryst., hardening due to oriented GP zones 80—55414
Al-Ge (2 wt.%), averaged, plastic flow mechanism 77—48507
Al-Mg, superconducting, yield stress increase by destruction of Cooper pairs by dislocations 79—43313
Al-Mg (1 wt.%), mechanisms of dynamic strain ageing and jerky flow 79—79024
Al-Mg (3 and 7 at.%) alloys, plasmon-dislocation interactions, electron microscope investig. 77—15421
Al-Mg (5 wt.%), static strain ageing at low temp. 79—29116
Al-Mg-Si solid solution under stress, solute atom clustering during ageing 78—31430
Al-Zn alloys, preprecipitation, elec. resist., microhardness meas., dislocation-growth distortion interactions *(Japanese)* 77—25053
$Al_xGa_{1-x}As$, point defects, recomb. enhanced interactions with dislocation networks 79—60398
α-Al_2O_3:$Cr^{3+}(Ti^{3+})(Ti^{4+})$, solid soln. hardening, yield stress conc. depend. 77—28823
Au bicrystals, interaction of lattice dislocations with grain boundaries, electron microscope obs. 78—51579
Bi, thermal cond. under plastic deform., phonon scatt. by dislocations and twin boundaries 77—11746

dislocation interactions continued
Cd, Cottrell-Stokes law, 4.2 to 300K, forest dislocations and other obstacles 77—43269
Cd crystals, X-ray topographic examination of basal dislocation glide, generation and locking 80—88156
Cd-Zn, cryst., internal friction, dislocation interactions 79—87673
CdTe, laser window material, vap. deposition, mech. props. 77—46776
CdTe, negative and positive photoplastic effect 79—51192
Co-Cr-C alloy, $M_{23}C_6$precip. mechanism 78—44130
Co-Ni-Cr superalloys, γ'-precipitation-strengthened, yielding 77—8894
Cu, cyclically deformed polycrystals, elastic limit, contribution of thermally active processes *(Spanish)* 79—91732
Cu, deformed, positron lifetimes, trapping model 77—15451
Cu, dislocation point defect sink strengths, mutual recomb. effects 79—73207
Cu, electron irrad., elastic point defect-dislocation interactions, defect dragging model extension 80—65050
Cu, electron irradiated, dislocation defect dragging, 4.2 to 350K 78—43027
Cu, electron irradiated, thermal variation of dislocation pinning by point defects 79—51150
Cu, electron-dislocation interaction, influence of mag. fields on flow stress meas. 77—31672
Cu, inhomogeneous clustering of radiation damage after neutron irradiation between 200 and 400°C 80—15161
Cu, near Σ9 grain boundary, structure and dislocation interactions 80—79808
Cu, neutron irradiation at 200 to 400°C, decoration of dislocations damage clusters 77—24332
Cu, plastic working of wires, high-density current appl. 79—57002
Cu plates, thin, dislocation-dislocation interaction inducing cross-slip, X-ray topographic anal. 80—49233
Cu, positron trapping rate by dislocations in plastically deformed sample, 6 to 77K 77—11592
Cu single crystals, positron trapping by edge dislocations, produced by bending 78—80606
Cu wires, electrolytic, Young's modulus, working temp. effects 80—50667
Cu-Al (10, 16 at.%), influence of jogs on extension of dislocation nodes 80—84176
Cu-Al (11 at.%) single cryst., dislocation reactions during deform. twinning 80—79795
Cu-Al alloy, lattice thermal cond. meas., 0.06-2K 77—15822
Cu-Au, (0.02-5 at.%), cold worked, internal friction peaks 79—11652
Cu-Au, cold worked solid solution, flow stress and activation volume 80—16393
Cu-Ni, cold worked solid solution, flow stress and activation volume 80—16393
Cu-Ni alloy, dil., dislocation damping, 95-297K, at high strain amplitudes 78—39824
Cu-Ni-Al (5, 2.5 at.%), precip. hardening *(Japanese)* 80—71663
Cu-Ni-Fe, age hardenable, dislocation interactions with internal coherency stresses 77—36528
Cu-O single crystals, shear stress measurement, solid solution strengthening 79—52225
Cu-Si (6.5 at.%) alloy, easy glide deform., obs. and mechanism 77—8887
Cu-Si (7 at.%), influence of jogs on extension of dislocation nodes 80—84176
Cu-SiO_2, in-situ deform. in HVEM 80—103338
Cu-Zn, cold worked solid solution, flow stress and activation volume 80—16393
CuAu, calc. of elastic interaction between locally transformed regions with screw and edge dislocations 78—83844
CuAu-type superstructure, interaction of reacting dislocations *(Russian)* 78—83814
Cu_3Au, flow stress 77—21231
Cu_3Au, superdislocation motion resistance due to atoms in incorrect positions *(Russian)* 79—99189
CuCoNi ferrite magnetoacoustic oscills. rel. to microstruct. 77—85536
Cu_2O, thermal activation of plastic deform. *(French)* 80—16394
Fe, Armco, rupture onset during cold rolling *(Russian)* 77—8904
Fe, domain wall-dislocation interaction, magnetoelastic damping 78—14980
Fe, high purity, dislocation-magnetic domain wall interaction, magnetomechanical damping expts. 78—39360
Fe, high-purity, magnetic 90° domain wall-dislocation tangle interaction, magnetomechanical damping expts. 79—78496
Fe, pure, deformed, internal friction, dislocation relax. and dislocation-defect interactions 79—29125
Fe whisker crystals, domain walls, interaction with dislocation bundle, X-ray topography obs. 79—87282
Fe-Al (40 at.%), ordered, plastically deformed, neutron irrad. damage and recovery, resist. meas. 77—19993
Fe-Ni (29 at.%), calc. of elastic interaction between locally transformed regions with screw and edge dislocations 78—83844
Fe-Ni alloy, N27T2 and N28, internal friction peaks after reverse martensitic transform. *(Russian)* 78—92287
Fe-Ni-C, martensitic, internal friction 77—16633
Fe-Ni-Mo-C, Mossbauer investig. of secondary hardening, dislocation mechanism *(Russian)* 77—44260
Fe-Si (3.5 wt.%), Barkhausen noise, strain depend., interaction of dislocations and domain walls 77—12155
Fe-Si single crysts., interaction of {110} 90° walls with lattice imperfections 80—39807
GaAlAs-GaAs heterostructures, electronic excitation effects on mobility of point defects and dislocations 78—2561
$Ga_{1-x}Al_xAs$, deep level-dislocation interactions, DLTS meas. 80—29357
GaAs, electron beam induced defect annealing 77—80790
GaAs:Te, phonon-dislocation interactions, nonstoichiometry effect *(French)* 77—43298
GaP, epitaxial layer, carrier recomb. at dislocations 77—20932
Ge (111)-amorphous film of SiO_2 or Si_3N_4, dislocation interactions, substrate bending and edge effects 80—39472
Ge chalcogenides, screw dislocations in layer crystal growth from vapour *(Russian)* 80—1953
n-Ge, current carrier-dislocation interactions, resistance in UHF range *(Russian)* 80—54732
Ge, doubly deformed, dislocation interaction obs. 79—73172
Ge, electron irradiated in HV electron microscope, defect form. and interaction with dislocation 77—19990

dislocation interactions continued
- Ge monocrystal, dynamic interaction of screw dislocations with flat clusters of dislocations on other slip planes *(Russian)* 79—86800
- Ge, phonon scattering and dislocation effect on low temp. phonon cond. 78—51754
- H assisted cracking, mechanisms, review 80—50721
- InGaAs-GaAs heterojunction with low misfit, misfit dislocation struct. 77—62783
- KBr, dislocation interaction with radiation-induced single halogen interstitials 78—34536
- KBr:Li, low temp. radiation hardening mechanism, dislocation-halogen interstitial interaction 79—23635
- $KNbO_3$, dopant effect on domain struct., etching study 79—56749
- $KNbO_3:Al^{3+}$, dopant effect on domain struct., etching study 79—56749
- $KNbO_3:Ba^{2+}$, dopant effect on domain struct., etching study 79—56749
- LiF bicrystal, high-angle tilt boundary and edge dislocation intersection effects 80—79836
- LiF, radiation induced voids, formation on dislocations 80—15159
- LiF, thermal phonon-dislocation interaction, thermal cond. and ballistic phonon propag. meas., 0.03-25K 79—95226
- Mg crystal basal slip, anal. of pairwise dislocation interactions and contrib. to flow stress 78—35440
- Mg-Cd single crysts, crit. resolved shear stress, temp. and comp. depend. 79—91659
- Mg-Mn-Ce alloy, MA8, dislocations at grain boundaries and grain-boundary glide 78—64605
- MgO crysts., geometrical-statistical parameters of dislocation interactions with point obstacles 80—103341
- $MgO:Fe^{3+}$, point defect complex-edge dislocation interaction energies, atomistic calc. 80—107314
- Mo, block boundary dislocation struct. singularities under high temp. steady state creep conditions *(Russian)* 79—90670
- Mo, deformed, dislocation-free channels prod. by heat pulses, electron microscope obs. and hardness meas. *(Russian)* 79—52251
- Mo, elastic aftereffect after fast neutron irrad. at 5K 77—89431
- Mo, He ion irradiated, ordered arrangement of micropores on dislocations 77—19943
- Mo single crystal dislocation interactions during parallel shear in (011) plane *(French)* 78—43029
- NH_4Br, dislocation influence on phase transition and light scatt. *(Russian)* 80—59648
- NaCl, γ-irrad., F-stimulated inversion of sign of dislocation charge 80—59475
- NaCl, neutron irradiated, induced flow stress and optical absorpt. 77—62569
- NaCl, point defect interaction with dislocations, internal friction meas. 79—90662
- Nb, electron drag on mobile dislocations, flow stress meas. 79—91197
- Nb, glissile dislocation interactions, TEM obs. 77—31666
- Nb, neutron irrad., embrittlement, yield stress, fracture stress and strain *(Japanese)* 77—76472
- Nb-Zr-C alloys, plastic deform. and annealing, dislocation struct. *(Russian)* 80—20951
- NbS_3, Peierls distortion, chain polytypism and dislocation coupling 78—79589
- Ni, cathodic charging of H_2, positron annihilation Doppler broadening obs. 79—83055
- Ni, creep, effect of AC mag. field, 1.5-4.2K *(Russian)* 79—11657
- Ni, dislocation intersection and solution strengthening, effect of solute on obstacle profiles 80—7590
- Ni, H-charged cold-worked, internal friction peak 80—107368
- Ni, neutron irradiation, low temp. recovery, effect of plastic deform. 78—51588
- Ni, plastically deformed, positron trapping rate, temp. depend. 80—71507
- Ni, rel. to alloying influence on recrystn. and grain growth *(Russian)* 80—81071
- Ni, rel. to mag. field effect on creep 77—16141
- Ni/Cr-Fe-C, Inconel, dislocation intersection and solution strengthening, effect of solute on obstacle profiles 80—7590
- Ni-Al-Cr-Co-Ti, Waspaloy, exam. of dislocation-precipitate interaction, cyclic stress-strain behaviour 78—84925
- Ni-Co, dislocation intersection and solution strengthening, effect of solute on obstacle profiles 80—7590
- Ni_3Al and $Ni_3(Al,Ti)$, deformation characts., temp., strain rate and orientation depend. 77—44320
- Ni_3Al, substitutional soln. and defect hardening mechanisms 77—21155
- Ni_3Fe, domain struct. after tensile deform., dislocation effects 80—71083
- Ni_3Ga, form. mech. of superlattice intrinsic stacking faults 77—27897
- Pb, rel. to hardening in intermediate state 78—47917
- PbS single crystals, plastic deform. thermal activation anal., dislocation behaviour, point defect influences 79—65095
- PbS-PbSe epitaxial bicrystals, direct scatt. of channelled He ions at dislocations 80—65110
- Pd, solubility of H, lattice defects influence, extended core model 80—88326
- Pt, neutron irradiation, low temp. recovery, effect of plastic deform. 78—51588
- Pt_2Mo-type superstructure, interaction of reacting dislocations *(Russian)* 78—83814
- n-Si, current carrier-dislocation interactions, resistance in UHF range *(Russian)* 80—54732
- Si, floating zone structural perfection changes by high temp. treatment, dendrites, dislocation interactions 80—29049
- Si, influence of imperfections on microplasma formation in p-n junctions 77—8177
- Si, near (111), fracture by painted indenter, SEM study 80—71734
- Si, plastically deformed, dislocations reactions obs. by X-ray topography 78—75691
- n-Si plate, rel. to influence of illumination on internal friction, 50-250°C *(Russian)* 77—20010
- Si:B, with insulating coating, mechanical stress influence on B diffusion, strained surface layers 80—29224
- Si:P, diffusional doping, diffusion-induced strain and dislocation effects 79—42084
- $SiTe_2$, dislocations and stacking fault energy 78—47378
- Sn chalcogenides, screw dislocations in layer crystal growth from vapour *(Russian)* 80—1953
- Ti, tensile properties and creep behaviour at high temp. 78—23773
- Ti-(Al)-Zr-Si (5, 0.5 wt.%), creep 77—36595

dislocation interactions continued
- TiO_2, rutile, single cryst., high temp. compression in O_2 atmosphere *(French)* 79—51194
- $TiS_{1.7}$, hexagonal polytypes form. mechanism 78—9990
- W, block boundary dislocation struct. singularities under high temp. steady state creep conditions *(Russian)* 79—90670
- W, plastic working of wires, high-density current appl. 79—57002
- W:Re, polygonisation in diffusion process, glide dislocation interactions 80—38998
- YIG, interaction force between 180° domain wall and edge dislocation 77—28408
- Zn, basal dislocation—prismatic dislocation ring interactions by method of moments *(Russian)* 80—10550
- Zn, Cottrell-Stokes law, 4.2 to 300K, forest dislocations and other obstacles 77—43269
- Zn crystals X-ray topographic examination of basal dislocations 80—88156
- Zn, density of basal dislocations, rel. to deforming stress, 1.5-300K *(Russian)* 80—29028
- Zn, dislocation interaction with 'forest' dislocation, TEM exam. 77—89440
- Zn, single crystals, positron trapping by edge dislocations, produced by bending 78—80606
- Zn-Al alloys, dislocations obs. in superplastic deformation 78—51549
- ZnS, interaction between charged dislocations and luminesc. centres *(Russian)* 79—56860
- ZnSe, electric charge transport by dislocations 80—103709

dislocation jog motion *see dislocation jogs*

dislocation jogs
- alloy, ordered, conservative jog slip on superpartial screw dislocations, work hardening 77—7731
- computer simulation of electron microscopic diffr. contrast 77—84750
- deformation kinetics analysis of stress sensitivity 77—3737
- double jog side-motion, elastic theory 80—84171
- edge dislocation, climb rate and core diffusion 80—10553
- FCC materials, jogs on extended defects, weak-beam electron microscopy technique 78—38713
- ice, edge dislocation dipole form. by heat treatment, X-ray diffr. topography 79—99203
- jog-kink interaction, nonlocal continuum theory 77—59043
- metal, FCC, climb model of extended dislocations 78—6059
- migration of steps on subboundaries 77—7721
- neutron irradiation, precipitation of point defects near grown-in dislocations 78—26600
- olivine, high temp. creep, edge dislocation control 79—79815
- repeated precipitation on edge dislocations, micromechanisms 78—95752
- Schmid's law deviations, in uni-directional strain 78—71783
- Al, creep and rupture, 77 to 273K *(Russian)* 79—43386
- Al, creep and rupture, in torsion, mech. *(Russian)* 79—5030
- Al, deformed, efficiency of dislocation as sink for vacancies, resist. obs. 77—36570
- Al, internal friction, dislocation glide and jog climbing *(French)* 78—11261
- CaF_2, plastic deform, work hardening regions, TEM obs. 80—3140
- Cu alloys, FCC, climb of extended dislocations due to irradiation in HVEM 80—103343
- Cu alloys, jog formation and glide on dissociated dislocations, direct obs. 77—68977
- Cu, cross-slip at low stresses 77—11564
- Cu, single crystals, dislocation breakaway, etch pit study 78—6064
- Cu-Al (10, 16 at.%), influence of jogs on extension of dislocation nodes 80—84176
- Cu-Al (15.8 at.%), extension of jogs on dissociated dislocations, electron microscopy obs. 79—95017
- Cu-Al alloy, irrad. in HVEM, climb of dissociated dislocations and point defect absorpt. 80—107257
- Cu-Si (7 at.%), influence of jogs on extension of dislocation nodes 80—84176
- α-Fe, creep and fracture, jogged screw dislocations, thermally activated motion 79—7649
- Ge, dissociated dislocations, constriction correlation with jogs 80—79801
- ^4He HCP crystals, US attenuation, dislocation damping 80—24711
- KCl, temp. depend. of dislocation charge, piezoelec. defect technique 78—22733
- MgO, electron irradiation damage, cryst. defects 80—107320
- Ni and Ni-Co, recovery of single crystal after varying amounts of cold work 79—100162
- Ni, electron irrad. in HVEM, interstitial loop growth 80—107326
- Ni-Al, solid soln. and solid soln. hardened, stead state creep 78—27578
- β'-NiAl, dislocation climb, hot stage TEM 77—24318
- Ni_3Fe, single cryst. ordered and quenched, stress relax. *(Russian)* 77—44282
- Se, undeformed rhombohedral, dislocations, electron microscope obs. *(French)* 78—51548
- Si, mobility of segments of dislocation loops, model of nonconservative dislocation motion 78—18647
- Si, self-diffusion and dynamical recovery at high temps., local equilibrium breakdown 79—69284
- Si, single crystals, dynamical recovery and self-diffusion 78—87816
- $(U,Pu)O_2$, thermal creep in 40 to 100 N/mm^2 stress range 77—28881
- UO_2, thermal creep in 40 to 100 N/mm^2 stress range 77—28881
- Zr_3Al, $L1_2$ phase, work hardening 78—23718

dislocation locking
- *see also Cottrell atmospheres*
- composite dislocations, asymm. equilib. positions and line tensions 79—51108
- metal, BCC, dislocation (100) stability, field stress effects *(Russian)* 80—10558
- Ag, elastic instability 79—82235
- Cd crystals, X-ray topographic examination of basal dislocations during microplastic deformation 80—88156
- Cu, elastic instability 79—82235
- Cu-Al (15 at.%), elastic instability 79—82235
- Nb-O, Snoek mechanism and long distance diffusion under strain ageing *(French)* 77—81279
- Si, mechanical strength, origin of difference in Czochralski grown and float-zone-grown cryst. 80—44212
- V, hydrogenated, grain size depend. of tensile strength 77—36657
- Zn crystals X-ray topographic examination of basal dislocations 80—88156

dislocation loops
  see also vacancy condensation loops
  acoustic emission from moving dislocations near crystal surface 78−87856
  alkali halide, crystal, irradiation-induced defects 80−107316
  alkali halides, surface step struct. 77−31853
  alloy, dispersion hardened, temp. depend. of work-hardening due to Orowan loops 79−91668
  alloy, dispersion hardened, work hardening due to Orowan loops, temp. depend. *(Japanese)* 80−66534
  alloy, overaged and dispersion hardened, dislocation bowing computed from Orowan relations 77−19949
  angular disclination and closed loop generation 77−51374
  anisotropic elastic medium, self-stress field singularity of plane loop 77−19952
  anisotropic linear-elastic medium, self-force on planar dislocation loop 77−35557
  anisotropic media, elastic energy of dislocation loops 78−38700
  BCC crystal, electron microscope image contrast, theoretical predictions for non-edge dislocation loops 80−24326
  BCC crystal, electron microscope image contrast from edge dislocation loops 77−76409
  BCC materials, small dislocation loop images 78−83823
  bounded media, dislocation loop growth and void swelling by charge particle damage 78−6110
  α-brass, quenched, secondary defect form. during ageing, TEM obs. 78−88482
  capture efficiency of dislocation loops, effect of nonlinear elasticity 80−59461
  coalescence of pores by dislocation mechanism, shape effect on charact. 77−73242
  creep, irradiation induced, correlation of theory with expt. evidence 80−88255
  creep and growth, radiation induced, fundamental mechanisms 80−92596
  cross slip dislocation self-interaciton, Orowan loops 80−24453
  cryst. with defects 78−60478
  crystal with island film, dislocations and stresses 79−87015
  crystalline materials, in situ deform. by high voltage electron microscopy 80−103352
  cubic crystal, image contrast of dislocation loops, elastic anisotropy depend. 80−103349
  cubic media, electron microscopy, black-white contrast 80−75234
  dark-field electron micrographs, defocused, for point defect accumulations investigation 79−99036
  dechannelling by dislocation loop, energy depend. 79−42127
  dechannelling due to dislocation loops 79−19299
  defect clusters, in particle-irradiated crysts., TEM identification 79−69108
  defect clusters, nucleation and growth due to energetic particle radiation, chemical rate reaction theory, computer program 80−49263
  deformation conditions and initial defect struct. effects on dislocation multiplication 78−30614
  deformation due to stress induced perferred adsorption induced dislocation anisotropy 80−75265
  deformed crystal, theory of X-ray scatt. *(Russian)* 80−70077
  diamond, planar defects, in {100} planes, electron microscopy 77−11569
  diamond, platelets, giant, on cube planes, electron microscopy 77−84765
  dilation due to dislocation made up of straight segments 77−47455
  dislocation motion, thermal activation through random point obstacles 79−1434
  dispersion hardened alloy, calc. of back stress decrease, due to Orowan dislocation loop climb 78−83812
  displacement field construction from angular dislocation segments, electron microscope image simulation 80−6325
  double cross-slip mechanism 78−22720
  double jog side-motion, elastic theory 80−84171
  elastic fields near stress-free surface, loop-point defect interaction 79−4301
  elastic interaction between disclination loops and straight disclinations 80−2015
  elastic wave interaction defects of finite vol. and defect mutual interactions 78−32676
  elastically nonlinear medium, self action force of dislocation loops *(Russian)* 79−27979
  electron microscope diffr. contrast 78−83700
  electron microscope dynamical image contrast, small lattice defects 77−15422
  electron microscope image calc. and Burgers vector sign determ. 77−59017
  electron microscope image contrast of small dislocation loops 80−6326
  electron microscopy of dislocation loops, direction of black-white contrast 77−15423
  fatigue, dislocation behaviour, loop patch props. in fatigue cycling 79−90725
  FCC crystal, field-ion images, computer simulation of contrast of dislocation loops 77−11561
  FCC metals, dislocation loops and voids, growth kinetics, role of divacancies 79−99196
  FCC metals and alloys, elastic energies of dissociated Frank loops 78−75671
  ferromagnetic resonance line, uniform, at finite temps., dislocation broadening 78−19334
  forest dislocations, motion of train through forest modelling methods 80−107238
  Frank-Read source, kinetics, quasistatic nucleation and expansion of dislocation loops 80−33999
  gliding, by-passing of hardened particles, coplanar Orowan loops form., stress-strain curves 80−49226
  grain boundary sliding, containing particles, during diffusional creep, dislocation bowing 79−37712
  graphite, fast neutron irrad. damage, chem. rate theory applic. effect of annealing and thermal equilib. defect concs. 77−67804
  graphite, fast neutron irrad. damage theory and modifications 77−67805
  graphite, point defects and self diffusion 78−63758
  hardening during creep, effect of interstitial and vacancy dislocation loops *(Russian)* 77−81271
  hexagonal crystals, intraction of flexible dislocations in intersecting slip planes 77−39592
  HV electron microscope irrad., dislocation loop growth 80−2018
  ice, dislocation form. kinetics, computer simulation 78−30622

dislocation loops continued
  ice, monocrystalline, radiation damage, 100 keV proton channelling 80−34102
  identification using computed electron micrographs 77−51383
  III-V compounds, dislocation half-loops, nucleation and generation 79−95009
  interstitial and vacancy dislocation loops, diffusion growth in supersaturated soln. of point defects 77−68974
  interstitial loop finite, modelling of growth under irrad. 79−23607
  intrinsic point defect-impurity atom mobile complex formation *(Russian)* 79−90653
  irradiation creep mechanisms, theoretical assessment 79−55817
  irradiation effects, low dose, void incubation, rate theory approach 79−77635
  linear isotropic elasticity, boundary problems, book contrib. 80−39092
  local heating at low temps., parallel glide planes, temp. distribution *(Russian)* 80−29020
  loop-length distribution and frequency-dependent damping form for small impurity concs. 80−49232
  martensite nucleation mechanism, kinetics 77−36504
  mean strain in crysts. containing prismatic dislocation loops 77−7720
  metal, BCC, dislocation (100) stability, field stress effects *(Russian)* 80−10558
  metal, FCC, climb model of extended dislocations 78−6059
  metal, FCC, dislocation behaviour at high strain rates, US detection method, data analysis basis 80−85136
  metal, hardening due to increased subgrain boundary stability 78−52934
  metal, irrad., containing pre-existing dislocations, interstitial loop form. kinetics 80−65040
  metal, irradiated, triangular Frank loop dissociation 77−11599
  metal, oxidation of high temp. material, lattice vacancy effect 77−70203
  metal, polycrystalline, strain hardening, dislocation link length model 80−84953
  metal, radiation damage effects, neutrons and heavy ions, rel. to reactor technology, review 77−43255
  metal, single crystal, dislocation loop formation, during deformation in quantising mag. fields *(Russian)* 80−103354
  metal, thermodynamics of electrons, dislocation dipole and prismatic dislocation loop effects *(Russian)* 79−56161
  metal, void swelling and dislocation loop growth on fast particle irrad. *(Russian)* 77−59047
  metals, interstitial loop growth, pulsed irrad. effects 80−88210
  metals, mechanical multipole moments determ. 78−55868
  metals, point defect and microstruct. behaviour during irrad., appl. to fusion reactors 79−23638
  metals and alloys, FCC quenched, form. of prismatic loops 77−65979
  mobile pinning points on dislocations, equilibrium distrib. 80−79792
  molecular crystal with point and linear defects, Rayleigh scatt. 77−44011
  neutron damage simulation, using HVEM, state-of-the-art 77−51417
  neutron irradiated, 573 to 923K, damage struct. 79−99247
  neutron-bombarded, diffuse X-ray scattering *(Russian)* 80−92560
  Nimonic PE16, He injected, bubble-void transitions in Ni ion bombard. 80−34095
  nucleation of defect clusters in crystalline solids 79−42051
  octadecanol, normal, single cryst., lattice defects, X-ray topographic obs. 78−18650
  ordered alloy, noncoaxial dislocation loop behaviour 77−11549
  Orowan loop storage capacity, system containing ellipsoidal particles 77−76402
  oxides, dislocation climb model 80−100230
  Peierls model, dislocation core energies 79−27984
  planar elliptical, stress field 77−47453
  point defect migration into dislocation loops, finite difference calc. 80−54225
  point-force array description 78−18646
  pore healing under press., initial stage of dislocation config. form. *(Russian)* 78−10050
  precipitate and dislocation loop strain and stress field calcs. using affine transformations 80−106722
  precipitation of point defects into dislocation loops, diffusion-controlled 77−62529
  quartzite, naturally deformed, textural and microstructural development, metallurgical approach 79−83228
  rare earth garnets, preparation, substrate and epitaxial layer surface quality control, X-ray topography *(German)* 77−55432
  sapphire, work hardening 77−16604
  semiconductor, recomb.-enhanced defect reactions 77−51377
  semiconductor, STEM spectroscopic techniques for simultaneous electronic and defect obs. 80−100145
  semiconductor, zincblende struct., dislocation climb model, appl. to degradation of lasers and LED's 77−1125
  n-Si:B, ion implanted, rapid identification of faulted loops 79−19254
  sink strength of dislocation loops, growth in irradiated materials 79−99246
  slip system, self-energy effects on choice 79−27982
  smectic A-nematic transition, breakup of order by smectic dislocation loops, defect model 79−14916
  solid-solid interface, circ. prismatic dislocation loop 79−82468
  sound emission, pile-up formation by Frank-Read source, emission of sound 79−37705
  spring constant between edge dislocation and loop *(French)* 80−54280
  stacking fault, antiphase boundary energies, investig. methods, review, appls. to FCC metals *(French)* 79−42080
  statistical approach to dislocation multiplication 80−49230
  stearic acid, microscopic obs. of cleaved surface 79−95248
  steel, austenitic, gas implantation effects, fusion reactor first wall damage simulation 80−29079
  steel, austenitic 316, displacement energy determ., HVEM obs. and electron bombardment 78−6100
  steel, austenitic stainless, irrad. creep of type 316 in HVEM 80−97523
  steel, austenitic stainless, neutron-irradiated, gamma-alpha transformation 79−96027
  steel, austenitic stainless, type 800, tensile creep props. rel. to intergranular microstruct. at 800°C, TEM study 79−38885
  steel, high C, high alloy, $M_{23}C_6$ type carbides, effect of alloying elements on defect struct. and hardness 80−16481
  steel, low C, hysteresis loop behaviour under fatigue load, dislocations model 79−74197
  steel, microstructure of 0Kh16N15M3B after creep tests in BR-10 reactor, electron, microscope invest. *(Russian)* 80−92531

dislocation loops continued
steel, pearlitic, deform. microstruct. and cementite fracture, −196 to 700°C 78−27576
steel, stainless, electron irrad. in HVEM, radiation damage obs. 77−50233
steel, stainless, He effects on microstruct. in ion-irrad. 80−29078
steel, stainless, He ion bombard., in situ electron microscope examination 80−34094
steel, stainless, irradiation creep and swelling, microstructural modelling 77−52407
steel, stainless, laser fusion reactor first wall, void growth charact. 80−34042
steel, stainless, neutron irradiated, stress effects on microstruct. 77−47490
steel, stainless, radiation damage by 1 MeV electrons, dislocation struct., brittleness *(Russian)* 80−75226
steel, stainless, solution treated, irradiated to low doses with 22 MeV C^{2+} and 46.5 MeV Ni^{6+} ions, interstitial loops 79−14855
steel, stainless, type 304L, neutron irrad., rel. to ferrite formation 79−42112
steel 0Kh16N15M3B, neutron irradiated, kinetics of nucleation and growth of vacancy pores and dislocation loops *(Russian)* 77−51408
steels, stainless, electron irradiated, dislocation damage, HVEM study 80−103389
stress fields generated by defects in continuum 79−69104
superconductor, critical temperature mag. field depend., strong diamagnetism *(Russian)* 80−7022
TEM black-white contrast images, loop analysis and identification 80−103350
TEM image black-white contrast figure vector 79−7609
TEM observations *(Japanese)* 79−82130
tetrahedral semiconductor, interstitial type dislocation loop form. by vacancy precipitation 78−67715
thin plate, behaviour of circular prismatic dislocation loops, using linear theory of elasticity *(Japanese)* 79−4302
triglycine fluoberyllate, deuterated, dislocation line defect X-ray topographic analysis 80−59465
two- and three-layer faulted defects, two-Shockley unfaulting 77−55292
two-phase material, circular glide dislocation loop 77−27881
Udimet 520, γ' distribution in slip plane, dislocation loop form. during creep *(Japanese)* 79−42075
Zircaloy-2, interstitial/vacancy nature of neutron induced dislocation loops, TEM study 79−42110
Zircaloy-2, irradiation growth, shape and volume changes 80−92562
Zircaloy-2, neutron irrad. damage, TEM characts. 80−107332
Ag, fatigued single crystal, annealing of deform. struct. 78−3204
Ag halide crysts., dislocations, survey of post-war research 80−62449
Al, [111] single crystal, in situ deform., HVEM obs. 78−52886
Al {111}, X-ray Huang diffuse scatt. from dislocation loops 80−79797
Al, acoustic emission from moving dislocations during tensile tests 77−19964
Al alloy D16, supersaturated solid soln., decomp. process, electron microscope obs. and acoustic anal. *(Russian)* 79−15650
Al alloys, dil., quenched, foreign element effects on dislocation loop form. 80−54239
Al and Al alloys, quenched, multiple-faulted dislocation loop config., TEM 77−27887
Al, dechannelling of α-particle by dislocation loops *(French)* 79−95056
Al, deformed in uniaxial and equibiaxial tension, dislocation arrangements 80−108516
Al, dislocation and point defect interactions, US study under quasistatic stress *(French)* 80−2061
Al, dislocation loops, interstitial, size distrib. for metal irradiated in high voltage electron microscope *(Russian)* 80−103335
Al, dislocation loops and pores due to 23 MeV proton irrad. *(Russian)* 80−54235
Al, electron irrad., interstitital loop nucleation at impurity site *(Japanese)* 77−43247
Al, foil, influence of O_2-pressure on oxidation rate, TEM study 80−104355
Al foil, quenched, anomalous annealing phenomena, quantitative study 78−80565
Al, internal friction due to dislocation-loop interaction *(French)* 79−79017
Al, laser strengthening, struct., hardness and dislocation density *(Russian)* 80−76399
Al, mechanical multipole moments determ. 78−55868
Al, pipe diffusion along segment of faulted dislocation loops during annealing 80−107256
Al, prismatic dislocation loops, (g.b)s product sign determ. *(Russian)* 78−38705
Al, pure, electron irradiation damage 77−19988
Al, quenched, diffusion solution for point defects in stress field, steady state and transient 78−30780
Al, quenched, vacancy annihilation at surface and dislocation loops 79−60351
Al thin foil, thin foil, electron irrad., observation of triangular loops at twin boundaries 80−34005
Al:^{12}B, relax. mechanism for polarised implant 78−87693
Al-Al_2Cu, aligned eutectic, precipitation, TEM and microhardness meas. 78−27529
Al-Cr, quench hardened, Cr effects on resoftening 77−66657
Al-Cu (1 wt.%), electron irradiated, dislocation damage, HVEM study 80−103389
Al-Cu (4 wt.%), reversion charact. *(Japanese)* 77−21150
Al-Cu (4 wt.%) alloy, neutron irrad., weak-beam dark-field obs. of dislocations near θ' precipitates 80−107333
Al-Fe alloys, dil., quenched, secondary defects, Mossbauer spectroscopy 77−28491
Al-In alloy, dilute, electron irradiation, interstitial dislocation loop obs. 78−18681
Al-Li (1.3 wt.%), prismatic dislocation loop rows due to precipitation *(Japanese)* 79−52220
Al-Li alloy, dil., quenched and irrad., recovery, resist. and internal friction obs. 78−52848
Al-Mg, dilute, dislocation loops, interstitial, size distrib. for metal irradiated in high voltage electron microscope *(Russian)* 80−103335
Al-Mg, foil, oxidation in O_2 atm., TEM study 80−104356
Al-Mg, oxidation induced stresses, dislocation network form., HVEM obs 80−14978

dislocation loops continued
Al-Mg 0.1 at.%, neutron-irradiated, dislocation loop characterisation by TEM 79−23614
Al-Mg (5.5 wt.%), effect of stress changes during creep on dislocation struct., TEM study 79−74214
Al-Si (1.2 wt.%), dispersion hardened, temp. depend. of work-hardening due to Orowan loops 79−91668
Al-Si (1.2 wt.%), dispersion hardened, work hardening due to Orowan loops, temp. depend. *(Japanese)* 80−66534
Al-Si alloy, dilute, electron irradiation, interstitial dislocation loop obs. 78−18681
Al-SiO_2 interface, stress and microstruct. via TEM 78−26797
Al-Zn-Mg-(Zr), low cycle fatigue, grain refinement effect 77−44345
Al-Zn-Mg-(Zr) alloy, microstruct. effect on fatigue crack growth 80−3164
$Al_{0.36}Ga_{0.64}As$, LPE films, Te-induced defects 78−43037
$Al_xGa_{1-x}As$ DH laser material, Ar laser induced catastrophic damage 79−86178
Al_2O_3, alumina, deformed by prismatic slip, HV TEM obs. of dislocations 80−108517
Al_2O_3, defect microstructure due to ion bombardment, TEM study 80−34100
Al_2O_3, sapphire, edge dislocation loop obs. by high resolution lattice imaging 80−103346
Au, electron irradiated, interstitials and their clusters, diffuse X-ray scatt. study 80−33997
Au foil, radiation damage, in situ study by HV electron microscopy 78−6101
Au-Cu, dil., electron irradiated, interstitials and their clusters, diffuse X-ray scatt. study 80−33997
Bi, low temp. plasticity, strain hardening, slip *(Russian)* 77−31713
Bi, US propagation anomalies, under hydrostatic press. *(Russian)* 78−83884
Cd, electron radiation damage in HVEM, nature of defect clusters 78−59838
Cd, faceting of interstitial loops 78−47381
Cd, single cryst., Burgers vector determ. of perfect dislocations obs. by X-ray topography 79−37711
CdI_2 polytypes, defect struct., electron microscopy 79−14809
CdS, deformed, dislocation struct., TEM obs. 80−54250
Co, HCP, heavy-ion irrad., dislocation loops, TEM obs. 77−31667
Cu alloys, FCC, climb of extended dislocations due to irradiation in HVEM 80−103343
Cu, cubic crystals, anisotropic, dislocation loops, electron microscope image contrast 80−39101
Cu, defect clusters, electron microscope exam. 78−47380
Cu, electron irrad., secondary defect formation, effect of refl. condition *(Japanese)* 77−43248
Cu, electron irrad., void swelling and dislocation loops 79−99206
Cu, electron irradiated, small-angle X-ray scatt. investig. of stage III recovery 77−7763
Cu foil, electron irradiated at low temps., annealing, form. of clusters of atomic defects 77−15416
Cu foils, electron-irradiated, point defect agglomerates, HVEM invest. during in-situ annealing 80−84213
Cu, foils, faulted defect formation by moving boundaries 80−107281
Cu, Frenkel pair production threshold energy, temp. depend., exam. 78−51530
Cu, ion irrad., Frank loops, electron microscope image contrast 80−6326
Cu, ion radiation damage 78−22773
Cu, irradiated, small edge dislocation loops, electron microscope image contrast, Burger's vector determ. 77−76410
Cu, irradiation induced defects, electron microscope images 78−83854
Cu, neutron irradiation damage inhomogeneous clustering, TEM obs. 79−73223
Cu, neutron irradiation induced dislocation loops and point defects, temp. depend., 316 to 483K 77−51410
Cu, prismatic dislocation loops revealed by X-ray topography and etching 77−11563
Cu, prismatic dislocation loops, (g.b)s product sign determ. *(Russian)* 78−38705
Cu single crystals, climb rate of Orowan loop anal. by dislocation pipe diffusion 79−83211
Cu, very low atom displacement threshold energy, around ⟨110⟩ directions, direct evidence 78−14379
Cu, X-ray studies of fusion energy neutron damage 78−51593
Cu-Al, dislocations, dissociated, climb mechanism, nucleated loops, Burgers vectors 80−65002
Cu-Al (2, 6.8 and 15 at.% Al), electron irrad. at 300 and 575 kV, exam. of damage rate 78−47425
Cu-Al alloy, irrad. in HVEM, climb of dissociated dislocations and point defect absorpt. 80−107257
Cu-$Al_2O_3(SiO_2)(TiO_2)$ alloys, internally oxidised, plastically deformed, influence of particle form on primary loop nature *(French)* 80−103344
Cu-Cr-SiO_2 system, age and dispersion strengthened, dislocation struct. around SiO_2 particles 80−108468
Cu-Fe (1.5 wt.%), precipitation-effect on void formation during electron irradiation 80−84211
Cu-Ni alloys, dislocation climb sources activated by 1 MeV electron irradiation 77−89443
Cu-Ni alloys, electron irradiated, dissociated struct. of dislocation loops with Burgers vector a⟨100⟩ 77−89444
Cu-SiO_2, low-temp. recovery creep, Orowan loop accumulation 80−81126
Cu-SiO_2 (0.0052 vol. fraction), work hardened, low temp. softening, particle size effects 77−52342
Cu_3Au, 5-100 keV Cu^+ ion bombardment, displacement cascades, TEM investig. 77−11601
Cu_3Au, fast neutron irrad., displacement cascades 78−83852
Cu_3Au, heavy-ion or neutron bombardment, disordered zone form., TEM diffr. contrast 77−11600
Cu_3Au, TEM diffr. contrast of dislocation loop 77−24253
$CuFeS_2$, natural chalcopyrite, defect struct., TEM 77−62535
EuS, defect struct., etch pitting and electron microscopic obs. 79−27989
α-Fe, dislocation loops, equilib. shape under shear stress 79−7608
α-Fe, neutron irradiated, low temp. mag. relax. 79−8022
Fe, rel. to vacancy mobility determ., HVEM expts. 80−33993
α-Fe, TEM on struct. round fatigue cracks 77−12699
Fe:Bi, impurity site distrib., channelling and nucl. orientation obs. 77−15447

dislocation loops continued
Fe-Cr-Ni (19, 13 wt.%), austenitic, Ni$^+$ ion irradiated, multiple dislocation loops *(French)* 80—65064
Fe-Cu (0.34 wt.%), neutron irradiated, field-ion microscope detection of ultra-fine defects 79—42116
Fe-N, neutron irrad. effects on mech. props. 79—4338
Fe-Ni-Ti-C (31, 4, 0-18 wt.%), coherent precipitates in austenite, effect on martensite substruct. 77—52327
Ga$_{0.9}$Al$_{0.1}$As:Ge(Si) epitaxial layers, defect obs. by TEM 77—51618
Ga$_{1-x}$Al$_x$As DH injection laser diode, long-term-degraded, TEM obs. 78—71102
Ga$_{1-x}$Al$_x$As, degraded DH LED, defect struct. by electrolum. topography and TEM obs. 79—60369
Ga$_{1-x}$Al$_x$As LPE crystals for DH laser, LEDs, TEM obs. of Ge, Si-doped epitaxial layers 79—1556
Ga$_{1-x}$Al$_x$As, rapidly degraded LED, defect struct. of ⟨100⟩ dark lines 78—10052
GaAs, etched, saucer-pit defect identification 78—43021
GaAs heterojunction laser, origin of dislocation climb during laser operation 77—51380
GaAs, ion implantation damage, TEM exam. of variation with ion species and stoichiometry 78—59827
GaAs, point defect generation by electron-hole recombination at dislocations 79—37699
GaAs, rel. to dark defects in LEDs 77—80509
GaAs:S(Te)(Zn), dislocation-free, TEM study of microdefects 79—82213
GaAs:Se$^+$, TEM structural study, surface and interior damage 80—34025
GaAs:Si, ion implantation, thermal annealing, Hall meas., SIMS atomic profile meas. 80—75243
GaAs:Si, Li, IR absorpt., microstruct., charge compensation 80—107565
GaAs:Te, heavily-doped, annealing-induced prismatic dislocation loops and elec. changes 78—51546
GaAs:Te, LPE, Te induced defects, rel. to growth conditions 78—6067
GaAs:Te, preferential precipitation on dislocation loops 79—7612
GaAs:Te, solubility and point defect-dopant interactions 79—90687
GaAs-GaAlAs planar stripe DH laser, origin of dark line defects 77—75510
GaP crystal, structure defect formation due to annealing and stress, dendrites, slip, dislocations 80—29026
GaP, dislocation loops and bipolar obs. by chemical etching 78—55873
GaP, LEC growth of dislocation-free crysts., microdefects and striations 78—9974
GaP, substrate for LPE GaP, effect on epitaxial layer perfection 78—30843
GaP:S, defect struct. and tetrahedral precipitates, TEM study 80—107246
GaP:S LEC grown crystals, HVEM investig. of defects 79—60376
GaP:Te, defects formed due to precipitation of Te, metallography and TEM exam. 77—84769
Gd$_3$Ga$_5$O$_{12}$, decorated dislocations, large interstitial climb loops round precip. particles 77—19960
Gd$_3$Ga$_5$O$_{12}$ dislocation anal. at inclusions by repeated etching technique 80—29024
Gd$_3$Ga$_5$O$_{12}$, optical birefringence images of edge dislocations 77—1129
Gd$_3$Ga$_5$O$_{12}$, precipitates assoc. with dislocation climb trails *(German)* 77—35567
Gd$_2$(MoO$_4$)$_3$, electron microscope exam. of ferroelec. and ferroelastic props., domain walls and cryst. defects 77—69786
Ge crysts., electron beam induced changes of real struct., HVEM 80—103390
Ge, defect form. under radiation-accelerated diffusion conditions 80—19854
Ge, dislocation motion near surface 79—82219
n-Ge, dislocational microwave conductance anisotropy *(Russian)* 79—91092
Ge, electron irrad., defect growth, struct. rel. to temp. 77—11591
Ge, high-temp. radiation effects under HVEM obs. 77—89475
Ge, ion beam irrad., defects prod. by individual displacement cascades, TEM study 80—70265
Ge surface, line tension induced dislocation motion 79—82212
Ge, with screw segment, shrinkage vel. and cross slip freq., activation energies *(German)* 78—43028
Ge:As, containing dislocation loops, dynamic scatt. of X-rays, extinction effect 78—47384
Ge:Ga, heavily doped, structure defect evolution during heating *(Russian)* 78—43026
InSb, X-ray topographic evidence of asymmetrical pre-yield behaviour 80—75229
KCl, cryst. isolated pore healing under press., dislocation struct. evolution *(Russian)* 80—100245
KCl, motion of dislocation half-loops, influence of prestart loading and ensemble nature 78—71745
KCl, X-irrad. induced deform. effects, glow curves *(Russian)* 79—52022
LiF, irradiated at 20K, deformation under stress *(French)* 79—90715
Mg alloy, quenched-in defect behaviour, effect on flow stress 79—61625
Mg, dislocation loops induced by neutron irrad., TEM obs. 79—51113
Mg, electron irrad. damage, dislocation loop growth, in situ obs. 78—87715
Mg, electron irradiation damage 77—35587
Mg, melt grown by Bridgeman method, X-ray topography 78—59770
Mg, neutron irrad. damage, TEM obs. 79—46713
MgAl$_2$O$_4$, faulted defect aggregates prod. by neutron-irrad. 80—107331
MgO, crack tip dislocations and dislocation-free zones 80—96533
MgO, defect aggregation and thermal-electric breakdown, TEM obs. 79—42069
MgO, electron irradiation damage, cryst. defects 80—107320
MgO, precipitation on dislocations, ultramicroscopy and chem. etching 78—67720
MgO, residual image contrast of dislocation loops 78—47382
Mo, 29 MeV α-particle irrad. in He, micropore and dislocation loops form. 79—14859
Mo alloys, dil., HVEM bombarded, neutron damage simulation, defect cluster and dislocation obs. 80—107330
Mo, electron radiation damage and props. of point defects 77—11590
Mo, He ion irradiated, TEM 77—19994
Mo, ion bombardment by Ni^{2+}, TEM study of damage depth distrib. 78—10101
Mo, ion irrad., defect anal., electron microscopy, appl. of theory of non-edge loop image contrast 80—70200

dislocation loops continued
Mo, ion irrad., dislocation loops and stacking fault tetrahedra, electron microscope image contrast 80—6326
Mo, irradiated, small edge dislocation loops, electron microscope image contrast, Burger's vector determ. 77—76410
Mo, irradiated with fission fragments, creep, 20-30K *(French)* 77—48493
Mo, irradiation induced defects, electron microscope images 78—83854
Mo, neutron bombard., radiation damage, electron microscopy obs. *(Russian)* 80—44235
Mo, neutron irradiated, small angle X-ray scatt. and TEM study of voids 79—14849
Mo, slip rosettes and dislocation struct. formed by microindentations 78—14349
Mo, temp. depend. at crack tip, of fractured single cryst. 79—29210
Mo-Zr, heavy ion irradiated, void swelling, phase instability 80—29084
MoSe$_2$, imperfections from TEM study 80—79800
NaCl cleaved surface structure, electron microscope 79—7735
NaCl crystals, config. of screw dislocation halfloops *(Russian)* 77—89436
NaCl, dislocation half loop mobility 78—59817
NaCl, high resolution TEM and radiation sensitivity, dislocation obs. on deformed crysts. 80—107260
NaCl, interrupted neutron irrad. expts. involving dislocations 79—99208
NaCl, motion of individual surface dislocation semi loops *(Russian)* 78—51542
NaCl, spiral dislocation mobility depend. on elec. field, relaxation time 80—39105
NaCl whiskers, X-irrad., stress oriented dislocation loop nucleation 79—33213
Nb, 15 MeV and fission neutron displacement dqmage, TEM anal. 77—35592
Nb and Nb alloys, superconductor, flux pinning under heavy ion irradiation 78—52167
Nb, channelling study of ^{4}He$^+$ irradiation damage, effect of irradiation temp. 79—82271
Nb, cubic crystals, anisotropic, dislocation loops, electron microscope image contrast 80—39101
Nb film, sputter-deposited on stainless steel, electron microscopy and ESCA 77—52554
Nb, flux pinning by proton irradiation damage 77—47947
Nb, irradiated superconductor, fluxoid defect interactions 78—52166
Nb, neutron irradiated, TEM obs. of interstitial clusters 79—19288
Nb, proton irrad., dislocation loops and mag. flux pinning 79—56463
Nb-H system, accommodation effects during hydride precipitation, TEM 80—89218
NdGa$_5$O$_{12}$ wafer, dislocations, etch pits and birefr. obs. 78—83818
Ni, cubic crystals, anisotropic, dislocation loops, electron microscope image contrast 80—39101
Ni, electron irrad. in HVEM, interstitial loop growth 80—107326
Ni, Frank loops, growth kinetics and 'preference factor' during electron irradiation 78—22723
Ni plated Fe single crystal, deformed at 77K, surface obs. 78—19916
Ni, point defect-dislocation loop interaction, effect on dislocation loop growth kinetics 78—47415
Ni, self-ion irradiated, defect clusters, annealing 78—18687
Ni, transient irrad.-induced creep under D bombardment, mechanism 78—80597
Ni:Bi, impurity site distrib., channelling and nucl. orientation obs. 77—15447
Ni-Al alloys, effects of electron irradiation in precipitation, nucleation and dislocation loop growth, TEM study 79—42106
Ni-Al-Cr-Co-Ti, Waspaloy, exam. of dislocation-precipitate interaction, cyclic stress-strain behaviour 78—84925
Ni-Cr-Fe alloys, radiation enhanced precip. and dissolution of precipitates, point defect kinetics and dislocation obs. 80—108467
Ni-Si (12.7 at.%), heterogeneous precipitation at internal and external surfaces during Ni ion irradiation 79—77647
Ni-Si solid solution alloys, irrad., γ phase precipitation, interstitial dislocation loops 77—1839
β'-NiAl, dislocation climb, hot stage TEM 77—24318
NiAl, nonstoichiometric, interstital defect cluster obs. 80—107226
Ni$_3$GA single crystals, anomalous temp. depend. of strength, dislocation struct., optical and TEM 79—74228
PbNb$_2$O$_6$, ferroelectric thick crystals, domain formation and dislocation loops 78—60410
Sb, electron microscope irradiation effects, agglomeration of point defects, dislocation climb and loops *(French)* 80—59518
Si, A-swirls, self-diffusion mechanism on high temps. 77—80500
Si, ambient effect of O precipitation, self interstitial mechanisms, IR spectra, TEM study 80—66510
Si, B implanted layers, damage obs. by X-ray double refl. 77—15463
Si, crack-tip dislocation pattern, X-ray topography *(French)* 80—107253
Si, critical resolved shear stress, 800 to 1050°C indentation dislocation rosettes 79—24577
Si crysts., dynamic processes associated with stacking faults and deform. twins, HVEM in-situ obs. 80—103369
Si, Czochralski grown, dislocation free, swirl defect form., doping effect 80—92519
Si, Czochralski grown crystal, O precip., nucleation behaviour and dislocation loop form. *(Japanese)* 80—59664
Si, defect form. under radiation-accelerated diffusion conditions 80—19854
Si, dislocation formation, under high stress, low temp. 78—47386
n-Si, dislocation free, memory effect associated with appearance of prismatic dislocation loops 77—1130
Si, dislocation loops, creation in region of interface, after annealing 79—82210
Si, dislocation motion near surface 79—82219
Si, dislocation-free, O$_2$ precip., IR and TEM obs. 80—29173
Si, dislocation-free single crystals, growth microdefects, etching and X-ray expts. 78—47385
Si, dislocation-free single crystals, microdefect type by anomalous X-ray transmission 79—95019
Si, electron microscopy, spatial meas. using images corresponding to different reflexes 77—55216
Si, electron-hole droplets nucleation at swirl defects 79—15095
Si, electron-irradiated, {113} loops obs. 79—82225
Si epitaxial wafers, role of metallic contamination in formation of 'saucer' pit defects 77—39588
Si, Frank hexagonal interstitial loop, dissoc. energy 77—35556

dislocation loops continued
Si, growth and melting processes, origin of swirl defects 77—76407
Si, heat-treated dislocation-free, elec. props. of stacking faults and precipitates 77—39796
Si, interstitial swirl defect form. in dislocation free floating zone cryst. 77—7682
Si, ion beam irrad., defects prod. by individual displacement cascades, TEM study 80—70265
Si, ion implanted, complex annealing behaviour of amorphous layers, TEM obs. of defect struct. 80—107299
Si, ion implanted, damage struct. obs. using TEM and cross section specimens 80—107298
Si, ion implanted, defect struct., dislocation loops and elongated defects 80—107300
Si, ion implanted, interstitial generation and loop form. during annealing in oxidising medium 80—107225
Si, ion-implanted, defect struct., SEM, TEM and X-ray topography expts. 77—51399
Si, ion-implanted, secondary defects development, three-stage model 78—87725
Si ion-implanted laser-annealed solar cells 80—93881
Si, ion-implanted layers, residual defects after high temp. annealing 78—87695
Si, microdefect obs., using double cryst. X-ray topography 77—4105
Si, mobility of segments of dislocation loops, model of nonconservative dislocation motion 78—18647
Si, neutron transmutation doping, annealing, lattice damage 80—15163
Si, oxidation-induced Frank sessile dislocation loops, struct. change 80—75228
Si, P^+ implantation, induced disorders. 80—6422
Si, prismatic dislocation loops, (g.b)s product sign determ. *(Russian)* 78—38705
Si, slip, room temp., TEM obs. 80—79804
Si substrate, stress field, induced by Si_3N_4 film edge, indentation-injected dislocation half-loops obs. 78—30839
Si surface, line tension induced dislocation motion 79—82212
Si, swirl defects, formation by agglomeration of self interstitials 77—80507
Si wafer, dislocation propagation and emitter edge defects, appl. to transistors 77—1128
Si wafer thermal gradient induced slip, effect of starting cooling temp. 78—10057
Si, X-ray channeling technique anomalous transmission, appl. to microdefects induced by heat treatment 79—19124
Si:$Ar^+(Si^+)$. implantation effect on carrier lifetime, damage obs. by TEM 79—65493
Si:As, ion implanted, laser annealed, lattice defects, epitaxial regrowth 80—103334
Si:As, ion-implanted, dislocation loops and etch pits, X-ray diffr. and TEM obs. 79—42068
Si:As, ion-implanted and postannealed, TEM obs. 77—84776
Si:As, segregation and substructure, TEM obs. 77—63674
Si:As implanted emitters, oxidizing drive-in ambient deleterious effect 80—2044
Si:As^+, annealing by scanning Ar ion laser, dislocation loop density comparison 78—47438
Si:B, dislocation net form. during annealing 77—51385
Si:B, implanted, shrinkage of rod shaped defects 78—6061
Si:B, ion implanted, localised defects, TEM study 78—87699
Si:B, ion implanted, struct. of rod defects, TEM obs. 78—71744
Si:B, ion implanted, structure defects formation and behaviour under annealing in various ambients 80—65033
Si:B, ion-implanted, dislocation climb, TEM obs. 78—6062
Si:B, ion-implanted, rod-like defects, TEM obs. 77—68975
Si:B, microdefect depend. on doping, undecorated interstitial loops 79—69120
Si:B, TEM study of stacking fault form. and annealing 78—51566
Si:B(P), diffusion induced imperfections, laser annealing, rel. to junction characts. 78—75678
n-Si:Cs, ion implanted, minority carrier lifetime and defect struct., annealing effect 78—6395
Si:Cu, interaction between vacancy emitting absorbing precipitates and dislocations, TEM obs. 78—71755
Si:Ni, low temp. annealing effect on behaviour of Ni 79—10862
Si:O, annealed, minority carrier lifetime 79—23985
Si:O, annealed, precipitates, dislocation and stacking fault loops, TEM characterisation 77—4111
Si:O, cryst., annealed, struct. defects 78—75673
Si:O wafer, annealed, surface- and inner-microdefects, TEM obs. 80—54236
Si:P, distrib. depth for dislocation loops and P precipitates 79—55756
Si:P, incoherent light flash annealing, elec. props., backscattering spectra 80—97504
Si:P, ion implanted, regrowth of damage structs. by laser annealing 80—107289
n-Si:P, secondary defects produced by high-temp. electron irrad. 79—33017
Si:P, stacking fault and dislocation growth induced by P predeposition 77—59023
Si:P spherical defect cluster and dislocation loop analysis 78—14356
Si:P^+, misfit dislocation net propagation due to osmotic forces 79—65108
Si:P^+ ion implanted single crysts., secondary defects development during annealing 80—44228
Si:P(B), high temp. impurity diffusion via vacancies and self-interstitials 80—24667
Si:Sb, ion implanted and annealed, influence of implantation temp. on dislocation generation 80—88158
Si-P, dislocation networks due to ion implantation, TEM exam. 77—35563
SiO_2-Si interface, interaction of point defects, electron microscope exam. 77—7979
SmS, defect struct., precipitate colonies, dislocation loops, TEM obs. 80—44214
Ti, neutron irradiated, characterization of dislocation loops 80—88155
Ti, single crysts., recrystallised, X-ray topography obs. 78—10054
Ti-Al (14.4 at.%), void form. and solute segregation under Ni ion irradiation 79—42122
Ti-Al-V (6,4 wt.%), ion irradiated, microstruct. study using TEM 80—96572
Ti-Fe-C-N, ion irradiated, microstruct. study using TEM 80—96572

dislocation loops continued
TiC_x, effect of structural vacancies on neutron radiation damage 77—35591
UO_2, neutron and electron irradiated, imperfect dislocation loops *(French)* 79—7606
V_3Si, neutron irrad., grain boundary pinning, field-depend. change of crit. current density 80—65759
V_3Si, neutron irrad., volume pinning force, summation and saturation behaviour 79—95554
YIG, plastically deformed, TEM, dislocation Burgers vectors 77—11557
Y_2O_3, electron irrad., dislocations *(French)* 80—2076
Y_2O_3, plastically deformed monocryst., HV electron microscopy obs. of dislocation config. *(French)* 79—55747
Y_2O_3, polycrystalline, high temp. O ion bombard., TEM microstruct. investig. 77—27923
zircalloy-2, annealed, neutron irradiated, 573 to 923K, damage struct. 79—99247
Zn, basal dislocation—prismatic dislocation ring interactions by method of moments *(Russian)* 80—10550
Zn, electron radiation damage in HVEM, nature of defect clusters 78—59838
Zn, faceting of interstitial loops 78—47381
Zn, single cryst., Burgers vector determ. of perfect dislocations obs. by X-ray topography 79—37711
ZnO, dislocation loop nucleation on prismatic faults in high voltage electron microscope 77—72620
ZnO, irradiation in high voltage electron microscope dislocation loops study 80—88157
ZnSe, electron irrad., dislocation climb, TEM obs. 79—1461
ZnTe, real structure effect on luminescence and absorption spectra, dislocations 80—16085
ZnTe:Ag, containing dislocation loops, optical absorption-edge fine struct. 78—43905
ZnTe:Ag, dislocation loops creation in region of interface 79—82210
ZnTe:Ag, doped during frowth and by diffusion, defect form. 80—15129
ZnTe:Ag, real structure effect on luminescence and absorption spectra, dislocations 80—16085
Zr alloys, creep and growth, irradiation induced, rate theory approach 80—89294
Zr and alloys, neutron irrad. at 573 to 923K, damage struct. 80—107334
Zr, annealed, neutron irradiated, 573 to 923K, damage struct. 79—99247
Zr base alloys, irradiation growth, dislocation model 78—51595
Zr, foil, dislocation loop nucleation and growth during 1 MeV electron irrad. 80—88152
Zr, irradiation induced defects, electron microscope images 78—83854
Zr, neutron irradiated, dislocation loop nature 77—47489
Zr, point defect migration into dislocation loops, finite difference calc. 80—54225
Zr-Al (8.6 wt.%), dimensional stability struct. and mech. props, effects of neutron irrad. 80—92563
Zr-base alloys, annealed specimens, irradiation growth 80—49276
Zr-Nb (0.1, 2.5 wt.%), foil, dislocation loop nucleation and growth during 1 MeV electron irrad. 80—88152

dislocation motion
for dislocation relaxation see dislocation damping
see also dislocation climb; slip
acoustic emission from moving dislocations near crystal surface 78—87856
activation entropy, computation 80—39083
adhesive wear, in presence of magnetic field, model 77—28913
aggregate, polycrystalline, deform. 77—4816
alkali halide, screw dislocations in puncture rosettes, motion-starting-stresses, surface-active media effects *(Russian)* 78—10051
alkali halide conc. solid solns., hardening theory, dislocations, stress effects 79—32994
alkali halide crystals, F-spectrum, deformation induced voltage 79—56256
alkali halides, dislocation dynamics studied by nucl. spin relax. meas. 80—108091
alkali halides, dislocation motion, nucl. spin relax. study *(Dutch)* 79—78556
alkali halides, local vibr. modes excitation by ions, moving dislocation steps *(Russian)* 77—31696
alkali-halide crystals, plastic deformation, effect of solid film coatings *(Russian)* 77—25167
alkaline earth fluorides, crack propag., cryst. props. effects 78—75720
alloy, ordered, with LI_2 superstructure, plastic deform. with mobile and immobile dislocations, phenomenological theory 79—7602
alloy, two phase, deform. 77—8893
alloys, with ordered domains and disordered regions, critical shear stress *(Russian)* 80—107237
anisotropic elastic medium, appl. to martensitic transform. 77—28811
antiferromagnet, dislocation slowing down due to spin waves *(Russian)* 79—95584
antiferromagnet, moving dislocations, interaction with spin waves *(Russian)* 78—56303
bent single crystal, equilib. face, surface relief form. during annealing 78—47651
Bergers, W.G., and J.M., work on dislocation theory 80—62440
binary, ternary oxides, dislocation motion and high temp. plasticity 80—59468
book on effects of many dislocations 80—105441
α-brass, acoustic harmonic generation by long-range dislocation motion 79—42150
brass bicrystals, two-phase (α/β), interphase boundary sliding at high temperature 80—88164
β_1 brass containing α-precipitates, reversible shape memory effect *(Japanese)* 78—60711
bronze P, heavily cold rolled, yield strength enhancement mech. 77—36539
calcite, sound emission on dislocation annihilation *(Russian)* 80—54246
carburized single crystal sheets, lattice strain during interstitial diffusion *(Japanese)* 78—10220
charged impurity influence on dislocation motion in cryst. 80—103333
coherent, stress-free, ordered particles, dislocation interactions 79—27988
coherent motion, lattice dynamics 78—71738
collective behaviour, velocity of slip band and mobile dislocation densities, HVEM study *(French)* 80—65006
collective dislocation motion, dynamic effects 78—79632

dislocation motion continued
- computer simulation of straight dislocation line motion in concentrated solid soln. 77—15413
- consecutive energy barrier systems, deform. kinetics 79—77672
- contact film absorption on plastic deform. of contacting bodies *(Russian)* 80—93596
- continuous distributed dislocations, transport eqns. *(Russian)* 79—32997
- core struct., dislocation mobility by electron microscopy, review *(French)* 79—42071
- creep, phenomenological theory, dislocation kinetics 77—63755
- creep, transient and steady state, compatibility of dislocations model *(Italian)* 80—33487
- creep, transition between dislocation and diffusion 80—88253
- creep under cyclic stressing, physical model and theoretical eqns. 78—39833
- crystal cleavage due to dislocation tilt wall splitting 78—91377
- cubic crystal, high vel. screw dislocations motion and interatomic force law 77—43214
- cubic crystals, dislocation theory, soln. of eqns. *(German)* 78—38701
- cubic crystals, elastic strip, moving stress sources, boundary-value problem soln. *(German)* 78—38702
- cubic metals, reson. vibrs. of metal spheres, elastic consts. and internal friction 78—15443
- defect dynamics, closure of governing eqns., plastic state theory 79—37702
- defect superlattices, hardening influence, computer simulation *(Russian)* 79—83206
- density of mobile dislocations 79—7604
- diamond cubic structure, kink formation and migration, rel. to Fermi level 79—82218
- digital simulation of movement through random array of weak obstacles 78—30633
- discrete obstacle model, dislocation and stress field distrib. 80—79794
- discrete obstacle model, dislocation pile-up kinetics dislocation mobility activation parameters 80—29022
- dislocation, straight line, motion in conc. solid soln. computer simulation 77—81268
- dislocation damping during electron irradiation, new model for peaking effect 78—87683
- dislocation interaction with point obstacle in non-uniform stress field, localised force approx. 80—15150
- dislocation loop growth during intrinsic point defect-impurity atom mobile complex formation *(Russian)* 79—90653
- dislocation motion, lattice resist., effect of impurity interstitials 80—84170
- dislocation movement, in volume dispersion of obstacles, stochastic model, low temp. anomalies rel. to yield stress 79—60367
- dislocation-soft mode interaction in displacive transitions *(Russian)* 80—84172
- dispersion strengthening, dislocation interaction treatment, digital simulation models 78—31419
- dissociated dislocations in diamond cubic struct. 78—59806
- dynamic Peierls stress in cryst. model with slip anisotropy, screw dislocation motion 78—95056
- dynamic waves along dislocations overcoming local obstacles 80—29021
- edge dislocation, atomistic models for rectilinear motion 77—72193
- edge dislocation, displacement field, in elastic strip, Fourier transform technique 79—46658
- edge dislocation motion, glide and climb resist. due to dragging a Cottrell atm. 79—99194
- edge dislocation thermally activated motion, appl. to KCl-KBr solid soln., computer simulation 79—19249
- edge dislocations, nonlinear motion in atomic lattices, nonequilibrium mol. dynamics 79—55742
- elastically nonlinear medium, dislocation interactions *(Russian)* 79—42064
- elastically nonlinear medium, field of dislocation shifts, integral eqn. *(Russian)* 78—47374
- elasto-plastic metal-dislocation system, stress-activated dislocation motion, thermodynamic theory *(Chinese)* 78—83868
- elastoplastic relaxing media, shock waves struct., distribution model 80—58961
- electron microscopy, conf., Nancy, France (May 1978) *(French)* 79—41915
- electron microscopy, HV, in situ obs. techniques and applics,. review *(Japanese)* 80—59351
- electron solid, two-dimens., defects and implications for melting 80—39076
- epitaxial small islands, one-dimens. model of mobility, parabolic substrate pot. 79—95299
- fatigue crack, dislocation diffusion mech. of form. 78—60829
- fatigue crack initiation, rel. to grain boundaries, stress gradients and cross slip 77—27890
- fatigue crack propag., low temp. 78—72876
- FCC crystal, transient effects during tensile tests in model of correlated dislocation motion 78—38715
- FCC metals and alloys, deform. behaviour 77—8892
- f.c.c. polycrystals plastic deform. in microstrain region 77—1165
- ferrite, internal friction, rel. to dislocation movement *(Polish)* 79—95026
- ferrite, polycrystalline, ionic diffusion and dislocation movement during creep deform. *(Japanese)* 77—28039
- ferromagnet, dislocation motion, mag. moments around screw dislocations, spin waves retarding dislocations 78—87670
- ferromagnet, dynamic dislocation deceleration by spin waves *(Russian)* 77—28379
- ferromagnet, dynamic slowing down of dislocations near Curie point *(Russian)* 79—8036
- field equations, four dimensional space-time setting 80—96521
- fluctuational breakaway from pinning sites, effective temp. *(Russian)* 78—22716
- foil, push-pull straining device for h.v. electron microscope in-situ deform. 77—4875
- forest dislocations, motion of train through forest modelling methods 80—107238
- Frenkel-Kontorova dislocation dynamics in cryst. of finite length 80—24452
- gauge transformations admitted by the equations of defect dynamics 79—27981
- Ge, heavily doped, dislocation vel., electronic effects 77—11547

dislocation motion continued
- geological materials, dislocation dynamics studies via stress relaxation testing method 78—96309
- geometrical theory, four-dimensional 79—84954
- grain boundary sliding and its accommodation during creep and superplasticity 77—40436
- grain boundary soliton-like features, molecular dynamics computer simulation study 79—77610
- H_2O:HF ice, single crystal, velocity of individual dislocations by X-ray topography *(French)* 78—87677
- Haynes Stellite 6B, particle erosion damage, TEM obs. 78—88546
- hexagonal crystals, intraction of flexible dislocations in intersecting slip planes 77—39592
- high pressure effects on dislocation mobility 78—55869
- ice, quantum mechanical approach to velocity of dislocations 78—91339
- II-VI semiconductor, charged dislocation motion during plastic deform. 79—82233
- III-V semiconductor, dislocations, velocities and internal friction 79—82231
- impact testing, investigation of dislocation dynamic props. *(Russian)* 78—85069
- impure crystal, steady motion, stochastic theory 77—11548
- impurity crystal, microstructural plastic instability *(Russian)* 79—99190
- Incoloy 800, review of mech. props. up to 600°C 79—43368
- incubation period following stress reduction during creep 79—7603
- inertia, influence on movement near precipitates *(Russian)* 78—14346
- n-InSb, acceptor effect of plastic bending 80—6885
- internal friction, extended model of effects of point defect dragging 78—10083
- internal friction meas. during deform., Kê peak anal. 78—18705
- internal stress field effect, on deformation rate, kinetic anal. 80—25787
- internal stress field produced by dislocation motion and creation 77—62530
- interphase boundary dislocations and coherency concept 80—24447
- Invar, dislocation motion anomaly 80—10554
- ionic crystal, dislocation mechanism of electrification during cleavage 77—24353
- ionic crystal, point defect-dislocation interactions 78—63787
- ionic crystal defects, mag. reson. studies 80—108066
- ionic crystals, dislocations, review 80—107236
- isotropic polycrystalline plasticity, dislocation theory 79—14875
- kinematics, continuous distrib. of disclinations and dislocations 78—63764
- kinetics in Peierls pot. 79—99192
- kink spreading process, dislocation kinetics anal. 79—60366
- kink stationary propag. 80—2016
- lattice drag force on moving dislocation, zero temp. 79—95006
- lattice models of screw dislocation high velocity motion, lattice model effects 79—77600
- load dependence, motion through random array of point obstacles, stochastic averaging 77—7732
- local heating at low temps., parallel glide planes, temp. distribution *(Russian)* 80—29020
- low-temperature statistical characts. *(Russian)* 79—90654
- magnetically ordered cryst., dislocation drag, magnetoelastic waves 80—103332
- metal, annealing, struct. and grain boundary mobility 79—47728
- metal, BCC, deform. 77—4815
- metal, BCC, thermally activated motion of screw and 71° dislocations *(German)* 77—19950
- metal, BCC screw dislocation motion, under shear and uniaxial stress, computer simulation 77—4102
- metal, creep movement of dislocations, effect of stress distrib. at grain boundaries *(Russian)* 78—27564
- metal, dislocation kinetics of superplasticity and creep 77—76404
- metal, electron drag od dislocations 80—10961
- metal, finite elastic-plastic deformation at high temp., work hardening rule 77—4828
- metal, flow stress relation with thermal conductivity discontinuity at supercond. transition 78—60246
- metal, plasticity at very low temperature, dislocation motion, rel. to supercond. and tunnelling *(Czech)* 77—32630
- metal, small-angle boundary migration in steady creep state 77—39624
- metal, thermo-inertial mechanism of plasticity enhancements normal to superconducting transition *(Russian)* 79—47183
- metal and alloy polycrystals, internal friction amplitude depend. *(Russian)* 79—90726
- metal bicrystal, mech. behaviour, continuous theory of dislocations appl. 78—67717
- metal systems, high voltage electron microscopy of dislocation dynamics *(Japanese)* 77—47458
- metallic crystals, pulsed mechanical stressing equipment 79—52532
- metals, athermal region of plastic flow at intermediate temps. 77—48497
- metals, atomic mobility under pulsed loading conditions *(Russian)* 80—96684
- metals, BCC, effect of screw dislocations, on mech. props. *(Russian)* 78—60704
- metals, BCC, plastic deform., review 80—104213
- metals, BCC, solid soln. hardening, crystal resolved shear stress depend. on dislocations 80—40373
- metals, BCC and FCC, dislocation dynamics method appl. to plastic flow 79—47745
- metals, dislocation motion depend. on electrons *(Russian)* 79—65260
- metals, dislocation-core movement and frictional stress 80—92529
- metals, inductional dislocation braking in mag. field *(Russian)* 80—79791
- metals, research at Birmingham, (1945-55) 80—62444
- metals irradiated, heavily, exam. of percolative mass transfer 78—79639
- metals under load, plastic deform. local instability *(Russian)* 77—76415
- mobile dislocation density determ. from sound velocity 79—19258
- mobile pinning points on dislocations, equilibrium distrib. 80—79792
- mobility in inhomogeneous stress field, hardening effects 80—70219
- modified Frenkel-Kontorova model 78—2134
- multiple dislocation motion, exam. 78—51541
- Nabarro, F.R.N., dislocation physics research 80—62441
- Nimonic alloy reinforced Al, Cu and brass, laminated composites, low-temp creep singularities, structural defect changes *(Russian)* 80—11696
- nonstationary temperature field, dislocation struct. dynamics *(Russian)* 77—27884

dislocation motion continued
nonuniformly moving dislocations, elastic half space response to realistic faulting model 78—85486
normal metals and superconductors, effect of conduction electrons on dislocation mobility 79—7932
nuclear spin-lattice relax. investigation, theory 78—34512
ordered alloy, noncoaxial dislocation loop behaviour 77—11549
particle resistance to motion 77—62539
particle-strengthened materials, dislocation creep model 78—3182
percolation through absolute obstacles in impurity crystals *(Russian)* 80—70196
phonon-dislocation interactions, drag of phonon gas by moving dislocations 80—70218
physical model for crystal with high Peierls relief in brittle failure region *(Russian)* 79—65093
plastic deformation, cyclic, exam. of reversible strain, effect on dislocation motion 78—84892
plastic deformation, macroscopic theory, dislocation and disclination kinetics *(Russian)* 80—49225
plastic deformation, partial disclination dipole motion 79—73165
plastic deformation, phenomenological theory, with mobile and immobile dislocations 78—75714
plastic deformation, steady-state, irreversible thermodynamic description 78—72831
plastic deformation instability, effects of physical parameters 79—47758
plastic deformation theory, thermally activated dislocation transforms. 77—20008
plastic flow, order-disorder transform. effect on creep, traction and relaxation *(French)* 80—35180
plastic strain rate changes, transient functions 77—15480
plastically deformed crystals, nuclear spin relaxation study *(Dutch)* 79—78556
plasticity, polycrystalline, probabilistic approach, appl. 78—26622
polycrystalline aggregate, continuous distrib. of dislocations, stress fields, movements in elastic-plastic deform. 78—75709
polyethylene molecules, transportation along their axis, energetics of defect motion, point dislocation energy calc. 78—14294
polymer, crystallising, defects and mech. relax. *(Russian)* 78—22789
polymers, defect elementary movement orientation from acoustic expts. 79—94927
pore growth and healing under load, dislocation mechanism, barrier influence *(Russian)* 78—18634
precipitate hardened material, intergranular cavity growth inhibition 80—50677
quantum motion of dislocations through local barriers *(Russian)* 79—60363
rectilinear dislocation annihilation, acoustic emission, exact soln. 80—44209
resistance fluctuations, anal. independ. of thermal voltage noise 80—84495
Schmid's law deviations, in uni-directional strain 78—71783
screw, in simple cubic lattice, anal. of displacement field 77—11551
screw dislocation soliton-like motion, piecewise linear force model 78—2119
screw dislocation-phonon interaction in cryst. with anisotropic slip system 80—29137
screw dislocations, moving in elastic nonlinear medium, displacement field *(Russian)* 80—44206
segment oscillations, internal props., point obstacle collisions, glide plane motion *(Russian)* 80—39088
segments, pinned, effects of viscosity on quantum motion *(Russian)* 80—44207
semiconductor, dissociated dislocations, statistics of kink formation 79—82207
semiconductor, tetrahedrally coordinated, effect of doping on dislocation mobility 79—82550
semiconductor, tetrahedrally coordinated, models of dislocation struct. 79—82205
semiconductor crystal, physical nature of low temp. microplastic strain *(Russian)* 79—65094
semiconductors, covalent, quantum mechanics of dislocation kinks 77—19951
semiconductors, II-VI cpds., dislocation motion obs. by SEM in cathodolum. *(Japanese)* 79—46666
shock front propag. in solids, wall of dislocations model 79—90728
simulation appl. to materials, conf., Gaithersburg, USA (April 1976) 78—27387
single crystals, dislocation mobility under conc. loads at indentations 79—95015
solid soln., ductility, comp. effect *(Japanese)* 79—43334
solid soln., flow stress, temp. plateau 79—14877
solid soln. strengthening, conc. computer simulation 78—31420
solid solution, activation energy for dislocation motion, from crit. resolved shear stress data 77—55289
solid solution, influence of diffusion on dislocation motion 79—27983
solid solution hardening, dynamic simulation 79—11635
solid solutions, dislocation-core movement and frictional stress 80—92529
solid-state turbulence 80—92528
soliton, dimensioned profile for propagation *(French)* 77—35155
solution hardening theory 77—36530
Somigliani dislocation containing medium, mechanics and kinematic props. *(Russian)* 80—38250
source activation by load impulses 78—14350
start stresses of ensemble leading dislocations 80—92530
static flow stress, decrease, by superimposition of ultrasonics 79—7652
steel, 17249, creep and creep fracture *(Czech)* 77—86089
steel, acoustic emission sources and dislocation patterns 80—61040
steel, austenitic, dislocation struct. formed by interstitial diffusion of C 77—4223
steel, austenitic stainless, Cr-Ni-Ti, creep deform. effects on intergranular TiC dispersion stability 78—84912
steel, austenitic stainless, creep dependence on electron irrad., in type SS316 steel, dislocation motion *(Russian)* 80—108495
steel, austenitic stainless, embrittlement by α-particle irrad. 77—69015
steel, C, brazed butt joint, static torsional deform. 77—16657
steel, Cr-C, (2.14, 1.08 at.%) tempered, resistance to small plastic deformation, strain relaxation *(Russian)* 78—56698
steel, Cr-Mo, annealed, interaction solid soln. hardening, precipitation effects on creep 79—4974
steel, Cr-Mo-V, low alloy, V effect on creep *(Czech)* 77—86088

dislocation motion continued
steel, Cr-Mo-V pressure vessel, microstruct. parameters and yielding rel. to plastic deform. 80—89318
steel, CrMoV, low alloy, creep resistant, temp. and stress depend. of time to rupture *(Czech)* 77—70160
steel, high strength, dislocation sweeping model for hydrogen assisted subcritical crack growth 80—97577
steel, high-strength, strain relax., model *(Spanish)* 77—73296
steel, low C, effective stress determ. during the loading cycle 79—38879
steel, low C, yield point, effect of ageing stress 79—96091
steel, low C and alloy, serrated flow and thermomechanical treatment *(Korean)* 80—30026
steel, maraging, and HY-80, deform., hydrostatic pressure effect 77—36596
steel, martensitic transformation, lattice deform. 78—27511
steel, mild, elastic-plastic analysis of yield process 77—36571
steel, stainless, 316, creep and rupture, 525 to 900°C, creep rate 79—11678
steel, stainless, creep 78—64583
steel, stainless, grain boundary behaviour validity of coincidence site lattice model of grain boundary struct. 79—51120
steel, stainless 304, deformation twins contribution to yield stress, Hall-Petch law for inter-twin spacing 79—24588
steel, structural, exam. of mech. props. when under impulsive loading *(Czech)* 79—91742
steel USA, spheroidised pearlitic, superplasticity *(Russian)* 78—19826
stored energy determ., analytical method *(Russian)* 77—25096
strain rate, dislocation density, dislocation motion and dislocation constitutive eqns. 80—103329
straining experiments, in situ, strong frictional force, quantitative anal. 80—100244
stress field, diffusing elastic fluid, mechanical interaction effects 78—63766
stress relaxation in crystals, review 79—73248
stress-free motion of dislocation arrays 79—65083
subboundaries, collective effects accompanying migration *(Russian)* 78—14347
superconducting transition, dislocation mobility change 77—15993
superconductors 77—47929
superconductors 77—47930
supersaturation, of H, produced by dislocation motion 77—36640
TEM, work of Hirsch et al., (1946-56) 80—62445
TEM obs. of plastic deformation, conf., Clermont-Ferrand, France (June 1976) *(French)* 77—44298
theory, book contrib. 80—107240
theory, development, inc. work of C. Crussard 80—62443
thermal activation analysis, of plastic deformation and dislocation motion using stress and temp. jumps 80—74771
thermal activation and mechanical loading induced, description using diffusion eqns. 78—38697
thermal activation through random point obstacles 79—1434
thermal and thermoelastic fields around moving dislocations *(Russian)* 78—22731
thermal drag force on moving dislocation, non zero temp. 79—95007
thermally activated, double exponential rate eqn. 77—31660
thermally activated motion in periodic pot. 79—99193
thermally activated motion of dislocation group, exam. 78—87669
transient Snoek atm. 79—73166
two phase alloy hardening by second phase particle coalescence 80—7591
Udimet 520, γ′ distribution in slip plane, dislocation loop form. during creep *(Japanese)* 79—42075
ultrasound resonance absorption by moving dislocation 80—54318
unbounded elastically isotropic medium, fields generated by moving dislocations, multipole-moment expansion *(Russian)* 80—103330
velocity, determ. by nuclear spin-lattice relax. meas., theory and expt. 77—35566
velocity, thermal activation exam. of applied stress and temp. depend., expt. methods *(French)* 80—59474
viscoplasticity problem, analytical soln. 77—84832
waiting time calc. of dislocation motion for computer simulation 78—30638
X-ray diffraction topographic patterns, TV system for visualisation 77—58925
Ag and Ag-Sn(In)(Sb) dil. alloy, single crystals, dynamic dislocation behaviour 77—4108
Ag halide crysts., dislocations, survey of post-war research 80—62449
Ag single cryst., effects of impurities and prestraining on temp. depend. of yield stress *(Russian)* 77—47506
Ag single crystal, dislocation dynamics during stress rate changes 78—19813
Al, [111] single crystal, in situ deform., HVEM obs. 78—52886
Al, acoustic emission from moving dislocations during tensile tests 77—19964
Al, acoustic emission under plastic deform., spectral anal., dislocation mean free path 78—84934
Al alloy, acoustic stress wave emission during plastic deform., dislocation motion explanation 77—36697
Al alloy, precipitation hardening, creep deform. effect 77—16601
Al alloy 7075, acoustic emission sources during plastic deform. 78—27573
Al alloy 7075, serrated flow and thermomechanical treatment *(Korean)* 80—30026
Al and Al-Mn (1 wt.%), subgrain growth during annealing after cold work 78—56656
Al, dislocation line movement at low temp., obs. by US meas. *(French)* 79—95025
Al, dislocation velocity, from amplitude-dependent internal friction 79—11653
Al, dynamic defect annealing during plastic deform. 78—88478
Al foil, α-particle irrad. under fusion reactor conditions, He bubble alignment during deform. 80—107345
Al foil, quenched, anomalous annealing phenomena, quantitative study 78—80565
Al grain boundary behaviour validity of coincidence site lattice model of grain boundary struct. 79—51120
Al, grain boundary migration, TEM obs. on mechanism 80—79812
Al, lattice resistance stress, Bordoni relax., microdeform. and US attenuation results 80—25747
Al, mobile dislocation density determ. from sound velocity 79—19258
Al, pipe diffusion along segment of faulted dislocation loops during annealing 80—107256

dislocation motion continued
Al plastic deformation depend. on mag. field at 4.2K *(Russian)* 79—91754
Al, recovery annealing, exam. using in situ high voltage electron microscopy 80—7596
Al, resistivity decrement under torsional deform., impurity segregation at moving dislocations 77—4321
Al, thermoactivated creep and stress relax. 79—87692
Al, trial cuts at low speeds in relation with traction trials *(French)* 80—24448
Al-Ag, thin-layered laminates, yield strength rel. to dislocation generation and motion 79—20137
Al-Al_2O_3, dispersion hardened, creep *(Czech)* 80—108463
Al-Cu, thin-layered laminates, yield strength rel. to dislocation generation and motion 79—20137
Al-Cu (33 wt.%) eutectic, superplasticity, in-situ obs. by TEM 77—28876
Al-Cu-Mg, tpye RR55, high strength, creep behaviour, effect rel. to anodic coatings, SEM study 80—97542
Al-Li, cold worked neutron irrad. alloys, He bubble behaviour, microstruct. changes 77—54359
Al-Li, dil. alloy, cold-worked, annealing spectrum 78—39801
Al-Mg (0.3 wt.%) single cryst., dislocations obs. by high voltage electron microsc. 80—79796
Al-Mg (2 wt.%), steady creep characts., precip. effect 80—35189
Al-Mg (5.5 at.%), theory of internal stress for class I high temp. creep 78—19807
Al-Mg (5.5%), creep, absence of instantaneous plastic strain upon stress changes 78—75718
Al-Mg solid soln., AE during plastic deform. 78—64592
Al-Zn (6.5 at.%), fatigue props., effect of ageing and thermomech. treatment 78—27620
Al-Zn-Mg alloys, decomp. kinetics from Young's modulus obs., microprocesses *(German)* 78—64522
Al_2O_3, ambipolar diffusion in deformation mechanism maps 78—48454
Al_2O_3-SiO_2, sillimanite, lattice defects, crystallo-chemical model, TEM obs. *(French)* 78—26570
BN, cubic single crysts., dislocations and other defects, X-ray topography study 79—99207
BN, graphite-like, twinning and shear 77—4114
Be, forest dislocation effect on single twin layer development in single crystals 78—63775
Bi, low temp. plasticity, strain hardening, slip *(Russian)* 77—31713
α-brass, serrated yielding, tensile tests and TEM obs. 79—34110
α-brass, solid soln., ductility, comp. effect *(Japanese)* 79—43334
C, heat-treatment and neutron irrad. effects on US atten. and Young's modulus 79—11644
$CaCO_3$, plastic deformation in compression parallel to (111) 78—38709
CaO-MgO, doloma, composition effect on creep, impurity effects 79—43318
Cd, single cryst. stress relax. depend. on elec. current, electron plastic effect 79—79021
$Cd_xHg_{1-x}Te$, dislocation motion, effect of lattice defects on microhardness *(Russian)* 80—70220
CdS, acoustic wave attenuation, phonon viscosity and dislocation drag 80—70319
CdS, dislocation motion, TEM obs. 80—79799
CdS, photoplastic effect due to α, β dislocations, spectral depend. 77—90180
CdS, reversible hardening induced by electron-beam irrad. 77—62580
CdTe, crystal size depend. of photoplastic effect 80—92592
CdTe, crysts., mech. behaviour, yield stress function of temp., stress relaxation 79—60427
CdTe, negative and positive photoplastic effect 79—51192
CoO single crystal, compressive creep 78—11275
CsI, annealing effects on mech. and microstruct. props. 77—66686
Cu, brazed butt joint, static torsional deform. 77—16657
Cu, control of dislocation propagation and generation 78—3025
Cu, cracks in fatigue early stages, direct obs. of substruct. by electron microscope *(Japanese)* 78—7028
Cu, cyclically deformed polycrystals, elastic limit, contribution of thermally active processes *(Spanish)* 79—91732
Cu, dislocation mean free path at 77K under elastic deform. 78—44162
Cu, dislocation mechanism of luminescence during fracture 79—24376
Cu, dislocation motion in highly perfect crystals *(Japanese)* 79—60373
Cu, dislocation path length after pulse loading 78—30630
Cu, dispersion hardened, mobile dislocation density and length of slip lines 77—51387
Cu, electron irrad. at 100K, dislocation vel. meas. etch pit technique 80—49271
Cu, electron irrad. at 100K, comparison of irrad. hardening with dislocation vel. 80—54284
Cu, electron-dislocation interaction, influence of mag. fields on flow stress meas. 77—31672
Cu film, internal stress determ. by stress relaxation method *(Russian)* 77—62787
Cu, grain boundary behaviour, validity of coincidence site lattice model of grain boundary struct. 79—51120
Cu, grain boundary migration, TEM obs. on mechanism 80—79812
Cu, high-purity, grain size and strain rate influence on mech. behaviour, precursors existence 80—85016
Cu, highly perfect crystal, dislocation motion obs. *(Japanese)* 79—60372
Cu, internal stresses in plastically deformed crystals *(Russian)* 78—79615
Cu, low temp., internal friction and microplastic strain 77—84839
Cu, neutron irradiated, effect on internal friction 78—15445
Cu single crystals, climb rate of Orowan loop anal. by dislocation pipe diffusion 79—83211
Cu, stress component determination during loading cycle *(Czech)* 79—91725
Cu, thermoactivated creep and stress relax. 79—87692
Cu, thin interlayer between high-strength alloy rods, rel. to tensile strength *(Russian)* 78—19821
Cu-Al, single crystal, dislocation velocity meas. 78—3171
Cu-Al, single crystal, dislocation velocity meas. 78—3172
Cu-Al (10 at.%), single crystal, variation of flow stress after changes in strain rate 77—28879
Cu-Al (10.4%), creep, absence of instantaneous plastic strain upon stress changes 78—75718
Cu-Au, cold worked solid solution, flow stress and activation volume 80—16393

dislocation motion continued
Cu-Be, dynamic strain age hardening 77—52375
Cu-Ge, single cryst., dislocation motion obstacles, effective strength 80—15107
Cu-Ni, cold worked solid solution, flow stress and activation volume 80—16393
Cu-Ni alloys, electron irradiated, dissociated struct. of dislocation loops with Burgers vector a⟨100⟩ 77—89444
Cu-Zn, cold worked solid solution, flow stress and activation volume 80—16393
Cu-Zn (30 wt.%), slip band growth, thermally activated 80—40457
Cu_3Au, superdislocation motion resistance due to atoms in incorrect positions *(Russian)* 79—99189
α-Fe, alloying with Ti, V, G, Mo, W and Mn, effect on dislocation mobility *(Russian)* 77—31671
Fe and Fe-Cr, flow stress, effect of cathodic, H_2 charging *(Japanese)* 79—52313
Fe, Armco, stress relaxation expt., significance under strain ageing cond. 79—57039
Fe, cast, spherical, mech. behaviour, continuous theory of dislocations appl. 78—67717
α-Fe, crack initiation study at low-cycle fatigue using slip bands *(Slovak)* 79—38949
α-Fe, creep and fracture between 77 and 673K 79—7649
Fe, deformation, influence of crystallographic lattice type *(Russian)* 79—34106
Fe dislocation dynamics, HVEM in situ obs. 78—83822
α-Fe, internal friction for low temp. deform. 80—40420
α-Fe, screw dislocation motion, orientation depend., tight-binding type electronic theory 79—51109
Fe-Mo (1.8%), creep, absence of instantaneous plastic strain upon stress changes 78—75718
Fe-Ni-C (21, 0.6 wt.%), stress assited and strain induced martensite morphologies 78—3187
Fe-Si, glissile and twinning dislocation motion temp. depend., influence of grain boundaries *(Russian)* 77—47452
Fe-Si, low-temperature fatigue crack propagation 78—72876
Fe-Ti (0.056 at.%), mobile dislocations during stress relaxation 78—68721
Fe-Ti (0.056 at.%), mobile dislocations during stress relaxation 78—68722
Fe-Ti (0.056 at.%), stress relaxation curves, anal. interpretation 77—59847
Fe-Ti (0.056 at.%) alloy, mobile dislocations during stress relax. 77—7729
Fe-Ti (0.056 wt.%), mobile dislocations during stress relaxation, comment 79—74193
Fe-Ti (0.056 wt.%), mobile dislocations during relaxation, reply to comment 79—74194
GaAlAs-GaAs heterostructures, electronic excitation effects on mobility of point defects and dislocations 78—2561
$Ga_xAl_{1-x}As$-GaAs DH laser, degraded, nature of ⟨110⟩ dark-line defects, TEM 77—89439
GaAlAsP-GaAs T-Q DH laser, light induced misfit dislocation motion 77—75518
$Ga_{1-x}Al_xAs_{1-y}P_y$-GaAs heterojunctions, light-induced misfit dislocation motion, photoluminesc. and X-ray diffr. meas. 79—11200
GaAs cryst., creep and dislocation vel. at different doping and temps. 78—95783
GaAs LPE layers, X-ray topographic studies of defects 77—62772
GaAs, n- and p-type, velocities of α- and β-dislocations, double-etch method 77—51382
GaAs, travelling heater method growth, dislocation elimination 77—7684
GaAs:Si, single crysts., asymmetric deform., dislocation vel., mobilities 79—23616
GaAs-GaAlAs, DH laser material, rapid optical degradation 77—7083
GaP, mech. props. and photomechanical effect 77—84833
GaP:N LED, acoustic emission, NDT of dislocation motion 78—91759
GaSb, acoustic wave attenuation, phonon viscosity and dislocation drag 80—70319
GaSb, dislocation velocities, double etch technique exam. 78—30629
Ge, dislocation ensembles motion in neutron irradiated covalent crystals *(Ukrainian)* 80—10579
Ge, dislocation kink length and diffusion coeff., calc. from US absorpt. 79—69197
Ge, dislocation mobility 77—76413
Ge mobility of screw and 60° dislocation at low stresses 77—11554
Ge, motion of partial dislocations 79—82229
Ge, short dislocation line movement at low stresses *(Russian)* 77—47462
Ge, single cryst., effects of ultrasound 77—69119
Ge surface, line tension induced dislocation motion 79—82212
H_2 transport by dislocations 77—21263
^3He, BCC, plastic flow 79—46880
Hf-O(N), solid soln. hardening, impurity cluster and interstitial mechanisms 77—36523
III-V semiconductors *(Japanese)* 79—42074
In crystals, twinning dislocation motion 79—65098
InAs, dislocation velocities, double etch technique exam. 78—30629
InAs, undoped n-type single crystals, dislocation velocity 77—11559
InGaP-GaAs junction, effect of elastic strain on energy band gap and lattice parameters 79—24057
InSb, asymmetrical dislocation glide, expt. evidence for 79—82232
KBr:Li(Na), low temp. radiation hardening mechanism, single halogen interstitials as hardening agent, Ha annealing 79—23634
KCl, dislocation motion in micro-plastic region 78—91341
KCl, hardness increase mode, effect on dislocation mobility 79—51114
KCl, motion of dislocation half-loops, influence of prestart loading and ensemble nature 78—71745
KCl single crystal, dislocation velocity stress exponent estimation by stress relaxation and creep tests *(Japanese)* 78—55875
KCl, stepwise motion of edge and screw dislocations *(Russian)* 77—84748
KCl, strain hardening during relax. of deforming stresses 77—7786
KCl, thermal hysteresis in ionic cond., dielec. loss meas. 78—34652
$KCl:Br^{2+}$, solid solution periodic precipitation in inhomogeneous conc. field 80—103485
$KCl:Sr^{2+}$, polarisation-plastic effect 78—2794
KCl-KBr, solution hardening and softening at low temp. 80—108462
KCl-KBr conc. solid soln., edge dislocation motion in stress field *(Japanese)* 78—2138

dislocation motion continued
KCl-KBr single crysts., yield strength and dislocation mobility, solid soln. hardening model 77—72649
KCl-KBr solid soln., highly conc., computer simulation of dislocation motion *(Japanese)* 77—68972
KCl-KBr solid solution, yielding model on plateau stress 78—27568
KCl-KBr solid solution, thermally activated edge dislocation motion, computer simulation 79—19249
KCl(Br)(I) with alkali and halogen impurities, colour centre deformation induced nonradiative decay 80—7387
LiF crystal, dislocation movement study with new chem. polish 78—15614
LiF, deformed in liquid He, penetration of He, dislocation effects 77—20131
LiF, dislocation distrib. on surface parallel to Burgers vector 79—65090
LiF, dislocation mechanism of electrification during cleavage 77—24353
LiF, dislocation mobility near fast-moving crack tip 78—47389
LiF, γ-irradiated crysts., dislocation retardation centre 79—95051
LiF, hardness increase mode, effect on dislocation mobility 79—51114
LiF, plastic deform. and dielec. losses 78—19410
LiF, single crystal, dislocation generation, beneath static and rolling contact with sphere 78—87671
LiF, small-angle boundary migration in steady creep state 77—39624
LiF, strained, mean mobile dislocation velocity 78—18657
LiF, US attenuation, 4.2 to 300K 77—47513
LiF, viscous drag of dislocations exam., using mobility of individual dislocations 79—14814
LiF:Mg^{2+}, deformed in ^3He and ^4He, dislocation struct. characteristics 79—69112
Mg-Ag(Cd), anisotropic, dislocation interaction with tetragonal impurity, mobility 77—19953
MgO, a/2 ⟨110⟩ edge dislocations, lattice friction stress, atomistic calc. 78—18648
MgO crystal, yield strength and dislocation mobility 80—93601
MgO crysts., radiation damage influence on deform. in HVEM 80—103391
MgO, dislocation motion 79—4309
MgO, hardness increase mode, effect on dislocation mobility 79—51114
MgO, Peierls mechanism for dislocation motion, formation of double kinks 77—68973
MgO, point-obstacle distance distrib. during motion of screw dislocations 77—11744
MgO short time chemomechanical effects, dislocation generation and motion, drilling simulation 79—87749
MgO single cryst., internal stresses and dislocation mobility, stress relaxation method 80—6413
MgO, single crystals, deform., dislocation motion and multiplication in HV electron microscope 77—84754
MgO single crysts., dislocation processes, obs. by HVEM in-situ deform. 80—103340
$MgZn_2$, solid soln. softening in homogeneity range, dislocation density and velocity *(German)* 77—44264
Mo, block boundary dislocation struct. singularities under high temp. steady state creep conditions *(Russian)* 79—90670
Mo dislocation a ⟨100⟩ stability, plastic deform. at high-press. 78—43030
Mo, dislocation dynamics, HVEM in situ obs. 78—83822
Mo fibre reinforced Cu, rule of mixtures of deform. parameters in stage III 80—97532
Mo monocrystal, dislocation motion, study by internal friction *(Russian)* 77—1133
Mo single crystals, simulating initial stage of deformation in fatigue loading 80—35328
Mo, single crysts., work hardening and softening in cyclic strain 80—20957
Mo, strengthening by vacuum-deposited W film *(Russian)* 77—66714
NH_4Cl, acoustic absorption by soft modes of defects 80—59584
NaCl, bent single crystal, equilib. face, surface relief form. during annealing 78—47651
NaCl, changes in internal friction and discharge following plastic deform. 79—99191
NaCl, dislocation distrib. on surface parallel to Burgers vector 79—65090
NaCl, dislocation half loop mobility 78—59817
NaCl, dislocation microplasticity, internal friction expts. 78—47388
NaCl, dislocation mobility under high press., temp. depend. 80—75235
NaCl, dislocation motion in micro-plastic region 78—91341
NaCl, dislocation movement, effects of adsorpt. of octadecylamine *(Russian)* 77—51372
NaCl, dynamic dislocation retardation, impurities effect 78—26577
NaCl, edge dislocation displacement 77—62540
NaCl, γ-irrad., F-stimulated inversion of sign of dislocation charge 80—59475
NaCl, hardness increase mode, effect on dislocation mobility 79—51114
NaCl, high hydrostatic press. effects on dislocation mobility 78—14358
NaCl, internal stresses and dislocation mobility 78—48440
NaCl, interrupted neutron irrad. expts. involving dislocations 79—99208
NaCl, motion of individual surface dislocation semi loops *(Russian)* 78—51542
NaCl, moving dislocations, interaction with defects, elec. effects meas. in plastic deformation *(Hungarian)* 80—10572
NaCl, plastic deform. and dielec. losses 78—19410
NaCl, polarisation caused by charged dislocation motion 80—59463
NaCl, screw dislocation mobility under high hydrostatic press. 79—69109
NaCl, spiral dislocation mobility depend. on elec. field, relaxation time 80—39105
NaCl:NaBr crysts., dislocation motion under work hardening, transmission electron microscopy 77—51381
NaCl:Sr deformation control by thermally activated processes 195 to 300K 79—24570
NaCl:Tl, deformed phosphors, thermoluminesc., impurity conc. effects 77—63473
NaF, dislocation microplasticity, internal friction expts. 78—47388
NaF(Cl), dislocation velocity determ. by nuclear spin-lattice relax. meas. 77—35566
Nb alloys, solid solution hardening, crystal resolved shear stress depend. on dislocations 80—40373
Nb, deformed polycryst., γ-peak obs. and interpret. in internal friction, 300-500K 80—81098
Nb, neutron irrad. effects on mech. props. 78—91361

dislocation motion continued
Nb single cryst., slip localisation during discontinuous plastic flow at 4.2K *(Russian)* 77—69029
Nb, single crystal, surface oxide softening, TEM obs. 77—40462
Nb, superconducting state influence on dislocation motion *(Russian)* 80—70208
Nb, surface oxide softening, anisotropy 78—60716
Nb-H system, accommodation effects during hydride precipitation, TEM 80—89218
$NbC_{0.98}$ single crysts., rel. to creep, 1800-2700°C *(Russian)* 79—5005
Nb_xC powders, plastic deform. characts. on vibratory milling 78—11183
Ni, creep, single crystals, 1.5-50K, orientation effects *(Russian)* 79—15757
Ni, creep rates, stress depend., and activation energies, constant stress tests, comparison with dislocation creep theory 80—71708
Ni, cyclically deformed, polarisation stress field, dislocation shuttling, computer calcs. 79—96095
Ni, defect electronic struct., strength characteristics relation by positron annihilation 79—91526
Ni, deformation in const. mag. field, 4.2K *(Russian)* 80—29591
Ni, deformation twins contribution to yield stress, Hall-Petch law for inter-twin spacing 79—24588
Ni, dislocation dynamics, HVEM in situ obs. 78—83822
Ni, grain boundary migration during recrystallisation after cold drawing 77—73289
Ni, magnetic aftereffect reactivation of single crystal by plastic deform. 79—65697
Ni, magnetically ordered state, softening with varying mag. field *(Russian)* 78—35017
Ni, single cryst., cyclically deformed, HVEM in-situ deform. study 80—103339
Ni, transport of H, effect of plastic deformation 80—21044
Ni-Cr, (30 wt.%), collective dislocation movements, in situ study 80—100243
Ni-Cr-Ti-Al-Fe-Co (19.65, 2.40, 1.37, 0.78, 0.52 wt.%), strength of γ' hardened alloy, ageing exam. 78—88501
Ni_3 (Al.Ti), flow stress and work hardening, exam. of temp. depend. by tensile tests 78—84839
Ni_3Fe, nondislocation origin friction stress in alloys, deformation hardening 80—21050
Ni_3Fe, single cryst. ordered and quenched, stress relax. *(Russian)* 77—44282
Ni_3GA single crystals, anomalous temp. depend. of strength, dislocation struct., optical and TEM 79—74228
Ni_3Ga, stacking fault form. in situ obs. by stretching thin foils in electron microscope 77—62547
Pb, dislocation electron drag coeff. temp. depend., internal friction method, superconducting state 80—29031
Pb, single cryst. stress relax. depend. on elec. current, electron plastic effect 79—79021
Pb-In (5%), supercond. mobile dislocation density, instantaneous flux change meas. 80—15670
Pb-Sn(Ag), dil. alloys, dislocation motion and electron-dislocation interactions 77—7728
Pb-Tl, sliding and its accommodation during creep and superplasticity 77—40436
PbS single crystals, plastic deform. thermal activation anal., dislocation behaviour, point defect influences 79—65095
$Pb_{1-x}Sn_xTe$ LPE grown heterostructures, dislocation etch pitch, interfaces 80—2023
$PbTiO_3$, phase transform., different kinetic types 80—71347
Si, crystal, dislocation multiplication *(German)* 78—38721
Si crysts., in-situ HVEM obs. of dislocation processes during high temp. deform. 80—103342
Si, dislocation dissoc. and mobility of partial dislocations 77—68980
Si, dislocation dynamics in plastic deform., theoretical anal. 79—42077
Si, dislocation ensembles motion in neutron irradiated covalent crystals *(Ukrainian)* 80—10579
Si, dislocation formation, under high stress, low temp. 78—47386
Si, dislocation mobility 77—76413
Si, dislocation mobility and mech. behaviour 79—82208
Si, dislocation motion from indentation rosette 80—79798
Si, dislocation velocities as function of electronic doping 77—4117
Si, dislocation velocities meas. 79—82230
Si, dislocations, dynamic behaviour *(Japanese)* 78—38722
Si, doped, motion of partial dislocations 79—82229
Si, extended glide dislocations, motion obs. by high voltage electron microscopy 80—10555
Si, heavily doped, electronic effects on dislocation velocities 77—62531
Si, heavily doped, electronic effects on dislocation velocity 77—62532
Si, isolated dislocation motion, velocity determ. *(Chinese)* 80—107243
Si, mechanical strength, origin of difference in Czochralski grown and float-zone-grown cryst. 80—44212
Si, mobility of segments of dislocation loops, model of nonconservative dislocation motion 78—18647
Si, plastic properties, internal friction, dislocation motion *(Russian)* 80—54305
Si, screw and 60° dislocations velocities 79—86798
Si, simple scheme for describing dislocation motion 79—65259
Si surface, line tension induced dislocation motion 79—82212
Si surfaces, influencing microstruct. deform. process by impurity type *(German)* 79—65107
Si wafer, dislocation propagation and emitter edge defects, appl. to transistors 77—1128
Si wafers, dislocation dynamics during annealing, X-ray topography system obs. 77—76261
Si:O, crit. stress of dislocation movement, determ. new method 77—80503
Si:P, high dose implantation, outside dislocation generation 78—87672
Si:P^+, misfit dislocation net propagation due to osmotic forces 79—65108
Si:Sb, heavily doped, TEM obs. of impurity effects in dislocation motion 77—43220
Sn crystal, white, time-dependent internal friction 80—7610
Sn, white, single crystal, dislocation movement in pre-yield region, etch hillock technique 79—60371
Sn, white crystals, dislocation reactions 79—86796
Steel, C, fibre reinforced Cu matrix, deformation parameters controlling dislocation motion, flow stress, activation volume 79—57055
Ta, single crystal, microyielding microflow parameters 77—52395

dislocation motion continued
Ti, acoustic harmonic generation by long-range dislocation motion 79—42176
Ti and Ti–Nb, plastic deform. and thermal cond., 2.5 to 20K, dislocation pinning 77—35629
Ti–Al, age-hardened, deform., order effects in Ti₃Al and temp. effects 77—[illegible]
α-Ti–Al, stress strain curves 77—[illegible]
Ti–Al–V (6,4 wt.%) superplastic deform. 78—31471
ThO₂–W, ThO₂–W(s Al, Sc, Y or Er) system, dislocation mechanism of diffusion processes 79—[illegible]
V, different grain sizes, room temp. microstrain (German) 77—36614
W, block boundary dislocation struct. changes under high temp. short time creep conditions (Russian) 79—[illegible]
W, screw dislocation motion, orientation depend., high-climbing core structure theory 78—[illegible]
W polycryst., plastic deform. at different deform. speeds, dislocation [illegible] (Russian) 80—[illegible]
YAG:Nd, laser cryst., dislocations density and propag., rel. to Czochralski growth (Chinese) 77—11552
YIG, motion viscosity effect in dislocation motion 80—24451
YIG, single cryst., high temp. dislocation motion 79—[illegible]
Zn, dislocation mobility under action of current pulses, selective etching meas. 79—19251
Zn, forest dislocation effect on single twin layer development in single crystals 79—[illegible]
Zn, plastic deform., effect of hydrostatic press. stress relax. meas. (Russian) 79—[illegible]
Zn polycrystals, deformation, grain sizes effect at room temp. (Czech) 80—45551
Zn, pyramidal edge and screw dislocation mobility, compressional stress pulse technique 77—[illegible]
Zn single cryst., dislocation velocity and plastic deform. 80—[illegible]
Zn single cryst., yield stress depend. on elec. current, electron plastic effect 79—[illegible]
Zn, strengthening by electroplastic strain, [illegible] effect (Russian) 80—[illegible]
Zn, twinning, influence of dislocation drag, mag. field effects 80—59472
Zn, US attenuation under high hydrostatic press., dislocation mechanism 77—[illegible]
Zn–Ag [illegible] anisotropic dislocation interaction with [illegible] impurity [illegible] 77—[illegible]
Zn–[illegible] wt.%, [illegible] deform., dislocation effects 77—[illegible]
ZnO, [illegible] effects 78—[illegible]
ZnO, in situ TEM obs. of sel. slip traces 77—[illegible]
ZnS crystals, structural change under plastic deform., partial dislocation movement 80—[illegible]
ZnS, plastic deform., struct. changes due to partial dislocation motion 77—[illegible]
ZnSe, charged dislocation motion mechanism (Russian) 79—[illegible]
ZnSe cryst., elec. cond., dislocation motion effects 80—[illegible]
ZnSe, dislocation motion, influence of elec. cond. 79—[illegible]
ZnSe, electric charge transport by dislocations 80—[illegible]
Zr, structure changes during plastic deform. (Russian) 77—[illegible]
Zr, [illegible] behaviour [illegible] effects, dislocation [illegible] 77—[illegible]
Zr–[illegible] alloy [illegible], [illegible] mechanism 80—[illegible]

dislocation motion, nonconservative see *dislocation climb*

dislocation motion hindrance see *dislocation drag*

dislocation multiplication
alkali halides, exposed to US waves, dislocation multiplication in original stage 79—[illegible]
crystalline materials, in situ deform. by high voltage electron microscopy 80—[illegible]
deformation conditions and initial defect struct. effects on dislocation multiplication 79—[illegible]
double cross-slip mechanism 79—[illegible]
kinetics of development of dislocation struct. near cryst. surface 79—[illegible]
metal, dislocation [illegible] by current noise measurements 79—[illegible]
metal, dislocation kinetics of superplasticity and creep 77—76404
metal, FCC or BCC, dislocation annihilation during tensile and cyclic deform. and [illegible] 80—[illegible]
metal systems, high voltage electron microscopy of dislocation dynamics (Japanese) 77—47454
metals, BCC, dislocation processes, straining expts., electron microscope obs. 80—29025
metals, work-hardening, dislocation multiplication model 79—[illegible]
metals under [illegible] deform. [illegible] (Russian) 77—[illegible]
[illegible] single crystals, dislocation struct. [illegible] 79—[illegible]
[illegible] mechanism by which [illegible] dislocation [illegible] 77—[illegible]
slip band broadening, computer model 79—[illegible]
[illegible] approach to dislocation multiplication 80—[illegible]
steady state dislocation motion via mic. dynamics 79—10649
steel, C, strain ageing and fatigue limit 80—41974
steel, St3 and KhVG, rel. to strength variation under influence of shock waves (Russian) 79—92290
X-ray diffraction topographic patterns, [illegible] 77—[illegible]
Ag and Ag alloys, [illegible] (Russian) 79—52916
Ag and Ag–Sn–In (Sn [illegible]) alloy, single crystals, dynamic dislocation behaviour 77—[illegible]
Al, [illegible] mechanism 80—[illegible]
Al–Mg, plastic deform., separation of internal friction components (Russian) 79—[illegible]
Al–Mg (1.5 wt.%) single cryst., dislocations obs. by high voltage electron [illegible] 80—[illegible]
Cu [illegible] mechanism 79—[illegible]
Cu, dislocation [illegible] (Russian) 79—[illegible]
Cu single [illegible] 80—[illegible]
Cu–Al, single crystals, dislocation velocity meas. 79—[illegible]
[illegible] film, deform. in electron microscope, dislocation mechanism 79—[illegible]

dislocation multiplication continued
Fe, model for Lüders band formation and plastic instability related with strain softening due to Johnson-Gilman-Hahn theory 79—61676
Fe, pure, strain ageing and fatigue (Japanese) 79—20161
Fe-Cr-V alloy, Remendur, heat treatment effects on mech. and struct. props. 77—8846
Fe-Cr-Ni (19, 15 wt.%), austenitic, Ni⁺ ion irradiated, multiple dislocation loops (French) 80—65064
Fe-3Si, single cryst., asymmetric deform., Gilman Johnson model appl. 79—[illegible]
GaAs-Ga₁₋ₓAlₓAs, DH, dark line defects induced by mech. bending 77—[illegible]
GaAsP epitaxial film, TEM obs. of misfit dislocation arrays, nucleation and multiplication 77—39742
Ge epitaxial layers, on GaAs substrate, misfit dislocation multiplication mechanism 78—[illegible]
Ge-GaAs inter faces, heteroepitaxial, misfit dislocations, TEM obs. 79—[illegible]
InP/InGaAsP/InP double heterostructure, grown on InP(111)B substrate, threading dislocation multiplication 80—[illegible]
LiF, multiplication of screw dislocations during deform., yield stress depend. 77—24521
LiF single crystals, dislocation motion and generation on plate impact 79—[illegible]
LiF: Mg²⁺, deformed at ³He and ⁴He, dislocation struct. characteristics 79—[illegible]
MgO, compressive stress-strain behaviour at high temps. 80—25774
MgO, crack propagation during in-situ deform., plastic zone formation 80—[illegible]
MgO, single crystals, deform., dislocation motion and multiplication in HV electron microscope 77—84754
MgO single cryst., dislocation processes, obs. by HVEM in-situ deform. 80—[illegible]
MgSiO₃, [illegible], plastic [illegible] of dislocations, cross-slip-controlled creep and mantle rheology 79—[illegible]
MgO [illegible], single cryst., yield strength 77—[illegible]
Mo, [illegible] tensile [illegible], deformation effects, dislocation [illegible] (Russian) 80—[illegible]
Mo film, deform. in electron microscope, dislocation mechanism 79—[illegible]
NaCl, dislocation struct. of slip bands, hydrostatic press. effect 80—[illegible]
Nb film, deform. in electron microscope, dislocation mechanism 79—[illegible]
Nb–H system, temp.-controlled acoustic emission, hydride precip. 80—[illegible]
Ni₃Ga single crystals, anomalous temp. depend. of strength, dislocation struct., optical and TEM 79—[illegible]
PbS single crystals, plastic deform., thermal activation anal., dislocation [illegible] point defect influences 79—[illegible]
Si crystals, [illegible] (German) 79—[illegible]
Si cryst., in-situ HVEM obs. of dislocation processes during high temp. deform. 80—[illegible]
Si, influence of P, plastic deform. relax. and dislocation generation 80—[illegible]
Si, dislocation dynamics during plastic deform., stress-strain characts. 79—[illegible]
Te, deformed and annealed cryst., elec. props., directional depend. 79—[illegible]
α-Ti, plastic deform., [illegible] and [illegible] parameter 80—18146
Ti–Al alloy, VT5-1, rel. to strength variation under influence of shock waves (Russian) 79—92290
Zn, basal forest dislocation as source of pyramidal dislocations (Russian) 77—84754
Zn, dislocation mobility under action of current pulses, selective etching meas. 79—19251

dislocation nucleation
[illegible] yield stress 77—[illegible]
[illegible] production process [illegible] (Russian) 77—[illegible]
[illegible]-phase [illegible] induced [illegible]-phase 79—[illegible]
dissociated dislocations of diamond cubic struct., movement 79—59866
[illegible] crack growth prediction using dislocation model 79—[illegible]
Frank-Read source, kinetics, quasistatic nucleation and expansion of dislocation loops 80—[illegible]
generation mechanism in shock wave deform. 79—[illegible]
glass surface, peeling of rubber film, spontaneous creation of interfacial dislocations 79—[illegible]
[illegible] model of passage through plane dislocation [illegible] 79—[illegible]
[illegible] dislocation [illegible], computer simulation 79—[illegible]
[illegible] compounds, dislocation half-loops, nucleation and generation 79—[illegible]
[illegible] semiconductor epitaxial layers, dislocations nature, origin and effects 79—[illegible]
kinetics of development of dislocation struct. near cryst. surface 79—[illegible]
metal, FCC, climb model of extended dislocations 78—6059
semiconductor single crystals, [illegible] growth, dislocation creation by thermal stresses 79—[illegible]
steel, austenitic, [illegible] wt.%, containing N, electron microscope obs. of [illegible] precipitation (Japanese) 79—[illegible]
steel, austenitic [illegible] stress relaxation at grain boundaries dislocation struct., TEM study 79—43346
steel, St3 and KhVG, rel. to strength variation under influence of shock waves (Russian) 79—92290
[illegible] single crystals, [illegible], high amplitude damping 77—[illegible]
void sink strength depend. on mutual recombination, point defect loss to fixed sinks 80—[illegible]
Ag [illegible] boundaries of [illegible] type, electron microscope obs. (Russian) 79—[illegible]
Al, dislocation generation from grain boundary, in situ obs. 78—51547
Al thin foil, thin foil, electron irrad., observation of triangular loops at [illegible] boundaries 80—[illegible]
Al–Ag, thin-layered laminates, yield strength rel. to dislocation generation and motion 79—[illegible]
Al–Cu thin-layered laminates, yield strength rel. to dislocation generation and motion 79—[illegible]

dislocation nucleation continued
- Bi, strain hardening curve correlation with slip band nucleation stress spectra 80−70217
- CC Si:P, secondary defect generation suppression and diffusivity restraint by HCl oxidation 79−70191
- Cd crystals, X-ray topographic examination of basal dislocation glide, generation and locking 80−88156
- Cu, control of dislocation propagation and generation 78−3025
- Cu-Al alloy, irrad. in HVEM, climb of dissociated dislocations and point defect absorpt. 80−107257
- Fe, Ni-plated, surface film softening in single slip orientation 77−32719
- Fe-Ni-C (21, 0.6 wt.%), stress assited and strain induced martensite morphologies 78−3187
- GaAsP epitaxial film, TEM obs. of misfit dislocation arrays, nucleation and multiplication 77−39742
- $Ga_xIn_{1-x}P$, rel. to breakdown of coherent growth in LPE on GaAs 77−59229
- Ge, plastic deform. under laser irrad. rel. to diamond-type structure *(Russian)* 77−56023
- LiF, microindentation, dislocation rosette generation 77−27936
- LiF single crystals, dislocation motion and generation on plate impact 79−95011
- LiF single crystals, glide band sources, work hardening 80−34126
- LiF, strain hardening curve correlation with slip band nucleation stress spectra 80−70217
- MgO, crack tip dislocations and dislocation-free zones 80−96533
- NaCl, microindentation, dislocation rosette generation 77−27936
- NaCl whiskers, X-irrad., stress oriented dislocation loop nucleation 79−33213
- Nb_xC powders, plastic deform. characts. on vibratory milling 78−11183
- Pd, epitaxial film on Au, misfit dislocation nucleation and growth 77−1338
- Si, diffusion of P, dislocations, creation conditions 79−95039
- Si, dislocation formation, under high stress, low temp. 78−47386
- Si, dislocation generation, influence of film stress and thermal oxidation 79−23609
- Si, high-dose implantation, dislocation embryo damage peak 77−7743
- Si, low temp. relax. of local stresses, dislocation behaviour, X-ray obs. 79−69110
- Si, oxidation, oxidation-induced lattice defects, review *(Japanese)* 78−39931
- Ti-Al alloy, VT5-1, rel. to strength variation under influence of shock waves *(Russian)* 78−92299
- Y_2O_3, electron irrad., dislocations *(French)* 80−2076
- Zn crystals X-ray topographic examination of basal dislocations 80−88156
- Zn single crystal, rel. to discontinuous creep *(Russian)* 77−81292
- Zn-Al (10,22,50wt.%), low temp. mech. props. plastic deformation, glissile dislocation nucleation *(Russian)* 80−11695
- Zn-Al alloys, comp. effects on intergranular slip during superplastic deform. *(Russian)* 77−32633
- ZnO, dislocation loop nucleation on prismatic faults in high voltage electron microscope 77−72620
- ZnO, irradiation in high voltage electron microscope dislocation loops study 80−88157
- Zr, dissolution of γ-ZrH, in situ study, HVEM obs. 78−55951
- Zr_3Al, $L1_2$ phase yield strength 78−19811

dislocation pile-ups
- alloys, dislocation pile-up model, fatigue crack necleation at intermetallic particles 79−69189
- BCC metals, influence of screw dislocations on cryst. lattice rotations during deform. *(Russian)* 78−6966
- β_1 brass containing α-precipitates, reversible shape memory effect *(Japanese)* 78−60711
- calcite, sound emission on dislocation annihilation *(Russian)* 80−54246
- coherent phase form. at stress concentrators, effect of dislocation splitting, dislocation pile-ups, and phase elastic moduli *(Russian)* 80−49356
- crack analysis, concentric circular arc cracks in anti-plane strain, screw dislocation pile-up model 77−54927
- creep deformation model incorporating recovery and thermally activated glide 79−64534
- cross slip dislocation self-interaciton, Orowan loops 80−24453
- cubic crystal, distrib. of dislocations in intersecting pile-ups *(Russian)* 78−87668
- Debonding of circular second phase particles 78−5688
- deformable solids, fracture and hardening kinetics 80−35210
- discrete obstacle model, dislocation and stress field distrib. 80−79794
- discrete obstacle model, dislocation pile-up kinetics dislocation mobility activation parameters 80−29022
- dynamics of planar pile-ups 78−6058
- filler metal, deformation mechanism at brazed joint 78−80616
- formation, by Frank-Read source, emission of sound 79−37705
- gliding, by-passing of hardened particles, coplanar Orowan loops form., stress-strain curves 80−49226
- hydrostatically compressed crystals, crack nucleation mechanism 79−10893
- Incoloy 901, foil prep. for TEM exam. 80−88001
- isotropic limit in anisotropic dislocation theory, Green's functions 79−46656
- kinematic hardening rule in single crystals 80−10551
- martensite nucleation at dislocations, elasticity model 80−55393
- plane, elastic displacements, electron microscope contrast 78−27986
- plane-parallel, inertial mechanism of avalanche-like breakthrough 78−2121
- refractory composites, fibre reinforced, directionally solidified tensile tests, in HVEM, deform. and fracture *(French)* 78−68785
- screw dislocation, fatigue crack growth 77−3774
- slip and twinning relns. *(Russian)* 77−65982
- slip lines, average length, rel. to rate of dislocation pile-up *(Russian)* 77−76416
- steel, austenitic stainless, V alloyed, creep mechanism 77−48514
- steel, cold-worked, state of cementite, nucl. gamma reson. meas., plastic deform. *(Russian)* 78−68706
- steel, inclusions effect on distrib. of local microheterogeneous deform. *(Russian)* 78−80586
- steel, low C, high cycle fatigue, crack initiation model *(Japanese)* 80−104258
- steel, martensitic, delayed fractures suppression, by neutron irradiation *(Czech)* 78−67743

dislocation pile-ups continued
- steel, stainless, anelastic and non-ideal viscoplastic behaviour relations at low homologous temps. 77−63742
- steel, stainless, in-situ obs. of deform. in HVEM 80−103334
- steel, stainless, martensite formation, in situ obs. 80−25692
- steel, stainless, martensite nucleation and growth, expt. study 78−3125
- steel, stainless, martensite nucl. obs., role of defects in nucleation 80−25693
- steel, stainless, single crystals, shear cracks, electron microscope study 80−40522
- structural changes in single crystal under single electric impulse discharge *(Russian)* 78−[illegible]
- superconducting states, impurity effects *(Russian)* 80−[illegible]
- superconductive states in dislocation structs. 78−[illegible]
- superplastic flow in two-phase mats., role of interphase-boundary dislocations, ledges and diffusion 78−[illegible]
- Taylor model description of plastic deform. in polycrystals 78−[illegible]
- thermoelastic martensite crystal, dislocation representations of development kinetics 80−[illegible]
- void initiation in random distrib. of spherical particles 79−46651
- Al, surface strengthening of single crysts. on coating with evaporated films 77−8972
- Al-Cu (4 wt.%), AE during deform., effect of ageing at 170°C 78−64597
- Al-Li-Mn (2.8, 0.3 wt.%), recrystallised sheet, fracture behaviour, SEM and TEM study 80−97566
- Al-Mg (0.3 wt.%) single cryst., dislocations obs. by high voltage electron microsc. 80−79796
- Cu-Bi, grain boundary struct. intergranular fracture, segregation role 80−66645
- Cu-Ni-Al (5, 2.5 at.%), precip. hardening *(Japanese)* 80−71663
- $Cu-SiO_2$, in-situ deform. in HVEM 80−103334
- Fe alloy type G18, martensitic γ⇌ε transformation, dislocation pile-ups, ε phase nucleation *(Russian)* 80−55396
- α-Fe, distrib. of dislocations in intersecting pile-ups *(Russian)* 78−87668
- Fe-Ni (29 wt.%), martensite nucleation at dislocations, elasticity model 80−55393
- Fe-Ni-Al (18.2 wt.%) aged, fracture toughness and mode, grain size depend. 77−12790
- Fe-Ni-C (32.7, 0.01 wt.%), athermal martensitic transition investigation by acoustic emission *(Russian)* 79−91645
- KCl-KBr, dislocation rosettes, diffusion origin 78−83620
- KCl-NaCl, dislocation rosettes, diffusion origin 78−83620
- KCl(Br)(I), single cryst., quenched, microstruct. around indentations 80−7625
- LiF bicrystal, high-angle tilt boundary and edge dislocation intersection effects 80−79550
- MgO single crystals, crack formation process, micro-deformation and fracture *(Japanese)* 80−24530
- Mg_2SiO_4, dislocations revealed by etching 79−90190
- Mo, dislocation structure evolution near electro-eroded crater *(Russian)* 80−100237
- NaCl, dislocation ordering influence on integrated X-ray coeff. 80−103357
- NaCl, dislocation rosettes around Vickers diamond pyramid indents, quenching effect 80−11740
- Nb heteroepitaxial layers on sapphire, residual mechanical stress and strain influence on superconductivity 80−15644
- Ni, lattice defects, formation kinetics, work hardening and resistivity study *(Russian)* 80−10557
- Ni_3Al, noncoherent second phase particle effect on strain-hardening parameters *(Russian)* 79−47703
- Ni_3Fe, dislocations, rate of piling up, rel. to average length of slip lines *(Russian)* 77−76416
- Si crysts., in-situ HVEM obs. of dislocation processes during high temp. deform. 80−103342
- Si, extended glide dislocations, motion obs. by high voltage electron microscopy 80−[illegible]
- Si particle reinforced Al, internal stresses, X-ray diffr. meas. *(Russian)* 78−[illegible]
- Ti-11, unstable shear modes in fatigued β-annealed specimens 78−84984
- Ti-alloy, IMI-685, unstable shear modes in fatigued β-annealed specimens 78−84984

dislocation pinning
- *see also dislocation damping*
- bronze P, heavily cold rolled, yield strength enhancement mech. 77−36539
- creep and growth, irradiation induced, solute effects on defect precip. rate 80−88252
- damping peak, amplitude analysis, estimation of no. of pinning points per network length 77−27889
- diffusion along dislocations, effect on linear stress, internal friction *(Russian)* 77−[illegible]
- dislocation loop-length distrib. and frequency-depend. damping for small impurity concs. 80−49232
- dynamic waves along dislocations overcoming local obstacles 80−29021
- edge dislocation screening in metals and superconductors, metal softening *(Russian)* 80−[illegible]
- ferromagnetic crystal, magnetic damping due to pinned domain wall motion 78−[illegible]
- fluctuational breakaway from pinning sites, effective temp. *(Russian)* 78−[illegible]
- Friedel's theory of amplitude depend. damping 78−27552
- graphite, irradiation induced creep, UKAEA reactor group studies 77−42065
- impurity crystal, microstructural plastic instability *(Russian)* 79−99190
- internal friction and Young's modulus measurement using automated Marx's composite oscillator method 80−[illegible]
- metal, electron irrad., elastic pole, defect-dislocation interactions, defect dragging model extension 80−65081
- metals irradiated, heavily, exam. of percolative mass transfer 78−79630
- microcreep, low temp. quantum effects *(Russian)* 78−[illegible]
- mobile pinning points on dislocations, equilibrium distrib. 80−[illegible]
- motion of dislocation in impure cryst., stochastic theory 77−[illegible]
- oxides, dislocation point mode 80−[illegible]
- quantum motion of dislocations through local barriers *(Russian)* 79−60363
- scaling relations in mag., mechanical and superconducting pinning theory 77−76403

dislocation pinning continued
segment oscillations, internal props., point obstacle collisions, glide plane motion *(Russian)* 80—39088
segments, pinned, effects of viscosity on quantum motion *(Russian)* 80—44207
solid-state turbulence 80—92528
statistical theory, dislocation configs., in point obstacle random array 78—18645
steel, austenitic, Mn-Cr-C(20, 4, 0.5 wt.%), intrinsic stacking fault energy, temperature variation 77—31679
steel, austenitic stainless, dislocation damping, H pinning 78—15501
steel, Cr-Mn, effect of composition, plastic deformation, and heat treatment on martensitic transformation 79—100141
steel, CrMoV, quantitative stereological anal. and creep-resistance *(Czech)* 80—30030
steel, maraging, Cr-Ni-Ti, effect of Ti addition on hardness and energy scatt. 79—15687
steel, structural, fatigue softening, temp. and load freq. influence *(German)* 79—61614
strain ageing effect on strength and toughness, susceptibility to strain hardening 79—57028
superplastic flow in two-phase mats., role of interphase-boundary dislocations, ledges and diffusion 78—11295
TEM obs. of pinned dislocation arrangements 77—43217
transient dislocational internal friction, freq. depend., under periodic stress *(Russian)* 79—65092
US hardening kinetics rel. to dislocations 80—50644
Ag, electron irrad., elastic moduli and internal function *(French)* 78—87703
Ag, electron irradiated, thermal variation of dislocation pinning by point defects 79—51150
AgBr:Cd^{2+}(Sr^{2+}), single cryst., stress-induced migration and aggregation of solute ions, internal friction 79—51200
Al alloys, inelastic electron scattering by dislocations *(Russian)* 78—79988
Al, cold-worked, dislocation-pinning defects, US attenuation obs. 77—31673
Al, dislocation and point defect interactions, US study under quasistatic stress *(French)* 80—2061
Al, positron annihilation momentum spectra, specific trapping rate of dislocations 79—19948
Al, US hardening kinetics rel. to dislocations 80—50644
Al-Li, dil. alloy, cold-worked, annealing spectrum 78—39801
Al-Mg alloy, creep rate, effect of dislocation pinning by impurity atoms *(Russian)* 78—38719
Al-transition metal alloys, anomalous sp. ht. and nuclear spin-lattice relax. 79—46814
Au, work hardened, Hasiguti peaks, spectrum and recovery, impurity effects *(French)* 77—66670
Bi, dislocation internal friction, HF, rel. to temp., freq., amplitude *(Russian)* 78—26574
Cu alloys, inelastic electron scattering by dislocations *(Russian)* 78—79988
Cu, cold worked, determ., of dislocation pinning and unpinning stages, using internal friction meas. 78—92278
Cu, dislocation pinning rate, neutron and electron irrad., meas. by internal friction method 80—96570
Cu, electron irrad., elastic point defect-dislocation interactions, defect dragging model extension 80—65050
Cu, electron irrad., migration and thermal conversion of defects, 100 to 330K 80—59519
Cu, electron irradiated, thermal variation of dislocation pinning by point defects 79—51150
Cu, electron irradiation damage, dislocation pinning investig. of crowdion model 77—69000
Cu, electron-irradiation internal friction behaviour, shear modulus and damping meas. 80—55444
Cu, neutron and electron irrad., interstitial formation, dislocation pinning, internal friction meas. 80—100284
Cu, neutron irradiated, effect on internal friction 78—15445
Cu, US hardening kinetics rel. to dislocations 80—50644
Cu, ultrasonic velocity response to stepwise change of stress *(Japanese)* 79—38905
Cu-Al (10 at.%), single crystal, variation of flow stress after changes in strain rate 77—28879
Cu-Al (10 at.%) alloy, work hardening at high temp. 77—32589
Cu-Cd (1.0 wt.%), yield stress and flow stress 80—97524
Cu-Ni-Fe (26,8 wt.%), microduplex struct. form., recrystn. annealing *(Japanese)* 78—76659
Cu-Si(Ge), dissoc. dislocations pinning by Suzuki effect *(French)* 79—100223
Fe and Fe alloys, dislocation unpinning rel. to u.s. attenuation at large strain amplitudes 77—1182
Fe, Armco, stress relaxation expt., significance under strain ageing cond. 79—57039
α-Fe, influence of C and ZrH$_2$ on static and cyclic creep behaviour 78—39856
α-Fe, internal friction for low temp. deform. 80—40420
α-Fe, internal friction peaks from dislocation relax. in plastically deformed and/or neutron irrad. sample 78—48438
Fe-H, deformed, internal friction 79—57041
Fe-Si (3 wt.%), strain aged polycrystalline samples, AE study of deform. 77—63696
GaAs homojunction LED, mechanical stress induced degradation 80—2860
^{4}He HCP crystals, US attenuation, dislocation damping 80—24711
In, supercond. and normal states, internal friction hysteresis *(Russian)* 77—36023
KCl, dislocation motion in micro-plastic region 78—91341
LiF, crysts. containing rigid dislocation forest, mech. props. 79—99212
Mg, US hardening kinetics rel. to dislocations 80—50644
NaCl, changes in internal friction and discharge following plastic deform. 79—99191
NaCl, dislocation motion in micro-plastic region 78—91341
NaCl, interrupted neutron irrad. expts. involving dislocations 79—99208
NaCl, strain ageing exam. 78—56661
NaCl whiskers, internal friction, dislocation detachment from pinning centres 77—15727
Nb-O(N), dislocation pinning, impurity interactions, strengthening *(Russian)* 80—92532

dislocation pinning continued
NbN$_x$, solid soln, strain ageing, internal friction, elec. cond. kinetics *(Russian)* 78—76667
NbN$_x$O$_y$, solid soln, strain ageing, internal friction, elec. cond. kinetics *(Russian)* 78—76667
NbO$_x$, solid soln, strain ageing, internal friction, elec. cond. kinetics *(Russian)* 78—76667
Ni 200, C interstitial effect of yield point develop. during static strain ageing, model 78—88498
Ni, self interstitial migration and crowdion conversion, dislocation pinning expts. 77—84762
Ni-Be (2 wt.%), high-temp. radiation embrittlement, mechanical tests and TEM *(Russian)* 77—44331
Pb, US oscillations and dislocation unpinning in supercond. and normal states *(Russian)* 79—11648
Si wafer thermal gradient induced slip, effect of starting cooling temp. 78—10057
Si:O wafer, dislocation pinning effect of O atoms 77—89437
Ta-O(N), dislocation pinning, impurity interactions, strengthening *(Russian)* 80—92532
Ti and Ti-Nb, plastic deform. and thermal cond., 2.5 to 10K, dislocation pinning 77—35629
V-O, dislocation pinning, impurity interactions, strengthening *(Russian)* 80—92532
Zn, line energy of basal screw dislocation, exptl. determ. 80—88154
Zn, US attenuation under high hydrostatic press., dislocation mechanism 77—43284
Zn, US hardening kinetics rel. to dislocations 80—50644
Zn-Ag, dil., polycryst., amplitude-depend. internal friction *(Polish)* 79—96079
Zr, amplitude depend. damping 77—32617
Zr polycrystalline, low-temp. alternating deformation and annealing, yield stress, elec. cond. variation *(Russian)* 79—74199
Zr-Al (8.6 wt.%), neutron irradiation effect on tensile props., swelling 77—7768

dislocation relaxation *see dislocation damping*

dislocation scattering
used for carrier scattering by dislocations
alloys, effects of temp. an order-depend. elec. resist. 77—31992
anthracene, dislocations effect on elec. props. 77—35947
conduction electron motion in vicinity of isolated dislocation parallel to mag. field 77—66147
electron slowing down of dislocations in the ultraquantum limit *(Russian)* 79—4545
electroplasticity, skin effect 80—21046
Fermi's 'golden rule', correct appl. derived for line-defect scatt. 77—62884
grain boundary elec. resist., dislocation model 77—76800
Hamiltonian for describing multivalued elastic displacement fields 80—24862
helical electric current flowing along screw dislocation 78—51959
III-V semiconductor, anisotropic carrier mobility due to dislocations 78—60124
III-V semiconductor, local resist. near dislocations, eqns. 78—60123
inhomogeneous strain field scatt. deform. potential, theory 77—35905
junction current, luminesc. near dislocation, surface, integral representations, appl. to LED's 78—68079
metal, cond. electron relax. time, review *(Japanese)* 78—30910
metal, dislocated, Dingle temp. plots 77—59248
metal, dislocation elec. resist. and reson. scatt. 77—43550
metal, dislocation scatt. and de Haas-van Alphen amplitudes 78—63967
metal, elec. resist., comparison of two theories 78—6371
metal, electron anisotropic scatt. by dislocations, kinetic eqn. *(Russian)* 77—47802
metal, electron drag od dislocations 80—10961
metal, electron scatt., effect of surface on lattice defects, surface Landau level reson. 79—65534
metal, electron state effect on mech. props. and electroplasticity 78—14725
metal, electron-dislocation scattering and negative deviations from Matthiessen's rule 80—80248
metal, influence of long-range dislocation pots. on de Haas-van Alphen effect 77—8009
metal, Matthiessen rule deviations, electron scatt. by dislocations, impurities and phonons 78—19026
metal with dislocations, temp. depend. of elec. resist. *(Russian)* 78—39094
metals, cond. electron and spin scatt. due to dislocations 80—75856
metals, elec. resist. of dislocations 77—69310
metals, electron-dislocation scatt. anisotropy effect on electron-electron scatt. contrib. to elec. resist. 80—29398
metals, residual elec. resist., one-electron approx. *(German)* 80—39568
metals, scattering of conduction electrons with spin flip by dislocations 78—26852
metals with dislocations, elec. resist. temp. depend. 79—60819
MOST structures with process-induced defects, elec. props. 80—54788
noble metal, elec. resist. of dislocations, calc. *(Russian)* 78—60117
point defect electrons and vibrations, dislocation field effect, dislocation photoconduction spectrum *(Hungarian)* 80—51977
resistivity of grain-boundary joint by pseudopot. method *(French)* 79—51539
scattering phaseshifts and resonances for line defects 78—51953
scattering theory for crystal dislocations 77—69286
screw dislocation, electron scattering 78—60101
screw dislocation, scattering of tight-binding electrons, numerical solution of Schrodinger equation 79—51540
semiconductor, carrier scatt. and mobility transient processes, pulsed Hall photoeffect 80—15546
semiconductor, charge carrier scattering by dislocations 79—82583
semiconductor, dislocation cond. process at low temp. 79—99551
semiconductor, dislocation pot., free carrier absorpt. spatial orientation and freq. depend. obs. 80—39546
semiconductor, electron scattering by layer of dislocation lines 79—78091
semiconductor, electron scattering by layer struct., geometrical resonances, plasmon and free carrier freq. 79—56212
semiconductor, influence of long-range dislocation pots. on de Haas-van Alphen effect 77—8009
semiconductor, model describing removal and scattering of charge carriers by defect clusters 78—76069

dislocation scattering continued
  semiconductor and semimetallic thin films, dislocation superstructures and conduction electron kinetics *(Russian)* 79−19678
  semiconductors, current instabilities, theory and expts. *(Hungarian)* 77−39857
  semiconductors, free electron scattering and dynamical cond. 78−2476
  semiconductors, free-carrier mobility associated with dislocation strain fields 77−51738
  semiconductors, polycryst., with low angle grain boundaries, residual cond. 80−15525
  semimetal, intrinsic, dielec. and supercond. phase transitions 77−66111
  simple metals, mech. for transverse linear magnetoresist. 79−23949
  SOS MOS devices, elec. characts., cryst. defects and residual stress effects 78−34906
  spiral dislocation scattering, t-matrix 78−39101
  tight-binding electron scatt. off screw dislocations 79−91012
  Ag, elec. resistivity increment due to low temp. plastic deform. *(Russian)* 77−31990
  Ag, electrical resistivity, low temp., T^4 behaviour rel. to electron scatt. mechanisms 80−39552
  Ag, strained, anisotropic electron scatt. in elec. resist. 78−91656
  Al alloys, inelastic electron scattering by dislocations *(Russian)* 78−79988
  Al, electrical conductivity temp. depend., inelastic electron scatt. by dislocations *(Russian)* 77−69315
  Al, Fermi surface, scattering anisotropy of conduction electrons on dislocations *(Russian)* 78−60051
  Al, strained, anisotropic electron scatt. in elec. resist. 78−91656
  Al, with linear lattice defects, temp. depend. of magnetoresist. and Matthiessen's rule departure *(Russian)* 80−84456
  Au, electrical resistivity deviations from Matthiessen's rule due to dislocations 79−65425
  $Cd_xHg_{1-x}Te$, vac. evap. film struct. rel. to carrier scatt. 77−85116
  Cu alloys, inelastic electron scattering by dislocations *(Russian)* 78−79988
  Cu, electrical resistance of edge dislocations *(German)* 80−96859
  Cu film, electron transport props., struct. defects role 77−40117
  Cu-Nb multifilamentary composite, dislocation resistivity 80−70671
  n-GaAS, plastic deform. effect on elec. props. 77−28178
  GaAs, elec. props. of dislocations review *(Japanese)* 78−6325
  GaSb, sputtered films, on GaAs, growth, Hall effect, impurity levels 80−20334
  n-Ge, dislocational microwave conductance anisotropy *(Russian)* 79−91092
  Ge, Hall effect, influence of dislocations 79−82611
  Ge, low-temp. dislocation cond. mechanism in plastically-deformed pure samples 80−15527
  Ge, optical excitation of dislocation states 77−85265
  n-Ge, single cryst. with dislocations, UHF cond. *(Russian)* 79−78128
  n-Ge:Bi,O, plastically deformed, dislocation scatt. anisotropy, effect of state of O in Cottrell atm. 78−19028
  InSb film, heteroepitaxial, MBE growth and elec. props. 80−2301
  InSb, galvanomagnetic props. of annealed single crystals 80−96909
  p-InSb, influence of plastic bending on galvanomag. props. 79−28349
  K, electrical resistivity, low-temp., electron-electron contrib., sample depend. 80−24875
  K, electrical resistivity below 2K, temp. depend. 78−51969
  K, electron-dislocation scatt. anisotropy effect on electron-electron scatt. contrib. to elec. resist. 80−29398
  K, phonon-dislocation scatt. and phonon equilibration at low temp. 79−51561
  Mg, pure and dil. alloys, electron lifetime anisotropy, Dingle temp. due to dislocation scatt. 79−78082
  Mo, film, vacuum deposited, elec. cond., internal stresses, surface corrosion, MOS gate appl. *(Japanese)* 78−80073
  Na, electrical resistivity, low-temp., electron-electron contrib., sample depend. 80−24875
  Nb, elec. resist. changes with plastic deform. 77−89749
  Pb-Sn(Ag), dil. alloys, dislocation motion and electron-dislocation interactions 77−7728
  n-PbTe:In(Cu) epitaxial films, elec. transport props. 80−75659
  Pd, strained, anisotropic electron scatt. in elec. resist. 78−91656
  Si, electrical properties of single crystal, dislocation effects *(Rumanian)* 79−73504
  Si, electrophysical props. of single crysts. with and without dislocations 77−47812
  Si, Hall effect, influence of dislocations 79−82611
  n-Si, plastically deformed, donor action of dislocations, elec. props. 79−11126
  Si ribbons, capillary action shaping tech., lifetime charact. 78−34847
  Si:P, electrical conductivity oscillation, effect of dislocations 78−6388
  Si:P, heavily doped, influence of impurities and crystalline defects on electron mobility 79−78095
  Si:P dislocation p-n junctions, capacitive props. 80−20300
  Te, dislocations influence on galvanomag. props. 80−54722
  Te, hole mobility anisotropy in edge dislocated cryst. 80−24936
  Te, imperfect pure cryst., thermomag. effects, dislocation effects and Auth model 77−85248
  Te, piezoelectrical free-carrier scatt. by screw dislocations, Hall effect and cond. meas. 80−24926
  Te, screw-dislocation-induced scatt. and acceptor states, galvanomag. and optical expts. 77−28142
  Te:Sb, 96 to 500K, cond. Hall const., hole mobility, conc., dislocation effects *(Russian)* 78−64039
  $Ti_{55}Nb_{45}$, supercond., anomalous phonon thermal resist. 77−69451
  ZnSe, dislocation motion, influence on elec. cond. 79−15149

dislocation sources
  see also Frank-Read sources
  activation by load impulses 78−14350
  alkali halides, exposed to US waves, dislocation multiplication in original stage 78−47383
  dynamic behaviour, of dislocation groups, of opposite sign emitted from a stressed source, computer simulation 80−6406
  FCC metal, origin of dislocations during microdeformation tests, X-ray topography 79−82226
  grain boundary as dislocation source during high temp. deform. *(Russian)* 78−15453
  internal stress field produced by dislocation motion and creation 77−62530
  local heating in crystals during low-temperature deformation 78−67766

dislocation sources continued
  local heating in low temp. deform. of crysts. 78−18660
  nonstationary temperature field, dislocation struct. dynamics *(Russian)* 77−27884
  screw subboundaries as dislocation sources, creep 80−100234
  slip band, action of dislocation sources in irregular stress field *(Russian)* 77−15426
  steel, austenitic stainless, grain boundary as dislocation source during high temp. deform. *(Russian)* 78−15453
  steel, C, accelerated deform. by to H_2 absorption *(Japanese)* 79−70121
  steel, stainless, type 304, TEM study of dislocation emission from grain boundaries 79−66121
  surface, calc. of critical shapes and stresses 79−46659
  Al, annealing twin growth, obs. by synchrotron radiation X-ray topography 79−55753
  Al, crit. resolved shear stress, orientation depend. 80−21001
  Al-$CuAl_2$ lamellar composite, creep, microstruct. obs. 79−8331
  Bi, low temp. plasticity, strain hardening, slip *(Russian)* 77−31713
  Cu high purity, grain boundaries as dislocation sources in premacroyield strain region 79−34096
  Cu, polycrystalline, friction stress meas. during high temp. creep 79−1898
  Cu, single crystals, neutron irradiated, stresses and secondary slip between overlapping and dislocation arrays 80−88162
  Cu-Al alloy, low temp. deform., heating of dislocation sources 78−18660
  Fe alloy type G18, martensitic $\gamma \rightleftharpoons \epsilon$ transformation, dislocation pile-ups, ϵ phase nucleation *(Russian)* 80−55396
  Fe, BCC surface ledge simulation, dislocation-like relaxation 78−30620
  GaAs, Czochralski growth, melting and regrowth, inclusion density and dislocation generation 77−21016
  Ge-GaAs, heteroepitaxial systems, misfit dislocations obs. using HV electron microscopy 80−100242
  KCl crystal, use of photoelectrons to investigate surface charges 80−2444
  Nb_xC powders, plastic deform. characts. on vibratory milling 78−11183
  Pd, epitaxial film on Au, misfit dislocation nucleation and growth 77−1338
  Si, dislocation free, O_2 precipitation, stacking fault form. 78−38731
  Si, initial stage of plastic flow 78−64602
  Si, oxidation, oxidation-induced lattice defects, review *(Japanese)* 78−39931
  Si single crystal growth, Czochralski method, small-angle dislocation boundary form. anal. 80−89136
  SiC:N, impurity effect on stress gradients and dislocation development 77−4116
  Zn particulate composite, mech. props., microstruct. correlation, at low and high temps. 77−32624

dislocation structure
  alkali halide, deformed single cryst., dislocation struct. formation *(Russian)* 77−7733
  alkali halides, exposed to US waves, dislocation multiplication in original stage 78−47383
  alloys, $L1_2$-type superstruct., anomalous temp. depend. of deform. characts. *(Russian)* 79−20109
  amethyst crystals, dislocations, selective etch method 78−75674
  asymmetric Bragg condition for thick real crysts., applic. to dislocation networks *(German)* 78−67607
  austenitic steel, 45G17Yu3, structure and loss of strength after hot deform. by rolling *(Russian)* 78−39794
  BCC metals, vacancy-edge dislocation interactions, computer simulation 78−83845
  BCC metals and alloys plastically deformed, electron microscopy *(French)* 77−44299
  Bordoni relaxation, theoretical aspects, numerical calcs. from thermally activated double kink formation 78−63805
  Bormann topograms, diffr. effects obs. during X-ray transmission through a cryst. with dislocations in slip planes 79−4310
  boundary friction study by ultramicroscleromerty, dislocation generation 80−34131
  α-brass, dislocation struct., deform. *(Polish)* 80−24454
  α-brass, dislocation structure around crack tips in early stage of fatigue 78−60830
  α-brass, fatigue crack propag., role of dislocation substruct. 80−60963
  brass, fatigue crack propagation, effect of stacking fault energy as deduced from dislocation patterns, TEM study 79−61719
  brass, misfit dislocation struct. in interphase boundaries, electron microscope obs. 78−18649
  γ-brass type alloys, faulted defects, nature determ. by image matching technique 78−63777
  γ- brass type alloys, superstructures and defect obs. 80−107284
  brittle fracture in ductile material, model and applic. to H embrittlement 78−23814
  broken twist boundary, model 78−47394
  cell wall and lattice misorientation origin during deform. 80−71712
  ceramic oxide, TEM study of deform., review 79−87686
  continuum approach of physical line structs., appl. to dislocations 78−81859
  core, thickness periodicity of atomic-resolution images 79−27995
  corundum, bladed crystals, morphology and struct. 77−84680
  covalent crystal, creep and dislocation structure under tension *(Russian)* 78−19839
  crack motion effects 77−86182
  creep, dislocation struct. and stress/strain relations, thermodynamic theory *(Russian)* 79−43319
  creep, irradiation induced, correlation of theory with expt. evidence 80−88255
  cross slip dislocation self-interaciton, Orowan loops 80−24453
  crystal growth, creation of stress and dislocations *(Russian)* 80−103277
  crystal with island film, dislocations and stresses 79−87015
  crystalline materials, in situ deform. by high voltage electron microscopy 80−103352
  crystalline physiology, dislocations rel. to model for non-chemical lifeform 77−90978
  Cu-Al, FCC, study of dipoles using weak-beam electron microscopy 78−22724
  deformed crystal, theory of X-ray scatt. *(Russian)* 80−70077
  diamond, natural, defect struct., recent obs. by new methods 78−30628
  diamond cubic structure, kink formation and migration, rel. to Fermi level 79−82218

dislocation structure continued
diffraction contrast validity of assuming symm. Laue diffr. conditions 79—50961
discrete obstacle model, dislocation pile-up kinetics dislocation mobility activation parameters 80—29022
dislocation structure, high press. effects, plastic deform. *(Russian)* 80—88159
dispersed metallic film distrib. function, effect of substrate dislocation struct. *(Russian)* 77—35840
dissociated dislocations, weak-beam technique, appl. to quartz, Al_2MgO_4 *(French)* 79—42070
elastically-anisotropic cubic crystals, image contrast of inclined dislocations, electron microscopy 79—27991
electron microdiffraction patterns, point group symmetry from dislocation cores 80—100140
electron micrograph hybrid image processing 80—53224
electron microscope diffr. contrast 78—83700
electron microscope imaging, high-resolution, additional image peak interpretation 77—68978
electron microscopy, conf., Nancy, France (May 1978) *(French)* 79—41915
electron microscopy, dislocation core struct., conditions for obs. by multibeam interference *(French)* 78—26571
electron microscopy, high resolution, dislocation core studies, image calc. methods 80—96535
epitaxial islands, equilibrium struct., one-dimens. model 79—15035
epitaxy and misfit dislocations in large misfit systems 80—24767
extended growth defect characterisation, review 78—30649
fatigue, dislocation substructure effects 77—86140
fatigue crack init. 77—86161
f.c.c. alloy, rolling texture *(Russian)* 77—1843
FCC metals and alloys, plastically deformed, electron microscopy *(French)* 77—44301
ferromagnet, dislocation effects on phys. props. at $T \neq 0K$ *(Russian)* 77—8378
ferromagnetic crystal with dislocations, mag. anisotropy *(Russian)* 77—8377
film defect growth and nucleation, electron microscopy and diffraction exam. *(French)* 80—59824
film/substrate interface, misfit dislocation obs. using electron microscopy 80—103605
fine fragmented crystals, complex struct. analysis by electron microscopy 80—104416
fluorite, use of proton irrad. to reveal growth and deform. features 80—84216
foil, rel. to recrystn. during heating in column of electron microscope *(Russian)* 78—48421
fracture surfaces in fatigue, and dislocation structs. *(Japanese)* 80—65144
geometry, electron microscopy *(French)* 79—42072
grain boundaries, differential geometry 77—27893
grain boundaries, high angle, plane matching secondary relaxations, electron microscopy 80—103363
grain boundary, high-angle, nature of dislocations, calcs. 78—14361
grain boundary dislocation struct. 77—55283
grain boundary dislocation structure, atomistic computer simulation 79—60383
grain boundary dislocations, Burgers vectors, grain boundary dislocations 78—87680
grain boundary misfit dislocation, core structures, TEM obs. 79—90673
grain boundary misfit dislocation, core structures 79—90674
HCP lattice, dislocation nodes equilibrium config. *(Russian)* 78—38699
HCP metals and alloys, plastically deformed, electron microscopy *(French)* 77—44300
heteroepitaxial system, dislocation struct. at stress meas., theory 80—2017
ice, Antarctic deep core, X-ray diffr. topographic studies 78—63803
III-V compounds, lattice constant determ. of epitaxial layers and effect of misfit dislocations 79—19479
III-V quaternary-binary heterojunction, X-ray characterisation of defects 78—95239
impurity crystal, microstructural plastic instability *(Russian)* 79—99190
Incoloy, alloy 800, $M_{23}C_6$/austenite phase boundary defect struct. resolution by weak beam microscopy 80—3046
intercrystalline boundaries, continuous distrib. of dislocations 77—84745
interfacial dislocations, Burgers vector determ. using electron microscopy 78—34720
interphase boundary dislocations and coherency concept 80—24447
intrinsic boundary dislocation spacing meas. from electron micrographs 78—30632
intrinsic structure, in grain boundaries and boundary mobility 80—103368
ionic crystals, dislocations, review 80—107236
irradiation creep due to stress induced preferred absorption of point defects, anisotropic dislocation struct. effects 79—42140
kinetics of development of dislocation struct. near cryst. surface 79—73167
kink bands, dislocation structure and orientation gradient development 79—90667
Lang X-ray technique, image forces and dislocation config. 77—27785
layered structure materials, model for 6-fold ribbon 79—60364
like dislocations near interface in presence of lattice frictional forces 77—47454
liquid crystal, nematic, homogeneously oriented, neutron small-angle scatt. by dislocations 77—1077
martensitic steel, amplitude independ. internal friction obs. *(Bulgarian)* 77—19966
martensitic transformation, crystallography, describable by nonuniform lattice strain *(Russian)* 80—81056
martensitic transformations, electron microscope study of cryst. geometry *(Russian)* 80—108441
metal, BCC, computer simulation of twin boundary and twinning dislocation struct. 78—30644
metal, BCC, core structure of screw and 71° dislocations, kinks and constrictions *(German)* 77—24316
metal, BCC, geometry of slip systems *(Hungarian)* 77—47463
metal, degree of deform. effect on thermophys. props. at high temps. 78—26694
metal, ductile fracture, crack initiation at dislocation cell boundaries 77—66692

dislocation structure continued
metal, fatigue damage examination using two-crystal X-ray spectrometer method 79—52481
metal, FCC and BCC, high temp. creep, influence of dislocation splitting width *(Russian)* 79—5004
metal, influence on thermal desorption of adsorbed atoms 78—47670
metal, inhomogeneous dislocation struct., model 79—90655
metal, martensitic memory mechanism *(Russian)* 77—21217
metal, recovered dislocation substructure, prod. and utility, review 77—84749
metal, single crystal, dislocation loop formation, during deformation in quantising mag. fields *(Russian)* 80—103354
metal, X-ray diffr. exam. by vibrating crystal method *(Russian)* 78—34519
metal systems, pulsed laser generated shock wave, tangled disloc. network generation 77—48443
metallic polycrystals, deform. during cooling, revealed by deposited graphite layer *(Polish)* 80—25755
metals, FCC, deformed single crysts., struct. evolution at heating 80—103337
metals and alloys, relaxation, rel. to defect struct. *(Russian)* 78—19801
metals under load, plastic deform. local instability *(Russian)* 77—76415
mobility, core struct. by electron microscopy *(French)* 79—42071
model for interaction between tensile crack and hole 78—67092
neutron damage simulation, using HVEM, state-of-the-art 77—51417
Nimonic, ageing, role of quenched-in vacancies 77—52363
nonstationary temperature field, dislocation struct. dynamics *(Russian)* 77—27884
obstacle strength determ. in solid soln. 78—68704
olivine, naturally deformed, recovery process, rel. to Earth upper mantle mech. state 78—96202
olivine, plastic flow of oriented single crystals, dislocation struct. interpretation 78—36156
olivine, plastic flow of oriented single crystals, mech. data 78—36155
oxides, interaction between point defects and dislocations, cryst. plasticity 80—15149
Ozhennite, yield point, effect of ageing stress 77—21223
periodic misfit-dislocation networks, electron diffr. 78—59815
periodic planar networks, elastic props. calcs. 77—62527
plagioclase feldspar, deformed in compression, dislocation substruct. and slip, TEM obs. 77—43221
plastic deformation theory with account of dislocation transform. 78—38703
plasticity, polycrystalline, probabilistic approach 78—26621
point defects, stress induced absorpt. and emission by grain boundaries 80—39081
polyethylene crystal, preferred orientation relationship, epitaxy 78—67923
pore healing under press., initial stage of dislocation config. form. *(Russian)* 78—10050
quartz, etching technique for deformed grains 77—39590
quartz, fine structure under electron irrad. 80—70213
quartz, naturally deformed, dynamic recrystn. during creep, dislocation substruct., Mg alloy comparison 80—109142
quartz, resonator, X-ray double crystal topographic assessment of defects 79—50943
rigidly plastic media with hardening, shock-loaded, dislocation model and elastoplastic waves 79—86379
sapphire, profiled growth, struct. perfection 78—68621
semiconductor, dislocations studied by weak beam electron microscopy 79—82216
semiconductor, structures and elec. props. 80—70201
semiconductor, tetrahedrally coordinated, dislocation struct. 79—82206
semiconductor, tetrahedrally coordinated, models of dislocation struct. 79—82205
semiconductors, dislocation structure, optical microscopy obs. techniques 80—24458
silicate minerals, lattice imaging 78—30522
sodium tartrate tetrahydrate, gel-grown single crysts., charact. 77—90261
solid-solid interface, chemistry and physics, book contrib. 79—1551
sputtering induced topography on solids, energetics and kinetics 80—88220
statistical theory, dislocation configs., in point obstacle random array 78—18645
steel, 11423, cyclic stress anal. within hysteresis loop *(Czech)* 80—30031
steel, 45G17Yu3, deformed, influence of hot rolling on struct. *(Russian)* 77—25073
steel, alloy, type Kh16N11M3, struct. changes during thermocyclic working, dislocation struct. *(Russian)* 80—54243
steel, austenite/ferrite interface, struct. and diffr. effects, TEM exam. 80—16308
steel, austenitic, creep, low-temp., during dynamic relaxation, effect of dislocation struct. *(Russian)* 77—25103
steel, austenitic, dislocation struct. formed by interstitial diffusion of C 77—4223
steel, austenitic, dislocation structural changes on hot rolling *(Russian)* 77 59805
steel, austenitic stainless, defect structure, N content depend. *(Russian)* 77—59022
steel, austenitic stainless, microstructure and transient creep 79—61675
steel, austenitic stainless, partial dislocation separation and dislocation substructure, effect of applied stress 78—22727
steel, austenitic stainless, stacking fault energy, effect of N 80—107279
steel, austenitic stainless, type 316, irradiated with 46.5 MeV Ni^{6+} ions, soluble C effect on void swelling and low dose dislocation structs. 80—49280
steel, austenitic stainless, type 800, tensile creep props., coherent twin boundaries, TEM obs. 79—38885
steel, austenitic stainless, V alloyed, creep inhibition at grain boundaries, dislocation struct., TEM study 79—43346
steel, austenitic stainless AISI 304, dislocation substruct., carbide precipitation and deform. mech. map 77—70116
steel, C, fatigue crack propag., crack closure, dislocation struct., electron microscopy obs. *(Japanese)* 80—25845
steel, cold worked, original struct. effect on softening during heating 80—60882
steel, Cr (13 wt.%), abnormal behaviour of H_2 at low temps. *(Russian)* 77—24434
steel, Cr-Mo, toughness of heat treated steels of equal tensile strength *(German)* 80—25727

dislocation structure continued

- steel, Cr-Mo-V pressure vessel, microstruct. parameters and yielding rel. to plastic deform. 80—89318
- steel, Cr-Ni, martensite defect identification by positron annihilation 78—39867
- steel, CrMoV, quantitative stereological anal. and creep-resistance *(Czech)* 80—30030
- steel, diffusion of C after high-temp. thermomechanical treatment *(Russian)* 78—39813
- steel, low C, fatigue, low cycle, cyclic stress-strain curve eval. 77—44347
- steel, low C, hot rolling effects on struct. *(Russian)* 78—19793
- steel, low C, P, plastic anisotropy and mech. prop. dynamic strain ageing effect 78—64608
- steel, low C, weldable, precipitation hardening rel. to low cycle fatigue *(Czech)* 79—15686
- steel, low C Mn-V, VC effects on strength and brittleness 77—70055
- steel, low-alloy 12GN2MFAYu, heat treated, testing temp. influence on fatigue strength *(Russian)* 80—40501
- steel, low-C, ferritic, deform. microstruct., electron microscopy *(German)* 78—64589
- steel, maraging, investigation with lower Ni and Co contents *(Chinese)* 78—84812
- steel, microstructure of 0Kh16N15M3B after creep tests in BR-10 reactor, electron, microscope invest. *(Russian)* 80—92531
- steel, mild, with different grain sizes, surface strengthening by high frequency loading *(Czechoslovakian)* 77—28934
- steel, NiCrMoV, stress corrosion cracking, cold work effects 78—11383
- steel, quenched, exam. of phenomena taking place during tempering by positron annihilation *(Russian)* 79—24543
- steel, stainless, 304, annealed and 9% prestrained, cyclic hardening and softening, room temp. 77—52483
- steel, stainless, AISI 304, dislocation struct., carbides, deform. mech. map 77—16650
- steel, stainless, AISI 304, dislocation substruct. around fatigue cracks, SEM obs. 78—15516
- steel, stainless, dislocation struct. adjacent to fatigue crack tips 77—36643
- steel, stainless, dislocation structure, of $\Sigma=9$ related coincidence boundary 79—27994
- steel, stainless, electron irrad. in HVEM, radiation damage obs. 77—50233
- steel, stainless, Kh25T, impact strength and substructure produced by deform. during cold rolling *(Russian)* 79—24535
- steel, stainless, radiation damage by 1 MeV electrons, dislocation struct., brittleness *(Russian)* 80—75226
- steel, stainless 304, recrystallisation, effect of dislocation structure 77—32595
- steel, stainless 316, creep under high stress 78—52892
- steel, stainless 316, dislocation substruct. prod. by elev. temp. fatigue crack propag., TEM obs. 78—19863
- steel, stainless type 03Kh13AG19, deformation temp. influence on dislocation struct *(Russian)* 80—11698
- steel, strengthened by surface plastic deform., tempering effect on physicomech. props. *(Russian)* 78—35409
- steel, type 12Kh1MF, dislocation struct. changes after thermomechanical treatment *(Russian)* 80—66545
- steel cylindrical bar loaded by longitudinal impact, dislocation struct. and plastic deform. *(Czech)* 78—60713
- steel Kh18N10T, substructure after low-endurance fatigue in pure bending *(Russian)* 77—81311
- steel mild, plastically deformed, X-ray meas. of stress and TEM 77—48496
- steels, heat-treated, nature of high sensitivity to stress raisers 80—21051
- straight edge dislocations, nonlinear computation of anisotropic elastic fields 77—7718
- strengthening and thermomechanical processing, conf., Las Vegas, USA, Feb. (1976) 77—84760
- subboundaries, collective effects accompanying migration *(Russian)* 78—14347
- TEM images of dislocation core, optical filtering for noise removal 80—107254
- TEM obs. of pinned dislocation arrangements 77—43217
- TEM obs. of plastic deformation, conf., Clermont-Ferrand, France (June 1976) *(French)* 77—44298
- thinned semiconductor device, SEM, electron beam induced cond. of defects, rel. to TEM 80—107027
- two dimensional superlattice of misfit dislocations, possibility of X-ray and electron diffr. struct. determ. 80—54560
- two-dimensional Lennard-Jones model, computer calc. 77—11550
- web dendrites, dislocations, stacking faults, X-ray topographic study *(Chinese)* 80—88148
- X-ray diffraction image fine struct. using single-crystal interferometer 77—62537
- X-ray diffraction topographic patterns, TV system for visualisation 77—58925
- X-ray distrib. function *(German)* 78—63767
- X-ray line broadening, fragmented crystal containing blocks *(Russian)* 79—86643
- X-ray plane wave topography, dislocation image computer simulation 80—54234
- Zircaloy-2 and -4, ⟨c⟩ component dislocations from TEM contrast expts. 80—6412
- Zircaloy-4-O alloys, rapidly heated and quenched, transform. charact. 79—20041
- Ag and Ag alloys, yield stress temp. variation hysteresis *(Russian)* 78—52905
- Ag, cold rolled, weak beam method appl. to dislocation obs. *(German)* 77—84757
- Ag, deformed at room temp., glide on {001} planes, TEM obs. 79—19257
- Ag, dislocation recovery *(Russian)* 77—65980
- Ag, epitaxially grown, on (001) Fe substrate, interface struct. 77—55470
- Ag, fatigued single crystal, annealing of deform. struct. 78—3204
- Ag film, epitaxial growth, characterisation of [001] tilt boundaries 78—84097
- Ag film, vacuum deposited, internal friction vibr. reed technique 78—43276
- Ag halide crysts., dislocations, survey of post-war research 80—62449
- Ag, ion beam plating using mass analysed ions, SIMS and AES expts. 78—19673

dislocation structure continued

- Ag, multiply twinned particles, internal and surface struct. by electron microscopy 80—84189
- Ag, rolled, dislocation struct. and recovery during annealing *(Russian)* 79—29084
- Al, A999, US inspection of purity and dislocation struct. 79—70286
- Al alloy, two phase, strength contribution of particles and dislocations *(German)* 79—29080
- Al and Al alloys, quenched, multiple-faulted dislocation loop config., TEM 77—27887
- Al, annealing of lightly deformed samples, effect of press. *(Russian)* 78—39795
- Al bicrystal, high resolution electron microscopy obs. of dislocations 80—103347
- Al bicrystals, [011] low-angle tilt boundaries, high resolution electron microscopy 80—34012
- Al binary alloys, exam. of dislocation structure, using diffraction electron microscopy *(Russian)* 79—10857
- Al cell structures produced by cycling and monotonic creep 80—55452
- Al, coincidence site lattice and DSC dislocation network model of high angle grain boundary structure 80—54260
- Al, cold rolled, weak beam method appl. to dislocation obs. *(German)* 77—84757
- Al, cold rolling of 1100 plates, substruct. development 80—108476
- Al, creep, low-temp., during dynamic relaxation, effect of dislocation *(Russian)* 77—25103
- Al, creep and dislocation distribution, influence of electron irradiation *(Russian)* 78—95775
- Al, creep and dislocation struct., electron irrad. effects 80—49268
- Al, creep and rupture, in torsion, mech. *(Russian)* 79—5030
- Al, deformed in uniaxial and equibiaxial tension, dislocation arrangements 80—108516
- Al, dislocation behaviour at melting, HV electron microscope in-situ obs. *(Japanese)* 77—43216
- Al, dislocation struct. change during cyclic straining at high temps. 78—44218
- Al, dislocation substructure formation under hydrostatic extrusion 78—56696
- Al, fatigue induced dislocation struct. and hardening, exam. *(Japanese)* 78—64624
- Al foil, α-particle irrad. under fusion reactor conditions, He bubble alignment during deform. 80—107345
- Al, high purity 6061, thermomechanical treatment 77—44277
- Al, plasma-sprayed, effect of Si substrate surface conditions and impact velocity of sprayed particles 80—21145
- Al, plastically deformed single crystal, X-ray diffr. by defects 77—68976
- Al, screw dislocation core, atomic struct. calc., modified lattice-statics approach 78—75669
- Al single crystal, polygonisation at high press. kinetic regularities, dislocation struct. at 140°C 79—66070
- Al, stationary creep in HVEM, cell struct. evolution 80—104242
- Al, strength changes on US treatment in programmed loading *(Russian)* 77—32583
- Al, superpure, creep rate-controlling processes 80—85009
- Al, surface deformation and wear track obs. using analytical electron microscope 80—108687
- Al, thermoactivated creep and stress relax. 79—87692
- Al, work softening, microstruct. interpretation 77—32593
- Al-(Mg)(Fe), pure (dilute), large wire drawing plastic deform. 80—108508
- Al-Al_3Ni eutectic composite, substructural matrix hardening *(Russian)* 77—21162
- Al-Cu (4 wt.%), elastic accommodation of semicoherent θ' 78—64543
- Al-Cu (4 wt.%) alloy, neutron irrad., weak-beam dark-field obs. of dislocations near θ' precipitates 80—107333
- Al-$CuAl_2$, directionally solidified eutectic, structural changes during strength tests *(Russian)* 80—7543
- Al-Mg, recrystallised, grain boundary dislocation identification by computer simulation of TEM image *(Japanese)* 77—47457
- Al-Mg (5 wt.%), recovered dislocation substruct. during plastic flow 79—83273
- Al-Mg (5.5 wt.%), effect of stress changes during creep on dislocation struct., TEM study 79—74214
- Al-Mg_2Si(1.42 wt.%), aged, dislocation structs. caused by plastic deformation 80—25786
- Al-Ni (6 wt.%), fine-grained, deform. in tension and torsion 80—85008
- Al-Ni(Cd)(Fe)(Si), cold worked, struct. and props. 80—71666
- Al-Zn (11 wt.%), stress depend. of strain rate at elev. temps. 78—23757
- Al-Zn (3.9 wt.%), single crysts., fatigued age-hardenable, dislocation structure *(German)* 80—54247
- Al-Zn-Mg (2.1, 1.3 wt.%), single crysts., fatigued age-hardenable, dislocation structure *(German)* 80—54247
- Al-Zn-Mg (5, 1 wt.%), relation between mech. props., SCC and dislocation struct. *(German)* 77—81345
- Al-Zn-Mg alloy, thermomech. treatment, precipitation and strengthening 79—24527
- Al-Zn-Mg(3.2, 2.2 wt.%), deform. strengthened by Guinier Preston zones 77—52343
- Al-Zn-(Mg), age hardenable single crystal, fatigue and fatigue cracks *(German)* 77—16689
- $Al_2Be_3(Si_6O_{18})$, beryl single crysts., dislocations obs., X-ray topography *(French)* 79—37709
- $Al_2Be_4(Si_6O_{18})$, beryl single crysts., growth defects study using X-ray topography *(French)* 79—37710
- AlCu-NiCo (5 at.%), Θ' hardened, creep mechanism 80—85013
- Al_2O_3, alumina, deformed by prismatic slip, HV TEM obs. of dislocations 80—108517
- Al_2O_3, defect microstructure due to ion bombardment, TEM study 80—34100
- α-Al_2O_3, radiation damage in HVEM, at high temp. and high dose 79—46707
- $(Al_2O_3)_nMgO$, $n \doteq 1.1$, high temp. creep, dislocation behaviour 78—80593
- Au, atomic arrangements of defects, dynamic obs. of atom movement 80—39108
- Au bicrystal, core structs. of misfit dislocations in grain boundaries, TEM 78—14360
- Au bicrystal, dislocation networks in twin boundaries, TEM obs. 78—51556
- Au, bicrystalline, electron diffraction on networks of grain-boundary and interphase dislocations *(Russian)* 79—73168

dislocation structure continued
- Au, dislocation free bicrystal, DSC dislocation network generation in coherent twin boundary 77—62544
- Au, epitaxial, on vacuum deposited Fe, interfacial dislocations 78—30847
- Au, epitaxially grown bicrystal on (001) Fe substrate, interfacial dislocation behaviour 77—51622
- Au film, epitaxial growth, characterisation of [001] tilt boundaries 78—84097
- Au, ion beam plating using mass analysed ions, SIMS and AES expts. 78—19673
- Au, multiply twinned particles, internal and surface struct. by electron microscopy 80—84189
- Au, thin film bicrystal, diffraction effects from inclined grain boundaries 80—103362
- Au-Pd, bicryst. thin film couples, interphase interfaces, TEM 80—70540
- Au-Pt epitaxial film system, mismatch dislocations obs., electron microscopy 77—4268
- BN, dislocation struct., single crystals, positron annihilation study 78—11016
- Ba ferrites, lattice imaging 78—30522
- BaTiO$_3$, single crysts., electron microscope study of domain and defect structs. 79—15425
- Bi oxides containing perovskite layers, ferroelec. cryst., electron microscopy, dislocation and domain boundaries 77—52030
- Bi-Sb, bicrystal rearrangement of grid of nonconformity dislocations on (111) interface during heating 79—28215
- Bi$_2$Te$_3$ single crystals, melt grown, structural perfection 80—15101
- C, pyrolytic, spiral growth rel. to temp., press., flow conditions, dislocations, props. *(German)* 78—42931
- CaCO$_3$, plastic deformation in compression parallel to (111) 78—38709
- CaCO$_3$ single crystals, effect of defect struct. charact. on X-ray diffr. 79—65089
- CaF$_2$, plastic deform, work hardening regions, TEM obs. 80—3140
- CaF$_2$, single cryst., dislocation etch pit shapes, dislocation line inclination effects 77—7722
- Ca$_5$F(PO$_4$)$_3$, colour centre accumulation deformation effects 77—84743
- Ca$_3$Ga$_2$Ge$_3$O$_{12}$, substrate, electron examination of microstruct. and microsegregation 78—67919
- Ca$_5$(PO$_4$)$_3$F, dislocation struct. exam. *(Russian)* 78—63770
- Cd, control after prep. low angle boundary decomp. *(Russian)* 78—3142
- Cd-Zn single crystal, plasticity, 4 to 50K 79—43362
- CdI$_2$ polytypes, defect struct., electron microscopy 79—14809
- Cd(S, Se) film grown on InP substrate, mismatch dislocations and lattice distortion, dangling bond density 80—84406
- CdSe, X-ray topography 77—89441
- CdSe-Ge (111) heterojunctions, epitaxial, azimuthal rotation 78—84085
- CdTe films, structural imperfections depend. on crystn. temp. 79—90661
- CdTe, single crystals, plastic deformation and dislocation struct. 79—8321
- Co-transition metal, transition metal additives influence on struct., specific resistance, microhardness, mech. props., magnetic props. 79—29078
- CoO, pure and Li doped, dislocation spacing effect on high-temp. creep 78—35444
- Cr-Nb, dislocation cell growth kinetics by TEM during annealing *(Russian)* 79—65084
- CsI, mechanical props., effect of impurities 77—69034
- Cu, acoustic losses due to strong ultrasonic and static stress fields 80—79886
- Cu and Cu-Al alloys, mech. props. effect of free mean path 78—84945
- Cu, annealing of lightly deformed samples, effect of press. *(Russian)* 78—39795
- Cu, coincidence site lattice and DSC dislocation network model of high angle grain boundary structure 80—54260
- Cu, cold worked, dislocation production 77—32597
- Cu, continuously cast, O free, effect of nonmetallic inclusion on microstruct. and props. 77—81280
- Cu, cracks in fatigue early stages, direct obs. of substruct. by electron microscope *(Japanese)* 78—7028
- Cu, creep, low-temp., during dynamic relaxation, effect of dislocation struct. *(Russian)* 77—25103
- Cu, deformation in ultramicrotomy 77—8874
- Cu, deformed at room temp., glide on {001} planes, TEM obs. 79—19257
- Cu, deformed by hydrostatic extrusion, drawing or drawing under press., dislocation struct. obs. *(Russian)* 77—21213
- Cu, dislocation structure, around tips of propagating fatigue cracks 79—29211
- Cu, dislocation substructure formation under hydrostatic extrusion 78—56696
- Cu, electrochem. overgrowths, role of substrate dislocations and grain boundaries in nucleation and growth 79—51454
- Cu, erosive wear mechanisms, combined TEM and SEM obs. 80—108601
- Cu, extruded at 77K, defect struct. and elastic limit *(Russian)* 80—30016
- Cu, fatigue crack propag., role of dislocation substruct. 80—60963
- Cu, fatigued, early stage crack tip dislocation morphology, electron microscope obs. 78—27628
- Cu, fatigued, structural changes, damping and modulus 77—28906
- Cu, fatigued single crysts., temp. depend. of saturation stress and dislocation substruct. 80—44211
- Cu, friction mechanism, HV TEM expts. 80—35341
- Cu, hardness-flow stress rel. during strain-controlled bending fatigue 79—74245
- Cu, low temp., internal friction and microplastic strain 77—84839
- Cu mirror, microstruct. effect on Ag overlayer deposition, 10.6 μm reflectivity 77—42543
- Cu phthalocyanine, grain boundary struct., crystallographic planes 80—103366
- Cu polycrystal, fatigued, interior dislocation struct. 80—88147
- Cu, polycrystalline, friction stress meas. during high temp. creep 79—1898
- Cu, pure, fatigue crack propagation, effect of stacking fault energy as deduced from dislocation patterns, TEM study 79—61719
- Cu, rolled, dislocation struct. and recovery during annealing *(Russian)* 79—29084
- Cu, single crysts., deformed in [001] and [111] axes, cell structs., TEM 80—70209
- Cu, single crysts., dislocation cell form. during plastic deform., TEM obs. 80—60935
- Cu, strengthening by dislocation substructures 77—36538

dislocation structure continued
- Cu, tension deformed single crystal, dynamic recrystallisation 79—47716
- Cu, thermal stress role in dislocation form. during growth from melt 80—6374
- Cu, thermoactivated creep and stress relax. 79—87692
- Cu, whiskers, hardening during uniaxial extension, preliminary torsion deform. *(Russian)* 78—15420
- Cu-Al (15 wt.%) single crystal, steady state deform. at high temps. *(Japanese)* 78—19833
- Cu-Al (2.5 at.%), single crystal, steady state deform. at high temps. *(Japanese)* 77—52415
- Cu-Al (4.5 at.%), alloy, dislocation recovery anomalies *(Russian)* 77—21163
- Cu-Al-Ni (14.5, 3 wt.%), fatigued, polycrystn., pseudoelastic, dislocation and martensite substructs. 79—82223
- Cu-Be (2 at.%), plastic deform. and dislocation substruct. 80—76307
- Cu-Cd (0.03 at.%), single cryst., deformed, dislocation arrangement 79—10856
- Cu-Co, age hardenable single crystal., fatigue and fatigue cracks *(German)* 77—16689
- Cu-Co (2 wt.%), single crysts., fatigued age-hardenable, dislocation structure *(German)* 80—54247
- Cu-Cr (0.75 wt.%), deformation characts., fully reversed cyclic strain with fatigue cracks and dislocation struct. 80—81148
- Cu-Cr-SiO$_2$ system, age and dispersion strengthened, dislocation struct. around SiO$_2$ particles 80—108468
- Cu-Fe (1.5 wt.%), precipitation-effect on void formation during electron irradiation 80—84211
- Cu-Ni bicrystal, misfit dislocation config., moire patterns, interdiffusion effects 78—84110
- Cu-Si (6.5 at.%) alloy, easy glide deform., obs. and mechanism 77—8887
- α-Cu-Zn, whiskers, X-ray topography, substruct. 77—11831
- Cu$_3$Au, disordered [001]-orientated single crysts., plastic deform., TEM and slip line studies 80—97541
- CuFeS$_2$, natural chalcopyrite, defect struct., TEM 77—62535
- Cu$_2$MnAl, antiphase boundary energy, deformation behaviour prediction *(Russian)* 79—65085
- Cu$_2$Se, VPE on mica, defect struct., temp. depend. 77—35837
- Dy, substructural changes during plastic deform., stress-strain diagrams and microhardness meas. *(Russian)* 79—52296
- Er, substructural changes during plastic deform., stress-strain diagrams and microhardness meas. *(Russian)* 79—52296
- α-Fe, $(\bar{1}\bar{1}2)$ $[\bar{1}\bar{1}\bar{1}]$ anti-twinning slip system, low temp. strengthening, dislocation struct. 77—21164
- Fe, Armco, dislocation struct. after hot and cold rolling *(Russian)* 77—8847
- Fe, Armco, dislocation struct. effect on creep *(Russian)* 78—39841
- Fe, Armco, rupture onset during cold rolling *(Russian)* 77—8904
- Fe, BCC, computer simulation of entropy of $^1/_2\langle 111\rangle\{110\}$ edge dislocation 78—67716
- α-Fe, creep life, meas. by microstruct. changes 78—35443
- α-Fe, cyclically deformed, mag. props. 77—28412
- Fe, deformed, dislocation structure determ. from magnetic props. 78—55874
- Fe, dislocation struct. around fatigue cracks, exam. *(Japanese)* 78—64623
- Fe, dislocation struct. at tip of fatigue crack 77—4107
- Fe, dislocation struct. round fatigue cracks 78—48519
- Fe dissolution, morphology of differently oriented single crystal surfaces, dislocation effects *(German)* 77—9002
- Fe epitaxial layer on Au(111), misfit dislocation obs. 79—73415
- Fe, fatigue crack propag., crack closure, dislocation struct., electron microscopy obs. *(Japanese)* 80—25845
- Fe, foil, fatigue crack, low growth rate, microstruct. round top 77—16674
- Fe microcrystals, dislocation struct. singularities in early deform. stage *(Russian)* 77—55284
- Fe, microhardness of single crysts. effect of temp. on dislocation structure *(German)* 79—52357
- α-Fe, single crystal, Sb diffusion induced dislocations 78—30798
- Fe, single crystals, work hardening and behaviour and dislocation struct. during simple shear tests 78—95762
- Fe, single crysts., effect of hydrostatic pressure on plastic flow props., dislocation distribs. 79—38887
- Fe whiskers, cryst. morphology and dislocation struct. study using optical and SEM, X-ray diffr. topography 79—23876
- α-Fe whiskers, pure, ductile fracture, microscopic obs. of initiation mechanism 80—85044
- Fe whiskers, undeformed, X-ray topographic study 77—80716
- Fe-Al, single crystals, deform. at high temps. 80—81125
- Fe-Al(25 at.%), mag. anisotropy induced by plastic deform., dislocations, long-range order 77—4544
- α-Fe-C (0.03 wt.%), structural singularities of transition from thermally activated to force-induced fracture *(Russian)* 78—56731
- Fe-Co alloy, V addition effect on atomic order parameters, mechanical props. 79—91762
- Fe-Co-Ni-W alloy, 45KKhVN, plastic deform., electron microscope obs. *(Russian)* 78—80584
- Fe-Cr-Mn, influence of alloying with Ni, Mo, N on defect conc. energy *(Russian)* 80—54241
- Fe-Mo(4.1 wt.%), steady state creep at high temps. 80—89316
- Fe-Nb-C (0.04, 0.02 wt.%), strengthening, hot rolling *(Chinese)* 79—100154
- Fe-Ni, alloy 20N24, martensitic, exam. of structure after laser treatment, and recrystallisation *(Russian)* 79—11608
- Fe-Ni, hardening by plastic deform. during polymorphic transform., mechanical props. *(Russian)* 77—90345
- Fe-Ni (23 wt.%), struct., composition changes during α to γ transform., martensite plastic deformation influence *(Russian)* 80—11642
- Fe-Ni-C, martensitic, internal friction 77—16633
- Fe-Ni-C (24, 0.5 wt.%), recovery and recrystallisation of stable austenite after hot rolling *(German)* 77—32591
- Fe-Ni-Cr (25, 15 wt.%), high temp. creep, dispersed γ'-Ni$_3$(Al, Ti) effects *(Czech)* 78—64590
- Fe-Ni-Ti-C (31, 4, 0-18 wt.%), coherent precipitates in austenite, effect on martensite substruct. 77—52327
- Fe-Ni-(C), substruct. of ausformed martensite 77—36548
- Fe-Pt, nearly thermoelastic, irreversible lattice defects formed by martensitic transform. cycles 78—60671
- Fe-Si, dislocation struct. of plastic relax. zone at tip of brittle crack 77—77582

dislocation structure continued
Fe-Si (3 at%), deformation and electron bombardment, influence on dislocation struct., 20-500°C *(Russian)* 80–92536
FeAl single crystal, compressed, dislocation arrangement 78–14354
Fe_2MnAl, antiphase boundary energy, deformation behaviour prediction *(Russian)* 79–65085
$Fe_{40}Ni_{40}C_{14}P_6$ amorphous film, dislocation and mag. struct., neutron diffr. study 80–70956
FeS_2 (pyrite), glide elements study by electron microscopy and electron diffr. 78–83817
Fe_3Si, ordering energy, electron micrography determ. 78–14353
Ga, dislocation structure on melting of nearly perfect crysts., Borrmann topography 77–31663
$Ga_{1-x}Al_xAs$, degraded DH LED, defect struct. by electrolum. topography and TEM obs. 79–60369
$Ga_{1-x}Al_xAs$ LPE crystals for DH laser, LEDs, TEM obs. of Ge, Si-doped epitaxial layers 79–1556
$Ga_{1-x}Al_xAs$-GaAs, heteroepitaxial layers on GaAs(001), misfit dislocation asymmetry 77–47694
$Ga_{1-x}Al_xAs$-GaAs, injection lasers, defects, TEM anal. 79–23866
$Ga_{1-x}Al_xAs_{1-y}P_y$ epitaxial film, nonradiative recomb. at dislocations 80–44213
$Ga_{1-x}Al_xAs_{1-y}P_y$-GaAs quaternary heterojunction, misfit dislocation charact. by synchrotron radiation white beam topography 78–63771
GaAs crysts., IR light scattering and absorpt. microscopy study of dislocations 80–107249
GaAs degraded lasers, climb asymmetry, TEM obs. 80–79802
GaAs, dissociation of dislocations 79–46665
GaAs epitaxial multilayer photocathode structures, TEM obs. of dislocations generated 80–100241
GaAs, LPE layers, X-ray topographic exam. of defects 78–30844
GaAs:Si, hardening by solute-vacancy pairs 77–4794
GaAs:Sn(Te), epitaxial film, influence of impurities on stacking fault energy 80–103371
GaAs/AlGaAs DH wafers and lasers, defect struct., X-ray topography 79–50312
GaAs-GaAlAs LPE layers, laser material, shallow growth pits obs. 77–7985
GaAs-GaAlAs wafers, defects and degradation, transmission cathodolum. evaluation 80–65395
GaAs-$GaAs_xSb_{1-x}$, heteroepitaxial structs., mismatch dislocation nets 79–10855
GaAs-GaInAs structure, dislocation struct., TEM anal., appl. as IR LED 80–70206
GaAs$Ga_{1-x}Al_xAs$ DH laser material, rapid optical degradation obs. 77–75528
$GaAs_{1-x}Px$, heteroepitaxial solid soln., defects of struct 79–28223
$GaAs_xSb_{1-x}$-GaAs epitaxial films and multilayer heterostruct., SEM obs. under cathodolum. conditions 79–11023
$Ga_{1-x}In_xAs$-GaAs low-misfit epitaxial interface, electron microscope contrast 79–73416
GaInAsP-InP DH layers, lattice deform. and misfit dislocations 79–19473
$Ga_xIn_{1-x}P_yAs_{1-y}$, 111-A and 111-B faces, defect struct., etching and X-ray diffr. obs. 80–2026
GaP, crystal, growth conditions rel. to dislocation struct. 80–88151
GaP, dislocation structure, optical microscopy obs. 80–24458
GaP, large cryst., optical birefr. images of dislocations 78–30627
GaP single crystal, direct obs. of dislocations by birefringence 79–14810
$Gd_3Ga_5O_{12}$, substrate, electron examination of microstruct. and microsegregation 78–67919
Ge, amorphous, struct., dislocation model 78–42911
Ge bicrystal, high resolution electron microscopy obs. of dislocations 80–103347
Ge, bicrystal, sessile Lomer dislocations *(French)* 77–55286
n-Ge, dislocational microwave conductance anisotropy *(Russian)* 79–91092
Ge, dislocations, lattice images 79–82215
Ge, edge dislocation struct., lattice distortion and surrounding vacancy distrib. 77–19954
Ge, epitaxial, in situ X-ray topography, misfit dislocations 78–47671
Ge, high resolution electron microscopy, dislocation and grain boundary struct. 3-4 Å resolution 78–38707
n-Ge, plastically deform., dislocation state spectrum, photocond., elec. cond., and Hall const. meas. *(Russian)* 80–2362
n-Ge, plastically deformed, elec. cond., magnetoresistance, Hall effect study *(Russian)* 79–99568
Ge ribbon single crysts. grown from melt, dislocation struct. form. under thermal stress 80–107082
Ge, shaped crystals, grown by Stepanov method, struct. perfection 78–2123
Ge, single cryst., effects of ultrasound 77–69119
Ge single crystals, constitutional supercooling growth conditions, structural and chem. inhomogeneities 80–93473
Ge-As, supersaturated solid soln., dislocation form. during thermocyclic treatment *(Russian)* 80–3057
Ge-GaAs, heteroepitaxial systems, misfit dislocations obs. using HV electron microscopy 80–100242
Ge-GaAs heteroepitaxial system, dislocation struct. in stress measurements 80–29030
Ho, substructural changes during plastic deform., stress-strain diagrams and microhardness meas. *(Russian)* 79–52296
III-V semiconductors *(Japanese)* 79–42074
In, twin boundary movement by creep 80–24460
InGaAs-GaAs heterojunction with low misfit, misfit dislocation struct. 77–62783
$In_{1-x}Ga_xP_{1-z}As_z$-InP, LPE heterojunctions, lattice matching and dislocations 78–23150
InP, and InP_xAs_{1-x}, 111-A and 111-B faces, defect struct., etching and X-ray diffr. obs. 80–2026
InSb, dislocations due to thermal stress, single and composite crysts. 78–2124
InSb, plastically bent single crysts., dislocation struct. obs. 78–59816
InSb, X-ray topographic evidence of asymmetrical pre-yield behaviour 80–75229
InSb:Se, exam. of defects in crystal 80–6423
KCl, cryst. isolated pore healing under press., dislocation struct. evolution *(Russian)* 80–100245
KCl, Czochralski-grown, dislocation subboundary characts. 78–67718
KCl, US plastic deform., dislocation struct. 80–19809

dislocation structure continued
KCl:Ba^{2+}, localised stress relaxation in excess vacancy system, prismatic loops *(Russian)* 80–88160
KCl:Br^{2+}, solid solution periodic precipitation in inhomogeneous conc. field 80–103485
KCl-KBr, dislocation rosettes, diffusion origin 78–83820
KCl-NaCl, dislocation rosettes, diffusion origin 78–83820
Li, temp. depend. of dislocation behaviour between 90 and 300K 80–88146
LiF bicrystal, high-angle tilt boundary and edge dislocation intersection effects 80–79836
LiF, deformed, influence of surface on density of edge components of dislocations 77–31670
LiF, dislocation distrib., after deform. *(Russian)* 78–22732
LiF, dislocation structure, influence of variable deform. temp. 80–70211
LiF, electron irradiated, mech. characts. 78–26595
LiF, single cryst., impression creep 78–6986
LiF, strong reorientation resulting from creep, X-ray obs. 79–100228
LiF:Mg, slip band struct. changes with temp. 78–47390
LiF:Mg^{2+}, deformed in ^3He and ^4He, dislocation struct. characteristics 79–69112
LiF:Ni, dislocation behaviour in diffusion zone, Cottrell clouds *(Russian)* 80–70212
$Li_{0.5}Fe_{2.5}O_4$ milled ferrite powder, substruct. and sinterability 80–84894
α-$LiIO_3$, dislocation struct. 77–1132
Mg alloy, dil., dynamic recrystn. during creep, dislocation substruct., quartz comparison 80–109142
Mg, cyclic hardening of single crystal 78–64552
Mg, dislocation struct. after US deform. *(Russian)* 80–29027
Mg, melt grown by Bridgeman method, X-ray topography 78–59770
$MgAl_2O_4$ spinel, rel. to stacking fault energy 77–28853
MgO, a/2 ⟨110⟩ edge dislocations, lattice friction stress, atomistic calc. 78–18648
MgO, core struct. and energy of dislocations, breathing shell model calc. 77–39586
MgO, high temperature prestrain effect on plastic props., dislocation struct. 80–79866
MgO single crystal, dislocation struct. of slip lines, TEM 79–27990
MgO, single crystal, effect of heat treatment on mechanical props. 77–70070
MgO, subgrain boundaries form. obs. by TEM, diffusion coeff. determ. 80–79817
MgO:Ni, heavily doped, defect characterisation, rel. to use as laser material 80–65000
$MgO(Al_2O_3)_{1.8}$, spinel, X-ray refl. topography, dislocation substructures during creep form. *(French)* 78–68737
MgO.1.1 Al_2O_3 spinel, high temp. deform., cryst. orientation effect 80–107263
Mg_2SiO_4 crysts., dislocations configuration and cleavage steps dissoln. 80–107250
Mg_2SiO_4, forsterite, decorated dislocations 80–54245
Mg0 bicrystals, electron microscope exam. of secondary grain boundary dislocations in high angle twist boundaries 80–6415
Mo alloy, TsM-10, fatigue fracture mechanism, dislocation struct. *(Russian)* 77–32674
Mo, atomic structure of grain boundaries 79–33003
Mo, block boundary dislocation struct. singularities under high temp. steady state creep conditions *(Russian)* 79–90670
Mo, cellular structure, initial stages of formation in rolled single crystals 79–23611
Mo cold worked, dislocation struct. change during postdeform. at 493K 79–43271
Mo, creep deformed single crysts., subboundary struct. obs., dislocation sets 80–103348
Mo deformed single crysts., struct. state and dislocation splitting *(Russian)* 80–29029
Mo, dislocation (100) density variation, deformation effects, dislocation stability *(Russian)* 80–15108
Mo, dislocation structure evolution near electro-eroded crater *(Russian)* 80–100237
Mo, dislocation structure inhomogeneity in electromachining crater zone *(Russian)* 80–16326
Mo, dislocation structure of diffusional welding zone *(Russian)* 80–96531
Mo, fatigue of single crystals, dislocation struct. and strain localisation *(Russian)* 80–71741
Mo, foil dislocation struct. of rolling texture *(Russian)* 78–59810
Mo, irrad.-induced voids and dislocations, annealing, theory *(Russian)* 78–47418
Mo, macroscopic heterogeneity of plastic deform., metallographic examination *(Russian)* 79–100210
Mo, mag. field effect on mech. props. and dislocation struct. *(Russian)* 79–42818
Mo, mechanical props. and dislocation struct., mag. field effect 80–54935
Mo, plastic deform. by rolling at 293K, dislocation struct. *(Russian)* 77–48481
Mo, plastic deform. mechanism during hydrostatic extrusion *(Russian)* 77–8879
Mo polycrystn., cyclically deformed, dislocation arrangements 80–108506
Mo, pure and He doped, at. config. of $^1/_2\langle 111\rangle$ screw dislocation 79–65081
Mo, single and polycrysts., struct. change during work softening, HVEM 80–103336
Mo single cryst., laser induced dislocation struct. 80–70210
Mo, single crystals, creep deformed, Burgers vectors, block boundary struct. *(Russian)* 79–77603
Mo single crysts., substruct. variation during fatigue, kinetics *(Russian)* 78–60742
Mo, slip rosettes and dislocation struct. formed by microindentations 78–14349
Mo, structural singularities of plastic deform. at localised flow stage, TEM obs. *(Russian)* 78–6968
Mo, temp. depend. at crack tip, of fractured single cryst. 79–29210
Mo-O system, grain boundary segregation and intergranular fracture 80–55516
Mo-O-C system, grain boundary segregation and intergranular fracture 80–55516
Mo-Re alloy MR47-VP, dislocation struct. and fatigue damage during room temp. deform. *(Russian)* 79–20111

dislocation structure continued
Mo-Ti(B)-Zr(Al)-C, stress cycling at room temp. *(Russian)* 77−25148
Mo-Zr-C (0.63, 0.06 wt.%), quenched and deformed, structural changes during heating to ageing temp. *(Russian)* 79−1879
Mo-Zr-Nb-C and Mo-Zr-C, carbide precip. hardening kinetics, ageing singularities *(Russian)* 77−25059
β-$MoTe_2$, domain struct., dislocation fine struct., phase transitions 79−82332
β-$MoTe_2$, layer cryst., dislocations and domain struct. 80−39102
$NH_4H_2PO_4$, {100} faces cryst. growth kinetics, low supersaturations range, dislocations 79−56047
$NaBrO_3$, dislocation struct. inhomogeneity rel. to growth rate 77−47456
NaCl, and NaCl-NaBr, Ca-doped, dislocation struct., etch pit obs. 78−43020
NaCl, cleavage ledges and interface dislocations on Suzuki phases 79−90659
NaCl, deformed, influence of surface on density of edge components of dislocations 77−31670
NaCl, dislocation ordering influence on integrated X-ray coeff. 80−103357
NaCl, dislocation struct. of slip bands, hydrostatic press. effect 80−54249
NaCl, edge dislocation, core struct. and props., theory 80−70194
NaCl, effect of annealing and neutron irrad. on block struct. 80−29061
NaCl, plastic deformation influence on shape recovery effects 80−6684
NaCl, plastically deformed [001] oriented single crystals, TEM 77−36579
NaCl, strained in one glide system at 450°C, dislocation struct. 78−22728
NaCl type crystal, dislocations due to high temp. stress relax. 78−2126
NaCl:Fe(Mn), nucleation of Au, surface imperfection effects 77−15699
NaF, deformed, influence of surface on density of edge components of dislocations 77−31670
Nb, deformation at 77-158K, slip and dislocation struct. 79−83277
Nb, dislocation struct. after tensile creep test under reactor radiation conditions *(Russian)* 80−45348
Nb, mag. field effect on mech. props. and dislocation struct. *(Russian)* 79−42818
Nb, mechanical props. and dislocation struct., mag. field effect 80−54935
Nb, plastically deformed single crystal, low temp. thermal cond. 79−28336
Nb, single crystal, surface oxide softening, TEM obs. 77−40462
Nb single crystal, yield point and dislocation struct. temp. depend. *(Russian)* 77−81290
Nb-Mo solid soln., single cryst., yield point and dislocation struct., temp. depend. *(Russian)* 77−81290
Nb-Zr-C, strengthening phase struct. and morphology after prolonged high temp. stress in vacuum *(Russian)* 77−25065
Nb-Zr-C alloy, long term loading at high temps. effect on struct. and morphology of carbide phase 79−15754
NbN_x, solid soln, strain ageing, internal friction, elec. cond. kinetics *(Russian)* 78−76667
NbN_xO_y, solid soln, strain ageing, internal friction, elec. cond. kinetics *(Russian)* 78−76667
NbO_x, solid soln, strain ageing, internal friction, elec. cond. kinetics *(Russian)* 78−76667
Nb_xO_y, lattice imaging 78−30522
Nb_xO_y structures, dislocations and related defects 77−7724
$NbTe_2$, layer cryst., dislocations and domain struct. 80−39102
Ni, acoustic hardening, influence of US treatment temps. and material purity *(Russian)* 80−11656
Ni alloys, creep transients, friction stress and recovery, dislocation substruct. 80−60933
Ni base superalloy, single crystal, apparent and effective creep parameters, incubation period 77−63715
Ni, cavitation-erosive wear in surface-active media, dislocation struct. and fracture study by FMR *(Russian)* 79−52384
Ni, deformed, magnetic susceptibility anisotropic changes 78−27025
Ni, deformed, work-hardening, dislocation and mosaic struct., X-ray and electron microscopy 77−35625
Ni, deformed at room temp., glide on {001} planes, TEM obs. 79−19257
Ni, deformed by hydrostatic extrusion, drawing or drawing under press., dislocation struct. obs. *(Russian)* 77−21213
Ni, dislocation struct formed by C diffusion in single crystals, electron microscope obs. *(Japanese)* 78−10053
Ni, dislocation structure evolution after hydroextrusion *(Russian)* 80−96530
Ni, dislocation structure parameter determ. due to plastic deformation *(Russian)* 80−54242
Ni, dislocation substructure formation under hydrostatic extrusion 78−56696
Ni, electrochem. overgrowths, role of substrate dislocations and grain boundaries in nucleation and growth 79−51454
Ni electrodeposit on Cu, growth and microstruct. 77−11823
Ni, erosive wear mechanisms, combined TEM and SEM obs. 80−108601
Ni, high-purity, softening of strained single crystals *(Russian)* 80−40499
Ni, interstitial diffusion of C in single crystals, stress distrib. changes 77−47626
Ni, ion irrad. with 20 and 500 keV $^4He^+$, depth distrib. of cavities and dislocation damage 80−107346
Ni, magnetised mono- and polycryst., activation vol. var. during low temp. deform. *(Russian)* 78−3178
Ni monocrystals, struct., effect of stress applied during electrodeposition 78−26777
Ni, plasma-sprayed, effect of Si substrate surface conditions and impact velocity of sprayed particles 80−21145
Ni, plastically deformed, dislocation struct., mag. small angle scatt. of neutrons *(German)* 78−22730
Ni, polygonisation, high press. grain growth, dislocation struct., electron microscopic obs. 77−16613
Ni, powder, subjected to vibratory milling, exam. of plastic deformation, recrystallisation, sintering 80−16234
Ni, rolled, dislocation struct. and recovery during annealing *(Russian)* 79−29084
Ni single crystals, cyclically deformed, behaviour during annealing 78−71740
Ni, slip character, H effect 80−89287
Ni, splat quenched, gaseous impurities effect on struct. 77−4042

dislocation structure continued
Ni, structural changes, creep mechanism, multiple dislocation cross slip *(Russian)* 80−59476
Ni, structural singularities of plastic deform. at localised flow stage, TEM obs. *(Russian)* 78−6968
Ni/Ni_3Al-Ni_3Nb eutectic, directionally solidified, plastic deformation *(Russian)* 78−39843
γ,γ′-Ni-Al alloys, irrad. effects on precip. 77−8829
Ni-Al-Cr, strain hardening, participation of various slip systems *(Russian)* 79−24536
Ni-base superalloys, powder metallurgical, creep-rupture at intermediate temps. 80−97568
Ni-Cr-Co-Ti-Mo-W-Al (14, 9.8, 5, 4, 3.9, 3 wt.%), low cycle fatigue, prior heat treatment effect 80−60962
Ni-Cr-ThO_2(20, 2 wt.%), dislocation struct. after high temp. deform. 77−52393
Ni-Fe(Co) alloys, fatigued, struct. and cyclic stress strain, influence of stacking fault energy and atomic size-module-interactions *(German)* 79−42082
Ni-Mo (14.4 wt.%) single crystals, ordered phase precipitates influence on deformation character, mechanical props. *(Russian)* 79−74155
Ni_2Cr, fine-domain ordered alloy, early deform. stages, dislocation struct. and motion *(Russian)* 77−81291
Ni_3Fe, compression induced mag. anisotropy and superlattice dislocations, annealing effect 78−31067
Ni_3Fe, single crysts., long range order degree influence on strain hardening *(Russian)* 80−11660
$NiFe_2O_4$ milled ferrite powder, substruct. and sinterability 80−84894
$Ni_{0.33}Fe_{2.33}O_4$, {001} ⟨110⟩ glide system, room temp. TEM obs. 79−90660
Ni_3GA single crystals, anomalous temp. depend. of strength, dislocation struct., optical and TEM 79−74228
Ni_3Ga, with $L1_2$ struct., dissociated struct. of superlattice dislocations 79−37706
Ni_3Ge single crystal, yield stress, temp. and orientation depend. 77−90432
Ni_3Mn, dislocation struct. after heat treatments, TEM *(Russian)* 77−8848
Ni_4Mo, domain struct. on annealing, and dislocation struct. during deform. *(Russian)* 77−16640
NiO, single crysts., TEM of dislocations 79−4306
PbS, epitaxial layer, structural nonuniformities and dislocation struct. 79−23852
Pd_2Si films on Si, lattice imaging obs. of structural details 80−103604
Pt-Au bimetallic films, electron diffraction on networks of grain-boundary and interphase dislocations *(Russian)* 79−73168
ReS_2, layer cryst., dislocations and domain struct. 80−39102
$ReSe_2$, layer cryst., dislocations and domain struct. 80−39102
Sb, dislocation internal friction depend. on high ampliutde US vibrations *(Russian)* 79−90727
Sb, dislocation internal friction changes due to high-amplitude US oscills. *(Russian)* 80−10556
Sb, epitaxial growth on Bi substrate 78−95246
Sb_2S_3, film, defect struct., electron microscope mode 79−28224
Sb_2S_3 spherolite crysts., direct lattice resolution obs. of defect struct. 80−107255
Si, 60° dislocation, X-ray diffraction contrast, section topography 78−83819
Si, controlled dislocation formation, struct. density *(Russian)* 80−107244
Si, core structure of glide-set 90° and 30° partial dislocations 80−96523
Si, crack-tip dislocation pattern, X-ray topography *(French)* 80−107253
Si, Czochralski growth, drop form. and crystn. rel. to dislocation struct. 78−2030
Si, diffusion of ^{71}Ge and ^{32}P, effect of dislocation struct. on migration rate 77−51551
Si, dislocation structure, effect of induction heating *(Russian)* 77−21180
Si, edge dislocation struct., lattice distortion and surrounding vacancy distrib. 77−19954
Si epitaxial layer, on Si ribbon substrate, X-ray obs. 77−85102
Si film, polycryst., substruct. 79−23848
Si, HVEM struct. images of extended 60° and screw dislocations 80−59466
Si, ion implanted, complex annealing behaviour of amorphous layers, TEM obs. of defect struct. 80−107299
Si, ion implanted, defect struct., dislocation loops and elongated defects 80−107300
Si, plastic deformation, dislocation density in yield point area *(German)* 78−38720
Si, plastically deformed, dislocation structure with different sample orientation 80−70207
Si, plastically deformed monocrystal, X-ray topographical study *(German)* 78−59813
Si, ribbons produced through capillary action shaping, elec. and struct. characts. 78−47804
Si, screw dislocation networks, TEM study 80−70204
Si single crystal growth, Czochralski method, small-angle dislocation boundary form. anal. 80−89136
Si, snowflake defect due to annealing in H at 1000°C, X-ray topography study *(Chinese)* 80−49227
Si:B, dislocation net form. during annealing 77−51385
Si:Ne(Ar)(Kr), ion implantation damage, annealing, comparative study 79−10867
Si:P, dislocation dissoc. mode obs. by weak-beam TEM 80−107259
Si-Ge heteroepitaxial system, imperfections and morphology, electron microscope and electron diffr. obs. 79−42420
SiC-B eutectic alloys, struct. of crystallising graphite 79−38829
$SiTe_2$, dislocations and stacking fault energy 78−47378
$SmCo_5$, mag. domains structure rel. to crystal defects, electron microscopy 80−103856
SmS, mechanical polishing, stabilisation mechanism for metallic phase on surface 78−60015
SmS, single crystals, crystallographic slip 78−18659
Sn, white, configurations, formation and Burgers vector of coupled dislocations stradlling polygon wall 78−26569
$Sr_{1-x}Ba_xNb_2O_6$, and Nd doped growth of low dislocation density cryst., dislocation struct. 77−40348
Ta, Ta-Re, Ta-Re-N, deformed at 77K, dislocation substruct. 77−32647
Te, c-slip, asymmetry and orientation depend. 77−27888

dislocation structure continued
Te, dislocation density and config. effects on cyclotron reson. absorpt. 79−78526
Ti and Ti-Al (4,6,9 wt.%), X-ray line profile anal. 77−47459
Ti-M-V-Cr-Mo, RMI 38644, shock loaded, age hardening 79−29112
Ti-Ni, reversible shape changes during martensitic transform., dislocation struct. stability *(Russian)* 77−63666
Ti-Ni (51 at.%), plastic deform., two reversible form change effects *(Russian)* 77−8881
Ti-transition metal, transition metal additive effect on struct., specific resistance, microhardness, mech. props. 79−29078
Ti_3Al, cyclic deform., dislocation struct. 78−7003
TiO_2-Ga_2O_3, crystallographic shear planes and defect pair splitting, electron microscopy 77−76425
TiO_{2-x} reduced, crystallographic shear planes, dislocation struct. 80−107175
α-U, autoionic images of dislocation struct., computer interpretation 77−62453
α-U, polycrystalline, compressive deform. at low temps. 77−28856
UO_2, compressed, dislocation substructure obs. *(French)* 78−78461
V, polycryst., struct. changes during deform. *(Russian)* 78−48447
V, rolling textures, microstructure, micro orientation *(Russian)* 79−91663
V, slip geometry and dislocation struct., rel. to degree and temp. of deform. *(Russian)* 78−38717
V, strain hardening, screw dislocations and microtwinning *(Russian)* 80−29971
V-Ta (5 wt.%), strain hardening, screw dislocations and microtwinning *(Russian)* 80−29971
V_3Si, grown-in dislocations, diffr. contrast behaviour 79−86794
V_3Si, phase transition and transition temp., chemical comp. effects, defect struct. exam. 78−18651
W, block boundary dislocation struct. singularities under high temp. steady state creep conditions *(Russian)* 79−90670
W, plasma-sprayed, effect of Si substrate surface conditions and impact velocity of sprayed particles 80−21145
W, powder, subjected to vibratory milling, exam. of plastic deformation, recrystallisation, sintering 80−16234
W single cryst., dislocation effects on thermionic emission and work function 80−76129
W single cryst., high temp. creep and dislocation struct. 80−71715
W, single crystals, creep deformed, Burgers vectors, block boundary struct. *(Russian)* 79−77603
W, stripe field-ion contrast form., dislocations effect 78−18652
W, vapour deposited, dislocation struct., rel. to texture *(Russian)* 80−65394
W wire, cold drawn, dislocation processes occurring during tensile testing *(Hungarian)* 77−48450
W-Th, atomic structure of grain boundaries 79−33003
WC-Co and WC-Co-TaC-TiC-NbC cemented carbides, microstructure, high temp. deformation, uniaxial plastic compression 80−40451
YIG, deformed at high temp., subgrain boundaries and dissociations of dislocations, TEM obs. 79−90658
YIG, plastically deformed, TEM, dislocation Burgers vectors 77−11557
Y_2O_3, dislocation and plasticity dissociation 80−107247
Y_2O_3, plastically deformed, dislocations obs. by TEM *(French)* 78−51545
Zn, control after prep. low angle boundary decomp. *(Russian)* 78−3142
Zn crystal, $\{11\bar{2}2\}\langle 11\bar{2}3\rangle$ slip system, deform. stress, dislocation density depend. *(Russian)* 80−103353
Zn, dislocation interaction with 'forest' dislocation, TEM exam. 77−89440
Zn, dislocation struct. stability, effect of deformational and thermal annealing 78−64567
Zn, growth from melt, conditions influencing dislocation struct. *(Russian)* 80−97424
Zn, isothermal annealing effect at 400-410°C, on dislocation struct. in monocrystals *(Russian)* 79−20082
Zn, work hardened crystal, jump-like plastic deform., dislocation struct. instability 79−96094
Zn-Al (0.4 wt.%), intergranular slip during in situ superplastic deform. 80−96538
ZnSe, twinning on melt-growth under pressure 77−80515
ZnTe:Cu, voltage depend. on precip. contrast 79−1433
Zr base alloys, irradiation growth, dislocation model 78−51595
α-Zr, polycrystalline, cyclic deformation *(Japanese)* 78−68757
Zr, structural changes during plastic deform. *(Russian)* 77−8880
Zr-Nb-Mo-Re, alloying effect on dislocation core struct., determ. by discrete lattice modelling 78−30618
Zr_3Al, deformed and irrad., lattice defects obs., superlattice dislocations and defect clusters 80−107261

dislocation translation *see slip*

dislocations
For pipe diffusion, see diffusion in solids. See also dislocation ......
see also Bordoni effect; Cottrell atmospheres; disclinations; edge dislocations; grain boundaries; screw dislocations
actinide carbides, lattice defects and rel. to phys. props., review 77−27874
adhesive joint strengthening 77−89659
adsorbed monolayers, dislocation geometry 79−23604
alkali halide crystals, dislocation internal friction, orientation depend. 78−48439
alloy, cryogenic, creep, review 80−104222
alloys, Ll_2, superstructure, dislocation link strength and strain hardening at high degrees of deform. *(Russian)* 78−39792
alloys, precipitation hardened, dislocation struct. *(Hungarian)* 79−55746
amorphous structure model *(Japanese)* 79−42065
anelastic relaxations and magnetic aftereffects in solids, conf., Katowice, Poland (Jan. 1978) *(Polish)* 79−96072
anisotropic continuum theory 79−73162
anisotropic crystals, long-wave vibrs. localised near dislocations 80−59603
anisotropic elastic media, appl. of geometric theorem 78−30619
anisotropic media, elasticity theory, book contrib. 80−39091
anthracene, γ-irradiation influence on defects, luminesc. study *(Russian)* 80−55185
antiferromagnet, dislocations producing domains and disclinations *(Russian)* 77−32213

dislocations continued
antiferromagnet, phase transformations in strong mag. fields, mag. moments collapse, strengthened magnetoelastic links *(German)* 78−68227
antiferromagnet, rel. to domains *(Russian)* 77−51919
atomic dislocation modelling, flexible boundary conditions and nonlinear geometric effects 78−75667
atomistic computer experiments of point and extended defects 78−30610
austenite solid soln., decomposition, effect of struct. of initial state *(Russian)* 77−48442
austenitic stainless steel, type 316, anelasticity and creep transients 78−84880
behaviour at advancing grain boundary during recrystallisation 77−7734
behaviour in fatigue 77−24352
bis(p-toluene sulphonate) diacetylene, partially polymerised, defect-induced absorpt. and fluoresc. 77−44030
α-βbrass, interface struct. of two-phase bicrysts. made by solid state diffusion couple method, X-ray Laue and TEM study 79−28214
α-brass, metallographic and fractographic study of void formation during creep 80−16449
brittle fracture, elastic energy momentum tensor and crack propagation 80−69741
brittle fracture, statistical theory, dislocation mechanism, crack propagation *(Chinese)* 80−106755
brittle solid, atomically sharp cracks, TEM study 80−71729
Burgers' vector of boundary dislocation 78−43025
Burgers circuit, Volterra process and homotopy groups 77−62528
Burgers circuits associated with generalized distortions 80−2014
Burgers vector, determ. by weak-beam image in HVEM *(Japanese)* 80−70199
Burgers vector determ. from electron microscope images 80−2030
Burgers vector identification for grain boundary dislocations from electron microscopic images 80−19807
central-force interatomic pot. construction from whisker deform. data, crystal defect stress investigation 79−56103
characterisation by TEM, appl. of computer simulation 80−19679
charged particle motion in curved axial channel, effects of dislocation 77−55314
chemical potentials of structural elements of compounds and face or dislocation specificity, thermodynamic parameters 80−96514
cholesteric mixtures, quasithermal crystn. 80−92652
coatings, defects and their effect on props. 80−39474
collective vibrations of a dislocation wall 80−70346
composites, adhesion between two crystals, theory 80−104417
compressed crystals, dislocations and point defects *(Russian)* 78−75666
computer simulation, of dislocations, methods in X-ray topography 79−23484
conference, Masnuy-St-Jean, Mons, Belgium, Oct. 1979 80−82570
continuous plastic cracks in ordered alloys, discrete dislocation analysis 78−80625
contrast in X-ray synchrotron topographs 77−76408
contrast simulation, numerical calc. in X-ray transverse topographs 77−84572
corundum, packing errors in structure, X-ray diffr. obs., charact. features 79−46655
Cosserat's medium, linear and surface defects, stresses 78−83813
covalent or ionic-covalent crysts., dislocation-free contact 80−80096
crack behaviour, discrete dislocation analysis 78−22788
crack propagation, computer simulation 80−59573
cracks discrete dislocation anal. 79−64590
creep, dislocation, diffusion controlled 79−46745
creep, dislocations, diffusion controlled 79−46744
critical resolved shear stress, influence of finite size of impenetrable obstacles 78−2120
crystal growth, dynamic computer models 80−103284
crystal melting, pre-melting near dislocations 77−76524
crystal melting and glasses, dislocation theory 79−99298
crystal under high pressure, dislocation theory 78−55870
crystals, with diamond struct., vacancy formation energy rel. to plastic state transition temp. *(Russian)* 80−19795
crystals and dislocations, spontaneous breakdown of spatial translation invariance *(German)* 79−7653
cubic crystal, ⟨111⟩ line force, anisotropic elasticity theory 79−55741
4-cyano-4-n-cyanobiphenyl, smectic A mesophase, plasticity anal., defects motion, Grandjean wall form. 78−91227
cyclic function, displacement description of dislocation lines 80−10549
cyclic functions, displacement description of dislocation lines 80−10548
cyclopentane, extreme case of dispirated diamond, Volterra-Weingarten dislocations 77−84747
Debye-Sears cell lattices, DSC-1 and DSC-2, computation of coincident and near-coincident cells 77−84746
dechannelling, by dislocations *(Japanese)* 80−34106
defect diffusion, radiation effects 78−87827
diamond, dislocation growth degree of supersaturation determ. 80−88145
diamond cathodoluminesc. at dislocations 79−47524
diamond lattice, Burgers vestor of grain boundary dislocations *(Russian)* 79−73176
diamonds, topographically identifiable sources of cathodoluminescence 77−55836
dielectric crystal, dislocation detection by divergent polychromatic beam method 77−35568
differential geometry of deformed crystals 80−19867
diffusion length and lifetime meas. and assessment by SEM 80−96902
Dingle factor, dislocation pot. rel. to de Haas-van Alphen effect *(Russian)* 78−30885
disclinations, rel. to dislocations 78−22717
disclinations and dislocations in continuum mechanics model, geometry and forces *(German)* 78−34511
discrete models *(Polish)* 79−14808
dislocation Burgers vector exam., birefringence method 78−30626
dislocation reactions *(Hungarian)* 79−55745
displacement field prod. by dislocations in elastic half-space *(Russian)* 79−51107
displacive transformations, connection to dislocations and solitons 79−82300
dissociated, stacking fault width determ. from 224 reflections with g.b=0 78−59722
durene, aldehyde doped cryst., photolysis 10 to 20K, physical and chem. defects 79−52721
dynamic behaviour, of dislocation groups, of opposite sign emitted from a stressed source, computer simulation 80−6406

dislocations continued
dynamical theory of dislocation contrasts *(Hungarian)* 79−55744
early work on imperfections in crystals, and forerunners of dislocation theory 80−62450
Earth mantle peridotites, stress estimates from structural studies 78−69330
elastic crystal, relationship between dislocations and surfaces 80−24446
elastic displacement fields, around dislocation outcrop, X-ray plane wave obs. 80−39084
elastic field of dislocation segment in 3D 79−60365
elastic half space, dislocation layers and crack problem 80−33533
elastic half-space, dislocations and extended sources 79−35562
elastic interaction with disclinations and dispiration elastic energy 79−19248
elastic isotropic micropolar continuum, stress and couple stress fields prod. by circular dislocations 79−97209
elastic theory, book 80−36784
elastically nonlinear media, expressions for forces acting on dislocations *(Russian)* 79−51106
elasticity theory, book contrib. 80−39090
electron micrograph, computer simulation for crystal defect identification 78−30525
electron microscopy imaging, approx. for dynamical calcs. of microdiffr. patterns 78−26393
electron solid, two-dimens., defects and implications for melting 80−39076
electron-microscope image of dislocations, in anticlassical scattering region, dislocation axis contrast 80−38877
elemental semiconductors, hybridisation effect on dislocation electronic states 78−51936
elimination by recrystallisation *(German)* 78−51559
epitaxial film, interfacial boundaries and transition regions *(Russian)* 80−103596
exciton absorption spectra, dislocations effect on band profile 80−16070
fatigue crack, blunting and growth, prediction of threshold stress intensity using dislocation model 78−79662
fatigue crack, dynamic treatment of growth *(Japanese)* 78−34084
fatigue cracks, dislocation model, threshold stress intensity 78−18244
FCC alloy, hardening by spinodal modulated structure 80−60874
FCC crystals, deform. faceting of large-angle grain boundaries TEM 77−65984
ferrite, transform. kinetics, grain size, alloying element effect, carbide precip. 80−93560
ferromagnet, local variation in mag. anisotropy due to linear defects *(Russian)* 78−68214
ferromagnetic domain theory, quasi-dislocation theory appl. *(Japanese)* 80−60358
ferromagnets, easy plane, containing dislocations, static props. 79−95626
ferromagnets, spin wave excitation due to parallel pumping, mag. impurity interactions *(Russian)* 80−80497
Fick's equations solutions for impurity diffusion, dislocations, interstitials, vacancies 80−70469
field ion microscopy, developments, lattice imperfections 79−67445
finite solid, dislocations, disclinations and grain boundaries 80−2019
finite two-phase bodies, response to internal and external stresses, geometrical considerations 80−24741
fission reactor fed, effect of solid fission products and dislocations on swelling and fission gas release during fast overpower transient 78−8917
fission reactor materials, radiational growth due to diffusional anisotropy 79−71897
fragmented structures, dislocation and disclination kinetics *(Russian)* 80−79788
Frenkel-Kontorova system, discreteness effects, perturbation formalism, Peierls pot. and kink vel. reduction 80−34001
friction stress, and back stress from hysteresis loops, dislocation behaviour in fatigue 80−3176
n-GaAs:Te, interaction of positrons with dislocations 79−99974
gauge invariance in field theory formulation 79−27980
gauge transformations admitted by the equations of defect dynamics 79−27981
geometrical theory, four-dimensional 79−84954
grain boundaries, energy and fine struct., surface dislocation model 79−28002
grain boundary crack nucleation, and growth under low cyclic stresses, dislocation mechanism 80−19811
grain boundary dislocation spreading 78−38729
grain boundary dislocations, appl. of field-ion microscopy 79−73170
grain boundary dislocations, effects on grain boundary processes of the steps in boundary plane 80−79785
grain boundary dislocations, impurity influence on spreading temp. 79−77609
grain boundary energies, discrete dislocation anal. 79−51115
grain boundary surface dislocations, minimum energy configuration 80−49235
grain boundary unified theory, dislocation content 79−7616
graphite, elastic constant softening 79−51190
graphite fibres, elec. resist., mech. props. after nitration 77−32698
N-p-heptyloxylbenzylidene-p-heptylaniline, liq. cryst., dislocations obs. in smectic A and C mesophases 78−91230
heteroepitaxial layers, dislocation structures, problems of formation 80−15100
homotopy groups of condensed matter physics 78−63752
ice, dislocation creep, creep deform. predictions 78−19815
ice, dislocation processes and tensile crack formation in glaciers 78−20438
ice Ih, dislocations, effect on physical and mechanical props. *(French)* 77−55287
III-V compounds, piezoelec. coupling and dislocations 79−91377
III-V semiconductor, temp. distrib. around dislocations, due to Joule heating, calc. 78−71734
III-V semiconductors, manifestation of local vibrs. of dislocations in IR spectra 78−88339
image contrast, in TEM, dynamical analytical theory 79−95014
image contrast in electron microscopy and X-ray topography, elastic anisotropy influence 78−26573
images produced by piezobirefringence, simulation 78−30521
Inconel 600, S penetration leading to sulphide form. *(French)* 79−74306
n-indecyl-p-azoxy-α-methyl cinnamate, dislocations obs. in smectic A and C mesophases 78−91230

dislocations continued
insulating crystals, piezoelec. potentials of dislocations 80−20594
insulator, lattice thermal resist. due to core dislocations 80−29231
insulator, with dislocations, lattice thermal cond. 77−59157
interface, dislocation model for loss of coherence 78−6057
interfacial energy, surface energy, surface tension and lattice friction relation 79−69341
ionic electret behaviour, ionic thermoconductivity technique 80−7274
isotropic crystals, ang. glissile dislocations, method of moments theory and electron microscope obs. *(Russian)* 80−24449
isotropic medium, elastic vibrations localised near dislocation 80−79897
kinetics of continuously distributed dislocations in SCF approx. *(Russian)* 79−14806
lattice defects, characterisation 80−103320
lattice dislocation calcs., classical elastic line force solution 78−22718
lattice imaging by high resolution electron microscopy 79−77467
lattice transformations and dislocations, book contrib. 80−107242
layers, external crack extension condition derivation 79−68657
light scattering by excitons localised at dislocations 78−60479
liquid crystal, lyotropic, parabolic focal conic struct., disclination-dislocation relation 79−27909
lithium formate monohydrate, thermal dehydration, dislocation effects 80−3331
localised states of order parameter close to dislocation *(Russian)* 78−14905
martensitc transformations, inheritance of dislocations *(Russian)* 79−52211
melting, dislocation generation, anharmonicity and solitons 78−79746
melting, dislocation model, theory 78−83923
melting, dislocation theory 80−65198
melting, two-dimens., dislocation-mediated theory predictions, light scatt. use as probe 80−92651
melting in two dimensions, Kosterlitz-Thouless dislocation model 79−7677
melting mechanism, dislocation theory 77−35674
metal, BCC, viscous brittle transition during fracture, dislocation model 77−62582
metal, dislocation models of plastic deformation at elevated temps. 77−70139
metal, dislocations rel. to electron gas thermodynamics at $2^1/_2$th order transition *(Russian)* 78−51910
metal, effect on bulk material props. 80−34004
metal, impurity atoms, diffusion in region of dislocations *(Russian)* 80−24670
metal, microstructural evidence supporting SIPA creep mechanism 79−61679
metal, NDT using positron annihilation technique 78−3294
metal, US attenuation, quantum oscills. with dislocations under press. *(Russian)* 80−88273
metal matrix fibre reinforced composite, high tem. appl., creep, dislocation processes 77−48369
metal powder, method for TEM study 80−84038
metallic glasses, structures based on disclination-dislocation model 79−82159
metals, dislocation cell diameter rel. to free energy during creep 79−91756
metals, FCC, slip dislocation reactions at coherent twin boundaries, effect on work-hardening 79−1431
metals, FCC, twist boundaries, struct. invest. using computer simulation technique 80−84185
metals, phys. model of process of loss of mechanical stability and neck formation *(Russian)* 78−6969
metals, pure and alloyed, grain boundary relaxation model, *(Russian)* 80−39107
metals, research at Birmingham, (1945-55) 80−62444
metals, scoring resistance under dry friction *(Russian)* 79−99267
metals, single phase FCC, cyclic deform. long range stress changes 80−54308
metals, stress transients, at changes of electron drag during plastic deformation 79−61677
metals, structural state and physical similarity criteria *(Russian)* 79−52298
metals, with lattice of different types, theory of adhesion, incl. dislocations *(Russian)* 78−7165
mica glass-ceramics, near perfect shape-memory solid 77−48492
micromechanical modelling of interacting creep processes in polycrystals 78−30205
micropolar continuum, isotropic, elastic fields of dislocations and disclinations 77−68971
microscopic derivation of theory of extended objects in crysts. 79−37704
microscopic formulation of a lattice-defect model 80−44208
microscopic theory 77−80508
mineral, Burgers vector characterisation method using electron microscope contrast simulations 80−109141
minority carrier recombination at surfaces, dislocations and microdefects, luminesc. evaluation 78−6769
model system, two dimensional, computer calc. 78−30621
molecular crystal, dislocation excitons 79−65388
NaCl, dislocation charge photostimulated variation kinetics *(Russian)* 80−79806
naphthalene single crysts., surface active substances effect on plastic flow 80−44248
$NH_4H_2PO_4$, cryst. growth from aqueous solns., dislocation groups in (100) faces, kinetics 79−74072
Nimonic 80A, order hardening, comparison between revised theory and expt. 80−93565
nonlinear elastic problems, book contrib. 80−39093
nuclear oxide fuel element in fast overpower transient, effect of solid fission products and dislocations 80−623
olivine in Japanese peridotites, dislocation densities rel. to uppermost mantle differential stress lateral var. 80−98275
orbitally degenerate interacting impurity thermodynamics, stress field depend. due to point defects, dislocations 79−69477
ordered alloy, with $L1_2$ structure, dissociation of superdislocations and plastic deform. mech. *(Russian)* 78−52909
ordered regions near macroscopic defects and percolation phase transform. in crystals *(Russian)* 80−92665
Peierls force of boundary layer, theory 80−10552
phonon conductivity correction due to three phonon normal processes in presence of dislocations 80−15318

dislocations continued
- piezoelectric crystal, Gulyaev-Blustein wave excitation by developing defects *(Russian)* 78—56030
- piezoelectric powders, explanation of polarisation echo by dislocation mechanism *(Russian)* 77—36181
- pipe diffusion, calc. 79—82374
- plastically deformed compound semiconductors, electronic transport and opt. props. of dislocations 80—80212
- plasticity, Cosserat continuum, non-Reimannian geometrical theory of imperfections 80—53639
- plasticity, polycrystalline, probabilistic approach, appl. 78—26622
- plasticity, polycrystalline, probabilistic approach 78—26621
- PMMA, plastic deform. by crazing *(Japanese)* 80—93619
- point source modelling for extended source stresses 77—72609
- Poisson brackets, nonlinear hydrodynamics eqns. in condensed matter physics 80—54296
- polycarbonate, plastic deform. by crazing 79—52310
- polyethylene, crystalline, steric struct. modelling of end defects 80—6371
- polymer, crystalline, in hydrostatic tension, plastic deform. of model 77—59870
- polyoxyethylene dodecyl ether/water system, lamellar liq. cryst., solubilized hydrocarbon effect on struct. and dislocation pattern 79—94885
- post yield solutions for fracture mechanics analyses of cracks emanating from elliptic holes 79—68643
- pressurised metal, quantum oscillations of thermodynamic props. *(Russian)* 79—86899
- quantum field theory of crystals and extended objects, review 79—42164
- α-quartz:Al, γ-irrad., thermal cond. below 10K 79—51320
- quartz, Brazil twins, twinning prod. by successive shears 79—19263
- quartz, defects growth, study by X-ray diffr. topography *(French)* 80—39095
- quartz, dislocations, electron irrad. induced vitrification 80—107252
- quartz, dissociated 'a' dislocations, TEM exam. 78—47379
- quartz, natural, gamma-irradiated, stress effect on thermolum. sensitivity 80—11482
- quartz grains in Moine thrust zone, deformation-induced microstructs. rel. to differential stress 80—85652
- quasi-Newtonian force 78—63765
- rare earth metal based compounds, spin glasses 80—50132
- recovery of dislocations, in subgrains and subgrain coalescence 77—76398
- refractory alloys, creep mechanism and struct. changes *(Russian)* 79—52299
- RHEED, Bragg diffraction imaging of cryst. surface defects 78—9920
- rocks, microfracture *(Japanese)* 78—7020
- rocks of crystalline basement, dislocations rel. to ductile deform. zones and mylonites 79—53344
- sapphire, dislocation obs. by weak-beam TEM 77—47461
- sapphire :Ti^{4+}, deformation history effects on precipitation hardening 79—83209
- scattered wave functions of dislocated lattices 78—6326
- section topography as single-cryst. interferometry 78—47208
- seismology, use of dislocation theory, book contrib. 80—109119
- SEM, crystalline contrasts from defects in thin and thick specimens 78—22611
- SEM, fitted with field emission gun, for cryst. defect obs. *(French)* 77—35452
- SEM dislocation imaging, electron channelling appl. 80—70214
- semiconductor, defects, electron microscopy study 79—95021
- semiconductor, quenching of luminesc. by charged defects 78—23531
- semiconductor, recombination of nonequilib. carriers in presence of dislocations 79—82607
- semiconductor, SEM charge-collection images of dislocations, contrast and resolution 79—46662
- semiconductor, SEM electron beam induced current images of dislocations and stacking faults, computer simulation 80—70198
- semiconductor, TEM/SEM observations comparing diffr., elec. and luminesc. contrast from dislocations 78—38714
- semiconductor, tetrahedrally coordinated, dislocations, symposium, Hunfeld, Germany (Sept. 1978) 79—82214
- semiconductor, tetrahedrally coordinated, effect of disorder and long range strain field on electron states 79—82545
- semiconductor, tetrahedrally coordinated electron states associated with dislocations 79—82544
- semiconductor crystal defect obs. by TEM *(Japanese)* 77—84752
- semiconductor CW lasers, DH, with specific growth defects, degradation characts. 78—13713
- semiconductor devices dislocations and microplasma sites, STEBIC/STEM/EELS correlation 80—96528
- semiconductor epitaxial and diffusional interfaces, obs. of individual misfit dislocations 79—82222
- semiconductor light source degradation, review of recent expts. 78—82970
- semiconductors, appl. of analytical techniques for observation 80—73546
- semiconductors, recombination, conference, Southampton, England (Aug.-Sept. 1978) 79—38087
- semiconductors, zincblende struct., deep levels associated with 60° dislocations *(French)* 80—29352
- shift-type packing defects, involving dislocation representations, influence on diffr. pattern 80—107239
- Si:As$^+$(P$^+$)(Sb$^+$), removal of misfit dislocations by laser irradiation 79—74024
- Si:B(p), dislocated crystals, microwave cond., localised electron energy spectrum 78—14694
- Si, X-ray step scanning section topography, lattice imperfection characterisation, automatic Bragg angle control 79—60221
- SIPA irradiation creep, material with preferred direction for dislocation Burgers vector, cold worked 79—20118
- smectic C liquid crystals, elasticity and defects 78—91233
- smectic liquid crystals, acoustic emission, appl. to defect dynamics study 78—91232
- solid solution alloys, creep behaviour at intermediate stresses and creep power law breakdown 79—57058
- solid state physics, 1933-40, contrib. of Sir Nevill Mott 80—57055
- solid state physics, historical aspects, symposium, London, England (Apr.-May 1979) 80—56999
- Somigliana dislocations and pure inclusions, internal stresses 78—30615
- SOS films, cryst. quality improvement by Si ion channelling, annealing 80—44222
- spectroscopic techniques, with STEM for electronic props. of defects and impurities in semiconductors 79—14812

dislocations continued
- spinel-type lattice, determ. of stacking faults, diffr. effects, in presence of dislocations 77—55290
- stacking fault energy calc. from fault pairs, threefold extended nodes *(French)* 79—42081
- state of art review, book contrib. 80—39089
- stationary lattice defects as sources of elastic singularities 78—59800
- steel; low alloy, high strength, hot compression dynamic precip. and coarsening of Nb(CN) 80—97514
- steel, AISI 316, fast reactor irradiated, solution treated, struct. 77—69008
- steel, austenitic, Ni-Cr, neutron-irradiated solute segregation and void swelling 79—60407
- steel, austenitic and martensitic, structural sensitivity of Bauschinger effect *(Russian)* 79—52303
- steel, austenitic stainless, creep deform. effect on struct. of twin boundaries 79—8332
- steel, austenitic stainless, dislocation transport and H_2 embrittlement 80—30087
- steel, austenitic stainless, extrinsic grain boundary dislocations, effect on $M_{23}C_6$ precipitate nucleation 79—51118
- steel, austenitic stainless, grain boundary struct. changes during initial stages of recrystallisation 77—36559
- steel, C (0.2 and 0.45 wt.%), spheroidization at 680 to 690°C, struct. changes *(Russian)* 78—15431
- steel, cryogenic, creep, review 80—104222
- steel, H embrittlement mechanism, microcrack formation, dislocation model *(Russian)* 80—65143
- steel, high Nb, HSLA, low temp. fatigue props. 80—40490
- steel, low C, 10Kh2G3M, development of plastic deform., slip and dislocation struct. *(Russian)* 79—15722
- steel, low C, cold rolled sheet, Cu effect on recrystallization texture *(Chinese)* 79—74173
- steel, low C, hysteresis loop behaviour under fatigue load, dislocations model 79—74197
- steel, plastic deform. effect on third-order elastic moduli, dislocation anharmonism *(Russian)* 80—50786
- steel, stainless 316, recovery by annealing of creep produced dislocations 80—11702
- steel, V, precip. and transform. kinetics, effect of N 80—97485
- STEM microdiffraction patterns, effect of cryst. defects 78—22610
- STEM of cryst. specimens, image contrast *(German)* 77—24251
- substructure strengthening mechanisms, dislocation charact. 77—84761
- superconducting states, impurity effects *(Russian)* 80—11131
- superconductor, flux pinning summation curves 78—52165
- superconductors, plastic deformation, Cooper pair scatt. model 80—39709
- superconductors near critical temperature at acoustic frequencies, internal friction 80—100305
- tensile crack, dislocation model of plastic zone 77—84837
- TGS, autostabilised state, elec. second harmonic generation 80—103921
- TGS, pure and Cu doped, growth from soln., dislocation density 79—52096
- TGSSe, autostabilised state, elec. second harmonic generation 80—103921
- theory, rel. to X-ray topography data 78—64254
- thermal vibrations, mean-square displacement, double-time Green function technique 79—19345
- thermodynamic force on dislocation under pressure *(Russian)* 77—76400
- thermodynamics and thermal activation of dislocations, book contrib. 80—107241
- thermomechanical treatment on struct. and props. 79—29109
- thin crystals and films, nondestructive microhardness testing of near-surface layers 80—71829
- thin films cryst. defects obs. in SEM *(French)* 77—31662
- time-defect densities in tilt boundaries of f.c.c., b.c.c., h.c.p., crystals 78—2142
- topological theory of defects in ordered media 79—93072
- transition metal, d-series, distance separating dislocation, determ. by positron-electron annihilation method 79—14811
- TTF-TCNQ crystals, X-ray topographic study of cryst. perfection 80—96525
- twin interfaces, obs. using relative translations of adjacent crystals in TEM 78—75675
- two-dimensional space, differential geom. of dislocations, appl. to shell deform. 78—22719
- two-phase interfaces, differential geometry 77—51388
- two-phase interfaces, non-metric geometry 78—14343
- two-phase structures, high-temp. deform. 78—68738
- unifying concepts in the theories of elasticity, plasticity, and dislocations 79—77599
- vacancy formation energy and vibr. freq. of atom in dislocation core region 80—103322
- vacancy loss during quenching of low dislocation density cryst. 78—75656
- void swelling, effect of recombination of sink strengths in rate theory 79—14851
- wedge-shaped crack plastic zone, superdislocation model 79—94557
- whisker growth by vapour-liquid-solid mechanism, book contrib. 79—69383
- Wigner solid, two-dimens., melting temp., quantum effects 80—88491
- Wigner solid, two-dimens., melting temp. in strong mag. fields, quantum effects 80—88492
- X-ray, and neutron small-angle scattering, structural defect studies, review 79—10752
- X-ray and neutron section topography, cryst. dislocation and planar defect images, book contrib. 78—42863
- X-ray interferometer, LLL type, interfering beam phase rels. 80—90973
- X-ray plane wave topography, observation of dislocation in Si single cryst. 78—91342
- X-ray projection topograms for crystal with dislocations, calc. 79—86647
- X-ray projection topograph, residual contrast of dislocation, depend-on sign of Burgers vector 79—14638
- X-ray reflections, broadening, from cryst. containing excess of dislocation walls of same sign *(Russian)* 79—7509
- X-ray topography, contrib. of diffr. to the contrast of dislocations 79—23485
- X-ray topography, techniques and interpretations 79—67454
- yield surfaces, dislocation mech. study 77—14916
- Ag film, twin boundary faceted struct., struct. coarsening due to dislocations *(Russian)* 79—99215
- Ag, finite dislocation elements, isostress contours 78—71735

dislocations continued
- Ag plastically deformed crystal, exam. of dislocation dynamics during strain rate changes 78—88506
- Ag, plastically deformed crystals, exam. of dislocation dynamics during strain rate changes 78—88507
- Ag-Au(Cd), deviations from Matthiessen's rule 78—10420
- Ag-Zn (30 at.%), neutron irrad., at. mobility enhancement, Zener relax. meas. 77—1157
- AgBr:Sr, stress induced anomalies in internal friction, logarithmic decrement 79—66095
- Al alloy D16, supersaturated solid soln., decomp. process, electron microscope obs. and acoustic anal. *(Russian)* 79—15650
- Al alloys, thermomech. treatments, effects on microstruct. 80—100858
- Al and Al-Mg alloy N4, irradiation with 100 and 400 keV Al ions, obs. and analysis of damage struct. 77—4133
- Al, deformed, thermal recovery, microstruct. and stress-strain relations 80—16325
- Al, deformed surface layer, block misorientation 79—99405
- Al, dislocation activation, using UHV electron microscope const.-load tensile device 78—11462
- Al film, dislocation observation by electron microscope using convergent beam *(French)* 80—96532
- Al, film, single cryst., defects, residual gas effects, TEM obs. 77—39587
- Al high-strength alloy constitutive eqns. and high-velocity deformation *(Japanese)* 79—79029
- Al, melting transition, TEM 77—80603
- Al, plastic deform. effect on third-order elastic moduli, dislocation anharmonism *(Russian)* 80—50786
- Al, polycrystalline, acoustic emission energy release, grain size and flow stress depend. 80—11722
- Al sheets, dislocation obs. at high temp., annealing effect *(Japanese)* 80—34003
- Al single crysts., elastoplasticity, dislocation model, work hardening, tensile tests, stress/strain curves *(Japanese)* 77—52410
- Al, thermal cycle annealing of single crystal, subboundary obs. 77—55992
- Al, yield surfaces from dislocation mechanics 77—14917
- γ'-Al-Ag (15 wt.%), dislocation splitting mechanism, cessation above critical temp. 78—26572
- Al-Cr(Mn), cold-worked and homogenised, precip. kinetics, impurity resist. and TEM meas. 77—16596
- Al-Cu (3.93 wt.%), planar defects within theta precipitates 77—16583
- Al-Cu-Mg type 2036, thermomech. treatment, flow stress anal., effect in mech. props. 80—93584
- Al-Cu-Mg-(Ag), effect of addition on fatigue microstructure relationships 80—40483
- Al-Cu-Ni, alloy RR 350, θ'-hardened, deform. induced microstructural instability, high temps. 80—16321
- Al-Cu(Mg), low freq. internal friction during plastic deform. *(Chinese)* 80—103420
- Al-Mg (4.4 wt.%), Burgers' vector of boundary dislocation, electron microscope obs. 78—43025
- Al-Mg-Si, nucleation and precipitation growth on dislocations, electron microscope studies 80—3064
- Al-Mg-(Ag), effect of addition on fatigue microstructure relationships 80—40483
- Al-Zn-Mg, oriented growth of precipitates on dislocations, model 80—108448
- Al-Zn-Mg (3.87, 1.79 wt.%) TEM exam. of early stage precipitation, on dislocation lines 79—4972
- Al-Zn-Mg (6,3 wt.%) high-strength alloy, dislocations distrib., corrosive environment influence *(Russian)* 79—52442
- AlGaAs-GaAs lasers, defects and degradation *(Japanese)* 79—31899
- $Al_xGa_{1-x}P$, LPE, crystallographic obs. and electrolum. 80—88445
- α-Al_2O_3 CVD and Czochralski grown crysts., imperfection anal. comparison 79—78868
- Al_2O_3, dislocation creep, creep deform. predictions 78—19815
- Al_2O_3, surface microstructural changes due to reduction by C *(Russian)* 80—100378
- Al_2O_3.Si kyanite, dislocation dissociation 77—76412
- $Al_2(SO_4)_3$-$K_2SO_4.2PH_2O$, rel. between etch pits or growth hillocks and dislocations on (111) faces 79—77602
- Au, polycrysts., dislocation relaxation under high pressure 79—77605
- Au-Ag (35 at.%), dechannelling of energetic He ions at dislocations 80—70275
- BaF_2:La^{3+}, relaxation processes, studies by ionic-thermocurrent techniques 79—69769
- Bi, polycrystn., cold worked, plastic deformation and stored energy, dislocation characts. 79—43348
- $CaCO_3$, calcite, form of end of free elastic twin *(Russian)* 80—6416
- $CaCO_3$, with perfect struct., temp. depend. of rate of twinning 80—10561
- $CaMg(CO_3)_2$, dolomite, partial dislocations and stacking faults obs. 78—3761
- Cd, single cryst., Burgers vector determ. of perfect dislocations obs. by X-ray topography 79—37711
- $CdCr_2Se_4$ film, electron irradiated, struct. 79—15032
- CdI_2, polytypism, review 77—11498
- CdS, characts. of interaction of light with dislocations 78—2137
- CdS, dislocation effects on radiative recombination processes 79—8186
- CdS, dislocation emission, photoluminesc. spectra 80—16084
- CdS, dislocation structural optical absorpt., plastic deformation *(Russian)* 80—34959
- CdS, photoplasticity and photocond., excitation energy conc. near dislocations, hardening 77—24346
- CdS, stress-induced photolum. bands, photocond., rel. to dislocation electron states 80—25447
- CdS-Ge heterojunction, grown by chemical transport, props. 77—4422
- CdS(Se), small-angle boundaries, SEM obs. 80—24456
- CdS(Se), with dislocations, optical props. 79—83001
- CdS(Se)(Te), charged dislocations, flow of charge with plastic deform. 80—85010
- CdSe, recombination mechanism at dislocations, photoluminescence 80—103993
- n-CdTe, cathodoluminescence microscopy obs. of dislocations, compared with etch pit pattern 79—69105
- n-CdTe, photolum., plastic deform. effects 79—15509
- CdTe:In precipitation and out-diffusion of solute during cooling 80—100840
- $Cd_yZn_{1-y}S$-Cu_2S, heterojunction interface double layer, dislocation field, charge compensation 79—7855

dislocations continued
- Co-Ni-Cr-C, carbide precipitation 79—29065
- Co-V alloy system, Co rich, low temp. phase, electron microscopy 77—84766
- Cr coatings, electrodeposition, conditions rel. to H_2 conc., internal stresses 77—1933
- Cr, specific heat of strained and annealed samples 79—38331
- CsI crystals, relation of struct. and bond type to slip geometry 80—88165
- Cu, Borrmann transmission topography, for quantitative depth meas. of dislocations 79—86795
- Cu, cementation, characterisation of nucleation and growth from aq. soln., TEM and SEM study 79—28972
- Cu complex, bis-(alkylammonium) (11) tetrachloride, perovskite, lattice perfection 78—87633
- Cu crysts., thick imperfect, dynamical X-ray diffr., topographic effects 77—68898
- Cu, elastic modulus and internal friction during plastic deform., dislocation props. determ. 80—35244
- Cu electrolytic form. by electrodeposition, structural defects 77—39749
- Cu, grain boundaries, intrinsic struct., electron diffr. anal. 80—84186
- Cu, nucleation and growth of oxidation zones during diffusional creep *(Russian)* 79—52431
- Cu, plastic deformation, formation of double twist boundaries *(Russian)* 77—81295
- Cu single crystals, in high temp. creep, meas. of internal stress 78—80608
- Cu single crystals, neutron irradiated, secondary slip 80—88161
- Cu, zigzag stress-induced, X-ray topography obs. dislocations 79—99205
- Cu/Ni double layer evaporated film, misfit dislocation effect on strength *(Japanese)* 79—42425
- Cu-Al, dislocation core cut-off parameter, estimation from stacking fault nodes 80—103370
- Cu-Al(Au)(Ga)(Ni)(Pd)(Rh)(Zn) (4 at.%), anneal hardening mechanism 80—60879
- Cu-Au(Ni)(Zn), elastic modulus and internal friction during plastic deform., dislocation props. determ. 80—35244
- Cu-In, thermally cycled, effect on mech. props. and microstruct. 79—4987
- Cu-Ni, nucleation and growth of oxidation zones during diffusional creep *(Russian)* 79—52431
- Cu-Si (6.5 at.%), plastic deformation, HVEM study *(French)* 80—66605
- β_1-Cu-Zn mixed crystal, metastable structural Umklapp process, isothermal phase transform. *(German)* 78—22798
- Cu-Zn-Al, internally faulted martensite, TEM obs. 78—3124
- α-Cu-Zn(Al) fracture behaviour, effect of deform. temp. and alloying content *(Japanese)* 79—20159
- CuAu, exam. of streaming due to intrinsic fluctuations 79—11602
- $CuFeS_2$, natural chalcopyrite, defect struct., TEM 77—62535
- β(CuNi)Zn alloys, effect of normal stress on $\{112\}$ $\langle 111\rangle$ slip 79—47760
- Cu_2NiZn, characterisation of superlattice dislocations by TEM 79—55748
- Cu_2NiZn, superlattice dislocations 78—83816
- Cu_2O, epitaxial, on Cu (111), misfit dislocations, TEM obs. 78—14629
- Cu_2O polycrysts., dislocation obs. by elecron microscope *(Spanish)* 80—75230
- EuS, defect struct., etch pitting and electron microscopic obs. 79—27989
- EuS, single cryst., high-field susceptibility meas., temp. range 2.5 to 16.5K 80—84589
- Fe, [110] and [410] single crysts., push-pull fatigue, dislocation distrib., TEM obs. 79—74257
- Fe, annealed, and deformed, exam. of immobile dislocation distrib. *(Russian)* 79—32995
- Fe, Armco, cold-rolling cavity formation, TEM study 78—6947
- Fe, BCC, void nucleation following electron irrad. 80—29054
- Fe, deformed, deep trapping states for H_2 80—29045
- Fe, epitaxial growth on Au, two types, observed dependent on deposit thickness of dislocation *(French)* 77—85109
- Fe, H_2 charged, depend. of softening on specimen size, charging current density and strain rate 80—16455
- α-Fe, high temp. deform., Cottrell-Stokes law 79—83274
- Fe, high-purity single crystals, X-ray topography and double-crystal diffraction 80—92534
- Fe, internal friction in plastic deformation process *(Chinese)* 80—88259
- Fe, plastically deformed, high field suscept. anisotropy and domain struct. 78—15002
- Fe, thin foil, extrinsic grain boundary dislocations, low C content influence 80—107273
- Fe, volume changes and defect healing due to plastic deform. *(Russian)* 80—81139
- Fe-Al alloy, antiphase boundary energies 77—36460
- Fe-Au (111) bicrystal films, misfit dislocations obs., for 500°C substrate temp. 77—51624
- Fe-Au bimetal epitaxial films, examination of interaction at temps. $\geq$600°C 80—75482
- Fe-Co-V, ordered and disordered, dynamic ageing *(French)* 80—16355
- Fe-Co-V (2 wt.%), gamma phase 77—36514
- Fe-Co(-V) alloys, neutron irradiated, influence of dislocation doping on recovery 79—46715
- Fe-Cr (9 wt.%), extrinsic grain boundary dislocations, low C content influence 80—107273
- Fe-Mn (0.5 wt.%) alloy, Burgers vector of dislocation determ. by weak-beam image in HVEM 80—103351
- Fe-N, nucleation and precipitation growth on dislocations, electron microscope studies 80—3064
- Fe-Ni (4 wt.%), extrinsic grain boundary dislocations, low C content influence 80—107273
- Fe-Ni-C (24, 0.5 wt.%), struct. of burst and isothermal martensites 79—38825
- Fe-Ni-(C), thin foil martensite, TEM obs. 77—51378
- Fe-Ni-(Cr)(Ti)(Al) austenite, high N content, cryst. struct. electron diffr. and electron miscroscope anal. *(Russian)* 79—24490
- Fe-Si (3.25 wt.%), Burgers vector identification from electron microscope images 80—2030
- Fe-Si (3.5 wt.%) plastic deform., slip initiation, X-ray topography study 79—47750
- Fe_2O_3, twinning dislocations, electron microscopy obs. 79—99218
- δ-FeO(OH) crystallites, TEM imaging investigation 80—39096
- FeS_2, dislocations and stacking faults, TEM obs. *(French)* 79—99204

dislocations continued
GAP:N LED, acoustic emission study of defects 79—86799
Ga single crystals, rate equations for dislocation-free and dislocation-assisted growth 79—4262
GaAlAs, SEM defect study, transmission cathodoluminescence 79—64964
$Ga_{1-x}Al_xAs$ epitaxial layers, spectroscopic technique for imaging spatial distrib. of nonradiative defects 78—23498
GaAs degraded heterojunction lasers, TEM obs. of dark defects 78—14355
GaAs, dislocation states 79—60762
GaAs, during deformation, acoustic emission rel. to cracks, dislocations 80—35441
GaAs, elec. effects of dislocations 79—82586
GaAs, electronic states associated with 60° dislocations, tight-binding calc. 79—15114
GaAs, etch pit pattern made by light irradiated electrolytic etching 79—95012
GaAs, grain boundaries, extended Read model 80—96543
GaAs, highly deformed samples, absence of dislocation-induced luminescence 79—4835
GaAs, plastically deform., photocond., spectral response and decay process 80—29435
GaAs, SEM defect study, transmission cathodoluminescence 79—64964
GaAs, semi-insulating, optical and electron microscopy exam., line dislocation precipitates 80—70205
GaAs:Au, back surface gettering 80—10758
GaAs:Cr, gettering by back surface mech. damage 80—10759
GaAs:Cr substrates and LPE layers, Au film deposition and annealing, Cr redistrib. and dislocation form. 80—15312
GaAs:Te, microcathodoluminesc. of effect of struct. defects on radiative recomb. 79—11475
GaAs:Zn(Cr), As precipitation at dislocations, TEM study 80—79820
GaAs-$Ga_{0.7}Al_{0.3}As$ (001), (211), threading dislocation in single layer heteroepitaxial struct., bowing 79—65341
GaAs-$Ga_{1-x}Al_xAs$ DH lasers, X-ray topographic obs. of lattice defects rel. to degradation 77—15420
GaAsP epitaxial film, composition self modulation, defect struct. 80—34331
GaP, cryst., characterisation by light scatt. *(Japanese)* 77—35498
GaP, dopant dislocations, scanning electron micrographs, cathodoluminesc. 78—91340
GaP, electrical recomb. behaviour at dislocations 79—82606
GaP, epitaxial layers, dislocation recomb., SEM cathodoluminescence studies 79—42558
GaP, GPE layers, nonradiative dark regions along surface ripples 77—59600
GaP, green cathodolum. from cryst. defects, SEM, TEM study 80—80870
n-GaP, LPE, non-radiative recombination 78—19565
GaP, minority carrier lifetimes at dislocations, SEM meas. using photon counting 78—23109
GaP, non-radiative recombination and structural defects 78—19566
GaP, radiative and non-radiative recombination around dislocations 78—19576
GaP, SEM, cathodoluminesc., impurity and defect detect. 78—83695
n-GaSb, temp. distrib. around dislocations, due to Joule heating, calc. 78—71734
Gd, ferromag. reson. line width *(Russian)* 78—39406
GdGa garnet, Czochralski grown, substrate material dislocation propagation 78—59771
$Gd_3Ga_5O_{12}$ crystal growth from melt, X-ray topography meas. *(Hungarian)* 80—11556
$Gd_3Ga_5O_{12}$, Czochralski grown, effect of melt flow phenomena on perfection 78—88419
GdIG, local mag. anisotropy in stress field of single dislocation 80—88744
$Gd_2(MoO_4)_3$, and isotypes exam. of crystal growth, and defect generation 78—68617
$Gd_2(MoO_4)_3$, ferroelec. and ferroelastic, electron microscopic study 77—85675
Ge, amorphous, dislocation model 80—1929
Ge, amorphous, dislocation model 80—1930
Ge bicrystals, [011] tilt boundary, grain boundary stability 79—82240
Ge bicrystals, low angle [011] tilt boundary 79—82239
Ge, bound electron states close to conduction band due to 60° dislocations 77—28141
Ge, deep dislocation states 80—24836
Ge, deformed at relatively low temps., Hall effect 79—82612
Ge, diffusion of Ga along dislocations 79—82385
Ge, dislocation electron image filtering in electron microscopy 80—75129
Ge, dislocation electron states, from press. depend. of photocond. 80—96819
Ge, dislocation energy levels, Hall effect meas. 78—6328
p-Ge, dislocations, grown-in defects, electrical props., deep level transient spect., Hall effect 80—39524
Ge, dynamical recovery and self-diffusion 79—82379
Ge, electron states associated with core region of 60° dislocation 78—39057
Ge, electron states below cond. band originating from dissociated 60°-dislocations, calc. using effective mass method 79—19546
Ge epitaxial film, misfit dislocations, determination of Burgers vector *(Russian)* 79—33207
Ge, faulted dipoles, high-resolution TEM study 80—103345
Ge, high-doped single crysts., impurity atom distrib. changes around growth dislocations in thermocyclic treatment *(Russian)* 80—107307
Ge, plastically deformed, photocond. produced by polarised light 79—82641
Ge, recombination at dislocations 79—38023
Ge, stacking faults of dislocations, constrictions obs. using weak-beam electron microscopy 77—35576
Ge-GaAs heterojunction, elec. and recomb. props., interface defect effects 80—80365
Ge-GaAs inter faces, heteroepitaxial, misfit dislocations, TEM obs. 79—23610
H embrittlement, trap theory 80—89325
^{4}He HCP crystals, US vel., temp. and freq. depend. 79—56016
$(Hf_xZr_{1-x})_{80}Nb_{20}$, β-decomposition, effect of Hf additions 79—8304
In, dislocation obs. by X-ray topography *(French)* 79—46661
In_2Bi, pre-melting absorption of sound 80—88277

dislocations continued
$In_xGa_{1-x}P$-GaAs lattice mismatched heterojunction, recomb. props. 78—13707
InP, LEC growth of dislocation free crystals 80—89134
InP photodiodes, dark current and breakdown characts. 80—70806
InP:Zn heavily doped X-ray topography, cathodolum., and TEM obs. 79—99197
InSb, electrical effects of dislocation, galvanomag. props. 78—23119
KCl, γ-irrad., photoplastic effect and internal friction aftereffect 80—24529
KCl, premelting due to thermal form. of dislocations 77—11671
KCl with Al_2O_3 disperse spheres, dislocation mechanism for stress relaxation in cooling crystal *(Russian)* 80—54347
$KCoF_3$, flux-grown cryst., direction of dislocations, X-ray topography obs. 77—35565
KH_2PO_4, dislocation strain decoration and static central peak 79—99263
$KH_3(SeO_3)_2$, dislocation strain decoration and static central peak 79—99263
$KMg_3AlSi_3O_{10}F_2$, dislocations, subgrain boundaries, X-ray diffr. topography study *(Chinese)* 80—88149
$KNbO_3$ thick crystals, vol. nucleation of domains by impurities 77—73120
$KNiF_3$, flux-grown cryst., direction of dislocations, X-ray topography obs. 77 35565
LiF bicrystals, intergranular fracture due to single slip 78—34520
LiF, charged dislocations, comprehensive deform. effects on charge, elec. field 79—14815
LiF crystals, relation of struct. and bond type to slip geometry 80—88165
LiF, dislocation creep, creep deform. predictions 78—19815
LiF, manifestation of local vibrs. of dislocations in IR spectra 78—88339
LiF TLD, plastic deform. effects on thermolum. sensitivity, rel. to handling technique 77—16988
LiF:Co, flow stress changes during precipitation 80—92594
$LiFe_5O_8$, microstruct. and magnetic props., electron microscope obs. 79—87290
$LiNbO_3$, crystal defects, X-ray diffr. topographic study *(Chinese)* 80—84173
$LiNbO_3$ waveguide, diffusion of Ti, exam. by electron probe anal. and X-ray diffr. 78—47588
$(Mg,Fe)_2SiO_4$, dislocation recovery rate affected by high-press. 80—94515
Mg, deformed single crysts., stacking faults and dislocation dissoc. 77—31681
Mg-Al-Zn (94.3, 3.9, 1.8 wt.%), pricip. on dislocations, weak-beam TEM 80 76264
Mg-Ce, workability, aging characts. and tensile strength 80—55416
Mg-La, workability, aging characts. and tensile strength 80—55416
$MgAl_2O_4$, microplasticity at room temp., dislocations, TEM study 80—19805
MgO, cathodoluminesc. at dislocations 79—47524
MgO, cryst., cumulative deform. by softer sliders 77—4154
MgO, deformed, cathodlum. obs. by STEM 80—76088
MgO, dislocation creep, creep deform. predictions 78—19815
MgO, lattice misorientation and displaced vol. for microhardness indentation 78—64617
Mg_2SiO_4, microhardness variation, exam. using Vicker indentor 80—25849
Mo, BCC, void nucleation following electron irrad. 80—29054
Mo film, sputtered on Si, annealing effect on uniform and nonuniform strains 79—82504
Mo, fragmented struct. formed during plastic deform., TEM investig., dislocation model *(Russian)* 77—32634
Mo, localised electronic states near dislocations 79—33257
Mo single crystal, early stages of plastic flow 77—36584
Mo-Re, solid soln., dislocation internal friction *(Russian)* 78—23748
NH_4ClO_4, photothermochemical process, influence of phase transition 79 24770
$NH_4H_2PO_4$, defects, X-ray topographic study 78—26580
$NH_4H_2PO_4$, solution growth mechanism investig., growth spiral interactions 77—58963
Na-A zeolite, struct. obs. by high-resolution electron microscopy 80—84175
NaCl, deformed surface layer, block misorientation 79—99405
NaCl, etched cleavages, moisture effect on spiral and terraces steps 77—4251
NaCl, γ-irrad., photoplastic effect and internal friction aftereffect 80—24529
NaCl, high-temp. deformed, dislocation grain subboundaries *(Russian)* 80—96534
NaCl, premelting due to thermal form. of dislocations 77—11671
NaCl, single cryst., crack healing at low temp. 77—36622
NaCl, single cryst. in vac., influence of dislocations on evaporation 79—10935
NaCl:Ba, Ba precipitation at dislocations, kinetics, ionic cond. meas. 79—60510
NaCl:Cd^{2+}, dielectric loss following plastic deform. 80—84690
NaCl-KCl mixed crystal, growth, X-ray exam. and microstruct. 78—44001
NaCl-O^{2-} X-ray irrad., defect generation during radiolysis 80—7831
$NaClO_3$, dislocations rel. to growth mechanism from aq. soln., X-ray topography 80—59464
Na_2CoGeO_4 hydrothermal single crystals, X-ray topographic study of growth defects rel. to growth conds. 79—19166
Nb, BCC, void nucleation following electron irrad. 80—29054
Nb, bicrystal, parelastic interaction between grain boundary dislocations and flux line lattice 79—24114
Nb, catastrophic slip bands, fine struct. *(Russian)* 78—38718
Nb, supercond., field history effect of flux gradient 78—91828
Nb, superconducting, torque anisotropy due to defects flux line pinning 77—20509
Nb-H, behaviour of H in Nb, relation to mech. props. 78—80572
Nb-Mo steel, HSLA, low temp. fatigue props. 80—40490
$NbH_{0.3}$, α-α' phase transition, sp. ht. anomaly 78—39764
Nb_3Sn, TEM of radiation damage 79—65122
Ni, creep, struct. and activation characts., effective stress, electron microscopy and resistometric obs. *(Russian)* 80—40427
Ni, crysts., thick, imperfect, dynamical X-ray diffr., topographic effects 77—68898
Ni, electrodeposit, linear defect obs., TEM study 79—4304

dislocations continued
Ni electrodeposits on (001)Cu films, growth and mag. anisotropy 79–42810
Ni, foil, polycryst., channelling micrographs using accelerators, defects investig. 77–11445
Ni, H diffusion, trapping and mobility near vacancies, dislocations and cracks 80–49426
Ni, magnetic neutron scattering by dislocations, temp. depend. 80–103820
Ni, positron capture by dislocations, vacancies, rel. to temp. *(German)* 78–30606
Ni single crystal, compressed, strengthening and dislocation cells *(German)* 80–66536
Ni, stress induced crossover effect near Curie point *(German)* 80–103874
Ni, volume changes and defect healing due to plastic deform. *(Russian)* 80–81139
Ni-Al, order hardening, comparison between revised theory and expt. 80–93565
Ni-Al (6.35 wt.%) precipitate coarsening, redistribution and renucleation during ion irradiation 78–23709
Ni-Cr, partial dislocation, stacking fault TEM study *(Chinese)* 80–84174
Ni-Cr (33 at.%), plastic deformation, HVEM study *(French)* 80–66605
Ni-Ni$_4$Mo system, deformation microstruct. 80–93591
Ni$_3$Fe, superlattice dislocations, compression induced mag. anisotropy 77–85442
Ni$_{2/3}$Fe$_{7/3}$O$_4$, precipitation of α-Fe$_2$O$_3$, optical microscopy, SEM and TEM studies *(French)* 80–11650
Ni$_3$Mn, ordered at below Kurnakov temp. then deform., $a/2\langle 110\rangle$ dislocations and deform. antiphase boundaries *(French)* 77–51384
NiO, diffusion of Ni in bulk and along dislocations 79–82381
Ni$_3$V, dissociation of $^1/_2\langle 112\rangle$ perfect dislocations and nature of slip dislocations 78–43022
PLZT, fine grained 90° electric domain wall movement, interpretation of dielectric losses *(German)* 79–33646
Pb, dislocation inertial effects, internal-friction meas. on normal and superconducting states 79–38883
Pb, dislocation internal friction changes under the action of US vibr. 79–69630
Pb, plastic deform. rate rel. to supercond. transition, temp. depend. *(Russian)* 78–31015
Pb, positron annihilation, evidence for microporosity and dislocations 79–78786
Pb thin films, thermal strain, multiple cycling to 4.2K effects 79–90918
Pb-Cd(Tl) alloys, positron annihilation, evidence for microporosity and dislocations 79–78786
Pb-Sn, dil., dislocation inertial effects, internal-friction meas. on normal and superconducting states 79–38883
PbIn films strengthening, by preventing formation of misfit dislocations 80–84858
Pb$_3$(PO$_4$)$_2$, ferroelastic props., domain struct., electron microscopic study *(French)* 80–44216
PbS, crystals, relation of struct. and bond type to slip geometry 80–88165
PbSe-PbS(Te) and PbS-PbTe epitaxial layers, electron microscope contrast of misfit dislocations 77–85113
Pb(Zr,Ti)O$_3$, fracture and deform. 80–79870
Pd$_3$Fe, X-ray and electron microscope obs. of antiphase domains and superdislocations *(Russian)* 77–86017
RbMnF$_3$, antiferromag. domain struct., depend. on dislocations 79–69693
Sb, dislocations, contrast simulation *(French)* 79–60374
Sb, thin film, electron microscopy identification criteria of dislocations *(French)* 77–76411
Si, 60° dislocation, X-ray diffraction contrast, section topography 78–83819
Si, amorphous, small dia. laser beam annealed, temp. distrib. and microstructure 79–73098
Si, crucible grown, virgin and implanted laser irradiation effects on surface struct. 80–92768
Si, cryst. growth, float zone, low ohmic seeds and dislocations 78–27398
Si, crystal defects in integrated circuits, review 78–88547
Si crystal dislocation slip bands formation due to pores, nondestructive monitoring 79–55749
Si, Czochralski growth of dislocation-free (110) crystals 79–100042
Si, deep dislocation states 80–24836
Si, deformed, defect states associated with dislocations, capacitance transient spectroscopy 79–42483
Si, deformed, photo-EPR of dislocations 80–11267
Si, diffusion-induced lattice strain and dislocation obs. by X-ray diffraction *(Japanese)* 77–84753
Si, dislocation defect states, capacitance transient spectroscopy 79–82549
Si, dislocation electronic states, Schottky diode meas. 79–82548
Si, dislocation energy spectrum, appl. of EPR and elec. meas. 79–82547
Si, dislocation images, comparison of SEM and scanning optical obs. 79–51112
Si, dislocation luminesc. obs. 78–15217
Si, dislocation study by high voltage electron microscopy and SEM 79–82217
Si, dislocation-induced elec. pots., appl. 79–82551
Si, dislocations, EPR meas. 79–82871
Si, dislocations, stacking faults, swirl defects, production and mechanisms *(Chinese)* 79–46684
Si, dynamical recovery and self-diffusion 79–82379
Si, EPR and spin-lattice relax. of dislocation spin chains *(Russian)* 79–91291
Si, electrical recomb. behaviour at dislocations 79–82606
Si, electron states associated with core region of 60° dislocation 77–35887
Si, electron states associated with core region of 60° dislocation 78–39057
Si, electron-channelling imaging, defect obs. 80–10471
Si, epitaxial (111) surface, etching observation of stacking faults, dislocations, S-pits, etch pits *(Chinese)* 80–70197
Si, epitaxial film, struct. defects, effects on planar diffused p-n junction elec. props. *(Russian)* 78–60195
Si, extinction fringes and Burgers vector determ., single-crystal interferometric technique 79–95013
Si, float zone crystal, dislocation creation and elimination 80–107072

dislocations continued
Si, heat treated, spin-depend. recomb. at dislocations 79–47122
Si, heavily damaged ion implanted (100) and (111), development of secondary defects 79–51166
Si, high dose self-irrad., spatial correl. between primary and secondary defect profiles 80–59536
Si, ion implanted, extent of annealed or melted regions as function of pulsed laser irrad. energy 79–74025
Si, ion-implanted, laser irrad., characterisation by X-ray topography 79–74026
Si laser annealing of SiO$_2$ layers 80–97505
Si, mag. props. of dislocations, spin polarons 79–82531
Si, misfit dislocations removal by laser irrad. 79–83063
Si, P diffused sample, stacking faults and dislocations formation from interstitials 78–95059
Si p-n junction, charge carrier recomb. at dislocations, combined SEM and TEM study 80–15105
Si, p-n junction, current-voltage characts., misfit dislocations, high press. effects 80–65671
Si, photoelectret effect, plastic strain induced dislocation relax. time enhancement *(Russian)* 79–15397
Si, recombination at dislocations 79–38023
Si, single cryst. characteris. by SEM using Schottky barrier charge collection microscopy 77–4444
Si, spin effects in electron transitions via dislocation states 79–82642
Si, spin-depend. recomb. at exchange-coupled dislocation centres 77–89725
Si, structural defects on (115) plane 78–87675
Si, surface, pulsed electron beam processing, doping, annealing 80–75254
Si, surface layer defects, influence of multiple oxidation *(Russian)* 78–47650
Si, thermally induced microdefects, effect of C, TEM obs. *(Japanese)* 80–54244
Si wafer creep testing using stress provided by deposited Si$_3$N$_4$ film 77–66000
Si wafer stacking faults, preoxidation gettering by reverse side P diffusion-induced misfit dislocations 80–60988
Si wafers, Czochralski grown, crystal defects, photoluminesc. topographic obs. 79–1432
Si, with dislocations, noise spectrum 80–107881
Si:As, ion implanted, two-step annealing, TEM study 79–82249
Si:B, SEM obs. of dislocations using Schottky barrier EBIC technique 78–79614
Si:B,P, high conc. diffusion without disloc. generation 78–10072
Si:B(P), deformed, EPR fine struct. spectrum of dislocation 77–66422
Si:B(P), dislocated crysts., DC cond., Hall effect, and energy spectrum 78–10400
Si:Fe(Cu), impurity segregation and microstructural changes by pulsed laser irrad. 79–82254
Si:In, p-n junction, spin-dependent recomb. at dislocations, revealed at reverse current 79–24062
Si:P, heavily doped wafer, rel. to anomalous bending 78–10074
Si:P, strain-induced band-gap narrowing effect on P diffusion 79–55935
Si:P(As)(B), nonequilibrium solid solutions obtained by heavy ion implantation and laser annealing 80–92544
Si:Sb,P, double implants, residual defect reduction after damage anneal 80–88170
Si-SiO$_2$ interface, oxidation stacking faults, growth rel. to self-diffusion 80–49239
SiC ion implanted, laser induced ordering and defects 80–84754
p$^+$-Si$_{1-x}$Ge$_x$-nSi junction diodes, lattice misfit effects on I-V characts. 80–70804
Si$_x$Ge$_{1-x}$-GaAs, heterojunction, elec. and recomb. props., interface defect effects 80–80365
Si$_3$N$_4$ film on Si substrate, dislocation generation at film edge, suppression effect of SiO$_2$ 80–2025
Si$_3$N$_4$, reaction-sintered, non-axial dislocs. 77–19956
SiO$_2$ layers, dielectric strength, dislocation effect 78–31154
SmCo$_5$, single cryst., grown-in dislocations and stacking faults, TEM investigation 79–19253
Sn, $\beta\rightarrow\alpha$ polymorphic transformation, mechanism of growth of cubic modification nuclei *(Russian)* 77–44239
Sn, diamag. moment meas., dislocation supercond. above crit. temp. *(Russian)* 79–4619
Sn, superconducting and normal phases, damping of dislocations and supercond. attenuation 78–52155
Sn-In, dil., amplitude depend. US attenuation in normal and supercond. state 77–28299
SnTe-Sn epitaxial system, electron microscope contrast of misfit dislocations 77–85113
Ta, polycrystn., dislocation relaxation under high pressure 79–77605
Te, intervalence band absorption, press. and defects influence 80–55149
Te, negative photoconductivity, intraband absorpt. *(Russian)* 80–107854
Te, strained and unstrained, SHG and propag. of CO$_2$ laser radiation 80–58641
Ti, recrystallised, dislocation obs. and characterisation by X-ray topography *(French)* 78–22722
Ti, type 70A, containing 0-6000 ppm ^{3}He, sensitivity of tensile props. 80–39197
Ti, volume changes and defect healing due to plastic deform. *(Russian)* 80–81139
Ti-Al-V, containing 0-6000 ppm ^{3}He, sensitivity of tensile props. 80–39197
Ti-Mo-Zr-Sn (11.5, 6, 4.5 wt.%), β III, mech. props. rel. to heat treatment 80–84961
TiMn, faceted parent martensite interface 80–6417
TlCl$_3$.(TlCl)$_3$, labelled, exchange of Tl ats. rel. to γ-irrad., heat treatment, grinding 78–92470
UO$_2$, dislocation creep, creep deform. predictions 78–19815
V, coherent twin boundary structure *(French)* 79–60379
V, zone-refined, deform. behaviour, stress relax. and slip plane patterns 79–29163
VH$_x$, positron annihil. lineshape Doppler broadening, H conc. and temp. depend., 20-500K 79–61463
V$_3$Si, dislocations, obs. by TEM 77–59012
V$_3$Si plastically deformed cryst., lattice transform., Kossel technique 78–95153
YIG, domain wall mobility and mass meas. method *(Russian)* 80–108033

dislocations continued
  Zn, deformed single crysts., stacking faults and dislocation dissoc. 77−31681
  Zn, dislocation mechanism of Rose channel formation under impact loading conditions *(Russian)* 79−79073
  Zn, hexagonal networks in basal plane, TEM exam. 78−2132
  Zn, magnetic susceptibility behaviour, dislocation and elastic deform. effects *(Russian)* 77−80912
  Zn single crystal, US flow detection in dislocation relaxation investigations 80−29122
  Zn, single crysts., Burgers vector determ. of perfect dislocations obs. by X-ray topography 79−37711
  ZnO (1010) surface bias voltage effect on hardness, charge exchange near dislocations 78−52078
  ZnO(S)(Se)(Te), charged dislocations, flow of charge with plastic deform. 80−85010
  ZnS, polymorphic transition, ($\beta \rightarrow \alpha$) effect of mech. deformation 79−1858
  ZnS:Cu crystal, powder, epitaxial film, luminescence anomalous thermal 80−76077
  ZnS-O, single cryst., fast neutron irrad., optical props. 78−27331
  ZnSe, multiphonon ionisation of deep point centres in a charged dislocation field *(Russian)* 80−100281
  ZnSe, photoplasticity and photocond., excitation energy conc. near dislocations, hardening 77−24346
  Zr, void swelling during electron irrad., HVEM study 80−92559
  ZrC-TaC solid solns., high-temp. creep 79−11661

disordered systems, vibrational states *see vibrational states in disordered systems*

disperse systems
  see also aerosols; Brownian motion; colloids; dust; emulsions; foams; fog; gels; powders; smoke; sols; suspensions
  acrylic dispersions, conc., shear thinning and thickening rheology 77−48691
  acrylic dispersions, shear thinning and thickening rheology 77−52676
  adhesive forces, between solid particles in liq., hydrodynamic method of meas. 79−68826
  adsorption effects in interaction between solid particles 78−11569
  adsorption on hydrated solid phase surface exchange cations effect 78−64893
  agglomerate characterisation methods, review *(German)* 79−100443
  agglomerates of small spheres, scatt. efficiency factors 80−1131
  agglomeration principles, review *(German)* 79−100442
  agitated dispersion, breakage and coalescence processes, obs., data reduction 77−90645
  agitated dispersion, droplet breakage and coalescence rates during mixing 78−85205
  albumin, adsorption on SiO_2 80−10777
  alloy, disperse state formation *(Russian)* 78−52757
  anisodiametric particles, light scatt. functions 79−98286
  anisotropic ellipsoids, scatt. matrix comparable in size to light wavelength 80−1132
  aqueous colloidal particles, number fluctuation meas. using light scatt. 79−96371
  aqueous heterogeneous systems, NMR, substrate struct. and H_2O mol. relax. 78−7247
  asymmetric skinned synthetic polymeric membranes struct. 79−29417
  atomisation of liquid by impinging jets, expt. and theory 78−87373
  autohesive strength, meas. installation 80−40644
  azo pigments, dispersions in flow system, nucleation and growth kinetics meas. 77−63967
  bimodal systems, particle size distrib. meas., forward scatt. techniques 79−21699
  binary liquid mixtures, dispersion interactions, struct. effects 79−46535
  biphase liquid cylindrical vortex, mass force effect on dispersion phase distrib. *(Russian)* 80−79388
  biporous media, influence of double layer on dynamics of ion adsorption 79−11827
  brightening of disperse media, role of laser fluctuations 79−41405
  Brownian coagulation and diffusive deposition of monodisperse particles 78−23967
  Brownian motion, intensity fluctuation spectroscopy applics., review 80−52129
  bubble swarms, light transmission 77−79749
  butadiene-styrene block copolymer, viscoelastic props. 79−8336
  butyl rubber dispersion, electron-microscopic investigation 78−53268
  butyl rubber ethylene propylene ternary copolymer mixture, permeability, diffusion of gases and solvents 79−95217
  cement pastes, flow behaviour, specific surface and conc. of solids influence 80−65132
  ceramics containing metastable tetragonal ZrO_2, grinding induced tempering 80−89260
  charged particle, capture by large uncharged particle, in uniform external electrical field 79−66357
  chlorophyll pigments, aggregated forms in soln., spectral-luminesc. characts. *(Russian)* 78−23529
  clay-water systems, NMR, substrate struct. and H_2O mol. relax. 78−7247
  coagulating dispersions, light scatt. data, Fourier inversion anal. 78−76932
  coagulation, asymptotic analysis, systems with external source of particles 79−57300
  coagulation, non-diffusional, growth kinetics and soln. of microparticles *(Russian)* 77−32836
  coagulation, slow, turbulent 78−53259
  coagulation, with breakdowns, exact solution of integrodifferential equation 78−53272
  coagulation in finite systems 78−68933
  coagulation theory, new aspects *(Russian)* 79−8453
  coal dust aerocolloids, ignition inhibition, flame extinguishers effects 79−100375
  coalescence model for two dimens. constrained drop in close packed dispersion 80−14796
  coalescence redispersion model for drop-size distribs. in agitated vessel 77−1950
  coherent inelastic scatt. theory 79−50957
  coke-pitch system, viscoelastic props. 80−1500
  collection efficiency of grid filters, effect of Stokes and Reynolds numbers 78−61592

disperse systems continued
  colliding gas-slurry jets, dispersed material motion, numerical anal. *(Russian)* 79−32653
  composite, thermal diffusivity 79−55943
  concentrated, rheology and principle of minimum dispersed energy *(French)* 78−22313
  concentrated, shear thickening effect 77−7351
  concentrated disperse systems, min. energy dissipation principle 77−72339
  concentrated disperse systems, non-Newtonian shear viscosity in steady flows 79−81957
  concentrated disperse systems, non-Newtonian viscosity model 79−77231
  concentrated macromolecular solution, sedimentation behaviour rel. to particle shape 77−81428
  conducting fluid with solid particles, field disturbances modelling, conductometric probe analysis *(Russian)* 78−231
  contact of spherical particle with a droplet, approx. eqn. 79−60604
  continuous multi-particle crystal growth in vertical cone 77−69978
  continuous sedimentation theory, effects of density gradients and velocity profile 77−60125
  convection, forced, heat transfer in ultradeep boreholes 79−68762
  convective combustion of disperse systems 80−53835
  counter-current flow, discrete polydispersed model 80−14779
  counter-current flow, hold-up and particle size distrib. simulation 80−14780
  cryogenic liquids, dispersion analysis of cryosols and suspended microadmixtures using Doppler spectroscopic method 79−75535
  crystal single-particle model, thermodynamic props of disperse materials *(Russian)* 80−19894
  cylinder with high surface charge density, electrophoretic mobility 79−96373
  dense scattering media, anisotropy factor 80−87307
  dielectrophoretic forces, expt. anal. 78−64892
  dielectrophoretic levitation of spheres and shells 79−81318
  diffusion effects in solns. of Brownian particles, light scatt. theory 77−4939
  dilute system, orientationally induced conservative dichroism 80−102623
  diphasic structure, systematic anal. to determ. permittivity and elec. cond. from dielec. relax. 78−56423
  dipolar dumbbells in a viscoelastic Oldroyd liquid, dilute soln., electric field effect on rheological behaviour 80−6009
  disperse powder interaction in high temp. gas flow *(Russian)* 80−106830
  disperse reactive system, nonsteady heat exchange 80−26061
  dispersed flow, heat and mass transfer, phase transition effect 78−67252
  dispersed materials, effective thermal conductivity meas. *(Japanese)* 80−70485
  dispersed particles, in plastic matrix, contrib. of load transfer to internal stress, approx. method 80−21047
  dispersion resulting from flow through spatially periodic porous media 80−92216
  DNA, calf thymus, flexible polyelectrolyte, elec. birefr. meas. 79−16126
  drop dynamics in mixture with uniform temp., thermal diffusion effects 80−103097
  droplet, EHD produced, specific charge and size 79−32696
  droplets, atomized, polydisperse system, nonisothermal vaporisation, algorithm for calc. vaporisation parameters 80−48782
  droplets, kinetics of processes controlled by diffusion 79−11828
  drops, diffusiophoresis in viscous media 78−35731
  drops, size distrib. and phase surface, expt. determ. 80−53837
  dust-gas flows, steady and oscill., mean heat transfer 80−89536
  dusts, electrostatic precipitation *(German)* 80−89532
  dusty gas, weak wave, general decay law 78−5785
  effective thermal conductivity of dispersed materials *(German)* 80−33440
  effective viscosity and heat cond. coeffs. 80−89537
  ellipsoidal particles orientation determ. by spectral transparency 79−98287
  electric conductivity of dispersed mixtures containing high-conductivity components 80−92954
  electric relaxation in external fields, contrib. to elec. susceptibility 80−55720
  electro-optical effect, use of two-phase Rc field 79−55060
  electrochemical reaction kinetics, in presence of surface-active substances, eqn. selection 79−34322
  electrokinetic phenomena, sedimentation pot. 77−9090
  electrophoresis, aperiodic inertial drift, in inhomogeneous alternating fields 79−96317
  electrostatic deposition of thin particulate layer, resistivity meas. under ionic bombardment 80−68218
  electrostatic drop formation using liquid, expt. 79−57302
  electrosurface properties measurement 78−53249
  estuarine particle dynamics, math. model, phys. and chem. processes 77−21793
  ferroactive fluids, advanced appls. 80−80714
  ferrofluid, permeability in alternating mag. field 80−48808
  ferromagnetic dispersions, structural and magnetic characteristics, cinematography appl. *(Russian)* 78−16886
  filled polymer solution, structural strength 79−64973
  filtration coeffs. of polymer-modified dispersive systems 78−67264
  fine particle deposition, on rotating disc surface, convective diffusion under elec. double layer forces 78−61060
  fine particles aggregation, mechanism and rate at uniform shear field 80−101046
  finely-dispersed system, adsorption of water mols., dispersion medium density changes 77−9137
  flame, containing light scatt. particles, optical props. and temp. meas. method *(Russian)* 78−56894
  floc, settling velocity, rel. to permeability 79−43636
  flocculation of sterically stabilised dispersions under better-than-theta conditions 77−77810
  flotation, noninertial, effect of particle aggregation 80−55719
  flotation, thin film capillary hydrodynamic theory 79−56038
  flotation of fine particles, effects of size and charge 77−16865
  flotation of small particles, capture by bubble, theory 80−11959
  flow, cooperative phenomenon, theory 80−69878
  flow behaviour of disperse systems, the thixotropic compromise 79−77232
  flow kinetics, doublets of rigid spheres, calc. method 77−72344
  flow kinetics, doublets of rigid spheres, simple shear expt. 77−72345
  fluid flow, use of dispersion model 80−48784

disperse systems continued
- fluid interface dynamics 77—25313
- fluidisable cracking catalysts, microstruct. 77—28738
- fluorescence from molecules embedded in small particles, angular distrib. 78—76926
- fractal dimension characterisation, textured and structured particle profiles, dilation logic appl. 79—58673
- freezing dispersed medium, origin of water aspiration 77—60130
- gas bubble boundary surfaces in turbulent liq. flow, equivalence of photographic, chem. determs. *(German)* 79—32630
- gas-electrolyte dispersions, void fraction meas. using conductivity method 80—76525
- gas-liquid dispersion, comparison of methods for meas. of interface areas 77—63962
- gas-solid dispersions, heat exchange in uniform elec. field 77—11273
- gas-solid mixture hydrodynamics, use of relative velocity of gas to solids *(Croatian)* 80—14799
- glass, particle size influence on force moving particle in inhomogeneous elec. field, influence of field frequency 79—11795
- glass melt, multibubble dissolution 80—81371
- glass microspheres, interaction force meas. in dried atmosphere *(Japanese)* 78—20077
- glass powder, light scatt., close particle packing 78—1161
- glass-metal composite, heat conduction, memory switching 80—96703
- glycerine-water mixture, boundary surface velocity of rising air bubbles *(German)* 79—32631
- grain orientation in sheared dispersion, appl. to sedimentary and igneous rocks 80—3420
- granular material, dispersion of thermal waves 77—89001
- granular materials, pneumatic conveyance, pressure drop production *(German)* 79—50782
- graphite-air mixture steady and oscill., mean heat transfer 80—89536
- heat conduction at small Peclet no. 78—22254
- heat transfer between a dispersed system and a vertical heating or cooling surface 79—1069
- heterogeneous nucleation, appl. of thermodynamic pots. 77—7948
- heterogeneous system with chaotic structure, generalized conductivity coefficients, review 77—87708
- heterosteric stabilization and selective flocculation 79—24836
- n-hexane droplets coalescence in aq. electrolyte solns. 79—64742
- hindered settling in a multi-species particle system 80—14782
- histones, H2a and H4, aggregation ionic strength effect *(Russian)* 80—55697
- horizontal gas-liquid stream, flow vel. meas. 80—96301
- hydrocarbon system electrokinetic and polarisation phenomena *(Russian)* 79—83514
- hydrodynamics in EM field *(Russian)* 77—80222
- ice, melting, in porous solid, NMR and differential scanning calorimetry obs. 77—62621
- ice microcrystal dispersions, dielec. props. *(French)* 78—60374
- inclusions in gas-liquid mixture, effect on interphase heat and mass exchange 80—103059
- interfacial polarisation, dielec. consts. and relax. freqs., numerical estimation 77—32833
- inverse scattering in Rayleigh-Debye approx., diameter distrib. for thin circular discs 79—24840
- inverse scattering in Rayleigh-Debye approx., length distrib. for thin cylinders 79—24839
- inverse scattering problem, soln. in Rayleigh-Debye approx. for assemblies of long cylinders 77—48693
- inverse scattering problem, soln. in Rayleigh-Debye approx. for thin spherical shells 77—48694
- large interfacial area meas. by light attenuation 78—7248
- laser scattering, log-normal size distrib. 79—6079
- latex, monodisperse, phase diagram, spectroscopic study 78—85209
- latex, monodisperse, short-range order, spectroscopic study 78—85208
- latex+free polymer, dispersion flocculation, equilib. anal. 80—45574
- latex spheres in H_2O, photon correlation spectroscopy, diffusion coeffs. determ. 80—93802
- lecithin+cholesterol interaction, equilib., stoichiometry of complexes in bulk systems 78—68985
- lecithin+cholesterol interaction, equilib., surface film phase relations and cholesterol condensing effect 78—68986
- lecithin-water system, lamellar phase, rheology 80—89779
- light scattering, by small spherical particles, single to multiple scatt. shift process. calc. *(Japanese)* 77—65578
- light scattering, decay in orientationally induced var., Rayleigh approx. 80—45576
- light scattering, polydisperse system of coarse spherical particles 79—3633
- light scattering by layers with loosely or closely packed particles, spectral transmission variation *(Russian)* 77—23619
- light scattering data analysis for very polydisperse samples 78—50702
- light scattering in dynamical props. study, principles spectra derivation and applics. 80—53218
- lipid bilayer, of dipalmitoyl-lecithin, NMR dispersion of layers dispersed in D_2O 79—48223
- liquid atomisation developments 79—66360
- liquid crystal, lyotropic, dispersion on reaching solubilisation capacity 77—84628
- liquid crystal-rubber dispersions prep. and props. 77—27821
- liquid dielectric, charge transport by solid particles 77—4329
- liquid drop in immiscible liquid, evaporation, surface tension effects 77—47648
- liquid films, dynamic behaviour, surface mobility effects 80—88409
- liquid-liquid agitated dispersion, droplets transitional breakage probability 79—77219
- liquid-liquid dispersion, droplet size spectra in turbulent pipe flow 78—67247
- liquid-liquid dispersion, new drop size distrib. meas. technique 80—3419
- liquid-liquid dispersion, phase inversion characteristics 80—69898
- low angle X-ray diffr., pore or particle size distrib. calc. 77—39512
- lyotropic liquid crystal, struct. rel. to amphiphilic structure 78—51416
- macromolecular absorbed layer, energy of interaction between two spherical particles 78—53271
- macromolecules, polydispersity in nonlinear electric methods, nonlinear dielec. effect formulas derived 78—59730
- macroparticles; charged spherical, dilute soln., Rayleigh scatt. 80—84748
- magnetic separation, review of current activity 77—63961
- magnetic sparation, particle capture in axial filters, theory and performance 78—92515

disperse systems continued
- magnetic stabilization of the state of uniform fluidization 80—19484
- maleate-acrylate polyester resin, with phenol and glass microspheres, rheological behaviour 78—53267
- mass transfer props. of dispersed solids, kinetic methods 77—86387
- material particles movement, differential equation, numerical solution *(Croatian)* 79—25983
- mechanics, spatial averaging, cellular scheme 80—48788
- metal oxide smoke particles, prep. by burning metal in $Ar\text{-}O_2$ gas, electron microscope obs. 77—52238
- metal ultrafine crystallites, form. by gas evaporation technique, crystal habit 77—52239
- metal-dielectric mixture, effective dielec. const. derivation 77—28508
- metal-polymer deposit, simultaneous electrophoretic deposition and electrochemical precipitation 79—56938
- metallic particles, anomalous absorpt. in far IR region 78—56464
- metals separated by dielectric, electronic component of metal-metal interaction force, calc. 78—52056
- microemulsion, sound velocity and absorption 80—81374
- microparticles rapid anal. by laser diffractomer 79—66589
- mineral particulates, identification by selected area electron diffraction 77—90970
- mist formation in turbulent convection field, critical supersaturation model 80—64611
- mists, electrostatic precipitation *(German)* 80—89532
- moist dispersed solid, local Rebinder criterion determ. 77—89199
- moist porous materials, water content determ., rapid thermal method 77—86258
- moistened, permittivity 79—95304
- molecular attraction of crossed fibres, depend. on air gap width 77—27216
- monidisperse quartz fractions from soils in completely dry state, local stability criterion 77—49060
- monodisperse nonabsorbing particles, refractive index determ. by light scatt. *(Russian)* 77—5891
- monodispersed particles, angular distrib. of fluoresc. 78—76927
- motion in electric field of plane electrodes *(Russian)* 77—3527
- mullite-based dispersed refractory system, rheological props. at high temp. 77—16629
- multipole expansion calculation of slow viscous flow about spheroids of different sizes 80—33662
- multispectral extinction data, analytic inversion in anomalous diffr. approx. 78—87016
- N-particle system, Brownian dynamics with hydrodynamic interactions 78—91209
- nucleation, heterogeneous, appl. of theory of spherical film thermodynamics 77—15724
- oil shale retort dispersion, effect of particle size distrib. and flow nonuniformities 80—28560
- optical extinction measurements, forwardscattering corrections in aerosol media, monodispersions 78—94367
- ore in a gas flow, mixing stage calcs. *(Russian)* 80—106829
- Orientational optic effects from above Rayleigh particles 80—106453
- orthokinetic phenomena in shear flows 77—32838
- parallel cylinders radial size distrib. 79—100450
- particle adhesion upon impaction 79—52784
- particle analysis, using laser-Raman microprobe 79—43696
- particle and pore size distrib. curves quantitative evaluation, Fortran program *(Czech)* 78—80795
- particle charges and particle-substrate forces by optical transients 79—50218
- particle collisions in concurrent dispersed flows 77—15101
- particle concentration determ. by statistics 79—66370
- particle deposition, in laminar flow in tube, thermal effects 77—58764
- particle diameter spectrum determ. by light scatt. 80—61169
- particle dispersion coarsening, computer simulations 80—30289
- particle growth, mathematical modelling, continuity eqns. for particle distribs. 78—65863
- particle masses, self-similar singular spectra in coagulating systems 79—70379
- particle medium, refr. index determ. from angular, polarisation characts. *(Russian)* 77—34827
- particle separation property of impactor stage with nonstationary flow *(German)* 78—18335
- particle size and velocity distribution, in flowing media, meas. methods *(German)* 78—34213
- particle size determ. using conductometric method 79—35664
- particle transport to rotating disc surface under external force field 78—15718
- particle-size distribution functions, determ. from SAS data by indirect transformation method 80—38860
- particle/matrix interface, coarsening of disperse particles, diffusion control 80—30288
- particles of disperse material, and plasma fluxes, heat exchange calcs. *(Russian)* 80—23997
- particulate air pollution meas. 79—70502
- particulate materials, quantitative three-dimens. characters. using polished sections and computer-controlled SEM system 77—2714
- particulate systems, dynamic eqn., numerical soln., finite element anal. 79—5185
- particulates, frustrated total reflectance meas., interface model 77—71362
- perfect gas hydrodynamics, applicability to disperse media 80—33657
- permeable model floc, settling velocity 77—60126
- perturbed flow, moisture form. kinetics 80—79387
- phase boundaries and multiphase systems, conf., Tokyo, Japan (Sept. 1977) 79—29415
- phase size effect in highly dispersed systems 80—6488
- phosphate working in direct flow plasma reactor *(Russian)* 80—55663
- phosphatidylcholine dispersion, phase transitions obs. with interference refractometer 78—44459
- photophoresis, stable orbits, circular, cycloidal and oscillating *(German)* 79—80545
- planar particle aggregates, sampling by quadrats 79—17485
- plasmid DNA and DNA-histone chromatin-like complexes, conform. and soln. props. by laser light scatt. 80—55987
- plastic disperse systems, laminar flow in circular tubes 80—87798
- plastic non-Newtonian fluids in circular pipes, laminar flow stability loss 78—79342
- plastoviscous, cone plastometer for strength props. determ. 80—76426

disperse systems continued
- PMMA latex particles, laser light scatt. for visualisation in EHD 78—75236
- pollutant in lake, convection-diffusion equation, 1-D, finite elements method, weighted residuals 80—53775
- poly-m-phenyleneisophthalamide, sedimentation coeff. distrib. at 25°C *(Russian)* 77—63971
- polyamide mixtures, thermodynamically incompatible, composition-prop. relationship *(Russian)* 80—7872
- polyamide-polyurethane copolymer dispersions, structurisation and relax. props., coating from props. 80—76559
- polydisperse droplets, produced by EHD method, charge-to-mass ratio 78—76931
- polydisperse fluid, of hard or permeable spheres, scatt. function 79—86664
- polydisperse hard-disc systems, equations of state, particle size effects 78—73947
- polydisperse hard-sphere systems, equations of state, particle size effects 78—73947
- polydisperse layer, isothermal, thermal radn. 77—68374
- polydisperse media, optical characts., approx. representation 80—63922
- polydisperse particle size distrib. function, angularly scatt. light intensity profile meas. 80—13040
- polydisperse particle size distrib. function determ. from angularly scatt. light intensity profile 80—98879
- polydisperse particles, fractional anal. by ring method *(Russian)* 78—71035
- polydisperse polymer, anal. of mol. mass. distrib. *(Russian)* 77—31038
- polydisperse randomly branched polymer, sedimentation coeff. 77—63966
- polydisperse spherical particles, light scatt. extremum invariants 80—9809
- polydisperse system, rotatory diffusion const., electro- optic decay curve, size distrib. 78—20079
- polydisperse system, turbulent coagulation in force field 79—57297
- polydisperse systems, photon correlation spectroscopy, diffusion coeffs. determ. 80—93802
- polydisperse systems of nonadditive hard particles, thermodynamics 80—7863
- polydispersed flows, Doppler signal spectrum 80—103081
- polydispersion, moments determ. of size distrib. function in scatt. 79—18347
- polydispersion size distrib. function, light scatt. determ. 77—10834
- polydispersive cloudy medium, containing water droplets, brightening by intense monochromatic radiation 78—9407
- polyelectrolyte, cross-linked, dimensions of disperse forms, protein precipitants and flocculants 80—11957
- polyethylene, microfine powder prod. for dispersions *(German)* 80—29920
- polyethylene, mol. wt. averages determ. by temp. drop turbidimetry 79—39207
- polyethylene oxide, mol. wt. averages and polydispersity determ. by temp. drop turbidimetry 77—63959
- polyhedral particles, adhesion forces in liq. medium 79—70380
- polymer, polydisperse, hydrodynamic invariants *(Russian)* 77—19580
- polymer adsorption at interface, self-avoiding random walk anal. 77—1085
- polymer agglomerates, forces in dispersive mixing 77—29052
- polymer coated metal spheres, flow, degradation mechanism 77—9036
- polymer lattices, particle size control 79—38785
- polymer lattices, purification 78—7243
- polymer melt, polydispersity, estimation from rheological data 80—6535
- polymer mixture, molten, polydispersion effects, crit. behaviour *(French)* 78—42879
- polymer mixture, particle size in dispersed phase, effect of component viscoelasticity 77—44514
- polymer particle pigment agglomerate display, optical microscopy method 79—85177
- polymeric particles obtained by suspension polymerisation, particle size distrib. eval. using Coulter Counter data 80—76564
- polymeric systems, rheology, review 78—87317
- polymers, heterophase mixtures, excess energy 78—53264
- polystyrene, monodisperse latex, shear US meas. 78—31711
- polystyrene, polydisperse, quasielectric light scatt. obs., mol. wt. and polydispersity 79—96376
- polystyrene, sedimentation coeff. distrib. at 25°C *(Russian)* 77—63971
- polystyrene dispersion, sterically-stabilised, reversible flocculation 78—44411
- polystyrene latex, grain boundary struct. obs. and boundary diffusion 78—51552
- polystyrene latex, ordered monodisperse, lyotropic liq. cryst., mech. props. 79—98676
- polystyrene latex, particle size determ. by electron microscopy 79—21698
- polystyrene latex dispersions, aqueous, in presence of poly(vinyl alcohol), stability, crit. flocculation temp. 78—85207
- polystyrene latex particles from water, adsorption of poly(vinyl alcohol), influence of temp. 78—85206
- polystyrene latexes, soft X-ray scatt., struct. determ. 78—51395
- polystyrene latexes, viscosity meas. *(Japanese)* 79—55432
- polystyrene lattices, electro-flotation, collection efficiency 80—74946
- polystyrene microspheres, dye impregnated, fluoresc. spectra struct. resonances 80—50914
- polystyrene particles, monodisperse, dil. and conc. aqueous dispersions, elec. cond., surface cond. and double-layer polarisation 80—89533
- polystyrene-benzene, dil. solns., polymer excluded volume exponent, experimental verification of n vector model for $n=0$ 80—70104
- polystyrene/polyethylene blend, particle dimension as function of melt viscosity added graft copolymer conc. 77—52279
- pore catalysts effectiveness factors 80—16719
- powder particle motion and segregation by density difference in V-type mixer 80—45250
- powder polydisperse, heating and vaporisation in plasma stream *(Russian)* 77—59707
- powders, light scattering, close particle packing 78—1161
- production, stability and meas. of disperse systems reviewed *(German)* 77—66773
- prolate spheroidal primary particles, floc simulation 79—79302
- prolate spheroids, random, light scatt. characts., for turbidity spectrum calcs. 78—25801
- propag. in bodies with initial strains *(Ukrainian)* 79—30258
- protein dispersions, viscoelastic effects, shear viscosity and primary normal stress difference 80—87754

disperse systems continued
- pseudospectral dispersion model, inter grid sources representation 79—12259
- PVAC dispersions, US method of determining plasticiser content *(German)* 80—21257
- PVC in DMF, THF solns., mol. wt., aggregation, light scatt. investig. *(Polish)* 77—28587
- PVC latex size determ. by TEM, vertical shadowing technique 77—53857
- PVC plastisol pastes, dispersion and characteristic functions, review *(German)* 79—55015
- pyrene, S_1, fluoresc. decay in micellar and homogeneous liq. dispersions 77—75199
- radiant heat transfer, to dilute cloud of drops or particles 77—58537
- random dispersion of equal spheres, average nearest-neighbour spacing 79—58639
- refractive index and particle size, simultaneous determ. from scattered radiation characts. 80—27335
- rheology of concentrated dispersions, review 77—19578
- rheometer for the investigation of disperse systems 79—82012
- ruthenium trisbipyridyl ions in surfactant solns., excited state decay kinetics 80—83407
- scattering indicatrix, expansion coefficient through Mie coeff., anal. 80—18993
- Schulze-Hardy rule, theory 80—89540
- sedimentation of binary particle mixtures 80—40757
- semiconductor, polydispersed, surface elec. cond. of particles influence on dielec. characts. *(Russian)* 77—16270
- shock compressibility, brittle destruction 80—49303
- sludge, cohesive, dynamic props. *(Japanese)* 80—45580
- soft spheroids, light scatt. matrix calc. 80—1133
- soil, sandy moist, compressibility and plasticity during repeated shock loading 78—11885
- solid, electro-osmotic mass transfer, surface cond. influence *(Russian)* 80—76546
- solid, evolution of two-phase dispersed system *(Russian)* 77—16866
- solid disperse systems, thermal conductivity rel. to moisture content *(Russian)* 77—54864
- solid particle systems, high Reynolds number, momentum trasfer. Karman-Pohlhausen method 80—74947
- solid particle systems, high Reynolds numbers, mass transfer, Karman-Pohlhausen method 80—79378
- solidifying melt, particle engulfment, thermodynamic aspects 77—4184
- solids, multicomponent mixing index and contact number estimation by spot sampling 80—16214
- solubility increase, phase composition, size effect calcs. 80—70418
- soluble matter initial dispersion in three-dimensional flow 79—37387
- spectral transparency approx. by Legendre polynomials, distrib. density of particle size 80—95800
- sphere and half-space, van der Waals attraction energy 80—16735
- sphere radii moments, size distrib. 80—21329
- spherical cells, light scatt., eikonal approx. corrections 79—57304
- spherical droplet, evaporation and condensational growth, mass transport calcs. 80—97736
- spherical monodisperse latexes, light scatt. matrices 79—98285
- spherical particle, in stagnant bounded fluid, lateral migration 77—48695
- spherical particle dispersion, light scatt. and polydispersity 78—27241
- spherical particles, absorpt. cross-section *(Russian)* 77—83815
- spheroids in shear flow, light scatt., orientation correlation 78—76481
- sprays, blast wave propag. 79—34367
- steel, low alloy, at. absorpt. anal. using electrically dispersed sample 79—74459
- sterically stabilised dispersions, critical flocculation temperature, effect of dipolar substituent groups 78—61061
- sterically-stabilised, reversible flocculation 78—44411
- structure-forming solutions, double light refraction and viscosimetry 79—94745
- structuring dispersions, dynamic dielectric behaviour, meas. device 79—12816
- structuring dispersions, dynamic dielectric behaviour, reply to comments 79—35785
- sunlight scattering intensity fluctuations from asymmetric particles 79—98282
- surface area meas. by light transmission *(German)* 78—89431
- surface tension, solid-liq. interphase, thermal meas. procedure *(French)* 77—66072
- surface-active agents, determ. in waste waters, review 79—53007
- surfactant solutions, aggregation, micelle and microemulsion form. 80—89547
- surfactant solutions, review of concepts 80—89542
- suspended spheres, effective shear viscosity of regular array 78—51718
- Teflon spheres-nigrosin black dye-water dispersion, turbid laser backscatt. 80—1129
- temperature meas. from mag. props. variation near Curie pt. 78—9556
- thermal conductivity measurement, comparative method, solids and disperse materials, 0.1-80 $W\ m^{-1}\ K^{-1}$ 77—45835
- thermal conductivity prediction of heterogeneous mixture, digital simulation technique 78—87247
- thermodynamic theory of nucleation on charged particles 79—39216
- thermophoretic and diffusiophoretic particle deposition estimation 77—90644
- thermoplastic/unsaturated polyester resins, moulding materials *(Polish)* 80—66523
- thickness distrib. for randomly oriented, independently scatt. polydisperse systems of platelets 77—60132
- thixotropic, mech. props., structural hysteresis, statistical thermodynamic anal. 77—46978
- thixotropic structure formation in dispersed media, rel. to phase transitions of second kind 77—7355
- toner dispersions, positively charged, electrokinetic props., electrostatic image development 79—80713
- transport in heterogeneous media, random dispersed phase model 78—65885
- treating, using two-stream plasmatron *(Russian)* 78—22575
- tubes, single horizontal and bundles, vibr. fluidised disperse medium flow 80—33658
- turbid media, spatial struct., light scatt. meas., interferometric study 79—54178
- turbid media with specularly reflecting boundaries, optical props., biological appls. 77—75416
- turbidity of oblate particles, reciprocal problems 79—72496

disperse systems continued
turbidity spectrum, wave exponent, spherical particle size depend., Rayleigh-Gans approx. calcs. 78—46514
turbidity spectrum for oblate particles 79—64180
turbidity spectrum for parameters determ., allowance for nonspherical particles 78—55302
turbidity-spectrum method, scatt. functions for nonspherical particle systems 78—20078
two-dimensional fluid motions induced by motile particles, convection field and geotactic components 77—55080
two-phase conducting diamagnetic system, coeff. of EM ejection of particles *(Russian)* 78—94364
two-phase dispersed flow, relationship between radiation transmissivity and void fraction *(Japanese)* 80—100026
two-phase dispersion, size distrib. function of bubbles/droplets in thermodynamic equil. 80—7862
vapour-liquid mixtures, acoustic velocity, damping decrement 80—66881
velocity-voidage relations for sedimentation and fluidisation 80—24076
vibration-extrusion discharge, process optimisation 77—66772
vibrational compaction, of bulk materials 78—52701
warm fog and steam clouds, emission spectra variations, evidence for clusters in vapour phase 79—39849
waves, plane, nonlinear viscous multicomponent media 78—51228
X-ray small angle scatt. using synchrotron radiation, from polystyrene latex spheres on polycarbonate film 77—21425
Ag fine particles, X-ray Debye temp. determ. using solid-state detector and continuous X-rays 79—50944
Ag particles, lattice defect influence on size effect 78—88329
AgBr dispersion in gelatin, adsorbed S and Au, transient absorpt. spectra, latent image form. and decay 80—66837
Al powder, gas suspension, critical spark ignition conditions 79—100373
Al-Cu-Mg/mica particulate composite mech. props. 80—100919
Al-Mg-Mn alloy, disperse β-phase, kinetic laws of coagulation *(Russian)* 78—27519
Al-Mg-Si alloys, effects of dispersoids upon micromechanism of crack propagation 79—83286
Al_3N_4, dispersion in transformer steel for cubic texture formation *(Russian)* 78—80557
Al_2O_3 disperse spheres in KCl, cooling crystal dislocation mechanism for stress relaxation *(Russian)* 80—54347
Al_2O_3 dispersion in polycryst. NaCl, diffusive creep 80—97531
Al_2O_3-Cr(Re)(Nb)(Ta)(Ti)(V) heterophase films, elec. props. rel. to Al_2O_3 content 77—15969
$Al_4Si_4O_{10}(OH)_8$, kaolinite dispersion, adsorbed water, PMR exam. *(Russian)* 78—35058
As_2S_3 suspension dispersed in gelatin, photoinduced dichroism 79—98453
Au sol, grain boundary struct. obs. and boundary diffusion 78—51552
Au+Ag adsorbed layers on Si, dispersed struct. formation 78—22952
B_2O_3-Na_2O-SiO_2-Al_2O_3, effect of alumina dispersions on the thermal cond./diffusivity/stress resist. 80—39368
C black, in polymer particles, photomicrography of submicrometer birefringent contaminants 80—62757
C fine particle formation by C vapour condensation 79—52781
C particle formation,C_2+C_3 as possible first step 78—68876
C paste, viscoelastic props., depend. on coke grain size 80—1501
$Cd(OH)_2$, highly dispersed precipitate, microstruct. and exchange props. 77—36793
CdS, aq. dispersion, O_2^- generation by photolysis, spin trapping detect. 78—11538
Cr black solar selective absorbers, thermal degradation 80—61417
Cr-Cr_2O_3, black, electrolytic deposited, characterisation and thermal stability *(French)* 80—55898
Cr-Cr_2O_3 black, electroplated solar collector coatings, high temp. optical and struct. degradation 80—66995
Cr-Cr_2O_3 black solar absorber surfaces, microstruct. rel. to electroplating parameters 80—61418
$Cr_2O_3.SH_2O$, heat-treated, narrow particle size distrib., surface props. 78—85210
Cu alloys, dispersion type, with low temp. gradient of resist. 80—49686
Cu crystals, two-phase, recrystn. retardation, particle size, spacing effects 80—89242
Cu-Al_2O_3 powder, electrolytic deposition 78—84743
Cu-SiO_2, in-situ deform. in HVEM 80—103338
(Cu-Au)-Co, single crysts., solid soln. and particle strengthening, superposition 80—97495
CuCl, effect of dispersed Al_2O_3 particles on ionic cond. 80—24649
Fe oxides, disperse, chemical reduction in discharges *(Russian)* 78—95915
Fe-Cu: graphite-$BaSO_4$-$CuSO_4$, friction material, solid state sintering kinetics 80—104096
Ge, ultrafine multiply twinned particles, form. by gas-evaporation technique 78—63685
Ge, ultrafine particles prep. by gas evaporation in Ar 78—34455
^{4}He vapour, cryogenic, ion-droplet mobility 79—57308
Hg+water systems, drop fragmentation rel. to thermal explosion detonation requirements 78—71368
Mg, powder, gas suspension, critical spark ignition conditions 79—100373
Mn II-lecithin lipid-water system, NMR and EPR obs. 80—61168
Na salt crystals in aqueous slurries, particle size distrib. determ. 79—61918
NaA neolyte, Hg cluster transition to paramagnetic state due to mag. field *(Russian)* 80—60183
NaCl, with dispersed Au particles, age hardening of surface, double decoration obs. 79—11634
Ni, highly dispersed K_β emission spectra, cluster effects 77—28650
Ni powder, light scatt., close particle packing 78—1161
Ni-Cr-Al-Y_2O_3 superalloy, recrystn. and texture development 80—16328
$PbCrO_4$, paste, anomalous viscous flow 79—64617
Si, ultrafine particles prep. by gas evaporation in Ar 78—34455
SiO_2 dispersed particulate in CVD reactor, correlations with film characts. 80—76192
SiO_2, nonaqueous dispersions stabilised by terminally-grafted polystyrene chains 79—39219
SiO_2, small amorphous particles, high resolution TEM, prep. by vapour-phase hydrolysis and polymerisation, TEM study 79—82157
Ti-Er(Y), effects of Er and Y additives on deformation behaviour 80—81121
$TiC_{1-x}N_x$ formation in high temp. N flow, ultra disperse powder, thermodynamic anal. *(Russian)* 80—55325
TiN, highly dispersed, metallic thermo-EMF 78—43363

disperse systems continued
TiO_2 particles in hydrocarbon fluid, appl. of meas. method for particle charges and particle-substrate forces by optical transients 79—50218
TiO_2-SiO_2, submicron dispersion of impurity, chem. diffusivity and elec. cond. 79—1528
UAl_x dispersion nuclear fuels, development and irrad. performance 80—78368
UO_2, closed boiling system, effect of condensation on dispersion following LMFBR HCDA 78—8936
W, at. absorpt. anal. using electrically dispersed sample 79—74459
$ZnCl_2$-oil system, simulation of steel-slag, macrophotographic method of diagnosing disperse system 80—25952

dispersion (wave)
see also acoustic dispersion; optical dispersion
anisotropic moving media, polarisation relations and dispersion eqns. to EM waves 80—9779
atmosphere short internal waves, nonlinear dispersion eqn. and instability *(Russian)* 77—49107
Bleustein-Gulyaev waves, propag. and amplification in materials with strain depend. dielec. const. 79—41469
body waves in granular medium, dispersion and dissipation 77—23909
boundary-layer flows, neutral stability calcs., Taylor-series expansion of dispersion relation 80—53744
capillary wave dispersion relation, for isotropic liq., two-mode struct. 79—98741
composite, fibre-reinforced, layered, harmonic elastic waves, dispersion 78—63223
composite rods, strongly anisotropic, dispersion longit. waves *(French)* 78—12573
dispersive wave trains, near-linear, two-time procedure for higher order modulation 78—65788
dissipative and nonequilibrium media, pulse spreading 80—94961
Earth, surface waves phase vel. and attenuation simultaneous inversion, Love waves appl. 78—85491
Earth surface layer, EM wave refl. and transmission coeffs., linear ramp model 80—61759
education, Slinky as model for transverse waves in plasma 80—17741
elastic body dispersion spectra, freq. coalescence and conical points 77—46955
elastic shear waves propagation in fibrous composites 80—58963
elastic wave, edge localised vibr. modes on rectangular ridge 77—89629
elastic wave propagation, free surface of cryst., spatial dispersion 80—54310
elastic waves in model sediments, dispersion and attenuation 77—73672
EM monochromatic wave energy density in nonabsorbent medium with freq. and space dispersion *(Russian)* 78—74818
EM pulse dispersion in conducting medium *(Russian)* 77—38780
EM pulse in dispersing medium, conservation laws *(Russian)* 77—27221
EM surface wave, normal mode propag. at drift vel. tangential discontinuity 77—24076
EM wave propagation in inhomogeneous media, strong and weak inhomogeneities 79—31774
EM waves dispersion equations in moving media, relativistic electrodynamics 80—57089
EM waves in anisotropic loss-cone plasma, dispersion relations 77—87185
EM waves in atmosphere, appl. in multi-wavelength distance measuring instrument 77—29484
EM waves in inhomogeneous isotropic plasma layers, linear transformations *(Russian)* 78—18415
ferromagnetic film, with domain struct., magnetostatic oscills. 78—48010
ferromagnetic medium, magnetised, unattenuated refracted wave propag., optical modulation appl. *(Russian)* 78—25774
ferromagnetic slab, magnetostatic volume wave dispersion relations, metal effects 78—47963
granular solid, one-dimens., small amplitude wave behaviour 78—59339
gravitational waves dispersion in cold matter 80—12967
gravitationally unstable propagation, rot. and streaming effects 79—37293
gravity-acoustic waves, self-localisation, non-linear effect in non-uniform atmosphere 79—8761
group velocity, four-dimensional 80—17814
group velocity, W.R. Hamilton's investigation 80—17815
groups of waves, dispersion rel. to vels. and refr. laws 78—85575
gyromagnetic slab magnetised in arbitrary direction, magnetostatic mode characteristics 78—2670
helical spring of small pitch, free waves dispersion relations 78—9598
HF wave dispersion for complex wave numbers, ordinary waves 80—70740
hydromagnetic surface waves, dispersion relations, spatial extent and gas compression 79—25462
infinite cylindrical shell, dispersion curves and distrib. coeff. of elastic waves *(Russian)* 77—46964
ion beam, neutralised, LF plasma wave dispersion *(Russian)* 79—98888
ionosphere, directional dispersion of sporadic-E modes between 9 and 14 MHz 78—28412
LF in solids, determ. by transformation of complex permittivity *(German)* 77—90089
longitudinal carrier waves in solids, coupled mode anal. *(Korean)* 78—43403
M87, highly dispersed millisecond radio bursts discovery 80—73034
magnetised liquids, separated by thin elastic film, surface stability 79—94727
magneto-acoustic macroscopic soliton instability growth rate, dispersion eqn. *(Russian)* 78—59562
magnetosonic waves in solar wind due to alpha particle beams, EM dispersion relation 79—35089
magnetospheric noise, influence of CW whistler, dispersion eqn. 77—82087
mesosphere internal gravity waves, dispersion relation and propag. range *(Russian)* 79—16575
MHD, Lorentz covariant eikonal method, dispersion relation, for cold-one component plasma 77—27663
MHD solitons in solar wind, nonlinear dispersion eqn. qualitative anal. 80—4217
modulated electron beams, instability, spatially separated in plasma 80—70012
modulational instability expt. using nonlinear transmission line 77—82397
non-linear dispersive wave, coupled modes approach, effect of dissipation on recurrence 78—49670

dispersion continued
nonlinear dispersive system with small dissipation, statistical theory 78—70058
nonlinear dispersive wave eqns., modulational instability and envelope solns. 78—54199
nonlinear dispersive waves, bifurcation and symmetry breaking, four wave interactions 80—69855
nonlinear dispersive waves, statistical theory, based on Korteweg de Vries eqn. 78—16662
nonlinear interaction between strongly dispersive wave and weakly dispersive one 79—17242
nonlinear wave conservation laws group theoretic aspects 77—30016
ocean equatorial trapped waves, vertical eigenvalue problem and dispersion relations 80—56477
ocean trapped waves, wavenumber/freq. spectrum anal. and dispersion relations *(Russian)* 78—81189
ocean trench waves, dispersion curves and eigenfunctions 80—72547
Pacific crust surface wave dispersion 77—56604
periodic coupling of piezoelec. and magnetoelastic surface waves 78—10269
piezoceramic disc resonators, dispersion of thickness vibrs. 78—22237
plasma, electronic, classical, dispersion relation, RPA method 79—55481
plasma, ion-cyclotron wave spectra dispersion eqn. numerical soln. *(Russian)* 78—59561
plasma, lower hybrid waves in inhomogeneous mag. fields, propag. and mode conversion 79—37489
plasma, moving, covariant dispersion eqns. 79—37538
plasma, parametric excitation of backward ion cyclotron wave with a pump in the lower hybrid range 79—37490
plasma, stimulated Raman backscattering of circ. polarised EM waves 79—37465
plasma, two-temp., field eqn. of electron wave 80—28633
plasma waves propagating along mag. field in strongly anisotropic relativistic plasma, dispersion props. 80—67542
pressure-scanning millimetric-wave dispersion spectrometer expt. 80—61904
propagation of radiation in media with slowtime-varying refr. indexes, dispersive phenomena *(Russian)* 80—28152
PSR 1858+03, pulsar, dispersion measure rel. to distance 77—64785
pulsar dispersion data anal., scale height determ. 80—85965
pulsar radio emission scintillation, decorrelation bandwidth rel. to dispersion measure 80—85964
pulsars, low-latit., dispersion measures and distances rel. to interstellar electron density 80—101606
radio waves by solar wind, spectral broadening of Helios 1/2 and Pioneer 10/11 signals 78—28595
radio waves in F-region, pulse spreading as cause of unresolved spread-F 77—78557
Rayleigh wave dispersion, subsurface struct., estimation, dense data 77—39730
Rayleigh wave dispersion, surface layer struct. estimation, anal. theory for sparse data case 78—38928
Rayleigh wave flattening corrections 77—40987
Rayleigh waves on rough surface, model of surface layer 77—39727
rotating gas, perfectly conducting compressible in mag field under gravity, wave dipersion relations *(Chinese)* 80—77276
seismic dispersion curves, methods of computing partial derivatives 77—37149
seismic Rayleigh waves, dispersion in Walvis Ridge rel. to lithospheric struct. 80—41412
seismic SH wave equation soln. for scattered field near plane boundary 77—86788
seismic surface wave dispersion, resolving power of data simultaneous inversion 79—16699
seismic surface wave dispersion function, computations for unlimited freq. values 79—74848
seismic surface waves, dispersion across Iceland Plateau rel. to deep struct. 80—41413
seismic surface waves, inversion of dispersion data with random errors 77—73681
seismic surface waves anisotropic dispersion, isotropic inversion significance 78—96156
seismic surface waves dispersion curves, partial derivatives calc. *(Russian)* 79—34764
seismic wave dispersion, continuous representation technique 80—51334
seismic waves higher mode dispersion, meas. technique 79—39974
semiconductor thin films, effect of multilayer dielec. medium, anal. *(Russian)* 78—31004
SH waves in multilayered, laterally heterogeneous media, dispersion eqn. 77—73645
shear modes in anisotropic systems, dispersion curves 78—36107
shear SAW in periodic structures on solids 79—90055
slow MHD waves in ionosphere, dispersion relations 78—45093
solid, phase and group vels. determ. for dispersive waves 78—81848
solitons, in dispersive media, nonlinear evolution eqns. soln., review 78—60
spatial discretisation effect on steady state and transient solns. of dispersive wave eqn. 77—30014
stimulated EM shock radiation, by EM wave-fast electron interaction, freq. dispersive media 77—83796
surface wave propagation over liquid and crystalline layers, dispersion eqns. 80—76925
surface waves, inhomogeneous liq.-vap. interface, origin 78—75158
surface waves, method for separation of interfering waves and dispersion comp. 77—73649
surface waves propagation over liquid and crystalline layers, dispersion eqns. 80—76924
surface-wave dispersion in inhomogeneous medium, investigation by finite difference method 79—66631
thin walled elastomer tubes, dispersive effects in wave propag. 78—87289
three-frequency soliton solns. in second approximation *(Russian)* 78—57789
transient waves in fluid-filled porous media, refl., refr. and dispersion 77—49604
transition radiation in nucl. dispersive medium, nucl. levels and permittivity meas. *(Russian)* 77—59635
two-frequency dispersion interferometers for space plasma nonuniformity 79—70964
unsteady waves from initial, periodic and travelling disturbances, asymptotic anal. *(Russian)* 78—77254
viscoelastic fibre-reinforced composites, wave propag. 79—76992

dispersion continued
water surface, long-wave propag., modelling criteria, appl. to tsunamis 78—26132
water surface, oscillotory waves, Korteweg-de-Vries and Schrodinger eqns. solns. and expt. 78—26131
waveguide, plasma filled, EM wave freq. spectra dispersion eqn. numerical anal. *(Russian)* 78—59605
whistler dispersion, group delay automatic meas., ionosphere and magnetosphere electron density 78—93050
whistler dispersion measurement using five channels phase-locked loop discriminator *(Japanese)* 80—31143
whistler occurrence rate and dispersion real-time analyser 77—87129
whistlers, Dowden-Allcock approximation generalisation rel. to normalised dispersion values 80—51607
whistlers, low latitude, effect of ions 78—20575
whistlers observed at Sofia during decreasing solar activity period, dispersion characts. 79—8779
width-extensional vibration energy trapping by complex branches of dispersion curves 79—51911
zero sound, in classical liq., excitation, damping, memory function approach 78—67771
Bi, Bernstein waves, electrostatic wave dispersion relation in mag. field 80—34471
Co-P film, amorphous, spin wave dispersion law, spin wave reson. obs. *(Russian)* 78—88196
GaAs thin films, differential mobility anisotropy effect on wave propag. 78—88050
YIG film, dielec. layered struct., magnetostatic volume wave propag., dispersion eqn. 78—95426
YIG film, tangentially magnetised, magnetoelastic Lamb wave propag. 79—82856
YIG film waveguide, with periodic mag. struct., dispersion characts. anal. *(Japanese)* 79—42809
YIG, magnetised in raised cosine profile magnetostatic surface wave propag. 80—2567
YIG magnetostatic surface wave dispersion rel. to mag. saturation diffusion 78—2671
YIG sandwiched between grounded dielectric layers, magnetostatic bulk wave propagation 80—60380

dispersion hardening
see also precipitation hardening
acrylic bone cement containing second phase dispersions, strength 77—81663
alloy, dispersion hardened, particle size effect on fracture 79—43418
alloy, dispersion hardened, temp. depend. of work-hardening due to Orowan loops 79—91668
alloy, friction stress for high-temp. creep 78—11289
alloy, load type effect on yield stress 78—35458
alloy, overaged and dispersion hardened, dislocation bowing computed from Orowan relations 77—19949
alloy with dispersion precipitate of ordered phase, yield limit theory surmountable pair mech. *(Russian)* 77—1855
alnico, thermal magnetic hysteresis *(Russian)* 77—16119
bronze casting, graphite dispersed, graphite particle size effect on wear *(Japanese)* 79—15804
coarsening of dispersed particles, in solid matrices 78—56651
composite, soln. method of synthesis and crystn. 78—3076
digital simulation models, dislocation interaction treatment 78—31419
disperse particles concentration and spacings between them in Poisson point field model 78—39963
dispersion hardened metallic matrix composite, powder metallurgically produced effective interparticle distance effects *(German)* 78—52727
dispersion-strengthened alloys, threshold stress for creep 80—93626
earth reentry exposure, simulated, effect on mech. props., oxidation of ThO_2 dispersion hardened alloys 79—5086
electrical resistance alloys, oxidation mechanism *(Polish)* 79—79143
ferromagnets, hardening by non-mag. inclusions, meas. of coercivity 79—38841
glass-ceramic, dispersion strengthened glass matrix 77—40425
graphite particle-Al alloy composite, improved damping capacity and machinability 77—4786
Incaloy IN 738, dispersion hardened superalloy 78—11156
Incoloy, oxide-dispersion-strengthened, pulsed YAG laser welding 79—70075
kinematic hardening rule in single crystals 80—10551
metal, cast, oxide particle dispersion, new method of introduction 77—73283
metal, deformed, dispersion-hardening, theory of strength, *(Russian)* 78—35424
metal with dispersed oxide phase, charged particle theory of oxidation 78—19925
metallic materials, dispersion hardening *(German)* 80—50646
metallic materials, review *(German)* 80—45316
nearest-neighbour size correlation with grain size *(French)* 77—8843
Nichrome based dispersion hardened material, Ti, Y, Zr addition effects on crystallisation *(Russian)* 79—74143
Nimonic PE 16, γ' particle dispersion rel. to yield stress 79—29153
nucleation in recrystallisation, finely dispersed second-phase particles effect 77—8845
particle dispersed composite, fatigue life anal., reliability concept *(Japanese)* 79—29200
slip morphology in dispersion hardened materials 77—4785
stainless steel, ferritic SUS 410 type, coated with organometallic complexes and Ti alkoxides 80—34078
steel, alloy, transform. from austenite 77—25045
steel, austenitic, Kh12N20T3R, ageing, submicroscopic struct. role in dispersion hardening *(Russian)* 78—64549
steel, austenitic, metastable, hardening by cycling of martesitic transform. during rapid heating, in 30N24M4 and 50N21M3 *(Russian)* 79—20074
steel, C, coarsening of dispersed particles, in solid matrices 78—56651
steel, CrMoV, low alloy, dispersed phase of VC, hardening mechanism *(Czech)* 78—60676
steel, dispersion strengthened with Al_2O_3 or ZrO_2, by spray method into molten stream, exam. of mech. props. 79—11636
steel, ferritic, MA 956, oxide dispersion strengthened, mech. props. and damping behaviour 79—47702
steel, heat resistant, explosive loading effects on struct. and mech. props. *(Russian)* 78—39787

dispersion hardening continued

- steel, heat resisting, type 15Kh1M1F, exam. of structural stability and props. *(Russian)* 79—29104
- steel, hypoeutectoid, C22, recrystn., influence of carbides distrib., mech. props. meas. *(German)* 79—38850
- steel, intergranular fracture, impurity effects 77—8842
- steel, low alloy, ferritic-pearlitic, carbonitride hardening 80—104174
- steel, low C, NbN and VN dispersion hardening effect on mech. props. 78—3137
- steel, Mn-Si, 17G2S, VN and NbV dispersion hardening effect on mech. props. 78—3137
- steel, Ni-Mn-Al-V, nonmagnetic, ageing, dispersion hardening, microstruct., phase comp., mech. props. *(Russian)* 79—34046
- steel, stainless, Cr-Ni (20, 25 wt.%), TiN dispersion effect on oxidation 79—20279
- steel, stainless, Cr-Ni-Co (13, 4.5, 0 to 13.8 wt.%), Co effect on martensite ageing *(Russian)* 77—66660
- steel, stainless, ferritic, mech. props., impurity effects *(Russian)* 77—52403
- steel, stainless, oxide dispersed, prod. by spray dispersion method, mech. props. exam. of mech. props. *(Japanese)* 78—48419
- steel, Ti (0.1 to 0.55 wt.%), strengthening by carbide precipitation 77—25062
- steel, tool, maraging, based on N12M10, exam. of hardening, crack resistance and wear *(Russian)* 79—34047
- strengthening phase particle distrib., quantitative analysis 78—15629
- strengthening theories for dispersion hardened alloys 80—97498
- ticonal, thermal magnetic hysteresis *(Russian)* 77—16119
- yield stress of single crystals, temp. and strain rate depend. 77—48445
- Zircaloy, effect of dispersion and spheroidisation treatment of δ ZrH 79—76073
- Ag, with MgO particles, electrical contacts appl. *(Slovak)* 78—31544
- Ag-MgO, dispersion hardened, exam. of ductile fracture 79—34144
- Ag-MgO, laws of plasticity of dispersion strengthened materials 78—84832
- Ag-MgO (0.1 wt.%), intergranular cavity growth at elev. temps. 79—66068
- Al alloy, AK4-1, dispersion-hardening, US effects on ductility and thermal resist. *(Russian)* 77—32582
- Al alloy, dispersion strengthened, made by mech. alloying 78—3136
- Al alloy, graphite dispersed casting, damping capacity *(Japanese)* 79—96059
- Al alloy, particle strengthened, yield drop and creep minimum *(German)* 78—39881
- Al alloy, two phase, strength contribution of particles and dislocations *(German)* 79—29080
- Al, dispersion hardened, mech. props., effect of strain rate *(Czech)* 77—59865
- Al, dispersion hardened with refractory carbides, sintering 79—74118
- Al, dispersion hardening Al_4C_3 77—55978
- Al-Al_2O_3, dispersion hardened, creep *(Czech)* 80—108463
- Al-Al_2O_3 alloys, dilatometric method for studying relaxation of conc. of defects 77—55288
- Al-Al_4C_3, dispersion hardened physical props. meas. *(German)* 78—31415
- Al-AlN, disperse system prep. by heterogeneous reaction in molten metal *(Czech)* 77—85964
- Al-C, dispersion hardened, effect of processing parameters on mech. props. 80—20826
- Al-C alloys, dispersion hardened exam. of production method using pressed powders 80—16244
- Al-Cr-Zn (2.5, 1.5 wt%), phase equilibrium, solubility *(Russian)* 78—19723
- Al-Cu-Mg (4, 1.5 wt.%), mica dispersed, wear characts. and bearing performance 80—108591
- Al-Ge (2 wt.%), averaged, plastic flow mechanism 77—48507
- Al-Mg alloy, disperse β-phase, kinetic laws of coagulation *(Russian)* 78—27518
- Al-Mg-Mn alloy, disperse β-phase, kinetic laws of coagulation *(Russian)* 78—27519
- Al-Mg-Si alloy, Mg_2Si dispersion hardened US waveguides, concentrators *(Polish)* 80—89237
- Al-Si, deformed, local lattice rotations at second phase particles 80—25709
- Al-Si (1.2 and 0.6 wt.%), single crystal, dispersion hardened with SiC, Bauschinger effect and work hardening 79—43360
- Al-Si (1.2 wt.%), dispersion hardened, temp. depend. of work-hardening due to Orowan loops 79—91668
- Al-Si casting alloys, graphite-dispersed, mech. props. and wear resist. 77—4857
- Al-SiO_2 (2wt.%), dispersion hardened particulate composite, prep. 80—7588
- Al-Zn (21.8 at.%), elec. conductivity and α'-precipitates, 276-302°C 77—80758
- Al-Zn-Mg, plastic deform. influence on structural transform. and mechanical props. *(Russian)* 80—7623
- (Al-Mg-Si)-Al_2O_3, SAP type, ageing 79—96055
- Al_2O_3 dispersion hardened by Ba mica, thermal diffusivity 80—25713
- Al_2O_3-Cu composite, dispersion-strengthened, hardness, tensile strength and struct. 77—70063
- Al_2O_3-Cu composite, vapour deposition, microstruct., texture and surface topography 77—70001
- Al_2O_3-TiC, multiphase ceramics, mech. strengthening due to dispersion of non-metallic particles *(German)* 78—60674
- Al_2O_3-ZrO_2, dispersion hardened, fracture toughness improvement by induced microcracking *(German)* 78—31501
- Al_2O_3-ZrO_2, multiphase ceramics, mech. strengthening due to dispersion of non-metallic particles *(German)* 78—60674
- Al_2O_3-ZrO_2 dispersed system, fracture toughness, inclusion induced microcracking effect 78—11296
- Al_2O_3+TiC system, elastic and fracture charact. at elev. temp. *(German)* 79—43299
- Au-Cu alloy, internal oxidation, calorimetric meas. 79—43258
- Au-Mg alloy, internal oxidation, calorimetric meas. 79—43258
- Cd-B(W) particulate composite, dispersion hardening, grain size and texture strengthening 77—8840
- Co-Cr-Ta(Al) alloy, high temperature wear resistant coatings, CrO_2 hardened 79—24677
- Co-WC dispersion hardened alloy, tensile deform., volume fraction of second phase effect, simulation *(Japanese)* 79—70122

dispersion hardening continued

- CoCrAl alloy, Al_2O_3 forming, oxidation resistance improvement by dispersed oxide addition 79—83379
- Cr-AlN, dispersion hardened, erosion resistance 77—12637
- Cr-AlN, dispersion strengthened, hardness and oxidation rate, 1000 to 1500°C *(Russian)* 78—15574
- Cr-La-V-Nb-Ta, La, V, Nb Ta effect on hardness and strength *(Russian)* 79—34050
- Cr-Ti/MgO-NbC(TaC) dispersion-strengthened, high temp. wear and oxidation resist. 80—25877
- Cr-Ti/NbC(TaC) dispersion-strengthened, high temp. wear and oxidation resist. 80—25877
- Cr-V-Ce-N, (2.4 to 2.6, 1.7 to 2.3, 0.005 to 0.23 wt.%) V effect on hardness, and ductile to brittle transition temp. *(Russian)* 79—34138
- Cr-Y_2O_3 dispersion hardened, oxidation and nitridation resistance, embrittlement 78—44267
- Cr_2O_3-stainless steel system under fusion reactor first wall condition, oxide dispersoid stability 80—40374
- CsI:Na^+(K^+),(Cu^{2+}),(Tl^{3+}),(Eu^{3+}), crysts., influence of impurities on yield stress 79—15748
- Cu alloy, graphite dispersed casting, damping capacity *(Japanese)* 79—96059
- Cu based materials, sputter deposited at high rate, microstruct. and props. 78—22988
- Cu, dispersion hardened, mobile dislocation density and length of slip lines 77—51387
- Cu-Al, dispersion hardening by internal oxidation 78—56649
- Cu-Al_2O_3, dispersion strengthened, plasticity qualities, fractographical analysis *(Czech)* 80—50680
- Cu-Al_2O_3, dispersion-strengthened, vapour-deposited, tensile creep 78—11115
- Cu-Al_2O_3 (1 vol.%), effect of second phase particles on diffusional creep 78—31472
- Cu-Al_2O_3 coatings, electrodeposited, dispersion hardened, exam. of props. 79—34181
- Cu-Al_2O_3 composite coating, electrodeposited, exam. of particle-cathode adhesion during formation 79—33954
- Cu-Al_2O_3 dispersed system, electron beam evaporated thick film, struct./prop. relations 77—44198
- Cu-Al_2O_3 dispersion hardened wires, drawn, substruct. and strength 78—35405
- Cu-Al_2O_3 electrodeposits, dispersion hardened, props. 79—28258
- Cu-Al_2O_3 extruded bars, strength anisotropy 77—16597
- Cu-Al_2O_3(SiO_2) dispersion hardening single crystal, cyclic deform. *(French)* 79—1893
- Cu-Al-Ti-Zr, internally oxidized, morphology of precipitates and dispersion hardening *(Russian)* 79—52217
- Cu-Cu_2O crystallisation from melt, influence of crystn. conditions on struct. *(Russian)* 79—38814
- Cu-MgO, dispersion hardened, prep. by milling Cu and Mg oxidising atmos. *(German)* 78—64509
- Cu-MgO, dispersion hardened alloys, prep. and props. 80—40291
- Cu-SiO_2, deformed, lattice rotations at second phase particles 80—25709
- Cu-SiO_2, dispersion hardened, surface plasticity effect 78—52832
- Cu-SiO_2 (0.0052 vol. fraction), work hardened, low temp. softening, particle size effects 77—52342
- Cu-SiO_2 single crystals, dispersion hardened, exam. of yield stress between 77 to 1200K 78—76720
- Cu-Sn, graphite dispersed, wear, effect of graphite content *(Japanese)* 77—56114
- Cu-ThO_2(ZrO_2) alloys, dispersion hardened, electrical cond. and mech. props. 78—44133
- Cu-Ti-Fe (0.7, 0.9 wt.%) film, dispersion-strengthened, form. by high rate magnetron/plasmatron sputtering, and props. 80—25715
- $CuAl_2$, single cryst., embrittlement and subboundary hardening via interstitial segregation *(Russian)* 77—12679
- Cu_3Al-Al_2O_3 dispersion hardenend, short range order, quenching effect on yield stresS 78—35399
- Fe alloy, oxide dispersed, mech. alloying, microstruct. 77—25063
- Fe alloy MA-956E, oxide dispersion strengthened sheet, tensile and creep props. at 1365K 78—48470
- Fe based dispersion strengthened thick condensates, struct., mech. props. 77—90361
- Fe, softening vs. hardening effects produced by high fugacity H charging 79—74172
- Fe-BeO, dispersion hardened alloy, struct.-props. relationships 77—66652
- Fe-Cr, high temp. oxidation, internal stable nitride and oxide dispersion 79—39017
- Fe-Cr (13 wt.%)+polycarbosilane, powder metallurgy, characts. 77—85962
- Fe-Cr-Al-Y (Y-Al_2O_3)(Y_2O_3), preparation and exam. of mech. props. 78—52720
- Fe-Cr-Ti-TiO_2 (13, 2.5, 2 wt.%), dispersion hardened, ferritic alloy DT02, oxidation, 823 to 1123K 79—61803
- Fe-Mn-Nb-V, high Mn, dispersion strengthening 77—16602
- Fe-NbN-C-Mn-Si, dispersion hardening effect on mech. props. 78—3137
- Fe-Ni-Cr, austenitic, dispersion-hardened alloys, thermomechanical working *(Russian)* 77—66659
- Fe-Ni-Cr austenitic alloy, homogeneous and dispersion strengthened, internal stresses and high temp. creep 78—19841
- Fe-Ni-Cr based alloy, KhN35VTYu, temp. depend. of energy of fracture, influence of γ' phase *(Russian)* 80—81147
- Fe-Ni-Cr-Ti-Al Elinvar alloys, dispersion-hardened, structural transform. *(Russian)* 79—1872
- Fe-Ni-Mo-C, Mossbauer investig. of secondary hardening, carbide form. *(Russian)* 77—44260
- Fe-P (0.14 wt.%), cavity formation at grain boundary-subboundary interactions 77—86040
- Fe-refractory compound, dispersion strengthened, thick vacuum condensate, control of struct. and mech. props. 80—16324
- Fe-refractory compound condensate, struct. and mech. props., disperse particle content depend. *(Russian)* 78—19772
- Fe-VN-C-Mn-Si, dispersion hardening effect on mech. props. 78—3137
- Fe-VN(NbN)-(C), dispersion hardening effect on mech. props. 78—3137
- Fe-X-MoS_2 (X=WC, HfC, Al_2O_3, ZrO_2, HfB_2, ZrB_2), self lubricating coatings, exam. of props. 79—96217
- KCl:Ba(Ca)(Sr), microstruct. and hardness, impurity distrib. effects 79—24529
- Mg-Ga (6 wt.%), precipitation, lattice const., ageing effects *(Chinese)* 79—43279

dispersion hardening continued
MgO-ZrO_2, dispersion hardened, fracture strength and texture, rel. to temp. *(German)* 79—43378
Mo alloy, ZrC dispersion hardened, thermally activated plastic deform. *(Russian)* 77—36612
Mo alloys, dispersion-strengthened, plastic deform. and hardness, temp. depend. 80—3087
Mo and Mo superalloys high temperature properties 78—44173
Mo, dispersed nitride strengthening anomalies *(Russian)* 77—21154
Mo-AlN, dispersion hardened, erosion resistance 77—12637
Mo-Nb-TiN, dispersion hardened with strong interface, fracture mechanism 79—5058
Mo-TiC(ZrC)(TiN), phase diagram *(Russian)* 78—27476
Mo-TiN (3.5 vol.%), failure characts. exam. 78—68788
Mo-W-Mo (4.74, 2.17 wt.%), creep resistance in ultrahigh vacuum 79—5027
Mo-ZrC, internal oxidation, struct. formation law, microstruct. examination 78—84836
Mo-ZrO_2 dispersion hardened, rolled, grain struct. and props. 77—77492
Nb-Zr (1 wt.%), internal oxidation state of O_2, dispersion hardening by diffusion alloying, X-ray diffr. and internal friction *(Russian)* 79—70102
Nb-Zr-C alloy, strengthening phase, particle distrib. anal. *(Russian)* 79—15685
Nb-Zr-C alloys, dispersion-hardened with carbide phase, influence of hydrostatic extrusion on struct. and props. *(Russian)* 77—52338
Ni alloy EhI867, effect of structural state on fatigue and heat resistance *(Russian)* 79—34140
Ni alloy IN-738, Y_2O_3 (1.5 wt.%) addition, mechanical alloying 77—40427
Ni, oxide dispersion strengthened, creep and tensile props. 77—86042
Ni, oxide dispersion strengthened materials, effect of prior creep at 1365K on room temp. tensile props. 78—39857
Ni, sintered carbonyl type and with dispersed ZrO_2 inclusions, struct. effect on high-temp. ductility 77—63757
Ni superalloy, dispersion strengthened, creep stress component rationalisation *(Korean)* 79—66115
Ni-Al_2O_3, composite coating, electrodeposited, exam. of particle-cathode adhesion during formation 79—33954
Ni-Al_2O_3 alloy, electron beam evaporated, struct. and mech. props. 78—11114
Ni-Al_2O_3(ZrO_2), dispersion strengthened, thick vacuum condensate, control of struct. and mech. props. 80—16324
Ni-Al-Ti(Nb), heat-resisting dispersion-hardening alloys, props. and struct., γ'-phase comp. influence *(Russian)* 80—20943
Ni-Cr, dispersion strengthening, prep. from powder, mech. props. 79—91658
Ni-Cr, heat resisting, dispersion hardened, electrical resistance meas. *(Russian)* 77—66708
Ni-Cr, solid soln., exam. of back stress role in creep behaviour of particle strengthened alloys 78—52889
Ni-Cr alloy, dispersion-hardened, prod. by mech. alloying 78—15345
Ni-Cr alloy KhN70VMTYu, heat resistant, explosive loading effect on struct. and mech. props. *(Russian)* 78—39787
Ni-Cr powder mixture, dispersion hardened, homogenisation 77—12638
Ni-Cr-Al (15, 5 wt.%), oxide dispersion strengthened, effect of dispersoids on oxidation 78—80679
Ni-Cr-Al-ThO_2, hot corrosion, cyclic oxidation depth of attack determinations 80—11837
Ni-Cr-Al-Ti (Ti-Co), exam. of back stress role in creep behaviour of particle strengthened alloys 78—52889
Ni-Cr-HfO_2, dispersion-strengthened, hot rolling effects on props. *(Russian)* 77—59797
Ni-Cr-ThO_2 (20, 2 wt.%), dispersion hardened, model for high temp. deform. based on struct. obs. 78—19809
Ni-Cr-ThO_2(20, 2 wt.%), dislocation struct. after high temp. deform. 77—52393
Ni-Cr-Ti-Al-Fe-Co (19.65, 2.40, 1.37, 0.78, 0.52 wt.%), strength of γ' hardened alloy, ageing exam. 78—88501
Ni-Cr-ZrO_2, dispersion hardened, sintered, rupture 77—21272
Ni-Cr-(Al), oxide dispersion strengthened, creep and tensile props. 77—86042
Ni-Cr-(Al), oxide dispersion strengthened materials, effect of prior creep at 1365K on room temp. tensile props. 78—39857
Ni-HfO_2 (3 wt.%), dispersion hardened alloy VDU-2, thermal and mech. treatment 77—90376
Ni-HfO_2(2.14 wt.%), dispersion hardened, HfO_2 particle size effect on struct. and mech. props. *(Russian)* 80—20944
Ni-Mo-W, diagram of state, W solubility, dispersion hardening *(Russian)* 80—66477
Ni-SiC, electrodeposited, oxidation 78—64756
Ni-SiC(WC), dispersion hardened coating, chemically deposited using electroless baths, exam. of protection props. 79—34208
Ni-SiO_2 composite film, influence of hardening phase on yield stress *(Russian)* 79—5001
Ni-ThO_2, dispersion hardened, fracture mechanism map 78—60823
Ni-ThO_2, dispersion strengthened, high temperature cyclic deformation 80—16430
Ni-ThO_2, irradiated with 5 MeV Ni^{++}, ThO_2 redistrib. 78—71771
Ni-ThO_2 (2.51 wt.%), dispersion hardened, high temp.-strength, deform. method and annealing effects 79—1882
Ni-ThO_2 dispersion strengthened, high temp. strength, grain size and shape effects 77—48447
Ni-ThO_2(HfO_2) dispersion hardened alloys, recrystallisation during annealing, O_2 partical press. effects *(Russian)* 78—3140
Ni-WC, dispersion hardened, centrifugally cast metallurgical coatings for wear resistance in plastics molding machines 79—29285
Ni-ZrO_2, dispersed inclusions, effect on recovery and recrystallisation 77—25064
Ni-ZrO_2, dispersion-strengthened condensate, density and mech. props. 77—44196
Ni-ZrO_2, electron-beam-evaporated condensate, cold deform. and annealing effects on microstruct. 80—16331
Ni-ZrO_2, thin layers, vapour deposited, dispersion strengthened, exam. of struct., mech. props. 78—80554
NiCr-MoAl-ThO_2 (13,3 wt.%), powder, mech. alloying 78—84744
Ni_3Sn_2, single cryst. embrittlement and subboundary hardening via interstitial segregation *(Russian)* 77—12679
Nr-Cr-ThO_2 (20, 2 vol.%), Orowan stress/creep threshold stress comparison 77—8901

dispersion hardening continued
Pb-Al_2O_3 composites, mech. alloyed, hot hardness meas. *(Japanese)* 78—84830
Si_3N_4-ZrO_2, sintered and hot pressed, exam. of mech. props. 78—48509
TC-Co, nearest-neighbour size correlation with grain size *(French)* 77—8843
Ti sintered, struct. stability, effect of dispersed refractory compound inclusions 77—28825
Ti-Al (14.7 wt.%), sintered, mech. props., effect of alloying and dispersed ZrO_2 phase 77—12636
Ti-Al_2O_3 system mixed films, prep., phase comp., struct. and elec. props. 79 -37930
Ti-Al-Mo(Cr)(Fe), thermomechanical treatment effect on mech. props., strengthening mechanisms 80—55441
Ti-Mg-ZrC(HfC)(TiC)(TiB_2) sintered, friction and wear props. 79—70019
Ti-Nb-Ta-Ge (40,20,0.8 wt.%) foil, dispersion hardening, TEM and electron diffr. obs. *(Russian)* 79—1873
Ti-Y(Er), dispersoid effect on deform. 79—24530
TiC film, Au-dispersed, struct., hardness and wear rate 77—77493
V-Nb-Ti-N alloy, dispersion hardened, fracture characts. 79—15794
V-Si, strengthening by internal oxidation 80—55424
V-Zr, strengthening by internal oxidation 80—55424
W alloys, recrystallisation alloying effects of ThO_2, Mo-Re, HfC, NbC 77—70083
W, wire, doped, high temp. creep behaviour 78—88499
W-WC, activated sintering, mech. props. *(Korean)* 78—60622
WC-Co, nearest-neighbour size correlation with grain size *(French)* 77—8843
WC-Co alloys, P additions, effect on hot pressing, hardness and wear resist. 78—11162
Zircaloy, dispersion and spheroidisation treatment of δ ZrH, effect on corrosion resistance 79—76072
Zr-Dy dil. alloys, plastically deformed, mech. props. and microstruct. *(Russian)* 79—20112
ZrO_2-ZrO_2, multiphase ceramics, mech. strengthening due to dispersion of non-metallic particles *(German)* 78—60674

dispersion power, rotatory *see optical rotation*

dispersion relations
see also dispersion (wave); Kramers-Kronig relations; Mandelstam representation; N/D method; phonon dispersion relations; phonons; plasma instability; plasma waves; S-matrix theory
$\Delta\sigma_L$ (pp) between 400 and 600 MeV 79—45097
π+nucleus low-energy forward elastic scatt., dispersion relation anal. 77—14200
$\pi\pi$ scattering at high complex energies, amplitudes with isospin 1 or 2 77—67631
ϕ^4 Grinzberg Landau Wilson model, dispersion theory and ε expansion for $T>T_c$ 79—12753
acoustic pulse in medium with high thermal cond., dispersion relation 77—27409
Adler sum rule subtractions and charge symmetry violation 77—18202
amorphous ferromagnets, dispersion rels. and spin-wave spectroscopy *(Russian)* 79—7983
analytic bounds on Pomeron trajectory from dispersion inequalities 79—361
analyticity verification 77—30283
anisotropic moving media, polarisation relations and dispersion eqns. to EM waves 80—9779
atom, forward elastic electron scatt. amplitude, dispersion relation 78—90263
atom+electron scatt., static exchange approx., third-order pole in exchange amplitude 77—83735
atomic electron scatt., analyticity and dispersion relations 77—23561
atoms, dispersion relations and AC Stark effect 78—945
bar, rectangular cross section, dispersion relations of elastic waves 78—9585
baryon resonances and electromagnetic couplings 79—9384
Benjamin-Ono eqn., multi-soliton like solns. 78—28960
Benjamin-Ono equation, meromorphic solutions 80—31980
biexcitons recombination, polariton effects 78—23033
Bose gas, charged, in uniform mag. field, zero-temp. dielec. response 77—5758
bounded skewed shear flow, tensor form of bulk dispersion coeff. 78—73393
Brillouin scattering process kinematic dispersion relation, wave vector surfaces representation *(German)* 78—19492
capillary wave dispersion relation, for isotropic liq., two-mode struct. 79—98741
charge-density waves, lock-in transition, effect of thermal fluctuations on harmonics 79—19338
circumferential waves, cylindrical shell supported by a continuum 78—90564
coherent submillimetric Cherenkov radiation generated by relativistic electron beam 77—38793
collective excitations, brief review of expt. and theory 77—1381
complex reflectivity, phase and amplitude 77—65572
conference on few body systems and nuclear forces, Graz, Austria (Aug. 1978) 79—80880
conserved axial second class current, sum rule, commutation relations and axial formfactor 80—18090
Cottingham formula, nuclear Coulomb energy differences 78—37256
coupling constants from dispersion anal. of N and d scatt. amplitudes, ^{6}Li-α-d, ^{4}He-d-d, ^{3}He-d-p, ^{3}H-d-n, ^{2}H-p-n 78—29399
crystal electronic spectrum, EM wave influence, parabolic and spherical dispersion relations 79—33218
crystal lattice electron energy spectrum depend. on external electric field *(Russian)* 80—34498
cubic lattice, soluble dispersion reln. for 3-D band struct. 77—8007
cubic symmetry cryst., quadrupole exciton theory 80—103632
cyclotrons resonance maser, Vlasov-Maxwell eqns., guided wave field theory 80—14309
decay state interactions, autoionisation bands *(Russian)* 80—75486
dielectric film, reflectivity, polariton standing-wave struct. as test of boundary conditions for spatial dispersion theories 79—4865
dielectric function, inverse RPA calcs. at metal-vacuum interface 78—14789
digital spectral techniques in plasma fluctuation diagnostics 80—49003
directional wind wave spectrum meas., role of dispersion reln. 79—20860
Drell ratio and the existence of a second heavy lepton 79—13048

dispersion relations continued
drift wave instability, due to nonuniform density gradient in sheared mag. field 79—23415
education, dispersion eqn., long wavelength approx., appl. EM wave in plasma 80—17735
elastic wave propagation, influence of random porosity 78—90552
electrodynamics of moving media, drag effect involving dispersion term *(Chinese)* 78—12558
electron beam, relativistic, unmagnetised, stimulated scatt. anal. of HF incident pump wave 79—77345
electron Fermi gas, quasistatic surface wave spectrum 77—84434
electron gas, 2D, intermediate density region 79—60110
electron gas, multipole surface plasmons, bulk-selvedge coupling theory 79—28394
electron plasma, war, isotropic, drifting, waveguide modes, relativistic electrodynamical study 79—77393
electron waves in plane periodic system, linear theory 80—48130
electron-hole plasma current layering, electron cooling length, momentum scatt. 80—6890
electronic localised state at edge dislocations, parabolic dispersion law *(Russian)* 80—65479
electronuclear sum rules, generalised, from EM structure functions 78—89806
electrothermal waves, in nonequilibrium MHD plasma, dispersion relation 79—98904
elementary excitations, dispersion relations, with damping 78—14687
EM oscill. spectrum, toroidal plasma-containing system 80—79471
EM wave propag. in plasma with static magnetic field of arbitrary direction 79—68927
EM wave propagation, homogeneous electrically anisotropic medium, dispersion equations *(Czech)* 80—37938
energy bands and gaps, phase integral method, Mathieu pot. appl. 80—22224
energy dispersion relation in valence band of quantum pendulum, semiclassical calc. 78—41199
Erdogan-Chatwin nonlinear diffusion eqn., asymptotic solns., pipe flow solute dispersion 79—32673
exciton dielectric type system with doping, low freq. excitations *(Russian)* 80—15459
ferromagnets, exchange and dipolar coupled, spin wave renormalisation, Damon-Eshbach surface spin waves 80—2564
fixed-t, single π photo and electroprod., theoretical anal., fixed-t dispersion relations 77—22743
forward dispersion relations appl. to $^{12}C+K^{\pm}$ scatt. 77—18626
galaxies, dispersion relation of gravitating spiral system 77—87538
galaxies, tightly wound density waves, nonlinear self consistent theory 79—101206
galaxy, disc shaped, global dispersion reln. for density waves 79—62916
galaxy disc, Lin-Shu dispersion relation appl. to axisymmetric disturbances 79—21410
generalised optical theorem and dispersion reln. for $3\to 3$ forward amptitude 79—22079
ghost-pole subtraction and the σ-exchange NN potential 80—86819
graphite, diamagnetism with quasilinear dispersion law, orbital susceptibility, valence bands *(Russian)* 80—80475
Green's function calc. by coupling const. dispersion relations 77—45987
hadron+hadron elastic scatt., >100 GeV, asymptotic theorems review *(Czech)* 78—29357
hadron scattering amplitudes, integral axiomatic restrictions *(Russian)* 77—82685
haeme proteins, inversely polarized modes in reson. Raman scatt., depolarisation dispersion curves, vibronic interactions 78—78676
heavy ion forward scattering dispersion rels. *(Rumanian)* 80—47501
heavy quarks, widths of neutral vector mesons 78—8602
HF wave dispersion for complex wave numbers, ordinary waves 80—70740
high density plasma interaction with a strong EM wave, Green's function method calcs. 80—48885
high-density pulsed plasma, laser interferometry 78—67430
holographic unslanted transmission and reflection gratings, modal theory, EM wave propag. 80—83673
hydromagnetic waves in high β plasmas, dispersion relation rel. to wave propag. and damping 80—17482
I-beams, dispersion relations for normal modes 78—9597
inhomogeneous semiconductor plasma filled rectangular waveguide propagation 79—68928
interface dipolar plasmon in liq. multilayer struct., freq. and dispersion relations 77—59323
interior dispersion relations appls. to π photoprod. near threshold 78—93889
internal waves excited by travelling forcing effects, compressibility influence 78—61495
interplanetary scintillation velocities, dispersion depend. and scintillation pattern rearrangements 79—96879
ion-acoustic instability oscillations in collisionless single ended Q-machine 80—38731
Jeans' gravitational instability of an anisotropic plasma with generalised polytropic equations of state *(Italian)* 79—94780
K_L^0-K_S^0 transmission regeneration in H, comparison of expt. data and theoretical prediction *(Russian)* 77—49955
Kramers-Heisenberg dispersion formula, Dirac transformation generalisation 78—16960
laminated viscoelastic composite, wave propag., dispersion relations, mode shapes, variational methods 78—18215
layered cylindrical shell, circumferential waves 79—94533
layered cylindrical shells, normal modes 79—94548
liquids, simple, elementary-excitation dispersion relation 77—31816
localisable field theories *(Russian)* 77—74618
long range oscillating pots., scatt. theory and dispersion relations 80—22213
magnetic fields, twisted, dispersion relations and stability 78—45217
magnetised plasma, parametric instabilities with well separated freq. *(Chinese)* 80—106887
magnetised plasma stability in large amplitude circularly polarised wave, dispersion relations 80—59223
many-particle dispersion relations, Regge theory 77—10200
massless non-abelian gluon confinement and rising total cross sections 80—13264
massless $[g\phi^4]_4$ theory, functional integrals, complex instantons and asymptotic perturbation series 80—86571

dispersion relations continued
medium beta plasma with velocity gradients, dispersion relation for drift waves 80—64719
metal, APW dispersion relation for plasmons 77—69265
metal particles, spherical, surface plasmon dispersion relation, hydrodynamical model 78—84277
metal surface, with adsorbed at., XPS intrinsic plasmon satellites, dispersion and lifetime effects 79—56151
metallic ferromagnet, antiresonance region, EM wave propag., Maxwells' eqns. soln. 80—66038
metals, collective modes of void-surface coupled systems, surface plasmons 80—49642
metals, proper EM radiation on inelastic electron tunnelling with photon emission, cond. *(Russian)* 80—54765
MHD pulses in Sun, dispersion relations rel. to use as diagnostic technique 80—109405
mixed valence compounds, dynamic susceptibility, RPA study of Anderson lattice 80—97075
modified K-matrix formalism for meson-meson scatt. amplitudes crossing symm., unitarity 77—82774
monolithic crystal filter overtone mode analysis 77—39170
moving magnetoplasma slab, space charge waves propag. 80—38700
multichannel partial-wave dispersion relations, coincident thresholds, pole approx. 79—9293
nonlinear electron plasma waves in magnetised plasma waveguide 80—38662
nonlinear equations with soliton solns. 78—45467
nonlinear susceptibilities of solids, spectral representation, asymptotic relns. 77—50715
nuclear fission, Sommerfeld-Watson transformation *(Rumanian)* 78—86526
nuclear forces, dispersion theoretical approach to NN interaction 79—85380
nuclear form factors, dispersion relation approach, pole and quark-counting model 77—26568
nuclear matter, dispersion relations, HF method for hard core interactions *(German)* 78—54713
nuclear optical model potl. energy depend. anal. 77—30537
nucleon form factors, dispersion theory, review 77—34155
optical properties of rough surfaces, general theory and small roughness limit 77—75423
P-f identity hypothesis, resolution problems 79—75747
parametric interactions in inhomogeneous medium with abrupt boundaries 77—49606
partial wave amplitudes asymptotic behaviour, Regge models and dispersion relations 77—10204
phase transition, 1st order, ageing stage, kinetic instabilities 78—87765
photon dispersion in asymptotically strong magnetic fields 77—82697
photon reflection, phase-shift sum rules, for complex polarisation amplitude 79—69802
photon scatt., exchange effects, scatt. amplitude and integrated photoabsorpt. cross section 77—82910
piezoactive waveguide, anisotropic, normal waves propagation 77—88975
pion-nucleus s-wave amplitude, test of new threshold expansion using dispersion relns. 77—6325
pion-nucleus scatt. amplitude determ. using derivative sum rules and dispersion relations 77—10373
plane EM waves in moving lossy medium, relativistic dispersion relation 77—37764
plasma, Bernstein dispersion relation for oblique propagation 80—75052
plasma, dispersion relation for EM instability 80—64725
plasma, dissipative trapped electron instability dispersion relation, ion-ion collisions 78—34290
plasma, drift and Alfven modes, current driven, electron-ion collisions and full dispersion function, numerical anal. 80—64726
plasma, hot collisional uniaxial, guided waves, TM mode dispersion rel. 80—53995
plasma, instability hindrance in a magnetically confined plasma with finite press. 80—59221
plasma, ion-acoustic waves freq. and damping from dispersion relations 80—69991
plasma, kink mode, in presence of helical RF mag. field, dynamic shear stabilisation 79—50858
plasma, moving weakly nonsteady, plasma wave propag. 80—106918
plasma, of electrons, warm, transversely-drifting, in strong mag. field, waveguide modes 79—50861
plasma, self-gravitating, isotropic pressure, wave propag. and dispersion relation 80—72763
plasma, turbulent, parametric instabilities, anomalous energy absorpt., dispersion eqn. 80—92291
plasma, two-component, nonlinear waves 77—62354
plasma anisotropic jet, dispersion relation for stability 77—17353
plasma anisotropic longitudinal waves 80—14891
plasma drift instability in Hall current plasma accelerator 77—19705
plasma drift waves, instability in AC elec. field wave growth rate and dispersion relation 80—48886
plasma drifting, cold or hot, radiation potential of immersed point antenna, DRFT computation 80—14906
plasma electrostatic heat flux instabilities, linear Vlasov dispersion relation 78—79420
plasma electrostatic shear flow instability linear dispersion relation 80—96359
plasma interaction with strong EM wave, efficient transformation of radiation frequency 80—106931
plasma ion oscillation excitation by freely propagating electron beam *(Russian)* 80—1815
plasma resonant collective processes, wave and particle accel. into increasing plasma gradient 77—47153
plasma rotating layer, self-gravit. instability dispersion relation 80—56706
plasma sheet, current-carrying, stability 79—60133
plasma surface EM wave interaction with relativistic electron beam 79—60153
plasma wave packet propagation through infinite homogeneous plasma, dispersion relations 80—38653
plasma waveguide, collisionless, dispersion relations *(Chinese)* 77—58865
plasma-wave dispersion rels., modification due to magnetic monopoles, pulsar emission 79—75704
plasmon dispersion in simple metals 78—91629
plasmon surface polariton dispersion curve, optical obs., demonstration 80—101690

dispersion relations continued
polynomials, analysis methods 79—67141
polytypes, one-dimens. Kronig-Penney model and calcs. 80—75494
Pomeranchuk theorem inverse for log rising total cross sections 77—71546
proton Compton scattering, dispersion relation anal. 79—36084
pseudoscalar Dalitz decays, form factor slopes, VDM with subtracted dispersion relation 78—58181
randomly distributed dielectric scatterers, dispersion relations, coherent wave phase velocity and attenuation 79—72466
reflectivity, normal, superconvergent sum rules 77—85678
relativistic electron ring azimuthal oscillations in resonator with stabilising medium *(Russian)* 78—29889
relativistic Kelvin-Helmholtz instabilities in extragalactic radio sources, general dispersion relation 78—45419
relativistic nonlinear electron cyclotron waves in plasmas 80—10377
relativistic particle ring, coherent oscillations, radial mode dispersion relations 78—55060
relativistic plasma, nonlinear dispersion relation for transverse wave 80—87939
relativistic systems, Bogolyubov equation hierarchy, plasma wave radiation damping 79—77377
renormalisable field theory differential dispersion relations, theory of ψ particles 77—26535
renormalisation group equations homogeneous dispersion approach 77—41753
rotating electron-plasma column space-charge wave propagation 77—55137
Roy eqns., regularisation with smooth cut off 78—29271
s-channel resonance prod. in πN scatt., amplitude zeros in Mandelstam plane 80—73686
S-matrix theory of relativistic elastic scatt., crossed channel struct. effects *(German)* 79—58906
S-wave $I=0$ KN scatt. length and forward cross-sections 78—37231
scattering amplitude zeros 79—21983
semiconductors, EM wave interaction in weakly nonlinear medium with superlattice 80—93257
semiconductors, two-dimensional, Mott exciton formation in high mag. fields *(Russian)* 80—65467
skin impedance parameter dispersion and correlation 79—29518
soliton nonlinear refraction and self-focusing effects *(Russian)* 80—98805
soliton velocity and linear dispersion relation, higher order corrections 80—46826
surface plasmon dispersion relation in presence of spatial dispersion 79—42612
surface plasmon dispersion relation in presence of surface roughness 80—65650
surface plasmons on rough surface, dispersion relation splitting 79—60739
surface waves in prestressed body with cylindrical cavity *(Russian)* 78—63369
thin film rib waveguide, numerical anal. by mode-matching method 80—48421
thin stretched foils, membrane wave excit. 78—90578
thin strip vibrations, dispersion of flexural normal modes 78—1604
three gluon exchange contribution to forward high energy scattering 79—26310
transition metal spectral emissivity variation with temp. *(Japanese)* 79—1517
transverse wave packet, 3-dimens., nonlinear evolution in hot plasma, ion-acoustic wave effect 80—43899
tunnelling MIS structures photovoltaic energy conversion, band struct. 80—92995
turbulent plasma, ion-acoustic wave, dispersion relation calc. 78—26284
two dimensional dispersion relations, phase problem appl. 80—102631
two Maxwellian plasma, electron plasma wave, higher order Landau modes 80—38601
two-layer fluid, dispersion relns. for internal waves *(French)* 77—68602
two-temperature plasma electron-wave dispersion 79—86580
ultrashort laser pulses, interaction with condensed matter *(German)* 79—27335
unidirectional wave motions, book 78—77730
unitarity and crossing in high energy scatt., differential cross section in diffraction region *(Russian)* 79—80764
US excitation and detection in mag. polarised nonferromagnetic metals. 78—56856
vacuum polarisation, breakdown of normal threshold dispersion relation, naive quark model 77—2849
variational nature of eigenvalue problems with a parameter 79—77338
Velicky's method, appl. to GaAs optical properties calc. *(Spanish)* 77—90119
velocity dispersion of missing mass in solar neighbourhood, stability of N-component stellar disc 78—69886
water bag plasma, electron plasma wave, higher order Landau modes 80—38601
wave propagations in orthogonally reinforced fibre composites 78—41168
X-ray scattering, anomalous, Kramers-Heisenberg dispersion calc. 79—89628
Yang-Mills theory, large order calcs. 78—8511
cross sections in dispersion-relation anal., geometrical scaling 78—74260
d, charge form factor falloff at large q^2 in dispersion approach *(Russian)* 79—3027
D-meson, gauge theoretic formulation of $SU_2 \times U$, model, mass limit 78—70316
$(e^+d^- \rightarrow$-hadrons$)/(e^+e^- \rightarrow \mu^+\mu^-)$ cross sections ratio, differential dispersive anal., narrow resonances 78—37223
e^+e^- annihilation, charged energy fraction data, Drell ratio and second heavy lepton 79—13097
e^+e^- annihilation channel, differential dispersive theory of ψ/J 78—45933
$e^+e^- \rightarrow \rho\epsilon$, transition form factors, dispersion theory 79—63495
$e\pi$ inelastic scattering, asymptotic bounds on π form factor 78—12917
$\eta' \rightarrow \eta\pi\pi$, finite dispersion relation calc. of decay rate 78—41542
$f'(1514) \rightarrow 2\pi$, decay amplitudes, OZI rule, dispersion relations, intermediate states contribs. 79—383
$\gamma N \rightarrow N\pi$, P-odd multipole amplitude, dispersion relations *(Russian)* 79—93435
$\gamma N \rightarrow \pi\Delta(1232)$, multipole amplitudes, dispersion relations 80—5002
$\gamma N \rightarrow \pi N$, dispersion rels. by method of Pade approx. 77—34166

dispersion relations continued
$\gamma N \rightarrow \pi N$, P-odd partial amplitudes, dispersion relns. *(Russian)* 79—85304
$\gamma N \rightarrow \pi N$, resonance region photoprod., dispersion model, M1 and E2 photoexcit. $N \rightarrow \Delta(1236)$ 78—70377
$\gamma NN \rightarrow \gamma NN$ forward scatt. amplitude and generalised optical theorem, dispersion relations 79—93446
γp elastic scatt., <400 MeV, dispersion relation anal. 77—82744
γp elastic scatt., <450 MeV, dispersive anal. 79—396
γp interactions, Thomson limit calc. using rising total cross sections 79—22103
$\gamma p \rightarrow \pi^0 p$, high energies, semiempirical amplitude anal. dispersion relations and Regge poles 80—86726
γp scattering, proton polarisability determ. 78—17025
K form factor and charge radii, isovector part using dispersion relations 79—22096
$K^*(982) \rightarrow K\pi\pi$, finite energy sum rules and finite dispersion relns. 77—22731
$\bar{K}N$ interactions, low energy, K matrix and dispersion relns., $\Gamma(1405)$ resonance 78—70408
$\bar{K}N$ low energy scatt., dispersion relation constraints 77—13981
Kp total cross-sections, new tabulation suitable for dispersion relations 79—417
$K^{\pm}p$ forward scatt. amplitudes, dispersion anal., effective KNY coupling constant 80—22636
$N \rightarrow \Delta(1232)$ electromagnetic transition form factor and pion-nucleon dynamics at moderate energies 80—57598
N isovector form factors, dispersion theory calc. of inelastic contrib. 77—13950
Nd S-wave scatt., dispersion relation approach to three-body systems, unitarity approx. 79—506
NN, $N\bar{N}$ helicity non-flip forward scatt. amplitude 78—21447
NN and $\bar{N}N$ forward scatt. amplitudes 78—62337
NN $I=1$ amplitudes struct. at 6 GeV/c 78—70395
NN interactions, conf., Vancouver, Canada (July 1977) 78—62418
NN interactions, dispersion relation approach 77—22759
NN interactions and chiral symm., dispersion relation anal. 78—66048
NN potentials, based on meson exchange, discussion and appl. to nuclear matter 79—80815
$N\bar{N}$ resonance, Goldberger-Treiman relation corrections 78—463
NN systems, resonances due to annihilation, baryonium states, many channel N/D method 78—66143
np system, dispersion approach to the inverse scattering problem *(Russian)* 79—22128
$N\pi\pi$ dynamics, medium energy, dispersion relations, isobar expansion for πN 80—4917
pp, $^1D_2$ state, multichannel N/D formalism 79—63506
pp, 1 GeV, elastic scatt. amplitude, phase shift anal. *(Russian)* 80—86746
$\bar{p}p$ elastic scattering, repulsive long range force, dispersion relation calcs. 78—25061
pp helicity amplitudes at $t=0$, dispersion theoretic anal. 78—62340
$\phi(1020) \rightarrow 3\pi$, decay amplitudes, OZI rule, dispersion relations, intermediate states contribs. 79—383
π, photoproduction in $E<450$ MeV region, dispersion relations, CT invariance, review, book contrib. 80—47311
π dispersion relation in nuclear matter using ν+nucleus reactions 79—488
π dispersion relns. in nuclear matter, $\gamma \rightarrow \pi^+\pi^-$ and $\bar{\nu} \rightarrow e^+\pi^-$ decays 77—65209
π EM form factor, dispersion theoretic study, mass, charge radius 77—67652
π electroprod., light cone dispersion sum rules, axial vector currents 78—41556
π photoproduction amplitudes, Pade approximants and dispersion relation solns. 80—91096
π photoproduction on N, multipole $E_{1+}^{(3/2)}$ and its double zero at reson. $\Delta(1232)$ 79—40790
πK low energy scatt., dispersion relation anal. 78—33088
πK scattering amplitude, analytic continuation, chiral symmetry breaking 80—63027
πK scattering length, dispersion relation anal. of phase-shift 80—63026
πN backward scattering amplitudes, superconvergence and nonlinear dispersion relations 78—468
πN coupling constant determ. using forward dispersion relations 79—45098
πN interaction, Coulomb corrections, phase shift anal., S-matrix theory, below 300 MeV 79—85325
πN off-shell t-matrix, P-wave states calc. 77—61205
πN S-matrix, inelastic effects in sidewise dispersion relations for nucleon EM form factors 78—82212
πN scatt., partial conservation of axial vector current limit, on shell corrections 77—18201
πN scattering, partial wave anal., threshold to 10 GeV/c 77—22768
πN scattering amplitude at high energy in localisable quantum field theory *(Russian)* 77—74603
πN t-matrix, half-shell theory, generalised to all partial waves 79—85330
πNN form factor; relativistic calc. of $\Delta(1232)$ contribution to imaginary part *(Korean)* 80—47292
πNN form factors for one off-shell nucleon, dispersion relation calc. 79—9373
πNN vertex function and low energy πN scatt. 79—85332
πNN vertex function and off-mass-shell πN scatt. 80—73739
$\pi^- p \rightarrow \eta n$, tensor-exchange amplitude and polarisation determ. 78—45962
$\pi^- p \rightarrow \pi^0 n$, $\pi^- p \rightarrow \eta n$, 6-200 GeV, charge exchange amplitude energy behaviour 77—22800
$\pi^+ p$ phase shift anal., 1.3-2.4 GeV, continuum ambiguity 77—22778
$\pi\pi$, coupled integral eqns. for scatt. at all energies 78—49982
$\pi\pi \rightarrow K\bar{K}$ amplitude in the unphysical region, hyperbolic dispersion curves 79—9407
$\pi\pi \rightarrow N\bar{N}$, partial-wave amplitudes using hyperbolic dispersion relations 77—30284
$\pi\pi$ phase shift analysis, imposed analyticity effects 79—418
$\pi\pi$ S-wave phase shift, lower bounds, ϵ° and ρ poles 78—45953
$\pi\pi$ scatt. amplitudes, Roy's eqns., mathematical props. 77—71463
$\pi\pi$ scatt. length, interior dispersion relations 78—45952
$\pi\pi$ scattering, description in chiral symmetry *(Russian)* 79—93459
$\pi\pi$ scattering in 1 GeV region, partial wave dispersion relation with inelastic cut 78—4877
$\pi\pi$ t-channel isospin-1 scatt amplitude, crossing constraints 77—67592

dispersion relations continued
$\pi^0\pi^0$ scatt. amplitude, new method for deriving absolute bounds 77−6059
$\pi\pi N\bar{N}$ partial-wave amplitudes, interior dispersion relations 77−82758
$\psi(3100)$ N total cross section from modulus dispersion relation anal. of photoprod. 77−18300
$\psi \rightarrow 3\gamma$, dispersion sum rule charmonium theory, decay probability lower bound *(Russian)* 78−89716
$\psi \rightarrow 3\gamma$, dispersion theory of charmonium, self consistency test, decay probability *(Russian)* 78−89717
ψ propagator, relativistic dispersion anal. of R in 4 GeV region 77−45989
ψ/J hadronic decays, dynamics, SU(3) violation, dispersion relations, mass splitting 79−382
Σ^- mag. moment calc. from dispersion relations in t 78−82257
Υ particle at 9.4 GeV, differential dispersion relations theory of l^+l^- annihilation 78−86424
Ag, surface plasmon dispersion relation in presence of surface roughness 80−65650
Au, energy band structure, X-ray N-emission spectra, relativistic APW calcs. 80−70596
Bi, EM wave dispersion and damping, Voigt configuration, non-local calcs. 80−100475
Bi, superconducting transition temp., two-band model 80−25034
Bi, thermomagnetic wave dispersion, propagation *(Russian)* 80−49696
BiSb, alloys, semimetallic, camera, dispersion relations 80−59854
n-$Bi_{1-x}Sb_x$, determ. carrier dispersion relation parameters 79−38107
^{12}C(p,p) forward scatt., dispersion anal., ^{12}C and ^{13}N ground states 77−34297
$CdCr_2Se_4$, reactor radiation influence on ferromagnetic phase transform. *(Russian)* 80−75760
CdTe, exciton magnetoreflectance spectra, multicomponent polaritons, Zeeman splitting 80−88974
GaAs, field ionisation speed of shallow impurity levels, quantum-mechanical estimates 80−97412
γp scatt. in $\Delta(1236)$ resonance region, dispersion relation anal. 80−18140
H atom, forward electron scatt., total cross section calc. 78−29852
H atom, Stark energy shifts, dispersion relations 79−93952
H, elastic electron scattering, static exchange amplitude, dispersion rels. 78−66664
H electron scatt. forward elastic exchange amplitudes and forward dispersion relations, anal. props. 78−78812
H, Stark effect, dispersion relation, asymptotic formulae, ionis. rate, perturbation theory calc. 80−14106
He-He, dipole-dipole dispersion energy, potential energy curves, dispersion damping functions, Hartree Fock interaction energy 79−98176
He-He, dipole-octupole dispersion energy, potential energy curves, dispersion damping functions, Hartree Fock interaction energy 79−98176
He-He, dipole-quadrupole dispersion energy, potential energy curves, dispersion damping functions, Hartree Fock interaction energy 79−98176
He-He, quadrupole-quadrupole dispersion energy, potential energy curves, dispersion damping functions, Hartree Fock interaction energy 79−98176
^{3}He, asymptotic normalisations for S-state wave-function component 77−74777
^{3}He, liq., hydrodynamic modes, macroscopic dispersion relations, two fluid model 78−10242
^{3}He, liq., hydrodynamic modes, microscopic dispersion relations, transport coeffs. 78−10243
^{3}He, liquid, electrostatic image force depend. on spatial dispersion, energy spectrum *(Russian)* 80−107593
^{3}He, superfluid, magnetic relaxation and high amplitude spin waves *(Russian)* 80−92749
$^3He+\pi_3^{\pm}$, dispersion relations, determ. of π^3He^3H coupling constant 78−58307
^{4}He, liquid, electrostatic image force depend. on spatial dispersion, energy spectrum *(Russian)* 80−107593
^{4}He(p,p)^{4}He forward amplitude real part, 1.5-10 GeV, from dispersion relns. 77−314
$^4He(\pi,\pi)$, backward dispersion relations and phase shift anal. 79−63703
$^4He(\pi,\pi)$, dispersion relations for forward scatt. logarithm 78−17243
n-InSb, cond. electron spectra in quantised mag. field, impurity resonance scatt. *(Russian)* 80−93178
K, phasons, transverse, freq. dispersion relation in CDW state 80−96804
KN($\bar{K}$N) scattering amplitudes, resonance region, t-channel couplings, hyperbolic dispersion relations 80−57643
K_2SeO_4, lattice dynamics, displacive phase transform. 80−39248
$LiNbO_3$, Y-cut, SAW $\Delta V/V$ waveguides in arbitrary propag. directions 79−81602
PbI_2, photoexciton interaction, luminescence spectra, polariton dispersion diagram 80−93397
Pr, magnetic excitations, exchange, crystal field and magnetoelastic interactions 80−2563
SF_6 gas, dispersion relation of spontaneous oscill., unstable regions 80−1875
SiC, dielectric coating effect on surface polaritons, optical consts. *(Russian)* 80−88489
Tm-Zn, paramagnetism, mag. excitations, exchanges interactions 80−88718
YGaIG, magnetoelastic wave propagation time dispersion reduction 80−75836
YIG, magnetoelastic wave propagation time dispersion reduction 80−75836
ZnO, surface exciton polaritons, nonlinear optical excitation and dispersion relation 79−82657

dispersions *see disperse systems*

dispersoids *see disperse systems*

displacement measurement
1 MHz crystal anharmonic AT modes, holographic displacement amplitude meas. 79−54097
90° phase shift beam splitter for displacement interferometer 78−87145
below 50 mm, transducers available commercially, comparative survey 80−42214
A/D convertor with multichannel phase shifter 77−5823
absolute retardation accurate meas. using holography 79−27201
accelerometer, superconducting, using Nb-on-sapphire RF resonator 79−49210
alloys, normal and in-plane determ. by holographic and speckle interferometric methods 78−27688

displacement measurement continued
angle monitoring using diffr. gratings 77−33973
angular, by photoelec. amplitude-phase modulation method 78−16774
angular and longitudinal, digital, magnetic scale recording system 77−2635
biaxial laser-based displacement transducer 78−73967
bonding displacement meas. by He-Ne laser interferometer 77−37972
breath amplitude meas. optoelectronic displacement sensor 77−66868
cantilever plate, deflection meas. by holographic interferometry 79−94568
capacitance displacement transducers, effect of tilt and surface damage 78−54356
capacitive displacement system for UHV operation 80−31737
capacitive transducer, autocalibration *(Russian)* 80−36981
capacitive transducers, manufacturing error effect on accuracy 78−89467
circular hole, normal surface displacement, reflection holographic interferometry 78−57893
combined holographic and double-aperture speckle interferometry *(Japanese)* 79−80670
contactless meas. by fibre-optic and capacitive transducers 78−8400
contactless pick-up, operational description *(Russian)* 77−65020
contour holography of moving object, using injection locked flash pumped dye laser 78−50737
contraction recorders for animal nictitating membrane and skeletal muscle 77−48969
coordimeter, two-dimens. for displacement meas. in rock masses 79−35016
coplanar surface plane deviation meas. using micrometer *(German)* 78−163
cryogenics, linear variable differential transformer displacement transducer optimisation 80−86323
curved surface, displacement meas. using laser speckle interferometry 80−31712
cylinder, rectilinearity meas. using equal chromatic order fringes 80−27286
deformable materials application to elastoresistance and elastocapacitance meas. of deformation *(French)* 77−70564
deformation anal. with additional degrees of freedom during reconstruction by holographic interferometry 79−32411
deformation measurement, in-plane, by video-electronic hologram interferometry 80−106488
deformation measurement, out-of-plane, using holographic interferometry and speckle photography, comparative accuracy 80−78804
derived holographic interferometric methods *(German)* 80−91758
differential frequency angular rate and displacement sensor, construction *(Russian)* 78−70106
differential-capacity transducers, improving metrological characts. 79−75493
diffraction grating imaging anal., displacement transducer design appl. 79−86258
diffuse surfaces moving with high vel., interferometric method 79−6092
diffusely reflecting objects, deformation meas. by lasers, appl. of holography and speckle, review *(Japanese)* 80−9832
diffusely reflecting objects with time-varying surface microrelief, holographic interf. deform. recording 80−74322
diffusing object axial displacement detection, image plane speckle 79−85118
dimensional stability, long-term, meas. using elec. resistance strain gauges 77−49711
direct-reading displacement digitiser construction and coding *(Russian)* 77−9983
direction-sensitive displacement analysis by multiple freq. holographic interferometry 78−54338
disc memory recording heads, investigation of dynamic mechanical props. that appear as stresses during small motions 80−22422
double beam interferometer, fringe value changing 78−278
double beam Michelson interferometer meas. of small linear displacements 78−73966
double exposure interferometry through speckle photography *(French)* 80−83568
drive system, digital method *(Polish)* 80−86260
dynamic angular displacement measurements by interferometry 79−49276
eddy current methods, principles *(Chinese)* 79−71409
eddy-current angle displacement type, in 213-473K temp. range, types *(Russian)* 77−33974
electric field meas. using pressure sensitive elements and fibre optical transmission technique 79−97367
electronic speckle pattern interferometry apparatus with multichannel data acquisition 79−80671
EM micrometers, noncontacting position transducer dynamic characts. 78−41277
epoxy resins, strain anal. by fluoresc. meas. *(French)* 79−47846
extrapolation of strain and stress from holographically measured surface displacement 79−32410
eye movement recording using non-contacting US transducer system 78−7414
fast precision capacitance transducer, design procedure *(Russian)* 80−98884
fibre optic lever displacement transducer 80−5816
fine movement meas. by PZT ceramic disc stack 77−37843
fission reactor core, during reactivity pulse operation *(Japanese)* 77−54321
flux gradient accelerometer, working model tests 77−26274
Fourier spectrometer reflector displacement precision meas., photoelectric method 77−18107
fracture toughness value determination by compact testing 80−45451
fretting expt. slip meas., high resolution optical method 79−61830
general object deformation decomposition by speckle displacement 80−106486
general-purpose meas. microscope with photoelectric readout 79−71524
goniometer, electromech., for total motion knee goniometry 77−52902
heterodyne holographic strain and stress determ., accuracy 79−94562
high-temperature displacement meas. using capacitive transducers 78−172
high-temperature reactor structural displacement and strain analysis by picture processing *(Japanese)* 80−78352
hologram real-time observation with photothermoplastic film *(German)* 78−1182

displacement measurement continued
  holograms, double exposure, automatic meas. of 3D displacements by scanning technique 78—37844
  holographic displacement analysis using image plane technique 79—44901
  holographic interference, fringe contrasts, displacement gradient determ. *(French)* 77—61928
  holographic interference fringe assessment, surface displacement obs. 77—75444
  holographic interferogram quantitative evaluation, fringe dynamics *(German)* 77—10097
  holographic interferometric evaluation of rigid body displacement 80—105610
  holographic interferometry, 3-D distribution 78—13673
  holographic interferometry, deform. anal., reconstruction 77—38829
  holographic interferometry, errors in small vector displacements meas., statistical anal. 78—78953
  holographic interferometry, evaluation, general formulation 77—38830
  holographic interferometry, for displacement or flow velocity distrib. meas., fringe analysis 78—25820
  holographic interferometry, model interferogram construction 77—82592
  holographic interferometry, motion direction and fringe order determ. 77—18077
  holographic interferometry, quantitative evaluation *(German)* 77—18085
  holographic interferometry, rigid body motion compensation 77—26387
  holographic interferometry, surface displacement sign identification 77—75438
  holographic interferometry, triple exposure, for displacement vector meas. 79—75498
  holographic interferometry appl. to displacement, deformation and vibration meas. *(Italian)* 78—54337
  holographic interferometry for quantitative strain meas. 78—32794
  holographic interferometry of plastic parts 77—7037
  holographic interferometry technique, appl. to membrane flexing 80—8962
  holographic interferometry techniques 79—17397
  holographic interferometry with continuously scanning reconstruction beam 77—88664
  holographic interferometry with continuously scanning reconstruction beam 78—71055
  holographic method displacement field eval., 3 dimensional, exact general theory *(German)* 79—32409
  holographic moire pattern differentiation 79—59951
  holographic nondestructive test system, quantitative fringe interpretation 77—75454
  holographic nondestructive testing at Fourier plane 78—46536
  holographic recording of displacement field inside stressed sample 77—57299
  holographic technique, double exposure 79—40537
  holographic techniques, expt. comparison 78—71057
  holographic vibration analysis, computer-aided, for vectorial displacements of bladed discs 78—71056
  holographic zero order fringe identification, direction of motion detection 78—63044
  holographic-moire technique, extension to 3D, to separate patterns corresponding to components of displacement 79—35661
  image-shearing camera for surface strain direct meas. 79—58773
  impact force vs. displacement curves, expt. determ. 78—83344
  impulsive displacement, capacitive contactless meas. transducer 79—6111
  in-plane motion measurements with Fourier lensless holography 80—77746
  in-plane vibrational analysis, time-averaged moire method 79—68665
  inaccessible target, meas. via noninterferometric optical probe 77—74362
  indentation depth measurement in testing hardness 79—83418
  induction extensometer, temp. compensated, features 79—17394
  induction transducer displacement/voltage proportionality improvement *(Bulgarian)* 80—52183
  inductive displacement-measuring system synthesis using CAD 78—73982
  inductive magnetic transducer for ferromag./nonferromag. object displacement meas. 79—6154
  interferometer for precision linear displacement meas. 80—27285
  interferometers with electro-optical modulators *(Russian)* 78—12667
  interferometry, automatic fringe counting, independ. of signal level changes 78—58018
  interferometry, multimode fibre optic, applications 80—86387
  interferometry, two-wavelength investigation of deform. and vibration of objects 77—46976
  interior displacement and strain measurement using white light speckles 80—95064
  IR probe, for internal interfacial wave motion meas. 79—18981
  laser appl., three-mode, geodesic problems solution 80—77748
  laser beams, position-sensitive photodetectors, selection of parameters 79—17490
  laser heterodyne detect. of slowly varying displacements, interferometric technique 77—34019
  laser interferometer, two-frequency, small displacement meas. in LF range 79—30533
  laser interferometer appl. 79—6094
  laser interferometers, AM and FM operation and applications *(German)* 80—86389
  laser interferometric displacement meas. system for positioning of sphere and meas. roundness 79—97416
  laser interferometry measurement system 79—6171
  laser microstrain gauge principle and technique 77—68541
  laser speckle photographic technique *(German)* 78—1616
  laser speckle photography for in-plane displacement sign detect. 77—79140
  lateral motion analyser sensitivity stabilisation along ranging line 79—72694
  lateral motion and longit. rot. of diffuse surface by speckle photography 78—21235
  lateral shearing inteferometry for transparency distortion anal. 78—4684
  linear and angular microdisplacement instrument *(Japanese)* 79—21728
  linear displacement meas. accuracy meas. accuracy improvement under vibration 80—90815
  linear movement transducers, magnetic amplifier principles 80—22341
  linear variable differential transformer method 78—73978
  linear/angular, automatic method by simultaneous use of primary transducers, computer appl. 79—6084
  loudspeaker signal displacement meas., optical method 78—51023
  machine part, holographic interferometry meas. method 78—9348

displacement measurement continued
  machine tools control, multisectional linear metrological gratings prod. 77—3686
  magnetic amplifier linear movement transducer manufacture and static functioning 79—67279
  magnetic displacement sensor *(Japanese)* 79—12761
  mechanical displacement of specimens using laser 80—73309
  microinterferometer limiting sensitivity and accuracy characteristics 77—79142
  microinterferometer transducer, air-bearing, for use with universal inspection machines 78—57899
  microscope scanning stage lateral displacements 80—10055
  milling machine, sandwich hologram interferometry 77—88662
  moire fringes and holograms, displacement meas. 80—32936
  Moire method effects modelling using finite element method 78—38259
  Moire method using diffraction beams, compensation of errors 80—13068
  moire methods for contouring displacement, deflection, slope and curvature 79—80674
  Moire strip attainment at specified pt. on contour of stress concentrator 77—52573
  motion paths display, speckle photography, holographic reconstruction 77—18084
  moving coil linear variable differential transformer for displacement meas. at liquid helium temps. in strong magnetic fields 78—54415
  neutron spectrometer, angular-displacement precision control with fast error-signal transducer 78—186
  noncontact material testing using laser energy deposition and interferometry 79—34258
  noncontact material testing using laser energy deposition and interferometry 80—71846
  noncontact optoelectronic position transducers 79—50406
  object deformation, determ. of components from 1 double-exposure hologram 79—94193
  oceanic ice movement measurement, microwave radiometers *(Danish)* 80—26624
  optical alignment using He-Ne laser/polarimeter system 77—37967
  optical gauging by remote image tracking used in production 79—86264
  optical methods for determining strain and displacement, book 79—20331
  optical surface modal deformation sensor for heterodyne interferometry 80—31859
  optical system, trihedron, for linear displacement meas., accuracy estimation 80—101780
  optical ultramicrometer technique using composite diffr. grating 78—4589
  orientation of vibration test-bed, dynamic meas. using system of He-Ne laser and photodiode 77—49712
  PCB blind hole misalignment meas., dual microscope system 79—75586
  photoelectric transducer for linear displacement meas. 79—50404
  photoelectric transmitter using LED *(Hungarian)* 78—4606
  photomicrometry with moire 78—4690
  physiological movements, microwave interferometer appl. 79—25137
  piezoelectric micrometer for precision movement in optical alignment applics. 77—65017
  pipe under internal press., lens holographic moire technique for displacement component determ. 79—44900
  plastic plate velocity measurement, as continuum, by streak camera technique 78—37095
  polarisation interferometer, for small dynamic deform. meas. *(Russian)* 79—9205
  potentiometric displacement transducers, standards for specification and tests, book 79—2763
  pyroelectric detector of transmitted power, coordinate-sensitive, for laser beam displacement determ. 79—75599
  quartz, y-cut, impact, appl. of transverse-displacement interferometer 78—12747
  quartz tube, fused, in a dimensional stability test facility, thermal expansion 79—58779
  real-time measurement of in-plane translation and tilt by electronic speckle correlation 80—57252
  reflective object displacement and vibration meas. *(Russian)* 79—21695
  rigid body, parallel displacement meas. using polychromatic speckle patterns 77—41568
  rigid-body movement induced speckle motion 79—76590
  ring specimen deformation, stress relax., meas. method, increased accuracy 77—75863
  rotation measurement, in-plane, speckle photography appl. 80—31714
  rough object motion measurement, real time, speckle pattern correl. 77—10098
  sandwich holography, meas. of in-plane displacement and compensation for rigid body motion 79—98312
  sedimenting particles, measured using light interferometry 79—60086
  SEM beam splitting by HF square-wave deflection 79—75654
  single-channel optoelectronic raster-type displacement transducer 77—74384
  skin recoil characteristics, human, in vivo meas. apparatus 79—57698
  sliding bodies, friction apparatus for meas. normal displacement 80—99977
  speckle, affine geometry, tilt topology 77—19176
  speckle, photographic recording, Chladni method 77—604
  speckle applications *(French)* 77—67494
  speckle camera and analyser for surface displacement and tilt meas. 78—32790
  speckle correlation and interferometry for planar deformation analysis *(Dutch)* 80—32930
  speckle interferometric analysis of transient phenomena 80—105701
  speckle interferometry, decorrel. effects, machine induced strain obs. 77—45887
  speckle interferometry, displacement meas. errors rel. to camera displacements during exposure 79—17479
  speckle interferometry, one beam, smallest displacement 79—97427
  speckle interferometry, real-time meas. of vibrations and displacements *(Italian)* 78—54336
  speckle method for meas. mechanical translations (10^{-11} to 10^{-3} m) *(German)* 80—17924
  speckle pattern interferometer for measurement of displacements and surface tilt, book contrib. 79—20334
  speckle pattern TV interferometer, principle and appl. 78—58014
  speckle patterns, holographic projection appl. to remote metrology 80—14299

displacement measurement continued
speckle photographic technique, hybrid optical and electronic image processing 80—99976
speckle photographs, displacement measurement using electro-optical readout system 80—62708
speckle photography, defocusing problem 77—18083
speckle photography meas. of axial displacements of diffusing object 77—57301
speckle shearing interferometer using Savart plate 77—30199
speckle shearing interferometry, fringe parameters 79—220
strain meas. by holographic interferometry, mathematical formulation *(German)* 80—78815
strain measurement, full field optical method having postrecording sensitivity and directional selectivity 78—57892
stress analysis using holographic interferometry and speckle photography 78—70095
stress measurement by sandwich speckle photography *(German)* 80—10216
string linear displacement transducer design *(German)* 77—79085
subspeckle size changes meas. by laser-speckle photography 80—31853
surface displacement and strain anal. by speckle interferometry 80—14635
surface displacement and vibration meas. using laser speckle *(French)* 78—4686
surface displacement meas., coherent optical correlation technique 79—75499
surface rapid motion under dynamic loading, high speed photography of Moire fringes 78—32789
tensile deformation of flat samples, meas. equipment using exoelectron emission 77—77679
thin-walled cylinder, radial deform. meas. by Ligtenberg moire method 79—59949
third intracranial ventricle dynamic displacement detection 78—57035
thread gauges standardisation, w.r.t. inner-pitch error 77—79053
three dimensional anal. from image-plane hologram 79—17385
three-dimensional, from single image hologram, combined holographic and speckle interferometry 77—83831
three-dimensional, of twisted belt, by holographic interferometry *(Japanese)* 77—7029
tiltmeter, stability and thermal compensation of a test-cell for a Hg-level tiltmeter 80—36978
time-varying images, object displacement estimation adaptive algorithm 80—99668
tracking Michelson interferometer stability improvement *(Russian)* 78—29149
transducer, reluctance, 'Polfer' ferrite cores appl. *(Polish)* 78—29100
transducer for recording elec. and mech. chronic intestinal activity 77—44862
transducer using second harmonic type magnetic modulator 78—21115
transducers, for use below 50 mm, review 79—63200
transverse displacement of distant body, interferometric meas. 77—82488
tubular spring with extending endpiece, calc. *(Russian)* 80—52157
tuned equipment-structure systems, response spectra design methods 79—3952
ultraprecision spindle unit construction on aerostatic supports 78—77880
ultrasmall displacement meas. by interferometry 78—57897
ultrasmall displacements measurement, nonoscillatory and oscillatory motions 79—2748
vibrating capacitor displacement transducer, eqn. of state 80—57281
vibrating plate like struct., displacement and strain meas. using time average holography 79—46272
vibrational contact means of measuring small, complicated and inaccessible shapes 79—97353
vidicon television camera, movement meas. appl. 80—41333
viewing techniques and engineering display applications 79—50264
violin G-string, resonant response and excitation of wolf-note 80—53540
water wave amplitude, surface standing, using capacitance meas. circuit 79—50833
whisker crystals uniaxial deformation, at He temperatures in magnetic field, mechanical displacement transformers design 80—50788
zero position recording interferometer 77—71368
Al bicrystal, tensile and creep deform. obs. by holographic interferometry *(Japanese)* 77—56197

displacive transformations
see also martensitic transformations; polymorphic transformations; soft modes
alkali metal double salts, $MB'BX_4$ (M=alkali; M'=alkali or NH_4^+; $BX_4=SO_4$, BeF_4, etc.), theory of phase transitions 79—99837
alkaline earth feldspars, homogeneous and heterogeneous polymorphic transformations 79—15659
alkylammonium compounds with perovskite-type layer struct., symmetry of lattice vibrs. 78—22797
alloys, phase transition premonitory phenomena, exam. by electron diffr. and microscopy *(French)* 80—59651
ammonium double salts, MH_4 MBX_4, (M=alkali metal; $BX_4=SO_4$, SeO_4, BeF_4, etc.), theory of phase transitions 79—99837
anharmonic Brownian oscillator, canonical correlation function based on projection operator technique 78—55926
anharmonic crystal, lattice dynamics and stability 78—6129
antiferroelectrics, multicritical points in structural phase transitions, renormalisation 80—75982
CDW instabilities, incommensurate struct. phase transitions, neutron scatt. study, review 79—51231
chaotic states of anharmonic systems in periodic fields 80—22288
classification of struct. transforms., using coupled double-well model 78—14443
cluster phenomena, displacive to order disorder crossover 80—10629
cluster walls and phonons in structural phase transitions 79—77720
continuum ϕ^4 equation, kink-phonon and kink-kink interactions 80—70354
coupled fields in one dimension: cross-over from a continuous symmetry to a discrete one 78—87758
critical behaviour at displacive limit of structural phase transitions model 77—7826
critical dynamics and hydrodynamics, microscopic 1/n expansion 77—76518
crystal classification by transition mechanisms *(Russian)* 78—60401
cubic antiflourite structs., halogen NQR spectra, struct. information for R_2MX_6 compounds 80—71228

displacive transformations continued
D_{2d} crystals, structural phase transitions, soft modes, group theory 80—92638
de Gennes pseudospin model, lattice phonons tunnelling effects 79—73290
defect cell and neutron scatt. central peak 77—15531
defect-containing crysts., US absorpt. near displacive phase transitions, anomalous temp. depend. 80—92612
defects, localised modes and central peak 78—83905
dialkylammonium metal chlorides, soft modes, phase transitions 78—79723
diffusionless first order phase transform. eqns. appl. to liquid crystals and solids 78—30734
dimethylammonium manganese chloride, neutron diffr., 188K, cryst. struct. 77—47434
1,8-dinitronaphthalene, orthorhombic struct. determ., 22 and 97°C, rel. to phase transition mechanism 78—6048
dislocation-soft mode interaction in displacive transitions *(Russian)* 80—84172
displacive type ferroelectric, thermal expansion and effect of press. on transition temp. 78—72471
distortive phase transitions, order-disorder and displacive regimes, mol. dynamics study 80—75324
doped displacive ferroelectrics, sound attenuation constant, Green's function technique 79—11397
dynamic aspects, nuclear quadrupole relax. studies 78—76344
dynamical critical exponents, microscopic calc. 78—10163
dynamics, 1/n expansions 77—15530
electron spin-lattice relaxation, role of soft phonon modes 79—28590
ferrodistortive and antiferrodistortive transforms., expt. results, book contrib. 77—89518
ferroelectric, inelastic neutron scatt. cross section 77—36187
ferroelectric, mixed order-disorder displacive transition, model 77—59540
ferroelectric, unified theory, quantum limit, zero point energy 78—68461
ferroelectric, unified theory for order-disorder and displacive types 77—12329
ferroelectric semiconductor, magnetic field influence, ferroelectric transitions 80—55049
ferroelectric transition, tunnelling concept in general theory 77—63375
ferroelectric transition in system with strong electron-phonon interband interaction 77—66462
ferroelectric transition unified theory 77—20808
ferroelectric transitions, unified theory, quantum limit 78—27167
ferroelectricity, vibronic theory 79—38492
ferroelectrics, low-dimens., thermal cond. 79—61314
ferroelectrics, model, fluctuation effects 79—33063
ferroelectrics, order-disorder, displacive transformations, tunnelling, phonons 80—75975
ferroelectrics and antiferroelectrics, polaron state of electron near structural instability 79—33245
first order displacive transformations, localized soft modes and US effects 79—73281
gradient invariants and incommensurate phase transitions 78—22824
Hamiltonian model with scalar displacive transition, crit. dynamics, renormalisation 78—87766
impurity, soft, static and dynamic behaviour 77—72669
incommensurate crystal phases, symm. props., superspace groups 80—75195
incommensurate structural phase transformations, recent neutron scatt. studies, review 79—42205
inducing soft mode transitions by IR or lower freq. EM radiation 78—7421
IV-VI compounds, mag.-field-induced displacive phase transition 80—50278
kinks in one-dimens. model, statistical mechanical treatment 79—42203
lattice defects, behaviour models at structural phase transitions 78—83904
lattice dynamical system, displactive structural transition anal., mol. dynamics calc. 79—86865
lattice mode softening by high-power visible and IR laser radiation 78—71825
lattice model, classical, n-component, phase transitions near displacive limit 77—45807
lattice phonons in presence of non-linear excitations 80—44283
localised modes and central peak at displacive phase transitions 77—69064
malononitrile, ^{14}N PNQR obs. of phase transition press. depend., line splitting 77—77120
malononitrile, displacive phase transition, 294.7K, Raman and Brillouin-Rayleigh scatt. obs. 80—16047
martensite formation, and lattice props. rel. to elastic constants 80—50630
metal, HCP, development of Kronberg's model for $\{10\bar{1}2\}$ twins, extension to $\{11\bar{2}2\}$ twins 79—51119
metallic state, one dimens. model, stability *(Russian)* 77—85171
model theory of ferroelec. and first and second order struct. phase transitions 79—51915
molecular dynamics of structural phase transitions in two dimens. model 77—20038
molecular dynamics results, for one-component displacement modeL 78—14424
noncritical fluctuations and temp. depend. of order parameter 77—1204
one-dimensional chain, harmonically coupled particles, displacive transformation model, soliton-phonon interaction 78—22813
perovskites, Rayleigh scatt., crit. dynamics at struct. transition 77—12396
perovskites, struct. phase transitions, octahedral tilt systems 77—11655
perovskites, successive phase transitions, unit cell distortion and atomic displacements 78—2057
pinning of virtual domain walls and central peak 79—28074
polyhedral tilting, pure displacive transitions, rel. to analcite at high press. 80—6515
pressure effect on transition temps. *(Japanese)* 79—65814
quartz:Fe^{3+}, EPR for phase transform., reduced signal above 670K 77—90016
refractive index changes induced by struct. transitions 80—16000
rigorous bounds, quantum anharmonic phonon model 77—15541
semiconductor, localised states near displacive transition 80—70644
semiconductor thin films, ferroelectric properties, quantum size effect 80—97201

displacive transformations continued
- single-particle properties of systems undergoing struct. phase transitions 78−26654
- SnTe film, polycrystalline, anomalous resist. at struct. phase transition 80−29488
- soft displacive impurity dynamics in host lattice with displacive phase transition 80−34159
- soft mode, dipole relaxation 78−91409
- soft mode concept, role of competing forces 77−80599
- soft optical phonon mode, discontinuous freezing-out of local order 79−42204
- soliton lattice, connection between dislocation and displacive transitions 79−82300
- spin, discrete cubic model, displacive phase transitions 77−32198
- spin Hamiltonian of S ions, depend. on order parameter 80−70356
- spontaneously modulated materials, Raman scatt. 79−95739
- squaric acid, struct. transition, US vel. meas. 78−79770
- steel, bainite formation mechanism 80−108431
- structural transitions of antiferroelectric and displacive modulated type caused by electron-phonon interactions 78−43092
- superconductor, metal-insulator transition, electron pairing, effect on optical props. 80−60139
- surface phonons and displacive phase transitions in surface layers 79−65167
- TCNQ salt, K-TCNQ, spin-Peierls system, paramag. susceptibility, Heisenberg chains 79−38299
- 1,2,4,5-tetrabromobenzene, structural phase transition, Raman and IR spectra meas. *(French)* 77−66503
- 1,2,4,5-tetrachiorobenzene, structural phase transition, Raman and IR spectra *(French)* 77−66503
- TGS:Cr^{3+}, EPR obs. of fluctuations near phase transition 78−43820
- transition metal, 2H layer compound, theory of superstructures 79−99291
- transition metal pnictides, displacive and mag. transitions 80−59616
- transitions metal sulphides, displacive transitions, theory 80−59616
- TTF-TCNQ, lattice distortion, displacive transform., Landau theory 77−31743
- TTF-TCNQ, lattice distortion, displacive transform., Landau theory 77−84879
- tungsten bronze structure ferroelectrics, tetragonal, model of ferroelec. transition 77−28526
- tunnelling effects, self-consistent pseudospin-phonon formalism 79−55858
- vibronic theory of antiferroelec. and struct. modulated transitions, soft modes 78−79719
- virtual domain walls, dynamic struct. factor central peak correlations 79−95114
- Ag_3AsS_3, and Ag_3SbS_3, Raman spectra obs. of low-temp. phases 80−93327
- Al complex, Al urea$_6(ClO_4)_3$:Cr^{3+} structural phase transition, ESR meas. 77−20681
- $AlPO_4$, α-β cristobalite phase transition, Raman meas. 79−4799
- $AlPO_4$:Fe^{3+}, EPR, α-β phase transition 77−90016
- As, rhombohedral, electronic struct. and optical props. var. with internal displacement parameter 79−60702
- BN structure after high temp. shock compression 80−39220
- $BaMnF_4$, magnetic neutron scatt. from structurally distorted cryst. 80−93086
- $BaTiO_3$, displacive ferroelectric, effective charge determ. 80−97212
- $BaTiO_3$:^{89}Zr, electron capture decay lifetime, struct. environment effects 77−28523
- $Bi_2Bi_4Fe_2Ti_3O_8$, dielec. and magnetoelec. props. 78−95562
- $CaThNb_2O_8$, monoclinic-quadratic phase transform. *(French)* 77−27998
- $CaUNb_2O_8$, monoclinic-quadratic phase transform. *(French)* 77−27998
- $CdThNb_2O_8$, monoclinic-quadratic phase transform. *(French)* 77−27998
- $CoSiF_6.6H_2O$, effect of press. on struct. phase transition, 100 to 300K 77−80616
- $CoZrF_6.6H_2O$, effect of press. on struct. phase transition, 100 to 300K 77−80616
- $Co[Pt(C_2O_4)_2].xH_2O$, Co deficient, displacive periodic antiphase model 78−30753
- $Cr_xMn_{1-x}As$, mag. susceptibility anomaly at displacive phase transition 80−93091
- $CsCuCl_3$, Jahn-Teller induced phase transition, helical at. displacements 77−43301
- $Cs_2LiCr(CN)_6$, room temp. struct., phase transitions 78−51491
- $CsPbCl_3$, high-resolution elastic neutron diffr. study 80−28984
- $CsPbX_3$, (X=Cl,Br), anharmonic thermal vibrs., neutron diffr. study 80−29125
- $Cu_{0.5}NbS_2$ and $Cu_{0.5}TaS_2$, order-disorder and displacive transforms., domain-type microstruct. 77−4195
- $Dy_2[Pt(CN)_4]_3.21H_2O$, phase transitions, X-ray study and spectroscopic study 79−60506
- $Er_2[Pt(CN)_4]_3.21H_2O$, phase transitions, X-ray study and spectroscopic study 79−60506
- Fe $SiF_6.6H_2O$, phase transform., temp. depend. of Mossbauer parameters 77−73102
- Ga complex, Gaurea$_6(ClO_4)_3$:Cr^{3+} structural phase transition, ESR meas. 77−20681
- GeTe, Hall coeff., temp. depend. rel. to order parameter 80−96921
- GeTe-MuTe, temp. characts. of phase transition, MnTe influence 80−20926
- $HUO_2AsO_4.4H_2O$ and $HUO_2PO_4.4H_2O$ layered cpds., struct. investigs. below antiferroelec. transition temps., H bond ordered structs. 80−107416
- $HUO_2AsO_4.4H_2O$ and $HUO_2PO_4.4H_2O$ layered cpds., single and polycryst., proton cond. behaviour w.r.t. antiferroelec. transition temps. 80−107481
- Hg_2Br_2, sp. ht. near phase transition region meas. 78−38855
- In-Pb alloys, elastic consts. of three phases, acoustic mode softening 80−30006
- $K_2Cd_2(SO_4)_3$, piezoelectric, cryst. struct., near ferroelastic transition 78−42984
- KD_2PO_4, ferroelec., tetragonal$\rightleftarrows$monoclinic transition, neutron powder diffr. meas. 77−7693
- KH_2PO_4, D_2-impurities effect on Rayleigh central peak 77−81068
- $KMnF_3$, Mossbauer gamma quanta scattering near 186K transition 80−108126
- $KMnF_3$, precursor order and Raman scatt. near displacive phase transitions 80−45061
- $KMnF_3$, second-order displacive transition region, static and dynamic characts. determ. 80−70409
- $KNbO_3$, displacive ferroelectric, effective charge determ. 80−97212
- K_2OsCl_6, Cl NQR spectra by Fourier transform methods 80−75879
- K_2OsCl_6, ferrorotative transition, neutron scatt. expt., consistency with displacive and order-disorder models 78−51673
- K_2OsCl_6, low temp. sp. ht. and thermodynamic props. near phase transition 77−39655
- K_2OsCl_6, thermal expansion meas. 78−10188
- K_2ReCl_6, low temp. sp. ht. and thermodynamic props. near phase transition 77−39655
- K_2ReCl_6, structural phase transition, soft rotary mode, obs. by triple-axis neutron scatt. 79−1483
- K_2ReCl_6, thermal expansion meas. 78−10188
- K_2ReCl_6, thermodynamic relations at solid state phase transitions 80−29164
- K_2SO_4, displacive solid-state transformations meas., DTA method 80−218
- K_2SeO_4, incommensurate phase transition, stress depend. of T_c 79−4391
- K_2SeO_4, lattice dynamics, displacive phase transform. 80−39248
- K_2SnBr_6, transform. dynamics probed by Raman scatt. and microscopy 78−63832
- K_2SnCl_6, phase instabilities and mode softening X-ray and neutron diffr. 77−7830
- K_2SnCl_6, structural phase transitions, Raman spectra 77−73143
- $KTa_{1-x}Nb_xO_3$, quantum limit of ferroelec. transitions, dielec. and elastic consts. meas. 78−15128
- $La_3S_4(Se_4)$, structural transitions, symm. anal. 80−92671
- $Li_4B_7O_{12}Cl$, cryst. struct. and ionic conductivity 77−84690
- $LiND_4SO_4$, ^7Li and ^2D NMR exam. of high-pressure phase 79−11396
- $LiNbO_3$, ferroelec., displacive type phase transition, far IR reflection spectra 80−71339
- $LiTaO_3$, displacive ferroelectric, effective charge determ. 80−97212
- $LiTaO_3$, ferroelec., displacive type phase transition, far IR reflection spectra 80−71339
- MnAs, relation between displacive and first order ferromagnetic-paramagnetic transition 79−10908
- $MnAs_{1-x}P_x$, mag. susceptibility anomaly at displacive phase transition 80−93091
- $NH_4H_2PO_4$, phonon echo method *(French)* 78−6640
- NH_4LiSO_4, NH_4IO_3, phase transitions, SHG obs. 78−76398
- $(NaAl)_xSi_{2-x}O_6.H_2O$, analcite, polyhedral tilt transitions obs. at high press. 80−6515
- Na_2CO_3, modulation wave form, tenfold supercell approx. 79−95157
- Na_2CO_3, struct. changes at incommensurate phase transition 79−95158
- $NbSe_2$ (2H), charge density wave transitions, neutron diffr. exam. 77−89515
- $NbSe_2$(2H), Raman spectra of soft modes at CDW transition 77−16301
- Nb_3Sn, elastic instability in cubic to tetragonal phase transitions 78−39767
- $Ni_{0.25}Zn_{0.75}Fe_2O_4$, structural phase transition, X-ray and neutron diffr. study 80−79735
- (Pb, Sn)Te-type semiconductors, displacive ferroelec. phase transitions, vibronic theory 80−11354
- $Pb_5Ge_3O_{11}$ acoustic relaxation near ferroelectric transition 78−2814
- $Pb_5Ge_3O_{11}$, dynamic central peaks and phonon interactions 78−83903
- $Pb_5Ge_3O_{11}$, struct. of paraelec. phase, neutron diffr. meas. 77−84720
- $Pb_3(PO_4)_2$, phase transition at 180°C, dielectric meas. 79−37831
- $Pb_{1-x}Sn_xSe$, displacive transition, temp. and press. depend., elec. meas. 80−10672
- $Pb_{1-x}Sn_xTe$, band struct. changes due to displacive phase transition, Hall coeff. meas. 80−10671
- $Pb_{1-x}Sn_xTe$, effect of interband hybridisation 79−33233
- $Pb_{1-x}Sn_xTe$, soft-phonon-induced Raman scatt. 77−77209
- $Pb_{1-x}Sn_xTe$, soliton modulation widths for TO-phonons 77−80588
- $PbTiO_3$, single crysts., lattice parameters and birefringence as function of temp. 79−38517
- $PbTiO_3$, tetragonal deform. of TiO_6 octahedron 77−55759
- $PbZrO_3$, elec. field induced phase transitions 77−62643
- $PbZrO_3$:^{89}Zr, electron capture decay lifetime, struct. environment effects 77−28523
- $RbCaF_3$, precursor order and Raman scatt. near displacive phase transitions 80−45061
- $RbCaF_3$, struct., phase transitions, neutron diffr. study 80−33918
- $RbCaF_3$, thermal props. near phase transition 78−75850
- $RbCaF_3$:Gd_2O_3, Gd^{3+}-O^{2-} pair, EPR study of displacive transform. *(French)* 78−27088
- Rb_2ZnBr_4, incommensurate phase transition, neutron-scatt. obs. 79−4390
- Rb_2ZnBr_4, modulation phase transitions, neutron scatt. 79−95712
- Rb_2ZnCl_4, phase transitions, soft mode, Raman scatt. meas. 79−4389
- SF_6, matrix isolated, IR spectrosc., temp. reversible site structural changes 80−95613
- Sb_5O_7I, ferroelastic, Raman scatt. and symm. aspects of phase transition 77−8578
- SbSI, cryst. and vitreous, nonlinear light absorpt., effect of temp. and phase transitions 77−75604
- SbSI, crystal struct. in ferroelec. phase, displacive type transition 77−11515
- SbSI, Raman scatt., near tricritical point 78−15159
- SnF_2, phase transitions 80−100329
- SnF_2, second order $\beta\rightleftarrows\gamma$ transition, neutron diffr. and NMR obs. 80−107095
- $Sn_{1-x}Mn_xTe$, degenerate mag. semicond., thermoelec. power meas. 80−29392
- $Sn_2P_2(S_{1-x}Se_x)_6$, solid solutions, ferroelectric soft mode freq., displacive transformations 80−29701
- $(Sn_{1-x}Pb_x)_2P_2S_6$, solid solutions, ferroelectric soft mode freq., displacive transformations 80−29701
- SnTe, bond gap, phase transform., optical dielec. const. meas. 80−10630
- SnTe, displacive phase transition at 22K, Mossbauer spectra and elec. resist. meas. 80−6514
- SnTe, displacive transform., interband electron-phonon interactions, phase diagram 80−93252
- SnTe, light scatt. from soft modes, theory above and below displacive transform. temp. 79−95791
- SnTe, mag-props., effect of structure transition 78−6158
- $SrThNb_2O_8$, monoclinic-quadratic phase transform. *(French)* 77−27998
- $SrTiO_3$, anharmonic motion rel. to struct. transition 78−79718
- $SrTiO_3$, dynamic central peaks and phonon interactions 78−83903
- $SrTiO_3$, stressed, trigonal-to-tetragonal transition, EPR data, realisation of 3-state Potts model 77−28525

displacive transformations continued
$SrTiO_3$, thermal expansion near displacive phase transition meas. 77−12345
$SrTiO_3$, thermal motion at room temp., anharmonic or disordered 79−37805
$SrTiO_3$ under [111] uniaxial stress, neutron scatt. 78−67798
$SrTiO_3:Cr^{5+}$, nonlinear Jahn-Teller coupling, local dynamics, near struct. transition 80−2625
$SrTiO_3:Fe^{3+}$, displacive struct. transition, order-disorder behaviour, phonon softening, EPR obs. 79−23695
TaS_2 (1T) and (2H), bonding and charge density wave phase transitions 80−44282
$TaSe_2$ (2H), charge density wave transitions, neutron diffr. exam. 77−89515
$TaSe_2$(2H), Raman spectra of soft modes at CDW transition 77−16301
$Tb_2[Pt(CN)_4]_3.21H_2O$, phase transitions, X-ray study and spectroscopic study 79−60506
$TiSe_2$ (1T), phonons and CDWs, inelastic neutron scatt. meas. 79−28059
$TiSe_2$, semimetal, electronic props., superlattice form. 77−15532
$TiSe_2(S_2)$ (1T), electronic and vibronic struct. 80−44500
$TlCdF_3$, thermal props. near phase transition 78−75850
$TlMnCl_3$, perovskite cryst., antiferrodistortion transition, transition temp., variation with press. 79−7694
TlN_3, press. induced phase transition, Raman scatt. meas. 78−19468
TlN_3, press. induced transition dynamics, light scatt. 78−80362
γ-UO_3, neutron powder profile obs. 77−15337
W (001), displacive transition, H adsorpt. effects, theoretical model 80−65352
WO_3, condensed modes represented by normal modes in space group D_{4h}^{7} 79−90747
W(100) surface, instability, distortion and dynamics 80−84360
$Y_2[Pt(CN)_4]_3.21H_2O$, phase transitions, X-ray study and spectroscopic study 79−60506
Zr-Nb, stacking solitons in ω-phase systems and quasielastic scatt. 79−38822
ZrO_2:^{89}Zr electron captive decay lifetime, struct. environment effects 77−28523

display devices
AC electrodeless narrow gap discharge, anal. and plasma display design 80−70063
AC plasma display panel wall charge magnitude and distribution probe 78−67487
AC-operated plasma display panels, optimum composition of dielectric materials, CaO and SrO 80−14945
acoustic pitch, new contour display in connection with sound spectra *(German)* 77−833
anthraquinoide, electrochromism, display devices, multiplexing 80−45037
anthraquinone pleochroic dyes in liq. cryst. soln., photostability, appl. to liq. cryst. displays 80−88961
anticipatory, for communication by severely disabled nonverbal person 77−78002
autostereoscopic displays using stereo-pair of projected images 80−1296
beam-addressable optical display using supersaturated vapour photonucleation 80−4691
camera character-forming display, based on LEDs and internal or external timing circuits 79−9251
checkerboard pattern generator for vision research 77−40801
cholesteric films, absorpt. and contrast in dichroic liq. cryst. displays 80−75155
cholesteryl nonanoate-MBBA, liq. cryst. mixture, two colour display device 80−70116
cyanobiphenyl E-7 mixture, bistable cholesteric liquid crystal display 80−96437
p-cyanophenol mixtures, p-alkylbenzoates twisted nematic effect, appl. to digital display prep. 79−82947
design improvements, digital measuring instruments appl. *(Rumania)* 77−74451
diapositive graphical data stereoscopic indicator *(Russian)* 77−71308
diffraction grating, surface relief, for colour image storage and display 77−84004
digital readout format, new arrangement reduces observational error 77−5822
electrochromic cell with anodic IrO_x film electrodes 80−7329
electrochromic displays, technical aspects 78−65917
electroluminescent, review of principles and appls. of electrolum. 77−40288
electrooptic beam deflectors as streak cameras, theory 79−58809
electrophoretic image display, X-Y address technique, multilevel voltage select system 77−74381
electrophoretic image display medium, changing mechanism identification, IR method 79−74389
fluorescent liquid crystal-display, utilising elec. field induced cholesteric-nematic transition 78−16781
gamma camera image processing *(French)* 77−37038
garnet film, magnetic rag-domains, appl. to magneto-optical displays 78−91912
garnet film, numerical display element exploiting rag domains 78−68339
gas discharge cells in colour display panels, comparison of light output *(Japanese)* 78−62191
graphic processor for pseudo-colour images representation *(Italian)* 80−98562
grating patterns, moving digital technique for generation on oscilloscope 77−40957
high-speed SEM voltage contrast waveform display 79−67432
hologram electronic heterodyne recording and self-interference term rejection 80−91756
holographic Pancake Window reflective system 80−1165
holographic systems *(Japanese)* 79−68368
line printer displayed binary hologram generation by phase reference method 78−9344
line printer for image reconstruction from three-dimensional computer-generated holograms 77−42506
liquid crystal, alignment of director using submicrometre periodicity gratings 78−63666
liquid crystal, dichroic dyes for guest-host interactions 77−59554
liquid crystal, DVM applic. *(German)* 78−21165
liquid crystal, for real-time multichannel optical spectral analysis 78−38042

display devices continued
liquid crystal, mol. orientation, effect of deposition of SiO_2 films *(French)* 79−10789
liquid crystal, optical characterisation apparatus 77−7222
liquid crystal, smectic A phase, electrically induced scatt. texture and elec. reversal 78−83725
liquid crystal, twisted nematic, control and elimination of disclinations 77−68912
liquid crystal, twisted nematic, off-ninety degree, electro-optical colour effect 77−77172
liquid crystal, twisted nematic review of recent advances 79−99056
liquid crystal, using dichroic I polarising element 77−46807
liquid crystal cell, hybrid aligned, as multicolour display 77−4624
liquid crystal display, with dichroic dye guest, field-induced colour switching 80−1327
liquid crystal display elements, principles and applications *(German)* 80−86277
liquid crystal display technique 78−51419
liquid crystal displays with auxiliary nonlinear elements, series excitation control 77−5818
liquid crystal electro-optical appls. review 77−43136
liquid crystal electro-optical props. and applications 77−77174
liquid crystal electrothermo-optic effects, display appls. 77−11469
liquid crystal for UHF EM field pattern display, flow detection 80−104378
liquid crystal indicator of variable light-reading angle 78−57932
liquid crystal layer stabilisation additives 77−76305
liquid crystal light valve, fast photoconductor coupled 79−59805
liquid crystal properties rel. to molecular structure 78−55807
liquid crystal screen VHF field thermoindication, linearity *(Russian)* 79−1391
liquid crystal structure, properties *(Italian)* 79−82145
liquid crystal-fibre optic modulator for display 79−72718
LV dynamic scatt. display liquid crystal mixtures 77−77178
M 6000 display for spectrum reduction 80−42210
magnetic disaccommodation measurement, device, graphical or digital registration *(Polish)* 79−93180
mechanical pointer for communication with handicapped children 79−84013
metallisation patterns used in matrix displays, vacuum deposition, development of rib-supported mask struct. 78−23615
S-(+)-4-2′-methylbutyl phenol, cholesteric derivatives, appl. in display devices 79−19145
micromechanical light modulator array fabricated on Si, laser display appls. 78−9433
multiplexed liquid cryst. display, use of cholesteric-nematic phase change 80−107408
multiplexed twisted nematic displays, liq. cryst. material design 79−90533
nematic dynamic scattering display, flow direction rel. to dopant electrochem. props. 77−90130
nematic liquid cryst. cells, with twisted and tilted arrangements, guest-host interactions 80−34891
nematic liquid crystal, generation of arbitrary colour 80−5815
nematic liquid crystal acoustic image detector, resolution expt. 78−46871
nematic liquid crystal diaplay, thin film process to improve off axis viewing 79−4239
nematic liquid crystal display, capacitative anal. 77−43969
nematic liquid crystal display, twisted, ang. and voltage depend. of light transmission, two-layer model 80−76006
nematic liquid crystal matrix display, scanning capability improvement 77−55770
nematic liquid crystal mixture, for low voltage dynamic scatt. display 78−27184
numeric, effect of vibration on reading 80−104582
p-n-octyl-p′-cyanobiphenyl, thermally addressed liq. cryst. display, light scatt. and contrast 80−34892
optically pumped cell for visible display of inhomogeneous mag. field or RF freq. spectrum 77−65027
orientational bistability, nematic storage effects 80−70112
pattern display using sound localising effect 79−53284
4-n-pentyloxy-phenyl-4′-n-octyloxybenzoate, nematic, dielec. relax. and freq. depend. of threshold voltage 80−60497
phase imaging systems, chromaticity, luminous efficiency 78−33824
phosphor film electroluminescent devices, book contrib. 77−73176
photorefractive materials for optical storage and display 77−71961
picture taking parameters display in amateur cameras, review 78−89578
plasma, for large-area graphics, selection circuitry 78−38556
plasma devices *(Japanese)* 79−68961
plasma display panel, short-gap atm. discharge with needle-sphere electrodes 77−4008
plasma panel, AC, phase change meas. $<10^{-5}$Å, laser interferometer 77−18087
plastic optical components and systems 78−25967
pretilted liquid crystal structure formation and props. 77−76306
pulsed Doppler blood velocity meter readout 78−69158
quasi-analogue display for electronic clocks *(German)* 79−49207
radiotherapy Clinac-18, satellite digital display 78−3599
reversible electrodeposition display struct. having dynamic hysteresis characts. 79−49219
rotating prism display of multiple LED lines 79−93111
semiconductor photoelectrode, appl. in reproducible photoelectrochem. imaging 80−14446
seven-segment luminescent vacuum lamps for digital phase meter, counter scheme 78−4648
short circuit memory in electrochromic displays 80−97238
smectic A liquid crystal, scattering textures, appl. to display device 78−91236
smectic displays, thermo-optic and elec. field effects *(French)* 78−91223
surface-relief phase gratings for image recording and display 77−19429
three-dimensional display improvement 78−59225
three-dimensional optical display unit 80−1297
transmission light gate, using bistable electrets 77−50750
transparent conducting film surface resistance obs. 77−77313
twisted nematic display with cholesteric dopant, transmission characteristic temp. depend. compensation 80−103934
twisted nematic liq. cryst. matrix display, two-frequency 100-line addressing 79−54119
units and terminology used in light meas. rel. to photometry and displays 79−21691

display devices continued
- vacuum-deposited layers formation, use of borosilicate glass intermediate layer 80-80979
- Victoreen 555 integral and rate exposuremeter, digital display plug-in module 77-405
- video raster display control apparatus *(German)* 79-67265
- viologen display, mechanism of electrochromism *(Japanese)* 80-34893
- virtual image display using Fresnel lenses 80-1295
- volume hologram superimposed information display 80-78807
- X-ray image receptor, large area, with electrophoretic display 80-98091
- X-ray topographic images, direct display systems, review 77-68899
- Ag halide complexes electrodeposited on $In_{2-x}Sn_xO_{3-y}$ contacts, appl. to display struct. 79-15435
- $Cd_{1-x}Zn_xS$, electro-optical multilayer film, for data storage and display 78-71176
- $Cd_{1-x}Zn_xS$, RF sputtered electro-optical film for data storage and display 78-83047
- Cr film vacuum deposition on glass display panels 78-39694
- p-GaAs/heptyl viologen system, appl. in photoelectrochemical cells and photoelectrochromic displays 80-76640
- $H_3PO_4(MoO_3)_{12}.29H_2O$, electrochromic solid-state cells 80-2724
- $H_3PO_4(WO_3)_{12}$ electrochemichromic cells 79-15436
- $(H_3PO_4)(WO_3)_{12}29H_2O$, electrochromic solid-state cells 80-2724
- Hg-A discharge, positive column, scaling towards display cells 77-84565
- In_2O_3-SnO_2, magnetron RF sputtered electro-optical film for data storage and display 78-83047
- In_2O_3-SnO_2 electro-optical film, for data storage and display 78-71176
- $In_{2-x}Sn_xO_{3-y}$ film, deposited from organometallic composition, transparent cond. appl. 78-91793
- IrO_2 anodic films, electrochromium, on transparent substrates 79-19861
- IrO_2, anodic films, new electrochromic for nonemissive displays 79-99851
- IrO_2, electrochromic film, prep. by reactive sputtering 80-29876
- IrO_x anodic film electrochromic cell, fabrication and display device use 80-61320
- IrO_x anodic films, electrochromic props. and device uses 80-61319
- IrO_x film, anodic, electrochromism, pH effects on corrosion stability, coloration and bleaching mech. 80-2726
- Ne-Ar (0.1%) mixture, AC plasma panel, Paschen breakdown curves 77-11418
- PLZT ceramic photoferroelectric image storage and display systems 77-72084
- PLZT slim-loop and linear ceramics, longit. electrooptic effects, display appl. 80-80751
- VO_2 thin films, resist.-temp. characts. and structure at phase transition temp. *(German)* 77-28265
- WO_3 electrochromic amorphous films, colouring and bleaching, expt. and anal. 77-20829
- WO_3 electrochromic reaction kinetics 77-77176
- WO_3 film electrochemical colouration for displays 77-77170
- WO_3-$LiF(MgF_2)$, electrochromic display struct., efficiency and humidity depend. 79-81540
- n-ZnCdS-PTA, photosensitive powder mixed with electrochromic material, photoinduced coloration and electrochem. bleaching 77-81082
- $ZnS{:}TbF_3$ film between semicond. Y_2O_3 layers, bright green electrolum. 80-2859

display equipment *see display instrumentation*

display instrumentation
- *see also cathode-ray tube displays; display devices; radar displays; screens (display)*
- 3-D displays, autostereoscopic image synthesis from binocular stereoscopic images *(Japanese)* 79-31812
- 3D real time for US diagnosis 80-51182
- analogue digital double integration joulemeter, AC loss meas. in superconducting magnets 80-57325
- angle-resolved electron spectrometer with large-angle visual display 80-52808
- AS77 scanning analyser for measuring Si-SiO_2 structure electrophysical props. *(Polish)* 79-95498
- astronomy, photon counting and analogue TV systems with digital real time image processing 78-96402
- automatic fluorescence microscope photometry data processing and display *(German)* 80-86369
- biocular magnifier design for display system viewing 79-27361
- bioelectric signal measurement and processing instrument trends *(Croatian)* 78-44665
- biomedical US images, cine display 80-108984
- biostereometrics, three dimens. displays 78-81010
- blood pressure monitor, systolic-diastolic, using display stabilising circuit 78-40364
- blood velocity waveform display by spectrum analysers, direction Doppler signal preprocessing 79-34611
- Braille display cassette tape recording for text reproduction *(Spanish)* 79-39612
- calligraphic projection display resolution and contrast photometer and X-Y plotter 80-86373
- cardiovascular neurography: cardiac-rhythm based neurosignal distribution display 80-41351
- chart recorder, adaptor for converting single channel to multi-channel instrument 77-37874
- colour, image overlay with single projection lens 79-36973
- colour display technique for NMR imaging 77-57373
- colour meas. techniques, using colorimeters and spectroradiometers 79-40605
- communication device for mute paralytic 78-40420
- composite thermal/visual display superposition technique 78-77992
- computed tomography image display system 80-46039
- computerised tomographic image display by TV and photography 80-8129
- computerised tomography, multiple window display techniques 80-109010
- conference, Chicago, USA, 1979 May 80-17932
- constant-display frequency meter 79-21718
- DCF 77 standard time and frequency receiver, display ccts. *(German)* 77-13737
- differential diagnosis hand tremors, artificial limb tracking using data compression methods 77-86697
- differential temp. sensor with indicator system *(Spanish)* 79-54133
- diffraction pattern display using photodiode array 78-86069
- digital, calibration requirements 77-37907

display instrumentation continued
- digital, seven decade reversing counter cct., quadrupole mass spectrometer appl. 77-18129
- digital, with histogram output 77-41652
- digital counters and timers, accurate meas. techniques 78-45605
- digital display adaptor for Victoreen 440 survey meter 79-70644
- digital display for lecture hall use 78-86075
- digital display of neuronal average firing freqs. 77-5117
- digital display technological varieties 79-80587
- digital image display, interactive program *(Italian)* 80-98559
- digital panel meter planar gaseous discharge display, LSI, microprocessing techniques 77-37867
- digital photoelectric localisation of objects *(Slovak)* 77-18089
- digital scan convertor for use in medical US scanning 80-30816
- direct display of gas-gun projectile velocity 78-177
- display design, visual psychophysics appl. 78-65017
- Doppler US system, for internal organs imaging 79-5332
- dynamic data display on large screen by brightness enhancing system 77-58462
- ECG data interactive display system 78-53550
- echo display equipment for US testing, nonlinearity *(German)* 79-34222
- educational aids *(Japanese)* 78-20924
- EEG electronic recording and display systems *(French)* 77-13025
- EEG real-time display of 2-dimens. fields 78-44651
- electro-optical imagery display efficiency study using human visual system model 77-73531
- electro-optical readout system for analysis of speckle photographs 80-62708
- electrochromism, application *(Japanese)* 77-1656
- electronic communicator for disabled, Fingercom 80-17199
- emission spectrometry, current developments *(Japanese)* 78-86356
- epicardial mapping, computerised display system *(Japanese)* 80-101279
- expendable bathythermograph digital recording and display system 80-46318
- Fermilab, beam intensity and efficiency display system 79-72218
- fibre optics appl., West German developments 1978 survey *(Swedish)* 79-55209
- fibres, elastic moduli determ., automatic laboratory display unit 79-55349
- Fourier domain aliasing and quantization in efficient image display 79-81372
- gait instrumentation for foot/ground interaction meas. and display 79-96696
- gated cardiac studies, data processing system 79-25091
- Glossynograph system for presenting printed text synchronously with speech for hearing-impaired persons 80-56153
- HF Doppler obs., realtime display system 77-73887
- hologram viewing techniques and engineering display applications 79-50264
- holographic display, large scale, in photographic emulsion, image reconstruction 78-78974
- holographic displays, colloquium, London (1978) 79-50258
- holographic displays, conventional light sources 79-50261
- holographic head-up display 79-50266
- holographic projection-type displays 78-78972
- holographic stereogram imagery 78-78978
- holographic terrain displays in 3D 78-78979
- holography, large-scale reflection and transmission, for displays 78-78975
- human factor studies, conf., San Francisco, USA (Oct. 1977) 78-48742
- human visual system models for image enhancement and display design 77-58279
- image evaluation, psychophys. and visual aspects, conf., Rochester, USA, (Oct. 1977) 78-65016
- impedance camera for spatially specific meas. of thorax 78-53464
- information display technology, symposium, San Francisco (1978) 79-9209
- interferometric examination of lenses, mirrors and optical systems, 3D display 80-69497
- Large Azimuthal Telescope program control system 79-16829
- large format, generation of generalised psychophysical stimuli 79-44072
- large-aperture holographic visual simulator 80-102679
- large-variation phase object visualisation method 77-50637
- laser recorder of video signals, on dry-developed photosensitive paper *(French)* 78-92998
- laser scanned visual displays, pulsed light data extrapolation 80-3713
- laser-induced retinal morphological and functional changes and safe energy levels 80-3712
- LED counter synchroniser EMG data, cine film, rats appl. 77-81754
- LED temperature display with integrated window discriminator TCA965 77-128
- light column display of sound pressure levels 79-41536
- mass spectra, graphic display, dynamically refreshable controller with vertical line generator 78-314
- medical diagnostic techniques, picture-display systems, developments and limitations *(German)* 79-100705
- medical display system perceived dynamic range evaluation from receiver operating charact. curves 78-44662
- meteorological satellite Earth-based receiving stations, minicomputer appl. 77-78431
- METEOSAT interactive image system 80-109330
- microprocessor based interactive radiographic image display 79-25092
- microscopy, UV, with image intensification and TV image displays 77-5888
- minicomputer, real-time, portable, for dynamic ocean data acquisition and display 80-12552
- modules of 'Summa' system for information output to oscilloscope, digital display and digital printing 77-3244
- multichannel EKRAN installation for the treatment of random-process parameters 80-13047
- multipeak residual gas analysis monitoring system 79-79342
- NDT, A-scope display explanation using US wave visualisation as teaching aid 77-57136
- neutron detector, expt. control and data acquisition system 79-45589
- nuclear medicine, image processing system 80-41174
- nuclear medicine, precision computer display techniques 80-98100
- nuclear medicine, precision computer display techniques 80-109011
- nuclear medicine display systems 79-16298
- nuclear medicine hard-copy image display systems comparison 79-74744

display instrumentation continued
  nuclear reactor multivariable parameter meas. and display microprocessor solution 79—72221
  ocean digital survey fathometer, providing chart display and digital output 79—5665
  on-line display aid for bubble chamber film automatic meas. 78—5098
  optical data processing application examples 79—27183
  optical fibre pattern display using TV camera 78—33820
  optical spark chamber data automatic digitisation using CCD 79—89517
  plasma electron density display with resonance cone RF probe 77—62404
  plasmascope, opto-electronic method for vel. meas. in thermal plasmas 77—39462
  polarcardiography, triaxicardiometry and other displays 79—39581
  pulse dispersion test bench for optical fibre characterisation 77—50778
  Q data acquisition system for PDP 11 79—89545
  quasi-digital meter using LED's 77—37938
  radial metrological pattern generating engine for manufacture of masters including scales and gratings 80—57282
  radioisotope image magnifier/rotator for enhanced visualisation 78—15889
  radioisotope imaging, multi-element band display performance 77—56448
  real-time, for neurophysiology 77—2071
  sampled/raster displays, assessment of information visibility using signal detection model 80—19002
  scanning NQR spectrometer freq. marker system 78—21191
  scintigram preprocessing and display by microcomputer *(Hungarian)* 78—15881
  seismic wide angle refl. data from expendable sonobuoys, display and processing 79—39896
  SEM, stereoscopic observation and three-dimens. meas. instrument 78—21287
  SEM modification for simultaneous exposure numbering 78—62266
  simulation and image realism, seminar, San Diego, USA (Aug. 1978) 80—3639
  Skylab simulator visual displays and training for joint obs. programmes 77—60566
  solar-terrestrial environment monitoring and forecasting system, SEL-DADS, for radiocommunication appls. 79—58097
  solid state oscilloscope using 10 LED bars 78—21113
  SonoChromascope, US B-scan image acquisition, display and recording 80—30818
  speckle noise, min, detectable contrast 77—19411
  speech trainer for multihandicapped children, display method and control program *(Japanese)* 80—108922
  STEM image accumulation, storage and display system 80—37132
  stereophotogrammetry, digital profile to contour convertor, display 77—9501
  stereoscopic imaging synthesis allowing for real positioning of operator's head *(Russian)* 79—64391
  temperature measurement, using linearisation of Si junction characts. for direct display 77—53904
  Tesla-ammeter (F4354/1) with digital display, investigation of const. mag. fields 77—26364
  thermometer, acoustic, cct. and operation *(French)* 79—35739
  three dimensional display using stereograms and composite holograms 77—79921
  three dimensional imaging, conf., San Diego, USA (Aug. 1977) 78—78971
  three-dimensional multiplane liquid crystal matrix *(Russian)* 77—9995
  time-code clock, date display, BST switch and alarm add on circuits 77—53866
  tissue mutual impedivity spectrometry 80—17046
  TOMAX autostereoscopic display, three-dimens. viewing of tomographic data 78—85446
  tomography, computerised *(Japanese)* 79—70688
  TV analyser for interphase boundary anal. 77—40483
  TV monitor display using vidicon camera in pseudo real-time coded aperture, imaging system 77—31133
  TV monitor on Skylab Apollo Telescope Mount, for solar EUV image obs. 77—60600
  US blood flow spectrum, coherent optical anal. 77—40722
  US display system, using colour TV, tissue disease diagnosis appl. 79—29576
  US Doppler spectragrams refreshed display and haemodynamic parameter meas. 80—41152
  US multiple section tomogram simultaneous display equipment 78—61227
  US real-time B-scan machine attachment for three-dimensional display 78—61229
  US-field display device with transducer and LED linear arrays, appl. to US holography 80—23843
  UV polymer-film dosimeters, automatic read-out device 80—78455
  vector cardiograph for pacemaker pulse display 80—41325
  vectorcardiography, computerised meas. and display system 77—40864
  video displays, conventional or stereo, operator performance for perceptual tasks 78—80882
  video displays, conventional or stereo, operator performance for perceptual tasks 78—85314
  vision and display *(Japanese)* 79—70551
  visual evoked response meas. using versatile pattern-reversal stimulator 80—17177
  visual simulation techniques in military training devices 79—50413
  visual stimulus generator, electronically controlled 79—74817
  weighing system, electronic, digital transducer instruments 80—95076
  X-ray spectrometry, quantitative, comparison of mathematical models 79—17587
  SiC thin-film thermistors with high thermal response *(Japanese)* 80—105629

display instruments *see display instrumentation*

display systems *see display instrumentation*

display tubes, television *see television picture tubes*

displays, radar *see radar displays*

disruptive voltage *see electric breakdown*

dissemination of information *see information dissemination*

dissipation (heat) *see cooling*

dissociation
  see also electrolytic dissociation; heat of dissociation; ionisation; molecular dissociation; molecular dissociation energies; photodissociation
  air flows in triple point shock configurations, anal. thermodynamics *(Russian)* 79—32569
  alkali bromides, soln. in propylene carbonate, dissociation, radius and no. of ion solvation *(French)* 79—70319
  alkali halides, cohesive energy, atomisation energy 78—18576
  alkali metal solvent-ferrite quasibinary systems, dissociation 77—40573
  alkaline earth carbonate, thermal decomp. in vac., dielec. method appl. 77—16802
  alkyl halide, chem. struct. determ. using electron capture response 77—21428
  biopolymers, assoc.-dissoc. phenomena, review 79—11884
  Bray reaction, kinetics obs. *(French)* 80—7788
  $CaO-SiO_2-CO_2$, subsolidus and liquidus phase relationships to 30 kbar 80—85643
  cellulose fibre, moist, dielec. props. 78—76380
  chemically driven convection of dissociating Navier Stokes fluid, instabilities 80—59128
  chemonuclear fusion reactor, gamma-neutron, chem. reaction parameters 77—34466
  chromatographic support materials decomposition by ionising radiation *(German)* 78—92587
  coal, in organic solvents, fast-dump reactor apparatus for short reaction times 77—44575
  collision induced, $A+BC \rightarrow A+B+C$, statistical classical trajectory theory 77—28977
  competitive decomposition and stabilisation models for collisional efficiency in external activation systems 80—25989
  composite material, heat exchange during rupture *(Russian)* 77—48517
  concrete, thermal decomposition, empirical model for kinetics and stoichiometry 78—17386
  Coulomb gas, 2-dimens., dissociation at low temp. 77—31748
  crystalline solid, decomposition, kinetic parameters 79—15984
  decomposition reactions, endothermic, kinetics 79—52646
  degree of dissociation of congruently melting compound, calc. from liquidus curve 77—84892
  desorption kinetics with precursor intermediates 78—87876
  determination from curvature of liquidus line 78—22828
  di(alkylbenzylthio)ethane, oil additive, thermal stability determ. by chromatography, colorimetry 79—15969
  di-p-anthracene, electron beam induced monomerisation 77—12789
  diatomic clusters, break-up in thin films, particle energy distrib., central peak nature 80—50490
  dolomite, $CaMg(CO_3)_2$, kinetics and thermodynamics of decomposition to metastable solid product 78—80740
  educational model 77—26110
  endothermic solid-gas decompositions, activation energy, interpretation *(French)* 79—15981
  ethylene, adsorbed on Ni(110) 77—85071
  ethylene, chemisorption on Ni (110), adsorption and decomposition exam. 77—55459
  excited charge transfer systems, in polar solvents, dynamic behaviour obs. 78—58772
  explosives, secondary, thermal decomp., solid-state kinetics, differential scanning calorimetry 78—92449
  ferrite formation during calcining of sulphate mixture 77—63608
  ferrite systems, thermodynamic stability, dissociation and phase relations *(Japanese)* 80—55378
  formic acid, adsorpt. and decomp. over Ni surface, obs. using combined SIMS-FDS-AES system 78—40076
  E-glass fibre, silane coupling agent deposited on surface, hydrolysis and drying effect on siloxane bonds 80—85072
  gypsum, thermal conductivity thermal decomposition 78—2310
  heavy oil droplet with simultaneous cracking inside, combustion mechanism 79—74385
  hydrocarbon dissociation, diamond formation, Hugoniot data, high temp. and press. 79—47927
  inorganic solid, interfacial endothermic reaction, abnormal thermal decomp. rate 78—76852
  o-iodohippurate, ^{131}I labelled, in vitro stability 80—16668
  ionic solid volatilisation, surface charge effects 78—14457
  kaolinite, decomposition 77—52627
  lithium formate monohydrate, thermal dehydration, dislocation effects 80—3331
  metal chelates, prep. of colloidal particles 80—71953
  metal ion hydrolysis *(Chinese)* 78—85153
  metal oxides, chemical dissoc. under pressure as alternative to metallisation, feasibility study *(Russian)* 78—48553
  metal-halogen arc lamp, nonequil. comp. developed by slow chem. reactions *(Hungarian)* 77—47288
  methanol, chemisorption on Ni (111), decomposition, UPS and flash-desorption exam. 77—55455
  methyl methacrylate methacrylic acid copolymer, hydrogen bonding effect on mol. relax., IR obs. of dissoc. process 77—58959
  MHD generator channel electrode surface temp. selection, effect of working body props. 79—55573
  negative specific heat paradox, theory for dissociation appl. to phase transforms. 78—9557
  noncrystalline solid element, polymorphic bonding and thermal stability 77—31597
  organic compounds, hydrolysis in water, rate consts. 78—76856
  partially dissociated gas, homonuclear diatomic mols., one-dimens. model 77—15157
  pentlandite, prep., H_2 reduction with lime, to yield Fe-Ni alloy 78—85018
  phenolic, two-stage cured, molecular struct. of Novolac effect on thermal stability *(Japanese)* 78—3092
  phenoxyacetic acid, photoinduced selective isomerisation in comparison with X-ray induced decomp., aq. soln., 25°C *(German)* 77—63931
  photographic emulsion gelatin enzymic hydrolysis expts. 79—79311
  plasmon mechanism for energy loss, dissoc. and orientation of fast ions excited by grazing collisions 80—11523
  polyethylene, fine struct., prep., O_3 selective degradation, chromatographic obs. 78—92475
  polyiodides, cathodic materials in I_2-Ag current source, compatibility with solid electrolyte $RbAg_4I_5$ 77—40555

dissociation continued

- polymeric electret films, produced in HF discharge, props. *(Russian)* 80−20578
- polymers, solid interaction with SF_6 plasma, in glow discharge, emission spectrum 80−87960
- polymethylstyrene, mech. scission by US irradiation *(Japanese)* 78−59190
- polyorganosiloxane, thermogravimetric assessment of stability at high temps. 77−52704
- polyurethane foam, rigid, gaseous thermal decomposition products, IR anal. *(German)* 79−29348
- propellant decomposition kinetics, eqns. 79−91941
- PVC, gaseous thermal decomposition products, IR anal. *(German)* 79−29348
- radical species, tube electrode generation, laminar flow through EPR cavity, decomp., convection 77−24746
- radioactive waste, vitrification, thermal decomp. of nitrates and additives in glass-making *(Korean)* 78−86638
- rare earth dihydrides, lattice thermal expansion and thermal dissoc. 77−51524
- rare earth hexaborides, powders, evaporation 77−89535
- rare earth systems, RCo_3-H_2 (R=Ce, Pr, Tb, Dy, Er), phase equilibria, from dissociation isotherms 80−50591
- rare-earth compounds, reaction processes in solid phase *(French)* 78−30756
- rarefied gas flow with chemical reaction, Monte Carlo simulation of homogeneous dissociating diatomic gas 77−51128
- reacting gas, steady axisymmetric supersonic free jet, approx. analytical soln. 77−55099
- reaction rate calc. by differential quotient 80−25990
- reverse pulsed polarography, reversibility characterisation, electrode reaction product determ. 80−66889
- schoenite-type salt, formation of single phase ferrite powders 77−16524
- shock wave formation, in dissociating gases 79−60004
- solids, thermal dissociation, dynamics, study via time-of-flight mass spectrometer 77−74547
- solution ionisation, induced ion pair separation, Coulomb cage pair 79−11811
- sphalerite, dissolution in ferric chloride soln. 79−47919
- stalactites, chem. decomp., ESR obs. 80−15788
- steel, cold-worked, state of cementite, nucl. gamma reson. meas., plastic deform. *(Russian)* 78−68706
- steel, hypereutectoid, austenite dissociation depend. on strain at intercritical temps., pearlite transform. *(Russian)* 80−40362
- suspensions, appl. of Gibbs-Thomson eqns. to particles of dissociative and associative substances 77−4944
- tetrabutoxytitanium, thermal decomposition in MgO-Al_2O_3-SiO_2 glass, effect on crystallisation 78−87627
- thermal dissociation vibrational relaxation at high temps., ab initio calcs. 79−74367
- transformer oil diagnosis, computerised evaluation of results *(Czech)* 80−97744
- triamino-trinitrobenzene, UV and shock-induced decomp. XPS obs. 79−31595
- triatomic molecular systems, unimol. decomp., exit-channel coupling effects 80−25984
- tripositronium, probability of decomposition into an electron and a photon *(Russian)* 79−22866
- type B carbonate apatites, dehydration obs. *(French)* 79−66264
- unimolecular decomposition, least motion paths 77−21370
- vanadium bronzes of type $M_xV_{12}O_{30}$, synthesis and thermal props. of single crysts. 77−84717
- water, dissociation under solar illumination, band bend of surface of n-TiO_2 photoanode 78−91765
- water decomposition into H and O using solar energy, one-step effusional process 78−15672
- water thermolysis, solar furnace, thermodynamic analysis 79−83625
- n-xylene, C precipitate with preferred orientation [100] *(Russian)* 80−45484
- zircon, dissociated, form. in plasma furnace, comp. and microstruct. 77−36429
- $Ag/RbAg_4I_5/I_2$ solid state battery, low temp. degradation 80−61331
- $AgCl{:}CdCl_2$, point defect model, free energy and radial distrib. functions 80−44201
- AlBr solution, in propylene carbonate, dissociation, radius and number of ion solvation *(French)* 79−70319
- $AlFeF_5.7H_2O$, Mossbauer spectra, thermal decomp. products 78−80258
- AlH_3, I-V and relax. characts. in dark cond. 77−85235
- α-AlH_3, prep., thermal decomposition, transform., struct. *(French)* 80−3326
- $AlM_xH_{1-x}(SeO_3)_2.nH_2O$, M=alkali metal, hydrothermal crystallization, thermal decomp. 77−90265
- Al-AlOOH, disapore, superstructure form. on dehydration, electron microscopy obs. 80−3327
- $Al_2(SO_4)_3$, decomposition, charact. of gaseous and solid products 78−44374
- $Al_2(SO_4)_3.17H_2O$, precipitated from acetic acid soln., thermal decomposition 79−91934
- Ar-Cu, Cu diffusion coeff. determ. volatile salt dissoc. in pulsed discharge 80−33721
- Au contact films, dissociation of GaAs and $Ga_{0.7}Al_{0.3}As$ during alloying 79−79357
- Au_3Si, room temp. dissociation 78−35672
- BFHOH, transient mol. form., microwave spectroscopic obs. 78−74643
- $BH(OH)_2$, transient mol. form., microwave spectroscopic obs. 78−74643
- $BP+N_2(NH_3)$ 79−43627
- $BaBr_2.2H_2O$, dehydration kinetics, isothermal and nonisothermal kinetics 79−57227
- $Ba(N_3)_2$, thermal decomp., role of defects 78−73033
- $Ba(PO_3)_2$, hydrolytic decomp. 80−21271
- Bi_2Te_3-based solid solns., decomp. kinetics under flux layer 77−81205
- $CaCO_3+SiO_2$, in presence of NaF, thermal decomposition of Ca_2SiO_4 formation 78−68889
- $CaO.3B_2O_3$, form. by dehydration of hydrated calcium borates *(Japanese)* 79−74378
- $Ca_9(PO_4)_6.H_2O$, hydrolysis, activation energy *(French)* 77−73447
- $CaSO_3$, thermal decomp., enthalpy of form. 77−73460
- $CdCO_3$, topotactic decomp., X-ray diffr. obs. 77−44478
- $Cd(OH)_2 \rightarrow CdO$, decomp. reaction, crystallite fragmentation, critical sizes and shapes 78−23635
- $Cd(OH)_2$, decomposition into CdO, crystallite size and shape 79−57219

dissociation continued

- Cd(OH)Cl, temp. depend. of elec. cond., solid state thermal decomp. 78−19042
- CdS, thermal decomp. kinetics, in vacuo, free electron density depend. 77−59111
- CdSe, meas. of partial press., by optical absorption method *(Japanese)* 78−51661
- CdSe, partial press. meas. by optical absorption 80−15234
- CdTe, meas. of partial press., by optical absorption method *(Japanese)* 78−51661
- p-CdTe, nondoped, heat treatment in vacuum, dissoc. obs. effects on struct. and props. *(Japanese)* 80−60662
- CdTe, partial press. meas. by optical absorption 80−15234
- $CoOOH \rightarrow Co_3O_4$, morphology, topotaxy, comparison with $Co(OH)_2 \rightarrow CoOOH$ 77−16817
- α-$CoSO_4$, anhydrous, thermal decomposition, SO_3 evolution, gas equilib. and kinetic approach *(German)* 78−23943
- $(Co_{0.001}Zn_{0.189}Ni_{0.143}Fe_{0.667})SO_4.(NH_4)_2SO_4.6H_2O$, schoenite-type salt, formation of single phase ferrite powders 77−16524
- Cs_2CO_3 thermal decomp., low work function surface prod. 77−85882
- Cu-Ti alloys, CuTi, $CuTi_2$, solubility of H_2, decomp. reacts. 79−65197
- CuCr alloys, supersaturated solid soln. dissociation *(Russian)* 79−52201
- Cu(OH)Cl, temp. depend. of elec. cond., solid state thermal decomp. 78−19042
- $Cu_{0.5}Pd_{0.5}Ti_2$, solubility of H_2, decomp. reacts. 79−65197
- Cu_2S, $Cu_{1.8}S$, $\alpha \rightarrow \beta$ transition, thermographic investigation of heats, entropies and activation energies 80−88314
- Cu_2S-GeS_2 and Cu_2S-SnS_2 systems dissoc. of ternary congruently melting cpds. 79−87832
- $CuSO_4.5H_2O$ monocryst. platelets, dehydration into trihydrate, displacement rate modulation of reaction front 80−108711
- Cu_2Se-Cu_2Te, intermolecular interaction, thermodynamic anal. of dissociation pressure 80−53088
- Cu_2Se-$GeSe_2$ and Cu_2Se-$SnSe_2$ systems, dissoc. of ternary congruently melting cpds. 79−87832
- Eu-salt solutions, frozen, Mossbauer parameters depend. on pH and halide conc., Eu(III) complexes form. 78−3330
- $Eu_3Fe_5O_{12}$, thermodynamic stability 77−52662
- Fe, cast, Mg, isothermal dissociation of supercooled austenite, exam. of kinetics *(Russian)* 79−29013
- Fe chelates, prep. of Fe_xO_y colloid particles 80−71953
- Fe surface, form. and decomp. of nitrides 79−24831
- Fe-MgO system, decomp. reactions, ferromag. reson. obs. 77−9058
- $FeMF_5.7H_2O$ (M=Zn, Co, Fe), Mossbauer spectra, thermal decomp. products 78−80258
- $Fe_{1-x}O$, wustite, vaporisation, mass spectrometric analysis of gaseous phase 78−48652
- Fe_2O_3, plasma sputtered coatings, oxide dissociation, coating props., struct. and composition *(Russian)* 80−54577
- Fe_3O_4, magnetite, vaporisation, mass spectrometric analysis of gaseous phase 78−48652
- α-FeOOh, goethite, superstructure form. on dehydration, electron microscopy obs. 80−3327
- FeS_2-$CaCO_3$-C, reaction on heating, dissociation, reduction to Fe *(Russian)* 78−44041
- Ga-Te system cpds., degree of dissoc. from curvature of liquidus line 78−22828
- GaAs, $Ga_{0.7}Al_{0.3}As$, dissociation during alloying with Au contact films 79−79357
- Ga_2O, decomposition and desorption on Al_2O_3 $(10\bar{1}2)$ surface, effect of multiple binding states 78−44406
- $Gd_2Ga_5O_{12}$, cryst. growth by Czochralski technique, dissociation products calcs. 79−47615
- GdP, vapour comp. and dissoc. pressure 77−84916
- GeP, dissociation kinetics rel. to volatile component sublattice 77−84917
- H_2 dissociation poison and H_2 embrittlement 77−9079
- H_2, interstellar, ionisation, dissociation and heating efficiencies of cosmic rays 78−28454
- H_2CO_3, dissoc. reaction rate meas. using reference electrode liq. junction 77−4906
- $HNO_2+OH \rightarrow H_2O+NO_2$ react. kinetics, at high temps. behind shock waves 77−44477
- H_2O dissociation using solar energy for H prod. 80−30597
- $H_3O^+.nH_2O$ cluster ions, stability, assoc. and dissoc. 77−60055
- $H_3S^+.H_2O$ cluster ions, stability, assoc. and dissoc. 77−60055
- $H_3S^+.nH_2S$ cluster ions, stability, assoc. and dissoc. 77−60055
- H_xTaS_2, nonstoichiometric, incoherent neutron spectra, X-ray diffr. 78−42998
- In-Te system cpds., degree of dissoc. from curvature of liquidus line 78−22828
- InP, fused, SRO structure changes on heating 77−89367
- K_2CO_3 melt in combustion prods. medium, vaporisation of drops 79−57290
- $K_2Ca(SO_4)_2.H_2O$, thermal dehydration, isothermal kinetics 79−15982
- $K_2Mg_4Mo_4O_{16}.(OH)_2(H_2O)_2$, dehydration processes rel. to stoichiometry *(French)* 79−24734
- $KMnO_4$, thermal decomp., $K_3(MnO_4)_2$ intermediate phase 77−44479
- KNO_3 calcite-type crystals, topotaxial decomp. TEM obs. 80−108710
- K_2O, under vacuum, exam. of thermal behaviour *(French)* 79−19365
- K_2O-Al_2O_3-P_2O_5-TiO_2, structural role of Ti, kinetic study of chem. destruction 80−88055
- $K_2S_2O_8$, thermal transitions, catalytic effects of CuO and ZnO 79−15983
- $K_2SnF_6.H_2O$, crystallographic characts. *(French)* 78−10011
- $LaBO_3$ (B=V, Cr, Mn, Fe, Co, Ni), chem. stability X-ray and thermal anal. 79−79242
- $LaNi_{5-x}Al_x$-H_2 system, decomposition press. control rel. to metal hydride appls. 77−86308
- $La(OH)_3$, thermal decomposition, TGA, DTA, X-ray diffr. study *(Japanese)* 77−36436
- La_2O_2S-Ga_2S_3 system, phase diagram determ. by DTA and X-ray diffr. *(French)* 77−43309
- La_2S, unsaturated and saturated vapour press., 673-1173K, thermal dissoc. pattern 80−104457
- Li_2CO_3, decomp. and ferritisation, effect of initial Fe_2O_3 content 77−52269
- $LiCrO_2$, evaporation, as a corrosion product in compatability experiment of Li_2O pellets with Fe-Ni-Cr alloys, mass spectrometric study 79−73301
- $Li_2W_2O_7$ 77−48407

dissociation continued
- Li_2ZrO_3, thermal decomposition, enthalpy of formation 298.15K 78—61003
- Li_4ZrO_4, thermal decomposition, enthalpy of formation 298.15K 78—61003
- Li_8ZrO_6, thermal decomposition, enthalpy of formation 298.15K 78—61003
- Mg compounds, X-ray diffraction study of MgO substructures 77—12581
- $MgCr_2O_7.6H_2O$, dehydration, thermal decomposition, kinetics 79—11777
- $(MgO-Fe_2O_3-Cr_2O_3-TiO_2):Na_2O$, powder, prep., heat treatment, Na_2O impurity effect on props. 77—16528
- $Mg(OH)_2$, decomposition to MgO, mechanism, product crystallite size rel. to reaction rate 78—85152
- $Mg_2(OH_2)CO_3$, cryst. struct. rel. to artinite topotactic thermal decomposition 77—68952
- $MgSO_3.6H_2O$, thermal dissoc. *(Russian)* 79—66267
- Mn_2O_3, thermal decomposition, exam. by thermogravimetric methods 78—80743
- MoS_2 on Mo, cryst. struct. and thermal stability 77—52539
- $MoSe_2$, evaporation, mass spectroscopic investigation 77—76530
- NH_3, chemisorption and decomp. on clean and N-covered Fe (111) and Fe (100) 78—40077
- NH_3, decomposition, on supported FE catalyst, kinetics, IR obs. 79—11792
- NH_4NO_3 aqueous solution, enthalpies of dilution and relative apparent molar enthalpies, dissociated soln. case 80—50876
- $5(NH_4)_2O.12WO_3$, thermal decomp. 100-500°C 77—56223
- NO, in AC field, kinetics and energetics *(French)* 78—64824
- NO_2, in AC field, kinetics and energetics *(French)* 78—64824
- N_2O, decomposition on titanate catalyst, energy reson. hypothesis 78—95947
- N_2O_4 dissociating coolant, chemical reaction kinetics in transient regimes *(Russian)* 78—58344
- N_2O_4 dissociating coolant, O_2 generation time constant, enthalpy change *(Russian)* 78—58345
- N_2O_4, dissociating system, dynamic sorption of ^{131}I from gas phase *(Russian)* 78—58356
- N_2O_4, dissociation, reaction with H_2O, HNO_3, N_2O_3 *(Russian)* 77—86313
- N_2O_4, turbulent dissoc. flow, along heated tubes, heat transfer 80—63225
- $N_2O_4 \rightleftharpoons 2NO_2$ equilib. system, condensation heat transfer on horizontal tube bundle *(Russian)* 78—46970
- $N_2O_4 \rightleftharpoons 2NO_2 \rightleftharpoons 2NO+O_2$ dissociating system, behaviour with BaO *(Russian)* 79—20363
- Na vapour, heat cond., temp. discontinuity for dissociating gas 78—94887
- NaCl, interpolational eqn. of state with allowance for melting, vaporis., dissoc. and ionis. processes 80—24566
- NaCl-KCl, molten, alkaline earth oxides solubility products, potentiometric determ. 80—76488
- $NaCl-KCl-CaCl_2$, solid soln., X-ray examination of final decomp. stage *(Russian)* 77—63681
- $NaHCO_3$, thermal conductivity thermal decomposition 78—2310
- NaK, $a^3\Sigma^+$ state, laser induced fluorescence, $D^1\Pi$ to $a^3\Sigma^+$ transition, molecular constants, dissociation energies 79—98143
- NaK, $a^3\Sigma^+$ state, $X^1\Sigma^+$ state, fluorescence, visible spectrum 79—98114
- β-$Na_2O-Al_2O_3$, thermal dissoc. at high press. 77—36435
- β''-$Na_2O-MgO-Al_2O_3$, thermal dissoc. at high press. 77—36435
- $Na_2S_2O_8$, thermal transitions, catalytic effects of CuO and ZnO 79—15983
- $NbSe_2$, thermal dissociation 78—44370
- Ni (100), chemisorption and decomp. of formic acid -d_1 79—34361
- Ni (111), adsorption and decomp. of hydrocarbons, high resolution EELS study 80—40739
- Ni_3C film, thermal decomposition, AES meas. 78—56056
- NiP_4O_{11}, formation in phosphoric acid melts 78—27394
- NiSi, dissociation in presence of Ni film 79—47892
- Pb-Te-O, thermal stability 78—44104
- $Pb(HPO_4)_2.H_2O$, thermal stability, 20-1000°C, decomposition prod. struct. 79—11775
- PbO, stoichiometric deviations on heating in vacuum 77—25035
- PbO_2, thermal decomposition, heating rate effect, kinetics, mechanism, struct. 78—92473
- Pb(OH)Cl, temp. depend. of elec. cond., solid state thermal decomp. 78—19042
- PdGe, dissociation in presence of Pd film 79—47892
- Pt (111) and (100) superlattices formed by dissociative adsorption of HI, LEED, AES, and thermal desorption studies 80—55715
- $PtCl_2$, PtCl, decomposition equilibria by simultaneous torque Knudsen technique 77—29035
- PtSi, dissociation in presence of Pt film 79—47892
- Rb_2SnF_6, thermal stability and thermolysis *(French)* 78—10011
- Re_2, adsorbed on W (211) surface, dissoc., thermodynamics 78—87861
- ScD_2, surface, interactions with reactive gases 78—23964
- $Sc(H_2PO_4)_3$, synthesis, struct. and stability 77—47423
- $ScPO_4$, $Sc(PO_3)_3$, mass spectra 77—47567
- Si, reactions with metal oxides, general features, glass form. 79—11819
- Si-Al-O-N, ceramics, thermal decomposition 79—91936
- Si-H, amorphous, thermal stability and decomp. kinetics 80—24758
- SiO_2 surfaces, charging and dissociation, AES meas. 77—59650
- $SmCo_5$ based alloys, dissociation process *(Russian)* 78—27542
- SnO_2:Sb, transparent cond. film prep. by thermal decomp. of Sn salt of organic acid *(Japanese)* 77—90269
- $SnS(Se)(Te)(S_2)(Se_2)$, oxidation, thermal decomp., Mossbauer spectra 79—11713
- $SnSe-Tl_2Se$, phase diagram, DTA and X-ray diffr. peritectic decomposition *(French)* 77—51471
- $SrCO_3$, $NiCO_3$ impurity effect on dissoc. 78—27425
- Ta_3As, arsenic decomp. pressures and enthalpy of form. 77—70329
- Ta_2N film, high temp. nitriding kinetics depend. on press. *(Russian)* 80—50838
- $TaSe_2$, evaporation, mass spectroscopic anal. 77—76530
- ^{228}Th source, selective separation of ^{212}Bi 77—40566
- Ti alloy, type VTZ-1, two phase, mechanism and kinetics of metastable β and α'' phases dissociation *(Russian)* 79—74152
- Ti alloy, type VT8, two phase, mechanism and kinetics of metastable β and α'' phases dissociation *(Russian)* 79—74152
- $Ti(Al_xB_{1-x})_2$ (B=Cr, Mn, Fe, Co), $0<x<0.4$, influence of Al on H sorption props. X-ray cryst. struct. determ. 79—28198

dissociation continued
- Ti(C,N), hydrolysis 78—15713
- $TiCo_{1-x}Mn_x$, H absorption-desorption characteristics 80—96735
- γ-TiH_2, dissociation pressure, 20 to 70°C 78—85150
- TiN, powder defect struct., thermal and elec. props. 77—59286
- Tl_2SnF_6, thermal stability and thermolysis *(French)* 78—10011
- $U(H_2P_2O_5)_2$, prep., identification, thermal stability 79—15970
- $U(HPO_3)_1.2H_2O$, prep., identification, thermal stability 79—15970
- $U(H_2PO_3)_4.2H_2O$, prep., identification, thermal stability 79—15970
- VN powder, defect struct., thermal and elec. props. 77—59286
- $W(CO)_6$, decomp. under high field conditions, cathodic growth of W needles 80—76162
- $Y_2(C_2O_4)_3$, roasting effect of temp. on props. of Y_2O_3 77—8790
- $Y_2O_3.2SiO_2.Al_2O_3$ glass, thermal stability 77—44502
- ZnO, thin Zn or O rich layers, thermolysis, photolysis, SEM, XPS 77—11821
- $Zn_3(PO_4)_2.4H_2O$, thermal transitions, thermographic investig. 77—9063
- Zr(C,N), hydrolysis 78—15713
- Zr_3N_4, powder, form. by vapour phase reaction of $ZrCl_4-NH_3-H_2-N_2$ system *(Japanese)* 77—73247
- ZrO_2 $1.6H_2O$, anion defect formation and annealing during thermal decomp. in vacuum 77—51366
- ZrO_2-based solid solutions, effect of added B_2O_3 and Nb_2O_5 on sintering and stability 77—40410
- $ZrSiO_4$, Fe_2O_3 and TiO_2 additions effect on stability 77—48377
- $ZrSiO_4$, mechanochemical effect by mechanical grinding *(Japanese)* 78—84754

dissolution *see dissolving*

dissolving
- *see also solubility; solutions; solvation*
- agglomerate characterisation methods, review *(German)* 79—100443
- alcohols, dil. aqueous solns., isentropic compressibility behaviour from sound vel. meas., dissolution mechanism 80—30269
- alkali halide, irradiated crystal, recombination of radiation defects *(Russian)* 80—39151
- alkali halide crystal, irrad., chemiluminesc. process during dissolution *(Russian)* 78—92133
- alkaline cyanide soln., chalcocite dissolution kinetics 77—73463
- amino acids, technique for study of radiation in induced free radicals using lyoluminesc. 77—29230
- benzoic acid, dissolution, mass transfer at vibr. spheres 80—57220
- birefringent crystal faces, meas. method of growth and dissoln. rates 80—79719
- brass, sphere, dissolution in H_2SO_4 in elec. field *(Russian)* 77—4867
- bubble growth by expansion and dissolution in variable pressure field 78—15723
- calcite, marine, dissolution by fossil fuel CO_2, effect of sediment mixing 78—81212
- calcium oxalate trihydrate and monohydrate, dissolution kinetics charact. by SEM 79—42250
- carbon tetrabromide, cryst. growth from melt, dissolution morphology *(German)* 77—24283
- carbonate rocks, dissolution kinetics, lithology effects 77—78172
- ceramic compounds, lyophilisation parameters, freeze-drying synthesis 80—97453
- clay minerals, in seawater, dissolved Al conc. meas. 77—66928
- collagen, enzyme- and alkaline-soluble, optical rot. dispersion and circular dichroism 77—70411
- composites, planar, dissolution of precipitate plates, one-phase diffusion controlled 80—15244
- corrosion pit, convective diffusion 80—40601
- crystal growth, and dissoln. in suspension, kinetic expts. anal. 80—59414
- dielectric additive in ice-water system, interphase phenomena obs. *(Russian)* 77—8486
- disperse system coagulation, growth kinetics and soln. of microparticles *(Russian)* 77—32836
- DNA-cetavlate crystal growth and morphology 77—66583
- electron microscopy, decoration method, rel. to crystal growth *(German)* 80—103222
- furfural-water interface, anomalous mass transfer, coupling of heat and mass transfer 77—80626
- GaAs wafer, dissolution kinetics in undersaturated isothermal solns. in Ga-Al-As systems 80—80106
- gas bubbles, dissolution in liquid, theoretical and expt. obs. 77—15097
- gas bubbles dissolving in liq. 79—90319
- glass, dissolution rate control by H^+ mobility 77—55932
- glass melt, multibubble dissolution 80—81371
- glassy polymer multi-phase Stefan problem describing swelling and dissolution 78—2263
- graphite, dissolution rate in molten Si, Fick's law calc. 79—99319
- graphite surface, adsorbed Cs, dissolution, lamellar cpd. form. *(French)* 80—100399
- III-V semiconductor heterostructures, growth and dissolution kinetics by LPE 80—49543
- insulating coatings on Si, dissolution and corrosion in high temp. water and moisture 77—48564
- interfacial impedance of graphite electrode/graphite-βZnS mixture electrode in acidic aq. soln. *(Japanese)* 77—52648
- kinetics of dissolution 78—63686
- luminescence, measuring device *(Russian)* 79—93202
- metals, anodic dissolution, ionic mass exchange effects on hydrodynamic conditions 78—3349
- metals, dissolution of interstitial H_2 and D_2, diffusion coeffs., reverse isotope effect *(Russian)* 80—88368
- metals, sintering, surface oxide layer effects, oxide dissolution process, anal. 80—11588
- methyl iodide, dissolution into aqueous NaOH solns., fission reactor accident conditions 77—88236
- mineral, dissolution under Earth surface conditions, rate control 79—20817
- minerals, effects of stress on soln. rates 77—86865
- non-Newtonian fluid solution, film flow over soluble wall, solvent layer form 78—42634
- nonconducting drop motion and dissolution in current-carrying liquid 77—11275
- nonelectrolyte aqueous solutions, temp. of max. density rel. to partial compressibility, struct. strengthening 80—30270
- particle size distribution, continuity eqn. 80—55406
- pharmaceutical dissolution testing, microprocessor controlled sampling system 80—86273

dissolving continued
phosphate glass, thermal expansion and chem. durability 77—80636
polycarbonate, decomposition by H_2SO_4 and grinding by ball mill, exam. of molecular chain scission *(Japanese)* 78—64827
polymer, kinematics model and its expt. verification 78—26687
polymer solution, dissolution rates and polymer-solvent system phenomena *(German)* 80—13167
polyoxyethylene aq. soln., kinetics of soln. form. 78—64913
polysaccharide components dissolved into chlorite liquor according to the variation of treating conditions *(Japanese)* 80—3291
porous material, press. soln. thermodynamics, chem. and mech. forces interaction 77—60369
pseudocontinuum mass transfer in media with spatially periodic boundaries 79—86500
quartz, dissolution of grown synthetic quartz inside the autoclaves 78—63911
salts, dissolving and outwashing from soil and rock, hydromechanical treatment *(Russian)* 78—77279
sand, during glass melting, kinetic equation for interaction between grain material and liq. 80—84901
scalloping by flowing water, sizes rel. to eddy effects 79—27628
soil, ^{89}Sr and ^{90}Sr determ. using total sample decomp. 80—35808
solid solution form. in heat of combustion process *(Russian)* 77—66765
solid sphere,, mass exchange with elec. current carrying liq. 77—11274
soluble flat surface stability in turbulent flow 80—14676
soluble matter initial dispersion in three-dimensional flow 79—37387
sphalerite, dissolution in ferric chloride soln. 79—47919
sphalerite, kinetic study on press. leaching 77—4893
spherical particle in free-fall, time-to-complete-dissolution prediction 80—15245
steel, austenitic, 40Kh13N8G8, dissolution kinetics of carbide $Cr_{23}C_6$ *(Russian)* 78—48369
steel, C, dissolution of Cr_7C_3 in austenite *(Russian)* 80—103479
steel, Cr-Ni-Mo, resistometric study of austenitization and carbide dissolution preliminary annealing *(Czech)* 77—59829
steel, dissolution in HNO_3, thermometric method of rate estimation, a limitation 77—56138
steel, graphite dissolution, segregation and diffusion *(Russian)* 78—11201
steel, mild, cyclic strain enhanced dissolution in NH_4NO_3, corrosion fatigue props. 80—85083
steel, Ni-Cr, anodic dissoln. in NaCl solns. at high current densities *(Russian)* 80—76396
steel, Si, grain-oriented, high permeability, dissoln. and precip. of AlN and MnS 80—89223
steel, sphere, dissolution in H_2SO_4 in elec. field *(Russian)* 77—4867
steel, stainless, of Ti, dissolution kinetics *(Russian)* 80—34193
steel, stainless, stabilised, knife line attack phenomenon, dissoln. of carbides in thermal cycles *(Japanese)* 78—68701
steel, stainless stabilised, knife line attack phenomenon, dissoln. of carbide during isothermal heat treatment *(Japanese)* 78—72784
strontium calcium tartrate tetrahydrate, crystals grown by ion diffusion through silica gels, exam. of preps. 79—52102
two particle size powder dissolution, kinetic eqns. optimisation anal. *(French)* 78—19994
zircon, rate of dissolution in molten Fe_3O_4, porosity effects *(Japanese)* 77—11699
Ag film, photodissolution in amorphous As_2S_3 78—26737
Ag halide crystals, relative dissolution rates meas. by flow calorimetry 80—85220
Ag, photodissolution in amorphous As_2S_3 films, elec. resist. meas. 77—62786
Ag-As-Se system glasses, soln. rate 79—43456
AgBr emulsion, model system, Ostwald ripening obs. 77—2707
AgCl, ionic space charge and dissolution 80—107431
Al alloys, age-hardenable, precipitation and dissolution processes, positron annihilation and X-ray small-angle scattering comparison 80—89238
Al, anodic polarisation, charge transfer processes 77—16736
Al dissolution in HCl soln., inhibition by hydrazine derivatives 80—50759
Al, liq., of Co and Fe, dissolution rate, 700-900°C *(Russian)* 77—59119
Al, molten, dissoln. kinetics and diffusion coeffs. of Fe, Co and Ni 80—59666
Al, sacrificial anode dissolution, Hg effect study using ion implantation 79—39016
Al substitutional solid solution alloys, volumetric effect and props. *(Russian)* 80—39293
Al-Mg (2 wt.%), hardening and fracture characts., β-phase dissolution role 80—81178
Al-Mg (7 wt.%), bare surface reaction rates in aq. solns. 80—101022
Al-Si, dil., mechanism of dissolution of Si 79—19375
Al-Si (0.57 at.%), Si precipitate dissolution kinetics 80—84935
Al-Si hypereutectic alloy, dissolution and primary crystallization of Si *(French)* 77—59832
Al-Si(Mn)(Ti)(Cr)(Ni)(Cu)(Fe), liq., dissoln. and diffusion of alloying components, 700-1000°C *(Russian)* 80—15275
Al-Zn (11.8 at.%), growth and dissolution of metastable precipitates, neutron scatt. study 79—15671
Al-Zn-Mg (4.5, 2 to 3 at.%) solid state reactions by interrupted continuous heating 80—25737
Al-Zn-Mg (4.8, 1.1 wt.%), second phase dissolution, calorimetry study 79—100193
Al_2O_3 film on Al in oxalic acid bath, pH and conc. effects 77—16754
Al_2O_3 in Na_3AlF_6 *(French)* 77—51297
Al_2O_3-MgO-SiO_2, S-glass, solvent effect of water 77—4889
AlZn, homogenization processes, dendritic struct. 79—15700
As-Se and As_2S_3 films, electron-stimulated changes in optical props. and dissolution rate 80—29709
As_2S_3, amorphous film, photodissolution of Ag, struct. changes 77—11815
As_2Se_3, vitreous, effect of gamma-radiation on solution kinetics 77—19986
Au anode, chem. dissolution in aq. alkaline cyanide, electron stoichiometry 80—40697
Au, anodic dissolution in H_2SO_4, current-potential curves 79—70344
B_2O_3, molten, growth and dissolution of air, N_2, O_2 gas bubbles 77—20070
BaF_2 crystal, selective etching and dissolution kinetics 80—71775
BaFBr, single cryst. growth by flux method, dislocation etch pits on dissoln. 79—56925
C adlayer, dissolution into (110) face of Ni, 600-913K 80—49504

dissolving continued
C, dissolution mechanism in liquid Fe *(Russian)* 79—51264
C, dissolution rate in CaO-Al_2O_3 molten binary slag *(Japanese)* 79—23739
C, dissolution rate in molten Si, Fick's law calc. 79—99319
CaF_2, cryst., (111) faces, selective etch rate and etch pit morphology, acid conc. and temp. effect 80—96524
CaO-SiO_2-Fe_2O_3(MgO), melt, CaO dissolution *(Japanese)* 78—6909
$Ca_{10}(PO_4)_6(OH)_2$, dissolution in water at constant pH, exam. of kinetics 78—59949
$Ca_{10}(PO_4)_6(OH)_2$ dissolution kinetics, nucleation-controlled 80—59659
$Ca_{10}(PO_4)_6(OH)_2$ microcrystals, dissolution in non-stoichiometric solns. at constant pH 80—24597
$Ca_5(PO_4)_3OH$ bioceramic, material props. 80—93523
$CaSO_4$, dissolution kinetics on {111} faces of H_2SO_4 etched CaF 80—2028
$CaSO_4.2H_2O$, thermodynamic expression for crystal growth and dissolution affinity 80—24385
Cd-Mg, selective dissolution, static samples 80—65228
Cd-Mg, selective dissolution, rotating ring disc electrode 80—65229
$CdCr_2Se_4$, into Se melt, P-T phase diagram between 600 and 964°C 77—63636
CdTe:Cu films, impurity behaviour, Hall mobility and hole density meas. 80—80420
Co, anodic dissolution into silicate glass melt, exam. 78—88582
Co-Ca, liq. alloy form. kinetics *(French)* 80—96652
^{58}Co dissolution control by H_2O_2 addition in PWRs 78—21657
^{58}Co dissolution during PWR refuelling shutdown, control with H_2O_2 78—21698
Cr-W, anodic dissoln. at high current densities *(Russian)* 80—76395
CsI cryst., dissolution, selective etching rel. to $CuCl_2.2H_2O$ additive in ethanol 77—72618
CsI, selective etching, growth and dissolution in alcohols 78—71739
CsI:Tl, precipitation of Tl solid solns. 80—70419
Cu, creep rate, effect of surface anodic dissolution in acetate buffer soln. 78—3249
Cu diffusion layer cathodic deposition and anodic dissolution rates 80—93503
Cu, electrochem. dissolution and deposition kinetics, in aq. SO_4^{2-} soln. 78—27773
Cu, electrodissolution kinetics in acidic chloride solns. 80—16695
Cu, matte, thermodynamics of converting, distrib. of Au, Ag, Pb, Zn, Ni, Se, Te, Bi, Sb, As, Noranda process 79—47648
Cu single crystal spheres, dissolution, formation of etch pits, surface structure study using SEM 79—23735
$CuFeS_2$, exam. of dissolution kinetics, for dissolution in $FeCl_3$-HCl and $Fe_2(SO_4)_3$-H_2SO_4 solns. 79—11790
Cu_2O, layer-planes form. at anodic overpotential after dissolution of Cu hydroxy complexes on Cu amalgam 79—61865
CuS, covellite, dissolution in aq. NH_3 via hydrolysis of cupric amines 77—29004
Fe anode in H_2SO_4, passivation, dissolution model 80—35545
Fe, anodic dissolution in acidic chloride solns., exam. 78—92389
Fe based binary and ternary alloys, intercrystalline internal adsorption exam. by electrolytic dissolution *(Russian)* 78—35390
Fe, corrosion and passivation in LiCl soln., peripheral velocity effect 80—61000
Fe dissolution, morphology of differently oriented single crystal surfaces, dislocation effects *(German)* 77—9002
Fe, dissolution and passivation, effect of phosphate and chromate corrosion inhibitors 80—21152
Fe, dissolution and passivation kinetics in solns. containing O 80—76547
Fe dissolution kinetics, and passivation depend. on temp. and ionic strength 80—97626
Fe, dissolution under cathodic polarization 80—25899
Fe, exam. of graphite and cast Fe dissolution during sintering 79—33969
Fe in distilled H_2O, initial corrosion behavior, velocity and dissolved O_2, influence 80—35375
Fe, pure circular disc electrodes in (Na, H)ClO_4 solns., complex formation meas. 80—55569
Fe-Cr-Ni, corrosion behaviour in hot conc. NaOH soln. *(Japanese)* 80—85082
Fe-Cr(-Mo), passivated single crystal, selective dissolution and surface enrichment 80—16543
Fe-Hl (Si) (Ti) (V), molten, gaseous O_2 absorption 80—11836
Fe-Ni-Mn melt, thermodynamic dissolution of O_2 *(Russian)* 78—27473
Fe-Si(Ni)(Cu)(Mn)(C), dissolution rate into molten Al, convection mass transfer *(Japanese)* 78—71858
Fe_xO_y crystal dissolution, electrical potential effect, review 79—46809
Ga, cryst. growth from melt, dissolution morphology *(German)* 77—24283
Ga-GaAs melt, mutual diffusion from soln. kinetics, self-diffusion coeffs. 77—47608
GaAlAs, heterostruct. formed by LPE, growth and dissolution kinetics 79—99439
$Ga_{1-x}Al_xAs$ heterostructure, LPE prep., growth and dissolution kinetics, thermodynamic and kinetic models 80—75456
$Ga_{1-x}Al_xAs$ layer form. on GaAs during dissolution in Ga-Al-As soln. 80—10799
GaAs anodic oxide films, optical studies using rot. light-pipe reflectometer 80—76096
n-GaAs, preferential photoelectrochemical dissolution in Fe(III) based etches 78—7066
$GaAs_{1-x}P_x$ heterostructure, LPE prep., growth and dissolution kinetics, thermodynamic and kinetic models 80—75456
Ge-Ce liquid alloys, enthalpies of mixing, exothermal effects *(Russian)* 80—34192
GeO_2-Na_2O borosilicate glass fibre prod. by phase separation and leaching 80—69558
^4He, liq., upper limit for conc. of potential dissolved contaminants 80—39373
Hf electrode, surface oxide film, impedance and pot. behaviour 80—61001
In surface, impurity precipitation and resolution at melting point 78—14553
InGaAsP-InP DH lasers, perturbed InP growth, photoluminesc. study 80—106518
InSb, electrodes, anodic and cathodic processes 77—44487
KH_2PO_4, growth and dissolution kinetics, temp. and pH effect 80—88070

dissolving continued
KNO_3 pellet, dissolution in KNO_3 soln., mass transfer coeff. in crossed electric and mag. fields 78—48741
LiF, γ-irradiated, chemilum. during dissolution *(Russian)* 78—80427
Li_2O-GeO_2-Ga_2O_3, glass, electrode props., dissolution kinetics 80—89387
Mg, H_2 dissolution, resistometric study under press. 80—70417
MgO crystals, dislocation core energy from etching data 80—39100
MgO crystals, etching and polishing, inorganic or organic acids effect 80—40573
MgO crystals, kinetics and mechanism of dissoln., etch rates in H_2SO_4 solns. 79—79136
MgO, dissolution, surface roughening effects and mechanism distinction 79—47975
MgO, dissolution mechanism in acids 80—39296
MgO, etching in acids, kinetics and mechanism of dissolution 78—85014
MgO-$NaVO_3$(NaB_4O_7)($NaSi_2O_5$) melt, transport-controlled dissolution 79—90791
Mg_2SiO_4 crysts., dislocations configuration and cleavage steps dissoln. 80—107250
Mg_2SiO_4, single cryst., preferential dissolution in molten KOH (NaOH), etching obs. 78—34513
Mn-N, liquid, N soln. 79—99321
Mn_xN_y, prep., rate of formation, chem. stability 78—11185
Mo anodic solution kinetics, in KOH, for high current densities *(Russian)* 78—11523
Mo oxides, low-grade, soda roasting study *(Korean)* 80—93508
Mo_4O_{11}, anodic dissolution, periodic phenomena 77—16735
N_2 absorption at high temps., Cr-N phase diagram, solubility-temp. relation *(Japanese)* 79—43201
N_2, dissolution in metallurgical slags, CaO-SiO_2-Al_2O_3 77—21109
NH_4NO_3 aqueous solution, enthalpies of dilution and relative apparent molar enthalpies, dissociated soln. case 80—50876
NH_4NO_3, standard enthalpy of soln. in water, standard thermodynamic state search 80—50877
Na+water small-leak reaction in LMFBR steam generator, dissolution ratio of hydrogen 78—29545
NaCl, rock salt, progressively mined soln. cavities, struct. behaviour 78—61409
NaCl, solution in ethyl alcohol using uncommon complexes 77—25356
NaCl:Eu, secondary Eu phase dissolution, EPR and optical absorpt. study 80—96655
$NaClO_3$, growth and dissolution kinetics, diffusion and convection regimes 78—63684
Na_2O-SiO_2 glass melt, dissoln. of O_2 and CO_2 gas bubbles 80—79945
Ni, anodic dissolution into silicate glass melt, exam. 78—88582
Ni corrosion in 0.1 N $HClO_4$, Cl^- effect 79—39020
Ni, dissolution and passivation in acid medium, effect of S in solid solution *(French)* 78—64771
Ni, dissolution and passivation in acid environment, effect of P *(French)* 80—45440
Ni, dissolution in methanolic soln. *(Rumanian)* 79—74283
Ni-Cr, anodic dissoln. in NaCl solns. at high current densities *(Russian)* 80—76396
Ni-Cr electrochem shaping in nitrate and chlorate, hardening γ'-phase concentration influence *(Russian)* 77—8979
Ni_3S_2, heazlewoodite, dissolution in acidic ferric chloride soln. at 25°C 79—95172
O_2 bubbles in H_2O, mass transfer coeffs. for rising bubbles 79—41737
Pb, sphere, dissolution in H_2SO_4 in elec. field *(Russian)* 77—4867
Pb/$PbCl_2$ electrode, in chloride media, low temp. props. 78—68899
Pb-Au (0-0.0918 at.%), lattice parameter changes due to Au dissolution 79—77558
Pt, of O, preanodised or passivated, DTA 77—16733
PuO_2, dissolution in HNO_3-HF soln., effects of metal ion impurities 77—70295
PuO_2 refractory, dissolution in HNO_3-HF-H_2O at 100°C 77—18683
$^{239}PuO_2$, fragmentation of respirable particles in water by alpha decay 77—56487
PuO_2-Na_2O, biological solubility of aerosols in rats 78—96096
Si, dislocation free, C and O impurity clouds, heat treatment influence on light scatt. 80—6427
Si, dislocationless plates, microdefect dissolving due to high temp. annealing *(Russian)* 80—54378
Si, dissolution rates in KOH, orientation effect 77—36674
Si, liq., dissolution of quartz, effect of C, rel. to melt growth 80—70414
Si solubility and transport behaviour of water, dissolution 80—93801
p-Si-Al, ohmic contacts, Si dissoln. and recrystn. effects, computer calc. 80—103749
SiC, dissolution rate in molten Si, Fick's law calc. 79—99319
Si_3N_4, dissolution rate in molten Si, Fick's law calc. 79—99319
SiO_2, dissolution rate in molten Si, Fick's law calc. 79—99319
SiO_2 dissolution rate in molten Si 80—103481
SiO_2-Na_2O-K_2O-CaO-MgO-Al_2O_3 glass melt, anodic dissolution of Ti 80—19949
$SrFe_{12}O_{19}$, mag. props., effect of Sr dissolution by milling in water 77—25000
Ta-8W-2Hf wt.% (t-111) alloy, dissolution kinetics of small amounts oxygen, internal oxide disp. reactions, annealing 77—16612
(Th,U)O_2 reactor fuel, dissolution in HNO_3-HF mixtures, fuel reprocessing study 78—59951
Ti alloy in Al alloy melt, raction zone formation, component interaction *(Russian)* 80—54377
Ti, anodic behaviour, steady-state, in conc. HCl 80—45515
Ti in acidic chloride solns., anodic dissolution and passivation 80—35541
Ti:Pd, ion implanted, corrosion behaviour and Rutherford backscatt. anal. 80—71792
Ti-Al (40 wt.%), TiAl plate dissolution 79—66055
Ti-Al-V (6, 4 wt.%), friction characts. improvement by O_2 dissolution and controlled surface hardening *(French)* 80—45401
Ti-Cu dissolution mechanisms, photoelectron spectra study *(French)* 80—45198
$TiAl_3$ crystals dissolution in pure Al liq., grain refinement of α-Al solid-solution by Ti addition 80—35178
V_2O_5 electrode, anodic dissolution in aq. acid soln. *(German)* 79—91826
W monocrystals in alkaline electrolyte, surface orientation, effect on anode current *(Russian)* 80—75360
Y-Si melts, enthalpy of formation and dissolution, microinhomogeneous struct., interatomic interactions *(Russian)* 80—34206
Zn, intergranular dissolution of sacrifical anode in seawater at elev. temps. 79—96181

dissolving continued
ZnS, (111) face, flux-grown cryst. dissolution characts. 77—59014
ZrO_2, rate of dissolution in molten slag of polycomponent systems *(Japanese)* 78—22859

distance measurement
acoustic source passive location with symmetric line array, variance bounds 78—9480
astronomical distance determination, method for extragalactic objects with active nuclei *(Russian)* 80—51880
astronomical laser ranging equipment, computer system *(Japanese)* 78—89080
astronomical laser ranging equipment, photoelectric circuit *(Japanese)* 78—89075
astronomical laser ranging equipment, range gate *(Japanese)* 78—89076
astronomical laser ranging equipment, system controller *(Japanese)* 78—89079
astronomical laser ranging equipment, telescope drive *(Japanese)* 78—89078
astronomical laser ranging equipment, timing system *(Japanese)* 78—89077
atmosphere sound ranging, rangers and source on same level not assumed *(German)* 77—54824
ATS-5 location by L-band trilateration 77—9652
automatic differential variometer type equipment feasibility and preliminary design for big structure displacements remote measurements *(Italian)* 80—62623
biomembrane, distance meas. by radiationless energy transfer, transition probabilities 78—24187
casting process, mould/metal, gap var. with time meas. method 77—52608
caustics technique using ellipsoidal mirror and point light source 77—42595
Cepheid variable stars, intrinsic colours and colour excesses rel. to distance scale 78—28696
coincident gamma-ray technique using positron lifetime spectrometer 79—12765
cosmic distance measurement using Cepheid variables 79—84920
cosmology, Friedmann model, large distance meas. by triangulation 78—86047
critical gap meas. and adjustment instrument 78—62177
direction scintillation meas. with split image range finder *(German)* 78—83076
Earth surface intersite distances, using spaceborne laser ranging system, SPEAR 78—3978
electro-optical distance meas. nonperiodic errors rel. to use of plane mirrors *(German)* 77—9324
electro-optical distance measurement, appl. to water levels surveying obs. *(German)* 78—69280
electronic, using capacitive transducers, frequency superposition principle appl. *(German)* 77—53955
electronic distance meas. technology, surveying appl. 77—67410
electronic tachymetry, ten years of Zeiss equipment *(German)* 79—34999
electrooptical instruments, Zeiss ELDI 2 type, error anal. *(German)* 79—21081
EM distance measurement (EDM), single-wavelength, data ratios rel. to line length changes resolution 80—4143
EM transducers for recording translations and vibrs. 77—67421
exact fractions US interferometer algorithm and circuitry 77—39182
extended-range three-wavelength distance measuring instrument design 79—80053
extragalactic distance indicators, test of four techniques 77—91641
extragalactic distance scale, determ. from galaxies H II region dias. 80—41887
extragalactic distance scale, nearest groups and field galaxies distances from secondary indicators 79—8987
extragalactic distance scale, rel. to Hyades Cluster distance 78—8121
extragalactic distance scale, tertiary distance indicators 79—25708
extragalactic distance scale 77—91640
extragalactic distance scale calibration, appl. to distance of giant spiral galaxy (M 101) 80—67852
eye surface point distance to needle tip within eye, geometric meas. method 79—53273
fibre optic sensors appl. *(Norwegian)* 79—93121
FM-CW acoustic sounder resolution rel. to modulation noise *(Japanese)* 78—30137
galaxies, distance determ. from H I line profiles 77—29920
galaxies distance scale, determ. from IR magnitude/H I vel. width rel. to expansion rate outside Local Supercluster 80—105325
geodesic interference distance meas. using semicond. lasers 80—77175
geodesy, appl. of Very Long Baseline Interferometry (VLBI) *(German)* 78—45036
geodesy, base line estimation using single passes of laser data 80—3910
geophysical distance measurement, multi-wavelength instrument 77—29484
Geos 3 laser tracking sites, base lines determ. from satellite-satellite tracking data 80—3911
gyromagnetic ratio of proton and fine-structure constant redeterm., by meas. distance between wires, with aid of laser interferometer 80—74253
halaxies, H II regions rel. dispersions as distance indicators 80—31360
high accuracy distance measurement by two-wavelength pulsed laser sources 80—192
interferometer for meas. of space between reflecting surfaces 79—97354
interferometric methods for distance meas., recent crustal movements appl. 79—80057
IR, optocator system, precision measurements non involving contact *(German)* 80—82823
IR distance meas. instrument for geodesy and surveying 77—49201
LAMBDA laser distance and thickness meas. system *(German)* 78—32792
laser interferometer, principles and performance 78—89442
laser location for lunar ranging *(Polish)* 79—27311
laser lunar ranging, scientific progress, 1969-77 period 78—36476
laser range measurements, atmospheric correction determ. *(Russian)* 80—12674
laser rangefinder, AN/GVS-5 hand-held, production engineering techniques 78—59018
laser rangefinder, with improved accuracy 79—17384
laser rangefinder and 3D object recognition algorithm 80—96016

distance measurement continued
- laser rangefinder operating frequency selection 79—72691
- laser rangefinder radiometric efficiency, optomechanical tolerance analysis 79—21705
- laser rangefinder technology, present and future 77—34957
- laser rangefinder using pulsed CO_2 TEA laser 77—88926
- laser rangefinder using pulsed CO_2 TEA laser 78—46760
- laser ranging, time-of-flight, at very low signal levels, accuracy analysis 77—111
- laser ranging equipment, range meas. system *(Japanese)* 78—89074
- laser ranging system, effects of random path fluctuations 77—7094
- laser ranging system using non-Gaussian pulse shapes 77—10929
- laser ranging systems, ground based and space based 77—88925
- laser ranging systems, NASA applications 78—81527
- light rangefinder, pulsed phase, 750 MHz modulation of injection laser radiation 77—54804
- light rangefinder and profilometer, high-resolution gas laser 80—102754
- light rangefinder principle, construction and test results 79—27427
- lunar laser ranging, polishing and Foucault test of receiving telescope mirror *(Japanese)* 78—89065
- lunar laser ranging obs., universal time meas. results 78—85854
- lunar laser-ranging, review 77—5459
- Mars rover laser rangefinder accuracy estimate 78—24437
- microwave trilateration, in German Bight area *(German)* 80—8248
- microwaves non-conventional appl. survey *(Italian)* 80—13093
- mm wave expt. for up to 40 m distances *(Japanese)* 77—71298
- modular multi-axis laser distance measuring system of high accuracy *(German)* 78—77856
- Moon and satellite distance meas. by laser 77—9673
- NGC 2403, galaxy, distance determ. from Cepheids 77—2471
- object dimension meas. by computer-controlled laser beams 80—31715
- ocean digital survey fathometer, providing chart display and digital output 79—5665
- optical bench accessory for distance meas. and positioning 78—21111
- optical path difference meas. by double diffraction interferometer 78—24851
- optical path difference meas. by double diffraction interferometer *(Japanese)* 78—82025
- optical pulse receivers for distance meas., basic params. determ. 78—33843
- optical surface contract interaction zone, thickness calc. and distance meas. methodology *(Russian)* 80—99889
- optical surveillance radar, range meas. potential accuracy 77—7202
- optical technique *(Japanese)* 80—8960
- optical triangulation for real-time noncontacting distance meas. 77—5801
- optoelectronic meas. methods appl., with twin diodes *(German)* 80—13064
- parallax method, undergraduate expt. 77—60871
- parallaxes of objects at cosmological distances, meas. via radiointerferometric techniques 78—53796
- photographic contact copying process, film material gap meas. 79—26166
- phototachymeter, amplitude-time characteristics of photomultiplier 79—12850
- phototachymeter, pulsed phase, distance meas. accuracy, semicond. laser temporal characts. effect 78—70097
- planetary nebulae, distance scale 80—109521
- planetary nebulae, distances determ. through nebular ionised mass/nebula radius relation 80—101625
- planetary nebulae, new distance scale and galactic distrib. 80—67819
- point-surface distance meas. adjustment, geometrical aspects *(German)* 80—86255
- polyhedral objects measurement from loci of vertices 80—42195
- position indicator with freq. data transmission *(Russian)* 77—65019
- projector, development and use of special mirror, examination of recording heads 80—83657
- pulsars, low-latit., distances from H I absorpt. meas. 80—101606
- pulsed light rangefinder, amplitude error in presence of signal fluctuations 80—28332
- pupil, closed-circuit TV infrared electropupillometer design *(Japanese)* 77—66870
- quasars, distances from transverse vels. obtained from redshifts relativistic Doppler formula *(Chinese)* 80—105379
- radioisotope instrumentation, industrial appl. *(German)* 77—70245
- range estimation using acoustic sensor subarray parallax, passive 79—72759
- range finding, laser beam appl. *(German)* 78—5522
- range measurements to moon, subnanosecond laser 77—82126
- rangefinder with fluctuating phase shift, systematic averaging error elimination 77—67469
- ranging laser atmospheric transmissometer with retroreflector 77—21905
- refraction-free direction meas., coincidence method *(German)* 78—87124
- refraction-free directions, coincidence procedure 78—87125
- satellite range measurements, formula for refr. effects computation 78—73609
- SHF light rangefinder, optical elements, orientation errors effects *(Russian)* 80—64158
- short range, by EM phase comparison technique 77—87090
- Soviet instruments and meas. systems exhibition 80—52161
- stars, trigonometric parallaxes, systematic differences 77—78776
- surveying, micrometer errors and short period errors of graduated circles *(German)* 78—45038
- terrain profiler, pulsed GaAs laser system 77—91297
- terrain profiler, pulsed GaAs laser system 78—49145
- thick-section parallel membrane separation estimation 79—70718
- throwing distance, for the Olympic Games, Moscow 80—82743
- tongue motion tracking by optical distance sensing 79—57673
- triangulation, microwave distance meas. in German net *(German)* 78—88792
- triangulation ranging using beta density angular errors 79—72758
- underwater objects, depths determ. in presence of refr. 77—34986
- underwater sound, Gaussian quadrature ranges with observed sound-speed profiles 77—46851
- underwater sound, range information from approximate ray angle diagram 77—46843
- US device with decremental acquisition of the measuring results *(German)* 80—19199
- US time-coordinate convertor appl., design aspects *(Russian)* 78—77857
- very long baseline interferometry appl. to geodesy and geodynamics 77—56767
- Viking spacecraft, Doppler and range data rel. to geocentric gravit. const. evaluation 80—3891

distance measurement continued
- Virgo galaxy cluster, distance and redshift rel. to Hubble's const. 78—89265
- Zeiss Eldi 2 electro-optical rangefinder, accuracy and range *(German)* 77—68274
- CO_2 laser multiwavelength interferometry, absolute distance meas. 79—31974

distillation
- *see also isotope separation*
- acid-labile amino acid precursors in Murchison meteorite, chromatographic fractionation 77—64707
- alcohol fuel production, practical aspects of a fractional distillation column 80—55774
- benzene production, using process chromatographs, monitoring procedure for pure product 78—92583
- biological materials continuous flow electrophoretic separator, for sounding rocket expts. 78—85398
- biological materials fractionation in space by deflected lamina electrophoresis 78—85397
- coal liquefaction, low temp. chem. fractionation of H-rich components 80—30336
- column control, FRACTRONIC system, appl. and development 77—39672
- column control, material balance concept 77—43320
- cryogen separation of Kr and Xe from dissolver off-gas in fuel reprocessing plant 77—61590
- cryogenic distillation process for noble gas removal from gas streams at Japanese power stations 77—61538
- desalination plants producing deuterium as byproduct, feasibility study 77—67894
- distiller of alkali metals, construction, operation 78—80490
- fluidised bed evaporator, liq.-solid wall to liq. heat transfer 79—1245
- greenhouse solar distillation and cultivation materials 79—74496
- heteroazeotropic system, thermodynamics in Gibbs pot. metrics *(Russian)* 79—96355
- inert gas fission products, separation of ^{85}Kr from Xe *(German, English)* 77—61516
- isotope compounds, conversion to metals by reduction-distallation methods 80—23223
- liquid mixtures, decomposition into components by thermal action of continuous laser irradiation 79—19362
- LMFBR coolant, decontamination by low-pressure distillation 80—13694
- molecular fractionation and jet stills, working eqns. for quantitative design 77—59107
- oil prerefining, shale, in situ, hydrotreatment at 1500 and 2200 psig 79—48047
- polyethylene solutions, conc., flow behavior in laminar steady flow field, mol. wt. numerical freq. distrib. *(German)* 79—68673
- process control, analogue recursive computer appl. 77—43321
- process control equipment influence 77—39671
- PVC-THF-H_2O, precipitation fractionation, influence of stereoregularity 79—7046
- radioactive liquid scintillation counting waste vol. reduction by distillation 78—78556
- seawater, heavy water concentration, numerical model calc. 79—26514
- seawater, scale control, electrodeposition appl. 79—66302
- separation, partial condensation methods, thermodynamics *(German)* 78—20054
- solar, drinking water production in India, 5000 lit/day plant 80—61280
- solar distiller, multistage-inclined type, solar energy distribution determination 79—96423
- solar still, double basin, performance and periodic anal. 80—89671
- solar still, industrial, stepped oblique type, annual operating data 79—39318
- solar stills, basin-type, periodic anal. for estimating distillate output 80—45733
- thermal field-flow fractionation, peak broadening, plate height effects 78—20088
- Tokamak plasma exhaust, packed distillation column for isotopic enrichment 80—838
- trimethylacetic acid, purification by distillation for cryst. growth 77—55883
- vacuum freeze distillation determ. of tritium concentration in fission reactor fuel liquid waste 77—14255
- vaporizer which induces vapour flow pattern producing centrifugal field 80—86274
- vapour compression distillation unit, compressor and flow system matching 78—83931
- water distillation using basin-type solar stills, use of wood charcoal beds 80—7924
- CO, $^{13}C/^{12}C$ and $^{18}O/^{16}O$ liq.-vapour isotopic fractionation factors 79—90770
- Ge-As-Se, Se-As and Se-Ge glasses, for IR appl., prod. using H_2 distillation 77—32551
- ^{3}H-methyl acetimidate preparation for protein labelling 79—53246
- K, purification by vacuum distillation 77—66599
- ^{85}Kr radioactive waste gas recovery system using cryogenic distillation 77—54331
- ^{85}Kr/Xe separation from nucl. engineering off-gases, low temp. distillation *(German, English)* 77—18671
- ^{210}Pb determination in lake and marine sediments 79—48582
- Te, pure, prep. by combined method, vacuum distillation and double condensation 79—33956

distortion, electric *see electric distortion*

distortion measurement, electric *see electric distortion measurement*

distortive transformations *see solid-state phase transformations*

distributed Bragg reflector lasers
- beam divergence reduction by corner-reflector type Bragg mirrors 80—91822
- continuous injection laser with distributed Bragg mirrors, construction and operation *(Russian)* 78—29972
- corrugated dielectric waveguide, radiation loss calcs. 79—41461
- corrugated waveguides and lasers, improved coupled mode analysis 78—46842
- corrugated waveguides and lasers, improved coupled mode analysis for TM mode 78—83117
- curved-line grating form., use as reflectors and laser resonators 77—88971
- dye laser, tunable DFB, with fan-shaped grating 77—88739
- grating reflector for thin film Fabry-Perot laser 78—55471

distributed Bragg reflector lasers continued
holographic interference lithography for integrated optics 79—14116
hybrid modes in distributed feedback structures 79—27441
injection laser sources for integrated optics 78—42472
integrated twin guide lasers, axial mode selectivities 77—75519
mode separation and selectivity, depend. on reflector length calc. 78—22153
monolithic integration of LOC-DBR lasers and optical components 78—38081
optical resonator with distributed Bragg reflectors, response to light pulses 78—63141
radiating distributed feedback structures, calc. and optimisation of parameters 79—27438
saturable optical resonator with distributed Bragg reflectors, transient behaviour 79—23029
semiconductor laser, single mode criteria at high speed pulse modulation 79—10305
semiconductor laser, single-wavelength oscillation at high speed pulse modulation 79—7129
thin-film laser with spatially separated multiple-frequency outputs 80—43368
tunability by modulating refractive index in corrugated waveguide 77—79866
two-dimensional DFB laser with acoustic wave and Bragg reflectors 78—79043
two-dimensional waveguide analysis with misaligned or curved gratings 79—23092
AlGaAs CW injection heterostructure laser, with second order distributed Bragg reflectors, exam. 78—37907
AlGaAs heterostructures in integrated optics 77—75713
AlGaAs integrated twin guide laser with distributed Bragg reflectors 77—88744
AlGaAs transverse junction stripe laser 80—106535
(GaAl)As heterojunction laser with distributed Bragg refl., mode switching 80—43336
$(Ga_{1-x}Al_x)As$ LOC DBR laser integration with p-n junction detector 78—38066
$Ga_{1-x}Al_xAs$-GaAs laser, distributed Bragg confinement, room temp. operation 78—74907
$Ga_xAl_{1-x}As$ injection heterojunction distributed output laser, exptl. study 80—43369
GaAs distributed Bragg reflection lasers, large optical cavity, optimal design 80—38028
GaAs, optically pumped DFB laser, with two-dimens. Bragg reflectors 78—1252
GaAs, optically pumped laser, two-dimensional distributed Bragg reflectors, oscillation *(Japanese)* 78—42350
GaAs, periodic surface corrugation generation by holography 78—55469
GaAs, room temp. laser, highly collimated broadside emission 78—13721
GaAs-(Ga,Al)As light modulators and distributed Bragg reflector laser, monolithic integration 78—50944
GaAs-(GaAl)As LOC-DBR laser, high differential quantum efficiency 78—79031
GaAs-$Al_xGa_{1-x}As$, optically pumped taper coupled laser, second order Bragg reflector 78—50788
GaAs-$Al_xGa_{1-x}As$, film waveguide, heterojunction lasers with Bragg mirrors, threshold characts. 79—23095
GaAs-$Al_xGa_{1-x}As$ strip buried heterostructure laser with passive DBR 80—14352
GaAs-AlGaAs integrated twin-guide laser, temp. characts. 78—87064
GaAs-$Ga_xAl_{1-x}As$ injection laser, large-optical-cavity, with low-loss distributed Bragg reflectors 78—1244
GaAs-GaAlAs junction, grating coupled 78—17934
GaAs-GaAlAs large optical cavity injection layer with low loss DBRs 78—1430
GaAs-GaAlAs lasers, recent advances in integrated optics 77—75712
GaAs-GaAlAs room temp. DBR lasers, highly collimated broadside emission 78—1428
GaInAsP/InP 1.5-1.6 micron integrated twin-guide lasers with distributed Bragg reflectors 80—74380
GaInAsP/InP integrated twin-guide lasers with first order distrib. Bragg reflector, room temp. operation at 1.3 μ 80—64077
GaInAsP/InP integrated twin-guide lasers with distributed Bragg reflector, spectral behaviour 80—74381
GaInAsP-InP integrated twin-guide lasers with first-order distributed Bragg reflectors, 1.3 μm 80—58567
$Ga_xIn_{1-x}As_yP_{1-y}$-InP injection laser, partially loaded with distributed Bragg reflector 78—82986
$Ga_xIn_{1-x}As_yP_{1-y}$-InP injection laser partially loaded with first-order distributed Bragg reflector 79—98387

distributed feedback lasers
acoustic DFB laser, EM and acoustic wave refl., freq. and amplitude modulation 77—54717
Bragg interactions, in active medium, Floquet theory, index modulation effects 77—58231
Bragg interactions in active medium, first and second order 78—50747
Bragg-reflector laser amplifiers, distributed, analysis 77—19348
buried heterostructure DFB laser investigation 77—31102
buried heterostructures, discrete or DFB 78—5499
corrugated dielectric waveguide, radiation loss calcs. 79—41461
corrugated waveguides, effective index approach to distrib. feedback, TE polarisation 80—102859
corrugated waveguides and lasers, improved coupled mode analysis 78—46842
corrugated waveguides and lasers, improved coupled mode analysis for TM mode 78—83117
coupled wave analysis 77—27305
curved-line grating form., use as reflectors and laser resonators 77—88971
diode structure improvements using DFB, integrated optical elements suggested as alternatives *(German)* 79—89920
dye, intrapulse thermally induced wavelength shift 79—59692
dye, line narrowing and wavelength stabilisation technique 77—88783
dye, N_2 laser pumped, external mirror effect on characts. 78—42352
dye, simultaneous oscill. of independently tunable spectral lines 77—23673
dye activated CLC, distributed feedback, tunable radiation generation *(Russian)* 80—102720
dye DFB laser, N_2 laser pumped, tunable single ps pulse generation 79—55147

distributed feedback lasers continued
dye DFB laser, single-freq., 10 Å continuous pressure tuning 79—76705
dye DFB pulsed laser with high repetition rate 77—27300
dye high power DFB laser, tunable 7420 to 10500 Å 77—88782
dye laser, binary mixture, distributed second-order feedback *(Russian)* 78—29945
dye laser, cholesteric liquid crystal as resonator, theory 79—31956
dye laser, DFB, single-mode operation 80—74409
dye laser, distrib. feedback formed by diverging pump laser beams, tuning curves 77—83893
dye laser, dynamic DFB, output power 80—14336
dye laser, N_2 laser pumped, self Q-switched, tunable picosecond pulse generation 80—69432
dye laser, noncollinear wave interaction 80—99722
dye laser, optically induced distributed feedback prod. of single ultrashort pulse 80—64067
dye laser, ultrashort pulse generation, self Q-switching mechanism 80—58612
dye laser systems with dynamic DFB, freq. tunable over whole gain profile 79—50317
dye laser ultrashort pulse generation, using distributed feedback *(Russian)* 77—38883
dye laser with integrated Si and polyurethane channel waveguide 80—74373
dye lasers, thin film, dichromatic switching effect 79—10331
dye solution DFB lasers, development, theory *(Russian)* 78—13700
dye solutions, light-induced grating form. by two independ. laser beams, DFB effect 79—94230
dye tapered DFB laser as tunable picosecond pulse source 78—22150
Epitaxial waveguide laser with distributed second-order feedback by electron excitation *(Russian)* 78—29973
fibre waveguide photosensitivity, appl. to refr. filter fabrication 78—63171
fluoromethane DFB gas laser, construction and operation 80—23715
gas laser waveguide precision calc. and pulse energy obs. 80—58577
grating reflector for thin film Fabry-Perot laser 78—55471
Green's function approach to waveguide DFB laser theory 78—5504
heterojunction laser diodes, book contrib. 80—99733
holographic interference lithography for integrated optics 79—14116
injection laser with external dispersive resonator as narrow-line tunable emission source *(Russian)* 77—83898
integrated optics using periodic structures 77—39109
limiting spectral characts. 79—64197
parametric interaction system, transient effects and nonlinear conditions 77—79898
periodic corrugated waveguides, grating coupled radiation and distrib. feedback 78—59161
periodic fibre waveguide, mode coupling, appl. to DFB laser 77—27348
periodic media with gain or loss, higher-order Bragg coupling 77—54814
radiating distributed feedback structures, calc. and optimisation of parameters 79—27438
relaxation oscillations, freq. and damping 77—10960
resonators, dielectric waveguide with periodic surface inhomogeneity 77—7146
rhodamine B activated waveguide, amplification of narrow-band signal 79—36930
saturable resonator with distrib. Bragg reflectors, bistability, bleaching and loss effects 77—27309
self-induced distributed feedback, stability, in system without resonator 80—87368
semiconductor, operating in higher Bragg interaction orders 79—89933
semiconductor, population-inverted, resonant Brillouin scattering and photoelastic consts. 80—76042
semiconductor acoustic DFB laser, high speed repetitive Q-switching 78—83007
semiconductor DFB laser pumped by electron beam, temporal and spectral characts. 79—94238
semiconductor diode lasers, book contrib. 80—106525
semiconductor heterostructures, elec. and optical phenomena, discrete devices, review 78—72250
semiconductor junction lasers, resonant acousto-optic interaction in degenerate semicond. 80—19036
semiconductor laser, single mode criteria at high speed pulse modulation 79—10305
semiconductor laser, single-wavelength oscillation at high speed pulse modulation 79—7129
semiconductor laser diodes, present status and technology *(German)* 80—58561
semiconductor laser excited by electron beam, radiation coupling out 79—90038
semiconductor super-DFB single-mode laser with periodic stripe width variations 80—58574
semiconductors, population inverted, resonant Brillouin scatt., photoelastic consts. 80—89015
seminconductor laser with electron-beam-induced stripe waveguide 80—28237
sinusoidal interface light diffraction 79—13900
symmetric and antisymmetric modes, discrimination *(Russian)* 77—75573
thin film lasers and waveguides with arbitrary refr. index distribs., optical processes 77—79971
thin-film laser with a two-dimensional diffraction grating 80—9906
thin-film periodic structures, optoelectronic devices appls. *(Polish)* 78—50947
tuning using acoustic wave 77—58359
two-mode operation, index and gain grating configurations 80—69357
two-photon spatially periodic pumping, excitation threshold and output power *(Russian)* 78—13693
waveguide, hollow-core rectangular, propagation losses at 10.6 μm for distributed feedback appl. 80—38101
AlGaAs heterostructures in integrated optics 77—75713
CO_2, planar hollow-core doubling grating DFB laser, characts. 78—46673
GaAlAs based heterojunctions, integrated optics appl., technology advancements *(Slovak)* 80—33226
(GaAl)As heterojunction laser with distributed Bragg refl., mode switching 80—43336
$Ga_{1-x}Al_xAs$, channelled substrate, planar struct. and DFB lasers 78—79032
$Ga_xAl_{1-x}As$ injection heterojunction distributed output laser, exptl. study 80—43369

distributed feedback lasers continued
GaAs, optically pumped DFB laser, with two-dimens. Bragg reflectors 78−1252
GaAs, optically pumped laser with acoustic distributed feedback 78−82977
GaAs, periodic surface corrugation generation by holography 78−55469
GaAs, two dimensional DFB laser with distributed Bragg and acousto-optic reflectors 77−10946
GaAs/GaAlAs diode, for integrated optics 77−46721
GaAs-Al$_x$Ga$_{1-x}$As, integrated twin-guide laser with distrib. Bragg reflectors 77−19310
GaAs-Al$_x$Ga$_{1-x}$As channelled-substrate-planar-struct. laser with lateral-evanescent-field distributed feedback 79−98398
GaAs-Al$_x$Ga$_{1-x}$As strip-buried heterostruct. laser with distributed feedback 79−76696
GaAs-Ga$_{1-x}$Al$_x$As, DH distributed Bragg reflector laser, room temp. operation 77−7085
GaAs-Ga$_{1-x}$Al$_x$As buried DH diode laser fabrication 77−75565
GaAs-GaAlAs DFB and distributed Bragg reflector lasers, historical review 77−31102
GaAs-GaAlAs DFB diode lasers with separate carrier and optical confinement, room temp. operation 77−10926
GaAs-GaAlAs monolithically integrated DFB lasers as freq. multiplexing source 77−34958
GaAs-GaAlAs optically pumped DFB laser, wavelength tuning effect 78−82979
GaInPAs/InP heterostructure DFB laser under optical pumping, lasing characts. 80−87396
Ga$_{1-x}$In$_x$P$_y$As$_{1-y}$/InP DFB injection laser, one-step LPE 80−58575
InGaAsP/InP DFB injection lasers 80−5746
Pb$_{1-x}$Sb$_x$Te DFB laser, CW operation 77−58338
Pb$_{1-x}$Sn$_x$Te, DH, design, fabrication and characts. 77−10944
PbTe-Pb$_{1-x}$Sn$_x$Te-PbTe, coupling coeff. calcs. 77−14714

distributed parameter networks
acoustic wave propagation in composite thin-plates, equivalent microwave network analysis 79−3820
heat transfer electrical analogy, nonstationary heat transfer through walls *(Slovene)* 77−39191
vertebrate retinal horizontal cells, spatial integration, computer analysis of network model 77−36920
waves in nonlinear media, Poincare normal form method 80−36875

distributed parameter systems
aquifer permeability and storage identification by artificial recharge hybrid simulation 77−45043
control, conference, Coventry (1977) 79−3897
coupled-core nuclear reactor, distributed parameters identification, pseudorandom perturbation and correlation anal. 80−86966
end-temperature in semi-infinite rod, distributed parameter optimal control problem 78−13886
hand-arm system, distributed-parameter dynamic model 78−92663
heat diffusion process, parabolic boundary-value control problem, numerical treatment 77−847
heat exchangers, approx. of dynamics of method of weighted residuals *(Japanese)* 78−67024
heat exchangers, parallel and counter-flow, weighted residuals method and modal control 79−3898
identification using doubly cubic spline, underground aquifer appl. 78−69391
ion sources, geometry, pot. profiles, ion currents 77−35365
laminar boundary layer, optimal control, group theoretic approach 79−32452
LMFBR fuel rod subassembly, thermal-hydraulic anal. as distrib. parameter system *(Japanese)* 80−68736
multidimensional infinite mechanical oscill. system, resonance and controllability 80−33444
nuclear fuel fabrication control system for remote operation 80−18571
nuclear reactor distributed parameter optimal control methods 78−54858
nuclear reactor system pointwise control and observation problems 78−54859
nuclear reactor three-point model, neutron and delayed-neutron emitter behaviour, describing differential equations *(Spanish)* 80−22889
one dimensional distributed parameter system parameter and state estimation, heat conduction experimental result *(Japanese)* 80−83727
optimal control of 1-D linear distributed parameter systems with cost functionals 78−59257
optimal control of distributed parameter reactor core by function space method, numerical experiences 77−54317
optimal point controlled, multiple shooting and sweep algorithm 77−25728
parabolic boundary value problem optimal control, heating process 78−67021
parameters' correlation effect on meas. system output *(Russian)* 77−9980
prokaryote epigenetic control mechanisms, distributed model 77−77879
reactor dynamics optimal control, exact closed-form soln. for terminal cost problem 79−54472
rod, thermal conduction, dynamic behaviour of distributed systems *(Dutch)* 80−28407
seismic inverse problem appl. of control theory 79−2402
self-excited wave medium with memory 78−77034
Shiva laser computer control system 78−59034
suboptimal control of reactors with distributed parameters, computer model, singular perturbation theory 77−6530
tracking Michelson interferometer stability improvement *(Russian)* 78−29149
viscoelastic media in plane stress and strain, local memory system qualitative props. 77−11142
P control in estuaries, parallel shooting models, Corpus Christi Bay (Texas) and Jamaica Bay (New York) appls. 79−57521

distributed processing
see also computer networks; multiprocessing systems
CANDU distributed computer control systems 79−76105
cardiology applications of computers 78−81013
data acquisition system 79−89532
HISS computer facility 79−89559
microprocessor based system, for LMFBR subassembly fault detection *(Japanese)* 79−41002
National Synchrotron Light Source, distributed computerised control system 79−72086
Niels Bohr Institute on line data acquisition system 79−89557

distributed processing continued
system THESEUS for mag. field analysis 79−41293
wastewater treatment, distributed digital processing and closed loop computer control 80−45824

distribution networks
classical systems, particle distrib. function, theoretical method 80−64856
flashover voltage calc. of uniform-field gaps under steep-front impulse voltages *(Japanese)* 79−64932
fusion reactor, TEXTOR, poloidal coil system power distrib. system 80−102327
fusion reactor auxiliaries, power distrib. system 78−54962
Tokamak fusion test reactor, AC distrib. system for pulsed loads 78−54963

distributions, statistical *see statistical analysis; statistics*

distributive data processing
see also stock control data processing
radioactive material control on medical science campus 77−44759

district heating
100 MW fluidised bed combustion district heating plant burning high S content residual oils 80−108777
air pollution reduced in urban built-up area, Japan 79−21006
BWR, safety study of district heating network 78−62600
centralised heat supply from nuclear boiler units, technoeconomic assessment 80−7899
coal, fluidised bed firing, technological state and economic chances *(German)* 79−92050
geothermal aquifers, reservoir lifetime and heat recovery factor, for urban heating 79−74492
geothermal district heating system, planning assessment, financing and design optimisation 80−61279
heat-electric power station for Cologne *(German)* 79−20999
HTGR, low temp. heat prod., energy transport systems 78−41837
HTGR dual purpose plant for military installations 78−41855
IPWR, appl. to district heating and desalination 78−41852
LWR, effect of district heat prod. on reactor operation and safety 79−85624
nuclear, CANDU operation for electricity prod. and district heating 78−41835
nuclear district heating plant, safety 80−767
nuclear district heating schemes, heat transport and storage 79−39321
nuclear heat utilization in Italy, appl. of low-enthalpy content steam 80−7902
nuclear plant, safety evaluation 78−37422
nuclear power stations, technical and economical aspects *(German)* 77−352
nuclear reactor with heat exchanger, 70 MW, transportable 78−46159
nuclear reactors, future appl. *(Russian)* 79−97885
nuclear steam turbines for power prod., district heating, desalination 78−37438
powerstation, chemical water treatment pH value calc., computer-aided analysis *(Russian)* 79−43572
solar heating system, annual cycle thermal energy storage, sensitivity anal. 80−67007
steam turbine district heating plant, condensing and regenerating equipment 80−92029
steam turbines for district heating in nucl. power plants 78−37437
THERMOS reactors, district heating and desalination appl. 78−41853
WWER reactors for district heating appl. 78−41854
SO$_2$ air pollution, Helsinki study of district heating effect 79−21010

diversity reception
see also fading
COMSTAR beacon receiver diversity experiment 78−73421
equipment calibration using standard frequency broadcasts 79−67258
geostationary satellite ATS-6 results, 13/18 GHz range *(Italian)* 78−49072
ionospheric scintillation suppression 77−21995
optical heterodyne receivers in turbulent atm., signal current probability distrib., theory 78−78916
optical heterodyne receivers in turbulent atm., signal current probability distrib., expt. 78−78917
satellite communications above 10 GHz, rain effects 80−8410
satellite link, space diversity improvement, squall line direction effects 77−91205
satellite links rain attenuation and site diversity effect, statistical studies 78−88892
satellite-to-ground radio path, 12 GHz, low elevation-angle space-diversity expt. 77−70914

divertors
see also surge protection
collisional divertor scrape-off layer in Tokamak, plasma transport 80−28614
DIVA, metal-impurity, confinement, discharges 80−28843
impurity effects and control, neutral beam injection, computational models for large Tokamaks 80−28773
plasma chromatograph/mass spectrometer column overload prevention valve 80−16748
plasma stability, energy and particle transport, and hydrogen recycling 80−28834
resonant helical divertor 77−62411
T-12 Tokamak with two axisymmetric divertors, characteristics of divertor 80−28844
Tokamaks, divertor, refuelling methods, pellet-plasma interaction 80−28841

dividers, frequency *see frequency dividers*

dividers, voltage *see voltage dividers*

dividing circuits
digital phase shift for meter calibration 79−44898
semiconductor position detector analogue division cct. 77−54470

DNA
acridine complexes, laser-induced fluorescence decay obs. 79−66449
actinomycin-DNA bindings, first-neighbour specificities, circular dichroism 78−3442
adduct systems, binding geometry, determ. by induced circ. dichroism 80−55988
adenocarcinoma cells, population anal. of DNA content, flow microfluorometry obs. 80−16913
alkali-labile sites, gamma-ray induced, in single stranded DNA in aq. soln. 77−9170

DNA continued
alkali-stable, lesion excision repair by γ-endonuclease Y enzyme 79−92145
amoeba irradiated by thermal neutrons, absorbed dose estimation 78−53449
anthramycin-DNA adduct, proposed struct. 80−30658
atom-atom potential functions method, improved definition of A and B forms 78−96000
axially symmetrical ensemble stained with acridine orange, polarisation of fluorescence 79−92140
B form conformations, double-helix and side-by-side models, X-ray diffraction 80−78735
B-A transition enthalpy, water-ethanol solns. 77−70412
B-configuration double helix, interaction with H_2O, isoenergy contour maps 79−20504
B-DNA helix, guanine-cytosine base pair, electrostatic pot. 80−8003
B-form, closer definition of struct. from X-ray diffr. and energetic criteria 80−81533
backbone vibrational mode displacements of A-DNA and B-DNA 80−8000
bacterial spores, thermorestoration of mutagenic radiation damage 79−20524
bacteriophage, double strand breaks, protein cross-links, induced by fast neutrons, γ-rays 79−66446
bacteriophage, gamma-ray induced cross linkage of DNA and protein 77−21485
bacteriophage λ superinfecting E. coli, induction and repair of DNA strand breaks 80−72228
bacteriophage ϕX174 DNA, possible message from extraterrestrial intelligence 79−53738
bacteriophage DNA and protein cross-linkage by ^{60}Co gamma-rays 78−77002
bacteriophage S13, lethal effect of ^{33}P transmutation, mech. of DNA double helix rupture *(French)* 80−98018
bacteriophage S shape determ. from small-angle X-ray scatt. 79−39347
base damage detection method, UV induced pyrimidine dimers in human cells 79−44067
base pairs., Coulomb interaction energy calcs, electron correlation role 79−96509
bases, polarised fluoresc. and estimated lifetimes, room temp. and in −125°C soln. 79−39352
bases, selective electronic excitation using dye lasers 80−8012
bases, selective ps laser excitation in condensed phases 79−48217
bases, theoretical study of electronic spectra 80−30665
bases, thymine type, polarised fluoresc. in neutral aq. soln. 80−21445
benzo[α]pyrene-DNA complex, triplet state props., optically detected zero-field mag. reson. obs. 77−79636
benzo[α]pyrene-DNA complex, triplet state props., optically detected zero-field mag. reson. obs. 79−18222
binding to ethidium bromide derivatives, competitive and non-competitive bonds *(German)* 79−79446
bioelectret, sorption and desorption of water, thermal-stimulated press. and thermogravimetric anal. 80−8008
birefringence, induced, conformation and struct. 80−26201
bromodeoxyuridine substituted, photolysis using UV light source 78−22185
calf thymus, flexible polyelectrolyte, elec. birefr. meas. 79−16126
calf thymus binding to cis- and trans-dichlorodiammineplatinum(II) extended X-ray absorpt. spectra 78−85291
calf-thymus DNA soln., time depend. correlation functions meas., three relax. components 77−40631
cancer, DNA repair, radiation hazards assessment 80−41143
cancer cell cycle kinetics, flow microfluorometric DNA distribution representation 77−21669
cancer receptor sites, proof by MO method for interstrand guanine binding of DNA 80−30656
cell distributions automatic processing and interpretation 78−92757
cell division delay, effect of ^{125}I-UdR and ^{3}H-TdR 77−29179
cell kinetics stochastic model using DNA microfluorometric data 79−83723
cetavlon salt, cryst. struct., X-ray diffr. meas. 78−2105
cetavlon salt, struct., small-angle X-ray diffr. meas. 78−11609
cetavlon salt, twin struct. obs. 78−71746
chain growth in vivo in intestinal crypt cells, effect of ^{60}Co gamma and hydroxyurea 77−66795
chain maturation in Bloom's syndrome fibroblasts rel. to UV sensitivity 77−29185
charge origin and mobility, adsorbed water effects 79−92461
Chinese hamster cells, DNA replication after X-irradiation 79−11986
Chinese hamster ovary cells, DNA damage on X-irradiation after preheating 79−34493
Chinese hamster V79 cells grown as spheroids or monolayers, radiation-induced DNA damage 80−41130
chorionic gonadotropin, human, α-subunit, cDNA isolation, cloning and sequence anal. 80−3587
chromatin, DNA-protein complexes, electron microscope visualisation, book contrib. 79−5434
chromatin, neutron scatt. rel. to higher order struct. 79−11894
chromatin, nucleosomal arrangement DNA, histones and non-histones, review 79−79464
in chromatin, stereochem. model for superfolding 80−35829
chromatin extracted from cultured mammalian cells, gamma radiolysis, DNA alkali-labile strand damage 78−77003
and chromatin molecule preparation for electron microscopy 79−25171
chromatin nucleosome core particle, ^{31}P mag. reson. of DNA 78−40112
chromatin structure and thermal denaturation profiles 77−12881
chromatin subunits, in glycerol/sucrose solns. containing various D_2O/H_2O mixtures, neutron scatt. study 79−11893
chromatin-DNA cross-links formation, radiolysis of extracts from cultured mammalian cells 80−81655
chromosome autoradiograph analysis by computer 78−57071
chromosome inactivation in UV irrad. E. coli during growth 77−86551
circular superhelical, X-ray scatt. calcs. 80−56109
closed duplex DNA, struct., reactions, book contrib. 79−5248
compact form, tertiary struct., small angle X-ray scatt. 80−72129
complexes with Hg (II) and Ag (I) in soln., theoret. interpret. of elec. dichroism obs. 80−85347
conformation, influence of intermol. interactions 80−16900
conformation changes, soft modes 77−29097
conformation of native molecule, influence of solvent struct. 80−30655

DNA continued
conformational fluctuations, internal motion correl. times, ^{31}P NMR obs. 80−72135
conformational transitions of DNA in conc. solns. of neutral salts 80−81531
conformations, possible, calcs. 80−76705
costacking nucleotides, γ-irrad., charge-migration phenomena, EPR obs. 80−36015
CTA-DNA crystal growth and morphology 80−26198
cyclophosphazene-DNa complex, spectrofluorometric and spectrophotometrics investig. 80−95643
cytidine monophosphate, aq. soln., spectra, 300-450 nm, polarisation study 78−96015
cytidylyl-3′,5′-cytidine, aq. soln., spectra, 300-450 nm, polarisation study 78−96015
damage and repair in γ-irrad. rat brain tumour, detect. by S_1 nuclease 78−48838
damaged by UV or N-acetoxy-2-acetylaminofluorene, rate-limiting steps in excision repair 77−90865
degradation in Escherichia coli after UV irrad. 78−48841
deoxyribonucleoprotein, gamma-ray protein damage 78−53338
dielectric hysteresis loop 79−83691
dielectric properties of low-mol. wt. DNA in aq. solns. at low ionic strength 80−85330
diffusion coefficient of calf-thymus DNA using quasielastic light scatt. apparatus *(German)* 80−12314
diploid fibroblasts human, correls. after potentially lethal damage from UV 80−21493
distamycin A, analog cryst. and molecular struct. 79−88051
DNA single-strand breaks in preheated cells irrad. under N_2 and N_2O saturation 78−28017
DNA solution, thermodynamic props., phase transition, one-dimens. Ising model study 79−16125
DNA-acridine dye complex, fluorescence studies 80−37921
DNA-acridine orange complexes, energy transfer after dye laser excitation 79−2005
DNA-Au (III) interaction, rate consts., activation energies, pH, spectrophotometric obs. 80−30228
DNA-cetavlate crystal growth and morphology 77−66583
DNA-dye complexes, fluoresc. intensities, dye laser spectroscopy 77−86444
DNA-dye-complexes, UV excitation, energy transfer and mol. struct. 79−57578
DNA[Cu^{2+}], ^{111}In bound, rot. correl. times, from γ-ray perturbed angular correl. 80−94152
double helical fragment intercalator complex, molecular struct. 79−16140
double helical left-handed DNA fragment, mol. struct. 80−30659
double helix, breathing modes and induced resonant melting 79−62180
double helix supercoils, linking numbers, twist, writhing number 77−12882
double helix unwinding during RNA polymerase binding 79−70512
double strand breaks rel. to radiation dose, yeast cell obs. 80−72232
double-helical model, sedimentation coeff., X-ray scatt. 77−14629
double-strand break induction by binding with ^{125}I-iodoproflavine 78−20145
double-strand breaks, gamma-ray induced, temporal local denaturation 78−48754
double-strand breaks during γ-irrad. of Micrococcus radiodurans, O_2 effects 78−7393
double-strand breaks in irradiated yeast cells, survival and yield, O_2 influence 80−35992
double-stranded, ^{13}C NMR obs. 80−69281
double-stranded, radiolysis in presence of O_2 78−48760
dye labelled, elec. dichroism and birefringence, comparison with mol. props. from polarised fluoresc. 80−84785
E. coli, DNA repair in radiation resistant and radiation sensitive strains 79−34489
E. coli, relative rates of repair of single-strand breaks and postirradiation DNA degradation 79−16149
E. coli, repairability of chromosomal and cytoplasmic DNA after γ and UV irrad. 80−30796
E. coli, UV-induced recovery of γ-irrad. bacteriophage DNA 80−72214
E. coli, UV-irradiated, double-strand breaks from single photochemical events 79−16151
E. coli, UV-irradiated, single-strand breakds and alkali-labile bonds 79−16152
E. coli ^{125}I and X-ray damage, effect of cell DNA content 78−28006
E coli B/r, UV sensitivity rel. to DNA content obs. 80−108960
E. coli strains differing in DNA repair capability, survival after fission-spectrum neutrons irrad. 80−98031
E-coli, enzymatic activities in UV-induced DNA degradation 80−36011
effective force constant corrections, in redundant mol. coords. 78−13634
Ehrlich ascites tumour cell, thymidine transport kinetics and DNA synthesis, X-ray effects 78−20215
electron damage repair in E. coli mutants, appl. of rapid lysis techniques 78−31775
electron microscopic preparation on uncharged C films 80−12320
electronic interaction with N-methyl-N-nitrosourea, ESR obs. and INDO calcs. 80−94154
electronic transport mechanisms, asymmetry role 78−6370
end group characterisation after low dose γ-irrad. of thymocytes 78−11613
entrapment mechanism at air-water interface 77−60181
entropy nature of B-A transition 79−92130
epitaxial sandwich, DNA occluded in single cryst. Au film, electron microscope contrast 79−57568
erythrocyte nucleosomes, chicken, temp. dependence of ^{31}P-NMR spectra 80−94280
ethidium bromide E-DNA, intercalated birefringent fibres, microspectrophotometric investig. *(German)* 80−57392
eukaryotic cells, improved method to detect small amounts of DNA radiation damage 80−36205
fast neutron induced DNA strand breaks and repair obs., cultured mammalian cells 80−61651
film, dehydration and conform. state, differential scanning microcalorimetry 80−35830
film, sp. ht. in range 4.2-400K *(Russian)* 77−51511
filsm, X-ray induced luminesc. and optical absorpt. rel. to γ-induced free radicals 77−5033
flow cytometry histograms analysis, computer program 80−41337

DNA continued
fluorescence depolarisation, electrically-induced macromol. characteristics 77—27210
fluorescence depolarisation, twisting and bending, rot. Brownian motion 79—70509
fluorescent light induced DNA crosslinkage and chromatid breaks, mouse cells 79—96615
fragment length produced from deoxyribonuclease I digestion of chromatin 79—79467
free radical induction due to proflavine and light treatment, influence of DNA struct. 79—100573
gamma irradiated, 2-deoxy-D-erythro-pentonic acid isolation from alkali-labile site 78—20144
gamma irradiated at 77K, effect of visible light, EPR 77—52744
gamma irradiated biologically active double stranded, alkali labile sites, post irradiation effects 80—35991
gamma irradiation, N-formamido group formed in place of thymine fragment, evaluation method 80—30790
gamma irradiation damage in Escherichia coli DNA, enzyme labile sites 80—35993
gamma radiolysis products from N-glycosidic bond rupture in cytosine ^{14}C-2 labelled DNA 77—9171
gamma-irradiated, enzymatic digestion, separation by ion exchange chromatography 78—85290
gamma-ray effect on interaction with nucl. non-histone proteins 78—7401
gamma-ray effects on hydration, PMR of frozen and liq. solns. 78—27900
gamma-ray induced damage, electro-optic meas. 80—85452
globin genes, human fetal, charact. of deletions of DNA 79—70519
haemopoietic stem cell population and proliferation model 77—44610
helical to coiled relax., statistical mech. approach, appl. to DNA secondary struct. 78—3443
helix-ball transition, peculiarities due to Cu^{2+} and Mn^{2+} 79—70514
helix-coil transition, thermodynamics 79—11883
helix-coil transition in low counterion conc. with irreversible cross links 80—32860
helix-coil transition model 77—52734
helix-coil transitions in specific sequence biopolymers 78—35794
high molecular weight, sedimentation data, radiation-induced single-strand breakage, additives effect 80—30667
histone F2b-DNA interaction studied by X-irrad. of calf lymph nodes 78—85346
hybrid molecule construction and cloning 77—56559
hydrate, stability studied by thermogravimetry 80—30650
hydrate, struct. conversions of sugar phosphate chain and nitrogenous bases, IR spectra 80—81530
hydration characteristics, γ-irrad. effects, NMR of frozen H_2O and D_2O solns. 77—21484
hydration characts. in H_2O/D_2O frozen solns., γ irrad. effects, PMR 78—31772
hydrodynamic shearing, computer model 80—16895
hydrodynamic shearing model 79—39337
hypochromic effect, oscillator strength, perturbation theory calc. 79—96515
hypochromic effect in natural DNA 77—81467
hypochromism, perturbation theory *(Russian)* 77—56339
hypochromism of natural DNAs, dependence on content and sequence of nucleotides 80—76711
immunoglobulin light-chain genes, nucleotide sequences at somatic recombination sites 79—83701
in soln., duplexes, synthetic, struct., dynamics 79—57574
in vitro transformation, conf., Toronto, Canada (May 78) 80—67931
inactivation by γ-rays in vitro, O_2 effect in presence of metalloporphyrins 79—92303
inelastic electron tunnelling spectroscopy appls. 78—92770
interactions with cations, UV difference spectrosc. and Marcus theory 80—94153
interactions with water, review 78—44448
internal modes relaxation, near UV photon correlation spectra 79—75621
internal motions, ^{31}P NMR and PMR 80—97855
ion beam effects, review *(German)* 79—43968
iso-ionic solutions, anti-thixotropic props. 79—57680
kidney cells, hamster, photodynamic induction of oncogenic virus 79—25029
kinetoplast, ultrastruct., interpretation of dark field electron microscopy images of isolated purified networks 80—85369
laser multistep selective excitation of DNA and RNA fragments, uses 80—61122
laser radiation, selective excitation and bond breaking, review 80—7832
length measurement, appl. of random flight theory 78—35799
length measurement using random flight theory 77—64008
light induced diffusion in solutions due to laser cutting *(Russian)* 80—81646
linear dichroism, strand separation determ. 79—62188
linear dichroism in pulsed elec. field, meas. apparatus 80—90875
lipid interaction, IR spectroscopic obs., DNA compactisation on disperse particles 80—104550
luminescence, excitation wavelength depend. in UV/VUV region 78—31768
lung, late biochem. changes after hemithoracic irrad. of rat 77—5053
lymphocyte cell DNA damage by US diagnosis 80—67148
lymphocytes, human, effects of low-dose radiation on repair processes 80—98023
lymphocytes, in vitro ^{60}Co gamma-ray response of leucoagglutinin stimulated human cells 78—57041
mammalian cells, replicon sizes estimated by X-ray plus bromodeoxyuridine photolysis method 79—16353
mammalian cells, UV-irradiated, DNA repair kinetics 79—20513
mammalian cellular DNA; breaks induced by accelerated heavy ions, impaired repair capacity 80—41129
mammalian chromosomal DNA, single-strand breakage, sensitive detect. by sedimentation anomaly appl. 80—104825
mammalian DNA, viscoelastic behaviour, rat obs. 80—8078
melting, local stability correl. with environmental conditions 79—88048
melting curves, automatic recorder using real time processing, DNA derivate *(French)* 80—104833
melting of DNA-type macromols., low mol. wt. impurity effect 80—12050
melting profiles for RF II ΦX174 DNA 78—24027

DNA continued
membrane fatty acid composition effect on E. coli K-1060 radiosensitivity 79—92306
metal ions interaction, with nucleic acids, nucleosides and nucleotides, review 80—3577
Methanobacterium thermoautotrophicum, DNA organisation, evolutionary implications 80—30686
methyl green-DNA binding, linear dichroism anal. 77—88479
methylation after UV irrad. of HeLa cells 77—12979
6-methylmercaptopurine riboside, S-substituted nucleoside, ESR and ENDOR obs. 77—36766
mitochondrial DNA, nucleotide sequence in human, replication origin identification 79—29502
modified bases characterisation by mass-analysed ion kinetic energy spectrometry 80—3591
molecular electrostatic pots. of complementary base pairs 78—92597
molecular motions, investigated by ^{31}P and ^{13}C NMR relaxation 80—63657
molecular shape, form dichroism of cryst. 78—60417
molecular weight determ. by fluctuation spectroscopy 77—10800
monodisperse, rod-like mols., transient elec. dichroism 78—94344
mouse liver, time depend. correl. function, single clipped photon correl. 77—48748
murine leukemic lymphoblasts, deficient repair and degradation of DNA after X-irrad. 80—72249
murine leukemic lymphoblasts, deficient repair and degradation of DNA after X-irrad. 80—72253
mutation theory, physical model of genetic stability 79—8486
mutations, quantum theory, proton transfer by dynamic interactions 77—77868
native Hela, shear breakage, expt. determ. 79—16121
natural storage of information, comparison with digital mag. recording 79—2009
neuronal DNA damage accumulation rel. to death after whole-brain irrad., rats 80—76804
p-nitroacetophenone charge transfer reaction with triplet state of guanine for radiosensitisation 79—92146
NMR, high-resolution studies of double helical polynucleotides, review 77—86450
nuclear peripheral DNA critical site for radiation-induced reproductive death 79—88131
nuclear synthesis in yeast, UV and gamma-ray effects 77—56428
nuclei acid phosphate group, analytical atom-pair pot., SCF-LCAO calc. 79—70516
nucleic acid-dye complexes, energy transfer obs. using laser-induced fluoresc. 80—12054
nucleic acids, electron microscopy using basic protein film method 80—104844
nucleosomal, electro-optical props., relax. times and chain struct. 80—85350
nucleosome core particles of chromatin, struct., X-ray diffr. and electron microscopy 77—86440
nucleosomes, structs. and modes of interaction 79—62182
nucleotide sequences of the attachment sites of bacteriophage Mu DNA 79—79463
optical measurements in presence of phenol and protein impurities 77—56546
oriented DNA, hydration, neutron scatt. obs. 80—89714
oriented films, hydration, slow neutron scatt. obs. 79—57572
packing in fibrils of DNP of polytene chromosomes 80—30649
phage T7 RNA polymerase, base pair for recognition and initiation 79—74597
phase transition, ψ transition of single coils 80—26200
phase transitions, light absorption oscills. obs. in soln. 80—26197
phase transitions in water-ethanol solns. *(Japanese)* 80—89709
photoemission, absorpt. spectra and luminesc., 120 to 250 nm 77—81466
physical and biological science conf., Japan (Feb. 1979) 80—12846
picosecond relaxation measurements book contrib. 77—64166
plasmid DNA and DNA-histone chromatin-like complexes, conform. and soln. props. by laser light scatt. 80—55987
plasmid molecular weight determ. from UV sensitivities 78—44458
Poisson-Boltzmann equation and its application to polyelectrolytes 79—77483
polymerase RNA-DNA dependent, determ. of intersubunit distances and subunit shape parameters of neutron small-angle scattering 79—53038
polymerase-DNA complex, thiopyronine-sensitised photodynamic inactivation of RNA synthesis 77—29177
polymorphism, X-ray diffr. and computerised model building study 78—27894
polytene chromosome, stretched, stained with acridine orange, fluoresc. polarisation rel. to DNA packing 78—76995
postreplication repair enhancements in UV-irrad. Chinese hamster cells by irrad. in G_2- or S-phase 78—77085
prealbumin-DNA-hormone interactions, X-ray studies, review 78—53322
protamine cDNA plasmids, coding and non-coding nucleotide sequences, sequence divergence of rainbow trout protamine mRNA 79—74596
protein nucleic acid recognition, role of unspecific complexing 79—79449
protein-DNA cross linking mediated by X-rays 78—27898
protein-DNA interaction, biostereochem. modelling, interactive computer graphics 78—88693
protein-DNA interaction, effect of cooperativeness on recognition of specific sites 77—81463
proton magnetic relaxation, methyl group reorientation 77—64009
proton radiationless transitions for hydrogen bonds *(Russian)* 80—97857
proton transfers between base pairs, LCAO SCF all-electron PRDO method 78—80829
pyrimidine dimers, excision repair of UV damage in monkey kidney cells 78—53332
pyrimidine dimers non-random distrib. after UV irradiation 79—96628
pyrimidines, cryst., lattice dynamics 78—75766
quasielastic light scattering, in aq. soln., AC elec. field 79—62186
quinacrine mustard-DNA complex molecule, laser-induced fluorescence 77—60187
radiation biology conference, Rotterdam, Netherlands (Aug. 1980) 80—105425
radiation carcinogenesis, shape of dose-response curve, extrapolation to low doses 78—15866
radiation effects, additive action of ionising and non-ionising radiations, Chinese hamster cells 77—48845
radiation effects, physical, molecular, cellular and macrocolony level obs. 80—12193

DNA continued
radiation induced breaks in E. coli and superinfecting phage λ, repair rel. to buffer 77–25376
radiation induced double strand breaks, recombination, formation of chromosomal rearrangements 78–85289
radiation induced mol. size change, electron irradiated, effect of p-nitroacetophenone 80–89807
radiation induced properties changes caused by UV- and γ-irrad., electrochem. anal. 80–72271
radiation sensitivity, physical aspects 80–67162
radiation sub-letahl damage accumulation site, evidence for location in Chlamydomonas 78–7390
radiation theories, strand breaks 77–77943
radiation-damaged, UV and gamma, defective repair in Fanconi's anaemia 77–44725
radiation-induced 78–69147
radiation-induced break rejoining capacity rel. to mouse age 78–69148
radiation-induced double-strand breaks, repair in isolated nuclei of Physarum polycephalum 80–72248
radiation-induced non-rejoining breaks rel. to cell death, high-LET radiation 77–44596
radiation-induced strand breakage, prod. of monophosphate end groups 77–32873
radiation/Pt complex effects, anal. using mol. theory of cell survival 77–21565
radioactive labelled, effect on excision repair in UV-irrad. human fibroblasts 80–94289
radioiodination method and in vivo studies of tumour localisation 80–51249
radiolysis of DNA and other bipolymers 80–67163
radionuclides incorporated into mammalian cell DNA, microdosimetry 80–12191
radionuclides incorporated into stem cell DNA, biological damage, radiation protection implications 80–12187
radioprotection by oxide-reduction coenzymes 78–40274
radiosensitivity of Escherichia coli K-12 rec and uvr mutants, LET depend. 78–15874
reaction with muonium, rate consts. 79–57210
recombinant DNA, scientific and social perspectives 79–88047
repair after γ-irradiation, action of hyperthermia in HeLa cells 79–100577
repair competency changes after 5-bromodeoxyuridine pulse labelling and near UV light 79–83854
repair mechanisms, damage from ionising radiation 79–11987
repeated, homology between humans and simians 79–8474
replication and repair in human melanoma cell-line resist. to UV irrad. 77–44721
replication by quantum mechanical interactions 77–40626
replication fork struct. in UV irradiated human cells 79–88117
replication kinetics in X-irrad. Chinese hamster ovary cells 78–20226
replicon autoradiograms, computer-assisted measurement 78–92692
replicons of mammalian DNA, organisation of repeated nucleotide sequences 77–73506
RNA, molecular motions investigated by ^{31}P and ^{13}C NMR relaxation 80–63657
secondary structure, dependence on base sequence, theoretical conformational anal. 79–53032
sedimentation constants, direct meas. by analytical ultracentrifugation *(French)* 80–8004
SEM cathodoluminescence probing of biomol. species at 100 Å resolution or below 78–24197
side-by-side model, X-ray diffr. 80–35835
single and double strand radiation damage comparison 79–92153
single strand break yield and survival curves for E.coli B/r 80–26282
single-strand break repair after X-irradiation, cultured insect and mammalian cells 79–74725
single-strand breaks, ultra-fast repair in γ-irrad. Chinese hamster cells 77–21569
single-strand breaks in rat thymocytes due to irrad. histidine and γ-rays 77–56438
single-stranded, alkali-labile sites and post-irrad. effects induced by H radicals 78–68994
single-stranded, reaction of O_2 with radiation-induced free radicals 78–48759
solution, conc.-depend. collapse in presence of second polymer 78–56949
solution, elec. birefringence, stabilised induced dipole behaviour 80–85349
spreading of large associations, dark field electron microscopy 80–85563
strand break kinetics in soln., electron pulse radiolysis using light scatt. detect. 77–16910
strand breaks, lymphoma cells, detected by hydroxyapatite chromatographic technique 79–43819
strand breaks in ^{60}Co γ-irrad. thymocytes 78–7395
strand breaks in developing rat brains and their repair 80–30786
strand breaks induced by ^{125}I in cultured human kidney cells, repair 80–12192
strand breaks induced by γ-irrad. of deoxygenated aq. solns. 80–61649
strand-break repair in chick embryo Mullerian ducts 80–36020
structure, evidence from electron microscopy 79–24948
structure, supercoiling 78–31766
subchromosomal synthesis in X-irradited V-79 cells 80–41141
sugar ring non-standard conforms. in A and B structs. 78–80827
sugar-phosphate backbone, molecular electrostatic pots. calc. 80–9679
supercoiled torsional stress and local denaturation 80–72131
supercoiling, elastic model 78–15767
supercoils and torsional stiffness of DNA double helix 79–83702
superconductivity, dynamical model 79–62172
superhelical packing in nucleosomes *(German)* 79–53041
synergism of radiation and other DNA damaging agents 80–26299
synthesis by DNA-membrane complexes from electron irradiated E. coli 79–16167
synthesis in chick embryonic Mullerian ducts, X-ray dose response obs. 79–88130
synthesis in root meristem cells, 2 MHz US effects, Pisum sativum 77–9218
synthesis in testes of fish Oryzias latipes, fast neutron effects 77–86553
synthesis in vitro, UV induced mutagenesis 79–92149
synthesis in X-irrad. HeLa cells, depend. on dose and time after exposure 77–37025
synthesis inhibition in vitamin-E-depleted lymphosarcoma cells by X-rays and cytostatics 77–56429

DNA continued
T content in organs, and DNA of rat liver cells, after doses of tritiated food, protein or water 80–56226
Tetrahymena, γ-irrad., role of DNA damage and repair in eukaryotic gene function 80–104677
Tetrahymena, viscoelastic meas. 79–100570
thermal neutron effects combined with agents which interact with DNA 78–20219
thermal properties in wide range of concs. of ions of neutral salts and of polymer 78–80833
thermal transition midpoint, CAA 79–74593
thermodynamics and decoding of long molecules 79–31757
thymine base damage release, γ-irrad. Tetrahymena pyriformis 80–72268
thymine damage production and excision, mammalian cells, high-LET irrad. obs. 80–72261
thymine dimer excision from DNA of UV-irrad. plant seedlings 78–61221
thymine dimer excision kinetics in UV-irrad. human cells 78–53331
thymine dimer induction by UV as function of cell stage 79–57715
thymine fragment damage retained in DNA polynucleotide chain after γ irrad. in aerated soln. 78–31773
thymus, rat, DNA and chromosomal proteins syntheses after whole-body X-irradiation 79–34492
thymus dividing cells, recovery response, in whole-body gamma-irrad. mice 77–12968
torsionally stressed, equilibrium statistical mechanics of helix coil transition 80–67032
torsionally stressed, transitions between B- and Z-conformations, theoretical anal. 80–94166
transcription, UV and incubation effects on heterogeneous nucl. RNA size in murine cells 78–69139
transcription of λ DNA, effect of UV irrad. 77–66827
transforming, X-ray sensitivity rel. to presence of free radicals 78–68995
transmutation effects of incorporated ^{32,33}P 80–26283
trigeminal neurons, rat, effects of γ-irrad. 80–72270
tumour localisation expts. using heat-denatured radioiodinated calf thymus DNA 79–96651
unscheduled synthesis in diploid yeast after X-irrad. in different phases of cell cycle 77–44722
unscheduled synthesis in UV irrad. spleen lymphocytes after X-irrad., rat 78–69156
UV and psoralen effects, use as probe for study of protein synthesis control 77–66881
UV and X-ray damage, interaction in Chinese hamster cells 79–11977
UV damage, postreplication repair in mammalian cells, model 78–80918
UV inactivation curve shape for transforming DNA 77–66797
UV induced unscheduled DNA synthesis, chromosomal localisation 77–25520
UV irradiated normal human and xeroderma pigmentosum cells, strand breaking and rejoining 77–4986
UV irradiation, dNA repair and longevity assurance in Paramecium tetraurelia 80–3741
UV irradiation, mouse tissue DNA 78–11702
UV irradiation of Chinese hamster cells, postreplication repair enhancement 78–92678
UV sensitive mouse neuroblastoma cells, replication and repair 77–5027
viral DNA, nucleotide sequence 78–40114
viruses in biological fluids, real time meas. using virometer 78–48869
water interaction, single and double helix DNA 80–30646
water localisation in a DNA mol. by differential Fourier synthesis 80–94164
water salt solns., microcalorimetric investigation of phase transition and eutectic fusion 79–79448
water sorbed on DNA, temp. anomaly, IR spectroscopic obs. 80–51046
X-irradiated E. coli cells, influence of uvrD mutation on survival and repair 77–86540
X-irradiation, differential absorption in micro-organisms 79–11969
X-irradiation production of alkali-labile lesions 79–43820
X-ray diffraction, circular superhelical DNA at 300-10000 Å 77–9168
X-ray excitation of triplet state 77–9174
X-ray induced damage in rat cerebellar neurons and brain tumour cells 78–80922
X-ray induced mutations and target theory 77–5040
X-ray induced single-strand breaks, yield and repair, E. coli cells 77–9173
X-ray lesion production, role of radicals, E. coli X-ray endonuclease specificity 77–52745
X-ray struct. study using synchrotron radiation and multichannel detector 78–47210
Yoshida sensitive and resistant cells, dimer form., excision and DNA strand growth after UV irrad. 77–90858
^{111}Cd^{m} bound on DNA, perturbed, γ-γ ang. correlations 79–79457
CsDNA, absorpt. factor, X-ray diffr. study using 1.2 Å synchrotron radiation 78–76988
CsDNA of T2 phage, in classical crystn. B form, struct., amplitudes, synchrotron radiation diffraction 80–85335
^{3}H distribution in glycogen, haemoglobin and chromatin of mice drinking tritiated water 78–31910
HeLa cell chromatin, effects of hyperthermia on protein-to-DNA ratio 79–11905
HeLa cells, synchronised, DNA damage from UV irradiation 79–25034
^{125}I labelled, pot. tumour imaging agent 80–30892
^{125}I toxicity, mol. consequences of Auger effect, fate of iododeoxyuridine after ^{125}I decay 77–4982
^{125}I toxicity in cultured mammalian cell, primary site for division delay 77–52851
^{111}In bound, rot. correl. times, from γ-ray perturbed angular correl. 80–94152
Na salt, freeze-dried layers, unpolarised IR spectrum, temp. dependent spectral shift 77–48755

document retrieval *see information retrieval*
documentation *see information science*
documentation, program and system *see program and system documentation*
Doherty amplifiers *see power amplifiers*
domain boundaries
for boundaries between magnetic domains and electric domains see magnetic domain walls and electric domains walls respectively
see also antiphase boundaries
activation energy of thick domain walls 79–56751

domain boundaries continued

- adsorbed layer, commensurate-incommensurate transition and domain walls 80—107654
- benzil, structural transition model, cryst. symm. spontaneous strain components 80—2161
- brownian motion of a domain wall and the diffusion constants 79—37775
- copolymers, triblock, lamellar domain dimensions, prediction 77—39547
- copper phthalocyanin, thin film, thermal behaviour *(Japanese)* 80—24753
- ferrodistortive materials, dynamics of domain walls, theory 79—73282
- ferroelectrics, $BaTiO_3$ type, surface acoustic waves on domain boundaries 79—90860
- Heisenberg model, nonlinear excitations 79—78286
- kinks, solitons, and nonlinear transport in solids 80—65421
- lattice systems with scalar spin variables wall and boundary free energies 78—155
- liquid phase sintering, role of grain and phase boundaries 78—72747
- metamorphic plagioclases from Japan, modulated microstructure 79—96760
- Peierls force of boundary layer, theory 80—10552
- polyethylene single crystals, fold domain boundaries, diffr. contrast 77—15428
- quartz crystal, opalescence near α-β transition, static model rel. to domain wall form. 80—11420
- relative orientation of two crystals from analysis os spot diffr. patterns 77—47305
- single-phase domain boundary identification by X-ray diffraction line broadening 78—1949
- squaric acid, ferroelasticity, elastic hysteresis loop and domain struct. 79—55814
- thermal impurity depinning in two dimensions 79—73565
- virtual domain walls, dynamic struct. factor central peak correlations 79—95114
- Ag film, on mica, microstruct. changes 78—72013
- α-Al_2O_3 CVD and Czochralski grown crysts., imperfection anal. comparison 79—78868
- Au-Cu-Ni(Ag), phase precipitation on domain boundaries *(Russian)* 78—39777
- Au_4Mn, fully ordered, microstruct., high resolution electron microscopy 79—1439
- Au_5Mn_2, phase transformations and domain structures *(French)* 78—27509
- Au_5Mn_2, variants in domain struct. 77—43224
- $(Ba_3Nb_6Si_4O_{26})_n.Ba_3Nb_4Ti_4O_{21}$, multiple intergrowth and microdomains obs. by electron diffr. and microscopy *(French)* 78—95160
- $BiVO_4$, ferroelastic domains, electron microscopy and electron diffr. obs. 80—100254
- $Cu_{0.5}In_{2.5}Se_4$, transition state and domain struct. by electron microscopy and diffr. studies 80—15095
- $ErCo_6$, domain wall grooving due to mech. polishing 79—70232
- Er_2Co_{17}, domain wall grooving due to mech. polishing 79—70232
- Fe, oxidation and domain structure, electron microscope exam. *(Russian)* 79—1437
- Fe-Co (33 wt.%), oxidation and domain structure, electron microscope exam. *(Russian)* 79—1437
- $GdCo_5$, domain wall grooving due to mech. polishing 79—70232
- Ge:Cu, surface waves at static domain boundaries *(Russian)* 80—80288
- α-GeTe, diffraction contrast between inversion domains and at boundaries in TEM 77—62457
- H_3BO_3, ferroelastic state shift and domain wall angle 78—43063
- ^3He, superfluid, domain wall energy and spatial conformation in parallel plate geometry 80—96716
- $KFe(MoO_4)_2$, ferroelastic domain struct. *(Russian)* 79—90719
- $KIn(WO_4)_2$, ferroelastic domain struct. *(Russian)* 79—90719
- K_xVF_3 ($x=0.45$ to 0.56), non-stoichiometric, struct. depend. on composition 79—99152
- $LaNbO_4$ crystals, ferroelastic, w′ walls, temp. depend. 80—10560
- β-$MoTe_2$, layer cryst., dislocations and domain struct. 80—39102
- Na_xWO_3 bronzes ($0.4<x<1$), domain, surface and substrate structs. 80—34281
- Nb-H system, phase diagram and transforms., struct. obs. of various phases 80—104125
- $NbTe_2$, layer cryst., dislocations and domain struct. 80—39102
- $NbTe_2$, phase transformations and domain structures *(French)* 78—27509
- $NdNbO_4$, ferroelastic domain wall motion, stress-strain hysteresis curve 77—43271
- $Ni_3Ti_{0.5}Ta_{0.5}$, conservative domain struct., TEM study 80—79776
- $Pb_3(PO_4)_2$, ferroelastic domain struct., twinning analysis by pseudosymmetry 77—76421
- Rb_xVF_3, non-stoichiometric, struct. depend. on composition 79—99152
- ReS_2, layer cryst., dislocations and domain struct. 80—39102
- $ReSe_2$, layer cryst., dislocations and domain struct. 80—39102
- SbSI, cryst., low temp. dielec. anomalies and domain struct. 80—40035
- Se, amorphous film, crystn., thermal and photo-effects 77—47692
- Ta-N, domain configurations of new phase *(French)* 78—56648
- Tl_xVF_3, non-stoichiometric, struct. depend. on composition 79—99152
- ZrV_2, anomalous softening at martensitic transform. 80—93630

domains

- *see also antiphase domains; crystal microstructure; domain boundaries; electric domains; magnetic domains*
- adsorbed layers, commensurate-incommensurate transitions, substrate defects effect 80—75437
- alkali tungsten bronzes, dynamic fluctuations between local struct. states in supercond. Tl phase 78—26981
- benzil, ENDOR study of phase transition 79—73855
- bounded domain undergoing sequential crystallisation, stress and strain investigation 80—100183
- cholesteric liquid crystal, bubble domain texture, obs. of forming process 78—26431
- cholesteric liquid crystal, bubble domains, mol. alignment 77—39534
- cholesteric-nematic mixture, bubble domain struct. and props. 77—89373
- cholesterics, shear flow induced propagating domains 80—64887
- coherent domain structures from crystal transitions with related space groups 79—42002
- conjugate domains, eqns. of math. phys., soln. 78—20967
- crystals with dislocations, phase transitions of the second kind, dislocation superparamagnetism *(Russian)* 80—1957
- 4-cyano-4-n-octylbiphenyl, smectic A phase, focal conics motion and plasticity, stroboscope obs. 79—86692

domains continued

- elastomers, block copolymers, generalised elasticity theory, domain crosslinkage vol. 77—39229
- ferroelastic crystal, nonideal, domains struct. 78—2191
- film, domain size and internal strain, studied by electron diffraction line broadening 78—30840
- gamma-ray diffraction applications 80—14972
- gamma-ray diffractometry, phase transitions, domain structures, twinned texture studies 80—19678
- graphite intercalation compounds with $FeCl_3$, struct. expt. data for domain theory 78—30596
- gyrotropy, an implicity form of ferroicity 79—73286
- heat transfer in domains with sources having variable power, soln. 79—72891
- J-ferroics, rotational-invariant classification of structural phase transitions 80—70369
- liquid crystal, cholesteric, long pitch type, with homeotropic boundary alignment, elongated and spherulitic domain struct. 80—107047
- liquid crystals, domain instabilities in elec. and mag. fields 79—94875
- MBBA, positive space charge influence on texture, domain form. factor, polarised light study 80—88037
- MBBA domains, in presence of iminoxyl free radicals, elec. field influence 79—64992
- MBBA-cholesteryl chloride mixture, liq. cryst., bubble domain texture, obs. of interference fringes 79—23520
- MBBA/CC mixtures, cholesteric phase, torsional shear flow in elec. and mag. fields 79—86697
- modulated structures, review 79—94929
- nematic liquid crystal, critical radius for homeotropic domain 79—19148
- nematic liquid crystal, domain form. in AC, DC fields, threshold voltages *(Russian)* 77—39542
- nematic liquid crystal, parallel and cross-like domains due to DC and LF electric fields 79—46557
- nematic liquid crystal, positive dielec. anisotropy, Williams domains as mag. threshold effect 78—26435
- nematic liquid crystal in mag. field 77—58951
- nematic liquid crystal layer, twisted, elastic deform. energies and reverse twist domains 79—37617
- nematic liquid crystals, electric feield influence *(Russian)* 77—47340
- nematic liquid crystals, light diffr. by 3D domain structs. 79—64989
- nematic liquid crytals, in nonuniform elec. fields, mag.-field stabilisation 79—94901
- nematic oriented film, birefringent stripe pattern generation by ultrasonic waves 77—76301
- nematic suspended films under AC and DC fields 77—11470
- ordered superlattices, X-ray studies, rel. to microstructure 79—94844
- PAA, nematic, adjustable domain struct. in inhomogeneous elec. field, electro-optic props. obs. 80—10494
- pheophytin containing monolayers, phase separation and domain interaction, surface press. and fluoresc. meas. 79—100580
- poly-n-benzamide, lyotropic liq. cryst., structural orientation *(Russian)* 77—31593
- polyether-amidourethane, segmented, polymer domain struct., IR spectra and optical microscope *(Russian)* 78—51453
- polyethylene, uniaxially stretched, density fluctuations 78—75587
- polymer, amorphous, domain struct. determ. by electron microscopy and electron diffr. 77—84667
- polymer science, conf., Pittsburgh, USA, (June, 1975) 77—38756
- polymer transitions, domain size effects 79—69232
- polystyrene, Millar interpenetrating network, viscoelasticity and phase domain form. 78—83749
- polystyrene-poly(styrene-b-butadiene-b-styrene) polyblends, electron micrographs for struct. 78—51442
- polyurethane, segmented, domain struct., deform. effect 80—93623
- polyurethanes, domain struct. obs. by NMR 77—47355
- quartz, incommensurate phase near $\alpha\rightleftarrows\beta$ transition pt. 79—90748
- smectic C liquid crystal, storage effect, memorisation of oriented picture of EHD instability 79—37615
- sodium dodecylsulfate—H_2O system, X-ray anal. 80—1926
- sodium pentadecyl sulphonate, lyotropic liquid crysts., X-ray study of domain structure *(Russian)* 77—62469
- solid electrolytes with structural disorder, domain states, thermodynamic study 79—42307
- superionic crystal, domain formation, thermodynamic theory 77—84963
- TCNQ salt, HMTSF-TCNQ, lattice phase transitions and conduct. anomalies obs., elastic microdomain model 77—1226
- textured materials, diffraction broadening studies, coherent domain size and microstrain 79—73060
- TMMC, one-dimensional, EPR at HF and low temp. 78—80205
- transition, cell-preserving, space group theory of translation, twin and translation-twin boundaries 77—19892
- transition metal alloys, domain struct. of diffuse ω-phase formed in quenching, 1D model 78—27523
- transition metal dichalcogenides, octahedral intercalate ordering study by electron diffr. 80—15076
- transition metal oxide catalysts, reduction, cryst. defects influence, in-situ electron microscopy 80—81322
- TTF-TCNQ, lattice phase transitions and cond. anomalies obs., elastic microdomain model 77—1226
- TTF-TCNQ, phason and metal-insulator microdomain model, Young's modulus temp. depend. anal. 77—31964
- type I superconducting film, cylindrical domain struct. in mag. field 80—15666
- n-undecyl-p-azoxy-α-methylcinnamate, smectic C phase, domains, walls, and disclinations 79—86687
- Ag-Ge (4.5 at.%), FCC, vapour-deposited, lattice imperfections, X-ray diffr. 78—72032
- $AgBiS(Se)_2$, polymorphism and defects, electron microscopy 78—2254
- Al complex, Al $urea_6(ClO_4)_3:Cr^{3+}$ structural phase transition, ESR meas. 77—20681
- $Ba_{15}Ca_{27-x}Nd_xAl_{31}Be_{27}F_{231+x}$, $0\leq x<8$, optical props. and vitreous domain 79—65820
- $BaCl_2.2H_2O$, ferroelastic effect obs. 79—28033
- $CaAl_2Si_2O_8$, anorthite, quenched from 1530°C, struct. refinement 77—15355
- β-Ca_2SiO_4, stabilisation, IR and Raman spectra 79—42265
- Cd, thin film, vac.-deposited, X-ray diffr. struct. obs., props. 79—37937
- CdS, charge in energy gap caused by acoustic domains 77—20822
- Co-Pt, mag. annealing, form. of ordered phase, study using X-ray scatt. *(Russian)* 80—81052

- **domains** continued
  - Cr_3Si type phases, A-15, crystallographic interpretation of atomic volumes 79—10833
  - Cs_2CrO_4, polarised light exam. reveals domain struct., mechanical stress, ferroelastic behaviour 78—18702
  - Cu-Al, gamma-2 phase intermetallic cpd., mech. props., effect of inversion domains 79—61599
  - Cu-Mn alloys, Cu-rich, heat treated, segregation obs. *(Russian)* 78—27517
  - Cu-Pt, quenched, microdomain model anal. of diffuse X-ray scatt. 79—52276
  - Cu-Pt alloy, quenched, SRO, microdiffr. obs. 77—76360
  - Cu_3Au, flow stress 77—21231
  - Cu_3Au, metastable states domain existence, phase transition ordering energy, press. effect *(Russian)* 80—45303
  - Cu_3Ga, interpretation of diffuse contours in electron diffr. *(French)* 79—19377
  - $Cu_{0.5}In_{2.5}Se_4$, transition state and domain struct. by electron microscopy and diffr. studies 80—15095
  - $Cu_{0.5}NbS_2$ and $Cu_{0.5}TaS_2$, order-disorder and displacive transforms., domain-type microstruct. 77—4195
  - CuPt, quenched, state of local order 79—47722
  - $CuSO_4.5H_2O$, dehydration into trihydrate obs. using monocryst. platelets, product domains shape 80—71905
  - Fe-Si single crystals with cube-on-edge orientation, iron-loss-domain-struct. correls. *(Japanese)* 80—7534
  - Ga complex, $Gaurea_6(ClO_4)_3:Cr^{3+}$ structural phase transition, ESR meas. 77—20681
  - GaAs:O, slow domains, origin 78—60132
  - α-GeTe, diffraction contrast between inversion domains and at boundaries in TEM 77—62457
  - GeTe, effect of phase transition on mech. and elec. props. 77—51746
  - GeTe, high pressure effects on hole conc. and thermoelec. props. 78—26894
  - GeTe, low temp. alloys, microstruct. obs. *(Russian)* 78—19768
  - ^3He, superfluid, domain wall energy and spatial conformation in parallel plate geometry 80—96716
  - ^3He, superfluid A_1-phase, domain wall exam. 79—42332
  - ^3He, superfluid B-phase, domain struct., derived from Ginzburg-Landau eqns. 78—63896
  - $K_2Ba(NO_2)_4$, new ferroelastic, phase transitions, optical and electrical props., domain struct. 79—55887
  - KCl:TlCl, lattice defects, X-ray line profile obs. 80—24455
  - K_2CrO_4, polarised light exam. reveals domain struct., mechanical stress, ferroelastic behaviour 78—18702
  - KH_2PO_4:cation impurities, growth domains 79—99224
  - $K_4Zn(MoO_4)_3$, domain struct. and phase transition, ferroelastic behaviour 77—62581
  - $LaAlO_3$, Pm3m to R3c or R$\bar{3}$c phase transitions, TEM method for domain identification 80—14980
  - $Li_2Gd_4(MoO_4)_7$, Czochralski growth, struct. and optical props. 78—27397
  - Mn-Cu, shape-memory effect at martensitic transform., cryst. and mag. struct. 77—36610
  - β-$MoTe_2$, domain struct., dislocation fine struct., phase transitions 79—82332
  - $(NH_4)_2SO_4.Al_2(SO_4)_3.24H_2O:Cr^{3+}$, and deuterated derivative, structural transition studied by EPR 77—85553
  - $NaAl(MoO_4)_2$, ferroelastic, domain struct. obs. 77—15483
  - Na_xWO_3 bronzes ($0.4<x<1$), domain, surface and substrate structs. 80—34281
  - Na_xWO_3, domain struct., optical microscope obs. 79—19436
  - Na_xWO_3, dynamic fluctuations between local struct. states in supercond. TI phase 78—26981
  - Nb_2O_5-WO_3 system complex cpds. with TTB type subcells, HV superhigh resolution electron microscopy obs. of struct. 80—103311
  - $Ni_{1-x}Fe_x$, short range order exam. allowing for formation of structural domains *(Russian)* 78—6888
  - Ni_4Mo, quenched, short-range order, electron diffraction study 77—39560
  - NiPt, quenched, ordering kinetics and domain struct. form. during isothermal tempering *(Russian)* 80—66502
  - Ni_3V, ordered, domain size effect on mech. props. 79—79027
  - $Pb_2(PO_4)_2$, ferroelastic, switching processes 78—2192
  - $Pb_3(PO_4)_2$, ferroelastic, bending stress effect on domain struct. *(Russian)* 77—39623
  - $Pb_3(PO_4)_2$ ferroelastic, dielec. consts. and birefringence meas. 78—2793
  - $Pb_3(PO_4)_2$, ferroelastic, switching processes in pulse mech. field 78—59853
  - $Pb_3(PO_4)_2$, ferroelastic phase, structure domains, electron microscope obs. 79—42078
  - $Pb_3(PO_4)_2$-$Pb_3(VO_4)_2$, direct obs. of ferroelasticity 77—21203
  - $Pb_3(VO_4)_2$-$Pb_3(PO_4)_3$ solid solutions, ferroelastic, dielec. consts. and birefringence meas. 78—2793
  - $Pb_3(VO_4)_3$, ferroelastic, dielec. consts. and birefringence meas. 78—2793
  - $Pb(Zr, Ti)O_3$ internal struct., prep. effect, ionic shadowing obs. *(Polish)* 80—11612
  - Pt-Ir, structural phase transform., ion field emission microscopy obs. *(Russian)* 80—50628
  - $RbCaF_3$, influence of domains on struct. phase transition 79—28097
  - Rb_2CrO_4, polarised light exam. reveals domain struct., mechanical stress, ferroelastic behaviour 78—18702
  - $RbMnCl_3$, twinning struct., cryst. domains, orientation mag. transition *(Russian)* 80—107275
  - Si, on sapphire, early growth, TEM 77—24961
  - Si, on sapphire, early growth, models 77—24962
  - $Sr_2Nb_2O_7$, normal-incommensurate phase transition, electron microscopy and diffraction study 80—39277
  - $Sr_2Ta_2O_7$, structural phase transition to superlattice, electron microscopy and diffraction study 80—39277
  - $SrTiO_3$, defects grown by Verneuil method 77—51390
  - Ti alloys, domain struct. of diffuse ω-phase formed in quenching, 1D model 78—27523
  - V_2O_3, low temp. crystallographic struct. domains 78—83765
  - V_3Si, US anomaly when cooled below martensitic and supercond. transition temps. 80—20354
  - WO_3, reduction, defect role, in situ HVEM obs. 80—81323
  - YAG, interrelationship between mech. props. and elec. relief on surface layer 79—23821
  - Yb, film, energy-scanning X-ray diffr. technique *(French)* 78—43264
  - Zn film, vac. deposited, X-ray diffr. study of microstruct. 78—26796

- **domains** continued
  - Zn, film, vac. deposited, X-ray diffr. study of microstruct. 78—75966
  - Zr alloys, domain struct. of diffuse ω-phase formed in quenching, 1D model 78—27523
  - ZrO_2-CaO, microstruct., ordering, elec. props. 77—15374
- **domestic appliances**
  - *see also ovens; refrigerators*
  - acoustic emission determ. facility development 77—58507
  - cooking plates with high abrasion and corrosion resistance, plasma spraying technique appl. *(Japanese)* 80—55558
  - energy saving in domestic washing *(German)* 79—83688
  - heat pumps, gas versus electric *(German)* 79—57438
  - heat pumps for space heating appls. *(German)* 80—94099
  - pacemaker interference, body potentials and currents from ELF elec. fields and househould appliances 78—88770
  - solar, self sufficient, for use in India's rural areas 79—74510
  - solar energy for domestic dwellings, installation practice *(Italian)* 79—100499
  - solar water heater/steam cooker, design and trials 79—66402
  - sound rooms for noise measurements 79—18604
  - temperature measurement, using A/D convertors TL505/507 and TMS 1000 microprocessor *(French)* 80—57290
  - vacuum cleaners sound power level measurement 79—18647
- **doping, semiconductors** *see semiconductor doping*
- **doping profiles**
  - algorithm for calc. of impurity concentration from sheet resistivity and sheet Hall coefficient data 80—70246
  - anomalous avalanche breakdown, effects 80—80284
  - C-V measurement interpretation, determ. of doping profile in semiconductors 80—59510
  - capacitance-voltage profiling tech. 78—38749
  - channelled ion implantations, apparatus for spatially uniform doping 78—51569
  - chemical analysis, by secondary-ion mass spectrometry *(German)* 78—95978
  - coincidence measurements between scattered particles and X-rays to obtain high depth and mass resolution 80—54278
  - composite ion implantation profiles, computer simulation 77—80528
  - composite ion implantation profiles, computer simulation 77—84786
  - controlled implated doping profiles, angular sensitivity 78—30659
  - crystal growing from lightly doped melt 78—2039
  - depth distrib., secondary ion mass spectra 80—79829
  - diamond:Sb, ion implanted under channelling conditions, depth profile, distribution tail 80—2057
  - diffusion layer, method for determining dopant and defect distribs. using polishing agent 79—37727
  - direct-gap epitaxial layers, optical compensation profiling 77—76450
  - dose depend. in laser annealing 78—91354
  - double AC Hall effect system for profiling semicond. impurities 77—37924
  - dynamic profiling of D, using low energy D(d,p) 78—2153
  - dynamic-implant profiling by low-energy nuclear reaction spectroscopy 77—59037
  - electron beam induced current technique appl. to semicond. device characts., review 78—21302
  - epitaxial film, dopant profile and Schottky barrier height determ. by second differential method *(Chinese)* 80—49257
  - high implantation doses, impurity profile calc. 80—24490
  - high-resolution photoacoustic spectroscopy for dopant depth profiling 80—77883
  - hyperabrupt varactors, fabrication from vapour phase epitaxial GaAs 80—29288
  - III-V multilayer structs., contact resistance profiling method 78—56213
  - impurity profile control by ion implantation 79—82258
  - inhomogeneous media, ion implantation range distribs. 79—23625
  - ion implantation, depth distrib., analytical calcs. using inhomogeneous equations 80—84203
  - ion implantation, in crystals of diamond struct., computer modelling 77—43235
  - ion implantation angular sensitivity 79—55770
  - ion implantation depth distrib., calc. in path-length approx. 79—23626
  - ion implantation depth profiles, influence of straggling using backscatt. and nucl. reacts. 78—47401
  - ion implantation through thin film, profile calc. 78—18672
  - measurement principles, capacitive methods, and theoretical principles 78—18675
  - melt-grown crystal, effect of crysallisation front oscills. 78—52657
  - metal, ^2H dynamic depth profiling by deuteron irradiation 78—26602
  - metal-semiconductor thermoelectric coolers, effects of contact resist. and dopant conc. 80—81481
  - modal dispersion in optical fibres with any numerical aperture and doping profile 78—1391
  - MOS device, B isolation region, numerical estimation 77—80843
  - MOS diode, impurity profile effect on density of interface states 79—33359
  - MOS structure, B and P implantation profiles, junction depth meas. *(Japanese)* 77—39606
  - MOSFET, dopant profile determ. from enhancement mode DC meas. 78—30987
  - nonuniformly doped MOS devices with lateral symmetry 80—15606
  - optical fibre manufacture, quartz, CVD process refractive index profile, liquid doping *(German)* 77—62050
  - optical fibre preform core diameter and Ge doping profile meas., X-ray nondestructive method 80—64231
  - optical fibre refractive index profile distortion due to thermal stresses 80—58726
  - optical multimode fibres with index profiles varying along length, pulse propag. 80—87534
  - p-n junction, background dopant density calc. from C-V meas. 78—26936
  - p-n junctions, determ. of arbitrary doping profile, depletion layer capacitance meas. 78—88021
  - p-n junctions, determ. of doping levels using nondestructive IR emission meas. 78—95338
  - p-n shallow junction, differential spreading resist. data 77—7755
  - Pearson IV distrib., appl. to ion implanted depth profiles 80—88195
  - quartz glass, Ge and B dopants, OH impurities, preform material and fibre optic waveguide struct. 80—64173
  - quartz glass optical fibres, B and P radial doping profiles 77—50771
  - redistribution of dopant impurities in oxidising ambients 79—90695

doping profiles continued
Schottky diodes with deep acceptor impurities, inverse square capacitance curve, theory 80—2468
semiconductor, dopant, transverse inhomogeneity, effect on ambipolar drift and field effect 80—6834
semiconductor, doping inhomogeneity, meas. by low-field electrorefl. 77—11584
semiconductor, multilayer spreading resistance anal., high-speed implementation and expt. evaluation 79—4324
semiconductor, predeposition diffusion profiles, errors in iterative numerical calcs. 78—26591
semiconductor, surface depletion and inversion, arbitrary doping profile, theory 80—107912
semiconductor depth profiling by electron beam induced junction current meas. 80—96977
semiconductor dopant surface concentration determ. by IR reflectance 80—34036
semiconductor epitaxial layer, p-n junc. and Schottky barrier differential capacitance obs. 77—12036
semiconductor film, heteroepitaxial, on insulating substrates, characterisation, book contrib. 79—82497
semiconductor impurity profile determ., multilayer spreading resistance anal. using image method 77—68993
semiconductor materials, channelling-blocking measurements, (n,α) method for B-depth profiling 80—70276
semiconductor microstructure fabrication, ion channeling effects 80—70230
semiconductor spreading-resistance meas. for doping profile determ., preprocessing of data for resistivity calcs. 80—57265
semiconductor substrate-semicond. epitaxial layer, doping profile using ellipsometric meas. 79—99453
semiconductors, dopant distrib. from carrier drift distrib. in high elec. field 79—51140
semiconductors, doping uniformity assessment using fully automated four point probe method 77—59040
semiconductors, ion implantation, recent progress 79—14831
shallow-level concentration, instrum. for automatic meas. 80—105673
SOS films, impurity conc. meas. technique using C-V plots 77—11585
spreading resistance meas., multilayer correction factor calc. 77—76823
sputter depth profiling with low press. HF plasma 79—95041
steel, austenitic, Cr-Ni, ion-implanted N, chem. state study by AES and XPS 80—79825
steel, depth profiles of transition elements using (p,γ) react. 80—50910
stripe optical waveguide, formed by ion exchange, diffusion profile 78—87137
thin epitaxial layer surface As concentration meas. 79—95037
transition metals, implantation of He^+, range profiles and thermal release 80—39138
transverse junction stripe injection laser structural improvement 80—23687
two-step diffusion profiles calc. 78—30662
VPE impurity profile computer-aided control 80—2962
(Al,Ga)As:Zn planar stripe lasers with deep Zn diffusion, guiding mechanisms controlled by impurity concs. 80—78853
Al, polycrystalline, high dose implanted with Cu and Pb, doping profile after laser pulse irradiation 80—88194
Al-Xe film, ion implanted radiation enchanced Xe outdiffusion, Rutherford backscatt. 77—76609
p- (AlGa)As:Zn, MBE grown, elec. props., shallow junction solar cell use 79—91175
p-$Al_xGa_{1-x}As$:Be layer, MBE growth, Be doping and diffusion 77—51397
$Al_xGa_{1-x}As$:Mg doping characteristics, elec. props., effective hole masses 79—78117
α-Al_2O_3:Pb, implantation, lattice disorder 77—80525
BP, epitaxial growth on Si substrate, Si impurity profile, ion microanal. 78—87886
BP:Zn(Se)(Cd), epitaxial layers, ion implantation, defects and lattic locations, channelling obs. 80—88179
Be:Zn, lattice location of implanted Zn, ion-beam channelling meas. 77—68992
CdS, diffusion of In, 729-1411K 78—22895
CdSe:Cu, doping profile rel. to photoelec. props. in alloyed surface layers *(Russian)* 77—85268
CdTe, anodic oxidation as thin-layer removal technique for impurity distrib. profile determ. 79—34169
CdTe crystals, exciton luminescence spectra rel. to shallow impurity conc. 80—97335
Cu single crystals Au ion implanted, pulsed electron beam irrad. 80—65019
$CuInSe_2$, Zn implantation profiles by AES 77—31692
Cu_2S-CdS heterojunction interface, depth distribution profiles, Auger spectra 80—88622
$Ga_{1-x}Al_xAs$ junction-up TJS laser electron injection efficiency improvement 80—48300
$Ga_{1-x}Al_xAs$:Si, Si determ., spectrochem. method, photoluminesc. spectra, Hall effect meas. *(German)* 77—77851
GaAs, 40 keV N^+ implantation, disorder profiles meas. by Rutherford backscatt. and channelling 80—54270
GaAs, direct-gap epitaxial layers, optical compensation profiling 77—76450
n-GaAs, dopant conc. determ. using laser IR microscopy 79—86811
GaAs, dual implantation of C^+ and Ga^+, sheet resist. and Hall effect meas. 78—67728
GaAs epitaxial layer and Sn-doped bulk characterisation 79—82596
GaAs epitaxial layers, meas. of doping profiles *(Hungarian)* 80—70545
GaAs epitaxial layers, doping profile degradation due to ion implantation 80—84194
GaAs, epitaxial structures, impurity profile 77—39610
GaAs, interimpurity interaction effect on distrib. profiles of impurities diffusing simultaneously 77—76451
GaAs, ion implantation, range distrib. calc. 79—55760
GaAs, ion implanted, capless annealed and dielectrically annealed, comparison of doping profiles 80—100278
GaAs, ion implanted, laser annealing 79—69124
GaAs LSA diodes, current controlled LPE for optimum doping profiles 78—35318
GaAs MBE physical characteristics and applications *(German)* 79—7618
GaAs, modification of Zn diffusion profiles by proton irrad. 78—43043

doping profiles continued
GaAs multilayer with abrupt carrier conc. profile, vapour growth technique 78—11123
GaAs, qualitative anal. of oxygen in thin epitaxial layers by SIMS 79—5233
p-GaAs, VPE growth and characterisation, doping levels 80—10841
GaAs, VPE layer growth with abrupt doping profile 80—24746
n-GaAs vapour phase epitaxial film electrophysical props. rel. to growth temp. *(Russian)* 80—49961
GaAs, with nipi superstructures, production and appl. *(German)* 78—95064
GaAs:Ag, diffusion of Ag at 1000°C, profiles, Schottky barrier and Hall effect meas. 80—54435
GaAs:Be, ion-implanted, photolum. spectra, effects of implantant depth distrib. 78—27293
p-GaAs:Be layer, MBE growth, Be doping and diffusion 77—51397
GaAs:Cr, ion implanted, implantation damage profiles, laser annealing, ellipsometry study 80—79819
GaAs:Cr, low temp. gettering 80—96549
GaAs:Cr, Mg, ion implanted, elec. meas. and optical activation studies 79—86806
GaAs:Cr,Zn, implanted, doping profiles after laser annealing, elec. props. 80—2058
GaAs:Cr capless annealed, under As press., Cr redistrib., SIMS obs. 80—59503
GaAs:Ge, MBE layers, complex free-carrier profile synthesis 80—54266
GaAs:Ge, VPE, doping, electrophysical characts. meas. 78—43493
GaAs:Ge MBE power FETs with Sn surface impurities 80—80374
n-GaAs:O film, influence of O on elec. props. 79—11252
GaAs:S, implantation depth profiles of S^+ and $S_2{}^+$ using AES 79—55774
GaAs:Se, implanted, depth profile, SIMS obs. 78—30655
GaAs:Se, pulsed electron beam annealing, doping profiles 80—6421
GaAs:Se depth profiles, Cs^+ SIMS anal. appl. 79—39265
GaAs:Si, Cr, carrier concs. from Hall effect, microscopy, localised vibrational modes absorption meas. 78—56104
GaAs:Si, encapsulated by SiO_2 and Si_3N_4, ion-implanted As profiles 79—4319
GaAs:Si, ion implantation, thermal annealing, Hall meas., SIMS atomic profile meas. 80—75243
GaAs:Si, ion-implanted, depth distrib. profiles of Si ions 77—43230
GaAs:Si epitaxial films, elec. and photoelec. props., impurity distrib. 80—7006
GaAs:Si layers, MBE growth, elec. and optical props., doping characts. 80—10819
GaAs:Sn, influence of growth process in doping profile and mobility profile during LPE 79—70000
GaAs:Sn films, MBE grown, doping profiles, carrier mobilities, RHEED and AES obs. 79—1447
GaAs:Sn(Te), epitaxial film, influence of impurities on stacking fault energy 80—103371
n-GaAs:Sn(Te), pure and doped, diffusion of Sn, radiotracer profiles 79—23782
GaAs:Te, ion implanted, abrupt dopant profile 77—1143
GaAs:Te(Cd)(Mg)(B), ion implant depth distribs., AES and glow discharge optical spectroscopy meas. 80—65028
GaAs:Zn, depth profile, photoluminesc. obs., LED applic. 78—72587
GaAs:Zn, diffusion during LPE, impurity gradients and annealing effects 80—29882
GaAs-Si heterojunction, IR quenching of photocapacitance 80—92968
GaAs-Si ion implanted, impurity profiles elec. props. 80—96550
$GaAs_{0.1}P_{0.9}$:Zn, shallow Zn diffusion profile determ. using anodic oxidation and double radioactive tracer method 77—43239
$GaAs_{1-x}P_x$:Zn, diffusion profile determ., $^{32}P/^{65}Zn$ double tracer technique 78—55888
$GaAs_{1-x}P_x$-SiO_2:N,Zn ion-implanted multiple layers, ion range distribs., secondary ion microprobe meas. 79—42129
GaP, dopant dislocations, scanning electron micrographs, cathodoluminesc. 78—91340
GaP, effective partition coeffs. and elec. behaviour of group IV elements 77—7754
p-GaP, epitaxial layers grown from liq., overcompensated, doping levels 78—91353
GaP, interimpurity interaction effect on distrib. profiles of impurities diffusing simultaneously 77—76451
GaP, ion implantation, range distrib. calc. 79—55760
GaP, LEC, SSD and CVD samples, Zn tracer diffusion profiles in solids 78—95189
GaP:Cr epitaxial layers, Cr conc. profile determ. 80—65029
GaP:Mg, ion implanted, elec. profiles 79—77628
GaP:N, N doping profiles in GaP grown by LPE, cathodoluminesc. data 79—23631
GaP:N LED structures, local dopant conc. determ. using SEM cathodolum. spectra 80—101057
GaP:Te epitaxial layers, dopant distrib. obs. by amalgam polarography 77—39609
GaP:Zn, diffusion profile determ., $^{32}P/^{65}Zn$ double tracer technique 78—55888
GaP:Zn, dopant diffusion profiles at 900°C, radiotracer meas. 77—59147
GaP:Zn, shallow Zn diffusion profile determ. using anodic oxidation and double radioactive tracer method 77—43239
n-Ge, doped, dopant distrib. from carrier drift distrib. in high elec. field 79—51140
Ge, melt growth conditions and doping level influence on impurity distrib. ratio 77—12516
Ge:As, NMR, conduction electrons in impurity band, metal-nonmetal transition 79—78544
Ge:B, single crystals, grown by Czochralski method, exam. of B distribution ratio and diffusion coeff. 79—95042
Ge:Be single crystals, grown by Czochralski method, exam. of Be distribution ratios and solubility 79—95043
Ge:Mg, diffusion and p-type cond. 80—6419
Ge:Sb, dopant distrib. rel. to direction of cryst. growth 77—51400
Ge:Sb(As)(P), implantation doping, annealing and doping profile determ. 77—19972
H isotopes, nuclear reaction anal. techniques, implantation studies, appls. 78—3422
^2H depth profiling with $^2H(^3He,p)^4He$ react. 80—49262
n-InAs:Cr, Czochralski growth of high-resist. single crysts. 77—66587
In_2O_3:Sn films, doping profiles and elec. props., appl. to optoelectronic devices 79—38203

doping profiles continued
InP:Be, LPE, Be distrib. coeff., carrier conc. 79–90694
p-InP:Cd(Zn), single cryst. growth by temp. gradient method 79–28907
InP:Zn heavily doped X-ray topography, cathodolum., and TEM obs. 79–99197
InP-metal Schottky barriers, effects of heat treatment characterised by SIMS 78–6446
$LiNbO_3$, Ti diffused slab waveguide, mode control by doping 77–88903
$LiNbO_3$:Fe, ferroelectric, treated in Li_2CO_3, formation of Fe^{2+} state, Mossbauer effect 78–92003
$LiNbO_3$:Ti, dopant conc., refr. index profile rel. to integrated optics 78–5583
$LiNbO_3$:Ti optical waveguide diffusion profile, AES obs. *(German)* 78–33876
Mg:H, solid soln. produced by ion implantation 78–67733
MgO:Cu, dopant conc., refr. index profile rel. to integrated optics 78–5583
Mo, doped, surface tension driven flow in electron beam floating zone expts. 80–19731
Na_2WO_4, cationic transport props. and struct. 77–76601
Nb, of He, replacement of implanted ^{3}He by subsequent ^{4}He bombardment, and vice versa, using ^{3}He(d, α) 79–4325
Ne depth profiling with resonant ^{20}Ne 79–7621
Ni dilute alloys, implant profiles modification by radiation enhanced diffusion and segregation 80–88217
Ni:He, implanted, profile meas. technique 77–80524
Ni-Si:As(Sb), implanted dopant redistrib. after silicide form., appl. to ohmic contacts 79–37729
n-PbSe, heterodiffusion of Sn 80–34245
$Pb_{0.82}Sn_{0.18}Te$:Cd, effective distrib. coeff. of Cd *(Russian)* 79–73203
PbTe, ion-implanted, doping profile evaluation by Hall effect and sheet resist. meas. 78–59831
$PbZr_{0.95}Ti_{0.05}O_3$ ceramics, of ABO_3 type, dopant distrib. between A and B sites 79–42093
Pd-H system, lattice parameter increase and H conc. distrib., X-ray diffr. meas. *(German)* 77–62560
Pd-Si:As(Sb), implanted dopant redistrib. after silicide form., appl. to ohmic contacts 79–37729
Pt-Si:As(Sb), implanted dopant redistrib. after silicide form., appl. to ohmic contacts 79–37729
$(Sb,Bi)_2(Se,Te)_3$ profiled crystalline ingot continuous elongation 79–69975
Si, 40 keV N^+ implantation, disorder profiles meas. by Rutherford backscatt. and channelling 80–54270
Si, amorphous, implanted ion trajectory and spatial distrib., Monte Carlo simulation 77–11611
Si, amorphous film, sputtering by 0.5 to 5 keV Ar^+ ions 79–91550
Si, amorphous layer, ion-implanted, spatially controlled cryst. regrowth by laser irradiation 78–55810
Si, amorphous layers, laser induced As profile broadening 79–95045
Si amorphous p-n junctions, high current, characts. 80–70807
Si, As implantation profiles, calc. comparison with expt. 78–38748
Si, carrier lifetime depth distrib. due to Ar ion implantation 80–70232
Si, comparison of interactions between sequential Ga-P and Ga-As diffusions 77–80655
Si, deep diffusion of B and P, expt. results 80–54437
Si, determ. by DC MOSFET dopant profile method 80–70244
Si, diffusion layers, B distrib. 77–7753
Si, dopant distrib. in mono- and polycryst. samples, C-V technique 80–6425
Si, dopant segregation by pulsed-laser annealing, test case for thermal melting concept 80–24489
Si doping by ion implantation, atomic collision theory and range-energy relations 78–71753
Si, doping impurity distrib., during cryst. growth by Czochralski method *(Russian)* 80–100276
Si, epitaxial, minority carrier lifetime and impurity conc. meas. *(Japanese)* 80–25025
Si epitaxial layers, doping the P cpds., process parameters effect on electrophys. characts. 78–38734
Si epitaxial layers, meas. of doping profiles *(Hungarian)* 80–70545
Si epitaxial wafer, impurity profile meas. by multilayer spreading resist. anal. 77–76449
Si, epitaxy lateral autodoping kinetics 78–6087
Si films, polycrystalline, elec. props., grain size and dopant conc. influence 80–29492
Si, heavily doped, doping density striation effects in metal-nonmetal transitions studies 79–28383
Si, high sensitivity depth profiling of As and P, SIMS 77–7742
Si, implanted crystal, laser induced annealing and diffusion behaviour 80–88202
Si, impurity determination, by neutron activation analysis 78–11586
Si, ion implantation, channelling, alignment effects 80–88183
Si, ion implantation, off-axis channelling disorder anal. 77–24325
Si, ion implantation and pulsed laser annealing of group III and group V dopants, supersat. alloy form. 80–54267
Si ion implanted, doping profile meas. by He^+ backscattering spectra 79–60390
Si, ion implanted, laser annealing 79–69124
Si, ion implanted, laser annealed, elec. props. and annealing kinetics 79–69508
Si, ion implanted, laser-annealed, theoretical anal. of thermal and mass transport 78–91364
Si, ion-implanted, lapping and staining techniques, junction depth determ. 80–29468
Si, ion-implanted layers, impurity profile meas. after laser annealing 78–87702
Si, ion-implanted surface, profiling method 78–95075
Si LPE layers, dopant distrib., meltback effects 79–69151
a-Si, laser induced crystallisation mechanism, epitaxial regrowth 80–84962
Si layers, carrier profiling using four-point probe method 79–37732
Si layers amorphized by molecular ions, laser annealing 80–103379
Si, Li ion implantation, depth distrib. variation after heat treatment 79–86814
Si, MOS capacitor, nondestructive of P^+ and He^+ induced damage, doping profiles 80–34087
Si, melt grown crysts., impurity incorporation, calcs. 80–79718
Si multilayer structure dopant distrib. and minority carrier diffusion length, SEM obs. *(Russian)* 78–10543

doping profiles continued
Si, neutron transmutation doping, photoluminesc. characterisation 80–11453
Si, O content and depth profiling, $^{16}O(\alpha, \alpha)^{16}O$ reaction method obs. 79–34408
Si, oxide layer form. by O^+ ion implantation, Rutherford backscatt. and IR transmission obs. 79–51141
Si, polycrystalline, As segregation at grain boundaries, elec. props. meas. 80–75259
Si polycrystalline solar cells, ion implantation method and results 78–63784
Si, profile anal. using anodisation and stripping, computer algorithm 77–43241
Si Schottky barrier metallisation characteristics 77–76922
Si solar cells, experimental efficiency optimisation of n^+pp^+ and p^+nn^+ cells 80–30486
Si solar cells, ion implanted grating type 80–101102
Si, surface, pulsed electron beam processing, doping, annealing 80–75254
Si two-step impurity diffusion, effect of internal elec. field 77–76624
Si wafer, B predeposited, B anal. by combined ion beam techniques and X-ray microanal. 79–5238
Si wafer surface doping profile determ. by SIMS 79–77618
Si: As(Pb), high-dose ion implanted and annealed, implant redistribution 80–107309
Si:Al(Ga), spreading resist. calibration using Si:B 80–103690
Si:Ar, As, ion implanted, laser annealing, doping profiles, channelling 80–97506
Si:As, annealed, dopant profile parameter contactless probing by IR spectroscopy 79–77629
Si:As, depth profile detect. limit of 3×10^{15} atom cm^{-3} using Cs^+ bombardment negative SIMS 77–65988
p-Si:As, electrochem. doping, depth profile analysis 77–72630
Si:As, electrochemical doping 79–90684
Si:As, electrochemical doping profiles 79–90685
Si:As, implantation into polycryst. Si and diffusion into Si substrate 77–59025
Si:As, implanted, laser annealing reduction in defect conc. 77–62559
Si:As, implanted, thermal diffusion of As 80–39352
Si:As, implanted As redistrib. during annealing in oxidising ambient, carrier distrib. meas. 79–19275
Si:As, implanted through SiO_2 films, elec. props., defect struct. 80–54264
Si:As, ion implanted, anomalous diffusion of As 79–14842
Si:As, ion implanted, formation of As complexes 80–59511
Si:As, ion implanted, glow discharge optical spectroscopy 78–22755
Si:As, ion-implanted, laser annealing, channelling obs. of As cluster form. 79–69128
Si:As, ion-implanted, laser recrystallisation by freq.-doubled Nd:YAG laser 79–77613
Si:As, relation between total and electrically active As conc. produced by diffusion 79–55773
Si:As high-dose implanted single crysts., pulsed electron-beam annealing 80–103373
Si:As ion implanted layers, annealing by CO_2 laser, doping profile shift 80–84965
Si:As sputter rate meas. SIMS combination with Rutherford backscatter 80–21334
Si:As(B), heavy-doping effects and impurity segregation during high-press. oxidation 80–65014
Si:As(B), ion-implanted, scanned laser and electron beam annealing 79–73182
Si:As(B)(N)(P), conc. profiles of ions and recoiled N after implantation through Si_3N_4 films 79–55764
Si:As(B)(P), ion-implanted polycrystalline films, laser annealing 79–73181
Si:As(P), oxidation-enhanced diffusion of impurities 79–46840
Si:As(Pb), ion-implanted, impurity redistrib. during laser irrad. 80–100280
Si:As(Sb), implanted, pulsed ruby-laser annealing, Rutherford backscatt., TEM and ion channelling study 79–86805
Si:As(Sb), ion implant lattice location after pulsed ruby laser annealing 79–73204
Si:As(Sb), ion implanted, lattice location of impurities after pulsed laser annealing 80–88196
Si:As(Sb), ion-implanted, CO_2 laser annealing 79–73183
Si:As(Sb), MBE, n-type doping techniques 80–15126
Si:Au, diffusion, effect of C concentration 78–10076
Si:B, anomalous B profiles prod. by BF_2 implantation 80–75252
Si:B, conc. profile of implanted cryst., by $^{11}B(p,\alpha)$ chem. anal., annealing *(German)* 78–83843
Si:B, diffusion from BN source with H_2 injection, AES study 80–19986
Si:B, diffusion of As atoms from ion implanted layers, conc. profiles 77–43376
Si:B, dopant density determ. by nucl. track technique 78–55886
Si:B, He^+ irradiation-induced diffuiion, effect on impurity distrib. 80–70470
Si:B, hole mobility calc. for dopant density and temp. var., resistivity meas., effective mass calcs. 80–54703
Si:B, impurity range distrib. determ. by $^{10}B(n,\alpha)^7Li$ reaction 78–11585
Si:B, influence of proton beam irrad. on concentration profiles *(French)* 77–51402
Si:B, inhomogeneous surface layer, diffusion and implanted, X-ray rocking curves 80–6603
Si:B, ion implantation, channelling and random distrib. of B ions meas. 77–47473
Si:B, ion implantation using B_2O_3-B mixture, Auger spectra, channelling anal. 79–4317
Si:B, ion implanted, comparison of range and range straggling 77–55293
Si:B, ion implanted, depth and lateral profiles of B atoms, Monte Carlo simulation 77–55297
Si:B, ion implanted, laser annealed, thermal annealing effect 79–73191
Si:B, ion-implantation doped, influence of radiation dose on diffusion processes 77–1141
Si:B, P, long range enhancement of B diffusivity by P diffusion 80–103386
Si:B, p-n junction form. by B deposition and laser-induced diffusion 78–87690
Si:B, polycrystalline, depth profiles of implanted B atoms, meas. by secondary ion mass spec. *(Japanese)* 78–67734

doping profiles continued
  Si:B, redistrib. of B during thermal oxidation, numerical and analytical calcs. 80−49259
  Si:B, sputtering influence on distrib. profile of ion-implanted impurities 79−42091
  Si:B deposition diffusion from B_2H_6, AES analysis 78−6085
  Si:B diffusion at Si-SiO_2 interface, Auger spectra, Rutherford backscattering 80−70471
  Si:B high-temp. diffusion, glass layer formation obs. 78−7069
  Si:B photodiode front region collection efficiency models 80−96899
  p-Si:B-SiO_2 interface in MOS structures, carrier mobility and impurity distrib. 78−34902
  Si:BF_2^+, anomalous migration of F and electrical activity of B 78−34654
  Si:BF_2^+, recrystallisation of implanted amorphous layers, F migration 79−55763
  Si:BF_2^+(Si^+,B^+), recrystallisation of implanted amorphous layers, elec. props. 79−55762
  Si:B(Al), (P)(As)(In), ion implanted film, elec. prop. impurity depend. 80−24467
  Si:B(Be)(Li) ion implanted, channelling and random equivalent depth distrib. 80−100293
  Si:B(P), profile determ. by anodic oxidation 79−28010
  Si:B(P), proton-irrad., impurity uphill diffusion, vacancy mechanism 80−92719
  Si:B(P)(As)(Sb), ion implanted, redistrib. of dopants by pulsed laser annealing 79−7620
  Si:B(P)(As)(Sb)(Cu)(Fe), ion implanted, doping profile, pulsed laser annealing effects 80−88197
  Si:Be, ion implanted, correl. of atomic distrib. and implantation induced damage profiler 80−88199
  Si:Co, diffused distrib. and state of Co atoms, Mossbauer spectra meas. 77−1146
  Si:Co, implanted or diffused, and annealed, localisation of Co atoms, Mossbauer obs. 80−39140
  Si:Co, ion implanted, Co lattice location, channelling meas. 80−88201
  Si:D, ion implanted, D depth distribs., SIMS meas. 80−54279
  Si:D, ion implanted, struct. of impurity centre 79−7623
  Si:Fe, implanted, annealing and stripping, Mossbauer expts. 80−39141
  Si:Fe(Cu), impurity segregation and microstructural changes by pulsed laser irrad. 79−82254
  Si:Fe(Cu)(Pt), implant redistrib. and enhanced solubility following laser irrad. 79−69129
  Si:Ga, As, sequential diffusion, radiotracer obs. 78−10073
  Si:Ga, diffusion of impurity into cryst., doping profile 79−77621
  Si:Ga(Al), MBE, growth, struct. and elec. props. 77−89458
  Si:Ga(As), laser-doped, impurity distrib., Rutherford backscatt. and channelling anal. 80−59507
  Si:H, amorphous, dopant conc., glow discharge optical spectroscopy 80−49546
  Si:H, ion implanted, anal. of methods used for H profiling in materials using ion beams 79−5197
  Si:H, ion implanted Monte Carlo calcs. of profiles of H ions 78−55889
  Si:H amorphous film, H quantitative depth profiling by nuclear reactions and SIMS 78−14373
  a-Si:H film, glow discharge deposited, H profiles, doping level 80−84202
  Si:H(D), amorphous films, CVD, post-hydrogenation 80−54552
  p-Si:In, ion implanted, doping profiles from capacitance-voltage characts. 80−88203
  Si:In(Sb), incorporation of implanted impurities during amorphous layer regrowth 79−55761
  p-Si:Li, electrolytical doping, depth-profile anal. 79−77623
  Si:O, comparision of depth profiling techniques 80−29048
  Si:O, incorporation of O during pulsed-laser irrad. 80−96557
  Si:O, ion-implanted between 2 and 20 MeV, range and range straggling 80−44241
  Si:O_2^+, in-depth distrib., Cs^+ SIMS anal. appl. 79−39265
  Si:O(C), implant redistribution, annealing effects, SIMS meas. 80−96561
  Si:P, anomalous doping profiles, numerical anal. 79−73206
  Si:P, As, chem. etching, thick epitaxial layers prod. for dopant conc. investigations by neutron activation anal. 79−37728
  Si:P, Au gettering by P diffusion and P-induced dislocations 78−91346
  Si:P, BF_2^+ ion implantation, anomalous carrier profiles 80−2048
  Si:P, carrier mobility and distrib. rel. to annealing, 400-910°C 78−79995
  Si:P, characterisation by IR reflectivity 78−56501
  Si:P, doping element incorporation, temp. depend. in CVD epitaxy 80−45234
  Si:P, implantation depth distrib. meas. by neutron activation anal., SIMS, junction depth method 77−31693
  Si:P, implanted, pulsed electron beam annealing, Hall effect and sheet resist. meas. 80−34467
  Si:P, incoherent light flash annealing, elec. props., backscattering spectra 80−97504
  Si:P, ion implanted, lattice damage and electrical activation correlation 78−67726
  Si:P, measurement techniques for determining P densities 80−75262
  Si:P, neutron irrad. crysts., qualitative distrib. of P using autoradiography 80−24486
  Si:P, neutron transmutation doping distrib. by emitted β-radiation meas. 77−19977
  Si:P, neutron transmutation doped, EPR, electron trapping 79−73179
  Si:P, quantitative model for diffusion of P and emitter dip effect 77−76611
  Si:P, spin-on borosilica diffusion source, doping uniformity factors 77−76442
  Si:P implantation profiles, neutron activation anal. 78−7284
  Si:P^+, ions implanted through SiO_2 mask window, lateral spread 79−77627
  Si:P(As), conc. profiles of P (or As) and recoiled O atoms after ion implantation into SiO_2-Si, SIMS obs. 79−51138
  Si:Pb, lattice location of dopant and amorphous zones, by Rutherford backscatt. 77−68990
  Si:Pt, deep level, exam. by thermally stimulated current and capacitance techniques 79−1579
  n-Si:Sb, arbitrary doping profiles produced by MBE 79−7617
  Si:Sb, diffusional doping by doped oxide method 80−15127
  Si:Sb, dopant implantation, activation analysis errors due to isotope comp. *(German)* 80−34037

doping profiles continued
  Si:Sb, dopant microsegregation rel. to crystal and crucible rotation 78−11106
  Si:Sb, epitaxial layers, doping profile techniques 80−44231
  Si:Sb, in solar cell struct., heavily doped, dopant striation, SEM 79−39312
  Si:Sb, ion implanted, annealed, dislocation generation, channelling and Rutherford backscatt. meas. 80−88158
  Si:Sb, laser doping, evaporation loss and diffusion of Sb, under pulsed laser irrad. 80−59508
  Si:Sb, low energy ion implantation, profile determ. 80−88176
  Si:Sb, low energy ion implantation Schottky barrier diodes and resistors 80−88177
  Si:Sb, MBE film, doping technique 80−79821
  Si:Sb, produced by ion implantation and laser annealing, Sb behaviour above solid solubility 80−88200
  Si:Sb, vacuum deposition combined with ion implantation *(Japanese)* 79−28005
  Si:Sb crystal Czochralski growth, radial microsegregation analysis 78−11105
  Si:Te, ion implanted, laser annealed, lattice location of Te 78−67725
  Si:Te, laser melting, surface Te atom accumulation, profiles 80−100258
  Si-Au Schottky barrier solar cell fabrication, doping of a-Si 80−50969
  Si-Au-P system, partition coeff. of P, temp. depend. 79−43158
  Si-B, exam. of two stage diffusion of B, under a gas phase oxide film 79−95044
  Si-electrolyte contact, implantation profile meas. from capacitance-voltage characts. *(German)* 77−1145
  Si-P, excess carrier recomb., photocond. 79−65495
  Si-SiO_2, impurity redistrib. during oxidation, numerical soln. including interfacial fluxes 80−25888
  Si-SiO_2 interface, Au conc., effective impurity doping 78−52094
  Si-SiO_2 interface, Auger-sputter profiling obs. of P pileup 78−95240
  Si-SiO_2 structures, ion implanted, surface characts. 77−80850
  Si-SiO_2-Si structures, P, As depth profiles, ion microanal. *(Japanese)* 78−85251
  Si+Ga^+ ion implantation at high current density, lattice disorder, proton backscattering 80−34085
  α-SiC, epitaxial layer, impurity macroincorporation, distrib. of Al, B, N and P 77−69192
  SiC, N doping inhomogeneities due to growth conditions 78−22741
  SiC:Al epitaxial layers, growth, Al distrib. and solubility 80−15391
  SiC:B, impurity distribution determ. by neutron activation anal. 77−76452
  Si_3N_4-SiO_2:N,Zn ion-implanted multiple layers, ion range distribs., secondary ion microprobe meas. 79−42129
  SiO_2 coatings on SiO_2 substrate, cathodoluminescence spectra, electron irrad. 80−76085
  SiO_2 film, on Si, range distrib. of implanted As, He^+ backscatt. obs. 77−39611
  SiO_2:BF_2, ion implanted, F influence on oxidation-induced stacking faults 80−65011
  SiO_2:P, diffusion from spin-on source 80−44367
  Ta_2O_5, sputter depth profiling with low press. HF plasma 79−95041
  W (110) surface, D depth profiles using imaging field desorption 77−59038
  Zn:Al, ion implantation, temp. and time depend. 80−65013
  ZnS:Ag film, photocapacitance IR quenching, hole photoionisation energy and spectral distrib. 79−87127
  ZnSe-Si heterojunctions, IR quenching of photocapacitance 80−92968
  ZnTe, effects of Zn anneals in 400-550°C range on acceptor conc. 80−10571

Doppler broadening *see Doppler effect*

Doppler effect
  see also atomic spectra; red shift; spectral line breadth
  4 MHz range-gated US Doppler flowmeter design and application 78−59527
  32 kW Doppler sonar for ocean internal wave meas. 80−46296
  accelerated dielectric medium, relativistic study 78−81862
  accelerating atomic clock synchronisation by radiowave propag., one-way Doppler effects 80−13044
  acoustic Doppler effect for randomly moving scatterers and platforms 77−62093
  acoustic Doppler sounding of falling snow 79−53467
  acoustic wave multiple scatt. in randomly inhomogeneous medium 78−1461
  aerodynamic isotope separation technique based on vel. slip in freejet expansions 80−19441
  aerosol particle size meas., optical particle counter calibration by Doppler shift spectrometry 80−68173
  aerosol size spectrum determ. in turbulent medium using coherent Doppler meas. 79−96841
  alkali halide, gamma irradiated, positron annihilation 79−23643
  alkali halides, cryst., positron lifetime and Doppler broadening spectra 79−8208
  animal research, totally implantable directional Doppler flowmeters 80−67293
  anomalous, amplification of slow waves in electron beam, obs. 80−78463
  anomalous, analogy with negative energy waves 77−65881
  aperture synthesis by object rotation in coherent imaging 80−69336
  arterial haemodynamic transfer function calc. from Doppler US flowmeter waveforms 78−61235
  arterial wall movement monitoring by microwave Doppler radar 79−96647
  atmosphere, acoustic meas. of turbulent vel. and energy dissipation rates 77−66966
  atmosphere echo sounding, Doppler shift extraction hy adaptive linear-prediction filtering 77−64453
  atmospheric acoustic echoes, zero-crossing technique for Dopper vel. extraction 79−53542
  atom, collision and Doppler broadening of fluorescence and Raman scatt. 78−13465
  atom, collisional redistribution of fluorescence radiation 78−13464
  atom, two-photon resonance in coherent fields 80−63606
  atomic beam velocity regulation and meas., using Doppler tuning 77−19110
  atomic degenerate system, Doppler-free laser-induced dichroism and birefringence 78−82711
  atomic hyperfine transitions in buffer gas, quantum theory *(Russian)* 78−21881

Doppler effect continued
atomic system, photon echoes in standing-wave fields: time separation of spatial harmonics 80—9759
attenuation, γ-rays from slowing down of excited particles 77—26945
audio alarm remote control system 79—64477
aurora, Doppler vel. meas., radio aural spectral characts. and incident incoherent scatter meas. 80—56663
auroral forbidden O I emission, Fabry-Perot interferometer obs. for thermosphere wind and temp. meas. 80—101441
auroral ionosphere, radio investigations via VHF bistatic Doppler system 78—28387
bat Doppler echolocator, obs. of surroundings 77—70483
beam-foil spectra, Doppler shifted X-ray refl. 77—18821
beam-plasma instability singularities, anomalous Doppler effect 80—75040
bearing estimation bias resulting from source motion 78—29084
biomedical Doppler signal processing, swept-frequency transient signal filtering 78—48848
biomedical methods for quantitative meas. and localisation of peripheral arterial occlusive disease 79—96640
biomedical noninvasive pressure meas. appl., ventricular pressure in heart 79—5384
biomedical US diagnostic technique of carotid artery disease, objective feature extraction 80—72273
biomedical US real-time scanner with pulsed Doppler and T-M facilities, obstetrical appls. 80—67172
blood, US, Doppler-shift waveforms, physiological interpretation 80—89814
blood flow echography using Doppler techniques *(French)* 80—26303
blood flow meas. by laser Doppler system *(Swedish)* 80—51199
blood flow meas. from US Doppler signals, on-line computer system decoding 78—3570
blood flow velocity profiles, US MTI meas. 80—36033
blood velocimeters, US transesophageal meas. of human haemodynamic parameters 80—41146
blood velocity measurement, ultrasonic method *(Dutch)* 78—31832
blood velocity waveform display by spectrum analysers, direction Doppler signal preprocessing 79—34611
blood-flow velocity estimation, Kalman filters for Doppler ultrasonic meas. 79—62325
blood-velocity waveforms, real-time spectrum analyser 79—88145
breast carcinoma detect. by US Doppler signals 80—8110
broadened laser amplification line frequency characteristics meas. 78—59060
carbon tetrafluoride $^{12}CF_4$ laser, Doppler-limited absorption spectroscopy 80—74347
carotid arteries, normal and stenosed, local Doppler audio spectra 80—30811
carotid arteries, US imaging, using CW, pulsed Doppler and pulse echo techniques, book contrib. 80—36047
carotid artery imager, CW Doppler US and spectrum analyser 79—57731
channelling of electrons and positrons, radiation spectrum, complex and anomalous Doppler effect 77—84819
charged sphere, freq. shift of radiation from moving surface 77—57260
Cherenkov radiation, alternating electric field effect 78—20984
Cherenkov radiation, boundary effects in alternating electric field 80—37940
coherent two-photon reson. and Doppler free population inversion, perturbation anal. 77—643
conference on satellite Doppler tracking and geodetic appl., London, England (Oct. 1978) 80—77264
contactless speed meas., laser Doppler difference system *(German)* 77—17957
conversion electron spectroscopy following (HI,xn) reacts., kinematic Doppler correction method 79—54739
cosmological red shift, Doppler and gravitational components using Birkhoff's theorem 78—86041
coupled Doppler-broadened system, laser induced transients 77—3325
critical fluids, light scatt. in presence of uniform shear flow 79—78693
crosswind relations for troposcatter link 77—5303
cyclotron-wave instability freq. up-shift, on a relativistic electron beam 79—22883
de Broglie wave, relativistic Doppler shift for teaching 78—49613
deep ocean navigation by Parametric Array Doppler Sonar 77—3698
deflection effect of light reflected from moving mirror in ether theory 80—91749
difference signal, struct., autocorrel. function anal. rel. to laser anemometry 79—50830
differential measurements, continuous-wave transmitting projectile, passive array tracking 80—94955
diode laser, appl. of Doppler line convolution by Gaussian instrument function 80—82830
directional sea wave spectrum determ. using HF Doppler radar techniques 77—29476
discrete-time Doppler frequency meter for blood flow imaging 79—57704
Doppler less spectroscopy, wave front convolution in parametric nonmonochromatic wave interaction *(Russian)* 79—94280
Doppler microscope for flow velocity meas. in areas $<10\ \mu$ dia., signal-analysing system *(Japanese)* 78—22441
Doppler radiation associated with Cherenkov radiation in presence of alternating elec. field 79—59621
Doppler velocimetry for plasma vel. meas., review 80—48975
DSA meas., ion-atom interaction 79—749
DSA meas. of nuclear excited state lifetimes, centroid shift and line shape anal. *(Rumanian)* 77—46135
DSA study of ^{28}Si lifetimes in selected materials, theoretical stopping power predictions 78—74329
ducted whistler mode signals, Pc 4-5 pulsation effects on Doppler shift 78—4040
dynamical properties study using light scatt., principles spectra derivation and applics. 80—53218
dynamically focused array imaging systems, induced Doppler distortions 79—46117
echo-Doppler, range-gated, pulsed, review and evaluation 79—96642
education, acoustical second-order Doppler effect, introductory expt. for special relativity 78—49584
education, Doppler shift formula for radar echo without transformation eqns. 77—82344
education, Doppler shift of laser beam, expt. 78—69939

Doppler effect continued
education, homodyne microwave Doppler velocimetry, accel. meas. 77—78920
electrochemistry, optical experimental methods 78—20022
electron waves, Doppler shift calcs. *(German)* 80—18982
electron waves, Doppler shift illustration using electron mirror interference microscope 80—95783
electrostatic precipitator, particle velocity, laser Doppler anemometry study 80—59144
EM reflection from moving interfaces, influence of transition layer thicknesses *(Russian)* 78—46490
EM wave, Doppler frequency shift by fast moving boundary *(Japanese)* 80—18967
EM wave reflection from moving ionisation front 77—39430
EM waves generation and amplification based on Doppler effect 80—63902
EM waves scatt. by ocean ripples due to acoustic and capillary waves 78—3807
emission line shapes from a rotating ring radiator 80—83998
energy level transitions, excitation by monochromatic laser radiation, Doppler-broadened transitions 80—78582
ether theory, relativistic formula for Doppler effect *(French)* 80—105494
excited nuclear states, 10^{-18} to 10^{-6} s, lifetimes, direct meas. 79—30804
F_2-layer vertical sounding, radio signal Doppler spectrum and arrival angle meas. *(Russian)* 78—61651
falling objects accel. due to gravity, Doppler effect, student microwave expt. 80—105472
fetal breathing, in utero, CW US Doppler method for recording 80—41215
flow meas., laser Doppler anemometry 78—34227
flowmeters, digital 2D full range Doppler velocity meter for cardiovascular diagnosis 78—88731
fluid mechanics, photon correlation techniques, conf., Cambridge, England (March 1979) 80—56998
forbidden decay modes of one- and two-electron ions, book contrib. 78—82679
formaldehyde, IR Doppler-limited spectrum, wavenumbers, line strengths and assignments 79—72310
formaldehyde, mol. beam, vel. meas. by Doppler effect on RF spectrum splitting *(French)* 78—13627
Fourier transform Doppler spectroscopy, appl. to reactive collisions 79—80692
frequency modulation by p-i-n structure, optical waveguide with moving walls 80—19099
frequency shift laser meas. of water and wind velocities 77—39385
frequency standards using divergent beams, stability limits 79—26037
gas, inhomogeneous layer, transmission calc. for spectral line with Voigt profile 80—59164
gas, resonance four-photon shift, optimal focusing of high-power pumping 80—95574
gas laser regeneration mode with saturation effect taken into account 77—650
GCFR simulation central Doppler worth evaluation 79—9814
gravitational Doppler effect explored using geostationary satellite 80—109351
gravitational radiation, detection possibility, Doppler tracked spacecraft 78—45549
gravitational radiation background, detection using spacecraft Doppler tracking 79—80494
haemodynamic parietal friction meas. by pulse type Doppler velocimeter 80—17206
heart rate meas. (foetal), adoptive correlation ratemeter, US signals 78—88732
heavy collision systems, vacancy prod. in strongly bound quasimol. states, impact parameter depend. 78—22003
heavy ion collisions, Doppler shift of continuum X-rays from quasimols. 79—22808
heavy ion collisions, quasimol. KX-ray spectra, Doppler shift 77—19044
Hertzian waves, reflection and diffraction by moving layers *(German)* 80—87266
heterodyne correlation radiometry 78—77980
HF Doppler method studies of high-latitude ionospheric dynamics 78—73569
HF Doppler obs. over S.E. Australia during 1976 Oct. 23 total eclipse 78—61662
HF radar sea-echo Doppler spectra, extraction of wave height and period 77—78474
HF waves reflected from ionosphere, freq. var. *(Chinese)* 80—56665
high resolution spectroscopy of atoms and mols., without Doppler broadening, laser techniques 77—54631
high-power microwave generation by relativistic electron beams 78—5444
historical evidence for discovery by Friedrich von Hahn *(German)* 77—53727
holography through fog, coherence requirements for light source 78—58949
homopolar devices, rotation of DC glow discharge, Doppler shift of spectral lines 80—33838
human retinal blood flow meas. by laser Doppler velocimeter 79—79623
interferometer, Doppler beats and interference fringes 79—62957
interferometer system, laser, error sources analysis, meas. volume structure *(Russian)* 80—27336
interplanetary H I, Lα emission Doppler shifts anal. rel. to local interstellar gas temp. and vel. 80—105141
interstellar H I clouds in distant galaxies, colour pictures of Doppler shifts 77—17383
intra-ocular pressure measurement using sonics and coherent optics 77—81548
ion beam, fast, vel. meas. using Doppler shift method 80—9083
ionosphere, Doppler fluctuations and angle-of-arrival var. caused by scintillation 78—77411
ionosphere, Doppler shift meas. with rot. antenna, ordinary and extraordinary modes 80—17426
ionosphere, HF Doppler observations at Chubu Inst. Tech. (Japan) *(Japanese)* 80—31165
ionosphere, HF radio waves Doppler shifts rel. to bottomside mid-latit. trough 80—109300
ionosphere, oblique sounding signals Doppler freq. shift in disturbed region 79—53630
ionosphere plasma line, Doppler shift detect. rel. to auroral Birkeland current meas. 80—98507

Doppler effect continued
ionosphere soundings, MHD waves as cause of simultaneous F-region and geomag. oscills. 77—9615
ionospheric EM wave propagation in HF and MF bands, Doppler meas. accuracy 78—77417
IR spectrum deconvolution beyond the Doppler limit 80—86467
IR wind-sensing system, spaceborne, atmospheric effects 79—96828
Langmuir soliton weak EM wave scatt., Doppler shift and reflection coeff. calc. *(Russian)* 79—7467
laser anemometer Doppler system, optics and signal processor for turbulent low speed flows *(French)* 78—59521
laser anemometry, commercial LDA instruments *(Czech)* 79—46409
laser anemometry of high-temp. industrial gas flow *(German)* 79—10618
laser based on coupled transitions with arbitrary polarization of radiation 80—78827
laser bulk absorption homogeneity, Doppler interferometric meas. 79—14010
laser Doppler and time of flight combined anemometer 79—55434
laser Doppler anemometers, rot. diffr. gratings for use as beam splitting freq. shifters 77—68721
laser Doppler anemometry, instrumentation, appls., explanation using Moire patterns 77—7490
laser Doppler anemometry, practical considerations 79—27725
laser Doppler anemometry in internal combustion engine cylinder 79—77296
laser Doppler anomemeter for velocity fields meas. near prosthetic heart valves 79—57814
laser Doppler blood velocimetry *(Japanese)* 80—94310
laser Doppler flowmeter, LADO 1, non-contact meas. of liquid and gas flow rate 79—77305
laser Doppler microscope, vel. measuring device 80—68251
laser Doppler microscope for blood velocity meas. 79—62329
laser Doppler microscope period meas. signal analyser *(Japanese)* 79—88998
laser Doppler velocimeter, blood flow meas. in fish *(Japanese)* 79—84052
laser Doppler velocimeter calibration burst generator 79—77321
laser Doppler velocimeter for meas. of specified velocity vector 80—47040
laser Doppler velocimeter for turbulent flow velocity meas., redesign 78—1245
laser Doppler velocimeter signal analysis for pulsatile arterial flow meas. *(Japanese)* 79—2156
laser Doppler velocimeter with differential photodiode array 79—76743
laser Doppler velocimeter with variable frequency shift for combustion flow meas. *(Japanese)* 78—67294
laser Doppler velocimetry, high-temp., improved seeding method 78—9730
laser Doppler velocimetry technique for particle size distrib. meas. *(Japanese)* 78—24913
laser Doppler vibr. meas. system using bispectral anal. 80—38357
laser Doppler vibrometer, reflecting surfaces appl. 79—6117
laser frequency meas., interferometric method based on Doppler shift 77—165
laser meas. of biological cells, scattering characts. of intersecting beams *(Russian)* 80—3874
laser radiation, frequency shifting via rotating half-wave retardation plate rel. to ang. Doppler effect 80—9800
laser radiation, interaction with free atoms, review 78—13473
laser radiation freq. shifting by refl. from moving blazed grating 77—88822
laser spectroscopy, biology appls. 79—66598
laser spectroscopy, Doppler shifts and recoil effects 79—35846
laser velocimeter, optical Doppler frequency discriminator applic. 78—26220
laser velocimeter, principles of operation and applications 77—68712
laser velocimeter appl. *(Czech)* 79—23388
laser velocimeter instrumentation developed by Electricite de France Optical Applications Division *(French)* 78—75233
laser velocimeter measuring technique, mathematical anal. *(Russian)* 77—27245
lidar temperature profiling of planetary atmsopheres 77—33352
light beating spectroscopic instrument for continuous meas. of tissue blood flow 80—41160
light Doppler effect, absolute spacetime theory 78—69979
light having traversed moving prism, freq. shifts *(Spanish)* 77—88638
light reflection from moving corner reflector 77—37758
linear velocity meas. by YAG laser 79—26039
LMFBR, Na void and Doppler reactivities 78—8891
long-range sound propagation 78—30116
Loran-A (1.85 MHz) radio wave backscatter from ocean waves, Doppler spectra *(Japanese)* 78—85737
many-level atoms, Raman scatt. resons. in separated fields 79—31449
metal, Doppler-shifted cyclotron reson., excitation of dopplerons and Gantmakher-Kaner waves *(Russian)* 77—32261
metal vapour coherent two photon reson. third and fifth harmonic VUV generation 79—72627
metallic glasses, Doppler broadening of positron annihilation γ-radiation and elec. resist. 80—66321
metals, Doppler broadening of position annihilation line 79—43057
methane, electron impact, Balmer-α emission Doppler profile energy depend. 77—42423
methane, high-resolution coherent Stokes Raman scattering, of ν_1 and ν_3 bands 79—31981
methyl amine, photodissoc. products, Doppler spectroscopy 80—53124
micropulsations, Doppler effect rel. to wavelength and phase rel. 77—64511
microwave backscatter from intense relativistic electron beam 77—38794
microwave coherent scatt. from relativistic electron beams 77—42477
molecular beam irradiated with stationary wave, saturation effects *(French)* 79—81247
molecular beam RF spectroscopy, interference effects *(French)* 78—58669
molecular energy level transitions, excitation by monochromatic laser radiation, Doppler-broadened transitions 80—78582
molecular resonant CARS, line shape and Doppler broadening 79—94002
molecular spectral line breadth, combined effect of collision and Doppler broadening 77—71832
molecular system, coherent three-level beats, theory 77—23526

Doppler effect continued
molecules, 3-dimens. scatt., vel.-angle distribs., Fourier transform Doppler spectroscopy 77—49776
momentum-energy Minkowski and Abraham tensors 78—45825
Mossbauer effect, recoilless fraction and second-order Doppler shift anomalies 77—12279
Mossbauer effect, second order Doppler shift, press. depend. 80—66088
Mossbauer impurity atoms trapped by vacancies, resonance energy shift 80—25265
Mossbauer linewidth, thermal motion effect, second order Doppler effect *(German)* 77—43924
Mossbauer spectra, 2nd-order Doppler shift, 1-100K 79—91317
myocardial dimension measurement system using pulsed Doppler US 80—26313
myxomycetes plasmodium protoplasmic flow, laser Doppler anemometry obs. 79—57681
negative ions, positronium formation, Doppler broadened positron annihilation line shapes 80—45164
neutron spectroscopy Doppler broadening of resonance levels, substantial reduction during cooling 79—97932
noise, aerodynamically generated in jet *(French)* 77—75951
non-equilibrium gas, Doppler broadened spectral and time correl. functions 78—14122
nonlinear high resolution laser spectroscopy, review of techniques 78—29171
nonlinear laser spectroscopy, inside Doppler line *(Russian)* 78—21231
nonlinear spectroscopy, recoil effects on Doppler-free lineshapes 80—82829
nonresonant excitation transfer, Doppler profiles, donor levels *(French)* 77—30824
nonstatic universe, generalised Doppler formula 77—78900
nonstationary, freq.-phase methods of investig., control of production processes 80—45464
nuclear, meas. technique 77—50232
nuclear energy level lifetimes, new plunger device using Doppler effect and spectra, expt. testing 78—13375
nuclear lifetime measurements, attenuation factor calc., recoiling nuclei velocity calc. *(Rumanian)* 77—46134
nuclear spectroscopy techniques *(Hungarian)* 80—14036
ocean mooring monitoring, acoustic phase tracking technique 78—30138
ocean sediment free-fall penetrometer with Doppler telemetry 80—46320
ocean waveheight nondirectional spectrum from inversion of HF sea-echo Doppler spectrum 78—16203
oceanic waveguide, normal mode theory of acoustic Doppler effects 79—50497
ocular tonometry through sonic excitation and laser Doppler velocimetry 80—56152
opt. freq. shifting of light and laser beams for Rayleigh scatt. spectroscopy 78—79392
optical Doppler instrument for measuring small turbulent flow velocities 78—90838
optical Ramsey fringes in two-photon spectroscopy, time delayed pulsed Doppler free technique 78—82708
optical wideband ambiguity function generator with Doppler compensation 78—78936
particle flowmeter, microwave, approx. signal theory 79—94747
particle spectra line shapes after γ emission in flight 78—41665
particle-sizing spectrometer appl., for research and calibration 80—4827
phase meas. of interfering reflections from interfering objects 79—81340
photon kinetic equation, for Doppler broadening 77—74334
photon kinetic equation for Doppler line broadening, soln. 78—9751
photons, origin of increased energy explained by mechanics of source, teaching 78—28897
physical and technical acoustics, conf., Parnu, USSR (Apr. 1976) 78—1451
plasma, axially symmetric, Doppler broadened optical line emission interpretation model 78—75276
plasma, Brillouin and dielec. side-scatt. of 10 μm laser light 80—103156
plasma expansion in vacuum diode, study of spectroscopic method 79—55551
plasma XUV transition Doppler broadening suppression, collisional-radiative model 80—19614
plasmas, Tormac, Gaussian HeII 4686 Å spectral lines, Doppler and Stark broadening effect, turbulence 80—106980
PMMA Doppler scatt. optical determ. of US radiation patterns 79—76930
polydispersed flows, Doppler signal spectrum 80—103081
polyoxyethylene aq. soln., kinetics of soln. form. 78—64913
portable laser Doppler velocimeter for vibrating surfaces 79—68666
positron annihilation, 2-D Doppler broadened technique 78—70722
positron annihilation γ-ray spectra, deconvolution using solid state detector 78—72631
positron annihilation γ-ray spectra, Doppler broadening, parameters 78—72630
positron annihilation in rare gases, Doppler broadening meas., electron mom. distribs. 78—55131
positron annihilation radiation spectra measured with Ge(Li) detectors, iterative unfolding method 80—97373
positronium formation inhibition by solvated electron precursor scavenging, line shape Doppler broadening, lifetime spectroscopy 80—93784
Princeton Large Torus, unbalanced neutral beam injection, toroidal plasma rot., Doppler shift meas., confinement times 79—77400
probing of clear atmosphere using Doppler radar 79—66811
pulsed Doppler flowmeter, development and cardiac appls. *(Japanese)* 80—36037
pulsed laser Doppler velocimeter signal processing, FFT and pulse-pair estimation 79—77322
PWR core Doppler spatial weight factor 79—9713
quadratic, laser appl. to precision meas., review 78—42246
quantum theory of Cherenkov and Doppler effects, paradoxes 78—45824
quasar radio var. timescale, redshift effect 77—29947
quasars, line identifications, red shifted UV lines or violet shifted IR lines 80—8707
quasars redshifts, relativistic Doppler formula rel. to transverse vels. and distances *(Chinese)* 80—105379
radar backscatter from water waves, induced current effects on microwave backscatter, expt. 77—25688
radar echo Doppler shift formula by wave superposition 79—97147
radar echoes, type 1, from equatorial electrojet, with double-peaked Doppler spectra 80—67458
radar pulse Doppler processing with low-loss SAW delay line 77—31184

Doppler effect continued
- radiative hydrodynamics, opacity enhancement by Doppler shift 77—75991
- radio galaxies components, radio continuum spectra rel. to fly away velocities *(Russian)* 80—62306
- radiowave propagation in ionosphere, satellite expt. in presence of wave perturbs., modelling 79—8744
- Raman gain spectroscopy, stimulated, Doppler broadening at electronic resonance 80—38065
- real-time optical processing using the liquid crystal light valve 80—63936
- reconstructive tomography and applications to ultrasonics 79—66578
- reflection from a corner reflector moving at high velocity 79—30228
- refracting medium, classical and quantum interpretations *(Russian)* 79—13002
- relativistic, freq. conversion on relativistic electron beam front, exptl. obs. 77—34799
- relativistic Doppler shift in satellite tracking 80—46951
- relativistic dynamics, teaching 79—97164
- relativistic gas, Doppler shift distribs. 78—65492
- relativity, special, Doppler effect 80—82637
- research in the nineteenth century 80—86070
- resonance data set choice in unresolved resonance region, sensitivity study, calc. of central Doppler worth 80—52651
- resonance fluorescence, Doppler-free obs., fluorescence-line-narrowing method and improvement 79—13840
- resonance Raman scattering and resonance fluoresc., time and freq. resolved 77—75624
- resonance transition broadening, saturation kinetics *(Russian)* 77—38641
- RF target simulator using acousto-optical device 80—102843
- ring laser, relativistic Doppler effect, two-wave mode instability and optimum tuning 77—38940
- ripple-tank demonstration 80—82621
- rocket exhaust anemometry, Doppler difference and two focus methods, correlator and photon counting 79—60084
- rolling mill product speed and length meas. by laser velocimeter *(German)* 79—72614
- rough laser illuminated rotating cylinders, far field speckle and Doppler shifts 79—50216
- HM Sagittae, emission line star, spectral obs. rel. to lines Doppler broadening *(Russian)* 80—36648
- SARSAT, search and rescue satellite, ionospheric effects on Doppler frequency 79—58183
- satellite Doppler techniques, geocentric positioning of triangulation of Great Britain 79—29695
- satellite line shape, classical broadening theory including Doppler effect, pot. effect 79—22764
- sea echo radar spectra resolution limitation inferred from ionospheric Doppler broadening 78—81489
- sea state and wind sensing by HF skywave radar 78—24396
- sea state remote sensing, HF sea echo Doppler spectra statistical props. 77—29312
- sea wave space and time structure measurement from Doppler frequency shift 77—29482
- sea waves, height, length and velocity, radar and Doppler effect, OREME project *(French)* 80—94625
- six-dimensional space, hidden variables 80—82666
- six-dimensional space-time theory, experimental tests 79—58538
- solar coronal red line, Doppler shifts meas. and precise wavelength *(Russian)* 78—40899
- solar limb local radial velocities, Doppler shift meas. 77—17537
- solar line shift obs. interpretation 80—51714
- solar oscillations, Fe I 5124 Å Doppler shift obs. 78—53905
- solar photosphere, vel. gradients retrieval from line asymmetries, linearised approach 80—62093
- solar rotation induced Doppler spectral shift meas. by scanning Fabry-Perot interferometer 80—77298
- solar spectrum, Doppler shift meas. rel. to solar oscillations and Sun internal struct. 80—105226
- sonar controller 80—43575
- sonar Doppler phased array coherent imaging and processing by metaxial optics 79—72521
- sonar fish counting system, feasibility study 78—50980
- sonar ocean current profiles 80—46311
- sonar signal processing by chip slice microcomputer 79—94408
- sonar signals, low-freq., of dolphin Phocoena phocoena, tolerance to Doppler effect *(French)* 77—52809
- spacecraft tracking, phase-coherent dual-freq. radio link 77—60576
- spatial and temporal variation meas., differential Doppler technique using satellite 79—12311
- special relativity, for teaching 78—24609
- special relativity test 78—20963
- spectral line broadening, elimination problem, parametric soln. 80—62730
- spectral line collisional broadening, classical and quantum theories, radiator motion effect 78—86822
- spectral line profile, saturation, influence of atomic collisions 78—70792
- spectroscopy, gas phase, narrow nonlinear reson. production by modulated optical radiation *(Russian)* 77—67507
- spectroscopy, two-photon, Doppler-free *(Dutch)* 79—50167
- spectrum profiles in the presence of Stark, Lorentz and Doppler broadenings 78—86820
- speed meas. devices survey, industrial appl. *(French)* 79—93105
- spermatozoa motility meas. by light scatt., appl. to reproduction immunology *(French)* 79—34628
- SS 433, enormous periodic Doppler shifts obs. 80—17593
- Stark effect, two photon absorption spectroscopy 80—43126
- steel, positron meas., for trapping mechanism detection 80—84798
- stellar aberration and Doppler shift rel. to barycentric motion of Earth 80—8520
- stellar spectra, differential Doppler shifts rel. to atmospheres vel. gradients determ. 78—57538
- stellar spectrograms, relative Zeeman and Doppler shifts determ. via statistical approach 78—36467
- stimulated EM shock radiation, book contrib. 79—27149
- sub-Doppler laser spectroscopy of mol. ions in fast ion beams 80—9655
- sub-Doppler line shapes, saturation and two-photon spectra, elastic collisions, review 78—82697
- subDoppler Stark spectroscopy in crossed elec. and mag. field 78—948
- submillimetre wave generation, upshifted reflection, from moving ionisation front 77—34796

Doppler effect continued
- Sun, Doppler shifts meas. rel. to 7 to 70 minutes periods pulsations 78—93180
- Sun, structure from global studies of 5-min. oscills. 80—26838
- sunspot, molecular lines Doppler shifts rel. to solar rot. determ. 79—92745
- sunspot magnetic fields higher rot. rate at photosphere, Doppler meas. 80—46516
- superradiance, Doppler beat observation 78—66794
- supraorbital Doppler evaluation of blood flow in vascular surgery 79—88144
- surface current mapping by Coastal Ocean Dynamics Radar 80—46316
- surface wave, momentum exchange with moving atom 79—64359
- tachometer appl., using microwaves *(Italian)* 80—13093
- target ion spectroscopy as method of overcoming Doppler limitation in beam foil spectroscopy 77—83720
- teaching, acoustic formula derivation, on intuitive basis 78—24621
- three-level coupled Doppler-broadened system, optical time-delayed laser saturation spectroscopy 78—54472
- three-level spectra, lineshapes in intense laser field, theory 80—69109
- time varying inhomogeneous media, space-time considerations for Doppler effects 78—20965
- tissue characteristion, static and moving, high spatial resolution US meas. techniques 80—51187
- Tokamak plasma-wall interaction, appl. of fluoresc. spectroscopy 79—23451
- tornado-parent storm relationship from dual-Doppler radar anal. 77—21830
- torsional vibration meas. with laser Doppler system 78—45612
- tracking of spacecraft, gravit. radiation detect. possibility 79—30345
- transcutaneous blood flow measurements using pseudorandom noise Doppler system 80—36035
- trapped ion, laser cooling, theory 80—58414
- two level model theory, extended, appl. to Doppler-, laser and collision-broadened bound-bound multiphoton absorption 79—3423
- two-(three-)level systems, steady and transient behaviour 78—1200
- two-colour laser Doppler velocimeter *(German)* 80—10326
- two-level atom, influence of relaxation parameters and laser fluctuations 79—72273
- two-level atom, radiation by intense laser beam, resonance fluorescence, photon antibunching, Doppler shift 80—74146
- two-level system, Doppler broadened, vel. tuned reson. as multi-Doppleron process 77—79789
- two-level system, multi-doppleron processes, probe spectroscopy 79—81400
- two-level system, one-photon optical absorpt. theory 77—34651
- two-level system, saturation kinetics after Doppler broadening *(Russian)* 78—86921
- two-photon absorpt., collisionally perturbed, reson. profile and strengths, degeneracy and Doppler shift 78—55156
- two-photon absorption, cross-section magnification and line contraction due to Dicke effect 77—6744
- two-photon Doppler-broadened transitions, wave-front conjugation by four-wave mixing of monochromatic waves 80—28265
- two-photon resonant absorpt. line profile, quadratic Doppler effect 77—34590
- two-photon spectra, three-level atom, strong-field aspects 78—960
- ultra cold neutron prod. using Doppler shifted Bragg scatt. and intense pulsed neutron spallation source 80—14024
- ultrasonic Doppler flowmeter 79—68889
- undersea acoustic signal coherence fluctuations 80—46191
- underwater sound, source-motion effects on transmission in deep-ocean 77—62088
- US blood velocity meas., phase-locked loop technique 78—61234
- US digitiser/processor for extraction of clinical parameters from Doppler-shift waveforms 80—36042
- US Doppler blood flowmeter modulation *(Japanese)* 79—2115
- US Doppler blood velocimeters, max. freq. detector 79—53201
- US Doppler flowmeter average frequency processor 79—83873
- US Doppler returns from foetal heart, processing, valvular timing information extraction 80—101238
- US Doppler shift signal processing, maximum frequency follower 79—62320
- US Doppler signal LF spectral analysis for blood flow model 79—62312
- US Doppler signal time-domain frequency analyser, numerical assessment 79—92314
- US Doppler spectra, transit time and geometrical broadening 78—44576
- US Doppler spectragrams refreshed display and haemodynamic parameter meas. 80—41152
- US Doppler velocimetry for 3D blood flow meas. 78—88730
- US equipment design and biological applications *(Spanish)* 78—7409
- US flow transducer for human milk flow meas. 79—53200
- US flowmeter, new modulation method, blood flow meas. 80—45989
- US flowmeters, operating principle 79—50817
- US mean frequency Doppler modulator performance, blood flow meas. appl. 80—45991
- US probes for blood stream meas. using Doppler technique *(German)* 79—2113
- US pulsed Doppler technique for quantitative blood flow meas. 80—45990
- US pulsed technique, clinical usefulness in intracardiac blood flow visualisation *(Japanese)* 79—96638
- US signals, real-time spectrum analyser, medical appls. 80—36040
- US synchronized pulsed Doppler blood flow and dimension meas. in conscious dogs 79—62318
- US system for internal organs imaging 79—5332
- US wave 3D meas. in transparent solids, Doppler-shifted light scatt. technique 78—90613
- vaneless diffuser of centrifugal compressor, flow velocity meas. using laser Doppler anemometer 80—59147
- vascular system, US Doppler imaging, book contrib. 80—36045
- velocimetry within turbulent phase boundaries 77—11289
- velocity meas. sonar system, transfer function model 77—7275
- venous flow, mech. oscills., ultrasonic Doppler study 80—108931
- Venus, CO_2 line Doppler shift rel. to retrograde winds possible periodic vars. 79—25530
- vibration meter, laser, 100 Å to 10 cm *(French)* 78—30250
- VLF signals in magnetosphere, Doppler shift meas. by JIKIKEN (EXOS-B) satellite *(Japanese)* 80—94651
- wave and particle descriptions of light, equivalence, rel. to radar freq. shift 80—101692

Doppler effect continued
wave in time-varying inhomogeneous anisotropic medium 79–40016
weather radar, development of weather echo props. 80–26645
weather radar systems, receiver bandwidth effect on refl. and Doppler vel. estimates 79–53549
whistlers received at Siple Station, Antarctica 78–28429
wind measurements in clear air by microwave radar 77–13136
X-ray sources, binarity detect. via Doppler effect *(Russian)* 78–77623
zodiacal light Fraunhofer lines Doppler shift, interplanetary dust dynamics 78–45278
zodiacal light spectrum, Doppler shifts meas. 78–85904
Ag, Doppler factor, comparison between calculated values and measured results 78–54811
Ag, positron annihilation spectra, Doppler-broadened, temp. depend., 9 to 1098K 80–71510
Al alloys, precipitation hardening, positron annihilation investig. by γ-ray Doppler broadening 77–81174
Al, positron annihilation momentum profiles, Doppler broadening technique meas. 77–24908
Al, positron annihilation momentum spectra, two-detector Doppler broadening technique 79–19948
Al, quenched, positron annihilation Doppler broadening meas. 78–27348
Al-Cu samples (0.5, 2.0 and 4.0 wt.%) polycryst., precipitation, positron annihilation and TEM 80–50639
Al-Fe alloy, dil., quenched, second order Doppler effect and isomer shift meas. 77–28491
Ar plasma arc, wall-confined, nonequilibrium effects 80–70058
Ar XVIII Lyman-α line Stark broadening, hot dense laser-produced plasma 77–11402
^{39}Ar, lifetimes of high-spin levels meas. Doppler shift technique 77–61380
^{41}Ar states from ^{40}Ar(d,p), lifetimes meas. by DSA method 78–78308
Au, Doppler factor, comparison between calculated values and measured results 78–54811
Au, positron annihilation characteristics, 27 to 592K 79–91523
BO_2, Doppler free spectra, backscatter fluoresc. line narrowing, theory and obs. 80–53034
Ba^{+} ion cloud containment in RF trap, <50 ions, optical sideband cooling 78–75407
Be, Doppler effects in X-ray spectra excited by accelerated ions 78–86808
Be IV, line broadening and self-absorpt. in laser prod. plasma 78–17615
^{9}Be(p,α)^{6}Li, α ang. distrib. determ. by Doppler γ-line broadening method 77–61407
CO_2 laser Doppler system atmospheric attenuation 77–75601
^{12}C gamma line Doppler broadening in ^{12}C(n,n'γ)^{12}C and ^{9}Be(α,nγ)^{12}C, 4438 keV 80–91147
Ca 657.3 nm line saturated absorption spectroscopy, photon-recoil component resolution 80–86457
Ca, photon recoil splitting, line widths, Doppler effects, saturated absorpt. optical interference spectroscopy 80–52922
Cd, Doppler-shifted cyclotron reson. of holes, nonlinear effects *(Russian)* 77–8010
^{59}Co, excited states lifetimes, Doppler shift attenuation meas. 78–42009
Cs freq. standard, error due to second order Doppler shift 77–87745
Cs, photoplasma, optical excitation in radiation diffusion conditions 78–55227
Cu, deformed, temp. depend. of positron trapping 77–48270
Cu, positron lifetime, Doppler broadening of annihilation spectrum, temp. effect 78–2941
Cu:H, interaction of H and vacancies, positron annihilation, Doppler broadening 78–80434
Cu-Al-Ni, positron annihilation study of vacancies before and after martensitic transform. 79–99971
^{63}Cu, excited states lifetimes, Doppler shift attenuation meas. 78–42009
^{65}Cu, excited states lifetimes, Doppler shift attenuation meas. 78–42009
D_2, electron impact, Balmer-α emission Doppler profile energy depend. 77–42423
Fe, Doppler broadened positron annihilation lineshapes, prevacancy lattice expansion 78–27349
Fe_3Pt:Sn Invar alloy, Mossbauer shift temp. depend. 80–100626
Ge, electron-hole drop velocities as probe of phonons 78–68517
Ge, electron-hole drops, laser Doppler velocimetry 77–43504
GeH_4, IR laser sideband obs., ro-vibr. struct., isotope shifts, line widths 79–72306
Ge(Li) detector, relative ang. efficiency meas., Q_k factors and Doppler broadening 79–54750
H ions, velocity measurement by Doppler shift of H atoms line spectra after traversing thin C foil 78–16778
H, photon emission, Bohr theory covariant eqns., teaching 80–105482
H, Stark broadening by ion impact on moving emitter, Doppler H shift, theory 80–47940
H-like ions in laser-produced plasma, Balmer fine struct. (broadening) 80–48860
$H+NO_2 \rightarrow OH+NO$, vel. and angular distrib., Fourier transform Doppler spectrosc. obs. 79–80692
H_2, electron impact, Balmer-α emission Doppler profile energy depend. 77–42423
H_2, electron impact dissociative excitation obs. 78–1090
H_2O, D_2O, electron impact dissoc. excitation, Balmer-α emission obs., Doppler profile meas. 79–31706
H* translational energy distrib., in HCl electron impact dissoc., optical emission obs. 80–14238
Hα and Hβ, Stark profiles, ion-motion effect 80–63592
Hα-line, direct obs. of the transversal Doppler-shift 79–18151
He I line profiles with forbidden components induced by fluctuating fields in small theta pinch plasma 77–80353
He II, Doppler and Stark broadened lines, electron density and ion temp. meas. 78–67407
He, subDoppler lineshape obs., of IR mag. reson. Rydberg transitions, using motional Stark effect 78–947
He-Ne ring laser, unidirectional, modes 80–91818
^{3}He-^{4}He mixtures Doppler shift in third and fourth sound 78–56017
^{4}He, superfluid, film, third sound long pulse propag. 77–20148
H(n=4) Balmer-β emission, Doppler profile, in HCN electron impact dissoc. 80–28106
I_2 folded Doppler broadened system, interaction with two reson. laser fields 80–53007
I2 fluoresc., Ar^{+} laser excited, high resolution and sub-Doppler Fourier transform spectroscopy 80–43089

Doppler effect continued
In, positron annihilation line Doppler broadening, self-trapping and vacancy form. 77–40298
In, US wave polarisation plane and ellipticity rot. in mag. field, Doppler shifted acoustic cyclotron reson. *(Russian)* 79–15335
KCl crystals, positron annihilation, Doppler broadening 80–40180
^{41}K states from ^{40}Ar(d,n), lifetimes meas. by DSA method 78–78308
Kr+Xe, nonresonant excitation transfer, Doppler profiles, donor levels *(French)* 77–30824
Li+inert gas, Doppler and collisional broadening, correls. 77–14530
Mg atoms, cooling to broad band reson. light press. 80–48835
Mg, Doppler effects in X-ray spectra excited by accelerated ions 78–86808
Mg II, radiation press cooling of ions in Penning EM trap 78–66527
Mo, Doppler shifted cyclotron reson., doppleron-phonon reson. *(Russian)* 77–32262
NH_3, phase conjugation in an inhomogeneously broadened medium 80–83642
NH_3^{+}, fast mol., dissoc. in thin C foils, Doppler broadening obs. 78–22019
NO, γ-band collisional broadening parameters from resonance line absorpt. 77–10704
NO, mol. beam tunable diode laser sub-Doppler spectra, $^{2}\Pi_{1/2,3/2}$ Λ splittings 79–41180
Na atomic vapour, Doppler-broadened system, degenerate four-wave mixing, line shape and strength angular depend. 80–43391
Na+Ar, Na spectral lineshape, orientation and vel. relax. contribs., low press. region 80–5503
Na+Ne(Ar)(Kr)(Xe)(N_2)(CO_2), fine struct. changing collisions, vel. depend. 79–22803
Na_2, TOF spectra, molecular beam diagnostics with internal state selection 78–86968
Na($^{3}P_{1/2}$)+Ar$\rightarrow$Na($^{3}P_{3/2}$)+Ar, angular scatt. distrib., Doppler spectrosc. obs. 78–94309
Ne buffer gas line broadening in Cu vapour laser, gas temp. meas. 80–19020
Ne, optical transitions, Doppler broadening, compensation by vel. depend. light shifts 80–52930
Ne X Lyman-α line Stark broadening, hot dense laser-produced plasma 77–11402
Ne($^{3}P_2$) elastically scattered, metastable, ang. distrib., conventional rel. to Doppler shift methods 80–58418
^{22}Ne, lowest 4^{+} state lifetime meas. via Doppler shift technique 78–37307
^{22}Ne(4_1^{+}) from ^{4}He (^{19}F,pγ), lifetime meas. by high vel. coincidence DSA method 78–33148
Ni, cold-worked, impurity-induced vacancy clustering 79–99972
Ni, Doppler broadened positron annihilation lineshapes, prevacancy lattice expansion 78–27349
Ni+Ni(Nb), Doppler shift of continuum X-rays from quasimols. 79–22808
NiSb, dilute alloy, impurity-induced vacancy clustering 79–99972
O_2^{+}, predissociated b$^{4}\Sigma_g^{-}$ state, high resolution laser spectroscopy in fast ion beam 80–9656
OH_2^{+}, and OH_3^{+}, fast mols., dissoc. in thin C foils, Doppler broadening obs. 78–22019
^{31}P, precision Doppler-shift attenuation lifetime meas. from γ-ray lineshapes 79–36195
Pb, positron annihilation, Doppler broadening, 4.2 to 600K 79–47540
RbBr crystals, positron annihilation, Doppler broadening 80–40180
SO_2, 4 μm $\nu_1+\nu_3$ band, Doppler-limited and atmospheric spectra 77–27064
Se, Doppler effects in X-ray spectra excited by accelerated ions 78–86808
Si, electron-irradiated, annihilation of positrons, broadening measurements 78–87713
^{28}Si, precision Doppler-shift attenuation lifetime meas. from γ-ray lineshapes 79–36195
Sn, neutron cross section, filtered neutron beam technique, Doppler effect 80–52670
Sn, solid and liquid, neutron cross sections 80–22933
ThO_2, nucl. Doppler effect in fast and intermediate spectra measured by direct flux depression in neutron beam expt. 77–50232
Ti-Al-Mo-Sn alloy, elastically and plastically deformed, positron annihilation meas. of deformation 80–21038
Tl, sensitised fluoresc. in Hg-Tl vap., Doppler broadening 77–3314
Tl+H_2, Tl atomic fluorescence, pressure and Doppler broadening 80–5504
UO_2, nucl. Doppler effect in fast and intermediate spectra measured by direct flux depression in neutron beam expt. 77–50232
UO_2, nuclear doppler effects, hybrid static dynamic heating technique 78–25308
^{238}U Doppler effect obs. in advanced fuels critical assemblies 79–9739
^{238}U, Doppler reactivity worth meas. in GCFR critical assemblies 77–54336
^{238}U, energy-depend. Doppler effect calc. using collision probability method 77–57714
^{238}U in UO_2, Doppler effect in GCFR critical assemblies, 300-1100K 78–29574
^{238}U+n, Doppler effect meas. at 24 and 144 keV 79–97704
V, Doppler broadened positron annihilation lineshapes, prevacancy lattice expansion 78–27349
^{51}V(α,nγ)^{54}Mn, Doppler shift attenuation meas. of ^{54}Mn excited state lifetimes 78–17141
W, Doppler-shifted cyclotron reson. along nonprincipal cryst. directions *(Russian)* 79–4725
Xe, AC Stark effect, on saturated absorption line shape in partially Doppler-compensated system 79–45669
Xe+Bi, Bi Kα X-ray lines, Doppler broadening 78–62759
Zn, positron-electron annihilation spectra, Doppler broadened 79–65953
Zn-Fe alloys, dil., positron-electron annihilation spectra, Doppler broadened 79–65953

Doppler shift *see Doppler effect*

dopplerons
metal, Doppler-shifted cyclotron reson., excitation of dopplerons and Gantmakher-Kaner waves *(Russian)* 77–32261
metal, Gantmakher-Kaner effect in strong mag. field *(Russian)* 78–80015
metal film, surface impedance oscillation effects due to one sided RF excitation *(Russian)* 80–11106

dopplerons continued
- metal film, surface impedance oscills. in perpendicular mag. field *(Russian)* 78—76165
- metallic plate, electron refl. effect on EM field transmission *(Russian)* 77—11952
- metals, compensated, Gantmakher-Kaner effect in strong mag. fields 78—91595
- propagation in inclined mag. field spectrum, decay, polarisation study, Fermi surface model 80—44922
- two-level system, multi-doppleron processes, probe spectroscopy 79—81400
- Cd, Doppler-shifted cyclotron reson. of holes, nonlinear effects *(Russian)* 77—8010
- Cd, electron and hole doppleron oscills., temp. depend. 79—7822
- In, US wave polarisation plane and ellipticity rot. in mag. field, doppleron interactions *(Russian)* 79—15335
- Mo, Doppler-shifted cyclotron reson., doppleron-phonon reson. *(Russian)* 77—32262
- Mo, electron-electron scatt., doppleron damping meas. 79—37963
- Mo, longwave dopplerons, nonlocal Hall effect, surface impedance, size effect *(Russian)* 80—80253
- Mo, RF surface impedance, new type of oscills. 79—15070
- W, alternating sign Hall effect and doppleron spectrum 78—79981
- W, longwave dopplerons, nonlocal Hall effect, surface impedance, size effect *(Russian)* 80—80253
- W, RF surface impedance, new type of oscills. 79—15070
- W, RF surface impedance at different sample surface states 79—60911
- W, rot. of polarisation plane and ellipticity of US waves near doppleron-phonon reson. *(Russian)* 79—19325

dosimeters
- *see also dosimetry; thermoluminescent dosimeters*
- A-150 plastic-equivalent gas for ionisation chambers 80—81745
- absorbed dose determ. with ionisation chambers in e^- and photon beams, 1 to 50 MeV 80—18703
- acetylene, ionisation meas. and $\bar{W}_n$ derivation for neutron irradiation 79—36430
- acoustic noise dosimeters and noise exposure ratings 77—31173
- air monitoring systems for radioiodine and inert gases, evaluation 80—95480
- albedo, for personal neutron dosimetry, thermoluminesc. and track detectors *(Spanish)* 77—37056
- albedo dosimeter, calibration using Sb-Be neutron source 78—33394
- albedo dosimeter response to monoenergetic neutrons 77—90905
- albedo-type neutron dosimeter, description and calibration data 77—65389
- alkaline earth tetraborates, doped, radiothermoluminesc. detectors, dosimetric characts. 77—61665
- Andersson-Braun remmeter modifications for improved directional depend. and thermal neutron sensitivity 78—53499
- audio noise dosimeters, comparison of available equipment, ANSI standards, use in mines 79—1026
- beta-gamma survey meter with numerical display 77—64134
- beta-ray protection-level dosimeters, calibration quantities 77—52888
- beta-ray survey meter for meas. of absorbed dose rate independently of energy 80—106203
- Bonner sphere spectrometer, least-squares technique for extracting neutron spectra 78—33366
- bremsstrahlung dose measurement using convertor-detector system, electron dose determ. 80—91294
- calibration and meas. standards at Austrian Dosimetry Laboratory 80—5362
- calibration in terms of absorbed dose in water for ^{60}Co γ-radiation 80—18696
- calibration method for personal integral dosimeters *(Czech)* 80—27825
- calibration of environmental and personal dosimeters using ^{133}Xe 80—86992
- calibration of instruments used in radiology and radiotherapy, metrological problems *(Spanish)* 79—92377
- calibration problems rel. to radiation protection of nuclear facilities 80—9422
- calibration uncertainties, estimation of confidence levels 79—3247
- calorimeter for X-ray pulse dose determ. 77—21628
- capacitor chamber appl. 78—78509
- cellulose nitrate, effect of high γ-doses on etching characts., dosimetry appl. 79—31224
- cellulose nitrate, sensitivity to α-particle registration 78—17498
- cellulose nitrate α-particle detector for Rn short lived daughters, results and calibration *(Czech)* 78—62663
- cellulose nitrate CA8015, calibration for fast neutron dosimetry 79—49907
- cellulose nitrate film, neutron dosimeter 78—20280
- cellulose nitrate foils, personnel neutron dosimetry meas. by induced molecular wt. changes 79—59269
- cellulose nitrate LR115, neutron personnel dosimetry at high energy accelerators 78—20284
- cellulose nitrate track detectors, CA80-15 and LR-115, etch pits due to Rn and Tn alpha particles 78—855
- cellulose nitrate track detectors, direct dosimetry in π^- beams 78—20281
- charge to voltage convertor, for ionisation chamber dosimeters 78—78505
- chemical, aq. solns., comparison for absorbed doses of 10-1000 rads 78—41885
- chromium acetylacetonate, Mrad range dosimeter appls. 77—16997
- cloud chamber, low-pressure, ionisation distrib. analysis 80—9461
- cloud chamber, low-pressure tissue-equivalent gas for α-particle tracking 80—9462
- corrected calibration of Andersson and Braun type rem counter for divergently incident Am-Be neutrons 80—74031
- coumarin, aq. soln., response to high LET radiation from ^{10}B(n,α)^{7}Li reaction 78—24149
- coumarin, aqueous solution, fast neutron irrad., dosimetry appl. 78—44613
- coumarin aqueous system as low-range chemical dosimeter 79—79659
- coumarin in water and heavy water, fast neutron response 80—845
- DePangher precision long counter and neutron dose-rate meters, calibration 80—47822
- diamond, radiation dosimeters, evaluation 80—78456
- diamond tissue-equivalent dosimeter, for X-rays and gamma-rays 77—56477
- direct meas. of β absorbed dose rate by discriminator and filter *(Japanese)* 78—74511

dosimeters continued
- direct reading pen dosimeters, radiation exposure meas. aspects *(German)* 78—5050
- dose intensity meter NRG 302 *(Czech)* 79—22538
- electret dosimeter and its principles of operation *(Japanese)* 79—81092
- electret ionisation chamber dosimeter for long-term personnel monitoring 78—21810
- electron linear accelerator, dose monitoring system 78—92710
- electronic, compromise between accuracy and sensitivity *(Italian)* 80—63394
- EM radiation hazard instrums. 79—92378
- EM radiation probes, implantable, design factors 78—73258
- encapsulated liquid crystal, colour transition temp. rel. to gamma dose 77—38547
- environmental, international intercomparison 79—63817
- environmental radiation meas., instrument calibration 80—9426
- ermeter-dosimeter ERMD-1, UV intensity and dose meas. *(Russian)* 80—12261
- exoelectron dosimeters, reference dosimeter bank, storage, exposure and reading 80—5360
- exoemissive, automation of testing 79—6770
- extrapolation chamber meas. of electron depth absorbed dose distribs., 77—81573
- Farmer type 2502/3, electronic timer for use with, in radiotherapy units 79—25114
- fibre optic dosimeter on Navigational Technology Sattelite 2 79—22487
- fibre-optic, for large area radiation monitoring 77—46423
- film, calorimeter for calibration in high intensity electron fields 78—73257
- film, K nuclear emulsion, characts., neutron detection 78—20290
- film badge dosimeter for UVA radiation 80—61702
- film photon and electron absorbed-dose detector 80—91379
- film rel. to ion chamber systems for radiation therapy depth-dose, meas. 79—53255
- fluence of secondary photons generated by attenuation in thin walls 80—18699
- Fricke dosimeter, influence of methanol and t-butanol on ferric yield 78—11736
- Fricke dosimeter, wall effects in gamma-ray dosimetry 80—18697
- Fricke $FeSO_4$ solutions, G-value determ. for 20 MeV protons 77—52884
- Fricke type, mixed field of fast neutrons and γ-rays, absorbed dose meas. 78—74514
- gamma, energy relationship of effectiveness and error estimation 79—31225
- gamma, reference material based on silicate glass 80—78454
- gamma effect of air scattered radiation on exposure dose rate measurements 79—6774
- gamma photon energy spectra estimation based on 34×34 matrix 79—41059
- gamma radiation attenuation method using variable-thickness filter calibration 77—83110
- gamma radiation dosimeters, sensitivity of p-type channel MOS transistors 79—67966
- gamma-radiation absorbed dosage, differential microcalorimeter 0.01-10 W *(Russian)* 78—85385
- gamma-ray, using Si detectors, energy dependence of spectral sensitivity 79—68146
- gamma-ray dosimeter using polycarbonate plastic, high exposures 79—63815
- Geiger-Mueller counter γ dosemeters, fast neutron sensitivities, mixed field dosimetry 78—92705
- Geiger-Mueller counter for mixed n-γ dosimetry 78—25394
- Geiger-Muller counter, fast neutron sensitivity meas. technique 79—81096
- Geiger-Muller dosimeter and tissue-equivalent ionisation chamber, use in dose equivalent evaluation 80—51264
- Geiger-Muller gamma dosemeters, fast neutron sensitivities, 14.7 MeV 77—52880
- graphite calorimeter in water phantom for absorbed dose meas. 80—74032
- graphite radiation damage dosemeter, GAMIN 78—29657
- holographic method, for ionising radiation dosimetry 80—852
- infralow frequency signals, apparatus for running dose and mean value meas. 79—83936
- integrating radiation dosimeter, using polyethylene and Pirani vacuum gauge for range 10^4 to 10^8 rad. 79—747
- interface ion dose distrib. meas. apparatus *(German)* 80—9464
- international standard reference radiations and their application to the type testing of dosimetric apparatus 80—9416
- ion chamber pocket dosimeter, electret electrostatic generator 78—13382
- ion chambers, integrating, used in medical X-ray exposure survey, performance characts. 78—853
- ion chambers, photon dosimetry in phantoms, effective meas. point 80—78453
- ion injection type fast neutron dosimeter, fabrication attempts 77—81583
- ionisation chamber, Baldwin-Farmer, C_E, C_λ and effective wall material 79—22555
- ionisation chamber, C walled CO_2 filled, neutron sensitivity 79—22557
- ionisation chamber, compared with $FeSO_4$ meas. at 6 radiotherapy centres *(French)* 77—37057
- ionisation chamber, liquid-dielectric, appl. to ^{252}Cf dosimetry 77—13009
- ionisation chamber, parallel plate, thin-walled, for use with photon and electron beam dosimetry 80—78490
- ionisation chamber, tissue-equiv., response to 15 MeV neutrons 77—48874
- ionisation chamber dosimetry for photon and electron beams, C-values 77—81575
- ionisation chamber for absorbed dose calibration 77—40777
- ionisation chamber ion collection efficiencies in pulsed and continuous radiation beams 78—53505
- ionisation chambers, calibration methods for primary and secondary standards, in Hungary 80—5357
- ionisation chambers, cylindrical, effective meas. position in electron beam dosimetry 78—9023
- ionisation chambers, radiation exposure intercomparison 80—5363
- ionisation chambers, wall correction factors, ^{60}Co γ-ray beam standardisation, Monte Carlo calcs. 79—3288
- ionising chambers with electrostatic relays, investigation of stability, reproducibility, and orientation characts. 80—57966
- ionising radiation, metrology and calibration, French system *(French)* 80—5351

dosimeters continued
  ionising radiation, primary standards and transfer methods in France, review *(French)* 80—5352
  ionising radiation, traceability in meas. systems 80—5355
  ionising radiation calibration, meas. standards, CNEN, Italy 80—12273
  ionization-chamber-dependent factors for calibration of megavoltage X-ray and electron beam therapy machines 80—18704
  Keithley diagnostic ion chambers, energy depend. of correction factors 78—53507
  Kodak LR 115 cellulose nitrate films, fast neutron dosimetry 78—20279
  Kodak Type II film badges, gamma dose meas. in presence of thermal neutrons 79—39517
  laser light, dosimeter for health physics evaluation of operating conditions at laser installations 80—76835
  Lexan polycarbonate track detectors, direct dosimetry in π^- beams 78—20281
  lignocellulose polymer composites as γ-dosimeters in the kilorad range 80—95465
  linear accelerator beam profile scanner, medical appls. 80—101267
  liquid radiochromic dye dosimetry for continuous and pulsed fields over wide range 77—60255
  liquid scintillator determ. of dose rates from homogeneously distrib. β,γ- and EC,γ-emitters in phantom organs 78—53501
  low level radiation monitors, calibration accuracy and precision 80—9428
  low-energy direct-reading pocket dosimeters, correction factor energy depend. 78—24144
  luminescent detector efficiency for 600 MeV protons, mass stopping power calc. 80—99346
  lyoluminescence dosimetry in photon and fast neutron beams, using mannose 78—15902
  lyoluminescence of saccharides 77—52881
  Makrofol, neutron personnel dosimetry at high energy accelerators 78—20284
  measurement errors 79—93835
  measurement standardisation and calibration within the European Communities 80—9415
  medical dosimetry standards programme of the National Bureau of Standards, USA, review 80—8187
  medical X- and γ-ray dosimeter with digital display, portable and versatile 80—81744
  metal-nitride-oxide-semiconductor transistor as a radiation dosimeter detector 79—22486
  metaphosphate glass: Ag dosimeter, optical absorpt. and radiophotolum., effect of temp. 78—40333
  mica, for visualisation of electron isodose curves in a medium 80—99349
  microdosimetric measurements with spherical proportional counters and solid-state detectors, comparative study 80—109038
  microwave, evaluation of implantable elec. field probe within finite simulated tissues 78—40345
  microwave P-N avalanche diode as gamma-ray dosimeter 77—54408
  microwaves, whole-body biological dosimeter using drug-induced ectothermia in small mammals 78—40350
  MOS, series configuration, sensitivity increase *(Czech)* 79—36425
  MOS dosimetry unit development for use in space 79—22485
  MOS transistor appl., response functions obs. *(Czech)* 79—49874
  MOST suitability as γ-ray dosimeter *(Czech)* 77—86636
  moving electrode instrum. for radiation dosimetry and control 79—3244
  multiwire proportional counter for microdosimetric studies 78—20286
  neutron, digital portable battery-operated, design details 79—18052
  neutron, personnel, recent developments 79—63818
  neutron albedo track dosimeter 79—85816
  neutron dose meas. with B-doped cellulose nitrate film 79—31321
  neutron dosimeter and monitoring instrumentation calibration using ^{252}Cf and ^{238}PuBe sources 80—13946
  neutron dosimeter based on ^{237}Np fission, for personnel 79—13539
  neutron dosimetry, meas. standardisation for biological and biomedical appl. 80—12271
  neutron dosimetry with solid state nuclear track detectors, brief review 78—33299
  neutron dual response albedo neutron personnel dosimeter 79—93885
  neutron monitor calibration for radiation protection at 24.5 keV and 2 keV 78—89983
  neutron personal dosimeter based on track detector 77—70551
  neutron personal dosimetry system, ^{237}Np neutron induced tracks in polycrabonate 78—31908
  neutron personnel dosimetry using cellulose nitrate film and LiF as radiator and TLD 77—64132
  neutron personnel monitoring film, Kodak NTA, energy depend. 79—100753
  neutron response of solid state nuclear track detector 80—27876
  neutron sensitive instruments, calibration using novel source emitting neutrons around 0.5 keV 77—6615
  neutron/gamma sensitivity determ., comparison of spectral difference and Pb filtration methods 77—90915
  noise dosimeter response to impulsive noise, meas. errors 79—18646
  nuclear accident dosimetry system for criticality accidents 77—88288
  nuclear accident dosimetry systems, comparison 79—22496
  nuclear emulsion latent image fading, effect of dry N_2 desiccation 78—15903
  nuclear fuel movement monitoring 77—67899
  nuclear reactor criticality incident detect. with γ dose rate alarm 79—36423
  nuclear track detector, appl. as neutron dosimeter, reponse to standard neutron sources 80—5342
  nuclear track emulsion, NTA film, as personnel neutron monitor in criticality accidents 77—29208
  p-n junction detectors, low-level DC current amplifier 77—38573
  PAM microwave field dosimetric device 80—3818
  parallel plate ionisation chamber, absorbed dose meas. in polystyrene phantoms 80—72335
  pencil chamber for direct beam CT meas., evaluation 80—46056
  personal dosimeters, comparative evaluation 79—41042
  personnel dosimeter calibration, US NBS standard reference neutron fields 80—9417
  personnel dosimeter design and use, physical requirements for dose meas. 80—9424
  personnel dosimeters based on film badges and TLDs, appl. *(Russian)* 78—20293
  personnel dosimeters calibration techniques for electrons and photons 80—9419
  personnel dosimetry, criteria for testing of performance 80—23169

dosimeters continued
  personnel dosimetry intercomparison studies at the ORNL Health Physics Research Reactor 80—9427
  personnel dosimetry methods introduced in the Czechoslovak National Laboratory *(Czech)* 79—36426
  personnel dosimetry performance, testing standard 80—9421
  personnel dosimetry photon calibrations, use of phantom 80—9425
  personnel monitoring dosimeter intercomparison 77—40781
  personnel monitoring for radiological protection, current status and developments, review 79—22490
  Perspex, clear, effect of storage temp. on calibration 77—60256
  photon calibration of radiation protection instruments in an authorized metrology service 80—9423
  photon detector, MRM-3, measuring range expansion 78—879
  photon dosimeter, fast neutron sensitivity determ., modified Pb attenuation method 79—81095
  photon irradiator calibration, compensation for geometry induced errors 80—18702
  photons, 6-7 MeV, exposure rate and absorbed dose meas. 79—26766
  plastic foils for neutron dosimeters, electrochem. etching prep. techniques 79—76298
  plastic solid state nuclear track detector, large γ dose meas. 77—38559
  plastic solid state nuclear track detectors, Rn and Th dosimetry 78—20556
  plastic track detectors, Rn dosimetry 78—33298
  plastics, comparison of fast neutron induced tracks using electrochem. etching 80—23154
  pocket-sized electronic system 78—5100
  polyamide-film calorimeter for measuring local electron-beam absorbed doses 80—83227
  polycarbonate fast neutron dosimeter, development and comparison with conventional emulsion dosimeter 80—86990
  polycarbonate film dosimeter for high-level electron dose meas., optical density 77—25559
  polycarbonate foil electrochemical etching for dosimetry, bulk etching rate evaluation 78—78506
  polyfluoroethylenepropylene, prepared for dosimetry, thermocurrents 77—52877
  polymer sheets, calibration via differential calorimeter for electron radiation 79—6795
  portable neutron spectrometer/kerma-rate meter, design, performance 78—33361
  portable radiation meters, accuracy checking facility at Berkeley Laboratories, UK 78—74507
  portable spectrometer/dosimeter for low level neutron radiation meas. 79—49869
  primary standard for determination of absorbed dose in water for X-rays generated at potentials of 7.5 to 30 kV 80—5354
  primary standards for industrial radiation processing 80—5356
  proportional, cylindrical wall-less counter, characteristics 77—3224
  PTFE, prepared for dosimetry, thermocurrents 77—52877
  pulsed neutron dose rate meas. instrument, portable, microcomputer-based 80—86991
  pulsed radiation intensity meas. by counting delayed pulses produced in Geiger-Muller counter 77—46407
  pyroelectric radiation detector for dosimetry of pulsed γ-radiation 77—71725
  pyroelectric receiver, gamma pulse meas. 78—860
  quartz, thermoluminescence sensitivity change due to stress 77—59627
  radiation protection instruments for personnel dosimetry, area and environmental monitoring 78—66427
  radiation therapy, calibration and meas. standards in USA 80—8188
  radiation therapy, exposure timer for use with tele Co units 79—20684
  radiochromic dye film, calibration industrial dosimeter appl. 78—40330
  radiochromic dyed plastic thin films, for absorbed dose and dose distrib. meas. 77—67906
  radiological instrumentation calibration by British Calibration Service 80—8186
  radiophotoluminescent, with miniature detectors, for clinical use 79—8543
  radiotherapy machine calibration, instrumentation used by AAPM, Keithley-Farmer system 77—2055
  Regional Calibration Laboratory at the M.D. Anderson Hospital, Texas, USA 80—8189
  REM ratemeter, for mixed radiation, using two spherical ionisation chambers 78—96100
  REM ratemeter for direct reading of dose equivalent rate 78—53502
  rem-dose measurement of mixed p-n radiation using solid state detectors of fission fragments 80—36137
  remote-reading operational amplifier radiation dosimeter, elec. constancy check 78—3613
  response time constants of two dose-rate meters 77—13006
  rod dosimeter, use of evaluation device in process computer-aided personnel dosimetry monitoring *(German, English)* 78—17441
  rod dosimeters, automatic evaluation of staff dosimeters during reactor shut down *(German)* 79—67960
  Rossi counter for neutron equivalent-dose measurement 80—18678
  scintillation counter with pulse shape discrimination for neutron dose and spectra meas. in n-γ field 77—77992
  secondary radiation dosimeters, prep., sensitivity anal. and calibration 80—74034
  secondary standard NPL ionisation chamber, calibration program 77—38584
  secondary standard X- and γ-ray dose rate meter, protection-level, NPL 77—81579
  semiautomatic device for relative dose distrib. recording 78—85380
  semiconductor detectors for dosimetry in intense neutron-gamma fields 77—46460
  semiconductor devices, dose meas. using radiation induced changes *(Japanese)* 78—78504
  sewage sludge irradiation plant, dose and irradiation homogeneity 79—22489
  solid dielectric detectors with breakdown phenomena and their applications in radioprotection 80—91388
  solid state dosimetry, tissue-equivalent systems, review *(Hungarian)* 80—91291
  solid state track detectors, neutron fluence meas., international intercomparison 78—20283
  solid-state nuclear track detectors, development and use for reactor phys. expts. 78—41886

dosimeters continued

- solid-state track detectors, international α-particle registration intercomparison 78–17497
- sound level dosimeter, ear-borne 77–11099
- stack gas monitor, β scintillation detector+Ge(Li) detector system, environmental γ dose *(Japanese)* 79–3246
- standardisation, conf., Atlanta, GA, USA, Dec. (1977) 80–4469
- standardisation in Germany, electrons and photons 80–5353
- standardisation in Japan, review 80–5359
- standardisation program at US National Bureau of Standards 80–13943
- standardization in radiation dosimetry in the United Kingdom, review 80–5358
- superheated drop detector 79–72201
- surface barrier detector for beta dosimetry 80–57973
- survey meters for low γ-ray dose rate meas. 79–41081
- therapy-level dosimeters, choice of meas. quantity 79–92379
- thermally stimulated conductivity in poly-4-methylpent-1-ene 77–11905
- thermally stimulated exoelectron detection, electronic instrumentation *(Spanish)* 77–32958
- thermoelectret gamma radiation dosimeter, use of BeO 80–7270
- thermoluminescence, calibration, γ-ray irradiator *(Japanese)* 78–66452
- thermoluminescence neutron dosimetry 77–60262
- thermoluminescence reader, high sensitivity *(Japanese)* 78–66426
- thermoluminescent dosemeter, NRPB's new record keeping service 77–81577
- thermoluminescent dosemeter service in United Kingdom 79–59268
- thin dielectric track detector as particle discriminator, α dosimetry appl. 78–17511
- thoron content in exhaled air, meas. apparatus 79–34672
- tissue-equivalent ionisation chamber, photon calibration for neutron dosimetry 80–56221
- TLD, automatic readers for personnel monitoring 78–50408
- TLD, neutron dose monitoring using multiple LiF TLD badge 77–90907
- TLD processing using desk-top computer 77–81580
- TLD response to 14.7 MeV fast and thermal neutrons 77–66856
- TLD-04B reader, meas. of TL materials for health phys. appls. *(Russian)* 77–86648
- topaz, thermolum. props. 78–35957
- track etch detectors, neutron energy depend. and threshold energy 80–61703
- transit dosimeter system, for ^{60}Co rot. therapy, electronic modification 77–2053
- transportation, exposure during air and ground transit 77–16987
- transresistance instrumentation differential amplifier 79–22561
- ultra-thin dosemeter for skin dose assessment, development 80–57974
- UV, MDUV-1A miniature dosimeter *(Russian)* 77–90902
- UV, response correction, spectral distrib. of natural radiation under clear day conditions 77–41171
- UV, semiconducting dosimeter 78–74059
- UV, thermolum. of MgO single cryst. 77–16986
- UV, using LiF photostimulated thermolum. 77–16984
- UV natural radiation meas. in study of photodermatoses and drug photosensitivity 78–40339
- UV polymer-film dosimeters, automatic read-out device 80–78455
- UV TLD, direct-response dosimeter using MgO 77–13010
- Victoreen 440 survey meter, digital display adaptor 79–70644
- Victoreen 570 Condenser R-Meter, energy depend. of correction factor 78–3597
- Victoreen 666 Radiographic Health Survey System, energy depend. of correction factors 78–3596
- wall-less tissue equivalent counters, performance evaluation in microdosimetric work 79–13599
- walled tissue equivalent counters, performance evaluation in microdosimetric work 79–13599
- water calorimeter for absorbed dose meas. 80–76836
- whole body counter, portable chair type for in vivo internal contamination monitoring 78–61260
- wrist watch dosemeter for ionising radiations, practicality tests 80–57972
- X-ray, for routine meas. with therapy equipment between 10 and 250 kV 78–28084
- Zener diode dosimeter for high-level electron dose meas. 77–50331
- β-ray point source dosimetry using variable cavity chamber, appl. to protection instrument response 80–13942
- ^{222}Rn daughters exposure, electronic dosimeter 80–46054
- Al_2O_3, thermoluminescence, effect of heat treatment following gamma irradiation 77–59624
- Al_2O_3:Si,Ti photostimulated thermolum., and appl. to UV dosimetry 78–53511
- Al_2O_3:Si thermoluminescent phosphor, annealing characts. and nature of traps 77–85817
- $BaTiO_3$, rare earth doped ceramics, thermolum. and microwave induced thermolum. fading 79–1792
- BeO, ceramic and single cryst., EPR-ENDOR study of [Li]° centre 77–85569
- BeO discs, thermally stimulated exoelectron emission and thermolum. sensitisation 78–35277
- CO_2, ionisation meas. and $\bar{W}_n$ derivation for neutron irradiation 79–36430
- CaF_2:Dy (TLD-200), practical UV dosimeter 77–60258
- CaF_2:Dy dosimeter crystals, γ-irrad. dose effect on thermoluminesc. response 77–64135
- CaF_2:Dy(Mn), thermolum. induced by monoenergetic parallel beam 81 MeV diffr. neutrons 77–52883
- CaF_2:Mn TLD, internal background build-up 77–54399
- $CaSO_4$ with rare-earth and Y dopants, ESR, thermolum. correlation studies following gamma irradiation 77–59628
- $CaSO_4$:Dy photostimulated luminesc. 77–90910
- $CaSO_4$:Tm and nonluminous ^{6}LiF powders mixture, thermoluminesc. response to thermal neutrons 77–73588
- CdS γ-ray dosimeters with elevated stability under irradiation 80–86995
- CdS with Cu traces, γ-radiation dosimeter, prod. and characts. 78–8999
- CdTe photovoltaic mode γ- and X-radiation dosimeters 79–13594
- Ce^{4+}/Ce^{3+} dosimeter, adsorbed doses, potentiometric determ. 78–94146
- $Ce_2(SO_4)_3$ type, mixed field of fast neutrons and γ-rays, absorbed dose meas. 78–74514
- ^{60}Co radiation therapy, eval. of dosimetric accuracy and uniformity 80–12269
- $FeSO_4$, compared with ionisation chamber meas. at 6 radiotherapy centres *(French)* 77–37057

dosimeters continued

- $FeSO_4$-benzoic acid-xylenol orange, ^{60}Co teletherapy build-up dose meas. 78–28081
- $FeSO_4$-$CuSO_4$, intense γ-radiation field effects *(Spanish)* 77–48876
- ^{3}He-filled proportional counter, for sensitive dose or dose equivalent meter 79–45427
- Hg vapour monitor, personal piezoelec. cryst. dosimeter 77–21672
- In_2Te_3, photosensitivity on γ- and neutron-irrad., γ-ray dosimeter mat. applic. 77–85258
- In_2Te_3-type semicond. radiation-resistant fast-electron detectors 78–78559
- LiF dosimeter energy response to high energy electrons $<$30 MeV, Monte Carlo calc. 77–86637
- LiF dosimeters for high energy electrons, Monte Carlo calc. of energy dependence 77–46421
- LiF, response to high energy electrons, application of cavity theory 79–22493
- LiF TLD, accuracy of megavolt. radiation dosimetry 77–81574
- LiF TLD, anal. of energy response to high energy electrons 77–52882
- LiF TLD-100, thermolum. response to 5 to 30 keV electrons effect of annealing atm. 77–86638
- LiF thermoluminescence induced by 13.8 and 81 meV diffr. neutrons 77–56481
- LiF, thermoluminescence mechanisms following gamma irradiation 77–59625
- LiF, thermoluminescence response to gamma rays 77–59626
- ^{7}LiF TLD, efficiency for H^+ and Ar^{18+} detect. 78–53504
- LiF:Mg,Ti TLD based passive neutron spectrometer and dosimeter 77–54394
- LiF:Mg^{2+}, TLD-100, precipitation reactions and ionic cond. 77–56479
- LiF:Mg^{2+}, TLD-100, solution treatment temp. and ageing effects 77–56480
- Mg_2SiO_4:Tb TLD, supralinearity of response to electrons and X-rays *(Japanese)* 78–78503
- Mg_2SiO_4:Tb thermoluminescence phosphor, response to high energy electrons *(Japanese)* 78–78502
- ^{227}Np damage track detectors, effects of subthreshold fission on neutron dose meas. 78–33375
- ^{237}Np dosimeter and spark counting system, for routine personnel monitoring 78–89984
- ^{237}Np fission-foil dosimeter, calibration using Sb-Be neutron source 78–33394
- Pu dosimetry, calibration of whole-body counters 80–21547
- ^{222}Rn, passive environmental monitor based on exoelectron dosimeter 78–82523
- Se, differential dosimetric characts. w.r.t. γ-radiation 80–32529
- Si detector with p-i-n junction in pulse count mode for γ dosimetry 78–33386
- Si diffused n-P^+ junction miniature for electron meas. 77–30718
- Si diode as in vivo fast neutron dosimeter 77–73587
- Si diode detectors in radiological physics, energy compensating shield development 78–24142
- Si diode detectors in radiological physics, high-energy photon dosimetry 78–24143
- Si diode neutron detector for meas. near high-energy accelerator, photon and electron response 78–35963
- Si microcalorimeter dosimetry system for transient radiation effects, radiation induced temp. rise meas. 77–26885
- Si p-n junction, radiation detector DC cct., transient processes 77–70556
- Si p-n junction radiation detectors in DC mode, temp. response nonlinearity 77–38565
- Si p-n junction radiation detector behaviour in temp.-compensated cct. 78–33389
- Si photodiodes for neutron dosimetry 78–31907
- Si, proton beam dosimetry in C, Al, Fe, mylar, H_2O 80–47733
- X-ray dosimetry, intercomparison and standardisation 80–12270
- ZrO_2 TLD using stabilised single cryst., for high gamma doses 77–56476

dosimetry

- *see also dosimeters; radiation detection and measurement; radiation monitoring*
- α-particle stopping power and straggling in water and tissue-equivalent liquid 80–23274
- A_{eq} and A_c, meaning of 80–89867
- A-150 tissue equivalent plastic, chem. composition 77–21632
- A-bomb survivors radiation dose chromosome aberrations relationship 79–43835
- absorbed dose, bounded estimate using linear programming 78–37452
- absorbed dose calibration of high-energy X-rays, comparison of plastic and water phantoms 79–8548
- absorbed dose determ. with ionisation chambers in e^- and photon beams, 1 to 50 MeV 80–18703
- absorbed dose determination, fund. principles for radiation technology 80–95467
- absorbed dose estimeates in prolonged ^{137}Cs γ-irrad facility for mice 80–101233
- absorbed dose measurements using parallel plate ionisation chambers in polystyrene phantoms 80–72335
- absorbed dose of cylindrical rotating object in collimated electron beam 77–25558
- absorbed dose ratio, effect of diffuse radiation, Fricke dosimetry c.f. ionisation meas. 80–13948
- absorbed-dose computations for inhomogeneous media in radiation-treatment planning using differential scatter-air ratios 79–25115
- accelerators, international standards 80–51272
- accelerators used for high energy photon radiotherapy, dose levels due to neutrons 77–13008
- accident features affecting emergency measures 78–55055
- accumulation dose factor for scattered γ-radiation in two-layer cylindrical shielding blocks 79–18058
- actinide nuclear transmutation, photon and neutron surface dose rates for actinide containing fuel 78–66428
- actinides, inhaled, research at Nat. Radiological Protection Board 77–48879
- activity meter for nuclear medicine, ionisation chamber characts. 79–66558
- acute exposure to LET radiation, early mortality predictions 80–47751
- adrenal imaging, radiopharmaceutical distribution and dosimetry 79–29632

dosimetry continued
- air, secondary radiation from γ-ray interactions *(Czech)* 79—67967
- air traffic radiation safety, high-altitude 78—44620
- air-scattering dose rate calc. by single-scatt. approx. 80—41252
- airborne radionuclide release assessment, importance of vars. in deposition vel. 78—80979
- airport cargo workers, radiation exposure meas. 79—8544
- albedo neutron dosimetry, advances 80—57982
- albedo neutron dosimetry 77—90914
- alpha emitters, health effects, man-made actinides compared with natural radionuclides 80—61647
- alpha particle dose to respiratory airway epithelium 77—44756
- alpha particle stopping cross-sections in ethylene and polyethylene, 1.5 to 4.2 MeV 78—53510
- alpha particle stopping power, 0.5-8 MeV, in water and aq. tissue equivalent soln. 78—40334
- alpha particle stopping power and straggling in liqs., determ. by Si spectrometer 78—82563
- alpha particles in N$_2$, CO$_2$, methane, Ar, H$_2$ and tissue equiv. gases, energy depend. of W 79—6999
- alpha-dose rates, upper limit calc. method for aquatic organisms, re ^{239}Pu, plankton 79—2133
- alpha-emitting radionuclides in bone, particularly ^{226}Ra and ^{239}Pu 77—16993
- alpha-particle stopping cross section, 0.3 to 2.0 MeV, ice and water vapour 77—55313
- amoeba irradiated by thermal neutrons, absorbed dose estimation 78—53449
- aquatic food chains appl., dosimetry calculations due to radionuclides, NEPTUN interactive code in FORTRAN 80—109039
- Artronix PC-12 implant dosimetry program, stero rel. to orthogonal options 79—62371
- astronaut dosages, Apollo 7 to 14 and Soyuz 3 to 9 missions, TL meas. *(Hungarian)* 79—29639
- atmospheric emissions from nuclear plants, applications related concept for radiation exposure calc. *(German)* 78—82531
- atmospheric radioactivity, dose calcs., incurred from deposited activity and cloud activity 80—3551
- atmospheric radioactivity inside buildings, absorbed dose estimation *(Spanish)* 78—8998
- atomic-bomb survivors residing in USA 77—9260
- background radiation and estimated risks from low-dose irradiation 80—46058
- backscatter factors for X- and γ-rays, polynomial and power law of central axis values 77—2056
- benchmark experiments for nuclear data validation 77—23203
- Berger coeffs. for Eisenhauer-Simmons γ-ray buildup factors in concrete 78—78510
- beta dose in skin from gaseous radioactive reactor effluents 80—26364
- beta dosimetry, comparison of laboratory standards 77—66858
- beta dosimetry, dose function calc., eye applicators 77—60260
- beta emitters, insoluble, ingested, dose to gastrointestinal tract 78—65134
- beta radiation, absorbed energy distribs. in homogeneous media 80—109033
- beta ray plastic scintillator survey meter for directly absorbed dose meas. *(Japanese)* 80—848
- beta sources, depth dose distribs. in varous materials 78—17462
- beta-emitting radionuclides from reactor accident, ingestion, acute toxicity 78—65082
- beta-emitting volume-seeking radionuclides in human bone, mean skeletal dose factors 78—77115
- beta-ray absorbed dose rate, direct meas. using plastic scintillator *(Japanese)* 77—73589
- beta-ray dose rates in skin, conversion from values meas. in air 77—16996
- beta-rays, high-energy, hazards to eye lens and gonads 78—65131
- betatron, radiation protection meas. 79—29636
- betatron electron beam, characterisation for dosimetry calcs. 79—39519
- Bevalac radiotherapy facility, dosimetry and beam handling apparatus 79—79630
- Bikini population, dosimetric results for man-made radiation 80—85498
- biological alkaline phosphatases in serum, as indicators of radiation damage in rats 77—86556
- biological dose rates in and around JAERI fusion reactor shielding 78—54872
- biological effects of radiation, methods of safety estimation and problems encountered *(French)* 80—98003
- biological specimens, reduction of radiation damage in electron microscopic exam. 79—34718
- biological tissue, calc. of spectra and linear energy transfer for neutron irradiation 79—100659
- biological tissue, recoil nuclei specific energy losses, analytic representation 79—100680
- biomaterial microwave complex permittivity meas., noninvasive selective exposure 79—20729
- biophysical dose planning expts., appl. to radiation therapy 78—15879
- bladder wall dose after ^{99m}Tc-microspheres administration 80—109030
- bleomycin, effect of dose loading and double labelling with ^{57}Co and ^{125}I on animal tissue distrib. 80—67220
- blood adenylate energy charge changes of lymphocytes, platelets, erythrocytes after γ-irradiation 79—57718
- blood vessels, X-irradiation induced damage, mouse, dose-effect time relationship 79—34603
- bluegill ^{222}Rn, ^{226}Ra fractional retention 79—39506
- BN-350 reactor, radiation safety assessment at design stage *(Russian)* 79—97869
- bone, cortical, microstruct. model using ionising particle path length distrib. 77—40774
- bone, meas. of LiF powder packing density in trabecular bone cavities by radiography 77—66855
- bone, radial scanning of trabecular bone, path length probability distribs. 77—66854
- bone, surface and volume distribution of ^{239}Pu 79—8550
- bone Ca activation anal., prod. of uniform ^{38}K yield using range modulator 77—40735
- bone marrow cellular survival parameters, neutron kerma factors 80—51176
- bone marrow electronic cell sizing and counting, biological dosimetry of irradiated rat 79—100744
- bone radiosensitive tissues irrad. by surface deposited radionuclides, calc. dose factors 78—53512

dosimetry continued
- bone-seeking radionuclides, comparative study in man, rhesus monkey, beagle and miniature pig 80—72338
- bone-tissue interface, doese distrib. due to anisotropic electron emission 80—36144
- brachytherapy, radiation exposure of nursing personnel to patients 78—85384
- brachytherapy program used with the Philips Treatment Planning System 80—81738
- brachytherapy source, dose rate meas., fundamental accuracy limitation 80—3815
- brachytherapy source calibration using Fe(NH$_4$)$_2$(SO$_4$)$_2$-benzoic acid-xylenol orange dosimeter 77—5081
- brain computed tomograms, contrast dose for enhancement 79—88193
- brain computerised tomography, dose to thyroid and eye 79—92389
- brain low dose elective, in small cell lung carcinoma 80—67253
- breast dose and cancer risk due to fluoroscopic chest exams. of women with tuberculosis 78—65128
- breast radiography with Mammomat, skin exposure and absorbed dose 78—73245
- bremsstrahlung, thick-target spatial distrib. of energy transfer meas. with miniature dosimeter 78—15897
- bremsstrahlung beam, 1000 MeV, on Pb and W thick targets, meas. of surrounding doses 77—9265
- bremsstrahlung influence on γ dose buildup factors rel. to penetration depth *(Russian)* 79—13542
- bremsstrahlung X-ray spectra stripping up to 300 kVp on desk type computer 79—83846
- bremsstrahlung yield produced by 4 MeV linear electron accelerator calc. rel. to hazard in radiolysis 79—76181
- brom phenol blue aqueous soln., irradiation induced discolouring as dose meas. 78—41866
- bronchial epithelium, population average dose from Rn pollution 79—70485
- build-up curves of scanned high energy electron beams, Sagittaire linear accelerator 80—89864
- building materials, conc. of ^{232}Th, ^{226}Ra, and ^{40}K from gamma-ray spectra 77—38424
- BWR, shutdown dose rate of primary cooling system, prediction by empirical formula 79—22408
- BWR shutdown dose rate prediction, calc. code 80—23061
- BWR-6 computer anal. of fission product release to containment via press. suppression pool 79—59223
- C$_\lambda$ and C$_E$ reevaluation using extended cavity ionisation theory, ferrous sulphate G-values appl. 78—92706
- C$_\lambda$ experimental determination using an absorbed dose calorimeter 80—41249
- calibration and meas. standards, Regional Calibration Laboratory, Cleveland, USA 80—5364
- calibration and meas. standards at Austrian Dosimetry Laboratory 80—5362
- calibration for radiation protection in European community 80—58000
- calibration methods for primary and secondary standards, in Hungary 80—5357
- calibration problems rel. to radiation protection of nuclear facilities 80—9422
- calibration uncertainties, estimation of confidence levels 79—3247
- calorimetric dosimeters, automation of calorimetric measurements evaluation 79—67965
- calorimetric measurements in fast neutron and ^{60}Co gamma-ray fields 77—40787
- cancer induced by radiation, dose-effect relationship linearity 80—67157
- CANDU 600 MW(e) station, man-rem expenditures 79—13493
- carcinogenesis, stochastic model, obs. from chemical and radiation dose-response data 79—2110
- carcinogenesis, time and dose factors 79—70590
- cell lethality computation, dose-time relationship, fractionated radiation therapy 79—20598
- cell neoplastic transformation and dose fractionation, role of damage repair 80—72242
- cell survival dependence on radiation quality, models and exptl. data analysis 80—26287
- cellular irradiation, repair and prolonged hypoxia 79—74721
- cellular O$_2$ enhancement ratio, hypothesis test and microdosimetric implications 80—26212
- cellular radiation dose of labeled neutrophils and platelets 79—100749
- cellular repair rates determined by split-dose and dose-rate methods, comparison 80—104680
- cellulose nitrate, effect of high γ-doses on etching characts., dosimetry appl. 79—31224
- cellulose nitrate foils, personnel neutron dosimetry meas. by induced molecular wt. changes 79—59269
- cellulose nitrate solid state nucl. track detector, gamma dose meas. 78—73247
- cellulose-nitrate plastic track detectors, high-LET pion dose contours 79—39513
- centralized TLD service and record keeping in Canada 80—58003
- ceric/thallous dosimetry at less than 1000 rad 80—63400
- cervical spinal cord, radiation myelopathy, time, dose and volume factors 79—20658
- cervical stage III carcinoma treatment, two regimes with same TDF but differing morbidity 78—53474
- charged heavy particle therapy, desirability of treatment with multiple fields 78—73220
- charged particle beam, influence of thin inhomogeneities 78—69219
- charged particle beam, influence of thin inhomogeneities 78—69220
- charged particle detection by photographic recording systems, appls. 78—17527
- charged particle flux-at-a-point in complex geometries, numerical method 77—26249
- charged particle track evaluation, distance distrib. and intratrack dose 80—26368
- charged particle yields from π^- capture in biologically significant materials 80—12201
- chemical dosimetry, chloroform-paraffin system chem. changes after ^{60}Co γ-irradiation 80—30258
- chemiluminescence, measuring device *(Russian)* 79—93202
- chert artifacts, thermolum. determ. of prehistoric heat treatment 78—24914
- chest wall irradiation, technique to improve electron dose distrib. homogeneity 80—72332

dosimetry continued
chromosomal aberrations as radiobiological quantitative end-point 80—12188
chromosomally aberrant cells, Japanese A-bomb survivors, dose-response relationship of neutrons and γ-rays 80—94295
chromosome aberrations, dose-effect relationship, population exposed to increased natural radioactivity 80—72254
chromosome aberrations as biological dose-response indicator in U miners 80—17019
chromosome aberrations as dosimetric technique for fission neutrons at 0.2 to 50 rad 78—69145
chromosome aberrations of peripheral lymphocytes in rabbits exposed to whole body X-irradiation 79—43834
chromosome observation, estimation of radiation effects *(Japanese)* 79—83845
chronic radioactive release assessment, models and computer codes 80—13710
cineurethrocystography, gonad dose 78—35956
Clinac 4 skin sparing improvement using leaded glass electron filters 78—31885
Clinac-18, electron-beam energy charact. using magnetic anal. method 79—39514
Clinac-18 linear accelerator, dosimetry of 10 MV X-rays 77—21631
clinical nuclear medicine, internal dosimetry of ^{99m}Tc labelled radiopharmaceuticals 79—12007
cloud chamber, low-pressure, ionisation distrib. analysis 80—9461
cloud dose data file fast correction for changes in dispersion parameters 78—80969
coal fired power stations, EPA regulations and radiological dose commitment 79—52980
coal power station fly-ash and slag, natural radioactivity meas. 78—17442
collective dose commitment, evaluation problems *(French)* 80—47760
collective dose commitment for estimate of radioactive pollution, concept and calcs. *(German)* 78—74504
collective dose commitments from nuclear power programmes 79—26772
collective dose commitments from the release of radioactive nuclides to the atmosphere 80—3556
collective dose distribution anal. using census data, graphical method, computer-aided 77—6567
collective dose equivalent, cost anal. 80—47761
collective dose equivalent concept for population exposures 77—2059
collective dose rate commitment in nuclear power industry, appl. to future dose rate eval. *(Spanish)* 79—63816
colonic diverticular disease population survey, patient X-ray dose 78—61259
committed effective dose equivalent conversion factors for intake of selected radionuclides 80—67256
complex-shaped mats., absorbed dose distrib. determ. 77—70263
computed tomography depth-dose distribution, effect of slice thickness 80—46038
computed tomography scanner, fourth-generation, performance evaluation 80—46035
computed tomography scanner geometry optimisation 80—46037
computer as an active element 79—67961
computer programs for radionuclide pathway anal. calcs., RAMM system 77—13015
computer tomography, picture formation, patient dose reduction 80—46031
computer tomography head scanner, translate-rotate type with Xe detectors, performance characts. 80—46036
computer-controlled radiation therapy 79—92367
computerised dosimetry calcs., linear accelerator electron beam parametrisation 79—83945
computerised electron beam treatment planning algorithms 79—100733
computerised tomography, dose determ. method 80—21542
computerised tomography, dose reduction using a generalised filter 79—66557
computerised tomography, dose specification philosophy 79—16309
computerised tomography, EMI first generation scanner, dose rel. to collimator geometry 79—74760
computerised tomography, head scanner, dose distrib. 79—83940
computerised tomography, noise and dose comparison, conventional and energy selective systems 79—66540
computerised tomography, ultimate limit for spatial and density resolution 79—83935
computerised tomography, X-ray dose reduction using a generalised filter 79—83946
computerised tomography dosimetry, exposure meas. techniques 78—69212
computerised tomography of the trunk, body and gonad doses 79—66559
computerised tomography scan dose, meas. using pencil shaped ionisation chamber 79—20683
computerised tomography scanners, effect of X-ray source filtration on dose and image perform. 80—30865
computerized operation of a dosimetric service 80—58004
computerized tomography field measurement utilising the partial vol. effect 80—89865
concepts of radiation dosimetry, photon and charged particle dose meas., book 79—81101
concrete, gamma-ray buildup factors, Tchebycheff-fitted Berger coeffs. 79—31226
concrete buildup factors based on the American National Standard for flux-to-dose-rate conversion 80—47732
concrete Eisenhauer-Simmons γ-ray build-up factors, Taylor coeffs. 77—34394
conference, dose limitation systems, Vienna, Austria (Mar. 1979) 80—46736
conference, radiation physics, Calcutta, India (30 Nov. to 4 Dec. 1974) 77—54128
conference, radiation protection monitoring advances, Vienna, Austria (June 1978) 80—57007
conference on nuclear power systems, Washington, USA (1978) 79—41045
conversion factors C_λ and C_E 78—40341
conversion factors for absorbed dose in water 78—40338
corneas, canine, γ and negative pion irradiation of microvasculature 79—43964
cosmic high energy loss particles, high precision localisation methods, Biostack expts. 78—20235

dosimetry continued
cosmic high energy loss particles, radiobiology using visual track detectors in Biostack expt. 78—20234
cosmic particle dosimetry in nucl. emulsions for Apollo and Apollo-Soyuz Biostack expts. 78—20288
cosmic radiation dose field, meas. aboard Salyut-6 orbital station 80—89876
cosmic ray heavy nuclei, LET spectra vs. absorber depth 78—20296
cosmic ray high LET particle dosimetry, Biostack III Zea mays expt. 78—20287
cosmic ray neutrons, Ames collaborative study on mid-latitude flights 78—53538
cosmic rays, dosimetric significance at altitude of supersonic transport and in free space 78—20295
CR-39 plastic, electrochemical etching, dosimetry appl. 80—52824
cranial structure model exposed to microwaves, heat potential distrib. 79—2105
craniofacial anomaly assessment, computerised versus conventional tomography 78—73239
critical assembly, rapid calc. of neutron fluence and dose 77—38317
Critical Human Organ Radiation Dosimetry operators for cell survival models and insult assessment 78—20221
criticality accidents, dosimetry using activations of blood and hair 80—89857
criticality accidents at facilities processing fissile material, characts., detect. and action procedures *(French)* 78—55054
cutaneous human tumours, selective RF heating at 27.12 MHz 79—2123
cylindrical source shielding eqns. including buildup, lateral dose rate, compact function use 78—89982
cytogenetic dosimetry, human, dose response relationship for ^{241}Am α-particle 80—30895
cytogenetical indicator of radiation effect, chromosomal dosimeter *(Hungarian)* 80—94292
decommissioned nuclear facilities, radiation exposure pathways 80—13957
decommissioning, activation and dose rate calcs. 80—13958
decommissioning of nuclear facilities, deform. of acceptable residual radioactive contamination levels 80—13973
dental enamel, human, proton activation anal., exposure and damage 79—70608
dental patients, X-ray exposure obs. 80—104761
dental radiography, pantomographic and conventional, doses to patients 79—92375
dental radiography, phantom meas. of absorbed doses 77—81576
dental radiography, reduction of patient exposure 79—25106
dental radiological safety, pilot survey 79—43993
dental X-ray photographs, comparative study of patient exposure to radiation 78—92702
depth dose distributions in water phantom irrad. by teleisotope photon beam 80—81741
depth-dose curves of linear accelerator, improvement, Monte Carlo calcs. 79—20681
depth-dose distributions for isotropic and cloud source irrad. by monoenergetic neutrons and photons 78—24138
depth-dose relationships near the skin resulting from parallel beams of fast neutrons 80—30902
detector perturbations to neutron and gamma-ray spectra measurements in liquid air 79—59314
diagnostic radiology, mean active bone marrow dose to USA adult population 78—85382
diagnostic radiology, Sweden, patient exposure and radiation risks 79—53248
diagnostic X-rays, dose distrib. calc. method for bone- and lung-equivalent material *(German)* 80—61704
dichromate solutions for low-level dosimetry 79—29633
digital data logger, microprocessor-based, for radiation detectors 79—26848
direct reading pen dosimeters, radiation exposure meas. aspects *(German)* 78—5050
discharge counter for U in water determ. by fission track method 78—5108
dominant lethality in spermatogonia of mice after acute and chronic gamma-irradiation 79—25039
dose assignment criteria, beagles, bilateral exposure to ^{60}Co γ-rays 79—16305
dose calculation system, ^{192}Ir interstitial radiation therapy 79—16268
dose conversion factors for high energy electron and photon dosimetry, solid-cavity theory 80—13944
dose distribution, effect on induction of expt. lung cancer in Syrian hamster by α-radiation 79—16254
dose distribution studies, partial body irradiation of small animals 79—20670
dose equivalent for gamma rays *(Japanese)* 80—23158
dose equivalent index, practical implications 80—47778
dose equivalent index, practicality for regulations 80—47777
dose equivalent measuring instrument for rapid use in mixed radiation fields 78—15901
dose equivalent unit 79—79658
dose field monitoring by independent detectors in cassette 77—81578
dose limitation system, application problems 80—47767
dose rate, risk factors, natural and man-made radiation, Germany, (1974) *(German)* 79—9897
dose rate evaluation from radiation heating of sample during irrad. 77—50311
dose record keeping service, description 77—16990
dose-equivalent index, application to natural radiation background 79—5374
dose-modifying factors test 80—21544
dose-rate conversion factors, radiation from nuclear fuel cycle facilities routine releases 80—86993
dose-rate conversion factors for external exposure to photons and electrons, modifications to DOSFACTER code 80—104775
dose-rate model testing with Chlamydomonas reinhardi 80—21543
dose-response relationship of neutrons and γ-rays to leukemia incidence, atomic bomb survivors 80—36148
dose-response relationships for female Ra dial painters 80—21545
dosimeter-based adjustments of fast-neutron spectra 79—54611
dosimetry, automated data acquisition and anal. system at LAMPF pion therapy facility 78—53506
drinking water, Finland, internal radiation doses due to radioactivity 80—109029

dosimetry continued
Drosophila melanogaster, repair of electron irradiation damage 79—11983
ECG-gated radiography 80—26344
electret pulse-detector for fast neutrons 80—23260
electrets, radiation-induced charge storage and polarisation effects 80—80684
electrometer operation in ionizing photon radiation fields by compensation method 77—79110
electron, standardisation program at US National Bureau of Standards 80—13943
electron accelerator, shielding for high energy neutron dose 79—54609
electron beam, dose and shielding parameters of electron-photon stray radiation 77—57755
electron beam, pulsed high-intensity, self-focusing obs. in low-press. gas 80—32899
electron beam, sinusoidally modulated, absorption curves for various materials 77—24339
electron beam applicator, variable field, dosimetry evaluation 80—76839
electron beam dose distrib. modification by transverse mag. fields 78—65132
electron beam dose distribs., model for calculating effects of small inhomogeneities 80—76837
electron beam dose profiles, cumulative normal distrib. model 79—88199
electron beam dosimetry for treatment planning 80—3817
electron beam processing, dosimetry and quality control 79—49871
electron beam radiation processing on industrial scale, surface dose 77—73282
electron beam treatment planning, patient specific data acquisition 79—100731
electron beam treatment planning, symposium, Cincinnati, USA (July 1977) 79—100730
electron beam treatment planning and execution, for 10 to 35 MeV beams 79—100732
electron beam treatment planning for 1 to 10 MeV beams 79—100735
electron beam treatment planning system, absorption equivalent thickness factor 79—100734
electron beams, 15 to 50 MeV, calorimetric and ionometric meas. in graphite 77—2052
electron dose distrib. in radiation processing 79—49872
electron dose distrib. in radiation therapy, magnetic enhancement 77—81570
electron dose distribution in phantom, mag. enhancement 77—48872
electron dose from immersion in semiinfinite photon-emitting cloud 77—73583
electron dose reduction coeff., internal radionuclides, source free target, cylindrical geometry 78—92704
electron dosimetry, scatter effects, plane ^{90}Sr-^{90}Y medical applicator 80—61699
electron dosimetry below 50 MeV, Monte Carlo calcs. 78—7453
electron dosimetry in tissue equiv. phantoms 78—7454
electron dosimetry of irregular fields on the Clinac 18 79—100747
electron elastic and inelastic interactions with liq. water 80—9477
electron flux in slab geom., high-energy radiotherapeutic field 77—81585
electron interactions, low-energy, single and twin biological targets 80—12195
electron irradiated mats., at 10 MeV, dose distrib. determ. 77—70265
electron irradiated solid, dynamic and dosimetric characts., laser and holographic interferometry obs. *(Rumanian)* 80—90886
electron linear accelerators, regulations, standards, and guidelines for use in medical radiation therapy 79—53258
electron slowing down in water, spatial correlation of energy deposition events 80—9473
electron sources, plane infinite oblique, Monte Carlo calcs. on dose distribs. 77—65339
electron therapy beam dose profiles in tissue and air 77—40786
electron track end effects in water 80—11932
electron transport Monte Carlo calcs., orthogonal function expansion technique 77—26248
electron transport simulation in liq. water, appl. to microdosimetry and radiobiology *(French)* 80—12202
electrons, 15 to 39 MeV, cavity displacement effect and reference depths, using LiF 77—2057
electrons, 25 MeV, absolute meas. of absorbed dose in water in total absorption type calorimeter *(Japanese)* 78—78501
electrons, 25 MeV, lateral absorbed dose distrib. in water, least-squares fitting FORTRAN program *(Japanese)* 78—74505
electrons, high energy, depth absorbed dose distribs. 78—73256
electrons, high-energy, using ionisation chambers 77—40785
electrons, microtron beam depth absorbed dose distribs. rel. to dosimeter type 77—52887
EM, non-ionising, hazards in the laboratory and effects on skin and eyes 78—96064
EM absorbed dose in man and animals for plane wave irrad. condition at variable orientations 80—36141
EM dosimetry for human and animal models, numerical techniques review 80—36142
EM energy deposition in animals and human models, grounding and reflector effects 78—40346
EM energy deposition in biological tissue at 900 and 450 MHz 78—69222
EM field induced in tissue, theoretical model 77—12957
EM fields induced in human bodies, up to 500 MHz 78—24140
EM internal field and absorbed power density in human torso, 1 to 500 MHz EM waves 77—86631
EM non-ionising radiation, influence of quality on bioeffects, exposure standards 78—44558
EM plane wave irradiation of ellipsoidal model of man, long-wavelength anal. 77—9219
EM power absorption, long-wavelength, by ellipsoidal models of man and animals 77—12956
EM power deposition in prolate spheroid models of man and animals at resonance 78—31905
EM radiation biological effects, conf., Amherst, USA (Oct. 1976) 78—40243
EM scattering and absorption efficiencies for nonspherical dielec. objects, biological models 78—40241
EM waves, biological effects and medical appls. 79—48288
embryo, radiation absorbed dose estimates from some nuclear medicine procedures 80—104760
embryo doses from nuclear medicine procedures 77—5083

dosimetry continued
emergency conditions, monitoring and handling 78—57082
EMI computerised tomography brain scanner, patient dose 78—28080
emissions from alternative electricity generation fuel cycles, health hazards evaluation 78—11791
emitted radiation, clarification of concept, brachytherapy dosimetry appl. 80—76843
energy deposition rates, materials irrad. in large ^{60}Co facility 80—47728
energy deposition spectra and radiation therapy appl. 80—26363
energy imparted under nonequilib. conditions, definition 80—36145
energy sources, role of health physicist in development of safe sources 78—36088
energy transfer in biological model structs., X- and γ-rays *(German)* 78—15906
enriched heavy minerals in sand grains, enhanced natural radiation exposure *(German)* 80—51018
environmental and personnel monitoring, long-term, with solid-state dosimeters 77—50308
environmental effects from nuclear energy, effects of small radiation doses 79—2312
environmental external radiation levels in N Carolina 78—80968
environmental impact from radioactivity releases, dose commitments, how long 79—52960
environmental pollution, biophysical aspects of ^{241}Am, ^{241}Pu 79—39530
environmental pollution by nuclear fission products 78—85607
environmental protection, radioactive waste from power plants in USSR 79—26601
environmental radiation dose assessment of a growing nuclear industry 80—3553
environmental radiation meas., instrument calibration 80—9426
environmental radioactive releases from nuclear installations, computer simulation of effects 80—3550
environmental radioactivity, determ. for dose assess. 80—85321
environmental radioactivity, meas. of water, soil, and foodstuffs 79—5378
environmental radioactivity, methods for determ. of radionuclides in environmental samples 79—48202
environmental radioactivity, radiation dosimetry control, exposure rate monitoring of natural radiation reference field 80—67017
environmental radiological surveillance, relative importance of environmental media 79—66421
environmental thermoluminescent dosimetry, regulation compliance, data interpretation 80—57995
ERDA nuclear plants, radiation levels in environmental vicinity 78—9002
European neutron dosimetry intercomparison project results, recommendations for biological and medical appls. 78—82532
exoelectron dosimeters, reference dosimeter bank, storage, exposure and reading 80—5360
experimental radiation transport to large distances from a bare reactor 79—59275
external beam radiation dose distribution calculation, radiation therapy planning 79—62364
external beam radiotherapy, isodose planning, new suite of programs 80—41243
external beam radiotherapy optimisation, relative radiation effect and isoeffect pattern computer study 79—62368
eye dose during tomography of para-nasal sinuses, conventional vs. rare-earth screens 77—37055
eye shield for use during carotid angiography 78—44615
eye tumour treatment, computerised X-ray tomography for post therapy control *(German)* 79—100727
face, solar dosimetry, natural UV exposure rel. to basal cell carcinoma localisation 79—92382
fallout at Chilton, Oxon. (1951-1977) 79—6775
fallout nuclide determination for 19th Chinese nuclear test 79—54601
fast electron f(z) meas. using short accelerator pulses 80—12275
fast neutron, scatt. radiation from neutron collimater 77—40788
fast neutron beam, computer generation of dose distribs. 79—39510
fast neutron beam build-up and depth-dose characts. for radiotherapy 78—28072
fast neutron beams, linear regression anal. of γ-dose 80—89866
fast neutron depth-dose and neutron fluence-to-dose-index conversion factors calcs. 80—41250
fast neutron dose equivalent rates in heavy ion target areas 79—54606
fast neutron dose to the human body, contrib. for ^{39}K, ^{35}Cl and ^{32}S 80—51263
fast neutron dosimetry techniques 79—20677
fast neutron dosimetry using S activation in CaSO$_4$:Dy and Teflon dosimeters 78—70648
fast neutron facilities for radiobiological irrad. 80—109064
fast neutron fluence meas. technique, uses neutron irrad. effect on light absorption of cellulose acetate 78—13345
fast neutron irradiation of cells cultured in monolayer, dosimetric aspects 78—69218
fast neutron pulses, time distrib. of doserate behind polyethylene/Fe layers *(German)* 77—26886
fast neutron research reactor YAYOI core absorbed dose meas. by chemical dosimeters *(Japanese)* 78—86695
fast neutron sealed-tube radiotherapeutic installations, characteristics 79—20650
fast neutron therapeutic dosage schedule development 79—20678
fast neutron therapy, use of ^{10}B to enhance tumour dose 78—73249
fast neutron therapy beam intercomparison using mouse testes as biological test system 78—20225
fast neutron therapy beam prod. by 26 MeV protons on Be, dose meas. 78—28054
fast neutron therapy system using cyclotron beam, beam optics and shielding 79—57756
fast neutrons, 4 to 27 MeV, dosimetry using response of E.coli AB2463 recA 78—65077
fast proton track energy deposition and ionisation calc. and obs. 80—12196
fast reactor dosimetry using zero-power facility ZEBRA 79—3219
fathead minnow, effect of dose rate on survival time 80—30799
FBR accidental releases, implications of dose-mortality relationships 80—46064
fetuses, mouse, obs. after 2.45 GHz irradiation of mothers 79—20578
film dosimeter exposure anal. method *(Bulgarian)* 79—85831
film dosimetry, endurance of film in personnel monitoring 80—23171
film dosimetry of multiple electron beam ports with wedges 80—98138
film evaluation by neutron activation and X-ray fluoresc. anal. 79—63820

dosimetry continued
film exposure determ., comparison of X-ray fluoresc. and optical density 78—24137
finger doses received by radiologists during Chiba needle percutaneous cholangiography 80—81737
fission counters, high sensitivity, neutron spectroscopy and dosimetry appl. *(French)* 80—58078
fission fragment track and activation detectors, neutron fluence and reactor core centre flux mapping 78—13346
fission neutron spectra, light water-moderated, depth-dose characts. 80—106205
fission neutron spectra degraded through high Z shields, depth dose characts. 80—46053
fission neutron spectra degraded through low Z shields, depth-dose distrib. 79—39516
fission rates and ratios in, intermediate energy standard neutron field 78—21687
fission reactor materials, gamma heating-effects, meas. using calorimetric and dosimetric techniques 80—658
fission research reactor intercomparison using chem. dosimeters and Ni foil threshold detector 77—57753
fission track glasses, calibration of fission track dating parameters 77—41207
fluence device for precise radiation dosimetry 80—46059
fluence of secondary photons generated by attenuation in thin walls 80—18699
fluoroscopic unit, variable aperture, reduced patient exposure 79—92368
fluoroscopy, organ dose per unit exposure, estimation method for artificial pneumothorax 78—96097
fluoroscopy without the grid, dose reduction method 80—41240
foetus, human, effect of a high gamma dose from ^{226}Ra 79—25104
frame recording method for intermittent X-ray TV to reduce exposure dose in fluoroscopy *(Japanese)* 78—89607
French nuclear power plant occupational radiation exposure meas. and prediction 79—9900
Fricke dosimetry, determ. of molar extinction coeffs. of Fe^{3+} 80—13949
full flux covariance matrix calc. for NBS intermediate-energy standard neutron field 80—5348
fusion reactor design, nuclear data requirements 77—23291
fusion reactor irradiation test facility, higher energy neutrons, shielding calcs. 80—13786
fusion reactors, TFTR test cell, calc. dose rates from induced activity, Monte Carlo methods 80—57967
gamma, irrad. vessel wall effects in chemical dosimeters 80—18697
gamma and X-ray, phys. quantities used in radiation safety monitoring 80—99344
gamma dose intensity in dwelling places, dose conversion factors *(Hungarian)* 77—77990
gamma dose meas. in d(80)+Be neutron beam 79—70648
gamma dose to gastric wall, estimation after administration of ^{131}I *(Japanese)* 80—98141
gamma exposure rate, real time simulation by puff model 80—47618
gamma irradiation, human whole body, fluence and exposure-to-dose conversion 79—5371
gamma irradiation geometries for food preservation 77—70508
gamma irradiation of housefly larvae, influence of caffeine on dose fractionation sparing effect 79—100679
gamma ray sources for exposure rate meas. instrument calibration 80—32562
gamma sources, secondary standard preparation for low activity gamma spectrometry 80—18701
gamma spectrometry, low-level, in vivo, optimum detector size and position 78—28075
gamma spectrum average energy and numerical buildup factors meas. 77—54397
gamma-ray, using cholesteric liq. cryst. soln. colour transition 77—48877
gamma-ray backscattering, survey of principal research 77—65340
gamma-ray dose buildup factor functions, polynomial parameters 79—54607
gamma-ray dose rate conversion and buildup factors 79—34671
gamma-ray dosimetry, effect of buildup factors 80—18698
gamma-ray dosimetry errors with thermoluminescent dose meters 80—18705
gamma-ray emitters, point isotropic, dose in surrounding water 79—62363
gamma-ray external field meas. at Vermont Yankee BWR power station 77—54368
gamma-ray natural flux spectral distribution, analytical approx. 78—815
gamma-ray streaming through annular cylindrical duct, dose computation at exit 77—65342
gamma-ray streaming through ducts, spectral meas. 80—32523
gamma-rays albedo, number and energy calcs., Monte-Carlo calcs. 79—31221
gas-chemical dosimetry, limitations of use of strong pulse electron beams 79—31231
gastrointestinal tract, specific absorbed fractions for photons emitted in walls 77—90903
Geiger-Mueller counter for mixed n-γ dosimetry 78—25394
Geiger-Muller dosimeter and tissue-equivalent ionisation chamber, use in dose equivalent evaluation 80—51264
genetically significant dose due to medical diagnostic exposure to Italian population, (1974) 77—66850
geometric factors, relation for different media 80—109036
glass dosemeter reader, design improvements *(French)* 80—57970
glass lenses, effectiveness in reducing eye exposure 79—92394
gliomas, malignant, anal. of dose-effect relationship in radiotherapy 80—72331
gliomas, malignant, high dose radiation therapy 80—67254
global collective dose commitments, long lived radionuclide release 79—26780
glottic cancer, T3, anal. of close time-vol. factors 80—104764
gonad dose due to radioactivity of building mateials in Norway 77—44761
gonadal dose determ. in Turkish diagnostic radiology 79—79655
gonadal doses to 78070 patients undergoing diagnostic X-ray exam. 78—53503
graphite ionisation chamber with CO_2 filling, Monte Carlo anal. of fast neutron irradiation 78—82583
Hanford workers dying from cancer and other causes, radiation exposures, Richland USA 78—15893
head and neck, advanced cancers, low dose rate irradiation 79—34649

dosimetry continued
head and neck cancer, advanced and recurrent, short course high fractional dose irrad. 80—72297
health aspects of low-level radiation, radiation protection standards 80—26375
health physics conference, San Francisco, USA, June/July (1976) 77—16983
health physics in the Novazza (Bergamo, Italy) uranium mine *(Italian)* 79—74764
health physics quantities and units 80—8193
Health Physics Research Reactor, operating history and recent improvements 80—9382
heavy charged particle/water interaction, dose distrib. due to electrons, delta rays 80—13937
heavy ion and He dosimetry and instrumentation 79—20675
heavy ion beam linear energy transfer distribution calc. 79—20630
heavy ion peak-to-plateau relative biological effectiveness ratios, fractionation enhancement 79—62309
heavy ion track structure in tissue, microdosimetry 77—2032
heavy ions, high energy, dosimetry for radiobiology expts. 77—66849
heavy particle comparison for therapy, depth-dose distribs. for π^-, n, p, He, C, Ne and Ar ions 78—85379
heavy particle microdosimetric data with high intensity beams, pion appl. 78—40331
heavy particles, stopping in gases, $\bar{W}$-values expt. results 79—7000
Hela cells, recovery from sub-lethal damage when irradiated at ultra high dose rates 79—79608
heritable lesions, radiation induced, in proliferating mammalian cells, review 79—20602
high current relativistic electron beam, X-ray emission, pulsed dosimetry 79—81099
high energy photon and electron dosimetry with ionisation chamber, C_λ and C_E discrepancy 77—52885
high energy photon and electron dosimetry with ionisation chamber, C_λ and C_E discrepancy 77—52886
high energy X-ray and electron beams, appl. in radiotherapy, dose distribs. 79—53227
high intensity radiation equipment, radiation safety during operation, personnel dose 77—73601
high LET constraints on low LET survival of cells, RBE theory 78—92679
high LET radiation therapy beams, expt. microdosimetry 80—12280
high-energy accelerator fields, bevatron and linear accelerator comparison 78—25331
high-energy photon dose meas. using exposure-calibrated ionisation chamber 78—3607
high-energy X-ray beams, scatt. radiation rel. to leakage radiation 80—51266
high-level waste solidification plant, contribs. to risk evaluation 78—17356
hip dysplasia studies, infant, using image intensifier fluorography 79—48343
hip radiography, bull, skin and gonadal dose reduction, Pb sheeting and Cu filtration 79—100743
Hiroshima A-bomb survivors, whole-body doses estimation by chromosome aberrations 80—109035
Hiroshima mass radiologic gastric surveys, examinees' doses 80—89858
historical development of need for radiation protection and meas. in USA 77—37708
holographic method, for ionising radiation dosimetry 80—852
Howe Caverns, USA, doses to employees and public from Rn and Rn daughters 80—89859
HTGR, maximum pot. hazard of ultimate accident sequence initiated by PCRV leak 78—13278
HTGR refuelling, equipment safety, gamma dose meas. 80—47668
human body radiation monitoring, radioisotopes direct determination 79—54602
human exposure due to environmental radiation *(Japanese)* 80—72336
human marrow, radiation dose deposition calcs. 80—26365
hyperthermia dosage definition form in vitro thermal cytotoxicity data 78—24178
hyperthermia induced by microwaves, dose definition 79—2135
ICRP dose limitation system *(French)* 80—47753
ICRP new concept of person dose, related to film badge exposure 79—29631
ICRP recommendation implication in Israel 80—47773
ICRP recommendations, applications in practice 80—47771
ICRU phantom neutron fluence to dose index conversion factors 79—9909
ilium, exteriorised upper segment in rat, effects of X-irradiation on glucose, proline uptake 79—11984
image intensifier fluorography, image quality rel. to patient dose 80—17081
impulse fluxes of ionising radiation, use of microwave methods 77—25557
impulsive and continuous noise, combined dose meas. 80—102929
Indian Secondary Standards Dosimetry Laboratory, development and functions 80—41244
indoor natural radiation environment and dose distribution in man, multicompartment models 79—12015
industrial radiography, accidental over-exposure to ^{192}Ir source 77—56472
inhalation doses, airborne releases, estimation using gross monitors 79—13532
inhalation exposure of miniature swine 79—11976
inhaled natural radioactive nuclides, dose calcs. 80—26354
inner radiation belt, max. radiation dose following 1962 STARFISH explosion 78—69612
intake limits of radionuclides for workers 80—36134
integral dosimetry, use of lyoluminescence *(Czech)* 79—67964
integrator for use in bombardment experiments 79—18092
intense neutron source facility, skyshine anal. methods comparison 80—5349
intense photon flux absorbed dose meas. 78—41387
interaction with matter, review and bibliography *(Japanese)* 80—39149
interface, dose enhancement due to backscatt. secondary electrons 77—2058
interface energy transport by electrons 77—86647
interferometry and holographic interferometry appls. 80—42871
intermediate-energy secondary spectrum system, determ. of neutron characteristics, ΣΣ-ITN *(Rumanian)* 79—22355

dosimetry continued
  - intermittent gaseous release from nuclear plant, probability distrib. of atm. dispersion factor 78—11994
  - internal absorbed dose determ., computer method 78—15895
  - internal radionuclide point source microdosimetry, specific energy density calc. 80—26373
  - internal source microdosimetry 78—3615
  - internally deposited radionuclides 77—25553
  - International Commission on Radiological Protection, dose limits (1934-77) 80—12266
  - International Commission on Radiological Protection, recommendations 80—47752
  - international network of laboratories to improve standards of absorbed radiation dose meas. 77—67898
  - international radiation standards, role of ICRU 80—9414
  - international standard reference radiations and their application to the type testing of dosimetric apparatus 80—9416
  - interstitial dosimetry, utilisation of the computerised tomography scanner 80—104770
  - intestinal tolerance in mice, effect of dose rate, implications in radiotherapy 79—29568
  - intracavitary therapy, dosimetry of Cathetron applicators 78—69217
  - intracavity implant therapy, appl. of linear programming to dose optimisation 80—72329
  - intracavity radiotherapy, interactive treatment planning using CT 80—8145
  - ion beam monitoring using thin self-supporting reference foils 80—50911
  - ion energy deposition in simulated biological matter, Monte Carlo method 77—81584
  - ion implantation, dosimetry techniques, review 80—32527
  - ion implantation dosimetry, diagnostic test 79—90690
  - ion implantation system, high current, design of end station, appl. to Si:As, ion implantation system, high current, design of end station 80—34030
  - ion implanted impurities, absolute dosimetry using colorimeter-Faraday cup system 78—26590
  - ion implanters, electrostatic and mechanical scanning, high current dosimetry techniques 80—32528
  - ion pair formation, depend. of average energy on atomic number of heavy ions 80—18695
  - ionisation chamber conversion factors C$_\lambda$ and C$_E$ 77—86645
  - ionisation chamber dose meter unit for emergency operations *(French)* 80—57977
  - ionisation chamber dosimetry, Ar/propane, mixed X-ray/neutron fields 79—20682
  - ionisation chamber perturbation correct. factor for β-radiation fields 80—37704
  - ionisation chambers, depth dose distrib. of 9 MeV photons, comparison with phantom results 77—32957
  - ionisation smoke detectors, risks to humans 78—15909
  - ionising gases, meas. of m-values 80—18694
  - ionising radiation, detection device, electret based *(French)* 80—57971
  - ionising radiation, dose-effect relationship for quantifying health risks *(German)* 80—61644
  - ionising radiation, metrology and calibration, French system *(French)* 80—5351
  - ionising radiation, personnel exposures, dose limits 80—99350
  - ionising radiation, primary standards and transfer methods in France, review *(French)* 80—5352
  - ionising radiation, SI meas. system *(Hungarian)* 77—3167
  - ionising radiation, traceability in meas. systems 80—5355
  - ionising radiation calibration, meas. standards, CNEN, Italy 80—12273
  - ionising radiations, effects and sources *(French)* 79—66494
  - ionization-chamber-dependent factors for calibration of megavoltage X-ray and electron beam therapy machines 80—18704
  - ionizing radiation and cavitation threshold 78—94774
  - ions, energy loss per ion pair in Ar and tissue-equivalent gas 77—35312
  - IR spectroscopy appl. to charged part. dose meas. in cellulose triacetate 78—94145
  - irradiated tumours, dose/cure relationships, statistical anal. 80—46052
  - IRT 2000 reactor in Sofia, neutron spectra and doses in exptl. canals *(Bulgarian)* 78—82489
  - isodoses in human radiotherapy, automatic determ. using whole body computer tomography *(German)* 77—9236
  - kerma partition to account for energy deposition in matter 79—66482
  - KERMA values, consistent set for H, C, N, and O for neutrons from 10 to 80 MeV 80—68967
  - Kodak Type II film badges, gamma dose meas. in presence of thermal neutrons 79—39517
  - laser radiation dosimetry, standardisation of practice 77—16998
  - laser radiation dosimetry for eyes 80—12268
  - leaf, Saintpaula, dose-effect curve shape rel. to radiation-stimulated repair 80—26291
  - leukemia incidence in atomic bomb survivors of Hiroshima, Nagasaki 79—57722
  - leukemia risk from neutron exposure 79—39509
  - life-expired LWR, neutron activation product density and dose rate calc. 79—9908
  - lightning, thermoluminescent dosimetry measurement of radiation 80—36361
  - linear accelerator, field separation between lateral and anterior fields, dose distrib. 80—94336
  - linear accelerator calibration monitor with a memory 80—3821
  - linear accelerator dosimetry control system, solid state 80—94371
  - linear accelerator used in high-energy photon radiotherapy, 10 MV, neutron prod. 77—16995
  - linear accelerator X-ray beam energy at off-axis points, calc. technique for correct. 80—81742
  - linear attenuation coefficients of biological materials, extrapolation from diagnostic energies to megavolt range 78—24145
  - Lipowitz metal shielding thickness for dose reduction of 6-20 MeV electrons 80—76842
  - liquid acoustic dosimetry for ionizing radiation 79—18060
  - liquid air, energy spectra and doses of ^{252}Cf neutrons 77—67901
  - liquid air, transport of neutron and secondary γ-rays from 14 MeV source 78—50234
  - liquid irradiated, dosimetry by holographic interferometry *(Rumanian)* 80—9412
  - liver membranes, mouse, X-irrad., dose-rate effects 80—94293
  - LMFBR, Clinch River Plant, sensitivity for radiological consequences to var. in aerosol parameters 78—13294

dosimetry continued
  - LMFBR, determ. of ^{137}Cs conc. in Na heat carrier 79—41043
  - low dose/dose rate RBE of ^{3}H β-rays and other low LET radiations 80—12190
  - low level radiation monitors, calibration accuracy and precision 80—9428
  - low-dose radiation carcinogenesis 80—12198
  - low-energy electron processing systems, calc. 80—844
  - low-energy heavy charged particle stopping power, phase effects 80—23277
  - low-level radiation during development studies, implications for ICRP-26 80—51281
  - LR115 cellulose nitrate detector system for personal dosimetry near high energy accelerators 80—58081
  - LR115 red cellulose nitrate personnel neutron rem dosimeter, design 80—52826
  - Lucens reactor accident, alarm and surveillance 78—50283
  - lung, ^{218}Po, ^{214}Po, dosimetry in Syrian golden hamster 79—16304
  - lung, nuclear medical imaging, estimates of radiation absorbed doses from radioxenons 80—101269
  - lung burdens of low-energy photon-emitters, interlaboratory comparison of meas. techniques 79—20671
  - lung dose in half body radiotherapy, determ. by computerised tomography 80—104763
  - lung ventilation studies with ^{133}Xe, patient dose 78—24146
  - LWPR, radiological emergency monitoring and instrumentation, Federal guidance 80—57961
  - LWR, design meas. to reduce radiation dose to reactor personnel 79—3199
  - LWR core meltdown, activity release and aerosol characts. 78—82469
  - LWR pressure vessels, radiation embrittlement, role of ASTM 79—22435
  - LWR radiation control techniques 79—59184
  - lymphocyte, human, dicentric yield, γ dose rate dependence calc. 79—92294
  - lymphocyte chromosome aberrations in humans induced by photon and electron irrad., sublesion interaction model 80—26279
  - lymphocytes, human, chromosome aberrations induced by ^{252}Cf neutron radiation 79—16169
  - lymphocytes, human, homogeneous sensitivity to radiation-induced chromosome damage 79—53197
  - lymphocytes, human, prediction of dose-rate effects for dicentric production by X- and γ-rays 80—72226
  - lyoluminescence 78—20274
  - lyoluminescent, of ionising radiation 79—6769
  - magnetic modification of electron beam dose distributions 80—30893
  - Magnox reactors, influence of design and operation on personnel radiation dose meas. 80—5385
  - Makrofol polycarbonate, electrochemical etching of neutron induced tracks, appl. to dosimetry 78—20282
  - malignant melanoma, radiation treatment 80—94372
  - malignant melanoma, relationship between total dose, fraction number, fraction size 79—5341
  - mammacarcinoma conservative radiotherapy, computer assisted dosimetric soln. *(Dutch)* 80—36139
  - mammalian cells, Chinese hamster, human kidney, radiation studies with modulated C ion beam 79—11978
  - mammalian cells in culture, continuous and fractionated irrad., growth rate effect 79—66493
  - mammary gland cells, rat, survival after X-irradiation under different endocrinological conditions 79—34513
  - mammographic dose reduction, Kodak Definix Medical rel. to Kodak Min R film *(German)* 80—12243
  - mammographic image quality improvement by scattered radiation grids 79—92332
  - mammographic imaging, historical review in terms of image quality and reduced radiation dose 80—41229
  - mammographs, high quality low-radiation, tone reproduction system 80—41198
  - mammography, absorbed dose evaluation, Monte Carlo simulation studies 80—98143
  - mammography, backscatt. factors, var. with field diameter and half-value layer 78—3593
  - mammography, carcinogenic dose-effects relationship 79—70617
  - mammography, dose meas. with high-sensitivity coated-film system *(German)* 79—53257
  - mammography, image quality and dose requirements *(German)* 79—79646
  - mammography, survey of patient skin dose, New Zealand 77—90901
  - mammography with magnification and grids: detail visibility and dose measurements 80—41231
  - mamography, risks, radiation dosage and picture quality, review *(German)* 80—36103
  - management of an automated dosimetry and dose record keeping service 80—58006
  - manned space crew radiation, design and zero-G problems 77—30674
  - mannose, increased lyoluminescence response on storage 79—25112
  - marrow colony-forming units, dose-dependence of the split-dose response 80—61701
  - marrow dose estimation by ^{59}Fe uptake in normal and splenectomised rats, 1000 kVp X-irrad. 78—15894
  - maternal cancer, internal irradiation technique, dose calcs. *(Dutch)* 80—3816
  - maximum permissible conc. calc. using absorbed dose data of MIRD pamphlet 11 78—53516
  - maximum radiation exposure calc. around German nuclear plants 80—856
  - maximum tolerable radiation doses recommended by Israel Advisory Committee on Nucl. Safety 78—53517
  - Maxwell method for rapid neutron dose evaluation in overexposure cases 78—62664
  - measurement standardisation and calibration within the European Communities 80—9415
  - medical, using TLDs *(German)* 78—15904
  - medical dosimetry standards programme of the National Bureau of Standards, USA, review 80—8187
  - medical examination dose, from X-ray and radioisotopes, children 79—16308
  - medical facilities, US state and federal regulatory meas. responsibilities 77—40765
  - medical findings for GDR works, documentation to meet ICRP-26 80—51280

dosimetry continued
- medical imaging system evaluation by contrast-detail-dose analysis 80—98140
- medical linear accelerators, neutron dose equivalent rate obs. 79—70643
- medical neutron dosimetry, standards 79—12013
- medical physics conf., Atlanta, USA (July-Aug. 1979) 79—83858
- medical physics conference, Ottawa, Canada (Jul. 1976) 77—16897
- medical radiation practice, ICRP recommendations in worker medical monitoring *(French)* 80—51275
- medulloblastoma treatment technique and radiation dosimetry 78—35926
- megavoltage depth-dose value corrections due to reduced backscatt. thickness 77—48871
- megavoltage dosimetry, choice of reference point 80—30898
- meningioma irradiation, prototype circumscribed tumour for planning high-dose brain irrad. 78—35925
- metabolic model for Po 79—79657
- methane, electron transmission function and mean energy per ion pair, obs. 80—23566
- methane-based tissue equivalent gas, W_n and neutron kerma 80—104769
- method for calculating the dose commitment from bioassay data 80—109031
- microdosimetric characteristics of neutrons at energies between 50 eV and 10 MeV 80—27829
- microdosimetric distributions for small sites, Monte Carlo calc. 78—3617
- microdosimetric measurements of pretherapeutic heavy ion beams 80—72337
- microdosimetric results from ionisation chamber and proportional counter compared 80—9429
- microdosimetric studies with low LET radiation using cylindrical walled and wall-less proportional counters 80—36140
- microdosimetry, conf., Brussels, Belgium (May 1978) 80—4472
- microdosimetry, energy deposition distrib. patterns, biological effects of ionising radiations 79—20600
- microdosimetry, interpretation of instrument lines of ionisation pulse spectrometer 77—73595
- microdosimetry, role in radiobiology 80—61705
- microdosimetry, secondary electron emission and two-target theory 80—12274
- microdosimetry of the pion beam at TRIUMF 80—109037
- microtron, 22 MeV, for radiation therapy, design, beam transport, gantry and depth doses 77—81552
- microwave, 2450 MHz, dose rate and O_2 consumption rate in mice confined in small holder 78—11697
- microwave, 918 MHz rat irradiation, thermographic near field effects and behavioural studies, near field effects 78—7386
- microwave, applic. of thermoluminesc. fading in $BaTiO_3$ ceramics 79—1792
- microwave, long-term exposure effects in rats, simulation of chronic exposure of human body 80—35972
- microwave absorbed dose rate distrib. in phantom heads irrad. by aperture source 77—73581
- microwave and radiofrequency radiations exposure limits proposed, in Canada 79—5375
- microwave dosimetry, thermographic comparison of temp. probes 79—96521
- microwave dosimetry method for penetrating radiation pulses 80—32531
- microwave energy absorption by mice, effect of ambient temp. 78—40263
- microwave enzyme inactivation system, electronic control to reduce dose variability 78—40285
- microwave exposure, densitometry and dosimetry techniques in bioeffects research 77—78072
- microwave far-field, dosimetric meas. of full-scale man model 80—67255
- microwave irrad., heat dissipation rate determ., mice 77—81472
- microwave linear accelerators, systematic patient-dose errors 79—92387
- microwave measurements of ionizing radiation exposure rate 79—97908
- microwave plane-wave power density calibration using power eqn. techniques 77—71341
- microwave radiation, dose rate rel. to time of death and total absorbed dose in mouse 77—2024
- microwave radiation, emission and exposure standards 78—44619
- microwave radiation, protection standards and need for field measurements 80—26377
- microwave radiation of biologically active microorganisms, coherent elec. vibrs. 79—2106
- microwave radiation pattern meas. in presence of biological specimens 78—48828
- microwave radiation safety, meas. and instrumentation 78—44618
- microwave whole-body dosimetry in small animals, effect of body mass and exposure geometry 78—40348
- microwaves, meas. of energy absorbed by biological systems by anal. of heating and cooling data 78—40343
- microwaves, meas. of energy absorbed by biological systems by Dewar-flask calorimetry 78—40344
- minicomputer-based radiation protection networks for nuclear plants 80—855
- mixed β-γ dosimetry, ionisation and scintillation counters 80—57975
- mixed field, comparison of methods for neutron and γ components separation 80—36143
- mixed n-γ field microdosimetry and neutron/gamma discrimination *(French)* 80—12279
- mixed radiations, device for dose-equivalent index determ. *(Russian)* 80—57976
- mixed-field γ meas. with nonhydrogenous Rossi counter 80—9430
- mobile testing laboratory PPLII-3 for ionizing radiation 79—74761
- monitoring beta and photon radiations for radiation protection purposes 78—15908
- monkey mortality, X-ray and neutron exposure, effect of autologous bone marrow transplantation 79—29572
- Monte Carlo computer code for calc. of radiation dose from syringes 80—41246
- MPD reduction suggestion fo meet requirements of higher safety 80—85499
- multi-channel meas. device for environmental control network *(Hungarian)* 78—57072
- multicell spheroid low dose-rate irrad. 79—62304
- multichannel electrometer data-acquisition system 79—89564
- multidetector technique readings, interpetation for dose equivalent determ. 79—49875
- multimode time-varying enclosures for exposure and dosimetry in bioelectromagnetic experiments 80—85497

dosimetry continued
- myocardial imaging agents, comparison of ^{201}Tl, ^{129}Cs, ^{43}K, ^{81}Rb 77—2037
- natural and man made radiation exposure in daily life, review 77—49535
- natural gamma-ray dose rate distribs., effect of male-female body-size diff. 78—24139
- natural internal radiation dose to man 77—56475
- natural radiation dose, variability as comparison point for acceptable radiation risk 80—51282
- natural radiation exposure, New Zealand, soil survey and air doses for ^{226}Ra and ^{232}Th daughters and ^{40}K 78—88747
- natural radioactivity in underground cavities, gas conc. and exposure levels *(Spanish)* 79—39322
- naturally occurring radioactive sources, external environmental radiation levels 78—9001
- naturally occurring radionuclides in building materials, estimation and control of population dose 78—9000
- neuroradiology, radiation dose to critical organs of staff and patients 80—8184
- neutron, above 10 MeV, standards 79—13544
- neutron, dielectric track detectors appl. *(Czech)* 78—66425
- neutron, elec. conductivity meas. method 77—40776
- neutron, fast pulse reactor, standardisation 79—13543
- neutron, international intercomparisons 79—12014
- neutron, radioactive target preparation and characterisation 80—18734
- neutron, standardization, 0.001-14 MeV, description of sources 79—9919
- neutron, standardized techniques for appl. beyond reactor core 79—9920
- neutron, stripping-theory anal. of thick-target prod. using Be(d,n) 77—6600
- neutron activation cross section, integral tests in ^{9}Be(d,n) field 80—851
- neutron beam characterisation by radioactivation image transfer technique 79—88195
- neutron beam dosimetry, prod. by Be(p,n) and Li(p,n) reactions with 26, 35 and 45 MeV protons 78—28083
- neutron beam for cancer radiotherapy 77—81567
- neutron beam production at Ruder Boskovic Institute for radiobiology and dosimetry appl. 78—20273
- neutron beams from D+d reaction, 6.8 to 11.1 MeV, dosimetric props. 78—53509
- neutron beams prod. by Be+p, 30 and 40 MeV, polyethylene filtration 78—53494
- neutron beams prod. by protons and deuterons on Be and Li, dosimetry 78—24141
- neutron capture therapy of cancer in mice, long range effects, dose effect 78—48877
- neutron collimated beam RBE for cell survival rel. to lineal energy spectral differences 80—12200
- neutron collimated fast beam, radiation quality local distrib. 80—12247
- neutron collimator, fast and slow neutron and gamma-ray components of scatt. radiation 77—48870
- neutron contamination of 25 MV photon therapy beam from Varian Clinac-35, evaluation criteria 77—86628
- neutron cross-sections and kerma values for C, N and O from 20 to 50 MeV 80—101217
- neutron cross-sections for reactor dosimetry, status 77—23304
- neutron detection, using Dy_2O_3 activation detectors 80—887
- neutron dose and quality factor meas. by tissue equivalent proportional counters 80—58079
- neutron dose calc., using analytical function, health physics appl. *(Slovak)* 79—25111
- neutron dose determ. using calculated neutron spectra 77—60263
- neutron dose distributions in pion$^-$ irradiated tissue, Monte Carlo calc. 79—16310
- neutron dose equivalent, meaning *(Japanese)* 80—847
- neutron dose equivalent meas. using ^{3}He proportional counter 79—63875
- neutron dose levels of 8 MeV linear accelerator and 18 MeV betatron used in radiotherapy *(German)* 78—69221
- neutron dose meas. with B-doped cellulose nitrate film 79—31321
- neutron dose measurements in a dummy for test animal irradiation in a reactor 78—61218
- neutron doses to patients in high energy X-ray therapy 77—86642
- neutron dosimeter and monitoring instrumentation calibration using ^{252}Cf and ^{238}PuBe sources 80—13946
- neutron dosimetric meas. using mica and pyrex, fission fragment track technique 78—13347
- neutron dosimetric measurements using ^{3}He detects. 79—63819
- neutron dosimetric props. using D(d,n) reaction 79—70646
- neutron dosimetry, appl. of thermoluminescent materials 79—22497
- neutron dosimetry, basic constants and meas. principles 79—20676
- neutron dosimetry, dose distrib. depend. on linear energy transfer *(Czech)* 80—68965
- neutron dosimetry, importance of fast neutron scatt. cross sections *(German)* 80—23175
- neutron dosimetry, international intercomparisons 79—20636
- neutron dosimetry, meas. standardisation for biological and biomedical appl. 80—12271
- neutron dosimetry, photointerference corrections for reactor pressure vessel lifetime studies 80—99345
- neutron dosimetry, problems rel. to incorrect composition of tissue-equivalent gas 80—81743
- neutron dosimetry at JINR synchrocyclotron 80—57983
- neutron dosimetry characterization of spent thermal reactor fuel assemblies, using nondestructive methods 80—23164
- neutron dosimetry for radiation protection, European workshop 80—23177
- neutron dosimetry in high energy X-ray beams of medical accelerators 79—83942
- neutron dosimetry methods for accidental exposures, Czechoslovak intercomparison 78—57075
- neutron dosimetry system, based on fission counter for fuel processing plant 80—57981
- neutron dosimetry techniques for accelerator-based irradiation facilities 79—41041
- neutron dosimetry using photodiodes 78—31907
- neutron dosimetry with cellulose nitrate film 78—20280
- neutron dosimetry with solid state nuclear track detectors, brief review 78—33299
- neutron energy deposition in tissue-equiv. sphere, influence of collimation 77—56482
- neutron energy spectra and close distrib. spectra of cyclotron-prod. beams 77—70554

dosimetry continued
neutron energy transfer to H_2, 30 to 100 MeV 77—52890
neutron equivalent dose and dose rate units, USSR primary standards 77—32955
neutron exposure of reactor press. vessel steel, safety limitations *(German)* 77—34405
neutron field, comparison of single and multidetector systems *(Russian)* 78—33294
neutron field in fast reactor, spectral charact. *(Japanese)* 78—46222
neutron field produced by D gas target with compact medical cyclotron 77—73592
neutron fluence meas. with solid state track detectors, international intercomparison 78—20283
neutron flux absolute meas. at fast pulse reactors, calibration against ^{252}Cf source 77—23389
neutron flux density determ., thermal and intermediate energy, using Au foils 78—82536
neutron flux density for irradiation of human tissue, max. permissible dose calc. 79—43992
neutron flux density monitor of non-flux perturbing thin foil 80—32522
neutron flux spectral uncertainties in ENDF/B dosimetry cross section file benchmark spectra 77—23306
neutron flux-to-absorbed dose conversion factor 77—90908
neutron ionisation chamber mean energy deposition calc., 0.1 to 20 MeV 80—9467
neutron irradiation facilities, dosimetric meas. 80—104762
neutron irradiation facility, TRIGA Mk.II reactor, remodelling and dosimetry 80—56200
neutron irradiation of lymphocytes in vitro, dosimetry rel. to radiobiology 77—64095
neutron kerma factors for H, C, N, O and tissue, 20-70 MeV 77—73584
neutron leakage spectra from critical assemblies, depth dose, dose equiv. and quality factor 78—58504
neutron monitor calibration, standard fields at Physikalisch-Technische Bundesanstalt 80—57999
neutron personnel dosimeters, European comparisons 80—57980
neutron personnel dosimetry, need for improved standards 79—12012
neutron personnel dosimetry in criticality accidents, fast neutron dosimetry system 79—85817
neutron primary beam and shielding radiation quality and absorbed dose obs. 80—12281
neutron production by 25-55 MeV protons on Be, spectra and yield 77—70539
neutron radiation therapy, cyclotron biological intercomparisons 79—20589
neutron radiation therapy, treatment planning corrections 79—20637
neutron radiotherapy, 14 MeV, skin-sparing, effect of metal sheets 78—35923
neutron radiotherapy, nature and significance of radiation outside beam 78—53477
neutron radiotherapy beam, photon dose fraction meas. 78—3605
neutron radiotherapy beams, effects on cultured human kidney cell reproductive capacity 79—62307
neutron radiotherapy planning and radiation quality definition 80—12246
neutron reflection and transmission for homogeneous slabs, dosimetric quantities and spectra 77—38319
neutron response of solid state nuclear track detector 80—27876
neutron scatt., random sampling technique for choosing scatt. angle from ang. distrib. 77—61619
neutron secondary spectra prod. by high energy bremsstrahlung in C, N, O and tissue 80—41239
neutron skyshine from nucl. facilities *(Japanese)* 79—18054
neutron source, 14 MeV, skyshine anal., Monte-Carlo computer code 78—66429
neutron source engineering problems and dose distributions 79—20635
neutron source for radiotherapy, gas target, energy spectra, flux, dose rates 78—92698
neutron spectra, Q-factor calcs. for spectra below 4 MeV 79—79654
neutron spectra form reactor, depth dose, dose equivalent, quality factor for various reactors and shields 78—94143
neutron spectra in stopping pion field, meas. with multiple foil activation method 78—73248
neutron spectral meas. in intense photon field of high-energy X-ray therapy machine 78—24133
neutron standards and appl., conference, Gaithersburg, MD, USA (March 1977) 79—9581
neutron teletherapy, effects of filters and wedges on skin sparing and γ/neutron dose ratios 80—46029
neutron temmeter, lack of accuracy considerations 80—42869
neutron therapy, dosimetric props. of d(80)+Be and d(80)+(Be+Ta) neutrons 79—12009
neutron therapy beam, dosimetry and radiation protection 79—48342
neutron therapy dose changes due to inhomogeneities, correction factor calc. technique 79—39511
neutron therapy hospital staff, occupational exposure report 78—96098
neutron thermoluminescence dosimetry 77—60262
neutron tissue dose from collimated beams of monoenergetic neutrons 77—70557
neutron-gamma mixed field, dose distrib. meas. on phantoms, TLD, solid-state, photoluminesc. detectors *(Russian)* 78—33297
neutron-irradiated tissue and equivalent material recoil spectra 80—17022
neutrons, 14.1 MeV, estimated dose to bone and whole body via ^{40}Ca and ^{31}P 79—53256
neutrons, 14.8 MeV, dose via ^{56}Fe in man 78—20275
neutrons, 14 MeV, dose distribs. across air-tissue, polythene-tissue and graphite tissue interfaces 77—52889
neutrons, 14 MeV, thermal neutron distrib. in bone in paraffin phantom, Au wire activation meas. 78—3616
neutrons, fast, calcs. of charged particle recoils, slowing down spectra, LET, event-size distribs. 79—25040
neutrons, fast, in vivo meas. of lung corrections for radiotherapy 77—13007
neutrons, p(90)+(Be+Ta) and p(101)+(Be+Al), dosimetric props. 80—89861
neutrons, research associated with National Radiological Protection Board's accelerator 77—2060
neutrons from DT reaction for radiotherapy 77—81568
noise dose criteria for setting hearing loss risk estimates for industrial noise 78—1504
noise exposure meas. of varying levels by noise records 79—23141

dosimetry continued
nonperturbing dielectric microthermometer probes 78—11743
NRPB thermoluminescent dosimetry and dose record keeping service 80—91293
NRPB TLD and dose record keeping service 80—5344
N.S. Mutsu, radiation streaming, repair plan 78—21781
nuclear accident dosimetry, blood-Na meas. 80—57979
nuclear accident dosimetry, report on fourth IAEA intercomparison expt. at Harwell 77—38426
nuclear accident dosimetry intercomparisons at US Health Phys. Research Reactor (1965-1978) 80—32520
nuclear accident dosimetry system, Czechoslovakia 80—57978
nuclear accident dosimetry systems, comparison 79—22496
nuclear accident dosimetry systems, Czechoslovak-Hungarian comparison 79—45437
nuclear accident dosimetry systems, neutron and gamma-ray dose meas. 77—38425
nuclear and atomic data sources 79—25081
nuclear and space radiation effects, conf., Albuquerque, USA (Jul. 78) 79—19276
nuclear energy production, research review *(Hungarian)* 78—74414
nuclear industry, health risks from various power sources 80—57899
nuclear installations, ambient radioactivity, standards rel. to dose and radioactive waste limits *(Spanish)* 80—52789
nuclear installations, environmental surveillance programme, Spanish experience 77—65336
nuclear medicine, computer software package for internal dose calc. 80—98139
nuclear medicine, dose calc. from remaining body activity 79—83941
nuclear medicine, intrainstitutional mobile, health physics considerations 79—8546
nuclear medicine measurements, quality assurance 77—40764
nuclear medicine procedures, personnel doses anal. 79—70645
nuclear medicine procedures, screen for radiation dose minimisation to nursing staff 79—53259
nuclear power, environmental effects of radiation 77—50304
nuclear power plant, environmental radioactivity and dosage models *(Spanish)* 80—32518
nuclear power plant chronic aq. releases, calc. rel. to meas. doses 79—54605
nuclear power plants, personnel monitoring concepts 79—85822
nuclear power plants, radiation exposure and protection 78—25301
nuclear power reactor accidental release, isopleth method for population reaction 79—13533
nuclear power sites, low-level radiation dose meas. 79—85820
nuclear power station, personnel dosimetry and access monitoring by process computers *(German, English)* 78—17440
nuclear power station, radiation protection, recommendations review *(Hungarian)* 78—74508
nuclear power station accidental activity release, effect of meteorological parameters 80—17142
nuclear power stations, ambiental radiology, equipment and methods, review *(Spanish)* 79—45425
nuclear power stations, radiation dosage determination, monitoring and control for personnel safety *(German)* 80—842
nuclear power stations, radiation safety, doses to personnel, local population 77—71701
nuclear power stations containing VVER-440 reactors, radiation safety of personnel and local population 77—71700
nuclear reactor, corrosion product reduction program 78—21665
nuclear reactor accident, dosimetry calcs., comparison with expt. data 79—36422
nuclear reactor accident dosimetry system *(Japanese)* 77—3119
nuclear reactor personnel 77—42195
nuclear reactor post LOCA doses, effect of I plateout 77—88254
nuclear reactors, underwater repair for workers protection 79—3226
nuclear safety, radiation protection estimation of individual and collective equivalent dose *(Spanish)* 80—5336
nuclear ship streaming neutron meas. by two-detector method 77—46408
nuclear spent fuel assembly, gamma dose rate distrib. meas. with TLD 80—47735
nuclear track detector, appl. as neutron dosimeter, reponse to standard neutron sources 80—5342
nuclear track emulsion, NTA film, as personnel neutron monitor in criticality accidents 77—29208
nuclear-dockyard workers, radiation-induced chromosome aberrations 79—34606
obstetric radiography, fetal radiation dose 79—92376
occupational doses in Ontario Hydro nucl. power program 77—88285
occupational exposure, averaging, weighting, ICRP-2G recommendations 80—47781
occupational exposure, problems raised by International Commission on Radiological Protection recommendations *(French)* 79—26771
occupational exposure Taiwan (1973 to 1975) 77—16985
occupational radiation exposure at nuclear power plants, meas. and prediction 79—59182
ocular hazard of short pulse Ar laser irradiation, primates 79—25030
ocular lens dose estimation in cranial irradiation of acute lymphocytic leukemia 79—88198
oil, lubricating, radn. effects and radn. dosimetry appl. 80—2069
oncology, computer aided treatment and diagnosis *(Swedish)* 77—44763
open-ended waveguide probe/applicator combination *(French)* 80—3820
optimization of radiation protection 80—47757
oral mucosa, determ. of dose from, and content of, U in dental porcelains 80—89830
organ dose estimates for the Japanese atomic-bomb survivors 80—21541
organ dose from external γ-radiation, relation to exposure, nuclear lab. environment 79—12010
organ doses from isotropic γ-ray fields, review 80—109026
organ-specific radiological impact of airborne effluents from model PWR and FBR reprocessing plants 80—3825
orthovoltage X-ray therapy, TLD dose intercomparison 80—12272
output factors, scatter ratios, for radiotherapy units, ^{60}Co γ-ray and MV X-ray calcs. 78—92708
output factors and scatter ratios 79—83944
paediatric patient, radiation exposure from cardiac catheterisation and angiography 80—41241
paired LiF TLD 600, 700 technique, γ-dose in mixed n-γ radiation fields 79—45432
parabiont rat pairs, late effects of successive massive radiation doses 79—29573

dosimetry continued
Parker, H.M., biographical note on medical physics contribs. 80−12
particle accelerators, radiological safety in design and operation, American National Standard 79−89511
particle accelerators ionising radiation produced during operation, dosage and shielding *(Czech)* 79−89505
particle radiation therapy, low linear energy transfer alternatives 79−20648
particle track structure analysis advantages over classical microdosimetry 80−26284
particles and radiation therapy, conference, Berkeley, USA (1976) 79−20619
passive solid state dosimetry, develop. of ultra-high parity sapphire dosimeters 78−20274
patient dose from EMI brain and body scanners 79−48341
patient exposure to diagnostic X-rays, anal. of 1972-1975 NEXT data 79−39505
pediatric cardiac catheterisation, absorbed dose in presence of contrast agents 80−30897
pelvimetry, low radiation dose gridless method 80−46010
PEP IR hall scale model, neutron and photon dose equivalents meas. 79−31227
peripheral reticulocyte count as biologic dosimetry of ionising radiation, mouse expts. 80−46051
permanent implant dosimetry, time-dose factor anal. of dose rate effects 77−70549
person dose, ICRP concept, related to exposure in industrial radiography 79−5370
personal dosimeters, comparative evaluation 79−41042
personal dosimetry and dose equivalent index 80−109027
personal dosimetry instrument for airborne radon daughter meas. *(French)* 80−57989
personal dosimetry service testing and evaluation in 1976 in Michigan 78−53498
personal monitor for uranium and thorium in uranium mine dust 80−52792
personal monitoring, effect of environmental radiation, thermoluminescent dosimeter *(Japanese)* 80−61707
personal sampling devices for atmospheric contamination monitoring *(French)* 80−57986
personnel, Czechoslovak comparison of neutron and gamma methods 77−50302
personnel dosimeter calibration, US NBS standard reference neutron fields 80−9417
personnel dosimeter design and use, physical requirements for dose meas. 80−9424
personnel dosimeters, Cd-capture γ-ray exposure 79−67963
personnel dosimeters calibration techniques for electrons and photons 80−9419
personnel dosimetric control in Hungary *(Russian)* 78−20292
personnel dosimetry, criteria for testing of performance 80−23169
personnel dosimetry, data processing system, mini-computer appl. 80−58005
personnel dosimetry in USA, survey results 78−53500
personnel dosimetry intercomparison studies at the ORNL Health Physics Research Reactor 80−9427
personnel dosimetry methods introduced in the Czechoslovak National Laboratory *(Czech)* 79−36426
personnel dosimetry methods introduced in the Czechoslovak national laboratories 80−57969
personnel dosimetry performance, testing standard 80−9421
personnel dosimetry photon calibrations, use of phantom 80−9425
personnel exposure during cardiac catheterisation, calc. technique using time-lapse photography 79−39504
personnel external gamma dosimetry, meas. of weighted average whole-body dose 80−26367
personnel monitoring, automatic film-badge reading system 78−40335
personnel monitoring for radiological protection, current status and developments, review 79−22490
personnel monitoring measurements 77−40782
personnel monitoring performance standards 77−40783
personnel neutron dosimeters, calibration for use in different neutron fields 80−58001
personnel radiation minimisation in nuclear power plants 78−21663
phantom, perspex, for assessment of nuclear medicine imaging equipment 79−25089
phantom calibration, internal, TLD phosphor obs. 79−62372
phantom mathematical model for body and organ dose of Japanese adult 77−70552
Phenix LMFBR, radioactive effluent release, operating team irrad. results *(French)* 79−31163
phosphate fertilizers, occupational dose from natural radionuclides 79−100751
phosphate glass, appl. in gamma dosimetry *(Slovenian)* 80−32521
phosphorescent detectors and X-ray convertors, Symposium, Riga, USSR (Oct. 1966) 79−6243
photochemotherapy, absolute radiation dosimetry 79−12008
photochemotherapy, anatomical distrib. of UV radiation 77−86643
photographic emulsions, supralinear, radiobiological aspects of X-ray exposure 79−8549
photographic film dosimetry by low energy photon transmission 79−45433
photographic film response to 25 MV X-rays, sensitometric curves, relative dosimetry 80−52376
photon, standardisation program at US National Bureau of Standards 80−13943
photon, variation with organ mass, validity of reciprocity theorem 77−64136
photon and electron transport simulation, deceleration photons prod. using linear accelerator *(French)* 80−12282
photon attenuation and energy absorpt., coeffs. for ICRP Reference Man organs and tissues 77−73582
photon beam 18 MV, from Philips SL/75-20 linear accelerator, fast and slow neutron contamination 78−65127
photon beam absorbed dose determ., cavity chamber correct. factors study 80−37703
photon beam dose calcs., power law tissue-air ratio algorithm for inhomogeneity corrects., verification 80−56222
photon beams, high energy, depth of max. dose var. with fluid size 77−70555

dosimetry continued
photon calibration of radiation protection instruments in an authorized metrology service 80−9423
photon dose rate from induced activity in the beam stop of a 400 GeV proton accelerator 78−94144
photon dosimetry, practical problems 77−60261
photon interaction data of 69 ICRP reference man tissues, 4th order polynomial coeffs. 78−28077
photon irradiator calibration, compensation for geometry induced errors 80−18702
photon mass attenuation and mass energy-absorpt. coeffs. for H, C, N, O, Ar and mixtures, 0.1 keV to 20 MeV 77−61715
photon mass energy-absorption coeff. air/medium ratios for ionometric dosimetry, 0.1 keV to 20 MeV 77−40784
photons, 6-7 MeV, exposure rate and absorbed dose meas. 79−26766
photons, monoenergetic, microdosimetric meas. of ionisation 78−65133
pion$^-$, central axis depth-dose and stopping rate distrib. for radiobiology studies 77−52879
pion$^-$, in vivo dosimetry using Al activation 80−46060
pion$^-$, sensitivity of personnel monitoring film 78−28079
pion$^-$ beam stopping distrib. determ. by charge collector 78−53513
pion$^-$ beams, dose patterns in irrad. cylinders, effects of tissue inhomogeneities 77−9266
pion$^-$ broad therapeutic beams, microdosimetric characterisation 80−12277
pion$^-$ cancer radiotherapy, RBE in and near large beam 80−12245
pion$^-$ capture, charged particle emission, energy spectra, LET distribs. and W-value 78−40337
pion$^-$ irradiation, dose outside treatment volume 78−53508
pion$^-$ peak expansion to range of depths useful in radiotherapy, chromosome aberration meas. 78−20243
pion$^-$ radiation, uniform depth-dose distrib. technique and cell survival obs. 80−17139
pion$^-$ radiation therapy, dosimetry and treatment planning 79−20646
pion$^-$ radiation therapy dosimetry 79−20679
pion$^-$ radiotherapy, biological effect prdiction, star distrib. for high LET dose determ. 80−12248
pion$^-$ radiotherapy, dynamic rangeshifter for modifying depth-dose distribs. 78−3595
pion$^-$ stopped in tissue phantom, neutron and photon dose and LET distribs. 77−52878
pion$^-$ therapy, neutron energy spectrum in stopping pion field 78−85386
pion$^-$ therapy beams, LAMPF 78−3606
pion$^-$ W-values for CO_2, N_2, and tissue-equiv. gas 77−56473
pion, energy dependent mean free path length for star formation 77−23393
pion, simulated treatment planning for Stanford Medical Pion Generator 77−86634
pion applicator, meas. at πE^3 single beam correl. to dosimetry and therapy-planning 80−26361
pion beam therapy, meas. of effect of inhomogeneities and compensating bolus 79−39512
pion beam treatment planning, deep seated tumours, computerised tomographic scans 80−41180
pion dose contours, high-LET, in cellulose-nitrate plastic track detectors 79−39513
pion radiotherapy facility at TRIUMF, dosimetry and radiobiology 77−70526
pion radiotherapy studies with nucl. emulsions 78−73219
pion therapy controller designed for patient irradiation at the SIN π^--applicator 79−57754
planar implants, effect of crossing needle location on dose distribs. 79−100742
plastic track detectors for calib. of high-energy heavy particle beams 77−79525
plexiglass, red, gamma dose meas. by optical absorpt., elec. conductivity, and mechanical hardness 78−55045
plumes, well-established dose while travelling underneath during evacuation 77−54369
PMMA, constancy of composition obs. 79−60286
Pollen, Pinus Silvestris, effect of X, UV irradiation on NAD(P), NAD(P)H, hydroxyproline levels 79−20582
pollutant release assessment, JEREMIAH computational system environmental transport and dose calcs. 78−94150
polycarbonate foil, α-particle track prod., electrochemical etching 80−52825
polyester foil neutron track detection, dosimeter appl. 80−5439
polymethylmethacrylate, effect of accumulated charge on depth dose profile of electron beam 79−90700
polystyrene, constancy of composition obs. 79−60286
population dose estimates, significance of incorporating age-dependent data 80−46057
population dose from. atm. dispersion of radioactivity, calc. method 78−85381
population dose from commercial radioactive waste burial site 77−61618
population dose from LWR fuel reprocessing 80−46073
population doses from environmental γ radiation in Norway 78−11745
population doses from reactor operation, compliance with appendix I 77−46410
population exposure doses from USSR power plants, evaluation, prediction, regulation *(Russian)* 79−26776
population exposure due to radioluminous clocks in households 77−73586
population exposure standards, determination problems *(Russian)* 79−26778
population radiation exposure, radioactive effluent from nuclear facilities in West Germany 79−26781
portable radiation meters, accuracy checking facility at Berkeley Laboratories, UK 78−74507
positron emitters ^{11}C, ^{13}N, ^{15}O, absorbed dose comparison rel. to γ-ray emitters 79−70647
postero-anterior radiography, method for eye dose reduction 79−92388
power plant effluents, gaseous, AEOLUS code for dispersion during normal, sea-breeze, and accident conditions 78−11993
power station, personnel dosimetry monitoring, use of evaluation device for rod and process computer *(German, English)* 78−17441
power station ashes, Th, U, and K conc. meas., dose rates in Poland 79−100754
primary dosimetric standards at the Memorial Sloan-Kettering Cancer Center, NY, USA 80−8190

dosimetry continued
primary standard for determination of absorbed dose in water for X-rays generated at potentials of 7.5 to 30 kV 80—5354
primary standards for industrial radiation processing 80—5356
prosthetic silicone breast, dose obs. 80—98144
proton and heavy-ion fractionated radiation therapy experience 79—20631
proton dose distribution fattening for large-field radiotherapy 77—73564
proton local exposure, 200 MeV, contrib. of secondary particles to absorbed dose 79—100752
proton relative biological effectiveness, microdosimetric interpretation of biological data 79—62306
proton relative biological effectiveness, microdosimetric parameters 79—62305
protons, 185 MeV, dose buildup from secondary protons and recoil electrons 78—15898
protons, additivity of stopping cross-sections in hydrocarbon gases, 50 to 150 keV 77—66853
public health aspects of radiation 78—35895
public health aspects of radiation 79—88141
pulmonary ventilation studies using ^{133}Xe, personnel exposure from unshielded system 78—15899
pulsed radiation intensity meas. by counting delayed pulses produced in Geiger-Muller counter 77—46407
pulsed X-ray thermionic tube intensity and dose angular distrib. obs. 79—67450
PWR, calcs. of neutron environment inside containment 80—13676
PWR, fast-neutron dose rate meas. inside containment shell 80—13674
PWR, neutron streaming in upper reactor cavity, dose rate calc. 79—89365
PWR, occupational radiation exposure 78—21664
PWR, post LOCA accident doses to equipment 77—88255
PWR, survey of neutrons inside containment 80—13675
PWR spent fuel calcs., neutron multiplication and shielding problems 77—74951
PWR steam generator, γ-dose rate distrib. meas. 80—5382
Q-factor for charged particle recoils rel. to neutron energy 80—63397
quality factor recommendations and dose limits 80—26369
quartz, natural, dosimetric props., possibility of thermolum. dating of geological objects 79—12288
radiation and chemical pollutant effects, dose comparisons 79—88115
radiation beam characteristics of a 22 MeV microtron 80—51260
radiation biology conference, Rotterdam, Netherlands (Aug. 1980) 80—105425
radiation calorimetry of single electron pulses from a LINAC 80—42872
radiation chemistry in liq. phase using ^{85}Kr source 77—60091
radiation dose-response curves, hazard function method of resolution 79—66556
radiation doses to equipment inside containment of power reactors 77—88253
radiation exposure intercomparison with ionisation chambers 80—5363
radiation exposure limits, establishment bases 79—26770
radiation exposure meas. in aircraft from transported radioactive goods 79—22488
radiation exposure near nuclear power plants, remote monitoring system 79—18055
radiation exposure of UK population, review 79—62373
radiation exposure resulting from radioactive gases released near the NRI Rez *(Russian)* 79—36427
radiation exposures from film dosimeters, analogue computer anal. *(Bulgarian)* 79—85877
radiation facilities, external exposures control, designer-health physicist collaboration 77—81586
radiation field measurements, Vermont Yankee Nuclear Power Station 79—9893
radiation field of extended rectangular source, numerical integration 78—66424
radiation meas. bibliography (1972-76) *(German)* 80—95510
radiation process quality control 77—67905
radiation protection instruments for personnel dosimetry, area and environmental monitoring 78—66427
radiation protection progress report, EEC, 1978, book 80—22148
radiation protection survey of mobile mass-miniature radiography unit, TLD obs. 79—62375
radiation risk assessment, importance 80—47754
radiation safety, permissible dose estimation based on biological risk 78—40352
radiation testing of materials in reactors, measure of radiation effect, dosimetric information 78—79640
radiation therapy, algorithm for calc. of central ray TAR and TMR values 80—76844
radiation therapy, appl. of thermolum. dosimetry to pion beam 80—26362
radiation therapy, calibration and meas. standards in USA 80—8188
radiation therapy, chamber factor reliability review, United States institutions 79—20685
radiation therapy, comparison of methods of obtaining % depth doses 79—53250
radiation therapy, compensation for inhomogeneities using computerized tomography 79—25065
radiation therapy, computer control 79—25099
radiation therapy, computer program for negative pion beam calcs. 80—46061
radiation therapy, dosage calculation and compensation, basic data 80—104765
radiation therapy, dose calculations from computerised tomography data 79—25062
radiation therapy, dose distributions, wedge-shaped, computer-controlled collimator motion 79—5358
radiation therapy, dose perturbation from Au dental fillings 80—12265
radiation therapy, dose response curves, methods of extraction 80—94374
radiation therapy, dose/cure relationships study 80—56218
radiation therapy, dosimetric considerations of very large ^{60}Co fields 80—104766
radiation therapy, dosimetry study of split beam technique 80—12264
radiation therapy, electron beam dose distributions, magnetic field modification 79—5376
radiation therapy, electron treatment planning, air-gap correction 79—53254
radiation therapy, electron-dose distrib. in tissue, lung phantoms, magnetic modification 79—5377

dosimetry continued
radiation therapy, estimate of risk due to unwanted neutrons by dose calcs. 80—81714
radiation therapy, external, use of computerised tomography in treatment planning *(French)* 79—66553
radiation therapy, external beam, three-dimensional dose distribs. 79—25064
radiation therapy, fractionation in ^{60}Co teletherapy, weekly intervals 79—34650
radiation therapy, high energy photon beams, absorbed dose from secondary electrons 79—92380
radiation therapy, high-energy proton beam, physical meas. using tissue substitutes 80—81720
radiation therapy, interstitial, dosimetric localisation, use of computerised tomography scanner 80—21540
radiation therapy, orthogonal megavoltage field matching technique 79—88197
radiation therapy, photogrammetry use in absorbed dose determ. 80—12222
radiation therapy, pion$^-$ dose studies, influence of beam characts. and detector size 79—53253
radiation therapy, practical nomogram for correcting nominal standard dose *(Italian)* 77—81581
radiation therapy, procedures with electron and photon beams 80—101266
radiation therapy, proton beam absorbed dose determ. 80—46062
radiation therapy, scatter dose distribs. for 6 MV photon beams 79—62370
radiation therapy, squamous cell carcinoma of head and neck, time-dose factors anal. 80—72333
radiation therapy, tissue-maximum ratios/scatter-maximum ratios, indirectly ionising beams 79—39515
radiation therapy, tolerance dose, treatment field size relationship 79—5359
radiation therapy, total body techniques for bone marrow transplanation, review 80—104738
radiation therapy, treatment planning, depth dose scaling using computerised tomography scans 80—30899
radiation therapy, treatment planning system using computerised tomography 79—29588
radiation therapy afterloading system for oesophagus tumours 79—74742
radiation therapy beams, physical factors affecting skin absorbed dose 79—83937
radiation therapy electron accelerator target, depth-dose obs. 79—70618
radiation therapy machines, calibration discrepancies, US institutions, data anal. 79—20686
radiation therapy mantle fields, dose compensator for lymph bearing areas 79—43991
radiation therapy of breast and chest wall, comparison of radiation techniques 80—30837
radiation therapy of lymphomas, depth-dose factors using a 4 MV linear accelerator 79—25066
radiation therapy of pelvis, optimisation of box technique to reduce femur dose 80—12263
radiation therapy of uterine cancer, dosimetry effect of position change 79—62362
radiation therapy optimisation 77—86593
radiation therapy planning, revision of tissue-max. ratio and scatter-max. ratio concepts 80—76840
radiation therapy planning and dosimetry for pion applicator 80—26360
radiation therapy simulator and linear accelerator meas. and control by microprocessor 77—40902
radiation therapy treatment planning, absorbed dose calcs. method 79—92386
radiation transport in Earth for neutron and gamma-ray point sources above an air-ground interface 80—32526
radiation treatment of obstruction of superior vena cava, optimum schedule importance of ^{99m}Tc scintiangiograms 80—72334
radiation treatment planning, computerised, accuracy 80—72328
radiation worker health registry for AECL employees 79—88201
radiation-technological apparatus in COMECON countries, development of methods and standards for dosimetry 79—93836
radioactive cloud, external gamma dose model 79—85828
radioactive decay, standardised data sets for dosimetry calcs. 80—13945
radioactive discharges, airborne, use of census data in assessing collective doses 79—59271
radioactive effluent release reduction, Japanese LWRs 79—31078
radioactive impact of nuclear facilities, preoperational evaluation 80—3534
radioactive pollution consequences from liquid pathways due to reactor core meltdown accident 80—104778
radioactive pollution from nuclear facilities, T population dose in the Northern Hemisphere 80—104779
radioactive release from nuclear facility, dose calcs. using on-site meteorological data 77—40798
radioactive release into environment, limits, new derivation approaches 79—26773
radioactive releases from nuclear installations, eval. of accidental atmos. discharges 79—39529
radioactive seed implants, computation of dose distrib. 80—101265
radioactive waste, land disposal, repository, packaging and cost estimate, internal radiation dose *(Japanese)* 78—66351
radioactive waste, radionuclide migration resulting from site intrusion 80—13701
radioactive waste geologic repositories, computer anal. of long-term radiation hazards 80—18483
radioactive waste management, influence on standardised plant design 77—46307
radioactive waste processing, health physics implications 79—57727
radioactive waste storage, integrated biological dose evaluation 80—5379
radioactivity standards programme of the National Bureau of Standards, USA 80—18700
radiobiological data for clinical dosimetry in pion tumour therapy 80—26266
radiobiological effects and dose-LET spectra 80—26265
radiochemicals in aqueous soln., use of revised MIRD eqn. for phys. systems 77—66851
radiogenic cancer, estimate of life shortening per rem absorbed dose 79—11967
radiographic dose reduction 80—98087
radiographic exposure, influence of cassette front 79—25105

dosimetry continued
radiographic film/screen combinations and patient exposure, Nationwide Survey of X-ray Trends 78—73233
radiographic magnification technique for gallbladder imaging 78—69186
radiographic quality, tube potential, and patient dose 79—62349
radiography, contrast in computerised transverse axial tomography of brain 77—86608
radiography, dose distribution description by X-ray quality monitoring *(German)* 80—41251
radiography, epoxy resin based tissue substitutes 78—7424
radiography, exposure and working procedure with paediatric chest stand 79—48337
radiography, free-focus, using conventional films, exposures in a simulated clinical study 80—89835
radiography, patient exposure 80—46066
radiography, quantitative meas. for estimating patient dose *(German)* 78—57073
radiography, rare earth oxysulphide intensifying screens, resolution and dose 77—21597
radiography, reduced scatter, effect on information content and patient exposure 80—51225
radiography, US Nationwide Evaluation of X-ray Trends and state radiation meas. 77—40779
radioisotope dose rates to human thorax, low energy photon attenuation theory-expt. discrepancies 79—5373
radioisotope dosimetric data tables 80—105438
radioisotope transport in terrestrial food chains, dynamic modelling using RAGTIME code 80—104776
radioisotopes manipulated in syringes, radiation exposure obs. 80—67252
radiological impact of the Rhein-Maas region from nuclear facilities under normal operation 80—3535
radiological implications of Pu recycling in HTGR fuels 80—68777
radiological instrumentation calibration by British Calibration Service 80—8186
radiology diagnostic facilities, quality assurance programme, proposed recommendation 78—73235
radiolyoluminescence, appl. to dosimetry of ionising radiation 79—62374
radionuclide airborne release assessment, determ. of atm. stability categories 78—73504
radionuclide concentrations in food products, FOOD II interactive code calc. 79—48348
radionuclide dynamic studies of physiological processes 79—62353
radionuclide intake by man through terrestrial pathways, TERMOD II interactive code analysis 79—48349
radionuclide intakes by workers, limits, recommendation from ICRP 80—47762
radionuclide movement from hypothetical nuclear waste repository, numerical anal. 80—16853
radionuclide releases to atmosphere, dose reduction factors from indoor residence 80—56219
radionuclides incorporated into mammalian cell DNA, microdosimetry 80—12191
radiopharmaceutical investigations, appl. of ten-day rule 77—21633
radiopharmaceutical patient diagnosis, absorbed dose derivation techniques 79—12006
radiopharmaceutical preparation and injection, dose to hands 78—20276
radiopharmaceuticals in diagnosis, patient dose 78—35967
radiotherapeutic agents, props., dosimetry and radiobiologic considerations 80—36106
radiotherapy,, electron whole body superficial therapy dose distrib. anal. 77—86633
radiotherapy, ^{125}I interstitial implants, dose inhomogeneity 79—100746
radiotherapy, ^{60}Co total body irrad. at 220 cm source axis distance 80—104768
radiotherapy, adjacent field overlap, clinical complications phys. and technical considerations 78—11741
radiotherapy, automatic var. of field size and dose rate in rot. therapy 78—11720
radiotherapy, breast treatment with tangential fields using 4 MV X-rays, superficial doses 78—11740
radiotherapy, build-up effect with ^{60}Co radiation and fast electrons *(German)* 78—20271
radiotherapy, central axis electron depth dose distrib., analytic expression 80—3813
radiotherapy, clinical significance of non-compliance with prescribed irrad. schedules 78—11723
radiotherapy, computational anal. and dosimetric evaluation of commercial irregular-fields computer program 78—24147
radiotherapy, depth dose function concept, definition and values 80—3814
radiotherapy, dose calculation, based on computed tomography images use of scatt. radiation meas. 80—51265
radiotherapy, dosimetry procedures at Northwest Medical Physics Center, USA 77—40790
radiotherapy, external beam, optimisation using computer 77—86632
radiotherapy, high energy photon beams, advantages and props. 80—51238
radiotherapy, high-energy accelerators, mixed photon-neutron field meas. 80—51267
radiotherapy, intercomparison of prescription dose delivery in New England region 77—40791
radiotherapy, linear accelerator, SL 75-20, neutron and gamma doses in entrance mazes of treatment rooms 80—85500
radiotherapy, linear accelerator neutron sources and characts. 80—51239
radiotherapy, malignant melanoma treatment near optic disc using small ^{60}Co beams 78—35929
radiotherapy, mantle treatment, meas. in patients compared with dose planning 77—9258
radiotherapy, megavoltage, eqn. for scatter-air ratios 77—2054
radiotherapy, NBS electron beam dosimetry service 77—40792
radiotherapy, photon beams, high energy, electrons as cause of d_{max} shift 79—83938
radiotherapy, photon beams, high energy, improving buildup and depth-dose characts. 79—83939
radiotherapy, precision of dose meas. devices, therapy machines and patient dose delivery 77—40789
radiotherapy, secondary radiation from supervoltage accelerators rel. to patient protection 77—56471
radiotherapy, using irregularly shaped fields 77—70550
radiotherapy, uterine cervix carcinoma, high rel. to low dose irradiation 79—74759

dosimetry continued
radiotherapy 25 MV X-ray beam, fast and thermal neutron profiles 78—73246
radiotherapy accelerator neutron leakage survey 80—51269
radiotherapy accelerator primary beam neutron contamination 80—51268
radiotherapy accuracy, errors in patient set-up 78—11726
radiotherapy afterloading applicator, dose distrib. around 79—53249
radiotherapy arc technique for total-body irrad. by 42 MV betatron 78—24134
radiotherapy beam-flattening filter calcs. for high-energy X-ray machines 78—65126
radiotherapy betatron, 25 MeV, fast neutron component and patient dose 78—3592
radiotherapy by external ionising radiation beams, for teaching 78—49616
radiotherapy cervical intracavitary applicators, computer program for optimisation of source loading 77—13005
radiotherapy compensation filter for chest portals 78—31887
radiotherapy dosage calculations for inhomogeneous media, direct use of computerised tomography numbers 79—83943
radiotherapy dose calculations, megavoltage beam representation method 79—92374
radiotherapy electron accelerator neutron prod. 80—51240
radiotherapy electron accelerator neutron production, conf., Gaithersburg, USA (Apr. 1979) 80—46730
radiotherapy electron accelerator photoneutron prod., survey of European meas. 80—51241
radiotherapy hard X-ray machine, RT 305, phys. aspects and appl. 80—81709
radiotherapy high-energy linear accelerator photon beam exit design for neutron prod. minimisation 80—51242
radiotherapy intercomparisons, recurrence rate discrepancies rel. to clinically equivalent dose definition 78—7426
radiotherapy linear accelerator 5.5 MeV Neptune, phys. characts. of beam *(French)* 77—29196
radiotherapy moving-strip technique, comparison of ^{60}Co unit and Varian 4 and 10 MV linear accelerators 77—70553
radiotherapy neutron leakage characts. rel. to room shielding 80—51273
radiotherapy of hyperthyroidism, absorbed dose to ovaries and uterus 79—79656
radiotherapy of paediatric malignancies, set-up and treatment techniques 78—35927
radiotherapy photon beam, 10 MV, dosimetry characts. and computerised treatment planning 77—48875
radiotherapy proton beam localisation using ^{15}O activation, dose required 77—48862
radiotherapy quality control recommendations 77—40778
radiotherapy shielding, comparison of photoneutron and ^{252}Cf neutron spectra 79—59273
radiotherapy surface dose var. with number of layers of LIGHTCAST tape 77—86635
radiotherapy tissue compensators, use in improving dose uniformity in total body irrad. 80—104767
radiotherapy treatment plan selection, complication probability factor 78—53476
radiotherapy treatment planning, computer-aided 77—9268
radiotherapy treatment planning, FORTRAN program for optimisation using complication probability factor 80—81686
radiotherapy treatment planning, inhomogeneity correction methods compared with Monte Carlo data 80—61698
radiotherapy treatment planning, inter-hospital interactive computerised system 80—36068
radiotherapy treatment planning, phys. charact. of 45 MV photon beams 77—48873
radiotherapy treatment planning and follow-up of superficial tumours, US B-scan appl. 78—11721
radiotherapy treatment planning appl. of computed tomographic imaging 80—51232
radiotherapy treatment planning for irregular fields 80—81739
radiotherapy treatment planning interactive computer/ultrasound system 77—9269
radiotherapy treatment planning system, clinical experience *(German)* 77—77991
radiotherapy treatment planning system implemented in FORTRAN on interactive computer 77—5080
radiotherapy treatment planning using microcomputer 80—8191
radiotherapy treatment time and sub-lethal repair, CHO cell obs. 80—30773
radiotherapy treatment verification and recording using small computer 77—81554
radiotherapy underdosing due to lack of electronic equilib. in upper respiratory air cavities, 10 MV X-irrad. 78—11739
radiotherapy with electrons, up to 20 MeV, phys. aspects 80—85474
radiotherapy with fast electrons, computerised treatment planning, dose distrib. calc. 80—81740
radiowave energy absorption in tissue prolate spheroids, calc. by point matching method 78—44612
Rando phantom dosimeter placement 77—73591
reactor accident consequences, estimated, effect of appl. of surface depletion model 80—30622
reactor accidents, struct. shielding against gamma-ray sources, dose reduction factors 78—13251
reactor core dosimetry standards 79—9824
reactor core gamma dosimetry, solid state nucl. track detector appl. 80—95466
reactor core radiation transport code, comparison of electron transport models 80—23030
reactor near-stack dose calc., diffusion model applicability 78—94147
reactor release, population risk, implication of WASH-1400 in FRG 77—46351
reactor safety, quantifying plant availability, ALARA, and occupational radiation exposure relationships 79—59183
Reactor Safety Study (Wash-1400) and implications for radiological emergency response planning 78—50284
reactor technology, sources, phys. units and biological factors *(German)* 78—46180
real time offsite dose calc. 79—45429
REBEL-3, code for dose calcs., phantom standing in dwelling room 80—94377
reduced radiation dose with electroradiography *(Swedish)* 77—9259
reference Japanese man *(Japanese)* 78—35968

dosimetry continued
reference radiations for radiation protection dose meter calibration *(French)* 80—57998
reproductive death and chromosomal aberrations in mammalian cells, RBE/LET 80—12189
residual activity levels allowing radioactive waste to be considered inactive 80—13735
respiratory dose from Rn daughters, influence of room ventilation rate variations 79—92381
restricted energy absorption coefficients 78—80971
review of nuclear fuel cycles and waste management 78—54863
RF, average specific absorpt. rate in ellipsoidal conductor and dielec. models of humans and monkeys 78—40349
RF EM fields, review of effects and dosimetric data, safety standards development 80—67154
RF energy absorpt. of simulated body material using portable transmitters 78—44614
RF power absorption in biological specimens, meas., 10-100 MHz 77—90916
RF radiation and EM fields, induction of focal hyperthermia in tumour and body models 78—40244
RF radiation dosimetry handbook, descriptive summary 78—40347
risk assessment from radiation 79—25116
risk justification, theory and appl. 80—47755
rod dosimeters, automatic evaluation of staff dosimeters during reactor shut down *(German)* 79—67960
rodents inhabiting radioactive waste receiving area 78—85383
roentgen densitometer for detect. of congenital heart defects, patient dose 77—9239
root meristem cells, Vicia faba, subnuclear chromosome aberrations rel. to neutron energy deposition 80—26280
Rossi counter equivalent dose meas. in high-energy radiation fields 80—94376
sand, heated, thermoluminescence, appl. to radiation dosimetry 77—61613
scanning electron beam, semi-empirical model for dose distribs. generation 80—94373
scatter factor determ. at depth in walls of cylindrical chambers 79—49909
scintillation counter method, dose rates in mixed beta-gamma fields 77—60254
secondary standard laboratory organisation in India 80—5366
Secondary Standards Dosimetry Laboratory, review of role 80—5361
secondary standards laboratory, role in a nuclear power utility 80—5365
seed radiosensitivity of winter hexaploid triticale 79—20583
semiconductor detector for ionising radiation dosimetry, anisotropy of dose sensitivity 78—70705
semiconductor rectal dosimetry in treatment of cervical cancer, using RALSTRON technique *(Japanese)* 77—73594
Serpukhov proton synchrotron shield, mixed radiation dose equivalent outside 80—32530
sewage sludge irradiation plant, dose and irradiation homogeneity 79—22489
SI units *(Spanish)* 79—62365
SI units in radiological protection 78—86235
skeletal Ca estimation by exhaled ^{37}Ar meas., fast neutron dose requirement 77—16962
skin, α-irradiation, possibility of late effects, U miners 79—20584
skin γ and neutron responses, dose fractionation effects 79—20593
skin acute response, human, pion$^-$ relative biological effectiveness 79—20596
skin growth regulation, mouse, after X-irradiation, possible role of chalones 79—16168
skin injury, pig, relationship of acute to late injury in fractionated radiation doses 79—34604
skin injury, pig, relative biological effectiveness of neutrons and γ-rays 79—34605
skin nodules, comparative effects of pion and X-irradiation 79—20659
skin tumour, rat, following proton irradiation 79—11982
Skylab astronauts, high-LET particle exposure 77—29212
skyshine dose due to gamma-rays from nucl. power plant *(Japanese)* 79—29917
slow ion stopping power meas., multiple scatt. corrections 80—23278
small intestinal cryptogenic cells in W/W^v mutant mice, survival curves after X-irradiation 79—11980
Snyder mathematical phantom, additions 79—92384
soil micro-organism beta-particle dose rates from natural radionuclides 77—90913
soil residual contamination levels and decommissioning nuclear facilities, radiological criteria 78—11747
solar flare, 1972 August 4, calc. of radiation doses absorbed in near-Earth orbit 77—52892
solar flare, dose at Earth's surface 79—25109
solar flares near-Earth radiation hazard, dosage estimation technique 80—67482
solid cavity theory rel. to derivation of C_λ and C_E 77—86644
solid state ionisation current comparator 77—23383
solid state nuclear track detectors, conf., Neuherberg/Munich, (Oct. 1976) 78—17513
solid state nuclear track detectors, fast neutron dosimetry 78—20278
solid state nuclear track detectors, reactor neutron fluence meas. using Au and In foils 80—69035
solid state track detectors, use in neutron dosimetry, verification of possibilities *(Czech)* 78—82574
somatic dose index, human, diagnostic X-ray procedures 79—16306
sound exposure monitoring for an individual for one month 78—30124
Space Radiation Effects Laboratory 710-MeV He ion beam, biophysical aspects 80—30871
space station, radiation protection design considerations for man in geosynchronous orbits 78—28096
spectral and intensity distribs. of accelerator prod. neutrons in concrete room 79—49868
spectral parameter measurement for γ-rays using overtake effect 79—45436
spent nuclear fuel shipment, appl. of ALARA principles 80—37541
spent reactor fuel, risk analysis of alternatives from reactor pool until final disposal 78—17355
spontaneously fissioning material, Monte Carlo neutronic and electronic model for thermal-neutron coincidence counting 80—23165
spontaneously fissioning radionuclides, max. permissible conc. 77—73598

dosimetry continued
stainless steel, neutron dose determ., from isotope abundance ratio, mass spectra obs. 80—61220
standardisation, conf., Atlanta, GA, USA, Dec. (1977) 80—4469
standardisation in Germany, electrons and photons 80—5353
standardisation in Japan, review 80—5359
standardization in radiation dosimetry in the United Kingdom, review 80—5358
standards for people involved in more than one source of hazard *(French)* 80—47772
statistical errors of dose estimation in personnel neutron monitoring with albedo dosimeters 79—48344
steam generator, multiple tube rupture, radiological consequences 78—74452
sterilisation facility, in Medicor Works' Debrecen Factory of Surgical Instruments, test dosimetry 78—40336
stopping power for low energy heavy charged particles, similarity treatment of phase effects 78—50447
sublesion production and interaction, primary ionisation cluster nanodosimetry 80—26278
sugarcane, evaluation of mathematical methods for optimum γ-dose prediction 79—29630
surface contamination meter 79—22494
surface dose, meas. considerations 79—100748
surface dose product meas., for official ionising radiation practice *(German)* 79—2137
tail necrosis, mouse, multifraction X-irrad., dose-incidence curve steepness anal. 80—98035
technologically enhanced natural radiation, chemical problems, human exposure 79—96346
teletherapy, implementation of Philips treatment planning system 78—73244
teletherapy installations, ^{60}Co source, US national evaluation 79—5360
terrestial sources, possibility of estimating population exposure 80—89855
terrestrial beta radiation field in natural environment, numerical evaluation 78—81161
testes, morphological changes after long term γ-irradiation in mice *(Russian)* 79—20601
Therac 6 linear accelerator, computer controlled evaluation for X-ray therapy 79—5363
Therac 6 linear accelerator, field elongation effects on depth-dose curves, central-axis output of X-rays 79—5361
therapy, source motion, calc. in intracavity moving-beam and multipositional irrad. 80—104759
Theratron 780, empirical table of equivalent squares of rectangular fields 77—48856
thermal neutron beam response of hamster and HeLa cells containing various concs. of ^{10}B 78—73178
thermally stimulated luminescence application, radiation dosimetry, book contribution 80—80882
thermoluminescence, absorbed dose from ^{90}Sr-^{90}Y beta source, rel. to TL dating 77—90911
thermoluminescence, appl. to radioactive minerals prospecting 78—32244
thermoluminescence, automatic, for personnel monitoring *(German)* 77—10493
thermoluminescence dating, reassessment of fine grain dose-rate 77—34071
thermoluminescence dating, revised dose-rate data 77—34072
thermoluminescence dating of pottery, ^{87}Rb dose-rate contrib. 78—70242
thermoluminescence dosimetry in patients *(German)* 80—104758
thermoluminescence spectra estimation using colour transparency film 77—86646
thermoluminescent, archaeologic ceramic samples age determining *(Czech)* 77—5972
thermoluminescent, intensity depend. on heating rate, competing deep trap model 77—73590
thermoluminescent, mammography radiation dosage in different examination systems *(German)* 79—100750
thermoluminescent dosimeter monitoring post, concrete shielding to reduce background 78—817
thermoluminescent dosimetry, some problems in precision meas. 80—13936
thermoluminescent dosimetry, TLD 700, parameters affecting overall calibration accuracy 79—63821
thermoluminescent dosimetry system for high energy bremsstrahlung dosimetry 80—106209
thermoluminescent reader TLD-04B for research and routine dosimetry appls. 78—20291
thermoluminescent response to fast neutrons of mixture of $CaSO_4$:Tm and polyethylene 80—5340
thermostimulated processes appl. to radiation dosimetry and dating 78—11004
thick inhomogeneity effects on charged particle beams 79—25041
thoracic inlet tumours, new irradiation technique 79—34651
thorotrast and ^{224}Ra radiobiological significance 78—96076
thorotrast biological effects, conf., Alta, USA (July 1974) 78—96068
thorotrast cases, bone irradiation meas. results 78—96092
thorotrast patients, α-ray tissue dose 78—96093
thorotrast patients, Danish, malignancies 78—96074
thorotrast patients, endosteal α-particle dose 78—96094
thorotrast patients, German, malignancies and estimated tissue dose 78—96072
thorotrast patients, Portuguese, malignancies 78—96073
Thre Mile Island, Unit 2 accident, noble gas releases 80—47616
thymic region shielding in radiobiology expts., dosimetry in irrad. mouse cadavers 78—61257
thyroid, absorbed fractions of photons of ^{125}I and ^{129}I 80—109032
thyroid, high dose associated with adrenal scanning using ^{131}I 79—29629
thyroid, microscopic dose distribs. due to I isotopes 79—39522
thyroid, volume and dose estimation by ^{131}I scintigraphy 79—16302
thyroid cell survival after irrad., directly generated single dose survival curve 80—36014
thyroid dose evaluation from fission reactor spent fuel following loss of spent-fuel-pool cooling system 80—26366
thyroid irradiation and 1977 ICRP dose limits for medical radioisotopes 78—65135
thyroid protection during radioiodine-labelled pharmaceutical administration, computer simulation 78—44616
thyrotoxicosis therapy, dose determ. by thyroid uptake meas., effect of gland parameters 78—61245
time varying X-ray fields, digital acquisition system 77—57828

dosimetry continued
tissue absorbed fractions for very low energy photons 79—39508
tissue attenuation factors for human body omnidirectional γ-irradiation 79—92383
tissue equivalent gas, meas. of $\bar{W}$ for H^+, ^{4}He ions, ^{12}C ions 80—19550
tissue equivalent gas electron transmission function and mean energy per ion pair, obs. 80—23566
tissue equivalent phantom, dose distrib. calc. using Monte Carlo programme 80—78457
tissue equivalent torso phantom for transuranic nuclide counting facility calibration 80—67257
tissue heterodensity meas. for charged particle radiotherapy 79—20623
tissue inclusions, close from photon emitters in bone 80—36149
tissue inhomogeneity corrections to absorbed dose calc. 78—3610
tissue LET dose distrib. calcs. for 14 MeV neutrons 79—96664
tissue neutron and gamma-ray response function, mid-head, military appl. 80—8185
tissue neutron energy deposition spectra from improved cross-section values 80—26300
tissue section imaging by α and thermal neutrons 79—29591
tissue substitute material formulation using basic interaction data 77—86640
tissue substitutes in experimental radiation physics 79—20680
tissue-air ratios for whole body irrad. with ^{60}Co gamma-rays 78—61258
tissue-equivalent compensators for 4-MV X-rays, basic data 80—98069
tissue-equivalent gas, W-value for low energy electrons 78—15896
tissue-equivalent plastic A-150, density and composition uniformity 78—73252
tissue-maximum ratio expression fitted to Varian Clinac-6 and Clinac-4 accelerators 78—24148
tissue-maximum ratios for high-energy X-rays 78—3609
tissuelike medium α trajectory heavy secondary ion ejection 80—9466
tissuelike medium α trajectory production of δ-rays 80—9465
TL, mixed-field dosimetry, appl. to personnel dosimeter badges 80—23170
TLD, low level detection 77—61132
TLD, safety and reliability of decentralised reading in Sweden 77—40780
TLD, use in high level photon dosimetry 78—74503
TLD, X-ray quality and output determ. in diagnostic range 77—60241
TLD calibration procedures in the Studsvik standardized personnel dosimetry system, Sweden 80—9418
TLD data analysisusing a Texas Instruments programmable calculator 80—36136
TLD environmental meas. at nucl. facilities 80—42876
TLD evaluation of internal beta-dose rate for archaeological dating 80—98478
TLD in medicine and biology 79—74762
TLD personnel monitoring, occupational radiation exposure in Austria *(German)* 80—26352
TLD phosphors, use for high-level gamma-ray dosimetry 80—13934
TLD reader, improved S/N ratio for low dose meas. 79—76153
Tokamak fusion test reactor, cross section sensitivity, uncertainty anal. personnel dose rate 77—6554
Tokamak fusion test reactor, dose rates from induced activity in test cell 80—23144
tongue carcinoma, dose and dose rate in ^{192}Ir interstitial irradiation 79—16267
Toshiba LMR-16 linear accelerator, X-ray depth-dose characts. 79—62369
track detector direct dosimetry in fast neutron beams 78—20277
track structure theory in radiobiology and radiation detection 78—50446
transmission microscopy of unmodified biological materials, radiation dose with electrons vs. ultrasoft X-rays 78—11788
transport calculations for poins, neutrons, protons, α-particles, ions 77—25555
transport of radioactive material, statistical anal. of low-radiation packages 77—88286
transuranic elements in environment, recommendations for exposure of persons 79—93842
treatment planning, three dimensional model for CT radiotherapy 80—8192
treatment planning in ^{60}Co radiotherapy using computerised tomography techniques 78—35964
TRIGA core, gamma dose meas. by plastic detectors 80—9381
TRIGA-II Musashi reactor, neutron irradiation facility for medical purposes *(Japanese)* 77—56459
tritiated water intake, calc. of committed dose equiv. 79—16311
tritium distribution in technological systems of Novovoronezh nuclear power station 80—32533
tritium in rabbits after ingestion of freeze-dried tritiated food and tritiated water 80—21549
TRIUMF biomedical pion beam automated dose mapping system 78—73254
TSC in human nail, for dose estimation after accidental exposure 78—73253
UK nuclear power station radioactive effluent monitoring and public information 78—89992
ultrasoft X-ray microdosimetry and biological effectiveness comparison 80—26277
US imaging system for chest and other body organs 80—67174
USA diplomatic courier radiation exposures 78—28078
UV radiation source output monitoring detector for psoriasis photochemotherapy 78—53473
Varian 6 MV CLINAC-6X accelerator, beam characts. 78—3582
Varian Clinac 4 MeV linear accelerator, radiation from U collimators, and shielding 78—24135
very-low-dose ion implantation by scatt. attenuation 79—77617
VHF/UHF broadcast radiation, determination of population exposure in US 80—21551
VIPER reactor, neutron leakage spectrum and dose meas. 79—3243
W values and backscatt. coeffs. for slow electrons in air 80—19551
W-value determ. for α-particles in Ar and methane 79—39518
wall-less proportional counter internal microdosimetry 80—26372
walled and wall-less proportional counter characteristics and microdosimetry 80—26371
waste, long-term risk assessment of waste disposed in geologic formation 78—17361
waste air at nuclear plants, dose conversion factors for radiation exposure estimation *(German)* 77—70558

dosimetry continued
waste from nuclear power reactors, disposal into deep ocean, hazard assessment 77—88233
waste management policies, OECD countries 79—26596
water pollution by radioactive waste, computer anal. of relative potential hazards 80—21422
water vapour electron stopping power and energy degradation 80—23276
water/air mass stopping power ratios for megavolt. photon and electron beams 78—28082
wedged field characteristics for Clinac-18 10 MV X-rays 78—3608
Westinghouse PWR, radiation levels 80—5296
worker noise exposure, types of measurement and accuracy 80—23854
workers in isotope diagnostics and nuclear therapy, annual dose distrib. anal. 80—61706
working level months, uncertainties, statistical procedure 79—41044
X-irradiation late effects, evaluation by dosimetry intercomparisons 79—62361
X-irradiation of rats, partial body, dosimetry intercomparison 80—41247
X-radiation therapy, computer simulation of central axis dose distributions 79—8531
X-ray absorbed dose unit, 1 to 5 J/kg, USSR special standard 77—32956
X-ray attenuation, effect on dose distrib. and choice of quantities for protection standards 80—51277
X-ray attenuation coeffs. of materials meas. 78—84680
X-ray beam, 4 MeV linear accelerator, dosimetric aspects in radiation therapy 80—17140
X-ray beam characteristics, 25 MV, from a 35 MeV linear accelerator 79—25110
X-ray close enhancement at material interfaces, Monte Carlo calc. verification 79—22484
X-ray diagnosis of digestive tract, dose to patient and radiologist *(German)* 78—28086
X-ray dose mean value of specific energy, variational meas. 80—12276
X-ray dosimetry, appl. of cavity theory 80—13947
X-ray epilation for tinea capitis, dose var. 77—9267
X-ray equipment, scattered-radiation exposure 79—34670
X-ray fluoroscopy, acute radiation injury caused by faulty use during cardiac procedures 77—9272
X-ray high-energy therapy, activity induced in patients 77—40744
X-ray isodose curves in water phantom, for radiography machine 78—15892
X-ray microscopy using ultrasoft X-rays, specimen dosage 77—90972
X-ray radiation, long wavelength, dosimetry by thermoluminescent method 79—6768
X-ray radiation output constancy during diagnostic exposures 79—5340
X-ray source, industrial, use for electronic component radiation effects work, calibration 80—63402
X-ray units used outside radiology, dose obs. 80—89856
xeromammography, absorbed dose obs. 80—41242
xeromammography, dose to patient and image quality 79—100741
xeromammography, Monte Carlo calc. of integral radiation dose 80—41248
xeroradiography, negative development, doses and clinical indications in breast exams. 80—56217
xeroradiography, reduction of patient dose 79—16303
ZPPR at Argonne, gamma-ray response calc. for encapsulated solid-state dosimeters 77—46420
α-particle, range-energy relations and stopping power in tissue equivalent liquid 80—23275
β-ray point source dosimetry using variable cavity chamber, appl. to protection instrument response 80—13942
γ radiation dose rate calc. in building materials 79—18057
γ ray natural background, exposure rate variations in open air *(Czech)* 77—67900
n radiation, meas. standard for equivalent dose 80—102351
π^- beams, direct track detector dosimetry 78—20281
Al, blanket/shield designs, minimum-activity, for D-T and D-^{3}He fusion blankets 79—85796
Al, electron spatial absorbed-dose distrib. for 25 MeV beam 77—88289
Al min. activity blanket design for TFTR upgrade 78—58460
Al ultrasoft X-rays, phys. props. and Chinese hamster cell expts. 77—86542
Al_2O_3, UV dosimetry grade, thermolum. glow curves and emission spectra, 90-500K 78—72615
Am-Be, neutron fluence-to-dose conversion factors 79—6771
Am-Be neutron probe, underestimation of radiation exposure by film badges 78—15900
^{241}Am, gastrointestinal absorpt. in hamster 79—39520
Ar ions, high-energy, depth-dose meas. in tissue-equivalent liq. and water 78—3614
^{40}Ar 450 MeV/amu beam microdosimetry with wall-less proportional counters 80—26370
^{41}Ar dose distributions due to atm. release from HWR, including wind effects 77—14271
Au/Si interface, X-irradiated, dose profiles 79—24388
Ba isotopes, uptake and retention of ^{133}Ba and ^{140}Ba-^{140}La in mouse tissues, eye and skeleton doses 77—9276
Be+d neutron source, material damage study, He prod. and neutron fluence per neutron obs. in irrad. material 78—86710
BeO, exoelectron emission and radiation dosimetry *(Japanese)* 79—83110
^{9}Be(d,n), 40 MeV deuterons from ORIC, intense neutron source 77—83425
Be(d,n), activation cross-section, integral tests, dosimeter appl. 80—32553
Br^{6+}, 42 MeV, stopping power and radial dose distrib. obs. in tissue-equivalent gas 80—101218
C, electron spatial absorbed-dose distrib. for 25 MeV beam 77—88289
CO_2, electron transmission function and mean energy per ion pair, obs. 80—23566
CO_2-^{14}C animal exhalation meas. by liquid scintillation counting *(French)* 79—48384
^{12}C 400 MeV/amu beam microdosimetry with wall-less proportional counters 80—26370
^{14}C fallout from nucl. weapons testing, human radiation burden 77—64091
^{14}C labelled diethylenetriamine pentaacetic acid, dosimetry in the rat 79—62366
^{14}C, metabolism of low energy β-emitters 79—8551

dosimetry continued
^{14}C produced in advanced FBR fuels, potential radiation doses 77−40799
^{14}C production by nuclear power industry 77−54367
^{14}C production in reactors and explosions, population dose, health impact 77−14274
^{14}C released to atmosphere, dynamic model for estimating radiation dose to world population 80−89852
^{14}C released to atmosphere as CO$_2$, population dosimetry 78−35958
^{14}C-KCN, rat metabolism and internal dose 77−44754
CaS:Bi phosphors, UV dosimetry by thermolum. 80−55199
CaSO$_4$:Dy, Cd-covered TLD, thermal neutron dosimetry 77−90912
CaSO$_4$:Dy ribbon, dosimetric props. study 80−63395
CaSO$_4$:Dy sintered pellets, thermolum. response 80−93411
CaSO$_4$;Dy, multi-reading method 79−76154
CaSo$_4$, exoelectron emission and radiation dosimetry *(Japanese)* 79−83110
Cd covered Au foils, neutron spectra determination by resonance reactions 79−93837
^{141}Ce standard, measured by dose calibrators, simulated ^{99}Tc^{m} standard 78−61261
^{144}Ce, intravenous injection, wound site absorption, comparison of metabolic behaviours in rats 79−8545
^{144}CeO$_2$, repeated inhalation exposure of mice, retention and dosimetry 80−109034
^{252}Cf fission neutron, transmission through various shields, dose equivelent meas. 77−61620
^{252}Cf for interstitial radiotherapy implantations, clinical study 78−11722
^{252}Cf neutron source, dosimetry meas. technique tests 79−68113
^{252}Cf source in tissue-equivalent phantom, neutron absorbed dose obs. 80−12278
^{252}Cf source with high emission, n and γ dosimetry, safety *(Czech)* 78−33296
^{60}Co axial depth dose empirical formula 78−35965
^{60}Co beam lateral profile model 78−28085
^{60}Co beam model for radiotherapy treatment planning 77−66857
^{60}Co beams, appl. of a single model 79−39521
^{60}Co beams, cylindrical ion chamber A$_c$ and A$_{eq}$ factors exam. 79−81121
^{60}Co dosimetry for beagles in Collaborative Radiological Health Lab., long-term study 77−73585
^{60}Co gamma ray absorbed-dose standards, comparison 78−74512
^{60}Co gamma-rays, calibration in water vs. calibration in air for teletherapy units 77−21630
^{60}Co γ-ray scatt. in air, anal. by discrete ordinates transport codes 80−32525
^{60}Co γ-rays, LiF TLD meas. rel. to Burlin cavity theory 80−56220
^{60}Co hot cell accidental exposure 77−9261
^{60}Co irradiation sterilisation processing unequal mass interchange model verification 79−26759
^{60}Co irradiation sterilisation processing, unequal mass interchange model 79−26758
^{60}Co irradiation sterilisation processing, nonstandard double carton simulation 79−26760
^{60}Co, long-term retention in Indian workers, dose commitment 78−35960
^{60}Co photon beam dose distribs., oblique incidence correct., comparison of shift factors 80−76838
^{60}Co radiation therapy, eval. of dosimetric accuracy and uniformity 80−12269
^{60}Co radiotherapy, correction for inhomogeneities, appl. of ACTA scanner 77−60259
^{60}Co, shutdown dose rate prediction in BWR primary coolant circuit 78−74445
^{60}Co source irradiation of 2 media, absorbed dose in vicinity of an interface 80−30894
^{60}Co teletherapy, IAEA-WHO dosimetry service using mailed LiF, 1970-75 survey 77−16991
^{60}Co teletherapy, surface dose reduction using Ag filter 79−79641
^{60}Co teletherapy build-up dose meas. using FeSO$_4$-benzoic acid-xylenol orange dosimeter 78−28081
^{60}Co teletherapy dosimetry, USA nationwide survey 77−56478
^{60}Co, teletherapy dosimetry, USA survey (1974-77) 79−12011
^{60}Co teletherapy dosimetry survey of facilities 79−62367
^{60}Co teletherapy split fields, symm. and asymm. 78−3611
^{60}Co teletherapy unit dose calibration, comparison of methods 80−30900
^{60}Co therapy, use of electron filters to improve buildup characts. of large fields 78−3612
^{60}Co therapy for Hodgkin's disease, gonadal and eye doses 79−96665
^{60}Co total body irradiation, dose distrib. meas. using thermoluminescent dosimeters 80−41245
^{60}Co-charging of γ-irradiation installation *(Bulgarian)* 78−82558
Cs, in seawater, rapid determ. using Cs selective resin 78−85609
^{134}Cs, for treatment of cervical cancer, isodose curves 77−90876
^{137}Cs accumulation in rat liver, effects of altered thyroid states 78−24136
^{137}Cs body burden in Japanese from 1967 to 1975 77−9283
^{137}Cs contamination of external-radiation doses in USSR territory 78−86698
^{137}Cs gynecologic insertions, expt. derived algorithm for computer calc. dose rates 80−101264
^{137}Cs, long-term retention in Indian workers, dose commitment 78−35960
^{137}Cs, uptake by cotton rats inhabiting banks of radioactive liquid waste pond 79−25121
^{137}Cs-irradiation, fractionated high dose-rate and continuous low dose-rate effect on pig skin 80−41127
^{137}Cs-irradiation, response of pig skin, various schedules of irrad. 80−72237
Cu, metabolic model and dosimetric data 78−65130
^{144}e inhalation effect of influenza virus infection on pulmonary retention and mouse survival 78−85340
^{165}Er decay parameters and whole-body dose, for radioisotope scanning 77−70529
Fe radiation shielding, TLD meas. of neutron and gamma-ray energy deposition 80−23163
Fe slab *(Japanese)* 80−18595
FeSO$_4$ dosimetry by NH$_4$CNS method 79−2136
FeSO$_4$ dosimetry for electrons, a re-evaluation 80−68963
GaAs-ZnSe, X-ray cond. 5.4 to 17.5 keV, spectral and dosimetric characts. *(Russian)* 77−35964
H$_2$O, electron spatial absorbed-dose distrib. for 25 MeV beam 77−88289

dosimetry continued
HT single release in a room, radiation dose 78−74513
HTO incorporation in maize and barley 79−25107
HTO potential radiation dose to man, HT gas escape into forest ecosystem 78−96101
He accumulation fluence dosimetry for fusion materials neutron irrad. testing 80−32479
He ion beam therapy expts. and prospects 79−20633
He^{2+} 650 MeV beam relative biological effectiveness as function of depth 80−26281
He^{2+} 650 MeV ions study for possible radiation therapy applications *(French)* 77−66835
^{3}He-filled proportional counter, for sensitive dose or dose equivalent meter 79−45427
I, A=123 to 135, derived air concs. annual limits 78−31909
I radioisotopes, high efficiency mixed species air sampling, readout and dose assessment system 78−57074
I radioisotopes, meas. of crit. environmental exposure for reactor accidents 78−57081
^{121}I, production on Heidelberg compact cyclotron, dosimetry studies 80−21539
^{123}I, absorbed dose to thyroid from radioiodine impurities 77−29207
^{123}I labelled Hippuran dosimetry, physiological parameters 79−53251
^{125}I, determ. of exposure rate constant using a scintillation detector 80−89863
^{125}I, encapsulated, and other photon sources, microdosimetric props. 80−36146
^{125}I insulin, labelling using dimethylsulphoxide as labelling agent *(Korean)* 78−88746
^{125}I thyroid dose calc., air and water conc. limits 79−88195
^{125}I thyrotoxicosis management, dosimetry, radiobiology, clinical aspects 77−2048
^{125}I toxicity in cultured mammalian cell, primary site for division delay 77−52851
^{125}I uptake minimisation and thyroid monitoring 77−40796
^{129}I, dose to world population from nucl. power industry 80−47619
^{129}I, limits to radiological dose, dog retention data 77−60253
^{129}I, thyroidal burdens from dietary sources 77−44755
^{131}I airborne release from PWR, determ. of sources 80−17138
^{131}I dosimetry of the rat thyroid, accurate method 80−46063
^{131}I, environmental, in vivo thyroid monitoring 77−9264
^{131}I in tissue, specific energy calc. in accordance with crit. cell concept 77−2031
^{131}I labelled Hippuran dosimetry, physiological parameters 79−53251
^{131}I, long-term retention in Indian workers, dose commitment 78−35960
^{131}I, low level detection in milk rel. to population dose 78−31911
^{131}I measurement in human thyroid gland, use of NaI(Tl) scintillation survey meter 78−80970
^{131}I population thyroid dose in USA after Chinese atm. nucl. weapons tests 78−77116
^{131}I, radiation exposure dose determ., hot particle model 78−82520
^{131}I therapy, absorbed doses to marrow and blood 77−48869
^{131}I therapy of hyperthyroidism, gonadal dose and genetic significance 77−5082
^{131}I thyroid activity meas., improvement in precision 79−29635
^{131}I thyroid therapy, estimating doses recorded by personnel dosimeters 78−15891
^{131}I transport from pasture to milk, modelling Dresden-Monticello data 79−88203
^{131}I$_2$ transport via pasture-cow-milk pathway, stat. anal., thyroid dose uncertainty 79−83950
^{131}I-iodomethylnorcholesterol, human adrenals absorbed dose 79−79660
^{131}I-ortho-iodohippurate absorbed kidney dose calc., literature review 80−76841
^{131}I-therapy of cancer or hyperthyroidism, absorbed dose to ovaries or uterus 80−36138
^{111}In labelled human platelets, dose obs. 80−94370
^{115m}In specific activity determination, for nuclear accident dosimetry 79−3248
^{192}Ir, estimation of long-term biological elimination 79−70642
^{192}Ir radioactive sources, field determ. of output and effective size 80−30193
^{192}Ir radiographic source, radiation accident 78−53514
^{192}Ir, specific γ-ray constant and exposure rate constant 79−36187
^{40}K, natural content and internal radiation burden of Hungarian adult population 80−26355
^{79}Kr, kinetics after inhalation in man, rel. to internal dosimetry calcs. 78−28073
^{85}Kr, beta dose to crit. human tumour sites 78−28074
^{85}Kr extraction, occupational doses in gas liquefaction industry 78−15905
^{81m}Kr, for various source organ-target organ pairs 77−16989
^{81m}Kr radiation, internal conversion electrons, error in previous work 79−12005
Li-Al-borophosphate glass, activated with Ag, in-reactor dosimetry *(Russian)* 77−83113
LiF dosimeter, radiothermoluminescence dosimetry of 10 MeV electrons *(Italian)* 77−81582
LiF, dosimeter material, thermolum. non-linear response to sequential irrad. at different dose rates 79−1793
LiF, exoelectron emission and radiation dosimetry *(Japanese)* 79−83110
LiF:Mg,Ti detectors, depth dose distrib. of 9 MeV photons, comparison with phantom results 77−32957
LiF:Mg dosimetric cryst., light-sum storage during linear stage 79−8194
^{7}LiF-Teflon disc TLD, determ. of neutron fluence and γ-dose distribs. 79−45434
^{99}Mo, generation of ^{99m}Tc, influence of radiation dose on elution yield 79−29624
N ions, 3.5 GeV, vel. spectrometry vs. depth in polyethylene 78−48896
N$_2$ sphere surrounding D-T source, neutron and gamma-ray spectra 77−38422
^{13}NH$_3$ intravenous injection, absorbed radiation dose calcs. 80−94375
^{14}N(n,γ), gamma-field from monodirectional neutron source in air 77−67785
Na estimation in cotton clothing for use in neutron activation dosimetry 80−47729
^{95}Nb inhalation in beagle dogs, deposition and retention, dosimetry 78−35959
^{18}O ions, radial dose, LET and energy per ion pair in N$_2$ and tissue-equivalent gas 78−7452

dosimetry continued
^{32}P-diphosphonate dose determ. in patients with bone metastases from prostatic carcinoma 78–61251
Pb, dosimetric data and metabolic model 77–29206
^{208}Pb (p,p′), 635 Mell protons, meas. of energy spectra of secondary protons 79–97708
^{212}Pb inhaled body burden calibration, general phantom procedure 77–64138
^{212}Pb ion clearance from rabbit bronchial epithelium to blood 77–86641
^{147}Pm, in-vivo measurement by phoswich detector 78–28087
^{210}Po activity in Indian tobacco, meas. and lung dose calc. 77–9224
Pu assay, in vivo methods for humans 79–20674
Pu dose to lung and bone from contaminated soils, statistical uncertainties 80–109028
Pu dosimetry, calibration of whole-body counters 80–21547
Pu isotopes, maximum permissible inhalation values 79–70640
Pu, toxicity, cancer risk. calc. 77–2025
Pu toxicity hazards, cancer fatalities 77–66864
Pu(NO$_3$)$_4$, long-term effects of inhalation, influence of inhaled Ca-DTPA 77–66861
PuO$_2$ aerosol, acute inhalation, predictive model of early mortality 80–36028
PuO$_2$ air transportable package PAT-1, dose rate and criticality calcs. 80–13938
PuO$_2$ multiple low level exposure, case study 78–80967
^{238}PuO$_2$ particle inhalation, pulmonary tissue local dose computation 79–92385
^{239}PuO$_2$ inhalation, rat pulmonary connective tissue modification by internal α-irrad. 79–92302
PuO$_2$-Na$_2$O, biological solubility of aerosols in rats 78–96096
^{236}Pu, ^{239}Pu, ^{242}Pu, ^{244}Pu, distrib. in mice after injection 79–12001
^{237}Pu, ^{239}Pu, citrate, early retention in mature beagles 78–96095
^{237}Pu, intracardially injected in channel catfish, distrib. kinetics 79–20673
^{238}Pu, ^{239}Pu, ^{240}Pu, content in deer from integrated nuclear fuel cycle facility 79–57778
^{238}Pu, factors affecting particle mobility in rats 79–12003
^{238}Pu IV citrate chronic exposure effect on embryonic development of fish eggs 78–53447
^{239}Pu, cancer risk from ^{239}PuO$_2$, max. permissible conc. in air 79–25108
^{239}Pu citrate, internally deposited, pot. genetic dose, influence of testicular microanatomy 80–36147
^{239}Pu, distribution in mouse skeleton 79–12002
^{239}Pu distribution in mouse testis, significance of interstitial tissue ultrastruct. 79–57610
^{239}Pu, endosteal cell dose and relative distrib. factors compared to ^{226}Ra 78–96091
^{239}Pu, gastrointestinal absorpt. in hamster 79–39520
^{239}Pu in tissue, specific energy calc. in accordance with crit. cell concept 77–2031
^{239}Pu, influence of administered mass of cross-placental transfer in mice 79–20672
^{239}Pu localisation in bone using neutron-induced autoradiography 77–40773
^{239}Pu, lung burden, assessment of tissue substitutes for calibration purposes 79–16307
^{239}Pu lung dose after aerosol inhalation, effect of bronchopulmonary lavage and chelation therapy 77–9270
^{239}Pu, study of non-uniform distrib. in mouse testis 79–39507
^{241}Pu dosimetry, applicability of methods used for ^{239}Pu alphas 77–90906
^{241}Pu, uptake and redistribution within the gonads, hamster, rabbit 79–12004
^{226,228}Ra in humans, radiation induced malignancies 78–96075
Ra and daughter products, personal dosimetry and area monitoring *(Japanese)* 78–55044
Ra needle implants, computer program for reconstruction and dose-rate calc. 77–40770
^{224}Ra and daughters, radioactive props. and biological behaviour 78–96090
^{224}Ra biological effects, conf., Alta, USA (July 1974) 78–96068
^{224}Ra, endosteal cell dose and relative distrib. factors compared to ^{226}Ra 78–96091
Rn and Th, plastic solid state nuclear track detectors appl. 78–20556
Rn daughter concentrations in air of dwellings in Great Britain 78–77118
Rn, daughters, dose conversion factors 79–70641
Rn dosimetry using plastic nuclear track detectors 78–33298
Rn, inhalation of ^{222}Rn, ^{220}Rn and daughters 77–64133
Rn, moisture insensitive monitoring using solid detectors 79–31228
Rn water spas, TLD and solid state track detector direct dosage approach 80–68966
^{222}Rn concentration in N.Carolina groundwater supplies rel. to stomach dose and conc. standards 78–85612
^{222}Rn curved plesiotherapy applicators 80–51261
^{222}Rn daughter dose estimates from area sources 78–94151
^{222}Rn external plesiotherapy 80–36135
^{222}Rn released by uranium tailings piles, potential population dose 79–85824
Ru, hazards and control in nuclear fuel cycle, review 79–36392
^{106}RuO$_4$ in lung, in vivo meas. and dosimetry 78–53515
^{75}Se, whole body retention following intravenous injection as selenomethionine 77–90904
^{75}Se-Na-selenite distrib. in human body, and organ doses 78–48880
Si dosimetry diode, irrad. by γ-rays and fast neutrons, lattice defect annealing *(Czech)* 79–45570
Si/Au interface, X-ray dose enhancement, Monte Carlo calcs. 79–22484
^{90}Sr contamination of external-radiation doses in USSR territory 78–86698
T forms released from nucl. prod. complex, detection and meas. 77–54372
T health effects during normal and off normal release in CTR's 78–774
T radiation dose absorbed in rat organs, after feeding with organically bound T 80–51262
T, release from CTR, radiological dose calc. 78–78511
Ta$_2$O$_5$/Ta, heat-treated anodic film, exoelectron emission and radiation dosimetry *(Japanese)* 79–83110
^{96}Tc, as pertechnetate and erythrocyte label, dosimetry rel. to use in humans *(French)* 77–90909
^{95m}Tc, as pertechnetate and erythrocyte label, dosimetry rel. to use in humans *(French)* 77–90909

dosimetry continued
^{99m}Tc, atmospheric release, dose evaluation 79–25119
^{99m}Tc, automatic dispensing system, radiation exposure evaluation 79–96663
^{99m}Tc, beta-decay and dose calcs. 80–91154
^{99m}Tc, generation from ^{99}Mo, influence of radiation dose on elution yield 79–29624
^{99m}Tc-hepatobiliary agents, absorbed dose estimation 80–72330
^{99m}Tc-pyrophosphate, myocardial dosimetry for infarct imaging 77–40771
^{99m}TcO$_4$, radiation damage to mouse testis cells 78–24103
^{123m}Te-labelled adrenal-imaging agents, radiation dosimetry 80–101268
(Th,U) carbide fuel reprocessing, radiological assessment 80–52776
(Th,U)C advanced FBR fuels, radiological assessment of reprocessing 80–73983
^{232}Th, reevaluation of dose unit per unit intake 80–26356
^{232}Th, Thorotrast kinetics and radiation dose 79–39523
^{201}Tl emissions, nuclide parameters and S factors 77–13011
(U,Pu)O$_2$ fuel, criticality control, critical mass meas., fission rate distrib. by solid state dosimetry 80–13723
U mill tailings, radiation pathways and potential health impacts 79–85826
U milling operations, radiological assessment methodology 79–85827
U miners, lung cancer rel. to radiation exposure time distrib. 79–79605
U, miners Rn daughter inhalation and pulmonary cancer incidence 78–96080
U mines, dose limitations, ICRP recommendations, implementation problems 80–47769
U mining, exposure standards 80–46055
U mining in Canada, health hazards associated with Rn daughter inhalation 79–88140
U, natural, absorbed dose rate rel. to depth in tissue 79–88194
U surface mining, radiation exposures, meas. 77–64140
X-ray dosimetry, intercomparison and standardisation 80–12270
Xe probe for contamination monitoring 80–27826
Xe whole-body counting and dose determs. 80–89853
^{127}Xe, health physics, dose calcs. 80–98142
^{127}Xe, kinetics of total body retention and clearance after inhalation 77–37121
^{127}Xe maximum permissible conc. in air 78–61262
^{127}Xe whole-hody retention for dosimetry calcs. 77–60257
^{133}Xe, in meas. of skin blood flow 77–16994
Zn radionuclide dosimetry and permissible body burden ^{65}Zn and ^{69m}Zn 77–56474
Zn radionuclide dosimetry standards and crit. organs 78–35961
ZnSe, X-ray cond. 5.4 to 17.5 keV, spectral and dosimetric characts. *(Russian)* 77–35964
^{65}Zn whole-body retention in pregnant mice, and secretion into milk 79–88200

double nuclear magnetic resonance
see also INDOR
adamantane, heteronuclear spin coupling and decoupling dynamics 77–48066
alkali metal bromates and chlorates, alkali and ^{17}O NQR, spin echo double reson. method, electronegativity 80–54970
ammonium hydrogen oxalate hemihydrate, single cryst., DNMR obs., elec. field gradients, reorientation 77–85618
AX spin 1/2 system, double reson. interferometry, relax. times 78–6603
bacteriochlorophyll cation in soln., N atom ENDOR and proton triple resonance 78–96018
benzene, polycrystalline heteronuclear dipolar modulated chemical shift spectra, geometrical and orientational obs. 77–20750
benzene, solid, double-quantum cross-polarization in solids 80–100623
benzene-d$_6$, NMR double-quantum spin decoupling 78–88227
benzenes, monosubstituted, high resoln. ^{1}H coupled ^{13}C NMR, INDO calcs. 77–50457
book, principles of magnetic reson. 78–80189
bromomethanes, ^{13}C-Br spin-spin coupling consts., isotope effects 78–13522
calcium formate, polycrystalline, heteronuclear dipolar modulated chemical shift spectra, geometrical and orientational obs. 77–20750
calcium formate, selective high resolution ^{1}H NMR 79–61245
N-5-chlorosalicylideneaniline, H$^+$-^{14}N double reson. NQR spectra temp. depend. thermochromism and tautomeric mech. 78–70849
computer controlled wide line CW double NMR spectrometer 78–45667
coupled spin systems, relax. mechanisms and multiple quantum transitions 78–88211
coupled systems, A-line intensity, phase, oscill. with time, heteronuclear double reson. spectra 80–34823
coupling between rare and neighbouring abundant nuclei *(Russian)* 78–48083
cross polarisation in solids with flip-back of I-spin magnetisation 80–39894
cross relaxation, theory *(Rumanian)* 79–8072
cross relaxation modes, appl. to NaF 78–10803
cross-polarization double-quantum NMR in solids, theory 80–100623
crossed slotted tube resonator, double resonance NMR probehead 78–265
p-dichlorobenzene, nuclear dipole absorpt. signal, under quadrupole reson. saturation conditions 78–48082
1,1-dichloroethane, tilt-effect and interference with rel. sign determination in weak irrad. expts. 80–32742
1,2-difluorotetrachloroethane, mol. motions and Zeeman-quadrupole cross relax., NMR obs. 79–65751
dimethylsulphoxide-d$_6$, NMR double-quantum spin decoupling 78–88227
dipolar broadening in solids 79–61265
dipolar energy influence in nucl. double reson. 77–28482
double spin flips, in nucl. double reson., theory 80–66076
double tuned matching boxes for FT expts. at 94 and 100 MHz 77–45874
double-quantum spin decoupling 78–88227
EBBA, mol. order study by means of C^{13}-H^1 double resonance 79–60275
electron-nuclear-nuclear triple-reson. spectrometer 77–41662
ENDOR studies using K-band high-pressure cell 79–67336
2-fluoropyridine, natural abundance ^{1}H coupled ^{15}N NMR spectra, selective population transfer method 79–95682
formic acid, ^{13}C NMR spectra and relax. under intermediate decoupling power conditions 80–20515
formic acid, heteronuclear double reson., spin echo modulations 78–1009

double nuclear magnetic resonance continued
formic acid($-d_1$), dilute deuterated mixture, high-sensitivity NQR, double quadrupole reson. 78—68412
formic acid-d_1, NQR sensitive detection by double resonance with spin mixing by continuous coupling 77—77128
glassy polymers double NMR, appl. of cross relaxation dynamics in modulated systems 80—71242
heteronuclear cross-correlation spectroscopy, rot. frame coherence transfer theory 79—97412
heteronuclear dipolar modulated chemical shift spectra, double reson. multiple pulse NMR 77—20750
heteronuclear double-resonance spectra, modulations 78—86897
heteronuclear spin coupling and decoupling dynamics 77—48066
heteronuclear spin system, second moments of NMR spectra, calc. 79—73836
heteronuclear two-dimensional spectroscopy, indirect detection of NMR 77—90068
N-(2-hydroxythiobenzoyl)morphiline, ^{1}H NMR, spin decoupling by torsional transitions 78—62832
ice, ^{17}O, NQR spectrum by double reson. with coupled multiplets, fine struct. 80—54969
ice, high-pressure forms, ^{2}D and ^{17}O NQR from double reson. obs., quad. coupling consts. 77—90069
ice Ih, NQR of ^{17}O, double NMR for ^{1}H tunnelling, 1.3 and 4.2K 79—47353
ice II, NQR of ^{2}D and ^{17}O 77—1617
iodomethane, IR-RF double reson., NQR of spin-rot. coupling consts. 78—66569
low-temperature double electron-nuclear resonance obs. using 3 cm rectangular resonator 80—98956
motional effect 78—68413
multilevel spin systems, selective excitation and detection, single transition operators 78—2771
multiple quantum, tickling 80—23446
NMR-NQR double resonance, two-freq. methods, resonance spectrometers 80—20512
nonintegral spin systems, appl. of nucl. double reson. interference spectroscopy 79—4745
nonstationary nutations in heteronuclear double resonance 80—20516
NQR, sensitive detection by double resonance with spin mixing by continuous coupling 77—77128
NQR double resonance detection, principles and appl. to D 78—76354
NQR multiple resonances, phase eqns. 77—16202
NQR-NMR double resonance line intensities, level crossing method, two freq. saturation 80—20514
NQR-NQR double resonance, double quadrupole spin echo resonance 80—20513
nuclear quadrupole double resonance, review 77—36153
nuclear spin systems dynamics, review *(Rumanian)* 78—55189
PAA, liq. crystal, ^{14}N NQR freqs., double-reson. level crossing method 78—6602
phosphates, cellular, heteronucl. two-dimens. NMR as conform. probe 80—3590
polycrystalline solids, selective high resolution ^{1}H NMR 79—61245
probe circuit, single coil, with transmission-line tuning for NMR 77—26375
pulsed NMR in solids, survey 80—34782
pyridine, ^{13}C-^{1}H spin-spin coupling consts. 78—25562
pyridine and salts, deuterium NQR, double reson. method, ring charge distrib. 80—53015
pyrrole, natural abundance ^{1}H coupled ^{15}N NMR spectra, selective population transfer method 79—95682
quadrupole-Zeeman cross-relax. between two nucl. spin species, appl. to difluorotetrachloroethane 79—65766
β-quinol clathrate, single cryst., double NMR obs. of mol. motion of trapped methanol 79—87332
relaxation rate calculation, appl. to CaF 78—15060
resonant transfer of nucl. spin dipolar order in rotating frame 79—33564
rotating frame, effect of nonresonant oscillating field, modification of Zeeman energy 77—28454
rotating frame, experimental set-up *(Rumanian)* 79—58763
separated local field spectroscopy for D-H and H-H spin systems 80—2667
single coil probe for solid state studies 78—264
solid, mol. and complex ion intramolecular configs., nucl. quadrupole double reson. obs. intramolecular configs., nucl. quadrupole double reson. obs. 80—34821
solid torsional oscillators, rotating frame, nucl. spin polarisation losses, torsional spectroscopy 80—31821
solid-state expts., theoretical concepts and expt. results 78—76353
solid-state NMR, deuteron spin decoupling from protons 79—61266
solids, detections of low abundance nuclear isotopes, review *(Rumanian)* 79—15380
solids, pulsed NMR, conf., London, England (Dec. 1978) 80—31404
solids, selective double quantum NMR 80—97164
spectrometer for nuclear quadrupole double resonance with programmable calculator control 79—12830
spin 1/2 system, nuclear double resonance by longitudinal detection 78—78733
spin diffusion, influence on nucl. spin-lattice relax. due to impurity nuclei under magic angle conditions 78—15061
TBBA, smectic, proton ^{14}N nuclear double reson. 77—58947
TBBA, smectic phases, orientational order, ^{14}N NQR and double NMR obs. 78—94974
TBBA, smectic VI and H phases, orientational order, temp. depend. 79—46555
p-terephthal-bis-aminocinnamate, smectic phases, orientational order, ^{14}N NQR and double NMR obs. 78—94974
thermodynamic influence of spin-spin energy on cross-relax. and spin diffusion 78—76343
thymopoietin active fragment in H_2O, soln. conformation by DNMR spectroscopy 80—89710
torsional spectroscopy by NMR in rotating frame 78—27119
transport coefficients of dilute spins, for structural and dynamic information *(Rumanian)* 79—65767
trichloromethane glass:O_3, ^{17}O, NQR by proton double reson., broad reson. assignments 80—53014
trifluorobenzene, symmetrical ^{1}H and ^{19}F NMR, cross relax. 79—38406
2-tromopropane, tilt-effect and interference with rel. sign determination in weak irrad. expts. 80—32742
two-dimensional, state-of-the-art 78—74044

double nuclear magnetic resonance continued
two-frequency NMR-NQR double reson. 79—95683
two-spin system with chemical exchange, amplitude-modulated DNMR 79—93194
Varian HA-100D NMR spectrometer improvements for double NMR and ENDOR expts. 79—80651
AgF, heteronuclear spin coupling and decoupling dynamics 77—48066
$Al_2O_3:Cr^{3+}$, corundum and ruby, ^{27}Al quadrupole, transitions, acoustic and elec. saturation 77—90071
β-Al_2O_3-Na_2O, nucl. double reson. interferometry, satellite spectrum 78—31123
AlP, multiple pulsed double NMR and nucl. spin dynamics 77—16208
$B(OH)_3$, $^{1}H/^{2}H$ quadrupole reson. freqs. detected by double reson. with level crossing 78—84497
$Ba(ClO_3)_2.2H_2{}^{17}O$, fine struct. in quad. reson. of ^{17}O, DNMR 77—8453
^{13}C coupled with ^{1}H, spinor character for spin $^{1}/_{2}$ nucleus via NMR interferometry 78—17699
^{13}C-^{1}H long-range coupling assignment through selective ^{1}H decoupling 77—46582
^{13}C-^{1}H NMR in organic solids, spin decoupling dynamics 77—4582
^{13}CH fragment, selective population transfer expts., density matrix formalism appl. to NMR spectroscopy 78—15059
CaF_2, high resolution double NMR at low gyromag. ratio 78—25577
CaF_2, relaxation rate calculation 78—15060
CaF_2, solid, ^{43}Ca-^{19}F double NMR method, determination of ^{43}Ca 80—2668
CaF_2:Na, pulsed DNMR exam. 78—35066
CdF_2, high resolution NMR and chem. shifts of ^{111}Cd and ^{113}Cd, double reson. expt. 80—60460
Co complex $[Co(NH_3)_4CO_3]Br$, ^{14}N quadrupole interaction, $^{1}H/^{14}N$ double reson. 79—51882
D double-quantum NMR with magic angle spinning in solids 80—108120
DCl, orthorhombic, nucl. quadrupole double reson. obs. and interpret. 77—90070
dimethylammonium cadmium chloride, proton-^{14}N double reson. exam. of struct. phase transitions 77—4583
HIO_3, $^{1}H/^{2}H$ quadrupole reson. freqs. detected by double reson. with level crossing 78—84497
H_2O_2, ^{17}O pure NQR spectrum 80—9620
H_2SeO_3, $^{1}H/^{2}H$ quadrupole reson. freqs. detected by double reson. with level crossing 78—84497
^{2}H-^{1}H, double-quantum spin decoupling 78—88227
KAl_2Br_7, NQR double-reson., $Al_2Br_7{}^{-}$ ion in cryst. 78—91993
$KHCO_3$, $^{1}H/^{2}H$ quadrupole reson. freqs. detected by double reson. with level crossing 78—84497
KH_2PO_4, ^{39}K spin-lattice relax. time double NMR meas. 79—47358
$KHSO_4$, $^{1}H/^{2}H$ quadrupole reson. freqs. detected by double reson. with level crossing 78—84497
Li powder, cross relax. rates between ^{7}Li and ^{6}Li 77—40153
LiF, ^{7}Li and ^{19}F reson., existence of single nuclear dipolar spin temp. 78—35065
LiF, dilute paramagnet, ^{8}Li-^{6}Li cross relaxation *(Russian)* 79—4747
$^{7}Li_2O$, β-radiation detected NMR of ^{8}Li obs., double freq. irradiation, ^{7,8}Li hyperfine struct. anomaly 78—91994
$^{7}Li_2S$, β-radiation detected NMR of ^{8}Li obs. double freq. irradiation, ^{7,8}Li hyperfine struct. anomaly 78—91994
Mo complex, ^{97}Mo and ^{95}Mo nuclear elec. quadrupole moment, nuclear quadrupole double reson. spectra 78—10802
^{95}Mo, ^{97}Mo, quadrupole moments, hyperfine B factors, laser-Rf double reson. meas. 78—33452
NH_3, liq., contraction phenomenon in DNMR spectra, simulation obs. 77—88469
NH_4Cl, solid phase, resonant transfer of nucl. spin dipolar order in rotating frame 79—33564
NH_4I, torsional spectroscopy by NMR in rotating frame 78—27119
NH_4NO_3, NMR double resonance *(Rumanian)* 79—58763
NH_4NO_3, solid, nuclear double reson. cross-relax. 79—15379
$(NH_4)_2SO_4$, paraelectric, N-quadrupole coupling meas. 80—60459
NaF, DNMR cross relaxation modes 78—10803
NaF, relaxation rate calculation 78—15060
NaF:Li, pulsed double nucl.-nucl. reson. *(Russian)* 78—10804
$NaHCO_3$, $^{1}H/^{2}H$ quadrupole reson. freqs. detected by double reson. with level crossing 78—84497
$NaNO_3$, ^{23}Na spin-lattice relax., orientation depend. 78—23372
$NaNO_3$, double quantum nuclear magnetic resonance of ^{23}Na by double resonance, line shape 80—75886
^{23}Na spin-$^{3}/_{2}$ nuclei, double quadrupole resonance 80—32634
^{17}O, NQR at natural isotope abundance, double reson. new techniques, review 80—53013
^{17}O nuclear quadrupole double resonance spectroscopy, line shapes and examples 80—31820
^{31}P, obs. using RYa-2308 radiospectrometer with attachment 80—98957
Ta, NMR-γ double resonance, Mossbauer absorpt. spectra *(Russian)* 80—34824
$Te(OH)_6$, $^{1}H/^{2}H$ quadrupole reson. freqs. detected by double reson. with level crossing 78—84497
double refraction *see birefringence*
double refraction, electric *see electro-optical effects*
double refraction, magnetic *see magneto-optical effects*
double resonance, electron nuclear *see ENDOR*
doublet antennas *see dipole antennas*
DPPH, diphenylpicrylhydrazyl *see organic compounds*
drag reduction
aft-body drag reduction, combined boat-tailing and base blowing at M=3 77—23988
asbestos fibre suspension, in turbulent flow 79—68786
boundary layer turbulence, burst cycle and drag reduction 77—15003
boundary layer turbulence, diffusion of polymer soln. introduced via slit 79—68685
bubble rupture between two solid walls, effect of drag-reducing polymers on cavitation 80—106822
bubbly, droplet and particulate flows, drag coeff. and relative vel. relations 80—24072
cavitation onset on cylinder, effect of dil. aqueous polymer solns. 77—68645
cetaceans, drag reduction and self regulation of skin damping while swimming *(Russian)* 77—32918
compliant coatings, review 78—26115
compliant membranes, appl. of tension 77—31287

drag reduction continued
- compliant wall drag reduction 78—26193
- compliant wall motion 78—22336
- conducting fluid, uniform current, flow past conducting porous sphere 78—34204
- conference, drag reduction and turbulence struct., Washington, USA (June 1976) 78—22329
- creeping flow round sphere, fluid elasticity effect on drag coefficient 80—43742
- cylinder, perforated, circ., finite-aspect-ratio, drag coeff. 79—23360
- drag reducing agents, decreasing mass transfer rate for Cu corrosion inhibition in soln. 78—19920
- drag reducing flow, mean vel. and turbulent energy closures 78—22331
- drag reducing fluid, turbulent fluctuations in viscous wall region 78—26160
- drag-reducing flows, calc. of velocity profiles 77—35185
- drag-reducing polymers aqueous solutions, turbulent bursts rel. to wall friction 78—63454
- elastic surface, turbulent boundary layer, hydraulic drag reduction 80—33572
- electrochemical mass transfer, drag-reducing polymers, effects, comparative study 80—76528
- electrochemical mass transfer between rough surfaces and solutions containing drag-reducing polymers 80—19447
- enhancement by mol. aggregates 78—26161
- fibre suspension, dil., mechanistic aspects of drag reduction in turbulent pipe flow 80—6102
- fibre suspension, rheology, rel. to turbulent drag reduction 78—22315
- fibre suspension flow in pipes, transition regime analysis, drag reduction 77—89186
- fibre suspension in water, turbulent jet, analogous behaviour to polymer solns. 78—1732
- fibre suspensions, fibre degradation effects 79—72918
- fluidised bed, effect of particle proximity on drag force 80—96306
- gas and non-Newtonian liquid, stratified flow in horizontal pipes 80—48787
- gas-solid turbulent suspension flow, frictional pressure drop Prandtl's mixing length anal. 79—14458
- geostrophic wind speed rel. to momentum exchange, global maps *(German)* 78—44955
- hydroxypropylmethyl cellulose soln., drag reduction by centre line fibre injection 80—14749
- laminar boundary layer, elongational viscosity and secondary instability 77—23997
- laws of motion of solid particles in laminar flow 80—83779
- liquid system, turbulent flow, drag reduction, neutral stability 77—7380
- low eddy friction polymer soln. hydrodynamics 80—53818
- mechanism 78—26107
- oscillating flat plate with interface film 80—10268
- oscillatory flow in U-tube manometers, effect of drag reducing polymer additives 80—64584
- particle-fluid mixture, energy balance in turbulent flow 77—47076
- PEO 301, dilute soln., pipe flow turbulence struct. drag reduction 78—26196
- pipe flow, triggered laminar to turbulent transition, random coiling macromolecular soln. 78—26195
- pipe flow turbulent entrance region, drag reducing fluid, expt. and anal. 78—63458
- plate, with suction, three-dimens. fluctuating flow, heat transfer, skin friction 78—87389
- polyethylene oxide, dil. aqueous solns., dynamical shear characts. *(Russian)* 79—86393
- polyethylene oxide, drag reduction props., Congo Red additive effects 79—64717
- polyethylene oxide aqueous solns., spectroscopic obs. of structural variability WRT turbulent resistance reduction 77—7356
- polyethylene oxide soln., drag reduction of highest mol. wt. fractions 77—68636
- polyethylenoxide additive mixing, turbulent drag reduction, schlieren obs. 78—26163
- polyisobutylene in toluene solution, effect of capillary materials on drag reduction *(German)* 80—87785
- polyisobutylenes, dilute solns., turbulent drag reduction, influence of mol. wt. and mol. conformation 77—80189
- polymer, dil. soln., and burst cycle mechanism 78—26164
- polymer additive in helicoidal flow, screw pump press. head 78—26166
- polymer additive mech. mixing in turbulent drag reduction 77—68637
- polymer injection at high Reynolds number boundary layer flow *(Chinese)* 79—32582
- polymer soln. turbulent flow over plate, drag reduction 78—5768
- polymer solns., dynamical behaviour, mol. conformation and optical props., expt. and rheological model 79—60034
- polymer solns., mass transfer and drag reduction near wall, electrochemical methods 79—77138
- polymer solns., parameter affecting the onset of drag reduction 79—77189
- polymer solution, 1st normal stress difference meas., rel. to water 79—98829
- polymer solution, channel flow, drag reduction, viscous sublayer struct. 78—22385
- polymer solution, dil., turbulent flow behaviour in annulus 80—33633
- polymer solution, drag reduction, laminar to turbulent transition, rot. disc expt. 78—75173
- polymer solution, drag reduction in pipe flow, flow time scales 78—22386
- polymer solution, drag reduction in turbulent flow 78—26159
- polymer solution, drag reduction in turbulent flows, book contrib. 78—59432
- polymer solution, laminar wake, behind cylindrical body 79—37355
- polymer solution, mass transfer between solid surfaces and drag-reducing fluids 78—79339
- polymer solution, mechanical model for flow, extensional viscosity 78—22378
- polymer solution, molecular weight distrib. effect on drag reduction in turbulent stream 78—83437
- polymer solution, rheology, rel. to turbulent drag reduction 78—22315
- polymer solution, stability in Couette flow *(German)* 77—47047
- polymer solution, turbulence structure, drag reduction 78—22381
- polymer solution, turbulent boundary layer, drag reduction 78—22414
- polymer solution, turbulent jet behaviour 78—1732
- polymer solution, turbulent mass transfer to pipe flow 78—1695

drag reduction continued
- polymer solution pipe flow, drag reduction 78—42631
- polymer solutions, in U-tube 79—1217
- polymer solutions, Toms effect 79—81929
- polymer solutions, turbulent, mass transfer rate, frictional force *(French)* 79—37357
- polymer solutions, weak, flow anomalies *(Russian)* 80—19454
- polymers in liquid stream, Toms effect mechanism, turbulent drag decrease 80—79270
- Polyox, drag reduction meas. in square duct, anomalous effects due to polymer degradation 80—83824
- Polyox 701, aq. soln., spectral effects in turbulent press. suppression 78—5771
- Polyox coagulant effects on turbulent boundary layer 78—26165
- polystyrenes, toluene soln., turbulent drag reduction, mol. wt. and struct. influence 79—7373
- rotating disc in polymer solutions under a turbulent regime 80—33634
- sharp flat plate, drag reduction in rarefied hypersonic flow 79—94669
- ship hydrodynamics, drag on displacement ships, hydrofoils, hovercrafts 78—63423
- shockless near free molecular flow, drag reduction calc., profile optimisation 79—14435
- slip flow past tangential flat plate at low Reynolds numbers 78—47000
- solar concentrators, paraboloid type with reduced wind drag, design 77—23731
- spherical condensed phase, motion in uniform vapour gas flow, kinetic theory 78—1725
- spike, fluctuating pressure wind-tunnel meas. 78—30310
- toluene in polymers, drag reduction 79—32591
- transonic flow of perfect gas around uniformly expanding sphere 80—28528
- tube flow, drag reducing additives and sudden enlargement of diam. 79—37397
- turbulent boundary layer flow, drag reducing additives, 2-D channels and circular pipes 78—26167
- turbulent boundary layer with compliant wall 78—26193
- turbulent boundary layers 78—18317
- turbulent drag reduction by fibre injection 79—37298
- turbulent drag reduction in pipe flow due to nonuniform polymer conc. 79—27672
- turbulent energy dissipation model 78—79345
- turbulent flow, drag reduction scale-up criteria 78—22330
- turbulent flow with polymeric additives, convective heat transfer 79—77098
- turbulent fluctuations in viscous wall region 78—26160
- turbulent heat transfer in dilute surfactant or polymer solutions 79—77101
- turbulent jets, influence of drag reducing polymers on cavitation inception 80—106823
- turbulent pipe flow, use of eddy viscosity expressions for vel. profiles in Newtonian, non-Newtonian and drag-reducing flows 80—83789
- two circular discs in tandem, drag reduction, wakes 80—106795
- two-phase flow, turbulent boundary layer, drag reduction 78—22414
- uniqueness and drag for fluids of second grade in steady motion 79—32584
- viscoelastic and inelastic fluid flow past sphere, creeping and boundary layer flows, drag coeff. 77—51090
- viscoelastic flow in tube, eddy diffusion reduction for heat and momentum transfer 78—22382
- viscoelastic fluid, turbulent flow, frictional drag reduction 78—1696
- viscoelastic liquid injected into Newtonian turbulent pipe flow, diffusion and drag reduction *(German)* 79—77251
- viscous drag computation for axisymmetric bodies at high Reynolds numbers 80—19343
- viscous sublayer and near wall turbulence struct., stroboscopic visualisation 80—19349
- wall turbulent flows with drag reduction, Reynolds stress model 80—43695
- weak polymer solution in smooth pipes, turbulent wall motions 80—14823
- weak polymer solutions, flow props. in narrow channel between rotating and stationary discs *(Russian)* 80—59089

drawability *see ductility*

drawing (mechanical)
- alkali-$PbSiO_3$ optical fibres, high aperture, double-crucible preparation 78—1450
- anisotropic polycrystal, yield and tensile test meas. of plastic behaviour 77—32631
- axisymmetric drawing through curved dies, heat transport anal. 77—52432
- α-brass, drawability correlation with sheet metal texture 78—60683
- brass, fracture initiation and propagation during strip drawing 78—64663
- α-brass sheets, earing, R-values and 3-D orientation distrib. functions, comparisons 79—91702
- clad metals, deformation behaviour contrib. in rod drawing *(German)* 80—11684
- clad sheet metal, optimum combination of composing sheets for deep drawing 77—81241
- continuous drawing of liquids to form fibers, review, book contrib. 80—97444
- crystalline polymer, epitaxial crystallisation on surface of drawn polytetrafluoroethylene 78—14626
- cup wall ironing, stress calc. 80—29989
- CVD optical fibre, long length strength 80—58752
- deep drawing, energy saving, and role of friction in metalworking 80—76271
- deep-drawing curves, cryst. microstruct. during deform. *(French)* 79—20066
- draw resonance theory, Newtonian fluids 78—83350
- draw resonance theory, power-law and Maxwell fluids 78—83351
- E-glass fibre strength, effect of forming and ageing atmos. 78—92283
- ethylene-vinyl alcohol copolymer, drawn samples, annealing effect around T_g temps. on shrinkage and mol. orientation 80—79712
- explosive forming, computer numerical simulation 80—59560
- extrusion and forming of solids, plastic deform., nonNewtonian flow, numerical solns. 78—19824
- fibres, optical, from compound glasses, using double-crucible and glass-plastic methods 79—3815
- flange, rigid-plastic deformation in deep drawing process, finite element anal. 79—18735

drawing continued
  glass fibre, cooling during drawing 79—52253
  glass fibre, forming process, characts., anal. techniques 80—58827
  glass fibre, optical loss, effect of manufacturing conditions 77—21085
  glass fibre drawing process, characterization and control 80—58826
  glass fibre drawing process, extensional instabilities 80—89258
  glass fibre waveguide drawing using CO_2 lasers 79—59857
  glass fibreguides, for lighwave communication, fabrication and characteristion 80—50586
  glass fibres, stresses induced by draw force 79—47737
  glass optical fibre drawing, fluid-dynamic stability analysis 77—11053
  glass systems used for optical fibres, diffusion kinetics 79—90040
  ingot, continually cast, optimum conditions for variable drawing rate *(Russian)* 79—70056
  laser drawing limitations on optical fibres 78—1447
  Lawsonite end plates for working spaces of liq. H_2 targets, prep. technique 77—67926
  lightguide fibre, prototype drawing fascility 80—64229
  metal, axisymmetric drawing simulation, numerical method development 78—30206
  metal, fibres, cubic struct., texture form. in uniaxial deform. theory 79—24532
  metal electroplastic deformation meas. pulse generator *(Russian)* 80—25931
  metal forming process, forming conditions and material characts. 80—30032
  metal sheets sliding on dies under plane strain drawing, sliding surface damage obs. *(Japanese)* 77—44369
  metals, deformability, quantitative determ. in drawing 79—52229
  metals, residual stress on drawing calcs. by stress state changes variational principle *(Russian)* 80—65125
  Newtonian and viscoelastic liqs. isothermal spinning, draw reson. instability 79—60027
  nylon, steady-state deform. and its effect on struct. and morphology 78—15459
  nylon 66, doubly oriented, annealing of drawn and rolled samples, struct. 78—52859
  Nylon 6, small-angle X-ray scatt. struct. changes w.r.t. thermal and mech. history 79—41976
  Nylon 6 gut yarn, fine struct. change in twisting, annealing and untwisting, microbeam X-ray obs. 80—81026
  Nylon 6 gut yarn, fine struct. change in twisting, annealing and untwisting, X-ray and electron microscopy obs. 80—84904
  Nylon 6 yarns, NMR, fibre struct. rel. to annealing, drawing *(Japanese)* 77—32269
  optical, fibres with high tensile strength, furnace drawing method 78—68666
  optical fibre, diameter control 78—13794
  optical fibre, furnace drawn, tensile strength 80—58751
  optical fibre, mechanical strength, fractographical analysis, review *(Japanese)* 80—35319
  optical fibre coating with conical shape applicator 80—58820
  optical fibre crystals floating zone growth, for IR optical waveguides 80—79019
  optical fibre drawing, diameter control improvements 78—1445
  optical fibre drawing, double layer silicone coating with double cone nozzle 80—53488
  optical fibre drawing, neck-down shape prediction from furnace temp. distrib. 78—5594
  optical fibre drawing, semi-automatic machine development 79—27449
  optical fibre drawing process control, optimisation theory appl. 79—90039
  optical fibre drawing technique for bundle of 19 fibres drawn from double crucible 78—55480
  optical fibre drawing techniques for plastic-clad and doped-deposited silica fibres 79—37066
  optical fibre drawing using laser, galvanometer beam-scanning rotating lens system 79—41463
  optical fibre drawing using ZrO_2 induction furnace 78—1446
  optical fibre fabrication techniques 79—18557
  optical fibre formation of microcapillary by pulling from billet, azimuthal asymmetry effects, theory 78—87172
  optical fibre geometry specifications rel. to measured fibre statistics 79—27371
  optical fibre manufacture, effect of thermal fluctuations *(Japanese)* 78—37980
  optical fibre preparation methods and performance factors 80—69557
  optical fibre processing techniques, review 79—50460
  optical fibre waveguides with large-diameter core and low optical losses, prod. technology 80—14463
  optical fibres, control of diameter 79—50468
  optical fibres, cooling rates during drawing 80—66538
  optical fibres, drawing conditions influence on attenuation 78—68667
  optical fibres, drawing of several fibres from a double crucible 78—33920
  optical fibres, heat transfer in laser drawing 79—94377
  optical fibres, high temp. resistance oven 80—74491
  optical fibres, UV curable epoxy acrylate coated, long-term mech. behaviour 78—95802
  optical fibres pulled in graphite furnace, effect of drawing conditions on tensile strength 79—50469
  optical single mode fibres, homogeneous CVD fabrication and characterisation 80—69562
  optical-fibre loss for high-speed drawing 79—14095
  PA-6, polymer fibre, orientation changes during stretching, IR spectra 78—75568
  PET, filament form. from gels 78—80508
  PET films, one-way drawn, constant strain effects, IR meas. 80—60584
  plastic deformation incompatibilities, resulting from moderate cold drawing, X-ray line broadening determ. *(French)* 79—43265
  plastic light focusing fibre, heat drawing process prep. 77—14815
  PMMA, oriented, hypersound propag., elastic props. 78—75737
  PMMA, uniaxially drawn, shrinkage, continuum model *(German)* 78—76722
  β-poly(vinylidene fluoride) films, single cryst. orientation, piezoelec. 80—20591
  polyacetylene films, stretch-aligned, prep. and morphology 80—66471
  polyamide-6, fibrillar struct. and annealing, small-angle X-ray diffr. 78—75565
  polybutylene terephthalate, semicryst., mech. props., effect of annealing below glass temp. 77—25066

drawing continued
  polybutyleneterephthalate, drawn annealed, struct. and props., X-ray scattering 79—7552
  polycarbonate, highly hot-drawn, mechanical prop. and phys. struct. changes 78—14293
  polycarbonate (BPA), thickness depend. of G_c for shear lip propag. from single crack propag. 78—11305
  polycarbonate fibre, highly-oriented, drawing behaviour and mech. props. 78—76708
  polyester fibres, orientation in drawn fibres, birefringence meas. 78—35344
  polyethylene, dielectric props., investigation for morphology changes created by mechanical drawing and annealing 80—84697
  polyethylene, drawn, ultrahigh modulus, linear, melting behaviour 80—19916
  polyethylene, drawn low-density, mech. and transport props. 79—74210
  polyethylene, drawn polymer, fibre composite model 78—76719
  polyethylene, effects of mol. rot. and crosslink on specific draw ratios *(Japanese)* 79—96099
  polyethylene, elec. empulse breakdown strength, rel. to rate of drawing 80—15960
  polyethylene, fibre, phase structure and molecular mobility, broad-line NMR spectroscopy 78—14290
  polyethylene, filled with glass particles, uniaxially drawn, elastic constants, filler addition effect *(Japanese)* 78—95780
  polyethylene, high density, cold-drawn, IR spectroscopy and X-ray diffr. 77—4764
  polyethylene, high density, effects of draw rate and temp. on necking stress *(Japanese)* 79—91757
  polyethylene, high density, solid state coextrusion, technique for ultradrawing thermoplastics 80—84979
  polyethylene, high mol. wt., porous, hot drawing 80—60894
  polyethylene, high-density, dielec. loss, below 4.2K, antioxidant, annealing and drawing effects 78—84518
  polyethylene, high-density ultradrawn, extrusion ratio influence on tensile props. 79—61618
  polyethylene, highly oriented, fibre composite model 78—3183
  polyethylene, highly oriented, thermal conductivity 78—47614
  polyethylene, hot drawn, low density, stress relaxation 79—29121
  polyethylene, lightly crosslinked, processed under mol. orient., boiling H_2O resist. fibres prep. 80—38957
  polyethylene, linear, γ-irrad., plastic deform. 79—56996
  polyethylene, linear, bulk-crystallised, morphology study 79—32918
  polyethylene, linear, draw temp. and mol. wt. effect on draw ratio and Young's modulus 80—84998
  polyethylene, linear, films, elec. cond. rel. to drawing, annealing *(Japanese)* 79—15817
  polyethylene, low density, γ-irrad., unixial elongation effect on elec. cond. 80—25812
  polyethylene, microstruct. obs., variation during drawing and annealing, electron microscopy *(German)* 80—38944
  polyethylene, oriented, elastic stiffness constants, US meas. 78—76690
  polyethylene, steady-state deform. and its effect on struct. and morphology 78—15459
  polyethylene, stress rel. to draw ratio during ultra draw *(Japanese)* 79—91759
  polyethylene, ultra-high modulus, drawing behaviour, effect of drawing temp. 80—35232
  polyethylene, ultra-high modulus, micromorphology 77—63621
  polyethylene, ultra-high-strength filaments, soln. spun/drawn, mech. and thermal props. 80—40440
  polyethylene, ultra-oriented, prep. technique, extreme moduli 77—21086
  polyethylene, ultradrawing, effects of temp. and drawing rate *(Japanese)* 79—91760
  polyethylene, ultradrawn, electron microscope exam. of struct. after annealing 80—11662
  polyethylene, ultradrawn linear, kink bands by compression, interfibrillar motion 79—24581
  polyethylene, ultrahigh draw ratios, mol. wt. effects 79—74211
  polyethylene, ultrahigh modulus, drawing temp. effect on void form. and modulus 80—35241
  polyethylene, ultraoriented, fibrillar struct. 77—89389
  polyethylene fibre, high-strength high-modulus, morphology and tensile prop. relations 80—103264
  polyethylene filaments, ultrahigh-strength, from soln. spinning and hot drawing 80—45268
  polyethylene film, drawn, dielec. breakdown and morphological struct., dichroic ratio 80—25813
  polyethylene film, minimum running thickness, biaxial extensional flow study 80—100993
  polyethylene films, elongated, γ-irrad., TSC meas. 80—11324
  polyethylene melt, drawing filaments, surface instabilities 78—71305
  polyethylene surface-growth fibres, hot drawing 80—97517
  polyethylene terephthalate, fibre, melting in crystn., intermediate and amorphous phases 77—84898
  polyethylene terephthalate, stretching, heat effects, struct. transforms. 79—15735
  polyethylene terephthalate, tensile drawing behaviour 80—35279
  polyethylene terephthalate, uni- and biaxially drawn films, preferred planar orientation 78—80590
  polyethylene terephthalate yarns, NMR, fibre struct. rel. to annealing, drawing *(Japanese)* 77—32269
  polyethylene ultradrawn fibres, Poisson ratio from Michelson interferometry 78—80596
  polyethylenes, ultra-high modulus, manufacture by drawing through conical die 80—66583
  polymer, coorientation with low molecular organic substances *(Russian)* 77—21089
  polymer, crystalline, necking stress, thermodynamically derived equation *(Japanese)* 79—91758
  polymer, drawing properties, role of interfibrillar tie mols. 78—76706
  polymer, fibrillation during cold drawing *(Russian)* 77—63691
  polymer, fibrous, drawing and annealing 78—15458
  polymer, recrystallisation during drawing 78—76658
  polymer, ultrahigh modulus, production 77—52277
  polymer melt spinning, mechanics of nonisothermal process 77—51010
  polymers, crystalline, oriented, drawing, load elongation behaviour, fibre composite model 79—15691
  polyolefins, ultra-high modulus, production by tensile drawing and hydrostatic extrusion 80—81022

drawing continued
polyoxymethylene, ultra-high modulus, prod. by high temp. tensile drawing 79—43352
polypropylene, cold-drawn isotactic bars and thin films, microstruct. and annealing 78—95760
polypropylene, drawn fibres, SEM and US study 78—47249
polypropylene, drawn polymer, fibre composite model 78—76719
polypropylene, metallic glass filled, mech. props. rel. to temp., strain rate filler content *(Japanese)* 79—15742
polypropylene, monofilaments, drawing behaviour, melt-induced orientation effects 78—84922
polypropylene, oriented, compressive elastic modulus and yield strength 80—16385
polypropylene, oriented fibre drawing *(Russian)* 77—21088
polypropylene, reasons for disintegration under tension 78—84940
polypropylene, stretching flow for film prod., stretching over canonical mandrel 78—71304
polypropylene, ultradrawn fibres, Poisson ratio from Michelson interferometry 78—80596
polypropylene, ultrahigh modulus, tensile drawing, mol. wt. effect 80—104211
polypropylene monofilaments, draw rate effect on long period 79—47726
polypropylene monofilaments, tensile props., orientation degree depend., IR dichroism obs. 78—3163
polypropylene rods, prep. by die-drawing 80—45327
polypropylene sheet, deep drawing *(German)* 80—104114
polypropylene spherulites, refl. acoustic microscopy obs. 80—28922
polystyrene, oriented amorphous, supermol. structures rel. to mech. behaviour 78—22673
polystyrene filament, melt spun, struct. and mech. props., effect of drawing, twisting, annealing, untwisting 80—45331
polystyrene-poly(styrene-b-butadiene-b-styrene) polyblends, mech. props. 78—52919
porous deep drawn conical shells, permeability 80—11728
PTE, polymer fibre, orientation changes during stretching, IR spectra 78—75568
PTFE, oriented fibre drawing *(Russian)* 77—21088
PVC, cold drawn, plastic fracture around cavities 79—56994
PVC, filled, mol. orientation study by Raman spectroscopy 79—73919
PVC, oriented mouldings, struct. order 80—60896
PVC, uniaxial tension, deep drawing, rigidity *(German)* 78—64556
quartz glass, Ge and B dopants, OH impurities, preform material and fibre optic waveguide struct. 80—64173
Recalloy, Fe-Nb, semihard magnetic alloy, magnetic props., hardness, microstruct. 78—56660
round profiles, US perturbed, stresses during drawing *(Russian)* 80—59557
sheet drawing, slip line field for mid-plane cracking or splitting 80—50648
sheet metal deformation, criteria for determ. of deformation limit G *(German)* 80—21000
shell, fracture behaviour, forming severity and metal flow in deep drawing 79—38975
shells, plastic, explosive forming, computer numerical simulation 80—59560
short tube drawing from thin metal sheets 78—86248
silica fibre, plastic coated, furnace drawing technique *(Italian)* 78—55475
silica fibres, caustics occurrence in the drawdown zone 77—66617
silica fibres, contamination with furnace drawing, losses 77—42634
silica fibres, epoxy acrylate coated, tensile strength >500 ksi, km length prod. 77—11052
steel, bars after drawing, mechanical characts. *(French)* 79—91662
steel, C, microplastic deform. of drawn and undrawn samples *(French)* 79—1894
steel, C, microstructural inhomogeneity, influence on formability and fracture 80—11682
steel, C, X-ray line fitting by Gram-Charlier distrib., appl. to tension test *(French)* 79—15689
steel, C and alloy, cold formability *(French)* 78—60681
steel, cold worked, original struct. effect on softening during heating 80—60882
steel, high strength, treatment effect on ductility and strength 80—60880
steel, low C, capped, cold rolled sheet, deep drawability, effect of carbide size, cold reduction annealing 78—64559
steel, low C, cold rolled sheet, Cu effect on recrystallization texture *(Chinese)* 79—74173
steel, low C, deform. form effect on texture *(Russian)* 78—3141
steel, low C, hot rolled and cold deep drawn, nonmetallic inclusion distrib. in microcavities *(Russian)* 79—52265
steel, low C, texture hardening in maximum shear planes during expansion 79—91704
steel, low C hot rolled sheet, drawability improvement by Al addition *(Ukrainian)* 79—78996
steel, low-C, preliminary thermomech. treatment, cold deform. effect on struct. and props. 79—38847
steel, low-C contaning Ti, sheets, recrystn. texture effects on plastic strain ratio and deep-drawing *(Chinese)* 80—66527
steel, mild, cold rolled sheets, microstruct. and strain path in deep-drawing 78—19775
steel, pearlitic, struct. variations under plastic strain and subsequent heating, cementite decomp. *(Russian)* 80—84954
steel, plastic working of wires, high-density current appl. 79—57002
steel, quenched and tempered sheet, first operation cupping *(German)* 78—72788
steel, St 37 sleeve, deformation behaviour contrib. in rod drawing *(German)* 80—11684
steel, stainless, austenitic, Cr-Ni-Mn-Si-Mo-C alloy, 13Khi8N10G3S2M2, elastic moduli exam. after thermomechanical treatment *(Russian)* 79—24558
steel, stainless, clad Al, sandwich sheet material, forming limits 80—3131
steel, stainless, ferritic, high CR penny shaped central bursting defect in cold drawing 79—20071
steel, stainless, filament produced by glass coated melt spinning, new metastable tetragonal struct. 79—20072
steel, stainless, sheet, deformation charact. determ. test *(German)* 79—24569
steel, stainless, wire, axial texture after electroplastic drawing, X-ray struct. investigation *(Russian)* 80—104177
steel, stainless, wire, cold drawing 80—50650
steel, stainless, wire, effect of stress on phase transformations 78—44119

drawing continued
steel, stainless 12kh18N9T, wire, mechanical and heat treatment effect on static and cyclical strength *(Russian)* 78—35410
steel, stainless 18N10T, electroplastic drawing, deformation zone current delivery schemes 79—91761
steel, stainless electroplastic drawing 79—20142
steel, stainless ferritic, drawability, mech. props., and grain boundaries in 08Kh16AMT and 08Kh18T1 80—35270
steel, transformations, influence of type of cold plastic strain *(Russian)* 79—52232
steel 42NKhTYuA wire, hysteresis loop and differential permeab. after US and conventional drawing 79—15818
steel wire, magnetically hard Kh13N13M2-type, electroplastic drawing *(Russian)* 80—20967
steel wires, drawn and annealed, tensile fatigue and tensile strength under cyclic stress *(Japanese)* 78—15507
steels, C, H_2 embrittlement after patenting and cold deform. *(Russian)* 79—29175
styrene-diene triblock copolymer, hexagonal struct., flow props. of melt and fracture 78—76729
tension test with neck triaxiality reduction 78—7159
thermoplastic sheet, deep drawing *(German)* 80—104114
tube wall heating during steady state tube drawing *(German)* 78—84899
wire drawing, anal. of radial-mode US tool with statically loaded inner surface 78—183
wire drawing, die wear, review 80—30113
Ag, filament produced by glass coated melt spinning, mech. props. 77—86125
Ag-Cu alloy filaments, prod. by glass coated melt spinning, microstruct. and tensile strength 79—91667
Al alloy, 6061-T6, thickness depend. of G_c for shear lip propag. from single crack propag. 78—11305
Al alloy 6061-T6, fracture initiation and propagation during strip drawing 78—64663
Al sheet, speed effects in deep drawing *(Japanese)* 79—52241
Al single crystals, relation between axial orientation rotating and deform. banding 80—104206
Al wire, hot and cold deformation drawing strengthened, thermal EMF study *(Russian)* 80—54674
Al-(Mg)(Fe), pure (dilute), large wire drawing plastic deform. 80—108508
Al-Al_2O_3, recrystallisation nucleation in drawn wires, optical and TEM obs. 79—47709
Al-Cu-Mg, cold plastic deformation, stress/strain relations 79—56991
Al-Cu-Mg, tube drawing, tensile forces, plastic deformation *(French)* 79—70130
Al-Mg, cold plastic deformation, stress/strain relations 79—56991
Al-Mg cold drawn wires with FCC lattice, texture and structure 77—70067
Al-Mg-Cr, tube drawing, tensile forces, plastic deformation *(French)* 79—70130
Al-Mg-Si-Cu, cold plastic deformation, stress/strain relations 79—56991
Al-Mg-Si-Cu, tube drawing, tensile forces, plastic deformation *(French)* 79—70130
Al-Ni(Cd)(Fe)(Si), cold worked, struct. and props. 80—71666
Al_2O_3-SiO_2 clad with B_2O_3-SiO_2 effect of drawing tension on residual stresses 78—64554
Au, hardening mechanisms, grain size effect 80—35302
β-$CaSiO_3$ fibre, continuous unidirectional crystallisation from melt 78—95739
Cr-Co-Fe cold formable mag. alloys for use in telephone receiver 79—52227
Cu, cold-rolled, thickness depend. of G_c for shear lip propag. from single crack propag. 78—11305
Cu, deformed by hydrostatic extrusion, drawing or drawing under press., dislocation struct. obs. *(Russian)* 77—21213
Cu, drawability, mech. props., effect of O impurities 79—83272
Cu, electroplastic drawing, deformation zone current delivery schemes 79—91761
Cu, fibre texture of filament produced by glass coated melt spinning 77—85966
Cu, OFHC effect of cold drawing under combined stress 80—60912
Cu, plastic working of wires, high-density current appl. 79—57002
Cu, recrystallised, inhomogeneous deform. due to texture changes *(German)* 79—29158
Cu sheets, earing, R-values and 3-D orientation distrib. functions, comparisons 79—91702
Cu single cryst., drawing deform. band form., axial orientation force meas., X-ray pole figure determ. *(Japanese)* 78—76710
Cu, stress-strain behaviour over large strain range 79—15745
Cu, tough pitch wire, cupping fracture surface, SEM study *(Japanese)* 79—79087
Cu, types MOb and M1, primary recrystallisation kinetics depend. on state of impurities *(Russian)* 79—66069
Cu, wire, axial texture after electroplastic drawing, X-ray struct. investigation *(Russian)* 80—104177
Cu wire, ductile fracture in drawing process, defect exam. *(French)* 77—21242
Cu wire, electroplastic drawing X-ray diffr. anal. and mech. props. exam. *(Russian)* 79—29138
Cu, wires, effect of heat treatment during drawing 78—56659
Cu-Ag(Se)(Sn)(Ag-SeSn), Ag, Se, and Sn effects, singly and together, on recrystallisation 79—100164
Cu-Al_2O_3 dispersion hardened wires, drawn, substruct. and strength 78—35405
Fe, Armco, sleeve, deformed by cold drawing, exam. of surface and texture *(Russian)* 79—34057
Fe, fibre texture of filaments produced by glass coated melt spinning 77—85966
Fe ore super-concentrate, deep drawing props. by integrated powder technology route 80—100806
Fe-Mo(W), semihard magnetic alloys, magnetic, elec. mech. props. *(Japanese)* 79—70078
Fe-Nb(Ta)-Co, Recalloys, semihard mag. alloys, mag. and elec. props., hardness, thermal expansion *(Japanese)* 79—5066
Fe-Si (6.5 wt%) filament, formation by modified Taylor technique, and mag. props. 80—75795
Fe-Ta alloy, mech. drawn and aged, exam. of electrical resistivity, hardness, microstruct., and mag. props. *(Japanese)* 78—48545
GeO_2-B_2O_3-SiO_2 optical fibres, optical transmission loss as function of drawing conditions 79—32038

drawing continued
MgCd wire, elongation during disorder-order transform. *(Russian)* 80—104148
Mo, US working effect on single cryst. during deform., strengthening effect, plasticity resource *(Russian)* 79—34107
Na_2O-B_2O_3-SiO_2 low-loss optical fibre prep. by double crucible technique *(German)* 78—33929
Nb wire drawing, $NbFe_2$ layers form. by diffusion 79—28153
Nb-Ti, multifilamentary, Mirror Fusion Test Facility, superconductor core manufacturing and quality 80—93521
Nb-Ti, wire drawn and hydrostatically extruded supercond., crit. current density 79—38275
Nb-Ti (46%) composite superconductor, fabrication 77—24989
Nb_3Al, and $Nb_3Al_{0.76}Ge_{0.24}$, supercond. props. of cold worked core wires an basis of A15 phases 77—85369
Nb_3Sn, supercond. props. of cold worked core wires an basis of A15 phases 77—85369
Nb_3Sn-Cu superconducting composite with submicrometer filaments, fabrication and props. 79—38282
Ni, deformed by hydrostatic extrusion, drawing or drawing under press., dislocation struct. obs. *(Russian)* 77—21213
Ni-HfO_2 (3 wt.%), dispersion hardened alloy VDU-2, thermal and mech. treatment 77—90376
Ni-Ti/Cu composite, plastic deform. influence on internal friction *(Russian)* 80—100871
$PbMo_6S_6$, cold-worked core-wires, supercond. transition temp. and lattice instability 78—6469
Pd-Cu-Si glass, cold drawn, serrated plastic flow, optical and SEM study 79—79052
$Pd_{77.5}Cu_6Si_{16.5}$, cold drawn wires, surface markings, fracture stresses 79—56997
$Pd_{77.5}Cu_6Si_{16.5}$ metallic glass wire, cold drawing 80—50650
SiO_2 fibre, prep. from $Si(OC_2H_5)_4$ *(Japanese)* 79—70038
SiO_2 fibres, fused, drawn from rods, oxy-H_2 flame, prep., strength, dia. var. 80—102868
SiO_2, furnace drawn optical fibres, contamination reduction 78—33918
SiO_2 glass fibre drawing, caustic curves in solidified drawdown zones 77—39117
SiO_2, laser drawn fibers, tension rel. to drawing vel. and ultimate strength 78—74986
SiO_2, optical fibre, phys. behaviour of neck-down region during furnace drawing 78—83127
SiO_2, silica, optical fibre-drawing, vac. furnace 78—66960
SiO_2:F, silica fibres, numerical aperture and attenuation, drawing from preforms 78—1449
SiO_2-Al_2O_3-B_2O_3-CaO-Na_2O-K_2O system glasses, relax. of struct. stresses rel. to forming process 79—34088
U/(Zr-Cu-Mo alloy) welded joints, mech. characts. determ. 20 to 750°C 79—29113
U/Ti welded joints, mech. characts. determ. 20 to 750°C 79—29113
W, drawn wire, microstruct. effect on fracture 80—3177
W, electroplastic drawing, deformation zone current delivery schemes 79—91761
W fibre, KAl, KSi, KSiAl and KSiGa, addition effects on workability *(German)* 78—64557
W, plastic working of wires, high-density current appl. 79—57002
W, recrystallisation of commercially pure and doped wire drawn to high strain 79—100165
W, US working effect on single cryst. during deform., strengthening effect, plasticity resource *(Russian)* 79—34107
W wire, cold drawn, dislocation processes occurring during tensile testing *(Hungarian)* 77—48450
W-K-Si-Al doped wires, heavily drawn, fibre struct., annealed 79—56993
Zn alloys, deep drawing behaviour, exam. in binary and ternary alloys *(French)* 79—52325
Zn, deep drawing behaviour *(French)* 79—52325
drives
see also clutches; electric drives; propulsion
artificial heart operation and monitoring system *(German)* 79—8583
circulation assist equipment, improved electromechanical drive response 79—100790
diaphragm scanning system for Michelson interferometer 78—12764
displacement digital method *(Polish)* 80—86260
EM, for perfusion pump, features 78—7532
emergency protection drive, optimum ratio between operational component times 78—82474
harmonic drive as ultra high vac. rotary motion feedthrough 77—2661
harmonic gear transmission, vibrations anal. 79—88949
intra-aortic balloon heart assist device fluidic drive system 78—53566
irrigation pump, using solar turbopack based on organic Rankine cycle, thermodynamics optimisation 79—62019
repetitive photoelec. scanning system for high resolution optical spectra accumulation 78—54456
solar tracking system, heliotropic fluid-mech. drive system, dynamic response anal. 80—55823
solar turbopack, based on low-temperature Rankine cycle, low-cost design, centrifugal pump appl. 79—62021
Stirling stroke controlled engine, variable angle wobble plate drive 80—30543
three-dimensional optical display unit 80—1297
drop model (nuclear) *see nuclear liquid drop model*
droplets *see drops*
drops
accretion by snow crystals, growth 80—41495
accretion growth of ice crystals, grain size 79—79933
acoustic levitation technique appl. 79—44906
adsorbed layers, clustering, bulk vapour pressure behaviour 79—4473
aerosol drop, submicron size evap. in continuum and non-continuum regimes 79—43639
aerosol nonvolatile particles capture by growing or evaporating drops 77—36797
aerosol particle capture by drops, thermodiffusionphoresis and Brownian motion effects *(Russian)* 79—39791
aerosols, particle-droplet inertial collisions 79—47989
agitated dispersion, breakage and coalescence processes, obs., data reduction 77—90645
agitated dispersion, droplet breakage and coalescence rates during mixing 78—85205
air bubble entrainment in self-aerated flow, channel or pipe flow 80—106832
drops continued
air-atomised water mixture, high temp. surface impact, heat transfer *(French)* 79—4015
air-steam mixtures, heat transfer to moving droplets 78—90997
air-stream mixture, direct contact dondensation on single droplet 77—68370
air-water fogs, particle polydispersity rel. to audible sound propag. 78—1473
air-water mist flows, uniform heat flux wedge, heat transfer 79—23352
almost spherical viscous drops, time-depend., shear induced deformation 80—87794
annular flow through annulus, droplet deposition 79—90311
annular gas-liquid flow, drop sizes 77—51099
aqueous film, plane-parallel symmetrical, stability, non-spreading oil droplet effect 80—107620
aqueous fog form. in shock tube 80—19531
arc welding electrode metal drop free surface calc., MHD anal. *(Russian)* 78—5822
atmoisation, droplet distribution in liq. breakup 77—11246
atmosphere, charged conducting drop electrostatic interaction with aerosol dielectric sphere 77—25749
atomisation of liquid by impinging jets, expt. and theory 78—87373
atomised liquid dropwise evaporation, mist cooling 80—6506
binary liquid drops, nucleate boiling evaporation on heated surface 77—27531
binary mixtures, near critical, metastable, phase separation and nucleation and drop growth, rate eqns. 80—65232
binary vapour mixture condensation into immiscible liquids *(German)* 78—18760
blood droplet deformation in Courette flow suspension, expt. *(German)* 79—16227
boiling, gradient explosion, under conditions of bulk heat release 78—83226
break-up in stagnant fluids 78—75182
breakup, rel. to liquid jet penetration 78—94798
breakup of long slender droplets in 2-dimens. straining motion, hyperbolic flow 79—60062
bubble and droplet-type contactors, wake shedding 79—4060
bubbly, droplet and particulate flows, drag coeff. and relative vel. relations 80—24072
burning droplet, finite reaction rate model rel. to flame sheet model 79—34306
burning droplet-vapour flow, conservation eqns., mass transfer 77—39363
butane drops, nucleation in flowing water 79—1099
California coastal fog and stratus microstruct. 78—61505
capillary condensation, Kelvin eqn. direct exptl. verification 79—33159
capillary phenomena for fluid/fluid interface, review 80—70506
carbon tetrachloride, drops, on brass surface, Leidenfrost pt., press. effect 78—87784
carbon tetrachloride drops falling through H_2O, surfactants rel. to deform., oscill. *(French)* 80—66880
carbon tetrachloride-I_2-water system, mass transfer in pulsed perforated plate column 78—71385
charge to mass ratio of drops prod. by electric spraying of liqs. *(Japanese)* 78—17835
charged droplets evaporation and motion in electric field 78—42669
charged liquid drops, dynamics, symmetric and asymmetric stabilities 80—79366
charged particle, effect of electrostatic field on rate of evaporation 77—27585
chlorobenzene drops falling freely through water, breakup 80—69899
chloroform, drops, on brass surface, Leidenfrost pt., press. effect 78—87784
cholesteric liquid crystal, screw sense determ. by droplet method 79—90544
circular tube thermal entrance region, laminar droplet flow convective heat transfer 80—6049
cloud and rain drops, accel. to terminal vel. 77—78334
cloud chamber, coronal discharge effect on cloud droplet growth 77—34514
cloud chamber, low-pressure, ionisation distrib. analysis 80—9461
cloud chamber, thermal diffusion, continuous flow parallel plate type, analysis w.r.t. atm. water droplet growth 80—36416
cloud condensation nuclei, size distribs. effects on cloud droplet sizes 77—87006
cloud development in turbulent atm., drop spectrum evolution 78—81325
cloud drop growth by condensation, air parcel model 78—7729
cloud drop spectrum evolution rel. to collision efficiency 78—69415
cloud droplet coalescence growth, fast computational method for Telford's theory 78—69486
cloud droplet collision, numerical study of Stokes and Oseen flow approx. 78—16102
cloud droplet condensation growth in turbulent medium, hygroscopicity and surface tension effects *(Russian)* 77—33142
cloud droplet condensation process, parametrisation for clouds numerical models *(Russian)* 78—16091
cloud droplet distribution, microstruct. meas. in Kenya high-frequency hail area 79—53484
cloud droplet growth by condensation, parameterization 78—3869
cloud droplet nucleation, expts. with monodisperse NaCl aerosols 80—82003
cloud droplet size meas., comparison of electrostatic disdrometer with impactor slides 77—2278
cloud droplet size spectrum evolution, effect of surfactants 77—78340
cloud droplet spatial variability, cloud base meas. 80—12495
cloud droplet spectra, effect of nuclei spectra 77—64364
cloud droplet spectra evolution, effects of mixing, lab. expt. 77—70778
cloud droplet spectrometry using light scatt. technique 77—41219
cloud droplets, 8-12 μm radiant energy transfer effects on mass and heat budget 79—5571
cloud droplets, collisional problem in turbulent environment 77—5293
cloud droplets, effect of electric charges and fields on collision freq. 80—8401
cloud droplets, interception collection efficiencies 78—3381
cloud droplets, size distrib. models, and visible and IR volume extinction coeffs. 77—25750
cloud droplets, stochastic collection eqn., computational instability in numerical soln. 77—2211
cloud droplets concentration, microphysical model sensitivity to urban environment 80—82004

drops continued
- cloud drops, collisions with particles, effects of elec. fields and charges 77—25748
- cloud drops collision efficiency, elec. charges and vertical external elec. field effects 77—25738
- cloud drops spectrum, kinetic eqn. of stochastic coagulation clouds 78—92944
- cloud liquid water content measuring devices 77—41223
- cloud particle size distrib. meas. by optical array probes 77—41220
- clouds, directional light scatt. coeffs. in droplet and cryst. clouds *(Russian)* 78—96292
- clouds, drop size distrib., Keily probe assessment for ground-based meas. 79—12317
- clouds, drop size spectra modification by urban pollution aerosol, physical demonstration 80—56571
- clouds, electrical charges fate in evaporating droplets 79—48559
- clouds, ice particle/water droplet discrimination with an optical ice particle counter 79—100973
- clouds, ice-bearing cumulus evolution, numerical simulation and obs. 77—2216
- coagulating droplets, statistical distrib. 79—74425
- coagulation theory, new aspects *(Russian)* 79—8453
- coalescence, film drainage 78—71387
- coalescence at liquid-liquid interface, drop surface velocities 77—43406
- coalescence rate, ambient liq. viscoelasticity effect 78—67248
- coalescence redispersion model for drop-size distribs. in agitated vessel 77—1950
- coalescence time in close-packed dispersion during thin-film drainage 79—86486
- coaxial jet drop generator for holographic flow visualisation in water tunnels 78—5836
- cold liquid spray interaction with hot gas stream in channels 77—15108
- colliding droplets, coalescence and disruption expts. 79—68768
- colliding liquid drops, investig. of free fall behaviour, elec. changed drops, stability 78—38396
- collision coalescence in presence of electric field, water drops in oil 80—51516
- collision-induced breakup effect on drop size distrib. in steady state rainshafts 79—92574
- collisions of falling drops, satellite drop production 80—12492
- column, vertical, approaching interface, shape 79—32725
- combustion, unsteady temp. modelling criteria 78—38179
- concentrated cloud, approx. eqn. for mass and heat flux in constrained flow 77—47073
- condensation, dropwise, heat transfer 77—58531
- condensation, max. drop size rel. to heat transfer coeff. 78—94559
- condensation heat transfer, effect of surface thermal conductivity 78—22252
- condensation nuclei, size resolution via humidity gradient counter 78—81470
- condensation-evaporation of multidroplet system, by kinetic theory 80—7873
- condensing surface thickness effects, dropwise condensation 78—22250
- confined burning jet, droplet vaporisation, expt. and theory 78—94855
- contact of spherical particle with a droplet, approx. eqn. 79—60604
- convective diffusion to drop, large Peclet no., finite Reynolds no., asymptotic soln. 79—41742
- convective heat and mass exchange, $Pe \leq 1000$, in uniform (shear) stream 78—55683
- cooled pipe, droplets from vapour condensation, size distrib., laminar flow 80—79111
- cooling tower drift deposition, modelling and monitoring 79—20992
- creeping flow, in cloud of round drops of arbitrary size distribution 78—9677
- creeping flow mass transfer in size distrib. cloud drops, high Schmidt number 80—14783
- critical fluids, droplet model 77—53846
- cryogenic liquids, technique for producing uniformly charged drops 77—49733
- crystallisation under influence of AgI-type reagents, kinetic parameters *(Russian)* 77—81963
- cumulonimbus clouds, elec. field strength and raindrop spectra, study from mobile ground station 78—92943
- n-decane, emulsion drop, efficiency of capture by bubble in noninertial flotation 80—11956
- decane on Teflon FEP, effect of drop size on contact angle 80—2245
- deformation, shear and vorticity effects 80—87795
- deformation and breakup of a single slender drop in an extensional flow 78—67250
- deformation and burst of drop in extensional flow 79—32645
- deformation and orientation in shear and extensional flow fields, dynamic interfacial props. 80—107611
- deformation dynamics, vortical flow Lagrange function *(Russian)* 77—55007
- deformation in extensional flow 80—19449
- deformational breakup in wet-steam stream, differential eqns. 79—14462
- dew, K/Na ratios rel. to atmospheric aerosol comp. 77—91190
- diameter, hold-up and backmixing coeffs. in liq.-liq. spray columns 78—75183
- dichloroethane drops falling freely through water, breakup 80—69899
- dielectric, two dimens., in presence of electric field, fluid circulation, equilib. geometry 77—58797
- dielectric drop in electric field, low Peclet number heat and mass transfer 80—6050
- diesel engine transient fuel jet droplet photography using light pipes 80—23784
- diffusion to chain of drops at large Peclet numers 79—86489
- diffusional interaction of drops in a liquid 79—81947
- diffusophoresis in viscous media 78—35731
- dimpled draining film, axisymm., model 77—59180
- direct contact heat transfer with intermittent electric field 80—74869
- disintegration mechanisms of liquid droplets due to air stream 80—74959
- disperse drop composition meas. in two-phase stream 78—55682
- disperse system, fluid interface, dynamic properties 77—25313
- dispersed drop-vap. flow, heat transfer, wall deposition and boiling 77—75965
- dispersed droplet past-dryout regime, nonequilib. heat transfer model 80—64548
- dispersed fluid drops, size distrib. and phase surface, expt. determ. 80—53837

drops continued
- dispersed supersonic two-phase flow, shock characts., droplet size depend. at nozzle 80—106815
- dispersion produced by rotating perforated drum 77—11244
- draining film off plate rim, drop form. 78—46926
- drift droplets deposition estimation from natural draught cooling tower 79—16647
- drop of soln. moving in hot gas, solvent evaporation 77—65783
- drop of soln. moving in hot gas, solvent evaporation 77—68673
- droplet convection vaporization with unsteady heat transfer in circulating liq. phase 80—53771
- droplet disintegration distrib. function, nonequilibrium atomisation 78—38387
- droplet dynamic interaction, angle of collision effects 80—38475
- droplet generated by disruption of large charged drop, specific charge 77—40580
- droplet growth and initial dew point temp. accuracy in cloud chamber on space shuttle 78—96268
- droplet impact, high-speed, effect of gas medium on dimensions of contact area 77—28942
- droplet motion induced by weak shock waves 80—33627
- droplet transport in gases and liquids, gravitational and thermophoretic contribs. 80—100052
- droplet-vapour flow, normal shock waves 79—32651
- droplets, atomized, polydisperse system, nonisothermal vaporisation, algorithm for calc. vaporisation parameters 80—48782
- dropping Hg electrode, synchronisation in natural drop expts., high speed device 80—37049
- dropwise condensation, heat flux and drop size distrib. 79—50573
- drying of solute skin-covered soln. drop *(Russian)* 79—68561
- ducts, one-dimensional models for transient gas-liquid flows 80—64614
- dynamic liquid surface tension determ. from drop oscillation frequency and capillary jet instability 78—56026
- dynamics in diffusion cloud chamber, growth stabilization 79—47996
- dynamics in mixture with uniform temp., thermal diffusion effects 80—103097
- dynamics in shear fields, role of dynamic interfacial effects 80—107612
- eccentric spherical fluid shell, heat and mass transfer at large Peclet number 77—27520
- EHD flow, with small Reynolds number, resulting deformation 80—59126
- EHD produced droplets, specific charge and size 79—32696
- elastico-viscous liquid, atomisation, drop size rel. to elasticity 77—35220
- electric field enhancement of collision efficiency 80—61863
- electrification by evaporation or vapour condensation *(French)* 78—61511
- electrified pendent drops, axially symmetric, equilib. profiles 78—87846
- electrolyte, aq. soln., field-induced ion evap. from liq. surface at atm. press. 80—29859
- electrolyte, on heated metal surface, charge separation 80—88617
- electrolyte aqueous soln. drops, ion emission due to laser heating 78—59063
- electrostatic drop formation, effects of conductive liquid props. 78—1122
- electrostatic drop formation rel. to liquid viscosity 79—55024
- electrostatic drop formation using liquid, expt. 79—57302
- electrostatic droplet source suitable for laser targets 77—34074
- electrostatic ink jet drop formation characteristics *(Japanese)* 78—25766
- emulsified fuel drop, microexplosive boiling of metastable overheated water, microblast *(Russian)* 80—74930
- emulsion, dilute, straining motion, effect of inertia on dynamic viscosity 80—87797
- emulsion, hexadecane-H_2O-butanol-Brij 96, drop dia., comp. depend. light scatt. obs. 80—45573
- emulsion, hexadecane-H_2O-pentanol-Tween 60, drop dia., comp. depend. light scatt. obs. 80—45573
- emulsion, inverse-type, coalescence of drops in uniform elec. field 78—53265
- emulsion, relative drop-drop and drop-wall motions, slow 79—32641
- entrained, in annular two-phase flow, size distrib. and entrainment rate 80—43760
- entrainment of liquid from horizontal cylinder by air flow 77—15102
- errors in measuring the dimensions of drops by holographic methods 79—67252
- ethylene glycol on Teflon FEP, effect of drop size on contact angle 80—2245
- evaporating droplet in turbulent gas flow, aerosol particles precip. 80—7870
- evaporating droplets, radiative absorption 80—33426
- evaporating droplets in immiscible liq., theoretical anal. 79—23193
- evaporating droplets in immiscible liquid, comments 80—19482
- evaporating drops, in vert. hot air tunnel, heat radiation effect 79—46400
- evaporation, asymptotic, convection and Jakob number 77—59108
- evaporation, diff. coeffs., vap. press. and Lennard-Jones pot. function determ. 77—80262
- evaporation, diffusional, in EM radiation field 78—43112
- evaporation, modelled by wet porous sphere, heat-transfer meas. 78—59268
- evaporation from surface droplet, theory 79—59909
- evaporation in constant cross flow, with and without gas. chem. reaction 77—35214
- evaporation in diffusion regime of cloudy atmosphere, influence of optical consts. *(Russian)* 78—32145
- evaporation in vap., slow viscous flow, heat flow asymmetry effect 77—75966
- evaporation of atomised liquid *(Russian)* 78—38828
- evaporation of binary liq. mixtures under free convection conditions 77—84121
- evaporation of drop, in EM field, theory 79—72787
- evaporation of sessile and pendant drops in still air 77—85027
- evaporation on heated surfaces, theory 78—87785
- evaporation on shell, temp. fields 78—9546
- evaporation rate in forced convective flow with transverse sound fields 78—51224
- evaporation rate of large water drops falling at terminal vel. in air, wind tunnel investig. 80—56541
- evaporation under laser irradiation, explosive evap. criteria 77—953
- falling into still liq., vortex ring formation 78—90946
- fast flowing wet steam, electrical meas. of droplet size 80—64659
- ferrofluid droplet, interphase boundary hydrostatic characts. in uniform mag. field 80—33692

drops continued
- ferrofluid droplet dynamics in magnetographic printing 79−50772
- film, thermodynamic theory of clustering and percolation transitions 77−47697
- film boiling destabilisation, liq. drop falling onto hot liq. surface 78−94588
- Fisher's droplet model, pure filled vap.-liq. nucleation theory 77−62626
- fission reactor, postulated LOCA, de-entrainment phenomena from droplet cross flow in vertical bundles 79−89430
- fission reactor LOCA, creation and persistence of mist-laden containment atmospheres 79−89421
- fission reactor LOCA-generated drop size perdiction, thermal fragmentation model 79−89422
- fixed evaporating droplet, aerosol particles precip. 80−7869
- flame spectroscopy, droplet size distrib., impact beads, mixer paddle and oxidant effects 80−93810
- flow in reactive system, mass transfer interaction 79−64738
- flow of centrally-located drop with thin jet in infinite viscous fluid 79−32614
- flow produced by uniform translation along cylinder vertical axis *(French)* 78−90967
- flowing dispersed liquid, size spectrum and phase surface of drops calcs. from exptl. data *(Russian)* 77−31366
- fluid-liquid interface, approach of close-packed arrays of drops and spheres 78−84030
- fluidised bed, fluidisation uniformity, disturbance criterion with uniform coding medium flow distrib. 80−43772
- fog, droplet spectra, new meas. instrument 77−53219
- fog, microphysics and models 80−41517
- fog droplets, size distrib. models, and visible and IR volume extinction coeffs. 77−25750
- formation in liquid jets, book contrib., review 80−19467
- formation in supersaturated systems, reaction kinetics 77−66748
- formation of drops with non-wetting liqs. in capillaries and bores *(German)* 78−87370
- fragmentation by laser beam 79−7169
- free motion transition criteria for single bubbles and drops 80−64605
- free moving drop in pulsating liquid, mass transfer *(French)* 77−27588
- Freons, C51-12, 113, drops, on brass surface, Leidenfrost pt., press. effect 78−87784
- fuel, liq. droplet, combustion, quasi-steady analytical model predictions 78−35681
- fuel droplet, burning anal., quasisteady model *(Japanese)* 79−32712
- fuel droplet evaporation at elevated press. and temp., math. model investig. 77−52675
- fuel droplet on hot surface, evap. and ignition 79−96310
- fuel droplet on hot surface, evap. and ignition 79−96311
- fuel droplets, mathematical models of transient heat flow 79−18673
- fuel drops, liq., blast wave initiated detonation waves 79−64691
- gas bubbles, on liq. surface, bursting, jet and droplet form., math. model *(German)* 77−24012
- gas-droplet flow, particle-source-in-cell model 77−84313
- gas-liquid boundary layer, droplet precipitation enhancement 78−1735
- gas-liquid droplet system, phase transition kinetics and kinetic eqns. 78−83933
- gas-liquid flow, drop size spectrum 78−34187
- gas-liquid flow, holdup, expt. results 78−14063
- gas-liquid flow in triangular ducts, two-phase wall layers 78−90999
- gas-liquid two-phase bubbles in immiscible liq. media, configs. 79−4068
- gas-vapour droplets, nonuniform mixture, acoustic wave attenuation 78−83154
- generalised one parameter droplet size distrib. function 80−38459
- glycerine-alcohol drop, growth in castor oil, obs. by quantitative schlieren technique 77−11040
- glycerine-water drops, collision dynamics, ang. of incidence influence *(Russian)* 78−83461
- graupel formation and growth, wind tunnel investigation 80−17324
- growth, method for condensation eqn. soln. 78−7795
- growth and decay, moment and Fokker-Planck eqns. 80−82709
- growth in atmosphere by condensation, cloud physics appl. 79−44216
- gyrostatic liquid drops, captive between co-rotating parallel faces, shapes and stability, capillarity eqns. 80−64592
- haze droplets, effects on visibility in natural and treated warm fogs 79−100951
- heat and mass transfer during vapour absorpt. 78−63427
- heat and mass transfer in turbulent gas flow 78−22410
- heat capacity meas. of air-water droplet *(Russian)* 80−54395
- heat pipe wick, liq. evaporation, drop carry-over phenomena in capillary struct., obs. 79−18948
- heat transfer, electric field effect 78−59276
- heat transfer between a dispersed system and a vertical heating or cooling surface 79−1069
- heat transfer characteristics and dynamic behaviour of saturated droplets impinging on heated vertical surface 80−14688
- heat transfer in immiscible liquid, intermittent elec. field augmentation 78−94872
- heat transfer through drop condensate, differential inequalities anal. 78−18293
- heavy oil droplet with simultaneous cracking inside, combustion mechanism 79−74385
- heterogeneous photocondensation process initiation by laser radiation 80−67410
- n-hexane droplets, coalescence in n-alcohol aqueous solns. 79−87882
- n-hexane droplets coalescence in aq. electrolyte solns. 79−64742
- high speed droplet interaction, erosion test effects 80−48756
- high speed interaction of drop with solid surface, apparatus design *(Russian)* 79−27605
- hollow drop production by injection of gas bubbles into liquid jet and US excitation 78−1710
- holographic droplet image analysis by TV camera and table calculator via IEC-Bus 78−36337
- holographic method of small particle analysis 79−13924
- homogeneous vapour nucleation, in carrier gas, hydrodynamic theory 79−69236
- hot wall with impinging liq. droplet, transient temp. profile 78−75050
- humid atmosphere, water droplet vaporis. model with natural convection 78−33999
- hydrocarbons, levitated in water, acoustically forced shape oscill. 79−47987
- hydrodynamic crisis, in two-phase channel flow 78−14066

drops continued
- hydrodynamic interaction between drops at low Reynolds number 80−43749
- hydrodynamics at finite visible contact angles, interface motion, drop spreading, solns. *(Russian)* 77−27640
- hydrometeors in clouds, size, conc. and struct. meas. 77−41218
- ice splinter production from accreting drop 80−72585
- immiscible liquids, flow in helix, high press. boiler analogue 77−58763
- impact dynamics on solid surface 79−86488
- impact on hard surface, dynamics *(Russian)* 78−47005
- impact on hard surface *(Russian)* 78−9688
- impact on solid surface 79−64747
- impulse drive jet used in character printing, model for fluid ejection and refill 77−68656
- incompressible fluid, equilib. and stability analysis 80−59092
- inertial confinement targets, hollow H_2 droplet prod. by acoustic excitation of superheated liq. H_2 jet 79−85766
- ink jet drop formation, scale model 77−75952
- ink jet droplet charging, math. model 79−50184
- inorganic emulsions, hydrophile lipophile balance temperature 78−95961
- interaction force between droplet and condensating vapour 80−79113
- interaction of fast-moving drop with liq. film surface *(Russian)* 79−64756
- interaction with boundary layer on rot. disc 78−47020
- internal boiling and superheating in vaporizing multicomponent droplets 79−3906
- internal circulation in falling drops, boundary layer theory 77−66964
- invert emulsion, aggregation equilibrium 79−66356
- Ising cluster size and shape, Whitney polynomial 79−33080
- isobutene, droplet nucleation from crit. gas-phase + positive ions 79−39222
- jet, controlled break-up, droplet prod. by imposed flow perturbation 77−68667
- jet, liq., breakup, 3rd perturbation Cosserat soln. 79−32615
- jet droplets from bursting bubbles at air/water interface, electrification and size 77−48700
- jet drops from bubbles bursting in seawater, ejection height rel. to organic material 79−39727
- jets, drop formation, continuous phase mass transfer, perforated plate extractor column design 79−90299
- jets, nonlinear capillary instability, satellite drop formation and control 80−33646
- jets, nonlinear capilllary instability, behaviour effects before droplet formation 80−33645
- kerosene drops, direct contact cooling of crystallising brine 79−1053
- kinetics of processes controlled by diffusion 79−11828
- laminar condensation heat and mass transfer at stagnation point of droplet in ternary mixture 79−14227
- laminar gas flow, transverse migration of individual particles 80−96240
- Landau-Ginsburg model, droplets free energy, Jost function 79−40469
- large, volatile binary solution, theory of evaporation 79−10931
- laser anemometry, size and velocity meas. equipment 78−86238
- laser beam hygroscopic aerosol interaction 77−79888
- laser beam propag. in evap. liq. drop medium, wind refr. 77−5322
- laser particle size analyser, size estimated from diffraction pattern 79−6091
- Laval nozzle, two-dimens. two-phase flows with nonequil. phase transition 77−51101
- law of metastability, appl. to effect of mag. field on boiling liqs. 78−79199
- Leidenfrost phenomena, spheroidal state min. wall temp., total vaporisation times 80−38246
- liquid, collisions with elements of packed column, probability 77−15084
- liquid, equilibrium of, on nonhorizontal substrate, Gibb's criteria for advance over sharp edge 80−29249
- liquid, evaporation, idealised models for preheat stage 78−94586
- liquid, on solid substrate, deviations from Young's equation 77−66075
- liquid drop aggregate breakup in shock waves 80−24084
- liquid drop coalescence, effect on disperse-phase-controlled mass transfer rates 78−26185
- liquid drop in immiscible liquid, evaporation, surface tension effects 77−47648
- liquid drop motion in non-Newtonian media 78−75184
- liquid droplet, direct contact with high temp. surface, Leidenfrost temp. model 78−90666
- liquid droplet, surface thickness and surface oscillations, quantum and classical calcs. 78−91511
- liquid droplets, equilibrium radius from Thomson-Helmholtz eqn. *(German)* 80−53847
- liquid droplets, forced vibr., Raman scatt. obs. 80−34929
- liquid droplets in free-mol. stream, drop size distrib. 77−35211
- liquid drops moving in single file in liquid continuum, heat transfer 79−46367
- liquid dynamic surface tension meas. instrument 80−42313
- liquid fuel droplet heating with internal circulation 78−75194
- liquid fuel droplets, transient heat flow in combustion gases, models 78−63507
- liquid jet, capillary breakup, random initial perturbation, drop size distrib. 78−38380
- liquid jet satellite droplet formation 77−75953
- liquid metallic thin film, supercooling, electron diffraction study *(French)* 79−7676
- liquid spreading on solid surface, physical regularities *(Russian)* 77−62712
- liquid vibration 80−43559
- liquid-liquid agitated dispersion, droplets transitional breakage probability 79−77219
- liquid-liquid dispersion, droplet size spectra in turbulent pipe flow 78−67247
- liquid-liquid dispersion, new drop size distrib. meas. technique 80−3419
- liquid-liquid fluidised beds, drop coalescence 79−50783
- liquid-liquid interfaces in isolation and in interaction, review 77−47651
- LMFBR, Clinch River, humidity effect on burning rate of Na droplets, Fick's eqn. anal. 78−13297
- long slender drops in a simple shear flow, slow viscous motion 80−79365
- macroencapsulation, composite drop form., hydrodynamics 80−64603
- magnetic fluid, spherical drop, motion in rot. mag. field *(Russian)* 78−75212
- magnetic fluid drops in homogeneous magnetic field, shape *(Russian)* 79−877
- magnetised fluid drop in homogeneous mag. field, drop shape 79−76544

drops continued
- marine advection fog, water distrib. rel. to droplet size, salt particle nuclei 79−5570
- mass exchange for spherical particle in flow at high Peclet numbers and $Re \leq 100$ 77−54988
- mass transfer, surface-active agents effect 79−77218
- mass transfer accompanied by chem. reaction at surface 79−77290
- mass transfer and internal circulation in forming drops 77−35198
- mass transfer inside drop, influence of chemical volume reaction at large peclet numbers *(Russian)* 80−28508
- mass transfer inside drops in continuous fluid, effect of pulsation *(French)* 78−55686
- mass transfer to ambient liq., combination of resistances 78−83458
- metal drop-oxidizing slag, oxidation kinetics 78−11153
- metal drops in electrolytes, electrocapillary motion, elec. field strength effects 78−3346
- methanol-H_2O mixture, evaporating droplets in air, temp. modelling *(German)* 80−2243
- microdrop, energy and mol. structure, mol. dynamics method 79−11004
- microdrop, pressure tensor and surface tension, mol. dynamics method 79−11005
- microdrop, two-dimensional, on solid body surface, stability dynamics 78−51790
- microemulsion, border between lyophobic and lyophilic colloids, thermodynamic stability 80−40747
- microemulsion, struct. description of liq. particle dispersion, ultracentrifugation and small ang. neutron scatt. obs. 79−5184
- microwave attenuation by salt water droplets 78−7725
- mist flow, evaporation of droplets 77−55350
- mixed salt aerosols, phase transform. and droplet growth in moist atmosphere 79−52783
- mixed-salt particle suspension in moist air, phase transform. and growth 77−12832
- molecular dynamics simulation of a small drop 78−15719
- mono-disperse drop formation, from large orifices 77−65782
- monodisperse aerosol, uniform electrical charging 77−56256
- monodisperse cloud regarded as isolated system, drop growth and supersaturation 77−53150
- motion in electrically conducting fluid, EM field effects *(Russian)* 77−3878
- motion in flow with varying vel. 78−59457
- motion in free turbulent jet 78−5789
- motion in immiscible liquid, integral eqn. for Stokes flow 78−71389
- motion in inhomogeneous-in-temp. viscous liq. 77−39334
- motion in stream of viscous incompressible fluid 77−11252
- motion of deformable drop in second-order fluid 79−64754
- nematic liquid crystals, Marangoni effect 78−6009
- Nolan-Pollak condensation nucl. counter, droplet growth rate, supersaturation 77−60480
- non-Newtonian fluid, quadratic shear flow, rigid sphere and drop migration 77−84309
- noncirculating, direct contact condensation 78−94548
- nonconducting drop motion and dissolution in current-carrying liquid 77−11275
- nonequilibrium droplet evaporation and condensation, quasisteady theory 79−99394
- nonviscometric flow, drop suspension model, deformation and vorticity 79−60022
- nozzle flow of moist water vapour, drop size distrib. function 77−42904
- nuclear reactor spray droplet heat transfer in LOCA 80−32380
- nucleation, droplet growth in nonuniform vapour 77−47563
- nucleation, homogeneous in vap., microcluster metastable equilib. conc. 77−62627
- nucleation homogeneous, gasdynamics of supersonic flow with condensation 77−62292
- nucleation in finite systems, theory and computer simulation 80−26038
- nucleation of liq. droplet, stat. mech. treatment trans.-rot. paradox 77−62625
- nucleation processes, computer simulation, single spin flip kinetic Ising model 77−62613
- nucleation theory, atomistic models of microclusters, exact free energy barrier 77−62612
- nucleation theory, role of replacement free energy, review 77−62611
- ocean spray, effect on energy transfers across air-water interface at high wind speeds 78−85574
- oil, shape when suspended in aq. soln. with density gradient, meas. of low interfacial tension 79−77863
- oil drop spreading and wetting on submerged solid substrate, dynamics 79−46885
- oil drop spreading and wetting on submerged solid substrate, forced spreading 79−46887
- oil drop spreading and wetting on submerged solid substrate, static profiles 79−46884
- oil drop spreading and wetting on submerged solid substrate, drop dynamics 79−46886
- oil droplets, motion and optical props. by interf. method 78−67893
- oil drops, appl. to skin friction meas. by viscosity balance method 77−19645
- optical backscattering from water, ice or mixed phase drops 77−64426
- optical caustics in near field from liq. drops 78−37802
- optical motion control applied to Atmospheric Cloud Physics Laboratory on Shuttle/Spacelab 80−12634
- optically dense liquid crops, motion in laser radiation field 78−50842
- organic liquid surface, charged drop formation from bubble bursting 77−14634
- oscillating drop, immersed in 2nd fluid, induced flow field streaming 78−59454
- oscillating droplets, in stationary liq. phase, behaviour 78−1718
- oscillations of liq. drop with surface charge 78−18320
- paraffin drop striking solid plane, microscopic flow regimes, trapped air bubbles obs. 80−53843
- particle, EM wave irradiated, evaporation, diffusion approx. 80−44308
- particle collection efficiencies by single droplets, calc., inertial impaction, Brownian diffusion and electrostatics 79−57525
- particulate conc. in raindrops, electron microscopy study 77−81971
- pendant, profile area meas. 78−81943
- pendant, surface and interfacial tension determ. by drop shape meas. 77−59176
- pendant drop, glass spheres attachment, wetting perimeter 80−2251
- pendant drops, surface area meas. 78−30813

drops continued
- petrol surface tension and flow, high-voltage effects *(Russian)* 79−83464
- plane pendent drops, instability 80−29247
- pneumatic nebuliser efficiency enhancement through appl. of elec. field 78−95966
- polydisperse droplets, produced by EHD method, charge-to-mass ratio 78−76931
- polymer drop wetting solid surface, spreading index for polymer surface props. *(Russian)* 78−51802
- polymer mixing, breakup of anisometric drops 77−40578
- profile and volume, symmetrical about vertical axis, analytical soln. 77−72346
- profile area as useful pendent drop parameter 79−23806
- pulsating fluid, mass transfer to moving drops, renewal penetration model 77−31369
- pulsed extraction column, with perforated plates, efficiency 79−64809
- pulsed laser-induced shattering of water drops 80−50471
- quadrupole resonance of drops driven by modulated acoustic radiation pressure, experimental props. 80−33275
- quiescent liquid-liquid systems, low vel. drop formation 80−79364
- radiant heat transfer, to dilute cloud of drops or particles 77−58537
- rain, mixing with near-surface water 79−53371
- rain drop representation by use of bubbles in wind tunnel for flow visualisation 77−80238
- rain drop size spectra, in Buenos Aires 79−53485
- rain drop spectra and fine structure on different time bases *(French)* 78−53681
- rain size spectra and intensities at Praia, Santiago, Cape Verde Is. during 1973-74 period *(German)* 77−5306
- rainbow formation in pendant drops, angular scattering 79−96816
- rainbow phenomena and the detection of nonsphericity in drops 80−58456
- raindrop, single, growth by condensation and droplet capture, props. 79−12208
- raindrop charge and assoc. electric field for different rain types 78−44933
- raindrop growth physics, for teaching 79−35502
- raindrop interactions effect on drop size distrib. obs. at ground 78−44945
- raindrop sise distributions parameterisation 78−77301
- raindrop size distrib. expressions 77−25744
- raindrop size distrib. in hilly region of N.Wales 77−29390
- raindrop size distrib. shapes 79−20949
- raindrop size distrib. with collision breakup in axisymmetric warm cloud model 79−34918
- raindrop size distribs. from attenuation meas. at 94 GHz 79−16632
- raindrop size spectra and growth in cumulus cells, model 80−21800
- raindrop sizes and related parameters for GATE 80−41521
- raindrop sizes in mm radio attenuation, lognormal distribution 79−16635
- raindrop spectra evolution with collision-induced breakup 77−33152
- raindrops, EM scattering by dielectric spheroids and ellipsoids 78−85622
- raindrops, spreading of ellipsoidal raindrops orientation during intense rainfall, expt. results 79−16634
- raindrops of Pruppacher-Pitter form, scatt. and cross polarisation of radio waves 77−41129
- Raman scattering by forced surface oscills. in liquid drop 80−92763
- reaction between water droplets and molten sodium 78−71263
- rime growth, splintering mechanism 79−39788
- rotating liquid drops, asymmetric shapes and stability 80−87796
- rotating liquid drops, held together by surface tension, equilibrium shapes and stability 80−79367
- rotationally symmetric fluid bodies in gravit. field, thermodynamic treatment of capillary phenomena 78−10262
- saline drift deposition meas. from natural draught cooling towers 77−73825
- saltwater drop falling in organic phase, ice growth 80−15218
- saturated, impinging on heated vertical surface, heat transfer characts. obs. *(Japanese)* 80−10271
- sessile drops, equilib., stability 77−31376
- Sessile liquid drops, meas. of small contact angles 80−10749
- shape of drop on inclined plane, solar still aspects 78−79856
- shape oscillation and static deformation of drops driven by modulated acoustic radiation stresses 80−33274
- silicone oil drop spreading on horizontal surfaces 80−2250
- single-component system, modification of charact. functions by interphase boundary and surface tension 77−90647
- size and dielectric const. determ., active microwave system 78−54339
- size and dispersion in tubes and coils 77−39328
- size and falling velocity meas. using laser Doppler velocimeter 80−68185
- size distribution, least squares method for fitting exptl. data 77−39329
- size distribution, reduced function, determ. from local meas. 77−68717
- size distribution airborne meas. for drops >60 μm diameter 78−45008
- size distribution in liquid phase of two-phase flow effect on characts. 80−103070
- size measurement, spherical mirror method 79−64806
- size measurement in dense fuel sprays, by in-line holography 78−37827
- size measurement methods, review 80−17916
- size of drops prod. by plain-jet airblast atomizer 78−3375
- slow motions of liquid drop in viscous liquid, force of resistance 77−35217
- solloidal solution droplets, solid, particle form., heat and mass transfer 78−95967
- solution drop, slow evaporation 79−90847
- solution droplets in gas flow, heat and mass transfer during evaporation 78−90998
- solution droplets vaporisation, in high-temp. gas flow, heat and mass transfer 78−75191
- solution-melt drops, periodic instability of motion over crystal surface 78−47260
- sound, high-intensity, attenuation in droplet-laden gas 77−62082
- spherical, mass transfer and chemical reaction at transitional Reynolds number zone *(Russian)* 79−50814
- spherical drop combustion, asymptotic, drop shrinkage and flame movement, heat and mass transfer 77−81405
- spherical drop in infinite viscous fluid 79−1234
- spherical droplet, evaporation and condensational growth, mass transport calcs. 80−97736
- spherical droplets in vapour environment, time evolution, physical-mathematical model 79−68789

drops continued
spherical drops in Stokesian field, interfacial boundary conditions 80−74931
spherical particles, line of centre motion 79−4067
spherical solids melting in turbulent carrier fluid, deformation and breakup 80−92646
splashing on liquid layers 77−3852
spray, photomicrographic anal., droplet size and vel. spectra determ. by Dimant's rotating mirror microscope 77−36800
spray cooling, characts. and minicomputer control *(French)* 79−3889
spray from nozzle, drop size distrib. 79−32633
spray in atmospheric surface layer, lab. and oceanic results 79−70844
spray nozzle, transfer processes in droplet plume during counterdirectional atomisation in gas flow 77−24014
spreading on solid surface, initial stage characts. 80−59761
static, pendant, and resting at deformable interface, shape determ. 77−31846
static drop on inclined plate, shape, finite element method anal. 80−29245
steam, dropwise condensation, moving picture study 80−74863
steam, dropwise condensation on electroplated Au layer, thickness depend. 79−46791
steam, wet, drop coagulation in cross-over pipe flows 80−74982
steam droplets growth in Laval nozzle 79−32648
steam-water mixture, intensive drop condensation, flow boundaries 77−35204
steam-water mixture, upward flow in tube, liq. film-core mass transfer, liq. distrib. 78−75189
Stokes flow, Faxen relations generalisation 79−32438
stratocumulus water clouds, droplet distrib. rel. to radiation transfer 77−45146
submerged in unbounded arbitrary vel. field, low Reynolds no. motion 78−42646
sulphate particle formation by heteromol. nucleation and condensation in cavities 80−26183
supercooled cloud, drop size distrib. influence on secondary ice particles prod. during graupel growth 78−73481
supercooled droplets, bursting rel. to ice splinter production during riming 78−85662
supercooled water droplet surface effect on ice crystal kinetic formation *(Russian)* 77−13099
supercooled water drops, probability of ice nuclei form. 78−3909
superheated droplets, flash boiling, undergraduate student expt. 78−81748
superheated drops, boiling in immiscible liq. 77−31368
supersaturated gas mixture-small liquid droplets, energy and mass transfer anal. 77−62135
surface and interfacial tension determ., pendent-drop method 79−46891
surface energies, contact angle, wetting *(German)* 77−62710
surface polarisation from sessile drop contact angle meas. 77−85365
surface tension, size effect, self-consistent calcs. 77−51569
surface tension apparatus using drop vol. principle 77−59179
surface vibrations in EM field, Raman line splitting 77−69826
surface wetting, motion anal. 78−22934
suspension of spherical drops, mean drag and ave. velocity *(Russian)* 78−67259
temperature of evaporating drop in air stream, calc. *(Russian)* 78−38827
terminal vel. adjustment for cloud and precipitation drops 78−16103
thermal diffusophoresis of droplets of a liquid solution in a binary gas mixture 80−43766
thermodiffusiophoretic motion, weak solution in binary gas mixture 79−64744
thin liquid film, instability and rupture 80−34279
tracer dispersion in annular climbing film flow 79−64751
transient heat and mass transfer, in electric field 77−80226
transient heat-mass exchange 79−7276
transonic two-phase vapour-drop flow in channel, stability singular point 77−55078
transparent droplet diameter meas. by side reflection 78−59518
turbulent gas jet, evaporation of semidispersive drop system 77−55077
two-phase dispersed-annular isothermal flow, vel. distrib., phase conc. and droplet size distrib. in core 77−47064
two-phase dispersion, size distrib. function of bubbles/droplets in thermodynamic equil. 80−7862
two-phase flow, annular, crit. heat flux, swirl effect 80−10113
two-phase flow, droplet entrainment and deposition at boundary 77−62299
two-phase flow, mixing and condensation in high-speed flow, review 78−47014
two-phase flow particle interaction, coagulation and rebound calc. 79−98789
two-phase fluid equilibrium, thermodynamic functions and surface tension 78−2262
ultrasonically produced aerosol droplet size rel. to liquid viscosity 79−47998
uniform waterdrop atmosphere, sunlight transmission 78−36244
urban atmosphere, thin layer brown haze form. 77−56685
US apparatus for studying physical and chemical props. of chemically active drops 77−72122
US resonance driving of ellipsoidal oscillations of liquid drops 77−31164
vacuum oil drop electrification in elec. field 79−86101
vaporisation, effect on droplet interactions 80−24106
vaporisation in moderately-high temp. stationary media, Chang model 78−34609
vaporisation in two-phase, gas+solid particle, flow 78−55677
vaporising, in gas stream in channel laminar entry region 78−30347
vaporising, internal temp. field 78−51042
vapour generator for K, heat transfer with drop motion in tube in supercrit. region 80−23880
vapour-drop flow, effect of drop conc. and dispersions 80−24082
vapour-droplet flow field, one-dimens. motion eqn. 78−59455
vapour-droplet mixtures, small perturbation propagation 78−95111
vapour-gas mixture, condensation, effect of thermal resist. of drops on heat and mass transfer 77−15015
vapour-gas mixture, liq. drop growth rate on surface during vapour condensation 77−11779
Venus clouds, coagulation effects on droplet size distrib. 77−67056
vertically vibrated liquid column, surface disintegration, bubbles and drops 80−74943
viscoelastic droplet break-up, in nonuniform shear flow 80−64588

drops continued
viscosity of drop falling through liquid, for teachers 79−40331
viscous, free oscillations 77−51105
viscous drop, almost spherical, Brownian motion and fluctuating hydrodynamics 80−87787
viscous drop, almost spherical, in arbitrary flow of compressible fluid, Faxen's theorem 80−87786
viscous droplet, deform. due to deposition of surfactant 78−18876
viscous fluid, bubbling through of air, drop entrainment 80−14787
viscous fluid drop, induced flow field in oscillating fluid 78−90980
viscous fluid stream, nonstationary mass transfer *(Russian)* 79−10561
viscous liquid drop in immiscible liquid, normal-mode anal. of oscillations 80−74932
volatile highly thermally conductive spherical drop, theory of diffusiophoresis 80−14784
volatile liquid droplets, impaction on hot liquid surfaces 77−39330
volatile solvent, evaporation from multi-component droplets, in stream of air 77−56255
water, coalescence, theoretical model of approaching drops 78−32207
water, coalescence problem, efficiency 78−32208
water, collisions, coalescence efficiency, expt. evaluation 78−32206
water, collisions on elastically deformable media, simulation of erosion by rainfield 77−56113
water, drops, on brass surface, Leidenfrost pt., press. effect 78−87784
water, evaporation by 10.6 μm laser radiation 77−75589
water, holographic investigation of hypersonic target material subject to impact with water droplet 78−42306
water, ice envelope splitting during freezing *(Russian)* 77−27982
water, large drops accel. to terminal vel., drag coeff. 78−61506
water, laser induced evaporation, diffusion coeff. temp. depend. 77−20062
water, on HV overhead power lines, expt. 80−33851
water, optical props., comparison with atmospheric aerosols *(Russian)* 78−77328
water, sessile drops on inclined plane surfaces, shape 78−67891
water, size distrib. in mist, vol. extinction coeff. at visible and IR wavelengths 77−37287
water, supercooled, hydrodynamic behaviour, interaction with columnar ice crystals 78−32205
water, thermal explosion by high-power laser radiation 77−75590
water aerosol, evaporation during transport through atmosphere *(Russian)* 79−88408
water and ice particles, interpretation of foil impactor impressions, rel. to hail research 78−57356
water condensation number, from micron size drop evaporation and growth rate determ. 79−90774
water drop breakup, catastrophic, free flight meas. of particle sizes 77−31361
water drop impact at surface, Lagrangian code calc. 78−47025
water drop impact noise *(German)* 77−75736
water drop impact on rigid surface 77−85084
water drop impacted brittle materials, damage thresholds 80−81149
water drop on heated plate interferometric study using laser source *(Russian)* 78−37049
water drop vibration analysis in near-zero gravity 77−7426
water droplet, explosive vaporisation on 10.6 μm radiation exposure, inhomogeneous internal heat evolution 80−29162
water droplet, IR emissivity 80−36394
water droplet clouds, rate of evaporation, stability 79−52782
water droplet coalescence in turbulent clouds 77−45114
water droplet collision and coalescence for small Reynolds numbers 77−78326
water droplet conc. and size determ. from cloud liquid water content and extinction meas. 80−51579
water droplet evaporation, heat transfer characts., on heated surfaces 78−59269
water droplet evaporation and microclimatic modification 77−17248
water droplet forced convection and heat transfer rel. to vapour conc. *(Chinese)* 79−23185
water droplet freezing process under supercooled conditions 80−65192
water droplet growth rel. to condensation coeff. *(Russian)* 79−34901
water droplet interactions, expts. for educational use 78−4441
water droplet size distrib. spectra in cumulus clouds *(Russian)* 80−81991
water droplet spectra formation, numerical model for advection fogs at sea 79−34916
water droplet/ice crystal clouds, angular depolarisation and multiple scattering of polarised laser light 80−41549
water droplet/ice crystal clouds, angular scattering of polarised laser light 80−41548
water droplets, atmospheric, sources and effects of surface organic monolayers 78−69412
water droplets, ebullition under steady-state superheated conditions 80−74928
water droplets, ebullition under transient superheated conditions 80−74929
water droplets, initiation of optical breakdown in air 80−10352
water droplets, small, weakly absorbing, motion in bounded laser beam 79−12269
water droplets and glory formation by Airy-type diffraction 77−53191
water droplets in hot gas flow, transient cooling 79−1063
water droplets in mists, clouds, size, density distrib. meas., laser remote sensing technique *(Japanese)* 78−49175
water droplets in stratocumulus cloud, humid plume interaction *(French)* 79−16605
water droplets size distrib. in cloud bases 78−73458
water droplets suspended in turbulent flow, evaporation rate rel. to $Ca(CO_3H)_2$ soln. drops 79−90771
water drops, crystallisation on CuS aerosol prepared by burning pyrotechnic mixture 78−96279
water drops, evaporation and condensation in air, quasi-steady approximation 77−21854
water drops, impaction and electrical effects on collisions with spherical particles 78−28272
water drops, on DC transmission conductors, corona discharge and elec. charge 79−82114
water drops, size meas., evaluation of direct methods 77−22527
water drops collision efficiency in atmosphere 77−29378
water drops in stratosphere, size distrib. rel. to sulphate aerosol growth by condensation *(Russian)* 80−94566

drops continued
- water drops in subsaturated air, aerosol particle collection efficiency 78−28273
- water in multiphase flow systems, diagnostics, laser induced Raman scatt. 77−31373
- water on PMMA, effect of drop size on contact angle 80−2245
- water supercooled droplets, on ice substrate after low speed collision, freezing behaviour, cryst. struct. 80−29152
- water vapour, wet, boundary layer in compressible flow 80−10295
- water vapour condensation in rarefaction waves, homogeneous nucleation case 77−42869
- water vapour expansion with condensation, nozzle flow at high pressure 80−106828
- waterdrop interaction extps., review 78−11974
- wave beam distortion by thermal self-interaction in droplet medium 80−19082
- weightless liquid systems, acoustic manipulation in space 77−49716
- wet-steam flow, critical pressure ratio 77−84300
- wetting, mechanism, mol. dynamics 78−51789
- Wilson Cloud form. by low altitude nuclear explosions, water aerosol and droplets characts. 78−53704
- wind tunnel particle and droplet field holography 79−76642
- wind tunnel water droplet size distrib. interferometer 79−80673
- Ar jet, supersonic, electron beam-excited, continuous VUV emission spectrum origins 79−6964
- Ar, liq. nuclei, thermodynamic props. mol. dynamics calc. *(Russian)* 77−47325
- Ar phase stability boundary, nucleus surface tension rel. to surface radius of curvature 79−60603
- Cu exploding, wire accelerated evaporation of fast drops colliding with target *(Russian)* 77−15570
- Fe, adsorption on W foil, multilayer film, contraction into drops 79−15023
- H_2, drops form. for uniform solid spheres prod. 77−74409
- H_2O droplet growth in presence of soluble gases, expts. 80−21807
- H_2O droplets, subcooled, nucleation in Ar-H_2O vapour mixture, rate const. 80−61131
- H_2O drops, acting as capacitors in corona discharge *(Russian)* 77−62420
- H_2O, sessile drop impinging on heated surface, heat and mass transfer mechanism 78−90908
- H_2O-H_2SO_4-ion aerosol particles, ultrafine, stratospheric form., ion-induced nucleation 80−72608
- H_2SO_4-H_2O droplets in atmosphere, equilib. size and comp., quick estimation method 79−66767
- H_2SO_4-H_2O solution aerosol particles nucleation in stratosphere 77−56678
- He, condensing on positron, Monte Carlo lifetime spectra, temp. and elec. field effects 78−55263
- He, dense gas, positive ion excess, ion-induced droplets 79−14925
- He, superfluid, laser light scatt., multiplicative and additive stochastic processes 78−84596
- ^3He and ^4He microdroplets, momentum transfer in collisions with Xe and CO_2 beams 79−50113
- ^4He charged drops in cryogenic vap., He^+ mobility, 1.3-2.0K 79−32734
- ^4He, droplets, surface energy, tension, thickness 78−84015
- ^4He, heavy nucleus analogue 78−59992
- Hg, dropwise condensation, at Cu surface, heat-transfer meas. 77−75781
- Hg, film boiling 78−14453
- Hg, liquid structure, X-ray diffr. obs., 173-473K 80−14997
- Hg, optical consts. meas. from Hg-air interface, ellipsometry at spherical object 79−61326
- Hg+water systems, drop fragmentation rel. to thermal explosion detonation requirements 78−71368
- K_2CO_3 melt in combustion prods. medium, vaporisation of drops 79−57290
- Na droplet, preignition oxidation process, rel. to LMFBR accident 79−30996
- NaCl, monodisperse aerosol, preparation and growth 77−86389
- NaCl solution, evaporation in laminar gaseous stream *(French)* 77−51102
- NaCl-$CaCl_2$, electrolyte mixture, evaporation from multi-component droplets, in stream of air 77−56255
- Na_2O-SiO_2 glass drops, quenched from liq. state, thermally treated, density profile 80−81085
- Ni-Na-di-2-ethylhexyl phosphoric acid-H_2O system, droplet phenomena 77−48697
- ^{239}Pu and ^{233}U droplets burning in air, aerosol generation investig. rel. to inhalation hazards 79−67959
- S, single liq. droplet, optical transmission and elec. resist. changes on polymerisation 77−35460
- Si, preshaped single crystal prep. by pendant drop method *(French)* 78−64466
- Si-electrolyte interface, incident radiation image form. *(Russian)* 77−7199
- Sn droplets, on Bi, Zn and Al, heterogeneous nucleation 80−44294
- W, molten drop break up in gas flow, surface drag, capillary excitation *(Russian)* 80−100024

drying
- agricultural products, using solar energy, India's 1978 development trends 79−74509
- biological material, prep. for X-ray microanal. of diffusible elements, methods of drying ultrathin cryosections 78−77166
- biological material prep. for X-ray microanal. of diffusible elements, rapid freezing and ultrathin section prep. 78−77165
- biological microspecimen holder for processing and critical point drying 79−74822
- biological specimen freeze-drying process obs. by SEM 78−28142
- boiling point drying by volumetric abs. of RF and MW EM energy, heat and mass transfer characts. 80−79130
- capillary porous body, drying, X-ray absorption obs., radiometry, temp. control 78−67023
- capillary porous body, drying kinetics, infinite plate calcs. 77−46890
- cell drying, critical point drying alternatives for specimen prep. 78−24210
- ceramic, electrical transducers for automatic recording of mechanisms occurring during drying 77−52561
- ceramic powders, equipment for sublimation drying, exam. 80−25733
- ceramic suspensions, sputter drying *(Russian)* 80−55324

drying continued
- ceramics, tensometric equipment, for determ. of properties, during vacuum pulse drying 80−20965
- ceramics treatment methods, drying, cooling, heat treatment, reln. to material props. *(French)* 77−90296
- clays and ceramics, plasticity determ. using drying process and shrinkage 79−20307
- coal, low sulphur, US assisted drying in vacuum filtration 77−32539
- concrete, creep during drying and wetting 79−52319
- concrete, drying shrinkage due to wind action *(Japanese)* 79−61838
- corrosive materials, freeze-drying 77−41580
- critical point dryer, low-cost, with continuous flow dehydration attachment, for electron microscopy 78−53595
- critical point drying theory, practice and artifacts, review 78−24211
- cultured cells preparation for SEM by air drying from org. solvents 77−48965
- diffusion coefficient time depend. from single (de)sorption expt., step-by-step calc. method 78−87859
- diffusion problem, nonlinear, soln. with const. flux boundary conditions 77−75782
- disperse materials, conductive drying kinetics and dynamics 80−81278
- drop, drying of solute skin-covered soln. drop *(Russian)* 79−68561
- droplet, vaporising, internal temp. field 78−51042
- dryout in an SGHWR rod bundle, exptl. and calc. comparison 79−3192
- evaporation by air jets, hydrocarbons on surface 79−72919
- evaporation of organic solvents, internal heating by IR irrad. 78−87237
- evaporation-drying apparatus, design *(Russian)* 78−36990
- ferrite powders with high specific surface, manufacture using freeze-dry method *(German)* 77−63603
- fluidised beds of inert particles, moisture evaporation 77−15113
- foodstuffs and biological materials, information systems models relevant to developed freeze-drying systems 79−58727
- freeze drying, prod. of ultrafine ceramic powders 80−55336
- freeze-drying of food models, heat and mass transfer 79−1098
- gelatin hardened layer structuralisation, kinetic anal. using swelling 78−62255
- German solar flat plate air collector development 79−62075
- E-glass fibre, silane coupling agent deposited on surface, hydrolysis and drying effect on siloxane bonds 80−85072
- grain, using 25 kW photovoltaic plant, US expt. 79−70442
- gypsum, strength changes on setting *(Japanese)* 77−36619
- heat and mass transfer, optimal control 78−67006
- heat and mass transfer formulae, const. temp. and mass transfer pots. 77−84123
- heat pump, air-to-air, heating and drying appls. *(German)* 80−50995
- hygroscopic materials handling, method for drying and cooling chamber 77−61054
- insulating element, laminated, vac. drying in inert heat-transfer vap. 78−56875
- latex solids, agglomerating and dewatering 80−104470
- liquid flow through porous media, 20 kHz US stimulation 77−31385
- microspecimen suspensions, simple magnetic holders for critical point drying 77−52946
- moist dispersed solid, local Rebinder criterion determ. 77−89199
- moist material, external heat transfer, calc. methods, drying kinetics 78−59467
- moist materials, drying kinetics calc. method, heat (moisture) transfer 78−55555
- moisture transferability in plastic mass *(Japanese)* 78−19990
- multirow dry or wet heat exchangers, simulation 79−191
- multispecimen holder for materials processing and critical point drying for SEM exam. 77−57429
- oscillatory drying process optimisation 78−83215
- paints and varnishes, stress anal. during drying 79−34183
- PCA, dehydration effect on carbonisation process, high temp. resistant materials *(Russian)* 79−8269
- pharmaceuticals, freeze drying 77−70010
- plastics, thermolabile, drying, heat and mass exchange in vibro-rotational bed *(Russian)* 77−68377
- plate in fluidised bed, heat transfer during drying 77−11243
- polydisperse filter bed, immobile, heat and mass transfer eqns. soln. 77−7446
- polyolefine, deep drying, internal mass transfer 79−14239
- porous bodies, drying, internal mass transfer coeffs. calc. 78−67011
- porous bodies, theory and expt. verification 78−59278
- porous body, liq. elimination by fluidised porous particles system, kinetics 79−86510
- porous body drying in heated gas flow 79−90328
- porous media, heat transfer and moisture flow *(Hungarian)* 80−83839
- porous medium, drying, evaporation characteristics determ. *(Russian)* 79−37134
- powders, spray drying to minimize preferred orientation 80−3098
- pressure generation during the drying of a porous half-space 79−23187
- pressure gradients generated during the drying of porous shapes 79−68801
- radioactive waste, anal. of concentrating and drying processes in thin-film evaporator 79−59215
- radioactive waste solidification, spray calcination system 79−59212
- sediments, drying remanent magnetization 79−66681
- SEM, critical point drying, semi-automatic method 79−17406
- SEM specimen mounting epoxies, aerosols, and adhesive tapes 79−71580
- silica gel regeneration by adiabatic desorption mathematical model 79−1967
- solar, of agricultural crops, using no-glass flat plate collectors, analytical model 79−70465
- solar powered installation for drying tobacco 80−93850
- spray drying, of highly viscous conc. solns., heat and mass transport *(Russian)* 78−83230
- spray drying, prod. of ultrafine ceramic powders 80−55336
- sublimation drying in UHF EM field 78−83936
- temperature coeff. depend. on heat and mass transfer similarity criteria 78−83214
- thermolabile porous material in contact with sorbent vac. drying intensification 77−89641
- three-component system transport coefficient determ. 78−21082
- timber drying process, detection of acoustic emission 80−102940
- tissue dimensional changes during SEM specimen prep. 78−24209
- ultrathin cryo-section stabilization by freeze-drying 78−54349
- unified representation of molecular heat and mass transport *(German)* 79−32219
- vacuum freeze drying of food by zeolite *(Japanese)* 78−15645

drying continued
warm wet surfaces, wetting and evaporation mechanisms, spray evaporator for spacecraft thermal control systems 80—29160
wet granular material, heating rate during drying 77—89009
Al_2O_3, transparent, evaluation of freeze drying and spray drying for prep. 77—4761
β''- Al_2O_3-Na_2O-Li_2O (8.85, 0.75 wt.%) pressing powders, prep. by spray drying 80—40294
$3Al_2O_3.2SiO_2$, mullite, synthesis by freeze drying 80—16252
Mn-Zn ferrite powder, spray dried calcination 77—12558
$NiTiO_3$, synthesis from products of soln. spray drying, kinetics 77—16519
$Pb(Zr,Ti)O_3$, synthesis from cryochem. mixtures, chem. reacts. in sublimation drying 79—11538
^{99m}Tc-diethylentriaminepentaacetic acid freeze-dried kit prep. 79—88189
UO_2, sintered, production by gel calcination and drying, thermal anal. *(Czech)* 80—45260

dual resonance model *see duality and dual models*

duality (mathematics)
Abelian and non-Abelian models, dual transforms., phase transition points *(Russian)* 79—2735
chirality, self-duality, and supergravity counterterms, quantum corrections 79—75429
dual extremum principles for heat eqn. 78—70077
dual extremum principles for heat transfer problems with variable thermal props. 78—66999
dual series eqns. involving Konhauser biorthogonal polynomials 78—4464
dual variational principles 78—77676
Einstein eqns., reln. to Yang-Mills eqns. 78—8521
EM field equilibrium equations and duality 79—879
fundamental development 78—36788
Gaussian core model duality relations 79—93070
gravitational duality and Backlund transformations 80—12971
heavy chain rotating, duality principle for non-convex optimisation, calculus of variations 79—71237
incompressible flow fields, finite element dual variational anal. 79—40375
instantons of Yang-Mills eqn., rank 2 stable vector bundles 78—45774
interaction models, geometric and algebraic duality 77—9849
interfaces, duality, 2D Ising model 78—24741
Ising model, duality relations and replica method 80—77722
Ising models, blocked, duality 79—12735
linear shell theory, dual complementary variational principles generated from dual functionals *(German)* 79—97196
massive electrodynamics with magnetic charges, duality covariant form of Maxwell's eqns. 78—4495
massless scalar free field, local von Neumann algebras 78—45778
modular operator, local observables, in von Neumann algebras, duality in QFT, CPT invariance 78—81793
nonlinear self-dual network eqn., shock wave and hole type soliton 78—27
plasticity, dual extremum principles in rate boundary value problems 79—25845
Potts models, percolation, and duality 79—97312
rods, generalised conjugate analogy for arbitrarily curved rods 77—49588
self duality in 4-dimens. Riemannian geometry, Yang-Mills eqns. 78—78073
Serre duality for polarised symplectic manifolds 78—29004
Tomita-Takesaki theory, classification of type III factors 77—17756
variational inequality related to elasticity operator, soln., dual problem 79—9109
viscoplastic limit load problem, kinematic soln. method *(French)* 78—30195
von Neumann algebra of type III, structure, crossed products 77—17757
X-Y model, vortices and low temp. struct. 78—49777
Yang-Mills field, many-dimens. method based on inverse scatt. problem *(Russian)* 77—74600

duality and dual models
see also Veneziano model
1/N dual unitarisation, triple bare pomeron parameters of Gribov's Lagrangian 78—74232
1/N dual unitarisation convergence due to SU(4) breaking, charm and strangeness implications 79—6321
$\lambda\pi^4$ field theory with internal symm., string representation 78—70266
$\lambda\phi^4$ theory, dual string theory from Feynman graph expansion 78—54544
ν-dimensional Yang-Mills and (ν-1)-dimens. nonlinear σ-model connection, quark confinement, dual strings 80—90978
σ-models, nonlinear, classical two dimens., dual symmetry 79—80750
ϕ^4 field theory dual transforms., extension to 4-dimens. using renormalisation group eqns. 79—49393
Abelian gauge theories, dual transformation 79—63370
Abelian Higgs two-dimens. model, continuum and lattice version, dual transforms 80—4860
action principle for Neveu Schwarz Remond string and other systems using supernumerary variables 77—46030
Adler zero and dual peripheral model 78—78153
analytic model without signature degeneracy *(Russian)* 77—38140
associated strange and charm prod. in dual unitary approach 77—41824
associative algebra of tensor fields, duality and Dirac identities 79—71618
asymptotic energy scale factors for pseudoscalar meson scatt. and charmed meson couplings 78—8620
asymptotic freedom and local duality 77—71518
asymptotic props. of strong interactions, probability interpretation, Veneziano description *(Russian)* 79—93389
automodel asymptotics, Mandelstam analyticity *(Russian)* 79—93388
baryon+antibaryon annihilation model, high energy, multiperipheral interpretation of dual unitarity diagrams 77—18253
baryon and baryonium states with string junctions in dual unitarisation scheme 78—25021
baryon dynamics description in dual and gauge theories 77—65138
baryon exchange effects in dual unitarisation 77—34133
baryon model based on duality and unitarity 78—17000
baryon models and the planar bootstrap condition 79—3005
baryon nonleptonic decay, pseudo-connected line diagrams, duality requirement 78—45918
baryonium, geometrical approach 80—91065
baryonium, mass and selection rule, string model 78—29319
baryonium, review of QCD, duality, string models and bag models 78—78135

duality and dual models continued
baryonium, S-matrix representation 80—399
baryonium, spectrum and prod. mechanisms 78—74295
baryonium dual S-matrix approach 80—52526
baryonium interaction, dual amplitudes 78—25022
baryonium interactions, string model, dual amplitudes *(Russian)* 78—54620
baryonium spectroscopy based on duality and unitarity 79—58947
baryonium spectrum classification based on duality and unitarity 78—45869
baryons and baryonium, SU_6 symmetry, duality and unitarity 78—8622
Bloom-Gilman duality, scaling violations 78—21399
Bloom-Gilman duality and pion form factor 79—9352
bootstrap eqns., Pade approx. to dual multiperipheral model 77—30347
bootstrap model size of σ_{el}/σ_T anal. 77—22706
bootstrap models, solns. satisfying Lee-Veneziano relation 79—71729
bound-state/free-state duality, JWKB connection with radial wave functions 80—62950
bounds for Regge slopes and intercepts for ordinary and new hadrons 78—8627
charge and baryon transfers in dual unitary model 77—30337
charge-monopole duality and nonAbelian gauge theory phases 79—71625
charge-monopole duality in spontaneously broken gauge theories 79—267
charmed meson decay, SU(4) symm. breaking 77—26518
charmed meson mass via duality calc. 77—22697
charmed meson masses, duality predictions 78—8619
charmed mesons, nonleptonic decays, dual model current algebra relations and amplitudes 79—89132
charmed particle elastic widths, from dynamics and finite energy sum rules duality 77—38139
charmed particles, duality constraints on spectroscopy 78—21398
charmonium potential models, testing Q^2 duality 79—45082
chiral (γ_5) symmetry of massless fields, neutrino theory of photons 78—411
classical Euclidean Yang-Mills theory, self dual SU(2) solutions 79—2945
classical interacting strings, dimensional reduction, Abelian gauge fields 80—73685
classical null strings, free Nambu strings 78—12560
classically massless string, quark confinement 79—22041
closed string as source of Yang-Mills field, gluon gauge field vortex 78—41413
cluster formulation in the dual topological unitarization scheme 80—13293
coloured dual diagrams 79—22072
compact group gauge fields, breaking of symmetry and dual charges *(Chinese)* 79—35918
conformally invariant amplitudes and field theory in a spacetime of constant curvature 79—49395
covariant formalism for a relativistic string in a constant homogeneous electromagnetic field 79—21546
covariant inclusion of quark spin into the dual resonance model *(Russian)* 79—22074
current-induced reactions, dual unitarisation 78—74233
cylindrical mixing phenomena in dual topological unitarisation, pomerons, reggeons and gluonic states 80—86696
daughterless dual amplitude 78—4838
deep inelastic processes book contrib. 78—82222
diffractive bumps, gluonic excitation Regge trajectories from bag and dual models 79—2978
diffractive dissociation, duality and mass-slope correl. 77—82725
Dirac monopoles, invariance props. 77—61208
Dirac strings, monopoles, duality, triality 78—12864
disconnected quark diags., forbidden coupling and inhibited decay 77—22686
discrete and Abelian lattice gauge theories 79—9279
discrete lattice gauge fields, duality transformation, review 79—26236
dual absorptive model with peripheral pomeron, energy depend. of dip in pp elastic scatt. 77—79281
dual analytical model for pomeron *(Russian)* 77—13946
dual Deck model, three component, factorisation and double diffraction dissociation 78—8621
dual models of weak interactions of leptons and quarks 78—66070
dual multiperipheral model, Pomeron and Reggeon slopes 78—62379
dual multiperipheral model planar bootstrap 78—4837
dual Pomeranchuk amplitude contrib. to multi-Regge limit and pomeron sister absence 80—13237
dual resonance amplitudes, satisfactory invariant measure 78—66093
dual resonance models 77—10223
dual resonance Pomeron, intermediate mass distribution 78—25026
dual spinor model, low energy region, supersymm. Yang-Mills theory, supergravity theory 77—49923
dual string models with non-abelian colour and flavour symm. 77—2804
dual string theory, local currents *(Russian)* 78—25024
dual string with internal spin, second quantisation 78—440
dual strings, mass spectra 77—231
dual symmetry and magnetic charge conservation *(Chinese)* 79—80766
dual theory space-time geometry, graviton coupling to fermion string 77—18242
dual topological expansion, Reggeon and Pomeron slopes 80—102032
dual topological unitarisation, higher rank cylinder kernel 80—27492
dual topological unitarisation, review of S-matrix developments for hadron bootstrap theory 78—62381
dual topological unitarisation, singular cylinder kernel 80—27493
Dual Topological Unitarisation scheme, flavour symmetry breaking 80—102030
dual topological unitarization, glueball exchange effects, pomerons and reggeons 80—52482
dual two-loop graph double Pomeron region, particle prod. 79—75751
dual unified model and Pomeron-Reggeon amplitudes 77—57504
dual unitarisation, calc. of interference terms in multiperipheral resonance prod. model 77—41829
dual unitarisation, Reggeon, Pomeron and annihilation prod. processes 77—65143
dual unitarisation, renormalisation of pomeron trajectory 77—2806
dual unitarisation and baryon processes, S-matrix topological expansion 77—74662
dual unitarisation and baryons 78—16999
dual unitarisation approach to hadron reactions 77—38141
dual unitarisation scheme, Pomeron and f Regge pole prod. 78—41512

duality and dual models continued
- dual unitarity scheme, non-planar corrections to pomeron and reggeons 77—230
- dual unitarity scheme, single particle distrib., bootstrap eqn. 78—17002
- dual unitarization scheme with several trajectories, diffractive scatt. predictions 79—89133
- dual unitary scheme calc. of pp and $p\bar{p}$ scatt. 77—6168
- dual-resonance model, M-loop amplitudes for excited states 78—50019
- duality and dual models rho mesons diffraction model [Neveu-Schwarz dual model for $\rho\pi$ system] 78—82175
- duality between resonances and free quark-antiquark pairs 79—63448
- duality for non-abelian lattice fields 80—42431
- duality in field theory and statistical systems, review 80—73610
- dynamical point-like struct. and dual strings 77—67630
- dynamical symmetry breaking in dual resonance model, Regge meason trajectories total renormalisation *(Russian)* 77—82717
- dynamical threshold for baryon resonance prod., baryon exchange in dual unitarisation scheme 78—45884
- dynamical thresholds in dual unitarisation scheme, two body scatt. 77—49924
- electrodynamics with strings and monopoles, book contrib. 79—58916
- elementary length and time in the strong interaction, meson reson. width data 78—82189
- EM duality, secondary symmetry, magnetic current conservation 80—27431
- equal-time commutators in continuous dimensions 79—71730
- Euclidean gravity, asymptotically flat self-dual solns. 78—45834
- exchange degeneracy breaking, charge conjugation, in s-channel, unitarity, quark diagrams 77—22713
- exchange degeneracy breaking, hadronic selection rules 80—37248
- exchange-degeneracy breaking, connection with multiquark states, dual approach 79—93387
- flavour symmetry breaking and production processes in dual unitarisation, ϕ and ψ prod. 79—45080
- four-reggeon amplitudes 77—233
- functional bridge between gauge theory and strings in two dimens. 77—45966
- gauge fields as phonon excitations in a condensate of dual strings 79—35934
- gauge fixing ambiguities, flux strings, and the unconstrained Yang-Mills theory 79—35927
- gauge lattice systems, transition, duality 79—262
- gauge theories, dual charge and principle bundles, structure *(Chinese)* 77—71438
- gauge theories including EM-type fields with sources, duality invariance 80—27440
- gauge theory, sourceless, interaction among dual strings 80—42432
- gauge theory of dual resonance model, spontaneous symm. breaking 77—6092
- gauge theory phases 79—97486
- general relativity canonical formulation by analogy with elementary particle string model 78—8287
- generalized dual loop expansion of $U(N_c)$ gauge theory 79—93385
- geometric strings, quark binding, quantisation in GL(2,C)/SL(2,C) struct. group 79—40727
- geometrical Schrempp model, analytic extension 77—74659
- ghost-free string models, systematic search, struct. constants in gauge superalgebra 79—30719
- glueball singularity, flavour loops and the Harari-Freund picture 80—42433
- gluon chains and multiquark hadrons 79—93337
- gravitation duality in quantisation problem 79—30344
- group theoretical structure of dual current vertex 78—74229
- hadron nonlinear string model 77—87901
- hadron reactions, large, small momentum transfer regions, transition point for s-depend. 77—30339
- hadron spectrum, planar amplitudes without Regge cuts 80—27464
- hadronic amplitudes, diffractive contrib., Chew Rosenzweig pomeron soln. 78—62382
- hadronic collisions, jet structure, two-jet events, glueball-Pomeron identity, dual field theory 80—63051
- hadronic cross section strength, nonlinear unitarity eqn., internal symm. restriction 78—33042
- hadronic diffraction, elastic scatt. as tunnelling phenomenon, dual model relation 80—57575
- hadronic matter, critical point exponents 79—58944
- hadronic processes, large and small p_T behaviour 79—26268
- hadronic processes, small and large p_T behaviour, new particle-wave duality 79—45081
- hadronic reactions, trajectory slopes in gauge-dual-topological approach 80—18142
- hadrons and baryonium, geometrical approach 80—91065
- Hamilton-Jacobi formalism for strings, string-gauge theory link 80—78048
- hard processes, large rapidity separation of baryonic number, partons, and dual topology 80—95255
- heavy quark bound system, vibr. states 78—29300
- heavy quark system prod. in QCD, duality predictions 79—13074
- high energy behaviour of a double discontinuity and the bare Pomeron 78—82179
- high-energy behaviour of a double discontinuity and the bare Pomeron 79—17696
- inclusive electroproduction, local duality and precocious scaling, quantum chromodynamics 77—2842
- instanton soln., Dirac eqn. 78—82100
- instantons, description in self-dual Euclidean Yang-Mills fields 79—6256
- instantons and characters in non-Abelian Yang-Mills theory 79—63345
- instantons and Kahler manifolds 79—12925
- integral representation of dual resonance amplitudes with two off mass shell states 78—66094
- intermediate mass distribution of dual resonance pomeron, rel. to multiperipheral processes 78—50020
- internal symmetry, unitarity constraints 77—41825
- inverse scatt. problem, self-duality eqns. 78—29247
- inverse scattering problem and instanton construction by algebraic geometry, review 80—47203
- Ising field theory, Z_2 duality algebra in $D=2$ quantum field theory 79—75685
- isomorphic function and Fock space representations of dual model superconformal group 78—74230

duality and dual models continued
- isoscalar meson-nucleon couplings, finite energy sum rules, duality determ. 77—13940
- jet struct. of hadronic final states, Bose-Einstein effect 78—16994
- Klein-Gordon equation, stringlike solns. 78—82114
- lattice approach to string theory tachyon problem exhibited 78—4840
- lattice gauge theories, vortex free energy, strong and intermediate coupling string tension 80—105786
- lattice gauge theory, extreme environments and duality transform., review 79—13024
- lattice gauge theory, string model, hadron spectrum, Regge trajectories 77—57452
- lattice gauge theory and spin systems, review 80—22528
- lattice massive dual fields for gravity 80—105779
- Lee-Weinberg model of weak and EM interactions, string-like solns., vortices 80—47231
- lepton-nucleon deep inelastic scatt., SU(4) duality and quark parton models 77—61293
- line space construction of non-self-dual Yang-Mills fields 80—9103
- linear baryonic string model, dynamical SU(3) symmetry breaking 79—22036
- linear string model, baryon SU(6)×O(3) multiplets 78—8624
- local complex supersymmetry in two dimens., O(2) string model 77—45985
- Lorentz force in loop space, duality functional equations 80—78049
- lorentz invariance from classical particle paths in quantum field theory of electric and magnetic charge 79—49431
- Lorentz invariant dual string model dimens. regularisation by hyperfunctions 78—41510
- Lorentz invariant string regularised dimensionally using hyperfunctions 78—41511
- low mass diffractive dissociation in a simple t-depend. dual bootstrap model 79—13089
- low mass diffractive dissociation in a simple t-dependent dual bootstrap model 79—36042
- low multiplicity diffractive dissociation, 1/N dual unitarisation scheme 79—75753
- mass-sum rule, Veneziano-type amplitudes π and K mesons 78—74180
- massive string model of mesons and baryons 80—4970
- massless antisymmetric tensor gauge fields, second rank, free field theory quantisation 79—257
- meson form factor in dual model with spontaneous vacuum transitions *(Russian)* 77—49967
- meson radiative transition, symm. and duality constraints 78—78178
- meson reson. elasticities belonging to a dual spectrum, multipion channel coupling 77—38136
- meson resonances, high spin, natural parity, dual reson. model with non-degnerate Regge trajectories 79—359
- mesons, unnatural parity, in dual unitarization scheme 77—87951
- multi-instanton determinants for covariant laplacian D^2, 't Hooft solution extension 80—13216
- multi-instanton solutions of the duality equation and the inverse-scattering problem *(Russian)* 79—21591
- multicolour QCD as dual resonance theory, mesons on rising Regge trajectories 78—16987
- multiparticle production in multiperipheral resonance model complemented by duality 79—36050
- multiperipheral parton model, Reggeisation and dual unitarisation 80—37249
- multiplicities, inclusive distribs., in hadron or lepton induced reactions, quark jet universality 78—41476
- multiquark states, octonionic interpretation in dual string picture 79—49449
- multiquark states and the breaking of exchange degeneracy, dual approach 79—45061
- n-particle decay of dual resonance, decay width, multiplicity distrib., multipion channels 78—16997
- Nahn partition function of the dual spectrum 77—87952
- Nambu string model, reggeon and pomeron interactions *(Russian)* 80—13294
- Nambu string model, scatt. amplitude *(Russian)* 80—86695
- narrow states in $\bar{p}p$, $qq\bar{q}\bar{q}$ mesons, $\bar{B}B$ bound states, duality, expt. 78—62378
- Neveu Schwarz Ramond model, complete action for spinning string, field eqns., constraints 77—13943
- Neveu-Schwarz dual model, vac. transitions *(Russian)* 78—33046
- Neveu-Schwarz dual pion model, two new Regge trajectories 77—38138
- Neveu-Schwarz Ramond dual fermion model, inclusive single particle distribs. 78—86446
- new duality, asymptotic symm. for charmed and ϒ mesons 78—21348
- non-Abelian lattice fields, duality 79—93280
- non-Abelian theories, dual formulation 80—82902
- nonabelian gauge fields, soln. of finite string type *(Russian)* 78—391
- nonAbelian gauge groups, dual charge, mag. monopoles *(Chinese)* 77—34076
- nonhadronic duality and π^0 photoproduction 77—67661
- nonhomogeneous string model 78—12884
- nonlinear relativistic string, Euler equations, introduction of new Lagrangian 79—36045
- nonstrange exotic meson production via baryon exchange, cross section upper limit meas. 77—50015
- nucleonic form factor, pion exchange, model 80—22608
- off-shell amplitude singularities in position-space and momentum-space 77—13941
- off-shell dual amplitudes, functional method 78—29318
- off-shell dual strings, point-like struct. 77—71492
- off-shell states in dual model 77—2805
- open membrane classical theory 77—67629
- Oxford Rutherford type model, semianalytic treatment, dual unitarisation scheme, trajectory parameters 78—16996
- OZI rule violation, analyticity and duality 78—24978
- P+f diffraction model, two component duality and flavouring, Regge fits and pomerons 80—95261
- partition functions of dual strings, functional evaluation 78—74231
- pathological lattice field theory for interacting strings 80—47186
- PCAC and dual resonance amplitudes, old and new mesons, charm 78—45885
- phenomenological consequences of new Regge trajectories on pion trajectories, dual models 78—33045
- phenomenological duality, strong interactions description using finite energy sum rules 77—82716

duality and dual models continued
Poincare covariance of free massive two dimens. quantum string 77−6048
point electric and mag. charge, nonAbelian gauge invariant classical Lagrangian formalism 79−12627
pole-dipole relativistic string model 80−386
Pomeron coupling diag. to order 1/N 80−47263
Pomeron exchange, SU(3) props., dual unitarisation scheme 77−13945
pomeron-f identity hypothesis, test 78−45887
pseudoparticle field propagators 78−8513
QCD, equation for dual chords *(Russian)* 79−58936
QCD, hadron interaction effective string lagrangian, Regge slope, charmonium pot. model 80−4939
QCD, Migdal approx. and 1/N expansion, string tension 80−101992
QCD, string constant, Regge slope and Λ parameter, empirical quarkonium approach 80−91053
QCD and particle-string variables 78−24939
QCD $q\bar{q}$ running coupling constant, β-function from string model, Pade approx. 79−343
QCD spectrum, infinite number of colours at fixed coupling, interacting string model 79−2993
quantisation of system of three relativistic strings 77−41826
quantised dual string theory, string functional and propagators 80−32088
quantised strings and chromodynamic IR behaviour, Yang-Mills electric flux lines 77−30316
quantum chromodynamics, unified approach to gauge, dual, Gribov theories 77−18223
quantum field theory and dual resonance models 77−30236
quantum relativistic strings and the multiplicative dual model *(Russian)* 80−82958
quantum strings and boson spin 77−54087
quark and string interacting system, gauge theory for 2-D statistical mechanics 79−30713
quark confinement, Dirac's magnetic monopole string theory 77−13927
quark confinement, infinite momentum frame formulation 79−36026
quark confinement, parton-hadron duality 78−41484
quark confinement without van der Waals forces, link operator formulation and string breaking 80−101994
quark duality diagram struct. of particle prod. 77−22696
quark string model, hadron spectrum, semiclassical approach, baryons and exotic hadrons 79−40747
quark-confining string 78−25004
quark-parton model from dual topological unitarization 79−93361
quark-string model, meson mass spectra 78−33065
quarkonia, spectra, decays, levels, jets, sum rules 80−18112
Regge cut cancellation in planar amplitudes of dual unitarisation scheme 77−87954
Regge spectra, symm. breaking effects, decay rates of mesons in dual resonance amplitudes 77−82715
Regge trajectories, dual unitarisation scheme, SU(3)-breaking and baryon exchange effects 79−26316
Regge trajectories for old and new particles 78−12886
Regge trajectory intercepts and mass formulae relation *(Russian)* 79−85283
Regge-cut cancellations in dual unitarisation scheme planar amplitudes 77−10228
Regge-Regge amplitude duality and high-energy behaviour in dual reson. model 77−10222
reggeon amplitude from analyticity and planar unitarity 77−41828
reggeon and photon coupling relns. 79−13063
Reggeon phases and dual bootstrapping 77−34132
Reggeon vertices and finite mass sum rule, bootstrap eqn., dual resonance model 80−13292
relativistic motion of massive quarks joined by massive string 78−74206
relativistic string, geometric approach 79−36044
relativistic string in a constant homogeneous electromagnetic field 79−22073
relativistic string model generalisation in geometrical approach, Yang-Mills approx. 80−383
relativistic string model in differential form 80−105870
relativistic string quantized in four-dimensional space, supersymmetrical Lagrangian in QCD principles *(Russian)* 80−13276
relativistic string theory in external field 79−97574
relativistic strings, boson transformation method, energy, momentum 77−34135
relativistic strings and dual models of strong interactions, review 78−439
relativistic strings and electromagnetic flux tubes 79−49494
relativistic strings theory, nonvanishing mech. mass 77−34134
relativistic strings with massive end quarks, boundary condition solns. 79−49493
renormalisation of trajectories with zero quantum numbers in dual unitarisation 78−21400
review of tree and loop amplitudes *(German)* 77−65142
Rohrlich string, classical, gauge mapping theorem 78−17001
s-channel discontinuities of torus insertion, dual unitarisation scheme, ρ-A_2 exchange degeneracy breaking 78−93866
s-channel resonance prod. in πN scatt., amplitude zeros in Mandelstam plane 80−73686
S-matrix, planar, building of cylinder correction in topological expansion or dual unitarisation 78−62321
S-matrix theory dual chiral pion model, partially conserved axial-vector current 78−58175
scaling violation, two-component duality model, ν and μ interactions 78−8623
Schwinger model, equivalent boson theory, anomaly-free Ward-Takahashi identities 80−82873
selection rule as extension to OZI and FWR rules hadron interactions, string model 78−29343
self dual SU(2) fields in multicentre spaces 80−73600
self-dual gauge field, Green function 78−82099
self-dual gauge fields and space-times 80−9108
self-dual pseudoparticle fields with massless excitations, Dirac eqn. equivalence for spinor with chirality 78−4788
self-dual sector, field strength formulation 78−29256
self-dual SU(2) gauge field, Pontryagin density 78−66044
self-dual SU(2) gauge fields, Backlund transform. and Atiyah-Ward ansatze 78−21339
self-dual Yang Mills fields in Minkowski space 80−18078
self-dual Z(N) gauge theories, critical temp. 79−49375

duality and dual models continued
semi-local duality in inclusive e^+e^- annihilation, duality sum rule 77−49985
semilocal duality constraints for mesons, on-shell particles, masses, couplings 78−58174
sequential particle order, fundamental concept for hadron physics 79−80762
sequential particle order, fundamental concept for hadron physics, S-matrix theory 79−80763
Shapiro-Virasoro model, multi-Regge limit, pomeron sister trajectory 77−82720
simultaneous bootstrap of mesonic and baryonic trajectories in dual topological unitarisation 80−42429
single dual pomeron contrib. to inclusive distrib., triple-Regge, fragmentation, pionisation, regions 78−41509
small p_T hadronic collisions, jets, quark, fragmentation universality and rising rapidity plateaus 79−40734
space-time anomalous dimension in Venziano and Neveu-Schwarz models *(Russian)* 80−68434
spectrum generating partition function, comment 77−61261
spin in spectrum of states of dual models 77−38137
spinning string, local supersymmetry and reparametrisation invariant 77−18244
spinning string, quantisation by Grassmann variables conversion to Clifford algebra elements 78−66095
spinning string in orthonormal gauge, gauge mapping theorem 77−41823
spinor dual model and supergravity 77−13675
spontaneous symmetry breakdown in standard dual string model 78−41508
statistical bootstrap duality in inelastic scatt. 77−18239
string, relativistic, $SU_{3,1}$ in orthornormal gauge 78−437
string, with confined 3/2 spin field 77−41822
string and quark systems, statistical mech. treatment renormalisation group meth. 77−54075
string interaction, tachyon-reggeon scatt., dynamic effect of extended hadrons 77−18241
string interactions in quantum chromodynamics, string lagrangian construction *(Russian)* 79−63432
string junction in hadron reactions 77−49907
string junction model, large p_T hadron prod. 78−62380
string model, critical dimension, field theory in $2+\varepsilon$ dimens. 77−57503
string model, critical dimension 77−49925
string model, geometrical interpretation of reggeon and pomeron intercepts 77−26499
string model, Green's function struct. 77−18243
string model and QCD 79−26292
string model for fermions 77−2803
string model of mesons with two massive quarks 77−10212
string model of particles and compensation *(Russian)* 77−61260
string models, nonhomogeneous class 77−2802
string operator eqns. of motion in QCD 80−4953
string representations and hidden symmetries for gauge fields 79−49378
string state, WKB-like wave functional and path-dependent phase factor, colour flux 80−52481
string theory, relation to field theory, strong coupling expansion 77−87953
string type solns., in classical gauge field theories, broken gauge symmetry 78−62317
string-junction model and width of baryonium 79−58928
string-like configurations in Weinberg-Salam theory, Regge trajectories of excitations 78−16966
stringlike object in quantum field theory 77−2738
strings, bags, baryoniums 78−29307
strings, functional integrals for partition functions 77−67628
strings, interacting relativistic, noninstantaneous action-at-a-distance theory 77−74661
strings, spinning, spinning strings, addition of scalar and spinor fields 77−49833
strings, vortices, gauge fields 77−71493
strings from field theory, statistical approach 78−25023
strings in non-Abelian gauge theories 80−52403
strings on lattice, renormalisation group techniques 77−22654
strong gravity and elementary particle theory in general relativity 78−8315
SU_2 dual charges, U_2 (Q) invariance of principal bundles, and corresponding ang. operators *(Chinese)* 79−36043
SU(2)×U(1) gauge theory of weak, EM and dual EM interactions 80−52448
SU(2) classical gauge field eqn., self-dual static solns. 78−45792
SU(2) gauge theory instanton solns., duality condition, Lie group interpretation, quasiparticle soln. 79−6261
SU(2) Yang-Mills theory, self duality of solns. 78−37143
SU(4)×SU(4) current two point functions, meson decay consts. and bare quark masses from duality 78−8598
SU(4) broken symm., duality, baryon+baryon and baryon+antibaryon exotic mesons prod. 78−89629
$SU(6)_W$ structure of baryonic reson. photocouplings duality constraint 79−71649
$SU(6)\times O(3)_L$ multiplets, semilocal duality, quark-orbital Regge trajectories 80−27490
SU(6) multiplet, connection with semi-local duality in quark model 79−93386
SU(n+1) invariant chiral theory, duality eqns. soln. 79−9351
SU(N) lattice gauge model, weak coupling, monopole condensation and quark confinement 79−75683
superoperator generalisation of dual model with coloured quarks, three reggeon vertex *(Russian)* 78−74234
superspace and spinning string 78−4839
supersymmetric Ising field theory, 'doubled' model, and supersymmetric sine-Gordon kink struct. 79−71614
supersymmetrical string model, physical states *(Russian)* 79−67523
t-channel diffractive scatt., elastic peak and hadron size 79−45083
tetrahedron, semilocal duality in hadronic amplitudes 78−438
thermal props. of gauge fields and quark liberation 78−24936
topological dual bootstrap model and hadron collisions 77−22708
topological excitations in Abelian Higgs model 78−70275
topological expansion for baryons and mesons, reaction diagrams using coloured quark lines 77−82700
topological expansions incorporating baryons and mesons 77−57505
triple-Pomeron couplings in dual models 79−358
twist parameter J-depend. in dual unitarity 77−26500

duality and dual models continued
twistable relativistic string, dynamics 77−18240
U$_1$ gauge field in SU$_n$ gauge field, dual charges *(Chinese)* 78−86417
U(N) gauge theory, Nambu-Gato string like equation 80−105785
U(N) lattice gauge theories with quarks, string eqns., Dyson-Schwinger eqns. 80−4857
U(N) lattice gauge theory, string representation, Wilson loop amplitudes 80−4856
U(N) lattice Yang-Mills theory, Schwinger-Dyson eqns., string model equivalence 80−4855
unambiguous field-strength formulation and dual potentials for gauge theories 79−35938
unified theory of direct interaction between particles, strings and membranes 78−86433
unitarised, conventional, renormalisation of new trajectory 79−85281
vacuum singularities in dual multiperipheral model 77−34140
van der Corput neutralisers, use in modifying pole residues 77−6093
vector meson leptonic width, duality between vector mesons and perturbative QCD 80−57589
vertex bootstrap conditions in dual unitarisation scheme 77−38135
vertex bootstraps conditions in dual unitarisation 77−74660
virtual Compton amplitudes, duality props. 77−30388
vortex line models, slopes of Regge trajectories 77−18249
vortex string picture and large p_T reactions 79−63415
vortex strings, mag. monopoles in gauge field theory 78−70283
weak charmed-baryon resonance prod., neutrino inclusive interactions, scaling behaviour 78−8645
Weinberg sum rules, derivation of meson spectrum, duality unification with chiral symm. 78−29272
X-Y model, gauge theory analogue, 4-D self-dual gauge model, phases and transitions 80−27399
Yang's R gauge for self-dual SU(3) gauge fields 78−78088
Yang-Mills field, self-dual, parametric Backlund transformation 79−97503
Yang-Mills fields, ambiguous relationship for dual models 79−49495
Yang-Mills pseudoparticles, dual-charges *(Chinese)* 77−82684
Yang-Mills theories, quantum dual string wave functional 79−21921
Yang-Mills theory, Regeisation of scalars and dual model struct. 78−16927
Z(N) gauge theories, self duality 79−2919
zeta-function regularization and multi-instanton determinants 80−13215
Zwanzigers local Lagrangian quantum field theory, electric and mag. charge, Lorentz invariance 79−6286
Zweig-superconvergence relations in meson collisions 78−21397
$A_2 \to \pi\gamma$, suppression factors for VMD couplings calc., duality constraints anal. 77−13960
d inelastic screening, form factor at $t \neq 0$ 80−91070
$D \to K\pi(\pi)$, current algebra relations and dual model amplitudes 80−82969
$D\bar{D}$ molecular charmonium from dual diagram and Schrodinger eqn. 80−86660
$D\bar{D}^*$ production and decay, VDM, dual amplitude anal., e^+e^- annihilation 77−49992
e^-e^- annihilation, parton model, finite energy results 78−419
$e^+e^- \to$ hadrons, dual unitarisation and quartz model 77−10272
$e^+e^- \to$ hadrons, string model investigation 79−58946
e^+e^- annihilation, jet struct., test of QCD and quark-confining string 78−33040
e^+e^- annihilation, Q^2 duality test with nonrelativistic potentials 80−102011
e^+e^- annihilation, QCD and semilocal duality (hadrons/$\mu^+\mu^-$) cross section ratio 80−78085
$ep \to \pi^\circ X$, duality and finite energy sum rules 80−42477
η,η' mesons trajectory mixing scheme, dual planar theory 77−13942
$\gamma p \to \pi^\circ X$, duality and finite energy sum rules 80−42477
$\gamma_V p \to \pi^0 p$, phase shift anal., shrinking photon, geometrical duality 77−87983
$K^-p \to (\pi^+\pi^-)_{\text{s-wave}}\Sigma^0(1385)$ amplitude anal., additive quark model and duality diagram predictions 77−30430
$K^-p \to \Lambda +$anything, 4.2 GeV/c, dual anal. of target fragmentation 77−57561
$K^-p \to \Sigma^+ +$anything, 4.2 GeV/c, dual anal. of target fragmentation 77−57561
$N\bar{N}$ interaction, low energy, meson exchange forces, one boson exchange potential, dual quark models 78−62444
$\bar{N}N$ narrow meson resonances near threshold, theoretical approaches 80−9157
np elastic scatt. at high energies and dual absorptive model 80−102072
$\omega \to \pi\gamma$, suppression factors for VMD couplings calc., duality constraint anal. 77−13960
pp, dual model, vacuum exchanges, double pomeron poles with exotic Regge poles 78−89686
pp, smooth interpolation between Orear- and fixed angle scaling behaviour of the scattering amplitude 80−105873
$\bar{p}p$ annihilation relative multiplicity moments, dual unitarisation scheme verification 79−89203
pp elastic differential cross section break, 90° scatt., duality satisfying lepton-hadron relation 79−3035
pp large p_T reactions, jets, dual-string approach 80−32136
$pp \to pX$, Deck effect contribution 78−21471
pp scatt., exchange degeneracy violating A_1-Z Regge amplitude and dibaryon resonances 80−4971
$\phi \to \pi\gamma$, suppression factors for VMD couplings calc., duality constraints anal. 77−13960
$\pi N \to \pi\Delta$, finite energy sum rules and duality 77−22763
$\pi N \to \pi N$, finite-energy sum rules, three component duality 80−82996
πN scatt., low energy nonresonant amplitudes, t- and u-channel structure 77−38193
πN scatt. baryon reson. spectrum in dual model 77−18318
πN scattering, amplitudes, singularities of zero trajectories, dual model predictions 80−63021
$\pi\omega \to \pi\pi$, operator dual model for bound relativistic quark based mesons *(Russian)* 79−9408
$\pi^-p \to \phi n$, quark line rule, violations 80−52530
$\pi^\pm p$, <280 GeV/c dual absorptive model of elastic scatt. 79−63529
ψ meson spectroscopy, charmonium model, quark-confining string 78−8625
ψ spectroscopy, quark-confining string model 77−6094
$\psi' \to \psi\eta$, OZI rule violating transition, unitary corrections using dual model 79−26330
$Q\bar{Q}$ mass, approx. scheme is QCD 80−42398
$qq\bar{q}\bar{q}$, suppressed decays, strings, bags, baryonium 78−21385
Υ, vibrational states in string picture, mass and leptonic width 80−62949
υ prod. from duality and new quark charge 78−74224
$\bar{p}p$ annihilations, studied using topological cross-section differences between $\bar{p}p$ and pp at 48.9 GeV/c 80−83011

ductile-brittle transition
see also embrittlement
acoustic absorption during brittle-plastic transition, theory 79−27595
acrylic, denture base, tensile testing 80−16621
acrylic, ductile-brittle transition conditions 77−66001
Armco iron, effect of low temps. and heat treatment on growth rate of fatigue cracks 79−57027
atomistic simulation by computer, exam. of thermal activation of crack tip plasticity 78−60801
γ-brass, brittle to ductile transition under high hydrostatic pressure and high temp. *(Japanese)* 80−35305
brittle-plastic phase transform. 77−11630
cleavage initiation by ductile tearing 78−64656
complex loading, exam. of ductile-brittle failure 78−79664
covalent crystals rel. to covalent bond metallisation *(Russian)* 77−56071
discs, circularly symmetric, rupture, ductile-brittle creep 80−69735
dispersion hardened alloy, load type effect on yield stress 78−35458
ductile-brittle transition pressure, grain size effect *(Japanese)* 78−60745
energy scaling, size effects and ductile-brittle transitions in fracture 79−43394
epoxide resin, low temp. crack propag. 80−85020
failure of crystalline material in transition zone 78−14401
fatigue crack propagation in ductile-brittle transition temp. range 77−59929
fatigued steel brittle transition temp. meas. by hardness testing *(Japanese)* 79−87797
Incoloy 800, exam. of caustic stress corrosion cracking, comparison with type 304 stainless steel 79−29261
Inconel 600, exam. of caustic stress corrosion cracking, comparison with type 304 stainless steel 79−29261
ionic-covalent crystal transition to plastic state 79−90717
metal, BCC, viscous brittle transition during fracture, dislocation model 77−62582
metal structures, thin walled, crack growth problems 80−55527
metallic glasses, Fe, Co, and Ni based 77−4847
metals, BCC, low temp. softening 79−34113
metals, ductile-brittle transition temperature evaluation, as function of thickness 80−3261
metals and alloys, BCC lattice, crit. embrittlement temp., struct. parameters effect *(Russian)* 80−66618
neutron effects in pressure vessels for PWR, BWR, safety calcs., design, operation control *(German)* 77−34404
nuclear reactor materials, crack propag., fracture, and ductile-brittle transition *(Spanish)* 79−36316
Nylon 6, injection moulded, yield stress and fracture toughness 80−38951
PMMA, indentation fracture mechanics 78−35490
PMMA, slow to fast crack propag. transition 77−12687
PMMA, solid, stress-strain behaviour, strain rate and temp. effects, cryogenic temps. *(Japanese)* 78−11315
polycarbonate, dielec. relax. and ductile brittle transition 78−52438
polycarbonate, impact behaviour, effects of thermal pre-treatment and mol. wt. 78−95798
polycarbonate blends, yield and deform. behaviour, impact modification 77−36572
polymer, solid, impact compression crushing at low temps. *(Japanese)* 78−7032
polystyrene, effect of pressure and environment on fracture and yield 78−76757
polystyrene, high impact, under press., mech. behaviour 79−52305
polystyrene-polyolefin blends, mech. and swelling props. on heating 79−57053
power-law hardening material, pre-cracked plate, unstable fracture criterion 80−84238
PVC, solid, stress-strain behaviour, strain rate and temp. effects, cryogenic temps. *(Japanese)* 78−11315
serpentinites, Glenrock, New South Wales, foliation development 80−21738
small particles, ductile-brittle transition rel. to impossibility of comminution by compression 78−52709
steel, 18 Kh2N4MA, grain size effect on mech. props. 78−44207
steel, 24Kh2NMFA, crack resistance, yield strength, ductile-brittle transition temp., optimum tempering of 24Kh2NMFA 77−63787
steel, alloy, 30Kh2N2SMK5, temper brittleness of 79−96129
steel, austenite decomposition, controlled rolling rel. to substruct., props. 79−29014
steel, austenitic, fracture toughness props. of A533B, prior austenite grain size effect 78−60780
steel, austenitic, reliability of stress intensity factor values 80−55530
steel, austenitic stainless, reliability of stress intensity factor values 80−55530
steel, brittle transition temp. comparison of arc, gas-pressure and friction-pressure welded alloy by hardness measurements *(Japanese)* 79−11691
steel, C, 35, low-temp. fracture toughness, non-metallic inclusions influence *(Russian)* 79−52346
steel, C, composite layered specimen influence of contact strengthening by intermediate layer, on fracture toughness *(Russian)* 79−15768
steel, C, prestrain effect on non ductile transition temp. and bending speed relationship *(Japanese)* 78−84919
steel, C, weldable, ferrite-pearlite, Widmanstatten structs., resist. to fracture 79−29203
steel, cast automatic couplings, yield strength, crack propag. resistance and ductile-brittle transition temp. 80−104281
steel, constructional, impact strength/brittle fracture relationship in ductile-brittle transition zone 78−56740
steel, continuously cast, ductility near melting pt., hot tearing 79−83314
steel, Cr-Mo, grain size effect on ductile brittle transition 79−24615
steel, Cr-Mo, impact fatigue crack growth at low temps. *(Japanese)* 80−104266
steel, Cr-Mo (2.25, 1.0 wt.%), temper embrittlement, effect of P, Sn, comp. and carbide precip. 80−85036

ductile-brittle transition continued
- steel, Cr-Mo and Ni-Cr-Mo-V low-alloy, additive remedy for temper brittleness 80—66659
- steel, Cr-Mo-(Ni-V), temper embrittlement by P and Sn, effect of rare earth additives 79—61721
- steel, CrMo and CrMoV, creep resistant, ductile-brittle transition temp., precipitation effects *(German)* 78—19856
- steel, ferritic, Charpy impact testing criteria 79—47855
- steel, ferritic, Cr-Mo (18, 2 wt.%), cold work effect on 885°F embrittlement 77—77499
- steel, ferritic, criteria for Charpy impact testing 80—7752
- steel, ferritic stainless welds, type 444, ductility loss rel. to ductile-brittle transition temp. 80—85002
- steel, ferritic-pearlitic, low C, low alloy, low temp. effects on fatigue strength 79—5057
- steel, for PWR press. vessels, RT_{NDT} shift of ductile-temp. curve, correl. with neutron dose *(German)* 77—34388
- steel, lamellar pearlite, containing proeutectoid ferrite, prestrain effect on brittle fracture *(Japanese)* 80—45388
- steel, low alloy, brittle fracture, quenched and tempered 80—11677
- steel, low alloy, ferritic-pearlitic, carbonitride hardening 80—104174
- steel, low alloy, radiation embrittlement, heat treatment effects 78—19893
- steel, low alloy, toughness, effect of packet size and lath width 77—16677
- steel, low C, ductile-brittle transition behaviour, grain size effects 78—52942
- steel, low C, effect of grain size on transition behaviour and bending speed correl. *(Japanese)* 79—8345
- steel, low C, impact strength and crit. brittleness temp., sample thickness and notch radius influence 80—85018
- steel, low C, microalloyed, heat treatment, mech. props. 79—24551
- steel, low C, nil ductility transition temp. 80—100896
- steel, low C, non-ductile transition temp., tensile speed, effect of prestrain *(Japanese)* 78—72839
- steel, low-alloy structural, radiation hardening, rel. to embrittlement *(Russian)* 77—21243
- steel, low-C martensitic, Ni addition influence on toughness and ductile-brittle transition 80—30099
- steel, martensitic-bainitic, lath morphology effect on yield stress, martensitic and ductile-brittle transition temps. 79—100215
- steel, medium Cr, B effects on struct. and toughness 77—21265
- steel, medium strength plate, quenched and tempered, fracture toughness in ductile-brittle range 78—7036
- steel, mild, yield strength and fracture toughness, microstruct. effect, heat treatment 78—27615
- steel, Mn (1.10 to 1.55 wt.%), reactor vessel material, assessment of weld heat affected zone mech. props. 79—29217
- steel, Mn-Mo-Ni (A533 B), ductile-brittle transition, material fracture temp. depend., Gauss distrib. function 80—97574
- steel, Mn-Ni-Mo low alloy steels for nuclear appl., toughness and heat treatment 80—5239
- steel, Ni-Cr, exam. of caustic stress corrosion cracking, comparison with type 304 stainless steel 79—29261
- steel, Ni-Cr, temper embrittlement by Sn 77—86149
- steel, nil ductility transition temp., and Charpy V-notch fracture appear transition temp. relationship between them, determ. *(Czech)* 79—91783
- steel, notched bar impact bending test, Robertson test and drop-weight test relationship 77—81364
- steel, S45C notched specimens, Charpy impact tests, notch angle effects *(Japanese)* 80—85124
- steel, stainless, Cr-Mn (21, 14 wt.%), grain boundary precipitation and fracture *(Japanese)* 79—100149
- steel, stainless ferritic, 10 to 30 wt.% Cr, ductile-brittle transition temp. 80—30095
- steel, structural, classification according to ductile-brittle transition temp. 78—11298
- steel, structural, CrN-modified, tempering and quenching effects on struct. and props. 77—59835
- steel, structural, ductile-brittle transition, anal. soln. by deadweight tensile test method *(Slovak)* 79—79095
- steel, structural, effect of rare earth metals on cold temper brittleness 79—29202
- steel, structural, effect of stressed state nature on ductility and failure 79—57078
- steel, structural 15KhNMFA, resist. to weakening during tempering, high purity effect 80—76279
- steel 10GN2MFA, effect of low temps. and heat treatment on growth rate of fatigue cracks 79—57027
- steel 35KhGSA, resist. to fracture after low temp. temperating, P content and grain size effects *(Russian)* 78—48490
- steel 45, effect of low temps. and heat treatment on growth rate of fatigue cracks 79—57027
- steel for nuclear reactor press. vessels, criteria for brittle fracture, neutron effects *(German)* 77—34389
- steel St.3kp, ductile-brittle transition temp., variation with grain size 78—27640
- steels, brittle transition temp. determs. from impact ductility tests, comparative evaluation 79—15888
- steels, structural St 37-2, cleavage fracture, report 80—25868
- structural steel, microstruct. and brittleness, rel. to austenizing and heat treatments 77—56091
- thermal fluctuation fracture phenomena 77—15489
- thermoplastics, glassy, embrittlement mech. and inelastic deform. criterion for delayed failure 78—52940
- transition metal amorphous alloys with metalloid elements, embrittlement/crystn. relationship *(Japanese)* 79—96134
- Al-Zn-Mg (6,1.5%), influence of ageing and cold work on tensile and fracture props. *(Japanese)* 78—52842
- AlN, polycrystalline, stress-strain data up to 1.25 GPa 80—100899
- Be, technical grades, intergranular embrittlement *(Russian)* 78—3208
- BeO, polycrystalline, stress-strain data up to 1.25 GPa 80—100899
- Co-Cr(-Al-Y) coatings, hot corrosion resist., ductile-brittle transition 79—24674
- Co-Zr, amorphous phase form. in Zr-poor region, hardness and fracture strength *(Japanese)* 80—84914
- Cr, and Cr alloys, cast, B additions effect on struct. and props. *(Russian)* 78—19891
- Cr, anomalous US damping under hydrostatic press. 79—14890
- Cr, fracture during electrospark cutting *(Russian)* 79—87719

ductile-brittle transition continued
- Cr-Ce-N, Ce and N effects in ductile-brittle transition, microstruct., hardness, *(Russian)* 78—35497
- Cr-Fe (1 wt.%), fracture during electrospark cutting *(Russian)* 79—87719
- Cr-Ni VKh-4 alloy, deformation and fracture mechanism investigation *(Russian)* 80—11738
- Cr-V-B-Y system, fatigue strength and fatigue fracture at 20 and 1100°C, SEM study 80—3194
- Cr-V-Ce-N, (2.4 to 2.6, 1.7 to 2.3, 0.005 to 0.23 wt.%) V effect on hardness, and ductile to brittle transition temp. *(Russian)* 79—34138
- Fe, cast, nodular graphite, annealed, fracture behaviour at low temps. 78—72875
- Fe, commercial, ductile-brittle transition temp., variation with grain size 78—27640
- Fe, embrittlement, fracture mode transition as function of grain boundary sulphur 80—55520
- Fe, fatigue crack propag., low temp. 80—35311
- Fe, high-purity, notch toughness 77—44353
- Fe, strain hardening and rate sensitivity, effect on ductile-brittle transition temp. 78—39900
- Fe-Al-Si, bending test, mech. props. under high press. and temp. *(Japanese)* 78—76711
- Fe-Al-Si (6.22, 9.63 wt.%), bending test under high press., high temp. 80—85057
- Fe-C-Fe_xO_y, cleavage initiation by ductile tearing 78—64656
- Fe-CR (26 wt.%), role of C and N in brittle fracture 80—16456
- Fe-C(0.001 to 0.44 wt.%), C effect on low temp. brittleness *(Japanese)* 80—50711
- Fe-Cr (25wt.%), continuously cooled, embrittlement 77—36636
- Fe-Cr alloy, impact strength, rel. to '475°C brittleness' *(Russian)* 78—92323
- Fe-Cr-Mo, (30,2 wt.%) Bridgman-type, unexpected embrittlement phenomena, hydrostatic tensile test *(Japanese)* 80—55517
- Fe-Mn (up to 8 wt.%), microstructure, mech. props. and fracture *(Japanese)* 80—35304
- Fe-Ni, fracture toughness at cryogenic temp. 78—72878
- Fe-Ni-C (9, 0.1 wt.%), effect of intercritical tempering on impact energy, exam. of mech. props. 78—52861
- Fe-Si (3 wt.%), hot rolled sheet steel, ductile-brittle transition temp. *(Chinese)* 78—31498
- Fe-Si(Ni), fatigue crack propag., low temp. 80—35311
- Fe-Si(Ni), strain hardening and rate-sensitivity, effect on ductile-brittle transition temp. 78—39900
- Fe-Zr, amorphous phase form. in Zr-poor region, hardness and fracture strength *(Japanese)* 80—84914
- Fe_{40} $Ni_{40}B_{20}$, amorphous alloy, ductile-brittle transition temp., relation to composition 78—52972
- $Fe_{40}Ni_{40}P_{20}$, amorphous alloy, ductile-brittle transition temp., relation to composition 78—52972
- $Fe_{40}Ni_{40}P_{14}B_6$, amorphous alloy, ductile-brittle transition temp., relation to composition 78—52972
- $Fe_{40}Ni_{40}P_{14}B_6$, amorphous, annealed and unannealed, temp. depend. of flow stress and ductility 79—29119
- GeTe, stoichiometry deviations influence on mech. props., 25-500°C 80—103410
- InP single crystals, uniaxial compression deform. characts. 80—84991
- MgO, strength under confining press. of 250 kbar, brittle-ductile transition 77—47510
- Mo alloys, intercryst. fracture in ductile-brittle transition region, local internal stresses effect 80—81200
- Mo, anomalous US damping under hydrostatic press. 79—14890
- Mo, electron beam melted with C additions, mech. props. *(Japanese)* 77—48449
- Mo, fractographic peculiarities in ductile brittle transition 78—39910
- Mo, irrad. between 425 and 1000°C, ductility in bending 80—39164
- Mo, polycrystalline, fracture and ductile-brittle transition, hydrostatic press. effects 78—60735
- Mo, recrystallised sintered sheet, C addition effect on ductility 79—8319
- Mo-Nb-Ti-N alloy, with dispersed second phase, ductile-brittle transition 80—93653
- Mo-O system, grain boundary segregation and intergranular fracture 80—55516
- Mo-O-C system, grain boundary segregation and intergranular fracture 80—55516
- Mo-Ti, irrad. between 425 and 1000°C, ductility in bending 80—39164
- Mo-Ti-N alloy, with dispersed second phase, ductile-brittle transition 80—93653
- Mo-Ti-Zr alloy TZM, fatigue and plastic flow, irradiation effects 77—52466
- Mo-TiN (3.5 vol.%), failure characts. exam. 78—68788
- NaCl, strength under confining press. of 250 kbar, brittle-ductile transition 77—47510
- Na_2O-CaO-SiO_2 sheet glass, pristine and scratched, fracture behaviour during bending 78—23829
- Nb alloy, VN2AE, influence of nitriding on heat resist. and brittleness *(Russian)* 79—8380
- Nb, slow strain rate embrittlement by O_2 77—28902
- Nb-W-Zr-N alloy, with dispersed second phase, ductile-brittle transition 80—93653
- NbC, NbC-ArC, right-through sat. prep., strength and plasticity, temp. depend. 77—40432
- Nb_3Sn, hot isostatically pressed, plastic deform. 80—108510
- Ni-Cr-W-Mo-Al-Ti (15,6,3,2,2, wt.%), wrought, Si effect on transition brittleness *(Chinese)* 80—55491
- Ni-Zn ferrite, high temp. behaviour of grain boundaries under bending stress *(Japanese)* 77—1875
- Ni-Zr, amorphous phase form. in Zr-poor region, hardness and fracture strength *(Japanese)* 80—84914
- Si, ductile-brittle transform. hypothesis and temp. depend. of charge bond *(Russian)* 78—35484
- Si-B based CVD coating for gas turbine blading, props. 80—40615
- TZM, irrad. between 425 and 1000°C ductility in bending 80—39164
- TiC, mech. props., 1073 to 2273K *(Japanese)* 79—15732
- TiC single crystal, change in slip system near transition 79—100211
- TiC-TiB_2 alloys, composition effect on surface layer rupture at various temps. 80—25879
- U-Mo-(Zr), ductile-brittle transition *(French)* 77—66693
- UO_2 fracture strength meas. of sintered specimens by diametral compression testing, effect of temp. and deformation rate 79—79074

ductile-brittle transition continued
V-Nb-Ti-N alloy, with dispersed second phase, ductile-brittle transition 80—93653
W alloys, deformed, vacuum technology appl., mech. props. *(German)* 79—57046
W wire, doped, high temp. tensile behaviour, bubble dispersion effect 79—74237
ZN, anomalous US damping under hydrostatic press. 79—14890
ZrC, NbC-ZrC, right-through sat. prep., strength and plasticity, temp. depend. 77—40432

ductile fracture
see also ductile-brittle transition; notch ductility
acoustic emission, interpretation of ductile fracture processes 80—35300
adsorbed molecule vibr. excitation due to plastic deform. accompanying fracture 77—15488
alloys, two-phase, void growth, finite element anal. 80—64383
automotive materials, microfractography appl. to ductile failure, brittle fracture, crack studies 77—56199
beam (plate) pure bending, dynamic fracture, axial force effect 78—63385
α-brass, plane stress ductile fracture, prestrain effects 80—108532
α-brass, with few inclusions, shear mode of ductile fracture 77—36652
cast Fe, spheroidal graphite, hydrostatic pressure effects on ductile fracture 78—60779
cement and mortar, strength, fracture mode, statistical props. *(Japanese)* 78—31520
circumferentially notched tensile specimen, finite element anal. 78—67150
computational models for one and two dimens. wave propag. 77—11628
computer model based on plastic strain, fracture toughness prediction, comparison with steel data 79—32383
crack extension, evaluation of resistance in single notch edge specimens 78—68807
crack extension, hybrid displacement finite element model 80—28471
crack extension, initial stage in time depend. and/or ductile fracture 78—67107
cracked plate in fully plastic state *(Japanese)* 78—38253
criteria for blunting cracks 78—64657
cup and cone fatigue fracture, electron fractographic obs. *(Japanese)* 78—72838
damage-induced tensile instability 77—4854
Duralumin, effect of alloy purity and ageing on fracture mechanism, and resultant toughness 79—5049
elastic contact problems, in fracture mech., friction effects 78—67142
elastic vibrations propag., relation to fracture parameters, defects 77—75855
elastic-plastic fracture mechanics, crack separation energy rates 78—46915
elastic-plastic fracture mechanics for structure design 77—14961
elastic-plastic mechanics, internal variable approach 79—68651
elastoplastic fracture mechanics, finite element analysis *(German)* 77—54935
electronic devices, failure analysis of metal parts using fractography 79—61811
engineering structures, welded exam. of fracture processes, review 78—60777
epoxy resins, exam. of fracture energy above glass transition temps. 78—56743
ethylene-propylene rubber, highly deformable, fracture surface roughness 78—44197
failure analysis, ductile crack growth 79—90724
failure through crack growth, discussion of different stages 77—68536
fibrous polymeric material, molecular model of fracture 78—60768
fracture toughness parameters J and G^{Δ}, effect of load biaxiality 78—67128
glass fibre reinforced plastic/polyurethane foam/Al sandwich, flexural props. *(Japanese)* 78—56707
glass fibre reinforced polyester filament wound pipe, failure 78—44192
Hastelloy X, grain size effect. creep and creep-rupture *(Japanese)* 80—16382
hydrostatic pressure effects on fracture, exam. 78—60779
inclusion parameter, use of ductile rupture theory for definition, correlation with impact energy *(French)* 80—21091
inclusions, in ductile fracture process, quantitative study method 80—35318
inclusions taking part in process, quantitative study 78—27630
Inconel alloy 718, exam. of struct., properties and continuum synthesis of ductile fracture 78—76736
instability, ductile fracture and formability limit diagrams 79—64589
integranular, problem of nucleation of voids 79—79110
intergranular, discussion on mechanism 79—73250
J-integral, $J(\tau_0\gamma_0)/x_1x_2$ and theoretical and expt. proof of path difference *(Chinese)* 78—15487
linear elastic and post yield fracture mechs., thermal and residual stresses 77—89066
metal, ductile fracture, crack initiation at dislocation cell boundaries 77—66692
metal, ductile fracture criterion 78—60817
metal, ductile fracture mechanism, theoretical and expt. investigation *(German)* 77—70142
metal, ductility effects during plastic deform., rel. to struct. changes 78—23770
metal, fracture and ductile deform., microprobabilistic approach 78—64665
metal, fracture under influence of high power US waves *(Russian)* 79—5034
metal, high plasticity, fracture nature *(Russian)* 77—25149
metal, nonlinear mech. response, Swift effect 78—35433
metal panels, adhesively bonded, cracked, fracture anal., crack tip stress intensity factors 78—90792
metallic glasses, flow behaviour, entropy model 77—24345
metallic shell, explosive expansion, deform. and rupture modes and mechanisms 80—85064
metallic shell, explosive expansion, rupture behaviour 80—85063
metals, ductile, spall damage accumulation theory 77—70153
metals, liquid metal embrittlement, mechanism 79—43495
metals, void growth stress/strain relations *(French)* 80—19280
metals and alloys, FCC, tensile fracture mechanism, review of pressure effects 77—70155
method of potentials, appl. to fracture mechanics 78—51121

ductile fracture continued
microcrack formation, disclination mech. 79—23674
micromechanisms of crack extension, conf., Cambridge, England (March 1980) 80—105421
model studies, formulation 77—50992
notched fracture toughness specimens, instability prediction, approx. flow stress model 78—34082
nuclear reactor coolant circuits, fracture mech. appl. 79—43430
nylon 6, fibres, viscosity-average mol. wt. change during fracture 78—19882
nylon fibre reinforced polypropylene, enhanced fracture strain 78—15503
PET fibre reinforced polypropylene, enhanced fracture strain 78—15503
pipe, straight, fracture under large deflection, pipe pressures, finite difference code 77—58616
pipes, straight, fracture under large deflection conditions, structural deformation 77—58615
plane stress ductile fracture, essential work 77—80108
plastic instabilities and uniaxial tensile ductilities 80—79180
plastic materials under proportional straining, appl. to gray cast iron 77—35091
plastic materials under proportional straining, theory 77—35090
plastic tensile crack behaviour, discrete dislocation analysis 78—22788
PMMA, craze zones at crack tips at different temps., meas. correl. with Dugdale model 78—23826
PMMA, impact testing, elastic analysis of conventional test, reassessment of testing 78—60770
PMMA, isothermal and adiabatic effects assoc. with crack propag. 78—23827
polycarbonate, notched specimens, impact fracture behaviour 77—28888
polycarbonate, viscoelastic ductile, delayed yielding of plane stress viscoelastic Dugdale model 78—27569
polycarbonate (BPA), thickness depend. of G_c for shear lip propag. from single crack propag. 78—11305
polydimethylsiloxane networks, stress-strain isotherms at high elongations to rupture point 77—40433
polyethyl acrylate atactic networks, stress-strain isotherms at high elongations to rupture point 77—40433
polyethylene, high density, fracture buildup due to prolonged loading, exam. 78—68779
polyethylene, high-density, thin-wall tubes, deform. and fracture processes 79—100222
polyethylene, low density, highly deformable, fracture surface roughness 78—44197
polyethylene, medium density, impact testing, elastic analysis of conventional test, reassessment of testing 78—60770
polyethylene film, minimum running thickness, biaxial extensional flow study 80—100993
polymer, viscoelastic ductile, delayed yielding of plane stress viscoelastic Dugdale model 78—27569
polymer-based composite solid propellants, viscoelastic fracture mech. 79—43431
polymers, fracture, molecular interpretation 78—60769
polymers, fracture and fatigue, review 78—68781
polypropylene nonfilaments, highly drawn, plastic deform. 78—44174
polystyrene, effect of pressure and environment on fracture and yield 78—76757
polystyrene, isothermal and adiabatic effects assoc. with crack propag. 78—23827
polystyrene, plastic fracture near T_g at low strain rate 77—86178
polystyrene, rubber-modified, impact-strength analysis 79—38972
polytetramethylene terephthalate, injection-moulded, struct. depend. of fracture behaviour 77—8912
porous ductile media, rupture by void nucleation and growth, criteria and flow rules 77—52492
post yield fracture criteria assessment 77—35092
post-yield, numerical investigation 78—18249
pressure vessels, heat treated, fracture modelling, acoustic emission 80—35303
PTFE, impact testing, elastic analysis of conventional test, reassessment of testing 78—60770
PTFE, thin-wall tubes, deform. and fracture processes 79—100222
PVC, cold drawn, plastic fracture around cavities 79—56994
PVC, ductile fracture, SEM investig. 77—44343
PVC, highly deformable, fracture surface roughness 78—44197
PVC, rigid, tensile fracture morphology, rel. to mol. props. 77—59883
random distrib. of voids, computer simulation 79—90723
review 77—7788
rocks, hot, dry, hydraulically fractured linearly expanding cracks, eqns. *(Japanese)* 79—34809
rotating discs, burst strength and necking 78—79226
rubber, peeling initiation and propag. 78—76824
serpentinites, Glenrock, New South Wales, foliation development 80—21738
shell forming solidification, hot tearing, model 79—79062
silicide coatings, on steel, exam. of fracture processes 78—44206
Silumin, AlSi10Mn, struct. and mech. props., Na modification effects 77—63786
stability analysis, of catastrophic fracture, in fully yielded components 80—33531
stainles steel, type 316, irrad. in simulated environment, tensile props. 80—34076
stainless steel, 18Cr-11Ni, for nuclear reactors, mech. props., neutron effects 77—34383
stainless steel type 316, ductile crack initiation, detection and toughness characterisation 77—16662
steel, 18 Kh2N4MA, grain size effect on mech. props. 78—44207
steel, 30N9K4, effects of Mo, V, and N on grain growth, tempering, hardenability, strength and toughness 78—44202
steel, alloy, C-Cr-Mo-V, exam. of fracture toughness and critical flow anal. 78—72848
steel, alloy, Cr-Mo, alloy SCM3, hydrogen embrittlement, delayed fracture, exam. *(Japanese)* 78—64620
steel, alloy, ductility, hydrostatic press. effects 78—80615
steel, alloy, fatigue strength and fracture, diamond grinding effect 80—55532
steel, alloy, HY130, temper embrittlement due to Si intergranular segregation, effect on H_2 induced cracking 78—76735
steel, alloy, medium and low C, quenched and tempered, fracture resist., nonmartensitic transformation products effect 79—96054
steel, alloy, tension test, computer simulation of deform. to fracture 79—11667

ductile fracture continued
steel, alloy, toughness evaluation inconsistency of AISI 4340 austenitised at increasing temp. 78—52982
steel, alloy, type 52100, exam. of microstruct. and fracture, as function of austenitising in temp. range 800 to 1100°C 78—76673
steel, austenitic, intermittent loading effect on creep *(Japanese)* 79—29147
steel, austenitic, Mn-Al, low temp. appl. explosion test of fracture mode *(Chinese)* 78—31496
steel, austenitic stainless, cylindrical specimens with crack. fracture characts. in inelastic strain, test methodology 80—25839
steel, austenitic stainless, type 304, intergranular H_2 assisted fracture, exam. of mechanism 78—80644
steel, austenitic stainless low-cycle fatigue, effect of mean plastic strain and stress factor 77—63766
steel, austenitic-martensitic 0Kh15N5M, ductile fracture 78—3226
steel, C, cylindrical specimens with crack. fracture characts. in inelastic strain, test methodology 80—25839
steel, C, ductile fracture, role of hydrogen 79—57103
steel, C, ductile fracture criterion for cracked plate in fully plastic state *(Japanese)* 78—38253
steel, C, ductile fracture under cold forming conditions, press. effect 78—52938
steel, C, martensites, fractography, facets classification *(Slovak)* 79—20173
steel, C, microstructural inhomogeneity, influence on formability and fracture 80—11682
steel, C, plastic deform., study of loading surface 77—44322
steel, C, quenched and tempered, ductility, effect of hydrostatic press. 78—44190
steel, C, tensile fracture surface in high press. H_2 at room temp. *(Japanese)* 80—108540
steel, C, tensile props. in high press. H_2 at room temp. *(Japanese)* 80—108501
steel, C(0.45, 0.15 wt.%), ductile fracture, in situ obs. of microprocess of failure *(Chinese)* 80—55492
steel, C and low alloy, structural, ductile and brittle fracture resist. in stable crack growth stage 79—52369
steel, case-carburized, low alloy, rolling contact fatigue 78—35518
steel, cast high-strength, local integranular fractures, formation mechanism *(Russian)* 78—95795
steel, cavitation during superplastic flow, affecting factors 78—60728
steel, Cr-Mo (2.25, 1.0 wt.%), thermally aged and Na decarburised, stress-rupture props. 80—21102
steel, Cr-Mo-Ni-Nb, Nb effect on mech. props. *(German)* 80—30012
steel, Cr-Mo-V, 1% Cr, chem. comp. and struct. effect on deform. props. *(German)* 79—1888
steel, Cr-Mo-V, rupture ductility rel. to cavitation, density and SEM obs. 79—34142
steel, Cr-Mo-W-V, long term creep rupture props., turbine blade *(Japanese)* 77—59909
steel, Cr-Ni-Mo-V, ductile fracture during tensile loading 80—45381
steel, crack-resistance limit and stress analysis in the ductile state 80—81188
steel, dimple fracture, relation between inclusions and morphology *(Chinese)* 79—74231
steel, ductile fracture in presence of elongated sulphides *(French)* 80—45394
steel, ductile fracture under cold metal forming conditions, metallurgical struct. influence 79—34125
steel, ductile struct., crack propag. 78—68805
steel, effect of H_2 on phys. and mech. props. 80—101657
steel, ferrite-pearlite, ductile fracture, pearlite colony morphology and hydrostatic press. effect *(Japanese)* 78—15510
steel, ferritic martensitic, effect of ductility of second phase on ductile fracture 78—19847
steel, fracture ductility, determ. in bending tests and US emission 78—23899
steel, fracture mode, tearing topography surface fracture 80—7670
steel, high C, ductile fracture, role of second phase particles 79—52359
steel, high strength, low alloy, rare earth treated, ductile fracture mech. 78—64658
steel, high strength, state of stress effects on ductile failure initiation 77—56070
steel, high tensile, H embrittlement estimation from viscous failure 77—73335
steel, inclusion effect on cold formability 80—29975
steel, inclusions effect on distrib. of local microheterogeneous deform. *(Russian)* 78—80586
steel, ledeburite, fracture during hot plastic deformation exam. 78—56755
steel, low alloy, acoustic emission during ductile fracture, isothermal tempering effect 79—83241
steel, low alloy, isothermal tempering effect on acoustic emission during ductile fracture 80—85047
steel, low alloy, naval, stretch zone width meas., COD for ductile crack initiation 78—68813
steel, low C, crack initiation at root of circumferential notch of round bar specimens *(Japanese)* 80—60947
steel, low C, plasticity role during low temp. fracture 78—39905
steel, low C, strain ageing, essential work of plane stress ductile fracture 79—29187
steel, low C, type En3, high strain deform., struct. and props. 80—89301
steel, low strength, strain induced fracture 79—43382
steel, low-alloy, study of deformation and fracture processes by acoustic emission transient anal., SEM and optical microscopy study 79—43311
steel, low-C, S10C and 520C, tensile fracture at low temps. *(Japanese)* 80—81163
steel, medium C, low-cycle fatigue effect of mean plastic strain and stress factor 77—63766
steel, medium strength plate, quenched and tempered, fracture toughness in ductile-brittle range 78—7036
steel, mild, cold-rolled, rate-sensitive, fracture initiation, loading rate and temp. effects 80—40532
steel, mild, ductile fracture of cracked plates, nonlinear boundary-value problem 77—81318
steel, mild, plate, effect of striking velocity on perforation energy 78—68818
steel, mild, resistance to slow stable crack growth, use of J integral 78—68809
steel, mild, shear mode of ductile fracture 79—91785

ductile fracture continued
steel, Mn-B-V, low alloy, transform. singularities *(Russian)* 80—104116
steel, Ni (9 wt.%), tempered, mech. stability of retained austenite 79—24521
steel, Ni-Cr-Mo and Cr-Cu-Mo and sintered, ductile fracture, microvoid effects *(Japanese)* 80—108542
steel, non-metallic inclusions changes due to heating obs. *(Spanish)* 80—25744
steel, pearlite, deform. and fracture mechanisms, HV SEM obs. 80—104243
steel, pearlitic or spheroidal plastic deform. and fracture *(French)* 78—35448
steel, plastic deformation zone, caused by crack, extent determ. with microhardness, surface roughness, measurements *(French)* 80—7682
steel, plastic zone growth, quantitative evaluation of acoustic emission, book contrib. 79—100328
steel, press. vessel, acoustic emission and ductile crack growth 78—11320
steel, pressure vessel, A533B, ductile, plane strain crack growth 78—80621
steel, reheat cracking in weld zone, method for evaluating sensitivity to cracking 78—72855
steel, spheroidized, shear mode of ductile fracture 79—61714
steel, spheroidized AISI 1095, ductile fracture of U-notched bend specimens 79—24616
steel, stainless, 0Kh12G14N4Yu2, effect of plastic deform. on biphase struct. 78—44176
steel, stainless, ductile fracture, in situ obs. of microprocess of failure *(Chinese)* 80—55492
steel, stainless, fracture and crack tip plastic zones, in situ obs. 80—108686
steel, stainless, He ion irrad., fracture behaviour, in-situ HV electron microscopy 80—29089
steel, stainless, two-phase $(\alpha+\gamma)$, twin-related lath occurrence rel. to fracture elongation 77—90443
steel, stainless, type 304, exam. of H_2 induced cracking 78—76738
steel, stainless, type 316, LMFBR and P1 cladding tubes, burst tests 78—44210
steel, stainless type 304 attack morphology of stress corrosion cracking, TEM study *(French)* 79—83368
steel, static bend testing of cracked samples until failure, −60 to 20°C 78—23893
steel, structural, addition of solid SiO, effect on ductile fracture 80—16465
steel, structural, lateral notches rel. to ductile fracture characts. 79—43392
steel, structural, slow stable crack growth, exam. of crack profile 78—84965
steel, thin walled shell, failure of model when loaded by internal press. 77—11147
steel, type 316, wedge crack nucleation 77—73339
steel 18 Gps, rel. between plastic deform. in fracture zone and fracture characts. *(Russian)* 77—52457
steel 30Kh2NMFA, microstructure of cup and cone fracture surface, effect of size of disperse phase particles *(Russian)* 78—68762
steel components, safety anal. for loading conditions 78—39979
steel Cr-V (1.5, 0.5 wt.%), cavitation effect of temp. and C content 78—64638
steel fibre reinforced Ag, exam. of recrystallisation behaviour *(German)* 78—84849
steel low alloy, high strength, ductile failure criteria for blunting crack 78—64657
steel plates, C and alloy steels, comparison of dynamic tear and Charpy V notch impact props. 78—92357
steel spheroidised type AISI 1090, hot rolled H_2 promotion of plastic instability 78—60725
steels, structural, fracture initiation, exam. 78—60778
strain energy density fracture criteria, extension to brittle and ductile fracture 78—75102
strain gauge method for detecting initiation 78—85085
strain hardening and damage relationship 80—108564
strain-hardening material, ductile fracture, J-integral estimates 77—89064
stress analysis of cracks, elastoplastic range 78—67144
stress and deformation field, for cracks with two and three corners 78—34087
styrene-butadiene rubber, highly deformable, fracture surface roughness 78—44197
styrene-diene triblock copolymer, hexagonal struct., flow props. of melt and fracture 78—76729
submarine cables, wire fracture modes and mech. props. correl. with fatigue life 78—35520
surface, statistical characts. of microcracks *(Russian)* 78—23807
topography, geometrical contribs. and H_2 effects 79—83310
uniaxial deformation of plastic body, model with account of microcrack form. and growth *(Russian)* 78—26051
unstable fracture criteria under large plastic deformation 78—67143
viscoelastic system, fracture mechanics 78—67145
void-containing materials, ductile fracture, conditions for shear localisation 78—79663
W fibre reinforced Nb, plastic deform. and fracture 77—40438
yielding materials, review 78—31521
Zircaloy-2, effects of simulated fission products on mechanical props. 80—52740
Ag-MgO, dispersion hardened, exam. of ductile fracture 79—34144
Al alloy, 6061-T6, thickness depend. of G_c for shear lip propag. from single crack propag. 78—11305
Al alloy, ductility effects during plastic deform., rel. to struct. changes and hot forming 78—23770
Al alloy, void form. in defeated targets 77—15403
Al alloy 01205, mech. props. at cryogenic temps. 79—29206
Al alloy 2024-T4, ductile fracture, microvoid effects *(Japanese)* 80—108542
Al alloy 6061-T6 cylinder, dynamic fracture, expt. rel. to Mott's theory 78—64651
Al alloys, fracture toughness values, wide range specimen thicknesses, new rig design 77—60011
Al alloys aged, local plastic strain distrib. by selected areas channelling patterns 77—44349
Al alloys D1 and AK6, cylindrical specimens with crack. fracture characts. in inelastic strain, test methodology 80—25839
Al alloys grain size effect 78—60781

ductile fracture continued
Al, oriented single crystal, plastic deform. *(Japanese)* 79—43336
Al, torque and length change during fracture in torsion test *(German)* 79—24611
Al-Cu, effect of alloy purity and ageing on fracture mechanism, and resultant toughness 79—5049
Al-Cu (4.5 wt.%), cast alloy, ductile intergranular fracture 77—28908
Al-Cu-Mg (4,1 wt.%), behaviour during ductile fracture, SEM *(Rumanian)* 80—21062
Al-Cu-Si-Mn, type 2017S-T4, crack initiation at root of circumferential notch of round bar specimens *(Japanese)* 80—60947
Al-Cu(Zn-Mg), age hardening, conditions leading to localised plastic deform. and fracture in slip bands during fatigue 78—64670
Al-Mg, fracture during superplastic flow 78—60729
Al-Mg (1 wt.%), behaviour during ductile fracture, SEM *(Rumanian)* 80—21062
Al-Mg (4 wt.%), enhanced ductility at elevated temps. 77—63740
Al-Mg-Si (0.52, 0.58 wt.%), ductile fracture intergranular mechanism 79—15784
Al-Mg-Si alloys, ductile intergranular fracture mechanisms, void formation and nucleation 80—108578
Al-Mg-Si-Mn, Mn addition effects on fracture 78—60791
Al-Zn (22 wt.%), superplastic strain rate sensitivity, rel. to ductility 78—31478
Al-Zn eutectoid, superplastic, fracture, electron microscope obs. 78—31533
Al-Zn-Mg, ductile intercrystalline fracture obs. 77—77554
Al-Zn-Mg-Cu, age hardened, effect of strain rate, temp. and environment on ductility 80—45368
Al-Zn-Mg-Cu, alloy 7075, hydrostatic pressure effects on ductile fracture 78—60779
Al-Zn-Mg-Cu alloy, laminated, adhesively bonded alloy 7075-T6, exam. of fracture resistance 78—76754
Al-Zn-Mg-Mn, correlation of microscopic features, with macroscopic crack propagation 78—60800
Be crystal, failure on basal plane 78—15525
Be-Ni(Y)(Al), plastic deform., flow stresses, fracture *(Russian)* 80—108496
Co-WC dispersion hardened alloy, tensile deform., volume fraction of second phase effect, simulation *(Japanese)* 79—70122
Cr-Ni VKh-4 alloy, deformation and fracture mechanism investigation *(Russian)* 80—11738
Cr-Ni-Mn, type 4340, acoustic emission interpretation of ductile fracture processes 80—35300
CrC-Ni-(P), hard alloys, sintered, fracture props., P addition effects 78—60610
Cu alloy, ductile fracture during tensile testing 80—45381
Cu alloys, appl. of SEM to brittleness study 78—3214
Cu alloys, cavitation during superplastic flow, affecting factors 78—60728
Cu and Cu-Si, deformation and fracture under dynamic loading 78—35442
Cu, appl. of SEM to brittleness study 78—3214
Cu, bicrystal, intergranular fracture 78—39883
Cu, cold-drawn, low-cycle fatigue, effect of mean plastic strain and stress factor 77—63766
Cu, cold-rolled, thickness depend. of G_c for shear lip propag. from single crack propag. 78—11305
Cu, dislocation mechanism of luminescence during fracture 79—24376
Cu, fragmentation and dynamic recrystallisation after heavy and very heavy deform. *(Russian)* 78—39793
Cu, prestrained, tough pitch and sintered, ductile fracture, voids *(Japanese)* 77—52472
Cu, shear mode of ductile fracture 78—31525
Cu, sintered preform, porous, ductile fracture criterion, rel. to forging process 77—56105
Cu, tensile fracture mech. 77—63782
Cu wire, ductile fracture in drawing process, defect exam. *(French)* 77—21242
Cu-Al composite, simulation of tensile behaviour and fracture void initiation *(Japanese)* 78—52948
Cu-Al-Ni-Fe-Mn, cast Ni-Al bronze, fracture metallography 78—27597
Cu-Al-Si-C (95, 2.8, 1.8, 0.4 wt.%) fracture characts. of superplastic single phase, exam. 78—48500
Cu-Fe, composite, simulation of tensile behaviour and fracture void initiation *(Japanese)* 78—52948
Cu-Ni, powder, sintered, effect of cold and hot dynamic pressing, upon structure and props. 79—33970
Cu-Ni-Cr (28, 2.8 wt.%), spinodal alloy, microstruct. and tensile props. 78—39858
Cu-Sb solid solution, dil., FCC, intergranular solid shortness mechanism *(Russian)* 79—5032
Cu-SiO_2 alloy, fracture at elevated temp. 78—39896
Cu-Ti (1.07 wt.%), containing coherent precipitation, observations of flow and fracture 78—80643
Fe, Armco, microstructure in quasibrittle and plastic fracture 77—1863
Fe, Armco, rupture onset during cold rolling *(Russian)* 77—8904
Fe, cast, ductile, strain rate and temp., influence on strength, elongation and deformation *(Japanese)* 80—45356
Fe, cast, ferritic, ductile fracture initiation and propag. 78—84966
Fe, cast, ferritic SG ductile fracture initiation and propagation 78—64661
Fe, ductile fracture, fractographic characts. SEM exam. of fracture surface necking obs. 78—35506
Fe, gray cast, under proportional straining 77—35091
α-Fe, plastic deform. in neck leading to fracture 78—64655
Fe, pure, ductile fracture, effect of nonmetallic inclusions 78—64660
Fe, pure, mech. props. at low temps. 78—44219
Fe, pure ductile fracture analysis, allowance for discontinuity *(Russian)* 77—25133
α-Fe whiskers, pure, ductile fracture initiation, macroscopic obs. of deform. history and failure 80—85043
α-Fe whiskers, pure, ductile fracture, microscopic obs. of initiation mechanism 80—85044
Fe-C-Fe_xO_y, cleavage initiation by ductile tearing 78—64656
Fe-Cr-Mn (11.5, 3 wt.%), microduplex ferritic-martensitic steel, exam. 78—39862
Fe-Cr-Ni-C (17.2, 7.34, 0.2 wt.%) alloy, twin related laths, fracture elongation, TEM study 79—29192
Fe-Mn (32.5 and 38.3 wt.%), steel sheet, exam. of form limit diagrams and damage 78—48461

ductile fracture continued
Fe-Mn alloys, α, ε and γ, brittleness 80—35314
Fe-N, neutron irrad. effects on mech. props. 79—4338
Fe-Ni-Al, correlation of microscopic features, with macroscopic crack propagation 78—60800
Fe-Ni-Al (18.2 wt.%) aged, fracture toughness and mode, grain size depend. 77—12700
Fe-Ni-C, lenticular martensitic alloy, fractured at liquid N_2 temps., crack propag. mode *(Japanese)* 77—48524
Fe-Ni-C, martensitic delayed fracture *(Slovak)* 79—43401
Fe-Ni-Mo(13,3wt%), welded alloy, fracture and strength for cryogenic service 79—38930
Fe-Si (2.35 wt.%), misorientation dependence of grain boundary segregation, Auger spectroscopy exam. 78—76629
H_2 transport by dislocations to initiation sites 77—21263
Li_2O-Al_2O_3-$4SiO_2$, glass-ceramic, tensile creep and high temp. fracture 78—52914
MgO, adsorbed CO vibr. excitation on fracture 77—15488
Mo alloys, fractography of deformed samples *(Russian)* 78—19889
Mo, deformation and fracture patterns under complex stress conditions 77—70134
Mo, fracture surface, effect of plastic deform. by rolling at 950°C *(Russian)* 77—59893
Mo, microcrack formation, statistical description *(Russian)* 77—66689
Mo-Nb-Ti-N alloy, with dispersed second phase, ductile-brittle transition 80—93653
Mo-Ti-N alloy, with dispersed second phase, ductile-brittle transition 80—93653
Mo-Ti(B)-Zr(Al)-C, stress cycling at room temp. *(Russian)* 77—25148
Nb, low temp. annealing effect, precip. of Nb_2O_5 *(Russian)* 77—52456
Nb-W-Zr-N alloy, with dispersed second phase, ductile-brittle transition 80—93653
Nb-Zr-C, structural depend. of elasticity limit *(Russian)* 79—29171
Ni based superalloys 713C and Mar-M200, Si effect on oxidation, hot corrosion and mech. behaviour 78—39950
Ni, deformed in uniaxial tension, fracture map 78—56764
Ni-ThO_2, dispersion hardened, fracture mechanism map 78—60823
Ni_3Al, ductility in poly- and single crystals, compressive and tensile tests 78—56715
Pb-Sb (1 wt.%), highly averaged, fracture behaviour 79—8366
Pb-Sn eutectic, cavitation during superplastic flow, affecting factors 78—60728
$Pd_{80}Si_{20}$, plastic flow, fracture, slanted necking and elongation at high temps. 79—57057
Si-Al, composite, simulation of tensile behaviour and fracture void initiation *(Japanese)* 78—52948
Si_3N_4, struct. of slow crack interface, light and electron microscope obs. 78—68770
Ta, evidence for slow strain-rate embrittlement due to O_2, SEM study 79—79109
Ta_2O_5, anodic oxide film, adhesion, ductility and fracture, spectrophotometric thickness meas. and SEM obs. 79—99460
Ti, pure plate, silver band formation in ductile fracture process *(Japanese)* 80—16445
Ti, shear bands in cup and cone fracture in pure plate *(Japanese)* 79—15773
Ti-Al (14 at.%), with precipitate free zones, tensile props., grain size effects 77—16690
Ti-Al (6.1 wt.%), hot rolled sheet, ductile fracture nuclei, SEM obs. 78—64654
Ti-Al-Sn (5, 2.5 wt.%), ductile fracture at low temps. 78—64659
Ti-Al-Sn (5, 2.5 wt.%), fracture mechanism at cryogenic temps. 78—64642
Ti-Al-V, (6,4 wt %), fracture mode, tearing topography surface fracture 80—7670
Ti-Al-V (6, 4 wt.%), void formation and growth, tensile fracture, exam. 78—80637
Ti-Al-Zr (6,5 wt.%), alloy IMI 685, SEM exam. of crack growth 78—72849
Ti-Nb superconducting composite in Cu matrix, low temp. effects in ductility 79—57119
Ti-V (27 and 30 wt.%), fatigue crack propag., in single and poly. crystals 79—5048
U, two-dimensional expt. fracture map 78—95803
U-Mo (10 wt.%), commercial alloys, influence of metallurgical factors on fracture processes *(French)* 78—60751
U-Mo (1.5 wt.%), superplastic behaviour 450 to 720°C *(French)* 79—74203
U_3Si, tensile ductility from 25 to 320°C 79—74225
V-Nb-Ti-N alloy, dispersion hardened, fracture characts. 79—15794
V-Nb-Ti-N alloy, with dispersed second phase, ductile-brittle transition 80—93653
Zn monocrystal, cavitation induced multiple slip, twinning and fracture 78—39872
Zn, pure single cryst., fracture stress 80—104269
Zn, single cryst., in metal melt, plastic deform. and fracture obs. by acoustic emission *(Russian)* 78—56737
Zn-Al (22 wt.%), superplastic, eutectoid alloy, ductility and fracture 78—60819
Zr-Nb (2.5 wt.%), nuclear fuel channels, neutron effects on ultimate fracture strength, 293 to 573K 80—85054
Zr_3Al, ordered polycrystals, ductile fracture 78—64641
$ZrH_{1.92}$, plasticity 77—36569

ductility
see also ductile fracture; notch ductility
ABS mouldings, selective Cu plated in areas, effect on mech. props. 79—34182
acoustic emission and fracture of ductile materials 77—56059
ageing alloys, single cryst., deform. and hardening 78—23716
alloy, austenitic, mechanical changes after electrolytic quenching *(Russian)* 80—50653
alloy, heat-resistant, alloying and heat treatment effects on struct. and strength 78—95758
alloy, high temperature, mechanical, thermal and corrosion props. 78—95763
alloy, solid solution, large grained, creep ductility 78—48479
alloy, strain rate sensitivity rel. to ductility, anomalies 77—36590
alloy steels N30 and N29T, press. effect on reverse martensitic transform. and mech. props. *(Russian)* 79—38824

ductility continued
alloys of two ductile phases of unequal strength, deform. *(Japanese)* 78—11284
austempered reinforcing wire, tempering under stress, effect on mech. props. and relaxation resistance 80—100861
austenitic steel, hardened by thermomechanical treatment with ageing, influence of stabilisation on mech. props. *(Russian)* 77—52356
austenitic steel neutron-irradiated weld toughness rel. to ferrite content 79—83327
axially loaded butt joints, stress strain behaviour 79—74209
bainite, formed from deformed austenite, morphology and mech. props. 79—43345
borides, lightweight ceramic armour appls., ballistic tests, computer simulation, book contrib. 78—48556
brass, anisotropic bend ductility in single phase alloys 78—60726
α-brass, bicrystal, grain boundary fracture at intermediate temp. *(Japanese)* 79—15774
brass, hot ductility and torsional deform. *(Japanese)* 79—57069
α-brass, single crystal, deform. and ductility at elev. temps. *(Japanese)* 79—5012
brittle coating, ductility meas., four point bend test 78—48577
brittle metal, meas. under tension or compression at high press., apparatus *(Japanese)* 78—35617
bronze, anisotropic bend ductility in single phase alloys 78—60726
Burke-Nix ductility expression, modification 79—60426
carbide, effect of mech. props. on erosion resist. under spark machining conditions 78—11421
ceramic, polycrystn. creep stress exponents rel. to slip and ductility 77—90400
corundum, grinding material, review *(Polish)* 80—29917
crack extension rates in ductile materials 80—96230
criterion 78—63336
endosseous implant material, radiation processed alumina-polyacrylic acid composite 77—60308
engineering materials relation between deform., rupture, power-law creep 79—5020
epoxy resins, mech. and elec. low temp. props. 80—25814
failure criterion considering stress state at crack apex 79—57113
ferritic alloy, reinforced by dispersed oxide, mech. props., modification by recovery heat treatment *(French)* 77—59837
fibre reinforced epoxy, laminate, static and impact props. 77—63725
fibre-reinforced rigid-plastic plates transverse impact anal. 78—38211
graphite particle-Al alloy composite, prod. by pellet method, and mech. props. 78—27454
hardness and ductility 79—87025
Hastealloy X, relations between weld heat affected zone cracking and microstruct., Gleeble test *(Japanese)* 78—52858
Hastelloy X, high temp. low cycle fatigue tests, ductility, fracture 77—90523
Hastelloy X, mech. props. effect of solidification substruct. 77—25040
heterogeneous composite materials, influence of prestress and limited deformations 78—38205
heteroplastic material, plastic rate, effect of strain hardening *(French)* 77—63718
high-strength alloy filamentary crystal prep. from brittle high-strength mats., mech. props. *(Russian)* 77—59712
hydrogen embrittlement due to H-inclusion interaction 78—30664
Incoloy 800, creep rupture ductility, 500 to 600°C, hardness and metallurgic exam. 79—43435
Incoloy 800, from KFA experimental duct at 700°C and 480 d in DRAGON reactor, mech. props. before and after contamination 79—47777
Incoloy 800, mechanical props., heat treatment and appl., conf., Petten, Netherlands (March 1978) 79—43296
Incoloy 800, review of mech. props. up to 600°C 79—43368
Incoloy 800, use up to 550°C, creep ductility 79—43369
Incoloy 800 and 802, influence of carburisation on mech. props. 79—20254
Incoloy 800 for HTR appls., correlation of carburization behavior, mechanical property degradation, and exposure conditions 80—5244
Incoloy 903, microstruct. and effect of H_2 charging 77—86143
Inconel 706 and 718, relations between weld heat affected zone cracking and microstruct., Gleeble test *(Japanese)* 78—52858
inhomogeneous deformation of ductile single cryst., geometrical effects 79—46741
interface forces and interactions, roughness and ductility depend. 77—24476
iron, spheroidal graphite, deformation under compression rel. to ductility 77—16639
limiter materials, for Doublet III fusion research machine, selection 78—55026
measurement technique for high-strain rate ductility of metals 78—80694
metal, BCC, effect of screw dislocations on mech. props. *(Russian)* 78—60704
metal, brittle, ductility improvement by plating *(German)* 77—8954
metal, deposition condition relationship with struct. and props. 78—11369
metal, diffusional relaxation of stress conc. at second phase particles 79—1889
metal, ductile, jet-impingement solid-particle erosion testing, halo effect 80—76376
metal, ductility effects during plastic deform., rel. to struct. changes 78—23770
metal, fracture and ductile deform., microprobabilistic approach 78—64665
metal, plastic props. investig. at elevated temps. by torsional method, review 79—43509
metal, sintered, ductility, porosity effect 77—59875
metal, surface layer dissolution, effect of rate on softening during plastic strain 78—39957
metal film, tester 77—63864
metal heat resistant power installation elements, estimating strength, ductility, heat resistance diagrams 80—25770
metal targets, penetration by conical projectiles, ductile hole formation study 79—23220
metallic fibre knitted gauze permeable materials, mech. props. 80—66607
metallic glasses, mats. props. review 77—4043
metallic two-phase coating, ductility maximum, weakening and strengthening 79—11681
metals, brittle fracture, specimen dimensions influence *(Russian)* 79—52345

ductility continued
metals, determ. with pulsation attachment for TsDMU-30t test machine 79—52538
metals and alloys, strength/ductility relation *(Japanese)* 79—29145
microcrystalline alloys, metastable, rapidly quenched particulates, props. appl. and production 80—84887
mineral-fibre composites that resist fracture and cracking 77—8798
mylonites flow strength, role of grainsize reduction and grain boundary sliding 80—21721
Nimonic 105, creep and stress rupture props., trace elements influence 80—66602
Nimonic PE16, creep rupture props. in CO_2, air and vacuum environments at 700°C 79—74248
nonferrous metal, semi-brittle, high-speed backward extrusion using superimposed hydrostatic press. 80—84865
nuclear reactor materials, radiation damage, fast breeder and fusion reactors *(Japanese)* 79—81011
nylon fibre reinforced polypropylene, enhanced fracture strain 78—15503
PET fibre reinforced polypropylene, enhanced fracture strain 78—15503
plastic anisotropy theory based on yield function of fourth order 78—31457
plastic deforms ands rupture mechanisms, depend on B additives *(Russian)* 79—61650
plastic instabilities and uniaxial tensile ductilities 80—79180
PMMA, ductile glassy, notch brittleness under plane strain 80—100900
polycarbonate, dielec. relax. and ductile brittle transition 78—52438
polycarbonate, ductile glassy, notch brittleness under plane strain 80—100900
polycarbonate, particles, critical stress 77—28869
polyethylene, mech. and elec. low temp. props. 80—25814
polyethylene, oriented chain-extended, Young's modulus, fracture and compression behavior 80—11747
polyethylene, Raman spectra, drawing effect on longit. acoustic mode *(French)* 77—24828
polyethylene surface-growth fibres, hot drawing 80—97517
polypropylene-bitumen mixture, thermomech. investigation changes in viscosity, ductility, elasticity, mol. wt. effects *(German)* 78—35454
PTFE, crystalline, subject to simple plane loading, limiting resistant, time and temp. factors 78—23794
PVC, ductile glassy, notch brittleness under plane strain 80—100900
PVC sheet, notched, yielding 78—56708
reactor pressure vessel brittle fracture, safeguards, American and German ductility requirements *(German)* 79—41017
rock, deformation and fracture under general triaxial stress states, anisotropic dilatancy *(Japanese)* 78—56750
SAP 895 (Al-Al_2O_3) alloy containing ^4He and ^3H, tensile props. 80—34129
sheet metals, ductile, shearing process 78—84841
sheet metals, strain-induced changes in mech. props. and press formabilities 78—19781
solid soln., ductility, comp. effect *(Japanese)* 79—43334
steel, 12 MKh, strength, ductility rel. to H_2 corrosion at 1000 kg/cm^2 press., 450°C *(Russian)* 79—15723
steel, 12Kh18N9T-TiB_2, eutectic alloy, high temp. props. 78—84931
steel, 18 Kh2N4MA, grain size effect on mech. props. 78—44207
steel, 20Kh, warm extrusion effects on struct. and mech. props. 77—44311
steel, 40Kh, effect of deform. ageing *(Russian)* 78—31427
steel, 45 and U7, deform. microheterogeneity and ductility 77—73309
steel, Al-killed rolled sheet, plastic anisotropy theory based on yield function of fourth order 78—31458
steel, alloy, deformation, rapid dynamic, at −196°C 80—104220
steel, alloy, ductility, hydrostatic press. effects 78—80615
steel, alloy, maraging, 18% Ni, effect of solution and ageing treatments, on microstruct., tensile props., fracture toughness 78—80648
steel, alloy, maraging, 250-grade, ductility and toughness of hot isostatically pressed powder 78—52925
steel, alloy, Mn-Cr-Cu, exam. of ductility when deformed, alloying addition effects 78—44175
steel, alloy 4340, fracture and high temp. props., 533K to 1255K 78—60821
steel, alloy high-C, amorphous, mech. props. and thermal stability 80—76361
steel, austenitic, 30KhGSA, grain size before quenching rel. to mech. props. 79—24553
steel, austenitic, 30KhGSA, heat treatment, preliminary, cold deform., elec. heating rel. to mech. props. 79—24554
steel, austenitic, 33N25Yu3F, hardening, effect of quenching and ageing temps. *(Russian)* 77—81267
steel, austenitic, ageing and plastic deform. effect on struct. and mech. props. of N15Kh5G3T3 *(Russian)* 80—71691
steel, austenitic, ASTM A533B and A542, H_2 embrittlement behavior of unirrad. steels for nuclear reactor press. vessels 79—8340
steel, austenitic, Cr-Mn, Kh4G18F, microstruct. and mech. props. during tensile deform. *(Russian)* 79—20114
steel, austenitic, Cr-Mn, metastable, plasticity, contrib. of martensitic transform. during deform. *(Russian)* 80—30018
steel, austenitic, Cr-Ni (18, 11 wt.%), creep rupture *(German)* 78—11297
steel, austenitic, low-C, transform. kinetics rel. to temp., deform., struct., mech. props. 79—24519
steel, austenitic, precipitation hardened, ductility of grain boundaries and crack propag. *(German)* 78—52834
steel, austenitic, strength, ductility and fracture toughness, N and Cr effects 80—100878
steel, austenitic, tensile props. after corrosion by UO_{2+x} and fission products *(German)* 77—70216
steel, austenitic Cr-Ni (18,12 wt.%), containing coarse irregular carbide precipitates along grain boundaries, ductility 78—60718
steel, austenitic heat-resisting, deformation and fracture rel. to grain-boundary reaction nodules 78—80591
steel, austenitic stainless, Cr-Mn, austenite stability during deform. 77—70050
steel, austenitic stainless, fast neutron irrad., effect on mech. props. 78—92309
steel, austenitic stainless, fusion reactor first-wall and blanket material, mech. props. 80—34074
steel, austenitic stainless, mech. props. correl. methodology development for fusion environments 80—29068
steel, austenitic stainless, metastable, transform. depend. ductility, temp. and deform. effects 78—3185

ductility continued
steel, austenitic stainless, strain hardened containing N_2, low temp. props. 79—66128
steel, austenitic stainless AISI 304, dislocation substruct., carbide precipitation and deform. mech. map 77—70116
steel, austenitic stainless Ni-Cr, heat resist. and comp. of non-metallic inclusions, effect of La, Nd, Pr and Ce 80—76315
steel, austenitic stainless tensile ductility in air and H_2 77—66687
steel, austenitic-martensitic, phase comp., struct. and mech. props. 80—29974
steel, C1020, dual phase, mech. behaviours and structs. *(Korean)* 80—25779
steel, C, 20 and 22K, ductility, effect of temp., deform. rate and stress state *(Russian)* 78—35428
steel, C, plates, residual elements effect on through-thickness props. 80—66660
steel, C, quenched and tempered, ductility, effect of hydrostatic press. 78—44190
steel, C, relax. resist. rel. to struct. 78—23788
steel, C(0.2 wt.%), explosively strengthened, cause of anomalous increase in H_2 of low cycle endurance *(Russian)* 77—16729
steel, C-Mo-P, intergranular fracture and grain boundary segregation, P, H, Mo effects *(Japanese)* 79—15775
steel, carbide formation during tempering on martensite decomp. and ductility 78—23733
steel, cast automatic couplings, yield strength, crack propag. resistance and ductile-brittle transition temp. 80—104281
steel, cold drawn wire, anisotropic fracture *(Russian)* 77—1867
steel, continuously cast, ductility near melting pt., hot tearing 79—83314
steel, continuously cast, tensile strength and ductility above 800°C 80—55476
steel, Cr, previous deformation influence on strength, ductility, in biaxial tension, low temps. 79—90718
steel, Cr, type Kh, (GOST 5950-51), in biaxial tension, effect of charact. of preloading on low-temp. ductility and strength 79—15749
steel, Cr (13 wt.%), sintered, organometallic complex addition effects on mech. props. 80—25595
steel, Cr-C (1, 1 wt.%), hot ductility and S segregation 80—66594
steel, Cr-Mo(-V), ductility and heat resistant prop. prediction rel. to fine struct. and solid soln. state 79—15751
steel, Cr-Mo (1.25, 0.5 wt.%), creep, fracture, Ti and Ti+B effects 77—36603
steel, Cr-Mo (2.25, 1 wt.%) annealing, high strain rate tensile props. 77—25117
steel, Cr-Mo-(V) austenitic, creep resist., high-temp. props. residuals effect 80—66600
steel, Cr-Mo-V, strength and ductility in creep, purity influence 80—66598
steel, Cr-Mo-V (0.5, 0.5, 0.25 wt.%), creep crack growth at 565°C 77—73323
steel, Cr-Mo-V (0.5, 0.5, 0.25 wt.%), creep crack growth in notched bend test, microstruct. effect 77—21261
steel, Cr-Mo-V (1.35, 1.0, 0.25 wt.%) exam. of mech props, comparison with mathematical model predictions *(Czech)* 79—91740
steel, Cr-Mo-V low-alloy, high-temp. ductility and crack growth, impurities effect 80—66652
steel, Cr-Mo-V low-alloy, mech. props. and stress relief cracking, effects of impurities and deoxidation practice 80—66599
steel, Cr-Mo-V low-alloy with high residual element content, cavitation control 80—66663
steel, Cr-Ni, effect of tempering under load on mech. props. 80—16354
steel, Cr-Ni, hydrogen effect on strength, ductile and fracture characts. 79—38960
steel, Cr-Ni, rolled and sintered, to produce capillary structured filter material, exam. of mech. props., and production 80—16235
steel, Cr-Ni-C (3, 1, 0.6 wt.%), grain boundary sulphide precip. and hot ductility *(Japanese)* 80—71654
steel, Cr-Ni-Mo-Cu, ε phase particle precipitation from martensite, local internal stress relaxation *(Russian)* 79—78969
steel, CrMoV, failure in post yield regime using single edge notched tension specimens 78—68765
steel, deformability characts. in surface-active medium at decreasing temp., mech. working effect *(Russian)* 77—59851
steel, ductile structural, fatigue crack propag. rate and striation spacing 80—93635
steel, eutectoid, mech. behaviour, thermomech. treatment effects 80—84970
steel, fatigue life, structural parameters and chem. comp. effects, rel. to test parameters 77—59928
steel, Fe-Cr-C, austenitizing temp. effect on microstruct. and mech. props. 80—16341
steel, Fe-Mn-C austenitic, deform. twinning and mech. props. 77—59868
steel, ferrite and dual phase, mech. props., effect of Si and P 79—57063
steel, ferritic, creep resist., high-temp. props. residuals effect 80—66600
steel, ferritic, underclad cracking mechanism, effects of residual strain and heat affected zone ductility 77—25158
steel, ferritic martensitic, effect of ductility of second phase on ductile fracture 78—19847
steel, ferritic stainless, type 444 welds, ductility loss mechanism 80—85002
steel, ferritic/austenitic high Cr, development, mech. props. and corrosion resist. 80—45422
steel, high strength, failure stress, structural relationships 80—81190
steel, high strength, fatigue crack growth 78—64697
steel, high strength, low alloy, plate, impaired ductility in sheared edges 78—60727
steel, high strength, thermally strengthened by rolling heat, H_2 embrittlement *(Russian)* 77—77562
steel, high strength, treatment effect on ductility and strength 80—60880
steel, high-speed, cast, mech. props. at high temps. 79—20135
steel, high-strength tool steel D7KhFN, remelting effect on mech. props. 80—76284
steel, hypereutectoid type HF-1, microstruct. effects on fracture toughness, ductility, strength 79—74255
steel, large forging, mech. props. 77—4797
steel, low alloy, eutectoid pearlitic, exam. of microstructures dominating ductility *(Japanese)* 78—84917
steel, low alloy, rel. between over-heating embrittlement and behaviour of S, Gleeble tensile test *(Japanese)* 79—79088
steel, low alloy, S and Mn influence on high temp. strength and ductility after solidification from melt *(German)* 80—81106

ductility continued
steel, low alloy structural, type 30KhGSA, effect of thermomech. treatment on strength, fracture toughness and fatigue props. 80—11676
steel, low alloy type 12Kh1MF, effect of thermal cycling on life under creep conds. 79—57075
steel, low C, brittle fracture susceptibility, low temp. deform. effects 77—56103
steel, low C, cyclic plasticity and low cycle fatigue life 80—21058
steel, low C, dual phase structures (martensite and ferrite), effect of martensite composition on content, mech. props. 78—76717
steel, low C, low endurance fatigue at low temps. 77—21274
steel, low C, microalloyed, heat treatment, mech. props. 79—24551
steel, low C, plastic props., fracture, effect of strain rate in static tensile tests *(Czech)* 77—59866
steel, low C, thermomechanically processed, martensitic fibre development, fatigue fracture 78—64572
steel, low C hot rolled sheet, drawability improvement by Al addition *(Ukrainian)* 79—78996
steel, low-alloy, bearing, mech. props., carbide behaviour effect *(Korean)* 80—93615
steel, low-alloyed, C-content influence on high temp. strength and ductility after solidification from melt *(German)* 80—81105
steel, low-C, fully pearlitic, struct. and mech. characts. rel. to cooling conditions *(French)* 80—40425
steel, low-C, phosphorus effect on annealing texture, plastic anisotropy and mech. props. 77—25069
steel, low-C, preliminary thermomech. treatment, cold deform. effect on struct. and props. 79—38847
steel, low-C, with Nb-B addition, transform. characts. and mech. props. *(French)* 79—43253
steel, marageing, austenite formation, stability, transformation to martensite *(Russian)* 79—91646
steel, maraging, (18 wt.% Ni), solution annealed, exam. of cryogenic tensile, fatigue, and fracture props. 78—92311
steel, maraging, ductility and resist. to deform., −196-1000°C 80—89313
steel, maraging, inert gas atomised, hot isostatic pressing temp. effect 79—24460
steel, maraging, influence of microstructure, strain rate and temp., on tensile props. 80—11733
steel, maraging, notch strength 77—56056
steel, maraging, prior austenite grain size effect on tensile ductility and fracture toughness 79—100226
steel, maraging, steady state unidirectionally solidified, austenite reversion and determ. 77—25118
steel, maraging 350, produced by powder metallurgy, mech. props. 78—15334
steel, martensitic, corrosion resistant type 07Kh16N4B, long time strength and ductility, 340 to 450°C 79—100233
steel, martensitic stainless, in SO_4 solns., activation pH and susceptibility to H_2 assisted stress corrosion cracking 80—97619
steel, medium alloy, constructional, strength-toughness relationship 77—70137
steel, microalloy V-Nb, V, Nb effects on strength and formability of cold rolled sheets 77—55979
steel, Mn-B-V, low alloy, transform. singularities *(Russian)* 80—104116
steel, Mn-Mo, castings, mech. props., Cu and Sn trace elements effect 80—66596
steel, Mn-Mo-Nb, high strength, ductile, acicular ferrite struct. 77—21191
steel, Mn-Mo-Ni-Cr, bainitic, microstruct. and mech. props. *(French)* 80—16362
steel, Mn-Nb-Al-C, crack progag. and hot ductility during straightening concast strand 80—66646
steel, Mn-Sn(-Nb), extra low C, shear transformation struct. *(German)* 80—60873
steel, Mo-bearing, intercritically annealed dual-phase strip, props. and appl. 78—84858
steel, Ni, sintered, relation between microstruct., microchemistry and mech. props. 78—64504
steel, NiMoCr waterquenched, for BWR press. vessel, fast neutron fluence evaluation, irrad. behaviour *(German)* 77—34369
steel, nonmetallic inclusion, effect on hot ductility 80—29999
steel, nonmetallic inclusions effect on ductility 80—30042
steel, rare earth additions, effect on physicomechanical props. 77—12639
steel, Si (6.5 wt.%) Mn, Ni and Al additions influence obs., on mech. and magnetic props. *(Slovak)* 79—5064
steel, Si-Mn-C (1.6-2.0, 0.4-0.6, 1.1-1.4 wt.%), cast graphitised, heat treatment effects on mech. props. and wear resist. 79—96050
steel, silver, elastic limit, bending strength, and ductility rel. to tempering temp. after quenching 78—95764
steel, sintered, mech. props. 77—40439
steel, spheroidised, H_2 embrittlement, effect of cathodic charging on ductility 79—57109
steel, spring leaf retainer with variable ductility, processing error, cold working error *(German, English)* 79—70267
steel, stainless, 304, bend test ductility of irrad. specimens for LMFBR appls. 80—104235
steel, stainless, 304 and 316 elev. temp. tensile ductility minima 78—60730
steel, stainless, 316, creep and rupture, 525 to 900°C, rupture and ductility 79—8327
steel, stainless, cold-worked, 316, chem. comp. effects on rupture life, tensile props. 77—25152
steel, stainless, Cr-Mn (21, 14 wt.%), grain boundary precipitation and fracture *(Japanese)* 79—100149
steel, stainless, Cr-Ni type, low temp. plasticity, effects of deform. rate and cooling conditions 77—70099
steel, stainless, creep ductility, intergranular particle size and spacing effect 80—40461
steel, stainless, creep ductility, sigmal phase influence 80—55478
steel, stainless, creep limit, cyclic load component effect at high temps. 80—104231
steel, stainless, deformation, rapid dynamic, at −196°C 80—104220
steel, stainless, deformation temp. determ. for high yield strength 78—44177
steel, stainless, duplex, hot ductility and fracture mechanism 78—60731
steel, stainless, durability in H_2 up to 500°C 80—30170
steel, stainless, embrittlement due to soldering with Cu alloy solder, effect of alloying additions 79—47773

ductility continued
steel, stainless, fast reactor cladding tubes subjected to thermal transients, rupture behaviour 80−37465
steel, stainless, ferritic, Cr-Mo-Ni (29,4,2 wt.%) 77−44276
steel, stainless, ferritic, Ni-free, effect of V, Ti addition on ductility 79−79048
steel, stainless, Kh18N10T, struct. and mechanical props., effect of previous deform. in rolling *(Russian)* 79−29099
steel, stainless, stress corrosion testing, slow strain rate, elevated temp. and high press. study 80−97615
steel, stainless, type AISI 316, effect on props. of Zn transfer from galvanised wire at 550°C 78−88527
steel, stainless, type Kh17N13M2T, strengthening by plastic deformation and cold working *(Russian)* 78−52839
steel, stainless 304, thermally exposed, tensile props. 77−25083
steel, stainless casts, creep ductility, Auger spectroscopy study 80−60917
steel, stainless complex alloy, hot ductility, B effect 80−30038
steel, stainless ferritic, drawability, mech. props., and grain boundaries in 08Kh16AMT and 08Kh18T1 80−35270
steel, stainless type 316, set of master curves for creep ductility 79−66112
steel, strengthening by rapid electrothermal treatment 78−84870
steel, structural, effect of stressed state nature on ductility and failure 79−57078
steel, structural 15KhNMFA, resist. to weakening during tempering, high purity effect 80−76279
steel, thermomechanical treatment effect on mech. props. and microstruct. *(French, German)* 79−66090
steel, tool, high-strength, mech. props. in compression, tempering temp. effect 79−83240
steel, TRIP, powder processing, tensile strength, ductility 78−64499
steel, TRIP, warm extrusion, process control and tensile props. 80−16338
steel, two-phase austenitic-ferritic, plastic deformation under hot working conditions 77−48466
steel, type 15Kh2NMFA, strain ageing effect on strength and toughness, susceptibility to strain hardening 79−57028
steel, type 28Kh3SNMVFA, strain hardened martensite, resist. to tempering, exam. 80−16348
steel, type IN-787, for use in Arctic, low temp. effects on mech. props. 80−76310
steel, type Kh18N9T and 15Kh1M1F, study of long term cyclic strength under soft asymmetric and rigid loading 79−57076
steel, ultrahigh C, heat treated, mechanical properties and microstructure 79−57012
steel, V strengthened dual phase, deform. and fracture props. 78−48467
steel, W, high C, amorphous, rapidly quenched from melt, mech. and thermal props. 79−38874
steel, welded-joints, H_2 induced cracking, S content effect 80−97562
steel, white layers forming at high rates of friction, struct. props. *(Russian)* 79−15800
steel 12Kh18N10T, struct. and mech. props. after prolonged working at −183°C 77−55988
steel 14Kh17N2, ductility anisotropy 77−70119
steel 2Kh13, anisotropy of strength and ductility, elevated temp. effect 77−4825
steel 38KhC, medium C, ductility, fracture, effect of H_2 *(Russian)* 77−25131
steel fibre reinforced porous mat. prod., mat. props. 77−59723
steel H-beams, tensile samples shape influence on results of mech. props. determ. 77−52569
steel hardness and ductility variations and micrographs rel. to heat treatment and phase diagram obs. 79−87609
steel Kh18N10T, substructure after low-endurance fatigue in pure bending *(Russian)* 77−81311
steel U8, struct. and mech. props., effect of hydrostatic extrusion *(Russian)* 77−56022
steel welded joint impact strength, preheating and tempering effects 79−24542
steels, 45, Kh18N10T, and 30KhGSA, determining the relative elongation from a machine tensile curve 79−15927
steels, die, mech. props. high temp. thermomech. treatment 79−20086
steels, ultrahigh C, superplastic, mech. behaviour at elevated temps 80−21028
strain rate gradient development 79−46219
superconductors, type II, review of mechanical behaviour and stress effects 77−86083
superplastic materials, flow and failure, review 80−50690
tearing of ductile material, fracture strength determ. 79−43385
tension creep, finite element anal. of void growth 79−18739
thermomechanical treatment on struct. and props. 79−29109
β-Ti-Mo (15wt.%) metastable alloy, strength enhancement 77−66650
transition metal-metalloid glasses, struct., elec., supercond., and mech. props. 80−6365
TZM-Mo alloy, mech. props., effect of exposure to high temp. He containing O_2, room temp. study 80−93639
uniaxial tension, effect of material strain rate sensitivity and specimen heterogeneity *(Polish)* 78−84887
VT3-1, HTMT effects on struct. and props. 78−23740
Zircaloy, effect of dispersion and spheroidisation treatment of δ ZrH 79−76073
Zircaloy cladding, irrad., tensile props., effects of temp., strain rate and annealing 77−48463
Zircaloy-2, mech. props. after exposure to I_2-methanol solutions, SEM study 80−93689
Zircaloy-4, creep damage at LWR temp. 79−52312
zircaloy-4, oxidation in high temp. steam atm. effect on cladding ductility 79−26515
Zircaloy-4, oxide coating effect on ductility 79−47819
Zircaloy-4, plain strain ductility dependent of struct. and texture 77−8885
Zircaloy-4 cladding rubes, burst strain and stress corrosion cracking, I influence 80−3248
Zircaloy-4 PWR cladding, effect of oxide coating on ductility 79−89381
Ag composite, SiC whisker-reinforced, prep. aboard Skylab. 78−84741
Ag-Cu-Zn-(Cd)(Mn), solder, UTS, room temp. to 4.2K 79−57064
Ag-Pd alloy, for use as wire-spring relay contact material 79−52278
Ag_3Sn, dental alloy, prod. by melt extraction technique, exam. of mech. props. 78−48349
Al alloy, AK4-1, dispersion-hardening, US effects on ductility and thermal resist. *(Russian)* 77−32582

ductility continued
Al alloy, ductility effects during plastic deform., rel. to struct. changes and hot forming 78−23770
Al alloy, heat treatment of semifinished products of alloy 01420 before cold deformation 78−84873
Al alloy 01205, mech. props. at cryogenic temps. 79−29206
Al alloy 7075, fracture toughness, hydrostatic press. depend., tensile ductility 78−3209
Al alloy AZ5G, age hardening heat treatment effect on mech. props. microstruct. *(French)* 77−52370
Al alloy granules, rolling, temp. and speed effects 79−70015
Al alloys, neutron irradiation effects on microstruct., mech. props. and swelling 79−65121
Al alloys, preliminary forging effects on struct. and mech. props. of extruded sections *(Russian)* 78−80564
Al bronze, anisotropic bend ductility in single phase alloys 78−60726
Al bronze, G, Si additions, corrosion resistance 77−16714
Al foils, high strength, vapour deposited on curved surfaces, quantitative characterisation 80−80144
Al, high purity, cyclic torsional deform., factors influencing ductility 77−56031
Al high-strength alloy constitutive eqns. and high-velocity deformation *(Japanese)* 79−79029
Al, strain rate sensitivity and ductility, trace element conc. effect 80−66597
Al, wire, appl. of subgrain control 77−86060
Al-Al_3Ni, aligned, eutectic alloy, mech. behaviour at high strain rates 78−39855
Al-Cu (4.6 wt.%), cold work and ageing influence on ductility and fracture behaviour *(Japanese)* 80−89295
Al-Cu-Mg/mica particulate composite mech. props. 80−100919
Al-Cu(Ag), tensile ductility, effect of ageing and impact velocity *(Japanese)* 78−15465
Al-Fe-Si commercial alloy, elevated temp. low cycle fatigue behaviour under rotating bending 79−47766
Al-graphite particulate composite, exam. of friction, wear and tensile props. 78−72890
Al-Mg, AMg6 alloys, effect of chem. comp. on strength and ductility at low temps. 80−3148
Al-Mg, Mg effect on ductility, 25 to 250°C 79−100214
Al-Mg (4 wt.%), enhanced ductility at elevated temps. 77−63740
Al-Mg alloy, superplastic behaviour, effects of bidirectional twisting 77−70129
Al-Mg alloy AMg6, mech. props. of welded joints, impurity effects 78−95789
Al-Mg_2Si (0.95 wt.%), excess Si effect on ductility 78−27580
Al-Mg-Zn alloy 7179-T651, reduced ductility under tensile after exposure to water 80−11835
Al-Si alloys, eutectics and hypoeutectics, mech. props. and thermal cond., P impurity effect 79−83271
Al-Zn (22 wt.%), superplastic strain rate sensitivity, rel. to ductility 78−31478
Al-Zn (40 wt.%), mechanical properties after thermal cycling 78−3150
Al-Zn-Mg, duplex ageing effect on tensile props. 79−91721
Al-Zn-Mg, fatigue crack propag., stage I 77−36653
Al-Zn-Mg (6,1.5%), influence of ageing and cold work on tensile and fracture props. *(Japanese)* 78−52842
Al-Zn-Mg and Al alloy 7050, age hardenable, microstruct., effect of monotonic and cyclic straining 77−36633
Al-Zn-Mg-Cu, age hardened, effect of strain rate, temp. and environment on ductility 80−45368
Al_2O_3-AlN, creep 77−21235
α-brass, solid soln., ductility, comp. effect *(Japanese)* 79−43334
Be, polycryst. plasticity, cleavage strength, ductility transition temp. 80−44250
C fibre reinforced Al, interaction between components and compatibility, mech. props. effect 80−11761
C steel, impact-fatigue strength , notch strength, rel. to comp. and ductility of core 77−56093
Co, influence of FCC phase retained at room temp. on mech. props. 79−47677
Co-base superalloy, machine thixocast, mech. prop. deficiencies 79−74244
Co-Cr-Al-Y coating, Pt-modified, oxidation and hot corrosion resist. 78−11437
Co-Cr(VC)((Ti,V)C)-(Al), eutectic alloy, unidirectional solidification, oxidation and tensile tests 78−52790
Co-Ni-Cr (20,20 wt.%), internal oxidation, improvement of mech. props. *(French)* 77−16521
Co-Ni-Mo-C, amorphous alloys, med. props. and thermal stability *(Japanese)* 80−85049
Cr diffusion coating of C steel, types 45, 50, U8, U10 79−43357
Cr, floating zone-melting prep., ductility 80−29875
Cr, optimum alloying with rare earth metals, Ti, Zr, Hf, Nb, Ta 78−68651
Cr-Fe, magnetically insensitive Invar-type alloys *(Japanese)* 79−8034
Cr-Fe, with Si and Ta additions, metallurgical and mechanical characterisation *(Italian)* 77−66674
Cr-V-Ce-N, (2.4 to 2.6, 1.7 to 2.3, 0.005 to 0.23 wt.%) V effect on hardness, and ductile to brittle transition temp. *(Russian)* 79−34138
CsI, annealing effects on mech. and microstruct. props. 77−66686
Cu, bidirectional twisting, effect on elongation and ductility changes 77−44315
Cu, cold worked, grain size effects on short-term strength *(Russian)* 78−56693
Cu, continuously cast, O free, effect of nonmetallic inclusion on microstruct. and props. 77−81280
Cu, drawability, mech. props., effect of O impurities 79−83272
Cu, ductility minimum, strain rate depend. at intermediate temps. 79−79056
Cu, hot ductility and torsional deform. *(Japanese)* 79−57069
Cu, polycryst., creep and fracture behaviour, effects of prestrain and O 80−97544
Cu, sintered, deform., temp. and loading rate effects 77−77548
Cu wire, ductile fracture in drawing process, defect exam. *(French)* 77−21242
Cu-Al_2O_3, sintered, deform., temp. and loading rate effects 77−77548
Cu-Al-Fe, strength increase from intermediate annealing determ. of annealing temp. by recrystallisation 78−44136
Cu-based alloys, deposition condition relationship with struct. and props. 78−11369

ductility continued
Cu-Bi-Fe, Fe effects on embrittlement 77-28900
Cu-H, rolled sheet, plastic anisotropy theory based on yield function of fourth order 78-31458
Cu-Ni, cast, strength and hot ductility, alloying and residual elements effect 80-66595
Cu-Ni cast alloy, effect of alloying and residual elements 78-85033
Cu-Ni-Zn-Mn fine grained precipitation-hardenable alloy, high strength and ductility 80-100805
Cu-SiO_2 alloy, fracture at elevated temp. 78-39896
Cu-Zn (0.25 wt.%), ductility minimum, strain rate depend. at intermediate temps. 79-79056
$Cu_{60}Zr_{40}$, amorphous, ductility and stress relief, low-temp. annealing effects 80-76296
$Cu_{60}Zr_{40}$, stability, crystallisation, ductility meas. 78-47246
$(Fe, Co, Ni)_3V$, control of ordered struct. and ductility 80-21029
$(Fe,Ni,Co)_3V$, long-range ordered alloy for fusion reactor appl. 80-32481
Fe alloy MA-956E, oxide dispersion strengthened sheet, tensile and creep props. at 1365K 78-48470
Fe, Armco, deform. strengthening during low-cycle fatigue in H gas *(Russian)* 77-52460
Fe, Armco, rupture onset during cold rolling *(Russian)* 77-8904
Fe, Armco, screw dislocation effect on mech. props. *(Russian)* 78-60704
Fe, Armco, struct. and mech. props., effect of hydrostatic extrusion *(Russian)* 77-56022
Fe, Armco, texture role in prestrain embrittlement 78-60796
Fe atomised powder, sintering effect on recrystn., mech. props. 80-40292
Fe, cast, high-strength bainitic with spheroidal graphite, mech. props., isothermal transform. 79-96023
Fe, cast, Mg, Pb impurity effect on struct. and mech. props. 79-96089
Fe, ductile, influence of crack tip sharpness and morphology of graphite on K_{1c} *(Chinese)* 80-81144
Fe electrodeposited foils, microstruct., internal stress and mech. props. 80-20807
α-Fe, hydrostatic pressure effect on creep rate and failure time 78-92306
Fe, pure, neutron irrad. and H_2 absorption effects on mech. props. 78-34546
Fe, sintered and pressed, props., effect of atomised Fe powder particle size distrib. 80-11601
Fe-Al-Si, bending test, mech. props. under high press. and temp. *(Japanese)* 78-76711
Fe-Al-Si (6.22, 9.63 wt.%), bending test under high press., high temp. 80-85057
Fe-C-Mn (0.5, 0.6 wt.%), powder forged, mech. props. 80-21096
Fe-Co-Mo-C, amorphous alloys, med. props. and thermal stability *(Japanese)* 80-85049
Fe-Cr-Al, HOS 875, oxidation, cyclic, role of thermal shock 80-97640
Fe-Cr-Al-Ti-Y_2O_3 (20, 4.5, 0.5, 0.5) type MA956, strain rate effect on fracture behaviour at 1366K 80-16458
Fe-Cr-Co, ductile magnet alloys, mech. props. 80-85001
Fe-Cr-Co (28, 10.5 wt.%) ductile magnet alloy, humidity-induced H_2 embrittlement 80-89406
Fe-Cr-Co-V-(Ti) hard magnets, V and V-Ti effects on mag. and mech. props. 79-91810
Fe-Cr-Mn (11.5, 3 wt.%), microduplex ferritic-martensitic steel, exam. 78-39862
Fe-Cr-Mo, (30,2 wt.%) Bridgman-type, unexpected embrittlement phenomena, hydrostatic tensile test *(Japanese)* 80-55517
Fe-Cr-Ni-Ti-Al, superalloy, Ti, Ni, Al, H_2 variations effect on mech. props. 78-3188
Fe-Cu-Ti, improvement of irradiation-enhanced Cu embrittlement by Ti addition 79-43393
Fe-Mn, struct. and props., effect of Nb, C and Si alloying *(Russian)* 77-90360
Fe-Mo-CaF_2 sintered composite, struct. and mech. props., heat treatment effect 80-66526
Fe-Ni (25 wt.%), and single phase, solidified from undercooled melt, mech. props. 77-48540
Fe-Ni-Al-Co-Cu-Ti YuNDK type, S effect on mech. props. 80-60927
Fe-Ni-Al-(Cu) (12, 0.5, 0.5 to 3 wt.%), Cu addition strengthening at 77K, mech. props. 80-60875
Fe-Ni-C, ausformed, ductility of martensite *(Japanese)* 77-48490
Fe-Ni-C-Mn (3.56, 3.25, 0.6 wt.%), solid soln., quenched, changes during annealing to crystal structure, mech. props. *(Russian)* 79-34076
Fe-Ni-Cr, austenitic, creep strength and ductility, effect of γ′ precipitation 77-36597
Fe-Ni-Cr alloy 800, creep ductility decline 77-48502
Fe-Ni-Cr alloy 800, minor alloying element effect on creep, ageing microstruct. 78-27572
Fe-Ni-Cr-Mo superalloy, mech. props., η-phase form. effect *(Chinese)* 80-20925
Fe-Ni-Cr-Ti-Mn-Mo, (25.8, 14.04, 2.17, 1.27, 1.30 wt.%), superalloy A-286, precipitation hardening, exam. of fracture toughness and mech. props. 78-92355
Fe-Ni-Mn, martensite, aged, grain boundary embrittlement 79-96144
Fe-Ni-Mo, ferrite plus martensite structures, exam. of mech. props. 78-56709
Fe-Ni-Mo-C, amorphous alloys, med. props. and thermal stability *(Japanese)* 80-85049
Fe-Ni-Ti-(Cu) (12, 0.25, 2 wt.%), Cu addition strengthening at 77K, mech. props. 80-60875
Fe-Ni-V-(Cu) (12, 2, 2 wt.%), Cu addition strengthening at 77K, mech. props. 80-60875
Fe-Ni-(Cu) (12, 0.5 to 3 wt.%), Cu addition strengthening at 77K, mech. props. 80-60875
Fe-refractory compound, dispersion strengthened, thick vacuum condensate, control of struct. and mech. props. 80-16324
Fe-Si (6.5 wt.%), ductility and mag. props., Ni and Mn addition effects 78-76704
Fe-Si (6.5 wt.%), Ni, Al and Mn additions effect on mech. and mag. props. 77-12667
$(Fe_{100-x}Ni_x)_{83}B_{17}$, amorphous, crystn. 80-75176
$(Fe_{100-x}Ni_x)_{83}B_{17}$ glassy alloys, Ni content influence on crystn., and bend ductility changes, during annealing 79-73103
$Fe_{40}Ni_{40}P_{14}B_6$, amorphous, annealed and unannealed, temp. depend. of flow stress and ductility 79-29119

ductility continued
$Fe_{40}Ni_{40}P_{14}B_6$, Metglas 2826, stability, crystallisation, ductility meas. 78-47246
Fe_3O_4, film formed in caustic electrolyte, deform. 77-25181
Ir, fracture mechanisms, and cleavage criteria 79-74253
Ir-W (0.3 wt.%), P segregation to grain boundaries, effect on high temp. ductility 78-95754
Ir-W (0.3%), grain boundary comp., trace element additions effect 80-66661
Mg alloys, heat treated, neutron irradiation effects on microstruct., mech. props. and swelling 79-65121
Mg-Er (<25%) alloys, struct. and props. 79-96001
Mg-Ni-S, electroforming, mech. props. rel. to heat treatment 80-35133
Mg-Zn-Zr, cast, exam. of phase composition, mech. props. 79-100217
MgO, compressive stress-strain behaviour at high temps. 80-25774
MgO, MgO-CaO (58 wt.%), comparison of high temp. creep and fracture 77-16658
Mo alloy, long-term ageing effects on ductility and microstruct. 77-44348
Mo alloy:Re, effect of Re on mechanical props. 80-35196
Mo alloys, fusion reactor first wall and blanket material, props. for struct. appl. 80-30071
Mo, C doped sheet, electron beam welded, low temp. ductility 79-87685
Mo, electron beam melted, C charge effect on ductility *(Japanese)* 80-35264
Mo, exam. of H_2 embrittlement mechanisms, effect on mech. props. 78-39891
Mo fibre reinforced Cu, rule of mixtures of deform. parameters in stage III 80-97532
Mo fibre reinforced Cu with weak interfaces, stability of tensile deform. 80-97533
Mo, irrad. between 425 and 1000°C, ductility in bending 80-39164
Mo, mag. field effect on mech. props. and dislocation struct. *(Russian)* 79-42818
Mo, mech. props., effect of exposure to high temp. He containing O_2, room temp. study 80-93639
Mo, plastic deform. mechanism during hydrostatic extrusion *(Russian)* 77-8879
Mo powder, influence of powder reduction processes on props. 80-89175
Mo, recrystallised sintered sheet, C addition effect on ductility 79-8319
Mo, single crystal, ductility and high temp. strength in routine tests 77-90427
Mo-C-Zr-B (0.004, 0.12, 0.002 wt.%) effect of grain size, cellular dislocation structure, on mech. props. *(Russian)* 79-34105
Mo-C(Ti)(B)(Zr)(Ru)(Pt), electron beam melted, alloying addition effects on brittleness and ductility 79-61728
Mo-Ti, irrad. between 425 and 1000°C, ductility in bending 80-39164
$(Mo_{0.6}Ru_{0.4})_{82}B_{18}$, supercond. metallic glass, neutron irrad. effects 80-29060
Nb alloys, fusion reactor first wall and blanket material, props. for struct. appl. 80-30071
Nb alloys, long-term ageing effects on ductility and microstructure 77-44348
Nb, and alloys, interstitial impurity effects on strength 78-3194
Nb, H_2 embrittlement, macroscopic behaviour at low temps. 77-32665
Nb, mag. field effect on mech. props. and dislocation struct. *(Russian)* 79-42818
Nb, oxidation in imperfect vac., solute O_2 level change and ductility loss 79-52452
Nb, single crystal, surface oxide softening, TEM obs. 77-40462
Nb:He, mech. props. and microstruct. 80-85003
Nb-Fe(Co)(Ni)(Os), alloying element influence on strength, ductility, surface and grain boundary energies *(Russian)* 79-74234
Nb-low alloys, strength and ductility at high temp. and different strain rates 80-16401
Nb-Ni amorphous alloys, glass transition and ductility, O additions effect 80-75168
Nb-Si(-V)(Zr)(Mo)(Ta)(W)(C)(B)(Ge), ductile amorphous, superconductivity 80-60131
Nb-Ti(Zr), type II superconductor, mech. behaviour and stress effects 77-86083
Nb-W-Mo-Zr, long-term strength props., vac. level effect 80-55484
Nb-W-Mo-Zr-C, strength and ductility, prolonged high-temp. soaking effect 80-55483
Nb-W-Zr-Ta, long-term strength props., vac. level effect 80-55484
Nb-Zr-C alloys, dispersion-hardened with carbide phase, influence of hydrostatic extrusion on struct. and props. *(Russian)* 77-52338
Nb_3Sn filamentary superconducting composites, mechanical property variations between composites 79-57054
Ni base alloys, IN-702, IN-601, TD-Ni-Cr-Al, B-1900+Hf, oxidation, cyclic, role of thermal shock 80-97640
Ni base alloys EhI607A and EhI929VD, fatigue strength, temp. depend. 79-15791
Ni base superalloy, directionally solidified, struct. and props. *(Chinese)* 80-20918
Ni carbonyl powder, sheet filtration materials with metallic gauze backing layers, bending strength and ductility 78-60613
Ni coating, electron beam evaporated, ductility and struct. 78-11439
Ni, ductility and fracture, nonmetallic inclusions effect 80-104221
Ni, EP742 type alloys, optimum struct. for strength, heat resist. and ductility *(Russian)* 79-52250
Ni electrodeposits, influence of Ni sulphamate operating parameters on impurity content and props. 79-28971
Ni, sintered carbonyl type and with dispersed ZrO_2 inclusions, struct. effect on high-temp. ductility 77-63757
Ni-Al_2O_3 alloy, electron beam evaporated, struct. and mech. props. 78-11114
Ni-$Al_2O_3(ZrO_2)$, dispersion strengthened, thick vacuum condensate, control of struct. and mech. props. 80-16324
Ni-Al-Cr, precipitation-strengthened, mechanical props. 78-84968
Ni-Al-Cr-Mo-Ti-W-(Co) alloys EhI 826 and EhI 929, reverse elastic after effect under loading 78-39829
Ni-B, hydrogen embrittlement, effect of B additions *(Japanese)* 78-84973
Ni-base superalloys, powder metallurgical, creep-rupture at intermediate temps. 80-97568
Ni-based superalloys, hot workability, effect of S, Ca, Mg, Y and Zr minor elements 80-66552
Ni-Co (10 wt.%), cast single phase, solidified from undercooled melt, mech. props. 77-48540

ductility continued

- Ni-Co electrodeposit, strength, heat treatment and comp. var. effects 77−32660
- Ni-Cr, heat-resist., high-temp. ductility and embrittlement 80−76314
- Ni-Cr Nimonic alloys, mech. props., high-temp. irrad. effects 80−100885
- Ni-Cr superalloy, interactions between creep and low cycle fatigue *(Chinese)* 80−66572
- Ni-Cr-Al sintered alloy, hot vac. pressure, fracture and mech. characts. 80−66667
- Ni-Cr-HfO_2, dispersion-strengthened, hot rolling effects on props. *(Russian)* 77−59797
- Ni-Cr-W (20, 10 to 40 wt.%), phase composition, struct. and props. 80−21034
- Ni-Cr-W-Mo-Al-Ti (15,6,3,2,2, wt.%), wrought, Si effect on transition brittleness *(Chinese)* 80−55491
- Ni-Cr-W-Mo-Ti-Al alloy KhN67MVTYu, heat treatment effect on mech. props. 77−70082
- Ni-Cu (30 wt.%), cast single phase, solidified from undercooled melt, mech. props. 77−48540
- Ni-Fe metallic glass, METGLAS 2826, creep props. 79−15746
- Ni-Fe-Cr (18, 18 wt.%) superalloy, mech. props., 4-295K 77−44327
- Ni-Nb-Al, eutectic, thermal cycling effect on strength and ductility *(Russian)* 79−24601
- Ni-Nb-Al (21,2.5 wt.%), eutectic aligned alloy, mech. behaviour at high strain rates 78−39855
- Ni-Si-B, amorphous, thermal stability of ductility 80−76327
- Ni-ThO_2, oxidation, cyclic, role of thermal shock 80−97640
- Ni_3Al, ductility, tensile and compressive tests *(Japanese)* 77−52414
- Ni_3Al, ductility in poly- and single crystals, compressive and tensile tests 78−56715
- Ni_3Al, room temp. ductility improvement by ternary trace element addition *(Japanese)* 79−52315
- Ni_3Al-B, $L1_2$ type intermetallic cpd. room temp. ductility improvement by B addition *(Japanese)* 80−35263
- $Ni_{60}Nb_{40}$, stability, crystallisation, ductility meas. 78−47246
- Pb-Sn (62 wt.%), superplastic eutectic, exceptional ductility 78−27579
- Pd-H, mech. props., influence of dissolved H_2 *(Russian)* 80−81109
- Pr, mech. props. from 78 to 525K 77−21165
- α-Pu and δ-stabilised Pu-Ga alloy, strain rate effect on tensile props. 77−21284
- 239PuO_2, stoichiometric, high-temp. deformation 80−81111
- $^{239}PuO_2$, hypostoichiometric, high temp. deformation rel. to cryst. microstruct. 79−79041
- SiC fibre reinforced Al interaction between components and compatibility, mech. props. effect 80−11761
- TZM, irrad. between 425 and 1000°C ductility in bending 80−39164
- Ta single crystal, H_2 embrittlement *(Japanese)* 80−66636
- Ta_2O_5, anodic oxide film, adhesion, ductility and fracture, spectrophotometric thickness meas. and SEM obs. 79−99460
- α-β Ti alloy, fracture toughness rel. to microstruct. 77−16673
- Ti alloy, VT16, decomp. of α'' martensite during continuous heating *(Russian)* 78−48370
- Ti alloy, VT23, ht. treatment effects on fracture *(Russian)* 78−80623
- Ti alloy, VT3-1 mech. props. and low-temp. creep 77−44314
- α and $\alpha+\beta$Ti alloy of different stability, exponential law use for anal. of strain hardening process 79−15697
- Ti alloy VT16, strengthening heat treatment in vacuum 79−79013
- Ti alloy VT20, phase composition and structure effect on mech. props. 79−38958
- Ti alloy VT22, hardening during thermomechanical treatment, precipitate particle internal struct. *(Russian)* 79−91657
- Ti alloy VT3-1, large forgings, heat treatment, struct. and mech. props. 78−52864
- Ti alloys, AT3 and AT6, tensile props. prolonged oxidation effects 78−85050
- Ti alloys, ductility, for different phase comps. at low temps. 80−35273
- β-Ti alloys, ductility enhancement by hydrogen *(Russian)* 77−52459
- Ti and Ti alloys, struct. sensitivity of mech. props., alloying influence *(Russian)* 79−47748
- Ti, dynamic annealing, effect on dynamic strain ageing phenomena 80−7594
- Ti, high purity, flow stress relaxation *(French)* 77−86117
- Ti, high-temp. ductility in vacuum, air and liq. metals *(Russian)* 77−52537
- Ti, IMI-125, strain rate effect on mech. behaviour 80−3153
- Ti-Al-Cr-Fe-Si alloy AT6, and weldments, mech. and corrosion props. 77−90409
- Ti-Al-Cr-Mo-Fe(V)(Zr), effect of structure and heat treatment on tensile strength, ductility, fatigue limit and notch sensitivity 78−56711
- Ti-Al-Sn (5, 2.5 wt.%) alloy, fatigue under combined alternating bending and torsional stresses 77−8923
- Ti-Al-V (6,4 wt.%) superplastic alloy, maximum attainable ductility 80−60919
- Ti-Al-V-Cr-Mo-Zr (3,8,6,4,4 wt.%), beta-C, microstruct. effect on mech. props. 78−27577
- Ti-Al-V-Sn-Zr alloy TS5, annealing effect on ductility and strength *(Russian)* 78−35427
- Ti-Al-V-Sn(Mo-Fe), heavy section extrusion, fabrication and mech. props. 78−6985
- αTi-Fe, plastically deformed, $\alpha \rightarrow \omega$ transform. 78−3095
- Ti-Hastelloy-N, homogenization 79−61606
- Ti-Mo (Zr) (Nb), sintered, manufacture and exam. of props. 79−95975
- Ti-Mo (15 wt.%) alloy, metastable β-phase, deform. characts. 78−6975
- β-Ti-Mo-Cr-Al (8, 4.5, 2.5 wt.%), metastable, tensile ductility, α-phase morphology and distrib. effect 77−86098
- Ti-Mo-Fe-Cr-Al, alloy VT3-1, influence of constitution on fracture toughness *(Russian)* 77−77559
- Ti-Mo-Zr-Sn (11.5, 6, 4.5 wt.%), β III, mech. props. rel. to heat treatment 80−84961
- Ti-Nb superconducting composite in Cu matrix, low temp. effects in ductility 79−57119
- Ti-Ni amorphous alloys, glass transition and ductility, O additions effect 80−75168
- Ti-Pd (0.15 wt.%), IMI-260, strain rate effect on mech. behaviour 80−3153
- Ti-TiO_2-ZrO_2-Mo, sintered struct. and mech. props. 78−60618
- Ti-V-Si (30, 1 at%), quenched and aged, hardness, tensile behaviour and phase transform. 79−11646
- Ti-W(-Al), mech. props. and heat treatment 80−35274

ductility continued

- Ti-Zr-Mo alloy, effect of O_2 on elec. resistivity, microhardness, mech. props. 77−56092
- α-Ti-Zr-W, effect of W impurity on mech. preps. 80−16392
- $Ti_{50}Be_{40}Zr_{10}$, Metglas 2204, stability, crystallisation, ductility meas. 78−47246
- TiC, mech. props., 1073 to 2273K *(Japanese)* 79−15732
- α-U, strain rate effect on tensile flow and fracture 80−84992
- U/(Zr-Cu-Mo alloy) welded joints, mech. characts. determ. 20 to 750°C 79−29113
- U/Ti welded joints, mech. characts. determ. 20 to 750°C 79−29113
- U-Mo (2 wt.%), depleted, effect of microstruct. on mech. props. 80−108497
- U-Mo(Nb)-(Zr), gamma stabilised, internal H_2 embrittlement 77−28883
- U-Mo(2 wt.%), mech. props., effect of ageing 77−8914
- U-Ti(0.75 wt.%), mech. props., effect of ageing 77−8914
- U-V (0.2 wt.%), mech. and struct. props., effect of internal H *(French)* 77−21253
- U_3Si, tensile ductility from 25 to 320°C 79−74225
- V alloys, fusion reactor first wall and blanket material, props. for struct. appl. 80−30071
- V, polycrystalline, strength, ductility, 4.2 to 400K, O_2 effect 77−36529
- V-low alloys, strength and ductility at high temp. and different strain rates 80−16401
- V-Nb-Mo(Cr), corrosion in liquid Na, O_2 effects 77−8987
- V-Ti (20wt.%), corrosion in liquid Na, O_2 effects 77−8987
- W and alloys, wire, increasing plasticity, by electroplastic rolling *(Russian)* 79−29103
- W, high temp. strength and ductility 77−52406
- W sintered rods, hot rolling with four roll passes, effect on struct. and mech. props. 79−100195
- W-Mo, vapour deposited, long-term strength and thermocyclic creep 80−16405
- W-Ni-Fe(Co)(Cr), structural characterisation *(French)* 77−56074
- Y_2O_3-AlN, creep 77−21235
- Zn, oriented polycrystals, tensile behaviour under hydrostatic press. *(Japanese)* 77−52417
- Zn, wear resistant coating, effect of surface-active substances in electrodeposition on props. *(Russian)* 78−11359
- Zn-Al (10,22,50wt.%), low temp. mech. props. plastic deformation, glissile dislocation nucleation *(Russian)* 80−11695
- Zn-Al (22 wt.%) eutectoid, superplastic, factors affecting ductility 77−86097
- Zn-Al(Cu), dil. alloy, creep ductility 79−38899
- Zn-Al(22 wt.%), alloy sheet, superplastic, cold-rolling effects on mech. props. and microstructure *(Japanese)* 80−71671
- Zr-Al (8.6 wt.%), fast neutron irradiated, tensile props. and fracture toughness 80−84994
- Zr-Al(8.6 wt.%), mech. props., corrosion and fast neutron irrad. influence 78−84948
- Zr-Cu amorphous alloys, glass transition and ductility, O additions effect 80−75168
- Zr-Mo-Nb-V-Sn (1,2,2,2 wt.%), heat treatment, transform. reactions and mech. props. 79−24545
- Zr-Mo-Sn (3,2 wt.%), heat treatment, transform. reactions and mech. props. 79−24545
- Zr-Ru(Pd), heat treated, mech. props. and struct. 78−80571
- ZrC, high-temp. strength, affecting factors 77−63794

duplicating *see reproduction (copying)*

dusk *see twilight*

dust

see also cosmic dust

- AC test dust, particle size distrib. for filter media testing 78−53060
- actinide industrial dusts, lung clearance studies at NRPB 78−65137
- aeolian dusts and biogenic lipids in marine environment 77−64327
- aeolian sediments, Mahalanobis' D^2 distance appl. *(Portuguese)* 78−61388
- aggregates of submicron particles, acoustic coagulation 77−35011
- air dust, long-lived beta-activity, freq. distrib. anal. 77−73835
- air pollution, dust cyclone operation, anal. 78−57362
- air pollution meas. by laser *(French)* 77−64486
- air pollution sources and sinks, stochastic models for SO_4^{2-} particles and windblown dust 79−100930
- airborne, collection efficiency of directional dust gauges 77−37415
- airborne, dust fallout in Kuwait, summer 1978 obs. 80−81966
- airborne, field sampling techniques 79−12258
- airborne, Nigeria during dry dusty season 80−81960
- airborne, respirable fraction, performance characts. of samplers matched to them 78−53438
- airborne, Saharan dust affecting radiative transfer rates, model 80−90149
- airborne, worldwide data on reduced visibility 78−40662
- airborne dust, effects on anemometer modified for indoor climate research 77−3897
- airborne dust pollution monitor 80−55971
- airborne dusts collection by bluff bodies 79−4065
- airborne dusts transport in near wakes of bluff bodies 79−4064
- airborne soil particles mass mass concentration rel. to visibility 77−73849
- Antarctic snow surface dust contamination, climatonomical modelling of temp. response 78−24354
- asbestos, environmental pollution rel. to use of quarried serpentine rock 77−91261
- Ashkhabad 1975 dust storm *(Russian)* 77−29396
- atmosphere, activation analysis experience at Karlsruhe Nuclear Research Center 78−3941
- atmosphere, dust grains mean radius rel. to transparency meas. on Maidanak mountain *(Russian)* 80−72627
- atmosphere, dust haze of African Harmattan wind, 1962-1973 visibility obs. 80−61900
- atmosphere, dust transport in Maricopa County, Arizona 79−70824
- atmosphere, effect on IR cooling rates 78−88886
- atmosphere, Harmattan dust deposition rel. to visibility, wind and solar rad. 80−94578
- atmosphere, meas. at Algarve coast, Portugal 79−58062
- atmosphere, near IR absorpt. due to soot particles *(Russian)* 80−82055
- atmosphere, particulate conc. changes during precipitation, field studies 79−12167
- atmosphere, peak short term dustfall meas. from dust generating industry 78−81386

dust continued
atmosphere, planetary radiation balance, climatological consequences 78—36242
atmosphere, propagation calcs., use of average complex refr. index 78—57314
atmosphere, SO_2 adsorpt. and oxidation on particles 78—96287
atmosphere, turbidity meas. on Hulunbeier grassland and dust transport study *(Chinese)* 79—84485
atmosphere dust, eval. using nuclear methods *(French)* 80—7993
atmosphere dust, meas. via personal CIP type sampler 78—81469
atmosphere dust loading, 1923-54, pyrheliometric and circumsolar sky radiation obs. 80—46240
atmosphere observations at Kingston, Jamaica, using lidar system 78—36284
atmosphere pollution dust dynamics, study via ^{222}Rn descendants radioactivity meas. *(Rumanian)* 80—12524
atmosphere soil-derived dust, Christiansen effect in IR spectra, Rayleigh limit 80—105046
atmospheres, reflective dust blanket rel. to Earth albedo sudden change and ice age onset 79—44241
atmospheric, airborne metal conc. rels. in industrial district, nuclear anal. technique 80—72107
atmospheric, imaginary refr. index rel. to particle size 78—7763
atmospheric, IR laser energy absorpt., spectrophone meas. 77—9513
atmospheric dust, neutron activation anal. 77—70718
atmospheric dust and radioactive fallout in air and rain over United Kingdom 77—73847
atmospheric particles anal. by proton beams 77—70399
atmospheric smoke and dust clouds, lidar observation at 0.7 μm, 10.6 μm 78—49181
atmospheric thermally driven vortices, numerical model, dust-devil dynamics appl. 77—17191
atmospheric transmission at Mauna Loa, volcanically related secular trends 79—62585
atmospheric turbidity caused by air pollutants, assessment 79—100941
back discharge, flashover meas., streamer or steady glow mode, dust layer effects 78—59708
NW British Isles, dust fall on 1977 March 6 assoc. with short rain shower 78—57287
cement kiln dust emission control by electrostatic precipitator, meas. 79—52989
charged, rotating, cylindrically symmetric interior soln of Einstein-Maxwell eqns. 80—82688
charged grain, light scatt., quantum approach 80—48196
chemical analysis using LMA 10 laser microspectral analyser 78—24385
chimney discharges, dust level determination, equipment charact. *(French)* 78—3948
climatic fluctuations in 1870-1969 period, statistical study of likely causes 78—7751
clouds, industrial, existence of lightning-like discharges 78—14235
coal-dust aerosol, radiation-absorbing coeff., effect of spectral comp. of radiation and particle size 77—23859
collection by high capacity preseparator 80—16884
collection efficiency of directional dust gauges 77—70843
concentration measurement using beta gauge *(French)* 79—53012
contaminant particle microanalytical methods 80—86397
control equipment available in GDR *(German)* 79—74571
corona ion generator for removing dust and aerosol particles in rooms *(Finnish)* 77—66883
Couette flow, of dusty gas between two infinite coaxial cylinders 78—55685
deflection from optical components by 20 kV negative potential 79—76888
deposition, onto rot. disc, convective diffusion, external force field 78—40081
deposition rates on snow, satellite remote sensing of snow albedo 80—17385
destruction degree, determ. in mech. screening 80—66882
dewatered pipeline coal dust pollution model 77—37401
dielectric constant at X-band, effect of moisture content 80—72578
diffusion through gas in force field, theory 78—18366
dustfall from isolated cement works, implications for residential development 77—37403
dusty gas, weak wave, general decay law 78—5785
dusty viscous flow between oscillating coaxial circular cylinders 79—18928
Ekman boundary layer, suspended particles effect 78—24349
electret filters for high efficiency air cleaning 80—56569
electric breakdown of air, influence of dust particles under sustained appl. field *(German)* 79—94830
electrostatic precipitator, re-entrainment, particle trajectories and gas flow 78—13642
eolian sediment transport during dust storms, Slims River Valley, Yukon territory 79—5552
erosion by shock wave in air 78—42648
explosion, flame propag. vel., uniform dispersion of single sized particles 80—66803
filter type AFA in air, X-ray analysis 77—41142
filtration, specimen prep. techniques for anal. of dust distrib. in fabrics 77—56191
filtration efficiences of selected filter types 79—57551
filtration efficiency of granular bed, triboelec. effects 80—38487
flow, dusty plane viscous incompressible fluid, kinetic, kinematic props. 80—38482
flow of dusty gas, uniqueness criteria 77—31360
flue gas, radiometric monitoring method *(German)* 77—29452
fluid containing dust particles, laminar boundary layer flow, 2-D stagnation point near oscillating plate 80—64606
fly ash particles, water accretion, refract. index and accreted layer thickness 80—58462
gas flow dust content, temp. and speed meas. method 78—34216
gas-dust mixture, wave eqns. of one-dimensional motion 79—86496
gas-particle mixture, shock wave structs., particle specific heat effect 78—14072
gas-particle plumes from finite-size combustion sources, dynamics 78—30341
gauges, directional, analytic expression for collection efficiency 79—21062
general relativistic rotating dust cloud, stationary exact soln. 77—87675
glass fibre, flaw generation and strength, dust particle effects 77—23741
Great Plains, USA, dust storms, lessons 79—29486

dust continued
hemispheric mean temp. response to stratospheric dust 77—29419
hypersonic free-molecular heating of micron size particulate 79—4058
hypersonic wedge flow, dusty gas effect 80—6083
ignition and flame quenching 80—28577
impact on Au or W target, ion plasma comp. rel. to micrometeoroid detect. 77—39438
impairment of flat plate solar collector performance 79—62054
indoor-outdoor relationshiops for airborne particulate matter of outdoor origin 79—83654
interaction with rainwater 77—37326
IR spectra of soil-derived atmospheric dusts, Christiansen effect 80—26608
IR Test-1 lidar obs., transmission meas. 80—99625
lead content determ. using atomic absorption method *(Hungarian)* 77—21893
lidar obs. at 0.7 and 10.6 μm wavelength 78—69459
Liege industrial region, five year record of atmospheric fall-out 78—81375
limestone rock dust rel. to acid precipitation in central Texas 77—37329
in liquid solutions, correction for effects on light scatt. meas. 77—37959
loess geological environments, China *(Chinese)* 78—81156
marine aerosol, Bermuda, alkali and alkaline earth chemistry 77—70727
marine atmosphere, lightly polluted, dust gravimetric determ. rel. to dark smokes 78—81376
Mars, dust complex refractive index, wavelength depend. and comp. 77—29695
Mars, dust storm 1971-2, Mariner 9 IR spectra, composition and particle size distribs. 77—41345
Mars, dust storm obs., 1978, Jan. 78—24482
Mars, dust transport by winds, general circulation model 77—5480
Mars atmosphere, aerosol characts. from isophotes 77—29699
Mars surface, fine particles in drifts, Viking 1 obs. 77—17412
measurement 79—39331
measurement engineering, survey *(German)* 79—35712
measurement techniques in dust control *(Hungarian)* 80—35810
medical photomicrography, elimination of dust 77—70576
minerals, electron microscope anal., environmental monitoring 77—81877
minerals, health hazards 77—86732
minerals, in environment, health hazards 77—87068
nondestructive neutron activation analysis of environmental samples using low-energy photon spectrometry 78—3995
oceanic dusty atmosphere, model of surface absorption of short-wave radiation and albedo *(Russian)* 77—60415
oceanic dusty atmosphere, surface radiation *(Russian)* 77—60409
optical component protection in dusty environments, electrostatic techniques 80—58657
optical depth of Saharan dust, NOAA 3 VHRR reflected radiance meas. 78—65390
particle deposition in human respiratory tract, sampling apparatus 79—96719
particle diffusion in electrostatic precipitators 77—3526
particles, collecting, handling and mounting for SEM characterisation 79—21867
particles in atmosphere, effects and size distribution *(Dutch)* 79—52974
pollution control, polarisation and interference microscopy appls. 78—61544
pollution control using chemical retardants 78—3945
power plant effects on environment, protection measures *(German)* 80—26574
pulmonary fibrosing disease diagnosis, histological section SEM and energy-dispersive X-ray microanalysis 80—72314
radioactive dust captured by wind from Earth's surface, radioactive fallout *(Russian)* 80—16869
radioactive fallout investigations, 1973 to 1975, beta activity meas. *(German)* 77—64420
radioisotope absorption type measuring device, electronic circuit design *(Polish)* 78—29101
raingauge dust excluder 78—73548
rare earth rich submicron grains in Earth's atm., solar vs. terrestrial origin 78—12180
relativistic rotating dust cylinders 77—61000
respirable aerosol mass conc. meas., using piezoelec. microbalance 78—69518
respirable airborne crystalline silica, determ. polymorphs., silicosis 80—45832
respirable dust, Pu meas. using different size fractionation methods 79—66836
retention effect on pressure drop, in high vel. pulse-jet fabric filter 80—103072
rotating charged dust, Newtonian and general relativistic treatments 78—73908
Sahara as possible sink of trace gases 79—34888
Sahara dust mass in atm., satellite radiance meas. 77—9456
Sahara dust particles, effect on atmospheric turbidity 80—51536
Saharan, atm. aerosols in N. tropical Atlantic region 78—32188
Saharan aerosols, complex refractive index between 300 and 700 nm 77—81970
Saharan dust radiative characts. at solar wavelengths 77—81969
Saharan dust transport and deposition over Italy and S.Europe 80—41504
sampling system collection efficiency rel. to particle density and size 77—37456
sandstorms effect on microwave propagation 79—70834
Saturn, Axel dust props., Mie theory 77—37565
Sharav (Khamsin) dust storm, optical depth and particle size distrib. 80—90162
shock-induced turbulent air flow, dust entrainment 80—43763
smelting dust in oxygen blowing of Martin bath, phase comp. determ. 77—52705
smoke/dust cloud temporal analysis algorithm 80—98484
soil erosion, wind tunnel simulation, effects on fine dust production 79—20834
soil-derived atmospheric dusts, particle absorption contributions to mass extinction coefficients 80—61896
spark generator for dust explosion hazard assessment and gas ignition 78—57983
sphere, slowly rotating, maximal slicing condition, initial value equations 80—73246
spherically symmetric charged dust distrib., Einsteins theory generalised to Brans-Dicke theory 79—2694

dust continued
stack dust monitor based on particle counting and sizing 79—83683
storms, aerosol and momentum mixing, fast-response meas. 78—65364
storms, freq. and diurnal var. in contiguous United States 77—29353
storms, SW. United States, tropospheric aerosols 79—20932
storms, types, locations and mechanisms 77—9481
stratosphere, dust collected from interplanetary space, visible absorpt. spectra 80—101554
stratosphere, dust meas., (1970-1977) 78—73445
stratospheric dust from St. Augustine Volcano, ruby lidar meas. 77—29431
suspended dust deposition, wind speeds and particle concs. 78—40623
thin dust layers, particle size effects automatic correction, computer appls. in spectrometry 79—83539
Titan, Axel dust props., Mie theory 77—37565
trajectory photography for compressible flow velocity meas. 79—82008
troposphere, Sahara dust cont. over N.Atlantic from air cond. meas. 78—92897
troposphere over equatorial N.Atlantic Ocean, dust conc. rel. to Sahelian drought 77—78356
unsteady flow of dusty viscous fluid through uniform pipe 78—59450
urban air, total suspended matter estimation, comparison of three methods 77—37416
velocity measurement of charged dust particles using laser Doppler velocimeter 80—95083
virtual impactor for particle classif. and generation of test aerosols with narrow size distribs. 80—30626
viscous dusty fluid flow through rotating circular cylinder 77—68675
volcanic, effects on climate, statistical evidence from long-term temp. records 78—69439
volcanic activity dust veil index, apparent periodicity 79—92514
volcanic dust in atmosphere, correl. with N.Hemisphere average temps. during Little Ice Age 80—82050
volcanic dust in stratosphere, effect on radiation reaching Earth surface 80—82035
volcanic dust influence on N.American high arctic climate change and glacier mass balance 78—36214
volcanic dust rel. to N.Hemisphere temp. changes 78—36258
volcanic dust veil index rel. to N.Atlantic climatic change 77—78402
windblown, impact abrasion of minerals 77—70647
windblown particles in planetary atmospheres 77—45083
Fe dust particles, respirable, meas. of mass and thickness by SEM backscattered electron imaging 79—21707
Fe, tribothermoluminescence of flakes in grinding wheel, rel. to solar coronal dust radiation 78—68570
^{210}Pb, radiochem. determ. in U ores, air dusts 77—56266
Si-P dust, electrification and cond. 79—82662
$SiO_2+Al_2O_3$ particulate emission from calcining of clay, removal using electrostatic precipitator 79—24925
U ores, dusts and mill tailings, simultaneous determ. of ^{238}U, ^{234}U, ^{230}Th, ^{226}Ra, and ^{210}Pb 78—15736

dust storms *see storms*

dwarf stars
see also white dwarfs
accreting nonmagnetic degenerate dwarfs, X-ray and UV radiation 79—40184
AGK2+81°266, hot subdwarf, spectral type 78—45323
AE Aquarii, cataclysmic variable, IUE satellite UV obs. 80—72985
Aquila X-1, photometry and spectroscopy of optical counterpart, model 78—32614
atmospheric structure, mol. effects 80—21999
λ Aurigae, in ε Indi moving group, detailed anal. 78—85982
late B dwarf in circumstellar dust cloud, IR source coincident with OH 205.1—14.1 80—101630
Barnard's star, astrometric obs. 1916-1976, sexagintennial report 77—45432
Barnard's star, perspective secular changes in proper motion, radial vel. and parallax 77—91524
Barnard's star, spectrophotometry with Carnegie image tube 78—57466
BD+0°2989, late-type dwarf star, metal abundances 77—78779
BD+39°3226, BD+34°1543, hot subdwarfs, spectral types 78—45323
BD+75°325, hot subdwarf, UV spectrum obs. by International Ultraviolet Explorer (IUE) 78—96474
BD +11° 4571=ADS 15010, subdwarf binary, history of astrometric obs. 79—62874
BD-3°5357, eclipsing binary with hot subdwarf component 77—91574
black dwarf companions, detection by direct photometry from space telescope 79—71076
blue star in SNR 1006, spectral features and UBV photoelectric meas. 80—41830
ξ Bootis A, active dwarf star, chromospheric emission lines obs. 80—12762
ξ Bootis A, late-type dwarf star, mag. field obs. 80—72949
brown and black dwarfs, structure, evolution and missing mass contrib. 79—48800
brown dwarfs and black holes rel. to missing mass 78—61879
YZ Canis Minoris, red dwarf star, weak radio flares interferometric obs. 78—65633
YZ Canis Minoris, spectroscopic flare obs. 79—92780
α Canis Minoris (Procyon), CNO abundances from near IR spectrum 78—93222
β Canum Venaticorum, Mg II and Ca II emission line intensities 79—80306
OY Carinae, eclipsing ultrashort periodic dwarf nova discovery 79—53823
μ Cassiopeiae, subdwarf binary, spectroscopic orbit 78—8046
cataclysmic binaries, evolution and origin 80—56885
cataclysmic binaries, gas flow hydrodynamic calc. 77—57037
cataclysmic binaries, masses and evolution 77—57031
cataclysmic binaries evolution, ang. momentum loss 77—57032
CD—42°14462 (V3885 Sagittarii), dwarf nova in permanent outburst 78—53966
CD —31°622 as metal-deficient subdwarf 78—65618
CD-31°622, spectroscopic obs. of DC white dwarf candidate 77—67090
proxima=V645 Centauri, dMe flare star, quiescent corona, transition region, and chromosphere obs. 80—56850
α Centauri A, Be abundance and constraints on Be form. 77—41379
α Centauri A and B, IUE spectra and transition region models 80—46543
α Centauri binary system, spectroscopic chemical anal. 80—62128

dwarf stars continued
α Centauri C (Proxima Centauri), EUV flare obs. rel. to flare star scaling theory 77—45453
UV Ceti, anomalous flare activity obs. 78—89202
τ Ceti, Ca II 866.2 nm emission event 80—26860
κ Ceti, IUE obs. of far UV spectra of G-type dwarf 80—56831
κ Ceti, Mg II and Ca II emission line intensities 79—80306
UV Ceti, variations of Hβ emission line during large flare 77—45456
UV Ceti flare stars, magnetic field effects 79—62845
UV Ceti flare stars, review *(Russian)* 78—28685
UV Ceti stars, photometric features near flare initial phase 80—105252
UV Ceti type stars, weak Ca II triplet absorpt. lines *(Russian)* 79—88691
Z Chamaeleontis, cataclysmic binary, masses radii, and mass exchange rel. to gravit. radiation 80—4386
Z Chamaeleontis, monitoring of southern dwarf nova, 1954-76 period 78—93272
chromospheres, models and activity 79—48773
Ci 182354, astrometric anal. of unseen companion from 61 cm Sproul refractor plates 78—16459
close binaries, struct. and evolution 77—57019
close binaries evolution and gravit. radiation 77—57030
β Comae Berenices, Mg II and Ca II emission line intensities 79—80306
cool dwarf stars, neutral-ion spectral anomaly 78—7985
cool stars, local interstellar H and D Lyman α towards four objects 79—5886
cool stars, Ti isotopic abundance ratios 80—26840
CPD-26°389, hot subdwarf, spectroscopic binary within planetary nebula (NGC 1360) 77—45494
EM Cygni, cataclysmic variable, red and white dwarf binary, period change, B photometry 80—90434
SS Cygni, dwarf nova, ANS detection of both soft and hard X-ray emission 78—36579
SS Cygni, dwarf nova during outburst, accretion disk model 77—82247
θ Cygni, F-type dwarf star, spectral type of faint distant companion 80—90481
ss Cygni, hard X-ray source, obs., accretion onto white dwarf 79—30078
61 Cygni A, B, late-type dwarfs, metal abundances 77—78779
61 Cygni B, ^{24}MgH IR rot. band equivalent width calc. 77—18918
degenerate, props. of low temp. pure He surface layers 78—7994
degenerate star, accretion process giving rise to X-ray emission 80—90459
BY Draconis, dwarf binary, flare star, rotational hypothesis for quasi-sinusoidal light variations 78—4234
BY Draconis, flare star, coronal soft X-ray emission obs. by (HEAO 1) 79—101140
BY Draconis, late-type flare star, metal abundances 77—78779
CM Draconis, low dispersion spectrum, metal abundance of eclipsing binary 79—25636
BY Draconis, prototype spotted flare star, pre-main-sequence nature 80—36633
BY Draconis, UV Ceti variable, flares colour behaviour 80—22020
BY Draconis stars, angular momentum initial distrib. and evolution 80—85954
BY Draconis stars, photometric radii compared with luminosity class V stars *(Russian)* 78—57564
BY Draconis type variables, flare activity and quiescent variability 78—45338
BY Draconis type variables, photometry, amplitudes and phases 79—67038
BY Draconis-type stars, spectroscopic binary incidence 77—87401
dwarf novae, mass transfer instabilities and accretion disk structure 77—82243
emission-line late-type dwarfs in S Hemisphere, image tube spectrograms 78—8016
emission-line M-type dwarfs, Hα var., stellar surface phenomena 79—21313
ε Eridani, model chromosphere of K-type dwarf 78—65610
40 Eridani, triple star, X-ray emission discovery 79—97035
ε Eridani, UV spectrum obs. by International Ultraviolet Explorer 78—96475
extreme subdwarfs molecular band strengths, theoretical approach 78—93221
F, G, K-type stars, chromospheres, wave dissipation of mechanical energy 80—82340
F, G and K-type stars, chromospheric radiative losses in continuum 80—72924
F-, G- and K-type, in solar neighbourhood, absolute magnitudes 78—81632
F- and G-type, Mn/Fe abundance ratios 78—45325
F- and G-type stars, C and N abundances 77—91530
F-type, kinematical and photometric props. 77—29937
faint blue southern stars, Hβ photometry, metallicity, luminosity 77—41381
faint blue stars near galactic anticentre, UBV photometry 78—40932
faint blue stars proper motions near galactic anticentre. 77—87386
faint red dwarfs near north galactic pole, vel. dispersion 78—7989
faint red stars, photoelec. photometry of complete sample, space density 79—71034
faint red stars at intermediate galactic latit., UBVR photometric obs. 78—32457
flare star 2329—03, spectra, chromospheric emission 77—74070
flare stars, dM stars as source of interstellar ^{3}He 79—48810
flare stars, fast electron hypothesis 77—78796
flare stars, flare emission spectrum rel. to fast electron hypothesis 80—67731
flare stars, identification with transient soft X-ray sources questioned 78—96485
flare stars, large-scale winds driven by mass loss, effects on interstellar matter 78—32464
flare stars, mean colours of flare continuum 77—13349
flare stars, multichannel spectrophotometry 80—105256
flare stars, photoelectric monitoring (1974 to 1976) 79—44509
flare stars as candidates for new class of transient soft X-ray sources 78—45337
flare stars in Orion Nebula region, new objects and repeated outbursts 80—56852
flare stars in Pleiades, new discoveries *(Russian)* 77—13366
flare stars in Pleiades, possible cyclic recurrence of flare activity *(Russian)* 78—49443

dwarf stars continued
flare stars in Pleiades, spatial distrib. using recovery method *(Russian)* 80—94722
flare stars in Pleiades, UV and photographic obs. of flares *(Russian)* 77—13367
flare stars in Scorpius-Ophiuchus region, discoveries *(Chinese)* 80—77418
flare stars in Taurus Cloud, comparison with ρ Ophiuchi flare stars, visible obs. *(Chinese)* 80—85957
flare stars physical characts. 77—41383
foreground red dwarfs in M15 field, photometry rel. to density gradient 77—78834
G139-29, perturb. from rectilinear motion, astrometric red dwarf binary system with subluminous component 79—8910
G262—21/22, subluminous stars in common proper motion binary 77—33491
G77-61, dwarf C star, proper motion 78—4209
G 208-44/45, possible double flare star, spectral obs. 80—67727
G- and K-type dwarf, correl. between motions and CN anomalies 77—17566
G-type, macroturbulence and age anticorrel. 78—93226
G-type, Mg II and Ca II emission line intensities 79—80306
G-type, uvby $H\beta$ photometry 77—82275
G-type stars, far UV Si emission line analaysis 80—56829
galactic disc dwarf stars, evolutionary effects on metal abundance distrib. 79—88733
U Geminorum, 1978 February magnitude estimates 78—36589
U Geminorum, dwarf nova, M-type dwarf companion spectral type 79—62851
U Geminorum, dwarf nova, M-type secondary detect. and spectrophotometric parallax 79—67012
U Geminorum, dwarf nova, radial vels. from emission line obs. 77—57029
YY Geminorum, eclipsing binary, photometry and orbital period study 80—105287
GK-type dwarf stars, Mg isotopic abundances 80—51757
Gleise 490 AB (BD+36°2322), red dwarf binary, flares and starspots, rot. period determ. 80—77423
Gliese 82, dM4e star, flare activity discovery 77—91539
Gliese 867, flares obs. on both components of visual binary 79—48861
Groombridge 1830, Fe curve of growth split as function of atmospheric pressure 77—29794
HD 128220, peculiar spectroscopic binary, props. of hot subdwarf component *(French)* 77—57014
HD 142373 (χ Herculis), var. intrinsic polarisation obs. 78—12202
HD 175742, spectroscopic binary, orbit determ. with CORAVEL photoelectric radial vel. spectrometer *(French)* 80—36671
HD 17576, UV subdwarf companion discovery from uvbyβ photometry 78—96479
HD 206860, G0 V star, IUE obs. of active region 79—92766
HD 224085, spot-covered red dwarf, light curves 77—74093
HD 25329, subdwarf, metal deficiency from spectroscopic anal. 80—62122
HD 27561, Hyades cluster star, CNO abundances from near IR spectrum 78—93222
HD 40409, in ε Indi moving group, detailed anal. 78—85982
HD 45088, BY Draconis binary, surface activity from high rot. vel., visible obs. 80—77425
HD 45088, reticon obs. in red of dK3 spectroscopic binary 80—67778
HD 45166, dwarf in Wolf-Rayet clothing, spectrum anal. 79—5826
HD 49798, H-deficient subdwarf O-type binary, non-LTE spectral anal. 79—16978
HD 49798, strange composite sdO star, evolution and nature of companion 78—49435
HD 88230, dM0 star, high-dispersion photometric atlas from 3900 to 6000 Å 78—7996
HD 94028, subdwarf, Mn abundance and Mn/Fe ratio 78—45328
HDE 283048, hot subluminous star, spectrum 78—20823
14 Herculis, C/Fe ratio of K-type dwarf 78—93227
AM Herculis, IR spectroscopy, period, mass function 79—71066
AM Herculis, M-type component detect. from spectrophotometry at min. light 80—98692
DQ Herculis, red and white dwarf eclipsing binary, emission line eclipse phenomena 80—94800
AM Herculis (3U 1809+50), binary star model 77—71155
DQ Herculis (Nova 1934), spectrophotometry rel. to red dwarf companion nature and mass 80—22017
high galactic latitude stars, division into giants and dwarfs by proper motion *(Russian)* 80—109431
high-velocity metal-poor dwarfs, blue spectra abundance anals. 78—53933
hot subdwarfs in Carnochan and Wilson catalogue, UV spectra 80—82354
Hyades, abundances of HD 28068 and 28344 dwarfs 77—29890
Hyades cluster, possible members BVRI photometry 80—51821
Hyades dwarfs, Be abundances 77—53584
Hyades metal content and distance rel. to solar colour 80—101569
VW Hydri, light curves of dwarf nova 78—12245
HZ 22 (UX Canum Venaticorum), hot subdwarf binary, evolution and mass 79—12472
ε Indi, late type dwarf star, model atmosphere 80—90425
K dwarfs assoc. with X-ray transients A060—00 to A1742—28, visible and IR obs. 80—101653
K- and M-type, space motions rel. to stellar age 78—69846
K-dwarfs, mass estimation for 12 objects 77—29837
K-type subdwarfs, missing halo population 79—25595
Kapteyn's star and M subdwarfs, comp. 77—13330
Kuiper 41, orbit and flare activity of visual red dwarf pair 79—97032
EV Lacertae, flare star, hot-plasma model of strongest flares 78—20838
EV Lacertae, flare star, photometry and spectrum rel. to starspots and rot. period 80—98665
EV Lacertae, flare star, polarimetric and photometric obs. *(Russian)* 77—13368
EV Lacertae, UV Ceti variable, flares colour behaviour 80—22020
large proper-motion stars, luminosity and motions for stars with annual motion $>1''$ 79—71020
late type stars, Ca II H and K lines and nearby continuum photoelectric calibration 80—36617
late type temp. minima, chromosphere models 80—67717
late-type, accretion and abundance distrib. 77—2425
late-type, broad-band IR colours, CO and H_2O absorpt. indices 78—4218

dwarf stars continued
late-type dwarfs, parallaxes and proper motions 77—37595
late-type dwarfs, photometric metal abundance index and appl. to galactic evolution 77—60754
late-type main-sequence stars near Sun, intermediate-band photometry 78—53934
LB 3459, O-type subdwarf plus hot white dwarf eclipsing binary, photometry, anal. 79—48859
LB 3459, short period eclipsing binary system containing two O-type subdwarfs, uvby photometry 78—53987
LB 3459, subdwarf eclipsing binary, evolutionary model 80—51808
LB 3479, subdwarf eclipsing binary, evolutionary model comment 80—90426
LDS 720-BC, visual binary with flare star, orbit calc. 77—13391
LDS 720BC (CD—32° 16135), visual binary, orbit 78—32515
AD Leonis, flare conditions from photometry and spectra 79—92773
AS Leonis, flare star, chromospheric emission lines in nonflare red spectrum 79—21294
AD Leonis, flare star, $H\alpha$ emission short-period variability limits 79—48807
AD Leonis, UV Ceti variable, flares colour behaviour 80—22020
AD Leonis, X-ray emission from flares, HEAO 1 obs. 80—41837
EH Librae, dwarf Cepheid, BV photometry 77—82226
local missing, mass problem, undetected M3-M8 dwarfs 77—67123
LS 630, subdwarf O star, spectrum and absolute magnitude 77—17561
LTT 2437, most metal-deficient subdwarf, spectrum, photometry and Ca/H ratio 78—69797
in M31, inner nuclear regions, spectral features and dwarf content 78—86005
M dwarf distrib. at low z distances 78—12232
M-dwarf enrichment possibility in M31 semistellar nucleus 80—51862
M-type, FeH bands identification in spectra 78—7952
M-type, in solar neighbourhood, absolute magnitudes 78—81631
M-type, in South Galactic Pole direction, catalogue of 282 objects 79—5762
M-type, IR Fourier transform spectroscopy, abundance anal. 79—21279
M-type, IR photometry 80—41823
M-type, problems in standard star transformation to Johnson system 79—62876
M-type, spectrophotometry with Carnegie image tube 78—57466
M-type, undiscovered, rel. to local mass defect in Galaxy 77—91632
M-type dwarf stars in galaxy cluster Abell 2029, coronal X-ray emission rel. to SAS 3 obs. 80—82519
M-type dwarfs, near IR luminosity-sensitive spectral features rel. to M31 and (M32) 78—49431
M-type dwarfs, proposed identification of FeH 77—45418
M-type dwarfs, radii from Barnes-Evans relation, effects of atmospheric opacity sources 78—7984
M-type dwarfs, space densities derivation via new matrix method 80—85932
M-type dwarfs atmospheres, FeH column densities 78—24507
M-type spectra, population discriminant 77—29840
M-type stars in direction of N galactic pole, photometry and spectroscopy 77—37594
M-type stars in halo of galaxy NGC 4565, identification from grid photography 80—62261
M-type stars near north galactic pole, scanner obs. of spectra 77—78789
main-sequence stars in globular cluster NGC 6752, UBV photometry and metallicity 79—71079
dMe stars, survey of BY Draconis syndrome 78—16428
Me-stars, multiplicity 79—44544
Me-type, cyclical photometric vars. interpretation 77—74059
Me-type dwarf stars, long-term variability 78—93254
α Mensae, chemical composition of cool southern dwarf 77—22225
metal abundances of F- and G-dwarfs from CORAVEL radial vel. scanner 80—94791
metal-poor dwarf stars, abundance anals. of yellow spectra 79—92760
metal-poor stars, C/Fe ratio from CH features 79—16945
metal-poor stars, Fe/H abundances from red spectra of nine objects 80—51751
AT Microscopii, X-ray emission from flares, HEAO 1 obs. 80—41837
nearby main sequence stars, XUV radiation upper limits 79—12471
nearby stars brighter than tenth mag. 80—56825
NGC 6752, globular cluster, blue horizontal branch stars as B-type subdwarfs 78—49488
nova brightening, magnetic fields and outburst phenomena *(Afrikaans)* 78—32481
novae, effect of red dwarf companion on outburst 80—82394
novae, mass transfer in binaries 77—56962
novae, mass transfer instability in semidetached binary systems 78—8047
novae, nature, H accretion, mag. field, radiation mechanisms *(Russian)* 78—93277
novae, satellite UV obs., temp. calc. 77—57033
novae, spectrophotometric estimate of electron density in rapidly rot. accretion discs 79—16968
old disc population subdwarfs, CaH and TiO band strengths 78—40930
old dwarf stars, kinematics rel. to Galaxy initial contraction 80—62204
70 Ophiuchi A, late-type dwarf star, mag. field obs. 80—72949
70 Ophiuchi A, model chromosphere of K-type dwarf 78—65610
parallax and proper motion meas. for seven stars 80—62109
γ Pavonis, C and N abundances 77—91531
EQ Pegasi, active dwarf binary star, chromospheric emission lines obs. 80—12762
PG 1413+01, white dwarf-red dwarf eclipsing binary, photometry and spectral types 79—8944
SX Phoenicis, short period dwarf Cepheid, UBV photometric obs. 78—57561
planetary nebulae central stars, Cassegrain image-tube scanner obs. 77—22214
planetary nebulae central stars, temps. determ. rel. to nebulae evolution 80—67724
proper motion stars in direction of galactic centre *(French)* 80—77404
VV Puppis, polar, evidence for M-type companion from IR photometric obs. 80—98687
red degenerates, eleventh list 79—25596
red dwarf stars, origin, evolution and variability 79—16954
red dwarfs, double-peaked flare events and solar 'sympathetic' flares 77—56963
red dwarfs, nature of flares optical continuum *(Russian)* 80—109445
red dwarfs, systematic errors in evidence for high space density 77—5524
red dwarfs, X-ray flares rel. to galactic X-ray background 77—9755

dwarf stars continued
red dwarfs in southern hemisphere, absolute magnitude and distance, BVRI photometry 80—90419
red nearby star suspects selection from Luyten proper motion catalogues, use of Luyten's magnitude estimates 80—82353
red stars at north galactic pole, proper motions 78—4214
Ross 614, parallax, orbit and mass of astrometric binary 77—91565
rotational velocities, studies in lower main-sequence stars 80—51767
Rst 4036, red-dwarf binary star, orbital period and total mass 80—12780
WZ Sagittae, image-tube spectroscopic obs. of 1978 Dec. outburst 80—72958
scaling hypothesis, relativistic statistics and critical mass 79—16960
Scutum Cloud direction, main sequence stars density functions from RGU photometry 79—35242
solar companion star, existence and nature 78—12198
solar-type stars, in open clusters, spectroscopic differences from Sun 78—36560
solar-type stars, metal abundances, microturbulence, spectroscopic data 78—40943
solar-type stars, photoelec. scanner obs., search for solar spectral analogues 78—40938
southern dwarf novae, image tube spectra 77—56960
southern subdwarfs, UBV photometry, UV excesses 79—5818
starspot magnetic fields in red dwarfs 79—92758
Stepanyan's star, obs. of G8 V absorpt. spectrum and emission spectrum 80—67788
subdwarf bolometric corrections 79—75205
subdwarf ionization equilibrium 80—90421
subdwarfs, 37—45 excess calibration using Fe/H abundances 80—82363
subdwarfs, He abundance and galactic halo 80—22003
subdwarfs, masses and metal abundances from spectroscopic anals. 80—62122
subdwarfs, photometry rel. to compositions and kinematics 80—82364
subdwarfs, Population II, luminosity functions in SA 51, SA 57 and (SA 68) 80—98648
subdwarfs, UV excesses and metal abundances 80—17574
subdwarfs in 47 Tucanae, CN vars. 80—94794
V471 Tauri, eclipsing binary, K-type star chromospheric Mg II emission obs. 80—26912
45 Tauri, Hyades cluster star, CNO abundances from near IR spectrum 78—93222
thermonuclear bursts assoc. with chromosphere flares 80—98684
three-dimensional motion, of high-vel. and low-vel. dwarf stars 80—12754
triple close approaches effect on stellar system evolution, one-parameter family appl. 80—17618
UV 1758+36, He deficient hot subdwarf B star, atm. parameters, radial vel. 78—53944
van Bueren 62, 117, 121, dwarf stars in Hyades, spectroscopic orbits 79—5862
VB10, spectrophotometry rel. to low luminosity M-type dwarfs optical spectral classification 79—58339
EQ Virginis, dK5e star, new absorpt. line obs., possible infalling gas 77—37602
EQ Virginis, dwarf binary, flare star, rotational hypothesis for quasi-sinusoidal light variations 78—4234
EQ Virginis, late-type flare star, metal abundances 77—78779
W851, high-velocity subdwarf, parallax and tangential vel. 77—49387
Wing-Ford 9910 Å molecular band as mass function constraint in old galaxy populations 77—17673
Wolf 1062, astrometric anal. of unseen companion from 61 cm Sproul refractor plates 78—16459
Wolf 1062, red dwarf, astrometric perturbation 77—49439
Wolf 630, visual multiple system including dwarf or degenerate stars 79—17019
Wolf 922, nearby red dwarf, evidence for low-mass unseen companion 80—51809
1228, nearby red dwarf, evidence for low-mass unseen companion 80—51809

dye lasers
ablative flashlamps for pumping 77—79836
accessory invertor for LG-21 serial N_2 laser 77—68224
active medium, hydroacoustical perturbations *(Russian)* 78—82966
actively mode-locked, flashlamp pumped, streak camera obs. of pulses 78—22158
aerosols of dye solutions as active media 80—95887
air pollution monitoring by pulsed dye laser 79—48204
aliphatic tertiary amines, laser action feasibility, emission spectra, two photon excitation 80—23683
alternate-pulse wavelength switching, appl. to differential lidar system 78—25890
6-amino-7-hydroxy-4-methylcoumarin solutions, additions effect on fluoresc. 80—2833
4-amino-N-methylphthalimide in n-propanol, nanosecond laser fluorometry 80—102721
7-aminocoumarins, fluorescence efficiency of laser dyes 77—42531
amplfier, DC elec. field effects 80—64006
amplified spontaneous emission and spatial depend. of gain in dye amplifiers 78—42332
amplified spontaneous emission in dye solutions, effect of O_2 80—95885
amplified spontaneous emission in spherical and disk-shaped laser media 80—1177
amplified spontaneous emission with picosecond light pulses 78—82965
amplifier, high average power, efficient, pumping by Cu vapour laser 77—88755
amplifier system, multipass electro-optical injection 79—22975
analytical atomic spectrometry, appl., review *(Japanese)* 80—11990
angularly resolved coherent Raman spectroscopy, crossed beam config., 79—30570
anisotropic theory, oscill. model of complex mols. *(Russian)* 79—22948
anisotropy of amplifying props., dye laser oscillator and amplifier in liq. cryst. matrix 80—74355
anthracene derivatives in soln., fluoresc. and laser parameters 79—27251
anthracene derivatives in solution, polarisability and dipole moments, emission and absorpt. spectra obs. 80—69256
anthracene-perylene energy transfer dye laser, gain meas. 79—59695
applications 79—55130
approximate theory of laser with saturable absorber, stationary pulse parameters 79—3690

dye lasers continued
BBO solution, induced pump absorption, lasing threshold and efficiency 78—50773
BBOT dye, vapour phase, optical props. *(Japanese)* 80—9879
BBOT dye vapour single-pass gain obs. 79—55136
beam divergence, transverse mode saturation, kinetics *(Russian)* 78—74931
beam expander for short cavity dye laser 80—87532
beam expanind telescope, on-axis reflective, for pulsed dye laser cavities 79—41398
beam expansion with diffr. grating in dye laser cavity 78—66858
benzoxazole, aromatic derivatives, spectral luminesc. and lasing props. rel. to electronic struct. 80—99519
benzoxazole, laser action at 330 nm 78—29949
bicyclic dye, stability, photodegradation parameters 78—71098
bicyclic dye stability, photodegradation relationships 78—55349
binary dye mixture with distributed second-order feedback *(Russian)* 78—29945
binary solutions, pulsed excitation, energy transfer and laser action 77—75506
birefringent, tuning filters without secondary peaks 78—29994
bis-styryle dyes, lasing characts. 78—42333
bis-styryles, sulphonated, CW operation in blue and violet spectral region 78—42334
blue region tunable output, using Xe ion laser pump source 78—46621
blue-green laser technology for ocean optics 77—78458
blue-violet stimulated emission *(Russian)* 78—25874
book, quantum electronics 80—105442
book 78—22122
booster-active dye soln. mixtures, for efficient laser action 78—37879
broadband tuning using electrochem. reactions 78—9397
butyl-PBD, tunable narrow-band coherent VUV source for Lyman-α region 80—38070
carbazine 720, single freq. CW dye laser operation in 690-700 nm gap 80—99719
carbocyanin dye, amplification and absorpt. from excited state *(Russian)* 77—54707
carbocyanine dye, tunable emission by pumping with Nd:YAG laser 79—950
carbocyanine dye CW laser emission, spectral range extension up to 1020 nm 78—74901
carbocyanines, dye laser appls., soln. chem. 77—40568
cavity, pulsed, concave grating for beam expansion and spectral dispersion 79—59721
cavity dumped flashlamp pumped dye lasers 79—13987
cavity dumping, efficient operation with 20 nsec output pulses 78—46684
chlorophyll and Mg-free derivatives, lasing and stimulated emission 77—52742
chlorophyll-a, laser action and excited singlet state absorpt. 77—27288
coaxial flashlamp pumped dye laser *(Chinese)* 79—55144
coherent optical image amplification by injection locked dye amplifier 80—19041
commercial dye laser design and pumping configurations 78—25889
complex molecule solutions, stimulated emission, light quenching *(Russian)* 78—33735
complex molecules, photoinstability and quenching effect on laser generation kinetics 80—3390
complex organic laser active substances, props. *(Russian)* 78—74904
conference, laser and electro-optical systems, San Diego, CA, USA (Feb. 1980) 80—62392
conference, laser engineering and appls., Washington, USA (May-June 1979) 80—1216
conical scattering of laser beams in active dye solutions 79—94294
continuous jet dye laser, appl. to intracavity spectrometer *(Russian)* 78—70197
continuously pumped, pulse compression with slow saturable absorber 79—31959
continuously pumped actively mode locked laser, pulse props. 77—42546
continuously scanned tunable laser, for atmospheric pollutants detection 78—81362
continuum generation, near UV to near IR, by amplification of dye laser subpicosecond pulses *(French)* 80—5747
conversion of Cu vapour laser output to 5782 Å 80—48241
correlation functions, Fokker Planck equation 77—71969
coumarin, flashlamp-pumped, picosecond pulses at 520 nm *(French)* 78—42335
coumarin 481, mixed solvent systems for optimising output 79—13981
coumarin 6 dye mols. in liq. cryst., fluoresc. intensity, orientation control 78—82759
coumarin deriv. solns., mol. struct. effects on luminesc. and lasing characts. *(Russian)* 77—83873
coumarin derivatives in simple dye laser, pumping by N_2^+ ion laser 78—74903
coumarin dye laser, mode-locked flashlamp pumped, tunable blue ps pulses 79—13974
coumarin dye-doped polymer film laser, optical gain 77—61948
coumarin laser dyes, in methanol, ethanol, and water, fluoresc. lifetimes meas. 79—27252
coumarin laser dyes, stability, lasing characts. obs. 78—1223
coumarine dye laser, N_2 laser-pumped, pulse time behaviour 79—31894
coumarins (C-30, C-102, C-7), synchronous pumping and mode locking 79—45966
coupling reflector, involute-related, for flash lamp pumped laser systems 78—90425
cresyl violet in ethanol soln., and dye mixtures, excitation by Cu vapour laser 80—28230
cryptopleurine derivatives, absorpt. and fluoresc. obs. of photodecomp. processes, dye laser relevance 80—55686
cumarine derivatives, stimulated emission by laser and lamp excitation 79—72563
CW, beat freq. generation between He-Ne laser with 80-GHz freq. offset 80—1253
CW, emission freq. shift due to pump intensity changes 77—79817
CW, freq. locking to absorpt. lines of Ne discharge Faraday filter 77—79870
CW, freq. locking to Na D-lines by Faraday filter, single-mode oscill. 78—5487
CW, freq. locking to Ne absorpt. lines by Faraday filter 79—22989
CW, improved freq. stability using He-Ne lasers *(French)* 79—31935
CW, investigation of jet quality 79—94253
CW, oligo mode action, kinematic model 77—14707

dye lasers continued
CW, on-line computer control, laser isotope separation appl. 78—70948
CW, optogalvanic effect to freq. lock to discharge transition freqs. 77—19309
CW, output power, effects of gaussian depend. of fields 79—952
CW, RF tuning 80—1243
CW, spectral narrowing and continuous tuning by grating beam-expansion 79—59720
CW, synchronous pumping and passive mode-locking, for picosecond pulse generation 79—3727
CW, technology developments and appl. 80—43383
CW, tunable by holographic grating 79—27288
CW, tuning and spectral narrowing using low-loss diffr. grating 78—71109
CW commercial, freq. stabilisation for ultrahigh resolution spectroscopy 77—88802
CW digital wavemeter, moving cube-corner interferometer system 78—50840
CW double-mode-locked, config. for independent tunability 79—72590
CW dye laser, cavity configuration anal. *(Chinese)* 80—64010
CW dye laser control techniques 77—58347
CW dye laser single mode, tunable 80—106534
CW dye laser spectrometer with computer control 79—75618
CW frequency-locked mode-locked laser, for high resolution spectroscopy in freq. domain 80—43350
CW laser, mode locking wing externally modulated pumping laser 79—18456
CW mode-locked dye lasers, Raman dephasing dynamics 79—44942
CW mode-locked lasers, vac. UV ps. pulse generation 80—43355
CW mode-locked lasers for ultrafast spectroscopic studies 79—31960
CW narrow band dye laser quenching 77—50561
CW organic dye lasers with intracavity absorpt., rate eqn. models 77—19247
CW passively mode-locked laser, subpicosecond pulse generation and amplification 80—9907
CW single-mode, 'double Michelson' mode selector and press. scanning 78—46686
CW synchronously mode locked laser, cavity length detuning 80—5768
CW tunable dye laser, appl. to rot. anal. of $A^2\Pi$-$X^2\Sigma$ system of SrF 79—31563
cyanine dye laser excitation by giant single pulses *(Russian)* 78—46596
cyanine dyes, solns., excited states, duration meas. 77—65503
3-cyano-4-methylumbelliferone in ethanol containing water, acid or alkali, laser emission 79—955
cylindrical active element with sheath, radiation intensity distrib. calc. 80—58531
cylindrical slab dye laser 78—22146
cytochrome c, fast Raman spectroscopy using dye laser intracavity reson. Raman amplification 77—66794
DCM laser dye, spectral props., synthesis, broad tuning range, comparison with other dyes 79—76684
demonstration system for a dye laser, educational appl. *(German)* 80—51994
dermatology investigation and therapy with dye lasers 78—35910
deterioration of dye, effect on performance 77—83867
deterioration of dye, effect on performance 80—83602
DFB, as tunable picosecond pulse source 78—22150
DFB, intrapulse thermally induced wavelength shift 79—59692
DFB, line narrowing and wavelength stabilisation technique 77—88783
DFB, N_2 laser pumped, external mirror effect on characts. 78—42352
DFB, single-freq., 10 Å continuous pressure tuning 79—76705
DFB, single-mode operation 80—74409
DFB dye solution lasers, development, theory *(Russian)* 78—13700
DFB laser, N_2 laser pumped, self Q-switched, tunable picosecond pulse generation 80—69432
DFB laser, N_2 laser pumped, tunable single ps pulse generation 79—55147
DFB laser, noncollinear wave interaction 80—99722
DFB laser with integrated Si and polyurethane channel waveguide 80—74373
DFB pulsed laser with high repetition rate 77—27300
1,4-di(2-benzoxazolyl)-benzene vapour lasers, generating capacity, stimulated emission *(Russian)* 77—679
9,10-dichloroanthracene with iso-amyl acetate or esters as solvents, dye laser material 80—74354
dichromatic switching effect in two thin film DFB dye lasers 79—10331
1,1′-diethyl 2,2′-dicarbocyanine iodide, high power DFB laser, tunable 7420-10500 Å 77—88782
3,3-diethyl thiadicarbocyanine iodide dye, stimulated fluoresc. and stimulated reson. Raman scatt. relationship 80—91853
7-diethylamino-4-methylcoumarin acriflavine binary soln., stimulated emission 77—50670
3,3′-diethyloxadicarbocyanine iodide, lasing and photoisomerisation, conc. and temp. effects 77—7081
3,3′diethylthiacarbocyanine iodide-rhodamine 6G, mixed dye laser system, laser and fluorescence behaviour 78—25876
difference frequency generation, degree of conversion depend. on line-width 80—48347
4-dimethylamino-4′-nitrostilbene in solvent fluorescence lifetime meas. by picosecond optical amplification 79—81227
1,4-bis(2,5-dimethylstyryl)benzene, lasing characts. on UV N_2 laser excitation 80—32979
diphenyl with pyrene cryst., self induced transparency self stimulated excitation *(Russian)* 80—14403
diphenyl-stilbene dye, sulphonated, CW laser emission, tunable down to 390.4 nm 79—41379
2-4-diphenylyl-5-phenyloxazole vapour lasers, generating capacity, stimulated emission *(Russian)* 77—679
distributed feedback, cholesteric liquid crystal as resonator, theory 79—31956
distributed feedback, simultaneous oscill. of independently tunable spectral lines 77—23673
distributed feedback formed by diverging pump laser beams, tuning curves 77—83893
divergence of emitted radiation, excited transverse modes determ. 79—94228
DODCI in ethanol, DQOCI added, electronic energy transfer, real-time ps meas. 80—58311
DODCI in ethanol, malachite green added, electronic energy transfer, real-time ps meas. 80—58311
DOTC, emission at 810 nm, 0.1 J in 1 μs *(French)* 77—42549

dye lasers continued
double frequency dye lasers with continuously variable power ratio, designs 80—5755
double frequency narrow-band grazing incidence pulsed dye laser 79—36929
double grazing-incidence single-mode dye laser 80—95906
double mode locked CW laser, sub ps pulse generation 77—10939
double mode locking of CW laser, parametric study 79—45978
double mode-locked CW, pulse cross-correlation studies 80—69389
double pumping source *(Chinese)* 78—82960
double wavelegnth N_2 laser-pumped dye laser 79—94241
double wavelength operation using gratings at grazing incidence 80—53317
double-pass planar amplifier, two-wavelength operation 77—75538
double-wavelength electro-optically tuned synchronously pumped mode-locked CW 79—89924
dye activated CLC, distributed feedback, tunable radiation generation *(Russian)* 80—102720
dyes, absorption edge struct. in stimulated fluorescence spectra, Raman scatt. 78—55350
dynamic DFB, output power depend. on pump power and optical density 80—14336
dynamic DFB systems, freq. tunable over whole gain profile 79—50317
efficiency with 1,4-diphenyl butadiene butadiene additive 77—19249
efficient oscillator-amplifier, pumped by freq. doubled Nd:YAG laser 79—41389
electro-optically tuned, optical switching and bistability 79—59708
electrochemical pumping 77—27287
electrochemiluminescence, electrochem. oxidation reduction 77—70304
electrochemiluminescent organic dyes and new type of laser 77—678
electron beam excited laser vapour cell designs 79—13951
emission locking onto wavelength of I_2 mol. fluoresc. 80—99721
emission spectrum switching by external optical signal 80—9892
emulsion dye laser, pumped by N_2 laser 79—13962
energy transfer, computer simulation 79—13964
energy transfer dye lasers and laser induced intermol. and intramol. energy transfer processes 80—9647
energy transfer laser, intermol. interactions and spectral shifts 78—74902
enhanced total reflection with surface plasmons, dye in contact with Ag film 79—59694
erythrosin in water-acetone, subnanosecond fluoresc. lifetime meas., environmental effects 78—5268
erythrosine B, dye soln., transient dichroism, rot. diffusion anomalies 79—87414
esculin in ethanol, coherent pumping, intracavity absorpt. anal. method sensitivity 79—57328
ethyleneglycol dye laser, conversion efficiency and tuning, solvent effect 79—55131
excitation conditions effect on lasing, discharge source 77—3582
excited singlet-state absorpt. effect on lasing 78—17930
Fabry-Perot with short pulse lasers, spectral selection and analysis in dye lasers 78—46669
fast mode-locking dyes, IR fluoresc. and laser action obs. 80—102717
flash frequency and fluid filtration effects, laser dye stability 77—19246
flash lamp, 1 kJ per pulse, for tunable organic-dye laser 79—36907
flash lamp pumped, mode locking, picosecond, pulse generation 78—71131
flash lamp pumped, tuning by grazing incidence grating technique 80—95914
flashlamp pumped, active mode locking by saturable absorber loss modulation 77—72002
flashlamp pumped, construction and performance of laser and pumping source *(Japanese)* 77—58341
flashlamp pumped, freq. tunable ns duration pulses by pulsed Q-modulation 79—41403
flashlamp pumped, injection locking without longit. mode matching 78—33760
flashlamp pumped, nanosecond pulse shaping 77—5928
flashlamp pumped, relative-gain curve determ. method 78—25878
flashlamp pumped, SHG *(Japanese)* 78—90459
flashlamp pumped, simultaneous tunable two-wavelength operation, cavity config. 77—3610
flashlamp pumped dye laser synchronisation, CW laser injection, spectral purity *(French)* 78—63118
flashlamp pumped dye ring laser, injection of N_2 laser excited oscillator beam 80—5754
flashlamp pumped high radiance laser, beam quality 78—29970
flashlamp pumped intense subnanosecond pulse generation, 0.58 to 0.80 μm 78—90422
flashlamp pumped UV laser driven by Marx-bank generator 77—19311
flashlamp-pumped, birefr. filter for tuning, theory and design 78—74914
flashlamp-pumped, high power *(Japanese)* 78—17933
flashlamp-pumped, pump source for colour centre laser 80—102737
flashlamp-pumped, two-stage amplification, for SHG 78—74922
flashlamp-pumped, using small-bore coaxial flashlamp, negative effect of cyclooctatetraene 77—14708
flashlamp-pumped dye lasers, 100 W 77—19334
flashlamp-pumped solutions, thermal effects 77—10917
flashlamps, coaxial and preionised linear, comparison as pumping sources for high power dye lasers 80—102730
fluorescein dye laser, solvation effects on tunability 80—53285
fluorescence decay, aggregation effects 78—25879
fluorescence efficiency of laser dyes 78—35205
fluorescent dye medium, short laser pulse superposition, numerical anal. 79—31891
fluorol 7GA, flashlamp pumped, passive mode-locking in green spectral region 77—38922
fluorometric system, nanosec. time-resolved spectrometry with tunable dye laser and pulse-gated photon counter 80—11968
forced mode locked CW system 77—38880
forced oscillator, efficient, to meas. upper atmospheric Na layer 80—41563
frequency control by piezo mirror translator 79—72582
frequency conversion to generate vacuum UV and IR radiation *(German)* 77—7132
frequency locked single mode pulsed dye laser appl. to tunable UV generation 77—42547
frequency locking by injection, CW and delta pulse regime anal. 80—87389
frequency locking by intracavity stimulated Raman scatt. 78—79050
frequency locking by selective refl. at glass-Na vap. interface 78—29992

dye lasers continued
  frequency locking to Na flame atomic transitions 78—50795
  frequency locking using absorbed atoms on glass 77—14755
  frequency mixing with N_2 laser in $NH_4H_2PO_4$ for 0.68-1.1 μm output 77—27314
  frequency shifting using stimulated Raman scatt. in H_2, tunable UV source 80—9963
  frequency stabilisation, wide bandwidth feedback loop 77—83891
  frequency stabilised CW laser, spectroscopic and metrological appl. 78—9395
  frequency sweeping, rel. to pumping conditions 77—61946
  gain measurements using amplified spontaneous emission 80—37986
  gas, excitation by elec. discharge, electron beams, optical stimulation *(Czech)* 78—79016
  gas phase and other new dye laser developments 79—958
  gas phase chemical reactions, laser obs. *(German)* 79—29365
  grazing incidence grating efficiencies, rel. to dye laser tuning 79—36990
  grazing-incidence pulsed, operation in single longit. cavity mode 78—94398
  heating effect minimization 80—1198
  1,3,3,1′,3′,3′-hexamethylindotricarbocyanine iodide, laser dye, ultra-fast excited state absorpt. spectroscopy 77—30876
  high average power, pumped by vortex stabilised flashlamp 77—14749
  high power CW dye laser configuration 78—50806
  high-power, at 6700 to 7700 Å, longit. pumping by Nd:YAG and dye lasers 77—3612
  high-power, single-mode, CW dye ring laser 78—13731
  highly synchronous CW double mode-locked, picosecond pusle shape meas. 79—64257
  hydrocyanic acid laser, 0.337 mm, for interferometric plasma density meas. 78—5922
  hydroxycoumarin dyes, laser emission 78—82962
  in-resonator isotopic filtration of radiation *(Russian)* 77—54752
  induced pump absorption, lasing threshold and efficiency 78—50773
  injection locked flash pumped, for contour holography of moving object 78—50737
  injection locked system, narrow-band tunable subnanosecond pulse generation 77—3611
  injection-locked dye laser pumped by Xe ion laser, 4-mirror ring-cavity 80—48280
  interference filters, nonlinear, spectral characts. in strong fields *(Russian)* 77—54718
  interference metrological applications, spectral kinetic characts. *(Russian)* 79—27253
  intermolecular and intramol. energy transfer 79—72562
  internally pumped mode-locked CW, theory 80—91787
  intracavity absorption, CW dye laser, Ba at. beam line shape obs. 80—47120
  intracavity absorption model in CW multimode dye laser 80—47119
  intracavity absorption of I_2 vapour 79—22992
  intracavity absorption spectroscopy at reduced pressures, using dye laser 80—47118
  intracavity absorption spectroscopy utilizing sweep dye lasers 79—89015
  intracavity dye laser quenching, quantitative detect. of Na absorpt. 77—36817
  intracavity dye laser spectrometer, double beam, flash lamp pumped 79—75620
  intracavity dye laser technique for spectroscopic and kinetic meas. of transients 78—62239
  intracavity enhancement of absorpt. in nanosecond regime 78—78839
  intracavity intensity modulated, 0.01 Hz to 1.2 GHz 79—41400
  intracavity method of analysis sensitivity *(Russian)* 78—46680
  intracavity SHG in CW dye laser 77—88842
  intracavity spectroscopy, spectrometer based on continuous jet dye laser 79—52831
  intracavity spectroscopy rel. to laser spectral characts. *(Russian)* 78—46561
  intraresonator absorption effect on laser characts. with forced mode synchronisation 80—78873
  IR, 685-965 nm, high power CW emission 77—42550
  IR, Nd:YAG laser pumped, continuously tunable 10810 to 12160 Å 78—22139
  IR, pulsed, tunable, pumped by flashlamp-driven dye laser 78—94400
  IR, simple grating tuned, IR N_2 laser as pump 77—61969
  IR source, tunable, efficient 80—5789
  isotope separation appl., system requirements 77—46405
  jet, pumping by Cu vap. laser 77—7128
  jet stream, CW, appl. of viscosity raising additives 77—10953
  jet stream, thickness meas. in real time, by optical technique 78—82975
  jet stream dye laser, mode locked synchronous pumping, near IR ps pulses 78—17948
  ketocyanine dye, lasing under lamp excitation 78—82964
  ketocyanine solutions, absorpt., luminesc. and lasing characts. 77—75502
  kilowatt average output dye laser development 77—54708
  kinetic spectroscopy of molecules 79—94110
  kiton red S, mol. fluoresc. decay time, self-absorption 79—68255
  laser dyes, photochemical quantum yield determ. using fluorescence data 80—55685
  lasing and amplified spontaneous emission on excitation by high-power N_2 laser *(Russian)* 78—25869
  lasing characteristics, at high levels of coherent excitation *(Russian)* 79—27254
  lasing characteristics, with high levels of coherent excitation 80—28229
  light-induced grating form. in dye solns. by two independ. laser beams, DFB effect 79—94230
  liquid crystal matrix dissolved dyes, laser emission obs. 79—41376
  liquid crystal planar dye lasers 77—3578
  liquid crystal solvent, threshold power for laser emission 77—14705
  long pulse, using resonator with spherical mirror and thermal lens 78—22149
  longitudinal mode selection due to saturable absorpt. 78—63143
  longitudinally pumped, simultaneous two-wavelength operation using intracavity prism *(French)* 79—970
  luminescence conference, Szeged, Hungary (Aug. 1976) 78—27279
  lysozyme protein solution, threshold power for laser operation 79—68391
  magnetic tuning system 77—75541
  malachite green in glycerol, subnanosecond fluoresc. lifetime meas., environmental effects 78—5268
  metal complexes containing methyleneiminobisacetic acid group 77—58324
  metastable state relaxation time determ. 80—102719

dye lasers continued
  3-methoxybenzanthrone in ethanol, photoprotolytic reactions, spectra, rate consts. and lasing thresholds 80—43327
  N-methylphthalimide in ethanol soln., gain and induced absorpt., struct. props. 77—24890
  N-methylphthalimides, laser, lamp-pumped, solvent and temp. depend. 79—3692
  1,4-bis(2-methylstyryl)benzene, picosec. gain kinetics 79—45940
  β-methylumbelliferone, amplification spectra, triplet-triplet absorpt. 77—31101
  β-methylumbelliferone in ethanol solns., spontaneous luminesc. kinetics 80—74192
  metrological interference measurements 80—28250
  mixed-dye laser tuning properties 79—59693
  mixture of dyes, possibility of tunable multiple wavelength output 80—23684
  mobile resonances, appl. to freq. stabilisation and tunability 77—7138
  mode selection by nonlinear absorber 77—705
  mode self-synchronisation in dye laser with continuous pumping 80—83605
  mode-locked, generation subpicosecond light pulses 78—42354
  mode-locked, synchronously pumped, pulse-width stabilization 80—83622
  mode-locked CW, prod. of picosecond and subpicosecond pulses *(French)* 79—31961
  mode-locked CW, subpicosecond pulse generation with slow saturable absorber 80—9915
  mode-locked dye laser and single pulse amplification 79—27255
  mode-locked dye lasers, exponential SHG autocorrelation function rel. to pulse to pulse var. 80—9920
  mode-locking, absorpt. expts. to explain action of DODCI 77—9098
  multilayered structures containing optically active medium, absorption and amplification of light *(Japanese)* 80—19052
  multimegawatt tunable IR source up to 7.7 μm, using dye laser and H_2 78—1301
  multimode beam, spectral distrib. meas. using speckle patterns 77—14730
  multiple system, flashlamp pumped, energy transfer 77—88720
  nanosecond, short constructional length with folded mirror beam expansion system 80—53328
  nanosecond laser fluorometry, spontaneous and stimulated emission kinetics 80—102721
  nanosecond pulse production using CW dye laser and pulsed dye amplifier 77—14756
  naphthalimide derivatives, solutions, lasing characts. in green spectral region, photostability 80—32978
  naphthyl 1,3,4 oxadiazole derivatives, lasing ability rel. to struct., appl. as UV dye laser 77—7080
  narrow band CW oscillator/pulsed amplifier system for precision nonlinear spectrosc. 80—53318
  narrow linewidth short pulse operation, using dual prism beam expander and grating 79—971
  narrowband CW, high output power, piezoelec. mirror translator for stabilisation 80—33036
  near IR tunable high output laser 79—36926
  nematic liquid crystal solvent, generation of induced radiation *(Russian)* 77—3583
  nonlinear transmission including stimulated emission influence 80—99720
  α-NPO solution, induced pump absorption, lasing threshold and efficiency 78—50773
  α-NPO-Ar mixture, vapour phase laser, electron beam pumping 78—63097
  α-NPO-inert gas vap. mixture, electron beam pumping 77—42535
  open dye stream, pumped by pulsed Xe ion laser 79—81448
  operation principles and tuning methods 77—10914
  optical, gain and saturation considerations 78—94393
  optical pumping, approx. analytic solns. 79—31890
  optical pumping by gigawatt monopulse laser radiation 79—55133
  optical pumping by hollow or coaxial pulse tubes, comparison *(Russian)* 77—83870
  optical resonator for pulsed dye laser pumped by powerful N_2 laser 79—94260
  optically induced distributed feedback prod. of single ultrashort pulse 80—64067
  organic compound laser, limiting length, stimulated radiation reabsorpt. by unexcited and excited singlet mols. 80—48240
  organic compound lasing ability *(French)* 79—31893
  organic compounds as active media in lasers *(Russian)* 80—38015
  organic dye solution laser, radiation characts. rel. to pumping intensity in long-time operation *(Russian)* 77—68214
  organic dyes, stimulated fluorescence, energy level scheme, photoisomerisation effect 77—70310
  organic scintillators, vap. phase dye laser media, photophysical parameters 80—95884
  organic solutions, lasing, excitation by excimer laser radiation 80—64007
  oscillator-amplifier MW system for high resolution spectroscopy 79—41393
  oscillator-amplifier system, for high resolution and coherent pulse spectroscopy 77—83892
  oscillator-amplifier system, high power, pumped by Nid-YAG laser 79—18443
  oscillator-amplifier system second harmonic generation using laser-flashlamp hybrid pumping 80—14359
  output coupling, optimisation by consideration of spatial gain distrib. 80—83603
  oxazine 1 and 9 laser dyes, absorpt. and gain with picosecond pumping 79—55134
  oxazine 720, single freq. CW dye laser operation in 690-700 nm gap 80—99719
  oxazine dyes, comparative photostability 80—3376
  oxazine dyes, fluorescence efficiency of laser dyes 77—42531
  oxazine dyes, orientation of $S_1 \rightarrow S_n$ transition moments, continuous ps photometry 79—10152
  oxazine-1-perchlorate mode-locked CW dye lasers, tunable near IR ps and subps pulse generation 79—45972
  oxazole scintillator solns., two- and three-component, laser emission spectra 80—32980
  parametric frequency conversion, of CO_2 laser, by radiation mixing *(Russian)* 78—22175
  parametric/dye laser amplifier combination, to overcome gain limitation 79—55177
  paraterphenyl, dye vapour, intense multistep photoionisation 79—10298

dye lasers continued

- paraterphenyl, efficiency, 323-364 nm tuning 77—14752
- paraterphenyl, UV lasers pumped by KrF, XeBr excimer lasers 79—10301
- paraterphenyl pumped by pulsed laser radiation, photodissociation 79—98353
- passive laser pulse compression in a fluorescent dye medium 79—98351
- PBD, and p-terphenyl mixtures, tunable narrow bandwidth 2 MW lasers 79—41378
- perylene, vapour phase, N_2 laser excited, quantum efficiency and thermal stability 78—50771
- perylene, vapour phase excitation energy transfer from pyrene 77—12802
- 2-phenyl-5(4-difluoromethyl-sulfonylphenyl)oxazole, stimulated emission, laser pumped 77—75504
- phenyloxadiazole derivatives, pumped by KrF laser, 3500 Å range 77—42532
- phenyloxazolyl pyridinium salt dye lasers, flashlamp pumped, blue-greenlasing 80—95886
- photochemical hole-burning memory magnetic and electric field addressing 79—81371
- photochemical stability of inert gas halide laser pumped dyes 78—33733
- photodecomposition of rhodamine dyes, spectroscopic investigation *(Russian)* 77—29017
- photodegradation of lader dye mixtures 80—9880
- photodermatological uses of dye lasers, erythema production, psoriasis treatment, tumour destruction *(German)* 80—56164
- photon distributions of lasers with first-order phase-transition analogies 80—23659
- photon statistics 77—727
- photon statistics for first and second order phase transitions 78—22121
- photonic efficiency of dye laser amplifiers *(French)* 78—59004
- phthalimide derivatives, solutions, lasing characts. in green spectral region, photostability 80—32978
- phthalimide solutions, fluoresc. optical quenching by ruby laser rad. *(Russian)* 77—12437
- phthalimides, solns., solvent effects on absorpt. spectra and fluoresc. 77—34650
- phthalimides, spectrum luminesc. props., laser generating capacity and generation features *(Russian)* 79—31897
- phthalocyanines, dye laser appls., soln. chem. 77—40568
- phthalocyanines, lasing props. obs. 78—17931
- picosecond light pulse techniques and applications, book 77—61137
- picosecond photochronoscopy, generation and meas. of pulses from mode-locked lasers 79—76734
- picosecond pulse emission, stable, multifreq., phase-locked radiation pumped CW dye laser 80—91789
- picosecond pulse generation, excitation by passively mode locked Ar laser 80—95930
- picosecond pulse generation methods, book contrib. 77—61138
- picosecond pulses generation and meas. 79—41401
- polarisation of stimulated emission *(Russian)* 78—25872
- polaristion rotation *(Russian)* 77—58325
- polymer films, prep. and characts. *(Japanese)* 78—5551
- polymethine, IR-140 laser dye, photoisomerisation processes 78—27800
- polymethine dye behaviour in lasers, efficiency and photoisomer generation 80—14335
- polymethine dye laser, near IR, optimal molecular struct. and lasing characteristics 80—19026
- polymethine dye lasers, mode-self-synchronisation, broadband, picosecond pulses *(Russian)* 78—29946
- polymethine dye lasers, optical absorpt. 80—64009
- polymethine dye nonequilib. protolytic forms, lasing, fluoresc. and nonradiative transitions 80—102722
- polymethine dye unstable photoisomers, superluminesc. and stimulated emission 79—31896
- polymethine dyes, excited mols., photoisomeric transformations 79—87854
- polymethine dyes, highly excited states, absorption and fluoresc. *(Russian)* 77—19248
- polymethine dyes, laser action and photoisomeric transforms. 79—89905
- polymethine dyes, mol. struct., lasing props. 79—3693
- polymethine dyes, relax. mechanisms in picosecond range *(German)* 78—33737
- polymethine dyes, ultrafast absorpt. spectra 77—18934
- polymethine dyes development for CW infrared output 78—1224
- polyphenyl 1 laser dye for pulsed and CW operation in UV 80—78850
- POPOP, vap., electron energy loss spectra rel. to lasing 78—29947
- POPOP, vapour phase, N_2 laser excited, quantum efficiency and thermal stability 78—50771
- POPOP+Cd(5^3P_1), vap., electronic energy transfer, laser appl. 77—30980
- POPOP dye vapour laser excited by N_2 laser, temp. depend. 79—81423
- POPOP dye vapour lasers, optical and electron beam pumping, review 80—48237
- POPOP laser, bleaching of vapour 80—19027
- POPOP pumped by pulsed laser radiation, photodissociation 79—98353
- POPOP solution, induced pump absorption, lasing threshold and efficiency 78—50773
- POPOP solution dye lasers, multiplate reflectors 80—83606
- POPOP vapour, electron beam excited superradiance 78—66820
- POPOP vapour, fluoresc. meas. buffer gases effect 77—75503
- POPOP vapour, induced losses mechanism 77—75505
- POPOP vapour, picosecond generation of radiation 80—48238
- POPOP vapour lasing, buffer gases influence, theory 80—91790
- POPOP-Ar-N_2, electron beam pumped, intense laser emission at 381 nm 78—74898
- POPOP-inert gas vap. mixture, electron beam pumping 77—42535
- power scaling effects under high power laser excitation 78—46595
- PPD pumped by pulsed laser radiation, photodissociation 79—98353
- PPP calculations of ground and excited states, triplet yields and efficiency 80—37743
- pressure tuned narrow band, Doppler limited resolution description 79—47931
- prism beam expander for dye laser, dispersion 78—17968
- prism beam expander in N_2 laser pumped dye laser, prism material dispersion 79—27285
- prism used as beam expander in N_2 laser pumped dye laser, dispersion 78—74924
- pulse distortion, in dye laser resonator with slow saturable absorber *(German)* 78—33732
- pulse duration, subps, of passively mode-locked laser 79—45979

dye lasers continued

- pulse generation, time correlated, picosec., appl. to dye lifetime meas. *(German)* 79—27045
- pulse generation and meas., 0.2 psec., from passively mode locked dye laser 78—50830
- pulse generation- subpicosecond relax. times meas. in rhodamine 6G, B *(Czech)* 78—78838
- pulse output, accurate numerical simulation 79—41380
- pulse structure and cavity length determ., synchronously pumped picosecond laser 80—95935
- pulse width influence on power output of PMMA Modular matrix dye laser 80—28247
- pulsed, beam divergence *(Russian)* 78—25902
- pulsed, design for nonlinear spectroscopy 77—79852
- pulsed, electronic tuning by piezo driven grating with etalon 77—42544
- pulsed, high efficiency flash lamps as pumping sources 77—14710
- pulsed, high energy, moderate energy, coaxial flashlight pump, applications 77—23681
- pulsed, light polarisation, solvent viscosity effect 80—32977
- pulsed, light polarisation with thin wedge plate in cavity 78—55394
- pulsed, mixed solvent systems for optimising output 79—13981
- pulsed, mode competition with Na coloured intracavity flame 78—46594
- pulsed, reliable high average power laser 78—29966
- pulsed, spectral narrowing by tuning elements *(French)* 78—46616
- pulsed, spectral props. and function of time 77—88718
- pulsed, transient behaviour 80—69388
- pulsed, without intracavity beam expansion, narrowband operation 78—17957
- pulsed absorption spectroscopy of metastable and excited Hg atoms 79—26924
- pulsed and CW laser comparison for reaction product excitation spectra meas. 80—76574
- pulsed narrow-band, construction and performance characts., review 77—10915
- pulsed opto-acoustic spectroscopy 80—62743
- pulsed oscillator-amplifier system, high power narrowband, design and operation 80—58570
- pulsed output, mode locking with synchronous-pumping 80—5760
- pumped by Nd:YAG, stimulated Raman scattering appl. 80—69451
- pumped by XeF, KrF excimer lasers *(Chinese)* 80—1234
- pumped generation by UV N_2 laser in 420-470 nm range *(Russian)* 77—88719
- pumping, synchronous, extension of spectral range 80—5731
- pumping at 248 nm with KrF* discharge laser, efficient emission characts. 79—954
- pumping by high power Ar^+ laser, CW 77—7130
- pumping by Nd:YAG laser freq. doubled output 78—59090
- pumping by wall ablation lamps, high energy design 78—29961
- pumping by XeCl excimer laser 79—59691
- pumping characterisation using KrF excimer laser at 248 nm 80—1199
- pumping in coaxial cell with external irrad., radial distrib. calc. 80—53308
- pyrene, vapour phase, N_2 laser excited, quantum efficiency and thermal stability 78—50771
- Q-switching transition-metal dithiene complex dyes for 0.9 to 1.4 μ lasers 80—1200
- quadraxial high repetition rate adapter for coaxial flashlamp pumping of laser dyes 79—45949
- p-quaterphenyl vapour laser, optically excited, laser action obs. at 350 nm 79—7123
- quenched fluorescein solution, lasing props. *(Russian)* 77—27286
- quenched soln., lasing action *(Russian)* 78—25873
- quinolone laser dyes, stability, lasing characts. obs. 78—1223
- quinoxalinones, new class of high-efficiency laser dyes 78—46597
- radiation directivity improvement due to pumping uniformity 77—72003
- radiation frequency capture, near at. absorpt. lines in elec. discharge *(Russian)* 79—27299
- Raman generated pulses amplified by dye amplifier, for laser-matter interaction diagnostics 79—41414
- Raman spectroscopy, semiconductors *(German)* 79—28729
- rate equations, nonstationary solns. 79—27250
- rate equations, spiking phenomenon 78—55351
- rate equations 78—82961
- reference wavelengths, two-photon transitions to Rydberg levels 78—94221
- relaxation oscillation use for generation of subnanosecond single pulses *(German)* 78—37877
- reliable high average power, four-fold symm. pumplight geometry 77—88756
- repetitively pulsed flashlamp-pumped dye laser *(Chinese)* 80—43329
- resonance fluorescence diagnostics, of high temp. H_2 plasma 80—48971
- resonant Rayleigh-type mixing spectroscopy using picosec. dye laser system 79—44944
- resonant Rayleigh-type mixing spectroscopy using ps light pulses, ultrafast relax. study 80—91834
- resonator, CW, astigmatism compensation using lenses 78—29978
- resonator modes of N_2 laser pumped dye laser, internal Fabry-Perot etalon effect 78—25896
- retroreflecting mirror for dynamic compensation of optical inhomogeneities 79—31970
- review, spectroscopic props., tuning, laser and flashlamp pumping 77—38884
- review of dye laser devices, book contrib. 80—106517
- rhodamine, 6G, laser, lamp-pumped, solvent and temp. depend. 79—3692
- rhodamine, activated 6G top layer in slab-type directional coupler, amplified oscill. 80—99718
- rhodamine, B, spectra of lowest excited singlet states 79—81424
- rhodamine, induced losses in active medium during incoherent excitation *(Bulgarian)* 79—10297
- rhodamine, pinacyanol as mode locking saturable absorber 77—42554
- rhodamine, solns., lasing characts., diphenyl polyene addition effects 77—3581
- rhodamine, synchronously pumped, electronically tunable pulse prod. 79—76698
- rhodamine 590 picosecond transverse-flow flashlamp-pumped dye laser 80—38025
- rhodamine 69, soln., bleaching and laser props., detergent effects 79—59697
- rhodamine 6G, amplifier system, pumped by TEA N_2 laser 78—82984
- rhodamine 6G, aqueous soln., absorpt. spectra, ground and triplet state photoprotonation pH depend. 80—42961

dye lasers continued
rhodamine 6G, B in ethanol soln., and dye mixtures, excitation by Cu vapour laser 80—28230
rhodamine 6G, Cu vap. laser pumped, axial mode struct. 77—23671
rhodamine 6G, CW, travelling wave oscills. 77—23699
rhodamine 6G, CW jet stream laser, high output power in visible and near UV 78—1249
rhodamine 6G, CW laser, passive-active mode locking 78—29993
rhodamine 6G, CW synchronously mode-locked, subpicosecond pulse generation 78—71128
rhodamine 6G, emission kinetics in ps. range 78—13699
rhodamine 6G, excited singlet-state absorpt. effect on lasing 78—17930
rhodamine 6G, fluoresc. polaris. spectra in glycerol soln. 79—76458
rhodamine 6G, halo laser device 79—72597
rhodamine 6G, in glycerine-water solns., anti-Stokes fluoresc., conc. quenching 79—24349
rhodamine 6G, in organic solvent, hot luminesc. 79—4842
rhodamine 6G, in Triton X-100 water soln., energy migration and laser performance 77—71982
rhodamine 6G, inductive storage bank for laser pumping 80—5742
rhodamine 6G, intracavity laser spectroscopy, absorpt. line profiles determ. 78—12776
rhodamine 6G, laser props., effect of cyclooctatetraene 78—13698
rhodamine 6G, long pulse, high average power 77—58342
rhodamine 6G, mol. fluoresc. decay time, self-absorption 79—68255
rhodamine 6G, photoreaction mechanisms, effect of pumping spectral composition *(Russian)* 77—70323
rhodamine 6G, preferential doping in polyurethane optical solid cct. 77—62075
rhodamine 6G, ring struct. laser emission, resonator exit mirror effect 77—38941
rhodamine 6G, SHG for high power tunable UV source 77—42565
rhodamine 6G, short-cavity, excited by electron beam pumped CdS laser 78—25887
rhodamine 6G, soln., triplet state lifetime determ., solvent effect 78—1225
rhodamine 6G, spectra of lowest excited singlet states 79—81424
rhodamine 6G, spectral line tuning using partially selective resonator *(Russian)* 77—61980
rhodamine 6G, sub ns dye laser with optical pumping, spectral width, efficiency, tuning *(Russian)* 78—29974
rhodamine 6G, superluminesc. band structureless spectra 79—7124
rhodamine 6G, synchronized CW psec. pulse train generation at 2 independently tunable wavelengths 78—33758
rhodamine 6G, tunable freq. doubled CW laser using ADA 78—17965
rhodamine 6G, tunable UV radiation prod., intracavity freq. doubling in $NH_4H_2PO_4$ 77—3628
rhodamine 6G, ultrashort pulse generation in resonator *(Russian)* 79—50289
rhodamine 6G activated polymer (liq.) films adjoining amplifying media, emission characts. 78—17932
rhodamine 6G amplifier, amplified spontaneous emission and spatial depend. of gain 78—42332
rhodamine 6G and 4B, amplification spectra, triplet-triplet absorpt. 77—31101
rhodamine 6G aqueous solution, surfactant effect on fluoresc. intensity *(Japanese)* 77—42536
rhodamine 6G dissolved in liq. cryst. hosts, laser emission obs. 79—41376
rhodamine 6G doped polyurethane film, fluoresc., photoinduced effects 77—1727
Rhodamine 6G doped polyurethane film coated with CF_3 coumarin-doped PMMA film, emission characts. 77—83868
rhodamine 6G dye amplifier, flashlamp pumped, gain meas. technique 80—1208
rhodamine 6G dye in ethylene glycol, broadband optical diode, one directional traveling wave operation of ring laser 80—58606
rhodamine 6G dye in quartz glass microcomp. matrix, as tunable solid laser 80—99734
rhodamine 6G dye laser, degree of polaris., solvent effect 79—41375
rhodamine 6G dye laser, induced radiation spectral characts., effect of vibr. relax. 80—64008
rhodamine 6G dye laser, N_2 laser-pumped, pulse time behaviour 79—31894
rhodamine 6G ethanol soln., absorpt. and luminesc. spectra using picosecond excitation 80—106351
rhodamine 6G in aq. and alcohol solns., thermooptical inhomogeneities, μ second pumping 77—75501
rhodamine 6G in ethanol, injection locked ring amplifier 77—88788
rhodamine 6G in ethanol, photobleaching mechanism *(Russian)* 78—48680
rhodamine 6G in ethanol dye soln., lasing props. recovery after photolysis 77—34888
rhodamine 6G in polyurethane film, etched cavity 77—7140
rhodamine 6G in soln., photochem. stability 78—37878
rhodamine 6G jet stream, CW 33 W output power 77—61968
rhodamine 6G jet stream CW laser, tuning range, mode competition effects 78—50791
rhodamine 6G laser, appl. to quantitatively analysing spectroscopy of atm. pollutants 77—78486
rhodamine 6G laser, pumping efficiency enhancement using luminesc. filters 77—38882
rhodamine 6G laser, radially nonuniform lamp pumping, lasing power 79—64220
rhodamine 6G laser amplifier pumped by N_2 laser, sub nsec pulse generation 80—1232
rhodamine 6G laser radiation interaction with Al 80—97387
rhodamine 6G laser with lamp excitation, cavity thermooptical distortions effect 79—55135
rhodamine 6G laser with lamp pumping, spatial coherence 77—50669
rhodamine 6G pulsed dye laser, locking by anomalous dispersion in vapour cell 79—7163
rhodamine 6G soln., cyclooctatetraene effects on laser props. *(Russian)* 78—25875
rhodamine 6G solns., acousto-optical distortions induced by pump lamp radn. 79—73898
rhodamine 6G solns., picosec. kinetics of emission 79—76685
rhodamine 6G solution, absolute fluoresc. quantum yield determ. by calorimetric method 80—78851
rhodamine 6G solution, flashlamp pumped, inductive storage units for laser pumping 79—89916

dye lasers continued
rhodamine 6G solution, induced pump absorption, lasing threshold and efficiency 78—50773
rhodamine 6G solution, pulsed high energy, freq. shift due to RI changes 77—7078
rhodamine 6G solution, stimulated emission under internal refl. conditions 77—58327
rhodamine 6G solution laser, pulse tube pumping *(Russian)* 77—88785
rhodamine 6G synchronously mode locked CW laser, pulse width depend. on intracavity bandwidth 78—66821
rhodamine 6G synchronously pumped laser combined with external compressor, sub-ps pulse generation 79—55148
rhodamine 6G thin film ring laser, emission features 79—64221
rhodamine 6G water soln. laser with spatial lamp pumping, spatial coherent emission 78—82963
rhodamine 6G-isopropyl or ethyl alcohol solution, flashlamp pumped laser, photochem. effects 80—53287
rhodamine 6G-ketocyanine mixed solns., wideband lasing 79—957
rhodamine 6G-safranin-T mixed dye laser energy transfer, 31 nm tuning range 80—58532
rhodamine 6GDN, synchronous tunable ps laser 77—75560
rhodamine 6Zh pulsed laser, simple transverse mode observation *(Russian)* 79—72565
rhodamine (6G-DTDC and 6G-CV) in alchohol solns., energy transfer by means of photobleaching 79—23031
rhodamine B, excited singlet-state absorpt. effect on lasing 78—17930
rhodamine B, laser, lamp-pumped, solvent and temp. depend. 79—3692
rhodamine B, mol. fluoresc. decay time, self-absorption 79—68255
rhodamine B, soln., bleaching and laser props., detergent effects 79—59697
rhodamine B, tunable freq. doubled CW laser using RbH_2PO_4 cryst. 80—53372
rhodamine B activated waveguide, amplification of narrow-band signal 79—36930
rhodamine B and 6G, fluoresc. decay time meas. in different solns. 80—9637
rhodamine B and 6G, laser wavelength and dye conc. 78—50770
rhodamine B dye laser, N_2 laser-pumped, pulse time behaviour 79—31894
rhodamine C and 6G, strong base solns., electronic spectra, temp. depend. 79—85987
rhodamine dye, coherent ellipsometry determ. of third order polarisability 79—71511
rhodamine dye, intercombination conversion rate consts. from triple quenching by 1,4-diphenylbutadiene 79—956
rhodamine dye soln. series, flashtube-pumped, calc. and expt. generated quantum power 78—50772
rhodamine dye solns., amplified spontaneous emission 79—45941
rhodamine dyes, amplified spontaneous emission, picosecond pulse generation 79—3691
rhodamine dyes, methanol-water solns., triplet state EPR spectra, aggregation, mol. orientation 77—48031
rhodamine dyes, soln. induced singlet-singlet absorption spectra 78—46363
rhodamine G, in glycerine-H_2O mixture, fluoresc. polarisation spectra, 350 and 540 nm excitation 79—98139
rhodamine G in ethanol, flash-lamp pumped, intracavity absorpt. anal. method sensitivity 79—57328
rhodamine G solutions, LiCl and $NaClO_4$ electrolyte influence on its lasing props. 80—91788
rhodamine GG tunable narrowband subnanosecond dye laser, optical pumped 79—81445
rhodamine laser light shifting into blue-green, using parametric amplifiers 79—18471
rhodamine R derivatives, water (heavy water) detergent solns., luminesc., lasing 79—56836
rhodamine solution, picosec. spectroscopy with antiStokes excitation, orientational rearrangement *(Russian)* 79—42984
rhodamine Zh, isomer separation, identification and emission efficiencies *(Russian)* 77—83871
rhodamine-6G mode locked dye laser pulse width monitoring by rapid scan autocorrelator 80—87421
rhodamine-B solutions, thermochromic and hyperchromic effects 79—91977
rhodamines, solns., amplification and induced absorpt., cross-sections, spectra 77—68208
rhodamines in ethanol soln., gain and induced absorpt., struct. props. 77—24890
ring, optical bistability and first order phase transition 80—95918
ring CW laser, high efficiency, tunable single-freq. radiation over visible spectrum 79—72589
ring laser, CW, feedback controlled pulse self-excitation 78—22152
ring laser, CW, optical diode to enforce one-direction travelling wave operation 80—69427
ring laser, CW, second-harmonic, single, freq. UV type 79—41392
ring laser, new high efficiency system *(German)* 79—10325
ring laser, performance and appl., internal freq. doubling possibility *(German)* 79—36927
ring laser with saturable absorber, pulse train generation *(German)* 77—38936
ring resonator CW laser, mode selection 80—14371
ring travelling-wave CW laser, mode locking 80—43354
saturable absorbed properties of laser dye, stimulated propag. of pump flux 79—41377
saturable absorber laser and dye laser, comparison of time depend. density matrix eqns. 79—86176
saturable absorbing dye, intense picosec. pulse photodynamics 77—34887
secondary fluorescence, of dye under very powerful pumping, fine struct. spectra 77—58383
selection criteria for tunable lasers, product survey 77—79849
self frequency locking, strong field effect on intracavity atoms 79—86198
self-injected laser-pumped, nanosecond pulse generation by cavity flipping 79—18457
SHG, automatically tunable 79—985
SHG, computer controlled intracavity, in CW ring dye laser 80—91841
short cavity blue dye laser, nearly transform-limited pulses 79—45965
short cavity design with multiple prism beam expander, high performance 78—1250
short resonator, tunable, pumped by travelling wave N_2 laser 80—48291
short tunable pulses from dye lasers pumped by N_2-laser 77—7126
short-cavity picosecond dye laser design 79—41390

dye lasers continued
short-pulse generation, simple and reliable technique 77—38909
simmer-enhanced flashlamp-pumped, efficiency improvement 79—64240
simultaneous 2 or 3 band tunable emission, band competition 77—7082
single mode operation of standing wave laser, using intracavity Michelson reflectors 79—89918
single pulse extraction from mode locked train using dye amplifier 77—19314
single pulse spectral distrib. meas. 79—3732
single-frequency pulsed dye laser with injection of low-power radiation 80—99756
single-mode, precise freq. tuning 78—33752
single-mode and multimode CW, as sources for obtaining power-squared corrected two-photon spectra 80—78849
six-level model, triplet-triplet pumping 78—25870
small linewidth, N_2 laser pumped *(German)* 78—1246
spark pumped compact modular design with high peak power 77—10950
spatial mode structure, thermal effects 79—36943
spatial-frequency selector, $LiNbO_3$ volume holographic grating 80—53240
spatially inhomogeneous gain saturation due to amplified spontaneous emission 77—42534
spectral characteristics of laser with modes locked to atomic absorption lines 80—9881
spectral condensation of dye laser emission near absorpt. lines of intracavity atoms 80—53286
spectral evolution, analytical eqn. 77—3580
spectral kinetics of complex org. mol. soln. lasers with tube pumping *(Russian)* 77—46719
spectral narrowing by intracavity Na atomic beam 79—55159
spectral narrowing by two-stage injection locking, flashlamp-pumped high-energy laser 79—81450
spectral narrowing on N_2 laser pumping 78—25903
spectral properties, hole-burning effects 80—102718
spectral selection and tuning using thin layer Fabry-Perot interferometer *(German)* 79—94242
spectrally narrow pulsed, without beam expander 78—79028
spectrometer, high resolution, for meas. of isotope, isomer shifts and hyperfine struct. 77—61141
spectrometer, two-photon, based on flashlamp-pumped dye lasers 78—16860
spectroscopic light source appl., props. *(German)* 79—12864
spectroscopic light source appl. *(German)* 78—89552
spectroscopy of biomolecules 77—86444
stability, input energy per flash, dye conc. and mirror reflectivity effects 77—31100
stability conditions for laser cavities with two foci 78—66850
stilbene laser dye picosec. laser obs. 79—36891
stilbene tunable narrowband subnanosecond dye laser, optical pumped 79—81445
stimulated emission, laser spectral kinetics 79—55132
stimulated emission from dye soln., amplitude-spectral asymmetry 79—10299
stimulated emission short-wavelength limit in dye solns., induced absorpt. spectra 79—59696
sub-picosecond optical pulses, generation and meas. 80—23731
subnanosecond dual freq. pulses from mm cavity laser using two dyes 78—17956
subnanosecond pulse generation with N_2 laser pumping, laser design 80—87403
subnanosecond radiation pulse formation mechanism, axial period *(Russian)* 77—50700
subnanosecond single photon counting fluorescence spectroscopy using tunable dye laser excitation 78—86355
subpicosecond laser directly pumped by mode-locked Ar laser 79—22969
subpicosecond pulse production 77—83906
subpicosecond spectroscopy, high intensity, broad wavelength tunability 79—44950
subpicosecond spectroscopy by passively modelocked continuously operated dye lasers 78—58066
superfluorescence influence on laser-dye amplifier system operation 79—10300
superluminescence pulses, waveform analysis *(Russian)* 78—22120
superluminescent laser theory for dye soln. *(Russian)* 79—951
superluminescent source of optical noise for nonlinear optics *(Russian)* 78—79033
superradiance and damping characteristics obs. 77—83869
superradiant dye laser, coherence and beam geometry 78—37876
synchronous mode locking, composite gain and absorber medium, sub ps pulses 78—79046
synchronous mode locking, two CW dye lasers sharing common amplifier medium 77—7119
synchronously mode-locked, used for material polaris. relax. meas. 79—44952
synchronously mode-locked CW laser, intracavity SHG in thin $NH_4H_2PO_4$ cryst. 80—95945
synchronously pumped mode-locked CW system, pulse characts., cavity detuning effect 79—3726
TEM_{00} tunable laser system high-power, with frequency-doubling crystal 79—50306
temporal compression of 5890 Å CW output, using Na vapour delay line 78—46688
p-terphenyl, and PBD mixtures, tunable narrow bandwidth 2 MW lasers 79—41378
p-terphenyl, flashlamp pumped, driven by Marx-bank generator 77—19311
p-terphenyl, narrow bandwidth pulsed UV laser, 3350 to 3450 Å 80—38032
p-terphenyl, substituted, dye laser and spectral characts., output power, conversion efficiency 80—23681
p-terphenyl, vap., electron energy loss spectra rel. to lasing 78—29947
p-terphenyl in cyclohexane, 1 MW laser, conversion efficiency and tuning curve 77—58323
p-terphenyl in p-dioxane, tunable UV emission, KrF laser pumped 77—7117
tertiary amines, lasing action feasibility, excited state absorpt., two step photoionisation 80—23682
3,6-tetramethyldiamino-N-methyphthalimide, in organic solvent, hot luminesc. 79—4842
thin film waveguide evanescent type, gain meas. 80—95908
thin-film laser with a two-dimensional diffraction grating 80—9906

dye lasers continued
thin-film laser with spatially separated multiple-frequency outputs 80—43368
thin-film ROROR dyestuff lasers *(Russian)* 79—7142
thin-film waveguide laser amplifier with lossy cladding 80—64074
three-stage birefringent filter, tuning over visible region 80—58667
threshold behaviour, second and first order phase transition analogy 79—953
threshold singularities of optically pumped dye lasers 79—3703
thyratron switched flashlamp pumped reliable dye laser 79—31930
time resolved spectra of spontaneous and stimulated emission 77—71983
TOPOT, 1,4-bi[2-(5-p-tolyloxazolyl)]benzene laser, bleaching of vapour 80—19027
TOPOT vapour dye lasers with multiplate reflectors 80—83606
TP-C-DMP, new bifluorophoric laser dye with intramolecular energy transfer, lasing characts. 78—74899
TP-CSC-DMP, bifluorophoric mol. ultrafast intramolecular energy transfer 78—74900
Transient pump absorption, generation threshold and efficiency of dye lasers *(Russian)* 78—25871
transverse flow, unstable resonator mode control 77—88789
transverse flow, unstable resonator mode control 78—46671
transverse pumping by frequency-doubled Nd:YAG laser 79—72561
travelling unidirectional light amplifier, operational characts. 78—13725
triaxial flashlamp-pumped dye laser, efficient high-energy SHG 80—38061
triazinyl-stilbene compounds, lasing characts. 78—29948
triazinyl-stilbenes, sulphonated, CW operation in blue and violet spectral region 78—42334
tricarbocyanine near IR dyes, flashlamp-pumped, photochemical stability 80—83604
triplet loss influence on relaxation oscills. 80—23680
triplet losses, six level model 77—14711
triplet state, rel. to chem. stability and H-bonding 77—75508
tunable, 545-680 nm radiation efficient conversion to 360-415 nm UV range 80—74439
tunable, flashlamp excited, triplet quenching effect 79—31892
tunable, for high resolution laser spectroscopy *(German)* 79—26138
tunable, improved freq. doubling for 217-360 nm 78—33781
tunable, N_2 laser pump for oscillator-amplifier system *(Japanese)* 79—68406
tunable, N_2 pumped, setting up, high resolution spectrosc. obs. 79—86177
tunable, O_2 quenching effect 79—72564
tunable, opto-galvanic effect in plasma, spectroscopy appl. 78—95977
tunable, simultaneous two wavelength operation *(French)* 78—29971
tunable blue picosecond pulses 77—88740
tunable coherent radiation source, 185 to 880 nm, stimulated Raman scatt. in H_2 79—31980
tunable CW mode-locked system, sub ps pulses 78—42362
tunable DFB, with fan-shaped grating 77—88739
tunable dye laser, dye dissolved in liq. cryst., second order phase transform. 80—43328
tunable dye laser, flashlamp pumped, ultra-narrow bandwidth 80—9897
tunable dye laser, for picosec. spectroscopy, 400-500 nm 78—82988
tunable dye laser, N_2-laser pumped, using single prism beam expander *(Chinese)* 80—74389
tunable dye laser fast light deflection, ultrahigh resolution 78—63178
tunable dye laser with laser pumping, integral radiation spectra, spectral kinetics *(Russian)* 77—54736
tunable dye lasers for future optical storage, patent 79—98301
tunable in 1.1 μm range, 13 MW peak power, Nd:YAG laser pump 79—86190
tunable in 1.1 μm region, picosecond laser, Nd:YAG laser pump 79—86191
tunable laser, undergraduate demonstration expts. 78—61988
tunable laser dyes, intersystem crossing rates and saturation paramaters in triplet state 77—36280
tunable laser excited by pulsed N_2 gas laser *(Korean)* 79—13963
tunable laser interferometry, oscillator strength meas. 80—105697
tunable laser with microcomposition matrix active medium 79—64238
tunable medium IR down conversion in GaSe using Nd^{3+}:YAG and dye lasers 79—55183
tunable picosecond UV dye laser pumped by third harmonic of Nd:YAG laser 79—31927
tunable ps high efficiency system for 340 nm to near IR 78—50789
tunable pulses, picosecond duration, production by synchronous pumping 79—22976
tunable single mode injection locked flashlamp pumped dye laser 77—19303
tunable source appl., capabilities extension and appl. 79—18495
tunable sources for vac. UV 77—68219
tunable superradiant emission, planar cell 77—7116
tunable ultrashort pulse generation 80—95931
tunable ultrashort pulse generation in N_2 laser pumped dye laser *(German)* 79—27275
tunable UV and visible lasers 78—59029
tuning, using tilted birefringent Fabry-Perot etalon *(Japanese)* 77—54735
tuning, wavelength shifts, surfaces model 77—7079
tuning and active mode-locking, interferometry technique 79—22982
tuning by birefringent Fabry-Perot etalon, electrooptic mechanical methods 77—75500
tuning by birefringent Fabry-Perot etalons *(Japanese)* 77—7125
tuning by dielectric interference filter-coated prism 79—10322
tuning by multistage interference polarisation filter 80—64091
tuning of emission freq. with cholesteric liq. cryst. Bragg mirror 79—89931
tuning of pulse radiation, up to 100 cm^{-1} 78—29986
tuning range extension using electrochem. reaction products 79—31895
tuning ranges in near UV, 390 to 333 nm, 266 nm pumped dyes 80—48239
tuning ranges of 355 nm pumped dyes from 410 to 715 NM 79—76683
tuning via high dispersion rutile prism 77—7107
tuning with stimulated electronic Raman scatt. in Cs vap. 78—1300
two wavelength outputs with orthogonal polarisations 78—50792
two-band stimulated fluorescence, laser action and bleaching effect in organic dyes 79—41190
two-wavelength double-pulse tunable dye laser for differential absorption lidar 77—21939
two-wavelength pulsed, spectroscopic applications 80—28246

dye lasers continued
two-wavelength single mode operation, using grazing incidence grating 80−53329
ultra-short light pulse generation, review *(Japanese)* 79−45973
ultrashort pulse formation mechanism rel. to peak transition process *(Russian)* 77−54745
ultrashort pulse generation, using distributed feedback *(Russian)* 77−38883
ultrashort pulse generation 80−58612
unfolded cavity using planoconvex lenses, for CW mode-locked dye laser 80−5765
unstable resonator, injection locking 79−979
unstable resonator calculation, laser operating on organic compound solution 80−58600
unstable resonators for annular gain vol. lasers 78−46672
unstable ring resonator, N_2 laser pumped 80−53326
uranin in ethanol soln., and dye mixtures, excitation by Cu vapour laser 80−28230
uranine, intercombination conversion rate consts. from triplet quenching by 1,4-diphenylbutadiene 79−956
UV, optically pumped by CO_2-laser-produced plasma 77−61947
UV irradiation of dye solns., bleaching and diffusion effects 77−42533
UV laser *(Japanese)* 79−3686
UV radiation prod., freq. doubling of N_2 laser pumped dye laser output 77−743
UV simultaneous tunable two-wavelength oscill., lidar source for atm. SO_2 detect. 77−88784
vapour, fluoresc. meas., buffer gases effect 77−75503
vapour dye pumped by N_2 laser, fluorescence and amplified spontaneous emission characts. 79−3694
vapour phase, down conversion of 351 nm radiation for fusion lasers 79−3695
vapour phase, molecular excitation and relaxation, discharge excitation 77−10916
vapour phase system using dye vapour-inert gas mixture, electron beam excitation 77−23672
velocimeter system, appl. to atom velocity meas. and flow speed meas. 78−46467
viscous media with induced absorption at stimulated emission wavelength, laser threshold 77−58326
VUV radiation, narrowband tunable, at Lyman-α wavelength 80−78907
water-soluble laser dyes, efficient in blue spectral region 78−33736
waveguide resonator for transverse mode control in high gain mm. bore laser 78−1268
wavelength, automatic reading by wavelength-modulation technique *(Japanese)* 78−1286
wavelength conversion of pulsed solid and gas lasers, organic dye attachment 79−7147
wavelength scanning with microcomputer control 79−94248
wavelength tuning by changing dye soln. conc. 78−17967
xanthene dye N-92+inert gas buffer, electron beam excited, fluoresc., energy transfer 78−25877
xanthene dyes, effect of pH on laser output power 77−38881
xanthene dyes, fluorescence efficiency of laser dyes 77−42531
xanthene-acridine dye mixture, flashlamp pumped, tuning props. 77−3579
xanthrene, dye soln., transient dichroism, rot. diffusion anomalies 79−87414
Cl_2, laser-induced fluorescence 79−45754
N_2 laser flash photolysis system, 5 μJ with 3 ns time resolution 80−1211
N_2 laser pumped, construction and performance of laser and pumping source *(Japanese)* 77−58341
N_2 laser pumped, single mode operation 78−87060
N_2 laser-pumped, subns. relax. oscills. 78−82959
Na fluorescein, laser wavelength and dye conc. 78−50770
Na fluoresceine, soln., lasing kinetics calcs. *(Russian)* 79−13778
Xe-ion laser pumped construction and performance of laser and pumping source *(Japanese)* 77−58341

dyeing
non-Newtonian fluids, particle movement, appl. to dyeing and haematology *(German)* 78−87369
polymer, dye conc. distrib. determ., microdensitometry *(German)* 77−37962
solar energy applications, hot water systems, dyeing, in textile industry, commercial aspects 79−83576
ZnO dye sensitisation in electrostatic photography 79−67404

dynamic braking *see braking*

dynamic nuclear polarisation
see also CIDNP; Overhauser effect; solid effect
^{1}H and ^{19}F dynamic polarisation, Cl scalar coupling enhancement 78−66568
anthracene: phenazine, optical nuclear polarisation, 1.4 to 300K *(German)* 77−63321
aromatic molecular crystals, optical nuclear polarization by optically excited triplet states 79−19804
aromatic molecules in cryst. lattice, phosphoresc. intensity and optical nuclear polarisation, level anticrossing effects 78−91992
cyclohexane, plastic-phase, NO-doped, heterogeneous solid soln., mag. reson. evidence 78−34449
di-t-butyl nitroxide, in benzene, solvent-solute interactions, ESR, DNP 78−17698
1,4-dibromonaphthalene, proton spin relaxation by optically excited triplet states 79−19810
dichlorofluoromethane, ^{1}H and ^{19}F dynamic polarisation, Cl scalar coupling enhancement 78−66568
dielectrics, solid, dipole electron-nucleus interaction, review 80−29649
dynamic magnetoresonance effects in solids 80−20447
dynamic polarisability, TDHF theory and RPA sum rules 78−78292
EPR line saturation, electron dipole reservoir cooling and dynamic polaris. of nuclei *(Russian)* 79−87331
EPR saturation spectrum, effect of strong microwave field 80−15785
fluorene:acridine (phenazine)(anthracene), optical nuclear polarisation, non-crossing rule, guest-host complex 77−42339
fluorene, optical polarisation of H nuclei, 4.2K *(Russian)* 77−12255
free radical solutions, relaxation process effect on coefficient of dynamic polarisation *(French)* 78−39446
Haupt effect, coupled rotational and dipolar relaxation of methyl groups 77−32292
hexafluorobenzene+bisdiphenylenephenylallyl radical, solvent effects on collisions, dynamic nucl. polaris., spin-lattice relax. 77−63303

dynamic nuclear polarisation continued
imidazoline nitroxide radical, H-bonding with H donors, NMR, DNP and spin lattice meas. 79−15971
line broadening effects associated with cryst. imperfections, theory 78−35021
nonlinear effects on time taken to establish steady state 80−11293
nuclear relaxation, spin temperature, solid effect, and thermal mixing, review of principles 78−64297
nuclear relaxation under ESR saturation conditions 77−8451
optical nuclear polarisation, field and orientation depend., non-crossing rule, perturbation anal. 77−42337
optical nuclear polarisation, the non-crossing rule, electronic relax. perturbation anal. 77−42338
organic free radical solutions, mol. motions 78−91991
polyacetylene and polyacetylene: AsF_5, one-dimens. spin diffusion, NMR T_1 and dynamic nuclear polarisation meas. 80−44946
propanediol, behaviour of nucl. spins near highly polarised paramag. centres 77−77127
radiation resistant materials, dynamic polarisation 79−31283
RF saturation spectroscopy, optical nucl. polarisation detect., excited state NMR and ESR transition mechanisms 80−54995
ruby, correlated ESR and NMR c-axis variation effect, dynamic nuclear polarisation 78−72436
ruby, dynamical polarisation of ^{27}Al, appl. of NMR line acoustic saturation in quantum strain detector 77−51009
ruby, ESR and NMR correl. line broadening effect assoc. with external mag. field inhomogeneities 80−50227
ruby NMR laser, spontaneous nucl. spin system self organisation 79−916
semiconductor, dynamic polarisation of nuclei due to optical orientation of conduction electrons 78−19376
semiconductor, luminesc. polarisation jumps and oscills. *(Russian)* 77−85619
semiconductor, spin polarisation induced by optical pumping 79−95681
single crystal, correlated ESR and NMR c-axis variation effect, dynamic nuclear polarisation 78−72436
speed of DNP, impurity acting as centre of polarisation coinciding with reson. freq. of distant nuclei *(French)* 78−91990
steady state nuclear and electronic subsystems by dynamic cooling of nuclei *(Russian)* 77−63322
Suhl-Nakamura interaction effects, nuclear spin motion in strong RF field 77−43905
TCNQ salt, K^+TCNQ^-, temp. depend. of dynamic nucl. polarisation enhancement of protons 78−6601
TCNQ-DIP Φ_4, electronic diffusion coeffs. in chains, proton spin-lattice relax. and dynamic nucl. polarisation 80−25241
TCNQ-potassium, dynamic nucl. polarisation exam., temp. depend. 78−39447
1,2,4,5-tetrachlorobenzene, proton spin relaxation by optically excited triplet states 79−19810
toluene, dynamic polarization in radiation resistant materials 79−31283
TTF-TCNQ, dynamic nucl. polarisation exam., temp. depend. 78−39447
TTF-TCNQ, temp. depend. of dynamic nucl. polarisation enhancement of protons 78−6601
$Al_{0.25}Ga_{0.75}As$, optically oriented electron, nuclear spin systems, local anisotropy effects on states, resonances *(Russian)* 78−43679
Al_2O_3:Cr^{3+}, solid-state nuclear spin-flip maser pumped by dynamic nuclear polarisation 77−31084
Al_2O_3:Fe^{3+}, dynamic nuclear polarisation, correl. ESR and NMR strain-broadening effects 77−48090
^{27}Al, distant ENDOR and dynamic nucl. polarisation 80−2664
CaF_2, spin-diffusion const. 77−66432
CaF_2:Tm^{2+}, single cryst., ^{19}F nucl. spin cooling of Tm^{2+} electronic spin *(French)* 77−66440
CdSe, optically pumped, dynamic polarisation of nucl. moments 78−68411
^{112}Cd, pionic atoms, dynamical nuclear polarisation, nuclear structure effects 79−94113
Cr complex, Cr(V)-dimethylformamide, proton dynamic polaris. and relax. 78−91988
Cr complex, Cr(V)-fluoroorganics, proton and ^{19}F dynamic polaris. and relax. 78−91989
Cr(V) complex, paramagnetic, dynamic polarisation of protons and deuterons 79−36453
Fe complex $Fe(NO)[S_2CN(C_2H_5)_2]_2$ in frozen toluene, for dynamically proton polarised target 78−52378
GaAs-AlAs mixed crystal, optical obs. of multiple-photon absorpt. NMR *(Russian)* 77−90073
HD, solid, enhanced nucl. polarisation of D 77−8450
^{1}H, scalar dynamic polaris. in trifluoroacetic acid solns. 78−23371
LaF_3:Pr^{3+}, $^1D_2$ metastable state, hyperfine splittings, enhanced and saturated absorpt. spectra 78−43694
LaF_3:Pr^{3+}, hyperfine splitting of $^1D_2$ metastable state, RF optical double reson. 78−35067
LaF_3:Pr^{3+}, nuclear quadrupole interaction, optical-RF double reson. meas. of ground electronic state 77−48092
$La_2Mg_3(NO_3)_{12}.24D_2O$:Nd, dynamic polarisation of deuterons in individual sites 77−59484
$La_2Mg_3(NO_3)_{12}.24H_2O$:$Nd^{3+}$, polarised neutron diffr. from dynamically and statically polarised protons 80−44078
LiF, behaviour of nucl. spins near highly polarised paramag. centres 77−77127
LiH, F-center, dynamic and NEDOR polarisation meas. *(French)* 77−28481
LiH, nucl. antiferromag. struct., neutron diffr. and dynamic polarisation *(French)* 78−88226
LiH, nuclear antiferromagnetism, dynamic nuclear polaris., NMR 79−1724
LiH, nuclear antiferromagnetism studied by neutron diffr. 79−11358
$LiTmF_4$ Van Vleck paramagnet, electron and nuclear spin-lattice relaxation of Er^{3+} ions 79−95643
^{6}LiD, polarised target material, DNP 80−87007
Mg_2SiO_4, NMR of ^{29}Si and ^{25}Mg with dynamic polarisation technique 78−56405
NH_3, solid, proton irradiated, dynamic nucl. polarisation below 0.5K 79−78569
^{110}Pd, pionic atoms, dynamical nuclear polarisation, nuclear structure effects 79−94113
^{104}Ru, pionic atoms, dynamical nuclear polarisation, nuclear structure effects 79−94113

dynamic nuclear polarisation continued
Si, compensated, ^{29}Si dynamic polarisation by optical pumping in weak mag. field *(Russian)* 77—40152
Si, compensated, ^{29}Si nuclei optical polarisation, nucl. relax. effects *(Russian)* 77—43907
Si, nuclear polarisation due to optical pumping, weak mag. field *(Russian)* 79—19805
Si, optically pumped, distrib. of polarisation of electrons and nuclei 77—59485
Si, optically pumped, dynamic polarisation and mag. relax. of ^{29}Si 78—48081
Si:Au donor and acceptor centre obs. using IR absorpt. and dynamic nucl. polarisation with optical pumping 80—54639
Si:Bi(,As), optical polarisation of ^{29}Si nuclei, nucl. relax. due to optical pumping 80—2665
Si:Ho(Gd)(Yb), impurities behaviour, dynamic nucl. polarisation 79—78568
Si:P, Gd, optical orientation of ^{29}Si nucleus, effect of donor level implantation depth *(Russian)* 77—8452
n-Si:P, optical orientation of ^{29}Si and its depend. on pumping light intensity *(Russian)* 77—4581
Si:P, spin relax. time of electrons determ., dynamic polarisation of ^{29}Si nuclei 77—55730
Si:P(Sb), electron-nucl. interaction under optical pumping, ^{29}Si optical polarisation meas. 79—95680
^{29}Si, nuclear dynamic polarisation, impurity centre photoionisation, extrinsic light absorpt. *(Russian)* 79—15378
^{150}Sm, pionic atoms, dynamical nuclear polarisation, nuclear structure effects 79—94113
^{119}Sn free radicals, dynamic nucl. polarisation in solution 77—88475
^{48}Ti, pionic atoms, dynamical nuclear polarisation, nuclear structure effects 79—94113
ZnTe:Mn^{2+}, forbidden transitions of Mn^{2+} induced by hyperfine interactions 80—60458

dynamic programming
see also integer programming
Attached Processor for Speech 80—96145
automatic speaker verification by cepstral analysis 80—91998
automatic spoken word recognition using linguistic information 79—55274
bar optimal design by dynamic programming *(Polish)* 79—64542
classical relativistic dynamics fundamentals revisited *(French)* 78—62074
compressed rod with large deflections, optimal design by dynamic programming *(Polish)* 78—22286
continuous speech recognition system for data base consultation 80—91990
electrocardiological diagnostic efficiency improvement by cardiovascular system model dynamic optimisation 79—39569
electron optics, mag. field with min. spherical aberration 78—9313
electron optics optimisation using dynamic programming 77—61907
electrostatic immersion lens with minimum spherical aberration, dynamic programming search 78—25789
flexible bar, min. vol. design by dynamic programming *(Polish)* 78—13965
general inverse problem, appl. of dynamic programming 78—45475
lungs long-term forced ventilation control excitation 77—60296
modular solar collector development for large solar generators 79—96467
multiplicative Markov decision chain recursions 77—53758
multispectral radiance method for temp. distribution meas. *(Japanese)* 78—77912
nuclear reactor closed-loop control system synthesis 77—3117
nuclear reactor fuel replacement, optimal strategy *(Czech)* 77—42112
optimal control of anaesthesia administration 77—5107
optimum control theory, Hamilton-Jacobi theorem, canonical transforms 78—20962
PWR steam supply control system optimisation 78—50251
radiation therapy of malignant growths, optimisation 79—5337
reservoir management stochastic model 77—73776
respiratory airflow pattern modelling by optimisation criteria 78—80898
rhythm analysis, long-term ECG data storage and multipass scanning 79—39578
scan-rescan process anal. *(Japanese)* 78—3602
shells of revolution, stability, dynamic programming 79—32270
spaceship, fission-engined series-staged, propulsion system model 77—2321
spatial reactor control methods 77—83056
stochastic reservoir optimisation, discrete representation of storage 77—64354
syllable-based recogniser for continuous speech 80—91986
SO_2 gas pollution of Osaka city, optimal discharge control 79—52993

dynamic response
anemometer, paired Gill-type propeller, effective response 77—70846
artificial satellite with gravitational attitude control, dynamics 77—25905
audiometric impedance meas. instrumentation 77—78005
beam dynamic deflection under external force of time-dependent frequency 78—83289
biodynamic subminiature piezoresistive accelerometer performance evaluation 78—20340
bone mechanical properties characterisation by dynamic response 80—76782
BWR, HDR reactor, design of blowdown loading expts., dynamic response of PWR-vessel internals 77—88204
cable-stayed cantilever beam dynamics 78—46889
cardiac assistance, in-series, by intra-aortic balloon pumping, haemodynamic responses, computer model 79—96711
circular plates subjected to transient loads, nonlinear dynamic response 78—16648
complex dynamic systems, elements of statistical energy anal. 77—75740
composite plates with cut-outs, clamped 78—30222
composite plates with cut-outs, simply-supported 78—30221
continuous systems with distributed parameters, displacement excitation 77—39254
cylindrical shell to conc. impact load 78—67072
cylindrical shells, dynamic response to concentrated impulse loads 78—22259
cylindrical shells, moving ring load effects 77—31218
EEG data compression via computer-generated evoked response to sensory stimuli 78—36016
elastic continuum, determ. using modal anal. 78—8242
elastic half-space containing cylindrical inclusion, axisymmetric waves 78—5684
elastodynamic equation on sphere, tensor spherical harmonics appl. 80—98296
electrosensory afferent, dogfish, adaptation, neuron discharge regression anal. 78—35833
EM micrometers, position transducers, contactless displacement meas. appl. 78—41277
errors in response calcs. for nonclassically damped structures 78—9587
flow rate transducer dynamic error determ. 77—72386
fluid flow in semicircular canals, utricle effect 77—86517
fluid-structure interaction, dynamic response 77—50917
fluidic element nonstationary flow meas. by laser Doppler velocimeter with frequency tracker *(Japanese)* 78—55707
foundation dynamic interaction with viscoelastic half-space *(German)* 78—79228
free water jet, investigation using high speed motion picture anal. and conventional pressure transducer 77—37842
haemodynamic response to ventricular pacing 77—81525
head viscoelastic model, impact response 78—40234
helical springs, numerical soln. of dynamic response 78—67026
high cycle fatigue diagram based on dynamic severity criterion 78—60759
hot-film anemometers, freq. optimisation theory for dynamic response 78—26218
industrial aerodynamics, conference, Aachen 80—17712
inertial seismographs, sensitivity and dynamic range 79—39910
LMFBR, dynamic response of containment vessel and coolant wave propag., REXCO-EUR code manual 78—58349
loaded thin circular plate stability criterion 78—77700
LWR core barrel model, circular cylindrical shell, dynamic response to nonaxisymm. loading 77—88247
matrix exponential method, dynamic response via digital simulation 77—72149
measuring instrument averaging time as equivalent dynamic parameter *(Polish)* 78—29081
model and full-scale cooling tower resonance tests 78—83291
multilayered spherical vessel, elastoplastic response to intermittent internal blast loading 77—65705
nerve impulse equation, dynamic responses of impulse 78—64972
nonlinear, finite element analysis 77—27469
nuclear containment vessel, dynamic response to fluid pressure pulses 78—26077
nuclear plant design, seismic response spectrum normalisation 78—50415
nuclear plant equipment response to aircraft impact 78—50416
nuclear power plant, dynamic response to earthquake, aircraft impact, soil structure interact. 79—3208
nuclear power station response to aircraft impact 78—41875
nuclear reactor, dynamic response of ducts to press. pulses, expts., finite element calcs. 77—3124
nuclear reactor, LMFBR, HCDA, structural response calcs., methods, codes development 77—3126
nuclear reactor, structural shock tests, prototype FBR MONJU scale models, computer code verification 77—3131
nuclear reactor fuel assembly 77—46265
nuclear reactor system anal., empirical modelling appl. 78—25284
nuclear reactor vessel dynamic response to HCDA in LMFBR 77—71674
ocean current sensors, EM- and acoustic-types, performance assessment 79—25345
ocean wind wave elevation sensor array system 80—46322
offshore tower, dynamic response to ocean waves 77—80058
optical fibre drawing, diameter control improvements 78—1445
optical fibre drawing process control, optimisation theory appl. 79—90039
peak harmonic response of locally non-linear systems 78—51109
pin-ended rod under parameter excitation, partial differential eqns. appl. 77—74199
piping systems under seismic excitation, modal anal. 80—33512
prestressed beam, dynamic bending response 77—39230
prestressed cablenets, 3-D, finite element anal. 78—5650
pupillary escape, positive off-diagonal kernels as correlates of dynamic process 80—26229
pupillary system, human, same-signed 1st and 2nd degree kernels 80—26228
reactor containment, nonlinear dynamic response, seismic analysis 77—3180
retinal horizontal cell receptive field centre/surround interaction model 77—86497
rock specimens impulse response estimation, numerical method and appl. to laboratory data 79—80049
seismic wide-band recorders specification 79—39908
skirt-supported pressure vessel free vibrations, finite element analysis 79—68632
sonar towed array modelling, transverse dynamic motion study 78—30112
structural panel, rectangular, with elastic edge constraints, dynamic response, Bolotin's asymptotic method 78—75091
submerged hemispherical shells, dynamic response to earthquake motions 78—51110
tensile testing machine with automatic null-balancing load meas. instrument, dynamic behaviour investig. and control *(German)* 77—60006
two-way continuous rectangular plate free vibration theory 79—68631
upper-limb prosthesis neuroelec. control 78—44704
urethane prosthetic compound, dynamic mode determ. 79—48376
variable section rod subject to longitudinal impact with flexible load 77—89036
wind turbine generator dynamic stability, digital simulation 79—96415
Wirbelrespirometer, improvements *(German)* 78—28099
NaOH-8% $NaNO_3$ phase change thermal storage for solar total energy system 79—57481
Pt thin wire resistance thermometer dynamic response 77—22549

dynamic stability *see stability*

dynamic testing
see also fatigue testing
abrasive wear testing under conditions of rolling friction 79—15894
alloy testing for use in heat treatment furnace, disc tribometer with high temp. pin 78—95900
alloys, shape memory effect, device for testing in bending 80—66723

dynamic testing continued
apparatus, for adherence, wear resist. and thermal shock meas. of thin films 78—72943
bar-to-block based testing method for materials characteris. in high-vel. tension 80—85133
bending, three point, at large deflections as elastic moduli meas. method 78—27699
biaxial loading techniques and apparatus, cruciform specimen, elec. motor and hydropneumatic based devices 80—85129
blood vessel walls, dynamic test apparatus 80—41354
bone, spongy, dynamic elastic props., determ. techniques 80—56326
brass, crack initiation at high strain rates, uniaxial and biaxial tests 80—85141
bronze, Al and Ti, sintered frictional material, wear resistance, effect of matrix struct. 77—28911
Charpy impact test instrumentation with capacitative displacement meter *(German)* 77—28959
circular membranes, clamped under impulsive load, charact. method *(Japanese)* 77—28952
coherent-optical materials, defect magnitude effect on vibration pattern *(German)* 77—77655
coke, metallurgical, industrial strength meas. methods, critique 80—85117
column buckling criteria determ. using vibr. data 78—34098
compliance determ. of hydraulic tensile testing machine, comparison of methods *(German)* 77—21332
composite bar technique for Young's modulus and internal friction meas., multiple reson. 78—35612
composite material, compression testing fixture, new 77—77688
compression test, determ. of accurate flow props. 78—27718
concrete, damping meas., expanded hysteresis loop method 77—12665
crack growth recording, automatic, elec. resist. method 79—39070
crack opening displacement testing 77—36722
cryogenic heat pipe/radiator dynamic testing 78—94532
cushion dynamic props. by mech. impedance method 78—72953
cyclic loading phenomena simulation in nonlinear hardening model 77—21158
cyclic microstrain meas. in tension and compression 77—74389
cyclic strain diagrams recording under nonisothermal conditions, review 80—71830
damping meas., vibration excitation method, equipment 79—1928
damping props. investigation, material in bending oscillations, new method 77—21340
deformation, cyclic, static, meas., recording, automatic system 79—15893
deformation heat attachment for scanning electron microscopy *(German)* 79—20297
dental crown restoration fixation, dynamic shear testing 78—36068
device for applying dynamic torsion and static tension 79—34214
diamond, mechanical strength depend. on thermal working parameters, microcracks *(Russian)* 80—55501
discontinuous fibre reinforced composites 80—21235
elasticity constants meas. device, use at 4.2 to 1000K 78—23898
electromagnetic device for loading and measuring wear in vacuum 78—56841
electron microscope, UHV, const.-load tensile device and appls. to materials science 78—11462
EM flowmeter dynamic calibration device 80—43817
epoxy based structural adhesives, time-temp. cure behaviour, torsional braid anal. 80—55621
epoxy resin, cure history effect on dynamic mech. props. 80—54356
erosion tests, comparison of results from various methods and sources 79—61819
experimental device for measuring friction between ski and snow 78—92410
falling-weight equipment pressure pulse parameter calc. 77—67425
fatigue crack growth testing, computer-controlled stress intensity gradient technique 80—76432
fatigue loadings, random signal analysis applic. 77—44453
FFTF dynamic modelling and sensitivity analysis 79—605
fibre reinforced plastic, dynamic strain investigation using EM wave method 79—20321
fibres, high-strength and high tensile, equipment for testing elongation 78—56844
film and fabric materials, unit for testing under cyclic loads 78—7120
flat plate solar collector dynamic evaluation 79—62044
forced vibration technique for meas. of material damping 78—19964
fracture evaluation at high loading rate by extrapolation method 77—36723
fracture toughness, conf., London, England, (July 1976) 77—36714
fracture toughness, correl. with static testing 77—60022
fracture toughness, using compact tension tests 79—34218
fracture toughness determination, by instrumented impact tests 78—68861
fracture toughness meas. 77—36721
fracture toughness test evaluation 77—36715
use of frequency convertors with mechanical resonators 77—73400
friction, wear testing in various media, device 79—29319
friction and wear testing equipment for use at high temp. in air 78—56839
GFRP laminate, damage assessment by stress wave emission and dynamic mech. meas. 78—11461
glass fibre, elastic moduli, thermal history depend. *(Japanese)* 80—45333
glass fibre reinforced composite plate, under vibr. load, strength testing, device 79—29318
glass fibre reinforced epoxy laminate, tensile testing, monitoring cond. effect on stress wave emission data 79—87814
glass fibre reinforced plastics, exposed to liq. media, dynamic high-speed Young's modulus determ. *(German)* 80—85123
hard coating on metal surfaces, abrasive wear resist. meas. 79—20327
heat cycle test of stainless hollow, O-ring for ultrahigh vacuum *(Japanese)* 80—13084
hermetically sealed box, dynamic testing system, vacuum or controlled environment *(French)* 80—61060
high strain rate behaviour, incremental elastic-viscoplastic constitutive eqns. integration 80—85138
Homalite-100 plates, modified compact-tension specimens, dynamic anal. 80—97561
hot metal, dynamic yield characts. during multistage deform., plastometer design 80—85135
hot twisting, shearing stresses, anal. determ. 78—60900

dynamic testing continued
impact, of resilient materials, testing machine and expt. results 77—25223
impact force measuring system, instability *(Japanese)* 77—25222
impact testing equipment for small specimens 77—52578
impact torsional test accuracy determ. using simulation *(Japanese)* 77—56198
instrumented impact testing, critical review 77—36725
internal friction in inorganic materials, programmed controlled test equipment 77—90541
laminated plates subjected to transverse dynamic loading, stress anal. for transient response 77—31245
laminates, exposed to liq. media, dynamic high-speed Young's modulus determ. *(German)* 80—85123
limestone tubes, dynamic torsional failure obs. 80—85648
linear viscoelastic behaviour simulation using simple electrical device 79—57179
liquid system monitoring for particulate contamination 77—28956
LMFBR fuel pin plenum press. transducer 78—8884
load relaxation testing for superplastic superalloys 77—40507
load release device, instantaneous, for mech. tests 79—52524
lumbar vertebra cortical surface strain distribution tests 78—11692
mechanical analysis appl. to materials testing 79—15911
mechanical impulse testing techniques, computer evaluation, high-speed film recording 78—44343
mechanical props. of nonmetallic materials, testing installation, +600 to −190°C 78—15633
melt dynamic viscosity meas., vibr. method 77—90519
metal, deform. resist. determ., plastometer 78—7121
metal, FCC, dislocation behaviour at high strain rates, US detection method, data analysis basis 80—85136
metal, strong, compressive stress/strain props. meas. at very high strain rates, modified Hopkinson bar system 80—85128
metal thermoelastic coeff. meas. by strain gauges 78—56853
metallic materials, dynamic hardness testing, energy meas. principle 80—21241
metallic thin spring strip, bending test device 80—61052
metallurgically bonded plates, structural integrity determ. by high energy impulse 79—39111
metals, alloys, unit for dynamic testing over wide temp. range 78—60908
metals, dynamic compression testing, mech. behaviour 80—40464
miniature test-pieces, multipurpose apparatus *(Russian)* 77—52558
MOS structure dynamic volt-capacitance characteristic meas. 78—60207
motor vehicle in impact test, force meas. *(German)* 79—34271
multimaterial impact, dynamic yield point 77—32731
nonlinear materials, dynamic testing using harmonic excitation, jump phenomena 78—51141
notched and bend specimens with equivalent geometries, cyclic deform. *(German)* 77—86271
nuclear power plants, PWR, model validation 77—3087
nuclear power station, Caorso plant, dynamic tests and seismic records of RHR building 78—41872
nuclear reactor, nonlinear structural dynamics of fuel elements, press. pulses, struct. models, expt. verification 77—3125
nuclear reactor dynamic loading of press. suppression containment blow-down, power station expt. data 77—3133
particulate materials, dynamic shear strength and flow behaviour, shear cell meas. 78—53048
phenolformaldehyde resin moulding compounds, dynamic testing *(German)* 78—76699
piezoelectric dynamometer for dynamic force meas. *(Hungarian)* 78—65918
plasma coating, fused, strength of adhesion to base by gas flame soldering 78—23894
plastic ligaments and tendons, dynamic motion simulator for testing *(German)* 78—81070
plasticity experiments, review 80—35288
plastics, stress relax. estimation for elec. connectors, expt. 77—21206
plastics, stress relaxation testing method 77—52576
plastics testing, automation 80—76443
plexiglass, shock loading, method for producing isentropic compression 77—44424
Poisson's ratio determ. in coarse grained materials 77—86244
poly(di-n-heptyl itaconate), alkyl side chain independent relax., double glass transition 80—59636
polyamide 6 , glass fibre reinforced, response function characterization of thermal state in dynamic testing 79—18680
polyamides 6 and 66, response function characterization of thermal state in dynamic testing 79—18680
polybutadiene, complex modulus meas. using forced vibrations at ultralow frequency 77—70258
polycarbonate plates, modified compact-tension specimens, dynamic anal. 80—97561
polyethylene, expanded, dynamic model rel. to drop impact 78—7160
polyethylene, high-density, impact fracture behaviour, adiabatic heating at crack tip 80—85142
polyethylene, linear, draw temp. and mol. wt. effect on draw ratio and Young's modulus 80—84998
polyethylene, rheological behaviour at high shear strain rates *(French)* 80—66574
polymer, complex dynamic Young's modulus measurement equipment 78—1615
polymer, reciprocating impact wear testing apparatus, results 78—15639
polymer, stress-relaxation apparatus, stress and vibration relaxation in sound frequency range 77—1905
polymer, viscoelastic prop. meas. method in fluid and highly elastic states using forced vibrations 77—70258
polymer, wear testing of bearing material, new sliding bearing test facility 78—95862
polymer multilayer composite, wire-reinforced, dynamically loaded, crack propagation and arrest 80—97567
polymer relaxation props., automatic assembly for exam. over wide range of temp., and medium moisture contents 80—7739
polymer thin film, tensile testing multiposition unit, for testing in vacuo and gaseous media 78—11478
polymeric systems, supported on inert substrates, dynamic thermomech. study 80—55623
polymers, amorphous, semi-cryst., mech. motions, review 77—32616
polymers, apparatus for determ. of volume stress/strain state 78—23896
polymers, torsion pendulum dynamic mechanical testing 80—55620

dynamic testing continued
- polyoxymethylene copolymers, response function characterization of thermal state in dynamic testing 79—18680
- polypropene-alt-1,4-butadiene and hydrogenated derivative, mol. relaxations in glassy state 80—53177
- polystyrene melt, carbon-black filled, rheological study 80—48665
- polystyrene-b-isoprene and hydrogenated derivative, mol. relaxations in glassy state 80—53177
- porcelain-metal cermet, stress determ., meas. method *(German)* 80—76425
- post yield fracture mechanics analysis of 3-pt bonding specimens rel. to toughness testing 77—56168
- processing results of dynamic force meas. *(Hungarian)* 77—117
- PVC, tensile tests at low strain rate, secondary instability form. *(German)* 77—66727
- radial expansion technique for fracture strain meas. at high strain rates 80—85134
- rain impact damage to supersonic missile radomes simulation 77—40500
- random vibration simulator, practical realisation 80—53732
- reciprocating impact wear testing apparatus 78—15639
- refractory, resonant frequency meas. apparatus, elastic props. investigations 77—19576
- refractory, strength determ., taking account of stress/deform. relation 77—28965
- refractory, thermal shock resistance by resonant frequency expt. *(German)* 77—9009
- refractory metals, internal friction meas. from 20 to 2000°C in superhigh vac. 77—86249
- reverse torsion testing for Bauschinger effect investig. 78—7133
- rocks, hyraulic press 79—87789
- rod, strain meas. with capacitive strain gauge 77—16774
- rubber, nonlinear dynamic props. meas. under steady vibr. 80—55602
- rubber, vulcanised, device for dynamic modulus of elasticity determ. *(Polish)* 77—28963
- SEM specimen chamber use for dynamic expts., state-of-the-art review 78—23918
- servocontrolled hydraulic hot-torsion machine for hot working studies 78—27698
- sheet steel, mechanical anal. of internal friction meas. apparatus 77—32752
- shock absorber, elastic damping props. determ. unit 78—5703
- shock compression testing instrument, for microsamples, exam. of design 79—52525
- shock-loaded material, self-consistent technique for estimating dynamic yield strength 78—80692
- sinusoidal and nonsinusoidal narrow band loads, equivalence 77—70266
- soft viscoelastic material, complex modulus of elasticity determ. 77—62221
- solid cylinder, annealed, dynamic forming by compression *(Japanese)* 77—70267
- split Hopkinson pressure bar application to fracture dynamics 80—85140
- split Hopkinson pressure bar use in obtaining dynamic stress/strain data at const. strain rates *(Japanese)* 80—16630
- stator end winding under short circuit, dynamic deform. and strength *(Japanese)* 78—11465
- steel, C-Mn, types SA-516-70, SA-105-B, fracture energy criterion determ. by static and dynamic testing 80—40651
- steel, dynamic fracture toughness meas. by instrumented impact bend and compact K testing 77—36718
- steel, dynamic testing by resonant flexion, energy consumption for degradation *(French)* 78—19961
- steel, fracture toughness dynamic, interlaboratory data, statistical analysis 77—36717
- steel, low alloy, S and Mn influence on high temp. strength and ductility after solidification from melt *(German)* 80—81106
- steel, low and medium C, dynamic and static strength, strain rate and temp. depend. of flow stress 80—85139
- steel, low-alloyed, C-content influence on high temp. strength and ductility after solidification from melt *(German)* 80—81105
- steel, mild, plastic flow, photoelastic investigation of temp. and strain rate effects 77—86238
- steel, mild, plastic flow localisation under dynamic torsional loading, crit. variables 80—85015
- steel, mild, welded struct., dynamic initiation of brittle fracture, testing 77—36716
- steel, S45C and SS41 types, dynamic yield condition under dynamic torsion and static tension 79—34214
- steel, stainless, 316, ductile, prestrained, method of J_Q and δ_i determ. 77—36724
- steel, stainless, austenitic, dynamic uniaxial and biaxial stress-strain relationships 80—81122
- steel, tensile testing, effect of specimen form, specimen prep., testing velocity, straining amount *(German)* 77—16764
- steel, tensile testing of ultra high tensile roping wire 77—44426
- steel, tool, chipping resistance testing method for blanking punches *(Japanese)* 79—100308
- steel, types S25C and S45C surface damage produced by pulsating impact contact load *(Japanese)* 80—104263
- steel *(German)* 80—100869
- steel cylindrical shells, external static+pulsed press., stability *(Russian)* 77—46952
- steel granular model material, equipment for shear deform. investigation *(German)* 80—35449
- steel stretch-bend test strain distribution obs. 77—70243
- steel-concrete composite T-beam, third point loading tests, ultimate flexural strength determ. 77—86252
- steels, wave propag. effects on dynamic loading of pressure vessels 77—3090
- strain gauges, resist., in alternating sign deform., calibration 79—15901
- stress corrosion cracking test machine, design and construction, appl. to Fe-Cr-Ni alloys 80—97649
- structural deformation under dynamic loading, state variable description of material behaviour 80—85137
- structural dynamics, modal anal. 78—39993
- structural freq. response testing, impulse technique 78—39992
- styrene-isoprene triblock copolymer, mol. relax. in glassy state 80—53177
- superconductors, test facility for dynamic stress effects 77—77698
- superplastic flow, activation enthalpy determ. from strain rate changes in tensile tests 80—81127
- tear test method evaluation 77—77686

dynamic testing continued
- tensile impact tests with rupture diagram recording on pendulum machines, testing procedure 79—29313
- tensile test, alignment problems 77—16759
- tensile test piece, profile of contracted part after the beginning of necking *(German)* 77—86269
- tensile test specimen contour, expt. and calc. comparison *(German)* 77—86233
- tensile testing at const. true strain rates, test machine 79—34262
- tensile testing machine, dynamic response estimation, valuation of different methods *(German)* 77—9018
- tensile testing machine with automatic null-balancing load meas. instrument, dynamic behaviour and optimal adjustment *(German)* 77—60005
- tensile testing machine with automatic null-balancing load meas. instrument, dynamic behaviour investig. and control *(German)* 77—60006
- tensile testing of small animal ligaments, gripping device 80—81791
- tension tests, analysis of misalignment 80—11864
- thermoset and coating technology, torsional braid and thermal anal. 80—55622
- thermosetting materials, formation and props., phase diagram and torsion pendulum anal. 80—55381
- threadlike crystals, precision method of internal friction investig. 78—36997
- thremosetting resin quality control by dynamic mechanical analysis 79—74319
- torsion bomb machine for dynamic stress/strain measurements under superimposed high press. 80—85130
- torsion deformation test apparatus for 0-1150°C range in different gaseous atm. 78—7123
- torsion pendulum, automatically driven, for continuous meas. of amplitude and amplitude-independent damping 77—35099
- torsion pendulum for damping capacity meas. and related phenomena 77—77687
- torsion pendulum oscillations recording equipment for internal friction meas. 78—36998
- torsional oscillation test instrument with process computer control *(German)* 77—21344
- tower extensometer 79—83410
- triaxial testing large specimens, machine for dynamic and static testing 79—83407
- tubing, testing and failure localisation by electrodynamic method 77—63847
- uniaxial strain conditions in modified Kolsky apparatus, dynamic material behaviour meas. 78—85070
- Universal bearing H-piles, dynamic and static stress charact. method 79—70270
- US grey scale scanner dynamic range testing 78—69169
- vertical test machine for tension at speeds up to 25 m/sec 78—39968
- vibration simulating system, optimisation 80—53729
- vibration test rig for wear meas. of granules 78—56840
- vibration-simulating systems optimisation, rel. to efficiency and cost 80—53728
- viscoelastometer, dynamic, direct reading, automation, appls. to polymer films, fibres 79—3980
- volume compression sensors, sensitivity under cyclic load 79—29315
- Zircaloy-4, techniques of impact and sliding wear study 79—74337
- Ag, granular thin film, adhesion measurement 80—50807
- Al alloy, crack initiation at high strain rates, uniaxial and biaxial tests 80—85141
- Al alloy, fracture toughness determ., dynamic mode II 77—36720
- Al, annealed, dynamic testing of rate sensitivity *(Japanese)* 77—70267
- Al, pseudo-brittle fracture, aspect of impact testing 79—79111
- Al-Si-Mg (1, 0.6 wt.%), plasticity due to superimposed macrosonic and static strains 78—60719
- C fibre reinforced composite, split Hopkinson press. bar test, opt. and strain gauge methods comparison 80—85132
- Cu alloys, stress relax. estimation for elec. connectors, expt. 77—21206
- Cu, annealed, dynamic testing of rate sensitivity *(Japanese)* 77—70267
- Cu, high-purity, grain size and strain rate influence on mech. behaviour, precursors existence 80—85016
- Fe, soft, annealed, dynamic testing of rate sensitivity *(Japanese)* 77—70267
- α-Fe-Mo (1.5 and 1.8 at.%), deform., testing mode effect at stages prior to steady states 77—66721
- K, device for press. variation of yield stress, elastic constants 78—53047
- SiC, instrumented Charpy impact testing 77—36719
- Si_3N_4, HS-130, dynamic mode I fracture toughness and flexural strength 77—21248
- Si_3N_4, hot-pressed, fracture mech. parameters, indentation-precracking and double-torsion methods 80—104364
- α-U, mech. props. at very high strain rates, double-notch shear test use 80—85131

dynamical symmetry
- 27-plet mesons, mass sum rules using SU_4 dynamical-group scheme 77—26505
- ζ-function regularisation, symmetric spaces of rank 1, physical instabilities 80—57519
- σ model, vacuum stability, strong dynamical symm. breaking 77—13856
- Abelian theory, stability of solns. with dynamically broken symm. *(Russian)* 77—38093
- atomic and molecular physics, dynamical groups 80—42362
- baryons, SU(1,4) dynamical group, anal. of discrete representations, mass formulae 77—45982
- boson sd model of nuclei, group O(6) 78—33132
- bound state spectra in ϕ^4 theory and Gross-Neveu model, temp. depend. 78—4770
- breaking, renormalisation group appls. 77—57461
- broken symmetry and phase transition in early hot universe 77—22661
- charmed baryons, dynamical group selection, SU(1.4) 78—37178
- composite fields, improved effective-pot. formalism, symm. breaking renormalisation group 77—6033
- cosmology, Lagrangian or Hamiltonian formulations, shift vector field restrictions, symmetry group 80—67923
- dual resonance model, dynamical symmetry breaking, Regge meson trajectories total renormalisation *(Russian)* 77—82717
- dynamical groups of completely integrable eqns., nonlinear realisations 80—4885
- dynamical lattice theory 79—21933
- dynamical quark mass generation and the mean instanton density 79—54305

dynamical symmetry continued
extended structs. generation in field theory, dynamical symm. breaking 77−6026
fermion system with higher symmetries, energy spectrum 77−5698
filling U(4) multiplets by hadrons *(Russian)* 79−22076
first integrals and differential forms of dynamical systems 80−77983
first integrals and symmetries, geometrical obtention 80−22535
free particle, Hamiltonian mechanics, Lie theory of extended groups 80−77982
gauge field in stability subgroup of vacuum in nonlinear realization 78−390
gauge symmetry, dynamical symmetry breakdown, appl. to intermediate vector boson mass relations 79−54269
Hamiltonian mechanics, Lie theory of extended groups 80−77982
hidden symmetries in dynamical systems 80−37168
inclusive cross sections in scatt. angle, anal. props., ladder models with dynamical symmetry 79−93390
infinite macrosystems in standard representation, dynamical symmetries 80−4590
infinitesimal symplectic relations and generalized Hamiltonian dynamics 79−25878
invariant sets of dynamical system 80−57518
isotopic symmetry group in strong interactions, possible geom. origin 79−17628
ladder models, dynamical symmetry and asymptotic scale invariance 79−21959
Lagrangian density determination from transformation group 80−18084
lattice gauge theories, chiral symmetry dynamical breaking 80−99061
left-right symmetry breaking and fermion masses 80−105810
Lewis Riesenfeld harmonic oscillator, unitary declension of dynamical symmetries 79−89074
Lewis-Riesenfeld time-depend. harmonic osc., dynamical symmetries 80−4588
Lie group framework for composite particles and mass spectrum 79−97608
light quarks and QCD Boson representation, dynamical symmetry breaking 80−52472
local QFT, higher symm. interpretation, spontaneous symm. breaking, quarks and flavours 78−16942
massive Thirring model, quantized renormalized, dynamical charges, soliton, antisoliton, breather states 77−18171
massless quarks in QCD, dynamical symmetry breakdown 80−52471
meson-meson interactions, symmetry restoration in $\lambda\Phi^4$, and large NO(N) σ-models 77−5989
mesons, $SU_{1,4}$ as dynamical group, discrete representations anal., masses 77−74642
models of dynamically broken gauge theories 80−77974
N-dimensional oscillator, time-depend., SL(N+2, R) symmetry group 80−46851
narrow resonances, dynamical model, mass mixing and splitting in degenerate multiplet states 78−93813
non-Abelian symmetries, spontaneous breaking in SU(2) and SU(2)×SU(2), observable consequences 79−26252
nonlinear dissipative classical systems, time-depend. canonical transforms. 80−62885
nonrelativistic particle in spherical space, dynamical symmetries 79−26255
Poincare covariance of free massive two dimens. quantum string 77−6048
Poincare symmetry gauge theory, Einstein-Cartan theory 77−22463
projective symmetries of dynamical systems, infinitesimal symm. transforms of vector field 78−32650
pseudosymmetries and first integrals of dynamical systems 80−57517
QCD, 1+1 dimens., dynamical symmetry breakdown 80−82949
QCD, dynamic symmetry breaking *(Chinese)* 79−22050
QCD, dynamical chiral symmetry breaking and explicit breaking due to current quark masses 79−71717
quantum chromodynamics psi-spectroscopy model *(Hungarian)* 79−13068
quark-diquark model with broken colour symmetry, hadron spectrum 78−12874
quarkonium, observed dynamical groups 80−9149
relativistic composite systems, dynamical groups for motion 80−9115
relativistic harmonic-oscillator model for extended particles with SO(3,2) internal symmetry 80−18121
renormalisation group anal. of massless field theories, dynamical mass generation 77−6027
rotational symmetry in Hamiltonian dynamics 78−74134
Schrodinger equations, 3-D, rotationally invariant time-dependent potentials, degeneracy and dynamical algebras 80−62510
second order differential equations, symmetries and invariants 80−82915
second order systems, conserved quantities 79−71651
SL(2,R) dynamical Lie group, hyperbolic transforms 80−57515
SO(4,2) dynamical symmetry, unified description of bradyons and tachyons, book contrib. 79−44834
Sp(3,R) matrix elements, recursion formula 80−62878
SU_3 symmetry breaking, dynamical 78−21346
$SU(3)_E$-invariant form factor for pseudoscalar mesons 77−61288
SU(3) colour gauge theory, effective scale depend. quark masses in chiral limit 77−18222
SU(N) symmetric quantum dynamical systems, $N \to \infty$, energy spectrum for singlet and adjoint states 80−62880
systems with SO(4) and SO(3,1) symmetry 80−22534
U(N)-symmetric gauge theory in 1/N expansion, dynamical symmetry breaking 77−6006
unified theories of strong+weak+EM interactions, Weinberg angle, dynamical symm. breaking *(Russian)* 78−413
unitary representations of general covariant group algebra, Lie algebra 78−58136
weak interaction orientation to strong interaction, quark mass spectrum, dynamical symm. breaking 77−74640
weak interaction theory review, dynamical symmetry breaking 78−78131
Z_N dynamically broken symmetry, electric quark confinement in 2+1 dimens. 79−85263
Q, axial vector mesons, dynamical mixing model 78−24973
H, n-dimensional atom, Kepler problem, dynamical symmetries 80−58121

dynamics
see also ballistics; fluid dynamics; force; friction; haemodynamics; impact (mechanical); kinematics; resonance; rotating bodies; rotation; vibrating bodies; vibrations
analogy to statics, related by variational techniques 78−28934
aspherical clusters of galaxies, dynamical friction effects 78−16547
astatic gyroscope with elastic cardan suspension, dynamics *(Russian)* 78−63273
axisymmetric body under high dynamic press., integration of eqns. of motion *(Russian)* 77−50874
axisymmetric rigid body, periodic motions in gravit. field of sphere 78−36446
binary galaxies, dynamics 78−4354
binary galaxies, late type, mass-to-light ratios from luminosity-weighted averages 78−8113
brachistochrone, arbitrary initial vel. object, for teachers 79−21500
cable, nonlinear, finite segment approach 77−2532
cD galaxy in Abell 2029, envelope spectra rel. to dynamics and struct. 79−92850
Centaurus galaxy cluster, galaxy dynamics rel. to Virgo cluster redshifts 78−54061
chain of flexible bodies, appl. to NASA Space Shuttle remote manipulator arm 80−94953
chaotic behaviour in simple system, continuous Euclidean dynamics 77−60046
circulant and near circulant systems 79−12585
clusters of galaxies, dynamical evolution 78−12384
clusters of galaxies, dynamical evolution rel. to density and Bautz-Morgan type 78−28804
clusters of galaxies, tidal forces in inhomogeneous cosmological models 80−62338
clusters of galaxies, very rich, dynamics from photometric study 79−21448
cohomology of action differential forms 77−33832
Coma galaxy cluster, dynamics rel. to mass segregation and missing mass 80−98730
completely integrable classical systems connected with semisimple Lie algebras 77−17805
connectance of dynamical systems with increasing no. of degrees of freedom 78−81831
connection between symmetries and first integrals 77−67269
conservative dynamic systems, search for cyclic coords. *(Russian)* 78−65764
conservative systems, integrable by separation of variables, properties *(Italian)* 77−5656
constrained material continua, eqn. formation 79−40360
constrained material continua, functional formation of dynamics 79−40359
continental shelf dynamics and topographically trapped coastal waves 78−16057
cosmic virial theorem 77−17726
coupled linear chains, dynamics 78−89403
crawl swimmer, six-stroke, dynamics, mathematical model *(German)* 78−90702
cultivator, relative movement under random stationary ergodic load *(Rumanian)* 78−34003
cylinder, partially full of mag. liquid rolling in mag. field 77−19515
cylindrical shells, finite difference computation 78−9586
deterministic dynamics to probabilistic descriptions 80−68029
difference dynamical systems, determ. of global regions of asymptotic stability 77−67225
disc galaxies, stability anal. of finite uniformly rotating disc 79−88732
disc galaxy, axisymmetric disturbances growth rates 79−21410
double radio galaxies, symmetry rel. to dressed slingshot effect 78−12359
education, circular motion with friction, numerical and analytical solns. 80−57029
education, dynamics of variable mass system, flexible inextensible rope 78−86071
education, falling domino chain, expt. and computer program 78−62009
education, Galileo and Aristotle, re-assessed 77−49541
education, particle motion in noncentral pot., action-angle formalism 77−78922
education, work and kinetic energy, automobile min. stopping distance 77−78929
elastic structures, quadratic transformation of Gaussian process applied to stochastic dynamics *(French)* 77−54917
elastic three-body linear collision, inverse scatt. problem, for teaching 79−35468
elastodynamic equations of motion 77−42766
elastodynamics, appl. of Ritz theory to Hamilton eqn. 77−50977
elastodynamics, numerical boundary integral eqn. method 79−63036
elastodynamics, vel. pots., stress functions 78−93534
elliptical protogalaxies, dynamical evolution 78−32571
equilibrium configurations and small oscillations of some dynamical systems 79−25832
equivalent Lagrangians and quasicanonical transformations 77−33861
extragalactic radio sources, supermassive objects dynamics rel. to aligned double struct. 77−45582
fault motion in presence of friction and inhomogeneous initial stress, rupture propag. 77−86835
flat galaxies dynamics, integral eqn. for normal modes in matrix form 77−33637
fluid-structure coupling method in dynamic analysis of structs. 79−7322
force determ. in dynamical system 80−39
frontal solution algorithm for finite element frequency analysis 79−3942
fundamental principles generalisation, appl. to motion of disc on ice surface *(Russian)* 78−65762
galactic density waves, excitation at Lindblad and corotation resons. by external potential 80−22072
galactic disc, dynamical friction theory 79−35367
galaxies, cool stellar discs equilib. 78−54037
galaxies, criteria of local gravit. instability of double gaseous discs *(Chinese)* 79−17099
galaxies, extent of bars 80−46666
galaxies, free collapse of stars rotating sphere 78−93325
galaxies, numerical models and spiral struct. variability 79−25725
galaxies, origin of spiral arm instability 77−13456
galaxies, radial oscill. modes of cool stellar discs 78−57628
galaxies, tidal disturbances of material arms and star clusters by spiral density waves *(German)* 79−17086

dynamics continued
- galaxies, tidal interactions, rel. to massive halo hypothesis 77—91625
- galaxies binary systems, luminosity/separation correl. as dynamical friction effect 80—36700
- galaxies distribution, N-body model computations rel. to hierarchical clustering pattern stability 78—86026
- galaxies inner Lindblad resonance, response density in nonlinear theory 79—35366
- galaxies spiral density waves, response near corotation radius to central bar 77—17689
- galaxy aggregates, dynamics rel. to main galaxy dynamics 77—5577
- galaxy cluster interaction with supercluster, model of Emden sphere embedded in background 80—62296
- galaxy clustering evolution, cosmological N-body simulations 78—96550
- galaxy clusters, effects of long-wave primordial gravit. radiation interaction with galaxies 80—17661
- galaxy clusters, first brightest galaxy multiplicity rel. to galaxies merger time scales 79—92873
- galaxy clusters, struct. and dynamics distortion by inclusion of spurious clusters 80—101643
- Galaxy disc, local K_z-force field rel. to interstellar matter z-distrib. 80—62271
- Galaxy dynamics, appl. of generalised twice restricted three-body problem *(Russian)* 80—51643
- galaxy formation, dynamical development and struct. of six collapsing models 79—25710
- galaxy groups, mass-to-light ratios and crossing times 77—45572
- galaxy groups, virial props. 79—9010
- galaxy merging, cosmological N-body simulations 80—56922
- Gauss' principle of least constraint, appl. to dynamical systems 77—17811
- general inverse problem, appl. of dynamic programming 78—45475
- general relativistic, new Hamiltonian structure 77—45745
- general shell and axisymmetric shell elements, diagonal lumped mass matrix formulation 79—3911
- genetic systems, dynamics of neutral mutation 78—86220
- globular cluster cores evolution, life and death matters 79—25653
- globular clusters, space distrib. and galactic dynamics 79—2560
- gravitational system dynamics, two-dimensional simulation rel. to Universe large-scale struct. form. 80—98749
- gyrostat, ang. mom., kinetic energy, and generalised inertia forces 77—19517
- Hamiltonian dynamics, for closed system of N particles in mutual interaction 78—62070
- Hamiltonian dynamics formulated in Lagrangian submanifolds *(French)* 77—5657
- Hamiltonian dynamics in symplectic phase space, Nambu's formulation 77—26168
- Hamiltonian systems, first integral 77—60926
- Hamiltonians perturbed by pulses, quantum dynamics 80—17829
- hidden symmetries in dynamical systems 80—37168
- homoclinic and heteroclinic points in Hemon mapping, analyticity 80—82634
- impulse dynamical equations, nonholonomic system, solid on plane, rolling without slipping *(Italian)* 78—57769
- inhomogeneous spherical gravitating systems dynamics, simplest hydrodynamic models 80—17620
- interplanetary particle dynamics 78—57501
- interstellar large globules, struct. and dynamics 80—62246
- interstellar medium, two-phase model and intercloud wind 78—85991
- interstellar ramjet probe, relativistic flight dynamics 77—25909
- Ising models, stochastic dynamics 77—49690
- isolated star clusters statistical theory of stellar escapes *(Polish)* 78—16466
- Kepler problem, formal equivalence with Maxwell fish-eye theory 78—81733
- Kepler problem, Lorentz and anti-de Sitter group 78—36817
- kinetic energy of rotating wheel, expt. using rocket accel., for teachers 79—17168
- Kolmogorov eqn., separation of variables *(Russian)* 77—78970
- Lagrangian equations of motion analysis for systems with extremely heterogeneous inertia props. 77—53775
- Lagrangian mechanics, consts. of motion anal. 78—81829
- Lagrangian-Hamiltonian systems, partial quantisation *(Portuguese)* 80—77653
- librational, of satellites with thermally flexed appendages 78—7868
- linked rigid body systems, nonlinear eqns. of motion *(German)* 78—87254
- LMC, kinematics and dynamics compared to galaxies of Magellanic type *(German)* 80—105348
- M31, vel. dispersions in nucleus and bulge 77—26049
- M32, orbit and gravit. effect on M31 spiral arm pattern 79—21408
- M82, Ne II 12.8 micron emission obs. and galactic dynamics 79—17082
- M87, dynamical evidence for central mass concentration 78—49529
- Mach's principle, gravity and inertia, Leibniz invariant theory 77—41426
- Magellanic Stream, simulation to estimate total mass of Milky Way 77—91622
- manipulator and man's hand purposeful motion, modelling 77—78969
- mass point displacement under effect of forcing conditions *(German)* 78—86149
- method of action-angle variables and the classical dynamics of a nonlinear Lagrangian 78—77702
- MHD generator channel, liquid metal piston dynamics, math. model *(Russian)* 80—74996
- Monoceros R2 cloud, near IR and mol. obs. of rot. collapsing cloud 77—78840
- Morse-Smale inequalities for dynamic systems in a banach manifold *(Russian)* 79—12591
- motion of solid body with elastic and dissipative elements *(Russian)* 78—65763
- motion rigidity *(Russian)* 79—9099
- mud thrown from wheel, critical speed, for teachers 78—12493
- multibody system equations of motion, computer-aided formulation *(German)* 78—39
- N70, giant filamentary shell in LMC, dynamics 80—90511
- Newton's first law of motion, formulation and interpretation in various languages *(Czech)* 78—45481
- Newtonian dynamics of systems of extended bodies 79—21160
- NGC 1023 galaxy group, H I radial vels. rel. to group membership and mass/light ratio 80—82521

dynamics continued
- NGC 3686 galaxy quartet, crossing time from galaxies surface photometry 80—62297
- NGC 741, 1316, 7626, radio galaxies, dynamics 80—94871
- nondissipative system, universal properties, bifurcation phenomena and universal numbers 80—68035
- nonholonomic Chetaev systems, Lagrange eqns. derivation from modified Pontryagin maximum principle 78—12557
- nonholonomic system, motion eqns. derivation *(Russian)* 78—20956
- nonholonomic systems of higher order, Mangeron-Deleanu eqns. in Poincare-Chetaev variables 77—33853
- nonlinear structural, Newmark's algorithm stability 77—26166
- W.North Atlantic Ocean, mesoscale motion space and time scales 78—49035
- ocean, unsteady currents 78—16054
- ocean dynamics, coastal jet conceptual model for shallow seas 78—16051
- ocean wind waves generation theory, dynamical eqns. *(Russian)* 78—44840
- once-through steam generator, dynamics and control studies 77—88271
- one-dimensional self-gravitating isothermal systems, stability 80—73008
- open star clusters assoc. with interstellar gas-dust clouds, dynamics 80—101622
- orbital dynamics and rigid body dynamics, analogy 80—98537
- Orion Molecular Cloud, new dynamical model 78—93373
- Periodic Comet Taylor (1916 I), nuclei separation vels. during disintegration 78—61812
- periodic solns., numerical extrapolation 78—69663
- perturbed motion stability anal. *(Russian)* 78—16640
- Pfaff's equations of motion in dynamics, appls. to satellite theory 79—12386
- phase space methods and the Hamilton-Jacobi form of dynamics 79—21542
- planetary satellite ejecta, effect of proximity to Roche limit on dynamics 80—98592
- Poincare canonical momenta and Nambu mechanics 78—77701
- point mass systems, dynamically and kinematically controlled, motion *(Russian)* 77—33858
- projectile motion, computer programs for high-school expts. 78—86094
- projective symmetries of dynamical systems, infinitesimal symm. transforms of vector field 78—32650
- PWR power plant dynamics, math. model *(Polish)* 79—63800
- quasi Lagrangian dynamical systems, generalisation *(French)* 77—33854
- radio sources, extended, statistical evidence on dynamical evolution 79—88757
- radio sources, extended internal dynamics and brightness distribs. 77—22323
- reduction of dynamical systems 79—63011
- reinforced concrete structs., initial stress approach to nonlinear dynamic anal. 77—83036
- rigid body dynamics, nonexistence of single valued integrals and branching of solns. *(Russian)* 79—9098
- rigid body with one fixed point, motion 77—78972
- ring galaxies, dynamical problems of form. and evolution 77—33635
- rotational frames and Euclidean connection 77—60907
- rotationally periodic large space structures, finite element transfer matrix dynamic analysis, 100 m parabolic dish 80—74731
- satellite stabiliser system with 2-stage suspension *(Russian)* 79—32222
- self-gravitating star system dynamics, time depend. soln. 80—4405
- shaft, rotating, with single disc, nonlinear inner damping forces *(German)* 78—1562
- Shahbazian 1 group of galaxies, dynamics from spectroscopic, obs. 80—67878
- solar quiescent corona, dynamics 78—40885
- solar surges, dynamics of descending stage *(Chinese)* 80—105221
- spring-mass systems, transfer props. of nonlinear resonators *(German)* 80—98793
- star cluster dynamics, evolution and statistical methods *(French)* 77—71133
- star cluster models dynamical evolution, early stages 79—8958
- star clusters, dynamical evolution with changing gravit. const. 79—17030
- star clusters, evolution, Fokker-Planck eqn. numerical integration 80—36675
- star clusters, test computations on dynamical evolution 77—49445
- star clusters dynamics, higher order fluid eqns. for multicomponent nonequilib. systems 80—105156
- star systems, purely discontinuous random processes in field of irregular forces *(Polish)* 78—16465
- stars, solns. for dynamical rupture of equilib. 77—56913
- state space, Heisenberg equations 77—37782
- statistical mechanical relation 78—49748
- stellar clusters, nonexistence of additional integral of motion of star 78—65663
- stellar orbits in rotating galactic bar, isolating integrals of motion 80—4404
- stellar system dynamics, field of directions of motion in Contopoulos potential *(Russian)* 80—62205
- stellar systems, dynamical evolution anal. rel. to hidden masses *(Russian)* 77—91583
- stellar systems, two component Emden sphere theory 80—22045
- stochastic processes in dynamical systems *(Russian)* 79—12718
- string with variable mass, nonlinear dynamics *(Polish)* 78—12553
- structural analysis, dynamic, soln. of quadratic eigenproblems 77—89017
- structural analysis, dynamic condensation method 79—3943
- structures dynamic problems, eigenvalue economisation, program *(Italian)* 79—35544
- submerged elastic cylindrical shell, initially stressed, axisymmetric dynamic response 79—18715
- system theoretic representation of mechanical systems 79—17342
- systems of solid bodies with combined control *(Russian)* 79—17209
- systems theoretic representation of mechanical systems, stochastic interpretation 79—17343
- tank with fluid, variational anal. of dynamic reaction *(Ukrainian)* 79—32234
- teaching approach to mechanics *(Hungarian)* 79—17157
- teaching laws of dynamics in Soviet schools *(Hungarian)* 78—9
- teaching spontaneous reasoning in elementary dynamics 80—4482
- thick anisotropic shells, dynamic eqns. *(Russian)* 77—58547
- thick circular plates, sector finite element for dynamic anal. 79—72845
- train, stability of unperturbed motion *(Russian)* 78—18160
- uniform acceleration, student laboratory expt. 79—40326

dynamics continued
- Venus atmosphere, dynamical processes rel. to thermal balance 77—73994
- Venus atmosphere, dynamics, winds, circulation and turbulence 77—78706
- Venus rotation, possible dynamical evolution since formation 80—56742
- Virgo galaxy cluster, galaxy dynamics rel. to redshift controversy, evidence from Centaurus 78—54061
- viscoelastic body with stripwise loading *(German)* 78—87281
- viscoelasticity, dynamical problems, approx. soln. of integral eqns. 80—10164
- Wick's theorem, relation between canonical and Fokker-Planck dynamics 79—17329

dynamometers
- *see also force measurement*
- calibration, for exact meas. up to 10 N *(German)* 77—53897
- chassis, features and appls. 80—52195
- conductive paper transducer output signal fluidity reduction 77—57318
- DC, features, control systems and standard ratings 80—52194
- digital, DE 1, mass diagnosis locomotor and nervous system disorder appl. 77—40854
- digital, using period transducers, noise action *(Russian)* 79—88944
- EDDIC eddy current type electric instrum., construction and performance 80—52192
- electrodynamometer modification for realization of ampere at NBS 80—98938
- FREC, features, construction and regulation 80—52193
- hydraulic universal testing machine, K value determ. *(German)* 80—90836
- multicomponent, practical experimental designs for calibration 79—35729
- performance evaluation by compensation curves *(German)* 78—192
- piezoelectric dynamometer for dynamic force meas. *(Hungarian)* 78—65918
- reference equipment for measurement of large forces, metrological provisions in COMECON member countries 79—75523
- standardisation machine calibration method *(French)* 77—53894
- strain gauge, effect of temp. on characts. 78—93677
- strain gauge, wind tunnel dynamometer, five component 78—54361
- strain gauge sytem, body of rotation form, non axially symm. load 80—73350
- strain-gauge type for aircraft rudder-bars *(French)* 78—49825
- tensile test diagram remote recording device 78—7139
- three-dimensional flow structure in circular cylinder, meas. *(French)* 77—23941
- time ageing determination using bonded resistance foil strain gauges 79—35726
- transducers, granular, based on conducting material contact resistance 79—35706
- two-string balance microprocessor operation *(German)* 78—57936

dynamos *see d.c. generators*

dysprosium
- *see also nuclei with ......*
- absorption of H_2, Mossbauer study 80—44987
- adsorption and absorption of $H_2(D_2)$ 77—4257
- adsorption on W, field emission electron study 80—100393
- antiferromagnetic, thermal expansion, US attenuation anomalies 79—47319
- atom, excited state lifetime meas. using cw dye-laser 79—89636
- atom, isotope separation, laser excitation, charge exchange with Cs^+ ions 80—83512
- atom, isotope shifts and hyperfine structs. 78—37600
- atom, K-shell ionisation and X-rays 79—93960
- atom, photoabsorpt. spectra 77—88417
- atom, photon-bound-electron scatt. meas. 77—14394
- atoms, prod. in nucl. reaction, K-shell ionisation cross-sections meas. 80—78687
- atoms, visible spectra obs., hyperfine struct., mag. dipole and electric quadrupole interaction const. anal. 80—91698
- Auger spectra, effect of mode of d-hole formation *(French)* 77—36356
- critical exponents and amplitude ratios from elec. cond. data, theoretical model 80—50126
- crystal hyperfine fields at positive muons 79—56662
- crystal structure, P-T phase diagram 78—84776
- Curie-Weiss law anisotropy, paramag. susceptibility meas. 80—15686
- domain effects near order-disorder and order-order ferromagnetic transitions 80—65886
- domain wall dynamics, NMR 77—69614
- elastic constants, in paramag. temp. range, magnetoelastic contrib. 77—4538
- elastic constants, magnetoelastic contrib. 80—15777
- electrical resistivity, high-precision meas., 1-4K 77—15817
- electron energy loss spectrum and surface electron states 77—85860
- electron irradiated, defect annealing, recovery spectra 79—23648
- EXAFS, white lines, interatomic distances 77—40302
- fan phase, hexagonal anisotropy 77—77051
- ferromagnetic, magnetoresist., fields up to 75 kOe, 1-70K 77—20297
- film, discontinuous electronic conduction mechanism 79—87169
- film, elec. resist., thickness depend., effect of presence of dihydride 77—51829
- film, elec. resist. results 78—84326
- film, Hall effect meas. in para- and ferromag. regions 77—55622
- film, helimag. order, surface deform., exchange and single-ion magnetocrystalline anisotropy energy 77—66390
- film, magnetoelastic waves, GHz, excitation, field depend. 78—72378
- film, O_2 and H_2 contamination effect on elec. resist. 77—80856
- film, thermoreflectance dispersion curves at 315K and 97K 80—7332
- film, vacuum deposition, using liq. He cooled cryopumping panel 78—56581
- film, vacuum-evaporated, thickness depend. of elec. resist. 77—39967
- fluoride, $MF_2:Dy^{3+}$, (M=Ba,Ca,Cd), far IR Stark and Zeeman splitting 77—48190
- foil, average thermal neutron flux determ. method 78—73112
- galvanomagnetic effect, longit., in single crystals *(Russian)* 78—56132
- helical antiferromagnetic phase, basal plane anisotropy 78—84412
- hexagonal-orthorhombic transition temp., effects of press. and crystallinity 80—24585
- hyperfine field at positive muon 80—40029
- hyperfine structure of odd isotopes, two step photoionisation, mass filtration *(Russian)* 77—46550

dysprosium continued
- impurity in nonmag. host, anisotropic exchange Hamiltonian, rel. to ESR spectrum 77—20696
- internal fields, positive muon investigation 78—68438
- interstitial site determ., μSR technique 80—71287
- ion implanted into Ni, annealing study by Rutherford backscatt., TEM, and total current spectroscopy 79—4343
- isotope separation, laser two-step photoionisation 78—46461
- liquid, mag. susceptibility, elec. resistivity 80—20377
- liquid, struct. factors, high temp. X-ray diffr. obs. 79—7544
- magnetic aftereffect obs. 77—8364
- magnetic anisotropy 77—69539
- magnetic anisotropy and ^{161}Dy Mossbauer effect 78—92001
- magnetic anisotropy constant, basal plane, field depend., 4.2-120K 77—63165
- magnetic characteristics in strong magnetic field 77—89936
- magnetic domain structure, hysteresis, thermal modulation study 80—71082
- magnetic phase transitions, field-induced 79—24161
- magnetic phase transitions, helical state, field induced 78—72349
- magnetic phases, US study 78—31101
- magnetic transitions and internal friction temp. depend. *(Russian)* 78—39317
- magnetisation, change in easy axis 77—8306
- magnetocaloric effect and mag. phase transitions, 80 to 300K 80—60279
- magnetocaloric effects between 84 and 280K 79—73721
- magnetocrystalline anisotropy, perturbation theory 78—2675
- magnetoelastic effects in mag. ordered regime 78—15003
- magnetoplastic deformation, 70-90 kOe, 4.2K 77—8376
- magnetostriction meas. re-analysis, domain effects corrected by phase theory 78—6555
- metastable high-pressure phase, conversion into stable phase 77—55357
- muon spin rotation; freqs., and relax. rates 80—55006
- muon spin rotation in ferro- and antiferromag. phases, local fields 78—43763
- neutron radiographic film imaging systems, MTFs and resolution capabilities 80—66758
- Oklo natural fission reactors, migration in core sample, appl. to dating of reactions *(French)* 80—21760
- paramagnetic phase, anomalous thermal expansion, up to 273K 79—7967
- parasusceptibility meas., 4.2-130K, spin wave anal. 79—95583
- phosphate glass:Sb^{3+},Dy^{3+}, fluorescence and energy transfer obs. 78—6778
- plastic and magnetoplastic deform. of single crystal 77—63713
- plastic deformation, substructural changes, stress-strain diagrams and microhardness meas. *(Russian)* 79—52296
- point defect production during electron irrad. at low temp. 80—49273
- resistance and mag. structure. near Neel point *(Russian)* 79—47074
- resistivity, crit., rel. to antiferromagnetism 79—47077
- resistivity anomalies at mag. transitions, sp.ht. 80—39785
- specific heat, mag. contrib. 79—28538
- spectral emittance above 1000K 77—4211
- spin fluctuation resistivity near T_N, theory 77—40071
- spin wave exam. 78—56306
- surface ionisation on W (110) 79—87142
- thermal expansion, interferometric meas. 78—52333
- US attenuation in mag. field 77—40104
- US attenuation maxima in mag. field 77—16140
- X-ray cross sections, L-shell, proton induced, 1 to 3 MeV range 79—1799
- X-ray diffraction obs. of magnetostriction and phase transitions 77—73068
- X-ray L_{III} absorption discontinuity, bidirectional orbital interpretation 77—16423
- Ag:Dy, orbit-lattice coupling, nonuniform strain effects 78—88182
- Al:Dy, orbit-lattice coupling, nonuniform strain effects 78—88182
- Al-Al_2O_3-Al junctions, Dy doped at Al_2O_3-Al interface, electron transport mechanisms and barrier height 78—91778
- Al-Al_2O_3-Dy junctions, steady state and nonsteady state behaviour 79—78205
- Al-Al_2O_3-Dy thin junctions, Poole-Frenkel effect obs. and cause 80—80398
- Al_2O_3-Dy_2O_3, phase diagram at high temps. *(Japanese)* 79—38810
- $BaF_2:Dy^{3+}$, far IR absorption 80—40143
- $Bi_{12}GeO_{20}:Dy$, luminesc., emission and excitation spectra 80—103975
- $Bi_4Ge_3O_{12}:Dy^{3+}$ crystal growth, spectral and laser props. 80—45115
- CaF:Dy, dimer reorientation activation volume 80—107285
- $CaF_2:D^{2+}$ submm. magnetospectroscopy, tunable far IR laser potential 78—52481
- CaF_2:Dy, colour centres, antiresonance-type phenomenon in external fields 78—68529
- CaF_2:Dy, cryst. fields, overlap and covalency contribs. 77—1397
- CaF_2:Dy, TLD-200, thermolum. phosphor, photolum. and absorpt. spectra, thermolum. mechanisms 80—97321
- CaF_2:Dy, thermolum. induced by monoenergetic parallel beam 81 MeV diffr. neutrons 77—52883
- CaF_2:Dy, thermolum. induced by 254 nm UV photons 80—55204
- CaF_2:Dy crystal with M centre, antiresonance line, mag. field effect 80—55138
- CaF_2:Dy dosimeter crystals, γ-irrad. dose effect on thermoluminesc. response 77—64135
- CaF_2:Dy sensitivity to UV and ionising radiations, temp. treatment effect 79—26763
- $CaF_2:Dy^{3+}$, ^{19}F NMR studies 80—60429
- $CaF_2:Dy^{3+}$, cubic cryst. field effects 80—2368
- $CaF_2:Dy^{3+}$, cubic sites, Γ_7 state energy, e.p.r. 77—1590
- $CaF_2:Dy^{3+}$, EPR of colour centres, spin-spin interaction of pair of Dy^{3+} ions *(Russian)* 79—69751
- $CaF_2:Dy^{3+}$, fluoresc. spectra, A-centres and B-centres, Stark levels 80—25428
- $CaF_2:Dy^{3+}$, Γ_8 quartets, orbit-lattice interaction, e.p.r. under stress 77—1591
- $CaF_2:Dy^{3+}$, high temp. fluorescence using Ar^+ and N_2 lasers 78—56514
- $CaF_2:Dy^{3+}$, Mossbauer obs. 78—64303
- $CaF_2:Dy^{3+}$, spin-lattice interaction in Γ_8 quartets, models tested for EPR data 78—23336
- $CaF_2:Dy^{3+}$, thermolum., associated luminesc. centres and traps 77—28638
- CaF_2:Dy(Ho)(Pr)(Tb), V_k-centre recomb. kinetics, phosphoresc. 77—55817
- CaO:Dy, thermolum. induced by 254 nm UV photons 80—55204

dysprosium continued
CaO-Li$_2$O-B$_2$O$_3$, calibo glass, Dy^{3+}→Ho^{3+} non-radiative energy transfer, diffusion limited relaxation 79−65925
CaO-Li$_2$O-B$_2$O$_3$:Dy^{3+} glass, optical excitation energy transfer from Dy^{3+}→Nd^{3+} 79−15515
Ca$_5$(PO$_4$)$_3$OH:Dy^{3+}, thermolum. props. 80−2877
CaS:Bi,Dy phosphors, thermoluminesc. 77−69921
CaSO$_4$:Dy, α and γ thermoluminescence response comparison 79−85814
CaSO$_4$:Dy, Cd-covered TLD, thermal neutron dosimetry 77−90912
CaSO$_4$:Dy, competing deep trap model for thermoluminescence 79−83039
CaSO$_4$:Dy, cryst. growth from soln., thermoelec. and thermoluminesc. props. 79−56923
CaSO$_4$:Dy, gamma-irradiated valency conversions in rare-earth ions 80−55198
CaSO$_4$:Dy, γ-ray induced sensitization, competing trap model 80−2881
CaSO$_4$:Dy, high exposure UV response and sensitisation 79−91506
CaSO$_4$:Dy, phosphor, X-irrad., thermoluminesc., role of Na$_2$SO$_4$ as charge compensator 79−78764
CaSO$_4$:Dy, photo-stimulated thermolum., for high-exposure dosimetry 77−9262
CaSO$_4$:Dy, phototransferred TL studies 80−80875
CaSO$_4$:Dy, TLD during irrad. by γ-rays, X-rays, electrons, ambient atm. effect 78−19578
CaSO$_4$:Dy, TLD phosphor response, heating rate effect 80−26359
CaSO$_4$:Dy, TLD-900, thermolum. stability at low radiation doses 80−101272
CaSO$_4$:Dy, thermolum. origin, test of model on CaSO$_4$:Eu 77−85813
CaSO$_4$:Dy, thermolum. induced by 254 nm UV photons 80−55204
CaSO$_4$:Dy, thermolum. phosphor, photolum. and absorpt. spectra, thermolum. mechanisms 80−97321
CaSO$_4$:Dy, thermoluminescent glow peaks, post γ-irrad. annealing study 80−89077
CaSO$_4$:Dy embedded Teflon TLD phosphor photon energy dependence obs. 79−26761
CaSO$_4$:Dy phosphor powder, effect of grinding on thermoluminescent sensitivity 79−33852
CaSO$_4$:Dy phosphors, photomag. susceptibility 78−2724
CaSO$_4$:Dy phosphors, dosimetric appls. 79−76154
CaSO$_4$:Dy photostimulated luminesc. for radiation dosimetry 77−90910
CaSO$_4$:Dy ribbon, dosimetric props. study 80−63395
CaSO$_4$:Dy sintered pellets, thermolum. response 80−93411
CaSO$_4$:Dy TLD, temp. effect during UV and gamma irradiation 79−38684
CaSO$_4$:Dy TLD phosphor, γ radiation changes in glow curve 80−60688
CaSO$_4$:Dy Teflon TL dosimeters, thin, development for β-dosimetry in personnel monitoring 80−63399
CaSO$_4$:Dy Teflon TLD discs, graphite-mixed, for beta dosimetry 77−86639
CaSO$_4$:Dy Teflon TLD discs, thermal history and reusability 79−89507
CaSO$_4$:Dy thermoluminescent props. of non-commercial phosphors 78−58550
CaSO$_4$:Dy thermoluminescence sensitivity and glow curves, 700° to 1300°C 79−85815
CaSO$_4$:Dy thermoluminescent phosphor, effect of sensitisation on energy depend. 80−26358
Cu:Du^{3+}, EPR, g-factor, hyperfine struct. 77−48046
^{161,163}Dy, hyperfine struct. and hyperfine anomaly for fine transitions, high resolution meas. 77−88416
Dy I, hyperfine struct. and isotope shift, fluoresc. meas. on at. beam 78−9109
Dy I excited states, lifetime meas. using single photon counting method 78−70793
Dy II spark spectrum, isotope shift, config. mixing 78−58628
Dy III lines in spectra of Ap and Bp stars 80−12764
Dy, isotope shift meas. using laser atomic beam technique specific mass shift determ. 80−91497
Dy$^+$ spectra, exam. of 4f^{10}6s and 4f^{10}5d configs. *(French)* 77−50385
Dy^{3+} activated vanadates, photoluminesc. meas. 77−77277
Dy^{3+}, free-radical relax. agent in biological tissues 78−81090
Dy^{3+}, impurity ion in frozen aq. solns., effect on Fe^{3+} spin-spin relax., Mossbauer obs. 79−33573
Dy^{3+} in molten LiNO$_3$-KNO$_3$, transition probabilities in absorpt. and fluoresc. spectra 79−50085
Dy^{3+}, in soln., non-radiative transitions as Forster's energy transfer to solvent vibrations 80−1014
Dy^{3+}, in Van Vleck paramagnets, EPR meas. 77−12199
Dy:^{111}Cd(^{177}Hf), polycryst. ferromag., impurity hyperfine field polarisation, TDPAC and IPAC 77−73106
Dy:^{181}Ta, ferro- and antiferromag. phases, temp. depend. of mag. hyperfine field, TDPAC obs. 77−36165
Dy^{3+}:oxide glass, intensity parameters and laser transitions 79−50300
Dy+H$^+$ ionisation, induced L-shell alignment 80−32813
Dy^{3+}+O$_3$(SO$_5$$^{2-}$)(SO$_2$), in H$_2SO_4$ soln., electrochemiluminesc. emitters quenching by electrolysis products 79−1794
^{160}Dy ion, electronic config. after β-decay of ^{160}Tb in TbSi$_2$ 79−59340
^{161}Dy, ^{163}Dy, HFS, isotope shifts and hyperfine splittings 78−37595
^{161}Dy, calibration of isomer shifts by conversion electron spectroscopy 80−39918
^{161}Dy polarised nuclei system, nonthreshold and amplification *(Russian)* 79−98332
GaP:Dy, photolumines. spectra 79−52015
GaP:Dy epitaxial films, photoluminesc. spectra 80−66294
Gd$_2$(MoO$_4$)$_3$:Dy^{3+}, cryst. field parameters 77−66142
GdPO$_4$:Dy^{3+}, Bi^{3+}(Sb^{3+}), energy transfer from sensitiser to activator, intermediate role of Gd^{3+} 80−50389
H, and He, stopping powers meas. 80−42904
LaBe$_{13}$:Dy, ESR, crystalline field single ion effects 78−84481
LaCl-Dy, mech. for X-ray luminesc. and thermolum. 79−8170
LaF$_3$:Dy, cryst. field anal. of triply ionised ion spectra 80−2796
LaF$_3$:Dy^{3+}, ^{4}F$_{9/2}$ and ^{4}I$_{15/2}$ levels, radiative decay rates 79−61415
LaF$_3$:Dy^{3+}, high temp. fluoresc., Dy^{3+} G-level emission 78−27295
LaF$_3$:Dy^{3+}, laser excited fluoresc., lifetimes meas. 79−24353
LaF$_3$:Dy^{3+}, laser excited fluoresc. rise and decay meas., expt. 80−22448
LaF$_3$:Dy^{3+}, magnetospectroscopy with optically pumped far IR laser 79−33737
LiYF$_4$:Dy^{3+}, ESR, nonlinear effect of elec. field 80−2635
LiYF$_4$:Dy^{3+}, spectrum, Stark struct. 77−85756
LuBe$_{13}$:Dy, ESR, crystalline field single ion effects 78−84481
MgAl$_2$O$_4$:Dy, US attenuation 77−89500
MgB$_4$O$_7$:Dy, TLD phosphor development 79−79661

dysprosium continued
MgSiO$_4$:Dy, thermolum. induced by 254 nm UV photons 80−55204
PrSb:Dy, ESR of non S-state ions 77−43881
SnO$_2$:Dy^{3+}, luminesc. and charge compensation 78−76532
SrF$_2$:Dy, far IR spectra 79−33736
SrF$_2$:Dy^{3+}, cluster form., IR absorption study *(French)* 80−108240
SrF$_2$:Dy^{3+}, nuclear spin-lattice relax. anisotropy, 78 to 300K 79−38395
SrF$_2$:Dy(Ho)(Pr)(Tb), V$_k$-centre recomb. kinetics, phosphoresc. 77−55817
TbO$_2$:Dy^{3+}, mag. hyperfine interaction, PAC expt. 78−35069
ThBe$_{13}$:Dy, ESR, crystalline field single ion effects 78−84481
TmBi:Dy, ESR of non S-state ions 77−43881
Y, recrystallisation *(Russian)* 77−24946
YAG:Dy, US attenuation 77−89500
Y$_2$O$_3$:Dy^{3+}, conc. quenching of X-ray and UV-excited luminesc. *(Russian)* 77−55829
ZnO:Dy, electrolum. brightness, field strength and freq. depend. 80−100696
ZnO:Dy, phosphor, electrolum. and photolum. spectra 78−80421
ZrO$_2$:Dy, thermoluminescence, traps and emission centres 79−24373

dysprosium alloys
dilute, ESR linewidth of rare-earth ions 78−68373
dilute, fan phase, hexagonal anisotropy 77−77051
DyNi$_{3.4}$, magnetisation data 77−32177
DyZn, exchange coulombic contrib. of cond. electrons to cryst. elec. field 79−95376
rare earth intermetallics, RAl 2-Dy, dil., (R=La, Yb, Lu), EPR and mag. susceptibility 80−15797
Ag-Dy, dil., cryst. field and spin exchange parameters, susceptibility and ESR expts. 77−40129
Ag-Dy, dil., EPR linewidth anisotropy and mag. field depend., internal stress effects 79−33532
Ag-Dy, dil., Schottky effect, sp. ht. meas. 78−34633
Ag-Dy, dil., thin films, ESR spectra, stress effects 80−39866
Ag-Dy alloy, dil., magnetoresistance meas., contrib. from quadrupole and exchange scatt. 79−78078
Ag-Ho, dil., high field magnetoresist. 80−15503
Al-Dy, dil., ion implanted, crystal hyperfine field interaction, Mossbauer spectroscopy study 80−44968
Au-Dy, dil., hyperfine interaction of Γ_8 quartet, Mossbauer expt. 78−43718
Au-Dy, dil., hyperfine interaction, Mossbauer study, Kramers quartets 80−66083
α-Ce-Dy, dil., ESR study of mag. prop 78−39398
Co$_{35}$Dy$_{65}$, metallic glass, internal friction peaks 80−25753
D-$_{12}$Fe$_{32}$O$_2$, anomalous magnetisation, compensated to uncompensated mag. arrangement transition 78−52254
Dy-Al$_2$, cubic Laves phase compounds, exchange striction determ. 80−44895
Dy-Au, dil., Mossbauer exam. of mag. hyperfine field at ^{197}Au impurity 78−88244
Dy-Bi, heat of formation 77−86349
Dy-Cd, dil., elec. field gradient, at ^{111}Cd impurities, temp. depend. 79−28642
Dy-Co amorphous film, prep. by dual-source evaporation, mag. props. 77−89988
Dy-Cu, amorphous, mag. phase diagram, magnetisation and sp. ht. meas. 80−80532
Dy-Cu amorphous mag. alloy, linear sp. ht. due to single-ion excitation 78−91874
Dy-Er, Kaufman approach to calc. of intra-rare earth phase diagrams 80−25657
Dy-Fe, amorphous, random anisotropy effects 78−68223
Dy-Fe, amorphous ferrimag. film, mag. props. and Curie point writing 77−12164
Dy-Fe, amorphous film, Kerr readout characts. 79−15439
Dy-Fe film, amorphous, contact printing 77−73061
Dy-Fe$_x$Ni$_{1-x}$ system, mag. hyperfine field, influence of lattice struct. and substituent 77−8058
Dy-Fe-Al, pseudobinary alloy, struct. exam. 77−58979
Dy-Fe-Al, pseudobinary alloys, mag. props. 77−59397
Dy-Fe-O system, O-stabilised intermetallic Dy$_{12}$Fe$_{32}$O$_2$, prep. and characterisation 77−8956
Dy-Ho, Kaufman approach to calc. of intra-rare earth phase diagrams 80−25657
Dy-Ho dil. alloy, nucl. spin-lattice relax. of ^{165}Ho 78−48069
Dy-Sc, magnetic relax. phenomena 79−33579
Dy-Sm, elec. resist. singularities and mag. transitions *(Russian)* 79−47075
Dy-Sm, magnetic moment growth due to Sm addition *(Russian)* 80−34608
Dy-Sm(Eu), mag. props. at low temp. in high mag. fields 79−56570
Dy-Sn, hyperfine fields acting on diamag. impurities and anisotropic exchange, Mossbauer spectra 77−1625
Dy-Ta, dil., elec. field gradient at ^{181}Ta, temp. depend., TDPAC meas. 79−95689
Dy-Th, single cryst., mag. susceptibility, transitions, anisotropy 80−54873
Dy-Y, magnetisation and hysteresis, temp. depend. 79−69673
Dy-Y, paramag. susceptibility in basal plane and hexagonal axis 77−20548
Dy-Y, scatt. of cond. electrons by spin disorder 78−47778
DyAg, amorphous, bulk mag. props., field, time and temp. depends. 77−89932
DyAg$_{1-x}$In$_x$, elec. and Hall resist. 80−96844
DyAl$_2$, anisotropic magnetostriction, temp. depend. 80−39841
DyAl$_2$, conduction electron spin and orbital polarisation effects 78−80228
DyAl$_2$, cryst. field volume magnetostriction calc. 79−8029
DyAl$_2$, first order transition and tricrit. points, three-state Potts model 78−43589
DyAl$_2$, hyperfine field, NMR spectra, effect of substitution of Sc, Y, La, Lu 80−15811
DyAl$_2$, sp. ht. and thermal props., 5 to 300K 77−43342
DyAl$_3$, polytypism, high resolution microscopy and electron diffr. obs. *(French)* 77−11503
Dy$_3$Al$_5$O$_{12}$, antiferromag., optical birefringence in fields along [111] meas. 77−28540
DyAu$_2$, long-duration pulsed mag. field appl. to magnetisation meas. 79−61183

dysprosium alloys continued
$DyAu_3$, mag. props. *(German)* 79—51761
$DyAu_{3.6}$, ordering temps. and effective moments 78—60283
$DyAu_6$, mag. props. temp. depend. *(French)* 77—51879
Dy_2Au, mag. props., 4.2-300K 79—7972
$DyAuNi_4$, mag. props. 77—20595
DyBi, electronic struct., LCAO calc. *(Russian)* 77—39777
DyC_x, $0.28<x<0.53$, cryst. struct. and Curie temp. 79—86741
$Dy_xCe_{1-x}Ru$, supercond., mag. order 79—87189
$Dy_xCe_{1-x}Ru_2$, supercond., mag. props. 79—11267
$Dy(Co,Ni)_2$, intrinsic mag. aftereffect obs. 77—63237
$Dy(Co,Ni)_2$, intrinsic mag. aftereffect meas., domain wall motion 80—71121
$DyCo_2$, elec. resistivity, thermopower, X-ray struct. meas. 80—24874
$DyCo_2$, field induced vol. magnetostriction 78—91920
$DyCo_2$, H_2 absorpt., Mossbauer study 80—44987
$DyCo_2$, magnetocryst. anisotropy props. by ^{57}Fe Mossbauer spectroscopy 77—63328
$DyCo_2$, spontaneous vol. magnetostriction and thermal expansion meas. 77—12183
$DyCo_2$-$DyAl_2$ system, mag. and structural studies 80—108006
$DyCo_3$, amorphous, mag. struct. and moments 77—66260
$DyCo_3$, effect of absorbed H_2 on mag. behaviour 79—33483
$DyCo_3$, mag. and quad. interactions, Mossbauer spectra 77—12267
$DyCo_3$, X-ray absorpt. edge shifts 80—25483
$DyCo_3$-H_2, phase equilibria, from dissociation isotherms 80—50591
$DyCo_{3.4}$, amorphous, mag. props. 77—32177
$DyCo_5$, mag. moment orientation, anisotropic mol. field model 77—89950
$DyCo_5$, rotational type spin reorientation, collinear to canted spin struct. change 77—63214
$DyCo_{5.3}$ noncollinear mag. struct. appearance in mag. fields, magnetostriction meas. *(Russian)* 80—100607
$Dy_{0.25}Co_{0.75}$ film, amorphous, displacement of mag. compensation temp. by elastic stress *(Russian)* 78—19284
Dy_2Co_{17}, and $Y_{2x}Dy_{2(1-x)}Co_{17}$, magnetocryst. anisotropy, 77-383K 77—89949
Dy_2Co_{17}, domain wall behaviour, TEM expts. 77—4524
Dy_2Co_{17}, hyperfine interactions and cryst. field effects, Mossbauer spectra 80—2369
Dy_4Co_3, cryst. field effect on mag. moment direction, neutron diffr. meas. 78—80132
DyCoAl, mag. props. 78—2659
DyCu, direct Coulomb contrib. of cond. electrons to crystalline elec. field 77—76784
DyCu, direct coulombic contrib. of cond. electrons to cryst. elec. field 79—91005
DyCu, exchange coulombic contrib. of cond. electrons to cryst. elec. field 79—95376
DyCu film, amorphous, asperomagnetic domains, Barkhausen jumps in hysteresis loop 80—75822
Dy_xCu_{1-x}, amorphous film, magnetisation meas., local anisotropy effects 78—68309
$DyCu_4Ag$, mag. props. and cryst. struct. 77—20562
$Dy(Fe,Al)_2$, saturation and remanent magnetostriction meas. 77—63256
$Dy_2(Fe,Co)_{17}$, mag. anisotropy fields by singular pt. detection 79—24156
$Dy_2(Fe,Co)_{17}$, magnetic anisotropy meas. by singular point detection method 77—63170
DyFe amorphous film, Mossbauer and mag. meas. 80—15844
$DyFe_2$, amorphous, mag. struct., US meas. 79—99683
$DyFe_2$, amorphous, struct. determ. EXAFS exam. 78—51421
$DyFe_2$, amorphous, ultrasonic exam. below T_c 79—73793
$DyFe_2$, and $Dy(Co_{0.98}Fe_{0.02})$, magnetostrictive material, changes in vibr. modes near mag. phase transition 79—90736
$DyFe_2$, crit. phenomena, Mossbauer effect 78—52403
$DyFe_2$, electronic heat capacity coeffs. 80—39787
$DyFe_2$, H_2 absorpt., Mossbauer study 80—44987
$DyFe_2$, high field magnetostriction and magnetisation 78—84471
$DyFe_2$, highly magnetostrictive props. 77—12180
$DyFe_2$, hyperfine interactions 80—44549
$DyFe_2$, magnetisation and magnetic anisotropy 78—91862
$DyFe_2$, phonon softening below Curie temp., Mossbauer effect 77—4589
$DyFe_2$ powders, mag. and hysteresis props. *(Russian)* 79—42800
$DyFe_2$, spontaneous magnetoelastic distortion, X-ray diffr. expts. 77—63253
$DyFe_3$, amorphous, mag. struct. and moments 77—66260
$DyFe_3$ and Dy_6Fe_{23}, magnetostriction, room temp. to 80K 80—65993
$DyFe_3$, effect of adsorbed H on mag. props. 77—63129
$DyFe_3$ hydrides, desorption isotherms 80—103565
$DyFe_3$, Mossbauer spectra, easy magnetisation axis temp. rot. 80—15859
$DyFe_{3.4}$, amorphous, mag. props. 77—72985
$DyFe_{3.4}$, magnetisation data 77—32177
$Dy_{1-x}Fe_x$, amorphous film, cosputtered, struct. and mag. props. 78—60323
$Dy_{1-x}Fe_x$, mean mag. moment calc. 79—82761
Dy_2Fe_{17}, domain structures and anisotropy constant. 80—93136
Dy_2Fe_{17}, hyperfine interactions and cryst. field effects, Mossbauer spectra 80—2369
Dy_xFe_{1-x} amorphous film, crystn., TEM obs. 79—87019
DyFeAL, scatter order cpd., mag. props. 77—51891
$DyFe_4Al_8$, mag. props. 78—52250
$Dy_2(Fe_{1-x}Co_x)_{17}$, hyperfine interactions, Mossbauer effect 78—2780
$DyFe_2H_x$, thermodynamic props., H_2 desorption isotherm meas. 80—89516
$Dy(Fe_{1-x}Mn_x)_2$, phase struct., mag. and Mossbauer meas. 77—20563
$Dy(Fe_xNi_{1-x})$, mag. interactions, mol. field model 77—73010
$Dy(Fe_xNi_{1-x})_2$, mag. behaviour, susceptibility and Mossbauer expts., 4.2-1300K 78—52235
$Dy_2(Fe_{1-x}Ni_x)_{17}$, Mossbauer spectra, hyperfine field interactions 78—6614
$Dy(Fe_xRh_{1-x})_2$, mag. props., Mossbauer spectra 80—25108
$Dy_2Fe_4Si_9$ and $DyFeSi_3$, cryst. struct. and mag. suscept., temp. depend. *(Russian)* 78—34957
DyGa, ferromag., mag. props., 4.2 to 350K 77—63230
$DyGa_2$, mag susceptibility, 1.5-300K and Neel temp. 78—68184
Dy_xGd_{1-x}, mag. anisotropy energy, composition depend. 77—16071
$Dy_{1-x}Gd_xAl_2$, ferromag, easy axis rot., ^{163}Dy NMR obs. 79—78562
$Dy_{1-x}Gd_xAl_2$, ordered alloys, ^{163}Dy NMR, hyperfine field 78—10801
$Dy_{1-x}Gd_xAl_2$, ordered alloys, hyperfine field, anomalous con. depend. NMR 80—75868
$Dy_{1-x}Ho_xNi_2$, cryst. field quenching of Dy^{3+} 4f shell, Mossbauer effect meas. 78—39480

dysprosium alloys continued
$DyIn_3$, magnetisation 80—25106
Dy_2In, mag. props., 4.2 to 270K 79—56512
Dy_2In, mag. props. 80—108009
Dy_3In, mag. props. 80—108009
Dy_5Ir_2, cryst. struct. 80—96473
DyM_2Si_2, (M=Mn, Fe, Co, Ni, Cu), Mossbauer spectra 80—20558
DyMg, mag. props., neutron diffraction and magnetisation meas. 77—16045
DyMg, Mossbauer spectroscopy and mag. props. 77—85624
$DyMn_{12}$, mag. interactions, mag. meas. and neutron diffr. 77—63103
$DyMn_2$, H_2 absorpt., Mossbauer study 80—44987
Dy_6Mn_{23}, magnetic moments, magnetisation 80—25094
Dy_6Mn_{23}, noncollinear mag. struct., magnetization meas. 79—78322
$Dy_{50}Nd_{50}$, mag. struct. and ordered moments, neutron diffr. data 77—66252
$DyNi_2$, H_2 absorpt., Mossbauer study 80—44987
$DyNi_2$, Mossbauer effect of ^{57}Fe 77—69743
$DyNi_2$, single cryst. mag. props. 77—24684
$DyNi_3$, amorphous, mag. struct. and moments 77—66260
$DyNi_3$, amorphous, resist. meas., 1.2-290K 78—19015
$DyNi_{3.4}$, amorphous, mag. props. 77—72985
$DyNi_5$ crystal, basal plane anisotropy, torque meas. 80—65857
Dy_2Ni_{17}, hyperfine interactions and cryst. field effects, Mossbauer spectra 80—2369
Dy_2Ni_{17}, magnetic struct. by neutron diffr. and Mossbauer spectra *(French)* 77—32165
$Dy_{69}Ni_{31}$, amorphous, Curie temp., mag. susceptibility and coercive force, 4.2 to 300K 80—93092
$DyNiSi_3$, mag. susceptibility, 80-1200K *(Russian)* 77—66281
Dy_3Os, cryst. struct. 80—96474
Dy_5Pd_2, mag. props. 77—20547
$Dy_{50}Pr_{50}$, mag. struct. and ordered moments, neutron diffr. data 77—66252
$DyPt_5$, low temp. mag. susceptibility 80—93075
Dy_2Pt, mag. susceptibility meas., mag. transitions obs. 80—60222
Dy_3Pt_4, mag. props., 4.2 to 160K 79—78343
Dy_5Pt_4, isotypic with Pu_5Rh_4, X-ray cryst. struct. refinement anal. 79—4271
DyRh, direct Coulomb contrib. of cond. electrons to crystalline elec. field 77—76784
DyRh, direct coulombic contrib. of cond. electrons to cryst. elec. field 79—91005
DyRh, exchange coulombic contrib. of cond. electrons to cryst. elec. field 79—95376
$DyRh_{1.1}Sn_{3.6}$, new supercond./mag. cpds., X-ray powder diffr. data 80—100215
DySb, quadrupole scatt. anisotropy, magnetically ordered material 78—64034
$Dy_{1-x}Sm_x$, magnetoresist. of polycryst. specimens in fields up to 44 kOe *(Russian)* 80—92880
$Dy_{0.7}Tb_{0.3}Fe_2$, magnetostrictive material, liq. phase sintering 78—64493
$Dy_xTb_{1-x}Fe_2$, and $Ho_xTb_yDy_{1-x-y}Fe_2$, high magnetostriction cpd., mag. anisotropy origins 78—68217
$Dy_xTb_{1-x}Fe_2$, single cryst., torque meas. 80—65877
$DyTe_2$, magnetostriction in polycryst. samples 77—73065
$Dy_{1-x}Y_xAl_2$, cryst. field quenching of Dy^{3+} 4f shell, Mossbauer effect meas. 78—39480
$Dy_{1-x}Y_xAl_2$, ordered alloys, ^{163}Dy NMR, hyperfine field 78—10801
$Dy_xY_{1-x}Al_2$, domain wall dynamics, NMR 77—69614
DyZn, direct Coulomb contrib. of cond. electrons to crystalline elec. field 77—76784
DyZn, direct coulombic contrib. of cond. electrons to cryst. elec. field 79—91005
DyZn, magnetoelastic consts. 78—15005
Fe-Dy, dil., implanted impurity hyperfine interaction 78—68417
$Fe_2(Tb_{0.2}Dy_{0.22}Ho_{0.58})$, highly magnetostrictive alloy, vibrating-reed meas. of ΔE effect and internal friction 79—42819
Ga-Ni-R, (R=Dy, Ho, Er, Tm, Lu), struct. determ. by X-ray powder method *(Ukrainian)* 80—39001
$(Gd,Dy)Al_2$, spin adjustment, NMR spin echo obs. 78—15058
Gd-Dy, dil., impurity component of elec. resist. meas. 1.5 to 390K 77—39831
Gd-Dy, galvanomag. effect, longit., in single crysts. *(Russian)* 78—56132
Gd-Dy, mag. anisotropy, magnetisation meas. 77—12115
Gd-Dy, magnetic and electric hyperfine fields at Gd, NMR spin echo 77—77123
Gd-Dy, magnetostriction contrib. to thermal expansion *(Russian)* 77—12184
Gd-Dy alloy, magnon contribution to electrical resist. *(Russian)* 78—39087
$Gd_{1-x}Dy_xAl_2$, EPR bottleneck, Dy substitution effect 77—63281
$Gd_{1-x}Dy_xNi$, FeB-CrB type stacking variations, cryst. struct. 80—64952
$Gd_{0.5}Dy_yY_{0.5-y}Ir_2$, effect of dil. Dy substitution on Gd ESR 79—82868
Ho-Dy-Sm, magnetic moment growth due to Sm addition *(Russian)* 80—34608
$Ho_xDy_yTb_{1-x-y}Fe_2$, Laves phase cpds., anisotropy and magnetostriction 77—63167
$Ho_{0.58}Tb_{0.20}Dy_{0.22}Fe_2$, magnetoelastic surface wave propagation, mag. field depend. 77—85535
$(Ho_{0.58}Tb_{0.2}Dy_{0.22})Fe_2$, microwave mag. props. 80—65860
La-Dy, elec. resist. temp. depend. 78—2462
Mg-Dy, dil., macroscopic shape effect due to quadrupole orientation, magnetostriction and thermal expansion meas. 80—60396
$MnCu_{1-x}Dy_xBi_{0.86}$ film, mag. and magneto-optic props., appl. as storage medium 77—8550
Nd-Dy, elec. resist. temp. depend. 78—2462
Nd-Dy HCP struct., mag. props. 77—63177
$Nd_{1-x}Dy_xCo_5$, rotational type spin reorientation, appl. to thermomagnetic generator 77—85451
Ni-Dy, annealing behaviour of implantation damage, Dy outdiffusion, TEM obs. 77—77505
Ni-Dy, dil., implanted impurity hyperfine interaction 78—68417
Pr-Dy, HCP struct., mag. props. 77—63177
Sc-Dy, dil., high field magnetisation 78—56292
Sm-Dy (3 wt.%), electrical resistivity, Neel temp., 15 to 300K 80—54672
$Sm_xDy_{1-x}Co_5$, temp. compensated magnetic material, mag. and struct. characterisation 78—68177

dysprosium alloys continued
- $Sm_{0.6}R_{0.4-x}M_xCo_5$ (R=Gd, Dy, M=Pr, Nd), temp. coeff. of magnetisation 80–34688
- (Tb,Dy)-Fe amorphous films prep. by cosputtering, magnetoelastic props. 80–97429
- $(Tb,Dy)Fe_2$ alloys, giant magnetostriction *(Chinese)* 79–51830
- Tb-Dy-Ho, phase diagram, alloy struct. *(Russian)* 77–25016
- $Tb_{0.24}Dy_{0.73}Fe_{1.95}$, magnetostrictive underwater sound transducer 78–13881
- $Tb_{0.26}Dy_{0.74}Fe_2$, temp. depend. of magnetomechanical coupling factor 77–90002
- $Tb_{0.27}Dy_{0.13}Fe_{1.98}$, grain-oriented, permeability, magnetomechanical coupling and magnetostriction 79–78491
- $Tb_{0.27}Dy_{0.73}Fe_2$, anomalous thermal expansion and magnetostriction 77–90003
- $Tb_{0.27}Dy_{0.73}Fe_2$, domain configurations, obs. by Kerr effect and synchrotron radiation topographs 78–64215
- $Tb_{0.27}Dy_{0.73}Fe_2$, LF magnetoelastic effects 78–68348
- $Tb_{0.27}Dy_{0.73}Fe_2$, magnetisation and magnetic anisotropy 78–91862
- $(Tb_{0.27}Dy_{0.73})Fe_2$, magnetisation, ferromag. domains 80–25162
- $Tb_{0.27}Dy_{0.73}Fe_2$, perpendicular suscept., magnetomechanical coupling and shear modulus 78–91918
- $Tb_{0.27}Dy_{0.73}Fe_2$, vertically zoned, magnetomechanical coupling and magnetostriction 80–65999
- $Tb_{0.3}Dy_{0.7}Fe_2$, elastic vs. magnetoelastic anisotropy 78–68347
- $Tb_{0.3}Dy_{0.7}Fe_2$, magnetoelastic coupling meas. by US method 77–69652
- $Tb_{0.3}Dy_{0.7}Fe_2$, magnetostrictive, resonant coupling of shear waves 79–33517
- $Tb_{0.3}Dy_{0.7}Fe_2$, prep. by powder metallurgy, magnetostrictive props. 80–75826
- $Tb_{0.3}Dy_{0.7}Fe_2$, sound velocity mag. field and temp. depend. elastic moduli calcs. 80–39839
- $Tb_{0.3}Dy_{0.7}Fe_2$, US velocity and attenuation obs. 77–28423
- $Tb_{1-x}Dy_xFe_2$, pseudobinary Laves cpds., spin-orientation diagram, Mossbauer effect meas. 77–55739
- $Tb_xDy_{1-x}Fe_2$, Laves phase alloy, magnetostriction depend. on powder orientation before sintering 78–76284
- $Tb_{0.20}Dy_{0.22}Ho_{0.58}Fe_{1.95}$, grain-oriented, permeability, magnetomechanical coupling and magnetostriction 79–78491
- $Tb_xDy_yHo_zFe_2$, temp. depend. of magnetomechanical coupling factor 77–90002
- Th-Dy, dil., supercond. Th, paramag. relax. of Dy moments, Mossbauer study 80–39957
- Th-Dy, dil., type I superconductor, paramag. Dy moment relax., Mossbauer spectra study 80–65755
- Th-Dy (1 at.%), Heisenberg exchange, residual resist. meas. 80–75558
- Y-Dy, mag. susceptibility, 4.2 to 300K, Neel temps. 79–19735
- $Y_{0.98}Dy_{0.02}$, spin glass, calorimetric exam. 78–68270
- $Y_{1-x}Dy_xCo_5$, NMR meas. of ^{59}Co 77–85585
- Zr-Dy dil. alloys, plastically deformed, mech. props. and microstruct. *(Russian)* 79–20112

dysprosium compounds
- *see also dysprosium alloys*
- ethylsulphate, pure dipolar Ising ferromag., critical thermodynamics 77–16095
- type II antiferromagnet with bilinear and biquadratic coupling, magnetic excitons in cubic cryst. field 79–78353
- Al_2O_3-Dy_2O_3, phase diagram at high temps. *(Japanese)* 80–50619
- CdF_2:DyF_3 films, electroluminesc. meas. *(French)* 79–11471
- $Ce_xDy_{1-x}C_2$, mag. props. 80–108008
- $CeDyS_3$, cryst. struct. determ. *(French)* 78–6034
- $CsDy(MoO_4)$, permittivity temp. depend., polymorphic transition 80–92670
- $CsDy(MoO_4)_2$, effect of 38K phase transition on phonon spectrum, IR reflection spectra *(Russian)* 79–10902
- $CsDy(MoO_4)_2$, trivalent ion impurity effects on structural phase transition temp., new transition 20-30K *(Russian)* 79–19367
- Dy complex, acetoacetic ether, luminesc. spectral band intensities, solvent effects *(Russian)* 78–84653
- DyAG, adiabatic magnetisation, optical obs. 78–88283
- DyAG, antiferromag., induced staggered mag. fields 80–65810
- DyAG, antiferromag., induced staggered magnetic fields, microscopic mech. 80–80527
- DyAG, crit., tricrit., and crossover phenomena, light scatt. 78–68251
- DyAG, cubic antiferromagnet, multiaxis phase transitions 79–78377
- DyAG, electrostatic model of cryst. field 80–59945
- DyAG, forced magnetostriction meas. 78–68349
- DyAG, induced staggered mag. fields and order parameters 77–63099
- DyAG, light scatt. from metamag. domains, crit. exponent determ. 77–66482
- DyAG, magnetic tricriticality nonuniversality 79–78392
- DyAG, single cryst. growth by Czochralski method 78–95690
- DyAG, tricritical crossover exponent 77–4239
- DyAg, neutron diffr. expts. in external mag. field, temps. below 1.2K 79–61067
- $DyAl_2$, magnetisation, three-state Potts model 79–42804
- DyAlG, tricrit. wing exam. 77–73026
- $DyAlO_3$:Yb^{3+}, Mossbauer relax. 80–15875
- $Dy_3Al_5O_{12}$, Czochralski growth, interface shape transitions 78–59772
- $Dy_3Al_5O_{12}$, magneto-optical rotation in transverse field 79–73902
- $Dy_3Al_5O_{12}$, magnetostriction, role of order parameter 79–73796
- $Dy_3Al_5O_{12}$:Ca^{2+}, optical absorpt. spectrum, strong crystal field of tetragonal symm. 77–32410
- $DyAl_3[BO_3]_4$, thermal stability, X-ray struct. anal., refractive indices 79–4297
- $DyAsO_4$, cooperative Jahn-Teller phase transitions, dielec. anomalies 78–64312
- $DyAsO_4$, cooperative Jahn-Teller transition, optical study 80–15240
- $DyAsO_4$, cryst. struct. by X-ray diffr. co-operative Jahn-Teller transition 77–89411
- $DyAsO_4$, ferroelectricity, dielec. meas. 80–60515
- $DyAsO_4$, first order Jahn-Teller phase transition, sp. ht. and refr. index meas. 80–59645
- $DyAsO_4$, first-order cooperative Jahn-Teller phase transition, dielec. suscept. studies 80–19940
- $DyAsO_4$, phase transitions obs. 80–70412
- DyB_{12}, nature of magnetism *(Russian)* 78–31049
- DyB_4, antiferromag. props. *(French)* 77–20566
- DyB_4, cryst. and mag. struct., neutron diffr. meas. 80–15692
- DyB_4, mag. and elec. props., metallic character 80–20386

dysprosium compounds continued
- DyB_4, mag. behaviour, in strong mag. field *(Russian)* 78–88119
- DyB_6, form. mechanism, reduction of Dy_2O_3 by B, DTA appl. 80–55643
- Dy_xB_y, prep. and props., DTA study 80–20859
- DyBi, mag. behaviour 80–71025
- DyBi, thermal expansion, thermal cond., 300-900K 78–91453
- DyC_2, mag. susceptibility, temp. depend. 79–87239
- Dy_2C_3, cryst. struct., mag. struct. and props., 1.6 to 300K 79–11296
- $DyCl_3$, aquo complex form., in aq. chloride soln., coord., X-ray diffr. obs. 79–64975
- $DyCl_3$, vapour press. and sublimation thermodynamics, mass loss effusion meas. 80–88313
- $Dy(ClO_4)_3$, osmotic coeffs. 80–45556
- $DyCl_3.6H_2O$:Gd^{3+}, spin Hamiltonian parameters EPR meas. 77–36128
- $DyCoO_3$, anomalous $^{57}Fe^m$ charge states, Mossbauer study 80–40017
- $DyCo_2Si_2$, mag. props. 80–107988
- $DyCrO_3$, Cr^{3+} exciton-Dy^{3+} spinflip absorpt. 77–73153
- $DyCrO_4$, determ. of mag. struct. by neutron diffr. 79–51753
- $DyCrS_3(Se_3)$, prep., elec. and thermal props. 78–43390
- DyD_2, cryst. elec. field transition, neutron energy loss spectra meas. 79–78059
- $Dy_xEr_{1-x}FeO_3$, transition to antiferromag. state, Dy^{3+} conc. effects 77–66319
- DyF_3, bomb calorimetric determ. of enthalpy of formation 80–50879
- DyF_3, crystal growth by Bridgman-Stockbarger method and Czochralski method 78–52660
- DyF_3, thermodynamic props., galvanic cell meas. 80–21316
- DyF_3, transferred hyperfine interaction, NMR study 78–68393
- DyF_3:Tb^{3+}, cryst. fields, luminesc. spectra 78–19563
- DyF_3-CsF, phase diagrams and ternary fluorides *(French)* 80–81040
- DyF_3-KF, phase diagram, cryst. symmetry and lattice constants of phases *(French)* 79–65171
- DyF_3-RbF, phase diagrams and ternary fluorides *(French)* 80–81040
- $DyFe_2B_2$, compounds with $CeAl_2Ga_2$ structure type *(Ukrainian)* 79–32970
- $DyFe_{0.998}Co_{0.002}O_3$, mag. transition, NMR meas. 78–27036
- $DyFe_{0.998}Co_{0.002}O_3$, orthoferrite, freq. and relax. of ^{57}Fe NMR signal near Morin spin-reorientation phase transition 79–69744
- $DyFe_{0.998}Co_{0.002}O_3$, orthoferrite, domain struct. near mag. transitions 80–2599
- $DyFe_{1-x}Co_xO_3$, magnetostriction, thermal expansion and elastic moduli near Morin point 77–8383
- $DyFe_2H_2$, mag. props., ^{57}Fe and ^{161}Dy Mossbauer spectra and magnetisation meas. 79–78579
- $DyFeO_3$, bubble domain struct. temp. depend. 77–69647
- $DyFeO_3$, field induced spin reorientation, Mossbauer spectroscopy 80–65878
- $DyFeO_3$, influence of mag. field on Faraday effect 78–27196
- $DyFeO_3$, mag. field induced intermediate state, magneto-optical effect meas. 77–55672
- $DyFeO_3$, magnetic intermediate state at antiferromag. to weakly ferromag. transition *(Russian)* 77–40059
- $DyFeO_3$, non Heisenberg R-Fe exchange interaction, behaviour in mag. field *(Russian)* 80–2568
- $DyFeO_3$, orthoferrite, domain struct. and hysteresis props. 77–77071
- $DyFeO_3$, phase domains, polarisation microscope obs. 77–28407
- $DyFeO_3$, Raman scatt. from magnons, anisotropy consts. determ. 80–66178
- $DyFeO_3$ single crystal, mag. domain width, temp. depend. 4.2 to 293K 77–40100
- $DyFeO_3$, spin reorientation, Faraday rot. meas. 77–8547
- $DyFeO_3$, spin reorientation near Morin temp., magnetooptical exam. 78–68284
- $DyFeO_3$, spin reorientation transitions induced by magnetic fields, Mossbauer study 80–71246
- $DyFeO_3$, spontaneous magnetostriction 79–56599
- $DyFeO_3$, weak ferromagnet, μSR study 80–93226
- $DyFeO_3$:Al^{3+}, Morin transition, mag. vacancies effect *(Russian)* 78–27039
- $Dy_3Fe_5O_{12}$, formation mechanism from metallic oxides 77–48376
- $Dy_3Fe_5O_{12}$, thermodynamic props. 79–77771
- $DyFeO_3$; linear dichroism influence on Faraday effect 80–2737
- Dy_2FeSbO_7, supertransferred hyperfine mag. fields and relax. of Dy^{3+} ions by Mossbauer spectroscopy of ^{57}Fe 77–59494
- $Dy_2Fe_3Si_5$, cryst. struct. determ. 78–18620
- $Dy_3Ga_5O_{12}$, crystal field effect on paramag. props. of Dy^{3+} ion 80–50040
- $Dy_3Ga_5O_{12}$, dipolar magnet, sp. ht. and magnetisation meas. 80–60344
- $Dy_3Ga_5O_{12}$, sp. ht. meas., 0.4-90K 77–55680
- $Dy_3Ga_5O_{12}$, sp. ht. meas, 37mK-2K 77–85476
- $Dy_3Ga_5O_2$, induced staggered mag. fields, neutron diffr. study 80–60196
- $Dy_2Ge_2O_7$, opt. absorpt. spectra, cryst. field parameters 77–48196
- DyH_2, lattice thermal expansion and point defect form. energy 77–51524
- DyH_2, mag. and crystal field props. from ^{161}Dy Mossbauer studies 79–95692
- DyH_2, mag. and electronic props., ^{161}Dy Mossbauer spectroscopy 78–80262
- DyH_3, mag. and crystal field props. from ^{161}Dy Mossbauer studies 79–95692
- $Dy_{0.5}Ho_{0.5}FeO_3$, mag. transitions, influence of Dy^{3+}, Ho^{3+} ground states 77–89955
- $Dy_{0.5}Ho_{0.5}FeO_3$ orthoferrite, domain struct., temp. depend. 80–71086
- DyI_3/CsI/Hg arc, oscillations induced by external mag. field, arc constriction 79–60205
- DyI_3-Hg arc discharge plasma, spectroscopic study 80–54033
- DyIG, mag. and magnetooptical props., temp. and field depends. 77–89927
- DyIG, magneto-optical absorption, near IR 80–40094
- DyIG, mol. field coeffs., magnetisation and mag. susceptibility anal. 78–95406
- DyIG, non-cryst., Mossbauer and magnetisation studies 80–44979
- DyIG, noncrystalline, Mossbauer and magnetisation data 80–34828
- DyIG, spontaneous Faraday rot. rel. to sublattice magnetisation 80–66159
- DyIG, thermoelectric power, elec. cond. charge carrier conduction mechanism 80–34441
- $Dy_{0.7}La_{0.3}FeO_3$, reorientational phase transitions, influence of La^{3+} ions 80–7108
- $Dy_2(MoO_4)_3$, cryst. growth and props. 79–55727

dysprosium compounds continued
- $Dy_2(MoO_4)_3$, DC electrical cond., 650 to 1150K 79—60831
- $Dy_2(MoO_4)_3$, mag. susceptibility, ferromagnetism, mol. field theory 78—34966
- Dy_2MoO_5, cryst. struct., IR spectra, elec. and mag. props. 80—33954
- $DyMo_6S_8$, long range mag. order in supercond. state 79—65653
- $DyMo_6S_8$, supercond. and antiferromag. coexistence, neutron study 78—95401
- $DyMo_6S_8$, superconductor, neutron scatt. exam. of mag. phase 79—73680
- $Dy_{1.2}Mo_6S_8$, long-range mag. order and supercond., neutron diffr. obs. 79—78320
- $Dy_{1.2}Mo_6S_8$, low temp. heat capacity anomaly rel. to antiferromag. transition in supercond. state 80—25044
- $Dy_{1.2}Mo_6S_8$, low temp. magnetisation meas., and supercond. props. 79—8018
- $Dy_{1.2}Mo_6S_8$, mag. ordering in supercond. state, resist. and AC susceptibility meas. 78—19194
- DyN, miscibility with UC *(German)* 80—96654
- $Dy(NO_3)_3$ in nonaqueous solvents, anharmonic vibrs. in electronic energy degradation 77—23541
- $DyNbO_4$-$CaWO_4$, phase transitions of fergusonite-scheelite *(French)* 80—19942
- $Dy_3Ni_7B_2$, struct., space groups, X-ray study *(Ukrainian)* 80—39029
- $DyNi_2Si_2$, mag. props., 4.2-200K 80—84602
- DyO, UV emission spectrum, high resolution, band systems and isotopic shifts 80—87146
- Dy_2O_3, ^{161}Dy hyperfine parameters for C_2 and C_{3i} site symmetries, Mossbauer obs. 77—20770
- Dy_2O_3, 300 to 900K, mag. susceptibility and Curie temp. meas. 78—56288
- Dy_2O_3, activation detectors for thermal and fast neutron detection 80—887
- Dy_2O_3, EXAFS and chemical shift 77—81176
- Dy_2O_3, electron microscopy, contrast near bend contours of upper Laue areas 79—55621
- Dy_2O_3 film, phase transforms. on annealing 79—95285
- Dy_2O_3, influence of upper Laue areas on fine struct. of bend contours near high symmetry axis 78—38596
- Dy_2O_3, lattice conservating twin, bend contours due to upper Laue zones 80—15113
- Dy_2O_3, powdered cryst., high resolution optoacoustic spectroscopy 80—31898
- Dy_2O_3, reaction with liq. Li and liq. Li-N 79—66276
- Dy_2O_3 reduction by B, DyB_6 form. mechanism, DTA appl 80—55643
- Dy_2O_3, soln. in $K_2O.2(3)MoO_3$, rel. supersaturation and supercooling 80—40245
- c-Dy_2O_3, transmitted intensity depend. on thickness, incident beam parallel to crystallographic axis 78—63644
- Dy_2O_3, XPS, charging effects on core-level binding energies 79—24409
- Dy_2O_3-based ceramic, preparation, mech. props. 77—24998
- Dy_2O_3-HfO_2, kinetics of initial stages of formation of solid soln. 77—48617
- Dy_2O_3-K_2O-MoO_3, melt, viscosity meas. 79—99346
- Dy_2O_3-TiO_2, high refractive index film growth by sputtering, waveguide appl. 77—48341
- Dy_2O_3-TiO_3 sputtered film, optical waveguide with high refractive index 79—3797
- Dy_2O_3-ZrO_2 phase diagram and long range ordering 80—93542
- $Dy(OH)_3$, Mossbauer spectra, cryst. field and mag. props. 80—15873
- $Dy_2O_2SO_4$, antiferromag., specific heat, 0.6 to 30K 79—33487
- $Dy_2O_2SO_4$, antiferromag., mag. props. and Zeeman effect meas. 79—33464
- $Dy_2O_2SO_4$, mag. ordering, magnetisation, AC susceptibility and Zeeman effect meas. 80—60205
- $Dy_2O_2SO_4$, magnetic struct. in antiferromag. and ferrimag. states 80—15695
- DyO_2X, X=S,Se,Te, mag. and quadrupole hyperfine interactions 77—63336
- $DyPO_4$, IR and Raman spectra 80—34904
- $DyPO_4$, mag. phase diagram and crit. exponents, MCD obs. 77—66307
- $DyPO_4$, mag. transitions under hydrostatic press., neutron diffr. study 80—71030
- $DyPO_4$, magnetic materials, transparent, optical studies of phase transitions 77—66481
- $DyPO_4$, metamagnet, mag. phase transitions, elastic neutron scatt. study 79—78371
- $DyPO_4$, metamagnet, phase diagram, influence of internal strains 79—28544
- $DyPO_4$, susceptibility near mag. phase boundaries 78—52258
- $DyPO_4$-$Pb_2P_2O_7$, solubility curves for high temp.-melts for growth of single crysts. 78—95687
- DyP_5O_{14}, luminesc. spectra 77—52155
- $Dy(ReO_4)_3.4H_2O$, $(ReO_4)^-$ ion vibrs. rel. to static field, Raman investig. *(Russian)* 78—76470
- $Dy(ReO_4)_3.4H_2O$, Raman spectra, $(ReO_4)^-$ ion normal vibrs. rel. to static field 79—65858
- $DyRh_4B_4$, cryst. struct., X-ray diffr. 77—89423
- $DyRh_4B_4$, ferromag. Curie temp. 77—89893
- $DyRh_4B_4$, NMR and sp. ht. in supercond. and mag. ordered phases 80—7037
- Dy_5Ru_2, Mn_5C_2-type struct., X-ray cryst. struct. determ. 80—96483
- Dy_2S_3, optical props. and electronic struct. in fund. absorpt. region 80—80817
- Dy_2S_3, polymorphic transforms. on impact compression 77—47575
- Dy_2S_3, semimetallic, elec. and thermal transport meas. 78—10442
- Dy_2S_3, vibr. spectra, factor-group anal. 80—80793
- Dy_2S_3-Ga_2S_3 system, phase diag. *(French)* 78—3108
- DySb, biquadratic exchange interactions, magnetisation above Neel point 77—69533
- DySb, magnetic excitations 79—78358
- DySb, magnetisation study, intermediate metamagnetic phase transitions 79—99698
- DySb, quadrupole interactions above T_N 79—78304
- $DySbO_3$, single crysts., hydrothermal synthesis and crystallographic characteristics 79—95916
- DyScFe garnets, mag. props. 77—47979
- DySe, formation and crystallographic charact. of thin film phase 78—91574
- Dy_2Se_3, mag. susceptibility 77—40032
- $Dy_2(SeO_4)_3.8H_2O$, thermal decomp. and IR spectra 80—3319
- E-$Dy_2Si_2O_7$, single cryst. flux growth 79—52097

dysprosium compounds continued
- $Dy_2Sn_2O_7$, supertransferred hyperfine mag. fields and relax. of Dy^{3+} ions by Mossbauer spectroscopy of $^{119}Sn^m$ 77—59494
- $Dy_2Sr_3(BO_3)_4$ dielectric thin films from vaporisation by cathode ray and HF ion-plasma methods 77—77380
- $DyTaO_4$, heat of form. 79—83494
- $Dy_xTb_{1-x}FeO_3$ orthoferrites, Dy^{3+} and Tb^{3+} contribs. to anisotropy const. *(Russian)* 77—89946
- $DyTiO_3$, bulk mag. and struct. props., ferrimag. order 80—107993
- $Dy_2Ti_2O_7$, neutron irrad., structural and volume changes 77—51416
- $Dy_2Ti_2O_7$, pressed powder, low temp. thermal cond., mag. field depend. 79—23789
- $Dy_xTm_{1-x}FeO_3$, transition to antiferromag. state, Dy^{3+} conc. effects 77—66319
- $DyVO_4$, antiferromag.-ferromag. structural phase transition induced by elec. field *(Russian)* 79—46802
- $DyVO_4$, basal plane magnetisation anisotropy under Jahn-Teller distortion 78—68222
- $DyVO_4$, centrosymmetric exhibiting cooperative Jahn-Teller effect, dielec. props. 79—28694
- $DyVO_4$, cooperative Jahn-Teller distortion, mag. field depend. 77—47777
- $DyVO_4$, cooperative Jahn-Teller phase transitions, dielec. anomalies 78—64312
- $DyVO_4$, cooperative Jahn-Teller transition, optical study 80—15240
- $DyVO_4$, cooperative Jahn-Teller phase transition, linear birefr. meas. 80—88960
- $DyVO_4$, dielec. anomaly and improper antiferroelectricity at Jahn-Teller transition 77—24802
- $DyVO_4$, electric field influence on elastic props., electron state initial splitting 80—34123
- $DyVO_4$, Green's function theory of phase transitions 79—38340
- $DyVO_4$ Jahn-Teller crystal, deform. induced transitions, elastic and dielectric characts. *(Russian)* 80—80726
- $DyVO_4$, Jahn-Teller domains obs. by cryogenic X-ray topography 77—39507
- $DyVO_4$, Jahn-Teller distortion, mag. field depend. 78—79733
- $DyVO_4$, Jahn-Teller phase transition and improper antiferroelectricity *(Japanese)* 78—80294
- $DyVO_4$, phase transitions obs. 80—70412
- $Dy_2(WO_4)_2$, mag. props., 300 to 900K 79—28510
- Dy_2WO_6, growth from soln. in melt 77—1806
- Dy_2ZrS_5, mag. and sp. ht. meas. on polycrystalline samples 78—23253
- $Dy_2[Pt(CN)_4]_3.21H_2O$, phase transitions, X-ray study and spectroscopic study 79—60506
- $Er_{0.8}Dy_{0.2}FeO_3$, mixed orthoferrite crystals, ^{57}Fe NMR in spin reorientation range 78—15039
- ethyl sulphate, uniaxial ferromag., nonuniversal props. in dipolar crit. region 77—24703
- Fe_2O_3-Dy_2O_3-Na_2O-B_2O_3 glass, AC mag. susceptibility, antiferromag. interactions 77—32179
- $Gd_xDy_{1-x}C_2$, solid soln., mag. susceptibility, temp. depend. 79—87239
- HfO_2-DY_2O_3 solid solns., prep., crystn. 78—42909
- $Ho_{0.5}Dy_{0.5}FeO_3$ orthoferrite, domain wall struct., stability conditions, Morin transition, anisotropy const. 80—34684
- $KDy(MoO_4)_2$, polarised IR and Raman struct., $^{92}Mo/^{100}Mo$ isotope effect 80—108198
- $KDy(PO_3)_4$, cryst. struct. 77—43188
- $KDy(WO_4)_2$, low temp. phase transitions *(Russian)* 78—87787
- $KDy(WO_4)_2$, phase transition mechanism, absorpt. spectra, symmetry props. *(Russian)* 80—55130
- KF-BeF_2-DyF_3, crystalline and vitreous phases of cross sections 78—44096
- KF-BeF_2-DyF_3, phase diagrams, intensification region 78—44097
- KF-BeF_2-DyF_3 system, KBe_2F_5-DyF_3 cross section phase diagram, vitreous phases struct. 77—24383
- $RbDy(MoO_4)_2$, Dy^{3+} doublets, temp. anomaly in splitting separation due to structural phase transformation *(Russian)* 80—39274
- $RbDy(MoO_4)_2$, low temp. phase transitions *(Russian)* 78—87787
- $RbDy(WO_4)_2$, cryst. struct. and refinement 77—65969
- Sc_2O_3-Dy_2O_3, solid solution, use of segregation phenomena to exam. solidification phase diagrams *(French)* 79—8293
- $TlDy\ (WO_4)_2$, fluoresc. spectra at 77, 300K 79—56848
- $TlDy(MoO_4)_2$, fluoresc. spectra at 77, 300K 79—56848
- $TlR(MO_4)_2$, R=Eu, Dy, Er; M=Mo, W, luminesc. *(Russian)* 78—48229
- YC_2-DyC_2, solid solution, antiferromag. props. 79—91230
- ZrO_2-Dy_2O_3 eutectic, unidirectional solidification, microstruct. and crystallographic characterization 80—35176
- ZrO_2-Dy_2O_3 solid solns., prep., crystn. 78—42909

E-layer *see E-region*

E-region
- *see also sporadic-E layer*
- acoustic-gravity waves, relaxational dissipation 78—4018
- anomalous ionisation at high latits., ground based sounding obs. 77—60523
- artificial quasiperiodic inhomogeneities formation due to powerful radiowave 79—84585
- auroral absorption event, lower ionosphere ion prod., density and comp. 80—36443
- auroral E-layer, plasma lines meas. 79—25386
- auroral E-layer, seasonal vars. 79—8746
- auroral E-region, enhanced plasma line spectra meas. 80—98507
- auroral E-region, irregularity drifts comparison with F-region plasma drifts 77—33262
- auroral E-region, Pc 5 micropulsation reson. region examination by dual auroral radar system 78—65454
- auroral E-region, possible nature 78—45088
- auroral E-region fine structure obs. in substorm 80—36452
- auroral electrojet, altitude differences for eastward and westward currents 77—87163
- auroral electrojet, solar flare effects 78—49198
- auroral electrojet, spectral struct. estimate of elec. field 78—40732
- auroral substorm expansion phase, ionospheric currents and elec. field vars. assoc. with absorpt. spikes 79—35039
- auroral zone, ion comp. and NO profile 77—41258
- auroral zone E-region, atmospheric motions deduced from spaced receiver obs. 77—87172
- auroral zone neutral wind and current meas. by incoherent scatt. radar 77—70927

E-region continued
cosmic noise absorption, F-lacuna and slant-E condition rel. to E-region Farley-Buneman instability 78—73563
cosmic radio noise 'absorbed' by E-region plasma waves 80—82139
cosmic radio noise absorpt. events meas. on riometers, due to backscatt. by E-region irregularities 77—25831
critical frequency changes during 1968 Sept. 22 solar eclipse *(Chinese)* 77—22154
critical frequency computation, comparison of formulae 78—45109
critical penetration freq. var. with solar activity 78—7828
cross polar cap horizontal currents, rel. to mag. disturbances and elec. fields 78—77405
cross-polar cap horizontal currents, rel. to mag. disturbances and measured elec. fields 77—45230
crossfield and two-stream instability spectral characts., rocket borne obs. 77—87180
day-night conductivity gradient effect on polar cap convective flow 78—45121
daytime drift obs., tests of electrodynamic consistency 77—70934
daytime E-region, geostationary satellite signals mid-latit. scintillation at 937 MHz 79—25388
daytime positive storm effects at middle latits., prod. by travelling atmospheric disturbances 79—25394
discrete auroral arcs and currents, review 80—77190
distortion effect of Sq current 77—45237
disturbances induced by F-region ion cloud releases 78—61657
drift above Ibadan 79—5711
drift and anisotropy parameters of small-scale irregularities at Waltair, India 77—13176
drift meas. and geomag. field vars. at tropical latits. 79—88528
drift meas. at Ahmedabad (1970-75) 78—40727
drift meas. over Ahmedabad, India, 1970-75 period 79—53637
drift meas. over Tiruchirapalli, India, 1972-75 period 79—53638
drift meas. over Udaipur, harmonic analysis 78—16233
drift speeds, magnetic activity effects 79—88541
drift variability above Tiruchirapalli, rel. to electrojet strength 80—82129
drifts over Tiruchirapalli, India, daily variations 79—84580
E-layer crit. freq., geomagnetic east component, and sunspot number relationships 78—65461
E-layer drift and anisotropy parameters, meas. from Waltair 77—70920
eastward electrojet position rel. to energetic electrons trapping boundary and aurora 77—25822
effective electron collision frequency 79—58153
electric fields, meas. in diffuse aurora 77—82077
electrodynamic state, horizontal mag. field component influence *(Russian)* 78—73556
electrojet, equatorial, plasma instability and electron density irregularities, HF radar obs. 80—105112
electron conc. profiles during sunrise and sunset 79—88526
electron concs. above Arecibo 79—101014
electron densities, diurnal, seasonal and solar cycle vars. 77—33267
electron density and recomb. coeff. profiles calc. rel. to absorpt. and rocket meas. 78—69559
electron density inhomogeneities prod. by auroral particles injection 78—45095
electron density model distribs. over Delhi 79—88536
electron density profile, distortion meas. using group and phase height meas. 80—109299
electron density profile from energetic particle and spread-F obs. 78—36383
electron density space-time vars. 77—17282
electron density variations during geomag. disturbances 78—69567
electron temp. compared to neutral temp., 100-120 km altitude 80—77211
electron-neutral collision frequency upper limit 79—84573
electrostatic waves, obs. in unstable polar cap ionosphere 79—29927
equatorial, Cherenkov radiation prod. by unstable plasma wave coupling 79—40003
equatorial, over India, turbulence obs. in electron density fluctuations 77—9609
equatorial, vars. rel. to interplanetary mag. field vars. 79—84572
equatorial counter-electrojet, two-stream instability, HF radar meas. 80—26671
equatorial E-region, dynamics 78—36369
equatorial elec. fields during mag. disturbances, auroral and equatorial meas. 80—31160
equatorial elec. fields during mag. disturbances, interplanetary mag. field effect 80—26676
equatorial electrojet, electron density profile changes 77—45234
equatorial electrojet, equivalent circuit anal. of neutral wind effects 78—57392
equatorial electrojet, HF oblique radar obs. of plasma instabilities over Africa 78—49205
equatorial electrojet, India, internal induction field from surface and satellite geomag. obs. 77—60535
equatorial electrojet, radar obs. of two dimens. turbulence, nighttime type 1 waves 79—35038
equatorial electrojet, radar profiles over Africa 77—21976
equatorial electrojet, two-stream irregularities, neutral atm. motions effects 79—16742
equatorial electrojet, type II gradient drift irregularities, numerical simulations 77—70926
equatorial electrojet, type II gradient drift irregularities, power spectrum studies 79—75016
equatorial electrojet and assoc. plasma instabilities 79—8750
equatorial electrojet axis in India, position variability 79—35046
equatorial electrojet longitudinal differences, radar studies review 78—36371
f0E, storm time var. at low latit. station 79—44295
fading records over Tiruchirapalli (1973-5), cross spectral anal. 80—101478
fading records over Tiruchirapalli (1973-5), full correl. anal. 80—101473
general circulation at altitudes >100 km, empirical model 78—61664
geomagnetic storm sudden commencement, uniform ionosphere transient response rel. to preliminary reverse impulse 80—8477
gravity waves at E-region heights, obs. of Es 80—72657
gravity waves during winter anomaly, evidence from lower thermosphere daytime neutral wind meas. 78—45071
H_E scatter signals power calc. 77—60520
height, calc. errors 77—22346
height variations, influence of lunar tides 78—77382

E-region continued
HF oscillating echoes from polar E-region 78—57390
HF radio wave absorption at mid-latits., temporal vars. 77—53305
high-latitude overhead horizontal current, discrepancy with mag. D-component vars. 79—75037
horizontal drifts at Ibadan, for solar cycle var. 78—36390
inhomogeneities drift in geomagnetic field 79—88546
ion production function from meteor particles 79—12336
ion velocity distributions for polarisation collision model 77—45241
ionisation, by solar flares X-ray and EUV emission, models 77—5515
ionisation, effect of neutral atmosphere seasonal vars. 79—12331
ionisation vars. and mag. disturbances in polar region 77—13151
ionization by solar UV and X-rays 77—17278
ionization correl. with solar flares X-ray and UV radiation 77—25815
ionization due to low level meteors, contrib. to LF propag., radio and optical obs. system 79—84514
irregularities, drifts, simultaneous obs. by different techniques at low and mid-latits. 77—53303
irregularities meas. by spaced receiver technique 79—53633
large-scale horizontal winds in presence of vertical vel., relaxation time 77—78561
layer structures, density response to gravity waves 78—81290
LF signals nocturnal amplitude correl. with neutron monitor count 78—40741
lightning location and ionospheric refl. heights from two-station mag. field meas. 79—70845
low latitude dynamoc current system, seasonal vars. near solar max. 80—8479
low-latitude E-region, ionisation by energetic ring current particles 78—77415
magnetic disturbance effects on daytime critical freq. 77—64527
metallic species, chemistry, problems 79—35035
MF absorption nocturnal var. and nighttime E-region 77—29563
MF pulsed transmissions, method for separating D- and E-region contribs. to toal absorpt. 78—69593
mid-latitude E-region electron density, geomag. storms effect 79—44294
midlatitude nighttime model including metallic ions 77—45249
mutual interaction between E- and D-regions during solar flare 77—45236
neutral wind obs. during equatorial electrojet 77—45210
neutral winds, comparison of Chatanika radar and optical meas. 78—32272
neutral winds and ion drifts in polar region 77—87173
night-time E-region, mid-latit., ionisation by charged particle precip. 79—44291
nightglow, diffuse Lyman alpha and beta and O I 5577 Å line radiation 79—66853
nighttime E-region, occurrence rel. to night-sky emission *(Russian)* 77—45223
nighttime E-region at Halley Bay, Antarctica, influence on Pi 2 pulsations polarisation and phase 79—21107
nighttime E-region valley, ionisation layers obs. above Arecibo 77—29569
nighttime electric fields and conductivity rel. to magnetosphere-ionosphere-atmosphere coupling 79—35034
nighttime Hall and Pedersen cond. comparison 77—41260
nighttime ionization by energetic particles, 120-200 km altitude 79—62666
nighttime ionization during meteor showers 77—29560
nighttime neutral conc. vars. meas., expt. method 77—45200
NO height distribution from rocket ion comp. results 80—26674
Pedersen current, effects on Perkins spread-F instability 78—40755
phase height var. and vertical drift 78—40747
plasma interaction with electron beam, beam energy distrib. appl. to ionosphere 80—103163
plasma measurements, during Western European Winteranomaly Campaign 78—45125
polar cap unstable region, rocket-borne wave, field and plasma obs. 77—21978
polar electron density fluctuations, gravity wave interpretation *(French)* 80—46334
polar slant-E condition, rel. to polar cap plasma flow entry region longit. position 80—67472
polar substorms, equatorial-auroral ionosphere coupling 78—32291
pulsating auroras, evidence for noncollisional thermalisation of precipitating electrons 79—96851
radar echoes from E-region, height shift around morning and evening electrojet reversals 79—66871
radio waves reflection from E-region arrival direction meas. system 79—25387
radiowave absorption, correl. with O I green line airglow emission 78—45075
radiowave absorption freq. var., model 77—13169
radiowave absorption meas., differences between sporadic-E and normal E-layer refls. 78—40734
radiowave absorption meas. at Waltair, India, D- and E-region models 77—13173
radiowave absorption near 100 km height, travelling (wave) disturbances 79—25392
radiowave propagation, quasi-periodic artificial inhomogeneities, formation *(Russian)* 79—21093
radiowave scatt. by anisotropic inhomogeneities oriented along geomagnetic field 78—53771
radiowave scintillation studies using ATS-6 radio beacons at Delhi 78—69600
random and anisotropic irregularities at low latits. 79—88532
recombination coeff. at midlatitudes, determ. from daytime N_e profiles 79—5700
small amplitude short period waves from radio reflection virtual height meas. 77—73906
solar tides, electrodynamic effects, equatorial electrojet 77—9611
solar tides, electrodynamic effects, Sq current system 77—9610
solar tides and electrodynamics, polarisation elec. field calc. 78—36391
solar X-rays, intensity in E-region meas. by rocket-borne proportional counters 78—45072
structure, calc. and obs., AE-C satellite and incoherent scatter radar obs. 78—49203
SW radio propag., weak large-scale inhomogeneities effect of auroral ionosphere 79—101017
temperature and wind measurement Fabry-Perot-interferometer imaging system appl. 80—101441

E-region continued
temperatures and collision freq. in polar regions, incoherent scatter meas. 80—72688
thermal electrons energy distrib. distortion near focus of S_q current vortex 79—35053
time comparison of JJY signal reception via the E-region 78—65910
travelling planetary scale waves 77—9612
vertical drift effect on absorpt. and phase height change of refl. 79—101003
VHF backscattering from irregularities near mag. equator 77—33248
VHF radar aurora and strong HF backscatt. comparison 80—61960
VHF radar echoes from equatorial E-region irregularities, sudden disappearance 78—40738
VHF radar partial reflections from equatorial plasma density gradients 77—25828
whistlers at low latitude, banded struct. origin on refl. from E-region 80—101476
winds and electric fields meas. over Malvern 78—49206
winter anomaly, as result of upper atmosphere seasonal vars. 79—53613
wireless transmission, 1900-1935, early ionospheric research 79—9070
MgO, wavelengths and relative intensities of IR bands 79—2407
NO density in lower E-region, diurnal and seasonal effects at low latits. 78—88976
NO density variations in E-region, theory, ion-neutral chem. constraints 79—75027
NO global morphology in lower E-region 78—88975
NO var. with solar activity 78—49207
O I 5588 Å green line airglow emission rel. to HF wintertime absorption in D-region 79—58148
O_2^+ source rel. to charge exchange of $O^+(^2D)$ metastable ions 79—58141
S chemistry 79—96854

ear
see also hearing
acceleration effects, +Gz influence on semicircular canal function, aircraft appl. 80—94245
acoustic impedance meter, principle aspects of development 79—24999
acoustic nerve paths, hearing analysis appl. *(Italian)* 80—94218
acoustic reflex, factors influencing acoustic-immittance characts. 80—56062
acoustic reflex, statistically based measure and relation to stimulus loudness 77—32907
acoustic reflex adaptation in humans 79—2082
acoustic reflex threshold, variability of measurements 77—16938
acoustic-reflex dynamics for pulsed signals 79—20549
acoustical research into life sciences, review 80—97925
actin in the inner ear, struct. of the stereocilium 80—108918
action potential responses to tone bursts in human and guinea pig cochlea 77—12930
action potential tuning curves, normal and pathological human ears 78—20184
anatomical and physiological basis of auditory information 79—11944
anterior semicircular canal units of anaesthetised pigeon, point process anal. 78—24079
artificial, for insert-type earphones 77—32904
artificial ear for sensitivity/frequency meas. for telephone use 78—63255
artificial middle ear, and problems with hearing aids 79—84009
audibility relative magnetic threshold meas. *(Croatian)* 78—11673
audiometric impedance meas. instrumentation 77—78005
auditory nerve, encoding of steady-state vowels, representation in terms of discharge rate 79—92230
auditory physics, hearing theory physical principles 80—85410
auditory system of crickets, acoustical analysis 79—92226
aural reflex, influence on sound transmission in the inner ear *(Japanese)* 80—81620
barotrauma, new aspects in oto-rhino-laryngology 79—11946
basilar membrane, anisotropic rigidity components evaluation 79—79569
basilar membrane, electrical model giving displacement 77—90810
basilar membrane, nonlinear electric circuit model, distortion 77—25459
basilar membrane displacement, electronic model 77—29159
basilar membrane displacement rel. to masking-period patterns produced by VLF maskers 77—56383
basilar membrane model, nonlinear, meas. apparatus and circuits *(Japanese)* 78—35868
basilar membrane model using digital filter for voice features extraction 78—77069
basilar membrane motion in alligator lizard, relation to tonotopic organization and freq. selectivity 80—76753
basilar membrane motion linear and nonlinear models 77—90800
basilar membrane nonlinear model assessment, spatial differentiation as auditory second filter 77—36949
basilar membrane nonlinearity 77—25461
behavioural, unit and AP thresholds, relationship in normal and abnormal ears 78—92642
bleeding, inner-ears of chinchillas, caused by simulated sonic boom 79—16247
brain stem electric response audiometry and middle ear effusion 80—56151
caecilian ear, sensitivity, electrical potential of cochlea 77—36959
caloric nystagmus, air and water, mathematical model 79—24983
canal temperature meas. in cattle, telemetry 77—86714
cat, action potentials at low intensities, thresholds, latencies and rates of change 79—11942
cat eardrum model as thin shell using finite element method 78—65036
central denervation hypersenstivity in auditory system of cat 79—96575
chamber microvasculature, rabbit, radiation damage and subendothelial repair 77—52847
chemical and physical aspects *(Dutch)* 77—9188
cochlea, 3-dim. model, point-impedance charact. of basilar membrane 78—57009
cochlea, disc model rel. to hydrodynamics in gap between cover membrane and organ of Corti *(German)* 77—86505
cochlea, hydroelastic modes 77—77915
cochlea, mammalian, fluid flow permeability through hair cell cilia 79—53157
cochlea, mathematical model for influence of spiral coiling on basilar membrane motion 79—5298
cochlea, stiffness gradient along basilar membrane as basis for spatial freq. analysis 79—24995

ear continued
cochlea, two dimensional model, method for computing motion 78—65037
cochlea 2-D model, heuristic approach and numerical results 77—16937
cochlea alternating elec. resist. changes caused by acoustic stimuli in guinea-pig 77—86507
cochlea as Laplace analyzer for optimum signals 78—35865
cochlea frequency response and tectorial membrane, math. anal. 80—26240
cochlea hair cell tuning props. 77—64054
cochlea mechanics, modes and waves 79—92232
cochlea mechanics, transmission line theory appl. 78—35866
cochlea model, acoustic wave reflection and resonance 80—61581
cochlea model, for signal anal. 77—26281
cochlea of guinea pig, comparison of spectra of cochlear microphonic and sound-elicited electrical impedance changes measured in scala media 79—96567
cochlea of guinea pig, spectral content of cochlear microphonic measured in scala media 79—96566
cochlear, evoked mech. response and the auditory microstruct. 80—94223
cochlear, struct. and functional changes following US irrad. 80—89791
cochlear action potential threshold and single unit thresholds 79—43927
cochlear compound action pots., tuning curves and delay times 80—94230
cochlear development, crit. period for acoustic trauma, hamster 77—90809
cochlear encoding, reverse correlation technique 78—40183
cochlear endolymph Ca content 78—61203
cochlear excitation, electric circuit model and overpressure meas. in guinea pigs *(French)* 78—85316
cochlear fibre responses in guinea pigs with well defined cochlear lesions 80—94226
cochlear fluid, two dimensional model 77—32906
cochlear fluid mechanics, flows on a cusp catastrophe 77—77903
cochlear fluid mechanics, kinetic theory 78—53440
cochlear fluid mechanics, signal anal. by Hopf bifurcation 80—26241
cochlear hydrodynamics model, digital simulation 78—31821
cochlear injuries rel. to CM pots. 80—94229
cochlear inner and outer hair cell selective destruction, freq. discrimination 78—77067
cochlear LF variable geometry model for morphological disorder compensation 78—40182
cochlear mechanics, 5 decade or research 80—76749
cochlear mechanics, nonlinear behaviour in 2-tone responses 80—76751
cochlear mechanics, some obs. 78—92643
cochlear mechanics freq. sensitivity anal. 78—24078
cochlear mechanism theory based on slow fluid waves 80—56057
cochlear micromechanics, mechanism for transforming mech. to neural tuning within cochlea 78—11666
cochlear micromechanics and anatomy, review 80—76750
cochlear microphonics induced by 918 and 2450 MHz pulsed microwaves, cat and guinea pig 78—40258
cochlear model, three-dimens., comparison of WKB calcs. and experimental results 79—70556
cochlear model, two-dimens., comparison of WKB and finite difference calcs. 79—70555
cochlear model vibration mode visualisation by holographic interferometry 79—2083
cochlear models, 2-tone suppression and second filter 80—76752
cochlear models—1978 80—94221
cochlear nonlinear phenomena in two-tone responses 80—94225
cochlear partition vibration, recent views 80—81617
cochlear potentials, effect of ethylendiaminetetraacetate in the scala media 80—16952
cochlear summating potentials, effects of crossed olivocochlear bundle stimulation 77—52800
cochlear temperature depression in guinea pig caused by anaesthesia and ventral ear surgery 80—97938
cochleas of different lengths from chinchillas, location of structurally similar areas 79—92229
compound PST histogram rel. to neural activity in cochlear 80—94148
cubic difference tone production, spectral transform. by infinite clipper 77—9212
Deiter's cells of organ of Corti, well developed gap junctions 77—29155
densitogram, use in ambulatory noninvasive monitoring of physiological data, recording systolic time intervals 79—66574
differential electrical excitation of auditory nerve 80—67092
discriminating ability during phase switching, function of sound pressure level and tone pulse freq. 77—60220
eardrum acoustic admittance and reflex threshold for impulses 77—64052
eardrum vibration meas. using electronic speckle pattern interferometry 80—67209
earplugs, real-ear noise attenuation and effectiveness 78—87199
electrocochleography, tone-burst, interpretation of action pot. off-effect 77—56386
electronystagmography system for vestibular testing, microprocessor-based 4-channel 80—41293
equilibration, physiopathology in aerospace medicine 79—11950
evoked brain stem response, cochlear processes affecting wave V latency 80—16958
frequency acoustic reflex, multiple probe meas. 80—56065
frequency discrimination capacities in goldfish, phase-locking in saccular nerve fibres 78—88720
frequency response of external ear and artificial ear model *(Chinese)* 80—56063
guinea pig, method for gaining access to auditory nerve 78—85455
guinea pig outer ear, transfer function *(French)* 79—24994
hair cell, vertebrate, response to controlled mechanical stimuli 78—15852
hair cell receptor pot., ionic basis in vertebrates, bullfrog obs. 80—26239
hair cells, inner, role of in hearing 79—43932
hair cells, mechanism of production of summating potential, elec. cct. model 80—72176
hair cells, vertebrate, response latency 79—83794
hair cells of organ of Corti, thermal noise 78—15845
hearing nonlinearities model described by active processes with saturation at 40 dB 80—56058
hearing protectors, rating method 77—7271
HF audiometry and stapedius muscle reflex thresholds in juvenile diabetics 80—85411
holography in otology 80—67206

ear continued
- human, ipsilateral stimulus intensity, tympanometry 80—104592
- impedance changes elicited by tactile and electrocutaneous stimulation 80—56066
- impedance matching by combined effects of outer and middle ear 79—96571
- impedance meas. instrument *(Hungarian)* 78—36012
- implantable middle ear, development prospects *(Japanese)* 80—81775
- inner, sound-induced resistance changes 80—81618
- inner ear impulse response and basilar membrane modelling 79—34570
- internal sound pressure monitoring, appl. to noise exposure meas. 77—52799
- interneurones, locust, time-intensity trading obs. 80—26238
- intracochlear acoustic pressure measurements in guinea pigs 80—94228
- intracochlear interference effect applicability for personal sound protection *(German)* 77—66816
- ipsilateral acoustic reflex artefacts measured in cadavers 80—85414
- isobaric counterdiffusion, middle ear gas exchange 80—81798
- labyrinth caloric test, estimation of stimulus strength 78—40210
- laser applications in otology, review 78—48860
- lateral line microphonic response to high-level stimuli, analytical model 80—61580
- level dependent freq. selectivity model *(German)* 77—64038
- mammalian, psychophysical tuning curves and auditory thresholds after hair cell damage 79—96564
- mathematical survey of modern theory of nonlinear systems applied to human hearing 78—40195
- microwave auditory perception, contrib. of middle-ear structs. 80—67097
- microwave induced hearing 77—2010
- middle, and sinuses, ventilation and clearance using ^{133}Xe 80—98075
- middle ear and acoustic reflex, development of electroacoustic analogue model 79—83798
- middle ear systems simulation from physiological data 78—44514
- middle-ear admittance development in hamsters 79—88088
- middle-ear muscle contraction, influence on auditory threshold 78—85319
- minimum audible pressure, revised estimate 78—65040
- model of auditory system from middle ear to primary auditory nerve 77—29158
- models and signal processing, conf., Munster, Germany (Sep. 1978) 80—90610
- movement of human ear, electronic speckle pattern interferometry in vivo 80—109083
- multifrequential impedance meas. 80—17031
- multisensory orientation stimuli, semicircular canal and otolith information integration 78—20199
- myringoplasty, comparison of implant materials after tympanic membrane perforation in rat 79—39597
- negative middle ear press. rel. to conductive hearing loss in children 80—12164
- neonatal acoustic reflex, static and dynamic impedance obs. 80—104597
- nerve fibre model 80—94227
- noise effects, and acceptable levels and meas. *(Spanish)* 78—15857
- noise effects, specific and nonspecific, human hearing system *(French)* 77—21538
- oculomotor control system, expt. set-up for clinical investigation, visual, acoustic, vestibular stimulations 78—80990
- organ of Corti, guinea-pig, rectangular arrays of intramembranous particles at zonula adherens 77—70480
- otolith membrane, finite element model, computer soln. of differential eqns. 77—40636
- peripheral auditory adaptation, dependence on recording site 80—81613
- physical principles of audiology, book 80—82592
- primary neurons, comparative physiology 80—94224
- protection systems, attenuation produced at each normal freq., Noise Reduction Rating calc. *(Spanish)* 80—109041
- protectors, meas. of real-ear attenuation, SABS 572 1973 80—53581
- protectors, relation of attenuation to noise spectra 80—96100
- rabbit ear chamber for continuous microscopy of implanted biomaterials 77—81755
- radiographic observations, clinical experience with the Optiplanimat 79—62339
- receptor pattern in herring 79—96579
- reflex threshold shift in chinchillas following a prolonged exposure to noise 79—100631
- review of physical aspects of hearing 77—90808
- review of sound anal. by the ear 80—104593
- round window, radiological anatomy review 79—62332
- scala tympani electrode for auditory prostheses, 8 channel 80—36194
- Schroeder-Hall hair-cell model, further investigations 79—70554
- semicircular canal afferent response system identification 78—27927
- semicircular canal primary afferents, impulse weight functions, frog 78—69116
- semicircular canals, flow of endolmph 79—92258
- semicircular canals, unsteady fluid dynamic response, math. model 77—9216
- simulators, constants meas., for earphone calibration 78—27960
- skin, mouse, fractionation effects in response to combined heat and X-rays 80—76805
- sound pressure in insert earphone couplers and real ears 78—65152
- sound pressure level transformation from diffuse sound field to external ear, body and head 79—68523
- sound transmission and cochlear microphonic characts., gerbil and guinea pig 77—32909
- sound transmission from mech. part of nerve endings model 79—57667
- source elevation illusions, created by spectral manipulation using monaural hearing 78—3510
- Sphenodon punctatus, ear anatomy and hearing 77—40681
- stapedial reflex in noenates 79—92236
- stapedial reflex thresholds and tympanometric compliance values, age and sex variations 80—41049
- stapedius muscle, fatigue and recovery of acoustic reflex in industrial noise 79—53159
- stapes footplate movement, holography 77—44690
- static acoustic-immittance measurements 80—76758
- stereophonic equalisation of artificial heads without exact replication of eardrum impedance 80—81614
- stimulated acoustic emission from human ear 79—100629
- stimulated acoustic emissions from within the human auditory system 79—11941

ear continued
- subcutaneous tissue gas space pressure during superficial isobaric counterdiffusion 80—30968
- susceptance tympanograms, asymmetry obs. 80—41051
- thermal resistance induced in mouse ear 79—48220
- thermal resistance induction, heating time rel. to temp 80—3595
- tonotopic organization in guinea pig cochlea damaged by kanamycin 79—96569
- transformation characteristics of external human ear up to 15 kHz 77—86508
- travelling waves and cochlear resonance 80—94222
- tympanic contactless membrane thermometer 79—34692
- tympanic membrane acoustic admittance in aging ear 79—100630
- tympanic membrane investigations in living man using holographic interferometry 80—67207
- tympanic membrane perforations, expt. induced, in cats, middle ear transmission loss 77—32908
- tympanic membrane vibr. studies in living man using holographic interferometry 80—67208
- tympanic membrane vibration study, phase sensitive holographic technique *(German)* 78—3513
- tympanic membrane vibrs. in human temporal bones, double pulsed holographic anal. 78—40289
- tympanic phonocephalography, passive noninvasive technique, normal tracing 77—81618
- tympanometric asymmetry 78—27963
- tympanometric screenings of 2-year-old children, repetitive obs. 80—85412
- tympanometry, interactions among variables 78—27964
- tympanometry in 3 year old children, seasonal influences 80—41052
- tympanometry in 3-year-old children, correl. with findings at paracentesis 80—85416
- tympanometry in normal neonates 80—3651
- vascular permeability in rat ears after X-irradiation 79—5330
- vestibular apparatus, transform. of angular accels. by system of semicircular canals 77—16943
- vestibular control of oculomotor and postural mechanisms 80—72151
- vestibular mechanisms, rel. to eye movement control, book contrib. 79—96588
- vestibular nystagmus, Alexander's law model 80—35878
- vestibular nystagmus, computer anal. of irregularities indicating central vestibular disorders 78—81036
- vestibular system, model of influence on blood press. during sleep 77—25410
- vibration measurement on human ear drum, electronic speckle pattern interferometry 79—53205
- vibration measurements, using light scatt. heterodyne interferometer 77—2073
- vibration waveform measurement using temporally modulated holography 80—67212
- X-irradiation damage, thermal enhancement in mouse, effect of prior heat treatment 79—48291
- Mo-Ti-La-C, influence of high pressure on mech. preps. after nitriding *(Russian)* 79—57137

ear microphones *see microphones*

earphones
- *see also hearing aids; telephone sets*
- audiometric, influence of cushion dimensions on output 79—41547
- audiometric circumaural earphones, calibration using damped flat-plate coupler 79—86316
- calibration, ear simulator const. meas. 78—27960
- circumaural headset for hearing testing, calibration 77—9211
- coupling device for transfer characteristics measurement *(German)* 77—75756
- electrodynamic earphone, mag. field probe 79—34690
- flying helmets, active noise reduction system 79—18602
- free-field characteristics, electrodynamic and electroacoustic type comparison *(German)* 78—33976
- group delay distortions in electroacoustical systems 78—69105
- insert-type, artificial ears 77—32904
- piezoelectric plastic film transducer theory 80—43582
- pocket Geiger counter for β detection *(Spanish)* 80—14051
- reference equivalent threshold sound pressure levels, audiometric zero 79—3872
- sound pressure in insert earphone couplers and real ears 78—65152
- stereophonic reproduction with control of special transfer functions through head movements *(German)* 78—20182
- Telex 1470-A audiometric, calibration data 80—74685

Earth
- *see also Earth composition; Earth rotation; Earth structure; earthquakes; geochemistry; geochronology; geodesy; geomagnetic variations; geomagnetism; terrestrial atmosphere; terrestrial electricity; terrestrial heat*
- 1978 annual review of Earth and planetary sciences 79—5437
- absolute motion and relict radiation *(Czech)* 80—31394
- absolute velocity meas. using one-way velocity of light 79—44924
- albedo, anthropogenic changes and effects on climate 80—81893
- albedo, anthropogenic effects 78—28238
- albedo, zonal and global, depend. on reflectivity regional vars. 80—17377
- albedo contrast due to continental drift, rel. to glaciation 79—74950
- albedo model in spherical harmonics 80—41445
- albedo monitoring technique from LANDSAT data 77—78516
- asteroid 1685 Toro, orbital resonances with Earth and Venus 79—2513
- astronomical parameters corrections determ. ill-conditioned systems least squares soln. 80—26747
- astronomical theory of climatic fluctuations geographical support 80—72509
- attenuated white noise statistical gravity model 80—30977
- attenuation models 78—61367
- barycentric motion rel. to stellar aberration and Doppler shift 80—8520
- best-known figure, three-dimensional geodesic mapping equations for non-rigid Earth models *(German)* 78—73304
- bodily tide and yielding due to tidal loading 78—36091
- catastrophes, theory incorporating galactic modulation 80—31043
- chemical composition, rel. to Moon and eucrite parent body comps. 77—60636
- chemical history, rel. to Moon and parent body of achondrites 77—60639
- circumterrestrial debris belt, creation by artificial satellites collisions 78—89035
- Clairaut eqn., connection to satellite geodesy and Jupiter 78—11795

Earth continued

- climate, astronomical theory, teaching approach 79—84891
- closest approaches of Mars 79—16866
- colour photographs from space probe *(German)* 77—53445
- comet impact, explanation of Cretaceous species extinction 80—76977
- contraction and palaeomagntic data, comments 79—34739
- contraction rel. to solar day and synodic month vars. from fossil record 78—11794
- daily free nutation parameters, determ. technique 78—96126
- decade fluctuations in rot. rate redeterm. for 1861-1978 period 79—84073
- density, min. depth of lateral inhomogeneities 78—7596
- density and composition, comparison with Venus 77—29680
- density distrib., inverse problems, max. entropy method, extreme models 78—65230
- dynamic processes, extraterrestrial causes, rel. to extinction of life 78—92820
- dynamical evolution of Earth-Moon system from shell growth rings 78—96122
- early history, review 79—20739
- early regolith formation 78—85698
- Earth/Moon system, satellite aided capture of external body 79—75087
- elastic tides and natural oscills. with Coriolis force included 77—37122
- ellipsoidal density distrib. model *(Russian)* 79—20741
- elliptical orbital elements long term vars. 77—64625
- equilibrium figure, integro-differential eqns. 79—44077
- evolution of interior, atm., ocean, Viking mission Mars information, appl. to Earth 77—78709
- expansion, rel. to form. of dolines *(French)* 77—86826
- expansion due to secular decrease in gravit. const., evidence from Mercury 77—32972
- expansion limits from palaeomag. data and gravit. constant changes 78—28155
- expansion of Earth or new global tectonics, comparison *(Russian)* 78—28211
- external gravitational fields screening by Earth's mass, effects on Earth tides obs. *(Russian)* 78—88787
- feature identification and location experiment, Space Shuttle remote sensing appl. 80—56657
- figure and gravit. field determ., least-squares collocation method 79—48392
- forced nutation, study via astronomical time meas. 77—52956
- free oscill. data inversion, eigenvalue problems, angular order spectra 79—8602
- free oscillation, radial mode Q-value using 1977 Indonesia earthquake data 80—67346
- free oscillation data inversion, asymptotic approach 79—92624
- free oscillations, amplitudes of split normal modes 78—40508
- free oscillations, attenuation data inversion, fundamental and first higher modes 77—78113
- free oscillations, general aspherical perturb. effects 78—48984
- free oscillations, perturb. theory, surface waves group vel. formulae 78—61349
- free oscillations, rot. and elliptical splitting 79—88257
- free oscillations attenuation in viscoelastic Earth, theoretical contrib. 80—21652
- free oscillations due to earthquake, complex eigenfreqs. improved resolution in analytically continued seismic spectra 78—36106
- geocentre position variation determ. using geostationary satellite obs. 80—82083
- geocentric gravitational constant, evaluation from Viking Doppler and range data 80—3891
- geocentric gravitational constant (GM), determ. from satellite-satellite tracking data 80—3911
- geodesy and geodynamics, reference frame establishment 80—21601
- geoid, longitude-averaged meridional profile of pear-shaped section 80—94450
- geoid figure determ., dynamic method 78—16175
- geoid shape anomalies *(Hungarian)* 78—15944
- geologic evolution of terrestrial planets 77—53442
- global heat balance, annual var. 78—73300
- gravimetric density formula for Earth of spherical shells 78—61303
- gravitational field, loci of nongravitational foci, apsides of set of paths analysis 78—7867
- gravitational field, stationary points coordinates 78—53805
- gravitational potential at physical surface, satellite model applicability 79—62774
- gravitational potential energy spherical harmonic eqn. 80—21613
- gravity, education as point mass, conical shell derivation 77—78928
- gravity anomalies and tectonics, review 80—98593
- gravity tide and ocean tide interaction, Ross Sea area, Antarctica 77—86903
- gravity tides in Japan, ocean tides effects 77—60342
- gravity tides spectrum, 1 to 4 cycles/day 78—20345
- gravity values at poles, rel. to equator, density effects 80—46758
- halo orbits in Earth-Moon restricted three body problem 80—36483
- heating by impact of accreted bodies 79—74868
- hydraulic fractures mapping technique 78—69543
- hydrostatic tides, theory, Earth, planets and satellites appl. 79—84075
- ice ages and biological catastrophes rel. to solar system encounter with nearby supernova 77—29662
- ice ages and orbital vars., theory and numerical modelling 80—56598
- ice cover and climatic models, sensitivity to external forcing 80—82049
- inertia tensor, change due to earthquakes rel. to Chandler wobble amplitude 77—90990
- interior phase change and shrinking effects on lunar motion 80—46182
- interstellar cloud encounter, terrestrial consequences 78—57292
- IR radiation pressure on Castor satellite, meas. from Cactus accelerometer results 80—77251
- Jupiter as source of electrons 80—90357
- kilometric radiation polarization, Voyager 1 and 2 direct meas. 79—12373
- Landsat views of Earth, book 78—7643
- libration points of Earth-Moon system, search for assoc. natural or artificial objects 80—98647
- local vectors connection in actual gravity field of Earth, model field, disturbing pot. 78—61297
- lunar palaeotides and Earth-Moon system origin 79—62769
- mass and moment of inertia 77—86735
- E.Mediterranean and Levant fracture zone, tectonics of continental collision 78—69319

Earth continued

- meteoric material distrib. near terrestrial planets, methematical modelling 79—96976
- microwave remote sensing, theory for thermal microwave emission from bounded medium containing spherical scatterers 77—87071
- momentum of inertia, effects of gravit. const. vars. 78—49302
- monitoring environment, Earthnet satellite programme 78—88921
- Moon, fission theory origin and geosynchronous release 80—101536
- Moon origin from Earth mantle, geosynchronous phase, consequences for Moon 80—101537
- motion, numerical theory using radar, optical and Venera satellite obs. data 78—16325
- motion through cosmic blackbody radiation 79—84887
- natural freq. spectra, information content of different angular numbers 78—61344
- natural vibration freqs. of Earth including ocean 79—62449
- normal mode excitation by collapsing cavity 78—7583
- normal mode oscillations, tensor spherical harmonics appl. to anisotropic Earth model 80—98296
- normal modes of laterally homogeneous Earth, one dimens. example 78—88797
- normal modes of rotating Earth model, excitation by earthquake fault 78—73312
- normal modes of simple Earth models, variational type finite element solution 78—11817
- nutation, appl. to latti. var. and national ephemerides calc. 78—88776
- oblateness, first-order effects on coasting bodies 77—60582
- oblateness effects on lunar ephemeris, corrections 77—22043
- obliquity of ecliptic, historical obs. anal. 79—44076
- obliquity of ecliptic 2000 years BP, calc., error correction 79—29688
- obliquity of ecliptic in geological time *(Chinese)* 78—69270
- optical-mechanical scanners for Earth observation *(Russian)* 78—96321
- orbit, determ. from radar obs. of Venus in 1962-1977 period 79—88570
- orbit determination on basis of radar and visible observations 80—90323
- orbital changes affecting climate Milankovitch model, review 78—44975
- orbital eccentricity correl. with palaeoclimate and palaeomagnetism 77—78093
- orbital eccentricity fluctuations, effect on climate and palaeomagnetic intensity, mechanism, discussion 79—88466
- orbital elements, long term changes rel. to Quaternary climatic var. 79—88469
- orbital elements, periodic vars. influence on insolation *(Russian)* 78—53605
- orbital elements rel. to caloric insolation long-term vars. 78—73502
- orbital motion, analemma, photographic representation inc. year-long solar images 80—12649
- orbital motion calc. method 77—53411
- orbital motion from self consistent FORTRAN subroutines 80—85845
- orbital parameter var., energy balance climate model sensitivity 80—12537
- orbital variations, cyclic, detect in S.Australian beach ridges chronology rel. to Milankovitch ice age theory 80—98307
- orbital variations, rel. to climatic change 77—13114
- orbital variations, rel. to Pleistocene ice fluctuations 77—37346
- orbital variations, support for astronomical theory of climatic change 77—87058
- orbital variations 80—51531
- origin and composition models 77—25663
- origin and history to earliest geological times, rel. to origin of life 78—69923
- origin from solar nebula, book 80—17266
- oscillations, corrections to eigenfreqs. due to dynamic shear modulus 77—81800
- oscillations, split normal modes, theoretical amplitude and Green's dyadics 80—101341
- oscillations, unresolved split normal mode multiplets spectra 79—74845
- polar g-values 78—81727
- precession, lunisolar, determ. via obs. of extragalactic radiosources 77—5129
- precessional constant and general catalogue for southern stars, proper motions in α *(Russian)* 79—92685
- precessional corrections to AGK3 system in polar region, rel. to stellar proper motion system anal. *(Russian)* 80—12647
- primitive abiogenetic organic synthesis involving Hg 77—37173
- primitive amino acid formation, prebiotic synthesis by ionising radiation 77—37410
- primitive Earth, chemical evolution and energetics of reactions in aqueous solns. 77—33189
- primitive water masses, amino acid formation in ultrasound 77—37409
- proto-Earth, melting due to primordial dense atmosphere blanketing effect 79—57935
- protoplanetary nebula formation of inhomogeneous Earth 80—90348
- pulsation and expansion rel. to Phanerozoic tectonics and volcanism *(Russian)* 79—2202
- punctuated evolution of tectonic style 79—16432
- Q frequency depend. in Earth rel. to mantle rheology and Chandler wobble 79—84190
- radial oscillations, core and upper mantle struct. effects 80—12347
- radial vibrations of a gravitating sphere with a material boundary 79—41609
- radiance meas. from Miranda (X4) satellite, IR expt. design and performance 80—72745
- radiation budget, fluxes simulation and accelerometric meas. *(French)* 79—84482
- radiation environment, for near-Earth, review 79—12359
- radiative balance, absolute meas. instrument *(French)* 79—29900
- radius var. and palaeogravity since late Precambrian kimberlite nodule data 78—24217
- relativistic effects verification, comparison of obs. results with theoretical data *(Russian)* 79—80209
- remote sensing by satellite, periodic coverage pattern quantisation and symmetry 77—78444
- research programme of ESA 80—109251
- resource imagery data processing techniques *(Italian)* 77—82063
- response to long-period geomagnetic fluctuations, phase 79—88239
- rotation pole secular trend, consideration of motion of latit. observatories 77—86734
- shadow radius during total lunar eclipse of 1974 November 29, obs. in Ussuriisk 77—67051
- shell of uniform layers, asymptotic distrib. of torsional eigenfreqs. 78—92797

Earth continued
shoreline information in artificial satellites autonomous navigation problems 78—53732
siderophile and volatile elements rel. to origin of Earth, Moon and C1 chondrites 78—7892
size measurement, from sunset obs., for teaching 79—35459
solar-lunar tidal force calc. accuracy *(Russian)* 80—61813
solotone effect and torsional eigenfreqs. of spherical shell 78—92798
spheroidal eigenoscillations, freqs. and corrections to interior struct. 77—52996
statistical model from gravity anomalies and HB$_1$ model 78—61306
Sun-Earth-Moon system, stability limits for restricted three body problems 79—75084
supernova causing shower of lunar ablation debris 80—56731
surface, radiance of natural formations 79—62515
surface, structure, atmosphere, magnetic field, development *(Hungarian)* 77—73987
surface air survey methods *(Dutch)* 78—3972
surface albedo, vars. during recent Sahel drought (1967 to 1974) 80—76981
surface albedo effects in satellite auroral photometry 77—56737
surface gravitational potential, satellite model error estimation 79—96935
surface thermal radiation interpretation, emissivity correction 80—82092
terrestrial kilometric radiation, spatial struct. 77—25873
thermal evolution of planet growing by planetesimal impacts 79—70968
thermal history, rel. to time-varying gravitation in Newtonian theory 78—93592
tidal deformations and pot. vars., relation between Love numbers and load factors 78—61305
tidal evolution of Earth-Moon system 80—82240
tidal friction with Moon changing Earth moment of inertia 80—81803
tidal potential, multiple expansion 79—12062
tidal-friction theory of the Earth-Moon system 80—81802
tide obs., ocean tides effect in near zones 77—32974
tides, anal. of obs., least squares methods *(French)* 77—87078
tides effects on artificial satellite orbits 77—87243
tides in new USSR Universal Time system, 1955-74 period *(Russian)* 78—69279
toroidal free oscillations, upper mantle discontinuity effects 79—29713
torsional eigenfreqs. of spherical shell, asymptotic distrib. 78—88800
torsional eigenfrequencies, effects of density and shear vel. discontinuities on asymptotic overtone struct. 77—78111
torsional normal modes eigenfreqs., asymptotic overtone struct., model study 77—78110
torsional vibrations, damping effect 79—44121
transient and impulse responses of one-dimens. linearly attenuating medium, analytical results 78—32687
transient and impulse responses of one-dimens. linearly attenuating medium, parametric study 78—32688
tropical year, its astronomical meaning, for teachers 79—97136
Universal view 79—5438
viscoelastic model, appl. to Earth tides theoretical study 80—67333
volatile outgassing vel. to Viking rare gas abundances on Mars 77—45342
whole-Earth dynamics, variational method 77—60340

earth (electric) *see earthing*

earth (soil) *see soil*

Earth age *see geochronology*

Earth atmosphere *see terrestrial atmosphere*

Earth composition
see also Earth structure
S.African kimberlites, ^{40}Ar/^{39}Ar anals. of phlogopite nodules and phlogopite-bearing peridotites 79—34769
Alpine tectonite lherzolites, Sr isotope comp., evidence for mantle origin 78—65302
Amitsoq gneiss, W.Greenland, initial Pb isotopic comp. and implications for Earth age 78—20371
andesitic and alkaline provinces in Mexico and central America 79—57880
anorthosite complexes, Marcy (New York) and Morin (Quebec), rare earth element abundances 77—78177
anorthosite gneisses, trace element comp. rel. to petrogenesis 78—65224
Antarctic Peninsula igneous rocks, transverse geochemical vars. rel. to calc-alkaline magmas genesis 80—56466
apatite in ijolitic and carbonatitic igneous rocks, comp. vars. 79—57929
Arakapas fault belt, Cyprus, sedimentation and metallogenesis along fossil oceanic fracture zone 79—29769
Archaean mantle, siderophile and lithophile trace element evolution 80—46147
Archaean metasedimentary rocks from Kambalda, Western Australia, rare earth element geochemistry 80—109143
Archaean migmatites in Lofoten-Vesteralen, Norway, Nd, Sr and Pb isotope data interpretation 79—34773
Archaean plutonic rocks, Pb isotope comp. 78—65223
Archaean precious-metal hydrothermal systems, Ontario, alteration patterns and metal distrib. 80—12382
Archaean precious-metal hydrothermal systems, Ontario, rare earth element and 0 isotope relations 80—12383
Archaean rocks of E.Lac Seul region, English River subprovince, NW.Ontario, Rb-Sr isotopic study 80—94486
Archaean volcanic rocks S content rel. to ocean floor basalts 78—88824
Archean greenstone belts, Nyanzian System, W.Kenya, trace element model study 77—60375
Archean sedimentary rocks, Kalgoorlie, Australia, rare earth elements and crustal evolution 77—60374
N.Atlantic mantle, chemistry and Pb, Nd, Sr isotopic correl. 80—90023
N.Atlantic recent sediments, volcanism effects on mineral comp. 78—44802
Mid Atlantic Ridge, 22 to 30°N, magmatic process var. and upper mantle heterogeneity 79—88334
Atlantic salt deposits distrib. 77—21752
Australian Zn-Pb-Ba deposit, primitive Pb determ. 78—11900
Azorean lavas, REE and LIL element compositions 77—25669
Baikal rift zone, petrochem. of Cenozoic basalts and assoc. rocks 78—36171
basalt, ^{238}U/^{235}U ratio and comparison with chondritic meteorites 80—85903
basalt glasses from FAMOUS area, Mid-Atlantic Ridge, regional var. and petrogenesis 80—31041

Earth composition continued
basalt glasses from Mid-Cayman Rise spreading centre, geochemical var. and petrogenesis 80—101364
basalt magma sources during opening of N.Atlantic, Nd and Sr isotopic comp. 79—100821
basalts, deep sea, statistical anal. of clinopyroxenes 78—88828
basalts, deep sea, trace element distrib. pattern, neutron activation anal., rel. to genesis 78—11879
basalts, oceanic, noble gas abundance patterns controlling factors 78—65220
basalts, Palaeocene, of Mull and Skye, immobile trace elements rel. to palaeotectonic affinities 79—34816
basalts and mantle derived materials, K and Rb relations rel. to phlogopite source 77—5165
basalts from DSDP Leg 37 cores, Pb and U isotopes 77—91123
basalts from DSDP site 332, evidence for chemically distinct magma chambers 77—91126
basalts from E.Pacific Rise—Galapagos Rise system, major element comp. rel. to mag. anomalies 78—73331
basalts geochemistry from back-arc spreading centre, East Scotia Sea 80—3989
basalts of Iceland and Reykjanes Ridge, F contents and outgassing 79—57900
Bay of Islands ophiolite complex Nd and Sr isotopic study rel. to midocean ridge basalts source evolution 80—85651
beach and dune sands on Goa coast, mineralogy 77—41028
big river sands, modern, petrology and chemistry 79—25274
biotites, Alpine, excess Ar evolution from ^{40}Ar-^{39}Ar anal. 80—94521
Black Sea sediment cores, organic geochemistry rel. to comp. differences 78—49040
Bouvet triple junction, S.Atlantic Ocean, geochem. and petrology of dredged basalts 78—11877
N.Britain, crustal layering, rel. to seismic vels. of Lewisian metamorphic rocks at high press. 79—84137
bulk composition, rel. to chemical heterogeneity of Archaean mantle and mantle evolution 78—11844
Caledonian granites in Britain, geochemical and geophysical evidence on geothermal pot. 79—74486
Caledonian granites of Scotland, Nd and Sr isotope study rel. to provenance 80—109146
S.California, crustal comps. from teleseismic Rayleigh waves anal. 79—92510
Canadian Precambrian Shield, N.W.Ontario, ^{18}O/^{16}O ratios 77—78130
Canadian Shield surface crystalline rocks, O isotope comp. 79—62496
Cantal continental volcanic system (France), ^{87}Rb-^{87}Sr constraints on genesis and evolution 79—88327
Caroline Plate, petrochem. of troughs and crustal accretion 80—12385
Central American andesites, Sr isotope evidence for mantle petrogenesis 79—20833
chemical and thermal struct. of deep interior, obs. constraints 79—53323
chemical evolution rel. to $^{206/207/204}$Pb ratios 79—88315
chevkinite from Oslo region, Norway, cryst. struct. and chemical comp. 78—85533
Clearwater Lake impact structures, Quebec, meterotic component and impact melt comp. 78—65314
clinopyroxenes from deep-sea basalts, statistical anal. of chemistry 80—41437
composite dike geochemistry, light rare earths partitioning between coexisting acidic and basic melts 79—2233
composite dike geochemistry, magmas commingling model for coexisting acidic and basic melts 80—12391
continental and oceanic basalts, ^{143}Nd/^{144}Nd ratio vars., rel. to magma sources and mantle struct. 77—21708
continental crust, constraints on comp. and nature of lower crust from mantle Nd-Sr isotope correl. 80—94498
continental crust, evolution age and isotope evidence 78—65233
continental crust, heat-producing radioactive elements distrib. and redistrib. 78—65232
continental crust modelling, structural and chemical constraints 79—16420
continental crust root zones, comp. rel. to thickness and thermal history 79—88320
continental shields, Curie temp. depth, compositional boundary 79—53330
continental tectosphere comp. and development 78—81133
core, comp. rel. to dynamics of fluid core with inward growing boundaries 80—76934
core, H contrib. to density deficit 77—66895
core, K content rel. to heat source and thermal model 78—15982
core, monosulphide solid soln. in Fe-Ni-S system 80—90038
core, Ramsey phase-change hypothesis 79—66662
core chemistry, review 77—13070
core composition, implications of Fe close-packed phases eqns. of state 79—20780
core-mantle boundary, nature of transition 77—78137
Cretaceous mid-ocean ridge basalt (MORB), Nd and Sr isotopic comps. and rare earth element abundances 80—94520
crust, chemical balance 77—86831
crust, chemical balance rel. to time scales and dynamic models of deep-sea sedimentation 78—15988
crust, isotopic comp. and trace elements concs. rel. to mantle and crustal reservoirs mean age 80—51359
crustal rocks, isotopic ratios rel. to rel. to mantle chemical evolution 80—90043
deep sea sediment cores, Au, Pd, Ir, Mn sources, neutron activation anal. 80—17247
deep-sea basalts, He and Xe as measure of magmatic differentiation 80—31040
Denchai Basalt, N.Thailand, paleomagnetism, age and geochemistry 80—41421
desert varnish of Sonoran Desert, comp. from optical and electron probe microanal. 79—79834
diamonds, rare gas isotopic compositions, rel. to atm. comp. 78—24270
diamonds from Lesotho kimberlite pipes, isotopically light C obs. 79—48487
Disko Island, Greenland, native Fe occurrences 77—81893
DSDP Leg 37 rocks, O isotope geochemistry 77—91072
dunite-peridotite mixed-oxide compositional models rel. to mantle temp. 77—2124
Duxbury massif (2.5 Ga), Quebec, initial ^{87}Sr/^{86}Sr rel. to remobilised pre 3.0 Ga sialic basement hypothesis 80—76970

Earth composition continued
environment evolution, available elements during Earth history rel. to life evolution 79—80030
evolution of Earth with non-Fe core 77—70621
ferromanganese nodules, oriented, U-Th series nuclides rel. to growth rates and turnover times 79—29740
Floridan Aquifer rocks, Sr content rel. to dolomitisation 79—53346
fumarole B isotope composition, Satsuma Iwo-Jima, Japan 80—67358
Galapagos Rise hot spring field, radionuclide ratios rel. to clam growth rate determ. 79—84300
garnet lherzolite, high-press. phase equilibria and Mg^{2+}-Fe^{2+} partitioning among constituent minerals 79—66687
gas-mineral equilibria and Earth interior chemical model 77—9411
Gondwanaland lithosphere, vars. in chemistry from Rb-Sr mantle isochrons 78—28201
granites of E.United States, radioactive elements concs. rel. to low-temp. geothermal resources 80—85264
granitic basement, ^{87}Sr/^{86}Sr for fracture-filling calcite 77—29267
granitic magma of Bushveld Complex, trace element abundances rel. to crystallisation history 80—109145
granitoid rocks, Nd-Sr isotopic relationship and continental crust development, chemical approach to orogenesis 80—94522
groundwater ^{14}C content, possible subsurface prod. rel. to dating 80—85690
halogen content of ultramafic nodules, determ. by gamma-ray spectroscopy and radioactivity meas. 80—76945
Hawaii xenolithic dunites, excess ^{129}Xe and high ^{3}He/^{4}He ratios 79—34814
hornblende, grunerite and garnet comp. in Archean Fe formation, Canada 78—7630
hydrocarbon bearing anticlines, pattern space of seismic anomalies, location tool and theory 80—17234
hydrosphere, seawater and river water comp. rel. to water-rock partition coeffs. 79—44200
hydrothermal mounds near Galapagos Rift, chemistry 79—29739
hypersthenic magmas, water contents 80—72507
Iceland, Hg natural conc. 77—64244
E.Iceland lava, ^{40}Ar/^{39}Ar dates and ocean ridge growth 80—36273
Icelandic mantle plume, Cl and Br abundances from Iceland and Reykjanes Ridge basalts 78—36136
W.Indian Ocean, mantle uplifted block 79—25228
SE.Indian Ridge, seafloor mag. anomalies rel. to chem. of mid-ocean ridge basalt 80—109102
inert gas composition, Earth's origin from solar nebula 80—61785
inner core, Poisson's ratio compatible with rigid metal 80—56438
inner core composition, Ni_2Si hypothesis 80—8266
inorganic gas chromatography for determ. of H_2O and CO_2 in rocks and minerals 80—85767
interior shells, chemical composition, analogous to components of hightly reduced enstatite chondrite meteorites 80—85624
isotopic equilibrium, regional and local, in mantle, from volcanic rocks comp. 78—65216
Japan, granitic rocks rel. to country rocks 78—81119
Josephine Peridotite, mineral comp. rel. to partial melting 77—81880
Jurassic seafloor, Point Sal, California, rare earth and trace element geochem. 78—32094
K-rich ultramafic magmas from peridotitic mantle source 79—2200
Kapuho lava, Hawaii, olivine phenocrysts excess ^{129}Xe and high ^{3}He/^{4}He ratio 79—34814
Karroo rhyolites, Swaziland, isotopic evidence of crustal contamination 80—21666
post-Kenoran upper crust, composition and evolution 79—92511
Kerguelen igneous rocks, petrology and isotopic geochemistry rel. to continental or oceanic character 79—57924
Kilauea fumaroles, He/CO_2 ratios as premonitors of volcanic activity 80—26482
kimberlite nodules, upper mantle petrology and geotherms 78—65310
Kimmeridgian black shales, N Atlantic region, rare earth elements distrib. 79—44187
Lakes Ontario and Erie, comparison of bluffs and sediments composition 77—5248
large impact craters, meteoritic material detect. and chemistry 78—57208
Lassen Park volcanic gases, He isotope ratios 79—16425
Lewisian gneisses, Sm-Nd systematics and implications for granulites origin 79—20777
liquid metals equation of state parameters rel. to core energetics 77—15536
lithosphere, present struct. and struct. evolution *(Russian)* 80—81857
Loc Uisg granophyre, Isle of Mull, isotopic and chem. evidence for origin 78—65303
Louvem volcanogenic Cu deposit, Quebec, lithogeochem. anomalies 79—5480
lower continental crust, comp. from granulite xenoliths in Lesotho kimberlites 78—24268
lower continental crust model, comp. and struct. 77—81840
lower crust, O isotope study of xenoliths showing heterogeneity 80—89992
lower mantle, convection, composition and thermal state 80—21678
magma mixing, petrological process and volcanological tool 77—37201
magma mixing at mid-ocean ridges, evidence from Mid Atlantic Ridge basalts 79—88335
magma series erupted in different marine tectonic settings, trace element anal. 80—21667
magmas, influence of volatile components 80—41418
magmatic rocks, anchieutectic comp. 80—12381
magmatic rocks, petrographic study of Indian Ocean floor 79—20807
Manicouagan impact melt, Quebec, chemical interrelationships with basement rel. to form. processes 78—81165
Manicouagan impact melt, Quebec, stratigraphy, petrology and chemistry 78—81164
mantle, 650 km discontinuities, implications of high press. phase transitions in MgO-SiO_2 system 79—90780
mantle, ^{3}He/^{4}He ratio in injected volatiles in Gulf of California, meas. in Guaymas Basin 80—85640
mantle, equilibrated Nd and unequilibrated Sr isotopes in xenoliths 80—98321
mantle, isotopic composition, advection effects 79—66656
mantle, mixed oxide and perovskite structure model 78—85507
mantle, Nd and Sr isotope content of diopsides from kimberlite pipes 80—51363

Earth composition continued
mantle, noble gases, abundances and isotopic compositions 78—85521
mantle, siesmic discontinuity at 650 km depth 79—44143
mantle, sub-Andean, ^{87}Sr/^{86}Sr ratio from Sr isotope anal. of Cerro Galan Calc-alkaline volcanic rocks 80—98318
mantle, upper, constitution, structurology of peridotite xenoliths in S.African kimberlites *(French)* 78—11889
mantle chemical heterogeneity, evidence, conf., Nov. 1978, London 80—85623
mantle chemical stratification 80—21687
mantle composition, derivation from comp. of lherzolites 80—76940
mantle composition from Pacific Ocean Basin basalts Sr isotope comp. 78—65218
mantle composition rel. to ocean ridge basalts trace elements 78—65219
mantle differentiation and crustal growth, geochem. model 80—21684
mantle evolution, implications from Sm-Nd isotopic investigations of Isua supracrustals 78—36129
mantle fluid comp. buffered by carbonates in peridotite-CO_2-H_2O 77—70644
mantle fluid phase, trace elements 79—34779
mantle melting, past and present, isotope and trace element evidence 78—65238
mantle Nd and Sr isotopes, differentiation occurring in episodes 80—67352
mantle partial melting and mineral-stability boundaries, rel. to seismic exploration of lithosphere, Canada 78—36121
Marda calc-alkaline suite, rare earth elements, Archean geochem. analogue of Andean-type volcanism 78—11898
marine minerals exploration, Mobile Initial Condition Indicator approach 79—5687
Matushiro fault zone, Japan, He spots caused by diapiric magma from upper mantle 79—8618
metabasalt block from Mid Atlantic Ridge, metamorphic mineral data 77—64279
metals, pressure depend. of melting 78—85517
methane, outgassing from Earth interior 78—92809
methane, profiles in marine sediments rel. to prod. and consumption 80—12373
Michigan Basin deep hole metagabbro, mineralogy and geochemistry compared to seawater hydrothermal alteration 79—39710
Mid-Atlantic Ridge basalts, geochem. variation along length of ridge 80—90027
Mid-Atlantic Ridge mafic and ultramafic rocks, Pd, Ir and Au contents 77—91073
mid-ocean ridge basalt, composition restrictions, fluid dynamical model 80—90025
mid-ocean ridge basaltic glasses, U-Pb, Sm-Nd and Rb-Sr systematics 80—36277
Middle America Trench offshore Guatemala, seismic refr. and refl. meas. 80—26493
minerals, magnetic trends on alkali-Fe-Mg diagrams 78—85551
Mistastin Lake crater, Labrador, Sr isotopes and trace element geochem. of impact melt 78—32105
models for origin and composition, core K hypothesis 77—25663
Mount St. Helens, Washington, Ca, Fe and K in glass shards from set-W tephra 78—24274
muscovite in medium to high grade metapelites of NW.Maine, comp. var. 79—62493
S Nain, complex, Labrador, anorthosite and assoc. plutons comps. 79—20825
SW Newfoundland, ophiolites rel. to tectonic models 77—17103
Nigorikawa geothermal area, Japan, rare gas isotopic anomalies 79—88314
Norwegian eclogites, Nd and Sr isotopic comps. rel. to crustal origin 80—76978
ocean floor basalts and ferromanganese deposits, Pb, Nd and Sr isotope comp. 78—61395
ocean major and minor elements balances, role of ridge crest hydrothermal activity from Galapagos data 80—41459
oceanic basalts, differential Sm/Nd evolution 78—61391
oceanic crust, structure, composition and origin 77—29268
oceanic crust basalt, U abundance, heat flow implications, fission track anal. 80—8287
oceanic crust layer 2 S distrib., effect of low temp. seawater-basalt interaction 80—41432
oceanic mantle, evidence for enriched mantle sources from Nd isotopic study of Kerguelen Islands igneous rocks 80—98319
oceanic tholeiites siderophile contents compared with lunar highland rocks 80—8562
oceanic upper mantle, comp. from petrology of ultramafics from Owen fracture zone, NW Indian Ocean 80—94519
ophiolites, N.W.Syria, rel. to Tethyan oceanic crust evolution during Mesozoic 77—81896
ophiolitic metabasalts in Mediterranean area, clinopyroxene comp. 79—57925
Ordovician volcanic rocks, N.Maine, magmatic affinity and tectonic significance 77—44984
orthopyroxene, occurrence and origin in some lavas from the French Massif central 78—96203
outer core, eqn. of state of liq. Fe rel. to comp. 77—73694
pelitic sediments, Sr and Ar isotopic homogenisation during low grade regional metamorphism 79—62511
perrierite from Oslo region, Norway, cryst. struct. and chemical comp. 78—85533
petrogenetic mixing models and Nd-Sr isotopic patterns 80—3965
phase boundary motion caused by surface temp. and press. excitations, rel. to vertical crustal movements 77—49040
phase transitions and matter differentiation in interior during formation 77—56610
phengite and eclogite in Xingyang metamorphic belt, tectonic significance *(Chinese)* 79—84264
phenocrystic minerals, Ca-Mg-Fe ratios, pyroclastic deposits correl. in S.Kyushu, Japan *(Japanese)* 77—64278
pigeonite, occurrence and origin in some lavas from the French Massif central 78—96203
planetary-type rare gases in an upper mantle derived amphibole 78—96167
plutonic granitic rocks, O and H isotope comps. 78—65221
polycyclic aromatic hydrocarbons in recent sediments, global distrib. 78—57192

Earth composition continued
- polymorphic phase boundaries effects on mantle vertical and horizontal motions 77−9395
- potassic igneous rocks from Roccamonfina volcano, Roman comagmatic region, Italy,, O isotope geochemistry 80−41420
- Precambrian basement of W.Canada, Hg and As distrib. and abundance 80−56419
- precious metals, values in interflow sedimentary rocks from Kambalda (W.Australia) komatiite sequence 79−20830
- primitive mantle structure, Pb isotope study of layered intrusions 80−81847
- rare earth elements, partitioning between hydrous silicate melt, amphibole and garnet peridotite 79−20775
- rare gas fractionation rel. to Earth-atmosphere evolution model 77−13077
- Recent andesites in Ecuador and N.Chile, Sr isotope data 78−32042
- rivers, evidence for higher natural U content 79−44208
- Rochechouart meteorite crater, France, projectile identification 77−33025
- Rogue and Galice formations, Klamath Mountains, element abundances rel. to Jurassic island arc sequence identification 79−100836
- sandstones of Califorinia Late Cretaceous fore-arc basin, petrofacies and petrologic evolution 79−2232
- E.Scotia Sea, back-arc basin, volatiles in submarine volcanic rock 80−67353
- NW Scotland Tertiary continental volcanics, Nd and Sr isotope evidence for crustal contamination 79−66693
- sedimentary deposits composition, geological records coding mech. *(Russian)* 80−17383
- sedimentary rocks, Th and U abundances rel. to crustal evolution and sedimentary recycling 80−85654
- sediments, H_2S contaminated, stagnation coeff. and appl. in palaeogeographic reconstruction 80−36291
- silicate melt inclusions in volcanic rocks, samples of early magmatic liquid 77−37202
- soils of New Zealand, ^{238}U, ^{226}Ra, ^{232}Th and ^{40}K radionuclide conc., rel. to Fe, K content 77−86867
- sphalerite, FeS content as geobarometer, experimental extension to 10 kbar 78−85703
- spilite and keratophyre from Oregon-Idaho Permo-Triassic volcanic arc, comp. and petrogenesis 79−20826
- spilitic rocks, rare earth element mobility and geochem. charact. 77−86887
- spinel lherzolite xenoliths, implications of texture composition depend. 79−25244
- spinel lherzolites from S.Rio Grande Rift, evidence for underlying oceanic mantle 79−29724
- submarine lithosphere, geophys., geochem. and petrological model 80−3994
- superheavy element search in Earth samples, meteorites and cosmic rays *(Russian)* 79−84277
- superheavy elements, detection by fission activity detect. *(Russian)* 79−13358
- superheavy elements search in terrestrial substances *(Chinese)* 79−84281
- tephra attributed to Glacier Peak, Washington, Ca, Fe and K contents 78−24273
- terrigenous and volcanogenic deep sea bottom sediments chem. comp., Sea of Japan 77−21758
- tholeiitic basalts, rare earth elements behaviour during submarine weathering 78−73369
- tholeiitic basalts from Japan, geochemical types 78−96206
- titanite, lanthanides, relative concs. rel. to host rock type 79−62492
- trace element geochem. of peridotite-gabbro-basalt suite, DSDP Leg 37 site 79−34793
- transitional basalts and tholeiites from E.Pacific Rise at 9°N 79−84218
- Troodos ophiolitic complex, major oxide geochemistry and origin 80−98317
- Ukrainian Shield, gravity and heat model rel. to lower crust basicity increase *(Russian)* 78−48991
- Ukrainian Shield, rock mag. props. map rel. to composition and metamorphism 80−17229
- ultramafic nodules, from Kimberley pipes, South Africa 79−34821
- ultramafic xenolith petrology and upper mantle processes, Kapfenstein, Austria 80−76973
- ultramafic xenolith suite from Tahiti, petrology and genetic significance 80−90086
- ultramafic xenoliths rel. to tectonites *(French)* 79−44141
- upper mantle, ultramafic xenoliths from Elwin Bay kimberlite rel. to Fe enrichment 77−91078
- upper mantle transition region, eclogite abundance 79−84192
- volcanic gases erupted in November 1978 fissure eruption in Afar, comp. 79−57912
- volcanic rocks, Tetagouche Group, Canada, geochem. rel. to origin 78−65298
- volcanic rocks, W abundances 79−16468
- volcanic rocks from Aleutian Islands and Pribilof Islands, Alaska, Pb and Sr isotopes 78−57185
- volcanic rocks of Marcus-Necker Ridge, comp. and stages of development 80−36282
- Vredefort structure, S.Africa, comp. of spherules on shatter cone surfaces 79−29773
- Yellowknife, Northwest Territories, Canada, Archaean granite, rare earth and trace element data 80−4007
- Yellowstone Park volcanic gases, He isotope ratios 79−16425
- Zhamanshin impact structure, USSR, impact glass chemically similar to tektites 80−51358
- zircon, element distrib. from proton multiprobe and fission track techniques 80−17261
- zone regining below lithospheric plates, steady state astheriosphere model 79−88326
- zoned steady-state magma chamber comp. var., evidence from Mid Atlantic Ridge 79−88336
- Al_2O_3 content of enstatite as geobarometer for plagioclase and spinel lherzolite 77−2142
- ^{27}Al, use as probe nucleus in NQR techniques appl. to geosciences 80−67426
- ^{36}Ar in primordial mantle from Arkansas diamond comp. 80−94493
- ^{40}Ar concentrations in sialic crust and atmosphere, rel. to form. from upper mantle 79−44153
- ^{40}Ar, mobility in metamorphic terrain, excess in biotite 80−17260

Earth composition continued
- B, content in bottom sediments interstitial waters on trans-Pacific profile 80−36289
- C in upper mantle, implications for plate tectonics 80−81845
- C, organic, dissolves and particulate, in marine environment, stable isotope comp. 79−20862
- CO_2 gas seep from seabed, Norton Sound, Alaska 80−67361
- CO_2 in upper mantle, fugacity at high temps. and press. from decarbonation reactions 79−16439
- Ca, isotope fractionation on Earth and other solar system materials 79−20835
- $Ca_2Al_2SiO_7$, gehlenite, new high-press. phase, rel. to Earth interior 79−29753
- Ca_2GeO_4, with K_2NiF_4-type struct., high press. decomp. 79−1507
- Ca_2MnO_4, with K_2NiF_4-type struct., high press. decomp. 79−1507
- Cr content of magnetite from Bushveld Complex upper zone, vars. rel. to magma chambers heterogeneity 80−56421
- Fe containing minerals in oil-impregnated sedimentary rocks 77−53053
- ϵ-Fe, vol. eqn. of state under static press. conditions, rel. to Earth core-mantle models 80−19904
- Fe-Ni-Si core, form. and comp. 78−12112
- Fe-Ti oxide minerals from Asama volcano, Japan, in 1973 eruption 77−17065
- FeS_2, pyrite, eqn. of state, rel. to constraints on Earth S content 79−70789
- $Fe_{0.9}S$, pyrrhotite, eqn. of state, rel. to constraints on Earth S content 79−70789
- He in Earth interior, incorporated from immature Sun *(Russian)* 80−81856
- He survey in S.India for structural mapping, water sample obs. 80−8261
- K abundance, implications of K solubility in Fe-S and silicate-K-(Fe-S) equilibria 78−11843
- K depletion inferred from mantle heat loss estimate 80−76943
- $MgSiO_3$, perovskite, synthesis and cryst. chem. charact., rel. to mantle mineralogy 78−65266
- Mg_2SiO_4, forsterite, single-cryst., shock wave compression 79−84242
- Mg0, vol. eqn. of state under static press. conditions, rel. to Earth core-mantle models 80−19904
- Mn nodules, mineralogy and comp. changes from long-term seafloor mineral exposure expts. 79−5471
- ^{92,94}Nb prediction in crust by cosmic-ray muons 77−49045
- Nd, Sr isotope geochemistry of hydrous mantle nodules and host alkali basalts, rel. to mantle heterogeneities 80−56420
- Nd-Sr isotopic correlation in mantle materials, geodynamic consequences 79−92512
- Nd-Sr isotopic var. implications for crustal and mantle chemical evolution 79−66655
- Pb, concs. and comp. in DSDP Leg 37 cores 77−91074
- Pb isotope inhomogeneity in Precambrian igneous K-feldspars 78−32095
- Pb-Zn belts and their origin 79−48427
- ^{206}Pb/^{204}Pb evolution during crust development, rel. to U, Th and Pb fractionation 79−57879
- ^{187}Re/^{186}Os in Earth mantle, rel. to use of Os isotopes as petrogenetic and geological tracers 80−89989
- Rn lognormal distrib. in soil 77−5205
- ^{222}Rn enhancements and gas upflow possibility 79−74893
- Sr evolution in W.Greenland-Labrador craton, early Rb depletion in mantle 78−69304
- Sr, Pb, isotope geochemistry rel. to catastrophic or continuous core form. 78−57178
- ^{87}Sr/^{86}Sr initial ratios and Rb-Sr ages, from Oxford Lake-Knee Lake greenstone belt, N.Manitoba 80−94485
- ^{87}Sr/^{86}Sr ratio in volcanic rocks from W.Pacific island arcs 77−33031
- ^{87}Sr/^{86}Sr ratio reduction during hydrothermal alteration of basalts 79−16446
- U analysis in geological samples, delayed neutrons method *(Rumanian)* 79−88507
- U and Th abundance in Precambrian basement, W.Canada, petrologic and tectonic controls 80−17257
- U and Th abundances in Indian kimberlites 77−60376
- U, conc. in mantle rel. to Earth thermal evolution 80−89988
- U, concs. in oceanic rocks of (DSDP Leg 37) 77−91075
- U, geochemical cycle, mantle and crust content 79−84275
- U in sandstone-type ore from Pakistan, assessment by charged particle track analysis 80−91405
- U prospecting by γ-ray logging of borehole, factors affecting resolution 80−98463
- Xe, fissiogenic isotopes in CO_2 well gas 78−73374

Earth core
- anti-dynamo theories, compressible flow effect 80−56361
- axisymmetric inertial fluid oscillations in cylindrical cavity during spin-up from rest 78−5750
- boundary irregularities influence on liquid vel. and mag. field 77−13065
- bumpy core-mantle interface, effects on variable geomag. and gravit. pots. 79−79771
- catastrophic or continuous formation, Sr and Pb isotope geochemistry constraints 78−57178
- celestial mechanics of Earth-Moon system, new kind of three-body problem 78−45210
- chemical and thermal struct. of deep interior, obs. constraints 79−53323
- chemical composition, analogous to components of hightly reduced enstatite chondrite meteorites 80−85624
- composition, eqn. of state of liquid Fe in core conditions 77−73694
- composition, H contrib. to density deficit 77−66895
- composition, monosulphide solid soln. in Fe-N-S system 80−90038
- composition, review 77−13070
- conductivity profile of core-mantle system 80−36238
- conference, Potsdam, Germany (Oct 1979) 80−86034
- convective dynamo, models 78−89090
- cooling by subsolidus mantle convection 80−36278
- core-mantle boundary, amplitudes of long period PcP 77−37143
- core-mantle boundary, layered transition zone rel. to seismic waves long distance propag. *(Italian)* 79−12071
- core-mantle boundary irregularities, effect on fluid speed and geomag. field 78−73333
- core-mantle boundary roughness, seismic array evidence 79−20781
- core-mantle boundary thermal interaction rel. to geomagnetic field long term behaviour 77−52981
- crystallization at inner core boundary under isochem. conditions, causing changes in dimens., stress and gravit. energy 79−84191

Earth core continued
- day length irregular variations, core-mantle coupling 77—64186
- density model, variational approach *(Russian)* 78—28191
- discovery, historical aspects 80—105486
- dissipative core-mantle coupling in nutation theory 77—64188
- dynamo model of magnetic field, self-consistent treatment 80—81808
- dynamo theory for mag. field generation *(German)* 78—40852
- early Earth, core form. rel. to Moon fission origin timing 78—85867
- earthquake magnitude calibration function for core phases, PKP1-PKP2 caustic 78—40509
- earthquake prediction methods, state and movement of Earth core *(Russian)* 79—84162
- electric current strength and mag. fields at top of core 80—36240
- electrical conductivity, determ. from geomag. field dynamics 79—12066
- electrically conducting fluid core location from external mag. obs. 78—32248
- electrically conducting rot. sphere behaviour in time-independ. homogeneous external mag. field 78—49309
- energetics, rel. to geomag. field generation and heat flow 77—73638
- equation of state (thermal), calc. method 80—90029
- equation of state fit to outer core 78—85522
- eutectic region between liquid and solid core 77—70624
- evolution of Earth with non-Fe core 77—70621
- fluid circulation around null-flux curves at core-mantle boundary 79—79764
- fluid core with inward growing boundaries, dynamics 80—76934
- fluid motion, interaction with bumpy core-mantle interface rel. to geomag. and gravit. fields 77—2085
- fluid motion, thermal and mag. instabilities 80—81850
- fluid oscillation of core, effect of Earth rot. 80—89965
- fluid velocity and mag. field bounds imposed by MHD $\alpha\omega$-dynamo 78—36101
- formation, examination of various hypotheses 79—44149
- formation, history and energetics 79—84694
- formation, in Earth and other terrestrial planets 80—17514
- formation and evolution, model 80—51367
- formation in undifferentiated Earth, chemical reactions thermal effects 79—25218
- formation simulation for originally homogeneous planets 80—90041
- free oscillation of Earth, radial mode, damping by bulk attenuation 80—76928
- geodynamo behaviour during reversal, model 79—88240
- geomagnetic data rel. to core physical characts. 79—79765
- geomagnetic dipoles, resolution of secular vars. into fields of separate centres *(Russian)* 79—96738
- geomagnetic dynamo, characts. during mag. field transition periods 79—8598
- geomagnetic dynamo, gravitationally powered, thermal consequences 79—39687
- geomagnetic dynamo action in rotating shell 80—81807
- geomagnetic dynamo theory, MHD, book contrib. 78—61331
- geomagnetic field, comparison of offset dipole and zonal nondipole models from Icelandic palaeomag. data 79—57852
- geomagnetic field 60-year variations, models rel. to mantle elec. cond. 79—8596
- geomagnetic field current loop models 80—21623
- geomagnetic field generation by battery effect, comparison with Ap-type stars *(Russian)* 77—17591
- geomagnetic field of crust and core, spherical harmonic spatial power spectra 80—104882
- geomagnetic field origin, homogeneous axisymmetric generator model 80—8251
- geomagnetic field polarity transition records and geomag. dynamo 77—91007
- geomagnetic field short-period variations, electromechanical effects 79—57847
- geomagnetic field struct. and secular variation, mathematical-physical anal. and interpretation *(German)* 79—34742
- geomagnetic non-dipole field, origin rel. to secular vars. during last 25000 years 77—32983
- geomagnetic non-dipole field, westward drift rel. to field vector counter-clockwise precession 79—57853
- geomagnetic source, EM induction in rot. cond. Earth 78—44764
- geomagnetic source models for Lake Mungo palaeomag. excursion and their implications 77—86771
- geomagnetism, example of nonlinear dynamo action 77—73637
- geomagnetism, kinematic dynamo of three spherical eddies 79—8597
- geomagnetism by scale model, transient magnetic effects 78—48969
- global geodynamics, Canadian contribs., 1971-79 period. 80—8262
- gravitational settling driving dynamo, theory 80—36246
- gravitationally powered dynamo 78—77199
- gravitationally powered dynamo model 79—84102
- gravity waves in liq. outer core, theory 80—36274
- Gruneisen parameter, generalisation of Vashchenko-Zubarev formula 80—90030
- Gruneisen parameter, melting curve and adiabatic gradient 80—90028
- Gruneisen parameter, reevaluation 79—39685
- inner core, Q-factor from seismic body wave studies 79—39682
- inner core, second high Poisson's ratio, second order elasticity theory 80—56438
- inner core boundary, discontinuous vel. increase, full wave theory 77—73674
- inner core eqns. of state 77—73695
- inner core rel. to nutation in obliquity and longitude 78—85510
- inner core-outer core discontinuity, Fe electronic struct. transition theory 77—1356
- interaction with mantle, effect on rotation 79—66601
- internal waves, in fluid outer core 77—91082
- K content rel. to heat source and thermal model 78—15982
- kinematic dynamo problem, role of mean circulation in parity selection 78—7566
- liquid core, dynamical effects and luni-solar nutation tables 80—98210
- liquid core convection model 78—28193
- liquid core dynamical effects, nutations 77—86736
- liquid core inhomogeneity rel. to nontidal gravity field change 79—92463
- liquid core model rel. to westward drift of magnetic field 77—81794
- liquid metals equation of state parameters rel. to core energetics 77—15536
- lower mantle convection requiring core heat supply 80—76944
- magnetic field, screening by mantle when elec. cond. is concentrated near core boundary 79—12064

Earth core continued
- magnetic field intensity at liquid core 80—36239
- magnetic field source 79—74837
- magnetic waves and Braginsky's stability conditions, comments 78—44770
- magnetic waves in fluid core and torsional oscills. 80—89993
- mantle boundary roughness, PKKP wave scattering 80—56437
- mantle interface friction effect on geomag. secular variation 80—98218
- mantle-core boundary, magnetic contour map 80—104880
- mantle-core boundary, nature of transition 77—78137
- mantle-core boundary irregularities, effects on fluid vel. and mag. field 78—44792
- mantle-core EM interaction when elec. cond. concentrated near core boundary 77—91001
- mantle-core interface, differentially heated cylindrical annulus model 78—28194
- mantle-core interface, topographic coupling 78—44794
- material properties by dynamic compression expts. 80—98315
- mean-field electrodynamics, and dynamo theory of Earth's mag. field 77—73636
- minerals, thermodynamic functions from eqns. of state for end members 80—90084
- models, core form. effects 78—61368
- Molodensky model of mantle/core rel. to Chandler wobble period *(Russian)* 79—92475
- outer, Gruneisen γ function for liquid Fe 79—84186
- outer core, application of liq. state theory 80—56439
- outer core structure from SKS amplitudes and travel times 78—65208
- oxides (FeO and CaO), eqn. of state at high press. 80—109122
- P- and S-waves diffracted around core, attenuation 79—53312
- P- and S-waves diffracted around core, rel. to mantle base vel. struct. 79—53313
- P-waves anomalous vels. in outer core rel. to struct. 79—48436
- paradox of thermal convection, Gruneisen's parameter vol. depend. theory from melting point curves 80—90033
- phase-change hypothesis, appl. to Sun and Moon accels., gravit. const. and orgin of mountains 79—8592
- phase-change hypothesis, rel. to struct. of terrestrial planets 77—87298
- PKKIIKP wave detect. and damping in inner core 80—104925
- PKP precursor data comparison from seismic arrays 79—25208
- proto-Earth, melting and core form due to primordial dense atmosphere blanketing 79—57935
- Ramsey phase-change hypothesis 79—66662
- relativistic spin-spin interaction theory for two concentric shells 80—46148
- rigidity of uppermost core layer, seismic models 80—56380
- rotating self-gravitating fluid sphere with uniform distrib. of heat sources, MHD convective instability 77—29264
- seismic core waves, Bangui obs. *(French)* 80—56396
- seismic long-period P-waves diffr. by outer core, obs. at Matsushiro *(Japanese)* 79—96744
- seismic precursors to PKKP, rel. to core-mantle boundary struct. 79—48409
- seismic wave scattering by rough core-mantle boundary 78—61345
- seismic wave velocity, below E.Australia and SW.Pacific 80—36279
- seismic waves, attenuation coeff. distrib. 80—90035
- solid core motion effect on global magnetic field 79—84104
- solid-Earth geophysics, bibliography 77—2078
- stability and Earth tides 77—9320
- static core paradox, physical explanation 79—8614
- stratification in early history, heat generation and heat-mass transfer 80—90040
- structure effects on radial oscills. 80—12347
- structure rel. to geomag. secular var. 79—39647
- structure vars. due to evolution 78—85512
- synthetic seismograms, full wave theory and reflectivity method 80—61777
- temperature distribution of outer core, Gruneisen's parameter vol. depend. theory 80—90033
- theoretical problems, conf., Aug. 1978, Caracas, Venezuela 80—51400
- theoretical seismograms of core phases from freq.-depend. full wave theory 78—7581
- thermal evolution 80—21674
- thermal-convective instability through porous medium 80—53769
- thermodynamics appl. to fundamental Earth physics 78—36125
- torsional MHD oscillations, induced by Sun 78—44793
- transition zone between core and mantle, seismological significance *(Italian)* 77—70618
- whole-Earth dynamics, variational method 77—60340
- Fe alloy core containing slurry layers, motion and thermodynamics, seismic wave propag. 78—48993
- Fe close-packed phases, eqns. of state and implications for Earth core 79—20780
- Fe, Curie point and A-γ transition to 53 kbar 79—56529
- Fe melting and adiabatic temp. distribs. in outer Earth core 77—70626
- Fe, melting temps. depend. on interatomic pots. choice 79—74863
- Fe melting under core conditions in shock wave expt. 80—104931
- Fe slurry layers, seismic wave attenuation 78—44789
- Fe thermal props. at high-press., from shock wave data 80—21683
- Fe, thermodynamical Gruneisen function 78—61361
- ε-Fe, vol. eqn. of state under static press. conditions, rel. to Earth core-mantle models 80—19904
- Fe-Ni-Si core, form. and comp. 78—12112
- Fe-S eutectic, Lindmann's melting law, solid-liquid core boundary, core mantle boundary 78—18743
- FeS_2, pyrite, eqn. of state, rel. to constraints on Earth S content 79—70789
- $Fe_{0.9}S$, pyrrhotite, eqn. of state, rel. to constraints on Earth S content 79—70789
- K content rel. to Earth origin and comp. models 77—25663
- ^{40}K fractionation in Fe-S liq. outer core, implications of solubility and chemical equilib. expts. 78—11843
- ^{40}K, pressure-induced changes in electron-capture decay const., theory 80—22771
- Mg0, vol. eqn. of state under static press. conditions, rel. to Earth core-mantle models 80—19904
- Ni_2Si, chemical composition of Earth's inner core 80—8266
- Pb isotope evolution during core formation time 78—7601

Earth crust
see also geology; oceanic crust
Absaroka Mountains, Wyoming, basalt flows palaeomagnetism and Eocene pole position 77—86765
Aburatsubo Crustal Movement Observatory obs. of tidal gravity 80—101316
abyssal fracture detection in Mountain Crimea region using Rayleigh wave amplitude spectra 80—89969
accretion at trenches, model, rel. to subduction complexes tectonic evolution 79—20797
active faults, aerial photographs interpretation *(Japanese)* 78—96124
active faults, research in urban areas, Japan 79—62471
active hydrothermal systems, intrinsic fluid and rock resistivity anal. 78—40480
active margin, gravity and struct., British Columbia and Washington 79—92516
active margins 78—57191
Adirondacks, geomag. fluctuations gradient anal. 80—89947
Adirondak mountains, deep crustal elec. cond. obs. 80—89946
Adriatic subplate, averaged model 79—44159
advective folding deformations, modelling and natural analogues 77—81858
Aegean region, crust and upper mantle struct. from deep seismic sounding 78—69308
N.Aegean region, evidence of crustal shortening 77—53028
Aegean region, geodynamics 78—69307
Aegean Sea and surrounding regions, active tectonics 78—96181
Afar depression, Ethiopia, an Atlantic type continental margin in the making 77—21692
Afar depression, palaeomagnetism of axial zone lavas rel. to tectonics 77—37126
Afar region 80—56364
Afar region plate tectonics, seismic and volcanic evidence 80—21700
Afar region rifting, geodetic evidence and elastic-brittle model 80—21697
Afar triangle, geodetic evidence for rifting, model for vertical displacements 80—98295
Afghan Pamir, geology and tectonics of Himalayas 80—72513
E.Afghanistan, Logar ultrabasite massif, geology and geomag. 80—72512
S.Africa, principal horizontal stresses 77—91093
S.Africa, resistivity soundings and continental crust 77—29252
African Archaean mobile belts and granite-greenstone terrain 77—33074
Pan-African fracture system, expansive brittle deformation 80—61788
African lithospheric thickness from teleseismic delay times 78—11847
African plate, stress system rel. to mantle convection pattern 77—81859
E.African Rift, cross-cut by volcanic chain in N.Tanzania, gravity survey 80—98301
E.African Rift models, discrimination via seismic ray tracing 78—11846
E.African rift system, structure rel. to Martian canyons 79—40111
E.African rift system, tectonic history, theory and laboratory expts. 80—21669
E.African Rift valley, seismic wave travel times 80—98238
African/Adriatic promontory, rel. to Alpine orogeny and Carpatho-Balkan region plate movements 77—9394
aftershock region of Off-Izu Peninsula earthquake, 1974 May 9, seismic waves attenuation 80—76926
aging and strain softening model for episodic faulting 79—79777
Al Jubail, Saudi Arabia, evidence for recent coastal uplift 79—79799
Alabama Piedmont, structural development 78—65290
Alaska, 1964 earthquake faulting mechanism regional var. from static displacement data anal. 80—30998
central Alaska, Bouguer anomaly map rel. to plate tectonics 80—51380
SE Alaska, megalineament marking Coast Range batholithic complex SW edge 79—62495
central Alaska, N.Pacific plate tectonics rel. to earthquake focal mechanisms 79—79806
Alberta, Canada, crustal stress evidenced by bore hole asymm. 80—21671
Aleutian arc, tectonic blocks, episodic subduction, strain diffusion and magma generation 77—33037
central Aleutians, double Benioff zone and lithosphere unbending 78—32047
Alleghany orogeny structural stages 79—88348
Alpine fault, New Zealand, frictional metamorphism, Ar depletion and tectonic stress 80—41440
Alpine geology, resoln. of fundamental questions *(French)* 78—24281
Alpine Longitudinal Profile 1975, first results 77—49172
Alpine metamorphism, thermal budget 78—61373
Alpine region, tectonic stress directions, correl. with joint orientations 80—105052
Alpine structures between Mont-Blanc, Petit-Saint-Bernard and Valgrisanche *(French)* 79—79758
Western Alps, axial culminations and depressions *(Italian)* 79—25210
Alps, continental convergence 77—78149
Alps, foreland folding model 78—81141
E.Alps, HD-profile (Vicenza to Innsbruck) preliminary interpretation 79—34765
Alps, Longitudinal profile (Judenburg to Hozzupereszteg), refr. seismic meas. *(German)* 80—76916
E.Alps, mag. and gravity anomalies correls. *(German)* 79—53327
S.Alps, Permian volcanics palaeomag. props. rel. to S.Alpine block plate tectonics 80—89948
Alps, precision levelling and recent vertical movements *(German)* 77—2139
Alps, shearing subductions mechanisms *(French)* 78—20376
Alps, tectonic progradation rel. to plate tectonic evolution 80—56452
Alps in Valais-Valle d'Aosta area, formation *(French)* 79—2206
N.America, effect of craton on distrib. of seismicity and intraplate stresses 80—98248
N.America, in situ stress data compilation 79—29728
N.America, Lower Palaeozoic tectonics rel. to New Brunswick rock units palaeomagnetism 79—100809
N America, possible Proterozoic plate boundary 77—91079
S.America, seismic wave propag. in Nazca plate, Altiplano and continental margin 80—36264
N.American continental margin in Nevada during Late Cambrian 79—48472
N.American Cordillera near Fortieth Parallel, tectonics and chronology 78—81138
N.American intra-plate crustal deformation, implications of VLBI meas. 80—51379

Earth crust continued
N.Anatolian fault zone, Plio-Pleistocene reversal of displacement 80—94512
Anchorage, Alaska, postseismic crustal uplift 77—86849
ancient metamorphism and charnockite formation in S.India 79—44154
ancient oceanic lithosphere, mag. props. as alteration indicators, Othris ophiolite example 80—8297
ancient shields, crustal magnetic model construction problems *(Russian)* 77—32985
ancient structure and ring magnetic anomalies *(Russian)* 77—33019
Ancona (Italy) area, strain meas. 77—86742
Ancona region, Italy, seismo-tectonic considerations *(Italian)* 78—40492
central Andes, Plio-Quaternary tectonics and volcanism rel. to plate tectonics 77—29273
andesitic island arcs of SW.Pacific, peralkaline rhyolites origin rel. to tectonics 78—32043
andesitic volcanism and crustal evolution 78—85524
anisotropic dynamic elasticity, tensor spherical harmonics appl. 80—98296
anomalous geomagnetic field, nature and interp. 77—86762
anomalous geomagnetic statistical props. rel. to crustal struct. 77—86761
anomalous strain before 1923 Kanto earthquake, Japan 80—85616
Ansei earthquake, Japan, 1854 December 23, tsunami and crustal deform. *(Japanese)* 77—41001
W.Antarctic, isostatic readjustment affecting ice grounding line 80—51445
E Antarctic craton sedimentary basins from seismic, mag., gravity and radar obs. 77—21733
Antarctic Peninsula igneous rocks, transverse geochemical vars. rel. to calc-alkaline magmas genesis 80—56466
E.Antarctica, age from Rayleigh wave dispersion meas., Precambrian shield 79—92513
Antarctica, distrib. of seismicity 77—86803
Antarctica, palaeomag. results and test for oroclinal bending 78—73311
Antarctica, subglacially erupted rocks of Early Miocene 80—98287
Anti-Atlas, Morocco, Pan-African province geodynamic interpretation from geology and geochronology *(French)* 80—76952
N.Apennine chain, heat flow meas. of folded continental arc 77—86841
Apennines, anticlockwise rot. rel. to Tuscan anatectic magmatism eastward migration 79—16428
N Apennines, obs. rel. to lithospheric split in descending plate 80—85639
Apennines, Rayleigh wave study of crustal and upper mantle structure 80—46153
NW.Apennines, seismicity and relation with surface structs. 79—34749
Appalachian foreland fold and thrust belt, New York State, deform. nature 80—3973
Appalachian orogen western margin, basement slice at Saint-Malachie, Quebec 79—20824
Appalachian salients and recesses, Lake Precambrian continental breakup and Iapetus Ocean opening 77—17057
Appalachians, recent thrusting 79—79836
Appalachians, structural trends NE of Newfoundland and Trans-Atlantic correlation 80—85656
Appalachians, tectonics in St. Dominique region, Quebec *(French)* 77—78144
N Appennines, collisional orogen model 79—92515
Apuane Alps structural evolution, continental margin deform. in N.Appennines, Italy 79—25245
aquifer water extraction leading to land deformation 80—105003
Archaean continental geothermal gradients 78—40525
Archaean crust, geothermal heating rel. to vertical tectonism in greenstone belts 80—81861
Archaean greenstone belt, Island Lake, Manitoba, diapiric structs. and regional compression 79—57922
Archaean greenstone belt, Yellowknife, Canada, structs. induced by granite diapirs, rel. to tectonics 77—81892
Archaean greenstone belts, tectonic hypothesis rel. to Agnew belt, Australia 80—94507
Archaean lithospheric/crustal thickness from volcano spacings 78—65225
Archaean rocks of Limpopo Mobile Belt, crustal thickness ~3, 100 Myr B.P. 80—94502
Archaean sialic crust, southern West Greenland, chemical and thermal evolution 80—31016
Archaean supracrustal relics of Sierra Leone, Liberia, Guinea and Ivory Coast, zonation 78—44815
Archean continental crust, magma genesis by crustal anatexis, garnet-pyroxene thermometry and barometry 78—65236
Archean greenstone belt, NW. Ontario, Zr-U-Pb geochronology 80—98272
Archean sedimentary rocks, Kalgoorlie, Australia, rare earth elements and crustal evolution 77—60374
Archean supracrustal Rb-Sr ages, Rocks and Amitsoq gneisses, Isua, Greenland 78—16013
Arctic Basin, tectonic evolution, Jurassic to present 79—48446
Arctic crustal studies, review 79—48439
Arctic Ocean, crustal struct. review 79—48456
Arctic Ocean Basin, plate tectonic evolution 80—76953
Arctic regions, gravity from 60°N to North Pole, rel. to crust and mantle density struct. 79—48391
Arctic regions, heat flow north of 60°N 79—48438
SE.Arizona, Laramide folding and faulting, basement cored uplift model 80—8272
E.Arizona, USA, heat flow rel. to subsurface struct. 80—21686
Armenia, crustal stress state and seismic wave vel. anisotropy 79—44123
Armenia, tectonic fault zones, geophysical investigations *(Russian)* 77—9386
Armenian territory foundation, new struct. and age data *(Russian)* 79—74874
Asal-Ghoubbet rift zone, Afar, 1978-9 geodetic survey after seismo-volcanic activity 80—46164
Asama Volcano, Japan, geodimeter survey during 1977, ground deform. *(Japanese)* 79—70732
ascending andesitic magma, cooling model 78—65239
aseismic ductile shear zones, dynamic model 79—79763
aseismic uplift prior to earthquakes 78—7575
central Asia, active faulting and Cenozoic tectonics of Tien Shan, Mongolia and Baykal 80—8278
Asia, central and south-central, large-scale Cenozoic tectonics as prods. of continental collision 80—17246
S.E. Asia, crustal tectonic stress field details *(Chinese)* 80—56414

Earth crust continued
- Asia, evidence for large Cainozoic crustal shortening from palaeomag. data 78—57189
- central Asia, seismic moments of major earthquakes and average slip rate 77—86796
- Asia, slip-line field theory and large-scale continental tectonics 77—5173
- Middle Asia seismoactive regions, geomag. investigations 80—26464
- Aso earthquake, Japan, 1975, focal mechanism rel. to active fault system *(Japanese)* 77—2107
- astroblemes on Earth's surface, review 80—98324
- astrons, cosmic impact features, role in geological evolution 77—56632
- asymmetric folding and monoclinal kinking of compressible elastic multilayers 77—17093
- Atlantic and Gulf coasts of USA, continental shelf bathymetry 77—70635
- Atlantic and Gulf coasts of USA, inshore bathymetry systematic regional vars. 77—70636
- Atlantic continental margins, obs. and ideas 77—21691
- Atlantic equatorial fracture zone trends, plate kinematic implications 78—85527
- S Atlantic Ocean, age of opening from palaeomag. of Cretaceous Pirgua Subgroup (Argentina) 77—90998
- Atlantic Ocean crust layer 2, oblique seismic expt. on DSDP leg 52 80—36275
- Mid-Atlantic Ridge, geophysical and petrological constraints 78—85508
- Atlantic type continental margins, conference, Sao Paulo, Brazil, (13-18 Oct. 1975) 77—21690
- Atlantic-type continental margin off New York, subsidence 79—29722
- Atlantic-type continental margins, distinction of two basic struct. types 77—21741
- Atlantic-type continental margins, geodynamic development and crustal struct. 77—21737
- Atotsugawa Fault, Japan, seismicity and focal mechanism of local earthquakes *(Japanese)* 80—94482
- Aulneau batholith, Ontario, subcritical seismic crustal refl. survey 78—65213
- NW.Australia, crustal profile across Archaean cratons 80—51352
- Australia, earthquakes and crustal stress meas. 80—51354
- SE.Australia, explosion seismic profiles and crustal evolution 80—51332
- Australia, geophysical profile along 29°S 80—72460
- Australia, isostasy and evolution of compensation mechanism 78—65252
- Australia, isostatic compensation of topography 80—72479
- SE Australia, long-range seismic profile 77—44945
- Australia, stress state of upper crust 77—9387
- Australia, tectonic, igneous and metallogenic provinces rel. to mantle convection and subcrustal stresses 80—72484
- SE Australia, thrust faulting, crust and upper mantle struct. 77—44944
- Australia and Timor Trough, facies rel. to topographic wave migration during past 3 million years 78—49018
- Australia continental slope and shelf, sedimentary basins evolution from Mesozoic times 78—96175
- N.Australia Precambrian shields and platforms, struct. and tectonic style 80—3982
- average dislocation temporal and spatial vars. before and after large earthquakes *(Chinese)* 78—61334
- b-values and seismic source models, tectonic stress vars. along active crustal fault zones 79—84150
- back-arc basin basalt, compositional evolution of mantle source 80—72471
- Baffin Bay continential margin and Lancaster Sound, seismic refr. meas., continental/oceanic crust boundary determ. 78—20368
- Baikal and continental rift zones, deep struct. from seismic data 78—36130
- NE Baikal region, regional gravity anomalies and seismicity 80—98217
- Baikal region, USSR, geoelectrical model 80—56365
- Baikal region hot springs *(Russian)* 80—94551
- SW Baikal Rift, crust and upper mantle struct. according to seismic data 80—94503
- Baikal rift valley system, structural features 78—40528
- Baikal rift zone, fault evolution 78—36132
- Baikal rift zone, heat flow rel. to neotectonic activity 78—36135
- Baikal rift zone, petrochem. of Cenozoic basalts and assoc. rocks 78—36171
- Baikal rift zone, recent crustal movements, precise levelling data 78—36139
- Baikal rift zone, relationships between geologically young and ancient structures 78—36133
- Baikal rift zone, rifting mechanism and deep struct. 78—36131
- Baikal rift zone, seismicity and earthquake focal mechanisms 78—36115
- Baikal rift zone, seismotectonics 78—36134
- Baikal rift zone, windows into Earth interior, geophysical exploration *(Russian)* 80—12364
- Baikal rift zone and adjacent area, mag. anomalies 78—36103
- Balcones Fault Zone Texas, fracture patterns, field study 78—73337
- Balei gold region (E.Transbaikalia), structural features and tectonics 80—98300
- Baltic Shield, lithospheric thickness from S-wave anal. 80—3978
- Baltic Shield, Proterozoic tectonics from palaeomag. study of Swedish rapakivi suite 80—56346
- Baltic shield and Barents Sea, crust and upper mantle struct., Rayleigh waves dispersion 78—77204
- Banda Arc, continent-island arc collision 79—84211
- Banda Sea (E.Indonesia), subducted lithosphere geometry from seismicity and fault plane solns. 78—81131
- barrier islands, global distrib. in terms of tectonic setting 79—2214
- basalt magnetic properties rel. to crust and upper mantle struct. and development 79—79816
- basalt sheets, thermal effect on adjacent rock, heat flow model 80—46181
- basic intrusions emplacement mechanism 78—61374
- Basin and Range province, heat flow and thermal effects of tectonic extension 79—70763
- Basque Provinces, Pyrenean folding, deep geomagnetic sounding *(French)* 80—67351
- Bay of Biscay, rifting, crustal attenuation and subsidence 79—2209
- Bay of Islands ophiolite complex Nd and Sr isotopic study rel. to midocean ridge basalts source evolution 80—85651
- Beaufort Sea area, earthquake data, tectonic setting and stress study of continental slope 80—3931
- bedded formations, modelling of structure-forming props., results *(Russian)* 79—48429

Earth crust continued
- Beijing, China, crust and upper mantle three dimens. P-wave vel. struct. *(Chinese)* 80—104894
- Beijing area, earthquake stress field direction, composite nodal plane solns. *(Chinese)* 80—76910
- bending stress and temp. at consuming plate margin, rock mechanics 80—31021
- Benin Gulf, Africa, struct. and sedimentation of continental margin 77—21693
- Benue Trough, Nigeria, early Cretaceous basalt volcanism and initial continental rifting 78—61417
- Benue Trough, Nigeria, gravity field rel. to tectonic evolution 80—21701
- Benue Trough, stratigraphic evolution and implications for W.Africa Upper Cretaceous palaeogeography 79—2230
- Bering Island, tectonic struct. of mountainous region 80—90045
- Bermuda geomorphology, results from satellite imagery 79—5470
- Black Sea basin, crustal struct. from Love and Rayleigh waves dispersion *(Russian)* 78—28192
- Black Sea crust, nature of mag. anomalies *(Russian)* 78—85473
- Black Sea NW shallow and nearby land areas, appl. of seismic multidimensional vel. generalisation *(Russian)* 80—105068
- block faulting mechanism, geological and expt. studies 79—66692
- block folding, mechanical model 77—81841
- block tectonics analysis in Mongolia, appl. of two-dimensional autocorrelation anal. 80—56469
- Blue Mountains, Oregon, Jurassic plutons tectonic rot., palaeomagnetic obs. 80—109099
- Blue Ridge and Piedmont provinces, recent vertical crustal movements from levelling surveys 79—79794
- Bohemian Massif, heat flow pattern, rel. to tectonic struct. 77—64241
- Bohemian Massif and W.Carpathian border, recent crustal movements 79—79791
- Bohemian Massif and W.Carpathians, geothermal models 77—81848
- Boksburg, S.Africa, dyke strain relief meas. near mine working 80—17263
- Bonnet Plume Basin, Yukon Territory, Canada, gravity profile anal. as aid to coal basin evaluation 80—76898
- borehole γ-ray logging, exact inverse filters 80—94609
- Borrowdale Volcanic Group, English Lake District, palaeomag. results rel. to polar wander 77—32984
- Botswana, dyke swarm interpretation as failed Gondwana spreading axis 78—57180
- Bournac, Haute-Loire, heat flow determ., geotherm proposal 80—8259
- Brawley, California, surface faulting assoc. with 1975 January earthquake swarm 77—9349
- NE.Brazil, Post-Palaeozoic volcanism and tectonic significance 77—21735
- SE.Brazil and SW.Africa, geotectonic features correl. 77—21703
- E.Brazil continental margin, salt distrib. and crustal models 77—21698
- S Brazil intracratonic and marginal basins tectonic evolution 77—21743
- Brazilian Continental Margin, melting assoc. with Panafrican thrusting 77—21769
- S.Brazilian continental margin, preliminary structural study 77—21694
- Brazilian Highlands, crustal heat flow obs. 80—109124
- Brevard ductile deformation zone, N.Carolina, struct. and seismic refl. study 78—65289
- Briones Hills, California, geodolite meas. near earthquake 78—92803
- Briones Hills, California, tilt obs. near earthquake 78—92802
- N.Britain, crustal layering, rel. to seismic vels. of Lewisian metamorphic rocks at high press. 79—84137
- N.Britain, crustal struct. from Lithospheric Seismic Profile in Britain (LISPB) 78—73329
- Britain, palaeoclimatic and geomorphic implications of ^{230}Th/^{234}U dates on speleothems 78—36128
- British Columbia, geotectonics of Cretaceous and Eocene plutons, palaeomag. fold test 77—91090
- British Columbia, north-central, northward displacement during late Cretaceous/early Tertiary 80—76955
- British Columbia, struct. from seismic refr. profile 80—17236
- British Isles 80—109086
- brittle fault zones, grain size as shear strain indicator 77—17062
- brown coal basins of Hungary, Eocene, geophys. exploration *(Hungarian)* 80—104938
- Bulgarian continental shelf, morpholithodynamic study 80—26495
- bulk densities measurement, gravity borehole data accuracy 79—5632
- buried conducting dykes, resistivity anomalies, model tank expts. 80—85582
- Burma and S China, seismicity and tectonics 80—89983
- Bushveld Complex, geology, eastern compartment emplacement model 80—94505
- Bushveld Complex Main Granite, magma crystallisation history from trace element abundances 80—109145
- Bushveld Complex upper zone, magnetite Cr content vars. rel. to magma chambers heterogeneity and convection 80—56421
- Cabo-Ortegal mafic/ultramafic massif, emplaced nappe, gravity data 80—21689
- calc-alkaline igneous rocks, Sr isotope data and crustal contamination model 79—79762
- calc-alkaline volcanic rocks of Cerro Galan, NW.Argentina, Sr isotope evidence for crustal contamination 80—98318
- Caledonian granites, isotopic evidence for continental crust provenance 80—109146
- Caledonian orogenic belt, palaeomagnetism and tectonic implications 79—88244
- Caledonides of N.Britain, struct. contrast, seismic wave interpretation 80—3975
- California, crust tectonic tilt rate, lake level obs. 80—90065
- S.California, crustal deformation model 80—51377
- California, earthquake swarms and local crustal spreading along major strike-slip faults 79—66645
- S.California, N.Peninsular Ranges province early 20th century upwarping 79—79796
- central California, preliminary stress meas. by hydrofracture 77—91097
- S.California, regional S-wave struct. from anal. of teleseismic Rayleigh waves 79—92510
- central California, seismic vel. structure of metamorphic belt 80—98270
- S.California, strain accumulation and stresses across thrust faults 77—53033
- S.California, strain and uniaxial N-S regional contraction 79—74883
- California coast, 1941-1978, land and sea level changes 80—21610
- California Coast Range, seismic vel. struct. model 80—61783

Earth crust continued
  S.California uplift, geodimeter meas. of strain 79—48434
  S.California uplift area, Recent vertical movements four-dimensional modelling 79—80055
  S. California uplift rel. to dilatancy hypothesis 77—49056
  Canada, lithospheric features correl. with long-wavelength mag. anomalies 80—85594
  Canada, P-wave residuals rel. to struct. 77—91037
  E. Canada, sedimentary cover thickness meas. by aeromag. survey 80—77138
  Canada, seismic techniques for crustal struct. study 77—45169
  E Canada, struct. from PP waves travel time residuals 77—9354
  E. Canada, thermal struct. of upper crust 80—31013
  Canada, vertical crustal movements, map 80—109130
  Canada Maritime Provinces, heat flow 79—100819
  E.Canada tectonically active region, magnetotelluric fields time depend. 80—26451
  Canadian continental margins, evolution and geophys. features 80—8274
  Canadian Cordillera, Mesozoic-Tertiary basin models, geological constraints 78—28232
  Canadian Cordillera geomag. transition anomaly, lateral cond. changes 77—64200
  Canadian precise gravity networks for crustal movement studies, instrument evaluation 79—79724
  Canadian Shield, electrical resistivity structure, layer Earth models 79—48396
  NW Canadian Shield, geochronology of Bear-Slave provinces granite rel. to crustal breakup 77—91080
  Canadian Shield, structure of Archean basin-craton complexes 78—61412
  Canadian Shield surface crystalline rocks, O isotope comp. 79—62496
  Canadian Shield tholeiitic basalt-rhyolite magmatism and massive sulphide deposits 80—36298
  Canary Island palaeomagnetism, and continental margin evolution 80—56363
  Canary Islands, palaeomagnetism and early magmatic history 80—72431
  Cantal continental volcanic system (France), ^{87}Rb-^{87}Sr constraints on genesis and evolution 79—88327
  N.Caribbean, crustal plate subduction history 80—41429
  Caribbean Basin, transitional intercontinental sutural geostructure model 80—31015
  Caribbean plate seismic wave attenuation near Lesser Antilles Island arc 77—40990
  Caribbean-North American plate boundary, Quaternary faulting in Central America 79—79804
  Caroline plate existence, from marine geophys. and seismological data 79—29731
  Carpathian Mountains, disjunctive dislocations revealed by interpretation of space television photographs *(Russian)* 80—104958
  Carpathian Mountains, secular geomag. field vars. characts. 79—53301
  Carpathian region and Ukrainian shield adjacent slope, basic crustal surfaces, seismic obs. 80—89995
  Carpathian region sedimentary cover, elec. conduction 80—89940
  Carpathian regional lithosphere, geoelectric model from data along deep seismic sounding profile *(Russian)* 80—104934
  Carpathians, character of seismic processes before 1977, March 4 earthquake *(Russian)* 78—48985
  E.Carpathians, complex model of lithosphere *(Russian)* 78—85511
  W.Carpathians, Czech Massif and Saxon Turing zone, crustal model 80—89994
  Carpathians, recent vertical crustal movements, geoid residual local undulation *(Russian)* 78—15987
  Carpathians deep crustal struct., elec. cond. anomaly, numerical electromagnetic modelling 80—31008
  Carpathians internal region, in depth dynamics and tectonic movements *(Russian)* 79—48444
  S.Caspian depression, density variation in Upper Neogene deposits *(Russian)* 77—70661
  Caucasus, Alpine history, example of active continental margin evolution 77—78147
  cavity research with geoelectrical resistivity methods, theoretical and exptl. investigations 80—56625
  central Alps, Infrahelvetic complex, fold strain analysis 80—61787
  Central Alps, structual zones and continental collision 78—81124
  Central Alps, Switzerland, heat flow, heat prod. and vertical crustal movements 77—81847
  Cerro Galan Caldera, NW.Argentina, tectonic setting 78—85523
  Cerro Prieto geothermal field, conf. at San Diego, (Sept. 1978) 80—94911
  Cesano geothermal field, Italy, geological study 80—76975
  Chad basin, Africa, active intra-continental sedimentary basin 77—21726
  Chagos-Laccadive Ridge (Indian Ocean), geophysical study 77—44952
  Chaine des Puys, France, elec. cond. anomaly, struct., active magma chamber 79—2185
  Charlevoix impact structure, Quebec shock-diminished palaeomagnetic remanence 80—26441
  chelogenic cycles in continental crust evolution *(Chinese)* 80—89984
  chemical balance, rel. to time scales and dynamic models of deep-sea sedimentation 78—15988
  chemical balance 77—86831
  chemical evolution, mantle and crustal reservoirs mean age 80—51359
  chemical evolution, Nd-Sr isotopic var. implications 79—66655
  chemical evolution and sedimentary recycling, evidence from Th and U abundances in sedimentary rocks 80—85654
  chemical evolution from Early Archaean rocks comp. 78—65222
  Chibougamau pluton, Quebec, Precambrian Rb/Sr geochronology 80—98273
  Chilkat Peninsula, Alaska Upper Triassic rocks, regional implications 80—98271
  China, active faulting and tectonics 77—86848
  China, crust and upper mantle struct. study by converted siesmic waves *(Chinese)* 79—12093
  China, crustal stresses rel. to earthquake sources *(Chinese)* 77—91016
  NE China, propagating deform. front rel. to Haicheng earthquake prediction 77—49028
  China, seismic surface wave study of crust and mantle 80—104916
  China, tectonic deform. characts. from seismological data *(Chinese)* 80—76951
  China, tectonic stress field rel. to plate movement 79—62478
  China, tectonics structure *(Chinese)* 77—73702
  S China and Burma, seismicity and tectonics 80—89983

Earth crust continued
  China region, plate tectonic stress field, numerical simulation *(Chinese)* 80—90055
  circular structures of large scale and great age, possible meteorite impact craters 78—28237
  Clarno Formation, central Oregon, volcanism on thin continental margin 77—29296
  Clearwater Lake impact structures, Quebec, meterotic component and impact melt comp. 78—65314
  coal prospecting by seismic profiling, new technique testing 80—17404
  E.Colorado, electrical and seismic sounding of low-resistivity low-velocity materials 78—3711
  Colorado plateau, crustal struct. from seismic waves high-resolution group vel. anal. 78—81111
  Columbia Plateau, basalt flow, contact zone remanent magnetisation 80—81881
  composition and Earth origin models 77—25663
  conducting channel between India and Sri Lanka, effects on equatorial electrojet 79—25189
  conductive bodies, single and multiple, scale model results of inductive logging 79—16696
  conductivity profile of core-mantle system 80—36238
  contemporary crustal movements in Canada 80—8273
  contemporary structural and structural evolution of lithosphere *(Russian)* 80—81857
  continent formation due to geosynchronous revolution of Moon 80—101348
  continental basement exploration by seismic reflection profiling 78—96172
  continental blocks rotational motions, evidence from terrestrial objects astronomical azimuths 78—53613
  continental convergence zones, temp. modelling 77—81850
  continental crust, constraints on comp. and nature of lower crust from mantle Nd-Sr isotope correl. 80—94498
  continental crust, evolution age and isotope evidence 78—65233
  continental crust, heat-producing radioactive elements distrib. and redistrib. 78—65232
  continental crust, tectonics and seismicity review 79—44160
  continental crust, thermal struct. and extension of oceanic heat flow-age relation 77—21696
  continental crust and root zones, thickness and thermal history 79—88320
  continental crust development, implications of Nd-Sr isotopic relationship in granitoid rocks 80—94522
  continental crust development, use of Os isotopes as petrogenetic and geological tracers 80—89989
  continental crust evolution, granitic rock formation and destruction rel. to U deposits 79—84201
  continental crust evolution by tectonic processes 77—64255
  continental crust formation in Precambrian shields *(Russian)* 77—33021
  continental crust modelling, structural and chemical constraints 79—16420
  continental crust rel. to ocean and margin formation 78—11851
  continental crust shortening, by reactivated basement reverse faulting 80—36284
  continental crust transformation to oceanic type 80—89997
  continental drift, Arthur Holmes' convection hypothesis 79—12559
  continental drift, high-latit. continents as cause of glaciation 79—20961
  continental drift mechanisms, review 78—92813
  continental drift motion of latit. observatories, rel. to rotation pole secular trend 77—86734
  continental evolution, basement and sedimentary recycling 80—56430
  continental geotherms during Archaean, upper limits 79—34780
  continental growth, influence of gravit. differentiation effects on mantle convection 80—51371
  continental growth and emergence timing 78—11867
  continental lithosphere, vertical temp. distrib. limits 78—65207
  continental lithosphere thermal evolution 78—65234
  continental lithosphere thickening model 78—77200
  continental lithospheric boundary layer, liability to sink into less dense asthenosphere 80—56447
  continental margin, possible mode conversion between Rayleigh and Love waves 78—73314
  continental margin morphology 79—12098
  continental margins, stress state 78—3742
  continental margins, vertical evolution 77—21739
  continental plates, ages rel. to P-wave travel time residuals 79—62439
  continental platform subsidence mechanisms and eustatic sea level changes 77—21718
  continental rift fault patterns, analytical model 79—79805
  continental rifting mechanism and crustal doming 78—49002
  continental shear zones, geological aspects of deform. 78—3768
  continental shelf, bottom topography alongshore vars. rel. to ocean shelf waves generation 80—51424
  continental shelf, isolated topographic irregularity scatt. of ocean shelf waves 80—51423
  continental shelf and slope deep terraces off N Labrador 78—65255
  continental shelf zones development and sedimentogenesis 77—64263
  continental shields, Curie temp. depth, compositional boundary 79—53330
  continental structure development and gravit. instability, synthesis 78—48995
  continental tectosphere comp. and development 78—81133
  continents, secular changes in marine inundation of USSR and N.America during Phanerozoic 78—3735
  convection fluid dynamics in a model of a fault zone in the Earth's crust 79—34778
  convective heat transfer model for lithospheric thinning and crustal uplift 79—84199
  convective hydrothermal geothermal reservoirs, balance laws and constitutive relations 78—61379
  cooling plutons, transport phenomena in assoc. hydrothermal systems 78—36206
  Coosa Valley, Alabama, struct., folding and thrust faulting 78—65291
  Coral Sea, crustal struct. from seismic data 80—72459
  Cordillera evolution 79—62475
  W.Cordillera of N.America, plate linkage mechanism rel. to oroclinal deform. 77—66901
  cordilleran tectonics, alternative to interarc spreading rel. to subducted oceanic lithosphere age 79—29732

Earth crust continued
Cornwallis Fold Belt, Canada, history and mechanism of basement uplift 77—91091
coseismic steps recorded on creep meters along San Andreas fault 77—53006
Coso geothermal area, underlying low-vel. body, teleseismic evidence 80—90005
Coso Range, California, structure, tectonics and stress field 80—90003
cratering by meteorite impact 79—21244
cratering record, crater prod. rate 79—66699
cratering record, current obs. status 79—66698
craters, evolutionary tracks 77—91134
creep deformation model, deformation due to geologic load 80—104939
Cretaceous oceanic crust, isotope study of petrogenesis and hydrothermal alteration 80—46177
Crimea, crustal tectonic stresses rel. to weak earthquake foci *(Russian)* 78—11862
Crimea, new data on Earth crustal structure *(Russian)* 79—8616
E.Crimea, new evidence for deep crustal struct. *(Russian)* 80—104933
Crimean mountains, crustal structure from deep seismic sounding *(Russian)* 78—3732
crystalline basement, seismic anisotropy 77—64221
crystalline foundation, anomalous high conductivity bands discovery *(Russian)* 78—96137
Cuba crustal struct. study, earthquakes exchange waves method appl. *(Russian)* 79—44158
N.Cuddapah basin, granite domes on eastern margin 77—53019
Curie depth determination from aeromag. spectra, W.USA 77—60349
Dahomeyide orogenic belt, geology and struct. correl. with Volta Basin 80—109121
Dalradian slide, NW Ireland, strain history from deformed pebbles 80—4013
DC resistivity modelling for axially symmetric bodies, finite element method appl. 79—5445
Dead Sea Rift and adjoining areas, gravity rel. to crusted density distrib. 79—57893
Dead Sea Rift and N.Israel, mag. and gravity obs. and interpretation 80—98233
Dedham granodiorite, E.Massachusetts, Rb-Sr age and relation to Avalonian orogenic belt 77—81835
deep crustal magnetic anomalies, mineralogical constraints on Curie isotherms 78—44805
deep EM sounding and profiling 77—9326
deep EM sounding of Earths crust, pulsed MHD generator 79—48589
deep geological structure, appl. of Bouguer regional anomalies reduction *(Russian)* 78—48958
deep seismic zone, Tohoku, Japan, freq.-magnitude obs. rel. to geochem. changes 80—72447
deep structure, seismology beneath Wind River Range, Wyoming, USA 80—46141
deep structure model of East European Platform *(Polish)* 77—21706
deep zones, composition from elastic props. of rocks *(Russian)* 79—48460
deformation, transition between regimes dominated by intercrystalline diffusion and creep 77—53047
deformation analysis, models for estimation of parameters *(German)* 80—101319
deformation and resulting local gravity changes 79—48389
deformation assoc. with fault form., finite element estimation *(Japanese)* 79—70759
deformation at Middleton Is. 10 years after 1964 Alaskan earthquake 77—91018
deformation at Nagano, central Japan, 1969-77 tilt obs. *(Japanese)* 80—41425
deformation before and after 1975 Feb. 4 Haicheng earthquake, China *(Chinese)* 78—24222
deformation by dilatancy model, earthquake precursors 80—51347
deformation due to atm. cyclones 77—53018
deformation following filling of Lake Kariba 77—9391
deformation from Turgen' Geophysical Observatory data 80—76935
deformation in S.Kanto, Japan, at Philippine Sea-Eurasian plate boundary 78—40533
deformation meas. of crustal movements *(German)* 77—33220
deformation meas. using underground optical waveguides 77—53230
deformation measurement, line length changes resolution by EM distance meas. ratio method 80—4143
deformational history of the Delhi rocks around Biliawas, Central Rajasthan 79—25246
Denali fault system, Alaska and Canada, displacement history 78—88805
Denali fault system, geological history rel. to S.Alaska tectonic development 78—81137
density, rigidity and incompressibility rel. to seismic vel., model 80—89990
density logging, influence of standard material comp. on readings *(Russian)* 79—74989
descending lithosphere thermal regime, effect of varying angle and rate of subduction 78—77206
Devonian alkalic basalt dykes, NE.Newfoundland, tensional environment 78—88826
Devonian Millboro Shale, Appalachian Plateau, slip planes, discfold anal. 78—65293
Diablo Plateau, W.Texas, contemporary uplift from levelling meas. 79—20798
Diablo Plateau region, W.Texas, new evidence for tectonic uplift 80—72481
Diablo Range, California, P-velocity models from earthquake and explosion arrival times inversion 79—12094
diapir formation, finite element model of density instability 80—51366
dielectric constant at high temps., determ. from electrical parameters of Ukrainian shield rocks *(Russian)* 79—8628
dike burial depth estimation by mag. palaeogeobarometric method 80—98220
dilatancy and short-period geomagnetic var. 77—2096
dilatancy-magnetic effect, local mag. vars. assoc. with earthquakes *(Chinese)* 78—61333
dislocation modelling of creep-related tilt changes 78—92801
displacements produced in porous elastic half-space by impulsive line load, non-dissipative case 77—23908
disturbance in semi-infinite poroelastic medium prod. by surface load 77—19533

Earth crust continued
Djibouti Republic, magnetic anomaly map and tectonic interpretation 80—61753
Dnieper-Donets depression, deep struct. from magnetotelluric sounding data *(Russian)* 78—96170
Dnieper-Donets depression, sedimentary cover struct. along Jagotin-Baturin profile *(Russian)* 78—92806
dolines, terrestrial and lunar, form. *(French)* 77—86826
doming and rifting mechanism, Upper Rhinegraben rift development appl. 78—61387
Don Basin, deep struct. investigation via combined gravity and seismic methods *(Russian)* 79—74987
Donets Basin, crustal evolution *(Russian)* 78—69302
double seismic zone in downgoing slabs and mesosphere viscosity 80—26472
drill holes, vertical, natural convection effect on temp. 77—78135
W Dronning Maud Land, Antarctica, radio echo sounding during (1974) 77—86838
dunite complex, S.Shetland Islands, deform., serpentinisation and emplacement rel. to fracture zone tectonics 78—44814
Duxbury massif (2.5 Ga), Quebec, remobilised piece of pre 3.0 Ga sialic basement 80—76970
dynamic rupture on three-dimens. fault with non-uniform frictions 78—77186
dynamic shear crack propag. mechanics, earthquake source model 79—84147
earthquake cycle, asthenosphere readjustment effects on free surface deform. 78—85490
earthquake cycle in underthrust zones, model 80—26457
earthquake focal depth determination method 80—56389
earthquake swarms, model involving dike clusters 77—44934
earthquakes, centrifuge modelling 78—81429
earthquakes, two-dimensional horizontal ground motions rel. to engineering structs. design 79—48419
East Africa, isostatic compensation 79—8623
Eastern Rift, Africa, volcano spacings and lithospheric attenuation 77—5167
eclogite production in overthrust orogenic zones, metamorphism 79—44142
Ecuador and N.Chile, Sr isotope data for Recent andesites rel. to continental crust contrib. 78—32042
El Pilar fault zone, NE.Venezuela, brief review 79—79775
elastic characteristics of rocks at high-press. and temp. *(Russian)* 80—76933
elastic medium wave propagation from spherical sources 80—3941
elastic plate, earthquake stress drops and plate driving stresses 77—91100
elastoplastic ground motion during earthquake *(Japanese)* 79—70748
Elberton pluton, Georgia, USA, palaeomag. of granite 80—72423
electrical conductivities, mapping via multifreq. airborne EM system 79—5446
electrical conductivity, evidence for water 77—70593
electrical conductivity, from spectral characts. of geomag. field vars. 77—87179
electrical conductivity, model for quantitative interpretation of towed-bird airborne EM system meas. 79—5447
electrical conductivity anomalies 79—53303
electrical sounding, elec. fields in random cond. layered Earth 80—77171
electrical sounding, theoretical apparent resistivity curves calc. *(Italian)* 78—40472
Ellsworth Mtns. crustal fragment, Antarctica, age and tectonic posn. 77—29262
EM wave refl. and transmission coeffs., linear ramp model 80—61759
energy changes due to mining 77—64236
NE.England, granite plutons effecting surface heat flow 80—94490
NW.England Carboniferous Limestone, crack anisotropy, in-situ seismic methods 80—17240
Eolian Islands, S. Thyrrenian Sea, basement structural trends from aeromagnetic and gravimetric data 78—40519
equatorial regions, struct. and topography effect on equatorial electrojet longit. differences 78—36371
SW.Ethiopia, dating of volcanic and rifting history 80—51369
Ethiopian rift geodimeter survey 77—70633
Ethiopian rift valley, present day strain rates 78—32051
Etna volcano, shallow geological struct. by elec. sounding 80—41419
Eurasian and North American plates, relative rot. pole determ. 80—85637
central Europe, active or residual tectonics stresses 77—91094
N.W.Europe, marine tides and crustal struct. interaction with Earth tide 77—86739
Europe, preliminary heat flow map and tectonic and geophysical implications 79—70765
Central Europe, tectonic units rel. to mantle heat flow and geotherms 79—70767
E.European platform, peculiarities of geoelectrical section and zonation of Volyn-Podolian margin *(Russian)* 78—48964
E.European shields, EM study of underlying asthenosphere 77—53021
European territory crustal struct. rel. to heat flow 79—96751
European USSR, heat flow map rel. to structural features 79—70766
W.Eurpoe and E.Canadian continental shelves, basement fractures, trans-Atlantic correls. 78—73327
Evia and Crete, crustal struct. from deep seismic sounding 77—64239
evolution in silicate planets, review 78—61774
evolution of surface features of Earth, endogenic and exogenic forces 80—3972
evolution rel. to rare earths in Australian post-Archaean sedimentary rocks 77—41015
Fairweather fault Late Quaternary offsets and crustal plate interactions in S.Alaska 78—88804
Falkland escarpment and Agulhas fracture zone, boundary between oceanic and continental basement 77—21700
Farallon plate fragmentation by pivoting subduction 78—77208
fault creep events, empirical law 78—3745
fault creep records and long-baseline strain data, Hollister, California 79—79776
fault displacement in Peking district *(Chinese)* 79—62462
fault growth dynamics, physical basis for aftershock sequences 77—21688
fault mechanics and earthquake prediction, conf., Stanford, California, USA (Dec. 1977) 79—84143

Earth crust continued
- fault motion and earthquake occurrence, numerical and lab. simulation 79—100815
- fault motion in presence of friction and inhomogeneous initial stress, rupture propag. 77—86835
- fault rupture model for seismic risk anal. 78—11810
- fault slip episodes near Hollister, California 77—86800
- fault slips, processes 80—8263
- fault strain field, included rectangular fault in semi-infinite media 80—98261
- fault termination deformation, normal fault in shade 80—90048
- fault zone with finite thickness, frictional heating, comment 79—25215
- faulting analysis in three dimens., strain field 78—77225
- faulting and gravitational energy 79—84121
- faulting model of earthquake 80—109114
- faulting processes in prestressed self-gravitating rotating Earth model, energy release 78—40499
- faulting rupture process, plane shear faulting model of earthquake *(Chinese)* 80—104893
- faults, local gravit. field effects on cloudiness distrib. 78—32136
- faults and other linear features, detect. from LANDSAT images 80—77177
- faults and shear zones, assoc. deep focus earthquakes 80—61786
- faults prospecting via seismic refr. method, model expt. and features of seismograms *(Chinese)* 79—12286
- Fennoscandian Shield and Danish Embayment, crust and upper mantle geothermal models 77—49044
- Fiji-Tonga deep focus earthquakes, relative teleseismic P-wave residuals interpetation 78—36111
- N.Finland, magneto-telluric expts. 79—44093
- Fiordland, New Zealand, crustal struct. 79—88325
- fluid flow through large vertical crack, geothermal heat extraction appl. 77—33027
- fluid-filled fracture, mechanical interaction with Earth surface 79—79779
- Fohnsdorf tertiary basin, Styria, in situ tension measurements *(German)* 80—21665
- folded and crystalline basements of deep cavities, determ. from seismic data *(Russian)* 79—39692
- folding, three-dimens. strains in hinge zones 77—81863
- folding of single viscous layer, exact infinitesimal-amplitude soln. 77—73729
- folding of single viscous layer, role of initial perturbs., finite element anal. 78—49003
- folds, non-Newtonian 79—88349
- forearc basins development, implications of large thrust earthquakes and tsunamis 79—57905
- Foredobrogen area, USSR abyssal elec. cond. 80—90000
- formation of continental crust, Sm-Nd and Rb-Sr chronology 79—12100
- fracture water, radioisotope long-term vars. rel. to earthquake prediction 79—62451
- fracture water radioisotope abundances for earthquake prediction 79—44124
- fracture water radioisotope vars. and earthquake prediction 79—44204
- fractures and photogeology 77—44954
- fractures generated in branching process, sizes, elementary anal. *(Japanese)* 79—70750
- France, heat flow rel. to deep struct. and mantle convection 80—98291
- Franciscan formation, California, pedestrians guide to rock exposures 80—81849
- Franciscan melanges, comparison with olistostromes of Taiwan and Italy 78—81159
- Frankische Alb, slope forms in Al(1) clay, statistical investigation *(German)* 78—57211
- free surface, effects on seismic moments and corner freqs. determ. 78—85492
- free surface effect on calculated stress drops 78—65193
- French Alps, relations between tectonic stresses and mag. props. of Guil valley Permian volcanics *(French)* 77—25679
- frictional heating on fault zone with finite thickness 78—36124
- Friuli, Italy, tectonic stress revealed by aftershocks 80—85597
- Friuli focal area, Italy, seismic body-wave dispersion 80—36267
- Fruili, crustal structure from 1976 October 13 aftershock 78—24265
- Fuji river, active faults anal. by track etch method *(Japanese)* 80—109127
- Gabilan Range, central California, pressure-induced seismic vel. gradient 80—21635
- Garm geodynamic polygon, surface deformation 79—79792
- Garm region, crustal fracturing rel. to weak earthquakes space-time sequence 80—21653
- Garm region, temporal changes in elastic wave vel. 80—104914
- Garon Lake Archaean geothermal system, Matagami rock-water interaction 80—98283
- geochemical model of crustal growth and mantle differentiation 80—21684
- geodesy applied to crustal movement measurement, instrumentation trends and prospect 79—29738
- geodetic measurements for crustal movements monitoring, statistical anal. 79—79726
- geodetic reference systems for crustal motion studies 79—79720
- geodynamics and palaeomagnetism 79—79737
- geoid anomalies and lithospheric thickness 79—84077
- geological faults, fracture, creep and strain 78—69345
- geological sections, props. determ. via combined spectral anal. of seismic records *(Russian)* 78—40696
- geological-geophysical zoning possibility 78—57342
- geomagnetic depth sounding, use of vertical component 77—91290
- geomagnetic field of crust and core, spherical harmonic spatial power spectra 80—104882
- geomagnetism, crustal field struct., mathematical physical anal. and interpretation *(German)* 79—34742
- geomechanical model of alpine valley, crustal plasticity 79—96754
- Georges Bank, NW.Atlantic, seismic vel. of sediments to 1.4 km depth 80—21644
- geostructures formation, mechanical modelling rel. to interpretation of regional gravity anomalies *(Russian)* 78—49154
- geosyncline processes, energy aspects *(Russian)* 78—96182
- geothermal energy resources in Oregon, USA, elec. and EM sounding obs. 80—97761
- geothermics, Southwestern Germany and Switzerland *(German)* 78—53633

Earth crust continued
- Geotraverse Rhenoherzynikum, fault zones investigation by seismic refl. and refr. studies 80—90046
- German Democratic Republic, geomag. secular var. anomalies rel. to crustal movements and heat flow 80—26449
- N.German sedimentary basin, cond. distrib. from widely spaced areal magnetotelluric meas. 79—74833
- glacial continental shelves, marginal longit. channels struct. and origin 77—64261
- glacial deposits of Brecon Beacons, S.Wales, Loch Lomond Stadial 80—105005
- glacial isostatic adjustment and sea level, global finite element model 79—20800
- global density and inhomogeneities determ. by terrestrial and satellite gravity obs. 79—62592
- global isostatic overcompensation 79—62474
- global plate reorganization during early Cenozoic 79—34788
- global plate tectonics, rel. to pole secular motion 78—65172
- Gondwana, tectonics from Alcaparrosa Formation (Argentina) palaeomagnetism and K-Ar age 78—96135
- Gondwana configuration in Early Palaeozoic, palaeomag. study of Argentina 80—89938
- Gondwanaland, breakup rel. to evolution of Indian Ocean 80—41428
- Gondwanaland, crustal evolution from Rb-Sr isochrons and lithosphere chemistry vars. 78—28201
- Gondwanaland, India and Madagascar fit based on matching Precambrian lineaments 79—62477
- NW Gondwanaland Proterozoic tectonics, new evidence from E Newfoundland 79—57908
- Gondwanaland reconstruction 77—66903
- Gondwanaland reconstruction from lower Palaeozoic sequence of N. Victoria Land, Antarctica 77—17069
- Gow Lake, N.Saskatchewan, terrestrial meteorite impact crater 78—7640
- graben containing high-resistance intercalation, magnetotelluric field calc. and anal. *(Russian)* 78—48965
- graben-type sedimentary basins form. by continental crust extension 77—25665
- grabens of Canyonlands National Park, Utah, geometry, mechanics, kinematics 80—21728
- Gran Canaria/Tenerife mag. discordance rel. to NW.African continental margin form. 78—85478
- granite magmatism initiation and thermal diversity 78—65240
- gravimetric and deep seismic sounding, data interpretation *(Russian)* 79—39937
- gravimetric and seismic methods combination for initial seismic data crustal vel. sections 80—105070
- gravimetric geoid over Alps, and tectonic interpretation *(French)* 79—66600
- gravity anomalies, logarithmic pot. from anomalous masses of variable density 77—52961
- gravity anomaly due to geologic contact, Fourier transform method for horiz. profile 80—94447
- gravity complex fields interpretation via minimisation method, automated system appl. *(Russian)* 79—35006
- gravity data inversion by compressed mass plane method *(Chinese)* 77—64175
- gravity gliding tectonics, orogenic wave simulation, model 80—94506
- gravity secular variations, due to water quantity vars. in lithosphere *(Russian)* 78—53609
- gravity sounding, calc. of gravity field of three-dimensional masses 80—94451
- Great Barrier Reef, Holocene sea level changes, interpretation rel. to hydro-isostatic flexure 79—84295
- Great Basin of Nevada and W Utah, struct. from seismic surface waves 78—73336
- Great Britain, Earth strain tides survey 79—44080
- E Greenland, continental rifting rel. to struct. of coastal dyke swarm and assoc. plutonic intrusions 80—56467
- W Greenland, crustal uplift, palaeomagnetic obs. 78—15954
- E.Greenland, Jurassic basin evolution 78—73344
- E Greenland, southern Caledonian fold belt polyorogenic nature from isotopic age study 80—76938
- S.E.Greenland, struct. of continental margin 77—33014
- E.Greenland dyke swarm offshore continuation, rel. to N.Atlantic Ocean formation 78—73352
- greenstone belts, ancient marginal basins or ensialic rift zones 78—61418
- greenstone belts, Archaean, thermal modelling rel. to komatiite generation 79—70762
- greenstone belts from Superior Province in Manitoba, tectonic evolution 79—62497
- Gregory Rift Valley, Kenya, magnetotelluric and magnetovariational study 77—91000
- Grenville Belt, Rb-Sr and palaeomag. evidence from Sweden rel. to magnetisation age and tectonics 77—81839
- Grenville Front Zone, Precambrian geological struct. of Labrador 80—98274
- Grenville Province as shear zone 77—53020
- Grenvillian palaeopoles, calibration by ^{40}Ar/^{39}Ar dating 79—20778
- ground cracking, instrumentation and field monitoring 79—79729
- Guadeloupe, seismic profiles of superficial structs. *(French)* 80—76932
- Guaymas Basin, Gulf of California, basaltic sill intrusion into sediments, hydrothermal activity 80—46154
- Gulf of Aqaba, sinistral movement rel. to Red Sea opening 80—76954
- Gulf of California, transform fault position and tectonics from 1975, July 8 earthquake aftershocks 78—20363
- Gulf of Mexico-Caribbean area, Permian-Triassic continental reconstruction 80—56431
- Gulf of Oman, fold development 78—15984
- Gulf of Oman, sediment deform. and plate tectonics 77—5176
- W.Gulf of Oman, tectonics 80—8279
- Gulf of Papua, crustal struct. from seismic data 80—72459
- Hackett River greenstone belt, Slave Province, NWT, regional deforms. and granitoid plutons emplacement 79—100834
- Harp Lake Complex, Labrador, palaeomagnetism and Precambrian polar wandering path 77—90997
- Hawaiian Ridge, vel. struct. from earthquake travel times, Tau Inversion method 79—62467
- heat flow, global scale pattern *(Russian)* 80—98284
- heat flow in continent, tectonic age and thermal evolution effects 80—72472

Earth crust continued
heat flow in Malaysia offshore areas, estimation in exploration wells 80–67349
heat flow of continental crust affected by erosion 80–89991
heat flow rel. to crustal thickness in USSR European section *(Russian)* 79–20772
heat loss of Earth, review 80–98286
heat production, linear relationship for exponential model 79–66660
heat production model for continental crust 80–21690
Hellenic Arc, dynamic model deduced from geophysical data 77–21734
Hellenic Arc, recent Quaternary tectonics from geological obs. on land 79–79797
Hellenic arc and trench system, key to E.Mediterranean area neotectonic evolution 80–56451
Hellroaring Plateau area, Beartooth Mountains, Montana, Rb-Sr dating of deformation 80–17238
Hercynian Front in Ireland, probably local feature 78–32035
heterogeneities beneath Gauribidanur seismic array (S.India), quantitative assessment 78–32033
N. Hida region, Japan, seismicity and focal mechanism of local earthquakes *(Japanese)* 80–94482
Hidaka mountain region, Hokkaido, Japan, unusual seismic waves from shallow quakes *(Japanese)* 80–94477
W.Himalaya, Central Crystallines, geology and tectonics 80–72516
Himalaya, intracontinental subduction initiation mechanics 79–16431
Himalaya, Tethyan and Higher, geological description 80–72515
Himalaya, two intracrustal boundary thrusts 80–104948
Himalaya, uplift and cooling rates from geochronological data 80–85627
Himalaya and Indo-Gangetic Plains, geology and pre-Mesozoic orogeny 80–72514
Himalaya and Tibet Plateau region, tectonic history 80–72486
Himalayan basic volcanic formation, palaeomagnetic study 80–51328
Himalayan mountain range central portion crustal struct. and geological significance *(Chinese)* 77–91066
Himalayan Suture Zone, Landsat picture obs. 80–76948
Himalayas adjoining Tibetan Plateau and Chinese mountains, crustal struct. 78–7600
Himalayas region, conf., Mar. 1978, Katmandu, Nepal 80–72523
Hindu Kush region, microearthquake seismicity and fault plane solns. 80–72446
Hindukush region, crustal struct. from body wave data 79–96752
Hinterland Belt, Canadian Cordillera, deformation episodes 78–88825
SW.Honshu, Japan, crust Q-factor derived from explosion seismic waves 80–17242
NE.Honshu, Japan, crust vel. struct. from earthquake data 80–76937
Honshu, Japan, crustal movement data from strain meas. 80–8277
SW.Honshu, Japan, crustal struct. derived from explosion seismic waves 79–74862
Honshu, Japan, deep seismic zone and plate tectonics 80–8269
horizontal crustal deformation from historic geodetic measurements in southern California 79–84197
horizontal stresses from satellite pictures *(Russian)* 79–20791
hot spots, sublithospheric upwelling distrib. 80–109126
Hyderabad, India, peninsula shield crustal struct. from long period P-waves spectra 79–66667
hydrocarbon bearing anticlines, pattern space of seismic anomalies, location tool and theory 80–17234
hydrothermal convection, theoretical study rel. to Cyprus ophiolitic sulphide ore deposits origin 79–29761
Iberian margin ocean-continent boundary struct., discovery of serpentinite diapir W. of Galicia Bank 80–94489
Iberian Peninsula crustal structure from seismic wave dispersion *(Spanish)* 80–36269
SW. Iceland, axial rift zone, seismic crustal study 80–90014
Iceland, continuum model of crustal generation, kinematic aspects 80–90059
Iceland, crustal stress, hydrofracture meas. rel. to tectonics 77–91098
NE.Iceland, elec. resist. model from magnetotelluric obs., correl. with temp. 80–89954
Iceland, geothermal activity rel. to geological struct. 78–61376
N Iceland, gravity and height vars. during present rifting episode 80–90060
Iceland, lateral magma flow within rifted crust 78–73339
NE Iceland, mag. anomalies (ΔZ) and interpretation based on rock magnetic investigations 80–89951
Iceland, magnetotelluric investigation of lower crust and upper mantle 79–66612
N.Iceland, microearthquakes rel. to geomorphology and tectonics 77–81801
Iceland, seismic structure along RRISP-Profile I 80–90018
Iceland, tectonic spreading, problems and mechanism 78–36137
N Iceland, vertical crustal movements from height meas., (1965 to 1977) 80–89931
Iceland crust above layer three, seismic structure 80–90015
N.Iceland fissures, relative movements and tile changes 80–90062
E.Iceland lava, $^{40}Ar/^{39}Ar$ dates and ocean ridge growth 80–36273
Iceland magnetic layer, mag. studies of basalts from deep drill holes 77–60365
NE Iceland rift zone, geodetic meas. and horizontal crustal movements 80–89930
N.Iceland rift zone, seismic study of crust struct. 80–90013
Iceland-Faeroe Ridge, subsidence history rel. to Lower Tertiary laterite and Thulean land bridge 78–85514
Icelandic plate boundary rift and earthquake activity *(German)* 79–5467
Icelandic thermal area rock stress implication for oceanic lithosphere 80–90012
Immiter Gabbroic Complex, Morrocan Atlas Mts., petrography and geochem. 80–41442
impact craters, modification by fallback ejecta 80–82317
impact craters and astroblemes, morphology and struct. *(Russian)* 77–45000
impact structs., so called, non-random geographical distrib., implications 79–34825
Imperial Fault, California, large creep events, 1975-77 period 79–12096
in situ stresses relationship with depth, trends 79–29729
N.E. India, and N. Burma, seismicity, gravity and tectonics 77–25654
India, Bouguer gravity anomaly map and tectonics 80–61791
India, Holocene deform. and crustal movements in type areas 79–79793
India, peninsular, fan faults rel. to origin of Himalayas 80–85630

Earth crust continued
S.Indian Craton, Archaean gneiss Rb-Sr date of 3360 Myr old 80–46155
S.Indian craton, tectonic-framework deduced by LANDSAT imagery 80–98290
Indian intra-cratonic sedimentary basins, deep struct. features and evolution 77–21728
Indian Ocean and surrounding areas, contemporaneous tectonic events 77–64256
Indian Shield, deep seismic study 80–12358
Indian subcontinent collision with Eurasia 77–78146
Indo-Australian plate, evidence for internal deform. 80–109134
Indo-Gangetic Plains and Himalaya, geology and pre-Mesozoic orogeny 80–72514
inferred from Nevada Test Site (NTS) explosions Rayleigh-wave signatures 79–66632
inflection surfaces, use in descriptions of folds 79–88324
inter-arc basins, kinematic model 78–81127
intersite distance meas. using spaceborne laser ranging system, SPEAR 78–3978
intra-plate volcanism during Cainozoic, rel. to mantle convection 80–98293
intracratonic basin, formation model involving deep metamorphism 80–85618
intraplate volcanism, geological and geophysical parameters 78–65243
intraplate volcanism, magma flow through lithospheric fractures, tensional tectonics 78–65242
Iran, seismotectonic implications of relocated aftershock sequences 79–44119
Iran plateau, crustal struct. from seismic waves high-resolution group vel. anal. 78–81111
Iranian Makran, Recent faulting episode 78–32038
Iranian segment of Tethys, Jurassic ophiolite Ar isotope age 80–46156
island arc development, obs. expts. and speculations 80–98298
island arcs, sources as indicated by Nd and Sr isotopic studies of lavas 78–32044
island-arc volcanism, magma formation and ascension due to sinking of tectonic plates 79–100823
isostacy and long term flexural rigidity of crust 80–46161
isostasy investigation, correl. coeffs. between elevations and Bouguer anomalies 77–86850
isostasy of plain regions *(Russian)* 78–85525
isostatic and dynamic processes rel. to viscosity 77–21745
isostatic compensation and viscosity differences between crust and asthenosphere 80–104947
isostatic compensation on continental scale, local and regional mechanisms 78–11859
isotopic ratios of trace elements, rel. to mantle chemical evolution 80–90043
central Israel, crustal structure for magnetotelluric data inversion 79–2196
central Israel, evidence for pre-Late Jurassic east-west fossil continental margin 79–34766
Israel, Mesozoic palaeomag. results and inferences for microplate struct. in Lebanon 80–61760
N.Italy, crustal deformation after Friuli earthquake 78–24267
N.Italy, crustal structure and seismicity 78–24264
Italy, crustal structure from deep seismic soundings 80–56417
S.Italy, crustal structure from seismic refraction profile 77–33013
Italy, fault-plane solns. and stress regime 78–69299
Italy, heat flow meas. rel. to tectonic features 79–70769
N.Italy area, earthquakes max. magnitude prediction by geotectonic method 78–40493
Itapicuru greenstone belt, Bahia, Brazil, mag. survey for ore bodies 80–81879
Iwate-Oki (Japan) earthquake, 1968, June 12, focal mechanism and sea bottom crustal deform. 77–78123
Izu Block, Japan, accommodation of colliding plates 80–41424
Izu Peninsula, Japan, active faults in Amagisan area *(Japanese)* 78–96164
Izu Peninsula, Japan, crustal uplift, Mogi model, related gravity change *(Japanese)* 78–96165
Izu Peninsula, Japan, earthquake swarm epicentres distrib. rel. to Bouguer anomaly *(Japanese)* 78–96144
Izu peninsula, Japan, elec. resistivity along Inatori-Omineyama fault *(Japanese)* 80–46121
Izu Peninsula, Japan, geodimeter surveys, horizontal strain meas. *(Japanese)* 78–96163
Izu Peninsula, Japan, gravity change assoc. with earthquake swarm *(Japanese)* 78–96123
Izu Peninsula, Japan, gravity obs. rel. to Jan. 1978 quake *(Japanese)* 80–41394
Izu Peninsula, Japan, resistivity meas. in crustal uplift area *(Japanese)* 78–96127
Izu Peninsula, Japan, shear waves used to construct underground struct. *(Japanese)* 80–41387
Izu Penisula, active faults anal. by track etch method *(Japanese)* 80–109127
Izu-Oshima-kinkai earthquake, Jan. 1978, fault mechanism 80–41390
Izu-Oshima-kinkai earthquake, Japan, 14 Jan. 1978, seismic waves anal. *(Japanese)* 80–41385
Izu-Oshima-kinkai earthquake, Japan, Jan. 1978, associated surface faulting 80–41408
Izu-Tokai District, Japan, tectonic activity rel. to earthquake prediction *(Japanese)* 78–96145
Jamaica, blueschists, coaxial pure shear rel. to deform. assoc. with subduction 79–2236
Japan, crust horizontal deform., first-order triangulation meas. 79–79727
Japan, deep crustal structure, determ. via nearby earthquakes converted seismic waves 80–30999
NE.Japan Arc, deep seismic zone double-planed struct. 78–77203
Japan geosyncline outer margin, structural characts. and tectonisms around microcontinent 78–81139
Japan islands and Sea of Japan, seismic structure 78–92807
Japan Trench, evidence for eastward extension of Honshu *(German)* 79–84200
Japanese and Izu-Bonin Islands junction, gravity meas. rel. to plate tectonics 77–78085
Japanese Islands, compilation of eleven new heat flow meas. 80–67350

Earth crust continued
  Japanese Islands region, geophysical data compilation *(Japanese)* 80−67332
  Jharia coalfield of India, survey of struct. and geol. 80−76972
  Jharia Gondwana sedimentary basin, India, heat flow meas. and basement rocks heat prod. 80−98276
  Jordan-Dead Sea Rift, crust and upper mantle struct. from seismic refr. data 80−26474
  Josephine Peridotite, alpine-type peridotite, effect of partial melting on mineral comp. 77−81880
  Jotunheimen Caledonian structure, geological evidence 79−25222
  Jura folds development 77−41013
  Jura type platform folds, centrifuge expt. 78−49001
  Jurassic rock in N.Armenia, palaeomagnetic directions rel. to remanent magnetisation 80−104870
  Kamchutka, volcanic zone, tectonic tilt meas. 80−3984
  Kandalaksha Bay, White Sea, crystalline basement struct. from seismoacoustic profiling 77−86854
  Kangzhuang-Dachang region near Peking, deep struct. and earthquake foci *(Chinese)* 80−56415
  S.Kanto area, seismic waves vel. change meas. from Tateyama explosions *(Japanese)* 80−67338
  S.Kanto district, Japan, crustal struct. by explosion seismology *(Japanese)* 80−51368
  S. Kanto Region, Japan, crustal struct. from body wave propag. derived from earthquakes initial motion *(Japanese)* 80−94481
  Karelia magnetic anomalies rel. to crustal structure *(Russian)* 77−32986
  Karroo rhyolites, Swaziland, isotopic evidence of crustal contamination 80−21666
  post-Kenoran composition and evolution of upper crust 79−92511
  Kenya rift valley, geophysics 77−86825
  Kerguelen, continental fragment or oceanic island, petrology and isotopic geochemistry evidence 79−57924
  Kharkov-Yalta profile, crustal structure *(Russian)* 80−85622
  Kilauea volcano, Hawaii, three-dim. crust and mantle struct. 78−28205
  Klamath Falls, Oregon, heat flow data and obs. geothermal phenomena 77−5158
  Klamath Mountains, Oregon, Jurassic island arc sequence identification in Rogue and Galice formations 79−100836
  Komyo Fault, central Japan, fault-forming process 77−2129
  Krafla Caldera, NE Iceland, gravity and elevation changes caused by magma movement 80−90052
  Krafla fissure swarm, Iceland, surface deform. in rifting events 80−90061
  Krafla volcano area, N. Iceland, horizontal magma flow rel. to subsidence events, (1975 to 1979) 80−90053
  Kupjansk-Novoazovskoe profile quasiperiodic gravity anomalies and structural confinement *(Russian)* 78−85465
  Kuril Trench, lithosphere elastic-perfectly plastic bending under generalised loading 78−73341
  La Malbaie area, Canada, upper crustal struct. lateral vars., teleseisms meas. 78−28187
  Labrador Sea earthquake, 1971, December 7, surface wave study and focal mechanism 77−91040
  Labrador Trough, Canada, early recumbent folds in northeastern part 78−65300
  E.Lac Seul region, English River subprovince, NW.Ontario, crust form. history from Rb-Sr isotopic study 80−94486
  Lachlan Fold Belt, SE.Australia, deep crust. struct. 80−56436
  Lachlan Fold Belt in New South Wales, description, tectonic history 78−96211
  Lageos for crustal movement meas. 78−65441
  Lake Biwa, Japan, secular gravity change meas. rel. to vertical crustal movement 78−40463
  Lake Eyre North, S.Australia, bottom profile and tectonic grooves 78−69376
  Landsat satellite observations of Earth 79−84280
  Laramide orogeny, seismic profiles in Wyoming, USA 80−85626
  Laramide Wind River uplift, Wyoming, USA, gravity and seismic refl. data 80−21679
  Lassen Volcanic National Park, California, 1976-8 seismic events 80−36257
  Late Cretaceous astroblemes in western Canada 77−44999
  Late Cretaceous fore-arc basin, N. and Central California, petrofacies and petrologic evolution 79−2232
  Late Quaternary uplift in New Hebrides, U series ages 78−3741
  lava flow terrain, radar imaged by satellite 80−98285
  Lepontine Alps, temporal changes in heat flow distrib. assoc. with metamorphism 80−101347
  Lewisian gneisses, Sm-Nd systematics and implications for granulites origin 79−20777
  LF tunnel waves propag. through subcrustal lithosphere, numerical expt. 77−49025
  Liaoning Province, China, crustal struct. from gravity data *(Chinese)* 77−5142
  Liaoning Province, China, crustal thickness from gravity and seismic obs. *(Chinese)* 80−12349
  E. Ligurian Apennines, ophiolitic breccias comparison with rifted oceanic ridges 77−86881
  Ligurian Sea area, crustal and upper mantle structure 78−65209
  Limpopo Mobile Belt, Rb/Sr ages and geological setting of Sand River ancient dykes 77−56611
  lineament, joint and drainage densities, rapid determ. method 78−32255
  Lipari, Eolian Islands, crustal struct. from seismic response of local earthquakes 78−40494
  liquid-filled vertical crack propagating due to hydrostatic press. 80−72505
  lithosphere, ancient, role in young continental volcanism 77−2133
  lithosphere, compression and extension rel. to gravity nontidal vars., appl. to Hungarian depression *(Russian)* 79−8621
  lithosphere, heterogeneities rel. to P-wave time and amplitude anomalies interpretation 78−96153
  lithosphere, isostatic disturbances rel. to elastic stresses 77−81842
  lithosphere, lower, structure in USSR from explosion seismology 77−86836
  lithosphere bending at trench, elastic-perfectly plastic anal. 78−81135
  lithosphere beneath New Madrid seismic zone, three dimens. vel. model 78−7573
  lithosphere elastic expansion caused by groundwater depletion 80−31010

Earth crust continued
  lithosphere plates, accretion and subduction effects on shallow global mantle flow 79−44163
  lithosphere rheological models 77−21716
  lithosphere-mantle decoupling, role of shear heating 79−20790
  lithospheric downgoing slabs, temps. rel. to seismic zone lengths 79−25212
  lithospheric materials, microscopic intracrystalline cavities *(French)* 77−9400
  lithospheric necking and slowly accreting plate boundaries 79−2208
  lithospheric plates movement, influence on mantle convection 79−74880
  Lithospheric Seismic Profile in Britain (LISPB), crustal shear waves studies 78−73313
  lithospheric strain model using generalised Norton-Hoff law *(French)* 78−88809
  loading effects of quarter-diurnal oceanic tides by Ligurian Sea 78−61308
  longitudinal folds, high-amplitude, form. and stress state 77−9382
  Los Angeles basin (California) SW block, thermal subsidence and petroleum generation 80−3967
  Love wave mode conversion at continental margin 77−40986
  low-velocity zones, compressional wave vels. meas. in rocks at high temps. and press. 80−41435
  lower continental crust, comp. from granulite xenoliths in Lesotho kimberlites 78−24268
  lower continental crust, model 77−81840
  magma, ascending, heat and mass transfer 79−34768
  magma chamber, fluid dynamics model of differentiation and layering 80−76939
  magma trapping by lithostatic control, influence of crust density struct. 79−66669
  magma traps theory, appl. to W.Greenland Cretaceous-Tertiary volcanic region 79−70776
  magmagenesis 79−12103
  magmatic arcs, arc-trench gap accretion and episodic plutonism 80−76956
  magmatic diapir folds evolution, influence of temp. and heat exchange with crustal rocks *(Russian)* 80−104957
  magnetic anomalies, estimation of cover thickness above magnetised mass *(Russian)* 80−105069
  magnetic anomalies, satellite data inversion 80−12563
  magnetic anomalies caused by two-dimens. vertical faults, direct interpretation method 78−77181
  magnetic anomalies in crustal abyssal zones *(Russian)* 77−73631
  magnetic anomalies of long-wavelength for deep struct. 80−72430
  magnetic anomaly due to 2-D assym. triangular prism, expression for total field 80−94457
  magnetic anomaly sources in crust of Siberian platform *(Russian)* 77−32987
  magnetic depth sounding by induction arrow representation, review 80−98486
  magnetic model under Ukrainian Shield 78−61313
  magneto-telluric response dispersion relations, inversion problem theory 80−104861
  magnetostatic anomaly field problem, soln. in high susceptibility case via method of subsections 80−105065
  magnetotelluric method for investigation of media with monotonically changing cond. 77−78439
  N.Maine, USA, palaeomagnetism of Devonian rocks and Avalon microcontinent 80−41373
  major continental blocks, drift since Devonian 78−11864
  Makran coast, Iran and Pakistan, large-magnitude earthquakes recurrence, crustal uplift 79−79754
  Manic 3 reservoir, Quebec, regional stresses rel. to induced seismicity 79−66636
  Manicouagan impact crater, gravity study and upper crust density contrasts 78−81170
  Manicouagan impact crater, Quebec, investigation 78−81163
  Manicouagan impact melt, Quebec, chemical interrelationships with basement rel. to form. processes 78−81165
  Manicouagan impact melt, Quebec, stratigraphy, petrology and chemistry 78−81164
  Manicouagan impact melt sheet, Quebec, thermal history 78−81167
  Manicouagan Impact Structure, Canada, formation *(French)* 79−88355
  Manicouagan impact structure, Quebec, melt rocks petrogenesis 78−81166
  Manicouagan melt sheet, Rb-Sr isochron age 78−81168
  Manicouagan structure, Quebec, central mag. anomaly 78−81169
  marginal basins, formation rel. to relative plate motions 80−41427
  marine seismic surveying, potential efficiency of shot grouping *(Russian)* 78−40702
  mass redistribution due to continental drift, influence on true polar wandering 79−44079
  mechanical models for absolute plate motions in Early Tertiary, mechanical models 77−33036
  E.Mediterranean, crustal struct., sedimentary layers 78−69311
  E.Mediterranean, crustal structure model 78−24263
  E.Mediterranean, deep struct. and tectonics 78−69309
  E.Mediterranean, struct. and tectonic setting of Levant continental margin 78−69310
  Mediterranean Alpine Belt, geodynamics of eastern region 77−13071
  Mediterranean and marginal seas origin 78−69322
  E.Mediterranean gravity anomalies, volcanic activity rel. to tectonic development 78−69318
  E.Mediterranean region, heat flow rel. to crustal thickness 79−70770
  Mediterranean region, Holocene eustatic changes and coastal tectonics, crustal consumption 78−81201
  Mediterranean region, struct. and tectonics, conf., Haifa, Israel (Aug.-Sep. 1976) 78−69306
  Mediterranean Ridge, young submerged chain assoc. with Hellenic arc, struct. and tectonics 77−53014
  E.Mediterranean Sea, tectonic elements and crustal struct. 78−44801
  Mekometer measurements in Imperial Valley, California 79−79728
  Mesozoic volcano-tectonic rift zone and back-arc basin development, South America 79−29762
  Messejana Dolerite fault-dike system (Iberia), age and origin rel. to N.Atlantic Ocean opening 79−2198
  Messina Layered Intrusion, Limpopo Mobile Belt, S.Africa, tectonic setting, geology and age 80−76969
  metadolerite dykes and assoc. folds, Caledonides of Finnmark, Norway 78−61375

Earth crust continued
- metallic mineral deposits of Australia mag. induced polarisation survey results 80—98223
- metamorphic bathozones and bathograds, meas. of regional scale post-metamorphic uplift and erosion 78—81113
- meteorite crater structures, Kola Peninsula 79—70802
- meteorite craters, form., props. and catalogue 78—96411
- meteorite craters, geophysical and geomechanical aspects 80—17265
- meteorite craters, Morasko, Poland 79—20837
- meteorite craters probable number in USSR, calc. 77—66921
- meteorite falls and crater formation *(Polish)* 79—88630
- meteorite impact, craters, internal struct. model 78—44825
- meteorite impact and explosion craters 78—45296
- meteorite impact crater, central Alaska, possible glacial origin 79—25249
- meteorite impact crater discovered in central Alaska with LANDSAT imagery 77—91136
- meteorite impact structure, Gosses Bluff, Australia 80—72520
- meteorite impact structures, catalogue of 230 sites 77—73741
- trans-Mexican volcanic belt, seismic refl. and geomag., leg 17 of project CICAR *(Spanish)* 80—36280
- N.Mexico, Mesozoic rocks palaeomagnetism rel. to N.American craton struct. 77—2099
- Michigan Basin, crustal stress meas. 79—39681
- Michigan Basin, deep borehole results 79—39679
- Michigan Basin, evidence for crack free rocks at 5.3 km depth 79—39705
- Michigan Basin, gravimeter survey in deep borehole 79—39634
- Michigan Basin, Keweenawan turbidites as foundered basin sequence developed during protoceanic rift system evolution 79—39712
- Michigan Basin, thermal and mechanical evolution, lithosphere elastic flexure 77—21719
- Michoacan, Mexico, seismic gap, length of earthquake-free period 80—76919
- microtremor sequences and tilting in deep mine 79—84125
- microtremours, 1 to 5 s, earthquake engineering appl., Tokachi-oki 1968 earthquake long-period accel. 79—16387
- Mid-Atlantic Ridge, fault mechanisms and sub-crustal seismic vel. 80—36265
- mid-ocean ridge basaltic glasses, U-Pb, Sm-Nd and Rb-Sr systematics 80—36277
- Middle America arc, focal mechanism solns. and tectonics 78—77191
- mining tectonical forecast maps, geoelectric bed sounding method *(Hungarian)* 80—105075
- Minnesota, crustal struct. and seismicity, rel. to historic earthquakes 78—11840
- models with single crust-mantle discontinuities, ray-mode duality for SH waves 78—77183
- Moho, dip and strike determ. from array anal. 79—66821
- Moho, magnetic boundary 79—96748
- Moho, seismic detect. by time fields method *(Russian)* 79—35010
- Moho depth, determs. from spectral-ratio anal. of NORSAR long-period P-waves 77—86814
- Moho dip beneath Scotland, by PS reflections 80—41409
- Moho P-wave velocity depth, regional distrib. from Rumania earthquake (1977 March 4) *(German)* 80—98256
- Mohorovicic discontinuity relief, determ. methods *(Russian)* 78—48992
- Mohorovicic relict discontinuities, correl. with tectonic cycle recurrence *(Russian)* 77—44947
- Moine Thrust Zone, Eriboll, Scotland, palaeostress estimates 79—79835
- Mole (Haute-Savoie, France), geological profile of south flank rel. to struct. and tectonics *(French)* 78—69348
- Mongolo-Okhotsk mobile belt, rift formation and tectonic history 80—90066
- SW.Montana, Yellowstone Nat. Park, Snake River Plain, recent vertical crustal movement 78—28212
- Morasko, Poland, craters due to meteoritic shower 79—70801
- Motagua Fault and Guatemala earthquake (1976, February 4), seismological aspects 78—85493
- motions detect. using spaceborne laser ranging systems 78—92995
- Mount Carmel, struct. and extension into E.Mediterranean, marine geophys. survey 77—33026
- Mount Rainier, Washington, underlying struct. from teleseismic body waves 80—31011
- mountain peaks uplift determ. by three dimens. triangulation *(German)* 77—52966
- mountain ridges, effect on atmosphere frontal waves development, numerical simulation *(Russian)* 78—53701
- mountains origin, implications of Sun and Moon accels., appl. to gravit. const. var. 79—8592
- movement, measured by geodesic networks, design *(German)* 80—76897
- movements, conf., Palo Alto, California, USA (July 1977) 79—79785
- movements observation for earthquake prediction *(Japanese)* 78—28180
- mud volcano in Trinidad, gravity anomaly model 80—56442
- multi-layered geothermal reservoir, natural convection 80—8347
- multiple refraction layer overburden, blind zone problem soln. 80—17241
- multispectral photography from space *(Russian)* 78—16198
- Munich-Milan Alpine section, active faulting and tectonics, LANDSAT imagery 77—53037
- Nain anorthosite (Labrador), palaeomagnetic results and tectonic implications 78—77178
- Nambucca slate belt, plate tectonic significance of structural succession 78—81140
- Nelson River gravity anomaly, SE.Saskatchewan, seismic survey 78—28153
- Nepal, basic intrusions of volcanic origin 80—72477
- Nepal Himalaya, body waves from earthquakes, focal mechanism and tectonics 80—72455
- Nepal Himalaya, struct. geology of Kusma-Sirkang section 80—72478
- N.-central Nevada, faulting patterns and crustal strength 80—72467
- Nevada Test Site, geology effect on absolute travel-time residuals 79—16391
- New Hebrides island arc, earthquakes precise relocation rel. to seismotectonics 79—16404
- New Hebrides island arc, fracture zone and aseismic ridge subduction rel. to 1969 January 19 earthquake 78—73342
- New Madrid seismic zone, wave vel. determ., crustal model 77—73652
- N.New South Wales, continental shelf development 80—51353
- New York area, seismicity and lithospheric stress 78—36113
- New Zealand (N.Island), plate boundary microearthquake study 80—109131
- New Zealand plate boundary distortion *(German)* 78—20382

Earth crust continued
- New Zealand soils, survey of naturally occurring radionuclude conc. 77—53057
- E. Newfoundland, aborted Proterozoic rifting 78—57200
- Newfoundland, Early Palaeozoic plate tectonic model 80—94509
- Newfoundland, gravity zoning 77—52965
- Newfoundland, Hercynian activity, geochronology 77—29263
- SW Newfoundland, Proterozoic-Palaeozoic thermal history from Grenville basement rocks ^{40}Ar/^{39}Ar ages 79—20771
- Newfoundland Basin, Mesozoic evolution 78—32045
- NE.Newfoundland continental shelf, ancestral relationship to Charlie Fracture Zone 77—25664
- Newfoundland lithosphere structure from teleseismic PP-wave refls. 78—65210
- Newfoundland Ridge, multichannel seismic refl. profiles of subsided continental crust 78—15980
- Nias Island, Indonesia, sedimentology and palaeobathymetry of Neogene trench-slope deposits 80—104950
- Nias Island, Indonesia, structural geology implications for subduction zone tectonics 80—109120
- N.Nigeria, pipe in schist belt, geophys. anomaly study 80—76971
- Nigerian and Sergipe-Alagoas sedimentary basins, Cretaceous transgressions 77—21701
- noncylindrical flexural slip folds, in nature and expt. 77—53024
- nonparallel stratified models, scattered EM radiation field 78—44773
- nonparallel stratified models, scattered surface wave 78—40489
- Nordlinger Ries giant meteorite impact crater, K-Ar and fission track dating 78—28236
- Norris Geyser, Yellowstone Park, USA, microseisms of geothermal area 80—104909
- W.North American plate, intraplate tectonics 77—41017
- North Sea, Buchan and Witchground Grabens, seismology study 80—51364
- North Sea basin, subsidence in post-mid-Cretaceous 80—109133
- N.Norway, continental margin crustal struct. and tectonic history 80—51360
- W Norway, Devonian basins subsidence and sedimentation 77—21727
- N.Norway, palaeomagnetic evidence for movement on Trollfjord-Komagelv Fault 78—40535
- Norwegian eclogites, Caledonian Sm-Nd ages and crustal origin 80—76978
- Norwegian gneiss eclogites, giving evidence for Precambrian continent-continent collision 77—49057
- Nova Scotia, tidal loading response, results from improved ocean tide models 78—92821
- Nova Scotia crustal struct. and NW.Atlantic M$_2$ tide from tilt and gravity obs. 78—40464
- Novaya Zemlya crust and upper mantle model from Rayleigh wave dispersion data 79—84187
- Novaya Zemlya nuclear explosions, P-wave travel time residuals vars. in central California 77—25658
- ocean basins, origin 77—91085
- ocean basins, primordial, form. 79—20770
- oceanic crust, serpentinite protrusions 77—5149
- oceanic ridges and trenches, polar wander excitation 79—16367
- Oita, Japan, tectonic topography rel. to 1975 April 21 earthquake *(Japanese)* 77—2109
- Oita earthquake, Japan, 1975, damage and ground disturbance rel. to Quaternary faults *(Japanese)* 77—2108
- Oita earthquake, Japan, 1975, focal mechanism rel. to active fault system *(Japanese)* 77—2107
- Olinghouse fault zone, Nevada, strike-slip fault 79—79840
- olivine, shock deform. expts., Hugoniot data implications 80—94497
- NW.Ontario, Canada, trondhjemitic basement enclave near Archaean Favourable Lake volcanic complex 80—94518
- Onverwacht Group, Transvaal, sedimentology rel. to early Earth characts. and evolution 78—44812
- open hydraulic fractures, form and stability 77—5157
- ophiolite complex of Point Sal, California, seismic vel. struct. 80—109110
- ophiolite emplacement on continental margins, similarity to thrust faulting 77—2136
- ophiolite nappes emplacement, Mesozoic-Cenozoic examples 77—41012
- ophiolites of S Quebec, oceanic crust of Betts Cove type *(French)* 79—57923
- ophiolitic melange of Late Precambrian, Egyptian desert, formation process 80—81884
- ophiolitic rocks tectonic emplacement in Precambrian Mona Complex, Anglesey 79—8631
- ophiolitic sulphide deposits in Cyprue, ^{87}Sr enrichment confirms ore form. by circulating seawater 77—81887
- ore-deposition through geological time, review 78—77235
- Oregon, structure from teleseismic P- and S-waves received at Corvallis 77—91067
- origin at spreading axes, rel. to thiocyanate in Red Sea brine and origin of life 79—57975
- orogenic belt, numerical expts. on migmatite rise based on continuum dynamics 80—51381
- orogenic regions deep crustal probing by natural EM fields surface impedance vars. 77—13060
- orogenic volcanism caused by thermal runaways? 80—90057
- Oroville, California, crustal shear wave vel. struct. determ. from 1975 August 1 earthquake 79—16417
- Oroville, California, crustal stresses due to artificial lake rel. to seismicity 77—9347
- Oroville, California, surface faulting assoc. with 1975 August 1 earthquake 77—9345
- Oroville earthquake, California, 1975, Aug. 1, geodetic meas. of assoc. deformation 77—53008
- oscillations caused by var. mantle pressure *(Russian)* 79—29735
- Oshima Island, Japan, crust struct. and aftershock activity *(Japanese)* 80—41384
- Oslo Rift, crustal structure from seismic refr. study 78—32037
- Otago schist megaculmination, origins and tectonic significance in New Zealand Rangitata Orogen 78—81142
- overthrusting, model of const. thickness overthrust on visco-plastic sole 80—51378
- Owen Basin, Arabian SE margin, and Owen Fracture Zone evolution 79—84217
- Oxford Lake-Knee Lake greenstone belt, N.Manitoba, Rb-Sr ages 80—94485

Earth crust continued
- P-wave abnormal delays in The Geysers-Clear Lake geothermal area, California 79—74860
- P-wave amplitude anomalies, interpretation 80—56386
- P-wave initial pulse widths rel. to anelastic props. and surface geology, central California 78—44778
- P-wave vel. struct to depth of 150 km, Kanto District, Japan *(Japanese)* 80—94475
- P-wave vels. in NORSAR area 78—3728
- SW.Pacific, Eocene subduction zone, disruptive ophiolitic belt evidence 80—104949
- Pacific plate, Neogene motion relative to mantle and Earth spin axis 79—44167
- Pacific plate subduction *(Japanese)* 80—94514
- Pacific plate subduction beneath Japan Islands, 3-D seismic struct. 80—51376
- E.Pacific Rise, hydrothermal vents on seabed issuing H_2 and methane 80—41422
- Pacific subduction zones, great earthquakes recurrence 77—17045
- palaeocontinental maps for Early Phanerozoic and Proterozoic 79—44150
- palaeocontinental slopes of East Coast Geosyncline, Canadian Atlantic Margin 78—36141
- Palmahim structure in SE Mediterranean off Israel, continuous tectonic activity since Upper Miocene 79—34790
- Palmdale, California, crustal resist. changes 79—16373
- Palmdale, California, P-wave millisecond travel time vars. systematic monitoring 79—57863
- Palmdale uplift, gravity changes and thrust faulting 78—44757
- SE.Pamir Mountains, geology and geochronology *(Russian)* 80—12392
- Pamir-Himalayan deep fault zone description 79—39676
- Pamir-Hindu Kush region, seismicity and fault plane solns. 80—72445
- Pan-African mountains, no evidence of 500 Myr detrital zircons 79—84213
- Panamint Valley fault zone, W.Basin and Range province, California, Holocene offset and seismicity 79—79802
- Pangaea, reconstruction for Permian period using mag. field configuration calcs. 77—56577
- Pangaea and movement of crustal fragments on shrinking Earth 78—57187
- Papua New Guinea, delayed partial melting of subduction-modified mantle 78—57183
- Papuan Ultramafic Belt, crustal structure 77—37166
- paraffin model experiment of plate tectonics 77—13073
- passive continental margin, evolution in light of drilling results 80—76942
- passive continental margins, isostatic gravity anomaly rel. to ocean-continent boundary evolution 77—81777
- Pearson Formation (Great Slave Supergroup, NWT), palaeomagnetism and Coronation loop 78—77179
- Peking region, convection-generated stress concentration and Tangshan earthquake seismogenic models 79—92507
- Peking-Tientsin area, China, crustal struct. from gravity data, rel. to seismicity *(Chinese)* 78—61357
- Pelusiam Line, major transcontinental shear 77—53034
- permeable formation with crack, nucl.-explosion induced, gas flow 78—61372
- Peru, 1969 Pariahuanca earthquakes, superficial deform. struct. anal. 77—53012
- Peruvian continental margin, Andean geosynclinal pair 77—21724
- petrogenetic mixing models and Nd-Sr isotopic patterns 80—3965
- petrovelocity model for Ukrainian Shield 78—7597
- Phanerozoic palaeomagnetic restructurings, chronological distribution curves 79—53302
- Phanerozoic sedimentary basins, Australia, tectonic implications 78—96174
- phase boundary under surface loads, dynamics 78—85509
- W.Philippine Basin, DSDP sediments palaeomagnetism, mag. anomalies phase shifting and Basin rots. 77—86764
- Philippine Islands, tectonic struct. revealed by seismicity and volcanicity 80—94511
- Philippines, microearthquake survey of tectonic features 80—81827
- Philippines, subduction zone south of Mindanao, evidence from 1976 August 16 earthquake 79—44117
- Phlegraean fields, Italy, intercrustal hydrodynamic correlation with geodynamics 77—2138
- Phlegrean Fields, Naples, geodetic and geophys. meas., elevation changes 79—29734
- piezomagnetism, response depend. on depth rel. to tectonomagnetism as earthquake precursor 80—26465
- Pine Mountain block thrust sheet, USA, energetics of driving force 80—21730
- plate motion and thermal instability in asthenosphere 77—17073
- plate motions, rel. to asthenosphere flow model 78—96180
- plate resting on deformed incompressible elastic halfspace, axisymm. flexure 77—46913
- plate tectonic explanation of Earth struct. 80—81855
- plate tectonics, roles of boundary friction, basal shear stress and deep mantle convection 78—57188
- plate tectonics evolution, rel. to prebiotic chemical evolution 78—40666
- plate tectonics in Phanerozoic 78—92812
- plates ridge and trench boundaries, appl. to individual plate absolute motion determ. 78—85529
- plutonic environment, contrasted magmas commingling in Nain anorthositic complex, Labrador 80—104959
- plutons, thermal evolution, parameterised approach 80—90042
- Point Mugu earthquake, California, 1973 Feb. 21, epicentral region elevation changes 77—56587
- point pulse source in elastic anisotropic half-space, propag. of vibrs. 78—57174
- Poland, heat flow map and Europe geothermal field *(Polish)* 77—21707
- polycrystalline cores, creep laws for various stress states *(French)* 77—53077
- porosity and permeability, rel. to transport phenomena in hydrothermal systems 78—36205
- post glacial uplift mechanism, phase boundary reaction to medium press. changes 80—90058
- postglacial tilting of Akpatok Island, Northwest Territories 79—57901
- postglacial uplift of crust, mechanism 80—104943
- postseismic surface deformations due to lithospheric and asthenospheric viscoelasticity 79—57884
- postseismic surface stress, viscoelastic model 80—98278

Earth crust continued
- postseismic viscoelastic surface deform. and stress, theory 80—94496
- Precambrian basement of W.Canada, Hg and As distrib. and abundance 80—56419
- Precambrian crust, seismic refls. study 78—32034
- Precambrian dykes, preferred orientation of intrusion 78—88829
- Precambrian geodynamics, palaeomagnetic data for Africa, Australia and N.America 77—66889
- Precambrian geologic history 77—2131
- Precambrian mobile belts of Africa, crustal evolution towards plate tectonics 77—66906
- Precambrian schist belt, Karnataka, India, struct. from aeromag. anomaly harmonic inversion 79—44094
- Precambrian shield of Liberia, heat flow 80—98279
- Precambrian thermal regimes 78—65235
- premonitory crustal deformations, strains and seismotectonic features (b-values) preceding Koyna earthquakes 79—79755
- preseismic crustal deformations, gravity vars. 79—70734
- pressure-temperature conditions modelling, appl. of rocks elastic props. experimental studies *(Russian)* 78—96207
- pretlercynian continental configuration, palaeomag. data from NW.France 80—72414
- primary stresses, meas. at Eisenhower Memorial Tunnel, Colorado 79—29727
- principal stress axes rotation caused by faulting 79—57886
- propagating fault, one-dimens., with nonuniform stress and strength, dynamic soln. 79—84149
- Proterozoic anorthosite massif of Labrador's Nain complex, magma origin 80—94500
- Middle Proterozoic continental arrangement, based on palaeomag. of Coronation Geosyncline 80—94456
- Proterozoic crust, gravit. instability inferred from mantled gneiss dome pattern 80—81848
- proterozoic intraplate deformation, comparison with SE Asian neotectonics 78—65250
- PS-waves refl. from Moho 77—86809
- Pyramid Lake fault zone, Walker Lane, strike-slip fault 79—79839
- Pyrenean mountains, explosion seismic sounding of continental Moho throws and dips 80—85620
- Pyreness, subduction and collision model 77—81854
- quartzite, deformation in Earth crust, dislocation climb mechanism 79—60425
- quartzites, microscopic deform. and flow laws, South Mountain Anticline 78—77220
- Quebec, LG-3 dam fault average net slip, dome and basin structs. *(French)* 77—73732
- N.Queensland, Australia, crust struct. from gravity survey 80—72458
- radioactive heat production in crustal rocks, exponential relationship with seismic vel. 79—70793
- radiogenic heat generation in old platform crusts 80—89996
- radiogenic heat production, depth depend. modelling by variational approach 80—72464
- radiogenic heat production, vertical distrib. 80—85619
- recent movements as determined by geodetic meas. 77—44960
- rectangular structures EM sounding, multi-freq. EM system response numerical modelling 80—56623
- Reggio Calabria earthquake, 1975 Jan. 16, seismological results and geostructural appl. 77—49007
- regional strain analysis, geometric interpretation 77—73705
- regional stresses determ. from seismic b-value scanning, appl. to earthquakes development modelling *(Chinese)* 79—12072
- regional studies, nonlinear interference anal. of seismic data 79—25217
- residual gravity anomalies interpretation *(Russian)* 79—88232
- resistivity sounding, technique for obs. crustal dilatancy prior to earthquakes 79—92609
- resistivity sounding data from South Africa, ridge regression inversion appl. 78—7561
- Reydarfjordur area, E.Iceland, dyke magnetisation and upper crustal struct. 77—78139
- Reykjanes Ridge Iceland Seismic Experiment (RRISP 77), for crust struct. 80—90017
- Rhenish Massif, recent vertical crustal movements determ. 79—79789
- Rhenish Massif/Rhenohercynian zone, W Germany, crustal struct., seismic refr. data 79—48435
- rheology based on long-term creep tests of rocks 79—79828
- Rhinegraben, differential geomag. sounding 79—74832
- Rhinegraben, geodetic high-precision meas. in active tectonic area 79—79788
- Rhinegraben area, gravity anomalies and geothermal implications 80—104852
- Rhinegraben geothermal anomaly at Landau oil-field, model 80—98281
- Rhinegraben rift system, Holocene movements and stress state 79—79801
- rhyolitic ignimbrites origin, Batopilas area, Mexico, Sr isotope study 80—94501
- Ries impact crater, siderophile and volatile element anal. 80—17552
- Ries impact crater, thermal events, age and intensity 79—79760
- rift structure in S.Ethiopia 78—61377
- rifted arch basins and post-breakup rim basins on passive continental margins 77—81861
- rifting and volcanism relative timing and tectonic implications 78—81129
- rifts at high angles to orogenic belts, origin, Upper Rhine Graben example 78—48989
- ring structures nature and origin in USSR *(Russian)* 78—16018
- Rio Grande rift, USA, deep crust struct., magnetotelluric interpretation 80—104878
- Roccamonfina volcano, Roman comagmatic region, Italy,, country rocks assimilation rel. to potassic igneous rocks form. 80—41420
- Rochechouart crater, Massif Central, France, shock zoning study 77—81897
- Rochechouart meteorite crater, France, projectile identification 77—33025
- rock bodies, cooling, residual stress development 78—88819
- rock crack mapping by obs. of seismic velocity anisotropy 80—98253
- rock fracture prediction problem 79—25230
- rock movement monitoring using inclinometers and tiltmeters 78—28318
- rock props. from 4000-6000 m deep cores *(Rumanian)* 79—57892
- rock sheet, Dent-Blanche, stressing subductions and Eocene flexure *(French)* 78—24282
- rock strain, estimation from deformed ellipsoidal objects, algebraic method 77—21766

Earth crust continued
rock stress measurement, hydrofracturing method and recent field results 79−29885
rockfall from cliff face, seasonal variation obs. in N.Ireland 80−105001
rocks, seismic anisotropy meas. under high-press., high-type conditions 77−49059
Rocky Mountain Trench near Radium, BC, gravity evidence against high angle fault 77−44940
N.Rocky Mountains, British Columbia, Canada, structural interpretation 79−100835
Rumania, geothermal regimes of tectonic units 79−70768
Rumania, lithospheric microplates rel. to regional gravity anomalies *(Rumanian)* 78−20380
central Russia, circular structures, possible meteorite craters *(Russian)* 77−9385
Russian platform sedimentary basins development dynamics 77−21729
S-waves vertical distrib. of vel. at Iwatsuki Deep Borehole Observatory, Japan 79−62457
Sagatu Ridge dyke swarm, Ethiopian rift margin 77−37170
Saguenay area, Quebec, gravity survey rel. to crustal models 77−52958
Sainte-Marie-aux-Mines observatory, underlying crustal struct. from analysis of converted P_s waves *(French)* 77−73666
salt dome dynamics, finite element analysis 79−20789
salt domes, N.Louisiana, imaging radar mission 79−66833
salt glaciers of Iran, seasonal movement obs. 80−104942
Salton Trough, California, deform. meas., 1973-77 period 79−84079
San Andreas and Calaveras fault region, crustal deformation, 1971-8 obs. 80−56428
San Andreas fault, California, bimodal distrib. of creep event amplitudes 77−78145
San Andreas Fault, California, in-situ stress meas. 79−79767
San Andreas fault, California, short-period nonseismic tilts rel. to episodic slip 77−29276
San Andreas fault, continuous strain meas. during and preceding episodic creep 78−36127
San Andreas fault, coseismic tilt changes assoc. with local earthquakes 78−36112
central San Andreas fault, creep, tilt, strain and water level var. 77−91023
San Andreas fault, fault creep obs. rel. to local mag. field meas. 80−85629
San Andreas Fault, geodetic tilt obs. 80−81800
San Andreas fault, local mag. field vars. and stress changes near slip discontinuity 80−26448
San Andreas fault, lower crustal structure determ. method 77−91284
San Andreas fault, Parkfield, repeated creep events, strainmeter array meas. 79−20762
San Andreas fault, Rn emanation vars. meas. 78−32022
San Andreas fault, shear stress meas. profile at shallow depth 80−76947
San Andreas fault, slip assoc. with great 1857 earthquake 79−66633
San Andreas Fault, stress accumulation and release mechanisms 79−84194
San Andreas Fault, vel. contrast, P-wave nodal plane distortion 78−65188
San Andreas Fault, wire strainmeter data subject to meteorological noise 80−81831
San Andreas fault (central California), mag. field local vars., creep rate changes and local earthquakes 80−26450
San Andreas fault strain accumulation 1964-1977 near 1976-7 earthquake swarm 80−36272
San Andreas fault stress pattern, near-surface in situ meas. 79−48433
San Andreas fault system, local stress field and kinematics modelling 79−79778
San Andreas fault zone, central California, source processes of earthquake sequences 77−2111
San Andreas fault zone, constitution at depth 79−12097
San Andreas fault zone, rocks NRM stress sensitivity meas. using cryogenic magnetometer 80−26506
San Andreas transform, geometry of related triple junctions 79−57904
San Andreas transform, geometry of subducted slab 80−98297
San Francisco Bay region, landslide hazard 77−70665
San Francisco earthquake, 1906, kinematic viscoelastic model 77−73671
San Jacinto fault, Riverside, California, strain accumulation 77−25633
Sanriku-Oki region, Japan, 1965-1970 shallow earthquake source characts. 80−12346
W.Santa Ynez fault system in S.California, struct. and neotectonics 79−79774
S.Saskatchewan, seismotectonics 79−20757
Scandinavia, Blue Road area, crustal model and isostatic state 77−64240
N.Scandinavia, compressional and shear wave anal. of lower lithosphere fine structure 80−3979
Scandinavian Caledonides, nappe displacement 78−81143
Scotland, elec. cond. rel. to Caledonian tectonics 77−44920
Scotland, electrical model of crust and upper mantle 80−98234
Scotland, imbricate thrust model of Southern Uplands 77−53031
NW.Scotland, Pb isotopes in Lewisian gneisses rel. to age and sialic crust form. 77−70625
NW Scotland Tertiary continental volcanics, Nd and Sr isotope evidence for crustal contamination 79−66693
SW. Scottish Highlands, temporal changes in heat flow distrib. assoc. with metamorphism 80−101347
screw dislocations in vertical slab with shear modulus contrast, shear stress, strain and displacement 77−56594
sea bottom feature off Charleston, S.Carolina, Gulf Stream deflection 79−53365
Sebakwian group, Selukwe, Rhodesia, Early Archaen age 77−13067
sedimentary basin on viscoelastic lithosphere, evolution 79−8615
sedimentary basins, development in Archaean rel. to lithosphere thickness 80−89986
sedimentary basins, form. with finite crustal extension rates 80−89987
sedimentary basins development, role of continental lithosphere stretching 79−29719
sedimentary basins of continental margin and craton, conf., Durham, England (Apr. 1976) 77−21715
sedimentary basins subsidence mechanisms, review 77−21746
sedimentary rock faulting and folding, strain hardening theory 80−85628
seismic anisotropy, investigations in USSR 77−49038
seismic anisotropy, review 77−49011
seismic anisotropy of crust and upper mantle, deep seismic sounding 77−70855

Earth crust continued
seismic attenuation in rocks, role of grain boundary friction 79−34755
seismic body waves, attenuation from inversions of high freq. $Q_\gamma^{-1}(f)$ 77−33000
seismic boundary, essentially nonplane, supercritic al reflected waves record peculiarities *(Russian)* 79−8606
seismic fracture zones, effects of groundwater hydrostatic press. vars. on seismicity *(Russian)* 80−104913
seismic ground response near Long Beach, California 80−61775
seismic Lg propagation and lateral variations in crustal structure in Asia 77−33008
seismic P-waves from mining explosions, search for time-depend. travel times 78−44788
seismic quality factor and effective viscosity relationship 80−12360
seismic reflection studies, Canadian Shield, weighted vertical stacking 77−87089
seismic section migration, summation base restriction *(Russian)* 78−40701
seismic shear-wave attenuation, 0.05-25 Hz 80−36268
seismic shear-wave travel time for Earth struct. 80−81817
seismic strong motion attenuation, regions of USA 80−81834
seismic vel. anisotropy correl. with in situ stresses 77−91045
seismic vel. anomalies in lithosphere, P-time residual data inversion 77−73877
seismic velocity depth dependence, prediction from minerals effective vels. var. with press. 79−44179
seismic velocity inversion in upper crust *(Japanese)* 80−94478
seismic velocity time variance from multiple explosive sources, Hollister, California 78−44779
seismic vertical time-depth curve, automatic approximation via successive layer detect. *(Russian)* 78−40700
seismic wave diffraction, using Earth crust models 80−98239
seismic wave field assoc. with fine structured Moho in continents and oceans 80−12361
seismic wave reflection at wide angles, travel times 78−65202
seismic waves, shear modes propag. in anisotropic systems 78−36107
seismic waves diffraction by finite crack, appl. to location of magma lens 79−16416
seismic waves propagation, integral spectrum parameters appl. to geological section prediction *(Russian)* 79−8705
seismology, implications of dilatancy-fluid diffusion theory for aftershock sequences 80−85604
Senegal, telluric current variation obs. *(French)* 80−76903
sequential deformation in central Appalachians 78−65294
SH waves due to shearing-stress discontinuity in viscoelastic half-space, displacement 80−56405
SH-waves ray-mode duality in Earth models with crust and mantle discontinuities 79−25213
shallow crustal vels., phase time inversions 80−21634
shallow earthquakes, seismic efficiency, radiated seismic energy, fault motion energy balance 80−76927
shallow structure in S.Central America from seismic data 77−56609
shear cracks nucleation and initial propag. 79−81804
shear deformation zones, along major transform faults and subducting slabs 78−73330
shear stress on base of lithospheric plate 77−91099
Shepetovka-Chernobyl seismic profile, petrovelocity crustal model and nature of M discontinuity *(Russian)* 77−44948
Shikoku district, Japan, upper crustal struct. from seismic anal. *(Japanese)* 80−94508
Shizuoka district, Japan, crustal struct., explosion seismology data 80−12359
short period P-waves, crustal struct. from spectral ratio response 77−73688
sialic crust and atmosphere system, form. from upper mantle 79−44153
SE Siberia, crust struct. and role of Archean folded ovals 80−101349
Siberian platform, main structures development history and dynamics 77−21732
W Siberian platform development history and dynamics 77−21731
Sicily, Mesozoic continental margin, palaeomagnetism and deformation 80−61761
Siebengebirge, Germany, K-Ar age of Tertiary volcanics 80−98280
Sierra Nevada, California, crustal movement anal. using repeated geodetic levelling data 79−79795
Sierra Nevada, California, regional deform. on conjugate microfault sets 80−21729
Sierra Nevada batholith, elec. conductivity of crust 80−72411
Sierra Nevada-Walker Lane region, recent crustal movements, rate and style of deform. 79−79838
E.Sierran Front, shallow crustal conductors under Coso Range, DC conc. 80−89942
sign-variable movements, possible mechanism *(Russian)* 78−3733
Sigsbee Scarp, Gulf of Mexico, salt tectonism and evolution 77−73714
Sila nappes (Calabria), palaeomag. evidence for non-Apenninic orign 80−56369
simulated upper crustal conditions, transient effect in rock samples 77−29293
Sinai subplate margins, Late Holocene tectonic activity 79−57907
Singhbhum thrust belt (India), results of geothermal studies 77−49050
Slate Islands, Lake Superior, probable meteorite impact structure 77−9427
Slate Islands structure, partially submerged meteorite impact crater in Lake Superior 77−78183
Slave craton-Churchill craton collision tectonics, Canadian Shield 78−24278
slip faulting, far-field body waves generated by elliptically expanding rupture 77−81804
slip monitoring along major faults in southern California 79−48388
Snake Bay-Kakagi Lake greenstone belt, NW.Ontario, expanding spread seismic refl. survey 80−12356
soft basin, seismic wave propag. determ. by glorified optics technique 79−66629
soils electrical properties, investigation of seasonal variations, in 10-1000 kHz band 78−88796
solid three dim. models of gradient media by precipitation 77−64235
solid-Earth geophysics, bibliography 77−2078
Souss Basin, S.W. Morocco, mag. survey and crustal struct. 80−89958
South America, origin of compressional intraplate stresses 78−61385
South Fork Mountain Schist (N Coast Ranges, California), early Cretaceous metamorphic age 78−81114
southern continents palaeopositions, revised reconstruction 78−92805

Earth crust continued
S.Spain, crustal struct. from deep seismic sounding *(Spanish)* 78—44795
S.Spain, deep seismic soundings 78—7587
SE.Spain, Quaternary strike slip faults 79—79798
Spanish Peaks, Colorado, stress state rel. to dike pattern 77—91095
spectrum characteristics, appl. to seismic stations calibration *(Russian)* 78—49158
sphene in high-pressure partial melting of hydrous mafic compositions 79—44174
spherical ore-bodies, total field mag. anomalies interpretation via zero-line method 79—39973
spreading shear faults stabilization by coupled deform. diffusion effects 77—17056
St. Vincent's Gulf, South Australia, Island and coast effect in geomag. vars. 80—72426
statistical model from gravity anomalies and HB_1 model 78—61306
Stonely waves, direct meas. at Ni-Pyrex rel. to crustal seismic waves 78—10268
strain accumulation, triggering factor for shallow intraplate earthquakes 79—39661
strain measurements by bore-hole strainmeter at Matsushiro, seismic waves response *(Japanese)* 79—96745
strain obs. with Cambridge laser strainmeter 77—44895
strain softening prior to two-dimensional strike slip earthquakes 79—70755
strains and tilts on continental crustal blocks 79—79773
stress accumulation in lithosphere 77—17071
stress and fault patterns rel. to Wind River Mountains 77—91096
stress assoc. with plateau uplift, continental splitting mechanism appl. 79—34777
stress changes, in situ monitoring 79—29884
stress corrosion cracking theory, geophys. appls. 77—62212
stress determ., statistical anal. 80—81852
stress drop of earthquake sources *(Chinese)* 79—62438
stress field, in situ determ. via hydrofracturing, fracture mechanics approach 78—81435
stress field anal. of northern Hsiaokiang fault, Yunnan *(Chinese)* 79—62464
stress field and ground surface deform. assoc. with vertical tension crack *(Chinese)* 79—62463
stress field of Tangshan area before and after 1976 July 28 earthquake *(Chinese)* 78—61358
stress fields, plume generated, expressed in Hawaiian rifts and recent Icelandic volcanism 80—90051
stress meas. limits 79—48588
stress measurement by overcoring, diagnostic stress-relief curves 79—29886
stress measurements in north China *(Chinese)* 79—88312
stress rel. to steady state flow of rocks 77—91120
stress state, review 79—5465
stress state and olivine flow laws 77—91121
stresses and displacement distrib. in body with system of parallel shear cracks 78—49012
strike slip fault, three dimens. viscoelastic model 77—56591
strike slip faulting in downward varying crust 79—84154
strike-slip fault, earthquake instability 79—84144
strike-slip faults in continental crust, length and offset correl. 77—41011
structural and vibr. bedrock props. in Sweden, seismic events 79—16402
structural geology, conf. (1978), Toronto, Canada 80—101666
structure, investigation via seismic reverberation 79—66820
structure, role of intercrustal convection 77—17061
structure along international DSS profile VIII from Russian to Poland 77—21705
structure and evolution, review of problems 79—96749
structure estimation from acoustic reflection meas., Cramer-Rao bound 77—5369
structure formation using plate tectonics and rotation hypothesis *(Russian)* 78—15986
structure from EM freq. sounding 78—49167
structure from seismic surface wave obs. 78—73323
structure modelling using teleseismic body-wave conversions 77—91283
structure models rel. to focal depth determ. for Friuli earthquakes 78—24243
structure rel. to longitudinal seismic wave arrival directions *(Russian)* 78—11850
structure rel. to quasi-periodic gravity vars. *(Russian)* 78—69275
structure under Canadian Rockies, seismic refraction survey 77—53015
subcrustal lithosphere structural variation, explosion seismic profiles 80—3974
subducted lithosphere, correl. with positive geoid height anomalies 80—90056
subducting lithosphere, heat transfer with continental asthenosphere 80—94510
subducting lithosphere boundary determ. using ScS to P conversions 78—7572
subducting lithosphere in Japan region, seismic wave vel. anomalies 79—92489
subducting slab undergoing upper surface melting, thermal field 80—85638
subduction, P.J. Holmquist theories 78—20379
subduction angle, in plate tectonics 78—11865
subduction angle, influence of mantle flow press., non-Newtonian corner flows theory 79—39695
subduction zones, material transport within accretionary prisms and 'knocker' problem 80—101353
subduction zones, shallow seismicity meas. 79—16401
submarine landslides, North American east coast and upper rise 79—20815
submarine sedimentary basins, seismic vels. meas. by sonobuoy 77—86852
subsurface electrically excited conductors, pot. field mathematical model 80—98230
subsurface EM profile from HF meas., reconstruction technique algorithms appl. 77—45199
subterrestrial fluid convection, appl. to Rn long-distance migration 77—37246
Sudbury irruptive, depth of burial from remanent magnetisation 77—44942
S.Sulaiman Range, Pakistan, struct. and seismicity rel. to tectonics 79—39715

Earth crust continued
Sulawesi (E Indonesia) western arc, palaeomag. studies and fission-track dating rel. to tectonic history 80—89957
sulphide mineralisation in Rajasthan, and Gujarat, India, induced polarisation surveys results 79—39714
sulphide prospect in California copper belt, broadband EM study 80—72503
Superior Province, Canada, shallow crustal sounding by audio freq. magnetotellurics 79—57882
Superior-Churchill boundary zone extension into S.Canada 80—26468
Superior-Churchill provinces boundary zone, S.Canada, cooperative seismic surveys 80—89985
surface albedo change, monitoring by LANDSAT 78—32104
surface deformation due to volcanic eruptions, piezomag. field assoc. with Mogi model 80—67334
surface heat flow, geotherms and lithospheric thickness regional var. 77—53025
surface tidal tilts, influence of atmospheric press. fluctuations *(Russian)* 78—88790
Surkhob fault zone, crustal deformations 78—15979
Surkhob fault zone, USSR, tidal deform. determ. for crustal movement anal. 80—104944
Sverdrup Basin, Arctic Canada, evolution, subsidence and uplift 77—25673
central Sverdrup Basin, crustal struct. from seismic refr. data 80—12355
Swaziland Ancient Gneiss Complex, Rb-Sr age and source of bimodal suite 80—51395
Sweden, crustal struct. rel. to earthquakes focal depth distrib. 79—79756
Sweden, deep-seated fracture zones in crust 79—66666
Sweden, Proterozoic rocks indicating subduction zone 80—46162
Switzerland, siting criteria for heat extraction from hot dry rocks 79—39275
Tabas-e-Golshan earthquake, Iran, Sept. 1978, faulting and bedding thrust 80—81826
SW Tadzhikistan, earthquake energy rel. to lithosphere thickness, forecasting 77—9367
Tashkent Palaeozoic crystalline basement, tectonic struct., gravity survey *(Russian)* 78—53610
Tasman Fold Belt System in New South Wales, description 78—96210
Tasman Fold Belt System in Tasmania, description 78—96209
Tasman Fold Belt System in Victoria, evolution, tectonics, deform. 78—96212
Tasman Orogenic Zone, description of eastern part 78—96214
Tasman Orogenic Zone, Thomson Orogen, tectonically active area 78—96213
Tasmania, two heat flow values 77—33018
Tataria, USSR, lithological data from seismic refl. of longit. and transverse waves *(French)* 80—101335
Tauern, Austria, deformed pillow lavas rel. to origin of epidote-banded greenstones 79—79833
Tauern Window, role of buoyancy in exotic eclogite blocks preservation 79—88350
tectonic deformation, migration 79—79800
tectonic dislocations prospecting in complex media, appl. to seismic surface waves correl. method *(Russian)* 79—8605
tectonic features, rel. to seismic anisotropy of subcrustal lithosphere 77—49039
tectonic fracture system, statistical anal. *(Chinese)* 80—41417
tectonic movements, recent, estimation, geodetic obs. goodness concept restatement 79—57840
tectonic plates driving force, induced suction phenomenon 78—40534
tectonic provinces, correl. with lateral heterogeneity of upper mantle, multiple ScS meas. 77—29259
tectonic strains and stresses in seismically active regions, calc. 79—79744
tectonic system development, new rotation hypothesis 77—81857
tectonics conference on passive margins, Jun. 1978, Nova Scotia, Canada 80—36774
tectonomagnetics and small scale secular variation, symposium, Seattle, Washington (1977 August 22) 80—22133
tectonomagnetism, implications of magnetite mag. susceptibility under hydrostatic press. 80—26504
teleseismic short-period P-waves propag. through crust 77—56590
temp. gradient distrib. and geological struct. Izmir-Seferihisar geothermal area, Turkey, relation between temp. gradient distrib. and geological struct. 80—56441
temperature distrib. and electrically conducting zone formation 78—85519
temperature-depth profiles, Poland, from geothermal and deep seismic sounding data 78—48988
E.Tennessee, palinspastic map 78—65295
Tennessee, seismic characts., surface wave dispersion study 79—48426
Tennessee Valley and Ridge, folding 78—65292
terrain evaluation methods, Mackenzie Transportation Corridor, Canada 78—20344
terrain relief, effect on gravimetric meas. polyhedron approx. 80—3895
Texas shelf zone, crustal struct. from sonobuoy and ocean bottom seismograph data 79—5462
Thelon metamorphic front, cryptic suture in Canadian Shield 77—53023
thermal evolution during magmatic accretion and metamorphism 80—46150
thermic state and continental crust structure *(Italian)* 79—20769
thermoelastic strains and tilts, anal. of coupling between thermal boundary layer and topography 78—20346
thickness in N.Nevada from seismic refr. profiles 79—48425
three dimensional seismic struct. of the lithosphere 77—33023
thrust sheet deformation at ramp, mech. model 79—70779
Tibet, active tectonics, LANDSAT imagery 79—20794
Tibet earthquake, 14 July 1973, source mechanism and seismic wave attenuation 80—36252
Tibetan Plateau, crustal structure from surface wave study 77—91068
Tibetan Plateau, late Cenozoic tectonics, LANDSAT imagery 79—20795
Tibetan Plateau, Rayleigh wave attenuation 77—33028
Tibetan Plateau underthrust by India, palaeomagnetic constraints 80—56449
tidal deformation of sea floor and continents, ocean tides effects *(Russian)* 77—29308
tidal displacement, Geos-3 laser ranging obs. 80—3913
tidal forces deforming crust, causing orogeny 80—85625
tidal strain, topography, geology and cavity effects 77—44896
tidal tilt obs. in N.Wales mine, strain-tilt coupling and Earth model 80—89926

Earth crust continued
tidal tilts, parallel recording through digital print-out and photorecording channels *(Russian)* 78−88785
tides, long water-tube tilt meter 79−100959
W.Tien Shan, crustal movements from geology of palaeomagnetic data 77−9392
Tien Shan region, contemporary tectonics 79−29733
tilt meter observations at Berezovaya Rudka station, results *(Russian)* 78−88783
tilt meter observations harmonic anal., influence of S_1 diurnal meteorological wave *(Russian)* 78−88788
tiltmeter obs. near 1976 February 4 Guatemala earthquake 79−16363
Tjornes Fracture Zone, N.Iceland, N.American-Eurasian plate boundary 78−3740
Tohoku district, Japan, crustal movements during 1900-1975 and tectonic implications 80−56453
Tokyo, base rock depth, seismic wave obs. from explosions *(Japanese)* 77−64232
Tokyo, base rock struct. from seismic waves from Yumenoshima explosions 79−66654
Tokyo, underground struct. from Yumenoshima explosions seismic waves obs. *(Japanese)* 77−41000
topographical features effects on earthquake induced damage *(Japanese)* 79−70752
topography, effect on EM fields in three-dimensional cond. model 77−25639
topography effects on cyclogenesis and anticyclogenesis, optimum modelling 78−28256
topography effects on ionospheric electron density inhomogeneities, airborne soundings 78−69579
topography rel. to lightning frequency *(French)* 78−3845
Torlesse Terrane, New Zealand, exceptionally large steeply plunging folds origin 80−12388
Transcarpathian deep fracture, elec. cond. anomaly detect. from geomag. field repeated obs. *(Russian)* 79−96736
transform fault, quasistatic creep slippage inherent instability 79−84193
transversal bent fold, stress and strain rate, stress relax. effect 79−66651
Transverse Ranges, California, tectonics from recent seismicity in San Fernando region 79−66634
Transverse Ranges, S.California, lower crust low-resistivity region, magnetotelluric meas. 77−37127
trench/island arc/marginal sea systems, underlying mantle density inhomogeneities 80−21676
Triassic Hound Island Volcanics, Alaska, crustal movement from palaeomagnetic obs. 80−89945
Trivandrum, crust-mantle structure from Indian geomagnetic data 78−85520
Troodos ophiolitic complex, major oxide geochemistry and origin 80−98317
Turanian platform, regional struct. and development 77−21730
W. Turanian platform, seismic crustal models of major structural zones *(Russian)* 78−40526
Turkey, seismotectonic implications of relocated aftershock sequences 79−44119
Turkey-Iran, crustal thickness and uppermost mantle P-wave vels. 80−72462
W.Turkmenistan, density model of crustal structure *(Russian)* 78−69303
two-dimensional geological structures, geometric characts. via magnetotelluric tensor anal. 78−40471
two-dimensional strike-slip fault, static deform. of laterally inhomogeneous half-space 80−31012
S.Tyrrhenian Sea region, seismic wave study of crustal struct. 80−41380
Ukraine, crusted struct. from combined deep seismic sounding and gramimetry data 80−21845
Ukraine, heat flow meas., radioactive elements distrib. in upper crust 77−86842
Ukraine, recent vertical movement *(Russian)* 77−73699
Ukrainian Carpathians, crustal interface, phase substance transformation contrib. 80−89999
Ukrainian Precambrian Shield, deep fractures analysis *(Russian)* 79−20773
NW Ukrainian Shield, abyssal fractures obs. from deep seismic sounding data *(Russian)* 79−96746
Ukrainian Shield, comparison of gravity and heat model with deep seismic survey profile *(Russian)* 78−48991
Ukrainian Shield, deep structure from seismic studies *(Russian)* 79−48428
Ukrainian Shield, geothermal survey peculiarities rel. to search for fracture waters *(Russian)* 80−104935
Ukrainian Shield, regularities in distrib. of dike complexes *(Russian)* 77−44995
Ukrainian Shield, rock mag. props. map rel. to composition and metamorphism 80−17229
Ukrainian Shield, thermal model from deep seismic sounding profile *(Russian)* 78−28190
ultramafic xenoliths rel. to tectonites and lower crust composition *(French)* 79−44141
Umbrian pelagic carbonate rocks, Italy, mag. stratigraphy of Early Cretaceous 80−36229
Umfraville gabbro, Ontario, palaeomagnetism rel. to Grenvillian plate tectonics 78−92777
underwater margins of W.Spitsbergen, glacial morphogenesis and sea floor morphology 80−26494
uniaxial stresses, effects upon remanent magnetisation rel. to seismomag. earthquake precursors 80−26505
W.United States, collided Palaeozoic microplate (Sonomia) 80−41415
NE United States, crust and mantle struct. by seismic vel. 80−56429
United States, lithosphere tectonics rel. to regional free air gravity anomalies 79−57906
W United States, plate absolute motion and interaction constraints from Cenozoic igneous activity 79−2207
E.United States, seismic struct., shear wave vel. 80−56385
United States, western region, strain accumulation rates, 1970-78 period 80−21607
United States Atlantic continental shelf, US Geological Survey core drilling 80−72511
central United States crustal velocity models, theoretical seismogram constraints 79−39693
United States east coast, recent vertical crustal movements 78−32052

Earth crust continued
Uordan-Dead Sea rift, crust and upper mantle seismic study, transition towards Mediterranean Sea 79−79766
upper lithosphere stress concentration caused by underlying viscoelastic creep 78−20374
Upper Proterozoic apparent polar wander, analogous loops from Laurentia, Fennoscandia and Africa 80−56360
Urach region, Germany, very abnormal temp. field investigation at great depths 79−48440
Urals, geodynamics 77−5175
Urals, geomag. secular var. anomalies rel. to aseismic geodynamics 80−26447
NW USA, evolution from oceanic to continental crust 77−86847
W.USA, vertical crustal movement, anal. of levelling survey 80−72409
USSR, tectonics and mineral resources *(Russian)* 78−40536
SW.Utah, two areas of probable Holocene deform. 79−79803
Utah seismic refr. profile DELTA-W, crustal phases 80−56384
Vancouver Island, 1946 earthquake mechanism, geodetic study 80−61770
Vancouver Island region, terrestrial EM induction 80−104879
velocity anomalies determ. in Mugodzhary from seismic rays emergence angles and azimuths 79−25206
velocity model, from seismic data, Kurinian depression example 79−39678
Venice historical centre, altimetry rel. to defences against high water and subsidence *(Italian)* 77−86740
Ventura, California, high rates of vertical crustal movements 77−56614
vertical crustal movements, interpretation in time-space domain 79−80056
vertical crustal movements, solvability and multiquadric anal. appl. 79−79787
vertical crustal movements in Atlantic coastal plain, USA 79−79790
vertical motions, vel. during rock mass seismic flow 77−33035
vertical movement detection, noise reduction in sea-level records 79−2395
vertical movements, Carpathian area of Rumania *(Rumanian)* 80−8281
vertical movements, rel. to gravity and height vars. *(German)* 78−15949
vertical movements, rel. to surface relief in Bulgaria, statistical investig. 78−81126
vertical movements and regional tilt, precise levelling error propag. 77−44884
vertical movements in N.W.Europe, gravity and altitude vars. meas. *(German)* 78−15948
vertical movements rel. to phase boundary motion in mantle 77−49040
vertical orogenetic profile, relation between terrestrial heat flux and rocks mechanical characts. *(German)* 78−81123
vertical seismotectonic motions in Baykal rift zone 79−79783
Viljuy syneclise, common depth point data digital processing technique *(Russian)* 79−74875
Villalvernia-Varzi-Bobbio Line (N.Apennines), geomorphological evidence of neotectonic deform. *(Italian)* 79−8624
visco-elastic modelling of tectonic systems, by finite element anal. 80−104930
viscoelastic deformation, by finite quasi-static sources 79−39686
viscoelastic stiffness model of seismicity 79−20764
Volta Basin, geology and struct. correl. with Dahomeyide orogenic belt 80−109121
Voronezh Crystalline Massif, seismic vels. significance of mineral substance inhomogeneous compression 80−94504
Vredefort structure, S.Africa, comp. of spherules on shatter cone surfaces 79−29773
S.Wales, deep geologic struct. by explosion seismology 80−36261
W.Washington, structure from Puget Sound earthquake 77−91026
water, isentropic decompression from crustal and mantle press., thermodynamics 79−79769
wave dielectric log curves in formations of limited thickness, interpretation *(Russian)* 79−74990
weathered layer, seismic wave front eqn. and travel time 77−78122
well logging data correction, shallow vel. struct. prediction *(Russian)* 77−86837
Wellington region, New Zealand, seismicity within plate convergence zone 79−16398
wells, bottom-hole temperature stabilisation model 80−51356
Western Australian Shield, struct. and tectonic style 80−3983
Western Cordillera, Colombia, upper crust seismic vel. 80−81819
Wilkes Land, Antarctica, evidence for possible hypervelocity impact crater 77−17059
Wilkes Land, Antarctica, large gravity anomaly, no evidence for meteorite crater 80−26512
Wolf Creek crater, Western Australia, gravity investigation 79−100838
world-wide belts in geomag. field, rel. to tectonic features 79−39651
Wyoming, Wind River Mountains stress system 80−94492
S.Yamanashi Prefecture, Central Japan, crustal movements changes rel. to microearthquake activity *(Japanese)* 80−67343
Yamasaki fault, SW.Japan, seismic activity and crustal movement, predictions 79−57872
Yap arc-trench system, metamorphic rocks rel. to tectonic history 78−32093
Yellowknife, Northwest Territories, Canada, Archaean granite, rare earth and trace element data 80−4007
Yellowknife supergroup, Northwest Territories, volcanic rock density determ. from gravity obs. 80−98320
Yellowstone hot spot, tectonics and crustal props., earthquake and aeromag. data 78−48996
Yellowstone Park hot spot, volcanic and tectonic evolution 80−56472
Yong Shan-Da Guan, Yunnan earthquake (May 19, 1974), main shock source multiplicity *(Chinese)* 79−12075
Yoshioka-Shikano Fault, seismically active fault along Japan Sea coast, geomag. induction study 80−26475
Yunnan Province, China, 1976 May 26 earthquake, crustal deform. time characts. from tilt recording 78−40511
Zagros collision orogeny, finite element modelling of deformation 79−20803
Zagros Mountains, geological comparison with island arcs 79−2231
Zagros Mountains, Iran, seismicity depth 79−34751
Zambia, crustal struct. and tectonics from gravity survey 77−40969
Zambia, heat flow and prod., evidence for lithospheric thinning 77−86840
Zendan Fault region, Iran, struct. lineaments, interpretation of Landsat 1 obs. 80−104941

Earth crust continued
- Zhamanshin impact structure, USSR, impact glass chemically similar to tektites 80—51358
- zone regining below lithospheric plates, steady state astheriosphere model 79—88326
- CO_2 gas seep from seabed, Norton Sound, Alaska 80—67361
- CO_2, isentropic decompression from crustal and mantle press., thermodynamics 79—79769
- CO_2 production associated with tectonic processes 80—94470
- He survey in S.India for structural mapping, water sample obs. 80—8261
- ^{92,94}Nb production by cosmic-ray muons 77—49045
- O isotope study of lower crust xenoliths 80—89992
- ^{206}Pb/^{204}Pb evolution during crust development, rel. to U, Th and Pb fractionation 79—57879
- Rn flow, simple model rel. to soil Rn conc. temporal and spatial var. 80—33671

Earth electricity *see terrestrial electricity*

earth electrodes
- electrosurgical passive grounded electrode/patient equivalent circuit analysis 77—78025
- tree root potential meas. electrode earthing method *(Russian)* 80—26420

Earth heat *see terrestrial heat*

Earth interior
- *see also Earth core; Earth crust; Earth mantle; tectonics; volcanology*
- acoustic Gruneisen parameter for high-temps. 79—39691
- anelasticity, physical dispersion in surface wave and free oscill. problems 77—64231
- attenuation models 78—61367
- chemical evolution, mantle and crustal reservoirs mean age 80—51359
- chemical reactions in undifferentiated Earth, thermal effects 79—25218
- composition and Earth mean density, comparison with Venus 77—29680
- composition and Earth origin models 77—25663
- conductivity, piecewise homogeneous ground models for sky-wave mixed-path loss and antenna elevation patterns 79—66774
- connection, models having multiplicity of large horizontal scales 79—16430
- continental crust and root zones, thickness and thermal history 79—88320
- convective models and radiogenic heat production constraints 80—90006
- convective stability, with radioactive heat sources 77—9381
- cooling rate of Earth, reappraisal 80—76943
- core fluid motion, thermal and mag. instabilities 80—81850
- core-mantle coupling rel. to Earth rot. due to zonal tides 80—104850
- crystalline layers, elastic consts. rel. to surface waves propag. 80—76924
- daily rotation variations, correl. with secular geomag. field vars. 78—73302
- deep magnetic-variation sounding, geoelectric and geothermal interpretation of results 78—44765
- degassing and thermal history, simple calcs. 80—98282
- density discontinuities, effect on asymptotic overtone struct. of Earth torsional eigenfreqs. 77—78111
- density distribution, determ. from gravity logging data *(Russian)* 78—92999
- density model, based on gravimetric data *(Russian)* 80—31009
- density structure, resolving power of seismic data simultaneous inversion 79—16699
- density structure determ. by max. entropy spectral anal. method 77—64465
- differentiation processes of interior, trace elements as probes, review 80—98584
- discontinuities, evidence from asymptotic overtone struct. of Earth torsional normal modes eigenfreqs. 77—78110
- dynamic shear modulus corrections for Love numbers 78—85513
- dynamo action in conducting sphere and Backus' condition 78—28195
- early evolution and thermal history 77—44950
- early evolution model, thermal history 77—86845
- education, Earth's interior and const. gravity models 77—45645
- elastic characteristics of rocks at high-press. and temp. *(Russian)* 80—76933
- elastic prestress in Earth interior, effects 78—77202
- elastic relaxation coefficients for spherical cavity in prestressed medium of arbitrary orientation 77—73692
- elastic wave propagation in anomalous layers, variational approach 79—44260
- elastic wave velocity at high-press., using Debye theory of sp. ht. 80—89979
- elasticity imperfection 79—8613
- elasticity inverse problem, soln. using amplitude and natural freq. data 77—2119
- electrical transients, from two horizontal thin conducting strata *(Russian)* 78—40485
- ellipsoidally anisotropic media, seismic waves refl. and transmission coeffs. 79—84136
- EM induction one-dimensional problem, model refinement 79—44096
- EM sounding, iterative ray tracing between boreholes for underground image reconstruction 80—98466
- energy balance 77—81851
- equation of state (thermal), calc. method 80—90029
- equations of state, theoretical, comparison using high-compression exptl. data 79—20779
- evolution of Earth's interior, heat generation and heat-mass transfer 80—90040
- evolution of interior structure 77—53444
- evolution of internal struct., calc. 77—82137
- ferroelectric phases, high press. studies 78—69334
- fluid distrib. in partial melt, mech. and thermodynamic constraints 80—21685
- formation of core and mantle, simulation 80—90041
- free oscill. spectra, coupling and attenuation of near reson. multiplets 80—61778
- free oscillation of Earth, attenuation of radial modes 80—89966
- free oscillation of Earth, radial mode, damping by bulk attenuation 80—76928
- free oscillations in gross Earth models, effect of attenuation 77—53005
- gas-mineral equilibria and Earth interior chemical model 77—9411
- general equation of state of matter 78—43095
- geodynamic, hydromagnetic convection, thermally driven, in rapidly rotating sphere 80—14548

Earth interior continued
- geoelectric deep sounding, appl. of elec. potentials and their derivatives *(German)* 80—56626
- geoelectric section model, elec. conductivity profile 78—44768
- geomagnetic dynamo, MHD convection in rapidly rot. fluid layer, stability 79—50808
- geomagnetic dynamo action in rotating shell 80—81807
- global problems of fluid dynamics 78—96173
- gravitational instability and continental struct. development, synthesis 78—48995
- Gruneisen function evaluated in harmonic approx. 80—72474
- Gruneisen parameter, derivation from seismic data 79—96753
- Gruneisen parameter, influence of press.-induced phase transitions 79—1497
- Gruneisen parameter of lower mantle, evidence for approximation $\gamma\rho$=-const. 80—3970
- heat generation, rel. to European territory heat flow date 79—96751
- Hildebrand equation of state, appl. to minerals of Earth interior 80—56464
- induced polarisation parameters, freq. depend. *(Russian)* 79—74836
- inertia and gravity in deep interior, effects of convection 80—98269
- Kenya Rift, induced currents mapping rel. to elec. cond. 77—73628
- layered transition zone between mantle and core seismic waves long distances propag. *(Italian)* 79—12071
- lithosphere flow and rupture, analogy with creep rupture in cold ice sheet 79—2306
- lithosphere slab subduction under Tohoku district, Japan, rel. to crustal movements (1900-1975) 80—56453
- Love number k, determ. from time-service obs., tides and nutation effects 79—96733
- Love waves, in stratified magnetoelastic solid with material boundary 78—32015
- magma, solubility and saturation of apatite, laboratory expts. 80—72504
- magnetic anomaly of circular lamina, derivation 79—88247
- magnetic field as probe of interior structure 80—36528
- magnetic secular variation, modelled on mantle elec. cond. inhomogeneity *(German)* 80—81806
- magneto-telluric surface impedance, calcs. by layered Earth model 80—56349
- magnetothermoelastic plane Lamb's problem in initially stressed conducting medium 78—67077
- mantle, seismic vel. variations, origins 80—81854
- mantle convection driven by radioactive energy, model for decaying source 80—72461
- mantle solidus curve beneath mid-ocean ridge, double partial melt zone 80—104940
- mantle viscosity, derived in convective plate tectonic model 80—85634
- mass distributions, modelling by gravimagnetic fields 79—96750
- material properties by dynamic compression expts. 80—98315
- melting of metals, pressure depend. 78—85517
- methane, outgassing rel. to geological phenomena and pot. fuel supplies 78—92809
- Mie-Gruneisen eqn. of state, generalisation 78—96194
- Mie-Gruneisen equation of state, appl. to planetary interiors 78—29072
- mineral composition of rocks at great depths, prediction from longit. elastic wave vels. *(Russian)* 80—104956
- models, core form. effects 78—61368
- Moho reflection from suppression of long-decay long-delay multiple reflections by predictive deconvolution 79—84133
- Mohorovicic discontinuity depth, vars. determ. via Bouguer anomalies reduction *(Russian)* 78—48958
- Mohorovicic discontinuity relief, determ. methods *(Russian)* 78—48992
- non-homogeneous internal stratum between two elastic media, Love-type waves propag. 78—32016
- nonlinear α-effect dynamo eqns., numerical solns. 77—56576
- ocean EM induction affecting Sq during IGY 80—72428
- ohmic region effect on geomagnetic vars. *(German)* 79—29708
- olivine, dislocation recovery rate affected by high-press. 80—94515
- olivine, shock deform. expts., Hugoniot data implications 80—94497
- P- and S-waves of deep interior, max. vel. amplitudes 80—98262
- phase transformations of minerals and Earth's deep interior materials *(Japanese)* 78—28225
- phase transitions and matter differentiation in interior during formation 77—56610
- prebiological compounds, form. in Earth interior rel. to presence in volcanic bombs. 78—40667
- Q-factor, freq. depend. rel. to seismic pulse propag. 80—72438
- Q-factor, results from seismic studies 79—39682
- radial expansion of Earth, effect on palaeomagnetic data 80—56422
- radial overtone eigenfrequencies, prediction for specified Earth model 80—104889
- radioactive heat generation, variation with depth 79—84202
- radioactive heat generation in crust, model 80—85619
- rare earth geochemistry and mineralogy, book contrib. 80—46157
- resistivity finite-difference modelling, practical approach 79—29878
- rock melts, prediction of major element mineral/melt equilibria 80—109125
- rotational deformation 77—13069
- seismic body waves, attenuation mechanism using point defect increases *(Spanish)* 77—9376
- seismic body-wave inversion method for Earth struct., using travel time and amplitude data 80—109108
- seismic boundary delineation, with respect to reflecting areas preassigned parameters *(Russian)* 79—74857
- seismic refl. and refr. of magnetoviscoelastic waves at welded contact 80—89967
- seismic reflection coefficients, determ. from waves 79—44115
- seismic SH-waves propag. in stratified medium with local inhomogeneities, finite element treatment *(Russian)* 79—34763
- seismic shear waves, Q estimation from S-SS spectral ratios 77—64218
- seismic sounding, iterative ray tracing between boreholes for underground image reconstruction 80—98466
- seismic velocity changes in deep interior, press. and temp. induced phase transitions 80—90034
- seismic wave propagation and damping coeff. in electrically charged water-saturated rock 80—76921
- seismic wave radiation pattern 80—56404
- seismic wave reflectivity, information extraction via minimum entropy deconvolution 78—81423
- seismic wave travel-time problem, new approach 80—51339

Earth interior continued
seismic waves reflecting area, parameters estimation allowing for amplitude characts. correl. *(Russian)* 79—74856
shear velocity discontinuities, effect on asymptotic overtone struct. of Earth torsional eigenfreqs. 77—78111
shear wave velocity, resolving power of seismic data simultaneous inversion 79—16699
shear wave velocity structure for spherically averaged Earth 79—92504
stratum velocities determination using seismic data, iterative method convergence *(Russian)* 79—74982
stress/strain relation for anelasticity 80—26471
structure for seismic wave source antipodal region obs. 80—89972
structure rel. to geomag. secular var. 79—39647
structure vars. due to evolution 78—85512
thermoelastic deformations of half-space, strains and tilts, Green's functions 78—36092
tidal tilt obs. in N.Wales mine, strain-tilt coupling and Earth model 80—89926
tide in solid Earth, dynamic shear modulus influence 80—76901
tides in solid Earth, review *(Chinese)* 80—89925
upper mantle physical conditions, Walsh's model 80—90047
Vashchenko Zubarev formula for Gruneisen parameter, generalisation 80—90030
viscoelastic model, appl. to Earth tides theoretical study 80—67333
viscoelastic response to deglaciation, causing Earth rot. change 80—85576
$Ca_2Al_2SiO_7$, gehlenite, new high-press. phase, rel. to Earth interior 79—29753
CaO, eqn. of state at high press., appl. to core and mantle 80—109122
CaO, solid, phase transition at high-press., lower mantle implications 80—79876
FeO, eqn. of state at high press., appl. to core and mantle 80—109122

Earth lower mantle *see Earth mantle*

Earth magnetic field *see geomagnetism*

Earth magnetic field variations *see geomagnetic variations*

Earth mantle
absorption of longitudinal waves in upper mantle 80—46145
Adriatic subplate, averaged model 79—44159
Aegean region, crust and upper mantle struct. from deep seismic sounding 78—69308
Aegean region, geodynamics 78—69307
SW.Africa, asthenolith intrusion rel. to evolution of continental margin 77—21740
S.Africa, upper mantle heterogeneity from Pb and Sr isotopes in kimberlites 77—60372
central Alaska, N.Pacific plate tectonics rel. to earthquake focal mechanisms 79—79806
central Aleutians, double Benioff zone and lithosphere unbending 78—32047
Alpine orogeny, Europe, upper mantle horizontal inhomogeneities, P-wave obs. 80—98268
Alpine tectonite lherzolites, Sr isotope comp., evidence for mantle origin 78—65302
sub-Andean mantle, partial melting as source of Cerro Galan calc-alkaline volcanic rocks 80—98318
Andean Wadati-Benioff zone morphology, andesitic volcanism, Nazca plate tectonic features 78—32039
andesite magma and ignimbrite petrogenesis 79—44146
anelasticity, physical dispersion in surface wave and free oscill. problems 77—64231
anomalous regions from S times for deep-focus Indian earthquakes 78—77188
anorthite, thermal eqn. of state up to 120 GPa 80—109136
Antarctic Peninsula, enriched sub-continental mantle rel. to igneous rocks transverse geochemical vars. 80—56466
Apennines, Rayleigh wave phase vels. rel. to upper mantle struct. 78—53618
Apennines, Rayleigh wave study of crustal and upper mantle structure 80—46153
Archaean convection, effects on ocean chemistry and biological evolution 77—56653
Archaean mantle, chemical heterogeneity rel. to Earth comp. and mantle evolution 78—11844
Archaean mantle, siderophile and lithophile trace element evolution 80—46147
Arctic Ocean, sediment thicknesses and upper mantle temps. from magnetotelluric soundings 79—48454
Arctic regions, gravity from 60°N to North Pole, rel. to crust and mantle density struct. 79—48391
ascending andesitic magma, cooling model 78—65239
asthenosphere, convective stability with radioactive heat sources 77—9381
asthenosphere, elec. cond. and struct.-sensitive physical props. of partially melted rocks 79—12116
asthenosphere, electrical conductivity data and partial melt content 78—85518
asthenosphere, flow rel. to plate motions 78—96180
asthenosphere, frictionally heated shear flows stability 79—44164
asthenosphere, influence on Himalaya intracontinental subduction initiation 79—16431
asthenosphere, kinematic viscosity rel. to median valley of Mid-Atlantic Ridge 80—90071
asthenosphere, of E.European Platform, study by EM sounding 77—53021
asthenosphere, stresses and effective viscosities 78—65229
asthenosphere, thermal stability or instability of shear flow 78—20370
asthenosphere conductivity meas. by ocean floor magnetotelluric sounding under N. central Pacific 77—86772
asthenosphere readjustment during earthquake cycle, effects on free surface deform. 78—85490
asthenosphere thermal instability and tectonic plate motion 77—17073
asthenosphere thermal instability beneath moving plate 80—31007
asthenospheric counterflow, kinematic model 79—25220
N.Atlantic, chemistry and Pb, Nd, Sr isotopic correl. 80—90023
equatorial Atlantic (7 to 10°N), fracture zones lithospheric struct. *(Russian)* 80—104932
N.Atlantic basalt geochemistry rel. to mantle heterogeneity 79—29745
Atlantic fracture zones in equator region, gravimetric model 80—72483
N.Atlantic region, gravity anomalies, regional elevation and deep struct. 79—16421

Earth mantle continued
Mid Atlantic Ridge, 22 to 30°N, magmatic process var. and upper mantle heterogeneity 79—88334
attenuation models 78—61367
attenuation of body waves, magnitude corrections 79—66642
central Australia, elec. conc. profile from geomag. induction meas. 80—72424
SE Australia, long-range seismic profile 77—44945
Australia, mantle convection and subcrustal stresses 80—72484
SE Australia, thrust faulting, crust and upper mantle struct. 77—44944
N.Australia, upper mantle P-waves vels. in long-range seismic profile 79—16419
Azores, evidence for mantle plume from Sr isotope geochemistry in Central North Atlantic 77—5179
back-arc convection and marginal basin formation 79—25219
Baikal and continental rift zones, deep struct. from seismic data 78—36130
Baikal region, USSR, geoelectrical model 80—56365
SW Baikal Rift, crust and upper mantle struct. according to seismic data 80—94503
Baikal rift zone, heat flow rel. to neotectonic activity 78—36135
Baikal rift zone, rifting mechanism and deep struct. 78—36131
Baikal rift zone, windows into Earth interior, geophysical exploration *(Russian)* 80—12364
Baltic shield and Barents Sea, crust and upper mantle struct., Rayleigh waves dispersion 78—77204
Baltic zone, upper mantle model from Novaya Zemlya underground explosion P-waves obs. 79—84115
Banda Sea (E.Indonesia), subducted lithosphere geometry from seismicity and fault plane solns. 78—81131
basalt magma sources during opening of N.Atlantic, Nd and Sr isotopic comp. 79—100821
basalt magnetic properties rel. to crust and upper mantle struct. and development 79—79816
basalts and mantle derived materials, K and Rb relations rel. to phlogopite source 77—5165
base lateral heterogeneity from PKP phases amplitudes 80—21675
Bay of Islands ophiolite complex, Newfoundland, seismic vel. struct 80—21688
Beijing, China, crust and upper mantle three dimens. P-wave vel. struct. *(Chinese)* 80—104894
Bermudas, upper mantle electrical conductivity 78—40482
Black Sea, mantle material intrusion age rel. to mag. anomalies nature *(Russian)* 78—85473
N.Britain, upper mantle struct. from Lithospheric Seismic Profile in Britain (LISPB) 78—73329
S.British Columbia, upper mantle struct. from Love and Rayleigh wave obs. 77—78131
bumpy core-mantle interface, effects on variable geomag. and gravit. pots. 79—79771
S California, upper mantle seismic velocity, regional variations 80—109111
Canada, P-wave residuals rel. to mantle inhomogeneity 77—91037
E Canada, struct. from PP waves travel time residuals 77—9354
Canadian palaeogeotherm, from ultramafic xenoliths in Elwin Bay kimberlite 77—91078
Carpathian regional lithosphere, geoelectric model from data along deep seismic sounding profile *(Russian)* 80—104934
Central American andesites, Sr isotope evidence for mantle petrogenesis 79—20833
chemical and thermal struct. of deep interior, obs. constraints 79—53323
chemical composition, analogous to components of hightly reduced enstatite chondrite meteorites 80—85624
chemical composition heterogeneity, beneath Iceland 80—21725
chemical evolution, implications from Sm-Nd isotopic investigations of Isua supracrustals 78—36129
chemical evolution, mantle and crustal reservoirs mean age 80—51359
chemical evolution, nature and timing of mantle's differentiation 80—90043
chemical evolution, Nd-Sr isotopic var. implications 79—66655
chemical evolution from Early Archaean rocks comp. 78—65222
chemical heterogeneity, evidence, conf., Nov. 1978, London 80—85623
chemical stratification 80—21687
China, crust and upper mantle struct. study by converted siesmic waves *(Chinese)* 79—12093
China, seismic surface wave study of crust and mantle 80—104916
circulation with partial shallow return flow rel. to oceanic plates 78—40520
Colombia deep earthquake, 1970, July 31, spatio-temporal history 77—86813
composition, derivation from comp. of lherzolites 80—76940
composition, rel. to ocean ridge basalts trace elements 78—65219
composition and Earth origin models 77—25663
composition from Pacific Ocean Basin basalts Sr isotope comp. 78—65218
conducting channel between India and Sri Lanka, effects on equatorial electrojet 79—25189
conductivity anomaly interacting with ionosphere current to form geomag. variation 80—30985
conductivity in deep regions, geomagnetic impulses 78—28200
conductivity rel. to geomagnetic secular variation impulse 80—98236
conference, Potsdam, Germany (Oct 1979) 80—86034
continental and oceanic basalts, $^{143}Nd/^{144}Nd$ ratio vars., rel. to magma sources and mantle struct. 77—21708
continental basement exploration by seismic reflection profiling 78—96172
continental crust and root zones, thickness and thermal history 79—88320
continental drift and large-scale polar wandering 79—79719
continental lithosphere, age and thickness rel. to P-wave travel time residuals 79—62439
continental lithospheric boundary layer, liability to sink into less dense asthenosphere 80—56447
continental mantle, heat flow var. with age, appl. to lithosphere thermal models discrimination 79—70764
continental upper mantle, P_n vel. anisotropy 77—49013
continental upper mantle anisotropy, evidence from explosion seismology 77—49014
convection, Benard problem with viscosity depend. on temp. and press. 78—69317

Earth mantle continued
  convection, countercurrent accompanying descending Pacific lithosphere beneath Japan *(Japanese)* 80—94514
  convection, depth extent from seismic energy release of deep and intermediate earthquakes 80—41404
  convection, influence of moving lithospheric plates 79—74880
  convection, nonNewtonian theory *(German)* 77—70631
  convection, numerical anal. 80—51371
  convection, parametrised model rel. to Earth thermal history 79—16429
  convection, rel. to crustal stress concentration and Tangshan earthquake seismogenic models 79—92507
  convection, rel. to inertia and gravity asymmetry 80—98269
  convection, scale rel. to plate motion 77—44963
  convection, seismic focal mechanisms and thermal boundary layer 77—17070
  convection, simple plate models 79—25221
  convection, solid-state, rel. to Earth thermal evolution 80—89988
  convection, surface deform. and gravity anomalies 77—44893
  convection, viscoplastic, with phase transitions and shearing processes 78—3738
  convection and stress field under Pacific plate, from geopot. harmonics 77—9393
  convection and thermal structure of plates 79—2197
  convection currents influenced by subduction zone heat balance 80—94510
  convection currents rel. to plate tectonics 77—29265
  convection depth 79—48432
  convection driven by radioactive energy, model for decaying source 80—72461
  convection in Canadian Shield, structure of Archean basin-craton complexes 78—61412
  convection in high Prandtl number fluid with strongly temp. depend. viscosity 77—3823
  convection in lower mantle, rel. to geoid 80—31023
  convection model, finite element method 80—67354
  convection model, plate tectonics mechanism 77—81860
  convection model entailing moving surface plates 80—85634
  convection models, laboratory expt. 77—9396
  convection pattern and stress system under African plate 77—81859
  convection pattern and subcrustal stress field under Asia, rel. to seismicity 78—57190
  convection processes rel. to plate tectonics 79—5464
  convection rates of viscous fluid, upper mantle and continental drift appl. *(Russian)* 80—1581
  convection rolls, stability anal. 80—76957
  convection shaping by tidal bulge, rel. to global tectonics 78—32048
  convection system, spin-symmetric, rel. to Phanerozoic plate tectonics 78—92812
  convective instability of many-layered models 79—25216
  convective instability of multilayered and nonhomogeneous models 79—62476
  convective instability of two layer models 77—78136
  convective instability of upper mantle, thermomechanical model 80—90063
  convective instability of upper mantle models 79—88323
  convective stability of upper mantle viscosity jump effect 77—70620
  cooling rate of Earth, reappraisal 80—76943
  Cordilleran granites, mantle origin 77—21710
  core cooling by subsolidus mantle convection 80—36278
  core interface friction effect on geomag. secular variation 80—98218
  core-mantle, interface, topographic coupling 78—44794
  core-mantle boundary, amplitudes of long period PcP 77—37143
  core-mantle boundary, layered transition zone rel. to seismic waves long distance propag. *(Italian)* 79—12071
  core-mantle boundary, magnetic contour map 80—104880
  core-mantle boundary, nature of transition 77—78137
  core-mantle boundary irregularities, effect on fluid speed and geomag. field 78—73333
  core-mantle boundary irregularities, effects on fluid vel. and mag. field 78—44792
  core-mantle boundary roughness, PKKP wave scatt. 80—56437
  core-mantle boundary thermal interaction rel. to geomagnetic field long term behaviour 77—52981
  core-mantle EM interaction when elec. cond. concentrated near core boundary 77—91001
  core-mantle interface, differentially heated cylindrical annulus model 78—28194
  core-mantle interface, irregularities rel. to correl. between gravit. and geomag. fields 77—2085
  creep in geodynamic processes 78—3744
  creep laws 78—69305
  creep rate, influence of natural radioactivity 79—92520
  Crimea, Moho surface relief rel. to crustal struct. *(Russian)* 79—8616
  crust hot spots, and sublithospheric upwelling distrib. 80—109126
  crust to mantle transition zone, seismic profile of Aleutian crustal section 77—33017
  Cuba upper mantle study, earthquakes exchange waves method appl. *(Russian)* 79—44158
  day length irregular variations, core-mantle coupling 77—64186
  Dead Sea Rift and adjoining areas, gravity rel. to upper mantle density distrib. 79—57893
  deep EM sounding and profiling 77—9326
  deep mantle convection and lithosphere basal shear stress, roles in plate tectonics 78—57188
  deep mantle geodynamics, rel. to vertical evolution of continental margins 77—21739
  deep seismic zone as upper mantle reflector of body waves 78—44790
  degassing and thermal history, simple calcs. 80—98282
  degassing by volcanism, rel. to oceanic Cl and Br origin 78—65342
  density, rigidity and incompressibility rel. to seismic vel., model 80—89990
  density anomalies of lower mantle, derived from geophys. data 80—89927
  density inhomogeneities of mantle 80—21676
  density inversion in upper mantle, rel. to seismic waveguides 79—12099
  density model, variational approach *(Russian)* 78—28191
  descending lithosphere thermal regime, effect of varying angle and rate of subduction 78—77206
  diamond with garnet inclusion originating in mantle 80—46172
  diamonds, rare gas isotopic compositions, rel. to atm. comp. 78—24270

Earth mantle continued
  differential stress in uppermost mantle, lateral var. across SW.Japan island arc 80—98275
  differentiation history revealed by mid-ocean ridge isotope abundances 80—36277
  differentiation occurring in episodes, Nd and Sr isotope evidence 80—67352
  discontinuities in upper mantle and P′P′ precursors 77—86806
  discrete islands formation in linear island chains due to discrete mantle plumes 78—44796
  dissipative core-mantle coupling in nutation theory 77—64188
  double partial melt zone beneath ocean ridge 80—104940
  double seismic zone in downgoing slabs and mesosphere viscosity 80—26472
  DSDP Leg 37, upper mantle melting rel. to U concs. in oceanic basalts 77—91075
  DSDP site 332, chemically distinct magma chambers rel. to basalts geochemical characts. 77—91126
  earthquakes, intermediate and deep focus, temporal var. of activity 80—3943
  earthquakes in mantle, spatial distrib. in Japan and Aleutian arcs 80—81820
  earthquakes near junction of Kurile and northern Honshu arcs, mechanism 77—81805
  Easter volcanic chain, S.E.Pacific, mantle hot line 77—70628
  electrical conductivity, distrib. rel. to core mag. field screening 79—12064
  electrical conductivity, interpretation from heat transport processes 80—3929
  electrical conductivity, rel. to geomag. field 60-year vars. 79—8596
  electrical conductivity anomalies 79—53303
  electrical conductivity model, effect of partial melting 80—76936
  electrical conductivity of lower mantle, theory of EM induction in rot. conductive Earth 78—44764
  electrical conductivity of lower mantle determ. from geomag. field dynamics 79—12066
  electrical conductivity of materials containing partial melt, simple model from Archie's law 79—100810
  electrical conductivity of upper mantle, interpretation of N.E.Japan Anomaly 77—78097
  enstatite-pyrope system, high press./temp. phase behaviour rel. to Earth mantle 78—11882
  equation of state, rel. to stresses due to phase changes in subduction zones 77—73718
  equation of state (thermal), calc. method 80—90029
  equation of state fit to lower mantle 78—85522
  equation of state of lower mantle 80—90032
  Eurasia, lateral var. in struct. of upper mantle 77—33016
  Eurasia, upper mantle anisotropy from polarisation of higher mode seismic surface waves 77—49015
  N.Europe, Benelux region, upper mantle struct. from seismic data 80—21691
  Central Europe, mantle heat flow and geotherms for major tectonic units 79—70767
  central Europe, upper mantle conductivity anomaly rel. to geomagnetism and secular var. *(German)* 78—7565
  W.Europe, upper mantle from Rayleigh mode dispersion 77—73693
  W.Europe, upper mantle P-wave vel., large scale variations 80—109112
  E. and central Europe, velocity-depth distribution in upper mantle 80—3980
  Europe and Eurasia, inferences from higher mode seismic data 80—72436
  European upper mantle struct. from Vranch earthquake seismic wave travel-time curves 80—89998
  evolution beneath mid-ocean ridges 77—44962
  evolution model, from oceanic basalts Pb isotope comp. data 78—65217
  Fennoscandia, subcrustal lithosphere seismic investigations 80—90009
  Fennoscandian Shield and Danish Embayment, crust and upper mantle geothermal models 77—49044
  ferroelectric phase transitions, significance for Earth and planetary interiors 77—53045
  ferroelectric-like phase transformation of pyroxene in mantle 78—61362
  ferrosilite, FeSiO$_3$, high pressure and temp. phases rel. to Earth's mantle 77—9403
  Fiji Plateau, underlying upper mantle struct. from second P-wave arrivals 77—60359
  finite deformation during fluid flow, theory 79—92519
  flood basalts from Siberian Platform, Nd isotopes and mantle sources 80—56435
  flow, one-dimensional modelling 79—39698
  flow and convection, inference from obs. of meteorite high-press. minerals 80—85909
  flow pressure rel. so subduction angle, non-Newtonian corner flows theory 79—39695
  flow two-dimensional beneath rigid accreting lithosphere 79—12102
  fluid circulation around null-flux curves at core-mantle boundary 79—79764
  fluid composition buffered by carbonates in peridotite-CO$_2$-H$_2$O 77—70644
  fluid phase, trace elements 79—34779
  Fogo seamounts, anomalous upper mantle struct. indicated by P-wave rel. delays 78—85515
  Foredobrogen area, USSR abyssal elec. cond. 80—90000
  formation, examination of various hypotheses 79—44149
  formation simulation for originally homogeneous planets 80—90041
  forsterite, glissile splitting of dislocations, cross-slip-controlled creep and mantle rheology 78—61406
  France, heat flow rel. to deep struct. and mantle convection 80—98291
  free oscillations attenuation in viscoelastic Earth, theoretical contrib. 80—21652
  G-type seismic waves generation 79—66624
  Galapagos hotspot, spreading centre jumps and subaxial asthenosphere flow 77—33042
  Galapagos Rift, mantle He in hydrothermal plumes 77—64259
  garnet lherzolite, in upper mantle, melting from expts. on fluorites and fluoroberyllates 77—51475
  geochemical model of mantle differentiation and crustal growth 80—21684
  geomagnetic secular variations, constraints on elec. cond. 80—61754
  geothermal gradient at 1000 km depth 80—8260
  global Earth tides and upper mantle struct. 79—25182

Earth mantle continued
global geodynamics, Canadian contribs., 1971-79 period. 80—8262
global gravity anomalies and two-scale mantle convection 77—17067
global tectonics rel. to mantle flow pattern 78—88810
Gondwanaland, Rb-Sr mantle isochrons and lithosphere chemistry vars. 78—28201
Gorringe Bank, oceanic mantle and crust, geological survey 78—53632
gravity anomalies source depths 77—44892
Great Basin of Nevada and W Utah, struct. from seismic surface waves 78—73336
Greater Antilles, mantle melting as source of the Late Cretaceous granodiorites 79—57927
W.Greenland Cretaceous-Tertiary volcanic region, magma traps theory appl. 79—70776
greenstone belts, Archaean, mantle diapirs and melting rel. to komatiite generation 79—70762
Gregory Rift Valley, Kenya, upper mantle elec. cond. 77—91000
Gruneisen parameter, generalisation of Vashchenko-Zubarev formula 80—90030
Gruneisen parameter, melting curve and adiabatic gradient 80—90028
Gruneisen parameter and eqn. of state determ. at press. induced phase transition 80—90031
Gruneisen parameter is upper mantle, influence of press.-induced phase transitions 79—1497
guide channels for seismic energy, transverse waves in upper mantle *(Italian)* 78—61355
H-polarisation induction over ocean edge coupled to mantle by conducting crust 77—48994
Hawaii Island, mag. induction fields rel. to oceanic mantle elec. cond. struct. 78—40477
Hawaiian hot spot, Neogene motion rel. to Pacific plate and Earth spin axis 79—44167
Hawaiian Ridge, vel. struct. from earthquake travel times, Tau Inversion method 79—62467
heat flow, map 77—37161
heat flow from old platform mantle 80—89996
heat transfer, consequences of gravitationally powered geomag. dynamo 79—39687
Hellenic Arc, mantle plume model deduced from geophysical data 77—21734
heterogeneity and mislocation patterns for seismic networks 77—81843
high Prandtl number convection, geophs. appl. 79—81875
high-pressure phase transformations of fluorite-type dioxides 80—101363
Himalaya and Tibet Plateau region, tectonic history 80—72486
Honshu, Japan, deep seismic zone and upper mantle struct. 80—8269
horizontal inhomogeneities influence on tidal oscill. amplitudes 78—57159
hotspots, correl. with positive geoid height anomalies 80—90056
NE.Iceland, elec. resist. model from magnetotelluric obs., correl. with temp. 80—89954
Iceland, magnetotelluric investigation of lower crust and upper mantle 79—66612
Iceland, seismic structure along RRISP-Profile I 80—90018
Iceland and Reykjanes Ridge, mantle heterogeneity rel. to basalts F contents 79—57900
Iceland Plateau, deep crust and mantle struct. from surface waves dispersion 80—41413
Iceland plume, rel. to sea floor morphology and mag. anomalies N of Iceland 80—89953
India, upper mantle struct. lateral vars. from Gauribidanur seismic array data 77—49016
Indian deep-focus earthquakes, P-wave travel times 79—2193
Indian geopotential anomaly, seismic and gravity data anal. 80—90037
NW Indian Ocean, crust and upper mantle density section construction *(Russian)* 79—48431
W.Indian Ocean, mantle uplifted block 79—25228
Indo-Gangetic Plains, shield-like upper mantle vel. struct. 77—29257
induced electrical currents below ocean bottom with vertical water flow 80—104863
interaction with core, effect on rotation 79—66601
intraplate volcanism, magma flow through lithospheric fractures, tensional tectonics 78—65242
island arcs, sources as indicated by Nd and Sr isotopic studies of lavas 78—32044
isostatic and dynamic processes rel. to viscosity 77—21745
isostatic compensation and viscosity differences between crust and asthenosphere 80—104947
isostatic rebound and power-law flow in asthenosphere 77—78133
isotopic composition, advection effects 79—66656
isotopic equilibrium, regional and local, in mantle, from volcanic rocks comp. 78—65216
N.E.Japan, upper mantle regionality from explosion seismic obs. 77—37167
NE.Japan Arc, double-planed deep seismic zone and upper mantle structure 78—77198
Japan trench, microearthquake activity in oceanic lithosphere off Sanriku 77—81803
Japan-Bonin trench, crustal and upper mantle changes 80—72466
Japan-Kurile Arc, upper mantle P-wave vel. model 77—78132
Japanese Arc, multiple ScS waves attenuation rel. to mantle anelastic props. 79—92508
jointed blocks of peridotite xenoliths in basalts and mantle dynamics 80—61796
Jordan-Dead Sea Rift, crust and upper mantle struct. from seismic refr. data 80—26474
Juan de Fuca hot spot, basalts comps. and mag. anomalies 77—29242
K-rich ultramafic magmas from peridotitic mantle source 79—2200
kaersutite, sound vels. and anisotropy, rel. to upper mantle seismic struct. 80—26501
Kamchatka active zone, Q-factor of upper mantle 77—44929
Kangzhuang-Dachang region near Peking, deep struct. and earthquake foci *(Chinese)* 80—56415
Kenya rift valley, geophysics 77—86825
Kilauea volcano, Hawaii, three-dim. crust and mantle struct. 78—28205
kimberlite nodules, upper mantle petrology and geotherms 78—65310
kimberlite volcanism, nature of mantle rock specimens 79—2205
kinematic models of large-scale flow 79—70777
Kuril Trench area, evidence for high vel. zone from ocean bottom seismometer obs. 78—48999
large-scale heterogeneities from P wave travel times 77—33022

Earth mantle continued
Lassen Park volcanic gases, mantle He component from He isotopic ratios 79—16425
lateral density anomalies in upper mantle 77—29261
lateral heterogeneity of upper mantle, determ. from travel times of multiple ScS 77—29259
lateral variations from LF eigenspectra data 78—36123
lateral variations in lower mantle, seismic array evidence 79—20781
Lehmann discontinuity, mantle props. beneath continents 80—56425
Ligurian Sea area, crustal and upper mantle structure 78—65209
LIL-element enrichment rel. to ^{143}Nd/^{144}Nd and ^{87}Sr/^{86}Sr ratios in Azore basalts 79—74873
lithosphere, compression and extension rel. to gravity nontidal vars., appl. to Hungarian depression *(Russian)* 79—8621
lithosphere, heterogeneities rel. to P-wave time and amplitude anomalies interpretation 78—96153
lithosphere anisotropic layering, effects on seismic waves propag., review 77—49012
lithosphere bending at trench, elastic-perfectly plastic anal. 78—81135
lithosphere slab, penetration into lower mantle beneath Sea of Okhotsk 77—73700
lithosphere structure from seismic refr., influence of lateral vars. 77—21686
lithosphere subduction beneath active margins, implications of earthquake foci three-dimensional projection 80—72453
lithosphere-asthenosphere boundary beneath S.America from converted phase wave obs. 77—64226
lithosphere-mantle decoupling, role of shear heating 79—20790
lithospheric formation, thermal boundary layer 77—73696
lithospheric split in descending plate, obs. from N Apennines 80—85639
long-period reflected and converted upper mantle phases 78—92786
low velocity zone, interpretation in terms of thermally activated point defects 78—88806
low viscosity zone, sublithospheric, rel. to convection models having multiplicity of large horizontal scales 79—16430
low-vel. zone inversion, Weichert-Herglotz integral 80—21829
low-velocity zone, parameters determ. as functions of focal depth 77—86828
low-velocity zone, seismic data simultaneous inversion 79—16699
low-velocity zone, stability from melt/solid segregation theory 79—40144
lower, convection, composition and thermal state 80—21678
lower, elec. cond., comments and reply 80—30988
lower, implications of fluorite isotype of SnO_2 and new modification of TiO_2 78—61371
lower, thermodynamically based eqn. of state 80—26473
lower mantle, MgO elastic consts. and internal friction 77—78165
lower mantle composition, implications of polycrystalline stishovite elasticity meas. 77—5189
lower mantle convection, inferred from low Q zone 80—76944
lower mantle Gruneisen parameter, evidence for approximation $\gamma\rho$=const. 80—3970
lower mantle inhomogeneities characts. from scatt. waves, correction 77—49042
lower mantle minerals, evaluation of finite strain eqns. of state using lattice models 80—96620
lower mantle shear-wave velocity, by diffr. SH wave data 80—56380
magma, lava lakes of Kilauea, Hawaii 80—26483
magma generation, evidence from ophiolite suites, oceanic lithosphere generation appl. 78—65311
magma genesis conditions, H_2O and CO_2 solubility, petrological implications 78—11886
magma migration beneath ocean ridge mantle convection 80—12366
magmas in upper mantle, high press. expts. 77—29291
magmas of upper mantle, struct., density and viscosity, expts. on $NaAlSi_2O_6$ 77—29290
magnetic secular variation, modelled on mantle elec. cond. inhomogeneity *(German)* 80—81806
magnetotelluric fields modelling above heterogeneities in conducting base 77—52979
magnetotelluric method for investigation of media with monotonically changing cond. 77—78439
Magnitskiy-Birch additivity hypothesis, shock adiabat testing 77—9379
marine refraction seismology, interpretation techniques 77—64230
Massif central, France, upper mantle struct. and dynamics from basalt xenoliths obs. *(French)* 79—48424
Massif Central, upper mantle regional struct. and geodynamics 78—81120
material properties by dynamic compression expts. 80—98315
Matushiro fault zone, Japan, He spots caused by diapiric magma from upper mantle 79—8618
E.Mediterranean, deep struct. and tectonics 78—69309
W.Mediterranean Basin, upper mantle structure from seismic profile 78—11841
melt production in mantle, by viscous dissipation 80—72463
melting, past and present, isotope and trace element evidence 78—65238
melting point estimation using Uffen method, remarks 78—20367
metal oxide-SiO_2 systems, phase diagrams calc. from high press. phases stability study 79—90779
metasomatically veined mantle, heterogeneities from nodules and alkali basalts Nd, Sr geochemistry 80—56420
meteorite craters geomechanics, lithosphere-asthenosphere evolution model 80—17265
Michigan Basin, thermal and mechanical evolution, lithosphere elastic flexure 77—21719
micropolar fluid with stretch, convection, appl. to asthenosphere 78—51202
Mid-Atlantic Ridge, crust and upper mantle struct. at 45°N 78—73332
Mid-Atlantic Ridge basalts, geochem. variation along length of ridge 80—90027
Mid-Atlantic Ridge N of Azores, upper mantle struct. from compressional waves obs. 77—73691
mid-ocean ridge basalt, mantle origin, composition restrictions 80—90025
mid-ocean ridge basalt (MORB) sources, heterogeneous sources mixing rel. to Nd and Sr isotopic comps. 80—94520
mid-ocean ridges, serpentinite protrusions from upper mantle 77—5149
Middle America Trench offshore Guatemala, seismic refr. and refl. meas. 80—26493
midocean ridge basalts, source evolution from Bay of Islands ophiolite complex Nd and Sr isotopic study 80—85651
mineral phases, bulk modulus-volume relationship, for cation-anion polyhedra 80—41434

Earth mantle continued

- mineralogy, interionic repulsive force and ion compressibility theory 77—11500
- mineralogy and chemistry above 1000 km 77—33015
- mineralogy of upper mantle, implications of monticellite ($CaMgSiO_4$) high-press. phase transforms 80—17255
- minerals, thermodynamic functions from eqns. of state for end members 80—90084
- mixed oxide and perovskite structure model 78—85507
- models of upper mantle structure *(Russian)* 77—73697
- models with single crust-mantle discontinuities, ray-mode duality for SH waves 78—77183
- Moho, dip and strike determ. from array anal. 79—66821
- Moho, magnetic boundary 79—96748
- Moho, seismic detect. by time fields method *(Russian)* 79—35010
- Moho depth, determs. from spectral-ratio anal. of NORSAR long-period P-waves 77—86814
- Moho dip beneath Scotland, by PS reflections 80—41409
- Moho P-wave velocity depth, regional distrib. from Rumania earthquake (1977 March 4) *(German)* 80—98256
- Mohorovicic discontinuity relief, determ. methods *(Russian)* 78—48992
- Mohorovicic relict discontinuities, correl. with tectonic cycle recurrence *(Russian)* 77—44947
- Molodensky model of mantle/core rel. to Chandler wobble period *(Russian)* 79—92475
- Moon origin from Earth mantle, geosynchronous phase, consequences for Moon 80—101537
- Mount Rainier, Washington, underlying struct. from teleseismic body waves 80—31011
- New Hebrides, hydrous mantle melting rel. to geochemistry of Quaternary volcanism 78—20375
- New Hebrides island arc, earthquakes precise relocation rel. to seismotectonics 79—16404
- New Hebrides island arc, upper mantle struct. in arc convex side 79—74861
- Newfoundland, Bay of Islands ophiolite complex, upper mantle exposure 78—40506
- noble gases, abundances and isotopic compositions 78—85521
- nonlinear stress propagation in Earth upper mantle 79—16422
- nonNewtonian antiplane flow, appl. to tectonic plate deform. 77—73704
- normal mode attenuation, Q mode of mantle 78—61343
- W North America, low-Q and low-vel. zones from surface wave vel. and attenuation inversion 78—85491
- North America, S and P station anomalies 80—94460
- North Sea region upper mantle struct. from Rayleigh wave dispersion 78—36122
- Novaya Zemlya crust and upper mantle model from Rayleigh wave dispersion data 79—84187
- ocean basins upper mantle, isotropic inversion of anisotropic surface-wave dispersion 78—96156
- ocean ridge thermal evolution, affected by spreading rate 80—56424
- oceanic lithosphere mechanical behaviour, implications of two earthquakes seaward of Tonga Trench 79—16405
- oceanic mantle, discovery beneath S.Rio Grande Rift 79—29724
- oceanic mantle, evidence for enriched mantle sources from Nd isotopic study of Kerguelen Islands igneous rocks 80—98319
- oceanic Sa seismic waves, appl. to mantle struct. determ. 77—73670
- oceanic upper mantle, comp. from petrology of ultramafics from Owen fracture zone, NW Indian Ocean 80—94519
- oceanic upper mantle, seismic anisotropy of ophiolite peridotite 78—53645
- oceanic upper mantle intrinsic heterogeneity effect on Rayleigh wave phase vels. 77—49022
- oceanic upper mantle seismic anisotropy, evidence from ophiolite complex 80—21677
- olivine, creep mechanisms 78—69332
- olivine, naturally deformed, recovery process, rel. to Earth upper mantle mech. state 78—96202
- olivine, shock deform. expts., Hugoniot data implications 80—94497
- olivine and ultrabasic rocks, diffusion and diffusion creep, rel. to upper mantle deform. 77—9409
- olivine to spinel transition kinetics, rel. to deep focus earthquake genesis 77—5190
- olivine-rich rocks, activation vol. for creep, rel. to upper mantle 79—44184
- Oregon, structure from teleseismic P- and S-waves received at Corvallis 77—91067
- oxides (FeO and CaO), eqn. of state at high press. 80—109122
- P_n vel. in USA, indicator of upper mantle anelastic quality factor 77—13064
- P_n velocity anisotropy studies in Britain and USA 79—53314
- P_n velocity rel. to partial melting in upper mantle 78—3729
- $P'P'$ precursors, origin in mantle seismic scatt. 77—37144
- P to SV converted waves, detect. rel. to mantle boundaries 77—81810
- P- and S-waves diffracted around core, rel. to mantle base vel. struct. 79—53313
- P-signal complexity from nuclear explosions and upper mantle struct. 77—56596
- P-wave amplitude anomalies, interpretation 80—56386
- P-wave model catalogue for upper mantle 77—17028
- P-wave refraction, hydrophone recordings of underground nuclear explosions 80—98257
- P-wave travel time anomalies rel. to epicentral distance to African stations 80—98237
- P-wave vel. struct to depth of 150 km, Kanto District, Japan *(Japanese)* 80—94475
- P-wave velocities, in uppermost mantle beneath Turkey and Iran 80—72462
- P-wave velocities in upper mantle, model for E. and S.Africa 79—44135
- P-wave velocity anisotropy, inversion 77—49017
- P-waves, evidence of vel. increase at about 770 km depth 77—2118
- P-waves, short-period, anisotropic scatt. in upper mantle 79—16377
- P-waves, short-period, attenuation in USA from P-wave spectra of SALMON nuclear explosion 77—25650
- P-waves, short-period, regional amplitude anomalies rel. to anelastic rel. to anelastic attenuation, North America 78—44777
- P-waves, travel times in Europe and W.Russia 77—33001
- P-waves in lower mantle, amplitudes and magnitude corrections for deep focus earthquakes 77—86797
- P-waves in upper mantle, vels. in Japan using time-term method 77—37145

Earth mantle continued

- W.Pacific, HF P_n and S_n phases obs. at great distances, spectral anal. 78—77195
- NW Pacific, HF P_n waveguide 77—91057
- W.Pacific, high shear vel. layer 78—3734
- W.Pacific, multiple ScS travel time implications on mantle heterogeneity 80—72443
- NW Pacific, upper mantle struct. and deep processes 77—37160
- Pacific, W. edge, new $dt/d\Delta$ profile for lower mantle 77—9380
- NE.Pacific asthenosphere, magnetotelluric sounding obs. 80—46123
- Pacific Basin, shear waves polarisation anisotropy 77—49018
- Pacific Ocean, deep EM sounding near Californian coast, interpretation 77—9383
- E.Pacific Rise, synthetic seismic profile 79—12095
- Pacific upper mantle, compressional wave anisotropy 77—17040
- Pacific upper mantle regionalized shear vel. models from Love and Rayleigh wave dispersion 79—53321
- palaeoanisotropy in upper mantle 78—7602
- palaeomagnetic field, time-averaged, anomalies rel. to lower mantle 78—11808
- Pamir-Hindu Kush, upper mantle high-Q zone from earthquakes spectral content 77—86795
- Pamir-Hindu Kush region, seismicity and fault plane solns. 80—72445
- Pamirs-Hindu-Kush region, mantle intermediate seismic zone 77—53011
- Pamirs-Hindu-Kush upper mantle, vel. inhomogeneity, mapping by graphical method 80—77146
- Papua New Guinea, delayed partial melting of subduction-modified mantle 78—57183
- partial meltin in upper mantle rel. to mineral comp. in Josephine Peridotite 77—81880
- partial melting, Ni distrib. and partitioning between forsterite and aluminous silicate melts, pressure depend. 79—44176
- partial melting and mineral-stability boundaries, rel. to seismic exploration of lithosphere, Canada 78—36121
- partial melting under oceanic spreading ridges 78—65237
- partial melts liquid distrib., effect of gravity field 80—81851
- peridotite, high-temp. anelasticity and elasticity 80—17256
- peridotite, petrogenetic grid and conditions for magma generation 77—5137
- peridotite equilibration conditions in upper mantle, exptl. determ. of geochemical parameters 77—2130
- peridotite-CO_2-H_2O and carbonatitic liquids in upper asthenosphere 77—29294
- peridotites, origin of olivine subgrain boundaries 78—85544
- Peru-Chile Trench basalts, fractionation and mantle heterogeneity 78—53626
- phase boundary distortion causing gravity anomalies 77—52963
- phase boundary equilib. position under horizontally varying surface loads 77—53017
- phase boundary motion caused by surface temp. and press. excitations, rel. to vertical crustal movements 77—49040
- phase boundary under surface loads, dynamics 78—85509
- phase separation surfaces shapes, material parameters effects 80—90036
- PKP precursor data comparison from seismic arrays 79—25208
- planetary-type rare gases in an upper mantle derived amphibole 78—96167
- plate tectonic driving forces, heat flow and tidal drag 78—32050
- plate tectonic explanation of Earth struct. 80—81855
- plumacy problems, graphic solns. 77—91081
- plumes, crustal radial stress fields rel. to Hawaiian rifts and recent Icelandic volcanism 80—90051
- plumes, fluid-dynamic model of ascending flow 80—12370
- point pulse source in elastic anisotropic half-space, propag. of vibrs. 78—57174
- Point Sal ophiolite, California, rare earth and trace element geochemistry rel. to mantle melts fractionation 78—32092
- Poland, heat flow map and Europe geothermal field *(Polish)* 77—21707
- polymorphic phase boundaries effects on mantle vertical and horizontal motions 77—9395
- porous flow model for magma migration in asthenosphere 78—40522
- postseismic surface deformations due to lithospheric and asthenospheric viscoelasticity 79—57884
- postseismic viscoelastic surface deform. and stress, theory 80—94496
- pressure solution creep in mantle evidenced by peridotite compositional layering 80—56471
- pressure vars. and forced lithospheric oscills. *(Russian)* 79—29735
- primitive mantle structure, Pb isotope study of layered intrusions 80—81847
- PS-waves refl. from Moho 77—86809
- Pyrenean mountains, explosion seismic sounding of continental Moho throws and dips 80—85620
- pyrope garnet-ilmenite transition 77—49063
- pyroxene-garnet solid-soln. equilibria in $Mg_4Si_4O_{12}$-$Mg_3Al_2Si_3O_{12}$ and $Fe_4Si_4O_{12}$-$Fe_3Al_2Si_3O_{12}$ systems 77—81895
- Q_{ScS} frequency dependence 80—56381
- Q frequency depend. in Earth rel. to mantle rheology and Chandler wobble 79—84190
- Q-factor of lower mantle, body wave results 79—39682
- radiative transfer of lower mantle, spectral obs. of shock compressed MgO-Fe^{2+} 80—90039
- radioactivity, rel. to geosynclinal processes energy sources *(Russian)* 78—96182
- radiogenic heating in convecting mantle, rel. to oceanic bathymetry flattening 80—85642
- rare earth elements, partitioning between hydrous silicate melt, amphibole and garnet peridotite 79—20775
- Rayleigh wave attenuation and group vel., regionalisation and pure path models 79—12091
- Rayleigh wave dispersion along Reykjanes Ridge rel. to lithosphere age 79—88267
- Rayleigh waves, great circle attenuation and group vel. for 150-600 s periods 77—49030
- Rayleigh waves, group vel. distribs. and upper mantle models, Pacific Ocean *(Japanese)* 79—70747
- Rayleigh waves, phase velocity and Q 79—74846
- Rayleigh waves, regional differences in phase velocity and Q-factor 79—16413
- Rayleigh waves higher modes to determine upper mantle struct. 80—104890
- Rayleigh waves under Pacific Ocean, group vels. and response 80—41398

Earth mantle continued
Recent andesites in Ecuador and N.Chile, Sr isotope data rel. to mantle origin 78—32042
regional studies, nonlinear interference anal. of seismic data 79—25217
relativistic spin-spin interaction theory for two concentric shells 80—46148
return flow and non-linear rheology 80—46152
Reykjanes Ridge, lithosphere lower boundary temp. from heat flow obs. 80—90011
Reykjanes Ridge, Profile I on SE. flank, seismic struct., RRISP 80—90019
Reykjanes Ridge and Iceland volcanism, Cl and Br rel. to degassing and mantle sources 78—36136
Reykjanes Ridge Iceland Seismic Experiment (RRISP 77), for mantle struct. 80—90017
Reykjanes Ridge Iceland Seismic Project 1977, first results 79—57889
rheological behaviour from creep eqns. of olivine, steady state flow 80—104924
rheology of upper mantle, micromechanisms of flow and fracture 78—69331
rheology rel. to absolute plate motions and intraplate stress 77—33046
Rhinegraben area, gravity anomalies and geothermal implications 80—104852
Rhinegraben area, heat and matter transfer in upper mentle 80—104927
rocks, partially melted, rheology, critical phenomena 78—32080
rocks, seismic anisotropy meas. under high-press., high-type conditions 77—49059
rocks physical props. under mantle conditions, conf., Durham, England (Aug. 77) 78—69333
roll cell convection under Pacific plate, evidence from bathymetry and heat flow 78—73345
Rumania, upper mantle processes rel. to gecthermal regimes of tectonic units 79—70768
S-wave velocity, lateral var. in upper mantle, Rayleigh mode data 79—66643
S-wave velocity model, based on great circle Rayleigh waves 80—109107
Scotland, electrical model of crust and upper mantle 80—98234
ScS multiple waves, attenuation operator 77—52995
sedimentary basins development, lithosphere stretching and asthenosphere upwelling 79—29719
seismic anisotropy in upper mantle, investigations in USSR 77—49038
seismic anisotropy in upper mantle, review 77—49011
seismic anisotropy of crust and upper mantle, deep seismic sounding 77—70855
seismic anisotropy of subcrustal lithosphere rel. to dynamical processes in upper mantle 77—49039
seismic body waves in upper mantle, parameters in Crimea-Vrancha-Bohemia geological traverse *(Russian)* 79—53316
seismic compressional and shear vels. in lower mantle, radial var. 78—73316
seismic discontinuities, rel. to garnet lherzolite high-press. phase equilibria 79—66687
seismic discontinuity at 650 km depth 79—44143
seismic precursors to PKKP, rel. to core-mantle boundary struct. 79—48409
seismic quality factor and effective viscosity relationship 80—12360
seismic S_n waves, propag. through Bering Sea and NW.Pacific Ocean 80—51346
seismic shear-wave attenuation, 0.05-25 Hz 80—36268
seismic shear-wave travel time for Earth struct. 80—81817
seismic vel. anomalies below Colorado Rocky Mountains 80—81853
seismic vel. variations, origins 80—81854
seismic velocity anomalies in mantle under N.Atlantic 77—49024
seismic velocity discontinuities, evidence of multiplicity in P-waves travel time curves 77—81809
seismic velocity of lower mantle, meas. using wide aperture array 80—105071
seismic velocity radial anomalies in lower mantle, identification using interference method 79—25209
seismic velocity structure below Hawaii island from local earthquake data 79—84195
seismic wave field assoc. with fine structured Moho in continents and oceans 80—12361
seismic wave reflection at wide angles, travel times 78—65202
seismic wave scattering by rough core-mantle boundary 78—61345
seismic wave vel. variation, method for quantitative estimation 77—44932
seismic wave velocity variations, below E.Australia and SW.Pacific 80—36279
seismic waveform synthesis, generalized ray and reflectivity methods comparison 79—84501
seismic waves, upper mantle vels. on N.Cocos plate 79—57858
seismic waves, very long period, charact. of upper mantle *(French)* 77—78107
seismic waves absorption in partially melted medium 78—85488
SH waves for epicentral distances greater than 90°, rel. to lowest mantle struct. 77—81811
SH-waves ray-mode duality in Earth models with crust and mantle discontinuities 79—25213
shallow, global mantle flow due to lithospheric plates accretion and subduction 79—44163
shear flow beneath oceanic plates and olivine rheology 78—40521
shear heating instability in upper mantle 79—20783
shear stress on base of lithospheric plate 77—91099
shear wave velocity and attenuation models, great-circle Rayleigh waves inversion 79—12090
shear wave velocity structure, evidence for lateral vars. 79—92504
shield-like upper mantle struct. from long-period surface wave dispersion 77—56608
single-cell convection, rel. to geoid 77—60362
solid three dim. models of gradient media by precipitation 77—64235
solid-Earth geophysics, bibliography 77—2078
solid-state convection, obs. evidence 79—84692
W.South America, volcanism, seismicity and anelasticity interrelationships 77—33044
Sp waves, from upper-lower mantle transition cone, seismogram calcs. 80—104901
Spanish deep-focus earthquake, 1954 March 29, source process and tectonic implications 77—9375
spin-pairing transition favours small mean atomic weight 78—61364
spinel disproportionation reactions, elasticity and phase equilibria 77—78158

Earth mantle continued
spinel lherzolite nodules from Pleistocene cinder cone, upper mantle origin 78—65299
spinel lherzolite xenoliths, implications of texture composition depend. 79—25244
spinel lherzolites in upper mantle, petrogenesis, magmatic model 77—86875
spinel-garnet peridotite transitions in upper mantle, evidence from harzburgite xenolith 78—65309
Stillwater complex, USA gabbro Sm/Nd age and mantle evolution curve of Nd 80—41410
stishovite (SiO_2), single cryst. anal. of struct. 78—53648
strain tide spectroscopy, interaction Earth mantle, liquid core appl. 79—5440
stratification in early history, heat generation and heat-mass transfer 80—90040
stress estimates from structural studies in some mantle peridotites 78—69330
stress measurement, applicability limits of grain size geopiezometer 78—85715
structural superplastic creep and linear viscosity 77—5155
structure and HF spheroidal modes 79—8603
structure beneath Japan Sea 78—81118
structure effects on radial oscills. 80—12347
structure from P-residuals azimuthal var. in southern California 80—3954
structure from seismic surface wave obs. 78—73323
structure models from flood basalt isotopic abundances of Nd and Sr 80—72475
structure of upper mantle beneath Eurasia and N.Atlantic and Arctic Oceans 78—85506
structure peculiarities rel. to nature of excess quadrupole moment 78—73334
structure under Canadian Rockies, seismic refraction survey 77—53015
structure under north central Italy, Rayleigh waves 80—3977
structure vars. due to evolution 78—85512
subcrustal earthquake location and mislocation 78—85498
subducting oceanic crust, thermodynamic consequences of minerals dehydration, high press. and temp. 78—69301
subduction angle, in plate tectonics 78—11865
subduction zone, thermal model with dehydration in downgoing slab 79—79784
subduction zone, thermal structs. evolution 80—56440
subduction zone dip angles and flow driven by plate motion 79—20801
subsolidus convection and cooling, lower mantle viscosity constraint 77—9384
Sunda trench and forearc basin, seismic study 80—72470
Takayama volcanic area, Japan, upper mantle S-wave anisotropy 80—90024
tectonic plate driving forces 77—64249
tectonics, plate motions and asthenosphere convection 80—41418
teleseismic Sn, guided wave in upper mantle 78—11823
temperature distrib. and electrically conducting zone formation 78—85519
temperature vars., radical and lateral, geophysical constraints 77—5141
temperature-depth profiles, Poland, from geothermal and deep seismic sounding data 78—48988
temperatures from dunite-peridotite mixed-oxide compositional models 77—2124
thermal convection, mechanical boundary conditions 79—20782
thermal convection, time dependent simulation 80—101352
thermal convection, two-scale flow model rel. to plate tectonics 78—73348
thermal domes, CO_2-rich mantle fluid heating possibility 79—66659
thermal evolution of differentiated upper mantle 80—98288
thermal gradients estimation, geological problems 77—5138
thermal history model with parameterized convection 80—26470
thermoconvective waves, propag. without attenuation 80—90064
thermodynamic properties of relevant substances at high press. and temp. 80—81874
thermodynamics appl. to fundamental Earth physics 78—36125
Tibet, active tectonics, LANDSAT imagery 79—20794
tidal tilt obs. in N.Wales mine, strain-tilt coupling and Earth model 80—89926
tide of solid Earth, mantle anelasticity influence 80—76900
Timano-Pechora province, USSR, seismic profile, upper mantle stratigraphy *(Russian)* 77—70616
time dependent flow, model 78—20369
N.Tonga region, Wadati-Benioff zone morphology and complicated subduction closure model 80—90010
topography of ocean bottom rel. to lithosphere viscosity 77—64250
topolgy of ray surfaces in low-velociy zones 80—21633
trace element diffusion and separations, appl. to asthenosphere and mantle diapirs 77—41008
transition zone between core and mantle, seismological significance *(Italian)* 77—70618
Transverse Ranges, S.California, upper mantle low-resistivity region, magnetotelluric meas. 77—37127
Trivandrum, crust-mantle structure from Indian geomagnetic data 78—85520
two-phase media, effective shear modulus and struct., rel. to seismic wave propag. 77—50949
two-scale convection, rel. to global gravity anomalies 78—85528
S.Tyrrhenian Sea region, seismic wave study of crustal struct. 80—41380
Ukrainian Carpathians, crustal interface, phase substance transformation contrib. 80—89999
ultramafic xenolith petrology and upper mantle processes, Kapfenstein, Austria 80—76973
ultramafic xenoliths, mantle-derived, from Tahiti, petrology and genetic significance 80—90086
ultramafic xenoliths rel. to tectonites and upper mantle composition *(French)* 79—44141
W.United States, 3-D mantle struct., P vel. study 80—85621
W United States, asthenosphere-oceanic crust contact rel. to Cenozoic igneous activity 79—2207
NE United States, crust and mantle struct. by seismic vel. 80—56429
E.United States, seismic struct., shear wave vel. 80—56385
W.United States, upper mantle P-wave vel. structure 78—61363
United States, upper mantle seismic struct., inversion of body wave arrival times 79—53322

Earth mantle continued
Uordan-Dead Sea rift, crust and upper mantle seismic study, transition towards Mediterranean Sea 79−79766
upper, beneath New Madrid seismic zone, three dimens. vel. model 78−7573
upper, complex structures modelling by finite-element methods 77−5164
upper, constitution, structurology of peridotite xenoliths in S.African kimberlites *(French)* 78−11889
upper, convective stability 79−74870
upper, discontinuities effect on toroidal free oscills. 79−29713
upper, global density inhomogeneities determ. by terrestrial and satellite gravity obs. 79−62592
upper, nonlinear stress propagation 77−17058
upper, seismic body waves attenuation from inversions of high freq. $Q_\gamma^{-1}(f)$ 77−33000
upper, structure in USSR from explosion seismology 77−86836
upper, thermal and mechanical struct., continental and oceanic models 77−37169
upper, thermomechanical models, plate vel. changes rel. to magnetic activity 78−65231
upper, travel-time branches from Yellowknife seismic array data 78−65211
upper, vel. cross sections from deep seismic sounding data 79−39677
upper, viscosity, non-Newtonian fluid 79−79770
upper layer, heat convection rel. to viscoelastic instability 77−41010
upper mantle, continent-ocean differences rel. to ScS travel time residuals 77−29253
upper mantle, degassing rel. to atmosphere and sialic crust system form. 79−44153
upper mantle, diffusion of Ca, Sr, Ba and Co in basalt melt 78−28223
upper mantle, partial melting and electrical conductivity anomalies 78−28199
upper mantle, struct. from inversion of surface wave dispersion data with random errors 77−73681
upper mantle density and surface wave inversion problem 77−17039
upper mantle heterogeneities beneath Gauribidanur seismic array (S.India), quantitative assessment 78−32033
upper mantle of Carpathians internal region, dynamics rel. to tectonic movements *(Russian)* 79−48444
upper mantle physical conditions, Walsh's model 80−90047
upper mantle transition region, eclogite abundance 79−84192
upper structure of Caucasus and Carpathians from seismic data 77−41009
E.USA, seismic vel. profile of upper mantle 80−81818
USA east coast P-wave vels. 77−86792
velocity-depth structure, Central Europe 80−3976
visco-elastic modelling of tectonic systems, by finite element anal. 80−104930
viscosity, calc. from gravity pot. model 80−21613
viscosity, rel. to Earth tides theory assuming Earth as viscoelastic body 80−67333
viscosity deduced from deglaciation Earth rot. effects 80−85576
viscosity-depth profile, polymorphic phase transition effects 78−48998
viscous flow under moving lithospheric plates and under subduction zones 77−56613
volcanism, continental, role of ancient lithosphere 77−2133
Voronezh Crystalline Massif, seismic vels. significance of mineral substance inhomogeneous compression 80−94504
Walvis Ridge, anomalously low mantle shear velocity from Rayleigh wave dispersion meas. 80−41412
Walvis Ridge, heat flow profile rel. to mantle hot spot origin 77−86827
Walvis Ridge, seismic refr. obs., crust and mantle struct. 77−78153
W.Washington, structure from Puget Sound earthquake 77−91026
water, isentropic decompression from crustal and mantle press., thermodynamics 79−79769
whole mantle convection rel. to plate tectonics 77−44957
xenoliths, equilibrated Nd and unequilibrated Sr isotopic comp. meas. 80−98321
xenoliths, mantle-derived, from S.Africa 79−34775
xenoliths underlying Sierra Nevada batholith, anisotropic elastic vels. 77−64225
Yellowstone caldera, seismic evidence for chem. mantle plume 77−2105
Yellowstone National Park, USA, teleseismic delay anal., structure 80−3981
Yellowstone Park volcanic gases, mantle He component from He isotopic ratios 79−16425
zone regining below lithospheric plates, steady state astheriosphere model 79−88326
^{36}Ar in primordial mantle from Arkansas diamond comp. 80−94493
^{40}Ar/^{36}Ar trapped in Cretaceous deep-sea basalts 79−16423
C in upper mantle, implications for plate tectonics 80−81845
CO_2 in upper mantle, fugacity at high temps. and press. from decarbonation reactions 79−16439
CO_2, isentropic decompression from crustal and mantle press., thermodynamics 79−79769
Ca diffusion in silicate melt 79−90809
$Ca_2Al_2SiO_7$, gehlenite, new high-press. phase, rel. to Earth interior 79−29753
Ca_2GeO_4, with K_2NiF_4-type struct., high press. decomp. 79−1507
Ca_2MnO_4, with K_2NiF_4-type struct., high press. decomp. 79−1507
CaO, solid, phase transition at high-press., lower mantle implications 80−79876
ε-Fe, vol. eqn. of state under static press. conditions, rel. to Earth core-mantle models 80−19904
Fe-S eutectic, Lindmann's melting law, solid-liquid core boundary, core mantle boundary 78−18743
Ge/Si and Ga/Al ratios vars. along Reykjanes Ridge and Iceland 79−8617
He from mantle, presence in Red Sea brines, ^{3}He/^{4}He ratio meas. 77−25693
^{3}He injection in Gulf of California, meas. in Guaymas Basin 80−85640
LiF-MgF_2, high-pressure phase relations rel. to mixed oxide zone of Earth mantle 77−37193
MgO, bonding, pressure effects in lower mantle 80−72491
$MgSiO_3$, perovskite, synthesis and cryst. chem. charact., rel. to mantle mineralogy 78−65266
$MgSiO_3$ perovskite polymorph, high-press elastic consts. determ. 77−51428
Mg_2SiO_4, forsterite, single-cryst., shock wave compression 79−84242
$2Mg_2SiO_4.3Mg(OH)_2$, possible mantle mineral phase, cryst. struct. 80−39028

Earth mantle continued
Mg0, vol. eqn. of state under static press. conditions, rel. to Earth core-mantle models 80−19904
$NaAlSiO_4$, (nepheline), transform. to Ca ferrite isotype rel. to mantle Mg_2SiO_4 struct. 77−64270
Nd and Sr isotope composition of diopsides from kimberlite nodules 80−51363
Nd-Sr isotope correlation, constraints on continental crust comp. and nature of lower crust 80−94498
Nd-Sr isotopic correlation in mantle materials, geodynamic consequences 79−92512
^{187}Re/^{186}Os ratio, rel. to use of Os isotopes as petrogenetic and geological tracers 80−89989
Si-O bonds, cryst. chem. at high press., rel. to Earth mantle mineralogy 79−48470
Sr evolution in W.Greenland-Labrador craton, early Rb depletion in mantle 78−69304

Earth rotation
see also time and latitude
20 year variations in diurnal rot. vel. rel. to sunspot numbers and geomag. vars. 78−32005
acceleration, nontidal secular vars. correl. with secular geomag. field vars. 78−73302
accelerations of Sun and Moon, rel. to gravit. const. and origin of mountains 79−8592
angular momentum correl. with geomag. field, theory 80−67337
angular velocity variations, influence of geosynclines pot. energy changes *(Russian)* 78−96182
annual polar motion, many-year var. rel. to atmospheric circulation many-year fluctuation *(Chinese)* 80−104848
annual wobble, affected by wind stressed sea level 80−36221
Archean apparent polar wander curve from Abitibi greenstone belt palaeomag. results 77−70596
atmosphere, ang. rot. vars. rel. to zonal circulation model, numerical expts. *(Russian)* 78−81295
atmosphere, critical levels in a vertically rotating compressible atmosphere 80−6073
atmosphere, equatorial gravity waves generation 78−36232
atmosphere, gravity waves generation at solar terminator rel. to E_s-layers form. 79−12337
atmosphere, middle, superrotation rel. to damped planetary wave interaction with zonally averaged circulation 80−109217
atmosphere, solar modulation of lunar tide 80−94593
atmosphere disturbance production, allowance for slope of terminator boundary 77−91208
atmosphere stratified flow over obstacle, influence of Earth rot. *(Russian)* 78−24291
atmosphere super-rotation, effect of momentum of meteoroids 77−56877
atmosphere tides in joint presence of friction and rot., f-plane approximation 79−66847
axis of figure, motion determ. from N solid bodies mutual gravit. pot. 79−12390
axis of figure, precession and mutation 78−65167
axisymmetric convection in rotating sphere, non-slip surface effects 79−64657
BIH data (1962-79) 80−101314
celestial pole, exact definition 79−53703
Chandler, annual and semiannual wobbles and mean latitude, anal. of 1957-77 data 80−30974
Chandler tides, comments and reply 79−88424
Chandler wobble, amplitude rel. to energy release in great earthquakes 77−86798
Chandler wobble, correl. with intermediate and deep focus earthquake activity temporal var. 80−3943
Chandler wobble, excitation by earthquakes and meteorological sources 77−78083
Chandler wobble, excitation-dissipation problem, ellipticity 77−64189
Chandler wobble, optimal complex ARMA model 78−61304
Chandler wobble, seismic excitation 80−26437
Chandler wobble, theory of amplitude 77−90990
Chandler wobble, tidal admittance of induced pole tide in ocean 77−9443
Chandler wobble affected by pole tide, theory 80−51318
Chandler wobble and rotation rel. to large energy release from earthquakes 78−28186
chandler wobble period and Moledensky model of mantle/core *(Russian)* 79−92475
Chandler wobble Q 80−21604
clock synchronisation in rotating frame of Earth, time discontinuity obs. 77−60333
core fluid oscillations, transverse motion, Earth rot. effects 80−89965
core-mantle interaction effects 79−66601
Coriolis force, rel. to spatial problem of influence of orography on air motion *(Russian)* 80−94565
crustal structure formation using plate tectonics and rotation hypothesis *(Russian)* 78−15986
daily free nutation parameters, determ. technique 78−96126
daily latitude variations anal. 80−21891
day duration rel. to solar activity 80−104853
day length and zonal tides, effect of core-mantle coupling 80−104850
day length changes rel. to atmospheric angular momentum fluctuations 80−85715
day length irregular variations, core-mantle coupling 77−64186
day length tidal fluctuations, comparison with self-consistent equilib. ocean tides 78−96218
daylength variations, prod. by short-period geomag. vars. electromechanical effects 79−57847
days in synodic month, palaeontological data on Earth-Moon system history 80−17224
deglaciation effects, viscoelastic response to unloading 80−85576
diurnal latitude vars. spectra based on obs. at Gor'kii 79−35100
diurnal polar motion and latitude vars. *(Russian)* 80−51641
early Earth, dynamical and secular stability rel. to Moon fission origin 78−85867
Earth liquid core dynamical effects, nutations 77−86736
Earth-Moon system, palaeodynamics from nautiloid growth 80−41713
effect on long baseline radio interferometer, classical response 78−61733
electrically conducting rot. sphere behaviour in time-independ. homogeneous external mag. field 78−49309
electrostatic field generation, Earth as unipolar generator 78−44771

Earth rotation continued
elementary oscillation of elastic rot. Earth, ordinary differential eqns. 79−39632
ellipsoid of inertia, axis posns. from satellite obs. 78−20343
EM induction, in rot. conductive Earth 78−44764
enhanced pole tide rel. to Chandler wobble period and damping 80−21778
Ephemeris and Universal Time, empirical difference from polynomial approx. 80−17223
ephemeris time, correction determ. from photographic obs. of Sun annular eclipse (1976, April 29) *(German)* 79−44335
forced nutation, study via astronomical time meas. 77−52956
Foucault pendulum model 79−58472
free oscillations of Earth, rot. and elliptical splitting 79−88257
gas deposits, distribution related to Earth's rotation and local geological conditions *(Russian)* 79−83545
geodesy, Molodensky's problem in gravity space for rot. Earth 78−65173
geodetic reference frames, polar motion effects 78−69272
geological time and tidal friction, evidence for Earth deceleration 80−3916
geomagnetic dynamo, MHD convection in rapidly rot. fluid layer, stability 79−50808
geomagnetic reversals, possible influence of ice ages on Earth rotation 77−56578
geophysical causes and consequences, book 80−76902
global geodynamics, Canadian contribs., 1971-79 period. 80−8262
Gor'kii latitude observations, half-year nutation wave terms errors 79−62728
gravitational field, local vanishing due to left turning motion *(Japanese)* 80−98798
gravitational shift due to Earth's rot., verification 77−2579
gravity tides, amplitude of diurnal waves rel. to Earth's rotation rate *(French)* 80−8245
gravity vars. rel. to irregular rotation 79−92473
Greenwich Obs., Time Report (1976, Jan.-March) 77−45293
Greenwich Obs. Time and Latitude Service, Time Report (April-June, 1977) 78−69661
Greenwich Obs. Time and Latitude Service, Time Report (January-March 1977) 78−57431
Greenwich Obs. Time and Latitude Service, Time Report (January-March 1978) 79−25453
Greenwich Obs. Time and Latitude Service, Time Report (January to March 1979) 80−72749
Greenwich Obs. Time and Latitude Service, Time Report (July-September 1976) 78−20624
Greenwich Obs. Time and Latitude Service, Time Report (July-September 1977) 78−73619
Greenwich Obs. Time and Latitude Service, Time Report (July-September 1978) 79−62729
Greenwich Obs. Time and Latitude Service, Time Report (October to December, 1977) 78−89046
Greenwich Obs. Time and Latitude Service Time Report (April-June 1979) 80−72750
Greenwich Obs. Time and Latitude Service Time Report (October-December 1976) 78−24443
Greenwich Obs. Time and Latitude Service Time Report (October-December 1978) 79−101053
Greenwich Observatory, 1976 April to June time report 77−70581
Hadrynian Polar Track discovery rel. to Grenville problem 77−48991
Huronian polar wander and Thessalon volcanics palaeomag. 79−5444
interior deformation, ellipticity anal. 77−13069
ionospheric valley, electron density inhomogeneities prod. by movement of terminator in atmosphere 77−91348
irregular variations in diurnal rot., correl. with solar wind vel. 79−8591
irregularities, amplitudes of components of ΔTs, depend. on observatory geographic position *(French)* 77−86741
Large Numbers Hypothesis implications 79−12063
laser satellite tracking techniques for Earth rotation meas. 77−41206
latitude variation, computation for national ephemerids calc. 78−88776
latitude variation, polar motion and declination, effects of Oppolzer terms *(Chinese)* 80−76891
length of day, Sun-induced vars. 77−90981
length of day fluctuations and geomag. dipole field vars., spectral line similarities 77−32993
liquid core effects, luni-solar nutation tables 80−98210
magnetosphere, elec. field around rot. mag. dipole 78−45141
mean pole position from star pair latitude obs. anal. 80−21892
mean solar time on Greenwich meridian, definitions and terminology 79−21155
Merate Observatory, time and latit. results of astrolabe obs. (1977) 79−40061
meteorological and climatic effects, contribution of space technology *(French)* 79−74827
moment of inertia change due to Earth-Moon tidal friction 80−81803
moment of inertia tensor, changes due to earthquake 79−44106
Moon, fission theory origin and geosynchronous release 80−101536
mountain wave drag, influence of Earth's rotation 79−88440
multiyear variations excitation, role of terrestrial atmosphere 79−96734
nearly-diurnal wobble effects in time and latit. obs. 77−56566
neutron interferometry, Earth rot. affecting wave function phase 79−54012
Newtonian gravitation field of internal bodies, rot. motion analysis *(Russian)* 77−37123
nighttime darkness, variation of duration with latit. 77−25632
nonuniformity, possible connection with Sun high-latit. mag. field 80−46119
nonuniformity spectra from International Time Service data 77−78086
normal modes of rotating Earth model, excitation by earthquake fault 78−73312
nutation amplitudes, annual Z-term of latitude var. anal. *(Chinese)* 80−8244
nutation in obliquity and longitude rel. to nature of inner core 78−85510
nutation theory with dissipative core-mantle coupling 77−64188
obliquity of ecliptic, historical obs. anal. 79−44076
ocean, slope currents on a rotating globe 79−100867
ocean stratified flow over obstacle, influence of Earth rot. *(Russian)* 78−24291
oscillations of a gravitating and rotating uniform liquid sphere 79−44082
Paris astrolabe observations, time and latitude (1976) *(French)* 77−78078

Earth rotation continued
Paris astrolabe time and latitude obs. for 1977-8 period *(French)* 79−101051
periodic satellite coverage pattern generation computer graphic system 77−37496
periodical fluctuations due to lunar tides, calc. by Einstein *(German)* 77−67169
Phanerozoic history and climatic instabilities 77−66981
plate tectonics, Phanerozoic, control by spin-symmetric mantle convection 78−92812
polar free wobble, 1900-1976, harmonic anal. *(Chinese)* 79−96732
polar large-scale wandering and continental drift 79−79719
polar latitude variations, VZT obs. at Cagliari *(Italian)* 79−21153
polar motion, coordinates 1949 to 1976, periodic and secular components *(Chinese)* 80−12327
polar motion, International Latitude Service Observations (1899-1977) anal. 80−104851
polar motion, random exciting process *(Chinese)* 79−20740
polar motion analysis by radio interferometric surveying, POLARIS project 79−79721
polar motion annual period and Chandler wobble calc. *(German)* 77−70582
polar motion determ., satellite Doppler tracking, MEDOC 80−101445
polar motion determ. by Doppler satellite obs. 77−44887
polar motion estimation from Doppler obs. of artificial satellites *(Polish)* 79−57843
polar movements, sea level response 78−53608
polar position, motion due to Earth's rot. Gen-3 laser ranging study 80−3912
polar wander excitation, effects of ridges and trenches 79−16367
polar wander paths, palaeomagnetic, deficiency of high-latit. poles 78−65181
polar wander paths from Lower and Middle Cambrian sedimentary rocks from Nevada 80−21620
polar wander paths from Upper Precambrian sedimentary rocks from Nevada 80−21621
polar wandering, influence of continental drift 79−44079
pole annual motion, vars., 1846 to 1971, and period anal. *(Russian)* 78−40461
pole posn. and rotation from lunar laser range-differencing 80−101312
pole secular motion, rel. to global plate tectonics 78−65172
pole secular trend, consideration of motion of latit. observatories 77−86734
pole-tide signal at low-latitude coastal station 78−61322
Poltava latitude differences from obs. of bright zenith stars 78−28488
positional astronomy and definition of ephemeris pole 78−93078
positive leap second on 1979 December 31, announcement 79−100808
Late Precambrian era, Earth rot. rate vars. effects on climate 80−4097
precession and nutation precision estimation from radio interferometric obs. 77−73623
precession and year length rel. to old calendar systems 79−48693
precession angle of rot. axis, effect of harmonics in gravit. pot. of Earth, Moon and Sun 78−48953
precession change, revision of IAU System of Astronomical Constants 77−17331
precession constant, new adopted value and effect on stellar proper values 79−25459
precession determ. from Lick proper motions referred to galaxies 78−65487
precession matrix based on IAU (1976) system of astronomical constants 79−48653
precessional corrections to AGK3 system in polar region, rel. to stellar proper motion system anal. *(Russian)* 80−12647
precessional rotation, determ. rel. to astrometric fundamental coordinate system rot. 79−62727
Q frequency depend. in Earth rel. to mantle rheology and Chandler wobble 79−84190
quadrupole moment excess and mantle struct. peculiarities 78−73334
radio interferometric systems, meas., appl. 79−25375
reference frame for positional astronomy, appl. of lunar laser ranging 77−64618
rigid Earth, theory of rot. 77−60332
Santiago astrolabe, time, latit. and radius obs. (1968 to 1971) 78−12077
Santiago astrolabe observations from 1972 to 1976, results 80−46363
satellite laser tracking for polar motion, Earth tides and latitude determ. 77−56570
secular polar motion, low frequency spectrum anal. *(Chinese)* 80−104849
slowing during Earth history, rel. to evolution of lunar orbit 77−29671
solar cycle modulating rotation period 80−56336
solar day length, palaeontological evidence rel. to rate of var. of gravit. const. 77−45307
solar hour angle, formula rel. to latit.-independ. sundial construction 78−81549
spin axis, Neogene motion rel. to Pacific plate and mantle 79−44167
spin axis location, control by subducted lithosphere and hotspots mass anomalies 80−90056
stratified ellipsoids of revolution, inertial frame dragging effects 79−2573
tidal friction [conference, Bielefeld, Germany (Sep. 1977)] 79−88234
time adjustment on 1978 December 31, positive leap second 78−93079
time and latitude, astrolabe obs. at Merate Observatory for (1976) 78−12078
time-service observations, tides and nutation effects 79−96733
Tokyo Astronomical Obs., Time and Latitude Bulletins (1976 April-June) 77−64619
Tokyo Astronomical Obs., Time and Latitude Bulletins (1976 Jul.-Sept.) 77−70982
Tokyo Astronomical Obs., Time and Latitude Bulletins (Apr.-June 1978) 79−101052
Tokyo Astronomical Obs., Time and Latitude Bulletins (April-June 1977) 78−45203
Tokyo Astronomical Obs., Time and Latitude Bulletins (April/June 1979) 80−72752
Tokyo Astronomical Obs., Time and Latitude Bulletins (December 1975) 77−2335
Tokyo Astronomical Obs., Time and Latitude Bulletins (Jan.-March 1976) 77−70983
Tokyo Astronomical Obs., Time and Latitude Bulletins (Jan-Mch. 1978) 80−17476

Earth rotation continued
- Tokyo Astronomical Obs., Time and Latitude Bulletins (January-March 1977) 78—45202
- Tokyo Astronomical Obs., Time and Latitude Bulletins (Jul-Sep 1979) 80—82177
- Tokyo Astronomical Obs., Time and Latitude Bulletins (July-September 1977) 78—73618
- Tokyo Astronomical Obs., Time and Latitude Bulletins (July-Sept. 1978) 80—4239
- Tokyo Astronomical Obs., Time and Latitude Bulletins (November 1975) 77—2334
- Tokyo Astronomical Obs., Time and Latitude Bulletins (Oct.-Dec. 1976) 77—87242
- Tokyo Astronomical Obs., Time and Latitude Bulletins (Oct.-Dec. 1978) 79—84646
- Tokyo Astronomical Obs., Time and Latitude Bulletins (October 1975) 77—2333
- Tokyo Astronomical Obs., Time and Latitude Bulletins (October-December 1977) 79—5736
- Tokyo Astronomical Obs., Time and Latitude Bulletins (September 1976) 77—2332
- Tokyo Astronomical Observatory Time and Latitude Service, Bulletin (January to March 1979) 80—72751
- Universal Time, short period terms anal. *(Chinese)* 79—8589
- Universal Time and polar motion determ. from lunar laser ranging and laser obs. of artificial satellites *(Polish)* 79—57844
- Universal Time in China, short-period terms 80—12648
- universal time system (TU2), differences anal. rel. to Earth rotation nonuniformities 78—65174
- Valinhos astrolabe obs. (April 1974-December 1977) *(French)* 79—70944
- variability, meteorological and oceanic causes and consequences 77—56571
- variations, secular and periodic, rel. to gravitation and inertia corpuscular model *(Russian)* 79—40439
- variations due to continental drift of islands 80—94445
- variations due to sectorial and tesseral harmonics 77—90987
- variations due to upper stratosphere zonal winds 80—81804
- variations in rotation rate within 10-100 years range, rel. to sunspot numbers and K_p-index 77—90980
- velocity irregular variations rel. to global atm. circulation anomalous changes 78—32000
- velocity variations anal. *(Russian)* 79—20743
- VLBI appl. to geodesy, Earth rot. and network geometry optimisation 78—92996
- westward drift of magnetic field rel. to liquid core model 77—81794
- whole-Earth dynamics, variational method 77—60340
- wobble and nutation, elastic gravit. normal mode theory 77—60341

Earth satellites *see artificial satellites; Moon*

Earth structure
- *see also Earth composition; Earth interior*
- abyssal fractures rel. to tectonics *(Russian)* 78—3731
- active margin, gravity and struct., British Columbia and Washington 79—92516
- active margins 78—57191
- Aegean area, crustal struct. from deep seismic sounding 77—64239
- Aegean region, crust and upper mantle struct. from deep seismic sounding 78—69308
- southern Africa continental margins, continental breakup and deep crustal struct. 77—21742
- E.African Rift models, discrimination via seismic ray tracing 78—11846
- E.African rift system, structure rel. to Martian canyons 79—40111
- Alabama Piedmont, structural development 78—65290
- Alboran Sea, crustal seismic profiles 78—61370
- Alpine structures between Mont-Blanc, Petit-Saint-Bernard and Valgrisanche *(French)* 79—79758
- ancient crustal structure and ring magnetic anomalies *(Russian)* 77—33019
- ancient Earth elastic parameters, appl. to lunar capture hypothesis 78—81570
- anelasticity, from inversions of high freq. $Q_\gamma^{-1}(f)$ 77—33000
- anelasticity model constraints rel. to complex propag. function 78—88802
- anisotropic layering, effects on seismic waves propag., review 77—49012
- anisotropic media, elastic wave propagation, point pulse source 80—3939
- anomaly source models, statistical parameters rel. to pot. fields obtained by superposition *(German)* 79—34783
- E Antarctic craton sedimentary basins from seismic, mag., gravity and radar obs. 77—21733
- Antarctic plate boundary near Bouvet triple junction, tectonic structure 78—53639
- Apennines, Rayleigh wave phase vels. rel. to upper mantle struct. 78—53618
- Apennines, Rayleigh wave study of crustal and upper mantle structure 80—46153
- Archaean lithospheric/crustal thickness from volcano spacings 78—65225
- circum-Arctic Ocean region, tectonic plates struct. rel. to Arctic Basin form. 80—98294
- Arctic regions, gravity from 60°N to North Pole, rel. to crust and mantle density struct. 79—48391
- SE.Arizona, Laramide folding and faulting, basement cored uplift model 80—8272
- asthenosphere, stresses and effective viscosities 78—65229
- N.Atlantic crustal structure, deep drilling results 80—26478
- N.Atlantic region, gravity anomalies, regional elevation and deep struct. 79—16421
- Mid Atlantic Ridge, 45°N, seismic vel. struct. of crust 79—25214
- Atlantic type continental margins, struct. from geophysical meas. 77—21702
- attenuation models 78—61367
- Aulneau batholith, Ontario, subcritical seismic crustal refl. survey 78—65213
- N.Australia, long-range controlled source seismic profile 79—16419
- SE Australia, long-range seismic profile 77—44945
- SE Australia, thrust faulting, crust and upper mantle struct. 77—44944
- Azov-Kuban' oil-gas basin structure from seismic data *(Russian)* 80—85601
- Baikal and continental rift zones, deep struct. from seismic data 78—36130
- Baikal rift valley system, structural features 78—40528
- Baikal rift zone, rifting mechanism and deep struct. 78—36131

Earth structure continued
- Balcones Fault Zone Texas, fracture patterns, field study 78—73337
- Balei gold region (E.Transbaikalia), structural features and tectonics 80—98300
- Baltic Shield, lithospheric thickness from S-wave anal. 80—3978
- Baltic Shield, petrological model *(Russian)* 77—33020
- Baltic shield and Barents Sea, crust and upper mantle struct., Rayleigh waves dispersion 78—77204
- basalt magnetic properties rel. to crust and upper mantle struct. and development 79—79816
- Basque Provinces, Pyrenean folding, deep geomagnetic sounding *(French)* 80—67351
- Baykal regions, 1962-71 epicentre field structure 77—33006
- Bihar mica belt, two catazonal granite plutons, mode of emplacement 79—44157
- Black Sea basin, crustal struct. from Love and Rayleigh waves dispersion *(Russian)* 78—28192
- Black Sea basin formation *(German)* 78—3737
- Black Sea NW shallow and nearby land areas, appl. of seismic multidimensional vel. generalisation *(Russian)* 80—105068
- Bournac, Haute-Loire, heat flow determ., geotherm proposal 80—8259
- Brevard ductile deformation zone, N.Carolina, struct. and seismic refl. study 78—65289
- British Columbia, crustal structure from seismic refr. profile 80—17236
- Caledonides of N.Britain, struct. contrast, seismic wave interpretation 80—3975
- S.California, regional S-wave struct. from anal. of teleseismic Rayleigh waves 79—92510
- central California, seismic vel. structure metamorphic belt 80—98270
- E Canada, crust and mantle struct. from PP waves travel time residuals 77—9354
- E. Canada, thermal struct. of upper crust 80—31013
- SE.Canadian Cordillera, structural evolution 78—88808
- Canadian Rockies, seismic refraction survey and crust and upper mantle structure 77—53015
- Canadian Shield, electrical resistivity structure, layer Earth models 79—48396
- Canadian Shield, structure of Archean basin-craton complexes 78—61412
- Cape Verde archipelago, underlying crustal struct. from seismic, mag. and gravity data 77—17052
- Carpathian system, geophysical data and Earth structure *(Hungarian)* 77—86829
- E.Carpathians, complex model of lithosphere *(Russian)* 78—85511
- Central Alps, structual zones and continental collision 78—81124
- chemical and thermal struct. of deep interior, obs. constraints 79—53323
- Cocos Plate, lower oceanic crust fine struct. 79—88337
- Colombia basin, Caribbean Sea, crustal struct. from profiler-sonobuoy meas. 78—28198
- Colorado, cond. anomaly rel. to geomag. field gradient meas. 77—29249
- Concepcion Bank, off Morocco, crustal struct., tectonic unit of volcanic origin 79—39689
- conductivity struct. determ., source field effects on EM transfer functions at mid-latits. 79—74831
- conference on plateau uplifts, Flagstaff, Arizona (August 1978) 80—57004
- conference on satellite Doppler tracking and geodetic appl., London, England (Oct. 1978) 80—77264
- continent formation due to geosynchronous revolution of Moon 80—101348
- continental basement exploration by seismic reflection profiling 78—96172
- continental crust, role of intercrustal convection 77—17061
- continental crust thermal state and structure *(Italian)* 79—20769
- continental plates, Archaean nuclei rel. to P-wave travel time residuals 79—62439
- continental structure development and gravit. instability, synthesis 78—48995
- continents, deep structure 79—66665
- Coosa Valley, Alabama, struct., folding and thrust faulting 78—65291
- core and upper mantle struct. effects on radial oscills. 80—12347
- core boundary irregularities influence on liquid vel. and mag. field 77—13065
- core catastrophic or continuous formation, Sr and Pb isotope geochemistry constraints 78—57178
- core physical characts. from geomag. data 79—79765
- core-mantle boundary, nature of transition 77—78137
- core-mantle transition zone, seismological significance *(Italian)* 77—70618
- cosmological change of gravitational const. rel. to Earth struct. 77—73626
- Coso geothermal area, underlying low-vel. body, teleseismic evidence 80—90005
- Coso Hot Springs, Known Geothermal Resource Area, model 80—90004
- Coso Range, California 80—90003
- Coso Range, California 80—90049
- Crimean mountains, crustal structure from deep seismic sounding *(Russian)* 78—3732
- crust, density struct. rel. to magma traps 79—66669
- crust, quasi-periodic gravity vars. *(Russian)* 78—69275
- crust and upper mantle structure from seismic surface wave obs. 78—73323
- crustal, deep structure to NW of Cape Verde Islands 79—2201
- crustal deep structure model of East European platform *(Polish)* 77—21706
- crustal geological-geophysical zoning possibility 78—57342
- crustal structure, investigation via seismic reverberation 79—66820
- crustal structure along international DSS profile VIII from Russian to Poland 77—21705
- crustal structure from EM freq. sounding 78—49167
- crustal structure modelling using telesiesmic body-wave conversions 77—91283
- crustal structure models rel. to focal depth determ. for Friuli earthquakes 78—24243
- crustal structure rel. to longitudinal seismic wave arrival directions *(Russian)* 78—11850
- crustal structures, inferred from Nevada Test Site (NTS), explosions Rayleigh-wave signatures 79—66632
- crustal velocity model, from seismic data, Kurinian depression example 79—39678

Earth structure continued
- crystallization at inner core boundary under isochem. conditions, causing changes in dimens., stress and gravit. energy 79—84191
- Cundeelee area, W.Australia, regional geology and gross structure 79—2194
- Danakil Depression and Dead Sea Rift, comparative study of sedimentary fills 78—69347
- deep crustal struct. inferred from mag. anomalies of long-wavelength 80—72430
- deep horizons, seismic refls. unravelling via seismic stripping 79—34970
- density inversion in upper mantle, rel. to seismic waveguides 79—12099
- density model, based on gravimetric data *(Russian)* 80—31009
- density model, variational approach *(Russian)* 78—28191
- density models, appl. to geoid anomalies computation 80—3897
- density of Earth and crust, Bouguer formula rel. to gravity corrections 79—29692
- density structure, max. entropy inversion 80—67602
- descending lithosphere, effects of accretion on geometry 77—29275
- dilatant regions in layered Earth, electrokinetic and mag. anomalies rel. to earthquake prediction 79—39658
- dynamic shear modulus, rel. to corrections to oscills. eigenfreqs. 77—81800
- early Earth, dynamical and secular stability rel. to Moon fission origin 78—85867
- early evolution and thermal history 77—44950
- earthquake foci beneath active continental margins, three-dimensional projection 80—72453
- earthquake zones, pore fluids and Q rel. to brittle fracture model 79—39671
- earthquakes focal regions, inhomogeneities and tectonics rel. to P-wave amplitudes regional anomalies 79—79751
- N Egypt, shear zones from gravity data 78—28208
- elastic homogeneous layers laterlally varying boundaries, volume and surface seismic sources 79—16397
- elastic spheroidal Earth, Green's function for deformation eqns. 77—81779
- elasticity imperfection in interior 79—8613
- elastodynamic propag. matrices, stratified Earth models 78—77197
- electrically conducting fluid core location from external mag. obs. 78—32248
- ellipsoidal model, exact and asymptotic synthetic multiplet spectra 80—21673
- Eltanin fault zone, Pacific Ocean, crustal struct. from petrographic data 80—12376
- Eolian Islands, S. Thyrrenian Sea, basement structural trends from aeromagnetic and gravimetric data 78—40519
- middle Europe, Rayleigh waves phase vel. investigations 79—44136
- E. and central Europe, velocity-depth distribution in upper mantle 80—3980
- E.European Platform, study of asthenosphere by EM sounding 77—53021
- European upper mantle struct. from Vranch earthquake seismic wave travel-time curves 80—89998
- Explorer ridge, off W.Canada, marine geophys. survey 79—25224
- fault models, elastic wave radiation expts. 80—3938
- faults, size and distrib. rel. to earthquake elastic energy release and heat prod. 79—44106
- Fiji Plateau, underlying upper mantle struct. from second P-wave arrivals 77—60359
- Fiji-Tonga deep focus earthquakes, relative teleseismic P-wave residuals interpetation 78—36111
- fine-laminar section, rel. to seismic waves absorpt.-conditioned transition functions estimation *(Russian)* 79—53318
- fission theory for Moon origin 80—101536
- folded and crystalline basements of deep cavities, determ. from seismic data *(Russian)* 79—39692
- free oscillation data inversion, asymptotic approach 79—92624
- free oscillation of Earth, attenuation of radial modes 80—89966
- free oscillations, rot. and elliptical splitting 79—88257
- free oscillations of Earth, finite element modelling 80—51338
- Friuli area, LANDSAT-2 imagery of linear features 78—24284
- Fruili, crustal structure from 1976 October 13 aftershock 78—24265
- Galapagos Rift at 86°W, regional morphological and struct. anal. 80—26491
- Galapagos Rift at 86°W, rift valley sheet flows, collapse pits and lava lakes 80—21708
- Galapagos Rift at 86°W, volcanism struct. and evolution of rift valley 80—21707
- geoid anomalies and lithospheric thickness 79—84077
- geologic evolution of terrestrial planets 77—53442
- geological section prediction, appl. of seismic waves integral spectrum parameters *(Russian)* 79—8705
- global Earth tides and upper mantle struct. 79—25182
- Gondwana configuration in Early Palaeozoic, palaeomag. study of Argentina 80—89938
- gravimetric and deep seismic sounding, data interpretation *(Russian)* 79—39937
- gravitational field, external. of three-dimensional body, analytic continuation into interior *(Russian)* 79—34731
- gravity anomalies, Geos 3 satellite altimeter data 80—21612
- gravity anomalies, surface harmonic expansion coeffs. from orthogonal collocation calcs. 80—81801
- gravity anomaly from masses distributed over infinite regions, interpretation theory 80—82103
- gravity anomaly interpretation, direct and inverse problems soln. for hemispherical bodies *(Russian)* 79—35012
- gravity data inversion by compressed mass plane method *(Chinese)* 77—64175
- gravity field anomalies sources, depths determ. 79—16366
- gravity model improvement using Geos 3 (GEM 9 and 10) 80—3909
- Great Basin of Nevada and W Utah, struct. from seismic surface waves 78—73336
- Gutenberg model, corrections from freqs. of spheroidal eigenoscillations 77—52996
- Hawaiian Ridge, vel. struct. from earthquake travel times, Tau Inversion method 79—62467
- Himalayan mountain range central portion crustal struct. and geological significance *(Chinese)* 77—91066
- Himalayas adjoining Tibetan Plateau and Chinese mountains, crustal struct. 78—7600
- Hindukush region, crustal struct. from body wave data 79—96752

Earth structure continued
- SW.Honshu, Japan, crustal struct. derived from explosion seismic waves 79—74862
- horizontally layered isotropic media, long wave anisotropy study 80—12343
- horizontally stratified media sounding, geophysical problems unification 80—56622
- Hyderabad, India, peninsula shield crustal struct. from long period P-waves spectra 79—66667
- Iceland, crustal mag. layer thickness from studies of basalts from deep drill holes 77—60365
- Iceland, Skagi and Langjokull volcanic zones, petrology and structure 79—2195
- Iceland Plateau, deep crust and mantle struct. from surface waves dispersion 80—41413
- impact craters and astroblemes, morphology and struct. *(Russian)* 77—45000
- impulse response, seismic wavelet estimation via short-time homomorphic signal anal. 78—81426
- inclined media interface, effects on ground surface displacements due to longit. incident wave *(Russian)* 78—85485
- Indonesia, 1977 August 19 earthquake, IDA network obs. of attenuation and splitting, Earth struct. determ. 79—34754
- induced polarisation sounding, response of polarisable inhomogeneous sphere 79—44092
- inner core, Earth-Moon system three-body problem 78—45210
- inner structure and static deform., caused by external forces *(Hungarian)* 80—21606
- interior density determ. by max. entropy spectral anal. method 77—64465
- interior struct. rel. to geomag. secular var. 79—39647
- interior structure evolution 77—53444
- interior structure from seismic wave source antipodal region obs. 80—89972
- internal structure evolution, calc. 77—82137
- internal structure vars. due to evolution 78—85512
- inverse logarithmic-potential problem for contact surface, solvability in finite form 77—82025
- island arcs, curvature rel. to convergence vel. and subduction angle 78—81128
- central Israel, crustal structure for magnetotelluric data inversion 79—2196
- N.Italy, crustal structure and seismicity 78—24264
- Italy, crustal structure from deep seismic soundings 80—56417
- S.Italy, crustal structure from seismic refraction profile 77—33013
- NE Italy, piedmont area stresses and strains rel. to Friuli fault-plane solns. 78—24266
- NE.Italy, surface geology rel. to seismically active tectonic structures 78—24286
- N.E.Japan, upper mantle regionality from explosion seismic obs. 77—37167
- NE.Japan Arc, deep seismic zone double-planed struct. 78—77203
- NE.Japan Arc, double-planed deep seismic zone and upper mantle structure 78—77198
- Japan geosyncline outer margin, structural characts. and tectonisms around microcontinent 78—81139
- Japan islands and Sea of Japan, seismic structure 78—92807
- Japan-Kurile Arc, upper mantle P-wave vel. model 77—78132
- Jordan-Dead Sea Rift, crust and upper mantle struct. from seismic refr. data 80—26474
- Karelia magnetic anomalies rel. to crustal structure *(Russian)* 77—32986
- Kharkov-Yalta profile, crustal structure *(Russian)* 80—85622
- Kurile trench-Hokkaido rise system, flexure profile by plate model 80—72482
- La Malbaie area, Canada, upper crustal struct. lateral vars., teleseisms meas. 78—28187
- Laccadive uplifting zone, crustal struct., gravity field modelling *(Russian)* 80—3966
- Lake Baikal rift system 77—37163
- Laramide Wind River uplift, Wyoming, USA, gravity and seismic refl. data 80—21679
- lateral density inhomogeneities, min. depth 78—7596
- lateral inhomogeneities, detect. via seismic three-component registrations anal. *(German)* 78—32017
- lateral variations from free oscills. and surface waves 78—88799
- laterally inhomogeneous media, seismic body waves ray amplitudes calc. 79—44118
- layered Earth model, appl. to buried electrode resistivity data 79—29701
- layered Earth model, seismic prospecting inverse kinematic problem soln. using reciprocal points *(Russian)* 79—44268
- layered Earth model, seismic wavefront curvature 79—29712
- layered Earth model for resistivity sounding 80—85583
- layered model, synthetic seismograms for body waves in anisotropic media 77—49021
- layered transitional Earth, resistivity sounding 80—85584
- Lesser Antilles island arc, crustal struct., seismic refr. expt. 79—84139
- Liaoning Province, China, crustal struct. from gravity data *(Chinese)* 77—5142
- Liaoning Province, China, crustal thickness from gravity and seismic obs. *(Chinese)* 80—12349
- Ligurian Sea area, crustal and upper mantle structure 78—65209
- Liguro-Piemontes Alps, struct. anal. from terrestrial mag. field *(French)* 79—57896
- line masses depth estimation from residual Bouguer anomalies, via Backus-Gilbert min. distance criterion 79—44257
- linear inverse theory with a priori data 79—53580
- lithosphere, heterogeneities rel. to P-wave time and amplitude anomalies interpretation 78—96153
- lithosphere, lower, structure in USSR from explosion seismology 77—86836
- lithosphere, review of seismic anisotropy 77—49011
- lithosphere structure from seismic refr., influence of lateral vars. 77—21686
- lossless layered media, synthetic seismograms, time-domain state space models 80—12342
- Love number, determ. from random function of universal time 80—46120
- Love number changes during Earth model variations in static theory of tides 77—44951

Earth structure continued
Love number k, determ. from time-service obs., tides and nutation effects 79—96733
lower mantle inhomogeneities characts. from scatt. waves, correction 77—49042
magnetic anomalies due to inhomogeneities in Earth spherical model, results of mag. var. soundings 77—13056
magnetic anomaly field vertical intensity, autocovariance function analytic derivation for sources statistical distrib. *(German)* 79—34746
magnetic anomaly interpretation, bidimensional inhomogeneous problem soln. via Cauchy integrals *(Russian)* 79—35013
magnetic bodies, numerical soln. for inductive magnetisation and palaeomag. sounding inverse problem *(Russian)* 79—34747
magnetic field as probe of interior structure 80—36528
magneto-telluric surface impedance, calcs. by layered Earth model 80—56349
magnetometric resistivity anomalies, two-dimensional struct., mag. field determ. method 80—12334
magnetotelluric sounding, soln. for horizontally-inhomogeneous media using finite differences method *(Russian)* 79—44102
Malaguide complex, structural facing and Palaeozoic rocks 77—49046
Manicouagan impact crater, gravity study and upper crust density contrasts 78—81170
mantle, convective instability of many-layered models 79—25216
mantle, lower, compressional and shear vels. radial var. 78—73316
mantle, lower, lateral vars., seismic array evidence 79—20781
mantle, lower, struct. from radial seismic vel. anomalies identification 79—25209
mantle, seismic vel. variations, origins 80—81854
mantle, time dependent flow model 78—20369
mantle, upper, constitution, structurology of peridotite xenoliths in S.African kimberlites *(French)* 78—11889
mantle, upper, thermal and mechanical struct., continental and oceanic models 77—37169
mantle, upper, vel. cross sections from deep seismic sounding data 79—39677
mantle, velocity-depth structure, Central Europe 80—3976
mantle base lateral heterogeneity from PKP phases amplitudes 80—21675
mantle conductivity anomaly interacting with ionosphere current to form geomag. variation 80—30985
mantle discontinuities and P′P′ precursors 77—86806
mantle discontinuities effect on toroidal free oscills. 79—29713
mantle heterogeneity and mislocation patterns for seismic networks 77—81843
mantle lateral variations from LF eigenspectra data 78—36123
mantle plumes rel. to plate tectonics, graphic solns. 77—91081
mantle structure beneath Japan Sea 78—81118
mantle structure from P-residuals azimuthal var. in southern California 80—3954
mantle structure peculiarities rel. to nature of excess quadrupole moment 78—73334
mantle structure under north central Italy, Rayleigh waves 80—3977
mantle upper structure of Caucasus and Carpathians from seismic data 77—41009
media with inclined boundaries, seismic screening *(Russian)* 78—92794
E.Mediterranean, crustal struct., sedimentary layers 78—69311
E.Mediterranean, crustal structure model 78—24263
E.Mediterranean, deep struct. and tectonics 78—69309
E.Mediterranean, struct. and tectonic setting of Levant continental margin 78—69310
W.Mediterranean Basin, upper mantle structure from seismic profile 78—11841
Mediterranean region, struct. and tectonics, conf., Haifa, Israel (Aug.-Sep. 1976) 78—69306
meteoritic Earth model validity *(Italian)* 77—44982
Mid Atlantic Ridge, SW of Azores, deep seismic sounding results 78—3747
Mid-Atlantic Ridge, struct. at 45°N 78—73332
Mid-Atlantic Ridge crest at 37°N, crustal struct. 77—9378
Middle America Trench offshore Guatemala, seismic refr. and refl. meas. 80—26493
model based on torsional oscill. eigenperiods 80—90044
modelling, seismic sections construction using stacked recordings of controlled directional reception *(Russian)* 79—39960
models of upper mantle structure *(Russian)* 77—73697
models with single crust-mantle discontinuities, ray-mode duality for SH waves 78—77183
Moho, continental, throws and dips sounding by explosion seismology 80—85620
Moho P-wave velocity depth, regional distrib. from Rumania earthquake (1977 March 4) *(German)* 80—98256
monolayer model, calc. of surface seismic waves dispersion curves partial derivatives *(Russian)* 79—34764
Mossbauer effect appl., conference, Kyoto, Japan (Aug.-Sept. 78) 80—7199
Mount Rainier, Washington, underlying struct. from teleseismic body waves 80—31011
multilayered elastic medium, reflection seismograms for explosive source, theory 80—17233
New Hebrides arc-trench system, structure 80—72465
New Hebrides island arc, upper mantle struct. in arc convex side 79—74861
Newfoundland, Bay of Islands ophiolite complex, seismic vel. structure 78—40506
Newfoundland lithosphere structure from teleseismic PP-wave refls. 78—65210
Ninetyeast Ridge, seismic sounding with bottom seismographs and air guns 78—3748
nonspherical thermoelastic deformations of nonuniformly heated Earth 79—74869
north magnetic pole, 1975 position analytical determ. 78—92778
North Sea region upper mantle struct. from Rayleigh wave dispersion 78—36122
Norway, Moho depth determs. from spectral-ratio anal. of NORSAR long-period P-waves 77—86814
Novaya Zemlya crust and upper mantle model from Rayleigh wave dispersion data 79—84187
ocean basins, primordial, form. 79—20770
oceanic crust, evidence for low velocity layer at base 77—37164
oceanic crust, seismic vel. evolution 79—5457

Earth structure continued
oceanic crust, structure, composition and origin 77—29268
oceanic crust, structure from refraction expts. 80—3952
oceanic crust *(Russian)* 79—100822
oceanic lithosphere, apparent seismic velocity meas. rel. to struct. 77—2117
oceanic lithosphere, thickness from geoid anomalies across fracture zones 79—88231
oceanic ridges and trenches, polar wander excitation 79—16367
oceanic upper crustal structure from variable angle seismic reflection-refraction profiles 79—70761
oceanic upper mantle intrinsic heterogeneity effect on Rayleigh wave phase vels. 77—49022
Okhotsk and Japan Seas abyssal depressions, struct. and origin 77—37168
Ontong Java and Manihiki Pacific oceanic plateaus, seismic struct. 80—21680
Oregon, crustal and upper mantle structure from teleseismic P- and S-waves 77—91067
orogenic regions deep crustal probing by natural EM fields surface impedance vars. 77—13060
Oroville, California, crustal shear wave vel. struct. determ. from 1975 August 1 earthquake 79—16417
Oslo Rift, crustal structure from seismic refr. study 78—32037
outer core structure from SKS amplitudes and travel times 78—65208
outer core thermal regimes, consequences of gravitationally powered geomag. dynamo 79—39687
outer layers, lateral inhomogeneities rel. to surface wave propag., ray tracing appls. 79—66630
P-signal complexity from nuclear explosions and upper mantle struct. 77—56596
P-waves anomalous vels. in outer core rel. to struct. 79—48436
NW Pacific, upper mantle struct. and deep processes 77—37160
Pacific Ocean, Pn waves propag. rel. to lower lithosphere struct. 80—26459
E.Pacific Rise crest, crustal struct. vars. from seismic travel time inversion 77—60357
E.Pacific Rise crest structure from multichannel seismic reflection 78—40523
Pacific sea-floor topography and isostatic compensation mechanism (Hawaii region) 80—104945
Pacific upper mantle regionalized shear vel. models from Love and Rayleigh wave dispersion 79—53321
palaeoanisotropy in upper mantle 78—7602
Pamirs-Hindu-Kush upper mantle, vel. inhomogeneity, mapping by graphical method 80—77146
Papuan Ultramafic Belt, crustal structure 77—37166
Peking-Tientsin area, China, crustal struct. from gravity data, rel. to seismicity *(Chinese)* 78—61357
phase boundary equilib. position under horizontally varying surface loads 77—53017
phase boundary motion caused by surface temp. and press. excitations, rel. to vertical crustal movements 77—49040
PKP precursor data comparison from seismic arrays 79—25208
planar dipping structure effect on source and receiver responses for const. ray parameter 78—7571
plate tectonic explanation of Earth struct. 80—81855
potential field anomalies geodynamic interpretation, physically based source models *(German)* 79—34782
primitive mantle structure, Pb isotope study of layered intrusions 80—81847
PS-waves refl. from Moho 77—86809
Q-factor, determ. from Moon tidal accel. 79—16849
radial expansion of Earth, effect on palaeomagnetic data 80—56422
random inhomogeneities, seismic waves attenuation and scattering *(Hungarian)* 77—86791
refraction seismology, time term method anal. 79—66838
Reggio Calabria earthquake, 1975 Jan. 16, seismological results and geostructural appl. 77—49007
Reis crater, struct. from geoelec. Schlumberger soundings *(German)* 77—64207
Reykjanes Ridge, crustal struct. at 63°N from seismic meas. 79—66661
Rhenish Massif/Rhenohercynian zone, W Germany, crustal struct., seismic refr. data 79—48435
Sakhalin, magnetotelluric investigations, induction effects detect. methods and appl. *(Russian)* 79—39642
San Andreas fault, lower crustal structure determ. method 77—91284
satellite geodetic meas. methods and geophysical appl., review 79—66835
N.Scandinavia, compressional and shear wave anal. of lower lithosphere fine structure 80—3979
ScS multiple waves, attenuation operator 77—52995
sedimentary basins of continental margin and craton, conf., Durham, England (Apr. 1976) 77—21715
sedimentary layers, energy resource exploration via refl. seismology, book 78—96162
seismic anisotropy, investigations in USSR 77—49038
seismic body wave data and Earth models linear relationship 79—57885
seismic body-wave inversion method for Earth struct., using travel time and amplitude data 80—109108
seismic boundary images reconstruction, numerical models appl. *(Russian)* 79—39923
seismic bright spot anomalies, refl. waves spectral characts. *(Russian)* 79—53319
seismic determination, admissibility of soln. to multilayered dynamic problem without consideration of multiples 77—73668
seismic exploration travel times meas. method of seismically conjugate points 77—9368
seismic high-frequency Pn,Sn phases on ocean bottom seismographs, high efficiency propag. 79—16400
seismic investigation, new methods using common-point obs. *(Russian)* 79—74981
seismic precursors to PKKP, rel. to core-mantle boundary struct. 79—48409
seismic reflecting-refracting surface, binary holography kinematic principle *(Russian)* 78—92795
seismic reflectivity function, extraction via data deconvolution, book contrib. 79—92635
seismic refractor velocity determ., cause and nature of errors 80—56621
seismic sections, automatic transform. of seismograms and images *(Russian)* 78—49155
seismic shear-wave travel time for Earth struct. 80—81817

Earth structure continued
seismic velocity anomalies in mantle under N.Atlantic 77—49024
seismic velocity determination, overlying sequence stratification effect *(Russian)* 79—39961
seismic velocity structure, rel. to body waves focusing at epicentre antipode 79—16399
seismic wave field assoc. with fine structured Moho in continents and oceans 80—12361
seismic waves scattering, elastic scatt. theory rel. to coda of P 77—73684
seismology, appl. to Earth interior struct. determ., book 80—41962
seismology, rel. to body wave and free oscill. interpretations 77—73689
seismology, transmission synthetic seismograms direct inversion 79—29877
SH-waves ray-mode duality in Earth models with crust and mantle discontinuities 79—25213
shallow crustal struct. in S.Central America from seismic data 77—56609
shear deformation zones along major transform faults and subducting slabs thermal-mechanical struct. 78—73330
shear wave phase velocity and Q^{-1}, determ. from surface wave vel. and attenuation inversion 78—85491
shear wave velocity structure for spherically averaged Earth 79—92504
shield-like upper mantle struct. from long-period surface wave dispersion 77—56608
Shizuoka district, Japan, crustal struct., explosion seismology data 80—12359
Slate Islands, Lake Superior, probable meteorite impact structure 77—9427
W.Slovenia, tectonic structures, rel. to macroseismic effects 78—24254
solid three dim. models of gradient media by precipitation 77—64235
S.Spain, crustal struct. from deep seismic sounding *(Spanish)* 78—44795
strain tide spectroscopy, 30 m laser system, interaction mantle, liquid core 79—5440
strain tides, spectroscopy rel. to struct. and reson. behaviour 78—73301
stratified bodies, analytical interpretation of gravity and mag. $V_{zz}(V_\Delta,Z_a)$ anomalies *(Russian)* 79—39968
subcrustal lithosphere structural variation, explosion seismic profiles 80—3974
subducting lithosphere boundary determ. using ScS to P conversions 78—7572
subduction zones, three-dimensional struct. from stereoviews of seismicity 80—72452
submarine lithosphere, geophys., geochem. and petrological model 80—3994
subsurface EM profile from HF meas., reconstruction technique algorithms appl. 77—45199
Sunda trench and forearc basin, seismic study 80—72470
surface deformation detect., 500-m base laser interferometer 80—105087
surface ridge, scatt. of Rayleigh waves 77—78125
surface-wave phase vel. inversion for anisotropic structure 78—85482
Tadzhik depression and Glissar range, earthquake focus orientation, effect on P-wave 80—3940
Tashkent Palaeozoic crystalline basement, tectonic struct., gravity survey *(Russian)* 78—53610
tectonic provinces, rel. to mantle Rayleigh waves phase vel. and Q 79—74846
Thelon metamorphic front, cryptic suture in Canadian Shield 77—53023
thermal model 78—15982
thermal structure of plates and mantle convection 79—2197
thin surface sheet of variable integrated elec. cond., two-dimensional EM induction 79—16372
three dimensional seismic struct. of the lithosphere 77—33023
Tibetan Plateau, crustal structure from surface wave study 77—91068
tidal tilt obs. in N.Wales mine, strain-tilt coupling and Earth model 80—89926
Tirumalai hill range AP, porphyritic granite fracture pattern interpretation 79—44156
Tokyo, base rock depth, seismic wave obs. from explosions *(Japanese)* 77—64232
Tokyo, underground struct. from Yumenoshima explosions seismic waves obs. *(Japanese)* 77—41000
N.Tonga region, Wadati-Benioff zone morphology and complicated subduction closure model 80—90010
transversely layered isotropic media, seismic wave vel. calcs. 80—12344
Trivandrum, crust-mantle structure from Indian geomagnetic data 78—85520
SW.Tunguska syneclise, platform structure from gravity surveys 80—98289
W.Turkmenistan, density model of crustal structure *(Russian)* 78—69303
two-dimensional heterogeneities, linearised direct and inverse problems for plane SH waves *(French)* 79—84131
Ukrainian Shield, deep crustal structure from seismic studies *(Russian)* 79—48428
Ukrainian Shield, deep seismic sounding profile reinterpretation 80—56407
underparameterised models, anal. of linear inference theory 78—49000
United States, upper mantle seismic struct., inversion of body wave arrival times 79—53322
Uordan-Dead Sea rift, crust and upper mantle seismic study, transition towards Mediterranean Sea 79—79766
upper mantle, complex structures modelling by finite-element methods 77—5164
upper mantle, structure and HF spheroidal modes 79—8603
upper mantle, travel-time branches from Yellowknife seismic array data 78—65211
upper mantle beneath Eurasia and N.Atlantic and Arctic Oceans 78—85506
upper mantle of W.United States, P-wave vel. structure 78—61363
velocity-depth structure, using waveform inversion method 80—105060
Walvis Ridge, lithospheric struct. from Rayleigh wave dispersion 80—41412
Walvis Ridge, seismic refr. obs., crust and mantle struct. 77—78153
W.Washington, 1965 April 29, from crustal and upper mantle structure Puget Sound earthquake 77—91026
Wilkes Land, Antarctica, large gravity anomaly, no evidence for meteorite crater 80—26512
Wyoming, Wind River Mountains stress system 80—94492
Yakutia, magnetotelluric investigations, induction effects detect. methods and appl. *(Russian)* 79—39642

Earth structure continued
Yellowstone caldera, seismic evidence for chem. mantle plume 77—2105
Yellowstone National Park, USA, teleseismic delay anal., mantle structure 80—3981
Fe-Ni-Si core, form. and comp. 78—12112

Earth third layer *see Earth mantle*

Earth upper layer *see Earth mantle*

earthing
see also earth electrodes
birth monitoring by cardiotocography, interference effect by infusion pumps *(German)* 78—85416
checking instrument, meas. of resist. of ground at various levels and of earthing connections *(German)* 80—98936
choke-earthed surgical diathermy circuit analysis 79—20705
defibrillator ground-loop current elec. skin burn computer simulation 77—78039
ECG, grounded, resistance to coherent mains interference, exptl. evaluation 78—85419
ECG, grounded, standardisation of resist. to external cophasal power line interference for isolated patients 78—57085
electrical safety, one-day seminar for nurses 77—37701
electronic diagnostic apparatus, input earth isolation 77—48905
electrostatic kilovoltmeter errors in unearthed circuits 77—13773
fusion reactor, JT-60, fault current anal. in grounding system 80—99307
fusion reactor, JT-60, grounding system design 80—102313
fusion reactor, JT-60, grounding system pot. rise during lightning strike, anal. 80—102314
guarded double insulation, reduction of shock hazard of grounded elec. systems in hospitals 77—56497
ion plating, induction-heated source, arcing elimination by top coil grounding 79—47639
lightning protection, general principles 79—48536
patient's virtual earth and electrical interference monitor, electrophysiological signal degradation reduction 79—57800
Shiva laser, 25 MJ energy storage and delivery system 78—59038
spacecraft external surfaces, conductive materials for grounding 78—45187
PbSnTe-PbTe heterostructs., effect of electrical grounding on electron irrad. 78—60194

earthquake recorders *see seismometers*

earthquakes
see also seismology
Acapulco, 1974 October 6, short-period surface waves, strong ground motion 79—84124
acceleration hazard map, sensitivity to input seismic parameters 79—44111
acceleration simulation, random process 79—2186
accelerograms, amplitude spectra, statistical properties 79—44122
accelerograms, spectrum compatible, generation method 80—3933
acoustic emission techniques appl. to rock mechanics, rel. to earthquake prediction *(Chinese)* 78—24279
active continental margins, earthquake foci three-dimensional projection 80—72453
Aegean Sea and surrounding regions, earthquakes rel. to active tectonics 78—96181
E.Afghanistan, shallow earthquakes and tectonic activity 80—72444
aftershock bursts, as long-term precursors of strong earthquakes 80—41406
aftershock sequences, implications of dilatancy-fluid diffusion theory 80—85604
aftershock sequences, physical basis fault growth dynamics 77—21688
aftershock sequences, relocated, in Iran and Turkey, seismotectonic implications 79—44119
aftershock sequences, sidereal periods, χ^2 test 78—53622
aftershocks, stochastic modelling of earthquake freqs. *(Japanese)* 80—94480
aftershocks as Green's functions 78—44787
aftershocks of San Andreas fault system, viscoelastic stress recovery theory 80—36249
aftershocks with different focal mechanism to main quake, causes *(Chinese)* 80—89960
Agua Caliente Springs, California, 1973 September 13, aftershock series 79—12084
Alaska, 1964, deformation at Middleton Is. 10 years later 77—91018
Alaska, 1964, March 28, static displacement data inversion anal. 80—30998
Alaska, 1964, split free oscill. amplitudes 77—91024
Alaska, 1964 March 28, aquifer response to tidal forcing 78—73407
Alaska, 1964 March 28, attenuation meas. of split normal modes 79—84120
central Alaska, earthquakes focal mechanisms rel. to N.Pacific plate tectonics 79—79806
Alaska, Saint Elias earthquake within seismic gap (Feb. 1979) 80—109116
N.E.Alaska, telemeter obs. of seismicity 77—64217
Aleutian arc, tectonic blocks, episodic subduction, strain diffusion and magma generation 77—33037
Aleutian subduction zone seismicity, volcano-trench separation, rel. to great thrust-type earthquakes 80—21655
E. Alpine region, seismicity and earthquakes assoc. with Bohemian Massif-Carpathians contact zone 80—104888
Alpine region, tectonic stress directions, correl. with joint orientations 80—105052
Alps and adjacent areas, assessment of max. earthquakes 80—3950
S.America, earthquake migration, spectral anal. 80—85614
N.America, effect of craton on distrib. of seismicity and intraplate stresses 80—98248
N.W.America, peak acceleration, velocity, and displacement from strong-motion records 80—98246
S.Central America, shallow crustal struct. from seismic data 77—56609
E.Anatolia, 1976 November 24, field investigations 78—15974
N.Anatolian fault zone, earthquake migration and seismic gaps 80—85613
Andulasia, 1884 December 25, focal parameters, aftershock sequence 79—84178
animal behaviour before quakes, alternative explanations 80—85599
animals unusual behaviour before earthquakes, positive and negative reports 80—26455
anomalous aftershock sequences, physical model 78—77194

earthquakes continued
anomalous Eurasian earthquakes, spectral and magnitude characts. 77−73656
anomalous seismicity changes prior to rock bursts rel. to earthquake prediction 77−91052
Ansei, Japan, 1854 December 23, tsunami and crustal deform. *(Japanese)* 77−41001
Antarctica, seismicity meas. 77−86803
antiseismic calc., stochastic model appl. 78−96139
Asama Volcano, spectral studies of explosion earthquakes assoc. with 1973 eruptions *(Japanese)* 80−67340
aseismic uplift prior to earthquakes 78−7575
central Asia, age determ. via lichenometry 79−92505
central Asia, seismic moments of major earthquakes and average slip rate 77−86796
Aso, Japan, 1975 January 22 and 23, focal mechanisms rel. to active fault system *(Japanese)* 77−2107
Aso, Japan, 1975 January 23, seismic intensity distrib. *(Japanese)* 77−2106
N. Atlantic, 1972 May 13, focal parameters from Rayleigh wave study *(Spanish)* 77−86823
Mid Atlantic plate boundary between Iceland and Azores, seismicity and earthquakes 79−88266
atmosphere blow-off mechanism 77−29524
Atotsugawa Fault, Japan, seismicity and focal mechanism of local earthquakes *(Japanese)* 80−94482
Attica, New York, 1966 January 1 and 1967 June 12, source parameters 79−16379
Auburn Dam, case history for earthquake evaluation 79−88284
Australia, earthquakes and crustal stress meas. 80−51354
Australia, fault-plane solns. for three events, implications 80−46140
Australia, siesmic risk estimates 77−53009
Australia, stress state of upper crust 77−9387
automatic recognition and timing from single traces 79−66822
average dislocation temporal and spatial vars. before and after large earthquakes *(Chinese)* 78−61334
axisymmetric seismic response of thick circular plate supporting many rods, nuclear power plant appl. 80−1458
Azores (1980 January 1), aftershock sequence and present day tectonics 80−104911
b-value changes during movement on cut surfaces in granite, lab. expt., rel. to earthquake prediction 79−12109
b-values and seismic source models, tectonic stress vars. along active crustal fault zones 79−84150
Badra area, Iraq, microseismicity 80−56413
Baikal rift zone, seismicity and earthquake focal mechanisms 78−36115
Balkan earthquake provinces, largest magnitudes third asymptotic distribs. 79−39669
Balkan region, statistical estimation of largest possible earthquakes 77−21680
Baltic earthquake, October 1976, source mech., surface wave study 80−81830
Banda Sea (E.Indonesia), seismicity and fault plane solns. rel. to subducted lithosphere geometry 78−81131
barriers on earthquake fault, characterisation 80−21657
Basel, 1356 October 18, review, basic data 79−84181
beams, eqn. of motion of large amplitude vibration of beams *(Japanese)* 80−33511
Beaufort Sea area, tectonic setting and stress study 80−3931
Beijing area, earthquake stress field direction, composite nodal plane solns. *(Chinese)* 80−76910
Bellingshausen Sea earthquake, Feb. 1977, ocean ridge generated compression mechanism 80−46142
Bengough (S.Saskatchewan), 1972 July 24, seismotectonics 79−20757
biaxial slip of mass on foundations subjected to earthquake motions 77−54915
Blanco fracture zone, microearthquakes location determ. using sonobuoy arrays 78−40504
block faulting mechanism, geological and expt. studies 79−66692
Bob-Tangol, SE.Iran, 1977 December 19, surface rupture and mechanism 79−44114
body wave ground motion, generation of audible acoustic press. waves 77−9351
body wave spectral structure from WWSSN stations long period records 78−28174
body-wave magnitude, rel. to modified Mercalli intensity 80−36259
Bonin Is. earthquakes, two-parameter scaling of source spectra of Love waves 77−73642
book 79−12092
Borgarfjordur, W.Iceland, 1974 earthquake series, focal mechanisms and faulting 77−52988
Borrego Mountain, 1968 April 9, source model from body wave data 77−25644
Borrego Mt., California, earthquake, 1968 April 9, strong ground motion 77−73644
Brawley, California, 1976 November 4, strong ground motion modelling 78−92782
Brawley swarm, California, 1975 January, surface faulting 77−9349
Brawley swarm, California, 1975 January, tectonic implications 77−9348
Brawley swarm, California, 1975 January 25, strong-motion accelerograms 77−9350
Brawley-Imperial Valley swarm, 1975, Jan., source parameters 77−91051
Briones Hills, California, 1977 January 8, locations and magnitudes of earthquake swarm 78−65187
Briones Hills, California, geodolite meas. near earthquake 78−92803
Briones Hills, California, tilt obs. near earthquake 78−92802
E British Columbia, 1918 February 4, earthquake location and magnitude 80−3932
British Columbia, 1946 June 23, focal parameters redeterm. 79−16380
brittle fracture model, rel. to pore fluids and Q 79−39671
Burma and S China, seismicity and tectonics 80−89983
Burma-India border, 1970 July 29, source parameters from body waves 79−66649
California, 1857 January 9, assoc. slip along San Andreas fault 79−66633
California, 1857 January 9, felt effects, isoseismal map 79−84128
California, 1857 January 9, foreshocks 79−84129
California, 1906 April 18, strong motion recordings, reanalysis 77−91017

earthquakes continued
central California, 1972, February 24 and September 4, source parameters 77−2112
California, earthquake swarms and local crustal spreading along major strike-slip faults 79−66645
central California, self-potential vars. preceding earthquakes 77−52977
California 1857 earthquake, body-wave magnitude estimate 80−81840
California earthquake parameters, statistics and model 80−104891
Californian earthquakes, strong motions, Fourier and response spectra 77−56597
Canada, 1968 catalogue 77−49035
Canada, 1971 catalogue 78−85500
Canada, 1972 events 79−34757
Canada, 1973 annual list 77−91059
Canada, 1974 catalogue 78−40517
Canada, 1975 records 79−34758
Canada, 1977, catalogue 79−84164
E.Canada, passive margin, focal mechanisms 79−96741
W.Canada, seismicity, 1899-1975 period 79−5452
Canada, seismological research in Charlevoix region *(French)* 77−78116
Canadian earthquakes, 1976, catalogue 79−44139
Canal de las Ballenas, Gulf of California, 1975, July 8, aftershock obs. 78−20363
Caracas, Venezuela, 1967 July 29, multiple source event, tectonic implications 79−20761
Carlisle, 1979 December 26, fault plane soln., aftershock study 80−89977
Carpathian region, expected earthquakes, max. magnitude, seismo-tectonic anal. 77−53002
Carpathians, 1977, March 4, seismic processes charact. in preparation period *(Russian)* 78−48985
catalogue, global seismicity aspects 79−53320
catalogues, geographical distrib. of detectability of ISC data 80−109117
catastrophic earthquakes in Iceland 79−84175
catastrophic earthquakes occurrence and distrib. in Europe 79−88262
catastrophic earthquakes prediction, development monitoring via seismic b-value time and space scanning *(Chinese)* 79−12072
Caucasus, magnitude estimation of max. poss. earthquake 77−64219
Caucasus, max. possible earthquake and shakeability maps 77−70607
Central Asia seismicity, historical and modern data 80−36254
Central Mississippi valley, evaluation of earthquake hazard 78−11833
centrifuge modelling, experimental results 78−81429
Chagos-Laccadive Ridge, earthquake swarm and tectonic implications 79−16395
Chandler wobble, excitation by earthquakes and meteorological sources 77−78083
Chandler wobble, seismic excitation 80−26437
Chandler wobble excitation, theory of amplitude 77−90990
Charleston-Summerville area of South Carolina, Geological and geophysical studies of seismicity 78−11837
Chile, 1960, split free oscill. amplitudes 77−91024
Chile, 1960, time-domain obs. of split spheroidal and torsional free oscills. 79−12079
s. Chile, 1960 June 6, anomalous slow earthquake characts. 79−39662
Chile, 1960 May 22, attenuation meas. of split normal modes 79−84120
China, catalogue of historical earthquakes from 1177 BC to 1899 AD 77−40996
China, catalogue of instrumentally determined earthquakes 79−12081
China, crustal stresses rel. to earthquake sources *(Chinese)* 77−91016
China, earthquakes correl. with heliocentric planetary alignments 77−5136
China, earthquakes rel. to active faulting and tectonics 77−86848
China, geophysical methods of seismology and earthquake prediction *(Rumanian)* 80−8257
China, history of people's struggle against earthquakes *(Chinese)* 77−67171
China, investigation of sunspot period stability by anal. of ancient earthquake records *(Chinese)* 79−21253
China, isoseismals for large magnitude earthquakes 78−92788
NE.China, major earthquake occurrence rel. to Japanese activity *(Chinese)* 80−56370
China, pre-quake signs given by subterranean fluids *(Chinese)* 80−56409
China, prediction using probabilistic regressional estim. *(Chinese)* 77−91013
W. China, seismic vel. anomalies before and after strong and moderate earthquakes *(Chinese)* 77−91009
W China, seismic wave vel. anomalies before and after strong and moderate earthquakes *(Chinese)* 77−9340
China, seismicity and Quaternary faulting 77−40995
China, seismicity and seismotectonics characts. *(Chinese)* 79−16406
China, tectonic stress field rel. to plate movement 79−62478
S.W. China, tectonic stress field rel. to recent tectonic activity *(Chinese)* 77−91089
S China and Burma, seismicity and tectonics 80−89983
N.China precursory vars. in seismic b-values before large earthquakes *(Chinese)* 79−12073
S.China Sea, 1965 October 7, intraplate thrust earthquake 80−26461
Chinese earthquake catalogue for evaluation of seismic risk 80−36258
Chinese earthquake history, point process anal. 80−85612
Chu basin, weak earthquakes focal parameters spatial distrib. rel. to strong earthquakes 78−61348
Chu depression basin, seismicity changes with time 77−53003
Cienaga Road, California, 1972 December 12, small earthquakes high-freq. radiation directivity 79−66625
circular sources, source dimension, stress drop and radiated energy 80−98240
classification of earthquakes 79−74851
coda waves from local earthquakes, spectral anal., decay characts. 79−66639
Colima earthquake, Mexico, Jan. 1973, source mech. and aftershocks 80−81823
Collin, GDR, microearthquake records, event criteria *(German)* 78−57170
Colombia, 1970, July 31, spatio-temporal history of deep earthquake 77−86813
Colombia, 1970 July 31, isotropic seismic source observability 79−39663
Colombia (1970, July 31), deep earthquake source mechanism from free oscill. data 79−16394
column section seismic design subjected to three components of earthquake 77−38355

earthquakes continued
- computer modelling of strong motions 79−88296
- computer simulation 78−48987
- conditioning improvement by scaling the eqns. of condition 77−40998
- Conference, New Delhi, India (March 1978), prediction 80−85602
- coordinates determ. using Mir-1 computer of Urgent Reports Service 77−78440
- Corsica, 1978 April 3, seismotectonic anal. *(French)* 79−74838
- coseismic steps recorded on creep meters along San Andreas fault 77−53006
- cosmological apsects 79−57856
- Coyote Lake, California (1979 August 6), local magnitude and seismic moment determ. 80−104904
- crack propagation in rock, branching model 77−23918
- Crimea, crustal tectonic stresses rel. to weak earthquake foci *(Russian)* 78−11862
- crustal deformation, viscoelastic, by finite quasi-static sources 79−39686
- crustal deformation assoc. with fault form., finite element estimation *(Japanese)* 79−70759
- crustal fracture water, radioisotope long-term vars. rel. to earthquake prediction 79−62451
- crustal movements, conf., Palo Alto, California, USA (July 1977) 79−79785
- crustal structure under Sainte-Marie-aux-Mines observatory from analysis of converted P_s waves *(French)* 77−73666
- Cuba, seismic risk estimation 79−74852
- Dagestan, 1970 May 14, precision in hypocentre and dimens. determ. 78−57172
- damage for buildings caused by shaking, new data *(German)* 79−62444
- deep earthquakes, origin of P-signal complexity 77−52994
- deep-focus earthquakes, genesis rel. to olivine-spinel transition 77−5190
- deep-focus earthquakes, GH branch confirmed from PKP obs. 78−61341
- deep-focus events, theory of subduction slab 80−51375
- Delhi region, seismotectonics, earthquake data, strain distribs. 77−17044
- descending slab stress state, anal. of seismic source parameters 80−104946
- deviatoric stresses and earthquake occurrence at outer rise of oceanic trenches 79−84196
- Diablo Range, California, P-velocity models from earthquake and explosion arrival times inversion 79−12094
- differential thermal expansion of pore fluids, fracture propag. and microearthquakes 77−70641
- dilatancy induced fluid migration and vel. anomaly 77−33065
- dilatancy model of crustal deformation, precursory events 80−51347
- dilatancy rel. to earthquake prediction *(Chinese)* 79−88254
- dilatancy-magnetic effect, local mag. vars. assoc. with earthquakes *(Chinese)* 78−61333
- dilatancy-magnetic effect to explain earthquake assoc. mag. variation *(Chinese)* 80−56374
- dip slip fault, ground motion 80−72440
- disaster mitigation, USA-Japan cooperative research 78−36119
- dislocation distribution and static source parameters, nonuniform initial stress 79−79747
- dislocation source in heterogeneous crust, propag. study using dislocation model 80−101340
- dislocation source model in multi-layer medium, long-period surface vels. and accels. 78−11829
- displacement field close to focus of earthquake, calc. *(Russian)* 78−65204
- displacement potentials for motion in homogeneous isotropic elastic medium 80−21649
- Duhamel's integral numerical evaluation, earthquakes response spectra calc. appl. 79−21035
- dynamic faulting in half-space, three-dimens. numerical simulation 79−16376
- dynamic field of Haskell's rectangular dislocation fault model 79−48403
- dynamic parameters of seismic sources 79−84141
- dynamic rupture on three-dimens. fault with non-uniform frictions 78−77186
- dynamic shear crack propag. mechanics, earthquake source model 79−84147
- Earth tremors true velocities, determ. from seismograms 79−96743
- earthquake prediction, implications of crustal deform. migration 79−79800
- earthquake wave analysis program WAVE, DEMOS-E library program 78−92800
- Echzell/Wetterau, 1975 November 4, seismotectonics 78−40512
- Edo, Tokyo, 1855 November 11, study of historical documents *(Japanese)* 78−11814
- Edo, Tokyo, history of disastrous earthquakes *(Japanese)* 78−11815
- effects, 8th meeting of US-Japan Panel (Gaithersburg, MD, 18-21 May 1976) 77−78395
- El Golfo, Mexico, 1966 August 7, source mechanism 79−66627
- elastic energy release, heat prod., and Earth inertia tensor changes 79−44106
- elastic half space response to realistic faulting model 78−85486
- elastic plate, earthquake stress drops and plate driving stresses 77−91100
- elastic prestress in Earth interior, effects 78−77202
- elastodynamic near field of finite propag. transverse shear fault, comments 78−40507
- elastodynamic near-field of finite propagating tensile fault, correction 78−7577
- elastodynamic radiation from slip zone, ray method 78−73322
- elastoplastic ground motion during earthquake *(Japanese)* 79−70748
- electromechanical effects, model 78−32026
- electromechanical phenomena assoc. with earthquakes 78−36108
- elementary catastrophe theory modelling of Duffing's equation for seismic excitation of nuclear power facilities 79−31240
- EM precursors, appearance time rel. to earthquake energy 77−13061
- Emperor Trough, N.Pacific Ocean, 1968 April 28, example of intraplate seismicity on bathymetric features 80−30997
- energy and prediction rel. to quasi-periodic gravity vars. *(Russian)* 78−69275
- energy coupling between tectonic processes and earthquakes 78−73321
- energy rel. to lithosphere thickness in SW Tadzhikistan, forecasting 77−9367
- energy release rel. to plate motion, Chandler wobble and Earth rotation 78−28186
- energy spectra and data systems 77−41005

earthquakes continued
- energy-moment tensor relation for seismic energy estimation from point and line sources 78−7584
- engineering activity induced earthquakes, tectonic and tectonophysical conditions for occurrence 77−81802
- epicentral parameters determ., software package 79−48585
- epicentre and origin time determ. accuracy, Turkey 77−41002
- epicentre determ. using P-wave arrival-time differences 80−101328
- epicentre field structure in Baykal regions 77−33006
- epicentre location procedure for RESMAC seismic array 80−56616
- Essex, England, 1884, intensity and peak accelerations 77−70601
- Etorofu (Kurile Islands), 1958 November 6, great earthquakes stress drops, wave spectra and recurrence intervals 79−44116
- Eurasian earthquakes and explosions, discrimination using P codes spectral characts. 78−7576
- Europe, large earthquakes of 20th century 79−84165
- Explorer ridge, off W.Canada, marine geophys. survey 79−25224
- Fairbanks, Alaska seismic zone, earthquake migration 80−101330
- Farallan Escarpment, 1977, April 30, earthquake characts. and escarpment seismicity 78−32018
- fast epicentre location program 77−73653
- fault gouge composition effect on frictional sliding stability 78−3759
- fault mapping in Japan *(Japanese)* 80−51348
- fault mechanics and earthquake prediction, conf., Stanford, California, USA (Dec. 1977) 79−84143
- fault model, frictional, earthquake sequence 80−30992
- fault model (stochastic) 80−109114
- fault model for strong motion short period accel., vel. and displacement 80−104918
- fault motion, energy balance 77−56593
- fault motion and earthquake occurrence, numerical and lab. simulation 79−100815
- fault parameters, time-domain determ. from short-period P-waves 77−25643
- fault plane solution of shallow earthquake, using P and sP amplitudes 80−51335
- fault plane solution optimum search procedure using wave-amplitude data 78−45011
- fault plane solution using theoretical P-wave seismograms 78−11822
- fault plane solutions, from relative amplitudes of P and pP 77−73669
- fault plane solutions near Vancouver Island 80−12341
- fault plane with barriers, model 78−36110
- fault rupture model for seismic risk anal. 78−11810
- fault rupture propagation, theory 80−104910
- fault slip episodes near Hollister, California 77−86800
- fault slip stabilisation by coupled deformation-pore fluid diffusion 80−56378
- fault unstable slippage, facing media of different elastic consts. 80−72506
- faulting, HF seismic waves from crack models 78−11821
- faulting, simulation, expt. thermal fragmentation 78−96160
- faulting and gravitational energy 79−84121
- faulting inception in rock mass with weakened zone 77−33064
- faulting mechanism, role of inhomogeneities 80−51342
- faulting model, energy balance 77−44926
- faulting process and prediction using fracture mechanics *(Chinese)* 77−91012
- faulting processes in prestressed self-gravitating rotating Earth model, energy release 78−40499
- faulting rupture process, plane shear faulting model of earthquake *(Chinese)* 80−104893
- Fennoscandia seismic risk, by recurrence periods 80−21664
- Fiji-Tonga, 1957-71 deep-focus earthquakes, P-wave spectra 77−56600
- Fiji-Tonga, relative teleseismic P-wave residuals interpretation 78−36111
- fission reactors, structural anal. of lifting-off 79−596
- fluid-saturated rocks, elastic dilatancy and earthquake dynamics 77−21683
- focal coords. determ. in area of unknown crustal parameters 78−7585
- focal depth determ., indeterminacy elimination 77−73660
- focal depth determ. from long-period P-waves signal characts. 77−9355
- focal depths of distant earthquakes, determ. from fundamental mode and harmonic Rayleigh surface waves 80−21654
- focal mechanism changes rel. to revived faults 79−62450
- focal mechanism consistency, new parameter describing seismic activity *(Chinese)* 79−12074
- focal mechanism effect on P-waves dynamic parameters and magnitudes from longit. waves 78−73318
- focal mechanisms, classical seismological study techniques 80−76918
- focal mechanisms in Hollister area, S.Coast Ranges, California 79−79752
- focal process and frictional characteristics of deep-focus earthquakrs 79−44127
- focal processes for $M\leq7.5$ earthquakes 80−46143
- foci motion, typification technique, seismotectonic problems soln. 78−61350
- foci parameter determ. and seismic source spectral theory *(Rumanian)* 77−33010
- focus fracture vel. and body wave seismograms 77−70606
- foreshock sequence features rel. to ordinary earthquake swarm *(Chinese)* 77−86782
- foreshocks, characts. rel. to earthquake prediction and premonitory slip on faults 80−3944
- foreshocks, differentiation from earthquake swarms via seismic waveform variability *(Japanese)* 80−67342
- foreshocks spectral features 78−96147
- Fort Ross, California, earthquake sequence, March-April 1978 80−81824
- Fort Tejon, California (1857), tree ring growth and seismic disturb. 80−98259
- Fort Yuma, Arizona, 1852 November 29, location and intensity 79−16382
- Fourier amplitude spectra of strong ground acceleration rel. to MMI and geology 79−62442
- fracture at weak shock sources before and after strong earthquake 78−85487
- fractures generated in branching process, sizes, elementary anal. *(Japanese)* 79−70750
- frequency and energy relations 80−8258
- frequency data, anal., San Andreas fault region 78−44781
- frequency-magnitude distribs., universal shape regularity obs. 80−101333
- frequency-magnitude distributions 79−66648

earthquakes continued
frequency-magnitude relation, statistical parameters rel. to seismic zoning problems 79—44112
frequency-magnitude relations, in NGSDC earthquake data file 80—81838
frequency/magnitude prediction for selected surface regions 79—16415
friction and earthquake mechanics 79—20766
frictional heating on fault zone with finite thickness 78—36124
Friuli, 1975 and 1976 aftershocks and fault plane solns. 78—24251
Friuli, 1976, magnitudes and max. intensities 77—49034
Friuli, 1976 earthquakes, spatial and temporal distribs. 78—24242
Friuli, 1976 earthquakes, spectral analysis of aftershocks 78—24240
Friuli, 1976 earthquakes and aftershocks, epicentre migration 78—24237
Friuli, 1976 epicentre distrib. and focal mechanism 78—24241
Friuli, 1976 fault-plane solns. rel. to piedmont area stresses and strains 78—24266
Friuli, 1976 May 6, conf. (Udine, Italy, 1976 December 4-5) 78—24226
Friuli, 1976 May 6, excited soil accel. 78—24260
Friuli, 1976 May 6, fault area, dislocation, stress drop and seismic moment 78—24236
Friuli, 1976 May 6, field meas. of ground motion 78—24253
Friuli, 1976 May 6, focal mechanism 80—85603
Friuli, 1976 May 6, geology survey and landslide inventory 78—24249
Friuli, 1976 May 6, geotechnical aspects 78—24250
Friuli, 1976 May 6, German macroseismic intensity map 78—65203
Friuli, 1976 May 6, isoseismal map 78—24245
Friuli, 1976 May 6, macroseismic effects, European obs. 78—24247
Friuli, 1976 May 6, macroseismic effects in N.Slovenia 78—24254
Friuli, 1976 May 6, macroseismic obs. and isoseismal maps 78—24246
Friuli, 1976 May 6 aftershocks v_p/v_5 ratio and hypocentre determs. 78—24258
Friuli, 1976 May 6 and Sept. 15, focal mechanism computations 78—24256
Friuli, 1976 May 6 and Sept 15., liquefaction of sands and liquefaction during Friuli 1976 earthquakes 78—24280
Friuli, 1976 May 6-Sept. 15, revised hypocentres and magnitudes 78—24239
Friuli, 1976 May-Sept., strong motion records in Yugoslavia 78—24252
Friuli, 1976 October 21-26 aftershocks on Gemona-Trieste profile 78—24257
Friuli, 1976 strong shocks, focal mechanism solns. 78—24238
Friuli, crustal deformation in N.Italy 78—24267
Friuli, Italy, 1976 May 6, fault area, dislocation, stress drop, seismic moment 78—48975
Friuli, Italy, 1976 May 6, focal mechanism *(Italian)* 78—48974
Friuli, Italy, 1976 May 6, hypocentral parameters *(Italian)* 78—48972
Friuli, Italy, 1976 May 6, macroseismic data, hypocentral parameters *(Italian)* 78—48973
Friuli, Italy, 1976 May 6, macroseismic fields of main shocks 79—84173
Friuli, Italy, 1976 May 6, past and future seismicity, plate tectonic model 79—79753
Friuli, Italy, 1976 May 6, space-time distrib. 79—84116
Friuli, Italy, May 6, 1976, earthquake sequence 80—81822
Friuli, Italy, small shocks total durations and local magnitudes 79—34750
Friuli, Italy, tilting vars. and seismicity preceding 1976 May 6 earthquake *(Italian, English)* 78—48971
Friuli, level of macroseismic field from 1967 events 78—24259
Friuli, N.Italy, 1975-6, intensity, aftershocks and focal mechanism 77—49033
Friuli, response spectra analysis for different sites 78—24248
Friuli, safe areas following 1976 earthquakes, geological survey 78—24285
Friuli, stricken zone, geological emergency interventions 78—24287
Friuli 1976 precursors in Trieste horizontal pendulum obs. 78—24216
Friuli (1976, May 6), main earthquake isoseismals map 79—44137
Friuli (1976, May 6), precursory aerosol anomalies 79—16407
Friuli accelerogram processing and analysis, strong motion records 78—24231
Friuli aftershocks, focal depth determ. using late arrivals 78—24243
Friuli aftershocks, temporal var. of V_p/V_s ratio *(French)* 77—70600
Friuli aftershocks of 1977, fault-plane solns. and hypocentral distrib. 80—85597
Friuli earthquake, 1976, seismic response of different recording sites 80—41379
Friuli focal area, Italy, seismic body-wave dispersion 80—36267
Friuli shocks recorded in Netherlands 78—24255
Friuli-Venezia Giulia region, A.D. 365-1976 earthquake catalogue 78—24230
Fruili, crustal structure from 1976 October 13 aftershock 78—24265
Fruili, Italy, 1976 May 6, seismic study, geodynamics 79—84174
fusion reactor, finite element anal. of structural response of superconducting magnet 77—3166
G-type seismic waves generation 79—66624
Galway Lake, 1975 June 1 aftershocks, hypocentres and shallow crustal vels., phase time inversions 80—21634
Galway Lake earthquake, California, 1975, search for P-wave vel. variations before and after 77—40997
Garm region, weak earthquakes space-time sequence 80—21653
Gazli, 1976 May 17, geomag. field vars. obs. 79—57859
Gazly, 1976 May 17, search for seismomagnetic effect 80—26463
Gediz, Turkey, 1970, March 28, resonant period effects 77—70602
Gemona-Fruili, 1976 May 6, engineering seismology aspects 78—24228
generation mechanism *(Japanese)* 78—28178
Genroku, Japan, 1703, tsunami inundation heights on South-Kanto coast *(Japanese)* 77—2121
geodesy, artificial satellite laser ranging, high precision, earthquake anal. 80—98215
geodesy contributions to geodynamics *(German)* 78—81101
geodynamic monitoring and earthquake research, radiointerferometry appl. 80—31151
geological conditions rel. to max. accel., max. vel. and source distance 77—9360
geological faults, fracture, creep and strain 78—69345
geological faults and shear zones, assoc. deep focus earthquakes 80—61786
Georgia Strait, British Columbia, seismic risk maps 79—88274
geothermal steam, ^{222}Rn emanations, rel. to seismic activity 78—11832
Geysers geothermal field, California, explosions and microearthquakes study 80—3964
global geodynamics, Canadian contribs., 1971-79 period. 80—8262

earthquakes continued
global location using minimum information *(German)* 80—56627
global variation of great shallow quakes, space-time distrib. 80—21662
Goat Mountain earthquakes, California, 1975, search for P-wave vel. variations before and after 77—40997
Gorda Ridge spreading centre, microearthquakes and active faulting, sonobuoy array meas. 78—85494
Gore Range (Summit County, Colorado), Quaternary geology, surface faulting and earthquake hazard 79—2238
granite microfracture, source process rel. to earthquake prediction 80—104919
gravity effects on earthquake sources exhibiting anelastic vol. changes 78—57176
gravity variations before and after 1975 Haicheng and 1976 Tangshan earthquakes 79—57842
great earthquake occurrence, chaos theory of fault block behaviour 80—72448
great earthquakes, chaotic behaviour, coupled relax. oscillator model, billiard model and electronic circuit model 80—94462
great earthquakes, R-waves initial phase anal. 80—41405
great shallow earthquakes, 1953 to 1977, magnitudes 80—85617
great shallow-thrust earthquakes rel. to volcanic activity at convergent plate margins 78—7588
Greece, lithospheric model for earthquake interp. 78—3726
Greece area, shallow earthquakes intensities attenuation with distance 79—44107
ground motion, mechanisms and prediction 78—40516
ground motion *(Japanese)* 78—28179
ground motion parameters for moderately strong earthquakes 79—88305
ground motion simulation and spectral representation using non-stationary amplitude modulated mathematical model *(Spanish)* 80—56397
ground movement reconstruction from earthquake recording 78—49165
ground-response maps for Tonopah, Nevada 79—12086
Guatemala, 1976 February 4, aftershocks 77—9364
Guatemala, 1976 February 4, rel. to Quaternary faulting along Caribbean-North American plate boundary 79—79804
Guatemala, 1976 February 4, secondary faulting at end of strike-slip fault 80—21636
Guatemala, 1976 February 4, tectonic aspects 77—2137
Guatemala, 1976 February 4, tiltmeter obs. 79—16363
Guatemala (1976, February 4), seismological aspects 78—85493
Guatemala City, 1976 February 4, landslides, implications for seismic hazard reduction 79—88276
Gulf of California spreading centres, earthquake swarms study 77—52987
Gulf of California transform fault aftershock sequences, sonobuoy and teleseismic study 77—25651
Haicheng, 1975, Feb. 4, V_P/V_S variations before and after *(Chinese)* 77—37140
Haicheng, 1975, Feb. 4, variations in teleseismic P-wave residuals during previous months *(Chinese)* 77—37139
Haicheng, 1975, February 4, rupture analysis method *(Chinese)* 80—76911
Haicheng, 1975 February 2, associated gravity field vars. *(Chinese)* 78—61332
Haicheng, 1975 February 4, spectral changes of foreshocks and aftershocks *(Chinese)* 77—91010
Haicheng, China, 1975 February 4, dislocation model of foreshocks *(Chinese)* 77—9338
Haicheng, China, 1975 February 4, ground surface deform. *(Chinese)* 78—24222
Haicheng, China, 1975 February 4, obs. of prior anomalous meteorological phenomena *(Chinese)* 78—24224
Haicheng, China, 1975 February 4 prediction, US report 77—78109
Haicheng, China, source processes of Feb. 1975 event 80—81828
Haicheng, Liaoning Province, 1975, Feb. 4, focal mechanism *(Chinese)* 77—37138
Haicheng, source parameters for small earthquakes *(Chinese)* 77—91014
Haicheng (China) 1975 February 4, physical interpretation of prediction 77—49028
Haicheng Earthquake, 1975, precursory sea level changes *(Chinese)* 80—51331
Hawaii, 1975 November 29, strong motion and damage report 77—73658
Hawaii, 1975 November 29, tsunami numerical anal. by finite-element method 80—72449
Hawaii, Honomu, April 26, 1973, subcrustal quake 80—81821
Hawaii earthquake, Nov. 1975, low dip angle faulting mechanism 80—56406
Hawaiian Ridge, vel. struct. from earthquake travel times, Tau Inversion method 79—62467
hazard mapping, Bayesian model 80—56391
hazard model for Reno, Nevada 79—88285
hazards 79—62441
hazards warning, US Geological Survey's role 79—84488
Hebgen Lake, 1959, recent vertical crustal movement 78—28212
Hellenic arc earthquakes, fault plane mechanisms rel. to E.Mediterranean area neotectonic evolution 80—56451
Hengill-Hellisheidi area, SW. Iceland, seismicity obs. 80—89976
HF coda waves of local earthquakes, Stone Canyon, California, temporal trend in attenuation 79—57861
N. Hida region, Japan, seismicity and focal mechanism of local earthquakes *(Japanese)* 80—94482
Hidaka mountain region, Hokkaido, Japan, unusual seismic waves from shallow quakes *(Japanese)* 80—94477
Himalayan, body wave and local magnitudes relationship 77—66890
Himalayan mountain front NW termination, active tectonics from microearthquakes 78—40505
Himalayan region, body waves spectral anal., earthquake source parameters 79—39660
Himalayas, seismicity, earthquake mechanisms and tectonics 78—40514
Himalayas adjoining Tibetan Plateau and Chinese mountains, crustal struct. 78—7600
Hindu Kush region, microearthquake seismicity and fault plane solns. 80—72446
Hindukush, Baluchistan arc, seismotectonics and struct. (1890-1970) 80—104922
Hollister, California, 1974 November 28, preceding microearthquakes fault-plane solutions 80—3936
Hollister, California, 1974 November 28, teleseismic residuals 77—9356

earthquakes continued
- Hollister, California, time and magnitude relations for three microaftershock series 77—56585
- Hollister, California (1974, November 28), localised geomag. field vars. as precursors 80—104912
- NE.Honshu, Japan, crust vel. struct. from earthquake data 80—76937
- Honshu, Japan, deep seismic zone and plate tectonics 80—8269
- Hopei Province, China, earthquake risk *(Chinese)* 77—91015
- horizontal ground acceleration, Fourier amplitude spectra estimation 79—16389
- horizontal ground motion, two-dimensional, evaluation for structs. design 79—48419
- Horse Canyon earthquake, California, stress-release process 80—56387
- hydrodynamic press. on sloping dams during earthquake, momentum method 78—73412
- hydrodynamic press. on sloping dams during earthquake exact theory 78—73413
- hypocentre and dimensions determ., precision 78—57172
- hypocentre coordinates and longit. wave vel. determ. *(Russian)* 79—66623
- hypocentre location, resolution of small ocean bottom seismic networks 78—85713
- hypocentre parameters in Kanto District, Japan *(Japanese)* 80—94475
- hypocentres inverse problem soln. for local tridimensional network *(French)* 77—56738
- Hyuganada, Japan, 1961 and 1968, assoc. local sea level changes 77—17042
- Iberian Peninsula, 1977 earthquakes and seismicity *(Spanish)* 80—36270
- Iceland, 1976 January 13, focal mechanism solns. 77—81812
- Iceland, 1976 January 13, focal mechanism solns. reanal. 79—44140
- N.Iceland, major rifting episode with intense earthquakes, ground deform. and magmatism 77—37175
- N.Iceland, microearthquakes 77—81801
- Iceland, statistical anal. of damaging earthquakes and volcanic eruptions, (1550 to 1978) 80—89975
- Iceland, weak earthquakes in northern part of rift zone 78—85496
- Icelandic plate boundary rift and earthquake activity *(German)* 79—5467
- identification of $m_b \geq 4.5$ earthquakes, adequacy of available data 78—11809
- Idrija, Yugoslavia, 1511 March 26, seismological parameters reconstruction 79—84180
- imminent earthquake precursors, anomalies and errors statistical anal. *(Chinese)* 80—104895
- Imperial Valley, California, 1973, microearthquakes assoc. with Mesa geothermal anomaly 77—52992
- India, focal mechanism solns. rel. to south-central Asia large-scale Cenozoic tectonics 80—17246
- N.India, magnitude, intensity and radius of perceptibility relations 78—32021
- NE.India, seismicity and focal mechanisms rel. to faults and tectonics 78—24221
- India, seismotectonics 78—44782
- NE.India, teleseismic P-wave residual anal. at Shillong, rel. to earthquake prediction 80—104921
- Indian deep-focus earthquakes, P-wave travel times 79—2193
- Indian deep-focus earthquakes, S times 78—77188
- Indian Ocean triple junction region, microseismicity 78—32020
- Indian subcontinent collision with Eurasia 77—78146
- Indonesia, 1977 August 19, Earth free oscill. Q-value 80—67346
- Indonesia, 1977 August 19, effects in W.Australia 80—46139
- Indonesia, 1977 August 19, IDA network obs. of attenuation and splitting, Earth struct. determ. 79—34754
- Indonesia earthquake exciting free modes, 19th Aug. 1977 gravimeter obs. 80—61767
- induced versus natural earthquakes in geothermal area, discrimination 80—101332
- instability on strike-slip fault 79—84144
- intensity determ., oscillation duration effect 78—24262
- intensity of earthquakes, concept and appl. *(Chinese)* 79—62437
- intensity prediction, fallacies in current methods 79—88292
- intraplate, apparent stress and stress drop 77—91050
- intraplate earthquake swarms in Greenland and adjacent continental regions 80—26466
- intraplate seismicity, zones of weakness, alkaline magmatism and tectonism 79—74882
- ionospheric disturbances accompanying earthquakes and explosions 80—36451
- ionospheric plasma disturbance due to earthquakes and volcanic eruptions 80—36453
- Iran, attenuation of intensities 79—92497
- W.Iran, earthquake swarms, 1971-73 period *(French)* 78—32028
- Iran, premonitory crustal vel. ratio changes 78—32029
- Iran, relocation of epicentres 78—40501
- Iran, seismic waves from Iranian quakes, excitation and attenuation 80—104900
- S.Iran (1976, March 16), seismic waves group vel. anal. rel. to crustal struct. 78—81111
- Iran and Turkey, focal and seismicity depth determ. errors 80—61779
- Iranian earthquakes, instrumental and relocated epicentres evaluation 79—88258
- Iraq, Badra area, (1975 November-1976 March) microearthquake study 79—88268
- Iraq, microearthquakes recording 77—21689
- Iraq, seismicity and seismotectonics, 1900-72 period 77—73665
- N Italy, 1976 May 6, fault-plane soln. and Eastern Alps tectonics 77—64228
- Italy, earthquake prone areas, pattern recognition 80—56411
- Italy, isoseismic area and earthquake magnitude relations 78—65196
- Italy, precursory seismicity to strong earthquakes 80—104884
- S.Italy, seismic risk map preliminary results 79—44113
- Iwate-Oki (Japan), 1968, June 12, focal mechanism 77—78123
- Izu Peninsula, 1974, May 16, aftershocks spectral anal. 77—56606
- Off-Izu Peninsula, 1974 May 9, seismic waves attenuation in aftershock region 80—76926
- Izu Peninsula, Japan, active faults in Amagisan area *(Japanese)* 78—96164
- Izu Peninsula, Japan, crustal uplift, Mogi model, related gravity change *(Japanese)* 78—96165

earthquakes continued
- Izu Peninsula, Japan, earthquake swarm epicentres distrib. rel. to Bouguer anomaly *(Japanese)* 78—96144
- Izu Peninsula, Japan, earthquakes induced by 1974 May 8 Izu-Hanto-oki earthquake 79—66650
- Izu Peninsula, Japan, field work on recent crustal activity, rel. to earthquake prediction *(Japanese)* 78—96140
- Izu Peninsula, Japan, geomag. variations rel. to earthquakes *(Japanese)* 80—41396
- Izu Peninsula, Japan, gravity change assoc. with earthquake swarm *(Japanese)* 78—96123
- Izu Peninsula, Japan, gravity obs. rel. to Jan. 1978 quake *(Japanese)* 80—41394
- Izu Peninsula, Japan, groundwater geochem. in crustal uplift area, rel. to earthquake prediction *(Japanese)* 78—96242
- Izu Peninsula, Japan, obs. of earthquake swarm, 1975-77 period *(Japanese)* 78—96141
- Izu Peninsula earthquake mechanisms, Japan 80—12345
- Izu-Hanto-oki, Japan, 1974, precursors 77—53010
- Izu-Hanto-Oki earthquake, May 1974, precursory resist. changes 80—51336
- Izu-Oshima earthquake, Japan, Jan. 14 1978, 'quake parameters 80—61763
- Izu-Oshima kinkai earthquake, 1978, fore- and aftershock distrib. *(Japanese)* 80—41383
- Izu-Oshima-kinkai earthquake, 14 Jan. 1978, aftershocks and crust struct. *(Japanese)* 80—41384
- Izu-Oshima-kinkai earthquake, 14 Jan. 1978, parameters of event 80—41381
- Izu-Oshima-kinkai earthquake, 14 Jan. 1978, seismic intensity and damage questionnaire survey *(Japanese)* 80—41388
- Izu-Oshima-Kinkai earthquake, 1978, foreshock and aftershock activity *(Japanese)* 80—51349
- Izu-Oshima-kinkai earthquake, accompanying tsunami, source mechanism 80—41393
- Izu-Oshima-kinkai earthquake, Jan. 1978, associated 73 Hz elec. resist. changes *(Japanese)* 80—46133
- Izu-Oshima-kinkai earthquake, Jan. 1978, damage, intensity and faulting *(Japanese)* 80—46136
- Izu-Oshima-kinkai earthquake, Jan. 1978, fault mechanism 80—41390
- Izu-Oshima-kinkai earthquake, Jan. 1978, foreshocks of Oshima Volcano *(Japanese)* 80—46138
- Izu-Oshima-kinkai earthquake, Jan. 1978, groundwater chem. and temp. changes *(Japanese)* 80—46134
- Izu-Oshima-kinkai earthquake, Jan. 1978, precursory elec. fields obs. *(Japanese)* 80—46131
- Izu-Oshima-kinkai earthquake, Jan. 1978, precursory elec. resist. of Oshima Volcano *(Japanese)* 80—46132
- Izu-Oshima-kinkai earthquake, Jan 1978, precursory geomag. variations *(Japanese)* 80—41369
- Izu-Oshima-kinkai earthquake, Jan. 1978, precursory groundwater level changes *(Japanese)* 80—41391
- Izu-Oshima-kinkai earthquake, Jan. 1978, precursory mag. field changes *(Japanese)* 80—41395
- Izu-Oshima-kinkai earthquake, Jan. 1978, precursory mag. variations and electricity *(Japanese)* 80—41397
- Izu-Oshima-kinkai earthquake, Jan. 1978, road cutting landslips *(Japanese)* 80—46137
- Izu-Oshima-kinkai earthquake, Jan. 1978, surface rupture obs. *(Japanese)* 80—46135
- Izu-Oshima-kinkai earthquake, Jan. 1978, tsunami source mechanism *(Japanese)* 80—41392
- Izu-Oshima-kinkai earthquake, Japan, 14 Jan. 1978, seismic waves anal. *(Japanese)* 80—41385
- Izu-Oshima-kinkai earthquake, Japan, Jan. 1978, aftershocks and main shock ground accel. *(Japanese)* 80—41386
- Izu-Oshima-kinkai earthquake, Japan, Jan. 1978, associated surface faulting 80—41408
- Izu-Oshima-kinkai earthquake (1978), precursory Rn changes 80—94472
- Izu-Oshima-kinkai earthquake of Jan. 1978, pre- and post-event seismicity *(Japanese)* 80—41382
- Izu-Tokai District, Japan, tectonic activity rel. to earthquake prediction *(Japanese)* 78—96145
- Jan Mayen, 1975 April 16, focal mechanism solns. reanal. 79—44140
- Japah, earthquake records in 'Diary of Librarians of Edo Bakufu (Feudal Government)' 78—65200
- Japan, 1974 to 1975, converted waves appl. to deep crustal struct. determ. 80—30999
- central Japan, conductivity anomaly changes rel. to earthquake occurrences 77—2102
- Japan, deep seismic zone cross-section beneath NE Honshu 80—3951
- Japan, geomagnetic secular change anomalies rel. to tectonic activities 77—2091
- Japan, historical earthquake records 77—25659
- SW.Japan, intraplate seismicity before and after great earthquakes 80—21663
- SW.Japan, major earthquake focal mechanisms rel. to tectonics 78—11827
- Japan, major earthquake occurrence rel. to NE.Chinese activity *(Chinese)* 80—56370
- Japan, map of historical earthquake disaster areas 77—41003
- Japan, nontidal gravity changes during earthquake activity 79—92471
- Japan, regional distrib. of earthquake risk 78—36116
- Japan, regional distrib. of max. earthquake motions 79—62461
- Japan, seismic activity research using catalogues of destructive earthquakes *(Japanese)* 77—17037
- Japan, seismicity index maps, rel. to earthquake risk 78—36117
- Japan, statistics of earthquakes energy release (1915 to 1978) 80—94471
- Japan, strongest possible earthquake determ. 77—9365
- NE.Japan Arc, deep seismic zone double-planed struct. 78—77203
- NE.Japan arc, seismic activity, earthquake prediction research 79—57875
- Japan arcs, time-predictable recurrence model for large earthquakes 80—85598
- Japan Sea, 1973 September 29, higher-mode Rayleigh waves studied as individual seismic phases 79—62440
- Japan Sea, historical tsunamis behaviour and source a areas 78—65198
- Japan seismicity, 1885 to 1925, catalogue of $M \geq 6$ earthquakes and smaller, damaging, earthquakes *(Japanese)* 80—67341
- Japanese earthquakes, 1901 to 1925, instrumental magnitudes *(Japanese)* 80—94484

earthquakes continued
  Japanese Islands region, earthquakes and mechanisms data compilation *(Japanese)* 80—67332
  Japanese prediction studies, building design and location, review 78—32014
  Jordan Rift Valley, macroseismic study and structural damage of major earthquakes 78—65190
  Kaj Darakht, Iran, 1923 May 25, epicentre determ. 79—84113
  Kalapana, 1975 November 29, intra-plate event rel. to geothermal processes 79—39664
  Kalapana earthquake, Hawaii, localised compressional vel. decrease 78—65206
  Kamchatka, 1964 December 26, anal. of oceanic Sa seismic waves 77—73670
  Kamchatka-Commander region, focal mechanisms 77—91048
  Kandalaksh Gulf region, White Sea, earthquake recorded in 1542 79—74854
  Kangzhuang-Dachang region near Peking, deep struct. and earthquake foci *(Chinese)* 80—56415
  Kanto, Japan, 1923, Sept. 1, anomalous crustal strain before quake 80—85616
  Kanto, Japan, 1923, tsunami inundation heights on South-Kanto coast *(Japanese)* 77—2121
  Kanto Distict, Japan, earthquakes rel. to countercurrent accompanying descending Pacific plate *(Japanese)* 80—94514
  Kanto district, definition and characts. of seismically active regions *(Japanese)* 78—96148
  NW Kashmir, 1972 September 3, aftershock sequence 77—49005
  Kawazu, Japan, 1976 August 18, damage and seismic intensity *(Japanese)* 78—96142
  Kawazu, Japan, 1976 August 18, damage and seismic intensity distrib. *(Japanese)* 78—96143
  Kern County, 1952 July 20, analysis of source and medium effects on strong motion observations 79—88299
  Kern County, California, 1952 July 21, local magnitude determ. 79—12087
  Kern County, California, (1952, July 20) precursory seismicity and small quakes 80—104902
  Khurgu, Iran, 1977 March 21, field report, seismotectonics 79—12083
  kinetic shear resistance, fluid pressures and radiation efficiency during faulting 77—91054
  Kinnaur, Himachal Pradesh, India, 1975 January 19, fault-plane soln. 78—96161
  Kirishima volcanic area, Japan, 1975-76 earthquake swarms *(Japanese)* 77—64211
  Komyo Fault, central Japan, fault-forming process 77—2129
  Koyna, 1967 December 10, temporal var. of body waves travel time ratio 79—5456
  Kuril Trench area, evidence for high vel. zone from ocean bottom seismometer obs. 78—48999
  Kurile Island earthquake, seismic quiescence precursory 80—85610
  La Malbaie, Quebec (1924-1978), epicentre relocation 80—104903
  Labrador Sea, 1971, December 7, surface-wave study 77—91040
  Lacq, France, petroleum exploitation rel. to non-natural earthquakes *(French)* 80—104892
  Lake Jocassee, S.Carolina, seismicity rel. to Rn content of groundwater 80—94466
  Lake Jocassee area, S.Carolina, seismicity, earthquake prediction algorithms 80—51345
  Lake Keowee, S.Carolina, USA, 1978 earthquake swarm 80—36255
  Lake Mead, Nevada-Arizona region, earthquake monitoring 77—25653
  Lake Ontario, 1967 June 13, source parameters 78—36105
  Lake Oroville, reservoir-induced pore pressure and seismic activity 79—2190
  large thrust earthquakes and tsunamis, implications for fore arc basins development 79—57905
  Lassen Volcanic National Park, California, 1976-8 seismic events 80—36257
  Lesser Kurile Ridge region, 1973 June 17, focal mechanism 77—53001
  Liaoning Province, China, crustal thickness from gravity and seismic obs. *(Chinese)* 80—12349
  Lice, E.Turkey, 1975 September 6, faulting mechanism 77—78128
  light emission by atmosphere, explained by chemiluminesc. of gas released from rocks 80—61906
  Lima, Peru, 1974 October 3, damage distrib. 78—44785
  Lima, Peru, 1974 October 3, intensity distrib. 78—44784
  Lipari, Eolian Islands, seismic response of local earthquakes rel. to crustal struct. 78—40494
  Lisbon, 1955, isoseismal map from Spanish data 79—84179
  Livermore, California, 1977 June 22, strong motion records 79—16390
  local coda mag. rel. to duration, moment and local Richter mag. 80—21632
  local earthquakes coda, Q-estimates 80—104899
  local magnitude, determination method from seismoscope records 80—56393
  local magnitude determ. from strong-motion accelerograms 79—12290
  local seismic foci, soln. of inverse problem 79—53582
  location accuracy depend. on number of seismic stations 78—32025
  location of strong earthquakes using information processing 77—73856
  Lompoc, California, 1927 November 4, epicentre location 79—84127
  Lompoc, California, 1927 November 4, source mechanism from geodetic data 79—84126
  Lompoc, California, 1927 November 4 earthquake and aftershocks 80—21638
  longitudinal and transverse wave characts., shearing motion along pre-existing fracture 77—64220
  Love waves, contribution to strong ground motions 79—88302
  Lubin, Poland, 1977 March 24, source study of mining tremor 80—41377
  macroseismic aspects of event intensities 78—24232
  macroseismic data processing and interpretation 78—61583
  magnitude 8 earthquakes off Pacific coast of Japan, possible prediction *(Japanese)* 77—86824
  magnitude calc. method for seismograph recordings during early 20th century *(Italian)* 79—84118
  magnitude calibration function for core phases, PKP1-PKP2 caustic 78—40509
  magnitude correl. with focal parameters, theoretical basis 80—101338
  magnitude determ. from PKIKP calibration curve 77—64222
  magnitude determ. from seismograms by Fourier anal. 77—73655

earthquakes continued
  magnitude determ. from surface and body waves, calibrating curves for different instruments 78—57173
  magnitude determination from longit. core waves *(German)* 77—70603
  magnitude of great earthquakes, 1837-1974, from tsunami data 79—79745
  magnitude rel. to rupture length, regional variations 80—81837
  magnitude rel. to tsunami height, empirical relation 80—94461
  magnitude scale, renormalisation 78—15977
  magnitude scale based on strong-motion horizontal particle vel. 80—81836
  magnitude scale structure from filtered broadband P-wave records 79—92509
  magnitudes from ultralong period seismometer records 77—44928
  Makran coast, Iran and Pakistan, large-magnitude earthquakes recurrence, crustal uplift 79—79754
  Makran region, seismicity var. rel. to large earthquakes 80—85611
  Malibu earthquake, Jan. 1979, precursory Rn changes 80—94464
  Maniwaki, Quebec, 1975 July 12, focal parameters, intraplate seismicity 79—16378
  mantle convection, seismic focal mechanisms and thermal boundary layer 77—17070
  mantle earthquakes, spatial distrib. in Japan and Aleutian arcs 80—81820
  mantle earthquakes near junction of Kurile and northern Honshu arcs, mechanism 77—81805
  Markansu Valley earthquake, Tadjikstan, USSR, 1974 August 11, seismotectonics 80—21659
  Matsushiro, interpretation of local geomagnetic var. 77—2097
  Matsushiro swarm, Japan, 1965 Aug.-1967 Oct., rel. to Asama-yama Volcano inactivity 77—70599
  Matushiro fault zone, Japan, He spots caused by diapiric magma from upper mantle 79—8618
  maximum ground acceleration determ. for large earthquakes *(Japanese)* 80—101453
  maximum magnitude prediction, geotectonic method and appl. to N.Italy area 78—40493
  maximum regional magnitude, freq.-magnitude relation 78—24220
  mechanical model for earthquake statistics 77—91033
  mechanical models and statistics 78—15968
  mechanism leading to P-wave first arrival sign distrib. 80—94474
  Mediterranean and Middle East, seismic moment, source dimens. and stress determ. 77—44925
  Mediterranean earthquake catastrophes, statistics 80—3955
  meizoseismal shaking of long-period, for strike-slip event 80—81814
  Meloy, N.Norway, intraplate earthquake sequence 79—74855
  Messina, Italy, 1908 December 28, seismotectonic study 79—84177
  Mexico, 1911 June 7, epicentre relocation rel. to Michoacan seismic gap 80—76919
  micro, space time correlations anal. 78—65184
  microearthquake activity adjacent to Rockin pluton, California 78—92791
  microearthquake activity around Japan trench, off Sanriku, ocean bottom seismographic network obs. 77—81803
  microearthquake location using max. likelihood processor 77—17033
  microearthquake research, methods and meas. errors 79—39987
  microearthquake survey in N.W. British Columbia and S.E. Alaska 77—25652
  microearthquakes, correl. with geomag. activity 79—66638
  microearthquakes near St. Paul's Fracture Zone, depth determ., lithosphere thickness 78—48980
  microseism variations before major earthquakes *(Chinese)* 77—64209
  microseisms at Palisades, source location and propag. 78—85495
  microseisms influence on terrestrial quartz gravity meters, mechanism *(Russian)* 79—39967
  microseisms vars. before earthquakes *(Chinese)* 79—62436
  microtremor sequences and tilting in deep mine 79—84125
  microtremour site anal. study, Beatty, Nevada 79—16386
  microtremours, 1 to 5 s, earthquake engineering appl., Tokachi-oki 1968 earthquake long-period accel. 79—16387
  microzonation, application of regionalized variables 79—88288
  microzoning for earthquake risk reduction 79—88290
  microzoning methods, need for experimental evidence 79—88514
  Mid-Atlnatic Ridge, ocean-bottom seismograph obs. near 45°N, results 78—96157
  Middle America arc, focal mechanism solns. and tectonics 78—77191
  Mindanao, 1976 August 16, preliminary seismological assessment 79—66635
  Minnesota, crustal struct. and seismicity, rel. to historic earthquakes 78—11840
  Miyagi-Oki, Japan, 1978 June 12, rupture process 80—98263
  Miyagiken-oki, 1978 June 12, accompanying tsunami *(Japanese)* 80—41400
  Miyagiken-Oki, Japan (June 12, 1978), report 79—88291
  Miyagiken-oki (1978, June 12), aftershock spectral anal. 80—109118
  modelling in homogeneous half-space 79—12078
  Modified Mercalli and JMA intensity scales, peak acceleration comparison 79—62443
  Modified Mercalli Intensity attenuation with distance in USA 79—48414
  modified Mercalli intensity scale, re-evaluation 77—81827
  modified Merco Mercalli intensity scale, modification 80—36260
  Mogod, 1967 January 5, focal mechanism and parameter determ. 80—3937
  Mojave desert, hypocentres and shallow crustal vels., phase time inversions 80—21634
  moment magnitude scale 79—84157
  moment tensor inversions and source models 78—28175
  moments and corner freqs., effects of free surface on body waves 78—85492
  Mongolia, 1905 July 9 and 23, surface-wave investigation, comment 79—29711
  Mongolia (1905, July 9 and 23), surface wave investigations 77—37142
  Monte Settepani, Italy, 1972 Jan. 16-Feb. 22 swarm, stress conc. in Maritime Alps 77—86781
  Moxa, GDR, microearthquake records, event criteria *(German)* 78—57170
  Murray-Darling river system, Australia, symposium (Melbourne, 13 October 1977) 79—92556
  Nankaido earthquakes correl. with Shikoku seismicity characts. 80—101339

earthquakes continued
  nanogravity survey in Canada rel. to tectonic movement detect. due to groundwater movements 77—33038
  natural seismic events and underground nucl. explosions, distinction *(French)* 78—20364
  Nazca plate subduction beneath Peru, earthquake spatial distrib. 79—66671
  N.China, seismic gaps prior to large earthquakes *(Chinese)* 79—20755
  near-field of seismic source in irregularly layered medium 77—78112
  Near-field source parameters by finite-source theoretical seismograms 77—91022
  Nemaha Uplift in Oklahoma, Kansas and Nebraska, geological survey of seismicity and tectonic rels. 78—7589
  Nepal Himalaya, body waves from earthquakes, focal mechanism and tectonics 80—72455
  Nevada, seismic cycle rel. to earthquake potential 77—73659
  New England earthquake hazard based on 1725-1974 seismic data 77—37159
  New Hebrides, dispersion of first and second Rayleigh modes, periods greater than 50 s *(French)* 77—64212
  New Hebrides (1969, January 19), focal mechanism and source characts. rel. to fracture zone subduction 78—73342
  New Hebrides island arc, earthquakes precise relocation rel. to seismotectonics 79—16404
  New Madrid, 1811-1812, archaeoseismology 79—84130
  New Madrid, 1975 June 13, parameters from seismic wave data 77—56586
  New Madrid seismic zone, focal mechanism studies 79—48410
  New York State, earthquakes related to hydraulic mining and natural seismic activity 78—48986
  New York State, spectral anal. of two small earthquakes 79—48412
  New Zealand, Main Seismic Region, var. of energy release, occurrence rate and b-value 79—39665
  New Zealand, plate tectonics developments 79—84208
  New Zealand, South Island, regional travel time ratio and near source V_p/V_s ratio 78—40500
  Nicaragua earthquake, Dec. 1972, redetermination of local magnitude 80—56393
  Niigata, 1964, June 16, seismo-magnetic effects 77—2093
  Ninetyeast Ridge area, seismicity and tectonics, Indian plate internal deform. 78—73343
  Ninghe aftershock, 1977 May 12, epicentral intensity lowering *(Chinese)* 79—88252
  Nobi, Japan, 1891 October 28, faulting mechanism 77—9374
  nonstationary model identification, nonlinear filtering approach 79—5458
  Nootka Fault Zone, new plate boundary off W.Canada, earthquake epicentres distrib. 79—92518
  NE. North America, spectral moments, magnitudes and intensities 77—91020
  E.North American earthquakes, surface wave focal mechanisms with tectonic implications 80—3942
  North Cascades, 1872 December 14, location from attenuation structure 80—21642
  North Island, New Zealand, axial tectonic belt 79—2173
  nuclear power conf., Chicago, United States, July 1979 80—794
  nuclear power plant, dynamic response to earthquake, aircraft impact, soil structure interact. 79—3208
  nuclear power plants, seismic safety, review 77—374
  nuclear power station, aseismic design, using rubber mounts 77—79470
  nuclear power station design engineering for earthquake loads 78—66431
  nuclear power station protection, design *(French)* 77—54332
  nuclear power stations, applications of multi-directional seismic inputs in the design of components 79—31238
  nuclear power stations, earthquake damage in UK, estimation of probability 79—93844
  nuclear power stations, risk due to seismic activity in New York and New Jersey 79—8611
  nuclear power stations, seismic safety margins research program of the US Nuclear Regulatory Commission 80—99229
  nuclear reactor probable risk assessment, seismic research programme 80—797
  numerical simulation of earthquake sequences, one-dimens. fault model 78—44780
  Oaxaca, Mexico, prediction using seismic gap obs. 80—85609
  Oaxaca, Mexico, seismicity gap as prob. precursor to large earthquake 77—91053
  Oaxaca earthquake, Mexico, aftershocks in former seismic gap 80—98265
  observation techniques *(Japanese)* 78—28340
  occurrence frequency, anal. of theory of extremes 78—36109
  occurrence probability from geophys. and geological characts. 77—78119
  ocean bottom hydrophone array obs. of P and S waves, wave train characts. 80—104898
  oceanic long-period Rayleigh group vel. dispersion curve from HF Doppler sounding of ionosphere 79—70756
  oceanic transform earthquakes, source parameters rel. to plate vel. and transform length 78—53620
  oceanic trench earthquakes, props. rel. to plates bending at trenches 80—41426
  Odawara City, Japan, 1853 March 11, intensity, damage and magnitude from old documents *(Japanese)* 78—96146
  offshore building structure, earthquake resistant design 79—12089
  Oita, Japan, 1975, maximum ground acceleration determ. using overturned gravestones *(Japanese)* 80—101453
  Oita, Japan, 1975 April 21, damage and ground disturbance rel. to Quaternary faults *(Japanese)* 77—2108
  Oita, Japan, 1975 April 21, focal mechanism rel. to active fault system *(Japanese)* 77—2107
  Oita, Japan, 1975 April 21, regional tectonic topography *(Japanese)* 77—2109
  Oita, Japan, 1975 April 21, seismic intensity distrib. *(Japanese)* 77—2106
  Oita-Chubu, Japan, 1975 April 21, structural damage *(Japanese)* 77—2120
  Okhotsk Sea and Kuril Islands, magnitude determination, body wave anal. 80—4139
  Onikobe earthquake, Japan, ground motion deduced from damage, source model *(Japanese)* 80—94479
  Oroville, California, 1975, Aug. 1, geodetic meas. of assoc. deformation 77—53008

earthquakes continued
  Oroville, California, 1975, August 1, surface faulting near Lake Oroville 77—9345
  Oroville, California, 1975 August 1, characts. 77—9343
  Oroville, California, 1975 August 1, crustal shear wave vel. struct. determ. 79—16417
  Oroville, California, 1975 August 1, fault plane 77—9344
  Oroville, California, 1975 August 1, focal mechanism 77—9346
  Oroville, California, 1975 August 1, precursory P-wave travel-time vars. 77—56580
  Oroville, California, 1975 August 1, strong-motion accelerograms of aftershocks and peak accel. data 79—16381
  Oroville, California, 1975 August 1, surface wave constraints on source parameters 77—56579
  Oroville, California, 1975 August 6, strong-motion accelerograms of aftershocks 80—101331
  Oroville earthquake, USA, foreshock identification 80—56379
  Osaka region, microzoning in Japan 79—88283
  P- and S-waves spectral content, from Garm, Tadjikistan local earthquakes 79—48406
  P- and SV-wave corner freqs., possible discriminant for earthquake source theories 77—56605
  P-delays temporal var. in S.California, rel. to earthquake prediction 79—57873
  P-phases, anal. of short-period waveforms, from deep focus earthquakes beneath Fiji Islands 79—25200
  P-wave amplitudes and sources of scatt. in m_b obs. 77—86807
  P-wave codas, spectral composition of earthquakes and explosions 80—21640
  P-wave signals, multivariate autoregressive model, short-period discrimination appl. 79—16385
  P-wave travel time anomalies rel. to epicentral distance to African stations 80—98237
  P-wave travel times from deep earthquakes 77—25648
  P-waves records complexity appl. for discrimination of artificial and natural seismic sources 80—12340
  W.Pacific, HF P_n and S_n phases obs. at great distances, spectral anal. 78—77195
  Pacific subduction zones, great earthquakes recurrence 77—17045
  Pamir-Hindu Kush intermediate depth earthquakes, spectral content rel. to upper mantle high-Q zone 77—86795
  Pamir-Hindu Kush region, seismicity and fault plane solns. 80—72445
  Pand S-phase data from local earthquakes, California, 1966-75 period 79—12088
  Papua New Guinea-Solomon Islands region, 1964-1973 earthquakes, seismotectonics 80—8270
  Pariahuanca, Central Peru, 1969 Jul. 24 and Oct. 1, superficial deform. struct. anal. 77—53012
  Parkfield, 1966 June, ground displacement and vel., dislocation model 80—21658
  Parkfield, California, 1966, strong-motion accelerograms, statistical analysis 80—98245
  Parkfield earthquake, USA, foreshock identification 80—56379
  Parkfield earthquakes, California, comparison of 1966 and 1934 sequences 80—56412
  Pasadena magnitude scale based on vertical ground accel. 80—51344
  peak ground accel. rel. to seismic intensity and other parameters 77—91035
  periodicities of Alaskan and central American earthquakes 78—53621
  periodicity rel. to lunar sidereal period 78—53844
  periodicity rel. to variation of gravitational const. 78—3724
  S.Peru, 1965, shallow seismicity meas. in subduction zone 79—16401
  Peru, microzonation methods and techniques 79—88513
  Peru, Oct. 3 1974, numerical seismogram dispersion curves computed by normal modes 79—16403
  Peru, seismic gaps and source zones 80—85607
  Petatlan (Guerrero, Mexico), 1979 March 14, first report 80—76920
  Philippine earthquake, 1976 August 16 evidence for subduction zone south of Mindanao 79—44117
  Philippine Islands, tectonic struct. revealed by seismicity and volcanicity 80—94511
  Philippines, ground motion attenuation 79—88278
  Philippines, microearthquake survey of tectonic features 80—81827
  physical source parameters determ. from free oscill. data, numerical method 78—11820
  Picton, Australia, 1973 March 9, crust and upper mantle struct. 77—44944
  piezo-magnetic effect to explain earthquake assoc. mag. variation *(Chinese)* 80—56374
  plane strain shear cracks, rupture vel., rel. to earthquakes 77—17043
  planetary gravitational forces, effect on earthtides and earthquakes 79—100817
  plate boundary quakes, magnitude-freq. relation 80—56390
  plate boundary seismic pot., major boundaries 80—85606
  Pocatello Valley 1975 March 28, source model 80—104896
  Point Mugu, California, 1973 Feb. 21, aftershocks 77—40992
  Point Mugu, California, 1973 Feb. 21, epicentral region elevation changes 77—56587
  pore water pressure changes in sand deposits 79—88308
  postseismic surface deformations due to lithospheric and asthenospheric viscoelasticity 79—57884
  postseismic surface stress, viscoelastic model 80—98278
  postseismic viscoelastic surface deform. and stress, theory 80—94496
  pre-seismic sound *(Chinese)* 79—34760
  precursor theory, dilatancy-creep model of source development, rel. to prediction *(Chinese)* 79—20754
  precursors, classification 79—88264
  precursors, seismic wave propag. through cracked solid, model 78—61342
  precursors from Earth tilt obs. corrected for rainfall 79—8609
  precursors search in central California 78—7590
  precursory acoustic emission, sound source direction formula *(Chinese)* 80—89961
  precursory changes of groundwater Rn content 80—94467
  precursory CO_2 changes, tectonic processes causing release from rocks 80—94470
  precursory earthquake swarm, characts. and appl. to earthquake long-range forecasting 78—15975
  precursory effects due to pore fluid stabilization of weakening fault zone 79—84145
  precursory He changes of soil, limitations imposed on method by daily variations 80—94469

earthquakes continued
  precursory phenomena, conf., Jan. 1977, Tokyo, Japan 80—46146
  precursory rainfall to San Andreas fault quakes 80—85615
  precursory Rn changes in California Transverse Ranges 80—94464
  precursory Rn changes in shallow subsurface of New York State 80—94463
  precursory Rn changes in soil before San Jacinto Fault, California 80—94468
  precursory Rn episodic outgassing, active faults of California 80—94465
  precursory rock cracking, size estimation of preparation zone 80—76930
  precursory seismicity burst, long-term prediction of strong quake 80—72441
  prediction, appl. of geodetic research *(German)* 80—101317
  prediction, appl. of intersite distance meas. by spaceborne laser ranging system 78—3978
  prediction, appl. of uniaxial stress changing rock remanent magnetization 78—20393
  prediction, as stochastic process 77—49029
  prediction, based on geochem. meas., conf., San Francisco, USA (Dec. 1980) 80—90606
  prediction, biosystem behaviour as precursor 79—39673
  prediction, changes in chemical composition, subterranean waters and gases *(Russian)* 79—84163
  prediction, continuous method for Rn measurement in groundwater and springs 78—88924
  prediction, data evaluation and exchange problem 80—3957
  prediction, depth calc. of piezomagnetic effect 78—11816
  prediction, elec. resistivity sounding of prior crustal dilatancy 79—92609
  prediction, electrokinetic and magnetic anomalies associated with dilatant regions in a layered Earth 79—39658
  prediction, empirical model 79—62453
  prediction, international cooperation *(Japanese)* 77—86812
  prediction, interpretation of vertical crustal movements in time-space domain 79—80056
  prediction, long- and short-term, in Kamchatka 77—41007
  prediction, long-range, based on single predictor 80—26454
  prediction, observational basis, conf., Durham, England (Aug. 1977) 79—57867
  prediction, overview and recommendations 79—8703
  prediction, P-wave mean travel time residuals, systematic variations 78—3727
  prediction, precise recurrence model for steady-state seismic slip 77—33003
  prediction, probabilistic significance 77—56589
  prediction, problems, rel. to elastic wave parameters time vars. 79—57870
  prediction, radio emergency warning system *(Japanese)* 78—85497
  prediction, rel. to ocean-bottom seismograph system off Pacific coast of Honshu, Japan 79—62628
  prediction, rel. to temp., rainfall and soil tilt 77—91058
  prediction, risk forecasts 79—79746
  prediction, rock dilatancy and vel. anomalies 79—16458
  prediction, search for time-depend. P-wave travel times from mining explosions 78—44788
  prediction, success of current methods *(Russian)* 79—84162
  prediction, uzing He/Ar and N_2/Ar ratio vars. in fault zone groundwater air bubbles 78—88803
  prediction, velocity anomalies prior to rock failure and violent slip 79—16409
  prediction, via continuous meas. of Rn in groundwater 77—44935
  prediction, via mag. behaviour of magnetite and rocks stressed to failure 78—32068
  prediction, via Rn long-distance migration in Earth, subterrestrial fluid convection hypothesis 77—37246
  prediction, water ^{222}Rn conc. rapid meas. with commercial liq. scintillation counter 78—28339
  prediction, workshop, Strasbourg, France, (1980 January 31 to February 1) 80—62396
  prediction *(German)* 80—98267
  prediction and American studies of rock mechanics 79—16449
  prediction and crustal fracture water radioisotope vars. 79—44204
  prediction and geophysical data processing 77—91061
  prediction and warning, theoretical review 79—5455
  prediction based on dilatancy induced seismogram polarisation anomalies 80—101342
  prediction based on tectonics *(Chinese)* 78—61335
  prediction based on tilt anomaly 80—104917
  prediction by crustal movements continuous observation *(Japanese)* 78—28180
  prediction by EM phenomena meas. *(Japanese)* 78—28182
  prediction by geochemical study via radon monitoring *(Japanese)* 78—28181
  prediction from pseudo-periodicity of strong aftershocks *(Chinese)* 80—76913
  prediction from V_p/V_s vars., case history, Chinese earthquake 1976 November 79—57869
  prediction information classification for practical use 78—57177
  prediction of large earthquakes on San Andreas fault, shear stress meas. profile at shallow depth 80—76947
  prediction research, Japan 79—62456
  prediction research in E.Canada 79—62454
  prediction system *(Japanese)* 77—86802
  prediction using automated Rn-Th monitor 78—73532
  prediction using crustal fracture water radioisotope abundances 79—44124
  prediction using scale invariant inclusion theory 77—49032
  predictions for Romania 79—62452
  premonitory changes in fault gouge 79—12110
  premonitory crustal deformations, strains and seismotectonic features (b-values) preceding Koyna earthquakes 79—79755
  premonitory processes, fluid-infiltrated rock 78—51073
  premonitory slip, creep and stable sliding 79—16410
  preseismic crustal deformations, gravity vars. 79—70734
  preseismic fault slip and earthquake prediction 79—2189
  prestressed media with moving phase boundaries, dynamics, continuum theory of failure 78—18238
  principal stress axes rotation caused by faulting 79—57886
  propagating fault, one-dimens., with nonuniform stress and strength, dynamic soln. 79—84149
  propagating strike-slip fault in elastic half-space, near-field motions 78—7568

earthquakes continued
  Puget Sound, 1965 April 29, crustal and upper mantle structure 77—91026
  Q-frequency depend. of coda, surface-body wave hypothesis 80—21660
  Qiaojia and Shimian, China, small earthquakes source parameters and potential danger *(Chinese)* 77—9341
  Quebec, 1975 October 23, induced by reservoir filling 78—40502
  radiant flux as guide to relative seismic efficiency 79—66646
  rapid mode II shear crack with finite cohesive traction, stability, earthquake model 79—84148
  Rat Island sequence, 1965, seismic scaling information 79—12076
  ray parameter-epicentral distance curves for point source on boundary 78—61336
  Rayleigh, surface waves, principal mode and harmonics obs. for focal depth determ. 78—61351
  Rayleigh wave amplitude meas. from earthquakes in distance range 0-150° 78—48979
  Rayleigh-wave radiation pattern, for small earthquake mechanism 80—61764
  reactor struct. seismic response, modal response method 77—83059
  reconnaissance microearthquake survey, Bucaramanga, Columbia 79—62448
  records, optimal digitisation 77—91044
  recurrence intervals and plate tectonics 79—92490
  recurrence of large events, semi-Markov model 80—98247
  recurrence rate curves and Rautian K energy class 77—56601
  recurrence relations 79—39672
  Reggio Calabria, 1975 January 16, macroseismic study *(Italian)* 77—49006
  Reggio Calabria, 1975 January 16, seismological results and geostructural appl. 77—49007
  regional focal mechanism solns., probability models 80—98244
  repetitive earthquake source model 77—53007
  resistivity changes as earthquake precursors 77—78121
  RESMAC seismic array, interactive epicentre location procedure 78—65395
  response calcs. using shear wave vels. from down-hole meas. 77—70849
  response of nonlinear plates to random loads 78—94604
  response spectra for nucl. plant design 78—41871
  response spectrum amplitudes, probabilistic computation 79—8610
  Reykjanes Peninsula, Iceland, 1972 September earthquake swarm and tectonic significance 77—33009
  Reykjanes Ridge at 59°N, microearthquake epicentres and seismic vel. 80—89964
  Reykjanes Ridge crest studied by surface waves with an earthquake-pair technique 80—90021
  Ridge Basin, S.California, earthquake focal mechanisms and hypocentres, tectonics 80—21695
  ridge-crest and transform earthquakes source parameters rel. to oceanic lithosphere thermal struct. 79—88265
  risk in S.Europe through to India, using Gumbel's third distrib. of extreme values 80—21648
  risk maps for Western Central Europe *(German)* 79—8600
  rock failure, scale invariant properties 78—3758
  rock fracture prediction problem 79—25230
  rock friction and earthquake prediction, conf. (Stanford, 28-30 April 1977) 79—16448
  rock friction modelling, expt. results and constitutive eqns. 79—84240
  rock friction modelling, preseismic slip simulation 79—84241
  rock masses seismic flows, deform. vels. calc. 79—74850
  rock rupture rel. to Rn content var. before earthquakes, model expt. *(Chinese)* 78—24225
  rock samples with saw cut, fracture and frictional sliding, earthquake prediction appl. *(Chinese)* 79—100825
  rock volume changes during fracture and frictional sliding 79—16450
  Rumania, 1977, March 4, long period effects 77—73686
  Rumania, 1977 March 4, P-waves obs. rel. to Moho vel. depth distrib. *(German)* 80—98256
  Rumania, 1977 March 4, rupture process, fault-plane soln. 78—65201
  Rumania, 1977 March 4, rupture rel. to fault plane soln. and multiple-event analysis *(Rumanian)* 79—57876
  Rumania, 1977 March 4, specific defect of area *(Rumanian)* 79—20768
  Rumunia, 1977 March 4, Bucharest strong ground motion record analysis 80—21641
  rupture inception, precursory processes, theory 80—8255
  rupture incoherence influence on seismic directivity 79—12077
  rupture velocity and radiation efficiency 77—9352
  S-wave far-field spectra, corner freqs. and pulse shapes 79—84153
  S-waves means free path under Kanto district, Japan 79—79748
  Sagami Bay and off Bose Peninsula, seismic activity during 1971, ocean bottom seismometer obs. 79—79749
  Salton Sea geothermal area, California, microearthquake study 79—12085
  San Andreas and Calaveras fault region, crustal deformation, 1971-8 obs. 80—56428
  San Andreas Fault, 1973 January 15, section seismicity and failure 80—101329
  San Andreas Fault, 1977 December 15, negative result for resistivity and self-potential vars. 79—57860
  San Andreas fault, California, Palmdale Bulge as precursor event, review 78—36114
  San Andreas fault, coseismic tilt changes assoc. with local earthquakes 78—36112
  San Andreas fault, local seismicity rel. to Rn emanation vars. 78—32022
  San Andreas fault, microearthquake activity 79—92493
  San Andreas fault, stress accumulation and release 77—91056
  San Andreas Fault, stress accumulation and release mechanisms 79—84194
  San Andreas fault near Palmdale, 1976-7 earthquake swarm 79—34756
  San Andreas fault slip and prehistoric large earthquakes 79—2188
  San Andreas fault strain accumulation 1964-1977 near 1976-7 earthquake swarm 80—36272
  San Andreas fault zone, central California, source processes of earthquake sequences 77—2111
  San Fernando, 1971 February 9, aftershock zone recent seismicity and Transverse Ranges tectonics 79—66634
  San Fernando, 1971 February 9, analysis of source and medium effects of strong motion observations 79—88299
  San Fernando, 1971 February 9, dynamic source model 79—84119
  San Fernando, 1971 February 9, particle velocity attenuation relations 78—11811

earthquakes continued
San Fernando, 1971 February 9, site transfer functions, preliminary evaluation 79—88301
San Fernando, 1971 February 9, source finiteness, teleseismic body waves 78—92781
San Fernando, 1971 February 9, source mechanism and aftershocks anal. 77—49023
San Fernando, 1971 February 9, strain-softening instability model 80—3949
San Fernando, 1976, Feb. 9 preceding spatio-temporal seismicity variation 77—86793
San Fernando, California, 1971 Feb. 9, static and dynamic finite element anal. 77—49010
San Fernando, California, 1971 February 9, foreshock activity 79—66626
San Fernando earthquake, California (1971), dislocation fault model, tectonic significance *(Japanese)* 80—104923
San Fernando earthquake, strong ground motion, ray models 80—61762
San Francisco, 1906, April 18, viscoelastic relaxation model for postseismic deform. 77—91055
San Francisco, 1906, kinematic viscoelastic model 77—73671
San Francisco, 1906, source mechanism 78—85499
San Francisco, 1906 April 18, strain accumulation and release mechanism 79—20765
Sanriku, 1933 March 2, dislocation model consistent with tsunami waves 80—31000
Sanriku coast, Japan, seismic risk to large quake 80—51337
Sanriku district coast, earthquake fault models from tsunamis simulation *(Japanese)* 78—65199
Sanriku-Oki region, Japan, 1965-1970 shallow earthquake source characts. 80—12346
scientific and economical aspect of earthquake engineering 80—81844
Sea of Okhotsk, 1970 August 30, source process of large deep-focus earthquake 77—9372
Sea of Okhotsk, 1971, January 29, evidence for lithospheric slab penetration into lower mantle 77—73700
seafloor earthquake meas. system, development 79—5689
seismic acoustics and earthquake prediction *(Chinese)* 79—34759
seismic activity and large earthquakes, Sanriku district, Japan *(Japanese)* 79—70749
seismic activity rel. to source power 79—44125
seismic amplitude measurements, focal mechanisms of fore and aftershocks 79—20767
seismic body waves, focusing at epicentre antipode 79—16399
seismic discrimination improvement using pattern recognition 78—40694
seismic driving stress, stress drop and efficiency 79—84152
seismic energy dissipation during propag., by solid friction 80—109106
seismic energy flux, space-time energetics model 77—9369
seismic events identification, appl. of non-linear stochastic models 79—16396
seismic focal process, unexpected earthquakes occurrence *(German)* 79—66644
seismic gap quiescence duration determ. method 80—26627
seismic gaps, two types of definition 80—85608
seismic instrumentation for nuclear power plants in Germany, review 79—620
seismic magnitude using statistical models 80—51343
seismic microzoning, mapping method based on subsoil conditions 79—44108
seismic moment, method of determination from seismological bulletin data 80—89980
seismic moment, source radius and fracture energy for shallow events 78—20358
seismic moment and stress drop relations in presence of stress and strength heterogeneity 79—84151
seismic moment calcs. WWSSN instrument appl. of AR method 80—21828
seismic moment determ. for local earthquakes using coda characts. 77—9534
seismic moment tensor elucidation from teleseismic data 80—104915
seismic moments beneath island arcs, phase changes and subduction vels. 77—33007
seismic pattern recognition, fundamental problems 78—81428
seismic radiation pattern theory 80—61780
seismic risk anal., renewal process model *(Japanese)* 79—84159
seismic risk analysis, of discrete system of sites 77—86785
seismic risk in linear source regions, San Andreas fault appl. 77—56588
seismic risk map, new proposal for Japan 79—88281
seismic safety factor for nuclear siting in earthquake zones 78—11839
seismic shocks, location with imperfect knowledge of seismic wave path hodographs *(Russian)* 79—35009
seismic signals, preprocessing of signals prior to input to pattern recognition scheme 79—62631
seismic sources, spectral theory and determ. of parameters of earthquake foci 77—21687
seismic spectra, earthquake strength anal., predictions *(Chinese)* 77—49009
seismic velocity structure below Hawaii island from local earthquake data 79—84195
seismic wave onset detection, computing 79—80059
seismic wave traces, multivariate autoregressive feature extraction and the recognition of multichannel waveforms 79—39878
seismic waves, very long period, charact. of upper mantle *(French)* 77—78107
seismic waves attenuation and azimuthal depend. in SE United States 78—65185
seismic waves travel-time anomalies, statistical anal., rel. to earthquake prediction 79—57868
seismic waves velocity anomalies before and after earthquakes, curvature vars. of wadati diagrams *(Chinese)* 79—62435
seismic zoning, contrib. of geophysical methods, conference (Erice, Italy, 13-23 April, 1977) 79—44104
seismic zoning map, new elements 79—44105
seismicity, model and observed, represented in two-dimens. space 78—53619
seismicity associated with subduction zones, stereoviews 80—72452
seismicity fluctuations before major earthquakes 77—49027
seismological equipment, possibilities of development 77—53228
seismological precursors in island arc 79—57874
seismomagnetic effects, space correl. method rel. to earthquake prediction *(Chinese)* 78—3719

earthquakes continued
Sendai, Honshu, 1978 June 12, balloon-borne magnetic survey *(Japanese)* 80—30990
SH sudden crack, displacement far-field spectrum, earthquake appl. 77—25641
SH-wave travel times and amplitudes for two well-constrained earthquakes 79—48407
shallow earthquake and precursors, generation mechanism 78—15972
shallow earthquakes, seismic efficiency, radiated seismic energy, fault motion energy balance 80—76927
shallow earthquakes occurrence, statistical study 78—96155
shallow events, 1904-52 magnitudes 77—91019
shallow focus earthquakes, implications of in situ seismic vel. study in San Andreas fault zone 79—57865
shallow intraplate earthquakes triggering factor, strain accumulation 79—39661
Shamil-Siahou, Iran, 1977 March 21, regional seismicity, ground movements, major shocks, aftershocks 79—48422
shear wave travel time residuals from oceanic earthquakes 77—64224
Shikoku, Japan, shallow earthquakes focal distrib. rel. to upper crustal struct. *(Japanese)* 80—94508
Shikotan, 1968 January 29, surface waves initial phase and phase vel. 78—92793
Shimane, SW.Japan, 1978 June 3, preceding seismic activity pattern 79—39659
Shioya-Oki, 1938 May and November, tectonic implications 77—81814
Sierran foothills near Oroville, California, regional seismicity 79—48411
Sinfengkiang Reservoir impounding earthquake, precursory V_P/V_S variations *(Chinese)* 78—3720
single-station fault-plane solution method 79—44263
Sinkiang, China, earthquake swarm (1974), source mechanisms from surface waves anal. 78—81427
Sitka, Alaska, 1972 July 30, changes in direction of mag. vector of short-period geomag. vars. 80—76923
slip of friction-controlled mass excited by earthquake motions *(Japanese)* 79—70753
small earthquakes, detailed spatial distribs. of foreshock and aftershock activities *(Japanese)* 80—94483
Snyder, Texas, USA, 16th June 1978, seismic activity 80—56395
soils, non-linear seismic response and liquefaction 79—57862
Solomon Islands, earthquake doublet mechanism in subduction zone 80—56410
Sonora, Mexico, 1887, historic fault scarp identification 78—11812
source development, model, rel. to precursory phenomena *(Chinese)* 77—9339
source dynamics, role of shear Mach number 77—40983
source mechanism and intensity distrib. *(Chinese)* 77—64208
source mechanism model, for pre-stressed self-gravitating, thermo-visco-elastic Earth 80—104886
source mechanism studies, surface wave data inversion 77—33204
source parameters, importance of receiver crustal struct. 77—73643
source parameters, relation to magnitude 78—96154
source parameters and magnitudes, scaling relations 77—25645
source parameters rel. to tectonic field, dynamical process of fault motion 78—88801
source spectra scaling law, regional var. 78—92783
source spectrum determ. using code of seismic oscills. 79—48405
source time function depend. on tectonic field 78—92799
South America, origin of compressional intraplate stresses 78—61385
South Sandwich arc, moderate and large earthquakes, tectonic var. along subduction zone 80—26458
Spain, 1954 March 29, source process and tectonic implications of deep-focus earthquake 77—9375
spatial distribution of earthquakes, two-point correl. function 80—89963
spectral anomaly estimate, appl. to prediction 79—57871
spectral modal analysis, dynamic anal. program *(Japanese)* 77—86784
split free oscill. amplitudes for 1960 Chile and 1964 Alaska earthquakes 77—91024
spontaneous rupture propagation, two-dimens. model, numerical study 77—78159
St. Elias, Alaska, 28 Feb. 1979, 1974-9 tilt obs. 80—81841
St. Elias, Alaska (1978 February 28), body wave anal. 80—104897
St-Donat, Quebec, 1978 February 18-23 sequence 80—26453
statistics, truncated exponential frequency-magnitude relationship 78—65191
stick slip earthquake, rupture propag. and energy focusing in foam rubber model 80—3947
stick-slip sliding dynamic props. appl. to earthquakes 78—48983
stochastic characterization through response spectrum 79—20758
strain softening prior to two-dimensional strike slip earthquakes 79—70755
strains and stresses in seismically active regions, calc. 79—79744
stress concentration mechanism for intraplate earthquakes 78—81112
stress corrosion cracking theory, geophys. appls. 77—62212
stress corrosion theory of crack propag. 78—24235
stress drop models for stress drop inversion from seismic observations 77—91049
stress drop of earthquake sources *(Chinese)* 79—62438
stress redistrib. by slow earthquakes 79—2191
stress relaxation models, finite difference calc. 77—73682
strike slip fault, ground motion 80—72439
strike slip fault, three dimens. viscoelastic model 77—56591
strike-slip failting, in crust of horizontally variable rigidity, model 80—56377
strike-slip fault in laterally inhomogeneous region 78—7591
strong aftershocks temporal distrib. of major earthquake sequence, theory *(Chinese)* 79—88253
strong earthquake foci dynamic parameters, from longit. wave spectra 78—57171
strong earthquakes, rel. to solar activity *(French)* 77—17027
strong earthquakes occurrence time forecasting results of expt. 79—53315
strong ground acceleration, empirical model for scaling Fourier amplitude spectra 77—9361
strong ground motion, prediction using small earthquakes 79—88297
strong ground motion characterisation, uniform risk functionals 78—92789
strong ground motion duration rel. to MM intensity and recording site geology 77—91036
strong ground motion representation and simulation 79—16388

earthquakes continued
strong ground motions along principal axes, anal., 1971 February 9 San Fernando earthquake appl. 80—3934
strong ground motions along principal axes, simulation, 1971 February 9 San Fernando earthquake appl. 80—3935
strong ground motions at short epicentral distance, simulation 80—104906
strong motion earthquake records, horizontal components duration characts. 79—66637
strong motion prediction for pot. earthquake fault, barrier model 80—105053
strong motions, estimation with regard to fault rupture 79—88307
strong volcanic earthquakes assoc. with lateral eruptions, dynamic focal parameters 78—61347
strong-motion accelerograms, vertical component characts. 79—62458
strong-motion accelerograph data management 78—36332
strong-motion accelerograph maintenance and data processing Japan 78—36330
strong-motion accelerograph network, USA, field operations 78—36331
strong-motion accelerograph records, statistical anal. 79—62459
strong-motion data management developments 79—62629
strong-motion earthquake observation, historical development, NTT records 77—17041
subcrustal, location and mislocation 78—85498
subsoil liquifaction during earthquakes in Japan 78—36118
Summerville, South Carolina, 1975 April 28, intensity survey 77—73663
Sunda Arc earthquake foci distrib. rel. to backarc area rotation 78—20381
surface motion of layered half-space calc. by Laplace transform method 78—7570
surface seismic Rayleigh waves, amplitude spectra in Mountain Crimea region 80—89969
surface wave contrib. to dislocation source in superficial multi-layers 79—44126
surface waves, importance in strong ground motion 79—84185
Svalbard, 1976 January 18, focal mechanism solns. 77—81812
Svalbard, 1976 January 18, focal mechanism solns. reanal. 79—44140
Svalbard archipelago, intraplate earthquakes in continental-type crust 80—26460
Sverdrup Basin, Arctic Canada, 1972 November and December, focal parameters 78—36104
Swabian Jura, 1911 November 16, seismotectonic concepts 79—84176
Swabian Jura earthquake of Sept. 1978, macroseismic field obs. 80—72451
swarm earthquakes, differentiation from foreshocks via similarity of seismic waveform *(Japanese)* 80—67342
swarms, model 77—44934
swarms, stochastic modelling of earthquake freqs. *(Japanese)* 80—94480
Sweden, deep-seated fracture zones in crust 79—66666
Sweden, seismicity map, earthquake catalogue for 1951-76 period 78—96159
Sweden, suspected periodicities of earthquakes 79—66647
Sweden (1951-76), error anal. of source parameters 80—104920
Swedish earthquakes, focal depth distrib. 79—79756
Szombierki coal mine, Upper Silesia, Poland, mining tremors, freq.-mag. relation 80—41378
Tabas, Iran, 1978 September 16, field report, damage 80—26456
Tabas-e-Golshan earthquake, Iran, Sept. 1978, faulting and bedding thrust 80—81826
Tabas-e-Golshan earthquake, Iran, Sept. 1978, mechanism and aftershocks 80—81825
Tadzhik depression and Gissar range, focus orientation, effect on P-waves 80—3940
Taft, California, 1952, strong-motion accelerograms, statistical analysis 80—98245
Taiwan, seismic zonation risk model 79—88277
Tajikistan, 1974 to 1977, precursory tectonomagnetic vars. 80—26446
Tango, 1927, conjugate fault system model, geodetic data inversion 78—88779
Tangshan, 1976 July 28, Earth tides anal. in Peking region, rel. to prediction *(Chinese)* 80—3892
Tangshan, 1976 July 28, seismogenic models rel. to convection-generated stress concentration 79—92507
Tangshan, 1976 July 28, short duration resistivity vars. before earthquake *(Chinese)* 79—88235
Tangshan, 1976 July 28, stress field of area before and after earthquake *(Chinese)* 78—61358
Tangshan, China, 1976 July 27, detailed analysis 79—92495
Tangshan, China, 1976 July 27, seismograph data of Polish Seismological Network *(Polish)* 77—78106
Tangshan, China, 1976 July 28, source parameters for small earthquakes *(Chinese)* 78—24223
Tangshan, China, elec. resisitivity anomaly in epicentral area prior to 1976 earthquake *(Chinese)* 79—20744
Tangshan, Hopei Province 1976, July 28, background and seismic activity *(Chinese)* 77—37137
Tangshan earthquake, China, related geomag. field variations *(Chinese)* 80—56372
Tashkent, 1966, main tremor Fourier and response spectra 77—56597
technique for parameter determ. by computer *(Chinese)* 80—77126
tectonic patterns and earthquakes, central Mississippi valley 78—85504
tectonoelectricity, review 78—36095
Tehran region, Iran, microearthquake survey 77—25656
teleseismic body wave radiation from seismic source in layered medium 77—9363
teleseismic magnitude relations, extension of Zurich magnitude recommendations (1967) 80—109105
temporal variation, of intermediate and deep focus earthquake activity 80—3943
Tennessee, seismic characts., surface wave dispersion study 79—48426
Texas-New Mexico Permian Basin seismicity rel. to hydrocarbon recovery operations 80—36256
theoretical problems, conf., Aug. 1978, Caracas, Venezuela 80—51400
thermomagnetoelastic model of source mechanism 79—70758
Thessaloniki, 1978, activated faults, intra-plate deformation 79—39697
Thessaloniki area, Greece, 1978 May-June major shocks, surface fault traces and fault plane solns. 79—84166
Tibet, active tectonics, LANDSAT imagery 79—20794
Tibet and Himalaya, long-term premonitory seismicity 80—72442
Tibet earthquake, 14 July 1973, source mechanism and seismic wave attenuation 80—36252

earthquakes continued
Tibetan Plateau, late Cenozoic tectonics, LANDSAT imagery 79—20795
tidal triggering in Swabian Jura 80—12348
Tien Shan region, fault plane solns. rel. to contemporary tectonics 79—29733
time and latitude residuals anomalies correl. with earthquakes *(Chinese)* 79—62725
Tohoku, Japan, intraplate seismicity correl. with interplate earthquakes 78—92787
Tokachi-oki, 1968, May, post-seismic microearthquake activity around Japan trench 77—81803
Tokai district, Japan, probability of great earthquake recurrence 78—3730
Tokyo, liquefaction of the ground during earthquakes 79—88309
Tonankai (Japan), 1944, source model for accompanying tsunami *(Japanese)* 80—67344
N.Tonga region, earthquake distrib. geometry and complicated subduction closure model 80—90010
Tonga Trench seaward side, earthquakes implications for oceanic lithosphere mechanical behaviour 79—16405
Tonga-Kermadec region, deep and intermediate earthquakes energy release rel. to mantle flow depth 80—41404
Tonghai, China, fault parameters determ. from ground deform. data *(Chinese)* 79—20753
topographical features effects on earthquake induced damage *(Japanese)* 79—70752
torsional spectrum for earthquake motions 79—2187
Torud, Iran, 1953 February 12, ground deform., saturated desert deposits liquefaction 79—84117
transform fault, quasistatic creep slippage inherent instability 79—84193
transient sliding motion under idealized dry friction, earthquake faulting appl. 78—34093
travel-time inversion method, for earthquake location and vel. struct. 80—109109
tree ring growth, affected by Fort Tejon 'quake, California 80—98259
triangular networks relative performance in regional seismic sources location 79—84523
Trichonis region, Greece, recent earthquake activity and tectonic significance 79—84114
triggering and rupture propag. rel. to prediction based on premonitory phenomena 79—84146
true ground motion reconstruction from earthquake records using Fourier transforms 77—86787
tsunami earthquakes and subduction processes near deep-sea trenches 79—84155
tsunami magnitude and wave source regions, N.E.Japan, 1611-1901 period *(Japanese)* 77—2122
tsunami risk, estimation via stochastic model 77—21685
tsunami type plane wave, Coriolis force effect *(Russian)* 78—77193
tsunami-generating earthquakes, ionosphere detect. method 79—44681
tsunamis, Nankaido, Japan, historical monuments, inundation heights rel. to 1946 tsunami *(Japanese)* 79—70751
tsunamis in Kanto, 1677 and 1703, behaviour along Kujukuri-hama coast from old monuments *(Japanese)* 80—67339
Turkey, microearthquake rupture length determ. from cepstrum anal. 77—81826
Turkey, seismic risk calc., preliminary approach 79—57878
N.W. Turkey, tectonomagnetic effects 77—2094
Turshiz, 1903 September 25, rel. to seismicity of Iran 77—49008
Tyrrhenian region, deep earthquake focal depth determination 80—56389
underground reactor installations, earthquake computations 78—25336
underthrust zones, earthquake cycle, model 80—26457
underwater microearthquakes, infrasonic sea noise meas. 78—11902
United Kingdom, perceptible earthquakes 78—77189
W.United States, horizontal ground accel. attenuation rel. to magnitude 80—104905
United States, national seismic hazard and zoning maps status and prospects 79—44109
N.E. United States and S.E. Canada, earthquake scaling by Lg waves 77—25646
United States Earthquake Hazards Reduction Act 79—48415
United States seismic hazard maps, prospects for geological data appl. 79—44110
Upper Amur region USSR, seismicity, tectonic features and earthquake epicentre confinement 80—101343
Upper Rhine graben, seismic risk evaluation 79—25207
upthrow of objects, vertical ground accels. 78—44783
US catalogue for 1568-1850 period 80—21643
US National Earthquake Information Service seismic data acquisition 77—29446
SE.USA, attenuation of Lg phase and determ. of m_b 79—92487
S.E.USA, earthquake activity data and seismic zones 78—11838
USA, East-Central, geological perspectives of earthquake hazards 78—11834
N.E.USA, rel. of seismicity to geology 78—11836
N.E.USA, seismic risk analysis in rel. to nuclear plant siting 78—11835
W USA, tectonomagnetic effects assoc. with earthquakes 77—2092
USA-Japan studies on wind and seismic effects, conf., Tokyo, Japan (May 1975) 78—36252
USSR, correl. between seismicity and underground water regime *(Russian)* 80—104913
Ust'-Kamchatka, 1971 December 15, P-wave study 78—73317
V_P/V_S ratio spatial and temporal changes before earthquakes in Kamchatka 78—32027
v_P/v_S ratio spatial and temporal vars. prior to strong earthquakes, Kamchatka 79—39657
Vancouver Island, 1946 earthquake mechanism, geodetic study 80—61770
central Vancouver Island, 1946 June 23, landslides 80—21637
Virgin Islands, tectonic struct. and earthquake swarms, seismic network obs. 80—89973
visible earthquake waves, stroboscopic effect explanation 77—25660
Vladivostok, 1973 September 29, seismic moment from P-waves and mantle Rayleigh waves 78—61354
Volvi-Langadhas earthquake, Greece June 1978, source parameters 80—56394
Vrancea, 1977 March 4, aftershocks and seismic activity migration 79—84172
Vrancea, 1977 March 4, anomalous seismicity pattern, rel. to earthquake prediction 79—88263
Vrancea, 1977 March 4, isoseismal map 79—84168

earthquakes continued
Vrancea, 1977 March 4, macroseismic field 79—84167
Vrancea, 1977 March 4, multiple seismic event, seismotectonic implications 79—84171
Vrancea, 1977 March 4, multiple seismic event 78—65205
Vrancea, 1977 March 4, recording peculiarities and source parameters 79—84170
Vrancea, Romania, 1977 March 4, successful prediction 79—62452
Vrancea, Rumania, 1977 March 4, seismic gap, anomalous activity 79—92498
Vrancea, Rumania, 1977 March 4, seismic waves and intensity recorded in Poland 78—92779
Vrancea, Rumania, intermediate earthquakes 80—3930
Vrancea, seismic source parameters of five large earthquakes 79—84169
Vrancea Rumania (1977 March 4), precursors to S and SKS waves, seismogram calcs. 80—104901
Vrances, 1977 March 4, and seismic microzonation of Bucharest 79—88280
Vranch earthquake seismic wave travel-time curves giving European upper mantle struct. 80—89998
Wakayama city, central Japan, micro-earthquake obs. rel. to earthquake prediction 80—31001
Warrnambool, 1903 July 14, isoseismal map 79—92506
wave anal. program *(Japanese)* 77—86783
wind and seismic effects, conf., Tokyo, Japan (May 1977) 79—62569
Xing tai, 1966 March, structural damage and ground displacement near faults *(Chinese)* 79—20756
Xingtai, 1966, March aftershock freq., rel. to subsequent N.China strong earthquakes *(Chinese)* 80—76912
Xingtai, 1966 March, hypocentral distrib. and tectonic stress field *(Chinese)* 77—91011
Yakataga Gap, Alaska, seismic history and earthquake pot. 80—109115
S.Yamanashi Prefecture, Central Japan, microearthquake activity *(Japanese)* 80—67343
Yamasaki fault, SW.Japan, seismic activity and crustal movement, predictions 79—57872
Yan-Yuan earthquake of 1976, stress field of source *(Chinese)* 80—56373
yearly seismic energy release, world totals versus ridge system total 77—2113
Yellowstone, Wyoming, 1975 June 30, event and precursive spectral stability 78—61352
Yellowstone hot spot, tectonics and crustal props., earthquake and aeromag. data 78—48996
Yellowstone Park, 1975 June 30, intensity studies 79—92494
Yong Shan-Da Guan, Yunnan earthquake (May 19, 1974), main shock source multiplicity *(Chinese)* 79—12075
Yongshan-Daquan, 1974 May 11, seismo-tectonic struct. *(Chinese)* 77—91008
Yunnan Province, China, 1976 May 26, crustal deform. time characts. from tilt recording 78—40511
Zhangjiakou-Huairou region, China, microearthquakes focal parameters *(Chinese)* 77—9342
Zhao-Tong earthquake, China, May 1975, focal process *(Chinese)* 80—56371
Zhaotong, Yunnan Province, 1974, May 11, rupture mechanism *(Chinese)* 77—37141
zonation for critical facilities based on two-level earthquakes 79—88286
NWSyria, seismic risk to large quakes 80—72454
EAS *see cosmic ray showers and bursts*
Eberhard effect *see photographic materials*
ebullition *see boiling*
e.c.g. *see electrocardiography*
echelons *see diffraction gratings*
echo
see also anechoic chambers; architectural acoustics; clutter; reverberation; sonar
acoustic imaging, phased array for medical diagnostics, dynamically focused insonification 80—89813
acoustic pulse-echo technique for determ. of parameters of liquid-filled shells 78—1462
acoustic radiation and scatt. anal., use of linear system theory 77—75729
acoustic sounder array, for atm. surface layer vorticity meas. 78—7810
acoustic sounding of atmosphere, refr. effects, multilayer model appl. 77—84041
air pollution meteorology, use of sodar acoustic echo sounder, low level stability and wind velocity monitors 80—108828
atmosphere echo sounding, Doppler shift extraction hy adaptive linear-prediction filtering 77—64453
atmospheric echo sounding, effects of phase-front distribs. on antenna radiation patterns 77—39123
auroral radar echoes drift meas. using radar auroragraph 78—65436
auroral radio echo, ion-acoustic, short term characts. 78—45080
automatic simple pulse echo tracking apparatus, US absorpt. meas. appl. 77—22571
bat detection instruments 80—69609
bat echolocation system, optimum phase modulation for insensitivity to acceleration 79—53163
broadband target classification using bionic sonar 78—18123
circular and rectangular transceivers, effect of range on US echo 79—94434
circumglobal signals in Atlantic equatorial zone *(Russian)* 78—69585
continuous noncircular cylinder, echo signal calc. using Kirchhof integral *(Russian)* 79—68453
convection, instability, crit. slowing, config. inversion acoustic obs. 78—34133
d-region absorption and forward-scatter radio-meteor data 79—75033
Demey metro station, noise level increase due to echoes from passing vehicles *(French)* 80—69600
diffraction by rigid elliptical cylinder, echo signal determ. using Kirchhoff integral *(Russian)* 78—13833
digital reverberation and echo apparatus *(German)* 79—50554
dynamically focused array imaging systems, induced Doppler distortions 79—46117
echoencephalography, US pulsatile, prototype instrument and trial obs. *(Russian)* 80—17174
electroacoustic echo in piezoelectric and ferroelectric materials 78—95549
electronic echo and reverberation generation, ccts. *(German)* 79—32138
EM wave scatt., echo width meas. 79—3614

echo continued
F-region, high latit., fixed freq. sounding echo rel. to gravity waves 79—25390
glasses, echoes and elec. dipole echoes at low temps. 79—69771
Hertzian waves, reflection and diffraction by moving layers *(German)* 80—87266
HF oscillating echoes from polar E-region 78—57390
HF peculiar lunar echoes, guided wave propag. in ionosphere and magnetosphere 78—93032
HF radar sea-echo Doppler spectra, extraction of wave height and period 77—78474
HF radio meteor echoes duration rel. to dense trains deionisation 79—5697
icebergs underwater profiling using unmanned submersibles, echo sounder and scanning sonar 79—5673
interior spaces, impulse response and echo patterns 80—28383
inverted echo sounders, for meas. thermocline depth vars., MODE results 77—87108
ionosphere, absorpt. events at high latits. 77—21987
ionosphere, equatorial, theoretical model of spread-F echoes in HF and VHF bands 78—85764
ionosphere, pulse synthesis technique for improving ionosonde resolution 78—28411
lightning radar echoes and simultaneous elec. field changes 79—84372
magnetosphere radio echoes rel. to plasma density, GEOS-1 relaxation sounder meas. 79—35072
Mars, surface props. obs. by Earth-based radar at 70, 12.5, and 3.8 cm wavelengths 77—91457
mesosphere, equatorial, multiheight radar echoes rel. to waves and winds over Jicamarca 78—36230
metallic powders, echo effect at low temp. *(Russian)* 78—34853
meteor trail radar echo, maximum ionization height detect. method 80—8487
meteor trails, radio echoes rel. to thermal diffusion 77—21955
meteoradiolocator echo signals, optical spectral processing *(Russian)* 79—100968
meteors, echo drift deceleration 78—36538
meteors, head echo heights 78—36537
meteors, heights obtained from decay rates of 18000 radar echoes 77—82175
meteors overdense trails, diffusion coeff. and initial radius from radio echoes 77—13140
noncircular cylindrical shell, plane acoustic wave refl. calc. 77—68291
ocean wave height meas. with satellite radar altimeter 79—44253
ocean wave spectra derivation by integral inversion of second order radar echoes 77—78475
ocean waveheight nondirectional spectrum from inversion of HF sea-echo Doppler spectrum 78—16203
piezoelectric powder, echos, theory *(French)* 78—72462
powder, three pulse echo, mechanism contribs. 78—68444
powdered materials, nonlinear mechanism leading to polarisation echoes 78—87739
power cepstrum for echo detect. in multi-peaked wavelets 77—14855
pulse Doppler radar obs. of severe thunderstorms 78—85651
pulse echo method for acoustic vel. meas., transducer effect 77—42676
radar, Doppler shift formula derivation without transformation eqns. 77—82344
radar echoes, type 1, from equatorial electrojet, with double-peaked Doppler spectra 80—67458
radar echoes from E-region, height shift around morning and evening electrojet reversals 79—66871
radar meteor echo rates, correl. with zonal winds at 95 km altitude 80—56775
radio auroral signals, maximum entropy spectral anal. 78—93006
radio echo sounding of ice sheets, internal props. var. with depth 80—26633
radio echo sounding through ice, obs. in W Dronning Maud Land, Antarctica (1974) 77—86838
radio signal transmission, long-delay echoes generation, models 80—26670
radio sources, superluminal, energy echo model rel. to Hubble's const. doubling 78—81722
rectangular room, instantaneous excitation of one-dim. sound waves *(German)* 78—87201
round-the-world echo signals, height factor estimate from expt. results 77—13159
scattering by random fluctuating surface, statistical model *(French)* 77—11066
sea echo radar spectra resolution limitation inferred from ionospheric Doppler broadening 78—81489
seismic reflection profiles of marine sediments, statistical anal. 79—2385
shear wave, from subsurface planar flaws, calc. model 77—25228
signals propag. characts., 10 and 15 MHz 78—69574
single-transducer coupler for diagnostic pulsed Doppler or pulse-echo US instrumentation 78—61236
sonar, incoherent and coherent processing against echo fading in shallow water 80—19142
sonar target recognition experiment 79—86298
sounder transducer field plotter 78—59238
speech intelligibility, time delay effect experiment 80—91996
spherical shell scanned by directional pulse, acoustic refl. 77—68292
stratosphere and mesosphere, UHF radar echoes, for wind and turbulence obs. 77—33135
subjective preference tests for musical sound fields with single echo 78—31819
time delay detection, effect of zero singularity smoothing 78—90605
troposphere, pulse compression radar echoes rel. to strong wind shear obs. 78—32193
troposphere VHF radar echoes, appl. to velocities and irregularities study 79—16701
underwater broadband echo ranging system for freq. charact. meas. of fish schools 79—64390
US echo pulse shape improvement in low impedance materials 78—1489
US liver sector scans, echoes across diaphragm 78—69165
US pulse-echo scanning, echo struct. 77—52857
US spatial echo distrib. processing for interface props. determ. 78—1490
VHF radar echoes from equatorial E-region irregularities, sudden disappearance 78—40738
VHF radar partial reflections from equatorial E-region plasma density gradients 77—25828

echo continued
VHF radar signals, partial refl. and scatt. from clear atmosphere 78−81278
VHF radar signals partial refl. from troposphere 78−85656
VHF radiowave ionospheric propag., equatorial spread-F scattering 78−61661
weather radar echo, receiver bandwidth effect on refl. and Doppler vel. estimates 79−53549
$LiNbO_3$:Fe, polarization echo signals amplification *(Russian)* 78−43780
SiO_2:OH^-, vitreous, elec. dipolar echoes 78−52430

echo suppression
cartography radar image interpretation, line detection technique 78−61630
interdigital transducer design and component specification tradeoffs 77−27455
SAW transversal equaliser using SAW tapped delay line and PIN diode control ccts., characts. 79−68532

ECL *see emitter-coupled logic*

eclipses
see also solar eclipses
1977, April 3-4, amateur obs. of partial eclipse 77−73985
1980, British Astronomical Association Handbook 79−96893
ζ Aurigae, 1974 eclipse, Ca I 6752 Å circumstellar line obs. 77−17619
VV Cephei, spectroscopic obs. during 1976/77 eclipse ingress phase 78−45359
31 Cygni, 1972 eclipse, Ca I 6752 Å circumstellar line obs. 77−17619
V444 Cygni, IR eclipse obs. and Wolf-Rayet wind structure 78−45357
66 Eridani, spectroscopic binary star, search for eclipses 78−32524
Galilean satellites, eclipse spectrophotometry 79−96949
Galilean satellites, eclipses rel. to improved ephemerides 80−62066
Galilean satellites, eclipses rel. to light hesitation determ. by Romer *(Danish)* 77−57140
Galilean satellites, photometric eclipses anal. rel. to theory of motion 78−53864
Galilean satellites mutual eclipses, ephemerides correction rel. to Jupiter oblateness 77−29715
historical accounts, solar and lunar 79−80411
Iapetus, eclipse by shadow of Saturn and rings (19-20 October 1977) 78−16342
Iapetus, eclipses by Saturn and its rings, 1977, Oct. 77−91471
Iapetus, eclipses by Saturn and rings, 1977 Oct. 19-20 and 1978 Jan. 7-8 predictions 77−53467
Iapetus eclipses by Saturn's ring A, photometric conformation of Encke division 78−45273
Interkosmos 7, photometry of eclipses observed in situ 77−91408
Jupiter, eclipses of Galilean moons, obs. program 77−9703
Jupiter's satellites, mutual phenomena (1973 Sept.-1974 Jan.) 79−40129
Jupiter inner satellites, mutual eclipses and occultations in 1979, ephemerides 78−53866
LMC X-4 eclipse and A0538−66 burst coincidence, Ariel 5 obs. 77−82321
lunar, 1974 November 29 total eclipse obs. in Ussuriisk 77−67051
lunar, 1975 November 18 total eclipse, obs. in Tadzhikstan 77−67052
lunar, brightness of eclipsed Moon due to cosmic dust *(French)* 77−37519
lunar, occultations of planets during eclipse, 100 BC to 3000 AD period 77−49319
lunar eclipses, Danjon relation correl. with gegenschein brightness *(French)* 79−96968
lunar eclipses, transitory phenomena obs. on Moon 78−61770
lunar total eclipse, 1975, May 24-25, UBV photometry 77−22126
Mercury, transits in 1677-1973 period, collected obs. of internal contacts 77−25964
Mercury transit, 1973 November 10, photographic obs. at Pulkovo *(Russian)* 78−28562
Moon, 1978 March 24 total eclipse, 3.4 mm obs. 80−31220
Moon, 1978 March 24 total eclipse, S.African obs. 79−44384
Moon, observational and theoretical temps. for total lunar eclipse 77−41328
171 Ophelia, lightcurve analysis, possible eclipsing binary asteroid 80−36549
Pluto, 1978 P 1, possible satellite, orbit and eclipses ephemeris 78−93152
pre-telescopic obs., uses in modern astronomy 79−96930
satellites of Jupiter and Saturn, eclipses and occultations *(Swedish)* 79−92695
Saturn satellites, mutual eclipses and occultations in 1979-1980, ephemerides 78−53868
Titan (Saturn VI) eclipse, 1979 December 20, photometric obs. 80−31250
Titan by Saturn, light curve obs. rel. to Saturn upper atmosphere struct. 80−90362
Wolf-Rayet binaries, interpretation of eclipses at emission-line freqs. 77−17596

eclipsing binary stars
2A 0311−227, AM Herculis type binary star, IR photometry and polarimetry 80−77517
2A 0311−227, high-speed photometry of AM Herculis-type binary 80−41912
2A 0311−227, new AM Herculis-type system, optical identification 79−101211
2A 0311−227, optical counterpart, AM Herculis type eclipsing binary, V-band obs. 80−101617
2A 0311−227, soft X-ray emission from AM Herculis-type system 79−101219
2A 0311−227 optical counterpart, simultaneous photometric and spectroscopic obs. 80−90572
2A 0526−328, optical counterpart, eclipsing binary, visible emission line variability 80−73075
Abell 46, planetary nebula, nucleus, hot component UV continuum obs. by IUE 80−98693
Algol, orbit, lightcurve and struct. review 80−109460
Algol, X-ray spectral obs., description and interpretation 80−105283
Algol type star, accretion and chem. struct., evolutionary calcs. 80−109481
Algol type stars, H I α obs. 80−109484
Algol type stars, mass loss and transfer 80−109480
RT Andromedae, light curve anal. of short period eclipsing binary 80−46603

eclipsing binary stars continued
RT Andromedae, three-colour photoelectric obs. and improved ephemeris 80−22043
ο Andromedae, UV spectrum 77−45485
RT Andromedae, V photoelectric obs. and lightcurve 79−71073
AB Andromedae, W Ursae Majoris type star, 1.2 and 2.2 micron light curves 79−84822
apsidal motion, discrepancy with main-sequence homogeneous stellar models 80−82413
EE Aquarii, UBV photometry of β Lyrae-type eclipsing binary 79−84817
V342 Aquilae, period and light curve changes, (1966 to 1976) 80−67791
V889 Aquilae, photometric obs. of eclipsing binary, apsidal motion 79−25640
KO Aquilae, UBV photoelectric study 80−62198
T Aquilae (Nova 1891), spectrophotometry of shell 80−72955
V603 Aquilae (Nova 1918), IUE obs. of periodic light vars. 80−105251
V603 Aquilae (Nova 1918), old nova, eclipses obs. 80−90476
V603 Aquilae (Nova 1918), periodic light vars. detect. 80−82391
V535 Arae, A-type evolved contact system 78−65650
V535 Arae, absolute characts. of W Ursae Majoris system 79−58373
V539 Arae, photometric analysis of B-type double lined eclipsing binary 79−44535
ζ Aurigae, 1973 to 1978, photoelectric obs. 79−84819
WW Aurigae, Am eclipsing binary, spectrographic obs., radial vel. curves 77−33559
ε Aurigae, astrometric study from Sproul 61-cm refractor plates 78−89219
BF Aurigae, B-type semidetached system, photoelectric obs. 79−44522
ζ Aurigae, Ca I 6752 Å circumstellar line obs. 77−17619
ε Aurigae, distance from astrometric obs. 79−53859
ε Aurigae, dual aspect of wavelength depend. fluctuations 80−62190
SX Aurigae, early-type semidetached binary, UBV photometric anal. 79−44521
ζ Aurigae, eclipse data rel. to radius change of K-type supergiant component 79−84820
T Aurigae, eclipsing binary nova, times of minima 77−22267
ϵ Aurigae, fine analysis of atmosphere of primary F-type supergiant 78−85976
AR Aurigae, Hg star, peculiar spectral var. during eclipse 80−98679
ε Aurigae, International UV Explorer obs. 79−17027
IU Aurigae, light curve study of early-type close binaries in triple systems 78−89222
SX Aurigae, light curves anal. by automated Fourier techniques 79−92798
IU Aurigae, massive triple system, obs. 77−64798
ε Aurigae, peculiar binary system, circumstellar dust and gas disc model 77−9771
EO Aurigae, revised elements from light curve anal. 80−90471
IU Aurigae, revised photometric elements 79−101175
CQ Aurigae, RS Canum Venaticorum type eclipsing binary, photoelectric obs. 79−40218
ε Aurigae, semi-detached system with accretion disc questioned 77−78824
SX Aurigae, semidetached massive binary system, period changes 79−25637
ε Aurigae, spectrum outside eclipse 77−71129
LY Aurigae, tidal effects in O-type eclipsing binary system 79−25638
IU Aurigae, two-colour photometry rel. to presence of third body 80−36669
ζ Aurigae, UV obs. of supergiant atmos. 80−94836
ε Aurigae, UV spectrum using IUE 79−71071
IU Aurigae, variable light curve 77−17627
T Aurigae (Nova 1891), old nova, photometric and spectroscopic obs. 80−90446
average absolute brightness of components *(Polish)* 77−17630
BD-3°5357, eclipsing binary with hot subdwarf component, photometry and spectrum 77−91574
ZZ Bootis, double spectrum eclipsing binary, revised spectrographic and photometric elements 78−61885
i Bootis, light curve and period vars. of W Ursae Majoris type star 80−4398
SS Bootis, UBV obs. and Fourier anal., RS Canum Venaticorum type star 80−17613
44=i Bootis, variable light curve obs. and implications 78−61887
TZ Bootis, W Ursae Majoris system, spectroscopic and photoelectric obs. 78−69832
AC Bootis, W Ursae Majoris system, V photoelectric photometry 77−64800
44 i Bootis, W Ursae Majoris type star, 1.2 and 2.2 micron light curves 79−84822
TZ Bootis, W Ursae Majoris type system, photoelec. obs. 80−73001
SZ Camelopardalis, early type close eclipsing binary, UBV light curve anal. 77−45486
SV Camelopardalis, eclipsing binary containing BY Draconis variable, motion round third component 79−67055
AY Camelopardalis, eclipsing variable, element determ. by Fourier anal. of light curve 77−45484
AS Camelopardalis, light curves Fourier analysis, appls. to eccentric orbits 79−25630
SZ Camelopardalis, semi-detached eclipsing binary, UBV lightcurves 80−85974
SS Camelopardalis, UBV photometry and light curve soln. for eclipsing RS Canum Venaticorum binary 80−41854
S Cancri, close eclipsing system, freq. domain anal. of light changes 77−53638
AH Cancri, contact binary in M67, spectrum and photometry 79−40222
WY Cancri, light curve of eclipsing system, UBV photometry 77−37619
UU Cancri, long-period eclipsing binary, radial vel. meas. 77−74096
WY Cancri, obs. 79−92799
RU Cancri, RS Canum Venaticorum type eclipsing binary, photoelectric obs. 79−40218
UW Canis Majoris, BV light curves of close binary 79−12496
UW Canis Majoris, mass flow anal. and circumstellar component from UV spectrum 80−109429
R Canis Majoris, multiband photoelectric photometry 77−53633
UW Canis Majoris, O7f supergiant, mass loss rate meas. 80−67736
UW Canis Majoris, O-type massive evolved contact system 78−65651
CW Canis Majoris, UBV photometry 77−37615
R Canis Majoris type, struct. and dimens. 80−82423
R Canis sMajoris stars, photometric elements 79−58371

eclipsing binary stars continued
RS Canum Venaticorum, explanation of observations 79—84826
RS Canum Venaticorum, intrinsic linear polarization 80—4394
RS Canum Venaticorum, out of eclipse light var. and comparison with similar stars 80—109489
VZ Canum Venaticorum, photometric elements and intrinsic variability 77—45487
RS Canum Venaticorum, quiescent X-ray emission obs. 78—81659
RS Canum Venaticorum, radio flare obs., (1979, February 6) 79—40220
RS Canum Venaticorum, spectrophotometric obs. of light curve wave distortion 77—33562
RS Canum Venaticorum binaries, effects of tides and flares 79—71068
RS Canum Venaticorum binaries, multiple periodic behaviour 77—87479
RS Canum Venaticorum binaries, observational selection and evolution 78—89208
RS Canum Venaticorum binaries, possible origins 77—57060
RS Canum Venaticorum stars, intrinsic light vars. due to starspots, model 79—35295
RS Canum Venaticorum type binaries, evolutionary status 79—67029
RS Canum Venaticorum type binaries, Hγ line vars., chromospheric diagnostics 80—62181
RS Canum Venaticorum-type binaries, evolutionary status 77—33570
δ Capricorni, Am primary component metallicism var. 77—67115
OY Carinae, eclipsing ultrashort periodic dwarf nova discovery 79—53823
OY Carinae, white dwarf cataclysmic, eclipsing binary, parameter determ. 80—82385
QZ Carinae (HD 93206), massive multiple system in great Carina Nebula, spectral types and orbits 79—97027
QZ Carinae (HD 93206), O-type quadruple eclipsing system, spectroscopic and radial vel. study 80—105275
SX Cassiopeiae, Algol type binary, spectrophotometry 77—2454
TV Cassiopeiae, Algol variable, UBV photometric obs. 79—35306
RZ Cassiopeiae, Algol-type binary, period vars. 77—13394
CW Cassiopeiae, anal. of V light curve 77—57009
V523 Cassiopeiae, BV photometry of W UMa type system *(Russian)* 79—92807
YZ Cassiopeiae, Fourier analysis of light curves for transit eclipses 78—96506
AO Cassiopeiae, intrinsic linear polarization, rel. to circumstellar envelope 77—17618
TV Cassiopeiae, light curve, long period var. interpretation 79—101174
TV Cassiopeiae, light curve and orbital elements of eclipsing binary 77—49430
AB Cassiopeiae, light vars. preliminary study 80—94831
BM Cassiopeiae, long-period eclipsing binary, radial vel. meas. 77—74096
AZ Cassiopeiae, long-period eclipsing system, photoelectric obs. 80—46608
TV Cassiopeiae, mass transfer from period vars. 79—84818
AO Cassiopeiae, O-type evolved contact system 78—93302
MN Cassiopeiae, orbital elements 77—71127
OX Cassiopeiae, photometric elements 80—56877
TV Cassiopeiae, revised photoelectric elements *(Russian)* 79—92808
HT Cassiopeiae, spectroscopic obs. of dwarf nova 79—88668
RZ Cassiopeiae, spectroscopic orbit 80—22040
AR Cassiopeiae rel. to supernova remnant Cassiopeiae A 80—72792
cataclysmic binaries, connection as source of accretion disc viscosity 78—93307
cataclysmic binaries, disc and hot spot eclipses anal. for circumstellar matter parameters determ. 80—109492
cataclysmic variables, apsidal motion and evolution 79—62834
cataclysmic variables, hard X-ray obs. 78—36732
cataclysmic variables, pulse timing meas., accretion disc models 79—62831
cataclysmic variables, review of structure 77—26018
cataclysmic variables, theoretical UBV colours of accretion discs 78—61865
CD—42°14462 (V3885 Sagittarii), dwarf nova in permanent outburst 78—53966
SV Centauri, early-type contact binary, evolutionary models 80—4403
BH Centauri, early-type contact system in IC 2944 open cluster 77—33552
SZ Centauri, eclipsing binary, four-colour photometry, photometric elements, dimensions and He content 77—41391
V78 in ω Centauri, light curve anal. in freq. domain by automatized Fourier technique 80—22039
SV Centauri, period changes of β Lyrae-type 77—33575
V78 in ω Centauri, radial vels. and circular orbit 79—97030
in ω Centauri, search for new variables 78—61895
V346 Centauri, spectroscopic orbit 79—58378
V748 Centauri (Centaurus X-4?), high-latit. eclipsing system, VBLUW photometry 79—44529
Centaurus X-3, accretion disk evidence from month-long X-ray obs. 79—44636
Centaurus X-3, long-term studies with Ariel 5 All-Sky Monitor 79—30146
Centaurus X-3, neutron star characts. from correlated spin-up and X-ray luminosity meas. 80—101648
Centaurus X-3, pulsation period and orbital elements 77—49494
Centaurus X-3, spectroscopic obs. of Krzeminski's star 79—53934
Centaurus X-3, stellar wind vel. change during transition 80—12829
Centaurus X-3, X-ray binary, tidal friction effects 77—57013
central star of Abell 46, eclipsing binary 80—73027
VV Cephei, 1976 November obs. in UBV rel. to eclipse start 77—9774
U Cephei, accretion discs obs. 80—82412
U Cephei, Algol type binary, spectrophotometry 77—2454
EI Cephei, Am eclipsing binary, light curve anal. 77—33560
U Cephei, anal. of radial velocity curve of B9 component 80—94829
EM Cephei, B-type eclipsing binary system, investigation of period and min. 80—17614
U Cephei, chem. comp. of secondary component of close binary system 79—35308
ER Cephei, contact binary in open cluster NGC 188, BV light curves 78—77580
VW Cephei, contact eclipsing binary, polarisation obs. 77—45489
VV Cephei, distance from astrometric obs. 79—53859
VW Cephei, evidence for circumstellar matter 77—33563
U Cephei, gas stream effects in UV spectrum, IUE obs. 80—26898
VV Cephei, Hα region spectra and system analysis 77—78823
U Cephei, hot/cool spots obs. in UV light curves 78—57577

eclipsing binary stars continued
CW Cephei, in III Cephei association, distance 79—21326
EM Cephei, light curve and spectrum *(Russian)* 77—64803
NY Cephei, massive eclipsing binary star, progress report from UBV photometry 80—67789
CQ Cephei, narrowband photoelectric obs. *(Russian)* 77—22278
EE Cephei, obs. of long period eclipsing binary *(Italian)* 78—93319
EI Cephei, occultation at primary minimum 77—9770
U Cephei, outbursts in 1969 and 1974, period change 77—87475
U Cephei, period changes in 1972-7 interval 80—8657
VW Cephei, periodic vars. in light curve of W Ursae Majoris system 80—36667
XY Cephei, photoelec. elements of semidetached binary system 80—31327
U Cephei, photoelectric obs. of recent eclipses 79—67061
U Cephei, primary eclipses obs., recent period behaviour 77—74087
EM Cephei, spectroscopic obs. of shell *(Russian)* 78—57587
VV Cephei, supergiant, UV spectrum 80—82415
U Cephei, three colour light curve perturbations and orbital element determ. *(French)* 80—67787
VW Cephei, transportation of masses in close binary *(German)* 79—58383
VV Cephei, UB photoelec. obs. 77—17633
EM Cephei, UBV, photometry rel. to constancy or variability of period 80—105286
VV Cephei, UBV obs. 77—2456
VV Cephei, UBV obs. 80—17611
U Cephei, UBV photometry, light curve solns. 79—67054
U Cephei, UV excess, mass transfer in eclipsing binary system 77—33555
VV Cephei, UV spectrum in 1978, flux distrib. 79—88698
VV Cephei, UV spectrum obs. during chromospheric eclipse phase 80—109498
VW Cephei, W Ursae Majoris star, identification with faint X-ray source 80—51913
VW Cephei, W Ursae Majoris star, orbital period decrease and B-V colours rel. to physical status 80—109495
VW Cephei, W Ursae Majoris star, rot. line broadening rel. to shape and mass ratio 80—109494
VW Cephei W Ursae Majoris system, period and colour change mass transfer model 80—77453
TV Ceti, F-type eclipsing binary, four-colour photometric obs. 79—40217
TV Ceti, light curves, photometric elements and He content 79—44526
XY Ceti, light vars. of eclipsing binary with Am spectra 78—93310
XY Ceti, revised photometric elements 80—109458
TX Ceti, UBV obs., photometric elements 79—8950
Z Chamaeleontis, cataclysmic binary, possible gravit. radiation emission 80—4386
Z Chamaeleontis, eruptive binary, model from photoelectric data anal. 80—72961
RS Chamaeleontis, four-colour photometry rel. to photmetric elements, absolute dimensions and He abundance 80—67783
Z Chamaeleontis, gravitational waves from eclipsing cataclysmic binary 80—90439
RS and RZ Chamaeleontis, photometric elements of detached systems 80—90473
Z Chamaeleontis, photometry of dwarf nova 79—67028
RS Chamaeleontis, uvby photometry of bright double-lined A-type eclipsing binary 78—69833
Circinus X-1, semiperiodic pulsations 79—48963
close binaries, distortion effects on struct. 78—57584
close binaries, form. by two-body tidal capture 77—33556
close binaries, gaseous circumstellar discs obs. 77—57043
close binaries, mag. fields generation *(Russian)* 77—17591
close binaries, mass flow, binary X-ray sources appl. 77—57039
close binaries, mass loss and parameters 77—13397
close binaries, narrow-band photometry and differential effects 80—67780
close binaries, nonradial radiative transfer 77—91567
close binaries, period distrib. from secondary maxima 80—109467
close binaries, review 77—33573
close binaries, rotational angular momenta 77—57057
close binaries, satellite UV obs. 77—57033
close binaries, struct. and evolution 77—57019
close binaries, unsteady mass loss 77—57049
close binaries accretion processes rel. to binary X-ray sources 77—57034
close binaries in globular clusters rel. to nature of cluster X-ray sources 77—41396
close binaries linear polarisation 77—49435
close binaries with mass transfer, particle motion 77—5545
close binary components, model atms. 79—62869
close binary stars props. before and after mass transfer, obs. and theory comparison 80—62187
close binary systems, convergence of Kopal's iteration method for light curve soln. *(Chinese)* 79—62872
close binary systems, neutron stars tidal disruption by black holes 77—13387
close binary systems, polarimetric determ. of revolution directions and spatial orientations 79—35309
close binary systems, precession and nutation 77—13392
close binary systems, problem of components oblique rot. axes 78—96509
close eclipsing binaries, J-integrals numerical evaluation 77—9668
close eclipsing binaries, recursion formulae for J-integrals 77—9666
close eclipsing binary stars, near IR photometry rel. to mass transfer rates 80—67784
close low mass binaries evolution and gravit. radiation 77—57030
close low-mass binary system, evolution with mass exchange and gravit. radiation losses 77—53631
close low-mass binary systems, evolution, unsteady mass loss, contracting secondary star 77—17617
close low-mass binary systems, evolution into contact 77—33557
close neutron star binaries, evolution, gravit. radiation and mass transfer 77—78821
close systems, mass transfer and accretion disk flow 77—82280
close systems including black hole, circumstellar gas motion 77—17628
close X-ray binaries, ellipsoidality effects and linear polarisation 77—78898
CC Comae, W Ursae Majoris star, proper motion 77—74099
CC Comae, W Ursae Majoris type binary, photometry and geom. elements 77—22272

eclipsing binary stars continued
CC Comae Berenicis, UBV photometry of shortest period contact binary 77−57055
common envelope binaries, evolution 77−57025
contact binaries, common convective envelope 77−57048
contact binaries, cyclic thermal instability 77−57050
contact binaries, energy transfer problem 77−57052
contact binaries, envelope energy transfer model 80−90478
contact binaries, evolution rel. to light curve and period changes 77−57054
contact binaries, gas circulation 77−57017
contact binaries, orbital periods sudden changes due to third component 80−109497
contact binaries, solar type, ang. momentum controlled evolution 80−36670
contact binaries, solar type, initial mass ratio distrib. function 80−109496
contact binaries, theoretical atlas of light curves and rot. broadening functions 80−17610
contact binaries, theories of struct. 80−109493
contact binaries, unstable mass outflow 77−57018
contact binaries of low mass, evolutionary fate 77−2453
contact binaries with age-zero components, secular stability 80−67786
contact binary, particle motion from L_2 Lagrangian point, elliptic orbits 77−91579
contact binary stars, discontinuity model internal inconsistencies 80−46613
contact binary stars, temp. discontinuity maintenance 80−8655
contact binary systems, possibility of convective energy transfer between components *(Russian)* 77−17615
contact systems, evolutionary tracks 77−57053
contact systems, massive zero-age binaries 77−57058
ε Coronae Austrinae, polarimetric obs. 80−56888
ε Coronae Austrinae, W Ursae Majoris type star, spectra, radii, masses 79−71069
α Coronae Borealis, UV spectrum 77−45485
corrected light elements for nine objects 77−37620
AI Crucis, revised photometric elements 80−109459
cyclotron self-absorption in accretion columns of magnetic degenerate stars, X-ray sources appl. 80−12760
31 and 32 Cygni, ζ Aurigae stars, UV spectroscopic obs. 80−109499
32 Cygni, λ6575 and λ4870 light curves anals. 79−88700
V1073 Cygni, A-type evolved contact system 78−65650
31 Cygni, Ca I 6752 Å circumstellar line obs. 77−17619
EM Cygni, cataclysmic variable, red and white dwarf binary, period change, B photometry 80−90434
CG Cygni, changing light curve obs. 79−48857
V477 Cygni, close binary system, apsidal motion 77−57011
SS Cygni, colour variations during dwarf nova outbursts 80−46576
SS Cygni, dwarf nova, hard X-ray emission 78−93275
EM Cygni, dwarf nova, photographic study 77−33529
V453 Cygni, in cluster NGC 6871, distance 79−21326
V1016 Cygni, IR spectrum and evidence for cool star 78−93266
32 Cygni, IUE obs. and effects of B-type star within late-type supergiant upper chromosphere 80−22036
V382 Cygni, IUE spectra of massive close binary 80−8659
V1143 Cygni, light curves Fourier analysis, appls. to eccentric orbits 79−25630
V444 Cygni, new light curve anal. techniques appl. 80−82417
V729 Cygni, O-type evolved contact system, masses 78−93309
32 Cygni, opacity wavelength depend. in atm. of K-type supergiant component 78−73741
GO Cygni, orbital period changes 80−72999
V444 Cygni, orbital period var. rel. to Wolf-Rayet star mass loss *(Russian)* 79−101178
SW Cygni, period changes, mass transfer and third body effects 80−62183
V388 Cygni, photoelectric obs. 77−37617
MR Cygni, photometric elements, period changes 78−61884
CC Cygni, photometric obs. of RS Canum Venaticorum type binary, interpretation 80−62182
V380 Cygni, revised photometric elements 80−109458
SW Cygni, semi-detached Algol type binary, period study, photometry and spectra obs. 80−82424
V367 Cygni, spectroscopic study 78−53984
CG Cygni, spectroscopic study of close eclipsing binary 79−97031
UZ and VW Cygni, UBV light curve solns. 80−41855
V1329 Cygni (HBV 475), symbiotic variable, photometric and spectroscopic history 80−62148
CI Cygni symbiotic star, UV and optical spectrum changes during eclipse 80−105258
31 Cygni-type, UV line predictions 77−78787
Cygnus X-1, distortion of absorpt. line vel. curves due to X-ray heating 77−29878
Cygnus X-3, efficient particle acceleration 80−31391
Cygnus X-3, X-ray polarisation obs. from OSO 8 80−90571
detached, period variations, review 80−109474
detached double-lined eclipsing binaries, revised photometric elements 78−61886
detached eclipsing binaries, erratic orbital period fluctuations 77−74085
detached systems, revised photometric elements for 8 double-line biuaries 80−46610
discoveries by John Goodricke, history 79−49005
distance determ. using Barnes-Evans relation 77−45482
distances, masses, radii and absolute magnitudes of 96 stars 79−44520
double-lined binaries, photometric elements of 14 detached systems 78−69834
AR Draconis, BV light curves and orbital elements 79−101173
BS Draconis, BV photometry 79−44536
CM Draconis, low dispersion spectrum, metal abundance 79−25636
AI Draconis, period and spectroscopic orbit of eclipsing binary 78−89221
RZ Draconis, photoelectric light curve and orbital period study 80−109461
WW Draconis, RS Canum Venaticorum type star, two-colour photoelectric lightcurves and elements 80−46606
BV Draconis (ADS 9537A), W Ursae Majoris type star, photoelectric photometric obs. 79−35296
BW Draconis (ADS 9537B), W Ursae Majoris type star, photoelectric photometric obs. 79−35296
dwarf novae, EUV obs. from Apollo-Soyuz Test Project 78−93252

eclipsing binary stars continued
dwarf novae, hard X-ray emission from 47 objects 78−93275
dwarf novae, HEAO-A2 soft X-ray survey during optical outburst 80−46574
dwarf novae, outbursts, accretion model 79−88680
dwarf novae, photometry of rise to max. and decline 77−9753
dwarf novae, soft X-ray emission 77−45457
dwarf novae, spectrophotometry, 1250-7500 Å region 80−46577
early-type contact binaries, uvby beta photometry 78−53981
eccentric orbit binaries, components min. projected distance calc. 80−26904
eclipsing binaries, orbital inclination, polarimetric determ. for five systems 78−45358
WX Eridani, light curves, period, orbital elements 80−26902
CD Eridani, photometric soln. for eclipsing binary system 80−62185
extragalactic distance indicators 78−93396
Fourier anal. of light curves, geometric elements soln. 79−25634
Fourier anal. of light curves, photometric perturbs. for partial eclipses 79−25635
Fourier anal. of light curves 77−87474
Fourier anal. of light curves 78−69830
Fourier anal. of light curves 78−93311
Fourier anal. of light curves 79−25632
Fourier anal. of light curves 79−25633
Fourier anal. of light curves 79−30088
Fourier anal. of light curves of eclipsing variables with extended atms. 80−46604
Fourier analysis, $B_{n,m}{}^q$ integrals explicit expression 79−35298
Fourier analysis of light curves, error anal. in freq. domain 80−31214
Fourier analysis of light curves, photometric perturbs. 78−96507
Fourier analysis of light curves 79−8945
Fourier analysis of light curves 79−8946
Fourier analysis of light curves of eclipsing binaries for transit eclipses 78−96506
U Geminorum, dwarf nova, radial vels. from emission line obs. 77−57029
U Geminorum, dwarf nova, times of minima 77−22267
RW Geminorum, element determ. by Fourier anal. of light curve 77−45484
U Geminorum, HEAO 1 obs. of hard X-rays 79−21299
U Geminorum, HEAO obs. of low-energy X-ray emission 79−21298
U Geminorum, magnitude estimates for 1978 Oct. 78−96493
U Geminorum, model of disk and accreting stream 77−82246
YY Geminorum, photometry and orbital period study 80−105287
U Geminorum, radial vel. meas., rot. accretion disc and hot spot model 77−33561
U Geminorum, soft X-ray emission and visual magnitude estimates 77−91544
U Geminorum, V mag., primary eclipse and visual mag. estimates 79−44505
U Geminorum, visual magnitude estimates during outburst (1980 Oct.) 80−109439
U Geminorum, visual magnitudes for 1978 Jun. 78−65627
YY Geminorum, VRI photoelectric photometry and absolute dimensions 78−69827
in globular clusters, preliminary report on eclipsing binaries and cataclysmic variables 80−109505
X Gruis, Algol variable, mean light curve and photometric solution 77−64799
HD 101799, W Ursae Majoris star, contact system anal. 77−22274
HD 152667=OAO 1653−40, physical parameters 79−17021
HD 152667 (V861 Scorpii), eclipsing binary X-ray source, possible black hole 79−53858
HD 153919, HDE 226868, X-ray sources, IUE UV spectrum obs. 78−96569
HD 153919, Of X-ray binary, narrow band photoelectric photometry 77−60761
HD 153919(3U 1700−37), coronal emission line search 79−35302
HD 153919 (3U 1700−37), binary X-ray source, radial vel. data in blue spectral region 78−61888
HD 153919 (3U 1700−37), X-ray binary, UV photometric obs. 77−45490
HD 153919 (3U 1700−37), X-ray binary uvby photometry 77−17624
HD 153919 (3U 1700−37), X-ray eclipsing binary, VBLUW photometric obs. 79−17135
HD 153919 (3U 1700-37), X-ray binary, five colour photometry 77−29877
HD 153919 (4U 1700−37), optical oscills. obs. 78−96572
HD 153919 (=4U 1700−37), supergiant-neutron star, optical variability 80−82419
HD 197406, WN7 type binary orbital data, UV obs. 80−85952
HD 3765, variability due to eclipsing star or planetary system, BV photometry 80−17615
HD 77581 (4U 0900−40), apsidal motion test 80−51908
HD 77581 (4U 0900−40), optical pulsations from eclipsing binary 79−48951
HD 77581 (Vela X-1), discovery of optical pulsations 77−82327
HD 77581 (Vela X-1), four colour photometric obs. and light curve anal. 77−17621
HD 77581 (Vela X-1), radial vel. curve distortions due to tidal deform. 77−53640
HD 77581 (Vela X-1), X-ray binary, photometric obs. 77−41392
HD 77581 (Vela X-1), X-ray obs. and UBV photometry 78−65722
HDE 226868 (Cygnus X-1), extended secondary envelope with eclipsing region, V-polarization obs. 79−35433
HZ Hercules, (Hercules X-1), X-ray spectra, pulse phase depend. on high-energy continuum 79−17128
HZ Hercules (Hercules X-1), 70 day period refuted 80−56975
Hercules X-1, 64 keV line feature in X-ray spectrum 77−78895
Hercules X-1, accretion disc viscosity determ. using slaved disc model 80−62110
Hercules X-1, cyclotron self-absorpt. in accretion column of mag. degenerate star 80−12760
Hercules X-1, evidence for 35 day precession in orbit 77−37667
Hercules X-1, Fe line emission discovery in low-state spectrum by (HEAO-1) 79−5922
Hercules X-1, high-energy X-ray spectrum 78−93473
Hercules X-1, long-term studies with Ariel 5 All-Sky Monitor 79−30146
Hercules X-1, obliquity 77−13390
Hercules X-1, precessing accretion disc with 70 day period 77−33693
Hercules X-1, X-ray emission behaviour 77−87569

eclipsing binary stars continued
Hercules X-1, X-ray pulsation obs. by SAS-3 during 1975, July 77−60793
Hercules X-1, X-ray spectra near turn-on in 35 day cycle 77−60794
Hercules X-1 (HZ Herculis) binary system, pre-supernova parameters 80−62318
Hercules X-1 (HZ Herculis) mass determ. 77−78891
Hercules X-1 binary system, possible third star existence 77−33572
Hercules X-1/HZ Herculis, evaporative winds 77−78888
HZ Herculis, 0.8 day periodicity in line emission 77−74089
AM Herculis, 1.2 and 2.2 μm light curves interpretation, model parameters 79−8949
HZ Herculis, 1978 UBV photometry of active state 80−62189
68=μ Herculis, ^{3}He identification 77−57045
HZ Herculis, abnormal N III emission lines in 1978 Aug. spectrum 78−81661
AM Herculis, accretion onto highly magnetised white dwarf 79−92764
AK Herculis, anal. of light changes in freq. domain 77−53635
HZ Herculis, Bowen fluorescence mechanism evidence 78−53985
u Herculis, BVR lightcurves interpreted 80−41856
AM Herculis, cyclotron lines in spectrum of nova-like star *(Russian)* 80−67753
DQ Herculis, emission line eclipse phenomena, visible spectra obs. 80−94800
DQ Herculis, emission lines phase depend. in accretion disc 77−74095
HZ Herculis, energy transport by circulation from illuminated region 79−71070
AM Herculis, evidence on nature of soft X-ray source from HEAO 1 obs. 79−17134
AM Herculis, hard X-ray spectrum 79−17022
DQ Herculis, He II 4686 Å line phase shift from spectrophotometry 79−21296
HZ Herculis, heliocentric pulse period, OSO 8 obs. 77−91573
AM Herculis, high speed photometric obs., 186 min. var., dwarf nova model 77−64806
AM Herculis, high-speed circular polarimetry 79−25629
AM Herculis, IR and visual monitoring, model constraints 79−17018
AM Herculis, IR spectroscopy, period, mass function 79−71066
AM Herculis, IUE UV obs. 79−67051
AM Herculis, J and K light curves 77−74091
HZ Herculis, light curve, radiation pressure effects 80−105280
HZ Herculis, light curve interpretation rel. to disclike envelope struct. 78−65658
AM Herculis, light curves and Fourier analysis 78−49483
AM Herculis, low-mass X-ray binary, radial vels. and line intensities 77−78826
AM Herculis, multicolour photometry, slow optical pulsar 78−28693
AM Herculis, narrow-band photoelectric obs. *(Russian)* 78−77565
68 Herculis, nature of He I line shifts 77−25999
HZ Herculis, nonperiodic optical flickering obs. 78−53988
HZ Herculis, orbital precession from Doppler modulation of pulsation arrival times 77−13398
AM Herculis, OSO-8 X-ray obs., 2-250 keV energy range 79−71075
AK Herculis, photoelec. obs. and period study, possible visual companion 79−67065
AM Herculis, photometric and polarimetric obs. 78−65657
AM Herculis, photometric and spectrographic obs. 77−45492
u Herculis, photometric elements, period changes 78−61884
LT Herculis, photometric elements 80−31328
DQ Herculis, photometric study of light curve 71 s oscill. 78−93259
AM Herculis, polar, IR photometric obs. 80−98687
AM Herculis, possible cataclysmic variable of Z Camelopardalis type 77−33497
HZ Herculis, pulse profile in hard X-rays 77−9811
AK Herculis, R and I light curves, B and V light curves comparison, starspot 79−67064
HZ Herculis, refl. effect turn-off *(Russian)* 78−69840
DI Herculis, relativistic motion of periastron 80−94830
HZ Herculis, spectrograms, radial vels. and equivalent width meas. 77−74094
AM Herculis, spectrophotometric obs. at min. light min. light 80−98692
AM Herculis, spectroscopic obs., H lines and He II 4686 Å line intensities 78−57589
AD Herculis, spectroscopic obs. and orbital elements 78−73738
u Herculis, synthetic light curve soln. of OAO-2 UV light curves 80−4399
u Herculis, two new light curves 80−90472
AM Herculis, UBVRI light curves 78−85972
AM Herculis, UBVRI photometric and polarimetric obs. 79−5861
AM Herculis, visual magnitude estimates (1977, April-May) 77−53642
AM Herculis, visual magnitude estimates (1980 March-June) 80−82428
AM Herculis, X-ray binary, emission lines, radial vel. var. 77−33567
AM Herculis, X-ray binary, optical light curve 77−33566
AM Herculis, X-ray binary, optical variability 78−53952
AM Herculis, X-ray binary, polarization obs., mag. compact star discovery 77−33569
AM Herculis, X-ray binary, spectroscopy and photometry, model 77−33568
AM Herculis, X-ray eclipsing binary, UV and visible spectra anal. 80−109563
AM Herculis, X-ray light curve 77−45491
DQ Herculis, X-ray obs. from Ariel 5 satellite 77−37671
AM Herculis (3U 1809+50), eclipsing binary, review of obs. 77−71155
AM Herculis (3U 1809+50), polarimetry and spectrophotometry rel. to mag. field 80−94835
AM Herculis (3U 1809+50), simultaneous three-channel photometry rel. to optical flickering mechanism 80−82411
AM Herculis (3U 1809+50), single accretion column model 78−57578
AM Herculis (3U 1809+50), soft X-ray results from OSO-8 Wisconsin Expt. 78−36722
AM Herculis (3U 1809+50), UV spectrum obs. 80−67782
AM Herculis (3U 1809+50), X-ray eclipsing binary, multicolour photometry 77−78887
AM Herculis (4U 1813+50), narrow-band photoelec. obs. *(Russian)* 79−88767
AM Herculis (4U 1813+50), rapid light variability obs. *(Russian)* 80−8662
AM Herculis (4U 1814+50), X-ray emitting mag. white dwarf binary, review of props. 80−105403
AM Herculis (=3U 1809+50), near IR and violet mag. obs. 77−53643

eclipsing binary stars continued
HZ Herculis (Hercules X-1), 2-6 keV pulse profiles, Uhuru data 79−17129
HZ Herculis (Hercules X-1), 35 day clock mechanism 80−73070
HZ Herculis (Hercules X-1), Ariel V X-ray spectra 80−90580
HZ Herculis (Hercules X-1), coordinated optical and X-ray pulsations obs. 80−51909
HZ Herculis (Hercules X-1), Copernicus and Ariel V obs. 77−45609
HZ Herculis (Hercules X-1), cyclotron line form. by reson. Compton cyclotron scatt. 80−8711
HZ Herculis (Hercules X-1), high-energy pulsed X-ray spectrum from OSO 8 obs. 79−92888
HZ Herculis (Hercules X-1), implications of cyclotron features in X-ray spectrum 80−86015
HZ Herculis (Hercules X-1), IUE obs. spectrum and light var. 80−73069
HZ Herculis (Hercules X-1), IUE UV spectrum obs. 78−96569
HZ Herculis (Hercules X-1), optical and UV obs. 80−109487
HZ Herculis (Hercules X-1), optical behaviour, 1976 Aug.-1977 Nov. 79−53855
HZ Herculis (Hercules X-1), optical pulsation theoretical calcs. 78−57580
HZ Herculis (Hercules X-1), optical pulsations rel. to accretion disc/mag field interaction *(Russian)* 80−51799
HZ Herculis (Hercules X-1), optical pulsations spectrum meas. 77−33685
HZ Herculis (Hercules X-1), orbital precession 78−65718
HZ Herculis (Hercules X-1), periodic mass transfer rel. to X-ray light curve 80−51911
HZ Herculis (Hercules X-1), precessing twisted accretion disks 80−56973
HZ Herculis (Hercules X-1), pulse phase spectroscopy, 6-60 keV 79−84870
HZ Herculis (Hercules X-1), search for X-ray polarization 80−4457
HZ Herculis (Hercules X-1), soft X-ray results from OSO-8 Wisconsin Expt. 78−36722
HZ Herculis (Hercules X-1), Sonneberg photographic obs. 77−37618
HZ Herculis (Hercules X-1), UBVR photometry during 1977 Jul.-Aug. *(Russian)* 79−17028
HZ Herculis (Hercules X-1), X-ray binary, tidal friction effects 77−57013
HZ Herculis (Hercules X-1), X-ray continuum and Fe line emission during X-ray low state 80−105393
DQ Herculis (Nova 1934), extended nova shell spectra 78−93253
DQ Herculis (Nova 1934), high time resolution spectrophotometry 80−22017
DQ Herculis (Nova 1934), light curve and double maxima 77−82255
DQ Herculis (Nova 1934), masses of interactive binary 79−97029
DQ Herculis (Nova 1934), short-period oscills. modulation and pulsed emission lines asymmetry interpretation 80−22044
DQ Herculis (Nova 1934), UBV photometry of visual binary 80−8661
AM Herculis type binaries, cyclotron self-absorption in accretion columns of magnetic degenerate stars 80−12760
AM Herculis/3U 1809+50 X-ray binary, rot. mag. white dwarf model 77−33571
hot stars, IR photometry *(Italian)* 79−53829
HR 1099, quiescent X-ray emission obs. from RS Canum Venaticorum star 78−81659
HR 3872, discovery during photometric search for β Cephei stars 79−71040
HR 5110, Algol type RS Canum Venaticorum star, Hα, yu photometry obs. 80−105276
HR 9049, (HD 224113), eclipsing spectroscopic binary star, period determ. 80−46609
EX Hydrae, 2:3 period ratio in light curve 80−46580
TT Hydrae, absolute dimensions of β Persei type eclipsing binary 80−62184
EX Hydrae, dwarf nova, hard X-ray emission 78−93275
EX Hydrae, dwarf nova, IR and optical light curves 80−67747
EX Hydrae, dwarf nova, times of minima 77−22267
EX Hydrae, dwarf nova lightcurve, periodic and secular vars. 80−77413
χ^2 Hydrae, four-colour photometry, orbital elements, dimensions and He abundance 78−65653
AI Hydrae, light curves and photometric elements of eclipsing binary 78−65652
HS Hydrae, photometric elements of detached system 80−90473
EZ Hydrae, photometric obs. and primary min. ephemeris 78−73737
EX Hydrae, soft X-ray emission during optical quiescence, HEAO-A2 obs. 79−71054
EX Hydrae, spectra of dwarf nova 80−98670
VZ Hydrae, transit or occultation at primary minimum 77−9770
TT Hydrae, UBV photometry, improved light elements 78−69837
AI Hydrae, uvby photometric obs. of eclipsing F-type binary 78−69835
VW Hydri, cataclysmic variable, light curve superhumps model 80−4381
VW Hydri, colour variations during dwarf nova outbursts 80−46576
VW Hydri, dwarf nova, IR light curves 80−67747
VW Hydri, outbursts of dwarf nova, long and short eruptions comparison 79−88669
HZ 22 (UX Canum Venaticorum), hot subdwarf binary, evolution and mass 79−12472
HZ 29, binary white dwarf system, evolution and gravit. radiation 77−57030
instantaneous spectra determ. by inversion technique 80−82218
JHKLM photometry of close systems 80−46614
SW Lacertae, contact type polarisation obs. 77−45489
AR Lacertae, Hα spectrogram following radio outburst, results 77−49432
AR Lacertae, period vars. 77−37616
AR Lacertae, photometric obs., intrinsic variation 77−22271
RT Lacertae, RS Canum Venaticorum binary, radio emission obs. 79−58379
AR Lacertae, times of minima, photoelec. obs. 77−57012
CM Lacertae, transit or occultation at primary minimum 77−9770
SW Lacertae, W Ursae Majoris star, photoelectric obs. and epochs of min. light 80−62196
SW Lacertae, W Ursae Majoris type star, 1.2 and 2.2 micron light curves 79−84822
late-type, mass-luminosity and radius relations, chem. composition 78−28728
LB 3459, O-type subdwarf plus hot white dwarf eclipsing binary, photometry, anal. 79−48859

eclipsing binary stars continued
LB 3459, short period eclipsing binary system containing two O-type subdwarfs, uvby photometry 78—53987
LB 3459, subdwarf eclipsing binary, evolutionary model 80—51808
LB 3479, subdwarf system, evolutionary model comment 80—90426
XY Leonis, light curve synthesis for contact binary 79—12494
20 Leonis, possible eclipse obs. in triple system 78—12298
T Leonis Minoris, Algol-type semi-detached binary system 77—91580
δ Librae, revised photometric elements 79—101175
libration in close binary systems, effects on light curves 78—57579
light and velocity curves simultaneous solution, eccentric orbit generalisation 80—36664
light curve analysis, Fourier techniques 79—58261
light curve analysis by Fourier techniques 80—72993
light curve analysis by Fourier techniques 80—72994
light curve Fourier analysis, eclipse parameters, geometric determinacy 78—96503
light curve solution by Kopal's iterative process 79—35310
light curves, Fourier analysis for partial phases 79—21350
light curves, Fourier analysis techniques, series expansions 79—75248
light curves, Fourier analysis techniques and light changes 79—75247
light curves Fourier anal. 77—9769
light curves Fourier analysis, appls. to eccentric orbits 79—25630
light curves linear analysis, fractional light loss anal. 80—82416
light curves soln. using LIGHT computer program 80—77454
light loss analysis, Fourier techniques 79—58262
line profile calc. for close systems with mass transfer 80—41860
LMC X-4, Ariel 5 obs. of eclipses and identification confirmation 77—74161
LMC X-4, identification with eclipsing binary system, review *(German)* 78—81713
LMC X-4, spectroscopic obs. and orbit 79—9028
LMC X-4 optical candidate, binary nature 77—64879
LMC X-4 optical counterpart, photometric and spectroscopic obs. 77—49431
low mass close binary evolution, catastrophic mass loss 77—33554
RR Lyncis, Am eclipsing binary, photometry and spectroscopy, abundances 77—33558
SW Lyncis, close binary, orbital elements 77—74090
β Lyrae, CNO abundances in atmosphere, IR spectra *(Russian)* 80—67794
β Lyrae, current knowledge 80—105289
β Lyrae, emission sources and gas streams *(Russian)* 79—92802
β Lyrae, H emission profiles rel. to pattern of gaseous flow in system 78—57576
β Lyrae, high time-resolution spectroscopy at Hα 77—13388
β Lyrae, intrinsic linear polarisation in Hα, Hβ emission lines 77—41390
β Lyrae, narrow-band photometry in (1971) 80—46605
β Lyrae, orbital period variability 80—72997
β Lyrae, random vars. in UV spectrum 77—22273
β Lyrae, secondary star spectral type and struct. of system *(Russian)* 79—97036
AY Lyrae, soft X-ray emission detect. from dwarf nova, H1839+37 79—75227
β Lyrae, UV line emission of ionised Fe 77—13364
β Lyrae evolution, accretion onto ZAMS secondary and contact binary stage 79—66994
in Magellanic Clouds, tabulated light curves 78—16536
magnetic X-ray binaries, synchronous rotation appl. to AM Herculis 79—62867
massive Algol-type systems, evolutionary status 77—57047
massive close binaries, evolution of systems with primaries of 10-15 M⊙ 77—87473
massive close binaries, post-supernova stage, tidal instability 77—57024
massive close binary systems, evolution 77—57022
massive close binary systems, late evolutionary stages 77—57023
massive X-ray binaries, evolution of optical components 80—41857
massive X-ray binaries, lifetimes 77—45608
massive X-ray binary systems, pulsars rot. history 77—49412
TY Mensae, contact eclipsing binary, evolutionary stage from UBV light curve anal. 80—105278
AU Monocerotis, cyclic variation in period 77—33565
AU Monocerotis, mathematical anal. of photometric peculiarities 80—77448
VV Monocerotis, orbital elements and dimensions *(French)* 78—89225
AU Monocerotis, photoelec. obs. 80—73002
VV Monocerotis, RS Canum Venaticorum type eclipsing binary, photoelectric obs. 79—40218
neutron star binaries, observational constraints on masses 77—5543
OB binary stars, evolutionary sequence to X-ray stars and pulsars, tugboat model 77—56915
UZ Octantis, W Ursae Majoris system, UBV light curves 80—22042
V2051 Ophiuchi, AM Herculis-type variable, spectrum scans 77—45492
V1010 Ophiuchi, early-type contact system, two-colour light curves 77—33553
U and V451 Ophiuchi, late-type, mass-luminosity and radius rels., chem. composition 78—28728
V566 Ophiuchi, light curve 77—71130
U Ophiuchi, massive eclipsing binary star, spectrophotometry 80—26900
RZ Ophiuchi, orbital elements from new obs. 79—21327
V566 Ophiuchi, period change, UBV photometry 77—29883
U Ophiuchi, photometric anal. 77—53628
V1010 Ophiuchi, short period close binary, radial vel. curve 77—29884
V566 Ophiuchi, W Ursae Majoris binary, synthetic light curve calc. 77—74097
V1010 Ophiuchi as massive zero age contact binary 77—57058
orbits, appl. of Kalman filter to light curves 77—5546
θ^1 Orionis, period determ. 77—2455
θ^1 Orionis A, photographic photometric obs. 79—58380
θ^1 Orionis A, UBV photoelec. obs. of primary eclipse 77—91576
η Orionis A, UV spectrum 77—45485
MW Pavonis, UBV light var. and orbital elements 77—49429
MW Pavonis, W Ursae Majoris system, evolutionary stage from UBV light curve anal. 80—105278
BB Pegasi, BV photoelectric lightcurve analysis 80—62194
BX Pegasi, photoelectric photometry of totally eclipsing W Ursae Majoris systems, 1978 Oct. to Nov. *(Chinese)* 80—31330
AQ Pegasi, UBV light curve solns. 80—41855
period distrib. 78—69829
period distribution, statistics 80—36662
period-mass ratio relations for objects with periods <5 days 78—57585

eclipsing binary stars continued
β Persei, 4.8 μ photometry 77—74092
X Persei, gaseous ring struct., H I alpha obs. 80—109482
AG Persei, in II Persei association, distance 79—21326
AG Persei, late-type, mass-luminosity and radius rels., chem. composition 78—28728
RT Persei, light curve analysis by automated Fourier technique 79—17020
AG Persei, massive eclipsing binary star, spectrophotometry 80—26900
β Persei, Mg II 280 nm line profile, calcs. and UV obs. 80—82421
β Persei, partially eclipsing binary, freq. domain light curve anal. 77—53639
β Persei, soft X-ray image 77—53627
RY Persei, spectroscopy and physical parameters of atmospheres 80—101618
β Persei, study of light curve at 3428 Å 77—53634
AG Persei, two-colour photometry of eclipsing binary system, apsidal motion 78—96504
RW Persei, UBV photometry of semidetached binary system 79—25639
β Persei, UV obs., from TD-1A satellite 80—77447
RT Persei, V light curve 77—53636
RY Persei, visible spectra obs., model 80—67795
X Persei (4U 0352+30), absence of ellipsoidal light vars. 79—80337
β Persei (Algol), detection of B component, mass determ. 78—65654
β Persei (Algol), general problems and history *(Swedish)* 77—22268
β Persei (Algol), light curve at 10 μm near scondary min. 78—93315
β Persei (Algol), orbital inclination and masses determ. from speckle interferometry 80—36668
β Persei (Algol), orbital period (1964 to 1978) 79—58377
β Persei (Algol), primary component rot. 80—72996
β Persei (Algol), radio outbursts and possible period change 80—26907
β Persei (Algol), X-rays detect. 77—9773
β Persei (Algol) eclipsing binaries, mass loss and mass transfer theory 80—62191
β Persei (Algol) system, gravity darkening 79—44525
β Persei (Algol) type semi-detached binaries, rotational vels. 78—89220
GK Persei (Nova 1901), visual magnitude estimate for 1978 July 78—69807
β Persei field, Asiago Schmidt obs. and new variables *(Italian)* 77—91547
β Persei type systems, orbital period changes and evolutionary status 80—4396
β Persei-type eclipsing binaries, mass transfer rates from period changes 77—57040
β Persei-type eclipsing binaries, red spectra, element abundances and neutrinos 77—57041
PG 1413+01, white dwarf-red dwarf eclipsing binary, photometry and spectral types 79—8944
ζ Phoenicis, late-type, mass-luminosity and radius rels., chem. composition 78—28728
AI Phoenicis, orbital elements and dimensions *(French)* 79—71074
AE Phoenicis, W Ursae Majoris type system, orbit 78—85970
AE Phoenicis, W Ursae Majoris-type star with elliptical orbit 77—57010
photoelectric lightcurves of possible sd-d systems, revised elements 80—56879
δ Pictoris, β Lyrae-type eclipsing binary, satellite UV obs. 77—57033
RR Pictoris (Nova 1925), spectrophotometry of surrounding filaments, abundances, ionization 79—40194
SZ Piscium, RS Canum Venaticorum star, photometric obs. rel to starspot model 80—109490
UV Piscium, short period eclipsing binary, light and colour curve obs. 79—88697
Princeton-Pennsylvania-Florida card catalogue 77—78666
pulsating binary X-ray sources, periodic timing residual 78—65718
RX Puppis, 2 μm spectroscopy, H_2O and CO absorpt., symbiotic binary model 79—67032
AU Puppis, A-type evolved contact system 78—65650
VV Puppis, AM Herculis type binary, accretion column absorpt. spectrum obs. 79—101176
VV Puppis, AM Herculis type binary, optical absorpt. spectrum, cyclotron intepretation and models 80—73003
VV Puppis, AM Herculis type binary spectrophotometric obs. 79—5860
VV Puppis, AM Herculis-type variable, spectrum scans 77—45492
V Puppis, B-type semidetached system, photoelectric obs. 79—44522
VV Puppis, brightening of magnetic variable (1978 March) 78—36595
VV Puppis, circular polarimetry in active state and evidence for two accreting poles 79—48854
V Puppis, circumstellar matter obs. 77—13385
VV Puppis, dwarf nova, spectroscopic obs. during active phase 79—80322
V Puppis, light curve study of early-type close binaries in triple systems 78—89222
VV Puppis, linear and circular polarisation during active phase 77—37621
VV Puppis, obs. in faint state 79—25643
VV Puppis, photometric activity, flickering 77—67112
VV Puppis, polar, IR photometric obs. 80—98687
VV Puppis, proper motion meas., distance and luminosity 78—96510
VV Puppis, spectroscopic obs., broad absorpt. features discovery 79—44502
TY Pyxidis, light curve of RS Canum Venaticorum type binary 79—25641
radial velocity curves of close binary systems, anal. 80—90470
radii, comparison with radii of single main sequence stars (A0 V to G2 V) 80—51758
review, of surveys and obs. of eclipsing variable stars 80—12772
WZ Sagittae, 1978-9 outburst of dwarf nova, spectra 80—94801
U Sagittae, Algol type binary, spectrophotometry 77—2454
WZ Sagittae, BV photometry and magnitudes (1978 Nov.-Dec. outburst) 79—12484
WZ Sagittae, cataclysmic variable, light curve superhumps model 80—4381
UU Sagittae, eclipsing binary, central star of Abell 63 planetary nebula 78—93304
U Sagittae, elements determ. from light changes anal. in freq. domain 77—53637
WZ Sagittae, eruptive binary, model from hot spot eclipses anal. 80—72962
WZ Sagittae, image-tube spectroscopic obs. of 1978 Dec. outburst 80—72958
HM Sagittae, IR spectrum and evidence for cool star 78—93266

eclipsing binary stars continued

WZ Sagittae, orbital parameter determ. for recurrent nova 78—93317
WZ Sagittae, outburst of December 1978, UV obs. 80—72982
WZ Sagittae, period change and magnitudes (1978 Dec.-1979 Jan.) 79—21309
V Sagittae, periodicity disclaimed due to telescope periodic drive error 79—92763
U Sagittae, photometric study of eclipsing binary 77—22270
WZ Sagittae, physical parameters from eclipse anal. 79—80336
WZ Sagittae, recurrent nova, IUE obs. in outburst 80—109448
WZ Sagittae, recurrent nova, physical parameters, present state, past and future evolution 78—85948
WZ Sagittae, recurrent nova, spectroscopic obs. and model for superhump phenomena 80—82368
WZ Sagittae, recurrent nova, spectroscopic obs. during 1978 outburst 80—26862
WZ Sagittae, recurrent nova, spectroscopic study during 1978 outburst 80—56849
U Sagittae, secondary mass from vel. curve 79—97025
WZ Sagittae, spectroscopic obs. (1978 December 1 and 2) 79—16983
WZ Sagittae, spectroscopic obs. and photoelectric V-magnitudes 79—16984
U Sagittae, theoretical light curve of contact system 78—77578
WZ Sagittae, time of minimum light, period, magnitudes 79—21353
WZ Sagittae, time-resolved broadband obs., optical pulsations, period 79—92781
WZ Sagittae, UBV photometry and spectroscopy of 1978 Dec. outburst 79—12483
WZ Sagittae, visual magnitude 1979 April 8 79—44508
WZ Sagittae, visual magnitude estimate 1979 June 20 for recurrent nova 79—84800
WZ Sagittae, visual magnitude estimates, 1978 Nov., 1979 Jan.-Feb. 79—30075
WZ Sagittae, visual magnitude estimates, (1978, November 28 to December 11) 79—12481
υ Sagittarii, absorpt. lines identification as Fe II high level transitions 78—93316
XZ Sagittarii, Algol system, UBV photometric investigation 80—22041
μ Sagittarii, eclipse of unseen companion, obs. 80—4401
V1647 Sagittarii, light curves, photometric elements and apsidal motion 77—60795
V356 Sagittarii, massive eclipsing binary star, spectrophotometry 80—26900
υ Sagittarii, UV spectrum 79—35300
V1357 Sagittarii, visible obs. 80—77452
μ Sagittarii primary eclipse prediction (for 1979 March 10) 79—35307
V861 Scorpii=OAO 1653—40, physical parameters 79—17021
μ^1 Scorpii, B-type semidetached system, photoelectric obs. 79—44522
V701 Scorpii, dimensions and evolution of early-type contact binary 80—62188
V861 Scorpii, IR obs. of black hole candidate 79—44538
V861 Scorpii, near IR meas. rel. to orbital phase 78—93324
V861 Scorpii, not associated with 38.22 second X-ray pulsations from OAO 1653—40 vicinity 80—27014
V861 Scorpii, not identical with pulsating hard X-ray source (OAO 1653—40) 79—67118
V861 Scorpii, upper limit on X-ray emission, and non-coincidence with (OAO 1653—40) 80—73072
μ^1 Scorpii, UV obs. from TD-1A satellite 80—77447
V861 Scorpii, X-ray emission from unseen companion 78—89226
V861 Scorpii (HD 152667), eclipsing binary, identification with X-ray source (OAO 1653—40) 78—69838
V861 Scorpii (HD 152667), X-ray binary, behaviour of Hα 79—101171
V861 Scorpii (HD 152677), Hα emission features vars. 78—77579
V861 Scorpii (OAO 1653-40?), simultaneous UV and X-ray obs. 80—17616
V701 Scorpii as massive zero age contact binary 77—57058
RT Sculptoris, close eclipsing binary, uvby light curves 77—60798
RY Scuti, β Lyrae system, optical and radio spectra 79—30090
RY Scuti, ephemeris and UBV photometry 80—94832
RZ Scuti, JKL IR obs., light curves 80—101615
RY Scuti, silicate grains IR emission from early-type supergiant binary system 80—41827
in Scutum-Vulpecula regions, visual minima obs., 1920-1950 period 77—33564
sd-d type, struct. and dimens. 80—82423
semi-detached systems, revised photometric elements for 8 single-line binaries 80—46611
semi-detached systems, revised photometric elements for 9 binaries 80—46612
semidetached binaries, mass transfer and impact-driven accretion discs 77—57036
semidetached systems, revised photometric elements 80—62193
CV Serpentis, BVRI photoelectric obs., but no eclipse 78—85971
CV Serpentis, IR photometry and CRL 2120 identification 77—78825
W Serpentis stars, new class, accretion onto nondegenerate stars 80—109483
Y Sextantis, W Ursae Majoris system, UBV obs., light curve soln. by computer program 80—77454
Sk 160, optical counterpart of SMC X-1, VBLUW photometry 77—82277
SMC X-1, distortion of absorpt. line vel. curves due to X-ray heating 77—29878
SMC X-1, observational constraints on mass 77—29957
SMC X-1, pulsation period and orbital period decrease 77—49499
SMC X-1, soft X-ray emission detection, 2-day flaring period 79—35432
SMC X-1, spin-up rate of X-ray pulsar 77—29956
SMC X-1, X-ray binary, 5 colour photometry 77—17622
SMC X-1 (Sanduleak 160), binary system, orbital elements and masses 77—9815
solutions, coeffs. of approx. polynomials 77—17380
southern spectroscopic and eclipsing binaries, cooperative obs. feasibility 78—69681
Stepanyan's star, obs. of G8 V absorpt. spectrum and emission spectrum 80—67788
Stepanyan's star, possible cataclysmic variable, eclipses obs. and orbital period refinement 80—62195
Stepanyan's star, spectrophotometric and photometric obs., 228-min period 80—56883
Stepanyan's star found to be eclipsing binary, possibly cataclysmic 80—51806

eclipsing binary stars continued

V471 Tauri, BV photometry of white dwarf eclipsing binary, light curve vars. 78—96508
RW Tauri, elements determ. from light changes anal. in freq. domain 77—53637
RW Tauri, gaseous ring struct., H I alpha obs. 80—109482
CD Tauri, intermediate-band photometric anal. 77—13389
λ Tauri, mass loss from UV spectra obs. 80—109485
λ Tauri, massive eclipsing binary star, spectrophotometry 80—26900
CD Tauri, orbital element determ., BV photometer obs. 80—73000
V471 Tauri, period var. and light curves of eclipsing binary system 80—22038
V471 Tauri, U photometry of eclipses and flares 79—71072
RW Tauri, UBVRI light curves of Algol-type eclipsing binary 77—91577
V471 Tauri, white dwarf eclipsing binary, IUE UV spectra 80—26912
V471 Tauri (Bd+16°516), Ca II H and K and Hα line vars. 79—67063
V471 Tauri (BD+16°516), eclipsing binary white dwarf, spectroscopy and photometry rel. to evolution 77—57028
V471 Tauri (Nova 396 AD), identification of possible outburst *(Russian)* 79—101162
BL Telescopii A, yellow variable supergiant near Cepheid instability strip, VBLUW photometry 80—98672
tidal friction in close binary stars, theory 77—57013
RW Trianguli, nova-like binary, radial vels., dimens. from visible spectra 80—82418
RW Trianguli, nova-like variable, eclipse timings 79—21357
AQ Tucanae, UBV photometry, light curves 79—8951
3U 0900-40 (HD 77581), X-ray to binary, orbital elements and pulsational period increase 77—64877
4U 1538—52, binary X-ray pulsar, early B-type supergiant as counterpart 78—93472
4 U 1538—52, corrections to ephemeris and revised period 79—25760
4U 1538—52, eclipsing binary pulsating system, position meas. by HEAO-1 78—96570
4U 1538-52, optical counterpart spectroscopy and system parameters 79—5924
4U 1700—37, binary X-ray source, X-ray position 78—54094
3U 1700—37, further Copernicus X-ray obs. 78—96568
4U 1700—37 (=HD 153919), X-ray obs. 80—86016
4U 1700—37 (HD 153919), X-ray binary, high-energy X-ray obs. 80—86014
4U 1700-37 (HD 153919), uncertainty of 97 min. periodicity 79—40295
4U 2129+47, X-ray light curve and binary model 80—46704
UBV photometric programme at Palomar and Kitt Peak 77—64796
ultrashort period binaries, obs. and theoretical problems *(Polish)* 79—58381
RU Ursae Minoris, photometric obs. of contact binary 77—74088
Ursa Major stream eclipsing binaries, ages and absolute dimensions 79—92800
UX Ursae Majoris, anomalous 1977 period change for nova-like eclipsing binary 78—85956
VV Ursae Majoris, BV photometry and elements of eclipsing binary 77—26026
TX Ursae Majoris, close eclipsing system, freq. domain anal. of light changes 77—53638
XY Ursae Majoris, constant orbital period 77—74085
W Ursae Majoris, contact eclipsing binary, polarisation obs. 77—45489
AN Ursae Majoris, emission lines and radial vel. curve 77—33514
AW Ursae Majoris, light curve anal. of contact binary 80—56875
XY Ursae Majoris, light curve changes, starspot activity 77—57044
W Ursae Majoris, OAO-2 UV photometry 77—13393
XY Ursae Majoris, observational evidence for large-scale spot activity on primary component 80—109491
UX Ursae Majoris, period changes 77—64805
AN Ursae Majoris, polar, IR photometric obs. 80—98687
AN Ursae Majoris, polarisation meas. of nova-like object 77—29851
AN Ursae Majoris, polarisation of AM Herculis-type nova-like binary 78—85958
AN Ursae Majoris, similarity to AM Herculis 77—91582
AN Ursae Majoris, soft X-ray flux detected 80—4400
AN Ursae Majoris, steady low luminosity state 79—40219
AW Ursae Majoris, theoretical light curve of contact system 78—77578
W Ursae Majoris, uvby obs. 79—44533
XY Ursae Majoris, variable light curve 77—91568
W Ursae Majoris, vars. of period and light curve of eclipsing binary *(Italian)* 78—93318
W Ursae Majoris binary stars, synthetic light curves calc., appl. to V566 Ophiuchi 77—74097
W Ursae Majoris metal-poor systems, evolution models 79—25628
W Ursae Majoris stars, A-type, radii and evolutionary state 79—8943
W Ursae Majoris stars, atm. parameters of A-type systems 80—36672
W Ursae Majoris stars, Fourier analysis of light curves 79—21349
W Ursae Majoris stars, nonradial radiative transfer, appl. to bolometric refl. effect 77—91567
W Ursae Majoris stars, rot. line broadening functions rel. to stellar shapes 80—109494
W Ursae Majoris stars, theory of light curves 77—57008
W Ursae Majoris systems, struct. and evolution 77—45488
UX Ursae Majoris time series photometry 80—77446
W Ursae Majoris type binaries, evolutionary models 77—53644
W Ursae Majoris type binaries, mass ratio function 79—8947
W Ursae Majoris type contact binaries, theories, observational tests 79—97026
W Ursae Majoris type stars, secular stability of contact binaries with age-zero components 80—67786
W Ursae Majoris type systems, UVBY photometry 77—57056
RT Ursae Minoris, photoelectric obs. of eclipsing binary 77—82276
V444 Cygni, light curve anal. by new method 80—109374
V80 in dwarf spheroidal galaxy in Ursa Minor, eclipsing binary star with RRc primary 80—109505
V 78 in ω Centauri, cluster membership determ. 78—73743
variable stars, Fourier anal. of light curves 77—49428
Vela X-1, long-term studies with Ariel 5 All-Sky Monitor 79—30146
Vela X-1 (3U 0900—40), Ariel V Sky Survey instrument obs. 77—45495
Vela X-1 (HD 77581), X-ray binary, uvby obs. 77—37668
CV Velorum, light curves, photometric elements and absolute dimensions 77—60796
BF Virginis, β Lyrae-type eclipsing binary, light curves 77—13395
CG Virginis, soln. of photoelect. light curve *(Chinese)* 79—53857
α Virginis, UV spectrum 77—45485

eclipsing binary stars continued
  AH Virginis, vars. of light curve and period 77—78822
  visual minima, Cracow Observatory obs. 77—74086
  DR Vulpeculae, apsidal motion 77—57011
  BS Vulpeculae, photoelec. photometry, light curve, period 79—21351
  ER Vulpeculae, W Ursae Majoris star, rot. line broadening rel. to shape and mass ratio 80—109494
  VV Puppis, 3470 Å emission as cyclotron line 80—36673
  Wolf-Rayet binaries, interpretation of eclipses at emission-line freqs. 77—17596
  WRA 795 (Centaurus X-3), search for X-ray polarization 80—4457
  X-ray binaries, axisymmetric accretion theory 77—33334
  X-ray binaries, constraints on apsidal motion 77—87571
  X-ray binaries, distortion of absorpt. line vel. curves due to X-ray heating 77—29878
  X-ray binaries, lifetimes 77—9812
  X-ray binaries, limitations on nature and evolution 77—82273
  X-ray binaries, matter supply mechanisms 77—9813
  X-ray binaries, review of new developments 77—71154
  X-ray binaries, test of quark bags and interacting neutrons models 77—78812
  X-ray binaries rel. to OB stars and pulsars, tugboat model for evolution 77—56915
  X-ray binary source in stellar wind, variable spectral features interpretation 77—17716
  X-ray binary sources, properties and models 77—41419
  X-ray binary sources rel. to old novae 77—87576
  X-ray binary sources with OB supergiant companions, possible mass transfer mechanism 77—9809
  X-ray binary stars, observational evidence for black holes 77—57007
  X-ray binary system, Fe fluoresc. line struct. 77—78889
  X-ray binary systems, accretion discs, observational appearance *(Russian)* 77—87477
  X-ray binary systems, evaporative winds 77—78888
  X-ray binary systems, K-fluorescence lines in spectra 78—93456
  X-ray binary systems, massive, gas streams and accretion discs 78—93464
  X-ray binary systems, models, X-ray transfer, Monte Carlo study 78—93463
  X-ray bindary systems, X-rays polarisation from mag. accretion disc *(Russian)* 77—87575
  X-ray burst sources, magnetised accretion disc model 77—53702
  X-ray burst sources, properties, binary systems *(Russian)* 78—93477
  X-ray burst sources, simple physical model 77—29960
  X-ray pulsars, accretion torques 77—49505
  X-ray pulsars, review 77—29869
  X-ray pulsars, role of Alven surface in X-ray pulses form. 77—78899
  X-ray sources, binarity detect. via Doppler effect *(Russian)* 78—77623
  X-ray sources, review of current knowledge in 0.5 to 10 keV range 78—69915
  X-ray sources, spin up as indicator of normal component evolution *(Russian)* 77—74100
  X-ray sources with repeating bursts, magnetospheric accretion model 77—5597
  X-ray transient sources, close binary star model 77—33695
  X-rays from radio binary systems 77—33700
  Be stars and shell stars, possible interacting binaries 77—57041
  SS Cygni, soft X-ray emission detect. during optical outburst 80—46574
  U Geminorum, soft X-ray emission detect. during optical outburst 80—46574

ecology
  alternative energy sources and environmental problems, Ispra Research Centre activities, w.r.t. EEC policy 79—97770
  aquatic organism tolerance and response to solar UV radiation 80—45974
  biophysics of living organisms communities in natural state, pollution effect 77—73503
  biosphere and active solar processes link, role of Earth's natural electromag. field 78—61211
  calcareous plankton in early Cenozoic Atlantic Ocean, palaeobiogeography rel. to climatic fluctuations 78—16143
  catastrophes, comets and ice ages 78—53714
  compartmental analysis in biology, medicine and ecology, mathematical foundations 78—68978
  computer-aided instruction, appl. to ecological population dynamics 79—30166
  cone pigment ecology in teleost fish 78—69041
  conference, Osaka, Japan (Nov. 1979) 80—98756
  coral growth form, light control, computer simulation 77—2076
  distributed trigger system, non-linear stability, biological barrier 79—92117
  diversity indices computation, FORTRAN program 77—33076
  Douglas fir ecosystem, acid rain and cation leaching 77—78392
  dynamic processes on Earth, extraterrestrial causes, rel. to extinction of life 78—92820
  ecosystem succession detection by aerial IR photography 78—81459
  environment, resistance to technogenic action *(Russian)* 79—88044
  environmental background monitoring program 80—81518
  environmental control, ORAKEL experimental conferencing for citizen participation 79—57499
  freshwater food chains contamination by ^{60}Co, direct water borne contamination of organisms *(French)* 79—20688
  fusion reactor materials resource cycle, environmental impact 80—18616
  global sea pollution, ecological aspects 78—3826
  inland aquatic ecosystems, chemical effects 77—70706
  intertidal ecosystems, ecological effects of petroleum, field expts. 79—66420
  Lake George ecosystem management model development 78—36217
  lake runoff management, ecosystem model WINGRA III 78—36216
  Lake Superior, primary production model including circulation influences 78—49041
  lakes and reservoirs, time and length scales for one-dimens. assumption, math. ecological models 80—12455
  leaf optical system modelled as stochastic process 77—44877
  leaf radiation stochastic model 77—32880
  life support system with autonomous control employing plant photosynthesis 77—25563
  limnological ecosystem modelling, real-time estimation methods appl. 79—5541
  lumped system in conflict with environment, Liapunov type design 79—57498
  marine particulate plume density and distrib., acoustic assessment 80—45843
  mathematical modelling, Conf. on Earth resources electronics Rome, Italy (Mar.77) *(Italian)* 77—82056
  modelling, temperate ecosystem, literature review 80—81949
  multicompartment systems, analytical techniques 79—83689
  nondestructive neutron activation analysis of environmental samples using low-energy photon spectrometry 78—3995
  nuclear energy centres, power development, economic and ecological problems, USSR *(Russian)* 79—31149
  nuclear energy effects on tradescantia, indicator for ecological effects *(Dutch)* 80—45967
  nuclear plant fuel cycle closing, radioactive materials reprocessing and disposal *(German)* 77—54344
  nuclear power stations, long term radioactivity values, meas. in marine life *(Spanish)* 80—7962
  nuclear waste ponds and streams, Hanford, ecological search for radiation effects 80—89804
  ocean dumping of high level radioactive waste 80—32376
  OTEC power system development and environmental impacts 80—66990
  palaeoclimatology and vegetation ecology *(French)* 78—88901
  photobiological conversion of solar energy *(German)* 79—2013
  photosynthesising organisms, remote laser probing by fluoresc. technique 79—66434
  plant uptake of transuranics, techniques for long term field studies 79—57821
  proton activation analysis of environmental and ecological pollution determ. 78—3994
  quantitative cartographic analysis, SYMAP auxiliary programs, geoenvironmental appls. 79—70469
  radioactive effluent, Pu and Am inventory of ecosystem near a nuclear facility 80—97820
  renewable energy sources and the environment 79—79411
  replicated diversity indices computation for random samples of specified size 77—37197
  review of ecology and systematics (book) 80—67945
  Satellite Power Station microwave health and ecology programme 79—70443
  shelly beaches, Victoria, Australia 79—92525
  sludge disposal in coastal waters, Philadelphia study 78—3823
  solar town in Iran, conceptual development 79—57408
  sonic boom of supersonic transport aircraft, effects on ecological environment 80—106661
  system model sampling/identification, input signal anal. 78—69267
  thermal insulation of animal coats and human clothing, review 78—73139
  thermal plant siting, regional policy and ecological aspect of landscape 80—862
  transformation systems direct and inverse regulation control 78—11606
  tree rings, long term environmental pollution histories, neutron activation analysis 79—92107
  tree rings, trace element distribs. using neutron activation 78—3939
  tropical rain forests, exploitation causing destruction *(German)* 80—101137
  urban flood control programs, ecological and social aspects 79—2316
  vegetation thermal IR emissivity, ecological variations 80—104557
  Volterra systems of N≥2 interacting species, evaluation of phase integrals 77—33932
  water, multielement instrument neutron-activation analysis, ecology appl. 80—40946
  Pu, Am release into estuarine-coastal sea ecosystem, assessment methodology 79—70471
  Pu dynamics in deciduous forest ecosystem, linear compartment donor-controlled model 78—85392
  Pu ecological export from reprocessing waste pond 78—53533

econometrics *see economic cybernetics*

economic and sociological effects
  see also demography; personnel; social aspects of automation
  academic physics community and industrial perspective 78—62032
  academic research and graduate education, effect of Department of Defense funding 78—62031
  agricultural effects of 1975-76 drought in United Kingdom 78—57298
  air pollution, material damage functions 80—76693
  air pollution damage, economic evaluation 80—76692
  American space programme, benefits 77—73930
  astronomy, sociology of innovation in modern science 78—12108
  Brecht's Galileo, changing perceptions of Galileo Galilei as scientific exemplar 80—51996
  bumpy torus reactor, beam driven 80—42859
  cancer management, potential impact of particle radiation therapy 79—20620
  CANDU, heavy water reactor system, political and economic uncertainties 79—85758
  chemistry, macromolecules, and the needs of man 78—95907
  climatic change effects on food production, statistical models limitations 78—57303
  climatic zoning criteria for housing standardization 78—3917
  comparative social impact of alternative electrical energy generating technologies 78—9003
  computer trends, effects on society 80—47590
  conference, physics in industry, Dublin, Ireland (9-13 March 1976) 77—60887
  crop response to hail suppression seeding, Nelspruit project, South Africa 78—57257
  Czechoslovakia, scientific degree recipients, 1953-1976 78—16619
  decommissioning of commercial power reactors, environmental, economic and sociological effects 79—67901
  decommissioning of commercial power reactors, technical feasibility, cost, environmental effects 79—67902
  democratic control of science and technology 79—75316
  driven magnetic fusion reactors, conf., Erice-Trapani, Italy (Sept. 1978) 80—41948
  dust storms, Great Plains, USA, lessons 79—29486
  earthquake prediction and warning, techniques and social effects 79—5455
  education, physics and society for nonscience undergraduates, course description 79—97128

economic and sociological effects continued
education in developing countries, the American science educator 79—2
electric utilities, impact of noise control regulations 78—33958
energy contribution to anthropogenic climatic fluctuations, 21st century problem 78—57299
energy crisis, exponential growth 78—86049
energy development, social impact mitigation planning for coal and nuclear plants 79—61938
energy modelling and forecasting at US ERDA 78—49629
energy related health effects, control technology, societal impacts 79—52865
energy requirements in United States in year 2000 for stable social progress 79—79385
energy storage, social implications 80—67001
epidemiology, causality, and public policy 79—97177
European agriculture rel. to climatic change 78—85679
European energy strategy, fusion research programme 80—45652
European physics publication output, by country 79—88776
Federal funding policy in physics and politics 78—62033
flash floods, American National Weather Service (NWS) warning and disaster preparedness program 79—25289
French plan VII, energy forecasting 78—49628
fuel supply, implications for national defence, social, economic and political well-being 80—3500
fusion reactor, beam and plasma direct converters 80—42861
fusion reactor, field-reversed mirror 80—42857
fusion reactor, Tandem Mirror Reactor power plant, maintenance and handling economics 80—102311
fusion reactor, using toroidally-linked mirrors 80—42858
fusion research, philosophy 80—42854
geothermal resources utilisation, systems aspects, computerised decision anal., social-economic anal. 80—30380
global problems soln., scientific and social approaches 77—74185
graduate PhD student subfield choice and employment prospects 78—65747
hail suppression, crop protection, involvement of society 79—8677
high school mathematics and science courses, participation rates 78—81737
historic climate correl. with wheat prices and wages 78—81346
human judgment, rel. to integration of scientific facts and social values 77—9847
India, science and technology policy, secondary information sources 79—49009
India, scientists' view of first Indian nuclear explosion 77—82362
Indian scientists' role in policy making process, critical assessment 80—90653
industrial noise control, choice of engineering or administrative controls or personal protection 78—33956
industrial noise control, costs and legal requirements 78—33957
information technology, conference, London, England (Nov. 1979) 80—90599
International Solar Energy Congress, New Delhi (1978) 79—57357
Israel, water shortage and supply, long-run policy for agriculture 78—61454
materials conservation ethic 79—44700
medical electronics, worlwide inequalities and development prospects *(French)* 79—70660
mirror reactors, economic significance of Q 80—47722
MIT undergraduate physics students, goals, aspirations and attitudes 80—57022
natural disaster fallacies, Sahel drought example 78—57302
natural resources, satellite remote sensing issues 78—12022
New England, economic and social effects of year without summer (1816) 80—4089
New York City blackout (1977 July 13) economic and social costs 79—24894
nuclear energy, German public relations campaign 77—37709
nuclear energy strategy, Japan, possibility of FFHR 80—42868
nuclear fuel, cycles, global optimisation, resource utilisation and nonproliferation 80—42783
nuclear fuel reprocessing, USA policy analysis 79—85737
nuclear nonproliferation, fuel cycle economics, numerical estimates 80—51982
nuclear power, Conference on Nuclear Power and the Public, September 1977, Geneva, brief report 78—29520
nuclear power, environmental issues 80—94121
nuclear power, public reaction to developments in Canada 77—33825
nuclear power, United Kingdom view 77—33826
nuclear power and nuclear weapon nonproliferation, United States policy, overview 80—3484
nuclear power development 77—33823
nuclear power plant site selection, social aspects 78—5062
nuclear power plant siting, risk-benefit evaluation, practical calcs. for Helsinki 77—54375
nuclear power station, operation, socio-economic effects on demography, finance and local activities of region *(French)* 80—74038
nuclear power station construction, minimisation of adverse effects 77—33828
nuclear power station development, public attitudes in Switzerland 77—33824
nuclear proliferation morality 77—53731
nuclear reactor remote siting as risk-reduction method, cost effectiveness 77—67178
nuclear technology transfer to developing countries, IAEA's contribution 80—13952
nuclear war, global consequences 77—57148
oceanographic microwave remote sensing 80—56612
petrochemical industry, prevention of water pollution 77—70705
physics, frontiers, roles in society 79—49008
physics and arms race, physicists participation explored for general education students 80—57023
physics in Europe, bibliography 79—40341
politics, science policy and research support 77—9848
power station siting, internalising social costs, United States experience 77—33827
public policy careers in the USA 79—5954
PWR decommissioning, safety, cost and occupational radiation exposure estimates 79—67903
radioactive waste, disposal, economic considerations, transportation, land burial and containers 78—17393

economic and sociological effects continued
radioactive waste management schemes, criteria for assessing societal, moral and political implications 78—13270
radioactive waste repository siting, socioeconomic impacts, environmental decision making 79—49715
recombinant DNA, scientific and social perspectives 79—88047
Regional Activities Model for economic and environmental impact evaluation 77—37376
renewable energy source utilisation in developing countries 79—57351
resources, nonrenewable, depletion rate 79—62966
resources, nonrenewable, depletion rate for teaching 79—62966
road traffic noise, a socioeconomic approach to subjective responses 80—67022
satellite communication systems in developing countries, fundings 77—64604
science and society, AAAS president's lecture 78—77660
science and society, research aspects 79—80412
science anxiety, a course for university entrants 78—77637
scientific career migration, bibliography 79—71220
seasonal storage of solar energy 79—57472
seismic trip system, risk assessment for power reactors 78—17377
SI system introduction into Poland *(Polish)* 77—67407
Soddy, F., nuclear science, economics and social responsibility, holistic approach 80—90640
solar energy consumer profile and application incentives 79—57391
solar energy utilisation 79—52888
solar power, social and economic implications for Australia 79—83568
solar satellite power system technology, environmental and societal impact 80—30386
solar water and space heating, economic feasibility 80—7920
space research payoffs 77—17328
stratospheric O_3 monitoring, satellite benefit assessment 77—78613
thunderstorms, severe, nature and effects on society 79—5560
tornadoes, distrib. of death and damage in United States 78—69397
transportation effects, public, future outlook 80—35621
urban flood control programs, ecological and social aspects 79—2316
US 94th Congress (1975-6), discussion of arising science issues 79—97176
US energy strategy, role of hybrid nuclear reactors 80—42743
USA-Japanese cooperation in science and technology 79—58518
walking appliances for paraplegics, misuse of technology 78—41132
water pollution abatement benefits in Merrimack River Basin, survey results 78—61456
weather forecasting, prospects and methods of improvement 78—69394
weather forecasts for West African Sahel 77—70729
weather modification, economic context 79—20936
weather modification, insurance perspective 79—20937
weather modification, national policy 79—20938
wind energy utilisation in rural areas 79—70416
wind power devices and their utilisation 80—45625
wind power generation in North Sea, feasibility and economics 80—97759
workplace noise exposure control, costs and benefits 77—23809
world predicament and climatic change, need for interdisciplinary research 78—57300

economic cybernetics
catastrophy theory appls., book 78—32665
energy policy process models, oil price decontrol and synthetic fuels commercialisation 79—83546
gasoline consumption, structural/econometric model 79—79366
long-term regional development, macromodel 79—12562
natural gas demand forecasting in California 79—79367
water pollution control, energy anal. 80—26180
water resources management, systems anal. and modelling techniques appl. 79—5518

economics
100 MWe commercial power plant, technical feasibility and economics 77—23778
accelerator magnet systems, piggy back power supplies advantages 77—83365
acoustic planning of plants, technical and economic advantages 80—3561
air to water heat pump and solar installation for single family house *(German)* 79—87968
air to water heat pump and solar water heating, dual purpose installations for family house *(German)* 79—87969
air-conditioning, energy saving control system, using heat storage tank *(Japanese)* 80—72087
all solar power supply for France, technological forecasting *(French)* 79—100497
alternative energy sources, energy accounting study 80—76589
alternative energy sources, feasibility and cost anal. of solar systems 80—50939
alternative energy strategies 80—30424
artificial satellites, future applications, reliability and cost considerations *(Italian)* 80—109334
aspheric optics production costs, instrumental and photographic applications 80—28308
atomic energy in USSR in ninth five year plan 77—23316
Austrian solar energy R&D activities and international cooperation 79—57374
autonomous and hybrid solar thermal electric plant energy storage requirements 79—57494
Belgian solar heating systems, economic feasibility 79—57443
boiler, P-67 type, operational efficiency increase, air-water heat exchanger application 79—68710
Brazil's energy consumption, oil resources and economic and technical difficulties *(French)* 80—55777
breeder reactors, long term economic forecast and place in French and worldwide energy needs *(French)* 80—47687
brown coal, 60 years supply at Hambach open cast mine *(German)* 79—57352
building insulation optimisation, w.r.t. internal and solar gains 79—62147
BWR, fuel cycle cost sensitivity anal. 79—31104
BWR, improved fuel utilisation 80—732
BWR, optimum fuel loading and operation planning, FAPMAN model 80—47606
Canadian solar energy competitiveness rel. to government incentive policy 79—57393
CANDU, economic aspects 77—38382
CANDU, energy, water, tritium budgets for Perch Lake 1975 78—29563

economics continued
CANDU nuclear stations, decommissioning 77—74973
CANDU operation for electricity prod. and district heating 78—41835
CANDU PHWR, Wolsung nuclear power plant, fuel cost anal. 78—54832
CANDU-PHW, decommissioning cost, environmental impact hazards and size 77—61598
capacitive energy stores, ultrapowerful, improved service life development problems 79—81089
cardiac pacemaker patients, late survival prognostic determinants 77—81693
cellulosic waste disposal by conversion to ethanol 80—61502
central receiver solar power systems, terminal concentrator concept analysis, economic aspects 80—26116
chemonuclear synthesis, product purification, cost anal. 79—61889
coal, fluidised bed firing, technological state and economic chances *(German)* 79—92050
coal conversion processes, appl. of non-fossil-derives H_2 for synthetic fuel manufacture 79—74483
coal gasification, catalytic, preliminary research 79—52871
coal gasification, underground, US Department of Energy status 79—48054
coal mining, processing and transportation in Western US, impact 80—45621
coal-fired power stations, financial impact of air pollution control costs 80—3497
compressed air energy storage concepts utilising thermal energy storage, cost anal. 80—30581
compressed air energy storage electric power systems, conceptual design 79—88006
computerised tomography, functional principles and applications *(French)* 79—70691
computerised tomography scanning evaluation, cost containment 80—36117
concentrator/photovoltaic system design for electricity and heat generation 79—61997
COS-B satellite, ESA extraterrestrial gamma radiation obs. project *(German)* 79—21151
cost estimation of solar thermal electric power system in Japan *(Japanese)* 79—79381
cost-effectiveness analysis applied to radioactive effluents *(French)* 79—93840
CVD SiHCl$_3$ process, for low cost solar grade Si 79—62007
cyclotron applications, case study at Crocker Nuclear Lab. 79—54723
Danish solar water heating system economics 79—62047
data management systems in economic geology 77—53201
denatured Th cycle in symbiotic systems, potential role 79—26484
desalination, PWR appl. 78—37461
desalination, solar powered electrodialysis appl. 80—55805
desalination plant coupling to solar collector systems, low-temperature multiple-effect type, technical and economic evaluation 80—55804
desalination plants, MSF, solar powered 80—61281
developing countries' solar energy evaluation by energy balances 79—57388
diamond tool bit machining, comparison with conventional optical process 80—69569
district heating from Kaiseraugst nuclear power station 78—37462
district heating in Stockholm, nuclear power and oil-fired plant comparison 78—37458
district heating systems, combined generation by fossil fired and nuclear power plants 78—37457
domestic water and space heating by new technologies, energy and direct economic effects, evaluation 79—92049
domestic wind, solar, wind and solar heating systems, economic evaluation 79—43744
Earth satellite power stations (Powersats), economic assessment 77—91404
economic growth and energy consumption, in Britain, 1700-1975 79—79364
electric utility load management, thermal storage systems appls. 80—16845
electrification of rural areas, energy economies and national policies, in developing countries 79—48042
electrochemical processes, energy use analysis *(Dutch)* 80—72019
electrochemical processes, energy use optimisation *(Dutch)* 80—72020
Elmo bumpy torus reactor, economics 78—54994
energy, forecasting of future requirements 79—57348
energy accumulators, flywheel, stationary, for industrial undertakings *(German)* 80—35757
energy conservation, hard and soft paths compared 80—89584
energy conservation, on-stream ion chromatography appl. 80—55737
energy conservation in Britain, main options 80—76620
energy consumption, primary, in UK, changing structure of final demand 80—26101
energy conversion systems, coal based, for electric power generation, economic potential 80—16774
energy cost analysis, selection of discount rates using discounted cash flow and revenue requirement methodologies 80—3498
energy demand and conservation in USA, in residential and commercial buildings, National Energy Plan impact 80—26121
energy future concepts, Conf. London, England (Jan.-Feb. 1979) 79—43709
energy models combination, reduced form approach, methodological issues 79—79386
energy planning in Arab world, with aid of computer 80—26122
energy resources, alternative technologies cost analysis 79—48041
energy resources, economic choice for rural India, methodology 80—104499
energy resources, non-nuclear, non-fossil, utilisation, W.Germany *(German)* 77—9426
energy schemes assessment, domestic solar heating appl. 79—48044
energy sources, renewable, assessment for UK power supply system 79—48043
energy sources, UN Economic Commission for Europe report, book 79—100544
energy storage devices assessment 79—48183
energy storage systems, compressed air, optimum design 80—26167
energy storage systems, economic assessment and optimisation 80—40909
energy supply, ECE (Economic Commission for Europe) policy 80—26119

economics continued
energy supply and demand, United States government analyses, review 80—30320
energy technologies assessment, based on renewable resources 79—48045
energy transfer by electric power generation and utilisation, economic case 80—16777
energy utilisation and economics, effects of US National Energy Act 80—3499
energy-political questions nationally and internationally for West Germany *(German)* 80—101072
environment monitoring system, benefit assessment 78—73507
environmental dispatch simulation and emission dispersion modelling 78—32221
European computer network, engineering design computer packages, teaching 80—31465
European Economic Community member states' nuclear achievements *(French)* 79—89490
evacuated heat pipe solar collector, rectangular, performance characts., trap mechanism 80—3531
exponential function, growth and compound interest 77—5637
FBR, 1300 MW demonstration commercial fast reactor CFR 1, UK 77—3168
FBR radial blanket, comparison of economic perform. for LMFBR and GCFR 79—49654
fibre optic market trends, worldwide 80—58699
fibre optical links, Canadian development 78—42408
finance for space research, the role of private funding in European space ventures 80—77121
fission reactor fuel preparation and reprocessing, aspects 77—88267
fission reactor occupational radiation exposure, ALARA inplant design, cost-benefit anal. 80—18547
fission reactor radiation protection, ALARA, effectiveness of design modifications 80—18546
fission reactor radiation protection, ALARA occupational radiation exposure, utility design viewpoint 80—18548
fission reactors, fast breeder, using uranium-plutonium cycle, Na-cooled, technical and economic viewpoints of application *(German)* 80—99202
fission-fusion hybrid energy storage system, economic feasability 78—796
fission-fusion hybrid power plant economics 78—789
fixed tilt solar collector with reversible vee-trough reflectors and vacuum tube receivers, economic evaluation 79—100539
flat solar collector, energy and economic analyses 78—83236
flat-plate non-tracking ground mounted photovoltaic array structures, cost reduction anal. 80—94038
flat-plate photovoltiac array design optimisation 80—94037
floods in United States, management and economic aspects 77—41073
flywheel and hot water storage systems for 10 kWe solar power pack 79—57469
flywheel energy storage and conversion system for photovoltaic appl., economic anal. 80—94116
French energy research projects *(French)* 79—74497
fuel, liquid and gaseous, from waste, economics, critical analysis 80—7893
fuel adjustment clause for collecting nuclear fuel costs 79—31105
fuel cells, H_3PO_4, technology advances 79—48122
fuel cycle and nuclear power plant development in USSR, economic aspects 79—644
fuel cycle optimization with nonproliferation objectives 80—730
fuel reprocessing plants, economic anal. of alternate location strategies 79—59235
fusion commercialisation, generalised requirements and R&D 77—34462
fusion energy, utility requirements and economics 79—76145
fusion mirror reactor studies 77—74980
fusion plant, inertial confinement, commercialisation anal. 78—58410
fusion plant design costs 78—791
fusion power, economic and environmental consequences 78—33285
fusion power, parametric anal. of utility operations 78—58409
fusion power plant, inertial confinement type, target prod., costs 78—58488
fusion power plants, engineering limitations 78—74473
fusion power station 78—788
fusion power stations, recirculating power, unit cost, thermal pollution 78—29643
fusion reactor, Culham Conceptual Tokamak Reactor Mk II, reactor costs and maintenance 77—74978
fusion reactor, inertial confinement, parametric studies 80—32507
fusion reactor, inertial confinement economics 80—32506
fusion reactor, LARTS, extended burn operation, physics, engineering and economics 80—95440
fusion reactor, multiple mirror, coil design and economic optimisation 80—99284
fusion reactor, ohmic heating energy storage for power reactor, costing 78—58495
fusion reactor, TNS, electrical design costing 78—55014
fusion reactor coil design, cost anal., for neutral beam magnets 78—55005
fusion reactor costing methods 78—790
fusion reactor design and economics, confinement physics effects 78—50358
fusion reactor toroidal field coil stress anal., cost effective procedures for TFTR 78—50379
fusion reactors, committed site development, technical and economic aspects 80—95437
fusion reactors, symbiotic energy system, U fuelled, economic anal. using SYMECON code 80—106172
fusion reactors, Tokamaks, maintenance design requirements and economics 80—99285
fusion symbiotic system, managing fusion burn, economic analysis 80—106173
fusion-driven symbiotic energy systems, economic anal. of fuel cycle and power costs 80—23141
fusion-fission hybrid system using divertored Tokamak, optimisation 78—798
gas, unconventional resources, public sector R&D investment allocation 79—79365
GCFR radial blanket, optimum management scheme 77—42126
GCR implementation strategy anal. using MCFLOW program 77—57733
geophysics, reflection seismic exploration 78—96325
geothermal binary cycle calc., hydrocarbon working fluid selection 79—48091

economics continued
- geothermal electricity generation costing methods, quantitative comparison 80—3487
- geothermal energy extraction and utilisation in France *(French)* 79—39276
- geothermal energy resources for electricity generation, discounted cash flow anal. 80—85263
- geothermal energy utilisation thermodynamic aspects *(German)* 79—96416
- geothermal plant optimum design conditions, Geysers Unit 16, Northern California (USA) 79—52877
- geothermal power generation, direct-flash steam and steam binary cycles comparison, effect of noncondensable gases 79—52878
- geothermal power stations, economics and risk assessment 80—30378
- geothermal power utilisation, in evaporation/crystallisation industry 79—48086
- geothermal resources for power generation 80—35635
- Go-ri nuclear power plant, fuel cycle schemes, economic comparison 78—54831
- graphic arts imaging material and laser source cost tradeoffs 80—14383
- Hagerstown, MD, instructional TV system cost analysis 78—12501
- hail-prevention operations, cost effectiveness estimation methods anal. 78—93013
- heat pumps, compression, optimised heat utilisation *(German)* 79—96483
- heat pumps operation and prospects *(Italian)* 80—45722
- heat pumps with internal combustion drives, economic advantages *(German)* 79—74535
- heliothermal power stations, 100 to 1000 kWhr 79—61960
- horizontal-axis wind-turbine system for pumping duties in Third World agriculture, economic aspects 80—61259
- household fuel uses, ORNL model 79—79387
- HTGR, economies in U reserve use 77—42175
- HTGR, low temp. heat prod., energy transport systems 78—41837
- HTGR, prebreeder fuel optimization, symbiotic combinations, comparative evaluations 78—29605
- HTGR dual purpose plant for military installations 78—41855
- HTGR fuel reprocessing plant, cost and environmental impact of radioactive waste treatment 77—46380
- HTRs, current development and commercial advantages *(German)* 78—37433
- HWR, fuel cycle cost anal. using computer code HWRCOST on-power refuelling 77—83051
- hybrid geothermal/coal fired power plant, site specific economic anal. 79—24887
- hybrid passive/active solar system: performance and cost 80—45635
- hybrid solar photovoltaic/solar thermal electric power system, simulation 80—94025
- hydraulic coal trunk pipeline transport systems, methods of improving economic effectiveness 80—106837
- hydro-photovoltaic plants, peak power generation economics and reliability 80—45706
- hydrocarbon oils as thermal storage media for solar central power appls., specific heat variations and their economic implications 79—100540
- hydrometeorological information in USSR, economic effectiveness 79—29909
- hydropower potential in Austria, current assessment *(German)* 79—87962
- hydropower reservoir lakes and dams construction, environment protection aspects *(German)* 80—30373
- indoor sports centre heating by heat pump, economic aspects *(German)* 80—16829
- induction heating, underground coal gasification, technical and economic advantages 80—3476
- industrial cost-effective noise control 78—55515
- inorganic chemicals industry, water pollution and solid waste disposal 77—70704
- integrated energy systems, environment impacts 78—73506
- integrated photovoltaic/thermal system with faceted-mirror sunlight concentrator 79—62010
- interfuel substitution, effects on electric power industry, in United States 79—87942
- international symbiotic nuclear energy parks using breeders and advanced convertors, economic feasibility 80—57825
- ion-beam fusion reactor, first wall costs 78—811
- irradiated fuels reprocessing, French and European policies *(French)* 80—809
- irrigation plants using solar or wind power, comparison w.r.t. cost, maintenance and reliability 79—70425
- JET pulse power supply system 78—25327
- Kitt Peak National Observatory telescopes, cost effectiveness in terms of publications and citations 80—90334
- KS-7F solar kitchen, economic effects on economy 80—89590
- large scale functional film coating systems, selection 77—69985
- laser fusion breeder, impact on nuclear economy 78—50336
- laser fusion breeder-fission converter system economics 79—85790
- laser fusion power plant, capital cost data base 80—32504
- laser fusion system studies model, TROFAN 80—32505
- laser U enrichment plant, optimum operating conditions 79—54578
- light-water waste management systems, vol. reduction 80—9367
- linear accelerator, energy doubling using coupled cavities *(Russian)* 78—70652
- LMFBR, development and Pu allocation, optimal policies 80—725
- LMFBR, energy investment 78—78512
- LMFBR, fuel cycle cost optimisation anal. of core design modifications 80—22900
- LMFBR, heterogeneous carbide-fueled reactors, thermal and economic performance 79—93703
- LMFBR, nucl. design and economic comparison of conventional and bullseye core 78—13222
- LMFBR bullseye core, performance, design characts. and economic anal. 79—59121
- LMFBR principles and potential advantages 79—81072
- LMFBR steam cycle conditions, comparison 80—18406
- low level radioactive waste volume reduction and cost savings 79—36360
- low-cost encapsulation materials for terrestrial solar cell modules 80—3522
- low-level radioactive waste management complexity and cost-effectiveness 78—94117
- LWR, alternative fuel cycles containing Th 80—37510
- LWR, fuel cycle *(French)* 80—682

economics continued
- LWR, heat supply for desalination, economics 78—41851
- LWR, optimum fuel loading and operation planning, FAPMAN model 80—47607
- LWR, Pu recycling, technical and economic study 80—720
- LWR, sensitivity of fuel cycle cost to uncertainties in nucl. data 80—680
- LWR 1300 MWe system, design of containment to withstand core melt 78—66335
- LWR alternative fuel cycles, sensitivity to data uncertainties 80—22934
- LWR diversion resistant processes and cycles 78—86677
- LWR fuel, future trends to improve U utilisation 79—85634
- LWR fuel containing Pn, waste treatment cost/benefit anal. 77—46378
- LWR fuel fabrication plant, cost of controlling inorganic chemical releases 78—5003
- LWR fuel reprocessing plant, radioactive waste treatment costs and environmental impact 77—46379
- LWR plant, decommissioning 78—29603
- LWR plant, economic effect of increased seismic load on design and construction costs 78—66432
- LWR power stations and fuel cycles, economic indices improvement *(Russian)* 79—26744
- LWR spent fuel, economics of away-from-reactor water storage basin 79—59201
- LWRs, Pu, commercial recycling assessment 79—71935
- magnetic levitation methods for tracked high-speed traffic 79—49011
- measurement standards in flow rate meas. improvement, cost analysis 77—80239
- medical microprocessor applications and costs 79—44011
- metallurgy, automatic barrel line type ATS closed system, small parts electroplating, after-treatment and drying *(German)* 80—84861
- meteorological radar system synthesis, economical aspects 79—62543
- MHD generation, open-cycle, 1978 reappraisal in United Kingdom 79—48140
- MHD steam power plant optimisation, computer-based model appl. 79—52942
- microwave appl., in industry, science and medicine 80—3754
- mixed oxide fuel cycles, cost sensitivity anal. 79—89369
- monetary system, analogy with electric current flow in circuit 78—54144
- motor fuel, technico economic study of the use of hydrogen and methanol for road transport 79—74512
- multipurpose water projects, efficiency and equity of cost allocation methods 79—88017
- municipal water treatment levels differences 79—83649
- NASA budget rel. to 1979 space missions 78—45195
- NASA remote sensing technology transfer to State of Georgia, cost anal. 78—73519
- neutral beam, pulsed, arc (arc filament) power supplies, for fusion reactor 78—70637
- neutral beam filament supply, 15 V 10^3 A, programmable, regulated, for fusion reactor 78—70630
- neutral beam source, cryopumping and mag. shielding, fabrication and operating cost 80—106229
- neutron activation analysis, cost minimisation 78—48728
- noise control in industry, costs 80—16877
- nuclear electric power plants, economic anal. c.f. fossil fuel plants 79—92057
- nuclear energy complexes, economic and ecological problems of nuclear power development 79—645
- nuclear energy for combined electricity and district heating prod. 78—37459
- nuclear fuel, financing and accounting, effects of Pu uncertainty 78—13243
- nuclear fuel, management and accounting, need for amortization 78—13241
- nuclear fuel accounting and rate making, regulatory issues 78—13242
- nuclear fuel accounting practices at Duke Power Company 78—13244
- nuclear fuel accounting system, nuclear inventory and management system program 78—13245
- nuclear fuel cycle, benefit-cost analysis 78—8957
- nuclear fuel cycle, core design optimisation 78—82420
- nuclear fuel cycle, economic analysis of 18 and 12 month fuel cycles 80—22957
- nuclear fuel cycle, international market development 77—33821
- nuclear fuel cycle, tutorial paper 78—17446
- nuclear fuel cycle cost sensitivity anal. of alternative reactor fuel cycles 79—89368
- nuclear fuel cycle cost sensitivity to data uncertainties, interactive graphic computation 79—9837
- nuclear fuel cycle management, with aid of computer 77—14241
- nuclear fuel cycle sensitivity anal. system for LWR 77—42119
- nuclear fuel cycle strategy in Korea, probabilistic anal. 77—57726
- nuclear fuel recycle facility, utility ownership 79—31099
- nuclear fuel services, analysis, costing and economics of cooperative facilities 77—57772
- nuclear fuel transport by air, feasibility and economics 78—94154
- nuclear fusion reactor materials, social aspects *(Dutch)* 80—106153
- nuclear international fuel exchange agreement, economic benefits 80—37462
- nuclear optimal cycle coastdown at San Onofre unit-1, reduced enrichment requirements 77—42118
- nuclear power, economics 79—22499
- nuclear power, U enrichment, market survey *(German)* 78—4999
- nuclear power, w.r.t. West German Government expenditure *(German)* 80—23180
- nuclear power appl. to district heating systems 78—37454
- nuclear power conf., Chicago, United States, July 1979 80—794
- nuclear power development in US, Pu recycle's influence 79—36394
- nuclear power economy, simulation 77—79486
- nuclear power plant, in-service inspection methods and limitations 77—3169
- nuclear power plant cost reduction by containment elimination 79—13467
- nuclear power plant siting evaluation, w.r.t. safety, comparison with coal-fired power station *(Czech)* 78—50266
- nuclear power plants, mathematical modelling methods 77—23315
- nuclear power reactors in elec. utility system, short range system analysis method 77—50252
- nuclear power research and development in Japan, aspects 80—47701
- nuclear power station outages, turbine-generator reliability assurance through large scale test facilities 77—3151

economics continued
nuclear power stations, combined heat and power, fusion reactor appls. *(German)* 79—67935
nuclear power stations, cost comparison of PWR and PHWR in Korea 80—57821
nuclear power stations, Swedish *(Swedish)* 77—79472
nuclear reactor, fuel savings by ‘stretch out’ operation *(German)* 78—86632
nuclear reactor, MSR strategies, fuel conservation effect, utilisation of convertors starting with Pu *(Japanese)* 77—50207
nuclear reactor, multigoal fuel cycle optimization including nonproliferation objectives 80—52764
nuclear reactor, Th based cycles relative worth of ^{233}U and ^{235}U 80—37511
nuclear reactor fuel cycle costs 77—6575
nuclear reactor pump coolant tests, computerised monitoring 78—70585
nuclear reactors, cost-benefit anal. of LMFBR programme 77—38392
nuclear science and technology, role in national economy of USSR 77—23314
nuclear spent fuel storage, design studies, cost estimates 78—29615
nuclear spent fuel storage, high-density, economic evaluation of alternatives 78—21732
nuclear system with advanced reactors, feed and enrichment requirements 77—61624
nuclear wastes as heat source 78—41838
nuclear water cooled channel reactor, electrical energy cost of change in fuel component 80—37480
O'Neill space colonies, economics rel. to realisation prospects 77—87230
ocean measurement remote data access systems 77—41172
ocean thermal energy conversion, OTEC power modules optimisation 79—83615
ocean thermal energy conversion, OTEC system development, Conf. Houston, TX, USA (Nov. 1978) 79—83611
ocean thermal energy conversion, US OTEC development programme overview 79—83613
ocean wave power, assessment 79—34422
oil supply and demand model structure 79—79369
optical bench base selection, accuracy/cost tradeoffs 79—27447
optical component manufacture, cost reduction 80—1361
optical fibre, cost models for A-7 aircraft ALOFT project 78—59131
optical fibre communication, A-7 ALOFT economic analysis, EM interf. and pulse tests 78—42448
optical fibre communication system, cost model 78—42447
optical fibre cost considerations 78—1389
optical fibre transmission systems, 1.2-1.5 μm, economic evaluations and forecasts 80—87533
optical fibreguides, costs 77—11017
optical instrument developments, economic potential 80—31841
optical precision instrument manufacture, microcomputer appl. *(German)* 80—95116
optical shop interferometric instrumentation as a cost-effective production tool 80—74535
optical telescopes and radiotelescopes, cost-scaling laws 80—41722
optics tolerancing tradeoffs for mass production economies 80—48473
osmo-hydro power system, using aqueous saline solutions, technical and economic feasibility 79—52916
panel-type solar thermoelectric generator, water-lift appl., technical and economic eval. 79—83619
passive solar heating systems design, microeconomic anal. methodology 80—35744
PBHTR, fuel cycle costs, bred fuel value of ^{233}U 77—42125
photoelectric conversion, MIS structures utilisation, and manufacture, photoelectric parameters *(Czech)* 79—83595
photomultiplier assemblies and associated electronics for high energy physics large counter expts. 77—83469
photovoltaic cells, current production and future prospects *(French)* 79—100531
photovoltaic concentrating array, using point focusing acrylic Fresnel lense 79—52937
photovoltaic conversion of concentrated solar radiation, feasibility assessment 79—57436
photovoltaic energy generation integrations into electric grid systems, general methodology 80—45647
photovoltaic generator operation and cost simulation 79—61975
photovoltaic power generation, modules fabrication cost analysis 80—45674
photovoltaic power supplies, self-contained, cost minimisation 79—48098
photovoltaic solar cell arrays, parametric cost analysis 79—100535
photovoltaic system sizing anal. 80—94039
photovoltaic systems, all component optimisation, theory and appls. 79—29475
photovoltaic systems break-even cost anal. for rural Mexico 80—94027
plasma confinement, quasisteady, scaling laws rel. to fusion reactor operation 79—27812
plates design, circular, rigid-plastic, w.r.t minimum-cost variational formulation 77—68440
pollution control, air, optimal timings and number of observations determ. 79—88026
pollution control capital costs by industry 79—79413
pollution problems from fertilizer manufacture 79—34450
polymer-concrete composites, civil engineering appls., technical, processing, economic merits 79—11545
power generation, hydroelectric, economic assessment of fuel savings *(Russian)* 80—97760
power plant availability improvement by surveillance techniques 79—9812
power reactor underground siting feasibility, Californian programme 79—13399
power reactors, min. unit generation cost 80—734
power stations, steam-gas combined, based on natural gas resources from North Sea, economics and possibilities *(Norwegian)* 80—101073
pressurised heavy water Candu nuclear power plants, cost aspects *(French)* 80—18463
primary and secondary batteries, performance limits, economic factors 80—45657
PWR, development and Pu allocation, optimal policies 80—725
PWR, economics of fuel cycle options 79—31102
PWR, optimal fuel loading and operation planning 78—50276
PWR, planned cycle stretchout 79—31103
PWR 18 month fuel cycles, core design operation and economics 79—85591

economics continued
PWR containment isolation using butterfly valves 78—13256
PWR nuclear steam supply system for district heating and elec. prod. 78—37466
quality health care and cost containment, conf., Washington, USA (Mar.-Apr. 1978) 79—39333
radiation shielding, sanitary-safety zone, cost optimization of structural design for particle accelerators 78—17443
radioactive low level contaminated metal waste volume reduction by melting 79—89412
radioactive solid wastes disposal, benefit-cost anal. 80—18556
radioactive waste, conditioning and storage costs estimation *(Italian)* 78—25303
radioactive waste, volume reduction and solidification systems 78—17396
radioactive waste depository in West Germany, advance payment from users, legal aspects *(German)* 79—71903
radioactive waste disposal, ^{85}Kr encapsulation in amorphous alloy 80—47589
radioactive waste management systems, economic considerations 79—54575
radiograph quality control programme, economic analysis 78—73236
radiographic equipment servicing by hospital-based group 78—69247
radiography, cost-effectiveness considerations in evaluation of new technology 78—69192
radiology diagnostic facilities, quality assurance programme, proposed recommendation 78—73235
reactor decommissioning, cost anal. for complete removal 79—67904
reactor radial blankets, economic anal. for LMFBR and GCFR 79—59163
reactor refuelling frequency, economic optimisation 80—731
reactor safety, quantifying plant availability, ALARA, and occupational radiation exposure relationships 79—59183
reference mirror hybrid fusion-fission reactor design 78—801
regional wastewater management systems, chance constrained approach 79—57513
regional water quality management, goal programming approach 79—57514
relativistic electron beam hybrid reactor, economic model 78—58412
remote heat supply from nuclear power stations *(German)* 77—352
remote inspection of ground sites, cost/effectiveness model 77—91319
residential solar energy systems, tax credit incentive costs and impacts 79—57450
review of energy and materials 77—77350
road traffic, cost and safety aspects of quiet tyres use 77—65652
rotating mirror deflector design cost/performance tradeoffs 77—58485
rotating mirror scanners, technology and market rel. to price 79—27362
Shiva laser, 25 MJ energy storage and delivery system 78—55015
SLAC, control and monitoring system, use of microprocessors, cost 77—83177
small village solar electrification economics 79—57387
soil warming, waste heat from nuclear power station 78—37463
solar absorption cooling systems, small scale, feasibility study 79—74502
solar air heater cost-effective optimum design 79—62039
Solar Assisted Gas Energy domestic hot water system installed costs 79—57447
solar cell arrays, economics modelling of photovoltaic module manufacturing, SAMICS methodology developments 80—55860
solar cell costs in 1985, forecast *(Swedish)* 80—7919
solar cell fabrication, photovoltaic process based on thick film technique 80—94016
solar cells, developments, appls., and economics of solar photovoltaic conversion *(German)* 80—26132
solar cells, technical and economic assessment 79—34433
solar cells, thin film, performance analysis employing loss minimisation of essential characteristics 80—45682
solar cells, thin film, technical and economical eval. 80—94012
solar collector, flat-plate, below atmospheric pressure, distributed-flow, modules integration into arrays 80—26153
solar collector construction and utilisation for low-temp. heating 79—57442
solar concentrating collectors, single axis, orientation, economic criterion 80—40907
solar domestic water heaters on Swiss central plateau, net heat output, economic evaluation *(German)* 79—100498
solar domestic water heating systems, in Great Britain, economic aspects 80—40835
solar energy, Middle Eastern research programmes 80—66939
solar energy concentrator/solar cell array systems, economic assessment 79—43770
solar energy concentrators, low cost-low ratio systems design 80—7928
solar energy cost calculation standard procedure proposal 79—57389
solar energy earth storage and utilisation, technical and economic aspects 79—57475
solar energy residential applications, life cycle costing assessment 79—57445
solar energy system components, cost effectiveness 80—45651
solar energy system with dual-source heat pump and long-term storage 79—57453
solar energy use in plating shop, 1979 prospects 80—3490
solar energy utilization, direct and indirect *(German)* 80—3489
solar enhanced oil recovery; an assessment of economic feasibility 80—40832
solar flate plate evacuated collector design 79—62099
solar grade Si prod., using Dow Corning process 80—29894
solar heating, of houses with swimming pool, Austrian development 79—57413
solar heating and cooling of buildings, economic problems 79—57451
solar heating and electricity generation, retrofitting of existing residence, expt. results and economic assessment 79—61952
solar heating of buildings, thermal performance evaluation, with aid of computer 79—57467
solar heating of public swimming pools, feasibility 79—87978
solar heating system for administrative building, for winter use, technical and economic feasibility 79—62136
solar input and solar data computation for engineering of solar systems, transients simulation 80—94060
solar investment decision criteria, appl. to space and water heating systems 80—35643
solar photoelectric conversion cost reduction *(Italian)* 80—30479
solar photovoltaic arrays, optimisation of total annual energy output from constant/adjustable tilt systems 80—94059

economics continued
solar photovoltaic cells production technology, future systems efficiency and cost effectiveness 80—16799
solar photovoltaic power systems for rural areas of developing countries, technology, reliability, economics and appls. 80—61286
solar pond experimental and economic aspects 79—62076
solar power, global energy option *(French)* 79—100496
solar power, technical-economic validation of resources as energy sources 80—89593
solar power, technological economics, current criteria based *(French)* 79—100495
solar power generating systems assessment, generalised methodology 79—52913
solar power generation, survey, vapour-tubine units, using organic working fluids 79—83618
solar power industry, economic considerations and feasibility in Britain 80—26111
solar power investment programme for small national state or political subdivision of large state, review 79—66403
solar power satellite, technical considerations 79—34425
Solar Power Satellites, energy anal. 80—50937
solar power stations, current projects *(French)* 80—55803
solar power stations, medium power heat and electricity production development program, economic requirements and technical options *(French)* 79—100493
solar power stations, tower type, economic aspects, power station construction and installation site *(French)* 79—100491
solar power systems, economics 77—73798
solar power utilisation in office complex design, up to 70% energy savings 80—40831
solar power verus heatpumps for domestic space and water heating, appraisal 79—74494
solar powered Rankine cycle system, digital simulation 79—52911
solar powered residential water heating 80—61311
solar radiation geometric Brownian distribution, implications for economical solar heating system 79—83571
solar residential heating system life cycle cost analysis 79—57444
solar space heating, interface with alternative auxiliary supply systems 79—57407
solar space heating systems, load optimisation algorithms 80—45643
Solar Thermal Electric Power System technical and economic evaluation for Japan 79—57441
solar thermal electric power systems, line focus collectors, economic comparison 79—70435
solar thermal power plants, dispersed, performance and economic risk evaluation, by computer Monte Carlo simulation 79—52902
solar thermal power plants for Iran, evaluation 79—74500
solar thermal-electric power plants, distributed-collector, comparative evaluation 79—52908
solar thermoelectric generators, metallic thermo-electric materials utilisation, economic characts. 80—101122
solar voltaic power systems, comparison to fuel energy, for telecommunications 80—61381
solar water heaters, aluminium alloy rolled-welded heating panels production and use 79—96421
solar water heaters, commercialisation in Florida 79—57460
solar water heating for swimming baths *(German)* 79—92061
solar water heating systems, economic assessment based on measured performance 80—97807
solar water pumps, comparison with wind power, petrol engine and electric water pump 79—74507
solar-electric power generation in remote locations, costs comparison with diesel generators 80—55813
solid waste utilization in integrated community energy systems 79—100359
space colonisation, preliminary cost benefit anal. 77—87231
space heating, photovoltaic and thermal collector system design and testing 80—45675
space heating, solar collectors combined with ground heat pumps, advantages *(German)* 80—76605
space research, forward-looking financial planning in ESA 80—4221
space research, investment planning in ESA 80—4222
space-manufactured satellite power systems, costs anal. using lunar materials 80—97767
spectral shift controlled reactor, SSCR, Pu fuel cycles 80—47608
sports centre all-electric with heat pump, economic aspects *(German)* 80—16827
static condensation stress recovery algorithms, cost comparison 78—41145
steel, MHD industrial smelting, techniques, economics *(Russian)* 77—24980
streamflow data network design, economics of resource information systems 77—73893
superconducting power transmission lines, He refrigerators optimisation 78—24802
superconductive energy storage magnet, single layer, design and cost-related parameters 80—108815
symbiotic system economic evaluation using SYMECON 80—106177
synthetic fuel, alternative programmes, decision anal. 79—83548
tandem mirror fusion-fission system studies 80—37607
teaching projects, distance (broadcasting), cost effectiveness evaluation 79—40312
terrestrial solar generators, design, fabrication, testing and economic power generation 80—45672
terrestrial solar modules, sandwich type glass encapsulation, climatic parameters effect, economic anal. 80—45673
thermal reactors, international fuel cycle centres, economies and financing 77—46374
thermionic power plant, design point selection impact 79—48155
thermionic topped steam power plant, conceptual design using advanced boiler concept 79—48156
thermochemical production of H_2, process economics *(French, English)* 77—86309
thermocouple alloys, Nicrosil-Nisil, for furnace control Chromel-Alumel thermocouple replacement 78—49831
Thermos pool reactor, heat generation application *(French)* 77—74967
thin sheet Fresnel solar collector-concentrators, features and economic benefits 79—79402
Tokamak, fusion power plant economics, effect of major design parameters 79—76141
Tokamak fusion power generation 78—74472

economics continued
Tokamak fusion power plant, cost sensitivity anal. 78—17412
tokamak fusion power plants, major cost drivers 78—58443
Tokamak fusion power reactors 78—21764
Tokamak fusion power stations, economic evaluation 79—76147
Tokamak fusion reactors, commercial feasibility 78—58406
Tokamak ignition test reactor, scoping studies 78—793
tokamak next step designs, system size and cost trends 78—58416
Tokamak power plants, impact of major design params. on economics 78—792
Tokamak power systems, economics 78—54993
Tokamak reactors with elongated plasmas, parametric and economic anal. 78—795
transducers of electrical variables, modular, third-generation individual and group arrangements, NC series *(Czech)* 80—62645
UK Post Office junction and trunk network applications for optical fibre systems *(German)* 78—38016
underground pressurised saturated hot water storage for peak lopping appls., economic aspects 80—76653
university engineering education courses economics 80—67973
USA National Energy Plan impact on solar home heating economics 79—57446
vacuum seal for borosilicate glass, use of Ni-In protective coating on Kovar *(Italian)* 80—40621
WAK reprocessing plant, a design basis for large-scale reprocessing plant 80—5310
waste disposal, with recovery of useful materials, industrial heating appl. *(Spanish)* 79—57419
wave energy system, optimum annual load factors estimation 79—43732
wave power generation viability 79—43728
weather modification economics, review, future anal. 79—20927
wind as energy source, for electric power generation 79—61941
wind energy conversion, toroidal accelerator rotor platforms appl. 79—48073
wind energy conversion system, low-cost, for domestic premises appl. 79—43716
wind energy conversion systems, value to electric utility, economic model 80—61257
wind furnace systems, advanced, for residential and agricultural heating and power supply 79—48070
wind power, recent developments aid economic aspects 80—61238
wind power electricity for high rise flats, economic feasibility *(German)* 77—70739
wind power plants, integration into existing power systems, implications 80—61258
wind turbine generator system, optimum selection 80—40818
windmill using sail-type Savonius rotor, low-cost water pumping appl 80—21367
windmills, horizontal axis, cost effectiveness evaluation 79—70421
windpower generation in combination with conventional systems, economic assessment *(German)* 79—66398
world oil markets and the business cycle 80—21359
CdS-Cu$_2$S thin-film solar cells, low-cost manufacturing process outline, economic anal. 80—93930
D enrichment by CW vibr. photochem. of methane, economic aspects 80—11920
D-T Tokamak reactor, costing and sizing using COAST code 79—76142
H thermochemical production using air blown coal gasification, economics 80—35790
H_2 production by water electrolysis, economics and technology *(French)* 79—100543
H_2 storage using cryoadsorbents, 65 to 150K, comparative evaluation 79—74548
Li, ores in United Kingdom, brief assessment 79—48476
Li requirements for fusion power plants, aspects 79—45401
Li resources, energy reserves of D-T fusion, recovery costs 78—46162
LiAl/FeS batteries, principles and construction, load levelling of nuclear stations 80—21392
Mn nodules, on deep ocean floor struct., composition, economic pot. 79—29747
Ni foil solar collector selective surface performance 79—62078
Pu fuel cycle back end services, utility optimisation model 78—41845
Pu recycle and nuclear proliferation, economic analysis 80—5302
Pu, reprocessing and recycle, economic and environmental benefits 77—46372
Si, crystalline sheets production, low cost, crystal growth techniques comparison 80—35083
Si photovoltaic industry, environmental control, economic and ecological requirements 80—94026
Si production, low-cost low-energy processes 78—11126
Si ribbon growth, technology assessment 1978-1986, computer anal. using PECAN 79—8244
Si solar cell production, Union Carbide Corporation Silane Process, cost analysis 80—21403
Si solar cells, crystal growth, heat exchanger method, fixed abrasive slicing technique 80—35082
Si solar cells, low cost processes for fabrication 80—94013
Si solar cells, low-cost fabrication processes *(Japanese)* 79—83600
Si solar cells with concentrating collectors and integrated heat use system 80—45701
Si solar photovoltaic cells, large scale production, materials, efficiency and economics 80—50970
T breeding costs in critical fission reactor 78—58456
Th fuel cycle role in thermal and fast reactors 79—13420
Th fuel cycles in pebble bed nuclear reactors 77—42124
ThO$_2$ nuclear fuel production, economic and environmental anal. 80—18575
U, enrichment methods, efficiencies and costs *(Dutch)* 80—37634
U isotope separation in countercurrent vortex tube, energy consumption *(German)* 79—27099
U isotope separation processes *(French)* 80—806
U, mining, processing and transportation, in Western US, impact 80—45621
U ores, lower grade, cost saving techniques 77—34418
U resource information economic value estimation 79—83547
U tailings management, economic impact on nuclear fuel cycle 80—18494
U/Pu coprocessing, impact on ore, conversion and enrichments costs 79—89475
^{233}U, symbiotic fast thermal fuel cycles, economic implications 80—726

economics continued
  ^{235}U enrichment by laser isotope separation process, cost anal. 77—42160
  ^{235}U to ^{238}U enrichment, ultracentrifuge, gas diffusion and nozzle separation techniques comparison 77—18680

eddy current losses
  Bloch walls, irreversible movements, loss contribs. from correlations 77—85483
  circular loop induced eddy current distrib. and loss calc. 80—9771
  conducting half-space, with adjacent filaments carrying AC current 80—53184
  conducting rectangular cylinder, losses due to finite length coils, exact analysis 77—10806
  crack detection in conducting material 78—19965
  domain structure dynamics, EM losses 79—87281
  domain wall dynamics, eddy current dominated, and magnetisation losses 80—88778
  electrical Fe sheet, single sheet tester for 20 Hz to 20 kHz range *(Japanese)* 77—70251
  electrotechnical steel, quality significance on energy and materials savings in magnetic circuits *(Czech)* 80—20947
  estimation method, in large steel plate having one-phase excitation *(Polish)* 80—93145
  ferromagnetic conductor, microscopic analysis of eddy current losses 77—85484
  ferromagnetic cylinders, sinusoidally varying end fields, eddy current phenomena numerical calcs. *(German)* 79—94131
  in ferromagnetic media, calc. *(French)* 79—69697
  ferromagnetic plate, due to currents in parallel conductors *(Polish)* 78—29877
  ferromagnetic plates eddy current phenomena numerical computation method *(German)* 80—65952
  ferromagnets, domain struct. effects on dynamic props., review 80—34678
  fusion reactor, TFTR, eddy current theory for structural materials 80—95427
  HF mag. pulse train diffusion into extended conductors, power calc. 77—27219
  long magnetic conductors, estimation of TE- and TM-mode losses 78—91891
  magnetic fields, eddy current losses in thin conducting coatings *(Polish)* 79—98263
  magnetic sheet with simple bar-like 180° domain structs. 80—39808
  MHD convertor channel and regions, eddy current losses due to magnetic field variations 80—40874
  microwave conductivity determ. from eddy current losses in planar specimens of high cond. 80—47077
  microwave conductivity measurement by eddy current loss method, effect of permittivity 78—24817
  multifilament superconductor, longitudinal field losses, freq. depend. 77—63037
  multifilamentary superconductor, AC losses, mag. field depend. of loss-freq. charact. 79—33384
  plane loop, power dissipation and inductance calc. method *(German)* 78—58881
  plate, nonmagnetic, thin, with multiparallel system of conductors, losses calc. 80—78743
  rare earth-Fe rod, US resonance with large eddy currents 80—54933
  semi-infinite shielded/unshielded mag. solid due to AC in parallel conductors with mag. shunt *(Polish)* 80—37929
  semiconductor microwave conductivity meas. by eddy current loss method 78—8417
  shielded magnetic solid, due to AC in parallel conductors *(Polish)* 80—32873
  steel, non-oriented, texture and mag. props., effect of Mn and S content 77—86047
  steel, transformer, anisotropy of temp. depend. of mag. props. *(Russian)* 78—39362
  steel, transformer, EM losses, influence of charact. of substruct. distrib. *(Russian)* 78—7058
  steel plate, fundamental and harmonic flux, sinusoidal applied mag. field 78—2708
  superconducting coil, electronic apparatus, for loss meas. 77—26361
  superconducting coil, multifilamentary composite losses 78—62637
  superconducting composite, multifilamentary, AC losses in transverse AC mag. field 80—34568
  superconducting composite 78—62636
  superconducting pulsed solenoid ORPUS-1, poloidal field coil performance 77—26352
  superconducting solenoid, 60 Hz AC loss meas. 77—26362
  superconductors, composite, and normal conductors, transient loss analysis and measurements using equivalent circuit technique 79—60978
  thin conducting sheets, variational estimation 79—41296
  thin laminations, minor loop hysteresis loss calc. 78—90342
  Tokamak toroidal field coil shielding calc. 79—31212
  transformer, EM losses, effect of degree of perfection of crystallographic texture *(Russian)* 78—60309
  A, magnetoresistance, field strength function, electrodeless methods 79—91026
  $CdCr_2Se_4$:Ag, ferromag. linewidth and eddy current losses 79—33541
  Fe alloy wire, glassy, shape, energy, eddy current loss and relax. damping of mag. domain walls 77—89975
  Fe, ferromagnetics, conductive, anal. by saturation/hysteresis simulation 77—12153
  Fe powder-plastic composite, soft mag. material, mag. and mech. props. 80—75812
  Fe-Ni, low frequency power losses 78—95466
  Fe-Si, low frequency power losses 78—95466
  Fe-Si (3 wt.%), domain wall drift due to nucleation during cyclic magnetisation 78—95461
  Fe-Si (3 wt.%), EM losses, effect of bending of 180° domain boundaries *(Russian)* 78—39357
  Fe-Si (3 wt.%), grain oriented, domain wall variation throughout magnetisation cycle 78—95459
  Fe-Si (3 wt.%), grain oriented, power loss depend. on domain wall bowing 78—95460
  Fe-Si (3 wt.%), grain-oriented, domain struct. regulation and power loss reduction 80—88779
  Fe-Si (3 wt.%), grain-oriented, power loss and domain wall variation with lamination thickness 80—88814

eddy current losses continued
  Fe-Si (3 wt.%), grain-oriented, energy loss reduction by lowering sheet thickness 80—88816
  Fe-Si (3 wt.%), loss prediction, from distorted waveforms 78—76273
  Fe-Si (3 wt.%), oriented, losses and domains, mech. stress effects 80—88852
  Fe-Si (3 wt.%), role of domain struct. *(Russian)* 77—80961
  Fe-Si (3 wt.%) alloy, domain structure influence obs. and calc. *(Slovak)* 79—4693
  Fe-Si (4 wt.%), freq. depend. of Fe losses in single crysts. with (100) [001] 79—51803
  $Fe_5Co_{70}Si_{15}B_{10}$, amorphous ribbon, zero magnetostriction, low residual mag. loss 77—12157
  In, resistivity measurement by eddy current decay method *(Korean)* 80—27275
  Li, resistivity measurement by eddy current decay method *(Korean)* 80—27275
  $Mn_{0.7}Zn_{0.1}Fe_{2.2}O_4$, temp. depend. of microwave resistivity 79—69540
  Nb-Ti, multi-filamentary superconducting wires, mag. field dependence of AC losses 78—60256
  Nb-Ti superconducting single layered multifilamentary coil, eddy current loss depend. on demagnetisation 80—97040
  Nb_3Ge film, CVD on inside of Cu tube, AC losses 77—28312
  Nb_3Sn-Cu composite superconductors, in-situ, AC losses 79—38283
  $Ni_xFe_{3-x}O_4$, $x<1$, anomalous microwave loss 79—69540
  YIG:Ca eddy current damping 80—39876

eddy currents
  see also induction heating
  3 GeV proton synchrotron magnet design and meas. 79—31303
  amplitude phase methods of testing, design relationship for eddy current transducers 78—53152
  brain tumour destruction by 8 MHz implanted metal powder eddy currents *(German)* 79—16337
  Burrows permeameter, eddy current error reduction 77—10067
  coating, steel plate induction heating 80—77775
  complex shape product inspection, local eddy current transducer 80—108671
  conducting cylinder with transverse mag. field, eddy current induction 78—74815
  conducting cylinders in field of conductors perpendicular to side surfaces *(German)* 80—106415
  conducting liquid, eddy current induced pumping, longit. current in corrugated tube *(Russian)* 78—75216
  conducting liquid, in cylindrical induction furnace, velocity and EM field distrib. calcs. *(Russian)* 77—47106
  conducting media, eddy current phenomena, neglect of displacement current 79—13868
  conducting slab, electrodynamic forces on coil, anal. *(German)* 77—58226
  conductivity meas., contactless, eddy current interactions *(German)* 80—31788
  conductor, current carrying, finite element analysis of skin effect 77—83785
  conductors in steady motion, solution in theory of eddy currents and forces 78—62970
  corrosion monitoring 78—88584
  crack detection and meas. technique 79—43500
  critical evaluation of test results, representation, processing *(German)* 78—7145
  cylindrical conductor with surface crack, eddy currents calc. 80—23601
  cylindrical products, diameter meas., interfering factors elimination 80—77755
  defectoscope performance analysis with series tank circuit in input stage 78—53106
  defectoscopy appl., using nonsinusoidal EM fields *(Czech)* 79—20311
  defectoscopy of permanent magnets, using electromagnetic method 78—39998
  destructive materials testing anal. by nondestructive electromagnetic methods *(German)* 77—86267
  display with heat-sensitive liq. cryst. colour change, for teaching demonstration 77—33804
  double-ended eddy current transducers, signal calc. for nonferromag. cylindrical products 80—89443
  dual energy methods of calculation 78—78859
  eddy current flaw detector for revealing fatigue cracks 79—66244
  eddy current inspection, possibilities of phase generator circuits 78—88614
  eddy current inspection system with simulated signal, calibration 78—3285
  education, eddy currents, levitation, metal detectors and induction heating 78—61967
  electrical donductivity meas., standard models 80—86343
  electrically conducting spherical specimens, electromagnetic control 78—53138
  electromag. convertor, forming part of unbalanced bridge circuit, exam. of characts. 78—85100
  electromagnetic flaw detector, differential eddy current transducer asymmetry effect on sensitivity 79—39092
  electromagnetic inspection review 80—35468
  elongated part of noncircular cross section, straight through eddy current transducer inspection 79—47860
  EM field induction in vacuum by US wave in magnetostrictive conductive half space, anal. 77—73415
  EM NDT phenomena, fissile element modelling 80—40633
  EM suspension field calc. using computer *(Russian)* 79—59616
  EM wave propag., self-consistent approach 78—51920
  fastener hole inspection, computer automation of eddy current inspection, exam. 78—53040
  fastener hole tester, improved design 80—30194
  fatigue crack growth monitoring with eddy current transducer 80—45460
  feed through eddy current transducer, numerical anal. or operating mode during ferromagnetic rod inspection 80—108670
  ferromagnet, dynamics of domain struct. and microeddy currents in HF fields *(Russian)* 77—80957
  ferromagnetic cylinders, sinusoidally varying end fields, eddy current phenomena numerical calcs. *(German)* 79—94131
  ferromagnetic cylinders with field intensity-dependent permeability, anal. *(German)* 77—40088
  ferromagnetic half space, density induced by a transient magnetic field 78—71002

eddy currents continued
  ferromagnetic metal, dragging of domains by temp. gradient 80—34425
  ferromagnetic plates eddy current phenomena numerical computation method *(German)* 80—65952
  ferromagnetic probe, with square cross section, numerical computation *(German)* 78—77951
  FFTF-type eddy-current flowmeter performance in SLSF P-series test trains 79—9669
  field weakening effect of rect. cond. cylinders in air gap *(German)* 79—86105
  flaw detection, suppression of interf. parameters 80—89442
  flaw detection of long ferromag. products, magnetizing device parameters 80—89447
  flaw detector appl., feedback phase effects on response to displacements 77—73418
  flaw detector for detecting electricaly conducting inclusions in UO_2 fuel element cores 77—90560
  flowsensor using eddy currents of conducting fluids, model 78—5829
  force effects calc., induced in thin plate by cylindrical magnetic field 80—14269
  fracture toughness testing, fatigue crack sensor for Al, Ti alloys 80—45459
  Fredholm integral equations in computational methods for solving static field and eddy current problems 79—68344
  fuel elements, quality inspection by eddy currents, unit 79—100315
  fusion reactor eddy current analysis, finite element circuit method 78—66373
  fusion reactor eddy currents, 3-dimens., perturbation-polynomial expansion calcs. 78—66372
  geometric distortion by eddy currents in cylindrical conductors 77—50584
  graphite reinforced epoxy, NDT 79—96254
  heat exchange tube thickness meas. by eddy current for corrosion testing, computer study 78—68852
  HFEF/N irradiated fuel element eddy-current exam., cladding performance 79—9750
  hot-rolled rods, surface defect detection without scale removal by NDT 78—95890
  imaging flaw detection system 80—89426
  Incoloy 800, eddy current testing *(German)* 79—96257
  induced, time const. determ. using EM field theory *(German)* 77—19130
  induction in thin curved sheets, calc. 79—41299
  inspection equipment, circuit for selecting signals in specified phase range 78—56863
  integral equation calculations 77—83783
  intermediate conducting solid, microwave eddy currents and EPR 77—80996
  irradiated fuel rod NDT using encircling and probe eddy-current systems 79—9751
  irregularity shaped plates, slow ramped field, eddy current heating, anal. 80—91722
  in laminated Fe cores, calc. in arbitrarily shaped three-dimens. cores, appls. *(German)* 79—45886
  liquid crystals *(Russian)* 77—39541
  magnetic domain wall effective mass, eddy current contrib. 80—29570
  magnetic field distribution, in conducting plate, computer soln. *(Polish)* 78—29878
  magnetic field time constant calc *(Polish)* 77—83779
  magnetic measurements, eddy currents 78—12730
  magnetometer, rotating sample, role of eddy currents in studies of magnetic anisotropy 79—63278
  magnetostrictive, transducer in presence of eddy currents, mobility analogy equivalent cct. 80—48540
  materials testing, numerical and expt. investigation *(German)* 77—12763
  materials testing appl., response approx. for primary eddy current transducers 77—73419
  Maxwell's eqns. in electromech., numerical resolution by finite element anal., eddy current effects *(French)* 79—30269
  metal, eddy current response to solidification in one dimension 80—104140
  metal, mag. domain wall mass, press. due to eddy currents 77—12144
  metal, nonferromagnetic polycryst., EM-acoustic oscills. during EM field emission by inductive convertor *(Russian)* 77—11638
  metal, packed powder, induction heating mechanism *(Japanese)* 79—59615
  metal fatigue, eddy current sensors, tuning method 80—21231
  metal object in media, depth measurement instrument, eddy current transducer 79—39091
  metal particles, ultrafine, eddy current nonlocal calc. 79—60744
  metallic crystal, perfect, mag. domain wall bowing, rel. to eddy current field 77—1566
  metallic lamination, domain wall bowing, simulation using new spline model 79—51807
  metallic objects with complex shape, eddy-current inspection 80—89446
  metals, eddy-current contactless method of temp.-depend. elec. resist. meas. 78—21171
  meter standards 78—27709
  MHD channel, anisotropically conducting plasma in inhomogeneous elec. and mag. fields, current calc. *(Russian)* 80—74995
  microwave ferromagnetic resonance probe, for eddy current detection of surface flames in metals 79—34254
  modulation type defectoscope, signal and sensitivity calc. 78—44327
  moving conducting ribbon, interaction with ferromag. inductor field *(Russian)* 78—94359
  multifrequency eddy current inspection with continuous wave methods 80—71844
  NDT, automatic combined inspection line for type 3102 bright steel bars 77—77714
  NDT, detection limit, comparison with US methods 78—60957
  NDT, electromagnetic methods, use in anal. of destructive materials testing *(German)* 77—73396
  NDT, equipment for production line inspection 79—29320
  NDT of tubes, rods and wires *(German)* 80—25971
  NDT probe, high saturation with internal reference, design and specifications 80—40658
  network analogy for three dimensional eddy current problems *(Japanese)* 79—81325
  non-contact displacement meas., principles and methods *(Chinese)* 79—71409

eddy currents continued
  non-magnetic tubular conductors, eddy current study *(French)* 80—83541
  nondestructive evaluation, finite element analysis appl. 80—35439
  nondestructive inspection unit of petroleum pipes, based on eddy current modulation unit 78—76814
  nondestructive materials testing, pulse-excited systems frequency spectrum analysis *(Czech)* 79—39071
  nonferromagnetic film sheet resistance meas., eddy-current method 78—45658
  nonferromagnetic solid eddy currents, three-dimensional calc. *(French)* 79—41301
  nonmagnetic conducting tubes appl., special study *(French)* 80—83540
  nonmagnetic conductors, three-dimensional eddy current calc. *(French)* 80—14270
  nonmagnetic electrically conducting rod, section shape effect on eddy current transducer parameters with uniform field 78—53132
  nonmagnetic strip in transverse uniform alternating magnetic field 78—94362
  nuclear power station heat exchangers, eddy current probe for nondestructive testing of transfer tubes *(Japanese)* 80—81246
  nuclear steam generators, inservice inspection, book contrib. 79—100322
  numerical anal. of eddy-currents induced within a metal cylinder by parallel ACs *(Polish)* 78—78856
  numerical solution eddy-current problems, including moving Fe parts 78—90340
  paramagnetic metals, EM excitation of sound, Mossbauer study *(Russian)* 79—99794
  phase sensitive eddy current detectors, effect of compensation conditions, on transducer-product clearance inductions 78—85103
  phase thickness gauge, automatic error corrections 79—9204
  plate, metallic, eddy current distrib. after step function of external magnetic field 80—69293
  plate fixed in air-gap between salient poles, eddy current induced *(German)* 79—86106
  Poisson's ratio, eddy current determination 80—65116
  polymer mixture, metal fraction contents and properties meas. method *(Russian)* 80—76571
  pressure transducer elastic elements characts. optimisation *(Russian)* 78—77890
  probes, rotary, for defects scanning and detection 77—90557
  probes, thickness measurement of plating layers *(German)* 79—85112
  problem soln., integral eqn. method developments 79—41292
  prolate spheroid, eddy current distrib., anal. *(German)* 78—37784
  pulse eddy current methods, appl. to NDT *(German)* 77—90533
  pulsed eddy current testing, for smooth and ribbed tubing 78—23906
  pulsed method of testing, theoretical and expt. foundations *(German)* 79—15920
  rare earth-Co permanent magnet EM acoustic transducer design 77—19508
  reciprocating magnetic refrigerator for 2-4K operation 80—2577
  resistance introduced by a defect in modulation inspection method 79—91892
  rotating probe for tubular condenser examination *(German)* 77—1897
  semiconductor-ferrite layer structure, EMF created by spin-wave, effect of current 80—11072
  shear modulus meas. under press., EM method of induced eddy currents 77—31709
  sheet conductor, induced eddy currents, IR meas. 80—37933
  skin effect transients on hollow sphere in plane field of system of conductors *(German)* 80—37927
  soft magnetic metals, ideal, AC response 78—64223
  solid cylinder fixed in air gap *(German)* 79—89827
  spatial harmonics, spectra density meas. 78—53141
  speed meter operating characteristic analysis 79—40543
  stamped disc surface inspection by automated eddy current unit 78—92430
  steady-state eddy-current dominated magnetic domain wall motion with severe bowing and necking 79—91248
  steel, austenitic, eddy current testing of welds, cladding and cast materials *(German)* 78—44293
  steel, austenitic weld joints and surface claddings, eddy current testing *(German)* 77—1895
  steel, C and Mn, rails, surface crack exam. by eddy current technique 77—9007
  steel, cold-rolled, isotropic, specific magnetic loss meas. at high frequency 80—101808
  steel, eddy current surface crack detection *(French)* 79—61831
  steel, ferromagnetic round bar, eddy current crack detection *(German)* 79—91880
  steel, square parts, surface inspection, defect depth meas., eddy current method 79—29307
  steel, stainless, Cr-Ni, low temp. plastic deformation, in mag. field 79—83256
  steel, structural ties, NDT by eddy current transducer, optimum parameters and capabilities 80—108669
  surface currents induced by perpendicularly incident point charges, anal. *(German)* 77—42461
  surround coil transducers, optimisation for eddy current testing 80—31728
  teaching laboratory demonstration of eddy current forces 79—62967
  temperature measurer, exam. of design 79—12803
  tester for crack detection, of nonferrous tubes and rods 78—85099
  testing, signal to noise ratios and sensitivity increase 77—73393
  testing devices, operation, appl. set up and evaluation, Verimet method *(German)* 79—70263
  testing of wire and bar 80—71819
  thermoelectric currents and eddy thermoelements 77—8126
  thermoelectrically anisotropic inhomogeneous media, eddy thermoelec. currents 77—55555
  thermoelectrically anisotropic media, thermoelec. eddy currents mechanisms, self consistant temp. and current distrib. 80—44626
  thickness gauge, total factor experiment exam., metrological characteristics determ. 78—39999
  thin conducting plate moving in mag field, calc. using scalar pots. *(Polish)* 80—32874
  thin conducting plates, variational techniques for eddy current calc. 78—90341
  thin cylinder of finite length with driving fields of ramp time depend., calc. 77—6966

eddy currents continued

- thin film, integro-differential eqns. soln. by finite element method 78—90343
- thin plate, lateral mag. skin effect 77—10811
- thin walled bearing races eddy current inspection of hardening and tempering quality 78—95892
- thin-film transducer, for temp. meas. *(Russian)* 77—26294
- three dimensional eddy current problems, numerical soln. *(Japanese)* 79—81324
- three- and two-dimensional eddy current problems, Fredholm integral eqns. 79—41298
- through type transducer, operating condition simulation when inspecting ferromagnetic rods 78—53077
- Tokamak, Texas exptl., homopolar generator, eddy currents, EM forces (torques), due to misalignment 78—54953
- Tokamak device, eddy currents induced in vacuum vessel, anal. 80—1832
- Tokamak fusion reactor vacuum vessel, eddy currents when plasma current is disrupted, calc. *(German)* 80—68937
- Tokamak machines, eddy currents, numerical and exptl. anal. 78—66374
- toroidal deflection yokes, eddy current compensation 80—95762
- transducer, electrical conductivity meas. of coatings, tuning out of gap instability 78—36994
- transducer, feed-through, approx. calc. of mag. field, non ferromag. media 80—78746
- transducer, matrix eddy-current, with magnetic circuit, design and construction 80—68228
- transducer, part geometry effect on inspection 78—53078
- transducer calc. of response, comparison with computer results 78—36995
- transducer of arbitrary form located parallel to multilayer medium, EMF 79—2762
- transducer of complex geometry, calculating added resistance 79—97375
- transducer with electrical commutation of excitation field, NDT 80—105633
- transducers, applied, resistance due to cracks, eddy current calc. and hodograph 78—53095
- transducers, for meas. thickness of lacquer coloured coating on mag. base 78—85101
- transient, distribution in plate of finite thickness due to coil of arbitrary shape *(German)* 79—27129
- transient distribution in two insulated coils embedded in conducting medium *(German)* 79—41282
- transient skin effect in laminated cores with sectionally different material props. *(German)* 79—41280
- TTF-TCNQ, microwave eddy currents and EPR 77—80996
- tube flaw detection by annular US transducers 78—60971
- tubular conductors, non-magnetic, study *(French)* 80—5659
- two-dimensional steady-state and transient eddy current problem soln. 79—41289
- ultrasonic and eddy current testing of welded titanium tubes *(Japanese)* 80—108651
- unbounded two-dimensional linear eddy current algorithm 79—41300
- Young's modulus, eddy current determination 80—65116
- Zircaloy-UO$_2$ fuel rods, eddy-current testing of claddings using encircling and probe coils 80—21245
- Al alloy cylindrical parts, crack detection by two channel eddy current inspection unit 78—72998
- Al alloys, crack opening stress level in fatigue, determ. by eddy current technique 80—16617
- Al, magnetoplastic effect and eddy current heating *(Russian)* 77—43858
- Al wires, eddy current effects on NMR 80—2645
- Be bronze, BrB2 grade, heat treatment quality evaluation, using eddy current device 77—90562
- Co-P, amorphous foil, complex permeability and eddy currents, annealing induced short-range order 77—8360
- Fe, cast, grey, eddy current test for hardness certification 80—7733
- Fe, saturable solid, calc. methods *(German)* 77—54644
- Fe, three dimensional arbitrarily shaped cores, eddy currents calc. *(German)* 80—18956
- Fe-Ni-Mn, Invar, RF collapse and thermal effects, Mossbauer study 80—100624
- Fe-Si (3.5 wt.%), dynamic neutron depolarisation meas. of ferromag. domain struct. 79—82812
- Ge, Foucault currents in electron-hole drops *(Russian)* 77—8030
- Hg arc plasma, azimuthal RF cond. meas. by eddy current effect, expt. 77—1029
- Li wire, NMR line shape, eddy current effect in presence of self-diffusion 80—54955
- Ni films on stainless steel, electroless, internal stress meas. by proximity method, eddy current detector appl. 79—64611
- Ni, magnetoelastic effects, ΔE-effect and macroeddy current damping, internal friction meas. 78—64253
- Ni, magnetoplastic effect and eddy current heating *(Russian)* 77—43858
- NiFe tape, rapid surface and vol. magnetisation, eddy-current-limited domain wall motion 77—12159
- Pb-Sn (20wt.%), eddy current study of solidification 80—104141
- Si monocrystal peripheral fusion channelling under HF heating *(Russian)* 80—59627
- Ti-Al-V (6, 4 wt.%) effect of high temp. oxidation on eddy current conductivity 78—76770

edge dislocations

- alkali halide, doped single crystals, plastic anisotropy 78—26575
- alkali halide, morphology of growth and evaporation surface 78—79544
- alkanes, thin plate microcrystals, transmission electron diffraction intensities 78—83821
- amorphous Lennard-Jones solid, edge and screw dislocation, stability, elasticity, simulation 80—15099
- anisotropic crystals, infinite rectilinear dislocation, vibrs. 80—44210
- atomistic models for rectilinear motion and vibration 77—72193
- BCC crystal, electron microscope image contrast, theoretical predictions for non-edge dislocation loops 80—24326
- BCC crystal, electron microscope image contrast from edge dislocation loops 77—76409
- BCC metal, discrete-continuum hybrid method for dislocation-point defects interaction 77—89467
- BCC metals, vacancy-edge dislocation interactions, computer simulation 78—83845
- bimaterial interface, wave propagation in non-uniform motion of displacement discontinuities 80—19264

edge dislocations continued

- bonded anisotropic bodies, arbitrarily oriented crack near interface *(Japanese)* 78—9611
- 4-n-butyloxyphenyl-4′-nonyloxybenzoate, edge dislocations in smectic C mesophase 78—91231
- cholesteric, liquid crystals, disinclinations, rotation defects, topology *(French)* 80—79679
- climb, numerical anal. 78—71736
- climb process, of edge dislocation, effect of glide forces 80—70195
- climb processes in high temp. recovery-creep 77—19965
- climb rate and core diffusion 80—10553
- coherent precipitation near dislocations 79—95016
- coincidence site lattice, differential geometry 79—28000
- collective dislocation motion, dynamic effects 78—79632
- β-copper phthalocyanine, dislocation detection *(German)* 78—63773
- crack propagation effect of 2- or 3-dimensional macrodefect *(Japanese)* 80—104261
- cracks, plane elasticity, curvilinear crack edges concentrated forces and edge dislocations, numerical soln. 80—58970
- critical resolved shear stress, from misfitting particles 78—79613
- crystal elastic and plastic anisotropy and dislocations *(Japanese)* 79—95069
- cubic crystal edge and screw dislocation—point defect elastic interactions 80—15151
- dechannelling mechanism due to dislocations, anal. 80—59538
- diamond, natural, dislocation-N$_2$ impurity interaction, photoconductivity spectra, resistivity 79—91097
- diamond crystals, synthetic, etch-pit formation on cube faces, electron microscopy obs. 80—75232
- diffraction, optical analogue using simulated models 78—38723
- disclination dipole of infinitesimal width and straight dislocations 79—51104
- dislocated ferromagnet, inhomogeneous magnetisation near dislocation effect on FMR linewidth 80—25213
- dislocation motion, straight line, in concentrated solid soln., computer simulation 77—15413
- dispersion-hardened single crystals, theory of high-temp. strength 77—48445
- displacement field, in elastic strip, Fourier transform technique 79—46658
- displacements in elastic strip, Fourier transform method 79—21553
- elastic half-plane, wave propagation for non-uniform motion of displacement discontinuities 80—1478
- elastic stress field shape change kinetics depend. on inclusion-edge dislocation interaction 79—86815
- elastically nonlinear medium, dislocation interactions *(Russian)* 79—42064
- electron micrograph, theoretical, foil surface stress relax. effect 77—31665
- electron microscope image calc. and Burgers vector sign determ. 77—59017
- electron microscopy, high resolution, dislocation core studies, image calc. methods 80—96535
- electronic localised state at edge dislocations, parabolic dispersion law *(Russian)* 80—65479
- energy and displacement field around edge dislocation, Ritz method 78—14344
- fatigue cracks, initiation, rel. to grain boundaries, stress gradients and cross slip 77—27890
- FCC materials, dissociated dislocation dipoles, weak-beam electron microscopy technique 78—34516
- finite-two phase bodies, response to internal and external stresses, numerical considerations 80—24742
- free surface in undeformed and deformed crystals, differential geometry, distortion, torsion, Burgers circuit 80—64996
- grain boundary dislocation struct. 77—55283
- grain boundary dislocations structure, atomistic study 80—15110
- graphite, fast neutron irrad. damage theory and modifications 77—67805
- HCP crystal, dislocation-point defect interactions, anisotropic elasticity theory, appl. to Zr 77—11588
- HCP crystals, dislocation-point defect interactions in slip systems 78—47417
- ice, edge dislocation dipole form. by heat treatment, X-ray diffr. topography 79—99203
- III-V compounds, stacking fault energy and ionicity 78—30651
- III-V crystals, piezoelectric effect due to dislocations 77—81059
- III-V semiconductor, anisotropic carrier mobility due to dislocations 78—60124
- III-V semiconductor, local resist. near dislocations, eqns. 78—60123
- III-V semiconductor, temp. distrib. around dislocations, due to Joule heating, calc. 78—71734
- image and surface dislocations models, comparison 79—23605
- interaction with interstitial atoms, influence on Peierls stress 78—34537
- interactions in infinite array, elastic energy 78—55871
- interface tractions induced by edge dislocation 78—14345
- intrinsic point defect-impurity atom mobile complex form., influence on defect diffusive fluxes 80—2063
- Invar, deformed, magnetism and temp. depend. of effective field on ^{57}Fe *(Russian)* 79—24234
- Invar, dislocation motion anomaly 80—10554
- ionic crystal, solid soln. hardening by aliovalent cations 77—44265
- ionic crystals, adhesion energy, calc. for NaCl type crysts. 77—43437
- irradiated materials, cascade damage and self-ion injection effects on swelling 78—34549
- irradiation creep due to stress induced preferred absorption of point defects, anisotropic dislocation struct. effects 79—42140
- irradiation creep mechanisms, theoretical assessment 79—55817
- irradiation induced creep, point defect absorption at dislocations 78—19842
- isotropic and anisotropic crystals, stress fields around defects of dislocation-aggregate type 77—39591
- lamellar liquid crystal, biaxiality due to oriented defects 79—41945
- laser optical simulation of diffr. from distorted lattices 79—23612
- lattice defects, high resolution microscope images, calc. and interpretation 79—73075
- lattice model near surface 77—7719
- localised electron states, extended Huckel theory 78—18999
- magnetically ordered cryst., dislocation drag, magnetoelastic waves 80—103332
- metal, BCC, cryst. lattice change during deform., influence of boundary dislocations with different Burgers vectors *(Russian)* 77—21219

edge dislocations continued
metal, BCC, relation between elastic energies of dislocations and choice of slip system *(Japanese)* 78—18656
metal, dislocation scatt. and de Haas-van Alphen amplitudes 78—63967
metal, dislocation scattering and de Haas-van Alphen effect 79—77982
metal, FCC and BCC, self-diffusion along edge dislocations by vacancy mech. *(Russian)* 78—87810
metal, FCC and BCC, vacancy diffusion along single edge dislocations, computer modelling *(Russian)* 77—47612
metal, FCC or BCC, dislocation annihilation during tensile and cyclic deform, and limits of dislocation densities 80—34007
metal, HCP, atomic struct. of defects 78—30611
metal, plastic flow, role of osmotic forces in low cycle fatigue, vacancy generation *(Russian)* 79—60430
metals, BCC, dislocations, anisotropic elasticity theory *(Japanese)* 79—10853
metals, BCC, solid soln. hardening, crystal resolved shear stress depend. on dislocations 80—40373
motion, glide and climb resist. due to dragging a Cottrell atm. 79—99194
non-hardening material, under plane strain, rel. to stress distrib. around crack tip 80—10189
nonlinear motion in atomic lattices, nonequilibrium mol. dynamics 79—55742
nonlocal hexagonal elastic crystal, edge dislocation 79—51105
4-n-octyloxy-4′-cyanobiphenyl, smectic A liq. cryst., elastic modulus determ., stress/strain relationships 78—91229
octyloxycyanobiphenyl, smectic-A phase, dislocation effects on viscoelastic props. 77—84633
olivine, high temp. creep, edge dislocation control 79—79815
Peierls model, dislocation core energies 79—27984
plastic relaxation in shock wave, slip mechanism 79—41605
plastically deformed crystal, lattice defects influence on axial shadow figure *(Russian)* 80—25508
point defect diffusion in stress field of edge dislocation of irrad. solid 78—51720
point defect-edge dislocation interaction near solid surface 80—79834
polystyrene latexes, edge dislocations 79—96370
quartz, synthetic, line defects, etch tunnels and X-ray topography 77—76406
quartz crystal, synthetic, dislocations obs. by light scatt. tomography 80—49229
repeated precipitation on edge dislocations, micromechanisms 78—95752
sapphire, work hardening 77—16604
screening in metals and superconductors, metal softening *(Russian)* 80—64997
semiconductor, electron multiphonon capture by edge dislocation *(Russian)* 79—86861
semiconductor, tetrahedrally coordinated, effect of doping on dislocation mobility 79—82550
semiconductor crystal, positron annihilation with electrons bound in edge dislocations 79—47539
semiconductor substrate surface, low loss electron and Auger images correl. 78—22944
semiconductors, free-carrier mobility associated with dislocation strain fields 77—51738
semiconductors, polycryst., with low angle grain boundaries, residual cond. 80—15525
smectic liquid crystal, edge dislocations obs. by polaris. microscopy 79—7547
smei-infinite solid, edge dislocation behaviour with surface energy effects 79—55743
solid soln. strengthening, conc. computer simulation 78—31420
spinel oxide, dissociation of dislocations and plastic deform., temp. effects 79—7613
spring constant between edge dislocation and loop *(French)* 80—54280
stability under shear stress, hydrostatic press. 80—59462
steady state dislocation motion via mol. dynamics 78—10049
straight edge dislocation in nonlocal elasticity, stress field, elastic energy 77—35555
straight line, motion in conc. solid soln. computer simulation 77—81268
stress field of edge-dislocation lying in plate 79—23603
stress field-point defect elastic interaction energy 79—77631
superconducting filament formation near edge dislocation *(Russian)* 79—4635
superconductors, type II, vortex pinning at edge dislocations, electrostatic mechanism 80—103802
superdislocations, resist. to motion, temp. depend. expressions *(Russian)* 80—79789
superstructure, interaction between superdislocations of opposite signs gliding in parallel planes *(Russian)* 77—80506
surface dislocation model, Z-phase interface boundary problem 80—39085
surface dislocations, universal concept, rel. to disclinations and grain boundaries 80—100231
TGS, effect of edge dislocations on shapes of moving domain boundary 80—20602
thermal and thermoelastic fields around moving dislocations *(Russian)* 78—22731
thermally activated motion, appl. to KCl-KBr solid soln., computer simulation 79—19249
triglycine fluoberyllate, deuterated, dislocation line defect X-ray topographic analysis 80—59465
two-face dislocation boundary, energy and induced stresses *(Russian)* 80—103331
type II superconductor, dielastic interaction of flux line lattice with internal stresses of cryst. imperfections 78—56270
web dendrites, dislocations, stacking faults, X-ray topographic study *(Chinese)* 80—88148
X-ray diffraction distortion distrib., behaviour from mixing near low Fourier orders *(German)* 79—37583
X-ray line broadening, fragmented crystal containing blocks *(Russian)* 79—86643
Ag, CESR due to edge dislocations 78—19328
Ag, elastic instability 79—82235
Ag film, elongated epitaxial (111) island growth on Cu(001), interface misfit, dislocations 79—82493
Al and Al-Mg alloys, thermal generation of vacancies involving dislocation climb 77—59808
Al bicrystal, high resolution electron microscopy obs. of dislocations 80—103347

edge dislocations continued
Al bicrystals, [011] low-angle tilt boundaries, high resolution electron microscopy 80—34012
Al, CESR due to edge dislocations 78—19328
Al, cold-worked, plastically deformed, internal friction spectrum, Hasiguti peaks associated with dislocations 80—7618
Al, plastic flow, role of osmotic forces in low angle fatigue, vacancy generation *(Russian)* 79—60430
Al-Mg (0.3 wt.%) single cryst., dislocations obs. by high voltage electron microsc. 80—79796
Al-Mg (5.5 wt.%), effect of stress changes during creep on dislocation struct., TEM study 79—74214
Al_2O_3, sapphire, edge dislocation loop obs. by high resolution lattice imaging 80—103346
Au, serration and dissociation of edge dislocations in low-angle tilt boundaries 77—72621
Au/Cu, bilayers, interdiffusion phenomena, lattice dislocations, TEM obs. 80—59736
Ba ferrite compounds, microsyntactic intergrowth and cryst. defects, TEM obs. 79—10858
$Ba_xSr_{1-x}Nb_2O_6$ crystals, optical defects and edge dislocation distributions 80—19806
Bi anisotropic crystal, dislocation wall stress field and strain energy 80—100233
$C_{12.6}AuCl_3$, intercalation compound, struct. *(French)* 78—42982
CESR due to edge dislocations 78—19328
$CaCO_3$, growth dislocations obs. using Lang X-ray topography 78—2133
$Ca_5(PO_4)_3F$, dislocation struct. exam. *(Russian)* 78—63770
CdS, acoustic wave attenuation, phonon viscosity and dislocation drag 80—70319
CdS, dislocation charges determ. 78—2136
CdS, epitaxial layers on (111) Ce, growth and defect struct. 78—18920
CdS, plastically deformed, optical and electronic transport anisotropies 77—8611
CdSe, deep dislocation levels, TSC and luminesc. obs. 77—8050
CdTe, aB glide dislocations, dissociated into two Shockley partials, stacking fault energy 78—43024
Co-Ga β' quenched single crystals, annealing-out of point defects 80—55426
Cu alloys, FCC, climb of extended dislocations due to irradiation in HVEM 80—103343
Cu, continuum representation of computer simulated dislocations 78—30623
Cu, cubic crystals, anisotropic, dislocation loops, electron microscope image contrast 80—39101
Cu, elastic instability 79—82235
Cu, electrical resistance of edge dislocations *(German)* 80—96859
Cu irradiated, exam. of dislocation bias for interstitials to edge dislocations 78—79612
Cu, irradiated, small edge dislocation loops, electron microscope image contrast, Burger's vector determ. 77—76410
Cu, layered cell structures and slip lines in deformed cryst., TEM obs. 79—99209
Cu, neutron irrad. cryst., edge and screw dislocation groups, mean vel. 79—7607
Cu, single crystals, neutron irradiated, stresses and secondary slip between overlapping and dislocation arrays 80—88162
Cu single crystals, positron trapping by edge dislocations, produced by bending 78—80606
Cu, single crysts., cyclically and unidirectionally deform. X-ray diffr. study 80—89319
Cu-Al (10.5 at.%), dislocation generation and displacement in single crystal in bending 79—60368
Cu-Al (15 at.%), elastic instability 79—82235
α-Cu-Al (15 at.%) alloys, effects on low temp. neutron irrad. induced point defects behaviour 77—43251
Cu-Cd (1.0 wt.%), yield stress and flow stress 80—97524
(Cu-Au)-Co, single crysts., solid soln. and particle strengthening, superposition 80—97495
CuAu, calc. of elastic interaction between locally transformed regions with screw and edge dislocations 78—83844
Cu_2NiZn, separation of partials of superlattice dislocations, anisotropic elasticity theory, ordering 79—65082
Cu_2O, epitaxial, on Cu(111), misfit dislocation annealing, TEM obs. 79—82228
Cu_2O, laminar growth on (111) Cu single cryst. surface, microstruct. 78—72025
α-Fe, a/2 $\langle 111\rangle$ $\{110\}$ edge dislocation, at. simulation 77—89435
Fe armcotype, Mossbauer spectrum linewidth, influence of dislocations 79—99806
α-Fe, atomic dislocation modelling, flexible boundary conditions and nonlinear geometric effects 78—75667
Fe, BCC, computer simulation of entropy of $^1/_2\langle 111\rangle\{110\}$ edge dislocation 78—67716
Fe, BCC, vib. entropy of $^1/_2$ $\langle 111\rangle$ $\{110\}$ edge dislocations 78—63768
Fe, BCC containing impurity atoms, Peierls energy of $1/2\langle 111\rangle\{110\}$ edge dislocation, temp. effect 77—84751
Fe, deformed, dislocation structure determ. from magnetic props. 78—55874
Fe, deformed single crystal, dislocation distrib. 77—59880
Fe, epitaxial growth on Au platelets, dislocations 80—96760
Fe epitaxial layer on Au(111), misfit dislocation obs. 79—73415
Fe, FCC, grain boundary struct. and energy, computer expt. 78—30643
α-Fe, He atom clustering at $^1/_2\langle 111\rangle\{110\}$ edge dislocation, calc. 78—2154
Fe, quenched-in hydrogen, yield stress decrease of prestrained specimens 80—16454
Fe, softening and hardening by H_2 charging during tensile deformation 80—16453
α-Fe:He, impurity clustering in vacancies bound to edge dislocations 78—91358
Fe-Al, single crystals, deform. at high temps. 80—81125
Fe-Ni (29 at.%), calc. of elastic interaction between locally transformed regions with screw and edge dislocations 78—83844
Fe-Si (3 wt.%), degeneration of slip on ($\bar{2}11$) planes *(Russian)* 78—80587
Fe-Si (3.25 wt.%), dislocations in twin boundaries, electron microscopic images 80—34006
FeAl single crystal, compressed, dislocation arrangement 78—14354
$Ga_{1-x}Al_xAs$-GaAs, heteroepitaxial layers on GaAs(001), misfit dislocation asymmetry 77—47694

edge dislocations continued
$Ga_{1-x}Al_xAs_{1-y}P_y$ epitaxial film, nonradiative recomb. at dislocations 80−44213
$Ga_{1-x}Al_xAs_{1-y}P_y$ epitaxial layer heterojunction, nonradiative recombination at misfit dislocations 80−96901
GaAs, piezoelec. coupling and dislocations 79−91377
GaSb, acoustic wave attenuation, phonon viscosity and dislocation drag 80−70319
n-GaSb, temp. distrib. around dislocations, due to Joule heating, calc. 78−71734
$Gd_3Ga_5O_{12}$, optical birefringence images of edge dislocations 77−1129
Ge, bicrystal, dislocation core structure *(French)* 78−26571
Ge bicrystal, high resolution electron microscopy obs. of dislocations 80−103347
n-Ge, deformed, 0.1 eV optical transition, interpretation using electronic states theory for Si 77−20261
Ge, dislocation energy band width, carrier lifetime anal. 77−11874
Ge, dislocations, lattice images 79−82215
Ge, dissociated dislocations, constriction correlation with jogs 80−79801
Ge, edge-type dislocations, energy spectrum 80−24842
Ge, elastic moduli, drag coeffs. and Keating's parameters 79−73238
n-Ge, electron occupancy of dislocation levels 77−15795
Ge, electronic states associated with 60° edge dislocation 77−89724
Ge, energy spectra of dislocations 80−70637
Ge, optical excitation of dislocation states, photocond. meas. 77−69273
Ge, optical excitation of dislocation states 77−85265
Ge, vacancy distrib. and lattice distortion calc. 77−19954
InP, damage induced during handling for TEM obs. 80−2024
p-InSb, influence of plastic bending on galvanomag. props. 79−28349
InSb, plastically bent single crysts., dislocation struct. obs. 78−59816
KCl, elec. field effect on flow stress, charged-dislocation model 77−27935
KCl, stepwise motion of edge and screw dislocations *(Russian)* 77−84748
KCl, temp. depend. of dislocation charge, piezoelec. defect technique 78−22733
KCl-KBr conc. solid soln., edge dislocation motion in stress field *(Japanese)* 78−2138
KCl-KBr single crysts., yield strength and dislocation mobility, solid soln. hardening model 77−72649
KCl-KBr solid soln., highly conc., computer simulation of dislocation motion *(Japanese)* 77−68972
KCl-KBr solid solution, thermally activated edge dislocation motion, computer simulation 79−19249
LiF, (100) face, surface layer and dislocation etch pits 77−19962
LiF bicrystal, high-angle tilt boundary and edge dislocation intersection effects 80−79836
LiF crystal, contact damage obs. by cathodoluminesc. 80−71728
LiF, deformed, influence of surface on density of edge components of dislocations 77−31670
LiF, dislocation distrib. on surface parallel to Burgers vector 79−65090
LiF, dislocation structure, influence of variable deform. temp. 80−70211
LiF, radiation induced voids, formation on dislocations 80−15159
$MgAl_2O_4$, dislocations, sessile dissoc. 79−46663
MgO, a/2 ⟨110⟩ edge dislocations, lattice friction stress, atomistic calc. 78−18648
MgO, atomistic breathing shell model calcs. of dislocation core config. 77−35558
MgO, core struct. and energy of dislocations, breathing shell model calc. 77−39586
MgO crystal, contact damage obs. by cathodoluminesc. 80−71728
MgO crystal, yield strength and dislocation mobility 80−93601
MgO, electron irradiation damage, cryst. defects 80−107320
MgO, interaction energies between vacancies and edge dislocations, shell-model calc. 78−22759
MgO, single cryst., tensile creep, stress induced dislocation structs. 80−96539
MgO single crysts., dislocation processes, obs. by HVEM in-situ deform. 80−103340
$MgO:Fe^{3+}$, point defect complex-edge dislocation interaction energies, atomistic calc. 80−107314
Mg_2SiO_4, etch pits in cleaved faces, revealing low angle boundaries 79−14818
Mo, dislocation ⟨100⟩ density variation, deformation effects, dislocation stability *(Russian)* 80−15108
Mo, irradiated, small edge dislocation loops, electron microscope image contrast, Burger's vector determ. 77−76410
Mo, localized electronic states near ⟨100⟩ edge dislocation compared with perfect lattice 78−30888
Mo, monocrystalline, exam. of microplasticity at ambient temps. *(French)* 78−52888
Mo:He, interaction of He with edge dislocation, influence of interatomic pot. 79−33014
NH_4Cl, transitional plasticity, light scatt. study 79−77674
Na, energy and displacement field around edge dislocation, Ritz method 78−14344
NaCl, deformed, influence of surface on density of edge components of dislocations 77−31670
NaCl, dislocation density in monocrystal deformed under high hydrostatic press. 80−70216
NaCl, dislocation distrib. on surface parallel to Burgers vector 79−65090
NaCl, dislocation half loop mobility 78−59817
NaCl, dislocation mobility under high press., temp. depend. 80−75235
NaCl, dislocation ordering influence on integrated X-ray coeff. 80−103357
NaCl, edge dislocation, core struct. and props., theory 80−70194
NaCl, edge dislocation dissoc. energy, atomistic calc. 77−27883
NaCl, edge dislocation displacement 77−62540
NaCl, edge dislocation dissoc., computer simulation of core struct. 79−37703
NaCl, electric field gradients near dislocations, resulting NMR lineshapes 80−75225
NaCl, high resolution TEM and radiation sensitivity, dislocation obs. on deformed crysts. 80−107260
NaCl, integrated intensity of X-ray diffr. by polygonization walls 77−89447
NaCl, plastically deformed [001] orientated single crystal, glide props. and X-ray topography 77−21228
NaCl, plastically deformed, integrated X-ray reflection coeff. determ. 77−65981

edge dislocations continued
NaCl, polarisation caused by charged dislocation motion 80−59463
NaCl-type crystals, donor levels due to dislocations, calc. 80−6771
$NaCl(:Mn^{2+})$, influence of elec. field on flow stress 79−51193
$NaClO_3$, dislocations rel. to growth mechanism from aq. soln., X-ray topography 80−59464
NaF, deformed, influence of surface on density of edge components of dislocations 77−31670
Nb alloys, solid solution hardening, crystal resolved shear stress depend. on dislocations 80−40373
Nb, cubic crystals, anisotropic, dislocation loops, electron microscope image contrast 80−39101
Nb, plastic deform., Shubnikov phase penetration, Faraday effect obs. 79−82731
Nb, single crystal, surface oxide softening, TEM obs. 77−40462
Nb, surface oxide softening, anisotropy 78−60716
Ni base superalloy, internal stresses due to dislocation walls around second phase particles 79−99210
Ni, cubic crystals, anisotropic, dislocation loops, electron microscope image contrast 80−39101
Ni, deformed, magnetic susceptibility anisotropic changes 78−27025
Ni, stacking fault energy, by electron microscope obs. of dissoc. edge dislocations and faulted dipoles 77−72627
Ni-Cr, movement and dislocations using SEM and diffr. contrast method *(Chinese)* 79−51110
Ni-H, thermally charged, serrated yielding 80−85007
Si (100), P implanted, dislocation dechannelling, obs. by backscatt. spectrometry and TEM 79−4308
Si, (111) surface, annealing of scratches 79−60609
Si, birefringence of dislocation lines in (111) wafers 79−61332
Si, Czochralski grown crystals, swirl-type defect obs. 80−100236
Si, dislocation generation in local oxidation 80−107245
Si, dislocation growth during laser melting and solidification 80−2022
Si, edge dislocation, crystal surface interception, X-ray diffr. obs. in Bragg case 80−49228
n-Si, edge dislocation and stacking fault defect electrical recombination efficiency 80−15106
Si, edge-type dislocations, energy spectrum 80−24842
Si, electronic states associated with 60° edge dislocation 77−20261
Si, energy spectra of dislocations 80−70637
Si, filamentary crystals, branching and bending obs. 77−7954
Si, spin dependent recomb. at dislocations, EPR and photocond. 79−38095
Si, stacking fault energies, intrinsic and extrinsic, by TEM 80−10562
Si surface defects, influence on MOS radiation sensitivity 77−20445
Si, two-step photoconductivity by dislocations 78−14761
Si, vacancy distrib., and lattice distortion calc. 77−19954
Si wafer, defect studies by ASLEEP, SEM and scanning AES 79−19256
Si:P, dislocation dissoc. mode obs. by weak-beam TEM 80−107259
n-Si:P, edge dislocation energy level, differential capacitance meas. 79−23927
$Si:P^+$, misfit dislocation formation mechanism, effect of implantation temp. 78−38708
Sn, edge dislocation walls with Burgers vector 1/2⟨111⟩ 79−99202
Sn, single crystal, dislocation walls consisting of double arrays 79−46664
Sn, white crystals, dislocation reactions 79−86796
$Sr_{0.75}Ba_{0.25}Nb_2O_6$, large cryst. growth, control of opt. defects 78−76595
Ta, transmission channelling of MeV ions to study edge dislocations, expt. setup 80−29098
Te, a-edge dislocated crystals, mobility anisotropy 80−107781
Te, hole mobility anisotropy in edge dislocated cryst. 80−24936
Ti, single crysts., recrystallised, X-ray topography obs. 78−10054
TiO_2, crystal dislocations, elastic parameters, elastic energy, stress field, anisotropic elasticity theory 79−95008
TiO_2 rutile single crystals, stoichiometric, dynamic strain ageing 80−50661
V, slip geometry and dislocation struct., rel. to degree and temp. of deform. *(Russian)* 78−38717
W single crystal, creep, excess edge and screw dislocation density calc. *(Russian)* 78−34519
YAG crystals, dislocations and inclusions, birefringence topography obs. 80−107248
YIG, distrib. of easy magnetisation axes near edge dislocation *(Russian)* 80−44891
YIG, interaction force between 180° domain wall and edge dislocation 77−28408
YIG, phonon viscosity effect on dislocation motion 80−24450
Y_2O_3, electron irrad., dislocations *(French)* 80−2076
Zn, dislocation damping on $\{\bar{1}2\bar{1}2\}\langle\bar{1}2\bar{1}\bar{3}\rangle$ slip system above Debye temp. 77−62538
Zn, line energy of basal screw dislocation, exptl. determ. 80−88154
Zn, pyramidal edge and screw dislocation mobility, compressional stress pulse technique 77−19957
Zn, single crystals, positron trapping by edge dislocations, produced by bending 78−80606
Zr alloys, creep and growth, irradiation induced, microstruct. depend. 80−93602
Zr, creep, optical and electron metallographic anal., 473 to 873K 78−39986
Zr, irradiation growth, reaction rate theory calcs. 80−88212

education
see also computer science education; educational administrative data processing; educational aids; educational courses; teaching; training
academic motivation, objective measurement 79−17154
academic research and graduate education, effect of Department of Defense funding 78−62031
ACS Tenth Biennial Education Conference on Safety and Health in Academic Lab., recommendations 79−80387
Adams, Roger, his role in American chem. education and research 80−4497
air-dielectric interface, EM wave reflection and transmission in terms of polarisation 80−105458
algorithms, implication for instructional design 78−81735
algorithms, suggested uses 78−49578
alternative energy sources, solar and atmospheric 78−69951
American Journal of Physics, nature of journal 79−58456
angular momentum operators, derivation in spherical polar coords. 77−78932

education continued
- Appalachian Education Satellite Project activities and outcomes 78—12450
- Aristotle's theory of falling bodies, pre-sixteenth century objections, for teachers 78—62026
- astronomy, Crab Nebula age and distance determ., student exercise 78—12520
- astronomy, education by radio programmes 77—67157
- astronomy, education in India 79—62947
- astronomy, education in US schools, reasons for decline 79—84882
- astronomy, pulsar period, distance and dispersion calc. exercises 77—53725
- astronomy, review of Canadian activities 77—45626
- astronomy, test item file construction and use 78—86054
- astronomy at Florida's Brevard Community College 79—12557
- atomic fluorescences spectroscopy, review of principles, instrumentation, methodologies, appls., teacher education appl. 78—69927
- atomic theory, spontaneous emission and superradiance, coherence effects, semiclassical 77—82347
- auroral science role and physics textbooks contrib. 80—4493
- behavioural objectives, classes of statements 79—92908
- bioengineering education, position in Hungary 79—67127
- biomedical engineering, prod. of practical engineer in developing country 78—28884
- biomedical engineering, professional society emphasis areas 80—27069
- biomedical engineering, Spanish and foreign professional and educative trends *(Spanish)* 79—83964
- biomedical engineering health care role fostered by hospital based student training 77—41433
- biomedical engineering in developing countries, Yugoslavia and Egypt 78—28882
- biomedical engineering in Sweden and other Nordic countries 77—71169
- biomedical engineering programs, accreditation 80—27070
- biomedical engineers, education and certification in Canada 79—80389
- biomedical engineers, W.Germany 78—41106
- biomedical equipment technician certification, status and trends 77—37683
- black hole energy emission, Heisenberg's uncertainty principle 80—105454
- CANDU reactor core, materials and design criteria for fuel, cladding, and fuel channel 78—13238
- career opportunities for physicists, discussion 78—61966
- chemical, paper-pencil inventory for cognitive functioning assessment 79—80386
- chemical bonding in inorganic complexes, quantum mech. ideas development and use 80—12878
- chemical bonding in inorganic complexes, quantum mech. ideas development and use 80—12879
- chemistry, heterogeneous reactions, bimolecular, following Langmuir-Hinshelwood mechanism, rates 79—84907
- chemistry, undergraduate education, future changes 78—69929
- class notetaker, rotating assignment of student 78—81734
- clinical engineer, education to continue his/her career 80—17733
- clinical engineering, cost effective community hospital internships 79—97132
- clinical engineers' acceptability to hospital administrators 77—21640
- CMOS logic, basics 77—78925
- cognitive level and college physics achievement 79—84877
- colour, chemical origins 79—21479
- community college, educational management system 79—35446
- competence concept, operational definition 79—92905
- competency-based programmes, faculty workload formulas 79—48982
- computer-aided ship structural design for diploma and undergraduate courses 79—35494
- computer-assisted learning in the University of Surrey Chemistry Department 79—30167
- computer-based examination system, CMI 79—48983
- computers in educational technology 78—49615
- conservative discrete models, difference eqn. formulation, nonlinear solid, fluid phenomena, computer calc. 77—78924
- corrosion education and role of professional societies *(Japanese)* 77—26105
- crisis question technique 78—81738
- crystallography, conference, International Crystallography Congress, Warsaw, Poland (Aug. 78) 79—23481
- cybernetic methods, pupil learning and teacher activity algorithms 78—49577
- cybernetic principles appl., comparison with other educational methods *(Croatian)* 80—12866
- Czechoslovakia, scientific degree recipients, 1953-1976 78—16619
- damped oscillator motion, expansion in normal modes 80—67951
- de Broglie waves, dispersion relation 80—67949
- dehumanisation, risk involved 79—17155
- demonstration problems, homework assignment for introductory physics course 77—71166
- developing countries and the American science educator 79—2
- developing countries educational broadcasting, case for use of satellites 80—4485
- developing-country university, physics teaching 79—35458
- dynamic electric and magnetic field evolutions, visualisation using computer graphics display 80—46776
- Earth's core discovery 80—105486
- Einstein, character rel. to scientific contributions 80—36828
- electrical and electronic engineering design education and training conference, London, England 80—67971
- electrical and electronic engineering undergraduate courses, engineering design importance 80—67972
- electrical/electronic engineering, conf., Portland, Ore., USA, May, 1977 77—81598
- electron-dipole system, min. dipole moment for binding, historical development 77—78926
- electronics design course curriculum study, overview 80—27063
- electrostatic potential, laboratory and theoretical comparison 80—105461
- elementary particles, individual properties, theory 78—57721
- elementary school science project assessment 77—33730
- energy crisis, exponential growth 78—86049
- energy from nuclear sources, outline for secondary school students 79—80975
- energy option for undergraduates 80—31447
- engineering design, creativity testing 80—27062
- engineering design curricula, computer appls. 80—27065

education continued
- engineering education, importance of research and design for satisfying industrial needs 80—67974
- engineering education, perspective and some current problems 79—10
- engineering project, submarine radiometry and physical environment monitoring 79—12555
- engineering-science summer programme 79—2588
- Euler's three-body problem, eqns. of motion 80—67953
- European computer network, engineering design computer packages, teaching 80—31465
- EUV generation of coherent radiation 79—76758
- evaluation of process-oriented problem solving skills 79—71172
- examination mark adjustment appl. of least-squares estimation 79—80402
- examination marks, reliability, in electronic engineering educational courses 79—75305
- examinations, two-trial system, general physics course 78—49612
- experimental design and statistical analysis of data, measurement of period of simple pendulum 80—42017
- extremum sufficient condition in classical action integral, eigenvalue problem 80—105462
- Fermilab summer programme for minority physics students 78—24594
- Finnish education system, school TV and radio broadcasts *(French)* 79—17171
- fission reactor in-core fuel management educational module 80—36804
- fluorescence spectrometry, anal. appls., historical review 78—93507
- formal reasoning patterns, study using Piagetian tasks, appls. to science education 80—77560
- frontiers in education, conference, Urbana-Champaign (1977) 78—81779
- geology, crystallography course 79—58459
- geology, students' success rel. to spatial abilities, aptitudes, and attitudes 77—5611
- Glasgow University, computer-aided learning project in maths 77—71168
- Government organisation of education in USA 79—1
- grade system improvement 77—53720
- gravitation, should Einstein's or Newton's theory be taught in secondary schools? *(Hungarian)* 79—88780
- gravity, Earth as point mass, conical shell derivation 77—78928
- group problem-solving sessions, in personalised system of instruction courses 78—61954
- hadronic atom strong interaction induced level widths and shifts, WKB calc. 77—78923
- Hagerstown, MD, instructional TV system cost analysis 78—12501
- Heisenberg theory of ferromagnetism, const. coupling approx. 77—78919
- higher education normatives at Jena University Dept. of Physics, planning *(German)* 77—22351
- hospital engineering, conf., Lisbon Portugal (May, June 1978) 79—79667
- hospital engineering education in the USA 79—79668
- hydrology of unsaturated zone, United States educational effort 78—81224
- illustrations for instructional texts 79—48990
- imaginative engineering through education and experience, conference, Williamsburg (1977) 77—71164
- inservice training, in special education 79—48981
- integrated problem sets, generation and reproduction using computer program 79—58479
- interactive computer assistance with calculations arising in undergraduate laboratory experiments 79—35493
- interactive learning, the Millikan Lecture 78, educational uses of computers 79—25785
- International Commission on Physics Education, activities 80—101682
- Japanese photographic education history and status 79—92910
- Kittel, Charles, 1978 Oersted medalist of the AAPT 79—97124
- Kittel, Charles, the conceptual problems of new discoveries 79—97125
- Klopsteg, Paul E, 1978 Oersted Medalist of the AAPT 79—97126
- Landau, L.D., attitudes and advice to students 77—60885
- Lawrence Bragg's advice to a lecturer 79—40314
- lectures, presentation technique 77—53719
- lesson design for computer-based instructional systems 79—35490
- linear algebra, book 78—12532
- LMFBR fuel pin failure monitoring, cumulative mech. damage function from materials data 78—13262
- Lorentz transform law for EM field, fluxoid motion example 80—67954
- lunar tide, semidiurnal, basic physics 80—31449
- Macquarie University lectures, tape recording via dual channel microphone amplifier 79—71210
- magnetic field from charges in arbitary motion 80—105460
- magnetic multipole expansion 80—105456
- malpractice suits problem in instructional technology 79—92907
- mathematics learning, effect of specially constructed advance and post-organisers 79—35452
- mathematics module, description and evaluation 80—86056
- maximization of comprehension, using typographical cueing systems 79—48988
- Medical College Admission Test, 1977, America, physics content evaluation 79—35462
- medical radiological physics education based on nucl. engineering 80—31448
- meteorology, survey of weather forecasting games at American Universities 80—98770
- microscopy, course at North Carolina State University 80—95135
- Millikan, Robert A., contribs. to physics teaching 78—69956
- MIT undergraduate physics students, goals, aspirations and attitudes 80—57022
- models and their use in chemistry teaching 78—86064
- models as a pedagogical tool 78—86065
- models in science, philosophical discussion 78—86108
- molecular excited state relaxation processes, oscillatory versus dissipative limits, education appl. 80—31468
- monkey/hunter problem and possible solutions 79—75306
- monosyllabic word discrimination, classroom acoustics effects 79—53160
- multiple choice examination, entropy state and evaluation of understanding 79—58457
- national science curriculum, impact on content-free cognitive outcomes, in Tasmania 80—77559
- natural philosophy teaching in 1800 A.D., Patrick Copland 78—12452
- natural sciences curriculum evaluation, cognitive preference meas. 80—27060
- natural sciences school curriculum, review *(Hungarian)* 79—71167
- New York Regents examination 78—28875
- New York Regents physics examination, misleading questions 78—28876

education continued
Nigerian local radio strategy, rural communities education 79—40313
nMTCB task analysis of nuclear medicine technology 80—8753
nondestructive testing qualifications, redefinition 79—9048
nonlinear oscillators, turning point approx. and appl. 80—67952
nonmathematical review of gravitational capture 80—26734
nuclear controversy in Canada, educational responsibility 77—37711
nuclear controversy in Europe, future educational plans 77—37712
nuclear educator involvement needs for nucl. controversy 77—37710
nuclear engineering, education facilities and problems in India 77—37680
nuclear engineering education and training with JASON low power reactor 77—41431
nuclear engineering in Japan *(Japanese)* 80—27067
nuclear fuel, solvent extraction and ion exchange learning module 80—36803
nuclear fuel cycle facilities design 80—36801
nuclear in-core fuel management computer system 80—36826
nuclear instrumentation, standard microprocessor based 80—36822
nuclear laboratory instruction with multichannel analyser/microcomputer system 80—31471
nuclear nonproliferation, fuel cycle economics, numerical estimates 80—51982
nuclear radiation detection lab., desk top calculators 80—36821
nuclear reactor fuel management calcs. 78—17298
nuclear reactor safeguards and waste management 80—36802
numerical electronic technique, in physics education 80—46777
objectives selection, four-step process 79—92909
observational astronomy teaching, report on symposium 79—71208
obstetric practice, the place of real-time and static B-mode scanning, educational syllabus 80—86057
oceanography 79—80393
optometry as remediation and education 80—12082
optometry in Nigeria, three year programme 79—25781
optometry opportunities, trends in higher education and health 80—8756
oral examination as follow up to written exam., report 78—61953
pacemaker patient and medical education journal 77—81700
participation rates in high school mathematics and science courses 78—81737
particle in selfgravitating spherical dust shell, adiabatic invariance 80—105459
particle motion in noncentral pot., action-angle formalism 77—78922
peer managed assessment of competencies 79—35443
personalised instruction system, evaluation, unit perfection requirement 78—24592
personalised system of instruction, comparative research, 1967-74 77—13516
personalised system of instruction, for low-enrolment years 78—61955
Physical Sciences Building, Washington State University 79—21499
physical sciences in medicine diploma 80—31444
physical understanding or mindless programming of students? 78—81739
physics, advanced placement examination, multiple choice component validity obs. 78—16596
physics, computer-graded homework for introductory courses 78—12453
physics, decentralisation of research and teaching facilities in Mexico 77—13517
physics, education and employment, situation and prospects 78—61963
physics, history and quasi-history 79—97130
physics, human resources and career opportunities 78—61962
physics and arms race, physicists participation explored for general education students 80—57023
physics careers, employment and education, conf., Pennsylvania, USA (Aug. 1977) 78—62034
physics careers, employment and education, conf., Pennsylvania, USA (Aug. 1977) 79—2591
physics education versus job training 78—61965
physics in Europe, bibliography 79—40341
physics in schools and universities in FRG, student numbers *(German)* 79—40315
Physics Manpower Panel of American Physical Society, employment and education trends 78—65735
physics syllabuses in schools, review 79—62952
physics teaching, recent advances, syllabus, apparatus, demonstration 77—22350
Piaget level correl. with end-of-semester grades, questionnaire and anal. 77—87587
Piagetian criteria as predictors of success in first year courses 77—13529
post-doctoral appointments, tenure and multiple appointments 78—61964
power industry, need for continuing education 77—45633
PSI system for reducing teaching loads in small depts. 78—49575
PWR fuel assembly design, stress, temp., radiation and chem. environment effects on performance 78—13310
PWR pressure vessel safety, term paper from course at Georgia Tech 78—58379
quality control of mandated programmes, model 79—35449
quantal tunneling through a rectangular barrier using $|\psi|^2$ and flux 80—105457
quantum oscillators, matrix element diagrams 80—105455
race, intelligence and education 80—4486
radioactivity, learning in secondary education *(Japanese)* 80—4484
reactor simulators and nuclear power plants, mutual dependency of numbers *(Czech)* 79—35499
reasoning development, influence of studying physics 77—29971
remote sensing/photogrammetry education in USA and Canada 77—74174
residential field centres for environmental education 80—31464
resistive hose instability in relativistic electron beam 80—67947
Rosenstiel School of Marine and Atmospheric Science, University of Miami, review 80—8755
rotation matrix formalism for rots. 77—82349
satellite telecommunications and educational expts. 77—60861
school curricula, science and mathematics development 80—86055
school physics, elementary presentation by theory of heat, thermodynamics, and thermometry *(Danish)* 80—4483
schools specialised in physics and mathematics *(Hungarian)* 80—67956
Schrodinger equation, exactly soluble with bistable pot. 80—67950
science, aims and social implications 79—35457
science, engineering, post-graduate educational system in North America rel. to Muslim graduate student 78—65736
science, role in modern society 79—80392
science anxiety, a course for university entrants 78—77637
science career facilitation project in energy-related fields 78—61959

education continued
science education, computers and intuition 78—81740
science education in Britain, a comparative study 78—28874
science education in Europe at secondary school level 80—22170
science projects, assessment of performance 80—27084
science teaching rel. to Piaget's cognitive psychology 79—58460
scientific, sequential examination processes appl. *(German)* 80—4487
scientific investigation experiment, development of theoretical model 78—86066
Scripps Institution of Oceanography, research projects and education review 78—69464
secondary education, the importance of expts. in physics education 79—71170
semiclassical quantization, Bohr-Sommerfeld quantization rule 77—78930
sixth form physics, proposed core syllabus 79—5934
social effects of microelectronics *(Dutch)* 80—20
sociotechnical systems: the new engineering frontier—a sketch for an engineering school plan 80—31445
solar energy R&D importance for university education and development in Sweden 79—57382
speech training system for deaf children *(Japanese)* 77—86515
spring-mass oscillator, parametric instability 77—78921
structured tutorials to develop students' creative thinking, problem-solving and formulation 79—35451
student and teacher perception of physicist's image 78—62030
student assessment techniques in cognitive domain, taxonomy 79—35444
student attitudes to physics as a subject 77—9833
suggestopaedia, training technique 79—17153
systems approach 79—35450
teacher effectiveness, self-determined change 78—54106
teacher training, using closed circuit television 79—80388
teacher/administrator training, educational computer use 79—35489
teaching at an independent day school in USA, a typical day 80—57045
teaching electromagnetism, to undergraduates, showing practical appls. 78—20922
teaching techniques, discussion methods, summary 79—48984
test-taking techniques, multiple-choice and advanced placement exams. 78—77654
textbook-integrated problem sets 77—67154
Third World, approaches to physics research and education 79—48987
time measurement experiment in phys. education, mass and charge meas. using electronic time counter *(Japanese)* 78—41127
tutorial modules, humanized instructional packages 79—48980
TV educational programmes, problems encountered in Bulgarian People's Republic 79—17170
undergraduate, history of science 80—12864
Universe structure, open and closed curved spaces 78—77652
university engineering education courses economics 80—67973
university entrants, cognitive level by Piagetian tasks 79—4
university lecturer, volunteer, experience in Fiji 78—61961
university physics, educational technology, aims and evaluation 77—33732
university physics curricula, review 79—62953
University physics education, South-East Asian Regional Conf., Penang, Malaysia (May 1977) 78—81732
Universum, Swedish astronomical information project *(Swedish)* 78—86048
USSR, educational TV and radio programme development *(French)* 78—89286
vacuum technology, medium, high and ultrahigh, conf., Oxford, England (Apr. 1978) 79—63242
verbal computation problem-solving, hierarchical struct. of learner abilities rel. to material strength 79—35453
vortex flowmeter for student laboratory use 79—7424
water moderated reactor, 10 W, construction, student project *(German)* 78—33238
work and kinetic energy, automobile min. stopping distance 77—78929
nabla^2 derivation in cylindrical and spherical polar coords. 77—78927

educational administrative data processing
DIAGNOSE, computer-based reporting of student test performance 79—17156
large self-paced courses, automated record keeping 78—12451
qualitative data analysis, networks anal. 80—31721

educational ADP *see educational administrative data processing*

educational aids
see also student laboratory apparatus
ammeter, demonstration apparatus, forces between parallel wires, calibration 77—33757
astronomy, Hubble's law as laboratory exercise 78—65740
astronomy, Ken Mattingly Planetarium 79—84921
atomic line spectra display, push-botton exhibit 77—57127
atomic movements in solids, illustration model for univ. students 77—49531
atomic orbital cross-sections, bonding interactions, spring model, teaching aid 78—93503
audio-visual, for teaching and examination, microprocessor applic. *(Hungarian)* 77—53723
audio-visual aids, synchronising visual to audio material 77—57135
audio-visual learning aids laboratory in teaching of analytical chemistry 80—94944
auscultation, portable clinical electronic device for simultaneous multiple auscultation 77—56507
ball-bearing electric motor construction 80—67997
BASIC interactive image processing for landuse anal., teaching appl. 77—74176
bi-lingual audio-visual aids for technical education in developing Arab countries 80—94943
CAI, audible, use of audio or video recordings 80—42008
calculator, programmable, as physics teaching aid, numerical intergation appl. 78—86083
castor oil dielectric fluid, microwave propag., permittivity effect, demonstration 80—105468
chemical equilibrium teaching, computer method using minimisation of free energy 79—30168
chemical spectroscopy teaching, computer-assisted learning methods 79—84906
chemistry course for artists, art buffs 79—84880
chronology of historical, scientific and technological events 77—41444
classical mechanics, possibilities of zero-g film making 78—12508
closed circuit interactive TV, inservice training 79—48981

educational aids continued

- college astronomy and physics texts, readability 80−77583
- compact solar camera, student project 80−67975
- computer assisted learning in nuclear engineering 77−13557
- computer graphics and electromagnetic fields 77−33781
- computer terminal to audiovisual device interface 80−67986
- computer usage in chemical education, state-of-the-art 80−4488
- computer-assisted-learning agency, staffing needs and position in vertical organisational struct. of educational institution 80−42007
- computer-simulated laboratory experiments, in chemical spectroscopy 79−40339
- crystal model, unit cell construction with polystyrene ball on rods 77−60882
- crystallographic point groups, symmetry, teaching aid 78−77650
- didactic microcomputer *(German)* 79−80396
- digital timer with memory, appl. to dynamics experiments, principles of electronic circuitry 80−67994
- display systems *(Japanese)* 78−20924
- ECG arrhythmia simulator, cct. description 77−73608
- Einstein, Albert, colour film footage 78−62001
- Einstein and Brownian motion, student project 80−68000
- electric current notation, positive and negative charges in electronic devices 78−12494
- elementary particle interactions, review 78−16615
- engineering education, modern methods and instructional media roles 80−27064
- films, utilisation in teaching 77−22354
- Foucault's rotating mirror method for meas. speed of light 80−67996
- fracture, recognition from stereo photographs 78−54140
- generalised mean of two numbers, simple examples 78−16609
- gravitation, as Newton saw it, historical background for teachers 78−4436
- gravitational problems, programmable pocket calculator appl. 78−4438
- hand calculator, appls. 78−12483
- handicapped child communication unit, portable 77−9287
- harmonic force acting on free mass, soln. of differential eqn. and simple analogue computer 78−28893
- Harris data memory, operation and educational uses 80−17779
- hazemeter for window pollution assessment 80−67995
- heliostat design teaching aids and demonstrations 79−62126
- HMO theory, student use, computerised visual aids 78−77649
- holographic beam splitter, optical problems 77−68182
- holographic movie camera and projection system 80−78808
- hospital safety design, probabilistic approach, use of basic n-element configurations for safety education 77−57137
- human retina model for props. of vision 78−77655
- illustrations for instructional texts 79−48990
- information technology, conference, London, England (Nov. 1979) 80−90599
- intra-aortic balloon pump simulator for dynamic demonstration and teaching 77−56537
- IR technology, educational film 77−45658
- Kelvin-Thomson atom, theory for teachers, expt. simulation 78−4439
- landform photograph three-dimensional projection system 77−74181
- lap dissolve projection 79−40333
- least square fitting, pocket calculator program with variable precision 80−67976
- light velocity fibre optic wink-around expt. 80−90628
- line-of-sight transparency for astronomy 79−35508
- Lissajous figures, generation tech. 78−77656
- lung phantom, dynamic, use as educational tool 80−8757
- materials science, use of closed circuit TV as teaching aid 79−71209
- mathematics, heuristic model evaluation, appl. to geometrical problem 79−80385
- mathematics teaching by computer, long-division practice program in BASIC 80−98775
- maximization of comprehension, using typographical cueing systems 79−48988
- mean electrical axis of heart trace on CRT, electronic technique, teaching aid 77−13022
- media effectiveness comparison, video tape, audio tape and printed transcript 79−80403
- microcomputer, educational computing 79−48989
- microcomputer applications in physics teaching, review 79−30171
- microcomputer systems, appls. for chemistry CAI 80−57042
- microcomputer systems, comparative eval. 79−30173
- microcomputer use in high school physics 79−30172
- microcomputer-based multiboard communication system for nonverbal handicapped children 78−57126
- microcomputers in education, hardware, software and personnel problems 80−98771
- microcomputers in schools, software and equipment choice 80−98772
- microneurology, appl. of colour TV as surgery teaching aid 78−40396
- microphone amplifiers, dual channel, for Macquarie University lectures tape recording 79−71210
- Miller Index concept, teaching aids 79−84910
- minicomputer, educational computing 79−48989
- models of dynamical chemical concepts 77−26110
- molecular model of t-RNA, appl. as teaching aid 77−78936
- molecular models based on Petri dishes stereochem. appls. 78−73817
- molecular vibration, model of AB_2 mol. 78−32633
- mud thrown from wheel, critical speed 78−12493
- music practice rooms, user requirements 80−74606
- NDT, US wave visualisation 77−57136
- neurophysiology, electronic model of neuron 78−85301
- Newton, particles and concepts of force, discussion for teachers 78−4437
- Newton's laws of motion, planets and rocket dynamics 78−12509
- Newton's telescope, review of design 78−8187
- nodal slide, experimental and theoretical thick lens parameters comparison 80−67998
- nondestructive testing, scientific film for science and engineering students 79−80395
- nuclear engineering, probabilistic systems reliability analysis for students 77−37698
- nuclear engineering teaching laboratory, development at Ecole Polytechnique 78−4444
- nuclear reactor engineering, undergrad. lab. course 77−37697
- numerical analysis, interactive teaching package 80−86058
- ophthalmological instruments and eye models in teaching, training and education 80−51993
- optical-to-tactile convertor 80−57041

educational aids continued

- oscilloscope trace photography in high school lab. using polaroid camera 77−41443
- overhead projection, transparencies for action effects 79−40330
- PET 2001, multidisciplinary summer course for schoolchildren 80−98774
- photosynthesis, carbon fixation cycle, model, teaching appl. 78−73806
- physics teaching aids, convention of secondary school physics teachers *(Hungarian)* 80−67957
- physics teaching using SWTP 6800 system in BASIC 80−98776
- physics tutoring, personal computer feasibility 79−30174
- planetarium, mobile equipment for Alberta, Canada 79−58508
- planetarium design, model from Mesquite Schools, near Dallas 78−81777
- power station game for physics teaching appl. 79−62949
- programmable calculators for elementary physics teaching 78−12506
- projection plotter system, for classroom demonstrations 79−33
- projector, overhead, adaptor device for horizontal to vertical stage conversion, cradle device 79−58500
- quantum mechanics in films and graphical representations *(German)* 77−49534
- radio transmissions at FM sub-carrier freqs. 79−35488
- radiology teaching, slide console 78−4435
- reactimeter, microprocessor based, nucl. engineering lab. class enhancement 80−36825
- resource letter on environmental noise control 78−61949
- Rutherford scattering formula, small-angle end 78−16608
- satellite broadcasts, use in education in developing countries 80−4485
- satellite transmission, distribution of sound, graphical pictures 80−31463
- scanning electron microscope appl., ISI Model (7) 79−89044
- Schrodinger eqn., harmonic oscillator, numerical soln. 78−8188
- Schrodinger equation, soln. for linear pot. hill 78−12492
- shuttlecock, terminal vel. in vertical fall 80−90627
- slide/tape modules use in teaching SEM 80−68005
- slide/transparency presentation of history of physics in high school course 77−41442
- spark tape anal. and mech. energy expts. 78−81758
- special relativity and Michelson-Morley experiment, history of physics, role in education 80−8759
- speech trainers, with visual display system, systematic use for hard of hearing children *(Japanese)* 79−39596
- speech trainers using visual display system, for hard of hearing children *(Japanese)* 79−39595
- stereographic projection model construction, for cryst. symmetry demonstration 78−86086
- stereoscopic diagrams prepared by desk calculator and plotter 77−37692
- strain gauge data logger, for educational purposes 80−73353
- student experiment, evolution of theoretical models *(Polish)* 80−36819
- student laboratory exercise, simple harmonic motion, to waves 77−60880
- tactile aids and equipment for physical science course for visually impaired students 78−8183
- Tasmania, TV programme storage systems 79−80404
- teaching aids and materials 80−94942
- televised educational programming 79−35485
- television in physics teaching, some suggestions for demonstrations 78−28895
- textbook survey in meteorological education 78−16087
- thermoelectric effects and contact pots., general theory 78−4440
- trajectory model device 80−46759
- TRS-80, teaching at Keene High School 80−98773
- tutored videotape instruction advantages for science and engineering courses 78−8194
- tutorial modules, audio, visual, films 79−48980
- TV appl. in colleges, closed-circuit system preparation and installation *(German)* 78−12521
- TV application to personalised system of instruction model 79−92912
- TV display of diffr. and interference 77−5613
- TV lecturing system using frame multiplexing technique 78−28887
- TV microscopy system for teaching and quality control 80−82817
- ultrasound propagation in liqs., undergraduate expt. 80−69608
- university engineering course, first semester subjects and projects *(French)* 80−27066
- University of Lowell Reactor utilisation 79−9857
- unsteady flow in open channels, num. analysis method, teaching aid paper 77−29972
- video applications in education 79−35491
- video recorders *(German)* 78−69954
- video studio, in-lab, of modest cost and mobile 77−67165
- video tapes in SEM teaching, evaluation 80−68004
- video technology uses in college of education 79−92913
- videotape instruction in physics, low-cost systems 79−29
- visual speech vocoder as teaching aid for deaf 78−36069
- wattmeter, static, for use in educational establishments 78−45656
- weather forecasting games at American Universities, survey 80−98770
- X-ray crystallographic computations for students using programmable calculator 80−36811
- zero-gravity environment, possible expts. for films 78−12507
- Zimdex audio indexing system, efficiency 79−92915

educational computing

see also computer-aided instruction; educational administrative data processing

- astronomy, use of computers in schools 80−73126
- calculator, programmable, as physics teaching aid, numerical integration appl. 78−86083
- data manipulation and handling, for teachers 80−4489
- instrument simulator, design and use 80−4490
- Kirchoff's laws of spectral analysis, computer laboratory exercises 78−73790
- luminescence decay time evaluation, computer programs, student expts. 77−26115
- microcomputers in education, hardware, software and personnel problems 80−98771
- molecular electronic structure theory, computer program for graduate instruction 77−78937
- nuclear instrumentation, computer-based data acquisition system for multi-station teaching laboratory 78−4446
- orbital motion on an interactive-graphics terminal 80−73152
- physics, computer-graded homework for introductory courses 78−12453
- physics laboratory experiments, graphic computer simulations 80−105470
- science education, computers and intuition 78−81740

educational computing continued
stratospheric photochemistry, computer simulation 79—21481
student appraisal system, computer automated sign-on, item anal. 80—62430
teacher training with computers 77—33734
test generation program design for astronomy courses 80—90622
test scoring system, micro-computer based 78—81757
unit teaching improved using the computer 77—53721

educational courses
advanced laboratory-research course for nonphysicists 79—25792
advanced student lab. course simulating research conditions, heuristic 77—87591
advanced undergraduate physics laboratory, industrial research roleplaying 78—36755
Age of Newton workshops in optics, mechanics and mathematics 77—87586
alkali metals, cohesive energy 80—90630
applied science CNAA degree course at Kingston Polytechnic 79—35454
approximation methods for 80—105474
architects, physics course description 79—25779
arts, rel. to physics of sound and light 77—22340
astronomy, university courses and career prospects 78—69931
astronomy examination, two-part scheme for varying mathematical abilities 79—71169
astronomy liberal studies course 79—71171
astronomy-astrophysics, courses, new approaches 79—3
astrophotography, exptl. summer course 77—64902
bioengineering curriculum enhancement through collaboration in rehabilitation medicine 77—81596
biological instrumentation, physical principles 78—40436
biomedical electronics, BSc level option, Lanchester Polytechnic, England 79—17158
biomedical engineering, France 78—73807
biomedical engineering, training experience at Ecole National Superieure des Telecommunications *(French)* 77—40817
biomedical engineering for physicians, at Federal Institute of Technology, W.Germany, doctor degree *(German)* 78—3627
biomedical engineering undergraduate degree program, state university approach 78—77646
biomedical engineering undergraduate programmes in USA, career prospects 78—28877
biomedical engineers and technicians in developing countries, training 80—62408
career oriented physics for the nonscience major 79—71168
chemical laboratory course, for intellectual skills development 79—21484
chemistry course for artists, art buffs 79—84880
chemistry teaching, courses, laboratories, for nonscientists, bibliography, 1968-1977 79—84881
clinical engineering, advantages of cooperative education between hospital and college 78—28879
clinical engineering internship at Ohio State University 77—41432
clinical engineering introductory course 78—28880
clinical engineering practicum, laboratory course 78—28878
computer interfacing, with laboratory expts., undergraduate course 77—13524
computer physics, elementary concentrated one-week course 78—73799
computerised test generation program design for astronomy courses 80—90622
cooperative education programs in Omaha Public Power District 78—4429
course development by team, human factors 78—49580
cross-disciplinary, physics, history and society 77—33726
crystallography education, a survey in the USA 79—9047
electrical safety, one-day seminar for nurses 77—37701
electronics, undergraduate laboratory course 80—105478
electronics laboratory course, for the non-physics specialists 79—71197
electronics unit for physics students, systems analysis approach 77—45625
electrooptics for electrical engineers, undergraduate curriculum 79—11
elementary particles, introductory course for liberal arts students 79—25780
energy overview course for general audiences 77—37681
energy projects, undergraduate physics 77—13530
engineering, for professional engineers, economic costs and course contents considerations 79—80414
engineering and physical science careers advisory program 78—69932
engineering education, modern methods and instructional media roles 80—27064
engineering electronics: An alternative degree program for departments of physics 79—9046
engineering physics, role and education 77—5610
environmental science and engineering interdisciplinary curriculum, faculty requirements 79—12553
environmental sciences, curricula for undergraduate courses 78—77644
European science study tour 77—33725
fibre optical communications, course status and effectiveness 80—62413
flexible, inquiry-based physical science course for education students 77—33727
fluid mechanics and heat transfer computer-assisted learning source for final year B.Sc. students 77—60877
forced pacing method of instruction calculus-based freshman physics course 78—61951
forensic science, for criminal justice students 79—48986
fusion design team, undergraduate education 78—58469
geophysics, applied MSc programme in Nigeria 80—105463
geophysics, for physics students 77—67155
graduate laboratory teaching assistant course 78—41105
health care deliverty data processing course 79—80394
health physics, Faculty Institute in Applied Health Phys. at Oak Ridge National Lab. 78—49581
health physics technicians, uniform approach for on-site training and qualification 77—64900
Hi-Fi sound reproduction fundamentals physics course 77—33733
high school science course for academically unsuccessful students 77—71170
history and physics, educational course 77—41429
history of physics in high school course, slide/transparency presentation 77—41442
history of science and technology in Polish higher education 78—32638
Illinois, staffing of new courses 77—22341

educational courses continued
Illinois staffing norms 77—22342
individualised laboratory system 78—36760
industrial hygiene training at Quinnipiac College, USA 79—84879
industrial internship programme in nuclear engineering education 78—4432
instructional evaluation by students, appl. in teaching diagnosis, improvement 79—35448
instrumentation in undergraduate engineering curriculum 78—8206
instruments in advanced physics, a final year undergraduate course 79—21486
integrated optics graduate survey course at Georgia Inst. of Technology 80—62414
interdisciplinary, physics, energy and environmental technology 78—61958
interdisciplineary general education science course 77—78908
introductory biophysics, personalised system of instruction course 79—5929
introductory physics, core plus branch struct., self selection 78—61950
introductory physics courses, college students' cognitive level 79—84900
introductory physics for non-science students, term projects 77—33729
introductory physics for nonscience students, comparison of concrete versus formal instruction 77—87588
introductory university physics, using small group approach 79—97127
Jamaican solar energy training seminar programme 79—57395
Keller plan course improvement 77—49518
laboratory course, individualized, first year undergraduate 79—21489
large self-paced courses, automated record keeping 78—12451
liberal arts physics course in holography 78—73798
liberal arts technology, history 78—86061
liberal arts-engineering courses, interaction with a physics dept. 77—64898
lifelong learning adapted to adults, principles and practice, University of Mid-America 79—12
localised interference fringes 80—101680
lower division physics, multiple level lecture series 78—61952
macromolecular solns., educational courses, integration with phys. chem. 78—77642
marine science courses evaluation 78—53657
master's level graduate training in medical physics at the Univeristy of Colarado Health Sciences Center 80—82603
mathematical education development, M.Sc. course, for teachers 79—80384
mathematical methods, for mixed-discipline undergraduate classes 79—80382
mathematical physics, personalised system of instruction course, problems in developing country 79—5930
mathematics, remedial work for university students in engineering courses 80—86054
mathematics, self-study programme with unusual topics, for undergraduates 79—80383
mathematics courses, effect of class evaluation method on learning 78—57719
mathematics for engineering students, student and teacher perceptions of degree of difficulty 78—57712
measurement oriented basic physics laboratory 79—25790
measurement theory, for student physics labs., university level 78—24601
medical instrumentation, using guided design format 78—28881
medical physics, four year baccalaureate course (undergraduate) 78—54107
Mendeleev law student laboratory exercise 77—26112
Modern Optics Project Laboratory course at MIT, programme 80—62421
molecular biophysics, protein crystallography, interdisciplinary course 77—33720
molecular electronic structure theory, computer program for graduate instruction 77—78937
M.Sc. theses, for pedagogical direction of studies *(Polish)* 78—73808
musical acoustics, role of demonstrations, source material 78—49576
musical acoustics, room reverberation time meas. 80—42000
musical acoustics, teaching of blind students 80—77584
musical acoustics for the musician 79—71205
nomograms role is physics undergrad. courses 77—49519
nonscience majors, innovative course based on mass-radius diagram of states of matter 78—62002
nonscience majors, professionally oriented astronomy laboratory course 80—51981
nonscience students, one-semester broad coverage course 78—36751
nuclear criticality safety workshop for graduate students 77—37699
nuclear energy peaceful uses, high school curriculum in Japan 77—37682
nuclear engineering, cooperative utility programs at North Carolina State University 78—4430
nuclear engineering, graduate cooperative program with industry, experience over 3 years 78—4434
nuclear engineering, teaching laboratory for expansion of student knowledge horizons 78—4445
nuclear engineering, teaching project management as part of international technology transfer 78—4428
nuclear engineering, training of existing staff for new nuclear units at university 78—4431
nuclear engineering, undergraduate cooperative industrial program at Cincinnati University 78—4433
nuclear engineering computer instrumentation, laboratory instructional programs 80—31472
nuclear engineering course, incorporation of commercial reactor codes 78—4448
nuclear engineering design, one term vs. one year projects 77—45632
nuclear engineering design at Idaho State Univ. 77—45631
nuclear engineering design course at Ohio State Univ. 77—45630
nuclear engineering design curriculum at Univ. of Illinois 77—45628
nuclear engineering design education of Mississippi State Univ. 77—45629
nuclear engineering programme, eval. for accreditation, design component role 77—41430
nuclear fuel cycle education module on nuclear criticality safety 80—36798
nuclear fuel cycle management, interdisciplinary approach in education and research activities 77—38433
nuclear fuel design module 80—36800
nuclear fuel management analysis core, computer code for teaching assistance 78—4449

educational courses continued
nuclear instrumentation, computer-based data acquisition system for multi-station teaching laboratory 78—4446
nuclear instrumentation laboratory course, computer based data acquisition and anal. 80—36820
nuclear laboratory course at Purdue University 78—4443
nuclear physics course, computer simulation techniques 80—36823
nuclear reactor engineering, undergrad. lab. course 77—37697
nuclear reactor safety, nucl. engineering programme at UCLA 78—58377
nuclear reactor safety education at Northwestern Univ. 78—58376
nuclear reactor safety educational programme at Purdue 78—58380
nuclear reactor safety instructional programs at RPI, LWR and FBR appl. 78—58375
nuclear reactor safety teaching, MIT nucl. engineering dept. courses, USA 78—58378
nuclear science, undergraduate teaching, courses, facilities 80—27086
optical design education program, desktop computer appl. 79—84922
optical engineering education at Carnegie-Mellon University, programmes review 80—62419
optical radiation detector laboratory, graduate-level, expts. 80—62432
optics, graduate training at Optical Sciences Centre, programmes 80—62418
optics and lasers, San Diego State University, programme 80—62423
optics at Texas Tech. University, programme methods 80—62424
optics education, graduate, at Air Force Inst. of Technology, programme 80—62417
optics education at Georgia Tech, development and current status overview 80—62420
optics graduate degree programme, on-site, case study 80—62416
optics laboratory, undergraduate, in American universities, status 80—62411
optics programmes and opportunities in US 80—62412
optics programmes in US, attacks and recommendations 80—62409
optics teaching by faculty of Inst. of Optics, profile 80—62422
optics technology programmes in US, development 80—62410
optometry, future of public and community health 80—12084
optometry, interdisciplinary course with vision training specialisation 79—40311
organic chemistry for master's degree, Keller method 79—58461
origin of life, molecular evolution and exobiology, interdisciplinary course 79—21485
personalised system of instruction, for low-enrolment years 78—61955
photography, course for fine arts students 77—33731
photointerpretation and photogrammetry teaching in natural resources field 77—74175
physical chemistry teaching, macromol. principles 78—77643
physical science, undergraduate major course, broadening 78—61960
physical science course for visually impaired students 78—8183
physical sciences, integrated applied programmes 80—41977
physical sciences at Lanchester Polytechnic 79—44658
physical theory in biology 79—58462
physics, A-level, computer managed independent learning 79—62948
physics, computer-graded homework for introductory courses 78—12453
physics, factors influencing New York State secondary school enrollment figures 78—24595
physics, for non-science students, rel. to history and arts 77—71165
physics, future changes, discussion 78—61956
physics, joint honours degree course at Manchester University 79—35456
physics, medical education, premed requirements 79—58458
physics, middle school course curriculum development 77—57115
physics, philosophical approaches 78—81791
physics, Piaget-type questionnaire assessment 78—81731
physics, self-paced introductory course at Cornell Univ., 8-year progress report 78—16597
physics, self-paced learning, testing of mastery concept 77—64899
physics, teacher effectiveness, self-determined change 78—54106
physics, two-trial examination system, results 77—67156
physics 13: teaching modern physics through science fiction 80—90626
physics and chemistry in archaeology, nonscience undergraduate course 77—26104
physics and engineering at Loughborough University of Technology 79—35455
physics and society for nonscience undergraduates, course description 79—97128
physics career-oriented pretechnical minicourse project, Dallas highschools, evaluation 78—24590
physics curricula design and development 79—97131
physics curriculum, theory 79—97129
physics for journalism 78—36754
physics for liberal arts majors, Piagetian styled process-based course 78—73800
physics for non-science students, enrolments of Southern Illinois University 77—49517
physics independent study, high school course 77—49520
physics minicourses 77—33723
physics Ph.D., industrial training option 78—61957
physics success rate, rel. to math. skills, testing 77—60860
physics teaching curriculum development, systems approach *(French)* 77—9834
physics with application to police science, US university course 77—45627
physics-chemistry project for Danish Folk School, Ask-nature project 78—8184
practical physics course for undergraduates 77—9836
PSI, objectivity in reporting 77—78909
PSI, review of courses reported 77—78907
PSI at Tuskegee Institute 77—33728
PSI introductory physics, comparison with lecture-discussion method, long range effects 78—49574
pulmonary function testing, training course features 78—24169
quantum mechanics, PSI, with optional lectures, on videocassettes 77—64951
radiation and the environment, undergraduate course evaluation 78—1
radiation health physics, graduate educational program to prepare science majors for career 78—4427
remedial physics course, for engineering and science students, Piaget theory 77—74173
remote sensing, individualised short course 77—74182
resources and costs, optimisation 77—33724
sandwich course merits 79—92911

educational courses continued
science anxiety, a course for university entrants 78—77637
science in society, a 6th form course 79—17161
scientific method illustrated by paraphysical and neuroscience topics 78—24591
scientific revolutions, Einstein and Lorentz examples 80—82594
secondary-school students, talented, university summer science course 78—89282
self-paced freshman physics laboratory and student assessment 80—51989
self-teaching laboratory course, first year undergraduates, inception, use and evaluation 78—4442
SEM coordinated, multidiscipline courses 80—67965
solar eclipse predictions using vector method for intermediate level astronomy courses 80—105452
solar energy concepts, in chem. teaching 78—73805
solid surfaces, surface processes, and solid/gas interactions 80—73125
sound, sixth form physics course 79—62973
special relativity, teaching module 79—21483
special relativity for general students 78—73791
spectroscopy quantum chem. teaching, fluctuating elec. dipoles, light absorpt. 78—73802
statistics courses classification 77—29970
student experiment design, course for high school teachers 78—36752
students in electronics and physics, examination, reliability 77—26103
Tao of Physics, course in modern physics and Eastern mystical philosophy 80—17730
tutored videotape instruction advantages for science and engineering courses 78—8194
underdevelopment of a course 79—35445
undergraduate engineering education, physics requirements 79—44656
undergraduate preparation for career in physical oceanography 79—12554
university engineering course, first semester subjects and projects *(French)* 80—27066
vacuum science and technology, undergraduate and post-experience courses 79—62954
wind energy as alternative energy source, energy science course material 78—61973
X-ray science, survey of former students of Oregon State University 79—9
Yugoslav university training of biomedical engineers 79—35442
^{11}B, NMR, for senior level inorganic courses 78—4424
U, nature and exploration in US sandstone deposits 80—36799

e.e.g. *see electroencephalography*

effective mass (band structure)
alkali metals, density of states effective masses, liq. and solid phases, model pseudopot. calc. 77—76738
anthracene, cryst., cyclotron reson. and carrier scatt. 77—76746
conduction and valence band effective mass parameters 79—60689
crystals, dipole-impurities, free-carrier absorpt. and dielec. losses calc. 77—63363
cubic semiconductor, Zeeman split acceptor levels, calc. method 79—28322
p-CuInTe$_2$, single cryst., IR study of lattice and free carrier effects 80—45074
cyclotron resonance meas., electron effective mass localised above liq. ^{4}He surface *(Russian)* 77—11756
D$^-$-state in semiconductors *(Japanese)* 77—85178
de Haas-van Alphen effect, FFT anal. 79—42434
diamagnetic band structure, second order calc. using Landau functions, cyclotron mass determ. 80—24784
diamond, natural, electron effective mass and lattice scatt., Monte Carlo anal. 80—44484
diamond, natural, lattice scattering and effective mass of holes 79—60842
diamond, semicond., energy band struct., elec. and optical props., review 77—35862
diamond, semiconducting, electron-hole liquid formation conditions and parameters 79—78013
dilute alloy, mag. ordering rel. to effective mass on Fermi surface 77—20550
dilute alloys, mag. impurity ordering 77—28370
electron effective mass calc. by pseudopot. theory, self-consistency 79—77990
electron specific heat and effective mass, temp. depend. *(Russian)* 78—59958
electron tunnelling, two band calcs., Gamow formula applications 80—54665
electron-hole plasma current layering, electron cooling length, momentum scatt. 80—6890
electrons in helical mag. fields, quantum theory 79—80470
elemental semiconductor, polarisability of donors 78—14693
exchange interactions in semiconductors and insulators, mean free path and energy gap effects 80—88522
exciton motion depend. on lattice vibr., inner potential energy, ground state, effective mass *(Chinese)* 80—54610
ferroelectricity, vibronic theory, developments 79—33620
ferromagnetic metal, freq. depend. elec. cond. 77—66181
films, semicond. and insulator, effective electron mass determ. 77—1506
gapless semiconductors, screening effects on electron-electron interaction 80—49647
graphite, neutron irradiated, effect on quantum limit Shubnikov-de Haas oscills. 78—95304
graphite acceptor intercalation cpds., C$_n$Br and C$_n$NO$_3$H, electronic struct., quantum-magnetothermal oscills. 80—44478
graphite intercalated with AsF$_5$, quantum oscillatory phenomena 80 -107823
graphite intercalation compounds, a-axis conductivity model 78—10435
graphite intercalation cpds., K-point effective masses and Fermi level shifts, magnetorefl. study 80—50305
graphite surface, adsorbed He, band struct. and thermodynamic props. 80—80349
Hall effect coeffs., linearised Boltzman eqn. solved 79—1595
heavily doped semiconductor, activity coeffs., for electrons with small effective mass 77—39837
II-VI compounds, doubly ionisable centre binding energy 79—65405
III-V semiconductors, k.p perturbation theory 77—43484
III-V semiconductors, sphaleritic structure. relation with forbidden bandwidth and lattice constant *(Slovak)* 78—51879

effective mass continued
impact ionisation thresholds, as generalisation of van Hove singularities 77—77295
inert gas solid, electronic struct. of self-trapped excitons 79—19525
inert gas solids, exciton states, nonstructural theory using effective mass approx. 78—84147
inert gases, solid, electronic excitations, nonstructural theory 78—79942
insulator-metal transition, electron-phonon interaction, electronic transport props. 77—89702
insulators, improved effective mass for impurity levels 78—87941
interface effect on effective mass approximation 78—64082
inversion layers, carrier effective mass, contribs. of electron-electron and electron-phonon interactions 78—64087
many-valley semiconductor, dispersive screening and Bloch function interference, large binding 79—51525
many-valley semiconductor, effective mass theory of intervalley mixing 77—47763
many-valley semiconductor, electronic structure of D^- ion 79—95369
many-valley semiconductors, space charge, contrib. of different charge carriers *(French)* 80—34458
metal, EM generation of ultrasound in static mag. field 78—14768
metal, work function, pseudopot. calc. 80—96970
MOS structure, 2D electron gas, for IR Faraday rotation 80—80389
MOSFET, ionic scatt. effect on Shubnikov-de Haas amplitudes in Si inversion layers 79—42653
multivalley semiconductor, rel. to donor binding energies, variational calc. 78—23041
narrow band gap semiconductor, electron-phonon interaction, effective mass of carriers determ. 79—11058
narrow band semiconductor, transport phenomena electron energy spectrum *(Russian)* 79—51616
negative effective mass carrier contribution to EMF, sign *(Russian)* 78—26886
neutral bound excitons, accurate binding energies, variational method calc. 80—107715
nonradiative transitions at impurity centre with participation of short-wavelength phonons 80—16099
piezopolarons and condensons, temp. and screening effects on effective mass 77—43521
plasmon refl., 86 to 320K 80—50346
polar crystal, Frenkel exciton effective mass temp. depend., lattice displacement interactions *(Chinese)* 80—84429
polar crystal, polaron effective mass temp. depend., electron interaction *(Chinese)* 80—84436
polar semiconductors, chemical shift of Zeeman masses 78—10338
polar semiconductors, hot exciton scatt. accompanied by transitions to excited states, phonon interactions 80—44516
polar semiconductors, peak electron velocity, simple method for estimation 77—8129
polaron model, Froelich Hamiltonian, perturbation theory calcs. 79—33247
polarons, effective mass and optical absorpt. spectrum, f-sum rule 77—43520
polarons, Feynman effective mass, Frohlich model, path integral method 79—69440
polymer, fragment method, nonempirical, electronic struct. determ. 77—89684
polyquinoline carboxylic acid film, effective electron mass determ. from IV characts. 77—85135
polytypes, one-dimens. Kronig-Penney model and calcs. 80—75494
pyrolytic graphite, magnetoresistance positive-negative transition *(Russian)* 80—96923
rare earth metal, effective-mass anal. carrier spectrum gap anisotropy 79—69494
rare-earth, light-heavy alloys, resistivity, mag. contrib. to resist. and Neel temp. 78—51971
semiconductor, acceptor binding energies 77—69270
semiconductor, bound exciton recombination, phonon replicas 79—38649
semiconductor, carrier relax. time and effective masses determ. by microwave photocond. meas. *(Russian)* 78—19071
semiconductor, core excitons, binding energy in effective mass approx. 80—24808
semiconductor, elec. cond., hopping model, semi-classical, effective mass and carrier mobility calc. 80—96872
semiconductor, light pulse propag. inducing transitions between bands with different effective masses 80—34871
semiconductor, multiband calcs. by pseudopot. method 77—51644
semiconductor, shallow impurity levels, effective mass approx. 80—6781
semiconductor, shielding by electron gas in magnetic field 80—107727
semiconductor, surface state excitons 77—51799
semiconductor, tetrahedral, bond orbital model on CNDO basis 77—47720
semiconductor, uniaxially stressed, zincblende struct., band edge Landau levels using effective mass Hamiltonian 79—60706
semiconductor, zincblende-type, valence band effective mass strain depend. 78—51880
semiconductor film, size-quantised with tilted valleys, two-photon absorpt. 79—95869
semiconductor in mag. and US fields *(Russian)* 77—62801
semiconductor solid solution, compositional disorder, free carrier absorpt. 78—64387
semiconductor superlattice, transverse electron effective mass 80—100429
semiconductor-insulator boundaries, impurity electron states near interface 78—95320
semiconductor-insulator interface, effective-mass approx. 79—99629
semiconductors, binding energies of core excitons, effective mass approx. 79—73439
semiconductors, ferromagnetic multivalley anisotropic, electron autolocalisation *(Russian)* 80—92848
semiconductors, graded mixed, effective mass theory for carriers, spin effects 77—85208
semiconductors, non-parabolic, average energy of conducting electrons 77—55521
Shubnikov-de Haas quasi-periodic oscill. curves, harmonic analysis, computer method *(Russian)* 78—39132
Si:Sb(P)(As), shallow donor states with strong central cell perturbation theory 78—51933
Si-SiO_2 double barriers, reson. tunnelling, effective mass of tunnelling electron determ. 77—80846
singularities of the small polaron effective mass 78—63989
superconductor, effect of varying electronic density of states 80—75672

effective mass continued
superlattice semiconductor impurity photoconductivity electron spectrum reconstruction 80—24966
transition metals, 4d, electron-phonon mass enhancement and supercond. 77—62811
tunnelling MIS structures photovoltaic energy conversion, band struct. 80—92995
two dimensional electron spectrum spin splitting, specified by surface potential *(Russian)* 80—15583
two-dimensional electron gas, electron-phonon interaction and cyclotron reson. 80—25014
two-dimensional surface layer, ground state energy and effective mass of polaron 79—23910
two-polaron bound state, strong and weak coupling approx. 78—39039
two-valley semiconductor, hot electron instability, intervalley scatt. *(Russian)* 80—92921
Wannier-Mott exciton decay, on acoustic phonons, in thin semicond. wire *(Russian)* 78—72075
wurtzite-type crystals, deform. effects on biexcitons, Bir-Pikus Hamiltonian 77—52038
zinc blende structure semiconductors, cyclotron reson. *(German)** 78—10337
Al, anisotropic Fermi vel., surface Landau level reson. 78—10333
Al, quasi-particle properties, anisotropic, electron-phonon interaction study 77—43480
Al_2O_3 film, effective electron mass determ. from current-voltage characts. in thermionic region 77—85135
As, interband, magnetorefl. for circularly polarised radiation 78—2840
Au film, rel. to microwave skin effect in mag. field up to 40 kOe 77—12032
Au-SiO_2-Si system, oxide film 16-36 Å thick, tunnel currents 80—70842
Be, spin susceptibility, electronic effective mass, spin density functional calcs. 78—43291
Bi film, rel. to microwave skin effect in mag. field up to 40 kOE 77—12032
Bi:Sn(Pb), carrier dispersion law, hole cyclotron masses rel. to Fermi surface vol. 77—20345
Bi-Sb, semiconduct., e.m. wave propag. perpendicular to mag. field 79—82517
n-BiSb, cyclotron mass meas., high hydrostatic press. 79—77991
$Bi_{1-x}Sb_x$, far IR magnetoabsorption, band struct. study 80—50351
$(Bi_{0.25}Sb_{0.75})_2Te_3$, opt. props. of bulk and films 78—27206
$(Bi_{1-x}Sb_x)_2Te_3$, highest valence band struct., Shubnikov-de Haas effect 78—14661
$Bi_{2-x}Sb_xTe_{3-y}Se_y$ solid solution, density-of-states effective mass, carrier mobility temp. depend. 80—24931
n-Bi_2Se_3, nonparabolicity of cond. band and anisotropy of electron effective mass 79—60692
BiTeI, layered cryst., rel. to anisotropy and temp. depend. of mag. susceptibility 79—73673
$Bi_2Te_{3-x}Se_x$ solid solution, Hall effect anisotropy parameter, thermoelectric power, depend. on carrier density 79—69536
Cd, de Haas-van Alphen effect and mag. breakdown *(Russian)* 77—80722
Cd, Fermi surface, 3rd band sheet, electron effective mass and relaxation time 79—11056
Cd_3As_2, band struct. from Shubnikov-de Haas and de Haas-van Alphen effects 80—49597
Cd_3As_2, band structure, Kane model, magneto-Seebeck and Hall data 77—62821
Cd_3As_2, electron effective mass. temp. depend., Hall effect and thermoelec. power meas. 80—39613
Cd_3As_2, electronic g-factor, effective mass and density of states 79—60691
Cd_3As_2, low-temp. energy band struct. and depend. of direct gap on press. and temp. 77—62822
$Cd_xHg_{1-x}Se$, derived from elec. props., 77-400K *(Russian)* 78—2485
n-$Cd_xHg_{1-x}Te$, conduction band struct., IR refl. spectra obs. 80—39502
$Cd_xHg_{1-x}Te$ epitaxial graded gap layers, plasma reflection and magnetoreflection 80—71391
$Cd_xHg_{1-x}Te$, Fermi level calc., temp. depend. of heavy-hole effective mass 77—55481
$Cd_xHg_{1-x}Te$, graded gap epitaxial layers, elec. and photoelec. props. 77—85362
$Cd_xHg_{1-x}Te$ layers, epitaxial graded-gap, nonlinear elec. effects 80—100468
n-$Cd_xHg_{1-x}Te$, thermal EMF, in transverse quantised EM field *(Russian)* 79—23993
$Cd_xHg_{1-x}Te$, x=0, x=1, effective mass of heavy holes, 4.2 to 300K 77—1353
CdS, average B band hole mass calc., exciton energy levels 79—51494
CdS, magneto-optical effects in field up to 200 T 77—52059
n-CdS, polaron effective mass, DC Hall effect meas. 78—39037
p-CdSb, elec. props. at low temp. 77—62866
p-$CdSnAs_2$, Hall effect, thermo EMF, thermomagnetic effects 80—107822
p-$CdSnAs_2$, heavily doped, elec. transport props. under elastic deformation 80—96915
n-$CdSnAs_2$, optical absorption rel. to energy spectra *(Russian)* 78—75994
n-$CdSnP_2$, Hall coeff. and elec. cond. meas., 24-900K 80—54721
CdTe:Li(Cl), acceptor states study by donar acceptor pair excitation luminesc. 80—100683
CdTe-HgTe superlattice on CdTE layers, evanescent states, tight binding calcs. 80—70611
$Ce_{3-x}S_4$, $Ce_{3-x}Sm_xS_4$, elec. cond. mechanism, thermoelec. power, Hall and absorpt. coeffs. 77—24559
Co, de Haas van Alphen oscill., effective mass 78—87900
$Co_{1-x}Ni_xSi$, IR refl. spectra in plasma refl. region 78—27233
CoS_2, galvanomagnetic effect of single cryst. 80—96912
CoSi, IR refl. spectra in plasma refl. region 78—27233
$Cr_{1-x}Mn_xSi_7$, semicond. props. 78—79992
$CrSi_2$, semicond. props. 78—79992
Cr_3Si, specific heat at low temps., electron density of states, Debye temp. *(Russian)* 80—54398
Cs, Fermi surface, de Haas-van Alphen meas. 78—2411
Cu (111) surface, high resolution photoemission spectra 79—52082
Cu, cyclotron masses using tetrahedron method 79—90946
Cu, energy band dispersions and lifetimes using angle-resolved photoemission 79—77998

effective mass continued
  Cu, Fermi surface, electron mass enhancement, orthornormal function enhancement 80—96777
  CuCl, energy bands and effective mass 80—10859
  CuCl, exciton spatial dispersion determ., two-photon Raman scatt. via excitonic mol. state 80—60595
  CuCl, exciton spectra, extended effective mass theory 79—69424
  n-$CuInSe_3$, from IR free carrier Faraday rot. meas. 77—55783
  $Cu_2Mo_6S_8$, normal state and superconducting property measurements 78—91660
  Cu_2O, exciton spectra, extended effective mass theory 79—69423
  Cu_2O:Fe, impurity scatt. effect on cyclotron reson. 79—56614
  $Cu_{2-\delta}(S+Se)$ solid soln., deviation from stoichiometry, effective hole mass 77—31775
  $Cu_{2-x}Se$, elec. props. and band struct. 79—73513
  Cu(111) surface 77—62979
  EuSe, annealed, AC conductivity and dielectric anomaly 80—34445
  EuSe, polarisability of shallow donors, permittivity meas. 80—24833
  $Ga_xAl_{1-x}As_x$ photodetector diode on GaAs substrate dark currents, tunnelling, energy gaps, effective masses 80—70805
  n-$Ga_{1-x}Al_xSb$, transport phenomena in low and high mag. fields 78—80007
  GaAs, conduction band effective mass, influence of high uniaxial stress 80—80162
  n-GaAs, conduction band nonparabolicity and coupled plasmon-phonon modes, IR refl. spectra 80—55110
  GaAs, effective mass, Raman spectrum determ. 80—24797
  GaAs, electron effective mass, temp. depend. for various degrees of doping and compensation *(Russian)* 78—79923
  GaAs, heavily doped, electron effective mass, Kane equation calcs. 79—77989
  GaAs, hole effective mass, press. depend., theory and tunnelling expts. 78—75986
  GaAs, interband tunnel current, influence of press. 77—76910
  GaAs, lower cond. band struct. 78—6271
  GaAs, Schottky barrier diodes, strain sensitivity mechanism 79—38165
  GaAs:C, Zeeman effect of effective mass acceptor, polarised luminesc. 79—4541
  GaAs:Cr, electroabsorption spectra obs., reduced effective mass determ. 80—50301
  GaAs-$Al_xGa_{1-x}As$ differentially doped heterojunction interface, two-dimens. electron gas obs. 80—49886
  GaAs-$Al_xGa_{1-x}As$ heterojunction interface, two-dimensional hole gas obs., Shubnikov-de Haas meas. 80—80357
  GaAs-$Ga_{1-x}Al_xAs$ heterostructures, quantum size effect in superlattices, electronic props. 80—29471
  GaAs-$Ge_{1-x}(GaAs)_X$ n-p heterojunctions, hydrostatic press. effect on elect. and photoelectric props. 80—20304
  $Ga_{0.47}In_{0.53}As$, LPE growth and characterisation 80—10845
  $Ga_xIn_{1-x}As_yP_{1-x}$, epitaxial layers on InP, expt. determ. of effective masses 79—65370
  $Ga_xIn_{1-x}As_yP_{1-y}$, electron effective mass, cyclotron reson. and magnetophonon effect meas. 80—103618
  $Ga_{1-x}In_xP_{1-y}As_y$, electron transient drift vel., influence of effective mass and alloy scatt. 80—2384
  GaP, density of states effective mass and cond. band energy minima 77—28101
  GaP, effective mass anisotropy at X_{1c} and X_{3c} minima of conduction band, optical absorpt. spectra 77—8021
  GaP, influence of shear deform. on interband interaction 78—39116
  GaP, polar semicond., radiative recomb., electron-phonon interaction effects, calc. 80—49631
  n-GaP, uniaxially deformed, piezoresist. exam. of donor levels 77—4346
  n-GaSb, Shubnikov-de Haas effect, effective mass, Dingle temp., and g-factor 79—51602
  GaSe, layer, upper valence bands using bond-orbital model 79—15078
  p-GaSe, resist. and Hall-mobility meas. at 77-850K 77—59295
  Gd-Ni, ferromag., elec. resist. temp. depend. 80—96843
  Ge, acceptor ground state, stress effects 80—34385
  Ge, bound electron states close to conduction band due to 60° dislocations 77—28141
  Ge, carrier density in electron-hole drops, plasma reson. determ. 77—24522
  Ge, diamagnetic excitons, fundamental absorption edge, Faraday config. 79—8144
  Ge, donor polarizability, multivalley effective mass calc. 80—96817
  Ge, effective masses of heavy and light holes, from ohmic mobility data 80—80160
  Ge, electron states below cond. band originating from dissociated 60°-dislocations, calc. using effective mass method 79—19546
  n-Ge, HF plasma oscills. in external mag. field 80—54731
  n-Ge, heavily doped, negative magnetoresistance model, spin-up spin-down electron effective mass variations 79—95423
  Ge, IR absorption coeff. by holes, temp. depend., effective mass *(Russian)* 80—50350
  Ge, localised states due to isocoric donor impurities 77—76768
  Ge, magnetodipole reson., 0.6 to 1.35 mm wavelength *(Russian)* 77—80736
  Ge, magnetoplasma resonance in electron-hole drops *(Russian)* 78—79944
  Ge, screw dislocations, effect of dislocation dissociation on localised electron and hole states 79—82546
  Ge, sum rule for intraband optical absorpt. of shallow acceptor impurities 79—28793
  p-Ge, uniaxial compression influence on carrier heating by weak electric field 80—10978
  Ge, valence band effective mass strain depend. 78—51880
  Ge:As(Se^+), energy spectra, multivalley effective mass calcs.. 77—59266
  Ge:Cu, press. effect on energy spectrum of carriers, elec. cond. and Hall coeff. expts. 79—23930
  GeS film, effective electron mass determ. from current-voltage characts. in thermionic region 77—85135
  GeTe, effective masses for cond., density of states 80—88472
  GeTe-Sb_2Te_3, solid solutions, cond., density of states 80—88472
  $Hg_{0.82}Cd_{0.18}Te$, electronic anomalous mass near reson. acceptor level, Shubnikov-de Haas meas. 80—80163
  $Hg_{1-x}Cd_xTe$, cyclotron reson., 337 μm transmission expts., 77 to 150K 78—34750
  $Hg_{1-x}Cd_xTe$, far IR cyclotron reson., band edge effective mass and relax. time 79—19781
  $Hg_{1-x}Cd_xTe$ films, Tamm surface states, Kane model 79—28395

effective mass continued
  $Hg_{1-x}Cd_xTe$, Tamm surface states 77—55595
  $Hg_{1-x}Cd_xTe$, zero-bandgap state induced by press., galvanomag. props. 77—47725
  HgI_2, electrons and holes cyclotron reson. 78—72061
  HgI_2, exciton study by wave length modulated reflectivity, band parameters 77—51667
  HgI_2, photoexcited, Hall effect, magnetocond., and cyclotron reson., carrier mobility and effective mass 77—59294
  HgI_2, stimulated emission at high exciton density, temp. depend. 78—84608
  $Hg_{1-x}Mn_xSe$, band struct. from anomalous Shubnikov-de Haas effect 80—20080
  HgTe, mobility of electrons and holes, 4 to 100K 80—107821
  HgTe, zero-gap semiconductor, variational approach to resonances 79—82559
  In-Mn, dil., film, ion implanted, supercond, and mag. props. 77—15987
  InAs, band gap and effective mass, depend on impurity conc. 79—69412
  n-InAs, magnetophonon resonance under hydrostatic press. 77—47832
  n-InAs, Shubnikov-de Haas effect, effective mass, Dingle temp., and g-factor 79—51602
  InAs:Zn, optical absorpt. and refl. spectra 79—91479
  InAs/GaSb (001) superlattices, electronic struct., two dimensional effects 80—11064
  InAs-GaSb (001) superlattices, two-dimens. effects and effective masses 80—49883
  InAs-GaSb superlattice, cyclotron resonance, energy level quantisation 79—73430
  $InAs_{1-x}\ P_x$, magnetophonon effect 79—65500
  $(InAs)_x(CdTe)_{1-x}$, band gap and effective mass, IR spectra obs. 78—56491
  $InAs_{1-x}P_x$, electron effective mass cyclotron reson. and magnetophonon effect 80—24786
  $InAs_{1-x}P_x$, evidence for reduction in momentum matrix element P^2 due to alloy disorder 79—65853
  $In_{0.9}Ga_{0.1}As_{0.22}P_{0.78}$, effective mass meas. by Shubnikov-de Haas oscills. 78—34754
  n-$In_{1-x}Ga_xAs_yP_{1-y}$, cyclotron reson., cond. band nonparabolicity 80—29311
  $In_{1-x}Ga_xAs_yP_{1-y}$, electron effective mass from Shubnikov-de Haas meas. 80—80298
  $In_{1-x}Ga_xAs_yP_{1-y}$, evidence for alloy scatt. from press. induced changes of electron mobility 80—88548
  $In_xGa_{1-x}As_yP_{1-y}$ photodetector diode on InP substrate dark currents, tunnelling, energy gaps, effective masses 80—70805
  $In_xGa_{1-x}P_yAs_{1-y}$, electron effective mass and Dingle temp., Shubnikov-de Haas oscills. 80—59859
  In_2O_3, Seebeck coeff., density of states effective mass 78—56171
  In_2O_3:Sn films, RF reactive sputtered, optical props. rel. to band struct. 79—91515
  InP, electroabsorption spectra obs., reduced effective mass determ. 80—50301
  InP, free excitons in high mag. fields, band struct. 77—52129
  n-InP, high field props. under high press. 78—26872
  InP, oscillatory interband magnetoabsorption meas. 79—73909
  InSb based MIS structs., charge accumulation in insulator layers 80—6993
  n-InSb, conduction band effective mass anisotropy and nonsphericity 79—69414
  n-InSb, doping and strain depend. of quantum props. 79—60690
  n-InSb, effective mass and Lande factor, stress depend. calcs. *(German)* 79—95313
  n-InSb, elec. cond., press. dependence 80—6830
  InSb, film, E_0, E_1 absorption edge size quantisation, optical and electroreflectance spectra 80—34998
  p-InSb, magnetophonon reson. of holes 79—95424
  InSe, high field magnetoabsorpt. of hydrogenic excitons at second direct gap 80—6729
  In_6Se_7, single cryst. prep. and electrophys. props. 79—43129
  K-Na, dil., dynamical props. of quasiparticle excitations, de Haas-van Alphen effect meas. 78—84128
  Li, analysis of optical consts. 77—40201
  Mg, spin susceptibility, electronic effective mass, spin density functional calcs. 78—43291
  Mo, cyclotron effective mass and identification of carriers on Fermi surface 79—65372
  Mo, density of states, optical mass and DC elec. resist., Slater-Koster interpolation 77—15731
  Mo, effective mass meas. and electron velocities 80—96773
  NaCl, conduction band struct. from first principles 79—65379
  Nb, band effective mass, Animalu TMMP theory 80—29312
  Nb, de Haas-van Alphen study of Fermi surface, cyclotron effective masses, mag. breakdown effects, KKR calcs. 78—43288
  Nb, density of states, optical mass and DC elec. resist., Slater-Koster interpolation 77—15731
  Nb, electronic structure, APW calcs., self-consistency and exchange effects 77—66109
  Nb, Fermi surface, electron mass enhancement, orthornormal function enhancement 80—96777
  Ne, solid, hole band struct., Bratsev wave function calcs. *(Russian)* 80—65437
  Ne, solid, large-gap insulator, valence excitons, integral eqn. method calc. 77—11858
  Pb, effective cyclotron masses of central and noncentral ζ orbits, de Haas-van Alphen effect 78—63968
  Pb/oxide/InAs structure, effective mass determ. by tunnelling spectroscopy *(Russian)* 80—44482
  $Pb_{1-x}Cd_xS$ epitaxial layer, metastable, optical props. and electronic struct. 79—15543
  $PbCl_2$:NaCl, trapped exciton states, absorption spectra 80—50383
  p-$Pb_{1-x}Ge_xTe$ film, cyclotron reson. above and below struct. phase transition 80—88879
  $Pb_{1-x}Ge_xTe$, n- and p-type, effective masses 80—44481
  PbI_2 (2H), electronic transport and cyclotron reson. 79—28369
  PbI_2:KI, trapped exciton states, absorption spectra 80—50383
  $PbMo_6S_8$, normal state and superconducting property measurements 78—91660
  PbS, anomalous magnetoresist. 80—107813
  p-PbS, dispersion law investigation, valence band density of state effective mass 79—95314

effective mass continued
- PbSe, electron gas magnetisation, energy band parameters determ., use of Faraday effect 80—45047
- p-PbSe, valence band structure, IR refl. and absorpt. meas. 77—55791
- $Pb_{1-x}Sn_xSe$, band struct. parameters, thermoelectric power meas. in strong mag. fields 79—51474
- $Pb_{1-x}Sn_xSe$, band struct. and transport props., hydrostatic press. effects 80—15452
- $Pb_{1-x}Sn_xSe$, energy band parameter determ. from Shubnikov-de Haas effect 77—69227
- $Pb_{1-x}Sn_xSe$, plasma reflection spectra, carrier effective masses and relax. times determ. 78—2858
- $Pb_{1-x}Sn_xSe$ solid solns., photoluminesc. spectra, energy band parameter determ. 80—71484
- $Pb_{1-x}Sn_xSe$, thermomag. effect meas. 77—24572
- p-$Pb_{0.65}Sn_{0.35}Te$, transport coeffs. and dispersion law 80—44629
- $Pb_{0.72}Sn_{0.28}Te$, Hall effect and elec. cond., 77 to 480K, energy band struct. 77—76817
- p-$Pb_{0.8}Sn_{0.2}Te$, magnetophonon effect obs. 78—23115
- $Pb_{0.8}Sn_{0.2}Te$, susceptibility effective mass, carrier conc. depend. 80—20069
- n-$Pb_{0.82}Sn_{0.18}Te$, conduction band struct., determ. by Shubnikov-de Haas meas. 78—2504
- $Pb_{0.82}Sn_{0.18}Te$, narrow-gap, Hall effect quantum oscillations *(Russian)* 77—4377
- $Pb_{0.82}Sn_{0.18}Te$, thermomagnetic, thermoelectric props., valence band struct. *(Russian)* 80—54724
- $Pb_{1-x}Sn_xTe$, basic electrons energy spectrum near mag. phase transition *(Russian)* 79—90955
- $Pb_{1-x}Sn_xTe$, diamag. reson. *(Russian)* 78—23347
- $Pb_{1-x}Sn_xTe$, effective mass of holes, thermoelec. power, Hall coeff., carrier conc. 79—65371
- $Pb_{1-x}Sn_xTe$, electron-phonon interaction 78—71819
- $Pb_{1-x}Sn_xTe$, energy band parameters from IR Faraday rotation 78—48154
- $Pb_{1-x}Sn_xTe$, epitaxial layers, photolum. in mag. field 79—83033
- $Pb_{1-x}Sn_xTe$, hole effective mass near zero bandgap, IR refl. study 80—108205
- $Pb_{1-x}Sn_xTe$, lattice and electronic props. and g-value 80—80161
- $Pb_{1-x}Sn_xTe$ narrow gap solid alloys, hole Fermi surface, galvanomag. and oscill. effect obs. *(Russian)* 77—69345
- PbTe, electronic struct. near band gap 77—69226
- p-PbTe, Fermi surface parameters depend. on carrier density, Shubnikov-de Haas oscills. 79—42435
- p-PbTe film, for IR magneto-optics, 8-30K 78—23543
- p-PbTe film, magnetophonon effect obs. 78—23115
- p-PbTe, relax.-time anisotropy 77—35954
- PbTe, struct. of second valence band 77—89697
- PbTe-based solid solns., 79—23990
- Pd, electron effective mass, press. depend. 79—11055
- Pd, Fermi radii, Fermi velocities and many body enhancement 79—65363
- Pt, rel. to de Haas van Alphen obs. of Fermi surface 78—91601
- Rb-K, dil., dynamical props. of quasiparticle excitations, de Haas-van Alphen effect meas. 78—84128
- Re, RF size effect, Fermi surface dimensions determ. 78—91598
- Rh-Fe, dil., anti-Kondo effect, de Haas-van Alphen obs. 79—73427
- $(SN)_x$, electronic props., ab initio LCAO HF orbital calc. 77—51635
- $(SN)_x$ polymer, quasi-one-dimens. and metallic behaviour *(Japanese)* 77—43577
- Sb, carrier energy spectrum, effect of hydrostatic pressure 78—87903
- Sb, de Haas-van Alphen effect, effective mass, Fermi levels 78—75982
- Sb, partial Fermi levels of electrons and holes, press. depend. 77—43490
- Sb:Te, de Haas-van Alphen effect, effective mass, Fermi levels 78—75982
- Sb-Sn, dil., de Haas-van Alphen effect, effective mass, Fermi levels 78—75982
- ScN_x, region of homogeneity, physicochem. props. 78—52018
- Si (100) inversion layers, effective masses, Shubnikov-de Haas oscills. under mechanical stress 77—43625
- Si, (100) surface, effective mass and collision time 78—64081
- Si, amorphous, effective mass theory, impurity states in band gap 79—77992
- Si, atomic wave functions localisation and band struct., LCAO calcs. 77—51648
- Si, deep-level point defects, effective-mass nature 80—59922
- Si, donor polarizability, multivalley effective mass calc. 80—96817
- Si, donors, dispersive screening and Bloch function interference, large binding 79—51525
- n-Si, effective mass from intraband Faraday rot. and Hall effect 77—52049
- Si, effective mass from Kramers-Kronig analysis for various doped crysts. 77—31942
- Si, effective masses of heavy and light holes, from ohmic mobility data 80—80160
- Si, electron and hole effective mass, intrinsic conc., temp. depend. 80—107692
- n-Si, Faraday rot. temp. depend., effective mass determ. 80—71392
- n-Si, HF plasma oscills. in external mag. field 80—54731
- Si, heavily doped, characts. of distrib. of density of states 79—15072
- p-Si, heavily doped, intra- and interband Raman scatt. by free carriers 80—108208
- n-Si, heavily doped, negative magnetoresistance model, spin-up spin-down electron effective mass variations 79—95423
- Si, intrinsic, electronic properties, temp. depend. *(German)* 77—76822
- Si, inversion layer, dynamic conductivity of electrons, temp. depend. 78—19115
- Si inversion layers, effective mass variation 79—24050
- Si inversion layers, stress effects on electronic props. 78—43476
- Si, local pseudopotential, Gaussian band charge model 80—88477
- Si, localised states due to isocoric donor impurities 77—76768
- Si on sapphire thin film, Hall effect, magnetoresistance *(French)* 80—65601
- Si p-channel MOS structure, stress effects on elec. props., press. transducer props. 80—100526
- Si, spherical effective impurity electron mass 77—24532
- n-Si, surface-barrier electroreflection, polarisation anisotropy 79—24295
- Si, transverse effective mass of E_1 and $E_1+\Delta_1$ transitions, rel. to band struct. 77—80725
- Si:B, hole mobility calc. for dopant density and temp. var., resistivity meas., effective mass calcs. 80—54703

effective mass continued
- Si:Li, electron-phonon scatt., in intermediate conc. region 80—65180
- Si:O, electrial and infrared spectroscopic investigations 80—34389
- Si:Sb(P)(As), shallow donor electrons, hyperfine interactions, reply to Onffroy's calcs. 78—51934
- Si-Al_2O_3, inversion layer subbands, magnetocond. oscills. 78—64124
- n-SiC (6H), density of states effective mass determ., high temp. meas. of elec. props. 79—15073
- n-SiC (6H), doping effect on birefingence dispersion, effective electron mass 79—69807
- SiC (6H), epitaxial film, electronic props. 79—60942
- β-SiC, deform. potential and effective mass anisotropy, Hall constant 79—90949
- SiC polymorphs, widths of first minibands and effective masses, resist. anisotropy 80—20071
- SiC:N, refr. index dispersion, effective electronic mass determ. 78—84548
- Si(100) inversion and accumulation layers, effective mass and collision time of electrons, oscillatory magnetoconductance 78—34909
- Si(100) inversion layers, effects of uniaxial stress on cyclotron reson. 80—20322
- SmS, metallic, determ. from transmission, refl. and absorpt. spectra 78—19587
- SmS, metallic, thermal modulation of reflectivity, 1.2-3.8 eV 79—99909
- SmS, semicond.-metal transition, cond. band type, deform. pot. determ. 79—69417
- Sn, liq., optical props., 0.62-3.7 eV 80—75996
- Sn, white, band masses and deformation pots., OPW pseudopotential model 80—100430
- Sn, white, cyclotron effective masses, US attenuation meas. 77—15753
- SnO_2 film, doped, electron effective mass and elec. props., carrier density depend. 77—43750
- SnSe, electron and hole effective masses, depend. on electron field orientation 79—69848
- p-SnTe, cathodoluminescence and Fermi level hole effective mass, determ. of Fermi-level effective masses of holes 80—25467
- SnTe, self-consistent relativistic energy bands 80—10870
- Ta, density of states, optical mass and DC elec. resist., Slater-Koster interpolation 77—15731
- Ta, electronic structure, APW calcs., self-consistency and exchange effects 77—66109
- Tb-Y, magnon component of elec. resist., effective cond. electron mass 77—15827
- TiO_2, resolved quadrupolar transition, absorpt. spectra obs., 1.6K 78—27259
- α-U, Fermi surface and effective masses, de Haas-van Alphen meas. 80—65426
- UGe_3, mass enhancements, band struct. calcs. and de Haas-van Alphen meas. 77—20225
- V, band effective mass, Animalu TMMP theory 80—29312
- V, electronic density of states, effective mass, electron-phonon interaction, Coulomb pseudopot. *(Russian)* 78—26804
- V, electronic structure, APW calcs., self-consistency and exchange effects 77—66109
- V, electronic structure, model potential calcs. *(Russian)* 80—100431
- V, Fermi surface area, effective heat, optical masses, surface anisotropy critical temp. depend. *(Russian)* 79—90943
- $V_{1-x}Fe_xO_{2-x}F_x$, $0<x<0.20$, magnetic susceptibility and electron cond. *(German)* 80—39754
- W, density of states, optical mass and DC elec. resist., Slater-Koster interpolation 77—15731
- Y_3Se_4 powder, prep. and optical props. 77—28771
- $Zn_{0.1}Hg_{0.9}Se$ type alloy, dispersion law of cond. band *(Russian)* 77—1366
- $Zn_xHg_{1-x}Se$, galvanomagnetic effects, Shubnikov-de Haas oscill. determ. of band struct. 80—6884
- $Zn_xHg_{1-x}Se$ semimetal-semicond. transition, thermo-EMF in mag. field and Hall expts. *(Russian)* 77—15881
- n-ZnSe crystals, electron scatt. mechanisms, high mobility 80—34433
- ZnSe, polar semicond., radiative recomb., electron-phonon interaction effects, calc. 80—49631
- ZnSe, two-photon absorpt. spectra, effective-mass parameters from energy splitting 77—52124
- p-ZnTe, cyclotron resonance from photoexcited electrons, polaron effective mass determ. 79—69723

effusion
- beam source, heterogeneous reaction type, chem. equilib. 80—52362
- corpuscular diagnostic method of metastable atoms in glow discharge plasma, review *(Czech)* 80—24241
- dynamic torsion-effusion pendulum, video obs. 77—61077
- education, mol. beam effusive flow, vector flux density distrib. calc. for any aperture 80—22165
- equilibrium pressure of gaseous components, metallic refractory compounds, determ. by Knudsen method 79—52529
- glass optical waveguide fabrication by effusion 80—5850
- high temperature gas and vapour characterisation, conf., Gaithersburg, USA (Sept. 1978) 80—53910
- Knudsen effusion cell, high temp. mass spectroscopy, thermodynamic and physicochemical behaviour, review 80—52354
- Knudsen effusion chamber with low axial temp. gradient for high temp. thermodynamic tests 77—71329
- Langmuir torsion effusion meas., recoil force correction factors 78—75929
- mass spectrometer effusion for thermodynamic props. determ., surface evaporation effects and elimination 77—184
- oxide system, complex, mass-loss Knudsen effusion method for phase equilib. determ. 77—11668
- rare earth nitrides, Knudsen effusion press., vaporization enthalpies 79—10936
- review of effusion and related surface processes 77—51151
- 3,3,4,4-tetrahydrothiophene-1,1-dioxide, vap. press. by effusion method 78—26680
- thoria effusion membrane, production techniques based on that of incandescent gas mantles 78—39724
- torsion-effusion method, vapour press. meas., automatic data acquisition 80—52188
- torsion-weighing effusion vapour pressure measurements, appl. to organic compounds 77—89530
- vapour pressure computer-automated meas. by simultaneous Knudsen torsion-effusion method 80—73334

effusion continued
vapour pressure measurement, effusion method, review 80—51995
water decomposition into H and O using solar energy, one-step effusional process 78—15672
Al-B, enthalpies and free energies, effusion and mass spectra, phase diagram 78—23665
β-B, rhombohedral, sublimation, 1823 to 2253K, torsion-effusion and mass spectroscopic meas. 77—39673
$CaSO_4$, thermal decomposition, torsion-effusion cell obs. 77—77741
Cu-Ni textured alloys, grain boundary effusion of Ni to surface 79—90680
Fe-Zn, homogeneous phases, Gibbs free energies of form., Knudsen effusion method 80—66481
In-Zn, liq., Zn activity meas. by Knudsen torsion-effusion method 79—10950
IrS_2, thermodynamic props. by effusion technique 77—40570
K_2SO_4, effusion studies of vaporisation/decomposition 79—95153
Li-Pb, thermodynamic study using Knudsen effusion mass spectrometry 80—24578
$MgSO_4$, thermal decomposition, torsion-effusion cell obs. 77—77741
Mn, vaporization, thermodynamic study by Knudsen-cell mass spectrometry, congruent effusion 79—10937
Mo_3Sb_7, Sb decomp. press. and enthalpy of form., Knudsen effusion meas. 79—87840
Ni-S system, Knudsen effusion and thermodynamics 78—79759
$PrCl_3$, sublimation press. and thermodynamics, mass loss effusion meas. 79—99307
RbI, vaporisation thermodynamics, mass-loss Knudsen effusion, mass spectrometry 79—28093
Sc_xS, high temp. vaporisation, enthalpy, atomisation, dissoc. energies 77—1223
TiS, vaporisation chemistry and thermodynamics, computer-automated simultaneous Knudsen-torsion effusion 80—48837
URu_3, sublimation thermodynamics 80—97722

EHD *see electrohydrodynamics*

EHT calculations
ω-β-variable method, convergence props. 77—18792
AB_4, non-transition element complexes, shapes and other props. 78—82648
AB_5, non-transition element complexes, shapes and other props. 78—86790
AB_6, non-transition element complexes, shapes and other props. 78—82647
acetylene, chemisorbed on Pt (111), self-consistent EHT studies 79—61896
acetylene, dissoc. chemisorption on Pt (111) surface, EHT calcs. 79—39190
adsorption of H on Ni substrate, extended Huckel theory calc. 78—10286
alkanes, H^+ chemical shifts, extended Huckel calcs. with gauge in variant atomic orbitals 80—102449
benchrotrene, EHT method calcs., parametrisation, population anal. *(French)* 80—58157
benzene, H^+ chemical shifts, extended Huckel calcs. with gauge in variant atomic orbitals 80—102449
benzene, SCF-EHT polarisability calc. 80—47895
benzene-benzene (anthracene) dimers, ground and excited states, EHT calc. 79—36553
benzenoid-o-quinoidal systems, valence isomerisation, EHT calcs. 77—77757
benzothiazole, and homologues electronic struct., photoelectron spectra and MO calcs. *(French)* 79—31598
trans-butadiene, polarisability, nonlinear elec. susceptibility, SCF calcs. 80—95547
charge transfer complexes, geometries, CNDO/2 and EHT calcs. 79—36530
chemisorption, iterative extended Huckel theory, INDO and CNDO methods 79—87875
chemisorption of acetylene on Pt (111) surface, EHT calcs. 77—62733
diamond, defect states, extended Huckel Hamiltonian calc. 79—7802
diamond, electronic energy bands of diamond-type crysts., appl. of EHT method 78—87907
diamond-type crystals, LCAO band structure, overlap and distant neighbour effects 80—49585
dibenzylchromium, EHT method calcs., parametrisation, population anal. *(French)* 80—58157
dimethyl sulphide dimerisation, S lone pair nonbonded contacts, EH, MINDO/3, CNDO/2 calcs. 79—773
double charge transfer and two to one charge transfer adducts, energetics 79—82561
edge dislocation, localised electron states 78—18999
electrostatic correction, deduced from Hartree energy, appl. to stretching problems 78—17573
ethylene, polarisability, nonlinear elec. susceptibility, SCF calcs. 80—95547
ethylenic compounds, H^+ chemical shifts, extended Huckel calcs. with gauge in variant atomic orbitals 80—102449
ferrocene, EHT method calcs., parametrisation, population anal. *(French)* 80—58157
haemin, hyperfine interactions and related props. 78—44451
haemoglobin derivatives, hyperfine interactions and related props. 78—44451
haloalkanes, max. overlap approx., heat of form. and dipole moment 78—94198
halogens, solid, intermolecular bonding influence on nucl. quadrupole interaction tensor 77—62882
hexatriene, polarisability, nonlinear elec. susceptibility, SCF calcs. 80—95547
HF wavefunctions, restricted and unrestricted, convergence problem 77—418
hydrocarbon, conjugated, nonlinear susceptibility, extended basis set calcs. 79—27107
III-V compounds, (110) surface, energy distrib. of dangling-orbital surface states 80—80347
intramolecular electron transfer rate, purely electronic effects, simple model Hamiltonian 77—10592
large molecules, computer method 77—26982
linear homoatomic macromolecules, stability 79—10038
macromolecules, quantum chemical characteristics, extended Huckel calcs. 79—45874

EHT calculations continued
nicotinamide, and related compounds, dipole moments, electronic transitions, chemical and biological activity 78—90086
nicotinic acid, and related compounds, dipole moments, electronic transitions, chemical and biological activity 78—90086
NMR spin-spin coupling consts. calcs. 77—68060
nonbonded interactions, pot. energy curves, CNDO/2, INDO and extended Huckel calcs. 77—27140
nuclear magnetic shielding constant, calc. by extended Huckel method with expansion by Gaussian functions 77—79634
nuclei acid base stacked dimer, origin of excimer states in extended Huckel method 80—35832
nucleic acid bases, excited states formation, EHT calc. 79—13651
organometallic compounds, EHT method calcs., parametrisation, population anal. *(French)* 80—58157
overlap and electron interaction effects, rel. to NDO LCAO theories 80—95536
oxalyl chloride, rot. isomerism, CNDO and EHT-type methods 78—58591
polarisability of hydrocarbons, static and dynamic, comparison with PPP calcs. 79—98242
trans-polyacetylene, electronic energy band struct., extended Huckel and MNDO studies 80—20065
polyacetylene, trans- and cis-isomer, electronic struct. calcs. 80—24788
polydiacetylene, model chain, band struct. calcs. 77—8016
polymer primary structures ESCA and EHCO methods 78—52630
polypropylene, isotactic, conformational origin of peak struct. in XPS spectrum 79—89819
population analysis and bond lengths forecasting 80—18800
α-quartz, CNDO/2 calcs., electronic props. of perfect cluster, EPR parameters of O^- vacancy 80—107701
radical and unsaturated polymer interactions, MO calcs. 77—44481
relative Raman line intensities, extended Huckel valence basis sets 80—106329
relativistically parameterized extended Huckel theory, appls. 79—49924
rubredoxin, reduced analogue, EHT calc., Mossbauer parameters, zero field splittings 77—79544
self-consistent charge Xα method, appl. to small mols. 80—91449
self-consistent charge Xα method, theory 80—91448
semiconductors, amorphous, electronic structure, chem. bond approach 79—65374
Si (111), surface relax., EHT and cluster calcs. *(Chinese)* 80—59762
structurally disordered systems, with diagonal and off-diagonal disorder in non-orthogonal basis set, numerical study 79—69387
$(TCNQ)_2$, dimeric interactions, MO calcs., applicability to crystal struct. 80—75215
TCNQ dimers, extended Huckel hamiltonian supermol. CNDOS calcs. 80—27953
tempered orbital energies, SCF calc., relation to Mulliken-Walsh ordinate and extended Huckel orbital energies 79—763
tetrazaporphin, coord. polymer with transition metal, one-dimens. conductor, band struct., EHT theory 79—90941
TGS:Cr^{3+}, EPR obs. of ferroelectric monocrystals, fine struct. EHT-SCCC-MO calcs. 79—19769
transition metal clusters, particle size rel. to bulk metallic props. 80—44490
transition metal complexes, counterintuitive orbital mixing in semiempirical, ab initio MO calcs. 78—90078
transition metal trinuclear carbonyl complexes, electronic structures. and spectra 79—59480
$(TTF)_2$, dimeric interactions, MO calcs., applicability to crystal struct. 80—75215
TTF-TCNQ, dimeric interactions, MO calcs., applicability to crystal struct. 80—75215
TTF-TCNQ, TCNQ and TTF bandwidths, extended Huckel and CNDO/2 calcs. 79—7771
Ag cluster 78—33646
Ag, cluster and microcrystal, matrix isolated, optical absorpt. spectra, photolysis and plasmon absorpt. 79—89820
Ag latent image particles, electronic effects 80—82840
$As_2S_3(Se_3)(Te_3)$ glass, electronic struct. calc. 78—23012
BeH radical, hyperfine splitting const., electronic energy, UHF-type, CCI calcs. 80—52909
CO, chemisorbed, CNDO calcs. of mol. struct. *(German)* 79—96368
CO_2, anomalous energy minima surfaces 78—86791
$Ca_3Fe_2Si_3O_{12}$, andradite, hyperfine parameters, Huckel theory calc. 80—39542
$CdCr_2S_4(se_4)$, ferromag. semicond., band struct., EHT calc. 80—54608
$CsPO_3$, He(I) photoelectron spectra, UTARC calc., assignments 79—72357
Cu, atomic clusters, struct. and electronic props., Mulliken-Walsh diagrams, extended Huckel procedure 78—46479
Cu, clusters, size, geometric effects, catalysis implications 78—73131
Cu metal cluster, adsorption of CO, mol. orbital calc. 78—18895
Cu surface, (001), electronic struct. of steps 78—34884
Cu, surface, (111), (100), (110), energy band parameters 78—34883
$Cu(NO_3)_2$, electronic struct., relative energies, iterative EHT calculations 77—38615
Fe complex, $Fe(dithiocarbamate)_2X$, X = NCS,Cl,Br,I,NO, elec. field gradient, HMO calc. 80—39543
Fe crystallites, vacancy diffusion and vacancy lattices semi-empirical mol. orbital calcs. 77—1121
$Fe_4S_4(SH)_4^{0,2-,3-}$, HFS-LCAO calcs., 4-Fe active site model in high pot. Fe protein and ferredoxin 80—42929
GaAs (110), surface electronic struct. calcs. 80—80343
GaAs, (110) surface structure, rotational relaxation, cluster model *(Chinese)* 80—107621
GaAs, electronic structure of (111) and $(\bar{1}\bar{1}\bar{1})$ surfaces 79—87137
GaAs, energy bands and pressure dependences *(Japanese)* 78—34747
GaAs, pure and N depend, extended Huckel theory appl. 80—59916
GaAs surface, cluster model approach for electronic struct. 78—56205
GaP, energy bands and pressure dependences *(Japanese)* 78—34747
GaP, pure and N doped, extended Huckel theory appl. 80—59916
Ge, electronic energy bands of diamond-type crysts., appl. of EHT method 78—87907
Ge, energy bands and pressure dependences *(Japanese)* 78—34747
Ge, LCAO band structure, overlap and distant neighbour effects 80—49585
Ge surface, Cl chemisorption, cluster calc. by iterative EHT 77—32062
Ge, surface, cluster model approach for electronic struct. 78—56205
H-bonded complexes, geometries, CNDO/2 and EHT calcs. 79—36530

EHT calculations continued

- InSb, zincblende and rocksalt type struct., semiempirical LCAO band struct. calc. 77—72816
- KPO$_3$, He(I) photoelectron spectra, UTARC calc., assignments 79—72357
- Li, cluster and microcrystal, matrix isolated, optical absorpt. spectra, photolysis and plasmon absorpt. 79—89820
- Li clusters, semiempirical calcs. equilib. struct. comparison to ab-initio and SCF-Xα-SW *(German)* 78—29874
- Li$_n$, equilibrium struct., effect of p-functions *(German)* 79—89823
- LiNO$_3$, electronic struct., relative energies, iterative EH calcs. 77—38615
- (Li$_2$SiO$_3$)$_x$, bond length variations, mol. orbital study 78—26500
- NH$_3$-lithium halide complex, ab initio calcs., Li bond rel. to H bond 77—14343
- Na, cluster and microcrystal, matrix isolated, optical absorpt. spectra, photolysis and plasmon absorpt. 79—89820
- NaPO$_3$, He(I) photoelectron spectra, UTARC calc., assignments 79—72357
- NbSe$_3$, electronic struct., chem. interpret. of geom. deform., oxidation state formalism 80—107690
- Ni, adsorption of H$_2$, activation mechanism, extended Huckel calc. *(French)* 79—42379
- Ni crystallites, vacancy diffusion and vacancy lattices, semi-empirical mol. orbital calcs. 77—1121
- Ni metal cluster, adsorption of CO, mol. orbital calc. 78—18895
- Ni-H interaction, 0.75 Å$\leq$R$\leq$5 Å, NiH form. effect of inner orbitals *(German)* 78—29752
- NiO$_2$, Ni(O$_2$)$_2$, coordination of mol. O$_2$ with Ni, EHT calcs. 77—18795
- Pd, clusters, size, geometric effects, catalysis implications 78—73131
- Pd^{2+}-L-Cl$^-$, model fragment (L=Cl$^-$, F$^-$, OH$^-$, H$_2$O, NH$_3$) bond strengths, EHT calcs. 77—23434
- Pt electrode, compact layer struct., absorpt. EHT calcs. 77—16828
- Pt^{2+}-L-Cl$^-$, model fragment (L=CL$^-$, F$^-$, OH$^-$, H$_2$O, NH$_3$), bond strengths, EHT calcs. 77—23434
- Pt(O)-Pt(O) dimers, bounding in a d^{10}-d^{10} system 78—74579
- RbPO$_3$, He(I) photoelectron spectra, UTARC calc., assignments 79—72357
- (SN)$_x$ chain, isolated, effect of (SCH$_2$)$_2$ impurities, on electronic props., EHT calcs. 79—15067
- Si (111) surface, with Al overlayers, electronic states 80—11061
- Si, divacancy, positive, EHT calcs. 79—99184
- Si, electron states associated with core region of 60° dislocation 77—35887
- Si, electronic energy bands of diamond-type crysts., appl. of EHT method 78—87907
- Si, energy bands and pressure dependences *(Japanese)* 78—34747
- Si, extended Huckel theory calc. of hyperfine interactions of positive divacancy 77—89742
- Si, extended Huckel theory calculations for positive divacancy 78—87938
- Si, He impurity props. investigation by EHT calcs. 79—99183
- Si, impurity interstitials, EHT calcs. 80—24845
- Si, matrix isolated cluster, otpical absorpt. extended Huckel calcs., electron energy levels 80—16045
- Si, neutron irrad., EPR, ⟨100⟩ split di-interstitial, positive charge state 77—20698
- Si surface, Cl chemisorption, cluster calc. by iterative EHT 77—32062
- Si, surface, cluster model approach for electronic struct. 78—56205
- SiO$_2$, g-tensor and ^{29}Si hyperfine tensors of E$_1$'-centre for model of O$^-$ vacancy 79—19777
- Si(111) surface, interpretation of intrinsic surface states 78—6423
- α-Sn, electronic energy bands of diamond-type crysts., appl. of EHT method 78—87907
- TcCl$_8^{3-}$, metal-cluster, EHT calcs. of electronic struct., metal-metal bonding *(Russian)* 77—61687
- Te, trigonal nucl. elec. field gradient ellipsoid, LCAO and extended Huckel approx. calc. 77—55736
- TlNO$_3$, electronic struct., relative energies, iterative EH calcs. 77—38615
- V$_2$, formation, spectra, electronic struct. 77—54642
- W (100) surface, chemisorption of CO, mol. orbital study 78—71995
- YIG, hyperfine parameters, Huckel theory calc. 80—39542
- ZnSe:Mn^{2+}, ligand HFS calcs., comparison with other methods and expt. 77—55501

eigenfunctions *see eigenvalues and eigenfunctions*

eigenvalues and eigenfunctions

- $\phi_1{}^4$ field theory, eigenvalues, Schwinger functions, critical behaviour 77—45931
- 't Hooft-Polyakov monopole, zero energy eigenvalues for quantum fluctuations, quantisation 79—9318
- acoustic destabilization of vortices 79—32533
- acoustic motional source transfer function characts., ocean profile anal. appl. 78—66982
- acoustic signal processing, eigenvector decomposition of correlation matrices 80—96118
- acoustic wave propag. in shallow water, soln. of wave eqn. based on eigenfunctions of Schrodinger eqn. *(French)* 79—41505
- acoustic wave propagation in bilinear medium, mode theory, WKB approx. 77—7229
- acoustics, eigenmode analysis of the interference patterns in reverberant sound fields 80—96112
- aerial photograph statistical spatial filtering 79—13908
- aeroelastic system, flutter eigenvalue problem, rigid-body degrees of freedom elimination 79—98651
- aerofoil flutter, vibration and stability of a bar in a stream of gas *(Russian)* 79—32548
- alpha-decay, complex energy eigenvalue theory 78—41678
- analytic continuation of a group of eigenvalues 79—6010
- Anderson localisation, transport props. of 2D disordered electron systems in strong mag. fields 78—95318
- anharmonic oscill., residue-squaring diagonalisation meth. 77—49635
- anharmonic oscillator, computation of energy eigenvalues of Hamiltonian 80—12925
- anharmonic oscillator, eigenvalues, eigenfunctions 78—36883
- anharmonic oscillator, modified perturbation theories using Riccati eqn., energy eigenvalues 79—12644
- anharmonic oscillator, moment recursions and the Schrodinger problem 79—35584
- anharmonic oscillator, quantum mechanical, eigenvalues of secular eqns. 78—49698
- anharmonic oscillator, thermodynamic properties 79—55321

eigenvalues and eigenfunctions continued

- anharmonic oscillator with polynomial pot., asymptotic forms of energy eigenvalues 78—45509
- anharmonic oscillators, transition moments 78—12601
- anharmonic potential models, exactly soluble, const. and soln. 78—54221
- anharmonic-oscillator energies using operator recursion mech. 77—22443
- anharmonically coupled oscillators, semiclassical calcs. of eigenvalues 80—95514
- anisotropic 3-D Ising lattice 79—156
- anisotropic and laminated plates, dynamic response, variational method, general functional 77—3770
- anti-commutative, self-inverse matrices and transformations in eigenvalue problems *(Chinese)* 80—101951
- arbitrary square matrix with multiple eigenvalues, analytical function evaluation 77—74188
- asymmetrical Ising model, phase transitions 80—17891
- asymptotic distribution of eigenvalues for the multidimensional Schrodinger equation 80—94985
- asymptotic eigensolutions of fourth and sixth rank octahedral tensor operators 79—93975
- asymptotic eigenvalue-distrib. for class of random matrices 77—5618
- atom, contact interactions, parity-violating and parity-conserving, new evaluation techniques 79—26872
- atom, three-level, continued fraction transition theory, reson. lineshape 78—33473
- atom+atom collisions, fine-struct. transition cross sections, eigenphase formulation 78—25651
- atomic collisions, two-state approximation in the adiabatic and sudden-perturbation limits 79—22780
- atomic eigenfunctions, nodal structure 80—57122
- atomic electron binding energies, determ. from relaxed-orbital relativistic Hartree-Fock-Slater calcs. 77—42255
- atomic one-electron model hamiltonians with STO eigenfunctions 77—3269
- atomic potentials with Coulomb tails, eigenenergy calc. 79—58560
- atomic relaxation, collisional and radiative eigenstates 78—29827
- atomic scattering amplitudes, two-cluster, partial-wave, analytic continuation 80—52045
- atomic system, two-electron, Schrodinger local energies 79—41090
- atoms and molecules, total SCF electronic energy rel. to eigenvalue sum 79—9993
- atoms total Hartree-Fock energy-eigenvalue sum relationship 79—59338
- bar on elastic foundation, buckling strength *(German)* 79—64546
- baroclinic waves growth rates and phase speeds, multilevel models 79—58022
- basis states generation by variational methods 78—78295
- Be, Rayleigh-Schroedinger perturbation calculations 78—9064
- beam, doubly tapered, transverse vibrs. 77—68511
- beam, subjected to elastic constraints, free vibrs. 78—83309
- beam in transverse vibr., optimisation of higher order eigenfrequencies 77—78971
- beams, linearly tapered, transverse vibr. 80—48627
- beams flexural-torsional problem by series expansion in eigenfunctions 80—83732
- Bell-Lavis 2-D bonded lattice model, critical behaviour 79—17356
- benzene, photoelectron and optical spectra, occupied virtual orbital energies and eigenvalue ordering, CNDO/S calc. 77—61796
- Bethe-Salpeter eqn., eigenvalue, asymptotic expansion, weak binding approx. of Wick-Cutkosky model 79—2925
- bifurcation problems, left branching soln., appl. to nonlinear buckling 77—67222
- bilinear functionals, upper-bound estimations 77—67796
- bimolecular reactions, rot.-vibr. symmetry correlation, building-up principle from mol. fragments 78—76849
- biological systems, symmetry 80—81519
- Birman-Schwinger bounds for the Laplacian with point interactions 80—137
- Blasius boundary layer, Orr-Sommerfeld eqn., temporal eigenvalue spectrum 78—42589
- Blasius profile, eigenvalues determ. using Riccati transform. method 77—65731
- Bloch electron continuous spectrum instability, N-band Stark ladder 77—57220
- Bloch Hamiltonian one-dimens. bands by fibres 77—31934
- block diagrams, divergence cancellation in energy level perturbation theory 79—80751
- Block-Stodola eigensoln. technique for large algebraic systems with non-symmetrical matrices 77—26163
- bodies disposed from aircraft, dynamic flight characteristics *(Polish)* 78—18311
- Boltzmann eqn. eigenvalues 79—80549
- Boltzmann equation, eigenvalue precision, influence of boundary conditions 80—27689
- Boltzmann equation, eigenvalue precision, influence of boundary conditions 80—27690
- Boltzmann equation, two-vector, analytical solns. in nonplanar geom. 77—65246
- Boltzmann equation for neutron transport, eigenvalue defn. and use 77—54275
- Boltzmann neutron transport operator, dominant eigenvalue determ. for inhomogeneous body 79—13377
- bond order, maximum principle, LCAO formalism 78—29728
- Born series, 2 cluster→2 cluster scatt., two, three, four particle Schrodinger operators 79—49072
- boson and fermion systems, eigenvalue spectra widths, symmetry, Wigner coeffs. 80—18213
- boson field, damping superoperator eigenvalue problem, direct soln. 80—57180
- boson model, interacting, shell-model basis, correspondence between fermion and boson states and operators 80—52593
- bound state wave function explicit normalisation, decay widths calc. 80—18116
- boundary layer, stability theory, high viscous eigenstates 77—907
- boundary-layer flows, neutral stability calcs., Taylor-series expansion of dispersion relation 80—53744
- branching diagram and Serber type spin functions, construction algorithms 79—6828
- Bravais-lattice operator in one band of solid 80—10519
- Brownian motion, Smoluchowski equation in presence of hydrodynamic interactions, Chapman-Enskog method 80—46979

eigenvalues and eigenfunctions continued
- Brownian particle, desorption from surface, one-dimensional time-dependent escape problem 80—29278
- buckling, bifurcation and limit point instability of dual eigenvalue third order systems 80—87727
- buckling, cylindrical shell and spherical panel, stability, critical loading density 80—53664
- buckling of elastic bar with varying stiffness, coupled boundary conditions 77—31231
- buckling of elastic beams, analysis using theory of quadratic operator pencils 80—48607
- building structs., eigenvalue routines 78—26078
- cantilevers, joined by a rigid connector nat. freq. determ. 78—83298
- Casimir operator eigenvalues and Lie algebra canonical realisations 77—5697
- Casimir operators of orthogonal and symplectic groups 77—71178
- Chandrasekhar's X-function, reln. to eigenvalues of integral operators with difference kernels 77—71280
- linear Chapman-Enskog procedure, evolution equations of hydrodynamic variables 80—49075
- characterisation, orthonormality-constrained variation method 78—45457
- charge changing collisions of ions, relative populations 80—52835
- charged particle scattering in homogeneous mag. field, transition amplitude 79—10218
- charmonium models, energy perturbation series from Schrodinger eqn. 79—6005
- charmonium spectroscopy, explicit soln. of wave eqn. for arbitrary power pots. 80—403
- Chebyshev polynomial method for computing analytic solns. to eigenvalue problems, appl. to anharmonic oscillator 78—62058
- chemical kinetics, eigenvalue and eigenfunction anal. of Kramer's theory 79—29330
- chemical reaction diffusion equation, nearly degenerate bifurcations, mode interactions 80—85149
- circle theorems for inviscid steady flows 80—59043
- circular plate bending under eccentric loads, elastic buckling eigenfunction method *(Japanese)* 78—22285
- clamped rectangular orthotropic plates, natural freqs. of vibr. upper and lower bounds 78—83284
- clamped square plates, Rayleigh-Ritz vibration analysis with modified Bolotin flexural freq. estimates 78—42563
- classical coupled dipole oscillators, optical props., normal mode treatment 79—36611
- classical groups, invariant operators 79—21585
- classical Liouville operators, eigenvalue problems 77—26228
- classical nonlinear σ-model, two dimens., scatt. of massless lumps, nonlocal charges 78—62300
- Clebsch-Gordan coeff. of symm. group, arranged into eigenvectors of propagation matrices 79—19175
- climatology of global solar radiation in California and an interpolation technique based on orthogonal functions 80—67402
- coherent multiphoton intense interactions, convergent perturbation anal. 80—1037
- coherent non-stationary superpositions of atomic eigenstates, beam-foil spectroscopy 77—38748
- coherent states, time-dependent invariants 79—44791
- collisionless drift waves in Tokamaks analytic eigenvalue eqns. 80—6246
- column critical buckling load, approximate eigenvalues 79—64551
- completeness value for eigenfunctions of second order differential eqns. 80—31564
- complex energy eigenvalues of a zero-range atom in a uniform electric field 79—72227
- complex matrices, location methods 78—36790
- complex poles residues of outgoing Green function, eigenfunction expansion involving resonant states 77—82885
- complex quadratic eigenvalue soln. of pipe flow 77—13614
- composite beams, vibration and buckling anal. 79—1123
- composite wall, constant props., transient heat cond. problem *(French)* 78—87229
- configuration interaction method formulation for triplet states 78—37536
- confined solutions of multidimensional inversion equations 78—77678
- confining pot., eigenvalue problem for Schrodinger operator 80—27154
- conservative discrete system, upper and lower bound eigenvalues 77—89020
- conservative discrete-continuous system, free vibration *(Russian)* 80—23950
- continued fraction solutions to systems of linear eqns. 77—2506
- continuity of generalised eigenfunctions of Schrodinger operator 78—45511
- convection, natural, over uniform heat flux vertical surface, higher-order approx. 78—59388
- convection-diffusion problem, singular perturbation problem with nearly resonant operator 78—22352
- convergence of eigenfunction expansions assoc. with vector matrix differential eqn. 78—69965
- convergence properties of the Pade approximants on a lattice 79—17615
- cosmological models, eigenvalue problem formulation, from Einstein eqn. 78—16704
- Coulomb potential with cut-off, exact eigenvalues 78—62692
- coupled large linear damped structures, eigenvalue anal. 78—1561
- coupled oscillator natural orbitals 77—57853
- coupled second-order differential eqns., numerical soln. method for eigenvalue problems 80—94976
- coupled vibration systems, eigenvalues, semi-classical SCF calcs. 80—27929
- coupled-channel Schrodinger eqn. bound states, renormalised Numerov method 79—13627
- covariance matrices eigenvectors, for interpretation of remote atm. radiance obs. 77—5341
- covariant EM projection operators, covariant description of charged particle guiding centre motion 78—58145
- crystal symmetry, implications in charge density studies 78—71694
- crystal vibrations, matrix paradox, for teaching 78—49611
- cubic crystal Zeeman anisotropy in absorpt., emission and MCD, eigenfunctions 77—55773
- cubic crysts., perfect, nonBloch electron state density 80—75487
- cubic harmonics computation, using point groups and an algorithm 78—20994
- cyclotron reson. at model interface in transverse mag. field 79—4726
- cylinder, circ., elastic, axial eigenfunctions orthogonality 78—51080
- cylinder, orthogonality of elastodynamic eigenfunctions 80—5940

eigenvalues and eigenfunctions continued
- cylindrical orthotropic shell stability problems, spectrum singularities 80—99950
- cylindrical shell of variable thickness, natural frequencies *(Russian)* 77—50967
- cylindrical shell with cutout, dynamic behaviour 77—75735
- cylindrical shell with elastic filler, eigenfrequency spectra, dynamic instability regions, nonaxisymmetrical vibrations 78—63367
- damped and constrained least squares method with application to gravity interpretation 79—66830
- damped double solitons in the nonlinear Schrodinger equation 79—64853
- damped linear systems, freely vibrating, eigenvalue lower bounds 79—27569
- Davidson's algorithm with and without perturbation ocrrections 80—27570
- decay-scattering systems, resonances and their eigenfunctionals in Friedrich's model 80—8847
- degenerate oblique derivative problem with interior boundary conditions, unique solvability theorem 77—67188
- delta wing equations, high freq. solns. 79—46337
- demagnetisation eigenfunctions anal. of linear transverse magnetisation in long, thin stripes 80—34687
- determination by continued fraction 80—105490
- diatomic molecule, rot. perturbed Morse oscillator, eigenfunctions and Franck-Condon factors 77—42309
- diatomic mols., spurious avoided crossing detection 80—87057
- diffusion, two-way, separation of variables, decaying and growing eigenfunctions 80—62594
- diffusion and convection in parallelogram cross-section pipe with plug flow *(German)* 80—100000
- diffusion equation, from space-time transport eqn., for anisotropic random media 80—62595
- diffusion of H_2 towards crack in stressed solid, eigensoln. 77—24446
- diffusion process with critical point, eigenvalues discretisation technique 80—172
- dimensional continuation for relativistic bound state problems 77—18159
- dimensional regulation, SU_2 gauge theory, instantons 80—18066
- Dirac eqn. with oscillating pot., scatt. problem *(Russian)* 77—79225
- discrete systems, conservative dynamic, K-Quotient for determ. of upper bound 79—18777
- discrete-continuous system, vibrations 80—23951
- dislocation scattering, new Hamiltonian for describing multivalued elastic displacement fields 80—24862
- domain monotonicity of first eigenvalue of boundary value problem 77—5638
- double well anharmonic oscillator, no horn of singularities 78—73884
- double well Schrodinger operators 80—90698
- doubly anharmonic oscillator, class of exact solns. 80—105531
- doubly connected membranes governed by Helmholtz eqn., eigenvalue determ. 79—23253
- drift wave eigenvalues, variational calc. 79—68920
- drift wave equations, numerical solution by invariant bedding 80—10374
- drought in upper Midwest, USA, 1931 to 1969 period 79—70880
- dynamic system, classical quantisation conditions with stochastic behaviour anal. 80—8922
- Earth, shell of uniform layers, asymptotic distrib. of torsional eigenfreqs. 78—92797
- Earth ellipsoidal model, exact and asymptotic synthetic multiplet spectra 80—21673
- Earth free oscillations, amplitudes of split normal modes 78—40508
- Earth free oscillations due to earthquake, complex eigenfreqs. improved resolution in analytically continued seismic spectra 78—36106
- Earth mantle lateral variations from LF eigenspectra data 78—36123
- Earth oscillations, corrections to eigenfreqs. due to dynamic shear modulus 77—81800
- Earth radial oscillations, core and upper mantle struct. effects 80—12347
- Earth torsional eigenfrequencies, effects of density and shear vel. discontinuities on asymptotic overtone struct. 77—78111
- Earth torsional normal modes eigenfreqs., asymptotic overtone struct., model study 77—78110
- education, eigenvector of general rot., geometrical construction 80—57025
- education, Sturm-Liouville problem, eigenfunctions normalization 77—78910
- eigenstate decay into continuum in presence of elec. field 77—13631
- eigenstates calc. for system of core and two valence nucleons 80—42606
- eigensystem derivatives, convergence of iterative method 78—28926
- eigenvalue eqns., appl. to fast and thermal neutron systems 78—50231
- eigenvalue multiplicity of nonradial stellar oscills. 80—51740
- eigenvalue perturbation theory, remarkable examples 78—93558
- eigenvalue problem, continued fraction solns. in degenerate perturbation theory 77—17840
- eigenvalue problems of domains without classical symm., possible appl. of group representations 77—13571
- eigenvalue problems of domains without classical symm., second and third type, group representations 77—13572
- eigenvalue problems of domains without classical symmetry, appl. of group representations 77—13580
- eigenvalue spectrum of homogeneous multiplying systems for monoenergetic neutrons with anisotropic scattering 79—22353
- eigenvalue spectrum of large symmetric random matrix with finite mean 78—32646
- eigenvalue systems of second order differential eqns., numerical soln., matching method 78—8232
- eigenvalues of graphs with twofold symmetry (molecular configuration) 79—72437
- eigenvector derivatives, banded eqn. soln. algorithms 77—22367
- Einstein eqns., classification system for one Killing vector solns. 78—93579
- Einstein stationary axially symmetric eqns., complete integrability 79—63099
- elastic collisions of three spheres in a line, eigenvalue and difference eqns. solns., for teaching 77—33786
- elastic composites, 3-D, harmonic waves 77—891
- elastic curved body, reson. mode eigenfrequencies of creeping vibrs. 77—50817
- elastic layer in acoustic medium, wave dynamical characteristics *(Russian)* 79—76995
- elastic quadrilateral plates 79—46201
- elastic rod, perturbation methods for soln. of linear eigenvalue problem *(German)* 78—18175

eigenvalues and eigenfunctions continued
elastic rotating Earth, elementary oscill., ordinary differential eqns. 79−39632
elastic shell, cylindrical, isotropic, elastic stability, critical load analysis 80−83744
elastic stability of linear system, simplified algorithm 77−62180
elastic wave scatt. from cylindrical cavity, nuclear resonance theory 78−87290
elasticity, equivalent inclusion method and impotent eigenstrains 79−97203
elastomechanical systems, theoretical models correction method *(German)* 78−38
elastoplastic non-isothermal deform., bifurcation of equilib. 78−79220
elastostatic anal. of transversely isotropic finite cylinders 78−51074
elastostatic end problems for finite cylinders semi-analytical finite element anal. 80−10143
elastostatic strip and wedge, Green's functions, bi-linear forms and eigenfunction completeness 79−97205
electric normal modes at small polyhedral particles, eigenvalue schemes 77−58225
electrohydrodynamic instability 80−14832
electrohydrodynamic stability in rigid cylinder, dielectric viscous fluids, eigen wavenumbers 78−59497
electron, free, motion in uniform mag. and elec. fields, Schrodinger eqn. soln. 78−24985
electron, nonrelativistic, and Euclidean massless Dirac particles, paramagnetism 79−63396
electron beam, thin, field-aligned in plasma, eigenfunctions 77−76124
electronic structure, Hartree problem, iterative diagonalisation soln. 79−6829
electronic wave functions, iterative scheme for simultaneous calc. of m 1st eigenstates of real symmetry matrix 79−85888
electrostatic Trivelpiece-Gould modes in a torus 80−38609
ELF eigenvalues approx. determ. in Earth-ionosphere waveguide 79−8763
ELMO bumpy torus, macroscopic MHD stability and beta limit 79−31186
EM cavity eigenfrequency density oscills. and lattice sums 77−65556
EM fields, real eigenfunction expansion for symmetric complex operators 77−71906
EM fields of embedding class one 78−36914
EM resonator eigen-oscillations, variational treatment *(Russian)* 77−79730
EM scatt. integral eqn. resonant solution elimination 79−45895
EM wave in random media, degeneracy and inhomogeneity in transport theory 78−62982
Emden-Fowler eqns., nonlinear boundary and eigenvalue problems by group methods 79−71224
empirical eigenfunction anal., appl. to prediction of beach changes in S.California 80−98305
energy eigenvalue problem, adiabatic perturbation theory using QFT techniques 78−93551
energy eigenvalues, pocket calculator determ., radial Schrodinger eqn. conversion to recursive eqn. 77−57215
energy eigenvalues lower bounds for quantum Hamiltonians in lattice field theories 78−45575
energy eigenvalues of Coulomb and oscillator potentials, connections 79−12637
ensemble of two-body random Hamiltonians, nonzero mean matrix elements, eigenvalue density, Monte Carlo calcs. 78−81920
EPR, eigenvalues and eigenvectors, error anal. 79−51840
equivalent nuclei, ENDOR fine struct., exact solns. 77−6811
ergodicity, classical, quantum mech. implications 80−8898
ergoregion instability of rotating stars, eigenfrequency calc. 79−8835
Euler buckling eigensystem for a nonprismatic strut 79−18764
evolution equations, nonlinear, inverse spectral transform, generalisation of Klein-Gordon problem 80−68055
evolution systems and convection-diffusion, stiffness and stability, Gershgorin theory 80−77626
extreme eigensolution calculation method for high order real symmetric matrix 80−90703
extremum sufficient condition in classical action integral, eigenvalue problem, education 80−105462
factorization theorems, stability and repeated bifurcation 78−65751
Faddeev eqns. approx. solns., possibility of complex eigenvalues 77−9909
fermion field with broken SU_2 symm., two-dimensional isotopic model *(Russian)* 80−73616
fermion reduced density matrices 78−16731
fibre optics, uniform asymptotic theory 80−28323
field problem structure, equilibrium, eigenvalue and propagation problems *(Rumanian)* 78−45520
finite chain, with random dil. impurities, localisation characts., amplitude anal. 80−96825
first-order linear differential eqns., optimum integration operators 77−78962
flat conduit, mass transport, asymmetrical boundary and starting conditions *(German)* 77−35236
flexure of clamped rectangular plates resting on Winkler foundations 80−5934
flow, in annulus, axial, numerical stability anal. 78−83363
flow, oscill., forced, of gas (liq.), in tube, linearised treatment 79−50744
flow-duct acoustics with eigenvalues depend. boundary conditions, eigenfunction expansion 77−50787
fluid, classical one-dimens. Lennard-Jones type, eqn. of state 80−24562
fluid, cold, displacement by hot fluid in porous medium, stability 79−27691
fluid dynamics, Poiseuille flow in circular pipe, linear stability 80−79399
fluid dynamics, stationary supersonic gas stream conical flow about plane wedge and circular cone 80−74912
fluid structure vibr. eigenvalue problems, finite elements, modal methods 80−96269
fluid-structure coupling method in dynamic analysis of structs. 79−7322
fluids, miscible, interface electrohydrodynamic instability in collinear field-cond. gradients 78−26199
flywheel, buckling and vibr. of rotating spoke, anal. 78−71288
Fokker-Planck equation, inhomogeneous, eigentheory 78−29068
four particle systems, eigenfunction/eigenvalue problem, effective Hamiltonians in paired channels 78−13037
four vector components, eigenvalues and -functions for spin 0 and 1 78−49720
fractal resonators, mode distribution 80−8782

eigenvalues and eigenfunctions continued
free oscill. data inversion, eigenvalue problems, angular order spectra 79−8602
Friedrichs model unitary regularisation for many particle system 80−32039
frontal solution algorithm for finite element frequency analysis 79−3942
fuel storage pool criticality calc., transport-consistent diffusion algorithm 79−9721
fully developed turbulent flow, between parallel plates, heat transfer in entrance region 78−1658
g- and p-modes of non-adiabatic self-gravitating fluid, perturbational-variational expansion 78−32337
galaxies, global instability of polytropic gaseous discs with Toomre density distrib. 80−98725
Galerkin's method, non-uniform convergence 78−83304
gas mixtures, eigenfunctions positivity in time depend. kinetics theory 77−19660
gas model of rigid spheres, Boltzmann eqn., eigenvalues eigenfunctions of Hilbert operator 77−26250
Gel'fand invariants for unitary, orthogonal and symplectic group 78−32651
Gel'fand-Levitan equation, non-self adjoint operators, eigenfunctions, spectral representations 80−86131
general anharmonic oscillator, eigenvalue calc. 79−6015
general nonlinear differential-difference equations, integrability by inverse scattering method 79−12575
general relativity, spin coefficient equations with nongeodesic eigenrays 79−25941
general relativity, SU(1,1) spin coefficient equations with nongeodesic eigenrays 79−25942
general SCF coupling operators, arbitrariness 80−99439
global gravitational instability of disc galaxies 79−48931
global gravitational instability of gaseous discs 79−48932
graph theory, of MO, symmetrical analysis and calc., eigenpolynomials 78−29729
gravitational radiation and invariants of curvature tensor in general relativity 78−57836
Green's function defined in phase space, using Wigner operator eigenfunctions and eigenvalues 78−24728
Green's function for surface physics, partial differential eigenvalue eqn. 80−6929
Green function expansion into eigenfunction set 80−22205
ground state properties, energy level lower bounds, particle in mag. field and external pot. 78−8260
ground state properties of Lipkin Meshkov Glick model using atomic coherent states, nuclear phase transitions 78−62489
gyroscopic effects in micropolar elasticity 79−30247
gyroscopic systems solution, with real symmetric matrix of same dimension 80−12895
gyrotron, freq. characts. determ. *(Russian)* 79−14241
hadronic atoms in momentum space, Dirac, Schrodinger and Klein-Gordon eqn. eigenvalues 79−872
hadronic matter, string junction model and spectrum energy density of string 80−57556
hadrons, extended, second-quantisation of strongly interacting fields 80−13270
Hamiltonian, complex-rotated, reson. props. 79−31427
Hamiltonian, information content of exact eigenfunction of physical system 79−30280
Hamiltonian eigenvalues in Weyl correspondence limit, Turschner's formula 79−84988
Hamiltonian of single variable systems, asymptotic behaviour of bound eigenfunctions 78−77754
Hamiltonian $P^2+A|X|^\nu$, exact eigenvalues 79−40392
Hamiltonian with stochastic trajectories, spectrum and eigenfunctions 79−54013
harmonic oscillator, ground and first excited state energies, $g\phi^4$ quantum field theory 80−62839
harmonic oscillator, vibr.-rot. interaction eigenvalue estimate 79−12628
harmonic oscillators, position and momentum eigenstates, superposed coherent states 80−57135
harmonic quadrupole collective Hamiltonian, exact soln. 78−37301
harmonic vibrations, one-dimens. incommensurate lattice 78−38788
Hartree-Fock theory, time depend. 77−42241
heat and mass transfer systems, modelling of eigenvalues and eigenfunctions 77−14872
heat conduction in composites, Sturm-Liouville problem eigenvalue bounds 79−50568
heat equation, pseudo-similarity solutions, in presence of moving boundaries 80−27240
heavy positive ions, total energy, rel. to eigenvalue sum and chem. pot. 80−47858
Heisenberg chain, explicit Plancherel theorem for ground state representation 77−89921
Heisenberg exchange interaction Hamiltonian, eigenvalues and eigenvectors 79−78289
Helmholtz equation eigenvalues calc., using simplified integral equation method 77−78964
Helmholtz-eqn., eigenvalues by boundary integral eqn.-finite element method 77−71195
Henon-Heiles Hamiltonian system, vibr. energy levels in quasiperiodic and stochastic regimes, props. 80−91529
Hermite polynomials, matrix eigenvectors 79−49013
hermitian matrix, large, eigenvectors determ., new approach 77−37717
Hermitian matrix, low lying eigenvectors, pseudo-convergence in iterative method 79−92970
Hermitian operator low lying eigenvalue calcs., iterative method 77−60965
hermitian operators, upper and lower bounds to eigenvalues, variational calcs. 78−36882
higher order modified pot. for effective phase integral approx. 79−44779
Hilbert spaces, nested, spectral props. in class of operators and group representations 78−4459
Hubbard model, computer renormalisation-group technique, eigenfunctions and eigenvalues in finite energy range 79−19716
Hubbard model, ground state energy, using degenerate perturbation theory 78−18938
Huckel matrix, degenerate eigenvalues investigated under insertion of additional bond or centre 80−78542
Hulthen potential energies for $l\neq0$, screening parameter 80−101731

eigenvalues and eigenfunctions continued
- hydrocarbon, conjugated, nonlinear susceptibility, extended basis set calcs. 79—27107
- hydrocarbons, mol. graphs, eigenvalues 77—26996
- hydrodynamic oscillations in Gentilly-I steam mains by inertial analysis 78—89944
- hydrodynamic stability, open disc theorem, upper bound of eigenvalues 78—59370
- hydroelastic systems, spectrum and normal modes 77—68494
- hydromagnetic thermal instability of rotating fluid layer, Hall current effects 79—27699
- hypervirial scaling iterative method 80—73196
- ideal string, extremal solutions of inverse eigenvalue problems with finite spectral data 80—101712
- image methods for constructing Green's functions and eigenfunctions for domains with plane boundaries 80—94979
- image processing and eigen representation 78—55312
- image restoration by Gauss LU decomposition 79—76600
- independent partitioning and direct minimisation of SCF theory 77—26970
- induced potential problem in 3-D, functional analytic approach 78—58880
- infinite sector problems, direct method of calc. of eigenvalues 78—81807
- infinite systems of linear eqns., eigenvalue problems 77—78956
- inhomogeneous circular waveguide, asymptotic eigenvalues 80—53442
- integrable system, finite dimens., scatt. behaviour 77—82415
- integral representation and generating functions for the polynomials $U_n^{(\alpha,\beta)}(x)$ 79—53957
- integro-differential eqn. of nuclear theory, numerical soln. *(Russian)* 77—57641
- interacting particle system with Lennard-Jones pot., Schrodinger eqn. eigenvalues 79—71292
- invariance principle in scatt. theory, proof 79—75378
- invariant operators of unitary groups U(n) and SU(n) 78—8555
- inverse eigenvalue problem of order four—an infinite case 79—9084
- inverse eigenvalue problem of order four 77—22389
- inverse eigenvalue problems, ideal soln. with finite spectral data 79—34974
- inverse iteration method convergence, for nonlinear elliptic eigenvalue problems 79—40353
- inverse scatt. problem, quantum mech. systems with discrete spectra 77—78995
- inverse scattering transform, Wronskian technique, isospectral flow eqn. 78—8275
- iosperimetric inequality for first eigenvalue of boundary value problem 77—67220
- irregular finite element meshes, grading rules 80—68045
- irregularly shaped clamped plates, free vibration 79—37231
- Ising model, 2-D, metastability 79—58648
- Ising system, periodically layered, cooperative effects in crit. phenomena in sp. ht. 78—23284
- Ising system, two-dimens., transverse field crit. props., renormalisation and scaling 78—21080
- isospectral matrices, finite transforms 80—105529
- IU(n) and IO(n) invariant operators and their eigenvalues 79—30194
- J^2 eigenvalues 80—17742
- Jacobi matrices, rational, asymptotical eigenvalue density 78—81794
- Jahn-Teller E-e problem, diagonalisation by means of transformed basis 79—82566
- jet, free, turbulent flow, large scale struct., discrete values meas. 78—90840
- Jordan's five dimensional theory, stationary axially symmetric solns. 79—88863
- Josephson junction, current biased, eigenstates and eigenvalues 80—60148
- Jost functions, S-matrix of massive Thirring model, relativistic field theoretic model 78—54552
- JWKB quantisation condition, appl., breakdown and near-dissoc. behaviour 78—58571
- Kalman filter technique, eigenfunction expansion, neutron flux core distrib. 78—54839
- Kirchhoff plate, eigenvalues with nonlinear spline functions, matrix displacement method *(German)* 80—33446
- Klein Gordon eqn. (1+4)-dimensional invariant expansion of soln. in orthogonal coord. system *(Russian)* 77—13875
- Klein-Gordon equation, inverse spectral transform 80—68055
- Klein-Gordon particles in deep square wells 80—31982
- Kramers equation, eigenvalues calc., Fokker-Planck eqn. for Brownian motion in a potential 80—86215
- Kramers theory of friction and vel. in chemical kinetics 80—50826
- laminate, 3-phase, longitudinal heat propag. at high exciting freqs. 78—90684
- laminates, piecewise continuous eigenfunction solns. 78—18178
- Lanczos method, method of moments, tri-diagonalisation of a matrix 78—58240
- Lanczos tridiagonalisation in bounding eigenvalues 77—53798
- Landau levels, analytic function theory, energy eigenvalues and eigenfunctions determ. 77—69259
- landscape multispectral data, Karhunen-Loove analysis 80—48164
- Laplace's tidal eqn. asymptotic eigensolns. 77—33166
- Laplace operator on spherical domain, fundamental eigenvalue numerical determ. 77—87628
- large real symmetric matrices, generalised eigenvalue problem, group coord. relax. method 78—16622
- large scale general eigenvalue problem iterative method for soln. 78—89318
- large symmetric matrices, ensemble averaged eigenvalue spectrum 78—132
- laser cavity resonator, nonconfocal, with output-coupling aperture *(Japanese)* 79—55163
- laser modelocking, soln. of 2nd order integro-differential eqns. 78—66796
- laser nonconfocal resonator with output-coupling aperture, matrix eigenvalue analysis 79—72600
- laser theory integral eqn., concept of 'approx. eigenvalue' 77—67217
- layered composites, heat conduction eigenvalue problems 80—74702
- layered elastic composites, harmonic wave frequency estimation, eigenfrequency bounds 79—46252
- level spacings, lower bound for single particle in neg. potential 77—22430
- Lie algebras, solitons and pseudopotentials 77—26131

eigenvalues and eigenfunctions continued
- Lie group matrix eigenvector determ. using identity spectral resolution 77—53740
- Lie groups, Casimir invariants and vector oprators 78—28911
- Lie linear groups, Casimir operators 77—2509
- light propag. in birefringent cryst., projection dyadic treatment for teaching 77—33789
- linear differential eqns. with separated boundary conditions, Riccati transformations for eigenvalues 77—38
- linear differential equation with two strong singularities, second order, iterative numerical soln. method *(German)* 77—30000
- linear eigenvalue problem properties describing non-radial stellar oscillations, model 80—17571
- linear harmonic oscillator on lattice, wave functions, energy eigenvalues, Pade approximant method 78—57817
- linear mechanical boundary and eigenvalue problems with symmetries 77—72154
- linear microscopic equations in irreversible thermodynamics, eigenvalue problem 80—57227
- linear potential, energy eigenvalue eqn. 79—2646
- linear potential eigenenergy equation, $K_n(3l')$ coeffs. 79—44762
- linear structures, complex, eigenvalues numerical bracketing *(French)* 80—42053
- linear transport equation, continuously varying spatial media, elementary solns. 80—86229
- linear transport operator spectrum, semi-infinite medium 77—2626
- linear transport operator with periodic boundary conditions, spectral decompositions 77—33961
- linear transport theory, singular eigenfunction expansions 80—13523
- linearised Boltzmann eqn., constructive soln., scalar BGK model eqn. 79—161
- Liouville-Green uniform asymptotic method, used to obtain eigenvalues of Schrodinger eqn. (3-d), with a radial Gaussian pot. 78—20995
- Lippman-Schwinger equation, soln. for n delta-shell pots. 78—41112
- Ljusternik-Schnirelman theory applied to unlimited variations *(German)* 79—85009
- loaded thin circular plate stability criterion 78—77700
- locally modified structs., derivatives of eigenvectors 78—5651
- Lorentz Fokker-Planck, kinetic theory 79—46413
- lower bounds for quantum Hamiltonians, classical limit of quantum theories 78—41200
- lower bounds to ground state eigenvalues, Pade approximants 78—49722
- lung compartmental models, steady state inert gas exchange 80—26249
- magnetic elastic system, one-Fermion-one-Boson model 78—43539
- magnetic resonance results, eigenvectors and eigenvalues, error estimation by linear data-fitting technique 80—68018
- magnetosphere, two-dimens. model, eigenvalues, magnetotail currents 79—53662
- magnon-magnon interaction in square lattice 78—2669
- many electron atomic Hamiltonians spectral props., method of configuration interaction 79—59368
- many-electron atoms, energy eigenvalues and eigenfunctions, CI method 77—50370
- massive Thirring model, explicit diagonalisation of Hamiltonian 79—21918
- massless electrodynamics, vacuum instability, bare coupling constant Gell-Mann-Low eigenvalue condition 78—89643
- matrix computation methods and applics., book 77—37721
- matrix eigenvalues sensitivity 78—89295
- matrix generalised eigenproblem developments for numerical weather simulation 77—25760
- matrix operator $S.\pi$ eigenvalues, spins 1/2, 1, 3/2, const. mag. field 78—32712
- MC-SCF equations, restricted, open- and closed-shell, soln. algorithm 79—63891
- mechanical systems, follower load type, time invariant functionals 80—77609
- membranes, vibrating fixed, on the first eigenfunction 77—50980
- membranes, vibrating wedge-like, isoperimetric norm bounds for first eigenfunction 77—14950
- meson wave functions in 1+1 dimens. QCD 78—54559
- metastability in macrosystems, eigenvalue problem 77—9977
- MHD diffuser flow across homogeneous magnetic field 79—1262
- MHD equilibria, by secondary bifurcation, rectangular boundary conditions 78—42673
- MHD instability, helical symmetry, linear theory 79—94729
- micropolar fluids, stability of laminar flows between parallel walls 79—1160
- Micu-type invariants of simple Lie algebras 80—12934
- Milne problem for two half spaces in two group transport theory 77—67784
- minicomputer open ended configuration interaction program, BERKELEY 78—37563
- mitral valve vibration anal. to detect first heart sound freq. 78—40233
- mixtures of reacting gases, extension of Chapman Enskog method *(Russian)* 78—57878
- mode calculations in interferometer, eigenvalue translation method 79—71515
- molecular bond order orbitals and eigenvalues 79—41088
- molecular dynamics, semiclassical study of bound states 80—9693
- molecular energy levels 80—58123
- molecular ground, excited states, doubly excited configurations in density-matrix method 77—3280
- molecular open shell systems, orbital energies, semiempirical calcs. 77—3272
- molecular orbitals, conjugated molecules 80—14078
- molecular orbitals, localised, population calc. method from given SCF eigenvector matrix, appls. 80—14063
- molecular potentials with Coulomb tails, eigenenergy calc. 79—58560
- molecular vibration, semiclassical eigenvalues in nonseparable systems, good action angle variables 79—13694
- molecular vibrational wave functions, semiclassical Gaussian basis set method 80—9583
- molecule, diatomic, electronic pot. rot.-vibr. eigenfunction, analytic expression 80—52964
- molecule, nonrigid, sum of states, isometric group, symmetry no., thermodynamic functions 80—58186
- molecule, quartic potential function with finite BE, props. 79—26913
- molecules, natural orbitals, Brillouin-Levy-Berthier theorem, multiconfigurational SCF optimisation 80—27936

eigenvalues and eigenfunctions continued
  momentum eigenfunctions in complex momentum plane, Hartree Fock functions 80—63517
  momentum eigenfunctions in complex momentum plane, secondary singular points 79—68179
  monoenergetic neutron systems, quadratically anisotropic scatt., influence on decay const., transport eqn. eigenvalues 78—46122
  monoenergetic neutron transport equation, existence of complex eigenvalues 77—345
  Morse oscillator, matrix elements calcs. with Sturm-Liouville eqn. eigenfunctions 79—2660
  moving electron in field of two Coulombic ions fixed in space, rel. to H_2^+ line spectrum 80—42083
  multilayered cylinders, nonstationary temp. fields with rotational symmetry *(German)* 78—79190
  multilayered laminated disc, orthogonality reln. for stress anal. 79—98621
  multiparticle scatt., ghost bound states and Pauli principle *(Russian)* 79—9152
  multiplicative stochastic processes in statistical physics, appls. 80—22289
  multiplicative stochastic processes in statistical physics 79—25980
  multipole fields in finite, spherically symmetric region 80—36881
  multiregion problems in plane geometry for neutron transport 78—17274
  multivariate master eqn. diffusion operator, reaction diffusion system eigenfunctions 78—29077
  N-body Schrodinger operators, eigenfunctions, wave packets, pointwise bounds 79—12634
  N-electron atomic Hamiltonian first eigenvalue, Hartree-Fock approx. method 78—90062
  n-electron atoms, compactness proof for infinite systems of linear equations 79—72247
  N-electron system, Schrodinger eqn. soln. using antisymmetrisation 80—106246
  N-group neutron transport theory, criticality problem in slab geom. 77—65243
  N-mode laser, emitted light correlations 78—63051
  narrow resonances, high energy mag. resonances, exactly soluble model 80—86134
  neural networks with random topology randomness of generated eigenvalues 80—22291
  neutral atoms, total energy and eigenvalue sums 78—21835
  neutral molecules, total energy and eigenvalue sums 78—21835
  neutron diffusion modelisation, optimal design and eigenvalue problems 78—66329
  neutron hot perfect fluid relativistic stars, asymptotic eigenfrequency distrib. for even parity perturbations 78—49668
  neutron multigroup transport operator spectrum for bounded spatial domains 79—97742
  neutron pulse behaviour in multizone breeder system, two-zone system pulse method 78—86574
  neutron transport, 2-D, diffusion synthetic acceleration method 79—22357
  neutron transport, one-dimens. transport equation soln., local separation of angle and energy 77—65248
  neutron transport, two-group transport transforms, comput. merit in finite nonplanar media 77—65247
  neutron transport eqn. with anisotropic scatt., discrete eigenvalues 80—553
  neutron transport integral eqn., iterative and direct approaches to critical dominant eigenfunction 77—38313
  neutron transport multigroup theory 80—13525
  neutron transport operator for medium with central spherical cavity, spectral props. *(Chinese)* 77—26817
  neutron transport theory, ω mode transport eqn., asymptotic soln. 80—102231
  neutron transport theory, homogeneous cylinder, numerical anal. 79—17953
  neutron transport theory, three dimens. integral monoenergetic, initial value problem 77—344
  NMR analysis system, LAOCOON3-type, reliability efficiency and error estimates 78—258
  non-separable bound system, semiclassical eigenvalues from classical trajectories, higher energy levels 77—50342
  nonlinear birth and death processes, relaxation mode anal. 77—49681
  nonlinear diffusion eqns., evolution of stable profile 79—17363
  nonlinear eigenvalue problem method 79—17208
  nonlinear eigenvalue problems, approx. method of first eigenvalue 77—64921
  nonlinear eigenvalue problems, asymptotic linearity 77—67186
  nonlinear evolution equations, integrable, inverse scatt. method 80—12913
  nonlinear heat generation eigenfunctions 77—49553
  nonlinear medium is form of complex structures, burning 79—18688
  nonlinear oscillators, normal modes, uncoupling and stability 80—27115
  nonlinear second order system, eigenfunction expansion solutions of Fokker Planck eqn. 80—73172
  nonlinear structural eigenvalue calcs., mode finding 78—51102
  nonlinear transformations, universal metric props. 80—52000
  nonradial pulsations of massive stars, stability coeffs. and eigenfreqs. 77—56908
  nonselfadjoint operator eigenvalues approx. 77—54952
  nonseparable bound system, quantisation rules, classical trajectories, degenerate case 77—9904
  nonstationary physical systems, mathematical model 79—84985
  nonvanishing potentials, eigenvalue problem 77—74270
  normal modes of laterally homogeneous Earth, one dimens. example 78—88797
  normal modes of self-gravitating fluids in perturbed configurations, perturbational-variation procedure 78—32336
  nuclear fuel lattice eigenvalue as function of buckling, perturbation theory correction 79—59118
  nuclear octupole vibration, collective, wave functions, spherical harmonics 80—68532
  nuclear states, SU_3 representation 80—42552
  nuclear structure, quasiclassical soliton solutions of Hartree eqn., Newtonian interaction with screening 80—68569
  numerical integration leading to Bohr-Sommerfeld formula, alternative to JWKB calcs. 80—86119
  numerical inversion of Laplace transform and Fredholm integral eqns., eigenvalues and eigenfunctions 78—81800

eigenvalues and eigenfunctions continued
  numerical solution of problems in unbounded regions, use of coord. transforms 78—8219
  O(N), eigenvalues of invariant operators 79—71652
  ocean, S.Sicily Basin eigenperiods rel. to 'Marrubbio' phenomenon 77—53062
  ocean equatorial trapped waves, vertical eigenvalue problem 80—56477
  ocean internal wave climate near NW.African coast during JOINT-I 79—20840
  ocean trench waves, dispersion curves and eigenfunctions 80—72547
  trans, trans-1,3,5,7-octatetraene, low freq. normal modes, CFF-π calcs. 79—68217
  off energy two body t-matrix in the R-matrix theory *(Russian)* 80—22780
  one dimens. symmetrical quantum systems, exact local states 80—46870
  one dimensional Ising system with random long-ranged interaction, density of eigenvalues of random matrix PV 79—12733
  one-dimensional classical spin chain with random interactions, exact calcs., transfer kernel eigenvalue 79—4687
  one-dimensional diffusion, soluble model potentials 79—35649*
  one-dimensional model system, Stark effects eigenvalues, Pade approximants calcs. 80—4561
  one-dimensional polaron, asymptotic spectrum of momentum eigenstates 79—56143
  Onsager-Casimir symmetry, geom. of roots of matrices 79—100
  operator eqns., solution by numerical means 79—84936
  optical bare resonator eigenvalue analysis, matrix methods 80—78927
  optical cavity with output coupling, one-dimens., quasimodes as field eigenvalue 80—9911
  optical fields, broadband coherence-separable, free-space propag. model 80—78763
  optical inhomogeneous circular waveguide, asymptotic eigenvalues of vector waves 80—96010
  optical leaky dielectric waveguide, planar hollow structure, eigenmode analysis 80—78973
  optical resonator nonsymm. eigenvalue problems, numerical solns., Prony method 78—82992
  optical system, noisy image restoration, eigenfunction expansion technique 78—63020
  optical-fibres, graded-index, mode eigenfunction computation, propagating beam method 80—95988
  OPW method, instability rel. to error in core eigenvalues 78—63963
  orbital angular momentum eigenvalues, integralness calcs. 80—67977
  orbitals, max. and min. overlap, localised, and hybrid, orthonormality-constrained variation method 79—6830
  ordinary differential eqns., invariant imbedding, Riccati transformations and eigenvalue problems 77—37
  Orr-Sommerfeld eqn., eigenvalue series representation 79—7364
  Orr-Sommerfeld eqn. eigenvalues, series representation 78—38280
  Orr-Sommerfeld problem, approx. to eigenvalue reln. 79—3995
  orthogonality properties of optical resonator eigenmodes 80—38042
  oscillating system, light damping, influence of eigenvalues *(German)* 80—31490
  oscillator, quartic, zeta function 80—62532
  oscillators, quartic, eigenfunction zeroes 80—73197
  oscillatory damped linear systems, eigenvalue bounds and subcritical damping 79—77005
  pairing Hamiltonian, general, approximate solns., by variational method 78—36931
  paramagnetic ion, eigen-value problem in crystalline and mag. field 79—7954
  parameter-dependent system, energy soln. method 80—8828
  partition functions, coherent states and upper bounds in Hilbert space 80—57173
  Pauli equation with differential operators for the spin *(German)* 79—2664
  periodic helical flow in pipe, linear stability, Hermitian forms and eigenvalue bounds 79—37401
  periodic potential energy levels, late terms, asymptotic expansions 79—25895
  perturbation theory, stationary state function ambiguity, resolution, for teaching 78—24603
  perturbed eigenvalues, perturbation expansions and variational constraints 78—16670
  perturbed ladder operator method, analytical determ. of generalised central field energies and wavefunctions 78—32704
  perturbed molecular system, eigenvalues and eigenvectors, method of generation 79—41094
  perturbed oscillator energies, numerical calc. method 79—58580
  physical systems instabilities, variational principles for complex eigenvalues 79—21527
  piecewise continuous eigenfunctions, extension of theorem of orthogonality 80—31541
  plane elastostatic boundary value problems, integral operators, eigenvalue num. calc. 80—36848
  plane elastostatics, numerical props. of integral eqns. describing boundary value problems 78—34013
  plasma, collisionless drift modes, graphical method for finding complex roots of nonlinear eqn. 80—33762
  plasma, collisionless universal instability, stability of bound eigenmode solns., convective modes 78—71472
  plasma, confined, drift and trapped electron instabilities, in systems with mag. shear 80—28648
  plasma, current-driven drift-wave eigenmodes, stability criteria 79—32769
  plasma, ion cyclotron beam-whistler mode instability in parallel shocks 78—14148
  plasma, ion resonance instability, strong self-elec. field influence, nonneutral column 78—34301
  plasma, MHD turbulence, three-dimens. soln. in cylindrical geometry 78—67351
  plasma, oscillations of radially confined round beam, stability and distrib. function 80—53966
  plasma, Scyllac ordering, instabilities, sharp-boundary dynamical model 77—51216
  plasma, stimulated backscattering nonlinear theory, eigenfunction 77—7547
  plasma, trapped-electron cyclotron instability, in Tokamak, 2-dimens. eigenvalue problem, analytic soln. 78—30434
  plasma, Vlasov type, inhomogeneous, localised modes 78—83563

eigenvalues and eigenfunctions continued

- plasma drift waves, eigenmodes with arbitrary radial wavelengths, stability 80—64710
- plasma instabilities, resistive-g and ion temp. gradient in sheared magnetic field 80—64708
- plasma MHD waves segregation in ideal medium 78—87440
- plasma oscillations, Vlasov theory, linear approx., electron distrib. initial value problem 77—84423
- plate, circular, with annular circle constraints, vibrs. and buckling 79—98652
- plate, completely free, rectangular, free vibr. analysis by method of superposition 78—83300
- plate, eigenvalue problem, bidimensional approximation *(French)* 80—33445
- plate, orthotropic multilayered, acoustic transmission loss 78—83143
- plate, orthotropic multilayered, vibr. modes, acoustic transmission 78—83142
- plate, polygonal, clamped, free vibrs. analysis 79—94523
- plate, rectangular, with clamped/simply supported edge conditions, free-vibr. anal. 78—59340
- plate, thick infinite, transversely isotropic, containing circ. hole, end effects 79—27510
- plate, thin, thermally stressed, vibrations 80—48628
- plate, thin elastic, buckling problem, eigenvalue eqn. positive soln. appl. *(German)* 79—68610
- plates, dynamic instability anal. by finite element method 77—3769
- plates, rectangular stepped thickness, with edges elastically restrained against rotation, vibrations 78—90740
- plates, rectangular thin, effect of different edge flexibility coeffs. on transverse vibrs. 78—83294
- Poiseuille flow, at large Reynolds numbers, Navier-Stokes eqn. soln. *(Russian)* 78—59364
- Poiseuille flow, plane, horiz., rot., stability, effect of Coriolis force 78—67203
- polarons, energy eigenvalue, systematic calculation procedure 80—84439
- polyatomic molecules, applic. of classical perturbation theory of good action-angle variables 80—23481
- polyatomic molecules, isotopic reduced partition function ratio approx., by polynomial perturbation method 78—66530
- polychromatic speckle pattern, dominant eigenvalues to evaluate intensity probability density function 80—106451
- polymer, derective, freq. branch calc. of n-paraffins, fatty acids, and glymes 79—31747
- polymer diffusion equation with hydrodynamic interaction, equiv. normal coord. 80—79966
- polymer solution, flexible mols., dynamic intrinsic viscosity, hydrodynamic interaction 78—47548
- position space LCAO wave function, momentum space variation approx., many centre integrals 80—27926
- post-buckling behaviour of structures using a finite element-nonlinear eigenvalue technique 80—92078
- potential problems, non-local, Perey effect, WKB method 80—68077
- potential scattering, partial waves with nonzero ang. momentum, zero range pot. method *(Russian)* 78—29006
- predissociating harmonic oscillator, relative line widths and level shifts 80—23469
- pressure vessel with hemispherical head, shell intersection, elastic stress anal., homogeneous eigenfunction method 77—23884
- projector variation method, general outline 79—97244
- propagation operators, eigenfunction orthogonality *(Russian)* 77—49613
- proportionally damped dynamic systems, eigenvalues *(German)* 79—21540
- pseudo Coulomb problem, group O(2,1), irreducible representation 80—73209
- PWR, internal vibration calc. rel to operational safety condition *(Czech)* 78—8915
- PWR core, variational estimate of eigenvalue of neutron diffusion eqn. 78—58322
- QED without divergence, fine structure constant, Ward-Takahashi relation and eigenvalue eqn. 79—17648
- quadrupole-phonon states, fifth label generating operator, props. and eigenvalues 80—79887
- quantum chemistry, spin-free, alternacy, quantum no. assignment 79—9988
- quantum decay models, complex energy eigenstates for pot. scatt. 79—6011
- quantum energy levels, statistical mechanics method, perturbative variational approach 80—62513
- quantum field theory, inverse problem method 80—68377
- quantum Hamiltonian on lattice, estimation of eigenvalues 79—40669
- quantum mechanical particle in random potential, inverse participation ratio in $2+\varepsilon$ dimens. 80—36908
- quantum mechanical systems, moment method of eigenvalue and expectation value determ. 80—62534
- quantum mechanics, decaying states in rigged Hilbert space formulation 80—62521
- quantum mechanics, group representation theory, intuitive approach for teaching 79—25804
- quantum pendulum, representation of canonical relns. 80—42084
- quantum pendulums, classical, semiclassical and quantum aspects, teaching 80—101679
- quantum scattering problem as eigenvalue problem 78—28971
- quantum system, jarring and corresponding stimulated transitions 80—17839
- quantum tunnelling, reaction coord. method 80—62500
- quark confinement, coupling constant inverse, energy perturbation expansion and eigenvalue 80—86658
- quark confinement, Dirac equation with quadratic scalar potential 80—27459
- quartic anharmonic oscillator, non-perturbative soln. of eigenvalue problems 77—33900
- quartz crystal resonator nonlinear analysis 79—55299
- quartz SAW velocity/temperature dependence calc. 79—56062
- quasi-degenerate Rayleigh-Schrodinger perturbation theory, calc. of effective Hamiltonians 79—71284
- quasiclassical estimates on moments of the energy levels 80—98806
- radial matrix element generating function for mol. vibr. calcs. 77—18904
- radial Schrodinger equation, eigenvalues, matrix elements, phase shifts 80—86133
- radial wave equation, particle in asymptotically Coulomb pot., eigenvalues and eigenfunctions calcs. 77—57214

eigenvalues and eigenfunctions continued

- radiation field in flat parallelepiped, ideal photon gas eigenvalue spectrum 78—8344
- radiative transfer albedo problem in inhomogeneous isotropically scatt. atmospheres 80—36398
- radiative transfer integral equation spectrum, eigenfunctions asymptotic behaviour 80—67540
- radiowave propagation in isotropic inhomogeneous atmosphere with refractive index arbitrary profile, appl. *(Japanese)* 78—44968
- random chain, low-energy density of states and long-time behaviour, scaling approach 79—25994
- random Hamiltonian eigenvalues by tridiagonalisation, density of states 80—39493
- random matrix ensembles, joint eigenvalue distrib. 80—101748
- random sparse matrix block triangularisation 79—44703
- reactor core, uniform infinite lattice eigenvalue as function of buckling 79—609
- reactor spatial control during nuclear station load cycling, multivariable control algorithm 79—13490
- real-space renormalisation group transformation based on cumulant expansion 79—12730
- recirculation maths. and cardiac output meas. 77—56404
- rectangular plate with thermal gradient vibration anal. 79—27567
- reduced eigenvalue method use in finite element thermal transient problems 77—3711
- reflected cylindrical reactor, eigenfunction and numerical solns. to critical problem 78—58326
- relativistic π-mesic atom, eigenfunctions and eigenenergies, N-space dimensions calcs. 80—41988
- relativistic single-particle two-body bound-state integral equation, numerical solutions 80—52389
- relativistic Wigner superoperator and its distribution 77—33897
- relativity, spherically symmetric space-times with vanishing curvature scalar 80—68096
- repulsive quadratic potential, energy eigenvalues determ. 79—9136
- rescaling Schrodinger eigenvalue problem perturbation series 79—92980
- resonance eigenvalues, accuracy criteria 80—91423
- resonance theory in indefinite metric spaces 80—101730
- resonator, marginally stable, gain effect on electrodynamics 80—53339
- Riccati method for difficult eigenvalue problems 77—64937
- Riccati transforms., eigenfunctions of linear differential eqns. with separated boundary conditions 77—64936
- rigid rotor in electric field, energy eigenvalues, Brillouin-Lowdin perturbation expansion 78—62690
- rigorous lower bounds to energy levels, Brillouin Wigner perturbation theory, finite summations 78—54216
- ring laser, open cavity matrix eqns. in diffraction theory 80—69429
- Ritz approximation, convergence theorem for eigenvalue calcs., appls. 77—75042
- Ritz-Givens-Householder method, anharmonicity type λx^{2m}, Schrodinger operator energy levels 78—28970
- rotated coordinate method use, rel. to stabilisation method 80—37845
- rotated hamiltonians, complex-coordinate rotation and least-squares variational method 80—68075
- rotating (kerr) black hole perturbations, spin weighted spheroidal harmonics 78—4277
- rotating cylinders, Taylor vortex form. and spectral props. of boundary value problems 79—90262
- rotating harmonic oscillator, eigenvalues 80—82675
- rotating harmonic oscillator, eigenvalues of radial Schrodinger eqn. 79—67184
- rotating stars, normal modes, general variational principle 80—12750
- rotating stars, perturbs. and stability, eigenvalues and perturb. theory 80—46538
- rotating stars, perturbs. and stability, eigenvectors and variational principle 80—46537
- rotating strings, elastic, heavy, nonlinear eigenvalue problems, bifurcating branches of solns. 80—73174
- rotating structure eigenvalue problem, stationarity principle 77—35027
- roto-translations, method of conditioned observations 78—12531
- S-matrix theory, determinant and its relation to number of eigenvalues due to perturbation 78—58132
- sandwich beams, tapered symmetric, frequency and loss factors 78—38247
- scalar diffraction, inverse theory, eigenvalue formulation 80—102613
- scalar fields, non-null eigenvalues 79—21623
- scalar wave scatt. by slender body of revolution 78—81857
- scattering, relativistic, separable representation of square well potential 80—82922
- scattering theory, existence and completeness of wave operators, eigenvector orthogonal complement 79—9150
- scattering theory for oscillating potentials 80—52072
- Schlesinger systems, isomonodromy deformation, integrable Hamiltonian systems 80—22229
- Schrodinger eigenstates, pointwise bounds, probabilistic approach 78—93544
- Schrodinger eigenvalue problem for N-particle system, survey of general results 77—45713
- Schrodinger eigenvalue problem soln. with long range pots. 80—83
- Schrodinger eqn., complete exact solution to the translation-invariant N-body harmonic oscillator problem 80—31558
- Schrodinger eqn., one dimensional, gap between asymptotic degenerate eigenvalues, quantum and semiclassical methods 78—57803
- Schrodinger eqn., $r^{-(s+2)}$ type, SL(2,R) acting on quaternions 80—57125
- Schrodinger eqn., solution method for special class of potentials 80—36897
- Schrodinger eqn. eigenvalue and eigenfunction computation by stepwise potential function approximation 77—17853
- Schrodinger eqn. eigenvalue nonexistence condition 78—24682
- Schrodinger eqn. eigenvalues for particle in monotonic pot. 79—40412
- Schrodinger eqn. with double-minimum potential, numerical integration 78—58573
- Schrodinger eqn. with logarithmic pot., soln. for quark model particle spectroscopy 80—32065
- Schrodinger eqn. with singular pots., scatt. phase shifts and eigenvalues 78—62102
- Schrodinger eqns. in exterior domains, nonexistence of nontrivial solns. 78—65819
- Schrodinger equation, applications of perturbation theory to numerical integration methods 80—12926

eigenvalues and eigenfunctions continued
Schrodinger equation, eigenvalue bounds, method for obtaining formulae 79−75392
Schrodinger equation, eigenvalues in singular perturbation problem 79−49088
Schrodinger equation, energy approximants and perturbation theory 80−22232
Schrodinger equation, exactly soluble with bistable pot. 80−67950
Schrodinger equation, existence of eigenvalues of infinite multiplicity 80−94989
Schrodinger equation, linear potential wavefunctions, generalised hypergeometric functions 80−62512
Schrodinger equation, momentum space, bound-state energies and eigenfunctions 79−92972
Schrodinger equation, nonlinear field equations, quantum inverse scattering transform method, 2-D ice and ferroelectric lattices 80−68348
Schrodinger equation, nonseparable, series solns. and variational principle, appl. to H_2^+ and He 79−36504
Schrodinger equation, numerical integration, using WKB approx., eigenvalue estimates 78−12486
Schrodinger equation, one-dimensional eigenvalue problem, bound state solns. 78−20992
Schrodinger equation, polynomial factor eigenfunctions, corresponding pots. *(Chinese)* 80−22236
Schrodinger equation, soln. for $\lambda x^2/(1+gx^2)$ interaction with g small and λ large 79−92967
Schrodinger equation, solution by hand-held calculator 80−52052
Schrodinger equation, three-body problem with hard cores, 1-D, reduction to 2-D Helmholtz eqn. 80−62523
Schrodinger equation, three-body problem with hard cores, 1-D, eigenvalue lower bounds 80−68069
Schrodinger equation, wave functions, generalised wave operators for system of three charged nonrelativistic particles 79−75398
Schrodinger equation eigenvalues, perturbation theory calc. without complete set of eigenfunctions 80−105519
Schrodinger equation nonseparable potentials, vibr. energy level semiclassical calc. 80−8832
Schrodinger equation with an anharmonic oscillator potential 80−27163
Schrodinger equations, three-body problem, bound state eigenvalues lower bounds, upper bounds by Rayleigh-Ritz method 80−68068
Schrodinger operator, eigenfunctions expansion 77−74260
Schrodinger operator, interaction of type $\lambda x^2/(1+gx^2)$ 79−91
Schrodinger operator, point spectrum, non-existence of eigenvectors of compact support *(French)* 80−68063
Schrodinger operator eigenvalue calc., linear error minimisation *(German)* 77−33880
Schrodinger operator eigenvalues, proof of nonexistence 78−81878
Schrodinger operators, weakly coupled and one-dimensional, asymptotic behaviour of ground state 80−22220
Schrodinger-Infeld-Hull factorisation, quantisation condition, matrix elements and selection rules 78−41909
second-order linear differential equations 77−9852
self-adjoint, semi-bounded operator in Hilbert space, computational method 77−26206
self-adjoint operator, eigenvalue bounds, variational approach *(German)* 79−25886
self-avoiding random walks, eigenvalues Monte Carlo determ. 78−57849
self-conjugate and positive definite operator, simultaneous calc. of eigenvalues *(Ukrainian)* 78−54154
semi-classical bounds for eigenvalues of Schrodinger operators 78−70010
semi-simple Lie groups, Casimir operator eigenvalues, symmetric power sum expansions 80−86604
semiclassical eigenvalue problem 77−23404
semiclassical for pot. functions, on finite interval, WKB soln. to one dimens. Schrodinger eqn. 78−28978
semiclassical perturbation expansion of the multichannel scattering matrix 79−49410
semiconductors, deep impurities, evanescent states and complex bound structure 80−34387
semiinfinite strip with clamped sides, bending, Papkovich-Fadle eigenfunction completeness 80−58929
sequential decays of open quantum systems 80−8851
Serber-type spin eigenfunctions, generation by projection operator method 77−30028
shaft, whirling motion, stability analysis 78−13894
shear flow stability, modified Tietjens function for asymptotic anal. 77−65733
shell, cylindrical, nonuniform axial edge load, thermal load, linear buckling 78−63345
shell model eigenvector components, distrib., invariance props. of random matrices ensemble 78−62492
shells, conical and cylindrical, effect of rib stiffness on buckling under external pressure 77−3757
shells of revolution, Ritz-Galerkin method *(Russian)* 77−80062
sine-Gordon equation, nonlinear field equations, quantum inverse scattering transform method, 2-D ice and ferroelectric lattices 80−68348
sine-Gordon soliton, adiabatic behavior in presence of perturbations 79−49093
single eigenvalue distrib. for non-zero mean matrix ensembles, correct form 80−73198
singular boundary points, behaviour of eigenfunctions of BEP and HEP 80−4920
singular integral operators with integral eigenvalues and polynomial eigenfunctions 79−62997
singular perturbation theory, eigenvalues that do not tend to unperturbed values 79−92976
singular potentials, inhomogeneous boundary value problem, eigenvalue equation 79−58530
singular Schrodinger operators, eigenfunction expansions 77−53793
singularity at corner of wedge shaped punch or crack 78−83252
skew-symmetric eigenvalue problem, algorithmic formulations 78−77673
slab, zeroth order variable eigenvalue approach to melting or solidification 77−67392
SO(N) grand unified gauge theories, eigenvalue conditions and asymptotic freedom 79−22010
solar flares, soft X-ray flux eigenvectors from principal component anal. 80−41781
solar intense magnetic flux tube, convective instability 79−30038
solitary Rossby waves in zonal shear flows, interactions, terrestrial atm. appl. 79−7379

eigenvalues and eigenfunctions continued
soliton, extended particle, quantisation, degeneracy of eigenstates 80−73594
soliton eqns., Lie group framework 78−24635
solotone effect and torsional eigenfreqs. of spherical shell 78−92798
solution of the Dirac equation with anomalous magnetic moment 78−82133
sound propagation in parallel sheared flows in ducts, mode estimation 80−79026
Sp(2n), eigenvalues of invariant operators 79−71652
spacecraft, flexible, eigenvalues and eigenvectors for hybrid coordinate eqns. of motion 79−75085
spectral modal analysis program DYNA-M, structures containing up to 40 lumped masses, DEMOS-E library program 78−92800
spectral props. of many electron atomic Hamiltonians, appl. to 2-electron atoms 79−63922
spectral theory of $(p^2+m^2)^{1/2}$-Ze^2/r operator 77−45719
spherical dome, three-dimens. elasticity soln. and edge effects 78−59306
spherical top mols., vibr.-rot. eigenvalue spectrum; energy level cluster anal. 79−18174
spin Hamiltonian consts., computation from EPR single cryst. data 77−90013
spin system, isotropic, N-component, with long- and short-range interactions, crit. behaviour 78−76256
spin system, transient phenomena, soln. using eigen-coordinate system of magnetisation vector 80−25116
spin-1 mixed states orbits of rotation group on density matrices 77−74612
spin-extended Hartree-Fock method, approx. variant 77−79531
spin-weighted angular spheroidal functions 78−8222
spinor-spinor Bethe-Salpeter eqn. 78−29238
spurious avoided crossings of pot. energy curves, eigenvectors and representation space 79−68286
stability problem, lateral, with free-flying column, asymptotic solns. 79−14242
star counts, eigenvectors anal. for space densities derivation 80−85932
Stark effect, perturbation and variation treatments, appl. to H(1s) reson. 80−14105
static screened Coulomb potential, high-accuracy eigenvalues 79−40403
stationary axially symmetric Einstein eqns., linear eigenvalue problem, complete integrability 78−77780
statistical analysis of ground wind vector, wind speed and direction prediction 80−17347
Stekloff type boundary-value problems, Green's functions, asymptotic formulae *(Russian)* 77−22379
stellar low-frequency gravity modes, eigenfreqs./rot. general relation 79−16934
stellar magnetic configurations linear oscills., eigenfreqs. and eigenfunctions 79−44461
stellar models, nonradial oscillations of generalized Roche series 80−21992
stellar nonradial oscillations, avoided level crossing 80−31294
stellar response functions and secular modes 80−17572
stochastic differential operator eigenvalues, approx. soln. of mean problem *(German)* 78−12540
stochastic eigenvalue problem, limit distribution *(German)* 80−52134
Stokes flow in a trench between concentric cylinders 78−83360
Stokes flow in conical trenches 78−83413
stratified flow of two fluids between vertical planes, interface stability *(French)* 78−38382
string with time-varying length 79−50620
structural analysis, dynamic, soln. of quadratic eigenproblems 77−89017
structural analysis, dynamic condensation method 79−3943
structural dynamics, vibrs., eigenrelations 78−1589
structures dynamic problems, eigenvalue economisation, program *(Italian)* 79−35544
Sturm Liouville eqns., numerical anal. and eigenvalue problems 80−90655
SU(2), eigenstates of complex linear combinations of J_1, J_2, J_3 78−58139
SU(2)×U(1) gauge model, eigenvalue condition for Weinberg mixing angle, new leptons and quarks 78−41463
SU(2) gauge fields, eigenspinor-eigenvalue eqn. 78−78076
SU(N) gauge theories, 1/N expansions, singular integral operator 80−57511
SU(N) symmetric quantum dynamical systems, $N \to \infty$, energy spectrum for singlet and adjoint states 80−62880
Sun oscillations, eigenfreqs. and eigenfunctions for 1968 nonstandard solar model 79−35218
Sun radial oscillations, first twenty modes of 1968 non-standard solar model 77−41371
superlinear Hammerstein operators and nonoccurrence of secondary bifurcation 78−16641
superposed Yukawa and inverse square potentials, eigenenergy expansion 79−30281
supersonic flow of nonstationary boundary layer with self-induced pressure near vibrating wall 79−86459
supersonic flow past conical parawings with small camber, trailing edge slope and membrane weight effect *(German)* 77−31331
surface waves, existence in nonhomogeneous elastic semi-space 78−67071
surface-fluid-shell system, finite element anal. of dynamically coupled motion 77−19536
symmetric eigenproblem partial soln., truncated Lanczos method 77−5649
symmetry in classical eigenvalue anal. 78−36827
Temple's lower bound, generalisation 79−88823
tensor spherical harmonics on S^2 and S^3 as eigenvalue problems 79−17324
theory, book 78−12532
thermal convection in closed gas centrifuge, eigenvector soln. of linearised eqns. 80−83797
thermoelastic stress in cylinders, Lanczos-Chebyshev method 80−33458
thermosphere, structure and dynamics rel. to tides and diffusion waves 79−35026
thin plate Semiloof element for structural anal. 79−3913
Thirring model, massive, static localised soln. 78−16930
three body problem for hyperbolic and Coulomb potentials 80−22223
three magnon bound state eqn., physical eigenstate 79−4663
three-body eigen wave function of a continuous spectrum, asymptotic form 79−5994

eigenvalues and eigenfunctions continued
  three-body problem, number of discrete levels 77—49636
  three-body problem, variational method appl. to He atom *(German)* 77—33881
  three-body system, computation method for eigenvalues and eigenvectors 78—24681
  three-body systems, number of bound states and Efimov's effect 80—31536
  three-particle reson., eigenvalues of Faddeev eqn. kernel determ. 77—2565
  tight lower bounds to eigenvalues of the Schrodinger equation 80—94984
  time asymmetries and classical and quantum physics 80—22216
  toroidal resonators for EM waves, Maxwell eqns. for toroidal geometry 80—102598
  torsional eigenfreqs. of spherical shell, asymptotic distrib. 78—88800
  torsional vibration natural freq. sensitivity anal. 77—74218
  torsional wave propagation in elastic inhomogeneous cylinders 77—80104
  transport problem stationary, generalised, Laplace operator eigenfunction series soln. *(Russian)* 78—81931
  trial wave functions, by off-diagonal hypervirial theorem 79—22578
  triatomic molecules, rotating, semiclassical eigenvalues 80—9588
  tropical troposphere, Fourier component eigenvalue anal. of CISK-induced disturbances 77—2199
  tunnelling in double-well potentials, symmetric and asymmetric, periodic orbit theory 80—23488
  two-body coordinate transform., laboratory to centre of mass coordinates 78—21345
  two-centre generator coordinate model functions, ang. momentum eigenstates projection 78—12994
  two-centre molecule-like states, generator coordinate wave function projection 78—12995
  two-dimensional Wigner-crystal-liquid-surface system, eigenmodes and instability of charged liq. surface 80—10896
  two-electron atom, energy eigenvalues and eigenfunctions, CI method 77—50371
  two-electron system, natural orbitals, pseudo-eigenvalue eqn. and long-range behaviour 79—85886
  two-point boundary-value problems with eigenvalue parameter in boundary conditions 78—73830
  two-site Hubbard Hamiltonians with arbitrary electron density, solution 77—74210
  two-well oscillator, eigenvalues, scaling properties, WKB approx. 79—25897
  unbounded Hermitian operators, low-lying eigenstates, method 80—98812
  uncertainty measure for compact Lie group, minimised for max. weight vectors 78—20996
  unified theory of atoms and atomic aggregates, self consistent theory 80—102418
  uniform potential vorticity flow, wave interactions model 79—12196
  uniform theory of inhomogeneous waveguide modes near cut-off 80—28324
  unstable resonator, half-symmetric, with coated rear cone, polarisation effects 80—74402
  unstable resonators, ε-approx. eigenvalues and eigenfunctions *(Chinese)* 80—5766
  van der Waals molecules, higher-order vibr. eigenvalues calcs. 79—36722
  variable-thickness elastic orthotropic annular plate nonlinear oscillations 79—68630
  variational interpolation of linear functionals of inhomogeneous eqns. 78—49638
  variational methods for complex eigenfrequencies 80—28631
  variational principle for spinning liquid-filled solid bodies 80—43609
  Varshni V and Lennard-Jones pots., 3rd order WKBJ eigenvalues 79—6982
  vector spherical harmonics of unit hyperboloid in Minkowski space 78—32732
  vector wind meas., principal components anal. 79—39807
  vibrating plates, reposing on springs, numerical solutions and eigenvalues *(French)* 78—79245
  vibrating system of finite degrees of freedom, linear, numerical solution 78—24656
  vibrating systems with mixed boundary conditions, nonorthogonal eigenfunctions 77—14941
  vibrating thin rectangular plates, influence of thermal grad. on natural freq. 79—32353
  vibration, transverse, of rectangular plate with eccentric circular inner boundary 80—106737
  vibration problems, element spaces and separation for determining bounds to eigenvalues 79—14317
  vibration problems of continuous systems, discrete models 77—89057
  vibrational systems of multi degrees of freedom subject to arbitrary force, response analysis 80—12912
  vibrations of plates, circular and annular, with ring mass *(Japanese)* 79—18783
  vibrations of string with time-varying length 79—25870
  virial theorems, generalised and pointwise 79—30354
  viscoelastic body eigenfrequency determ., finite element method *(German)* 79—23270
  viscoelastic fluid, stability of laminar boundary layers *(German)* 77—72335
  viscoelasticity equations, numerical soln. via eigenvalues expansion 77—89042
  viscous flow in channel, existence theorem of eigenvalue problem 77—33871
  Wangerin differential eqns. for capacity of charged disc or sphere in concentric hole of grounded sheet 77—14635
  water waves, discontinuous Steklov problem 79—98739
  wave coupling in an anisotropic medium 79—55514
  wave eqn., one-dimensional, asymptotic formulae for eigenvalues *(Japanese)* 79—25869
  wave equations, numerical solns. for real or complex eigenvalues 77—33877
  wave functions, Serber-type spin-adapted, and time reversal 78—5117
  wave propagation, random periodic structure, statistical properties 77—75392
  wave propagation in stratified media, matrix anal. 79—12618
  waves, shallow water, with quasi-periodic boundary conditions, eigensolutions of elliptic problem 80—83804
  weak quantization in a nonperturbative model 79—88825
  wedge field, composite truncated, Dirichlet problem, point source appl. 77—5676

eigenvalues and eigenfunctions continued
  Weinberg functions, Born approx. in scattering problems, phase shift 80—32248
  whispering-gallery waves, polarisation and losses along twisted trajectories 80—9798
  Wick-Cutkosky model, asymptotic behaviour of eigenvalues for large principal quantum no. 77—10177
  Wick-Cutkosky model, eigenvalue refl. symmetry 77—61193
  Wigner representation, semi-classical ergodicity of quantum eigenstates 80—8833
  Wigner-Weisskopf model form factor construction from eigenfunctions 77—78995
  wind, empirical eigenvector anal. of vector obs. 77—86990
  wind generator oscillation modes in large power systems 79—29446
  WKB approx. and scaling behaviour for Hellmann-Feynman and virial theorems 78—86193
  WKB eigenvalues, asymptotically exact, upper and lower bounds 77—3250
  x^4 potential, associated ground state wavefunction, sum rules 79—45036
  zeta-function regularization and multi-instanton determinants 80—13215
  $\Theta_2{}^4$ quantum field theory, numerical methods, anharmonic oscillator approx. 80—52390
  Be, atom, ground state, accurate CI wavefunction 77—42245
  C, first-principles pseudopotential in the local-density-functional formalism 79—59328
  Ca_2, rot. perturbed Morse oscillator eigenfunctions and Franck-Condon factors 77—42309
  ^{40}Ca, vibrating nucleus, eigenvalues of Baranger-Veneroni operator, RPA solns. 79—40863
  Cu IV, wavelength region 700-1200 Å, extended analysis 80—99473
  Fe, spin 3/2, in strong crystal field, axial and rhombic symmetry, EPR parameters 79—28591
  H atom, eigenfunctions in spherical and parabolic coords., relationship coeffs. 77—82409
  H atom spectra, homogeneous mag. field, variational approach 79—22629
  H, degenerate 3s-3d levels, in mag. field, eigenvalues, Bender-Wu formulas 80—83275
  H, eigenfunctions and eigenenergies, N-space dimensions calcs. 80—41988
  H, eigenvalue resonances in Stark effect and perturbation theory 78—90118
  H hyperfine splitting inside paraboloidal surfaces 80—99445
  H + positron, S-wave scatt., lowest reson. calc. 78—37743
  H_2, 3d-triplet complex, Zeeman effect, eigenvectors and g-factors, rovibronic states 79—72353
  $H_2{}^+$ three lower states, three body problems, separations of variables 80—36903
  H_2 + Ar, 4500K shock wave expt. simulation, vibr. state changes and dissoc. 79—61850
  H_2O, excited stretching vibrs., quantum mechanics. 80—91535
  He atoms, S-state eigenfunctions, Konishita's expansion 78—16674
  He, energy eigenvalues and eigenfunctions, CI method 77—50371
  He^+, electron impact excitation cross-sections, reson. parameters calcs. 80—91686
  He-He, Born-Oppenheimer pot. using Hylleraas-type electronic wave functions 79—31438
  HeH^{2+}, lowest 20 states, eigenvalues, electronic wavefunctions, w.r.t. internuclear separation 77—18811
  $He(1s2p)^1P$, eigenvalues and eigenfunctions, time-depend. HF calcs. 77—42241
  $He(2^{1,3}S)$ + H, autoionising system, Siegert eigenvalues, variational calcs. 79—50106
  HgH, predissoc. by rot., continuous rot.-vibr. spectrum, resons. and eigenvalues, Weyl's theory 77—18997
  N_2, rot. perturbed Morse oscillator, eigenfunctions and Franck-Condon factors 77—42309
  NO, v=0,1 states, spectroscopic data calc. 78—86851
  Na_2, rot. perturbed Morse oscillator eigenfunctions and Franck-Condon factors 77—42309
  NiVI, sixth spectrum analysis 220-335 and 890-1325 Å regions 80—95565
  ^{16}O, vibrating nucleus, eigenvalues of Baranger-Veneroni operator, RPA solns. 79—40863
  SF_6, ν_3 band high-J manifolds, eigenvalues use second-order perturbation theory 79—36702
  SO(2), infinite-well pot., for teachers 77—33791
  UO_2-water tightly-packed lattices, ENDF/B-IV data evaluation 79—9805
  W, first-principles pseudopotential in the local-density-functional formalism 79—59328
  YIG thin film gyromag. waveguide, on GGG substrate, optical propag. props. Faraday effect 80—74513
eigenvectors *see eigenvalues and eigenfunctions*
eightfold way *see SU_3 theory*
Einstein-de Haas effect
  see also gyromagnetic ratio
  history, Einsteins' expt. work 80—98783
  measurement, balance appl., thermal noise effect 78—65906
einsteinium
  see also nuclei with ......
  film, preparation and characterisation 80—15405
  ^{249}Es, K-shell fluorescence yields from Auger electrons and X-rays, precision meas. 79—31462
  ^{253}Es, separation and α-spectra identification following neutron irradiation of Cf 78—17435
einsteinium compounds
  aqueous solution, electrochem. props., thermodynamic props., radiopolarography 77—29040
  X-ray powder diffr. 80—2002
  $EsCl_2(Br_2)(I_2)$, prep., characterisation and decay of Es(II) 80—16727
  $^{253}EsBr_x$, spectral and X-ray diffr. data, 25 to 700°C 77—28584
  $^{253}Es(NO_3)_3$, inhaled by rats, late effects 80—30781
elastic aftereffect
  cylindrical shell, submerged 79—18715
  metal porous strip, metal pressure in cold rolling in elastic aftereffect zone 80—40421
  metal strip, porous, elastic aftereffect in cold rolling 80—11689
  steel, C, spring, compressed, patented wire, reverse elastic aftereffect and fatigue strength 79—38881

elastic aftereffect continued
- Ag-Zn (30 at.%), electron irrad. exam. of defect supersaturation by elasticity, and creep meas. 78−47366
- Ag-Zn (30 at.%), electron irradiated, atomic mobility, elastic after-effect meas. *(French)* 78−63874
- Al, electron-irradiated, anelastic relax. due to single self-interstitial atoms 77−39627
- Al, electron-irradiated, anelastic relax. due to clustered self-interstitial atoms 77−39628
- Cu, aftereffect deformation, creep duration effect on structure, rupture time 79−91766
- Cu-Zn-Al, Zener relaxation *(Russian)* 77−21198
- α-Fe, neutron irradiated, mobile C atom trapping, anelastic and magnetic relaxations 80−100306
- Fe powders, cold-pressed, props., effect of air 80−100810
- Mo, elastic aftereffect after fast neutron irrad. at 5K 77−89431
- Nb, relaxation from room temp. to 114°C, computer optimization of elastic aftereffect curves 77−90390
- Nb-H, incoherent spinodals, meas. by Gorsky effect 78−19712
- Nb-H, spinodals and diffusion coefficients of H, sample shape depend. 78−19713
- Ni-Al-Cr-Mo-Ti-W-(Co) alloys EhI 826 and EhI 929, reverse elastic after effect under loading 78−39829
- Ta-H, incoherent spinodals, meas. by Gorsky effect 78−19712
- Ta-H, spinodals and diffusion coefficients of H, sample shape depend. 78−19713
- Ta-H(D), anelasticity due to long-range diffusion 80−60904
- TiNi, imperfect elasticity, elastic after-effect on basis of martensitic transformation theory *(Russian)* 79−100198
- V, diffusion of O and N, elastic aftereffect meas. 78−38881
- V-H, incoherent spinodals, meas. by Gorsky effect 78−19712
- V-H(D), anelasticity due to long-range diffusion 80−60904

elastic constants
- *see also elastic moduli*
- acrylic gel, US observation of critical behaviour *(French)* 79−29414
- alkali halide, interionic potentials, based on elastic consts. and equilib. eqns. 77−47374
- alkali halide, many-body effects and press. derivative 77−35621
- alkali halide, overlap repulsion and pot. energy function for Bohr-like atoms 77−15344
- alkali halides, elastic constants, temp. depend., pseudopot. calc. 80−65120
- alkali halides, free energy of formation of vacancy determ. 77−76597
- alkali halides, interionic potentials, completely independent specification of Born-Mayer potentials 78−55828
- alkali halides, photoelastic consts., short range polarisability effect 80−80748
- alkali halides, three-body interactions, effect on electronic polarisabilities and photoelastic behaviour 79−47382
- alkali hydride, repulsion interaction 78−26488
- alkali hydrides, bulk props. prediction from molecular behaviour 78−51468
- alkali metal, Ashcroft pseudopotential, unified study of props. 80−39239
- alkali metal, bulk properties, computer simulation 78−30729
- alkali metal, thermal expansion, elastic constants, phonon freq. anisotropy *(Russian)* 79−1516
- alkali metal halides, elastic consts., anomalous temp. depend., phonon-lattice interaction 80−107354
- alkali metals, effective ion-ion potential, compressibility and force consts. 80−70158
- alkali metals, elastic and thermal props. by pseudopotential method 80−19899
- alkali metals, elastic constants, temp. depend. 78−51603
- alkali metals, electron fluid model 78−75738
- alkali metals, energy-independ. model pseudopot., second-order elastic consts. 77−62890
- alkali metals, Gruneisen parameter and temp. depend. of elastic consts. 80−39317
- alkali metals, Gruneisen parameters calc. in terms of elastic consts. 77−1242
- alkali metals, phonon dispersion binding energy, compressibility, elastic consts. electron screening and Ashcroft pot. calcs. 80−65174
- alkaline earth chalcides with NaCl-type structure, third-order elastic consts. 80−70292
- alkaline earth oxides, analysis of press. derivatives of second order elastic consts. 77−35618
- trans-p-n-alkoxy-α-methyl cyanophenyl cinnamates, elastic consts. and orientational order parameters 80−44244
- 4′-n-alkyl-4-cyanobiphenyls, elasticity, orientational order, and nematic-isotropic transition 77−84643
- 4′-n-alkyl-4-cyanobiphenyls, nematic, elastic and optical props. 77−11613
- alloys, hot plastic strain, stress- strain-time dependences *(Russian)* 80−40430
- alloys elastic const. meas. technique 78−7164
- almandine-pyrope garnet, elastic consts. from rectangular parallelepiped resonance method 77−56625
- Anderson-Gruneisen parameter for cubic crystals 78−79672
- anharmonic crystal, lattice dynamics and stability, self-consistent phonon theory 79−51209
- aniline hydrobromide, ferroelastic, acoustic softening near transition temp. 80−96617
- anisotropic media, US determination of second-order adiabatic elastic coeffs. 79−73256
- anisotropic medium, perturbed, propag. of elastic waves *(French)* 79−42144
- anthracene, lattice parameters press. depend., elastic consts. 78−38686
- Armco iron specimen, elastic const. meas., X-ray diffr. technique 78−5714
- azoxybenzene, nematic liq. crystal, elastic consts., varying mag. field and temp. 78−18540
- BCC crystal, elastic constants, thermal expansion and bulk modulus 80−6452
- BCC lattice, deform. potential calc. 79−55806
- benzene, Brillouin scatt., cryst. at 0°C, elastic consts. 78−43882
- benzene, Brillouin spectra, elastic consts. and intermol. pot. 79−42977
- bimaterial full-plane with crack at any angle to interface 77−14965
- biological soft tissues, large deform. anal. 77−5018
- biphenyl-d_{10}, Brillouin scatt. at room temp. 80−71433
- bone, human cortical, US properties and microtexture 80−51144

elastic constants continued
- bone, piezoelectric, dielectric and elastic constants, rel. to temp. and hydration 77−16946
- β-brass, cryst. struct., elastic consts., central force model 78−51637
- brass, elastic constants, third order, from US velocity meas. 78−76687
- α-brass, reson. vibrs. of metal spheres, elastic consts. and internal friction 78−15443
- β-brass (40 to 50 at.% Zn), elastic shear consts., comp. depend., pseudopot. calc. *(Russian)* 80−24525
- butadiene-styrene block copolymer, viscoelastic props. 79−8336
- calcite, anisotropic elastic const. meas. by uniaxial compression test *(Japanese)* 79−79822
- carbon fibre reinforced composites, filament-wound, thermal residual stresses 80−49290
- Cauchy relations, sufficiency for central pot. determ. 79−46735
- CBOOA, nematic, mag. field depend. of laser light scatt., interf. rings 78−26434
- CBOOA, nematic phase laser light scatt., mag. field depend., crit. deform. *(Japanese)* 78−2826
- CBOOA, nematic-smectic transition, singularities, elastic const. var. 77−39537
- CBOOA, smectic A-nematic transition, X-ray and light scatt. obs. 79−95129
- ceramic, elastic behaviour, finite element anal. model, thermal props. 78−31449
- cerebro-spinal specific elastance in cats, in vivo determ. 78−40236
- chevron notched short bar specimens, compliance and stress intensity coefficients 80−96232
- 2-chloronaphthalene, elastic props. exam. by Brillouin scatt., rel. to polymorphism 79−77669
- cholesteric liquid crystal mixture, with positive dielectric anisotropy influence of external fields *(Rumanian)* 78−59751
- cholesteric liquid crystals, mol. model, temp. depend. of pitch and elastic consts. 79−77510
- clinical support surfaces, mech. compliance evaluation 80−92053
- Co-base metallic glasses, elastic const. 77−66671
- coesite, elasticity meas. on 100 μm cryst. 77−44978
- compact tension specimens, stress intensity and crack openings 80−1474
- compliance, review and extension of information for common crack growth specimens 79−3974
- compliance and K_I calibration of double cantilever beam specimens 78−55598
- compliance calibration, expt., of WOL specimen 78−19798
- composite materials, determ. methods, review 77−42746
- composite materials, elastic constant estimation, elastic wave scatt. theory 80−34114
- composites, three-dimensional structure, mech. characts. 80−38266
- conical inclusions, singularity values for ranges of elastic constants 78−51071
- COOB, smectic A-nematic transition, X-ray and light scatt. obs. 79−95129
- coplanar Griffith cracks in infinite elastic medium, dynamic stress conc. 79−46270
- Coulomb vector gas in two-dimens., melting 79−69449
- crack at the boundary between two materials with a branch into one of them in the case of antiplane strain 80−79231
- cracked elastic solid, 3-D wave propagation 79−46251
- critical behaviour near elastic phase transitions 80−100299
- crystal, stressed, elastic const. determ., static method 80−49291
- crystals, deformed, hydrostatic pressure, invariance relations for acoustic waves 79−95087
- crystals, rel. to surface waves propagation over liquid and crystalline layers 80−76924
- cubic crystal, acoustic waves, Christoffel elastic eqns., and elastic consts. 79−51205
- cubic crystal, phase transitions with three-component order parameter, elastic anomalies *(Russian)* 79−37837
- cubic crystal, stressed, second and third order elastic consts. 79−82274
- cubic crystal, temp. depend. of third-order elastic consts. 78−18699
- cubic crystals, third-order elastic consts., determ. method 77−80566
- cubic ionic crystal, photoelastic shear consts. 79−86833
- cubic solids, Debye temp., elastic consts. averaging 80−54332
- 4-cyano-4′-octylbiphenyl, bend mode elastic const., single power law behaviour 79−73297
- N-p-cyanobenzylidene-p-n-octyloxyaniline, smectic-A liq. cryst., nematic pretransitional mech. effects 77−11481
- cyanobiphenyls, 80CB and its mixtures with 7CB, orientational order and elastic consts. 78−91245
- cyclohexane, plastic phase, Brillouin scatt., elastic consts. determ. 79−24324
- cylinders, perfectly conducting arrays, transport prop. investig. 80−13011
- DC Bi:Te, elastic consts., electronic contrib. 77−84826
- deformation potential of crysts. formulation *(Russian)* 77−19894
- di-n-decyl azoxy methyl cinnamate, smectic-A liq. cryst., anisotropic US propag. 79−55829
- diamond, acoustic phonon geometric propag., anisotropic continuum acoustics 77−4170
- diamond, Cosserat continuum model, elastic props., lattice dynamics 80−59552
- diamond, yield stress from Hugoniot elastic limit and elastic consts. 79−83261
- diamond, zone-centre optical phonon, effect of uniaxial stress, elastic consts. determ. 78−91399
- dicalcium lead propionate, ferroelec., piezoelec. and elastic props. 78−84528
- dicalcium strontium propionate, elastic stiffness consts., determ. in US freq. region 79−37752
- dicalcium strontium propionate, temp. depend. of elastic const. c_{16} 79−28029
- dielectric, many-body theory, appl. to NaCl-structure 78−38805
- p,p′-diheptylazobenzene, nematic, physical props. 78−79524
- dimethylammonium manganese tetrachloride, elastic props. 79−60418
- dislocation energy and line tension, effect of dissociation 79−27985
- dislocation self-energy effect on choice of slip system 79−27982
- DOBAMBC, chiral smectic C-phase ferroelectric liq. crystal film, classical X-Y system, props. 80−44123
- dynamic modulus and compliance, loss and storage component relations *(German)* 79−32268
- EBBA, IR absorpt. spectra, elec. field effects, orientational order parameter determ. by IR dichroism, bend elastic consts. 80−80778

elastic constants continued

- elastic coefficients, independent 4th-order for all cryst. classes, numerical methods anal. 79—69219
- elastic-plastic solids, effective shear modulus, effect of rotation of principle axes *(French)* 77—68409
- elastomeric block copolymer properties obs. 78—27560
- entangled polymers, viscoelastic props., transient network model 78—13918
- epoxy resin-ferroelectric Pb(Zr,Ti)O_3 composite, dielec., elastic and piezoelec. consts. 77—8515
- fatigue crack growth, mechanisms 78—64703
- fatigue crack propag. meas. and crack closure at low stress intensity level by unloading elastic compliance method *(Japanese)* 77—9016
- FCC polycrysts., under hydrostatic pressure 80—107356
- Fe, pure, cubic, single cryst. elastic constants from mech. and X-ray elastic constants of polycryst. *(German)* 80—10591
- ferrobielastic poling, differing stiffness coeffs. of domain states 77—16102
- ferroelectric, order-disorder type, piezoelec. and elastic props. 77—12318
- ferroelectric, uniaxial, crit. behaviour, electrostrictive coupling role 80—71329
- ferroelectric ceramic, polycryst., elasticity props., neutron bombardment effects 80—79856
- ferroelectric ceramics, elastic and piezoelec. eigenstate spaces 79—42901
- ferroelectrics, low lying vibrational modes, crit. behaviour of uniaxial materials 78—84539
- ferromagnet, itinerant electron, magnetoelastic contribs. to US vel., elastic consts., and susceptibility 80—75829
- ferromagnetic metal, band struct. contribs. to shear consts., deform. pot. formalism and Stoner model 79—91280
- fibre cross-reinforced layered composites, moment effects in plane problem 80—64393
- fibre reinforced composite, containing voids, elastic consts. and US velocity, theory 77—89498
- fibre reinforced composites, three-dimensionally reinforced with short fibres, effective elastic consts. 80—58910
- fibre reinforced composites, transverse plane, elastic, failure behaviour *(Japanese)* 78—48510
- fibre reinforced composites, US diagnosis of elastic characts. and struct. parameters 80—40663
- fibre reinforced composites calculation of stress distrib. and X-ray elastic consts. *(German)* 78—52883
- fibre reinforced materials, therm. stresses in unit cell 80—10160
- fibre reinforced polymer matrix composites, space environmental effects 80—71721
- fluorite crystals, Brillouin scatt. and high temp. disorder 78—80365
- fluorite crystals, disorder at high temp., Brillouin scatt. 78—2866
- fluorite structure solids, long wavelength behaviour, elastic consts. 79—87441
- fluorite structured crystals, high temp. disorder and elastic consts. 78—30689
- forsterite, elastic constants of single crystal, temp. var. 78—92818
- fourth order, general method for determ. and appl. 80—34119
- fourth order coeffs., independent, for 32 cryst. classes, computer calcs. *(French)* 80—34117
- fourth-order, determ. 78—6958
- fourth-order elastic coefficients, for all cryst. classes, numerical methods anal. 79—69219
- fourth-order independent elastic coeffs. for trigonal and hexagonal symmetry classes 79—77665
- frontal method for structural mechanics, algorithm for excluding unknowns 80—79157
- Galois unsolvability of anisotropic crystal elasticity sextic equation 79—37170
- garnet solid soln. series, elastic props. inferred from expts. on pyrope 80—76968
- garnet solid-soln. series, elastic props. 78—40550
- glass, inorganic, calc. of microhardness and glass transition temp. 79—5059
- glass, inorganic, cylindrical shell, with initial geometric imperfections, precritical deform. under external hydrostatic press. 77—81306
- glass, laser, elastic, elasto-optic consts. and extinction coeffs., Brillouin scatt. meas. 79—11429
- glass fibre reinforced epoxy composite, mech. and photoelastic props. at high temps. 78—19799
- glass-ceramic, machinable, elastic const. temp. depend. 80—79852
- glasses, strain interactions, low-temp. props. 79—42269
- granular medium, compressibility and force transmission, discrete probabilistic model 78—15448
- graphite, elastic constant softening 79—51190
- graphite, self-consistent calcs. 77—27933
- hard sphere crystal, thermoelasticity in relation to melting 80—107353
- 2,4-hexadiine-1,6-diol-bis(p-toluene sulphonate), cryst., polymerisation, elastic consts., Brillouin scatt. 79—1950
- hexagonal crystals, under press., finite strain theory *(French)* 79—1475
- hexagonal material, Δs effect, anisotropic contrib. 77—90005
- homogeneous isotropic material, high press. eqn. of state and sound vels. to fourth order elastic consts. 79—37806
- III-V compounds, rel. to lattice constant determ. of epitaxial layers 79—19479
- incoherent ellipsoidal precipitate, re-exam. of elastic strain energy 78—51676
- Inconel X, X-ray study of stress meas., elastic const. *(Japanese)* 79—66092
- inert gas solid, long range forces, book contrib. 77—51347
- inner elastic constants, general expressions 79—60419
- inner elastic constants, symm., depend. on symm. of interlattice tensors 79—28028
- inner elastic constants, tensor notation and relation to lattice dynamics 79—28027
- Invar, phase stability, spinodal decomposition 80—88327
- invariance relations for elastic waves in crystals 80—84250
- ionic crystals, eval. of 3rd order and press. depend. of 2nd order elastic consts. 79—77668
- ionic crystals, structurally modulated, elasticity and its limits, yielding and melting 80—49295
- ionic solid, many body effects on fourth order elastic coefficients 77—72647
- ionic solids, many-body effects on fourth-order elastic consts. 77—76483
- ionic solids with NaCl struct., third order elastic consts. 77—35620

elastic constants continued

- Ising spin system, coupled to acoustic and optic lattice modes, critical behaviour 80—71044
- isopropyl ammonium chloroplatinate and chlorostannate, ferroelastic transition, thermal, optical, and elastic meas. 79—28096
- isotropic materials, continuum mechanics in space of any dimension *(Japanese)* 78—41161
- Jahn-Teller cooperative systems, low-freq. dynamics 79—82565
- Jahn-Teller cooperative T-systems, dynamics, elastic props. 80—65511
- Kroner limits of technically important materials, low order limit comparison *(German)* 79—33029
- laminate, calculation of stress distrib. and X-ray elastic consts. *(German)* 78—52883
- laminated beam, 3 component, strength props. *(German)* 80—35269
- layered or reinforced composites, elastic constants and stress-strain parameters *(Russian)* 79—46209
- liquid crystal, tensor field of weak inhomogeneous orientational ordering *(Russian)* 78—67640
- liquid crystal theory, phenomenological and microscopic approaches connection 79—4248
- liquid crystals, NMR spin-lattice relax. time near phase transitions 80—71222
- liquid crystals, prep. and phys. props., book 80—105444
- liquids, US vel. meas. method for elastic const. determ. w.r.t. temp. and pressure 80—15177
- lithium ammonium tartrate, ferroelectric and ferroelastic transitions, Brillouin scatt. meas. 79—33716
- low trigonal symmetry crystals, method for elastic const. determ. 78—2187
- lung parenchyma described as prestressed compressible material 77—90837
- machine-made paper orthotropic US plate wave theory and expt. 79—68460
- magnetic contributions, cooperative, exchange striction mechanism 77—40108
- magnetic crystal, sound velocity temp. depend. anomaly 77—72891
- magnetic symmetry groups, higher order elastic coeffs. calcs. 80—28939
- martensite formation, and lattice props. rel. to elastic constants 80—50630
- MBBA, Frank elastic const. ratio determ. by Rayleigh scatt. 79—99059
- MBBA, IR absorpt. spectra, elec. field effects, orientational order parameter determ. by IR dichroism, bend elastic consts. 80—80778
- MBBA, nematic liq. cryst., elastic consts. determ. 77—27824
- MBBA-CPB nematic complex, dielec., elastic and electro-optical props. 77—32350
- mechanical anisotropy of texture effect on X-ray stress measurement *(German)* 79—29091
- metal, asymptotic ion-pair pots., contrib. to lattice energy, elastic consts., phonon dispersion 77—19898
- metal, cryst. equilib. and Cauchy deficiency 79—19328
- metal, cubic, HCP, non-central, non-isotropic interactions, third-order elastic const. determ. 79—10474
- metal, HCP, atomic struct. of defects 78—30611
- metal, lattice dynamics model *(Hungarian)* 77—27952
- metal, Morse parameter calc., elastic const. evaluation 77—7692
- metal, simple, phase stability and elastic const. 78—31387
- metal, textured cubic, residual stress evaluation 80—89435
- metallic materials, mech. stressed, lattice strain distrib., X-ray elastic const. calc. *(German)* 78—52884
- metals, BCC, ang. forces in lattice dynamics, rel. to elastic consts. 77—84870
- metals, cubic, vol. depend. contrib. to elastic consts., pseudo-pot. theory 77—72646
- metals, d band, reson. model pot. binding energies and elastic consts. calc. 77—69263
- metals, d-band, force fields, elastic consts. predicted 79—33051
- metals, elastic constants and moduli of axial textures 80—75286
- metals, FCC, elastic const. in pair potentials calc., appl. to point defect props. 80—19798
- metals, HCP, electrostatic contrib. to second- and third-order inner elastic consts. for different axial ratios 79—51186
- metals, lattice dynamics and three body interaction 78—10139
- metals, Morse potential appl. in molecular-metallic framework 80—79742
- metals, resonance method for determ. within 80-300K temp. range 78—46918
- metals, simple, interion interaction and interion force constants, effective pots. in nonlocal pseudopot. method *(Russian)* 78—22684
- methylammonium aluminium sulphate, third order elastic consts. from stress shifted reson. freqs. 78—55905
- microinhomogeneous media, appl. of random functions theory *(Russian)* 78—63280
- micropolar circular cylinder, flexural rigidity 79—18724
- mode I stress intensity factors, method of caustics 80—38364
- molecular crystal, anomalous thermoelastic behaviour and orientational transition 77—76334
- molecular crystals, polariton spectra and lattice dynamics 80—49313
- Morse model cubic crystals under hydrostatic pressure, stability 80—19870
- multiphase materials, finite element anal. 77—3717
- naphthalene, lattice parameters, elastic consts., press. depend., neutron diffr. obs. 78—26558
- nematic layers, optical phase difference and capacitance, elec. and mag. field depend. 80—28911
- nematic liquid crystal, anamalous stiffness and tilt angle from nonuniform attachment angle 79—86688
- nematic liquid crystal, capacitance response to elec. and mag. fields, appl. to elastic const. determ. 79—90545
- nematic liquid crystal, elastic consts. determ. 77—27824
- nematic liquid crystal, flexural elasticity meas. *(Dutch)* 80—34112
- nematic liquid crystal, twisted, phase transition like instability in static samples with surface induced tilted alignments 78—26667
- nematic liquid crystals, Frank elastic consts., statistical mech. theory 80—29104
- nematic liquid crystals, IR absoprtion, strong positive dielec. anisotropy, elastic consts. 78—75545
- nematic liquid crystals, molecular structure and elastic consts. 79—77512
- nematic liquid crystals, orientation fluctuations in high mag. field, quenching, birefringence effects 80—64892
- nematic liquid crystals, shear flow in presence of electric AC field, elastic and viscous const. determ. 77—43144

elastic constants continued
neopentane, diamond force const., rel. to crystal elastic consts., Raman freq., bulk compressibility and freq. assignments 80—65183
nephrite, mech. props. 77—44295
noble metals, electronic properties, form. factors, phonon freq. and elastic consts. 77—4168
non-elastic phase transitions, elastic const. crit. behaviour 80—100298
non-piezoelectric crystals, consts. determ. by method of homogeneous deformation 77—80570
non-piezoelectric crystals, elastic constants anal. 77—84827
non-piezoelectric crystals, long-acoustic wave phase velocity governing by elastic consts. 77—80571
noncontact material testing using laser energy deposition and interferometry 79—34258
noncontact material testing using laser energy deposition and interferometry 80—71846
8OCB, nematic-smectic A transition, impurity effects 78—47507
7-8-OCB mixture, nematic-smectic A transition, impurity effects 78—47507
4′-n-octyl-4-cyanobiphenyl, interlayer elastic const. meas. close to smectic-A to nematic transitions 77—80606
octyl-cyano-biphenyl, elastic props. near smectic-A nematic transition 79—23704
octyl-cyanobiphenyl, elastic props. near nematic-smectic A transition 78—59756
octyl-cyanobiphenyl, smectic A-nematic transition, X-ray and light scatt. obs. 79—95129
optical waveguide, thin film, Brillouin scatt. obs. 78—35153
optically isotropic mats., stress intensity factor determ. by dynamic method of caustics 80—33546
orthoenstatite 78—85546
orthorhombic crystals, elastic consts. determ. from free vibr. of rectangular parallelepiped cryst. 77—84849
orthotropic composite model materials, photoelastic calibration 80—87715
oxide minerals, elastic constant systematics 79—69177
paramagnet, elastic modes in applied mag. field 79—60423
paramagnetic metal, band struct. contribs. to shear consts., deform. pot. formalism and Stoner model 79—91280
partially disordered crystal, lattice dynamic model 78—83897
pentyl-cyano-biphenyl, nematic, hydrodynamic parameters meas. with and without applied elec. field 80—100297
phase transition point, elastic anomalies *(Russian)* 77—80621
phenomenological theory of elastic constants anomalies near struct. transition 78—67765
phenylcyclohexanes, p-disubstituted, elastic consts. and diamag. anisotropy 79—65639
phonon focusing and cond. in orthorhombic and tetragonal crysts., boundary scatt. regime 79—42162
physisorbed layer on elastic substrate, commensurate-incommensurate phase transition 79—56074
piezoceramic elastic compliance and mechanical Q-factor at high drive levels 78—60395
plastic, fibre-glass reinforced, flat stressed state, strength and deformation props. function of reinforcement struct. 80—19866
poly(4-methyl-1-pentene), semicrystalline, bulk and film, surface effects in terms of compressional and shear consts. 79—42982
polycrystal, US scatt. by grains 80—2122
polycrystals, single phase, stress strain relations by X-ray diffraction *(Russian)* 80—5999
polycrystals with axial texture, heterogeneity of props. *(Russian)* 80—29192
polydimethylsiloxane end-linked chains, nonGaussian effects 80—65127
polydomain ferroelec. crysts., phys. consts., self consistent calcs. 80—88942
polyethylene, low density melts, temp. depend. of the elongational behaviour 80—6012
polyethylene, oriented, elastic stiffness constants, US meas. 78—76690
polyethylene terephthalate, extruded, elastic consts. meas., mech. anisotropy 78—44155
polyethylene terephthalate, shear compliances meas. of oriented sheet 80—104363
polyethylene terephthalate, sheet, extensional compliance normal to sheet 77—12664
polyethylene terephthalate, sheet, mech. anisotropy meas. by optical technique 77—12662
polyethylene terephthalate, sheet, Poisson ratio compliance consts., interferometry 77—12663
polymer, crosslinked, probabilistic theory of structural and physical characteristics 80—5649
polymer complex dielec. permittivity and compliance, algorithm for calc. freq. dependence 78—68442
polymer films and fibres, compliance constants meas. 78—38261
polymer with hollow spherical inclusions filler, elastic and strength props. 80—35245
polypropylene, extruded, elastic consts. meas., mech. anisotropy 78—44155
poroelastic discs or slabs, dynamic response to harmonic loading 79—41578
Potts model, three state, order-disorder structural transform. exam. 78—83918
precipitate, cuboidal, in anisotropic matrix, elastic strain field calc. 78—48416
PVC, filled, with varying plasticiser content, deformative props. in highly elastic state, temp. depend. 79—20099
pyrazine, thermal diffuse scattering corrections, choice of elastic constants in evaluation 79—32849
pyrope garnet, elastic consts., pressure and temp. depend. 77—70643
pyrope-almandine garnets, elastic consts. temp. depend. 80—17251
quantum crystals, phonon spectrum, rel. to elastic consts. 77—11766
quartz, α-β phase transition, lattice dynamical study 79—65168
quartz, AC and BC crysts., rotated elastic consts., coupling factors and conversion efficiencies 79—19838
quartz, acoustic phonon geometric propag., anisotropic continuum acoustics 77—4169
quartz, elastic constants and piezoelec. props. 80—92590
quartz, electroded doubly-rotated thickness-mode resonators, temp.-induced frequency 79—55298
quartz, fundamental elastic consts., first temp. derivatives 79—77667
quartz, independent fourth-order elastic coeff. determ. 77—20003
α-quartz, interatomic forces and lattice dynamics 77—7802
quartz, piezoelectric, var. of elastic consts. under gamma irradiation 77—36180
quartz, synthetic piezoelectric, precision meas. of elastic characts. 78—6638
quartz fundamental elastic constants, temp. derivatives 79—55810
α-quartz plate frequency changes rel. to electroelastic tensor and second-order phenomena 78—60398
quartz resonator, nonlinear thermoelastic couplings *(French)* 80—34118
quartz SAW velocity/temperature dependence calc. 79—56062
quasi-isotropic crystals, singular approx. and self-consistent calcs. 77—11623
rare earth alloys, cryst. field effects on thermal props. 77—12072
rare earth garnets, prep. and props. book contrib. 80—44193
rare earth intermetallics, structural instabilities 80—24587
rare earth metals, paramag., c_{11}, c_{33}, mag. field depend. 77—16143
rare earth-iron alloys, elastic vs. magnetoelastic anisotropy 78—68347
rare gas crystals, lattice heat capacity, thermal vibrations, Lindeman parameter, lattice dynamic model *(Russian)* 80—29141
rare gas crystals, three-body forces and third-order elastic consts. 79—51185
relaxation of third-order elastic const. in crystal with point defects 77—8873
rock like material, anisotropic elastic const. meas. by uniaxial compression test *(Japanese)* 79—79822
rocks, meas. at high press. in cubic press. 78—69337
rubber, vulcanised, biaxial deformation study, isotopic tensor function *(German)* 79—70129
sapphire, acoustic phonon geometric propag., anisotropic continuum acoustics 77—4169
tris-sarcosine calcium chloride, elastic props., US damping 80—84229
Schiff's bases, nematic phase, relation between elasticity and mol. struct. 79—90711
second-order, of solids with ZnS struct., many-body effects 78—10116
semiconductor alloy, pseudobinary, phase diagram calc. 78—52786
semiconductors, covalent and ionic, surface (110) atomic struct. bulk elastic consts. and phonon freqs. 79—69331
semiconductors, resonance method for determ. within 80-300K temp. range 78—46918
shallow thin shell finite element, stiffness matrix development 78—90705
shell, reinforced plastic, optimisation with allowance for geometrically nonlinear factors 80—38270
silicate minerals, elastic constant systematics 79—69177
simple crystalline lattice with central force bonds, thermal eqn. of state and elastic consts. *(Russian)* 78—14437
simple metals, volume forces 80—15178
single cryst. elastic constants from mech. and X-ray elastic constants of polycryst. *(German)* 80—10591
single crystal, rel. to vibr. behaviour, supercond. 78—10114
sintered two phase material, calculation of stress distrib. and X-ray elastic consts. *(German)* 78—52883
smectic liquid crystals, acoustic props., US velocity and anisotropy in mag. fields *(Russian)* 79—90547
sodium ammonium tartrate, crysts., temp. depend. of elastic compliances at phase transition 79—15409
sodium ammonium tartrate, improper ferroelec. transition anomalies 78—19430
sodium magnesium aluminium oxdate, elastic consts., Debye temp. 79—82275
solid state phase transformations, thermodynamic relations, appl. to K_2ReCl_6 80—29164
spherical precipitates in anisotropic matrix, elastic interaction energy 80—3049
squaric acid, layered, antiferroelec., phase transition mechanism 80—97210
squaric acid, structural phase transition, US vel. meas. as function of temp. below and above T_c 79—14927
squaric acid, two dimensional antiferroelec., Brillouin scatt. at structural phase transition, hypersonic elastic consts. determ. 80—71430
static geometric and elastic stiffness matrices of finite element hybrid displacement models 78—18173
steel, 1045, elastic const. meas., X-ray diffr. technique 78—5714
steel, austenitic, X-ray elasticity constants *(German)* 80—30004
steel, austenitic stainless, N-alloyed 80—108490
steel, austenitic stainless, tensile prestrained, X-ray elastic const. meas. *(Japanese)* 79—66093
steel, austenitic stainless, X-ray elastic constants, determination by ψ_0 oscillation method *(Japanese)* 78—64575
steel, cantilever bend specimen, side grooving effect on compliance relationships 78—35472
steel, Cr-Mn (13, 19 wt.%), elastic const. behaviour, anomalous, low temp. 80—97521
steel, elastic moduli, temp. depend., −196 to 1000°C 80—6451
steel, elastic moduli, temp. depend. *(Japanese)* 77—59840
steel, eutectoid, anisothermal strain with phase transform., effect on tensile strength *(Russian)* 80—40431
steel, ferritic-pearlitic, X-ray elasticity constants *(German)* 80—30004
steel, hardened, X-ray elasticity constants *(German)* 80—30004
steel, low C, influence of cold rolling reduction on elastic stored energy 79—91731
steel, Mo and Cr-Mo, X-ray elasticity constants at high specimen temp. *(German)* 80—35239
steel, Mo and MoCr, X-ray elastic consts. as function of plastic strain *(German)* 78—31436
steel, stainless, Cr-Mn, N strengthened, anomalous low temp. elastic behaviour 77—77524
steel, stainless, polycrystalline, elastic consts., inelastic coherent neutron scatt. meas. 80—34122
steel, temper embrittlement, fracture mech. of grain boundary segregated phases 78—48531
steel plate, thin, in compression, initial deflection and postbuckling behaviour analysis 80—50666
steel plates, hot rolled, anisotropic texture, exam. of elastic deformation behaviour *(Japanese)* 78—64586
steel railway line, acoustoelastic and third-order elastic constants meas. 77—4798
steel St 52, textured, rolled, REK and lattice strain distrib. *(German)* 79—29095
steels, hot plastic strain, stress- strain-time dependences *(Russian)* 80—40430
stiffness, exact straight line element calc. 80—79138

elastic constants continued
strain measuring instrument, low stiffness, three component, for tubular specimens 77—32749
stress inteisity factors, time depend., singular finite element 80—1471
stress intensity factor for a flat elliptical crack in an elastic solid under uniform tension 79—27525
stress intensity factor for crack in sphere embedded in infinite medium 79—27585
stress intensity factors, UNCLE finite element system calcs., appls. in fracture mechanics 78—67098
stress intensity factors for self similar cracks derived from path independ. integrals 79—23213
stress intensity factors in plane or axisymmetric problems, calc. using weight function concept and crack closure 78—67102
stress intensity factors of point loaded circular disc with two diametrical cracks 79—27589
stressed anisotropic solid, Rayleigh wave vel., third-order elastic constants 77—11772
stressed crystal, adiabatic and isothermal elastic consts. 79—65137
superconductor, type II, fluxoid lattice, plausible arguments for large elastic reponse 77—63040
ternary chlorides, ferroelec., birefringence, twinning and structural phase transitions 79—38480
p-terphenyl(-d_{14}), Brillouin scatt. at room temp. 80—71433
tetragonal crystal Debye temp. calc. from elastic consts. 80—29143
TGS, deuterated, Brillouin spectra and elastic consts., behaviour near T_c 78—15178
TGS, elastic and dielec. consts. from Brillouin scatt. 77—48180
TGS, paraelec. phase, elastic and thermoelastic consts. 77—47503
TGSe, acoustic and thermal anomaly correlation near ferroelec. transition 79—4775
TGSe, ferroelec., effect of gamma irradiation on dielec., piezoelec. and elastic props. 77—43943
thermal diffuse scattering corrections, choice of elastic constants in evaluation 79—32849
thermodynamic theory for cryst. props. behaviour near structural transitions *(German)* 78—38809
thermoplastic based composites, mean stiffness 80—11693
thin annular plate, inner clamp carrying bending moments 77—89031
thin film elastic constants and SAW velocity and attenuation meas. 79—56101
third and fourth order elastic consts. *(French)* 80—34116
tourmaline, elastic consts. by US phase-comparison method 80—2108
tourmaline, resonator, electroelastic constants, elec. field induced freq. shift study 80—20597
trabecular bone from human vertebral body, elastomech. props. 80—67141
transition metal, BCC, phonon dispersion curves and elastic, calc. using cohesive energy 78—59885
transition metals, elastic constants, temp. depend. rel. to conduction electron density of states *(Russian)* 78—38769
translation and rot. dynamics, microscopic Hamiltonian anal., inelastic neutron scatt. elastic consts. 78—38632
transversly isotropic symmetry materials, third order elastic consts. 77—39621
tris-sarcosine calcium chloride, ferroelec., US attenuation and vel., elastic consts., and permitt. near Curie temp. 79—37761
TTF-TCNQ, elastic- and inelastic-neutron scatt. study 79—69208
two-phase material, circular glide dislocation loop 77—27881
type II superconductor, dielastic, interaction of flux line lattice with internal stresses of cryst. imperfections 78—14906
uniaxial crystals, third-order elastic consts., review 80—65119
uniaxial ferroelectrics, microscopic theory, crit. behaviour and anomalous elastic consts. 79—38463
valve tissue, glutaraldehyde preserved, stress/strain and fatigue behaviour 78—40217
vinylidene fluoride-trifluoroethylene film, cryst. phase transition 80—66120
wurtzite and zincblende structure materials, relation between elastic constants from Keating's valence-force field 79—51188
wurtzite-type crystals, lattice dynamics including the effect of electronic extension 80—59586
X-ray diffraction errors due to TDS, calc. from elastic const. 77—19819
X-ray tensometric measurement, reliability *(Czech)* 80—27382
Zerodur, glass-ceramic, thermoelastic props. 78—27550
zincblende and wurtzite structure materials, relation between elastic constants from Keating's valence-force field 79—51188
Zircaloy-2, elastic const. determ. 78—11257
Ag, FCC, dynamical study for Gruneisen parameters 77—47594
Ag, second-order elastic consts., method of homogeneous deform. 79—55808
Ag, single cryst. elastic consts. 77—1164
Ag, third order elastic constant 79—51184
Ag-halides, photoelastic const. calc. 77—76484
Ag-Sn(In), single cryst. elastic consts. 77—1164
AgBr-AgCl mixed crystal, elastic consts., temp. and press. derivatives 77—11620
AgCl-AgBr mixed crysts., elastic consts. and cryst. symm. 80—70290
AgCl-AgBr mixed system, third order elastic consts. 79—90713
AgI, B1 phase, high press. elastic props., thermally activated rel. anomaly 80—44261
Al alloy, elastic moduli, temp. depend. *(Japanese)* 77—59840
Al alloy, precipitation hardened 2014 and 2219, temp. depend. of elastic constants 77—66673
Al alloys, elastic moduli, temp. depend., −196 to 1000°C 80—6451
Al, elastic constants, temp. depend. 80—2109
Al, elastic consts., third order, pseudopotential calc. by method of homogeneous deformation 80—29106
Al, elastic properties *(Russian)* 78—56678
Al, energy and elastic constants 80—59435
Al, FCC, dynamical study for Gruneisen parameters 77—47594
Al, metallic, phonon freq., binding energy, compressibility, elastic const. and energy band gap calcs., linear pot. 80—88284
Al, polycrystalline, elastic consts., inelastic coherent neutron scatt. meas. 80—34122
Al, reson. vibrs. of metal spheres, elastic consts. and internal friction 78—15443
Al, third order elastic constant 79—51184
Al, US velocity, depend. of applied stress and third order elastic const. *(Japanese)* 79—29124
Al-Mg, single crystal, ultrasonic meas. during ageing 78—11263

elastic constants continued
Al-SiC fibre reinforced materials, therm. stresses in unit cell 80—10160
Al_2Cu crystal, Young's modulus, Poisson ratio, elastic consts. determ. by extensometry and US meas., anisotropy discussion *(French)* 79—50683
Al_2Cu, single cryst. elastic consts., 4.2-300K 78—72803
Al_2O_3, elastic behaviour, finite element anal. model, thermal props. 78—31449
Al_2O_3, single crystal, fracture mirror formation, anisotropy of fracture surface energy and elastic constants 78—68824
Al_2O_3 sintered, and hard metal alloys, comparison of stress intensity factor depend. on notch base dia. *(German)* 78—35470
Al_2O_3+TiC system, elastic and fracture charact. at elev. temp. *(German)* 79—43299
$Al_2(SO_4)_3$ soln., adiabatic and apparent molal compressibility determ. from US vel. meas. 78—63797
Al_2SiO_5, sillimanite and andalusite, elastic constants, cryst. struct. 79—60422
Ar, solid, phonon dispersion, many body pot. assuming variable at. polarisability, mech. props. 79—55840
Ar, solid, thermal eqn. of state and elastic consts. *(Russian)* 78—14437
Ar, solid, vol. depend. lattice dynamics, pseudo-harmonic approach 79—99260
As, interlattice displacement and second-order elastic consts. 80—34121
As, rhombohedral crystals, slip dislocations and slip systems 79—23617
As, zone centre phonons and elastic consts., hydrostatic press. depend. 78—59905
As_2Ge_2SeTe, semiconducting glass, elastic props., US vel. meas. 78—26628
$As_2Ge_3T_{15}$, semiconducting glass, elastic props., US vel. meas. 78—26628
AsGeTe, semiconducting glass, elastic props., US vel. meas. 78—26628
As_2S_3 glass fibre, elongation, force depend., deviations from linearity 80—45334
As_2S_3, semiconducting glass, elastic props., US vel. meas. 78—26628
As_2Se_3, semiconducting glass, elastic props., US vel. meas. 78—26628
Au, FCC, dynamical study for Gruneisen parameters 77—47594
Au, pseudopotential, fitted to elastic data 78—75705
Au, third order elastic constant 79—51184
Au-Ag-Cd alloys, martensitic phase transition, elastic anomalies and mode softening 79—91647
Au-Cd (47.5 at.%), single cryst., temp. and press. derivatives near martensitic phase transform. 77—63667
B fibre reinforced Al, orthotropic elastic stiffness consts., US vel. meas. 80—49289
B-fibre reinforced Al, elastic props., 300-4K 77—86066
BN films, elastic stiffness and thermal expansion 80—49559
BN, hexagonal, long optical vibrs., elastic consts. from valence force consts. 78—51621
BN, Raman scatt. exam. of high press. effects on force const. anisotropy 79—38542
B_2O_3 glass fibre, elongation, force depend., deviations from linearity 80—45334
BaClF, cryst., elastic consts. 80—19863
BaF_2, third-order elastic consts. from Lundqvist pot., many-body effects 80—39201
$Ba(NO_2)_2.H_2O$, hexagonal, piezoelec., electro-optic, dielec., elastic, thermoelastic props., space groups 78—76388
BaO, NaCl struct., elastic props., US meas. 78—18697
BaO single crystal, temp. depend. of bulk modulus 78—27549
$Ba_2Si_2TiO_8$, elastic consts., thermal expansion and piezoelec. props. 77—85651
$BaTiO_3$, dielec. and elastic consts., temp. depend. *(Russian)* 78—64307
$BaTiO_3$, ferroelectric ceramic, dielec., piezoelec. and elastic props., orientational contrib. 78—68468
$BaTiO_3$, paraelectric crystal, nonlinear props. 80—84699
$BaTiO_3$, polycrystalline, exam. of effect of freq., temp. and DC electric field strength, on elastic consts. 79—1890
$BaTiO_3$ polydomain crystals, dielec. props. 78—43827
$BaTiO_3$, polydomain ferroelec. crysts., phys. consts., self consistent calcs. 80—88942
$BaTiO_3$, pure, dielectric const. and elastic compliance temp. depend. for various phases 79—19830
$Ba_2TiSi_2O_8$, fresnoite, Czochralski growth and phys. props. 78—3026
$BeAl_2O_4$, Czochralski grown single crystal, hardness, thermal expansion, concl., elastic const. 79—52353
BeO, wurtzite-type crystals, lattice dynamics including the effect of electronic extension 80—59586
Bi, interlattice displacement and second-order elastic consts. 80—34121
Bi, rhombohedral crystals, slip dislocations and slip systems 79—23617
Bi, US propagation anomalies, under hydrostatic press. *(Russian)* 78—83884
Bi, zone centre phonons and elastic consts., hydrostatic press. depend. 78—59905
Bi:Sn(Pb)(Sb)(Te) polycrystal elastic constants for US velocity obs. 79—69180
$Bi_{12}FeO_{20}$, longitudinally vibrated bars, reson. freq., DC elec. field effects, elastic coupling polarising correction terms 80—60503
$Bi_{12}GeO_{20}$, elastic and piezoelectric consts., thermal expsn. 78—31157
$Bi_{12}SiO_{20}$ crystal, piezoelec. and saw props. 80—75949
β-CO, single cryst., adiabatic elastic consts., at triple pt., Brillouin scatt. obs. 79—47466
CaF_2, third-order elastic consts. from Lundqvist pot., many-body effects 80—39201
CaO, modified electron gas theory, high press. effect 77—19899
CaO, NaCl struct., elastic props., US meas. 78—18697
Cd, under press., finite strain theory *(French)* 79—1475
CdF_2, elastic constants. and Debye temp., 4.2-295K 78—38770
$Cd_6Ge_3As_{11}$, press. depend. 78—72064
$Cd_6Ge_3As_4$, semiconducting glass, elastic props., US vel. meas. 78—26628
$Cd_xHg_{1-x}Se$, phase transition and elastic consts., US vel. study 80—75354
$CdIn_2S_4$, Brillouin scatt., elastic and photoelastic consts. determ. 80—60619
CdS, elastic, piezoelec. and dielec. props. 80—108157
CdS, elastic, piezoelectric, and dielec. props., 4.2 to 300K 80—60508
CdS, resonant Brillouin scatt., photoelastic const., imag. part contrib. 80—108218
CdS-ZnTe, acoustoelectric domain injection across interface, propag. loss, elastic consts. 77—51778
$CdS_{1-x}Se_x$, mixed crystals, deformation effects on free excitons 80—76073

elastic constants continued
CdTe, lattice dynamics and phonon parameters bond bending force model 80—59595
γ-Ce, lattice and spin dynamics, inelastic neutron scatt. obs. 79—86859
$CeAl_2$, mode softening due to magnetoelastic interaction, elastic consts. meas. 1.5 to 280K 77—32233
$CePd_3$ single crystal Czochralski growth and characterisation 80—60767
$Ce_2(SO_4)_3$ soln., adiabatic and apparent molal compressibility determ. from US vel. meas. 78—63797
$CeSn_3$, mode softening and elastic consts., acoustic vel. meas. 80—88242
Co, Anderson-Gruneisen parameter, temp. depend., third-order elastic consts. calc. 79—46776
Co based metallic glass, B and P glass former additions, elastic consts., flow behaviour correlations 78—44154
Co, lattice dynamics and compression curves 78—38793
Co, martensitic HCP-FCC transition, neutron scatt. obs. 79—51252
Co-powder, isostatic compaction, mech. and elec. props. *(French)* 80—40285
$CoCl_2$, acoustic phonon dispersion determ. from neutron scatt. 77—39645
CoF_2, elastic constant determ. by US pulse echo overlap 79—14874
Cr, lattice dynamics, improved Fielek model 80—59598
Cr, spin-flip transition temperature, press. depend. from elastic const. meas. 80—65944
Cr_2O_3, elastic consts., distance depend. of mag. interactions, US vel. meas. 77—4539
$CsAl(SO_4)_2.12H_2O$, third order elastic consts. from stress shifted reson. freqs. 78—55905
CsBr, lattice statics and dynamics, deformation shell model 77—20034
CsBr, thermodynamic props., lattice dynamical calc. 77—20090
$CsCdF_3$, nonlinear elastic behaviour, US velocity, 1 bar-3 kbar 78—59851
CsCl structure solids, many-body effects on elastic consts. 77—1163
CsCl type crysts., elastic consts. Cauchy discrepancy, three-body force shell model 77—20004
CsCl-structure compounds, lattice energy and elastic consts. for 3-body Van der Waals interaction 77—72580
CsD_2AsO_4, ferroelec., elastic consts., HF meas. 77—8524
CsH_2AsO_4, Mandelstam-Brillouin spectra and US vel. meas. near ferroelec. Curie point 79—38553
CsH_2AsO_4, piezoelec. coupled soft mode, Brillouin scatt. near Curie temp. obs. 77—52109
CsI, thermodynamic props., lattice dynamical calc. 77—20090
$CsMnCl_3.2H_2O$, diagonal elastic const., thermal expansion coeffs., ultrasonic velocity meas. 80—79853
$Cs_2NaM^{3+}Cl_6$ (M^{3+}=Bi,Nd,Pr), ferroelastic phase transitions, thermal expansion, elasticity, and X-ray anal. 80—70393
$CsPbBr_3$, critical thermodynamic props. around successive phase transitions 79—33627
$CsPbBr_3$, US vel. around successive phase transition points 77—80581
$CsPbCl_3$, critical thermodynamic props. around successive phase transitions 79—33627
$CsPbCl_3$, elastic constants and thermal expansion, near struct. transitions 78—59849
$Cs_2S_2O_6$, hexagonal, piezoelec., electro-optic, dielec., elastic, thermoelastic props., space groups 78—76388
Cu alloys, elastic moduli, temp. depend., −196 to 1000°C 80—6451
Cu, elastic constants, up to 2500 bar, −196-25°C, US pulse echo obs. 79—87680
Cu film, effect of thermal strain on orientation 80—49294
Cu free electrolytic films, tensile creep for various film thicknesses calcs. *(Russian)* 80—11697
Cu, nonlinear acoustics, third-order elastic const. meas. 80—33292
Cu, pair potentials calcs., elastic props. calc. 80—49176
Cu, polycrystalline, elastic consts., inelastic coherent neutron scatt. meas. 80—34122
Cu, second-order elastic consts., method of homogeneous deform. 79—55808
Cu, third order elastic constant 79—51184
Cu, US velocity, depend. of applied stress and third order elastic const. *(Japanese)* 79—29124
Cu, zero to first sound transition, inelastic-neutron scatt. data 77—31738
Cu-Al-Ni, elastic const. behaviour near Ms 77—12623
Cu-Cd-Cr, precipitation hardened, low temp. elastic props. 77—73299
Cu-Ni system, composition depend. of third-order elastic consts. 77—62579
Cu-Sn (15 at.%), temp. depend. of elastic consts. above martensitic transition temp., US exam. 78—76695
Cu-W sintered materials, porous, mech. and X-ray elastic const. *(German)* 77—81288
Cu-W(Fe)(Ag), biphase material X-ray stress determ. *(Russian)* 79—5097
Cu-Zn-Al (19.3, 13.0 wt.%), effect of hydrostatic or uniaxial stress on elastic consts., near martensitic transformation point 78—76697
Cu-Zn-Al martensite, β-phase, single cryst., elastic waves behaviour as function of temp. 79—55807
$Cu_3B_7O_{13}Cl(Br)$, piezoelectric, elastic and electromechanical coefficients *(French)* 78—39504
CuCl third-order elastic and piezoelec. constants 79—46739
Cu_2MnAl, Heusler alloy, magnetisation mag. anisotropy, magnetostriction and elastic consts. 78—23318
$Cu_{2-x}O$, nonlinear elastic props., nonstoichiometry effects *(French)* 80—34133
D_2, solid, elastic constants and anisotropic pair correls. 79—33042
D_2, solid, HCP, density depend. of elastic consts. 80—6589
D_2, solid, HCP, effect of internal strains on elastic consts. 77—24343
D_2, solid, phonon absorption line shape as function of density 80—50329
Dy, elastic constants, magnetoelastic contrib. 80—15777
Dy, magnetic phases, US study 78—31101
Dy, paramag., magnetoelastic contrib. 77—4538
Er, Anderson-Gruneisen parameter, temp. depend., third-order elastic consts. calc. 79—46776
Er, elastic constants, magnetoelastic contrib. 80—15777
Er-Tb, elasticity modulus, ΔE-effect, internal friction, magnetic transformations *(Russian)* 79—91723
Fe based metallic glass, B and P glass former additions, elastic consts., flow behaviour correlations 78—44154
Fe, elevated temps., US vel. obs., transmitting receiving pulse method 78—75830
Fe, powder-forged, elastic consts., density depend. 80—84987
Fe, reson. vibrs. of metal spheres, elastic consts. and internal friction 78—15443

elastic constants continued
Fe, third order elastic constant 79—51184
Fe-B, binary alloys, giant ΔE effect and Elinvar characts. 78—76291
Fe-base metallic glasses, elastic const. 77—66671
Fe-C (graphite, 0.3 wt.%), powder-forged, elastic consts., density depend. 80—84987
Fe-Ni(Pt) Invars, elastic and mag. props., magnetoelastic interaction effects *(Russian)* 80—84631
Fe-Si, 6.3-25 at.% Si, single crysts., adiabatic elastic consts., room temp. US pulse echo meas. 77—48467
Fe-Si, elastic consts., temp. depend., 77 to 300K 77—70089
Fe-Si (0-25 at.%), composition depend. of elastic consts. at 0K 77—84830
$(FeCo)_{80}B_{20}$, glass, elastic consts. 79—83249
$(FeNi)_{80}B_{20}$, glass, elastic consts. 79—83249
Fe_3O_4, magnetocrystalline anisotropy, anomolies in magnetostriction and elastic constants 80—60244
Fe_3Pt, Invar alloy, theory of elastic-anomalies 78—95505
Fe_3Si, single cryst. elastic consts., polycryst. elastic moduli 77—39815
GaAs crystal growth, thermal and elastic const. evaluation 80—92586
GaAs, lattice dynamics, phonon freq., bond bending force model calcs. 80—70335
GaAs, lattice vibration, thermal expansion and pressure effect 80—39233
$GaAs_xP_{1-x}$, elastic consts. and Debye temp. determ. 77—4142
GaN, elastic constant calc., elastic wave propag. vel. 78—87734
GaP, elastic moduli, 80-700K, and elastic consts. 79—73245
GaP, lattice dynamics and phonon parameters bond bending force model 80—59595
GaP, thermal expansion below room temp., press. depend. of elastic stiffness consts. and phonon frequencies 80—79963
GaS, anisotropic phonon dispersion 77—84864
GaS, lattice dynamics parameters, X-ray diffr. study *(Russian)* 80—29146
GaS(Se), Brillouin scatt. by pure transverse phonons, elastic consts. obs. 79—78696
GaS(Se), layer compound, long-wavelength phonons and elastic consts. 80—65175
GaSb, anharmonic force consts. from third order elastic consts. at 300K 77—59074
GaSb, lattice dynamics, phonon freq., bond bending force model calcs. 80—70335
GaSb, lattice vibration, thermal expansion and pressure effect 80—39233
GaSe, lattice dynamics and elastic props., Born-von Karman model study 80—70337
GaSe, lattice dynamics parameters, X-ray diffr. study *(Russian)* 80—29146
GaSe, layer cryst., elastic props. rel. to zone-centre phonon freqs. 79—46736
GaSe, layer struct., fine independent elastic const. using Brillouin scatt. 79—19896
Gd-Tb, elasticity modulus, ΔE-effect, internal friction, magnetic transformations *(Russian)* 79—91723
Gd-Y (40 wt.%) alloy, magnetic phase transitions, elastic consts. meas. 78—14957
Ge, acoustic phonon geometric propag., anisotropic continuum acoustics 77—4170
Ge, extended Born-Von Karman scheme for lattice dynamics 77—27953
Ge, lattice dynamics using Born-van Karman model 79—73271
Ge, nonlinear acoustics, third-order elastic const. meas. 80—33292
Ge, thermal expansion coeff. and Gruneisen const. 77—59128
Ge, third order elastic constant 79—51184
GeO_2 glass fibre, elongation, force depend., deviations from linearity 80—45334
H, metallic, cubic structure, mechanical stability 77—4242
H_2, phonon absorption line shape as function of density 80—50329
H_2, solid, elastic constants and anisotropic pair correls. 79—33042
p-H_2, solid, elastic consts., Brillouin scatt. obs. 79—8149
H_2, solid, HCP, density depend. of elastic consts. 80—6589
H_2, solid, HCP, effects of internal strains on elastic consts. 77—24343
HCN crystals, polarition spectra and lattice dynamics 80—49313
He, solid, theory and thermodynamic props., book contrib. 77—47646
^{4}He, FCC quantum cryst., lattice dynamics 79—77859
^{4}He, HCP, pulse echo expts. 78—38910
Hf, HCP, lattice dynamics, thermal and elastic props., model 80—34155
Hg, rhombohedral crystals, slip dislocations and slip systems 79—23617
Hg_2Br_2, ferroelastic phase, softening of acoustic and optical modes 79—33064
$HgCl_2$, second order phase transition, elastic consts. meas., Brillouin scatt. 78—10908
HgO_2-Y_2O_3, solid soln., elastic and photoelastic props., Mendelstam-Brillouin scatt. 78—6693
Ho, 80-140K, 95K anomaly and annealing 79—46734
Ho, bulk modulus, thermal expansion, third order elastic constants 77—84875
Ho, magnetoelastic coupling in paramag. region 77—80984
Ho, magnetoelastic interactions 78—64252
Ho, paramag., magnetoelastic contrib. 77—4538
Ho-Tb (50 wt.%) alloy, mag. phase diag. from anomalous US propag. 78—6526
$HoAl_2$, magnetoelastic effects on elastic consts., 4.2-280K 78—72385
In, elastic consts., from room temp. to MP, US pulse echo meas. 77—24342
In-Pb alloys, elastic consts. of three phases, acoustic mode softening 80—30006
In-Tl, BCC alloys, stability and elastic consts., US vel. 79—42133
InP, lattice dynamics and phonon parameters bond bending force model 80—59595
InSb, lattice vibration, thermal expansion and pressure effect 80—39233
InSb, third-order elastic consts. meas. at 300, 80K 77—31711
InSe, layer compound, long-wavelength phonons and elastic consts. 80—65175
K, anharmonic lattice dynamics 78—18720
K, appl. of model pseudopot. to elastic consts. 80—59845
K, device for press. variation of yield stress, elastic constants 78—53047
K, elastic constants, cryst. equilib. and electronic contrib. 79—73243
K, pair potentials calcs., elastic props. calc. 80—49176
$KAl(SO_4)_2.12H_2O$, third order elastic consts. from stress shifted reson. freqs. 78—55905
$K_2Ba(NO_2)_2$, elastic props. 80—96588
$(K_{3/4}Bi_{1/4})(Zn_{1/6}Nb_{5/6})O_3$, cation disordered perovskite, elastic consts. and thermal expansion 80—96587

elastic constants continued
$KBr_{1-x}(CN)_x$, mixed mol. cryst., coupled rot. and translational modes 80—84267
KCN, Brillouin line width of phonons 78—80370
KCN, cubic, third-order elastic consts., nonlinear behaviour 79—28026
KCN, dipolar impurity tunnelling model, elastic interaction and const. 78—71826
KCN, elastic anomaly at 168K 78—27242
KCN, inelastic neutron scatt. by coupled rot. and translational modes 80—79895
KCN, order-disorder transition, press. and temp. depend. of soft elastic const. 78—79769
KCN, single cryst., orientationally disordered, Brillouin scatt., elastic consts. 77—85732
$(KCN)_x(KBr)_{1-x}$, Brillouin scatt. of elastic anomaly 79—28779
KCl, TSM study of lattice statics and dynamics 79—82292
KCl, thermodynamic props., lattice-dynamical calc. 77—35715
KCl-KBr mixed crystal, elastic consts. press. derivative 77—11619
$KCl_{1-x}CN_x$, dipolar impurity tunnelling model, elastic interaction and const. 78—71826
KCl(F)(Br)(I), elastic constants, temp. derivatives at constant volume 80—59549
KD_2PO_4, acoustic phonon dispersion, elastic stiffness, light scatt. obs. 80—103966
$KD_3(SeO_3)_2$, acoustic phonon softening and spontaneous strains 78—26652
$KD_3(SeO_3)_2$, phase transition, neutron scatt. study 80—75351
KH_2PO_4, appl. of γ-ray diffractometry to twinned crystals study 79—68987
$KH_3(SeO_3)_2$ and $KD_3(SeO_3)_2$, ferroelastic phase transition, mech. stress effect 80—70394
$KH_3(SeO_3)_2$, ferroelastic, low-frequency elastic props., −190 to 50°C 79—37759
$KH_3(SeO_3)_2$, phase transition, acoustic phonon softening 77—27997
$K_2Hg(CN)_4$, third order elastic consts. 80—84231
$K_{2.89}Li_{1.55}Nb_{5.11}O_{15}$, elastic and piezoelec. props. 79—15403
$K_2Mn_2(SO_4)_3$, elastic props. using piezoelec. reson. and US vel. meas. 80—15180
$K_2Pt(CN)_4Br_{0.3}.3H_2O$, lattice softening, temp. depend. of elastic consts., US meas. 78—14432
$K_{0.5}Rb_{0.5}I$, mixed cryst., phonons, neutron scatt. 77—1192
K_2ReCl_6, softening of acoustic modes, obs. by Brillouin scattering 80—71440
K_2ReCl_6, thermodynamic relations at solid state phase transitions 80—29164
K_2SO_4-$ZnSO_4$ system, glass formation and phase diagram study, physical props. 78—27500
K_2SeO_4, elastic props. at commensurate-incommensurate transition, Brillouin scatt. and US study 80—93248
K_2SnCl_6, elastic consts., inelastic neutron scatt. and US meas. 80—59553
K_2SnCl_6, softening of acoustic modes, obs. by Brillouin scattering 80—71440
$KTa_{1-x}Nb_xO_3$, quantum limit of ferroelec. transitions, dielec. and elastic consts. meas. 78—15128
$KTa_xNb_{1-x}O_3$, ferroelectric transition, US attenuation, elastic consts., soft modes 78—23411
$K_2Zn(CN)_4$, third order elastic consts. 80—84231
Kr, solid, phonon dispersion, many body pot. assuming variable at. polarisability, mech. props. 79—55840
$LaAg_xIn_{1-x}$ alloys, structural instability 78—79562
$LaAg_xIn_{1-x}$, phonon dispersion, elastic consts. and struct. instability, soft mode behaviour 80—103436
LaB_6, elastic consts. at room temp., US vel. meas. 77—43268
LaP_5O_{14}, continuous ferroelastic transition elastic and mechanical props. 80—92668
LaP_5O_{14}, coupling effects between soft optic and acoustic modes at ferroelastic transition 80—70358
LaP_5O_{14}, ferroelastic transition, soft acoustic mode 77—11656
LaP_5O_{14}, ferroelastic phase transition, thermal expansion and elastic consts. tensors 79—42236
Li, energy and elastic constants 80—59435
Li single cryst., US attenuation and vel. measurements in vicinity of martensitic phase transformation 80—75358
LiCl(F)(Br)(I), elastic constants, temp. derivatives at constant volume 80—59549
$LiClO_4.3D_2O$, hexagonal, piezoelec., electro-optic, dielec., elastic, thermoelastic props., space groups 78—76388
$LiClO_4.3H_2O$, hexagonal, piezoelec., electro-optic, dielec., elastic, thermoelastic props., space groups 78—76388
LiF, revised data up to 650°C 78—14397
Li_2GeO_3, acoustic props., intrinsic piezoeffect, US absorpt. coeffs. *(Russian)* 80—29692
Li_2GeO_3, components of elastic, piezoelec. and permittivity tensors meas. 77—8518
LiH(D), elastic constants, lattice dynamics and phonon dispersion 78—30711
$LiIO_3$ crystal elastic, piezoelec., dielectric and acoustic props. 79—46740
$LiNbO_3$, piezoelectric stress const. determ. by impact loading technique 77—69778
$LiYF_4$, elastic consts. and acoustic symm. 80—15182
^6Li, and natural Li, elastic consts., temp. and press. depend. 78—30692
^7Li, lattice dynamics, temp. depend., 110-424K 77—20033
Lu, lattice dynamics, heat capacity, thermal expsn. 79—86857
metals, model pseudopotential calcs., elastic consts., spin susceptibility, Fermi surface distortions 78—79922
Mg, under press, finite strain theory *(French)* 79—1475
MgF_2, elastic const. C_{44}, depend. on temp. 79—73239
MgF_2, elastic constant determ. by US pulse echo overlap 79—14874
MgO, fourth order elastic constants and temp. variation of second order elastic constants 79—19306
MgO, modified electron gas theory, high press. effect 77—19899
MgO, second-order Raman scatt. 78—10894
MgO, single crystal, elastic consts. and internal frictions meas. by rectangular parallelepiped reson. 77—78165
$MgSiO_3$ perovskite polymorph, high-press elastic consts. determ. 77—51428
Mg_2SiO_4, fosterite, lattice dynamics, IR and Raman spectra meas. 79—65153
Mg_2Sn, third-order elastic constant, low temp. limit of Gruneisen parameter 79—73280
Mn-Cn (25, 62 wt.%), temp. depend., 170-300K *(Russian)* 80—81095

elastic constants continued
Mn-Ni, single cryst. or polycryst., elastic anomalies at antiferromag. transition 78—14972
MnF_2, elastic constant determ. by US pulse echo overlap 79—14874
MnO, antiferromag., temp. depend. of elastic consts., US study 80—79854
MnO, first order mag. phase transition, elastic consts. meas. 77—66316
MnO, multidomain single cryst. and monodomain cryst., crit. and elastic behaviour, T_N to 300K 77—66407
Mo, lattice dynamics, improved Fielek model 80—59598
Mo, pair potentials calcs., elastic props. calc. 80—49176
Mo, sample chamber for ultrasonic vels. and elastic consts. meas., 4.2 to 300K *(German)* 78—46868
$MoS_2(2H)$, elastic consts., from dispersion curve and linear compressibility data 77—11618
$MoSi_2$ film, elastic stiffness and thermal expansion coeffs. 80—107451
ND_4Cl, order-disorder transformation, elasticity and heat capacity temp. depend., US obs. 78—71851
ND_4Cl, ultrasonic exam. near order-disorder transition, elastic consts. 79—46799
$NH_4Al(SO_4)_2.12H_2O$, third order elastic consts. from stress shifted reson. freqs. 78—55905
$(NH_4)_2BeF_4$, elastic compliance, US attenuation and piezo-coeffis., 170 and 190K 79—51918
$(NH_4)_2BeF_4$, elastic props., US damping 80—84229
$(NH_4)_2BeF_4$, ferroelectric, Brillouin scattering study 79—15470
NH_4Br, order-disorder phenomena, high press. US investigation 79—37835
$NH_4Br_xCl_{1-x}$, cryst., order-disorder phase transitions, US investig. 80—6378
NH_4Cl, λ-type phase transition, hypersonic study using Brillouin scatt. 80—34165
$NH_4H_2PO_4$, improper antiferroelec. phase transition, elastic props., free energy, thermodynamic theory 78—80299
$(NH_4)_2SiF_6$, softening of acoustic modes, obs. by Brillouin scattering 80—71440
$(NH_4)_2SnCl_6$, softening of acoustic modes, obs. by Brillouin scattering 80—71440
Na, appl. of model pseudopot. to elastic consts. 80—59845
Na, linear potential and phonons 79—82293
NaCN, Brillouin backscatter spectra of (100) LA phonons, elastic consts. determ. 79—65886
NaCN, cubic, KCN-type anomalous thermoelastic behaviour 77—84823
NaCN, cubic, third-order elastic consts., nonlinear behaviour 79—28026
NaCN, elastic const. temp. depend., Brillouin and US exam. 77—80572
NaCN, order-disorder transition, press. and temp. depend. of soft elastic const. 78—79769
NaCN, single cryst., orientationally disordered, Brillouin scatt., elastic consts. 77—85732
NaCl, calc. of third- and fourth-order elastic constants 79—10891
NaCl, changes in internal friction and discharge following plastic deform. 79—99191
NaCl, cubic cryst., temp. depend. of third-order elastic consts. 78—18699
NaCl, high press. eqn. of state and sound vels. to fourth order elastic consts., 270 kbar 79—37806
NaCl, interrupted neutron irrad. expts. involving dislocations 79—99208
NaCl, thermodynamic props., lattice-dynamical calc. 77—35715
NaCl type crysts., elastic consts., Cauchy discrepancy, three-body force shell model 77—20004
NaCl(Br) (F) (I), lattice dynamics and statics, three-body-force shell model 80—49323
NaCl(F)(Br)(I), elastic constants, temp. derivatives at constant volume 80—59549
$NaClO_3$ single crystals, change of elastic constants by gamma radiation 78—63800
Na_2CoGeO_4, single cryst. growth and study of their piezoelec. and elastic props. 79—4906
$NaH_3(SeO_3)_2$, dynamics of α-β transition, Brillouin scatt. meas. 77—8526
$NaH_3(SeO_3)_2$, ferroelectric, electromechanical props. near Curie point 80—29690
NaN_3, orientational motion and elastic anomaly 79—46803
NaN_3, struct. phase transform., microscopic model 79—65022
$NaNO_2$, adiabatic and isothermal elastic compliances, critical behaviour 78—92031
$NaNO_2$, elastic constants and US attenuation coeffs., anisotropic charact. 78—63809
Na_2O-CaO-SiO_2, double torsion specimens, compliance and fracture load as crack length function 78—48508
Na_xWO_3, elastic consts., composition depend. Brillouin scatt. meas. 79—61388
Nb, density, rel. to elastic const. calc. from US meas. 77—86079
Nb, elastic constants, 0K to melting point 79—38882
Nb, elastic constants up to melting point, US meas. 77—86081
Nb, reson. vibrs. of metal spheres, elastic consts. and internal friction 78—15443
Nb third-order elastic consts. using nonlinearity parameter 78—75733
Nb-H system, lattice dynamics, local frequency spectrum, mean thermal displacement of H 80—59604
Nb-H(D) system, anelastic behaviour, 0.5-15K 80—49300
Nb-Zr, effect of band structure on elastic constants and superconductivity 79—8313
Nb-Zr, elastic constants, 0K to melting point 79—38882
Nb-Zr alloys, BCC phase, 4.2-300K 77—81285
Nb-Zr(Hf)(W) alloys, single cryst. elastic consts. 77-298K 78—84879
NbC, physicomechanical props. within the homogeneity range 77—1848
NbH_2, harmonic and anharmonic elastic props. 80—10589
NbO_2, low temp. elastic consts. and Debye temp. 78—47463
NbO_2, semicond. cryst., elastic props. 79—19308
NbO_2, semiconducting, elastic const., press. depend. at 296K 79—23672
$NbSe_2(2H)$, elastic consts., from dispersion curve and linear compressibility data 77—11618
Nb_3Sn, A-15 compounds, interlattice displacements, elastic consts. 78—55906
$Nb_{53}Ta_{47}$, effects of hydrostatic pressure on changes in elastic consts. caused by addition of H 80—75287
$Nb_{53}Ta_{47}$, pure and hydrogenated crysts., effect of pressure on elastic consts. 80—7614
NbTi filament reinforced Cu, superconducting composite, elastic const., temp. depend. 78—68717

- **elastic constants** continued
  - NbTi/Cu composite superconductor, room temp. elastic consts., US determ. 77–59839
  - Nd, elastic constants, low-temp., mag. field depend. 78–76290
  - Nd, higher order elastic consts. of double HCP cryst., calc. 79–51189
  - Nd, mag. ordered, single cryst. elastic consts. meas., 4-50K 77–63249
  - Nd, single cryst. elastic consts., 4.2 to 300K, mag. ordering effects 77–15477
  - $NdAl_2$, elastic constants, 4.2K to 280K, crystal field effects 77–11615
  - $Nd_3Ga_5O_{12}$, elastic and thermoelastic consts., US meas. *(German)* 77–59061
  - $NdVO_4$, elastic modes in applied mag. field 79–60423
  - $NdVO_4$, magnetoelastic interactions, finite strain and rot. effects, elastic consts. 79–87303
  - Ne, solid, phonon dispersion, many body pot. assuming variable at. polarisability, mech. props. 79–55840
  - Ne, solid, phonon-dispersion, mode Gruneisen parameters and elastic consts. 77–11651
  - Ni, computer simulation of point defects and planar defects 78–43013
  - β_2-Ni-Al, supersaturated thermal vacancy effects 80–54298
  - β_2-Ni-Al (47.6 to 60.5 at.% Ni), elastic stiffnesses −196 to 400°C 78–27556
  - Ni-base metallic glasses, elastic const. 77–66671
  - Ni-Cr(V)(Co)(Mn)(Mo)(Ru)(Fe), spin wave stiffness consts., RPA CPA band model 79–61088
  - Ni-Ru (3.3 at%), magnetisation, magnetocrystalline anisotropy, magnetostriction and elastic consts., thermal variations 79–28563
  - Ni_3Fe, Debye temp. determ. from elastic consts. and X-ray meas., effect of configurational order 78–30727
  - NiO, phonon dispersion relations, neutron scatt. meas. 79–42181
  - $Ni_{1-x}S$, metal-semimetal transition, lattice dynamics and thermodynamic props. 80–29324
  - $NiTe_2$, acoustic phonon dispersion, inelastic neutron scatt. meas., elastic consts. and sound vels. 79–95098
  - NiTi equiatomic alloy, single cryst. elastic consts. near martensitic transform. 80–75283
  - O_2, solid, lattice dynamics 79–95095
  - PAA, nematic liq. cryst., elastic consts. determ. 77–27824
  - Pb, elastic consts., from room temp. to MP, US pulse echo meas. 77–24342
  - Pb, elastic properties *(Russian)* 78–56678
  - Pb, filamentary crysts. third-order elastic consts. combinations 80–92585
  - PbF_2, elastics consts., acoustic phonon modes up to high temps., neutron scatt. meas. 79–33052
  - PbF_2, inelastic neutron scatt. study of phonon dispersion relation, elastic constants calc. 78–30712
  - PbF_2, phonon temp. depend., neutron scatt. study 79–60450
  - PbF_2, US vel. near press. induced cubic-to-orthorhombic transform. 80–103476
  - $Pb_5(GeO_4)(VO_4)_2$, $Pb_5(SiO_4)(VO_4)_2$, and Pb_5GeO_{11}, elastic nonlinearity and acoustic losses 80–59554
  - PbI_2, cubic, elastic consts., hydrostatic press. effect, US vel. meas. 80–49292
  - $Pb(Mg_{1/3}Nb_{2/3})O_3$, cation disordered perovskite, elastic consts. and thermal expansion 80–96587
  - $Pb_3MgNb_2O_9$ diffuse phase transition, Brillouin scatt. and acoustic phonons 78–76401
  - $Pb_3(PO_4)_2$, temp. depend. of lattice parameters and spontaneous strain 80–29170
  - $Pb_3(P_xV_{1-x}O_4)_2$, ferroelastic phase transition, DTA, dilatometric and Brillouin scatt. study 80–70398
  - $PbS-As_2S_3$ glass, elastic props. temp. depend. 78–71780
  - $PbSe_xTe_{1-x}$ epitaxial layers, growth, struct., elastic strain and Hall mobility 77–15717
  - $Pb_5(SiO_4)(VO_4)_2$ cryst. growth and elastic props., appl. in acousto-optical devices 78–19660
  - $PbTiO_3$, ferroelectric ceramic, dielec., piezoelec. and elastic props., orientational contrib. 78–68468
  - $Pb(Zn_{1/3}Nb_{2/3})O_3$, cation disordered perovskite, elastic consts. and thermal expansion 80–96587
  - Pd, elastic consts. 4 to 300K 80–6455
  - Pd-D alloys, phonon dispersion relation meas., elastic constants and Debye temp. 78–26639
  - Pd-H system, lattice dynamics, local frequency spectrum, mean thermal displacement of H 80–59604
  - $Pd_{0.96}Ag_{0.04}$, phonon dispersion curves at 296K 80–24546
  - β-$PdH_{0.66}$, elastic consts. 4 to 300K, Debye temp. 80–6455
  - $Pd_{0.9}Rh_{0.1}$, lattice dynamics, inelastic neutron scatt. meas. at 296K 80–29135
  - $Pd_{0.95}Rh_{0.05}$, exchange-enhanced, phonon dispersion relations exam. 77–84868
  - Pd_2Si and PdSi films, on Si, stress obs. 80–80145
  - Pr, elastic constants, magnetic effects 78–68355
  - Pr, higher order elastic consts. of double HCP cryst., calc. 79–51189
  - Pr, magnetoelastic effects, zero field single cryst. elastic consts. meas. 77–66403
  - $PrAl_2$, elastic constants, 4.2K to 280K, crystal field effects 77–11615
  - $PrCu_2$, Jahn-Teller transition, susceptibility, elec. resist., thermal expansion and acoustic meas. 77–20276
  - $PrSn_3$, thermal expansion and transverse elastic const. near mag. phase transition 80–60394
  - Pr_3Tl, thermal expansion and transverse elastic const. near mag. phase transition 80–60394
  - PtSi films, on Si, stress obs. 80–80145
  - Pu-Ga (1 wt.%) alloy, single cryst. elastic consts., US wave vel. meas. 77–20005
  - Rb, elastic constants, cryst. equilib. and electronic contrib. 79–73243
  - Rb, lattice dynamical props., conduction-core exchange, Lindgren approx. 79–1481
  - $RbAg_4I_5$, 208K phase transition, Jahn-Teller-like model 77–35694
  - $RbAg_4I_5$, third order elastic consts. at room temp. using 110 cut 78–59848
  - $RbAg_4I_5$, US attenuation near 208K phase transition 79–33085
  - RbCN, cubic, temp. and press. derivatives of elastic consts. 80–6456
  - RbCN, cubic phase, temp. depend. of elastic consts., Brillouin spectra obs. 79–56805
  - $RbCaF_3$, elastic consts. near phase transition by Brillouin scatt. 78–38844
  - $RbCaF_3$, first order improper ferroelastic phase transition at 194K, phenomenological description 80–70397
- **elastic constants** continued
  - $RbCaF_3$, nonlinear elastic behaviour, US velocity, 1 bar-3 kbar 78–59851
  - $RbCdF_3$, nonlinear elastic behaviour, US velocity, 1 bar-3 kbar 78–59851
  - RbCl, thermodynamic props., lattice-dynamical calc. 77–35715
  - RbCl, third order elastic constants 78–6117
  - RbCl(F)(Br)(I), elastic constants, temp. derivatives at constant volume 80–59549
  - $Rb(H,D)_3(SeO_3)_2$, improper ferroelec. phase transition, anomalous elastic props. 79–33634
  - $RbH_3(SeO_3)_2$, phase transitions, elastic compliance temp. depend. 77–90116
  - RbI, elastic constants determ. by inelastic neutron scatt. 78–79659
  - $RbNO_3$, cubic to rhombohedral transition, X-ray diffr. obs. 78–22681
  - $RbNO_3$, cubic to rhombohedral transition induced by orientation-shear strain coupling 78–22682
  - Re, Anderson-Gruneisen parameter, bulk modulus and compression curves 78–30690
  - Re, lattice dynamics, third order elastic consts. and thermal expansion 77–76505
  - ReO_3, elastic consts. determ. 77–11617
  - ReO_3, elastic stiffness const. determ. by Brillouin scatt. 78–19494
  - Ru, Anderson-Gruneisen parameter, temp. depend., third-order elastic consts. calc. 79–46776
  - Ru, lattice dynamics, thermal expansion and bulk modulus 77–59079
  - Sb, interlattice displacement and second-order elastic consts. 80–34121
  - Sb, rhombohedral crystals, slip dislocations and slip systems 79–23617
  - Sb, zone centre phonons and elastic consts., hydrostatic press. depend. 78–59905
  - Sc, HCP, lattice heat capacity, third order elastic consts., thermal expansion 79–82352
  - Sc, lattice dynamics, sp.ht. and bulk modulus 78–71814
  - Sc_2O_3, Mandelshtam-Brillouin spectra, transverse phonon contrib., elastic and photoelastic consts. 77–81115
  - Se, amorphous, elastic props. at high press. 79–37753
  - Se, Debye temp. calcs. using elastic consts. and Kopp-Neumann relations 78–2220
  - Se, elastic and piezoelec. consts., US phase vel. meas. 79–86834
  - Se, trigonal, low temp. sp. ht. and elastic consts., piezoelec. effect influence on phonons 80–54404
  - Se, trigonal or amorphous, thermal expansion and Gruneisen coeffs., 10-300K 78–22870
  - Si, acoustic phonon geometric propag., anisotropic continuum acoustics 77–4170
  - n-Si, deform. pot. shear const. determ. 77–15763
  - n-Si, degenerate, density of states from elastic consts. 80–6690
  - Si, lattice dynamics using Born-van Karman model 79–73271
  - p-Si, low temp. depend. of elastic const. c_{44} 77–84831
  - Si, thermal expansion coefficient and Gruneisen const. 77–59128
  - Si, third order elastic constant 79–51184
  - Si:B(P)(Ge), strain distrib. rel. to dopant conc., accurate determ. by X-ray Bragg reflection 77–19835
  - Si:H, amorphous, Brillouin scattering from acoustic bulk and surface waves 80–11425
  - SiN film, elastic stiffness and thermal expansion coeffs. 80–107451
  - Si_3N_4 film, elastic stiffness and thermal expansion coeffs. 80–107451
  - SiO_2, fused, US study by harmonic generation, elastic consts., Gruneisen parameters 78–83735
  - SiO_2 glass fibre, elongation, force depend., deviations from linearity 80–45334
  - $SmCo_5$, single-cryst. and liq. phase sintered, elastic stiffness consts., US velocity obs. 77–73066
  - $Sm_3Ga_5O_{12}$, elastic and thermoelastic consts., US meas. *(German)* 77–59061
  - $Sm_{0.75}Y_{0.25}S$, mixed valence, phonon dispersion theory 80–34153
  - Sn, grey, lattice dynamics and elastic consts. 77–84865
  - Sn, white, elastic stiffness consts. calc. 78–39825
  - $Sr_{0.5}Ba_{0.5}Nb_2O_6$ crystals, ferroelec., dislocation free, pyroelec. props. 79–42907
  - $SrCl_2$, elastic constants and acoustic wave velocity, temp. variation 78–6118
  - SrClF, cryst., elastic consts. 80–19863
  - SrF_2, third-order elastic consts. from Lundqvist pot., many-body effects 80–39201
  - $Sr_2Nb_2O_7$, phase transition at 215°C, physical props. obs. 79–56744
  - SrO, NaCl struct., elastic props., US meas. 78–18697
  - $SrTiO_3$, critical elastic compliance, acoustic resonance meas. 80–65118
  - TGSe, domain-wall orientations and wall energies 78–23420
  - TGSe:D,L-α-alanine crysts. with large unipolarity, dielec., piezoelec., elastic props. and internal friction 79–33615
  - Ta, density, rel. to elastic const. calc. from US meas. 77–86079
  - Ta, reson. vibrs. of metal spheres, elastic consts. and internal friction 78–15443
  - Ta, shear elastic constant, anomalous temp. behaviour, US study 80–79855
  - Ta, temp. depend., H_2 effect 77–32610
  - Ta-H system, lattice dynamics, local frequency spectrum, mean thermal displacement of H 80–59604
  - $TaSi_2$ film, elastic stiffness and thermal expansion coeffs. 80–107451
  - Tb, elastic constants, magnetoelastic contrib. 80–15777
  - Tb, ferromagnet, field depend. of elastic const. c_{66} 80–15181
  - Tb, magnetic phase diagram, US meas. of elastic const. 80–15721
  - Tb, paramag., magnetoelastic contrib. 77–4538
  - Tb, third order elastic consts. and thermal expansion 77–80569
  - Tb-Ho, US attenuation and elastic consts. in 3 mag. phases, 4.2 to 300K 77–72645
  - Tb-Ho alloy, influence of internal strain on Neel temp., thermal expansion and elastic const. meas. 77–63176
  - $Tb_{0.3}Dy_{0.7}Fe_2$, elastic vs. magnetoelastic anisotropy 78–68347
  - Te, Debye temp. calcs. using elastic consts. and Kopp-Neumann relation 78–2220
  - Te, elastic and piezoelec. consts., US phase vel. meas. 79–86834
  - Te-Se, Debye temp. calcs. using elastic consts. and Kopp-Neumann relation 78–2220
  - TeO_2, paratellurite, single crysts., third-order elastic constants 80–88243
  - TeO_2, press.-induced ferroelastic transition and internal displacement, soft effective elastic const. meas. 79–73240
  - Th single crystal, 4.2-300K, effect of C addition 77–90386
  - $ThC_{0.063}$ single crystal, 4.2-300K 77–90386

elastic constants continued
- α-Ti alloy, rolled, elastic stiffness and Bauschinger effect accompanying anisotropic hardening *(Russian)* 80—40435
- Ti alloy TA6V, fatigue, low cycle, and microfractography *(French)* 77—70168
- Ti alloy VT20 and VT22, yield strength anisotropy and durability after cyclic loading *(Russian)* 78—27565
- α-Ti alloys VT1 and VT5, struct. and phys. props., H_2 effect 80—108576
- Ti, lattice specific heat and thermal expansion 79—73318
- α-β Ti Widmanstatten alloy interfaces, elastic interact. stresses, effect on plastic flow onset 80—104218
- Ti-Al-V, rolled, elastic stiffness and Bauschinger effect accompanying anisotropic hardening *(Russian)* 80—40435
- Ti-Al-V (6, 4 wt.%), compliance calibration results 78—19798
- Ti-V-H system, BCC, hydrogen effects on anisotropic elastic props. 79—24565
- TiO_2, elastic const. C_{44}, depend. on temp. 79—73239
- TiO_2, rutile, ferroelectric ceramic, dielec., piezoelec. and elastic props., orientational contrib. 78—68468
- Ti_2O_3, press. depend. of elastic consts. at 296K. 79—42134
- $TiSi_2$, film, elastic stiffness and thermal expansion coeffs. 80—107451
- $(Tl,NH_4)_2Cd_2(SO_4)_3$, langbeinite type mixed cryst., ferroelec. transitions, dielec. and elastic meas. 78—2810
- Tl, thermal and elastic props., lattice heat capacity, elastic constants and thermal expansion, model 80—39321
- Tl-halides, photoelastic const. calc. 77—76484
- $TlCdF_3$, elastic consts. near phase transition by Brillouin scatt. 78—38844
- $TlCdF_3$, nonlinear elastic behaviour, US velocity, 1 bar-3 kbar 78—59851
- $TlCdF_3$, third and fourth order elastic consts., press. depend. near phase transition *(French)* 80—34116
- $Tm_{0.82}Lu_{0.18}VO_4$, elastic consts. at 9 GHz 77—62576
- $TmPO_4$, Jahn-Teller induced elastic constant changes, 4.2 to 300K 78—79657
- TmSb, cryst. field effects on elasticity, rot. and higher order interactions 77—63251
- TmSe, first obs. of negative elastic const. 80—103409
- $TmVO_4$, elastic consts. at 9 GHz 77—62576
- TmZn, magnetic-ion-lattice interactions, cryst. elec. field 77—4540
- UAl_2, temp. and mag. field depend. 80—55450
- UN, antiferromag., mag. susceptibility, elec. resist. and elastic consts. meas. 77—69510
- UN, sound velocity temp. depend. anomaly 77—72891
- UN, sound velocity temp. depend. anomaly in elastic consts. determ. 77—72892
- UO_2, elastic props. at high press., US meas. 77—4141
- US, elastic consts. temp. depend. in para- and ferromag. regions 79—77666
- V, density, rel. to elastic const. calc. from US meas. 77—86079
- V, effects of hydrostatic pressure on changes in elastic consts. caused by addition of H 80—75287
- V, pure and hydrogenated crysts., effect of pressure on elastic consts. 80—7614
- V, pure and with O_2 additions, single cryst. elastic consts., 4.2 to 300K, and hardening 79—90712
- V, reson. vibrs. of metal spheres, elastic const. and internal friction 78—15443
- V, shear elastic constant, anomalous temp. behaviour, US study 79—28031
- V-H single crysts., elastic consts., temp. depend., H effects 80—66563
- V-H system, lattice dynamics, local frequency spectrum, mean thermal displacement of H 80—59604
- V_3Ge, Anderson-Gruneisen parameter, from 3rd order elastic const. data 79—33059
- V_3Ge, third order elastic consts. 78—88490
- V_2O_3, US vel. and elastic const. meas., 150-273K 77—15478
- V_2O_3:Cr, pure and doped, sound vels. and elastic consts. from phonon dispersion curves 79—55844
- V_3Si, Anderson-Gruneisen parameter, from 3rd order elastic const. data 79—33059
- V_3Si, anharmonic contrib. to mode softening 79—73241
- V_3Si, third order elastic consts. 78—88490
- $V_3Si(Ge)$, A-15 compounds, interlattice displacements, elastic consts. 78—55906
- W, reson. vibrs. of metal spheres, elastic consts. and internal friction 78—15443
- WC, single cryst. elastic constants from mech. and X-ray elastic constants of polycryst. *(German)* 80—10591
- WO_3, acoustic instability near monoclinic orthorhombic phase transition, X-ray scatt. 80—65215
- WSi_2 film, elastic stiffness and thermal expansion coeffs. 80—107451
- Xe crystal, elastic consts. determ. by Brillouin scatt., comparison with neutron scatt. data 77—39622
- Xe, solid, elastic consts., thermodynamic props., Monte Carlo simulation 77—62575
- Xe, solid, phonon dispersion, many body pot. assuming variable at. polarisability, mech. props. 79—55840
- Y, elastic consts., 4 to 300K 80—39200
- Y, thermal and elastic props. 79—33027
- YB_{68}, melt grown, props. meas. 77—11518
- $Y_3Fe_{5-x}Ga_xO_{12}$, inhomogeneous stress effect on ferromagnetic resonance 79—24219
- YIG, elastic and thermoelastic consts., US meas. *(German)* 77—59061
- Y_2O_3, Mandelshtam-Brillouin spectra, transverse phonon contrib., elastic and photoelastic consts. 77—81115
- Zn, elastic properties, compilation and review 78—27551
- Zn single cryst., diffuse X-ray scatt. determ. 78—11255
- ZnF_2, elastic constant determ. by US pulse echo overlap 79—14874
- ZnF_2, elastic props., 4.2-300K, incipient ferroelec. transition 78—30691
- ZnF_2, press. depend., 0-10 kbar 78—10117
- ZnO, elastic, piezoelec. and dielec. props. 80—108157
- ZnO triode sputtered film elastic props. rel. to structure and composition 79—46988
- ZnS, lattice dynamics, phonon freq., bond bending force model calcs. 80—70335
- ZnS struct. solids, second and third order 78—63799
- ZnS type structure solids, contrib. of many body forces to elastic consts. 78—2188
- ZnS-MgS, exam. of piezoelectric props. and elastic compliances, as function of MgS conc. 79—95709

elastic constants continued
- ZnS(Se)(Te), thermal expansion and lattice dynamics under press. 80—100316
- ZnSe, lattice vibration, thermal expansion and pressure effect 80—39233
- ZnSe, photoelastic and elastic constants determ. using thermal Brillouin scatt. *(Japanese)* 79—51974
- ZnTe, Brillouin scatt. spectra, elastic and photoelastic consts. 77—59585
- ZnTe, lattice dynamics and phonon parameters, bond bending force model lattice dynamics and phonon parameters bond bending force model 80—59595
- ZnTe, lattice vibration, thermal expansion and pressure effect 80—39233
- Zr sheet, elasticity coefficient computation by use of pole figure data 77—77521
- Zr-Nb-Mo-Re, alloying effect on dislocation core struct., determ. by discrete lattice modelling 78—30618
- ZrN, physicomechanical props. with the homogeneity range 77—1848
- Zr_2Ni, search for soft phonon modes, neutron scatt. 79—23686
- ZrO_2-Y_2O_3, solid soln., elastic and photoelastic props., Mendelstam-Brillouin scatt. 78—6693
- $ZuCuZn_2$, martensitic transition, shear elastic const. meas. 77—28810

elastic deformation
- *see also bending; elasticity; electrostriction; stress/strain relations; torsion*
- abdominal aorta wall, human, after endarterectomy, deform. and strength 77—25497
- absorbing media, acoustic pulse deform., numerical calc. algorithm *(Russian)* 80—96591
- adhesion of elastic particles to solid surface, electrostatic rel. to mol. component 77—42787
- adhesive contact during the oblique impact of elastic spheres 79—77027
- adhesive contact of elastic solids, tangential force effect 77—62216
- adhesively bonded sheets, fracture anal. 77—50996
- aeolotropic cylindrical shell, nonhomog., hollow, thick-walled, torsional stresses 78—75068
- alloys, machining damage, depth of surface layers determ. 80—85094
- amorphous materials, deform. processes 77—4813
- anelastic deformation, generalised representation by num. sol. of initial boundary value problems *(German)* 79—12610
- anisotropic cantilever plate with variable rigidity, stress and deflection anal. 79—59927
- anisotropic cone, axisymmetrically loaded, stress state *(Russian)* 77—68413
- anisotropic elastic deformation, effective stress law, appl. to saturated porous rocks 80—51385
- anisotropic elastic slab, stress field and crack energy 77—50908
- anisotropic elastic slab containing crack, deformation 79—68570
- anisotropic elliptical layered plates, deflection, interlayer shear effects 79—98622
- anisotropic materials, determ. of mutual influence coeffs. 77—75862
- anisotropic media, elastic strain energy of precipitates, and periodic distrib. inclusions 78—84810
- anisotropic medium, perturbed, propag. of elastic waves *(French)* 79—42144
- annular elastic membranes, large deflections, theoretical and expt. exam. 78—30186
- annular plate of inhomogeneous material, varible loading and heated conditions 78—94594
- annular rotating disc 77—23888
- annulus, infinite, with two pairs of cracks at inner boundary, plain strain problem 77—14963
- anti-plane shear for compressible materials in finite elastostatics 78—13900
- antiphase problems in linear elasticity theory *(French)* 78—87268
- antiplane deform., soln. representation for nonlinear elastic media *(Russian)* 77—84145
- antiplane deformation state for elastic body, potential function representation *(French)* 79—37176
- anvil, truncated, compressive strength, high press. apparatus appl. 78—84906
- arches, curved beams, rings, treatment of extensional deformations for bending 77—58556
- arterial grafts, in vivo mech. props., biological vs. synthetic grafts 77—37002
- arterial wall axial deform. and anisotropy *(Japanese)* 78—53437
- artery, finite deform. elastic model, large amplitude oscills. 77—37000
- artery pressure-radius relationships, comparison of elastic tube models 77—64077
- artery pressure-radius relationships, comparison of theory and expt. for rubber tube 77—64078
- articular cartilage in uniaxial tension, large deform. nonhomogeneous and directional props. 80—3696
- articular cartilage under compressive stress, elastic behaviour 77—73536
- asymmetric elastodynamics with homogeneous initial conditions, Boggio's type theorem 78—26037
- axisymmetric elastic bodies subject to cyclic loadings *(Russian)* 77—75800
- axisymmetric problems, scatt. light photoelasticity for stress and strain determ. 77—72168
- axisymmetrical homogeneous elastic solid with internal circular cracks, energy release rates 78—67139
- bar, curved, in-plane vibrs., shear deform. and rotatory inertia effects 80—43646
- bar structures, large deflection anal. 79—98606
- bar with space curve axis, loaded bar shape calc. 78—51069
- bars, literature review and bibliography on finite elastic deflections 77—84140
- bars, phase boundary propagation, dynamic elastic bar theory, sound wave interactions 80—69706
- beam, deflection under equally spaced moving loads, analytical approx. *(German)* 77—75835
- beam, elastic, on elastic half-space support, forced flexural vibr. 78—63353
- beam, rotating, nonlinear flap-lag-axial eqns. derivation 77—84134
- beam, thin wall, bending stiffness 80—28425
- beam, Timoshenko's shear coeff. variation with frequency 79—32367
- beam boundary conditions vibratory identification 77—27480
- beam dynamic deflection under external force of time-dependent frequency 78—83289
- beam dynamic loading, large elastic-plastic deform., numerical anal., expt. meas. 78—1574

elastic deformation continued
beam modelling, linear shape function for axial displacement approx., finite element anal. 80−69665
beam nonlinear elastic optimal design for minimum compliance 79−1108
beam on elastic medium, force distrib. change effects 79−55326
beam-columns, optimal design 80−10142
beam-like lattice trusses, numerical analysis, shear deformation 80−14566
beams, 1-D, stability in torsional extension *(German)* 78−87270
beams, curved, large deflections, equilibrium positions *(German)* 77−14901
beams, elastic straight slender undergoing small strains and rots., nonlinear behaviour 79−64518
beams, heterogeneous anisotropic almost cylindrical, Saint-Venant problem 77−39220
beams, orthotropic almost cylindrical, loaded on lateral surface and ends 77−42736
beams, spatially curvilinear elastic, geometrically nonlinear theory 80−96189
beams, straight, finite displacements and small deform., asymptotic anal. *(French)* 78−90716
beams, straight, homogeneous and isotropic, linear flexural theory *(French)* 80−74743
beams, thin walls, stress-strain state determ., method of segments 80−28424
beams and plates, lateral deflection, determination by iterative method 80−19241
beams subjected to nonconservative compressive follower loads, lower bound theorem 77−68459
Beltrami-Michell and Beltrami-Michell type eqns. in static and dynamic elasticity 77−53782
bending, finite, existence-uniqueness results 77−75811
bending of elastic plates, resolution of elliptic problems 79−64538
bending of rectangular form optimal plates *(Russian)* 77−23882
bending of ring of micropolar elastic material, displacement soln. 77−19535
bent crystal, X-ray Laue diffraction, integrated intensity 79−23492
bi-material, elastic composite, Southwell's analogues for plane and bending problems 78−87265
biological soft tissues, large deform. anal. 77−5018
biological soft tissues, stress response anal. 77−90845
blister test specimen, effect of adhesive layer elasticity 77−16778
bodies with periodic microstructure, asymptotic solns. *(Russian)* 78−41158
bone, elastic and damping props. of human femur in bending 77−25489
Boussinesq problem for material with different moduli in tension and compression 78−55564
brittle abrasive material, rating capability for elastic deformation 78−56680
brittle materials, splitting of fracture toughness into two terms, elastic deform. and plastic deform. *(German)* 78−35468
brittle solids, unstable growth of thermally induced interacting cracks 78−63374
buckling, nonlinear, appl. of bifurcation problem left branching soln. 77−67222
buckling of elastic bar with varying stiffness, coupled boundary conditions 77−31231
buckling of elastic beams, analysis using theory of quadratic operator pencils 80−48607
buckling of elastic-plastic cylindrical panel under axial compression 78−1584
buckling of rotating rod, critical rotation speed, extended Galerkin method 77−35064
buckling strength of orthogonally stiffened plates under uniaxial compression 80−5964
Burgers circuits associated with generalized distortions 80−2014
butadiene-styrene block copolymer, viscoelastic props. 79−8336
cable-bar trusses, static anal. 79−98609
cantilever (Timoshenko), elastically restrained, with attached masses, follower force stability 78−63347
cantilever beam, distorted isoparametric elements 79−27526
cantilever beams, inelastic large deforms. 77−50913
cantilever curved beam, stress singularity anal. 79−23214
channel, straight (buckled), two-dimens. flow, stability anal. 78−59490
Chromel alloy, influence of elastic strain on oxidisability *(Russian)* 79−70116
circular cylinder, micropolar, elastic, flexure problem 78−51083
circular plates, elastically restrained, of variable thickness, static and dynamic behaviour 77−75841
circular ring plates, finite deflections 79−27533
circular sliding contact on transversely isotropic spheres, stress field 79−18833
circular tube fibre reinforced sector, elastic deform. 77−72164
clamped columns, single and bimodal optimum buckling loads 77−62182
clamped plate, asymmetric deform. 80−10147
clamped rectangular plates, bending anal. 77−68435
clamped skewed plates, elastic deformations by dynamic relaxation 78−34049
classical impact theory, Carnot functional *(Russian)* 79−25856
collagen with planar crimp, tensile deformation 80−84235
colloidal systems, surface forces, direct meas., elastic deform. effect 80−93805
complementary energy principle, finite elasticity solns., hybrid finite element anal. 79−32274
complex idealised bar, deformation processes, bifurcational elastic eqn. soln., pseudobifurcation *(Russian)* 80−58945
composite Cosserat elastic cylinders, deformation 79−37178
composite material, longitudinally cracked, exam. of plane deformation 78−67096
composite micropolar elastic cylinders, Saint-Venant's problem 79−46206
composite ribbed multilayer cylindrical shells, stability and optimal design 80−58949
composite rod, small deformations, initial stresses effect 78−63284
compressibility, finite element displacement model 77−867
compressible elastic solids, finite plane strain problems, analytic soln., volume changes 77−68452
compressible elastic solids, finite plane-strain problems 77−14900
compressible hyperelastic solid, failure of ellipticity of eqns. for finite elastostatic plane strain 77−54875

elastic deformation continued
compressible rubberlike materials, determination of elastic potential function 80−10159
compressible solids, finite plain strain problems 79−10479
computational methods of treating nonlinear and special linear problems 77−74226
comressible circular block, bending into a spherical shell 80−1437
concentric impact of pointed bodies 79−41604
concrete, compressive strength and ultimate strain under impact loading 79−70128
concrete, cracking along anchored deformed reinforcing bars 79−96122
concrete, deformation under complex loading, mathematic description 80−25783
concrete, plain, deform. and fracture 79−70167
conic body torsion, double series method *(Russian)* 79−23206
conical punch pressing into elastic layer 77−13612
conical shells, axially compressed with edge constraint, elastic and plastic buckling 78−63341
conservation laws of J-integral type 77−49598
consolidating semi-space, axisymmetric punch problem with mixed boundary, permeability conditions 78−51087
consolidation in compressible mixtures 79−46271
constant-stress surfaces and stress conc. minimisation 77−869
contact, frictionally heated, thermoelastic deform. 80−83764
contact between sphere and semi-infinite transversely isotropic body 77−31217
contact problem, elastic layer on rigid foundation with cylindrical hole 77−72252
contact problem, half-space indented by truncated conical stamp 79−98672
contact problem, non-axisymmetric cylindrical 77−19574
contact problem of half space pressed onto rigid base with cylindrical protrusion or pit 79−37249
contact problem with friction, solution using nodal parameters *(French)* 78−63401
contact problems involving a cooled punch 79−32390
contact stress minimisation by contour design 78−63396
contacting asperities, theoretical analysis of elastic-plastic deformation 79−95076
continuous flexible member, shooting method with Newton-type iteration 80−48575
core supported structure, stability 79−98607
Cosserat type solid, continuity eqns. and Cesaro type formulae 77−50903
coupled elastic-plastic boundary-value problems, rock mech. appl. 77−14918
crack, oblique edge, in semi-infinite plate, stress anal. 80−64463
crack closure in bending, elastic plates, sixth order anal. 80−96231
crack development, radial, elastic antiplane deformation conditions, self similar problem 78−5698
crack energy in initially stressed neo-Hookean anisotropic infinite medium 80−48642
crack tip singularity, order changing at discontinuity 78−59345
cracked stiffened panels, biaxially loaded, elastic and elastic-plastic analysis, using finite element method 79−68656
cracks, coplanar Griffith, in infinite elastic layer under torsion 78−1610
cracks, curvilinear, star-shaped array in infinite isotropic elastic medium 78−55609
cracks, model deduced from thermodynamics *(French)* 78−63386
cracktip under incipient creep deform., stress field and modified J-integral *(Japanese)* 80−103411
critical equilibrium states of nonlinear elastic systems, unified method of computation 79−98610
crosslinked elastomer, adsorption of Rn 80−10775
cruciform crack, unsymmetric, soln. in infinite plane isotropic elastic medium 79−14342
crystal, diffusional motion and distortion of macroscopic inclusions under influence of elastic stresses *(Russian)* 77−66676
crystal, elastically bent, dynamical Bragg diffr. of X-rays 79−14639
crystal, relationship between dislocations and surfaces 80−24446
crystal, stressed, elastic const. determ., static method 80−49291
crystal plates, higher-order effects of initial deform. on vibrs. 77−46862
crystalline particles at sphere-plane contact, nondiffusional deform. under capillary forces 78−15329
crystalline solids, absolute strain rate in elastic deformation, model 78−75073
crystalline solids, discontinuous nature of elastic deformation 78−75072
crystals, device for low temp. uniaxial compression 78−49809
crystals, Laue groups, hydrostatic pressure deform., acoustic waves invariance relations 79−95087
crystals, monatomic, nonlinearly elastic, twinning 80−58903
cubic boxes subjected to pressure, exptl. stress and strain anal. 78−59307
curves of strengthening construction from bend tests, deformation curves *(Russian)* 79−59928
curvilinearly aeolotropic thin rubber tubes, forced oscillations soln. 78−9589
cylinder, circ., elastic, axial eigenfunctions orthogonality 78−51080
cylinder, circular embedded in resisting medium, twisting, stress anal. 80−53637
cylinder, clamped heterogeneous, stresses and displacement anal. 80−14571
cylinder, compressible, under uniform compression, stability *(Russian)* 78−55577
cylinder, elastic, equilib. difference scheme, deformation tensor approx. 79−41583
cylinder, hollow, end effects *(Russian)* 79−10487
cylinder, infinite, solid, diametrically opposite conc. load deform. and stress 78−63287
cylinder, thin, deformation due to band press. 78−94595
cylinder embedded in elastic half space, Reissner-Sagoci type problem 79−27524
cylinder penetration of thin obstacle, 1-D approx. anal. *(Russian)* 78−30246
cylinder with internal hole, dynamic excitation 79−18712
cylinders, axially compressed, comparative study of elasticity, shell and boundary layer solns. 77−89029
cylinders, deform. anal. in modified Bessel functions *(Russian)* 79−10478
cylinders and plates, dynamic deform. at high frequencies *(Russian)* 78−18223

elastic deformation continued
cylindrical elastic tube torsional oscillations under large internal and external press. 78—79249
cylindrical membrane, non-uniform inflation, direct determ. of strain energy function 77—75805
cylindrical rod, linearly elastic, elastic waves anal. from two-point strain meas. 77—72211
cylindrical shell, stretching, bending, twisting and flexure 77—11125
cylindrical shell, thin walled, stability under external pressure, linearised theory *(Ukrainian)* 79—98645
cylindrical shell, transverse shear effect on axial crack 78—67090
cylindrical shell with circular cut out, uniform bending, strength and flexural rigidity 78—87282
cylindrical shell with wind load, membrane/bending forces ratio anal. *(German)* 77—31211
cylindrical shells, dynamic behaviour under transient inner pressures 79—23215
cylindrical shells, finite element anal. of stress deform. states *(Russian)* 79—14256
cylindrical tubes, compressible, wire-layer reinforced, inflation and extension 79—3922
damage accumulation in nonstationary low cycle rigid loading 77—16686
defect dynamics, field equations, four dimensional space-time setting 80—96521
deflection analysis for large heated elastic plates by constant deflection line method 80—14641
deformable body three dimensional stability theory, variational principles 80—38300
deformable body with central vertical crack, destruction in homogeneous force field *(Russian)* 79—27554
deformation wave processes, corrected nonlinear eqns., stresses and strains 80—102998
diamond composite with Cu-Ti matrix, microstresses, X-ray diffr. exam. 78—56679
diatomic crystals, strain energy functions, crystal symmetry constraints 78—47467
diatomic solids, thermoelastic, continuum theory 80—53635
dielectric, polarised, small longitudinal vibr. 79—18772
dielectric elastic half space with point charge, stress and polarisation anal. 77—83776
dielectric shell, thin, EM interactions and small elastic deformations 80—53624
dielectric shell, thin, EM interactions and small elastic deformations, technical theory and Love's approx. 80—53625
differential geometry of deformed crystals 80—19867
dipolar solid microdeformation field in nonlinear theory 77—75794
director rod, elastic instability 78—63292
discrete spectra for elastic plates without deflection, mixed boundary conditions *(German)* 79—27579
discretised stress, strain, eqns. and theorems 77—49596
discs, anisotropic, singular integral eqn. anal. *(German)* 78—87272
dislocation layers and crack problems in elasticity theory 80—33533
dislocation scattering, new Hamiltonian for describing multivalued elastic displacement fields 80—24862
p-disubstituted phenylcyclohexane, liq. cryst., investigation of elec. field induced deform. by capacity measurements 79—4234
ductile materials, tearing, fracture strength determ. 79—43385
dynamic coefficient of an elastically supported, pre-stressed beam 79—14306
dynamic crack system interactions, elastic antiplane deformation conditions 78—9609
dynamic props. of impulsive-type loading 79—70106
dynamic response of variable section rod subject to longitudinal impact with flexible load 77—89036
dynamic rigid indentation induced by sliding frictionless contact 78—75107
Earth, surface waves phase vel. and attenuation simultaneous inversion, Love waves appl. 78—85491
Earth crust, free surface deform. during earthquake cycle, asthenosphere readjustment effects 78—85490
Earth lithosphere bending at trench, elastic-perfectly plastic anal. 78—81135
edge dislocation screening in metals and superconductors, metal softening *(Russian)* 80—64997
elastic behaviour of elastic materials, thermodynamical bounds, thermoelasticity, deformation 79—41576
elastic circular plate subject to nonuniform load, instability 77—62178
elastic creep fatigue rules fo ASME B&PV code case 1592 78—44211
elastic solid, cracked or notched, general numerical method for three dimensional singularities 78—67137
elastic-plastic torsion, nonlinear boundary value problem 77—89043
elasticity, annealing and deformation effects, with and without texture 79—52274
elastohydrodynamic contacts, ellipsoidal solids subjected to Hertzian contact stress, surface deform. 77—35097
elastomeric network, finite linear viscoelastic theory, time-depend. deform. behaviour 80—38292
elastomers, strain-energy function theory 77—11133
elastomers, vulcanised, tensile failure and network fracture mechanism, particle reinforcement 80—41928
electric conductor, elastic strain state, contact phenomena effects *(Russian)* 78—9564
electrically conducting elastic plate, vibrs. in transverse mag. field, shear deformation *(Russian)* 79—81756
ellipsoidal inclusion in anisotropic material, stress and strain concs. factors 77—50900
elliptic crack and punch problems, Lame polynomial solns. 78—75069
elliptic infinite bar, impulsive loads, three dimens. elastic stress-strain anal. 78—87259
elliptic plate, heated, deflection under uniform load 77—35040
elliptic plates on elastic foundation, anal. of large deflections 77—50914
elliptical contact deform. between elastic solids, simplified soln. 78—55616
epoxides, dielectric relax. and deform props., cross-link density effect *(Russian)* 80—60942
epoxy polymers, dense-network, elastic deform. rel. to props. *(Russian)* 80—40468
epoxy resins, alteration by reactive elastomers *(German)* 79—100106
estimation of parameters for a beam on an elastic foundation with large deflections and built in at both ends 79—27520
Euler buckling eigensystem for a nonprismatic strut 79—18764

elastic deformation continued
Euler column Lyapunov stability analysis 78—71285
evolving shells, postcritical deformations *(Ukrainian)* 79—32310
exceptional wave propagation in continuous medium, finite deform., evolution of discontinuities, elastic pot. determ. *(Italian)* 78—54202
expansion process, associated differential geometry 79—67159
eye, elasticity of sclera and choroid in humans, rel. to scleral rigidity and accommodation 78—80907
fatigue, hydrostatic stress-sensitive relationship for biaxial stress conditions 80—74805
fatigue crack, low cycle, test machine rigidity effect on kinetics 78—15632
FCC polycrysts., under hydrostatic pressure 80—107356
ferromagnetic beams, prismatic elastic, deformation by external mag. field 80—34749
fibre reinforced composite, energy release rate for cracks 77—66690
fibre reinforced composite, stress boundary value problem for finite plane deform. 80—48583
fibre reinforced composites, deformability determ. by stiffness averaging method 80—3115
fibre reinforced composites, stress redistribution dynamics during fibre rupture 80—64394
fibre-reinforced composite, small vibr. propag. in static deformation 77—42775
fibreglass composite, oriented, model, conditions of monolithicity, exam. 78—67044
filaments, slender, with planar crimp, tensile deformation 80—84235
finite deformation crack in infinite body under antiplane simple shear 78—18242
finite deformation elastoplasticity, strain measure decomposition 79—23223
finite elasticity for small superimposed deforms., self-adjoint differential eqns. 77—78982
finite elasticity with general loading, uniqueness for deformed surface 80—79153
finite hyperelastostatics, continuous dependence result for mixed boundary value problem 79—68574
finite strain coordinates and stability of solid phases 77—7306
flat elliptic paraboloid shells subjected to uniformly distrib. horizontal load at edges *(German)* 79—27518
flexibility matrix for skew-curved beams 79—98620
flexible plate sealing incompressible liquid, removal of anomaly in perturbation anal. 78—38201
flexible string under transverse impact, dynamic deform. and possible unwinding from drum *(Russian)* 78—22279
flexure, Scholnikoffs method 79—21552
flexure of clamped rectangular plates resting on Winkler foundations 80—5934
flow surface of solids, nonlinear elasticity *(French)* 77—68397
fluid saturated porous solid, fundamental solns., deformation, pore-fluid diffusion, soil mechs. 77—84160
fluid-infiltrated elastic materials, deformation of cavities and inclusions 78—51073
fluid-structure coupling problem soln. using boundary-integral eqn. method 77—54920
fluid-structure interaction, dynamic response 77—50917
follow-up loading determ. at small deform. *(Russian)* 77—19529
fourth-order elastic constants, determ. 78—6958
fracture zone analysis of fission reactor elastoplastic materials *(Spanish)* 79—66139
frictionless indentation by an elastic punch: a dynamic Hertzian contact problem 79—32389
frictionless indentation by rigid wedge, effect of tangential displacements in contact zone 79—37250
fundamental theory, and applications, book 80—22158
fusion reactor coil, multilayer structs., laminated beam theory anal. 78—55011
gas-saturated porous media, deform. theory *(Russian)* 77—41483
gels, non-linear behaviour under strong deform. 78—7240
geometrical nonlinear shell theory, continua with warped cross section *(German)* 79—23210
glass, adsorption of Rn 80—10775
glass, deformation in glass transition interval 79—66137
glass, viscous deformation during heating and cooling 80—89314
glued joint, axially symmetric, stress determ. for torque loading *(Polish)* 78—79287
granular elastic layer underlain by smooth rigid base, surface load 77—14905
granular material with no intergrain slip, elastic zone 79—34087
Green's function of elastic plate in the shape of epitrochoid of order-3 and clamped along the boundary 79—17220
grinding, role of elastic and plastic behaviours *(Japanese)* 80—100868
ground surface profile, crest and trough height distrib., Monte Carlo simulation *(Japanese)* 79—34180
ground surface profile power spectrum, Monte Carlo simulations *(Japanese)* 79—34179
Guinier-Preston ellipsoidal zone model of X-ray scatt. *(French)* 77—84568
gyroscope drift, elastic deform. effect on rot. gimbals with base vibr. *(Russian)* 77—14894
gyroscopic problems in elasticity, orthogonality principle 79—17218
half-bounded medium, unidimensional deformation under vibr. loading *(Ukrainian)* 80—5933
half-planes, distributed load end values by optical caustics technique 79—18851
half-space, coupled thermoelastic problems 78—59300
half-space subjected to sinusoidally distrib. strip load, two-dimensionality 77—65685
half-space transient motion, numerical inversion method *(Russian)* 77—54877
hard-alloy/U8 C alloy steel weld, local internal stress region boundaries 77—59846
hardness testing, scale effect during indentation, role of elastic strains *(Russian)* 79—39062
Hencky's approximate strain energy function for moderate deformations 79—63045
heteroepitaxial film deformation, causes and countermeasures *(Russian)* 80—49561
hinged strut, large elastic deformations *(German)* 79—81725
holes with loaded boundaries in elastic plane, anisotropic property optimisation *(Russian)* 79—46208

elastic deformation continued

- hollow sphere with stamps on external surface, creep stresses 77—84152
- hollow thick-walled cylinders, stress-deformation, limiting state anal. *(Russian)* 79—27538
- holographic interferometry, study of elastic and plastic deform. 77—62223
- homogeneous simple strain in elastic-plastic media, necessary and sufficient conditions 80—28427
- horizontal falling wire, max. strain due to instantaneous avert of its ends 80—28418
- hybrid deformation elements for elastic media 80—92049
- hydroelastic shell opening in fluid flow numerical soln. *(Ukrainian)* 79—50592
- hydrogels, two-component, elasticity theory and compress. meas. 80—44246
- hyperelastic bodies, isotropic, deformations, extension of Ericksen's theorems 80—31507
- hyperelastic composite reinforced by inextensible fibre, first- and second-order constitutive eqns. *(German)* 78—18174
- hyperelastic compressible medium with cylindrical cavity, finite dynamic expansion under sudden press. 78—79213
- hyperelastic compressible spherical shell, dynamic expansion 77—72165
- hyperelastic isotropic behaviour laws for large deform. *(French)* 78—77715
- hyperelastic materials, anisotropic, compressible, finite plane strain, universal deformations 80—69667
- hyperelastic systems, discrete and continuum mech. 77—864
- hypo-elastic materials with internal variables, shear 77—31221
- hypoelastic materials undergoing uniform rectilinear shear, rotation and stress rate anal. 79—98604
- hypoelastic materials with internal variable, work-hardening, hysteresis, fracture law 77—62177
- ice, columnar grained, rheology 79—57044
- ice, floating sheet, viscoelastic response under prolonged loading 78—51093
- ice sheet deflection by submerged gas source 77—80120
- ideal elastic fibre-reinforced slab, dynamic flexural deformations, flexural wave propag. 80—33510
- III-V compound heteroepitaxial interface mech. and crystallographic props. 77—76706
- III-V epitaxial pseudobinary compounds, lattice deform. determ. by X-ray diffraction 78—6242
- impact, elementary analysis of elastic longitudinal impact problems 79—72809
- impact attenuation system using plastic deform., effect of strain-rate sensitivity 77—23890
- impact on thin flexible struct., dynamic contact *(French)* 77—68408
- impact problem, stress wave elementary analysis 79—50628
- incoherent ellipsoidal precipitate, re-exam. of elastic strain energy 78—51676
- incompressible elastic material finite anti-plane shear study 78—13899
- incompressible elastic materials with different moduli in compression and tension, dynamic problems 80—79141
- incompressible finite elasticity, method for numerical soln. of problems *(French)* 80—42062
- incompressible isotropic material, speed of propagation of waves 78—54201
- incompressible isotropic solids, plane deformations 78—38194
- indentation, dynamic, of elastic half-space by rigid punch, numerical method 78—1612
- indentation hardness and hot pressing, calc. methods 80—58981
- indentation of elastic half-space by rigid rectangular punch 78—18167
- indentation testing, mech. characts. calcs. inc. elastic strains *(Russian)* 78—95863
- indenter moving on an anisotropic elastic half-space 79—37248
- inextensible material, uniqueness of displacement boundary-value problem 78—54195
- infinite elastic solid with spherical inclusions, linear elasticity eqns., stresses, displacements 78—65773
- infinite elastic thick plate, axially symmetric loading, numerical method *(Japanese)* 78—9568
- infinite plate, axisymmetric interaction with elastic halfspace, influence of Mindlin force 78—38193
- infinite plates clamped along inner curvilinear edges, Green's functions 78—38191
- infinitely long trapezoidally corrugated plates in shear, elastic buckling 79—32315
- inhomogeneous materials, elastic deform. under multiaxial stress, analytical relations 80—44247
- inhomogeneous materials, elastic deformation under multiaxial stress, constraint ratio 80—19235
- inhomogeneous materials, with ellipsoidal inclusion, and polycrystals, elastic deform. 78—15451
- initial stress problems, stress function appl. 79—18722
- integral equation formulation of plane deform. of isotropic incompressible solid 78—51081
- interface separation for elastic layer on rigid plane, leaded by rigid stamp 78—87307
- internal friction measurement by resonant specimen with a dumb-bell shape 80—48660
- internal stress determ. by deform. mechanics model *(Russian)* 80—54300
- ionic crystals, structurally modulated, elasticity and its limits, yielding and melting 80—49295
- Ising systems, compressible, elastic anomalies inducing first order transitions 79—47288
- isochoric deforms., strain invariants 77—50901
- isotropic bodies, stability under all-round compression by dead load *(Russian)* 77—42762
- isotropic elastic body, displacement tensor representation by Piola stress tensor *(Russian)* 77—42743
- isotropic linear viscoelastic material, connection between shape and volume change *(German)* 79—27531
- isotropic thin shells with circular hole, stress state, numerical investigation 80—48586
- j integral applications for short fatigue cracks at notches 80—38332
- laminated anisotropic plates, transverse shear deformation effect 80—19237
- laminated anisotropic shells, transverse shear stiffness calc. 78—42526
- laminated composite, dynamic response under large deformation, nonlinear mixture theory 78—56717

elastic deformation continued

- laminated plates, symmetric, specially orthotropic, thermoelastic anal. 80—92058
- laminated rectangular antisymmetric angle ply plates, shear deform. effects on vibr. 78—63356
- laminated rectangular plate on elastic foundation, uniform loading, computer anal. 77—46915
- large deflection analysis of plates and shells by discrete energy method 79—3918
- large deflection of a shallow spherical shell subjected to uniform normal pressure and heating 78—94593
- large deform. three-dimens. anal. of thin walled beams 77—11126
- large plane bending deformation anal., approx. solution *(German)* 78—5674
- lattice-parameter determ., elastic deform. effect 77—72524
- layer interface, SH type disturbance due to shearing stress discontinuity 78—34011
- layer pressed against substrate, separation and slip caused by tensile load 80—96536
- layered elastic quarter space, transient contact shear stress under anti-plane loads 77—14936
- layered half-space, transient response under reciprocating anti-plane shear load 77—14935
- linear Cauchy and Piola-Kirchhoff constitutive theories for stress in solids 79—37173
- linear elastic, material of hexagonal symm., half-space, indentation by circular punch 78—34020
- linear elastic arbitrary deformable bodies, iterative method *(Polish)* 79—10476
- linear elastic half-space, frictional unloading problem, variational soln. for stress analysis 78—59350
- linear elastic incompressible solid, stability of void growth under uniaxial tension and shear 79—76972
- liquid drop collisions on deformable media, simulation of erosion in rainfield 77—56113
- liquid-filled circular cylinder, influence of bulge terms on section and deform. *(German)* 78—90717
- liquid-saturated porous media theory with account of simultaneous deform. of structure and liq. *(Russian)* 77—41482
- lithosphere, elastic-perfectly plastic bending under generalised loading, appl. to Kuril Trench 78—73341
- lithosphere, subducting, dynamic support of ocean trench outer rise 78—81116
- LMFBR piping components, resistance to bending moments 77—6505
- long flexible cylindrical panel deform., temp. field effect *(Ukrainian)* 79—90128
- Long-life notch strength reduction due to local biaxial state of stress 78—9612
- long-wave quasiparticle states localized at screw dislocation *(Russian)* 78—95126
- LORA—an accurate four node stress plate bending element 79—27527
- lung, deforms. at minimal vol. 80—97977
- lung, gravitational deformation, excised canine lungs, linear elasticity soln. 80—30747
- lung membrane indentation anal. on elastic half space 79—20522
- lung parenchyma anisotropic props. 78—31842
- lung parenchyma described as prestressed compressible material 77—90837
- magneto-elastodynamics, boundary-value problems 79—49046
- magnetoelastic buckling of rectangular plates, edge effect influence 77—80988
- magnetosolid mechanics, semi-infinite cylindrical shell with strain depend. permeability, torsional response 79—94483
- magnetostrictive cylinder, torsional deformation 80—53636
- magnetostrictive viscoelastic cylinder, nonhomogeneous, torsional deformation 79—37169
- massive designs, investigation of large deformations using finite-element moment system 79—41580
- matrix formulation of large deformation analysis using computers 79—98608
- matrix methods, appl. to bent beam *(Dutch)* 77—41451
- maximum-energy-release-rate criterion applied to a tension-compression specimen with crack 79—23212
- MBBA, liq. crystal, hydrodynamic instabilities and elastic deformation created by US 77—19873
- membrane, elastic, rigid centre, press. gradient, large deflections *(Russian)* 78—5662
- membrane, elastic support, mixed boundary-value problems, variational principles and hypercircle 78—57749
- membrane, rectangular under uniform pressure, large deflections 78—55560
- membrane, slack circular, under point load 77—46911
- membrane deformations, constitutive relation effects 79—14269
- membranes, elastic, universal deforms. 78—67048
- membranes, isotropic elastic, large deform., static solns. 78—13903
- membranes for pressure meas., nonlinear characts. calc. *(Czech)* 79—26021
- metal, elastically strained, elec. field gradients on nuclei, calc. *(Russian)* 78—60096
- metal, HCP, self-migration energies, elastic calc. 79—95205
- metal, polycryst., free surface influence on mutual restriction between grains 77—51431
- metal, surface strain meas. by intensity of reflected light flux 77—17972
- metal-composite shell, three-layer, stochastic formulation of optimisation using heuristic methods 80—38268
- metallic materials, mech. stressed, lattice strain distrib., X-ray elastic const. calc. *(German)* 78—52884
- metallic structures, magnetostriction method of measuring elastic stresses 78—72985
- metals and alloys, polycrystalline, LF viscosity meas. 78—80576
- microflow, activation volume, meas. impracticality *(French)* 80—52026
- microhardness, Knoop numbers, correction factors, elastic recovery 78—72952
- micropolar circular cylinder, flexural rigidity 79—18724
- micropolar elastic almost cylindrical beams, deformation 79—37177
- micropolar elastic thick-walled tube under forces and moments 77—865
- mineral dispersed macromolecular matrix, holographic interferometric meas. of displacement vectors on boundaries 79—79015
- mirror, nonaxisymmetric, fabrication by stressed mirror polishing 80—99885
- mitral valve vibration anal. to detect first heart sound freq. 78—40233

elastic deformation continued
mixed boundary value problems, numerical scheme 78—26038
mixed boundary-value problems soln. by direct variational method 78—83331
Mooney-Rivlin materials, superposition of finite deforms. 77—65681
Mooney-Rivlin rubber-like materials, finite element anal. 78—46894
multi-support sandwich beams, calc. *(German)* 79—98612
multiconnected shell, closure conditions for surface deformations *(French)* 77—23887
multilayered inhomogeneous packet of elastic strips on elastic half-plane, contact stresses *(Russian)* 77—75796
muscle, force-length relations of glycerinated rabbit psoas 77—48828
muscle contraction, math. model with account of excitability 77—25417
muscle fibres, Ca^{2+}-activated, effect of MgATP on stiffness meas. at 5 and 100 Hz 78—48822
neo-Hookean elastic layer, Griffith cracks, plane strain problem 79—50666
Nimonic type, elastic interphase strains on ageing effects on extinction *(Russian)* 77—66646
non-associated plasticity and elastoplasticity, rate boundary value problems, variational principles 80—87726
non-homogeneous hollow cylinders stress determ. *(French)* 79—32423
non-homogeneous medium, coupled deform. waves *(Russian)* 80—48635
non-linear viscoelastic behaviour, numerical anal. 78—59318
non-uniform motion of thin smooth rigid inclusion through elastic solid 79—32267
nonconservative elastic systems, branching anal. at coincidence buckling loads 77—80090
nonhomogeneous cylinders and cylindrical shells, torsional oscillations anal. 79—18768
nonhomogeneous elastic layer bonded to nonhomogeneous half-space, torsion by circular die 78—87263
nonlinear beam of thin-walled open cross-section, sectorial coord. 77—35036
nonlinear beam structures, finite element method for deformation, kinematic functions *(German)* 79—37167
nonlinear cantilever beam statics *(German)* 80—106726
nonlinear discrete continuous model of elastic layered body, homogeneous deformation 79—23207
nonlinear dynamic mech. moduli 78—60693
nonlinear elastic half-space, dynamic contact stresses due to axisymmetrical projectile impact 78—42573
nonlinear elastic half-space and slab, anal. of moving line force 78—13944
nonlinear elastic medium, mutual focusing of sound waves *(Russian)* 78—26001
nonlinear elastic membranes, large finite strain effects, asymptotic solns. 79—50597
nonlinear elastic stability problems using a finite difference perturbation method 78—83273
nonlinear elastic systems, incremental approach to the solution of snapping and buckling problems 79—76975
nonlinear elastic tubular membrane, limiting pressure in simultaneous elongation and inflation 79—37166
nonlinear elasticity, integral estimates for displacement and strain energy, body force 77—54882
nonlinear elasticity for nearly incompress. rubber like materials, large strains, finite element anal. 80—19238
nonlinear elasticity incremental eqns., bifurcation of pressurised spherical shells 79—17225
nonlinear elasticity incremental eqns., membrane theory 79—17224
nonlinear elasticity strain energy, integral bound for displacement boundary value problem 79—37171
nonlinear elasticity theory, generalised plane deform. *(Russian)* 77—46922
nonlinear finite elasticity, uniqueness condition, work theorem 78—57784
nonlinear flexural oscillations of orthotropic shallow spherical shells 79—3939
nonlinear isotropic medium, symmetric spherical wave propagation eqns., permissible transform. *(Russian)* 78—87292
nonlinearly elastic body at eqn., relation between stability and continuous dependence 80—92063
nonlinearly elastic plates, buckled states 79—1118
nonlocal thin elastic plates, impact by cylindrical projectile, shearing stress anal. 79—10467
nylon, oriented, transverse compression 78—68728
Nylon 6, oriented, extensional deformation, and effects 80—7613
open shells, prebuckling state, bending stability, contour deformation effect 79—94519
optical fibre preform rod, refractive index profile meas. by transverse differential interferogram 80—64141
optimal anisotropy of elastic shafts under torsion *(Russian)* 79—23211
optimal design of bending elements 79—10470
optimal strain paths in linear viscoelasticity 80—5956
ordered regions near macroscopic defects and percolation phase transform. in crystals *(Russian)* 80—92665
orthodontic appliances, 3-dimens. large displacement anal. 77—29228
orthotropic cantilever beams, Rayleigh-Ritz determ. of upper and lower bounds 78—59298
orthotropic cylindrical shell acted upon by local load 80—43617
orthotropic plate, twisting in large deflection regime 77—23870
orthotropic shell with elastic filler under external press., stability *(Russian)* 77—19528
Pacific lithosphere, flexure seaward of Bonin and Mariana trenches 79—57903
panels, stiffened, eight-stringer, with rectangular cut-out, stresses and deformations, eccentric tensile load *(Japanese)* 80—64467
particle adhesion, effect of elastic contact deformation 77—29048
particle falling in viscous fluid, deform. 80—79149
particle system to continuum model transition 77—854
penny-shaped crack problem, deformed incompressible elastic solid 80—92085
perfect single crystal, elastic instabilities and plastic modes *(French)* 79—28034
PET, oriented, extensional deformation, and effects 80—7613
PET, rigid, unoriented, prefracture state study, forced high-elastic deform. 77—59931
piezoelectric plate, infinite, on elastic medium, transient response to pot. pulse 78—52442
piezoelectric thin plates, integer polynomial solns. *(Russian)* 78—52444

elastic deformation continued
plain strain displacement and stress field in transversely isotropic elastic solid 79—14340
plane deformation, isochoric solids, volume changes under plane strain 79—50596
plane strain, alternative approach 77—50899
plane wedge under large deform., eqn. of compatibility *(German)* 77—23889
plane with heat-permeable curvilinear cut, limiting equilib. *(Russian)* 79—50576
planetary bodies, ancient, deform. energy rel. to lunar capture hypothesis 78—81570
plastic clay body, mech. behaviour, retarded elastic deform. *(Japanese)* 77—32622
plate, arbitrary shape, weight optimality condition *(Russian)* 77—23879
plate, circ., thin, elastic, containing Griffith crack, in infinite elastic medium, stress distrib. 79—32374
plate, circ. isotropic, compressible, bending into ellipsoidal shell 79—32252
plate, circular, laterally loaded, elastic instability initiation 77—50936
plate, deformation instability in brittle fracture mechs. problems 78—63382
plate, elastic, infinite, thick, fixed, subject to axially symmetric load, numerical stress anal. *(Japanese)* 79—50600
plate, elastic circular cylindrical, with arbitrary transference, stress-strain state *(Russian)* 80—23895
plate, elastic deform. due to axisymmetric punch 78—75065
plate, heated equilateral triangular, large deflection, uniform load, temp. distrib. 78—83250
plate, homogeneous high-order deformation theory 78—63308
plate, infinite, concentrated load, stress anal., numerical method *(Japanese)* 78—22273
plate, laminated, high-order deformation theory 78—63309
plate, orthotropic, irregular, on elastic foundation, vibrs. under in-plane forces 78—79251
plate, orthotropic, transient response to uniformly distributed transverse load, computer calcs. 77—68503
plate, plane rectangular hydrostatically acted, clamped and supported edges, exact calc. 77—39256
plate, relaxed by holes, elastic-plastic deformation, stress state *(Russian)* 79—27545
plate, right angled isosceles triangle, on Pasternak-type viscoelastic foundation, deflection 78—75075
plate, round, nonlinear deform. anal. *(Ukrainian)* 79—98618
plate, round, viscoelastic, deformation and creep *(Russian)* 79—32291
plate, round compressible, stability under uniform loading *(Russian)* 79—27522
plate, semi-infinite, with strip mound, stress analysis 80—10139
plate, simply supported rectangular under axial compression, creep buckling and deformation 79—68605
plate, thin, homogenisation in bending, periodic and symm. structure *(French)* 77—39222
plate, thin, under elastic bending, optical method for slope and curvature contours 79—37259
plate, thin circular, bending, parabolic loading over concentric elliptic limacon 78—59299
plate, thin elastic, with hypotrochoidal hole, under uniform press., stresses 79—98617
plate, unsymmetric angle-ply rectangular, under edge moments, large deflection anal. 77—68420
plate bending, numerical soln. by general boundary integral formulation 80—1422
plate bending, reduced and selective integration techniques in finite element analysis 78—42552
plate bending, transient problem, variational and reciprocity principles 77—50898
plate bending theory, optimal thickness distrib. *(Russian)* 78—63295
plate boundary and extension problems, stress intensity factors, finite element anal. 79—55341
plate deflection theory, soln. of biharmonic eqn. 77—80068
plate flexure, Castigliano's principle *(Russian)* 79—18718
plate problems, novel finite element method 77—35063
plate resting on deformed incompressible elastic halfspace, axisymm. flexure 77—46913
plate sealing incompressible liquid, finite deflections 77—50915
plate with circular hole reinforced with strained annulus, stress distrib. in bending *(Ukrainian)* 79—50591
plate with circular hole under dynamic loading, comparison of deform. and flow theories 79—23228
plate-cylinder intersection, elastic, three-dimensional anal. by boundary-point-least-squares technique 77—58558
plates, deform. by concentrated loads 77—870
plates, tapered, circular, with affine imperfections, large deflections, stresses 78—75070
plates, thick, bending anal. *(Russian)* 79—10485
plates, thick circular, axially symmetric vibration, elastodynamic deformation 79—37214
plates and pivots, elastic stability under heterogeneous precritical states *(Ukrainian)* 80—48573
plates with linear constraints of deform. *(Polish)* 78—13901
plexiglass composite, long term strength and durability 80—75294
PLT toroidal field coils, operational deflection meas. 78—62627
PMMA, atactic, elastic strain detection by X-ray scatt. 80—25751
PMMA, glassy, photoelasticity 80—45034
PMMA, nonlinear dynamic mech. moduli 78—60693
point contact elastohydrodynamic lubrication, surface deform. calc. 78—18255
polybutene-1 film, tubular-extruded, light scatt. from crystn. superstruct. 77—55796
polycrystal, elastic deform., effect of Young's modulus, shear modulus, Poisson's ratio 77—24344
polycrystals, bond between deformation and stress *(Russian)* 79—33031
polycrystals, intensity and lattice strain distrib., calc. from inverse pole figures *(German)* 78—52885
polydimethylsiloxane, stress-strain props., cross link functionality 79—46575
polydimethylsiloxane end-linked chains, nonGaussian effects 80—65127
polyester resin, PN-3, creep, effect of temp. and moisture 77—4820
polyethylene, crysts., subject to fold-surface tensile stress, elastic deform. 78—76712

elastic deformation continued
  polyethylene, hard elastic fibres, deform. and struct., −196 to 80°C 78−51437
  polyethylene, high density, film, melt growth, cryst. superstruct., small angle light scatt. 77−31602
  polyethylene, low density, isotropic, extensional deformation, and effects 80−7613
  polyethylene extrudate, transverse compression 78−68728
  polyethylene films, hard elastic, deform. mechanism 77−32652
  polyethylene melt, lightly crosslinked, crystn. under uniaxial compression, stretching 80−38957
  polyethylene terephthalate, stretching, heat effects, struct. transforms. 79−15735
  polyethylenes, u.h. modulus linear, cryst. modulus 77−4799
  polyethyleneterephthalate-polycaproamide melts, two-phase blend, rheological props. *(Russian)* 80−58997
  polyhedral sandwich domes, elastic behaviour, failure, practical investigation and numerical simulation 78−59309
  polymer, crystalline, dynamic mech. props., influence of struct. 79−4991
  polymer elastic deform. meas., occurring under reversible slippage, friction method 77−52598
  polymer film between two rigid or quasirigid bodies, memorised mechanical birefringence *(French)* 80−43677
  polymer materials, hysteresis flow model applicability for degree of inelasticity 80−28422
  polymer melts, elastic, uniform extension by const. force, rheology 80−43682
  polymer network, crosslinks and trapped entanglements, two-network model 80−38962
  polymer network formation, struct. and mech. props., computer simulation 80−38965
  polymer network in solution, free energy of deform. 80−38900
  polymer networks, deformation free energy, vol. depend. 80−40454
  polymer-metal sliding, wear eqn. in terms of fatigue and topography of sliding surfaces 80−108597
  polymeric joist, bending calcs. *(Rumanian)* 77−68396
  polymeric structures, contractile, rel. to artificial muscles 77−25595
  polymers, cryst., hard-elastic fibres, morphology mech. props., mechanisms, review 77−32612
  polymers, glassy, viscoelastic relaxation processes role in macrodeformation 79−72825
  polymers, partially crystalline, nonlinear mech. relax. *(Russian)* 80−40467
  polymers, solid, mech. deform., model 79−20120
  polymers, viscoelastic, deform., depth of polymerisation 80−40414
  polypropylene, oriented, thermooxidative degradation kinetics, durability, influence of mech. initiated processes *(Russian)* 79−24591
  polypropylene fibre, hard elastic, macroscopic deforms. in lamellae 79−96097
  polypropylene films, hard elastic, gas permeability, extension effects 80−40412
  polysilicane gel on glass plate, elastic deformation in adhesion of solids 78−60010
  polystyrene, high impact, hard elastic behaviour 79−57036
  polystyrene, wood filled exam. of reversible elastic deformation 78−48437
  polystyrene spheres, crystallised suspension, gravitational compression 78−23975
  polyurethane, segmented, domain struct., deform. effect 80−93623
  polyurethanes, vapour press. of solvent above swollen crosslinked networks rel. to rubber elasticity theory 80−45536
  polyvinyl-pyrrolidone/polyethylene glycol oligmers, elasticity theory, and compression meas. 80−44246
  poroelastic medium, semi-infinite, disturbance produced by surface load 77−19533
  porous body in rigid sheath, energy expenditure in densification 80−16216
  porous elastic half-space, displacements prod. by impulsive line load, non-dissipative case 77−23908
  porous elastic soil, finite consolidation theory 77−46916
  postbuckling behavior of thin-walled open cross-section compression members 80−5963
  postbuckling of elastic structs., mode imperfection anal., imperfection sensitivity 77−89048
  pre-stress, influence on imperfection sensitivity 78−67035
  pre-twisted beam vibrs., elements based on approximation of displacements in fixed directions 77−75843
  predeformed elastic systems, deflected and compressed bar *(German)* 77−19523
  press fitting thick cylinder into outer housing of octagonal form, finite element anal. 79−50603
  pressure between elastic bodies having a slender area of contact and arbitrary profiles 79−64596
  pressure vessel, stress concentrations around multiple windows photoelastic anal., strain gauge tests 77−72254
  pressure vessel heads, torispherical, elastic instability and with triangular thin shell finite elements 77−58576
  pressured shells, stress intensity factors for very short cracks 77−50997
  prestrain effect on dynamic modulus of elasticity and attenuation coeff. in nonconducting materials 80−29110
  prestressed thermoelastic media, seismic-dislocation theory 77−86811
  prism bending to helical form, formal perturbation scheme 78−55558
  prismatical beams, torsion and flexure 79−18711
  propagating rectangular fracture in semi-infinite elastic medium 78−57168
  pseudo-elastic analysis of plastics, validity in load-bearing appl. 78−39868
  pseudoplane equilib. state, stress eqns. 77−50889
  punch on elastic layer overlying elastic foundation 77−39228
  punch-elastic body dynamic contact, superseismic stage, exact soln. 78−55614
  PVC, antiplasticised, linear-nonlinear viscoelasticity transition 79−5015
  PVC, filled, with varying plasticiser content, deformative props. in highly elastic state, temp. depend 79−20099
  PVC, mech. behaviour in nonlinear viscoelasticity range 79−4996
  quartz, ceramic, elastic property changes on sintering 77−90301
  quartz, synthetic, growth boundary between −X and Z sectors 78−59775
  quartz, synthetic, growth sector boundary between −X and Z sectors 78−59774

elastic deformation continued
  quasistatic problem of mechanics of deformable body in stresses 79−37179
  radial deformation of nonhomogeneous spherically anisotropic media 77−11128
  randomly nonhomogeneous elastic body, parametrix method for determ. of effective elastic moduli 77−54884
  rectangular bar, semi-infinite, longitudinal impact, elasticity eqns. anal. 78−90703
  rectangular electrode frame prestressing and deformation in MWPC and spark chamber appl. 78−29708
  rectangular Mooney sheet, large plane deformations 77−14912
  rectangular parallelepiped compression, small elastoplastic deformation, variation anal. *(Russian)* 79−32294
  rectangular plate, simply supported, shear deform. effect on transverse displacement 78−38202
  rectangular plate, stability, mechanical props. dependent on strained condition *(Russian)* 79−10494
  rectangular plate of variable thickness, vibrating, approximate strain energy expression 80−38317
  rectangular plate on elastic foundation subjected to transverse load, evaluation 78−34019
  rectangular plate resting on Pasternak-type elastic foundation, large deflection 78−38215
  rectangular plates on elastic foundation, approx. large deflection anal. *(French)* 77−68463
  rectangular plates with rectangular inserts, stress distrib. by finite element anal. 77−23876
  rectangular punch on elastic half-space 77−65686
  red blood cell, using membrane model 77−56400
  red blood cells, minimum energy anal. of membrane deform. 80−72141
  regularly layered half-space, deformation, vibrational loading 80−99933
  regularly multilayered rectangular elastic plates, post-buckling behaviour 79−98643
  Reissner-Sagoci problem for a non-homogeneous large thick plate, soln. using Fredholm integral equations 79−90132
  resonance phenomena in multi-degree of freedom systems, effects of geometrical nonlinearities 79−98648
  restrained beam, stability with nonordinary boundary conditions 77−50941
  rhombic plates uniformly loaded over concentric circle, Taylor series expansion of Schwarz-Christoffel transformation 80−5962
  rigid body impact on elastic half-space, Fourier synthesis of steady state vibr. 77−80101
  rigid circular punch on elastic halfspace, Mindlin force 79−18716
  rigid indentation and plane crack extension 79−18835
  ring, plane deformation, determ. of stresses and displacements, composite boundary conditions *(Russian)* 80−74738
  rock, fracture, role of crack inertia 80−109138
  rocks, time-dependent deform. not purely elastic specimens 78−32075
  rod, curved, deformed by end loads *(Russian)* 80−74745
  rod, elastic, approx. soln. to deformation problem *(Russian)* 79−64511
  rod with helical anisotropy 77−62155
  rods, ideally elastic, nonlinear bending, discrete anal. 77−46953
  rods axisymmetric motions, experimental assessment of Mindlin-McNiven rod theory 78−1595
  rotating disks, elastic and elasto-plastic, with temp. gradient, stress distrib. determ. *(Italian)* 79−41633
  rotating viscoelastic tapered cantilever, circulatory force at free end, influence of angle of attack on stability 80−69686
  rotation of nonhomogeneous composite cylinder, plane strain problem 77−72161
  round bars, endurance limit under combined tension and torsion 79−32387
  rubber, natural, crosslinked by dicumyl peroxide, modulus, swelling relations 80−59551
  rubber, synthetic, nonlinear anelastic behaviour at finite strains 79−3923
  rubber, thick tube, large elastic deform. theory and unstable deformations 77−73298
  rubber, vulcanised, biaxial deformation study *(German)* 79−70129
  rubber, vulcanized, rheological props., stress-strain rels. 77−32608
  rubber balloon, internal press. eqn., for teachers 79−14
  rubber belt, cord reinforced, finite cylindrical deformation, stresses 78−38203
  rubber covered rolls, contact and deformation nonlinear elastic problem, stress anal. 80−79239
  rubber cylinder, circular, uniformly heated, combined extension and torsion 80−92057
  rubber half-cylindrical tube compressed between parallel plates, load-deformation relation 77−50999
  rubber in uniaxial extension, hysteresis, test of Fitzgerald's concept *(Russian)* 77−86065
  rubber sheets, circular, elastic deformation profiles 79−66481
  rubber shell, spherical, mode of loading effect on stability 80−24528
  rubber stress/strain relations, uniaxial extension and compression 78−80578
  rubber under biaxial strain, non Gaussian theory, mechanical props. 80−16366
  rubber under biaxial strain, nonGaussian theory, optical props. 80−16367
  rubber under cyclic compression, heat generation and thermal conduction 79−52283
  rubber-elastic networks, stress-deformation behaviour, steric hindrance *(German)* 80−35277
  rubber-like solids, anisotropy of compressibility 79−43302
  rubber-like solids, associated volume changes 77−68447
  rubber-like solids, biaxial deform. 80−1431
  rubberlike solids, nearly isochoric deform., anal. of volume changes 79−10471
  rubbers vulcanized, biaxial finite deformation props. *(Japanese)* 78−84939
  Saint-Venant's principle for mixture of elastic media *(Russian)* 77−72174
  Saint-Venant's problem for micropolar elastic cylinder 77−3719
  sandwich disc, axisymmetric deformation 80−10148
  sandwich plates, orthotropic, theory of stretching *(Polish)* 80−10151
  sandwich plates with thick faces, orthotropic, hybrid stiffness matrix 77−80072
  sandwich strips, plane deform., Saint Venant end effects 78−46893
  scale single flat spring fulcrum deformation, second approximation *(Japanese)* 79−184

elastic deformation continued
- semiconductors, subsurface strain, reconstruction induced, theory, appl. to Si (100) 78–63914
- semiinfinite elastic cylinder indenting elastic half space 80–53722
- shafts, with abrupt changes of section, flexibility of shafts 78–90711
- shallow spherical shells, deflections and internal forces, finite element anal. *(Chinese)* 79–68583
- shear, effect on flat sandwich arches, stability analysis 80–48570
- shear deformations, generalised, for isotropic incompressible hyperelastic materials 78–94599
- sheet, plane elastic, containing circular hole or inclusion, radial deformation 79–41575
- shell, circular cylindrical under tension, stresses around rib-reinforced elliptic hole 77–58557
- shell, consistent second approx. to elastic strain energy 79–81732
- shell, cylindrical, nonlinear theory, displacement field definition 77–41484
- shell, deposited in vacuum, elastic characts. meas. by short time static extension *(Russian)* 78–39961
- shell, nonlinear elastic cylindrical biharmonic excitation, parametric vibrations *(French)* 78–87294
- shell, spherical, non-shallow, torsional axisymmetric deform. subprogram 80–43607
- shell, spherical, with rigid core, deform. under effect of plane press. wave *(Ukrainian)* 77–31239
- shell, thin walled axisymmetric, elastic deformation, nonlinear numerical anal. method *(French)* 79–41584
- shell, uniqueness and existence theorem for linear model *(French)* 77–39223
- shell equations via extended variational principle *(German)* 77–72166
- shell of revolution, stability of nonlinear local axisymmetrical strains 77–35042
- shell structures, large elastic deformations 79–98611
- shell theory *(Ukrainian)* 78–83244
- shell wall anal., circular tanks under axisymmetrical pressure 79–46202
- shells, axially compressed cylindrical and conical, post buckling behaviour, large elastic deflections 80–33490
- shells, cylindrical, large elastic deflections, numerical anal. 79–98613
- shells, deform. by concentrated loads 77–870
- shells, finite cylindrical, of various wall thicknesses, flexural vibrs. and displacement patterns 78–1588
- shells, highly stressed nonhomogeneous thick-walled cylindrical and spherical, radial oscillations 77–3768
- shells, isotropic thin elastic, nonlinear theory *(Russian)* 80–79147
- shells, large elastic deflections of axially compressed cylindrical and conical structs. *(Polish)* 78–13937
- shells, layered thick-walled cylindrical, large amplitude radial oscillations 77–72215
- shells, thin shallow axisymmetric, strain displacement equations, incremental anal. 80–53628
- shells, thin walled, elastic, Rayleigh method anal., energy calcs. 77–65677
- shells, transversely isotropic, elastically deformed, optimal reinforcement of openings 80–38269
- shells of revolution, max. principles and pointwise error estimates for torsion 78–18180
- shells of revolution, postbuckling finite-element analysis 77–62185
- short sandwich beams, extension and shear rel. to vibrs. 77–75842
- Si crystal, elastically bent, strain distrib. determ. by X-ray intensity meas. 79–50928
- single crystals under large loads, theoretical elastic behaviour, review and appl. 80–71681
- singularity at corner of wedge shaped punch or crack 78–83252
- size effect, model of dynamics, generalised thermodynamic forces 80–53627
- size effect, thermodynamical model for constrained and unconstrained bodies 80–58900
- skew plates, shear and rotatory inertia effects on large amplitude vibr. 77–75734
- skin, living, human, constant strain rate, hysteresis and stress relax. behaviour 78–40237
- slightly compressible materials finite deformation theory 78–45485
- snap-buckling of orthotropic shallow spherical shells 79–23234
- soft elastic block bonded to rigid end plates, plane strain rotation moduli 79–90135
- soil, drained and undrained behaviour, anal. 77–3720
- solid, finite stressed, surface dislocation model 79–73247
- solid bodies, elastoplastic and isotropic elastic deform. eqns. 79–86348
- solid lubrications dynamics, obs. using Micro Contact Imager 78–85002
- spacecraft, flexible, in gravitational field, stability 77–25906
- sphere, deformation and sticking to a rigid plane, mol. force effect 80–106720
- spheres and rough planes, in contact with normal load, numerical analysis and expt. verification *(Japanese)* 77–19575
- spherical rubber balloon, aspherical deform. under inflation 77–46914
- spherical shell, internal weak shock wave action *(Russian)* 77–68497
- spherically symmetric elasticity problems, finite element soln. 78–63293
- spot weld between elastic plates, near field stress anal. 77–11160
- spring, complex arch type, movable, snap-through action characts., appl. to microswitches 78–63339
- spring, complex arch type, movable, snap-through action characts., microswitch appls. 78–63340
- springs, thin, of constant cross section, elastic behaviour calc. and obs. *(German)* 78–87269
- square plate, large deflection, behaviour according to Foeppl and Von Karman 78–63296
- stability, buckling and postbuckling 80–1454
- stability predictions through a succession of folds 79–76991
- stamp problem, elastic layer or half space, variational formalism, numerical soln. 79–1106
- statics of stationary and non-stationary three-dimensional systems using dual deformation vectors (deformation screws) *(German)* 80–38257
- steadily moving load, elastic strip on rigid foundation, noncontact regions, displacements, contact press. 78–87264
- steel, austenitic, types A533B and A508, acoustic emission during tensile tests, elastic and plastic deformation processes 79–74212
- steel, C, X-ray line fitting by Gram-Charlier distrib., appl. to tension test *(French)* 79–15689
- steel, Cr-Ni, martensite defect identification by positron annihilation 78–39867

elastic deformation continued
- steel, flat bars, stress meas. and calc. around drilled hole, with hole-gage-rosettes aid *(German)* 80–25757
- steel, mild, temperature monitoring system used during mech. deform., stress anal. appl. 79–12796
- steel plates, hot rolled, anisotropic texture, exam. of elastic deformation behaviour *(Japanese)* 78–64586
- steel shell, mech. behaviour during solidification 80–81043
- steel SW7M, low-cycle fatigue at high hardness levels *(Polish)* 80–89323
- stiffened panels with rectangular cut outs, stresses and deform. *(Japanese)* 79–3977
- stiffened plate, model studies of elastic buckling 77–7324
- stiffened plates, linear and nonlinear anal. 77–89026
- stiffened shear webs with skin stabilisation, optimum design 77–892
- stochastically inhomogeneous solid with opening, plane deform. problem 79–86337
- strain energy of solids with different moduli in tension and compression, small strain theory *(French)* 78–87261
- stress and configuration, elastic and plastic strain increments 80–87718
- stress and deformation rate calcs., finite element anal. *(German)* 79–50602
- stress and strain anal. by approximation method *(German)* 79–76978
- stress concentration factors and stress distribution around sharp corner elastic inclusions 77–84164
- stress distribution of frictional bonds, computer model *(Hungarian)* 79–14275
- stress field, surface deformation in half-space with cuboidal zone 79–18721
- stress measurement, temporary and residual stresses, high-temps. 80–64498
- stressed crystal, adiabatic and isothermal elastic consts. 79–65137
- stretched plates weakened by inner curvilinear holes 78–55567
- strip, arbitrarily oriented crack distrib. *(Russian)* 78–63378
- strip rolling, appl. of elastostatics element method to determine elastic behaviour of 4 high stands *(German)* 77–36541
- strip with one-sided constraint under moving load 77–7305
- structural anisotropic domes, deformation anal., fission reactor appl. *(Slovenian)* 80–48577
- structural systems, elastic critical loads 79–18754
- styrene-acrylonitrile copolymer, amorphous, rubbery state, nonequil. tensile deform., effects of temp. and strain 80–40442
- sub-structure analysis for elastic fields with stress singularities, hybrid formulation 77–3730
- superconducting rings, linked chain, with trapped mag. flux, elastic length change *(Russian)* 77–63039
- superposition principle in the solution of contact problems taking friction forces into account *(Russian)* 79–7343
- surface deform. of opt. flats and Fizeau method for film thickness meas. 78–77970
- surface dislocation anal. of elastically bent cryst. 80–2019
- surface instability, nonlinear problem in elastic half-plane *(Ukrainian)* 80–5961
- surface loads, reciprocating dynamic stresses produced in elastic half space 78–9562
- surface ripples, periodic, of elastic skin 77–31845
- surface roughness, mathematical models 79–82428
- temperature gradient, X-ray diffr., infringement of Friedel law 77–31554
- temperature monitoring system used during mech. deform., stress anal. appl. 79–12796
- tendon, viscoelastic deform. obs. 80–101211
- tensile conc. optimisation using iterative method *(German)* 78–87271
- tension determination in elastic element on motionless sheave, hybrid calculator appl. *(Bulgarian)* 80–23894
- test machines, elastic yielding determ. 79–70251
- textiles with planar crimp, tensile deformation 80–84235
- texture, influence on mech. and phys. props. 79–83224
- thermal flexure of an infinite plate with a doubly periodic array of holes 79–68586
- thermodynamics, eqn. of state for solids 80–96589
- thermodynamics of non-simple elastic materials 77–14904
- thermoelastic deformation, second order effects 80–92051
- thermoelastic effect, lattice dynamics and energy channelling 78–22786
- thermoelastic solids, thermomechanical constraint, internal, constitutive equations, material anisotropy 80–58897
- thermoelasticity, anisotropic, crack problems, temp., displacement, stress field 77–80105
- thermoelasticity, stability of some plane deform. states 80–43634
- thermoelasticity of anisotropic cylindrical shells 80–92059
- thermoelastoplastic medium, variables for universal deform. representation 78–49666
- thick layer blastodynamics, semi-3-D soln. to axisymmetric problem *(Ukrainian)* 77–68402
- thick orthotropic plates stretching *(Polish)* 78–13902
- thick plate, containing eccentric spherical cavity, stresses under uniaxial tension 77–23873
- thick plate, with spherical cavity, stresses under transverse bending 77–23874
- thick plates, 3-dimens. refined elasticity theory, bending and torsion 80–64375
- thick walled sphere, nonsteady hydroelastic oscills. 78–18227
- thick-walled tube, micropolar, generalised Lame problem and torsion *(Polish)* 77–54886
- thin circular quadrant, singularly loaded, with clamped radial edges and free circular edge 78–63300
- thin elastic shells, stability, variational method *(Russian)* 79–32321
- thin shells, heterogeneous stress/strain state, stability eqns. for small deformations *(Russian)* 80–1426
- thin wall beams with deformable contour, stress/strain state 79–94500
- thin-walled beams with initial stresses and initial deformations, lateral buckling 80–1448
- Timoshenko beams on Pasternak foundations, shear deform. rel. to natural freqs. 77–60938
- toroidal shell of revolution, axisymmetric deform., limit state anal. 79–94498
- toroidal shells and tubes, flexible shell theory and buckling 79–23231
- torsion free axisymmetric deformations, two function expression for displacements 80–64367
- torsion in open sets with holes, problem homogenisation *(French)* 77–67288

elastic deformation continued
torsion of elastic layer, by annular die, Fredholm integral equation anal. 79—3969
torsion of elastic layer by two circular discs 77—35037
torsion of truncated elastic core, mixed boundary value problem 77—46908
torsional oscillation of inhomogeneous elastic half space *(Russian)* 77—19559
transient response of half-space due to reciprocating antiplane shear load 77—46963
transition metal carbides and nitrides, solid soln. formation, elastic lattice deform. energy 77—84927
transverse deformations associated with rectilinear shear in elastic solids 78—86162
transverse flexure of rectangular plate of arbitrary stiffness *(Russian)* 78—51084
trapezoid plate, freely rotating, mechanical effects, calc. method *(German)* 80—106728
trigonal monocrystals, classes 3 and $\bar{3}$, elastic potential and yield condition *(Russian)* 80—29108
tube, cylindrical, thick-walled, finite twist and external press., stability, vibrs. 78—83286
tube and spherical shell, incompressible elastic, response coefficients and controllable deformations 79—68580
tubes, thick-walled, bifurcation under axial loading 80—79150
turbulent flow, press. fluctuation spectrum, elastic boundary compliance effect 78—63422
twist and stretch of circular bar of rate sensitive material 80—23912
twisted bar, elliptic, stress and deform. states produced by axisymmetric elastic torsion *(Italian)* 78—22262
twisting, differential geometry 77—84834
two flat surfaces in contact, thermal conductance with applied load, variation, determination for elastic surface deformation 79—72782
two parallel elastic plates with ribs, deformation, stationary problems, differential eqns. 80—33465
uniformly loaded plate, interaction with isotropic elastic halfspace 80—23966
urinary bladder interferometry, holography of bladder deforms. in vitro, rabbit expt. 80—67201
urinary bladder interferometry, tumour and lesion detect. by holography 80—67202
uterine deformation during labour, thin shell model and kinematic analysis 79—2090
V-notched elastic half-plane problem, plane stress and strain 79—68571
vacancy formation vol. in solids, stress-assisted diffusion theories 79—95201
viscoelastic $^1/_2$-space, glass ball adherence, coming-on-expts. *(French)* 79—1113
viscoelastic cracked linear bodies, stress and strain under tension and compression 77—7342
viscoelastic cylindrical shells, forced axisymmetric motions 77—89038
viscoelastic deformation, finite, one-dimens., impulsive response, constraints *(French)* 78—51092
viscoelastic media, deform. theory with account of thermodiffusion *(Ukrainian)* 78—67052
viscoelasticity, nonlinear, estimate for work 78—55572
viscous fluid slow flow, inhomogeneity finite deform. 77—7425
viscous incompressible two dimensional slow flow, finite deform. of ellipsoidal inhomogeneity 77—51013
wave propagation in deformed compressible elastic material 79—14338
wedge stroke blow, along membrane at surface of incompressible liquid *(Russian)* 78—55561
wetting, elastically deformable bodies, influence of vol. deform. of solid 79—11008
wetting of elastically deformable bodies, reduction of effects of deform. to line tension 79—11007
whisker crystals uniaxial deformation, at He temperatures in magnetic field, mechanical displacement transformers design 80—50788
Winkler layer, axisymmetric deform. by internally loaded elastic half-spaces 78—26044
wood, load bearing capacity, and deformability, evaluation of timber structure safety *(German)* 78—39983
wood particle board, method of mech. testing, elastic deform. meas. 78—56837
woven fabrics, partially set, finite axial extension, elastic deform. anal 80—19240
X-ray diffraction, integrated intensity 78—34383
X-ray dynamic scatt. in elastically bent cryst., quasiclassical approx. 77—4022
X-ray elasticity method for stress and deform. meas. 79—43506
Ag-Cu (39.9 at.%), eutectic composites, solidification and deform. *(Czech)* 77—59773
Ag-Pd-Cu, contact-spring props., fatigue and spring limit *(Japanese)* 79—29117
(Al,Ga)As/GaAs, LPE grown heterostructures, X-ray diffr. exam. of interfacial elastic strains 78—72019
Al, polycrystalline, probabilistic micromech. theory 77—863
Al, US velocity, anomalous response to applied stress 78—63811
Al-Zn, Guinier-Preston ellipsoidal zone model of X-ray scatt. *(French)* 77—84568
Au diffusion, and elastic strain, influence on O_2 state in Si *(Russian)* 79—69181
B fibre reinforced Al, stress redistribution in fibre elastic deformation failure *(Russian)* 79—47740
β-BaF_2, stress wave profiles 80—96593
$BaTiO_3$, deform. and stress relax. of single crysts. 77—59542
Bi, energy spectrum changes under strong uniaxial compression, Shubnikov-de Haas effect 77—28098
Bi, Fermi surface changes due to strong elastic tensile strains *(Russian)* 77—85133
$Cd_xHg_{1-x}Te$, low temp. piezoresistance, Hall effect, elec. cond., plastic flow 80—6844
CdS, exciton optical and luminescence spectra characts. near dislocation slip bands 80—45111
CdS, low resist. single cryst., photodeform. mechanism 77—89806
CrO_2 semidry refractory, struct. and mech. props., surface-active agents effect 80—89304
CsI, and Na doped sample, elastically loaded, effect of annealing on optical absorption 77—44034
Cu, cyclic straining anal., discrete polycrystal model 77—47507

elastic deformation continued
Cu, deformed, intensity and lattice strain distrib., exam. *(German)* 78—52885
Cu, elec. resist. under torsional deform., impurities and tensile strain 78—30898
Cu, electrode potential, transient response to elastic straining rel. to reaction kinetics 79—70212
Cu film, effect of thermal strain on orientation 80—49294
Cu, polycrystalline, probabilistic micromech. theory 77—863
Cu, theoretical strength 80—104229
Cu-Al-Ni, formation of martensitic phases during deform. by extension 79—20048
Cu-Al-Ni alloy single crystals, anomalous elasticity orientation depend., martensitic phase struct. during strain 79—87634
Cu-based alloys, orientation dependence of mechanically induced transformations 79—87660
Cu-Sn, deformed, martensitic transformation *(Russian)* 79—15668
Cu-Zr amorphous alloys, mech. props. *(Japanese)* 77—86179
Fe, Armco, H_2 diffusion 0 to 300°C, effect on elongation tension *(Russian)* 77—66044
Fe, elastoresistivity effect, meas. of resistance at 4.2K and 300K, using mag. field method 78—72132
Fe whiskers, elastically and plastically deformed, mag. domain structs. 80—15752
Fe-Co-Cr-W-Ni-C, alloy KKhVN, transforms. during annealing and nature of hardening *(Russian)* 78—56653
Fe-Mo-Au, orienting of precipitating Au particles by external elastic stress 77—73279
Fe-Ni alloys props. of materials used in electromechanical filter resonators *(Czech)* 80—76318
Fe-Ni-Si, double spontaneous reversible deformation during thermal cycling 78—84942
Fe-Si (3 wt.%) alloy, nonuniform deform. in grains *(Russian)* 78—35415
GaAs-$Ga_xIn_{1-x}P$ heterostructure, elastic stresses and substrate/epitaxial film mismatch, X-ray diffr. method 80—92794
Ge, deformation, annealing characts., X-ray study 78—75713
n-Ge, elastically deformed, anisotropy of thermoelec. effect 78—19066
Ge single crystals, photopiezoelectric effect under elastic deform. 80—107856
KCl, pure and Ba doped, symm. of elastic fields due to defect displacements, diffuse X-ray scatt. 80—70256
MgO, precipitate morphology, strain energy effects 80—40358
Mo, siliconised thermal stress and thermal expansion 77—21324
NaCl, electric field induced by homogeneous stresses 80—11343
NaCl, monocrystalline, defect struct. and intrinsic ionic cond. relationship 79—95211
NaCl whiskers, X-irrad., stress oriented dislocation loop nucleation 79—33213
Na_2O-CaO glass, crack nucleation during indentation, micromechanics 80—30069
Na_2O-SiO_2 glass, scoring, deform. and fracture mech. approach 80—89332
Nb, elastically deformed, quadrupole effects, NMR line intensity *(Russian)* 78—56400
Nb_3Sn, supercond. transition temp., deform. effects 77—12051
$NiFe_{2-x}Al_xO_4$, LPE grown films on $ZnGa_2O_4$ substrates, tensile strain due to elastic deformation 79—28238
PLZT ceramics, stress-induced ferrelec. transition, pseudoelasticity and shape memory, bending meas. 79—24274
Pd alloys, effect of alloying on activation energy of H_2 diffusion 80—107571
Si crysts., deformed, strain distrib. characterisation, annealing response 77—70140
Si, deformation, annealing characts., X-ray study 78—75713
Si, diffusion of P, elastic deform. relax. and dislocation generation 80—79997
Si, elastically bent cryst., intensity of diffracted beams in general case of diffr. 79—50935
Si, elastically bent crystal, with large strain gradient, X-ray diffraction study 80—44073
Si, electron-hole liquid and exciton and biexciton gas in elastically deformed cryst. *(Russian)* 78—34782
Si, oxidised on one side, elastically flexed, dynamic X-ray scatt. *(Russian)* 77—43115
Si, plastically deformed, hot-exciton luminesc. as function of strain 78—88361
Si, single crystal, depth profile of radiation damage using lattice deform. study *(German)* 77—39618
Si, stretched, lattice vibr. anharmonicity, influence of stress on elastic moduli, Raman spectra 80—80791
Si wafer creep testing using stress provided by deposited Si_3N_4 film 77—66000
n-Si:P, piezoresist. under strong uniaxial elastic deform. 77—15858
SiC single crystals, friction, deform., and fracture, crystal orientation effect 79—96150
Ti alloy TA6ZrSD, low cycle fatigue at 450°C *(French)* 79—70169
Ti-Al-Mo-Sn alloy, elastically and plastically deformed, positron annihilation meas. of deformation 80—21038
TiO_2-Fe_2O_3, strain energy pot. well oscills. rel. to crystallographic shear orientations and comp. waves 78—43034
U-Nb-Zr (7.5, 2.5 wt.%), elastically bent, ageing induced shape instability 77—16622
V, elastically deformed, quadrupole effects, NMR line intensity *(Russian)* 78—56400
W, Fermi surface, uniaxial strain depend., quantum oscills. in magnetostriction, US vel., with torque 77—28094
WO_3, reduced, elastic strain energy of crystallographic shear planes 77—69026
Zn, elastic properties, compilation and review 78—27551
Zn, magnetic susceptibility behaviour, dislocation and elastic deform. effects *(Russian)* 77—80912
Zr, elastically deformed, positron annihilation, Doppler broadening study 79—69900
α-Zr, some stress change expts. on creep 80—3125
Zr-Sn alloys, mathematical models for transient deform. 78—86616
ZrO_2, porous, sintered stabilised microspheres, strength and fracture studies 80—85019

elastic hysteresis
analytical description 77—3764

elastic hysteresis continued
bimodular columns, buckling and immediate postbuckling behaviors 79—23232
cyclic plasticity and masing behaviour in metals and alloys 78—64616
cyclic strain hysteresis loop, width and area determ. 78—26056
dislocation behaviour during fatigue, friction stress and back stress from hysteresis loop anal. 79—42076
endochronic theories of material behaviour, uniqueness and stability 79—18752
epoxy resin, hardening, mechanical and dielectric losses 78—48115
ethylene-propylene copolymers, mech., photoelastic props. rel. to chain microstruct. 77—48468
ethylene-propylene rubber, highly deformable, fracture surface roughness 78—44197
fatigue specimen, nonsteady temp. field computation, rel. to thermal part of mech. hysteresis 79—3905
fatigue testing, hysteresis energy-temp. rise relation *(Japanese)* 77—77682
fibre reinforced composite, mech. behaviour, axial residual stress effect 77—36573
fibre reinforced silicone rubber composites, interfacial slip and damping 79—5010
fine ceramic masses, organic plasticizer, plasticity model and plastic behaviour meas. by cyclic shear test *(German)* 79—96080
geological media, hysteresis behavioural effects 80—21712
glass fibre reinforced vinyl ester matrix, axial fatigue failure sequence and mechanism 78—68773
heat energy relaxed due to deform., thermocouples obs. 80—21214
hypoelastic materials with internal variable, work-hardening, hysteresis, fracture law 77—62177
impact vibration, steady, body with impact hysteresis characts., stability anal. 78—51099
Incoloy 800H, high temp. low cycle fatigue, ageing and cold working effect 79—43277
internal friction, complex theory 79—18746
internal friction, determ. from dynamic hysteresis loop area and specimen cross section in deform. 78—23897
linear models of frequency-independent internal friction *(Russian)* 79—18834
nonlinear behaviour in 1- and 2-dimens., elastoplastic hysteresis, flow and relaxation *(French)* 79—46229
nonlinear nonideally elastic materials, relationships between stresses and strains *(Russian)* 80—90675
nonlinear viscoelasticity variational formulations of boundary problems *(Russian)* 79—18749
nylon 6 fibres, dynamic mech. props., interpretive nonlinear viscoelasticity 79—4994
polyethylene, low density, highly deformable, fracture surface roughness 78—44197
polymeric materials, inelasticity degrees estimation, hysteresis friction model appl. rel. to US testing 80—3136
polymers, inelasticity, estimation using hysteresis friction model 80—7617
prismatic bar hysteretic behaviour, yield condition under repeated axial loading 77—62167
PVC, highly deformable, fracture surface roughness 78—44197
rigid slider, deformational contact and friction on viscoelastic substrates 79—50677
rubber, hysteretic behaviour, thermomech. study 78—76692
rubber in uniaxial extension, hysteresis, test of Fitzgerald's concept *(Russian)* 77—86065
screw connections, bend and tension loaded, hysteresis *(German)* 78—87312
shafts, noncircular cross section, effect of external forces and internal friction on rotary motion *(French)* 78—63274
shock absorber, elastic damping props. determ. unit 78—5703
skin, living, human, constant strain rate, hysteresis and stress relax. behaviour 78—40237
squaric acid, ferroelasticity, elastic hysteresis loop and domain struct. 79—55814
steady impact vibration of body with quadrilateral hysteresis loop for restitution force 77—23905
steady state response of systems with hardening hysteresis 78—60680
steel, 0Kh16N15M3B, irradiation effects on resistance to cyclic elastoplastic deformation 79—91767
steel, age hardened, dynamics of cyclic plasticity *(Czech)* 80—108464
steel, Cr-Cu-Mn, fatigue crack propag. rate eval. by J integral method *(Japanese)* 79—8346
steel, Cr-Mo-V, cyclic deformation under out-of-phase loads 80—40428
steel, low C, effective stress determ. during the loading cycle 79—38879
steel, low C, ferrite grain size effect on cyclic stress-strain response 79—100203
steel, low C, hysteresis loop behaviour under fatigue load, dislocations model 79—74197
steel, low C, hysteresis loop initiation mechanism under repeated load *(Japanese)* 78—39851
steel, low C, low cycle fatigue, cumulative damage, absorbed plastic energy anal. 79—38932
steel, low C, temp. effect on hysteresis loop under cyclic load *(Japanese)* 79—20096
steel, medium C, S 45 C, influence of mean strain on low-cycle torsional fatigue life *(Japanese)* 79—8348
steel, mild, ground/sandblasted interfaces, tangential displacement, contact press. and lubricating film distrib. effect 80—16484
steel, mild, two sandblasted interfaces, tangential displacement, contact press. and lubricating film distrib. effect 80—16484
steel, stainless 304, cyclic plasticity, exponential stress-strain law 77—25157
steel, type AC/HT-2, grain diameters, US attenuation 80—89429
steel, type Ck22 and St52-3, under cyclic stress, damping behaviour and fatigue strength correlation *(German)* 80—39211
steel reinforced concrete, local bond-stress/slip relationships under repeated loading 79—20123
styrene-butadiene rubber, highly deformable, fracture surface roughness 78—44197
vibration decrement determ. of nonlinear hysteresis type system from resonance peak width 77—84191
Al bronze, superplastic low cycle fatigue 78—27632
Al-bronze, input energy, hysteresis, and fracture in low cycle buckling fatigue, superelastic range 78—31527
Al-bronze, single crystal rod, energy dissipation, deformed by cyclic buckling in superelastic range 78—31479

elastic hysteresis continued
Al-Mg single crystal, fatigue deform. 79—91747
Cu, fatigue of single crystals and low const. plastic strain amplitude 79—20174
Cu, high purity, low cycle fatigue, cumulative damage, absorbed plastic energy anal. 79—38932
Cu, stress component determination during loading cycle *(Czech)* 79—91725
α-Cu-Al, single crystal, low cycle fatigue 79—43405
Cu-Al-Ni alloy, thermoelastic transformation hysteresis loop width strain rate depend. *(Russian)* 79—100138
β-Cu-Zn-Al pseudoelasticity 79—29126
Fe, cast, with uniaxial loading, changes in ultrasonic waves vel. and attenuation 79—15756
$Gd_2(MoO_4)_3$, crysts., elastic props. during domain switching under mech. loading 79—55809
HfO_2, monoclinic, microcracking, elasticity, internal friction, thermal expansion meas. 79—29195
$K(D_xH_{1-x})_3(SeO_3)_2$, ferroelastic, anelastic and elastic infra-low freq. props. 80—70304
Mn-Cu, shape-memory effect at martensitic transform., cryst. and mag. struct. 77—36610
$Pb_3(PO_4)_2$, ferroelastic, deform. hysteresis loop. 77—51432
SiO_2 fibres, fused, load-elongation curves, elastic hysteresis, tensile testing machine 79—1891
steel, C, annealed S45C, multiple repeated low cycle torsion fatigue under controlled strain *(Japanese)* 78—27610
$Tb_2(MoO_4)_3$, crysts., elastic props. during domain switching under mech. loading 79—55809
Ti-Ni (51 at.%), martensitic transformation, thermoelastic, hysteresis, exothermic and endothermic effects *(Russian)* 78—19749
V_3Si, mixed state, hysteresis in elastic characteristics *(Russian)* 80—103799

elastic limit
brass sheet, in-plane stretching, limit strain meas. 78—80573
bronze, Be, elastic elements made from spring alloy bands 79—87678
heterogeneous composite materials, influence of prestress and limited deformations 78—38205
hyperbolic paraboloids elastic stability analysis, using reduced scale models 79—3910
nondestructive hardness test, determ. of elastically homogeneous struct. elastic limit 77—66719
paper strip reinforced paraffin, model composite, optimum reinforced plates, tension/compression tests 77—86124
PMMA, activation parameters of creep 79—38925
PMMA, laser damage mechanism rel. to viscoelastic props. 80—55233
PMMA glasses, crosslinked, strips, sheets, compression, tensile testing, mech. props., plasticiser effects *(Russian)* 77—32621
polycrystal, HCP, microstress and starting boundary of plasticity *(Russian)* 78—30695
polymer, rigid, prefractured states study, elastic limit and strength 77—70092
polyvinyl butyral, activation parameters of creep 79—38925
resolution method for second problem of elastic limits for plane *(French)* 78—57779
shell stability during axial compression, hardening beyond elastic limit 80—99931
steel, 4340, quenched, tempered, and austempered, effect of plastic strain followed by ageing on elastic limit 78—31446
steel, C, mech. props. rel. to heat treatment, ferrite-pearlite transform. *(French)* 79—20043
steel, deoxidised, AlN and V carbonitrides precip. effect on mech. props. *(French)* 80—45311
steel, high strength, sensitivity to stress concentration with various H content *(Russian)* 79—15724
steel, low alloy, type 4340, quenched and tempered, effect of plastic strain followed by ageing, on torsion fatigue resistance 78—92360
steel, sheet, in-plane stretching, limit strain meas. 78—80573
steel, silver, elastic limit, bending strength, and ductility rel. to tempering temp. after quenching 78—95764
steel, stainless, elast elements made from spring alloy bands 79—87678
steel, stainless Kh15N9Yu, elastic limit, effect of microstruct. and heat treatment 79—83251
steel, structural, elastic limit determ. by acoustic emission 80—66716
steel 65G, elastic props., effect of additional tempering temp. 77—21192
stress relaxation effect *(Japanese)* 79—98632
stress-strain curve from continuous indentation test 77—90396
thin plates, limit load and elasto-plastic bending, finite element anal. 79—27544
thin walled bar, subject to bending and mixed torsion, expt. *(Croatian)* 77—35060
tubes, infinitely long cylindrical elastic, collapse under bending, press. and axial loads 78—18204
Ag-Pd-Cu, contact-spring props., fatigue and spring limit *(Japanese)* 79—29117
Al bronze, elastic limit after repeated transverse deformation *(Russian)* 77—66668
Al sheet, in-plane stretching, limit strain meas. 78—80573
Al-Cu (4 wt.%), with θ' precipitates, relation between elastic limit and hardness *(French)* 79—5018
Al-Cu (4wt.%), elastic limit, precipitation effects *(French)* 79—47738
Be bronze, struct. and props. after ageing under load 78—84932
Be bronze BrB2, quenched deformed, substruct. and props., effect of prerecrystallisation annealing *(Russian)* 78—60677
Cu, cyclically deformed polycrystals, elastic limit, contribution of thermally active processes *(Spanish)* 79—91732
Cu, dislocation mean free path at 77K under elastic deform. 78—44162
Cu, extruded at 77K, defect struct. and elastic limit *(Russian)* 80—30016
Fe, cast, contact deformation, reverse slipping effect *(Russian)* 80—97591
Fe, stress relaxation in high purity single crystal with controlled amounts of C *(French)* 79—70105
Fe-Ni (1 to 5 at.%), mech. props. below 300K *(French)* 79—8314
$LiNbO_3$, shock-wave compression, 2.4-44 GPa 80—34139
Nb-O, Snoek mechanism and long distance diffusion under strain ageing *(French)* 77—81279
Nb-Ti-Al alloy, effect of heat treatment on strength and elastic props. 77—55976

elastic limit continued

- Nb-Zr-C, structural depend. of elasticity limit fracture features *(Russian)* 79-29171
- Ni, microscopic elastic limit, effect of preliminary plastic strain *(Russian)* 77-76485
- $Pb(Zr_xTi_{1-x})O_3$, meas. of Hugoniot curve with commercial manganin stress gauges 80-70362
- Ta wire, strain ageing by return of elastic limit method *(French)* 78-68713
- Ta-O, BCC, Snoek type reordering during strain ageing *(French)* 79-8312
- Te, c-slip, asymmetry and orientation depend. 77-27888
- α-Ti, determination of microflow parameters from compression tests 80-66584
- Ti, high purity, flow stress relaxation *(French)* 77-86117
- WC-Co, elastic and plastic charact. 80-35280
- Zr-Cu-Ti (2.5, 0.15 wt.%), indentation irregularity at elastic limit after heat treatment *(French)* 79-79004

elastic moduli

see also Poisson ratio; shear modulus; Young's modulus

- A15 compounds, linear muffin tin orbital band results by press. calc. 79-65356
- A15 compounds, supercond. rel. to struct. transform. 78-14873
- A-15 compounds, struct. transformations and soft phonon modes, microscopic theory *(Chinese)* 79-37803
- acrylate adhesive coating on glass substrate, mech. props. determ. using transfer functions of US oscillations *(Russian)* 79-87644
- adamantane, elastic props., press. depend. rel. to intermol. forces 80-54297
- adhesion joints, calc. of internal stresses under temp. variation *(Russian)* 77-70273
- alkali halide, dielec. const., press. depend. from ionic polarisability and bulk modulus 79-19828
- alkali halide, melting, mechanical instability 77-89524
- alkali halide, static and dynamic props., appl. to KCl 77-7798
- alkali halide, static dielectric const. temp. depend. 78-43770
- alkali halide crystal, fourth order elastic moduli 78-91373
- alkali halide crystal, vol. damage anisotropy under laser irrad. 77-89469
- alkali halide elastic dielectrics, Gruneisen parameter, effective ionic charge volume derivative 80-84273
- alkali halides, bond forces, parameterless calc. 78-47275
- alkali halides, mixed, bulk modulus, temp. variation 80-92588
- alkali halides, repulsive hardness parameters, crystal-independent 80-64947
- alkali halides, repulsive softness parameter anal. 80-107102
- alkali metal halides, interionic repulsive force and ion compressibility rel. to bulk moduli 77-11500
- alkali metal hydrides, bond forces, parameterless calc. 78-47275
- alkali metals, atomic properties, pseudopot. calcs. 77-89512
- alkali metals, bulk modulus and eqns. of state under press. 80-88293
- alkali metals, equation of state and vol. depend. of thermodynamic props., pseudopot. theory 78-18738
- alkali metals, third order elasticity moduli, temp. depend. *(Russian)* 78-63798
- alkali silicate glasses, secondary relax. transitions 80-88261
- alkaline earth-silicate glasses, elastic props. and struct. 77-24273
- amorphous structure, computer simulation of deformation 79-7647
- Anderson-Gruneisen parameter for 16 cubic symmetry crystals 80-24556
- Anderson-Gruneisen parameter for cryst. of cubic symmetry, determ. using elastic moduli 78-79713
- aneurysm of ascending aorta in patients with and without Marfan's syndrome 77-37001
- anharnomic crystal, violation of Cauchy relations for elastic moduli 79-69179
- anisotropic composites, bounds and self consistent estimates for overall props. 78-5654
- anisotropic elastic half-space, plane indentation by moving punch 78-18181
- anisotropic medium, US diffr. expt., cryst. elastic anisotropy theory verification 77-84846
- annealing and deformation effects on elasticity, with and without texture 79-52274
- antiferromagnet, magnetoelastic coupling in nonlinear acoustic phenomena, exchange interaction effects *(Russian)* 77-90010
- Araldite, neutron irradiation, elastic moduli effects, hardener conc. depend. 79-55804
- aramid fibre reinforced acrylic bone cement, tensile strength and fracture toughness, SEM study 79-29667
- arteries with nonlinear elastic modulus, press. pulse propag. 78-44550
- bakor beams, residual thermal stresses, expt. determ., theoretical anal. 77-66667
- Barre granite, prop. determ. and wave propag. 77-56617
- BCC crystal, elastic constants, thermal expansion and bulk modulus 80-6452
- bimolecular lecithin membranes, artificial, rheological and viscoelasic props. 80-26252
- biomembrane elasto-viscous properties determined from bilayer meas. 80-30671
- biotissues, physicomech. props. rel. to selecting alloprosthetic material 77-25596
- blood vessels, medium sized, mech. characts. 80-41101
- body loading with cracks, energy conditions for brittle failure *(Russian)* 80-96234
- bone, compact, fracture mechs., effects of density and specimen thickness 78-3534
- bone, human, demineralized, deform. props. on stretching 80-3703
- bone, human vertebrae, depend. on age and density 77-36985
- bone, rel. to composition 78-31835
- bone, tensile strength rel. to strain rate, microstruct. and density 77-44703
- bone, US transducer, shear-wave vel. meas. 78-83201
- bone callus, dynamic characts. determ. by induced vibr. method 79-62284
- bone china body, MgO effect on vitrification mech. props. *(Japanese)* 79-78922
- bone elastic and strength props., 3-point bending tests using canine long bones 77-64080
- bone transverse elastic coeff. determ. 78-27985
- Born-Durand melting hypothesis for vol. depend. 79-60420

elastic moduli continued

- borosilicate glass containing simulated high level radioactive waste, characterization *(Japanese)* 79-93745
- Boussinesq problem for material with different moduli in tension and compression 78-55564
- bovine hip bone, compression tests, effect of specimen shape and size on mech. props. and fracture mode 78-69132
- brain elastic response in vivo, influence of methylmethacrylate 77-90818
- brain tissue, nonlinear constitutive relations 77-40707
- brass, creep of β and β' phases, influence of order *(French)* 79-38921
- Brillouin scatt. and refr. index measurements 80-76035
- brittle composite, local crack-driving force, elastic and thermal mismatch 78-7017
- bulk moduli, Wachtman's eqn., and temp. depend. 78-75799
- butadiene nitrile, soot filled, thermal treatment influence on mech. props. *(German)* 80-30000
- butyl rubber vulcanisation with resins, mech. props. *(Polish)* 79-74129
- calcified tissue, role of collagen 78-3539
- carotid arteries of dog, longitudinal stretch effect on dynamic elastic props. 78-27977
- ceramic, elastic behaviour, finite element anal. model, thermal props. 78-31449
- ceramic multilayer capacitors, fracture mechanics approach to structural reliability assessment 80-89328
- ceramics, elastic moduli, effect of inhomogeneous porosity distrib. 79-87674
- ceramics, high temp. props., conf., Baden-Baden (Feb. 1978) *(German)* 79-70135
- close-packed $A^{8-n}B^n$ lattices 78-18700
- close-packed crystals, elastic moduli of polytypic modifications 79-51187
- coherent phase form. at stress concentrators, effect of dislocation splitting, dislocation pile-ups, and phase elastic moduli *(Russian)* 80-49356
- coke, metallurgical, industrial strength meas. methods, critique 80-85117
- collagen and muscle, rel. to phonons, Brillouin spectra 77-52824
- collagen fibres, of dermis, structural and mech. charact. and natural interweaving 78-48824
- collagen structures, piezoelec. effect, in rel. to mol. struct. 80-41100
- colloids, model, elastic moduli, Monte Carlo methods 80-108754
- composite, multimodulus material, apparent flexural modulus and strength 77-28845
- composite elastic medium, effective bulk and shear moduli 80-99927
- composite material, arbitrarily shaped inclusions in infinite elastic medium, effective moduli 77-72172
- composite materials, fracture, elastic mismatch and interfacial bonding influence 80-40506
- composite materials, laser beam determination, of elasticity-compressibility modulus, during compaction 79-43542
- composite materials, two-component systems, comment 80-23896
- composites, overall elastic moduli prediction 80-75285
- compressed crystals, dislocations and point defects *(Russian)* 78-75666
- concrete, compressive strength and ultimate strain under impact loading 79-70128
- concrete, creep, elasticity and strength in tension and compression 78-11287
- concrete, elastic modulus variations, gauge meas. by embeddable-strain-units 78-84878
- concrete, elasticity modulus and strength, aggregate conc. effect 80-66591
- concrete, flowing, expt. studies *(Japanese)* 80-89298
- concrete, high strength, made with a special cement admixture, mech. props. *(Japanese)* 80-89297
- concrete, strain rate effect on strength and deform. during hardening process *(Japanese)* 80-93616
- concrete, unsaturated, dynamic props. of impulsive-type loading 79-70106
- concrete creep under nonuniform temp. distrib., linear viscoelastic analysis 77-62172
- covalent crystal, resistance to microindentation 78-60753
- cracked material, elasticity parameters calc. 79-55346
- cranial bone, fetal, elastic modulus obs., appl. to fetal head moulding biomechanics 80-67128
- cross-plied factors controlling transverse cracking 77-77566
- crystal, elastic moduli, calc. from interatomic forces 79-95071
- crystal classification by acoustic props. 78-79547
- crystals, strain wave vels., Poisson ratios and elastic moduli 78-51609
- cubic crystal, surface contribution to low temp. sp. ht., elasticity theory 78-18790
- cubic crystals, theoretic props. at arbitrary press., density and bulk modulus 78-51606
- cushion dynamic props. by mech. impedance method 78-72953
- cylinder, thick orthotropic circular, bimodulus elasticity, thermal stress 77-23885
- cylinder, thin-walled, laminated, non-uniform, elastic equilib. with surface loads and displacements 80-69671
- cylindrical three layer pipe, stress-strain state, filler compressibility effects *(Russian)* 80-58901
- deformation and temp. depend., quasi-harmonic approx. 77-69068
- dental restorative materials, empirical eqn. including fracture toughness for friction 78-61283
- diamond, compressibility, appl. of Murnaghan eqn. of state, Morse pot. 80-79861
- diamond, effective supersystem cryst. simulation method, geometrical parameters, bulk moduli, impurity levels calcs. *(French)* 80-15430
- diaphragm for loudspeaker, using carbon reinforced olefin polymer, with high specific modulus, flexural rigidity and loss factor *(Japanese)* 80-53596
- diaphragm muscle, canine, in vivo stiffness props., obs. and meas. system 80-97988
- dipalmitoyl phosphatidylcholine(-cholesterol) aligned multilamella lipids, elastic props., Brillouin spectra 79-5255
- disordered materials, bounds for effective elastic moduli 78-4486
- double cantilever beam, fracture studies 80-53708
- double lapped composite joints, efficiency in bending, of steel/B reinforced Al or epoxy adherends 78-68870
- ductile materials, tearing, fracture strength determ. 79-43385
- E-glass epoxy beams, dynamic mech. behaviour, meas. and analysis 77-28844
- E-glass fibre reinforced epoxy, room temp. curable, mech. props. and thermal conductivity 78-68669
- ebonite, viscoelastic, linearity conservation 80-108492

elastic moduli continued
- elastic deformation, thermodynamics of, eqn. of state for solids 80—96589
- elastohydrodynamic lubrication, low elastic moduli material, elliptical contact 79—90198
- elastohydrodynamic lubrication of elliptical contacts for materials of low elastic modulus 79—20214
- elastomer, filler effect on mech. behaviour 79—91729
- elastomer, relaxation processes, statistical description *(Russian)* 79—23229
- elastomers, filler type, effect on concentration rel. to equilib. swelling in solvents 79—64979
- elastomers, rel. between relax. behaviour and tensile strength *(German)* 80—66604
- elastomers, soot filled, mech. relax. behaviour *(German)* 80—84985
- electron-ion metal system, dynamics eqns. in microscopic theory *(Russian)* 80—15198
- Elinvar, Cr addition effect on modulus of elasticity and thermoelastic coeff. 77—90387
- enstatite, elastic modulus and internal friction in single crystal 78—85550
- epichlorohydrin/bisphenol A epoxy polymer concrete, viscoelastic props. 80—45340
- Epon 828 epoxy, composite three dimensional model for photoelasticity 78—52871
- epoxide resin, struct. and elastic moduli 77—85984
- epoxy resin, deform. rate depend. of mech. props. at cryogenic temps. 80—55456
- epoxy resin, filled and unfilled, subjected to extensional creep, dynamic props. 80—71697
- epoxy resin, low temp. irradiation effects on mechanical props., use in superconducting magnets 78—60737
- epoxy resin, powder filled, exam. of mech. props., thermal contraction 80—25821
- epoxy resins, relationship between struct. and mech. props. *(Japanese)* 78—31438
- epoxy structural adhesives, tensile tests, stress/strain relations, stress relaxation 78—60702
- epoxy/E-glass continuous fibre composite type 3M Scotchply, complex moduli, comparison of meas. with estimated bounds 80—93590
- ethylene copolymers, partially crystallised, quasistatic moduli at small strains *(German)* 78—76700
- ethylene-vinyl alcohol (<36.3 mol.%) copolymer, elastic moduli of crystalline region *(Japanese)* 79—15715
- ethylene-vinyl alcohol (>40 mol.%) copolymer, elastic moduli of crystalline region *(Japanese)* 79—15716
- FCC cryst., theory of response to [110] uniaxial loading 79—19310
- FCC lattice, uncorrelated-pairs approximation for anharmonic free energy, tests 78—59920
- ferroelastic transitions, order parameter symm., free energy expansions 80—49164
- ferroelectric, elastic nonlinearity near phase transition, effect of elec. field 77—24804
- ferroelectric transition region 78—6646
- ferroelectric with piezoeffect in paraphase, third order, elastic moduli near second-order phase transition, temp. depend. 78—19429
- ferromagnets, easy plane, containing dislocations, static props. 79—95626
- fibre reinforced composite, unidirectional, representative volume, elastic moduli, calcs. by photoelasticity *(Russian)* 79—34094
- fibre reinforced composite with viscous matrix, random stresses in components, laws of distrib. 79—23226
- fibre reinforced composites, approx. formulae 77—66672
- fibre reinforced composites, elastic moduli and shrinkage factors, calc. taking account of anisotropy 79—52291
- fibre reinforced composites, materials properties, unsolved problems, review 77—4843
- fibre reinforced composites, mech. props. 79—52329
- fibre reinforced composites, overall moduli, effect of fibre length, self-consistent method 79—76977
- fibre reinforced ionomer composites, fatigue strength, dynamic viscoelastic props. and fracture surface exam. *(Japanese)* 78—92339
- fibreboard, made from Asplund pulp-PMMA composite, props. *(Japanese)* 80—7664
- fibrous composite material, estimate for composites isotropic on the average 78—51077
- filled polymer, elastic reinforcement theory, filler orientation distrib. anal. *(Japanese)* 78—39734
- filled polymer mechanical properties, particle shape effect, review 80—100864
- film on cylinder, calc. of moduli *(Russian)* 78—63304
- fluoride crystals, rutile-type, interionic pots., cohesive energy, bulk modulus, calc. 80—79741
- forsterite, elastic modulus and internal friction in synthetic polycrystal 78—85550
- frozen sand-argillaceous rocks, elastic moduli 77—9406
- furfuralacetone resin, filled, elastic modulus calc. 79—57030
- garnet solid soln. series, elastic props. inferred from expts. on pyrope 80—76968
- gels, dynamic light scattering in poor solvent 78—88318
- glass, device for temp. depend. meas. at low pressures 80—30183
- glass, internal friction in region of transition to viscous-flow state 79—66101
- glass bead reinforced nylon, design parameters, fibre orientation effect 80—81141
- glass bead reinforced polycarbonate, design parameters, fibre orientation effect 80—81141
- glass bead-reinforced epoxy resin composite, bulk and shear elastic props. 78—6959
- glass ceramic, machinable, elastic moduli press. and temp. derivatives, specific heat 78—52873
- glass fabric reinforced phenol resin, effect of thermal loading on physicomech. props. 79—24622
- glass fibre, elastic moduli, thermal history depend. *(Japanese)* 80—45333
- glass fibre, reinforced filled resin, analytical method of determ. 79—100201
- glass fibre reinforced epoxy, struts for superconductive storage magnets, mech. props. 80—25824
- glass fibre reinforced nylon, design parameters, fibre orientation effect 80—81141

elastic moduli continued
- glass fibre reinforced plastic, flexural fatigue props. *(Japanese)* 79—20171
- glass fibre reinforced plastic, strength dispersion, statistical anal. *(Japanese)* 79—61655
- glass fibre reinforced plastics, ageing by boiling in water, effect on physicomech. props. 80—60892
- glass fibre reinforced plastics, laminated ring with extra steel pin radial reinforcement, mech. props. 80—11714
- glass fibre reinforced plastics, microstructure rel. to mech. props. 80—11685
- glass fibre reinforced plastics, under compressive load *(Japanese)* 78—92301
- glass fibre reinforced polycaproamide, viscoelastic, linearity conservation 80—108492
- glass fibre reinforced polycarbonate, design parameters, fibre orientation effect 80—81141
- glass fibre reinforced polyester, behaviour under bending load *(Japanese)* 79—38904
- glass fibre reinforced polyester, struts for superconductive storage magnets, mech. props. 80—25824
- glass fibre reinforced polyester filament wound pipe, failure 78—44192
- glass fibre reinforced polyurethane foam fracture toughness, modulus increase 78—44196
- glass microsphere reinforced, composite, mech. charact. calc. 78—64578
- glass/C reinforced epoxy resin, hybrid effects, conditions for positive or negative effects vs. rule of mixtures, mech. props. 78—68769
- grade n material, tensor of effective elastic moduli 79—10473
- grain boundary internal friction in magnetics, elastic moduli anomalies *(Russian)* 77—35633
- granular medium, shear modulus, rel. to void ratio *(Japanese)* 79—32401
- graphite, irradiated ultimate tensile bending and compressive strength charact. 78—15479
- graphite, neutron induced changes, exam. of lattice consts., elastic modulus, elec. cond 79—95053
- graphite, pyrolytic, thermal expansion coeff. rel. to temp. 78—43147
- graphite, pyrolytic commercial, high-temp. thermal and mech. props. 80—75372
- graphite, recompressed expanded, thermal conductivity, elastic moduli, density effects *(French)* 78—26744
- graphite fiber reinforced epoxy, transversely isotropic moduli 79—83246
- graphite fibre, transversely isotropic moduli 79—83246
- graphite fibre filled polyimide composite laminates, space environment, phys. and mech. response 80—81140
- graphite fibre reinforced epoxy laminates, expt. investigation of tensile moduli and strength 78—52870
- graphite fibres, elec. resist., mech. props. after nitration 77—32698
- hard sphere fluid, elastic modulus and viscosity coeff. 77—30086
- hardened components, residual stress, elastic characts. after surface plastic stress 78—60901
- hardness, elastic moduli, density, cryst. temp., mech. props., for flywheel appl. *(Dutch)* 78—52878
- Hashin Shtrikman bounds, effective elastic moduli, hexagonal, trigonal and tetragonal polycrysts. 80—75282
- Hashin-Shtrikman bounds, effective elastic moduli, monoclinic polycrysts. 80—70291
- heat resistant weld seam metal, tensile strength, thermophysical characts. 79—91769
- hollow viscoelastic cylinder, plane nonaxisymmetric deform., dynamic behaviour 79—98635
- honeycomb based composite, deform. theory 80—35250
- hybrid glass fibre/C fibre reinforced epoxy-phenolic, elastic characts. prediction 80—108491
- II-VI semiconductors, electronic theory, cryst. energy and bulk modulus 78—72104
- III-V semiconductor, electronic theory, cryst. energy and bulk modulus 78—72104
- incoherent ellipsoidal precipitate, re-exam. of elastic strain energy 78—51676
- incommensurate two-dimensional crystal, ground state, spectrum, phase diagram 79—19458
- incompressible elastic materials with different moduli in compression and tension, dynamic problems 80—79141
- internal friction peaks, dislocation-defect elastic force in dragging model 80—39104
- intervertebral joint, systems identification for material props. 78—69125
- Invar, stainless, thermal expansion, elastic props. and Mossbauer effect 79—56502
- Invar alloys, bulk modulus anomaly, rel. to itinerant electron model of ferromag. 77—48025
- Invar alloys elastic and magnetoelastic effects 79—56589
- Ising systems, compressible, elastic anomalies inducing first order transitions 79—47288
- isoprene rubber elastomers, thermal treatment influence on mech. props. *(German)* 80—30000
- isotropic composite material containing spherical inclusions at nondilute concs., effective elastic moduli 78—67037
- isotropic materials, continuum mechanics in space of any dimension *(Japanese)* 78—41161
- Jahn-Teller crysts., ferroelec. transitions, elastic and dielec. anomalies, microscopic model 80—71332
- Kevlar/epoxy composites, elastic props. rel. to thermal expansion 80—24622
- Kovar, effect of magnetic electrons on atomic interactions 77—43820
- Kroner limits of technically important materials, function of temp. *(German)* 79—28032
- laminate, anisotropic layers, fibre reinforced, effective moduli of elasticity 77—4802
- laminate, post-failure behaviour, no stress conc. 77—28895
- latex, shear waves, elastic modulus determ., light scatt. 80—58956
- Lennard-Jones fluid model, bulk and shear modulii determinations, computer experiments *(Spanish)* 79—60417
- lethicin, bilayer membrane, elastic props., in direction perpendicular to membrane plane 79—57602
- Lexan, optical and phys. parameters 79—32004
- lipid bilayer, freq. depend. 78—48762
- lipid bilayer, saddle splay instability, crit. elastic modulus 78—44462
- liquid, Gruneisen parameter rel. to Rao's acoustical parameter 80—92581

elastic moduli continued
liquid metal, bulk modulus, calc. using press. fluctuation in microcanonical ensemble 80—2106
low-dimensional crystals, SAW propagating along free boundary 79—73388
magnetically ordered cryst., dislocation drag, magnetoelastic waves 80—103332
MBBA, nematic mesophase, struct. of flow in cylindrical capillary 77—7671
measurement, via automatic internal friction and modulus apparatus using phase-locked loop 78—13981
melting, dislocation model, appl. to FCC cryst. 78—26658
metal, damageability determ. by meas. of elastic, inelastic, internal friction charact. 79—66133
metal, limiting elastic moduli, Morse pot. appl. 77—69025
metal mechanical property effects on frictional behaviour 80—55548
metallic glass, hardness, elastic moduli, density, cryst. temp., mech. props., for flywheel appl. *(Dutch)* 78—52878
metals, cubic, ionic overlap interaction energy, press. and bulk modulus 80—29340
metals, dynamic elastic moduli of finite temps. *(Russian)* 79—14873
metals, elastic constants and moduli of axial textures 80—75286
metals, Hume-Rothery's class I, Engel-Brewer theory and related phys. props. 78—2059
metals, interatomic potentials of Na, K, Al, Cu, Fe from phonon spectra 80—19744
metals, polycryst., elastic moduli rel. to those of single crysts. 79—23671
metals, simple, elastic moduli, chem. trends, pseudopot. method 80—107355
metals, static and dynamic isothermal elasticity moduli *(Russian)* 80—24524
metals and alloys, EM acoustic reson. for elastic moduli meas. 80—15573
metals and alloys, hexagonal cryst. struct., anisotropy of elastic props. calc. *(Russian)* 78—23749
methane, crystalline, struct. and compression at high press., room temp. 80—107199
minerals, bulk modulus-volume relationship, for cation-anion polyhedra 80—41434
minerals relevant to Earth interior geophysics, Hildebrand equation of state 80—56464
mucus mechanical props. rel. to mucociliary transport, effect of pharmacologic interventions 80—3663
muscle, elastic and viscous props. of resting frog skeletal muscle 77—44700
muscle, glycerol-extracted fibrillar fibres, cross-bridge slippage induced by AMP-PNP and stretch 78—77075
muscle, mech. pulse propag. vel. meas. using piezoelectric crystals, elastic moduli 78—92668
Nb carbides, nonstoichiometric, elastic props., 20-2000°C 77—12661
non-randomly cracked body, elastic moduli 79—23209
noncubic materials, temp. depend. *(French)* 79—65135
nonlocal elasticity, rel. with lattice dynamics 77—84824
nonlocal moduli for elastic medium determ. *(Russian)* 77—35622
Nylon 6, fibre, crystallite dimensions, effect on struct., mech. and diffusive props. 78—11273
Nylon 6, oriented, extensional deformation, and effects 80—7613
nylon 6 (polycaproamide), salted, glass transition temp. and elastic modulus, moisture effect 80—103465
nylon 6 fibres, dynamic mech. props., interpretive nonlinear viscoelasticity 79—4994
oblate spheroidal inclusion, internal stress, misfit, inhomogeneity and plastic deform. 78—60701
4-n-octyloxy-4′-cyanobiphenyl, smectic A liq. cryst., elastic modulus determ., stress/strain relationships 78—91229
orbitally degenerate interacting impurity thermodynamics, stress field depend. due to point defects, dislocations 79—69477
oriented fibres and films 78—38261
orthorhombic symmetry polycrystals, Hashin-Shtrikman bounds on effective elastic moduli 80—19864
orthotropic incompressible arteries, incremental elastic modulus 80—30751
oxide crystals, rutile-type, interionic pots., cohesive energy, bulk modulus, calc. 80—79741
oxides on Al alloys, mech. props. and influence on substrate fatigue 77—44408
paper sheet, elastic props., inhomogeneity with reference to basis wt. depend. of elastic moduli *(Japanese)* 80—2110
peridotite, elastic modulus and internal friction 78—85550
PET, fibre, crystallite dimensions, effect on struct., mech. and diffusive props. 78—11273
PET, oriented, extensional deformation, and effects 80—7613
Pierre clay shale, longit. modulus meas. at varying strain rates 77—53038
piezoelectric cryst., excitation and energy flux of acoustic harmonic, amplitude depend. on elastic nonlinearity 79—15404
piezoelectric hexagonal crystals., elastic wave propag. *(Russian)* 77—69777
piezoelectric solid, appl. of hardened elastic moduli to elastic wave propag. and interaction with charge carriers *(Russian)* 78—35095
pivalolactone-α-methyl-α-propyl-β-propiolactone copolymers, struct., thermal and mech. props. 79—43582
plasma sprayed materials, control of mech. props. 80—11560
plastic, flexural fatigue props. *(Japanese)* 79—20171
plastic, static strength determ. from elasticity and internal friction 77—70094
plastic elasticity, hardness, creep, and relaxation meas. with Vickers indenter by electroacoustic method *(German)* 78—48584
plastic powder compact rheological characteristics *(Japanese)* 78—95770
plastics, randomly reinforced, elastic constants calc. *(Japanese)* 78—31437
platelet reinforced media, effective moduli and isotropic props. 80—40422
plates, elastic, optimum bending and extension *(Russian)* 80—38259
platilon UO1, use in artificial blood pumps, fatigue resist. and mech. props. 79—84026
Plexiglas 55, optical and phys. parameters 79—32004
plexiglass composite, long term strength and durability 80—75294
plywood shallow shells, orthotropic, mech. charact., effect of restraint of sliding or expansion *(Japanese)* 77—77522
PMMA, visoelastic props., γ-irrad. influence *(Russian)* 78—88492

elastic moduli continued
Poisson ratio/elastic modulus ratio, optical expt. method 79—82273
poly(cis 1,4-isoprene), cryst. phase, elastic modulus 79—57037
poly(p-benzamide), highly oriented, ultimate mech. props. 79—91751
poly(p-phenylene terephthalamide) fibres, chain orientation distrib., and elastic props. 78—75566
poly(p-phenyleneterephthalamide), highly oriented, ultimate mech. props. 79—91751
poly(vinylidene fluoride) piezoelectric film, Lamb and shear wave propagation *(French)* 80—44256
polyacrylamide-water gels, copolymerised with N,N-methylene bisacrylamide, dynamic light scatt. 78—60477
polyamide, aromatic, fibre, high modulus, mol. and supramol. struct. 80—79710
polyamide, test pipes, static tensile strength, equipment effect on tension-extension diagram *(German)* 78—35453
polyamide, viscoelastic, linearity conservation 80—108492
polyamides, extended chain aromatic, fibres, tensile strength and moduli 80—81021
polyamides, preoriented, method for increasing elastic moduli 77—80425
polyaryleneimides, oriented, elastic props. 80—40416
polybutadiene, complex modulus meas. using forced vibrations at ultralow frequency 77—70258
polybutadiene, hydrogenated, linear and star branched, melt rheology 80—23978
polybutadiene, linear and star branched, rheology 80—23977
polycaproamide, oriented filaments, mech. props. 80—66550
polycarbonate, glassy, rolled, craze initiation *(Japanese)* 77—8969
polycrystal, linear, E and G moduli, crystallisation effect *(German)* 80—59556
polycrystal, US scatt. by grains 80—2122
polycrystal elasticity theory, role of Gruneisen elastic parameters 79—95070
polycrystalline aggregate, with fibre texture, coincidence of bounds 79—28030
polycrystalline cubic and hexagonal substances, eqns. for effective moduli of elasticity 77—15474
polycrystalline material, scatt., lattice representation 78—65774
polydimethylsiloxane, end-linked chains, model elastomeric networks, Gaussian, nonGaussian and ultimate props. 80—103260
polydimethylsiloxane, end-linked model network, elastic modulus and equilib. deg. of swelling 77—35616
polydimethylsiloxane, stress-strain props., cross link functionality 79—46575
polydimethylsiloxane chains, end-linked, swollen model networks, stress/strain isotherms and elastic modulus 80—79668
polydimethylsiloxane chains, with known radiative side chain amounts, model elastomeric networks prep. by sel. crosslinking 79—73106
polydimethylsiloxanes, rubbery and liq., hypersonic sound vel., Brillouin spectra meas. 80—75308
polyester resin, unsaturated, chalk filled, props. *(German)* 80—104228
polyester resin concrete, effects of styrene-unsaturated polyester ratio on props. *(Japanese)* 80—89299
polyester/E-glass chopped fibre composites types PPG SMC-R25 and PPG SMC-R65, complex moduli, comparison of meas. with estimated bounds 80—93590
polyester/E-glass hybrid chopped/continuous fibre composite type PPG XMC-3, complex moduli, comparison of meas. with estimated bounds 80—93590
polyethylene: (Dy_20_3), mech. props. and transfer to steel surfaces 80—16496
polyethylene, deformation, Hartree-Fock SCF calcs. 80—18949
polyethylene, direct ram extrusion, correl. between chain folding and tensile modulus 77—44209
polyethylene, dynamic mech. behaviour, longitudinal cryst. thickness 78—76691
polyethylene, dynamic modulus under high press., nature of high press. phase *(Japanese)* 80—3120
polyethylene, filled, model, effect of stiff fillers on elastic modulus 78—68720
polyethylene, filled with glass particles, uniaxially drawn, elastic constants, filler addition effect *(Japanese)* 78—95780
polyethylene, high density, monodisperse system mol. wt. effect on dynamic elastic modulus 77—70093
polyethylene, high density, solid state coextrusion, geometric factors effect 80—71704
polyethylene, high density extruded fibres, morphology effect on physical and mech. props. 79—83235
polyethylene, lamellar structs. nucleated onto fibrous substrates for high modulus 78—75578
polyethylene, linear, injection moulded at high press. struct. 79—11640
polyethylene, linear, melt rheology 80—23976
polyethylene, low density, isotropic, extensional deformation, and effects 80—7613
polyethylene, orthorhombic and triclinic lattices, eqns. of state 79—28069
polyethylene, solid-state extruded, exam. of props. 80—11669
polyethylene, ultra-oriented, prep. technique, extreme moduli 77—21086
polyethylene, ultrahigh modulus, drawing temp. effect on void form. and modulus 80—35241
polyethylene, ultrahigh-modulus, thermal cond. in region 2 to 100K 77—62690
polyethylene, ultraoriented high-density, annealing characts., tensile modulus meas. 77—8852
polyethylene electrets, charge trapping mechanism, TSC, DTA and optical meas. 80—11322
polyethylene fibres, high density, ultra oriented, physical, mech. props. 80—25649
polyethylene flow crystallisation, in extensional flow developed by convergent capillaries, props. 80—84111
polyethylene oxide, cryst., lowest laser Raman active accordion oscillations, elastic moduli effect 80—29734
polyethylene terephthalate, effect of excess thermodynamic props. versus struct. form. on dynamic moduli 77—86053
polyethylene terephthalate fibres 79—79019
polyethylenes, u.h. modulus linear, cryst. modulus 77—4799
polyimides, cryst. lattices elasticity and mech. props. 80—20995
polyimides, DFOPF and DFOB, X-diffr. exam. of structure and elasticity 80—6370
polymer, fibrous, drawing and annealing 78—15458
polymer, linear viscoelastic model and dynamic behaviour, elec. transmission line representation *(Spanish)* 77—72185

elastic moduli continued
- polymer, microinhomogeneous, elastic props. description rel. to crystallinity 79—19307
- polymer, nonoriented partially crystalline, elasticity and strength 77—52386
- polymer, particle-filled, elastic moduli, interfacial slippage effect anal. 78—76688
- polymer, physical problem determ. problems, tensile strength, elastic moduli *(German)* 78—15470
- polymer, rigid, prefractured states study, elastic limit and strength 77—70092
- polymer, yield stress and elastic modulus power law relationship 79—47752
- polymer films and sheets 78—80590
- polymer fluids, complex modulus, freq. depend. var. during extensional flow 79—55351
- polymer gel, quasielastic laser light scatt. theory 79—82986
- polymer materials, hysteresis flow model applicability for degree of inelasticity 80—28422
- polymer networks, stochastic cross-linked, modulus of elasticity, functionality effects *(German)* 80—59555
- polymer-metal sliding, wear eqn. in terms of fatigue and topography of sliding surfaces 80—108597
- polymers, accordion-type laser-Raman oscills., elastic moduli 79—55854
- polymers, composite three dimensional model for photoelasticity 78—52871
- polymers, elastic moduli, press. depend. 78—52877
- polymers, filled, elastic moduli, effect of particle shape at finite conc. 79—15712
- polymers, glassy, Gruneisen const. calc. from thermoelastic meas. 79—14945
- polymers, mech. props., at 4.2K depend. on chemical struct. and physical struct. form. 77—28847
- polymers, mech. props., temp. dependence of polymers of different struct., 4.2 to 300K 78—68746
- polymers, multicomponent, props. and struct., review 78—44076
- polymers, partially crystalline, nonlinear mech. relax. *(Russian)* 80—40467
- polymers, unoriented, temp. depend. of elastic modulus 80—39202
- polymers filled with agglomerated particles, dynamic mech. props. 80—66569
- polymers in glassy state, calc. method from chem. struct. *(Russian)* 78—75707
- polymethylpentene, LF acoustic relaxation 78—38784
- polymethylpentene, visoelastic props., γ-irrad. influence *(Russian)* 78—88492
- polymide, elasticity of crystal lattice 78—3164
- polyolefin, filled, appl. of reduced conc. principle, generalised elastic modulus 77—8871
- polyolefines, filled, struct.-mech. props. relation *(German)* 78—35451
- polyolefins, ultra-high modulus, production by tensile drawing and hydrostatic extrusion 80—81022
- polypropylene, oriented, compressive elastic modulus and yield strength 80—16385
- polypropylene fibres, homologue mixtures, props. 78—76709
- polysiloxane dizwitterionomers, mech. props., microstruct. 80—49131
- polystyrene, atactic, effect of excess thermodynamic props. versus struct. form. on dynamic moduli 77—86053
- polystyrene, cryogenic foam insulators, low temp. props. 80—25818
- polystyrene, microcryst. cellulose filled, glass transition temp. shifts 78—95144
- polystyrene, viscoelastic, linearity conservation 80—108492
- polystyrene melt, carbon-black filled, rheological study 80—48665
- polystyrene-polypropylene(polyethylene) mixtures, elastic moduli, phase struct. effect *(Polish)* 79—70107
- polystyrene-tetrachloroxylene(tetrachlorobenzene) glassy solns., additive morphology rel. to mech. props. 79—65007
- polystyrol, test pipes, static tensile strength, equipment effect on tension-extension diagram *(German)* 78—35453
- polystyroles, filled, struct.-mech. props. relation *(German)* 78—35451
- polyurethane, cryogenic foam insulators, low temp. props. 80—25818
- polyurethane foam, SiO_2 particulate filled, mechanical props. 79—11666
- polyvinylidene fluoride, film, piezoelec., pyroelec., thermal expansion, elastic consts. 78—84529
- porous ceramics with non-spherical holes, effective elastic moduli and US wave vel. 77—60031
- porous material, strength, elastic modulus, exponential porosity depend. 77—36563
- Portland cement-fly ash, physico-mech. props., SEM and X-ray diffr. anal. 79—74239
- prestrain effect on dynamic modulus of elasticity and attenuation coeff. in nonconducting materials 80—29110
- prolate spheroidal inclusion, stress conc. 78—67042
- PTFE and filled PTFE, nonlinear creep, compression bulk modulus 80—66593
- PVA, microcryst. cellulose filled, glass transition temp. shifts 78—95144
- PVC, at 10-90 kHz range 77—86235
- PVC, crosslinked, mech. and thermal props. with plasticisers *(Japanese)* 79—15741
- PVC, test pipes, static tensile strength, equipment effect on tension-extension diagram *(German)* 78—35453
- PVC block copolymers, physical props. and morphology 79—82166
- PVC plastisol films, thermally hardened, struct. and props. *(German)* 79—70097
- PVC-chlorinated PVC mixtures, compatibility, mixing techniques, elastic modulus determ. 79—4943
- PVC-ethoxymethylmelamine blends, dynamic mech. props. *(Japanese)* 79—96063
- pyrope, elasticity of single cryst., implications for garnets 80—76968
- PZT, polycrystn., thermal expansions, elasticity and internal friction 80—35238
- quartz, fused, second press. derivatives of elastic moduli, US vel. meas. 79—23670
- quasi-isotropic crystals, singular approx. and self-consistent calcs. 77—11623
- random media, effective moduli, unified calc. of bounds and self-consistent values 78—91372
- randomly nonhomogeneous elastic body, parametrix method for determ. of effective elastic moduli 77—54884
- rare earth cobalt intermetallics, RCo_2, elastic moduli, 4.2-300K 78—52332

elastic moduli continued
- rare earth hexaborides, obtained by melting, micromech. props., rel. to bonding 80—21082
- rare earths, elastic and mechanical properties, review 79—70132
- rare gas solids, third order elastic consts., second order elastic const. press. derivatives 80—70501
- red cell membrane elastic area compressibility meas., osmotic correction 78—20147
- refractory wear-resistant coatings, composite struct. develop., props. 77—63618
- resonance method for meas. complex elastic moduli of polymer films 77—67426
- rocks, Murnaghan constants evaluation as function of pressure 80—31037
- rocks, porous, self-consistent imbedding and ellipsoidal model 80—26503
- rosette cylinder, elastic response under axisymmetric loading 77—58549
- roving glass cloth fibre reinforced plastic, fracture mech., time depend. *(Japanese)* 80—55508
- rubber, network entanglement contrib. 80—39203
- sandwich composite beam, impact bending behaviour *(Japanese)* 80—55468
- sandwich composite beams, stress distrib. meas. under four-point bonding, multilayer builtup theory 80—96190
- schorl tourmaline, elastic const. 78—68718
- second-order phase transitions in crystals, equilibrium configurations, thermoelasticity theory 80—70364
- semiconductor, Anderson-Gruneisen parameter, bulk modulus temp. depend. 78—10154
- shell, conical, stress distrib. near hole, orthotropy effect 80—43630
- shell, cylindrical, viscoelastic core, parametric vibrations 77—27489
- shell, cylindrically compressed, with varying elastic props. along length, optimisation 77—27472
- shell of revolution high modulus material shape of wound membrane rationalization 77—27473
- Sialon, reaction sintered, mech. props., effect of composition and X-phase 77—56013
- silicate, glass, elastic modulus temp. depend., metal oxides effect 79—61637
- silicate glasses, longit. and transverse elastic wave vels., temp. and comp. variations 80—88258
- silicate glasses, vol. of fluctuation microcavities calc. 79—65000
- silicone rubber vulcanisates, as alloprosthetic material 77—25596
- simple metals, volume forces 80—15178
- single crystals under large loads, theoretical elastic behaviour, review and appl. 80—71681
- soft elastic material dynamic props. determ. *(German)* 78—71297
- soft-sphere, model, bulk and shear modulii determinations, computer experiments *(Spanish)* 79—60417
- soil, layered, effective moduli theory appl. *(Polish)* 79—25237
- solids, evaluation of finite strain eqns. of state using lattice models 80—96620
- specific heat, const. press., press. variation of vacancy contrib. 79—1510
- spinel disproportionation reactions, elasticity and phase equilibria 77—78158
- β-spodumene-mica glass ceramic, thermal expansion thermal shock and moduli of rupture and elasticity 78—60736
- spring-loaded mass system vibration analysis *(German)* 80—96224
- square well fuild, elastic modulus and viscosity coeff. 77—30086
- Steatit ceramic strength determination by measuring US dynamic elastic modulus *(German)* 79—43301
- steel, 110G13L, P content, effect on elastic moduli and internal friction 78—23753
- steel, 12X2H4A, nonmetallic inclusion effect on plasticity and impact strength *(Ukrainian)* 78—92296
- steel, austenitic stainless, fast neutron irrad., effect on mech. props. 78—92309
- steel, austenitic stainless, porous fibre, sintered and compacted, mech. props. 79—15623
- steel, austenitic stainless, types 304 and 316, environment effect on crack growth, under creep and fatigue conditions 80—85035
- steel, C, antifriction material, sintered, determination of elastic moduli 79—96070
- steel, C, fatigue strength and damping capacity, short term cyclic overload effect 79—66157
- steel, die type 5KhNM, stressed state effect on softening 79—66168
- steel, electric arc sprayed coating on wire, elastic and elastic-plastic props. *(German)* 79—34089
- steel, graphitised, elastic modulus and internal friction, temp. depend. 80—35242
- steel, high-strength reinforcing, 20GS2, local microstresses on creep strength in hydrogenating media *(Russian)* 77—52462
- steel, mild, plastically pretorsioned, dynamic props. 79—83267
- steel, Ni, antifriction material, sintered, determination of elastic moduli 79—96070
- steel, plastic deform. effect on third-order elastic moduli, dislocation anharmonism *(Russian)* 80—50786
- steel, stainless, austenitic, Cr-Ni-Mn-Si-Mo-C alloy, 13Khi8N10G3S2M2, elastic moduli exam. after thermomechanical treatment *(Russian)* 79—24558
- steel, temp. depend. of elastic, moduli US obs. *(Japanese)* 80—25750
- steel fibre reinforced Al, vacuum hot pressing, strength *(Czechoslovakian)* 77—32543
- steel wire reinforced Portland cement mortar, wire pull out, inelastic behaviour 78—56681
- stochastically inhomogeneous structures, macroscopic third-order elastic moduli 80—69672
- stresses in cylindrical welded rod with interlayer of lower elastic modulus, stresses in tension 79—24557
- substitutional impurities in solids, entropy and volume of solution 80—15253
- technological strength and nondestructive methods of testing during heat treatment 78—85090
- Textolite, mech. props. in elastic symmetry planes 77—21211
- TGS, large scale inhomogeneity effect on ferroelectric transition *(Russian)* 78—76411
- TGS, sound group vel. vector direction, temp. depend. 78—67774
- thermal stress distribution associated with elastoplastic deform. 77—19549
- third order, alkali metals, calc. *(Russian)* 77—51427
- Thornel 300/Fiberite 1034 graphite epoxy composite, elastic moduli, environmental effects 77—86068

elastic moduli continued
- three layer cylindrical shell having low stiffness filler, resistance to axial compression 79−86353
- Ti alloys, commercial, elastic modulus at low temps. 79−66100
- transition metal, 2H layer compound, theory of superstructures 79−99291
- transition metal, 3d and 4d, local density theory, mech. and mag. props. evaluation 78−91630
- transition metal, BCC isothermal compression to 100 kbar 78−43069
- transition metal, bulk modulus, effect of correlations and ferromag. order 78−34564
- transition metal, cohesive energy, lattice consts. and bulk modulus, renormalised atom method 77−43170
- transition metal, magnetic ground state props., simple one-electron theory 77−63063
- transition metal alloys, cohesive properties and press.-vol. relation 80−92476
- transition metal alloys, elastic properties, vol. depend. 78−95103
- transition metal carbides, elastic moduli, scratch geometry, micromech. tests 78−35416
- transition metal carbides, nitrides, and borides, d-band contraction upon metalloid formation, resolution of bonding controversy 79−87041
- transition metals, correl. effects, bulk modulus and equilib. lattice spacing 78−10115
- transition metals, elastic constants, temp. depend. rel. to conduction electron density of states *(Russian)* 78−38769
- transition metals, solubility of H_2 and bulk modulus 78−55950
- triglycine selenate, elastic moduli matrix, and temp. depend. of elastic moduli 79−46738
- trigonal monocrystals, classes 3 and $\bar{3}$, plastic potential and yield stress *(Russian)* 80−29109
- type II superconductor, low-flux density, shear modulus of flux-line lattice 77−1528
- type II superconductor vortex state, elastic energy calcs. on high inductions 77−36030
- type II superconductor vortex state, elastic energy calcs. on low inductions 77−36031
- undirectional fibre composites, anisotropic constituents, effect elastic moduli and other props. 80−58911
- US propagation in cryst. under quasihydrostatic compression, elastic characts. 77−51445
- viscoelastic fluid theories based on left Cauchy-Green tensor history 80−4534
- viscoelastic material, failure and instability in tension 80−87720
- viscoelastic materials, error anal. in complex moduli investig., coated beam method 79−27565
- viscoelastic materials, true moduli determ. using superposition method 79−18744
- wire for high-speed matrix printers *(Japanese)* 80−55540
- wood, impulse method of determining moduli of elasticity, shear moduli 77−77661
- wound healing, var. of mech. props. in different areas 78−27984
- Zircaloy-4, elastic props., O additions effect 80−66565
- Ag, Bordoni effect during recrystallisation 77−90388
- Ag, electron irrad., elastic moduli and internal function *(French)* 78−87703
- Ag halides, quadrupolar deformability theory by tight binding method 80−10614
- Ag, halides, strain derivatives of elastic and dielectric consts. 79−60421
- Ag-Pd, composition modulated foils, layer struct. and mech. props. 79−95300
- AgBr, bulk modulus fall, curvature of conductivity plots, consequence of anharmonicity 78−79800
- AgBr, interionic forces, cohesive energy, bulk modulus calcs. 79−82176
- AgCl, bulk modulus fall, curvature of conductivity plots, consequence of anharmonicity 78−79800
- AgCl, interionic forces, cohesive energy, bulk modulus calcs. 79−82176
- AgF, interionic forces, cohesive energy, bulk modulus calcs. 79−82176
- AgI, sound vels. and bulk moduli near phase transitions with negative dP/dT 78−83885
- Al alloy 7075, fracture toughness, hydrostatic press. depend., tensile ductility 78−3209
- Al alloy rod, elastic moduli determ. from shock wave profiles 78−6125
- Al, deformation, internal friction, dynamic modulus and creep meas. 79−91727
- Al, elastic properties *(Russian)* 78−56678
- Al, liquid, bulk modulus, calc. using press. fluctuation in microcanonical ensemble 80−2106
- Al, mechanical deformation with superimposed insonation, volume effects 78−60723
- Al, plastic deform. effect on third-order elastic moduli, dislocation anharmonism *(Russian)* 80−50786
- Al, pure, Bordoni effect during recrystallisation 77−90388
- Al-Mg solid solns., decomposition studied by ultrasonic meas. of elastic props. 80−35184
- Al-Mn profiled alloy components pulled from melt, physicomech. props. 78−3175
- Al-Zn (20 (30) (35) (40) (60) at.%), effect of UTS on cyclic creep strength *(Korean)* 80−25778
- Al_2O_3, deform. curve and modulus-temp. relation *(Russian)* 78−35613
- Al_2O_3, elastic behaviour, finite element anal. model, thermal props. 78−31449
- α-Al_2O_3 fibre FP reinforced Al and Mg composites, fabrication and props. 80−81004
- Al_2O_3, mechanical props. charact. by dynamic elastic modulus meas. up to 1400°C *(German)* 79−70101
- Al_2O_3-SiO_2 refractory concrete, elastic props. 80−89280
- Al_2TiO_5, grain size pseudobrookite oxide, microcracking relations 79−29194
- Ar, liq., elastic modulus and stress relaxation 79−19304
- Ar, solid, equilib. props., uncorrel. pairs approx. 80−84303
- Ar, solid, self consistent field calcs. of isotherms and thermodynamic props. *(Russian)* 80−10633
- Ar, solid, thermodynamic props. under press., multiparametric pairwise and Lennard Jones potential calcs. 80−39316
- As, elastic moduli, calc. from interatomic forces 79−95071
- As_2S_3, chalcogenide glass, effect of press. on elastic props. 80−10590
- As_2S_3:Ag, amorphous US props. 78−51616
- $As_2S_3(Se_3)$ glasses, elastic moduli, hydrostatic press. effect, US wave vel. meas. 80−34115

elastic moduli continued
- As_2Se_3 glass, mech. props. var. due to high press. phase change 77−76481
- As_2Se_3:Ag, amorphous, US props. 78−51616
- Au, lattice vibr., electron press., central pair pot. model calc. 78−75749
- Au-Ni, composition modulated foils, layer struct. and mech. props. 79−95300
- Au-Ni, supermodulus effect, one-dimens. modulated structs. 79−95068
- Au-Ni foil, composition-modulated, elastic modulus enhancement 77−52382
- B fibre reinforced epoxy resin, anisotropic laminate, effective modulus of elasticity 77−4802
- B fibre reinforcement of thermoplastics, creep resist. and elastic moduli 80−55458
- B fibres of various diameters, tensile strength, elasticity, elongation 78−3189
- B, liq., thermoelastic props. near melting point 80−19862
- B-B_4C materials, hot-pressed, elastic modulus and flexural strength rel. to grain size and porosity 79−79018
- B-fibre reinforced Al, elastic props., 300-4K 77−86066
- B_4C fibres, yarn prep. from C fibres, mech., chem. props., struct., book contrib. 78−48365
- BN fibres, prep., struct., thermal, mech. and elec. props., appls., book contrib. 78−48360
- BN, polycryst. cubic, props. 80−21013
- Ba, elastic properties, Debye temp., 20°C, 20 to 70 kbar, US wave velocity meas. 78−87735
- BaF_2, fluorite-struct. compound, high-temp. elasticity, US pulse meas. 77−81878
- $Ba(NO_3)_2$, press. derivatives of elastic-moduli, ultrasonic velocity meas. 78−95102
- BaO single crystal, temp. depend. of bulk modulus 78−27549
- Bi, deformation calculations, band struct. variation, electron phase transitions due to deform. *(Russian)* 80−65137
- Bi, elastic moduli, calc. from interatomic forces 79−95071
- $Bi_{12}GeO_{20}$, third-order elastic moduli determ. 80−65121
- $Bi_{1-x}Sb_x$, deformation calculations, band struct. variation, electron phase transitions due to deform. *(Russian)* 80−65137
- $Bi_{12}SiO_{20}$, third-order elastic moduli determ. 80−65121
- C adsorbent, granules and artifacts, strength, mech. characts. 78−23771
- C fibre, as-processed, diamag. studies 77−25165
- C fibre, mech. prop. determ. from C fibre reinforced plastics 77−81287
- C fibre, Ni coated, high-temp. compatibility 78−19829
- C fibre, physicomechanical props. stability, tensile strength versus fibre cross section 77−52387
- C fibre reinforced composites for spacecraft use, prep., props. and struct. 80−71625
- C fibre reinforced epoxy and C fibre, elastic moduli 77−86069
- C fibre reinforced nylon, design parameters, fibre orientation effect 80−81141
- C fibre reinforced plastic, modulii meas. *(Russian)* 80−39199
- C fibre reinforced polycarbonate, design parameters, fibre orientation effect 80−81141
- C fibre reinforced polyethylene, for medical appls., tensile and flexural props. 78−31969
- C fibres and C fibre reinforced epoxy phenol, oxidation, effect on props. 80−40574
- C, isotropic pyrolytic, for biomedical devices, mech. props. 78−65150
- C, modulus of elasticity, interrelationship with crystalline struct., heat and irradiated effects 77−21210
- C, ribbon, high modulus, strength, prep. 77−21062
- C-C composite material, syntactic-foam type properties 78−44169
- CaF_2, fluorite-struct. compound, high-temp. elasticity, US pulse meas. 77−81878
- $CaMgSi_2O_6$, diopside, elasticity, Brillouin scatt. meas. 80−6454
- CaO, elastic moduli, pressure and temp. derivs. 77−62577
- β-$CaSiO_3$ fibre, continuous unidirectional crystallisation from melt 78−95739
- CdS, elastic wave propag., in hexagonal piezoelec. crysts. *(Russian)* 77−69777
- CdS, elastic wave propag. and interaction with charge carriers, appl. of hardened elastic moduli *(Russian)* 78−35095
- p-CdSb, elastic moduli depend. on hydrostatic press. up to 17 kbar 79−37755
- CdSb, elastic moduli temp. depend. 77−51430
- CdTe, temperature variation in bulk moduli in solids 79−73237
- $CeH_{1.98}$, $CeH_{2.98}$, elastic props. at high press. 77−84825
- Co, ferromagnetic, anomalies in thermal expansion and heat capacity 79−73744
- Co, thermal expansion and bulk modulus 77−31788
- Co-Mo-Cr-Si, plasma and detonation coatings, Laves- and carbide-strengthened, comparative props. 78−15562
- Cr, electrolytic, bending modulus, −200 to 800°C *(Russian)* 77−39626
- Cr, paramagnetic, elastic moduli meas., comparison with Ti-V, V-Cr, rel. to bandstructure 80−7615
- Cs, absolute zero isotherms and polymorphic transition 79−73310
- $CsCuCl_3$, phys. props. 77−62511
- CsH_2AsO_4, elastic props., photoelasticity near ferroelectric phase transition 80−29107
- $CsPbCl_3$, $O_h{}^1$-$D^5{}_{4h}$ transition, US and thermodynamic props. 78−67826
- Cu alloys, flat spring, mechanical props. in bending, stress relax. test, 23 to 232°C 78−72806
- Cu, amplitude depend. modulus effect 78−64573
- Cu, elastic moduli rel. to Gruneisen elastic parameters 79−95070
- Cu, elastic moduli second press. derivatives 79−96058
- Cu, elastic modulus and internal friction during plastic deform., dislocation props. determ. 80−35244
- Cu, electron irradiated, dislocation defect dragging, 4.2 to 350K 78−43027
- Cu, electron irradiation damage, dislocation pinning investig. of crowdion model 77−69000
- Cu, fatigued, structural changes, damping and modulus 77−28906
- Cu, modulus meas. during high frequency fatigue *(German)* 77−59938
- Cu, pair potentials, elastic props. calc. 80−49176
- Cu, US attenuation, nonlinearity parameter temp. depend. 79−42152
- Cu-Ag (0.1 wt.%), cold-worked, internal friction peaks in kHz range 80−89276
- Cu-Au, elastic modulus and internal friction during plastic deform., dislocation props. determ. 80−35244
- Cu-BeCo (1.85, 0.29 wt.%), type CA172 (TH04), strengthened by spinodal decomp., stress relax. in bending 80−7616

elastic moduli continued
Cu-Ni, foils, supermodulus effect, one-dimens. modulated structs. 79—95068
Cu-Ni-Sn (4-15, 4-8 wt.%), strip strengthened by spinodal decomp., stress relax. in bending 80—7616
Cu-Ni(Pd), composition modulated foils, layer struct. and mech. props. 79—95300
Cu-Ni(Zn), elastic modulus and internal friction during plastic deform., dislocation props. determ. 80—35244
Cu-Pd foil, composition-modulated, elastic modulus enhancement 77—52382
β-Cu-Zn-Al pseudoelasticity 79—29126
$CuCl_2.2H_2O$, magnetoelastic props. under press., antiferromagnetic resonance, lattice parameters 80—29598
D_2, solid, equation of state, at high pressure 79—46781
$DyFe_{1-x}Co_xO_3$, magnetostriction, thermal expansion and elastic moduli near Morin point 77—8383
$DyVO_4$, electric field influence on elastic props., electron state initial splitting 80—34123
$DyVO_4$ Jahn-Teller crystal, deform. induced transitions, elastic and dielectric characts. *(Russian)* 80—80726
Er, lattice dynamics, thermal expansion, bulk modulus calcs. 77—20022
Eu_2O_3-Ta_2O_5, microcracking, elastic props., internal friction 78—92326
Fe and related compounds, bulk moduli from hydrostatic compression 78—83862
Fe, cast, ferritic grey, exam. of ordering kinetics by elastic modulus meas. 79—100136
Fe, cast, grey, electric arc sprayed coating on wire, elastic and elastic-plastic props. *(German)* 79—34089
Fe, cast grey, effect of quenching conditions, on elastic modulus 78—56675
Fe, glassy, heat of crystn., and bulk modulus, calc. using struct. model 78—51428
α-Fe, lattice wave dispersion, lattice consts., elastic consts. 80—24545
Fe single crystals (111), elasticity modulus variation, depend. on external mag. field *(Russian)* 79—82849
Fe-Al (12 wt.%) alloy 23 kHz US transducer piezomagnetic props. 78—59240
Fe-B alloy reinforced polysulphone exam. of tensile and flexure props. 78—72823
Fe-B metallic glass, hardness, elastic moduli, density, cryst. temp., mech. props., for flywheel appl. *(Dutch)* 78—52878
Fe-Co-Cr-W-Ni-C, alloy KKhVN, transforms. during annealing and nature of hardening *(Russian)* 78—56653
Fe-Mn alloys, elasticity modulus anomaly and magnetoelastic effect *(Russian)* 79—28578
Fe-Mn-Cr(Ni), mag. and crystallographic transformation depend. on Cr-Ni addition *(Russian)* 79—83334
Fe-Ni, thermodynamic props., anomalous 80—39313
Fe-Ni alloys props. of materials used in electromechanical filter resonators *(Czech)* 80—76318
Fe-Ni Invar alloy, bulk modulus anomaly, mag. effect 79—91728
Fe-Ni system, constant modulus alloys for mech. oscillators 79—61641
Fe-Pt Invar alloy, bulk modulus anomaly, mag. effect 79—91728
$Fe_{0.7}Ni_{0.3}$, Invar alloy, bulk moduli, pressure effect on lattice spacing 79—55805
α-Fe_2O_3 (haematite), X-ray diffr. compression studies under hydrostatic isothermal conditions 78—85539
Fe_3Si, single cryst. elastic consts., polycryst. elastic moduli 77—39815
Fe_2SiO_4, spinel, isothermal compression up to 75 kbar hydrostatic press. 77—43280
Fe_2TiO_5, grain size pseudobrookite oxide, microcracking relations 79—29194
Ga, elastic moduli, temp. depend., anharmonic effects *(Russian)* 77—31708
GaP, elastic moduli, 80-700K, and elastic consts. 79—73245
GaP, elastic moduli and attenuation of elastic waves 77—51429
n-GaP:S, elastic moduli and mode gammas 79—73242
GaSe, isolated layer model, lattice dynamics and elastic props. 80—24547
$Gd_2(MoO_4)_3$, crysts., elastic props. during domain switching under mech. loading 79—55809
Ge, amorphous, elastic moduli, random network model, calc. 78—6119
Ge, elastic moduli, drag coeffs. and Keating's parameters 79—73238
Ge, pure and n-type, US velocity and attenuation, second and third order elastic moduli 80—70325
Ge-Se glass, elastic props. under press., US interferometry 78—79658
GeS_2 glass, temp. and press. depend. of elastic props. 77—15476
H_2, solid, equation of state, at high pressure 79—46781
HfO_2, monoclinic, microcracking, elasticity, internal friction, thermal expansion meas. 79—29195
HfO_2, stabilised comps., elastic props. rel. to porosity and temp. 80—81096
HfO_2:$Er_2O_3(Y_2O_3)(Eu_2O_3)$, elastic props., sonic reson. meas. 80—7612
Hg_2X_2, X=Cl, Br, I, acoustic props., cryst. lattice bonds 78—30700
$Ho_xTb_{1-x}Co_2$ lave phase compounds, elastic props., temp. and magnetic field dependence 80—60393
InSb, US attenuation and Akhieser loss, temp. depend. 79—86842
InSe, elastic props. temp. depend. 78—10119
K, absolute zero isotherms and polymorphic transition 79—73310
K, electrical and thermal resistivity determ. from first principles 79—69493
K pair potentials, elastic props. calc. 80—49176
K, self-diffusion, high temp. bulk modulus determ. 80—79976
K, thermodynamic props. at high press. *(Russian)* 78—47536
$KBrO_3$, trigonal, elastic, thermoelastic and dynamic piezoelec. props., US vel. meas. 77—32328
KCN, elastic functions meas. by US pulse-echo method and Brillouin scatt. 77—84829
$K(CN)_{1-x}Cl_x$, elastic functions meas. by US pulse-echo method and Brillouin scatt. 77—84829
KCl, meas., appl. of piezoelec. method, for small sandwich specimen 77—54939
KCl(Br), elastic moduli, quadratic fit against temp. 78—14397
$KCl_{1-x}Br_x$, bulk modulus, room temp. to 400°C 80—92588
K_2CuF_4, Brillouin scatt. and US meas. of phonons, elastic moduli and Debye temp. calc. 79—87454
KDP crystal, third-order moduli of elasticity 79—46737
$KMgF_3$, elastic moduli, press. and temp. depend., US technique 80—6453
$K_2Pt(CN)_4Br_{0.3}.3H_2O$, spin-lattice model for elastic anomalies 80—15179

elastic moduli continued
$LaH_{2.96}$, elastic props. at high press. 77—84825
Li, phonon limited resistivity struct. depend., Umklapp scatt., elastic consts. 80—88532
Li, thermodynamic props. at high press. *(Russian)* 78—47536
LiAl(In)(Zn), elastic moduli and Debye temp., US meas. 79—91724
LiF, high-temp. behaviour of elastic moduli, comparison with MgO and CaO 77—11621
LiF, inverse moduli, up to temp. of 650°C 78—14397
Li_2GeO_3, pure, and Si- and Mg-doped, impurity effects on elastic and piezoelec. props. 79—47388
$LiNbO_3$, γ-irradiated and annealed, elastic and piezoelectric props. 78—2807
$LiNbO_3$, LF sound attenuation, internal friction 78—63804
$LiNbO_3$, polydomain, nonstoichiometric crysts., elastic, piezoelec., dielec. constants. 77—8513
$LiNbO_3$, shock-wave compression, 2.4-44 GPa 80—34139
Li_2O-Al_2O_3-SiO_2, glass ceramic, elastic props. at high press., US meas. 78—83863
Li_2O-Al_2O_3-SiO_2, glass, study of elastic props. 80—104205
Mg-Zn metallic glass, hardness, elastic moduli, density, cryst. temp., mech. props., for flywheel appl. *(Dutch)* 78—52878
$Mg(Al,Cr,Fe)_2O_4$, spinel, elastic moduli calc. 78—6960
$MgAl_2O_4$ spinel, single cryst., fracture behaviour, temp. depend. 80—40503
MgF_2, polycrystalline, elastic moduli, press. and temp. depend. US meas. 77—21202
MgO, compression to 8 GPa, bulk moduli and press. derivatives 77—89496
MgO, hot-pressed, elasticity props. of polycrystals and single crystals 80—54301
MgO polycrystals, hot-pressed, changes in elastic moduli on annealing 79—34073
$MgTi_2O_5$, grain size pseudobrookite oxide, microcracking relations 79—29194
γ-Mn-Ni-C, elastic anomalies, martensitic transformation in Mn rich alloys 78—84807
MnAs, second-order phase transition, elastic anomalies 79—10908
MnO, elastic props. singularities near phase transition 77—16093
Mn_5Si_3, elastic moduli, phase transitions, ultrasonic velocity 80—92589
Mo and Mo superalloys high temperature properties 78—44173
Mo, binding energy, lattice parameters bulk modulus, self-consistent pseudopot. calc. 79—60748
Mo, elastic moduli meas. *(Russian)* 78—75704
Mo, electric arc sprayed coating on wire, elastic and elastic-plastic props. *(German)* 79—34089
Mo, pair potentials, elastic props. calc. 80—49176
$(NH_4)_2BeF_4$, Mandelstam-Brillouin and US exam. of phase transitions 77—12347
$(NH_4)_2SO_4$, pure and Rb doped, ferroelec. transition, light scatt. meas., dielec. and elastic props. 78—43822
Na, electrical and thermal resistivity determ. from first principles 79—69493
Na, phonon limited resistivity struct. depend., Umklapp scatt., elastic consts. 80—88532
Na, thermodynamic props. at high press. *(Russian)* 78—47536
NaCl, elastic props. at press. up to 9 GPa, ultrasonic wave velocities 79—95073
NaCl, Gruneisen γ and other thermodynamic props., vol. depend. 77—76577
NaCl, US vel., Poisson's ratio and shear modulus meas., 9 GPa 77—4140
$NaClO_3$ temperature variation in bulk moduli in solids 79—73237
NaF, high-temp. behaviour of elastic moduli, comparison with MgO and CaO 77—11621
NaF, US vel., Poisson's ratio and shear modulus meas., 9 GPa 77—4140
NaF(Cl), elastic moduli, quadratic fit against temp. 78—14397
NaIn(Tl), elastic moduli and Debye temp., US meas. 79—91724
$NaND_4SeO_4.2D_2O$, nonlinear electromechanical props. above Curie temp. 79—33610
Na_2O_3-B_2O_3-SiO_2, glass, effect of composition on mech. props. 78—48435
$Na_2O_3(CaO)$-Al_2O_3-SiO_2, effect of composition on mechanical props. 78—48435
Nb, density, rel. to elastic const. calc. from US meas. 77—86079
Nb, elastic constants, 0K to melting point 79—38882
Nb, polycrys., high temp. elastic props. 80—30007
Nb-Mo, elastic moduli of single crystals 77—31712
Nb-Mo BCC, press. derivatives, Fermi surface topological changes, band struct. 79—61639
Nb-Mo monocrystal, elastic moduli, 4.2 to 300K *(Russian)* 77—52381
Nb-Ni metallic glass, hardness, elastic moduli, density, cryst. temp., mech. props., for flywheel appl. *(Dutch)* 78—52878
Nb-Ti-Al alloy, effect of heat treatment on strength and elastic props. 77—55976
Nb-Zr, elastic constants, 0K to melting point 79—38882
Nb-Zr alloys, BCC phase, 4.2-300K 77—81285
Nb_3Ge A15 cpd., bulk modulus 80—7611
NbSn multifilamentary superconducting composites, micromechanics 79—38878
Nb_3Sn, elastic instability in cubic to tetragonal phase transitions 78—39767
Nb_3Sn, electronic props. calc. 79—7780
Nb_3Sn, softening of surface phonons in (100) plane 80—107627
Nd, higher order elastic consts. of double HCP cryst., calc. 79—51189
Ni ferrites, internal friction and modulus defect at US freqs. 79—19762
Ni, ferromagnetic, anomalies in thermal expansion and heat capacity 79—73744
Ni, porous, internal friction and effective elasticity modulus, temp. depend. *(Russian)* 79—29118
Ni-Al, electronic, mag., and cohesive props. 80—44491
Ni-based TaC eutectic, directionally solidified, elastic moduli 80—84984
Ni-Cr-Mo-Mn alloy 02KhN40MB, corrosion-resist, heat-resist., phys. and mech. props. 80—35411
Ni-Cu-Al(Si), spinodal decomposition, morphology of microstructure, elastic strain energy anisotropy effect 78—15354
Ni-Mo-Cr-Si, plasma and detonation coatings, Laves- and carbide-strengthened, comparative props. 78—15562
Ni-Zn ferrite, elastic moduli temp. and composition depend. 78—26617
NiF_2, press. depend. of elastic moduli to 10 kbar 77—35619

elastic moduli continued
- NiTi, thermoelastic martensites, cyclic stress-strain curves obtain in tension compression 79−29166
- α-Np, bulk and shear moduli, 77 to 373K 77−20009
- PVC-Cu, particulate composite, mech. props. effect of particle size 78−95799
- Pb, elastic properties *(Russian)* 78−56678
- Pb impregnated porous Ni, porous, internal friction and effective elasticity modulus, temp. depend. *(Russian)* 79−29118
- $Pb_5Ge_3O_{11}$ acoustic relaxation near ferroelectric transition 78−2814
- $Pb_5(GeO_4)(VO_4)_2$, elastic and dielectric props. 77−7782
- $Pb_{1-x}Ge_xTe$, TO phonon interaction with acoustic phonons near phase transition temp. 79−90776
- $Pb(NO_3)_2$, press. derivatives of elastic-moduli, ultrasonic velocity meas. 78−95102
- PbS, first-principles calc. of eqn. of states 80−49649
- PbS, thermomech. props., SCF Xα scatt. wave theory 78−71704
- $Pb(Zr,Ri)O_3$:Ni-silicon rubber flexible composite pyroelectric, dielectric props. 80−80704
- $Pb(Zr,Ti)O_3$ ceramics with ladder type struct., prep. and props. 80−75945
- Pd alloys, effect of alloying on activation energy of H_2 diffusion 80−107571
- Pr, higher order elastic consts. of double HCP cryst., calc. 79−51189
- ε-Pu, BCC phase in equil. with liq. phase, calc. vs. meas. value 77−19866
- α-Pu, sound vel. meas., press. to 50 kbar 77−20015
- Pu-Ga (1 wt.%) alloy, polycryst. consts. calc. from single cryst. data 77−20005
- Rb, absolute zero isotherms and polymorphic transition 79−73310
- $RbHSO_4$, acoustic and dielectric props. near phase transition 80−55053
- $RbMnCl_3$ crystal, structural phase transition, birefringence, elastic moduli and Raman spectra 80−15243
- S-based composite, engineering props. 77−86093
- Sb, elastic moduli, calc. from interatomic forces 79−95071
- ScM, (M=Ru,Rh,Pd,Ag,Mo), self-consistent local density functional calcs., LMTO method 79−11059
- Se, amorphous, elastic props. at high press. 79−37753
- Se, trigonal, normal mode calcs. 80−84259
- Se, trigonal or amorphous, thermal expansion and Gruneisen coeffs., 10-300K 78−22870
- Si, amorphous, elastic moduli, random network model, calc. 78−6119
- Si, compression to 8 GPa, bulk moduli and press. derivatives 77−89496
- Si, effective supersystem cryst. simulation method, geometrical parameters, bulk moduli, impurity levels calcs. *(French)* 80−15430
- Si, ground state props. in density-functional pseudopot. approach 80−92803
- p-Si, photosensitivity of elastic moduli and surface tension 78−83864
- Si, pure and n-type, US vel. and attenuation, evaluation using elastic moduli 80−70325
- Si, stretched, lattice vibr. anharmonicity, influence of stress on elastic moduli, Raman spectra 80−80791
- Si, structural props., self-consistent calc. 80−28947
- Si, temperature variation in bulk moduli in solids 79−73237
- Si, total energy calcs. by r-space method, Wannier functions 80−88503
- Si/SiC ceramic composite, elastic moduli and bend strength meas., anisotropy 77−59838
- Si/SiC ceramic composite, room temp. props., effect of SiC content and orientation 78−27599
- Si-Ge, solid soln., vol. effect on bulk modulus 80−24526
- SiC, mechanical props. charact. by dynamic elastic modulus meas. up to 1400°C *(German)* 79−70101
- SiC polytypes, effect of degree of hexagonality 77−59845
- SiC-coated C fibre, compatibility with Al *(Japanese)* 80−71700
- Si_3N_4, bending strength, deformability, elastic moduli and brittleness 80−81191
- Si_3N_4, mechanical props. charact. by dynamic elastic modulus meas. up to 1400°C *(German)* 79−70101
- Si_3N_4, reaction bonded, fracture mech. pararucters, microstmet. amd temp. effect 79−24598
- Si_3N_4, reaction-sintered, elastic moduli, fracture mechanics parameters, and strength 77−28889
- Si_3N_4-MgO (2-5 wt.%) hot pressed, tensile creep testing 80−40423
- SiO_2 concrete, elastic moduli meas. during heating and cooling 80−55451
- SiO_2-Al_2O_3-Cu_2O glass alkaline durability, corrosion rate, heat capacity and elastic moduli 80−93673
- SiO_2-Al_2O_3-Y_2O_3-La_2O_3-TiO_2 glasses with high elastic moduli, alkaline durability 80−85071
- SiO_2-M_2O (M=Na,K) glasses, temp. depend. of elastic modulus 80−40410
- SmS, f-d hybridisation, valence fluctuation and phonon spectrum, Raman scatt. expts. 78−60464
- Sn, Fermi surface, dilational strain depend., elastic moduli and torque obs. 80−70586
- SrF_2, fluorite-struct. compound, high-temp. elasticity, US pulse meas. 77−81878
- $Sr(NO_3)_2$, press. derivatives of elastic-moduli, ultrasonic velocity meas. 78−95102
- $SrTiO_3$, crit. behaviour under stress 77−31745
- Ta, acoustic emission induced by hydride formation 80−76257
- Ta, density, rel. to elastic const. calc. from US meas. 77−86079
- Ta, elastic moduli, effect of H and UHV annealing 77−90389
- Ta, lattice parameter, X-ray meas., rel. to density and elastic moduli 77−89406
- Ta, polycrys., high temp. elastic props. 80−30007
- Ta-W, BCC, press. derivatives, Fermi surface topological surface, band struct. 79−61639
- $TaSe_2$ (2H), thermal and elastic props., X-ray diffr. exam. 79−37754
- Tb, US meas. using CdS transducer, mag. field effect 77−11151
- $Tb_{0.27}Dy_{0.73}Fe_2$, perpendicular suscept., magnetomechanical coupling and shear modulus 78−91918
- $Tb_{0.3}Dy_{0.7}Fe_2$, magnetoelastic coupling meas. by US method 77−69652
- $TbFe_2$, magnetic field dependence, acoustic transducer appln. 80−87698
- $Tb_2(MoO_4)_3$, crysts., elastic props. during domain switching under mech. loading 79−55809
- $Tb_2(MoO_4)_3$, nonlinear elastic props. near phase transition 79−73244
- (Ti,V)C carbides, prep. and mech. props. 78−64518
- α-Ti alloy, VT1-1, cold rolled, recrystn. texture and prop. anisotropy 78−52846

elastic moduli continued
- Ti alloy β III, precipitation of α and ω phase, evolution of mech. props. *(French)* 77−16591
- α and $\alpha+\beta$Ti alloy of different stability, exponential law use for anal. of strain hardening process 79−15697
- Ti alloys, data handbook of low temp. mech. and phys. props. 80−22153
- Ti and Ti alloys, mechanical, thermal and elec. props., data sheet 79−43317
- Ti, high purity, data handbook of low temp. mech. and phys. props. 80−22153
- Ti, mechanical deformation with superimposed insonation, volume effects 78−60723
- Ti-Al-Mo-Zr alloy, VT9, decomp. kinetics of metastable β-phase, X-ray and mech. props. obs. *(Russian)* 78−48368
- Ti-V, elastic moduli, comparison with paramag. Cr, V-Cr, rel. to band-structure 80−7615
- Ti-V (40 wt.%), effects of H on anisotropic elastic props. 79−74192
- Ti-V-Cr, BCC, press. derivatives, Fermi surface topological changes, band struct. 79−61639
- TiAl, Ti_3Al-(Nb) dynamic elastic moduli 77−86070
- Ti_3Al, phase transitions and physical props. 77−25068
- TiC coating on C fibre, by CVD TiC coated C fibre compatibility with Al *(Japanese)* 79−78898
- TiC, polycrystalline, elastic props. 78−27547
- TiC_xNy, elastic props., 290K 77−52379
- TiC_xO_y, elastic characts. 77−80568
- TiN_zO_y, cubic, thermal expansion coeffs., Ti-Ti bond screening 79−10970
- Tl halides, strain derivatives of elastic and dielectric consts. 79−60421
- TlBr-TlI(Cl) crystals, photoelastic moduli 80−97230
- UC-NbC, UC-ZrC and UC-ZrC-NbC, solid soln. strengthening rules, physicomech. prop. changes 77−28826
- UO_2, in-reactor meas. of modulus of elasticity, US spectroscopic method 77−23210
- V, density, rel. to elastic const. calc. from US meas. 77−86079
- V, determination of effect of H based on US vel. meas. 80−75288
- V, polycrys., high temp. elastic props. 80−30007
- V-Cr, elastic moduli, comparison with paramag. Cr, Ti-V, rel. to band-structure 80−7615
- V-Cr, elastic moduli, US pulse echo meas. 78−84881
- V-H single crysts., elastic consts., temp. depend., H effects 80−66563
- $(V_{1-x}Cr_x)_3Si$, elastic moduli, 4.2 to 290K, softening near supercond. transition *(Russian)* 80−92582
- V_3Si, exam. of superconductivity and props. 79−1649
- V_3Si, magnetic susceptibility, density of states model for lattice transformation in A-15 compounds 80−65219
- V_3Si, mixed state, hysteresis in elastic characteristics *(Russian)* 80−103799
- V_3Si, neutron irrad., sound velocity, magnetic susceptibility and upper critical field 78−88074
- W, lattice wave dispersion, lattice consts., elastic consts. 80−24545
- W, self-diffusion, high temp. bulk modulus determ. 80−79976
- WC-Co, elastic moduli and their press. derivatives 79−83248
- Y_2O_3 ceramics, strength under mech. and thermal actions 80−97554
- ZnF_2, elastic props., 4.2-300K, incipient ferroelec. transition 78−30691
- ZnF_2, press. depend., 0-10 kbar 78−10117
- ZnP_2, Brillouin scattering and optical props. meas. 80−76041
- ZnS, elastic moduli of polytypic modifications 79−51187
- ZnSe, elastic moduli, temp. depend., 293-973K, electrostatic reson. determ. 78−59850
- ZrC-NbC-MoC_{1-x} alloys, physicomech. props., comp. depend. 79−66097
- $ZrC_{0.97}$-$NbN_{0.93}$, $Zr_{0.5}Nb_{0.8}C_xN_{0.98-x}$, solid solns., elastic props. expansion and hardness 77−52380
- ZrO_2, porous, sintered stabilised microspheres, strength and fracture studies 80−85019
- $ZrSiO_4$, compression to 8 GPa, bulk moduli and press. derivatives 77−89496
- $ZrSiO_4$, natural zircon, nucl. radiation effect on elastic moduli 77−11616

elastic moduli measurement
- acoustic insulating material complex elastic modulus meas. and transfer function theory *(Hungarian)* 80−106765
- acoustic resonance method, temp. depend. 78−18264
- alloys, elastic const. meas. technique, for X-ray diffr. stress meas. calibration 78−7164
- anelastic relaxations and magnetic aftereffects in solids, conf., Katowice, Poland (Jan. 1978) *(Polish)* 79−96072
- aortic compliance meas. from transthoracic admittance plethysmogram, dog expt. 78−31925
- apparatus, for elevated temps. *(Polish)* 79−96279
- arterial elasticity, transcutaneous assessment by US Doppler flowmeter 77−77948
- arterial elasticity determ. and transcutaneous continuous pressure monitoring analysis 79−53179
- arterial elasticity measurement in vivo using transit-time US micrometer 77−40719
- bending, three point, large deflections as elastic moduli meas. method 78−27699
- bone, elastic props. of cortical bone of female human femurs, noninvasive meas. 77−21552
- bone, US longitudinal and shear wave velocity meas. 77−25623
- brittle materials, normal elasticity modulus, strain gauge meas. 80−55601
- bulk material rigidity determ. using capacitive transducer 78−19977
- canine aorta Young's modulus, 10 MHz US meas. 79−57836
- ceramic layers on metallic substrates, mech. props. meas. *(French)* 80−104375
- circular plate, elastic moduli meas., appl. of contactless vibr. excitation and detection method *(Polish)* 79−94571
- coatings, machine attachment for eliminating error in load-meas. device 77−25218
- compensation for temp. effects, cable capacitance and hysteresis in strain gauge meas. *(German)* 80−31734
- complex elastic modulus, temp. freq. var. for soft elastic materials *(German)* 80−106764
- complex shear modulus, meas. by fully automated torsional pendulum, in range −180 to 250°C *(German)* 80−17935
- composite, meas. reliability establ. 77−52574
- composite bar technique for Young's modulus and internal friction meas., multiple reson. 78−35612

elastic moduli measurement continued
composite of uniform thickness, analysis of determ. methods of shear moduli 77−63873
concrete, elastic modulus variations, gauge meas. by embeddable-strain-units 78−84878
constructional materials, pulsed method of determ. 80−8955
coral skeleton US velocity and Young's modulus anisotropy obs. 79−57837
cylindrical specimens, measurement of dynamic shear modulus using closed-loop vibration system with PLL 79−61827
damping capacities, cantilever beam tests *(Japanese)* 79−91869
device, use at 4.2 to 1000K 78−23898
dielectrics, elec. and mech. props. at increased temps., meas. equipment 77−71342
dynamic, use of capacitance sensor for monitoring resonance vibr. amplitude 77−23923
education, coefficient of restitution of bouncing ball expt. 78−86074
elastometer probe system for localised in vivo compliance meas. 78−31960
fatigue crack closure determ. using elec. pot. method, cf compliance method 78−5701
fibre reinforced composite, fatigue damage, early detection by NDT 77−28951
fibres, automatic laboratory display unit 79−55349
Fourier transform method for elastic consts. and internal friction meas. in small specimens 79−14357
fused quartz, determ. of acoustic and acousto-optical parameters using acoustic interferometry 79−41532
glass fibre reinforced plastics, effect of deform. rate *(German)* 78−64796
high-temperature US apparatus for elasticity characts. and thermal cond. meas. of materials 78−5705
inhomogeneous material structural characts., automatic NDT system 78−48586
insulating thin films, Young's modulus measurement by micromechanics 80−33548
isotropic materials, rod shaped, elastic moduli and Poisson ratio determ. method 80−55606
isotropic materials, third-order elastic moduli meas. using Rayleigh waves *(Russian)* 80−50786
isotropic materials, Young's modulus determ., kinematic excitation of resonance oscillations 80−25958
isotropic solid, viscoelastic characterisation using harmonic dispersion of longit. reson. 79−10538
laser energy deposition method 79−20309
laser-target technique, for glass, over wide temp. range 77−27497
linear isotropic viscoelastic material, exptl. determ. of relaxation modulus 79−61810
liquid, complex apparatus for viscous and elastic prop. meas. at high press. 78−9734
liquids, complex shear modulus meas. by Ni-tube resonator in kHz range 80−17936
material elastic anisotropy, analysis, by acoustic ellipsometry 79−47864
metallic glasses, small samples, Young's modulus meas. by impulse induced resonance technique 80−40411
metals, thermal props. at high temps. meas., acoustic method 79−14222
Michelson interferometer, Poisson ratio compliances meas. 77−12663
multiphase material, X-ray determ. of elastic moduli *(German)* 79−91876
muscle, skeletal, deriving viscoelastic modulus from transient pulse propag. 78−77077
optical technique, Poisson ratio and extensional modulus meas. 77−12662
orthorhombic crystals, elastic consts. determ. from free vibr. of rectangular parallelepiped cryst. 77−84849
piezoelectric method, for small sandwich specimen, 30-200 kHz 77−54939
piezoelectric transducer automatic setup, for continuous meas. of internal friction and elastic moduli of solids 80−108652
plasma coatings, elastic properties, acoustic meas. *(Russian)* 80−97519
Poisson's ratio determ. by Moire method 78−51137
Poisson ratio, optical method of exptl. determ. 79−43523
polymer, oriented, dynamic shear modulus determ. by acoustic method 78−23911
polymer, precision meas. using reson. method *(German)* 78−76823
polymer complex dynamic Young's modulus measurement equipment 78−1615
polymer soft lossy, viscoelastic props. determ. from torsional vibr. of laminated bar 77−62218
polymers, dynamic shear modulus 78−60916
polymers, elastic and creep moduli meas. by contact methods 80−11852
polymers, testing using Rayleigh surface waves 79−70249
poroelastic material dynamic characterisation, complex, modulus meas. 80−14640
refractories, test unit for up to 1500°C 79−57167
refractories, US method for up to 2000K *(French)* 80−104373
refractory, resonant frequency meas. apparatus, elastic props. investigations 77−19576
refractory ceramic, deform. test apparatus and method *(Russian)* 78−35613
resonance method for determ. within 80-300K temp. range, for metals, and semiconds. 78−46918
rheological spectrophasemeter, for polymer systems meas. 80−33547
rocks elastic properties determination, modified borehole jack method 78−81448
rubber, vulcanised, device for dynamic modulus of elasticity determ. *(Polish)* 77−28963
shear modulus, low frequency, meas. during tesile creep *(French)* 78−23913
shear modulus under press., torsional vibr. excitation by induced eddy current method 77−31709
sinew dynamic elasticity modulus meas. apparatus *(German)* 79−2167
soft viscoelastic material, complex modulus of elasticity determ. 77−62221
steel, elastic consts., meas. app. 77−33739
steel, low C, Young's modulus, apparatus for elevated temp. meas. *(Polish)* 79−96279
steel, wire, dynamic moduli of elasticity meas. by travelling normal wave method 78−53110
4-sulphone diglycidyl ether, on Al alloy D16T alloy base, dynamic shear modulus determ., −80 to −180°C 78−60916

elastic moduli measurement continued
technique, and appl. to PVC, 10-90 kHz 77−86235
thremosetting resin quality control by dynamic mechanical analysis 79−74319
torsional oscillation test instrument with process computer control *(German)* 77−21344
transducer, viscoelastic, in-situ, Duomorph, appl. to polymeric materials 79−30463
transparent materials, low-modulus, mech. props. determ. method 78−5704
travelling normal wave method for thin wire 78−53110
vibrational-frequency meas. errors 77−74391
viscoelastic properties dynamic evaluation for use in cardiac prosthetics 78−40405
waveguide slow torsional wave sensors 79−46748
X-ray anal., conf., Denver, USA (Aug. 1976) 77−70382
X-ray diffr. residual strain meas., elastic const. meas., material errors 78−5714
Young's modlus, meas. apparatus for brittle materials 77−27499
Young's modulus, measurement using automated Marx's composite oscillator method 80−37151
Young's modulus meas. using audio generator amplifier and speaker 80−62427
Young's modulus measurement, laboratory instrument design and construction 77−82350
Young's modulus of thin plate, measurement by composite vibrator method *(Japanese)* 78−11463
Al-Si alloy, rod, tensile loaded, internal friction and Young's modulus measuring equipment, inelastic phenomena exam. *(Hungarian)* 79−52546
Al_2Cu crystal, Young's modulus, Poisson ratio, elastic consts. determ. by extensometry and US meas., anisotropy discussion *(French)* 79−50683
Al_2O_3, US method for up to 2000K *(French)* 80−104373
Au, rod, tensile loaded, internal friction and Young's modulus measuring equipment, inelastic phenomena exam. *(Hungarian)* 79−52546
Cu, rod, tensile loaded, internal friction and Young's modulus measuring equipment, inelastic phenomena exam. *(Hungarian)* 79−52546
Cu, thin conductor, dynamic moduli of elasticity meas. by travelling normal wave method 78−53110
β-Cu-Zn-Al, US elastic const. meas. near martensitic transform. temp. 78−39827
$Fe_{0.49}Ni_{0.415}Mo_{0.095}$, Vibralloy, high-temp. vibrating reed meas. 79−55811
Tb, US meas. using CdS transducer 77−11151

elastic scattering of atoms and molecules
adiabatic approximation, energy-modified 79−59523
angular correlations, summary of review papers 80−63757
angular distribution, in complex angular momentum theories, calc. method 79−76483
asymmetric scattering, spin-1 particle by non-central field 78−55214
atom+atom, small angle differential cross section, semiclassical description 80−28086
atom+atom collisions, fine-struct. transition cross sections, eigenphase formulation 78−25651
atom+atom scattering 79−86029
atom+diatom, body-fixed formulation for close-coupling calc. 78−78768
atom+diatom, collinear, quasiclassical collision dynamics, direct histogram method 78−42151
atom+diatom, degeneracy averaged scatt. cross-section calcs. 79−89735
atom+diatom, scatt., l_z-conserving sudden approx. calcs. 78−66628
atom+diatom, scatt., opacity functions, J_z-conserving approx. calcs. 77−6878
atom+diatom, stochastic one-dimens. model 78−42159
atom+diatom, T-matrix element approx., j_z-CCS calcs. 77−19003
atom+diatom scattering, field theoretic calcs. 77−50484
atom+diatom scattering eqns., generalised phase shift, semiclassical series soln. 80−43142
atom+harmonic oscillator, radial Schrodinger eqn., propag. method, appl. to close coupled eqns. 80−42096
atom+ion, rainbows, interference, and diffr. effects *(Dutch)* 79−50110
atom+rigid rotor, differential scatt. cross-section, quantum mech. inversion, IOS approx. calcs. 79−89736
atomic, fine struct. transitions, collision cross section calc. 78−25652
atomic, molecular and solid-state theory, conf., Flagler Beach, Florida, USA (Mar. 1978) 79−31356
atomic and molecular collisions, book 80−27058
atomic and molecular collisions in intense light beams, quantum aspects *(Russian)* 79−6903
atomic dipole moments induced by collisions, multipole expansion procedure 79−64069
atomic metastability exchange collisions, Pauli principle effects 80−99536
atomic physics, conf., Riga, USSR (Aug. 1978) 80−22141
atomic resonance interaction, photon echo meas. 79−27061
atomic spin exchange collisions, Pauli principle effects 80−99535
atomic systems, scattering amplitude, Glauber approx. 79−59531
atoms, charged and neutral, direct scatt. theory 80−23483
benzene+bromomethane, microwave line width and quadrupole moments, perturbation theory 80−69190
benzene+OCS, microwave line width and quadrupole moments, perturbation theory 80−69190
binary collisions, time correlation functions, influence of bounded trajectories 80−43143
body-fixed theory, two-system collision, arbitrary ang. momenta 78−25642
born-Huang expansions in the generator coordinate method of molecular dynamics 79−31646
charged particle potential scattering in laser field, eikonal theory 79−81249
charged particle scattering, Schwinger variational principle 79−45780
chemically reactive system, elastic scatt., parametrised S-matrix models 79−79225
classical differential scatt. cross section, asymptotic expression 77−68090
classical many-body collision model incorporating Heisenberg and Pauli principles 80−63511
collision effects on nonreson. interactions, nonlinear spectrosc. obs. 80−23496
collision induced transition probabilities and line width parameter of rot. transition 79−22776

elastic scattering of atoms and molecules continued
complex molecular systems, collision phenomena by stochastic model, observables distribs. and information entropy 78-25640
complex potential from elastic differential cross sections 77-23534
complex scaling transformations in stationary and scattering problems 79-18124
conducting spheres, polarisability spatial extension in two body collision induced light scattering 79-98174
diabatic and adiabatic representations 79-45795
diatom, phase shift difference, trigonometric pots. in radial Schrodinger eqn. 79-22787
diatomic mol. scatt., Tietz phase shift differences, semi-empirical relations, Varshni and Hulbert-Hirschfelder pots. 80-9673
diatomic one-electron mols., wavefunction calc., collision matrix elements, computer program 78-50457
differential cross section deconvolution by iterative van Cittert process 78-17746
differential cross-sections, factorisation, sudden approx. calcs. 80-18902
differential cross-sections, from classical trajectory studies, Legendre polynomial series 78-17738
dipole-dipole elastic scatt., second-order perturbation theory 78-5317
distorted-wave amplitudes, sensitivity of cross-section and ang. correl. to scatt. parameters 80-5596
electronic and at. collisions, conf., Kyoto, Japan (Aug.-Sept. 1979) 80-57011
electronic and at. collisions, conference, Kyoto, Japan (Aug.-Sept. 1979) 80-62394
energy moments of final state distrib., direct moment method 78-33562
ethylene dimer, exchange forces, Hellmann-Feynman theorem calc. 77-54589
exchange forces, Hellmann-Feynman theorem calc. 77-54589
excited atom exchange interaction with molecules, calc. using electron scattering data 77-58125
exponential model, two-state, comment on Stueckelberg phase calcs. 79-3514
Faddeev equations, off-shell matrix elements evaluation 77-67336
field theoretical method for mol. scatt., distorted wave formalism 79-3513
fluids, atomic and molecular, collision induced light scatt. *(German)* 79-27057
gas kinetic theory, elastic cross-section analytical approximation *(Russian)* 78-75248
gasdynamic equations, multiatomic gases with different elastic and inelastic rates 79-81993
Glauber approx. for particle-atom collisions 77-10716
graphite, diffraction of He atoms by (0001) basal face, bound state resonances 79-47575
heavy particle scatt., independent electron approx., semiclassical derivation 77-83673
hexafluorobenzene+bisdiphenylenephenylallyl radical, solvent effects on collisions, dynamic nucl. polaris., spin-lattice relax. 77-63303
high energy higher order Born approx., differential cross section series approx. 79-72417
high momentum transfer, semiclassical model cross sections 77-19004
hole burning into molecular velocity distribution due to monochromatic radiation and molecular elastic collision 80-43116
inert gas+inert gas, total cross-section, glory struct. meas. apparatus 80-18901
inert gas hollow cathode arc, mol. beam sampling of metastable atoms as electron temp. probe 80-43967
ion+atom, inversion problem, quasi-potential method 80-37850
ion+atom collision, nonadiabatic transitions between decaying states *(Russian)* 77-10754
ion+molecule, classical differential cross-sections, anisotropic pots. 78-66627
ion + molecule, elastic collision frequency, determ. by Fourier transform ICR spectroscopy 79-50105
ionosphere, effect of ion-neutral collisions on ion vel. distrib. 77-29565
large asymmetric mol. interaction with small mol., target factor, mixture thermodynamic props. 78-26225
large-angle elastic scattering, in reactive systems, interference effects, Regge pole anal. 77-58123
laser field, multimode, intensity time variation on mol. collision processes 79-31620
light scattering, collision-induced and multiple, by simple fluids 80-53919
many channel scattering model, exactly soluble 80-43127
methane, narrow reson., elastic scatt., spectroscopic studies 80-53094
methane, saturated absorpt. reson. shape, geometry and field intensity effects *(Russian)* 80-32778
mixing and quenching cross-sections for atomic collision processes 77-61821
modulated perturbation theory, mol. interactions, STO expansions nonlinear parameter minimisation 77-57871
molecular bound states, semiclassical study 80-9693
molecular collisions, projection operator formalism, stochastic reductions 77-65521
molecular collisions, stochastic theory in perturbation limit 78-1042
molecular collisions, turning point region, approx. method 79-72373
molecular collisions in laser field, basis set selection and rotating-wave approx. 80-58341
molecular scattering amplitude, j_z=conserving approx., space- and body-fixed formulation 78-21987
molecular scattering wavefunctions, algebraic approx. 78-78780
molecular translation factor, parameter-free, semiclassical approach 80-23482
molecule, zero point vibr. effect in low energy scatt. 79-22832
Monte Carlo averaging technique, for anal. of laboratory differential cross section data 78-21997
multiple scattering in molecular gases, target at.+energetic ion spatial correlation influence 79-27062
multistate mol. treatment, impact parameter approx., computer program 77-38705
near-adiabatic collisions, theory, electron translation factor method 78-81889
near-adiabatic collisions, theory, scatt. coord. method 78-81890
neutron detection, recoil atoms (mols.) meas. by laser spectroscopy 79-22864
nonadiabatic reactions, rate const. temp. depend., influence of charact. features of elastic scatt. 80-37852

elastic scattering of atoms and molecules continued
noncrossing interactions, Rosen-Zener model, differential cross-section calcs. 77-46621
nonlinear resonance profiles at low press. *(Russian)* 79-68295
nonlinear spectroscopy, diffr. effects in mol. collisions 79-36731
orientation and alignment, collisional transfer, single-mode laser-excited atom. 80-23495
partial wave parameters in CS and IOS approx., mag. transitions 79-10164
partially redistributed resonance radiation, ang. depend. 77-42285
phaseshifts, pot. determ., generalised WKB method 77-58116
photon-echo technique, feasibility of appl. to atomic collision studies *(Russian)* 77-79673
polyatomic molecular mixtures, Waldmann-Snider collision integrals, transport phenomena study 80-18900
polyatomic molecule+atom, many body approach 79-31645
positron scattering by atoms, computer simulations, review 77-79692
potential scattering, refined Born approx. 80-77
potential scattering theory, anisotropic, classical, small-ang., comparison with $Li^+ + N_2(CO)$ results 80-1043
potentials, anisotropic, from rotationally inelastic and elastic cross sections, direct inversion method 80-69090
prior statistical distributions implied by dynamical threshold laws for molecular collisions 78-86928
quantum-mechanical streamlines and classical trajectories in elastic scattering 78-70898
rainbow maxima, pot. well depth determ. method 77-14527
rainbow scattering, Regge pole anal. 78-58774
redistribution of scattered radiation by collisions in nonimpact region of spectral line profile 79-35109
Regge pole analysis of differential cross sections for elastic molecular scattering 79-3523
resonance width, stabilisation method, variational calc. 77-19011
ring laser, collision model, averaged, in active medium polarizability theory 80-95924
ring laser, effect of elastic collisions on drift splitting of opposite wave frequencies 80-14370
rotational infinite-order sudden-approximation, low energy appls. 78-1052
Rydberg atoms, expts., metastable states, multiphoton ionisation, spectroscopy, Stark struct., collisions, polarisability *(Dutch)* 78-5160
S-matrix factorisation, in mol. collision problems 79-72380
scattering amplitudes, Regge representation calcs. 78-58770
scattering cross sections, phase shift calc. 78-78767
semiclassical collision theory, breakdown of integer Bessel uniform approx. for elastic transitions 79-36730
semiclassical S-matrix, by generalised phase shift approach 79-89725
single elastic scattering cross-section from multiple scatt. distrib. function, inversion formula 77-34716
slow atoms, inverse scatt., semiclassical approx. calcs. 78-17747
spectral line shapes, linear and nonlinear, atom or mol. cross sections 78-70899
SPF-Dunham expansion for interat. pot., systematic anal. of elastic beam scatt. cross sections 77-50491
stopping cross-section, target atom Z depend., Hartree-Fock calcs. 77-10725
sub-Doppler line shapes, saturation and two-photon spectra, elastic collisions, review 78-82697
theory, review 78-1043
three body problems with Coulomb interaction, adiabatic representation, two-level approx. 80-47861
translational energy distribution, Brownian motion model 77-50483
translational nonequilibrium in reson. EM field, rel. to atom-buffer gas collision cross-section differences 80-96340
two-level system, saturated lineshape, collisional and radiative damping effects 77-58124
vibration-rotation lineshapes, effect of elastic and reorientation collisions 79-89712
wavefunction, total ang. momentum body frame radial, coupled states and infinite order approxs. 78-25641
$\mu d + d$ elastic scatt. cross section for muonic d 79-89811
$\mu p + p$, elastic scattering cross section of muonic H atoms 80-69278
Ar, collision induced light scatt. spectra, pair polarisability 78-55135
Ar-Xe mixture, microwave absorption, collision-induced 79-22626
Ar+Ar(Kr)(Xe), total cross section, glory struct. 80-23494
Ar+Kr, elastic collision total cross-section, low energy 80-5603
Ar+methane, low energy collision, close coupling and coupled states, rot. transitions 78-78784
$Ar + N_2$, polarisation in elastic scatt., close-coupling calcs. 78-25650
$Ar + N_2(TlF)$, scatt., l_z-conserving sudden approx. calcs. 78-66628
$Ar + O^+(^4\Sigma^-)$, differential elastic cross sections, 2-20 eV, interatomic pot. 77-6885
$Ar^+ + Ar$, elastic scatt. and charge exchange, differential cross section, 2.7-20 eV 78-66660
$Ar^+ + He$, integral elastic scatt., repulsive potentials derivation 80-63744
$Ar^*(4s^3{}_{2,0}) + Kr(Xe)$, elastic and reactive scatt., ang. distribs. 77-6919
$Au^+ + X$, $X = H, H_2$, He, C, N, O, cross-section, closure-Born approx. 78-66630
B^++inert gas atom, pot. interactions 78-55219
$Br^- + K$, differential cross-section, small angle scatt. 79-98186
$C^+ + H$, fine structure transition of C^+, collision cross section calc., validity of current approx. 78-25652
CO, collision-induced reorientation, direct meas. by IR double reson. 80-32800
CO_2, narrow reson., elastic scatt., spectroscopic studies 80-53094
CO_2, optical reson. widths, nonlinear press. depend. 77-42358
Cl+Xe, elastic scatt. for interaction pot., $Cl(^2P) + Xe(^1S)$ 79-27059
$Cl^- + Na(K)$, differential cross-section, small angle scatt. 79-98186
$Cl^- + Xe$, elastic differential cross-section, 250-500 eV, well depth of 79-86027
$Cs + H^+$, elastic scatt., differential cross-section calc., 13.4-24.2 eV 79-59530
Cs+inert gas, three body interaction, fluoresc. spectra principal series lines and secondary satellites 80-83313
$Cs^+ + X$, $X = H, H_2$, He, C, N, O, cross-section, closure-Born approx. 78-66630
CsF+Ar, elastic and rot. inelastic scatt., quantum mech. calcs. 77-14525
CsI+Ar(He), elastic and inelastic scatt. 77-58119
D, muonic, proton scatt., Schwinger variational principle 79-45780

elastic scattering of atoms and molecules continued
$D+H_2$, pot. surface, isotropic part determ. 79–36729
$D+HCl(HBr)$, elastic scatt., van der Waals pot. meas. 77–58120
D_2+D_2, total scatt. cross-section, below 10 meV 80–28087
$D\mu^-+H^+$, Schwinger variational principle 79–45780
$F^-+Na(K)$, differential cross-section, small angle scatt. 79–98186
F^-+Xe, elastic differential cross-section, 250-500 eV, well depth of XeF^- 79–86027
H, positron elastic scattering, S-wave phase shifts calc., least squares method 80–106374
H+ charged particle, Glauber approx. scatt. amplitudes 80–14191
$H+H_2$, elastic differential cross section high resolution meas. 78–50610
$H+H_2$, integral cross section meas. at thermal energy 77–10724
$H+HCl(HBr)(HI)$, elastic scatt., <50 meV, Van der Waals pot. 79–54937
H+He, D+He, low energy elastic scatt., pot. well depth determ. 77–6884
H+He, elastic scatt. cross-section, using model pot. 79–13786
H+He(Ne)(Ar)(Kr)(Xe), low energy elastic scatt. cross section MCSCF calc., van der Waals forces 78–70897
H+Hg, differential cross sections, orbiting contribution 79–41221
H+positronium elastic scatt., electronic $S=1$ state 77–512
H^++Cs, elastic and charge exchange collisions, projected valence bond method 78–78804
$H^++Cs(6s)$, elastic scatt., pot. determ. from differential cross-sections meas. 78–78778
H^++H_2, elastic of rot. excitation, semiclassical treatment 79–31657
H^++H_2, elastic scatt. and rot. excitation, multistate semiclassical orbital method 79–27058
$H^++H(D)$, elastic scatt., rainbow struct. and g-u-interference effects 77–6886
$H^++H(D)$, elastic scatt. and charge exchange, resonances 78–78777
$H^++H(D)$, low energy elastic cross sections, impact parameter calc. 77–14526
H_2, D_2 and HD, intermol. collision process obs. using light scatt. expts. 80–53001
H_2, interstellar, effects of departure from translational equilib. on collision rates 78–8081
H_2, short range intermolecular forces, scattering of molecular beam 79–36727
H_2+D_2, differential cross section data for intermol. pot. 78–5311
H_2+H_2, elastic scatt., rigid rotor approx. 79–31642
H_2+H_2, total scatt. cross-section, below 10 meV 80–28087
H_2+Kr, elastic total cross section, orbiting effects, Regge theory 78–82814
$H_3{}^+$ fast molecules, transmission through thin C foils 79–76484
HCl+Ar, differential cross section, quasiclassical close coupling approx. 80–63743
HCl+Ar, elastic and rot. inelastic collisions, quasiclassical and quantum mech. results 77–79679
$HD+D_2$, rot. inelastic differential cross sections, diffr. oscills. in elastic and inelastic scatt. 78–74743
HD+HD, total scatt. cross-section, below 10 meV 80–28087
HD+Ne, $j=0$ to 1 scatt. differential cross section, interaction pot. anisotropy 77–42382
$HF(^1\Sigma^+)+Xe(^1S_0)$, expt. and computational study, 0.044 and 0.153 eV 79–89748
$(H_2O)_2$, exchange forces, Hellmann-Feynman theorem calc. 77–54589
H(1s), electron impact, elastic phase shift, post-adiabatic approx. calcs. 78–58827
H(1s)+Cs, differential electron attachment and elastic scatt., 30-528 eV 80–63745
$H(1s)+\mu^+\rightleftharpoons Mu(1s)+p$, thermal collision, quantal calc., elastic and transfer cross sections 77–42446
$H=H^+$ collisions, H(2s), H(2p) production, 1-7 KeV, differential, total cross sections 80–32818
He beams, scattering by crossed at. and mol. beams, elastic differential cross section 79–10171
He, Glauber scatt. amplitude, numerical method in Lommel function 79–22795
He-Ar(Kr)(Xe), 208 and 707K, intermol. forces, virial, diffusion, and viscosity coeffs. 77–75256
He+Ar, interatomic pot. well depth, SPFD pot., diffusion, viscosity and second virial coeff. 80–5599
He+Ar, scatt. pot., He in (2^3S) state, 0.02-0.12 eV 79–54938
He+CO, polarised mol., differential scatt. cross-sections calcs. 79–89733
$He+H_2$, averaged definite parity j_zCCS approx. calcs. 77–34710
$He+H_2$, exchange forces, Hellmann-Feynman theorem calc. 77–54589
$He+H_2$, mag. transitions, close coupling calcs. in uncoupled space frame 78–17769
$He+H_2$, scatt., opacity functions, j_z-conserving approx. calcs. 77–6878
$He+H_2(\mu H)$, interaction pots. and rot. scatt. calcs. 80–43158
$He+H^+$, differential scatt., 1-12 eV, high resolution beam meas. 80–58348
$He+H^+$, elastic scatt. and 2^1s and 2^4p excitation cross-sections 79–36747
$He+He^+$, cross-section oscills., 5 to 40 keV 79–45785
He+methane $(NH_3)(H_2O)(SF_6)$, differential scatt. cross-section, intermol. pot. 79–36728
$He+N_2(O_2)(CO)(NO)$, anisotropic intermol. pots., crossed beam expts. 79–31639
$He+Na_2$, elastic scatt. and rot. excitation, model pot. energy surface 77–6895
He+NaK collisions studied using circularly polarised laser fluorescence, molecular reorientation obs. 80–69215
He+Ne pot., differential cross section, quantum mechanical inversion 78–70896
He+Ne(Ar)(Kr)(Xe), absolute total elastic cross sections 77–30953
He^++H, unpolarised and spin-change collision, low energy 78–86943
He^++He, elastic scatt. and charge exchange. differential cross-section, 0.4-30 eV 78–66659
He^++He, $He(2^3S)$ formation, elastic and resonance charge exchange perturbations 77–42386
He^++He, high-energy collisions, experimental device for study of elastic and inelastic diffusion *(French)* 78–22053
He^++He, low energy cross section, calc. 79–55447
$He^{2+}+He$, 5 to 100 keV, elastic and double charge exchange, mol. treatment 78–82813
$He^{2+}+He(1s^2)$, differential and total cross-sections 80–23506

elastic scattering of atoms and molecules continued
$He^{2+}+N_2$, 200-600 eV, 0-20°, comparison with $He^{2+}+Ne(Ar)$ 78–74732
He_2, exchange forces, Hellmann-Feynman theorem calc. 77–54589
$^3He+{}^3He$, collision cross-sections, Ramsauer-Townsend effect 77–6892
$^4He_2+{}^4He$, zero-energy, Faddeev-unitary pole expansion theory 78–37572
$^4He+{}^4He$, collision cross-sections, Ramsauer-Townsend effect 77–6892
He*+Ar, complex potential from elastic differential cross sections 77–23534
He*+Ar(Kr)(Xe), elastic scatt., repulsive rainbows and optical pots. 79–840
$He^*(2^1S)+Ne$, elastic and reactive scatt., ang. distribs. 77–6919
$He(2^1S, 2^3S)$, transition probs., pots. 80–58371
$He(2^3S)$ collisions, elastic scatt., Penning ionisation, polarisations *(Russian)* 78–70922
$He(2^1S)+Ar$, optical interaction pots. from differential cross sections 77–30956
Hg, slow atoms, inverse scatt., semiclassical approx. calcs. 78–17747
Hg+Ne(Na)(K)(Rb), elastic scatt., interatomic pots. 77–58122
$H(muonic)+H^+$, elastic scatt., cross section 79–871
I_2, angular momentum transfer, elastic, inelastic collisions, orientation and polarised fluoresc. 78–90271
I_2, coherent optical transients and optical dephasing in mol. collisions 80–9966
I_2, laser fluoresc., relax. of oriented ground and excited mols. 78–46390
I_2, resonance Raman scatt. and collision-induced redistrib. scatt. 77–14439
I_2+I_2, collisional energy transfer, selection rules for elastic collisions 77–50467
I_2+I_2, optical coherent transients detected by frequency-switched tunable laser 77–54762
$K+Br_2$, nonreactive differential scatt., 0-10 eV, scatt. angle 78–42156
K+inert gas atom, ground-state pots. from elastic cross sections 77–75258
K^++Cu crystal, ang. and energy relationships, 1-3 keV *(Russian)* 79–78802
Kr+carbon tetrachloride, differential elastic scatt. cross-section 79–45784
Kr*+He, persistence of velocity following elastic collisions 78–78779
Li+He, elastic scatt., fine-struct. transition cross sections, eigenphase formulation 78–25651
Li^++H_2, elastic scatt. and rot. excitation, multistate semiclassical orbital method 79–27058
Li^++inert gas, elastic differential scatt., diffr. effects 77–511
Li^++Na, charge transfer and elastic scatt., two state model 78–58805
Li^++X, $X=H$, H_2, He, C, N, O, cross-section, closure-Born approx. 78–66630
Li_2, circular polarisation of emission, influence of nucl. hyperfine interactions and elastic collisions 80–9635
Li_2, emission circ. polaris., hyperfine coherence and elastic collisions effect 79–3471
Li_2+inert gas, energy and ag. momentum transfer, polarised laser fluoresc. obs. 79–31590
Li^+H_2, elastic of rot. excitation, semiclassical treatment 79–31657
N_2, liq. spontaneous Raman scatt., vibr. dephasing, review 77–28568
N_2+Ar, total differential cross section, diffr. oscills. quenching 78–66625
Na, slow atoms, inverse scatt., semiclassical approx. calcs. 78–17747
Na+Ar, differential cross-section at thermal energy, Na-Ar ground state pot. 78–58769
Na+Ar, scatt. cross-section, thermal energy, interaction pot. for $Na(3^2P)$ 79 - 27060
$Na+Ar(0_2)(N_2)(He)(H_2)$, total elastic cross sections meas. 77–30954
Na+He, collisional freq. redistrib. of scatt. laser light 77–30815
Na+Ne, differential cross section at thermal energy, expt. and theoretical results comparison 80–37851
Na^++Cu crystal, ang. and energy relationships, 1-3 keV *(Russian)* 79–78802
Na^++He (Kr) thermal, two trajectory model from meas. cross-sections 77–75257
Ne-Xe mixture, microwave absorption, collision-induced 79–22626
Ne+Ar(Kr)(Xe), elastic scatt. absolute total cross section, long range interaction 78–58768
Ne+Ar(Xr)(Xe), total cross section, glory struct. 80–23494
Ne+Ne, total cross-section, 0.5-1.4 km s^{-1}, long range pot. 79–13787
Ne^++Ar integral elastic scatt., repulsive potentials derivation 80–63744
Ne^++D_2, elastic scatt. at small angles, 1.3-3.5 keV, scaling law 78–82812
$Ne(^3P_2)$ elastically scattered, metastable, ang. distrib., conventional rel. to Doppler shift methods 80–58418
Ne*+Ne, differential elastic scatt., rainbow max., mol. states 77–38710
$O^-+Ne(Ar)(Kr)$, 0.2-1 keV, elastic and inelastic reduced differential cross-sections 80–32829
O^++inert gas, potential energy curves from elastic scatt. cross sections 80–23502
O_2, liq. spontaneous Raman scatt., vibr. dephasing, review 77–28568
O_2+inert gas atom, absolute total elastic cross sections 78–9220
OCS, microwave rot. transitions, phase shift effect, collisional effects 79–98073
$O(^3P)$+inert gas atom, absolute total cross sections, 0.6-2.0 km sec^{-1}, model pots. 77–19010
Rb+inert gas atom, ground-state pots. from elastic cross sections 77–75258
Rb^++Cu crystal, ang. and energy relationships, 1-3 keV *(Russian)* 79–78802
SF_6, narrow reson., elastic scatt., spectroscopic studies 80–53094
U+Kr, momentum transfer cross-section, 0.1 eV 79–45783
$U^++U(U^+)(U^{2+})$, elastic scatt. in plasma, interaction pots. and momentum transfer 80–38534
Xe, 3.51 μm line press. broadening 77–14390
Xe three-level system, collisional effects on optical coherence 79–93954
Xe+He, saturated absorpt. of 3.51 μm line, vel. changing collisions by line width 78–86819
Xe+ion $(1\leq Z_1\leq 90)$, 2.5-400 keV, 1-6°, effective interat. pots. 80–23492

elastic scattering of electrons by atoms and molecules
see also gas phase electron diffraction
absolute cross sections meas. 77–42411
adiabatic approximation, energy-modified 79–59523

elastic scattering of electrons by atoms and molecules continued

- alkali atom, positron and electron low energy scatt., JWKB approx. 77—14579
- alkali halides, electron impact, elastic scatt., model, static and static exchange calcs. 78—94321
- alkali metal, polarised orbitals method modification 79—22835
- alkali metal atom, positron elastic scatt. cross-sections, vel. distrib. functions 78—42218
- alkali metal plasma, effect of elastic electron scatt. by at. excited states on conductivity 78—42715
- analyticity and dispersion relations in forward e-atom scatt. 77—23561
- Ar, electron shadow scattering, cross-sections calcs. 79—59575
- asymptotic solutions for coupled eqns., calc. program 80—53129
- atom, angle depend. resonance profile parameter 77—88563
- atom, bremsstrahlung spectrum, low-energy theorem for soft-photon end pt. 78—17796
- atom, dispersion relations, static exchange approx. 77—83735
- atom, effective pots. below inelastic thresholds, asymptotic forms 77—83728
- atom, eikonal approx. for collisions in elec. field 78—33607
- atom, exchange amplitude for elastic forward scatt. of electrons *(Russian)* 78—46447
- atom, forward elastic electron scatt. amplitude, dispersion relation 78—90263
- atom, independent particle model pot. calc. of differential shielded cross section, keV range 79—13824
- atom, intermediate changes in high-energy charged particle scatt. 80—14234
- atom, one-electron, scatt. asymmetry and spin polaris. 78—58820
- atom, spin polarisation, density matrix formulation *(Russian)* 77—31003
- atom, theoretical models, review 77—58166
- atom+foreign gas, absorpt. spectrum shift near series limit, K-matrix anal. 77—10731
- atom in resonant EM field, elastic and inelastic scatt. cross sections 77—14574
- ATOM programme package for atomic calculations 79—10010
- atomic and molecular collisions, book 80—27058
- atomic collisions, experiments, review 79—81256
- atomic continuum processes, R-matrix method, program 78—74558
- atomic electron (positron) elastic (inelastic) scatt., 5-500 eV, perturbations treatments, review 77—30997
- atomic electron (positron) scatt., eikonal theory, review 78—25707
- atomic electron scattering, in IR radiation field, theory 80—83487
- atomic electron scattering, intermediate energy approx. 78—22030
- atomic electron scattering, many-electron correlations 77—42409
- atomic electron scattering, two-pot. intermediate energy approx., ang. depend. 78—25701
- atomic electron shadow scattering, cross-sections calcs. 79—59575
- atomic ion, electron scatt., S-matrix calc. 79—45847
- atomic long-range forces, contrib. to low-energy phaseshifts 78—5344
- atoms, electron and positron forward scatt. amplitudes, anal. behaviour 78—58829
- atoms, electron scatt. in strong radiation fields, review 80—63801
- atoms, scattering of fast electrons and positrons 78—62918
- bicyclo(4,2,0)octane, cis and trans isomers, struct. mol. mechanics and electron diffr. 77—54608
- binding energy of electron in elec. dipole field 79—98220
- Born partial wave amplitude for any electrostatic multipole field 80—53128
- bremsstrahlung, electron+atom, 1-500 keV, bremsstrahlung ang. distrib. prediction 79—41312
- bremsstrahlung cross-section, near HF limit 79—18288
- butane, gas, electron drift vel., Ramsauer-Townsend minima in electron scatt. 78—87427
- n-butane, vibr. shrinkages, mol. struct., electron diffr. obs. 77—50535
- carbon tetrachloride, mol. characts. from fast low-angle scatt. 77—50537
- charged particle potential scattering in laser field, eikonal theory 79—81249
- charged particle scatt., exact results for three particles 79—81309
- charged particle scattering, Schwinger variational principle 79—45780
- coaxial electron and atomic beams sequential multiple scatterings, random walk approach 80—99574
- complex angular momentum theories, background integral evaluation 79—6986
- computational atomic and molecular physics, conf., Nottingham, England, (Sept. 1978) 79—59567
- conference, electronic and atomic collisions, Paris (July 1977) 78—58758
- conference, physics of ionised gases, Dubrovnik, Yugoslavia, (Aug.-Sep. 1976) 77—42961
- continuum Dirac electron, Coulomb field, simple asymptotic wave function 78—41455
- continuum state, electron scatt. in intense radiation field, time-independent methods 78—25705
- continuum wave functions, discrete basis set method 79—22829
- cross section calculation, radial integrals of parametric functions 80—9737
- DC Fano effect polarised electron source appl. to electron-atom scatt. 78—66689
- diatom, phase shift difference, trigonometric pots. in radial Schrodinger eqn. 79—22787
- diatomic molecular gas, electron elastic scatt. intensity calc., vibr. coord. averaging method 77—68114
- diatomic molecule, electron scatt., low energy, multichannel variational calcs., static exchange approx. 80—83483
- diatomic molecule, electron scatt., low energy 80—53132
- diatomic molecule electron scatt., iterative static exchange method 80—53155
- diatomic molecules, electron elastic scatt. cross-sections calcs. 80—48088
- diatomic molecules, equilibrium parameters and Morse anharmonic consts., electron diffr. determ. 78—58818
- diatomic polar molecules, electron scatt., calcs., Born approx. limitations 78—17794
- diatomic polar molecules, electron scatt., frame transformations treatment 80—23553
- dichlorodinitromethane, mol. struct., electron diffr. investig. 78—86950
- diffusion theory and Monte Carlo calcs. of electron transport, depend. on initial ang. distrib. of injected electrons 80—53136
- distorted wave eikonal approx. for elastic electron-atom scatt. 77—83731
- distorted wave matrix elements for inverse power pots., approx. analytic evaluation 80—83442

elastic scattering of electrons by atoms and molecules continued

- distorted-wave amplitudes, sensitivity of cross-section and ang. correl. to scatt. parameters 80—5596
- dosimetry of electrons, scatter effects, plane ^{90}Sr-^{90}Y medical applicator 80—61699
- effective pot. approach to mol. electron scatt. theory 80—53131
- eikonal exchange amplitudes 80—69235
- electron and positron scatt. by atoms, cross sections, review and expt. conditions 78—58828
- electron bremsstrahlung energy spectra above 2 MeV, partial wave interpolation 79—72416
- electron scatt. and photoionisation, shape-resonance enhanced nuclear motion effects 80—63603
- electron scatt. reson. using dilatation transforms., dilatation stability condition 78—46445
- electron scatt. using dilatation transforms., restricted perturbation methods 78—50639
- electron-atom collision theory, soln. of coupled integro-differential eqns. by computer program 78—86948
- electron-matter interactions rel. to electron microscopy 80—89097
- electronic and at. collisions, conf., Kyoto, Japan (Aug.-Sept. 1979), 80—57011
- electronic and at. collisions, conference, Kyoto, Japan (Aug.-Sept. 1979) 80—62394
- elementary atomic processes, threshold behaviour 80—23546
- ESP detector for 300-2000 eV electron, optimum conditions theory *(Japanese)* 78—66693
- ethane, gas, electron drift vel., Ramsauer-Townsend minima in electron scatt. 78—87427
- ethane, Ramsauer-Townsend minimum in electron scatt. cross section 77—89821
- ethinyltetrafluorophosphorane, mol. struct., electron diffr. obs. 79—50133
- exchange amplitude, for forward electron-atom scatt., analyticity 77—58161
- exchange forward scatt. amplitude singularities *(Russian)* 77—54611
- exchange perturbation theory for electron scatt., appl. elastic scatt. from H 80—78709
- excited atom exchange interaction with molecules, calc. using electron scattering data 77—58125
- Feshbach resonances at 1 meV resolution 78—58831
- finite range problem, electron atom scatt. below inelastic threshold, effective pots. 78—25704
- first row elements, ground state, self-consistent orbitals with uniform long-range behaviour 80—9485
- fixed scatterer approx. simple form 77—50544
- forward atomic electron scattering amplitude, anal. struct. 77—14577
- forward scattering, complex energy plane, analytic props. 78—29851
- free particle Green's function, Gaussian matrix elements 79—2667
- free-free transition of electron, in presence of atomic system, multichannel theory 78—1078
- free-free transitions, mutiphoton, energy absorption laser pulse shape-independ. 80—43184
- gas in SEM sample chamber, electron scatt., appl. to N_2 79—49342
- gases, multiple scatt. effect on electron mobility 80—58383
- Glauber eikonal approximation for low and intermediate energy mol. electron scatt. 80—53130
- Glauber-Ochkur exchange amplitude, validity 77—23562
- halogen atoms 80—9736
- high energy higher order Born approx., differential cross section series approx. 79—72417
- HV electron microscopy, total scatt. cross-section obs. 79—21859
- hydrocarbons, gas phase, thermal electron interactions, drift vel. meas. 78—62919
- inert gas, effective collision cross sections 79—98222
- inert gas, positron elastic scatt., polarised orbital approx. 77—30996
- inert gas low energy electron elastic scatt. effective cross section, time of flight meas. 79—13823
- inert gas-positron total cross-sections at intermediate energies meas. 77—3456
- inert gases, computer anal. of differential cross section 77—58160
- inert gases, optical model, differential and inelastic cross-sections, spin polarisation 77—75299
- inert gases, positron scatt., low energy, semiempirical polarisation pot. calcs. 80—9735
- ionosphere, electrons collision freq. and transport props. 79—80079
- ionosphere photoelectron flux, anisotropic electron-neutral cross sections 79—21103
- Jahn-Teller mols., fast electron scatt. theory 79—89784
- laser field affecting scattering from atoms, many-body Green's function 79—31679
- laser field atomic electron scatt. without optical pumping, reson. state coupling, theory 78—17804
- laser induced free-free transitions, differential sum rule, anal. 80—23372
- laser induced one-photon transitions between two short-lived negative ion states 80—9731
- light atom, intermediate energy, differential cross-sections calc. 80—106394
- light atoms, intermediate energy, review 79—856
- light element microanalysis 79—61935
- light elements, electron backscatt. rates, Moliere approx. calcs. *(German)* 78—82841
- local optical pot., second order partial wave amplitude 78—25703
- low energies, phaseshift evaluation by pseudopotential method 79—22830
- magnetic and laser fields simultaneously influencing potential scattering 79—81248
- many-body theory, second-order 80—32832
- many-electron atom-unbound electron system, normalisation of wave function 77—68123
- matrix variational calcs. of electron-atom scattering, review 79—59577
- metal atom, collision cross sections 77—42410
- metal vapour, elastic and inelastic scatt. 78—58830
- methane, elastic and inelastic electron scatt. differential cross section, obs. and calc., struct., binding energy 80—28110
- methane, elastic scattering of electrons, differential cross-sections 79—89780
- methane, gas, electron drift vel., Ramsauer-Townsend minima in electron scatt. 78—87427
- methane, large angle elastic and inelastic electron scatt. differential cross section, exchange corrections 80—28111
- 2-methoxacyclobutane, mol. struct., electron diffr. obs. 80—1065
- minimum-variance method, discrete-basis-set approach 77—83734

elastic scattering of electrons by atoms and molecules continued
- molecular electron scatt., ab initio theory including polarisation 78—50640
- molecular electron scatt. resons. near threshold, vibr. induced narrowing 80—91673
- molecular gases, positron scattering, 50-800 eV, total cross-section meas. 79—31680
- molecular scattering theory, review 80—32847
- molecule, adiabatic nuclei theory 79—45846
- molecule, diatomic, R-matrix theory 77—75298
- molecule, local exchange approx. 78—17791
- molecule, polar, electron scatt. symmetry 80—32834
- molecule, polar, slow electron scatt. 80—1064
- molecule, resonances, use of high-Rydberg at. as spectroscopic probe 77—58162
- molecule, Schrodinger eqn. Fourier transform 79—64105
- molecule, semiclassical perturbation theory 78—58825
- molecule, zero-radius potential appl. to molecule comprising spin-1/2 atoms *(Russian)* 77—34771
- molecule characts. from fast scatt. 77—50536
- molecules, close coupling method, elastic and rot. excitation 79—10202
- molecules, intermediate energies, general theory 77—10757
- molecules, one- and two-electron characts. determ. 79—31691
- molecules, scatt. mechanisms and calcs. 80—17721
- momentum space, electron molecule. scatt. 80—48087
- momentum-transfer cross sections 79—25777
- multicentre molecules, intratarget diffr., extended Glauber theory 80—58380
- multiphoton free-free transitions in scatt. electrons induced by laser pulses 78—62917
- N-body scatt. in two-cluster region 78—28975
- negative atomic ion, correl. effects, Bethe-Goldstone calc. 79—54967
- negative ions, Feshbach type reson. scatt., Glauber approx. calcs. 80—102570
- neopentane, gas, electron drift vel., Ramsauer-Townsend minima in electron scatt. 78—87427
- nonpolar molecules, slow scatt. 80—91666
- one-electron model from $1/r_{12}$ partition, applic. to scattering from rare gas atoms 77—14572
- open-shell target, electron scatt., orthogonality constraints 77—71869
- optical model in atomic physics 79—98223
- optical model in electron-atom scatt. 78—5345
- optical model theory, electron and positron scatt., intermediate energy 77—30990
- partial resonance widths, Siegert eigenvalues, basis-set calc. 80—37880
- phase shifts calc. perturbation theory, one-electron target computer program 78—50637
- photoelectric effect and electron diffusion in gases 78—81745
- plasma, at. elastic electron scatt. cross section, Glauber approx. modification 78—25700
- polar molecule, electron scatt. cross sections, threshold behaviour *(Russian)* 78—5347
- polar molecule, fast scattering, intensity approx. 77—46640
- polar molecule electron scatt., excitation and scatt. cross sections 78—58826
- polar molecule electron scattering, exam. of models 80—37898
- polar molecules, differential cross sections 77—38735
- polar molecules, elastic and inelastic electron scatt. 78—94322
- polar molecules, electron impact, elastic scatt. and vibr. excitation, effective range theory 80—83485
- polar molecules, electron scatt., orthogonalisation and model exchange pots. calcs. 80—23552
- polar molecules, electron scattering, αr^{-s} pot. effects 80—9733
- polar molecules, thermal electron scatt. 77—58163
- polarisation, comparison in optics and spin-$^1/_2$ particle assemblies, Stokes vector formalism 77—27181
- polarisation potential, quasi-adiabatic, appl. to electron-H-atom scatt. 77—30993
- polarisation potential, quasi-adiabatic theory 77—30992
- polarisation potential, quasiadiabatic, for elastic electron-atom scatt. 77—6929
- polarisation potential for electron-atom scatt. 78—42228
- polarised electrons, book 77—46679
- polyatomic molecules, electron elastic scatt., differential cross-section calcs. 80—48089
- polyatomic system, multiple scattering method for photoelectron and absorpt. spectra 77—88501
- positron + H(He), second-order nonadiabatic polaris. pot. for elastic scatt. 79—22836
- positron annihilation in matter, Monte Carlo calcs. 77—88558
- positron collisions in gases, low energy 78—13609
- potential scatt. in low freq. laser field, perturbation theory 80—43191
- potential scattering, refined Born approx. 80—77
- propane, gas, electron drift vel., Ramsauer-Townsend minima in electron scatt. 78—87427
- propane, Ramsauer-Townsend minimum in electron scatt. cross section 77—89821
- pseudostates wave functions determ. in modified close-coupling calcs. 80—99572
- R-matrix method, application to atoms and ions 78—58833
- R-matrix method, appls. to electron mol. collisions 78—58834
- R-matrix method, basic concepts, rel. to other theories 78—58832
- R-matrix theory, atomic continuum processes 77—83478
- reduced phase space approach calcs. 80—83438
- resonances during dilatation transformations, reson. eigenvalues stability 79—18291
- resonances in atoms and molecules 80—9734
- resonant phenomena, complex stabilisation method 80—78515
- resonant scattering, complex-coordinate method, using variational principle 79—86070
- review, of expt. and theory 78—25699
- review 77—34762
- scattering cross-sections, ab initio calcs., incl. polarisation 78—5341
- scattering T-matrix eqns., discrete basis function calcs. 80—23551
- second Born approx., small angle elastic electron scatt. from atoms, high energy limit 78—78811
- slow positrons and electrons, meas. of angular distribs. using TOF spectrometer 80—86496
- soft photon approx. accuracy for resonances in electron scatt. in laser field 78—70935
- spin polarisation processes in two-electron systems *(Russian)* 79—94085

elastic scattering of electrons by atoms and molecules continued
- strongly polar molecule, low energy electron scatt., dipole moment depend. *(Japanese)* 77—42405
- summation of partial wave expansions in scatt. by long range pots. 79—41239
- system of N charge particles in external Coulomb field, asymptotic form of wave function 77—71871
- tetrachloromethane, electronic characts. from electron scatt. meas. 79—59576
- 1,1,2,2-tetrafluoroethane, anti- and gauche-rotamers, struct., spectra, electron diffr. 77—50439
- tetrafluoromethane, elastic and inelastic electron scatt. differential cross section, obs. and calc., struct., binding energy 80—28110
- theory, review 78—1043
- theory and calc. techniques 80—63841
- total collision cross sections, for electron- or positron-atom scatt. in curved axial mag. field, transmission meas. 78—1082
- trifluorodimethylmercury, gas phase mol. struct., electron diffr. and microwave spectra obs. 80—78609
- trifluoromethyl sulphonyl chloride, mol. struct., electron diffr. obs. 79—7016
- two-state atom, in low-freq. laser field, charged particle scatt. 79—41241
- variational method, modified 78—1081
- variational methods, appl. to at. scatt., review 78—86951
- variational methods 77—42408
- variational principle for scatt. length, target ground-state wave functions imprecisely known 77—58164
- vibronic effects 78—9249
- μ^-p, electron scatt. length determ. 79—36801
- Al, electron scatt., transitions, oscill. strengths, config. superposition calcs. 77—6732
- Al, fast electron beam scatt. calcs. 77—65534
- Ar, 40 keV electron scatt. 7-200 mrad, relativistic and electron correlation effects 77—34760
- Ar, differential cross-section crit. position 79—54968
- Ar, elastic electron and positron scatt., optical model theory 77—19076
- Ar, elastic electron scatt., resonance struct. 77—50532
- Ar, electron and positron scattering, elastic, 100 and 500 eV, second-order eikonal approx. 78—78814
- Ar, electron elastic scatt., differential cross-section meas. 77—3458
- Ar, electron impact, elastic scatt. calcs. 78—25708
- Ar, electron pot. scatt., 100 and 500 eV, extended Glauber approx. calcs. 77—54610
- Ar, electron scatt., effective pot. calcs. 80—53131
- Ar, electron scatt., in laser radiation field, free-free cross sections meas. 78—74762
- Ar, electron scatt. and ejection, electron energy loss spectra 80—58394
- Ar, electron scatt. in laser radiation field, free-free cross sections, reson. struct. 78—74763
- Ar, electron scattering, elastic, at low-energy, polarised orbital calc. 78—82840
- Ar, electron scattering, elastic, low-energy, polarised-orbital calcs. 80—37882
- Ar, phaseshift anal. of ang. distribs. 79—22833
- Ar, positron annihilation decay rates, high temp. behaviour 80—58389
- Ar, positron differential cross-section, 2.2-8.7 eV 79—54939
- Ar positron scatt., elastic, diffusion and annihilation cross sections 79—36769
- Ar, positron scatt., total cross sections 78—22031
- Ar, positron scatt., total cross sections 79—86065
- Ar, positron total scatt. cross sections 77—14573
- Ar, positron vel. distrib. at equilib., elec. and mag. fields 77—71870
- Ar, total scatt. cross section, 20-3000 eV 79—36778
- Ar total scattering cross sections for low-energy electrons 80—58417
- Ar-Ne, positron vel. distrib. at equilib. elec. and mag. fields 77—71870
- BF, X-ray and high-energy elastic electron scatt., vibr. averages 79—81279
- Ba, electron scatt., elastic and inelastic (5^1D, 6^1P) cross sections, 20-100 eV 78—74769
- Ba, electron scatt. cross sections, close coupling calc. with CI 80—43180
- Ba, electron scattering, above ionisation threshold *(Russian)* 79—68317
- Ba, scatt. from excited atoms, 30 and 100 eV, inelasic and superelastic 78—86933
- Be, ^2P shape reson., electron scatt. calc. 79—41240
- Be^{2+} quantum defects rel. to angular momentum, nuclear charge, Coulomb-Born approx. method *(Japanese)* 77—50534
- β^{3+} quantum defects, rel. to angular momentum, nuclear charge, Coulomb-Born approx. method *(Japanese)* 77—50534
- C, cross sections 77—50538
- C, low energy elastic and inelastic scatt. Bethe-Goldstone and pseudostate approx. 77—68112
- C, low energy elastic scatt., pseudostate and Bethe-Goldstone approx. 77—68111
- CO, elastic differential cross-section, 3-100 eV, 15-130° 79—27086
- CO, electron elastic scatt., differential cross-section meas. 77—3458
- CO, electron elastic scatt., low energy, static exchange approx. calcs. 80—69236
- CO, electron scatt., absolute total cross-section meas. 78—74774
- CO, electron scatt., adiabatic polaris. pots. 79—10203
- CO, electron scatt., effective pot. calcs. 80—53131
- CO, electron scatt., low energy, multichannel variational calcs., static exchange approx. 80—83483
- CO, electron scatt. at low energy, mechanisms *(Russian)* 78—90306
- CO electron scattering, intermediate energy electrons 79—72418
- CO, low energy electron scatt., ab initio study, frame-transform. theory 77—83732
- CO, X-ray and electron scatt. first Born approx. calcs. 77—61867
- CO, X-ray and high-energy elastic electron scatt., vibr. averages 79—81279
- CO_2, 0.07 to 10.0 eV electrons, cross-sections by coupled-channel approach 77—75300
- CO_2, elastic and inelastic electron scatt. differential cross section, obs. and calc., struct., binding energy 80—28110
- CO_2, elastic electron scattering and rot. excitation calcs. 79—22834
- CO_2, electron elastic scatt., 0 to 100 eV 80—23547
- CO_2, electron elastic scatt. and vibr. excitation by 4, 10, 20 and 50 eV electrons 80—83484
- CO_2, electron energy deposition, rel. to Venus and Mars atms. 79—45857
- CO_2, electron impact, 3.8 eV resonance 77—42430
- CO_2, electron scatt., absolute total cross-section meas. 78—74774

elastic scattering of electrons by atoms and molecules continued
- CO_2, electron scatt., effective pot. calcs. 80—53131
- CO_2, electron scatt., Glauber eikonal approx. calcs. 80—53130
- CO_2, electron swarm parameters for high E/N, Monte Carlo simulation 80—19548
- CO_2, large angle elastic and inelastic electron scatt. differential cross section, exchange corrections 80—28111
- CO_2, scatt. electron angular distrib. 78—74766
- CS_2, electron elastic scatt., 0 to 100 eV 80—23547
- Cs, 0.8-20 eV, energy and angle depend. of cross section, reson. structs. 78—5353
- Cs, electron elastic scatt., polarisation and ang. distrib. meas. 79—89781
- CsF, electron impact, elastic scatt., model, static and static exchange calcs. 78—94321
- Cu, ang. distrib. for 98.6 keV electrons 79—18295
- Cu, atom, electron impact cross section, elastic and ^2P and ^2D states, inversion ratios 78—9256
- D_2, electron scatt., isotope effects 77—58188
- D_2, electron scatt., low energy, rot. resons. 78—33608
- F, electron scatt., d-wave resonances, close coupling calcs. 78—33610
- F, electron scatt., low energy d-wave resonances 78—33609
- F_2^-, absorption coeffs., shape resonance in e-F_2 scatt. 78—17792
- FH, X-ray and high-energy elastic electron scatt., vibr. averages 79—81279
- Fe, 1-8 keV, differential shielded cross section calc. 79—13824
- H, 2s state, elastic electron scatt. 77—50531
- H (2s) metastable state elastic electron scatt. 78—55238
- H, absolute elastic cross sections 77—50533
- H, Born amplitude, unitarity sufficiency condition 79—86068
- H, cross sections 77—50538
- H, differential cross sections calc. 78—90293
- H, dispersion relations, forward scatt. electrons, numerical study 77—68113
- H, dispersion relations, static exchange approx. 77—83735
- H, $E_e \geq 100$ eV, ang. distribs. calc. 80—74248
- H, e^+ scatt., two-pot. eikonal approx. 79—31685
- H, effective pots. below inelastic thresholds, asymptotic forms 77—83728
- H, eikonal-Born series and modified Glauber approach comparison 79—81281
- H, elastic electron (positron) scatt., relativistic Glauber amplitudes 79—31681
- H, elastic electron scatt., pseudostates wave functions determ. in modified close-coupling calcs. 80—99572
- H, elastic electron scatt., 20-50 eV, Born calcs. of differential cross section 80—102571
- H, elastic electron scattering, static exchange amplitude, dispersion rels. 78—66664
- H, elastic electron scattering, eikonal Born series calc. 79—36766
- H, elastic positron scattering, differential cross sections 79—86028
- H, elastic scatt. and n=2 states excitation, fixed-scatterer approx. 77—50544
- H, elastic scatt. of electrons and positrons 77—19075
- H, electron and positron scattering, elastic, 100 and 500 eV, second-order eikonal approx. 78—78814
- H, electron and positron scattering, second-order pot. method calcs. 79—72419
- H, electron elastic scatt., two-pot. Glauber-Born approx. calcs. 78—25706
- H, electron elastic scatt., differential cross section 78—33605
- H, electron elastic scatt., second Born amplitude calcs. 80—32833
- H, electron elastic scatt., exchange perturbation theory 80—78709
- H, electron elastic scattering, fixed scatterer approx. 79—10204
- H, electron exchange scatt., generalised Coulomb-projected Ochkur-Born approx. 77—83730
- H, electron scatt., dispersion relations 78—42216
- H, electron scatt., effective pot. calcs. 80—53131
- H, electron scatt., orthogonality constraints 77—71869
- H, electron scatt., polarisation potential 78—42228
- H, electron scatt. at intermediate energies, fixed scatter approx. 80—9740
- H, electron scatt. in EM field, reson. emission and absorpt. of photons 79—27087
- H, electron scatt. in presence of a laser field, theory 78—74767
- H, electron scatt. resons., coord. rot. method calcs. 77—83736
- H, electron scatt. total spin quantum number changes 79—54969
- H, electron scattering, differential cross-sections, eikonal approx. calcs. 79—81278
- H, electron scattering, inhomogeneous eqn. method 77—27182
- H, electron scattering, low-energy, 1S-approximation channel coupling array 77—10756
- H, electron scattering, low energy, R-matrix calc. 79—59571
- H, electron scattering, optical pot. methods 80—102569
- H, electron/positron elastic scatt., least squares calcs. 79—3572
- H, exchange amplitude, Glauber-Bonham-Ochkur approx., differential cross sections 77—19078
- H, exchange amplitudes and dispersion relations 77—79693
- H, finite range problem, electron atom scatt. below inelastic threshold, effective pots. 78—25704
- H, forward elastic exchange amplitude, Born approx. 78—5342
- H, forward elastic exchange amplitudes and forward dispersion relations, anal. props. 78—78812
- H, forward scatt., total cross section calc. 78—29852
- H, forward scatt. amplitude, dispersion relation 78—58823
- H, Fresnel and recoil corrections in Glauber theory 79—50131
- H, high energy higher order Born approx., differential cross section series approx. 79—72417
- H, high-energy behaviour of elastic and 2s excitation scatt. cross-sections 77—10763
- H, intermediate energies, modified Glauber theory 77—14575
- H, L=2, 3 phase shifts 78—37742
- H, local optical pot., second order partial wave amplitude 78—25703
- H, local pot. method, bound states 77—75296
- H, logarithmic ang. depend. at small scatt. angles 78—50638
- H, low energy elastic scatt., variable phase method, s-, p- and d-wave phase shifts 80—9732
- H, modified Glauber method, Glauber exchange 77—83733
- H, modified Glauber theory, intermediate states 80—53139
- H, modified Glauber theory with exchange 77—65533
- H, modified variational method 78—1081
- H, partial transition matrix elements, Faddeev approach 77—75297
- H, positron annihilation rate, p-wave contrib. 78—17790

elastic scattering of electrons by atoms and molecules continued
- H, positron elastic scatt. lengths and phase shifts, variable phase method 79—22838
- H, positron elastic scattering, low-energy S-wave phase shifts calcs. 78—78813
- H, positron P-wave scatt., elastic and positronium form. cross sections 77—3468
- H, positron scatt., analytic model, complex scaling 79—18257
- H, positron scatt., low energy, semiempirical polarisation pot. calcs. 80—9735
- H, positron scatt., modified Glauber method 78—17797
- H, positron scatt., optical pot. theory 80—43181
- H, positron scatt., Schwinger variational principle 79—45780
- H, positron scatt. and annihilation, s and p pseudo-states 78—42217
- H, quasi-adiabatic polarisation potential 77—30993
- H, scatt. phaseshifts, H-continuum frozen-core Hartree-Fock approx. perturbation theory 77—75295
- H scattering amplitude, left-cut contrib. to dispersion relation 79—59574
- H, scattering length calc. with imprecise target wave function, variation principle 79—72375
- H, source theory 78—46415
- H-like atom or ion, electron-electron interaction operator, dipole approx. 78—58821
- H-like atoms, electron exchange scatt., high impact vels. 79—22846
- H-like ions, elastic electron (positron) scatt., relativistic Glauber amplitudes 79—31681
- H-like ions, ground-state, elastic electron (positron) scatt., relativistic Glauber amplitudes 80—23550
- $H+e^-$ scatt., channel coupling array theory 77—19005
- $H+e^-$ scattering at low energy 77—30994
- $H+e^-(e^+)$, elastic and inelastic scatt., relativistic spin-dependent amplitude, Glauber approx. 80—63818
- $H+e^-(e^+)$, elastic scatt., asymptotic effective pot. 80—14233
- $H+e^-(e^+)$, S-wave phaseshifts bounds, least norm variational principle tests 80—5619
- $H+e^+$, moment T-matrix approach, ang. distrib., total cross section, below pickup threshold 79—3573
- $H+e^+$, moment T-matrix approach, elastic scatt., total cross section, intermediate energy 79—3582
- H+positron, S-wave scatt., lowest reson. calc. 78—37743
- H_2, 1 keV elastic scatt., Glauber model anal. 80—43178
- H_2, 100-2000 eV, scatt. amplitude and cross-section 80—87228
- H_2, 11-12 eV, variational calcs. of resonant states of H_2^- 79—3571
- H_2, 30, 50, 100, 200 eV, Glauber cross sections, independ. scatt. centres model calcs. 77—58165
- H_2, 50-400 eV, cross section calc. by potential scatt. formalism *(Japanese)* 77—42404
- H_2, absolute elastic cross sections 77—50533
- H_2, absorption effects calc., 30-200 eV 78—22029
- H_2, adiabatic polarisation, ab initio calc., static electric dipole polarisability 79—72229
- H_2, diffr. of medium energy electrons 78—9251
- H_2, elastic and rot. excitation, effective pot. theory 80—5627
- [CC H_2, elastic electron scatt., comparison of local exchange pots.] 78—5346
- H_2, electron elastic low energy scatt., ab initio pseudostates calc. 78—9247
- H_2, electron elastic scatt., free-electron-gas model exchange pot. 78—58824
- H_2, electron elastic scattering, intermediate energy, optical eikonal theory calcs. 79—72420
- H_2, electron energy loss spectra, $B^2H_u{}^+$ state cross sections, Franck-Condon factors 78—13616
- H_2, electron impact, elastic scatt. and rot. excitation, close-coupling calcs. 77—6949
- H_2, electron scatt., ab initio theory, elastic scatt. and rot. excitation 78—50640
- H_2, electron scatt., absolute total cross-sections, 0.2-100 eV 80—91674
- H_2, electron scatt., effective pot. calcs. 80—53131
- H_2, electron scatt., elastic and inelastic, Glauber approx. 80—91695
- H_2, electron scatt., Glauber eikonal approx. calcs. 80—53130
- H_2, electron scatt., isotope effects 77—58188
- H_2, electron scatt., iterative static-exchange calc. 79—18290
- H_2, electron scatt., low energy, rot. resons. 78—33608
- H_2, electron scatt., low energy, multichannel variational calcs., static exchange approx. 80—83483
- H_2, electron scatt., Schwinger variational principle, static-exchange approx. 80—63820
- H_2, electron scattering, low energy, R-matrix calc. 79—59571
- H_2, electron total scatt. intensity, first Born approx. , SCF CI calc. 77—10755
- H_2, exchange effects in independ. atom model 79—22837
- H_2, Gaussian basis Glauber approx., elastic and vibrorotational excitation cross sections 80—58399
- H_2, intermediate and high energies, independ. at. model 80—37884
- H_2, modified Glauber theory 78—94320
- H_2, positron scattering, 50-800 eV, total cross-section meas. 79—31680
- H_2, static exchange approx., variational correction 79—7015
- H_2^+, electron elastic scatt., two-centre variational calc. of s-wave phaseshift 79—3570
- H_2^+, electron elastic scatt., phaseshifts, quantum defect and two electron excited states 80—91671
- H_2^+, electron scatt., Schwinger variational principle appl. 80—48086
- H_2^+, electron scatt. eqns. convergence, H_2 continuum states, appl. to photoionis. 78—66663
- H_2+e, elastic scatt., incident energies, 100-2000 eV, calcs. 78—55237
- HBr, electron scatt., elastic rot. scatt. and vibr. excitation 78—58822
- HCN, elastic electron scatt. differential cross section, 3-50 eV, 20-130°, rel. to He 78—90291
- HCN, electron elastic scatt., differential cross-sections, effective range theory 80—83485
- HCl and HBr, low-lying reson. states in 0.25-1.15 eV electron scatt. 79—45844
- HCl elastic electron scatt., short-lived resons., theory 77—14578
- HCl, electron elastic scatt., exchange and polarisation 80—91668
- HF, elastic electron scatt., short-lived resons., theory 77—14578
- H_2S, electron impact, vibr. elastic scatt. and vibr. excitation 79—13822
- H(1s), electron elastic scatt., semiclassical and quantal treatments 77—38733
- H(1s) electron scattering, variable-charge Coulomb-projected Born approximation 80—58392

elastic scattering of electrons by atoms and molecules continued
H(2s), optical model approach to elastic scattering of electrons, polarisation effects 80—58382
He, 0-16.5 eV electron scatt., R-matrix calc. 79—36768
He, 0.00136 to 50.40 eV, adiabatic exchange approx. 77—30991
He, absolute total scatt. cross sections, 0.5 to 50 eV 78—74765
He, angle depend. resonance profile parameter 77—88563
He atoms, matrix effective potential for electronic response in 30-400 eV electron scatt. 80—58388
He, Born approx. 77—57217
He, differential cross-section, 2-19 eV 79—54966
He, effective collision freq. of electrons 79—3566
He, elastic electron scatt., resonance struct. 77—50532
He, elastic electron scatt. phaseshifts, 2s2p ^{3}P autoionisation, 1s2s ^{3}S→1sεp ^{3}P triplet continuum photoionisation 79—31480
He, elastic electron scatt., differential cross sections, eikonal approx. 80—53138
He, elastic scatt. of electrons and positrons 77—19075
He, elastic scatt. of electrons in second-order eikonal approximation 80—91667
He, electron and positron elastic scatt., DWBA 77—30995
He, electron and positron elastic scattering, 100 and 200 eV, differential cross section 79—98221
He, electron and positron scattering, second-order pot. method calcs. 79—72419
He, electron and positron total scatt. cross sections, positronium form. 78—62916
He, electron elastic and inelastic scatt., Glauber eikonal series 80—43183
He, electron elastic cross sections, 0.04-1.5 eV 78—42214
He, electron elastic scatt., p-wave reson., Breit-Wigner formula calc., perturbation method 77—38731
He, electron elastic scatt., 50-500 eV, optical model semiclassical wave-function approx. 78—22030
He, electron elastic scatt. at low energy, exchange effects, natural boundary conditions methods 79—22831
He, electron elastic scatt., 5 to 200 eV, cross-sections meas., calibration 80—63822
He, electron elastic scatt., two-pot. eikonal approx. calcs. 80—99573
He, electron elastic scattering, intermediate energy plane wave approx. calcs. 77—10758
He, electron elastic scattering, intermediate energy 78—22032
He, electron elastic scattering, 100-500 eV, optical model, two-pot. approx., ang. depend 78—25701
He, electron elastic scattering, total cross-section calcs. 78—42220
He, electron elastic scattering, improved second Born calc. at intermediate energies 79—36770
He, electron scatt., effective pot. calcs. 80—53131
He, electron scatt., Glauber-Bonham-Ochkur exchange amplitudes 80—69237
He, electron scatt., He$^-$ resonances in post collision interaction 79—13820
He, electron scatt., ionisation, elastic and inelastic collisions, many body theory appl. 80—48093
He, electron scatt., momentum transfer cross-section, 4 to 12 eV 77—68115
He, electron scatt., near 2^1S-state threshold, S-matrix obs. 77—10761
He, electron scatt., total cross-sections, meas. apparatus 77—54628
He, electron scatt. resonances during dilatation transformations, reson. eigenvalues stability 79—18291
He, electron scattering, by long-range pots. summation of partial wave expansion 79—41239
He, electron scattering, differential cross-sections, eikonal approx. calcs. 79—81278
He, electron scattering, elastic, at low-energy, polarised orbital calc. 78—82840
He, electron scattering, intermediate energy, absolute total cross-section meas. 80—18926
He, electron scattering, low energy, R-matrix calc. 79—59571
He, electron scattering, optical pot. methods 80—102569
He, electron scattering amplitudes for energies less than 19 eV 79—45845
He, electron scattering length, using effective range theory, 0.009-0.4 eV 78—17793
He, electron scattering total cross sections, 0-3000 eV 78—25709
He, electron shadow scattering, cross-sections calcs. 79—59575
He, excited, optically-allowed, long-range interaction pots. with electrons, protons and atoms 77—14520
He, Glauber scatt. amplitude, numerical method in Lommel function 79—22795
He, local optical pot., second order partial wave amplitude 78—25703
He, low energies, phaseshift evaluation by pseudopotential method 79—22830
He, low energy positron scattering 79—89786
He, many-body method, 30-200 eV 80—5620
He, many-body method, 30-200 eV 80—5621
He, minimum-variance method, discrete-basis-set approach 77—83734
He, modified Glauber approx. 78—74764
He, phaseshift anal. of ang. distribs. 79—22833
He, positron and electron elastic scatt., 100-700 eV, optical model calcs. 77—34761
He, positron annihilation, average energy, lifetime spectrum, Monte-Carlo calcs. 77—88558
He, positron diffusion in gas, annihilation and scatt. 77—19074
He, positron elastic S-wave collisions, optical pot. formulation 77—14576
He, positron elastic scatt., polarised orbital approx. 77—30996
He, positron elastic scattering, total cross-section calcs. 78—42220
He, positron s-wave scatt., total cross sections 77—42406
He, positron scatt., intermediate energy, total cross sections, modified Glauber amplitude 80—23549
He, positron scatt., low energy elastic cross-sections 78—5343
He, positron scatt., polarisation effects, orbitals calcs. 77—3457
He, positron scatt., total cross section 78—70933
He, positron scatt., total cross section meas., with positron TOF spectrometer 79—3568
He, positron scatt., total cross sections 79—86065
He, positron scatt. cross sections 79—3569
He, positron total scatt. cross sections 77—14573
He, positron total scatt. cross sections 77—83729
He quantum defects rel. to angular momentum, nuclear charge, Coulomb-Born approx. method *(Japanese)* 77—50534

elastic scattering of electrons by atoms and molecules continued
He, s- and p-wave scattering T-matrix eqns., discrete basis function calcs. 80—23551
He, scattering, differential cross sections, variational calc. electron elastic scattering, differential cross sections, variational calc. 79—89785
He, Schwinger variational principle, including exchange 79—81277
He, slow positron elastic scatt. phase shifts, simplified RPA calcs. 77—10759
He, total cross section 80—37881
He, total scatt. cross sections for low-energy electrons 80—58417
He, zero-energy Born exchange amplitude 77—38732
He$^+$, electron scatt., elastic, ^{1}P continuum phaseshift, autoionis. state 77—88561
He$^+$, electron scatt. ^{1}S reson., restricted perturbation scheme calcs. 77—83736
He$^+$, modified Coulomb-Glauber approx. 78—86949
He(2^1S, 2^3S), elastic electron scatt., 7-500 eV Glauber cross sections 77—19077
Hg, absolute total cross section 79—59570
Hg atoms, elastic electron scatt., relativistic effects 80—102568
Hg, electron drift vel., momentum cross-section, theory 78—30404
Hg, electron elastic scatt., 4-6 eV, reson., scatt. ang. and spin polaris. spectra 78—25702
Hg, electron elastic scattering, 8 to 18 eV, electron spin polaris. 80—91669
Hg, electron impact spectra, intermediate energy 78—82842
Hg electron resonant elastic and inelastic scatt. *(Russian)* 80—78710
Hg, electron spin polarisation, detector, experimental exam. 78—32927
Hg, positron scatt. at low energy 80—91670
I_2, equilibrium parameters and Morse anharmonic consts., electron diffr. determ. 78—58818
K, electron elastic and inelastic scatt., 54.4-217.7 eV, 2-145° 80—1067
K, normalized momentum-transfer, differential and integral cross sections, 6.7, 16 amd 60 eV 77—68117
KI, electron impact, elastic scatt., model, static and static exchange calcs. 78—94321
KOH, electron collisions, integrated and momentum transfer cross sections, cond. integrals 79—41238
Kr, elastic positron scatt., phaseshifts and elastic, diffusion and annihilation cross section 80—53134
Kr, electron pot. scatt., 100 and 500 eV, extended Glauber approx. calcs. 77—54610
Kr, electron scattering, elastic, low-energy, polarised-orbital calcs. 80—37882
Kr, large angle elastic and inelastic electron scatt. differential cross section, exchange corrections 80—28111
Kr, total scatt. cross section, 20-3000 eV 79—36778
Li, adiabatic exchange approach, integral form 79—31684
Li, electron and positron scattering, second-order pot. method calcs. 79—72419
Li, electron elastic scatt., differential cross-section, local optical pot. calcs. 77—10760
Li, electron elastic scatt., two-pot. eikonal approx. calcs. 80—99573
Li, polarised orbitals method modification 79—22835
Li$^+$ quantum defects rel. to angular momentum, nuclear charge, Coulomb-Born approx. method *(Japanese)* 77—50534
Li_2, electron scatt., effective pot. calcs. 80—53131
LiF, elastic and rot. excitation cross sections for electron scatt. 78—46446
LiF, elastic electron scatt. intensity, rel. to electron density distrib. 78—1079
LiF, electron elastic scattering, by highly polar mols., chem. bond effects 78—9248
LiF, electron elastic scatt. cross sections 78—50641
LiF, electron elastic scatt., differential cross-sections, effective range theory 80—83485
LiF, electron impact, elastic scatt., model, static and static exchange calcs. 78—94321
LiF, electron scatt., orthogonalisation and model exchange pots. calcs. 80—23552
LiF, electron scatt., quasiclassical close-coupling approximation 79—81280
LiF, electron scattering; differential cross sections, three part hybrid method 80—58381
LiH, electron elastic scattering, by highly polar mols., chem. bond effects 78—9248
LiH, electron scatt., low energy, multichannel variational calcs., static exchange approx. 80—83483
LiH, electron scatt., orthogonalisation and model exchange pots. calcs. 80—23552
LiH molecule, fast electron elastic scatt. intensity calcs. 77—3459
Li_2O, elastic electron scatt. intensity, rel. to electron density distrib. 78—1079
Li_2O, electron elastic scattering, by highly polar mols., chem. bond effects 78—9248
Mg, ^{2}P shape reson., electron scatt. calc. 79—41240
Mg, cross sections 10, 20, 40 eV 78—70940
Mg, electron scatt., effective pot. calcs. 80—53131
Mg, electron scatt. cross sections, close coupling calc. with CI 80—43180
Mn, elastic and inelastic electron scatt. 10 to 100 eV 78—70934
N, cross sections 77—50538
N, effective collision freq. of electrons 79—3567
N, elastic electron scatt., low energy, linear algebraic method 77—88562
N, electron elastic scatt. resonance, neutral bremsstrahlung 77—46639
N isoelectronic sequence ions, atomic struct. and electron scatt. data 80—51649
N, low energy elastic and inelastic scatt. Bethe-Goldstone and pseudostate approx. 77—68112
N, low energy elastic scatt., pseudostate and Bethe-Goldstone approx. 77—68111
N$^-$, continuous absorption coeffs., from elastic e-N scatt. data, target wavefunction effect 78—9128
N_2, 50 eV, centrifugal-dominant channel decoupling, INDOX polarised SCF model 80—32831
N_2, computer anal. of differential cross section 77—58160
N_2, differential cross-section, 0-30 eV 78—78815
N_2, discharge, excitation efficiency of rot. and vibr. levels, heating due to elastic collisions and relax. 80—38751
N_2, eigenphase sums 77—42407
N_2, elastic and inelastic electron scatt. differential cross section, obs. and calc., struct., binding energy 80—28109

elastic scattering of electrons by atoms and molecules continued
N_2, elastic and inelastic electron scatt., state to state cross section 80—78708
N_2, elastic electron scatt., total cross-section, 0-1000 eV 78—17795
N_2, elastic electron scatt. from 0 to 1000 eV, energy dependent exchange pots., continuum multiple scatt. method 80—43182
N_2, electron elastic low energy scatt., ab initio pseudostates calc. 78—9247
N_2 electron elastic scatt., differential cross-section meas. 77—3458
N_2, electron elastic scatt., discrete basis static exchange approx. calcs. 78—42219
N_2, electron elastic scatt., free-electron-gas model exchange pot. 78—58824
N_2, electron elastic scatt. differential cross section 79—86067
N_2, electron elastic scatt. cross-sections calcs. 80—48088
N_2, electron impact, differential cross-section, converged close-coupling calcs. 78—90290
N_2, electron impact rot. and vibr. excitation, elastic scatt., close coupling and Born approx. 80—28108
N_2, electron scatt., 50-500 eV, two-pot. approach 79—41242
N_2, electron scatt., absolute total cross-sections 80—83486
N_2, electron scatt., effective pot. calcs. 80—53131
N_2, electron scatt., elastic and inelastic, Glauber approx. 80—91695
N_2, electron scatt., Glauber eikonal approx. calcs. 80—53130
N_2, electron scatt., iterative static-exchange calc. 79—18290
N_2, electron scatt., local exchange pot. comparison 80—78707
N_2, electron scatt., low energy, multichannel variational calcs., static exchange approx. 80—83483
N_2, electron scatt., total cross-sections, meas. apparatus 77—54628
N_2, electron scattering, 13.6 eV, coupled channel treatment calcs. 79—64106
N_2, electron scattering, charge polarisation effects, SCF treatment 79—50132
N_2, electron scattering, low energy, R-matrix calc. 79—59571
N_2, electron swarm parameters for high E/N, Monte Carlo simulation 80—19548
N_2, large angle elastic and inelastic electron scatt. differential cross section, exchange corrections 80—28111
N_2, low energy electron scatt., N_2^- resonance at 2 eV as energy standard 77—71872
N_2, low-energy elastic scatt. cross sections 78—42213
N_2, multiple scatt. method, scatt. cross section calc. 80—63816
N_2, R-matrix, low-energy scatt., static-exchange approx. 78—13601
N_2, total cross section 80—37881
N_2, X-ray and electron scatt. first Born approx. calc. 77—61867
N_2, X-ray and high-energy elastic electron scatt., vibr. averages 79—81279
NH_3, 35 keV electron elastic differential cross section, bond formation, independent atom model 79—31683
Na, 54.4-150 eV differential cross-sections, 12-140°, optical model calcs. 78—74761
Na, efficiency laser ionisation via superelastic collisions and reduced ionisation pot. 77—79588
Na, electron drift vel., momentum cross-section, theory 78—30404
Na, electron scatt., crossed beam study 80—91672
Na, excited, electron scatt. at low energy, total cross section 80—63821
Na, slow electron scatt., computer calcs. 77—50530
Na^+, electron scatt., reson. rel. to $2s2p^63s^2$ term position and width 79—59347
$Na(3^2P_{3/2})$, electron total cross section, at. beam recoil technique 77—27186
Ne, 10^2-10^3 eV, direct, exchange, and polaris. effects, cross sections calc. 78—42215
Ne, 40 keV electron scatt., 7-200 mrad, relativistic and electron correlation effects 77—34760
Ne, effective collision freq. of electrons 79—3566
Ne, elastic electron scatt., resonance struct. 77—50532
Ne elastic electron scattering, crit. point 80—5622
Ne, electron and positron elastic scatt., DWBA 77—30995
Ne, electron and positron total scatt. cross sections, positronium form. 78—62916
Ne, electron elastic cross sections, 0.04-1.5 eV 78—42214
Ne, electron elastic scatt., differential cross-section meas. 77—3458
Ne, electron scattering, elastic, at low-energy, polarised orbital calc. 78—82840
Ne, electron scattering, elastic and inelastic, reson. spectra, R-matrix calcs. 79—72421
Ne, electron shadow scattering, cross-sections calcs. 79—59575
Ne, low energy positron scattering 79—89786
Ne, phaseshift anal. of ang. distribs. 79—22833
Ne, positron and electron elastic scatt., 100-700 eV, optical model calcs. 77—34761
Ne, positron elastic scatt., close-coupling calc. 78—90292
Ne, positron scatt., total cross sections 78—22031
Ne, positron scatt., total cross sections 79—86065
Ne, positron scatt. and annihilation 78—33606
Ne, positron total scatt. cross sections 77—14573
Ne, positron vel. distrib. at equilib. elec. and mag. fields 77—71870
Ne, total scatt. cross section, 20-3000 eV 79—36778
O, cross sections 77—50538
O, effective collision freq. of electrons 79—3567
O, low energy elastic and inelastic scatt. Bethe-Goldstone and pseudostate approx. 77—68112
O, low energy elastic scatt., pseudostate and Bethe-Goldstone approx. 77—68111
O, low-energy elastic scatt. cross sections 78—42213
O, low-energy electrons integral scatt. cross section 78—69556
O_2, differential and integral cross sections 79—10216
O_2, interactions with slow electrons 79—45848
O_2, low-energy elastic scatt. cross sections 78—42213
O_2, X-ray and electron scatt., first Born approx. calcs. 77—61867
O_2^-, $A^2\Pi_u$ state pot. energy curve, MCSCF calcs. 80—63565
O_3, low energy elastic and inelastic electron scatt., rot. transitions, close coupling calc. 80—78706
OCS, electron elastic scatt., 0 to 100 eV 80—23547
OCS, electron scatt., absolute total cross-section meas. 78—74774
Rb, differential spin exchange, differential cross section 77—535
SF_6, electron elastic scatt., total cross-section, multiple scatt. calcs. 79—7014
SF_6, electron elastic scatt., shape resonances 79—18289
SF_6, electron elastic scatt. resons. 80—53133

elastic scattering of electrons by atoms and molecules continued
SF_6, electron impact, elastic scatt., absolute differential cross-sections meas. 79—36767
SF_6 electron scatt., total absolute cross sections, 0.5-100 eV, incl. reson. struct. 79—45843
ScOH, electron collisions, integrated and momentum transfer cross sections, cond. integrals 79—41238
Si, scatt. of slow electrons 77—88564
T 79—45757
Tl vapour, electron drift vel., momentum cross-section, theory 78—30404
U, atomic model 79—41095
U^+, atomic model 79—41095
W, fast electron beam scatt. calcs. 77—65534
Xe, 5-300 eV, 30-120°, scattered electrons spin polarisation 80—23548
Xe atoms scattering, expt. 79—857
Xe, elastic electron scatt., 2-300 eV, ang. distrib. 80—43179
Xe, elastic positron scatt., phaseshifts and elastic, diffusion and annihilation cross section 80—53134
Xe, electron scattering, elastic, low-energy, polarised-orbital calcs. 80—37882
Xe, polarisation of elastically scatt. electrons, 150-1200 eV 77—38734
Xe, Ramsauer effect enhancement in mag. field 80—53137
Xe, total scatt. cross section, 20-3000 eV 79—36778

elastic waves
see also acoustic waves; Love waves; magnetoelastic waves; Rayleigh waves; seismic waves; vibrations
absorbing boundary conditions for wave equation 78—59320
absorbing media, acoustic pulse deform., numerical calc. algorithm *(Russian)* 80—96591
acceleration one-dimens. waves, chemically reacting elastic materials 77—75829
acceleration wave reflection in elastic-plastic medium 79—7331
acceleration waves at boundary between two nonlinear elastic materials, reflection and refraction 79—98650
acceleration waves in anelastic bodies, propag. conditions 77—1169
acceleration waves in binary elastic materials, effect of memory, diffusion, multiple temp. 79—50640
acceleration waves in constrained elastic rods 80—53672
acceleration waves in deformable dielectrics with memory 77—1170
acceleration waves in elastic dielectrics with internal state variables 79—47396
acceleration waves in thermoelastic incompressible solids, propag., amplitude 77—19555
acoustic beam interaction with elastic hollow sphere in acoustic fluid *(Ukrainian)* 80—69710
acoustic emission leak detection, attenuation of elastic waves in pipelines 78—27711
acoustic liquid, thermoelastic scatt. effect on wave processes in piecewise inhomogeneous space with plane interface *(Russian)* 77—55317
acoustic method for determ. biaxial residual stresses *(Russian)* 77—19560
analytic quantisation 79—88815
anisotropic materials, propag. from spherical and cylindrical cavities 77—72213
anisotropic media, asymptotic equipartition of kinetic and strain energy 80—92081
anisotropic media, criteria for cusp points on elastic wave surfaces 79—37236
anisotropic media, elastic wave propagation, point pulse source 80—3939
anisotropic medium, perturbed, propag. of elastic waves *(French)* 79—42144
anisotropic two phase media, freq. depend. of elastic wave velocity and attenuation 79—50644
Armenian basic and ultrabasic rocks, elastic wave vels. at high pressures 77—44972
asymmetric elastodynamics with homogeneous initial conditions, Boggio's type theorem 78—26037
asymmetric impact of finite bars, finite element method 77—75847
asymmetry-axis waves for transversely isotropic media 77—68500
bar, nonuniform elastic, longit. vibr. dynamics of impact excitation 78—75086
bar, phase velocity of longitudinal impact wave, tensor wave theory *(Japanese)* 77—72228
bar, rectangular cross section, dispersion relations of elastic waves 78—9585
bar with various bends, dynamic stress conc. due to flexural wave propag. 77—23904
Barre granite, prop. determ. and wave propag. 77—56617
bars, phase boundary propagation, dynamic elastic bar theory, sound wave interactions 80—69706
bars with central circular holes, dynamic response to longit. impact 77—65703
BCC crystal, elastic constants, thermal expansion and bulk modulus 80—6452
beam, composite anisotropic, torsional vibration, torsional wave dispersion *(French)* 77—14934
beam, short rectangular, bidimensional anal. of longitudinal vibration *(French)* 77—7328
beam, thin, semi-infinite, transversal displacement 80—74802
beam, Timoshenko's shear coeff. variation with frequency 79—32367
beams and rods, dispersive waves, experimental study using FFT 79—46275
Beltrami-Michell and Beltrami-Michell type eqns. in static and dynamic elasticity 77—53782
bending waves in thin shells 77—50971
BKZ viscoelastic fluids, acceleration waves of arbitrary form 77—62224
bodies with initial stresses, elastic wave propag., review 80—38323
body waves, short period, propag., isotropic scatt. model including wave conversions 78—40510
bonded dissimilar half planes having Griffith crack at interface, elastic wave interaction 78—67091
bone, wave propag. in piezoelectric two-layered cylindrical shell with hexagonal symmetry 78—55487
bore hole explosion, elastic wave emitter model 77—33005
borosilicate glass, interaction between EM and elastic waves at low temps. 77—31724
boundary friction effects on elastic wave propag. 79—46242
Bragg light scattering at elastic waves, acoustic activity in crysts. *(Russian)* 77—62587
brittle materials, water drop impacted, damage thresholds 80—81149

elastic waves continued
buried impulsive load, effect on viscoelastic layer on elastic half-space 80−28428
cantilever follower force problem, non-conservative load, boundary conditions and stability 77−46956
capacitative excitation of elastic oscillations 80−71862
cenotypal volcanogenic rocks under hydrostatic press., longitudinal wave vel. *(Russian)* 77−73722
characteristic eqns. for homogeneous elements of mechanical structures 79−30265
charged particle beams in liqs., elastic wave excitation, microscopic bubble acoustic emission 80−43516
circular discontinuity in elastic plate dynamic stress conc. during passage of cylindrical wave 77−62191
circular rod, controlled impact on isotropic, elastic half-space 79−90167
circular viscoelastic porous shell, dispersion of longitudinal waves *(Russian)* 78−42556
circumferential waves, cylindrical shell supported by a continuum, dispersion relations 78−90564
classical Lamb problem, time-harmonic soln. for elastic head waves 78−63215
colliding elastic bodies, nonlinear surface waves *(Ukrainian)* 79−32331
composite, fibre-reinforced, layered, harmonic elastic waves, dispersion 78−63223
composite material, modelling as interpenetrating solid continua, plane wave solns. 78−13895
composite materials, 3-D, harmonic waves 77−891
composite materials, elastic constant estimation, elastic wave scatt. theory 80−34114
composite materials, fibre reinforced, rectangular rods, elastic wave propagation *(French)* 80−83749
composite panel under fluid loading, reflection and free wave props. 80−14603
composite semi-infinite rod, wave propagation 80−10180
composites, fibrous, elastic shear waves propagation 80−58963
compressible hyperelastic solids, spherical wave propag. analysis 77−58588
compressional and shear waves in saturated rock during water-steam transition 80−30995
compressional impulse interaction with slot normal to surface of elastic half space 79−50626
compressional wave vel. temp. depend. in anisotropic dunite 78−77224
conical bar, transients propag. treated by Rayleigh's correction 79−81749
conservation laws, Riemann problem 80−42059
constant Q-wave propagation and attenuation 80−30996
controllable propagations, finite deformations, cylindrical shell 77−7329
Cosserat medium, hemitropic, propag. of plane, cylindrical and spherical waves 78−20968
couple stress effects on elastic waves and vibr. 79−14307
couple stress effects on wave prop. in elastic layer immersed in infinite liquid 79−1126
coupled dynamic thermoelasticity problem for a half space with thermal 'memory', thermoelastic waves 80−83753
coupled solid/fluid/surface wave dynamic interaction problem, improved fluid superelement 78−81108
crack characteristics from elastic wave scatt. using quasistatic approx. 79−37241
crack scattering in polycrystalline media, ultrasonic attenuation meas. 78−75089
crack tip elastodynamic fields, stress intensity factors 77−68535
cracked elastic solid, 3-D wave propagation 79−46251
cracks, action as elastic wave radiation, rel. to AE signal charact. 78−60952
cracks, Rayleigh scatt. of elastic waves 79−55343
creeping locomotion kinematic modes, ideally elastic model 78−15853
creeping waves on curved body, rel. to normal modes of vibr. 77−50817
critical reflections of axially symm. waves in isotropic hollow cylinder 77−31242
crystal, elastic wave theory *(Russian)* 79−7320
crystal, hexagonal, and tranversally isotropic media, transient displacement field 77−75846
crystals, special surfaces and directions, elastic surface wave existence 80−92604
crystals, strain wave vels., Poisson ratios and elastic moduli 78−51609
cubic crystal, acoustic waves, Christoffel elastic eqns., and elastic consts. 79−51205
curved fluid-solid interface, shock wave front propagation 77−46962
cuspidal edges for wave surfaces in cubic crystals 77−51436
cyclic stress amplitude meas. by time-averaged photoelasticity 78−18261
cylinder, elastic, of finite length, free oscill. calc. 77−35078
cylinder, surface impact, numerical soln. 80−38274
cylinder, torsional vibr. superposed on finitely deformed state 80−19263
cylinders and plates, dynamic deform. at high frequencies *(Russian)* 78−18223
cylindrical anisotropic waves propagation in nonhomogeneous material 79−32364
cylindrical cavity in absorptive medium, elastic wave reflection 78−55582
cylindrical cavity in anisotropic elastic material, impact-initiated wave propag. 78−13943
cylindrical impact waves in inhomogeneous viscoelastic media 79−14295
cylindrical non-axisymmetric wave propagation in laminated medium, continuum theories 79−14293
cylindrical rod, linearly elastic, elastic waves anal. from two-point strain meas. 77−72211
cylindrical rod, periodic structure, torsional vibrations, interfacial elastic parameters 80−96215
cylindrical shear wave propag., inhomogeneous viscoelastic solids 78−75090
cylindrical shell, longitudinal wave propagation *(Russian)* 77−65714
cylindrical shells with finite regions of structural discontinuity, wave propag. 78−13841
deformation wave processes, corrected nonlinear eqns., stresses and strains 80−102998
deformed compressible elastic material 79−14338
deformed material, speed of propagation of waves 78−54201
deformed Mooney-Rivlin material, transverse waves 77−26178
diatomic elastic solids, nonlocal continuum theory, kinematics, balance laws, wave propag. 78−9559
diatomic solids, thermoelastic, continuum theory 80−53635

elastic waves continued
diffraction, two-dimensional, for semi-infinite plane screen *(Russian)* 78−28955
diffraction at a spherical cavity, stress field, finite difference method *(Russian)* 79−68617
diffraction at segment, exact solns. 77−84189
diffraction by a crack of a cylindrical longitudinal pulse 80−92082
diffraction by cracks, surface-wave rays 78−79161
diffraction by cylindrical cavity in half-space 79−23110
diffraction by semi-infinite solid's periodic rigid boundary 78−90768
diffraction by small cylindrical cavities 79−68636
diffraction by wedge, three dimensional nonstationary problem 80−69723
diffraction of longitudinal waves at elastic circular inclusions (fibres) *(Russian)* 78−63368
diffraction of spherical wave at wedge *(Russian)* 77−35073
diffraction of stationary and nonstationary waves, survey *(Russian)* 79−18795
dilatant (nondilatant) media, shock wave propagation 80−14608
discontinuity wave propagation in elastic body with dislocations 79−18787
discrete wave number representation of elastic wave fields, three-dimensional generalisation 80−3945
dislocations moving nonuniformly, elastic half space response to realistic faulting model 78−85486
dispersion spectra, freq. coalescence and conical points 77−46955
displacement field due to P or SV incident waves on elastic sphere *(French)* 80−36847
dissipative media, hyperbolic elasticity and wave propag. modes 77−45699
DNA film, vel. of propag. *(Russian)* 77−51511
dolomite, compressional wave data rel. to strain rate depend. 77−44977
dynamic axisymmetrical elasticity problems soln. using factorised differential systems of second-order accuracy *(Russian)* 80−8796
dynamic contract of elastic bodies, direct connection and feedback mechanism *(Russian)* 79−50670
dynamic response of variable section rod subject to longitudinal impact with flexible load 77−89036
dynamical contact problem, shock waves in elastic layer after impact *(Russian)* 80−23964
dynamical problems, radiation condition *(Russian)* 78−20973
dynamics of elastic layer, approx. eqns. 79−7326
edge effect analysis of the linear theory of elastic continua mixture *(Ukrainian)* 80−69711
edge notched brittle plates, virgin waves and boundary reflections at fracture 80−79233
edge waves under biaxial initial stresses 78−79248
eigenvalues of stochastic differential operator, approx. soln. of mean problem *(German)* 78−12540
elastic impact problem, stress wave elementary analysis 79−50628
elastic laminated composites, transient wave propagation 79−50630
elastic layer in acoustic medium, wave dynamical characteristics *(Russian)* 79−76995
elastic material, non-linear, thermodynamic theory, considering thermal vel. waves 77−62189
elastic materials, strongly anisotropic, wave propagation 79−14300
elastic media, longit. shear fracture, dynamical problem for region with curvilinear cuts 78−81842
elastic plastic half-plane under movable loads, propag. of plane waves *(Russian)* 78−5685
elastic strip with fluctuating parameters, flexural wave characts. 79−23116
elastic wave propagation, influence of random porosity 78−90552
elastic-plastic, propagation, influence of energy dissipation 77−7326
elastic-plastic wave propagation, transmission of elastic-plastic boundaries 77−62188
elastic-viscoplastic materials delayed behaviour of double shear perturbations 78−45483
elastic-viscoplastic skewed plates, impact, anal. of combined pressure-shear waves 77−65712
elastic/viscoelastic bar interface, impact wave behaviour 78−26075
elastic/viscoplastic plate, combined longitudinal/torsional stress wave propag. *(Japanese)* 78−38227
elasto-plastic half-plane generated by supersonic variable load *(Russian)* 79−10526
elasto-plastic medium, compressible, coupled dilatational and shear waves, proagation speeds 77−893
elastodynamic diffraction, by periodic rough surface (stress-free boundary) 78−13826
elastodynamic diffraction, two-dimens., by cracks, matched asymptotic expansions 80−1468
elastodynamic stress intensity factors, ray theory approach 79−7339
elastodynamics with rigid inclusions, identities 79−10422
elastoplastic spherical and cylindrical waves, interface existence 77−7331
electroelastic plane wave propagation in piezoceramic medium *(Russian)* 77−55752
electromagneto-thermoelastic plane wave propag. phase vel. and attenuation coeff. 80−48621
ellipsometer for meas. of material property variations 79−46143
elliptic thin cylindrical shells, hydrostability 77−75830
elliptical cylinders, free harmonic waves propag. *(German)* 77−62186
elliptical cylinders, scatt. matrix for elastic waves 78−59324
EM transducer with periodic permanent magnets, horizontally polarised shear elastic wave excitation 79−76932
emission by small sources in heterogeneous elastic media 77−56599
end-fire piezoelectric transducers, wideband excitation of surface elastic waves in microwave range 80−10105
equipartition of energy in elastic wave propagation 79−64570
Eulerian computation technique for domains with moving boundaries 77−53779
exceptional surface waves in triclinic crysts., existence problems, general props. 80−92603
exceptional wave propagation in continuous medium, finite deform., evolution of discontinuities, elastic pot. determ. *(Italian)* 78−54202
excitation and proagation of elastic waves, book 80−94937
excitation by laser beam, through thermoelastic effect 80−103503
explosion-generated longitudinal and surface waves, mutual conversion 77−70610
extensional stress pulses, energy transmission from bar to helix of small pitch 77−19564
ferrite, magnetoacoustic reson. in strong mag. field 80−11309

elastic waves continued
ferromagnets, higher order surface couplings 78—79212
fibre composites, orthogonally reinforced, wave propagations 78—41168
fibre reinforced composite, dynamic model 77—68496
fibre reinforced composites, Longitudinal wave behaviour at low and high frequencies 78—38246
fibre reinforced composites, surface wave propag., load transfer from reinforcement to matrix 78—46904
fibre reinforced composites, ultrasonic vibrs. propagation velocity, dependence on composites elastic props. 80—5975
fibre reinforced composites, wave guide-type propag., microstruct. theory 78—83279
fibre-reinforced composite, mixture theory for longitudinal waves in rectangular fibre arrays 78—9590
fibre-reinforced composite, small vibr. propag. in static deformation 77—42775
fibre-reinforced continuum, wavefront motion *(German)* 77—35068
finite amplitude, in nonlinear elastic half-space, numerical method 77—48
finite amplitude standing waves in compressible elastic solids 79—18784
finite disc, thermal shock, finite integral transform method 77—3765
finite plate, propag. mode III crack, dynamic stress intensity factor, reflected stress waves 80—103001
flexural vibr. of elastic plate, energy flux vector *(Russian)* 77—42773
flint glass, dense, nonlinear elastic props. *(French)* 80—34132
fluid and isotropic solid acoustic harmonic generation 77—27417
fluid filled cavities in elastic solids, fluid identification using resonance method 80—64452
fluid filled elastic tubes, effect of governing eqns. nonlinearity 77—89055
fluid saturated porous elastic solid, wave propagation 79—81750
fluid-filled porous media, response to transient input 77—31244
fourth order, general method for determ. and appl. 80—34119
fracture, ductile, relation to elastic vibr. emission, defects 77—75855
free wave motion in periodic systems with multiple disorders 79—23247
frictional boundary, transmission (reflection), approx. anal. method 78—63371
frictional interface, elastic wave reflection, refraction and absorption, SH motion 80—64437
front excitation and diffr., by point source with semi-infinite shield 80—79202
fundamental symmetric Lamb wave, refl. at edge of semi-infinite plate, variational anal. 77—78987
gas, press. var. along longit. standing wave, teaching 78—12514
gas filled tube, pressure waves *(German)* 78—87295
general electromechanical reciprocity relations applied to the calculation of elastic wave scattering coefficients 79—56729
generalized orthogonality relation for rectangular strips in elastodynamics 79—64567
generation in elastic half space by thermal excitation of finite duration 80—33517
geophysical elastodynamics, group theoretical formulation, seismic sources 77—78126
glass fibre reinforced plastic, dynamic stress conc. around defects, discrete model 80—30024
glass prisms, vel. meas. by pulse technique and propag. theory 79—18636
granular medium, body waves propag. 77—23909
gravitational and acoustic waves in elastic medium, relativistic eqns., neutron star appl. 78—24712
Griffith crack-antiplane shear wave interaction at interface of two bonded elastic half-spaces, geophys., seismological appl. 80—92087
guided waves in wire with weak surface corrugation, mode coupling 80—33271
Hadamard material, dynamic axial shear 77—80102
Hadamard materials, elastic plate waves, dispersion relations 77—50962
half space, plane elastic wave scatt., reciprocity and power flow theorems 80—102997
half-space containing cylindrical inclusion, axisymmetric waves, singularities and wave fronts 78—1603
half-space containing cylindrical inclusion, axisymmetric waves 78—5684
half-space containing cylindrical inclusion, dynamic surface stresses 78—90748
half-space with cavity, SH wave excitation, dynamic stress conc. 77—62194
harmonic wave diffraction at axisymmetric inhomogeneity, polynomial approx. *(Russian)* 77—50968
harmonic wave propagation in a periodically layered, infinite elastic body: plane strain, analytical results 79—64574
harmonic waves in elastic sandwich plates 79—37235
hemitropic micropolar thermoelastic continuum, static and dynamic problems 78—22293
homogeneous anisotropic medium, propag. of wavefront produced by nonstationary source *(Russian)* 77—41489
homogeneous isotropic viscoelastic medium, wave propagation eqns. with time lag 79—35573
hypo-elastic transverse surface waves in internal stratum 77—27481
hypoelastic compressible rate-sensitive material flow, integrable generalized wave eqns. 78—38213
ideal elastic fibre-reinforced slab, dynamic flexural deformations, flexural wave propag. 80—33510
impact, high velocity, three dimens. finite element anal. 77—65674
impact, internal meas. of shear and compression waves, gauge lead effects 80—74817
impact force meas. by elastic stress wave obs. 79—34215
impact of linearly elastic rod on thin linearly viscoelastic target 79—81793
imperfectly periodic structures, random evolution approach 79—14339
impulse attenuation, waves emanating from cylindrical cavity in anisotropic media 77—46954
inclusions, thin, elastic wave scatt. 80—65151
incompressible elastic solids, finite amplitude circularly pol. elastic wave reflection and transmission 80—64448
incompressible isotropic elastic material, Hadamard criterion, wave propagation 79—27571
indentation with perfect adhesion, wave propag. anal. 77—23919
inert gas solid, non-linear and dispersive elastic continuum, wave eqns. of motion 80—15187
infinite cylindrical shell, dispersion curves and distrib. coeff. of elastic waves *(Russian)* 77—46964
infinite elastic bar, induced oscills., normal and associated wave propagation 80—5980

elastic waves continued
infinite elastic medium, diffraction of torsional waves by flat annular crack 80—64447
infinite elastic space with cavity and shell, micropolar elastic wave propag. 80—58950
infinite elastic space with cavity and shell, micropolar torsional elastic wave propag. 80—58951
infinite medium with cavities, response to impact load 77—50945
inhomogeneous anistropic elastic media, cylindrically symmetric waves, propagation and reflection 79—21559
inhomogeneous elastic slab impedance soln. 79—44745
inhomogeneous elastic structures, active compensation of vibrs. 78—18103
inhomogeneous viscoelastoplastic media, wave propagation *(Russian)* 79—32337
interacting finite amplitude waves, reflection and distortion, initial boundary value problem 80—53699
interaction with defects of finite vol. and defect mutual interactions 78—32676
interface of two solids, sliding mechanism without slipping 78—51136
interface separation caused by a plane elastic wave of arbitrary form 79—50643
interface wave guided by thin film between two solids 80—100385
interface waves and sliding between two solids 79—18800
interface waves for nondestructive inspection of engineering materials 77—40481
interface waves involving separation 77—80100
interfacial waves in pre strained neo-Hookian body, biaxial strain states 80—48630
interfacial waves in pre-strained neo-Hookian body, triaxial strain states 80—48631
internal friction measurement by resonant specimen with a dumb-bell shape 80—48660
inverse problem soln. using J-fraction expansion 78—11819
isotropic elastic body, asymptotic distrib. of natural freqs. *(Japanese)* 78—30121
isotropic elastic half-space, response to nonuniformly expanding surface loads, wave fronts 79—81751
isotropic elastic medium, finite deformation shock waves, centric cumulation 80—53673
isotropic half space with embedded anisotropic layer, elastodynamic Green's tensor 80—69732
isotropic homogeneous medium, elastic wave scatt. by circular cylindrical flaws and inclusions 79—86369
isotropic isoceles right-angled triangular plate on elastic foundation, thermal-shock induced vibr. 77—35070
isotropic medium, elastic wave scatt. from flaws, long-wave approx., appl. to ellipsoidal voids and inclusions 79—86368
isotropic medium, elastic waves, mag. field effects 80—58955
isotropic medium, propag. crit. of accel. waves 77—62190
isotropic solid half-space, Rayleigh and leaky surface waves 77—50974
jets produced by shaped explosive charges, particle size distribution in breakup 80—23957
jointed granite in situ, compressional vel. and transport props. 77—66909
Lamb and SH wave propag. in layer with initial stresses 77—35076
Lamb wave propag. on isotropic plates, second harmonic acousto-optic interaction 80—34886
Lamb waves, leaky, in solid plate with water loading on one side *(Japanese)* 77—3690
laminated, initially strained medium 80—38321
laminated composites, mechanics of homogenisation and random evolutions 80—28423
laminated composites, simulation of effect of bonding materials on dynamic behaviour 79—46216
laminated rectangular antisymmetric angle ply plates, shear deform. effects on vibr. 78—63356
laminated viscoelastic composite, wave propag., dispersion relations, mode shapes, variational methods 78—18215
laminates, comparative study of subsonic transverse elastic wave propag. theories 79—14324
laminates, periodic and disordered, wave propag. 77—42768
latex, shear waves, elastic modulus determ., light scatt. 80—58956
layered composites, continuum modelling, SH-wave propag., filtering 77—887
layered cylindrical shell, circumferential waves 79—94533
layered elastic composites, harmonic wave frequency estimation, eigenfrequency bounds 79—46252
layered elastic quarter space, transient contact shear stress under antiplane loads 77—14936
layered half-space, transient response under reciprocating anti-plane shear load 77—14935
layered hyperelastic half-space, one-dimens. propag. of weak discontinuities 78—30226
layered medium, transient wave propagation normal to layering 80—53676
layered systems, film-substrate characts. of phase-velocity dispersion and struct. of waves 80—59775
lenticular martensite growth by transformation wave propag. 80—81055
lexan, stress wave propagation 78—46910
limestone, crystalline, variation of elastic wave velocity *(Japanese)* 78—11887
linear elastic continuum, book 79—25862
linear isotropic dielectric, inhomogeneous plane wave solns., energy flux and group velocity 79—53987
linear isotropic elastic solid, inhomogeneous plane wave solns., energy flux and group velocity 79—53987
linear viscoelastic waves, theory of diffraction *(Russian)* 78—65787
linear wave motions study using FFT, NDT appl. 80—92038
linearised inverse problems, variational approach 79—71259
linearized theory of elastic wave propagation in initially stressed bodies *(Russian)* 78—83318
liquid, three-dimensional gravitationally-elastic, gravitationally-capillary surface waves *(Russian)* 79—32537
liquid flow in viscoelastic tube, wave propag. 78—9714
liquid-filled porous solid, first strain gradient theory of thermoelasticity 77—53783
locally simple unsteady deformations 77—68506
long elastic wave scatt., inverse problem 79—55819
longitudinal, transversally isotropic cylinder with initial stress 80—99934
longitudinal elastic waves, harmonics generation 77—79991

elastic waves continued
  longitudinal propag. theory in solid cylinder under initial stress 78—51116
  longitudinal wave diffraction, geometrical theory for three-dimensional elastodynamics 77—46829
  longitudinal wave propagation in circular cylinder with Cauchy's initial stress 79—37217
  longitudinal wave vel. and absorpt. in rocks and minerals at high press. and temp. 79—39704
  Love waves, propgation and attenuation in elastic solid-liquid-isotropic solid medium 80—17811
  magnetised liquids, separated by thin elastic film, surface stability 79—94727
  magnetoelastic/piezoelectric composite media, SH-type guided elastic waves, transmission line model 78—27069
  magnetostrictive media, slow wave with struct. of EM wave *(Russian)* 77—16251
  magnetothermoleastic waves, propag. in initially stressed conducting layer 79—63
  magnetoviscoelastic initially-stressed conducting medium, plane Lamb's problem 79—37183
  martensitic transformation, elastic wave generation comparable to Bain deform., role of multiphonon processes *(Russian)* 80—84246
  material containing rigid spheres, dynamic model for wave propagation 79—51199
  matrix method of optimal truncation, appl. to scatt. from voids and rigid obstacles 80—62480
  matrix theory of scatt., conservation law 78—63217
  membrane dynamic response to expanding ring load 77—46957
  metal, nonferromagnetic polycryst., EM-acoustic oscills. during EM field emission by inductive convertor *(Russian)* 77—11638
  metal, plastic impact, energy absorbed by elastic waves 80—5972
  metal, polycrystalline, elastic precursor wave model in shock loading 78—1601
  metal, spalling produced by elastoplastic waves 77—80574
  metal and alloy, characts. and effects of laser generated stress waves 79—69192
  metal-liquid interface, laser generated MHz elastic waves 79—73387
  metallurgically bonded plates, structural integrity determ. by high energy impulse 79—39111
  metals, ultrasonic inspection, echo-mirror method with transform. of elastic waves 80—108663
  metals under contact explosion loading, shock damping process 80—54309
  metamorphic rock mass, elastic wave vels. from seismoacoustic methods 77—81871
  micropolar elastic bars with rectangular cross section, wave motion and vibrs. 79—77000
  micropolar elastic cylinder, free vibrs., wave propag., asymptotic anal. 78—51111
  micropolar elastic half space, steady state response to moving loads 77—58577
  micropolar elastic layer, asymptotic anal. of vibr. 77—89061
  micropolar elastic media, anisotropic, propag. of shock and acceleration waves 79—30242
  micropolar elastic solid, wave generation due to action of concentrated forces and body couples 77—22426
  in micropolar elastic solid under conc. forces and body couples 77—889
  micropolar elastic waves in cylindrical bore containing fluid 78—51107
  micropolar elastic waves in cylindrical fluid filled bore 78—46903
  micropolar space with cylindrical or spherical hollow, elastic wave propagation 80—87731
  micropolar sphere, harmonic wave propagation 79—27560
  mixed method in elastodynamics, appl. to plate theory 77—65709
  model sediments, elastic wave propag. 77—73672
  multidimensional wave radiation from source with Gaussian time variation and Gaussian approx. distrib. about spherical sheet 78—45487
  multiple scattering by elastic ellipsoidal inclusions, self-consistent approach 78—63372
  neutron beam channelling and focusing in ferromagnets *(Russian)* 80—107351
  non-homogeneous medium, coupled deform. waves *(Russian)* 80—48635
  non-piezoelectric crystals, long-acoustic wave phase velocity governing by elastic consts. 77—80571
  noncentrosymmetric crystals, effect of electric field on elastic wave propag. rate *(Russian)* 77—85654
  nonhomogeneous elastic rods, similarity soln. of wave propagation 78—59323
  nonhomogeneous media, one dimensional response to acoustic sources 78—18083
  nonhomogeneous viscoelastic media, propag. of initially plane waves 77—11145
  nonlinear aftereffect medium, longitudinal one-dimens. wave propagation 80—5974
  nonlinear deform. wave propagation in dissipative medium, interaction and reverse problems 78—53
  nonlinear dispersive and dissipative wave propagation 77—74231
  nonlinear dispersive elastic solid, standing waves 77—41488
  nonlinear elastic half-space and slab, anal. of moving line force 78—13944
  nonlinear elastic laminated composite, wave propag., geometrical acoustics anal. 77—42774
  nonlinear elasticity of geological media with phase microheterogeneities *(Russian)* 77—73719
  nonlinear hereditary elastic medium, longitudinal wave weak distortion process 80—62473
  nonlinear hyperelastic medium, wave front intensity, ray method calc. 80—43639
  nonlinear isotropic medium, symmetric spherical wave propagation eqns., permissible transform. *(Russian)* 78—87292
  nonlinear mechanics eqns. and entropy growth across a shock, symmetric form 80—69705
  nonlinear mode coupling, numerical investigation 79—7240
  nonlinear mode coupling 77—79990
  nonlinear progressive waves in finitely deformed elastic materials 77—68507
  nonlinear strain waves in viscoelastic rod *(Russian)* 80—1460
  nonlinear transient deformation, multidimensional approach *(Russian)* 77—57203
  nonlinear viscoelastic media, 1-dimens. deformation waves 79—50645
  nonlinear viscoelastic wave of very small amplitude *(French)* 80—8803

elastic waves continued
  nonlinear viscoelastic wave propag., effect of time dependent compressibility 77—39244
  nonlinear wave equns. in Hilbert space, bounds for solns., appl. to nonlinear elastodynamics 77—13618
  nonlinear waves in homogeneous and heterogeneous elastic solids 80—34134
  nylon 6 fibres, dynamic mech. props., interpretive nonlinear viscoelasticity 79—4994
  oblique compression of two elastic spheres 79—27564
  one dimensional plastic materials with work hardening, acceleration waves 79—32339
  one domain ferromagnetic insulators, spin wave and elastic wave interactions 79—73700
  one-dimensional, in continua, non-propagative modes *(Japanese)* 80—4539
  one-dimensional propag., finite element anal. *(Japanese)* 78—28961
  ordered and disordered materials, frequency spectra 77—1168
  orthorhombic ferrimagnets, domain wall motion at near sonic velocity, magnetoelastic interactions 80—34683
  orthotropic regularly layered elastic half-space, elastic wave reflection 80—33522
  P and SV wave scatt. by rigid elliptic cylindrical inclusion in elastic medium 79—76999
  P-pulse propag. in elastic media, finite difference modelling 77—73868
  P-wave scatt. by random distrib. of inclusions 77—886
  P-wave seismograms from continuously varying transition zones, elastic media 78—20362
  perfectly conducting elastic sphere, in vacuum, radial vibr. freq., mag. field effects 80—58955
  periodic elastic media, wave dispersion 79—17244
  periodic heterogeneous ring, harmonic vibrs. *(French)* 79—50621
  periodically layered composites in plane strain, dispersion eqn. for waves 80—79212
  periodically layered medium, wave propag. normal to layering, viscoelastic analogy 80—48636
  periodically reinforced elastic body, wave propag. in plane strain state 79—81803
  perturbation of front of flat plastic wave 79—5980
  piezoelectric crystals, elastic surface waves 80—103558
  piezoelectric crystals, of classes 422 and 622, transverse-transverse elastic polarisation waves 79—95077
  piezoelectric hexagonal crystals., elastic wave propag. *(Russian)* 77—69777
  piezoelectric infinite plate, critical reflection of antisymm. SH waves 77—34990
  piezoelectric media, slow wave with struct. of EM wave *(Russian)* 77—16251
  piezoelectric medium, semibounded, body waves and quasi-body surface waves 80—107367
  piezoelectric medium, wave propag. 79—28042
  piezoelectric plate, infinite, on elastic medium, transient response to pot. pulse 78—52442
  piezoelectric plates, elastic wave vel. control *(Russian)* 79—61310
  piezoelectric solid, appl. of hardened elastic moduli to elastic wave propag. and interaction with charge carriers *(Russian)* 78—35095
  piezoelectric wave, transient scattering from crack 80—43499
  pink westerly granite, wave propag. study by holographic interferometry 78—20536
  plain strain displacement and stress field in transversely isotropic elastic solid 79—14340
  plane circular shearing, incompressible fluids and solids 77—75822
  plane compressional wave attenuation by random distrib. of thin circular cracks 79—27561
  plane elastic standing waves of finite amplitude 78—18218
  plane elastic waves, reflection and refraction at elastic solid plane interface, initial stresses 79—72838
  plane harmonic elastic P and S wave scatt. by spherical inclusions and cavities 78—89353
  plane harmonic waves in pre-stressed heat cond. elastic material 80—62
  plane progressive waves in linear elastic material binary mixture 79—32357
  plane wave diffraction by two parallel half-planes 80—5858
  plane wave propagation in thermoelastic solids with Tolotti's isothermal pot. 79—18786
  plane wave reflection and refraction at elastic interface, initial stress effects 79—62445
  plane wave reflection under initial stresses at free surface 78—55581
  plane waves in generalised thermoelasticity, stability and propagation 79—50618
  plane waves scattering by finite obstacle, reciprocity relations 77—49602
  plasticized epoxy polymer rods, stress wave propag. 79—19322
  plate, deformed elastic, thickness oscillations 80—64439
  plate, rectangular, variable thickness, stability and vibr. anal., finite element method 77—54918
  plate, surface wave generation by turbulent boundary layer flow 80—74843
  plate, thermoelastic, deflection under point heat source 79—32261
  plate, thermoelastic deflection under point heat source 79—32260
  plate, thin elastic, suddenly punched hole, plane stress unloading waves 80—69729
  plate kinematics in oscillatory bending, particle trajectories *(Russian)* 79—37209
  plate-impact recovery expt. using star-shaped flyer 78—18262
  plates, counter elastic waves *(Russian)* 78—14402
  plates, elastic homogeneous and isotropic, transient and time harmonic wave propagation 79—50633
  plates, travelling edge waves 77—27484
  PMMA, stress wave propagation 78—46910
  Poisson's ratio determ. in coarse grained materials 77—86244
  polyvinylidene fluoride piezoelectric film, Lamb and SH wave attenuation *(French)* 80—79196
  poro-elasticity, disturbance due to expanding ring and disc load 78—79250
  poroelastic layered media, waves and apparent additional mass effect 80—53675
  poroelastic medium, semi-infinite waves prod. by surface load 77—19533
  porous elastic half space, Lamb's line load problem 79—30248
  porous elastic half-space, waves prod. by impulsive line load, non-dissipative case 77—23908

elastic waves continued
porous material, long wavelength press. waves and transient regimes *(French)* 77—62193
porous rock, shear propagation of longitudinal wave *(Russian)* 77—54912
porous structure, water-saturated, elastic wave speeds, Biot's theory confirmation 80—103418
prestressed isotropic elastic bodies, exact relativistic theory of principal wave fronts propagation *(French)* 77—67356
prestressed nonlinear elastic solids, exact relativistic theory of wave propag. 79—1124
prestressed relativistic elastic body, principal infinitesimal waves *(French)* 77—67294
progressing torsional loads along a bore in an elastic medium 80—79197
propagation, in thin-walled nonuniform tubes containing incompressible inviscid fluid 77—79981
propagation from moving normal point loads in layered media 77—37157
propagation heterogeneous bars with varying cross-section 77—65707
propagation in cylindrical coord. systems 78—88798
propagation in discrete random medium 77—19554
propagation in highly scattering medium, diffusion approach 77—86804
propagation in infinite bar, elliptical cross section 78—67073
propagation in layered media with lateral inhomogeneities, modal methods 77—73676
propagation in oceanic model sediments 77—44966
propagation in solid layer-liquid system 80—31522
propagation in two-phase media, interaction model 78—18213
propagation in vertically inhomogeneous media 77—73675
propagation of weak waves in elastic-plastic and elastic viscoplastic solids with interfaces, Al calcs. 78—18216
propagation rel. under model and natural conditions, similarity criteria in comparative anal. 79—96742
propagation when negative slope region in stress/strain diagram *(Russian)* 78—79255
pulse propag. in media with freq. dependent Q, theory 80—72438
quantum effects of lattice elastic surface waves 77—1290
quantum elasticity theory, resolving functions and potentials for linearised eqns. 77—22425
quantum theory, natural vibrations of rectangular parallelepiped and plate 77—27483
α-quartz, acoustic activity, elastic wave polarisation plane rotation, Bragg scatt. of light investigation 79—65142
quartz, shock-loaded, y-cut shear-wave particle vel., interferometer technique 79—99268
quasilayered elastic strip, modulated propagating normal wave transform. 80—74800
quasivolume surface waves, in low-symmetry crysts. 77—28070
radiation from spherical wave sources, seismic model 79—8612
random media, coupled EM and elastic waves 79—28579
rarefaction-wave splitting in polarizable solid media in outer electric field 79—90168
Rayleigh wave, propag., isotropic elastic material with homog. strain 78—94460
Rayleigh wave scatt. by thin surface layers, singular perturbation anal. 78—58
rectangular bar, semi-infinite, longitudinal impact, elasticity eqns. anal. 78—90703
rectangular cross section solid waveguide, nondispersive propag. of elastic strain waves 79—18565
rectangular ridge, edge localised vibr. modes 77—89629
reflected wave field changes in cylinder caused by surface curvature changes *(German)* 80—106767
reflection and refraction of elastic waves in presence of separation at solids interface 77—75848
reflection-refraction wave fronts at nonlinear elastic media boundaries *(Russian)* 79—32336
refracted transverse, influence of adjoining media characts., on the amplitude 78—94614
relativistic elasticity of dissipative media, wave propagation modes 78—4485
relativistic hypoelasticity, characteristic manifolds, wave propagation *(French)* 79—30227
relativistic initially stressed elastic solids, infinitesimal discontinuities 77—45775
relativistic magneto thermo viscoelastic medium, effect of mag. and thermal fields on plane wave propag. 79—2637
relativistic magnetoelasticity, infinitesimal discontinuities *(French)* 79—25853
ring subjected to time-depend. fluid pressures, dynamic behaviour 77—65704
rock, plane wave propag. in anisotropic jointed media 77—68501
rock elastic wave absorption meas. and recording instrument *(Russian)* 79—29891
rock rupture by elastic shock wave superposition in multiple detonations *(Russian)* 77—35082
rock samples, dry and water-saturated, at high press., elastic wave vels. and v_P/v_S ratio 79—92529
rocks, cylindrical stress waves generated by moving axisymm. superseismic pressure pulse 77—44979
rocks, longitudinal wave vels. during nonelastic deform. 78—61402
rocks, quartz-bearing and quartz-free, high temp. and press. effects on compress. wave vel. 78—32081
rocks, transverse wave vels. in dry and water-saturated samples, up to 2 kbar press. *(Russian)* 78—28219
rocks, ultrabasic xenoliths, wave vels. up to 10 kb pressures 77—56624
rocks, wave vels. rel. to deep crustal composition *(Russian)* 79—48460
rocks sound velocity determination, suggested methods 78—81433
rod, elastic, nonlinear modulation of torsional waves 77—62195
rod, elastic oscillations, wave operator fundamental solutions; asymptotic formulae 80—69722
rod, nonhomogeneous elastic, with varying cross section, pulse propagation 79—46257
rod, nonlinear hyperelastic, decay of acceleration waves 79—1125
rod, straight linearly elastic, axially loaded, dynamic response 79—68635
rod, stress-wave detection of an edge crack 78—30236
rods, coupled thermoelastic wave propagation, asymptotic theory 79—12609
rods, elastic, linear, nonhomogeneous, propag. and decay of shock and accel. waves 78—83278
rods, elastic with multiple wave speeds, wave propagation 79—72850
rods, propag. anal. using numerical method, impact motion 79—32352

elastic waves continued
rods, simple orthotropic elastic, shock waves and wave-type instability 80—48622
rods and clad rods, elastic waves anal., tutorial review 78—94608
rods and plates, strain-rate-sensitive material, elastic-plastic wave propag. mech. 80—69724
rods with variable cross section, elastic wave propag. 80—64450
rotary shear waves in initially stressed neo-Hookean material, radial propag. 77—35071
rotors, elastic wave stability 78—87297
rubber balloon bursting under biaxial strain, tear behaviour 80—19287
rubber bands and filaments, length oscill. pulse generation, instabilities *(Russian)* 78—30227
rubber cylinder, effect of stretch on wave speed 80—1467
sapphire, absorbing microdefects effect on anisotropy of optical strength 78—2952
sapphire rod, numerical description of torsional vibrs. 77—51435
sapphire rod, torsional waves at low freqs. 77—84053
sapphire rod, wave propag. 77—51434
scalar-wave propag. in random elastic layer 80—83754
scattering by bounded obstacles, multiple 80—43496
scattering by edges of thin surface layers at oblique incidence 78—18085
scattering by elastic sphere embedded in isotropic elastic medium 80—96214
scattering by flaws, Born approx. 77—79984
scattering by randomly distributed and oriented scatterers 79—50483
scattering from cylindrical cavity, nuclear resonance theory 78—87290
scattering from heterogeneous material 78—32674
scattering from localised defects in solids, long-wavelengths 79—87794
scattering from weak inhomogeneities, deterministic inverse problem 80—75300
scattering of elastic waves, reciprocity relations, forward amplitude theorems 77—49605
scattering of elastic waves by an elastic sphere 80—83747
scattering of P and S waves by spherical inclusions and cavities 79—81776
scattering of plane waves by crack of finite width 77—80092
scattering of plane waves by rigid strip 77—80093
scattering theory for anal. and design of flaw characterisation expts., long-wavelength limit 79—83408
sea ice in Gulf of Bothnia, flexural waves meas. *(Japanese)* 78—96225
sedimentary rocks fluid saturation effects on dynamic elastic properties 77—17082
seismic exploration, elastic wave source and receiver grouping *(Russian)* 77—9563
seismic vels. in rocks before earthquakes 80—8256
seismic wave generation, explosive versus nonexplosive sources *(Russian)* 77—9377
seismic waves, fault models 80—3938
semi-infinite elastic media, harmonic wave generation at unbonded interface 79—23237
semi-infinite elastic strings, interactions between stretching and deflection waves 77—45703
sH wave diffraction by spherical stratified medium *(French)* 80—53674
SH wave propag. in laterally and vertically heterogeneous media due to line source 79—81800
SH wave propag. in medium with step-shaped discontinuity 77—56602
SH wave scatt. by spherical layer 79—27562
SH wave scattering by thin semi-infinite inclusions 80—43655
SH waves, multiple scatt. by arbitrary cross section cylinders 78—63216
SH waves due to shearing-stress discontinuity in viscoelastic half-space, displacement 80—56405
SH-surface waves, scatt. and excitation in mass-loaded elastic half-space 77—14933
SH-wave diffraction by edge crack in elastic medium 79—64573
SH-waves incident on cylindrical tunnel dynamic stress anal. of elastic liner 80—79201
shear, and compression wave propag. in impacted solids 80—83755
shear normal mode diffraction by surface crack in elastic plate 79—94549
shear wave propag. in trilaminated waveguides, continuum mixture theories 78—33935
shear wave propagation in an elastic two-component quater space, solution by Volterra method *(Russian)* 80—42064
shear wave propagation in layered elastic medium, dispersion eqn. 79—17245
shear wave scattering by cracks in elastic medium, stress intensity factors 80—74787
shear waves, diffr. at row of round elastic fibres 78—67083
shear waves, horizontally polarised, finite crack in linear elastic media 79—68652
shear waves, horizontally polarised, generation in ferromagnets using magnetostrictively coupled meander-coil EM transducers 79—46144
shear waves in an elastic-plastic material due to a supersonic surface step load 80—102999
shear waves in an infinitely extended medium perforated with a row of cylindrical ducts 79—32116
shear waves in presence of couple stresses 77—31233
shear-wave scattering from spherical fluid obstacles in solids, resonance theory 80—43497
shell, cylindrical, dynamic stability under periodic axial load 79—14302
shell, cylindrical, inhomogeneous, thermoelastic torsional waves 79—92952
shell, elastic, containing ideal fluid, nonaxisymm. vibrs. 77—35077
shell, infinite cylindrical, in elastic medium, action of moving load, pressure waves *(Russian)* 79—81754
shell, orthotropic cylindrical, interacting with a fluid, nonaxisymmetric elastic wave propag. 80—33518
shells, cylindrical, containing swirling fluid flow, dynamic stability 77—68510
shells, three-layer cylindrical, axisymmetric free waves 80—5982
shells, two fluid-coupled cylindrical elastic, transient response to incident press. pulse 80—58966
ship propeller shaft dynamics, forces between shaft and bearings, root bearing rigidity depend. 79—81801
shock formation in elastic solids in relativity *(French)* 80—31496
shock wave decay in elastic rods 79—41603
shock waves, propag. in elastic rods. 77—60939
shock waves in isotropic elastic space 80—28448
shock-loaded solid, longit. and shear waves 77—11633
short waves grazing incidence on slender cavity 80—5983

elastic waves continued
- silicate glasses, longit. and transverse elastic wave vels., temp. and comp. variations 80−88258
- simple harmonic waves in infinite nonhomogeneous elastic medium, diffr. by Griffith crack, rigid strips 77−54913
- singular reflection and refraction of elastic waves due to separation 79−32358
- singular wave surfaces in linear inelastic media 79−81799
- slip zones along interface, caused by plane horizontally polarised SH stress pulse 80−53648
- small amplitude propag. in thin pre-stressed elastic plates 77−39245
- smectic B_A, B_C and E_A liquid cryst., transmission of US shear waves *(French)* 77−51309
- soil interaction with surface mounted struct. under excitation by plane SH wave 78−22292
- solid, surface stress effects on plane wave propag. 77−3761
- solid layer, field of elementary source of elastic strain waves 79−18561
- solid-nematic interfaces, reflection and refraction of obliquely incident shear wave 79−86691
- solids, inhomogeneous linearly elastic, parabolic theory of stress wave propagation 78−38243
- solids, symmetric backward first-order Lamb wave 79−60433
- solids, transition matrix for correl. scatt. wave coeffs. to incident wave coeffs., using Betti's identity 78−90744
- solitons and weak shock waves, short-wave asymptotics 77−37763
- spark sources, grouping technique *(Russian)* 77−7630
- specific directions of plane elastic waves in thin quartz crystal plates 80−92601
- sphere, elastic, inverse normal mode problem *(French)* 79−41610
- spherical cavity in infinite medium, radial vibr. freq., mag. field effects 80−58955
- spurious reflection in nonuniform finite element grids 79−14303
- statistics of longitudinal nonlinear waves *(Russian)* 78−42565
- steel, wave propag. effects on dynamic loading of pressure vessels 77−3090
- steel layer types St3+0Kh13, acoustic emission parameters, brittle fracture, crack propagation *(Russian)* 80−93633
- steel layers, types St3+Kh18N9T, acoustic emission parameters, brittle fracture, crack propagation *(Russian)* 80−93633
- stimulated acoustooptical effects due to nonlinear photoelasticity 80−103941
- Stoneley wave meas. using differential interferometric optical scanning system 78−75919
- Stoneley wave on the fluid and preliminarily stressed body interface *(Ukrainian)* 80−69708
- Stoneley waves, effect of gravitational force in the liquid layer 79−3968
- Stoneley waves at (001) interface between cubic symm. cryst. 80−100388
- Stoneley waves at interface between two hexagonal crystals *(French)* 77−31859
- Stoneley waves propag., effect of liquid layer overlying a thermoelastic halfspace with an embedded spherical cavity 79−1134
- strain measurement in rod, electron inertial effect, shock loaded rod 78−51139
- strain wave propagation in visco.elastic bars due to longitudinal impacts anal. *(Japanese)* 80−96223
- strain waves, in solids, third approx. effects, asychronous interactions and self-action 77−1171
- stratified media, elastic waves at normal incidence, inverse problem 80−33509
- stratified media, Hamiltonian formalism for nonlinear wave propagation *(Russian)* 77−45705
- stratified medium with spherical symmetry, incident P and SV fields, resulting field *(French)* 80−46806
- stratified shear flow, wave breakdown 77−31358
- strength of materials, empirical determ., cleavage fracture in plane waves 80−96225
- stress intensity factors for semi-infinite crack under 3-D loading 77−80115
- stress wave dislocation damping, strain-amplitude depend., KGL String model 77−4101
- stress wave generation in metal by electrons excited by nucl. fission fragments 79−37747
- stress wave penetration in plates 77−78983
- stress wave propagation calcs., effect of material constitutive models 78−90769
- stress wave propagation following explosion, spatial front anal. *(Polish)* 80−19275
- stress waves focusing in viscoelastic solid cylinder *(Russian)* 79−27535
- stress waves in heterogeneous media, Laplace transform inversion 77−80103
- stretched elastic sheet, punched hole, wave propagation 79−10524
- string, flexible elastic, simple wave interaction 77−68509
- strip, thin, transversally loaded, dynamic stress analysis, solution by physical discretisation 77−50943
- strong discontinuity wave in initially strained elastic medium 79−14301
- structural foundations, excitation by seismic surface wave 80−10182
- supersonic flow past slender body, wave system 77−31327
- surface elastic waves, surface effects theory 79−90171
- surface loads, reciprocating dynamic stresses produced in elastic half space 78−9562
- surface of crystal, elastic wave propagation, spatial dispersion 80−54310
- surface ripples, periodic, of elastic skin 77−31845
- surface thermoelastic waves in the regular layered half space *(Ukrainian)* 79−50625
- surface wave guidance by stress free crack 79−46250
- surface waves, existence in nonhomogeneous elastic semi-space 78−67071
- surface waves, isotropic elastic semispace with small nonhomogeneity 77−68473
- surface waves, leaky, in isotropic solid 77−14949
- surface waves at hexagonal surface and interface, thermodynamic and dynamical props. 79−69338
- surface waves guided by edge of semiinfinite slit 78−1457
- surface waves in a pre-stressed elastic body 79−59940
- surface waves in generalized thermoelasticity 78−87291
- surface waves in prestressed body with cylindrical cavity *(Russian)* 78−63369
- surface waves in two component mixture of elastic materials *(Russian)* 78−59335

elastic waves continued
- surface waves of elastic medium in presence of inviscid flow field 77−49603
- surface waves on interface of pre-stressed elastic bodies *(Ukrainian)* 80−10176
- surface-wave dispersion in inhomogeneous medium, investigation by finite difference method 79−66631
- surfaces waves, effects of gravity and viscosity 77−81797
- symmetry relations between reflection and transmission coeffs. 78−26080
- temperature compensation and travel times of waves 80−69731
- tensile cracks and shear faults, elastic wave radiation 79−16411
- tetragonal media, elliptical conical refraction 80−5976
- thermo-elastic wave propag. in micropolar layer 77−35066
- thermo-piezoelectric material, time depend. harmonically changing plane wave propag. anal. 80−15977
- thermodynamic effects of shock waves in elastic fluids 77−15061
- thermoelastic dielectric, linear, wave propag., singular surfaces 77−72216
- thermoelastic dielectrics, constitutive eqns. determ. 78−18170
- thermoelastic half-space, dynamic response to energy flux, stress wave evolution *(French)* 80−74795
- thermoelastic plane Lamb's problem with gravity 77−29241
- thermoelastic Rayleigh-type surface waves, retrograde modes 79−77888
- thermoelastic steady state response to moving load, effect of gravity and temp. 77−23871
- thermoelastic surface waves in micropolar elastic solid medium 77−72206
- thermoelastic wave propag., critical thermal load 78−30228
- thermoelastic-plastic coupled medium, accel. and shock wave propag. 77−58578
- thermoelasticity, coupled problems, wave propags., effect of second order time derivatives 77−42772
- thermoelasticity, nonlinear theory, propagation of mechanical and temp. acceleration waves 79−75346
- thermoelastodynamics mixed boundary value problem, algorithm *(French)* 77−50979
- thermoviscoelastic materials, thermodynamics of nonlinear single integral representations, appl. to one-dimensional wave propag. 77−68438
- thin elastic plate of const. width, vibr. energy propag. 78−9599
- thin layer surface inhomogeneity effect on dynamic surface response 79−7288
- thin plate optimal design using Prager's theorem *(Russian)* 77−39247
- thin stretched foils, membrane wave excit. 78−90578
- thin walled elastomer tubes, dispersive effects in wave propag. 78−87289
- thread, nonlinear elastic, cone-induced shock, self-similar problem soln. *(Russian)* 80−53677
- three-layer structures, phase vels. of antisymmetric modes, freq. depend. 77−50975
- torsional wave propagation in elastic inhomogeneous cylinders 77−80104
- torsional waves in two-layered circular cylinder with imperfect bonding 77−14948
- transient analysis of three dimens. plate, ray grouping technique 78−22294
- transient and impulse responses of one-dimens. linearly attenuating medium, analytical results 78−32687
- transient and impulse responses of one-dimens. linearly attenuating medium, parametric study 78−32688
- transient disturbance prod. in elastic half-space by impulsive shearing traction 78−57786
- transient response of half-space due to reciprocating antiplane shear load 77−46963
- transient response of inhomogeneous thermoelastic media to a dynamic input 79−27532
- transient waves in fluid-filled porous media, refl. and refr. 77−49604
- transient waves in medium with axisymmetric cavities, stress anal. *(Ukrainian)* 80−33503
- transtropic thick plates, multiply-connected, forced oscills. *(Russian)* 77−39241
- transverse, reflection from cylindrical defect 78−47472
- transverse vibr. of systems with account of inadequate material elasticity *(Ukrainian)* 77−68475
- travelling waves in hyperelastic rods 79−49051
- triclinic crystals, elastic waves, general theory and degeneracy 80−39215
- triclinic crystals, elastic waves, polarisation fields topology and general theorems 80−39216
- truss joints, elastic and plastic wave distrib. *(German)* 79−18769
- tube, cylindrical, thick-walled, finite twist and external press., stability, vibrs. 78−83286
- tube filled with streaming incompressible fluid, pressure wave propagation 80−96228
- tubes, fluid filled, transients produced by longit. impact 77−72212
- tubes, liquid filled Al and PMMA longitudinal wave experiments, laminar flow 79−64604
- tubes, liquid filled elastic and viscoelastic, longitudinal waves theory 79−64562
- two bonded elastic solids interface, penny shaped crack, torsional wave interaction 80−64484
- two-dimensional wave propagation in a micropolar thermo-elastic layer with stretch 79−94527
- two-layer fluid, waves caused by periodic press. near thin wall *(Russian)* 77−27541
- two-layer strip, harmonic wave propagation *(Russian)* 77−35080
- ultrasonic pulse propagation in elastic waveguides *(Russian)* 79−18576
- unconsolidated porous sand reservoirs, elastic props. 78−61400
- unilateral interface, elastic wave interactions, frictional slip effects 79−94542
- unloading waves, elastic-plastic wave propag. in semi-infinite rod 77−35079
- Van der Waals moment between anisotropic bodies, calc. 79−94547
- vibrating elastic solid due to scattering of elastic waves by pores 79−86372
- viscoelastic bar, transient wave propag. 80−106745
- viscoelastic fibre-reinforced composites, wave propag. 79−76992
- viscoelastic fluid, circular and elliptic polarised shear waves 79−60024
- viscoelastic fluid flow between parallel plates, inertia elasticity and shear thinning props. *(German)* 78−55665
- viscoelastic layer, anisotropic, nonstationay torsional waves problem *(Russian)* 80−53678
- viscoelastic layered composites, wave propag., dispersion and dissipation effects 80−102982
- viscoelastic media, stress wave propagation 78−46910

elastic waves continued
- viscoelastic media, two-dimensional wave problem, Volterra method solns. 80—69727
- viscoelastic plate, guided harmonic waves 80—79194
- viscoelastic rod with temp.-depend. props., propag. theory 77—54822
- viscoelastic solid, plane and spherical wave propagation 80—106738
- viscoelastic surface waves on clamped boundary 78—90767
- viscoelastic surface waves on standard linear solid 80—28461
- viscoelastic wave propagation, integration contour deform. for Laplace transform inversion 80—74801
- viscoplastic medium, wave-barrier interaction 80—14609
- viscoplastic-elastic media, waves under complex strain *(French)* 79—27570
- viscous materials, heat-conducting, with hidden variables, shock waves and acceleration waves 80—74788
- water layer between solid plates, elastic wave propag. 77—4158
- waveguide slow torsional wave sensors 79—46748
- weak explosion in deformed elastic material 77—56598
- weak nonlinear waves in homogeneously deformed heat-conducting elastic materials 80—48632
- weakly anisotropic elastic bodies with cubic symmetry, surface waves *(Russian)* 80—79198
- wedge, mixed boundary value problem 78—28952
- wedge region with mixed boundary conditions, elasticity theory, dynamic problems soln. 80—43641
- wedge under surface press., elastodynamic response 78—18169
- wood, impulse method of determining moduli of elasticity, shear moduli 77—77661
- Al alloy 6061-T6 cylinder, dynamic fracture, expt. rel. to Mott's theory 78—64651
- Al, pressure-shear waves due to oblique plate impact 77—65713
- Al rod, exponentially varying shape, impact by steel spheres, elastic wave propagation 80—74791
- Al, stress wave propag., transmitted wave profile 77—80578
- Al_2O_3 ceramics, elastic props. meas. in 100 to 300°C range 80—55445
- Al_2O_3, dynamic deform., stress-wave response 80—21020
- $BaTiO_3$, elastic props., singularities near tetragonal-cubic phase transition 80—70303
- $BaTiO_3$, piezoceramic, elastic normal wave propagation, phase transitions *(Russian)* 80—40067
- Cd US attenuation due to conduction electrons 79—46754
- CdS, elastic wave propag., in hexagonal piezoelec. crysts. *(Russian)* 77—69777
- CdS, elastic wave propag. and interaction with charge carriers, appl. of hardened elastic moduli *(Russian)* 78—35095
- CdS, flexural waves in resonator platelets, synchronous amplification and generation 78—84527
- CdSe, wave propag. 79—28042
- Cu_2O, single crystal, thermoelectric behaviour *(French)* 78—71786
- $Cu_{2-x}O$, nonlinear elastic props., nonstoichiometry effects *(French)* 80—34133
- $Fe_{65}Ni_{35}$ ferromagnetic alloy, zero sound anomaly, inelastic neutron scatt. 79—46764
- GaN, elastic constant calc., elastic wave propag. vel. 78—87734
- GaS, elastic prop. anisotropy, Debye temp. *(Russian)* 80—88244
- GaS(Te)(Se), elastic characteristics, Debye temp., ultrasonic study *(Russian)* 80—79872
- Ge-Pb-Bi-O glass, photoelasticity, glass transition limits 79—33670
- He, bulk, Kapitza conductance, acoustical mismatch 77—76637
- KD_2PO_4, neutron scattering from coupled polar-elastic waves 80—92623
- $LiNbO_3$, damping of elastic waves at 36.5 GHz 77—39632
- $LiNbO_3$, ion implanted, acoustic model of SAW delay lines *(French)* 78—55540
- $LiNbO_3$, piezoceramic, elastic normal wave propagation, phase transitions *(Russian)* 80—40067
- $LiNbO_3$ piezoelectric plate, direct and indirect elastic wave excitation *(Russian)* 80—34858
- $LiNbO_3$, thin crystal plates, specific directions of plane elastic waves 79—82281
- $LiTaO_3$, near ferroelec. transition, elasticity, photoelasticity 78—88268
- $LiTaO_3$, thin crystal plates, specific directions of plane elastic waves 79—82281
- Mg US attenuation due to conduction electrons 79—46754
- $MgAl_2O_4$, damping of elastic waves at 36.5 GHz 77—39632
- MgO, longitudinal elastic vels. to 360 kbar 77—70642
- MnO, elastic props. singularities near phase transition 77—16093
- Mo magnetoacoustic effect shear wave selectivity 79—47131
- NaCl-NaBr, elastic wave damping, 300 to 1500 MHz, impurity effects 80—92602
- $PbMoO_4$, elastic wave excitation and amplification by laser radiation 80—103419
- $Tb_2(MoO_4)_3$, nonlinear elastic props. near phase transition 79—73244
- W, elastic wave scatt. from oblate spheroidal WC inclusion 80—65151
- W magnetoacoustic effect shear wave selectivity 79—47131
- YAG:Er, elastic wave damping, 300 to 1500 MHz, impurity effects 80—92602
- YIG, parametrically excited reson. magnetostatic modes of spin, elastic and magnetoelastic waves 79—56523
- Zn US attenuation due to conduction electrons 79—46754

elasticity
- *for crack problems in elasticity see crack-edge stress field analysis*
- *see also elastic constants; elastic moduli; elasticity of liquids; elastoplasticity; photoelasticity; rheology; thermoelasticity*
- α-quartz, constitutive eqns. by group theoretic methods 80—1954
- A15 compound, superconducting transition depend. on non-hydrostatic stress 80—107948
- acceleration waves at boundary between two nonlinear elastic materials, reflection and refraction 79—98650
- acoustoelasticity, general stress-velocity expressions 79—81722
- acoustoelasticity, theory, natural modes and forced response to sinusoidal excitations 77—84058
- active damping of vibrations in elastic systems with distributed parameters, active stabilisation *(Russian)* 79—27577
- adhesive bonded lap joints, elastic stresses theory 78—55563
- adhesive contact of elastic solids, tangential force effect 77—62216
- aeolotropic elasticity, semi-infinite medium, axisymmetric problem solns. *(French)* 80—8795
- aeroautoelasticity, active control and suppression of flutter in aircraft *(Russian)* 78—67079
- aerodynamics, unsteady, modelling, for arbitrary motions 78—14033

elasticity continued
- aeroelastic analysis of subsonic aircraft *(Italian)* 79—41598
- aeroelastic behaviour, large Darrieus rotors derived from behaviour of 5.5 m rotor 80—61251
- aeroelastic stability, large wind turbines 80—61249
- aeroelastic stability of wide span surface structs., wind vels., flutter, binary divergence 78—26083
- aeroelastic system, flutter eigenvalue problem, rigid-body degrees of freedom elimination 79—98651
- aeroelastic vibr. elimination, appl. of Pontriagin max. principle 78—55584
- aeroelastic vibr. elimination, optimal control method 80—33514
- aeroelasticity, flutter testing, modal parameter identification 79—3938
- aeroelasticity in separation streamline flow 80—5979
- aeroelasticity of unsteady aerodynamics, force calc. methods *(French)* 78—75095
- ageing, hereditary solid, optimum form for system with reinforcing elements *(Russian)* 79—81727
- aircraft wing weight optimisation with static aeroelasticity constraints *(Russian)* 79—23240
- alkali metal halides, strain derivative of static dielectric constant 77—72579
- alkoxyphosphazene polymer, elastic and thermoelastic props. 77—56014
- allowable representations of appropriate small groups, calc. of system coords. and physical props. 79—2595
- aluminates with perovskite struct., elasticity meas. to 6 kbar 77—51428
- analytical continuous solns., harmonic displacement field representation 80—62472
- angular disclination and closed loop generation 77—51374
- anisotropic, elastic crystals, Rayleigh wave speed, secular eqn. 79—77889
- anisotropic, Saint-Venant's principle and end effects 78—38198
- anisotropic, stress concentration around holes, formulation of problems 79—64509
- anisotropic composite cantilever, bending and torsion, mathematical formulation 79—18708
- anisotropic elastic fields around straight edge dislocations, nonlinear computation 77—7718
- anisotropic elastic medium, elastic field prod. by straight dislocation dipole 79—99195
- anisotropic elastic medium reinforced with thin tapes, model 80—38276
- anisotropic elastic state, plastic-strain mechanism 78—42530
- anisotropic elastodynamics, linear theory, stability anal. 77—13610
- anisotropic inhomogeneous bodies, convergence rates for elastic solutions method and variable elasticity parameters *(Russian)* 79—44740
- anisotropic inhomogeneous rods, eqns. of theory 77—14906
- anisotropic material, different moduli in traction and compression, stress-strain laws in small strain theory *(French)* 78—90704
- anisotropic materials, elastic and plastic pots. *(German)* 77—46926
- anisotropic media, roots of characteristic eqn. *(Russian)* 79—17221
- anisotropic media, stability criteria 80—1455
- anisotropic media, stress anal. by integral eqn. method 77—72176
- anisotropic media dynamics, solns. to system of second order partial differential eqns. *(Russian)* 77—23878
- anisotropic media oscillations *(Russian)* 78—87293
- anisotropic medium containing ellipsoidal medium, uniform strain field 77—53785
- anisotropic medium under polynomial form applied stress, elliptical crack elastic field 79—46263
- anisotropic multilayer shell, refined linear theory 77—58555
- anisotropic nonhmogeneous elastic media, radial deform. and stresses 78—51079
- anisotropic plate with curvilinear holes, plane elasticity problem, soln. approach *(Russian)* 80—33457
- anisotropic plate with curvilinear holes, plane elasticity problem, comment *(Russian)* 80—38260
- anisotropic plate with curvilinear holes, plane elasticity problem, basis of soln. *(Russian)* 80—38261
- anisotropic point load solns., appl. of boundary integral eqn. method 77—68431
- anisotropic strip with elliptic aperture, successive approx. method for determ. of elastic equilib. *(Russian)* 78—13907
- annealing and deformation effects, with and without texture 79—52274
- annular disc analysis, in-plane edge load 80—38264
- annular plates, nonsymmetric postbuckling behaviour, numerical analysis 80—102968
- annulus, circular, elastic contact problems, approx. soln. 80—38349
- anti-median elastic problem, N-harmonic solutions 80—99928
- antisymmetric stresses in plane elastostatics, rel. to displacements and stress functions *(German)* 77—35038
- aortic-iliac junction, geometry and elastic response 80—16977
- aperture in elastic body, optimal form *(Russian)* 78—22270
- approximate method to 3-D problems *(Russian)* 78—16651
- arches, flat, sandwich-type, stability analysis 80—48570
- aromatic polyesters, broad-line NMR, dynamical mechanical behaviour 77—55718
- arterial system, elastic non-uniformity using hydraulic model 77—29164
- arteries, human, intracranial and extracranial, stiffness and elastic behaviour 80—85436
- arteries, small, pulmonary, elasticity in the cat 80—108942
- artery, mechs. of corrugated collagen fibrils 77—48823
- articular cartilage, asymptotic theory for thin layers with appl. to knee joint 78—44537
- artificial satellite, gravitationally oriented, spatial oscills. and stability of relative equilib. 78—4068
- aryloxyphosphazene polymer, elastic and thermoelastic props. 77—56014
- astatic gyroscope with elastic cardan suspension, dynamics *(Russian)* 78—63273
- asymmetric elastodynamics, domain of influence theorem 79—59925
- asymptotic theory of 3-D elastic plate problem 80—5946
- automorphic functions in plane theory *(Russian)* 79—35563
- axial impact buckling of a column with random initial imperfections 79—18762
- axisymmetric bodies with arbitrary boundary conditions, boundary integral approach 79—75344
- axisymmetric concentrated load problems, solns. with singularities 79—50588
- axisymmetric disturbance due to shearing stress discontinuity propag. in elastic medium 78—67075
- axisymmetric elastic problems, stress function solns. *(Japanese)* 80—64371

elasticity continued
axisymmetric problem, appl. of method of invariant submersion *(Ukrainian)* 79—97200
axisymmetric problems, numerical soln. using integral eqn. method 77—22421
axisymmetric shrink fit problems of cylinder of finite length 77—75803
axisymmetric thermal stresses in transversely isotropic circular cylinder with spherical cavity 77—17824
axisymmetrically loaded circular plates, Reissner nonlinear eqns. *(German)* 77—22423
band plate anal. as constrained body *(Polish)* 80—10153
bar, elastic, resonant longitudinal vibrs. *(German)* 79—90178
bar, elastic and viscoelastic, impact loading model 77—23911
bar, homogeneous isotropic, shearing stress in Saint-Venant torsion, integral eqn. method 79—80445
bar, impact excitation, longitudinal vibr. 78—94606
bar, phase velocity of longitudinal impact wave, tensor wave theory *(Japanese)* 77—72228
bar, prismatic, with rigid ends, lower and upper bounds for torsional rigidity 80—48568
bar, thin curvilinear elastic; natural freq. of vibr. optimisation *(Russian)* 80—19266
bar optimal design by dynamic programming *(Polish)* 79—64542
bar structures, exact anal. with nonlinear eqn. system, stresses 79—81731
bar under tension, torsion appl., 2nd order effects, energy method 80—79158
bar with space curve axis, loaded bar shape calc. 78—51069
bar with two natural freqs., minimum mass design 79—46246
bars, spatial modes of buckling *(Russian)* 77—885
bars, thin, variational method *(Russian)* 79—23216
beam, cracked, dynamic weight function from finite element soln. 80—79234
beam, cracked, transverse loading by stamp, stress and fracture anal. 80—10187
beam, dynamically loaded circular, on elastic foundation, natural freqs. 80—79209
beam, flexural vibrs., method of asymptotic expansions *(French)* 78—51112
beam, homogeneous, initial boundary value problem of transverse vibr. 79—41601
beam, homogeneous, initial boundary value problem of transverse vibr. 79—40367
beam, initially stressed hyperelastic, incremental motion from variational principle 79—68638
beam, large displacement-small strain anal., finite elements with rot. degrees of freedom 78—86161
beam, short rectangular, bidimensional anal. of longitudinal vibrations *(French)* 77—7328
beam, simply supported on nonlinear elastic foundation, equilibrium paths and buckling 79—81747
beam, simply supported thin elastic, parametric instabilities under stochastic loading 79—68582
beam bending on Pasternak foundation, reciprocal variational inequalities 80—92091
beam containing fluid flow, on elastic base, flexural vibration stability 79—46248
beam element in space, geometrical stiffness, virtual work approach 80—14567
beam formation, eccentric, error anal. 79—3920
beam formulation, eccentric, error analysis 77—89028
beam of minimum weight, optimal design, quasioptimal soln. *(Russian)* 77—72158
beam of stepped thickness, Timoshenko theory 78—94600
beam on elastic foundation subjected to nonconservative load, stability 80—79191
beam resting on elastic foundation, optimum shape design with normal stress restrictions *(Polish)* 78—22267
beam with different moduli of elasticity in tension and compression, three-point bending 79—81729
beam-truss gridworks, design formulae for exact elastic analysis 77—50870
beams, 1-D theories of motion 78—18179
beams, accuracy of elementary, and Timoshenko theory 77—80076
beams, curved, shear stress formulas and shear centre 79—18726
beams, elastic structures, optimal rigidity *(French)* 78—59305
beams, finite, curved, stress anal. under general equilib. loading 79—14258
beams, rectangular, of arbitrary depth, free vibr. 79—98647
beams, skew-curved, static anal. for loading and response, closed form soln. 80—64368
beams, spatially curvilinear elastic, geometrically nonlinear theory 80—96189
beams, straight, homogeneous and isotropic, linear flexural theory *(French)* 80—74743
beams, thin walled elastic, as directed curves 80—1421
beams, uniform elastic, lateral buckling, perturbation methods 80—64417
beams. elastic, under tension, nonlinear transverse vibrs. 80—74803
beams hung at both ends, lateral buckling, variational anal. methods 79—86361
beams subjected to successive loading, bending, stability eqns. *(German)* 78—26045
beams subjected to vertical and follower forces, lateral stability and eigencurves 77—68394
Beck's column, harmonic nonlinear response to lateral excitation 79—10517
Beck's column subjected to vertical+follower forces, vibr., stability 78—9583
Beltrami-Michell and Beltrami-Michell type eqns. in static and dynamic elasticity 77—53782
bending, axisymmetric elastic bodies with arbitrary boundary conditions, semianal. boundary integral 80—102969
bending of plates and shells, small parameter method 80—99930
Bergman operator method and anti-plane contact problems involving an inhomogeneous half-space 79—14353
bicrystal, elastic incompatibility stresses *(Japanese)* 80—107361
bifurcation of non-differentiable operators, appl. to elasticity 77—46945
bifurcations, singular perturbations 78—16626
biharmonic function difference eqn., improved, appl. for elasticity 77—68411
bimaterial composite, influence on elasto-dynamic stress intensity factors of crack straddling interface 77—68532

elasticity continued
bimaterial problems and cracks, integral equations 79—44741
biological tissues, LF acoustic characts. 77—25496
biwedge, stress singularities under various boundary conditions 79—12601
blood vessel compliance, theoretical investigation 80—41091
blood vessels, exam. of mech. props 80—12175
bodies coupled by elastic spherical hinge, eqns. of motion *(Ukrainian)* 79—50590
body with array of fine elastic inclusions, elongation and stress concentration 80—33466
body with plane cracks of normal fracture, 3D problems *(Russian)* 80—79219
bonded orthotropic strips with cracks, elastostatic problem 79—81809
bonded sector plates, stress anal., soln. of elastostatic boundary value problems 80—1425
bonded wedge shaped stamp apex singularity, Green's functions for elastic half space 80—64489
bonded wedges, plane problem *(Russian)* 79—23284
bone, elastic characts. of compact bone tissue of human tibia, differences and correls. 77—25490
bone, spongy, dynamic elastic props., determ. techniques 80—56326
bone, stress distrib. in long bone due to prosthesis positioning 77—36984
bone remodelling, adaptive elasticity theory 79—25016
bone remodelling, small strain adaptive elasticity 77—16949
bone surface remodelling, math. theory 78—31847
boundary elements in potential and elasticity theory 79—35560
boundary integral eqn. method in stress anal., resolution of tension discontinuity problem *(French)* 77—71215
boundary problems in static elasticity, distortion trivector pot., variational principle *(Russian)* 80—79146
boundary value problems in 1-D 79—30236
boundary-value problems and 2-D theory soln. with ad hoc assumptions 77—75808
Boussinesq-Papkovich displacement functions, generalisation to anisotropic medium 78—12570
Boussinesq-Papkovich stress functions for linear elasticity 79—68579
brain tissue elastic response props. in vivo 78—31840
brittle elastic body, stability and post-critical growth of system of cooling or shrinkage cracks 80—1486
brittle material, dynamic solid particle damage, elastic and elastic-plastic response regimes 77—8910
bronchial tree axial forces 77—90830
buckled elastica at contact: a perturbation analysis 79—98646
buckling and post-buckling behaviour in elastic structures *(Chinese)* 79—72832
buckling load of elastic struct., upper limit from Timoshenko coefficients *(French)* 79—68609
buckling models for higher order catastrophes in elastic structs. 79—1122
buckling of elliptical plate, simply supported, under compression 77—17826
buckling with mode interaction, asymptotic expansion appl. 80—14592
bulk constitutive relations for cracked materials 80—8790
buried impulsive load, effect on viscoelastic layer on elastic half-space 80—28428
canonical model, dynamical processes in elastic isotropic medium *(Russian)* 79—25855
cantilever beam shape optimisation *(Polish)* 78—79203
cantilever column, elastically restrained, subjected to follower force, instability 78—63299
cantilever column post-buckling, Galerkin finite element analysis 77—54907
cantilever under multiple loads, postbuckling and stability anal. 80—48617
cantilevers, flutter load, discontinuity, variational technique 80—58944
cap, cracked, transverse shear and material orthotropy effects 80—10144
caps, thin elastic spherical, stability curves, boundary value problems 79—81745
cardiac muscle series elasticity, effects of mech. history and time in twitch 77—37004
cascade airfoil aerodynamic design, exact method based on conformal transformation *(Italian)* 79—41599
Cauchy bodies, Darboux classification 77—75801
Cauchy elastic materials, canonical representation using Darboux classification theorem 80—83735
Cauchy problem for a system of equations for plane dynamic elasticity theory *(Russian)* 79—5983
caustics equations for crack and dynamic plane elasticity problems 80—43669
centre cracked plate under quadratic thermal gradient, stress intensity factors analysis 80—43665
centred finite difference scheme for 3-D eqns. of elastodynamics, stability 78—63294
ceramics, effects of additives on elastic properties, elastic property-porosity data 78—88533
ceramics, mechanical behaviour, book 79—38983
circular bar in elastic half-space, longitudinal harmonic excitation 79—10518
circular cylinder with prolate spheroidal cavity under tension, stress distribs. 80—19236
circular disk resonators in vicinity of thickness resonance, vibration mode anal. 80—48634
circular elastic ring free vibrations, accurate nonlinear eqns. and perturbation soln. 79—64576
circular plate of variable thickness, bending with symmetrical loading 80—69699
circular plate on elastic foundation, bending and contact problems 80—96235
circular plates, elastically restrained, of variable thickness, static and dynamic behaviour 77—75841
clamped heterogeneous circular cylinder, torsion problem, stresses and displacement 79—32278
clamped-free rod subjected to tangential follower forces, variational principle 79—50594
classical elastodynamics as linear symm. hyperbolic system, differentiability of solns. 78—57783
closed-end cylindrical shell under line load along a generator, elastic anal. based on discrete element method and Vlasov eqns. 80—69675
co-existent phases in the one-dimensional static theory of elastic bars 80—52023

elasticity continued
coal formations, elastic props. rel. to interference waves appl. in seismic tracing *(Russian)* 79—74858
coated inclusion in elastic medium 78—79215
coiled multilayer shell, stress anal. of elastic and elastoplastic work 80—79156
colliding cylinders, resulting stress field for linearly elastic material *(Russian)* 80—79237
column, elastic, axially loaded, optimum linear tapering design 80—64379
column, non-uniformly compressed, optimal shape and non-homogeneity 80—10145
column, stochastically imperfect finite, on nonlinear elastic foundation, buckling 80—48619
columns and plates, lower bounds to fund. freq. and buckling loads 79—10469
combined mode cracks, energy fracture criteria, complex variable method 79—27596
complementary energy principle, finite elasticity solns., hybrid finite element anal. 79—32274
complementary energy principle in nonlinear shell theory *(French)* 80—43611
complex elastic systems, appl. of generalised functions to analytical methods of study *(Ukrainian)* 79—35537
complex elastic systems, unsteady vibrs. method of dynamic compliances generalisation *(Russian)* 79—81755
composite, steady creep bending stresses 78—71280
composite, tape disc, chord winding, elastic props. 79—87679
composite, thick walled rings, calc. taking into account deformation nonlinearity 77—58565
composite body homogenisation under action of large spatial freq. forces *(French)* 80—42061
composite cylinders, St. Venant torsion warping and stress functions 79—32265
composite cylindrical shell, stiffened and stable, rational design using elasticity 80—5954
composite dislocations, asymm. equilib. positions and line tensions 79—51108
composite elastic system, interface flaw, appl. of dynamic Green function method 77—84153
composite material, arbitrarily shaped inclusions in infinite elastic medium, effective moduli 77—72172
composite material, mechanical behaviour, book 80—94935
composite materials elastic characts. by vibr. tests and discrete conservative model calcs. *(French)* 80—45337
composite materials with periodic structure, homogenisation, functional anal. appl. *(French)* 77—67292
composite mechanics, nonlocality and size effect 77—65675
composite media, self-consistent field approx. for elastic props. 78—51078
composite micropolar elastic cylinders, Saint-Venant's problem 79—46206
composite nonlinear media, effective characteristics *(Russian)* 77—58553
composite plates with smooth or rough interfaces, stress singularities at vertices 77—7348
composite rib stiffened constructions, design criteria 80—102977
composite shell structs., stress-strain state, elastic equilib. 80—74748
compound elastic systems, natural frequency spectra *(Russian)* 79—17230
compressed crack development at circular inclusion boundary with elastic medium *(Russian)* 79—46265
compressed laminar structures, stability *(Russian)* 79—18759
compressible bodies under all-around compression, stability for rods and plates 80—43633
compressible elastic solids, finite plane-strain problems 77—14900
computer automated synthesis for minimum struct. weight of elastic structures 78—34015
concavity techniques, point mass impact on elastic, viscoelastic or nonlienar elastic rod 79—37172
concrete, workability, predictions from viscosity-elasticity analogy, effect of aggregate volume conc. 77—25087
concrete reactor vessels, behaviour of perforated slabs under temp. and external load 79—30917
cone cylinder jointed shell, ring stiffened, external hydrostatic pressure, elastic stability *(Chinese)* 80—64412
conference, computational methods in nonlinear problems in mechanics and engineering, Austin, Texas, USA (March 1979) 80—51945
conical inclusions, elastic stress singularity 78—51071
conical shell, anisotropic, stress conc. new hole *(Ukrainian)* 78—83247
conical shell, impact anal. *(Russian)* 77—895
conical shell, skew, truncated, external hydrostatic pressure, elastic stability *(Chinese)* 80—64413
conical shell of compressible nonlinear elastic material, axisymm. proper vibr. 78—30211
conjugate gradient solutions, finite element elastic problem with high Poisson ratio 78—90707
connectivity theory, boundary element methods systematic formulation 79—63035
connectivity theory for formally symmetric operators 78—49651
connector choice in finite element anal. 78—45
conservative elastic continua, stability anal. with adjacent equilibrium method 78—28951
constant deformable dielectrics, coupled mechanoelectric fields, piezoelectricity and Lamb problem 80—58899
constrained material continua, eqn. formation 79—40360
construction element, optimal design in case of impulsive loading 79—86382
contact between flexible plate and isotropic elastic halfspace 80—43679
contact of two discs, method of caustics study 79—59948
contact of two plane bodies, loading distrib. intensity, slope and curvature discontinuities 79—86386
contact on a transversely isotropic half-space, or between two transversely isotropic bodies 80—64488
contact pressure attainable using indentor which is body of revolution 77—11127
contact problem, conjugation of bi-analytical functions *(Russian)* 77—53780
contact problem for a layer with two stamps 80—69653
contact problem for cylinders, approx. soln. of Shtaerman's eqn. 80—38355

elasticity continued
contact problem for dissimilar semi-infinite elastic strips 78—55615
contact problem for rigid cylinder pressed between two elastic layers 77—65723
contact problem of elasticity for space with spherical hollow *(Ukrainian)* 79—50669
contact problem of semi-infinite strip and half plane, plane soln. 77—46924
contact problems, mixed approach using finite element methods *(Chinese)* 80—5995
contact problems, soln. by finite element displacement method 77—31261
contact problems involving forces and moments for elastic incompressible body, rigid punch problems 80—53719
contact problems involving friction, finite element soln. using nodal variables *(French)* 77—72183
continuous beam resting on tensionless elastic foundation, soln. 79—46238
continuous elastic systems under multiple loads, postbuckling anal., stability theory 80—48616
continuum mechanics, introduction, book 79—30234
continuum model, ordered and disordered materials 77—1168
contour integral method for computation of singularity intensities 77—72180
cooling tower supporting columns and reinforcing rings, displacement analyses 78—38187
coplanar Griffith cracks in infinite elastic medium, dynamic stress conc. 79—46270
Cosserat's medium, linear and surface defects, stresses 78—83813
Cosserat linear theory, existence and uniqueness of solns. 77—57189
Cosserat plate, governing eqns., inherent dualities 77—19531
Cosserat strip under tension, effect of couple-stresses on stress conc. around rigid circular inclusion 78—13898
Cosserat surfaces, simple problem reduction to ordinary differential eqns. 77—50894
Coulomb friction, elastic theory 80—33539
coupled bending-torsion flutter in cascades, aeroelastic stability boundaries 80—64424
crack, stress concentration near apex, elasticity theory and photoelastic expts. 80—23959
crack at the boundary between two materials with a branch into one of them in the case of antiplane strain 80—79231
crack behaviour model, from thermodynamic considerations *(French)* 79—10534
crack dynamics for elastic body *(Russian)* 80—1480
crack emanation, from circular hole in infinite sheet, Green's function methods 80—92084
crack growth thermodynamics for elastic, almost elastic and viscous bodies *(Russian)* 80—1481
crack propagation in non-proportionally scaled elastic structures 79—18807
crack tip lattice trapping, relation between macroscopic and microscopic thermodynamic surface energies 80—59572
cracked elastic body statics, three-dimensional problem *(Russian)* 78—73858
cracked hollow elastic solid, torsion anal. 78—51134
cracked infinite elastic wedge loaded by rigid punch, stress intensity factors 79—77019
cracked material, elasticity parameters calc. 79—55346
cracked medium, nonlinear elasticity 79—64581
cracked members, anal. by optimisation techniques 80—1470
cracks, circular, forced torsional oscillations at low frequencies 80—53703
cracks, edge, interface, energy release rate calc. based on M-integral 80—87742
cracks, penny-shaped, in elastic sphere embedding in infinite elastic space, thermal stresses 80—64460
cracks, penny-shaped, transverse tension, stresses, micropolar elasticity 80—64459
cracks, plane, occupying two-connected domain, elasticity theory problems *(Ukrainian)* 80—74804
cracks, plane elasticity, curvilinear crack edges concentrated forces and edge dislocations, numerical soln. 80—58970
cracks, soln. by superposition of finite elements and singular fields 78—38249
cracks dynamic propagation in anti-plane shear, anal. by finite differences 80—84240
cracks with a corner point, stress intensity factors, modified Lobatto-Chebyshev method 80—99972
creep buckling of complete spherical shell, perturbation method 77—19552
critical loads for elastic bodies, lower bounds, stability 80—79185
cross-spring hinge problem, 2-D, use of minimization methods in solving 78—18163
crowdion elastic interaction with extended at. defects in isotropic media 77—76454
crystal, point defects, anisotropic cubic elastic Green's tensor function, elastic energy coeff., Algol 60 program 77—11537
crystal elastic and plastic anisotropy and dislocations *(Japanese)* 79—95069
crystal surface elastic props., surface tension tensor, volume stress *(Russian)* 80—100389
crystalline solids, theory *(German)* 77—63706
crystallographic point groups, Cauchy symm., elastic work functions 77—72644
crystals, cubic-tetragonal transitions, symmetry anal. 80—10636
crystals, quasicontinuum theory 77—855
cubic box subjected to conc. loads, elastostatics 77—50909
cubic cavity weaken elastic space, stress state *(Russian)* 80—1430
cubic crystal, ⟨111⟩ line force, anisotropic elasticity theory 79—55741
cubic crystal edge and screw dislocation—point defect elastic interactions 80—15151
cubic crystals at arbitrary pressure, shear moduli and relative elasticity 79—42132
cubic elastic material, circles on slowness surface 80—36853
cubic single crystals, hardness meas. by spherical indentation 80—16622
cuboid surrounded by infinite elastic space, stress field due to initial strains 78—55565
curved bar with linear elastic props., eqns. of motion *(French)* 79—94495
curved orthotropic body, approx. soln. for canonical regions *(Russian)* 79—17229

elasticity continued
- curved sandwich beam, finite elements for linear static elastic anal. 77—62153
- curvilinear crack along the interface of two plane isotropic elastic media 79—37246
- curvilinear crack theory *(Russian)* 79—46266
- curvilinear elastic rods, vibrations 80—57095
- cylinder, circular, transversely isotropic, concentrated loads, 3-D anisotropic elasticity theory 80—83734
- cylinder, clamped heterogeneous, stresses and displacement anal. 80—14571
- cylinder, composite of compressible elastic materials, second order torsion 79—72808
- cylinder, elastic, equilib. difference scheme, deformation tensor approx. 79—41583
- cylinder, elastic thin walled, vibrations under axial stress 79—59937
- cylinder, orthogonality of elastodynamic eigenfunctions 80—5940
- cylinder, thick-walled heteromodular, subjected to underwater waves, numerical calc. 80—74746
- cylinder, thin, deformation due to band press. 78—94595
- cylinder, thin-walled, laminated, non-uniform, elastic equilib. with surface loads and displacements 80—69671
- cylinder, torsional vibr. superposed on finitely deformed state 80—19263
- cylinder, transversally isotropic with initial stress, longitudinal waves 80—99934
- cylinder, transversely isotropic with circumferential edge crack, singular stresses 80—19284
- cylinder containing radially stretchable disc, axisymmetric problem 77—58551
- cylinder dynamic behaviour in the vicinity of the fundamental radial-mode frequency *(Ukrainian)* 80—69709
- cylinder elongation, containing periodically located disk-shaped cracks 79—90186
- cylinder on elastic support, excitation by harmonic Rayleigh waves, free surface effects *(German)* 78—87296
- cylinder under torsion elastic, spherical cavity effect in stress-strain state 80—101717
- cylinder with inserts and holes, torsion problem, integral eqn. soln. method 80—106717
- cylinder with oblate spheroidal cavity or internal penny shaped crack under tension, stresses 80—69736
- cylinders, anisotropic homogeneous circular, Saint-Venant's problem and bending 80—53622
- cylinders, constrained, elastic stress analysis by special finite element method 80—106718
- cylinders, elastic doubly connected hollow, min. weight design for given torsional, flexural rigidities 78—18172
- cylinders, fibre-reinforced, singular stress layers 79—14268
- cylinders, noncompressible, under all-round compression *(Ukrainian)* 78—90708
- cylinders, solid or hollow, approx. separation of variables appl. to vibr. problems 78—1605
- cylinders, stiffened, subjected to pure torsion, min. weight design 78—1582
- cylinders bonded to rigid end plates 79—76976
- cylinders in elastohydrodynamic contact, lubricant layer thickness and resistance to rolling 80—96236
- cylindrical cavity in elastic half-space, Rayleigh wave loading, stress spectral representation 80—64453
- cylindrical elastic bodies, damping rate of stresses 77—53786
- cylindrical elastic tubes, collapse and buckling under combined bending and pressure loads 78—83277
- cylindrical inclusion, motion in dislocation strain field, diffusion theory *(Russian)* 78—18676
- cylindrical panels, nonlinear buckling and stability 79—72835
- cylindrical resonator in liquid filled cavity, natural frequencies *(Russian)* 80—38303
- cylindrical shell, radial loading through plate brackets 77—89032
- cylindrical shell, thin, instability rel. to mechanical anal. of geologic structs. *(Chinese)* 78—73364
- cylindrical shell, with non-small holes, elastic equilib., integral representations method *(Ukrainian)* 79—32256
- cylindrical shell and belt, interaction contact stresses, elastic layer model 80—33543
- cylindrical shells, moving ring load effects 77—31218
- cylindrical shells, orthotropic, noncircular, problem solubility *(Ukrainian)* 79—32255
- cylindrical shells, stress conc. anal. by integral eqn. method 77—75806
- cylindrical shells under internal pressure, approx. anal. 80—5943
- cylindrical tube, isotropic elastic, holographically meas. surface displacement, stress/strain extrapolation 80—64374
- damaged zone steady state dynamic propagation *(French)* 80—74737
- De Giorgi's counterexample, linear elastostatics 77—50907
- debond dynamics of elastic strip, simple transient motion 78—67040
- deflection analysis for large heated elastic plates by constant deflection line method 80—14641
- deformable shell containing compressible fluid and gas, spectral anal., vibr. modes *(French)* 77—72209
- deformable solid, stress calc., finite element basis *(German)* 79—50602
- deformed Mooney-Rivlin material, transverse waves 77—26178
- developing shells, buckling elastic strain energy 79—86363
- diaphragm supported cylindrical shells, static anal. using curved finite strip 79—27507
- diatomic elastic solids, nonlocal continuum theory, kinematics, balance laws, wave propag. 78—9559
- diatomic solids viewed as directed media, generalised continuum model 77—69051
- p-p′-dibutyl-azoxybenzene, DIBAB, light scatt. studies *(Dutch)* 80—33885
- dielectric, elastic, containing 2 rigid spherical conductors, electrostrictive stress conc. 77—23883
- dielectric, isotropic elastic thin shells, nonlinear electrodynamics 77—88626
- dielectric comprising several molecular species, field eqns. 77—5668
- dielectric isotropic nonlinear elastic shells, electrodynamics, eqns. of motion 77—88627
- dielectric isotropic nonlinear elastic shells, electrodynamics, constitutive eqns. 77—88628
- dielectrics, constitutive eqns. 77—8512
- dielectrics, elastic, stress tensor, polarisation vector, electric tensor 80—55018

elasticity continued
- dielectrics, electric, optical and acoustic interactions from Lagrangian representation, book 80—2715
- dielectrics, group theoretic methods 80—1954
- dielectrics, hyperelastic, with saturated polarisation, variational and invariance principles 80—74730
- dielectrics with polarisation gradient, boundary value problem exact soln. 80—58898
- directionally dependent lineal porosity materials, continuum theory from isothermal elasticity 80—48588
- Dirichlet problem of classical elasticity, method of integral eqns. validity *(French)* 79—17217
- disc, circular, edge cracked, plane stress under symmetric pin loading 79—50595
- disc, circular, linearly elastic, radial edge crack, const. internal press., stress anal. 77—54932
- disc, constant stress, quasi-isotropic laminate, longitudinal and transverse stresses *(Italian)* 79—41573
- disc, high freq. torsional oscills., Reissner Sagocci problem 78—26082
- disc, spinning, with transverse load system, stability anal. 77—19562
- disc and coaxial ring, partial contact, loaded by external pressure *(Russian)* 80—74814
- disc inclusion, rigid, embedded in with transversely isotropic elastic medium 80—83763
- disclination loops and straight disclinations, elastic interaction 80—2015
- discontinuous deformation gradients near crack tip in finite anti-plane shear 80—58973
- discrete dynamic system with series structure, non-linearity of vibration 78—28935
- discrete equations of fluid flow and elasticity 78—65781
- discrete lattice model transition to continuum limit, invariance conditions 77—861
- discrete models of two-dimensional continuum, side (deformation) effects 79—58
- discrete spectra for elastic plates without deflection, mixed boundary conditions *(German)* 79—27579
- discrete systems with random excitations, random excitations 77—41537
- discrete theory, displacement functions 77—74228
- discs, axisymmetric planar vibr. HF spectrum *(Ukrainian)* 78—83283
- dislocation interactions spring constant between edge dislocation and loop *(French)* 80—54280
- dislocation layers and crack problems in elasticity theory 80—33533
- dislocation lines, appl. of cyclic functions 80—10549
- dislocation lines, cyclic functions 80—10548
- dislocation motion, effect of anisotropic elastic medium, appl. to martensitic transform. 77—28811
- dislocation networks, periodic planar, elastic props. calcs. 77—62527
- dislocation shifts in elastically nonlinear medium, integral eqn. *(Russian)* 78—47374
- dislocation stress field, diffusing elastic fluid, mechanical interaction effects 78—63766
- dislocation theory, nonlinear elastic problems, book contrib. 80—39093
- dislocations, elasticity theory, book contrib. 80—39090
- dislocations in anisotropic media, elasticity theory, book contrib. 80—39091
- dislocations in solids, book 80—36784
- dislocations of elastic materials 78—12567
- disordered materials, bounds for effective elastic moduli 78—4486
- disperse system, fluid interface, dynamic properties 77—25313
- displacement field due to P or SV incident waves on elastic sphere *(French)* 80—36847
- displacement fields, representation by three harmonic functions 79—97208
- displacement stress reln. evaluation *(German)* 79—12603
- displacement theories for straight and circ. curved members *(Japanese)* 80—43615
- dissipative media, hyperbolic elasticity and wave propag. modes 77—45699
- dissipative system subjected to time depend. force, equilibrium stability *(Italian)* 77—71214
- dolphin fins, controllable hydroelastic effect *(Russian)* 80—41062
- dual elastic continuum model, internal mobility induced consolidation 79—14352
- dual elastic continuum model of media with quasicracks, tensional medium with mobility effects 77—72153
- dual integral equation solns. *(Ukrainian)* 79—88809
- dual theory for media with regularly distributed cracks 77—68534
- ductile metals, spontaneous void growth in elastic and elastic/plastic media 80—48567
- dynamic 3-dimens. problems, partial solutions for eqns. of motion *(Russian)* 79—63042
- dynamic axisymmetrical elasticity problems soln. using factorised differential systems of second-order accuracy *(Russian)* 80—8796
- dynamic contract of elastic bodies, direct connection and feedback mechanism *(Russian)* 79—50670
- dynamic elasticity, irregular finite element meshes, grading rules 80—68045
- dynamic elasticity, linear, discrete time approx. of initial boundary value problems, error estimates 80—73175
- dynamic elasticity, tensor spherical harmonics appl. to Navier eqn. 80—98296
- dynamic indentation of elastic plate by rigid punch, numerical soln. 79—14260
- dynamic linear dipolar elasticity eqns. soln., convergence to classical elastodynamic solns. 77—888
- dynamic modulus and compliance, loss and storage component relations *(German)* 79—32268
- dynamic poroelasticity, fundamental soln. rel. to pore fluid effects on seismic wave propag. 79—74847
- dynamic problem of theory, soln. in curvilinear co-ord. 77—46961
- dynamic problems, generalised orthogonality of homogeneous solns. 78—28954
- dynamic response of a slab of elastic-viscoplastic material that exhibits induced plastic anisotropy 80—83737
- dynamic response of elastic continuum, determ. using modal anal. 78—8242
- dynamic response of elastic shell of revolution in acoustic medium 77—19566
- dynamic shear loading at boundary between elastic space and cylindrical rigid enclosure *(German)* 80—58896

elasticity continued
  dynamic surface tension, oscillating jet method, effect of surface elasticity 80−10743
  dynamic universal solns. for fibre-reinforced incompressible isotropic elastic material 77−14925
  dynamical problem for region with curvilinear cuts 78−81842
  dynamics of elastic layer, approx. eqns. 79−7326
  Earth, inverse problem soln. using amplitude and natural freq. data 77−2119
  Earth interior, elasticity imperfection 79−8613
  edge cracked sheets with mixed boundary conditions, stress intensity factors, displacements, stresses 80−64477
  edge dislocation interactions in infinite array, elastic energy 78−55871
  edge function method, appl. to elastostatics 77−68427
  edge-dislocation displacements in elastic strip, Fourier transform method 79−21553
  education, homogeneous ellipsoidal inclusions, general theorems, Poisson theorem, dielectric polarisation, conduction and elasticity 78−61979
  effective properties of random elastic media 79−68575
  Einstein eqns. for spherically symmetric elastic body, exact solns. *(Russian)* 79−88854
  elastic beam with steadily moving load resting on tensionless Winkler foundation 79−64519
  elastic beams of various orders 79−76968
  elastic behaviour of elastic materials, thermodynamical bounds, thermoelasticity, deformation 79−41576
  elastic body cryogenic gravitational wave antennae, sensitivity 79−12705
  elastic body stability under isotropic uniform compression 80−4531
  elastic circular cylinder, axisymmetric end-problem solns. 79−18700
  elastic contact problem, automatic anal., point-matching method 77−31213
  elastic contact problems with friction, nodal parameter soln. *(French)* 79−10475
  elastic continuum penetrated by elastic tube, biaxial stress field, appl. to concrete pressure vessel 77−46921
  elastic cubic crystals, Dirichlet problem soln. uniqueness 79−75345
  elastic cylinder under stress, biharmonic problem solution 80−4532
  elastic dielectrics, nonlinear compatibility equations and Bianchi-type identities 79−41574
  elastic discs, high frequency vibr. spectra, second order approx. theory potentiality *(Russian)* 79−10515
  elastic lateral torsional buckling of unbraced and braced planar frames 79−46236
  elastic mechanical systems, design sensitivity analysis, adjoint variable methods 78−90706
  elastic mechanical systems, vibr. damping by dampers with filled voids *(Russian)* 80−58954
  elastic ring indentation by rigid roller system 80−36854
  elastic shell, stable solutions of simplified problem *(French)* 79−5984
  elastic shell revolution, transient motion in acoustic medium 79−7333
  elastic strip pressing against elastic half plane, strain anal. 79−7345
  elastic strip with periodically spaced holes, surface integral method 77−50911
  elastic tube, cylindrically symmetric vibr. *(German)* 79−7330
  elastic tube conveying compressible flow, 2-dimens. model nonlinear stability anal. 79−64547
  elastic wedge, mixed boundary value problem 78−28952
  elastic-ideally-plastic beams, sectorial coord. 77−68406
  elastic-liquid systems, dynamical strength *(Russian)* 78−51085
  elastic-plastic materials, dynamic behaviour *(German)* 79−14271
  elastic-plastic struct. cyclic thermomech. loading 79−7299
  elastic-plastic-creep-large strain analysis at elevated temperature by the finite element method 79−37185
  elastic-viscoelastic correspondence principle for harmonic oscills., alternative representation 77−65710
  elastic-viscoelastic-elastic beams, compressional damping in vibratory response 79−32323
  elastic-viscoplastic boundary value problem, stress anal. variational method 77−35051
  elastic-viscoplastic materials, hardening parameters 78−46895
  elastic-viscoplastic materials delayed behaviour of double shear perturbations 78−45483
  elastically loaded polycrystal, stress state by contact problem theory 80−14573
  elastodynamic equations of motion 77−42766
  elastodynamic fracture analysis of plane crack extension 78−5693
  elastodynamic stress intensity factors, ray theory approach 79−7339
  elastodynamics, appl. of Ritz theory to Hamilton eqn. 77−50977
  elastodynamics, general representations of soln. of steady-state elastic vibr. eqns. 77−894
  elastodynamics, linear, stability theorems for abstract eqn. in Hilbert space 78−36832
  elastodynamics, mixed method, appl. to plate theory 77−65709
  elastodynamics, numerical boundary integral eqn. method 79−63036
  elastodynamics, time harmonic, pointwise variational principle for mixed boundary value problems 80−31510
  elastodynamics, vel. pots., stress functions 78−93534
  elastohydrodynamic lubrication at high press., mineral oils between disks 78−34094
  elastohydrodynamic oil film, shear behaviour 77−68635
  elastokinetics and elastostability, equation structure from D'Alemberts principle *(German)* 79−63046
  elastomers, block copolymers, generalised elasticity theory, domain crosslinkage vol. 77−39229
  elastomers, tackiness, fracture mechanics theory *(French)* 80−38344
  elastostatic end problems for finite cylinders semi-analytical finite element anal. 80−10143
  elastostatic strip and wedge, Green's functions, bi-linear forms and eigenfunction completeness 79−97205
  elastostatics, appl. of modified integral eqn. method 79−14254
  elastostatics, body force integral 77−64947
  elastostatics, combination of boundary and finite elements 79−92941
  elastostatics, error estimates of finite element approx. 80−8793
  elastostatics, singularity methods 77−13609
  elastostatics, variational and minimal theorems 79−88807
  elbow, in-plane bending behaviour, finite element anal., pipeline design 78−18166
  electrically conducting elastic plate, vibrs. in transverse mag. field, shear deformation *(Russian)* 79−81756
  electrodynamics of moving media, Minkowski formulation 77−78992

elasticity continued
  electroelasticity for piezoelectric medium with cuts, 2-D boundary value problems 80−71319
  electron beam curing, beam voltage effects on mech. props. and chem. struct. 77−70201
  electronic structure and solid props., rel. to chemical bonding, book 80−86044
  elementary elasticity 79−81721
  ellipsoid, displacement fields for double forces 79−37168
  ellipsoidal inclusion, external elastic field 78−55566
  ellipsoidal inclusion elastic field, appl. to martensite formation 77−48436
  ellipsoidal inclusions in anisotropic material, numerical evaluation of stresses and strains 77−68410
  elliptic hole, under uniform tangential force in homogeneous isotropic compressible medium, in second order elasticity 77−31216
  elliptic inclusion in anisotropic medium, antiplane strain problems 78−38200
  elliptic plate, with curvilinear cracks, elastic equilibrium *(Ukrainian)* 77−68521
  elliptic stamp, stress and displacement anal., mixed boundary value problem 79−75342
  elliptic stamp moving at constant speed on an elastic half-space 80−69654
  elliptical punch, elastic contact problems 78−9613
  elstic-plastic crack and hole interaction in elastic medium under uniform shear load 78−51117
  end-loading ring in rigid cavity, elementary catastrophe theory modelling 79−68585
  energy estimates analogous to Saint-Venant's principle 80−36856
  energy for hypoelastic constitutive equations 79−92940
  entropy existence in classical thermodynamics, efficiency of cyclic processes 77−57290
  epicentre motion of elastic halfspace due to suddenly applied buried point source 79−72840
  epoxy resin, low temp. thermal props., phonon states and crosslinked struct. *(German)* 78−75846
  epoxy systems, thermoreactive, elasticity modulus, change on curing *(Russian)* 79−64521
  equilibrium and elastic stability problems, appl. of triangular facet shell element method, TRUMP 77−46946
  equilibrium determination given the stress on a contour *(German)* 80−105505
  equilibrium finite element methods 80−28421
  equivalent inclusion method and impotent eigenstrains 79−97203
  estimation of parameters for a beam on an elastic foundation with large deflections and built in at both ends 79−27520
  ethylene-CO copolymer, highly alternating, melting and internal motion 77−51474
  ethylene-vinyl acetate copolymers, extrusion and heavy duty films, radiation crosslinking, struct. effect 80−66844
  Euler method application for case of follow-up load preset on part of body surface *(Russian)* 78−28948
  Eulerian computation technique for domains with moving boundaries 77−53779
  evolution equations, appl. of well-posed quasi-linear second order hyperbolic systems 77−53743
  existence theorems for solution of fundamental static problems of transversally isotropic body 77−75812
  expansion bellows, elastic flexibility of axially loaded omega and toroidal bellows, review 79−32266
  expansion of thin-walled hyperelastic spherical shell 78−55576
  explosive shock wave on elastic plate 77−89060
  extended anistropic body, equations of equilibrium, polynomial solutions *(Russian)* 80−42063
  extremum problem for distributed parameter, and determ. of optimum props. 79−88811
  extruded billets, residual stress determ. from acoustoelastic meas. 80−76467
  fast reactor, dynamic elastic response of subassembly ducts to impact loading, finite element anal. 80−18536
  fatigue cracks, elastic transpositions, numerical calc. 80−74809
  fatty acids, long chain, spread monolayers, rheological behaviour 79−95245
  femur, canine, in-depth mech. props. anal. 80−16979
  ferromagnet, uniaxial, domain struct. and elastic props. in orientation region of phase transitions *(Russian)* 78−19270
  ferromagnets, higher order surface couplings 78−79212
  ferromagnets, itinerant electron, lattice props. depend. on cond. electron magnetisation, elastic props. 79−61035
  fibre reinforced composite, fibre geometry and filler vol. influence on fracture stresses 80−45397
  fibre reinforced composite, nonlinear elastic props. *(Russian)* 77−19532
  fibre reinforced composite, nonlinearly elastic in transverse direction, programmed winding of articles 79−86339
  fibre reinforced composite waveguides, axisymm. elastic vibrs. 80−102995
  fibre reinforced composites, applicability of generalised continuum theories 77−859
  fibre reinforced composites, surface wave propag., load transfer from reinforcement to matrix 78−46904
  fibre reinforced composites, wave guide-type propag., microstruct. theory 78−83279
  fibre reinforced elastic slab subjected to axial loads, instability and buckling 80−64420
  fibre reinforced laminate, elastic law for materials with different tensile and compressional moduli 80−11713
  fibre reinforced materials, macroscopic elastic props. *(Russian)* 78−59304
  fibre reinforced prestressed elastic circular cylinder, stability 78−79234
  fibrous composite materials, models for composites with different props. in tension and compression 78−35417
  field theory problems, alternating continuity principle in piecewise solutions 79−84959
  filler containing beam reinforced three layer plates *(Russian)* 80−43613
  film on cylinder, calc. of moduli *(Russian)* 78−63304
  finite anti-plane shear for compressible elastic circular tube 79−97206
  finite deformation crack in infinite body under antiplane simple shear 78−18242
  finite dimension body, elasticity theory soln. 78−13908
  finite elasticity, compatible perturbation method, traction boundary value problem 79−63043

elasticity continued
finite elasticity, equilibrium shocks, dissipation inequality 79—68634
finite elasticity, nonlinear two-point boundary-value problems 78—9566
finite elasticity, stability and uniqueness 80—31509
finite elasticity for small superimposed deforms., self-adjoint differential eqns. 77—78982
finite elasticity solns. using hybrid finite elements, complementary energy principle, incompressible materials 79—63044
finite elasticity theory, optimal control problems for Mooney-Rivlin type materials 80—28419
finite elasticity theory, research directions 77—68416
finite elasticity with general loading, uniqueness for deformed surface 80—79153
finite elastodynamics, uniqueness theorem for displacement problem 77—50887
finite element, transition from fine to coarse grid 78—26043
finite element anal. of crack problems 78—67146
finite element analysis of elastic behaviour near an open circular hold *(Japanese)* 80—74750
finite element formulation, variational technique 78—69985
finite element method, continuous elements 78—24668
finite element method, reduced integration, appl. to elastostatics 78—75066
finite element stiffness matrices, incompletely integrated shape functions, numerical stability 78—1567
finite element stiffness matrix, symbolic generation 79—32244
finite elements equivalence for nearly incompressible elasticity 77—68421
finite elements method, iterative algorithm for continuous stress field anal. 77—72179
finite extension of an elastic strand with a central core 79—46217
finite hyperelastostatics, continuous dependence result for mixed boundary value problem 79—68574
finite incompressible elastic body, Hadamard theorem of integral inequality in bifurcation 77—41485
finite-amplitude oscillations of a spherical cavity in a nearly-incompressible elastic material 79—64553
flagella bend propagation, derivation of eqns. of motion and simulation 78—77074
flat elliptical crack, behaviour in an anisotropic elastic body 79—7336
flat spring strip elasticity characteristics for balances *(Polish)* 78—21129
flexible body dynamics, finite element anal., Hamilton's principle 78—24667
floating finite-width plate in a periodic pressure system 80—6070
fluid bi-inclusion in elastic solid, geometry and mech. props. from US pulse scatt. 77—21348
fluid filled cavities in elastic solids, fluid identification using resonance method 80—64452
fluid filled porous medium, thermal behaviour, thermoconsolidation eqns. for elastic lattice 79—72933
fluid impregnated solids, elastic and dynamic response regimes 78—90713
fluid loaded elastic plate, intersection of dispersion curves 79—77003
fluid saturated porous elastic cylinders, vibrations 79—10521
fluid saturated porous elastic solid, equil. soln. 77—65683
fluid saturated porous elastic solid, tensorial eqns. of motion 79—40366
fluid saturated porous elastic solid, wave propagation 79—81750
fluid saturated porous solid, eqns. of motion 78—79208
fluid-elastically coupled coaxial cylindrical shells, response to external flow 77—89063
fluid-saturated rocks, elastic dilatancy and earthquake dynamics 77—21683
force transmission through incompressible viscous fluid-isotropic elastic solid interface 78—43252
forced 2-D oscillations of rigid strip in smooth contact with elastic half space 77—50963
fracture, brittle, energy release rate, equivalent to Rice integral *(French)* 80—64457
fracture criterion of Sih, formal extension, elastic stress field near crack *(German)* 79—1139
fracture mech. techniques, review 79—41635
fracture mechanics, K_{Ic} values determ. in elastic-plastic material behaviour range 80—45376
fracture mechanics problem, two-dimensional, Green's function method 79—23272
fracture of solids containing arrays of cracks 80—1473
frameworks' stability analysis, w.r.t. sway excess of columns 78—51098
Frank disclinations in isotropic elastic micropolar continuum, stress and couple-stress fields 77—72245
Fredholm conditions in Signorini's perturbation method 80—62471
Fredholm linear eqns. of first kind, failure to satisfy Picard's condition 79—2601
frequency anal. of unsupported structures 79—32333
frictional interface, elastic wave reflection, refraction and absorption, SH motion 80—64437
frictionless contact problem for elastic layer under axisymm. loading 78—83341
frictionless elastic contact problems, approximate soln. 78—16646
frictionless stamp impression in elastic half space, contact problem with semiunknown boundary of the contact region 80—69744
fully stressed state of an elastic continuum 80—92050
functions of two complex variables appl. to elasticity theory 78—5660
fundamental frequency of vibration of a rectangular plate on a nonlinear elastic foundation 80—69712
fundamental laws and constitutive equations, in space of any dimension *(Japanese)* 78—41160
fundamental theory, and applications, book 80—22158
Galois unsolvability of anisotropic crystal elasticity sextic equation 79—37170
gas diffusion in linear elastic solid, stress-assisted 80—65294
gels of rodlike macromolecules, nonlinear elasticity in condensed state 80—104199
general physics and heat, book 79—25814
general problem, 1- or 2-dimens. asymptotic approximations 79—80444
general relativistic elastomechanics, compatibility relations *(German)* 78—81902
general relativistic formulation, elastic rotating cylinder 80—82642
general relativity 78—70025
general relativity theory, props. of gravi-inertial reference system *(Russian)* 77—53810
general relativity theory, refractive index of gravit. waves interacting with elastic body *(Russian)* 77—2584
general solution for unified theory of elasticity eqn. systems *(Chinese)* 79—71251
generalised displacement functions, elastic continuum 79—7289
generalised stress intensity factors, numerical determ. method, crack problem appl. 79—72851
generalized orthogonality relation for rectangular strips in elastodynamics 79—64567
geometrical nonlinear shell theory, dual extremum and complementary stationary principles 80—4526
geometrical stiffness, appl. to beam and shell problems 77—33869
geometrically nonlinear anal., correlation of finite element notations 78—42527
geometrically nonlinear elasticity theory, dual variational principle 80—94958
geometrically nonlinear finite element behaviour using buckling mode superposition 80—1449
geometry of motion of single elastic body point 78—49662
geophysical media, boundary conditions rel. to instability of finite difference schemes 77—21912
GFRP, shrinkage stress calc. 78—19869
glass, mechanical properties, review 78—3162
glass, narrow sandwich seals, shape factor, finite element anal. 78—75111
glass fibre reinforced composite, three-dimensional effect of high modulus and hollow fibres 77—4803
glass fibre reinforced epoxy composite, unidirectional, hygroelasticity, angular depend. 80—50663
glass fibre reinforced plastic, cemented joint of cylindrical shell with cover, stressed state 80—69668
glass fibre reinforced polyester, filament wound pipe, winding angle effect on failure 79—43379
glass narrow sandwich seal, correction factor for thermal expansion mismatch 78—75110
glasses, polymerised, statistical thermodynamics, short and long range props. 77—27834
grain boundary drift diffusion under influence of stress fields 79—77835
granular half-space axisymmetric contact problem, stress and normal displacement 77—57196
granular layer, axisymmetric contact problem, stress singularity under stamp 77—57195
granular layer on elastic foundation, axisymmetric contact problem 79—27600
granular media, nonlinear elasticity *(Polish)* 77—54885
graph theoretic field model, modelling and formulations 79—67165
graph-like state of matter, electrical cond. of random networks, gelation and elasticity 78—65875
gravitational and acoustic waves in elastic medium, relativistic eqns., neutron star appl. 78—24712
gravitational wave effects *(German)* 78—81904
Green's matrix for two elastic half-spaces, frictionless sliding *(German)* 78—62083
Green's tensor, elastodynamic, for 2D half-space 79—68581
griffith crack in an infinite nonhomgeneous elastic medium under shear 78—87300
Griffith crack in transversely isotropic material stress anal. 79—64583
Griffith crack opened by thin symmetric wedge, stress intensity factor 77—75807
Griffith crack problems in non local elasticity, solutions for one and two dimensional problems 78—51125
Griffith crack system stress field, at 2-bonded dissimilar elastic halfplane interface 79—64584
Griffith crack-antiplane shear wave interaction at interface of two bonded elastic half-spaces, geophys., seismological appl. 80—92087
Griffith cracks, coplanar opening in infinite medium 79—32379
Griffith cracks, in infinitely long elastic strip, stress intensity factors for variable pressure 79—77022
Griffith energy criterion of fracture for edge cracks 80—5992
grillages, min. weight design *(French)* 77—68407
guided launch vehicle misalignments, static aeroelastic anal., matrix formulation 79—14313
gyroscope on elastic suspension, principle resonance *(Russian)* 79—30461
gyroscope with tuned elastic suspension, dynamical characts. 80—79133
gyroscopic effects in micropolar elasticity 79—30247
gyroscopic eigenvalue problems in elasticity, nonconservative 80—101708
gyroscopic problems in elasticity, orthogonality principle 79—17218
Hadamard's theorem, appl. to thin elastic plates 78—16650
Hadamard conditions in nonlinear elasticity theory *(Russian)* 79—46207
half space, elastic, edge cracks, dynamic growth 80—58972
half space, elastic field due to ellipsoidal inclusions with uniform dilational eigenstrains 80—58913
half space, rectangular cylinder penetration, contact problem, stress fields 80—64490
half-plane with internal line crack, elastic problem, stress intensity factors and crack form. energy 77—42782
half-space, axisymmetric body force problems 77—42738
half-space, dislocations and extended sources 79—35562
half-space, epicentre solns. for pt. multipole sources 79—81798
half-space, mass-loaded, SH-surface waves scatt. and excitation 77—14933
half-space, ring shaped punch contact stress determ. 80—38356
half-space, singularities in elementary soln. of boundary value problems *(French)* 77—71218
half-space, steady state vibr. elastic contact problem, dual integral eqns. appl. 78—18219
half-space containing embedded rigid block 80—23890
half-space with crack nonperpendicular to edge, exact soln. and stress intensity factors *(Russian)* 80—53711
half-space with cylindrical cavity, pure shear under tangential load 80—33464
half-space with spherical inclusion, eigenstresses 77—11131
hardness law for inelastic deformation, elastic-viscoplastic constitutive eqns. 78—46896
harmonic holes, inverse prob. anal. 77—17821
harmonic holes for nonconstant stress fields, deloids and cardeloids 80—64373
harmonic wave propagation in a periodically layered, infinite elastic body: plane strain, analytical results 79—64574

elasticity continued
- harmonic waves in elastic sandwich plates 79—37235
- HCP crystal, dislocation-point defect interactions, anisotropic elasticity theory, appl. to Zr 77—11588
- head, spheroidal model, effect of bending on axisymm. vibrs. 77—29168
- heated electric plates, large deflections, constant deflection line method 79—32277
- helical compression springs, finite elements for dynamical anal. 80—96191
- hemispheres, thin elastic spherical, stability curves, boundary value problems 79—81745
- heparinised elastomer antithrombogenicity and mech. props. for artificial heart *(Japanese)* 80—12296
- hereditary elasticity, integro-differential problems 79—67162
- Hertz problem for finite linear and nonlinear elastic bodies 77—54938
- Hertzian impact of two elastic spheres in the presence of surface damping 80—69743
- heterogeneous solid media, statistical continuum theory, information theory approach, static field theory 80—22198
- heterophase systems, pressure-induced elastic fields, effective inclusion method 79—10502
- historical development during the 17th and 18th centuries 79—17167
- hole in heavy semi-plane, optimal form *(Russian)* 79—10486
- holes with loaded boundaries in elastic plane, anisotropic property optimisation *(Russian)* 79—46208
- hollow elastic cylinder, axisymmetric mixed problem, Legendre polynomial soln. 78—81840
- hollow thick-walled cylinders, stress-deformation, limiting state anal. *(Russian)* 79—27538
- homogeneous elastic matrix containing short fibre, stress state *(Russian)* 77—68412
- homogeneous elastic sphere, spheroidal mode props., displacement radial depend. special reference 79—14312
- homogeneous elastic sphere in its own gravit. field, general relativistic calc. 77—67344
- homogeneous isotropic compressible elastic media, circular concentric ring, second-order torsion problem 79—32276
- honeycomb sandwich beams with laminated faces, flexural wrinkling 80—79183
- Hooke's law, potential energy curve 80—67961
- hoop stresses at tee intersections of cylindrical shells, approx. prediction 80—5942
- horizontal axis wind turbine blades, aeroelastic stability and response 80—61250
- hybrid many body systems, elastic part guided motion, vibr. behaviour *(German)* 79—90175
- hybrid oscillation systems with elastically coupled rigid bodies, eigenvalue problems *(German)* 79—90176
- hydrodynamic analogy *(Russian)* 80—31514
- hydrogels, two-component, elasticity theory and compress. meas. 80—44246
- hyperbolic balance laws in continuum physics 80—4525
- hyperbolic paraboloids stability analysis, using reduced scale models 79—3910
- hyperboloid, elastic parted, mixed axisymmetrical problem *(Russian)* 78—36831
- hypercircle method in the problem of a case-bonded cylinder in the gravity field 78—45484
- hyperelastic bodies, isotropic, deformations, extension of Ericksen's theorems 80—31507
- hyperelastic bodies, Lyapunov stability sufficient criteria 79—12604
- hyperelastic boundary value problems, dual extremum principles and global error bounds 79—30253
- hyperelastic compressible medium with cylindrical cavity, finite dynamic expansion under sudden press. 78—79213
- hyperelastic materials, anisotropic, compressible, finite plane strain, universal deformations 80—69667
- hyperelastic rod dynamics, second-order theory 78—77717
- hyperelastic spherical cavity, finite amplitude oscillations 79—32332
- hyperelastic systems, discrete and continuum mech. 77—864
- hypo-elasticity with internal variables and derived failure condition 77—33868
- hypoelastic materials with internal variable, work-hardening, hysteresis, fracture law 77—62177
- hypoelastic solid, oscillatory shearing 79—88810
- hysteresis damping, continuum description 78—67078
- impact damage in elastic response regime 78—71785
- impact load impulse form determination by the displacements and strains of a circular plate *(Russian)* 80—74751
- impact loading of disc by radial force 79—14298
- impact phenomena with elastically deformable stricker and solid obstacle 78—77703
- imperfection sensitivity of semisymm. branching, rel. to catastrophe theory, stiffened plate appl. 77—84170
- inclined crack in orthotropic strip, elastostatic problem 79—64594
- inclusions in anisotropic solids, generalised plane problems 77—17823
- incompatible basis functions in boundary value problems, variational techniques appl. to thin elastic plate 80—48587
- incompressible elastic materials with different moduli in compression and tension, dynamic problems 80—79141
- incompressible elastic solids, finite amplitude circularly pol. elastic wave reflection and transmission 80—64448
- incompressible elasticity, two dimens., conforming finite element method 79—63039
- incompressible finite elasticity, method for numerical soln. of problems *(French)* 80—42062
- incompressible isotropic elastic material, Hadamard criterion, wave propagation 79—27571
- indentation of elastic half space, numerical method *(French)* 79—50673
- inextensible elastic materials, general solns. in equilib. theory 79—12602
- infinite dimensions and the fold catastrophe, particle modelling 80—8788
- infinite elastic bar, induced oscills., normal and associated wave propagation 80—5980
- infinite elastic dielectric with Griffith crack, EM wave propag., Voigt-Toupin model 80—1469
- infinite elastic medium, diffraction of torsional waves by flat annular crack 80—64447
- infinite elastic medium with cylindrical inclusion, axisymmetric external crack stress intensity 79—72859
- infinite elastic medium with cylindrical inclusion, external crack in torsion, stress distrib. 80—79216

elasticity continued
- infinite elastic solic containing spherical cavities, stress distrib. 79—98616
- infinite elastic solid, with two spherical cavities, asymmetric problem 77—31212
- infinite elastic solid with doubly periodic array of cracks, fracture mechs. 78—34085
- infinite elastic solid with spherical inclusions, linear elasticity eqns., stresses, displacements 78—65773
- infinite elastic space with cavity and shell, micropolar elastic wave propag. 80—58950
- infinite elastic space with cavity and shell, micropolar torsional elastic wave propag. 80—58951
- infinite elastic strip, circular inclusion undergoing dimensional changes, stress components 80—48590
- infinite isotropic elastic medium, crack and misfitting inclusion interaction 79—37244
- infinite isotropic solid, with curvilinear cuts, elasticity theory *(Ukrainian)* 79—32257
- infinite plane with crack in nonuniform steady field, stress intensity coeffs. 80—38343
- infinite plate with parabolic crack, stress anal. 78—30239
- infinite transversely isotropic solid, containing penny-shaped crack, stress intensity factor 80—69738
- infinite transversely isotropic solid containing penny shaped crack, stress intensity factor *(French)* 80—43663
- infinite wedge, first boundary value problem *(French)* 77—35041
- inflated, thin walled elastic circular cylinder under axial loading, bifurcations, membrane theory 80—19246
- inhomogeneous bodies, finitely deformed, effective stress/strain relations 77—75809
- inhomogeneous bodies, static and dynamic elasticity, rel. between stress states 77—14907
- inhomogeneous elastic material, antiplane crack problems 79—14343
- inhomogeneous media, strong ellipticity and van Hove's lemma 78—49
- inhomogeneous medium, high freq. Reissner-Sagocci problem, exam. of stress singularity 78—83239
- inhomogeneous solid weakened by circular slit, vibrs. problem 79—86381
- inhomogeneous strip, boundary value problem spectra props. in elasticity theory 80—31512
- inhomogeneous strip, resonance props., boundary value problem formulation 80—31513
- inhomogeneous strips, elastic equilibrium, stress *(Russian)* 80—19244
- inhomogeneously compressed rods, crit. loads, two-sided estimates 78—62082
- instability of evolving systems 78—44442
- integral eqns., variational formulation *(French)* 77—72181
- integral eqns. in which boundary values and solns. defined on different curves 77—68428
- integral equation, solution, boundary-value problem, index of integral operator *(German)* 80—5945
- integral method for plane stress and strain problems 77—68433
- interface crack, singularity anal. 80—10201
- interface crack tip, adhesion loss model 80—38335
- interface separation for elastic layer on rigid plane, leaded by rigid stamp 78—87307
- interference fits in cylinders with concentric and eccentric holes, stress anal. 77—50916
- internal plane crack in elastic half-space, integral eqns. 80—38336
- internal stress fields caused by lattice defects, entropy 80—39067
- internally loaded elastic plate, containing infinite row of closely spaced parallel cracks, approx. anal. 79—68644
- inverse problem in 2-D theory *(Russian)* 78—22269
- ionic crystal, solid soln. hardening by aliovalent cations 77—44265
- isoparametric shell elements study *(Japanese)* 78—34016
- isothermal one dimensional problem in contact hydrodynamics, correct formulation 79—86387
- isotropic body with different moduli *(Russian)* 79—30249
- isotropic body with sharp elastic inclusion, longitudinal shear *(Ukrainian)* 77—68401
- isotropic composite material containing spherical inclusions at nondilute concs., effective elastic moduli 78—67037
- isotropic elastic half spaces with circular crack, stress at interfaces *(Russian)* 79—27582
- isotropic elastic half-plane, curvilinear crack system 79—81806
- isotropic elastic half-space, response to nonuniformly expanding surface loads, wave fronts 79—81751
- isotropic elastic medium, finite deformation shock waves, centric cumulation 80—53673
- isotropic materials, continuum mechanics in space of any dimension *(Japanese)* 78—41161
- isotropic micropolar continuum, stress and couple stress fields prod. by circular dislocations 79—97209
- isotropic plate, stresses under concentrated forces 80—48572
- isotropic thick plates, review of problems of plates with geometric, and load discontinuities 79—46218
- iterative algorithm for continuous stress and displacement solns. 79—1109
- justification of the von Karman equations *(French)* 79—49047
- Karman-Foppl eqns., energy approach 79—12607
- Kolosov-Muskhelishvili functions in generalized symmetrical problems of elasticity theory *(Ukrainian)* 79—75340
- Lagrangian formulation for continuous media 77—57192
- Lamb's problem, generalisation to class of inhomogeneous elastic half-spaces 78—32023
- Lamb's problem, line load suddenly applied on micropolar elastic half-space 80—12907
- Lame eqns., fundamental soln. to displacement and strains 79—35559
- Lame eqns., mixed problem in R_+^3, explicit soln. 77—60937
- laminar slab, boundary value problems 77—35047
- laminate, static problems *(Russian)* 78—30187
- laminate cylindrical shells, prepared by continuous filament winding calc. of strength and reliability 80—10194
- laminated beam, steady-state response to moving load 78—26030
- laminated composites, mechanics of homogenisation and random evolutions 80—28423
- laminated composites, mixture theory for dynamic response 79—49049
- laminated composites, simulation of effect of bonding materials on dynamic behaviour 79—46216
- laminated composites, transient wave propagation 79—50630
- laminated reinforced elastic shells, stability 80—58948

elasticity continued
laminated sandwich short beams, departure from classical beam theory 78—26034
laminates, multilayer, thick, hybrid-stress finite element formulation 80—92043
laminates, piecewise continuous eigenfunction solns. 78—18178
large strain inelastic analysis, quasi-static problems, finite element anal. 80—14568
lattice dislocation calcs., classical elastic line force solution 78—22718
lattice shells under axially symmetric load, field eqns. 78—79209
lattice-parameter determ., elastic deform. effect 77—72524
layer dynamics, homogeneous axisymmetric problems, eqns. and solns. *(Ukrainian)* 80—5932
layer on substrate, frictional slip caused by normal load 80—33541
layered cylindrical pressure vessels, shell theory, comparison with uniformly valid theory 79—64516
layered elastic materials, homogeneous continuum model 77—58546
layered materials, stress free and problem, plane elastostatic problem, crack across interfaces 78—34076
layered plates approximate theories, accuracy and applicability estimation 80—43620
layered rod on sagging elastic supports, aeroelastic stability, vibr. modes 78—51115
layered system, thermal stresses and displacements 80—23891
left ventricle active model deform., nonlinear finite element anal. 78—35877
line and point loads on a non-homogeneous incompressible elastic half-space 79—40371
linear, two dimens., Saint-Venants principle for non-striplike domains 78—54188
linear Cauchy and Piola-Kirchhoff constitutive theories for stress in solids 79—37173
linear Cosserat plate, practical appls. 80—23892
linear dynamic theory of elasticity, minimum principles 78—57781
linear elastic beams, shells and plates, elementary theories review 80—69677
linear elastic body, disclination dynamics 78—34510
linear elastic continua, variational principles, finite element techniques *(German)* 79—9113
linear elastic half space, frictional unloading problem 80—33542
linear elastic helical spring, Saint-Venant's principle 79—18720
linear elastic solid, expanding crack under conc. load, dynamic problem 79—68646
linear elastic solid with mass addition, stresses and displacement eqns. 77—55955
linear elastic three layered rings, transient response 77—80075
linear elasticity, finite error approx., error estimates for continuous time approx. 80—52024
linear elasticity in exterior domains, continuous dependence theorems 79—46204
linear elasticity systems, finite equilibrium element models *(French)* 79—21550
linear elastodynamics, Galerkin-type tensor soln. 77—17815
linear elastostatics, boundary-integral approach for mixed boundary-value problems 79—64508
linear elastostatics, combined boundary integral eqn./finite element anal. of cracks 77—72178
linear elastostatics, Liouville theorems, uniqueness, analytic continuation, continuous dependence 80—64372
linear elastostatics, unified boundary-integral eqn. method 80—57092
linear elastostatics, uniqueness theorems for displacement fields with locally finite energy 79—97201
linear hemitropic micropolar isotropic elastostatics, Green functions 78—49661
linear isotropic elastic solid, inhomogeneous plane wave solns., energy flux and group velocity 79—53987
linear isotropic elasticity, boundary problems, book contrib. 80—39092
linear programming approach for second-order elastic plane frame anal. 77—39231
linear reinforced composite material with anisotropic structural components *(Russian)* 79—30250
linear theory, refinement of comparison theorems 79—75347
linear theory, with point Maxwellian sources of stress relax., numerical solns. 79—5982
linear theory of, shift function derivation 78—4484
linear theory of elastic beams, construction of optimal admissible extension *(French)* 79—90131
linear theory of elastic shells *(French)* 77—54883
linear theory of plates and shells, numerical method *(Russian)* 77—17819
lipid bilayer, curvature elasticity, vesicle shapes 77—21493
lipid bilayers, curvature elasticity 79—48222
liquid carrying pipe on elastic foundation, dynamic stability 79—90161
liquid crystal, polymeric nematic, Frank elasticity and light scatt. 77—68916
LMFBR beam-type core components separated by thin fluid layers, transverse impulsive motion, Timoshenko beam anal. 77—88203
local effects and energy methods *(Chinese)* 80—42060
long thin profiled strips, numerical soln. *(French)* 77—72182
longitudinal-shear crack refraction, Wiener-Hopf method calcs. 80—87743
Love-Kirchhoff plate, homogeneisation *(French)* 77—68398
lubricant, shear rheological behaviour at high press. 80—35342
lubrication of point contacts, elasticity effects 79—52379
lung, dynamic compliance, freq. dependence, anal. from 1 breathing cycle 80—97967
lung, nonlinear mathematical model, parameter tracking adaptive algorithm 77—60227
lung elastic recoil rel. to ageing healthy males and females 80—67117
lung elasticity in regional and diffuse pulmonary fibrosis 80—30742
lung structure and elasticity, 3-dimens. modelling 77—36992
machine vibrations anal. and obs. block deformability influence *(Italian)* 78—51108
magnetic tape, coil, determ. of stressed-strained state 79—14283
magneto-elastic plates under mixed boundary conditions 79—7328
magneto-elasticity, stresses in plate with holes 77—866
magneto-elasto dynamics, mixed initial and boundary value problems, vibr. circular plate in mag. field 78—67034
magnetoelastic bodies, homogeneous isotropic with couple stresses, spherical inclusions, boundary value problems 77—46917
magnetoelasticity, two-dimens. boundary value problems 77—19525

elasticity continued
magnetoelastodynamics problem with mixed boundary conditions 80—1466
magnon-phonon coupling, continuum approach, general eqns., background soln. 79—95622
magnon-phonon coupling, continuum approach, hexagonal symmetry, wave propagation 79—95623
manipulator compliance, kinetostatic error distrib. 79—18697
martensite nucleation at dislocations, elasticity model 80—55393
material characteristics, determination from phase shift in sinusoidal stress, strain, device for measuring 79—52518
Maxwells stress function representation, completeness 80—36851
medium thickness shell, elastic and elastoplastic contact problem, variational approach 79—64599
membrane, prestressed, dynamic loading 78—51068
membrane dynamics, non-univariable automodel problem *(Russian)* 78—42529
membrane models in shell theory, existence theorem *(French)* 80—17801
membranes, elastic and isotropic, universal solns. 77—84139
membranes, stability of nonlinear oscillations from Liapunov method 80—96212
membranes and cords as slender bodies, dynamics 77—50878
membranes for pressure meas., nonlinear characts. calc. *(Czech)* 79—26021
metal, BCC, ⟨111⟩ screw dislocation—vacancy interaction energies 77—15415
metal, BCC, atomic displacement about ⟨111⟩ screw dislocations 77—15414
metal bending spring, effects of stress, temp., thermal and mech. treatment on non-elasticity *(German)* 77—77531
metal specimen, ultrasonic technique for stress anal. 78—64790
metal-hydrogen system, 2-dimens., elastic interaction, spinodal temp. and density modes 77—69072
metals, atomic interaction force characts., association with struct., mech. props. 80—49172
metals, BCC, under elastic stress, Snoek peak height determ. 80—65153
microcontinuum theory for elastohydrodynamic inlet zone of line contact, lubricant film 77—50998
microelasticity, construction of static and dynamic Green tensors 77—27470
micropolar, stress concentration around elliptic hole 78—5658
micropolar, theory of multiple stresses, phys. foundation 77—45
micropolar continua, generalisation of Saint-Venant's principle 77—68395
micropolar continua, static problems, nonhomogeneous eqn. of equilibrium, Green's functions and Fourier transforms 80—58905
micropolar continuum, 2-D model 77—74227
micropolar continuum, isotropic, elastic fields of dislocations and disclinations 77—68971
micropolar current and heat conducting magnetically-saturated solid, field eqns. 78—36845
micropolar elastic bars with rectangular cross section, wave motion and vibrs. 79—77000
micropolar elastic cylinder, free vibrs., wave propag., asymptotic anal. 78—51111
micropolar elastic half space with suddenly applied line load, Lamb's problem 79—98614
micropolar elastic half-space, body-force and couple effects 77—50896
micropolar elastic media, anisotropic, propag. of shock and acceleration waves 79—30242
micropolar elastic plates and rods, eqns. of motion *(German)* 80—53643
micropolar elasticity, 3-D finite element approach to static and dynamic problems 78—34014
micropolar elasticity, mixed problem 78—54189
micropolar elasticity, uniqueness for anti-plane crack problems 79—30235
micropolar elasticity theory, uniqueness of 2-D boundary value problems 78—54192
micropolar elastodynamics, harmonic solns. 80—36852
micropolar elastostatics, J-integral type conservation laws 79—18710
micropolar half space, soln. of source problem 79—30238
micropolar half space, uniqueness of soln. of mixed boundary value problems *(Polish)* 79—63041
micropolar half-space disturbance due to axially symmetric source of finite length 79—30239
micropolar media, elastostatics, J-type conservation laws *(French)* 79—17227
micropolar space with cylindrical or spherical hollow, elastic wave propagation 80—87731
micropolar theory, axisymmetric problem for half-space 77—50895
Mindlin plate elements, free vibration anal. 79—46244
Mindlin plates, finite element displacement formulation 80—10154
mineral oil lubricants, behaviour in line contact and oscillatory movement *(Spanish)* 79—98671
minerals, elastic props., chemical comp. and crystal struct. 77—86862
misfitting elastic inclusion in infinite plane containing crack 77—65718
mixed boundary-value problems, orthogonal polynomial solns. 78—54193
mixed periodic problems, quadrature solution 80—86088
mixed problem, plane theory of elasticity of truncated wedge 80—43619
mixed problem, St. Venant principle 78—16654
mixed spatial elasticity problems, variational soln. *(Russian)* 79—9110
mixed-boundary value problems, numerical scheme 77—68432
mixture of two elastic solids, variational theorem in linear theory for quasi-static case 78—9561
mixtures, with 2-phases, closed system of eqns. *(Russian)* 78—16652
mixtures with long range spatial interaction 79—12600
mode I loading three-dimensional elastostatic problems, soln. method 80—92086
monodromic Galois groups of the sextic equation of anisotropic elasticity 79—97207
monolayer, elastic, of dipalmitoyl lecithin, dynamic surface potentials 80—3603
motion of solid body with elastic and dissipative elements *(Russian)* 78—65763
moving elastic strip, attenuation of conc. loads 77—19522
moving load on elastic strip on elastic half plane, steady soln. 80—10215
moving thin elastic strip subjected to random parametric excitation, dynamic stability 80—48618
multi-part mixed boundary value problems, numerical solns. 77—68430
multicomponent-medium, macroscopic stresses *(Polish)* 79—63040

elasticity continued
- multilayer cylindrical shell, theory in inhomogeneous temp. field 80—1434
- multilayer cylindrical shell, with elastic core, bending under local radial load 77—27474
- multilayer foundations of complex struct., method of flexibility functions *(Ukrainian)* 79—76969
- multilayer stress displacement calc. by double layer method *(Chinese)* 79—37162
- multilayer systems, elastic fluid motion *(Russian)* 79—46211
- multilayered shells, nonlinear anal. 78—18168
- multiparametric discrete-continual elastic systems, characteristic series coeff. *(Ukrainian)* 79—40368
- multiparametric elastic system, lower frequencies and crit. loadings *(Russian)* 79—44739
- multiply connected domains with cyclic and mirror symmetry, plane elasticity problem 80—96188
- multiply connected region, two-dimens. elasticity problems, numerical soln. 80—33463
- multiply connected thick plates, oscillations, elastic medium model anal. *(Ukrainian)* 79—94525
- multistorey elastic frames, critical load numerical determ. *(French)* 79—14262
- multiwedge corner, singular stress field, boundary value problem elasticity solns. 79—37174
- muscovite, exam. of dislocations and props. using elasticity theory *(German)* 79—10854
- natural stress rate, three-dimens. defn. 77—67291
- Navier, and Beltrami-Michell eqns., fundamental solns. in deform. of elastic space, dynamical case 80—12908
- Navier's eqn. soln. in cylindrical coords. 79—44744
- Navier equations of elasticity, iterative solns., depend. on Poisson's ratio 79—1107
- nematic liquid crystal-anisotropic crystal interface, influence of second-order elasticity on local Frederiks transitions 78—1982
- nematic liquid crystals, flexoelec. polar deform. and second order elasticity 78—1979
- neo-Hookean elastic layer, Griffith cracks, plane strain problem 79—50666
- neo-Hookean incompressible materials, finite elasticity theory exact solns. 79—63037
- neutron stars, relativistic elasticity 78—12267
- non-conservative stability, appl. of iterative Ritz procedure 77—22422
- non-homogeneous elastic shells transient displacement and stress 77—65684
- non-piezoelectric crystals, consts. determ. by method of homogeneous deformation 77—80570
- non-piezoelectric crystals, elastic constants anal. 77—84827
- non-sloping circular arc, large deflections, parametric extension *(Russian)* 80—1429
- non-standard anal. methods 77—47
- non-standard analysis method 77—46
- nonconservative autonomous and nonautonomous systems, stability, energy approach 78—51097
- nonconservative circulatory systems, variational formulation 80—48584
- nonconservative continuous elastic systems, post-buckling behaviour 79—3931
- nonconservative elastic systems, induced oscillations, transition through resonance *(Ukrainian)* 79—98654
- nonconservative elastic systems, stability under periodic effects *(Ukrainian)* 79—32309
- nonconservative systems which are conservative in a higher sense, Hamiltons variational principle extension 79—44742
- nonhomogeneous elastic layer bonded to nonhomogeneous half-space, torsion by circular die 78—87263
- nonhomogeneous medium, shock wave refl. from movable partition 79—7327
- nonhomogeneous medium under shear, elasticity theory 78—86166
- nonlinear, complementary energy and Reissner's principle relation 78—32678
- nonlinear, complementary energy principle 77—67289
- nonlinear, continuous dependence of solution on given data 78—18182
- nonlinear, effect on capture efficiency of dislocation loops 80—59461
- nonlinear, existence of solns. to elastostatic problems 79—75341
- nonlinear, existence theorems for various equilibrium boundary-value problems 77—58550
- nonlinear, potential wells and stability 79—9111
- nonlinear bending of elastic plates, lumped mass approx. *(Japanese)* 77—78984
- nonlinear boundary-value and evolution problems, Galerkin approx. 77—33870
- nonlinear boundary-value problem, incremental var. formulation, rel. to elasticity *(German)* 77—33866
- nonlinear Cauchy elastodynamics, global soln. nonexistence 80—31508
- nonlinear conservative systems, equilibrium anal., mixed method *(Russian)* 77—57193
- nonlinear Dirichlet problems, exponential decay estimates, elasticity and heat conduction 79—92939
- nonlinear discrete continuous model of elastic layered body, homogeneous deformation 79—23207
- nonlinear discrete-continuous model of an elastic layered medium 78—81844
- nonlinear elastic bodies, of different tensile and compression-strengths, stress and strain *(Ukrainian)* 80—69661
- nonlinear elastic body, stress/strain deviator ratio *(Russian)* 79—25854
- nonlinear elastic continuum, comparison of Runge-Kutta-Nystrom method and Newmark method *(German)* 78—87273
- nonlinear elastic continuum, one-dimens. description *(German)* 80—106725
- nonlinear elastic cylinder, parametric biharmonic vibrs., reson. modes *(French)* 79—10522
- nonlinear elastic dispersive media, interaction of solitary waves *(Russian)* 80—42076
- nonlinear elastic media, second order phase transitions *(Russian)* 80—24583
- nonlinear elastic rods, shear and necking instabilities 77—65682
- nonlinear elastic shells, stability loss *(Ukrainian)* 79—32308
- nonlinear elastic strings, multiple equilibrium states 80—27131
- nonlinear elastic systems, linear damping coefficients, experimental determ. 79—50680

elasticity continued
- nonlinear elastic tubular membrane, limiting pressure in simultaneous elongation and inflation 79—37166
- nonlinear elasticity, boundary value problems, finite element anal., recent developments 79—44737
- nonlinear elasticity, boundary value problems, numerical anal. 79—92945
- nonlinear elasticity, extremum principles, appl. to composites 78—51072
- nonlinear elasticity, integral estimates for displacement and strain energy, body force 77—54882
- nonlinear elasticity, relaxed continuity requirements, generalised variational principles 79—92942
- nonlinear elasticity, two-point boundary-value problem 77—75804
- nonlinear elasticity for nearly incompress. rubber like materials, large strains, finite element anal. 80—19238
- nonlinear elasticity incremental eqns., membrane theory 79—17224
- nonlinear elasticity strain energy, integral bound for displacement boundary value problem 79—37171
- nonlinear elasticity theory, generalised plane deform. *(Russian)* 77—46922
- nonlinear elastodynamics which conserve energy,,finite element methods 79—18723
- nonlinear finite elasticity, uniqueness condition, work theorem 78—57784
- nonlinear flexural vibr. of elastic ring 79—18805
- nonlinear hereditary elastic medium, longitudinal wave weak distortion process 80—62473
- nonlinear hyper-elastostatics, boundary value problem of space and traction, error energy, and error norm 80—53631
- nonlinear hyperelastic medium, wave front intensity, ray method calc. 80—43639
- nonlinear hyperelastic problem, soln. analyticity *(French)* 79—32249
- nonlinear hyperelasticity, finite deformations in constructive method *(German)* 77—41486
- nonlinear materials with different moduli in tension and compression 78—16649
- nonlinear nonideally elastic materials, hysteresis, relationships between stresses and strains *(Russian)* 80—90675
- nonlinear plate and shell theory problems soln. 77—53784
- nonlinear plate problems, unconditional stability of finite element scheme, nonlinear vibrs. *(Japanese)* 79—77004
- nonlinear rectangular elastic plate, instability 79—32316
- nonlinear shell analysis via mixed isoparametric elements 78—1566
- nonlinear shell theory, boundary value problem solutions 80—57094
- nonlinear structures, progressively changing equilib. eqns. soln. 78—1581
- nonlinear theory, dynamic problems, existence and uniqueness theorem 80—69658
- nonlinear theory of elastic materials with voids 80—53623
- nonlinear theory of simple dipolar elastic solid, successive approx. method 77—39221
- nonlinear Timoshenko beam, dynamic buckling 80—23928
- nonlinear wave propagation in relativistic continuum mechanics, applications in elasticity 80—22203
- nonlinearly elastic body at eqn., relation between stability and continuous dependence 80—92063
- nonlocal, 1-D models 79—40365
- nonlocal, fundamental 1-D solns. 79—67163
- nonlocal, static lattice defects props. 79—46743
- nonlocal elastic half space, boundary forces in solvable integral model 79—35558
- nonlocal elastic half-space, Lamb problem 79—98615
- nonlocal elasticity, rel. with lattice dynamics 77—84824
- nonlocal elasticity straight edge dislocation anal. 77—35555
- nonlocal elastodynamics, reciprocal theorems and var. theorems 78—9588
- nonlocal hexagonal elastic crystal, edge dislocation 79—51105
- nonlocal theory, appl. to point defects interaction 77—860
- nonlocal theory, stationary boundary problems, reciprocity principle and Green's tensors 80—68046
- nonplanar stamps, contact area determ., variational aspects 80—36855
- nonsymmetric structs., static and dynamic imperfection sensitivity, buckling model modification 80—79190
- notch stress anal. in elastic bodies, energy variations 80—64378
- numerical anal. in applied engineering science (conf. May 1977) 77—67249
- numerical estimation of boundary stiffness *(German)* 79—10466
- numerical methods for integral eqns., anal. of three-dimens. elastic solids 77—17818
- numerical treatment of boundary integral eqns., three-dimens. elastostatic anal., fracture mechs. appls. 77—46909
- oblique compression of two elastic spheres 79—27564
- oceanic lithosphere mechanical behaviour, implications of two earthquakes seaward of Tonga Trench 79—16405
- one-dimens. problems, diagonal mass matrices and finite element eqns. 78—73857
- one-dimensional wave propagation in materials with different moduli in tension and compression 80—83746
- opening mode crack problems, Westergaard method, critical re-examination 80—38337
- optimal control of dynamically controllable motions, appl. to hollow cylinder deform. 78—79214
- optimal design of freely vibr. elastic bodies *(German)* 78—65775
- optimal design of one-dimens. structures with linear or rotational displacement, iterative solutions 80—23887
- optimal design problems with singularities, soln. 77—72151
- optimal elastic design for prescribed maximum deflection 79—75343
- optimality criteria methods in elastic struct. design 78—83253
- ordered cubic alloys, reversible martensitic transformations 78—27516
- orthogonal polynomial solns. to crack and frictionless punch problems 77—75857
- orthogonal polynomials in elasticity theory 80—36857
- orthorhombic crystal, Hugoniot curves, elastic anisotropy effect *(French)* 78—18735
- orthotropic bridge decks with closed stiffeners, anal., behaviour 78—18164
- orthotropic layer weakened by double periodic plane cracks, compound problem of theory of elasticity 79—90139
- orthotropic medium of revolution in plane deform. state, law of behaviour *(German)* 77—23866
- orthotropic parallelepiped, weakened by double periodic plane cracks, theory of elasticity 79—86340
- orthotropic regularly layered elastic half-space, elastic wave reflection 80—33522

elasticity continued
orthotropic shell with tangential and normal strain, engineering theory eqn. 78—63303
orthotropic solid, rigid elliptic inclusions, soln. method 79—32275
orthotropic strip, stress intensity factors and crack opening displacements 80—53710
oscillation of rectangular elastic body framework model 79—41607
P and SV wave scatt. by rigid elliptic cylindrical inclusion in elastic medium 79—76999
panel structural optimisation under supersonic flutter conditions *(Italian)* 79—41600
particulate material, stress dependent behaviour 77—90398
peeling mechanics of elastic strip from rigid substrate, large bending 77—80122
penny-shaped crack, sudden twisting in a finite elastic cylinder, stress calcs. 78—67110
penny-shaped crack in elastic cylinder bonded to elastic surrounding material 80—19285
penny-shaped crack problem, deformed incompressible elastic solid 80—92085
perfect single crystal, continuum model of many-body interactions 79—35564
peridotite, high-temp. anelasticity and elasticity 80—17256
periodic elastic inclusion-rectilinear crack system in isotropic medium 79—41619
periodic heterogeneous ring, harmonic vibrs. *(French)* 79—50621
periodic problem in elasticity theory, soln. uniqueness 80—69674
periodic problems in elasticity theory *(Russian)* 79—9112
periodically reinforced elastic body, wave propag. in plane strain state 79—81803
perturbation method in solid mechanics, appl. to slack circular membrane 77—46911
phenol formaldehyde resin reinforced with chrysotile asbestos fibres, thermal expansion, specific heat 79—55908
physically nonlinear elasticity for small deform. anal. 77—74230
piecewise continuous elastic systems, eigenvalue lower bounds, stability and vibrations 79—50604
piecewise homogeneous bodies, two-dimens. elasticity theory stress problems 80—74749
piecewise homogeneous body, elasticity spatial problems, approx. solutions, R-functions 80—69670
piecewise homogeneous elastic medium, crack with finite branch, slip lines 80—38342
piecewise-homogeneous plate with slits on elliptic line separating materials 80—99932
piezoelasticity equations in stresses *(Russian)* 79—46210
piezoelectric cylindrical body with random anisotropy, elastic equilib. *(Russian)* 79—61308
pipe, layered, support layer thickness effect on stress-strain state *(Russian)* 80—43614
plane, and plate bending, finite element analysis 77—35033
plane, inclusion problem, numerical soln. of Cauchy-type integral eqn. 78—54194
plane, local trial functions in line soln. technique 77—14902
plane crack displacement field, integral eqn. formulation *(French)* 79—55338
plane crack of arbitrary configuration in elastic medium, stress concentration coeff. *(Russian)* 79—81805
plane crack problems in micropolar theory of elasticity 78—54191
plane elastic contact problems, pseudocaustics method 79—77034
plane elastic crack, dynamics under variable loading *(Russian)* 80—79222
plane elastic wave diffraction by wedge, three dimensional nonstationary problem 80—69723
plane elastic waves, reflection and refraction at elastic solid plane interface, initial stresses 79—72838
plane elasticity, cracks, Cauchy type integrals and integral eqns. with logarithmic singularities 79—30252
plane elasticity, mixed finite element method, convergence and performance 80—38258
plane elasticity, periodic contact and crack problems, closed form solns. 77—42783
plane elasticity, stress behaviour *(German)* 77—82394
plane elasticity of anisotropic media with antisymmetric stress tensor *(German)* 79—86338
plane elasticity problems, general bi-orthogonality condition 79—80442
plane elastostatic boundary value problems, formulation as integral eqns. by singularity method 79—35556
plane elastostatic boundary value problems, integral operators, eigenvalue num. calc. 80—36848
plane elastostatic boundary value problems, Rizzo's integral and Kupradze's functional eqns. 80—57093
plane elastostatics, boundary value problems, spectra of integral operators 78—57782
plane elastostatics, functional eqn. for static boundary value problem 79—80446
plane elastostatics, integral equations for mixed boundary value problem 80—79143
plane elastostatics, numerical props. of integral eqns. describing boundary value problems 78—34013
plane elastostatics, polynomial approx. in direct pot. method 77—72177
plane finite elastostatics, discontinuous deformation gradients, ellipticity failure and cracks 79—32264
plane harmonic Dirichlet problems, soln. for canonical domains 79—21548
plane isotropic elasticity, crack stress intensity factors using singular integral eqns. 79—72858
plane mixed boundary value problem, Legendre polynomials soln. 78—4487
plane momentum theory eqns. *(Russian)* 77—53787
plane problem formulation using dislocation layers, contact and crack problems 79—64507
plane problems, integral equation soln. 77—75810
plane problems of elastic half-spaces, Somigliana's method 77—13611
plane shearing stress meas. with wired strain gauges *(German)* 78—89471
plane steady solutions for stress-assisted diffusion 79—90136
plane theory, singular integral eqn. for mixed problem soln. *(Ukrainian)* 78—89339
plane theory problems, plane framework model for approx. soln. *(Russian)* 79—17223

elasticity continued
plane with const. tangential stress at free boundary, expt. stress anal. of subdomains 80—99978
plane-strain buckling of cracks in incompressible elastic solids 80—79186
planes, periodic contact problem *(Chinese)* 79—94487
plastic flow in thick-walled cylindrical shell, non-homogeneity effect, numerical calc. 80—19248
plastics reinforcement theory, functional model *(German)* 77—58564
plate, annular, bending anal., closed form solns. 80—38263
plate, annular, elastically supported, with central rigid mass, free vibrations *(Japanese)* 80—96226
plate, behaviour in limit of thin inclusion of high stiffness *(French)* 79—32250
plate, bounded by curvilinear contour, weakened by cracks, elastic equilibrium *(Russian)* 77—68524
plate, buckling, von Karman eqns., generic and nongeneric bifurcation 79—46239
plate, circular, elastically supported, free axisymm. vibr. 77—14942
plate, circular, elastically supported, with conc. mass at centre, large amplitude vibrs. *(Japanese)* 80—96227
plate, circular elastic, transient response to applied fluid pressure 79—64572
plate, deformed elastic, thickness oscillations 80—64439
plate, diagonal line-loaded, dynamic response 78—26036
plate, elastic, containing through crack, skew symmetric loading, transverse shear effects 80—64478
plate, elastic, infinite, thick, fixed, subject to axially symmetric load, numerical stress anal. *(Japanese)* 79—50600
plate, elastic, under aerodynamic tension, flutter, bending stiffness effect 78—30208
plate, elastic rectangular randomly inhomogeneous, free vibrs. 77—84180
plate, elastic with rib, vibr. freq., Weierstrass condition *(Russian)* 79—81757
plate, elastically supported, free vibr. 79—72836
plate, high freq. long wave vibrs., two-dimens. eqns. 78—83321
plate, impact force meas. method 80—79242
plate, infinite, with circular disc, tensile and compressive stress problems 80—38255
plate, laminated composite, under tension, interlaminar stresses around circ. cutout 78—34010
plate, linear elastic, classical boundary value problem 79—14261
plate, linearly elastic, free harmonic vibration fundamental frequency, approx. solution 79—46256
plate, obliquely stiffened, subjected to uniform compression, buckling strength *(Japanese)* 78—67067
plate, orthotropic, with small shift rigidity, stability eqns. construction method *(Ukrainian)* 77—31215
plate, prestressed elastic, homogeneous solns. for bending and stability 80—43610
plate, rectangular with asymmetrically reinforcing beams, contact interaction 80—99975
plate, rectangular with stiffening ribs, stress-strain state, elasticity eqns. *(Russian)* 80—1427
plate, relationship between centres of flexure and twist 79—86335
plate, semi-infinite with crack on end of stiffened edge, uniform tension 79—68659
plate, square with inset circular discs, elastic consts. effect on interference fit *(Russian)* 79—77031
plate, stability via Lyapunov's Second Method 77—54914
plate, thick, containing eccentric spherical cavity, transverse bending stresses 78—63288
plate, thick infinite, transversely isotropic, containing circ. hole, end effects 79—27510
plate, thin circular elastic material, Poisson's ratio effect on natural freqs. 77—84181
plate, thin elastic, buckling problem, eigenvalue eqn. positive soln. appl. *(German)* 79—68610
plate, thin elastic, Chladni patterns in random vibration 79—81714
plate, thin elastic, suddenly punched hole, plane stress unloading waves 80—69729
plate, variable thickness, Kirsh problem *(Russian)* 78—42528
plate, variable thickness, on elastic foundation, bending, closed form soln. 80—79179
plate aerodynamic stability in supersonic/hypersonic flow 79—14424
plate and shell theory, generalised two-dimens. theories generation 78—12569
plate bending elements, quadrilateral, finite element anal. with reduced integration 78—75071
plate bent with clamped edges, polyharmonic functions in elasticity theory 78—13927
plate incompressible isotropic, stability under all-round compression *(Ukrainian)* 79—37149
plate indentation by rigid punches 79—72807
plate of variable thickness, defined applied theories construction, asymptotic method *(Russian)* 80—53634
plate stability conditions, variational formulations 80—69701
plate stretched and compressed, geodetic lines *(Ukrainian)* 79—97199
plate theory, high order, stress soln. determ. 78—83248
plate theory, justification of nonlinear model *(French)* 79—25852
plate theory, nonlinear elasticity model, asymptotic expansion method anal. 79—44738
plate theory, nonlinear eqn., Cauchy problem, existence and uniqueness of smooth global soln. *(French)* 78—93513
plate theory, virtual work principle *(French)* 77—17817
plate with aperture, bending moments, exact. soln. 78—94598
plate with circular hole, axisymmetric stress distrib. 78—51066
plate with curvilinear elasticity, stress distrib. around hole, asymptotic method *(Russian)* 79—81726
plate with initial crack subject to extension, brittle fracture energy conditions *(Russian)* 80—103002
plate with rectilinear thin walled elastic inclusion, bending stress state *(Russian)* 79—81736
plate with two circular holes having tangential stresses, stress anal., electrostatics 80—48571
plate with unsymmetrical cruciform crack, stress distrib. 77—31256
plate-beam interaction, bending in plane of plate *(Russian)* 80—1428
plates, anisotropic skew, large amplitude vibrs., transverse shear, rot. inertia, theory 80—79207
plates, anisotropic skew, large amplitude vibrs., transverse shear and rot. inertia, numerical results 80—79208
plates, annular, dynamic stability numerical soln. *(Polish)* 80—10173

elasticity continued
- plates, complete solns. in linear theory *(French)* 80—52025
- plates, cracked, buckling under tension, finite element anal. 80—53666
- plates, elastic, optimum bending and extension *(Russian)* 80—38259
- plates, elastic homogeneous and isotropic, transient and time harmonic wave propagation 79—50633
- plates, loaded, thin elastic shell approx., energy conservation, stability eqns. *(German)* 77—873
- plates, rectangular clamped, elastic buckling 79—68606
- plates, rectangular elastic, secondary buckling states 80—74782
- plates, rectangular stepped thickness, with edges elastically restrained against rotation, vibrations 78—90740
- plates, ridigity matrix, triangular finite elements *(Russian)* 80—74739
- plates, semicircular, displacement due to concentrated force at a point, Green's function technique 80—58904
- plates, thick orthotropic on elastic foundations, freq. anal. using triangular plate bending element 79—46273
- plates, thin, circular, modal coeffs. for axisymmetric response 77—19537
- plates, thin elastic, large amplitude vibrs. by conformal transformation method 80—19262
- plates, thin heterogeneous, and sloping shells, elastic materials, exam. of theory 78—63307
- plates, thin rectangular elastic, bending, finite difference anal. 79—46181
- plates, thin rectangular elastic, response using Greens functions 80—1424
- plates, V-notched elastic, symm. loaded, stress intensity factors, caustic method 80—83770
- plates, vibrating elastic, transcendental equation solns. 79—53980
- plates and pivots, elastic stability under heterogeneous precritical states *(Ukrainian)* 80—48573
- plates and shells, random loading, soln. of boundary value problem *(Russian)* 77—57197
- plates laminated, shear deformations and correction factors, plate and elasticity theory 79—76963
- plates on elastic foundation, simplified finite element soln. 78—26041
- plates on elastic foundations, nonlinear dynamic behaviour 78—13956
- plates on elastic foundations, variational approach 80—79160
- plates on Pasternak-type elastic foundation, large amplitude free vibrs. 79—64556
- plates thin, third order elastic consts., effect on buckling 80—10172
- plates with pressed in solid discs, contact stresses *(Russian)* 80—43678
- PMMA, oriented, hypersound propag., elastic props. 78—75737
- Poincare elastic constant, increase for strongly starred domains *(Italian)* 80—23886
- point defect interaction with grain boundaries 80—59483
- point force soln. for infinite transversely isotropic solid 77—45701
- point source problems, differential transform technique in operational form 77—33865
- Poisson's equation solution, using curvilinear finite differences 78—28923
- Poisson brackets, nonlinear hydrodynamics eqns. in condensed matter physics 80—54296
- polarisable dielectric crystals, mean internal stress pot. *(Italian)* 79—65797
- polycrystal, elasticity, graded disorder, self-consistent scheme 79—10473
- polycrystal elasticity theory, role of Gruneisen elastic parameters 79—95070
- polycrystals, elastic stress and strain microinhomogeneity, finite element method 80—79155
- polydimethylsiloxane, rubber elasticity in uniaxial tension, compression 79—15714
- polydimethylsiloxane end-linked chains, nonGaussian effects 80—65127
- polyester laminates, glass fibre reinforced, enhanced elasticity, chem. resist. tests *(Polish)* 80—60901
- polyester resins unsaturated, enhanced elasticity, chem. resist. tests *(Polish)* 80—60901
- polyethylene, low density, melt elongation, stress and recovery maxima 79—90209
- polyethylene melt, applicability of statistical rubber elasticity theory 78—42579
- polyethylenes, extrusion and heavy duty films struct. parameters influence on cross-linking by radiation 80—66844
- polymer, elasticity of bulk and film from multipass Brillouin spectra 78—76485
- polymer, filled, solution, normal stresses and hyperelasticity under simple shear flow 80—1506
- polymer, microinhomogeneous, elastic props. description rel. to crystallinity 79—19307
- polymer chains 80—3116
- polymer composite anisotropic plates, stress conc. around holes with shear strain taken into account 80—43618
- polymer craze mechanics, elastic model 77—48519
- polymer films elastic anisotropy based on thermal shrinkage strains 77—86245
- polymer glass, isothermal struct. relax., in high elasticity transition region, mol. model *(Russian)* 78—87629
- polymer globule elasticity 77—70404
- polymer granules, compression, stress state 80—10218
- polymer materials, hysteresis flow model applicability for degree of inelasticity 80—28422
- polymer network junctions, elasticity, local constraints effects 78—2021
- polymer networks, effect of geometric constraints on junctions 78—75711
- polymer science, conf., Pittsburgh, USA, (June, 1975) 77—38756
- polymer solution, rheological eqns. of state, macromol. elasticity and internal viscosity effects 77—80127
- polymer structure and mech. props., book 78—83756
- polymer with spherical inclusions, slope discontinuity prediction in stress/strain behaviour 78—94596
- polymeric solids, mech. retardation time spectrum, thermostimulated creep 79—5014
- polymers, longitudinal acoustic mode in 79—73277
- polymers, thermoreactive, elasticity modulus, change on curing *(Russian)* 79—64521
- polynomial solutions for an ellipse on an anisotropic elastic half-space 79—10480
- polyoxymethylene, transitions and relaxation spectrograph 80—65204
- polyphase materials, effective tensors 79—81728
- polypropylene fibres, high strength, elastic 80—20992
- polypropylene monofilaments, tensile props., orientation degree depend., IR dichroism obs. 78—3163
- polypropylene-bitumen mixture, thermomech. investigation changes in viscosity, ductility, elasticity, mol. wt. effects *(German)* 78—35454
- polyurethane, stress plate in contact zone with solid indentor 78—1624

elasticity continued
- polyvinyl-pyrrolidone/polyethylene glycol oligmers, elasticity theory, and compression meas. 80—44246
- ponderable thick-walled hemispherical dome, elastic equilib. *(Russian)* 80—53632
- poro-elasticity, disturbance due to expanding ring and disc load 78—79250
- poroelastic cylinder, twisted pore effect on fluid flow, solid deformation and stress 80—64377
- poroelastic cylinders, torsional vibrs., wavelength, phase and group vel. 80—79214
- poroelastic hollow cylinders, torsional vibrs. 79—64557
- poroelastic semi-infinite cylinder, torsional vibr. 79—32334
- porous elastic half space, Lamb's line load problem 79—30248
- porous materials, self-consistent imbedding approx. in elasticity theory 77—33066
- porous media, elastic, variational theory 80—10146
- postbuckling analysis of elastic structures by the finite element method 80—96209
- postbuckling at coincident branching points, relation to energy surface umbilic point geometry 80—23926
- potential approach appl. 77—68429
- potential-type singular integral approx. algorithm 80—27132
- powder, temperature effect on flow and tensile strength 79—61668
- precipitate and dislocation loop strain and stress field calcs. using affine transformations 80—106722
- precipitate strain energy and elastic strains *(Korean)* 79—65201
- preconditioning of indefinite problems by regularization 79—46214
- pressure distribution and gap shape in a one-dimensional elastohydrodynamic contact 79—94526
- pressure vessel with hemispherical head, shell intersection, elastic stress anal., homogeneous eigenfunction method 77—23884
- pressure vessels, creep bounds and brittle damage estimates 80—23908
- prestressed concrete reactor vessels, perforated plate ligaments, time varying stress 79—49679
- prestressed elastic body, 3-D contact problem 80—69655
- prestressing in 2-phase media *(Polish)* 79—12605
- prismatic bar of linearly elastic material, maximum theorem appl. for complementary energy functional 80—83733
- prismatic bars, torsional stiffness of heterogeneous material and solid cross section 79—27519
- prismatic bars, torsional stiffness upper limit 79—32248
- prisms, minimum energy, St. Venant's solns. 80—52027
- prisms, periodic solns. 80—48582
- progressing torsional loads along a bore in an elastic medium 80—79197
- projective geometry determination of plasticity and elasticity coefficients *(Spanish)* 79—50605
- propagation of elastic waves in infinite bar, elliptical cross section, linear elasticity 78—67073
- propoxylated bisphenol A, mech. props., effect of polyester copolymers modified with polypropylene glycol addition *(Polish)* 80—60902
- propyl stearate monolayers, elasticity and viscosity determ. by laser light scatt. 77—72749
- pulmonary interstitial fluid space compliance, estimation in isolated perfused rabbit lung 80—104605
- pulsed excitation of flexural modes in infinite plates 80—38167
- punch, axisymmetric, contact with semi-infinite transversely isotropic elastic body *(French)* 80—23969
- quadrilateral plate anal. 79—46201
- quadrilateral shell element utilising isoparametric principles 78—34012
- qualitative methods, book 78—20969
- quantum theory, linearised eqns., acoustic tunnel effect 77—26188
- quantum theory, natural vibrations of rectangular parallelepiped and plate 77—27483
- quantum theory, resolving functions and potentials for linearised eqns. 77—22425
- quarter plate support, planar flexibility depend. on fillet radius 80—5944
- quartz, electron irradiation effects on optical, dielec., elastic props. 80—59521
- quartz plates, rotated-Y-cuts, high frequency vibrations 80—96216
- quasi-perfect elasticity, adiabatic temp. variations 78—32675
- quasi-state hyperelastic crack propagation, energy release rate 79—68661
- quasistationary Rayleigh waves on inhomogeneous anisotropic elastic body surface 80—69721
- radial cracks emanating from outer and inner surface of circular ring, elastic anal. 79—68645
- radial vibrations of a gravitating sphere with a material boundary 79—41609
- rare earth metals, elastic props., connection with electron struct. *(Russian)* 80—19895
- rare earth oxides, binary, struct. and props., book contrib. 80—45292
- ray theory in relativistic anisotropic elasticity *(French)* 80—36846
- Rayleigh waves, inelastic particle reflection 79—74022
- Rayner model, elastic sphere in general relativity theory *(Russian)* 79—92671
- reactor component-support impact dynamics, elastic anal. by model expansion method 79—45343
- rectangular orthotropic region, plane shear, stress free edge effects 79—18830
- rectangular parallelepiped, natural vibrs. from 3D elasticity and plate theory *(Russian)* 80—79199
- rectangular plate, initially stressed, forced motion, elasticity solution 78—38235
- rectangular plate bending, superpower degeneration of boundary layer of angular points *(Russian)* 80—74776
- rectangular plate with fins, stress anal. under bending, approximation theory *(German)* 79—90144
- rectangular plates with perforations, stability anal. *(Russian)* 79—32311
- rectilinear anisotropic solids, mixed-mode crack anal. using conservation laws of elasticity 80—84239
- rectilinear oscillations of a rigid spheroid in an elastic medium 79—71253
- reflex stiffness of man's anti-gravity muscles during kneebends while carrying extra weights 80—61601
- regularly layered half-space, deformation, vibrational loading 80—99933
- reinforced hollow spheres, dynamic behaviour 78—1577
- reinforced panels, variable stiffness, plane stress problem 79—94497
- reinforced shell under external press., max. stability 78—94597
- reinforced tube, bending and flexure 78—51076
- reinforcement material distrib. for specified stress field criteria, plane elasticity hybrid problem 80—64376

elasticity continued
relativistic, one dimensional nonlinear motion 79—84953
relativistic elasticity of dissipative media, wave propagation modes 78—4485
relativistic hypoelasticity, characteristic manifolds, wave propagation *(French)* 79—30227
relativistic initially stressed elastic solids, infinitesimal discontinuities 77—45775
relativistic theories of materials, book 78—81907
renormalisation method for unbounded media, elastic fields and effective moduli *(Russian)* 78—41162
representation theorem for isotropic linear constitutive relns. 79—17226
resolution method for second problem of elastic limits for plane *(French)* 78—57779
retina detachment, math. model 78—44536
rib rigidity distrib. on elastic plate, necessary optimal conditions *(Russian)* 80—53633
ribbed plate, optimal design 80—14578
rigid body displacement field 77—67293
rigid disc inclusion embedded in isotropic elastic medium, displacements for external force 80—48652
rigid indentor and elastic halfspace, dynamic contact with perfect adhesion and frictional slip 80—58980
rigid punch, flat-ended cylinder with elliptical cross section, Boussinesq problem 79—68663
rigid punch bonded to elastic half plane, stress singularities 80—64491
rigid punch problem on non-homogeneous elastic half-space 80—53720
rigid sphere embedded in elastic medium, response to incident stochastic waves 80—64451
rigid sphere on elastic half-space boundary with friction, equil. anal. *(Russian)* 77—80071
rigid stamp, elastic layer indentation under complete adhesion conditions 80—58979
ring, homogeneous isotropic compressible elastic, second order torsion problem 80—14570
ring, multilayer elastic, forced vibration, variational principle effectiveness in Ritz method *(Russian)* 79—68616
ring sector, mixed plane elasticity theory problem *(Russian)* 78—62080
rock, dry, quantitative model of dilatancy and appl. to Westerly granite 79—16445
rock bodies, cooling, residual stress development 78—88819
rock penetrator, initial response, elastic rod theory 79—32392
rocks, elastic props. experimental studies rel. to Earth crust press.-temp. conditions modelling *(Russian)* 78—96207
rocks, elasticity freq. depend. and seismic vel. dispersion 77—73727
rocks, Murnaghan constants evaluation as function of pressure 80—31037
rod, buckling under time-varying load 78—42551
rod, curved, deformed by end loads *(Russian)* 80—74745
rod, elastic, approx. soln. to deformation problem *(Russian)* 79—64511
rod, elastic oscillations, wave operator fundamental solutions, asymptotic formulae 80—69722
rod, fixed-free circular, soln. under various bad conditions 78—67047
rod, nonhomogeneous elastic, with varying cross section, pulse propagation 79—46257
rod, perturbation methods for soln. of linear eigenvalue problem *(German)* 78—18175
rod, short elastic, in viscous liquid axial flow, stability and transverse oscillations 80—33521
rod, straight linearly elastic, axially loaded, dynamic response 79—68635
rod, thin elastic, non-conservative torsion *(German)* 80—106723
rod, thin elastic, with causally mixed inputs, iterative numerical soln. 80—79161
rod, twisted axially loaded, nonlinear anal. 79—72811
rod, wave propag. 77—60939
rod central collisions soln. from impulse conservation *(German)* 78—22274
rod equations 79—40364
rod impact, numerical soln. using Volterra integral eqns. 77—68437
rod on viscoelastic half-space, forced longit. vibr., appl. to muscle study 78—44538
rod with clamped ends, axial and transverse loading, stability, plane elasticity theory *(Russian)* 80—79184
rods, elastic, high-freq. long wave vibrs. 80—96211
rods, elastic, large deflections and rots., asymptotic anal. 79—50584
rods, elastic with multiple wave speeds, wave propagation 79—72850
rods, initially stressed, curved, twisted, constitutive eqns. 79—27517
rods, simple orthotropic elastic, shock waves and wave-type instability 80—48622
rotating circular cylindrical elastic membranes bifurcation 80—33494
rotating circular elastic disc, diametral edge cracks, stress anal. 79—32386
rotating deformable elastic disc, vibr. stress anal. *(Russian)* 80—19265
rotating disc, elastic stress state distrib. calc. 79—37175
rotation effects on natural vibr. frequency *(Russian)* 79—7319
rotor, elastic, parameter excited vibrs. *(German)* 79—90179
rough curved surfaces, elastic contact stresses calc. 80—10213
rough elastic bodies, plane and axisymmetric contact problems 80—74812
rough materials, stressed state on contact 80—38352
rough spheres, elastic contact, anal. approx. 80—79240
rubber, natural, crosslinked by dicumyl peroxide, modulus, swelling relations 80—59551
rubber, network, highly swollen, long time dynamics 80—38291
rubber, props. prediction on basis of microscopic structure, small angle neutron scattering appl. 80—3113
rubber, rupture life calc. 77—59933
rubber, theory for highly entangled regime 77—90385
rubber covered rolls, contact and deformation nonlinear elastic problem, stress anal. 80—79239
rubber elasticity, Gaussian statistical and Mooney-Rivlin theories 77—46935
rubber elasticity, molecular aspects book contrib. 78—84886
rubber elasticity, new statistical theory 77—35623
rubber elasticity theories, statistical, applicability to polymer melts 78—42579
rubber network, mol. theory 80—38290
rubber seal technology, advances 80—93730
rubber sheets, circular, elastic deformation profiles 79—66481
rubber tube, inflation and extension, biaxial strain studies 78—83251
rubber-like elastic materials, stress-strain behaviour 78—67049

elasticity continued
rubber-like solids, biaxial deform. 80—1431
running crack, three-dimens. problem, elasticity dynamic eqns. 79—18811
Saint Venant's problem for inhomogeneous anisotropic Casserat elastic solids 78—42534
Saint Venant's solns. in rod and beam theories 80—69676
Saint Venant-von Mises materials, two-field variational methods *(French)* 77—17816
Saint-Venant's principle, elastic cylinder energy decay 79—14270
Saint-Venant's principle, in three-dimensional nonlinear elasticity 77—50888
Saint-Venant's principle for bodies of general shape 77—62157
Saint-Venant's problem for inhomogeneous anisotropic solids with microstruct. 77—74229
Saint-Venant principle in 2-D, for second order linear elliptic eqns. 77—26177
sandwich plates, finite element anal. 78—67046
sandwich plates with thick faces, orthotropic, hybrid stiffness matrix 77—80072
sandwich strips, plane deform., Saint Venant end effects 78—46893
sandwich structure stability, analog method 79—32314
sandwich type shells, elastic Cosserat surfaces, small bending and stretching 78—22264
saturated elastic half-space with partially embedded elastic bar, quasi-static bending 80—79145
screw dislocation, nonlocal elasticity 77—31659
screw dislocation in nonlocal hexagonal elastic crysts. 78—59807
second fundamental crack problem and the rigid line inclusion problem in plane elasticity 80—27129
second order, internal instability 79—60
second order beam theory 80—58908
second order effects in an elliptic hole stressed at infinity 80—96192
second order symm. tensors in compact Riemannian manifold, compatibility and orthogonal decomp. 77—57161
sector problem soln. using Mellin transform technique 79—97204
sector problem with arbitrary loads on edges 79—32263
semi-infinite crack, kinking under dynamic loading conditions, elastodynamic stress intensity factors 79—68660
semi-infinite elastic media, harmonic wave generation at unbonded interface 79—23237
semi-infinite medium with anisotropic elasticity, 1st and 2nd periodic fundamental problems *(Chinese)* 80—5931
semi-infinite plate subjected to increasing boundary force, dynamic response, ice sheets 78—83254
semi-infinite strip under symmetric load, stresses, elastic plane theory 78—59301
semi-infinite transversely isotropic materials, Green's function solutions 79—46205
semiinfinite elastic solid, frictional shear effect on dynamic stresses 79—10537
sethlets, generalised singular points 79—46
shaft, symmetrical, nonlinear elastic and internal damping props., flexural vibrations 78—71290
shakedown analysis, numerical, circular plates subjected to press and temp. cycles 77—3749
shallow anisotropic shells of double curvature, weakened by hole 79—90151
shallow arch under multiple loads, postbuckling and stability anal. 80—48617
shallow shell theory, admissible singular solns. 77—68419
shallow shell theory, existence problem of solns., effect of initial deflection 77—23872
shallow shell theory, series representation of fundamental solution 79—10468
shallow shells, force loading and temp. field effects, algorithm construction *(Ukrainian)* 78—89338
shallow thin shell finite element, stiffness matrix development 78—90705
shaping of adherends in bonded joints 79—27599
sharp edge in contact problems with friction, stress singularity 77—7313
shear crack, stress distrib., finite elastic anal. 78—51119
shear of infinite elastic space with plane crack *(Russian)* 77—75853
shear stress bounds in Saint-Venant's theory of flexure 77—13608
shear stresses induced by hydrostatic pressure near the surface of an inclusion 78—75074
sheel, cylindrical, closed, laminated, longitudinal crack, elastic eqn., energy approach *(Russian)* 80—87740
shell, aerohydroelastic opening of shell in nonstationary flow *(Ukrainian)* 79—32258
shell, axially stiffened, mode interaction in postbuckling behaviour 77—89046
shell, consistent second approx. to elastic strain energy 79—81732
shell, cylindrical, dynamic stability under periodic axial load 79—14302
shell, cylindrical, in vicinity of supporting elements, stress state 80—48585
shell, cylindrical, isotropic, elastic stability, critical load analysis 80—83744
shell, cylindrical, Rayleigh wave propag. using elasticity theory *(Russian)* 80—38307
shell, cylindrical elastic, dynamic response in potential fluid 80—64446
shell, elastic, cylindrical, stability, Liapunov's second method 80—64410
shell, elastic, smooth, materially uniform, field equations of motion 77—82389
shell, elastic anisotropic multilayered, improved linear theory 77—50906
shell, elastic cylindrical, impact on surface of compressible fluid *(Russian)* 79—37181
shell, elastic cylindrical, ribbed, with weight on springs, free vibr. freqs. 80—69725
shell, high-shallow, with rib of equal resistance, contact interaction, tangential stress distrib. *(Russian)* 80—87745
shell, infinite cylindrical, in elastic medium, action of moving load, pressure waves *(Russian)* 79—81754
shell, layered, refined theory *(Russian)* 77—35045
shell, multilayer orthotropic shallow, theory allowing for transverse shear deform. and normal stresses *(Russian)* 77—35046
shell, reinforced with zero Gaussian curvature, momentless stressed state 77—35043
shell, spherical transversally isotropic stability *(Ukrainian)* 80—10171
shell, supported cylindrical, interaction pressure variation 80—38354
shell, thin elastic, containing liquid, free vibrs. *(Russian)* 80—33505

elasticity continued
shell, thin elastic, equilibrium state, existence and uniqueness theorem 79—94493
shell, viscous plastic layers, viscous elastic filler, variable loading *(Russian)* 80—69695
shell buckling under creep conditions, sequential loading method, deformations anisotropy 80—33495
shell design by finite element method, deformation and elasticity theory 80—74747
shell of revolution, orthotropic, thick, stress-strained state, finite element method *(Russian)* 80—87713
shell of revolution in acoustic medium, steady state motion 79—18728
shell of rotation, existence and uniqueness of soln. for stress-strain state *(Russian)* 78—36830
shell problems, finite element anal. *(Ukrainian)* 80—69662
shell problems, finite element methods, numerical integration *(French)* 77—74206
shell stability during axial compression, hardening beyond elastic limit 80—99931
shell structure, 10 ft diameter, imperfection survey, buckling load 77—89023
shell surfaces calc., thick-walled, with axisymmetrical load using finite element method *(Russian)* 80—48569
shell theory, algebraic assumptions equivalent to Kirchhoff hypothesis 77—13606
shell theory, forms of eqns. 78—16653
shell theory, momentless *(Russian)* 78—51075
shell theory, two dimens., asymptotic expansions, error bounds 78—5661
shells, applicability limits for approx. theories *(Ukrainian)* 80—23933
shells, circular cylindrical, in axial compression, axisymmetric creep buckling, isotropic elasticity 80—69704
shells, conforming finite element methods, convergence 80—53630
shells, curvilinear tubular, elastic equilib., finite element anal. *(Russian)* 80—79148
shells, cylindrical, and of revolution, path independent integrals 80—87711
shells, cylindrical, diaphgragm-supported, static analysis using curved finite strip 77—89027
shells, cylindrical, dynamic stability, in-plane inertia and disturbance effects 80—79181
shells, cylindrical, finite element anal., solid of rev., thin shell and interphase elements 80—74744
shells, internally pressurised 2:1 ellipsoidal, elastic and elastic-plastic buckling 79—37206
shells, isotropic thin elastic, nonlinear theory *(Russian)* 80—79147
shells, Kirchhoff-Love, structural stability, mixed variational principles and non holonomeous constraints *(French)* 80—74779
shells, orthotropic, cylindrical, axial pressure wave effects 80—10183
shells, parabolic, shallow, thin, approximate calc. 79—57
shells, spatial stability problems in elastic systems, modified energetic procedure *(Russian)* 80—58943
shells, stable solutions, finite element and Newton-Raphson methods 80—14593
shells, thick cylindrical hyperelastic, large amplitude oscillations 79—64560
shells, thick hyperelastic, spherical, large amplitude free and forced oscillations 80—74794
shells, thin, doubly curved, numerical integration of triangular finite element 80—92044
shells, thin conic, with asymmetric edge loading, Newton polygon soln. *(German)* 77—57199
shells, thin elastic, recent advances in linear theory 79—59921
shells, thin elastic spherical, large axisymmetrical deflection states 80—79154
shells, thin orthotropic elliptical cylindrical, elastic collapse under combined bending and press. 80—48589
shells, thin walled, elastic, Rayleigh method anal., energy calcs. 77—65677
shells, three-layer cylindrical, axisymmetric free waves 80—5982
shells, two fluid-coupled cylindrical elastic, transient response to incident press. pulse 80—58966
shells, two-dimensional eqn. system *(Ukrainian)* 78—89342
shells, two-layer cylindrical, stress-strain state, elasticity theory eqns. 80—33462
shells of revolution, finite-difference method *(Russian)* 79—10477
shells of revolution, mixed finite element formulation for geom. nonlinear anal. 78—38189
shells of revolution, stability, dynamic programming 79—32270
shells of revolution, stability eqns., symmetry props. *(Russian)* 80—1450
shells of revolution with arbitrary loading, asymptotic integration methods *(Russian)* 77—58552
shells of rotation, limiting equilib. at low temps. 79—64512
shells of variable thickness, eqns. of motion *(Russian)* 77—39226
shells under external press., stability 80—23898
shells with curvilinear axis, geometric approach 79—32271
shells with tangential load, singular solns. to eqns. 80—23897
shock wave-acoustic wave interactions in elastic solids 79—32370
shock waves in nonlinear elastic media 80—48629
short column vibrator, apparent elasticity analysis and applications 78—59242
Signorini's perturbation procedure in elasticity, branching of solutions 80—27134
Signorini's problems, reciprocal variational inequalities soln. 79—41585
Signorini problem for a Cosserat plate 80—69666
Signorinis perturbation scheme for a general reference config. in finite elastostatics 78—83241
simple material without memory, elastic pot. existence, hyperelasticity 79—94486
single crystals under large loads, theoretical elastic behaviour, review and appl. 80—71681
single mass vibroimpact system, response to white noise random excitation 80—64454
singular integral eqns., regularisation for cubature formulae and approx. soln. methods 77—17820
singular integrals, 2-dimens., used in 3-dimens. elasticity 79—35561
singular stress field at crack front edge in elastic body, crack propagation 79—50656
singularity anal., boundary integral eqn. 77—68426
skeletal elastic structures, forced, damped vibr. anal. procedures 79—32330

elasticity continued
skew crack propagation, induced dynamic stresses, numerical soln. 79—1137
skin elasticity of living dolphins *(Russian)* 80—45926
skin wrinkling, human, using model of thin elastic shell on continuum foundation 77—52819
slamming safety membrane, stability loss in elastoplastic and elastic regions, expt. coeffs. 80—33496
slender damped structures, vortex excited aeroelastic oscills., mathematical model *(German)* 78—94616
slender Z-crack, elasticity problems 78—87304
slip friction characteristics in nonstationary motion *(Russian)* 80—43652
smooth circular plates, axisymmetric elastic contacts 80—19291
soft ferromagnetic elastic solid, magnetoelastic interaction with penny shaped crack in const. mag. field 79—18829
soft shells, geometrically nonlinear strain *(Ukrainian)* 79—50589
solid deformable body, residual stresses by creating holes, holographic interferometry appl. *(German)* 80—79243
solid mechanics, elements of elasticity *(Japanese)* 79—59932
solid with annular crack, bending effect 79—72806
space-time deformations of an elastic medium and the electrodynamic equations *(Russian)* 80—52028
spacial problems, appl. of theory of two complex variables *(Russian)* 77—57194
spatial curved bars, kinematic elements of mechanisms, movement equations 80—46809
spatial elastica theory with centreline compressibility 78—79211
spatial structures of shells and grids, statics 77—19526
sphere, composite elastic nonhomogeneous, with concentric spherical inclusion, opposite couple stress, displacement 79—94494
sphere, deformation and sticking to a rigid plane, mol. force effect 80—106720
spherical cavity in prestressed medium arbitrary orientation, elastic relaxation coeffs. 77—73692
spherical crack in elastic space *(Ukrainian)* 77—68522
spherical dome, three-dimens. elasticity soln. and edge effects 78—59306
spherical elastic shell, thick walled, transient response, ray theory determ. 79—10484
spherical inclusion embedded in bonded dissimilar half-spaces, eigenstresses 77—23886
spherical inclusions, stress concentrations between two 77—80077
spherical shell, axisymmetric forms of equilibrium *(Russian)* 78—87262
spherical shells, local stability 78—1587
spinning shells, Magnus characts., empirical calc. method 78—26072
spot weld between elastic plates, near field stress anal. 77—11160
springback in beams and plates, bending 80—38256
St. Venant planar theory, nonhomogeneous problem, logarithmic decrement *(French)* 78—49664
stability, response to finite strain 80—79187
stability of elastic incompressible bodies under isotropic compression 80—14597
stability of elastic systems with small internal friction *(Russian)* 79—17222
stability of incompressible body under uniform lateral pressure *(Russian)* 78—32680
stability of linear system, simplified algorithm 77—62180
stability theory, nonlinear partial differential eqns. *(Russian)* 79—9128
stability theory for plates with inhomogeneous precritical states *(Russian)* 78—49665
stannates with perovskite struct., elasticity meas. to 6 kbar 77—51428
star shaped membranes, new bounds of Poincare const. *(French)* 79—25860
static fields in inhomogeneous anisotropic medium *(Ukrainian)* 78—81837
static response rel. to fundamental freq. of undamped linearly elastic systems 77—68484
static-geometric analogy in thin shell struct. eqns. 77—80087
statistically homogeneous media, linear theory 77—862
stayed columns, concise buckling, vibration and static anal. 79—18755
steadily moving load, elastic strip on rigid foundation. noncontact regions, displacements, contact press. 78—87264
steady state crack propagation, media with variable elastic moduli 78—90783
steel, 40Kh, plastic-strain mechanism for work hardening 78—42530
steel, acoustoelastic stress field imaging technique, stress field contour plots 79—77033
steel, austenitic, martensitic transform. temp., singularities in 50Kh2N22 *(Russian)* 78—68689
steel, austenitic, type of Kh15N27T3MR, exam. of elasticity props. 78—56687
steel, correlation links between mech. props. controlled rolling effect 80—35234
steel, mild, residual stress meas., acoustoelastic, in a patch-welded disc 79—27604
steel, Ni (9 and 5 wt.%), for liquefied natural gas appls., material and weld props. 79—61736
steel, sintered, mech. props. 77—40439
steel, spring alloy, microstruct. and props. at low temps. 77—44286
steel, stainless, global bending response analysis of elastic and viscoplastic nuclear shipping cask structures subjected to impact loading 80—76301
steel, stainless 304, cyclic plasticity, exponential stress-strain law 77—25157
steel, type Kh12M, rel. between structural inhomogeneity and wear resist. *(Russian)* 80—66672
steel 60S2 and 55S2GF, elastic and fatigue charact. 77—21267
steel Cr-Mn (13, 19 wt.%), for liquefied natural gas appls., material and weld props. 79—61736
steel H_2, embrittlement resist., selection of test conditions *(Russian)* 79—15883
Steklov consts., bounds 79—25861
stiffness factor formulation, explicitly or using numerical integration 77—65676
stishovite, polycrystalline, elasticity 77—5189
stochastic excitation systems, identification of damping and stiffness parameters *(Polish)* 78—69973
stochastic medium, dynamics anal. with Markov approx. *(Russian)* 78—41163
strain energy of elastic prismatic bar, theorems *(German)* 80—79142
stress anal. in two dimensions, expt.-numerical hybrid technique 77—50910
stress analysis, improved equilibrium finite elements 78—75067

elasticity continued
stress analysis for an elastic half space containing an axially-loaded rigid cylindrical rod 80—1423
stress and crack-displacement intensity factors, in elastodynamics 78—67112
stress concentrations round cylindrical cavity in half-plane under tension, effect of couple-stresses 77—19524
stress distribution in elastic half-space, nonlocal effects 77—80070
stress in elastic wedge or notch loaded by localised internal source 77—42741
stress intensity and elastic equilibrium of a wedge with a crack 80—69733
stress intensity factor calcs. using elastostatics M-integral conservation law, plane cracks 78—46913
stress meas., nondestructive, acoustoelasticity appl. 79—34259
stress separation in photo-orthotropic elasticity, numerical method 78—59296
stress state of structural elements of vessels under external hydrostatic press. 77—14908
stress tensor, Kauderer's postulates *(German)* 80—64364
stress-deformation relns. inversion, associated inequalities 77—50904
stress-strain state at brittle crack vertex, geometric nonlinearity effects *(Russian)* 80—79221
stress/strain relations, materials with different moduli in tension and compression 77—42735
stressed rocks, crack induced anisotropy, effective elastic moduli and attenuation 80—56461
stretched elastic sheet, punched hole, wave propagation 79—10524
stretched finite elastic strip, central crack dynamic response 79—18826
string, stochastic vibr., mean displacement determ. by successive approx. 79—27523
string vibrating against rigid wall, partially elastic or anelastic impact, energy calcs. 78—67028
strip, elastic, Griffith crack interactions, mixed boundary value problem 80—58969
strip, thin, transversally loaded, elastic waves propagation solution, by physical discretisation 77—50943
strip or beam, state of stress, rectilinear thin walled inclusion effects 80—96187
strip with isolated crack, equilibrium 80—14620
strip with periodically spaced rigid framed holes of complex shape *(Russian)* 77—75797
strip with semi-elliptic notches or cracks, stress anal. by rational mapping function 79—14257
strips, mixed elasticity theory problems, appl. of dual trigonometric series *(Russian)* 77—71189
strips, seizure, elastic stresses, extra loading moments *(Russian)* 80—69664
structural dynamics, finite element reduction scheme, variational theorem 77—890
structural optimisation, homogeneous functionals 79—98619
structural stability anal., num. methods 79—94489
structures, elastic realisability of force and displacement systems 80—46808
structures, work hardening deflection stability 79—27528
structures with rotational degrees of freedom, large displacement-small strain anal. 78—89310
supports for straight fluid-carrying pipes, critical velocity calc., w.r.t. vibrations production *(German)* 80—58914
surface atom mean-square displacements, elastic continuum theory 77—76655
surface concentrated loading, axisymmetric problem for homogeneous medium *(French)* 80—92041
surface instability, nonlinear problem in elastic half-plane *(Ukrainian)* 80—5961
surface stress, equilib. shape of elastic cryst. 77—35030
surface-fluid-shell system, finite element anal. of dynamically coupled motion 77—19536
surfaces with metric and curvature tensors 79—71252
symmetrical branches at end of crack, effects on growth 80—103003
symmetrical free vibrations of a thin elastic plate with initial condition as a generalized function 79—59939
symmetry considerations for material surfaces 80—8794
tangential loading of two bodies in contact 77—19538
tapered beams, stress trajectories, stress contours 78—63305
teacher resource paper on entropy an rubbery elasticity 80—17777
telescope secondary mirror, flexure, elasticity theory *(French)* 77—14789
tensioned bar with initial curvature, parametric excitation 80—43654
tensionless contact without friction between elastic layer and elastic foundation 80—64487
tensors of fourth order 79—97202
theory, partial differential equations transformation into uniform system of equations 79—2630
theory for body with curvilinear cracks, integral eqn. construction, two dimensional problem *(Russian)* 77—27490
thermodiffusion in elasticity, vibr. boundary value problems 78—41164
thermodynamic behaviour of non-hyperelastic elastic materials, mathematical model 80—73290
thermodynamic fundamentals of continuum mechanics, equilibrium states 79—40373
thermoelastic material, deformed isotropic, thermal effect on acoustoelasticity 80—33276
thermomechanics, introduction, book 78—54187
thermoplastic elastomers, crosslinked by secondary valence interactions, elasticity and processing, crosslinking behaviour 80—40320
thick membrane strip, effect of shearing prestress, static case 80—10137
thick membrane strip, effect of shearing prestress on response, dynamic case 80—10138
thick multiply connected plates with nonsymmetric stress tensor, oscillations *(Ukrainian)* 79—41602
thick plate elastodynamics, soln. of 3-D axisymmetrical boundary value problem *(Ukrainian)* 80—10140
thick plate with spherical cavity, three-dimens. stress concs. under uniaxial tension 77—31214
thick plates, 3-dimens. refined elasticity theory, bending and torsion 80—64375
thick shells, stress-strain behaviour, analytical solns. in spherical coords. *(German)* 77—30010
thick spherical shells, eversion anal. for compressible bodies 80—33452
thick walled cylinder, internal or edge crack, stress intensity factors 79—18827

elasticity continued
thick-walled cylinder, stability loss, three-dimens. form 80—5965
thick-walled shells of revolution, axisymmetric problems soln. by design and exptl. methods *(Russian)* 78—73853
thin elastic bar, impact buckling, Monte Carlo calcs. 79—32317
thin elastic layer, bending by rigid die 80—14627
thin elastic pivots theory, nonlinear balance equations, constructive method *(Russian)* 79—49050
thin elastic plate, birfurcation theory for case of unilateral conditions 78—22283
thin elastic shells, general theory 79—25857
thin elastic shells, stability, variational method *(Russian)* 79—32321
thin electroelastic sheets, fluttering, thermodynamic effects *(German)* 80—106749
thin hyperelastic spherical shell, finite amplitude oscillations 78—93533
thin layer surface inhomogeneity effect on dynamic surface response 79—7288
thin plate dynamics, elastic asymptotic anal. of boundary and initial conditions 80—43640
thin plates, nonlinear dynamic stability 77—3759
thin shell, 9-node Lagrangian element 80—23888
thin shells, stability theory *(Ukrainian)* 79—76970
thin shells, variational analysis of nonlinear problems 78—5673
thin shells in Eulerian coordinates, eqn. of dynamics 79—17232
thin shells of resolution, torsion and Saint-Venant's principle 77—50912
thin tubes conveying fluid, hydroelastic stability, in plane boundary conditions, shearing loads 80—64419
thin walled shells, elastic stability theory *(Ukrainian)* 79—94515
thin walled sphere in contact with elastic or acoustic media, interior dynamics 80—5981
thin walled tubes, St.-Venants problems 79—94485
third fundamental problem soln. for doubly connected domains bounded by broken lines 80—4530
thorax, human, elastic finite element anal. models 78—3542
thread, nonlinear elastic, cone-induced shock, self-similar problem soln. *(Russian)* 80—53677
three dimensional mixed dynamic problem theory, new method 79—84958
three dimensional notch problems, elastic medium, book contrib. 78—94622
three-dimensional bodies with rigid inclusion or periodically spaced holes, macroscopic behaviour *(French)* 78—87260
three-layer plates, circular, stability 80—79188
three-phase anisotropic medium, antiplane line force 78—67041
Timoshenko beam, elastically supported, moving harmonic load 78—42566
Timoshenko beam, shear coeff. *(German)* 80—106729
Timoshenko beam, transverse vibr. without transverse deflection 77—50976
Timoshenko type shells, nonlinear theory *(Russian)* 78—63283
tissues, including muscle, elastic strain energy storage 77—16950
titanates with perovskite struct., elasticity meas. to 6 kbar 77—51428
torsion, axially symmetric, cylinder embedded in layered elastic half space 77—17822
torsion investigation by approx. methods for inhomogeneous elastic layer 80—98799
torsion of elastic sphere by elastic punches 80—99929
torsion problem for elastic cylinder with holes, integral eqn. method soln. 80—36849
torsion-free axisymmetric problems, equivalence between Boussinesq and Timpe approaches 79—86336
torsional oscillations due to rigid annular disc 78—28958
track compliance, influence on running, model and expts. 80—61602
traction problem, strain energy bound in finite elasticity with nonzero surface data 80—58909
traction problem in finite elasticity, integral bounds on strain energy 79—35557
transient elasto-dynamic response of circular crack in thick plate under torsion 80—5993
transient response of continuous elastic structures with viscous damping 79—46254
transition metals, cohesive and elastic props. model *(Hungarian)* 80—34120
transversally isotropic layer, soln. of three-dimens. problem of theory of elasticity 79—40372
transversely isotropic finite cylinders, elastostatic analysis 78—51074
transversely isotropic half space, elastic strain caused by rigid punch 79—59947
transversely isotropic half-space indented by a flat annular rigid stamp 79—55347
transversely isotropic medium with closed conical cavity, stressed state *(Russian)* 80—43616
transversely isotropic medium with cylindrical cavity and external crack, stress distrib. 78—79259
transversly isotropic half-space, Boussinesq and Cerruti solns. 78—55568
truncated cone, semiinfinite, nonaxisymm. end loading, total stress problems, equilib. 77—65678
truss, pin-jointed, with cyclic symmetry, structural rigidity, static and kinematic indeterminacy 80—58906
tube, compressible hyperelastic, combined torsional and telescopic shear 79—64520
tube, cylindrical, elastic, shearing oscills. *(Chinese)* 79—64555
tube, micropolar elastic circular cylindrical, flexural rigidity 79—81724
tube and spherical shell, incompressible elastic, response coefficients and controllable deformations 79—68580
tubes, infinitely long cylindrical elastic, collapse under bending, press. and axial loads 78—18204
tubes, liquid filled elastic and viscoelastic, longitudinal waves theory 79—64562
tunnel lining, bedding model using matched elastic springs *(German)* 77—35039
twisted elastic prismatic solid, torsion, Gohner-Giovannozzi stress anal. *(Italian)* 79—18766
twisted stiff chain, spatial quadrupole correl. function 80—27130
two bonded elastic solids interface, penny shaped crack, torsional wave interaction 80—64484
two material elastic media, stress computation by best fit strain tensors method 77—46910
two nonlinearly elastic bodies, impact-contact problem 79—98669
two parallel elastic plates with ribs, deformation, stationary problems, differential eqns. 80—33465

elasticity continued
  two phase periodic materials, mathematical model for linear dynamic behaviour 79—49048
  two-component systems, elastic moduli 78—59302
  two-dimensional problems, interferometry on transparent plates 77—75865
  two-layer transversely isotropic elastic plate, energy-asymptotic method *(Russian)* 78—13906
  two-phase anisotropic medium, interfacial dislocation, stresses, displacements and energy calc. 80—79786
  two-phase elastic bodies, coeff. of mutual penetration determ. *(Ukrainian)* 79—94491
  two-phase elastic isotropic bodies, dynamics eqns. for composites 80—33461
  two-phase transversely isotropic elastic materials, Green's function solns. 80—58912
  two-shell spatial structures with feathering, statics 77—39219
  type II superconductors, flux pinning by point pinning centres 77—28321
  ultramafic rocks elastic props. 77—9413
  unbounded body, weakened by circular cracks, elastic equilib. 80—53717
  unbounded contact between elastic and elastic-rigid media, variational calcs. 79—98670
  unbounded elastically isotropic medium, fields generated by moving dislocations, multipole-moment expansion *(Russian)* 80—103330
  undamped linear elastic systems, stability under follower forces, perturbation study 79—1110
  unified theory of elasticity and plasticity using rate theory type constitutive eqns. 78—9571
  uniform systems of elastic eqns., general solns., appl. *(Russian)* 79—14272
  uniform systems of elasticity eqns., general solns. 79—84957
  uniformly compressed elastic medium, brittle rupture, plane fracture wave *(Russian)* 80—53705
  unifying concepts in the theories of elasticity, plasticity, and dislocations 79—77599
  unilateral contact problem in linear elasticity 80—79238
  unilateral contact problem integral eqn. approach 80—8798
  unilateral problems, energy bounds 77—45698
  unilateral thin plates, optimal control 77—60935
  unitary eqn., soln. uniqueness 79—5981
  unloading wave propagation in cylindrical, semi-infinite, elastic-plastic rod, asymptotic behaviour 80—69659
  unsteady aerodynamic modelling for arbitrary motions 80—19433
  unsteady MHD forces on oscillating shell, transient soln. 79—64775
  unsteady thermal stress problems, numerical treatment based on Euler-Maclaurin summation formula 80—48580
  urethra, female, tissue elasticity and flow dynamics 77—81522
  V-notched elastic half-plane problem, plane stress and strain 79—68571
  vacancies in metals 77—27879
  valveless shock tube pumping mechanism 79—14337
  variational inequality related to elasticity operator, soln., dual problem 79—9109
  variational principle for simple elastic materials 77—71213
  vascular compliance interaction with const. vascular taper 77—36999
  vesicular lipid membranes, vol.-elastic props. determ., US obs. 80—45861
  vibrating heterogeneous string *(French)* 79—7317
  vibration, justification of two scale method for class of integro-differential eqns *(French)* 78—28947
  vibration of partially adhering stamp 80—69656
  vibration of viscoelastic cylinder with elastic shell when subjected to random forces 79—59941
  vibrations of plates and shells, method of edge-functions 77—72231
  vibroisolation parameter selection method and stability for two machines on elastic beam 80—87738
  vinylidenechloride-vinylchloride latex copolymers grafted on to elastomers, film struct. and props. *(Russian)* 77—21090
  viscoelasticity rods with nonlinear elasticity relation and nonlinear internal friction, parametrically excited oscills. 80—99947
  Vlasov and Kerr foundation models 77—14897
  Vlasov theory of cylindrical shells, boundary conditions 80—69660
  volume change in internal stress fields 79—90138
  wave generation in micropolar elastic solid under conc. forces and body couples 77—889
  wave propagation for non-uniform motion of displacement discontinuities 80—1478
  wave propagation in fluid saturation porous medium *(French)* 78—86165
  weakened elastic region with arbitrarily shaped hole, boundary integral approach 79—90137
  weakening of an elastic solid by a periodic array of penny-shaped cracks 79—68658
  weakly anisotropic elastic bodies with cubic symmetry, surface waves *(Russian)* 80—79198
  weakly rigid motions in linear kinematics of Cosserat surfaces, elastostatics 78—87267
  web structures between cavities, stress anal., appl. to struct. materials with microcavities 77—874
  wedge, 3-dimens., functional equations of static elasticity theory *(Russian)* 79—46203
  wedge, composite, plane elasticity stress singularities 80—38262
  wedge, elastic, shear of, mixed boundary value problem, use of Mellin transforms 80—23884
  wedge, infinite, stress distrib. 80—23885
  wedge, symmetric cracking by transverse displacements, stress intensity factors 80—79226
  wedge region with mixed boundary conditions, elasticity theory, dynamic problems soln. 80—43641
  wedge stress singularities, inversion theorem for conical regions, elasticity and fracture appls. 79—68578
  wedge-shaped straight elastic bars, new method for longitudinal and torsional vibration freq. calc. 78—59338
  weight functions from virtual crack extension 80—10188
  wrinkled membranes with anisotropic and nonlinear elastic props., tension field theory 77—31220
  Ag-Cu, highly deformed eutectic composite wire, anomalous props., fibre diameter and foreign atom effects *(German)* 77—36566
  Al, acoustoelastic stress field imaging technique, stress field contour plots 79—77033
  Al, elastic grain boundary responses, thermodynamic props., computer calc. 77—39593
  Al-Cu (4 wt.%), elastic accommodation of semicoherent θ' 78—64543

elasticity continued
  Al-Mg, elastic and anelastic props. in relation to Guinier-Preston zones, US investigation *(French)* 79—38833
  Al-Mg (4.4 and 6 wt.%), for liquefied natural gas appls., material and weld props. 79—61736
  Al-Mn alloys, study of solidification by rapid cooling *(Japanese)* 78—88459
  Al-W composite, mixtures theory, physical constants determ. from experimental dispersion curves 80—45338
  Al_2O_3-B_2O_3-SiO_2 sheet glass, solar energy appl., optical and mech. props. 80—87447
  Au, thin film, in Si detector, electrical contact at He temp. 78—37019
  Be-bronze BrB2, struct. and phase transform. during mechano-thermal treatment *(Russian)* 80—11667
  C and graphite, mechanical props., high temp., review 79—38897
  C fibre reinforced composites, mech. props., rel. to aircraft appl. 77—81289
  C fibre reinforced plastic, nonlinear stress strain relations, under continuous static loading 77—59872
  C fibre reinforced plastics, angle ply specimen, calc. of strength and elastic response 79—20108
  C fibre reinforced plastic, stress analysis of butt strap joint 79—43300
  $Ca_{12}Al_{14}O_{33}$, piezoelectric material, cryst. growth and characterisation 79—99825
  $CaGeO_3$ perovskite, elasticity meas. to 6 kbar 77—51428
  Cd, Hugoniot curves, elastic anisotropy effect *(French)* 78—18735
  CdSe, photosensitivity of elastic properties 78—92049
  Cu, elastic grain boundary responses, thermodynamic props., computer calc. 77—39593
  Cu, volume change due to point defects and He bubbles, isotropic elasticity theory 78—47445
  Cu-Al, dislocation core cut-off parameter, estimation from stacking fault nodes 80—103370
  Cu-Al-Ni, 2H to 6R lattice restructurization during deform., anomalous elasticity 78—19753
  Cu-Al-Ni, single variant twinned martensites, pseudoelasticity 77—28849
  Cu-Al-Ni (14.0 4.2 wt.%), two stage superelasticity, successive martensite to martensite transform. 77—8826
  Cu-Al-Ni alloy single crystals, anomalous elasticity orientation depend., martensitic phase struct. during strain 79—87634
  Cu-Be, elastic interaction energy calcs. for Guinier-Preston zones 79—11617
  Cu-Zn single crystal, pseudoelastic effects 79—47739
  Fe based amorphous alloys, Invar effects, mag. and elastic props. *(Japanese)* 79—20100
  Fe, cast, mech. charact. in plane stressed state of type SCh15-32 79—57072
  Fe-Al, single crystal, twinning and pseudoelasticity 79—15718
  β-Fe-Be, pseudotwinning and pseudoelasticity 79—96056
  Fe-N, single cryst., solid soln. softening, effect of interstitial N 80—97496
  Fe-Ni, FCC, elastic props. and stability near martensitic transform. temp. *(Russian)* 78—6921
  Fe-Ni alloys props. of materials used in electromechanical filter resonators *(Czech)* 80—76318
  Fe-Si, polycrystalline, exam. of stress-strain state of individual grains 78—80580
  KDP crystal, third-order moduli of elasticity 79—46737
  LiF(:Mg), shock waves in ⟨111⟩ direction, elastic precursor amplitudes 80—54314
  MgO, atomistic breathing shell model calcs. of dislocation core config. 77—35558
  Mn-Cu-Al alloy under torsion, anomalous elasticity and transformation plasticity obs. *(Russian)* 78—75834
  Na_2O-P_2O_5 glass, elastic and viscoelastic props. by Brillouin scatt. 79—51972
  α-Nb-H solid soln., BCC, const. vol. thermodynamic functions 79—61561
  Nb_3Sn fatigue effects in unidirectional composites, computer simulated model 80—35289
  Ni electrodeposition from alkaline citrate electrolytes, coating impurity quantities and props. *(Russian)* 79—8252
  β_1-Ni-Al, elastic softening and electron diffr. anomalies prior to martensitic transform. 77—8825
  Ni-base alloys, US vibration during crystallisation, effect on mech. props. *(Russian)* 78—19827
  Pu, elastic constants at elevated temps., noncontact meas. tech. 80—104405
  Si, local mechanical defects, annealing and effect on autoepitaxial growth *(Russian)* 80—7701
  Sn plate, quality evaluation method using elasticity characts. 77—52582
  $SrTiO_3$, critical elastic compliance, acoustic resonance meas. 80—65118
  Ti β III alloy, elastic and anelastic phenomena associated with α and ω phase isothermal precipitation *(French)* 79—52288
  Ti-Al-Zr (3,3 wt.%), W alloying addition effects on mech. props. *(Russian)* 77—59860
  TiNi, imperfect elasticity, elastic after-effect on basis of martensitic transformation theory *(Russian)* 79—100198
  V-O solid soln., BCC, modelling of interstitial solute behaviour 79—77748
  $V_3Si_{1-x}Ge_x$, elastic props., 77 to 290K, rel. to supercond. transition temp. *(Russian)* 80—66560
  $V_3Si_{1-x}Ge_x$ solid soln., longitudinal and transverse US wave propag. rate, 4.2 to 300K *(Russian)* 80—103423
  W wires monolayer tapes, mixtures theory, physical constants determ. from experimental dispersion curves 80—45338
  WO_3, reduced, elastic strain energy in cryst. shear planes 80—75239

elasticity of liquids
  see also compressibility of liquids
  acoustic levitation technique appl. 79—44906
  p-n-alkoxybenzoates of p-n-alkoxyphenyl, smectic A phases mol. struct. and elastic behaviour 80—59382
  4′-n-alkyl-4-cyanobiphenyls, elasticity, orientational order, and nematic-isotropic transition 77—84643
  4′-n-alkyl-4-cyanobiphenyls, nematic, elastic and optical props. 77—11613
  azoxy compound, liquid cryst. mixture, nematic, elec., optical and viscoelastic props. 79—55803
  CBOOA, liq. cryst., twist viscosity and mech. props. near smectic A-nematic transition 78—95136
  CBOOA, nonlinear elastic behaviour, near nematic-smectic-A phase transition 77—35679

elasticity of liquids continued
p-p′-dibutyl-azoxybenzene, nematic liq. cryst., elasticities and viscosities, light scatt. meas. 79—4245
DOBAMBC, ferroelectric liquid crystal film, freely suspended, polarisation, elastic consts. and viscosity meas. 79—55663
elastohydrodynamic lubrication, non-Newtonian effects of volume relaxation 80—103009
elastohydrodynamics, solns. to steady-state problems 77—35107
equations of state, crit. evaluation 79—78650
ferroliquids, phenomenological theory 79—16042
hexyl-azoxybenzene, liq. cryst., twist viscosity and mech. props. near smectic A-nematic transition 78—95136
Lennard-Jones fluid model, elastic modulii determinations *(Spanish)* 79—60417
lipid bilayers, saddle-splay elasticity and mol. asymmetry 78—92594
MBBA-CPB nematic complex, dielec., elastic and electro-optical props. 77—32350
measurement, complex apparatus for viscous and elastic prop. meas. at high press. 78—9734
4-methoxy-4′-azoxybenzene, nematic liq. cryst., elasticities and viscosities, light scatt. meas. 79—4245
nematic bend-splay elasticity near the nematic-smectic-A transition 80—24360
nematic layer, Freedericksz transition, first-order, second-order elasticity effect 79—99069
nematic liquid crystal, anamalous stiffness and tilt angle from nonuniform attachment angle 79—86688
nematic liquid crystal layer, twisted, elastic deform. energies and reverse twist domains 79—37617
nematic liquid crystals, nonlinear elastic behaviour, near nematic-smectic-A phase transition 77—35679
nematic liquid crystals, temp. dependent props., twisted nematic displays 79—32901
octylcyanobiphenyl, second sound propag. and smectic response function, forced Rayleigh scatt. obs. 79—86693
octyloxycyanobiphenyl, liq. cryst., twist viscosity and mech. props. near smectic A-nematic transition 78—95136
oscillating cup expt., shear elasticity in liqs. digital computer simulation 77—72190
pentylcyanobiphenyl, nematic, elastic and dielec. props. from capacitance-voltage curve 79—32894
poly-γ-benzyl-L-glutamate, lyotropic liq. cryst., trifluoroacetic acid effect on viscoelasticity, susceptibility 77—84644
polymer, isotropically swollen networks, vol. depend. of elastic eqn. of state 78—67832
polymer melts, elastic, uniform extension by const. force, rheology 80—43682
polymer network in solution, free energy of deform. 80—38900
polymer solutions, aq., capillary flow, thermal noise, low freq. oscills. 80—48754
polyoxymethylene-copolyamide mixtures, melt rheological props., extrudate microstruct. *(Russian)* 80—7530
primary normal stress function from shear viscosity data 77—68548
smectic C liq. cryst. film, mol. orientation fluctuations in two-dimens., light scatt. obs. 80—93355
smectic C liquid crystals, elasticity and defects 78—91233
smectic liquid crystals, mech. instability under dilative or compressive stresses 77—31583
soft-sphere model, elastic modulii determinations *(Spanish)* 79—60417
stability criteria for elastic mixtures 78—18514
$Al_2(SO_4)_3$ soln., adiabatic and apparent molal compressibility determ. from US vel. meas. 78—63797
Ar, liq., elastic modulus and stress relaxation 79—19304
B, thermoelastic props. near melting point 80—19862
$Ce_2(SO_4)_3$ soln., adiabatic and apparent molal compressibility determ. from US vel. meas. 78—63797

elasto-optical effects *see photoelasticity; piezo-optical effects*

elastomers
see also rubber
adhesive, mech. props. 77—16638
alkoxyphosphazene polymer, elastic and thermoelastic props. 77—56014
amorphous solids, time-temperature-pressure superposition phenomena, free volume theory 78—26059
artificial blood pump fabrication for durability 79—84026
aryloxyphosphazene polymer, elastic and thermoelastic props. 77—56014
block copolymers, generalised elasticity theory, domain crosslinkage vol. 77—39229
butadiene, durability, influence of intermol. interaction *(Russian)* 78—76746
butadiene acrylonitrile copolymer, raw elastomer, containing crosslinked particles, flow behaviour 79—37359
butadiene acrylonitrile elastomers, props. in glass transition range *(Polish)* 79—42223
butadiene nitrile, soot filled, thermal treatment influence on mech. props. *(German)* 80—30000
butadiene styrene elastomers, cross-linked, mech. relax. behaviour *(German)* 80—84986
butadiene-acrylonitrile elastomer, supramol. formations *(French)* 80—1941
butadiene-nitrile elastomers, high temp., and press. chem. transformations *(Russian)* 79—52659
cellular elastomer selection for use in biomechanical capacitive force transducers, measuring device *(German)* 80—85545
copolymers, block, strength and related properties 78—27560
crosslinked, adsorption of Rn 80—10775
diene oligomers with hydroxyl groups, prep. by rubber oxidation *(German)* 80—85175
dissipative rubberlike material rod, nonisothermal nonlinear waves 79—86380
elastomer-oligomer system, flow props. *(German)* 77—28868
elastomers, relax. transitions from relax. spectrometry and internal friction *(German)* 80—34136
epoxy resins, adhesion to metals fracture mech. study 77—4888
epoxy-polyglycol elastomers, fracture strength under compression 79—38929
ethylene-propylene-diene terpolymer, sulphonated, ionically cross-linked, foam elastomer, thermo-mech. props. 78—48362
filled, swollen state, network density determ. from stress/strain meas. 79—34112
filled, unfilled, Poisson ratio, dilatometric method 79—11733

elastomers continued
filler effect on network behaviour at high elongation 79—79049
filler type, effect on concentration rel. to equilib. swelling in solvents 79—64979
film casting method for electron microscopy samples, particularly elastomers 78—29213
finger prosthesis, elastomeric bearing as internal joint 79—92429
grinding technique, cryogenic 77—32555
heparinised elastomer antithrombogenicity and mech. props. for artificial heart *(Japanese)* 80—12296
integrated optical elastomeric modulators 77—75715
isoprene rubber elastomers, thermal treatment influence on mech. props. *(German)* 80—30000
laminated elastomeric bearings, high-capacity, finite-element anal. 80—96197
lattice model of ionic conductivity 77—4218
long-term oscillatory testing arrangement, flexometer *(German)* 79—52552
lubricated elastomers in contact with regularly spaced sliders, frictional dynamics 79—20213
mechanical behaviour, filler effect 79—91729
network, finite linear viscoelastic theory, time-depend. deform. behaviour 80—38292
O-rings for service in hot water, evaluation 79—29257
poly-2-hydroxyethyl methacrylate gel, thermoelasticity 77—84205
polybutadiene, C black filled, struct., Fourier transform IR obs. 77—50571
cis-1,4polybutadiene, lightly crosslinked, isothermal and nonisothermal creep 77—25106
polybutadiene, thermal cond. and sp. ht. 79—65265
polydimethylsiloxane, end-linked chains, elastomeric properties, dilution effects 79—90570
polydimethylsiloxane, end-linked chains, model elastomeric networks, Gaussian, nonGaussian and ultimate props. 80—103260
polydimethylsiloxane, end-linked model network, elastic modulus and equilib. deg. of swelling 77—35616
polydimethylsiloxane chains, with known radiative side chain amounts, model elastomeric networks prep. by sel. crosslinking 79—73106
polyether-polyester, differential scanning calorimetry, crit. points *(Japanese)* 80—75344
polyether-polyester, fine structure and mech. props. 77—59844
polyether-polyester elastomers, differential scanning calorimetry by using poly(oxy-1,4-butylene glycol) as soft segment *(Japanese)* 80—79916
polyether-urethane elastomers, crosslinked, three dimensional polymerisation, kinetics, gel. form., mech. props. *(Russian)* 80—7792
polyisobutylene-glass adhesion bond, macroscopic contact form. 79—39113
trans-1,5-polypentenamer, stress-opt. behaviour 77—90128
polytetramethylene oxide-polytetramethylene terephthalate, block copolymer, props. 78—51438
polyurethane, dithiodiglycol-plasticised, time-crosslinked density reduction, photochem. scission obs. 78—52920
polyurethane, heat treatment, physical and chemical mutual effects *(German)* 79—57229
polyurethane, strength and related properties 78—27560
polyurethane, TSD rel. to glass transition dipole relax. activation *(Russian)* 77—20793
polyurethane elastomers, hard segment struct., model 79—64131
polyurethanes, cross-linked, mol. mobility and struct., thermomechanical and NMR obs. *(Russian)* 80—69285
polyvinyl alcohol, atactic, thermoelasticity of networks swollen in water, polymer-diluent interactions 80—29102
prosthetics, in vivo method for evaluation of effects of materials on arterial thrombosis 78—81071
radiation mechanical props., creep *(Russian)* 77—16641
radiation vulcanisation, continuous, exam. *(German)* 78—92231
reinforcement, carbon black-polymer interaction 79—83171
reinforcement, role of particulate fillers, review 80—29921
relaxation behaviour, rel. to tensile strength *(German)* 80—66604
relaxation processes, statistical description *(Russian)* 79—23229
relaxation time spectra calc. from stress relax. data *(Russian)* 77—44288
repetitively impacted, mech. response and heat buildup 77—54889
Rutical optical processing capabilities 78—79140
seal, for valves, for high and ultrahigh vacuum 79—63246
segmented block, morphology, pulsed proton NMR study 80—33907
silastene seal, easily demountable for cryogenic appl. 79—207
silastic tubular electret, mag. polarised, thermal currents 80—40037
silicone, for teeth impressions, holographic interferometric meas. of dimens. variations 79—94195
silicones, dental impression materials, dimens. stability, holographic and interferometric study 80—67204
soot filled, mech. relax. behaviour *(German)* 80—84985
steric hindrance, rubber-elastic networks, stress-deformation behaviour *(German)* 80—35277
storage device evaluation for optical signal processing 80—48444
strain-energy function theory 77—11133
styrene polymers, elastomer toughening, grafting techniques 78—35347
styrene-acrylonitrile, plastomer and elastomer, styrene copolymer synthesis, props. rel. to composition *(German)* 79—66291
styrene-butadiene elastomers, testing by dynamic mech. anal. 80—16626
styrene-butadiene-styrene block copolymer, with reinforcing resins, effect of styrene domain structure 79—83317
surface roughness, friction and adhesion 80—66674
tackiness, fracture mechanics theory *(French)* 80—38344
TCNQ, elastomeric complexes, doped with pure TCNQ, elec. conductivity 78—84220
thermal defectoscopic study 80—89445
thermovacuum chamber, criteria for choice of elastomer seals 79—71466
thin walled elastomer tubes, dispersive effects in wave propag. 78—87289
urethane elastomer, thermoplastic, dilute soln., viscosity and sedimentation 80—103512
urethane elastomers, rheo-optical const., Young's modulus *(Polish)* 79—70108
urethanic polyester elastomers, dielectric relax., spatial network density *(Russian)* 80—71310
vacuum compatible, chem. character correl. with physical characts., review 78—24804
vacuum seal materials, practical selection 80—77797
vinylidenechloride-vinylchloride latex copolymers grafted on to elastomers, film struct. and props. *(Russian)* 77—21090

elastomers continued
viscoelastic and fracture behaviour similarities, activation energy, types SK30 and SKM10 *(German)* 79—57105
Viton A fluoroelastomer-EPDM blends, melt viscosities 77—7781
vulcanised, positron annihilation and positronium destruction 78—35221
vulcanised, tensile failure and network fracture mechanism, particle reinforcement 80—41928
B filled elastomer mould, surface coating for wear prevention in mould 78—64728
ZnO fibre reinforced elastomer, X-ray diffr. exam. of filamentary crystal distrib. 80—7738

elastoplasticity
$\sigma \sim \varepsilon$ relation variant for variable loading of elastic-plastic bodies 80—58933
acceleration wave reflection in elastic-plastic medium 79—7331
adhesion of solids, review of physical mechanisms *(French)* 78—6231
algorithm, finite difference and variational methods in flow theory models 77—871
antiplane elastoplastic strain of a solid with rigid fine inclusions *(Ukrainian)* 79—50607
approximation functionals, simplification in elastoplasticity theory *(Russian)* 78—63328
arches, shakedown anal., linear programming appl. 78—51091
array weakened by periodic system of round orifices, elastic-plastic problem *(Russian)* 79—50610
asymmetric cracked specimen under longit. shear, elastic-plastic anal. 77—14954
asymptotic behaviour of elastoplastic bodies under periodic loading 80—83740
axially symmetric body, subject to cyclic heat loading elastoplastic strain 78—5672
axisymmetric large elastoplastic strain problems, natural finite element anal. 78—83259
axisymmetric solids with material and geometric nonlinearities, finite element anal. 78—34037
bar, elastic-plastic, large deform. anal. under repeated axial loading, small deform. theory correl. 78—59310
bar, elastic-plastic cylindrical, Lipschitz character of stress tensor during twisting 79—46221
bar, rectangular elastic-plastic, necking in plane tension, boundary value problem 79—50608
bar (tube), compressible, combined loading, elastic-plastic problem 78—63311
bar semi-infinite prismatic, elastoplastic wave propag., intense load-release wave existence *(Russian)* 78—24671
bars, cylindrical, elastic-plastic torsion 80—33473
bars, cylindrical and prismatic, stochastic, holonomic, elastoplastic torsion *(German)* 79—37192
bars, instability modes *(Russian)* 79—10514
beam and frame structures, historical deform. analysis as parametric linear complementary problem 77—58563
beam columns and frames incremental anal. 79—3925
beam dynamic loading, large elastic-plastic deform., numerical anal., expt. meas. 78—1574
beams, elastoplasticity, flexural motion, finite element anal. 79—46223
beams, impulsively loaded, higher modal dynamic plastic behaviour 78—90721
beams, inelastic response, elasto-plastic transition effect 79—32300
beams, pure elastic-plastic bending diagram, general relationships 80—14588
beams and frames, large deflection anal. 77—19542
bending, isotropic/kinematic hardening 78—63312
bending of thick-walled tube, approx. determ. 77—882
bending plastic collapse, mm. cost in elastoplastic structs. 78—30197
bifurcation forms of deformation process under combined loading *(Ukrainian)* 79—98628
bifurcation in elastic-plastic solids, perturbed motion of stress axes 78—90730
bifurcation of deform. process and postcritical behaviour of plate model *(Ukrainian)* 79—41587
bifurcation theory of non-isothermic elastic-plastic deformations *(German)* 77—54892
body with period system of cracks laminar plastic zone development during longitudinal shear *(Russian)* 77—68442
body with slots strengthened at edges, antiplanar deform. *(Russian)* 78—34035
bonded bodies, internal stress/strain relations *(German)* 79—90143
boundary element method, initial stress approach 80—74762
bridge plate of pin joints, elastic-plastic anal., photoelasticity method *(Polish)* 79—64608
buckling of curved webs, Gauss-Seidel iterative procedure 78—34043
buckling of elastic-plastic cylindrical panel under axial compression 78—1584
buckling of thin torispherical shells 80—5967
bulk solids, coupling of elastic and plastic deform. 78—30198
cantilever beam method to investigate J_{Ic} and J_{Iscc} *(Chinese)* 78—15488
carbon steel, elastic-plastic plane waves with combined stresses 78—90764
cavity, cylindrical, stress distrib., photoelastic investigations, successive elastic solns. *(Polish)* 80—64391
chromorheology, exptl. verification of numerical solns. of elastic-plastic problems 80—48659
chromorheology, new exptl. method 80—48658
circular bar, tension and torsion 79—14285
circular bar of rate sensitive material, elastic-plastic tension-torsion 80—48602
circular elastoplastic torsional shaft, crack tip plastic zone propag. 80—48649
circular plates, nonlinear behaviour, equilibr. eqns. 79—14279
circular plates, numerical anal. under press. and temp. cycles 78—30199
clay, consolidation model, finite element anal. 79—18732
club sandwich, elasto-plasticity anal., comparison to shells 80—43625
coal pillars, elastoplastic anal. of stresses, finite element method 79—66691
coiled multilayer shell, stress anal. of elastic and elastoplastic work 80—79156
cold working, dynamic, struct. modification *(French)* 78—52847
columns, elastoplastic, thin and vertical, postbuckled, deflections 80—87728

elastoplasticity continued
combined elastoplastic and limit analysis via restricted basis linear programming 79—68595
composite, shell, rotation under axisymmetrical strain, elastoplastic edge effect 79—94509
composite materials, laser beam determination, of elasticity-compressibility modulus, during compaction 79—43542
composite media, elastic-plastic phases, constitutive law 77—875
composite medium, two-component residually stressed, elastoplastic crack model *(German)* 78—90790
composite spherical pressure vessels with hardening metal liners 80—7655
compound rotor, exam. of stress state, taking account of interference stresses, contact stresses 78—83342
compressible elasto-plastic medium, coupled dilatational and shear waves, propagation speeds 77—893
computational methods of treating nonlinear and special linear problems 77—74226
concentration factors, determination by deformation theory of plasticity 77—31225
concrete, reinforced, failed slabs, nonlinear analysis by finite element method *(Japanese)* 77—42785
conference, computational methods in nonlinear problems in mechanics and engineering, Austin, Texas, USA (March 1979) 80—51945
conference, reliability and stress anal., San Francisco, CA, USA, 1975 80—8740
constitutive eqn., admissible form 78—1573
constitutive theory, thermodynamic treatment 80—64390
continuous casting cylindrical ingot, development of elastic-plastic temp. stresses and deformations *(Russian)* 79—29151
convexity condition in an elastic-plastic material *(German)* 80—106734
coupled finite element-finite difference anal. of hydrodynamic and elastoplastic problems 77—71200
crack development kinetics, with varied rigidity under low cycle loading 77—90464
crack extension forces in elasto-plastic stress fields 78—18250
crack growth, elastoplastic finite element anal. 79—46260
crack growth, numerical model 78—55596
crack movement, isothermal conditions, heat liberation, finite element method *(Russian)* 79—27583
crack opening and plastic zone size depend. on stress state 79—14348
crack theory in elastic-plastic media, invariant integral 77—14966
crack tip characterisation, relation to R-clusters 78—56767
crack tip singular behaviour in elastic-plastic material with plastic orthotropy 79—81816
crack tip stress and strain fields and fracture behaviour, work hardening, finite element programme 78—22304
crack tips, blunt, elastic-plastic stress fiield, plane stress and plane strain *(Chinese)* 80—64469
crack tips, blunting during conc. plastic flow *(Russian)* 78—7013
crack-tip fields in steady crack growth with linear strain hardening 78—5695
cracked bar under torsion and shear, elastoplastic stress and strain calc. from screw dislocations 79—68654
cracked bodies, plane stress to plane strain thickness dependent transition, anal. model 78—67126
cracked thick walled cylinder, elastic plastic fracture anal. under displacement controlled loading 78—67119
cyclic elastoplastic bending, recording deform. curves and working life 79—52499
cyclic loading of struct. with kinematic hardening *(French)* 78—42537
cyclic loads, small displacement finite element analysis 77—62171
cylinder, elastoplastic, necking under uniaxial tension 78—63335
cylinder, subjected to heating and cooling, thermoelastoplastic soln. 79—72816
cylinder compression, at small elasticoplastic deformation *(Russian)* 78—42542
cylinder compression at small elastico-plastic deformations *(Russian)* 79—10497
cylinder expansion under finite plane strain 78—51094
cylinder under uniform pressure, transition functions 80—10158
cylinders, discretely stiffened, buckling under axial compression 80—64408
cylindrical bar, elastoplastic, with linear hardening, simultaneous torsion and tension 80—53658
cylindrical bar in tension, necking, num. anal. 79—90147
cylindrical ingot, continuous casting, elastic-plastic temp. stresses and deformation *(Russian)* 79—61576
cylindrical layer, two-component loading small curvature of strain trajectory *(Russian)* 80—48606
cylindrical shell under internal press. elastoplastic nonhomogeneity 79—37196
cylindrical thick shells, elastic-plastic creep anal. 80—5960
damaged body, unknown boundary value problem explicit solution *(French)* 80—79166
dangling spider problem for elastic-perfectly plastic material, ordinary differential eqn. 79—94502
defining relations for media whose elastic props. vary with plastic deform. and temp. 79—18751
deformable body three dimensional stability theory, variational principles 80—38300
deformation, finite homogeneous, bifurcation 77—62158
deformation process bifurcation under combined loading *(Russian)* 77—54888
deformations, dynamics of nonisothermal elastic-plastic media, constitutive equations and numerical soln. 80—31503
disc, annular, axially symmetric, with rigid inclusion, decohesive carrying capacity *(Russian)* 80—69688
discs, doubly-connected, elastoplastic, full yielding at collapse, noncircular shapes 80—74755
discs, doubly-connected, noncircular, full yielding at collapse, photoplastic verification 80—74756
discs, irregularly rotating elastoplastic, tangent tension optimisation *(Russian)* 79—50609
dissipation energy in shakedown of elastic perfectly plastic solids, local bounding principle 80—53647
double edge notched specimen, elastoplasticity, curved boundary shape anal. 79—72823
double-skinned composite circular cylindrical shells failure under external press. 78—75078

elastoplasticity continued
- double-skinned composite circular cylindrical shells under external press., experimental behaviour 78—75077
- doubly connected region, numerical solution of two dimensional elastic-plastic problems 80—99946
- ductile fracture mechanics, internal variable approach 79—68651
- ductile metals, spontaneous void growth in elastic and elastic/plastic media 80—48567
- ductile wire-through-glass seal, stress anal. 77—84161
- duralumin, elastic-plastic stress anal. by photoelasto-plastic method and X-ray method *(Japanese)* 78—13978
- dynamic, implicit and explicit computational schemes 78—34038
- dynamic deformation, internal state variables and internal forces 80—53660
- effective shear modulus, effect of rotation of principle axes *(French)* 77—68409
- elasti-plastic closed form stiffness matrix for axisymmetric finite elements 78—26048
- elastic viscoplastic disk, uniformly rotating, axially symmetric stress state *(Russian)* 79—50611
- elastic-perfectly plastic material, theory of stable crack growth 78—79272
- elastic-perfectly plastic solids subjected to variable loads, plastic strain upper bounds 79—86346
- elastic-perfectly plastic von Mises material, accuracies of numerical soln. constitutive eqns. 78—59315
- elastic-plastic boundary, photoelastic determ. 79—81739
- elastic-plastic crack problem, comparison of finite element soln. 78—79263
- elastic-plastic deformation stress-strain anal., parametric linear programming method 79—37194
- elastic-plastic fatigue crack growth under load cycling 77—59913
- elastic-plastic frames, deformation anal. Monte Carlo technique 79—7295
- elastic-plastic initial value problem, iterative numerical integration 77—62170
- elastic-plastic solids, crack tip deformation and fracture 79—27591
- elastic-plastic structure, shakedown anal., incremental procedure 79—23219
- elastic-plastic torsion, nonlinear boundary value problem 77—89043
- elastic-viscoplastic frames, dynamic responses, strain hardening effects 80—79178
- elastic-viscoplastic initial boundary value problem, soln. existence and uniqueness 80—28433
- elastic-viscoplastic materials, strain rate effects on necking 80—58918
- elastic-viscoplastic materials, stress concentrations determ. by integral eqn. methods *(French)* 77—72194
- elastic-viscoplastic materials, uniaxial cyclic loading, stresses, relaxation, creep 80—64402
- elastic-viscoplastic materials delayed behaviour of double shear perturbations 78—45483
- elastic-viscoplastic proportional combined twist and stretch of circular bar of rate sensitive material 80—23912
- elastic-viscoplastic skewed plates, impact, anal. of combined pressure-shear waves 77—65712
- elastic-viscoplastic structures, accommodation to periodic loading, stress and strain fields *(French)* 77—46928
- elastic-viscoplastic work hardened slab, indentation by rigid punch 80—53721
- elastic/viscoplastic plate, combined longitudinal/torsional stress wave propag. *(Japanese)* 78—38227
- elasto-plastic contact problem 78—46917
- elasto-plastic coupling, thermodynamic conditions resulting from Il'iushin's postulate 77—31224
- elasto-plastic flow in computer simulated, A533 steel 78—56720
- elasto-plastic metal-dislocation system, stress-activated dislocation motion, thermodynamic theory *(Chinese)* 78—83868
- elasto-viscoplastic analysis of large deform. problems, natural finite element formalism 78—83258
- elasto-viscoplastic thermal stress model, appl. to continuous casting of metals 79—18740
- elasto-viscoplastic-viscous theories of granular and porous media, soil mechanics appl. 79—76982
- elasto/visco-plastic finite element analysis, unconditionally stable algorithms 78—34030
- elastoplastic coupling within thermodynamic strain space formulation of plasticity 78—30189
- elastoplastically deformed strengthened material, stress deformed state during rolling *(Russian)* 80—54299
- elastoviscoplastic analysis for spherical or cylindrically symm. cavities in infinite media 78—79229
- elastoviscoplastic system, work hardening due to residual stresses constitutive eqns. for rates *(French)* 77—70068
- elongation, dynamic, of material, stress/strain curve up to scabbing, meas. method 79—7348
- elstic-plastic crack and hole interaction in elastic medium under uniform shear load 78—51117
- equilibrium models in finite element elasto-plastic analysis 79—81742
- equilibrium stability, Timoshenko's method *(Russian)* 79—10504
- Eulerian computation technique for domains with moving boundaries 77—53779
- existence and regularity of the solutions of plasticity equations *(French)* 79—21551
- existence-uniqueness result for some models of thermoplasticity 80—92077
- externally cracked cylinder, elastoplastic response anal. by method of lines, computer program 80—28435
- fatigue crack, low cycle, test machine rigidity check on kinetics 78—15632
- fatigue crack closure, and delay effects under mode I spectrum loading, elastic-plastic anal. 80—19282
- fatigue life estimation of structures from programmed elastoplastic loading results 77—56102
- FCC polycrystals, plastic flow self-consistent scheme extension 79—64530
- fibre reinforced composite with viscous matrix, random stresses in components, laws of distrib. 79—23226
- fibre reinforced composites, thermal cycling, elastoplastic strain calc. under action of external stresses *(Russian)* 79—38896
- fibrous composites, elastic-plastic behaviour 79—76985

elastoplasticity continued
- finite deformation elastoplasticity, strain measure decomposition 79—23223
- finite element anal. for large strains and displacement, natural factor displacement method 80—14580
- finite element analysis, interpolation vs. iterative soln. for Tresca yield condition 78—59312
- finite element approximations in thermo-plasticity 80—1435
- finite strain work-hardening theory for rate independent elasto-plasticity 79—76983
- fission reaction fuel, kinematic hardening rule of plasticity 80—42764
- fission reactor, FAXMOD anal. of creep and sheath ballooning 80—42759
- fission reactor fuel performance anal. by finite element method 80—42750
- flat ring subject to internal pressure, elastic-plastic anal. 78—13913
- flawed elastoplastic structure, method of lines applied to crack problem 79—46259
- flow, plastic, in thick-walled cylindrical shell, non-homogeneity effect, numerical calc. 80—19248
- flow rule for lowering buckling stresses *(Japanese)* 80—99949
- flow surface of materials with no elastic potl. *(French)* 77—65690
- formulation of laws for plastic anisotropic elastic materials in volume expansion *(German)* 80—106732
- fracture, estimation of load required to start a crack *(Russian)* 79—14346
- fracture and yield conditions elastoplastic solid 79—14344
- fracture criterion, J integral, thin section metals 77—56067
- fracture mech., linear elastic, appl. to crack stability in brittle struct., elastic-plastic conditions 78—90800
- fracture mechanics, elastic-plastic, for structure design 77—14961
- fracture mechanics, elasto-plastic, critical assessment 79—38943
- fracture mechanics, finite element analysis *(German)* 77—54935
- fracture mechanics, plasticity, finite element anal., review 79—41612
- fracture modelling, acoustic emission 80—35303
- fracture stress obtained from the elastic crack tip enclave model 80—71730
- fracture toughness parameters J and G^{Δ}, effect of load biaxiality 78—67128
- fracture toughness testing, elastoplastic range, computer simulation 80—21217
- fracture zone analysis of fission reactor elastoplastic materials *(Spanish)* 79—66139
- fracturing structures, elastoplastic, boundary value rate problem, extremum theorems 80—48596
- frames, elastoplastic anal., uniqueness 79—7297
- frames and beams, arbitrary cross-section, deflections at shakedown 78—34028
- glass (roving cloth) fibre reinforced plastics, yielding behaviour of plate with circular hole *(Japanese)* 79—8323
- half-spaces interface, oblique refr. of plastic wave, self-similarity problem *(Russian)* 78—20974
- hardening elastoplastic material, variational inequality 78—63320
- heat energy relaxed due to deform., thermocouples obs. 80—21214
- hereditary theory, taking temp. into account 78—26055
- high strain rate behaviour, incremental elastic-viscoplastic constitutive eqns. integration 80—85138
- high temperature deformation for nuclear reactor design 77—3094
- hollow circular cylinder, expansion and contraction, strain softening with finite elastoplastic strain *(French)* 80—38283
- hollow sphere exposed to radiation, thermoelastoplastic problem 77—14928
- homogeneous simple strain in elastic-plastic media, necessary and sufficient conditions 80—28427
- hybrid-stress models for elastic-plastic analysis by the initial-stress approach 79—32288
- hypoelastic compressible rate-sensitive material flow, integrable generalized wave eqns. 78—38213
- ideal compressible media, elastoplastic thin walled constructional elements and shock wave interaction *(Russian)* 79—68618
- ideal elastic-plastic materials, constitutive eqns. and thermodynamics 78—71272
- Il'iushin's postulate, thermodynamic conditions on elastoplastic coupling 78—18190
- Il'iushin's postulate, thermodynamic conditions on elastoplastic coupling 78—18191
- impact fracture in elastoplastic regime 78—51133
- impact problems, involving severe distortions 77—17825
- impact vibrations, steady, of body having hysteresis collision characteristics 80—14602
- incremental boundary-value problems for elastic-plastic coupling, rock mech. appl. 77—14918
- incremental elastic-plastic constitutive eqn., principal axes rotation, shear deformation 77—19545
- incremental finite element anal. 78—34034
- incremental formulation in nonlinear mechanics, large strain elasto-plasticity 78—77692
- indentation experiments 77—35054
- indentation hardness and fracture 78—34090
- inelastic constitutive equation, irreversible thermodynamic treatment 77—82391
- inelastic deformation of structures, repeated actions of load temp., structural model 77—3747
- inelastic material, effect of material struct. changes 78—12562
- inelastic material, ideal, theory of elastic and plastic distortions 78—12561
- infinite elastoplastic medium, bifurcations at a spherical hole 80—33493
- inhomogeneous viscoelastoplastic media, wave propagation *(Russian)* 79—32337
- integral I and elastic-plastic fracture criteria *(Chinese)* 78—75100
- integral J_{I}, calculation by finite element analysis 78—67129
- integrated load increment method for finite elasto-plastic stress analysis 80—92072
- integration algorithms for elastic-plastic models 80—5959
- interfaces, existence and uniqueness 77—7331
- internal struct. tensor 78—79227
- irradiated material in elastoplastic region, systems of remote meas. of forces and deform. in cyclic tests 77—90546
- isotropic elastic-plastic materials, thermodynamic theory, global entropy inequality 80—1436
- j integral applications for short fatigue cracks at notches 80—38332

elastoplasticity continued
J-integral determ. under elastic-plastic strain 79—64515
kinematic hardening rule in single crystals 80—10551
kinematically hardened structures, accommodation *(French)* 77—27475
laminar blocks with plastic deformations, instability 80—43629
laminate, shock wave propag., stress history recording 78—38242
large deformation elastoplastic analysis of arbitrary shells, triangular finite element 78—83257
large deformation finite element formulation 77—75819
large nonisothermic elastoplastic and elastic-viscoplastic deformations 77—75817
large strain problem, finite element formulation in terms of true stress and logarithmic strain 80—23901
limit surfaces for model bar, geom. effects *(Polish)* 80—10162
limiting equilibrium of elastoplastic bodies with cracks in complex states of stress 80—53715
linear models of frequency-independent internal friction *(Russian)* 79—18834
linear strain triangular element solns. 78—90719
LMFBR, dynamic response of containment vessel and coolant wave propag., REXCO-EUR code manual 78—58349
LMFBR shell structures, finite element elastic-plastic anal. 78—41804
load increment analysis, elastic-plastic analysis of anisotropic materials by variable stiffness finite element method 77—7319
localisation of deformation, bifurcation modes 80—79167
longitudinal shock-waves in an elastoplastic medium *(French)* 79—46249
matched asymptotic expansions, in nonlinear fracture mechanisms 78—51127
material with nonuniform mechanical properties, elastic-plastic deform. 79—92531
mathematical prgramming methods for deform. anal. at plastic collapse 78—1572
metal, dynamic and static response to simple compression, tension and torsion 77—28858
metal, finite elastic-plastic deformation at high temp., work hardening rule 77—4828
metal, model of elastic-plastic deformation *(Russian)* 77—48484
metal, spalling produced by elastoplastic waves 77—80574
metal, stress-induced EM effect, phys. model 78—55909
metal, Swift effect, in twisted tubes 77—28859
metal, Swift effect, rel. to stress/strain behaviour in simple compression, tension and torsion 77—28860
metal extrusion process, stress and deform. distribs., elastic-plastic anal. 77—48364
metallic materials, elastic-plastic transition behaviour model *(German)* 80—75295
metals, hardening response in small deform. 79—47719
metals, inelastic cyclic strain under nonuniform stress state conditions, residual stresses effect 80—81132
metals, residual stress and deformation, due to quenching, elastic-plastic anal. *(Japanese)* 78—83268
metals, vector props. at normal and low temps. 80—16406
metals in nuclear reactors, thermo-elasto-visco-plasticity and neutron irradiation 77—3111
metals under contact explosion loading, shock damping process 80—54309
metals with mixed hardening, finite element anal. of elastic-plastic materials 79—27543
microplastic regime in elastic-plastic media, shock layer struct. 79—76997
minimum principles, stress field derivation in elastic-perfectly plastic solid 77—878
minimum principles in elastic-plastic solid, stress and strain fields 77—879
mixed finite element method for elasto-plastic plates 78—28929
model, and analogy with liquid vapour phase equilib. 77—84155
multi-axial stress states, elasto-plastic stress-strain relationships 79—1115
multilayer cylinder with monolithic insert, exptl. study of stress/strain state 79—42139
multilayered packet, contact elastic-plastic problem 80—5997
multilayered spherical vessel, elastoplastic response to intermittent internal blast loading 77—65705
multistory frames, elastic-plastic anal., slope deflection method 77—11137
necked cylindrical bar, elastic-plastic, residual stresses after unloading 80—38284
non-associated plasticity, dual extremum principles in rate boundary value problems 79—25845
non-associated plasticity and elastoplasticity, rate boundary value problems, variational principles 80—87726
non-isothermal deform., bifurcation of equilib. 78—79220
nonisothermal elastic-plastic and elastic-viscoplastic deforms., stress/strain relations 78—22276
nonisothermal theories, of plastic flow and theory of work hardening in creep 79—57077
nonlinear behaviour in 1- and 2-dimens., elastoplastic hysteresis, flow and relaxation *(French)* 79—46229
nonlinear fracture mechanics, matched asymptotic expansions method, longit. shear of elastic-perfectly-plastic specimen 77—35087
nonlinear fracture mechanics, matched asymptotic expansions method, longit, shear of elastic work hardening plastic specimens 77—35088
nonlinear material and structural behaviors, soln. procedure, theoretical basis for program composite—III 78—30204
notch fatigue cracks, propag. and initiation, elastic-plastic fracture mechanics 80—38329
notch tip stress distrib. in strain hardening material 79—3927
notch-tip geometry, influence on stress and strain distrib. 80—33535
notched bars, elastic plastic stress and strain conc. factor *(Japanese)* 78—26052
notched plates, fatigue life estimation based on elastopolastic anal. *(Japanese)* 79—18814
notched plates, monotonic and cyclic loaded, exam. of elastic-plastic stress-strain behaviour 78—63390
nuclear fuel element behaviour in transients 77—88202
nuclear fuel pin inelastic modelling and stress analysis using FULMOD code 77—46233
nuclear reactor fuel hexcans, elastoplastic anal. 77—83027
Pacific lithosphere, flexure seaward of Bonin and Mariana trenches 79—57903
perfectly plastic medium, elastic-plastic field at tip of steadily growing crack *(Chinese)* 80—58968

elastoplasticity continued
perforated plane, thermoelastic-plastic problem *(Russian)* 78—55571
perforated plate, global stress strain behaviour 80—10169
perforated plates, finite element elasto-plastic anal. 80—10168
piecewise linear elastic-plastic analysis 79—55331
pipe, axial crack, elastic-plastic dynamic finite element anal. 77—3795
plain strain contained plastic deformation, elastic-plastic laws, finite element anal. 80—92073
planar shear specimen with V-notch, anal. of stress and strain conc. factor using finite element method *(Japanese)* 78—38212
plane elastic-plastic stress with variational problem in Hilbert space 77—13607
plane elastoplasticity, subject to large strains, finite element anal. *(Japanese)* 80—96207
plane V-notched specimen, elastic-plastic limit load anal. 80—69684
plane wave propagation in elastic plastic half-plane under movable loads *(Russian)* 78—5685
plane weakened by openings, periodic and inverse elastoplastic problems soln. 77—35055
plane-strain crack growth, comparison of theory and experiment 80—108560
plane-strain formulation of elastic-plastic constitutive laws 80—23918
plane-strain radial flow of plastic materials 79—64529
PLASTEF code, numerical simulation of thermoelastoplastic behaviour using finite element method 78—90731
plastic strains, upper bound principles in elastoplastic structure dynamic shakedown 79—76986
plastic/elastic transition, strains and stresses *(German)* 80—28431
plasticity equations, new functions framework *(French)* 79—21549
plate, 2-D high velocity impact problem *(Russian)* 77—50924
plate, elastic-perfectly plastic, dynamic hole expansion 79—46234
plate, elastic-plastic, flexed in its plane, stress concentrations, method of small parameter *(Russian)* 80—74759
plate, elastic-plastic circular, biaxially stretched, necking calcs. 78—5666
plate, inelastic thick, dynamic response, rectangular finite element development 79—94520
plate, interference fit fastener-filled hole, stress intensity factors for through cracks 77—58609
plate, radially stressed annular, elastic-plastic anal. 77—68456
plate, relaxed by holes, elastic-plastic deformation, stress state *(Russian)* 79—27545
plate, round, elastoplastic, plastic flow stability *(Russian)* 79—32293
plate, round uniformly loaded, of linearly strengthened elastoviscoplastic material, large flexures *(Russian)* 77—23894
plate, slim, relaxed by round orifice system, elasto-plastic problem *(Russian)* 79—32292
plate, thin, elastoplastic, buckling model *(French)* 80—74778
plate weakened by equal-armed cross-shaped crack, plastic strain and fracture 80—69740
plate with crack close to one edge, elastoplastic equilib. 80—14624
plate with periodic circular aperture system, elastoplasticity problem 78—9573
plates, elastic viscoplastic, transient dynamic large deflection anal., finite element method 80—69683
plates, elastic-viscoplastic analysis by finite element method 78—34031
plates, inelastic response, elasto-plastic transition effect 79—32300
plates, minimum principles 79—68593
plates, thickness tapered, elastoplastic large deflection anal. 80—23917
plates and shells, elastic-plastic, cyclic loading anal. variational method 79—37198
plates and shells under linear hardening, Bauschinger effect 80—23916
plates and shells with hydrostatic press. depend. mech. props., stability problem soln. *(Russian)* 80—53668
PMMA, stress fields round indentations 77—28861
polybutadiene rubber, modified with oligoester acrylate, plastic-elastic and rheological props. *(German)* 80—19871
polycrystal, elastoplastic, grain size effect on deformation curve *(Russian)* 79—51191
polycrystalline material, plasticity analysis using stat. model *(Russian)* 78—26619
polycrystals, constitutive relns. in elastic-plastic range 78—63801
polycrystals, large elastic-plastic deform. anal. with finite element method 78—26049
polycrystals elastic-plastic deformation, plane geometrical model and finite element calc. 80—79860
polymer, plastoelasticity theory 78—75712
polymer, viscoelastic-plastic, birefr. relation 77—31266
polymer melt, deformation, loss of fluidity 77—89078
porous bodies, stresses induced by drying, elastoviscoplastic model, finite element anal. 80—23904
porous metals, plasticity, stress-strain curves, yield stresses, strain vectors 80—83738
portal frame, elastic-perfectly plastic behaviour under column axial force variations 79—7296
power-law hardening material, small-scale yielding problem, soln. *(German)* 78—38210
Prantle-Reuss eqn. *(French)* 79—64526
pressure vessel heads, internally pressurized ellipsoidal and torispherical elastic plastic, nonsymmetric buckling 77—58575
prismatic bar, large deform. anal. for repeated axial loading 78—38207
prismatic bars, elastoplastic torsion by quadratic programming, finite element scheme 79—32251
quasi-bifurcation in dynamics 78—38223
quasistatic deformation of elastoplastic bodies, models, initial boundary value problems *(German)* 78—42549
Rakhmatulin elastic-plastic model, dynamic 3-dimens. eqns. 80—58927
rate boundary-value problem of elastic-plastic solid, operator method for variational principles *(Polish)* 77—54898
rate problems in finite strain classical elastroplasticity energy theorems, Lagrangians 80—74766
reactor fracture safe design, appl. to elastic-plastic fracture mechanics params. 78—30241
rectangular block, non-normality and bifurcation in plane strain tension and compression 80—19251
rectangular parallelepiped compression, small elastoplastic deformation, variation anal. *(Russian)* 79—32294
reinforced concrete, elasto-plastic anal. of plane frame *(Chinese)* 80—5950
reinforced masonry shear wall, elastoplasticity and crack-growth anal. *(Chinese)* 79—94506
relaxing media, shock waves struct., dislocation model 80—58961

elastoplasticity continued
rhomboidal steel panel, elastoplastic stress and strain diffusion 79—20128
rigid plate on elastic-plastic foundation, load-deflection, contact stress distrib. 77—46931
rigid-plastic dynamics, large deformation, extremum, principle 80—53642
rigidly plastic media with hardening, shock-loaded, dislocation model and elastoplastic waves 79—86379
rod, elastoplastic, dynamic bending and residual deformation *(Russian)* 80—75293
rod of rate-sensitive material, elastic-plastic tension-torsion analysis 80—83741
rods, quasi-bifurcation within axial plastic compressive wave 79—10513
rods and plates, strain-rate-sensitive material, elastic-plastic wave propag. mech. 80—69724
rolling disc, stress distrib., finite element anal. 77—68444
rotating discs, burst strength and necking 78—79226
rotating disks, elastic and elasto-plastic, with temp. gradient, stress distrib. determ. *(Italian)* 79—41633
screw connections, bend and tension loaded, hysteresis *(German)* 78—87312
seals behaviour obs., for high pressure techniques *(German)* 78—21160
semi-infinite rod, propag. of elasto-plastic waves in one-dimension 78—34036
separation energy rate for crack advance 78—56765
shakedown, partial, under thermomechanical loading path *(French)* 80—74757
shakedown analysis of elastoplastic structures 77—3745
shakedown problems for elastic plastic solids with piecewise linear yield surface 80—79173
shallow shells elastopolastic anal. using laminated element *(Japanese)* 78—63323
shear joint, discontinuous, holonomic elastoplastic anal. *(German)* 79—1117
shear waves in an elastic-plastic material due to a supersonic surface step load 80—102999
sheet metal stamping, finite element anal. 79—7344
shell, cylindrical, elastoplastic plastic buckling in pure bending 80—19257
shell, cylindrical, viscous, explosive squeezing and effects 79—86378
shell, finite circular cylindrical, rate formulation for elastic-plastic creep anal. 77—58568
shell, rectangular flexible elastoplastic, yield theory and deformation theory appl. 80—74773
shell bifurcation loads, variational principle *(German)* 77—42755
shell constitutive eqns. 78—18188
shell structures, elasto-plastic analysis 79—3926
shell surfaces calc., thick-walled, with axisymmetrical load using finite element method *(Russian)* 80—48569
shells, axially compressed circular cylindrical, elastoplastic buckling, nonlinear material behaviour 80—48615
shells, axisymmetric, unsymmetrical bending, elastoplastic anal. 80—92065
shells, elastic-plastic circular cylindrical, under internal pressure, bifurcation 80—64421
shells, flexible shallow elastic-plastic, natural vibrs. and buckling 80—33519
shells, internally pressurised 2:1 ellipsoidal, elastic and elastic-plastic buckling 79—37206
shells for explosion containment 77—58594
shells of resolution, ring-stiffened, dynamic nonlinear anal. by finite element program DYNAPLAS 77—3766
shells of resolution, transient dynamic and inelastic anal., survey of programs 77—3767
shells of revolution under nonaxisymmetric loading, elastic-plastic strain anal. 80—5958
simulation of inelastic material behaviour in struct. anal. 78—34041
slab with elliptical opening, flexed in its own plane, small parameter method *(Russian)* 80—74760
slamming safety membrane, stability loss in elastoplastic and elastic regions, expt. coeffs. 80—33496
slipbands, wedge shaped object, elasticity theory 80—38294
snow, volumetric constitutive law based on neck growth model 80—48595
soil, cohesionless with curved yield surfaces, elastoplastic stress-strain theory 78—18186
soil, deformation of compressible elastoplastic ground 78—96198
soil, incremental approach to elastoplastic hardening 77—75818
soil, pulverulent, homogeneous, stresses due to vertical local load *(French)* 78—61398
soil, wave interaction, stresses and strains 77—86801
soil mechanics, elastoplastic deformation, volumetric constitutive equation 80—53655
soil-struct., interaction initial stress finite element method 78—59313
solid, crystalline, finite strain, uniqueness criteria and minimum principles 78—51086
solid bodies, elastoplastic and isotropic elastic deform. eqns. 79—86348
solid containing holes in vicinity of crack tip, finite element anal. 78—67147
solid free boundary, slip line initial development, elastic-plastic problem 80—96196
solid mechanics, yield criteria and constitutive eqn. of elastic-plastic material *(Japanese)* 79—59933
spatial wave propagation, influence of energy dissipation 77—7326
sphere under external press., stability 78—94603
spherical body, instability under uniform loading 80—58946
spherical cavity in infinite elasto-plastic medium 77—50934
spherical cavity surrounded by infinite elasto-plastic medium, upper bound on asymptotic pressure 78—38214
spherical shells, internally pressurised, effect of thickness inhomogeneities on collapse 77—42761
springback in beams and plates, bending 80—38256
stability condition for elastic plastic structures 78—87284
stability of elastoplastic half-space around spherical cavity, rock deformation appl. *(Russian)* 79—27551
stability of thin-walled pressure vessels of elastic-plastic linear hardening material 80—92075
steel, 0Kh16N15M3B, irradiation effects on resistance to cyclic elastoplastic deformation 79—91767
steel, 40, elastoplastic bending of beams of various cross section 78—3196
steel, 45KhN, hardening by loading 77—86050

elastoplasticity continued
steel, austenitic stainless, high temp. low cycle fatigue resist. under superimposed stresses at two freqs. 80—25832
steel, austenitic stainless in liq. Na, mechanical props., review 79—20150
steel, C, elastoplastic stress anal. by photoelasto-plastic method and X-ray method *(Japanese)* 78—13978
steel, C, transform. kinetics, heat cond. and elastic-plastic stresses during quenching *(Japanese)* 80—25688
steel, Cr-Mo, constitutive eqn. model for high temp. behaviour of fast reactor structural alloys 78—66343
steel, Cr-Mo-V, cyclic deformation under out-of-phase loads 80—40428
steel, Cr-Ni-Mo-V, plate, type HY130, exam. of elastic-plastic R curve 79—29157
steel, elbow-pipe assembly, high-temp. elastic-plastic creep test 77—77551
steel, electric arc sprayed coating on wire, elastic and elastic-plastic props. *(German)* 79—34089
steel, flat bars, stress meas. and calc. around drilled hole, with hole-gage-rosettes aid *(German)* 80—25757
steel, free plate elastoplastic stress condition during phase transformation 78—95781
steel, high strength, shell, stress distrib. around notch, beyond fatigue limit 78—13928
steel, low alloy type 10KhSND, resist. to low-cycle deformation at low temps. 79—87696
steel, low C, annealed, fatigue crack propag. law under elastic-plastic and general yield conditions *(Japanese)* 77—48538
steel, low C, crack initiation at root of circumferential notch of round bar specimens *(Japanese)* 80—60947
steel, mild, elastic-plastic analysis of yield process 77—36571
steel, mild, Luders band front 78—3168
steel, mild, Luders bound front, elastoplastic anal. by finite element method 78—3169
steel, mild, with small flaws elastic-plastic anal. of fatigue limit 80—21069
steel, notched bar, plastic zone determ. near rupture *(French)* 78—88515
steel, plates, thin, welding residual stresses calc., elastoplastic thermal stress anal. 78—83262
steel, shock transition rise-time meas., limiting viscosity coeffs. 79—77680
steel, stainless, 304, beam, elastic-plastic response to impulse loads 79—34118
steel, stainless, type 304, elastoplastic fracture mechanics for reactor piping 78—68777
steel, stainless type 316, monotonic and cyclic biaxial loading at room temp. 78—52928
steel, structural, J-integral fracture toughness, specimen size effect, extension to elastoplastic region 78—68808
steel, transforms CC types M6 and M3N, elastoplastic bending, insulating coating influence on magnetic losses *(Russian)* 79—100284
steel, type 20 loading history effect on resist. to cyclic elastoplastic strain 80—16398
steel, type 33Kh3SNMVFA, high-strength, failure accompanying cyclical elastoplastic straining *(Russian)* 79—70152
steel, type 4052Kh, thermomechanical working influence on mech. props. *(Russian)* 80—93578
steel, type 4Kh5MFS, 5KhNM, 5KhNMFS, stress conc. effect on low-cycle fracture results 79—87697
steel 45, elastoplastic props. in explosive loading 78—6999
steel A533A, review of data in reln. to fracture toughness at upper shelf temp. 79—15797
steel case hardened cylinders, heat treated, residual stress fields 80—3102
steel casting, calc. method of thermal and thermo-visco-elasto-plastic processes *(German)* 80—79859
steel continuous casting, thermal, thermo-visco-elasto-plastic processes *(German)* 80—81044
steel ingot, state of viscoelasticoplastic stress deformation, in process of solidification *(Russian)* 80—45295
steel plates, explosively clad, fatigue crack propagation behaviour *(Japanese)* 80—104262
steel shaft, residual tangential stress determ. after elastoplastic twisting 78—60902
stiffened plates, structural and by finite element and integration methods 77—3753
stiffened thin shells, elastoplastic, buckling and stability *(Chinese)* 79—72824
strain diagram plotting from data obtained during elastoplastic bending or torsion 77—81371
strain eval. by strain gauge 80—28473
strain gauge meas. in cyclic elastoplastic tests, automatic processing on portable computer 77—5829
strain hardening structures under repeated loading, deflection analysis 78—63313
strain meas., elastic and residual components, single plate hologram interferometry 80—32932
strain uniqueness and min. principles 77—3734
strength of materials, empirical determ., cleavage fracture in plane waves 80—96225
stress analysis in elasto-plastic media using birefringent coatings *(French)* 79—18846
stress analysis of crack, elastoplastic range 78—67144
stress and strain fields, min. principles 77—3735
stress distrib. in array weakened by biperiodic system of holes *(Russian)* 79—46228
stress field approximation error anal. 78—1578
stress measurement, temporary and residual stresses, high-temps. 80—64498
stress wave propag. *(Czech)* 80—108507
stresses and strains during loading, mathematical programming, pivoting procedure 80—53641
strip or half-plane under moving load, residual stresses and plastic zones 80—53645
strip with circular hole, visco-elastoplastic stress conc. 77—68455
structural element design calc. under creep conditions 80—48598
structures at shakedown, maximum deflections, improved upper bound 79—27547
structures with overlay materials during cyclic loading, finite element anal. 80—38280
supplementary strain method, appl. 80—96205

elastoplasticity continued
- tensor dislocation density near crack vertex 78—26090
- theory, thermodynamic restrictions 79—3924
- theory of cracks, elastoplastic solns. special characts. *(Russian)* 79—32375
- thermal elastoplastic stress analysis based on initial strain method *(Japanese)* 80—77620
- thermal loads in elastoplastic stress finite element anal. 79—46225
- thermal stress distribution associated with elastoplastic deform. 77—19549
- thermal stress problem, numerical method of soln. 77—3742
- thermal stresses in axisymm. problems *(Japanese)* 78—51096
- thermoelastic wave propag., critical thermal load 78—30228
- thermoelastic-plastic coupled medium, accel. and shock wave propag. 77—58578
- thermoelastoplastic 3-D problem formulation by integral eqns. 79—7292
- thermoelastoplastic anal. for hollow sphere, incremental plasticity theory 77—62168
- thermoelastoplastic medium, variables for universal deform. representation 78—49666
- thermoelastoplastic solution for a circular solid cylinder subjected to heating and cooling 80—5952
- thermoelastoplasticity, doubly periodic, soln. 77—84165
- thermoelastoplasticity, planar, corrected boundary integral eqns. 77—46933
- thermoelastoplasticity three-dimensional integral eqns. *(French)* 78—90718
- thermoviscoelastic-plastic materials, constitutive reln. 80—58
- thick shell anal. by viscoplastic solid finite elements 78—38208
- thick spherical shell under thermal loading, numerical anal. 77—68445
- thick-walled sphere, nonlinear behaviour 77—50921
- thick-walled tube, two segment elastic plastic processes *(Russian)* 78—67063
- thin plate, elastic-plastic equilibrium, cracks running to orifice contour *(Russian)* 80—23956
- thin plate elastic-plastic buckling, Hencky effects, von Karman nonlinear strain *(French)* 80—58942
- thin plates, limit load and elasto-plastic bending, finite element anal. 79—27544
- thin skin structures, residual strength prediction, using crack resistance curves 78—90795
- thin wafer method, analytical examination for rate independ. and rate depend. materials *(Japanese)* 79—59931
- thin walled bar subjected to bending and mixed torsion, expt. *(Croatian)* 77—35060
- thin-walled structures, elastoplastic analysis by finite strip method *(Japanese)* 77—42753
- Timoshenko shells with curved openings elastic-plastic deformation under impulsive loading 80—33483
- torispherical vessel heads, elastic-plastic internally pressurized, stresses and buckling 77—58574
- torispherical vessel heads, internally pressurised, elastic-plastic buckling 78—79241
- torsion, elastic-plastic, variational inequality concept 80—23907
- torsion problems, zone estimates 78—67058
- torsion stress distribs. 77—50922
- transition metal carbides, X-ray investig. of abrasive action 77—52497
- trusses, with unstable bars, collapse anal. 78—90729
- tube, thick-walled, axisymmetric deformation in presence of upper yield point *(Russian)* 80—74758
- tubes, pressurised elastoplastic, large strain solution 79—64537
- tubes, thick-walled, thermoelastoplastic creep stress anal. 80—58922
- two layered parallelepiped under large elastoplastic deformations, deformation instability 80—33499
- U-shaped bellows design, low cycle fatigue life, elastoplastic anal. 79—37247
- unidirectionally reinforced metal composite, complex torsional and tensile loading 79—61669
- unloading waves, elastic-plastic wave propag. in semi-infinite rod 77—35079
- variational method using mixed finite elements *(French)* 79—72819
- velocity discontinuities, variational formulation of boundary-value problems *(French)* 79—32284
- virtual crack extension method, nonlinear material behaviour 78—18230
- visco-elastoplastic medium mechanical birefringence in loading and unloading processes 78—59314
- visco-plastic approach to plasticity and creep problems, involving geom. nonlinearities 78—26050
- viscoelastoplastic deformation of isotropic body, tensor laws of behaviour *(French)* 77—62160
- viscoplastic materials, elastic, rate-independent limit of constitutive eqns. 80—74753
- viscoplastic model, cyclic load, stress evolution, asymptotic behaviour *(French)* 80—64382
- viscoplastic/elastic media, constitutive eqn. covering wide range of strain rates *(Japanese)* 80—79862
- viscoplasticity anal., boundary integral eqn. method *(French)* 78—90728
- viscoplastoelastic material, plane wave propagation anal., upon shock loading 79—14336
- wave propagation, transmission of elastic-plastic boundaries 77—62188
- wave propagation, weak, in elastic-plastic and elastic viscoplastic solids with interfaces, Al calcs. 78—18216
- wave propagation in half-plane generated by supersonic variable load *(Russian)* 79—10526
- wire, locked coil rope, limiting moment calc. in torsion 79—10507
- work-hardened material, elastic-plastic stress distrib. near flat surfaced notch with cycloidal tip 77—35084
- Zircaloy-4 tubes, texture influence on anal. of thermoelastic/plastic anisotropy and initial yielding 80—35260
- Al alloy 7075-Tb, coldworked fastener holes, elastic-plastic boundary layer determ. 79—34066
- Al alloy D16, elastoplastic bending of beams of various cross section 78—3196
- Al, alloys, limiting plastic props. *(Russian)* 78—88504
- Al beam, exam. of elastoplastic contact strength law, using impact bending *(German)* 79—43365
- Al, plane stress calc. with two dimensional elastic-plastic computer program 78—35465
- Al, shock transition rise-time meas., limiting viscosity coeffs. 79—77680
- Al single crysts., elastoplasticity, dislocation model, work hardening, tensile tests, stress/strain curves *(Japanese)* 77—52410

elastoplasticity continued
- Al, use in design of composite superconductors in elasto-plastic region 77—28851
- Al-Cu-Si-Mg, deform. simulation using torsional test, elastoplastic constitutive eqn. 80—93594
- Al-Cu-Si-Mn, type 2017S-T4, crack initiation at root of circumferential notch of round bar specimens *(Japanese)* 80—60947
- Al-Zn-Mg-Cu (6, 2.5, 1.5 wt.%), deform. simulation using torsional test, elastoplastic constitutive eqn. 80—93594
- Cr-Mo-Nb, elastic-plastic mathematical model response on quasistatic loading *(Czech)* 80—29111
- Cr-Ni, elastic-plastic mathematical model response on quasistatic loading *(Czech)* 80—29111
- Cu, shock transition rise-time meas., limiting viscosity coeffs. 79—77680
- Fe, cast, grey, electric arc sprayed coating on wire, elastic and elastic-plastic props. *(German)* 79—34089
- Fe-Ni (15, 25 at.%), longitudinal forces in the hot torsion test *(German)* 79—38889
- $Fe_{40}Ni_{40}P_{14}B_6$, metallic glass, bending tests, evidence of ideal elastic-plastic deform. 80—97543
- Ge:Sb, shock polarisation anisotropy in elastoplastic compression range 77—16244
- Mo, electric arc sprayed coating on wire, elastic and elastic-plastic props. *(German)* 79—34089
- Mo, laser irradiation, shock wave formation relationships, surface propagation, elastoplastic wave effects 79—55825
- Ni-Cr-Fe-W, type EH1868, loading history effect on resist. to cyclic elastoplastic strain 80—16398
- Ni-Cr-Ti, type EH1698, loading history effect on resist. to cyclic elastoplastic strain 80—16398
- Ni-Mo-Cr steel, elastic-plastic material characterisation 78—72854
- SiC, identation plasticity and microfracture 79—70158
- Ti alloys, strength characts., elastoplasticity, creep 78—6976
- Ti-Al-Mo-Zr, type VT-9, creep eqns. rel. to extension and compression props. 80—100875
- Ti-Al-V (6, 4 wt.%) cylinders, residual stresses introduced by quenching elastoplastic anal. *(French)* 80—45355

elastoresistance
- heart electrical and mechanical monitoring on extensometer 80—45944
- piezoelectric thin plate, electroelastic equilib. anal. *(Russian)* 78—19417
- thin anisotropic layer, electroelastic equilibrium 80—28429
- TTF-TCNQ, and related cpds., elastoresistivity by strain gauge technique 80—24892
- TTF-TCNQ and related cpds., elastoresistivity 79—23956
- Ag film, Maxwell stresses at charged surface from elastoresistance 80—49957
- Al film, Maxwell stresses at charged surface from elastoresistance 80—49957
- Al film, single cryst., elastoresist. effect 78—84321
- Au film, Maxwell stresses at charged surface from elastoresistance 80—49957
- Bi, film, evaporated, elect. and elastoresistance props. 79—33367
- Cu, elastoresistivity of Frenkel pairs, defect migration *(French)* 80—2073
- Cu film, Maxwell stresses at charged surface from elastoresistance 80—49957
- Fe, elastoresistivity effect, meas. of resistance at 4.2K and 300K, using mag. field method 78—72132
- a-Ge, elastoresistive effects 79—60838
- Sb film, Maxwell stresses at charged surface from elastoresistance 80—49957
- p-Si film, on sapphire, elastoresist. coeffs., room temp. 80—34532
- Si on sapphire, residual strain effect on elec. props. *(Japanese)* 80—84522

ELDOR
- actomyosin, X-irradiated ENDOR and ELDOR obs. 80—63689
- ammonium acetate, irrad. crysts., freq. swept ELDOR obs. at 77K, resolution of spin packets 79—95686
- anthracene-tetracyanobenzene, triplet exciton annihilation, mag. double reson. *(Russian)* 78—19380
- d-camphor, NO diffusion, ELDOR, self-diffusion 77—1618
- cyclohexane, NO diffusion, ELDOR, self-diffusion 77—1618
- cyclohexane, plastic-phase, NO-doped, heterogeneous solid soln., mag. reson. evidence 78—34449
- diethylammonium manganese chloride, T_1 and T_2 meas. by LODESR 78—15064
- glycine-d_2 crystal, X-irrad., H-D exchange reactions 77—16837
- liquid correlation times, discriminating rot. and transl. components 77—1619
- longitudinal detection, electron-spin double reson., signal depend. on relax. times 77—81030
- magnetic field-pulsed ELDOR spectroscopy for electron spin-lattice relax. time meas. 79—93188
- 4-methyl-2,6-di-tert-butylphenol, γ-irrad. cryst., ENDOR transitions, ELDOR detect. 78—95531
- 3- methylhexane, glass, γ-irradiated, trapped electron-radical mag. energy transfer, ELDOR, cross relax. 77—16209
- 2-methyltetrahydrofuran, glass, γ-irradiated, trapped electron-radical mag. energy transfer, ELDOR, cross relax. 77—16209
- multi-level system, relax., double resonance, resistance network analogues 77—1583
- myosin, X-irradiated ENDOR and ELDOR obs. 80—63689
- polycrystalline dipeptides, X-irradiated ENDOR and ELDOR obs. 80—63689
- polymer chain motions, electron-electron double reson. obs. 79—69753
- polystyrene, soln., chain motions, electron-electron double reson. obs. 79—69753
- quinone anions, ELDOR study of nucl. spin exchange due to cation migration 79—68244
- review 78—39449
- smectic A mesophase, spin-probe longitudinal relax. 79—94871
- 2,2,5-trimethyl-1,3-dioxane-4,6-dione, cryst., X-irradiated, methyl group hindered rot. tunnelling, EPR, ENDOR, and ELDOR 79—68328
- $MgO:Fe^{3+}$, spin-lattice relax. 77—90037

electrets
- *see also dielectric devices; electrostatics; photoelectrets; thermoelectrets*
- abietic acid glass, corona-charged, TSC curves 77—55744
- alkaline earth phosphate ($MO-Al_2O_3-P_2O_5$) irradiated electret glasses, relax. of external field intensity on heating 80—25282
- anodic oxide films, space charge, TSC obs. 77—32326

electrets continued
applications to transducers, filters and pyroelectric devices, book contrib. 80−80709
aromatic copolyesters, charge storage props., electret stability 80−7277
bioelectrets, electrets in biomaterials and biopolymers 80−80686
bioelectrets, occurrence of electret state and appl. in mol. biophysics and bioengineering 80−8007
carnauba wax, electret states, role of crystallites 80−2686
carnauba wax, magnetoelectret state, mag. anisotropy, quantum mech. effect 77−59379
carnauba wax, orientation prod., by mech. press. or US waves 78−64314
carnauba wax, residual strain and crystal size of orienting crystallites and their effect on charge behaviour 80−11319
carnauba wax electret, effective charge rel. to polarisation tmep. 78−15086
carnauba wax magneto-electret, Struve function 78−76287
cellophane membrane, polarised, electret transport props., permeability coeff. 80−7860
cellulose, thermally stimulated discharge studies 80−11329
cellulose, TSC study 80−25284
ceresin wax magnetoelectret, X-ray diffr. pattern 78−6014
charge distribution, meas. technique 77−30184
charge meas., influence of meas. method *(French)* 77−41637
charge storage, charge transport and electrostatics conference, Kyoto, Japan (Oct. 78) 80−7252
cobalt naphthalate electret, thermally stimulated discharge, 55-75°C 80−25279
diamagnetic anisotropy of thermoelectret and magnetoelectret states 80−97053
dielectric electret effect, homo and heterocharge charge distribution 80−11317
dielectrics, conf., Sao Carlos, Brazil, Sept. (1975) 80−7251
discharge model, injection relaxation mechanism, space-charge cond. 78−80279
discharge model 80−88908
discharge model 80−88909
discharge theory 79−11380
EL2 telephone transmitter, technology development 80−83723
ferroelectrics, phenomenological theory of electret effects 78−88260
fibre, non-woven, high-efficiency filtering medium 80−76691
film, spatial charge distrib. meas. technique 77−32327
foil transducer eqns. using Lagrange's eqn. 78−83202
free energy and Gibbs energy determ. 77−28513
fundamental aspects of research, book 80−77552
generator for pocket ion chamber dosimeters 78−13382
glass properties obs., bonded, under corona discharge and electron irradiation conditions *(Russian)* 79−4759
4-n- heptyloxyphenyl 4-n-hexydexybenzoate, liquid crystal, freezing polarisation, electret effect *(Polish)* 80−10496
hexamethyldisiloxane plasma polymerised thin film, charge trapping characts. 80−96895
p-hexyloxyphenyl-p-pentoxybenzoate, nematic liq. cryst., elec. discharge meas. of persistent internal polarisation 80−10488
ionic electret behaviour, ionic thermoconductivity technique 80−7274
ionisation chamber dosimeter for long-term personnel monitoring 78−21810
lysozyme bound water, thermally-stimulated press. and current 78−15757
magnetoelectrets, possible mech. of biological effects of mag. fields 80−93157
magnetoelectrets, review 80−25289
measurement of rocket exhaust effluents from space shuttle model, electrets appl. 79−53548
metallised, mech. instabilities *(French)* 80−88906
naphthalene, mag. polarised electret, X-ray diffr. obs. 78−43775
naphthalene, single crystal, anomaly in permittivity due to thermodielectric space charge 80−7258
neutron detection, dosimeter 80−23260
novolac and novolac allyl ether electrets, thermal depolarisation, chem. struct. effect 80−71297
p-octyloxyphenyl-p-pentoxybenzoate, nematic liq. cryst., elec. discharge meas. of persistent internal polarisation 80−10488
Perspex magneto-electret, equiv. elec. field calc. from thermally stimulated discharge current 80−7259
photoresist, KTFR, thermally stimulated discharge current studies 80−75924
physical principles 80−80682
piezoelectric and pyroelectric props. 80−80685
plastic films, charge distribution determ. *(German)* 80−75920
PMMA, dielectric meas. at ultralow freq. by reheating 80−4741
PMMA, tubular magnetoelectrets, TSC obs. 78−88250
polar polymer, piezoelectricity and pyroelectricity 80−7267
polarized dielectric appl. *(French)* 79−51902
poly(alkyl-methacrylates), surface charge decay and TSC 80−11328
poly(vinyl halides), surface charge decay and TSC 80−11328
polyacrylonitrile, elec. polarisation 80−7275
polyacrylonitrile, polaris., pyroelec., electret film, solar energy conversion *(Russian)* 78−39507
polychlorotrifluoroethylene, TSC 80−7266
polychlorotrifluoroethylene electrets, TSC profiles, poling conditions depend. 78−10835
polyelectrolyte, membrane-type, energy storage appl. feasibility 80−26177
polyethylene, charge trapping mechanism, TSC, DTA and optical meas. 80−11322
polyethylene, tubular magneto-electret, surface charge characts., forming temp./mag. field depend. 77−32318
polyethylene electret, internal pot. topography, Raman and IR spectra 80−7362
polyethylene film, polarisation obs. and influence of wax impurities, TSC obs. and analysis *(French)* 80−44999
polyethylene terephthalate, formed by electron injection, TSC meas., space charge drift 80−11321
polyethylene terephthalate, TSC, due to injected charge 77−16242
polyethylene terephthalate, TSC spectrum from electron beam charging 77−77139
polyethylene terephthalate electrets, TSC due to injected charges, electron trapping props. 79−4566
polymer, charge dissipation, transport mechanisms 80−7268
polymer, electret, vapour-induced depolarization currents 79−87379
polymer, piezoelectricity and pyroelectricity, review 77−8514

electrets continued
polymer, thermally stimulated discharge, compatibility and impurity effects 77−4595
polymer film, absorpt. and relax. of charge 80−6942
polymer film, relax. mechanism of electret charge, at high humidity *(Russian)* 77−63360
polymer film, synthetic, acoustoelec. transducers appl. *(Italian)* 79−98577
polymer film electret, charge distrib., generalized model 80−6873
polymer films, electret state and adsorption during injection 79−69770
polymer foil, charge distrib. determ., thermal pulse technique, meas. accuracy 78−80287
polymer foil, electron irradiated, charge dynamics, computer simulation 79−82915
polymeric electret films, produced in HF discharge, props. *(Russian)* 80−20578
polymers, electrical phenomena, nature and appl., book contrib. 80−50254
polypropylene, electron bombarded, radical formation, piezoelectric and pyroelectric effects, ESR study 80−7169
polypropylene, electron bombarded electret, trapped charges ESR study 80−7170
polypropylene 78−27093
polypropylene electrets corona charged at high temp., TSC study 80−7261
polypropylene film, corona-charged, bistable electret, use in construction of transmission light gate 77−50750
polypropylene film electret, space charge injection induced pyroelectricity 77−12324
polystyrene film, thermally stimulated discharge currents 80−71300
polystyrene foils, breakdown-charged, surface charge densities and depths, TSC spectra 80−7260
polyvinyl acetate:Cu, and undoped, thermally stimulated currents exam. 78−35083
polyvinyl acetate film, charge retention, adsorbed water vapour effects, TSC obs. 77−32321
polyvinyl alcohol, bulk polarisation, thermally stimulated discharge current meas. 80−40039
polyvinyl alcohol-polyelectrolyte membranes, heterocharge electret form., divergence model 80−15943
polyvinyl fluoride film, electret effects 77−90094
polyvinylacetate film, effect of electrode metals on depolarisation current characts. 78−76387
polyvinylidene electrets, IR and Raman spectra 80−7359
polyvinylidene fluoride, dielectric relax. mechanism 80−55023
polyvinylidene fluoride, structure, and its electret, review *(Japanese)* 80−10510
polyvinylidene fluoride magnetoelectret, AF and RF charge and dielectric characts. 80−40038
prepolarised, meas. microphones appl. 80−74649
PTFE electrets corona charged at high temp., TSC study 80−7261
PTFE film electret, optical spectra, band theory interpretation *(Russian)* 78−88376
PVC, magneto-electrets, refr. index, temp. and mag. field effects 78−6655
PVC, magnetoelectret form., RF thermomagnetic treatment, dielectric aftereffects 78−6625
PVC, piezoelect. and pyroelec. response rel. to dipole polarisation 80−7267
PVC, rigid, physical ageing effect on elec. props. 78−10836
PVC, spontaneous current emission, various metal electrodes 78−43412
PVC magnetoelectrets, mag. susceptibility 80−2687
PVF$_2$, plastic film sensors 79−99826
PVFD, electret, polarisation process 80−7273
radiation-induced charge storage and polarisation effects 80−80684
RNA, solid hydrated samples, hysteresis loops, nonlinear dielectric properties 80−71294
shellac and bee's wax, orientation solidification in mag. field, magnetoelectrets, X-ray diffr. 77−12299
silastic, magneto-electret of tubular shape, surface charge 78−56419
silastic tubular electret, mag. polarised, thermal currents 80−40037
slot-effect transducer, appl. of energy principle for calc. force upon electret *(German)* 77−3706
spatial distribution of charges and dipoles, transient heating technique 77−12303
surface charge density determ., rel. to measurable parameters 77−48120
surface polarisation from sessile drop contact angle meas. 77−85365
Teflon FEP, annealed electret, charge stability 80−6943
Teflon FEP-A, corona and electron beam charged, TSC peak identification and surface-voltage stability 79−78614
Teflon-FEP, film, plate-electret, construction and use in condenser type headphone 80−5907
terylene film, electret state prod. using electrochem. injection, adsorbed states, frozen field 79−91344
TGS, conditions for electret state 78−43773
thermal pulsing technique for spatial distrib. of charge and polarisation 80−93235
thermally stimulated discharge 80−80683
thermodielectric electret, Costa Ribeiro effect 80−7272
US transducer performances and prospects 78−59244
vinylidene fluoride copolymer electret, charge and polarisation distribs. meas. 78−35081
vinylidenefluoride/tetrafluoroethylene copolymer, piezoelect. and pyroelect. response rel. to dipole polarisation 80−7267
Ag$_3$SbS$_3$, pyrargyrite, order-disorder phase transition and elec. polarisation 79−38468
BeO, thermoelectret props. 80−7269
BeO, thermoelectret state, effect of gamma radiation 80−7270
Ca(NbO$_3$)$_2$, thermally stimulated currents exam. 77−69766
KTaO$_3$, polarisation, dielectric. const., relax. effects, electret state 77−12302
KTaO$_3$:Li, polarised cluster stabilisation by Li defects, polar glass form. 79−91342
LiNbO$_3$:Fe, electron irrad., photoinduced charge transfer and hologram recording 79−36859
PVC, tubular magneto-electret, surface charge characts., forming temp./mag. field depend. 77−32318
S magnetoelectret, thermally stimulated discharge current 79−91341
SrTiO$_3$ glass ceramics, polarisation and dielec. const., 4-77K 77−32319

electrets continued
- $SrTiO_3$, thermal expansion near displacive phase transition meas. 77–12345
- ZnS:Cu, polycryst. electret, electroluminesc. light flash character *(Russian)* 77–55833

electric actuators
- artificial heart, electronic pressure control with fast variable aperture valve *(French)* 77–40928
- cardiac assist system, implantable pulsed solenoid device 77–44848
- deformable mirrors with bimorph actuators 80–33135
- differential ball screw actuator driven deformable mirror design and performance 80–33137
- discrete actuator deformable mirror 80–33133
- drip feed unit microprocessor control development 78–53563
- electromechanical actuator, vibr. linearisation of mag. hysteresis charact. *(Russian)* 79–12789
- thread grinder, high precision, laser interferometric auto-correcting system 80–90830
- three-actuator deformable water-cooled mirror 80–33134

electric admittance
- air blast circuit breaker, near current zero, local elec. props. 78–87516
- alkaline earth fluoride solid solns., MF_2-UF_4-CeF_3, surface degradation, complex admittance anal. 78–55980
- anisotropic body of arbitrary geometry, conductance and resist., variational calc. 80–32865
- axon asymmetry currents and admittance, squid 77–73518
- composite electrostrictive resonators, finite element simulation 78–59237
- discontinuous metal film, AC equivalent circuit anal. 79–51690
- electric cells, metal/β-alumina/metal, complex admittance diagrams, grain boundary effect *(French)* 80–45653
- electrolytes, in ethylene carbonate viscosity and conductance meas. at 40°C 79–28122
- electromechanical filter torsional mode transducer analysis 77–27436
- fused salt, simulation of high field cond. 80–54421
- hemispherical monopole surrounded by plasma layer, Tonks-Dattner reson. and input admittance 80–87887
- heterogeneous matrix system, generalised conductivity and loss, tangent 80–7289
- heterojunction, interface state parameters from differential admittance 77–15944
- hot carrier p-n junction as a contact with negative differential capacitance and conductance 79–69590
- impedance of a p-n junction by direct currents *(Russian)* 78–84285
- inhomogeneous continua with Hall effect, elec. fields and effective conductance tensor *(Ukrainian)* 77–50590
- interdigital transducer in layered anisotropic semiconducting struct., elec. input admittance matching 78–22238
- ionic conductor, AC props. 78–47578
- lipid bilayer membranes, pancuronium inactivation of alamethicin-induced conductance 79–39189
- macroion solutions, theory of effect of small ions on electrical admittance 80–71914
- metal-insulator-metal junction, hopping model of zero-bias tunnelling anomalies, mag. field effect 79–60936
- MIM structures, zero bias anomaly due to elastic tunnelling, calc. 80–2483
- MIS structure, semicond. surface states, capacitance, admittance, freq. depend. 80–49940
- optical cavity, one-dimens., with output coupling, thermal radiation, fluctuation-dissipation theorem 79–978
- p^+-n diode under forward bias, effects of radiation-induced deep levels on admittance 78–23157
- p-n heterojunction differential admittance theory in the presence of surface electron states 80–96981
- plane-parallel plasma waveguide iris admittance 77–84447
- polyvinyl chloride, dielec. props. at ULF, superimposed direct voltage *(French)* 78–15138
- ring aperture antenna in plasma, input admittance anal. 78–38542
- SAW IDT, input admittance calc. using moment-method technique 79–94439
- SAW propagation in admittance sheet deposited on piezoelectric substrate 77–80689
- Schottky diode, GaAs, trap levels, admittance spectroscopy 79–51672
- SCLC diode, influence of carrier transit time on small-signal admittance 77–85305
- SCLC diode with traps, small-signal admittance in high freq. range, negative conductance 79–11221
- semiconductor, surface-state props., using field effect anal. 79–24053
- semispherical monopole, immersed in plasma electrons, thermal noise *(Russian)* 77–76196
- tapered piezoelectric bar transducer with transversely polarised piezoceramic, capacitance and admittance 78–1537
- transient and AC steady-state response of solid with recombining space charge 77–51737
- $4AgI$-Ag_2XO_4, (X=Cr, Mo, W), ionic cond., complex admittance 77–84969
- $Al_xGa_{1-x}As$:O-n-GaAs heterojunction for MIS device, capacitance voltage meas. 79–87157
- β''-Al_2O_3-Na_2O, Li_2O stabilised, electrolyte polarisation anal. by complex admittance method 80–2689
- Au surface, iodide ion adsorption, depend. on electrode crystallographic orientation, admittance pot. curves 79–15020
- $CaF_{2-x}H_x$, ionic cond. determ. from admittance and dielec. loss meas. *(French)* 80–107479
- $Cd_xHg_{1-x}Te$ polycrystalline films, electrical props., rel. to struct. *(Polish)* 78–31002
- CdS, electron traps, admittance spectra on hetero- and Schottky junctions 79–56159
- CdS-Cu_2S single cryst. heterojunction, trap depths in depletion region 78–52064
- Cr, discontinuous thin film, AC equivalent circuit anal. 79–51690
- Cr-SiO_2-n-Si tunnel diodes elec. characts. meas. and modelling 77–39955
- GaAs MOS structure, small signal admittance study 80–2478
- GaAs-$Al_{0.5}Ga_{0.5}As$-Cr/Au MIS capacitors, characts. meas. 78–95371
- GaP diodes, TSCAP and admittance spectroscopy of gamma-ray induced defects 77–89472
- GaP, p^+-n diode junction, admittance meas. and carrier traps 78–91757
- Ge:Au, unipolar injection influence on high frequency conductance 80–34474

electric admittance continued
- InSb MOS capacitor, AC behaviour, semicond.-oxide interlayer effect 78–19151
- Nb-NbO_x-Pb tunnel junctions at 4.2K, conductance of oxide barrier 80–7046
- PbTe-ZrO_2 (SiO_2), epitaxial MIS struct., fabrication and elec. props. 80–2472
- Si, amorphous film, electron beam evaporated, freq.-depend. dielec. behaviour 79–99549
- Si ion-controlled diodes, acid-base exposure effects, Si-SiO_2 interface state density 80–96984
- Si MOSFET, conductance oscills., source-drain limited cond. 80–20316
- p-Si, neutron irrad. effects, admittance meas. of n^+-p diode 78–51587
- Si, p^+-n diode, neutron irrad., defect levels, G-T and C-T curves obs. 77–62986
- Si p-n junction, dielectric props., freq. depend. of capacitance and conductance 78–43469
- Si, polycrystalline, transconductance of boundaries passivated with H 79–56158
- Ta-Ta_2O_5-Au capacitive system, freq. depend. of dissipation factor, dielectric const., conductance *(Spanish)* 77–69426
- Ta_2O_5, amorphous and cryst., elec. cond. mechanism, admittance meas. 80–70705

electric admittance measurement
- AF impedance bridge, 4-terminal-pair, 40 Hz to 2 kHz 79–88978
- aortic compliance in living dogs measured by elec. admittance plethysmography *(Japanese)* 80–3748
- deep-level transient spectroscopy, using HP desk-top computer semiconductor processes and devices testing appl. 80–37091
- digital multimeter conductance function introduction 79–93167
- faradaic admittance, rapid drop time on-line FFT meas. 78–92544
- heterogeneous charge transfer kinetic effects, deconvolution by FFT faradaic admittance meas. 78–20091
- micro-organism enzymic activity indicator 79–57819
- microcomputer controlled bridge, for passive network testing 77–18037
- MIS structure wideband admittance meas. by phase-selective rectifier *(German)* 77–61089
- MIS/SIS solar cells, automated surface states anal. 80–93966
- photoelectric conductance submicrosecond relaxations, in semiconductors *(Czech)* 80–31804
- plethysmography, venous occlusion admittance automated monitoring system 78–31937
- plethysmography for limb blood flow meas., evaluation of theory and accuracy 78–31936
- semiconductor device, automatic display of CV and GV characts. at HF 77–26329
- semiconductor device C-V and G-V measurements using automatic technique, 50 Hz to 300 KHz 80–31800
- skin conductance meas. IC operational amplifier cct. 77–25566
- SYDAGES system, for on-line FET faradaic admittance meas. 78–20090
- transthoracic admittance plethysmogram meas. of aortic compliance, dog expt. 78–31925
- PbS-Si p-n heterojunctions, AC admittance meas. 80–96979

electric amplifiers *see amplifiers*

electric arc furnaces *see arc furnaces*

electric arc welding *see arc welding*

electric arcs *see arcs (electric)*

electric breakdown
- *see also electric breakdown of gases; electric breakdown of liquids; electric breakdown of solids*
- arc plasma flow-cold electrode gap, electric breakdown *(Russian)* 78–34280
- cathode prebreakdown field emission transition to vacuum breakdown 78–75462
- charge injection between concentric cylindrical electrodes 77–59514
- charge storage, charge transport and electrostatics conference, Kyoto, Japan (Oct. 78) 80–7252
- cohesive force and resistivity between electrostatically- precipitated particles 79–86102
- CTR devices, surface effects related to voltage breakdown 77–35356
- dielectric conduction and breakdown, conf., Gainesville, FL, USA (Oct.-Nov. 1979) 80–82564
- dielectric in vacuum, surface breakdown, dielectric strength calc., quantitative model 80–34855
- dielectric surface with accumulated air positive ions, vacuum breakdown obs. 78–75464
- discharge gap, high-vac., effect of transverse mag. field and geometry 78–38567
- discharges growth in short point-plane electrode systems, critical survey 79–4206
- field emitter vacuum breakdown, external mag. field effects, transition period 80–38824
- gelatin film, dielectric losses and breakdown, struct. effects *(Russian)* 77–52017
- heavy ion counters based on MOS structure 80–69032
- illumination, intense, of optically transparent medium, avalanche ionis., recomb. effect 80–7295
- ion beam extraction, computer simulation, finite element method 80–96387
- laser plasma-target interface breakdown 77–89282
- laser-induced breakdown, time-evolution of light emission 77–58836
- membrane, elec. excitable, phys. model, excitation mechanism 77–36902
- metal cathode, electrically stressed surface elec. phenomena, electrolum. and breakdown with medium gap spacings 80–20710
- numerical description of treeing for dielectric breakdown in polymethylmethacrylate 80–100633
- p-n junction thermal second breakdown prediction test 79–82668
- plasma sheath breakdown to glow transition in plasma filled gap 80–100105
- polysulphone, elec. appl., dielec. props. meas. 77–55750
- PWR containment vessel wall electrical penetration tests *(Japanese)* 79–6747
- snow, impulse breakdown characts. estimation *(Japanese)* 78–40669
- space charge field, spatio-temporal distrib. determ. in breakdown 80–38771
- testing, Voyager spacecraft, JPL, Pasadena, USA 80–92415
- tracking phenomena in solid dielectric materials under moist conditions, expt. 77–43934
- vacuum, implications for HV technology 78–30509

electric breakdown continued
vacuum, impulse breakdown initiation mechanism, microscopic obs. of vacuum gap electrodes 77—84554
vacuum breakdown, microparticles detection by laser scatt. 77—19787
vacuum breakdown, thermal anode instability in prebreakdown stage 79—77445
vacuum breakdown in DC electrostatic separator for high energy physics 77—26921
vacuum breakdown initiation, 4.2K, critical field emission currents 78—75459
vacuum gap, breakdown initiation, microparticles electrical charge 77—76231
vacuum gap breakdown initiation by microparticle impact 80—96413
vacuum gap breakdown strength, 200-500 kV pulses, anode grid 78—5980
vacuum gap with processed electrodes, atm. effects on dielectric strength 78—51389
vacuum gaps with conditioned metal electrodes, thermal press. effect 78—42843
vacuum insulation, elec. strength prediction *(Russian)* 77—15257
vacuum to gas breakdown transition, discharge phenomena 80—38825
Van de Graaff generator terminal discharges, transient radial elec. field in breakdown channel 79—22501
vertical single-pole earth sphere gap, voltage measurement influence of neighbouring surfaces *(German)* 78—29880
wire-plane electrodes, breakdown voltage, effect of vacuum conditions 80—64798
Al_2O_3 film, RF sputtered by planar magnetron, phys. props. 77—43448
As_2S_3 film, evaporated, switching effects 80—96952
C electrode breakdown voltage dependence on adsorbed gases 78—75465
Cu electrodes, breakdown voltage, prebreakdown current in vacuum, crossed elec. mag. fields depend. 80—79604
Kr-Ar, phase matched, generation of Lyman-α radiation 80—91845
Kr-Xe, phase matched, generation of Lyman-α radiation 80—91845
SF_6, compressed, influence of electrode macroscopic curvature upon surface roughness effects 80—40693
SF_6/N_2 pressurized mixtures, electric breakdown investigation 80—14877
Si, thermally oxidised-electrolyte system, features of cathodic breakdown *(Russian)* 80—107907
SiO_2 film formed by ion implantation, dielectric props. 78—35090
Ta_2O_5 film, temp. and time characts. of breakdown *(Russian)* 77—55751
TiO_2:Si(Fe)(Mn)(Cr)(Ni), anodes, low breakdown voltage due to electron tunnelling via grain boundaries 79—74407
Y-Y_2O_3-Au thin film capacitors, self-healing dielec. breakdown 80—11104

electric breakdown of gases
see also electron avalanches
aerosol, elec. breakdown, due to pulsed, RF, and static fields 77—76242
aerosol induced breakdown in air, two-dimensional modelling 79—90368
air, arc channel transient charact. under impulse voltage *(Japanese)* 78—5973
air, breakdown by pulsed laser radii 80—1731
air, breakdown in crossed elec. and mag. fields, modified Paschen's law 80—24121
air, breakdown near solid targets, by pulsed CO_2 laser radiation *(Russian)* 78—26362
air, breakdown near transparent dielectrics 78—34381
air, breakdown pot. reduction by pulsed lamp 79—94767
air, breakdown potential, pulse lamp irrad. effects *(Russian)* 78—83518
air, breakdown threshold meas. using pulsed HF(DF) laser 77—11423
air, breakdown voltages, from normal to cryogenic temps. 78—59692
air, compressed, uniform field gap spark breakdown 77—11410
air, dielectric stimulated arcs in lighting-arrestor connectors, substantial lowering of breakdown voltage 79—99013
air, elec. discharge, effect of long laser spark ionis. channel 78—67468
air, electric breakdown between coaxial cylinders in crossed elec. and mag. fields 78—5963
air, electric breakdown by long laser spark 79—64822
air, electric breakdown voltage hysteresis, electrode coating effects 78—87553
air, electrode surface roughness effects 80—84018
air, erratic breakdown due to sustained appl. voltage and presence of dust particles *(German)* 79—94830
air, focusing of laser beam as a whole 77—88875
air, formative time lag rel. to gap geometry, pressure, and overvoltage 79—18994
air, heated, breakdown parameters 80—103202
air, high temp. elec. breakdown characts., theory and obs. 78—87581
air, impulse breakdown processes at low press. 80—44021
air, influence of positive and negative impulses on breakdown voltage, obs. *(German)* 78—5981
air, laser breakdown, very long spark prod. *(Russian)* 77—1031
air, laser induced gas breakdown threshold at 1.06 micron 80—28594
air, laser-induced breakdown over long distances 80—33795
air, laser-initiated ionisation channels, form., characts. 77—89345
air, leader development and its mechanism in air under impulse voltages *(Japanese)* 77—80390
air, low threshold breakdown, near target, by pulsed laser radiation *(Russian)* 78—22594
air, microwave breakdown field calc., resonator and rectangular waveguide expt. 79—41789
air, negative point-plane corona, electrical characts. 78—71567
air, optical breakdown, initation by absorbing water droplets 80—10352
air, optical breakdown near metal target by laser beam 80—6209
air, optical breakdown threshold reduction near dielectric surface 77—51211
air, positive point-plane gap, critical press. prediction, v_c/press. characts. 78—87583
air, positive/negative leader breakdown process, problems 77—11427
air, submillimetric laser induced breakdown 78—67446
air, undervoltage breakdown between parallel plates 79—60099
air, unionized, enhanced light emission from positive corona 79—37568
air (dry), 6.2 MHz elec. field, perpendicular mag. field, 350 G, 500 G, 0.5-8 torr 77—35422
air at Ti surface, optical breakdown, interferometric investigation 80—100064
air breakdown by CO_2 laser radiation near solid target *(Russian)* 77—84472

electric breakdown of gases continued
air breakdown in homogeneous AC and DC fields, obs. *(German)* 79—86625
air breakdown in superimposed DC and HF electric fields 78—67571
air gap, point-to-plane switching surge breakdown 77—4005
air gap between electrodes, conducting body and space charge effect on breakdown 79—50919
air gaps, 1 to 9 cm, with heated electrodes, investigation *(German)* 80—107010
air gaps, pre-breakdown phenomena under impulse voltage, streamers obs. *(Japanese)* 78—5972
air gaps, schlieren studies of impulse breakdown 78—87518
air in long spark-gaps, breakdown voltage *(French)* 80—33828
air insulation gaps, critical impulse voltage stress determ., test 77—4018
air near Al, optical breakdown gasdynamic processes, recoil impulse 77—35370
air near solid dielectric surface, reduction of laser breakdown threshold 79—77446
air positive point-to-plane corona, continuous and pulse components 79—19119
air-gaps, ramped impulse voltage tests 77—15266
air-SF_6 mixture, breakdown voltage and discharge extension of long gaps 77—84550
atmospheric air, breakdown and corona characts. under AC voltage for rod to plane air gaps *(Japanese)* 79—84416
atmospheric negative ions, electron detachment rates, time lags to breakdown 78—87564
automobile ignition RFI suppression at distributor rotor gap 79—55586
benzonitrile, anodic polymer growths during electrical breakdown conditions, TEM study *(French)* 78—75960
boundary layers, multicomponent, in models undergoing breakdown 78—42588
breakdown development meas., elec. and optical methods 78—22584
breakdown voltage of air, effect of sand particle pollution 78—81363
breakdown wave propagation in ionised gas in nanosecond discharges 80—87890
butene-1, Townsend primary and secondary ioniz. coeffs. and sparking voltages 78—51372
coaxial cylinder geometry, cross-field breakdown 79—82029
coaxial plasma guns, breakdown phase, optical and elec. meas. 80—70036
compressed gas, electric breakdown, dielectric strength 77—31543
compressed SF_6, repeated breakdown field strength in uniform field perturbed by protrusion 80—96406
corona discharges in atmospheric air under AC voltage, observation *(Japanese)* 79—84417
corona onset and breakdown in non-uniform air gaps, physical models 77—15268
corona with heated discharge electrode, breakdown streamers, expt. 77—76228
crossed mag. field, characts. prediction 79—32839
crossed magnetic field, equivalent reduced electric field concept 80—64805
cryogenic gas, dielectric breakdown 80—40051
cyclotron resonant gas breakdown with 1.22-mm $^{13}CH_3F$ laser 79—55549
detonation products in discharge gap, electric breakdown 79—10736
detonation products of condensed explosives elec. stability 79—86635
dielectric gas, breakdown strength, electron impact ionis. and scatt. cross section 79—82031
dielectric gases and gas mixtures, maximum electric strength and vapour pressure relationships 80—92249
diffusion theory validity in RF breakdown, mol. gases in longit. mag. field 77—39491
discharge development in gas-filled gap *(Russian)* 78—22580
discharge in positive point-to-plane air gaps, obs. 77—35414
electric strength 78—83631
electron neutral collision frequency from breakdown measurements in crossed electric and magnetic fields 79—14517
electron velocity, general soln. in steady-state pre-breakdown region 77—11420
electronegative gases, sparking pots. and ionisation coeffs. 78—42705
electrostatic precipitators, air temp. influences on negative corona integral characts. *(Russian)* 79—41892
ethane, electron-mol. collision freqs. from breakdown data in crossed mag. field 80—43835
ethylene, Townsend primary and secondary ioniz. coeffs. and sparking voltages 78—51372
flame, ruby laser-induced gas breakdown thresholds 79—1951
flow rate meas. by multiple electric breakdown method 77—39371
flowing gas spark gaps, electric breakdown study, improved method 80—64821
fluorocarbon vapours, sparking potential meas. 77—65922
Freons and their mixtures with N_2 and SF_6, breakdown voltage in uniform electric field *(German)* 78—71423
gap between two spherical electrodes, breakdown voltage calc. 78—55763
gas breakdown, by combined laser and microwave irrad. 77—35434
gas-dielectric interfaces, initiation of low threshold breakdown 79—68900
gas-filled diode, rarefied gas breakdown time delay statistics 78—87571
gases as electrical insulators, nature and practice 78—83632
glow discharge, breakdown and extinction, tube wall role 80—44002
glow discharge breakdown, temporal development of electrode pot. 80—44003
glow discharge growth in two-dimensional geometry, streamer breakdown 80—24286
hexane, electric breakdown strength of vapour and liq., behaviour in critical region 77—47285
HF breakdown, lower-hybrid waves, focusing and channelling *(Russian)* 80—106890
HF discharge, in low press. gas, multipacting breakdown mechanism for teachers 79—97144
high press. gas discharge prebreakdown processes, electrode surface inhomogeneity effects 79—14628
high temp., 300-2100K, formulae and graphs for breakdown voltage *(Russian)* 78—51370
highly ionised gas flow, local elec. breakdown criterion 79—41894
homogeneous elec. field, physical aspects *(German)* 79—82108
inert gases, using single ps ruby laser pulses 77—19789
insulating replacement gases for SF_6 80—59313
insulators, initiation and propagation *(Japanese)* 79—19837
ionising wave propag. mechanisms 80—83941
large-area nanosecond discharge breakdown 78—71614

electric breakdown of gases continued
laser, electrically pumped, breakdown delay 77−27270
laser and microwave field induced gas breakdown, press. depend. 79−55446
laser beam with retractable focus, ionis. path form. in gases 79−18992
laser beam-plasma interaction, in mag. field, breakdown, heating, trapping, fusion, diagnostics, book contrib. 77−51196
laser gas breakdown, shock and ionisation waves, photographic absorpt. obs. 80−87967
laser induced, book contrib. 77−51256
laser radiation gas breakdown at high intensity *(Russian)* 79−98853
laser radiation-matter interactions, dissertation 79−86555
laser triggered fast-response sealed dischargers 78−51391
laser-induced, effective photon theory, critical analysis 77−68735
laser-induced, excitation, ionisation and energy loss processes 78−14126
laser-induced breakdown phenomena 78−75390
laser-induced gas-breakdown model 80−1821
laser-induced plasma, effects of spherical aberration and multiphoton absorpt. 77−84473
laser-supported breakdown, finite absorpt. length model 80−107005
laser-triggered breakdown in gases, basic processes responsible studies 80−38794
liquid metal cathodes, nanosec. discharge form. in H_2 atmosphere 78−87578
long air gap minimum breakdown voltage and time estimation 78−67575
long rod-to-plane air gap voltage/time characteristic for switching impulses 78−67576
in long tube in mag. field 80−24120
low pressure gases, dielectric breakdown model Hg, Ar appls. 78−9883
low threshold breakdown, near target, by pulsed laser radiation *(Russian)* 78−22594
low-pressure gas discharge, mean free path and viscosity, mag. field effects 80−24282
low-pressure gas gap, two breakdown voltages, breakdown prevention method 80−6207
metal carbonyl vapours, pulsed laser breakdown, ultra-fine metal particle form. 80−84881
metal-dielectric system, gas cavity initiation-discharges phenomena *(Polish)* 80−19660
MHD generator, plasma interelectrode breakdown, model 79−55572
microwave breakdown in gases, Schwinger variational princple 79−41788
microwave discharge, breakdown and maintenance electric fields meas. 78−22587
microwave gas breakdown, ionisation pot., qualitative theory 80−43837
minimum breakdown potentials in crossed elec. and mag. fields 78−67554
mixtures and unitary attaching gases, breakdown field strength 79−55445
molecular ion reactions influence on optical breakdown 80−96341
multiply-charged plasma, temp. kinetics and population levels *(Russian)* 80−106952
needle to plate spark gap, laser triggered in nonuniform field, charact. 77−7614
negative point to plane gap, in air, pulseless corona 78−47195
optical breakdown in intense annular beam from CO_2 laser, flow-concentration effects 79−64886
overvoltage breakdown development at high gas press. 80−84021
Paschen's law, modification 80−24121
Paschen law and HF breakdown 79−86624
photon-photon scattering, effective-photon theory for cross-section 78−58962
plasma propagation in gas breakdown near laser-irrad. target *(Russian)* 79−55476
point-to-plane air gap, corona onset, breakdown voltage 78−47194
point-to-plane gap corona and breakdown in supersonic airstream 78−67573
positive leader, in long nonuniform air gap, growth 78−75444
prebreakdown stage, review 80−106868
predischarge current meas. in compressed air 78−87555
propylene, Townsend primary and secondary ioniz. coeffs. and sparking voltages 78−51372
resonators, RF breakdown, rel. to lower hybrid reson. in Tokamak plasma 78−26364
RF breakdown, lower hybrid wave self-trapping 80−38850
RF breakdown, time-resolved studies 78−79485
RF breakdown in resonators for lower hybrid resonance plasma heating, 0.8-0.9 GHz 77−84564
rod-to-plane air gap breakdown under negative impulse voltage 78−67563
rod-to-plate system, initial corona voltage calculated according to Townsend's Theory *(Czech)* 80−87961
SF_6 compressed, breakdown threshold, surface roughness and pressure effects 78−75449
small spark gaps, optical investigation *(German)* 78−30497
space charge ionising waves, high velocity propagation 80−87889
spark, laser-produced, light pulse narrowing and power density increase 80−28862
spark, long, in reduced air density 77−35428
sparking potential in longit. mag. fields 80−106996
time lags, formative and total, calc. under uniform fields 80−49037
Tokamak discharge gas breakdown time model 78−67555
Townsend primary ionization coefficients and breakdown voltages of cycloparaffin vapours 80−79602
vacuum, DC breakdown, electrode vap. reson. radiation emission 78−14234
vacuum, delay time depend. on voltage pulse form *(Russian)* 77−4001
vacuum, static high-voltage breakdown in mag. field, Cu cathode pretreatment effect 77−19781
vacuum breakdown, Trump-Van de Graaff condition anal. 80−79613
vacuum breakdown in elec. field in range $(5\text{-}7)\times10^6$ V/cm 80−87973
vacuum gap, impulse breakdown 79−82112
vacuum gaps, influence of solid-state cohesion of conditioned metal electrodes on elec. strength 77−7618
vacuum gaps, long, with static uniform fields, time interval determ. 77−15267
vacuum to gas breakdown transition, discharge phenomena 80−38825
water vapour, microwave breakdown, 20 mtorr-22 torr 79−72983
weakly ionised gas, low threshold optical breakdown 79−27860
wire/plane electrode air discharges in strong nonuniform field *(Rumanian)* 79−68964
D_2, elec. breakdown, Paschen's law violations 78−87570

electric breakdown of gases continued
Ar, breakdown conditions with current present before breakdown 78−42841
Ar breakdown in superimposed DC and HF electric fields 78−67571
Ar, breakdown threshold meas. using pulsed HF(DF) laser 77−11423
Ar, breakdown waves 77−31542
Ar gap, low-press., with thermionic cathode, upper and lower breakdown voltages 78−79405
Ar gas breakdown for HF laser nanosecond pulse generation 79−81465
Ar, heated, breakdown parameters 80−103202
Ar, high press. gas discharge form. 78−87567
Ar high press. gases, laser spark, breakdown and radiation supported shock waves 79−32791
Ar, high temperature, up to 2400°C, breakdown voltage and voltage-current characts. obs. 78−87510
Ar, laser induced gas breakdown threshold at 1.06 micron 80−28594
Ar, laser-induced gas breakdown, wavelength depend. meas. of threshold 79−41895
Ar, microwave breakdown of nanosecond duration, calc. of threshold fields 78−94948
Ar, plasma, ion energy level populations in crossed elec. and mag. fields 78−67428
Ar plasma, RF breakdown pot. microwave scanning technique 80−64773
Ar, pulsed electrical breakdown at high temps. *(Russian)* 78−34379
$Ar\text{-}H_2$, time and space resolved spectra 78−18470
$CCl_2F_2\text{-}CO_2$ gas mixture, field breakdown gradients calc. method 80−92248
$CCl_2F_2\text{-}N_2$ gas mixture, field breakdown gradients calc. method 80−92248
CO, ionisation growth, spatial current growth meas. 77−19665
CO_2, $CO_2\text{-}CCl_2F_2$ under pressure, in uniform and nonuniform-elec. fields *(Rumanian)* 77−19782
CO_2 laser pulse breakdown of air, Ar, and He 80−6206
CO_2, negative point-plane corona, electrical characts. 78−71567
CO_2, Paschen curves *(French, English)* 77−76221
CO_2 photoionisation laser, breakdown effect on output 79−68379
CO_2, pulsed electrical breakdown at high temps. *(Russian)* 78−34379
CO_2 TEA pulsed, UV preionized, high power laser, development and performance 80−106539
H, HF discharge, gas breakdown, electron diffusion eqn. exact soln. 80−19658
H, laser-induced gas breakdown, wavelength depend. meas. of threshold 79−41895
H, RF induction discharge breakdown, diffusion theory 77−84562
H_2 6.2 MHz elec. field, perpendicular mag. field, 350 G, 500 G, 0.5-8 torr 77−35422
H_2, breakdown in crossed elec. and mag. fields, modified Paschen's law 80−24121
H_2, cyclotron resonant laser induced breakdown obs. 77−39499
H_2, elec. breakdown, Paschen's law violations 78−87570
H_2, Paschen curves *(French, English)* 77−76221
H_2, prebreakdown current growth, ionis. coeffs. 77−80385
He, breakdown by alternating electric field near ion cyclotron freq. 78−55765
He, cyclotron resonant laser induced breakdown obs. 77−39499
He, dielectric breakdown across epoxy insulation 78−62658
He, elec. breakdown by pulsed high freq. field, electron distrib. function *(Russian)* 80−14876
He, electron distribution function relaxation in high freq. gas breakdown *(Russian)* 80−14957
He, gas, laser-induced breakdown cyclotron reson. at low press. 79−60100
He, heated, breakdown parameters 80−103202
He, laser-induced breakdown 80−96339
He, laser-induced gas breakdown, wavelength depend. meas. of threshold 79−41895
He, microwave breakdown of nanosecond duration, calc. of threshold fields 78−94948
He, Paschen curves *(French, English)* 77−76221
He, pulsed breakdown at low temp. 80−103216
He, pulsed electrical breakdown at high temps. *(Russian)* 78−34379
He, RF induction discharge breakdown, diffusion theory 77−84562
He rise time and time-depend. spark-gap resist., microwave meas. technique 77−31538
He, supercritical, dielec. breakdown 79−65796
He-Ne mixtures, spark channel formation 78−1936
$KNbO_3$, single cryst., dielec. breakdown and electroluminesc. 78−2917
Kr, laser-induced gas breakdown, wavelength depend. meas. of threshold 79−41895
N, compressed, breakdown at cryogenic temp., obs. *(Russian)* 78−67448
N_2, breakdown in crossed elec. and mag. fields, modified Paschen's law 80−24121
N_2 breakdown in superimposed DC and HF electric fields 78−67571
N_2, breakdown threshold meas. using pulsed HF(DF) laser 77−11423
N_2, breakdown voltages, from normal to cryogenic temps. 78−59692
N_2, breakdown waves 77−31542
N_2, compressed, insulation breakdown at cryogenic temp., obs. 78−51368
N_2 discharge, flowing, electron-beam maintained, cathode shape effects 79−27850
N_2, elec. breakdown at high press. and field strengths, steady-state expts. 78−79488
N_2, electric breakdown, vol. discharge with external photoionisation, plasma focus spark channel *(Russian)* 80−38738
N_2, electric breakdown between coaxial cylinders in crossed elec. and mag. fields 78−5963
N_2, electric breakdown gas discharge, Paschen curve double minima 80−44036
N_2, electric breakdown in long high-voltage gaps with gamma and alpha particle irrad. 79−18993
N_2, formative time lag rel. to gap geometry, pressure, and overvoltage 79−18994
N_2, high temp. elec. breakdown characts., theory and obs. 78−87581
N_2, high temperature, up to 2400°C, breakdown voltage and voltage-current characts. obs. 78−87510
N_2, laser induced gas breakdown threshold at 1.06 micron 80−28594
N_2, pulsed electrical breakdown at high temps. *(Russian)* 78−34379
N_2, rise time and time-depend. spark-gap resist., microwave meas. technique 77−31538
N_2-filled diodes, breakdown time depend. on electrode temp. 80−1735

electric breakdown of gases continued
N_2-O_2 gas mixtures, elec. breakdown voltage, 113-293K 79—1363
N_2-O_2 gas mixtures, highly transient gas discharges, obs. 79—37562
N_2-O_2 mixture, impulse breakdown processes at low press. 80—44021
N_2-SF_6 mixture, breakdown voltage and discharge extension of long gaps 77—84550
N_2-SF_6 mixture, electrode surface roughness effect 77—39490
NO in AC field, kinetics and energetics *(French)* 78—64824
NO_2, in AC field, kinetics and energetics *(French)* 78—64824
Ne flash tube, investigation of forms. and decay mech. of internal fields 78—58552
Ne microwave breakdown field calc., Monte Carlo method 78—67551
Ne-Ar (0.1%) mixture, AC plasma panel, Paschen breakdown curves 77—11418
Ne-HCl mixture breakdown obs. 78—67553
Ne-Kr Penning mixtures, Townsend ionisation coeffs. and breakdown pot. meas. 80—19641
Ne-methane mixture breakdown obs. 78—67553
O_2 6.2 MHz elec. field, perpendicular mag. field, 350 G, 500 G, 0.5-8 torr 77—35422
O_2, cyclotron resonant laser induced breakdown obs. 77—39499
O_2, formative time lag rel. to gap geometry, pressure, and overvoltage 79—18994
O_2, negative point-plane corona, electrical characts. 78—71567
S_6, partial discharge disintegration product meas. *(Czech)* 78—67450
SC_6, electric breakdown voltage hysteresis, electrode coating effects 78—87553
SF_6 and SF_6-N_2 mixture, elec. breakdown and corona stabilisation obs. 78—87582
SF_6, at high pressure, breakdown voltage meas. *(German)* 77—55181
SF_6 avalanche breakdown as stochastic process 78—67574
SF_6, breakdown at high pressure, possible cosmic ray effects 78—87577
SF_6 breakdown at moderate temps., investigation 79—27863
SF_6 breakdown characts. in non-uniform field gaps, at 0.8-2 MV range 77—15269
SF_6, breakdown characts. for 0.8 to 2.6 MV range 78—87552
SF_6 breakdown distributions, low-value fractile determ. 78—67578
SF_6 breakdown field strength, electrode surface roughness tolerance 78—67577
SF_6 breakdown mechanisms, review 78—59699
SF_6 breakdown voltage calc. based on elec. field strength values *(German)* 77—15264
SF_6, breakdown voltages dispersion, anal. 80—38772
SF_6 coaxial gap breakdown probability determ., influence of meas. procedure 78—67579
SF_6, compressed, low probability first breakdown voltage determ. 80—38787
SF_6, compressed in positive rod-to-plane gaps, static breakdown anal. 80—38796
SF_6, contamination with metal particles, theoretical model *(Italian)* 79—64937
SF_6 corona-stabilised breakdown, computations and obs. 80—64804
SF_6, dielectric strength tests *(Czech)* 78—30498
SF_6 dielectric strength, conductor surface irregularities influence 80—14946
SF_6, discharge development, high speed elec. and optical temporal resolution 78—87584
SF_6, elec. discharges, expt. *(German)* 79—10726
SF_6 electric strength, electrode surface roughness effects *(German)* 78—63609
SF_6 electric strength as statistical charact. *(Russian)* 79—41787
SF_6, electrode surface and coating effect on DC breakdown voltages 78—87557
SF_6, electron beam irrad., delayed elec. breakdown 79—4200
SF_6, first breakdown voltages 78—87554
SF_6 high-temp. electrical breakdown parameters 78—67567
SF_6, impulse breakdown, polarity effect 80—38773
SF_6 impulse breakdown characteristics for nonuniform field gaps for switchgear design 80—84024
SF_6 in coaxial electrode arrangement, impulse breakdown anal. *(German)* 77—76219
SF_6, initial corona voltage increase, due to electrode surface roughness *(Croatian)* 80—54074
SF_6 insulation breakdown characts. under operating conditions in HV apparatus 80—96414
SF_6, laser-induced gas breakdown, wavelength depend. meas. of threshold 79—41895
SF_6, negative point-plane corona, electrical characts. 78—71567
SF_6, performance under mixed voltages *(German)* 77—3999
SF_6, positive point-plane gap, critical press. prediction, v_c/press. characts. 78—87583
SF_6 positive-point corona phenomena, breakdown voltage/press. characts. 80—38859
SF_6-air mixture impulse discharge characteristics of 30 cm gaps 78—67572
SF_6-gas mixtures 79—37438
SF_6-He(N_2)(CO_2), AC particle initiated breakdown, compressed gas mixture 78—87556
SF_6-N_2 mixture, discharge inception voltages, calc. 79—68966
SF_6-N_2 mixture in rod-plane gaps, static field breakdown 79—68965
SF_6-N_2 mixtures, effective ionisation coeff. and static breakdown voltage meas. 80—19549
UF_6+H_2, laser induced dielectric breakdown obs. 77—28992
Xe anode-directed streamer propagation simulation 78—67591
Xe lamp, pulsed, effect of gas heat capacity on characts. 78—42838
Xe, laser induced gas breakdown threshold at 1.06 micron 80—28594
Xe, streamer breakdown parameters 77—80388
XeCl discharge, KrF laser induced preionization 80—84020

electric breakdown of liquids
bubble creation in high elec. field, explained in terms of struct. 79—91370
bubbles behaviour obs. 80—71313
cryogenic liquid, dielectric breakdown 80—40051
dielectric breakdown influence of US excitation 80—15964
dielectric fluid, electro-dielectrophoretic forces acting on spherical impurity particles, analytical evaluation 78—88641
dielectric liquid high field carrier transport, electron multiplication and breakdown, mol. struct. depend. 80—84694
dielectric liquids, cond. and breakdown, conf., Mont-Saint-Aignan, France (July 1978) 79—91354

electric breakdown of liquids continued
dielectric liquids, corona light emission 77—8508
dielectric liquids, ion mobility meas. and breakdown process, optical methods 80—84692
dielectric liquids, prebreakdown phenomena in sphere-sphere electrode configurations 77—85647
dielectric liquids, qualitative model of elec. breakdown process, effects of external field 80—84693
dielectric tracking, in liq. He, supercond. magnet coolant 78—92022
dielectrics, magnetic field effect on breakdown voltage 79—42894
dimethyl silicone oil, laser-induced breakdown mechanism *(Japanese)* 77—43935
dynamics, parallel electrode expts. on liquid hydrocarbons 80—15962
electrical dispersion in different gaseous environments 78—88254
electrolytes, magnetic field influence obs. *(Russian)* 78—11521
electrostatically rechargeable liquids, max. discharge energy estimate *(German)* 80—38737
fluorocarbon, breakdown characts., comparison with hydrocarbon liqs. 79—91361
fluorocarbon liquid prebreakdown light emission obs. 80—15963
hexane, electric breakdown strength of vapour and liq., behaviour in critical region 77—47285
n-hexane, impurity particle motion, under DC and AC conditions, expt. results and computer simulation 78—88642
n-hexane, prebreakdown events, divergent field study 79—91371
high field conduction and breakdown in dielectric liquids 79—91355
high speed photography expts., breakdown mechanism obs. 79—91367
high-field conduction and breakdown in dielectric liquids, anal. 77—8506
high-field electron transport *(Japanese)* 78—2495
hydrocarbon, breakdown characts., comparison with fluorocarbon liqs. 79—91361
hydrocarbon liquids, elec. cond. at fields up to breakdown strength, crit. review 77—80787
hydrocarbons, electric breakdown, light emission investigation 80—93241
hydrocarbons, high speed laser schlieren techniques 78—15093
hydrocarbons, high-field carrier transport at pre-breakdown and breakdown regions 80—25305
hydrocarbons, liq., dynamics of elec. breakdown 78—88253
hydrocarbons, liquid, high-speed schlieren studies of elec. breakdown 77—89332
hydrocarbons, streamer breakdown in divergent field 80—25308
inelastic electron interactions in liq. dielec. obs. using FEM and energy analyser 79—91369
insulating liquid, bubble injection and elec. induced hydrostatic press. 77—81055
insulating liquid, electronic processes in elec. breakdown, streamer growth 77—89333
insulating oil, breakdown in long gaps, impurity effects 79—91359
insulating oils at solid-liquid interface with EHD motion, expt. 77—76226
insulators, initiation and propagation *(Japanese)* 79—19837
laser induced breakdown 77—81056
laser-induced breakdown, expt. results for various liqs. 79—91363
liquid dielectrics, electrical conductivity and breakdown, liquid impurity effects 80—11340
mechanical perturbation effects, theory and expt. 79—91366
mineral oil, apparent zero-gap breakdown voltage, surface oxide film effects 77—28519
mineral oil, breakdown voltage, live electrode polarity depend. for non-uniform field 78—75450
mineral oil, electrical breakdown under uniform fields 77—80387
mineral oil in large gaps, electric strength study 79—38452
n-hexane, chemically pure, influence of electrode material on time lag *(Russian)* 80—50265
organic liquids, polarity effect on breakdown voltage, comment on hyperconjugation 77—76229
organic purified dielectric liquids, expt. 78—84523
perfluoro-trans-4-methyl 2 pentene, liq. breakdown characts. *(Japanese)* 79—82925
polarity effect on breakdown voltage in inhomogeneous field 77—52018
polybutene oil, direct voltage elec. strength 79—91360
polymeric dielectric materials exposed to partial discharges, degradation product anal. 79—4765
prebreakdown events in liquid dielectrics, optical studies 77—20797
pulsed breakdown, interferomatic obs. 80—80696
silicon fluids, positive discharge propag., rel. to transformer oil 80—88926
silicon oil, behaviour under HV stress 79—91368
silicone fluid, discharge propag. 79—91362
transformer oil, influence of electrode material on time lag *(Russian)* 80—50265
transformer oil, optical obs. of pre-breakdown and breakdown 77—80386
transformer oil, positive discharge propag., rel. to silicone fluids 80—88926
trifluorotrichloroethane, liq., as insulating material and coolant, dielectric strength, HVDC convertor appl. *(German)* 77—76218
underwater arc, prebreakdown stage, energy characts. 78—5978
US effects on liquid dielectric breakdown characts. *(Korean)* 77—90101
water, electrical breakdown in μs regime with Cu, brass, steel and Al electrodes 80—103917
water, for applied electric fields in range 200-500 kV/cm in the 2-10 microsecond time domain 80—71316
water, obs. of prebreakdown during electrohydraulic forming *(Japanese)* 77—24977
water of increased conductivity, prebreakdown stage fundamental characts., calc. *(Russian)* 80—49019
Ar, cryogenic liquid, elec. breakdown, time lag 80—29684
Ar, high-field carrier transport at pre-breakdown and breakdown regions 80—25305
Ar, statistical and formative time lags 79—91364
D_2O laser induced breakdown, comparison with H_2O 78—68453
D_2O, single 1.06 μm picosecond pulse superbroadening, concurrence with dielec. breakdown 79—86223
H_2O, distilled, influence of electrode material on time lag *(Russian)* 80—50265
H_2O, laser induced breakdown, comparison with D_2O 78—68453
H_2O, pulsed elec. field applied to sharp point, prebreakdown field 80—6308
H_2O, short pulse strength investigation 78—9897
H_2O, single 1.06 μm picosecond pulse superbroadening, concurrence with dielec. breakdown 79—86223

electric breakdown of liquids continued
He, dielectric breakdown across epoxy insulation 78—62658
He, electrical strength, breakdown voltage depend. on electrode configuration 80—7293
He, high-field carrier transport at pre-breakdown and breakdown regions 80—25305
He, liquid, dielec. breakdown voltages, anomalous polarity effect 80—2695
He, statistical and formative time lags 79—91364
He, supercritical, dielec. breakdown 79—65796
KNO_3, aq. solns., laser induced breakdown 79—87530
KOH, aq. solns., laser induced breakdown 79—87530
N_2, breakdown by field induced microbubbles 79—91365
N_2, breakdown strength, in mm gap range, press. effects 79—91357
N_2, cryogenic liquid, elec. breakdown, time lag 80—29684
N_2, dielec. breakdown, press. depend. of polarity effect 80—75936
N_2, dielectric breakdown, using discharge figures 80—11338
N_2, discharge development in nonuniform elec. field 79—91358
N_2 electric strength determination 79—38451
N_2, high-field carrier transport at pre-breakdown and breakdown regions 80—25305
N_2, insulation characts. at cryogenic temps., polymer films 78—1920
N_2, liquefied, prebreakdown mechanism, intermittent electron emission obs. 77—32325
N_2, statistical and formative time lags 79—91364
NaCl(I), aq. solns., laser induced breakdown 79—87530

electric breakdown of solids
see also impact ionisation; partial discharges; Zener effect
alkali halide, DC breakdown strength at room temp., calc. 79—24260
alkali halide, X-irrad., elec. breakdown, temp. and F-centre conc. depend. *(Russian)* 77—8504
alkali halide crystal, activator centres, excited state transitions, bleaching dynamics 79—4527
alkali halide crystals, optical breakdown, role of colloidal particles 80—50270
alkali halides, laser induced breakdown, 10.6 μm, reproducibility 77—62023
alkali halides, laser induced damage *(Russian)* 79—43070
alkali halides, optical breakdown, 1.06 to 0.172 μm 78—35089
alkali halides, optical breakdown, damage threshold calcs. 79—95708
alkali metal halide optical breakdown, multiphoton carrier generation theory 79—19953
alumina film, anodic, 200-2500 Å thick 77—1637
aromatic copolyesters, charge storage props., electret stability 80—7277
avalanche ionisation, multiphoton ionis. *(Russian)* 79—51906
barrier oxide films, elec. breakdowns, theory 78—11391
cast-epoxy resins, AC breakdown-voltage characts. *(Japanese)* 80—88927
composite insulation breakdown under AC and impulse voltages 78—23398
corona charged insulating film high-field conduction and breakdown 80—15975
cross-linked polyethylene insulator breakdown by treeing *(Korean)* 79—91353
current runaway in insulators affected by impact ionisation and drift 78—39501
diamond, dielec. breakdown, two-photon absorpt. and other optical damage mechanisms 78—84684
dielectric, criterion for breakdown by single light pulse *(Russian)* 77—12311
dielectric, in vacuum, surface breakdown 78—64321
dielectric, surface vac. breakdown by ultrasoft X-rays 80—43989
dielectric materials, spacecraft, charging and discharging 80—71315
dielectric solids, electric breakdown 80—66111
dielectric surface, photoinduced surface discharge 80—88929
dielectric-gas interface, initiation of low threshold breakdown 79—68900
dielectrics, electric breakdown mechanism, discharge development, electron impact ionisation 80—15961
dielectrics, electron multiplication, phonon scatt., ionisation rate calcs., Markov processes 80—50267
dielectrics, inhomogeneous, model 80—50268
dielectrics, thermal breakdown, theory 80—75938
discharge breakdown, mechanism determ. in solid dielectrics using scanning electron microscope 77—85649
donors with excited states, non-equilibrium phenomena, theory of kinetics of electron transitions 78—79961
electret discharge model, injection relaxation mechanism, space-charge cond. 78—80279
electret discharge model 80—88908
electret discharge model 80—88909
electrode erosion in pulse discharge breakdown of multiple medium *(Russian)* 79—95707
electron and ion beam generation at high power, review 80—13988
electrostatic forces effect on vacuum breakdown 79—56724
epoxy polymers, unfilled and filled effect of specimen size on elec. strength expt. 77—8505
epoxy resin, electroluminesc. 78—56522
epoxy resin, partial discharge initiation phase, effects of field strength, temp. and internal mech. stresses *(German)* 78—72461
epoxy resins, phenomena and mechanisms of tree inception 80—29687
epoxy treeing breakdown, slit model 80—15970
ethylene propylene rubber, effect of electrode profile on dielec. breakdown voltage, epoxy resin insulation system 80—60502
excitonic insulator, tunnel breakdown theory *(Russian)* 80—29686
ferrite, surface metallisation via elec. discharges 77—77626
film, breakdown mechanisms 78—76385
films, breakdown voltage and self-healing effects mag. method 79—87388
gaseous model, macroscopic channel development in strong elec. field, tree growth and return streamer 80—84696
glass, ZhS-12 type, optical discharge, dynamics and props. 79—61471
hexatriacontane, single crystal, elec. props. *(Japanese)* 79—51592
hexatriacontane single cryst., elec. cond. and dielec. breakdown 80—6849
hexatriacontane single cryst., temp. depend. of dielec. breakdown 79—51905
high field conduction and breakdown in solid dielectrics, review 80—84691
ice and ice-silica compound system, electrical breakdown at cryogenic temps. 80—45007
III-V semiconductor, avalanche breakdown voltage for p-n junction, calc. 78—88020

electric breakdown of solids continued
insulating film, electrical breakdown by impact ionisation, models 79—91373
insulating film, statistical analysis 78—2603
insulating solid, elec. strength and degradation 78—83631
insulator, transparent, laser breakdown, acoustic characts. 80—50269
insulator, transparent absorpt. wave struct. associated with optical breakdown 78—68581
insulator flashover in HV vacuum transmission line, mag. effects 77—24236
insulators, detection of US emission prior to breakdown 80—88924
insulators, initiation and propagation *(Japanese)* 79—19837
insulators, prebreakdown phenomena, freq. dependent dielectric losses 80—45006
intense electric fields, tree-shaped phenomena in solid insulating materials *(Rumanian)* 80—63885
IR-optical material surface breakdown, adsorbed water evaporation model 80—35020
Kapton H, discharge area scaling and surface/subsurface damage due to electron beam irrad. 80—34853
laser damage, spot size and pulse duration depend. 77—61995
laser pulse produced breakdown, SHG increase evidence for large carrier conc. 80—102769
many-valley semiconductor, breakdown criteria 78—19046
metal powder direct resistance sintering, electric circuit components, breakdown voltage *(Ukrainian)* 77—70018
metal-dielectric-semiconductor structure, ponderomotive force effect on dielec. breakdown 79—15230
mica, pulse electric breakdown under pressure, lamination effects 80—66110
MOS capacitor breakdown voltage *(Rumanian)* 79—51677
MOS structure, electron trapping region to improve performance 78—19150
multilayer dielectric coatings, radiation breakdown and microinhomogeneities 80—7294
Mylar, discharge area scaling and surface/subsurface damage due to electron beam irrad. 80—34853
numerical method for computing the electrical stress in dielectrics 79—4767
nylon-6, ns breakdown voltage, polarity effect, mechanism 77—63367
one-sided abrupt junctions, distinction between avalanche and tunnelling breakdown 78—56211
optical glass irrad. with quasi-CW laser pulse, obs. of absorpt. waves 79—89952
p-n junction, planar, junction breakdown walkout exam. 78—60199
p-n junction microplasma, breakdown voltage 78—47854
paper, non-impregnated, non-destructive breakdowns 80—55035
Perspex, breakdown by treeing 78—84526
Perspex, dielec. breakdown and space charge, treeing 78—27160
photography of pre-breakdown luminescence in dielectrics, intensification of underexposed images 77—24793
physical basis dielec. localisation and memory track 80—88925
piezoceramic, statically compressed layer, electrical energy of instantaneous discharges *(Russian)* 78—39503
planar junction, oxide thickness and breakdown voltage relationship 79—99608
plasma jet formation *(Russian)* 78—22524
plastic insulation, of HV and MV cables, distribution law parameters estimation *(French)* 77—24794
Plexiglas, spark energy balance 79—23474
PMMA:butlacrylate, breakdown threshold to ns IR laser pulses *(Russian)* 77—81179
PMMA, immersion in high press. gaseous media, breakdown characts. for direct voltages with ripple 80—45009
PMMA, ns breakdown voltage polarity effect, mechanism 77—63367
PMMA, pulsed dielectric breakdown, mech. stress photoelasticity obs. *(Russian)* 78—2800
PMMA, thermochem. instability at Pt sphere inclusions caused by CW laser beam 80—29689
PMMA, treeing effects on electric breakdown *(Korean)* 77—81053
PMMA glass, electron bombard. induced elec. discharge, electromech. effects *(Russian)* 77—32324
pnp switching transistors, anomalous breakdown regions, laser scanning obs. 80—34854
polycaprolactam film, subjected to 9 kV elec. discharge, X-ray obs. *(Russian)* 79—23536
polycaprolactam film, temperature-time dependence *(Russian)* 78—76386
polyetheylene, charge carrier trapping phenomena *(Korean)* 77—89773
polyethylene:$Br_2(I_2)$, films, electron-beam induced carrier mobility and elec. breakdown 80—80429
polyethylene:NaCl, internal field strength, Raman spectra obs. 80—40061
polyethylene, accumulated charge profile during fast electron irradiations 77—4600
polyethylene, artificial voids, partial discharge charact. *(German)* 78—92023
polyethylene, cable grade crosslinked, effect of electrode profile on dielec. breakdown voltage, epoxy resin insulation system 80—60502
polyethylene, charact. *(Korean)* 78—2799
polyethylene, DC partial discharge and current 78—43790
polyethylene, DC treeing breakdown with space charge formation, expt. 77—24789
polyethylene, dielectric props., investigation for morphology changes created by mechanical drawing and annealing 80—84697
polyethylene, elec. empulse breakdown strength, rel. to rate of drawing 80—15960
polyethylene, elec. trees free radical ESR study 78—60393
polyethylene, electrical tree growth anal. using simultaneous meas. of light intensity and partial discharges 80—45008
polyethylene, electron beam crosslinking process for high voltage power cable 80—66846
polyethylene, halogen-doped, carrier transport and breakdown characteristics *(Japanese)* 80—96889
polyethylene, high field cond. current and elec. breakdown 77—76835
polyethylene, low density, water tree growth under DC voltage stress, expt. 77—77148
polyethylene, low-density in nonuniform AC fields, influence of temperature obs. *(German)* 80—29685
polyethylene, ns breakdown voltage, polarity effect, mechanism 77—63367

electric breakdown of solids continued
polyethylene, space charge effect on local electric breakdown 77—69773
polyethylene, tree initiation by DC and impulse voltage appl., expt. 77—24790
polyethylene, tree initiation under impulse voltage, effect of needle electrode materials 77—73112
polyethylene, treeing at 77K, expt. 77—24792
polyethylene, voltage-induced charge transfer and its effects on tree initiation 80—25307
polyethylene 50 Hz tree propagation between needle electrodes 80—15968
polyethylene and ethylene-vinyl acetate copolymer dielectric breakdown 80—15966
polyethylene cables carrying DC current, TSC and space charge effects *(French)* 80—40042
polyethylene film, dielec. breakdown sites 80—50266
polyethylene film, directional effect of impulse breakdown strength 77—20796
polyethylene film, drawn, dielec. breakdown and morphological struct., dichroic ratio 80—25813
polyethylene film, elongated, elec. impulse breakdown strength temp. depend. 20 to 80°C 77—73113
polyethylene film, partial discharge degradation, effect of discharge products in air *(Japanese)* 77—69774
polyethylene film, quenching effect 77—73114
polyethylene life test needle electrode selection 80—15969
polyethylene terephthalate film, nonlinear elec. cond. and space-charge effect 77—39980
polyethylene terephthalate polymer insulator, conduction and breakdown mechanism *(German)* 80—100469
polyethylene thin film, partial discharges energy content effect on breakdown *(German)* 77—81052
polyethylene treeing inception voltage, effect of blending and crosslinking 78—43788
polyimide film, in high-temperature region 78—84522
polymer, dielec. breakdown theories, mol. and morphological features rel. to elec. strength, review *(Japanese)* 80—60501
polymer, dielectric breakdown, DC trees caused by space charge accumulation, carrier injection and trapping effects 80—84695
polymer breakdown plasma analysis, mass-spectrometric installation 78—88670
polymer film, glow discharge polymerised, conditions for attaining perfect self-healing breakdown 80—20590
polymer film, partial discharges, HNO_3 absorption, expt. *(German)* 77—77147
polymer treeing resistance assessment 80—15971
polymeric, insulating materials, partial discharges, simulation and meas. *(German)* 77—77146
polymeric dielectric materials exposed to partial discharges, degradation product anal. 79—4765
polymeric insulating materials, water treeing initiation and growth, effects on cable service life 80—84698
polymers, elec. props. and morphology, correl. review 78—43786
polymers, space charge behaviour and luminescence at 77K 79—99947
polymers, streamer breakdown in divergent field 80—25308
polymers, tree initiation mechanism 77—24791
polystyrene:$Br_2(I_2)$, films, electron-beam induced carrier mobility and elec. breakdown 80—80429
polystyrene, halogen-doped, carrier transport and breakdown characteristics *(Japanese)* 80—96889
polystyrene, ns breakdown voltage, polarity effect, mechanism 77—63367
polystyrene, plasticizer effect on electric strength 80—29688
polystyrene film, glow discharge polymerised, conditions for attaining perfect self-healing breakdown 80—20590
polystyrene foils, breakdown-charged, surface charge densities and depths, TSC spectra 80—7260
polyvinylidene fluoride, dielec. breakdown and elec. cond., room temp. to 150°C 80—60500
PTFE, ns breakdown voltage, polarity effect, mechanism 77—63367
pulsed surface flashover mechanism involving electron-stimulated desorption 80—70055
PVC, ns breakdown voltage, polarity effect, mechanism 77—63367
PVC films, temperature-time dependence *(Russian)* 78—76386
quartz, fused, picosecond-pulse optical breakdown direct obs. of dynamics 78—6629
quartz, fused and cryst., laser pulse breakdown freq. depend., self-focusing elimination 77—55855
quartz glass, optical breakdown by sharply focused laser beam 79—69776
refractory oxide optical coatings, laser damage resist., spectral depend. 77—62022
secondary breakdown, microplasma effect *(Russian)* 79—56722
semiconducting plate, optical thermal breakdown, laser hysteresis 79—56889
semiconductor, optical thermal breakdown, fluctuations and wave processes 80—20587
semiconductor, secondary breakdown, hydrodynamic instability model *(Russian)* 78—43407
semiconductor devices, breakdown voltage, temp. effects 79—7882
semiconductors, effect of freq. on applied voltage 80—75592
sliding discharge, guided, explosive emission phenomena 80—19649
solid dielectrics, treeing 78—80285
statistical test of solid dielectrics in pulse irradiation regime 78—95548
stator windings, failure mechanisms under thermal cycling *(Japanese)* 80—104189
styrene films, glow discharge polymerized, self-healing breakdown 79—91374
surface discharge initiated breakdown, in high pressure gaseous mixtures 78—48117
surface impact on transparent dielectric, shock wave dissipation from imperfections 79—69925
Teflon FEP, discharge area scaling and surface/subsurface damage due to electron beam irrad. 80—34853
Teflon FEP, negative streamer development, computational model for electron irrad. dielec. 80—34852
transparent dielectric, absorpt. of laser radiation by defects in surface layer *(Russian)* 80—25497
transparent dielectric, laser damage, appl. of gas breakdown model 77—63496
transparent dielectric destruction by laser radiation, review 77—50702

electric breakdown of solids continued
transparent dielectric optical breakdown, thermal instability *(Russian)* 77—55854
transparent dielectric with metallic inclusions, light pulse shape effect on optical breakdown threshold 80—20588
transparent dielectrics, laser damage, electron avalanche and multiphoton ionisation roles 80—35016
transparent polymers, laser-induced optical breakdown, chem. reactions effects *(Russian)* 78—35676
transparent solids, role of thermal stresses in optical breakdown *(Russian)* 78—95547
treeing in organic insulating materials, tutorial 78—84524
treeing in solid extruded electrical insulation, bibliography 77—24788
Weibull distribution analysis, parameter estimation, dielectric life tests 77—77149
ALF_3, evaporated layers DC props. and α-particle scatt. 78—14845
AgN_3, dielec. breakdown by elec. induced chem. decomposition 80—20586
Al foil, elec. explosion, dielec. breakdown 78—67388
Al, foil, elec. explosion, immersion medium effects 78—67389
Al-CdSe-Ag dry air stabilised struct., elec. cond. mechanism, breakdown phenomena 80—34527
Al-Si_3N_4-Si, electrical strength effect of struct. defects in Si_3N_4 *(Russian)* 78—26955
$Al_xGa_{1-x}As$ native oxide, low leakage, MOS characterisation 78—91795
Al_2O_3, anodic oxide films, luminesc., breakdown and colouring 78—19528
Al_2O_3, anodic oxide films on superpure Al, growth kinetics and UV radiation effect, breakdown voltage 79—34190
Al_2O_3 composite films, elec. instability 78—68452
Al_2O_3, DC reactively sputtered, in MIS structs. optical and elec. props. 79—19486
Al_2O_3, dielec. breakdown mechanism determ. acoustic signature anal. techniques 80—11337
Al_2O_3, elec. breakdown during anodic growth 80—55034
Al_2O_3, film, CVD on Si, chem., phys. and elec. props. 77—12543
Al_2O_3 insulators, surface treatment with Mn-Ti, effect on voltage-holdoff in vacuum 79—24261
Al_2O_3 plasma anodised film on Si, breakdown strength 80—7722
Al_2O_3-BaO-SiO_2 glass coatings in fission and fusion reactors, permeation, elec. cond. and dielectric breakdown 80—18439
Al_2O_3-P_2O_5 glass, electron bombard. induced elec. discharge, electromech. effects *(Russian)* 77—32324
B_2O_3-SiO_2 glasses, phase separated, DC cond. and elec. breakdown 78—23400
$BaTiO_3$ ceramic, degradation under high AC elec. field 80—60499
$BaTiO_3$ films, ferroelec., effect of elec. field on dielec. props. 79—33642
$BaTiO_3$, single cryst., dielec. breakdown and electroluminesc. 78—2917
BeO, dielec. breakdown mechanism determ. acoustic signature anal. techniques 80—11337
Bi_2O_3 anodic film form. on Bi, electric breakdown 79—20377
Bi_2O_3 film, dielec. meas. 80—2696
CaF_2, picosecond laser-induced breakdown at 5321 and 3547 Å, freq. depend. 77—63495
CoO film, Poole Frenkel effect and elec. breakdown props. 77—85364
CoO film on thermally aged Co hardened Au, mech. film breakdown and ESCA, expt. 77—4436
Cr electrodes, arcing and breakdown meas. in vacuum 77—24238
Cu, cathode, ns voltage pulse breakdown of emitting sites, field emission microscopy obs. *(German)* 77—63547
Cu foil, elec. explosion, dielec. breakdown 78—67388
Cu, with Al_2O_3 inclusions, breakdown and emission props., effect of inclusions 79—87389
GaAs, laser-induced bulk breakdown and free carrier generation, photocond. meas. 80—35018
GaAs, oxide, charge density and breakdown voltage, depend. on annealing 79—66189
GaAs thermal oxide film, fabrication and characterisation 80—11808
Ge, epitaxial-diffusion p-n junction, inductive props. in secondary breakdown 80—15598
n-Ge, impurity breakdown field, temp. depend. 79—24263
Ge, impurity breakdown field increase due to strong compensation 80—20204
Ge, laser-induced bulk breakdown and free carrier generation, photocond. meas. 80—35018
n-Ge, many-valley semicond., elec. breakdown criteria 78—19046
Ge, p-n junction, I-V curve for microplasma breakdown, at. size difference effect 78—2550
p-Ge-n-GaAs diode, microplasma breakdown 79—91140
GeO_2, film, optical and electrophysical props. *(Russian)* 77—85821
KBr whiskers, electric breakdown mechanism 79—28679
KCl laser-induced breakdown fields rel. to wavelength and focal spot radius 80—35019
KCl, optical breakdown, γ-irrad. effects, rel. to appl. in high power lasers 77—8507
KCl, optical breakdown from 0.53-10.6 μm 80—7292
KCl, spark channel, plasma light absorpt. coeffs. 79—7501
KH_2PO_4, picosecond laser induced breakdown at 5321 and 3547 Å, freq. depend. 77—63495
LiF, picosecond laser-induced breakdown at 5321 and 3547 Å, freq. depend. 77—63495
LiF, pulsed dielectric breakdown, mech. stress photoelasticity obs. *(Russian)* 78—2800
$LiNbO_3$, light emission from surface on heating or cooling 78—64416
$LiNbO_3$, spontaneous elec. breakdown 77—66458
$LiNbO_3$:Fe, photorefr., surface recombination 79—56759
$LiTaO_3$, spontaneous elec. breakdown 77—66458
MgO, defect aggregation and thermal-electric breakdown, TEM obs. 79—42069
MgO, elec. field effects on cond. above 1300K, elec. breakdown 79—42551
Mo cathode, ns voltage pulse breakdown of emitting sites, field emission microscopy obs. *(German)* 77—63547
$MoSi_2$ oxide film, dielec. props. and growth kinetics 80—81215
NaCl, laser damage simulation, optical breakdown probability at 6943 Å 77—12470
NaCl laser-induced breakdown fields rel. to wavelength and focal spot radius 80—35019
NaCl, optical breakdown from 0.53-10.6 μm 80—7292
NaCl, optical strength, effect of irrad. in mechanically stressed state 80—80695

electric breakdown of solids continued
NaCl, picosecond laser-induced breakdown at 5321 and 3547 Å, freq. depend. 77−63495
NaCl, pulsed dielectric breakdown, mech. stress photoelasticity obs. *(Russian)* 78−2800
NaF_2, picosecond laser-induced breakdown at 5321 and 3547 Å, freq. depend. 77−63495
Nb_2O_5 amorphous films, switching phenomena and dielec. breakdown 77−24594
Nb_2O_5, polycryst. film, switching processes, dielec. breakdown 77−39981
Ni, anode, oxide growth, effect on breakdown voltage and efficiency 79−4766
Ni-Nichrome, MOM diode, breakdown effect in visible and near-IR regions 80−6999
NiO films, on Ni (100) electrodes, oxide defect sites role in breakdown 79−43587
PLZT, Sn substituted, antiferroelectric ceramics research and their applications *(Chinese)* 79−33617
PbN_x, pressed, lag time of breakdown and dielec. strength 77−36174
$PbO-SiO_2$ glasses, charge trapping and dielec. breakdown, radiation-induced, microphase separation 78−23399
$Pb(Zr,Ti)O_3$ ceramics, shock depoling, pulse charging of nanofarad capacitors 79−42913
Pt-n-GaAs Schottky diode, microplasma breakdown 79−91140
RbCl films, breakdown on appl. of electric voltage pulses 80−66109
Si, laser-induced bulk breakdown and free carrier generation, photocond. meas. 80−35018
Si oxide film, porous Si layer oxidation, dielec. props. 80−55556
Si p-n junction, subnanosec. current drops in delayed breakdown 80−75633
Si p-n junction, subnanosec. current drops in delayed breakdown 80−75634
Si p-n junction, unified approach to breakdown phenomena 79−42630
Si, p-n junctions, neutron transmutation doping, breakdown process 80−15600
Si p-n junctions, secondary breakdown, pre-mesoplasma state expsn. *(Russian)* 79−56723
Si planar semiconductor junctions, disruptive voltage calc., ionisation coeff. *(Rumanian)* 80−103746
$Si-SiO_2$ interface, electron injection into oxide due to mobile ion induced internal field 77−15963
$Si-SiO_2$ MOS capacitors, two-dimens. calc. of avalanche breakdown voltage 80−11096
$Si-SiO_2$ structures, scanning analyser of electrophysical parameters of MOS transistors *(Polish)* 79−91145
$Si-SiO_2$-polycryst. Si structs., field strength degradation exam. 77−4445
Si_3N_4, conditions for thermal current runaway and breakdown 77−43760
SiO thin film, elec. breakdown voltage vs. thickness 78−2602
SiO_2, dielectric breakdown, impact ionisation-recombination model 78−6633
SiO_2 film, dielectric breakdown and I-V characteristics 77−63368
SiO_2 film, effect of oxidation on dielec. strength 77−16249
SiO_2 film, electric strength in MOS structures obs., under unidirectional, laternating and combined voltages *(Slovak)* 78−88034
SiO_2 film, from oxidation, in dry O_2 and H_2O ambients, initial oxidation regime obs. 79−29240
SiO_2 layers, dielectric strength, dislocation effect 78−31154
SiO_2 layers, room temp. transforms induced by diethyl ether vapour 79−99456
SiO_2 on Si, thermally grown, breakdown, review 78−23172
SiO_2, picosecond laser induced breakdown at 5321 and 3547 Å, freq. depend. 77−63495
SiO_2, surface pot. during ion implantation 80−19826
SiO_2, thermal, elec. stressed film, dielec. breakdown 78−64322
SiO_2 thermally-grown, highly stressed ultrathin films, cond. and trapped of electrons 77−66216
SiO_2 thin film, elec. breakdown voltage vs. thickness 78−2602
SiO_2 thin film capacitors using polycrystalline Si and Al electrodes, dielec. breakdown 79−69600
SiO_2, uniform film prep. by pyrolysis of tetraethoxysilane 77−40379
SnO_2 coated glass, surface elec. breakdown 80−25303
Ta_2O_5, elec. breakdown during anodic growth 80−55033
Ta_2O_5 film, for MIS device, CVD and characterisation 77−4742
Ta_2O_5, reactive DC sputtering deposited films with magnetron-plasmatron, mechanical elec., optical props. 80−25566
Ti, anodic oxidation under high voltage, porous layers *(French)* 80−54574
TiO_2, reactive DC sputtering deposited films with magnetron-plasmatron, mechanical elec., optical props. 80−25566
Tm_2O_3 film, between Al electrodes, prep. and elec. props. 80−60103
Tm_2O_3 film, electron beam deposition, elec. props., and struct. 79−87580
VO_2, thermal mechanism of switching effect 77−15919
W-Ni, MOM diode, breakdown effect in visible and near-IR regions 80−6999
Y_2O_3 film in $Y-Y_2O_3$-Au junction, defect struct. and local conduction 78−26970
Yb_2O_3 film, amorphous, electron beam deposited, dielec. props. 79−91339
ZnO ceramic varistors, thermal breakdown 80−88928
ZnO piezoelectric film US transducers obtained by DC diode sputtering, dielec. breakdown props. 80−40066
ZnO varistors, statistics and grain size effects on breakdown characts. 80−34010
ZnO-based ceramic varistors, current-voltage characts., leakage and breakdown regions, 100 to 1300°C 79−56231
$ZnO-Bi_2O_3$, heterojunction, current-voltage characts. 79−56291
ZnS, current and refractive index oscills. in electric fields due to barrier instability 79−91372
$ZnS-MgF_2(SrF_2)$, dielec. films, transparent, microscopic inhomogeneities and optical breakdown 78−10844
ZnSe:In, highly compensated single crystals, thermally initiated current breakdown, current-voltage characts. 80−65579

electric cables *see cables (electric)*

electric capacity *see capacitance*

electric cells *see cells (electric)*

electric charge
see also space charge
aerosol, charge deposition on charged particles of arbitrary shape 78−3386

electric charge continued
aerosol, polydispersity, unipolar charging, charging mobility analysis 78−61059
aerosol, unipolar diffusion charging, particle dielectric constant and ion mobility effects 78−61058
aerosol particle, nonequilib. bipolar charging 78−3382
aerosol particle-small ion combination coeffs., size depend. 77−25320
arbitrary-shaped surface charge distrib., determination using numerical procedure 79−89825
bodies, electrical charging by removal of charged particles by hydrodynamic flow *(Russian)* 78−9292
capacitor, charge difference phenomena *(German)* 79−36810
carnauba wax electret, electric charge studied by TSC *(Japanese)* 78−6626
conducting body charge distrib. computation *(Polish)* 78−78850
conductor, elastic strain state, contact phenomena effects *(Russian)* 78−9564
contact charge density, true meas. using soft rubber 78−43462
cosmic systems charge polarisation, appl. to stars and universe 79−48771
cosmology of charged universe 79−25766
cryogenic liquids, technique for producing uniformly charged drops 77−49733
differential photoelectric charging of nonconducting surfaces in space 79−25439
double layer, aqueous, at charged plane interface, theories comparison 79−34317
droplet, EHD produced, specific charge and size 79−32696
droplet generated by disruption of large charged drop, specific charge 77−40580
drops prod. in electric spraying of liqs., charge to mass ratio *(Japanese)* 78−17835
dust in cosmic plasma environments, electrostatic charging effects 80−26930
Echo IV electron beam-emitting rocket, neutral N_2 cloud effect on elec. charging in ionosphere 79−75017
EHD flow, nonstationary, with charge diffusion, nonlinear and linear wave processes 80−59124
electrets, meas. of charge distrib. 77−30184
electrets in plastic films *(German)* 80−75920
equivalence charge concept, appl. to electrostatic energy of charges and multipoles 79−18323
ferroelectric, interaction energy between a charge and domain wall 80−88939
fibre charging in electroflocculation, expt. *(Russian)* 79−83515
flotation of fine particles, effects of size and charge 77−16865
force exerted when immersed in polarised nonconducting dielec. fluid 78−78872
fractional charge, $^1/_3$e, expt. determ. on Nb sphere 79−21694
fractional charge on matter, obs. by mag. levitation of Nb spheres 77−49709
glass, fracture, electrical energy losses and causes, atm. humidity effect 80−55498
Hertz Quincke effect 79−36808
ink jet droplet charging, math. model 79−50184
insulating film, electric charging by X-radiation *(Japanese)* 79−61488
interface, ionic distribution function, discreteness-of-charge effects 79−100399
interface, ionic distribution function, discreteness-of-charge effects in inhomogeneous dielectrics 79−100400
interstellar charged dust grains, motion in interplanetary space 80−4300
interstellar grains, charge rel. to thermal coagulation in dense clouds 79−53872
interstellar grains, effects of radioactivity on elec. charge 77−87499
jet droplets from bursting bubbles at air/water interface, electrification and size 77−48700
lightning stepped leader, excess charge distrib. rel. to return streamer EM radiation 79−8652
Lippmann eqn., statistical mech. deriv., dielec. const. 77−20404
liquid hydrocarbon filtration, generation of charge 77−55082
lunar surface, intense local photoelectric charging in sunset terminator region 77−45330
lunar terminator, localised photoelectric supercharging with progression of sunset 77−45331
material charging in space environment 80−109327
microscopic charge and current densities in terms of polarisation and magnetisation fields 78−8251
monodisperse aerosol, uniform electrical charging 77−56256
multipole and charge distrib., appl. of Dirac δ-function 77−75356
neutron star, rotating, with strong mag. field total charge and electron cap shape 78−12265
observable phase factors and symmetry of electric and magnetic charges 78−86428
paper sheets, charge decay and resistance parameters correlation determ. 80−70795
phosphate glass, electron-irradiated, charge accumulation, comp. depend. 78−2159
PMMA, electric phenomena in process of deform. and failure, role in fracture mechanism 77−44344
polymer film electret, charge distrib., generalized model 80−6873
powder-bead mixture, triboelec. charging, incremental charge-mass characterisation 78−17833
pulmonary regional electroaerosol deposition model 79−83842
PVC nascent particles during polymerisation 79−79249
PVC nascent particles in monomer during suspension polymerisation 79−79251
quantisation of electric charge in elementary matter, generalized quaternion struct. of general relativity 78−29013
radiating particles of finite size, Dirac's subtraction formalism *(German)* 80−91740
rocket payload, charge neutralisation during electron beam emission, laboratory studies 80−77258
satellite plasma sheaths, streaming instabilities, elec. equilib., one-dimens. particle simulation 77−22036
Space Shuttle Orbiter, elec. charging calcs. 77−25860
spacecraft, charge neutralisation via electron emitter *(Japanese)* 80−94673
static electricity, charge neutralisation on moving filament *(Russian)* 79−7876
SU(2), unification of isospin and hypercharge, electroweak interactions of leptons 80−27439
surface charge 80−36331

electric charge continued
surface polarisation from sessile drop contact angle meas. 77−85365
zodiacal dust cloud, charged dust particles motion in interplanetary space 80−4299
β-active aerosol particles, stationary charge distribution 79−92581
C blacks, surface polarity, surface activity, slurry pH, oxidation effects 78−68915
He, liq., charged surface stability *(Russian)* 77−35791
KH_2PO_4, powder sample, pyrocharge temp. depend. near phase transition 79−87399
LiF, electrification of crystals by cleavage 78−60189
$NH_4H_2PO_4$, powder sample, pyrocharge temp. depend. near phase transition 79−87399
$(NH_4)_2SO_4$, powder sample, pyrocharge temp. depend. near phase transition 79−87399
O ions, energetic, in radiation belts, charge states theory 78−77427
Se, amorphous, interface with poly-N-vinyl carbazole, photoinsulator-air gas-dielectric system, charges on surfaces 79−67407
Si-SiO_2 interface charge effects and related props. 78−10575
SiO_2, surface charge, effect of doping with P+B, differing vacuum deposition conditions *(French)* 77−85286
W particles, search for fractional charge 77−74349

electric coils *see coils*

electric condensers *see capacitors*

electric conductance *see electric admittance*

electric conductance measurement *see electric admittance measurement*

electric conduction processes *see electrical conductivity*

electric conductors *see conductors (electric)*

electric connectors
see also cable jointing
9th Annual Connector Symposium, Cherry Hill (1976) 77−22577
600 MW pulsed energy convertors for toroidal field coil, design philosophy 78−58496
additive-free hard Au appls. 80−108718
Al/Cu bimetal, galvanic corrosion elimination 80−35387
BNC-JJ coaxial floating shield bakable and coolable vacuum feedthrough useful from dc to 4 GHz 78−54381
cold formed wire connector 79−88929
feedthrough for gas pressures up to 10 kbar and low temps. 80−31787
fibre-optic interconnection advantages over conventional cabling 78−9442
free-moving mouse EEG recording and drug infusion technique 79−57831
fusion reactor magnet coil, 125 kG, 1 m, design, fabrication 78−55008
hardness and ductility 79−87025
hot filament connection 79−63273
hybrid fibre optic/electrical connector, environmentally sealed, multispin, cylindrical 79−41457
inlet for elec. conductor into high-pressure chamber 78−74016
lead-ins with composite seal for high pressure chambers 80−105665
leads, detachable, for superconducting magnet 79−75557
moulding compound, glass fibre reinforced low press. diallyl phthalate, props. 78−52750
nuclear reactor connector specification, performance, design and testing 77−23233
offshore seismic exploration streamer cable connector design and programming 77−25803
plastics, for transmission media, thermomech. reliability 80−40666
solar array repair, adhesive bonding, and interconnector developments 79−96455
solar cell interconnector fatigue resistance tests 79−96457
squirrel-cage photomultiplier base design, for nanosec. fluoresc. decay meas. 77−30204
stress relaxation estimation for Cu alloys and plastics, expts. 77−21206
student laboratory apparatus, crocodile clips and single sockets 77−61086
ultrahigh vacuum and cryogenic feedthrough, with 48 pins 79−97399
underwater electric cable terminations 78−45041
vacuum feedthrough, Burndy, bakeable 300°C quick contact 79−40582
vacuum leadthrough, heavy duty, for vapour deposition resistively heated box sources 79−40584
Cu-Ni-Sn spinodal substitute for Be-Cu alloy 80−35217
SnNi, metastable, possible underplate material for connector contacts, oxidation obs. 77−48575

electric control equipment
see also controllers; electric actuators; electric final control devices; electric sensing devices; switches; telecontrol equipment; telemetering equipment
35 mm camera control cct. for automated time-lapse photography 78−58076
above-knee prosthesis, myoelectric control system development 78−53575
bilateral shoulder disarticulated children's jaw-controlled manipulator 78−53578
CERN's 28 GeV proton synchrotron, RF system development 77−79488
electro-optic deflector using $Pb_3MgNb_2O_9$ crystal, design and adjustment 79−72690
electromagnet field control system 77−37950
electrostimulator three-mode control unit 79−20693
F-30 digital avometer, MUF-30 control module in CAMAC standard 79−88942
Large Space Telescope optimal fine pointing control using Annular Momentum Control Device 77−73934
laser beam intensity control circuit 78−9394
light control unit using logarithmic A/D convertor *(German)* 79−93117
LMFBR ML-3 Na circuit, electrical and control installations *(Spanish)* 80−57819
precision DC stabiliser based on P-136 stabiliser 78−8411
resistance furnace programmed temperature regulator 78−86256
Ritchey Chretien telescope, microprocessor control system *(German)* 79−53726
roller pump for pulsatile blood flow 78−44721
slide projector, dissolve control unit provides cross-fading and operational sequence recording 80−77833
spectral radiometer, high-speed, with full electronic control *(German)* 79−54169
splash down programmer unit for bathythermographic appl. 77−56759
thyristor controlled drive for machines for mechanical testing 77−25213
timer compatible with transistor logic and auxiliary equipment 77−67420

electric control equipment continued
two-laser frequency difference stabilisation electronic system 79−68401
video raster display control apparatus *(German)* 79−67265
vision experiments, rapid cycling dual shutter control system [for vision research] 80−41358

electric control gear *see electric control equipment*

electric current
see also arcs (electric); corona; critical currents; current density; current distribution; current fluctuations; eddy currents; electrojets; fault currents; leakage currents; short-circuit currents; sparks
Alaska oil pipeline, induced elec. currents meas. by gradient fluxgate and SQUID magnetometers 80−98231
Ampere's theorem appl. to magnetic effect of finite length line current 77−71905
Anderson-type elec. current shims for mag. field correction, role of image currents 77−49745
bipolar trickle reactors, electric current versus potential plots 80−76521
charged current loops around Kerr black holes, field and pot. 78−40988
circular electric current loop field representation of Earth's mag. field 80−12329
Comet Kohoutek (1973 XII), ionosphere current sheets rel. to HCN high speed jets 77−49332
comets, CO-rich, elec. currents rel. to struct. of ionospheres 77−29723
coronal-interplanetary space modelling, sheet-current approach 78−20807
cosmic plasmas, role of elec. currents 78−12094
current sheets, appl. to solar flares and magnetospheric substorms 77−17477
diaphragm-type electrolysis cells, current yields of alkali 79−100402
diffusion processes in rectangular conductor, equiv. time constant *(Polish)* 77−65008
equilibrium stability conditions for system of two ideal current rings *(Ukrainian)* 77−50583
ether, generation of magnetic field by electric current, Einstein early paper *(Russian)* 79−84925
heliosphere, elec. currents rel. to model of mag. field configuration 80−94670
HF surface currents excited by point source on concave perfectly conducting cylindrical boundary 79−64146
horizontal electric wire source of arbitrary length, EM fields 79−27130
ionosphere, current collection by long wire in near-Earth orbit 79−25438
ionosphere, currents distrib. rel. to polar-equatorial currents 78−93029
Jupiter magnetosphere, currents generation by Io interaction with plasma torus 80−98604
Jupiter magnetosphere, elec. currents assoc. with Io mag. flux tube, Voyager 1 obs. 80−26793
Jupiter magnetosphere, field-aligned current obs. by Pioneer 11 77−25975
lightning, current density in transmission line model with general vels. 77−33156
lightning, return stroke current and vel 79−25306
limiting current of electron in mag. field of conical electron beam 78−90348
magnetosphere, elec. currents over auroral arc 77−33296
metallic tethers in ionospheric plasma, current and pot. distrib. 78−69652
notation, positive and negative charges in electronic devices 78−12494
power transmission lines, elec. currents induced by auroral activity 79−62640
prebreakdown ionisation current spatial growth expts., initial photoelec. current changes 78−67566
solar atmosphere, current dissipation and electrostatic ion-cyclotron heating 80−51708
solar atmosphere, elec. currents as solar wind energy source 80−94768
solar corona, plasma heating by anomalous current dissipation 78−53895
solar flares, current sheet models 77−17475
solar flares, expt. on merging of two current carrying plasma columns *(Japanese)* 80−94775
solar flares nonthermal electron beams, reverse currents effects on dynamics and X-ray bremsstrahlung 80−51711
solar photosphere, elec. currents as energy source of flares 77−17483
solar quiescent prominences, elec. currents distrib. rel. to downward motions 78−20779
solar wind, thin layered field aligned currents distrib. 79−12375
solid electrolyte containing systems, electronic self-discharge currents 79−100502
space charge limited current flow in coaxial cylinders, potentials up to 15 MV 77−39477

electric current control
arc lamp current stabilisation, start control device 77−57362
automatic radiographic system and HT generator, for gastrointestinal tract exam. *(Japanese)* 79−88167
coercivity meter with automatic current setting and recording for heat treatment monitoring 77−87795
current-supply stabiliser, adjustable, for magnetic lens β spectrometers 78−74528
dental pain reliever with increased stabilisation of working current 77−48922
electron accelerator current source, dialable, with ovenless construction and ppm/h stability 77−50320
electropolishing, rectifier with thyristor current control 77−74377
electrosurgical load-independ. const. current generator 78−44684
flux pump power supply using inductive current transfer, primary current waveform control 78−12704
furnace power supply, transformerless 77−65035
glow discharge electrolysis, power supply unit, current regulator 77−39489
hot-filament device, electron current to anode stabilisation cct. 77−26341
impedance meas. equipment design *(Spanish)* 78−8421
iontophoresis device for safe elec. administration of ionised drugs 78−31965
magnet winding current regulated source based on industrial thyristor convertors 77−37921
microelectrode current and voltage clamp cct. for central nervous system neurons 78−24191
neutral beam, pulsed, arc (arc filament) power supplies, for fusion reactor 78−70637
phototransducers in tide-recording equipment, current and light output ratio stabilisation *(Russian)* 78−88949

electric current control continued
- plasma current multiplier, gas discharge device, current amplification 80—49018
- precision DC stabiliser based on P-136 stabiliser 78—8411
- pulse generator for pumping semiconductor lasers, amplitude control 77—27299
- respiration rate meter, corona discharge identification and ionisation current control *(French)* 79—92411
- semiconductor devices for generator current control and stabilization 78—21790
- semiconductor junction lasers, simultaneous feedback control of bias and modulation currents for injection lasers 80—43332
- superconducting solenoid, current regulated sweep unit 78—4659
- threshold current sensor, struct. and operational features 80—34689
- zone refiner, electron beam, improved emission current control 78—6844
- Ar laser, discharge current control using thyristor convertor 77—14747
- Ar laser power supply for discharge current and output power control 77—38912

electric current measurement
- *see also ammeters; galvanometers*
- AC, matching measurement sensing method to application 80—47072
- AC, multijunction thermal convertor, meas. errors 77—18033
- AC, precision direct meas. facility 78—49863
- AC, RMS value, use of digital multimeter *(German)* 77—5860
- AC, thermal current convertors for accurate meas. 77—18032
- AC, using magneto-optical methods, principles and advantages *(Polish)* 80—105676
- AC measurement, using digital instruments 78—93726
- AC unit, 40 Hz to 100 kHz, USSR special standard 77—30179
- AC/DC, up to 25 kA, using zero-flux current transformer 77—30177
- AF, high accuracy, using AC-DC comparator 77—18024
- ampere, absolute meas. using NMR 80—98941
- ampere absolute value improved realisation 78—93737
- ampere as standard electric current unit *(German)* 77—22574
- ampere realization and gyromag. ratio of proton meas. at NPL 80—98940
- ampere realization by means of current balance at NPL 80—105678
- ampere realization expts. at NBS 80—98938
- analogue detection device for mol. beam scatt. expts. and vel. anal. 78—33635
- arc discharge, cathode spot high current density meas., expt. 78—9879
- atmospheric conduction current, direct meas. 78—85637
- auto-zero electrometer for analytical electron beam instruments 78—12721
- automated controlled-current system, for coulometric, potentiometric and galvanostatic meas. 77—70353
- automatic range-changing amplifier, ionisation current pH and vacuum measurement appls. *(French)* 79—63262
- automotive distributor, arc initiating processes, EM radiation reduction 80—19665
- bipolar cell stacks. leakage currents 80—76526
- bipolar junction transistor, common-emitter current gain β, measurement of low values 79—63268
- calibrated current sources with direct radioactivity collection in vacuo 77—74449
- charged particle beam in range 100 μA-300 mA, magnetomodulation device 80—68993
- coaxial current shunt and resistor stack, current waveform recording in μsec region 78—21178
- contactless noncircuit-breaking method using magnetosensitive diode, 10-100 kA 78—8410
- coronasonde, balloon-borne, for thundercloud elec. field meas. 78—61577
- cryogenic current standard based on AC Josephson effect 77—82557
- current balance, modified, for elementary physics laboratory 77—67163
- current digitiser, 2×10^{-15} A to 2×10^{-10} A, ion chamber currents meas. appl. 77—61666
- current-to-frequency transducer systematic error and sensitivity threshold 77—79117
- cylindrical probe, electron current second derivative calc. algorithm 78—63594
- DC, 10^{-12} to 10^{-6} A, meter with automatic drift compensation *(Czech)* 78—883
- DC, 10^{-5} to 10^{-11} A range, portable picoammeter/teraohmmeter 79—17441
- DC and AC ammeter calibration using digital voltmeter *(Polish)* 78—45655
- DC currents, low, new system of meas. 80—82791
- DC Josephson current meas., automatic recorder 79—17444
- DC ratio standard using toroidal cryo current comparator 79—88977
- digital dynamic method for precise meas. of static characteristics 78—54389
- digital multimeter, general-purpose, design practice 77—57348
- digital multimeter, type Shch68003, with printer output, features 77—74437
- digital multimeter technology and future development 77—57345
- digital multimeters, MOS/LSI, mains/battery operated, construction and performance *(French)* 77—61090
- double constant current source for cyogenic current comparators, appls. 79—21775
- electro-optic voltage dividers, capacitor type, technique *(Italian)* 77—26339
- electrochemical measurement, microprocessor controlled potentiostat 79—85133
- electrometer/ratiometer of high sensitivity and precision 78—70154
- electrometers, high-speed general-purpose, features 77—74448
- electron beam current meas. fast response magnetic loop current monitor 79—35791
- electron beam deflection tube, circuit breaker current meas. 78—54393
- electrostatic precipitator with duct-geometry needle plate electrodes 78—16819
- Faraday cup, for laser produced plasma diagnostics 78—5941
- Faraday cup for simultaneous ion-beam current obs. and meas. 78—49865
- galvanic current meas. instrumentation, function of velocity of metal electrolyte 77—10040
- galvanomagnetic semiconductor voltage and current transducers, Gauss effect compensation 78—77892
- glow discharges, high-pressure, electro-optical meas. of current and voltage 78—37033
- HF current intensity unit, USSR state standard 78—36979

electric current measurement continued
- high current meas. instrum. using Faraday rotation effect 77—2669
- high potential circuits, contactless meas. instruments 77—26334
- high-power current pulse, precision measurement by Rogowskii loop with ferrite core 78—4639
- high-sensitivity, with modem amplifier 77—74447
- high-speed instrument for measuring small currents 79—75547
- HV electrical meas. by optical methods 78—24822
- in-circuit DC current measurement device for PCBs 77—18009
- indicator, quadrature, current and voltage, errors components determination 77—74442
- insulating materials under high elec. field, determination of complex permittivity *(French)* 80—98933
- ionisation current sources for electrometer calibration 77—79111
- iontophoresis circuit isolated current monitor for cell membrane studies 77—60311
- iontophoretic isolated current monitor for cell membranes 77—25626
- Kelvin vibrating capacitor with pot. difference amplifier for current meas. *(French)* 77—22572
- laser light measuring techniques *(Japanese)* 80—86342
- laser sensing system for elec. and mag. fields in power transmission 77—45870
- leakage currents, medical equipment safety aspects 78—11748
- lightning peak current meas. and recording device results *(Japanese)* 80—46288
- lightning stroke, automatic observation system *(Japanese)* 77—29506
- lightning stroke current meas. using optical fibre cable and optoelectronic conversion, rocket launched 78—92930
- low currents, instantaneous capacitor discharge, errors and nonlinearity 79—6142
- magnetic defectoscopes, nonsinusoidal periodic currents meas. 80—104386
- magneto-optic current measuring device using low-birefringence silicone-clad fused silica fibre 79—50425
- magneto-optic current sensing with birefringent fibres 79—75544
- maintenance, renovation and repair procedures for multimeters including Avo model 8 79—35795
- mass spectrometer, mag. scanning, ion current meas., computer controlled electronics 78—8464
- MHD generator chamber, current intensity meas. *(Polish)* 77—7602
- microchannel plate dark current meas. 79—81555
- microcoulombmeter, for accelerated ion beams meas., with mean current meas. facility *(Czech)* 77—67476
- minivoltmeter, electronic, in 10 nA range *(Spanish)* 78—54408
- molten semiconductors in strong electric fields, method of plotting volt-ampere characts. 77—87787
- MOS capacitor, TSC meas., suppression of meas. interferences from interface states and mobile ions 80—29479
- moving-coil expt. for meas. of current and EMF, vel. control technique 80—98939
- MP-Tandem at Munich, light link coupled current monitor 78—33311
- multijunction thermal convectors for AC-DC transfer standards 80—98874
- multimeter, automatic storage, for DC and AC signals *(German)* 77—10044
- noninductive current probe, construction 78—4663
- nonsinusoidal periodic current meas. using standard DC shunt with magnetic powder monitoring, frequency errors 80—104398
- optical fibre, current measurement appl. 80—96015
- optical fibre, single-mode, for current meas. system, birefr. induced by bends and twists 80—99832
- optical isolation operational amplifier, for current meas. in 10^{-11} to 10^{-6} A range 77—67473
- oscilloscope appl., conversion to proportional voltage signal *(German)* 77—13766
- Permalloy magnetoresistive mag. field and current sensor 77—10048
- photomagnetoelectric effect, contactless measurement apparatus, operation analysis using equiv. cct. 77—41655
- polyethylene charge carrier injection, contactless electrode expt. 80—15540
- polymer film, bulk elec. cond. parallel to film surface 79—87094
- primary standards, curved stabilisation, superconducting quantum interferometer design 77—53945
- PTFE film capacitors in low DC meas. ccts., temp. effects 79—6141
- pulsed beams of charged particles, liquid US meter 79—68110
- pulsed corona meas. in coaxial electrode structures 79—19114
- in pulsed X-ray device, voltage divider and Rogowski coil *(Japanese)* 78—93788
- quantum current-frequency convertor using optical orientation of ^{133}Cs *(Russian)* 79—10275
- reproduction of ampere at German ASMW 80—98944
- RF SQUID, narrow-band ultra-low current meas. 79—63274
- RMS, true value meas. methods, appls. *(Italian)* 79—21767
- RMS measurement errors quantified 80—57274
- semiconductor thermoelectric properties automatic meas. device *(Polish)* 77—69359
- servo-controlled balance, absolute ampere determ. 78—82003
- sheet conductor, induced eddy currents, IR meas. 80—37933
- shunt, made from composition resistor, for current pulse measurement 78—4640
- shunt heated by current pulse, iterative method for overcoming errors 79—21766
- SQUID arrays, for mag. field meas., geophysical, biomedical appls. 78—32830
- SQUID for AC current meas. down to 10^{-14} A 78—49859
- superconducting critical current, continuous meas. method for tapes and composites 77—24656
- suspension, in nonpolar dispersion media, particle size and number conc. meas. 80—9082
- techniques for minute currents *(German)* 79—54153
- transients, fast digital technique *(Polish)* 80—86340
- ultrashort current pulse generation and meas. using Josephson devices 80—90827
- wideband current and voltage comparators 77—57356
- Cu cathode with oxide film, emitting site lifetimes and current densities, meas. 77—27761
- Zn sulphate electrolyte cathodic-current 78—35707
- Zn sulphate electrolytes purity determ. 78—35706

electric discharge machining *see spark machining*

electric discharges *see discharges (electric)*

electric distortion
- *see also fading; reception*
- AM/FM radio signal diffraction in homogeneous dispersive medium, space time geometric theory 79—4149
- biopotential recording interference and motion artifact sources and suppression 77—81634
- integral pulse freq. modulator, spectral props., heart-rate variability meas. 77—90951
- low-distortion FM demodulator using SAW delay device 78—51014
- optoelectronic scanning device accuracy, raster distortion and instability effects 79—72697
- spectrometers, single peak output distortion due to electronic time consts. 77—2667

electric distortion measurement
- piezoelectric mirror-driving transducer for gas lasers, distortion measurement 77—10006
- waveform distortion anal. due to recording and playback speed instability 78—73981

electric domain walls
- activation energy of thick domain walls 79—56751
- benzil, phase transition study be simultaneous Raman-scatt. and domain-struct. investigations 79—60504
- boracites, spontaneous birefr., meas. and appl., statics and dynamics of domains and walls 79—15434
- ceramics, ferroelec., dielec. losses due to domain wall oscill. 78—84541
- coupled fields in one dimension: cross-over from a continuous symmetry to a discrete one 78—87758
- double quadratic kink soln. to ferroelec. domain wall dynamic polarisability 80—66135
- EM wave diffraction at domain wall in ferroelec. *(Russian)* 77—90118
- ferrodistortive materials, dynamics of domain walls, theory 79—73282
- ferroelastic, roughening transition suppression by long range elastic forces 80—75991
- ferroelastic crystal, struct. of Sapriel's w′-wall 80—34866
- ferroelastic-ferroelectric crystals, rel. to appl. in electronic micropositioning 79—17392
- ferroelectric, domain wall mobility, two-dimens. ordering effect 78—48137
- ferroelectric, interaction energy between a charge and domain wall 80—88939
- ferroelectric, kinetics of heterogeneous state *(Russian)* 80—45022
- ferroelectric, polarisation switching influence of mobile point defects 78—31165
- ferroelectric, SAW propagation along domain boundaries, low temp. sp. ht. contrib. 77—77158
- ferroelectric ceramic, mech. and elec. losses, correl., theory and expt. 80—66133
- ferroelectric ceramics, materials and dielec. props., review 80—75957
- ferroelectric crystal with defects, permittivity, nonlinearity 78—27170
- ferroelectric domain wall struct., and stability under competitive phase transitions 79—78639
- ferroelectric domain walls motion in strong fields and polarisation wave spectrum *(Russian)* 79—87409
- ferroelectric materials, repolarisation in SEM 79—15424
- ferroelectric narrow walls, steady-state motion 80—11356
- ferroelectric. surface EM wave propag. along domain boundaries 77—40195
- ferroelectrics, surface sound waves on domain boundaries, low temp. sp. ht. 78—71937
- ferroics, secondary, polycryst., poling effects 77—16102
- guanidinium aluminium sulphate, domain wall energies and domain structures 78—92039
- improper ferroelectric, domain wall theory using simple one-dimens. model 77—12349
- Ising model, temp. depend. of domain wall parameters 79—69797
- one-dimensional ferroelectric, quantum corrections 77—4609
- perovskite-type ferroelectric crystals, calc. of domain wall motion 77—90117
- piezoelectric ceramic, nonlinear charge release under uniaxial press. 80—80706
- point defect interactions, effect on dielec. loss and relax. of ferroelec. 77—32338
- quartz, ferroelastoelectricity, expt. 80—40078
- quartz ferrobielastic twinning coercive stress obs. 78—59854
- rare earth molybdates, cryst. growth, cryst. chem., and phys. props., book contrib. 80—44194
- roughening transition, Peierls force against Peierls divergence 80—75991
- Tanane, ferroelec. ferroelastic transition, X-ray and optical expts. 78—15110
- TGS:α-alanine, single crysts., dielec. spectrum in RF range *(Russian)* 80—66097
- TGS, acoustic emission, threshold electric field 79—60874
- TGS, domain boundaries, X-ray topographic study 78—48136
- TGS, domain growth shapes 78—27168
- TGS, domain nucleation in AC elec. fields 80—34867
- TGS, domain wall dynamics and small signal permitt., loss mechanism absence 78—43825
- TGS, domain wall thickness determ. from longit. US wave propagation meas. 77—66463
- TGS, effect of edge dislocations on shapes of moving domain boundary 80—20602
- TGS, exponential switching by sidewise domain wall motion 80—29703
- TGS, ferroelec., domain wall orientations and domain shapes 79—38508
- TGS, monocrystalline, ferroelectric, domain boundary dynamics contrib. to permittivity near Curie point *(Russian)* 79—73875
- TGS, pure and deuterated, domain wall thickness and surface energy 79—87408
- TGS, pure and doped, thermal diffusivity, domain wall thickness determ. 79—42324
- TGS, pure and nitroaniline-admixtured, longit. US wave propag., domain struct. effects 77—55322
- TGS, tan δ depend. upon sample thickness 77—59510
- TGS, X-ray topography 78—60409
- TGSe, domain growth shapes 78—27168
- TGSe, ferroelec., domain wall orientations and domain shapes 79—38508
- thiourea, ferroelec., soft mode and Debye relax., IR reflection spectra 77—90111
- triglycine selenate, sideways velocity anisotropy 79—8108

electric domain walls continued
- uniaxial ferroelectric, static and dynamic crit. phenomena, Larkin-Khmelnitzkii theory 78—64327
- uniaxial ferroelectric-crystal, with one-dimensional inhomogeneity, fluctuations of order parameter 80—15995
- BaT:O$_3$:Mn, ferroelec. domain stabilisation by bulk ordering of defects 79—42925
- BaTiO$_3$, deform. and stress relax. of single crysts. 77—59542
- BaTiO$_3$, electron microscopy investigs. of ferroelec. substances, review *(Japanese)* 80—71366
- BaTiO$_3$, ferroelec., elec. field in 90° domain walls 80—2713
- BaTiO$_3$, ferroelec., reduction of hysteresis losses 79—42926
- BaTiO$_3$, ferroelec. domain boundary struct., TEM 77—24806
- BaTiO$_3$, light emission during repolarisation 77—36299
- BaTiO$_3$, periodic domain struct. and opalescence at tetragonal to orthorhombic transition 80—66131
- BaTiO$_3$, polarisation reversal and surface neutralisation 78—27169
- BaTiO$_3$, single crysts., electron microscope study of domain and defect structs. 79—15425
- BaTi$_{0.98}$Sn$_{0.02}$O$_3$, ferroelec. film, switching process 80—60518
- Ba(Ti$_{0.98}$Sn$_{0.02}$)O$_3$ film, ferroelec., switching process in elec. field with rectangular impulses, domain wall nucleation and motion 80—2714
- Bi oxides containing perovskite layers, ferroelec. cryst., electron microscopy, dislocation and domain boundaries 77—52030
- CsH$_2$PO$_4$, domain obs. in paraelectric phase 79—24277
- Gd$_2$(MoO$_4$)$_3$, ferroelec., amorphous Si:H coating, domain wall motion, image scanning 80—83663
- Gd$_2$(MoO$_4$)$_3$, ferroelec. and ferroelastic, electron microscopic study 77—85675
- Gd$_2$(MoO$_4$)$_3$, ferroelec. ferroelastic, domain wall motion, crit. field var. 77—81075
- Gd$_2$(MoO$_4$)$_3$, matrix-addressed analogue ferroelec. memory 80—103926
- Gd$_2$(MoO$_4$)$_3$, prismatic domain exam. 78—56441
- Gd$_2$(MoO$_4$)$_3$, spontaneous birefringence, pulsed field switching, compression effect, domain movement 78—27187
- KH$_2$PO$_4$, and isomorphs, dielec. props. and birefr., simultaneous obs. 78—15130
- KH$_2$PO$_4$, dielectric const. at ultra low freq., domain wall relax. effects 77—12348
- KH$_2$PO$_4$, initial dielec. const. by thermal noise method, domain wall motion 77—16267
- KH$_2$PO$_4$, mobility, model 77—63385
- KH$_2$PO$_4$, rel. to amplitude depend. of permittivity and losses 79—99842
- KH$_2$PO$_4$-type crystal, domain wall mobility, two-dimens. ordering effect 78—48137
- KNbO$_3$, dopant effect on domain struct., etching study 79—56749
- KNbO$_3$ thick crystals, vol. nucleation of domains by impurities 77—73120
- KNbO$_3$:Al^{3+}, dopant effect on domain struct., etching study 79—56749
- KNbO$_3$:Ba^{2+}, dopant effect on domain struct., etching study 79—56749
- LiNbO$_3$, crystal defects, X-ray diffr. topographic study *(Chinese)* 80—84173
- LiNbO$_3$, damping of LF elastic vibrs., internal friction meas. 79—28043
- NaD$_{3x}$H$_{3(1-x)}$(SeO$_3$)$_2$, ferroelec. dispersion 80—66129
- NaNO$_2$, rel. to thermal history effects on temp. range of modulated struct. for 163°C transition 78—95563
- PLZT, fine grained 90° electric domain wall movement, interpretation of dielectric losses *(German)* 79—33646
- PLZT, mech. and elec. losses, correl., theory and expt. 80—66133
- PLZT, transparent, optical exam. of small signal behaviour, of 90° electric domain walls *(German)* 79—33645
- Pb$_5$Ge$_3$O$_{11}$, acoustic emission, threshold electric field 79—60874
- Pb$_5$Ge$_3$O$_{11}$, uniaxial displacive ferroelectrics, domain wall dynamics 79—73890
- PbNb$_2$O$_6$, ferroelectric strain polarisation interaction, domain wall formation 79—56750
- PbTiO$_3$, anomalies in elec., photoelectric and mechanical props. 80—55051
- PbTiO$_3$, ferroelec. domain boundaries, rigid body displacement of lattice 80—40079
- Pb(Zr,Ti)O$_3$, porosity-permittivity relations, depolarising factors determ. and pore effects *(Japanese)* 80—97189
- SbSI, max. vel. of domain boundaries in polarisation reversal, Barkhausen effect meas. 78—60411
- SbSI, single- and poly-domain, complex permitt. and dielec. relax. losses 79—28699
- SbSI, uniaxial displacive ferroelectrics, domain wall dynamics 79—73890
- Sr$_{0.5}$Ba$_{0.5}$Nb$_2$O$_6$, ferroelec., dielec. behaviour 78—80309
- TGSe, domain-wall orientations and wall energies 78—23420

electric domains
- *see also electric domain walls; ferroelectric materials*
- acceleration waves in elastic dielectrics with internal state variables 79—47396
- boracites, spontaneous birefr., meas. and appl., statics and dynamics of domains and walls 79—15434
- cholesteric, liquid cryst., nucleation of focal-conic domains in field induced nematic texture 78—34430
- di-1′,4″-octyloxybenzylidene-1,4-diaminochlorobenzene, nematic with some smectic ordering, EHD instabilities 77—84640
- dicalcium strontium propionate, ferroelec. domains, direct optical visibility 80—84704
- exciton dielectric, inhomogeneous current state phase transition, free energy *(Russian)* 80—84703
- ferroelec. crystal, Barkhausen effect study 79—38507
- ferroelectric, collinear, domain struct. changes on switching, liq. cryst. visualisation *(Russian)* 79—33648
- ferroelectric, struct. of domain boundaries, light diffr. 78—15135
- ferroelectric ceramic, shock induced polarisation 77—48133
- ferroelectric ceramic, tetragonal TsTS-23 and TBK-3, 90° domain rot. in fixed elec. field 80—7315
- ferroelectric crystals, Landau theory, phase transitions, surface symmetry 79—56741
- ferroelectric domain boundary quasielastic displacements 77—24807
- ferroelectric domain equilibrium configuration near Curie temp. 78—88270
- ferroelectric domain struct. obs. using TOF neutron diffractometer 79—51923
- ferroelectric improper, EM wave diffr. by domain walls 79—69799
- ferroelectric material domain struct., branching *(Russian)* 80—34868

electric domains continued
ferroelectric plate, domain struct. near first-order phase transition resembling second-order transition 80—93139
ferroelectric plate, polarisation distribution, permittivity, domain structure 80—29704
ferroelectric substances, electron microscopy investigations, review *(Japanese)* 80—71366
ferroelectric tetragonal ceramics, 90° domain-rot. fraction after polarisation, X-ray determ. 80—75992
ferroelectrics, domain structure as outcome state for poling procedure 80—80728
guanidine aluminium sulphate hexahydrate, ferroelec. cryst., growth, domain struct., dielec., switching props. 77—43950
guanidine aluminium sulphate hexahydrate, SEM obs. of ferroelec. domain struct. in single crysts. 80—97219
guanidinium aluminium sulphate, domain wall energies and domain structures 78—92039
guanidinium aluminium sulphate hexahydrate, surface obs., SEM and AES expts. 80—71362
guanidinium aluminium sulphate hydrate, ferroelec., decoration patterns on cleavage surface, domain obs. 80—97218
guanidinium uranyl sulphate hydrate, ferroelec., decoration patterns on cleavage surface, domain obs. 80—97218
guanidinium uranyl sulphate trihydrate, new ferroelec., dielec. props. 78—43824
Gunn diode, anode domain disappearance dynamics, computer simulation calcs. 80—6859
Gunn diode, domain instability at near-critical dopant conc. 79—23980
Gunn diodes, domain instabilities in transverse mag. field 79—23981
Gunn domain transient behaviour and associated equivalent circuits 78—19043
Gunn planar elements, stationary domains 79—56238
p,n-hepthyloxybenzoic acid, smectic C liq. cryst., coherent light diffr. 78—1999
Klein-Gordon nonlinear eqn., generalised susceptibility of solitary wave 79—75357
maximum electric field in high-field domain in Gunn devices 78—79996
MBBA, nematic liq. cryst., relaxation times for formation and break-up of Williams domains 78—34423
MBBA, nematic liq. cryst., temp. depend. of EHD instability 78—1998
metal, electric domains at low temp. 79—65368
metals, electrical domains at low temps. *(Russian)* 78—91687
multivalley semiconductor, domain instability, two-beam model 79—47116
nematic liquid crystal, domain structure of new type in dielec. region 77—11480
nematic liquid crystal, domains, of 2nd kind, form. with positive dielec. anisotropy *(Russian)* 78—18550
nematic liquid crystal, flexo-electric domains 78—43792
nematic liquid crystal, flexoelectric domains in thin layers *(Russian)* 78—18549
nematic liquid crystal, stimulated rearrangement of domain struct. 78—26438
nematic liquid crystal, temp. depend. of EHD instability 78—1998
piezoelectric semiconductor, shock waves and acoustoelec. domains 77—32049
planar Gunn diode, high-field domain dynamics anal. using stroboscopic SEM 79—56232
polydomain ferroelectrics, spontaneous polaris. screening *(Russian)* 79—91395
quartz ferrobielastic twinning, electrical and acoustic emissions 79—56731
α-quartz twinning and tailored domain patterns 77—40197
Rochelle salt, ferroelectric props., student expt. 79—97162
Rochelle salt ferroelectric surface creep discharge plasma channel and domain interactions 80—15996
rotational domains, electric polarisation *(Chinese)* 79—56747
semiconductor, basic shape of Gunn domain using $\mathcal{J}$ operator 77—55535
semiconductor domain instability and resistivity profile meas., universal capacitive probe 80—31796
semiconductor heating, thermal domain investigation, current voltage characts. 80—70711
semiconductors, current instabilities, theory and expts. *(Hungarian)* 77—39857
semiconductors, exciton and domain luminesc., book 80—82588
SLC, chiral structure in electric field, dielectric permeability, spontaneous polarisation *(Russian)* 80—75159
smectic liquid crystal, piezoelectric domains, free energy minimisation and Euler eqns. calc. 77—51319
smectic liquid crystals, ferroelec., submicrosecond bistable electro-optic switching 80—84051
surface potential between ferroelec. domains, electron microscopy 78—15132
TBK-3, ferroelectric ceramic, 90° electric domain processes, mech. stress, X-ray diffr. 78—72478
tetragonal ferroelectric irradiated by laser pulses, spatial temp. and bound-charge distrib. 80—103927
TGS, alignment on domains of nematic liq. cryst. 79—38506
TGS, correlation between domain struct. and dielec. props. 79—42927
TGS, domain growth shapes 78—27168
TGS, domain nucleation in AC elec. fields 80—34867
TGS, effect of Fe^{3+} admixture on phys. props. 80—76052
TGS, ferroelec. activation field change 80—71358
TGS, ferroelec. crystal, Barkhausen effect study 79—38507
TGS, ferroelec. domain struct., polarisation obs. *(Chinese)* 80—20603
TGS, ferroelectric, domain pattern using pyroelectric effect 77—40196
TGS, ferroelectric domain exam., decoration with auramine 77—16268
TGS, internal field prod. in layer periodical domain struct. by X-ray irrad. 80—71359
TGS, kinetics of domain formation during phase transition 80—66130
TGS, layered domain struct. form., theory and expt. 77—52029
TGS, piezoelec. RF reson. rel. to ferroelec. domain struct. 77—16269
TGS, pyroelec. signal, domain struct. determ. 77—43951
TGS, surface alignment of nematic liq. cryst. controlled by domain struct. 79—99068
TGS cleavage faces, ferroelec., oriented growth of Te 79—38509
TGS crystals, influence of domain struct. on pyroelec. props. 78—31159
TGS crystals, thermal props., γ-radiation defects and inhomogeneity of domain deposition 79—46810
TGSe, domain growth shapes 78—27168
TGSe, low freq. dielec. dispersion near Curie point 79—38432

electric domains continued
triglycine selenate, coercive field calc. using two-dimens. domain growth model 79—8108
triglycine sulphate, ferroelec., decoration patterns on cleavage surface, domain obs. 80—97218
TsTS-23, ferroelectric ceramic, 90° electric domain processes, mech. stress, X-ray diffr. 78—72478
uniaxial ferroelectrics, domain formation during second order phase transition 79—38505
uniaxial pyroelectric, rel. to nonlinear optical susceptibility 77—23705
Ag_3AsS_3, proustite crystals, stoichiometric composition derivation influence on phase transition 79—95715
$Ba_{0.92}Ca_{0.08}TiO_3$ ceramic, uniaxial stress effects, US dilatometric and dielec. meas. 78—52454
$Ba_2NaNb_5O_{15}$ crystal domains, amplitude modulation of light by diffr. 79—59832
$Ba_2NaNb_5O_{15}$, electrooptical diffr. by periodic domain struct. 80—40090
$Ba_2NaNb_5O_{15}$, ferroelec. conversion to single domain, elec. and photoelec. props. 78—88271
$Ba_2NaNb_5O_{15}$, kinetics of low temp. conversion into single domain form 77—43953
$Ba_{2.09}Na_{0.72}Nb_{5.02}O_{15}$, cryst. growth, monodomenisation, detwinning, optical homogeneity, composition, dielec., spectral props. 77—44151
$Ba_xSr_{1-x}Nb_2O_6$, nonequilibrium processes 78—48124
$BaTiO_3$, 90° electric domain processes, mech. stress, X-ray diffr. 78—72478
$BaTiO_3$ a-domain crystals, domain struct. influence on physical consts. 79—69798
$BaTiO_3$ ceramics, PTC-type, grain boundary study using TEM 80—107267
$BaTiO_3$, controlled surface layers 78—48120
$BaTiO_3$, domain structure obs. using SEM 77—1647
$BaTiO_3$, domain struct. characts. of unipolar ferroelec., photocarrier effects 78—19435
$BaTiO_3$, domain struct., formation at phase transitions 79—38510
$BaTiO_3$, doped, loss mechanism and domain stabilisation 78—84542
$BaTiO_3$, ferroelec., X-ray diffr. topographic study of polarisation reversal 79—38442
$BaTiO_3$, ferroelec. ceramic, 90° domain rot. in fixed elec. field 80—7315
$BaTiO_3$, ferroelec. domain form., X-ray topography 79—78638
$BaTiO_3$, ferroelec. inhomogeneous impurity distrib., distrib. of spontaneous induction 77—28530
$BaTiO_3$, ferroelec. to paraelec. transform., influence of domain boundaries on interface struct. 79—95718
$BaTiO_3$, ferroelectric domain struct. and cryst. struct. changes, X-ray diffr. 77—24803
$BaTiO_3$, ferroelectric ceramic, dielec., piezoelec. and elastic props., orientational contrib. 78—68468
$BaTiO_3$, ferroelectric domains, X-ray topography 79—65815
$BaTiO_3$, ferroelectric-paraelectric transform., basic struct. and characts. 79—95717
$BaTiO_3$, head to head and tail to tail domains 78—43826
$BaTiO_3$, martensite type phase transition 78—64326
$BaTiO_3$, periodic domain struct. and opalescence at tetragonal to orthorhombic transition 80—66131
$BaTiO_3$, periodic motion of laminar domains, const. elec. field 78—15133
$BaTiO_3$, photoferroelec., lighting effect on deform. and stresses 78—43802
$BaTiO_3$, piezoceramic, nonlinear piezoeffect 79—42900
$BaTiO_3$, planar phase boundaries and domain struct. 79—69795
$BaTiO_3$ polydomain crystals, dielec. props. 78—43827
$BaTiO_3$, polydomain ferroelec. crysts., phys. consts., self consistent calcs. 80—88942
$BaTiO_3$, pure and doped crysts., surface and domain struct., AES and SEM expts. 80—71363
$BaTiO_3$, secondary struct. periodic motion 80—15993
$BaTiO_3$, single crysts., electron microscope study of domain and defect structs. 79—15425
$BaTiO_3$, unipolar cryst., topography of defect. and thermodepolarisation currents 77—43954
$BaTiO_3{:}La_2O_3$ and $BaTiO_3{:}La_2O_3.3TiO_2$ capacitor, permittivity ageing obs. *(Korean)* 80—25325
$Bi_xTi_yO_z$, poling method 77—59544
$Ca_3(VO_4)_2$, new high temp. ferroelec., 180° domains 78—43811
$Cd_2Nb_2O_7$, Mn^{2+} ESR, hyperfine interaction const., ferroelectric domain orientation 80—54943
CdS, domain elec. instabilities, elec. field and temp. distribs., optical meas. 79—11405
CdS, lattice attenuation meas. by US injection method 78—76480
CdS, phase memory effect and vel. of trap-controlled high-field domains 77—47855
n-CdS, photocond. film, phase memory effect and deep levels 79—82556
CdS, recombination electric domains, production mechanism 80—29433
$Co_3B_7O_{13}Cl$, polydomain ferroelec., magnetoelec. effect below Neel temp. 78—10745
$Fe_3B_7O_{13}Br$, $Fe_3B_7O_{13}Cl$, polydomain ferroelec., magnetoelec. effect below Neel temp. 78—10745
$Fe_3B_7O_{13}I$, twinning in orthorhombic phase, ferroelec. domain struct. with switching 78—19434
Fe_3O_4, lattice parameters, NMR freqs., and magnetoelec. pots. near 12K 80—71146
n-GaAs, diffusion coeff., Monte Carlo calc., rel. to trapped domain behaviour 78—56152
GaAs, domain elec. instability in two-valley semiconds. 77—76842
GaAs, Gunn device, planar, domain dissolution for wide range of doping 77—8109
GaAs Gunn diodes, static domain form. 77—8111
n-GaAs, IR luminesc. emitted by travelling acoustoelec. domains 78—27329
n-GaAs, IR luminescence of acoustoelectric domains 78—31258
n-GaAs, two-valley semiconductor, domain instability *(Russian)* 77—62934
GaAs:Cr, single cryst., optical quenching spectrum, disappearance of stationary high-field domain 78—47830
n-$Ga_xIn_{1-x}Sb$ Gunn diode, high field domain characts. 80—59992
$Gd_2(MoO_4)_3$, domain structure obs. by GdF_3 decoration 78—84544
$Gd_2(MoO_4)_3$, electron microscope exam. of ferroelec. and ferroelastic props., domain walls and cryst. defects 77—69786
$Gd_2(MoO_4)_3$, electron microscopy investigs. of ferroelec. substances, review *(Japanese)* 80—71366
$Gd_2(MoO_4)_3$, ferroelectric domain decoration 78—10862

electric domains continued
$Gd_2(MoO_4)_3$, one-dimensional ferroelectric image sensor with polymer photoconductor 80—80729
$Gd_2(MoO_4)_3$, prismatic domain exam. 78—56441
Ge p-n junctions with hot carriers, current amplification, elec. domain form. 80—6966
Ge:Au, current-voltage phase shift, impedance of subthreshold domains 77—43609
Ge:Au, moving elec. domain, impedance 77—1429
Ge:Cu, surface waves at static domain boundaries *(Russian)* 80—80288
Ge:Cu photodetector, high field domains, rel. to I-V characts. 78—19141
n-Ge:Ni, negative differential conductance of surface channels 79—11134
GeTe, heterophase state, plasma refl. spectra, twinning domain distrib. study 79—69845
KCN-KCl mixed system, order-disorder transition, dielec. props. meas. 78—15112
KCN-KCl mixed system, order-disorder transition, Raman spectra obs. 78—15113
KD_2PO_4, domain structure obs. using SEM 77—1647
KD_2PO_4, ferroelec. domain struct. obs. using TOF neutron diffractometer 79—51923
KH_2AsO_4, domain struct. formation, opt. polarisation obs. 77—63381
$KH_{2x}D_{2(1-x)}PO_4$, domain struct. influence on switching processes 80—11355
KH_2PO_4 crystal, and deuterated cpd., optical meas. of phase transition point by domain obs. 77—40187
KH_2PO_4, differential γ-ray diffractometry, exam. of ferroelectric-ferroelastic cryst. in cyclic fields 79—38511
KH_2PO_4, ferroelastic cryst., appl. of γ-ray diffractometry 77—8533
KH_2PO_4, struct. memory effects in low temp. changes 79—28700
$KH_3(SeO_3)_2$, ferroelastic, low-frequency elastic props., −190 to 50°C 79—37759
$K_2Mn_2(SO_4)_3$, optical and dielectric props. 79—11403
$KNbO_3$, growth from soln. in melt and characterisation of optical quality cryst. 77—8741
K_2O-SrO-Nb_2O_5 system, selective delineation of dislocations by etching 77—72617
$(Li_2B_4O_7)_{1-x}(WO_3)_x$ dipolar glass, space charge injection, thermally stimulated depolarisation currents 80—66103
$LiNbO_3$, crystal defects, X-ray diffr. topographic study *(Chinese)* 80—84173
$LiNbO_3$, monodomain ferroelec. cryst., secondary electron emission coeff. 78—11032
$LiNbO_3$, polydomain, nonstoichiometric crysts., elastic, piezoelec., dielec. constants. 77—8513
$LiNbO_3$, reversed polarity layer at positive domain surface, heat-induced, etching investig. 77—63383
$LiNbO_3$, Ti diffused optical waveguide, ferrolectric domain inversion 79—94338
$LiTaO_3$, crystallographic features and domain struct. 78—34498
$LiTaO_3$ crystals for commercial SAW TV IF filters, fabrication 80—80961
$LiTaO_3$, multidomain cryst., birefringence, Tyndall cone struct. 77—4618
$LiTuO_3$, light scatt. from ferroelec. domains 78—80310
$Mg_3B_7O_{13}Cl$, pyroelec. effect, spontaneous polarisation, domain struct. 77—8520
NH_4Cl, electro-optical props. near order-disorder transition 78—31173
NH_4Cl, order parameter, electro-optic measurement 78—88280
NH_4Cl, order-disorder phase transform., effect of plastic deform. and electrooptic effect 79—33672
$NH_4H_2PO_4$, crystal, and deuterated cpd., optical meas. of phase transition point by domain obs. 77—40187
NH_4HSeO_4, ferroelec. props. rel. to struct. 80—71345
$NaAl(MoO_4)_2$, domain struct., phase transition, and dielec. props. 79—56748
$NaFe(MoO_4)_2$, domain struct., phase transition, and dielec. props. 79—56748
$NaH_3(SeO_3)_2$, domain struct. realignment and Barkhausen effect 80—71361
$NaH_3(SeO_3)_2$, ferroelec. crystal, Barkhausen effect study 79—38507
$NaNH_4SeO_4.2H_2O$, crystal struct. in ferroelec. phase, nature of transition 77—43946
$NaNH_4SeO_4.2H_2O$, ferroelectric crystal, effect of hydrostatic pressure on phase transition 78—52453
$NaNO_2$, ferroelec., X-ray obs. during polarisation reversal 79—51921
$Na_5W_3O_9F_5$, single cryst., prep., optical and dielec. studies *(French)* 80—15994
$NaZnGeO_4$:Mn, electrolum., ionisation domains 80—84787
Ni-I single crystals, mag. and dielectric props. 80—93095
$Ni_3B_7O_{13}Cl$, boracite, on Cr-Cl boracite, gas phase synthesis of epitaxial layers 79—60650
$Ni_3B_7O_{13}I$, magnetoelectric tensor component detection 79—95625
PLZT ceramic, dielectric anisotropy, role of 90° domain processes 77—63384
PLZT ceramic with memory, domain reorientation, alternating elec. field effect 79—47405
PLZT ceramic;, visible light scatt. depend. on photoferroelectric space charge fields 80—80806
PLZT ceramics, photoferroelectric effects, image storage device appl. 79—42924
PLZT ceramics, sp. ht., 2-25K, field depend., phonon modes 77—47586
PLZT composition, effect on its switching characts. 79—42917
PLZT, controlled light scatt. 78—10909
PLZT, ferroelectric domain struct. obs. by SEM and optical microscopy *(Japanese)* 78—15136
Pb, superconducting phase condensation in bulk sample *(German)* 79—56447
$Pb_5Ge_3O_{11}$, growth defects and polarisation switching 78—48132
$Pb_5Ge_{3-x}Si_xO_{11}$, ferroelec., switching vel. and spontaneous polarisation 78—84543
$Pb_{0.27}K_{0.56}Nb_{0.91}Ta_{4.15}O_{15}$, coupled ferroelastic-ferroelectric props. 77—59543
$Pb_2KNb_{5-x}Ta_xO_{15}$, ferroelastic-ferroelectric coupling, dielec. props. 79—38433
$Pb_{2.07}K_{0.56}Nb_{0.91}Ta_{4.15}O_{15}$, tetragonal tungsten bronze type, ferroelastic-ferroelectric coupling *(French)* 77—28522
$Pb_{0.97}La_{0.02}(Zr_{0.92}Ti_{0.08})O_3$, ferroelec. ceramic, stress effects 80—2119
$PbNb_2O_6$, ferroelectric thick crystals, domain formation and dislocation loops 78—60410
$PbNb_2O_6$ ferroelectric single crysts., domain struct., cryst. planes, twinning 78—64340

electric domains continued
$PbNb_2O_6$, surface (001), microstruct. obs. by optical, etching, and interferometric techniques 79—11399
$Pb_{0.99}Nb_{0.02}(Zr_{0.95}Ti_{0.05})_{0.98}O_3$, ferroelec. ceramic, stress effects 80—2119
$Pb_3(PO_4)_2$, ferroelastic, dielectric anomalies, phase transitions, permittivity, relaxation *(Russian)* 80—71293
n-PbTe film, epitaxial, hot electron transport effects 77—12035
PbTe, high field drift vel. and Hall coeff. 78—26875
$Pb(Ti, Zr)O_3$, piezoelectric-ferroelectric ceramic, polarisation processes, X-ray obs. 80—34847
$PbTiO_3$, anomalies in elec., photoelectric and mechanical props. 80—55051
$PbTiO_3$, crysts., X-ray investigation of 90° domain struct. 79—15426
$PbTiO_3$, domain struct. formation during jump motion of phase front 78—64339
$PbTiO_3$, domain struct., formation at phase transitions 79—38510
$PbTiO_3$, domain struct. form. during jump-like motion of phase boundary 79—69794
$PbTiO_3$, ferroelectric ceramic, dielec., piezoelec. and elastic props., orientational contrib. 78—68468
$PbTiO_3$, mechanical twinning, spontaneous polarisation shielding 79—42930
$PbTiO_3$, phase transform., different kinetic types 80—71347
$PbTiO_3$, single cryst., He^+ backscatt. shoulder spectra struct., domain struct. 80—35048
$PbTiO_3$, spontaneous polaris. shielding destruction by polishing and scribing 79—15427
$PbTiO_3$, switching, domain structure reorganisation and polarisation change 77—1645
$PbTi_xZr_{1-x}O_3$, ferroelec., electric field depend. of contour mode reson. 77—12351
$Pb(Zn_{1/3}Nb_{2/3})O_3$, electrostriction investigation, strain gauge method 79—87395
$Pb(Zr,Ti)O_3$ ceramic, X-ray investigation before and after polarisation *(Chinese)* 80—2712
$Pb(Zr,Ti)O_3$ ceramics, space charge field meas. by ferroelec. domain switching current, piezoelec. reson. freq. ageing characts. 80—7296
$Pb(Zr,Ti)O_3$, piezoceramic, nonlinear piezoeffect 79—42900
$Pb(Zr,Ti)O_3$, polarisation effect on deform. and strength, Curie pt. region 79—42902
$Pb(Zr,Ti)O_3$, tetragonal ferroelec. ceramic, 90° domain-rot. fraction after polarisation, X-ray determ. 80—75992
RbCN, molecular motion and ordering from dielec. and Raman techniques 79—73932
$Rb_2Cd_2(SO_4)_3$, pyroelectric and dielectric props., ferroelectric transitions 79—38458
$RbHSeO_4$, ferroelec. props. and domain struct. 79—78637
$RbHSeO_4$, ferroelec. props. rel. to struct. 80—71345
$RbH_3(SeO_3)_2$, ferroelec. domain struct., obs. using dew method 80—50283
$RbH_3(SeO_3)_2$, order parameter 77—66460
Rb_2ZnCl_4, incommensurate phase form., domain struct. near phase transition, NQR obs. 79—33643
Sb_5O_7I, polytypes 2MC and 2MA, photoferroelastic phenomena 79—95447
Sb_2S_3, crystal, domain structure 78—43828
SbSI, domain struct. relaxation 78—48135
SbSI, electroreflectance exam. 78—48145
SbSI, ferroelec. semicond., influence of internal fields on polarisation reversal process 79—38443
SbSI, surface layer exam. 78—48119
p-Se photocond. film, phase memory effect and deep levels 79—82556
Si (100) inversion layers, effective masses, Shubnikov-de Haas oscills. under mechanical stress 77—43625
n-Si, current instability due to temp.-elec. domain pulsations 77—43608
n-Si, current-voltage characts., static high field domains 78—84223
n-Si, field and current domains, at low temp. 80—6868
$Sr_{1-x}Ba_xNb_2O_6$, photorefraction in space charge field, phase transitions 80—97229
$Sr_xBa_{1-x}Nb_2O_6$, domain struct. influence on electrooptical props. 80—93283
$Sr_xBa_{1-x}Nb_2O_6$, neutron and light scatt. in phase transition region 78—64336
TGS, deuterised, growth in form of oriented blocks, domain struct. obs. 77—90266
Te, acoustoelec. domain induced transparency at 11 μm 78—27182
Te, acoustoelectric domain induced transparency near 11 micron 77—85727
TiO_2, rutile, ferroelectric ceramic, dielec., piezoelec. and elastic props., orientational contrib. 78—68468
VO_2 needles, switching, rel. to voltage oscills. 79—15199
VO_2 single cryst., switching, visual obs. of metallic and semicond. domains 78—52041
ZnS, prebreakdown electrolum., domain form. and negative resist. effects 80—84788
ZnS:Mn AC thin film devices, domain electrolum. 80—66303

electric double refraction *see electro-optical effects*

electric drives
see also clutches; electric propulsion
astronomical laser ranging equipment, telescope drive *(Japanese)* 78—89078
blood circulation apparatus, improved electromechanical drive regulator 80—3871
blood pump supply, biventricular, development and in vivo evaluation 79—53285
chart recorder timer control, pen overload protection systems, at. absorpt. appl. 77—73481
dual capstan drive tape recorder *(German)* 80—95092
electrodynamic scanning mirror drive system for fast-scanning Fourier spectrometer 79—75630
electromechanical mirror scanning devices 77—58477
EM self drives for captive liners, plasma compression appl. 78—9769
Fourier spectrometer, electrodynamic drive system 78—82059
heat pumps with electric drives and gas drives, comparison *(German)* 80—7952
laser grating mount, stepping motor controlled 80—87402
linear asynchronous motor drive system, for rotating optical components inside vac. system 80—102874
linear motor slide drive system for optical machining 80—1366
microprocessor-controlled tape drive 79—93123

electric drives continued
monochromator drive, using high-speed digital servo 78—36992
Mossbauer spectroscopy drive system, low cost, using μA747 ICs 79—89049
photographic emulsion spreading appl., operational principles *(Russian)* 77—79172
piezoelectric, implantable, for left ventricular assist device, invertor improvement 78—15927
solar tracking electronic servo 79—57433
stepper motor drives for use in synchronous interlock systems for cinematographic special effects 80—98991
stepper-motor 'shutter' drive, using monostables 78—35860
telescope drive, controlled 300 Hz freq. supply 78—61746
terrestrial solar panel design, construction and operation 79—96442
thyristor controlled, for machines for mechanical testing 77—25213
vacuum-tight drive, with gear pump for pumped circulation of corrosive liquids 77—74376
wheelchair, Emory detachable elec. powered drive 77—25606

electric field effects
see also acoustoelectric effects; discharges (electric); electrical conductivity; electro-optical effects; electrochemistry; electrodynamics; electrokinetic effects; electroluminescence; electromechanical effects; electromigration; electron field emission; electrophoresis; field emission ion microscopy; field evaporation; field ion emission; field ionisation; high field effects; magnetoelectric effects; particle optics
60 Hz electric field, 240 kV/m, long-term effects on mice 80—89784
60 Hz electric field effects on small birds and mammals 77—86538
60 Hz high intensity electric fields, behavioural and biological effects in living organisms 80—89740
400 kV substation electric fields, long-term exposure, epidemiologic investigation *(French, English)* 80—21599
AC on surface tension of liquids, distilled water and organic substances *(Russian)* 77—55417
Aerosil in cetane, suspension, thermal cond. rel. to elec. field, struct. form. 77—9138
aerosol particle charging by α-ionizing radiation in electric field 78—11566
aerosol particles, β-active, electrification, in external elec. field, influence of stopping power of gaseous medium 79—20473
air breakdown in homogeneous AC and DC fields, obs. *(German)* 79—86625
alkali metal chemisorbed on metallic surface, effect of field 77—7975
alkoxybenzylidenaminobenzonitriles, elec. field and press. induced transitions, transparency and texture 77—43317
alternating electric field effect 78—20984
aniline, liq., far IR absorpt. spectra, electric field effects 80—95625
atomic and mol. reson. states, electrostatically induced, perturbation theory, 1-D model 77—75077
atomic interactions, retarded energy shift and pair polarisability, field theoretical perturbation theory 80—102560
bacterial culture viability under negative ion irrad. in elec. field *(Russian)* 79—83855
behavioural effects of 25 kV/m 60 Hz field on rats 80—56108
biomolecular effects of 50 Hz EM fields, mechanism of effect *(Russian)* 80—51158
blood coagulation and fibrinolysis, DC effects 78—48766
boiling, in circuit system, effect of intense electric field *(Russian)* 78—46887
bone stimulation devices, anal. of sinusoidal EM fields 80—108990
capillary-porous bodies, internal mass transfer, influence of inhomogeneous elec. and mag. fields 80—6138
cerebral tissue, Ca^{2+} binding rel. to weak oscill. elec. fields 77—1984
chalcogenide glass, elec. field influence on crystn. process, 60-240°C 77—76315
charged particle, capture by large uncharged particle, in uniform external electrical field 79—66357
charged particle, effect of electrostatic field on rate of evaporation 77—27585
chemical equilibrium, displacement by elec. field *(French)* 77—25299
chemical thermodynamic equilibrium, and field chem. consequences 78—7224
chemical waves, multiple, induced by electric field 79—92047
chlorobenzene, liq., spin lattice relax. time, elec. field induced charges 80—44945
cholesteric liquid crystal mixture, with positive dielectric anisotropy influence of external fields *(Rumanian)* 78—59751
cholesteric positive dielectric anisotropy mixture, helix pitch increase below 20 kHz 80—15997
cholesteryl chloride-cholesteryl crotonate (75:25% wt.) mixture, cholesteric-nematic transition field effect temp. depend. 78—75813
colloidal particles in gap between nonconductive fibres, electroconcentration 80—11895
colloids, electrostabilisation effect in elec. field 79—39210
convection heat transfer enhancement, d.c. high voltage electric fields *(Japanese)* 79—98593
corona, positive, initiated by negative ion decay, expt. 77—55182
crystal surface, Shockley states in a semi-infinite Kronig-Penney model 79—73562
crystallisation, comp. control of crysts. grown in elec. and mag. fields 79—33920
crystallisation parameters of dielec., elec. field effect *(Russian)* 77—55338
4-4′-cyano-octyl-biphenyl, smectic A liq. cryst., elec. field effects, capacitance meas. 78—91237
4-4′-cyano-octyloxy-biphenyl, smectic A liq. cryst., elec. field effects, capacitance meas. 78—91237
cylinder in still air, DC corona cooling obs. 80—70071
dielectric, thermal explosion theory in strong elec. field 79—91954
dielectric crystallisation kinetics, electric field effect, nucleation 80—19919
dielectric film, formation during ion implantation, electric field effects 78—2801
dielectric fluids vapours condensation, heat exchange obs. *(Russian)* 79—1055
dielectric liquid, film condensation, heat transfer enhancement in elec. field 78—55551
dielectric liquid, surface tension, influence of HF elec. field *(Russian)* 80—49463
dielectric liquids, interfacial profile, elec. field effects theory 80—2244
dielectrophoretic levitation of spheres and shells 79—81318

electric field effects continued
diethyl ether, liq., spin lattice relax. time, elec. field induced charges 80—44945
dioxane, liq., spin lattice relax. time, elec. field induced charges 80—44945
DNA, soln., quasielastic light scattering, in AC elec. field 79—62186
DOBAMBC, ferroelec. liq. cryst., helical struct., elec. field depend. *(Japanese)* 80—38910
doubly rotated α-quartz plate vibration, polarising effect 79—14186
drop, heat transfer, electric field effect 78—59276
drops in immiscible liquid, intermittent elec. field heat transfer augmentation 78—94872
EBBA, nematic, mol. alignment, elec. and mag. field effects, dielec. const. obs. 77—11472
EHV transmission line ground level gradient, small plants and animals biological studies 78—31856
electrodynamics, evaluation of electrofluidic pumps and generators, appls. *(German)* 79—94724
electron mobility, trajectory curvature effect in strong elec. field 78—83517
electrons and phonons in strong const. elec. field, kinetic eqns. 80—34157
electrostatic precipitator, free-fall, motion of charged particles, determ. 78—71020
emulsion, inverse-type, coalescence of drops in uniform elec. field 78—53265
EPR method of appl. strong electric fields at low temp. 79—21792
extruded polymer soln. through capillary, flow instability and electrostatic effects 79—60035
ferroelectric crystal, displacive, effect of elec. field on thermal cond. 77—85002
flame, counterflow diffusion, struct. in elec. field, interferometric obs. 80—16685
flames, propag. rate and precombustion Joule heating 78—53207
fluid, promotion of combustion, vaporisation, and heat transfer 79—20370
fogging effect of an electric field on a photographic film *(Russian)* 80—62783
gas breakdown in homogeneous elec. field, physical aspects *(German)* 79—82108
gas bubble form. synchronised with AC pot. 80—24080
gas fluidised bed, heat transfer assisted by alternating electric field 78—9697
gases, dipole, nonlinear theory of complex dielectric constant 78—1787
glass, particle size influence on force moving particle in inhomogeneous elec. field, influence of field frequency 79—11795
heat pipes, electric field effects on characts. 80—83728
n-hexane, geminate ion scavenging yield, external elec. field effect 79—47909
n-hexane, heat transfer from horizontal wire, AC and DC electric field effect 77—31202
high electric field biological effects on human nervous systems 80—89739
hollow cathode lamp, spectral lines width and intensity, high freq. field effects 78—16856
human beings, effects of elec. and mag. fields, HV lines to 800 kV *(French, English)* 80—72209
HV transmission line, electrostatic field effects on human body *(French)* 77—21562
HV transmission line elec. and mag. field exposure effects and hazards 78—77083
hyperthermia, localised current field heating as an adjunct to radiation therapy 80—98056
ice crystals, epitaxial, influence of environmental saturation and elec. field on growth and evaporation 79—42408
impulse discharge treatment, of machine bearings coatings, wear resistance improvement *(Russian)* 79—1917
insulating liquid, small air bubble formation, under strong nonuniform electric field 79—46373
ionic conductor, quasielastic scatt. of light, neutrons and electrons, Debye-Huckel eqn. *(Chinese)* 78—68521
latent photographic images, erasion by electric field *(Russian)* 79—97462
light sensitivity of photographic films in an electric field *(Russian)* 80—290
linear response theory, macroscopic vs. microscopic, appl. to electron in periodic pot. 78—65813
lipid bilayer, alkane solubility modified by elec. field 80—97874
liquid gas interface, deform. in inhomogeneous elec. field *(Bulgarian)* 80—54474
liquids, potential and flux conserving static equilibria in elec. or mag. fields, determ. 80—88399
living organisms, static field perception and teratogenic effects of microwaves 77—81532
MBAB:cholesteryl chloride, thickness depend. of threshold elec. field for instabilities 79—32896
MBBA, mol. alignment in elec. and mag. fields 77—58956
MBBA, nematic, in alternating elec. field, two-dimens. lattice form. *(French)* 77—11473
MBBA, nematic phase, effect of elec. field on flow alignment angle 79—10792
metal, current pulse effects on structure at crack tip *(Russian)* 77—44332
metal-liquid insulator interface, in presence and absence of applied elec. field 79—19429
metallic film, carrier density, evaluation from transverse elec. field and cond. meas. *(French)* 80—39682
metallic thin films, dynamic coalescence origin *(French)* 77—51612
12-methylpentane, γ-irrad. glass, trapped electron yield, elec. field effects 77—16848
MHD channel, anisotropically conducting plasma in inhomogeneous elec. and mag. fields, current calc. *(Russian)* 80—74995
MHD generators, Window-Frame, with nonuniform velocity and conductivity in transverse plane, electric effects, anal. 79—68960
micro-organism electroretention effectiveness rel. to electrode type *(Russian)* 80—26419
micropolar effects in liquids, characts. evaluation under rotating electric field *(Polish)* 79—55638
natural convection heat transfer, nonuniform alternating field influence 77—50860
nematic liquid cryst., 3D convective instability in AC field 77—62475
nematic liquid crystal, capacitance response to elec. and mag. fields, appl. to elastic const. determ. 79—90545

electric field effects continued
nitrobenzene, liq., spin lattice relax. time, elec. field induced charges 80—44945
nuclear emulsion type BA-2, pulsed electric field effect on cosmic ray detection 79—26829
nuclear emulsions, heavy ion tracks separation from background 78—17491
oil film transient heat exchange in transverse electric field *(Russian)* 79—94607
organic halides, NQR shift in external elec. field, rel. to bonding 77—12237
organic liquids, boiling points 77—15566
orientation of long particles in a uniform electric field *(Russian)* 79—72451
particles suspended in electrolytes, in crossed elec. and mag. fields, trajectories, rel. to organisms' sensitivity to fields 78—48657
perturbed crystals in k q representation, in presence of homogeneous electric field 79—69386
photographic emulsion layers, sensitivity to elec. fields *(Russian)* 77—67524
photographic emulsions, effect of applied electric field on light sensitivity *(Russian)* 80—296
plant growth and development, effect of 60Hz elec. field 77—81534
plasma, non-isothermal, low-ionised, influence of HF elec. field on electron ensemble *(German)* 79—77383
poly(vinyl methyl ether)-polystyrene mixture, electric field depend. of cloud point temp., laser scatt. meas. 80—6519
polyethylene, elec. field effect on positron annihilation 79—4868
polyethylene, structural changes induced by high elec. field *(Japanese)* 79—23532
polymers, pure liquid, electric field dependence of the glass temperature 79—86875
porous solid layer form. on viscose fibre, EM field effect *(Russian)* 77—66595
positron in condensing He, Monte Carlo lifetime spectra, temp. and elec. field effects 78—55263
powder, disintegration of powder particle agglomerates under the action of an alternating electric field 78—68642
powder classification in electric field of plane capacitor 77—12775
powders, fine, electrogravitation classification by particle mass 79—61531
power line ground gradient simulation for biological effect exam. 77—86731
power-line elec. field interaction with human and animal organisms 79—66483
pulsars, particle acceleration by DC electric fields 80—31316
quartz crystals, Bragg reflection enhancement due to X-ray irradiation under high elec. fields 79—14643
R. sphaeroides, polarisation of photosynthetic membranes and reaction centres in elec. field 80—94277
rats, lack of effect of elec. field exposure, data re-evaluation 80—72210
rats influence of 45-Hz vertical elec. fields 80—76784
relativistic charged particle in electric field, spin rot., curved crystal p,e$^+$ channelling *(Russian)* 80—63907
retardation of electrolytic mass transport in collinear electric-magnetic fields 80—104443
secondary electron emission near dielectric-metal interface 79—38697
semiconductor, paramagnetism switching off in strong electric field *(Russian)* 78—80124
semiconductor junctions, electric field effect on thermal emission of traps 80—11073
skywave field strengths, effect of proximity to discontinuity in Earth's elec. props. 77—40974
soyabean oil, heat transfer from horizontal wire, AC and DC electric field effect 77—31202
spacecraft charging, positive ion beam system for charge ejection 79—12379
superionic conductor, phase transitions induced by elec. field 78—63856
surface tension of polar liq., elec. field effect 78—51791
swine, exposure method for vertical 60 Hz elec. fields 78—53587
TGS-type crystals:Cr^{3+}, radiospectroscopic studies, elec. field effects on EPR, EM EPR 79—15341
thermistor, heat transfer intensification effect in nonuniform elec. fields 77—57354
thermoelastic solids, field-matter interactions, book 79—30270
transmission electron microscope 80—4823
UHV transmission line, biological effects on animals and plants obs. 80—17003
vacuum deposited metal film, elec. field effect on residual struct. 78—51836
water droplet collision and coalescence for small Reynolds numbers, electric force effects 77—78326
water drops in oil, collision coalescence, elec. field influence 80—51516
weakly conducting fluid, separation by thermal diffusion in elec. field *(Russian)* 79—16117
Al_2O_3, α to γ transformations, electric field effects, proton gradient meas. by SIMS 79—52209
Ar, absorpt. spectra, field induced autoionisation near ionisation threshold 80—106301
Ar gas, high press., recombination luminescence in scintillation induced by alpha particles 78—50441
Au-Al system, influence of current on phase form. in diffusion layer *(Russian)* 78—52826
$BaMoO_4$ crystals, growth in SiO_2 gel under influence of elec. field 80—93469
BaO-SiO_2 glass ceramic, nucleation, effect of electric fields 78—83742
Bi and Bi-Sb (12 at.%), cryst. growth from melt, impurity distrib. control by electrotransfer method *(Russian)* 80—66418
$CaCO_3$, acceleration of growth of particles, Lorentz forces, electric and mag. field effects 78—51455
CaF_2:Gd^{3+}-M$^+$, (M=Li, Na, K, Rb, Cs, Ag), electric field effect expts., EPR line breadths, lattice distortions 78—80210
Cd, single cryst. stress relax. depend. on elec. current, electron plastic effect 79—79021
$CdBr_2$ and CdI_2(4H), electric field effect on NQR, elec. polarisation mechanism 77—20746
Ce^{3+}, local symmetry in frozen aq. solns., EPR and linear electric field effect 77—16169
Er^{3+}, local symmetry in frozen aq. solns., EPR and local electric field effect 77—16169
Fe alloy YuNDK35T5, mag., solidification, direct elec. current effect 79—78954
Fe, refining by electric fields in vacuum, surface active impurity elimination *(Russian)* 80—55563
GaAs epitaxial growth, in GaAs-$AsCl_3$-H_2 system, elec. field effect 80—2306
GaAs layers, grown by electroepitaxy and LPE, surface morphology 79—19478
Ga_2O_3-Fe_2O_3 system, anomalous Mossbauer line shapes, incomplete annealing 78—92006
Ge, adsorption of O, enhancement by elec. field of polarity facilitating field-ion emission 79—65325
H atom in box, 2-D Schroedinger equation, influence of constant elec. field, finite-element method 80—31544
H, in uniform electric field, level energies and widths 77—14378
H, photoionisation cross sections elec. field-induced oscills. 80—955
H$^-$, ion lifetime in elec. field 79—54986
H_2, nonempirical calc. for molecules in electric field 78—25459
He$^+$ Lamb-shift measurement by the quenching-radiation anisotropy method 80—18824
^{3}He, B-phase, superfluid, orientational electric field effect 79—46868
^{3}He, superfluid, distortion in elec. and mag. fields, NMR shifts 77—35780
n-InSb, acoustoelectronic interaction, effect of alternating electric field 79—11188
KCl, sublimation on (100) surfaces in elec. field 79—77739
Kr, absorpt. spectra, field induced autoionisation near ionisation threshold 80—106301
α-$LiIO_3$, in electrostatic field, X-ray double cryst. spectrometric investigation *(Chinese)* 78—67666
α-$LiIO_3$, lattice consts. variation due to electrostatic field *(Chinese)* 78—83787
MgO-Al_2O_3-SiO_2 glass ceramic, nucleation, effect of electric fields 78—83742
Mn thin films, vacuum deposited in elec. field, resist., struct. 80—103761
Mo, film, formation by reduction of $MoCl_5$ 80—93491
N_2, boiling liq., infuence of electric field on heat transfer 80—53770
N_2, liq., boiling, cryogenic, heat transfer rel. to sinusoidal elec. field 77—72135
N_2, nonempirical calc. for molecules in electric field 78—25459
NaCl (001) substrate, preferential epitaxy of evaporated films induced by electron bombard. or elec. field 80—10824
NaCl, spiral dislocation mobility depend. on elec. field, relaxation time 80—39105
$NbSe_3$, incommensurate CDW, X-ray scatt. and elec. field studies 79—42471
Nd^{3+}, local symmetry in frozen aq. solns., EPR and linear electric field effect 77—16169
Ni-Si melt refining by electric fields, ionic conduction of Ni, Si *(Russian)* 80—65273
O_2, nonempirical calc. for molecules in electric field 78—25459
Pb, single cryst. stress relax. depend. on elec. current, electron plastic effect 79—79021
$PbCl_2$ emulsion layer, effect of elec. field on microcrystal sensitivity *(Russian)* 79—58831
PbI_2(2H and 4H), layer cryst., elec. field effect on NQR, elec. polarisation mechanism 77—20746
$PbZrO_3$ crystal, structural phase transitions in very high elec. fields 80—15987
$PbZrO_3$, elec. field induced phase transitions 77—62643
Rb, photoionis. cross section, elec. field depend. 80—37796
Rb, π-photoionisation spectra in DC field, Fano profile 79—59410
Se, crystallisation kinetics correlation with molecular structure 78—94998
$Se_{0.95}Te_{0.05}$, glass crystallisation, effect of an alternating electric field 80—88054
Si, inclusion type defects removal from bulk of single cryst. by elec. fields 79—43126
p-Si, positron annihilation, effects of applied elec. field *(German)* 78—72634
Si:H, amorphous, plasma-deposited, effect of DC elec. field superimposed during deposition 80—44643
Si:In, backward wave phonon spectroscopy 80—2357
Sn film, vacuum deposited, substrate and substrate temp. effects on struct. 80—107677
Sr, autoionisation reson. states elec. field depend., three-photon ionisation 78—33478
$SrCl_2$:Mn^{2+}(Co^{2+}), cubic impurity EPR spectra, elec. field effect, mechanism 78—68361
$TlAsS_2$, glass, crystallisation, effect of an alternating electric field 80—88054
Yb^{3+}, local symmetry in frozen aq. solns., EPR and local electric field effect 77—16169
Zn, positron annihilation in plastically deformed sample, electric field effect 79—69899
Zn, single cryst. stress relax. depend. on elec. current, electron plastic effect 79—79021
ZnO, electric field dependence of photoconductivity *(Russian)* 80—49821
ZnS, photoluminesc. quenching by weak alternating field 77—85778
ZnS:Cu phosphor, electric field quenching of photoluminesc. and flashlike rise in luminesc. 78—2911

electric field measurement
see also field plotting
800 MHz portable transmitters, meas. of energy deposition in simulated human operators, comments and reply 79—57777
AC corona meas. using field-filter probes 80—47082
active C dust current, electrostatic field meas. using radioactive convertor 78—16812
airborne wave tilt meas. for reconnaissance mapping at poorly cond. areas 77—78473
aircraft EM environment meas. near thunderstorm cells 78—49180
antenna electric field intensity, conversion equations for meas. 77—26332
atmosphere, max. field intensity during thunderstorms, meas. over water 77—33160
atmospheric diffusion, tracking elec. charged air by ground level elec. field meas. 77—78450
cetyltrimethylammonium bromide, micellar soln., internal elec. fields, linear dichroism obs. 77—86325
circular discs and rectangular plates, shadow-side field meas. 77—79731
clouds, instrums. review 77—41226

electric field measurement continued
- coronasonde, balloon-borne, for thundercloud elec. field meas. 78−61577
- cylindrical electrode under corona discharge, elec. field intensity meas. 79−23473
- dielectric plate in const. current flow, appl. sea elec. field meas. *(Russian)* 77−65813
- dielectric tensor field determ. in weakly inhomogeneous anisotropic media 79−72492
- disturbances in conducting fluid modelling, due to solid particles, conductometric probe analysis *(Russian)* 78−231
- dosimeter, evaluation of implantable elec. field probe within finite simulated tissues 78−40345
- electrolyte internal electric field study by linear dichroism probes 77−86325
- electrostatic charge meter IEZ-P 79−75553
- electrostatic field, calibration of transducers for intensity and potential measurements 79−75551
- electrostatic field, effects of distortion on measurement 79−75550
- electrostatic intensity, electroluminescence method *(Russian)* 78−77934
- electrostatic precipitator with duct-geometry needle plate electrodes 78−16819
- electrostatic voltage sensor *(Japanese)* 80−105632
- fibre optic sensors appl. *(Norwegian)* 79−93121
- in finite heterogeneous biological bodies, using insulated elec. field probe 79−2170
- fluorocarbon vapours, sparking potential meas. 77−65922
- gas flows, particle-bearing, probe measurement of electrostatic fields 79−75552
- gaseous insulating materials, potential meas. by corona probe 80−82790
- HF short-term field-strength predictions, real-time 79−58180
- high-Q resonant probe for plasma wave diagnostics 78−9831
- influence E-field meter as sensitive measuring instrum. *(German)* 77−74425
- insulators, nondestructive acoustic elec. field probe 80−47076
- intensity unit, 30 MHz to 1 GHz, USSR special standard 77−30181
- interference electron microscopy, for elec. field distrib. meas. 79−17567
- International Sun-Earth Explorer 1 and 2, plasma wave investigation 78−85802
- ion analyzers for DC electric field and ion temp. meas. 79−21147
- isolated sciatic nerve in volume conductor 77−21505
- isotropic RF electric/magnetic field strength meter, design 80−82751
- laser sensing system for elec. and mag. fields in power transmission 77−45870
- magnetosphere, constant electric field strength vector meas. problems 78−16245
- magnetosphere, DC and low-freq. field instrumentation on International Sun-Earth Explorer A 78−85807
- magnetosphere, quasi-static and low-freq. fields meas. by International Sun-Earth Explorer-1 78−85808
- magnetosphere, quasistatic elec. fields meas. between 3-7 R_E 79−29942
- microfields, quantitative registration on solid surface, using raster electron microscope 80−31790
- microfields meas. with SEM attachment 79−2789
- microwave mapping of near-field pattern in simulated biological tissues 79−39445
- microwave meas. of high intensity elec. field using Ne gas-discharge tube 80−9006
- miniature ELF electric field probe 78−70160
- miniature probe, 60 Hz, laboratory investigation of electric fields generated by electrode systems appl. 78−77930
- ocean, baseless method of electric field meas. *(Russian)* 79−39900
- ocean electric field measuring system equivalent base for rectangular fairing *(Russian)* 79−34988
- ocean electric fields, EM phenomena accompanying movement of current fairing in sea water *(Russian)* 78−77361
- optical sensor for measurement of high electric field intensity 80−69509
- passive probe for free atmosphere electric field meas. 79−8710
- pressure sensitive elements, appl. 79−97367
- probes, widebandedness, influence of parasitic resonances *(Polish)* 79−2783
- probes for corona discharge field measurement 80−33822
- probing by electron reflection 80−31791
- pulsed field meas. in flux of penetrating radiation 77−57357
- pulsed field meas. using electro-optical device 78−4644
- RF fields, near-zone field-strength meter 80−52174
- RF industrial heaters, elec. and mag. field strengths meas. 80−52175
- scanning mirror electron microscopy, quantitative evaluation of elec. microfields 78−74110
- schlieren method for the determination of electric field distributions in dielectrics 80−31720
- secondary electron collector for local electric field meas. in REhM-200 raster electron microscope 78−4736
- semiconductor surface potential distrib. meas. using mirror electron microscope 79−35784
- solar wind, DC and low-freq. field instrumentation on International Sun-Earth Explorer A 78−85807
- solar wind, quasi-static and low-freq. fields meas. by International Sun-Earth Explorer-1 78−85808
- space simulation plasma chamber, elec. field meas. with double probes, atm. appl. 79−64909
- static probe for electric field meas., in presence of space charge 79−17448
- transient fields, measurement using electrostatic field meter of Smith type 79−21723
- VHF noise field strength at 95 MHz over India, meas. techniques and obs. 80−109294
- N-O mixtures, positive glow corona in quasi-uniform fields 80−100104

electric field strength measurement *see electric field measurement*

electric fields
- *see also electric field effects; electric field measurement; electromagnetic fields; electromagnetic waves; field plotting*
- analogies with temperature fields, engineering calc. appl. *(Czech)* 79−68343
- analysis and computation, computer appl. book 78−37787
- asymptotic behaviour near singular points of conductor surface 78−13641
- auroral forms, magnetic field aligned electric fields rel. to downward electron energy fluxes 79−53606
- auroral ionosphere, electric fields and conductivity in quiet periods 77−53280

electric fields continued
- auroral particle distrib., parallel electric field acceleration 80−12602
- auroral zone electric fields at 1 R_E altitude 78−57397
- auroral zone electric fields rel. to interplanetary magnetic field vars. 78−77431
- automatic computation, three methods, comparative study *(French)* 79−68346
- axisymmetric field problem soln. by Gaussian surface charge simulation 80−95758
- bevelled p-n junction in Si power device, elec. field in controlled region and blocking capabilities determ. 77−1474
- biological electric-field probes, effect of material interface on probing internal field 79−53204
- Bruce electrode, surface elec. field 77−75359
- C-CD, insulator-semiconductor interface, electrostatic field, Green's function calc. 77−76933
- calculation, approx. method for electric field distrib. with space-charges *(German)* 80−23595
- calculation by charge simulation, finite element, and Monte Carlo methods, comparison *(Italian)* 79−94124
- calculation by floating random walk method 80−95760
- calculation of three dimensional fields using multipoles, numerical method *(German)* 77−75358
- capacitor plate-plate electrical configuration with injected unipolar space charge *(Portuguese)* 80−28132
- capacity estimation by means of Ritz and Trefftz's methods 78−5387
- cathode, electric field averaging in space charge sheath 77−19806
- charge distortion on a wire in a warm plasma 78−55274
- charge superposition modified method for elec. field calc. 77−27218
- charged microparticles productions under high electric field intensity in ultra high vacuum, measurement *(Japanese)* 80−96411
- charged nonconducting disc and metal sphere, pot., field strength and charge 77−46668
- complex fields between electrodes in conducting media, numerical calc. 80−43227
- in composite dielectric arrangements, field behaviour near singular points 79−31763
- computation by charge simulation and finite element methods 80−95759
- computation using SCOFF program *(German)* 80−78740
- computer drawn fields for diverse configurations, program 77−22401
- conducting body charge distrib. computation *(Polish)* 78−78850
- conducting body in uniform electric field, computations of dipole moment *(Polish)* 79−76546
- conducting emitter, surface elec. field *(Russian)* 79−10242
- conducting plate with temp. depend. resistivity and surface heat loss, temp., current and elec. field distribs. 77−42696
- conducting sphere, dielectric-coated, modal and near field characts. 80−28144
- configurations, in 2- and 3-dimens. cond. distribs. and calcs. *(Russian)* 77−3515
- between conical electrode with hyperboloid end and earthed plate, mathematical formulation *(Czech)* 79−27125
- contactless suspension of objects, oscill. field stabilising effect 77−68150
- corners, elec. and mag. fields external to series of corners 77−75360
- cylindrical condenser, finite length, elec. field distrib. calcs. 77−5957
- cylindrical conductor, between conducting surfaces, electrostatic field 78−9293
- cylindrical particle analyser, fringing field 78−94165
- dayside magnetopause, electric field topology 78−57398
- dense gas nanosecond discharge, cathode region field amplification 80−38855
- dielectric, inhomogeneous, electrostatic pot., numerical soln., finite difference method *(Spanish)* 79−89824
- dielectric, inhomogeneous nonmatrix type, elec. field and effective dielec. tensor eqns. 78−52425
- dielectric, reflection in terms of polarisation 79−82916
- dielectric block, solid, between point-plane electrodes, treeing inception conditions calc. *(French)* 77−38771
- dielectric multilayers, laser damage, elec. field strength role 77−61993
- dielectrics, stability and growth estimates for elec. fields 79−71262
- difference frequency generation by stimulated Raman scatt. using inhomogeneous electrostatic field 80−95954
- dipole fields in conducting media, calc. by numerical methods 80−18957
- discharge, volumetric, semi-self-maintaining, excited by electron beam, current maintanance in cathode layer 80−59322
- discontinuous metal films, elec. and mag. field distrib., TEM obs. 79−95518
- dissipative media, field strength by equivalent cct., for teachers 79−40319
- drift diffusion unipolar conduction between parallel plate electrodes, closed form steady state solutions 80−91720
- dust clouds, industrial, existence of lightning-like dicharges 78−14235
- dyadic Green's function, direct derivation 77−14641
- dyadic Green's functions in source region 80−43229
- Earth as unipolar generator 78−44771
- education, demonstration of electrostatic dipole lines of force 77−78931
- Einzel-type electrostatic field with rot. symmetry, Fourier-Bessel soln. 78−82878
- electro-optical deflector with cylindrical electrodes, controlling field distortion 79−98493
- electrochemical electrodes linearly polarised, electrolyte stationary electric field calc. *(Russian)* 80−21289
- electrode fields calc., blade-type *(Czech)* 78−55273
- electrode system, for elec. quadrupole field prod. 77−54012
- electrofluid dynamic field calc., substitute-charge method 77−38767
- electron beam, nonuniform elliptic, inside hollow cond. of elliptic cross-section, elec. pot. and field *(French)* 77−50582
- electron beam, relativistic, electrostatic field rel. to propag. in strong mag. field *(Japanese)* 80−91737
- electron microscopy using electrostatic field on electron-charged dielec. *(German)* 78−82081
- electrostatic, two-dimensional, computerised solution using Sander's function 79−878
- electrostatic field equation, general orthogonal curvilinear coords., finite difference approx. 77−38770
- electrostatic fields, finite element anal., element function shape geometry *(Polish)* 79−3609
- electrostatic fields calc., finite element method using cubic potential distribution *(German)* 80−32872
- electrostatic problems in presence of linear and isotropic quadrupole matter *(German)* 80−37924

electric fields continued
enriched isotope target preparation, design of quasi-hyperbolic electrostatic fields 80—23597
EPR spectroscopy in strong elec. fields at 77 and 4.2K 78—86310
excitation of conductive body, covered with thin dielectric layer, integral equation solution *(Russian)* 79—18322
external physical fields of sources investigation, modelling devices construction 80—17817
F-region convective electric field determ. from rocket meas. of thermal ion spectra 78—57386
fast insulator surface flashover, investigation using electro-optical elec. field meas. 80—64820
FEM, local field strength and work function rel. to field emitters, analogue simulation on Teledeltos paper 77—41731
field analysis computers, colloquium, London, England (March 1980) 80—94964
field ion microscope, electric field distrib. 79—75658
finite elements in electrical and magnetic field problems, book 80—62399
flame, diffusion type, oppositely directed jets, elec. props. 78—56896
fluid nonpolar polarisable, local field at large distances from charge or dipole rel. to dielec. constant 80—83534
focusing field generation, geometric and analytic solns. *(Russian)* 79—64164
gap between flat plate and cylindrical electrode with cone-shaped end, calc. method *(Croatian)* 80—99600
Gaussian beam propagation beyond the paraxial approximation 79—72476
geomagnetic tail, electric field of a time-dependent Alfven-type neutral sheet 79—25403
guided electro-optic structures, distributions 77—72068
heterogeneous and anisotropic media, finite element anal. 77—34794
heterogeneous dielectric, bounds on energy and mean square fields 77—31042
heterogeneous dielectric, Dirichlet problem, Green's function method 78—37782
human heart consistent rectangular/spherical coordinate system for EEG and magnetocardiography 77—86679
HV field induced in humans, determ. using moment method 77—86535
inhomogeneous continua with Hall effect, elec. fields and effective conductance tensor *(Ukrainian)* 77—50590
inhomogeneous media, galvanomag., stratified, elec. fields 80—63888
insulating and semiconducting media, electric field numerical soln. *(Slovak)* 78—66710
intense electric fields, tree-shaped phenomena in solid insulating materials *(Rumanian)* 80—63885
intensity, numerical calculation methods *(French)* 80—106413
interacting gravitational and electron fields, Hamiltonian formulation, canonical form 79—17301
interfacial entropy, elec. and mag. interfacial polarisation *(French)* 79—7050
interplanetary elec. field penetration of magnetosphere, balloon meas. 78—57408
interplanetary electric fields, cosmic rays drift as essential energy loss process 80—8498
interplanetary magnetic holes, plasma sheath elec. field 79—29961
interplanetary shock wave, assoc. plasma wave turbulence obs. 79—53700
inverse problems, soln. *(Russian)* 80—1102
ion mass-energy spectrograph for space plasmas anal., double-focusing field geometry 77—53401
ionosphere, auroral zone electric fields, conductivities and currents, latitudinal distrib. 78—77399
ionosphere, elec. fields rel. to cond. and drifts 78—36366
ionosphere, electric fields and currents generated by field-aligned currents, TRIAD obs. 79—40013
ionosphere, electrostatic fields theory 78—36387
ionosphere, incoherent scatter radar studies 77—22001
ionosphere, transverse electric fields rel. to field aligned currents, model 78—77397
ionosphere equatorial field, coupling to high-latit. mag. vars. 78—93029
ionospheric generated large scale fields, penetration into lower atmosphere *(Russian)* 77—9606
Kerr black holes, charged current loop field and pot. 78—40988
laser damage protective coating, electric field interference 80—33062
laser window, elec. fields and power dissipation at oblique incidence 77—46746
leader channel temp. rise, initial stage, elec. field strength determ. *(Russian)* 77—35411
LF and MF ground waves in realistic terrain, field strength meas. at LF and MF 78—88795
lightning current, elec. field strength anal. *(Russian)* 79—88402
lightning discharge, elec. field strength at ground level, calc. *(German)* 78—28254
lightning leader stroke model, electric field strength computation *(Czech)* 79—5554
lightning stroke current, calc. 78—3860
long thin wire on half-space interface, series soln. 77—75364
lunar surface, intense local photoelectric charging in sunset terminator region 77—45330
macroscopic sphere above grounded plane in sinusoidal field, fields and forces 77—46669
magnetopause, tangential electric field, three-dimens. energetic ion obs. 79—40038
magnetosphere, GEOS-1 meas. of electric and magnetic wave fields and cold plasma parameters 79—48620
magnetosphere, ISEE-1 electric field meas. results 79—40037
magnetosphere, radial diffusion coeff. near L=6, field fluctuations 79—101022
magnetosphere, transverse electric fields rel. to field aligned currents, model 78—77397
magnetotail, substorm electric field effects on charged particles 78—77425
mapping theory of two-dimensional anisotropic regions 79—55022
Maxwell's equations as one quaternion eqn., appl. to wave propag., for teaching 78—54133
metallic conductor, hollow, image field produced by uniform or nonuniform beam 77—14638
MHD generator current density and elec. field dependence on plasma thermodynamic pulsation *(Polish)* 77—80268
microstrip anisotropic electrostatic field problems, Green's function technique 78—70998
monochromatic parallel beam uniformly polarised *(French)* 78—90339

electric fields continued
moving sources in conducting medium, multipole expansion 80—106417
multilayer, dielectric reflectors, simplified description 79—89984
multilayer, electric field distrib. and laser damage reduction 80—87420
multilayer resonance elements, elec. field distribution calc. *(Russian)* 78—78854
neuron electric potential field evaluation, with time-dependent surface potential, using hybrid computer 77—86478
nonlocal electrostatics, spherical interface 78—82880
numerical computation, using ELMAG program system *(German)* 77—3516
open electron optical system with rotational symmetry, Fourier-Bessel series soln. for pot. and field intensity 79—76570
optical film, electric field and absorption distributions 77—601
orientation of long particles in a uniform electric field *(Russian)* 79—72451
perception and generation by honey bees 78—15941
periodic electrode structure, analytic method of solving simultaneous eqns. 77—75362
permittivity meas., lumped-capacitance method, fringing field effect anal. 78—54392
phosphate glass, electron irrad., elec. flield, distrib. above surface *(Russian)* 77—43763
piezoceramic plate, electroelastic equilibrium *(Russian)* 78—43795
piezoelectric transducers, electric field, nonuniform, expt. study 80—102955
plane electron-optical system, electrostatic field anal. with integral eqns. of first kind 77—19157
plane electrostatic fields in doubly connected polygonal domains, anal. using conformal mapping 77—58223
plane meridional, between equipotential electrodes, analysis *(Russian)* 79—45880
plasma, collisionless, signature of parallel elec. fields 78—77439
plasma, electrostatic field struct. in wake of body in rarefied flow 77—91402
plasma, low-density, electrostatic field struct. in wake of sphere 77—60509
plasma electron velocity distrib. function relax., time depend. electric field *(German)* 77—31424
plotting, computer programs for high-school expts. 78—86094
points of equilib. in electrostatic fields 80—31453
polar cap electric field structures with a northward interplanetary magnetic field 79—44305
positive column, Ne, He, with diffusion loss, axial elec. field effects *(Japanese)* 78—47196
potential fields calc., plane-parallel, in mixed boundary conditions *(Rumanian)* 78—82877
power system, unloading charging voltages calc. using related maximum field strengths *(German)* 80—28130
powers determination using direct analogue method *(Czech)* 80—69290
pulsar magnetospheres with parallel electric fields 78—65643
pulsars, elec. fields rel. to amplified linear accel. radio emission 79—8936
quadrupole lens spatial field determ. 78—55292
quarter-wave dielectric reflector, spectral absorptance approximation 80—33131
in quiet plasmasphere, dynamo origin, whistler data 78—77426
reciprocity theorem for corrugated surfaces used in conical diffraction mountings 80—1333
relativistic vector formulation *(Italian)* 78—12448
ring, charged, insulated, potential calc. *(Czech)* 79—64142
ring conductor systems, maximum electric field intensity calculations *(Czech)* 79—81321
rotating magnetic dipole, elec. field components 78—45141
sea, electric intensity vector direction determ. device *(Russian)* 77—60490
singularities at edges in solving electrostatic problems by series method 79—86103
skin electric field intensity distribution due to external pot. 77—73553
small apertures in perfectly conducting wall, polarisability 77—19136
solar wind, bow shock, magnetosheath, magnetopause and magnetosphere, ISEE meas. 79—40053
solar wind, elec. field fluctuations rel. to plasmadynamical processes *(German)* 80—109323
solar wind, plasma wave elec. fields obs. by Helios 1 77—37492
source region, evaluation using tensor Green's function 77—75363
spinning magnetic field inducing elec. field, moving and non-moving force line hypotheses 78—9296
stars, elec. fields, accretion and stellar winds in He rich atmospheres 79—48772
static, near angular points of media interfaces, asymptotics *(Russian)* 77—10807
static electric field determ., numerical methods, monodielec./multidielec. regions, iterative solns. *(Spanish)* 80—106419
static field problems, numerical soln. algorithms 80—95757
stationary potential fields, theory, complementarity principle 80—63894
surface potentials of stratified spheroidal volume conductors excited by electric dipole source 80—32867
surface scattering from piecewise planar surfaces, algorithm 78—62983
synchronous machines, slot-less, armature and excitation field, analytical calc. method using polar coordinates *(German)* 80—32870
thermocouple branch, calc. 77—13751
three dielectric media image method for potential eqn., discussion and reply 79—3610
thunderstorm electric fields, 10-year study of Minneapolis area 78—57253
thunderstorms, electric fields produced in Florida 78—40621
transponder dipole antennas in and near three-layered body 80—98181
tube, ambient axial electric field, temp. depend. surface shielding effect 77—58221
two dimensional, computerised shape investigation *(Czech)* 79—27126
two spherical electrodes with equal radii, field calc. *(Japanese)* 80—28138
two- and three-dimensional in moving electromotive media, calc. methods *(Russian)* 77—53745
two-dimensional electrostatic field construction for energy analysis 80—9796
two-dimensional electrostatic quadrupole field, for ion beam deflection 78—5417
two-dimensional field with open boundaries, anal., exterior finite elements 78—22064
two-dimensional open boundary problems, finite element anal. 78—94354

electric fields continued
- variable space charge density, design, between hyperboloidal conic electrode and grounded plate *(Czech)* 80—87258
- variation during low solar activity *(Japanese)* 79—40032
- vertical single-pole earth sphere gap, voltage measurement influence of neighbouring surfaces *(German)* 78—29880
- weakly conducting layer, elec. field transient penetration 78—84525
- wedge in air-gap, resultant force anal. *(German)* 77—6967
- xeroradiography, physical theory and photon noise obs. 77—5072
- CO_2 laser, pulsed, elec. field distrib. in vol. discharge controlled by electron beam 80—58505
- ^{3}He, superfluid, B-phase, phase transition to inhomogeneous state induced by elec. field *(Russian)* 77—51566
- $LiNbO_3$ crystal, different interdigital electrode struct., electric field distrib. obs. 78—76433
- SF_6 breakdown voltage calc. *(German)* 77—15264
- SF_6 impulse breakdown characteristics for nonuniform field gaps for switchgear design 80—84024
- SF_6-N_2 mixture in rod-plane gaps, static field breakdown 79—68965

electric filters *see filters*

electric final control devices
- *see also electric actuators; electric motors; switches*
- static interruptor cct., triac, thermostatic and lighting control appl. *(Italian)* 78—73984

electric furnaces
- *see also arc furnaces; resistance furnaces*
- atomic absorption spectrometry, graphite furnace, atom loss mechanism 78—3389
- commercial, for case carburising 80—27310
- cylindrical induction furnace, velocity and EM field distrib. calcs. *(Russian)* 77—47106
- electrode heating, for electrolytic boriding 80—27309
- electrothermal atomiser using graphite braid, for at. absorpt. spectrosc. 79—34377
- emissivities of graphite, ThO_2 and W Knudsen cells heated by radiation *(Japanese)* 80—13073
- glass, melt, electrical resistance calc. in electric furnace 77—66165
- glass melting, 14 ton/day 79—58693
- glass melting process, TV monitoring, equipment protection 79—58756
- glass production 80—11620
- glass-melting, resist. between electrodes calc. 79—58690
- heat propagation in plane wall, temperature dependence on time and spatial coordinates 79—1054
- heating elements, SiC, elec. cond. 79—69510
- high-temperature, for NMR measurements up to 2000K 79—63214
- high-temperature minifurnace, homogeneous, 25 to 1600°C for NMR measurements 79—49235
- induction, cylindrical charge equivalent diameter *(Czech)* 79—50188
- induction melting, fluid velocity, large scale meas. and predictions 77—46985
- inductively heated high temp. furnace for photoelectron spectroscopy 77—82521
- laboratory, considerations for the prospective buyer 80—77788
- laboratory furnace, 2300K, oxidising atmosphere *(French)* 80—27311
- low-inertia reverb. furnace for alloy phase transforms. study by mag. method 79—2771
- MHD flow of liquid metal plane layer, industrial furnace appl. *(Russian)* 78—5817
- microprocessor triac interface, used to control kiln temperature 78—45632
- muffle type, automation of temp. regime 77—61068
- optical cuvette, high temp., for transmission spectra meas. over 2-13 μm, 300-1600K ranges 79—2839
- optical fibre drawing, neck-down shape prediction from furnace temp. distrib. 78—5594
- oxidizing furnace design, for integrated optics processing 78—9461
- plasma generation, investig. of gas conditions *(Russian)* 78—94921
- rotary hearth, modified SAZ 11.5.3/10 79—49232
- temperature control of suspended electric furnaces on tensile machines 77—82523
- thyristor power supply for optical glass melting 77—50780
- toroidal ellipsoid furnace, narrow zone heating by new radiation focusing 78—88424
- transformerless power supply 77—65035
- tubular furnace for thermal diffusivity meas., design 80—30182
- vacuum, for heat treatment 80—27308
- vacuum extraction device, with mass spectrum analyser, gas-forming admixture in metals determ. 80—22371
- vacuum furnace, optical fibre-drawing 78—66960
- vacuum furnace developments, heat treatment, high speed steels *(German)* 79—100174
- vacuum furnace for laboratory applications 79—71454
- vacuum furnaces for quenching developed in USSR 78—84872
- H high-temp. probe for proton magnetic resonance expts. 79—49234
- Pb crystal glass melting 79—58691
- ZrO_2 induction furnace for precision silica optical fibre drawing 78—1446

electric fuses
- coaxial high current discharge, exploding cylindrical foils in air, compression and expansion 80—38841
- constant current test method for fuseable links 80—73390
- high breaking capacity, arcing phenomena anal. 77—11425
- high energy Cu foil fuse for plasma implosion expt. 77—24218
- metal-filled epoxy resin, temp. variation, current interruption appl. 78—76124
- Al foil fuse, electrically exploded, surrounding medium effect 80—103207

electric generators
- *see also a.c. generators; d.c. generators; magnetohydrodynamic convertors; turbogenerators; Van de Graaff generators*
- cooling, H_2 production, onsite, by H_2O electrolysis 80—72097
- explosive electrical generator with resistive load, design and performance 77—55195
- explosive-magnetic generators, energy take-off to inductive load using circuit breaking 80—59323
- generator-motor model for physics classes 78—65739
- impulse current generators, H_2O as electrical insulator *(Russian)* 78—75430
- mains voltage generators, constructional theory and problems *(Slovenian)* 80—10451

electric generators continued
- radioisotope power generation, radiation techniques and technology development in the Soviet Union 79—685
- Stirling engine/generator for on-site electric power generation, pre-prototype perform. testing 80—30539
- superconducting, ht. transfer to liq. He in centrifugal acceleration fields, free convection and boiling regimes 77—89604
- wave energy conversion, directly driven generator design constraints 79—43725
- wind-powered, potential output calc. for USA 77—2205

electric glow *see corona*

electric heaters *see electric heating*

electric heating
- *see also dielectric heating; domestic appliances; drying; electric furnaces; heating elements; induction heating; ovens; radiofrequency heating; space heating*
- 10 kbar hydrothermal installation with internal heater 79—67333
- Auger electron spectroscopy blanking resistive heating cct. 77—29078
- blanking resistive heating for Auger spectroscopy and LEED using retarding field analyzer 78—54509
- coal gasification plant, high-temp. alloy evaluation for nucl. process heating 78—13237
- coal gasification plant using nuclear process heat, material corrosion 78—13348
- compound conductors, impulse heating, Cu vapour conc. determ. 80—75346
- continuous temperature gradient incubator, fungal growth 80—47044
- double helix vacuum resistance heater element design and construction details 78—49839
- electrolytic heating use in high-pressure chamber 80—17958
- finite cylindrical coil, temp. distrib. calc. *(Polish)* 77—54865
- fixed-pitch propellor wind-power plants, appl. 80—61260
- fluid heating mantle using heat-exchanger principles 78—93665
- fusion reactor, Doublet III, ohmic heating E-coil vacuum breaker system, function and operation 80—102323
- fusion reactor magnetic coil, Large Coil Program, test heater conceptual designs 80—91251
- heater, for static testing of riveted samples for short-term high-temp. strength determ. 79—87793
- Incoloy, evaluation for use in nuclear process heat appl. 78—13234
- industrial organic chemicals production, electrical power applications development *(French)* 79—96327
- latent cold work heat release kinetics meas. using adiabatic elec. heating 77—52344
- LMfBR, Na loop temp. control using 100 kW elect. heater *(Czech)* 80—5203
- LMFBR ML-3 Na circuit, electrical and control installations *(Spanish)* 80—57819
- long rod, direct-heating meas., interpretation 80—102964
- metal wire, heated by electrical current, steady-state thermal cond. 78—59285
- metals, heat content correlation under fast heating *(Russian)* 80—70426
- municipal wastewater treatment plants, mathematical modelling of electrical energy consumption and heating requirements 80—26194
- nuclear process heat system, material screening studies 78—13236
- nuclear steam gasification of coal, test and development of heat-exchanger alloy 78—15589
- ohmic heating system for TFTR Tokamak 78—55017
- optical communication fibre endface preparation by AC discharge heating and stretching 80—64232
- parallel connected ohmic heating coil for double Tokamak fusion reactor 78—54930
- pipe, of variable thermal and elec. conds., elec.-heated, flow-cooled, temp. distrib. 78—90626
- portable salt bath for rapid anal. of high speed steel, high frequency current heating 77—70256
- rapid heating attachment, for IMASh-5S installation 80—21230
- recreation centre, all-electric, camping ground water-heating systems *(German)* 80—16828
- regulator using a FET amplifier and Schmitt trigger convertor *(French)* 79—58681
- resistance thermometer sensor overheating, influence of meas. current *(Russian)* 79—26053
- SEM/STEM cold stage thick specimen heating model 78—61289
- sintering, ohmic, diffusion processes, temp. distrib. influence 80—92704
- steel, boiler, determ. of temp. distribution in specimens with thermal fatigue *(Russian)* 79—68542
- steel, high and low C, wires, electroheated, thermal cycling and corrosion behaviour 80—61006
- swimming pool outdoor, heating, heat pump appl. *(German)* 80—16781
- thermal length control, for lasers and etalons 78—87056
- thermal radiation sources, high-temp., for calibrating radiometers 80—17946
- thermoplastic sheet local fusion image recording and erasure *(Russian)* 77—57416
- utilization for energy conservation, review 79—24884
- window, thermal distortion 77—34952
- Cu wire, transient current pulsed heating, explosive inhomogeneous boiling explosive 78—38562
- MgO-spinel concrete, cast, hardening by elec. heating 80—21258

electric heating elements *see heating elements*

electric ignition
- automobiles, suppression of RFI at distributor rotor gap 79—55586
- discharge striking in highly inhomogeneous axisymmetric mag. field 78—75473
- low-pressure discharge striking in axisymmetric elec. and mag. fields 78—75472
- spark generator for dust explosion hazard assessment and gas ignition 78—57983
- thyratron ignition of gas lasers *(German)* 79—64245
- Xe lamps, for cine projection *(Russian)* 77—41719

electric immittance measurement
- *see also electric admittance measurement; electric impedance measurement*
- quartz crystal impedance and admittance bridge development 77—37944

electric impedance
- *see also electric reactance; electric resistance*
- alternating current electrode processes, review 80—61107
- anisotropic metals in perpendicular mag. field, surface impedance behaviour *(Russian)* 78—39145

electric impedance continued
- antenna in magnetoplasma, transmission line theory for impedance 77—39429
- antenna of revolution in cold collisional plasma, current distrib. and input impedance 77—24096
- antennas, horizontal, above infinite plane Earth, input impedance and current distrib. 80—90259
- antiferromagnetic superconductor, surface impedance 79—82709
- biological cell impedance transient response characterisation 79—53066
- blood impedance, effects of pulsatile flow *(Japanese)* 80—21513
- capacitor, coaxial and planar magnetoplasma, impedance characts. 78—42837
- cardiac impedance during elec. stimulation, depend. on electrode, pulse duration and acid-base balance 78—27929
- cardiac pacing, signal source impedance of implanted electrodes 80—56275
- chalcopyrite, nonlinear impedance of mineral-electrolyte interface 79—53338
- characteristic impedance of double line in front of dielec. wedge *(German)* 78—78855
- conducting ferromagnets, surface impedance resonance depend. *(Russian)* 79—91089
- conducting solutions, bridge method for meas. dielectric relaxation 80—82793
- cylindrical magnetic film, calc. of impedance and susceptibility *(Russian)* 77—89992
- cylindrically layered conductors, electromagnetic NDT 79—74318
- DC defibrillator discharge, contrib. of paddle electrode area and edge length to transthoracic impedance 80—3860
- dipole antenna in warm isotropic plasma, boundary-value problem, multiple water bag model 78—91115
- discontinuous metal film, AC equivalent circuit anal. 79—51690
- ECG electrode impedance and offset pot. 77—40874
- ECG electrode motion artifact reduction, electronic method 77—40872
- eddy current transducer, impedance introduced by nonmagnetic plate 78—60939
- eddy currents, calculation by dual energy methods 78—78859
- electric field probe, dielec. insulated, for field meas. in finite heterogeneous biological bodies 79—2170
- electrochemical cells, multicomponent impedance diagrams, resolution technique 80—66959
- electrochemical impedance, by rapid methods, transient Faraday process 78—27782
- electrochemical impedance simulation, by AC ladder networks 77—12806
- electrochemical kinetics at interface with space charge layer, appls. *(German)* 77—32807
- electrocrystallisation, impedance frequency dependence, in the case of DC superposition 78—51844
- electrode, corroding, impedance and polaris. resistance 79—83466
- electrodes, glassy-C, elec. props. 80—17157
- EM coupling, between two short circuited flat dipoles *(French)* 79—81320
- EM scattering, by slit infinite impedance plane 79—86110
- EM theory of surface impedance behaviour in vicinity of gratings 77—65557
- fuel cell, molten carbonate, scaled-up, performance and current distrib. model 80—55837
- galena, nonlinear impedance of mineral-electrolyte interface 79—53338
- glow discharge, tube impedance with and without metal cover 78—67508
- graphite, nonlinear impedance of mineral-electrolyte interface 79—53338
- hollandites, ionic cond., impedance, struct. 78—67856
- hollow-cathode arc discharge impedance/frequency characteristic obs. 78—67536
- human skin, experimental, theoretical study 77—81773
- impedance of a p-n junction by direct currents *(Russian)* 78—84285
- intestinal-prostatic impedance in bulls at ejaculation 78—40458
- ion-exchange membrane, all-round electrochem. investig. equipment 79—91970
- ion-selective electrodes, liq. membrane, free and supported, ion transport, bulk elec. props. 79—83534
- ion-selective electrodes, liq. membrane, free and supported, ion transport, interfacial kinetics, time depend. phenomena 79—83535
- ionic conductor, AC props. 78—47578
- Josephson-effect absolute noise thermometer, resolution of unmodelled errors 78—62196
- leg electrical impedance freq. characts. *(Japanese)* 80—56252
- liquid, small signal AC response, mobile charge recomb., theory 78—52005
- MBBA film, homeotropic nematic cell, subjected to ultrasound, impedance variations 79—41948
- metal, in mag. field normal to surface, reson. singularities of surface impedance 78—10495
- metal, surface impedance in mag. field, cyclotron waves 77—89787
- metal, surface impedance in mag. field 77—89786
- metal, surface impedance in magnetic field, Azbel-Kaner cyclotron resonance 78—87901
- metal, surface impedance near anomalous skin-effect limit, electron-electron N processes 80—100497
- metal electrodes, impedance props., chronic recording from mammalian nerves 79—12043
- metal film, RF impedance temp. and freq. depend. 77—4453
- metal film, surface impedance oscills. in perpendicular mag. field *(Russian)* 78—76165
- metal-metal point contact, α^2F depend. of electrical impedance 78—47848
- metals, surface impedance in mag. field, theory *(Russian)* 78—6427
- micropipet, for microvascular pressure meas., capacitive modulation 77—37080
- MISIM structure impedance and equivalent cct. 77—62998
- MOST, short channel, output impedance, thermal feedback effects *(French)* 80—15609
- moving lossy plasma, power reflection coeff. and surface impedance calc. 77—84445
- muffin tin struct., transverse shunt impedance of deflection waves *(French)* 80—5396
- NMR probe coaxial transmission line, optimum charact. impedance 77—53967
- organic molecules, adsorbed, Si-SiO_2 interface as electrode for electrical and ellipsometric meas. 80—15366
- p-n-p structure, variable-gap, impedance 77—43707

electric impedance continued
- piezoelectric transducer, eqn. for energy balance of piezoelec. medium 79—28684
- piezoelectric transducers, calc. using modified Auld's energy method 77—72126
- piezoelectric transducers, input electrical impedance expression, internal loss correction 78—53101
- piezoelectric transducers, surface-driven, input impedance calc. 80—35493
- plane wave at skew incidence on right-angled impedance wedge 78—90346
- plasma, complex nonlinear impedance of flat antenna 80—103130
- plasma probe, RF, ion sheath effects on impedance characts. 78—42818
- plasma triode ion beam production, anode design for reflex operation without impedance collapse 78—9862
- plethysmography, cuff blood press. meas. errors 77—40886
- plethysmography, pulmonary arterial press. rel. to thoracic baseline impedance 77—40888
- polyacrylonitrile, pyrolyzed, surface layer, anal. of elec. cond. mechanism by impedance diagram *(Japanese)* 78—23148
- polymer solutions, mol. diffusion coeff. meas. using impedance meas. technique 79—23328
- polystyrene, particles in dil. soln., bridge method for meas. dielectric relaxation 80—82793
- pyrite, nonlinear impedance of mineral-electrolyte interface 79—53337
- radiation and scatt. from wires and surfaces, free space impedance functions 78—86999
- reference electrodes for in vivo meas. 79—52687
- RF sputtering, impedance matching networks, experimental and design information 80—50555
- Schottkey barrier, high freq. rectification, transport theory 79—82660
- semiconductor diode, layer, HF characts. 79—7886
- semiconductors, antiferromagnetic resonance rel. to surface impedance, magnetoelastic contrib. 80—50200
- skin, simulation, equivalent circuit construction 77—5101
- skin impedance, Laplace plane anal. 79—39458
- skin impedance parameter dispersion and correlation 79—29518
- solenoid surrounding cylindrical conductor with surface crack, impedance and eddy currents calc. 80—23601
- solid, small signal AC response, mobile charge recomb., theory 78—52005
- sonar transducer, Langevin type, made from $Pb(Zr,Ti)O_3$ type 1 ceramic, performance characts. 80—79095
- steel, stainless, 18-8, impedance diagram in passive and transpassive state in Na_2SO_4 soln. *(Japanese)* 77—21318
- storage cell impedance theory and experimental data review 80—55667
- superconducting point contacts, Nb and Ta, 9 GHz complex impedance 77—28303
- superconducting weak link, RF impedance 78—14889
- superconductor, type II inhomogeneous, impedance in Shubnikov phase *(Russian)* 78—23212
- surface wave line, dielec. obstacle on impedance jump 78—18063
- tetrabutylammonium iodide/I solid/liquid electrolyte interface, impedance study 80—26031
- thin conducting films thickness meas. by skin impedance method 79—35673
- thin metal conductors, surface impedance oscills. in RF range *(Russian)* 79—91090
- thin-layer cell, concentration impedance, unequal diffusion coeffs. and 2nd-order reactions effects *(French)* 78—53214
- thin-layer cell, concentration impedance reactive and nonreactive diffusion effects *(French)* 78—53213
- thin-layer cell, fast reaction, kinetic consts., diffusion and conc. impedance 78—73053
- thoracic, model for cardiac-associated changes in man 79—25128
- thoracic electrical impedance camera for chest fluid meas. 77—40889
- thoracic electrical impedance sensitivity to blood volume changes 79—34543
- thoracic impedance cardiogram in acute exptl. aortic regurgitation 77—40890
- thorax impedance finite element model for cardiovascular and respiration meas. 77—40887
- transducer testing, using high-power DUMILOAD device 77—3707
- voltmeter, multiplier design 77—41649
- weakly polarised electrodes, faradaic impedance, elec. double layer effects 79—70351
- Ag/(α-AgI) interface, impedance meas., equivalent circuit parameters. calc., electrolyte defect struct. 78—59975
- Ag/$Na_2SO_4(WO_4)$, and Ag/$Ag_2SO_4(WO_4)$ solid cell systems interface form., intergrain contact growth 77—16827
- Al anode, implanted in heart-blocked dog, AC impedance and corrosion investig. 77—60297
- Al, anodisation, impedance meas. during 80—3236
- Al-CdS-Au structure, interfacial phenomena, complex impedance meas. *(French)* 79—42668
- β-Al_2O_3 polycryst. electrolyte containing cells, impedance and cond. relax. 79—100401
- β-Al_2O_3-Na_2O, electrolytes, electric modulus spectroscopy 77—84974
- β-Al_2O_3-Na_2O, single cryst., non-Debye capacitance 80—107497
- β-$Al_2O_3.Na_2O$ cryst. or sintered disc, Au electrode interface impedance rel. to roughness 77—4437
- Bi, surface impedance change, reflected RF EM wave interaction *(Russian)* 80—49867
- Bi_2O_3, anodic film, dielec. props. 77—20794
- $Ca_{1-x}Y_xF_{2+x}$, solid anionic conducting electrolytes, struct., elec. props. 77—84977
- Cd, electrodeposition on solid Cd or CdHg amalgam, rate, impedance meas. 78—52693
- Cd film, surface RF impedance in strong mag. fields *(Russian)* 80—92920
- Cd, surface impedance, Gantmakher-Kaner oscills. *(French)* 77—66195
- Cd, surface impedance, in mag. field *(Russian)* 78—19079
- CdS:Cu binder layer, photoactive, AC impedance meas. 80—25299
- CdTe, sputtered film, electrode effects in AC characts. from equivalence impedance meas. of metal-CdTe-Al struct. 79—82686
- Cr, discontinuous thin film, AC equivalent circuit anal. 79—51690
- Fe passive film AC electroreflectance and impedance obs. 78—7093
- GaAs electrodes, n- and p-type, freq. depend. of impedance 77—12001
- GaAs-AlGaAs DH laser, impedance meas. 78—17939
- GaAs-metal Schottky barrier diodes, impedance, freq. and voltage depend. 78—64114

electric impedance continued
$Ga_xIn_{1-x}P$, flat band pot., impedance meas. and photoelectrochemistry *(French)* 80—49894
GaP, n-, p-type, electrode, impedance in alkaline medium *(French)* 79—43586
GaP, single cryst. electrode, impedance, effect of freq., voltage and electrolyte comp. 78—19146
Ge:Au, current-voltage phase shift, impedance of subthreshold domains 77—43609
Ge:Au, moving elec. domain, impedance 77—1429
H_2 electrode, complex impedance *(French)* 78—27766
In, surface superconducting layer in high amplitude LF EM field *(Russian)* 79—78261
InSb, intrinsic capacitance in transverse mag. field *(Russian)* 79—91070
$Li_{1.8}N_{0.4}Cl_{0.6}$, fast ionic Li conduction, elec. conductivity and thermodynamic stability 79—65247
Mg-MnO_2 dry batteries, impedance parameters and state-of-charge 80—21390
γ-MnO_2 electrode, impedance in alkaline solns. 79—70350
Mo, RF surface impedance, new type of oscills. 79—15070
Mo, skin effect, Gantmakher-Kaner effect peculiarities *(Russian)* 80—49796
$Na_xIn_xSn_{1-x}S_2$, ionic conductors, ^{23}Na NMR and complex impedance meas. 79—91314
Nb film, superconducting surface impedance 79—24110
Nb, supercond. surface resistance derivative meas. for annealed and unannealed crysts. 79—33395
Nb_3Sn, vapour deposited, supercond., surface resist. and penetration depth 79—33392
Ni, electrocrystallisation, reaction mechanism, appl. of impedance meas. *(French)* 80—103597
Ni/Ni(II) electrode reaction in LiCl-KCl eutectic melt, impedance meas. *(Japanese)* 79—100392
$Ni_{1-x}O$, electronic cond. at high temp., complex impedance study, effect of defects *(French)* 78—79990
Pb-H_2SO_4 battery negative plates, impedance, theory 78—27771
$Pb_{1-x}Bi_xF_{2+x}$, solid anionic conducting electrolytes, struct., elec. props. 77—84977
β-PbF_2, complex impedance exam. 78—47579
PbI_2 single crysts., photo-induced AC impedance meas., photodielec. effect 78—52034
PbO_2(Pb) electrode, anodic impedance during suspension-electrolysis leaching of β-ZnS in 1N H_2SO_4 soln. *(Japanese)* 79—43594
PdO, free energy of form. using impedance dispersion analysis 80—108728
Pt electrode, H adsorption, dynamic impedance meas. 79—74393
Pt electrodes, elec. props., impedance meas. and time-domain anal. 78—40360
Pt microelectrode potentials and small-signal impedances 79—34716
Pt surfaces, oxidation by electrosorpt., of H_2, effect of soluble prods. *(German)* 80—55717
Pt/Y_2O_3-ZrO_2/Pt cell, Faradaic reaction kinetics, impedance dispersion anal., electrode/electrolyte interface process 79—11798
Se, amorphous, monostable switching, current noise 80—44682
Si, surface characterisation by Si-electrolyte interface impedance meas. 78—84291
Si:Zn, P^+-n-n^+ struct., deep doubly ionized centres, impedance calc. 79—11202
Si:Zn, reson. characts. of impedance near excitation threshold of recomb. waves 80—20301
Sn, surface impedance change, reflected RF EM wave interaction *(Russian)* 80—49867
Sn, surface superconducting layer in high amplitude LF EM field *(Russian)* 79—78261
Sn thin-film superconducting bridge microwave impedance anomalies 79—7942
ThO_2:Y_2O_3, electrochem. cell, complex impedance, temp. and freq. depends. 77—1458
TiO_2 electrodes, chemically modified, nature of surface states 80—107905
n—TiO_2-electrolyte interface, equivalent circuit elements from impedance meas. 80—39669
n-TiO_2-electrolyte interface impedance, freq. depend., equiv. cct. 80—100516
W film, surface RF impedance in strong mag. fields *(Russian)* 80—92920
W microelectrode potential and small-signal impedances 79—34715
W plate, impedance oscillations in mag. field 78—39140
W, RF surface impedance, new type of oscills. 79—15070
W, surface impedance and HF cond. in strong mag. field, thin single cryst. plates *(Russian)* 77—89831
W thin plate, oscillations of surface impedance in circularly polarised RF fields *(Russian)* 78—39144
WO_3 semiconducting electrode, influence of surface states, impedance meas. *(French)* 77—1468
WO_3 thin film, Li diffusion, appl. of AC techniques 80—70468
Yb_2O_3, electronic cond. rel. to partial press. of O_2 of high temp. *(French)* 80—59979
Zn, electrocrystallisation, reaction mechanism, appl. of impedance meas. *(French)* 80—103597
Zn-MnO_2 dry batteries, impedance parameters and state-of-charge 80—21390
ZnO pellets, and ZnO:Li single crysts., photo-induced AC impedance meas., photodielec. effect 78—52034
p-ZnTe, interface impedance in KOH electrolyte soln. *(French)* 77—51814
ZnTe, photoinduced dielec. loss and capacitance changes, rel. to space charge polarisation 80—2417
ZnTe-electrolyte interface, electrochem. behaviour of single crysts. 79—91138
ZrO_2-Y_2O_3 superionic cond. cell, complex impedance 80—10702

electric impedance measurement
see also electric reactance measurement; electric resistance measurement
abdominal fluid accumulation meas. 77—48912
AC impedance meter, battery-operated, for contact resist. determ. before patient monitoring 78—81006
acupuncture point location using elec. impedance meas., statistical anal. 78—44628
acupuncture points Li-4 and Li-12 Laplace plane analysis of transient impedance 77—81772

electric impedance measurement continued
AF impedance bridge, 4-terminal-pair, 40 Hz to 2 kHz 79—88978
arterial impedance plethysmographic signal quantitative interpretation 79—57742
bacterial growth detection by impedance meas., electrode characts. 77—60325
bioimpedance, four-point probe technique 77—17000
bioimpedance monitor 77—40845
biological impedance automatic recording system 78—44625
biological impedance meas. using 4-terminal instrumentation system for oedema detect. 78—48853
biological tissue, vector impedance meter 78—57138
biomedical plethysmography, origin of impedance changes measured in the human calf 80—56269
body fluids meas. by basal thoracic elec. impedance 78—48852
bone bending stiffness determ. by LF impedance probe 79—96695
brain impedance scanner principles and exptl. results 79—57804
brain impedograph, computerised 78—77139
brain tissue specific-impedance meas. four electrode method 78—3647
capacitor loss-angle and capacitance checking cct. 77—61085
coaxial waveguide wave impedance, USSR special standards 77—30182
complex impedances in RF range, meas. using Maxwell bridges 80—98931
complex mutual inductance concept for bioelectric impedance transformer bridge 80—63886
controlled-current impedance meas. equipment design *(Spanish)* 78—8421
cross-capacitor method *(Chinese)* 80—77815
cross-correlator for broad-band impedance meas. using high-speed CMOS switches 77—26324
cryotumourectomy control with LF impedance meter 77—25591
defibrillator electrode gel testing, meas. of impedance to transthoracic DC discharge 78—57056
disc impedance meas. and US transducer CAD program 79—46157
electrochemical impedance meas. method, automatic, computerised data anal. 77—70307
electrochemical system, LF impedance meas. technique using on-line computer 80—57339
electrode, accuracy of parameter meas. 80—61108
electrodes, using AC ohmmeter 79—67342
electrolytes, solid oxide, elec. props., study methods *(French)* 80—22386
electroplethysmograph for regional lung function evaluation 77—21647
exercise stress testing with continuous noninvasive cardiac monitoring 78—36000
high-quality voltage follower input impedance and transfer factor meas. 77—13772
impedance probe calibration, for vacuum meas. in single component two-phase mixture *(Italian)* 80—62677
implantable cardiac pacemakers, non-polarizable stimulating electrode development 79—92428
LF 4-probe meas. system for studying biological system 78—7554
limb pulse origin, separation of blood vol. and resist. change 77—40891
low impedance instrument using 1 KHz source *(German)* 77—13767
meter, high-speed, for electrochem. system obs. 79—30490
microprocessor-based instrument, method, advantages 78—89501
microwave losses in materials, by resonance input impedance method *(Czech)* 77—26326
natural VLF antenna, Deception Island, impedance meas. 79—48399
network parameter automatic meas. methods and systems 77—57363
oedematous tissue quantification by elec. impedance meas. 78—44630
oesophageal geometry changes in swallowing, transduction, for animal grazing studies 80—76888
pacing impedance determination in man from resist. meas. 78—40417
paediatric pneumogram patterns 80—3749
physiological tissues, guard ring appl., critique 78—7462
pipeline leak location by coaxial test cable characteristic impedance variation 77—57317
planar slow wave structures, interaction impedance meas., theoretical study 79—80586
plant water content meas. using high-sensitive impedance meter *(Japanese)* 77—5125
plasma sheath, metal probe-gas discharge plasma boundary, impedance parameter variations 77—58869
plethysmography, eval. for venous vol. meas. 77—40885
plethysmography, influence of erythrocyte vel. 78—61238
plethysmography and appl. of finite-element method, torso model and elec. potential distrib. 80—30958
pulmonary oedema detect. by quantitative elec. impedance plethysmography 78—31951
radial arterial deformation meas. based on impedance rheography 78—3545
radiating magnetostrictive transducers, impedance determ. 79—32173
rheography, integral method and electrode for exertion function tests 77—77995
rheoplethysmography, for study of artery function *(French)* 77—37075
rheoplethysmography with occlusion, for study of vein function *(French)* 77—37076
skin, human, circuit 79—20607
skin impedance dynamic meas. system 79—57744
solid electrolyte, polycryst., impedance and modulus spectroscopy 77—12309
superconducting thin film, RF complex impedance meas. 80—84573
thoracic impedance of humans, meas. using automatic recording device on defibrillator 78—61239
thorax, impedance camera for spatially specific meas. 78—53464
thrombophlebitis diagnosis, reliability of Doppler and impedance techniques 78—77144
tissue impedance meas. by phase-sensitive voltage and current detection 78—53602
tissue mutual impedivity spectrometry 80—17046
transthoracic impedance curve processing, patient-computer interface 79—34686
vaginal impedance meas., cattle, proposed instrumentation for optimum insemination time determ. 80—36210
waveguide impedance meter verification scheme 78—37035
waveguides, coaxial, analyzing errors of standard measures when calculating step discontinuities, 1 to 2 GHz 79—80643
Cu-Ni alloys 706 and 715, corrosion in flowing sea water, dissolved sulfide effect 80—35379
Ni-Cd battery, state-of-charge nondestructive determ. 79—57423
Pb-acid battery charge determ. from internal impedance 79—96436

electric impedance measurement continued
- Se photoconductive layers, impedance-freq. characts. meas. *(Japanese)* 79—38120
- Zn electrodeposit dendritic growth control using impedance meas. 78—84721
- ZnO-resin photoconductive layers, impedance-freq. characts. meas. *(Japanese)* 79—38120

electric load *see load (electric)*

electric locomotives
- *see also motorcoaches*
- aerodynamic noise generated by high speed electric train 79—18591
- traction motor, circuit fault detection by NDT method 79—39097

electric machine analysis computing
- Faraday-type MHD generator optimisation, using a computer method *(Polish)* 78—79476
- liquid metal MHD loop dynamic analysis 77—39479
- magnetic field calc., saturable, by finite element method, using scalar magnetic potential 77—38773
- magnetic field computation, conference, Grenoble (1978) 79—41262
- plane permanent magnet system field distrib. model *(Russian)* 80—28133
- slotted boundary machine field soln., conformal transformation and integral methods 79—41272
- turbogenerator, electrical and magnetic fields computation, using ELMAG program system *(German)* 77—3516

electric machine CAD
- diagonal-wall MHD generator design optimisation by nonlinear programming *(Polish)* 78—79477

electric machine computer aided design *see electric machine CAD*

electric machine testing *see machine testing*

electric machine theory *see machine theory*

electric machines
- *see also a.c. machines; d.c. machines; electric generators; electric motors; machine bearings; machine insulation; machine testing; machine theory; machine windings; rotors; small electric machines; stators; superconducting machines*
- acoustic noise generation mechanisms and characteristics, selecting quiet equipment and correcting noisy devices 80—64286
- acoustic noise meas. errors *(Hungarian)* 80—96102
- active parts electrodynamic equations general solutions using orthotropic modelling *(Russian)* 80—99601
- air cooler using evaporative thermosiphon, design nomogram 77—71194
- automatic testing, of rotational speed, using digital measurement method, in steady or transient regimes *(Czech)* 79—71419
- eddy current problems, three dimensional, network analogy *(Japanese)* 79—81325
- electric arc, self magnetic field, kink instability, plasma jets production *(Polish)* 80—19662
- end zone magnetic field calc. using approx. analytic method 80—106416
- ferromagnetic components, magnetisation characts. approximation *(Russian)* 78—31094
- noise control, conf., W.Lafayette, IN, USA (Apr/May 1979) 80—43526
- noise level meas., outside condensing power plant, with four 200 MW blocks *(Czech)* 79—57548
- nuclear power plant machinery surveillance and diagnostics automation 79—641
- power plant dynamics and control, conf. Hyderabad, India (Feb. 1979) 80—91215
- quasi stationary short arc, anode spot mathematical model temp. field calcs. *(Polish)* 80—19664
- rotating machine in nuclear power plants, vibration monitor 78—13299
- vibrations anal. and obs., block deformability influence *(Italian)* 78—51108
- volts-per-bar and flashover, causal mechanisms and preventive measures 80—92408

electric moments
- *see also atomic electric moment; molecular moments; nuclear electric moment*
- alkali halide:NH_2^-, paraelectric alignment, UV electroabsorpt. and Kerr effect 77—12413
- alkali halide, electric-dipole ordering of tunnelling impurity centres 80—2215
- baryon electric dipole moments in CP noninvariant Kobayashi-Maskawa theory *(Russian)* 80—105897
- bond polarity parameters, IR intensities, molecular orbital study 79—63914
- carnauba wax thermoelectret, mag. anisotropy evidence for dipolar orientation 77—16240
- colloids, macromolecules, particle size distribution, reduced electric dipole moments, polarisabilities using electric birefringence 78—95958
- current density and electric and magnetic multipole-moment operators in quantum mechanics 80—27433
- t-cyanobutane, dielectric relaxation study, complex permittivity 80—80688
- derivatives in IR intensity theory, with respect to symmetry coordinates *(French)* 77—88389
- dichlorophenol isomers, elec. dipole moments determ. *(Spanish)* 77—69762
- diffraction of electric dipole on system of two concentric spherical segments *(Ukrainian)* 80—23603
- 1,1-difluoroethylene, dipole moments in ν_4 and ν_9 states 79—36694
- dipolar crystal, surface local field effect, dipole moment, self consistent electric field calcs. 80—49178
- dipolar hindered rotators, dielec. response calcs. 77—24781
- dipole moment laboratory experiment 77—57116
- dipole pseudo-spin glasses, collective excitations 80—59617
- dipole relaxation in electric field, teaching 80—90625
- discrete stochastic electric double layer, electrostatic props. 79—96318
- disperse system, electro-optical effect, use of two-phase Rc field 79—55060
- DNA solution, elec. birefringence, stabilised induced dipole behaviour 80—85349
- education, electron-dipole system, min. dipole moment for binding, historical development 77—78926
- electric dichroism spectroscopy 78—1013
- electrolyte solution, second moment condition of Stillinger and Lovett 77—90609
- electron, elec. dipole moment, quantum supercond. interferometric meas. *(Russian)* 78—37158

electric moments continued
- EM interactions, gauge formulation, SU$_\tau$(2) internal symmetry and P- and CP-violation *(Russian)* 80—42368
- equivalence charge concept, appl. to electrostatic energy of charges and multipoles 79—18323
- fermions, information from potential scatt. *(Russian)* 79—5998
- ferroelectric, eight-site order-disorder model, influence of tunnelling 80—2709
- ferroelectric, ion-ion interaction due to soft phonon modes 79—99838
- fluoromethane, ν_3 band Lamb dips, effects of RF elec. field modulation on Stark spectra 80—52989
- frequency-dependent electric and magnetic multipole moments and Siegert's theorem 80—27432
- glasses, echoes and elec. dipole echoes at low temps. 79—69771
- heavy atom, parity violation in forbidden mag. transitions, chiral absorpt. of polarized light and circular dichroism in crossed DC fields 80—23370
- heavy ice Ih (D_2O ice), dielec. props. 80—29671
- hydrocarbons, IR intensities, polar tensors, atomic population densities 77—23497
- ice III, dipolar correlation factor and dipole moment of water molecule 79—77548
- induced neutron electric dipole moment, MIT bag model anal. 79—63430
- iodomethane-d_3, Stark tuned level crossings and saturated absorpt., RF elec. field modulation effects 80—52989
- ionic conductor, elec. dipolar coupling between intracell dielec. response and intercell hopping response 79—55918
- ionic crystal, surface stability 80—20016
- light emission by mag. and elec. dipoles, radiation patterns 80—32886
- linear gyrotropic media, E2, M1 moment contribs. to linear polarisation *(Russian)* 77—8540
- muon, electric dipole moment meas., new upper limit 78—37209
- neutron, and strong P and T noninvariances in gauge theories with manifest L-R symmetry 79—63372
- neutron, dipole moments and spin rot. meas. 79—36080
- neutron, electric and magnetic dipole moments 80—4993
- neutron, electric dipole moment, ultracold neutron technique *(Russian)* 79—75775
- neutron, expt. determ. and degree of precision, review 79—58961
- neutron, fundamental physics with reactor neutrons and neutrinos [conf. ILL, Grenoble, France (Oct. 1977)] 79—59112
- neutron, in SU(2)×U(1)×SU$_F$(2) gauge symmetry 79—89091
- neutron, prediction in six-quark model *(Russian)* 79—93379
- neutron dipole moment using ultra cold neutron source, expt. current status and results 80—37678
- neutron dipole moments and spin rotations 78—74296
- neutron electric dipole moment, expt. determ. of non-zero value employing ultra cold neutron storage methods 79—58963
- neutron electric dipole moment, expt. search 77—26555
- neutron electric dipole moment, search using ultra cold neutrons 79—67551
- neutron electric dipole moment in Kobayashi-Maskawa model 79—93417
- neutron electric dipole moment search with ultra-cold neutrons, expt. set-up 80—37270
- nonpolar molecules, adsorbed on metal surface, depolarisation interaction 78—51820
- nucleon structure function, quark and gluon moments, gauge theory 78—50036
- organic binary liq. mixture, relax. times and dipole moments, RF and microwave obs. 77—12308
- particles with anomalous moments, motion in external EM field *(Russian)* 79—9321
- polar liquid, electric double layer at surface 78—53212
- polar liquids soln., mol. electric dipole moments, extrapolation formula 79—38437
- polarizabilities of proton and pion, sum rule relation *(Russian)* 79—93420
- poly(1,3-dioepane), dipole moments, dielectric const. meas 80—66099
- polyacrylonitrile, elec. polarisation 80—7275
- polyelectrolytes, saturation of induced dipole moment, orientation mechanism and electro-optical effects 80—84785
- polynucleotide solution, elec. birefringence, stabilised induced dipole behaviour 80—85349
- polystyrene interfacial colloidal crysts., microscopic obs. 80—97737
- propanes, substituted, dielec. relax. in liquid state 77—8500
- proton electric polarisability 79—49524
- QCD, neutron electric dipole moment, chiral estimate, current algebra, CP violating reactions 80—27471
- quark electric dipole moment from CP noninvariant gauge theory, left handed currents *(Russian)* 78—74218
- quark electric dipole moment in Kobayashi-Maskawa theory with gluonic corrections *(Russian)* 80—86688
- quartz, smoky, γ-irrad., electric dipolar echoes 80—20604
- radially symmetric reradiating scatterers in EM fields, formulae for simple treatment *(German)* 80—87270
- radiowave propagation over curved anisotropic surfaces, fields for horizontal and vertical dipole excitations *(Japanese)* 78—42266
- Reissner-Nordstrom gravitational field, electric dipole *(Russian)* 79—21611
- Rochelle salt type cryst., dipole interaction symm. aspect 77—20805
- SU(2)×U(1) gauge theories of leptons, T violation, leptonic decay and dipole moment 79—299
- SU(6) exotic gauge model, neutron electric dipole moment upper bound estimate 78—12875
- thermodynamic properties of permanent dipoles on lattice 78—88246
- unstable particles in electric field, physical meaning of Zel'dovich dipole moment 79—36594
- unstable particles in electric field, Zel'dovich dipole moment 77—74627
- zeolite-S layers, high-temp. activated dipole moments in S clusters *(Russian)* 80—20575
- $\Delta(1236)$ M1 and E2 photoexcitation $N \to \Delta$ in $\gamma N \to \pi N$ 78—70377
- e dipole moment, experimental searches 80—77996
- μ dipole moment, experimental searches 80—77996
- $\mu^\pm$, anomalous mag. moment, elec. dipole moment, and test of relativistic time dilation 79—45088
- n electric dipole moment, CP violation in gauge theories 80—91041
- n electric dipole moment, quark and gluon corrections 80—4994
- π photoproduction on N, multipole $E_{1+}^{(3/2)}$ and its double zero at reson. $\Delta(1232)$ 79—40790

electric moments continued
ρ-meson, EM form factor, elec. quadrupole and mag. dipole moments 78—12913
Ar+N_2(O_2, CO), molecular fluid mixtures, equilibrium props. 80—64867
Au, surface dipole moment calc. 80—60060
BaF_2:R^{3+} (R=rare earth) dipole reorientation, ionic thermocurrents obs. 79—95705
GeH_2, centrifugal-distortion dipole moment, CO_2 laser spectroscopy 77—75331
H_2, quantum cryst., short-range corre. and motional renormalisation of anisotropic interactions as function of density 80—34272
KCl:CN^-, paraelectric reson. study, tunnelling parameters and elec. dipole moment 80—25326
KCl:Li^+, coherent excitation by EM and acoustic waves, induction and echo signal study 78—67773
n, electric dipole moment using ultracold neutrons 80—82974
N_2+O_2, molecular fluid mixtures, equilibrium props. 80—64867
NH_4Cl, Raman scatt. of light on limiting and nonlimiting dipole vibr. 80—11402
NH_2D, dipole moments effects of RF elec. field modulation on IR stark spectroscopy 80—52989
Pt, surface dipole moment calc. 80—60060
SiO_2 fused glass, coherent elec. echoes 79—61300
SiO_2 glass, Suprasil I, electric dipole moment distrib. of values 79—61299
SrO:Co, noncentral and interstitial ion complexes, ESR obs. 80—71169
W, surface dipole moment calc. 80—60060

electric motors
see also a.c. motors; d.c. motors; fractional-horsepower motors; linear motors; permanent magnet motors; stepping motors; torque motors
ball bearing electric motor, for teachers 79—21488
ball-bearing electric motor construction 80—67997
coal crusher, shaft breakage, US detection 77—77716
electromechanical deflector with quasi-time-optimal scanning control *(Russian)* 77—58431
electronic-micromechanical interactions, conference, Lausanne (1976) 77—30140
gearless telescopic drive, transference from elec. motor to polar axis 80—67571
generator-motor model for physics classes 78—65739
ribbed frames with external fans, heat transfer coefficient measurements *(Hungarian)* 80—87709
rotating mirror deflector motor and control system selection 77—58484
two-phase, AC, rotor vibration reduction method *(Japanese)* 77—45704
Fe-Si, non-oriented sheets, production and props. 80—88797

electric networks *see networks (circuits)*

electric noise measurement
300 MHz oscillators using SAW resonators and delay lines 78—59255
600 MHz to 1 GHz coaxial thermal noise standard 80—98875
amplifier, voltage sensitive 77—88353
amplifiers, noise figure, measurement by connecting source resistance between input and output *(French)* 80—68214
atmospherics, radiometer exp. at 30 GHz, ATS-6 satellite link appl. *(Dutch)* 78—7742
automatic anomalous noise meas. for ferroelectric capacitor parameters, not in equilib. *(French)* 78—74029
circuit component LF noise meas. arrangement 77—13776
composite amplifier-discriminator cct., RMS noise meas. 77—54473
education, elec. noise and Boltzmann's const. determ., absolute temp. scale noise thermometer 78—36767
frequency anal., optimized octave, half-octave and third octave bandpass filters *(German)* 79—64470
level meter error detection method *(Russian)* 79—67244
magnetoresistive head Barkhausen noise voltage meas. 79—82821
membrane noise analysis by integral spectrum procedure 77—48958
membrane noise spectral density measurement, use of octave filters 77—48957
microwave noise standards, Japanese, 10 GHz system *(Japanese)* 78—57985
MIM cathode, method and its appl. to Al-Si_3N_4-Al system 78—2998
noise immunity control and meas., methods *(Russian)* 77—42663
noise thermometer, thermodynamic temp. meas. of ^{4}He at various vapour pressures 80—27298
ohmic contact 1/f noise intensity and contact resistance analysis 77—62982
passive thermostat for electronic noise meas. 77—2654
phase noise meas. with high-resolution counter and online calculator 77—37945
photodetector noise power spectrum density meas. 78—21197
resistive channel, perturbation of homogeneous current path by stub 77—43677
rotating noise sources, correl. meas. method, math. model construction *(Croatian)* 77—39150
search coil magnetometer testing and calibration *(German)* 77—49754
semiconductor in nonlinear region, spectral noise meas. between 30 and 400 MHz, pulse technique device *(German)* 79—47134
solar cell device reliability estimation using noise spectral density meas. 80—93896
SQUID noise thermometer, future of superconducting instruments in metrology 79—26020
thermal noise, zero point energy noise term presence 80—68213
thermocouple time constant measurement by cross power spectra 77—30145
transistors, noise figure, measurement by connecting source resistance between input and output *(French)* 80—68214
for very low impedances using impedance transformers, freq. range 1 KHz to 1.5 MHz *(French)* 77—145
Al thin films 1/f noise, depend. on internal mech. stresses 80—65711
PbTe, semiconductor polycrystalline thin films, low-frequency 1/f noise meas. 80—15629

electric potential
see also contact potential; overvoltage; surface potential; voltage control; voltage measurement
anodic film form., electrode pot. variation rel. to nucleation, growth 78—68634
back diode amplifier, use at low temp. 80—57324
binary liquid alloys, electrode pot., rel. to intermetallic compound content 78—9940
capacitor, charge difference phenomena *(German)* 79—36810

electric potential continued
charge superposition modified method for elec. field calc. 77—27218
charged disc or sphere in concentric hole of grounded sheet, capacity 77—14635
charged nonconducting disc and metal sphere, pot., field strength and charge 77—46668
charged particles, equilibrium space distrib. *(Russian)* 79—22887
charging current generated during liquid hydrocarbon filtration 77—55082
collisionless magnetized cosmic plasmas, non-resistive electric potential drops 80—31204
computation of potential surfaces for diverse configurations, program 77—22401
conducting plane, infinite, nonuniform, with radial conductance distribution, calc. *(Russian)* 79—7051
constricted conducting cylinder, potential distrib. 77—88617
crack length determ. by electric potential meas., automatic instrument *(German)* 79—96258
cylinder, infinite length, Green's function anal. *(French)* 80—28140
dielectric, electrostatic potential distrib., new meas. method *(French)* 77—143
dielectric, potential distrib. determ., new method 77—26336
dielectric block, solid, between point-plane electrodes, treeing inception conditions calc. *(French)* 77—38771
dielectrics, potential distrib. determ., non-destructive method *(French)* 80—40060
dielectrics pot. perturbation, non-exponential decay and correlated systems dynamics 79—73882
distribution about point current source, numerical technique 79—92617
distribution in dielec. meas., radiation method 77—41640
Earth surface hydraulic fractures mapping technique 78—69543
ECG electrode impedance and offset pot. 77—40874
electrochemical systems, current and potential distrib. calcs. 77—21394
electrode resistance, effect on current density and electrode pot., rel. to cell design 77—60070
electrode-electrolyte systems, absolute half-cell EMFs and single ion free energy of solvation 77—73449
electrolysis in W-tube, anomalous pot. and temp. grads. 77—60073
electromotive force: Volta's forgotten concept 80—73143
electron beam, nonuniform elliptic, inside hollow cond. of elliptic cross-section, elec. pot. and field *(French)* 77—50582
electron optics device, pot. soln. for symm. rectangular stepwise const.-pot. boundaries 78—46506
electrostatic half-space lattice sums, new inversion formula 77—58224
electrostatic potential, laboratory and theoretical comparison 80—105461
electrostatics, influence of geometric and electric parameters of system *(French)* 80—48118
EM beam in circ. cylinder, reciprocity theorem derived from Green function *(French)* 78—42260
EMF, pot. difference, voltage, for teaching 79—58478
EMF, potential difference and voltage, definitions 78—12469
EMF production by shock compression of solids 77—31719
fatigue crack closure determ. using elec. pot. method, cf compliance method 78—5701
ferromagnets, cyclically remagnetised, discrete spectra of induction calcs., demagnetising factor 80—103859
force on conducting sphere due to charge on dielectric halfspace 77—3511
galvanic cell, reversible, thermodynamics, EMF rel. to temp. 77—1935
gap between flat plate and cylindrical electrode with cone-shaped end, calc. method *(Croatian)* 80—99600
gas flow, nonequilib. ionisation and Hall EMF 80—69981
glow discharge tube, EM MM-wave detection properties in mag. field 80—70059
graphite arc, in Ar flow, meas. of anode voltage drop 80—84022
heterogeneous dielectric, Dirichlet problem, Green's function method 78—37782
induction flow-meas. theory for poorly conducting fluids 78—38429
ion cyclotron resonance cell, elec. pot. improvement 79—2875
ionosphere, dynamo currents from EMFs at different latitudes 77—64524
ionosphere, high-latit., elec. pot. soln. for field-aligned current sources 80—72674
Kerr black holes, charged current loop field and pot. 78—40988
Laplace's equation, periodic Green's function, solution method 77—82370
limited ion-dipole system, screened pot. *(Russian)* 78—66707
lunar surface, intense local photoelectric charging in sunset terminator region 77—45330
lunar terminator, localised photoelectric supercharging with progression of sunset 77—45331
magnetosphere, electrostatic shocks, double layers and anomalous resistivity 78—45152
mapping theory of two-dimensional anisotropic regions 79—55022
Martin steel, thermoelectric determination of C content during melting 77—56276
membranes, mosaic, charged, thermal membrane pot. 79—34358
metal, EMF appearance due to mag. field and laser pulse irrad. 77—76797
metal-dielectric interface, static point charge in dielec., pot. distrib. *(Russian)* 80—60088
metal-polyethylene terephthalate metal system, electrochem. effects as source of EMF 79—87163
metal-polyethylene terephthalate-metal struct., electrochem. effects as source of EMF 78—72278
metal-polyethylene terephthalate-metal system, electrochem. effects as source of EMF 79—87162
metallic films, vapour deposited on polymer, ageing, adhesion, elec. cond., electrochem. pot. *(Russian)* 79—33362
metallic tethers in ionospheric plasma, current and pot. distrib. 78—69652
MHD conduction channel, optimal operating characts. calcs. *(Russian)* 78—47190
MHD generators, technique for boundary layer voltage loss determ. 77—72507
MHD generators, Window-Frame, with nonuniform velocity and conductivity in transverse plane, electric effects, anal. 79—68960
Moon, interaction with plasma sheet rel. to near-surface pot. at Apollo 14 site 77—2354
myoelectric multistate channel for multifunction powered prosthesis, signal processing 77—44837
normal modes at small polyhedral particles 77—58225
oxide-electrolyte interface, transition layer model 78—68895

electric potential continued
- phosphate ester, electrical prop. rel. to lubrication 79−38150
- photoelectret, internal counter-EMF determ. by pot. meas 80−45003
- plane-parallel potential fields calc., in mixed boundary conditions *(Rumanian)* 78−82877
- plasma, magnetised, double-layer characts. meas. 80−43874
- point source in angular region of heterogeneous media *(Chinese)* 79−68342
- potential distribution around point charge in three dielectric media, calc. using image method 77−42459
- potential theory, higher-order approximations for integral eqns. 79−22877
- potentiostat, microprocessor controlled, for electrochem. meas. 79−85133
- Procopiu effect EMF in ferromag. material under torsion *(Rumanian)* 78−86986
- pulsar polar caps, pot. drops and ultrarelativistic particle accel. along curved mag. field 78−53970
- resistive films, AC and DC characteristics, algorithm anal. *(German)* 77−55618
- RF discharge, electrode voltage drop 78−9875
- ring, charged, insulated, electric field calc. *(Czech)* 79−64142
- rocket carrying electron gun, electrical potential determ. device 79−21146
- rotation induced electromotive forces in normal and superconducting metals 79−24120
- satellite charging at geosynchronous orbit during eclipse 79−16792
- satellite plasma sheaths, streaming instabilities, elec. equilib., one-dimens. particle simulation 77−22036
- semiconductor, transverse pot. in acoustoelectric effect 77−35967
- skin potential artifact reduction in biopot. recording 77−40873
- stationary potential fields, theory, complementarity principle 80−63894
- sulphide melt, conc. EMF meas. using solid-electrolyte cell 77−40571
- Sylevester's criterion applied to Poisson's eqn., quantitative proof of Earnshaw's theorem 80−87261
- thermal energy, electrochem. conversion using cells with reversal of pot. with temp. 80−26124
- thermocouple transient EMF response under reactor conditions 77−71320
- thermocouples stability obs., Nicrosil-Nisil, 538°C to 1177°C, production furnaces appl. 80−68198
- thick ellipsoidal coil and ferromagnetic ellipsoid system, vector potential 79−41269
- three conduction sphere system, field potentials and forces *(Russian)* 80−37935
- two coaxial circular discs in a free space, electrostatic pot. problem 79−76542
- two spherical electrodes with equal radii, field calc. *(Japanese)* 80−28138
- two-dimensional potential fields in complex media *(Slovak)* 78−94351
- unit realisation progress *(German)* 78−160
- vanadate polystyrene based membranes, parameters, biionic pot. 79−57294
- zone electrophoresis, voltage gradient, rel. to resolution 78−31649
- Ag, electrode pot. effects on surface plasmon excitation 78−15149
- Ag filaments, cryst., electrolytic growth in Teflon capillaries, differential-capacity meas. 77−40552
- Ag-AgCl/KCl/AgCl-Ag thermocell, and thermal liq. junction pot. for KCl solns. at high temp. 80−16819
- Ag-β-Al_2O_3, test for solid electrolyte by EMF meas on Ag/Au couples *(German)* 80−104307
- Ag-Zn, molten, EMF meas. of activities using ZrO_2 solid electrolytes *(Japanese)* 80−88339
- AgBr crystals, electrical potential distrib. near interface, recording using automatic device 79−24759
- AlZnMgCuO.5, static crack growth, stress state effect, elec. pot. meas. 78−7007
- Au, electrode pot. effects on surface plasmon excitation 78−15149
- Au^-, electrochemical generation, oxidation, standard pot., in liq. NH_3 79−100386
- Au-Zn, molten, EMF meas. of activities using ZrO_2 solid electrolytes *(Japanese)* 80−88339
- $Ba_{100}Ti_{101-x}Sn_x$+0.3 at.%Sb, intergranular capacitor, effect of microstructure on electrical props. 79−34160
- Cd-Pb(Sn)(Bi) alloy, molten, EMF meas. of liquid separation 78−39747
- n-CdSe, partially illuminated single crystal, current-voltage characteristic and potential distrib. 79−65519
- Cu wire, drawn through diamond die, deformation zone EMF *(Russian)* 77−81327
- Cu/Cu+Fe low-temp. thermocouples thermo EMF, strong magnetic field effects 78−220
- Cu-Hg amalgam electrode, standard pot. 78−76874
- Cu_2O, standard free energy of formation, by EMF method with solid oxide electrolyte at low temps. *(Japanese)* 80−88338
- $Cu_3(PO_4)_2$, polystyrene based membranes, parameters, biionic pot. 79−57294
- Fe, cast thermoelec. method of Si, Mn, C content monitoring, thermo EMF meas. 77−73490
- Fe-Mo system, thermomech. props. 80−89208
- Fe-Mo systems, galvanic cell meas., 1160 to 1366K 78−61042
- Fe-Ni, liq. alloy, electrochem. meas. of O, thermodynamic props. at 1873K 80−30244
- Fe-Ni (32 wt.%), EMF appearance during $\gamma\rightarrow\alpha$ transform. *(Russian)* 80−89215
- Fe_3O_4, standard free energy of formation, by EMF method with solid oxide electrolyte at low temps. *(Japanese)* 80−88338
- Fe_xO, standard free energy of formation, by EMF method with solid oxide electrolyte at low temps. *(Japanese)* 80−88338
- Ge graded p-n junction, volume EMF of hot carriers 77−47895
- GeS amorphous layers between Al electrodes, dielec. relax. currents, pot. distrib. 77−16250
- He diffusion plasma column in coaxial cold cathode discharge, space pot. distrib. 77−51237
- Hg electrode, electroreflection spectra calc., electromodulation mechanisms 77−1658
- Hg/aqueous solution interface, elec. double layer in presence of adsorbed ions 79−83469
- Hg-Cd cell, EMF rel. to temp., thermodynamics 77−12805
- Hg-electrolyte interface, polarizable, dynamics of double layer 79−24756
- In-Hg amalgam, EMF meas. of In/$InCl_3$/amalgam cell and thermodynamic quantities 79−33999
- In-Te, molten thermodynamic props. determ. by EMF method 77−51504

electric potential continued
- Li^+, hydrated, polarisation model, review 80−54115
- Li-Te alloys, liq., electrochem. investig. of thermodynamic props. 77−1244
- Mo|Cr, CrF_2|CaF_2, CO|Mo galvanic cell, EMF meas., thermodynamic props. of CaF_2 determ. 77−7874
- Na-Sn liq. alloys, thermodynamic props. by EMF meas. with β-Al_2O_3-Ba_2 electrolytes 79−19379
- Na-Te system, liq., electrochem. determ. of thermodynamic props. rel. to temp. 77−1245
- Na_2O-B_2O_3-NiO melts, NiO activity and solubility meas. by EMF method *(Japanese)* 80−92677
- PbO, standard free energy of formation, by EMF method with solid oxide electrolyte at low temps. *(Japanese)* 80−88338
- $PbSO_4$-PbO.$PbSO_4$(PbS)(SO_2), solid, EMF determ. of O_2 equilib. press., 1000-1100K 78−48683
- Pd, H_2 diffusion, induced elec. pot. investig. *(French)* 77−43379
- Sb_2O_3, standard free energy of formation, by EMF method with solid oxide electrolyte at low temps. *(Japanese)* 80−88338
- Se, differential dosimetric characts. w.r.t. γ-radiation 80−32529
- $ZnCl_2$ in methanol-water mixtures, thermodynamic props. from EMF meas. 79−52735
- ZrO_2, electrochemical cells for O_2 sensing, EMF oscills. 79−47999

electric power generation
- *see also direct energy conversion; power stations; wave power generation*
- 5 kW photovoltaic generator system, analysis, design and realisation 80−45704
- 150 kW solar powered irrigation facility, design 79−96427
- 1978 state and long-term assessment, in US conditions 79−52863
- 2000 MW by water-moderated water-cooled reactor, development possibility 77−67865
- alternative resources exploitation, cost analysis 79−48041
- alternatives, evaluation rel. to environmental impact, capacity factor, public acceptance 79−87938
- American Power Conference, Chicago, Ill., USA, April 1976 77−46201
- breeder reactor programme in United States, near term objective 78−5009
- coal, fluidised bed gasification, power generation fuel gas manufacture for combined cycle gas turbines 80−26104
- coal underground conversion, integrated fuel-generation and power-generation concept, using electrochemical engines 79−48053
- coal-based, alternative processes development, IEA activities 79−48064
- commercial Tokamak hybrid reactor, fissile fuel and power prod. 80−13808
- compressed air energy storage electric power systems, conceptual design 79−88006
- developing countries, rural electrification, energy economics and national policies 79−48042
- diagonal-wall MHD generator design optimisation by nonlinear programming *(Polish)* 78−79477
- energy conversion engineering, alternative energy sources *(Japanese)* 80−26105
- energy conversion systems, coal based, for electric power generation, performance and economic potential 80−16774
- energy cost analysis, selection of discount rates using cash flow and revenue requirement methodologies 80−3498
- energy efficiency, problems and solns. 78−81762
- energy policy, climatic effects 78−61538
- energy storage technology and solar energy use, worldwide trends *(German)* 80−72086
- energy strategy, soft vs. hard energy technologies, review 79−24885
- energy transfer by electric power generation and utilisation, economic case 80−16777
- environmental dispatch simulation and emission dispersion modelling 78−32221
- FBR, appl. in Spanish electricity supply system, review *(Spanish)* 79−59115
- FBR, electric power generation, research, development and demonstration, risk and timing 80−57837
- FBR for electricity generation in UK 78−730
- fission product decay heat appl. to electrical energy and H_2 production 79−18005
- fission-fusion electric energy supply system modelling 78−740
- fuel cells, H_3PO_4 and molten carbonate fuel cell developments 80−66966
- fusion, inertial confinement, electric power generation 78−50314
- fusion power, future prospects, United States 77−10488
- fusion reactor, integration with closed Brayton cycle gas turbine, design study 77−38395
- fusion reactor blanket concept, 1500 to 2000K Li boiler for process heat/electric power generation 80−37633
- fusion reactors, light nuclei fusion of charged particles 79−18032
- gas turbine waste heat utilisation for elec. energy generation and desalination *(German)* 79−87936
- gaseous fuel reactor, appl., USA 77−79469
- geothermal energy, low grade, future uses in France *(French)* 77−53022
- geothermal energy potential 79−70427
- geothermal power at Geysers, Calif., USA, net energy anal. of elec. energy generated 80−45629
- geothermal resource field development 80−66934
- H-coal products appl. 79−48056
- heat-pipe nuclear power plants for reliable space power 80−18377
- helically-wound compressed mag. field generator, characts., 2-d MHD computational model 78−17838
- HTGR utilisation in technological processes and electric power generation, review 79−97886
- hydroelectric, economic assessment of fuel savings *(Russian)* 80−97760
- hydroelectric dams, surplus water discharged over spillway during heavy flow, electricity generation source 79−100481
- hydroelectric power, application potential 80−30372
- Iranian solar town conceptual development 80−35645
- laser fusion, electric power generation 78−50315
- LMFBR, for large scale generation, advantages 77−23244
- marine structures for energy conversion 79−43712
- medical aspects of power generation, present and future 80−36219
- metal hydride heat pump as topping cycle for power generation 80−40928
- MHD power generation, development of coal-fired plant 80−16818
- MHD power generation, future prospects 80−35700
- microwave induced plasma 77−80224

electric power generation continued
modular dish solar electric system, technical feasibility 77–23777
nuclear, laser fusion systems development 77–26867
nuclear and coal fuel for electric power generation 78–37455
nuclear reactor, types and development in Europe and USA *(German)* 78–29647
ocean thermal energy conversion, Early Ocean Testing Platform siting considerations 79–5506
ocean thermal energy conversion, electricity to shore schemes 80–16783
ocean thermal energy conversion, preliminary design of a cruising modular experiment 80–30505
ocean thermal energy conversion, status and prospects 79–5502
ocean wind waves, energy utilization, power generation 77–9446
osmo-hydro, a pressure retarded heat engine for prod. of elect. from low temp. waste heat 80–30528
Osmo-Hydro power, salinity gradient energy conversion feasibility and system design 80–45721
photovoltaic energy generation integrations into electric grid systems, general methodology 80–45647
photovoltaic generator operation and cost simulation 79–61975
photovoltaic power generation, modules fabrication cost analysis 80–45674
photovoltaic power system elements, efficiency and terminology summary 80–97790
photovoltaic solar cell array used for supplemental power generation 80–35686
PULSAR, pulsed power conversion system with inductive storage 78–55029
pulsed energy conversion with DC supercond. magnet 77–34426
PWR for commercial electricity generation in Britain, safety issues 77–79468
radioisotope-powered photovoltaic generator 79–22495
reactor hybrid-organic Rankine cycle power system for spacecraft power supply 78–8993
refuse fuel, conversion to elect. energy at St. Louis refuse fuel demonstration project 80–93846
reverse electrodialysis of brine solns., elec. cell design and cost 80–85271
risk assessment, conventional and non-conventional energy technologies comparison 79–52862
risk assessment of energy production *(Japanese)* 79–83543
rural electrification by solar power, photovoltaic arrays efficiency 80–66974
salinity gradient power utilising vapour pressure differences in water 80–76652
semiconductor devices for generator current control and stabilization 78–21790
SGHWR, Britain's controversial program 77–368
small nuclear reactors for power production and ship propulsion appl., prospects 77–10485
solar, compound parabolic concentrator, description and development 77–23727
solar electricity production by direct and indirect conversion schemes, review 80–50981
solar ponds, electric power generation at Salton Sea, CA, USA 80–94113
solar thermochemical electric power generation, reversible chemical reactions 80–61394
solid electrolyte fuel cell for electric utility power generation 80–30470
spacecraft, solar energy thermionic electricity generating plants 77–78603
Stirling engine combustion and heat transport system design alternatives for stationary power generation 80–30536
synthetic fuels R&D and electric power 80–35624
thermoelectrochemical cycles for power and hydrogen production 80–45718
thermomagnetic, appl. of spin reorientation phenomenon 77–4325
thermonuclear power plants, problems and perspectives *(Polish)* 78–54876
Tokamak fusion power generation 78–74472
two-stage refrigeration and power producing arrangement, with cooling tube and thermoelectric stage 78–21142
underground fusion explosion, use as geothermal energy source 78–46176
very high temp. nuclear reactor, graphite moderated He cooled 77–23247
wastes treatment and disposal, technological and economic aspects 79–48066
water power development, feasibility, economics 80–61274
wind energy for electricity production, windmill construction *(French)* 80–66925
wind power electricity for high rise flats, application *(German)* 77–70739
wind power generation in North Sea, feasibility and economics 80–97759
wind power plants, experimental projects in progress, design problems and results achieved *(Italian)* 80–72007
wind-powered generators, potential output assessment, in USA 77–2205
windpower in combination with conventional systems, economics *(German)* 79–66398
worldwide energy prospects, synthesis of studies published in 1976 and 1977 *(French)* 79–29443
Yugoslavia, energy conversions in the S.R. Croatia *(Croatian)* 80–3475
H_3PO_4 fuel cell designs for residential and commercial cogeneration 80–66970
Na-S batteries, energy storage for peak power generation 80–30455
Si photovoltaic cell system, 100 kW generation, costs and efficiency *(German)* 79–79398
U plasmas, fissioning, for space vehicle power, propulsion, terrestrial appls. 77–3145

electric propulsion
see also electric drives; electric vehicles; traction
air-scooping nuclear-electric propulsion for advanced orbital transportation missions 78–45188
automobiles, batteries, current designs and their limitations 79–66405
EM accelerators/launchers with pulsed energy storage 80–35756
fabrication of ionisers for electric propulsion *(French)* 79–56946
fuel cells for vehicle propulsion appls. technical and economic eval. 80–30475

electric propulsion continued
marine reactor systems, Monte Carlo reliability anal. of power and heat removal systems *(Japanese)* 78–58396
metal-air batteries for electric vehicle propulsion, comparison of Li, Al, Zn, Fe systems 80–30444
metal/air batteries, status and potential, review 80–55828
nuclear electric spacecraft propulsion, fast spectrum reactor core design 80–37440
nuclear-electric propulsion, fast numerical analysis for Jupiter orbiter mission 78–45189
secondary cells, Pb-acid, cylindrical, pure lead, design features and performance experiences in float service applications 80–55831
spacecraft solar electric propulsion, 25 kW solar array development testing 80–30500
Stirling engine powered total energy system for recreational vehicle appls. 80–30538
vehicle battery systems available and under development, review *(Dutch)* 80–72025
vehicle power sources, battery design requirements for commercial use *(Dutch)* 80–72024
vehicle power sources, fuel cell/secondary battery hybrid appls. *(Dutch)* 80–72037
vehicle secondary cell development program of US Dept. of Energy, review 80–30442
Li-Al/FeS cells for electric vehicle propulsion 80–30446
LiAl/FeS electric vehicle battery, charging system developments 80–30447
LiAl/metal sulphide high temp. battery with multi-foil insulation container for electric vehicle appls. 80–30448
LiAl(Si)/FeS(S_2) battery developments for electric vehicle propulsion and load levelling appls. 80–61325
Na/S traction batteries, development progress and problems, review 80–61326
Ni-Zn electric vehicle battery, performance characts. 80–30443
Pb-acid batteries, for elec. vehicle propulsion, heat transfer, math. anal. 80–3509
Zn-Cl_2 batteries for electric vehicles, battery design modelling 80–30452

electric reactance
see also capacitance; inductance
eddy currents, calculation by dual energy methods 78–78859
frequency derivative of input reactance of linear, passive, time-invariant system calc. 77–9892
GaAs solar cells, photoreactance of p-n junction diodes 80–81464
Si solar cells, photoreactance of p-n junction diodes 80–81464

electric reactance measurement
see also capacitance measurement; inductance measurement
HF, comparison by transformer bridges 77–82564
inductance bridge measurement methods and formulae for calculating inductance 79–44920
Q-meter, digital, automatic, design procedure 78–70155
resistors, reactive components, measurement using precision dielectric cell 79–49255

electric reactors *see reactors (electric)*

electric relays *see relays*

electric resistance
anisotropic body of arbitrary geometry, conductance and resist., variational calc. 80–32865
bevelled shallow junctions, spreading resistance data correction 80–80358
cell, capillary-Hg electrolyte, elec. characts. rel. to mag. field, gravity 77–1937
CL Al_2O_3, film, dielec. const. and resist., thickness depend. 78–39502
computer program for equiv. resist., for teaching 77–5615
continuous recording apparatus for resist. change during heating and cooling 77–22568
elastoresistance parameters change by physical distortion *(French)* 77–70564
electrode, impedance meas., accuracy 80–61108
electrodes, ellipsoidal, embedded in conductor, spreading resist. and 1/f cond. fluctuations 80–2435
electrolyte resistance polarisation in electrochemical potentiostatic meas., automatic compensator 77–21393
furnaces, glass-melting, resist. between electrodes calc. 79–58690
gas-cooled current leads, for superconducting magnets 80–37056
human body, electrostatic spark discharges obs., nature and incendiary behaviour 80–72406
human body, equivalent circuit *(Russian)* 79–53295
Josephson tunnel junctions, fabrication and four terminal resistance study *(Chinese)* 78–68116
liquid variable resistance, high-voltage technology appl. 77–37918
magnetic coated small dipole antenna, lowering of reson. freq. and improvement of radiative resist. *(Chinese)* 79–50193
membranes model using millipore-DOPH membrane, increase in elec. resist. with Ca^{2+} ions and its oscill. 80–40745
metals, temp. depend. qualitative anal. by audible demonstration 80–46775
micro plastic strain energy criterion applied to reversed biaxial fatigue 78–63391
microelectrodes, open tip glass, influence of diffusion, double layer, and glass conduction on elec. resistance 80–67300
MOSFET, piezoresistivity effects and use as press. transducers 80–4695
pressure catheters, resist rel. to applied volt., elec. shock risk 77–40818
quantum transport effects in DC elec. resistance of solids, review 79–40500
screw-fastened joints for thermal contact at low temperatures 79–35760
semiconductors, temp. depend. qualitative anal. by audible demonstration 80–46775
skin potential artifact reduction in biopot. recording 77–40873
skin resistance during square-wave elec. pulses of 1 to 10 mA, rel. to nerve stimulation 78–31929
solar cells, series resistance evaluation 79–61972
spreading resistance anal. using image method, semiconductor impurity profile determ. 77–68993
steel wire, drawn, age hardening props. obs., mechanical and electrical props. relationship 80–50662
toroidal field coils, EM parameters calcs. of current paths in homogeneous media *(Japanese)* 80–106155
transducers, applied, resistance due to cracks, eddy current calc. and hodograph 78–53095

electric resistance continued
Au-Al$_2$O$_3$-Al system, influence of mech. modulation on elec. transport 80—2481
n-GaAs, AuGe contact, temp. dependence meas. 78—76146
GaAs, p$^+$-n^0-n$^+$ struct., control of modulation of base resist. 79—91133
Na-S cells, factors affecting S electrode operation 79—29463
Na-S cells, S electrode resistance calc. 80—35667
Na-S interconnected cell performance 79—29464
Pt anode, impedance behaviour study in β-ZnS suspension-electrolysis leaching in 1N H$_2$SO$_4$ soln. *(Japanese)* 79—24754
Si:P. ion implanted, sheet resistance variations at elevated temps. 78—43041

electric resistance furnaces *see resistance furnaces*

electric resistance measurement
see also ohmmeters
1 Ω to MΩ resistance meas. bridge *(Spanish)* 77—74457
10 MΩ to 1 TΩ range, and new 1 GΩ resist. standard 77—82568
12 kHz IC resistance-frequency convertor *(Russian)* 78—81963
20 μΩ to 300 GΩ range, portable meter 79—17441
absolute ohm of ETL, determ. using calculable capacitance standard *(Japanese)* 79—6137
AC bridge for small resistance meas. at low temps. 79—67347
AC resistance bridge for low resistance meas. 77—26337
AF impedance bridge, 4-terminal-pair, 40 Hz to 2 kHz 79—88978
barrier resistance meas. in multifilamentary composite superconductor 79—30506
bimetal junction layer, low elec. resist. determ. method 79—49249
bridge ccts. for differential resist. meas., resist. thermometry appl. 77—79126
capacitive loss-angle resistor meas. bridge, 1 mHz to 100 Hz *(German)* 77—79125
circuit resistance measurement in inflammable atmosphere using meter employing pulse technique 79—63269
constant-current source appl., Tietze-Schenk *(German)* 79—88974
contact resistance analyser system 79—99605
contact resistance of metal-semiconductor interface 80—105672
corrosion kinetics, mass and resist. change techniques, comparison, for Permalloy film 78—27675
CRT tester based on ohmmeter and adapter 79—35711
data logger, 16-channel with multiplexing, and voltage pulse measurement 80—42203
DC bridges, high-resistance wide-range, measurement error 79—75548
DC galvanometer internal resistance meas. by potentiometer 77—13777
DC resistance decades, precision, integral verification 78—242
DC standard materials, physical and technological props. *(German)* 78—54400
defibrillator, damped sine wave, intact, evaluation of operating parameters 78—57120
dermal-resistance meter with high resolution *(German)* 79—84031
digital multimeter, general-purpose, design practice 77—57348
digital multimeter, type Shch68003, with printer output, features 77—74437
digital multimeter technology and future development 77—57345
digital multimeters, MOS/LSI, mains/battery operated, construction and performance *(French)* 77—61090
digital resistance comparator, type Shch68200, features 77—74438
double constant current source for cryogenic current comparators, standard resistor calibration appl. 78—93731
earthing checking instrument, meas. of resist. of ground at various levels and of earthing connections *(German)* 80—98936
electrically conducting surface coating, of linear induction accelerator tube, beam losses and coating inhomogeneity 78—5066
electrochemical meas. system, using phase-sensitive detector, control circuit *(Spanish)* 80—55671
ELF magnetic field effect on personal vegetative status meas. by elec. resist. between hands 77—81533
energy deposition measurement by thin film resistors 78—29719
epitaxial layers meas., based on spreading resistance probes *(Polish)* 79—88981
erythrocyte, human, dynamic osmotic haemolysis and ghost repair, resistive pulse spectra 79—62208
film, optical and elec. props. in situ determ. during deposition 77—59341
four-point sheet resist. meas., semicond. doping uniformity determ. 77—47475
freeze etching and related techniques, resist. monitor for automatic film thickness regulation 78—49810
fundamental ohm determ. by ASMW standardising office, status *(German)* 79—9221
gigaohmmeter, electronic, with controllable threshold sensitivity 78—74024
high, review of accuracy and sensitivity of various instruments and techniques 80—57331
high loss materials at high freqs. 80—62686
high resistance meas. circuit using matched pair of diodes 77—74455
high resistance measurement, for radiation detectors *(French)* 78—77929
high-resolution cryogenic resist. bridge using SQUID null det., construction and performance 79—2792
human body resistance measurements *(German)* 78—53541
human skin resistance transducer, psychophysiological studies appl. 77—86729
instrument for crack measurement 80—100984
internal resistance of energy source meas., student expt. 79—30176
Kelvin bridge, link resistance compensation 78—86292
linear scale meter, capacitance measurement included, transistor amplifier, improved cct. *(German)* 77—26327
loudspeaker moving coil temp. meas. systems *(Hungarian)* 80—106698
maintenance, renovation and repair procedures for multimeters including Avo model 8 79—35795
Manganin wire, resistance meas., with cubic-anvil type pressure apparatus 79—44919
metal samples high precision meas. and control in He II environment 78—54403
metal-gas systems, surface reaction rate meas., resist. relax. method 79—66355
metallic thermal connectors for use in nuclear refrigeration, elec. resist. meas. 78—224
metals, low-cycle failure investigation, elec. resist. meas. appl. 80—85109
metals and alloys, electrical resistance meas. at increased temp. under stress 77—56147

electric resistance measurement continued
meter construction accurate, low cost, 0 to 10 MΩ range 78—8423
meterless cct., ohm gnome, amateur constr. appl. 77—74456
multimeter, automatic storage *(German)* 77—10044
multimeter, microprocessor controlled *(French)* 77—74433
multiprobe measuring head for measurement of semiconductor electrical resistivity 79—49253
nonferromagnetic film sheet resistance meas., eddy-current method 78—45658
ohm, absolute determ. based on standard capacitors 77—82565
ohm SI unit realisation at National Physical Laboratory 78—89505
ohmic contacts to semiconductor, meas. of contact resistance using transmission line model 80—70826
Permalloy film corrosion characterisation by crystal oscillator microbalance and resistance meas. 78—7101
piezoelectric crystals, crystal bridge for equivalent electrical parameters meas. 78—54404
polymer, surface and bulk electrical resistance, screened meas. cell 79—49251
probe, ultra-high vacuum compatible, thin film supercond. meas. 78—49867
quantum transport effects in DC elec. resistance of solids, review 79—40500
rapid changes in resist., method and appl. to resist. decay obs. in deformed Al 79—49256
reproduction of ohm at German ASMW 80—98944
resistance standard unit transmission techniques 77—53854
resistance standards, group storage errors, statistical analysis 77—53853
rheographic electrode system for thyroid gland 79—57783
RLC bridge, with oscillator and having ten ranges 79—2785
semiautomatic bridge for high-precision DC resistance measurements on pure metals at low temperatures 79—35788
semiconducting ceramic, meas. cell and setup for elec. resist. meas. 300-1400°C 79—30488
semiconductor resistivity, spreading resist. calcs., role of source boundary conditions 78—89499
semiconductor sheet resistance meas. by four point probe technique *(Chinese)* 80—52262
semiconductor spreading-resistance meas. for doping profile determ., preprocessing of data for resistivity calcs. 80—57265
semiconductor thin rectangular samples, four-point sheet resistance correction factors 77—82547
skin resistance biofeedback, using frequency controlled oscillator detector 80—101156
small active resistance and inductance meas. AC bridge 78—86299
small value resistance, cct. 77—37941
soil resistance meter, geological and archaeological applications *(German)* 78—57361
solar concentrator cells, effects of temp. variations 80—93944
solid dielectric specific resistance meas. instrument 77—79109
solid dielectrics, surface resistivity meas. and calc. 79—1617
spark gap breakdown, time-resolved resist. meas. 80—19639
spreading resistance, multilayer correction scheme 78—247
spreading resistance meas., multilayer correction factor calc. 77—76823
SQUID resistance bridge, ultra high resolution 79—63275
standard representative of ohm and volt, January 1977, France *(French)* 79—26077
steel, low C, low-cycle failure investigation, elec. resist: meas. appl. 80—85109
steel tearing rate determ. *(German)* 78—15619
steel with Nb and V additives, critical temperature of precipitation identification *(Slovak)* 77—4781
strain gauge plethysmograph, automated 2-channel 79—29648
superconducting chopper amplifier for resistance meas., sensitivity and noise calc. 79—12817
superconducting transition meas., contactless, circuitry 79—17442
surface resistivity, at 890 GHz, using modified pyroelectric detector 77—34004
surface wave gauge, oceanographic appl., accuracy and calibration 80—24110
temperature dependence of thermoelectromotive force and resistance 80—57330
tenso-resistors, meas. using closed Wheatstone bridge *(Russian)* 79—12821
thermophysical meas. above 2500K, apparatus 77—45845
thermostat appl., precision 77—57355
vacuum gauge for 10^{-3} torr *(Polish)* 79—71472
Van der Pauw structure with finite contacts, anal. of Greek cross, sheet resistance meas. 80—22387
very high resistance, meas. device using operational amplifiers 80—42240
weak signal detection, circuits for resistance meas. and temp. control *(Chinese)* 79—30451
C resistance thermometers, determination of magnetoresistance in liquid He temp. range 80—31752
CdS evaporated films, growth rate and resist. determ., in situ meas. technique 79—77940
GaAs, epitaxial layers on conductive substrate, elec. characterisation 78—91790
Ge resistance thermometers, stability data at 3 temperatures 80—86307
Pt resistance standard capsule thermometer, for 13.81 to 273.15K, two-point calibration 79—206
Si, resistivity depth profiles calcs. from spreading resist. meas. using math. algorithm 80—2393
Si slices, application of capacity gauges *(Polish)* 79—2784
Si wafer, automatic meas. system for resist. profiles 80—39574
SiC heating element, resistance meas. instrument 77—71349
W, sintered metal resist. standard, resist. at high temp. 78—89427

electric resistors *see resistors*

electric sensing devices
see also instruments; measurement
acceleration sensor for heart implantation, heart attack warning *(German)* 79—57802
acceleration sensors, lower limiting frequency and indication threshold *(German)* 80—95093
air-intake flowmeter using corona discharge principle, automobile engine appl. 80—33716
analogue digital double integration joulemeter, AC loss meas. in superconducting magnets 80—57325
aperture diameter inductive meas. device 77—26268

electric sensing devices continued
- atmosphere temperature sensors, humidity effects and sea salt contamination 80—82095
- audio alarm remote control systems, using Doppler shift 79—64477
- balance, mechanical, with electronic displacement sensor, precision 78—77866
- biochemical sensor devices, review *(Japanese)* 79—12050
- bioelectrochemical sensor using immobilised enzyme electrodes *(Japanese)* 80—109071
- biomedical catheterisable sensors, PO_2 probes, press. transducer and photometers 80—46080
- biomedical system control sensors 79—48380
- bipolar IC temperature transducer, intrinsic bandgap voltage as reference, Fahrenheit, Celsius or arbitrary scale operation 80—82761
- bone stress wave detection using piezoelec. effect, non-invasive technique 78—31948
- butterfly-valve inductive orientation detector as means of measuring angular displacements 80—68193
- capacitance sensor, microstrip technique for theoretical capacitance determ. 80—198
- capacitance sensors, helical, for volume fraction determination, analysis and design 79—75516
- capacitance sensors for phase percentage determ. in multiphase pipelines 80—62625
- capacitive sensor, characts. linear approximation, in vicinity of working point *(Slovak)* 79—40547
- capacitive sensor of soil pressure, using polyurethane foam dielectrics *(Slovak)* 80—86281
- capacity gauge for resistivity meas. of semicond. slice *(Polish)* 79—2784
- cardiac sound and vibration recording, electro-optical sensor 77—21648
- catalytic sensor for gaseous mixture conc. fluctuation meas. 77—26291
- chromatography, liquid, detector characts. and use, book 78—15751
- CMOS, for diffusion pump monitoring 77—5855
- conductivity meter for in situ ocean meas., development, testing and calibration 79—5671
- conductivity probe design for use with bridge instrument, wide range of test solns. 80—95110
- contact cryogenic fluid level sensor 80—73371
- crack growth recording, automatic, elec. resist. method 79—39070
- crack length automatic recording in sheet samples 78—60907
- creep curves, multicycle, device for recording at elevated temps. 79—43512
- cryogenic temp. sensors, for use in EM fields 77—2655
- dielectric detector for automated LF permittivity meas. 78—29126
- differential frequency angular rate and displacement sensor, construction *(Russian)* 78—70106
- differential pressure transmitter, electronic, design and appls. 79—17435
- diode sensor and Norton amplifier for liquid nitrogen level control 78—29121
- eddy current probe, thickness measurement of plating layers *(German)* 79—85112
- eddy-current flowsensor, model 78—5829
- EEG automatic sleep staging detectors 78—53551
- electrochemical sensors for partial press. meas. in blood 80—67303
- electrochemical species-selective sensor, use of semi-permeable membranes in book, for teachers 78—8200
- electromechanical transducers in hostile environments, review 80—37019
- electronic gas detection, Pellistor, VQ and TGS sensors *(Spanish)* 80—93832
- electronic sphygmomanometer, direct and indirect methods for blood pressure meas. 79—25125
- electronic-micromechanical interactions, conference, Lausanne (1976) 77—30140
- electrostatic voltage sensor *(Japanese)* 80—105632
- EM coating thickness gauge calibration using air gap 77—57300
- EM device, noncontacting, for bone mech. props. in vivo determ. 78—77133
- EM instruments for use in liquid sodium, theoretical anal. 78—54857
- EM pulse measurement both inside and away from nuclear source regions 78—21773
- EM water current nonlinearity and sensitivity 77—5383
- emissivity meas. by thermoreceiver/gas heat exchange 77—22552
- energy loss measurement, in superconducting magnets 79—71489
- eye movement recording system for clinical appl. 78—3623
- fast reactor, EM temp. sensor in liquid sodium, performance 78—700
- ferroelectric sensor for linear temp./temp. difference detection 78—21136
- ferroelectrics hysteresis loop sensing *(Czech)* 80—82792
- ferromagnetic pick-up for iron sheet local magnetic properties *(Russian)* 78—77946
- flood prevention device for laboratory procedures 78—179
- for quartz thermometer 78—81967
- force sensor, inductively coupled, high bandwidth 79—6118
- galvanic coating thickness gauges using phase angle meas. 77—79114
- galvanic dissolved O_2 sensor, improved, activated sludge aeration appl. 77—70364
- gas bubble detection recording and measuring system with nanolitre resolution for use in liquid environment 78—31739
- gas chromatographic air analyser fabricated on Si wafer 80—73343
- gas detector, all-electric, using laser beam and Stark cell 80—74417
- gas sensor, SnO_2 thin film, prep. 80—39691
- gas sensor, using α-Fe_2O_3 semiconducting ceramics *(Japanese)* 80—61498
- gas-sensitive sensor with ultrafine particle film deposited on monolithic IC chip *(Japanese)* 80—105630
- Hall device for grain detection in Fe-Si sheets 78—11470
- heat flowmeter, battery, heat flux meas. using Kalman filter 79—37143
- HF magnetic field measurement appl. *(Polish)* 77—87797
- hot wire sensor, for liq. level detect. 77—17966
- Humiceram-III, ceramic sensor, multifunctional sensor to detect humidity and gases *(Japanese)* 80—105659
- humidity sensitive ceramic resistor device, characts. and appls. *(Japanese)* 77—71332
- humidity sensor, Al_2O_3, ageing improvement *(Japanese)* 80—100863
- humidity sensor, based on thin film capacitor, Finnish development of meteorological instruments 79—12310
- humidity sensor, capacitive, Panahume *(Japanese)* 80—105658
- humidity-sensing capacitance transducer, construction and characts. 80—4729
- image sensor, charge coupled device, microscope television for detection and meas. of nuclear emission tracks 79—3290

electric sensing devices continued
- inductive sensors for coating thickness meas., correction for thermally produced errors *(Russian)* 77—13740
- infrared detector, pulsed LED source detects objects on a conveyor belt 78—45700
- ion controlled chemically sensitive diodes 80—13066
- ionisation smoke detectors, risks to humans 78—15909
- isotropic RF electric/magnetic field strength meter, design 80—82751
- laser-operated, photographic paper quality improvement, colour spots detection *(German)* 80—57412
- leak detector, sparking, using semiconductor switching diodes 80—31774
- level and volume meas. in conductive liquids using array of point sensors 80—68177
- level detector, controller for liq. N_2 in cold traps 78—24805
- level detector for pumped bath of He II 78—49843
- level sensing in elec. conducting liquids using PTC thermistors 80—42209
- level sensor, for liq. N_2, PTC thermistor P310-C11. 80—52247
- line sensor used to monitor a distant transducer 79—6145
- line sensors for photographic slide scanners, P^2CCD *(German)* 79—49308
- linear rotary convertor angle meas. *(Russian)* 79—63192
- liquid chromatography detector based on dielec. const. meas. 77—21436
- liquid He depth gauge, level sensing circuit 77—82527
- liquid level measurement transducer, cascade transistor cct., level to freq. convertor 80—73310
- liquid N_2 two-level controller 80—52241
- load cell monitor for liquid N meas. with Li drifted Ge detectors 78—29122
- low temperature resistive pickup based on Ge-Si solid soln. layer on ceramic 79—88953
- magnetic displacement sensor *(Japanese)* 79—12761
- magnetic field sensor, Wiegand module *(German)* 80—62694
- magnetic flaw detector, using magnetic powder method 77—90571
- magnetic heading sensors, in towed hydrophone location system 79—2401
- magnetic induction gauge consisting of 3 Hall transducers 80—105682
- magnetic position sensor, differential, built with magnetic resistances *(Italian)* 79—85155
- magnetic sensor, high permeability metal core solenoid absolute sensitivity calibration 80—31133
- magnetometer, RF SQUID, construction, geomag. microfluctuation meas. appl. *(Japanese)* 79—5641
- mechanical compensation methods influence on error characts. of electro-mechanical sensors *(German)* 78—16786
- metal-film temp. and vel. sensors and self-propelled research vehicle stability evaluation for ocean turbulence meas. 79—5672
- microprobes, non-perturbing, based on cholesteric crystal and dielectric microthermometer 78—16791
- monitoring shock waves in liquids, new developments *(German)* 79—82001
- MOS gas sensor for combustible gas and vapour monitoring 79—16104
- multichannel synchronous detector for NQR signals 77—61098
- multislit screen induction phase shifter with increased electric reduction coefficient 77—5864
- nasal air emission in speech disorders, electrodynamometric evaluation 78—77134
- needle electrodes based instrument for flow props. and bubble vel. determ. in gas-liquid bed 77—72374
- nondestructive acoustic elec. field probe 80—47076
- NTC thermistor sensors, cct. designs and design calculation tables 80—68201
- ocean current sensors, EM-type, performance assessment 79—25345
- oceanographic buoys, electronics and telemetry developments 79—5659
- oceanographic instrument for vel., temp. and cond. microstruct. studies, sensors 79—5669
- offshore oceanographic buoy, telemetering sensors and new mooring design 79—5660
- optoelectronic two-component spirit-level for whole-arm prostheses *(German)* 79—8572
- particle size counter, $BaTiO_3$ dispersion effects 79—17383
- pH automatic control for electrolysis, instrumentation, appls. 77—63928
- photoelectric sensor, digital measurement, rotational speed, applications to automatic testing of electric machines *(Czech)* 79—71419
- photoelectric sensor, gas-filled, flame detector appl. 77—168
- piezoelectric pick-up, for pulsed pressures meas. 80—31778
- polarographic sensor with microwire indicator electrode, exam. of design 80—21340
- porosity meas. device for fluidised beds, exam. 78—60911
- pressure and differential-pressure sensors, seven types *(German)* 80—77772
- pressure quartz, qualification as deep sea gauge *(German)* 79—74980
- pressure sensor, semiconductor, two-conductor pressure-to-current transducer appl. *(Czech)* 79—97374
- propane gas detector using SnO_2 doped with Nb, V, Ti, or Mo 79—29426
- proportional temperature controller, using IC sensor diode and operational amplifiers 79—75515
- PVDF pyroelectric IR detector *(Japanese)* 80—105714
- pyroelectric polymer IR detector *(Japanese)* 80—105713
- pyrothermometer in scanning calorimeter, heat cond. eqn., model 77—10026
- quantum sensors, use in instrument for digital recording of submarine irradiance and photoperiod 80—98474
- rainfall intensity sensor 79—39888
- redox gas sensor of sintered SnO_2, for anal. of pathological lung gases *(German)* 78—85440
- remote temp. sensor using diode, cct. 77—53901
- resistance thermometer sensor overheating, influence of meas. current *(Russian)* 79—26053
- resistance vacuum meter, range extrusion method *(Polish)* 79—54148
- ring-core magnetometer sensor for articulatory meas. of jaw movements 80—101243
- rocket attitude control, solar sensor system pointing accuracy *(Japanese)* 78—24420
- rocket geomagnetic aspect horizontal component sensor *(Japanese)* 78—24421
- rocket solar sensor data processing cct. *(Japanese)* 78—24423
- rotation-angle pickup, for goniometer, using precision variable resistor 80—47047
- salinity/temperature sensor chain for estuarine meas. 79—5670
- SEM, wet, live and frozen objects, review 79—26183

electric sensing devices continued
- semiconductor, properties and appl. *(German)* 78−36991
- semiconductor and piezoelectric, development trends and appl. *(German)* 80−52186
- semiconductor gas detector, for gas chromatograph, electroadsorption phenomena *(Russian)* 78−7307
- semiconductor gas sensors, review *(German)* 80−55974
- semiconductor gas sensors, selectivity to CO and CH_4 79−34407
- semiconductor gas sensors *(Japanese)* 80−31736
- semiconductor pressure sensors, thin Si diaphragm form., piezoresistive and capacitive structs. 80−13065
- signal acquisition and processing in clinical cardiac catheterisation lab. 77−44768
- sleep EEG automatic K-complex detector 78−53557
- 'smart sensors', role in remote sensing of Earth from space, book 80−62402
- soil moisture gauges, testing procedure 77−78481
- solar flux mapping sensor, Si p-n junction, for high intensity appl. 78−40720
- solar heating systems, instrumentation principles for performance meas. 80−35743
- solenoid with ferrite core, for geomag. pulsations detect. 78−24384
- solid electrolyte galvanic cell for gas sensing, response speed 77−60149
- solid electrolyte gas sensor developments 80−61217
- solid-state, for high direct voltages meas. 79−44916
- sonic interface detection for multiproduct liquid transportation by pipeline, developments 80−33382
- sounding rocket three-axis attitude control system *(Japanese)* 78−24422
- spectrophone, low-noise, using continuous laser beam 80−74418
- speed meas. devices survey, industrial appl. *(French)* 79−93105
- speed sensing facility, electronically operated 79−30427
- splash down programmer unit for bathythermographic appl. 77−56759
- SQUID, appl. to cardiac recording, phase and amplitude relationships of elec. and mag. events 80−104695
- SQUID, RF sensor, automatic monitoring circuitry 77−18044
- SQUID arrays, for mag. field meas., geophysical, biomedical appls. 78−32830
- SQUID for gravitational antenna *(Russian)* 77−45773
- steel, detector designed to meas. retained austenite 78−35602
- superconducting fast-response thin-film probe, for detection of second-sound shock waves in superfluid He 79−63237
- superconducting quantum magnetometer with two-contact sensor, asymptotic characteristics 79−6155
- superconducting thin film probe, for detection of second-sound shock waves in superfluid He 79−73355
- temperature, monolithic transducer, LX 5700 A, for −100 to +150 degree C temps., operation *(French)* 77−67431
- temperature, with 4-bit A/D convertor *(German)* 78−12693
- temperature and thermal sensors, appls. and types *(Japanese)* 77−71318
- temperature fluctuation measurement in turbulent channel, sensor wire-supports cond. influence *(French)* 79−94751
- temperature meas. devices developments *(German)* 80−8986
- temperature regulator circuits, using thyristors and triacs *(Spanish)* 79−6115
- temperature sensing, use of LEDs 78−4619
- temperature sensors, determination of dynamic behaviour *(German)* 80−17940
- temperature sensors, elec. Japanese and international standards 78−65928
- temperature sensors, Pt-100, stability and calibration 20-273K range *(German)* 77−79094
- temperature sensors for flow meas. *(French)* 79−86536
- thermal diode sensor based on const. leakage current with negative temp. coeff. 10 V analogue output *(German)* 80−47052
- thermistor static voltage/current characteristic calc. 77−26286
- thermistor-respiratory flow sensor, shunted, characts. *(German)* 78−28097
- thermo-sensors utilizing temperature-sensitive magnetic characteristics *(Japanese)* 79−12790
- thermometer for 0 to 100°C, using Si transistor *(German)* 79−6122
- thermometer sensors, digital, in kit form *(French)* 80−4712
- thermoresistive, physical mechanism and appl. *(Italian)* 79−80617
- thin film temp. sensor with high temp.-resistivity 78−41308
- threshold current sensor, struct. and operational features 80−34689
- torque measuring contactless coupling, construction and testing *(German)* 77−13744
- trace-level sensors, chemically sensitive, semicond. 77−52720
- underground mines, flame sensor-trigger device for explosion barrier 80−52313
- underwater temperature meas. thermistor chain 77−5379
- vacuum gauge, Pirani type, with TaN thin films *(Japanese)* 80−52257
- visual prosthesis, processing and tactile stimulation of images *(French)* 79−100788
- VMOS transistors used to give linear thermal response characts. 79−9216
- water leak detector for water cooled electron microscope 78−21277
- water quality control, appl. of information transducing sensor using electrokinetic effects 79−70349
- water vapour sensor of P_2O_5 type 80−98907
- water wave probe, parallel wire type 79−18979
- Wiegand effect, influence on magnetic sensors *(Spanish)* 80−31735
- Ag^+ ion automatic sensor-analyser for photographic fixing bath regeneration systems *(Russian)* 80−95172
- AgBr-SiO_2, field effect potentiometric sensors 78−35691
- Al_2O_3 moisture sensor for sealed hybrid packages 77−87754
- $As_{10}Ge_{15}Te_{75}$, thermal memory switch development 78−89468
- $BaTiO_3$, temperature sensor using thick film techniques 79−93137
- C resistors as low temp. sensors in low temp. reactors, gamma, neutron irrad. investig. 77−45848
- $Co_{1-x}Mg_xO$ ceramics as O_2 sensors, phase stability, elec. cond. and thermoelec. power meas. 78−3420
- Cu resistance temperature sensors *(Polish)* 79−97388
- GaAs diode temperature sensors, characts. obs. at 4.2 to 393K 80−47054
- GaAs thermionic diode, temp. meas. appl., 1-400°C range 77−37886
- Ge sensors, He level gauge appl. 80−57277
- Ge:Au film strain gauges, press. sensor *(Japanese)* 80−105631
- H_2-sensitive Pd-gate MOS 78−2578
- Hg vapour conc. meter, construction and performance 79−2759
- $LiNbO_3$ sensor for elec. hygrometer *(Japanese)* 80−95103

electric sensing devices continued
- $MgCr_2O_4$-TiO_2 porous ceramic humidity sensors 80−86325
- N_2, liquid, sensor using domestic incandescent gas lighter element 79−63201
- O_2 analysis, electrochemical sensors 80−93816
- O_2 analysis, gaseous and dissolved, direct readout instrument 77−40606
- O_2 sensors, solid electrolyte, noncatalytic electrodes 80−76573
- PLZT pyroelectric detectors, delayed onset of piezoelec. oscills. 80−75953
- Pd gate MOS transistor, H_2 detection appl., characts., fabrication *(French)* 78−2569
- Pd MOS structure, surface chem. reactions, H_2 detection 77−73470
- Pd-TiO_2 Schottky barrier, work function depend. on adsorbed species, appl. as gas sensor 80−54782
- Pt resistance thermometers performance 80−27296
- Pt thin-film temp. sensor *(Japanese)* 80−105645
- Si diaphragm pressure sensor, integrated signal conditioning 80−76859
- Si diodes as low temperature sensors *(German)* 80−31744
- Si ion-controlled diodes, acid-base exposure effects, Si-SiO_2 interface state density 80−96984
- Si, on sapphire, Schottky magnetodiode, integrated mag. sensor 80−68223
- Si whiskers, as basis for low-temp. sensors of temp. and deformation 79−5095
- SnO_2, gas sensor, CO, H_2O vapour, surface temp. effect on cond. 78−76067
- SnO_2 gas sensor, fast-detecting, prep. 80−61497
- SnO_x thin-film conductance-modulation CO sensor, operation model 79−97371
- $SrTiO_3$, temperature sensor using thick film techniques 79−93137
- ZrO_2, electrochemical cells for O_2 sensing, EMF oscills. 79−47999
- ZrO_2-CaO thin film O_2 sensor, ionic transference number, cell design 77−70360

electric shielding, nuclear *see nuclear screening*

electric shocks
- *see also electrical faults; protection; safety*
- 50/60-Hz AC, ventricular fibrillation tests on animals *(German)* 80−101154
- current flow effects on human body 77−64084
- electroconvulsive therapy pulse instrument 78−53562
- electrosurgical hazard monitor 79−83882
- fibrillation threshold for intracardiac catheter, vs. current flow duration and electrode area 77−37101
- guarded double insulation, reduction of shock hazard of grounded elec. systems in hospitals 77−56497
- IC shock scrambler 78−48898
- instrument safety precautions, may result in health hazards 77−34001
- intensive care unit/coronary care unit safety 78−69252
- lightning strike and death of soldier in Singapore 78−44949
- line isolation monitor with adjustable alarm level for hospital elec. systems 77−56496
- micro-electrocution in medical apparatus, effects on human body 77−9295
- pressure catheters, resist rel. to applied volt., elec. shock risk 77−40818
- protection of people, safety curves as function of ambient conditions *(French)* 77−17012
- ventricular fibrillation for AC shocks at 50-60 Hz, threshold considerations 80−51065
- ventricular fibrillation/defibrillation threshold energy-time anal. 77−48924

electric spark machining *see spark machining*

electric sparks *see sparks*

electric strain gauges *see strain gauges*

electric strength
- *see also electric breakdown*
- air, erratic breakdown due to sustained appl. voltage and presence of dust particles *(German)* 79−94830
- air, predischarge-stabilised breakdown voltage *(German)* 78−63608
- ceramics, US investigation, porosity, mech. and dielectric strengths *(Polish)* 79−52565
- compressed gas, electric breakdown, dielectric strength 77−31543
- dielectric film, amorphous, covalent, disruption of stationary state and electrical breakdown 77−20332
- dielectric film, amorphous, ionic, disruption of stationary state and electrical breakdown 77−20333
- dielectric film, glow polymerised, struct. and props. *(German)* 77−20799
- dielectric films in MIS structures *(Slovak)* 78−56231
- dielectric gases and gas mixtures, maximum electric strength and vapour pressure relationships 80−92249
- discharge with external ionis., electric strength and elec. cond. 78−91180
- DOBAMBC, dielec. props. near ferroelec. smectic A to C transition 80−45015
- electron and ion beam generation at high power, review 80−13988
- epoxy polymers, unfilled and filled, effect of specimen size, expt. 77−8505
- epoxy resin, mech. and thermal props., amine hardeners, added softeners and filter effects *(Polish)* 78−68741
- epoxy resin cured with composite curing agents, arc resistance *(Japanese)* 78−92371
- ethylene propylene diene terpolymer, crosslinked, AC elec. breakdown studies 78−43787
- exploding wire, electric strength recovery rate, following explosion *(Russian)* 78−22592
- fluorocarbon liquid, breakdown characts., comparison with hydrocarbon liqs. 79−91361
- Freons and their mixtures with N_2 and SF_6, breakdown voltage in uniform electric field *(German)* 78−71423
- gas in crossed electric and magnetic fields, elec. strength calcs. 78−87568
- gaseous dielectric, electric strength and mol. props. correlation 77−76025
- gaseous dielectrics, electron-molecule interactions and negative ion resonances 78−75480
- gases as electrical insulators, nature and practice 78−83632
- hexatriacontane single cryst., temp. depend. of dielec. breakdown 79−51905
- high field conduction and breakdown in dielectric liquids 79−91355
- hydrocarbon liquid, breakdown characts., comparison with fluorocarbon liqs. 79−91361

electric strength continued
  insulating solid, elec. strength and degradation 78—83631
  insulation, dielectric internal discharge, apparent charge evaluation *(Polish)* 80—19659
  leader channel temp. rise, initial stage, elec. field strength determ. *(Russian)* 77—35411
  metal-dielectric system, gas cavity initiation-discharges phenomena *(Polish)* 80—19660
  MHD generator interelectrode gap, increasing its electrical strength by gas blowing 78—9854
  mica, pulse electric breakdown under pressure, lamination effects 80—66110
  mineral oil in large gaps, electric strength study 79—38452
  moving gas, electric strength calcs., gas vel. effects 78—87568
  oil for switching surges and long flash-over distances, expt. *(Czech)* 78—56427
  organic purified dielectric liquids, expt. 78—84523
  perfluorocarbon compounds, electron attachment obs., dielectric strength 79—36759
  polybutene oil, direct voltage elec. strength 79—91360
  polycaprolactam film, temperature-time dependence *(Russian)* 78—76386
  polyethylene, effect of Se on electrical and mechanical strength, after mechanical and electrical ageing *(Russian)* 79—52396
  polyethylene, elec. empulse breakdown strength, rel. to rate of drawing 80—15960
  polyethylene, influence of Se on mechanical and electrical strength *(Russian)* 79—11662
  polyethylene, polymer life eqn. appl. to dielec. strength 80—25304
  polyethylene film, dielec. breakdown sites 80—50266
  polyethylene surface field strength under DC stress 80—15967
  polyethylene terephthalate, polymer life eqn. appl. to dielec. strength 80—25304
  polymer, dielec. breakdown theories, mol. and morphological features rel. to elec. strength, review *(Japanese)* 80—60501
  polymer electric strength rel. to permittivity, loss-angle, and volume resistivity 78—6631
  polymers, reduction due to stretching *(German)* 79—43446
  polystyrene, plasticizer effect on electric strength 80—29688
  polysulphone, elec. appl., dielec. props. meas. 77—55750
  polyvinylidene fluoride, dielec. breakdown and elec. cond., room temp. to 150°C 80—60500
  PVC films, temperature-time dependence *(Russian)* 78—76386
  rare earth aluminate, scandate and zironate film coatings, electrophys. props. w.r.t. prep. technology 80—60781
  rubber, effect of Se on electrical and mechanical strength, after mechanical and electrical ageing *(Russian)* 79—52396
  silicone, film deposition, glow discharge polymerisation, elec. and thermal characts. 78—6467
  spark gap electric strength recovery after impulse current passage 78—67565
  spark gaps, SF_6, limiting sparkover voltage values determ. and dielectric strength testing in power equipment *(Czech)* 80—87962
  statistical test of solid dielectrics in pulse irradiation regime 78—95548
  styrene-butadiene copolymers, elec. strength meas. 78—15096
  surface finish effects, backscattered electron intensity meas. *(Japanese)* 77—66081
  surface vac. breakdown of dielectric solid by ultrasoft X-rays 80—43989
  synthetic insulating materials, correl. with other parameters, expt. 77—43933
  trifluorotrichloroethane, liq., as insulating material and coolant, dielectric strength, HVDC convertor appl. *(German)* 77—76218
  vacuum gap following high-current arcing, dielec. recovery strength 78—9891
  vacuum gap with processed electrodes, atm. effects on dielectric strength 78—51389
  vacuum gaps, influence of solid-state cohesion of conditional metal electrodes 77—7618
  vacuum gaps with conditioned metal electrodes, thermal press. effect 78—42843
  vacuum insulation, elec. strength prediction *(Russian)* 77—15257
  $Al-SiO_xN_y-Al$ structure, effect of fast neutrons on elec. strength *(Russian)* 77—85343
  Al_2O_3, anodic film, trapped O_2 and effect on dielec. stability 80—100634
  Al_2O_3, detonation coating, porosity, electrical strength, phase anal. *(Russian)* 77—69204
  Al_2O_3, film, CVD, props. rel. to deposition parameters 78—92197
  Al_2O_3, insulator, electrical puncture strength at high temps. *(German)* 79—70175
  $B_2O_3-SiO_2$ glasses, phase separated, DC cond. and elec. breakdown 78—23400
  $BaTiO_3$ ceramic films, dielec. strength, statistical anal. 80—75935
  $CCl_2F_2-CO_2$ gas mixture, field breakdown gradients calc. method 80—92248
  $CCl_2F_2-N_2$ gas mixture, field breakdown gradients calc. method 80—92248
  GaAs thermal oxide film, fabrication and characterisation 80—11808
  He, liquid, electrical strength, breakdown voltage depend. on electrode configuration 80—7293
  HfO_2 film, CVD growth, struct., elec. and optical prop. characterisation 77—55891
  $LiNbO_3$, optical strength anisotropy, excitation of second harmonic 79—69923
  N_2, compressed, insulation breakdown at cryogenic temp., obs. 78—51368
  N_2, dielectric strength, bubble-phase equilib., high press., low temp. *(Russian)* 77—20798
  N_2, gas, in crossed elec. and mag. fields, elec. strength calcs. 78—87568
  N_2, liq., breakdown strength, in mm gap range, press. effects 79—91357
  N_2, liq., determination 79—38451
  N_2, liq., discharge development in nonuniform elec. field 79—91358
  NaCl, optical strength, effect of irrad. in mechanically stressed state 80—80695
  PbN_x, pressed, lag time of breakdown and dielec. strength 77—36174
  SF_6 breakdown field strength, electrode surface roughness tolerance 78—67577
  SF_6, compressed, electrode surface roughness effects, model *(German)* 78—63609
  SF_6, conductor surface irregularities influence 80—14946
  SF_6, dielectric strength tests *(Czech)* 78—30498
  SF_6 electric strength as statistical charact. *(Russian)* 79—41787

electric strength continued
  SF_6, predischarge-stabilised breakdown voltage *(German)* 78—63608
  SiO supermultilayer dielectric film, elec. strength *(Russian)* 77—85648
  SiO_2 film, dielectric breakdown and I-V characteristics 77—63368
  SiO_2 film, effect of oxidation on dielec. strength 77—16249
  SiO_2 film, in MOS structures, under unidirectional alternating and combined voltages *(Slovak)* 78—88034
  SiO_2 film, thermally grown, pore size influence of punch-through voltage 78—6632
  SiO_2 layers, dielectric strength, dislocation effect 78—31154
  Ta_2O_5, film on Al, Cu, Au, Ag electrode, electric strength of MIS system 80—96999
  TiO_2 based ceramic dielec. materials, medium permittivity, elect. charact. 78—35086
  TiO_2, sintered ceramic, props. rel. to additives, impurities 78—35329
  WC-Co, conditioned metal electrode, effect on electrical strength of vacuum gap 79—90489
  ZrO_2 film, CVD from organometallic cpds. and characterisation 78—23626
  ZrO_2, plasma deposited, porosity, gas permeability and dielectric strength 79—52125

electric susceptance *see electric admittance*

electric susceptibility *see optical susceptibility*

electric switchgear *see switchgear*

electric transformers *see transformers*

electric utilities *see electricity supply industry*

electric variables control
  see also electric current control; frequency control; gain control; load dispatching; phase control; power control; voltage control
  clearing electrode control system for CERN ISR 77—38514
  conductivity, rectangular waveguide, control, rect. E_{112} mode resonator sensitivity analysis *(Russian)* 77—18052
  cytopherometer, field strength rel. to reproducibility improvement 77—52954
  linear accelerator, field control in standing wave structure at high average beam power 77—38486
  TEM, high resolution, electronic control systems 78—32939

electric variables measurement
  see also attenuation measurement; capacitance measurement; charge measurement; dielectric measurement; electric admittance measurement; electric current measurement; electric distortion measurement; electric field measurement; electric impedance measurement; electric noise measurement; electric reactance measurement; electric resistance measurement; electrical conductivity measurement; frequency measurement; gain measurement; high-frequency transmission line measurement; inductance measurement; phase measurement; power factor measurement; power measurement; Q-factor measurement; voltage measurement
  200 kW Gedser windmill in Denmark, performance meas. 80—61431
  A/D convertor with special appl. to medium precision Pt resist. thermometry 80—86297
  AC electrical load information recorder utilising standard multi-point chart recorder 80—42238
  AC thermopower measurement, method for semiconds. 80—44624
  AC/DC transfer measurements, wideband, automated 77—18035
  analogue conversion using transducer, synthesis principles *(Polish)* 77—53882
  back discharge in electrostatic precipitator, light meas. technique 77—76232
  battery load characts., alkaline, for camera appl., effect of discharge resistance obs. *(Polish)* 79—57420
  breakdown development in gases, elec. and optical meas. methods 78—22584
  carrier lifetime measurements from transient elect. photoresponses in solar cells 80—61346
  carrier modulation, operation and accuracy of meters 77—37912
  CEI standards for measuring instruments *(Italian)* 80—31789
  conference on precision EM meas., Braunschweig, Germany (Jun. 1980) 80—98903
  contact electrification of polymers, meas. using computer-controlled apparatus 80—86341
  discontinuous electrical phenomena measurement, digital techniques *(Rumanian)* 77—79120
  electrocapillary curves, automatic meas. eqpt. 78—40061
  electron beam recording, film speed choice, TV image appl. *(Russian)* 77—38049
  electronic industry, Spain measuring equipment choice, criteria *(Spanish)* 78—36963
  electronic measurements, book 80—31805
  electrostatic force meter, device for undergraduate laboratory 79—17164
  electrostatic properties of powders 80—52266
  EM meas. and instrumentation, conf., Ottawa, Canada, 1978 79—21731
  film, electrophysical properties measurement apparatus 78—4654
  free carrier profile measurement on thin-layers, fast current pulse MOS deep-depletion technique 78—80075
  Hall coeff. contactless meas. in materials of small Hall angle in skin depth regime 78—86303
  Hall coeff. of semiconductors, automatic device for temperature dependence determ. 80—52270
  Hall coefficient, resistivity, Van der Pauw method, contact position and sample geometry influence *(German)* 78—233
  Hall effect, measuring cell construction, for liquid metals and semiconductors 77—5866
  Hall effect measurement, liq. semiconds. 80—65594
  Hall mobility, microwave meas. method 79—54154
  high pressure chamber designed according to opposed anvil principles, thermoelectric force meas. *(German)* 80—90863
  hydrostatic pressure cell, up to 90 kbars, appl. 79—17436
  INI-3 measuring system for nanosecond pulses 79—35793
  instrument servicing and calibration *(German)* 77—2665
  insulating particles in insulating liquids, high field electrophoresis 80—90865
  Josephson AC effect applications in precision metrology and novel voltage source *(German)* 80—70902
  kinetic coeff. meas., universal electrical meas. installation 78—4645
  low-noise power supply for electrical transient meas. 80—52273
  LV short-circuit testing station, equipment and measurement methods *(Polish)* 80—77773
  magnetoresistance four-probe method for free carrier density and mobility meas. 77—43626

electric variables measurement continued
magnetoresistance measurements, influence of supercond. contacts 78−21184
MIS structure, elec. parameter meas. of second order equivalent ccts. 80−57332
model for 1/f noise 80−98945
m.o.s. capacitor C-V characts. meas. by nondestructive method using Au ball probe 77−1491
null apparatus for minority carrier lifetime meas. 78−56184
piezoelectricity, reson. method for determ. of small piezoelec. consts. *(German)* 78−92025
precision, conf., Brighton, UK (Sep. 1977) 77−82551
precision electrical meas. using superconductivity *(German)* 77−79124
precision EM measurements conference, Boulder, Colorado (June 1976) 77−18010
pyroelectric materials, automated simultaneous meas. of electrical properties 80−57335
quartz resonator parameters, high-accuracy bridge instrument 77−10056
quasistationary electrical quantities, digital techniques *(Rumanian)* 77−79120
Seebeck coefficient, AC method of meas. using laser beam, for semicond. 78−76096
Seebeck coefficient in solid biopolymers, meas. apparatus 78−21172
Seebeck coefficient measurement of disc-shaped samples by AC method *(Japanese)* 80−73392
semiconductor, piezogalvanomagnetic effects measurement at low temps., apparatus with stabilised dynamic load 77−67458
semiconductor deep level props. meas., capacitance spectrometer *(German)* 80−15471
semiconductor junction noisy transient meas. 78−62205
semiconductors, elec. props., mag. field effect determ., method 80−44623
semiconductors, temperature dependences of electric conductivity, Hall coeff. and magnetoresistance automated installation 80−31792
signal generator output measurement correction coefficient for waveforms, standard instrument *(Polish)* 77−53957
skin electrical quantities, frog, method for in situ meas. 80−36208
SQUID appl. to low temperature transport physics 79−26067
standardising laboratory for developing countries 80−101774
standards importance in International Organisation of Legal Metrology *(German)* 79−75486
standards progress and fund. consts. role *(Japanese)* 78−24760
sulphide melt, conc. EMF meas. using solid-electrolyte cell 77−40571
superconductivity, definition of terms for fundamental states, flux phenomena, meas. practices 78−34916
superconductivity appl. to metrology *(Japanese)* 78−37030
techniques for establishing echelon-I standards 78−24812
thermoelectric figure of merit, meas. for poor thermal conductors 77−28202
thermoelectric power, liquid metals and alloys 79−40591
thermoelectric power, meas. using analogue subtraction 78−244
transducers, third-generation, Czechoslovak (Metra Blansko) range *(Czech)* 80−73340
Wiltron bridge used for 70 MHz-4 GHz, oscilloscope indicator *(French)* 80−42241
work function measurement method for use in inert medium 79−49250
Si wafer, nondestructive method for meas. of spatial distrib. of minority carrier lifetime 80−13098

electric vehicles
see also electric drives; electric locomotives; electric propulsion; motor-coaches
assessment c.f. H_2-powered vehicles 80−16769
automobile propulsion batteries, current designs and their limitations 79−66405
batteries, criteria for electric vehicle and energy storage applications 80−72031
batteries development, Al-air, mechanically rechargeable 79−48103
batteries development, Fe-air, long-life 79−48118
batteries development, high temperature, Na/S 79−43757
batteries development, Japanese, advanced Fe-Ni battery *(Japanese)* 79−83589
batteries development, Li-Al/MS_x improved design 79−48116
battery, Pb-acid, response to chopper-controlled discharge 79−48120
battery systems available and under development, review *(Dutch)* 80−72025
battery-powered, cf. H_2 powered vehicles 80−45819
bipolar Li-Al alloy/FeS_2 battery appl., using LiCl-KCl eutectic or LiF-LiCl-LiBr melt, cycle life, self-discharge rates and edge losses obs. 79−48117
dispersed electrodes appl., Zn electrode development *(French)* 80−72023
energy conversion, Conf., San Diego, CA, USA (Aug 1978) 79−48038
flywheel energy storage system appl., composite, regenerative braking 79−48185
flywheel energy storage unit for a high power energy source for vehicular appls. 80−30580
fuel cells, Fiat research, Italy 80−35673
fuel cells for vehicle propulsion appls. technical and economic eval. 80−30475
high speed ground transportation vehicles gas-flow-controlled arcs for power collection 80−70054
mechanical energy storage systems for electric vehicles, effect on performance 80−30579
metal-air batteries for electric vehicle propulsion, comparison of Li, Al, Zn, Fe systems 80−30444
metal/air batteries, status and potential, review 80−55828
power sources, battery design requirements for commercial use *(Dutch)* 80−72024
power sources, fuel cell/secondary battery hybrid appls. *(Dutch)* 80−72037
propulsion, regenerative flywheel energy storage system 80−30564
road vehicles, energy economy aspects *(German)* 80−30427
secondary cell development program of US Dept. of Energy, review 80−30442
social implications of energy storage 80−67001
thermal management of battery systems for electric vehicles and utility load leveling 80−30458
utilization for energy conservation, review 79−24884
Li-Al/FeS cells for electric vehicle propulsion 80−30446
Li-FeS_2, battery appl., industrial participation in ANL development program 79−48113
Li-Si alloy/FeS battery appl., research and development at Atomics International 79−48115
Li-Si alloy/FeS_2 cells appl., high performance 79−48114
LiAl/FeS electric vehicle battery, charging system developments 80−30447
LiAl/FeS(S_2) battery developments for electric vehicle propulsion and load levelling appls. 80−61325
LiAl/metal sulphide high temp. battery with multi-foil insulation container for electric vehicle appls. 80−30448
Na/S cells appl., pulse characts. obs. 79−48109
Ni-Zn electric vehicle battery, performance characts. 80−30443
Pb-acid batteries, for elec. vehicle propulsion, heat transfer, math. anal. 80−3509
Pb-acid batteries appl., using high-rate tapered DC charge method 79−48111
Zn-Cl_2 batteries for electric vehicles, battery design modelling 80−30452

electric welding
see also arc welding; electron beam welding; resistance welding; welding electrodes
diffusion, surface treatment by glow discharge effect 78−7089
electroslag, using plate electrodes for Al busbar component parts welding 80−81083
fusion welding of Al alloys, weld susceptibility to hot cracking 80−81143
glow discharge as welding heat source, appls. review 79−73051
interferometric study using laser source *(Russian)* 78−37049
mild steel, effects of CO_2-O_2 mixture, compositions on hot cracking resistance 77−21239
quality monitoring, US testing 78−56854
seals high-temp. metal foil, formed by seam welding 79−80597
steel, G-Mo type, welded joints, thermal fatigue testing 78−3278
ultra pulse welding, heat transfer characts. 79−1047
welded joint non-metallic, inclusions anal. 77−76245
Au wire-semiconductor, elec. contacting by spark welding *(German)* 79−49215
Pt and Au threads in air, pull-off force, influence of electric charge 79−11196

electric wiring *see wiring*

electrical conduction in condensed matter
see also carrier density; carrier lifetime; carrier mean free path; carrier mobility; carrier relaxation time; dislocation scattering; electrical conductivity of liquids; electrical conductivity of solids; electrical conductivity transitions; electron density (metals); electron mean free path (metals); electron mobility (metals); electron-phonon interactions; electron relaxation time (metals); high field effects; hopping conduction; impurity scattering; Lorenz number; minimum metallic conductivity; minority carriers; mixed conductivity; negative resistance effects; one-dimensional conductivity; photoconductivity; point defect scattering; size effect; skin effect; small polaron conduction; space-charge-limited conduction; spin disorder resistivity; surface conductivity; surface scattering; thermally stimulated currents; tunnelling
Anderson localisation, self-consistent diagrammatic theory 80−107746
anisotropic medium, resistance, geometrical effects 79−28331
Boltzmann transport theory, temp. dependent energy levels effect 77−89743
bond-percolation conductivity, effective-medium approx. 78−29057
charge storage, charge transport and electrostatics conference, Kyoto, Japan (Oct. 78) 80−7252
conference, Krusevac, Yugoslavia, Sept. 1978 79−56104
disordered media, elec. transport theories, effective medium approx. improvement 79−47071
disordered system, scaling near mobility edge 77−11835
disordered systems, elec. transport mechanisms 79−69483
geminate recombination, time depend. Onsager problem anal. soln., critical elec. field 78−72446
Hubbard model, electrical conductivity calc. including electron-phonon interactions 77−47804
Hubbard model, electrical conductivity calculation, dielectric function and plasma oscillations 78−64020
inhomogeneous media, galvanomag., stratified, elec. fields 80−63888
inhomogeneous medium, effective cond., iteration series and variational estimates, Herring method 80−70663
isothermal local resistivity, theory 78−72128
MHD generator, open cycle, with shaped magnetic induction, theory of nonuniform electrical conduction 80−28831
micellar solution, micellisation kinetics, pressure-jump and stopped-flow methods 80−45564
Monte Carlo calc., book contrib. 80−100458
noninteracting electrons in correlated arrays of fixed scatterers, AC and DC cond. 78−51955
nonlinear response of some simple quantum systems 77−49620
particle conductivity in 2-dimensional random potential *(Russian)* 79−99523
quantum transport theory, CPA calcs. 77−85186
quantum transport theory in CPA, limit of small carrier number 77−69285
quantum transport theory in CPA, using diagrammatic expansion and resummation approach 77−69284
randomly-inhomogeneous conducting media, generalised charac. computation using random function theory *(Russian)* 80−75535
soliton in solids with chain structure *(Chinese)* 79−90931
spatially disordered system, two-dimens., localisation and conductivity exam. 78−18998
strongly correlated system, electronic transport 77−1401
Swiss Physical Society, autumn sessions 78−72053
H_2^+ system, quantum oscillations in tunnelling, oscill. freq., tunnelling currents *(Russian)* 80−60065

electrical conductivity
see also electrical conduction in condensed matter; electrical conductivity of gases; electron mobility; ion mobility; space-charge-limited conduction
alluvial aquifers, relation between resistivity meas. and hydraulic parameters *(Italian)* 77−53079
anisotropic porous media, degrees of anisotropy of fluid flow and diffusion (elec. conduction) 77−51109
auroral ionosphere, electric fields and conductivity in quiet periods 77−53280
bacterial suspension, physico-chem. changes on cooling, cell elec. cond. anal. 77−86458
biological specimen-conductivity problem in electron microscopy, review 78−24206

electrical conductivity continued
  conductance network, random, simple, triangular, site percolation, effective medium theory 79—12746
  disperse system, diphasic struct., systematic anal. to determ. permittivity and elec. cond. from dielec. relax. 78—56423
  disperse systems, depend. on conducting component content 80—92954
  Earth crust, cond. anomaly in N America rel. to possible Proterozoic plate boundary 77—91079
  Earth crust, in Gregory Rift Valley, Kenya, cond. from magnetotelluric study 77—91000
  Earth crust, in Scotland, cond. rel. to Caledonian tectonics 77—44920
  Earth crust, induced currents mapping around Kenya Rift 77—73628
  electrode resistance, effect on current density and electrode pot., rel. to cell design 77—60070
  electron transport over barriers of fluctuating height 78—56122
  erythrocyte membranes, human, ghosts and lipid bimol. membranes 77—9180
  erythrocytes of human blood, diameter meas. by specific elec. cond. 78—53353
  fluid system, electric conduction in relativistic thermodynamics 80—105498
  fluidised bed, electrical conduction theory 80—18988
  foam, rel. to degree of aeration 79—57299
  gas-liquid emulsions and foams, electrical conductivity 80—11961
  geological conductors, water-bearing and frozen, elec. props. investigations *(German)* 79—5472
  graph-like state of matter, electrical cond. of random networks, gelation and elasticity 78—65875
  heat and electrical transfer differential eqns. 78—67004
  heterogeneous system with chaotic structure, generalized conductivity coefficients, review 77—87708
  homogeneous materials, theory relating to Kirchhoff's method of determ. 79—64170
  inhomogeneous media, conductivity profile determ. by time domain reflectometry 79—36820
  ionosphere, elec. cond., field-aligned currents and electrojets 77—21974
  ionosphere, tensor conductivity 77—13172
  isothermal resistivity, interacting charged particles in contact with bath, Matthiesen rule 77—35904
  Kerr black hole, elec. and mag. cond. 79—25625
  Kubo-Greenwood formula for teachers 78—62017
  magneto-rheological suspensions, mag. field effects 80—11960
  microemulsion, stirred percolation model 79—79314
  modelling, arbitrary two-dimensional structures 79—92617
  multistate trapping model, rel. to continuous-time random walk model 78—93624
  nonlinear electrical conductivity theory based on integral Boltzmann eqn. 78—72125
  nonlinear electron transport in vac. diode 77—13718
  oceanic asthenosphere, deep EM sounding near Californian coast, interpretation 77—9383
  oceanic basalts, press. depend. of solidus temps. and elec. cond. during melting 77—91109
  packed bed, hold-up profile, elec. cond. meas. 77—35201
  permafrost active layer, in situ meas. of apparent cond. 77—64333
  polyhedral foams, limiting cond. at low density, theory 78—44410
  polystyrene particles, monodisperse, dil. and conc. aqueous dispersions, elec. cond., surface cond. and double-layer polarisation 80—89533
  porous electrodes, relative elec. cond. of soln. and matrix phases 79—52679
  quantum theory, appls. 78—84181
  resistivity logging tool response, sonde position effect 77—86759
  static conductivity of 1-D disordered systems 77—49697
  stratosphere at Syowa Station, Antarctica, cond. from vertical elec. fields and currents meas. 77—53142
  thermoelectricity, stationary interaction of temp. and elec. tension in 3-D body *(German)* 79—27497
  tissue microwave dielectric props. rel. to rot. mobility of tissue water 77—29092
  Cu particles in fluidised bed, electrical conductivity of electrodes, expt. meas. 77—48652

electrical conductivity measurement
  25 kV bias isolation unit for 1 MHz measurements using commercial C/G meter 78—54401
  AC conductance cell, appl. to phase transitions determ. 77—55341
  alkali metal glass, elec. cond. meas. method 79—66250
  alkaline frozen solutions, polycryst. and glassy, photocond. and radiometric obs. 80—45531
  anisotropic materials, measurement of resistivity using RF contactless method 79—67344
  anisotropic metals, eddy current method 77—67466
  anodic oxide film, ionic cond. determ., open-circuit transient method, rel. to other techniques 80—24650
  antistatic polymer film surfaces, microammeter meas. method 80—98932
  atmosphere, multielectrode ion mobility spectrometer construction 80—31145
  automatic conductometer, exam. 78—56933
  automatic resistivity, Hall mobility and thermopower meas. *(Polish)* 77—41638
  biological conductivity monitor for isolated nerve preparation expts. 80—67301
  blood cell aggregation, conductometric meas. 77—25614
  cardiac tissue resistivity, intramural meas. 79—39388
  catalyst, non-metallic, dynamic measurements during adsorption and catalysis using bifilar conductivity probe 80—13096
  cell for solid-phase 'anvil-toroid' apparatus, 8 GPa, 1500°C 80—31794
  ceramics, electron and ion conductivity, instrument for meas. up to 2000°C 79—96247
  chemical monitoring laboratory, installation 78—61123
  circuit breaking arc column electrical conductivity meas. *(French)* 80—28864
  coal, bituminous, meas. as function of freq., polarisation, EM wave direction and temp. 79—12113
  concrete electrical conductance meas., automatic instrument 77—77659
  conductance meter classification and quality assurance 77—12857
  conductivity meter for in situ ocean meas., development, testing and calibration 79—5671
  conductometer to record rapidly varying electrical conductivity 80—61184
  contact transducers, threshold sensitivity meas. 80—62688

electrical conductivity measurement continued
  contactless meas. method, cond. cylinder motion in solenoid field *(Russian)* 79—214
  contactless measurement of sheet conductivity and mobility of semiconductor wafer by using eddy current 80—62693
  contactless measurement of solid cylinder cond. in current ring 79—75554
  contactless measurements for solids using torsional resonance apparatus 79—75675
  contactless resistivity measurements, appl. for graphite intercalation compounds, review 80—37054
  core samples, methods using electrode configurations without necessity for access to sample end faces 79—67345
  cryogenic liquid, ionic mobility measurement, pulsed spacecharge technique 77—74420
  cryostat, for meas. on plastically deformed specimens at liq. He temps. 78—81985
  crystalline materials, high-pressure and temp. cell *(German)* 79—93162
  dark conductivity of solid discs and flakes, cell designs with variety of contacts 78—24816
  dielectrics, elec. and mech. props. at increased temps., meas. equipment 77—71342
  dry stress corrosion kinetic studies of threadlike metal specimens 79—83381
  Earth, DC resist. meas. interpretation 79—5449
  Earth's resistivity determination, by surface meas. 78—24393
  Earth conductivities, mapping via multifreq. airborne EM system 79—5446
  Earth conductivity, model for quantitative interpretation of towed-bird airborne EM system meas. 79—5447
  Earth interior resistivity distribution, in uppermost kilometres on continental areas 78—24219
  eddy current interactions in contactless meas., theoretical investigation *(German)* 80—31788
  eddy current transducer, electrical conductivity meas. of coatings, tuning out of gap instability 78—36994
  electrodeless conductivity probe for high-temperature and pressure measurements 80—52272
  electrodeless meter design, for electrolytic liquids 79—85153
  electrolyte flows, low-loss instrument IC with induction transducer 79—17439
  electrolyte solution, HF elec. cond. and dielec. const., determ. in RF region 77—21396
  electrolytes, solid oxide, elec. props., study methods *(French)* 80—22386
  electrolytes in H_2O, voltage amp. for temp. compensation *(German)* 78—54399
  electrolytic cell resistance meas., differential recorder 78—86297
  electrolytic conductivity of solutions, using multi-electrode equipment 78—21175
  electrolytic solutions, bridge cct. for cond. cell *(German)* 79—9220
  electron microscope, HV, in-situ elec. resistivity meas." 80—101893
  electrooptic crystal voltage-induced birefr. obs. for very high resist. meas. 80—73386
  electrophysical information collection, recording and processing system 78—8388
  epitaxial layer resistivity meas. using Hg—n-GaAs barrier contact 79—60945
  film, electrophysical properties measurement apparatus 78—4654
  films electrophysical properties, using automatic recording and expt. data analysis 79—17446
  fluids, simultaneous investigation of eqn. of state and elec. cond. 77—55337
  four probe AC conductivity meas. system 79—35792
  four-point probe meas. error factors, SEM obs. on Si 79—71484
  four-probe method for up to 50 kbar and 1000°C 78—57978
  gas chromatographic bipolar pulse differential electrolytic cond. detector 80—93814
  gas-electrolyte dispersions, void fraction meas. using conductivity method 80—76525
  general reciprocity theorem for conducting media 79—31770
  glass, ionic cond. meas. equivalent circuit for ohmic resist. meas. 79—33110
  glasses, electrical cond. meas. technique using thermally stimulated polarisation currents 79—99561
  glasses, sources of error in AC cond. meas. 78—76076
  ground, determination using EM methods, review 80—22382
  Hall measurements instrument, specimens in strong elec. fields 79—35779
  hardened concrete, specific resist. meas. *(German)* 79—97406
  heterogeneous dielectric, resistivity and static dielec. permittivity determ. in linearly time depend. elec. field 80—52268
  high-pressure measurements at low temp. using clamp cell 8 GPa, 77K 80—37047
  high-resistance specimen conductivity nonlinearity meas. instrument 79—67341
  hot gas conductivity meas. method 80—13104
  'Impul's' conductometer (USSR), elimination of dilute soln. instability 80—77813
  inductive oscillometry, field difference theory 78—51342
  instrument for loose materials 78—54395
  insulating materials, common, temp. depend. of elec. resist. determ., expt. *(Croatian)* 77—74426
  insulating materials, three-terminal cell for meas. over wide freq. and temp. ranges 80—37053
  ion exchange materials, elec. cond. meas. using isocond. pt. determ. method 77—52646
  ionic conductivity, four-probe AC bridge technique 80—57340
  ionic crystal, edge and surface effects 78—6177
  kinetic investigations in soln., high press., device for conductivity meas. 79—93161
  large conductances, meas. via modified commercial admittance bridge 78—4660
  LF electromagnetic wave meas. method, soil resistivity appl. *(French)* 78—24394
  liquid metal, simultaneous meas. of density, elec. cond., abs. thermopower at high temp. and high press. 77—1402
  liquid metals, contactless resistivity meas., impedance change of a coil 80—73388
  liquid semiconductor, resistivity temperature dependence, meas. apparatus for 10^{10} Hz freq. region 78—21169

electrical conductivity measurement continued
liquids, gases, conducting, high press., temp. elec. cond. meas., four electrode method 80—62685
metal dioxides, pure and mixed, conductivity meas. by new method 80—45517
metal resistivity in He II environment using computerised facility 80—31799
metal-semiconductor interface, meas. of resistivity 80—105672
metallic thin film, thickness dependence, quantum size affect *(German)* 80—86344
metals, continuous contactless meas. of temp.-depend. elec. resist. 78—21171
metals, liq., viscosity effect on cond. meas. by rot. mag. field method *(Russian)* 77—57349
metals, residual resistivity and thermal conductivity coeff., comparison of max. values as parameter of metal purity 79—65431
metals and alloys, critical temperatures determination, elec. resist. method, IMASh-5S-69 installation 80—71827
MHD generator chamber *(Polish)* 77—7602
micro-organism electrical characteristics meas., elec. cond. and dielec. props. *(Italian)* 78—3684
microwave conductivity determ. from eddy current losses in planar specimens of high cond. 80—47077
microwave conductivity measurement by eddy current loss method, effect of permittivity 78—24817
MISS, apparatus with automatic compensation for geometric capacitance, 1 Hz-100 kHz range 79—21780
narrow-band semiconductors, current-carrier conc. distrib. nonuniformity, contactless meas. 77—76853
ocean conductivity microscale studies, stable platform development 79—5669
ocean internal waves meas. with electrical contact device 80—12566
oceanographic in situ meas. instrument, development and operational experience 79—74970
organic charge transfer salts, voltage shorted compaction technique 78—43365
organic liquid conductivity and bulk charge determ. cell *(Russian)* 80—57328
oscillating conductivity probe, density and density gradient meas., hysteresis effect 78—32796
oxide electrolytes, solid, rapid method of control of conductance 77—52647
oxide melts, at 1000 to 1750°C, methods survey *(Slovak)* 80—47079
particulate layer, thin, under ionic bombardment 80—68218
patient electrical conductivity and permittivity imaging, computing tomography technique 80—98055
photoconduction decays, fast, measurement, DC-10 MHz low noise amplifier system 80—57326
photoconductive insulators, interdigital electrode method, current density and arrival time 79—33308
photoconductivity of solid discs and flakes, cell designs with variety of contacts 78—24816
point defect concentration monitoring during low-temp. irradiations and anneals 80—7741
poly- and single-crystalline solids in diamond anvil cell, DC 4-point probe method 79—6147
polymer film, bulk elec. cond. parallel to film surface 79—87094
polymeric insulators, controlled current DC meas. 78—57982
polymers, atuomatic device for measuring elec. direct current props. *(German)* 78—45647
potential single-sonde method for inhomogeneity meas. of InAs, InSb 80—65549
probe design for use with bridge instrument, wide range of test solns. 80—95110
properties of high-conductivity copper and copper alloy wires *(Japanese)* 79—91665
rapid conductivity meas. with electrolyte cond. probe, astable multivibrator freq. control 78—37029
reconstruction of spatial resistivity distribution of conducting objects from external resistance measurements 79—80648
rectangular pulse generator, calibrated, for conductor elec. props. meas. 78—8416
residual resistivity, meas. via medium temp. electron irradiation 77—54016
resistance changes, continuous recording apparatus 77—53931
resistance variation with temperature 80—77575
resistivity measurement, using spreading resist. method, automatic device 80—17959
resistivity measurement of thin square sample with square four-probe array 77—41654
resistivity measurements using high-pressure cell, 13 GPa, 1.2K 79—80637
resistivity relaxation measuring system, for surface reaction meas. 80—55718
rocks, elec. resistance and dielectric const. meas. method, appl. to Ukrainian shield *(Russian)* 77—73721
rotating sample magnetometer for contactless conductivity meas. 80—73391
salinity/temperature sensor chain for estuarine meas. 79—5670
salt concentration, monitored by one-chip conductivity meter 78—232
seawater, new meas. method, temp. effects 78—20531
seawater, using bathometer sonde 77—78480
seawater, using meters with automatic correction of characts. *(Russian)* 78—65426
seawater conductivity/temperature/pressure profiler errors 77—5377
SEM technique, appl. to TTF-TCNQ 80—86507
semiconductor, field depend. meas. by coaxial line method *(Russian)* 77—85206
semiconductor, molten, quartz cells for elec. cond. and thermo-EMF meas. 77—74439
semiconductor, waveguide method of measuring electric parameters at microwave frequencies review 79—93170
semiconductor contact potential and conductivity simultaneous automatic meas. 78—21118
semiconductor contact potential difference and surface cond., combined meas. method 77—18042
semiconductor epitaxial layers, resistivity and thickness monitoring, use of spreading-resistance method 80—47075
semiconductor film, cell for measuring electrophys. parameters over wide temp. range 77—51830

electrical conductivity measurement continued
semiconductor film X-ray and electrical characteristics meas. chamber 78—86396
semiconductor films, combined four-probe method 79—67348
semiconductor layers, resistivity meas. by four point contacts arbitrarily spaced on circumference 78—51983
semiconductor layers with inhomogeneous regions, four-probe meas. *(Russian)* 77—79104
semiconductor materials, high-resistivity, using EM methods with capacitance sensing element, computer-aided evaluation 79—80647
semiconductor materials temperature dependence meas., using automatic device 80—52270
semiconductor microwave conductivity meas. by eddy current loss method 78—8417
semiconductor resistivity, geometric factor in perpendicular four-point-probe meas. 77—67475
semiconductor resistivity, spreading resist. calcs., role of source boundary conditions 78—89499
semiconductor resistivity and Hall effect meas., nondestructive four-electrode characterization 80—49743
semiconductor resistivity meas., influence of space charge 78—23076
semiconductor resistivity meas., two dimensional plotting by SEM 77—39852
semiconductor samples pulse method for contact resist. and bulk resist. 78—52083
semiconductor structure, electrodeless meas. of resist. and spherical curvature 79—49252
semiconductor thin film conductivity monitoring by microwave resonator absorption *(Russian)* 78—23182
semiconductor volume and contact parameter determ. from V-I characteristic *(Russian)* 80—49912
semiconductor wafer resistivity distribution, contactless meas. *(Polish)* 77—79102
semiconductor-based HF meter, principles and advantages *(Hungarian)* 78—16815
semiconductors, airtight cell for simultaneous conductivity and thermo-EMF meas. 78—21168
semiconductors, high temp. conductivity and Hall effect meas. 77—87786
semiconductors, liq., viscosity effect on cond. meas. by rotating mag. field method *(Russian)* 77—57349
semiconductors, resistivity profile meas. using two-probe spreading resistance techniques 80—49742
semiconductors, SHF waveguide methods 78—95542
shallow-water mineral exploration by controlled-source audiomagnetotellurics and resistivity profiling 77—5356
silicone fluid conductivity meas. under DC field 80—15533
six solenoid oscillometer for non-intrusive LF positive-glow plasma diagnostics 78—51343
skin conductivity measurement, electrode materials *(German)* 78—85406
slice resistivity distrib., contactless meas. results *(Polish)* 77—89756
soil, bulk resistivity meas. method 78—24381
soil, SW measurement of dielec. const. and conductivity 80—22388
soil conductivity measurement methods *(Spanish)* 79—96831
solution conductivity measuring instrument, DG-1, features *(Polish)* 78—41330
solutions, in electrochem. cells, DC cond. meas. using rot. electrode 77—70362
Spar Buoy Oceanographic Telemetry System 80—46307
specific resistivity meter with logarithmic output for rock samples 79—35781
specimen preparation, by spark-cutter *(Japanese)* 80—22339
spherical metallic specimens, eddy-current probe method 78—53138
spherical samples measuring method 77—67464
spreading resistivity rel. to load applied to meas. probe 78—4647
SQUIDs, multiple mag. flux entry, cosϕ conductance exam. 79—4623
standard models for measuring elec. cond. 80—86343
standard reference mat., W, 4-3000K 77—45820
student expt. for resistivity meas. 78—16612
surface resistivity of Au at 890 GHz, using pyroelectric detector 77—34004
surfacing probe for ocean surface layer elec. cond. meas. 79—2392
thin liquid films on inaccessible surfaces, thickness meas. 79—30412
three-terminal test cell for rapid dielectric loss and resistivity meas. of oil samples 77—67465
transient, coaxial conductivity cells for subnanosecond time resolution 80—197
triaxial acoustic current meter for small-scale ocean turbulence resolution 77—41232
two-circuit system, resonant EM transducer sensitivity anal. *(Russian)* 79—213
ultracentrifuge with magnetic suspension, contactless meas., appl. 77—16776
ultrapure water electrolytic conductivity meas. 79—24755
universal bridge, digital meter used to measure L, R, and C 78—12715
Van der Pauw method, contact position and sample geometry influence *(German)* 78—233
Van der Pauw method, meas. of resistivity and Hall constant 77—67467
van der Pauw method, modified for appl. to powder compacts 78—32833
van der Pauw sample and its dual, elec. resistivity and Hall coeff. meas. 79—88984
wafer resistivity distribution, contactless meas. *(Polish)* 77—79102
water, monitoring using conductivity cell for wave height probe 80—57280
water, pure (10^{-1} μS/cm), at steady temperature and flow *(Czech)* 80—62684
water quality meas., continuous, in tubular columns, probes utilisation *(French)* 78—3836
water sample, automated anal., pH, conductivity, alkalinity 79—12287
Ag halide microcrystal, photoconductivity meas. by microwave technique 80—103719
Al-Al$_2$O$_3$ thin film system, electrical conductivity and I-V characts. meas. *(Polish)* 79—56310
Au wire-semiconductor, elec. contacting method, spark welding *(German)* 79—49215
Bi$_2$O$_3$-Ta$_2$O$_5$, sintered, high oxide ion cond. meas. 78—14503
CaF$_2$, elec. cond. at high temp. 78—72159
CdTe, charge carrier transport prop. meas. by time of flight technique 77—39850
Cu at MM wave freqs. 80--42235
Cu conductors used in coaxial cables, resistivity measurements *(French)* 79—69487

electrical conductivity of amorphous metals and alloys continued
Ni_xZr_{1-x} metallic glass, crystallisation kinetics, elec. resist. and mag. susceptibility meas. 80—103659
Pb-Si-Sb amorphous alloys, electrical resistometric detection of relaxation 79—60278
Pd-Au-Si, influence of struct. on elec. resist. of glass forming alloys 80—65518
Pd-Co-P amorphous alloy, mag. an elec. props. 77—40043
Pd-Ni-P, amorphous, elec. resistivity negative temp. coeff., CAP calcs. 79—42515
Pd-Ni-Si amorphous alloys, crystn. process during isothermal ageing 80—89275
Pd-Si(—Cu), glassy, liq. and cryst., mag. and elec. props. 77—66249
$Pd_{68.5}Cu_{15}Si_{16.5}$ glass, elec. resist., struct. and mag. props. 79—65423
$Pd_{80}Si_{20}$, amorphous, elec. resist. and magnetoresist. 80—49693
$Pd_{0.775}Si_{0.165}Cu_{0.06}$, glassy alloy, resist. minimum associated with mag. impurities 79—56187
$Pd_{82-x}V_xSi_{18}$, amorphous, effect of structural relax. on elec. resist. 79—56186
$Pd_{82-x}V_xSi_{18}$, metallic glasses, effect of press. on elec. resist. 80—6805
Pt-Sb, amorphous sputtered film, elec. props. 78—68006
$R_{1-x}Co_x$, rare earth amorphous alloys, thermal stability, elec. cond. enthalpy 80—100172
$Rb_{1-x}O_x$, metallic glass, prep., elec. props. and struct. 78—67652
Si-Au films, quenched condensed, elec. resist. and supercond. 80—54669
$Si_{100-x}Al_x$, RF sputtered, amorphous, props. 80—34754
Sn-Au, amorphous film, elec. resist., temp. depend. 79—91159
Ta-Co(Ni)(N)(Ar), amorphous metal films, struct. and elec. characterisation 79—87017
Ta-Ir(Rh) system glasses, form., crystn. and microhardness, resist. obs. 80—89178
$TbFe_2$, amorphous, Mossbauer spectra *(French)* 80—25261
Th-Fe (20 to 70 at.%), amorphous alloy, electrical resistivity and thermal stability 80—33901
Ti-Be-Zr base alloy, glassy rel. to suitability as active element of resist. thermometer 77—82532
Ti_2AlN, prep. and props. 77—28745
W-Cu(N) amorphous metal films, struct. and elec. characterisation 79—87017
W-Re, amorphous wire, elec. resist., 2-20K, dimens. and mag. field depend., quantum localisation 80—39547
W-Re amorphous alloys, phase-slip and localisation diffusion lengths 80—107747
W-Re films, amorphous, one-dimensional quantum localisation 80—80413
WSi_2, sputtered, props. for MOS IC appl. 80—70831
Zr-Co(Ni) amorphous alloy, thermal stability and electronic props. 79—73487
Zr-Pd, metallic glasses, electronic props. and supercond. 79—73486
Zr-Rh alloys, amorphous, thermal relax. effects on electronic and supercond. props. 79—65575
$Zr_{40}Cu_{60-x}Fe_x$, electronic and mag. props. 77—8271

electrical conductivity of amorphous semiconductors and insulators
see also carrier density; carrier lifetime; carrier mean free path; carrier mobility; carrier relaxation time; dislocation scattering; electrical conductivity transitions; electronic conduction in insulating thin films; high field effects; hopping conduction; impurity scattering; minority carriers; negative resistance effects; photoconductivity; point defect scattering; small polaron conduction; surface scattering
alkali metal glass, elec. cond. meas. method 79—66250
alkaline earth glasses, $RO\text{-}Al_2O_3$, $\text{-}P_2O_5$, $R = Mg, Ca, Sr, Ba$, exam. of electron beam irradiation effects 79—4253
aluminous porcelain, electrical conductivity of function of O_2 partial press. *(German)* 77—1419
amorphous, vac. evaporated, doping, transport and optical props. 80—49715
amorphous and liquid semiconductors, conference, Cambridge, MA, USA (Aug. 1979) 80—41933
amorphous film junction, I-V and C-V characts. 77—85307
amorphous semiconductor, electrical conductivity at strong elec. fields and high hydrostatic press. *(Czech)* 77—24560
amorphous semiconductor, localised gap states, hopping cond. and chem. bonding 78—23052
amorphous semiconductor film, ion bombardment effect on electronic props. 79—65125
amorphous semiconductors, props., principles, appls. review 77—4287
anomalous charge transport behaviour in amorphous materials 79—91048
anomalous transit time dispersion, Monte Carlo simulation 77—47827
aqueous glasses, electron trapping reaction kinetics, non-Gaussian diffusion model 78—34843
bonding and transport properties in amorphous semiconductor alloys 79—90950
carrier pulse propagation, macroscopic theory 78—72154
cathode, oxide type, conductivity model 79—15159
chalcogenide glass, AC conduction, theory 78—23077
chalcogenide glass, AC conductivity, temp. depend. 78—72153
chalcogenide glass, charge screening lengths 79—23974
chalcogenide glass, charged dangling bond model reassessment 77—72813
chalcogenide glass, elec. cond. mechanism, review of developments 78—26854
chalcogenide glass, elec. cond. parameters rel. to charge carriers 77—35970
chalcogenide glass, Fe, doped in equil. conditions, impurity cond. and Mossbauer effect 80—49726
chalcogenide glass, localised states role in cond. in high elec. fields 77—76841
chalcogenide glass, weakly freq.-depend. cond. 77—1425
chalcogenide glass films, high field, short pulse cond. expt. 80—49751
chalcogenide glass films nonlinear current voltage characts., Poole-Frenkel effect 80—7007
chalcogenide glasses:Cu(Mn), elec. cond. increase on impurity addition 77—11920
chalcogenide glasses, AC conduction mechanism, electronic versus atomic 80—29409
chalcogenide glasses, conductivity, doping effect 79—38062
chalcogenide glasses, defect pairing and effect on AC cond. 80—49725
chalcogenide glasses, elec. cond., press. effects 78—56142
chalcogenide glasses, elec. cond. at room temp., contact effect 77—20354
chalcogenide glasses, electronic gap states, origin, structural relax., electronic transport and trapping 80—54648

electrical conductivity of amorphous semiconductors and insulators continued
chalcogenide glasses, electronic transport mechanisms and coeffs. 80—80282
chalcogenide glasses, gap states electronic behaviour 79—87098
chalcogenide glasses, multicomponent, Hall-thermopower sign anomaly 77—35957
chalcogenide glasses, percolation-controlled elec. cond. 78—72150
chalcogenide semiconductors, elec. cond. freq. depend., hopping cond. contrib. 77—76856
chalcogenides, Poole-Frenkel effect, charged dangling bonds model 80—59994
computer simulation in quasi one-dimens. disordered system 77—4334
computer simulation in three-dimens. disordered system 77—4336
computer simulation in two-dimens. disordered system 77—4335
conference, Balatonfured, Hungary (Sept. 1976) 77—76802
covalent semiconductor, Hall effect sign in hopping cond. 77—72872
cupferron and complexes, amorphous, hopping cond., 0 to 150°C 79—60828
cytochrome c_3, anhydrous film, elec. cond., temp. and ambient press. depend. 80—85327
cytochrome c_3 film, anhydrous, elec. cond. 79—66439
DC conductivity using quasiclassical approx. 78—23080
dielectrics, radiation induced charging and discharging, analytic solution 79—78612
disordered and amorphous semiconductors, band conduction mech. 79—95414
disordered materials, thin films and wires, resist. and localisation 80—44537
disordered semiconductor, high-field cond. in random field 79—65489
dispersive transient transport in disordered solids, expt. and theory 79—28342
dispersive transport, computer simulation, time of flight signals 80—70696
doped amorphous semiconductors, electronic props. 80—80283
drift effect on carriers in amorphous semiconds. *(Russian)* 78—47789
E-glass fabric, acid-treated, elec. resistivity studies 79—70178
electronic properties and structure *(Japanese)* 79—47179
epoxy resin, mech. and thermal props., amine hardeners, added softeners and filter effects *(Polish)* 78—68741
epoxy resin, thermosetting, electrical props. during cure cycle 77—72864
film, hopping cond., thickness depend. 77—89887
films, threshold switching theory 80—2433
finite disordered system, resistance probability distrib. *(Russian)* 80—103657
fluorinated copolymers, mech. and elec. props., processing and appls. 78—84760
glass, elec. cond. on surface, effect of impurity adsorption *(German)* 78—30971
glass, electron migration and spectral relax., random-walk model 80—80280
glass, phase separated, EPR rel. to struct., elec. and opt. props. 78—23333
glass diode with electrothermal instability in switching channel 79—78238
glass transition temperature, determ from expansion and elec. cond. temp. depend. 80—19967
glass-metal composites, elec. cond. 80—10970
glasses, contact influence on AC cond. 78—76076
glasses, elec., mag., and optical props., conference, Troy, NY, USA (Aug. 1979) 80—105417
glasses, elec. props. 78—2479
glasses, electrical cond. meas. technique using thermally stimulated polarisation currents 79—99561
glassy polymers, elec. resist., corresponding states relationship 80—59704
graphite, anisotropic elec. cond. rel. to stacking disorder 80—34437
graphite-HNO_3 intercalation compound, in-plane elec. resistivity 80—34435
Hall conductivity in random-phase model 80—65599
hopping, variable range, freq. depend. 77—32008
hopping carriers, AC cond. and DC Hall mobility 80—44585
hopping cond., Kirchhoff equations, computer calc. 80—39579
hopping conduction, DC, photon- and US-induced, microscopic theory 77—76872
hopping conduction, DC, pre-exponential factor 78—76074
hopping conductivity in noncryst. system, freq. depend. 77—15853
hopping conductivity in ordered and disordered solids, review 77—1420
inhomogeneous semiconductor, acoustoelectric interaction, elec. cond. 79—95453
insulator film, high-field cond. 79—56320
intercalation inorganic-organic layered complexes, effects of intercalation on elec. and mag. props. *(Japanese)* 79—8255
Kaprolon, compressibility, elec. cond., sound vel. behind shock front 78—95105
Kapton, pyrolysed, cond. polymer, transport and mag. props. 80—96887
Lexan:triphenylamine, molecularly doped, hole transport by hopping 78—34831
Lexan:triphenylamine, photosensitisation using rhodamine B or thiapyrylium 78—34856
localised singly occupied gap states, variable range hopping, susceptibility and EPR 77—72866
localised states and cond. mechanism in amorphous semicond. *(Japanese)* 80—84467
localised states role, review 77—62871
magnetic substance with rare earth ion, low temp. specific heat, elec. resistance and US absorpt. *(Russian)* 79—19734
metallomacrocytes, mixed valent, cofacial assembly, cond. polymeric material 80—70143
nylon 6 block polyether amide blend fibres, fine struct. and elec. cond. *(Japanese)* 77—89769
nylon 6-LiCl mixtures, DC cond. and struct., Lill effects 80—44149
nylon (N12), uniaxially oriented, anisotropy of elec. cond. 79—87095
one dimensional periodic model, boundary condition, limiting processes 79—60825
optimal polynomials in calcs. of complex glass's properties 78—68026
oxide glass, elec. cond. parameters rel. to charge carriers 77—35970
oxide glasses, elec. cond., polaronic hopping model 79—65479
oxide glasses, elec. cond. and dielec. relax., correl. 78—79801
oxide glasses with Bi or Se granules, elec. props. and microstructure 78—2490
oxide semiconducting glasses, electronic cond. mechanism 80—65562
paraffin wax, elec. cond., 33-55°C and 1-2 kV cm^{-1} 79—99555

electrical conductivity of amorphous semiconductors and insulators continued
pentacene, evaporated film elec. cond. meas. for various temps., SCL 78—10584
perspex, electric conduction and isothermal dielectric relax. 80—80285
phosphate glass, electron-irradiated, charge accumulation, comp. depend. 78—2159
phosphate glasses: Ti^{3+}, $MO(M_2O)$-TiO_2-P_2O_5 M=K, Ca, Be, elec. resistivity *(Japanese)* 77—12719
phosphate-tungstate semicond. glass, W (V) complex, EPR and electronic spectra interpretation 77—69682
photoconduction, model involving capture and escape from multiple traps 77—76863
plastic clad metal, corrosion charact. by electrical resist. and capacitance meas. *(German)* 80—30171
plastics, pigmented elec. cond. depend. on mech. stress *(German)* 80—20264
plexiglass, red, gamma dose meas. by optical absorpt., elec. conductivity, and mechanical hardness 78—55045
poly(γ-methyl L-glutamate), electric conduction mechanism *(Japanese)* 80—54696
poly(alkyl methacrylate)s, corona charged, decay of surface charge and TSC *(Japanese)* 80—54712
poly(ethyl vinyl ketone) film, reacted with phosphoryl chloride, elec. cond. 80—97599
poly(p-phenylene), AsF_5 doped, highly cond. charge transfer complexes, elec. and optical props. 80—70778
poly-2-vinylpyridine-iodine, semicond. film, elec. cond., depend. on I conc. and temp. 79—73606
poly-α-naphthol film, SCL currents obs. 77—47910
poly-γ-methyl-L-glutamate, uniaxially oriented, anisotropy of elec. cond. 79—87095
poly-aryl-acetylene, elec. cond. of cis- and trans- stereo isomers *(German)* 78—84221
poly-N-vinyl carbazole, and Br-substituted derivative, transient hole hopping transport, 150-500K 78—39108
poly-N-vinyl carbazole, containing carbazylium cation radicals, synthesis and semicond. props. 77—85224
poly-N-vinylcarbazole, polymerisation, struct., props., elec. characts., review 79—41972
poly-N-vinylcarbazole thin amorphous film, hole drift mobility, mol. mass. depend. 80—75663
polyacene quinone radical polymers, elec. props. described by variable range hopping model 80—44588
cis-polyacetylene:AsF_5, conductivity meas., non-Ohmic effects 80—96891
polyacetylene:AsF_5, heavily doped, transport props., evidence for metallic state 79—87121
polyacetylene:Br(Pd), ion implantation effect on elec. props. 80—65026
polyacetylene:I, electric props. in semicond. and metallic regions 80—29432
polyacetylene:SbF_5, elec. cond. meas. 80—60055
polyacetylene, doped, p-n junction, elec. props., review *(Japanese)* 80—29410
polyacetylene, electrical conducting, current status 80—44579
trans-polyacetylene, halogen doped, elec. cond. 79—19589
polyacetylene, variable density, synthesis, elec. cond., thermopower 80—60016
polyacetylene film, $(CH)_x$, synthesis, struct. and elec. props., doped materials, review 80—15623
polyacetylene film, partially oriented, anisotropic elec. cond., quasi-one-dimens. behaviour of fully oriented doped material 80—11112
polyacetylene films, doping effect on elec. cond., chem. and optical props. 80—65572
polyacetylene films, electrical properties *(Japanese)* 80—96888
polyacetylene films, pure and doped, cond., ESR 79—82859
polyacrylonitrile, AC conduction mechanism, freq. and temp. depend. *(Japanese)* 80—54706
polyacrylonitrile, pyrolyzed, elec. cond. and dielec. const. in AC regime 78—60173
polybisaminophosphazenes, elec. cond. 77—32016
polycarbonate: tri-p-tolylamine, chemical control of conductivity 80—59984
polycarbonate:tri-p-tolylamine amorphous film, elec. and mag. props 80—49959
polycarbonate, and charge-transfer complex modifications, isothermal dark currents 80—88559
polyester polymer-C black composition, elec. cond. under press. 77—28224
polyethylene, conduction mechanism, expt. determ. *(German)* 78—76086
polyethylene, cross linking by energy rich radiation, mech. and elec. props. *(German)* 78—20035
polyethylene, DC partial discharge and current 78—43790
polyethylene, dielectric props., investigation for morphology changes created by mechanical drawing and annealing 80—84697
polyethylene, elec. cond. of high and low density samples, oxidation effects 80—107784
polyethylene, elec. props. and oxidation after electron beam irradiation and heat treatment 79—87092
polyethylene, electric field enhanced conductivity 77—35951
polyethylene, low density, γ irrad. effect on elec. cond. and temp. characts. 77—85221
polyethylene, low density, γ-irrad., unixial elongation effect on elec. cond. 80—25812
polyethylene, low density, dielec. behaviour, struct. props. influence *(German)* 78—92017
polyethylene 2,6-naphthalate, AC conduction mechanism, freq. and temp. depend. *(Japanese)* 80—54706
polyethylene charge carrier injection, contactless electrode expt. 80—15540
polyethylene film, quenching effect 77—73114
polyethylene film, uniaxially drawn low-density, pre-exponential factor in elec. cond. 77—21224
polyethylene films, low density, γ-irrad., elec. cond., effect of elongation 79—4564
polyethylene terephthalate, TSC due to mobile ions and ionic conduction *(Japanese)* 80—54432
polyethylene terephthalate polymer insulator, conduction and breakdown mechanism *(German)* 80—100469
polyethylene terephthalate under high elec. fields, γ-ray induced cond. 79—60840
polyglycine chain with hydrated side group, electronic struct., transport props. 79—16146

electrical conductivity of amorphous semiconductors and insulators continued
polymer, C black filled, DC conduction processes 79—56275
polymer, conductive, freq. depend. of elec. cond. and polarisation 77—11918
polymer, conjugated, synthesis and elec. props., review 80—15513
polymer, excess charges, band gap levels and elec. props. 78—23053
polymer, mobility edge, classical solns. and crit. exponents 80—10936
polymer film, bulk elec. cond. parallel to film surface 79—87094
polymer film, bulk elec. cond. parallel to film surface 80—92889
polymer foil, electron irradiated, charge dynamics, computer simulation 79—82915
polymer UV photoconduction expts. and electronic props. 80—15572
polymers, atuomatic device for measuring elec. direct current props. *(German)* 78—45647
polymers, book 80—7257
polymers, bulk controlled cond. mechanism 80—20182
polymers, electric phenomena, book 80—46746
polymers, electrical phenomena, nature and appl., book contrib. 80—50254
polymers, nonlinear electric behaviour interpreted through free vol. changes 78—84226
polymers, oriented, conduction anisotropy meas. *(Japanese)* 80—54707
polymers, self-consistent continued fraction theory of cond. 79—69482
polynaphthalene films, plasma polymerised, photovoltaic and photocond. props. 80—34479
polyphenylacetylene, crystallizable, DC cond., annealing and defect effects 77—62923
polyphenylacetylene films, phys. struct., AC and DC cond. 80—44750
polypyrrole films, electrochemical prep., chem. and phys. characterisation 80—70708
polystyrene, electron-beam-induced conduction 80—2397
polyvinyl acetate, thick film, pure and I_2 doped, electrical cond. 77—85234
polyvinyl fluoride film, pure and vanadyl ion doped, elec. cond., annealing 78—26859
polyvinylcarbazole, amorphous, hopping transport, reinterpretation of mobility meas. 79—42563
polyvinylidene fluoride, DC conduction characts. 78—2488
polyvinylquinazoline-I_2 complexes, absorpt. spectra and elect. cond. 80—92891
powder semiconductors, HF conductivity depend. on surface energy band bending *(Russian)* 77—15890
protein-methylglyoxal complex, electronic props., energy band cond. 79—24936
PTFE, mech. and elec. props., processing and appls. 78—84760
random field acting on charge carriers 80—44580
RC network model, based on percolation theory 79—4560
relaxation regime, generalised transport eqns. 78—56139
review *(Japanese)* 77—35943
review *(Chinese)* 79—82581
review of structural and electronic props. 80—64901
scintillating glasses, effects of temp. on pulse height and cond. 77—10547
semiconducting glasses, containing transition metal ions, elec. props. *(Rumanian)* 78—47791
semiconductor, amorphous, field effect and capacitance-voltage meas. anal., localised density of states 80—103686
semiconductor, amorphous, non-polaronic, cond. and thermopower near band edge 80—49719
semiconductor, amorphous or disordered, cond. mechanisms, model of medium-range comp. disorder 78—79994
semiconductor, cond. tensor, freq. depend. in presence of mag. field 80—44631
semiconductor, conduction mechanisms, comparison with amorphous Si and Si thin films 79—56214
semiconductor, crystal-glass transition influence on local struct., cond. and density 77—36163
semiconductor, current fluctuations and switching 79—87133
semiconductor, electrical conductivity, super-linear freq. depend. 79—28348
semiconductor, impurity control, elec. resist. *(Japanese)* 79—37722
semiconductor, local elec. field character, and electron transport mechanism 78—23088
semiconductor, thermopower, conductivity, statistical shift, doping effects 79—69537
semiconductor characterisation, cond. type determ. by pot. profiling 80—73387
semiconductor thin films, glassy-crystalline, with switching channel, electrothermal instability 80—15576
semiconductors, amorphous, electronic transport mechanisms and coeffs. 80—80282
semiconductors, conductivity, thermopower and statistical shift 79—95434
semiconductors, elec. and optical props., w.r.t. electronic band states *(Japanese)* 79—23979
semiconductors, electrical conduction in strong elec. fields, percolation mechanism 80—20206
semiconductors, electrical properties calculated from thermophysical and thermomagnetic effects 79—73535
semiconductors, temp. depend. electronic cond., review 80—59975
shellac, electrical cond. mechanisms, Schottky and Poole-Frenkel processes and work function 80—29402
shellac platina, elec. cond., temp. and thickness depends., mechanism 79—99645
a-Si:H_x structure, effect of H-Ar plasma contact on elec. props., and optical gap 80—34533
silicate glasses containing iron, switching and memory effects 77—8155
soda glass, ageing effect of HF discharge on conductivity and dielec. const. 78—39138
sputter-deposited materials, electrical and optical props. 79—47181
styrene acronitrile copolymer, glass transition temp. determ. by elec. meas. 78—47506
styrene-sodium methacrylate (9 mol.%) copolymer cond. relax. 78—38874
substantially doped, electronic props., review 79—87175
TCNQ salt, polyvinylcarbazole-TCNQ complex, elec. cond. meas. 80—34456
TCNQ salts organic semiconducting polymers, electron transfer mechanisms 79—42544
teflon, measuring technique *(French)* 78—77929
Teflon, non-destructive charge release 80—24946

electrical conductivity of amorphous semiconductors and insulators continued
temp. depend. of conductivity and photocond. at 632.8 nm *(Russian)* 80–44666
temperature dependences meas., automated installation 80–31792
p-terphenyl, hopping cond. among localised states 80–70861
tetracene, amorphous film, TSC meas., carrier traps 80–2496
tetracene, hopping cond. among localised states 80–70861
thermal mechanism for bias-induced switching effects in inhomogeneous thin films 80–11057
thermoelectric power and transport models 78–10482
threshold switching by computer simulation 78–88002
transition metal phosphate glasses, ohmic contact and dielectric. relax. 79–65795
tri-p-tolylamine and its paramag. radical cation, disordered mol. solid, direct obs. of superexchange 80–39848
trinitrofluorenone, amorphous, hopping transport, reinterpretation of mobility meas. 79–42563
vanadium phosphate glass, comp. depend. of elec. cond. 77–62922
variation due to crystallisation, model and its verification for Ge 77–20475
violanthrene-A film, amorphous and crystalline, carrier mobility differences 78–60125
wave packet propagation in random struct. at crit. energy 78–26855
Wiedemann-Franz law in semiconductor and metal glasses 79–65422
Ag-As-Te glasses, elec. props. *(Russian)* 77–85211
Ag_2O-B_2O_3 glasses, electrical props. and dielectric relaxation *(Japanese)* 80–20199
Ag_2O-P_2O_5 system, electrical conductivity and dielectric relaxation *(Japanese)* 77–66455
$AgPO_3$-Ag_2SO_4, new Ag^+ and Li^+ ion glass conductors, glass transition, Raman spectra *(French)* 79–47094
$AgPO_3$-PbI_2 system, elec. conductivity as function of composition and temp. *(French)* 77–69112
Ag_2Se thin film, switching and Ag movement, point contact technique 80–60107
Al-Sio-Al structure, with amorphous SiO, VLF behaviour 77–76946
AlF_3 film, dielec. characts. 77–85650
Al_2O_3, noncrystalline films, opt. and elec. props. 77–51627
α-Al_2O_3:Ca(Ce), semicond. props. 80–54684
Al_2O_3-Al, disordered, energy diagram model 79–56110
Al_2O_3-B_2O_3-P_2O_5 glasses, formation and props. 78–83737
Al_2O_3-B_2O_3-SiO_2 glasses, elec. cond. study, 700-1900°C 79–65487
As, AC cond. and photo-induced states 79–87128
As, amorphous, optical, vibr., transport and defect-related props., review 79–51935
a-As, opt. and elec. props. 77–39894
As:Ni(Ge)(S)(Se)(Te) film, amorphous, chemical modification of props. 80–49250
As-Ge-Te, chalcogenide glass, elec. cond. and dielec. const. 80–75567
As-S chalcogenide glass holographic recording efficiency, photocond. and annealing effects *(Russian)* 80–15556
As-S-Te, vitrification, density and elec. cond. measurements 79–7645
As-Se glasses, elec. transport studies 80–103695
As-Se:^{197}Au, glassy, Au impurity influence, elec. cond., optical absorpt. and Mossbauer meas. 77–24558
As-Se-Bi, semicond. chalcogenide glasses, crystallisation and electrophys. props. 78–9955
As-Se-Cu system glass films, elec. and photoelec. props. variation with photostruct. transforms. 77–76980
As-Se-Te glasses, electron transport props. 78–10439
As-Se-Te system glasses, AC cond. and permittivity, freq. and temp. depend. 77–76857
As-Te system glasses, DC and AC cond., thermo-EMF, 140 to 350K 79–42549
As-Te-Cu system glasses, DC and AC cond., thermo-EMF, freq. depend., 100 to 370K 77–76827
As-Te-Cu system glasses, elec. cond. and thermo-EMF 79–42540
As-Te-Ga, glass, elec. cond., 190-300K *(Russian)* 80–54702
As-Te-Ge system glasses, thin films, effect of S, Se, Sb, Bi, Tl on volt-ampere characts. 77–15976
As-Te-Si-Ge amorphous chalcogenide semiconductor, thin film interface, meas. *(Korean)* 80–97014
As-Te-metal amorphous film, switching, memory effects 80–44677
As_2-Se_3-Bi_x amorphous system, elec. and photocond. props. 79–51574
$As_{10}Ge_{15}Te_{75}$, glass, cond. and switching characts. 77–32054
$As_{10}Ge_{15}Te_{75}$:Ag glasses, elec. props. 79–91045
$As_xGe_{10}Te_{90-x}$ glass, cond. and dielec. const. from 77 to 383K and from DC freq. to 5 MHz 79–23964
$As_{10}Ge_{15}Te_{75}Ag_x$ glass, elec. and dielec. props., Ag additions effect 80–65558
$As_{2-x}S_{3+x}$, hydrogenated chalcogenide glasses, prep. by plasma decomposition 80–49735
As_2S_3 (Se_3), electron irradiated, effects on elec., photoelec. and optical props. 80–49806
As_2S_3, amorphous, AC cond. magnitude and variation *(French)* 79–47095
As_2S_3, bulk material and evaporated thin films obs. *(Japanese)* 80–11028
As_2S_3 glass, band gap determ. from elec. cond. 77–4337
As_2S_3 glasses, DC elec. cond. and thermo-elec. power 80–96865
As_2S_3, glassy, diffusion, elec. transport and first group impurities effect on elec. and opt. props. 77–76623
As_2S_3, glassy, thermally stimulated depolarisation 77–24782
As_2S_3, photodissolution of Ag, elec. resist. meas. 77–62786
As_2S_3, temp. dependence of high-frequency cond. 80–11027
As_2S_3, vapour-deposited, pure and doped, hole mobility 80–49728
As_2S_3 vitreous, Ag, Cu, Sn and Ge impurities infleunce on electrophys. props. 77–76826
As_2S_3 vitreous film, hole transport obs. 80–49727
As_2S_3:Ag, AC conductivity determ. 77–66167
As_2S_3:Te glasses, doping influence on AC conductivity, electron transport by hopping 79–78106
As_2S_3-PbS glass, DC elec. cond. and photocond. 78–39107
As_2S_3-Sb_2S_3, vitreous, dispersive charge transport analysis 79–95418
$(As_{0.4}S_{0.6})_{100-x}Cu_x$, glassy, struct. and elec. cond. study 80–59399
$(As_2S_3)_{0.55}(Sb_2S_3)_{0.45}$ vitreous film, dispersive charge transport, time-of-flight meas. 79–19594
$As_2S_3(Se_3)$:Ag glassy films, doped by photodiffusion and thermodiffusion, photocond. 80–29441
AsS(Se)I films, electrophys. and opt. props. 77–51741

electrical conductivity of amorphous semiconductors and insulators continued
$As_2S_{3-x}Te_x$, ternary chalcogenide glassy system, optical absorpt., mag. susceptibility and AC cond. meas. 80–55125
$As_4Sb_2Se_9$ glassy semiconductors, electronic props. 80–103712
AsSe-$GeSe_2$-PbSe, glass form., struct. defects, elec. cond., assoc. *(Russian)* 80–54144
$AsSe_{1.2}$:Fe, Fe effect on physiochem. props. of glass 80–24370
$AsSe_x$ amorphous films, high field behaviour 79–87172
$As_{2-x}Se_{3+x}$, hydrogenated chalcogenide glasses, prep. by plasma decomposition 80–49735
As_2Se_3, AC cond. and photo-induced states 79–87128
As_2Se_3, amorphous, AC cond. magnitude and variation *(French)* 79–47095
As_2Se_3, amorphous, DC Hall effect, elec. cond. mechanism 78–23121
As_2Se_3, amorphous, dark discharge, relaxation current meas. *(German)* 80–49760
As_2Se_3, amorphous, defect states, exptl. study. 80–54645
As_2Se_3, amorphous, electron and hole transport, charge defect model 79–15162
As_2Se_3, amorphous, field-depend. dispersive hole transport 78–14728
As_2Se_3, amorphous, hole mobility expt., transient photocurrent shape 79–99582
As_2Se_3, amorphous, photocond. and photoinduced optical absorpt. 79–82645
As_2Se_3, AsSe and As_3Se_2 films, photostimulated changes in opt. and elec. props. 77–76979
As_2Se_3 bulk glass, physical parameters anisotropy, cooling effects 77–36545
a-As_2Se_3 film, metallic impurity effect on transport props. 80–49963
As_2Se_3 glass, microwave elec. cond. and struct. 80–49793
As_2Se_3, glassy, elec. cond. meas. in high elec. field 77–4355
As_2Se_3, glassy, influence of oxygen added in As_2O_3 and SeO_2 forms on phys. props. 77–76314
As_2Se_3, glassy, with adsorbed $H_2O(NH_3)(NO_2)(O_2)(CO_2)(CO)$, surface cond., photocond. 78–80038
As_2Se_3 glassy films, current-voltage characts., temp. depend., SCL current 80–92902
As_2Se_3, solid and liq., elec. cond. meas. 77–28185
As_2Se_3, transient electrical transport, general and unified treatment 80–59977
As_2Se_3, transient hole transport props., trap controlled hopping model 77–47820
As_2Se_3, vitreous, elec. and opt. prop. changes on densification 77–11958
As_2Se_3, vitreous, hole drift mobility, temp. and field depend. 77–76830
As_2Se_3:Ag, doping effect of gap states and elec. cond., dielec. relax. and DC cond. meas. 79–47098
As_2Se_3:Ag amorphous, freq. depend. cond. 80–88565
As_2Se_3:Bi, annealing kinetics, cond. activation energy and density 79–73503
a-As_2Se_3:Mn(Fe)(Ni)(Cu)(Zn)(Ga)(Tn)(Il)(Na), hole drift mobility depend. on impurity conc. 79–60846
As_2Se_3:Pt, glass, effect of impurities on elec. props. 80–103699
As_2Se_3:X (X=Cu, Ag, Tl, I, Ge), effect of doping, NMR meas. 80–11282
As_2Se_3-As_2Te_3, solid and liq., elec. cond. meas. 77–28185
As_2Se_3-As_2Te_3, vitreous, localised states role in cond. in high elec. fields 77–76841
a-As_2Se_3-Au contact sandwich, response to voltage step in dark and with illum. 77–69431
As_2Se_3-Bi_2Se_3, semiconducting crystallized glasses, elec. conductivity mechanism 77–39843
As_3Se_2, electron irradiated, effects on elec., photoelec. and optical props. 80–49806
$As_2Se_3Ag_x$, optical absorpt. coeff. and DC cond. 80–54699
As_4Se_5Ge, glass, light irrad. induced changes in optical and elec. props. *(Japanese)* 78–68031
$AsSeI_x$, glasses, cond. and photocond. 80–20253
$AsSe_{1.1}Te_{0.2}$:Fe, Fe effect on physiochem. props. of glass 80–24370
$AsSe_{1.5-x}Te_x$ glasses, physical props. 78–68028
$As_2Se_xTe_{3-x}$ chalcogenide glasses, cond. meas., field strength and temp. depend. 78–84225
$As_{40}Se_xTe_{60-x}$ amorphous system, resistivity press. depend. 79–82592
As_2Te_3 and As_2Te_3Ge, amorphous, AC cond. at low temps. 80–80269
As_2Te_3, glassy, field depend. elec. cond. and localised states role 77–76829
As_2Te_3, solid and liq., elec. cond. meas. 77–28185
$As_2Te_3+Tl_x$, glassy system, composition depend. of activation energy, thermopower meas. 78–64052
$As_{50}Te_{50}$, amorphous semicond., elec. props. after heavy-ion irrad. *(French)* 77–72639
As_xTe_{100-x}, glassy system, composition depend. of activation energy, thermopower meas. 78–64052
$AsTeCu_x$ ($0 \leq x \leq 0.4$) glass, effect of Cu on elec. cond. and thermoelectricity, 100 to 370K 78–87978
$AsTeE_x$, E=S, Se, Sb, Bi, annealing effects on elec. cond. of films 77–43594
$(As_2Te_3)_{1-x}Ge_x$, amorphous, AC cond. magnitude and variation *(French)* 79–47095
$As_xTe_{90-x}Ge_{10}$, $As_{35}Te_{55}Ge_{10-x}Si_x$ glasses, elec. and optical props., comp. depend. 77–24555
$As_{35}Te_{28}Ge_{16}S_{21}$, chalcogenide semiconductor study of electric properties *(French)* 80–29414
Au_xSi_{1-x} amorphous films, phys. studies 80–75476
B film, elec. field effect on struct. 80–20050
B, hopping cond., book contrib. 78–47797
B_2O_3-CaO-Fe_2O_3 glasses, semicond., cond. models, electronic props., 77-800K 80–54688
B_2O_3-SiO_2 glasses, phase separated, DC cond. and elec. breakdown 78–23400
B_2O_3-V_2O_5-P_2O_5, glass, mech. and elec. props 80–84228
BaO-Al_2O_3-B_2O_3-V_2O_5 glass, spectra, oxidation-reduction behaviour, DC cond. 77–76814
BaO-B_2O_3-SiO_2 system glass, electronic cond. of Ti ions 78–23095
BaO-B_2O_3-SiO_2:Ti^{3+}, elec. cond., struct. 78–72148
BaO-B_2O_3-V_2O_5 glasses, polaron hopping cond., optical absorpt. and ESR spectra 79–23966
BaO-B_2O_3-$V_2O_5(Fe_2O_3)(Cu_2O)$, glass, resist. and activation energy, reduced valency 77–51749
BaO-CaO film, Cu-electrodes, DC props. 77–35997
BaO-K_2O-VO_2-SiO_2, glass, elec. cond. rel. to ion polarisability, polarons 80–49729

electrical conductivity of amorphous semiconductors and insulators continued
- $BaO-La_{0.6}O-VO_2-SiO_2$, glass, elec. cond. rel. to ion polarisability, polarons 80—49729
- $BaO-V_2O_5-CuO$, $P_2O_5-V_2O_5-CaO-CuO$ glasses, EPR, Cu impurity effect on elec. props. 79—51849
- $BaO-V_2O_5-CuO$ semiconducting glasses, impurity effects, elec. resist. and EPR study 80—103692
- n-$BaTiO_3$, elec. transport props., theoretical discussion and expt. 78—84215
- $BaTiO_3$, RF sputtered amorphous films, phys. and elec. characterisation 79—83119
- Bi-Sb alloy film, amorphous nature, AC and DC cond. and Hall coeff. obs. 80—11114
- C, anthracene, heat treated, AC cond., 100 to 400K, electron hopping and Mott-Davis models 80—34443
- C black-graft polymers crosslinked with epoxy resin, electrical props. *(Japanese)* 80—24920
- C blacks, powders, resistivity rel. to compression *(French)* 80—35349
- C disordered, variable-range hopping cond. and negative magnetoresist. 80—34436
- C, elec. cond. and Hall effect, temp. depend. 78—60141
- C, elec. cond. at low-temp. as function of freq. 79—23965
- C fibre, temp. dependence of electrical resistivity 77—20311
- C fibres, from mesophase pitch, resist. magnetoresist., EPR and mech. props. rel to struct. 79—78116
- C film, planar and transverse resist. 77—20474
- C film, struct. and semicond. props. and heterojunction form. with single cryst. Si 80—25002
- C, glassy, prep. and DC cond. at low temps. 79—95404
- C, glassy and fibrous, density of states, magnetoresistance theory appl. 80—44620
- C, prepared by glow discharge method, elec. and optical props. 77—21036
- C:H films, amorphous, elec. props., chem. modifications 80—84523
- C:H films, elec. cond. and optical absorpt. 80—49723
- CC NiO, amorphous, charge transport in band tails 78—76026
- $CaO-B_2O_3-Al_2O_3-V_2O_5$ glass, cond. mechanism, current carriers, V_2O_5 conc. effects 77—62668
- $CaO-B_2O_3-Fe_2O_3$ glass, electronic and dielec. props. meas. 77—24574
- $CaO-B_2O_3-Fe_2O_3$ glasses, effect of heat treatment on electronic props. 78—2480
- $CaO-Fe_2O_3-B_2O_3$ glasses, phys. props. rel. to struct. and comp. 78—23331
- Cd-Sb thin film prep. by vacuum deposition, elec. props. 78—92194
- CdAs, $CdAs_2$, elec. cond. and thermopower 80—49722
- $CdAs_2$ based glasses, AC cond. 78—39109
- $CdAs_2$ based glasses, cond. and permittivity, freq. depend. 77—76859
- Cd_3As_2 films, elec. resist., Hall mobility, temp. depend., cond. mechanism 77—76982
- $Cd_{0.96}Ga_2Te_{4.1}$, amorphous film crystallisation and conductivity switching 77—4459
- $CdGe_xAs_2$ glass, conductivity and Hall effect for x=0.1 to 0.8, 300 to 600K 77—69347
- $Cd_6Ge_3As_{11}$, DC cond., press. depend. 78—72064
- $(CdGeAs_2)_{1-x}D_x$ amorphous films, property control in common target sputtering, elec. cond. 80—7494
- $CdO-P_2O_5$ glass, thin film, elec. cond., high and low fields 80—80427
- $CdO-P_2O_5$ glasses, elec. props. at high elec. fields 80—39573
- $CdO-P_2O_5$ glasses, prep., density, elec. and optical props. 79—70033
- $CdO-ZnO-P_2O_5$ glasses, prep., density, elec. and optical props. 79—70033
- CdS film, microinclusion distrib. of high resist. phase and residual cond. 80—7008
- $CdSn_xO_y$, DC reactively sputtered film, elec. and optical props. 79—87022
- $CdSn_xO_y$ films, transparent conducting, deposited by RF sputtering from $CdO-SnO_2$ target 80—76179
- Cu-Ge codeposited film, elec. resist. and thermoelec. power, rel. to struct. 79—87168
- $Cu_{10}As_{31}Se_{38}O_{21}$, chalcogenide glass, exam. of electron mechanism of photo induced changes 78—87998
- $CuInTe_2$, vac. deposited film, growth, struct. and elec. characts. 77—69995
- $CuO-CaO-P_2O_5$ glass devices, memory switching 78—56192
- $CuO-CaO-P_2O_5$ system glasses, DC cond., hopping transport, 300 to 620K 78—23096
- $CuO-V_2O_5-P_2O_5$ glass, elec. cond. and switching *(Japanese)* 80—34492
- $FeO-P_2O_5$ glass, elec. props. effect of high energy γ-radiation 79—11173
- $FeO-P_2O_5$ glasses, electrical and mechanical losses 78—80283
- $Fe_2O_3-B_2O_3-PbO$ glass, semicond., elec. resist. meas. 78—95300
- $Fe(OH)_3$ thin films, elec. cond. var. with temp., amorphous struct. 80—75566
- $20Fe_2O_3.80[3B_2O_3.(1-x)PbO.xGeO_2]$ glass, phys. props. 80—49119
- Ga-Ge-Se chalcogenide glasses, rare earth element doped, elec. props. 80—96885
- GaAs amorphous film, EXAFS, optical and elec. props. 80—49547
- GaAs amorphous film, effective medium theory and freq. depend of conductivity 79—24090
- GaAs, amorphous state, thermal stability, elec. cond. obs. 80—33888
- GaAs:H sputtered films, high field cond. props. 80—44607
- GaP amorphous film, EXAFS, optical and elec. props. 80—49547
- GaP, effects of hydrogen incorporation during deposition by sputtering 79—69981
- GaP film, deposited by RF sputtering *(Czech)* 78—52667
- GaP, plasma deposition and elec. cond. 78—60585
- GaP, RF sputtering on glass and Au film substrates, struct. and elec. props. 80—2311
- GaSb amorphous film, elec. props. *(French)* 78—14843
- GaSb films, vac. evaporated, Elec. cond. thermoelec. power and optical absorpt. 80—2504
- GaSe film, I-V characts. in strong elec. fields, 173-373K 78—56248
- $Ga_{0.25}Te_{0.75}$ amorphous film, nanosecond switching, resist. fluctuations in low-resist. state 80—44676
- $Ga_{1-x}Te_x$ amorphous films, elec. cond., optical absorpt. and transparency, band gap energy 79—56335
- Ge alloys, amorphous film, crystn. transform. kinetics 78—22653
- Ge, amorphous, ionisation enhanced crystallisation, elec. cond. meas. 77—35481
- Ge, amorphous, O_2^+ ion implanted, influence on electrical and optical props. 77—89891
- Ge, amorphous, substitutional doping, electronic props. 77—1418

electrical conductivity of amorphous semiconductors and insulators continued
- Ge, amorphous and polycryst. layers, sputtered, elec. cond. and thermoelec. power 78—2586
- Ge, amorphous film, annealing, effect on localised states 79—4535
- Ge amorphous film, effective medium theory and freq. depend of conductivity 79—24090
- Ge, amorphous film, high freq. cond., AC loss 80—49792
- Ge amorphous film, ultra high vac. prep., DC elec. cond. 80—49721
- Ge amorphous films, high elec. field cond. and magnetoresist. at 4.2K 80—49748
- Ge amorphous films, self-ion bombard., electronic props. 79—28422
- Ge amorphous films, structural relaxation and crystallisation 80—100170
- Ge, ESR and DC cond. 77—48032
- Ge, effect of Au, fresh and aged samples 78—76161
- Ge, elec. and opt. props., review 78—23094
- Ge, electrodeposited, X-ray, electrochem., and electrorefl. characterisation 78—14624
- Ge film, AC cond., up to 200 kHz, 100-300K, role of contacts 77—76970
- Ge film, amorphous, O implantation effects on absorpt. edge and elec. cond. 77—39970
- Ge film, amorphous, vac. deposited, XPS and elec. props., evidence for polycryst. phase 77—28691
- Ge film, crystn. kinetics, elec. cond. obs. 77—62767
- Ge film, DC cond., Meyer-Neldel rule 78—64152
- Ge film, elec. cond. obs. of crystn., expt. verification of model 77—20475
- Ge, film, elec. resist. and struct., post-deposition heat treatment effects 79—78229
- Ge film, evap., structural aspects in electronic transport data interpret. 77—76977
- Ge film, freq. response characts. 79—56334
- Ge film, high field effects, 100-300K 77—24563
- Ge, film, laser pulse annealing 80—15006
- Ge film, prepared by evap. or sputtering, AC loss meas. 80—65560
- Ge film, thickness depend. of resist. 77—39978
- Ge, film, variable range hopping 78—76176
- Ge, lightly doped, heavily compensated by fast neutrons, electrical props. 77—89766
- Ge, Mott's parameters for hopping cond., effect of annealing 77—69324
- Ge:Al(Sb) film, amorphous, ion implantation, effect on cond. 78—83839
- Ge:Mn, amorphous, cond. increase by Mn doping 78—72155
- Ge:P, amorphous, electronic transport and photocond. 79—60834
- Ge:Sb, amorphous, electronic transport props. 80—44589
- Ge:Sb(Ga), amorphous, doping effects on Fermi level, electrical meas. 79—42546
- Ge-Al film, elec. resist. and IR transmission, comp. and substrate temp. depend. 78—52112
- Ge-As-Te glass, between metal electrodes, contact props. determ. 79—7908
- Ge-As-Te glass, thermoelec. power and DC cond., temp. depend. 77—62955
- Ge-Bi-S system, semicond., elec. cond., glass transition temp. and optical absorption meas. 77—16329
- N-Ge-Bi-Se glass, elec. and optical props. 80—65550
- Ge-Fe system, amorphous films, mag. and elec. props. 79—51695
- Ge-Ga amorphous alloy, co-evaporated elec. and optical props. 80—70860
- Ge-metal films codeposited, amorphous and polycryst., struct. and elec. props. 80—24766
- Ge-Mo amorphous semicond.-granular metal film system, elec. transport and thermopower 77—76984
- Ge-Pb-Se-Te, glass form., DC cond., and mole volume 79—90560
- Ge-S-Ga amorphous thin film, memory switching effects 80—88605
- Ge-S-In, chalcogenide glass, meas. of resist. 79—23526
- Ge-S-Sb glasses, microgravity effect on recrystn., optical and elec. props. 80—49127
- Ge-Sb-Se glass, elec. props, comp. depend. 80—70697
- Ge-Se, effect of Ag electrodiffusion on volt-ampere characteristics 79—7869
- Ge-Se-Fe phase system, amorphous films, mag. and elec. props. 79—51695
- Ge-Se-Te glasses, form. region, elec. props. 79—94904
- $Ge-SiO_2-p^+Si$ tunnel junctions, for determ. of AC cond. of amorphous Ge 77—24608
- Ge-Te alloy films, amorphous, semicond. props., refr. index, struct. study 78—26978
- Ge-Te film, electrical switching 77—4411
- Ge-Te-As-In quaternary compounds, elec. resist. of thin sheets, Mott's theory *(Spanish)* 77—69320
- $Ge_{100-x}As_x$ glass, elec. props. 77—76966
- n-$Ge_{20}Bi_{10}Se_{70}$ glass, preparation and elec. props. 79—74126
- $Ge_{20}Bi_xSe_{80-x}$, semicond. glass, resist., thermoelec. power, optical absorpt. 80—88555
- $Ge_{20}Bi_xSe_{70-x}Te_{10}$, n-type semiconducting glasses, resistivity and thermoelectric power meas. 80—54695
- $Ge_{20}Bi_xSe_{70-x}Te_{10}$, semicond. glass, resist., thermoelec. power, optical absorpt. 80—88555
- GeC_x, prepared by glow discharge method, elec. and optical props. 77—21035
- GeS_{11} glass, neutron irrad., thermal and elec. props. 79—19286
- $GeS_{1.35}$ glass, neutron irrad., AC elec. cond. 80—24924
- GeS_8 glass, activation energies after neutron irradiation, elec. cond. and transmission coeff. 78—83850
- GeS_x, neutron irrad., thermal and elec. conductivity and heat capacity 78—2165
- Ge_2S_3, electron irradiated, effects on elec., photoelec. and optical props. 80—49806
- $Ge_{42}S_{58}$, amorphous, bulk and film forms, elec. props. and ESR study 80—103691
- $Ge_{100-x}S_x(Se_x)(Te_x)$, amorphous film, effect of alloying chalcogen atom on elec. cond., optical transmission and ESR 79—78101
- $Ge_{2.33}SbSe_5$:Fe, Fe effect on physiochem. props. of glass 80—24370
- GeSe amorphous films in Al-GeSe-Al structs., AC cond. and capacity, thickness depend. 79—65566
- $GeSe_2$ amorphous semicond., DC conductivity, calorimetric, and X-ray diffr. meas. 79—78107
- $GeSe_2-As_2Se_3-Sb_2Se_3$ system glasses, vitrification and elec. cond. 79—50996
- $GeSe_2-As_2Se_3-Sb_2Se_3$, quenched glass system, elec. cond., low temp. heat treatment effect 80—39586
- $GeSe_2-As_2Se_3-Sb_2Se_3$, elec. cond. over wide range of temp. 80—88564

electrical conductivity of amorphous semiconductors and insulators continued
$Ge_{1-x}Se_x$ film, EPR, elec. and optical props. meas. 78−48038
Ge_xSe_{1-x}, amorphous, AC cond. *(Korean)* 80−44591
Ge_xSe_{1-x} amorphous film, photocrystn., elec. cond. and optical microscopy obs. 79−87024
Ge_xSe_{1-x}, amorphous semicond., elec. props. 78−84219
Ge_xSe_{1-x} chalcogenide glasses, trap-controlled carrier mobility, time of flight meas. 79−4557
Ge_xSe_{1-x} glasses, DC cond. and static dielectric const. meas. *(French)* 77−62925
Ge_4Se_5Te, amorphous layers, charge carrier transport mechanism 80−54708
Ge_4Se_5Te amorphous layers, prep. and elec. props. 80−97436
a-GeSi film with Mo contacts, AC performance *(German)* 77−63012
$Ge_{1-x}Sn_xTe$ film, amorphous, elec. cond. 80−93016
GeTe, amorphous film, annealing effects on resistivity, comparison with SnTe 77−66212
GeTe film, amorphous, evaporated and annealed, variable range hopping cond. 78−80077
Ge_xTe_{1-x} amorphous matrix with Te crystallites, effect of annealing 77−24274
H_xWO_3, amorphous film, electronic transport meas., insulator-metal transition 77−72923
H_xWO_y film, effect of struct. on optical and electrical props. 78−84671
HgSe film, anomalous photocond., electron microscope study 80−65623
In_2O_3:Sn, glass like thin film, electron evaporated, conductive transport *(Chinese)* 80−49960
In_2O_3:Sn, sputtered film, optical and elec. props. 78−76177
InSb amorphous film, effective medium theory and freq. depend of conductivity 79−24090
InTe thin films, flash evaporation, electrical props. 80−65722
$In_{0.25}Te_{0.75}$ amorphous film, nanosecond switching, resist. fluctuations in low-resist. state 80−44676
$In_{1-x}Te_x$ amorphous films, elec. cond., optical absorpt. and transparency, band gap energy 79−56335
La_2O_2S-AgS-Ga_2S_3, ionic conducting glasses *(French)* 78−79804
Li-graphite intercalation compounds, synthesis, elec. and optical props. 79−74108
LiCl-Li_2O-P_2O_5 glass system, vitreous domain, struct., elec. cond. *(French)* 80−70135
LiF-$NaPO_3$-MeF_x (Me=Mg, Ca, Al) glasses, IR spectroscopy study 80−16042
Li_2O-B_2O_3-P_2O_5, glass, mech. and elec. props 80−84228
$LiPO_3$-Li_2SO_4, new Ag^+ and Li^+ ion glass conductors, glass transition, Raman spectra *(French)* 79−47094
$Li_2Si_2O_5$-Li_2SO_4 glasses, electrical cond. and Raman study of struct. *(French)* 79−65482
$y(Mn_xFe_{3-x}O_4)$-$(1-y)B_2O_3$ glasses, elec. and struct. props., 400-1000K 79−51575
MnO_2 battery-grade, resistivity rel. to water content *(German)* 79−96431
MoO_3-P_2O_5, glass, DC conductivity meas. high temp. range 78−6376
Na_2O-$3SiO_2$:Fe^{2+}, Fe^{3+} glasses, Mossbauer and ESR spectra and internal friction 80−100865
Na_2O-Al_2O_3-SiO_2 glasses, elec. cond. and cation mobility 78−59973
Na_2O-B_2O_3 glasses, electrical props. and dielectric relaxation *(Japanese)* 80−20199
Na_2O-B_2O_3-Bi_2O_3, glass with metallic Bi granules, elec. cond. 80−84493
Na_2O-B_2O_3-P_2O_5, glass, mech. and elec. props 80−84228
Na_2O-B_2O_3-SiO_2-$As_2O_3(As_2O_5)$ glasses, DC and AC resist., bipolaronic hopping cond. 80−88558
Na_2O-K_2O-Al_2O_3-SiO_2 glasses, effect of Al_2O_3 77−8104
Na_2O-K_2O-B_2O_3-SiO_2, glass, character of elec. cond. 80−103516
Na_2O-Li_2O-NiO-Fe_2O_3-B_2O_3-SiO_2 glasses, thermally stimulated cond. studies of trapping centres 79−78113
Na_2O-SiO_2, (5.3, 94.7 wt.%) glass, liq.-phase separated, struct., heat treatment effect 80−16359
Na_2O-SiO_2 glass, OH^- content effect on mech. and other props. 80−89337
Na_2O-TiO_2-SiO_2 glass, elec. props. and energy gap 78−26921
Nb-Al_2O_3 composite, semicond. films, cond. on localised states 77−24628
Nb-N_x disordered thin films, thermometrical props., appl. as temp. sensors *(French)* 79−65558
NbH, internal friction 78−6962
Nb_2O_5 amorphous film, in Nb-Nb_2O_5-MnO_2 sandwich, elec. cond. variation during heat treatment 79−82593
Nb_2O_5-V_2O_5-P_2O_5, glasses and glass ceramics, elec. cond., struct. 80−84466
P, amorphous film, prepared by chemical transport in glow discharge, electronic props. 79−24011
P_2O_5-FeO glass, electrical cond., nonadiabatic hopping of small polaron 77−1417
P_2O_5-WO_3:CuO glass, EPR, Cu impurity effect on elec. props. 79−51849
$P_2Se_xS_y$ glass, thermophysical props., 303-413K, struct. interpretation 78−47615
P_2Se_xSy glass, vitrification temp., elec. props. and hardness meas. *(Russian)* 77−28177
PbO thin films, elec. props. *(Korean)* 79−60943
PbO-B_2O_3-Bi_2O_3, glass with metallic Bi granules, elec. cond. 80−84493
PbO-B_2O_3-Fe_2O_3-CuO glass, electric cond. and struct. *(Japanese)* 78−23093
PbO-SiO_2 glasses, charge trapping and dielec. breakdown, radiation-induced, microphase separation 78−23399
PbO-SiO_2-Fe_2O_3(0,2,10 wt.%), conduction process 77−8096
PbS film, form. by chem. spraying, elec. and optical props. 78−2588
PbSe-GeSe-AsSe, glass form., elec. cond., struct. defects, assoc. *(Russian)* 80−54145
$Ru_xTi_{1-x}O_2$ films, percolation elec. cond. in strong electric fields *(Russian)* 80−84471
S-based amorphous semicond. film, prep. by plasma decomp. of H_2S-N_2-NH_3, and characterisation 80−80422
$(SN)_x$ polymer, elec. props. of amorphous thin film and single crystal, role of chain breaks *(Japanese)* 78−68104
(SN)x, halogen-doped, temp. depend. of elec. cond. 79−65563
$SSe_{22.5}$, amorphous, photo-effect on crystn. kinetics, elec. cond. obs. 79−77522
$SSe_{22.5}$, amorphous-cryst. transition, light effect, rel. to polymer crystallisation 79−99076

electrical conductivity of amorphous semiconductors and insulators continued
Sb evaporated film crystallisation rel. to substrate temp., −50° to 170°C 78−47680
Sb-Ge-Se system glasses, activation energy of elec. cond. calc. 79−51568
Sb_2O_3-Na_2O-B_2O_3-SiO_2 glass, elec. cond. meas., −160 to 200°C 80−20190
Sb_2S_3, vitreous, prep. elec., opt. and struct. props. 77−76889
SbSe, amorphous thin film high field charge transport and quasi-Fermi level location 80−70863
Sb_2Te_3-Sb_2Se_3 thin layers, struct., phase comp., and elec. cond. 80−15389
Se, amorphous, AC cond. magnitude and variation *(French)* 79−47095
Se, amorphous, carrier lifetime and drift mobilities 78−87985
Se, amorphous, effect of doping on mol. struct. and valence alternation states 80−49249
Se, amorphous, elec. cond., activation energy, density, cryst. Se effect 80−65548
Se, amorphous, electrical transport, activation energy 79−95406
Se, amorphous, O impurity addition rel. to elec. cond. 79−38067
Se, amorphous film, AC conductivity at radio and microwave frequencies 79−11248
Se, amorphous film, dark and photoconductivities 79−87173
Se, amorphous film, photocond., dark cond., rel. to crystn. 80−88596
Se, amorphous thin film, elec. noise, monostable switching 80−44684
Se and Se-Ge system, press. depend. of AC cond. 77−76858
Se, bulk, DC cond. expts., cond. mechanism 78−43401
Se film, photocond. props. *(French)* 77−72886
Se, hole diffusion obs. 77−76828
Se layers, amorphous and partially crystallised, trap spectrum, TSC and I-V characts. 77−76981
Se, monostable switching, current noise 80−44682
Se, transient electrical transport, general and unified treatment 80−59977
Se:Ge(Si)(Sn), vitreous, crystn. kinetics study by elec. cond. meas. 79−65526
Se:O(Cl)(K) amorphous, elec. cond. increase on impurity addition 77−11920
Se:P, vitreous, crystn. kinetics study by elec. cond. meas. 79−64998
Se:P, vitreous, stabilisation of cond. 77−11910
Se:Te, amorphous, pure and doped, freq. depend. of elec. cond., 150 to 310K 79−42545
Se:Te, conductivity and activation energy depend. on dopant conc. 77−69325
Se:Te(Ag), amorphous film, elec. cond., 300 to 350K, transition 77−4454
Se-Fe system, amorphous films, mag. and elec. props. 79−51695
Se-Ge amorphous system, AC elec. cond., near T_g, temp. depend. 80−49791
Se-Ge-Te, chalcogenide glass, elec. cond. and dielec. const. 80−75567
Se-S, glassy alloy, order-disorder transition kinetics 78−67650
Se-Te-As-Ge glasses, elec. transport 79−60833
Se-Te-Ge and Se-Sb systems, amorphous, electrical transport, activation energy 79−95406
Se-Te-Sb glasses, electronic transport 80−88579
$Se_{1-x}Ge$, amorphous, AC cond. magnitude and variation *(French)* 79−47095
$Se_{1-x}Te_x$, amorphous, optical and elec. props. 80−84506
$Se_{1-x}Te_x$ amorphous films, sublinear and superlinear I-V characts. 79−82695
$Se_{1-x}Te_x$, film, struct. and props. 79−99079
$Se_{12}Te_{49}As_{29}Ge_{10}$ semiconductor amorphous films, field effect, trapping 80−84472
$Se_{60}Te_{30}Ge_{10}$, amorphous, neg. magnetoresist. 79−51603
Si, amorphised by ion implant., localised states and cond., irrad. and heat treatment, doping 80−39529
Si, amorphous, AC cond., bipolaron hopping 79−23928
Si, amorphous, doped, non-polaronic cond. and thermopower near band edge 80−49719
Si, amorphous, EPR and spin-dependent effects 80−80592
Si, amorphous, electrical transport and photocond. 77−85355
Si, amorphous, film, hydrogenation by H diffusion, effect on elec. cond., band gap *(Korean)* 80−45326
Si, amorphous, hopping model for activated charge transport 79−87099
Si, amorphous, hydrogenated pure and B doped, annealing effect on cond. *(Korean)* 79−15142
Si, amorphous, ion implantation method, B and P ions 80−100274
Si, amorphous, photo-induced changes in elec. props., defect states 79−82553
Si, amorphous, substitutional doping, electronic props. 77−1418
Si, amorphous co-sputtered doped, photovoltaic material appl. 80−93488
Si amorphous film, AC conduction 77−66213
Si, amorphous film, drift mobility and photocond. 79−15143
Si amorphous film, EPR rel. to elec. cond. 77−69692
Si, amorphous film, ESR, cond. secular change on annealing *(Japanese)* 79−15238
Si, amorphous film, heavily doped, glow discharge, AC cond. 80−49718
Si amorphous film, heavy doping by alkali ion implantation, cond. meas. 80−2045
Si amorphous film, hole carrier transport 80−2500
Si, amorphous film, in Ti-Si-Ti struct., elec. cond. processes and threshold switching 79−78207
Si, amorphous film, interface charge, influence on transfer meas. 79−15237
Si, amorphous film, oxidised, vacuum deposited, cond. change due to electron irrad. 78−10089
Si, amorphous film, RF plasma deposition from $SiCl_4$-H_2, characterisation 80−66435
Si amorphous film, sputter-deposited, elec., optical, and photoelectronic props. 79−24433
Si, amorphous film, TSC, density of localised states distrib. 80−65587
Si, amorphous films, halogenated and hydrogenated, elec. and optical props. 80−97016
Si, amorphous films, hopping conduction, dangling bond generation by high temp. annealing 80−60115
Si, amorphous films, ion implanted, elec. and photocond. props. 80−49717
Si amorphous films, RF sputtered, appl. as Schottky barrier solar cells 79−34434
Si, amorphous films, RF sputtering prep. at high Ar press., props. obs. 80−80418
Si amorphous films, self-ion bombard., electronic props. 79−28422

electrical conductivity of amorphous semiconductors and insulators continued
Si, amorphous glow discharge films, H_2 content, elec. props., and photostability 80—25577
Si, amorphous sputtered film, elec. cond. and photocond. 79—87097
Si DC sputtered, amorphous, dark conductivity and photocond. obs. *(French)* 78—64155
Si, discharge produced, reversible cond. changes 77—85256
Si, doped, density of states determ. from transport meas. 80—49720
Si, doped amorphous, transport props., conductivity, thermopower, temp. depend. 79—73512
Si, doping effects on cond. in hopping transport regime 79—28424
Si, ESR and DC cond. 77—48032
Si, elec. and opt. props., review 78—23094
Si, elec. props., effect of amorphous to polycryst. transition 79—28425
Si, elec. props., ion implantation effects 80—79828
Si, electron-beam-evaporated amorphous thin films, noise meas. 79—24091
Si film, amorphous, effects of annealing of gap states 78—72115
Si film, crystn. on annealing at low temps. in contact with Al 80—24765
Si film, electron beam evaporated, freq.-depend. dielec. behaviour 79—99549
Si film, evap., structural aspects in electronic data interpret. 77—76977
Si film, hopping cond. control by ion bombard. induced struct. modification 80—92898
Si film, RF-sputtered, influence of O_2 and deposition conditions, elec. cond., IR absorpt. and ESR 80—2949
Si film, sputtered amorphous, P and B doped, elec. cond. and thermopower meas. *(French)* 78—47403
Si film, variable range hopping 78—76176
Si, ion irradiated, elec. cond. 79—11127
Si, position of Fermi level, spectroscopic and transport determ. 80—6706
Si, solar cells, and photovoltaic devices *(Japanese)* 80—50965
Si, sputtered, resist. control by ion implantation 80—100262
Si, sputtered amorphous film, photocond. and electronic props., effects of annealing in plasma gas 80—44644
Si, substantially doped, electronic props., review 79—87175
Si, transient electrical transport, general and unified treatment 80—59977
Si, transport results, interpretation 80—80260
Si, transport results interpretation 80—44590
Si:Al(Sb) film, amorphous, ion implantation, effect on cond. 78—83839
Si:Au, O(H), film, amorphous, elec. cond. meas. 80—80423
Si:B, heavily doped, annealing characteristics obs. *(Japanese)* 78—18666
Si:B amorphous film, CVD prep., EPR, elec. and optical props. 79—4558
Si:BF_2^+(Si^+,B^+), recrystallisation of implanted amorphous layers, elec. props. 79—55762
Si:B(P), amorphous, photo- and dark conductivity 77—28216
a-Si:B(P), Hall effect and impurity cond. 77—72871
Si:B(P), ion implanted crystalline and amorphous laser annealing 80—97509
Si:F, amorphous, heat resistant, prep., elec. cond., IR absorpt., annealing 80—65719
Si:F, amorphous film, effect of F on elec. cond. 80—34444
Si:F, H amorphous films, optical props., photoconductivity, photostructural changes 80—11034
Si:F,H, glow discharge deposited elec. props. and device aspects 80—44744
Si:H, amorphous, discharge prod., optically induced cond. changes 80—96937
Si:H, amorphous, plasma deposited, cond. adsorbate and insulating layer effects 80—49749
Si:H, amorphous, Schottky diodes, elec. props., light-induced effects 80—103741
Si:H, amorphous, solar cells, carrier generation, recombination, and transport 80—55844
n-Si:H, amorphous, thickness depend. cond. 80—49724
Si:H, amorphous field induced and quenched-in excess cond. 80—24968
Si:H, amorphouse film, optical and elec. props. 79—82694
Si:H, Cl(F), amorphous, photocond., dark cond. and photoluminesc. 80—49802
Si:H, evaporated amorphous film, prep. elec. cond. and photocond. 79—38201
Si:H, model for variable gap intrinsic semiconductor 80—10988
Si:H, prod. by high temp. thermal decomp. of SiH_4, and photocond. 79—87585
Si:H, reactively sputtered, H content effect on props. 80—49714
Si:H,B, amorphous, field effect and thermoelec. power 80—96924
Si:H,Li, DC electrical conductivity, absorption edge and IR meas., role of H 80—54694
Si:H,P, amorphous, heavily hydrogenated, high gap state densities 80—49803
Si:H,P film, elec. cond., thickness and temp. depend. 80—65559
Si:H amorphous film, plasma-deposited, elec. and comp. heterogeneity 80—44745
Si:H amorphous films, conductivity and temp. dependence of optical gap 80—100462
Si:H amorphous films, ESR, optical gap and elec. cond. meas. 80—75842
Si:H amorphous films for solar cells, optical and elec. props. of RF glow discharge deposited films 80—54576
Si:H film, elec. cond., effect of adsorbed gases and illumination 78—88048
a-Si:H MIS junction, electronic struct. study by tunnelling 80—44729
Si:H(D), amorphous films, CVD, post-hydrogenation 80—54552
Si:In amorphous films, EPR, elec. cond., and magnetoresist. 80—50160
Si:Li, amorphous, elec. cond. and thermopower 79—73537
Si:Li, amorphous, thermopower and cond. meas. 79—69142
Si:Li, interstitial doping by in-diffusion and implantation and elec. characterisation 78—26585
Si:Li(Na)(K)(F)(Cl), amorphous, implantation effects on elec. props. 80—49716
Si:Mn, amorphous, cond. increase by Mn doping 78—72155
Si:Mn(Fe)(Ni) amorphous films, ESR and elec. cond. 80—50171
Si:Na(K)(Cs), ion implanted, control of cond. 79—60835
Si:Ne, implanted, cond. change 78—23097
Si:O, amorphous, sputtered, influence of O and deposition conditions 80—54693
Si:P, amorphous, CVD, defect compensation 80—54644
Si:P, amorphous, substitutionally doped CVD, electrical props. 79—99566
Si:P, heavily doped, glow-discharge-produced, elec. and optical props 80—2497

electrical conductivity of amorphous semiconductors and insulators continued
Si:P film, amorphous, unusual temp. depend. of thermoelec. power 77—59343
Si:Sb, amorphous, electronic transport props. 80—44589
Si-As-Te glass, thermoelec. power and DC cond., temp. depend. 77—62955
Si-B amorphous film, plasma deposited, characterization 79—69828
Si-Ge amorphous films, effects of annealing and crystn., ESR microstruct. and elec. meas. 78—26790
Si-Ge film, ESR line intensity anal., rel. to cond. mechanism 78—43645
Si-Ge:As,P, heavily doped, electron scatt., Hall coeff., Seebeck coeff. and resist. meas., 4-300K 77—4379
Si-H, amorphous, struct. and press. induced transition 80—44131
Si-H, RF sputtered amorphous alloy, influence of Ar press. on elec. props. and photoluminesc. 79—91585
Si-H amorphous film, reactively sputtered, prep. and props. 79—78889
Si-H:P amorphous film, dark cond., struct., Raman scatt. 80—88588
$Si_{1-x}B_x$:H, amorphous films, thermopower and cond. for mixed band and broad tail state cond. 80—49786
SiC amorphous film, elec. props. and hopping transp. 77—66211
SiC, sputtered amorphous film, struct., elec. and optical props. 79—78236
SiC_x, prepared by glow discharge method, elec. and optical props. 77—21035
$Si_{12}Ge_{10}As_{30}Te_{48}$ chalcogenide glass threshold switch conductivity in high ohmic state *(Russian)* 78—43502
$Si_{12}Ge_{10}As_{30}Te_{48}$, conducting filaments and switching phenomena 79—87134
$Si_{12}Ge_{10}As_{30}Te_{48}$ glass, nonlinear I-V characts. 79—99557
$Si_{12}Ge_{10}As_{30}Te_{48}$, vitreous, localised states role in cond. in high elec. fields 77—76841
SiH_x discharge produced amorphous film, gap state role in carrier transport 79—73608
a-$Si_{1-x}H_x$, oxygenated thin film, sputtered, elec. cond. and optical props. 79—15239
$Si_{1-x}H_x$:Al, amorphous, co-sputtered Al modification, electronic and optical props. 80—100461
Si_3N_4, amorphous, charge transport in band tails 78—76026
Si_3N_4, insulator film, high-field cond. 79—56320
Si_3N_4, unsteady cond. in high elec. fields 78—76152
Si_xN_y, prepared by glow discharge method, elec. and optical props. 77—21035
SiO amorphous thin film capacitor, EPR, elec. cond. 78—68358
SiO_2, amorphous, high-field transport of excess electrons and holes 77—89767
SiO_2, defect-controlled carrier transport 79—91049
SiO_2, elec. cond. mechanism, review of developments 78—26854
SiO_2, fused, as-received and irrad., dielectric props. 79—65786
SiO_2 layers, thermally grown, undoped and ion implanted, elec. props. 78—23187
SiO_2, transient electrical transport, general and unified treatment 80—59977
SiO_2-Li_2O-Al_2O_3-K_2O:Ag_2O(-CeO_4) (-Sb_2O_3), surface resist. meas. 80—44700
SiO_x, amorphous, ESR and hopping cond., He^+ irrad. effects 79—61213
$SiO_2B_2O_3$-K_2O-Al_2O_3-As_2O_3 glass fibres containing metallic granules, tensile strength, Young's modulus, DC conductivity 80—30023
$Si_{12}Te_{48}As_{30}Ge_{10}$ amorphous film, high-field transient conduction 78—43500
$Si_{12}Te_{48}As_{30}Ge_{10}$, amorphous film, elec. cond. mechanisms, temp. depend. *(Japanese)* 78—80078
$Si_{12}Te_{48}As_{30}Ge_{10}$ amorphous film, current-voltage characts. 79—87104
Sn-Se-P system, glasses, comp. depend. 77—84658
SnO_2 film, optical and elec. props., rel. to stoichiometric deviation and struct. 77—47701
SnO_2:P, CVD films, elec. props., cryst. to amorphous transition effects 80—107933
SnO_2:Sb film on glass substrates, elec. props. 80—88652
SnSe-$GeSe_2$-As_2Se_3 glasses, vitrification region and elec. cond. 80—15008
$SnSe_2$-$GeSe_2$-As_2Se_3 system glasses, vitrification and elec. cond. 79—50997
SnTe film, amorphous, evaporated and annealed, variable range hopping cond. 78—80077
Sr-Te-O system, amorphous thin film, vacuum deposited, elec. cond., current cut-off *(Japanese)* 77—24625
Ta_2O_5 anodic films, elec. cond. mechanism, admittance meas. 80—70705
$Ta_{16}W_{18}O_{94}$, characterisation of thermally contracting tungstates 78—63869
Ta_2WO_8, characterisation of thermally contracting tungstates 78—63869
$Ta_{22}W_4O_{67}$, characterisation of thermally contracting tungstates 78—63869
Te, evaporated film epitaxial and amorphous-crystalline phase transition growth and struct. 79—51449
Te, film, vac. deposited, phonon-assisted hopping cond. 80—2392
Te film in Sn/Te/electrolyte system 77—63923
a-TeAsSiGe film with Mo contacts, AC performance *(German)* 77—63012
$Te_{81}Ge_{15}As_4$, Hall effect in electrically switched memory state 80—2403
$TeSe_{20}$, vitreous alloy, elec. and thermal cond. during crystallisation 79—7550
$TeSe_{50}$, amorphous to cryst. transition, kinetics 79—73099
$Te_{50-x}Se_{50}Sn_x$, thin films, elec. cond. and thermoelectric power meas. *(French)* 80—80335
TiO_2-P_2O_5 reduced glasses, prep., elec. transport, chem. anal., DC, AC cond., seebeck coeff. 78—30924
TiO_2-SiO_2, semicond. glass, small polaron hopping cond. 78—60126
TiO_2-Ti_2O_3-P_2O_5, glass form., struct. and elec. props. 80—44592
$Tl_2Se.As_2Te_3$, vitreous, thermal switching process in high electric fields 80—2432
Tl_xTe_{1-x}, bonding and electrical conduction 79—90951
$Tl_2Te.As_2Te_3$, vitreous, temp. depend. of cond. and thermopower, electron energy spectrum 77—76831
VO_2, amorphous thin films, phase transition, resistivity and opt. transmission discontinuities 77—47871
VO_2, metal-semiconductor transition, effect of deviations from cryst. lattice periodicity 79—23898
VO_2, sputtered, switching effects in four-electrode structures 78—2596
V_2O_5, amorphous, electronic cond., effect of random glass struct. 79—23972
V_2O_5 amorphous layers, gel deposited, semicond. props. 80—92887

electrical conductivity of amorphous semiconductors and insulators continued
V_2O_5 layer, photocond. investig. using V_2O_5-n-Si system 77−76875
V_2O_5-As_2O_3-RO, R=Ba, Ca, Pb, semicond. glass, electronic props. 80−88557
V_2O_5-based glasses, amorphous, electronic cond. and related props. 79−99547
V_2O_5-GeO_2 glass, effect of thermal processing on elec. and thermal props. *(Russian)* 77−63814
V_2O_5-GeO_2-PbO glasses, memory and threshold switching 78−23142
V_2O_5-MoO_3-P_2O_5 glass, semicond., DC cond., dielec. props 79−91044
V_2O_5-P_2O_5, glass, DC cond. meas. high temp. range 78−6376
V_2O_5-P_2O_5 (70-30), electrical cond. and thermoelectric meas., Au-glass-Au sandwich 80−29403
V_2O_5-P_2O_5 glass, EPR investig., samples with varying V^{4+} content and cond. 77−8389
V_2O_5-P_2O_5 glass, electrical 1/f noise and DC cond. 79−91109
V_2O_5-P_2O_5 glass, splat-cooled, EPR of V^{4+}, polaron hopping and carrier localisation 77−28436
V_2O_5-P_2O_5 glasses, anomalous cond. mechanism 77−76832
V_2O_5-P_2O_5 glasses, secondary electron emission 79−87534
V_2O_5-P_2O_5 glasses containing metallic particles, elec. props. 79−42547
V_2O_5-V_2O_4-$BaZnO_2$ glass, V ion states, mag. and elec. props. 80−88556
VTe, mag. and elec. transport props. 80−92897
WO_3 amorphous film, elec. cond. and dielec. const. 78−60238
WO_3 film, evaporated, mech. of elec. cond. 80−44747
WO_3 film, sublimed under different conditions, elec. transport props. 80−7015
WO_3-B_2O_3-ZnO semiconducting glasses, DC cond. and optical absorpt. 80−107783
WO_3-P_2O_5, glass, DC conductivity meas. high temp. range 78−6376
WO_3-P_2O_5 glass, DC elec. cond., 100-400K 78−39106
Y-Si-Al-O-N glass, prep. and props. 80−25647
Y_2O_3-AlN-SiO_2 oxynitride glasses, elec. props. 80−80267
ZnO, CVD growth and elec. props. 77−76973
ZnO ceramic containing rare earth metal oxides and Co_3O_4, non-ohmic props. 77−76833
ZnO-SnO_2-M_xO_y, M_xO_y=glass-forming additive, I-V characts., heat treatment effects 77−43595
ZnSe, amorphous thin film, prep. and electronic props. 77−85350
a-ZnSe, elec. and optical meas., Mott-type model for amorphous semicond. 78−2414
ZrO_2 refractories, elec. cond. variation, gas flow effect 80−39581

electrical conductivity of crystalline metals and alloys
see also dislocation scattering; electron density (metals); electron mean free path (metals); electron mobility (metals); electron relaxation time (metals); electronic conduction in metallic thin films; impurity scattering; point defect scattering; surface scattering
1/f fluctuations *(Japanese)* 78−43448
A15-compounds, electron lifetime affecting electronic props. 79−15134
A-15 compounds, supercond. transition temp., correl. with resist. anomalies and defect struct. 77−47920
A-15 high-T_c supercond., apparent T^2-depend. of normal-state resist. and lattice sp. ht. 77−47921
actinide, transport props. and sp. ht., role of optical and acoustic phonons 77−15821
actinide alloy, resistivity temp. depend. due to localised spin fluctuations 77−8083
actinide non-stoichiometric intermetallic cpds., elec. resist. temp. depend. 79−1597
actinide systems, nearly ferromag., coupled d- and f-band model 77−63211
actinide systems, nearly magnetic, thermoelectric power determ. 78−56133
actinides, lattice vibrs. role in phys. props. determ. 77−28158
Al alloy AK4-1, acoustic investigation of ageing 79−34083
alkali metal, electron-phonon drag effects in elec. cond. and thermoelec. power 77−15824
alkali metal, ideal electrical resistivity, temp. depend. 78−64022
alkali metal, low-temperature elec. resist., empirical expressions, validity 79−23945
alkali metal alloy, charge-transfer state, from residual resist. of electronegative impurities 79−95372
alkali metal wire, low temp. elec. resist., size and temp. depend. 77−76958
alkali metals, electrical resistivity, data tables, 1-2000K 79−78072
alkali metals, electron relax. time energy depend., electron-phonon resist. 79−60805
alkali metals, electron-electron scatt., thermal and elec. resistivity 80−59956
alkali metals, heavy, supercond. and high temp. resist. at high press. 77−47917
alkali metals, liq., electrical resistivity and thermoelec. power, Harrison's method 79−78066
alkali metals, Matthiesen rule deviations rel. to CDW 80−29385
alkali metals, phonon-limited electrical resistivity 78−6346
alkali metals, phonon-phonon scattering relax. times, rel. to elec. resist. 77−39813
alkali metals, pseudopotential calcs. of binding energy, compressibility and resistivity 79−65025
alkali metals, thermopower and elec. cond., relationship at low temps. *(Russian)* 80−92882
alkaline earth elements, electrical resistivity; 1-1000K, data tables 79−78073
alloy, concentrated, electrical resist. and Hall coefficient, temp. depend. 78−39093
alloy, Debye temp., determ. from elec. resist. meas. *(French)* 77−4322
alloy, role of anisotropy in elec. resist. of Guinier-Preston zones 77−36515
alloy,dil., electrical resistivity, Kondo effect vs. spin glass behaviour 78−68269
alloy with arbitrary gradient of conc. and degree of order, residual elec. resist. 79−19569
alloys, effects of temp. an order-depend. elec. resist. 77−31992
alloys, highly resistive, temp. depend. on elec. resist. 78−91657
alloys, resistivity evolution during decomposition, theory *(French)* 80−75546
alloys, substitutional, electrical resist., long and short range orders effect 80−107761
alloys, with off-diagonal disorder, density of states and cond., CPA calc. 80−24780

electrical conductivity of crystalline metals and alloys continued
anisotropic materials, measurement of resistivity using RF contactless method 79−67344
anisotropy of electrical and mag. props., calc. for HCP metals and alloys *(Russian)* 77−66292
antiferromagnetic alloy, stoichiometric depend. of elec. resist. 77−69312
antiferromagnetic alloys, spin disorder resistivity, coherent potential approx. 78−14722
antiferromagnetic metal, crit. resistivity, appl. to Dy 79−47077
antiferromagnetic metals, electron scatt. features, s-d exchange model 77−8085
antiferromagnetic metals, two band model for elec. resist. 78−14720
band mixing, generalised Boltzmann theory 79−38060
binary alloy, elec. resist. due to crit. fluctuations near order-disorder temp., theory 77−40071
binary alloy, electronic transport in substitutionally disordered systems, MCPA and Monte Carlo calc. 78−84185
binary alloy, partially ordered, elec. resist., CPA calc. 78−43356
binary alloys, charge transfer and transport props. in tight-binding model 79−82577
binary alloys, elec. resist. near crit. point 80−96847
binary continuous solid solutions, elec. resist. and thermoelectric power behaviour 79−69492
binary disordered alloy with long range order, single band model 77−28154
binary ordered alloys, residual resist., s-d hybridisation effect 80−39559
Bloch theory agreement and limitations 79−28332
Bloch-Gruneisen formula validity for elec. resistivity, temp. depend 77−31991
borides, hexa- and di-, electronic structs., elec. props., book contrib. 78−47701
borides, hexa- and tetra-, prep., struct., elec., mag. props., book contrib. 78−47303
borides, ternary, struct. classification, props., book contrib. 78−47309
β-brass, disordering under γ-irrad., elec. resist. meas. *(Russian)* 77−48429
α-brass, electron irradiated, defect production and interdiffusion 78−67739
brass, LANKMts, solid soln. range of existence 77−12653
brass, recovery and recrystallisation of plastically deformed α-phase, comparison of positron annihilation, elec. resist. and microhardness 79−52240
brass alloys, thermal and elec. cond., 4 to 300K, Zn conc. depend. 80−29379
β_1 brass containing α-precipitates, reversible shape memory effect *(Japanese)* 78−60711
braze alloys, low vapour press., binary eutectic, props., thermionic converter appls. 77−90236
carboxylic acid metallic salts, laminated cpds., nature of cond. *(Russian)* 79−42512
cathode spots of the first kind, erosion rate resistivity and thermal cond. depend., explosive model 79−14630
coherent precipitates, particle size distrib. influence on extra-resist. 80−49689
coherently decomposing alloys, extra resistivity calc., X-ray small angle scatt. 80−92873
collision frequency of electron with positive ions, vel. to ionosphere collision freq. and recomb. coeffs. 79−8742
copper quaternary thiospinels, mag. and elec. props. *(French)* 80−65771
Cr-Au alloys, dil., elec. resist., 77-700K 78−64035
critical temperatures determination, elec. resist. method, IMASh-5S-69 installation 80−71827
cubic metals, monovacancy resist. using pseudopot. models 80−29378
cubic metals, relationship between defect resist. and bulk resist. at melting temp. 78−6344
deformation potential of crysts. formulation *(Russian)* 77−19894
deformed metal, kinetic eqn. *(Russian)* 77−35906
dilute alloy, electron scatt. by impurity cluster, lattice distortion and backscatt. effects 77−20306
dilute alloy, perturbation expansion for the asymmetric Anderson Hamiltonian 80−80202
dilute alloys, elec. transport and deviations from Matthiessen's rule 80−65524
dilute binary alloy, residual resistivity 77−1406
dilute magnetic alloy, reverse Kondo effect, magneto-transport theory 80−15509
dilute magnetic alloys, transport props. from Suhl's dispersion relations 77−62891
dirty metal, resist. temp. depend., causes of Matthiessen's rule deviations *(Russian)* 77−69291
dislocation elec. resistivity, comparison of two theories 78−6371
dislocation resistivity, inelastic scattering of electrons 78−26853
dislocations in metals, residual elec. resist., one-electron approx. *(German)* 80−39568
disordered alloy, electronic transport, effect of thermal and off-diagonal disorder 78−30902
disordered alloy, residual resistivity due to clustering, ageing effects 80−65521
disordered alloy, temp. and composition depend. anomalies, modified Evans-Ziman theory 77−69288
disordered alloys, frequency depend., abstract Hilbert space generalisation of perturbation theory 77−24542
disordered alloys, temp. depend. of elec. resist., elastic electron-phonon scatt., CPA calcs. 79−56185
disordered system, residual resistivity 78−87954
dynamic conductivity, generalised linear Boltzmann eqn. perturbation soln. 78−34818
electrical domains at low temps. in metals *(Russian)* 78−91687
electrically conducting spherical specimens, electromagnetic control 78−53138
electron scattering, relation between X-ray small-angle scatt. and elec. resist. 79−19125
electron theory, contrib. of Sir Rudolf Peierls, 1928-1935 80−57054
electron-dislocation scatt. anisotropy effect on electron-electron scatt. contrib. to elec. resist. 80−29398
electron-dislocation scattering and negative deviations from Matthiessen's rule 80−80248
electron-electron scatt. and elec. resistivity of metals 79−95396
electron-impurity scattering, lattice distortion effects, phase shifts, calc. 80−96860

electrical conductivity of crystalline metals and alloys continued
rel. to emissivity estimation, classical electron theory *(Russian)* 78—38859
eutectics, HgTe-PbTe and Au-PbTe, prep. and thermoelectric behaviour characts. 80—107774
FCC metals, high dose neutron irrad. effects, 4.6K 78—34548
FCC metals, props. of vacancies and divacancies 80—10545
ferrite spinel, DC resistivity depend. on substitutions 80—44565
ferromagnet, anisotropic, spin-fluctuation resist. 78—56137
ferromagnetic, elec. cond. review 77—31993
ferromagnetic binary alloy, elec. resist. temp. depend. *(Russian)* 79—1592
ferromagnetic binary alloys, narrow-band with random hopping, spin wave stiffness const. and elec. cond. 79—56524
ferromagnetic Fermi-liquid model, electron-impurity system hydrodynamics, elec. cond. 80—103835
ferromagnetic metal, electron scatt. by fluctuations of mag. moment near Curie temp. 79—73502
ferromagnetic metal, nearly and weakly ferromag., freq. depend. elec. cond., Drude's formula deviation 79—47091
ferromagnetic metal, uniaxial, anisotropic spin fluctuations and anisotropic band struct. effects on resist. near T_c 80—65543
ferromagnetic metal, with domain struct., resistivity 78—95285
ferromagnetic metals, resist. anisotropy, crit. behaviour and temp. depend. 80—96858
ferromagnetic metals, resistance meas. *(Dutch)* 77—8066
ferromagnetic metals, transport props., crit. behaviour 80—65522
ferromagnetic metals, with domain struct., low-temp. resist. 77—47791
fibre materials, thermal and elec. conductivities 78—10419
fine particles, tunnelling effects on props. 78—14704
foils, surface scatt. data table 79—60907
fracture mechanics test, electrical potential method, unusual potential drop 77—16761
HCP metals, and alloys, anisotropy of phys. props. rel. to texture 79—91700
heat-resisting alloys, VM-1 and VX-4, thermal fatigue rel. to struct. changes *(Russian)* 78—11302
hexagonal metals, deformed, resistivity changes calcs. 80—44564
high magnetic field behaviour of solids and plasmas, conference, Cambridge, MA, USA (Sept. 1978) 79—60667
highly resistive metallic alloy, elec. resist. calc. including Debye-Waller factor 77—66150
highly resistive metals, random phase model, negative temp. coeff. 78—47758
impure metals at low temperatures, conductivity 80—103669
Invar, effect of deform. by cold rolling 77—48556
Invar, elec. transport props. and Invar features *(Russian)* 78—14710
Invar, magnetoresist. and temp. variation of elec. resist. meas. 77—31999
Invar, resistivity temp. depend., 300-1300K *(Ukrainian)* 77—69290
Invar, ternary alloys based on Cr-Fe and 4d transition metals, magnetically insensitive 77—28026
ion polarisation and point defect resistivity in metals 80—103672
irradiated metal, containing self-interstitials and vacancies, electronic transport props. 78—60105
irradiated metal, elec. cond. tensor calcs. 79—87079
itinerant electron magnet, low temp. resist., collective excitations 77—72851
jellium residual resistivity of vacancies 78—6348
kinetic equation, iteration soln. 77—43564
Kovar, effect of magnetic electrons on atomic interactions 77—43820
lattice defects and diffusion processes in solids, book 80—107207
layered structure metals, transport props., book contrib. 77—43566
Linde law, validity in normal metal based alloys *(Russian)* 77—80759
linearized Boltzmann eqn. soln., resist. and deviation from Matthiessen's rule 80—65523
low temperature, Matthiessen's rule deviations *(Croatian)* 79—11099
low temperature depend. of elec. resist., mag. suscept., heat capacity, Hall const. *(Russian)* 78—30900
magnetic alloy, highly concentrated, elec. resist. 79—24134
magnetic alloys, dil., in finite mag. field, Suhl's dispersion eqns. 77—24673
magnetic metals, Neel temp. and crit. exponents determ. from electronic transport coeffs. 77—69556
magnetic ternary alloys, statistical theory of electrical resistivity 78—87969
many-band metals, elect. resistivity from force correlation function method 78—43357
Matthiessen rule deviations, electron scatt. by dislocations, impurities and phonons 78—19026
metal, BCC, temp. depend., anharmonic effects 78—76045
metal, Debye temp., determ. from elec. resist. meas. *(French)* 77—4322
metal, defect annealing study by positron annihilation, and elec. resistivity meas. 78—51584
metal, deformed, microcrack effect on elec. resist. temp. depend. 77—51726
metal, degree of deform. effect on thermophys. props. at high temps. 78—26694
metal, dislocation elec. resist. and reson. scatt. 77—43550
metal, elec. resist., correction from non-Hermiticity of pseudopotential 79—7815
metal, electrical resistivity changes during polymorphic transform. A1 to A2 and A3 to A2 77—48430
metal, electron Boltzmann eqn. solns., energy depend. 80—88537
metal, electron transport properties 79—19565
metal, electron-electron scatt. 79—38045
metal, ferromagnetic, dynamic scatt. effects on crit. transport props. 78—84239
metal, ferromagnetic resonance linewidth, interaction of spin waves with conduction electron current 80—25216
metal, impure elec. conductivity calc., effect of electron-electron correlation *(Russian)* 78—68010
metal, kinetic effects at high anisotropic strains, elec. transport props. meas. 78—54384
metal, localised atomic states, resist. and free energy calc. 77—8069
metal, low temp. impurity cond. temp. depend., kinetic eqn. *(Russian)* 79—7817
metal, low temp. phonon resist. 77—62888
metal, pinch effect on plastic deform. *(Russian)* 78—35426
metal, quantum kinetic equation for electrons 78—91686
metal, simple, vacancy, formation energy and residual resist. calc. 79—11077

electrical conductivity of crystalline metals and alloys continued
metal, with impurities, noise fluctuations, quaternary correlation function calc. 79—24041
metal film, d+inhomogeneous, elec. cond. determ. 77—15973
metal powder compacts, elec. resist., surface layer effect 80—34415
metal wires, DC resistance, size effect correction 78—91679
metal with dislocations, temp. depend. of elec. resist. *(Russian)* 78—39094
metal with unfilled f-shell, elec. resist. *(Russian)* 78—72141
metal-H systems, temp. depend. of impurity resist. 80—65529
metallic bicrystals, residual resistance theory, diffusivity, disorientation effects *(Russian)* 80—49875
metallic ferromagnet, antiresonance region, EM wave propag., Maxwells' eqns. soln. 80—66038
metallo-octaethyl porphyrins, I oxidation products, metallic cond., EPR and reson. Raman spectra 80—29610
metals, acoustoelectric current for conductivity electron arbitrary dispersion law *(Russian)* 80—49829
metals, elec. resist., intermediate temp., Bloch-Gruneisen formula, deviations 80—2375
metals, elec. resist. of dislocations 77—69310
metals, electrical and thermal resistance, influence of static atomic displacements 80—103674
metals, electrical conductivity, high pressure effects 80—92879
metals, electronic transport eqns., optical cond., number conserving relaxation time approx. calcs. 80—49681
metals, energy depend. relax. times in electronic transport props. 79—60804
metals, low temp. elec. resist., comparison between first principles form factor and empirical form factor 78—2463
metals, low temp. resistivity, electron-phonon scatt. anisotropy influence 79—60818
metals, normal hexagonal, temp. depend. anisotropy of phonon scatt. resist. 78—51967
metals, phonon limited resistivity, anharmonicity, Debye Waller factors, multiphonon terms 80—49691
metals, phonon-phonon scatt. role in lattice thermal cond., phonon drag, elec. cond. 80—70483
metals, proper EM radiation on inelastic electron tunnelling with photon emission, cond. *(Russian)* 80—54765
metals, pure, electrical resistance, exam at high temp. using inductive heating 79—7816
metals, quantum magneto-dimensional effects, open Fermi surfaces, conduction electrons *(Russian)* 80—80487
metals, two and one interstitial model explanation of elec. cond. variations 80—88143
metals electrical resistance at high temperature, $T^{3/2}$ depend. 77—43561
metals with dislocations, elec. resist. temp. depend. 79—60819
minimal metallic cond., localisation scaling theory *(Russian)* 80—103671
mixed valence cpds., elec. cond., periodic Anderson model, memory function approach 80—84458
monovalent metals, 1-4K, HF phonons role 77—15828
N-S boundary resistivity, tunnelling contact resistance *(Russian)* 80—93048
neutral and charged impurity scattering, Matthiessen's rule 79—47081
noble metal, elec. resist. of dislocations, calc. *(Russian)* 78—60117
noble metal alloys, dil., deviations from Matthiessen rule 80—65525
noble metal dilute alloy, residual resist. calc. 77—28156
noble metals, elec. resist., temp. depend. data 80—51967
noble metals, elec. resist. calc. using Animalu's model pot. 77—43558
noble metals, electrical resistivity, pseudoharmonic effect of phonons 80—34414
noble metals, electron relax. time energy depend., electron-phonon resist. 79—60805
noble metals, pure, low-temp. transport props. 77—8072
nonlinear effects due to coherent mag. breakdown *(Russian)* 78—76062
nonsimple metals, calc. of elec. resist. and thermoelec. power 78—19019
normal metals, low temp. resistivity, correl. with electron-phonon scatt. anisotropy 79—56190
one-dimensional metal, phonon drag and sliding CDW 80—20173
ordered alloys of CsCl type, change in resist. with degree of order *(Japanese)* 78—34817
paramagnetic impurity scatt., nonlinear elec. resist. 77—15826
phase comparisons for Sondheimer size effect oscills. 78—34823
phonon-phonon scattering, Peierls condition 77—62910
plane lattice defects contrib. to elec. resist. *(Russian)* 80—49688
polycrystalline materials, macroscopic elec. cond. determ. 79—99521
polycrystalline metallic conductivity, grain-boundary scatt. model 80—88530
polycrystalline metals, statistical model for grain boundary effects 80—6814
polycrystals with axial texture, heterogeneity of props. *(Russian)* 80—29192
polyvalent metal alloys, dil., deviations from Matthiessen rule 80—65525
polyvalent metals, electron relax. time energy depend., electron-phonon resist. 79—60805
polyvalent metals, Matthiessen's rule deviation crit. resist. 80—6811
powder metallurgy compact, elec. resistivity 78—64028
properties of high-conductivity copper and copper alloy wires *(Japanese)* 79—91665
pseudopotential investigation of phys. props. of metals and alloys 77—43526
pseudopotential study of electronic props. 80—20149
rare earth alloys, magnetic and electronic phase transitions 79—87254
rare earth alloys, RBe_{13}, XPS, resist. and susceptibility study 80—71565
rare earth alloys, RCo_2, elec. resistivity, thermopower, X-ray struct. meas. 80—24874
rare earth iron intermetallics, RFe_2, (R=Sc, Lu, Y), mag. props., 80-1300K *(Russian)* 80—75750
rare earth metal, anisotropy of magnetic component of electrical resistivity 79—69494
rare earth metal impurity in metallic host, exchange interaction, electrical resistivity 80—84453
rare earth metals, 80-1000K 77—43572
rare earth metals, anisotropy of elec. resist., scatt. mechanism 78—72134
rare earth metals, electrical resistivity, high temp., scatt. mechanisms 80—39553
rare earth metals, HCP, point defect production during electron irrad. at low temp. 80—49273
rare earth metals, mag. and transport props. 79—69658

electrical conductivity of crystalline metals and alloys continued
- rare earth metals and their alloys, resist. anomalies 78—19018
- rare earth monochalcogenides, 4f-6s excitation energy, metallic and insulating elec. props. 80—44603
- rare earth orthocobaltites, $R_{1-x}Sr_xCoO_3$ and $La_{1-x}M_xCoO_3$, itinerant electron ferromagnetism obs. 78—10660
- rare earth orthotitanates, $RTiO_3$, metallic and semicond. elec. and mag. props. 79—38068
- rare earth strontium vanadates, $R_{1-x}Sr_xVO_{3-0.1x}$, elec. cond. and mag. susceptibility, temp. depend., 77-300K 77—47816
- rare earth tetraborides, mag. and elec. props., metallic character 80—20386
- rare earth tungsten oxide bronzes, metallic, elec. props. meas. 78—30906
- rare earth-Al_2, cubic Laves phases, prep. and phys. props. *(German)* 78—23075
- rare-earth, light-heavy alloys, resistivity, mag. contrib. to resist. and Neel temp. 78—51971
- rare-earth alloys, quadrupole scatt. anisotropy, magnetically ordered material 78—64034
- Recalloy, Fe-Nb, semihard magnetic alloy, magnetic props., hardness, microstruct. 78—56660
- residual resistivity, meas. via medium temp. electron irradiation 77—54016
- residual resistivity and thermal conductivity coeff., comparison of max. values as parameter of metal purity 79—65431
- residual resistivity for electrons scatt. by spin-depend. potentials 77—39829
- resistance fluctuation spectroscopy, power spectrum of density fluctuations 79—65428
- resistivity, temp. fluctuations and 1/f noise effects 77—20373
- resistivity anomalies of ferromag. metals near Curie temp., itinerant mag. electron theory 78—95292
- resistivity anomaly at low temp. *(Russian)* 77—35918
- resistomatic studies of lattice defects review *(Japanese)* 78—59799
- resistor, metallic, nonlinear current fluctuations, microscopic calc., heating, perturbation theory 79—69484
- rotation induced electromotive forces in normal and superconducting metals 79—24120
- saturation effects in electron transport 78—76065
- saturation resistivity charges, ion and fission fragment irrad. induced 78—79643
- simple metals, energy-independ. model pseudopot. calc. 77—62890
- simple metals, model pseudopot. appl. to various props. 80—59845
- simple metals, screening of light impurities, residual resistivities 77—85177
- solid solution, dilute, residual resistance, pseudopotential calc. *(Russian)* 79—33276
- spin fluctuations, mag. field effect, electronic sp. ht. and elec. resist. 80—108026
- spin glass, resist. max. rel. to Kondo temp. and RKKY interaction 77—20307
- spin glass, resistivity below ordering temp. 78—51980
- spin glass Kondo transition resist. max. 79—19584
- spin glasses, resist. maximum, press. and conc. depend. 77—69300
- spin glasses, resist. maximum, s-d exchange interaction 77—69586
- spin glasses, review 77—69578
- spin glasses under high press., resist. meas. 78—52277
- spiral dislocation scattering, t-matrix 78—39101
- steel, alloy, Fe-C-Zn (0.45, 1.56 wt.%), pearlite transformation during continuous cooling 78—80538
- steel, alloy, thermal and electro-physical props. of various heat resisting stampings *(Russian)* 78—51698
- steel, alloy, type HSLA, exam. of NbCN precipitation by elec. resistivity meas. . 78—84822
- steel, austenitic, age-hardening kinetics, study by resistivity, Young's modulus and internal friction *(Czech)* 80—29970
- steel, austenitic stainless, Cr-Ni, elec. resistivity and struct.-mag. transitions at low temp. 79—99527
- steel, austenitic stainless, Cr-Ni, resist. damage rate during neutron irrad. at 23K 80—96571
- steel, austenitic stainless, structure phase transitions due to high energy electron irrad. *(Russian)* 80—7553
- steel, C, fracture criterion determination, using 3-point bending 79—29216
- steel, C, resistivity, thermal and elec., spin disorder scatt. anal. 78—76063
- steel, Cr-Ni-Mo, resistometric study of austenitization and carbide dissolution preliminary annealing *(Czech)* 77—59829
- steel, Fe-Al-C alloy, redistribution of C during tempering *(Russian)* 77—90371
- steel, high Cr, V additions effect on brittleness near 475°C *(Russian)* 78—19890
- steel, maraging, ageing kinetics and struct. of N12K7M5TYu, effect of high temp. deform. of austenite *(Russian)* 80—84960
- steel, maraging, plastic deform. effects on ageing kinetics *(Russian)* 77—77508
- steel, maraging 18%Ni, calorimetric anal. of ageing *(Japanese)* 80—89264
- steel, maraging Ni-Co-Mo, precipitation, elec. resist. meas. *(Japanese)* 78—11228
- steel, maraging Ni-Co-Mo, strengthening by repeated strain ageing *(Japanese)* 79—100157
- steel, microalloyed, alloy carbide precipitation during isothermal ageing 80—3077
- steel, N27Yu2T2B, elec. and thermal cond., 4.2 to 200K, Wiedemann-Franz law *(Russian)* 79—78076
- steel, Ni (19 and 24 wt.%), austenite thermal stabilisation at sub-zero temps. 77—52324
- steel, nonoriented, mag. props. texture, Cr addition effect 77—1880
- steel, Si and Si-Mn, non-magnetic, minimum electroresistivity, −268 to 0°C *(Russian)* 79—91021
- steel, stainless, low-temp. electroresistance anomalies *(Ukrainian)* 77—32006
- steel, stainless, maraging high strength, embrittlement on low temp. ageing *(Japanese)* 79—100155
- steel, type 55SM5FA, formation of hardened layer during burnishing 78—85046
- steel alloys, low and medium C content, relaxation phenomena in volume changes during tempering *(Russian)* 79—100176
- steels, ferritic and martensitic, C and N migration at low temps., monograph 80—22149

electrical conductivity of crystalline metals and alloys continued
- steels, tool, type U10A and R6M5, phase comp. and phys. props. after hydrostatic extrusion 79—96053
- superconducting B-W type compounds, resist. characts. in normal state 78—51963
- synthetic metals, anisotropy of elec. props. rel. to chem. bond struct. 80—24888
- temperature dependence, correl. with thermal cond. temp. depend. 77—8064
- temperature dependence, general formula 78—47757
- ternary alloy ordering, correlation effects, Kirkwood method calcs. *(Russian)* 79—66038
- thermoelectric materials, B_4C_x and $(B,Si)_4C_x$ P-type LaS_x N-type alloys, fabrication and thermoelectric props. 80—107771
- thermopower and resistivities, validity of Nordheim-Gorter relation 78—91671
- thin metal slabs, with rough surfaces, conductivity 80—2378
- thin metallic plate in strong mag. field, electron scatt. elec. cond. theory *(Russian)* 80—59974
- thin wires, exptl. study of Anderson localisation 80—96849
- thin wires, Kubo formalism for heavy elec. cond., heavy impurity electron scattering 79—56191
- transition metal, modified tight binding approximation, reexam. 78—43279
- transition metal, thermal and electrical conductivity at high temperature, interpretation of temp. depend. 77—35912
- transition metal alloys, anomalous behaviour of resist., alternative mechanism to spin scatt. 78—91690
- transition metal alloys, disordered, density of states, elec. cond., extended Hubbard model 79—37948
- transition metal alloys, ferromagnetic, low temp. resist. calc. 80—24919
- transition metal alloys, spin fluctuations effect on temp. depend. of elec. resistivity 78—47776
- transition metal based alloy, resistivity temp. depend. due to localised spin fluctuations 77—8083
- transition metal borides, cryst. struct., prep. methods, chem., elec., mag. props., appls., book contrib. 78—47307
- transition metal borides, refractory, single cryst. prep. methods and characterisation, book contrib. 78—48296
- transition metal compounds, saturating contrib. to elec. resist. from electron-phonon contrib. 80—2376
- transition metal double oxides, exam. of elec. cond. 78—51990
- transition metal germanium borides, metallic resist. mag. suscept. 79—42731
- transition metal magnetic alloys, dilute, props., review of theory 79—15282
- transition metal superconductor, normal state, anomalous temp. coeff. at high temp. 78—2458
- transition metal-H systems under high H pressure, phase diagrams., electrical cond., mag. props. 80—29923
- transition metal-simple metal disordered alloy, effect of electron correl. on elec. resist. 79—47076
- transition metals, elec. resist. calc. using Animalu's model pot. 77—43558
- transition metals, electrical properties, temp. depend. 80—15496
- transition metals, emissivity, temp. depend. from DC elec. resist. 80—10688
- transition metals, HCP, electrical resistivity high-temp. anisotropy 79—65429
- transition metals, impurity scattering and residual resistivity 79—56192
- transition metals, McMillan-Hopfield factor and ideal phonon limited resist. 78—64024
- transition metals, resistivity and superconductivity 79—51550
- transition metals, thermophysical data at high temps., submicrosecond-pulse-heating method 80—103459
- transition metals and alloys, BCC, electron lifetime affecting electronic props. 79—15134
- transition metals and their alloys, resist. anomalies 78—19018
- transport kinetic coeffs. quantum oscills. in mag. breakdown regime *(Russian)* 79—91035
- tungstates, hexagonal bronze type struct., cryst. struct., MP, dielec. const. and metallic elec. cond. 77—39574
- twin crystals, resistivity calcs. by pseudopotential technique *(French)* 80—2379
- two-component layered system, with interpenetrating components, thermoelec. and galvanomag. props. 78—79982
- vacancies and lattice elec. cond. determ. method at high temp. 79—37695
- very thin wires, effect of inelastic electron scatt. on cond. 80—80259
- VPE on sapphire, highly oriented film prod. 77—66097
- wire, cylindrical, elec. resist., scatt. processes, Monte Carlo calc. 80—75560
- Ziman's variational expression for resistivity, use 80—15494
- Ag alloys, dil., transport props. 78—76046
- Ag, cascade energy density effect on isochronal recovery 78—47431
- Ag, elec. resist., press. variation 78—84193
- Ag, elec. resist. meas., 293-908K 77—43559
- Ag, electrical contact material with liquid lubricant, prod. and appl. 78—10559
- Ag, electrical resistivity, low-temp. meas. 79—23944
- Ag, electrical resistivity, low temp., T^4 behaviour rel. to electron scatt. mechanisms 80—39552
- Ag, electron-phonon interaction determ. from current-voltage curve at 1.5K *(Russian)* 77—47789
- Ag, film, condensate obtained in electric field, anisotropy of elec. props. 80—44743
- Ag, lattice vibrations and ideal elec. resistivity 79—46770
- Ag, low temp. elec. resist. 78—51964
- Ag, low temp. resist. and thermoelec. ratio, electron-electron scatt. contrib. 80—70670
- Ag, metal and dil. alloys, electrical resistivity at low temp., ultra high resolution meas. 79—60795
- Ag, phonon limited elec. resist., temp. depend. 80—24876
- Ag, phonon-limited elec. and thermal resistivity 79—42517
- Ag, production and annealing of radiation defects 78—47362
- Ag, resistivity increment due to low temp. plastic deform. *(Russian)* 77—31990
- Ag, strained, anisotropic electron scatt. in elec. resist. 78—91656
- Ag, transport props. meas., 20 mK-4.2K 77—20292
- Ag, transverse electron focusing and specular refl. from cryst. faces 80—6823

electrical conductivity of crystalline metals and alloys continued

- Ag, virtual bound states due to 4d- and 5d-transition metal impurities 80−70667
- Ag-Au, dil., low temp. elec. resist. 78−51964
- Ag-Au(Cd), deviations from Matthiessen's rule 78−10420
- Ag-Au(Cu), residual elec. resist., pseudopot. calc. 80−6813
- Ag-Cr dilute alloys, elec. cond. meas., 1.5 to 30K 77−62914
- Ag-Cu, composite, fibre and layer structs., anomalous props. caused by internal phase boundaries 78−72754
- Ag-Ge alloy system, atomic struct. and electronic props. *(Russian)* 77−20289
- Ag-Hg alloys, thermopower, thermal cond., elec. resistivity 79−65439
- Ag-Mn, spin glass alloy, elec. resist. 77−8067
- Ag-Mn alloys, dilute, low temp. elec. resist. *(Russian)* 78−68024
- Ag-Ni, composite, fibre and layer structs., anomalous props. caused by internal phase boundaries 78−72754
- Ag-Pd system, low temp. resist., 1.5 to 40K 77−62887
- Ag-Zn (38 at.%), morphological and struct. studies of thermoelastic martensites 77−63669
- Ag-Zn(Cd), production and annealing of radiation defects 78−47362
- Ag-Zr(Nb)(Mo) film, dielec. const., optical props., DC resist. and thermoelec. power 77−85824
- $Ag_{1-x}Au_xYb_y$, thermopower and resistivity 79−65457
- $Ag_xAu_{1-x}Zn$, resistivity and X-ray diffr. 78−47283
- $Ag_{1-x}Sn_{1+x}Se_{2-y}$, supercond. and normal state props. 77−36008
- AgZn, β' to ζ_0 and β to ζ_0 phase transform. 79−34026
- AgZn, $\beta' \to \zeta$ transformation, effect of additional elements 80−66507
- Al alloy, dilute, Matthiessen's rule deviations in strong mag. field 80−44571
- Al alloy, dispersion strengthened, made by mech. alloying 78−3136
- Al alloy, mechanical properties, correlation with elect. cond. 79−34114
- Al alloy 7075, precipitation hardening, toughness and microstruct. *(Japanese)* 78−15509
- Al alloys, age-hardening, resistivity charge by low temp. deform. *(Japanese)* 78−84831
- Al alloys, effect of alloying elements on cond. 80−3205
- Al and Al-Cu (1.5 at.%), vacancy charact. study by electrical resistance derivative method, rel. to temp. 78−47361
- Al, atomized powder, metallic contact for hot rolling in air 77−73294
- Al, band struct. effects on electrical and thermal cond. 78−34820
- Al, cold-worked, transport props., 1.5-8.5K 78−7059
- Al, deformed, efficiency of dislocation as sink for vacancies, resist. obs. 77−36570
- Al, deformed, resist. decay, meas. of initial stages, method and results 79−49256
- Al, deformed in tension, elec. cond. changes at 78 and 283K, grain boundary effect *(Japanese)* 80−30029
- Al, diffusion coeffs. of Zn, Co, and Ni, resistometric determ. 79−51313
- Al dilute alloys, 3d transition metal impurities, residual resist., influence of multiple scatt. effects 79−19570
- Al dilute alloys, elec. resist., impurity and temp. depend. 80−65526
- Al, effect of microvoid size on positron annihilation and residual resist. 77−48272
- Al, elec. resist. and magnetoresist., anisotropic temp. depend. *(Russian)* 79−11103
- Al, electrical conductivity temp. depend., inelastic electron scatt. by dislocations *(Russian)* 77−69315
- Al, electrical resist. and magnetoresist., 2 to 40K, Matthiessen rule deviations *(Russian)* 77−31996
- Al, electrical resistivity of ultra pure samples at low temp. 79−60794
- Al, electron-phonon enhancement of electron-electron scatt., elec. and thermal cond. 80−49326
- Al, electroplastic effect 80−7647
- Al, film, adsorption of O_2 and N_2 77−24486
- Al, film, condensate obtained in electric field, anisotropy of elec. props. 80−44743
- Al film, neutron irradiated, increase of elec. resist. 78−26973
- Al films, N_2^+ and O_2^+ ion bombardment, structural and phase changes 80−2094
- Al foil, electrical conduction, electron mean free path, surface scatt. 80−88535
- Al, granular supercond., normal state cond. 80−88529
- Al, high purity, changes during cyclic torsional deform. 77−56031
- Al, low temp. electrical and thermal transport props., Matthiessen's rule breakdown 78−26847
- Al, low temp. resist. and thermoelec. ratio, electron-electron scatt. contrib. 80−70670
- Al powder, resist.-sintability *(Japanese)* 80−16228
- Al, press. depend. of electron-phonon interaction rel. to normal state resist. 79−28063
- Al, press. depend. of electron-phonon interaction, elec. resist. meas. 79−95106
- Al, quenched, irradiated, anisotropic electron scatt. on defects 79−95397
- Al, quenched, vacancy agglomeration, elec. resist., splat-cooling effects 77−51365
- Al, remanent supercond., effect on temp. depend. of normal phase resist. 79−56362
- Al, remnant superconductivity, temp. depend. elec. resistivity meas. 79−99529
- Al, resistivity, press. depend., calc. 80−20151
- Al, resistivity decrement under torsional deform., impurity segregation at moving dislocations 77−4321
- Al, resistivity temp. depend., evidence for electron-electron scatt. 79−69488
- Al, resistivity well above T_c, supercond. effect up to $2T_c$ 80−6810
- Al, self-interstitial interaction with solutes, resistivity meas. 78−47331
- Al, small spheres, bulk plasmons damping 80−75561
- Al, Sondheimer oscillation 79−87085
- Al, strained, anisotropic electron scatt. in elec. resist. 78−91656
- Al, vacancy formation energy and entropy, migration, quenched-in resist. meas. 77−11540
- Al, wire, appl. of subgrain control 77−86060
- Al, with linear lattice defects, temp. depend. of magnetoresist. and Matthiessen's rule departure *(Russian)* 80−84456
- Al-3d transition metal, dil., transport props., sp. ht. and supercond. ant. temp. calcs. 77−1393
- Al-Ag, dil., deviation from Matthiessen's rule at high temps. 77−69294
- Al-Ag, discontinuous decomposition *(Polish)* 78−52808
- Al-Ag (1.03 at.%) alloy elec. resist. meas. above room temp., Ag atom configuration correlation 78−35534

electrical conductivity of crystalline metals and alloys continued

- Al-Ag (4 wt.%), scattering of conduction electrons, effect of size and internal struct. of GP zones *(Japanese)* 77−21149
- Al-Ag (up to 40 at.%), exam. of anelastic phenomena and structural state 78−76693
- Al-Ag(Cu)(Zn), electrical resist. of Guinier-Preston zones during age-hardening 77−72848
- Al-Ag(Ga)(Ge) dil. alloys, Hall coeff., residual resist., and relax. times 79−11107
- Al-Ag(Ge)(Mg)(Zn) alloy, dil., electron-irradiated, impurity-interstitial interaction 77−15449
- Al-Ag(Mg)(Zn)(Ga)(Ge), dil., deviations from Matthiessens's rule, 4-OPW approx. calc. 79−19574
- Al-C, dispersion hardened, effect of processing parameters on mech. props. 80−20826
- Al-Co alloy, dil., fast neutron radiation damage, interstitial trapping, Mossbauer spectra and elec. resist. meas. 77−27914
- Al-Cr, Al-Mn, Al-Cr-Mn, dil. alloys, Hall coeff. and elec. resist. 77−11898
- Al-Cr (0.1 wt.%), exam. of pre precip. behaviour, by elec. resistivity meas. and TEM exam. 78−48406
- Al-Cr(Mn), cold-worked and homogenised, precip. kinetics, impurity resist. and TEM meas. 77−16596
- Al-Cr(Ti), electron irradiated, interstitial trapping and detrapping at undersized impurity atoms 78−47424
- Al-Cu (2-5 wt.%), precipitation total surface influence on resistivity *(French)* 80−71650
- Al-Cu (4 wt.%), reversion charact. *(Japanese)* 77−21150
- Al-Cu (4 wt.%) alloy, reversion characts. *(Japanese)* 79−56989
- Al-Cu alloys, anisotropy function determ. 77−43565
- Al-Cu dil. alloys, elec. resist. temp. depend. 77−8068
- Al-Cu-Mg, dil. alloys, ageing response *(Korean)* 77−28832
- Al-Cu-Mg(:Fe,Si) alloys, double-ageing, resist., hardness meas. 77−28822
- Al-Cu-Mn-Mg-Fe-Si (4.48, 0.66, 1.55, 0.43, o.23 wt.%), alloy D16, relationship between intercrystallite corrosion depth, and elec. cond. 79−20220
- Al-Cu(Ag)(Ge), dil., deviation from Matthiessen's rule at high temps. 78−64025
- Al-Cu(Zn, Ag, Mg_2Si), intermediate precipitates, stability, X-ray, elec. resist. and hardness study 80−3063
- Al-Ga, dil., neutron irrad., 4.2K, defect prod., recovery 77−1155
- Al-Ga(Mg)(Zn), electrical resist. and magnetoresist., 2 to 40K, Matthiessen rule deviations *(Russian)* 77−31996
- Al-Ge (0.2 at.%), exam. of interstitial trapping by X-ray diffuse scatt. 78−47363
- Al-Ge alloy, effect of high press. on phase equilibrium *(Russian)* 79−1844
- Al-Li (10 at.%), struct. changes on annealing, 25-500°C, Li atoms role 80−35183
- Al-Li alloy, annealing of vacancies and ageing, resist. and TEM obs. 77−21172
- Al-Li alloy, dil., quenched and irrad., recovery, resist. and internal friction obs. 78−52848
- Al-Li alloys, precipitating, annealing spectrum 78−31429
- Al-Mg, dil., neutron irrad., 4.2K, defect prod., recovery 77−1155
- Al-Mg, dil. alloy, residual resistivity, model pseudopot. form factors 77−8062
- Al-Mg (5.7 wt.%) alloy, pre-precipitation, elec. resist. investig. 77−32601
- Al-Mg alloys, cold-worked, transport props., 1.5-8.5K 78−7059
- Al-Mg-Ag, age effect on age hardening *(Japanese)* 78−52831
- Al-Mg-Mn alloys with high Al content, resist., 1.5 to 4.2K 78−26841
- Al-Mg-Si, Guinier-Preston zones, inception and effect on ageing, review *(Hungarian)* 79−11627
- Al-Mn, splat cooling and heat treatment effect on struct. and props. *(Russian)* 77−48456
- Al-Mn (0.35 wt.%), quenched exam. of Mn-vacancy interaction 78−76676
- Al-Pr (16 wt.%), resist. depend. on temp. and hot rolling *(Polish)* 80−39555
- Al-Sc, elec. resist. determ. 80−92876
- Al-Sc, solid solubility and residual resist. 79−51265
- Al-Si, magnetic susceptibility and elect. resistivity, 500 to 1000°C, struct. sensitive props. *(Russian)* 78−15550
- Al-Si-Cu-Zr, ageing kinetics *(Russian)* 80−76274
- Al-Sn, dil. alloy, vacancy-impurity interaction, exam. by electrical resistivity meas. at 77K *(German)* 78−83846
- Al-transition metal, dil., residual resist. of 4d and 5d impurities 77−28155
- Al-transition metal alloy, residual resistivity, effect of 4d and 5d transition metal impurities 79−60791
- Al-W(Mo)(Nb), struct. and props. of alloys obtained from granules 80−50717
- Al-Y, specific elec. resist., variation with Y conc. 80−84455
- Al-Zn, dil. alloy, ageing and reversion, annealing curves, X-ray obs. 78−88485
- Al-Zn, discontinuous decomposition *(Polish)* 78−52808
- Al-Zn, formation of Guinier-Preston zones, and their limit temp. *(Japanese)* 78−84861
- Al-Zn, GP zones, effect of Si, Ag, Mg on transport props. 77−16588
- Al-Zn, interdiffusion meas. by elec. resist. 80−49433
- Al-Zn, metastable solvus curve, struct. changes 77−55950
- Al-Zn, precipitation struct. and phys. props. effect of miscibility gap *(German)* 78−92265
- Al-Zn, resistivity anomalies in Guinier Preston zones *(French)* 78−6937
- Al-Zn, resistivity calc. for age-hardened alloy 77−73284
- Al-Zn (0.041 to 4.4 at.%), clusters, electrical resistivity meas. *(Japanese)* 77−21168
- Al-Zn (10 wt.%), ageing at low temp., solute conc. fluctuation effects *(Japanese)* 79−4969
- Al-Zn (10 wt.%), ageing at low temp., effects of fluctuation of solute conc. 80−76287
- Al-Zn (10 wt.%), ageing at low temp., effects of fluctuation of solute conc. 80−76288
- Al-Zn (10 wt.%), solute conc. fluctuation effects on ageing at low temp. 79−57023
- Al-Zn (2 and 4 wt.%), ageing and elec. cond. reversion *(Japanese)* 79−4983
- Al-Zn (21.8 at.%), elec. conductivity and α'-precipitates, 276-302°C 77−80758

electrical conductivity of crystalline metals and alloys continued
Al-Zn (6.8 at.%) alloy, elec. resist. temp. depend. rel. to ageing processes 77—77486
Al-Zn (6.8 wt.%), effects of ageing temps. on microhardness and resistivity *(Japanese)* 78—35408
Al-Zn (8-25 wt.%), solid solns., residual resist. during clustering 80—97483
Al-Zn alloy, resist. and X-ray small angle scatt. during GP zone form., theory *(French)* 79—29070
Al-Zn alloys, anisotropy function determ. 77—43565
Al-Zn alloys, preprecipitation, elec. resist., microhardness meas., dislocation-growth distortion interactions *(Japanese)* 77—25053
Al-Zn alloys, spinodally decomposing, resistivity behaviour 80—45271
Al-Zn-Mg, Guinier-Preston zones, comp. and contrib. to elec. resist. 80—16316
Al-Zn-Mg, heat treatment and inversion processes, elec. resist. study *(Hungarian)* 77—25078
Al-Zn-Mg, solid soln. decomp., 20 to 200°C 79—38830
Al-Zn-Mg, zone composition change during ageing 79—29110
Al-Zn-Mg (4.5 at.%, 2 to 3 at.%), decomp. behaviour during continuous heating 80—29922
Al-Zn-Mg alloy, Ag addition and pre-precipitation treatment, influence on GP zone growth 80—71658
Al-Zn-Mg alloy, elec. resist. of η' precipitates 77—48441
Al-Zn-Mg alloys, decomposition kinetics, resistivity meas., extended jump model 78—84766
Al-Zn-Mg alloys, extra-resistivity of coherent precipitates 80—3050
(Al-Mg-Si)-Al_2O_3, SAP type, ageing 79—96055
Al_2O_3-NiCr composite, plasma sputtering of electroheating coatings, elec props. *(Russian)* 80—108350
$Al_{10}V$, well defined local modes, resistivity meas. 78—26648
$Al_{10}V$-Ga, dil., well defined local modes, resistivity meas. 78—26648
AlZn, disordered, residual resistivity due to clustering, ageing effects 80—65521
Am, elec. resist. and sp. ht. 78—47762
^{241}Am metal film, resist. meas., 3.6 to 300K 77—28263
^{241}Am, temp. depend., 3.6-300K 78—6345
AsF_5-graphite intercalation compound, lamellar, highly two dimensional synthetic metal, room temp. elec. cond. 78—6349
Au alloys, electrical resistivity, deviations from Matthiessen rule and scattering anisotropy 78—76051
Au, deformed, annealing kinetics of vacancies, elec. cond. meas. and computer simulation 78—47353
Au, deformed, annealing kinetics of vacancies *(Japanese)* 80—88139
Au, elec. resist., press. variation 78—84193
Au, elec. resist. and vol. change due to lattice vacancy 79—51101
Au, elec. resist. exam. 79—38042
Au, electrical resistivity deviations from Matthiessen's rule due to dislocations 79—65425
Au, electron irradiated, interstitials and their clusters, diffuse X-ray scatt. study 80—33997
Au, electron-phonon interaction determ. from current-voltage curve at 1.5K *(Russian)* 77—47789
Au, ideal resist., 5.2-40K, deviation from Matthiessen's rule 79—99526
Au, lattice vibrations and ideal elec. resistivity 79—46770
Au, low temp. resist. and thermoelec. ratio, electron-electron scatt. contrib. 80—70670
Au, magnetoresist of quenched and annealed metal, defect scatt. 79—4981
Au, phonon limited elec. resist., temp. depend. 80—24876
Au, phonon-limited elec. and thermal resistivity 79—42517
Au polycrystalline wire, internal oxidation of impurities, rel. to resist. and magnetoresist. 78—83842
Au, proton irrad. at 0.3K, resistivity annealing 77—76475
Au quenched single crysts., vacancies, diffuse scatt. and resist. obs. 80—33994
Au, residual resistivity of ^{57}Co 78—71881
Au, resistivity and thermoelectric ratio at low temp., 0.04 to 7K 79—73497
Au, virtual bound states due to 4d- and 5d-transition metal impurities 80—70667
Au-^{171}Yb, dil., nuclear induced resistivity drop 78—10431
Au-^{174}Yb, dil., nuclear induced resistivity drop 78—10431
Au-Cd (47.5 at.%), effect of cooling rates on stress-strain behaviour 78—76721
Au-Cr, dil., elec. resist., generalised phase shift anal. of Kondo effect 80—75556
Au-Cr, dil., spin glass, elec. resist., press. and conc. effects 78—52278
Au-Cr, dil. alloys., elec. resist., deviations fro Matthiessen's rule 80—75541
Au-Cr(Mn), spin glass alloy, elec. resist. 77—8067
Au-Cu, dil., electron irradiated, interstitials and their clusters, diffuse X-ray scatt. study 80—33997
Au-Cu, residual elec. resist., pseudopot. calc. 80—6813
Au-Cu alloy, internal oxidation, calorimetric meas. 79—43258
Au-Fe(Co)(Mn), residual resistivity conc. depend. 80—2382
Au-Fe(Mn) dil. spin glass alloy, impurity-impurity interaction press. depend., resistivity meas. 77—20308
Au-Ga, resist. and supercond. meas., electron-phonon interaction and Coulomb pseudopot. determ. 78—43358
Au-Ge, liquid quenched, exam. of phase decomposition 78—48371
Au-Mg alloy, internal oxidation, calorimetric meas. 79—43258
Au-Mn-Cr(Pd) alloy, ferro- to non-mag. transform. 77—12117
Au-Pd (1(50) wt.%), quenched, vacancy annihilation and short-range order formation, elec. resist. 80—108487
Au-Pd-Pt-Ag, composition-property diagrams, mathematical models for diagrams *(Russian)* 79—11554
Au-Pd(Pt), elect. resistivity, temp. depend. between 1.6 and 4.2K *(German)* 79—28337
Au-Rh(Y)(Zr)(Nb)(Pd), dil., Friedel d-reson. scatt. and elec. resists. 80—44566
Au-Sn(Bi)(Ga)(Ni), elec. resist. in liquid and solid state *(Russian)* 79—51549
Au-transition metal alloy, residual resistivity, effect of 4d and 5d transition metal impurities 79—60791
Au_xAg_{1-x}, density of states and resist., CPA calc. 80—24780
Au(Pd)-Zn, martensitic transformation, Hall coeff., specific elec. resistivity and X-ray powder diffraction 78—72774
$Au_{50-x}Pd_xZn_{50}$, $(0\leq x\leq 15.02)$ β'-phase, Hall effect and elec. cond. 80—107768
$Au_{1-x}Sn_x$ liq./solid alloy, resist. and percolation 80—6804

electrical conductivity of crystalline metals and alloys continued
Au_4V, effect of structural changes on phys. props. 78—31400
Au_4V single crystal, ordered, mag, props., domain models 80—39770
$Au_{100-x}Zn_x$, $(47\leq x\leq 52)$, β'-phase, Hall effect and elec. cond. 80—107768
Ba, high-purity solid and liq. phases, elec. resist. and thermopower meas. 77—47799
Ba, transport properties, elec. resist., thermoelec. power, thermal cond. deviations from Matthiessen's rule 78—39086
$BaVS_3$, quasi-one-dimensional ferromag. or antiferromag., metallic cond. and mag. meas. 78—52233
Be, BCC, high-temp. resist. and band struct. 79—51551
Be, impure, resistance, anomalous temp. depend. *(Russian)* 79—51552
Be, longitudinal dielec. function calc. 77—1358
Be, resistivity minimum temp. depend., 4.2 to 40K *(Russian)* 79—87077
Be, sintered, physicomech. props. anisotropy, BeO inclusions effect 80—60804
Be, temp. depend. minimum in resist. *(Russian)* 77—35919
Be, wire, elec. cond., heat treatment and strain effects *(Russian)* 80—24870
Be wires and strips, elec. resist. at 77K, size factor *(Russian)* 80—24867
Bi whiskers, persistent metallic behaviour, elec. resist. meas. 80—75544
Bi wire, elastically bent, elec. resist. in mag. field 80—44568
Bi wire, field effect and magnetoresist., surface scatt. 77—43570
Bi-Sb (6 at.%) whiskers, persistent metallic behaviour, elec. resist. meas. 80—75544
Bi-Sn, thermoelec. props. from 2 to 300K 80—24872
Bi-Te, dil. alloy, elec. cond. depend. on Te conc. *(Russian)* 78—76042
CC Al-Mg-Si, precipitation of cube-shaped phases, electron diffr. study using TEM *(Japanese)* 79—43251
CU-Zr-(Cr), powder metallurgical alloys, thermomech. treatment effect on props. 80—50660
Ca, electrical resistivity and thermoelectric power 78—26846
Ca, transport properties, elec. resist., thermoelec. power, thermal cond. deviations from Matthiessen's rule 78—39086
CaSb, resist., susceptibility and thermopower rel. to electronic struct. 78—67935
Cd, electrical resist. and anisotropy at press. up to 80 kbar 77—43554
Cd, electron-electron scatt., RF size effect meas. 79—60821
Cd foil, monocrystalline, anisotropy of size effect 79—38048
Cd, Hall effect and elec. resist., temp. depend. 78—64030
Cd, Hall resistivity, importance of intersheet scattering 77—76794
Cd, recovery after 6.1 MeV α-particle irradiation at 4.2K 78—47441
Cd, resistivity, existence of Einstein type phonon mode 79—42519
Cd, single cryst., electrical resistivity and deviations from Matthiessen's rule 79—23943
Cd, stage III recovery, after α-particle irradiation 77—27924
Cd-Ag, polycryst. quenched foil, the influence of Ag on the recovery spectrum 78—76661
Cd-Ag, polycryst. wire, cold worked, resistivity changes 78—68827
Cd-Mg, dil. alloy, single cryst., electrical resistivity and deviations from Matthiessen's rule 79—23943
Cd-Mg alloy, dil., elec. resist., phonon local mode effect 78—6347
Cd-Sb, near CdSb, Hall coeff., resistivity 79—56216
Cd-Sb diffusion couple, layer growth of CdSb phase at high press., elec. meas. 80—2218
Cd-Zn, polycryst. wire, cold worked, resistivity changes 78—68827
(Ce, La)In_3, heat capacity and elec. resist. 80—71049
β-Ce, 2-300K, quenched Kondo scatt. 77—4320
Ce and Ce-Nd, reversible mech. memory effect, α to γ transition *(Russian)* 78—15396
Ce compounds, Anderson model, exchange parameter, Kondo temp., mag. susceptibility 79—1656
Ce, electrical resist. behaviour at press. induced α'-tetragonal phase transform. 77—35916
α-Ce, exchange-enhanced, elec. resist. T^2 depend., press. effect 80—96845
Ce, high temperature transport props., scatt. mechanisms, phase transitions 77—15825
γ-Ce, Kondo-like anomaly 80—96857
Ce, phase boundary between α' and tetragonal polymorphs, resistance anomaly meas. 79—60500
Ce, sp. ht. and temp. coeff. of resist., 20 kbar at 300K 78—83973
Ce, TCR up to 15 kbar *(French)* 79—95383
Ce-alloys, dil., elec. resist. in presence of external mag. field 78—19022
Ce-Co-Si, thermoelectromotive force and electrocond. *(Ukrainian)* 80—54670
Ce-Fe-Si, thermoelectromotive force and electrocond. *(Ukrainian)* 80—54670
Ce-La, mag. ordering, sp. ht., susceptibility and resist. 78—68238
Ce-La alloys, DHCP, low temp. mag. and elec. props. 77—62911
Ce-Ni-Si, thermoelectromotive force and electrocond. *(Ukrainian)* 80—54670
Ce-Pr powder, DHCP⇄FCC transition, X-ray, DTA and resistivity studies 80—50629
CeAg, mag. and structural phase transition at hydrostatic press., elec. resist. meas. 79—61102
$CeAl_2$, electronic transition under pressure, resist. meas. 79—33311
$CeAl_2$, press.-induced electronic transition 80—20147
$CeAl_2$, resistivity and volumetric meas., phase diagrams, comparison with CeS 80—107789
$CeAl_3$, effect of disorder on cond. transition into ground state 77—89755
$CeBe_{13}$, intermediate valence state, XPS, resist. and susceptibility study 80—71565
$CeCu_2Si_2$, resistivity, thermal conductivity and thermopower between 1.5 and 300K 78—87963
$CeCu_2Si_2$, transport anomalies 80—20148
Ce(In, Sn)$_3$, heat capacity and elec. resist. 80—71049
$CeIn_{3-y}Sn_y$, electrical resist. and thermal expansion meas., 1.5-300K 80—34400
$Ce_{1-x}La_x$, dil., $\gamma-\alpha$ transition temp. and press., elec. resist. meas. up to 10 kbar 80—59643
$Ce_{1-x}La_x$, electrical resist. T^2-depend. under high press. 80—29383
CeP(As), single crystals, low temp. thermal, electrical and mag. props. meas. 78—27051
$CePd_{3-x}Rh_x$, resistance behaviour and intermediate valence effects 79—78068
$CeTl_3$, mag. susceptibility, magnetisation, neutron diffr., elec. resist., and sp. ht. meas. 80—75733
^{244}Cm, electrical resistivity and mag. ordering 77—80760

electrical conductivity of crystalline metals and alloys continued
Co based alloys, resistivity magnetoresistance, s,p impurities in ferromag. host 78–68008
Co, Co alloys, electrical resistivity and specific heat meas., anomalies rel. to thermally excited states 80–6809
Co, electrical resist. temp. depend. near Curie point *(Russian)* 77–31989
Co, electrical resistivity, effect of domain wall orientation at 4K 78–91662
Co, impure, thermal cond., resistivity, total and spectral emissivity, linear expansion coeff., 300-1700K 77–47790
Co, low temp. electron irrad., elec. resist. recovery 77–35588
Co powder, isostatic compression, elec. cond., densification models *(French)* 80–55321
Co-C, ferromag., prep. by splat-quenching, obs. of electronic struct. of interstitial C 77–62868
Co-Cr-C eutectic alloy, thermal conductivity and electric resist. at high temp. 80–103668
Co-Cu, electrodeposited alloy, struct. and physicochem. props. 78–35327
Co-Cu(Ti)(Fe), neutron radiation stimulated diffusion, electrical resistivity exam. *(Russian)* 79–14959
Co-Fe, morphology and certain props. of α-and η-phase martensite *(Russian)* 77–1838
Co-Ga alloys, transition metal partially substituted, elec. resist. anomalies 79–38044
Co-Ga liquid and solid alloys, elec. resistivity at high temps., partial struct. factors 80–6806
Co-Mn alloys, Nernst-Ettinghausen effect and electrical resistivity *(Russian)* 78–14714
Co-Pd, transfer phenomena and association with electronic struct. *(Russian)* 79–91017
Co-Pd alloys, 0-70 at.% Pd, conc. depend. of anomalous Hall field and resistivity *(Russian)* 78–14713
Co-powder, isostatic compaction, mech. and elec. props. *(French)* 80–40285
Co-Ti (9 at.%), decomp. kinetics, elec. resist., hardness, and saturation magnetisation during ageing *(Russian)* 80–50587
Co-V (10 to 23 wt.%) system, phase constitution, X-ray and elec. resist. meas. 80–3007
$CoCl_2$ purification by H_2 reduction, of Co, exam. of conductivity *(Russian)* 79–28981
$CoCl_2$-NaCl purification by H_2 reduction, of Co, exam. of conductivity *(Russian)* 79–28981
$(Co_{1-x}Fe_x)_2Y$, substitutional Fe atoms effect on mag. and elec. props., paramagnon scatt. 77–36054
β-$Co_{52}Ga_{48}$, negative TCR obs. 80–75543
Co_xGa_{100-x}, electrical resistivity anomaly, spin cluster model 79–99531
$Co_2Ga_{2-x}Fe_x$, elec. resist., temp. and mag. field depend., mag. contrib. 80–96846
Co_5Ge_3, solid and liquid, physicochemical props. and structure 80–39548
$Co_{1/3}NbS_2$, intercalate, metallic cond., Hall effect and mag. props. 77–76789
$Co_x(Ni_{0.5}Cu_{0.5})_{1-x}Fe_2O_4$ ferrite, relation between elec. cond. and mag. anisotropy 80–75548
$Co(S_xSe_{1-x})_2$, galvanomag. effects, obs. and interpretation 80–70726
$CoSnTe_2$, thin films, metallic elec. props. 79–78212
$Co_2Ti(Y)(Zr)(Nb)$, Laves phase, elec. resist. rel. to mag. props. 77–59282
Cr, antiferromag., elec. resist. near Neel temp. 79–33278
Cr, critical coeff. of resistivity near Neel temp. 77–59417
Cr, high purity, 280-1000K 77–39816
Cr, neutron irradiated at 24.5K, elec. resist. exam. of radiation damage *(French)* 78–30671
Cr, volt ampere characteristics during electron melting process *(Russian)* 80–75336
Cr-Al, antiferromag., transport props., anomalous crit. behaviour 79–61108
Cr-Al, disordered alloy, effect of high press. on resistivity 78–95286
Cr-Co, dil., antiferromag., elec. resist. min., press. and impurity effects 80–59970
Cr-Co (4.0 at.%) alloy, antiferromag., disappearance of resist. min. under press., and press. coeff. of T_N 80–10960
Cr-Co (up to 8 at.%), antiferromagnetic, resist. minimum, Kondo effect by pairs of Co atoms 80–39566
Cr-Co-V alloys, dil., elec. resist. min. 80–54680
Cr-Fe, dil., antiferromag., elec. resist. min., press. and impurity effects 80–59970
Cr-Fe alloys, antiferromag., elec. resistivity, Kondo effect 79–60812
Cr-Fe-V, dil., V effect on para- to incommensurate and commensurate transitions 78–68260
Cr-Fe-V, effects of V on mag. transition, elec. and mag. props. 77–69554
Cr-Ga alloys, dil., Neel temp., elec. resist. and thermal expansion meas. 79–51778
Cr-Mn alloys, antiferromag. and weak ferromag., elec. props. 79–56514
Cr-Mn alloys, elec. resist. near T_N 77–69313
Cr-Mo, elec. resist. and thermo-EMF, conc. depend., 4.2 to 1500K *(Russian)* 80–80247
Cr-Mo, electrical resistivity, spin density wave gap, Neel temp. 80–88534
Cr-Ni, high temp. strength, interatomic bonds ionic component correlation *(Russian)* 79–15761
Cr-Os, magnetic transition T-P-C diagram, triple points *(Russian)* 80–54895
Cr-Re(Ru)(Os)(Ta)(V)(Nb), Invar alloys, thermal expansion, plasticity, elec. resist. and mag. suscept. *(Russian)* 79–55907
Cr-Sb alloy, dil., mag. phase diagram, elec. resist. and thermal expansion obs. 79–1669
Cr-Si (1.37 at.%), thermal and elec. props. 79–78071
Cr-Si-V, (2, 0.1 at.%), paramag. to commensurate spin density wave transition 80–65875
Cr-Si-V, dil., V effect on para- to incommensurate and commensurate transitions 78–68260
Cr-V-Fe alloy, resistivity minimum, press. effect 79–38043
$Cr_{99.94}Al_{00.6}$, thermal and elec. transport coeffs. near Neel temp. 79–78075
CrAs, high press. paramag. antiferromag. transitions, elec. props., band model development *(Russian)* 80–60277
$Cr_{0.5}NbSe_2$, cryst. struct., metallic cond., mag. and phys. props. *(French)* 80–33956

electrical conductivity of crystalline metals and alloys continued
CrO_2 and tetravalent Cr oxide derivatives, metallic, chem. and phys. props. review 78–31069
Cr_5Te_6, magnetoresist. in region of mag. phase transforms. *(Russian)* 77–66299
Cs, elec. and thermal resist. calc. using modified noncentral force model 79–91016
Cs, metal impurity effect on residual elec. resistance *(Russian)* 80–84457
Cs, supercond., elec. resist. and phase transforms. under high press. *(German)* 80–107763
Cs-Ag, dil., electronic struct., density functional approach, appl. to elec. and mag. props. 80–44492
Cu, 400 GeV proton irrad., resist. meas., supercond. magnet stabilising material 77–37948
Cu alloys, dil., transport props. 78–76046
Cu alloys, microconductors, cast, struct. and physical props. exam 78–44232
Cu alloys, reduction processes in sintering *(German)* 80–25597
Cu alloys, thermopower and resistivity, Nordheim-Gorter relation 79–65438
Cu based 3d-transition metal dil. alloys, residual resist., Dingle temp. 77–1409
Cu, cascade energy density effect on isochronal recovery 78–47431
Cu, compressed powder, elec. cond. −30 to +30°C *(German)* 79–28335
Cu, compressed spherical powder *(German)* 78–6343
Cu conductors used in coaxial cables, resistivity measurements *(French)* 79–69487
Cu, damage production by high energy d-Be neutrons, elec. resist. meas. 77–62564
Cu, deformed by hydrostatic extrusion, drawing or drawing under press., dislocation struct. obs. *(Russian)* 77–21213
Cu, deuteron bombarded, annealing elec. resist. changes freq. factors, activation energy distrib. 79–77648
Cu, effect of cyclic strains and work hardening at 4.2K 78–91655
Cu, elec. cond. exam. in solid and liquid phase *(Russian)* 77–62895
Cu, elec. resist., electron-electron scatt., Fermi surface calc. 78–64023
Cu, elec. resist., press. variation 78–84193
Cu, elec. resist. under torsional deform., impurities and tensile strain 78–30898
Cu, electrical cond., effects of impurities 78–43355
Cu, electrical resistance of edge dislocations *(German)* 80–96859
Cu, electrical resistivity, at low temp., temp. depend. 78–23071
Cu, electrical resistivity, linear strain effect at elevated temps. 79–91022
Cu, electrical resistivity changes at high temp. due to vacancies 78–26565
Cu, electron-phonon interaction, scatt. and transport props. 79–91037
Cu, electronic transport properties, OPW calcs. 77–43553
Cu films, ion plated on polyethersulphone, structural and resistivity study 79–42411
Cu, high purity crystal, resistivity changes with deform., subsequent recovery 77–52397
Cu, high-cond., high spt. ht., for cryogenic appl., prep. 78–76670
Cu, high-conductivity, treatment technique for low temp. applics. 78–27650
Cu, lattice vibrations and ideal elec. resistivity 79–46770
Cu, low temp. resist. and thermoelec. ratio, electron-electron scatt. contrib. 80–70670
Cu, microalloyed with B, elec. cond. and strength props. *(Polish)* 80–89285
Cu PM parts, improving cond. by pretreatment of green compact 80–20824
Cu, phonon limited elec. resist., temp. depend. 80–24876
Cu, phonon-limited elec. and thermal resistivity 79–42517
Cu, polycryst., low temp., plastic deform., structural defects, elec. resist. meas. *(Russian)* 78–39844
Cu, proton irradition, 10 to 16 MeV, resistivity changes 80–2082
Cu, resistance thermometer, heat shock influence on elec. cond. and thermophysical props. *(Russian)* 80–52210
Cu, resistivity and thermoelectric ratio at low temp., 0.04 to 7K 79–73497
Cu screw-fastened joints, low temp. thermal cond. and elec. resistance 79–95469
Cu, self-interstitial interaction with solutes, resistivity meas. 78–47331
Cu single crystal, weakly deformed, elec. resist. recovery, annealing effect 77–81304
Cu, sintered, in contact with ^{3}He, thermal conductance, rel. to elec. resist., heat flow model calc. 80–10728
Cu, Sondheimer oscills. in elec. resist. and Hall effect meas. 77–11896
Cu, thermal neutron irradiated, isochronal resist. recovery, 30-400K 79–19287
Cu wire, corrosion in $AgNO_3$ soln., elec. resist. variation, rel. to Gruneisen parameter 78–11404
Cu wire, electroplastic drawing X-ray diffr. anal. and mech. props. exam. *(Russian)* 79–29138
Cu wire, negative longitudinal magnetoresist. size effect 80–80252
Cu wire, residual elec. resist., size effect and grain boundary contribs., heat treatment effects *(Russian)* 78–56126
Cu, wire, residual resistivity reduction by internal oxidation 79–87747
Cu-Ag-P amorphous alloys, strain gauge factor and elec. props. *(Japanese)* 79–79130
α-Cu-Al, binary substitutional, short-range ordering kinetics, vacancy behaviour 78–55867
Cu-Al, internally oxidised, structural, elec. and mech. characts. 78–60761
α-Cu-Al, kinetic behaviour of vacancies and atoms 79–28129
Cu-Al, short range order and static distortion contribution to residual elec. resistivity *(Russian)* 80–70672
Cu-Al, sintering, reduction processes, resist. meas. *(German)* 80–25597
α-Cu-Al, solid soln., residual elec. resist. *(Russian)* 79–51547
Cu-Al (12 wt.%), acoustic emission related to props. 79–34032
Cu-Al (15 at.%), vacancy migration, and short range ordering, comparison of exp. results with theory 78–47356
Cu-Al (15 wt.%), residual resistivity, influence of short range order and size effect *(Ukrainian)* 79–99528
Cu-Al alloy, vacancy formation energy, determ., using new method, elect. cond. meas. 78–47345
Cu-Al alloys, internally oxidised, elec. resist. meas. 77–35753
Cu-Al films, elec. cond. of vacuum condensates depend. on composition, annealing *(Russian)* 80–65709

electrical conductivity of crystalline metals and alloys continued

- Cu-Al powder compacts, elec. resist., temp. depend. 80−49690
- Cu-Al-Fe-Mn (10,3,2 wt.%), phase comp. struct., continuous cooling from β-phase effect 79−24499
- Cu-Al-Ni, positron annihilation study of vacancies before and after martensitic transform. 79−99971
- α-Cu-Al(Fe) dil. alloys, Al ion charge screening, elec. resist. obs. 77−4500
- Cu-Au, dil., O_2 solubility, thermodynamic and residual resist. study 78−59952
- Cu-Au, dil., thermal neutron irradiated, isochronal resist. recovery, 30-400K 79−19287
- Cu-Au, dose depend. of recovery after thermal neutron irrad. 77−69011
- Cu-Au, pseudopot. calc., size effect and short range order *(Russian)* 78−2460
- Cu-Au, vacancies and divacancies, quenching effects and elec. resist. meas. 80−39072
- Cu-Au alloys, vacancy and divacancy migration activation energies, elec. cond. meas. 80−88140
- Cu-Au(Ga)(Ge)(Zn) alloys, dil., Matthiessen's rule deviations above room temp. 79−91023
- Cu-Be, electrical resist. of Guinier-Preston zones during age-hardening 77−72848
- Cu-BeCo (1.85, 0.29 wt.%), type CA172 (TH04), strengthened by spinodal decomp., stress relax. in bending 80−7616
- Cu-Ce(Y)(In), effect of alloying additions on electrical cond., and mech. strength 78−44233
- Cu-Co(Cr)(Ni)(Ti), (1-1.3 at.%), elec. cond. exam. in solid and liquid phase *(Russian)* 77−62895
- Cu-Cr, dil., spin glass, elec. resist., press. and conc. effects 78−52278
- Cu-Cr, dil. alloy, Kondo resist. at 35 GHz 79−60814
- Cu-Cr, vapour deposited, electron irrad., resistance behaviour *(German)* 78−47779
- Cu-Cr dilute alloys, elec. cond. meas., 1.5 to 30K 77−62914
- Cu-Cr dilute alloys, thermal and elec. cond. deviations from Wiedemann-Franz law 77−66151
- Cu-Fe, composite, fibre and layer structs., anomalous props. caused by internal phase boundaries 78−72754
- Cu-Fe, dil., internally oxidised mag. and electrical prop. 77−12100
- Cu-Fe, highly dil., mag. impurity scatt., and deviations from Matthiessen's rule 78−43371
- Cu-Fe, precipitation processes during aging, TEM, resistivity, hardness study *(Japanese)* 80−35221
- Cu-Fe, vapour deposited, electron irrad., resistance behaviour *(German)* 78−47779
- Cu-Fe system, ageing and reversion phenomena study 80−89274
- Cu-Ga (17 wt.%), elec. resist. and TEM studies 80−108604
- Cu-Ge(Sb) alloy systems, atomic struct. and electronic props. *(Russian)* 77−20289
- Cu-Mn, dil. alloys, conc. depend. of resist. maximum 77−62893
- Cu-Mn, spin glass alloy, elec. resist. 77−8067
- Cu-Mn alloy, manganin, hysteresis-corrected calibration under shock loading 80−74818
- Cu-Mn dil. spin glass alloy, impurity-impurity interaction press. depend., resistivity meas. 77−20308
- Cu-Mn-Ni alloy, Manganin, elec. resist. under static pressures up to 110 kbar, pressure gauge appl. 79−1594
- Cu-Nb multifilamentary composite, in situ formed, high temp. tensile strength 79−61602
- Cu-Nb multifilamentary composite, dislocation resistivity 80−70671
- Cu-Ni, bimetallic film, exam. of diffusion by electrical resistivity meas. *(Russian)* 79−14970
- Cu-Ni, cyclically deformed, electrical resistance changes 79−57096
- Cu-Ni, neutron irradiation, enhanced diffusion, elec. resist. meas. 80−6440
- Cu-Ni, neutron radiation stimulated diffusion, electrical resistivity exam. *(Russian)* 79−14959
- Cu-Ni (30-90 wt.%), elect. resist. rel. to cold working and heat treatment 80−71765
- Cu-Ni dil. paramagnetic alloys, sp. elec. resist., effect of Ni clusters *(German)* 78−95293
- Cu-Ni films, thickness depend. of Curie temp., resist. meas. 78−6545
- Cu-Ni-Fe, quenched and aged, deformed, low-temp. elec. resist. meas. *(Russian)* 77−52514
- Cu-Ni-P, precipitation hardening 77−12633
- Cu-Ni-Sn (4-15, 4-8 wt.%), strip strengthened by spinodal decomp., stress relax. in bending 80−7616
- Cu-Ni-Sn spinodal substitute for Be-Cu alloy 80−35217
- Cu-O, effect of Se, S, Pb impurities on annealability and resistivity 77−28834
- Cu-P wire, phosphor bronze, magnetoresist. upper limit 77−43567
- Cu-Pd alloy, pressure effect on β-phase transition by elec. resist. meas. 79−15660
- Cu-Sc alloy, dil., impurity effects on annealing and resist., vacancy-Sc interaction 79−51142
- Cu-Si-Zn wire, silicon bronze, magnetoresist. upper limit 77−43567
- Cu-Sn(5 wt.%), electrical resistivity, annealing, cold rolling 77−8070
- Cu-$ThO_2(ZrO_2)$ alloys, dispersion hardened, electrical cond. and mech. props. 78−44133
- Cu-Ti (5 wt.%), effect of cold work on ageing behaviour, study by elec. resist. and hardness meas. *(Japanese)* 79−78991
- Cu-Tl-S, phases, semiconductor and metallic behaviour *(French)* 79−96011
- Cu-transition metal alloy, residual resistivity, effect of 4d and 5d transition metal impurities 79−60791
- β-Cu-Zn, change in resist. with degree of order *(Japanese)* 78−34817
- α-CuAl, kinetic study of short-range ordering 78−23726
- CuAu, electrical resistivity meas. to detect phase changes 77−48425
- Cu_3Au, elec. resistivity, temp. depend. 79−47078
- Cu_3Au, electrical resistivity and LRO, energy gap formation in Fermi surface 80−88533
- Cu_5CdSb, electrophys. props. 78−27491
- $Cu_{1-x}Cr_2Se_4$, influence of excess Cu on physical props. 80−103836
- $CuGaSe_2$, single cryst. growth from melt, doping 77−12522
- CuMn, acceleration of coarsening by temp. changes, study by resistivity meas. 79−47718
- $Cu_{75}Mn_{25}$, concentrated spin glass, elec. resist., depend. on hydrostatic press. 79−69685
- Cu_2MnAl Heusler alloy, elec. resistivity 79−91020
- $Cu_{2.0}Mn_{0.94}In_{1.0}$, In-Heusler single crystal, elec. resist. 78−60107

electrical conductivity of crystalline metals and alloys continued

- $Cu_2MnIn_{1-x}Sn_x$ alloy, compositional SRO, hyperfine interactions 80−71065
- $Cu_2Mo_6S_8$, normal state and superconducting property measurements 78−91660
- Cu_xNi_{1-x}, low-temp. elec. resist. meas. *(Russian)* 77−52514
- Cu_2NiSn, Heusler alloy, elec. resist., 4.2 to 300K 80−75547
- α-CuNiZn alloys, Zener-relaxation effect 80−3121
- Cu_3P, single crystal, prep. and props. 80−40250
- CuPb, coexistence of ordered and disordered phases, elec. resist. meas. 77−85992
- CuPt alloy, equiatomic, ordering processes, anisothermal annealing exam. *(Japanese)* 78−39765
- CuPt equiatomic alloy, effects of quenching temp. on ordering, study by elec. resistivity meas. *(Japanese)* 79−43285
- $Cu(Rh_{1-x}Cr_x)S_4$, spinel system, susceptibility and metallic resistivity, anomalies due to s-d interaction 80−70958
- $Cu(SCN)_{1/3}$, synthesis and high elec. cond., activated and metallic cond. obs. 80−96957
- Cu_2TlX_2 (X=Se, Te), struct. and physical props., metallic conduction *(French)* 79−86758
- Dy, critical exponents and amplitude ratios from elec. cond. data, theoretical model 80−50126
- Dy, elec. resist. and mag. struct. near Neel point *(Russian)* 79−47074
- Dy, resistivity anomalies at mag. transitions, sp.ht. 80−39785
- Dy-Sm alloys, elec. resist. singularities and mag. transitions *(Russian)* 79−47075
- $DyAg_{1-x}In_x$, elec. and Hall resist. 80−96844
- DySb, quadrupole scatt. anisotropy, magnetically ordered material 78−64034
- electrical resistivity, relax. time near order-disorder transition 78−87788
- Er, Hall const. and elec. resist., 80-700K *(Russian)* 78−60110
- $ErFe_2$-YFe_2, and $ErFe_2$-$LuFe_2$, mag. props., 80-1300K *(Russian)* 80−75750
- $Er_xLa_{1-x}Cu$, and $Er_xY_{1-x}Cu$, antiferromag., mag. and resist. behaviour 80−34412
- $ErRh_4B_4$, magnetisation and elec. resist. at low temp. 79−56374
- $ErRh_{1.1}Sn_{3.6}$, synthesis, supercond. and mag. props. 80−100547
- ErSb, metallic, cryst. field effects on transport props. 78−72133
- Eu, electrical resistivity of solid and liquid phases, thermopower, melting temp. 80−59955
- Eu, high temperature transport props., scatt. mechanisms, phase transitions 77−15825
- Eu, resistance anomaly below Neel temp. 77−11889
- $EuB_{6-x}C_x$, mag. and transport props., metallic cond. 80−54689
- $EuGd_2S_4$, nonstoichiometric, elec. transport props., semicond. and metallic cond. 80−107786
- $Eu_{1-x}Sm_xS$, ESR, exchange interaction, susceptibility, elec. cond., thermoelectric power 80−93174
- Fe alloys, dilute, residual resist. in two-current model, impurity mag. moments 77−15818
- Fe, appl. of KUR LINAC to radiation damage studies 78−71760
- Fe based alloys, resistivity magnetoresistance, s,p impurities in ferromag. host 78−68008
- α-Fe, defect creation anisotropy in electron irradiated samples 77−31994
- Fe, effect of irrad. by fast neutrons and ^{235}U fission products at 20K *(French)* 79−51159
- Fe, elastoresistivity effect, meas. of resistance at 4.2K and 300K, using mag. field method 78−72132
- Fe, elec. resist. between 2 and 30K, deviations from Matthiessen's rule 80−10944
- Fe, electron irrad. damage, 20K *(French)* 78−2160
- Fe foil, electrodeposited, phys. and mag. props. 79−91275
- α-Fe, high purity, neutron and electron-irrad., interstitial migration at 200K 79−55920
- Fe, high-purity, H_2 charged resistivity recovery at low temps. 78−26729
- Fe, highly pure, temp. depend. 1.6 to 298K 78−84194
- Fe, isochronous annealing recovery, in cold rolled and explosively formed samples 79−100166
- Fe, oxidised powder, soft mag. props. oxide film-Fe composite material, magnetically soft, preparation, elec., mag. props. 77−8778
- Fe, porous, density, elec. cond., Young's modulus, toughness 78−64645
- Fe, powder, consolidated, exam. of mech. and electrical props. 78−56599
- Fe Powder, resist.-sintability *(Japanese)* 80−16228
- Fe, powder compaction, elect. cond. changes 79−66175
- Fe, proton irradition, 10 to 16 MeV, resistivity changes 80−2082
- Fe, purification, recrystn. temp. and elec. resistivity *(Japanese)* 80−100780
- Fe, quenched-in hydrogen, yield stress decrease of prestrained specimens 80−16454
- Fe, resistivity anomalies at mag. transitions, sp.ht. 80−39785
- Fe, single component, powder, compressibility and elec. resistivity in cold pressing under low press. 77−77444
- Fe, thermal cond., elec. resist., Lorenz number and magnetisation, crit. behaviour 77−4521
- Fe, vacancy recovery stage, radiation doping, elec. resistivity meas. 79−51102
- Fe, zone melted, H_2 diffusion, reversible lattice dilation 77−11732
- Fe-Al, deformed, low temp. recovery of elec. resist. *(Russian)* 80−7697
- Fe-Al, residual elec. resist., contrib. from static lattice distortions and short-range parameters *(Russian)* 79−51548
- Fe-Al (15 at.%), short range order form. kinetics *(Russian)* 78−3146
- Fe-Al (38.5-47 at.%), type B_2 ordered alloys, elec. resist. recovery stages after neutron irrad. *(French)* 77−69010
- Fe-Al (40 at.%), ordered, plastically deformed, neutron irrad. damage and recovery, resist. meas. 77−19993
- Fe-Al (40 at.%) and Fe-Al (50.5 at.%) ordered alloys, 20K neutron irrad. effects, stoichiometry depend., resist. obs. *(French)* 80−84215
- Fe-Al (40 at.%) B_2 type ordered alloy, C migration, resistivity meas. *(French)* 78−52868
- Fe-Al (40 wt.%), defect elimination by laser irradiation *(French)* 79−65960
- Fe-Al (50.5 at.%), ordered, neutron irrad. enhanced defect diffusion, resist. meas. 77−11598
- Fe-Al alloy, B_2-type, electrical resist. meas. 78−30917
- Fe-Al alloy, γ-ray effect on resistivity and configuration struct. *(Russian)* 78−43049
- Fe-alloy, FCC, Invar, thermally excited electron transitions 79−56559
- Fe-based alloy, effect of sp-3d impurity interactions in resistivity 79−46696

electrical conductivity of crystalline metals and alloys continued
- Fe-based alloys, volume interactions between substitutional sp and 3d solutes 79−78069
- Fe-C, ferromag., prep. by splat-quenching, obs. of electronic struct. of interstitial C 77−62868
- Fe-C (0.52 wt.%), FCC structure, exam. of electromigration of C by steady state method 78−75865
- Fe-C-Cr-Mn-Si-Ni (4.6, 38.7, 1.1, 2.0, 1.58 wt.%) alloy US-25, powder, compressibility and elec. resistivity in cold pressing under low press. 77−77444
- Fe-Co, partially ordered, elec. cond. 78−91663
- Fe-Co alloy, annealing of point defects produced by cold working *(French)* 78−72829
- Fe-Co-Mo-Nb(Ta) semihard mag. alloy, mag. props., thermal expansion, elec. resistivity and hardness *(Japanese)* 80−88789
- Fe-Co-Si-B sputtered amorphous thin film, coercivity, galvanomagnetic props., resistivity 80−29578
- Fe-Co-V, neutron irradiated, damage rates 79−77646
- Fe-Co-V (2%), annealing of point defects produced by cold working *(French)* 78−72829
- Fe-Co-V(2%) alloy, correl. of resistivity with microstructure 78−72896
- Fe-Co(Cr), electron state density and elec. resist. 80−39558
- Fe-Cr, single and two component, powder, compressibility and elec. resistivity in cold pressing under low press. 77−77444
- Fe-Cr-Al alloys, low temp. sp. ht., resistivity and coercive force 78−63866
- Fe-Cr-Co, effect of heat treatment on strain gauge factor 78−72802
- Fe-Cr-Co, heat treatment effect on strain gauge factor *(Japanese)* 78−6954
- Fe-Cr-Co phase diagram, lamination region, resist. meas. *(Russian)* 78−27479
- Fe-Cr-Ni, α-particle induced precip. and phase instability 79−1470
- Fe-Cr-Ni, electron irradiated, resistivity during annealing, 4.2-1300K 78−87962
- Fe-Cr-SiC-B_4C powder mixture, compressibility and elec. cond. in cold pressing under low press. 78−60609
- Fe-Cu (1.77%) alloy, influence of neutron irrad. on electric resist. *(Russian)* 79−38041
- Fe-H, recovery of hydrogenated and quenched alloy, solute diffusion 77−77510
- Fe-Mn-Cr(Ni), mag. and crystallographic transformation depend. on Cr-Ni addition *(Russian)* 79−83334
- Fe-Mn-Si-C, minimum of elec. resist. near LNT *(Russian)* 77−66707
- Fe-Mn(Ni), electron state density and elec. resist. 80−39558
- Fe-Mo(W), semihard magnetic alloys, magnetic, elec. mech. props. *(Japanese)* 79−70078
- α-Fe-N, supersaturated solid solns., N atom precip. kinetics, resist. meas. 80−60864
- Fe-N alloy, dil., galvanomag. effects, 4.2-250K 78−87964
- α-Fe-N solid soln., N precipitation kinetics, defects effect 77−59789
- Fe-Nb (3.1 wt.%), semihard mag. alloy, Recalloy, mag. props., elec. cond. *(Japanese)* 78−10723
- Fe-Nb(Ta)-Co, Recalloys, semihard mag. alloys, mag. and elec. props., hardness, thermal expansion *(Japanese)* 79−5066
- Fe-Ni, (35 wt.%), transport props. and Invar features *(Russian)* 78−51973
- Fe-Ni, α to γ transformation, changes in Young's modulus and electrophysical props. *(Russian)* 79−20042
- Fe-Ni, elect. phenomena rel. to martensitic avalanche *(French)* 78−68691
- Fe-Ni, electrical resist., 1000 to 1700°C *(Russian)* 77−85193
- Fe-Ni, $Fe_{65}(Ni_{1-x}Cr_x)_{35}$, low-temp. elec. and galvanomag. props. rel. to mag. boundaries *(Russian)* 77−35910
- Fe-Ni, thermodynamic props., anomalous 80−39313
- Fe-Ni (32 wt.%), martensitic transform., study by fast electronic amplification *(French)* 77−86028
- Fe-Ni alloys, enthalpy change between $\alpha' \rightarrow \gamma$ and $\alpha \rightarrow \gamma$ transformations 80−93550
- Fe-Ni alloys, reverse martensite start temp., heating rate effects *(Russian)* 78−6924
- Fe-Ni Invar, low temp. struct. 79−55856
- Fe-Ni Invar alloy, Curie temp. and elec. resist., effect of press. 77−85449
- Fe-Ni-C, martensitic transform., new investigation method *(French)* 79−91881
- Fe-Ni-Co-W(Mo) (18.65, 8.99, 4.87 wt.%), ageing characts., 380-530°C 80−60876
- Fe-Ni-Ti (25.9, 2.15 wt.%), exam. of effect of inhomogeneous solid soln., on martensitic transformation *(Russian)* 79−34034
- Fe-Ni-Ti (30, 3 wt.%), reverse martensitic transform. and memory effect *(Russian)* 79−87627
- Fe-Ni-V, austenite, martensite elec. cond. depend. on heating *(Russian)* 79−70177
- Fe-Ni-V, effect of low temp. ageing on props. during high temp. ageing *(Russian)* 78−39811
- Fe-Ni-V alloy, ageing of martensite *(Russian)* 78−39808
- Fe-P-Cu-SiO_2-$FeAl_3$-asbestos composite, thermal and elec. conds., temp. and composition depends. 77−66609
- Fe-Pd, anomalous elec. cond. near mag. phase transition point, α to γ phase transition 80−15722
- Fe-Pd, residual resist., s-d hybridisation effect 80−39559
- Fe-Pd Invar alloys, elec. and mag. props. and thermal expansion 80−75732
- Fe-Pt, high mag. field phase transition 77−66301
- Fe-Rh, mag. phase transitions, triple point 79−1672
- Fe-Si (3 to 5 wt.%) sinters, mag. props., Si and Fe-Si additions effect 80−71104
- Fe-Si-Al (6,4 wt.%), Sendust alloy, effect of Ni content on mag. props. 78−72897
- Fe-Si-Al Sendust alloy ribbon form, rapid quench prepared, elec. cond., coercive field, permeability 79−83151
- Fe-Si-Al-Ni alloy, Super Sendust, Ni content and thermomag. treatment effects 77−4861
- Fe-Si-Mn, effect of Mn addition on mag. props. and elec. resist. 78−91890
- Fe-Ta alloy, mech. drawn and aged, exam. of electrical resistivity, hardness, microstruct., and mag. props. *(Japanese)* 78−48545
- Fe-Ti, solubility and diffusivity of H and D in mixed crystal phase, elec. cond. meas. *(German)* 80−107575
- Fe-Ti (V)(W), dil., thermophysical props. and elec. cond., temp. depend. 80−96842

electrical conductivity of crystalline metals and alloys continued
- Fe-Ti(Nb), internally nitrided, mech. props. 77−44307
- Fe-V alloy, Curie temp. determ. using deviation from Mattheisen's rule 79−15306
- Fe-V alloy, elec. resist. between 78 and 1200K 77−8065
- Fe-V(Cr)(Mo)(W)(Ti)(Nb) alloys, split bands evidence from sp. ht. and elec. transport data 77−24515
- Fe-V(Nb)-N, precipitation study, 550 to 600°C *(German)* 77−90350
- Fe_3Al, electrical resistivity and LRO, energy gap formation in Fermi surface 80−88533
- Fe_3Al, order-disorder transform. effect on optical and elec. props. *(Russian)* 77−39820
- Fe_3Al, order-disorder transition, elec. resistance meas. 79−42518
- Fe_3Al, vacancy conc. and ordering conc. 78−18639
- FeC_x ($x \leq 0.05$), splat-quenched, struct., elec. and mag. props. 77−21187
- FeCo, neutron irradiated, damage rates 79−77646
- FeCo, ordered alloy, 550°C change, study through elec. cond. and specific heat meas. 78−56633
- FeCo, ordered and disordered alloy, annealing of point defects created by neutron irrad. at 20K *(French)* 79−1467
- $Fe_{50}Co_{50}$, neutron irradiation, close pair recombination *(French)* 80−39162
- $Fe_{68}Co_{32}$, ferromagnet, magnon heat cond. and lifetimes, 1-2 to 4.5K 77−16066
- $Fe_xCo_{1-x}Si(Ti)$, magnetic props., sp. ht. and resist. meas. 79−61120
- $FeCo_2V$, ordered and disordered alloys, annealing of point defects created by neutron irrad. at 20K *(French)* 79−1467
- $Fe_{49}Co_{49}V_2$, neutron irradiation, close pair recombination *(French)* 80−39162
- $(FeMn)_3$ Si alloys, mag. and crystallographic props. 77−59393
- $Fe_{1-x}Mn_x$, elec. resist., anomalies in temp. depend. 79−23942
- $Fe_{1/3}NbS_2$, intercalate, metallic cond., Hall effect and mag. props. 77−76789
- Fe_xNbSe_2, transport props. and mag. ordering 80−65527
- FeNi-Cu, composite fibre and layer structs., anomalous props. caused by internal phase boundaries 78−72754
- $Fe_{1-x}Ni_x$, elec. resist., anomalies in temp. depend. 79−23942
- $Fe_{40}Ni_{40}B_{20}$ alloys, crystalline and amorphous, resistivity minimum, X-ray, Mossbauer studies 79−73489
- $Fe_{40}Ni_{40}B_{20}$, amorphous and crystalline, resist. minimum 79−47079
- $Fe_{32}Ni_{36}Cr_{14}P_{12}B_6$, Metglas 2826A elec. resist. during crystn. 79−91014
- $Fe_{0.5}(Ni_xMn_{1-x})_{0.5}$, elec. resist., anomalies in temp. depend. 79−23942
- $Fe_{65}Ni_{28}Mn_1$, disordered, mag. struct. near ferro-antiferromagnetic transition 80−60211
- $(Fe_{1-x}Ni_x)_2P$, mag. props. 78−23248
- FeNiTe alloys, disordered, polycrystalline, elec. resist., temp. depend. 80−49692
- FeP, mag. suscept., resistivity and thermal expansion meas. 78−2661
- $Fe_{1-x}P_x$ dilute alloys, electronic struct., mag., elec. and struct. props. 79−37971
- $Fe_{25}Pd_{50}Au_{25}$, atomic ordering influence on mag. props. and elec. resistance *(Russian)* 80−7551
- Fe_3Pt Invar alloys, elec. resist. anomalous crit. behaviour 79−78067
- Fe_3Si, long range ordered cryst., 4.2-300K 77−39815
- $Fe_{3+x}Si_{1-x}$, electron transport 78−91669
- $Fe_{95}Si_5$, thermal and elec. cond., heat transport by spin waves 79−38047
- Fe_xSi_{1-x}, struct. exam. by electron diffr. and resist. meas. 77−89409
- FeTi alloy, elec. and mag. props. near order-disorder transition 79−82576
- B-Ga, metastable, elec. props. in normal and supercond. states *(Russian)* 80−65520
- Ga, ultra-pure, bulk residual resist. 80−10950
- Ga-In, dil., elec. resist., temp. and impurity depend., deviation from Matthiessen's b-axis crystals 78−51970
- Ga-Sn, dil., elec. resist., temp. and impurity depend., deviation from Matthiessen's b-axis crystals 78−51970
- Ga-Zn, dil., elec. resist., temp. and impurity depend., deviation from Matthiessen's b-axis crystals 78−51970
- Gd, elec. resist., 4.2-600K 78−14706
- Gd, ferromag., transport props., crit. behaviour 80−65522
- Gd, spin reorientation transition, crit. behaviour of elec. resist. 79−51787
- Gd, T>1100K 77−24548
- Gd, thermal diffusivity, conductivity and elec. cond. 110 to 2100K 79−42516
- Gd, transport props., anisotropy, high temp. obs. 78−26843
- Gd-Dy alloy, magnon contribution to electrical resist. *(Russian)* 78−39087
- Gd-Ni, ferromag., elec. resist. temp. depend. 80−96843
- $GdAg_{1-x}In_x$, elec. and Hall resist. 80−96844
- $Gd(Al_{1-x}Cu_x)_2$, C15 struct., elec. resist., comp. depend. 78−14705
- $Gd_{80}Au_{20}$, amorphous ferromag., mag. and transport meas. 77−89930
- $Gd_{67}Co_{33}$, amorphous ferromag., mag. and transport meas. 77−89930
- GdCu, electrical resistivity and length changes with temp., hysteretic behaviour 80−97600
- $Gd(Cu_{1-x}Gd_x)$, pseudobinary alloy, mag. susceptibility and elec. resist. at low temp. 80−34602
- $GdH_{2.92}$, electrical resistance anomalies at high pressures 80−29381
- $GdNi_5$, anomalous behaviour near Curie point 78−91880
- $Gd_{68}Ni_{32}$, amorphous ferromag., mag. and transport meas. 77−89930
- GdTb alloy, transport props., anisotropy, high temp. obs. 78−26843
- GdTb, elec. resist. and thermal diffusivity anisotropy *(Russian)* 77−85192
- $(Gd_xY_{1-x})_4Co_3$, Curie temp. and resist.-temp. curves, comp. depend. 80−71020
- $HfPt_3$, corrosion resist. and elec. cond., bulk and film samples 78−72285
- HfV_2, C-15 struct., phase transitions, elec. cond., crystal lattice parameters *(Russian)* 80−54826
- HfV_2, elec. resist. and mag. suscept., anomalous temp. depend. 79−69491
- $(Hf_xZr_{1-x})_{80}Nb_{20}$, influence of Hf additions to $Zr_{80}Nb_{20}$ on temp. coeff. of elec. resist. 79−8304
- Hg, electrical and thermodynamic props. in metal-semicond. transition range 80−20144
- Hg, solid, resistivity ratio, 1.65 to 234K 80−59952
- $Hg_{2.86}AsF_6$, elec. cond., pseudo-one dimens. 77−20304
- $Hg_{2.91}AsF_6$, elec. cond., pseudo-one dimens. 77−20304
- $Hg_xMo_6S_8$ Chevrel phase, synthesis, stability and characts. 80−71608
- $(Ho,Y)Co_2$, mag. props., elec. resist. and thermal expansion 78−76246
- Ho, Hall const. and elec. resist., 80-700K *(Russian)* 78−60110

electrical conductivity of crystalline metals and alloys continued
Ho-Cu intermetallics, resist. and magnetoresist., mag. ordering obs. 80—70677
$HoCu_2$, mag. struct. and elec. resist., neutron diffr. obs. 80—60206
HoSb, quadrupole scatt. anisotropy, magnetically ordered material 78—64034
$Ho_cY_{1-c}Sb$ system, magnetisation, elec. resist., and sp. ht. meas. 80—60213
I, metallic A1-type modification, normal conductivity and superconductivity 80—20348
In ultrathin films on TbTe and Te, prep. and characterisation 77—7995
In-Cd, high temp. deviation from Mattheissens rule 77—43560
InBi, anisotropy of temp. depend. elec. resist., 4.2-293K 78—43354
Ir, thermophysical props. at temps. up to 7000K 80—103497
K, cryst., elec. cond., temp. depend. calcs. 77—59276
K, elec. resist., effect of energy depend. of electron relax. time 77—69296
K, electrical and thermal resistivity determ. from first principles 79—69493
K, electrical resistivity, low-temp., electron-electron contrib., sample depend. 80—24875
K, electrical resistivity at low temp., phonon-dislocation scatt. 79—60820
K, electrical resistivity below 2K, temp. depend. 78—51969
K, electron-dislocation scatt. anisotropy effect on electron-electron scatt. contrib. to elec. resist. 80—29398
K, electron-electron scattering, elec. resistivity, thermal cond., thermoelec. power and Lorenz function 79—95382
K, ideally pure, anisotropy correction to elec. resist. 77—4317
K, low temp. resist. and thermoelec. ratio, electron-electron scatt. contrib. 80—70670
K, Matthiessen's rule, low temp. deviations 78—14724
K, metal impurity effect on residual elec. resistance *(Russian)* 80—84457
K, phonon-dislocation scatt. and phonon equilibration at low temp. 79—51561
K, residual-resistivity anisotropy using several impurity scatt. potentials 79—19571
K, resistivity, anomalous temp. depend. below 1.6K 79—78074
K, temp. depend., low temp. limit 77—11892
K, temp. depend. of elec. resistivity, free electron approx., anisotropic continuum dispersive model 77—43557
K, transport calculations, usefulness of theoretical form factor 79—23946
K, vacancies and elec. resist. 79—82575
K-Cs alloys, elec. resist., minima for K_2Cs, K_7Cs_6 concs. *(German)* 78—14708
K-Rb, dil., calc. of press. depend. of low-temp. transport props. 78—30905
$(La,Gd)Al_2$, reverse Kondo alloy, transport props. at finite mag. field 80—6812
$(La,Gd)Al_2$, very dil., resist. 79—23958
$(La, Nd)Sn_3$, cryst. field effects, normal and supercond. props. 79—60973
$(La,Nd)Sn_3$, reverse Kondo effect in presence of crystalline elec. field splitting 80—103684
α-La, elec. resist., 5-300K, rel. to β-phase 78—10417
La-Ce alloy, press. induced spin glass to Kondo phase transition, resist. meas. 79—24174
La-Dy, elec. resist. temp. depend. 78—2462
La-Gd (8 at.%), FCC, under hydrostatic pressure, resistivity meas., comparison with positive-J spin glasses 80—59958
$La_{1-x}Pr_xSn_3$, Kondo effect from excited cryst. field levels, elec. resist. 78—14723
LaAg, under hydrostatic press., supercond. and phase transform, elec. resist., 1-300K 78—10595
LaB_6 thermal and electrical conductivities, 1000-2100°C 77—69293
$La_xCa_{1-x}RuO_3$, metallic, mag., electronic and structural props., ^{99}Ru Mossbauer spectroscopy 77—48107
$La_{1-x}Ce_xPd_3$, resistance behaviour and intermediate valence effects 79—78068
$La_{1-x}Ce_xSn_3$, electrical resist. and thermal expansion meas., 1.5-300K 80—34400
$LaCu_2Si_2$, resistivity, thermal conductivity and thermopower between 1.5 and 300K 78—87963
$LaH_{2.98}$, electrical resistance anomalies at high pressures 80—29381
$LaNi_{1-x}Fe_xO_3$, semicond. and metallic phases, elec. and mag. props. 79—78102
$LaPt_5$, cryst. field effects on transport props. 78—72133
LaS, elec. cond. and diff. thermo-EMF in 77-300K range 77—24573
LaSb, metallic, cryst. field effects on transport props. 78—72133
$La_{1-x}Sm_xSn_3$, Kondo scatt. from Sm ions 77—51734
$La_xSr_{1-x}RuO_3$, metallic, mag., electronic and structural props., ^{99}Ru Mossbauer spectroscopy 77—48107
Li, effects of core and correl. corrections 78—64026
Li, elec. and thermal resist. calc. using modified noncentral force model 79—91016
Li, elec. resist., soln. of Boltzmann transport eqn. 78—39090
Li, electrical resistivity, non-alkali-metal behaviour 79—60793
Li, phonon limited resistivity struct. depend., Umklapp scatt., elastic consts. 80—88532
Li, resistivity measurement by eddy current decay method *(Korean)* 80—27275
Li, temp. depend. of elec. resistivity, free electron approx., anisotropic continuum dispersive model 77—43557
Li-B (0-60 at.%), density, elec. resist. and Hall coeff. 78—39089
Li-Mg, Mathiessen's rule, elec. and thermal deviations, impurity scatt. 80—88536
Li-Pt, phase diagram for comp. range 0-40 at.% Pt, mag. and elec. props. *(German)* 80—84912
LiAl, anomalous elec. resistivity near critical composition 80—103673
LiIn, electrical resist. and thermal expansion temp. depend., 30 to 400°C, vacancy form. 77—24547
Lu, Hall coefficient meas., 80 to 1000K 80—49694
Lu-Gd, dil., positive exchange Kondo system, magnetisation and resist. 78—68158
Lu-Gd, positive exchange const. Kondo system, resistivity meas. 78—47775
Lu-rare earth metal alloys, dil., elec. resist. 79—82578
Mg, H_2 dissolution, resistometric study under press. 80—70417
Mg, Hall effect and elec. resist., temp. depend. 78—64030
Mg, recrystallisation after straining by rolling, −25 to 100°C *(French)* 77—59815

electrical conductivity of crystalline metals and alloys continued
Mg, recrystallisation after cold rolling 78—72790
Mg-Al, dil. alloy, residual resistivity, model pseudopot. form factors 77—8062
Mg-Er (<25%) alloys, struct. and props. 79—96001
Mg-Fe alloy film, quench-condensed, resistance meas. 79—15235
Mg-Mn, dil. alloy, single impurity Kondo behaviour in elec. resist. *(French)* 79—60815
Mg-Nd-Zn dilute alloy, metallography and precip. kinetics 80—71655
Mg-Nd-Zr, phase diagram, Mg rich region, microscopic anal. and elec. resistivity meas. *(Russian)* 78—56619
Mg-Sm, solid soln., phase diagram *(Russian)* 77—25015
Mg-Y-Zr, phase equilib. and props. *(Russian)* 77—66626
Mg_2Sn, phase transition under hydrostatic pressure, Mossbauer effect and electric resistance 78—51665
α-Mn, spin fluctuations, temp. depend. of elec. resist. 77—62913
Mn-Ni-Ti (Zr) systems, and mech. props. thermal expansion for different heat treatments *(Japanese)* 79—29123
Mn-Pt, Elinvar props., −150 to 500°C *(Japanese)* 77—52385
Mn-Pt, exam. of Elinvar props., from −150 to 500°C 78—76684
$Mn_{2-x}Cr_xSb$ film, prep. and mag. props. 78—48009
$Mn_{17.5}Cu_{82.5}$, mictomag. process, susceptibility and resist. meas. 78—3157
$Mn_{5-x}Fe_xSi_3$, elec. resist. and mag. susceptibility, ferromag. to antiferromag. transition 80—80504
Mn_3Ge, elec. and mag. props. *(Russian)* 77—76792
Mn_5Ge_3-Mn_5Si_3, electrical resistivity meas., order-disorder transition 80—10945
$Mn_{1/3}NbS_2$, intercalate, metallic cond., Hall effect and mag. props. 77—76789
MnSb, resist., susceptibility and thermopower rel. to electronic struct. 78—67935
Mo, 14 MeV neutron damage 77—15460
Mo and Mo superalloys high temperature properties 78—44173
Mo, annealing in stage I, dose depend. and radiation doping defects 78—47422
Mo, density of states, optical mass and DC elec. resist. Slater-Koster interpolation 77—15731
Mo, effect of microvoid size on positron annihilation and residual resistivity 77—48272
Mo, elec. resist., quadratic contrib., 2 to 40K *(Russian)* 80—92874
Mo, electrical resistance data in the region 300 to 2800K 77—43555
Mo, electron irradiated, recovery studies of pure and radiation doped crystals 79—19280
Mo, high purity single crystal doped with C, low temp. mech. props. 77—77544
Mo, liquid and solid, thermophysical props. 78—75808
Mo, neutron dose depend. of elec. resist., vacancy-interstitial recomb. *(Russian)* 77—80546
Mo, neutron irradiated extended low temp. annealing 79—79014
Mo, porous, high temp. props. 77—11894
Mo, sintered, thermal and elec. conds., 50-800°C, microstructure 78—43352
Mo, temp. depend., electron-electron scatt. 78—68025
Mo, thermal conductivity and electrical resistivity, 300 to 2600K 77—35913
Mo, vacancy recovery stage, radiation doping, elec. resistivity meas. 79—51102
Mo, volt ampere characteristics during electron melting process *(Russian)* 80—75336
Mo-Al-Ge, new compounds, structure and props. 80—39003
Mo-Fe, spin glass and mictomag. regimes, sp. ht., resist. and susceptibility meas. 77—69581
Mo-Ni two phase alloys, elec. and mass transport *(Russian)* 78—76044
Mo-Permalloy, galvanomag. props. 77—39822
Mo-Re, σ phase alloy, critical mag. field, elec. resistance 80—54850
Mo-Ti-Zr (0.5, 0.7 wt.%) alloy TZM, props. and appl. *(German)* 80—21040
Mo-V, elec. resist. and thermo-EMF, conc. depend., 4.2 to 1500K *(Russian)* 80—80247
MoFe, occurrence of spin glass and mictomagnetic regimes, props. meas. 77—16085
Mo_3Ge, A15 cpd., normal state, low temp. resist. 80—107762
$Mo_{4.66}Rh_{1.33}Te_8$, synthesis, struct., and elec. props. 80—92877
$Mo_4Ru_2Te_8$, synthesis, struct., and elec. props. 80—92877
β-$MoTe_2$, metallic in-plane resistivity meas. indicate first-order phase transition 78—30903
Na, cryst., elec. cond., temp. depend. calcs. 77—59276
Na, electrical and thermal resistivity determ. from first principles 79—69493
Na, electrical resistivity, low-temp., electron-electron contrib., sample depend. 80—24875
Na, metal impurity effect on residual elec. resistance *(Russian)* 80—84457
Na, phonon limited resistivity struct. depend., Umklapp scatt., elastic consts. 80—88532
Na-Ga alloy, mag. susceptibility and elec. cond. *(Russian)* 80—29522
Na-Li (19.2 wt.%), elec. resistivity, immiscibility region 79—1593
Na-NaO-Na struct., inelastic tunnel effect, spectra, potential barrier parameters 79—95511
Na_xWO_3, metallic, transport props. near metal-insulator transitions 77—24596
Nb, damage production by high energy d-Be neutrons, elec. resist. meas. 77—62564
Nb, density of states, optical mass and DC elec. resist., Slater-Koster interpolation 77—15731
Nb, elec. resist. changes with plastic deform. 77—89749
Nb, elec. resist. due to interstitial H (D) 80—96848
Nb, high temp. elec. resist., supposed failure of Boltzmann eqn. 77—72849
Nb, high-purity, resistivity recovery following low temp. electron irrad. 77—27909
Nb, high-temperature nonlinear electrical resistivity, supposed failure of Boltzmann eqn. 78—91664
Nb, mobile interstitials after electron irrad., resistivity recovery meas. 79—55783
Nb, nonlinear resistivity, failure of Boltzmann equation 77—11893
Nb on sapphire, highly oriented film prod. 77—66097
Nb, plastic deformation effects on superconducting specific heat transition 80—20352

electrical conductivity of crystalline metals and alloys continued
Nb purification, using hot extraction of gases, from refractory metals under vacuum elec. cond. meas. *(Russian)* 79—56940
Nb, residual resistivity, effect of interstitial atoms of O, N and C *(German)* 77—11895
Nb, resistivity studies of interstitial He mobility 79—14800
Nb, resistivity variations caused by H and D interstitials, isotope effects 77—89750
Nb, specific elec. resistance, 200-2700K 78—39088
Nb spheres, residual resistivity ratio, prep. method effects *(German)* 79—8372
Nb, thermal and elec. cond., temp. depend., 900-2100°C, additive effects *(Russian)* 77—15816
Nb, thermal and elec. cond., 9-50K 79—87078
Nb, vacuum heat treatment effects on gas content and elec. and mech. props. *(Russian)* 79—43281
Nb, volt ampere characteristics during electron melting process *(Russian)* 80—75336
Nb:N, deviations from Matthiessen's rule 78—39092
Nb-Cu, neutron radiation stimulated diffusion, electrical resistivity exam. *(Russian)* 79—14959
Nb-D system, elec. resist. change with temp. at constant comp. *(Japanese)* 79—78936
Nb-Mo alloy, electronic density of states, temp. depend. of elec. resist. and mag. susceptibility 77—11891
Nb-Mo(Zr) alloys, vacuum heat treatment effects on gas content and elec. and mech. props. *(Russian)* 79—43281
Nb-Pt alloy, superconducting parameters of A15- and σ-phases 78—39242
Nb-Rh, σ-phase alloy, superconductivity and resistance behaviour 80—70882
Nb-Ru(Re)(Os), dil., impurities effect on elec. resist. at 0.4 and 77.3K *(Russian)* 79—91196
Nb-Ta(V)(Ti)(Mo), resistivity due to H incorporation 80—70666
Nb-Ti, metallurgical treatment, effects on props. 79—38846
Nb-Ti and Nb-Ti-Zr, low temp. resist., enhancement due to short-range supercond. order 77—28157
Nb-Ti-Al alloy, effect of heat treatment on strength and elastic props. 77—55976
Nb_3Al, A15 cpd., normal state, low temp. resist. 80—107762
Nb_3Al, temp-depend. of elec. resist. 80—103675
Nb_3Ga, Debye temp., determ. from elec. resist. meas. *(French)* 77—4322
Nb_3Ga, temp-depend. of elec. resist. 80—103675
$NbGe_2$ single crysts., elec. resist. and superconductivity 79—38233
Nb_3Ge, A15 cpd., normal state, low temp. resist. 80—107762
Nb_3Ge, effect of ^{16}O and ^{32}S ion irrad. and thermal recovery on T_c, residual resist. and slope of crit. field 79—56348
$Nb_3Ge(Al)$, anomalous resistivity, insight from band theory 78—60106
$NbS_2(Se_2)$ intercalation complexes with 3d transition metals, mag. and metallic transport props. 80—44814
$NbSe_2$ nonstoichiometry, electrical props. *(Japanese)* 78—10593
Nb_3Sn, A15 cpd., normal state, low temp. resist., disorder effects 80—107762
Nb_3Sn, Debye temp., determ. from elec. resist. meas. *(French)* 77—4322
Nb_3Sn, highly disordered, elec. resist. and supercond. T_c 78—52142
Nb_3Sn, neutron irrad., elec. resist., temp. depend. 79—91024
$(Nb_{0.99}Ti_{0.01})_{1-x}Ge_x$, high T_c, resist. meas. 80—88531
$Nb_{1-x}W_xSe_2$ $x=0$ to 0.15, elec. resist., mag. suscept., heat capacity, structural, supercond. transition *(Russian)* 78—31006
Nd, high temperature transport props., scatt. mechanisms, phase transitions 77—15825
Nd, magnetoresistance, mag. struct., elec. resistance at low temps. *(Russian)* 80—54936
Nd-Dy(Y), elec. resist. temp. depend. 78—2462
Nd-La, mag. ordering, sp. ht., susceptibility and resist. 78—68238
$NdSn_3$, elec. cond., cryst. field effect, spin disorder contrib. 80—65540
Ni, anomalous resistivity near Curie temp., band theoretical calc. 78—56127
Ni based alloys, resistivity magnetoresistance, s,p impurities in ferromag. host 78—68008
Ni, cathodically H charged, isothermal ageing 79—15703
Ni, deformed by hydrostatic extrusion, drawing or drawing under press., dislocation struct. obs. *(Russian)* 77—21213
Ni, diffusion of D, isotope effect, elec. resistivity meas. 79—86928
Ni, effects of grain size on resist. anomaly near Curie point *(French)* 77—4318
Ni, electrical resistance and H solubility at high press. *(Russian)* 79—91018
Ni, electrical resistance in DC mag. field after ultrasonic deform. *(Russian)* 80—54671
Ni, electrical resistivity and stress amplitude change during push-pull fatigue 79—91792
Ni, electroplated, fuchsin additive effect on low-temp. annealing characts., resist. meas. 77—32725
Ni, exploding wire, elec. resistivity in fast RCL circuit 77—31995
Ni, foil, electron bombard., impurity redistrib. during third stage of annealing, residual resist. meas. 80—6434
Ni, H diffusion in H_2 quenched sample, elec. resist. recovery 78—2299
Ni, high purity, quenching expts. 78—48432
Ni, high purity wires, elec. resist. determ. 77—39817
Ni, high-purity, softening of strained single crystals *(Russian)* 80—40499
Ni, laser irrad., elec. cond. recovery *(Russian)* 77—55512
Ni, lattice defects, formation kinetics, work hardening and resistivity study *(Russian)* 80—10557
Ni layer, vol. composition of sharp filamentary textures, elec. cond. meas. *(German)* 78—22978
Ni plated WC powder, detonation spray deposited hard alloy coating, electrical conductivity 77—12025
Ni powder, resist.-sintability *(Japanese)* 80—16228
Ni powders, stereological appl. in study of compacting process, elec. and mech. props. *(French)* 80—40286
Ni, push-pull fatigued polycrystals, point defects, elec. excess resist. meas. 80—100910
Ni, resistivity, thermal and elec., spin disorder scatt. anal. 78—76063
Ni, US deformation at low temps., elec. resistivity recovery *(Russian)* 79—11656
Ni, volume strained, sintered, porous, physicomechanical props., electrical resistivity 77—12572

electrical conductivity of crystalline metals and alloys continued
Ni:^{235}U (0.1 at.%), exam. of saturation defect conc. and elec. resistivity meas., for neutron irrad. at 7K 78—47435
Ni:H thin plate, recovery of quenched-in solute H 77—62673
Ni-Al (6.3 at.%), influence of localised order on thermo-EMF and Hall-EMF *(Russian)* 78—6951
β'-Ni-Al-Fe, mag. impurity states, resist. meas. 77—55519
Ni-Al-Fe(Co), electrical and mag. anomalies due to substitutional atoms 77—15839
Ni-Al-Si, β-phase stability *(Russian)* 78—39738
Ni-alloys with 3d- and 4d-metals, low temp. elec. resist. *(Russian)* 79—23941
Ni-C, ferromag., prep. by splat-quenching, obs. of electronic struct. of interstitial C 77—62868
Ni-Co, electrical resistance and H solubility at high press. *(Russian)* 79—91018
β-Ni-Co-Al, martensitic transform., metallographic, X-ray diffr., and elec. resist. obs. *(Russian)* 78—19748
Ni-Co-H system, phase transform. under high H_2 press., Co additive effects *(Russian)* 78—60645
Ni-Co-P, ferromag. film, amorphous to cryst. transition, diffr. and resistivity meas. 78—60587
Ni-Cr, heat resisting, dispersion hardened, electrical resistance meas. *(Russian)* 77—66708
Ni-Cr, high temp. wire resistance strain gauges 77—53896
Ni-Cr, residual resist., CPA calc. to muffin tin pot. 77—62892
Ni-Cr (0-35 at.%), neutron irrad. at 25K, damage, elec. resist. obs. *(French)* 80—54286
Ni-Cr (33.3 at.%) alloy, ordering after US deform., microhardness and elec. resist. meas. *(Russian)* 79—20113
Ni-Cr alloys, low temp. transform. mechanism, electrophys. props. obs. *(Russian)* 77—59777
Ni-Cr-Fe (75, 35, 12 wt.%), electron and α-particle irrad., positron annihilation and elec. resist. meas. 79—83054
Ni-Cr-MgO system, elec. resist. variation with comp. and prep. method 78—60637
Ni-Cr-Mo-Mn alloy 02KhN40MB, corrosion-resist, heat-resist., phys. and mech. props. 80—35411
Ni-Cr(-W) alloys, heat-resistant, integrated hemispherical degree of blackness, specific elec. resist., oxidised surfaces 79—86912
Ni-Cu, hydrogenated, Curie point, cluster magnetism 78—14960
Ni-Cu, Ni rich alloys, magnetic phase transition, elec. resistivity meas. 300-700K 79—82781
Ni-Cu, Ni-rich, temp. depend. resist. 80—10943
Ni-Cu, spin fluctuations effect on temp. depend. of elec. resistivity 78—47776
Ni-Cu alloys, short-range atomic clustering, residual resist. meas. 80—29386
Ni-Cu-H systems, Curie temp. during phase transitions under high press. H_2 80—71029
Ni-Cu-Si (38,5 at.%), changes in modulated struct. during ageing early stages *(Japanese)* 79—100183
Ni-Fe, residual resist., CPA calc. to muffin tin pot. 77—62892
Ni-Fe-Cr, extraordinary Hall effect, elec. and mag. meas. at 77 and 300K 80—34421
Ni-Fe-Mo-Cu (79, 16, 4.3, 0.7 wt.%) K-state formation, physical props. exam. 78—47761
Ni-Fe-Nb, Hardperm, origin of high magnetic permeability 77—8362
Ni-Fe-Nb-Mo (11.42, 6.92, 1.54 wt.%), Hardperm, high magnetic permeability alloys 77—8361
Ni-In(Sn), electrical cond. and magnetic susceptibility of B 8_2-compounds *(German)* 79—42520
Ni-Mn, low temp. anomalies of elec. resist. *(Russian)* 79—60788
Ni-Mn, low temp. kinetic props., 4.2-77.3K, resistivity *(Russian)* 79—19568
Ni-Mn base polynary alloys, magnetic and elect. props. *(Japanese)* 78—15551
Ni-Mn base polynary alloys, magnetic, and elec. props., composition and heat treatment effects 79—11710
Ni-Mn-CO(Fe), low temp. anomalies of elec. resist. *(Russian)* 79—60788
Ni-Mo-Al and Ni-Mo-Al-V, high-resist., struct. transforms., TEM *(Russian)* 78—19762
Ni-Re, dil. alloys, two-band Mott conductivity *(Russian)* 78—60118
Ni-Rh alloys, thermal EMF, elec. resist., mag. susceptibility, mag. moment and Curie temps., 18-500°C *(Russian)* 77—20288
Ni-S, defect control by heat-treatment in S atmos. 79—43293
Ni-S, S atom redistribution under high temp. electron irrad., residual elec. resist. reduction *(Russian)* 79—82256
Ni-S solid solns., residual elec. resist. *(Russian)* 80—70465
Ni-Sn(Sb), dilute ferromagnetic alloy, resistivity and magnetoresist. anisotropy 79—11106
Ni-Ti, Ni-rich, temp. depend. resist. 80—10943
Ni-Ti (0-1.5 at.%), elec. cond., mag. phase transition, 300-750K 78—2678
Ni-Ti (51.5 at.% Ni) metallide, thermal cond., elec. resistivity, 90-450K 78—68009
Ni-Ti (60 at.%) alloy, high stress effects on struct. and props. *(Russian)* 78—19838
Ni-Ti alloy, Curie temp. determ. using deviation from Mattheisen's rule 79—15306
Ni-Ti-Co, Co effect on martensitic transform. temp. and low temp. props. *(Korean)* 78—11224
Ni-transition metal, deviation from Matthiessen's rule in elec. resist. 77—4319
Ni-V, magnetocryst. temp. and conc. depends., rel. to resistivity 77—40052
NiAl, annealed near stoichiometric, elec. resist. meas. 77—8071
Ni_3Al-Ni_3Nb, directionally crystallised, thermal and electric cond., emissivity 77—43556
β'-$Ni_{48}Al_{52}$, 3d transition metal impurities, elec. resist. meas. 77—69295
$(NiAl)_{1-x}M_x$, M=3d transition metal, elec. resist. and magnetoresist. 77—43580
Ni_2Cr, neutron irrad., point defect prod. and annealing 78—87718
$(Ni_{1-x}Cu_x)Ti$, martensitic, shape memory effect kinetics and thermodynamics 80—3021
$Ni_3(Fe,M)$, M=Cr,Mo,W, elec. resist., temp. depend. anomalies, Hall and Nernst-Ettinghausen effects *(Russian)* 80—10942
$Ni_3(Fe,M)$, M=Cu, Cr, Mo, W, kinetic phenomena rel. to ordering and electron struct. *(Russian)* 78—76043
Ni_3Fe, atomic order, Mossbauer effect obs. 77—69736

electrical conductivity of crystalline metals and alloys continued
Ni$_3$Fe, effect of alloying with Cr, Mo, W or Cu *(Russian)* 78—39095
Ni$_3$Fe single crystals, longitudinal magnetoresist. meas. 80—70675
Ni$_3$Fe-Sn, dil., atomic order detection by ^{119}Sn spectroscopy 80—39993
Ni$_3$(Fe$_{1-x}$Nb$_x$), temp. and conc. depend. of anomalous Hall effect *(Russian)* 80—70674
Ni$_5$Ge$_3$, amorphous-crystalline transition, opt. and elec. characts. *(Russian)* 77—85191
Ni$_5$Ge$_3$, solid and liquid, physicochemical props. and structure 80—39548
NiH$_x$, magnetization, elec. resist., and non-occurrence of supercond. 79—56195
Ni$_3$(Mn,Cu), ordering kinetics, neutron diffr. and elec. resist. meas. *(Russian)* 77—47379
Ni$_3$Mn, elec. resist., relax. time near order-disorder transition 78—87788
Ni$_4$Mo, ordered, electrical resistivity and thermal EMF, temp. depend. *(Russian)* 77—55513
Ni$_{1/3}$NbS$_2$, intercalate, metallic, cond., Hall effect and mag. props. 77—76789
NiO, dipole orientation from bound polaron hopping 80—84437
Ni$_{76}$P$_{24}$, thermopower and resist. meas. 80—20145
NiPt, quenched, ordering kinetics and domain struct. form. during isothermal tempering *(Russian)* 80—66502
Ni(Rh$_{1-x}$Cr$_x$)$_2$S$_4$, ferromag. spinel system with metallic conduction 79—56513
NiS$_{2-x}$Se$_x$, sp. ht. and elec. resist. in metallic regime 77—69589
NiSb, resist., susceptibility and thermopower rel. to electronic struct. 78—67935
NiTi, martensitic, shape memory effect kinetics and thermodynamics 80—3021
NiTi, premartensitic transformation of B2 phase, shape memory 80—84931
NpSn$_3$, itinerant f-electron antiferromag. obs. 77—8315
Os, elec. resist., thermal diffusivity, and thermal cond., 290 to 3300K 79—11101
Os; electrical resistivity and thermal diffusivity meas. 80—15495
Pa, electrical resistivity meas., 0.90 to 300K 77—35915
Pb and Pb-Mg, dil., resistivity, multiple plane wave calc., Fermi surface, vel. and band struct. 77—51723
Pb, charged particle irrad., damage and recovery processes 77—69002
Pb, crystal defect accumulation after plastic deform. in normal and supercond. state resist. meas. 77—85196
Pb dilute alloys, solute resist. meas., multiple point defect form. 78—10433
Pb, electrical resistivity, 300-1050K 80—24868
Pb, electron irradiation at 4.7K and below 3K, annealing expts. 77—11595
Pb, melting curve, elec. resist. determ. at high pressure 80—49337
Pb, press. depend. of electron-phonon interaction rel. to normal state resist. 79—28063
Pb, solid solubility of Au, elec. resist. meas. 80—39298
Pb ultrathin films on PbTe and Te, prep. and characterisation 77—7995
Pb whiskers, grown from metallic vapour phase, whisker resist. 78—47686
Pb-As (~0.01 wt.%), enhanced precip. phenomena, invest. of mechanism by elec. resist. meas. 80—104162
Pb-Au, dil., solute resist. meas., multiple point defect form. 78—10433
Pb-Bi alloys, phonon-electron interaction, normal and supercond. state thermal cond. and elec. resist. meas. 79—60460
Pb-Cu, charged particle irrad., damage and recovery processes 77—69002
Pb-Sb battery grids, ageing behaviour obs., effects of casting and cooling 79—100517
Pb-Sb-As (1.1-1.8, ~0.01 wt.%), enhanced precip. phenomena, invest. of mechanism by elec. resist. meas. 80—104162
Pb-Sn system, soft solder, elec. and thermal cond. at low temps., superconducting transition temp. 80—20150
Pb(Ag) alloys, effect of Ag content on yield strength 80—76322
PbMo$_6$S$_8$, normal state and superconducting property measurements 78—91660
PbMo$_6$S$_8$:Fe, elec. cond. anomalous temp. depend., mag. moments *(Russian)* 80—92878
PbNb$_2$O$_6$, permittivity and elec. cond. meas., first order transition 79—24270
Pd alloy-H system, α-β phase transformations, hysteresis of press., elec. resistance, review 80—60859
Pd, elec. resist., temp. depend. data 80—51967
Pd, elec. resist. due to interstitial H (D) 80—96848
Pd, electrical resistance and H solubility at high press. *(Russian)* 79—91018
Pd, float zone purification, residual resistivity ratio 78—44008
Pd, hydride and alloys, electronic band struct., comparative study of electric and mag. props. 78—95259
Pd, liq. and solid, thermophysical props. 78—75808
Pd, strained, anisotropic electron scatt. in elec. resist. 78—91656
Pd, transport props. 40 mK-6K 78—51968
Pd-Ag alloys, elec. resist. meas., 300-900K 77—47792
Pd-Ag alloys, elec. resist. meas., density of states and Debye temp. 77—76715
Pd-Ag electrical resistivity, thermo-EMF and thermal diffusivity at high temps. *(Russian)* 80—6808
Pd-Ag microwires, electrical resistance, influence of gaseous environment in heat treatment *(Russian)* 80—20146
Pd-Ag-Cu (35,25 at.%), determ. of ageing transformations by resist. meas., metallography, TEM and X-ray diffr. 79—4967
Pd-Ag-Fe, (0.5, 1.0, 2 at.% Fe), elec. resist. reduction near ferromag. and spin glass ordering 77—69299
Pd-Co (0.1-45.7 at.%), thermo EMF at 4.2-300K *(Russian)* 80—92881
Pd-Cr, dil., temp. dependent scatt. 80—59973
Pd-Cr (11-18 at.%), resistivity comparison with canonical spin glass system 78—10432
Pd-Cr alloys, dil., elec. resist., 7.4 to 300K, anomalous temp. depend. associated with cond. electron scatt. 79—73491
Pd-Cu, H solubility enthalpy and entropy, effect on elec. cond. 77—35699
Pd-Fe, dil., transport props. at low temp. 0.05 to 5K 79—38046
Pd-Fe, very dilute, very low temp., spin glass-like behaviour 79—99708
Pd-Fe (0.54-8.0 at.%), thermo EMF at 4.2-300K *(Russian)* 80—92881
Pd-Fe-H, elec. resistivity, 4.2 to 300K *(Russian)* 79—7814
Pd-H, low temp. transport props., heterogeneous-mixture model 80—24871
Pd-H, nature of the 50K anomaly, residual resist. 79—7818

electrical conductivity of crystalline metals and alloys continued
Pd-H, temp. depend., H conc. var. *(Russian)* 77—39819
Pd-H system, α-β phase transformations, hysteresis of press., elec. resistance, review 80—60859
Pd-H(D) system, normal state phonon resist. and supercond. tunnelling density of states 79—56402
Pd-Mn dilute alloys, mag. ordering, sp. ht. calc. by Monte Carlo method 77—77030
Pd-Ni, neutron radiation stimulated diffusion, electrical resistivity exam. *(Russian)* 79—14959
Pd-Ni (15-90 at.%), thermo EMF at 4.2-300K *(Russian)* 80—92881
Pd-Pt, elect. resistivity, temp. depend. between 1.6 and 4.2K *(German)* 79—28337
Pd-Pt-Au alloys for low-temp. precision resistors 79—69490
Pd-Ru, electron transport props., 50 mK-4.2K 78—14707
Pd-Ru-W(V)(Ti), elec. resist. and thermal cond. *(Russian)* 78—19017
Pd-Si(−Cu), glassy, liq. and cryst., mag. and elec. props. 77—66249
Pd-Ti alloy, Matthiessen's rule breakdown 77—15823
Pd-W, elect. resist., mag. susceptibility, Hall coeffs., in plastically deformed state and after annealing *(Russian)* 79—66174
Pd-W (20 wt.%), permeability, diffusion, and solubility of H$_2$, elec. resist., heat treatment effects *(Russian)* 79—51307
Pd$_{50}$Fe$_{37.5}$Co$_{12.5}$, elec. resist., cond. electron scatt. and heterogeneities of spin system *(Russian)* 79—56189
PdFe$_{1-x}$Cr$_x$ ordering alloys, elec. resist., temp. depend. *(Russian)* 80—24866
PdH$_x$, PdD$_x$, ordering, resistivity, annealing and neutron diffr. obs. 79—34030
β'-PdIn, electrical resistance, mag. susceptibility and IR freq. dispersion *(Russian)* 80—107759
(Pd$_{95}$Rh$_5$)$_1$H$_x$, elec. resistivity studies 80—59957
Pd$_{0.97}$Sm$_{0.03}$ dil. alloy, assist. meas. 79—19583
Pd$_{0.97}$Tm$_{0.03}$, dil. alloy, elec. resist. meas. 79—19583
Pr, DHPC single cryst., Kondo-like resist. between 15 mK and 5K 79—60816
Pr, electrical resistance increase due to nucl. cooperative anomaly at low temp. 79—15133
Pr, high temperature transport props., scatt. mechanisms, phase transitions 77—15825
Pr, localised 4f shell breakdown under press. 80—70411
Pr, mag. scatt., effect of cryst. field levels 77—62904
Pr, resistance anomalies under pressure up to 40 kbar 79—65430
Pr-Ce(Tm), mag. order onset, elec. resistivity 80—20416
Pr-Nb alloy, elec. resist. and magnetisation 77—66367
Pr-rare earth dilute alloy, low field magnetic props. 78—84443
Pr-Tb, elec. resist. temp. depend. 78—2462
Pr-Tb alloy, elec. resist. and magnetisation, spin glass behaviour 77—66367
PrB$_6$, metallic, elec. resist., aspherical Coulomb and exchange scatt. of cond. electrons 77—51725
PrCu$_2$, Jahn-Teller transition, susceptibility, elec. resist., thermal expansion and acoustic meas. 77—20276
PrCu$_5$(Pt$_5$), cryst. field effects on transport props. 78—72133
PrIr$_2$(Pt$_2$)(Rh$_2$)(Ru$_2$), sp. ht., differential susceptibility and elec. resist. meas., 1.4-40K 80—71063
Pr$_3$Tl, resistivity and sp. ht. near threshold 79—78399
Pt, air annealed, ultralow temp. transport anomalies 77—69297
Pt, damage production by high energy d-Be neutrons, elec. resist. meas. 77—62564
Pt, electrical resistance and H solubility at high press. *(Russian)* 79—91018
Pt foil, quenched, 1.2 MeV electron irrad., subthreshold irrad. effects 78—51585
Pt, impurities on grain boundaries 79—87076
Pt, interstitial thermal conversion study by elec. cond. meas. 80—15096
Pt irradiated with 20/6 MeV deuterons, resistivity recovery and energy release 80—31756
Pt, quenched, deviations from Matthiessen's rule 77—69289
Pt, radiation damage, recovery of elec. resist., interstitial migration and clustering 77—11604
Pt, radiation damage recovery curves, evidence for two self-interstitial configs. 77—7773
Pt, recovery spectrum after thermal neutron irrad., resist. obs., Au addition effect and defect conc. depend. 80—65057
Pt, resistance thermometer, heat shock influence on elec. cond. and thermophysical props. *(Russian)* 80—52210
Pt, thermal and fission neutron produced defect configurations 78—47432
Pt wire, cold worked, recovery of elec. resist. 77—12643
Pt, wire, thermal cond., 900-1800K, elec. cond., 800-1800K 78—26845
Pt-Cr, elec. resist. meas. through percolation limit, mag. order onset 77—69298
Pt-Cr (0.3 and 0.5 at.%) anomalous resist. associated with conduction-electron scatt. from Cr impurities 79—99530
Pt-Cr alloys, (13-18 at.% Cr) resistivity and AC susceptibility, temp. 1.4—300K 78—2461
Pt-Cr alloys, dil., elec. resist., 7.4 to 300K, anomalous temp. depend. associated with cond. electron scatt. 79—73491
Pt-Fe alloy, ordered, T-c phase diagram, antiferro- and ferromagnetism *(Russian)* 80—65871
Pt-Mn dilute alloys, spin glass, low temp. resist. meas., cluster model explanation 78—26851
Pt-Rh, elec. cond., temp. influence *(Russian)* 80—39549
Pt-Rh alloys, low temp. resistivity 79—60787
Pt-Ti alloys, Matthiessen's rule breakdown 77—15823
Pt-transition metal, dil., impurity resist. 80—92875
Pt-V alloy, Matthiessen's rule breakdown 77—15823
Pt$_3$Fe, transport and mag. props. near Neel temp. 79—7976
Pt$_{37.5}$Pd$_{12.5}$Co$_{50}$, elec. resist., cond. electron scatt. and heterogeneities of spin system *(Russian)* 79—56189
Pt$_{12.5}$Pd$_{37.5}$Fe$_{50}$, elec. resist., cond. electron scatt. and heterogeneities of spin system *(Russian)* 79—56189
Pu and Pu-Np alloys, additional resist. due to self-radiation damage, Matthiessen's rule deviations 77—28170
Rb, elec. resist. and phase transforms. under high press. *(German)* 80—107763
Rb, metal impurity effect on residual elec. resistance *(Russian)* 80—84457
Rb, search for supercond. at high press., elec. resist. meas. 79—56359
Rb, temp. depend. of elec. resistivity, free electron approx., anisotropic continuum dispersive model 77—43557

electrical conductivity of crystalline metals and alloys continued
Rb, transport props. and electron-electron scatt. 79—73490
Rb_xWO_3, phase transitions, supercond. transition temp. and elec. props. 79—28431
Re, elec. resist., quadratic contrib., 2 to 40K *(Russian)* 80—92874
Re, elec. resist. and Hall effect at low temp. *(Russian)* 78—47760
Re, elec. resistivity temp. depend., plastic deform. effects *(Russian)* 77—35909
Re, electrical resistance anisotropy, temp. depend. *(Russian)* 78—76041
Re, electron-electron scatt. 78—68025
Re, single crystal, size effect in elec. resistivity *(Russian)* 78—87961
Re, specific heat, elec. cond., emissivity, 1600-2400K 78—67835
Ru, elec. resist., quadratic contrib., 2 to 40K *(Russian)* 80—92874
Ru, electrical resistance anisotropy, temp. depend. *(Russian)* 78—76041
Ru, kinetic and thermal props. at high temp., anisotropy 77—43563
Ru, single crystal, size effect in elec. resistivity *(Russian)* 78—87961
Ru, transport props., anisotropy, high temp. obs. 78—26843
$(SNBr_{0.4})_x$, metallic, transport and optical props. 77—85724
(SN)x, halogen-doped, temp. depend. of elec. cond. in metallic phase 79—65563
Sc, sp. ht. data rel. to electronic props. 78—83971
Sc thin films, obtained in vac. of 10^{-5}-10^{-6} Torr, struct. and elec. resist. 80—107931
Sc-Gd, dil., reverse resist. anomaly and negative magnetoresist. 80—84459
Sc-H, conc.-temp. depend. at room temp. of elec. resist. thermo-EMF, mag. susceptibility, and Hall coeff. 80—29382
$ScAl_2$-Eu, intermediate valence on Eu ions, Mossbauer isomer shift 80—84587
Sc_3In, itinerant electron ferromagnet, spin fluctuations 77—73096
Si, metallic, superconducting transition temp., press. effects, elec. cond. 80—103777
Si:P, ion implanted, ionisation enhanced annealing, resist. changes meas. 78—30667
Si-Au, solid soln., influence of precip. on relax. of ^{29}Si nucleus 80—11287
Sm, electrical resistivity, Neel temp., 15 to 300K 80—54672
Sm, electron radiation damage, elec. resistivity change rates 80—59954
Sm, magnetoresistivity and elec. resist., 4.2 to 300K *(Russian)* 80—88539
Sm, metastable phase modification formation during quenching from molten state *(Russian)* 79—91636
Sm, resistivity and thermopower anomalies at high temp. 78—64027
Sm-Dy (3 wt.%), electrical resistivity, Neel temp., 15 to 300K 80—54672
$SmCo_5$, specific heat and kinetic props. at elevated temp. *(Russian)* 79—28530
SmH_x [x=2.78, 2.85, 2.91], electrical resistance anomalies at high pressures 80—29381
Sn bronze, extruded atomized powders, struct. and props. 79—38763
Sn, electrical resist. and anisotropy at press. up to 80 kbar 77—43554
Sn, galvanomagnetic props., temp. depend. meas. in single cryst. 80—96850
Sn, monocrystals with impurities, elec. resist. anisotropy 78—79975
Sn, superconducting film, paraconductivity, above transition temp. 80—54845
Sn wire, elastically bent, elec. resist. in mag. field 80—44568
Sn-Pb alloy, dil., lattice dynamics, sp. ht., resist., thermal expansion and nuclear γ reson. expts. *(Russian)* 78—87749
Sn_xPg_{1-x}, thermal cond. and Lorenz function 78—51966
Sr, electrical resistivity and thermoelectric power 78—26846
Sr, transport properties, elec. resist., thermoelec. power, thermal cond. deviations from Matthiessen's rule 78—39086
$SrCoO_{3-\delta}$ $(0<\delta<0.5)$, ferromag., metallic elec. props. 80—70668
Ta, density of states, optical mass and DC elec. resist., Slater-Koster interpolation 77—15731
Ta, elec. resist. due to interstitial H (D) 80—96848
Ta, electrical and thermal resistance at low temp. *(Russian)* 78—68007
Ta, electrical resistance temp. depend. in solid and liq. states, 2200-4200K 78—10415
Ta, resistivity due to H incorporation 80—70666
Ta, resistivity variations caused by H and D interstitials, isotope effects 77—89750
Ta, singularities of elec. resist., 4.5-300K *(Russian)* 78—26842
Ta, thermophysical props. and neutron absorpt. 80—103488
Ta:H, recovery after cold working at 4.2K, resist. meas. 79—4977
Ta-D system, elec. resist. change with temp. at constant comp. *(Japanese)* 79—78936
Ta-H, N interstitial trapping of H, hydride precip., resist. meas. 77—20293
Ta-N (0.6 to 6.5 at.%), supersaturated solid soln., precipitation 79—96028
Ta-O solid soln., interstitial ordering and precipitation at 100 to 270°C, exam. 78—52813
Ta-Rh, σ-phase alloy, superconductivity and resistance behaviour 80—70882
Ta-T(D), diffusion and resistivity at low temps. 78—14511
Ta-W alloy, electronic density of states, temp. depend. of elec. resist. and mag. susceptibility 77—11891
TaS_2 intercalation complexes with 3d transition metals, mag. and metallic transport props. 80—44814
6R-TaS_2, metallic cond., resist. anomalies 77—11909
Tb, ferromag., electron-magnon interaction and elec. resist., 1.5 to 50K 79—60790
Tb, ferromag., spin wave resist., 1.5-50K 79—60813
Tb, high-precision elec. resist. meas., 1-4K 77—15817
Tb, transport props., anisotropy, high temp. obs. 78—26843
Tb-Gd, elec. resistivity and thermopower critical behaviour 80—15499
Tb-Gd alloy, single cryst., mag., magnetoelastic and elec. props. *(Russian)* 78—2677
Tb-Gd alloys, ferromag. monocrystalline, crit. behaviour of elec. resist. 77—62886
Tb-Y, Fermi surface topology var., mag. and elec. props. *(Russian)* 77—80723
Tb-Y, single cryst., magnon component of elec. resist. 77—15827
Tb-Y, single crystal growth from melt, X-ray obs., props. *(Russian)* 78—95689
$TbAg_{1-x}In_x$, elec. and Hall resist. 80—96844
$TbNi_{2-x}Cu_x$, elec. resist. and mag. props. 78—72348
TbSc, crit. scatt. of electrons near antiferromag. transition temp. 79—69505

electrical conductivity of crystalline metals and alloys continued
$Tb_cY_{1-c}P(As)$, singlet ground state systems, resistivities 77—62912
$Tb_cY_{1-c}Sb$, elec. resist., cryst. field and exchange interaction contribs. 80—39556
TbZn, elec. resist., behaviour at mag. crit. points 80—65901
TbZn, ferromag., elec. resist., just below crit. temp., effect of mag.-domains 80—39557
TbZn, ferromag. transition, transport coeffs. critical behaviour 80—15498
Th-Gd(Tb)(Dy)(Ho)(Er)(Tm)(Lu) (1 at.%), Heisenberg exchange, residual resist. meas. 80—75558
Th-Y alloys, resist., temp. coeffs. 77—20303
Ti 78—60602
α-Ti alloy, VT1-1, cold rolled, recrystn. texture and prop. anisotropy 78—52846
Ti alloys, data handbook of low temp. mech. and phys. props. 80—22153
α-Ti alloys VT1 and VT5, struct. and phys. props., H_2 effect 80—108576
Ti and Ti-Nb, mechanical, thermal and elec. props., 2.5 to 10K 77—35629
α-Ti, anisotropy of mag. susceptibilty and elec. resist. *(Russian)* 77—66292
Ti, $\alpha\rightarrow\beta$ phase transformation, elec. resistivity 79—15661
Ti, $\alpha\rightarrow\omega$ transform., pressure-induced, impurity effects and reaction kinetics 78—11220
Ti, electrical resistivity high-temp. anisotropy 79—65429
Ti, high purity, data handbook of low temp. mech. and phys. props. 80—22153
Ti, melting point, normal spectral emittance and elec. resistivity, pulse heating method 78—91423
Ti, neutron irradiated, relation between microstructure and recovery behaviour 77—15456
Ti, plastic deform. dynamics, mech. characts. and phys. props., effect of O_2 *(French)* 80—45353
Ti, polycrystal, discontinuous electrical resistivity, low temp. active straining *(Russian)* 80—103666
Ti powder, resist.-sintability *(Japanese)* 80—16228
Ti, resistivity, pulse heating method, 1500 to 1900K 78—43139
Ti-Al, phase diagram in Ti rich region *(Russian)* 77—25013
Ti-Al-V alloy, thermophysical meas. above 1450K, using subsecond transient technique 78—95161
Ti-Al-Zr alloy system, room temp. elec. resist. and thermal EMF *(Russian)* 77—20290
α-Ti-Fe, solubility, resistivity variation rel. to quenching temp. 79—99324
Ti-Fe alloys, elec. and thermal props. *(Russian)* 78—19020
Ti-Mn alloys, elec. and thermal props. *(Russian)* 78—19020
Ti-Mo, phase diagram investigation *(Japanese)* 77—63632
Ti-Mo-V-Al-Cr-Fe (4.8, 4.7, 5.2, 1.1, 1.0 wt.%), structural changes during heating up to 1000°C, DTA study *(Russian)* 80—93552
Ti-Nb-W, 20 to 1000°C, isothermal section, X-ray anal., microstruct., hardness, cond., transform. *(Russian)* 77—55947
Ti-Ni, multiplicity of structural transitions, phase diagrams, elec. cond. meas. 80—71649
Ti-Ni-Fe, multiplicity of structural transitions, phase diagrams, elec. cond. meas. 80—71649
Ti-Ni-Fe, plasticity, tensile stress-strain diagrams, ultimate tensile strength, elec. resist. depend. on temp. *(Russian)* 79—61652
Ti-Ru (0.05 to 90 wt.%) hardness, thermal EMF, electrical conductivity, in annealed or quenched state *(Russian)* 77—55998
Ti-V, anomalous elec. resistivity, mag. susceptibility, soft-phonon induced structural inhomogeneities 78—60104
Ti-Zr-Mo alloy, effect of O_2 on elec. resistivity, microhardness, mech. props. 77—56092
α-Ti-Zr-W, effect of W impurity on mech. preps. 80—16392
Ti_3Al, phase transitions and physical props. 77—25068
Ti_3Al-(Mo) (0.5 at.%), ordering, Mo effects 77—28841
$TiBe_2$, itinerant antiferromag., mag. susceptibility and elec. cond. meas. 79—19726
$Ti_{1-x}Co_x$, electronic struct. and anomalies of elec. and mag. props. 80—6710
$Ti(Fe_{1-x}Co_x)$, density of states estimation from magnetisation and resistivity meas. 78—84119
Ti_xGe_y, interrelationship of X-ray charact. with physical props. *(Russian)* 77—1765
$Ti_{0.5}NbSe_2$, cryst. struct., metallic cond., mag. and phys. props. *(French)* 80—33956
$Ti_{1-x}Ni_x$, electronic struct. and anomalies of elec. and mag. props. 80—6710
TiO_x, interstitial alloy, electronic state, XPS, mag. susceptibility and elec. resist. 77—12486
$Ti_{1+x}Se_2$, superlattice form., phase transform., metallic, resist. meas. 77—15383
$Ti_xZr_{1-x70}Nb_{30}$, ω phase precipitation 79—34042
Tl, electrical resistivity, 300-1050K 80—24868
Tl-Bi system, phase transitions near Tl_3Bi, elec. props. meas. 80—35181
Tl-Pb in solid and liquid state, specific electric resistance 80—103662
TlV_5S_8, prep., props. and cryst. struct., metallic behaviour 77—27864
Tm, Hall coefficient meas., 80 to 1000K 80—49694
Tm magnetic transitions, effect of H_2 in solid solns., elec. resist. meas. 80—100585
$Tm_y(La,Y)_{1-y}S$, microwave resistivity 77—11949
$Tm_y(La,Y)_{1-y}Te$, microwave resistivity 77—11949
TmS(Se), far IR refl. and DC resist., 1-300K, interconfig. fluctuation effects 78—35136
TmSb, metallic, cryst. field effects on transport props. 78—72133
TmSb, metallic, elec. resistivity, 4f-quadrupole charge distrib. 80—24873
TmZn, cooperative Jahn-Teller effect 78—67998
U-Cr(Mo)(Nb)(Zr) alloys, resist., temp. coeffs. 77—20303
U-Ga system cpds., resist. temp. depend. 77—20559
UAl_2, spin fluctuations, mag. field effect, electronic sp. ht. and elec. resist. 80—108026
UAl_2, transport props., susceptibility and sp. ht. 80—11174
UCo_2, elec. resist. and mag. susceptibility meas., non-stoichiometry influence 77—63088
$U(Co_{1-x}Fe_x)_2$, ferromag. onset, susceptibility and resist. meas. 80—70967
UMn_2, transport props., influence of lattice distortion 80—100452
UNi_2, mag. phase transition, elec. resist. meas. 80—97094
$UNi_{5-5x}Cu_{5x}$, NMR and press. effects 80—25230
UPd_3, anomalous behaviour in low temp. props. 79—28108
$U_{1-x}Th_xAl_2$, ferromag. spin fluctuation system, sp. ht. and elec. props. 77—20604

electrical conductivity of crystalline metals and alloys continued
$(U_xTh_{1-x})S$, metallic, 5f virtual bound states, elec. resist. and mag. susceptibility meas. 77−28363
$(U_xTh_{1-x})Se$, metallic, 5f virtual bound states, elec. resist. and mag. susceptibility meas. 77−28363
V,V-Zr (2 wt.%), internally oxidised, neutron irradiated, annealing effect on mech. props., elec. cond. and electron microscope obs. *(Japanese)* 79−15701
V, elec. resist. due to interstitial H (D) 80−96848
V, electrical resistivity, 200-2100K 79−33277
V, low-temperature thermal and elec. cond. 79−60792
V, resistivity variations caused by H and D interstitials, isotope effects 77−89750
V, thermal cond., elec. resist. and Seebeck coeff. meas., 6-300K 77−39818
V, thermophysical props. at temps. up to 7000K 80−103497
V, volt ampere characteristics during electron melting process *(Russian)* 80−75336
V-Cr alloy, electronic density of states, temp. depend. of elec. resist. and mag. susceptibility 77−11891
V-D system, elec. resist. change with temp. at constant comp. *(Japanese)* 79−78936
V-H, effect of neutron irrad. on electrical resistance, magnetic susceptibility 80−29063
V-H, phase diagram, resistometric contribution 78−15372
V-Mn-Cr, disordered BCC state, mag. phase diagram, mag. and elec. props. 77−63185
V-Ni-Al, phase equilib., elect. cond., hardness *(Russian)* 77−66627
V-Os system, equilib. phase fields, X-ray diffr., elec. resist., DTA, and EPMA meas. 79−47661
$(V_{1-x}Cr_x)_3Si$, single cryst., elec. resistivity, temp. depend. 79−56193
V_3Ge, low temp. props., mag. suscept. and resistance 78−19213
$V_3Ge_xOs_{1-x}$, low temp. props. 79−99652
$V_2(Hf,Zr)$, Laves phase compounds, temp. dependence with composition 78−76047
$V_{0.5}NbSe_2$, cryst. struct., metallic cond., mag. and phys. props. *(French)* 80−33956
VO_2, metallic phase, electronic props., plasma freq., Hall coeff. 78−84195
VSe_2, metallic behaviour obs., anomalous elec. and mag. props., temp. effects 77−15819
V_3Si, channelling, at displacements and electron phonon/defect interactions 77−84815
V_3Si, elec. resist. below 77K, phonon assisted interband scatt. 78−14703
V_3Si, neutron irrad., elec. resist., temp. depend. 79−91024
V_3Si, neutron irradiated single crystal, superconducting transition temp. widths, resistivity and heat capacity meas. 78−91802
V_3Si, neutron-irrad., ht. capacity and resistivity 78−88075
V_3Si, normal state resistivity as function of neutron irrad. 79−56194
V_3Si single crysts., elec. resist. and Hall coeff., temp. depend., 17-300K *(Russian)* 77−69292
V_3Sn, A-15 cpd., normal-state elec. resist. 80−75542
V_3Sn, $V_3Sn_{0.5}Al_{0.5}$, and $V_{2.5}Ti_{0.6}Sn$, elec. resist., temp. depend., T_c to 300K 79−65426
W, cyclically deformed, electrical resistivity 77−52491
W, elec. resist., quadratic contrib., 2 to 40K *(Russian)* 80−92874
W, elec. resist. below 1K meas. 77−15820
W, electrical resistivity -temperature scale and vacancy parameters 78−71727
W, electron-electron scatt. 78−68025
W, electron-electron scatt. 79−38045
W, electron-electron scatt. 79−60822
W, electronic transport below 1K 80−2377
W, low temp. transport props., phonon and impurity scatt. 78−10418
W, neutron irrad., at thermal energies, annealing exam. of recovery 78−47355
W, porous, high temp. props. 77−11894
W, porous, physicomechanical props. sintering effects 77−12575
W, resistivity min., thermoelectric anomaly correlation 78−2468
W, single crystals, electron irradiated, recovery of resistivity, 4.5-380K *(German)* 78−87714
W, sintered metal resist. standard, resist. at high temp. 78−89427
W, structural defect recovery after irradiation and cold work 78−47429
W, surface impedance and HF cond. in strong mag. field, thin single cryst. plates *(Russian)* 77−89831
W, thermal neutron irradiated, radiation damage and stage III defect annealing 78−51586
W, vacancy recovery stage, radiation doping, elec. resistivity meas. 79−51102
W, vacancy-defect clustering, due to annealing and quenching, TEM and elec. cond. exam. 78−47344
W, volt ampere characteristics during electron melting process *(Russian)* 80−75336
W, wire, elec. resistance, low-temp. continuous and cyclic heating effects, compared with W-Re 78−92370
W-Co, dil., excess resistivity, temp. depend., Kondo effect 78−68011
W-Fe, dil., excess resistivity, temp. depend. 78−68011
W-Fe, electronic transport below 1K 80−2377
W-Mo-Re heat resisting alloy MVR-27-VP2, high-temp. emissivity and resistivity 77−35727
W-Re, dil., excess resistivity, temp. depend. 78−68011
W-Re, wire, elec. resistance, low-temp. continuous and cyclic heating effects, compared with W 78−92370
W-Re alloy, effect of thermal prehistory on resistivity meas. 78−3241
W-Re alloy, elec. resistivity meas. near conc. anomaly, 300 to 1200K 77−35911
W-Re alloys, anomalous conc. depend. of elec. resistivity 77−35917
W-Zr (2.92, 7.42 and 10.02 wt.%), and W_2Zr, thermal expansion, elec. resistance, 100-900°C, crystallisation 78−91455
WC-Co (15 wt.%), detonation spray deposited hard alloy coating, electrical conductivity 77−12025
Y, electrical resistivity of solid and liquid phases, thermopower, melting temp. 80−59955
Y, electron radiation damage, elec. resistivity change rates 80−59954
Y, magnetic and elec. props., 100 to 900K *(Russian)* 80−25077
Y, transport props., anisotropy, high temp. obs. 78−26843
Y-Gd, dil., reverse resist. anomaly and negative magnetoresist. 80−84459
YNi_3, magnetism resurgence, neutron diffr. and mag. props. study 80−65819
$Y_{1-x}Th_xFe_3$ system, elec. resist. meas., 77-300K 80−34413

electrical conductivity of crystalline metals and alloys continued
Yb, electron radiation damage, elec. resistivity change rates 80−59954
Yb, shock compressed, elec. cond. behaviour and transitions, up to 220 kbar *(Russian)* 77−80761
$YbB_{6-x}C_x$, mag. and transport props., metallic cond. 80−54689
Zn, bicrystals, galvanomagnetic phenomena at common boundary, electric field potential distribution *(Russian)* 80−29388
Zn, electrical and thermal resist. calc. 79−69489
Zn, electrical resist. and anisotropy at press. up to 80 kbar 77−43554
Zn, electron irradiated, diffuse X-ray scatt. exam. of self interstitials 79−73213
Zn, electron irradiated, diffuse X-ray scatt. exam. of interstitial clustering during thermal annealing 79−73214
Zn, electron-phonon interaction anisotropy, microcontact spectroscopy *(Russian)* 79−37786
Zn, Hall effect and elec. resist., temp. depend. 78−64030
Zn, neutron irradiated, recovery of c-axis spacing and elec. resist. 80−34081
Zn, recovery after 6.1 MeV α-particle irradiation at 4.2K 78−47441
Zn, single cryst., contribution of basal dislocations to residual elec. resist. *(Russian)* 80−75539
Zn wire, elastically bent, elec. resist. in mag. field 80−44568
Zn:Al, residual resistivity, numerical calc., Fermi surface and multiple plane wave band struct. 77−51722
Zn-Bi(Sn) alloys, specific elec. resist., temp. and conc. depend., 20-800°C 79−82571
Zn-Mn, dil., Kondo effect and impurity interactions in resist., 0.05-14K 78−14721
Zn-Sb diffusion couple, layer growth of ZnSb phase at high press., elec. meas. 80−2218
Zn-transition metal alloy, residual resistivity, effect of 4d and 5d transition metal impurities 79−60791
Zr, low temp. deformed, O_2 effect on production and recovery of defects, elect. resist. meas. 79−47705
Zr polycrystalline, low-temp. alternating deformation and annealing, yield stress, elec. cond. variation *(Russian)* 79−74199
Zr, proton irradition, 10 to 16 MeV, resistivity changes 80−2082
Zr-H, effect of neutron irrad. on electrical resistance, magnetic susceptibility 80−29063
Zr-Hf, mag. susceptibility, elec. cond., Hall conc. thermoEMF conc. depend. *(Russian)* 80−39551
Zr-Nb(2.5 wt.%) alloy, effect of pre-irradiation on oxidation 78−88580
Zr-Ti, alloy, mag. susceptibility, elec. cond., Hall conc. thermoEMF conc. depend. *(Russian)* 80−39551
Zr_3Al, ordered, elec. resist. of LI_2 phase as function of temp. 79−19572
ZrC_x, x=0.99 to 0.13, elec. cond., supercond. state 78−43504
$Zr_{40}Cu_{60-x}Fe_x$, electronic and mag. props. 77−8271
$Zr(Fe_{1-x}Co_x)_2$, density of states estimation from magnetisation and resistivity meas. 78−84119
$Zr_xHf_{1-x}V_2$, polycrystalline superconductor, resist. and mag. susceptibility, transition temp., temp. depend. 80−25113
ZrN-NbC solid solns., mag. susceptibility and elec. resist. in 300-1300K range 77−24670
$ZrPt_3$, corrosion resist. and elec. cond., bulk and film samples 78−72285
$Zr(V,Al)_2$, struct., supercond. props., elec. resist. and mag. susceptibility, 4.2 to 300K *(Russian)* 79−15246
ZrV_2, C-15 struct., phase transitions, elec. cond., crystal lattice parameters *(Russian)* 80−54826
ZrV_2, elec. resist. and mag. suscept., anomalous temp. depend. 79−69491
ZrV_2, Laves-phase, cubic to rhombohedral transition, lattice electron instability 78−92261
$ZrZn_2$, weak itinerant electron ferromagnet, resistivity 77−72850

electrical conductivity of crystalline semiconductors and insulators
see also carrier density; carrier lifetime; carrier mean free path; carrier mobility; carrier relaxation time; dislocation scattering; electronic conduction in crystalline semiconductor thin films; electronic conduction in insulating thin films; high field effects; hopping conduction; impurity scattering; minority carriers; negative resistance effects; photoconductivity; point defect scattering; small polaron conduction; surface scattering
1/f fluctuations *(Japanese)* 78−43448
2,4-hexadiyne-1, 6-diol, bis(p-toluene sulphonate), dark-current meas. 80−15520
AC conductivity due to intimate pairs of charged defect centres 79−4563
AC response, influence of states in gap and generation-recomb. effects 77−4362
adamantine ceramic, structural, thermophysical and electrophysical props. 80−6918
β-Al_2O_3-Cu_2O, phys. and chem. props., use in determ. of thermodynamics of Cu-Sn alloys 80−107502
algorithm for calc. of impurity concentration from sheet resistivity and sheet Hall coefficient data 80−70246
alkali alkanoates, solid-state transitions, diffractometric and conductometric meas. 79−60507
alkali halide:VO^{2+}, impurity behaviour, elec. cond. and IR absorpt. obs. 77−8607
alkali halides, premelting elec. cond., heat capacity 78−91445
alkali metal aluminosilicates, $MAlSi_2O_6$, elec. cond. meas. 78−47787
alkali metal borides, prep., cryst. struct., thermal stability, phys. and chem. props., book contrib. 78−47304
alkali metal ferrisilicates, $MFeSi_2O_6$, elec. cond. meas. 78−47787
alkali metal-rare earth oxides, $MLnO_2$, Ln=Y or Gd, synthesis and physicochem. props. 77−48216
alkali metal-V_2O_5 bronzes, single cryst., elec. cond., 300 to 900K 77−20369
alkali perchlorates, elec. transport during struct. transforms. 78−59971
alkaline earth-ReO_6, ordered or perovskite type struct., magnetic and elec. props. 79−65053
alkaline-earth-Os ternary oxide system, solid state prep. and reactions, cryst. struct., mag. and elec. props. 79−24739
alloy, disorder scatt., Green's function calc. 77−11906
amphibole, electrical resist., up to 60 kbar *(German)* 80−31032
anodic oxide films on Cu, in neutral soln., resistometric study 77−16739
anthracene:rhodamine, triplet exciton density, isotope substitution effect, in weak mag. field 77−90184
anthracene, dislocations effect on elec. props. 77−35947
anthracene, drift mobility expts., arrival-time detection 79−33308
anthracene, impurity effects on elec. cond. *(Russian)* 77−62930

electrical conductivity of crystalline semiconductors and insulators continued
  anthracene, laser excited single crystal, numerical anal. for TSC results *(Japanese)* 80—34464
  anthracene, mol. cryst., elec. field independent electron drift mobility 79—51645
  anthracene, off-diagonal electron mobility and lateral space charge drift 78—72192
  anthracene, photo-oxidised, current oscills. due to recomb. instability in high field domain 77—4353
  anthracene, transient photocurrent, appl. of Scher-Montroll method 79—7851
  anthracene single cryst., injection of holes, current-voltage characts. *(Russian)* 77—1433
  anthracene single crystals, hole trapping by photo-oxidation products, injection currents *(Russian)* 80—92904
  azulene, drift mobility expts., arrival-time detection 79—33308
  bicrystal, charge carrier interface recomb., photocond. meas. method 79—99431
  bipolar conductivity investigs. using ohmic and acoustoelec. currents in Hall effect 77—32027
  Boltzmann eqns., soln. for electron-LO phonon scatt. 79—19586
  bone china body, MgO effect on vitrification mech. props. *(Japanese)* 79—78922
  bone tissue crystals, effect of compression 77—25492
  borides, hexa- and di-, electronic structs., elec. props., book contrib. 78—47701
  borides, hexa- and tetra-, prep., struct., elec., mag. props., book contrib. 78—47303
  borides, ternary, struct. classification, props., book contrib. 78—47309
  t-butyl bromide, elec cond., temp. depend. in liq. and plastic phases 80—1944
  t-butyl chloride, elec cond., temp. depend. in liq. and plastic phases 80—1944
  caesium propanoate, solid state transitions and melting process, diffr. and conductometric meas. 80—10670
  β-carotene, depend. on chemisorbed O_2, use as vacuum gauge *(Czech)* 77—139
  carrier scattering by lattice defects, nonlinear optical props. 80—29399
  celsian, with CaF_2 and ZnO additives, props. obs. *(Bulgarian)* 80—50579
  ceramic, electrical conductivity, porosity effects, 20 to 1000°C *(Polish)* 78—6385
  ceramics, electron and ion conductivity, instrument for meas. up to 2000°C 79—96247
  ceramics, TiO_2 based, variation of dielectric constant and resistivity with temp. 80—2683
  chalcogenide solid solutions thermoelectric materials, physico-chemical study 78—30945
  chalcopyrites, for electrolum. device appl., props. and technology, book contrib. 77—73175
  charge-transits, flash excited, electrode-edge effects, meas. 80—2396
  Chevrel phase supercond., resistivity meas. from 4.2 to 400K 79—56230
  chevrel phases, $A_xMo_3X_4$ (A=Cu, Pb, Zn and x=S, Se, Te), anomalous elec. resist. 79—56221
  Chevrel type compounds, single crystals, growth, stoichiometry, elec. resist. 78—92187
  collision frequency of electron with positive ions, vel. to ionosphere collision freq. and recomb. coeffs. 79—8742
  compensated semiconductor, cluster scattering, DC resist., energy-loss method 80—96862
  copper phthalocyanine, imperfect cryst., elec. transport phenomena, charge carrier conc. 77—1421
  copper quaternary thiospinels, mag. and elec. props. *(French)* 80—65771
  crystal-glass transition influence on local struct., cond. and density 77—36163
  cubic many-valley semiconductor, cond. in warm electron region, phenomenological theory 77—43586
  current instabilities theory and expts. *(Hungarian)* 77—39857
  cyclohexane, liq. and solid, mobility of excess charge carriers 78—2489
  dark conductivity anomalous temp. depend. 77—20319
  DBTTF halogen complexes, IR, UV spectra, EPR study 80—108215
  deep fast trapping dielectric, SCL current injection 80—6862
  deep impurities role, book contrib. 78—10403
  defect cluster scatt. and removal of carriers, model 78—76069
  defect semiconductor, or insulator, carrier densities, elec. cond. and Fermi level 77—43532
  degenerate polar semiconductor, asymptotic soln. to Boltzmann transport equation 77—4332
  degenerate semiconductor, p-type, hot carrier distrib. function and cond. 77—28190
  degenerate semiconductor, Sondheimer oscills., asymptotic behaviour 78—19059
  degenerate semiconductors, ionised impurity scattering cross-section, variational calc. 80—20180
  2,6-N,N-diacetyldiaminopyridine elec. cond., γ dose and temp. (303-363K) effects 80—103696
  diamond:B, B conc. and impurity-to-band activation energy 79—56165
  diamond:B, synthetic, current-voltage characteristics, temp. depend. *(Russian)* 79—7825
  diamond:B hopping conductivity in range 12 to 1300K 78—51994
  diamond:Ge(B)(B_4C), doping by diffusion at high temp. and press. 79—19273
  diamond:Li, ion implantation, Hall effect and elec. cond. meas. 80—15526
  diamond:Sb, implanted, radiation damage and annealing study 80—100263
  diamond, applications in electronics *(Czech)* 77—1414
  diamond, B doped, electron irradiated, defects at low temps., elec. resist. meas. 77—11593
  diamond, B doped, electron irradiated, threshold energy for atomic displacement, elec. cond. meas. 77—11594
  diamond, hard conducting C ion implanted layer, resistivity 77—15974
  diamond, natural, dislocation-N_2 impurity interaction, photoconductivity spectra, resistivity 79—91097
  diamond, natural, elec. cond. and thermoelec. power 78—39115
  diamond, semicond., electron irrad., charge carrier mobility 77—11921
  diamond, synthetic, elec. cond. 78—56144
  diamond, synthetic and natural, neutron irrad., optical and elec. props. *(Russian)* 78—59841
  diamond ceramic, elec. cond., temp., freq. depend. 80—54687
  diamond ceramic, elec. cond., thermal cond. rel. to temp. 79—15140

electrical conductivity of crystalline semiconductors and insulators continued
  2,6-N,N-dibenzoyldiaminopyridine elec. cond., γ dose and temp. (303-363K) effects 80—103696
  dielectric, irrad. by electron beams, effect of bulk and surface cond. on pot. 80—2446
  dielectrics, space charge studies of elec. phenomena 80—24939
  dielectrics containing impurities, carrier distribs. and currents, numerical simulation *(French)* 80—70718
  5,10-dihydro-5,10-diethylphenozinium-iodide, average struct. and props. 79—90636
  domain instability and resistivity profile meas., universal capacitive probe 80—31796
  dopant, transverse inhomogeneity, effect on ambipolar drift and field effect 80—6834
  doped semiconductor, tight binding approximation in Kubo formalism 79—60778
  doped semiconductors, variable range hopping, computer simulation 80—24929
  double injection structure, V-I characteristics and contact effects *(Russian)* 80—49911
  dyes, cond. type, I-V characts. 78—6391
  EBBA, solid and liquid states, temp. and freq. depend. *(Russian)* 78—72450
  electrical resistivity, Hall coeff. of samples dual to van der Pauw samples 79—88984
  electron beams as virtual electrodes, review 80—6861
  electron irrad., defects, elec. and optical props. 79—19282
  electron speed, technique for doubling 79—38076
  electron-hole pairing, collective modes, current states 77—39838
  electron-hole plasma and elec. field, stratification at low temp. 80—60020
  epitaxial layer resistivity meas. using Hg—n-GaAs barrier contact 79—60945
  epoxy resin based composites, superconducting magnet insulators, gamma-ray radiation effects 80—24495
  exciton gas, plasma model *(Russian)* 77—11860
  excitonic and optical insulator with nonequilibrium distrib. of quasiparticles 77—15888
  ferrite-semiconductor structure, EM wave excitation and amplification 80—6891
  ferrites, electronic cond. mechanisms, review 77—20314
  ferroelectric and antiferroelectric crystals, perovskite type structure, semiconductor props. *(Polish)* 78—56437
  ferroelectric ceramic, elec. and thermoelec. props. of grains and grain boundaries 78—43382
  ferroelectric semiconductors, props., book 80—82590
  ferromagnetic semiconductor, energy and mobility of spin polarons 80—70982
  ferromagnetic semiconductor, spin polaron props., effect on carrier scatt. 80—60233
  ferromagnetic semiconductors, conduction electron heating, critical scatt. effects 79—91040
  ferromagnetic semiconductors, hot electron relax. time 80—59996
  GaAs, polycrystalline, grain boundary resistance meas. effect on solar cell performance 80—93891
  galvanomagnetic-recombination field effect, theoretical model 78—43420
  gapless semiconductor, nonlinear effects in transverse quantising mag. fields 77—69353
  glass-epoxy laminate, superconducting magnet insulators, gamma-ray radiation effects 80—24495
  graphite, artificial, electrophys. props. 77—51745
  graphite, fusion reactor first wall appl., radiation damage 79—86822
  graphite, grain boundary scattering effect on temp. depend. of electroresistivity, galvanomagnetic effect *(Russian)* 78—56148
  graphite, neutron induced changes, exam. of lattice consts., elastic modulus, elec. cond 79—95053
  graphite, neutron irrad., microporosity, elec. resist., length, struct. changes 78—43051
  graphite, neutron irradiation, electron transport, annealing study 80—39165
  graphite, phonon thermal conductivity, rel. to elec. cond., possible supercond. 80—49434
  graphite, Poco AXM-5Q1, thermal and elec. transport props., 4-3000K 78—6375
  graphite, pressure-depend. conducting calcs. using band model 77—28171
  graphite, pyrolytic, extrinsic defect effect, on a-axis electrical resistivity, exam. 78—47784
  graphite, resistivity and magnetoresistance, 4.2 to 293K 80—100459
  graphite fibres, elec. resist., mech. props. after nitration 77—32698
  graphite intercalation acceptor lamellar cpds., charge distrib. and transport props. 79—95411
  graphite intercalation compounds, a-axis conductivity model 78—10435
  graphite intercalation compounds, alkali and halogen, electronic props., conductivity and optical reflect. *(German)* 80—49837
  graphite intercalation cpds., acceptor type, elec. cond. theory 80—44686
  graphite intercalation cpds. with K, Rb, or Cs, phase transitions, resistive anomalies, electronic props. 79—95405
  graphite-K intercalation compounds, electronic props., resistivity, Hall effect and magnetoresistance 80—75585
  graphites, electrical conduction in c-direction, rel. to struct. perfection 79—38069
  haematite, elec. resist. and phase transition under shock compression 80—72496
  heat treatment effects on elec. props. 78—43411
  heavily doped semicond., electronic sp. ht. and transport coeff., influence of band-tail parameters 79—14941
  heavily doped semiconductor, activity coeffs., for electrons with small effective mass 77—39837
  heavily doped semiconductor, conductivity electrons and elastic scatt. by static inhomogeneities *(Russian)* 80—29375
  heavily doped semiconductor, correction to static elec. cond. due to many-centre scatt. 80—2374
  heavily doped semiconductor, electron density dependent ordering parameter and role in elec. prop. anomalies *(Russian)* 77—43582
  heavily doped semiconductors, static conductivity in terms of transport relax. time 79—56213
  heavily doped semiconductors and devices, review 79—47039
  hexatriacontane single cryst., elec. cond. and dielec. breakdown 80—6849
  p-n hexyloxy benzylidine-p-toludine, liquid crystal, elec. cond. and dielectric constant, in solid phase 79—61293

electrical conductivity of crystalline semiconductors and insulators continued
  high magnetic field behaviour of solids and plasmas, conference, Cambridge, MA, USA (Sept. 1978) 79—60667
  hopping conduction, disordered systems, freq. depend. of cond. due to repeated jumps 80—15528
  hopping conductivity in ordered and disordered solids, review 77—1420
  hopping model, semi-classical, effective mass and carrier mobility calc. 80—96872
  ice Ih, dislocations, effect on physical and mechanical props. *(French)* 77—55287
  II-IV-V_2 phosphides, cond. compensation by electron bombardment 79—15151
  II-IV-V_2 semiconductors, resist., possible use in thermistors 77—4343
  III-V compounds, n-type, new meas. method for compensation and spatial fluctuations of impurities 78—6404
  III-V semiconductor, disorder scatt. 78—47780
  III-V semiconductor, temp. distrib. around dislocations, due to Joule heating, calc. 78—71734
  III-V semiconductors, conduction-band struct. from reflectivity meas. when subject to mechanical strain 79—42449
  III-V semiconductors, stress-induced elec. props. of point defects, piezoresistance effect 79—56726
  impurity conduction, at very low temp. *(Japanese)* 80—20200
  p-InSb:Cu, Ag, deep impurity centres, acceptor conc. effect on conduction type 80—44602
  p-InSb:Ge, single cryst. field dependence of Hall effect, cond. and carrier mobility *(Bulgarian)* 78—34848
  n-InSb, acceptor effect of plastic bending 80—6885
  insulators, transient radiation induced ionisation effects 77—80788
  ionic crystal, electron beam excited, luminesc. and cond. of nonideal degenerate electron-hole plasma 78—10488
  ionic crystals, nonstoichiometric, equilib. with gas phase in mech. vibr. field 78—43388
  ionic semiconductors, cyclotron resonance, elec. cond., electron-phonon interactions 80—93180
  ionisation rate, kinetic approach including acoustic phonon contrib. 79—56211
  IV-VI semiconductors, structural phase transitions, anomalous resist., electron-soft phonon interactions 80—108167
  jadeite, electrical resist., up to 60 kbar *(German)* 80—31032
  Kane semiconductors, transport props., kinetic integrals method 77—55525
  lattice defects and diffusion processes in solids, book 80—107207
  lattice parameters, mag. and elec. props. 80—100578
  layered semiconductors, transport props., book contrib. 77—43587
  lead acetate trihydrate:Mn^{2+}, ESR, elec. cond. 80—93165
  lead phthalocyanine:O_2(I), Schottky barrier effect on AC current response 80—75623
  lithium formate monohydrate, elec. props. 79—87371
  magnetites, cond. mechanisms *(Russian)* 79—42539
  metal colloids in ionic cryst., preparation, optical, mag. resonance, elec. props. 80—59459
  9-methyladenine single crysts., protonic cond. 77—55388
  $MgAl_{2-x}Fe_xO_4$ solid solution system, solid state properties study 80—93094
  mica, elec. cond. change and EM radiation during weakly bound water separation *(Russian)* 77—31779
  mica, EM effects during liberation of water of constitution from cryst. lattice *(Russian)* 77—31778
  mica, North American, electrical cond. rel. to chem. composition 77—29285
  α-MnS, elec. props. meas. 78—87971
  molecular crystals, electron mobility, temp. depend., hopping model 79—19588
  molecular crystals, electronic props. *(German)* 78—23089
  monocarbides of subgroups IVa and Va, kinetic props., review 78—47613
  n-type semiconductor with grain-boundary barriers, elec. cond. 77—55523
  naphthalene, charge carrier drift mobility, semi empirical anal. 80—65553
  naphthalene, electron and hole off-diagonal mobility component determ. 80—65552
  naphthoxazole derivatives, elec. cond., thermoelec. power, energy gap, absorpt. spectra 77—32053
  narrow band gap semiconductors, conference, Warsaw, Poland (Sept. 1977) 79—82582
  narrow band gap semiconductors, conference, Warsaw, Poland (Sept. 1977) 80—49703
  narrow band semiconductor, transport phenomena electron energy spectrum *(Russian)* 79—51616
  nematic liquid crystal, elect. conduct. based on injection-contact phenomena theory *(Russian)* 80—107807
  niobate based ceramics, synthesis, struct., elec. cond., mag. props. *(Czech)* 80—45259
  9-nitroanthracene, semiconductive props., gas adsorpt. effect 79—65471
  p-nitrophenyl p-n octyloxy benzoate, liquid crystal, elec. cond. and dielectric constant, in solid phase 79—61293
  non-linear transport theory, field depend. of carrier screening 80—29415
  non-stoichiometric phase, physico-chemical props. 80—29532
  nondegenerate strongly doped compensated semicond., electron props. *(Russian)* 77—11839
  nonhomogeneous semiconductor, galvanomagnetic effects 79—91077
  p-n octyloxy benzylidine-p-toludine, liquid crystal, elec. cond. and dielectric constant, in solid phase 79—61293
  oil shales, review of thermophysical properties 79—100479
  one-dimensional phenomenological transport equation set 78—39102
  organic free-radical solid conductors and semiconductors, electronic structure 79—35496
  organic molecular crystal, electron mobility, temp. independent, theory 79—69509
  organic molecular crystal, temp.-independ. mobilities, elec. field and defect scatt. effects 80—10963
  organometallic semiconductors, activation energy of elec. cond. rel. to press. 78—24811
  oxide, defect struct., nonstoichiometry and elec. cond., pentavalent oxide dopant effect 80—24442
  oxide ceramic, ferroelectric, with perovskite struct., cond. and polarisation 77—12325
  oxide semiconductor, gas adsorption effect on cond. *(Japanese)* 79—95408
  $Pb_{1-x}Sn_xTe$ film, conductivity dependence on applied strain 78—6465

electrical conductivity of crystalline semiconductors and insulators continued
  n-PbTe, dynamical cond. in freq. range of LO-phonon-plasmon excitations 79—19592
  periclase refractories, props. after testing at over 2000°C 80—104317
  perovskite oxides, ferroelec., point defects and elec. props. 79—42533
  perovskite oxides, point defects, elec. cond., and electron energy spectra 80—70706
  phenothiazine derivatives, semicond. elec. props., optical spectra, and EPR 80—103693
  phosphosilicate films, deposited, P conc. meas. 79—69014
  phthalocyanine-halogen complex, influence of halogen on elec. and optical props. *(Japanese)* 79—51586
  phthalocyanine-halogen complexes, elec. props. 80—29424
  phthalocyanines, elec. cond., compensation effect 80—100455
  picric acid-o-bromoaniline binary system, phase diagram and DC elec. resist. 77—15546
  plasma effects, strongly elongated electron distrib., normal oscills. 80—60021
  polar semiconductor, oscillatory electron drift rel. in non-ohmic regime at low temp. 79—33291
  polar semiconductors, anharmonicity influence on cond. in quantising mag. field 80—2406
  polar semiconductors HF conductivity at low temperatures, anal. *(Russian)* 77—8128
  poly(halo-N-vinylcarbazoles):2,4,7-trinitro-9-fluorenone charge transfer complexes, dark DC cond. 80—39626
  poly-N-vinylcarbazole, synthesis and photocond. props. 77—55563
  polyacene quinone radical copolymer, reversal of usual electric field effect and nomadic polarisation 77—12304
  polyacetylene:AsF_5, thermal decomp. kinetics, elec. cond., ESCA and mass spectra 80—50830
  polyacetylene:I, dc microwave cond., permittivity 80—107843
  polyacetylene, doping with AsF_5, mechanism, effect on elec. cond. and spectra 80—24473
  polyacetylene, pristine and acceptor doped isomers, EPR, DC cond., evidence against solitons 80—15782
  polyacetylene, pure and doped, electronic props. from one-dimens., tight-binding LCAO-SCF-MO calcs. 79—56123
  polyacetylene, pure and heavily doped, optical and IR studies, electronic struct. calcs. 80—7347
  polyacetylene film, heavily doped with AsF_5, conductivity and Hall effect meas. 79—28353
  polycrystalline materials, macroscopic elec. cond. determ. 79—99521
  polycrystalline semiconductor, phenomenological model 77—11908
  polycrystalline semiconductor, residual conductivity, low angle grain boundaries, theory 80—15525
  polycrystalline semiconductors, theoretical models and high-field behaviour *(Czech)* 79—42537
  polydiacetylenes, band struct., ab initio cryst. orbital method, and transport props. calc. 78—26811
  polyethylene, elec. cond. of high and low density samples, oxidation effects 80—107784
  polyethylene, inverse currents, applied voltage, electrode material depend. 78—84206
  polymer, in MIS struct, charge movement study using capacitance-voltage characts. *(French)* 80—39575
  polymer dielectrics, electrical conduction and polarisation phenomena at low fields 78—48113
  polymer films, superconducting magnet insulators, gamma-ray radiation effects 80—24495
  polystyrene, plasma polymerised, free radicals, transient elec. current, EPR, heat treatment 80—71178
  potassium acetylacetonate, polycryst., elec. cond., pyroelectricity, phase transition, UV spectrum 78—76392
  powder compact, appl. of van der Pauw method 78—32833
  PTZ:PMDA, purification, growth, struct., optical and elec. props. 80—54216
  pyrocarbon, Hall effect and conductivity of specimens deposited at 2000 and 2200°C 78—23112
  pyroxene, electrical resist., up to 60 kbar *(German)* 80—31032
  rare earth aluminates, effects of roasting in reducing and oxidizing media on elec. props. 78—52736
  rare earth chalcobismuthites, $RBiTe_3$, prep., elec. props., and crystallographic date 80—59981
  rare earth chalcogenides, cond. mechanism and thermoelec. efficiency 79—38110
  rare earth compounds, R_2MoO_5, cryst. struct., IR spectra, elec. and mag. props. 80—33954
  rare earth compounds, $R_2V_2O_7$, (R=Tm, Yb, Lu), physical props. 78—39320
  rare earth hydrides, props., book contrib. 80—45291
  rare earth monochalcogenides, 4f-6s excitation energy, metallic and insulating elec. props. 80—44603
  rare earth niobates, pyrochlore structure, synthesis and props., 79—11533
  rare earth orthotitanates, $RTiO_3$, metallic and semicond. elec. and mag. props. 79—38068
  rare earth orthotitanates and orthovanadates, interrelationship between cryst. struct., IR spectra and physiochem. props. 77—24835
  rare earth oxides, binary, struct. and props., book contrib. 80—45292
  rare earth oxides, perovskite-like, synthesis, struct., elec. props. 80—65554
  rare earth perovskites, prep. and props. book contrib. 80—44193
  rare earth pyrochlores, $R_2(V_{4/3}W_{3/3})O_7$, (R=Gd, Tb, Dy, Ho, Er, Tm, Xb, Lu), synthesis and elec. props. 80—29914
  rare earth strontium vanadates, $R_{1-x}Sr_xVO_{3-0.1x}$, elec. cond. and mag. susceptibility, temp. depend., 77-300K 77—47816
  rare earth sulphides, $EuRs_4$, R=La, Ce, Pr, Nd, Sm, Gd, elec. cond. meas. 80—65555
  rare earth tungstates, elec. cond. and thermoelec. power meas., band theory 80—20191
  rare earth tungstates and molybdates, A_2BO_6 type, elec. cond., and Meyer-Neldel rule 78—72157
  rare earth vanadites, RVO_3, extrinsic p-type cond. 77—11919
  rare earth-CrO_3, elec. transport 80—70700
  rare-earth-Cu double oxides, catalytic props., mag. props., elec. conductivity 79—66350
  refractory materials used in MHD generator channels, thermophysical props. 77—28054
  refractory oxides, high temp. elec. conduct. 77—28176
  relaxation of nonequilib. electrons at very low temps. 78—60121
  relaxation regime, generalised transport eqns. 78—56139

electrical conductivity of crystalline semiconductors and insulators continued
resistivity, temp. fluctuations and 1/f noise effects 77−20373
resistivity and Hall effect meas., nondestructive four-electrode characterization 80−49743
resistivity meas., two dimensional plotting by SEM 77−39852
resistivity profile meas. using two-probe spreading resistance techniques 80−49742
review, electronic transport in insulators *(Spanish)* 80−84464
rhodusite, electrical resist., up to 60 kbar *(German)* 80−31032
rubidium propanoate, solid state transitions and melting process, diffr. and conductometric meas. 80−10670
ruthenates, $ACu_3Ru_4O_{12}$, A=Na,Ca,Sr,Cd,La,Pr,Nd, synthesis, cryst. struct., mag. and elec. props. *(French)* 80−107151
rutile ceramic anomalous conductivity effect analysis 80−15512
second breakdown electro-thermal model, computer program 77−24561
semiconducting ferroelectric glass-ceramics, dielectric dispersion *(Russian)* 79−8097
semiconductor, absorption of strong EM waves, weak electric field effects 79−95400
semiconductor, anisotropic electrical conductivity, use in thermometry *(Russian)* 79−63211
semiconductor, carrier transport, in presence of temp. gradient, flux method 78−72144
semiconductor, current instability, bifurcation and stability of dynamical structs. 79−91071
semiconductor, degenerate electrons, relax. of spin and energy 80−10965
semiconductor, dislocation cond. process at low temp. 79−99551
semiconductor, dislocation pot., free carrier absorpt. spatial orientation and freq. depend. obs. 80−39546
semiconductor, elec. cond. in quantising mag. field, and electron heating, mutual electron-phonon drag 77−69355
semiconductor, electron quantum states, nonequilibrium current fluctuations in quantised mag. fields *(Russian)* 80−107704
semiconductor, electron scattering by layer of dislocation lines 79−78091
semiconductor, electron scattering by layer struct., geometrical resonances, plasmon and free carrier freq. 79−56212
semiconductor, electron transport phenomena, high-field transport and quantum transport in strong mag. fields *(Japanese)* 77−55526
n-semiconductor, electron-phonon drag in longit. quantising mag. field 77−76805
semiconductor, gapless, bottleneck effect at low temp., hole heating 78−10470
semiconductor, Gaussian diffusion determ., alternative method to angle lap and strain anal., sheet resist. 79−86925
semiconductor, hot electron distrib. in strong electric and quantised mag. fields 79−95417
semiconductor, impurity band props. 79−23888
semiconductor, inhomogeneous, anomalous elec. props. in mag. field 80−44621
semiconductor, inhomogeneous, elec. cond. 77−8087
semiconductor, inhomogeneous, theory of residual cond. 78−14739
semiconductor, nondegenerate, band electrons at arbitrary electron-phonon coupling, transport props. 80−39592
semiconductor, theory of charge transport partly dissociated excitons and impurity atoms 80−44581
semiconductor, with hot electrons, temp. superlattice, transport props. effects *(Russian)* 78−34839
semiconductor characterisation, cond. type determ. by pot. profiling 80−73387
semiconductor crystal, zone melting growth, process parameters influence on radial scatter of resist. 80−16174
semiconductor devices, resistivity and lifetime inhomogeneities, laser scanning method detect. 79−30489
semiconductor galvanomagnetic-effects in strong elec. field 78−56163
semiconductor impurity bands, one-dimens. AMO-MT model validity 79−33256
semiconductor physics, conf., Edinburgh, Scotland (Sept. 1978) 79−95303
semiconductor transport props., effect of temp. depend. band shifts 77−55522
semiconductor wafer resistivity distribution, contactless meas. *(Polish)* 77−79102
semiconductor with anisotropic conductivity, elec. and photoelec. props., review 78−10447
semiconductor with charged defects, elec. cond. and magnetoresist. 80−20225
semiconductor with energy-dependent relax. time, expression for cond. 79−56268
semiconductor with grain boundary barriers, thermal breakdown 78−39171
semiconductor with position depend. band struct., electron and hole currents 78−43377
semiconductor with superlattice, high freq. cond. 79−69542
semiconductors, differential conductivity with inelastic electron scatt. *(Russian)* 80−2399
semiconductors, elec. cond. in elec. and mag. fields, carrier scatt. mechanisms 79−65467
semiconductors, electrical properties calculated from thermophysical and thermomagnetic effects 79−73535
semiconductors, electrical resistance, exam at high temp. using inductive heating 79−7816
semiconductors, grain-boundary resist., DC voltage depend. 79−82597
semiconductors, kinetic effects at high anisotropic strains, elec. transport props. meas. 78−54384
semiconductors, n-type, metal-insulator transition and negative resist. effects 79−24026
semiconductors, nonequilib. electron and phonon fluctuations *(Russian)* 77−80770
semiconductors, temp. depend. electronic cond., review 80−59975
semiconductors, thermoelectrically anisotropic, carrier kinetics at low temp. 80−92893
semiconductors, thermoelectrically anisotropic 80−92894
semiconductors with grain-boundary barriers, boundary states' energy struct. influence on elec. cond. 79−11147
semiconductors with impurities, electron cond. temp. and freq. depend., two band model *(Russian)* 80−75564
semiconductors with neutral impurity, transverse cond. in quantising mag. fields, finite radius scatterers *(Russian)* 80−29400
semimetal, compensated, hydrodynamic cond., surface scatt. and phonon drag *(Russian)* 77−8088

electrical conductivity of crystalline semiconductors and insulators continued
semimetal, degenerate, anisotropic scattering at low temp. *(Russian)* 78−95298
semimetals, exciton phase, transport effect in strong mag. fields 78−87977
n-Si, elec. cond. in weakly heating alternating elec. field 79−23977
p-Si, interstitial Fe and thermal defects, Hall effect and resist. meas. 79−82200
Si poly-oxide leakage current and conductivity reduction expts. 77−76990
sisal wax, electronic conduction and persistent internal polarisation 78−80277
slice resistivity distrib., contactless meas. results *(Polish)* 77−89756
solid state physics, conf. Munster, Germany (March 1979) 80−41941
solid-state electronics, introductory theory, book 80−22160
soot, granulated, thermal and elec. cond. 80−24687
spinel ferrites, electrical resistivity and hardness 77−43596
spinel structures, electroconductivity and electron exchange 78−84207
spreading resistances, multilayer analysis, errors in resistivities 80−10964
spreading-resistance meas. for doping profile determ., preprocessing of data for resistivity calcs. 80−57265
Stark-Ladder current theory 78−68035
stilbene, single cryst., free charges and excitons generated by electron pulses 78−63988
sulphide group minerals, using four point probe technique, effects of cracks 78−64045
superlattice, nonlinear HF conductivity 77−15889
surface charges produced in photoconductor-air gap-semicond. system, calc. 80−6905
surface resistivity, effect of hydrofluoric acid treatment 78−10537
TCNQ, salt, DBTTF-TCNQ, elec. resistivity and thermoelec. power meas. 80−20193
$(TCNQ)_2$ benzacridinium, small bandgap semicond., cond. and thermoelec. power meas. 77−35946
TCNQ complexes with N-methyl derivatives of pyridine, cond. and thermoelec. power meas., band model anal. 80−10952
TCNQ salt, $(DEPE)(TCNQ)_4$, elec. props., semicond. behaviour obs., no stable metallic state 77−51772
TCNQ salt, $Cs_2(TCNQ)_3$, elec. cond. and elastic const., mol. bending *(Korean)* 78−23090
TCNQ salt, Rb-TCNQ-II, two carrier cond. 80−44625
TCNQ salts, elec. cond. spectrum fine struct. 80−96884
$TEA(TCNQ)_2$, elec. cond. and thermoelec. power under hydrostatic press. 80−11024
temperature dependences meas., automated installation 80−31792
p-terphenyl, carrier generation and transport, temp. depend. around phase transition at 180K 78−47783
tetraselenotetracene, electronic structure, conductivity studied by ESCA 79−4889
tetraselenotetracene iodides, struct. and physical props., DC electrical cond. and EPR linewidth meas. 80−103312
tetrathionaphthalene, electronic structure, conductivity studied by ESCA 79−4889
tetrathiotetracene, electronic structure, conductivity studied by ESCA 79−4889
TGS:nitroanilines, permittivity, elec. cond. and Curie temp. 80−25273
TGS, pure and with lattice defects, elec. cond. 79−42538
thallium hexanoate, soliton conduction, elec. cond. field and temp. depend. anomaly *(Russian)* 80−103703
thermal instability in semicond. based on effective thermal time const. 79−15155
thermal probe for cond. type determ. 77−37900
thinned semiconductor device, SEM, electron beam induced cond. of defects, rel. to TEM 80−107027
$(TMTSF)_2PF_6$ (AsF_6), linear-chain conductor, semicond.-metal transition in small elec. field 80−103730
transition metal chalcogenides, quasi-one-dimens., elec. mag., and supercond. props., review *(Russian)* 80−93022
transition metal compound refractories, electron and phonon behaviour 80−54624
transition metal dichalcogenides, physical props., review *(Japanese)* 80−33969
transition metal double oxides, exam. of elec. cond. 78−51990
transition metal intercalates of Ni and Ta dichalcogenides, Hall coefficient and resistivity 80−39610
transition metal pnictides, atomic volume, semicond. props. 78−59780
transition metal pyrites, mag. and elec. props., review *(Japanese)* 78−47941
transition metal sulphides, selenides and phosphides, NaCl struct., supercond. props., elec. resist. up to room temp. 79−4613
transition metal vanadates, elec. and mag. props., stoichiometry 78−51991
transmutation doped, stabilisation 78−10449
urea nitrate single cryst., elec. cond. anisotropy 78−79807
violanthrene-A film, amorphous and crystalline, carrier mobility differences 78−60125
volume and contact parameter determ. from V-I characteristic *(Russian)* 80−49912
W-dichalcogenide, valence band nature, elec. and mag. props 78−39014
wafer, influence of discontinuous resist. distrib. on results of four-point probe method meas. 77−39841
zeolite A, synthetic, with salt inclusions, elec. and thermal props. 79−55925
zinc blende semiconductors, small-gap, electron scatt. and transport props. 78−95294
zincblende narrow-gap mixed crystals, disorder scatt. 78−51985
n-ZnSe:In, highly compensated, freq. depend. of cond. 79−99548
Si:P, sheet resistance of Gaussian n-type ion-implanted layers 79−87103
Ag_3AsS_3, proustite, elec. cond. rel. to impurities, melt stoichiometry deviations 77−11914
Ag_3AsS_3, proustite, residual conductivity and low-temp. phase transitions 78−91729
Ag_7AsS_6, thermal, crystallographic and elec. props. *(French)* 80−40338
Ag_7AsSe_6, thermal, crystallographic and elec. props. *(French)* 80−40338
AgBr, reversible variations meas. 78−10588
$AgFeSe_2(S_2)(Te_2)$, elec. props., band gap *(Russian)* 79−11116
n-Ag_8GeSe_6, elec. cond. and photoelec. props. 77−69380
AgI group superionic conductor, phase transition detection by thermoelectric power method 80−92669

electrical conductivity of crystalline semiconductors and insulators continued
AgI-HgI$_2$, solid electrolyte, ionic and electronic cond., phase composition determ. 78−2296
AgN$_3$, high-resist. explosive cpd., elec. and galvanomag. props., temp. depend. 80−103728
Ag$_x$Na$_{2-x}$Te$_2^{IV}$Te$_3^{VI}$O$_{14}$, (x=0,4), mixed tellurate, cryst. chem. and elec. cond. *(French)* 80−107150
β-Ag$_2$S, electrogalvanic and elec. props., and range of existence *(French)* 78−43175
α-Ag$_2$S, electronic and electrogalvanic props. *(French)* 78−84237
Ag$_2$S, transport props., 700-1500K 78−47796
Ag$_2$S(Se)(Te), changes in elec. cond. and thermoelec. power at melting point 79−15147
β-AgSbS$_2$, phase transitions, electrophysical props. 80−44316
Ag$_3$SbS$_3$, pyrargyrite, elec. cond. rel. to impurities, melt stoichiometry deviations 77−11914
Ag$_3$SbS$_3$, pyrargyrite, electronic to ionic conductivity ratio *(Russian)* 77−80818
Ag$_3$SbS$_3$. piezoelec. semicond., residual cond., ultrasound photoabsorpt. *(Russian)* 78−72465
Ag$_2$Se(Te), single cryst. growth by chem. transport, and characterisation 77−36380
p-Ag$_2$Te, electrophysical props. 77−39842
Ag$_2$Te-Ag$_2$S system, elec. and thermal props. at 300K 78−64044
Al-anodised Ta$_2$O$_3$/native oxide-n-GaAs MOS structure evaluation 80−84514
AlB$_{12}$, α- and β-forms, elec. props. at high temps. and in strong elec. fields, thermistor appls. 80−92903
α-AlB$_{12}$, heavily doped, elec. props. 78−10446
α-AlB$_{12}$, prep. and electrothermal props. 80−20863
AlB$_2$ electronic struct. calcs. 78−2417
n-Al$_x$Ga$_{1-x}$As, electrical props. 78−6381
p-Al$_x$Ga$_{1-x}$As:Ge layer on GaAs substrate, Hall and elec. cond. meas., Hall mobility 80−2402
Al$_x$Ga$_{1-x}$As:Mg doping characteristics, elec. props., effective hole masses 79−78117
AlH$_3$, dark electrical cond., exam. 80−39624
AlH$_3$, I-V and relax. characts. in dark cond. 77−85235
Al$_2$In$_{12}$S$_{21}$, preparation, struct. and elec. props. 77−59685
Al$_2$In$_{12}$Se$_{21}$, cryst. growth from melt, elec. props. 79−56922
AlMgB$_{14}$, prep. and electrothermal props. 80−20863
Al$_{2+x}$O$_3$, nonstoichiometric, DC and AC cond., 20 to 1200°C 77−51740
Al$_2$O$_3$, acceptor-dominated polycrystn., cond. and creep 79−78109
Al$_2$O$_3$, conductivity near melting point 77−28176
Al$_2$O$_3$, elec. props. under isentropic compression up to 500 GPa 78−71789
Al$_2$O$_3$ film, Al embedded, non-ohmic conduction behaviour 78−64157
Al$_2$O$_3$ scales on Pt-Al alloy, elec. props. 79−20282
α-Al$_2$O$_3$, unintentionally doped, defect struct. 79−60755
Al$_2$O$_3$:Cr, pure and doped, electron irrad. induced cond., TSC and EPR study 80−80277
α-Al$_2$O$_3$:Ti, defect struct., electronic and ionic cond., optical absorption meas. 78−30603
Al$_2$O$_3$:Zr ceramic, elec. props., additives effect, and interaction with steel melt 80−104305
β-Al$_2$O$_3$-H$^+$(H$_2$O)$_n$, p-type conductor, stability *(French)* 79−38063
β-Al$_2$O$_3$-NH$_4^+$, p-type conductor, stability *(French)* 79−38063
As, electrical and thermal props. 78−14747
As, electrical resist., thermal cond. and thermopower, low temp. transport props. 80−49708
As, electrical resist. and anisotropy at press. up to 80 kbar 77−43554
As, electrical resistivity meas., 50 mK-7K 79−60839
As$_2$Se$_3$, crystalline, electron drift mobility and DC cond., trapping model 77−47815
As$_2$Te$_3$, phase transitions and elec. cond. 78−10440
AuBr, α, I, P and BCC forms, transitions 78−38836
B, β-rhombohedral, elec. props. at high temps. and in strong elec. fields, thermistor appls. 80−92903
B, β-rhombohedral, field effect on hopping cond. 79−82589
B filaments, CVD prep., elec. resist. 80−15523
B modifications, exam. of physical props. and electron structure 79−94954
B, preparation and purification, physical characterisation *(French)* 80−16189
B, purity evaluation by elec. meas. 78−59822
β-B, rhombohedral, AC cond. meas., 150 to 300K, hopping cond. mechanisms 80−15521
β-B, rhombohedral, EPR intensity correl. with elec. cond., book contrib. 78−48041
α-B, rhombohedral, elec. cond., thermoelec. power, and Hall coeff. 80−6843
β-B, rhombohedral, high field elec. cond., single voltage pulse meas. 80−20201
β-B, rhombohedral, influence of impurities on elec. cond. 77−4345
β-B, rhombohedral, Knoop hardness and room temp. resist., rel to purity 80−21084
β-B, rhombohedral, thermally activated hopping, 140-300K 80−20189
B, zone melting, solar energy appl., struct. and elec. props. 77−16492
B, zone-refined effect of Ni doping on conductivity type, microhardness and metallographic obs. 77−31682
BC, EPR, book contrib. intensity correl. with elec. cond., Hall coeff., book contrib. 78−48041
BC, sintered, struct. and props. 80−104181
B$_{12}$C$_3$, sintering and subsequent high temp. annealing, struct. and props. 80−20858
B$_4$C, thermophysical props. and neutron absorpt. 80−103488
B$_x$Cy, metal-insulator transition, elec. cond. and thermoelec. power, 80 to 700K 80−44673
BN fibres, prep., struct., thermal, mech. and elec. props., appls., book contrib. 78−48360
BP, cryst. growth from Cu-fluxed melt, and characterisation 77−85920
B$_{14}$Si, β rhombohedral, conduction mechanism, thermoelectric props. 80−24932
B$_{14}$Si elec. props., medium range disorder model 80−15522
Ba-ferrite, temp. range 303 to 353K 79−42564
Ba$_2$Bi^{3+}Bi^{5+}O$_6$, structure and elec., mag., thermal props. vs. temp. X-ray and neutron powder diffr. study 79−19189
BaCuO$_2$, prep. and props. *(French)* 77−43201
BaCuO$_{2+x}$ ($0 \leq x \leq 0.12$), study of mag. and elec. props. rel. to the non-stoichiometry *(French)* 78−95051
BaF$_2$, elec. cond. of shock-compressed monocrystals 77−9404

electrical conductivity of crystalline semiconductors and insulators continued
BaF$_2$, powder, elec. cond. transition under high press. *(Russian)* 77−20370
BaF$_2$ solid electrolyte, n-type electronic cond., 700-900°C 80−29448
BaFe$_{12}$O$_{19}$, ferrite, DC cond., dielec. props., lattice consts. 80−80272
BaFe$_{12}$O$_{19}$, Hall effect, magnetisation and elec. resist., 30 to 80°C 77−51766
BaHfO$_3$, BaSnO$_3$ and BaZrO$_3$, high-density ceramics prep. and elec. props. 80−60812
Ba$_x$I$_y$ cyclodextrin, quasi-one-dimens. cpd., synthesis, elec. and mag. props. 80−2380
Ba$_x$La$_{1-x}$CoO$_3$, x=0 to 0.5, structural, elec. and mag. props., Zener double exchange and Goodenough's model 79−65663
BaM$_2$(PO$_4$)$_2$, M=Co, Ni, Mg, Zn, dielec. permittivity and elec. resist., temp. depend. 77−59502
BaMoO$_3$, perovskite-type cmpd., metallic conductivity, room temp. to 2.5K 79−65483
Ba$_2$MoO$_5$, Ba$_3$MoO$_6$, electrophys. props., effects of thermophys. props. of medium in synthesis 77−48375
Ba(NO$_3$)$_2$, low temp. struct. changes, elec. props. 79−87377
BaNb$_x^{V}$Ti$_x^{III}$Ti$_{1-x}^{IV}$O$_3$, A and C-domain crysts., elec. cond. and absorption spectra 77−47805
BaO-SiO$_2$-Fe$_2$O$_3$ permanent mag. ceramics, exam. of phase diagram, using X-ray analysis, optical microscopy, electron probe anal., and thermal analysis *(German)* 79−29012
Ba$_3$Re$_2$O$_9$, cryst. struct., mag. and semicond. props. 79−10836
Ba$_3$Sc$_4$O$_9$, Ba$_3$Sc$_2$WO$_9$ and Ba$_2$ScTaO$_6$, elec. cond. nature, depend. on comp. and medium thermodynamic parameters 80−70773
Ba$_{1-x}$Sm$_x$B$_6$, prep., elec. cond. and thermoelec. props. 80−49697
Ba$_{0.5}$Sr$_{0.5}$Nb$_2$O$_6$, electronic props. and photoresponses 80−92925
Ba$_x$Sr$_{1-x}$Nb$_2$O$_6$, reduced, effect of oxygen vacancies 77−35939
BaTiO$_3$, acceptor doped, exam. of electrical conductivity 130 to 300°C 79−33286
BaTiO$_3$, acceptor-doped defect equilibria, elec. cond. 77−39579
BaTiO$_3$ and BaTi$_{1-x}$Fe$_x$O$_{3-x}$F$_x$, electrical, optical and mag. props., photoelectrolysis 77−47856
n-BaTiO$_3$, ceramic, expt. and theoretical investigation of grain-boundary resist. 79−56235
BaTiO$_3$ ceramic, PTC-type, voltage contrast imaging for low and high Ti excess 77−28183
BaTiO$_3$ ceramic, positive temp. coeff. resistivity, investigation as function of Ti-Ba ratio 78−72151
n-BaTiO$_3$, ceramic, systematic expt. and theoretical investigation of grain-boundary resist. 79−56236
BaTiO$_3$, defect chem., elec. cond. obs. 77−4097
BaTiO$_3$, defect chemistry and elec. cond. improved positive temp. coeff. model 77−39859
BaTiO$_3$, donor doped, elec. props., effect of kinetic processes 78−64042
BaTiO$_3$, donor doped, exam. of heterogeneous microstructure *(German)* 79−24632
BaTiO$_3$, exam. of PTC effect as function of Ti excess *(German)* 79−23960
n-BaTiO$_3$, grain boundary resistivities 77−80782
BaTiO$_3$, H$_2$-reduced, elec. cond. mechanism, EPR, resist. and Seebeck coeff. meas. 80−10976
BaTiO$_3$, perovskite structure, semiconductor props. *(Polish)* 78−56437
BaTiO$_3$, polycryst., elec. resist. anomaly in phase transition region 78−43381
BaTiO$_3$, single cryst., elec. cond., 800-1200°C, nonstoichiometric disorder 78−51989
BaTiO$_3$:C, solubility of C at low O$_2$ potentials, 800°C 80−100334
BaTiO$_3$:La, Sb, second phase effect on elec. and mag. props. 80−60986
BaTiO$_3$:La and undoped, defect chemistry elec. cond. at high temp. meas. 77−39858
BaTiO$_3$:Mn, polycrystn., annealing effect on transition temps. 80−3100
BaTiO$_3$:Nb, elec. props., contact material influence 80−70848
BaTiO$_3$:Nb, ferroelec. and paraelec. phases, props. 79−42919
BaTiO$_3$:SnO$_2$, transition temperature shift, resistivity anomaly obs. *(Korean)* 77−39856
BaTiO$_3$-Ni(Co, Mn)Fe$_2$O$_4$, ceramic, exam. of prep. and physical props. 78−68655
Ba$_{0.15}$VO$_2$, electrical cond., thermo-EMF, and lattice consts. 80−54685
BaVS$_3$, mag. and elec. props. 79−91214
BaV$_x$Ti$_{1-x}$S$_3$, mag. and elec. props. 79−91214
Ba$_2$XRuO$_6$(X=La,Eu), ^{99}Ru Mossbauer spectra and other techniques 80−29659
(Ba$_{1-x}$Y$_x$)TiO$_3$ ceramic, resistivity rel. to donor dopant content 79−65474
BaZrO$_3$-LaAlO$_3$ systems, sintering conditions, elec. props. 79−43184
Ba[Pt(CN)$_4$].4H$_2$O, DC elec. cond. props. 79−51582
(Be, Al)B$_{12}$, wide-gap semicond., elec. cond., refl. and absorpt. spectra 80−20188
BeTeI, cryst. struct., semimetallic nature, elec. resist. and Hall coeff. meas. 77−28788
Bi and Bi:Te, neutron radiation defects 78−47430
Bi, Bi-Pb and Bi-Sn, elec. cond. and thermal EMF at press. up to 12 kbar 77−47806
Bi, diffusion size effects 79−60824
Bi, elec. resist. meas., 1.1 to 100K 77−69321
Bi, electrical resist., thermal cond. and thermopower, low temp. transport props. 80−49708
Bi, electrical resistivity, electron-hole scatt. 77−4331
Bi, electrical resistivity due to electron-phonon scatt. on small cylindrical Fermi surface 79−4562
Bi, electron irrad., displacement threshold energy *(French)* 79−23649
Bi, growth of single cryst. wires with high resistivity ratios 78−68622
Bi microcontact, resistivity at low temp. *(Russian)* 78−80054
Bi, nonlinear properties under sound generation conditions 79−60845
Bi, phonon generation rate, nonreciprocity of current-voltage curve *(Russian)* 77−89776
Bi, polycryst., grain boundary scattering effect on temp. depend. of electroresistivity, galvanomagnetic effect *(Russian)* 78−56148
Bi, quenching and annealing of defects, elec. resist. meas. 78−87973
Bi, recrystn., effect of Sb, Sn and Pb 78−52841
Bi, resistivity at ultralow temp., high precision meas., scatt. mechanisms 77−80776
Bi, single crystal, drift velocity of charge carriers *(Russian)* 78−84208
Bi whiskers, elec. resist. under strain *(Russian)* 79−91164
Bi, whiskers, hardness, elec. props. *(Russian)* 78−51874
Bi:Sb(Te), quenching and annealing of defects, elec. resist. meas. 78−87973

electrical conductivity of crystalline semiconductors and insulators continued
Bi:Sn,Te, and undoped sample, low-temp. transport meas., electron scatt. 77–24551
Bi:Te(Sn) , elec. resist., 1.8 to 77K, electron-phonon scatt. mechanism 79–15144
Bi-Sb, semiconducting solid solution, forbidden band width Sb-conc. depend. 77–66117
Bi-Sb, single cryst., semimetal-semicond. transition. cond. 77–1459
Bi-Sb alloy films, quantum size effect *(Russian)* 77–85351
Bi-Sb alloys, thermomagnetic quality factor 77–15882
Bi-Sn, superconductive microsegregations, 3.7K resist. drop 79–69646
$Bi_{12}GeO_{20}$, electrophys., props. determ. *(Russian)* 78–51987
Bi_2O_3, polymorphic transformation and elec. resistivity *(Japanese)* 80–93555
Bi_2O_3, thermoelec. props., 500-1500K 80–29423
Bi_2O_3-Mo(W)O_3 system, elec. cond. and dielec. const. obs. 77–89816
Bi_2O_3-ZnO(CdO), elec. cond., dielec. const., mag. susceptibility meas., effect of melting transition 77–7849
Bi_2S_3-$CuPbBi_5S_9$, solid solution, semiconductor and dielectric props. 79–69511
$Bi_{0.88}Sb_{0.12}$, semiconducting transport props., 2 to 100K 80–59989
$Bi_{1-x}Sb_x$, elec. resist., 1.8 to 77K, electron-phonon scatt. mechanism 79–15144
$Bi_{1-x}Sb_x$, semicond. alloy, mag. freeze-out effect, superlow temps. *(Russian)* 77–89775
$Bi_{1-x}Sb_x$, semiconductor, anomalous conductance in strong electric and longit. quantised mag. field *(Russian)* 78–76084
$Bi_{1-x}Sb_x$, thin film, elec. props., composition variations *(Russian)* 79–7841
$Bi_{2-x}Sb_xTe_{3-y}Se_y$, elec. cond. and thermoelec. props., neutral defects influence 80–60017
$Bi_{2-x}Sb_xTe_{3-y}Se_y$ solid solution, density-of-states effective mass, carrier mobility temp. depend. 80–24931
ρ-BiSe, single crystal, synthesis and elec. props. 77–16490
p-Bi_2Se cryst. growth, elec. props. 77–8748
n-Bi_2Se_3, cryst. nonparabolic cond. band., IR refl. and Hall voltage meas. 77–31940
n-Bi_2Se_3, single cryst., new aspect of carrier scatt. 80–49707
Bi_2Se_3:Sn(Pb), dopant influence on elec. cond. 79–51569
$Bi_2Sn_2O_7$, polymorphic phase transition, X-ray, DSC, SHG, dielec. and optical obs. 80–44163
Bi_2Te_3, galvanothermomag. props. up to 14 kbar 77–47829
n-Bi_2Te_3, galvonomagnetic props., influence of hydrostatic press. 79–73536
Bi_2Te_3-Bi_2Se_3 solid solns., bladed cryst. growth, electrophysical props. 78–43387
Bi_2Te_3-Bi_2Se_3-Sb_2Te_3, solid solution, single crystal, elec. cond., thermoelectric props. 80–88550
Bi_2Te_3-InTe, thermoelec. props. 77–85250
Bi_2Te_3-Sb_2Te_3:Cu, electrical cond. and thermopower, disorder effects *(German)* 77–1422
Bi_2Te_3-$SbTe_3$, ordered structure formation, heat treatment effect on thermal cond. 80–54448
BiTeI, elec. props., crysts. grown from melt in excess iodine 79–4907
BiTeI-SbTeI solid solns., form., crystn., elec., thermal props. 78–44003
$(Bi_2Te_3)_{0.9}(Sb_2Te_3)_{0.5}(Sb_2Se_3)_{0.05}$ n-type alloy for thermogenerators, thermo-EMF, elec. cond. and thermoelec. efficiency factor, 300-600K 80–70735
$Bi_2Te_{3-x}Se_x$ solid solution, Hall effect anisotropy parameter, thermoelectric power, depend. on carrier density 79–69536
$Bi_4Ti_3O_{12}$, elec. characts., phase transition obs. 80–60517
$Bi_2(Ti_{1-x}S_x)_3$, thin crysts., adsorpt. effects on elec. cond. 78–19034
Bi_2WO_6, ferroelectric, dielectric props., elec. cond. and relaxation phenomena obs. 80–80692
C, diamond like, graphitisation, elec. resist. meas., 30-550°C *(Russian)* 77–39676
C fibre reinforced Al, mech. props. 80–11708
C fibre reinforced epoxy phenol plastic, resistance to interlayer shear and elec. resistivity 78–68752
C fibre reinforced plastic, deform. and failure using AE method *(Russian)* 80–40630
C resistors as low temp. sensors in low temp. reactors, gamma, neutron irrad. investig. 77–45848
C-C composites, existence diagram and properties *(French)* 78–64517
C-PVC composite, transport props. 79–38073
$C_{8n}AsF_5$, intercalation cpd., elec. cond. theory 80–44686
$C_8Br_xCl_{1-x}$ intercalate, crystallographic, elec., mag. props. 80–107184
$C_{24}Rb$, intercalated graphite, resistivity and specific heat anomalies 80–107440
$CaCO_3$, calcite, elec. cond., 300 to 1200°C at CO_2 pressure of 40 bars 80–20195
$CaCo_2(PO_4)_2$, dielectric permittivity and elec. resist., temp. depend. 77–59502
CaF_2 crystals, elec. cond., O^{2-} effect 80–2431
CaF_2, elec. cond. at high temp. 78–72159
CaF_2, elec. cond. of shock-compressed monocrystals 77–9404
CaF_2, powder, elec. cond. transition under high press. *(Russian)* 77–20370
$CaIr_xTi_{1-x}O_3$, semiconductor, struct., mag. and elec. props. 79–91046
$Ca_2LaFe_3O_{8+x}$, influence of O_2 partial pressure on nature of point defects, characterisation by elec. cond. meas. *(French)* 79–42055
$CaMnO_3$, microstruct., elec. cond., thermoEMF 78–23084
$Ca_2MnO_{4-x}F_x$, antiferromagnetic props. and elec. cond. *(French)* 80–29526
$CaMoO_3$, perovskite-type cmpd., metallic conductivity, room temp. to 2.5K 79–65483
$CaMoO_4$, electrical cond. and ionic transport number meas., defect struct. model 80–2388
$CaNd_{3/2}Nb_{3/2}O_7$, pyrochlore struct., synthesis elec. props. 79–42543
$CaSO_4$:Dy, cryst. growth from soln., thermoelec. and thermoluminesc. props. 79–56923
Ca_3SiO_5-$Cr_2O_3(Al_2O_3)(Fe_2O_3)$ solid solns., elec. cond., 800-1000°C, hydration 80–54683
$CaSnO_3$ and $CaZrO_3$, high-density ceramics prep. and elec. props. 80–60812
$Ca_{0.15}VO_2$, electrical cond., thermo-EMF, and lattice consts. 80–54685
$CaWO_4$, solid-phase synthesis, disordering and vacancy defect form. 77–8774
Ca_2XRuO_6 (X=Y,La,Eu), ^{99}Ru Mossbauer spectra and other techniques 80–29659
Cd-Sb, near CdSb, Hall coeff., resistivity 79–56216

electrical conductivity of crystalline semiconductors and insulators continued
Cd-Sb (53-100%), elec. resist. temp. depend. 77–59285
$CdAs_2$, synthesis, microstruct., hardness and elec. cond. 79–51268
Cd_3As_2, effect of annealing on elec. transport props. 80–49739
Cd_3As_2, elec. resist. and HF dielec. const. calcs. *(French)* 77–59284
$CdCr_2S_4$, $CdCr_2Se_4$, variation of elec. props. with chalcogen content of gas phase, 500-700°C 77–20310
$CdCr_2S_4$ crystal growth, structural defects, physical properties 80–60759
$CdCr_2S_4$ ferromag. semicond. film, props. 78–76175
p-$CdCr_2S_4$, single cryst., elec. cond. 79–15148
$CdCr_2S_4$:Cu, magnetic microregions caused by s-d exchange 77–77050
$CdCr_2S_4$:Gd, ferromag. reson. and electrical cond. 79–28626
$CdCr_2S_4$:In, single cryst. prep. and elec. props. 79–38727
$CdCr_2S_4$:In(Ga), resist. and magnetoresist. meas., effect of donor impurities 79–19608
$CdCr_2Se_4$, ferromag. semicond., conc. anomalies rel. to red shift of absorpt. edge 80–70732
$CdCr_2Se_4$, narrow conduction band, crit. behaviour of resistivity 79–78096
p-$CdCr_2Se_4$, resistivity anomalies at mag. transitions, sp.ht. 80–39785
$CdCr_2Se_4$ single cryst., photocond. in air, vacuum, mechanism 77–8138
$CdCr_2Se_4$, temp. depend. of resist. and magnetoresist., influence of Se vacancies 78–60130
p-$CdCr_2Se_4$:Ag, electrical props., 100-300K 80–54692
$CdCr_2Se_4$:Ag, magneto-electrical props. temp. behaviour depend. on dopant conc. *(Russian)* 80–11006
$CdCr_2Se_4$:Ga, sp. elec. resist., temp. and mag. field depends. *(Russian)* 78–26893
$CdCr_2Se_4$:In, elec. cond., annealing effect 79–87102
n-$CdCr_2Se_4$:In, electrical props., 93-168K 80–49713
$CdCr_2Se_4$:In, influence of Se-deficiency on props. 78–30921
$CdCr_2Se_4$:In (Ga)(Ag), and undoped, elec. prop., vac. heat treatment effect 80–15518
$CdCr_2Se_4$:In(Ga), elec. resist. and magnetoresist., 2 to 200K 80–96876
$CdCr_2Se_4$:In(Ga), temp. driven metal-semiconductor transition, temp. and mag. field depend. *(Russian)* 78–88003
$CdCr_2Se_4$:In(Ga)(Cu), magnetic microregions caused by s-d exchange 77–77050
$Cd_{1-x}Cu_xCr_2S_4$, temp. depend., behaviour at Curie point 77–62929
$Cd_{0.96}Cu_{0.04}Cr_2Se_4$, single cryst., elec. resis., depend. on Cu content and temp. 79–7848
CdF_2, conversion into semicond. by heating in H_2 atm., resist. meas. 80–20978
CdF_2, MnF_2 or rare earth fluoride doped, elec. cond. and electroluminesc. 79–87508
CdF_2: rare earth, electronic props., compared to CaF_2 *(French)* 80–49662
CdF_2:Eu(Gd)(Nd), semicond., symmetry of optical centres, optical and elec. props. 77–59592
CdF_2:Ge^{3+}, Ce^{3+}, in semicond. state, elec. cond. and Hall meas. 78–10443
CdF_2:Mn, Y, deconversion due to vacuum heat treatment, elec. resist. and electron probe meas. 79–24025
CdF_2:Mn^{2+},Y^{3+}, thermal stability under vacuum, effect of heat treatment on resist. 79–23969
CdF_2:YbF_3, conversion processes into semiconductor 78–14730
CdF_2-YF_3, thermal ionisation energy of monovalent centres 80–80207
$Cd_{1-x}Fe_xCr_2S_4$:Cu, effect of doping on elec. props. and Curie temp. 78–84214
$Cd_xFe_{3-x}O_4$, cond. mechanism, collective electron description 77–4588
$CdGeAs_2$, cryst. growth and elec. props. *(French)* 77–59682
$CdGeAs_2$, electron irradiated, change in electrical props. 79–7829
$CdGeAs_2$, optical and elec. props. 79–19590
n-$CdGeAs_2$:In(Te), resist. and Hall coeff. meas., influence of press. 77–47810
n-Cd_2GeO_4, electronic and cond. props. rel. to prep. conditions and defect struct. 80–107787
Cd_2GeO_4, n-type, prep. and photoelectronic props. 80–39628
$CdGeP_2$, cond. compensation by electron bombardment 79–15151
$CdGeP_2$:Cu, impurity behaviour 77–15857
$CdGu_2S_{4(1-x)}Se_{4x}$, opt. absorpt., elec. cond., spectral response, thermopower 77–72862
$Cd_xHg_{1-x}Se$, 77-400K *(Russian)* 78–2485
$Cd_xHg_{1-x}Se$, carrier mobility, 4.2 to 300K, scatt. mechanisms 79–4561
$Cd_xHg_{1-x}Se$, narrow band gap semicond., electron scatt., and transport phenomena 80–49706
$Cd_xHg_{1-x}Te$ crystals, donor compensation, low temp. cond. study 80–75571
$Cd_xHg_{1-x}Te$, electron irradiated, elec. and recomb. characts. 78–39113
$Cd_xHg_{1-x}Te$, epitaxial graded-gap layers, elec. transport props. 77–85358
$Cd_xHg_{1-x}Te$, fine-graded gap struct., electrophysical props. *(Russian)* 78–60144
$Cd_xHg_{1-x}Te$, IR detector appls., prep., elec. props. *(German)* 78–86332
n-$Cd_xHg_{1-x}Te$, in strong mag. field, current-voltage characts., current instabilities 78–87980
$Cd_xHg_{1-x}Te$, low temp. piezoresistance, Hall effect, elec. cond., plastic flow 80–6844
$Cd_xHg_{1-x}Te$, resistivity, Hall effect and magnetoresist. in strong elec. field 77–28199
$Cd_xHg_{1-x}Te$, solid solns., role of stoichiometry defects 77–47813
$Cd_xHg_{1-x}Te$, strong elec. field effect on galvanomagnetic effects 79–11159
$Cd_xHg_{1-x}Te$, zero gap semiconductor, interband optical-phonon scattering 80–6846
n-$Cd_{1-x}In_xCr_2Se_4$, effect of doping on elec. cond. and magnetoresist. 78–72174
$Cd_{1-x}In_xCr_2Se_4$, electric, photoelectric and mag. props., metal-semicond. transition *(Russian)* 80–54738
$CdIn_2O_4$, crystal growth from flux, elec. and struct. props. 77–81206
$Cd_{1-x}M_xS$ (M=Sr, Ca, Mg, Pb, Sn), solid soln., prep. and semicond. props. 80–2383
CdO, effect of compacting pressure on consolidation and elec. cond. 79–29007
CdO, elec. cond. and IR refl. spectra after sintering and compaction 79–56945
CdO, influence of initial compacting press. on elec. resis. Hall coeff. 80–20872
n-CdO, polycryst., 25-650°C, dependence on O_2 pressure 78–34830
$Cd_3O_2Cl_2$, electrical conductivity 77–43589

electrical conductivity of crystalline semiconductors and insulators continued
Cd_3OF_4, electrical conductivity temp. quasi-independ., novel semiconductor 77−43589
$Cd_4P_2Cl_3(Br_3)(I_3)$, elec. and photoelec. props. 80−34480
CdS, electron-exciton elastic scatt. cross sections, central field and exchange approxs. 77−62919
CdS, grown from high temp. alkaline solns. 77−52240
CdS, high pressure effects on electrical resistivity and structure 77−15574
CdS, obtained from CdS-Cr_2O_3 system, α-Cr_2O_3 effect on props. *(Russian)* 79−65469
CdS, plastic deform. and annealing effects 77−55534
CdS, plastically deformed, optical and electronic transport anisotropies 77−8611
CdS, plastically deformed, electronic transport and optical props. 79−73508
CdS, porous, dynamic phase transition at high press. 79−23723
CdS, prepared by ceramic Technol., physical props. 79−60837
CdS, semicond. piezoelec. crysts., US determ. of cond. 77−1456
CdS, single crystal, growth by modified Piper-Polich method, props. *(Japanese)* 79−100036
CdS thin layers, recryst. from CdS-Cr_2O_3 mixtures, phys. and photoelec. props. 80−96935
CdS, trapping level parameter determ., limiting current injection *(Russian)* 78−39129
CdS, vap. phase grown cryst., stoichiometry control, elec. cond. 79−100034
CdS, wide-gap extrinsic semicond., injection currents, theory 78−19052
CdS:Cd(In), Cu- or defect-compensated, optical ageing rel. to storage cond. 78−84247
CdS:Cl, impurity conductivities 78−91691
CdS:Cu(Cl), thin layer, electron pulse induced cond. relax. 80−2501
n-CdS:In, containing excess Cd, effects of In on elec. props. 79−56217
CdS:In, impurity resist., Matsubara-Toyozawa theory extension 80−80264
CdS:N photoluminescence, resistivity and photoconduction obs. 78−10965
CdS:Ni, dark cond. and photoconductivity 78−76110
CdS:Ni, elec., photoelec. and luminesc. props. *(Russian)* 78−84259
CdS:Ni, elec., photoelec. and luminesc. props. 79−95828
n-CdS:Te, grown from Te soln., elec. props. 79−65475
CdS-$NiCl_2$ interface, elec. props. using SAW techniques 79−56302
CdS_xTe_{1-x}, recryst. from CdS_xTe_{1-x}-Cr_2O_3 mixtures, photocond. props. 80−96936
CdS_xTe_{1-x}, surface layer conductivity type inversion by ruby laser radiation *(Russian)* 77−15948
p-CdSb, elec. props. at low temp. 77−62866
CdSb, phase diagram, region of homogeneity, elec. cond. 79−43219
CdSb resistance thermometer, characts. of cryogenic temps. 79−21760
CdSb:Au, solubility, thermal anal., microhardness, microstruct., elec. characts. 77−16557
CdSb:Ge, anisotropy of elec., mag. props. 78−34829
CdSb-Ag, thermoelectric, thermal defect relax., elec. cond. and thermo-EMF effects *(Russian)* 78−14749
CdSe, electrical cond. near metal-insulator transition 79−73550
CdSe, electron-exciton elastic scatt. cross sections, central field and exchange approxs. 77−62919
CdSe, epitaxial film, gas-phase comp. effects on elec. props. 77−85354
CdSe, epitaxial films, carrier scattering temp. depend. *(Russian)* 78−10583
CdSe, single cryst. elec. props., annealing in Se atm., expt. *(Japanese)* 77−1423
Cd_2Se_3, elec. resist., thermoelectromotive force, temp. depend., 300 to 1400K *(Russian)* 78−84243
p-$CdSiAs_2$, electron irrad. elec. props. annealing, lattice defects 80−100465
$CdSnAs_2$, electron induced defects, p- to n-type cond. inversion, Hall meas. 77−24557
p-$CdSnAs_2$, Hall effect, thermo EMF, thermomagnetic effects 80−107822
p-$CdSnAs_2$, heavily doped, elec. transport props. under elastic deformation 80−96915
$CdSnAs_2$, hydrostatic press. effect on resist. and Hall coeff., band struct. 77−47808
$CdSnO_3$ and Cd_2SnO_4, crystal growth by flux or high press. method, elec. and struct. props. 77−81206
$CdSnO_3$, single crysts., elec. props. 80−6978
Cd_2SnO_4, single crysts., elec. props. 80−6978
n-$CdSnP_2$, Hall coeff. and elec. cond. meas., 24-900K 80−54721
$CdSnP_2$:Cu, deep centres, emission transitions, polarisation *(Russian)* 78−84650
$CdSnP_2$-$CdSnAs_2$, and $CdSnP_2$-$CdGeP_2$, solid solution form. and elec. characterisation 78−43125
CdTe, compensated single cryst., impurity centre parameters, elec. cond. and galvanomag. props. *(Russian)* 77−47811
CdTe detectors, depletion layer extension 78−41891
CdTe, elec. and photoelec. props. due to double injection, quenching spectra 80−70765
CdTe, growth by travelling heater method, high resistivity charact., γ-ray detector appl. 78−84707
CdTe, growth from Te-rich soln. by travelling heater method, cond. and luminesc. 77−40351
n-CdTe, Hall effect and resist., close and distant donor-acceptor pairing effects 77−39881
CdTe, n- and p-type, elec. and galvanomag. props. 79−7830
CdTe, physical props., review 77−39833
CdTe, properties and appls., conf., Strasbourg, France (Jun-Jul 1976) 77−39832
CdTe, single cryst. sublimation growth, X-ray topographic characterisation 80−29866
CdTe:Cl, influence of lattice defects on electrical behaviour 78−2497
CdTe:Cl, localisation of electrons, temp. depend. of cond. and Hall effect 78−14732
CdTe:Cl, semi-insulating, Hall effect and cond. meas., carrier mobility 77−39849
CdTe:Cl, semiinsulating, Hall effect and elec. cond., impurity levels 77−55532
CdTe:Ge, dopant behaviour 78−22742
CdTe:Tl, growth by travelling heater method, elec. and optical characterisation 77−40356

electrical conductivity of crystalline semiconductors and insulators continued
CdTe-CdS heterojunctions, growth by closed-tube chem. transport, elec. props. 80−60070
CdTe-HgTe, neutron irrad. rel. to elec. props. 79−15141
CdTe-HgTe, semicond. solid solns., effect of reactor irrad. on electrophys. props. 77−51744
$CdTl_2Se_4$, single cryst., preparation, elec. cond. 77−24554
$CdTl_2Se_4(Te_4)$:Au, elec. cond., density, dielectric const., changes on fusion 80−88553
$Cd_2V_2O_7$, elec. props. and EPR meas. 79−11114
$Cd_{3-x}Zn_xAs_2$, cryst., two-band and impurity conduction, 1.8 to 370K 78−19057
$Cd_{1-x}Zn_xS$, film, technical data, for low cost solar cell 79−48127
$Cd_xZn_{1-x}S$ films, chem. sprayed, carrier density and mobility 80−60121
CeB_6, crystal preparation, elec. resistance, phase transitions 80−97427
$CeNb_3O_9$, $CeNbO_4$, $CeNbO_{7.6}$, electron config. of Ce ions, mag. sucept., L_3 absorpt. edge, resist. 79−43063
CeO_2, elec. cond. and dielectric props. at low temp. 78−72447
CeO_2 in O_2 atmos., adsorption and elec. cond. props. 79−23836
CeO_2, nonstoichiometric, defect struct. and elec. props. 79−60827
CeO_2:Nb_2O_5, sintered, elec. cond. and solid solubility, 800 to 1329°C 79−99546
CeO_2:S, acceptor properties of S, free electron concentrations 80−34395
CeO_2:S, in $O_2+CO_2+SO_2$ atmosphere, elec. cond. study 80−39583
CeO_2:S, influence of S on elec. props. *(Russian)* 79−51566
CeO_{2-x}, small polaron mobility, elec. cond. and nonstoichiometry meas. 78−47785
$CePd_3$-MPd_3 mixed valent systems, nonlinear conc. depend. of resist. 80−65528
CeS, resistivity and volumetric meas., phase diagrams, comparison with $CeAl_2$ 80−107789
$Ce_{3-x}S_4$, $Ce_{3-x}Sm_xS_4$, elec. cond. mechanism, thermoelec. power, Hall and absorpt. coeffs. 77−24559
$Ce_{3-x}S_4$, mag. ordering and elec. cond. 78−10681
Ce_2Se_3-$SnSe_2$, solid-solution region, physical properties 78−43391
Co complex, 2,6-N,N-diacetyldiaminopyridine-Co(II) elec. cond., γ dose and temp. (303-363K) effects 80−103696
Co complex, 2,6-N,N-dibenzoyldiaminopyridine-Co(II) elec. cond., γ dose and temp. (303-363K) effects 80−103696
$CoAs_3$, prep. and characterisation 77−77356
CoB_{12}, growth from melt and phys. props. 80−20782
$CoCr_2Te_4$, cryst. growth, struct., elec. props., Hall effect 78−43416
$Co_{1-x}Fe_xCr_2S_4$, ferrimag. spinel semicond., Curie temp. variation with composition and elec. props. 77−15849
$Co_{1-x}Fe_xSi$, elec. and optical props. 80−49740
$Co_2Ge_2Te_3$, struct., resist., and thermo-EMF 80−20908
$Co_{1-x}Mg_xO$ ceramics as O_2 sensors, phase stability, elec. cond. and thermoelec. power meas. 78−3420
$Co_{3-x}Mn_xO_4$, solid soln., synthesis, effect of Bi_2O_3 admixture upon props., thermistor appl. 78−15325
$Co^{2+}Mo^{4+}O_3$, defect spinel struct., elec. and mag. props. 80−70176
$CoMoO_4$, mag. susceptibility and electrical transport props. 79−56511
$Co_2Mo_6S_6O_2$, O-containing Chevrel phases, synthesis and props. 80−108368
$Co_{3-x}Ni_xO_4$, $0 \leq x \leq 1.1$, struct., semicond.-semimetal transition, Seebeck coeff. 78−87972
CoNiZn ferrites, Fe excess, complex permeab. var. with annealing temp. 77−89979
CoO, electronic cond., rel. to basic processes of Co corrosion 77−25198
CoO, electronic struct. calc. 78−43297
$Co_{1-x}O$, point defect struct., elec. cond. and Co tracer diffusion 79−10849
Co_3O_4 anode, wear-resistant, use in applied electrochem. 80−40701
Co_3O_4:S, defect struct. and elec. props., electron, hole conc. 80−44601
CoP_3, prep. and characterisation 77−77356
$Co_{0.83}(Pt(C_2O_4)_2).6H_2O$, cond., dielec. const., microwave obs. 80−44636
Co_2RhS_4, mag. semicond., mag. and elec. props. 80−93121
CoS_2, ferromagnet, elec. resist. and thermal expansion anomalies 80−15542
CoS_2, galvanomagnetic effect of single cryst. 80−96912
CoS_2, narrow-band ferromag., high press. effect on anomalous elec. resist. 80−70698
$Co(S_xSe_{1-x})_2$, $(0 \leq x \leq 1)$, mag. props. and elec. resist. 79−65657
$CoSb_3$, prep. and characterisation 77−77356
$CoSiF_6.6H_2O$, elec. resist. anomaly near struct. phase transition 79−95401
Co_2Z ferroxplana form. process peculiarities 80−89368
$Co_xZn_{1-x}Fe_2O_4$, ferrite, DC cond., dielec. props., lattice consts. 80−80272
Cr-Ge system, phase anal. and physical props. 79−24160
CrAl, semicond. solid solns., temp. depend. of elec. resist. at high temp. 78−67941
CrB_2, crystal growth by floating-zone method, elec. and mag. props. 77−1801
$Cr_xMn_{1-x}As$, antiferromagnetic-ferromagnetic transition, mag. moment and elec. resist. meas. 80−15718
$Cr_xMn_{1-x}As$, antiferromag. to ferromag. transitions, superexchange-double exchange mag. coupling, susceptibility and resist. obs. 80−50070
$Cr_{1-x}Mn_xSi_z$, semicond. props. 78−79992
CrN-MnN, synthesis and props. 77−40405
$CrNbO_4$, elec. cond. meas. 80−100463
Cr_2O_3 carrier mobility temp. dependence 77−35958
Cr_2O_3, dielectric const. and loss, cond., 10^2-10^7 Hz, 30-450°C 77−59504
Cr_3O_4:Li(Cr)(Al)(S), and pure Cr_3O_4, elec. cond. and thermo-EMF 80−20231
$CrPr_2S_4$, synthesis, single crystal growth, mag. and elec. props 79−78857
$CrPr_2Se_4$, synthesis, single crystal growth, mag. and elec. props. 79−78857
CrS-FeS, sulphorspinel, struct. and elec. props. 80−49834
Cr_2S_3, rhombohedral single cryst., AC cond., freq. and temp. depends. 77−76810
$Cr_2S_{3-x}Se_x$, elec. resist., thermal cond. and Seebeck coeff. meas. 80−24958
$CrSe_2$, layered, phys. and elec. props. 80−44594
$CrSi_2$ based solid solns., prep., elec. cond. and thermoelec. props. 80−49697
$CrSi_2$, semicond. props. 78−79992
$CrVO_4$, elec. cond. meas. 80−100463
CsBr, crystal, short range interaction polarization, dielectric const. loss, and elec. cond. 10^2 to 10^7 Hz 79−99814

electrical conductivity of crystalline semiconductors and insulators continued
- $CsClO_4$, AC elec. cond. temp. and freq. depend., obs. and unified defect struct. model 80–88554
- $CsCuCl_3$, phys. props. 77–62511
- Cs_xWO_3, normal phase and supercond. props 80–25035
- Cu-Tl-S, phases, semiconductor and metallic behaviour *(French)* 79–96011
- $Cu_{1-y}Ag_yInS_{2-x}Se_{2x}$, for solar photovoltaic cells 80–10982
- $CuAl_{1-x}Fe_xS_2$ system, delocalisation of d-electrons, mag., elec. and optical obs. 78–34804
- Cu_3AsTe_4, elec. and thermal conds., thermo-EMF, solid and liq. states, temp. depends. 78–43384
- CuB_{24}, elec. props. at high temps. and in strong elec. fields, thermistor appls. 80–92903
- $Cu_2^{I}B^{II}C^{IV}X_4$, (B^{II}=Zn, Mn, Fe, Co; C^{IV}=Si, Ge, Sn; X=S, Se), X-ray elec. and mag. meas. 79–65660
- $Cu_3B_7O_{13}Cl$, dielec. const. and elec. resist. 77–69783
- CuCl, optical microscopic, X-ray diffr. and elec. resist. studies at high press. 80–11051
- CuCl, pressure depend. of structural, chemical, elec. and mag. props. 80–96596
- $CuCrS_2$ single cryst., spectral study and phys. props. *(French)* 80–29002
- $CuCrSe_2$, influence of excess Cu on physical props. 80–103836
- $CuCr_2Se_4$, cryst., preparation, elec. cond., thermo EMF 77–8125
- $CuCr_2Se_4$, crystal growth from melt, exam. of props. 80–55283
- $CuCr_2Se_{4-x}Br_x$, elec. resistance, Hall const., magnetoresistance singularities *(Russian)* 79–91078
- $Cu_{0.67}Cr_{1.78}Se_{2.67}Br_{1.34}$, polycrystalline mag. semicond., mag. and elec. props. 79–7846
- $Cu_yCr_2Se_{4-z}Br_x$, degenerate ferromag. semicond., resist. minimum 79–73517
- $CuCr_2Se_4(S_4)(Te_4)$, binary and ternary solid solns., mag. and elec. props. 80–2407
- $CuFe_5O_8$, sintered, eutectoid decomposition study by elec. resist. meas. *(Japanese)* 78–19711
- $Cu_{1-x}Fe_{2+x}O_4$, elec. resist., Seebeck coeffs., 20 to 900°C, cation distrib. 79–4575
- $CuGa_xIn_{1-x}Se_2$, CVD, elec. and optical props., use as heterojunction solar cell absorber 79–52095
- $CuGaSe_2$, cryst. struct., X-ray powder data 77–39565
- $CuGaSe_2$ single crysts., Hall effect and resist., acceptor states 80–10975
- $CuGaSe_2$ single crystals, elect. and optical props. for solar cell appl. 80–10981
- $CuGaTe_2$, elec. and optical props. 80–6829
- $CuGdTe_2$, synthesis and elec. props. 78–26529
- $CuInS_2$ crystals, growth, struct., and elec. props. 79–38729
- $CuInS_2$:Cd(Zn), elec. props. 77–62927
- $CuInSe_2$, acceptor levels, elec. props. study 80–39578
- $CuInSe_2$, n- and p-type, elec. resist. and Hall effect, 80 to 500K 79–87096
- $CuInTe_2$ single crystals, directional freezing growth and doping, resist. changes on annealing 80–60768
- $Cu_3MTl_2X_4$ (X=Se, Te, M=Fe, Ga, Al), struct. and phys. props. *(French)* 79–86758
- $Cu_4Mn_2S_4(Se_4)(Te_4)$ spinel, prep. and elec. props., 100 to 650K 79–43127
- $Cu(Mo_2Re_2)S_8$, synthesis and electrical props. of mixed tetrahedral cluster phases 80–2971
- $Cu_2Mo_6S_6O_2$, O-containing Chevrel phases, synthesis and props. 80–108368
- CuO-CdO-Fe_2O_3, sintered ferrite, preparation, mag. susceptibility, DC resistivity 80–34598
- CuO-ZnO-Fe_2O_3, sintered ferrite, preparation, mag. susceptibility, DC resistivity 80–34598
- Cu_2O and CuO powders, contact resistance, temp. and pressure dependence, obs. *(German)* 79–4555
- Cu_2O, electron-exciton scatt. cross sections, central field and exchange approxs. 77–62919
- Cu_2O, positive and negative photomemory, IR luminesc. spectra, illum. effect 79–69557
- Cu_2O, residual conductivity, role of vacancies, photoluminesc. and photocond. 77–15901
- CuPbBiS, ferroelec. semicond., elec. cond., photocond. permittivity, phase transitions 77–47822
- Cu_2S, electromechanical props. *(Russian)* 79–11117
- Cu_2S, low temp. modification, elec. props. 77–8092
- Cu_2S, thermoelectric props. 80–54726
- Cu_2S:Cd(Zn), effects of doping on elec. and optical props. 78–38743
- Cu_2S-CdS heterojunction characteristics and CdS polarity *(Japanese)* 78–23154
- $Cu_{2-\delta}S$, $Cu_{2-\delta}Se$ and $Cu_{2-\delta}(S,Se)$, ionic and electronic cond., thermopower and Hall coeff. 77–20117
- $Cu_{2-x}S$ single crysts., comp. depend. 77–24302
- $Cu(SCN)_{1/3}$, synthesis and high elec. cond., activated and metallic cond. obs. 80–96957
- $Cu_2S(Se)$-Ge(Sn)S, phase diagrams 78–44100
- $CuSbS_2$ crystals, growth and characterisation 80–60770
- Cu_3SbTe_4, elec. and thermal conds., thermo-EMF, solid and liq. states, temp. depends. 78–43384
- $Cu_{1.8}Se$, I-V characts., switching effects, nonstoichiometry effects *(Russian)* 78–84266
- $Cu_{2-x}Se$, elec. props. and band struct. 79–73513
- $Cu_{2-x}Se$, electric, thermal and magnetic props. investigation in low temp. phase *(Croatian)* 79–11299
- $Cu_{1.7}Te$, and Cu_2Te, I-V characts., switching effects, nonstoichiometry effects *(Russian)* 78–84266
- Cu_2Te-Ag_2S, kinetic props. of solid solutions 79–7827
- $Cu_{2-x}Te$, x=0 to 0.3, elec. cond., Hall const., carrier mobility, conc., thermoelec., density, lattice parameter 77–11915
- $Cu_{2-x}Te$, $x<0.22$, phase diagram, electronic and ionic cond. meas. 80–6917
- CuV_2S_4, preparation, cryst. struct. and physical props. *(French)* 79–55714
- $Cu_{0.65}VS_2$, cryst. struct. and phys. props. *(French)* 79–60334
- $CuWO_4$, elec. cond., thermoelectric power and dielectric constant temp. depend. 80–96886
- Cu_2ZnGeX_4, (X=S,Se), optical and electrical props. 77–35941
- Cu_2ZnSiX_4, (X=S,Se), optical and electrical props. 77–35941
- $DyCrS_3(Se_3)$, prep., elec. and thermal props. 78–43390

electrical conductivity of crystalline semiconductors and insulators continued
- DyIG, thermoelectric power, elec. cond. charge carrier conduction mechanism 80–34441
- $Dy_2(MoO_4)_3$, DC electrical cond., 650 to 1150K 79–60831
- Dy_2S_3, semimetallic, elec. and thermal transport meas. 78–10442
- $Er_2(MoO_4)_3$, DC electrical cond., 650 to 1150K 79–60831
- ErO_x, nonstoichiometric film, short-range order characts. and its effect on elec. behaviour 79–99435
- Er_2O_3, mag. susceptibility, elec. cond. and dielectric const., hopping cond. 77–12083
- Er_2O_3:CaO, elec. cond. and nonstoichiometry 79–11112
- $ErRh_4B_4$, superconducting and normal state props. 79–73632
- ErS, heat carrier scatt., thermal and elec. cond. from 5-400K 79–14974
- Er_2Se_3, elec. resist., thermoelectromotive force, temp. depend., 300 to 1400K *(Russian)* 78–84243
- EuB_6, correlation between mag. struct. and elec. props. 77–63192
- EuB_6, electrical transport under press. 79–87101
- EuB_6, electronic struct., transport and mag. props. 80–96782
- EuB_6, growth by soln. method, struct., mech. and elec. props. 80–16168
- EuB_6, Hall effect and resistivity data, ferromagnetic ordering temp., pressure depend. 80–60010
- EuB_6, mag. and transport props. 80–54689
- EuB_6, pure single crystals, magnetic and electric props. 80–11260
- EuB_6, resistivity press. variation, lattice consts. 80–100456
- $EuB_{6-x}C_x$, magnetic and elec. props. 78–91842
- $EuBi_2Te_4$, elec. cond., Hall, thermo-EMF coeffs. determ., 300-1100K 78–43386
- $Eu_{1-x}{}^{2+}Eu_x{}^{3+}N_xO_{1-x}$, resist., pressure depend., semicond.-metal transition obs. 79–78104
- $EuGa(In)_2X_4$, X=S,Se,Te, prep. and props. 77–85214
- $EuGd_2S_4$, nonstoichiometric, elec. transport props., semicond. and metallic cond. 80–107786
- Eu_2IrH_5, prep., cryst. struct., mag. and elec. props. 80–88117
- $Eu_{1-x}{}^{2+}Nd_x{}^{3+}N_xO_{1-x}$, resist., pressure depend., semicond.-metal transition obs. 79–78104
- EuO, HF conductivity meas. 79–33304
- EuO, hydrostatic press. effects on elec. resist. in temp. range 3 to 300K 79–23968
- EuO, microwave and DC cond., dielec. const., 1.7 to 300K 77–20347
- EuO, microwave cond., influence of mag. ordering 79–69544
- EuO, nonstoichiometric film with excess EU, elec. resist. variation with lattice parameter 79–8204
- EuO, physical and physicochem. props., review 80–96875
- EuO:Gd, elec. cond. under hydrostatic press., Curie temp. 80–96881
- EuO:Gd, pure and doped, elec., mag., and optical props. rel. to electronic conc. 80–96880
- Eu_2O_3, elec. cond., thermoelec. power, dielectric const, 79–69763
- Eu_2O_3, thermophysical props. and neutron absorpt. 80–103488
- $EuO_{1-x}N_x$, ferromag. semicond., elec. and mag. props. *(French)* 78–79993
- EuO(S)(Se)(Te), cryst. and electronic struct., mag., elec., and optical props., book contrib. 80–39760
- EuO(Se), complex elec. cond. anomalies 80–107812
- EuO(s), mag. semicond., s-f model, intermediate coupling theory 79–95326
- EuS, pure and Gd doped, electronic struct., mag. exchange and elec. transport props. 78–87974
- Eu_2Sb_3, cryst. struct., elec. and mag. props. 80–33958
- $EuSb_2S_4(Se_4)(Te_4)$ elec. cond., Hall, thermo-EMF coeffs. determ., 300-1100K 78–43386
- EuSe, annealed, AC conductivity and dielectric anomaly 80–34445
- EuSe, HF conductivity meas. 79–33304
- EuSe, Hall effect, elec. cond. and magnetoresistance temp. depend. 79–33296
- EuSe, microwave and DC cond., dielec. const., 1.7 to 300K 77–20347
- $Eu_{0.98}Sm_{0.02}O$, ferromag. semicond., elec. cond. meas. 80 to 370K, press. effect to 20 kbar 77–51751
- $Eu_{1-x}Sm_xO$, ferromag. semiconductor with elevated Curie temp. 77–51903
- $Eu_xSr_{1-x}M_4O_{11}$, M=Nb, Ta, electrophys. and mag. props. 77–89760
- EuTe, magnetic impurity states, mag. and transport props. 80–96913
- Eu_2VO_4, prep. and props. 77–15379
- $Eu_3V_2O_7$, prep. and props. 77–15379
- $Eu_2(WO_4)_3$, mag. susceptibility, elec. cond. and dielec. const. meas. 77–11916
- $Eu_2(WO_4)_3$, molar mag. susceptibility, DC elec. cond., thermopower meas. 79–15172
- $Eu_{1-x}Yb_xO(S)$, solid soln., ferromag. semicond., increase of exchange interaction 78–88109
- $Eu_{1-x}Yb_xTe$, $(0<x<1)$, mag. semicond., elec., mag. and optical props. 80–97070
- $FEPS_3$, layered semiconductors, optical and electronic props. 80–70761
- $FeAl_{2-x}Cr_xO_4$, spinel, elec. cond. behaviour during oxidation 79–19593
- γ-$(Fe_{1/3}Al_{2/3-y}Cr_y)_2O_3$, lacunar spinels, elec. cond. behaviour during oxidation 79–19593
- $(Fe_{1-y}{}^{3+}Al_y{}^{3+})_2O_3{}^{2-}$, γ to α transform. elec. cond. study, oxidation initial stage kinetics, lacunar spinel form. 78–92384
- $Fe_{3-x}Al_xO_4$, cation distrib., mag. and other phys. props. 77–43818
- Fe_3BO_6, spin-reorientation, elec. resist. and microwave absorption 78–14751
- $Fe_3B_7O_{13}I$, spontaneous polarisation, dielec. const., d.c. resist., sp. ht. 77–1643
- $FeCoCrO_4$ spinel, elec. resistivity, temp. var. 79–38065
- $Fe_xCo_{1-x}Rh_2S_4$, spinel struct., X-ray, mag., elec. and Mossbauer spectra meas. 77–12278
- $Fe_{0.2}Co_{0.8}S_2$, narrow-band ferromag., high press. effect on anomalous elec. resist. 80–70698
- $Fe_{1-x}Co_xSi$ solid solution, semiconductor-metal transition 80–103627
- $(Fe_{1-y}{}^{3+}Cr_y{}^{3+})_2O_3{}^{2-}$, γ to α transform. elec. cond. study, oxidation initial stage kinetics, lacunar spinel form. 78–92384
- $Fe_{2-x}Cr_xO_3$, elec., optical and photocond. props. 79–56262
- $FeCr_2S_4$, elec. and galvanomag. props. 78–23111
- $FeCr_2S_4$, pure and doped, CVD grown, surface struct., elec. props. and band struct. 79–4905
- $FeCr_2S_{4-x}Se_x$, elec. props. 78–23083
- $Fe_{0.5}Cu_{0.5}Cr_2S_4$, ESR spectra, elec. and mag. props., Curie temp. 80–97137
- $Fe_{1-x}Cu_xCr_2S_4$, mag. semicond., mag. props. and elec. cond. *(Japanese)* 79–47111
- FeF_3 thin film, polarisation mechanism, AC and TSC study 80–66104

electrical conductivity of crystalline semiconductors and insulators continued
$(Fe^{2+}Fe_{2-x}{}^{3+}M_x{}^{3+})O_4{}^{2-}$, $(M^{3+}=Cr^{3+}$ or $Al^{3+})$, elec. cond., Verwey transition temp. *(French)* 79—60878
$Fe_{0.95}{}^{2+}Fe_{2.05}{}^{3+}O_4{}^{2-}$, magnetite, elec. resistivity above 300K 79—78099
$FeGa_2Se_4$, elec. cond., mag. susceptibility 80—88301
Fe_xI_y cyclodextrin, quasi-one-dimens. cpd., synthesis, elec. and mag. props. 80—2380
$Fe_{2-x}M_xO_4$, M=Al,Cr, time dependence of oxidation, elec. cond. obs. *(French)* 77—66710
$FeMnGaO_4$, X-ray study of cryst. struct. and ionic config., elec. resist. meas. 78—55851
Fe_2MoO_4, electron exchange between $Fe^{2+}-Fe^{3+}$ ions on tetrahedral and octahedral sites, Mossbauer spectra 79—78585
$Fe(Mo_2Re_2)S_8$, synthesis and electrical props. of mixed tetrahedral cluster phases 80—2971
Fe_xN_y, prep. by reactive sputtering, struct. and props. *(Japanese)* 78—92190
$Fe(Nb_{1-x}W_x)O_4$, mag. and elec. props. and Mossbauer effect 79—78590
FeO, electronic struct. calc. 78—43297
Fe_2O_3 based γ defective spinels, elec. cond. behaviour during transform. to α rhombohedral phases *(French)* 80—49354
α-Fe_2O_3, electrical conductivity 77—69365
α-Fe_2O_3, polycryst., pure and TiO_2 doped, flatband potentials, donor densities, photocurrent meas. 78—76089
Fe_2O_3-Al_2O_3 mixed oxide, X-ray diffr. and elec. cond. 80—79954
Fe_2O_3-V_2O_5 system, elec. transport 79—51576
Fe_3O_4, effect of residual stresses on sp. ht. and elec. cond. 77—59308
Fe_3O_4, magnetite, and related Jente spinels, mag. crit. point behaviour 80—60342
Fe_3O_4, magnetite, anomalous electrical conductivity, press. effects 79—56222
Fe_3O_4, magnetite, electronic cond. mechanisms, review 77—20314
Fe_3O_4, magnetite, Verweg transition temp., isotope effect, elec. resist. and DTA meas. 80—24976
Fe_3O_4, selective excitation double Mossbauer exam. of electron hopping 77—69750
$Fe_3O_{4-x}F_x$ substituted magnetite, low temp. resistivity, Seebeck coeff., thermopower 80—20234
α-FeP_4, diamag., semicond., Mossbauer study 80—50243
Fe_2P, magnetisation, susceptibility, thermal expansion and elec. resist. meas. 77—77037
$FePb_4Sb_6S_{14}$, photosensitive semiconductor, with high permittivity, elec. props. 79—65518
$FeRh_2S_4$, mag. semicond., mag. and elec. props. 80—93121
FeS, pressure effect on elec. resist. and thermoelec. power 80—70308
$FeSO_4.7H_2O$, single cryst., elec. and dielec. props., temp. depend. 79—19826
$FeSb_xO_{4-y}$, defect struct. and mag. transition, elec. transport and Mossbauer expts. 78—59803
$FeSb_2S_4$, berthierite cryst., anomalies in elec. and dielec. props. 77—47821
$Fe(Sb_{1-x}Te_x)_3$ system cpds., prep., cryst. struct., elec. and mag. characteris. 80—108349
Fe_7Se_8, 3c struct., spin axis transition 78—14967
$FeSiO_3$, UV and soft X-ray spectra, band gap determ. 79—61468
Fe_2SiO_4, elec. cond. under defined thermodynamic activities, up to 20 kbar, 340-1100°C 80—6832
Fe_2SiO_4, fayalite, elec. cond. obs. under shock compression 80—81873
Fe_2SiO_4 in solid media apparatus, high press. and temp., controlled O_2 fugacities, buffer techniques *(German)* 79—93162
Fe_2SiO_4, UV and soft X-ray spectra, band gap determ. 79—61468
1T-$Fe_xTa_{1-x}S_2$, Anderson localisation, elec. resist. and magnetoresist. meas. 80—44596
θ-$Fe_xV_2O_5$, spin glass and paramag. props., susceptibility, EPR and Mossbauer studies 80—75782
Ga chalcogenides, energy spectrum of local levels *(Russian)* 79—51517
Ga-Sb-Te, props. of ternary solid solution based on GaSb 79—7826
n-GaAS, plastic deform. effect on elec. props. 77—28178
GaAS, semiinsulating, heat treatment effects 78—6382
GaAS:Cr, mag. field depend. of single carrier parameters, mixed cond. anal. 79—91043
n-$Ga_{1-x}Al_xAs$:Si, room-temp. cond. and band struct. 80—96869
$Ga_{1-x}Al_xSb$, melt growth and elec. props. 79—65999
GaAs, conductivity of complementary error function n-type diffused layers 77—35944
GaAs, current controlled negative resist. at low temps. 78—39133
n-GaAs, current-voltage characts., dislocation etch pits and perfect cryst. 80—70695
GaAs, cylindrical and spherical localised inhomogeneities in mag. field, anomalous elec. prop. calcs. 80—44621
GaAs, Czochralski grown, pure and doped, elec. props. 80—10989
GaAs, defect clusters induced by γ-rays and neutrons, effect on elec. props. 80—29408
GaAs device isolation with deuteron bombardment 80—75248
GaAs diffusion of ion implanted Be, SIMS and electrical profiling 78—47605
GaAs, disordered, ion implanted, elec. props. 78—84212
GaAs, dual implantation of C^+ and Ga^+, sheet resist. and Hall effect meas. 78—67728
GaAs, elec. cond., effect of As vapour press. at 200-1000°C 77—15846
GaAs, elec. effects of dislocations 79—82586
GaAs, elec. props. of dislocations review *(Japanese)* 78—6325
GaAs, electrical conductivity and thermoelectric power charge due to melting 80—100490
GaAs, electron transport analytical model 79—91039
GaAs, epitaxial, residual donor identification by far IR photoconductivity meas. 80—103717
GaAs epitaxial layers, structural defect and conc. inhomogeneities influence on barrier diode I-V characts. 80—15602
GaAs, H^+ irradiation, effect on electrical props. 80—65567
GaAs, heavily doped, fluctuation-induced tunnelling cond. 80—65516
n-GaAs, heavily doped, impurity-band cond., DC cond., Hall mobility, and magnetoresist. meas. 80—49733
GaAs, high press. electron transport props., three band model 80—15516
GaAs, high-purity, residual donors, ionisation energies determ. 78—6333
GaAs, interimpurity interaction effect on distrib. profiles of impurities diffusing simultaneously 77—76451
GaAs, ion implantation, disordered layer physical props. 79—77624
GaAs, ion implanted, laser annealing 80—107296
n-GaAs, Landau level lifetimes for electrons 79—87112

electrical conductivity of crystalline semiconductors and insulators continued
GaAs, low temp. gamma irrad., donor-acceptor pair formation 79—69158
n-GaAs, mechanism of cyclotron reson. induced cond. 78—43396
GaAs, model relating elec. props. to impurity concs. 77—51697
n^+-GaAs, multiple energy proton bombard. effects on elec. characts. 77—39853
GaAs, p- and n-type, and Zn-diffused, spreading resist. meas. 79—28343
GaAs, photoelectric memory effect, effect of metallic island struct. on surface 77—55570
n-GaAs, piezoelectric semiconductor, influence of acoustic phonon disturbances on conductivity 78—91697
GaAs, plastic deform. prod. by thermocompression bonding, elec. props. 77—76807
GaAs, point defects, laser annealing 80—107224
GaAs, polycrystalline, carrier transport at grain boundaries 80—29411
n-GaAs, proton irrad., $E_p=30$ MeV, defect form., orientation depend. 78—55898
GaAs, semi-insulating, cond. mechanism, model explaining temp. depend. of elec. props. 79—51571
GaAs, semi-insulating, conduction model 80—10986
n-GaAs, shallow donors, elec. cond. and Hall coeff. meas. 77—11942
GaAs, shallow donors, screening, energy spectrum of electrons and cond. mech. 79—7831
GaAs, three level cond. band struct., uniaxial stress effects, resist. and Gunn effect threshold meas. 77—85137
GaAs, transmutation doping by thermal neutrons 80—10581
n-GaAs, uncompensated, mech. of energy relax. at low temps. 77—62921
GaAs:^{11}B, physicochem. and resistivity meas. 80—24933
GaAs:Be, implantation and annealing, elec. props. 79—99540
GaAs:Be, ion implanted, elec. profiling and optical activation expts. 77—89457
p-GaAs:Be, ion implanted, annealing characts., defect cond. profiling, electron diffr. obs. 79—4318
p-GaAs:C, ion implantation efficiency, elec. profile and compensation level meas. 77—27880
GaAs:Cd, lattice defects caused by quenching, elec. cond. 79—56160
GaAs:Cr, carrier equilibrium effects, impurity states, elec. resistivity 80—65488
GaAs:Cr, current voltage characterisation, deep levels and Fermi level determ. 79—7823
GaAs:Cr, high resistivity, specific resistance depend. determ. using impedance freq. depend. *(Czech)* 80—15536
GaAs:Cr, parameters determ. using cond., Hall-effect and magnetoresist. meas. *(Slovak)* 78—47802
GaAs:Cr, semi-insulating elec. compensation, Hall and resist. meas. 77—62855
GaAs:Cr, semi-insulating, I-V characts. and photocond. spectra dependencies on Fermi level 79—99576
GaAs:Cr, semiinsulating, I-V characts., photocond., Fermi level, and deep levels 78—39118
GaAs:Cr,O semi-insulating monocrystal development and four-level model 80—88191
GaAs:Cr semi-insulating wafer, heat treatment technique for no thermal conversion 80—100857
GaAs:Cr(W), deep trapping centre exam. by thermally stimulated capacitor discharge method and luminesc. 77—55495
GaAs:Ge, cryst. and epitaxial layers, ion-implanted, elec. props. 79—99542
GaAs:Mg(C)(Te)(Ge), ion implanted, laser annealing, ellipsometric and Hall meas. 79—73193
GaAs:Mn epitaxial layers, fabrication and electrical props. 77—80859
GaAs:O, annealing effects, optical absorpt. and I-V characts. 80—29037
GaAs:O, electrolum., photolum., negative differential resist. rel. to recomb. processes 80—66304
n-GaAs:O carrier removal profiles meas. 78—56154
n-GaAs:O film, influence of O on elec. props. 79—11252
GaAs:Se, Ga, dual species ion implantation, elec. characts. 80—103377
GaAs:Se ion implanted samples, Q-switched ruby laser annealing, improvement in elec. props. 80—100460
GaAs:Se^+, implanted semi-insulating, pulsed electron and laser beam annealing effects on elec. characts. 79—73196
GaAs:Si, ion-implanted, elec. props. 79—46686
GaAs:Si, ion-implanted, annealing with Nd:glass laser 79—73194
n-GaAs:Te, elec. cond. and Hall coeff. temp. depend. meas., three band model 79—33287
GaAs:Te, heavily doped degenerate semicond., anomalies in temp. depend. of resist. 79—61053
GaAs:Te, ion implanted, laser annealing 79—73192
GaAs:Te, recombination barrier, dark cond., photocond., and Hall mobility meas. 80—15559
GaAs:$Te^+(Se^+)(Sn^+)(Ge^+)$, ion implanted, laser annealing effect on elec. characts. 79—73195
GaAs:Zn, implanted, laser annealing, elect., Rutherford backscattering and SEM meas. 80—100273
GaAs:Zn, laser annealing of implanted layers 77—55296
GaAs:Zn, Se, double doping during LPE, exam. of elec. cond. and Hall effect 79—4923
GaAs-ZnSe, solid solution crystals, grown by Bridgman method, exam. of resistivity and Hall effect 79—95919
GaAs-ZnSe system, heterovalent solid solns. of substitution, prep. and investig. 77—24553
$GaAs_{0.6}P_{0.4}$:Be, implanted annealing studies, elec. resist., Hall effect meas. 78—84213
$GaAs_xP_{1-x}$, energy band struct., CPA based on LCBO *(Japanese)* 80—44495
GaAs;Cu, epitaxial and bulk conductivities compared *(Russian)* 78—10585
$Ga_{1-x}Mn_xSb$ alloys, mag. phase transition obs. 78—52248
$Ga_{1-x}Mn_xSb$, elec. cond., mag. susceptibility, Hall const., and thermo-EMF, 80 to 1000K *(Russian)* 80—88549
$Ga(Mo_2Re_2)S_8$, synthesis and electrical props. of mixed tetrahedral cluster phases 80—2971
GaN, epitaxial growth on sapphire substrates, elec. props., X-ray diffr. anal., photoluminescence spectra 79—4919
GaN:Mg, and undoped, epitaxial growth from vapour, orientation, elec. props. 77—4740
Ga_2O_3:Mg(Zr) single crystals, quenched, ionic and elec. props. 78—30922
GaP diodes, TSCAP and admittance spectroscopy of gamma-ray induced defects 77—89472

electrical conductivity of crystalline semiconductors and insulators continued
GaP, effective partition coeffs. and elec. behaviour of group IV elements 77—7754
GaP, epitaxial layer prep. and elec. props. 77—85096
GaP, influence of shear deform. on interband interaction 78—39116
GaP, interimpurity interaction effect on distrib. profiles of impurities diffusing simultaneously 77—76451
GaP:Cr$_2$O$_3$, growth, dopant distribution, elec. resist. 78—34531
GaP:Fe, diffusion, solubility, elec. activity and energy levels 77—55395
GaP:Fe^{3+}, deep impurity states investig. 77—15794
GaP:s, elec. props. following 1.7 MeV electron irradiation 78—80005
n-GaP:S, Hall effect and resistivity meas. *(Japanese)* 77—39840
GaP:Te, Hall effect and elec. cond., 80-400K 78—91705
GaP:Zn, Hall effect and elec. cond., 80-400K 78—91705
GaP:Zn, implanted, elec. profiling using anodic oxidation in N-methylacetamide 80—54690
GaS-YbS system, phase diagram, reacts., thermal, mag. and elec. meas. 79—11578
GaS$_x$Se$_{(1-x)}$ solid solns., electrical props. meas. 78—84216
p-GaSb, cond. mechanisms, uniaxial compression effects 77—20312
p-GaSb, elec. cond., Hall effect, mobility and carrier concentration *(Russian)* 79—19603
GaSb LEC single crystal growth, novel encapsulant material 80—93475
n-GaSb, stress-induced elec. props. of point defects, piezoresistance effect 79—56726
n-GaSb, temp. distrib. around dislocations, due to Joule heating, calc. 78—71734
GaSb, undoped, impurity band parameters calc. 79—51516
GaSb, undoped, intrinsic acceptors, parameters determ. 79—51515
GaSb:Cd(Zn)(Se)(Te), thermal sensitivity, −170 to +180°C, resist. meas. 77—39906
GaSb:Fe, shallow acceptor level, electrical meas. 79—11087
GaSb:S, cond. and Hall coeff. relax., impurity config. model 80—6786
n-GaSb:S, inhomogeneous, temp. depend. of elec. resist. 78—2482
n-GaSb:Se, resonant and bound impurity states, Hall effect and resistivity press. depend. 77—28143
n-GaSb:Te, Hall coeff., carrier conc. and mobility, elec. cond., 290 to 550K *(Russian)* 79—19604
GaSb-GaAs-Ge system, props. and struct. 80—20232
GaSe, high resistivity, electric field stimulated conduction 77—66172
p-GaSe, resist. and Hall-mobility meas. at 77-850K 77—59295
p-GaSe, resistivity, anisotropy 77 to 750K 79—4559
p-GaSe, single cryst., negative photocond. induced by elec. field 79—19623
Ga$_2$Se$_3$, solid solution, elec. cond. 80—88301
Ga$_2$Se$_3$-FeSe, phase diagram, elec. cond., mag. susceptibility 80—88301
Ga$_2$Se$_3$-In$_2$Se$_3$, semiconducting props. of four stable phases 77—55528
Ga$_2$Se$_3$-In$_2$Se$_3$ solid solution system, X-ray diffr. exam. 77—63639
GaTe, Hall mobility, resistivity anisotropy 79—11150
GaTe, resist. anisotropy in layer plane 79—51581
GaTe, transport properties under hydrostatic pressure 80—75589
Ga$_2$Te$_3$, single cryst., elec. cond. meas. 79—11124
Ga$_2$Te$_3$-Cu system solid solns., elec. cond. 78—51988
p-GaTe$_x$Se$_{1-x}$, resistivity and Hall effect meas. 77—24556
Ga$_x$V$_{1-x}$O$_2$, resistivity, EPR, enthalpy and entropy meas., rel. to semicond.-metal transition 78—88004
Gd-Dy, dil. alloy, impurity component of elec. resist., meas. 1.5 to 390K 77—39831
GdB$_6$, crystal preparation, elec. resistance, phase transitions 80—97427
Gd$_3$Ga$_5$O$_{12}$, elec. cond. meas. 79—23961
Gd$_2$GeSe$_5$, elec. props., 300 to 1100K 79—51585
GdIG, thermoelec. power, elec. cond., 500-1200K, ferrimag. Curie temp. 79—99543
Gd$_2$O$_3$, elec. cond., thermoelec. power, dielectric const. 79—69763
c-Gd$_2$O$_3$, electrical cond., dielectric const. mag. susceptibility, polymorphic transition 77—59505
GdP, electronic struct., mag. exchange and elec. transport props. 78—87974
GdS, electronic struct., mag. exchange and elec. transport props. 78—87974
Gd$_2$S$_3$, antiferromag. to ferromag. and semiconductor to metal transitions *(Russian)* 79—33485
Gd$_2$S$_3$, semimetallic, elec. and thermal transport meas. 78—10442
Gd$_{3-x}$S$_4$, ferromag., elec. props. near Curie temp. 80—107788
Gd$_{3-x}$S$_4$, mag. ordering and elec. cond. 78—10681
Gd$_2$(WO$_4$)$_3$, molar mag. susceptibility, DC elec. cond., thermopower meas. 79—15172
Gd$_{3-x}\square_x$S$_4$, transport and mag. props., mag. Wigner localisation 80—97069
Ge bicrystal, cond., Hall effect and Shubnikov-de Haas oscills. 80—10984
Ge, bicrystal, two-dimensional electronic phenomena at He temp. *(Russian)* 79—56273
Ge, chemomagnetic effect, elec. cond. change due to surface recomb. of H atoms 77—8086
n-Ge, current carrier-dislocation interactions, resistance in UHF range *(Russian)* 80—54732
n-Ge, D$^-$-band conduction 77—76821
Ge, DC cond., periodic explosions of electron-hole drops 77—11950
n-Ge, deformed, 1/f noise, resist., mobility, and carrier density 77—8161
p-Ge, dislocation microwave cond. and Hall effect meas. *(Russian)* 77—47848
p-Ge, dislocations, grown-in defects, electrical props., deep level transient spect., Hall effect 80—39524
n-Ge, elec. cond., effect of shock waves *(Russian)* 78—87979
Ge, electron irrad., light-sensitive defects 80—24498
n-Ge, electron irradiated, annealing at 6K, Watkins model explanation 78—47427
Ge, electron mobility in Δ_{1c} minima, temp. depend. 79—65473
Ge, electron mobility is semiconductors based on dielectric function modification of Dingle pot. 79—60836
Ge, electron-hole droplets, percolation theory of cond., expt. 80—92896
Ge film, polycrystalline, structural and elec. props. 78—76173
Ge, Foucault currents in electron-hole drops *(Russian)* 77—8030
Ge, galvanomagnetic-recombination field effect, theoretical model 78—43420
Ge, heavily doped, vacuum hot-pressing thermal and electrical props. 77—40400
Ge, heavily doped, vacuum hot pressing, effect on thermal, electrical props. 80—25594
Ge, high-purity dislocation-free, divacancy-hydrogen complexes 78—2449
electrical conductivity of crystalline semiconductors and insulators continued
p-Ge, hole drift vel. in high field 79—95415
Ge, hopping cond. at intermediate impurity concs. 80—6840
n-Ge, impurity breakdown field, temp. depend. 79—24263
Ge, impurity-ion potential, electron-conductivity mobility, spatially variable dielectric function calcs. 79—78105
Ge, irradiation at about 6K, low temp. annealing of defect 78—2162
n-Ge, irradiation induced compensation, elec. meas. 77—85225
n-Ge, laser irrad., accumulation of defects, effect on elec. props. 80—107317
Ge, lattice defects formed on γ-irrad., effect on elec. props. 80—19839
n-Ge, lightly doped, compensated by disordered regions, conductivity and Hall mobility 80—11016
Ge, lightly doped, nonohmic impurity cond. 78—14738
Ge, magnetoresistance of electron-hole liq., percolation model 80—96920
n-Ge, minority-carrier injection and extraction 80—49767
Ge, n- and p-type, fast neutron irrad. at low temp., resistivity, annealing characts. 77—89481
Ge, neutron irradiated, positron annihilation, ESR and resist. meas. 80—15160
Ge, nonuniformly deformed, electron-hole drop density depend. on size *(Russian)* 80—20092
Ge, optically injected carrier density and temp. depend. 78—68046
Ge, oscillatory exciton breakdown, microwave cond. 80—103716
Ge, p-type, and n-type converted to p-type by irradiation at 77K, defect form. mechanism 79—23651
Ge, p-type, hole conductivity anisotropy 77—4360
Ge, partly dissociated excitons and impurity atoms system, collisional processes, charge transport theory 80—44581
N-Ge, phenomenological cond. relax. time, uniaxial stress and electron-electron scatt. effects 77—15862
n-Ge, plastically deform., dislocation state spectrum, photocond., elec. cond., and Hall const. meas. *(Russian)* 80—2362
n-Ge, plastically deformed, elec. cond., magnetoresistance, Hall effect study *(Russian)* 79—99568
Ge, point defect creation by plastic deform., Hall const. electrical conductivity 78—6053
Ge, polycrystalline epitaxial film, exam. of growth kinetics and props. 80—55304
Ge powder, temp. and press. depend. 77—8090
Ge, quenched n- and p-type, intrinsic defects migrating near 100°C 77—62670
Ge, quenching temp. effect on annealing rate of quenched-in acceptors 79—82590
n-Ge resistance thermometer material for 14 to 300K *(Russian)* 80—49731
Ge slab, intrinsic, longit. cond., influence of surrounding gas *(French)* 78—10448
Ge, surface, high freq. cond. and cyclotron reson. 80—11273
n-Ge, surface electron mobility, Hall effect and cond. meas. 79—56281
Ge, thermal rectification and negative differential cond. 79—42554
Ge, transmutation-doped, impurity cond., 1.5-4.2K 77—89758
Ge, voltage-current curves, specimens of variable cross-section 77—8113
p-Ge:Ag, Sb, electron beam irradiation cond. characts. 80—19842
n-Ge:Au, current oscill. damping in weak transverse mag. field 77—4365
Ge:Au, Sb, Hall mobility, temp. dependence 80—96919
Ge:Au, trap charge exchange waves *(Russian)* 78—34846
Ge:Ba(Ca), elec. props. and effect of impurities on γ-radiation defect formation 78—10088
Ge:Be single crystals, grown by Czochralski method, exam. of Be distribution ratios and solubility 79—95043
Ge:Cu, deep-level impurities, insulating props. 78—39124
Ge:Cu, press. effect on energy spectrum of carriers, elec. cond. and Hall coeff. expts. 79—23930
Ge:Ga, cryst. defects due to neutron irrad., elec. cond. and annealing 79—55789
p-Ge:Ga, heavily doped, elec. resist., 40 mK to 300K 79—38071
Ge:Mg, diffusion and p-type cond. 80—6419
Ge:Mg, energy level behaviour, Hall coeff. and elec. cond. meas. 80—34396
Ge:O, elec. props., O donor levels determ. 77—8123
Ge:O, elec. props., O interaction with point defects 79—11081
Ge:O, slow thermal relax. of cond. rel. to donor complexes 80—70704
Ge:Sb, annealing stages of thermal defects, elec. meas. 77—55282
Ge:Sb, cryst. defects due to neutron irrad., elec. cond. and annealing 79—55789
n-Ge:Sb, electron irrad., impurity photoconductivity 77—15900
Ge:Sb, heavily doped, scatt. of electrons 77—59283
Ge:Sb, heavily doped semicond., scatt. mechanism, resist, and Hall coeff. maxima 80—75586
Ge:Sb, impurity conductivities 78—91691
Ge:Sb, low-freq., low temp. dielec. behaviour below metal-insulator transition 80—50250
Ge:Sb, neutron irradiated, hopping cond. between shallow defect levels 77—4347
n-Ge:Sb,Cu, exactly compensated, static photocurrent-voltage characts. 79—38131
Ge:Sb crystals, purification by zone recrystallisation with temp. gradient 79—4916
Ge:Sb(As), experimental data anal. 77—35933
Ge-In-Te system, homogeneity region, struct., electrophysical props. 78—44091
Ge-In-Te system, region of solid soln. of In in GeTe 77—51499
Ge-Si alloy, vacuum hot pressing, effect on thermal, electrical props. 80—25594
Ge-Si alloys, n-type, phosphorous doped, precipitation effects due to heat treatment 80—107833
Ge-Si:Sb, energy spectrum of Sb 80—34382
GeBi$_2$Te$_4$, Hall const., thermoelec. power, and elec. cond. 80—29407
(Ge$_{1-x}$Ga$_x$)$_{1-x}$Te, rhombohedral and cubic phases, transport effects 78—2481
(Ge$_{1-x}$In$_x$)$_{1-x}$Te, rhombohedral and cubic phases, transport effects 78—2481
Ge$_x$Ni$_{1-x}$O, crystallographic and elec. props. 77—32011
GeO$_2$, film, optical and electrophysical props. *(Russian)* 77—85821
GeS, interband transitions, intrinsic photocond., anisotropy 80—20244
GeS, Si doped and undoped, elec. cond. and thermally stimulated currents 80—20194
GeS$_x$Se$_{1-x}$, form. of solid soln. and phys. props. *(Russian)* 77—1232
γ-GeTe, anisotropy of elec. props. 79—73515
GeTe, effect of phase transition on mech. and elec. props. 77—51746

electrical conductivity of crystalline semiconductors and insulators continued
GeTe, elec. cond. and microhardness, thermal cycling effect *(Russian)* 78−35485
GeTe, high pressure effects on hole conc. and thermoelec. props. 78−26894
γ-GeTe, investigation by elec. resist., latent heat of phase transform. and plasma refl. of light 79−99317
GeTe, machining effects on electrophys. props. 77−86199
GeTe, quenched, phase transitions and electrophysical props. 79−51250
GeTe-Ga_2Te_3, electrophys. props. 77−48403
GeTe-MnTe, heat treatment effect on struct., elec. props. 80−54725
GeTe-MnTe-SnTe system, compds., GeTe phase transition temp., elec. props., thermal cond. 79−43220
α-$Ge_{1-x}Te_x$, anisotropy of elec. props. rel. to cubic phase transition and band struct. 77−76820
$Ge_{1-x}Te_x$, elec. cond., Hall effect in phase transition region 79−11113
$H_{1.6}MoO_3$, electronic props., mag. susceptibility and spectra 80−80266
HfC_x, electron energy spectrum and phys. props. in homogeneous region *(Russian)* 77−31941
$HfC_{1-x}N_x$, elect. resist. *(German)* 79−38064
HfO_2-PrO_x, phase equilibria and physicochem. props. in range 1000 to 1800°C 79−100117
$(HfO_2)_y(In_2O_3)_{1-y}$, bulk resistivity 77−35936
HfS, equilibria, nonstoichiometry and elec. props. temp. depend. *(French)* 78−64053
$HfSe_{2-x}Te_x$ and $HfTe_{2-x}$, elec. resist. and mag. suscept. studies 80−44599
$HfSi_2$, work function rel. to phys. props. 77−47887
Hg-Ar quench condensed system, annealing effects on elec. cond. 79−60880
Hg-S binary system, phase relations, bulk resist. meas. 79−66040
HgCdTe, electron irradiated, high temp. defects 79−78122
n-HgCdTe, photocond., Hall mobility and resist. 80−34478
$Hg_{0.79}Cd_{0.21}Te$, ion implanted, elec. props. 80−20184
n-$Hg_{0.8}Cd_{0.2}Te$, microwave bolometer heterodyne receiver based on magnetic field induced phase transition 80−13135
$Hg_{1-x}Cd_xTe$ epitaxial layers, elec. props. 80−96910
$Hg_{1-x}Cd_xTe$, resonant acceptor level, single and multiple scatt. effect 77−47767
$Hg_{1-x}Cd_xTe$-type semimetals, kinetic props., local acceptor level effects 80−65557
$Hg_{a-x}Cd_xTe$, ($x<0.16$), semimetallic phase, acceptor states and galvanomagnetic effects 80−6882
$Hg_xCd_{1-x}Te$, Hall effect and elec. cond., carrier density and mobility temp. depend. 77−4341
Hg_2Cl_2, elec., dielec., and thermophysical props. 79−10989
$HgCr_2Se_4$, cryst., preparation, elec. cond., thermo EMF 77−8125
$HgCr_2Se_4$, ferromag. semicond., transport props. 78−68039
HgI_2, cryst. growth from soln., doping rel. to elec. cond., phase transitions 77−55880
HgI_2, dielectric const., up to 500 bar, press. depend. 78−27153
HgI_2, single cryst. elec. and thermal props. 79−11111
$HgSb_4S_8$, photosensitive semiconductors with high permittivity, elec. props. 79−65518
HgSe, CVD crysts., electrophys. characts. 77−85910
HgSe, elec. resist., high press. phase transform., band gap 80−70707
HgSe, epitaxial growth on CdSe, struct. and electrophysical props. 77−12540
HgSe, point defect model rel. to elec. props. and phase diagram 77−4339
HgSe, press. induced phase transitions, nucleation, resistance discontinuity 77−27996
HgSe(Te), narrow band gap semicond., electron scatt., and transport phenomena 80−49706
HgTe, contrib. of resonant states to conductivity 79−51577
HgTe, electron conc. temp. depend., 1.6 to 32K, Hall effect and cond. meas. 80−24952
HgTe, mobility of electrons and holes, 4 to 100K 80−107821
HgTe, vacancy doping, effect on elec. characts. 79−82595
HgTe-type crystals, inverted band structure, influence of interband scattering on cond. *(Russian)* 79−51563
$Ho_2(MoO_4)_3$, DC electrical cond., 650 to 1150K 79−60831
Ho_2Se_3, elec. resist., thermoelectromotive force, temp. depend., 300 to 1400K *(Russian)* 78−84243
I_2:Li(Na) (K) (Cs) (Be) (mn) (Fe) (Cr), doping effect on elec. cond., semicond. props. 80−49732
In-CdS-In structure, volt-ampere characts., carrier tunnelling emission *(Russian)* 80−49914
InAs, elec. props. after heating for 300 to 900°C for 1 to 100 hours 78−47793
InAs, electrical conductivity and thermoelectric power charge due to melting 80−100490
InAs, exam. of decomposition of donors 79−1605
InAs, intrinsic point defects, nature and influence on electrophys. props. 78−79609
InAs, resist. inhomogeneity meas. with single-sonde potential method 80−65549
InAs, surface potential and surface states rel. to n-, p-, compensated n-type behaviour 77−15932
InAs, thin film prep. and elec. props. 79−1633
n-InAs, undoped, electron irrad., Hall coeff., elec. resistivity, optical absorption 77−89479
InAs:Cd, Te, donor-acceptor interaction, elec. cond. and Hall coeff. meas. 80−59988
InAs:Cd,Te interaction between impurities, effect on elec. props., Hall effect. 80−19832
n-InAs:Cr, Czochralski growth of high-resist. single crysts. 77−66587
InAs:Cr, high-resist., energy positions of deep levels, elec. and optical props. 79−7807
InAs-FeAs, eutectic, growth from melt, electrical props. 77−11911
$(InAs)_{1-x}(CdSe)_x$ solid solution, elec. props. 79−15146
InAs(P), electron irrad. at 50 MeV, elec. and optical props. 77−47486
$(In_{1-x}Ga_x)As$, scattering of electrons by potential clusters 77−15842
n-$In_{1-x}Ga_xP$ solid solns., electron scatt. mechanisms *(Russian)* 79−4568
$In_{1-x}Ga_xSb$ films, elec. props., preparation 80−100473
In_2O_3, polycrystalline, electron conc. and mobility, 25 to 700°C, O_2 partial press. depend. 77−76811
In_2O_3:Sn solar collector selective coating resistivity obs. 79−62034
n-InP, compensated impurity conduction and negative magnetoresist. 79−28360
InP, electrial props. at high temp. and in liquid state 77−11888

electrical conductivity of crystalline semiconductors and insulators continued
InP, electron transport props., mag. field and temp. depend. 80−92888
InP, free carriers, freq. depend. relax. time 80−2385
InP, growth and props. 79−1822
n-InP, γ-ray and electron irrad., annealing of radiation point defects, elec. cond. and Hall coeff. meas. 80−65051
n-InP, high resistivity layers produced by Fe^+ implantation 78−47404
InP, large size single crysts., synthesis, solute diffusion technique, elec. props. 79−33917
InP, n-type conductive regions produced by ion implantation 78−10067
InP, proton bombard. effects on resist. 77−80552
InP:Co(Cr)(Fe), Hall and resistivity meas. 80−10990
InP:Si, pulse electron annealing, carrier activation and mobility 80−15124
p-InP:Zn, electrical meas., doping levels hole conc. 78−14745
InP_xAs_{1-x} alloys, thermoelectric characts. 77−11947
$In_{2/3}PSe_3$, cryst. growth and characterization 77−77357
InS, prep., and elec. and optical props. 77−77361
In_6S_7, single crystal, switching effect and memory *(Russian)* 80−70774
n-InSb, compensated cryst., influence of surface cond. on Hall coeff. and elec. resist. 79−69579
InSb, conductivity anisotropy in strong electric field 78−19048
n-InSb, elec. props. changes during ht. treatment 77−85213
InSb, electron irradiated, kinetics of changes in carrier density 79−56228
n-InSb, freq. depend. cond. tensor in quantising mag. fields *(German)* 80−29419
n-InSb, helicon wave propag., quantum mechanical features 79−42571
p-InSb, high press. effect on elec. props., 50-300K 77−47807
InSb, high-purity specimen irradiated at 80K, transport prop. and defect annealing 78−95307
n-InSb, high-resist., prep. using radiation compensation 80−34016
p-InSb, influence of plastic deform. on elec. props. 80−103711
InSb, intrinsic and n-type, elec. cond., carrier wave instability in elect. and mag. fields 79−82617
InSb, intrinsic capacitance in transverse mag. field *(Russian)* 79−91070
p-InSb, ion bombardment using 30-80 keV ions, isochronous annealing, elec. props. obs. 79−19295
InSb, low-temp. annealing effect 77−8091
n-InSb, magnetophonon effect, temp. depend. below 90K 79−56247
InSb, neutron irrad., defect cluster form., effect on elec. props. 80−65062
InSb, quasi-static transport characts., expt. and explanation 77−20335
InSb, resist. inhomogeneity meas. with single-sonde potential method 80−65549
InSb, thermal cond., elec. cond., and thermoelec. power, press. depend. 80−59744
InSb, thermoelec. power and relative resist. at press. up to 35 kbar 79−65505
p-InSb, uniaxially stressed, elec. cond., Hall coeff. and photocond. at 15K 77−47828
InSb:Cd (Zn) (Ge), ion-irradiated, p-n conversion during heat treatment 80−96558
n-InSb:Cr, deep impurities, elec. cond. and Hall coeff. meas., 4.2 to 120K 80−107791
InSb:Cr, press. effects on transport props. 78−56146
InSb:Cr,Zn, transport props. meas. 77−1424
InSb:Cr:Zn, resist. in static and pulsed mag. field 79−15169
InSb:Cr(Zn)(Mn)(Ge), recombination of nonequilibrium carriers 79−65496
p-InSb:Cu(Ag), ionisation energy of multiply charged impurities, compensation effects 78−18996
InSb:Ge, uniaxially compressed, anisotropy of elec. props. 78−19035
InSb:S(Se)(Te), reson. states and reson. scatt., elec. props. 80−49738
InSb:Te, heavily doped degenerate semicond., anomalies in temp. depend. of resist. 79−61053
InSb-HgTe system solid solutions, elec. cond. and thermo-EMF 79−51570
InSb-MnSb eutectic alloy, temp. depend. of conductivity and Hall effect, field depend. of Hall coeff. 77−24566
InSb-NiSb, eutectic alloy, Te-doped, electrophys. props. 77−35955
InSb-type semiconductor, inelastic scatt. of electrons by optical phonons 78−76073
$InSbSe_3$, cryst. prep. and props., resistivity versus temp. study 230-400K 79−15601
$In_{1.8}Sb_{0.2}Se_3$, cryst. prep. and props., room temp. DC resistivity 79−15601
n-InSe, layered semiconductor, current-voltage characts. investig., 130 to 400K 77−4342
n-InSe, optical spectra, photocond. and resistivity 78−88321
InSe-SmSe system, microhardness and electrophys. props. 79−87093
In_2Se_3-Cu_2S system, electrophys. props., influence of 1-4% Cu_2S 80−20219
In_4Se_3 layer crystal, three-dimensionalization of transport effects 79−73514
In_6Se_7, single cryst. prep. and electrophys. props. 79−43129
α-In_2Te_3 single crysts., elec. and photocond., temp. depend., linear thermal expansion coeff. 79−42541
In_2Te_3-PbTe system, phase diagram, elec. props. 78−35361
In_2TeO_6, crystal growth by high press. method, elec. and struct. props. 77−81206
Ir metal double oxides 80−34438
$IrGe_{1.5}S_{1.5}(Se_{1.5})$, new skutterudite relation compounds, prep. and charact. 78−52700
IrP_2, prep. and characterisation 78−39679
$IrSn_{1.5}S_{1.5}$, new skutterudite relation compounds, prep. and charact. 78−52700
K, electrical conductivity, Toya's theory 78−51965
KBr(Cl), electron irradiated, electrotransport 79−69526
KCl, electron-irrad., positron-capture centres, thermal annealing kinetics 79−95875
KCl:$CdCl_2$, elec. cond., role of electrode material, surface precipitation effects 80−59985
$K_2Cr_2O_7$, polymorphic behavior, depend. on thermal and prep. history 80−34184
KD_2PO_4, high temp. phase transition, dielec. const., elec. cond. and IR refl. meas. 78−43118
$K_{1+x}Fe_yGa_{11-y}O_{17}$, electron hopping and excitation at room temp., ^{51}Fe Mossbauer spectra 80−25257
KH_2AsO_4, high temp. phase transition, dielec. const., elec. cond. and IR refl. meas. 78−43118

electrical conductivity of crystalline semiconductors and insulators continued
  $KNbO_3$, elec. and thermoelec. props., influence of O defects 80−29401
  $KNbO_3$ monocrystals, low freq. oscills. of elec. current 79−91053
  $KNbO_3$, perovskite structure, semiconductor props. *(Polish)* 78−56437
  $KTaO_3$, defect struct. and elec. props. 78−91695
  $KTaO_3$, pure and Gd_2O_3 doped, elec. cond. and sp. ht. 79−78097
  $K_2Te^{IV}Te_3{}^{VI}O_{12}$, mixed tellurate, cryst. chem. and elec. cond. *(French)* 80−107150
  $K_2[Pt(CN)_4].3H_2O$, DC elec. cond. props. 79−51582
  La compounds, plasma light reflection by free charge carriers 80−11403
  La_{1-x} Eu_x B_6 solid solutions, cryst. lattice defectiveness, mag. susceptibility and elec. conductivity 80−15083
  LaB_6, elec. cond. under hydrostatic press. 79−7832
  LaB_6 film, structure, stoichiometry, elec. properties 78−60043
  LaB_6, growth by soln. method, struct. mech. and elec. props. 80−16168
  $La_{0.003}Ba_{0.66}Sr_{0.34}TiO_3$ ceramic, positive TCR near Curie temp. rel. to charge dispersion *(Russian)* 80−16511
  $LaCO_{1-x}M_xO_3$, M=Mg, Ti, cryst. struct., elec. and mag. props. 79−86748
  $La_{0.9}Ca_{0.7}CrO_3$ polar semiconductor, elec. props., slight reduction effect 80−20183
  $La_{1-x}Ca_xVO_3$, struct., elec. and mag. props., temp. and conc. depend. *(French)* 77−4293
  $LaCrO_3$-Cr ceramic, prep., phase comp. and elec. cond. *(Polish)* 80−71621
  La_2GeSe_5, elec. props., 300 to 1100K 79−51585
  $3La(IO_3)_3.HIO_3.7H_2O$, pyroelec. p_3 and piezoelec. d_{33} coeffs. 79−19840
  $LaMnO_3$, O_2 environment, phase stability and nonstoichiometric behaviour, 1200°C 78−43134
  La_3NbO_7, weberite-type, elec., mag. and opt. props. 77−85212
  $LaNi_{1-x}Fe_xO_3$, semicond. and metallic phases, elec. and mag. props. 79−78102
  La_2O_3, elec. cond. and dielec. const., 400-1180K, phase transition 79−56224
  La_2O_3-Mn_2O_3-Cr_2O_3, synthesis and properties of solid solutions 78−44038
  $La_{0.65}Pb_{0.35}MnO_3$, transport props. near Curie points 78−88100
  LaS, heat carrier scatt., thermal and elec. cond. from 5-400K 79−14974
  $LaS_{1.47}$ elec. cond. and diff. thermo-EMF in 77-300K range 77−24573
  $La_{3-x}S_4$, mag. ordering and elec. cond. 78−10681
  $La_{1-x}Sr_xCoO_3$, $(0.5 \leq x \leq 0.9)$, ferromag., elec. props., itinerant electron model 80−107785
  $La_{1-x}Sr_xCrO_3$ $(0 \leq x \leq 0.4)$, localised level hopping transport 80−10974
  $La_{1-x}Sr_xCrO_3$, x=0-0.2, AC and DC cond., 77-1300K, hopping of polarons 78−2477
  $La_{2-x}Sr_xNiO_4$, $(0 \leq x \leq 1)$, cryst. struct. and elec. props. 78−2088
  $La_{1-x}Sr_xVO_3$, high-temp. transport meas. 77−11917
  La_3Te_4, thermal cond., thermoelec. power abd elec. cond. meas., 80 to 750K 78−18853
  Li ferrite, carrier mobility 78−19039
  LiAl, transport props., rel. to semimetallic band struct. 80−88581
  $LiBO_2$-In_2O_3, phase composition, mag. props, elec. cond. 80−55365
  LiCr ferrite, elec. resist., thermoelec. power and Nernst-Ettingshausen meas. near compensation point 78−10487
  LiF, effect of impurity traces on physical props. 77−12450
  $Li_{0.5}Fe_{2.5}O_4$, ht. treatment conditions effect on superlattice formation 77−84922
  LiH(D), electrical conductivity, effect of isotopic composition of H 79−15150
  $Li_{1-x}H_xIO_3$, cryst. growth from soln. and phys. props. 77−31634
  $LiNbO_3$, anomaly in elec. resist. 78−68030
  $LiNbO_3$ crystal, elec. cond., optical quality, impurity depend., space charge pyroelectric field compensation 79−64295
  $LiNbO_3$:Fe, elec. resist., temp. and conc. depend. 80−80275
  $LiNbO_3$:Fe, photovoltaic effect and charge transport mechanism 79−38123
  $LiNbO_3$:Fe, pure and doped, photocond. and dark cond. 80−29439
  $LiNbO_3$:Fe, temp. depend., electron cond., holography appl. 78−14731
  $LiNbO_3$-$3(Li_2O).Nb_2O_5$ eutectic, anomaly in elec. resist. 78−68030
  Li_2O-NiO-O_2, phase diagram and mag. props. of $Li_xNi_{1-x}O_{1 \pm y}$ 78−48380
  LiTiZn ferrites, elec. resist., mag. props., effect of Bi addition 78−95474
  LiV_2O_5, needle cryst. form. by reduction of molten Li_2O-V_2O_5, semicond. props. *(Japanese)* 78−3030
  $Li[Mn_2]O_4$ spinels, crystallographic, electronic and mag. props. *(German)* 79−60324
  $Li_2[Pt(CN)_4].3H_2O$, DC elec. cond. props. 79−51582
  Lu_2O_3, elec. cond. and dielec. const., 400-1180K 79−56224
  $LuRhO_3$, elec., mag. and photoelectrochemical props. 80−96925
  Lu_2Se_3, elec. resist., thermoelectromotive force, temp. depend., 300 to 1400K *(Russian)* 78−84243
  $MgAl_2O_4$, γ-irradiated crystal, TSC, thermoelec. power, thermolum. and afterglow 80−75583
  $MgCr_2O_4$-TiO_2, porous ceramics, humidity-sensitive electrical conduction 80−107782
  $Mg_xFe_{1-x}O$, diffusion of ^{59}Fe and elec. cond. 80−59700
  $MgIn_xFe_{2-x}O_4$ and $MgSc_xFe_{2-x}O_4$, Mossbauer spectra, elec. and mag. props. *(Russian)* 77−69737
  $MgM^{3+}{}_xFe_{2-x}O_4$, M=In,Al,Cr,Sc, comp. effects on ferrite characts. 78−52305
  MgMn ferrite, carrier mobility, temp. depend. 78−19039
  MgO, defect aggregation and thermal-electric breakdown, TEM obs. 79−42069
  MgO, elec. field effects on cond. above 1300K, elec. breakdown 79−42551
  MgO, sintered, refractories, props. after testing at over 2000°C 80−104317
  MgO, with paramag. surface defects, elec. cond., 20-250°C, H_2 atm. effects 77−20313
  MgO:Cr, elec. cond. at high temp. in oxidising atmosphere 77−69323
  MgO:Li, enhancement of elec. cond. by oxidation 80−44600
  5 wt.% MgO-Si_3N_4, hot-pressed, dielec. props. 78−10822
  MgO-Si_3N_4, hot-pressed, electrical props. 78−39136
  MgO-ZnO-Fe_2O_3, sintered ferrite, preparation, mag. susceptibility, DC resistivity 80−34598
  $MgSiO_3$, elec. cond. under defined thermodynamic activities up to 20 kbar, 340-1100°C 80−6832
  Mg_2SiO_4, forsterite, elec. props. 78−34833
  $Mg_2Si_2O_6$, enstite, elec. cond. var. with O_2 partial press., obs. and theory 79−1609

electrical conductivity of crystalline semiconductors and insulators continued
  $Mg_{0.25}Zn_{0.75}Fe_2O_4$, ferrite, DC cond., dielec. props., lattice consts. 80−80272
  $Mg[Pt(CN)_4].7H_2O$, DC elec. cond. props. 79−51582
  $(Mn,Zn)Fe_2O_4$:Si, Ca, Ti, second phase effect on elec. and mag. props. 80−60986
  Mn-Zn ferrospinels, carrier transfer phenomena 80−54727
  $MnAs_{0.95}P_{0.05}$, anisotropy of elec. cond. and Hall effect 80−92908
  $MnAs_{1-x}P_x$, high spin-low spin transition 77−20591
  $MnAs_{1-x}P_x$, low temp. resistivity minimum 77−8122
  $Mn_2As_xSb_{1-x}$, $x < 0.5$, temp. dependence, 78 to 400K 78−76248
  MnB_{12}, growth from melt and phys. props. 80−20782
  $MnCo_2O_4$ spinel, synthesis, effect of Bi_2O_3 admixture upon props., thermistor appl. 78−15325
  $MnCr_2Te_4$, elec. props., 100 to 650K *(Russian)* 79−11115
  $Mn_xFe_{3-x}O_{4+y}$, prep., resist., hysteresis loop and mag. disaccommodation *(Spanish)* 77−73045
  $Mn_{1-x}Fe_xSi_{1.7}$, solid soln. system, temp. depend of conductivity and thermo-EMF, conc. depend of Hall const. 77−11913
  $MnGa_2S_4$, synthesis electrophys. props. 77−51747
  $Mn^{2+}Mo^{4+}O_3$, defect spinel struct., elec. and mag. props. 80−70176
  MnO, electronic cond., rel. to basic processes of Mn corrosion 77−25198
  MnO, electronic struct. calc. 78−43297
  MnO-CoO-O_2, semicond. solid solns., ageing effects on elec. cond. 78−23085
  MnO_2, DC cond., water content depend. 77−80774
  MnO_2 powder electrical characts. obs. battery grade, highly hydrated 79−100501
  Mn_3O_4:Li(Cr)(Al)(S), and pure Mn_3O_4, elec. cond. and thermo-EMF 80−20231
  Mn_3O_4:S, defect struct. and elec. props., electron, hole conc. 80−44601
  MnP, elec. resist. of different mag. phases, temp. depend. 80−54691
  $MnSb_2S_4$, synthesis, electrophys. props. 77−51747
  MnSe, mag. suscept., thermal expansion and elec. resist. meas. 78−34964
  Mn_2SiO_3, effect of vibration during sintering, on electrical resistivity 80−16258
  MnTe, resistivity anomalies at mag. transitions, sp.ht. 80−39785
  $(MnTe)_{1-x}$-$(As_2Te_3)_x$ solid solns., thermoelec. props. 79−42567
  $(MnTe)_{1-x}(Bi_2Te_3)_x$ $(x \leq 0.05)$ solid solution, electrophys. props. 80−24925
  MnZn ferrite, gas phase fluorination for improved props. 78−52306
  MnZn ferrite, polycrystalline, doped, DC resist. 78−47788
  MnZn ferrite, props. rel. to raw materials *(German)* 77−21074
  MnZn ferrite, temperature dependence of Hall mobility 78−30944
  MnZn ferrites, elec. cond. mechanism in paramag. and ferrimag. phases 80−15524
  $Mn_{1.18}Zn_{0.06}Co_{0.01}Fe_{1.75}O_4$, transport props. near Curie points 78−88100
  $(Mn_{0.7}Zn_{0.3})_xFe_yO_4$, electromag. props. rel. to Fe content 78−43613
  Mo complex, $MoOCl_3.2Ph_2SO$, prep. and characterisation 78−30592
  Mo-dichalcogenide, valence band nature, elec. and mag. props. 78−39014
  Mo_2B_5 and MoB_4, thermal, elec., and mag. props. 80−20187
  Mo_5GaS_6, struct. transform. below 50K, mag. permeability and elec. cond. meas. *(Russian)* 77−7864
  MoO_2, MoO_3 and Mo_xO_{3x-1} single cryst. growth by chem. transport, elec. resist. meas. 77−59681
  MoO_3:Li, elec., catalytic props. 78−60122
  $MoRh_2O_6$, crystn. and cryst. struct., paramag. and elec. cond. props. *(French)* 77−80480
  $Mo_4Ru_2Se_8$, synthesis, struct., and elec. props. 80−92877
  MoS_2 (2H), elec. cond. press. depend. 78−43394
  MoS_2, elec. cond. and Hall coefficient temp. depend. 77−28180
  MoS_2 solid lubricant, antifriction and elec. props. depend. on oxidation temp., dopant influence 80−108584
  MoS_2, synthetic molybdenite single crystals, growth from vapour, elec. props. 80−34446
  Mo_6S_8 Chevrel phases with group IIIa metals, Nb, Hg, Pb and Cu, synthesis, stability and characts. 80−71608
  $MoSe_2$, elec. cond. and Hall coefficient temp. depend. 77−28180
  $MoSe_2$:Nb(Re), layered, elec. props., semicond.-metal transition 77−11922
  $MoSe_{2-x}$, transport meas. and band structure 77−69361
  $MoTe_2$, elec. cond. and Hall coefficient temp. depend. 77−28180
  $MoTe_2$, elec. cond. and thermoelec. power 79−91047
  $MoTe_{2-x}$, thermal switching mechanism 77−15920
  $MoTe_{2-x}$, thermoelec. power and resist. meas., band struct. 77−1438
  $Mo_{0.5}W_{0.5}Se_2$ single cryst. vapour growth, characterisation 80−93466
  $NH_4Cl:[MoOCl_5]^{2-}$, single cryst., struct. investigations 77−66524
  $NH_4Cl(Br)$, effect of $NH_4{}^+$ internal motion on elec. and optical props. 80−100454
  NH_4ClO_4, AC elec. cond. temp. and freq. depend., obs. and unified defect struct. model 80−88554
  $NH_4H_2PO_4$, high temp. phase transition, IR spectra, differential 80−25319
  $NH_4IO_3.2HIO_3$, dielec. constant, elec. cond. phase transition and cryst. struct. 80−1999
  $(NH_4)_2[Pt(CN)_4].2H_2O$, DC elec. cond. props. 79−51582
  $(NPCL_2)_3$, trimer and polymer, polycrystn., resistivity 77−51735
  Na, electrical conductivity, Toya's theory 78−51965
  $NaAl(MoO_4)_2$, domain struct., phase transition, and dielec. props. 79−56748
  NaCl, elec. cond. and distrib. of Ni^{2+} ions 79−33010
  NaCl, electron irradiated, electrotransport 79−69526
  $NaCl:S^{2-}$, enthalpy of anion vacancy migration 80−15309
  NaCl:Sr, solubility of free and assoc. Sr 77−62645
  NaCl:X (X=Ca, Sr, Ba, Mg, K, Li, Tl, Ag), impurity conc. effect on mech. and elec. props. 78−47469
  NaF:U, single crystals, variation with preparation procedure 78−72588
  $NaFe(MoO_4)_2$, domain struct., phase transition, and dielec. props. 79−56748
  $NaNO_3$, low temp. struct. changes, elec. props. 79−87377
  $NaNbO_3$, elec. and photoelec. props. near ferroelec.-antiferroelec. phase transition 80−15989
  $NaNbO_3$, elec. and thermoelec. props., influence of O defects 80−29401
  $NaNbO_3$, elec. cond., Hall mobility, thermoelec. coeff. 79−82584
  $NaNbO_3$, elect. cond. mech., resist., Hall coeff. and thermoelec. power meas. 80−65603
  $NaNbO_3$, perovskite structure, semiconductor props. *(Polish)* 78−56437
  $NaNbO_3$-based ferroelec. solid solns., morphotropic transitions and elec. props., enhanced vacancy conc. 80−55048

electrical conductivity of crystalline semiconductors and insulators continued
Na_2O-Ga_2O_3 system, new superionic conductor *(French)* 78—14504
Na_2SO_4, pure and K-doped, phase transforms., X-ray, DSC and elec. cond. obs. 79—33082
$Na_xVS_2(Se_2)$, mag. and elec. props. rel. to struct. transitions 78—91848
Nb carbide interstitial phases, elec. and mag. props., neutron radiation effects 79—77640
Nb complex, $NbOCl_3.2L$ ($L = Ph_2SO$, Ph_3PO and $(Me_2N)_3PO$), prep. and characterisation 78—30592
Nb complex, prep. by halide reaction with tetramethylurea and tetramethylthiourea, and characterisation 79—15972
Nb-N(-H) system, electrophys. props. of nitrides and hydronitrides 77—85215
Nb_3As, electronic and supercond. props. 77—16011
NbC, high-temp. plastic deform. effects on elec. props. 77—44370
NbC_x, reactor irrad. effects on elec. resist. and supercond. props. *(Russian)* 78—47895
NbC_x, thermophysical props. at high temp., thermal vacancies form. 78—43141
$NbCl_4$, high press. elec. resistivity 80—29404
NbI_4, NbI_5, Nb_3I_8, elec. cond., temp. and press. depend. 79—60830
NbI_4, quasi-one dimens., press.-induced metal-insulator transition 78—43447
NbN_x, solid soln, strain ageing, internal friction, elec. cond. kinetics *(Russian)* 78—76667
NbN_xO_y, solid soln, strain ageing, internal friction, elec. cond. kinetics *(Russian)* 78—76667
NbO, high press. elec. resistivity, semiconductor to semiconductor transition 80—29404
NbO_2, high press. elec. resistivity, phase transition 80—29404
NbO_2, on-state decay rel. to recomb. and nonlinear props. 80—84492
NbO_x, solid soln, strain ageing, internal friction, elec. cond. kinetics *(Russian)* 78—76667
$Nb_{12}O_{29}$-Nb_2O_5, oxide defect structures of stable and metastable phases, 800 to 1100°C 79—46651
Nb_2O_5, partially reduced, electrical conductivity 77—15918
Nb_2O_5, partly reduced, mag. and elec. props. 77—43593
Nb_2O_5-V_2O_5-P_2O_5, glasses and glass ceramics, elec. cond., struct. 80—84466
$NbSe_2$ solid lubricant, antifriction and elec. props. depend. on oxidation temp., dopant influence 80—108584
$NbSe_3$, CDW form., non-linear props., temp. and press. depend. 80—49753
$NbSe_3$, phase transitions, phys. props. meas. 77—8005
$NbSe_x$, $x = 1.48$-2.0, nonstoichiometric, elec. props., supercond. transition temps. 79—73624
Nb_3Si, electronic and supercond. props. 77—16011
$Nb_{1-x}V_xSe_2$, elec. and mag. anomalies at CDW transition 80—107722
Nd-Gd-Te alloys of R_2Te_3-T_3Te_4 region, physicochem. props. 78—52017
$Nd_{1-x}Ca_xVO_3$, solid solutions, elec. props. 80—96866
Nd_2GeSe_5, elec. props., 300 to 1100K 79—51585
$NdH_{2.82}$, high-pressure structural phase transforms., resist. meas. 78—10185
$Nd_2(MoO_4)_3$, mag. susceptibility, elec. cond. and thermoelec. power 78—88091
$Nd_{1/3}NbO_3$, $NdNbO_4$, structural characteristics and residual polarisation 77—15361
Nd_3NbO_7, weberite-type, elec., mag. and opt. props. 77—85212
Nd_2O_3, A-type, elec. cond. and dielec. const. 4.2-1200K 77—4340
Nd_2O_3, A-type, thermoelectric power, AC cond. 78—68044
Nd_2O_3, elec. cond., thermoelec. power, dielectric const. 79—69763
Nd_2S_3, semimetallic, elec. and thermal transport meas. 78—10442
$NdTlO_3$, physicochem. props. 80—25625
$Nd_2(WO_4)_3$, elec. transport and mag. props. meas. 77—24668
$Nd_2(WO_4)_3$, molar mag. susceptibility, DC elec. cond., thermopower meas. 79—15172
$Nd_2Zr_2O_7$-$Nd_2Hf_2O_7$, struct., elec. cond. and melting point 80—54197
Ni complex, 2,6-N,N-diacetyldiaminopyridine-Ni(II) elec. cond., γ dose and temp. (303-363K) effects 80—103696
Ni complex, 2,6-N,N-dibenzoyldiaminopyridine-Ni(II) elec. cond., γ dose and temp. (303-363K) effects 80—103696
Ni complex, $Ni(S_2C_2(CN)_2)_2{}^{1-}$, elec. cond. 79—73505
Ni ferrite, gas phase fluorination for improved props. 78—52306
Ni-Zn ferrite, electrical cond., Seebeck coeff. and saturation magnetisation 77—20315
Ni-Zn ferrites, hot-pressed, key props. 78—15348
$Ni_{1-x}Co_xS_2$, anomalous elec. props., polaron transport in highly correl. narrow bands 77—85222
$Ni_{1-x}Co_xS_2$, elec. cond., thermoelec. power and optical meas. 80—59986
$Ni_{1-x}Co_xS_2$, elec. transport and semicond.-metal transition 80—10985
$Ni_{1-x}Cr_xS$, elec. transport, mag. susceptibility and DTA meas. 80—96954
$Ni_{0.51}{}^{2+}Fe_{0.46}{}^{2+}Fe_{1.95}{}^{3+}O_4{}^{2-}$, elec. resistivity above 300K 79—78099
$Ni_{0.89}{}^{2+}Fe_{0.13}{}^{2+}Fe_{2.11}{}^{3+}O_4{}^{2-}$, elec. resistivity above 300K 79—78099
$NiFe_2O_4$, electronic phase transition 80—65640
$Ni_xFe_{3-x}O_4$, DC and low freq. cond. and influence of microstruct. 80—70699
$Ni(Mo_2Re_2)S_8$, synthesis and electrical props. of mixed tetrahedral cluster phases 80—2971
$Ni_2Mo_6S_6O_2$, O-containing Chevrel phases, synthesis and props. 80—108368
NiO catalyst, superparamagnetic, elec. props. 79—65506
NiO, doped and undoped, elec. props. and surface characts. 80—65571
NiO, elec. cond. and chem. diffusion coeff. at high temps. 79—23962
NiO, elec. cond. meas. at 1000°C 78—10451
NiO, elec. cond. under low O_2 press. 78—64041
NiO, elec. cond. variation with temp. *(French)* 79—60829
NiO, electronic cond., rel. to basic processes of Ni corrosion 77—25198
NiO, electronic struct. calc. 78—43297
NiO, localised charge carrier transport, Seebeck, resistivity meas. 78—72152
NiO, microwave cond. and DC cond. meas., 803-1873K 77—43638
NiO, physicochem. props. at high temps. *(French)* 80—39582
NiO scale on Ni, elec. cond. 77—48568
NiO, temp. and stoichiometry depend., antiferromag. T-domain influence 77—8332
NiO, thermodynamic study of point defects, anal. of elec. cond. results 79—23963
NiO_2, elect. cond. under low O_2 press., kinetics interpretation 79—82587
$Ni_{1-x}O$, electronic cond. at high temp., vacancies and interstitials effect *(French)* 78—79990

electrical conductivity of crystalline semiconductors and insulators continued
$NiPS_3$, layered semiconductors, optical and electronic props. 80—70761
$Ni_{1-x}Rh_xS$, nonvolume effect of Rh substitution on paramag. metal-antiferromag. nonmetal transition 79—28277
NiS_2, weak ferromagnetic semiconductor single crystal, elec. and magnetic props. 77—85226
$NiSO_4$:Li (10 at.%), powder, semiconducting, exam. of freeze drying rate in cryochemical prep. method 78—52706
$NiS_{2-x}Se_x$, elec. cond., thermoelec. power and Hall effect meas. 80—65561
Ni_2SiO_2, elec. cond. under defined thermodynamics activities, up to 20 kbar, 340-1100°C 80—6832
$NiWO_4$, AC elec. conductivity, thermoelec. power and dielec. const. 80—70736
$Ni_{0.4}Zn_{0.6}Fe_2O_4$, conditions for max. resistivity 77—21065
$Ni_{0.5}Zn_{0.5}Fe_2O_4$, Hall mobility, elec. cond. and carrier conc., 30 to 180°C 77—51765
Os metal double oxides 80—34438
PLZT, thin, elec. cond. and pyroelectric behaviour 80—75954
Pb chalcogenide, solid solution, thermoelectric efficiency 79—95429
Pb chalcogenides, warm electron cond. 79—91066
Pb-Sn-Te, solid solution, scattering mechanism of carriers 80—49710
Pb_y-$Sr_{1-y}(Zr_x$-$Ti_{1-x})O_3$:Cr_2O_3, ferroelec. ceramic, reversible characts. and dielectric losses *(Russian)* 78—84517
$Pb_{2-x}Ba_xLi_{0.5}Nb_{1.5}O_6$, elec. resistivity, Curie temp., $x = 0$-0.15, 50-350°C 78—2478
$Pb_{0.94-x/2}Ba_{0.6}Nb_xZr_{1-x}O_3$, Nb dopant morphology effect on microstructure 80—81005
$Pb_{1-x}Be_xTe$, anomalous resist. near ferroelec. phase transition 80—20196
$PbBr_2$, determ. of sign and drift mobility of majority carriers *(Russian)* 79—69512
$PbCl_2$, determ. of sign and drift mobility of majority carriers *(Russian)* 79—69512
$PbCo_2(PO_4)_2$, mag. susceptibility, elec. cond. and optical refl. 79—56495
PbF_2, superionic, electrical conductivity at high temp. 78—79798
$Pb(Fe_{1/2}Nb_{1/2})O_3$-$La_2O_3(CeO_2)$ ferroelec. ceramics, electrophysical props. 78—35099
$Pb_5(Ge,Si)_3O_{11}$, dielec. and elec. props., 20 to 250°C 80—29697
$Pb_5Ge_3O_{11}$, dielec. behaviour, 60 Hz-100 kHz, particle size effects 79—33638
$Pb_5Ge_3O_{11}$, ferroelec., elec. cond. meas. 79—65472
$Pb_5Ge_3O_{11}$, ferroelec., surface capacitance effect on dielec. props., DC cond. and dielec. const. meas. 79—91333
$Pb_{1-x}Ge_xTe$, ferroelec. phase transition, IR refl. and resist. meas. 80—11353
$Pb_{1-x}Ge_xTe$ solid solns., phase transition influence on elec. props., 77 to 450K 80—103689
$Pb_{1-x}Ge_xTe$, solubilities, elec. and optical props. 77—35940
$Pb_{1-x}Ge_xTe$:Ga, Fermi level stabilization, transport props. meas., 77-400K 78—56065
$Pb_{1-x}Ge_xTe$:Ga, influence of hydrostatic compression on elec. props. 79—73516
PbI polytypes, phase transforms. and electrical behaviour 78—47839
PbI_2, determ. of sign and drift mobility of majority carriers *(Russian)* 79—69512
PbI_2, dielectric props., elec. cond., space charge polarisation 80—100631
PbI_2, elec. props. rel. to polytypically modulated structs. 79—94971
PbI_2 polytypes, elec. cond., band gap reduction due to stacking fault levels 77—32015
$Pb_{1-x}In_xTe$, $0.01 \leq x \leq 0.2$, elec. cond., Hall coeff. liquid He temp. 78—47815
$PbLaZrNbO_7$, dielectric with zero temp. coeff. of dielect. consts., electrophys. props. 77—52010
$Pb_{1-x}Mn_xTe$ ($x = 0.005$, 0.001, 0.05), solid solns., exam. of electrical and thermal props. 79—1599
$PbMoO_4$, ionic and electronic cond. 79—91107
$PbMo_6S_6O_2$, O-containing Chevrel phases, synthesis and props. 80—108368
$Pb(NO_3)_2$, low temp. struct. changes, elec. props. 79—87377
$Pb_{0.98}Nb_{0.02}(Zr_{0.95}Ti_{0.05})_{0.98}O_3$, PZT 95/5, ferroelec. ceramic, resist. meas. under shock wave compression 78—19031
PbO single crystals, current-voltage characts., electrolum. *(Russian)* 80—2863
PbO_2, compressed powder, electric conductivity obs. 77—32013
$4PbO.GeO_2$, X-ray phase and thermal anal., new antiferroelectric 79—1744
PbS, hot-pressed compact, elec. behaviour, adsorbed atmos. gas effects 77—66601
PbS, low carrier conc., prep. and props. 77—39846
n-PbS, $PbS_{1-x}Se_x$ layers prepared by hot-wall epitaxy 77—16481
PbS, phase transitions under action of high press., elec. cond. meas. 77—4196
p-PbS, struct. of valence band, transport processes study 80—20081
PbS-Ni, phase diag., cpd. formation and electrophys. props. 77—85997
PbS-Sb_2S_3 semicond., optical and photoelec. behaviour 80—96938
$Pb_6Sb_{14}S_{27}$, zinkenite, electrophysical properties 78—34834
PbSe film, influence of pot. barrier on thermoelec. props., elec. cond., Hall coeff. and Nernst-Ettingshausen coeff. 78—39239
PbSe, Hall effect and elec. cond. under strong anisotropic pressure 77—55549
PbSe:Tl, scatt. of holes and phonons by impurities 78—19068
$Pb_{0.59}Sn_{0.41}Se$, struct. phase transition, temp and hydrostatic press. influence, Hall effect, resistivity *(Russian)* 78—51675
$Pb_{0.65}Sn_{0.35}Se$, solid soln., elec. props. 78—39112
$Pb_{1-x}Sn_xSe$, band struct. and transport props., hydrostatic press. effects 80—15452
$Pb_{1-x}Sn_xSe$, displacive transition, temp. and press. depend., elec. meas. 80—10672
$Pb_{1-x}Sn_xSe$, film struct. and elec. props. 77—80708
$Pb_{1-x}Sn_xSe$, n- and p-type, with band inversion, study of transport phenomena 80—49741
n-$Pb_{1-x}Sn_xSe$, single crysts. and diodes, elec. props. under high press. 77—47809
$Pb_{1-x}Sn_xSe$, transport phenomena in solid solutions with band inversion 80—107792
$Pb_{1-y}Sn_ySe$, electron-irradiated, elec. and recomb. props. 79—56227
PbSnTe, electron irradiated, high temp. defects 79—78122
$Pb_{0.41}Sn_{0.59}Te$, Hall coeff., elec. cond. meas. 80—44615
$Pb_{0.56}Sn_{0.44}Te$, press. induced ferroelec. phase transition 79—65809
$Pb_{0.72}Sn_{0.28}Te$, Hall effect and elec. cond., 77 to 480K, energy band struct. 77—76817

electrical conductivity of crystalline semiconductors and insulators continued
$Pb_{0.76}Sn_{0.24}Te$ single crystals, current-voltage characts. at He temps. 80—20197
$Pb_{0.82}Sn_{0.18}Te$, film, effect of hydrostatic pressure on props. 80—70862
$Pb_{1-x}Sn_xTe$, anomalous resist. near ferroelec. phase transition 80—20196
$Pb_{1-x}Sn_xTe$, Cd-In diffusion, changes in elec. props. 78—91348
$Pb_{1-x}Sn_xTe$, correlation between elec. props. and crystalline environment 77—80773
$Pb_{1-x}Sn_xTe$, diffusion of Cd, Hall effect, cond. and solubility meas. 79—69292
$Pb_{1-x}Sn_xTe$, electron-irradiated, elec. and recomb. props. 79—56227
p-$Pb_{1-x}Sn_xTe$, pressure-induced transition to zero-gap state, changes in energy band parameters 79—69413
p-$Pb_{1-x}Sn_xTe$, single crysts. and diodes, elec. props. under high press. 77—47809
$Pb_{1-x}Sn_xTe$, thermoelectric effects, characteristics at low temps. 80—107831
$Pb_{1-x}Sn_xTe$:Cd, deep energy level, temp. depend. of elec. cond. 78—18994
$Pb_{1-x}Sn_xTe$:In, dielectric state, avalanche breakdown in strong elec. fields *(Russian)* 80—92901
$Pb_{1-x}Sn_xTe$:In, high temp. Fermi level position 79—90948
$Pb_{1-x}Sn_xTe$:In(Ga)(Al), elec. props., dopant influence 79—51599
PbTe, diffusion of Cd, Hall effect, cond. and solubility meas. 79—69292
PbTe film, elec. transport props. 79—42679
n-PbTe, low temp. elec. cond. 80—20227
PbTe, struct. of second valence band cond. of warm carriers and magnetoresist. 77—89697
PbTe:Bi(Sb)(Cr)(Ag), thermoelec. props., thermal and elec. cond. 79—82616
PbTe:Ga, location, behaviour of Ga, electrophysical props. meas. 79—38016
PbTe:In, electron mobility, temp.-independent part, Hall effect and elec. cond. meas. 80—92914
PbTe:Ti, effect of impurities on transport props. 79—11158
PbTe:Tl, thermoelectric power, elec. cond., Hall coeff. and optical absorpt. coeff. 80—39584
PbTe-InTe system, phase interactions and solid soln. form., physicochem. and elec. characteris. 80—104129
$PbTe_{1-y}Se_y$:In, high temp. Fermi level position 79—90948
$PbTiO_3$, cryst., polarisation and resistivity, elec. field effects 78—64313
$PbTiO_3$, perovskite structure, semiconductor props. *(Polish)* 78—56437
$PbTiO_3$, struct. changes with temp. variation, rel. to elec. cond. 78—91437
$Pb(Ti_{0.47}Zr_{0.53})O_3$, elec. cond. rel. to O_2 partial press. 77—51742
$Pb(Ti_{0.47}ZrO_{.53})O_3$, small polaron cond. mechanism, elec. cond. and thermopower meas. point defects 78—43380
$PbWO_4$, ionic and electronic cond. 79—91107
$Pb(Zr,Ti)O_3$ solid soln., elec. cond. and Seebeck coeff. 79—51564
$Pb(Zr,Ti)O_3:Cr_2O_3$ ceramic, electrical cond. and dielectric const. meas. 80—2389
$Pb(Zr,Ti)O_3$:Fe(Nb) ceramic, elec. and electromechanical props., depend. on dopants 80—81212
$Pb(Zr,Ti)O_3:Nb_2O_5(Sc_2O_3)$, elec. cond. investigation with and without various dopants and stoichiometry 79—11120
$PbZrO_3$, perovskite structure, semiconductor props. *(Polish)* 78—56437
$PbZrO_3$-monocryst., elec. cond., permittivity, polarisation, para- and ferro-to antiferroelec. phase transistions 78—60402
$Pb(Zr_{1-x}Ti_x)O_3$, electrical conductivity and I-V charact., neutron effects 78—47781
$Pb(Zr_xTi_{1-x})O_3$, elec. props. effect of proportional composition, morphotropic phase boundary 78—35105
$Pb(Zr_xTi_{1-x})O_3$, elec. props. temp. and composition depend. 78—47817
$Pb(Zr_xTi_{1-x})O_3$ solid solns., elec. props. near morphotropic phase boundary 79—42566
$Pb(Zr_{0.47}Ti_{0.43}Sn_{0.10})O_3:Cr_2O_3$, ferroelec. ceramic, reversible characts. and dielectric losses *(Russian)* 78—84517
Pd metal double oxides 80—34438
Pr compounds, plasma light reflection by free charge carriers 80—11403
Pr_2 NiO_4, elec. props., 300 to 1000°C 78—91694
$PrFeO_3$, elec. props., 300 to 1000°C 78—91694
Pr_2GeSe_5, elec. props., 300 to 1100K 79—51585
Pr_6O_{11}, mag. and transport props., multiphonon hopping conduction 78—19211
PrS, heat carrier scatt., thermal and elec. cond. from 5-400K 79—14974
Pt complex, bis(1,2-benzoquinonedioximato)platinum(II), intrinsic elec. cond. 78—6377
Pt complex, $Pt(S_2C_2(CN)_2)_2^{1-}$, elec. cond. 79—73505
Pt, deuteron irrad., energy release and resist. recovery, self-interstitial-atom interaction energies 79—95002
Pt metal double oxides 80—34438
$PtSb_2$, high field elec. props., impact ionisation 80—96892
$RTiNbO_6$, R = rare earth, electrophys. props. 78—23388
$RbAg_4I_5$, solid electrolyte, electronic cond. meas. 78—2483
$RbAg_4I_5$, superionic conductor, phase transition detection by thermoelectric power method 80—92669
$RbClO_4$, AC elec. cond. temp. and freq. depend., obs. and unified defect struct. model 80—88554
RbH_2PO_4, high temp. phase transition, dielec. const., elec. cond. and IR refl. meas. 78—43118
$RbNO_3$, permittivity and dielec. cond. press. up to 5 kbar, antiferroelec. transition obs. 77—36183
$RbNO_3$, single cryst., DC cond., dielec. and thermophys. props., temp. depend., transitions interpret. 78—26682
Rb_xWO_3 bronze, elec. resist. meas., anisotropy 80—75569
Rb_xWO_3, resistivity, Hall effect and Seebeck coeff. from 1.5 to 300K 80—6879
$Rb_2[Pt(CN)_4].3H_2O$, DC elec. cond. props. 79—51582
Rh metal double oxides 80—34438
$RhGe_{1.5}S_{1.5}$, new skutterudite relation compounds, prep. and charact. 78—52700
Ru metal double oxides 80—34438
$Ru_2Ge_{3-x}Sn_x$, and $Ru_2Ge_{3-y}Si_y$, diffusionless phase transitions, elec. and mag. props. 80—96871
RuO_2, thermal conductivity meas., rel. to elec. cond. 80—65317
RuO_2-TiO_2 anode, wear-resistant, use in applied electrochem. 80—40701
RuP_2, prep. and characterisation 78—39679
S, flash-excited charge-transits, electrode-edge effects, meas. 80—2396
S, single crystal, photoinjection, electronic transport and Mott-Gurney transition *(Spanish)* 80—84464

electrical conductivity of crystalline semiconductors and insulators continued
$(SN)_x$ polymer, elec. props. of amorphous thin film and single crystal, role of chain breaks *(Japanese)* 78—68104
(SN)x, halogen-doped, temp. depend. of elec. cond. 79—65563
Sb, electrical resist., thermal cond. and thermopower, low temp. transport props. 80—49708
Sb, electrical resist. and anisotropy at press. up to 80 kbar 77—43554
Sb, mutual drag effect in ideal elec. and thermal resist. 79—73507
$(Sb_{1-x}Bi_x)_2Te_3$, δ phase, equilib. state, electrophysical props. 79—52178
$Sb_{1.48}Bi_{0.52}Te_3$, obtained by zone crystallisation, effect of extrusion and annealing on elec. props. 79—96038
$Sb_{1.5}Bi_{0.5}Te_3$ solid solution, temp. influence obs. *(Slovak)* 78—30946
Sb_2O_3, thermoelec. props., 500-1500K 80—29423
Sb_2S_3, cond. anomalies at phase transition pts. 77—43604
Sb_2S_3, defect drift in elec. fields and bistable switching 80—92947
Sb_2S_3, elec. and mag. props., carrier transport mechanism 78—47792
Sb_2S_3, galvanomag. props. and elec. resist., temp. depend. 78—43419
SbSI, electrical cond. and acceptor level shift temp. depend., para- and ferroelec. phases 77—28181
Sb_2Se_3 crystals, mag. and elec. props. 80—96873
Sb_2Se_3, energy gap, light absorpt., elec. cond., photocond. meas. 78—47826
Sb_2Se_3 film, struct. and photoelec. props. 77—85257
Sb_2Se_3 single crysts., phys. prop. anomalies, 400-450K *(German)* 79—38072
$(Sb_2Se_3)_x$-$(Bi_2S_3)_{1-x}$ single crystals, elec. and photoelec. props., stoichiometry deviations influence 79—60870
$(Sb_2Se_3)_{0.7}(Bi_3Se_3)_{0.3}$, solid soln., prep. and elec. properties of layered crystals 80—70762
Sb_2Te_3, mag. and elec. props., carrier excitation 78—43395
Sb_2Te_3, $Sb_{1.5}Bi_{0.5}Te_3$, Te- and Se-doped cryst. growth and elec. props. 77—48334
Sb_2Te_3, thermoelectric properties and phase transition, under hydrostatic pressure up to 9 GPa 80—65609
Sb_2Te_3-Bi_2Te_3 solid solns., bladed cryst. growth, electrophysical props. 78—43387
Sb_2Te_3-Sb_2Se_3, ordered structure formation, heat treatment effect on thermal cond. 80—54448
Sb_2Te_3-Sb_2Se_3 thin layers, struct., phase comp., and elec. cond. 80—15389
ScN_x, region of homogeneity, physicochem. props. 78—52018
Sc_2O_3, heat treated, elec. cond. rel. to O_2 partial press. 77—15845
Sc_2O_3, liq. and solid phase elec. cond., high temp. meas. 80—84468
Sc_2O_3, solid and liq. phases, thermophysical and electrophysical props. 80—103495
Sc_2Se_3, elec. resist., thermoelectromotive force, temp. depend., 300 to 1400K *(Russian)* 78—84243
Se, crystallisation kinetics correlation with molecular structure 78—94998
Se diode surface states determ. by conductance and capacitance 77—85318
Se, elec. cond., 0-500 kbar 79—99589
Se, electrical conductivity after X-ray irradiation 79—51567
Se, hexagonal, resistivity depend. on applied elec. field freq. during crystn. 77—35938
Se, liquid-crystal phase transition, elec. cond. changes 79—33310
Se, polycrystalline trigonal layer, freq. depend. elec. behaviour and its relationship to xerographic performance of Se particle contact photoreceptors 79—82640
Se powder compacts, sintered, electrical cond. 80—70693
Se, X-ray effects *(Russian)* 80—15519
Se:Ta, electrophysical meas. rel. to control of conductivity type 77—24323
Si, Ar and B implantation effects on cond. 77—80779
Si, As-doped, effect of elec. and struct. parameters on avalanche breakdown localisation 77—11926
Si, bicrystals, grain boundary states and varistor characts. 80—24829
n-Si, carrier recomb. and photoionisation via E-centre resonance state 79—60847
Si, charge transport properties, review 77—39851
Si circular slices, resistivity var. meas. using automated photovoltaic systems 80—52274
n-Si, complex defect production rate introduced by high energy electron irradiation 77—72635
P-Si, conductivity and carrier lifetime, high injection effects 80—70719
Si, conductivity of holes at low temp., electric field depend. 77—28179
Si crystal, impurities determ. and resistivity after reactor neutron irrad. 80—65563
n-Si, current carrier-dislocation interactions, resistance in UHF range *(Russian)* 80—54732
n-Si, current instability due to temp.-elec. domain pulsations 77—43608
n-Si, current-volt. characts. along ⟨110⟩ 79—78111
p-Si, Czochralski grown, microdistrib. of O, SEM and spreading resist. obs. 80—79830
p-Si, deformed, 1/f noise, resist., mobility, and carrier density 77—8161
n-Si, deformed, thermal treatment effect on elec. cond. and dislocation mobility 80—107265
Si, diffusion coeff. of Se, by sheet Hall coeff. meas. 79—46843
Si, divacancies due to proton irrad., IR absorpt., annealing effects rel. to resist. 80—20673
Si, elec. cond. between 500 and 1200°C 77—11923
n-Si, elec. cond. control by hot electron intervalley transfer 80—59993
Si, elec. props., plastic deform. and annealing temp. depend., dislocation effects *(Russian)* 77—89765
p-Si, elec. props. and thermal defects, influence of high temp. treatment 79—69531
p-Si, elec. resist., shock wave compression effects 80—80265
Si, electrical conductivity, inertia of electron heating, expt. and theory 80—65613
Si, electrical properties of single crystal, dislocation effects *(Rumanian)* 79—73504
n-Si, electron heating by static elec. field 80—96894
Si, electron irrad., limiting position of Fermi level, elec. cond. and optical absorpt. meas. 79—65484
Si, electron irrad., resistivity-fluence relation 80—54700
n-Si, electron irradiated, elec. props. 77—8041
Si, electron mobility is semiconductors based on dielectric function modification of Dingle pot. 79—50836
Si, electron-exciton elastic scatt. cross sections, central field and exchange approxs. 77—62919

electrical conductivity of crystalline semiconductors and insulators continued
Si, electrophysical props. of single crysts. with and without dislocations 77—47812
Si, enhanced conductivity in plasma hydrogenated films, thermionic emission 80—70692
Si, epitaxial layer thickness meas. using phase correction function of substrate resistivity *(Rumanian)* 80—90812
Si, floatzone, P doping by thermal-neutron irradiation 78—22750
Si, four-point probe meas. error factors, SEM obs. 79—71484
Si gas-sensitive microtransducer, cond. variation with pulsed ethanol adsorption *(Russian)* 80—50915
n-Si, γ-irradiated, with layer inhomogeneity, quantum current oscillations 80—11010
Si, γ-ray induced elec. cond. at low temps. 78—52002
n-Si, heavily doped, carrier conc., comparison of expt. and theory, screening effects 77—85216
Si, heavily doped, carrier mobility calc., 300K 79—56215
Si, heavily doped, carrier recomb. through shallow donor and acceptor states 80—15535
Si, heavily doped layer, electronic characts., electron beam induced current obs. 78—10473
Si, high O conc., electrical and mechanical props., influence of heat treatment 77—35934
Si, high resistivity, specific resistance depend. determ. using impedance freq. depend. *(Czech)* 80—15536
Si, high-resistivity layer form. during electron irrad. 80—80352
p-Si, hole drift vel. in high field 79—95415
Si, impurity-ion potential, electron-conductivity mobility, spatially variable dielectric function calcs. 79—78105
Si, influence of one-dimensional superlattice on two-dimensional electron gas 77—43683
Si ingots, polycrystn., growth and characterisation from metallurgical grade source material 79—87576
n-Si, inhomogeneous impurity distrib., elec. props., effect of γ-irradiation 77—55550
p-Si, interband transitions, contrib. to conductivity at submillimetre wavelengths 80—34473
Si, intrinsic, electronic properties, temp. depend. *(German)* 77—76822
n-Si, inversion layers, many-valley electron-phonon interactions, piezoresistance, anisotropic cond., Shubnikov-de Haas oscillations 78—52096
Si, ion implanted, laser annealed, elec. props. and annealing kinetics 79—69508
Si, ion implanted and laser annealed, characterisation 80—29043
n-Si, ion-implanted, elec. characts. after laser annealing 80—88562
n-Si, irradiated with 1.2 GeV, temp. depend. of cond. 79—51156
n-Si, irradiated with large neutron doses, defect annealing 80—19849
Si, laser annealed ion implanted, elec. props., melting threshold 80—10969
p-Si, laser irrad., accumulation of defects, effect on elec. props. 80—107317
Si, masking effects of Sb diffusion, from doped oxide source 77—15437
Si, metallurgical grade, purification and charact. 78—56573
n-Si, mobility and resist. as functions of dopant density and temperature 78—2487
Si monocrystalline rod growth from gas phase 78—64453
Si, multigrained, grain boundary elec. and compositional props., surface anal. 80—76575
Si, n-type, V-I response in epithermal electron range 77—4361
p-Si, neutron irradiated, elec. props. 78—51939
Si, neutron irradiated, resistivity and minority carrier lifetime, radial inhomogeneity *(Russian)* 78—26881
n-Si, neutron or γ-irrad., elec. props., in strong elec. fields 79—95416
Si, neutron transmutation doped, zero-bias resist. of grain boundaries 78—76072
Si, neutron transmutation doped, highly compensated, resistivity fluctuations 80—15531
Si, neutron transmutation doped, elec. props. 80—15532
Si, neutron transmutation doped, isochronal annealing of resistivity 80—19828
Si, neutron transmutation doping, annealing, deep defect levels 80—20123
n-Si, phenomenological energy relaxation time, temp. depend. 78—43409
n-Si, piezoresist. rel. to piezothermoelec. power, electron-phonon drag region 80—70737
Si, point defects, laser annealing 80—107224
Si, poly crystalline, electronic behaviour of grain boundaries, solar cell appl. 80—92859
Si, polycryst., elec. and photovolt. props., grain size effects 80—49800
Si, polycrystalline, neutron transmutation doped, grain boundary zero-bias resistance 79—15153
Si, polymorphism under high press. *(Russian)* 78—59947
Si, proton irradiation, energy depend. of rate of degradation of cond. 77—62944
Si, radiation defects, influence of dislocations on accumulation, elec. props. 80—92558
Si, radiation detector, barrier heights, electron and hole currents, Schottky contact effects 79—33293
Si resistivity and carrier mobility effects of dissolved interstitital O_2 77—76824
Si, resistivity and deep impurity levels at 300K anal. 77—43591
Si, resistivity depth profiles calcs. from spreading resist. meas. using math. algorithm 80—2393
Si, resistivity meas. simplified temp. corrections 77—26338
Si ribbon crystal evaluation for solar cells 77—76813
Si ribbons, roller quenching method of prep., grain sizes and carrier conc. 80—40275
Si, single crysts., devices for resistivity meas. *(German)* 79—12824
Si solar cells, low-cost sheet fabrication structural defects, effect on electronic props. and cell performance 80—50977
Si, spreading resistance calibration, effect of specimen preparations 78—10450
p-Si, surface elec. behaviour after chem. treatment 80—20185
Si surface layers, impurities, elec. and photoelec. props. 80—2298
Si, technology and physics, review 80—34353
Si, thermal donor generation in temp. range 600-800°C 79—11121
n-Si, uniaxially deformed, intervalley scatt., 78-300K 77—20330
Si, voltage-current curves, specimens of variable cross-section 77—8113
Si wafer, automatic meas. system for resist. profiles 80—39574
Si wafer, colour-banded, sheet resist. variation following high dose implantation at high dose rates 78—95074

electrical conductivity of crystalline semiconductors and insulators continued
Si wafers, Czochralski grown, minority carrier transport props., laser beam scan for homogeneity anal., photovoltaic cell appls. 80—92905
Si whiskers as basis for strain resistors 79—5094
Si with thermal defects, photocond., effect of annealing on elec. resist. 80—6837
p-Si, X-ray bombard. effects on elec. resist., and carrier density, annealing effect 77—4125
p-Si:Al, diffusion and incorporation of dopant in closed system, elec. props. 77—59026
Si:Al(Ga), spreading resist. calibration using Si:B 80—103690
Si:As, 1.5 MeV H^+ and He^+ irradiations of As diffused layers 78—47447
Si:As, diffused, laser irrad., stability study 80—65547
Si:As, effects of recoil-implanted O on elec. activation of As 79—99227
Si:As, heavily As-diffused, Hall mobility and resist. rel. to carrier conc. 80—107815
Si:As, high-dose implanted, irrad. time and subsequent heat treatment effects on laser annealing 80—29041
Si:As, implanted, spatially varied activation during regrowth of amorphous layers, sheet resist. and backscatt. obs. 78—71749
Si:As, implanted, thermal diffusion of As 80—39352
Si:As, implanted As redistrib. during annealing in oxidising ambient, carrier distrib. meas. 79—19275
Si:As, ion implanted, anomaly of elec. activation by additional Ne irradiation 78—84211
Si:As, ion implanted, low temp. thermal annealing 80—96552
Si:As, ion-implanted, laser recrystallisation by freq.-doubled Nd:YAG laser 79—77613
Si:As, laser annealing, channelling, optical obs., and resist. meas. 79—1444
Si:As, laser annealing of implanted layers 77—55296
Si:As, p-n junction form. by laser annealing, space charge region, effects on reverse current 80—54772
Si:As, relation between total and electrically active As conc. produced by diffusion 79—55773
Si:As^+, implanted, CW laser annealing, electron-beam induced current 80—100709
Si:As^+ sheet resistivity rel. to isochronal annealing and defect structures 77—76443
Si:Au, IR absorption and elec. resist. meas., impurity centres 79—38580
Si:Au(Zn) deep-level impurities, insulating props. 78—39124
Si:B, dopant density and temp. depend. of hole mobility and resistivity 79—38075
Si:B, heavily doped, annealing characteristics obs. *(Japanese)* 78—18666
Si:B, hole mobility calc. for dopant density and temp. var., resistivity meas., effective mass calcs. 80—54703
Si:B, ion implanted, comparison of range and range straggling 77—55293
n-Si:B, ion-implanted damage, positron annihilation and sheet resist. meas. 80—35003
Si:B, using oxidised BN dopant source, sheet resist., rel. to temp. and deposition time 77—43231
Si:B effect of elec. field on carrier capture by attractive centres. 79—11145
p-Si:B(Al), radiation defect form. and annealing study using Hall effect, cond. and carrier diffusion length 80—84214
Si:B(As), doped using new paint-on diffusion source, characterisation 77—4118
Si:B(P), dislocated crystals, DC conductivity, Hall effect, energy spectrum 78—10400
Si:B(P), dislocated crystals, microwave cond., localised electron energy spectrum 78—14694
Si:B(P), ion implanted crystalline and amorphous laser annealing 80—97509
Si:Cr, specific resistance, activation energy of deep levels, and carrier mobility *(Russian)* 78—72146
Si:Fe, interstitial form., Au dopant effect 80—29611
Si:Fe(Al), compensated substrates for solar cells, effects of Fe and Al 80—94009
Si:Gd, radiation defects effect on elec. props. 77—28184
a-Si:H alloys, sputter deposited thin film coatings, property-comp. relationships 80—80975
Si:Ir, precipitation of solid soln., photocapacitance, electrical resistivity meas. 78—47833
Si:Li, precipitation centres, elec. cond., Hall effect meas. 78—48417
p-Si:$N_2{}^+$, implanted, anneal behaviours of lateral photovoltaic method, sheet resist., junction conductance 79—14825
Si:Ni,Co,Mn, γ-irrad., interaction of deep-level impurity atoms with radiation defects 77—76457
Si:Ni(Co)(Mn), influence of neutron irradiation as elec. props. 78—55895
Si:O, annealing behaviour of O donor, conc. reductions via resistivity meas. 79—51129
Si:O, cryst., donor form. during annealing, elec. resist. study 80—49653
Si:O, electrial and infrared spectroscopic investigations 80—34389
Si:O, specific resist. rel. to annealing, Si-O complex form., O_2 distrib. *(German)* 77—72863
Si:P, amorphous, CVD, substitutional doping, electronic props. 79—23923
Si:P, amorphous, elec. cond. and thermoelectric power 77—89783
Si:P, amorphous, thermoelectric power and conductivity 77—89782
Si:P, annealing characteristics at low temp., elec. props. 78—63781
Si:P, carrier mobility and distrib. rel. to annealing, 400-910°C 78—79995
Si:P, Cu(Au) radiation-doped, influence of growth defects on elec. props. 79—69144
Si:P, Czochralski growth, dopant evaporation coeffs., resistivity distrib. 77—16487
p-Si:P, defect energy levels, ion implantation effects, Hall coeff., sheet resist. meas. 77—85173
Si:P, diffusion-doped laser irradiation effects, electrical reactivation of P 80—39124
Si:P, ESR-induced changes in DC resistance 78—35037
Si:P, electrical conductivity oscillation, effect of dislocations 78—6388
n-Si:P, electron mobility and resist., dopant density and temp. depend. 77—76816
n-Si:P, heavily doped, carrier conc., Hall coeff. and elec. cond. meas. 77—8094
n-Si:P, heavily doped, elec. cond. and Hall effect meas., impurity effects 78—19032

electrical conductivity of crystalline semiconductors and insulators continued
Si:P, heavily doped semicond., scatt. mechanism, resist, and Hall coeff. maxima 80—75586
Si:P, implantation damage of channelled P ions, elec. activity recovery stages 77—59034
Si:P, implanted, pulsed electron beam annealing, Hall effect and sheet resist. meas. 80—34467
Si:P, implanted low temp. annealed, elec. activation, damage depend. 80—88182
Si:P, impurity conductivities 78—91691
Si:P, incoherent light flash annealing, elec. props., backscattering spectra 80—97504
Si:P, ion implanted, laser and thermal annealing, elec. cond. and Hall effect meas. 79—69145
Si:P, ion implanted low temp. elec. cond. 79—56225
Si:P, low energy and high dose ion implantation, through SiO_2 film 77—15435
Si:P, neutron irradiated, influence of growth defects on change in cond. 78—39117
Si:P, neutron transmutation doping, elec. props. rel. to neutron fluence 80—96555
Si:P, neutron transmutation doping, resist. homogeneity rel. to compensation ratio 80—96556
Si:P, polycryst., grown in epitaxial reactor at 800°C, characterisation 77—1815
Si:P, strongly compensated, temp. depend. cond. meas. down to 1K 77—72865
Si:P, variable range hopping conduction, in lowest temp. region 79—73511
n-Si:P,V, degeneracy ratios and impurity levels of V, resist. and Hall effect meas. 77—20260
Si:P^+, highly implanted, two step annealing effect on crystallinity 77—31683
n-Si:P(B), elec. cond. oscills., electron instability effects due to dislocations 80—103704
Si:Se, energy levels, resistivity and Hall coeff. 79—69528
Si-Al-O-N ceramics, elec. and therm. cond. 79—86934
Si-Ge, heavily doped vacuum hot-pressing, thermal and electrical props. 77—40400
Si-Ge:Al(B)(P), hot-pressed alloy, thermoelec. props. 78—91711
$Si_{(6-z)}Al_zO_zN_{(8-z)}$, sialons, hot-pressed, dielec. props. 78—10822
$Si_{6-x}Al_xO_xN_{8-x}$, x=1.5, 3, 4, Sialon ceramics, elec., thermal cond. 79—33124
$Si_{6-z}Al_zO_zN_{8-z}$, hot pressed, DC elec. props., 18-500°C, fields up to 1.1×10^4 V cm^{-1} 78—26860
$Si_{(6-Z)}Al_ZO_ZN_{(8-Z)}$ 78—39136
SiAs, cryst. growth from melt, elec. props. 80—76170
SiC, 6H polytype, elec. and thermal cond., carrier concentrations 80—2223
n-SiC (6H), density of states effective mass determ., high temp. meas. of elec. props. 79—15073
SiC base material, electrical props., heat treatment effect 77—12645
β-SiC, cubic, elec. props. 78—51996
SiC, diffusion of B, elec. cond. meas. 80—96696
SiC, fusion reactor first wall appl., radiation damage 79—86822
SiC heating elements for elec. furnaces, elec. cond. 79—69510
SiC polymorphs, widths of first minibands and effective masses, resist. anisotropy 80—20071
β-SiC, pyrolytic, optical and elec. props. 79—78093
SiC, self-bonded, microstruct., electrical props., sintering effects 77—1822
SiC, self-bonded polycryst., electrophys. props. 80—10980
SiC-Si composite, bulk resist. of technical SiC powders 79—28350
Si_3N_4, and Si_3N_4-MgO, hot pressed, DC elec. props., 18-500°C, fields up to 1.1×10^4 V cm^{-1} 78—26860
Si_3N_4, hot-pressed, dielec. props. 78—10822
Si_3N_4, hot-pressed, electrical props. 78—39136
Si_3N_4, pyrolytic, prep. by CVD, bulk and coatings, exam. of electrical, optical and physical props. 79—95935
Si_3N_4 reaction bonded, microstructure, formation, properties, phase composition 79—56947
SiO, evaporated film, AC cond meas. 80—20236
SiO_2, transport of electrons at high electric fields 80—20208
SiO_2-Si, P ion implantation, electrical transport props. 80—39130
SiO_2-Si:A, effects of recoil-implanted O on elec. activation of As 79—99227
SiTe-GaTe, thermo-EMF, elec. cond. and solubility 77—20346
Si_2Te_3, passivated single cryst., elec. conductivity 78—95299
p-Si_2Te_3, photoelectric props., luminesc., hole lifetime and trapping 77—39892
SmB_6, crystal preparation, elec. resistance, phase transitions 80—97427
SmB_6, mixed valent, large low-temp. Hall effect and resist. 80—39611
SmB_6, mixed valent semicond., transport props. and electonic struct., review 80—96877
SmB_6, resistivity press. variation, lattice consts. 80—100456
$Sm_{1-x}Gd_xS$, metal-insulator transition, induced by temp. and press. *(Japanese)* 79—51488
Sm_2GeSe_5, elec. props., 300 to 1100K 79—51585
$Sm_xLa_{1-x}B_6$, solid solns., exam. of structure, elec. props. 80—39290
SmO, intermediate valence state *(French)* 80—20132
Sm_2O_3, elec. cond., thermoelec. power, dielectric const. 79—69763
SmS, first-order transition from semiconducting to metallic state 78—52040
SmS, physical and physicochem. props., review 80—96875
SmS, semicond., anomalously high magnetoresist., Hall coeff. and elec. resist. meas. 78—10479
SmS, semicond. phase, cond. band model, elec. and thermal cond. meas. 77—39854
SmS, semicond.-metal transition, cond. band type, deform. pot. determ. 79—69417
$Sm_2(WO_4)_3$, molar mag. susceptibility, DC elec. cond., thermopower meas. 79—15172
SnF_2, α- and γ-phases, elec. cond. characts. determ. *(French)* 79—47093
SnF_2, phase transitions, X-ray diffr., elec. cond. and thermal anal. studies 80—100329
$Sn_xGe_{1-x}Se$, ^{119}Sn Mossbauer and elec. conductivity study 79—19595
$Sn_{1-x}Mn_xTe$, $0.02<x<0.08$, transport and magnetic properties, low magnetic field 79—99569
SnO_2, film, diffusion of impurities, sheet resist. meas. *(Japanese)* 79—95218

electrical conductivity of crystalline semiconductors and insulators continued
SnO_2, gas sensor, CO, H_2O vapour, surface temp. effect on cond. 78—76067
SnO_2, heat treated film, electrical conductivity 77—8211
SnO_2 surface, interactions with O_2, H_2O and H_2, desorpt., ESR and cond. meas 80—10790
SnO_2 thermoelectrical properties, investigation 77—76852
SnO_2, transparent conductive film, prep. by magnetron sputtering and elec., optical and structural props. *(Japanese)* 79—8247
SnO_2:ThO_2, exposed to CO gas, self-oscill. phenomenon 78—68032
SnO_2:ThO_2, exposed to H_2, temp. depend. of resistivity 79—56219
SnO_2-based gas sensors, resist. temp. depend. on exposure to CO, H_2, and propane 80—103694
$Sn_{1-x}Pb_xTe$, film, production under quasi-equilibrium conditions 80—45241
SnS_2 polytypes, electronic bandgap meas. 80—34358
SnSSe, electron mobility, elec. cond. and Hall effect meas. 78—80004
$SnS_{2-x}Se_x$, electron mobility elec. resist. and Hall constants 79—28346
$SnS_{2-x}Se_x$ solid soln., resistivity, lattice parameter, comp. and temp. depend. 78—91693
SnSe, sublimation growth, deviation from stoichiometry, elec. props. 78—76594
$SnSe_2$-$GeSe_2$, phase diag., electrophys. props. of solid solns. 77—52306
SnTe, displacive phase transition at 22K, Mossbauer spectra and elec. resist. meas. 80—6514
p-SnTe, elec. resist. anomaly in vicinity of struct. phase transform. 79—19597
SnTe, isothermal meas. of galvanomag. and thermomag. effects *(Russian)* 78—56160
SnTe-In_2Te_3 system, thermoelec. props., phase diagram, transitions 78—43424
SnTe-MnTe, degenerate semicond., anomalous Hall effect 80—29420
$SrCl_2$, superionic, electrical conductivity at high temp. 78—79798
SrF_2, powder, elec. cond. transition under high press. *(Russian)* 77—20370
$SrFe_{12}O_{19}$:Si, Sr, second phase effect on elec. and mag. props. 80—60986
$Sr_2Fe_xRu_{1-x}O_4$ solid soln., Mossbauer spectrosc. study 80—50235
$SrGa_2Si_2O_8$-$SrGa_2Ge_2O_8$, solid solution, exam. of elastic and electrical props. 79—96057
$Sr_{0.3}La_{0.7}MnO_3$, neutron-irrad. induced phase transition 77—89952
Sr_2MNbO_6, (M=Ti, Zr, Nb), perovskite struct., synthesis, lattice constants and elec. props. 77—21369
$SrMnO_{3-x}$, O-deficiency induced polymorphs and elec. cond. 80—71643
Sr_2MnbO_6, M=Ti,Zr,Hf, semiconductors, elec. cond. 77—51748
$SrMoO_3$, perovskite-type cmpd., metallic conductivity, room temp. to 2.5K 79—65483
Sr_3MoO_6, electrophys. props., effects of thermophys. props. of medium in synthesis 77—48375
$Sr(NO_3)_2$, low temp. struct. changes, elec. props. 79—87377
$Sr_2Nb_2O_7$, electronic props. and photoresponses 80—92925
SrO-SiO_2-Fe_2O_3, permanent mag. ceramics, exam. of phase diagram, using X-ray analysis, optical microscopy, electron probe anal., and thermal analysis *(German)* 79—29012
$SrSnO_3$ and $SrZrO_3$, high-density ceramics prep. and elec. props. 80—60812
$SrTiO_3$, pure and Nb doped, heat treated, Hall effect, electrical cond., optical absorpt., defect states 78—47812
$SrTiO_3$, semicond., free carrier optical absorption and scatt. *(Korean)* 78—23489
$Sr_{0.15}VO_2$, electrical cond., thermo-EMF, and lattice consts. 80—54685
Sr_2YRuO_6, ^{99}Ru Mossbauer spectra and other techniques 80—29659
$Sr[Pt(CN)_4].5H_2O$, DC elec. cond. props. 79—51582
$(TSeT)_2Cl$ complex, metal-semimetal transition, magnetoresist. and cond. *(Russian)* 79—38138
$TTT_2I_{3+\delta}$ complex, influence of press. on metal-dielectric phase transition *(Russian)* 80—92818
Ta complex, prep. by halide reaction with tetramethylurea and tetramethylthiourea, and characterisation 79—15972
TaC, thermal and electrical conductivity, 1500-3000K 78—43385
α-Ta_2O_5, elec. cond. mechanism, admittance meas. 80—70705
TaS_2, 1T and 1H polytypes, fast neutron irrad., defect prod., effects on resist. and charge density waves 80—65060
TaS_2, 1T-, 2H-, 6R- thin cryst. polymorphs, anomalous resistivity, 0-350K 77—11909
TaS_2 (1T) electron irradiated, lattice contraction 80—59520
1T-TaS_2, and 1T-$TaS_{2\ x}Se_x$, Anderson localisation, elec. resist. and magnetoresist. meas. 80—44596
1T-TaS_2, pure and cation-doped, charge carrier localisation 80—44597
1T-$TaS_{2-x}Se_x$, electronic cond. process, resist. meas., 1.3-240K 80—44595
$TaSe_2$ (2H), sp. ht. and resist. near CDW phase transitions 78—34786
$TaSe_2$:Fe, competition between charge and spin density waves, Landau-Ginzburg theory 79—95352
$Ta_xTi_{1-x}Se_2$, cryst. struct. and elec. props. 79—47133
Tb-Sn-Se system, cross section Tb_2Se_3-$SnSe_2$ phase diagram, physicochem. anal. 79—87621
$TbCrSe_3$, prep., elec. and thermal props. 78—43390
$Tb(NO_3)_3$-$Fe(NO_3)_3$-$(NH_4)_2CO_3$-H_2O system, cpd. form., comp. and props. 80—100832
Te, a-edge dislocated crystals, mobility anisotropy 80—107781
Te, deformed and annealed crystal, depend. on stress 79—7847
Te, elec. cond., 0-500 kbar 79—99589
Te, elec. props. anisotropy, influence of deform. and annealing 77—15859
Te, energy gap under press., elec. resist. and Hall effect meas. 78—30926
Te, piezoelectrical free-carrier scatt. by screw dislocations, Hall effect and cond. meas. 80—24926
Te, screw-dislocation-induced scatt. and acceptor states, galvanomag. and optical expts. 77—28142
Te, undoped, elec. cond., magnetoresist. and Hall meas., hydrostatic press. effect 77—47830
Te:Sb, 96 to 500K, cond. Hall const., hole mobility, conc., dislocation effects *(Russian)* 78—64039
Te:Sb, impurity states and impurity conduction, hydrostatic pressure 80—39521
Te-$(Bi_xSb_{1-x})_2Te_3$ eutectic, electrophys. props., directed crystn. conditions influence and comp. depend. 80—107827
Te-based eutectics, crystn. rate effect on electrophys. props. mutual solubility effect 80—60774
$TeSe_{19}$, glasses, crystallisation kinetics, elec. cond. meas. 77—43155

electrical conductivity of crystalline semiconductors and insulators continued
Th_3As_4, prep. and semicond. props. 78−23087
Th_3As_4-U_3As_4 solid soln., electronic props. 80−34469
ThO_2 ceramics, CaO and Y_2O_3 stabilised density, elec. cond., permittivity 78−47838
ThO_2:Y_2O_3, electrochem. cell, complex impedance, temp. and freq. depends. 77−1458
Ti-O system, nonstoichiometry between Ti_3O_5 and TiO_2 comps. at high temps. 77−15594
Ti_2AlC, Ti_3AlC, TiC, phys. props. 77−43602
TiB_2, low-temp. neutron irrad., electrical resistance and stored energy 78−67744
TiC-TiN system, electro- and thermo-phys. props. 80−34210
TiC-VC, mag. susceptibility, elec. cond. and thermoelec. props. 80−50033
TiC-ZrC, mag. susceptibility, elec. cond. and thermoelec. props. 80−50033
TiC_x, electron energy spectrum and phys. props. in homogeneous region *(Russian)* 77−31941
TiC_xN_y, thermal cond., elec. cond., and thermal expansion 80−10714
TiC_xO_y, thermal cond., elec. cond., and thermal expansion 80−10714
$Ti_{1-x}Hf_xSe_2$ mixed cryst., elec. resist. and phase transition temp. 80−24928
TiN, powder defect struct., thermal and elec. props. 77−59286
TiN-Al_2O_3, exam. of sintering and densification kinetics, and physical props. 79−95986
TiN-AlN composites, struct. and props. 77−40413
TiN-CrN system solid solns., electrophys. and galvanomag. props., energy spectra 77−15847
TiN-VN refractory powder composite, resistors, produced in low temp. 78−11182
TiN_zO_y, elec. cond., conc.-temp. depend., 25-1000°C 80−34439
TiO_2, chemical implantation of 10-keV H^+ and D^+, resist. and optical absorpt. expts. 77−59031
TiO_2, elec. cond., temp. depend. resistivity meas. at 77 to 600K, unwsitched samples 80−20262
TiO_2, rutile, defect struct. and elec. cond. at 1273K 80−44604
TiO_2, rutile, deuteron and alpha-particle implantation, chemical effects, optical and cond. meas. 78−67755
TiO_2, rutile, oscills. in elec. resist. induced by solid/gas interactions 79−91068
TiO_2 rutile, single cryst., elec. cond. meas. rel. to O_2 press., temp. *(German)* 77−47823
TiO_2, sintering, hardness, density, elec. cond. and colour *(Japanese)* 78−68659
TiO_2, stoichiometric single crysts., anisotropy of ion transport 80−2206
TiO_2:Cr(Ta), slightly doped, elec. cond. and defect struct., charge compensation and point defect model 80−75568
TiO_2:Nb, rutile, elec. cond., 1273-1623K, O_2 press. depend., charge compensation mechanism 77−85217
TiO_2:Nb_2O_5(Ta_2O_5), conduct. rel. to defect structure, obs. 77−76392
TiO_2:S, acceptor properties of S, free electron concentrations 80−34395
TiO_2:S, in $O_2+CO_2+SO_2$ atmosphere, elec. cond. study 80−39583
TiO_2:Ta_2O_5(Nb_2O_5), rutile, defect struct. and elec. cond. at 1273K 80−44604
TiO_2:Zr, electronic conduction, temp. depend. 77−8099
TiO_2-RuO_2 anode, wear-resistant, use in applied electrochem. 80−40701
TiO_2-SiO_2, submicron dispersion of impurity, chem. diffusivity and elec. cond. 79−1528
TiO_{2-x}, reduced, cond. between elec. props. in equil. at 1100°C and after quenching, defects role *(French)* 80−44582
TiO_{2-x}, rutile, O chem. diffusivity, near stoichiometric ratio, elec. cond. meas. 77−11731
TiO_3:Cr_2O_3, dielec. consts., AC and DC resist. 80−20186
Ti_2O_3, cryst. growth by chem. transport and tri-arc methods, and characterisation 78−3003
Ti_5O_9, phase transitions, elec. cond., mag. susceptibility, sp. ht., EPR and struct. aspects 78−10526
TiP_2, synthesis and characts. 77−85953
TiS_2, elect. resist. at room temp., press. depend. to 80 kbar 80−49730
TiS_2, evidence for semicond. props., Hall coeff., refl., cond., thermoelec. power 80−20220
TiS_2, resistivity, Hall effect and mag. suscept. 78−79991
TiS_2, semicond. charact. under press., in-plane resist. and Hall coeff. meas. 78−23086
TiS_2, semimetallic charact. 77−62926
TiS_2, transport props. and semicond. nature 80−44598
TiS_2, transport props. under press. 79−95410
$TiS_2(Se_2)$, modelling contrasting semimetallic characters 78−43393
$TiSe_2$, CDW transition temp. and transport props. pressure depend. 79−99550
$TiSe_2$, IR reflectivity, phonons and free carriers 79−61379
$TiSe_2$ impurity effects on elec. props. 80−80263
$TiSe_2$, semimetal, electronic props., superlattice form. 77−15532
$TiSe_2$, semimetallic charact. 77−62926
$TiSe_2$, semimetallic charact. under press., in-plane resist. and Hall coeff. meas. 78−23086
$TiSe_2$, transport props. under press. 79−95410
$TiSe_2$:Ta(V), transport props. and phase transition 78−72149
Ti_xSi_y, work function rel. to phys. props. 77−47887
$Ti_{1-x}Ta_xO_2$, solid soln. formed in TiO_2-Ta_2O_5-Ta at 1100°C *(French)* 78−35375
$Ti_{1-x}V_xS_2$, resistivity, Hall effect and mag. suscept. 78−79991
$Ti_{0.99}V_{0.01}Se_2$, negative mgnetoresist. and nonlinear cond. 79−87105
$Ti_{0.99}V_{0.01}Se_2$, negative magnetoresist. and nonlinear cond. 80−44617
$Ti_{1-x}V_xSe_2$ ($0 \leq x \leq 0.1$), elec. resist. and Hall effect 80−2386
Tl-V-S system, crystallographic data and phys. props of some phases *(French)* 79−99163
$TlAsS_2(Se_2)(Te_2)$, elec. cond. and thermopower in solid and liquid states 77−89764
$Tl_2Cr_2O_7$, $Tl_2Mn_2O_7$, pyrochlore type, synthesis and physical props. 80−33963
$TlInS_2(Se_2)$, electrical cond. of single crysts. with symm. and asymm. Ag-In contacts 80−6835
$TlInSe_2$, single cryst., elec. cond., photocond. and IR spectra absorpt. spectrum 79−47097
$TlInSe_2$-$TlPrSe_2$ system, struct., elec. cond., and thermoelec. props. 79−87119
Tl_2MoO_4, prep., characterisation 78−63731
Tl_2O_3 single crystal, elec. cond., cryst. grown from vapour in air 77−85219

electrical conductivity of crystalline semiconductors and insulators continued
Tl_2O_3, single crystal, elec. cond., annealing at 923K in O_2 effects 77−85220
TlP_3, elec. cond. temp. depend., 77-590K 77−51743
$TlSbS_2$, phase transitions under action of high press., elec. cond. meas. 77−4196
TlTe, elec. props., cryst. growth *(Japanese)* 79−33907
TlTe single crystal, resistivity, Hall coeff., magnetoresistance, thermoelec. power 78−43418
Tl_2Te_3, exam. of electrical props., density and viscosity, for solid or liquid states 79−95431
Tl_2Te_3, exam. of electrical props., in solid, liquid state 80−54686
Tl_2Te_3:Ag(Sn), effect of dopant on electrical props., density and viscosity, for solid or liquid states 79−95432
$Tl_{0.33}WO_3$ bronze, elec. resist. meas., anisotropy, supercond. 80−75569
Tl_2WO_4, solid-state prep., cryst. struct. and props. 78−38673
TmSe, Anderson lattice resist. for antiferromag. ordering 80−65556
TmSe, intermediate valence state, resistivity of magnetically ordered ground state 79−1683
TmSe, mixed valence cpd., thermal, mag., and transport props. 79−61074
Tm_xSe, $0.87<x<1.05$, mag., thermal and transport props., comp. depend. 78−68239
Tm_xSe, low temp. props., effect of composition 77−80775
Tm_xSe, residual resistivity at very low temp., composition depend. 79−82588
Tm_xSe, valence instabilities, antiferromag. order 80−20128
$TmSe_{0.83}Te_{0.17}$, spontaneous magnetisation, mag. susceptibility, magnetostriction, elec. cond. 79−24146
TmTe, far IR refl. and DC resist., 1-300K, interconfig. fluctuation effects 78−35136
$Tm_xY_{1-x}Se$, Kondo effect, Van Vleck behaviour 80−25085
$(U,Pu)_{2+x}$, pure state and Mo addition influence, 350 to 750°C 77−20320
U dipnictides, elec. and mag. props. 78−84399
U-O system, phase equilibrium, thermal, X-ray and cond. meas. 78−35371
UC, quenched-in defects, formation, migration and resistivity 80−64990
UC-UC_2, alloyed, electron bombarded, enhancement of U_2C_3 deposition, resist. obs. 77−27911
UCN, quenched-in defects, formation, migration and resistivity 80−64990
UN, UP and $UC_{1-x}N_x$, low temp. elec. resist., temp. depend., 3 to 90K 77−20321
UO_2 pins, electrical resistance meas. at high temp. 77−15848
UO_2:Nb_2O_5, additions on elec. cond. 80−49712
UO_{2+x}, elect. cond. and thermoelectric power 78−52020
U_3O_8-Y_2O_3(Sc_2O_3), solid soln. electrode, high temp. electrochem. appl. 80−6828
$U_xPu_{1-x}O_2$, theoretical study of electronic thermodynamic and valence props. 79−37655
$(U_xTh_{1-x})S(Te)$ solid solns., electronic struct., mag. susceptibility and elec. resist. obs. 77−20551
VC, damage sustained during neutron irradiation 77−1841
$(V_{1-x}Cr_x)_2O_{3+y}$, elec. props. and struct. 80−84494
$V_xCr_{3-x}S_4$, elec. and mag. props. 79−28523
V_2D, elec. resistivity studies of order-disorder phenomena 79−78961
$V_{1-x}Fe_xO_{2-x}F_x$, $0<x<0.20$, magnetic susceptibility and electron cond. *(German)* 80−39754
$V_{1-x}Ga_xO_2$, phase transitions, semicond. metal transition, antiferromag. props. 77−11969
V_2H, elec. resistivity studies of order-disorder phenomena 79−78961
VN powder, defect struct., thermal and elec. props. 77−59286
VN-CrN system solid solns., electrophys. and galvanomag. props., 77 to 1300K 77−24567
VO_2, reactively sputtered film, influence of manufacturing parameters on film struct. and props. *(French)* 77−81218
VO_2, switching effect, temp. depend. 80−20259
VO_2:M^{3+}, M=Al,Ga,Fe, anisotropy of thermoelec. power, hole conductivity 77−11946
V_2O_{3+x}, $0 \leq x \leq 0.08$, mag. and elec. props. 80−49833
V_2O_5 bronze catalysts, α- and β-phase, rel. to decomp. mechanism determ. for isopropanol 78−11553
V_2O_5 cathode, used in Li-V_2O_5 reserve cells, microstruct. optical reflectance, elec. cond. meas., chem. anal., SEM obs. 79−43752
V_2O_5, ferroelec. semicond., dielec. and elec. meas. 80−60516
V_2O_5, thermoelec. props., 500-1500K 80−29423
V_2O_5:Na(Li), pure and doped, elec. cond. and thermoelec. power meas. 80−10987
V_2O_5-BaO-K_2O-ZnO glasses, elect. props. and struct. 80−15547
V_2O_5-based glasses, crystallised, electronic cond. and related props. 79−99547
V_2O_5-In(Tl)$_2O_3$, ceramic, elec. resist., dielec. props., porosity 77−8093
V_2O_5-MoO_3 solid solns., small polaron cond., elec. resist. and thermoelec. power meas. 80−34447
V_3O_5 single crysts., prep. by chem. transport reacts. props. 79−43115
VOCl, and $Li_{0.8}VOCl$ intercalation cmpd., magnetic, optical and electrical props. 79−95402
$V_{2-x}Sb_xO_4$, defect struct. exam., temp. depend. 78−18635
$(V_{1-x}Ti_x)_2O_3$, solid solution, phase transition exam. 77−15590
$V_xTi_{1-x}S_2$, elec. and mag. props. 79−65504
$V_xTi_{1-x}Se_2$, cryst. struct. and elec. props. 79−47133
W-complex, $WOCl_4.Ph_3PO$, prep. and characterisation 78−30592
WB_{12}, growth from melt and phys. props. 80−20782
WB_4 and W_2B_5, core of B filaments, elec. resist. 80−15523
W_2B_5 and WB_4, thermal, elec., and mag. props. 80−20187
WO_3, nonstoichiometric, elec. investig. of correl. between defects and O chem. pot. *(French)* 77−47817
WO_3 powders, hopping mechanism and Poole-Frenkel effect, elec. props. determ. 80−49734
WO_3:H^+, optical and elec. props., suggested band struct. model 77−4654
WS_2 solid lubricant, antifriction and elec. props. depend. on oxidation temp., dopant influence 80−108584
WS_2-NbS_2 system, compds., elec., antifriction props. 79−38066
WSe_2 (2H), elec. cond. press. depend. 78−43394
WSe_2, elec. cond. and Hall coefficient temp. depend. 77−28180
WSe_2, lubricant, prep. by self-propagating high-temp. synthesis, technological characts. 78−35338
Y oxides, perovskite-like, synthesis, struct., elec. props. 80−65554
YAG:Ce, γ-irradiated elec. cond. meas. 77−43601

electrical conductivity of crystalline semiconductors and insulators continued
YB_{68}, melt grown, props. meas. 77—11518
$YCrO_3$-$MgCr_2O_4$ sintered ceramics, elec. cond. 80—24927
$Y_2Cr_2O_7$, $Y_2Mn_2O_7$, pyrochlore type, synthesis and physical props. 80—33963
$Y_3Fe_{5-x}In_xO_{12}$, K absorpt. and Mossbauer spectra and other phys. props. *(Russian)* 77—32467
YFe_2O_4, parasitic ferrimagnetism 79—4703
YH_x ($x=1.92$ to 1.98), magnetic and elec. props., 100 to 900K *(Russian)* 80—25077
YIG, elec. props. 79—99552
YIG, elec. props. meas., 600-1500K 77—8098
YIG, nonstoichiometry and electronic defects, thermogravimetric expts. and anal. of elec. data 78—6050
YIG, substituted, effect of electron bombardment on mag. and elec. props. 79—42103
Y_2O_3 ceramic, elec. resistance rel. to density 79—82594
Y_2O_3, electrical conductivity of mono- and poly-crystalline substances 77—20322
Y_2O_3, liq. and solid phase elec. cond., high temp. meas. 80—84468
Y_2O_3-TiO_2 system, elec. cond. at 700-1000°C 79—78100
Y_2S_3, elec. cond. and thermoelectric power, p-n transition *(French)* 78—84264
$YV_{1-x}Cr_xO_3$ ($0 \le x \le 0.6$), room temp. elec. conductivity and mag. props. 79—23967
$Y_2(V_{4/3}W_{2/3})O_7$ pyrochlore, synthesis and elec. props. 80—29914
Y_6WO_{12}:$ZrO_2(MgO)(CeO)(SrO)(BaO)$, polycryst., elec. cond., 800-7400°C 80—15517
YbB_6, mag. and transport props. 80—54689
YbB_6, resistivity press. variation, lattice consts. 80—100456
$YbGa(In)_2X_4$, X=S,Se,Te, prep. and props. 77—85214
Yb_2O_3, electronic cond. rel. to partial press. of O_2 of high temp. *(French)* 80—59979
YbS_x, thermo-EMF, elec. and thermal cond., 300 to 1000K, comp. depend. 79—38111
Yb_2Se_3, elec. resist., thermoelectromotive force, temp. depend., 300 to 1400K *(Russian)* 78—84243
Zn-Ga-P-S quaternary system, p-type conductive alloys 78—39105
$ZnAs_2$, homogeneity region and electrophys. props. 80—60833
p-$Zn_{0.1}Cd_{0.9}Sb$, thermoelec. anisotropic semicond., carrier kinetics at low temps. 80—92893
$Zn_{0.1}Cd_{0.9}Sb$, thermoelectrically isotropic semicond., carrier kinetics in intrinsic cond. range 80—92894
$ZnCr_2Se_4$, electroconductivity, thermoelectromotive force, Hall effect *(Russian)* 80—70694
$ZnCr_2Se_4$:In, magnetoresist. and elec. resist. above and below Neel temp. *(Russian)* 80—88576
$Zn_xFe_{3-x}O_4$, cond. mechanism, collective electron description 77—4588
$ZnGeAs_2$, elec. cond. in solid and liq. state 77—11912
$ZnGeP_2$, cond. compensation by electron bombardment 79—15151
$ZnGeP_2$, electron irrad., elec. and optical props. 79—33743
$ZnGeP_2$, synthesis, characts., applic. to laser windows *(French)* 78—80467
$Zn_xHg_{1-x}Se$, band struct. and scattering mechanism, determ. from transport coeffs. 77—59254
$Zn_xHg_{1-x}Se$, galvanomagnetic effects, Shubnikov-de Haas oscill. determ. of band struct. 80—6884
$Zn_xHg_{1-x}Te$, impurity influence on thermomagnetic effects and elec. cond. 79—60856
$Zn^{2+}Mo^{4+}O_3$, defect spinel struct., elec. and mag. props. 80—70176
$Zn(Mo_2Re_2)S_8$, synthesis and electrical props. of mixed tetrahedral cluster phases 80—2971
ZnO ceramic, nonohmic, drift phenomena of capacitance and current 80—39587
ZnO ceramics, heat treatment effect on cryst. phases, microstruct. and elec. props. 79—100268
ZnO ceramics, non-Ohmic, cond. mech. 78—68034
ZnO ceramics, non-Ohmic transient cond. phenomena, current-voltage overshoots 79—91057
ZnO, chemisorpt. of water, cond. and ESR meas. 79—56072
ZnO, elec. cond. and oxidation kinetics of Zn in O_2-CO_2-SO_2 gas mixture 80—34448
ZnO, elec. cond. at high fields 80—80287
ZnO, electron-exciton elastic scatt. cross sections, central field and exchange approxs. 77—62919
ZnO epitaxial film electrical props. rel. to substrate orientation and growth conditions 79—56339
ZnO, epitaxial layers, influence of deposition conditions on luminescence, electrical props. 79—99924
ZnO non-ohmic ceramic, degradation props. under AC and DC bias 80—80262
ZnO, nonhomic ceramic, current oscillation phenomena 79—69515
ZnO, nonohmic ceramic, current creep 79—69514
ZnO, powder layers, conductivity, O_2 chemisorpt. and photodesorpt. effects 78—43441
ZnO, single cryst. growth in ZnO-H_2-H_2O-O_2 vapour, morphology, electrophys. and opt. props. 78—52649
ZnO, single crystal, excess Zn atom conc. and elec. cond. determ. 78—3435
ZnO single csytals quantised accumulation layers, Hall mobility of electrons 79—60909
ZnO surface extreme accumulation layers due to He^+ ions 77—72909
ZnO, temp. depend. elec. cond. 79—91041
ZnO varistor ceramics, current-voltage characts., inhomogeneities and single barriers 80—80273
ZnO:$^{31}P^+$ implanted nonlinear resistor production and characteristics *(Russian)* 80—49252
ZnO:Ba, Co, rare earth metal varistors, microstructure-prop. relations 80—100249
ZnO:Bi, Sb, Co, second phase effect on elec. and mag. props. 80—60986
ZnO-based binary semiconductor system nonlinearity prognosis *(Russian)* 78—43406
ZnO-based ceramic microstructure and nonlinear props., B diffusion effects *(Russian)* 80—49423
ZnO-Bi_2O_3, ceramic semiconductor, injection currents 79—11141
ZnO-Bi_2O_3-CoO-MnO-Sb_2O_3 (97.5, 0.5, 0.5, 1.0 mole%), exam. of elec. props. at different annealing temps. 80—3099
ZnO-CoO_4 (Fe_2O_3), ceramics, impurity at. states, elec. cond. 79—11130
α-ZnP_2, doped, single crystal, electrical properties 80—92892
ZnP_2, pure and doped, carrier mobility and conc., donor and acceptor energy levels, 190 to 380K 78—84217

electrical conductivity of crystalline semiconductors and insulators continued
Zn_3P_2, elec. cond., Hall effect, P interstitial effects 80—84465
Zn_3P_2 photovoltaic material and Schottky diode characteristics 78—64066
Zn_3P_2, single crystal, growth, electronic and device props. 80—25551
p-Zn_3P_2, temp. dependence of resistivity and Hall constant 77—35937
ZnS, current oscills., 300K, 1-6 s period *(Russian)* 77—80819
ZnS, low temp. equilibrium compensation limit of intrinsic-defect hole conductivity *(Russian)* 79—1598
ZnS:Ag, single crystal, ionisation mechanism of field trapping centres 80—45156
ZnS:Ag, TSC and induced impurity photoconductivity, existence of two electron trapping centres 80—44655
ZnS:Pb phosphor, ionisation mechanism of field trapping centres 80—45156
$(ZnS)_{0.2}(CdS)_{0.8}$, elec. props. effect of wurtzite-sphalerite boundary 77—55531
ZnSb, thermoelec. anisotropic semicond., carrier kinetics at low temps. 80—92893
ZnSe, cryst., elec. cond., dislocation motion effects 80—54710
n-ZnSe crystals, electron scatt. mechanisms, high mobility 80—34433
ZnSe, dislocation motion, influence on elec. cond. 79—15149
ZnSe, effect of In-doping and Zn-annealing, 300 to 77K 78—76075
ZnSe, elec. props. efect of wurtzite-sphalerite boundary 77—55531
n-ZnSe, impurity band, Hall effect, elec. cond., mobility and magnetoresist. expts. 77—35888
n-ZnSe, long persistent cond. relax. and frozen cond. 80—54735
ZnSe, phase transition, differential thermal analysis 77—7863
ZnSe, pure and Cu doped, elec. props. after heat treatment in Zn or Se vapour 79—99505
ZnSe single cryst. for LED, heat treatment effects on elec. props. 80—29406
ZnSe:Al(Mn), elec. and luminesc. props. 77—39844
ZnSe:Ga, defect struct., Hall effect and resist. meas. 79—1428
ZnSe:In, heavily compensated, galvanomag. props. and thermopower 79—51600
ZnSe:In, heavily doped, Hall effect and DC cond. expts., compensating acceptors 78—52013
ZnSe:In, heavily doped, impurity band cond., Hall coeff. and cond. expts. 78—72147
ZnSe:In, single crysts., new vapour phase growth method, elec. cond. props. and photoluminesc. spectra 79—19982
ZnSe:N, ion implanted cond. type conversion on annealing *(Korean)* 78—18668
ZnSe-HgSe, solid soln., defect distrib., elec. props., Hagemark's theory 78—64040
ZnSe(:Ga)(Al), effect of thermal treatment and doping on elec. props. 77—85223
$ZnSiAs_2$, cryst. growth and elec. props. *(French)* 77—76815
$ZnSiAs_2$, electron irrad., defects, elec. and optical props. 79—19282
p-$ZnSiAs_2$, electron irrad. elec. props. annealing, lattice defects 80—100465
$ZnSiP_2$, effect of crystal growth method, on physical props., effect of doping on physical props. *(German)* 79—52094
$ZnSiP_2$:Ga, effect of doping conc. on elec. cond. and Hall coeff. 78—76077
n-$ZnSiP_2$:Ga, elec. cond. and Hall meas., 77 to 1000K, scatt. mechanisms 79—11153
ZnTe, effect of quenching on electrical props. 79—1920
ZnTe, polymorphism at elevated temp., elec. resist. and X-ray diffr. under press. 80—49359
Zr carbide interstitial phases, elec. and mag. props., neutron radiation effects 79—77640
Zr hydride interstitial phases, elec. and mag. props., neutron radiation effects 79—77640
ZrC high-temp. plastic deform. effects on elec. props. 77—44370
ZrC_x, thermophysical props. at high temp., thermal vacancies form. 78—43141
$ZrH_{1.9}$, neutron irrad. induced defects, nature and thermal stability 77—50246
ZrN high-temp. plastic deform. effects on elec. props. 77—44370
ZrN, thermodynamic props. of vacancies 77—11539
ZrN-Al_2O_3, exam. of sintering and densification kinetics, and physical props. 79—95986
ZrN-Al_2O_3 sintering reaction thermodynamics 80—2989
ZrN-AlN composites, struct. and props. 77—40413
ZrO_2, elec. cond. at high temps. 78—6380
ZrO_2, elec. cond.-nonstoichiometry relationship, direct determ. 78—76079
ZrO_2 electrolyte cells, elec. props. 79—24477
ZrO_2, stabilised voltage-current-time charact. with point contact Pt electrode in Ar gas ambient 77—1461
ZrO_2:Nd_2O_3, in contact with $NdCrO_3$, electrical cond. meas. 78—76071
ZrO_2:Y_2O_3, in contact with $YCrO_3$, electrical cond. meas. 78—76071
ZrO_2-CaO-SiO_2, relationship between texture parameters, and sintering, elec. cond. and mech. strength props. *(German)* 79—24474
ZrO_2-CeO_2, semiconducting ceramics, electronic conductivity and oxidoreduction *(French)* 78—26919
ZrO_2-Y_2O_3 (10 mole%), electron transport, elec. induced p-n junction 77—43597
$(ZrO_2)_x(In_2O_3)_{1-x}$ ceramic, bulk resistivity 77—35936
$4.26ZrO_2.Nb_2O_5$, elec. cond. meas. 80—100463
$6.14ZrO_2.Ta_2O_5$, elec. cond. meas. 80—100463
ZrS, equilibria, nonstoichiometry and elec. props. temp. depend. *(French)* 78—64053
ZrS_3, quasi one-dimens. semicond., elec. transport props. 80—107790
$ZrSi_2$, work function rel. to phys. props. 77—47887
$ZrTe_5$, giant resistivity anomaly 80—107794

electrical conductivity of electrolytic liquids
see also electrochemical analysis; electrolytic ion mobility; Wien effect
1:2 electrolytes, conc. solns., vel. correls. calcs., diffusion, cond. and transference props. 78—85166
acids, conc. aqueous, amorphous protonic conductors, DC cond., glass transition and elec. relax. meas. 78—2290
alkali iodides in acetone, press. effects on Walden products, ion-solvent interactions 80—3398
alkali metal cations in aq. solns., limiting equiv. cond. rel. to water viscosity 77—1252
alkali metal fluorides, dil. aq. solns., conductance at 25°C 77—69105
alkaline earth halides, solns. in methanol, conductance data anal., assoc. consts. 78—71875

electrical conductivity of electrolytic liquids continued
S-alkyl-isothiouronium iodides in methanol-water mixtures, conductance at 25°C, solute-solvent interaction 79—95194
N-alkylpyridium halides, molten, and mixtures with $AlCl_3$, density, elec. cond. and viscosity meas. 80—24630
annulus flow electrolysis, solenoidal mag. field effect on ionic mass transport 80—26021
aqueous solutions, naturally recurring, activity coeffs. rel. to ionic diffusion 78—57224
concentrated electrolyte solution, cond. model 77—84957
conductance equation, compatibility with Onsager's reciprocal relation 78—31647
conductance equation, generalized, for strong electrolytes 78—31646
conductance meter classification and quality assurance 77—12857
conductance-concentration function for associated symmetrical electrolytes 77—21392
continuity eqn., boundary conditions for integration 78—3342
dielectric liquid with electrolytic dissoc. of additive, weak conductivity *(Russian)* 78—27161
dielectric liquids, ion mobility meas. and breakdown process, optical methods 80—84692
dissociation enhancement by field, and EHD instabilities *(French)* 77—62655
electrochemical electrodes linearly polarised, electrolyte stationary electric field calc. *(Russian)* 80—21289
electrochemical reactions, in conc. solns., ionic mass transport rates calc. method 79—70352
rel. to electrode current density *(Russian)* 78—64847
electrodeless meter design 79—85153
electrolyte solns., particle-particle interactions, velocity correl. coeffs. 78—64852
electrolyte solution, Brownian dynamics approx., time evolution and transport props. 79—37604
electrolytes, complete conductance eqn., hydrodynamic terms 79—23755
ethanol, alcoholic electrolytic solutions, Dielectric constants 79—99813
formic acid solvent system, behaviour of electrolytes 79—57239
fused salt, simulation of high field cond. 80—54421
galvanic current meas. instrumentation, function of velocity of metal electrolyte 77—10040
gas chromatographic bipolar pulse differential electrolytic cond. detector 80—93814
Hall effect, in flowing electrolyte, student expt. 79—21501
HF, and dielec. const., determ. in RF region 77—21396
impedance parameters for electrochemical systems exhibiting pseudoinductance 79—66303
ion-selective electrodes, liq. membrane, free and supported, ion transport, bulk elec. props. 79—83534
ion-selective electrodes, liq. membrane, free and supported, ion transport, interfacial kinetics, time depend. phenomena 79—83535
ionic melts, unusual elec. props., review 79—99338
isobutyric acid-water mixture, electrical conductivity near crit. pt. 77—15612
isothermal, electrolyte transport, irreversible thermodynamics calcs. 80—3364
measurement, multi-electrode technique 78—21175
measurement of conductivity, bridge cct. for cond. cell *(German)* 79—9220
methanol, alcoholic electrolytic solutions, Dielectric constants 79—99813
mixed electrolytes, conductance, relax. terms 78—67840
mixed halide melts, elec. cond., surface tension, density and viscosity, tables 79—60531
mixed strong electrolytes, relax. effects in limiting law region, integral representation 77—86322
model for electrolytic conductance 80—6533
molecular liquids, ionic cond. at high temps. 80—29195
molten salt, hydrodynamic correlation functions 77—31577
molten salts, ion mobilities, group vel. correl. function calcs. 77—89561
molten salts, transport coeffs., integral representations 78—67842
multicomponent electrolyte systems, elec. cond. and diffusion 78—71872
organic fluid charge carrier generation, role of molecular electroinduction effects *(Russian)* 79—96321
paired ion model, conductance-conc. function 79—37603
phenol-water mixture, pure and KCl-doped, electrical conductivity near crit. pt. 77—15612
pigments, photochemical ionisation reactions in soln., automatic conductimetric instrument for kinetic studies 77—4971
polar solvent, spherical ion radius and limiting elec. cond. Brownian motion 78—95168
poly(aminiumphosphate)s, mol. wts., and cond. studies 80—14264
polyelectrolytes, electric transport 78—31648
in porous body, electrolyte elec. cond. meas. 77—63927
quinone electrochemical reduction at packed, fluidised bed electrodes, kinetic behaviour 79—57235
rapid conductivity meas. with electrolyte cond. probe, astable multivibrator freq. control 78—37029
rare earth complex, $R(DMMP)_6(ClO_4)_3$ and $R(TBPO)_4(ClO_4)_3$, synthesis and characterisation 77—23498
rhodamine B in aq. LiCl soln., absorpt., pH, electric conductance 77—27079
small signal electrical response theory, generation-recomb. and trapping kinetics 77—89772
solutions, in ethylene carbonate viscosity and conductance meas. at 40°C 79—28122
solutions, mixed, electrical transport 80—3354
solutions, thermodynamics, transport props., semi-phenomenological approach including short range forces 80—3353
symmetrical electrolytes, conductance, relax. terms 78—67840
symmetrical electrolytes, conductance and model for ions in soln. 80—29197
TCNE electron donor/acceptor complexes, photoionic dissoc., photocurrents 77—14502
tetraalkylammonium bromide soln., conductance and viscosity, temp. and concentration depend. 80—6531
tetrabutylammonium iodide, in aq. proline soln., elec. conductance investigation 80—10692
tetrabutylammonium picrate, elec. cond. in nematic (smectic) 4-alkyloxy-4′-cyanobiphenyls, temp. (conc.) depends. *(German)* 78—55966
tetramethylammonium iodide, in aq. proline soln., elec. conductance investigation 80—10692
ultrapure water electrolytic conductivity meas. 79—24755

electrical conductivity of electrolytic liquids continued
unsymmetrical electrolytes, conductance, relax. terms 78—67840
water, Earth surface forms, at frequencies below 1000 GHz 78—24310
AgBr, molten, freq. depend. ionic cond. 77—7882
AgCl, molten, freq. depend. ionic cond. 77—7882
$AgNO_3$, solution, sono-conductance rel. to temp. 77—15496
Ag_2S, liquid, ionic and electronic cond., thermoelec. power 80—39329
Ag_2Se, liquid, ionic and electronic cond., thermoelec. power 80—39329
Ag_2Te, liquid, ionic and electronic cond., thermoelec. power 80—39329
$AlBr_3$, specific and equivalent cond. of aq. solns., viscosity 77—35736
$AlCl_3$-LiCl, molten mixtures, specific cond. meas., comp. and temp. depend. 80—15279
AlI_3, molten, electrical cond., press. effect, 0-1 kbar 78—55963
Ba soln. in liq. ammonia, conductance at −62.37°C 78—91459
$BaCO_3$, soln. kinetics and activation heat *(German)* 79—16031
$Ba(ClO_4)_2$, soln. in liq. ammonia, conductance at −62.37°C 78—91459
$BeSO_4$ soln., high press. conductance meas., transfer mechanism 77—76586
BiI_3, molten, electrical cond., press. effect, 0-1 kbar 78—55963
BiI_3-CdI_2, molten, elec. cond., temp. depend. 77—89562
$CaCl_2$, $CaCl_2$-CaF_2-CaO eutectic melts, specific cond. meas. 77—59131
$CaCl_2 \times 5.99,5.33H_2O$, molar cond., compressibility, expansivity 78—51712
CaF_2, melt, influence of B_2O_3, La_2O_3 and Y_2O_3 on elec. cond., ionic mech. 78—43157
$Ca(NO_3)_2.nH_2O$, aq. soln., conc., compressibility, elec. cond. 77—69024
CaO-SiO_2 melt, tracer diffusivity of Ca^{45} and elec. cond. 79—60532
CaO-SiO_2-MnO molten mixtures, struct. and phys. props. *(French)* 80—24635
$CdBr_2$-$BiBr_3$, molten, elec. cond., 500-870K, composition depend. 78—55965
CdI_2, aq. soln., isothermal transport props., 298.15K 78—18815
CdI_2, aq. soln., transport props., irreversible thermodynamic anal. 78—14490
CdI_2, molten, electrical cond., press. effect, 0-1 kbar 78—55963
$Cd(NO_3)_2$-XNO_3, (X=Li,Na,K,Tl), molten mixtures, electrical conductance, non-Arrhenian behaviour 78—43158
$Cd(NO_3)_2 4.1H_2O$-$CoCl_2$, melt viscosity, equivalent conductivity, glass transition temp. 78—75855
$Cd(NO_3)_2 4.1H_2O$-$NiCl_2$, melt viscosity, equivalent conductivity, glass transition temp. 78—75855
Cl^-, in aq. solns., limiting equiv. cond. rel. to water viscosity 77—1252
Co complexes, $[Co(H_2O)_x(NH_3)_{6-x}][Co(CN)_6]$, x=1,2, hydrogen bonding 77—42437
Co complexes, nitropentaammine and hexaammine Co(III) complexes, ion assoc. in aq. soln., conductance meas. *(Japanese)* 78—40059
Cr complexes, $[Cr(H_2O)_x(NH_3)_{6-x}][Co(CN)_6]$, x=1,2, hydrogen bonding 77—42437
Cs-Au, liq. alloys, ionic conductance 77—1251
CsBr-dioxane-H_2O solns., elec. cond. calcs., computer program, data anal. *(German)* 77—32806
Cu complexes of 2-amino-5-methyl-1,3,4-thiadiazole and 2,5-dimethyl-1,3,4-thiadiazole, conductometric and IR meas. 80—87121
Cu tripolyphosphate complexes, electrolyte development for direct deposition of Cu 80—45246
$CuSO_4$, aq. soln., electrolytic resistance variation in mag. field 80—11897
$CuSO_4$, aq. solns., densities, viscosities, elec. cond. meas., 20 to 70°C 80—59688
$CuSO_4$, effect of press. on ion pair dissoc., cond. of aq. solns. 78—53218
$CuSO_4/H_2SO_4$ electrolytes, densities, elec. cond., viscosities 80—107455
GaI_3, molten, electrical cond., press. effect, 0-1 kbar 78—55963
HCl-KCl-H_2O mixed electrolyte solns., elec. transport 80—3355
$HN(SO_2Cl)_2$, physical props. meas. 79—51293
H_3PO_4, aq. soln., elec. cond. and Raman spectra at high-press., 25°C 79—56220
$HgBr_2$-$BiBr_3$, molten, elec. cond., 500-870K, composition depend. 78—55965
HgI_2-BiI_3, molten, elec. cond., temp. depend. 77—89562
$Ho(NO_3)_3$ solns., f-f transitions, intensity anal., correl. with cond. and US absorpt. 80—97292
I_2, molten, electrical cond., press. effect, 0-1 kbar 78—55963
$InBr_3$, specific and equivalent cond. of aq. solns., viscosity 77—35736
InI_3, molten, electrical cond., press. effect, 0-1 kbar 78—55963
$In(NO_3)_3$, specific and equivalent cond. of aq. solns., viscosity 77—35736
KBr-Al_2Br_6 soln. in toluene, conduction mechanism 80—6870
$KBrO_3$, KIO_3 and K_2SO_4, in dioxane-water mixtures, ion-solvent interaction and conductance 79—34315
KCl, mol. dynamics study 79—28116
KCl, soln., elec. cond., dielec. relax., kinetic characts. 78—34641
KCl solution, elec. cond. obs. for seawater salinity scale 80—72646
$KClO_4$ soln. in liq. ammonia, conductance at −62.37°C 78—91459
KH_2PO_4, aq. soln., elec. cond. and Raman spectra at high-press., 25°C 79—56220
KI, soln. in organic solvents, elec. cond., shock compression effects 79—46822
KNO_2 pressures up to 6 kbar temp. range ~100K above melting temp. 77—15609
KNO_3-$Pb(NO_3)_2$ molten mixture, elec. cond., Tobolsky parameter *(German)* 80—15282
KNO_3-$Sr(NO_3)_2$ molten mixtures, electrical conductance 78—43159
La_2O_3-$Li_2B_4O_7$-Li_3AlF_6 melts, LaB_6 electrodeposition, pot.-current curves 79—20378
(Li-Cs)NO_3, molten, internal cation mobility meas. 79—60534
(Li-Rb)NO_3, molten, internal cation mobility meas. 79—60534
$LiAlCl_4$, solid and liq., ionic cond., 25-180°C 77—20114
LiBr, dil. aq. solns., conductance at 25°C 77—69105
LiBr, in anhydrous acetone, elec. conductance at high press., Shedlovsky method 78—53219
LiBr soln., conductance and viscosity, temp. and concentration depend. 80—6531
LiBr-Al_2Br_6 soln. in toluene, conduction mechanism 80—6870
LiCl, dil. aq. solns., conductance at 25°C 77—69105
LiCl-KCl, molten mixture, struct., diffusion, cond., mol. dynamics calc. 80—64871
LiCl-NaCl-$AlCl_3$ melt, elec. cond., 800 to 1200K *(Japanese)* 80—24633
LiF, dil. aq. solns., conductance at 25°C 77—69105
LiI, dil. aq. solns., conductance at 25°C 77—69105
$Mg(NO_3)_2.6H_2O$-NH_4NO_3 system, molten, elec. cond. 79—51288
$MgSO_4$, aq. soln., electrolytic conduct. affected by US waves 79—23997

electrical conductivity of electrolytic liquids continued
$MgSO_4$, soln., electrolytic cond. dispersion, 1-6 MHz, caused by US propag. 80—44343
$MnCl_2$-tetra-n-butylammonium halide melts, density, elec. cond., and viscosity 80—24631
MnO-SiO_2-TiO_2 melt, electrical cond. meas. and electrolytic anal. *(Japanese)* 78—38861
$MnSO_4$, effect of press. on ion pair dissoc., cond. of aq. solns. 78—53218
NH_4Br soln., conductance and viscosity, temp. and concentration depend. 80—6531
NH_4NO_3-$LiNO_3$-NH_4Cl-water system, cond. and viscosity *(French)* 79—51286
NaBr, n-propanol soln., cond. and transference no. meas., radioisotope method 77—35735
$NaBrO_3$, $NaIO_3$ and Na_2SO_4, in dioxane-water mixtures, ion-solvent interaction and conductance 79—34315
NaCl, stratified solutions, elec. cond. meas. instrument 77—52718
NaCl, water-HMPT soln., ionic diffusion coeffs. meas. *(French)* 80—65265
NaCl-CsCl-$MnCl_2$, molten salt system, molar volume and elec. cond. meas. 80—34218
NaCl-CsCl-$MnCl_2$, ternary molten salt system 80—34217
NaCl-KCl($MgCl_2$)-H_2O mixed electrolyte solns., elec. transport 80—3355
$NaClO_3$, pressures up to 6 kbar temp. range ~100K above melting temp. 77—15609
NaF-AlF_3 binary melt, density and elec. cond. *(Japanese)* 78—18814
NaI, dil. aq. solns., conductance at 25°C 77—69105
NaI, n-propanol soln. cond. and transference no. meas., radioisotope method 77—35735
$NaNO_2$, pressures up to 6 kbar, temp. range ~100K above melting temp. 77—15609
NaOH-KOH eutectic molten mixture, elec. cond. and sp. mass 79—82365
Na_3PO_4, aq. soln., elec. cond. and Raman spectra at high-press., 25°C 79—56220
PbO-SiO_2, melt, elec. cond. and struct. 80—88020
Tl_2S-Tl_2Se systems, melts, ion transfer, diffusion coeffs., elec. cond., density meas. 77—1253
UO_2^{2+}, aq. soln., ionic mobility meas., conductivity method 77—31791
UO_2^{2+}, n-propanol soln., ionic mobility and assoc. consts. 77—31792
$UO_2(NO_3)_2.2H_2O$, in n-butanol, ionic mobility determ. 78—34642
$UO_2(NO_3)_2.6H_2O$, in n-propanol, ionic mobility determ. 78—34642
$ZnSO_4$, effect of press. on ion pair dissoc., cond. of aq. solns. 78—53218

electrical conductivity of gases
see also space-charge-limited conduction
aerosol particles, charged, effect on thermal and elec. conds. of ionised gas 80—28593
air, conduction current, effect of cross mag. field 79—18990
air, humidified by boiling water, ion content, sensitive cell meas. 80—53913
alkali metal, dense vapour, anomalously large elec. cond., positive complex ions form. 80—19547
atmosphere, conductivity meas. in lower stratosphere over Poona 77—70750
bipolar current in dense gas without volume ionis. 80—6208
Boltzmann eqn., numerical method of soln., weakly ionised heterogeneous gas 77—49693
Boltzmann equation, time independent, gas mixture in elec. field, soln. using Fortran program BOLTZ 77—11304
butane, gas, electron drift vel., Ramsauer-Townsend minima in electron scatt. 78—87427
combustion products, seeded oxy-liq. petroleum gas system, elec. cond. meas. 77—58835
conductance for the gas flow of an accelerating tube 80—102359
cyclohexane, gaseous, crit. and liq., density and temp. effects on electron mobilities 79—27739
cyclopentane, gaseous, crit. and liq., density and temp. effects on electron mobilities 79—27739
dense gas, thermal electron drift, Boltzmann eqn. soln. 80—1734
electron drift velocities as function of elec. and mag. variables in several gas mixtures 78—71424
electron drift velocity, density dependence, high press., quantum mech. theory 79—1285
electron stream, diffusion in gas, elec. field effects near absorbing boundary 77—55127
ethane, gas, electron drift vel., Ramsauer-Townsend minima in electron scatt. 78—87427
ethane, gas, liq., and crit., electron mobility, density and temp. effects 80—92246
ethane, supercritical, electron mobility as function of density and temp. 80—59163
excited gas, resonant optical discharge 80—92343
field-dependent mobility at drift vels. near sound vel. 80—43840
flame plume behind bluff body with fuel injection, elec. cond. mechanism 79—39150
fluid, two dimens. motion, mag. field evolution, anti-dynamo theorem extension *(Russian)* 80—59127
n-hexane, gaseous, crit. and liq., density and temp. effects on electron mobilities 79—27739
hot gas, meas. method 80—13104
imperfect high temp. plasma, elec. cond. meas. *(Russian)* 80—100072
inert gases, partly ionised, minimisation of effective electron-neutral particle collision cross section 79—64821
ion transport, three-temp. theory generalisation, appl. to $Cs^+ + Ar$ 80—6202
ionised gas, slow electron momentum transfer cross section in mag. field, RF cond. meas. 79—82030
methane, fluid, electron mobility, density and temp. effects 80—10351
methane, gas, electron drift vel., Ramsauer-Townsend minima in electron scatt. 78—87427
methane, gas, electron transport, kinetic theory 77—84391
MHD duct flow, H_2O_2, two-dimensional calc. 79—83605
neopentane, gas, electron drift vel., Ramsauer-Townsend minima in electron scatt. 78—87427
packed bubble columns, holdup profiles, elec. cond. meas. 77—35201
partially ionised gases, magnetic inductive effect, Hall coefficient 77—19662
partially-ionised gas, elec. and computation 79—86563

electrical conductivity of gases continued
partly ionised multicomponent dilute gases under EM and graivity fields, kientic thoery 79—77328
pentane isomers, vapour and liq., electron mobility 79—72984
petroleum-acetylene-O_2 combustion products, seeded, elec. cond., for MHD power plant 78—34256
photoelectron injection in gases from thin metal films on quartz 79—68899
propane, gas, electron drift vel., Ramsauer-Townsend minima in electron scatt. 78—87427
Ramsauer-Townsend effect, partially ionised gas elec. cond. 78—67458
teaching, relax. approx. to Boltzmann eqn. approach 78—73804
test particle diffusion, in conservative field, integral Boltzmann eqn. solns. 79—97324
weakly ionised gas, relaxing, negative cond., kinetic eqn. anal. *(Russian)* 79—4101
Ar, fluid, dense, excess electron drift vel., hopping model 80—43838
Ar, ionised gas, high press. elec. cond. meas. 78—26233
As, crit. parameters determ. 77—47562
CO, electron scatt. cross sections for momentum transfer and inelastic excitation 79—36782
CO_2, electron and negative ion swarms 80—28595
CO_2 laser, glow discharges at high press., voltage-current characts. 78—87036
Cs, dense vapour, anomalously large elec. cond., positive complex ions form. 80—19547
Cs, saturation effect on thermo-EMF up to 1950°C and 140 atm. 77—51727
Cs vapour, elec. cond., tight binding approx. in Kubo formalism 79—60778
Cs vapour, electrical cond. near saturation point 80—69967
Cs vapour, nearly saturated, prebreakdown elec. cond. 80—48841
H_2, electron swarms, anisotropic scatt. model 78—91059
H_2, gas discharge, low press., emitted photon probe for electron swarm parameters 80—43839
H_2, lateral diffusion to electron mobility ratio 79—1284
H_2-O_2 seeded system for MHD generator, elec. cond. 80—76642
He, gas discharge, low press., emitted photon probe for electron swarm parameters 80—43839
Hg, dense vap., electron injection 77—47138
Hg, supercritical vap., semicond. model 77—51154
KOH, electron collisions, integrated and momentum transfer cross sections, cond. integrals 79—41238
N_2, electron transport coeffs. in crossed fields at low E/p 77—24050
N_2, gas discharge, low press., emitted photon probe for electron swarm parameters 80—43839
N_2, lateral diffusion to electron mobility ratio 79—1284
N_2O, mech. of thermal electron attachment, microwave cond. meas. 78—59536
N_2O, pure and in mixtures, electron attachment near 1 atm., microeave cond. meas. 80—1063
N_2O-hydrocarbon mixtures, mech. of thermal electron attachment, microwave cond. meas. 78—59536
O_2, electron and negative ion swarms 80—28595
O_2-CO_2 (ethylene)(neopentane), thermal electron attachment meas., microwave cond., pulse radiolysis 80—28592
SF_6, electrical conductivity calc., 2000 to 50000K 79—14512
SF_6, equilib. composition and transport props., 300 to 15000K 77—24051
$SF_6 + H_2$ mixture, equilib. composition and transport props., 300 to 15000K 77—24051
ScOH, electron collisions, integrated and momentum transfer cross sections, cond. integrals 79—41238
UF_6, thermodynamic functions and elec. cond. at 1000 to 11000K and 0.1 to 100 atm. 77—42964
Xe, electrical conductivity beyond critical point, intermediate density between gas plasma and solid *(Russian)* 80—20265

electrical conductivity of liquids
see also electrical conductivity of electrolytic liquids
acetone, macroscopic model for solvated ion dynamics, cation conductance calcs. 80—65261
acetonitrile, macroscopic model for solvated ion dynamics, cation conductance calcs. 80—65261
acetonitrile+CS_2 liquid mixture, elec. cond. crit. phenomena 77—4212
albumin, human serum, elec. cond. and dielec. const., 1 to 15 MHz 78—53315
alkali metal-ammonia solns., elec.-cond. and thermopower 77—1370
alkali metal-Au alloys, elec. props. 78—84187
alkali metal-NH_3 solution, Hall effect and cond. at metal-nonmetal transition 78—2530
alkali metals, calc. of enthalpy of soln. of nonmetals and elec. resist. 77—55225
alkali metals, elec. resist., exchange and correlations effects 77—1403
alkali metals, liq., Fermi energy, density of states, electronic props., exchange and correl. effects 80—96774
alkali metals, nonlocal harmonic model potential, appl. to elec. props. 80—6802
alkali metals, resist. and struct. factor, temp. depend. 77—62466
alkali metals, soln. chemistry as elucidated from elec. resist studies 77—52636
alkaline earth elements, electrical resistivity; 1-1000K, data tables 79—78073
p-n-alkoxybenzoic acid, elec. cond. anisotropy of nematic structs. 80—1928
N-4-n-alkoxybenzylidene-4′-n-butylanilines, elec. cond. in nematic and smectic phases *(German)* 77—15860
alloys, highly resistive, temp. depend. on elec. resist. 78—91657
aluminophosphate melts with V, Cr, Fe and Co oxides, resistivity, 800-1200°C 77—39903
aniline, in benzene, polar dielectric system, RF cond. and dipole moment 78—2788
anthracene, elec. current decrease due to electrode coverage form. 77—8108
azoxy compound, liquid cryst. mixture, nematic, elec., optical and viscoelastic props. 79—55803
baddeleyite-corundum refractories, fused, elec. resist., 1300-2300°C 79—28345
benzene, elec. current decrease due to electrode coverage form. 77—8108
benzene, gaseous, critical and liquid, electron transport 80—64673
benzol, liq., dark conductivity obs. *(Russian)* 77—55560

electrical conductivity of liquids continued
binary alloys, liq., calc. of electromigration forces and resistivities 79−82572
borosilicate glass containing simulated high level radioactive waste, characterization *(Japanese)* 79−93745
bromides, and mixtures, molten, elec. cond., density, viscosity, surface tension, review 77−80638
Brownian particles in periodic medium, cond. 79−49170
t-butyl bromide, elec cond., temp. depend. in liq. and plastic phases 80−1944
t-butyl chloride, elec cond., temp. depend. in liq. and plastic phases 80−1944
p-n− butyl-p′-methylhydroxyazobenzene/p-n-butylheptanoylazoxybenzene mixture, temp. depend of elec. cond. 80−1925
caesium acetate, molten, elec. cond. and density 77−15613
chalcogenide semiconductors, elec. cond. freq. depend., hopping cond. contrib. 77−76856
chemical kinetic investigation in soln., high press., device for conductivity meas. 79−93161
cholesteryl caprilate, conduction mechanism 78−64046
cholesteryl capsylate and laurate, and their mixtures, elec. cond. *(Rumanian)* 79−64988
cholesteryl laurate, conduction mechanism 78−64046
cholesteryl laurate-cholesteryl caprilate mixture, elec. cond. mechanism 79−10796
cholesteryl laurate-cholesteryl caprylate (75 wt.%), polymorphic behaviour, optical, elec. and dielec. meas. 80−65208
conference, Banff, Alberta, Canada, (5-11 Sept. 1976) 77−89680
p-cyanophenyl-p′-caproyloxybenzoate, charge carrier behaviour, thermal depolarisation current study 80−7283
cyclohexane, gaseous, crit. and liq., density and temp. effects on electron mobilities 79−27739
cyclohexane, liq., ion injection by metallic electrodes *(French)* 79−51289
cyclohexane, liq. and solid, mobility of excess charge carriers 78−2489
cyclohexane+acetic anhydride, elec. resist. near crit. soln. temp. 78−71874
cyclohexane-acetic anhydride, crit. resistivity, H_2O impurity effect 79−51565
cyclohexane-acetic anhydride binary liq. mixture, crit. behaviour of elec. resist. 78−6422
cyclohexane-acetic anhydride mixture, impurity effects on crit. behaviour of elec. resist. 79−65527
cyclopentane, gaseous, crit. and liq., density and temp. effects on electron mobilities 79−27739
trans-decaline-cyclohexane liq. mixtures, hole mobility, percolation model 80−65551
dielectric, charge transport by solid particles 77−4329
dielectric liquid, cond. effect on electroviscosity 78−1751
dielectric liquid, DC cond. due to impurity particles, computer simulation and comparison with expt. 79−91060
dielectric liquid, ionic mobility estimation from charge relax. 77−11719
dielectric liquids, cond. and breakdown, conf., Mont-Saint-Aignan, France (July 1978) 79−91354
dielectric liquids, cond. band minima, rel. to electron mobility maxima 78−80029
dielectric liquids, high-field cond. and breakdown, anal. 77−8506
dielectric liquids *(Slovak)* 79−51562
dielectric liquids electric conduction, thermal activation energy, anal. 78−43399
dielectric polar liq., electroviscosity rel. to cond. process, EHD model 78−1750
dielectrics, electric breakdown, impurity effects 80−11340
dielectrics, electrical model *(Russian)* 77−8101
diffraction model, critical test, elec. resistivity of amorphous and liq. metals 78−84191
dilute binary alloys, conduction electron scatt. cross section and component effective charges *(Russian)* 77−8082
diphenylanthracene in benzene soln., extrinsic photocond. kinetics 80−92691
disturbances in conducting fluid modelling, due to solid particles, conductometric probe analysis *(Russian)* 78−231
EBBA, liq. crysts., thin layers, addition of iminoxyl radicals, effect on elec. cond. *(Russian)* 78−67641
EBBA, nematic, linear and nonlinear relaxations of fluid dynamical motion 77−31585
EBBA, solid and liquid states, temp. and freq. depend. *(Russian)* 78−72450
EHD flow intensity and efficiency, low voltage liq. conductivity depend. 80−33699
electrical resistivity, data tables, 1-2000K 79−78072
electrification of fluids, rel. to fluid dynamics 78−26200
electronic states and transport 79−99474
electrophotographic liquid developer, permittivity and conductivity meas. *(German)* 78−62257
electrostatic drop formation, effects of conductive liquid props. 78−1122
elemental semiconductors, model pseudopotential, band struct. calcs., liquid semicond. resistivity calcs. 80−20075
emulsion of H_2O-alcohol, elec. cond. rel. to conc. 79−20471
ethane, gas, liq., and crit., electron mobility, density and temp. effects 80−92246
ethane, liq., photoelectric determ. of conduction state energies and electron ranges 77−89487
fluid, two dimens. motion, mag. field evolution, anti-dynamo theorem extension *(Russian)* 80−59127
fluoride-oxide slags, elec. cond., Al and Si addition agents influence *(Russian)* 80−39572
glass, liquid-phase separated, struct., use of elec. methods 79−66249
glass, melt, electrical resistance calc. in electric furnace 77−66165
glass melt, multiphase electric current field *(Czech)* 80−84310
graphite intercalation cpds. with H_2SO_4 and sulphuric oleums, elec. resist. evolution 80−45518
n-heptane+acetic anhydride, elec. resist. near crit. soln. temp. 78−71874
n-heptane-methyl alcohol, crit. resist. of binary liq., 10 Hz-100 kHz 78−76123
hexafluorobenzene liq., electron mobility, percolation model 80−65551
hexafluorobenzene-benzene liq. mixture, electron mobility, percolation model 80−65551
n-hexane, gaseous, crit. and liq., density and temp. effects on electron mobilities 79−27739
n-hexane, impurity particle behaviour and cond. pulses 79−91059

electrical conductivity of liquids continued
n-hexane, subjected to charge injection, low stress mobility, induced motion effects 79−91063
n-hexane-ethanol liq. mixtures, electron mobility, percolation model 80−65551
HEXOAB/7CBP, mixed crystals, induced smectic A phases, elec. cond. 78−76068
homogeneous solid, small signal AC response, mobile charge recomb., theory 78−52005
hydrocarbon liq., effect of mol. struct., temp. and elec. field on electron mobility 78−2535
hydrocarbon liquid, model for thermalisation of quasifree electrons rel. to electron mobility 77−40316
hydrocarbon liquids, elec. cond. at fields up to breakdown strength, crit. review 77−80787
hydrocarbons, high-field carrier transport at pre-breakdown and breakdown regions 80−25305
hydrocarbons, ion injection, low field elec. cond. 79−91064
hydrocarbons, localised and quasifree excess electron mobility, cond. state energy and temp. depend. 79−4588
hydrocarbons, saturated open-chain, transport behaviour of excess electrons and props. 80−39643
hydrocarbons liq., geminate pair of charges, neutralisation escape with field depend. electron mobility 78−26865
'Impul's' conductometer (USSR), elimination of dilute soln. instability 80−77813
inert gas, kinetic equation for electrons for strong ion-ion interaction 77−35908
inert gas, liq., photoelectric determ. of conduction state energies and electron ranges 77−89487
inert gases, liq., model for thermalisation of quasifree electrons rel. to electron mobility 77−40316
iodides and mixtures, molten, elec. cond., density, viscosity, surface tension 77−80638
ionic melts, unusual elec. props., review 79−99338
isolated ion pair, in irrad. medium, transport, transient elec. field effects 77−81419
liquid alloys, determ. of diffusion coeff. from meas. of resist. 77−55375
liquid film, wave parameter meas., local electrical cond. method 77−51141
liquid metal, electron states, esp. opt. and mag. props., review 78−2882
liquid metals, resistivity expression, electron kinetic eqn. 80−48857
low conductivity media, unipolar injection, forced diffusion model 80−92692
macromolecular solutions, light scatt., ionic charge effects calc. 77−79714
macromolecule in soln., spectroscopic meas. of energy barrier to electron transfer 77−38766
MBBA, doping effect on cond. anisotropy and dynamic scatt. 77−40208
MBBA, liq. crysts., thin layers, addition of iminoxyl radicals, effect on elec. cond. *(Russian)* 78−67641
MBBA, nematic, transient elec. current obs. 77−20324
MBBA, nematic liq. cryst., charge carrier drift mobility 78−87801
MBBA-EBBA mixture, nematic liquid cryst., anisotropic effects in dielec. cond. of thick samples 79−10795
MBBA-EBBA mixtures, quinone and hydroquinone doped, dynamic scatt., elec., electro-optical props. 79−37616
metal, anomalous temp. coeff. at high temp. 78−2458
metal, conductivity calculation with regard for nonlinearity of electron-ion interaction screening *(Russian)* 78−43351
metal, electrical resistivity in short mean free path regime 79−56184
metal, electroconductivity in mag. field *(Russian)* 78−39085
metal, electron transport, nonlocal pseudopot. calc., appl. to Cd 77−1404
metal, Hall effect theory 77−47797
metal, kinetic equation for electrons for strong ion-ion interaction 77−35908
metal, Lorenz no. and thermal cond., apparatus for meas. 77−51716
metal, resistivity, thermoelectric power, Harrison nonlocal pseudopot. calcs. 78−23069
metal, review of research, phys. aspects, Knight shift elec. resist. *(Dutch)* 77−7657
metal, simple, resistivity at MP, general model pseudopot. method 77−55508
metal, thermophysical properties meas. by submicrosecond-pulse-heating method 80−52220
metal, tight binding theory of transport props., Ishida-Yonezawa approx. for single-band model 78−84190
metallic liquids, resistivity, struct. factor calcs. 78−51962
metals, Ashcroft and Schaich, and Gyorffy theories equivalence 79−60693
metals, conductivity meas. by rot. mag. field method, viscosity effect *(Russian)* 77−57349
metals, effect of multiparticles interionic correls. *(Russian)* 79−28333
metals, monovalent, divalent and trivalent, resist. and thermo-electric power using corrected parameters of Shaw model 79−19566
metals, non-simple liq., electronic props. 77−47721
metals, polyvalent, electrical resistivity by harmonic model potential 80−54668
metals, pseudopotential study of electronic props. 80−20149
metals, resist. calcs. 77−85190
metals, resistivity as function of press., nearly-free-electron model 78−84192
metals, role of multiparticle effects *(Russian)* 79−91015
metals, spin-orbit coupling and resistivity 77−85189
metals and alloys, book 78−51406
metals and alloys, cond., Hall coeff. and thermoelec. power, tight-binding model 77−47798
metals of groups IIB, IIIB, and IV, thermoelectric power, pseudopotential calc. 80−59959
methane, compressed, excess electron mobility, density depend. 77−11924
methane, fluid, electron mobility, density and temp. effects 80−10351
methane, liq., drift vel. of excess electrons 80−54744
methane, liquid, photoelectric determ. of conduction state energies and electron ranges 77−89487
methane-ethane liquid mixture, field-depend. excess electron mobility 77−89822
methanol solution in benzene, dielec. relax. time by RF cond. meas. 80−71302
methanol-n-heptane, elec. resistance, crit. phenomena, freq. depends. 79−60884

electrical conductivity of liquids continued
MHD generators, Window-Frame, with nonuniform velocity and conductivity in transverse plane, electric effects, anal. 79—68960
micelle formation of cationic surfactants, influence of perfluorinated counter-ions *(German)* 79—74423
microemulsion system, existence of bicontinuous zone 80—104466
microemulsion type systems, percolative conduction 79—100452
microemulsions, elec. cond., stirred percolation situation *(French)* 79—83512
microemulsions, light scattering, rel. tp percolation phenomena 80—104467
naphthalene-I_2 soln., elec. cond., thermoelec. power, conc. depend., 120°C 77—39845
nematic liquid crystal, volt-ampere characteristic nonlinearity *(Russian)* 79—33292
nematic liquid crystal mixtures, charge carrier transport 78—51413
neopentane, liq., excess electron mobility, elec. field depend., parity and differentiability restrictions 79—38141
nitromethane+CS_2 liquid mixture, elec. resist. crit. phenomena 77—4212
nitromethane-CS_2, crit. resist. of binary liq., 10 Hz-100 kHz 78—76123
nitromethane-CS_2, elec. resistance, crit. phenomena, freq. depends. 79—60884
noble metals, elec. resist., temp. depend. data 80—51967
noble metals, pseudopot. exam. of electronic props. 78—51960
non-polar, elec. charges 80—20217
p-n-nonyloxybenzoic acid, nematic, cond. anisotropy, dopant effect 77—7667
p-octyloxyphenyl-p′-pentyloxybenzoate, charge carrier mobility and cond. in nematic and isotropic phases 80—44347
organic liquid conductivity and bulk charge determ. cell *(Russian)* 80—57328
PAA, nematic obs. of orientation in thick layers 77—15312
PCB liquid crystal, conductivity depend. on thickness and electrode molecular orientation 78—91248
PEBAB/HEXOAB, mixed crystals, induced smectic A phases, elec. cond. 78—76068
pentane isomers, vapour and liq., electron mobility 79—72984
pentyl-cyano-biphenyl, nematic phase, transport props. of dissolved ionic species, electrochem. meas. *(French)* 79—90811
phenyl benzoate liq. cryst., doping effect on cond. anisotropy and dynamic scatt. 77—40208
polar liquids, activation energy for viscosity, rel. to charge distrib. 79—37865
polar liquids in double layer capacitors, RF conduction, ion diffusion effect 80—107883
polar molecules, viscosity activation energy and relax. time, RF cond. meas. 80—96677
polar solvents, charge transfer, general oscillator model 77—21390
pyrene-I_2 soln., elec. cond., thermoelec. power, 155°C, conc. depend. 77—39845
pyridine, macroscopic model for solvated ion dynamics, cation conductance calcs. 80—65261
pyridinium molten salts, ^{1}HNMR rel. to transport props. 77—73087
rare earth, liquid, divalent electrical resist. 79—38039
rare earth, liquid, trivalent, electrical resist. 79—42514
rare earth metals, structure factors, calc. of temp. coeff. of resistivity, one component plasma model 79—32881
rare earth metals and their alloys, elec. resist. meas. 77—51718
rare earths, resistivity 80—24865
rare-earth metals, strong-scattering theory 77—59274
reduced density metals, screening, struct. and elec. resist. 78—19016
rubidium acetate, molten, elec. cond. and density 77—15613
rubrene, in benzene soln., extrinsic photocond. kinetics 80—92691
seawater, salinity rel. to specific electrical conductivity and temp. *(Russian)* 78—16039
seawater, standards, relative conductivity and density 77—64296
semiconductor, bonding and transport properties 79—90950
semiconductor, Hall conductivity in random-phase model 80—65599
semiconductor, molten, quartz cells for elec. cond. and thermo-EMF meas. 77—74439
semiconductor melts, metallic cond. at high temp. 80—49832
semiconductors, viscosity effect on cond. meas. by rotating mag. field method *(Russian)* 77—57349
sepiolite, clay mineral in suspension, elec. cond., depend. on length 79—38520
silicate melt, effect of CoO, MnO, NiO impurities on elec. cond. *(Ukrainian)* 77—69104
silicone fluid conductivity meas. under DC field 80—15533
silicone liquid film, cond. currents obs. 79—91062
silicone oil, ionic behaviour, carrier mobility and viscosity 80—107453
simple metals, elec. resist. and thermoelec. power calc. 77—76788
sodium-caesium acetate, molten mixture, elec. cond. and density 77—15613
sodium-rubidium acetate, molten mixture, elec. cond. and density 77—15613
solvent, ion migration and frequency-dependent dielectric loss 79—19832
suspension of charged particles in ionic solutions, elec. cond. 80—7866
tetramethylsilane, liq., electron drift vel. saturation, skeletal vibr. 80—34451
thermal props. at high temp. 80—75536
thin film thickness measurement, conductometric method 80—77751
Thomson model of ion conduction, steady state characts. 77—15606
Thomson model of ion conduction, transient state anal. 77—15607
tight binding approx., Kubo formalism 79—60778
toluene, gaseous, critical and liquid, electron transport 80—64673
transition metal liquids, electrical transport 79—38040
transition metals, electronic struct. and transport props. 80—29314
transition metals, liq., and their alloys, elec. resist. using t matrix 77—31988
transition metals, liq. and amorphous, elec. transport 77—51720
transition metals, structure factors, calc. of temp. coeff. of resistivity, one component plasma model 79—32881
transition metals and alloys, elec. resistivity, Hall coeff., mag susceptibility 78—95280
transition metals and their alloys, electronic struct. and elec. resist. 77—51647
trifluoromethanesulphonic acid monohydrate, electrochemical props. and use as fuel cell 79—61969
water, supercooled emulsified droplets, relative permitt. and cond., Maxwell-Wagner interfacial polarisation 78—52423

electrical conductivity of liquids continued
water-in-dodecane microemulsions, struct. transitions in liq. cryst. phase, dielec. props. 79—28669
water-toluene-sodium dodecyl sulphate-butanol 1 mixture, interface light scatt., interface tension meas. 80—76039
xylene liq. jets induced by electrostatic field, disintegration and convergence 79—81986
Ag-Sn(Sb), liquid alloys, anomalous behaviour of electrical resistivity and thermoelectric power 77—11901
Ag-Te, liq., struct. and elec. props. 80—49083
α-AgI, activation vol. for ionic cond., appl. to molten salts 80—59711
Ag_2S and Ag_2Se melts, electrotransfer, ionic component of elec. cond., Ag ion diffusion 79—51640
Ag_2S, liquid, ionic and electronic cond., thermoelec. power 80—39329
Ag_2Se, liquid, ionic and electronic cond., thermoelec. power 80—39329
Ag_2Te, liq., elec. cond. at high temps. and pressures 79—11119
Ag_2Te, liquid, ionic and electronic cond., thermoelec. power 80—39329
$AgTlSe_2$ and AgTlSe, elec. cond. and thermoelectric power, doping effects, rel. to pseudogap model 78—2506
Al determ. in Bayer liquors by elect. cond. meas. 77—73493
Al, model pseudopotential 78—91582
Al-Zn, physical props. study by electrodiffusion method *(Czech)* 77—84956
Al_2O_3, conductivity near melting point 77—28176
Al_2O_3, molten, specific elec. cond. up to 3000K 78—2273
Ar, α-irrad., free-ion yield, geminate recomb., track model 80—24983
Ar, α-irrad., geminate recomb. of charges, hot electron thermalization length 80—20266
Ar, condensed, electron drift, Davydov electron energy distribution function, diffusion *(Russian)* 80—80339
Ar, electron drift vel., mol. solute effects 77—4338
Ar, high-field carrier transport at pre-breakdown and breakdown regions 80—25305
Ar, liq., α-particle excited carriers, geminate recombination 78—34876
Ar, liq., drift vel. of excess electrons 80—54744
Ar, liq., electron mobility, role of shallow traps 80—34440
Ar, liq., electron mobility/diffusion coeff. 80—44593
Ar-methane, liq., drift vel. of excess electrons 80—54744
As, crit. parameters determ. 77—47562
As, liq., Anderson transition, cond., at high temp. and supercrit. press. 78—34869
As_2Se_3, liq., semicond.-metal transition at high temp. and press. 77—51784
As_2Se_3, molten, temp. depend. of 10^{10} Hz elec. cond. 77—4388
As_2Se_3, solid and liq., elec. cond. meas. 77—28185
As_2Se_3-As_2Te_3, molten semicond., thermoelec. power and elec. cond. near metallic cond. transition 78—10486
As_2Se_3-As_2Te_3, solid and liq., elec. cond. meas. 77—28185
As_2Te_3, molten semicond., thermoelec. power and elec. cond. near metallic cond. transition 78—10486
As_2Te_3, solid and liq., elec. cond. meas. 77—28185
Au, electron-ion pseudopot., form factor, liquid elec. cond., phonon dispersion 78—34785
Au-Ge-Si, influence of struct. on elec. resist. of glass forming alloys 80—65518
Au-Sn(Bi)(Ga)(Ni), elec. resist. in liquid and solid state *(Russian)* 79—51549
$Au_{1-x}Si_x$, liquid, elec. resistivity as function of temp. and comp. 79—56188
$Au_{81}Si_{19}$, optical refl., 0.5 to 6 eV, hall coeff. and elec. resist. 80—29755
$Au_{1-x}Sn_x$ liq./solid alloy, resist. and percolation 80—6804
Ba, high-purity solid and liq. phases, elec. resist. and thermopower meas. 77—47799
BaO-SiO_2-TiO_2, molten, ionic elec. cond., TiO_2 effects *(Japanese)* 77—51532
BeO, molten, specific elec. resist., melting temp. to 3000K, ionic character 79—82366
Bi, electrical resistivity with spin-orbit scatt. 78—64018
Bi, liquid, elec. cond. and assoc. optical scattering 78—76040
Bi-$BiBr_3$ liquid system, miscibility gap, elec. cond. meas. 79—90790
Bi-Se, liq. chalcogenides, elec. cond. and mag. susceptibility 79—51578
Bi-Te(Se), liq. chalcogenides, elec. cond. and mag. susceptibility 79—51578
Bi_2O_3-$Mo(W)O_3$ melts, electrophys. props. 77—89817
Bi_2O_3-ZnO(CdO), elec. cond., dielec. const., mag. susceptibility meas., effect of melting transition 77—7849
C liquid, metal-non-metal transition 79—60712
CS_2 binary liquid mixtures with acetonitrile, nitromethane and acetic anhydride, crit. behaviour of elec. resist. 78—6422
CS_2+acetic anhydride, elec. resist. near crit. soln. temp. 78—71874
Ca, elec. resist. and thermopower, meas. at melting temp. 79—99524
Ca-Ag(In), liquid alloy, thermodynamic exam 78—75848
CaF_2, melts, elec. cond., surface tension, viscosity, density *(Russian)* 80—92758
CaF_2-MgO-SiO_2, melts, elec. cond., surface tension, viscosity, density *(Russian)* 80—92758
CaF_2-MgO(SiO_2), melts, elec. cond., surface tension, viscosity, density *(Russian)* 80—92758
$Ca(No_3)_2.3.91H_2O$-$NiCl_2$ melts, glass forming, transport behaviour 78—59963
CaO-SiO_2-MgO melt, elec. cond. meas., MgO behaviour *(Japanese)* 78—75857
CaO-SiO_2-MnO systems, melts, elec. cond., struct. *(French)* 79—51287
CaO-SiO_2-NiO melt, viscosity and elec. cond., effect of NiO conc. *(Japanese)* 79—23760
CaO-SiO_2-NiO-MgO glass melt, interaction of NiO and MgO, elec. cond. and IR spectra obs. *(Japanese)* 80—24632
Cd, interference function temp. depend. from X-ray diffr., elec. resist. calc. 77—47332
Cd-Zn binary systems, melts, elec. resist., 0-700°C 80—65517
$CdTl_2Se_4(Te_4)$:Au, elec. cond., density, dielectric const., changes on fusion 80—88553
Ce, liquid, resist. and thermoelec. power, t-matrix calc. 78—26840
Ce-Sn, liq., elec. resistivity negative temp. coeff., CPA calcs. 79—42515
Co, amorphous and liquid states, electronic states and transport 79—99474
Co, exploding wire, elec. resist. at high temp., submicrosec. pulse heating meas. 77—89747
Co-Ga liquid and solid alloys, elec. resistivity at high temps., partial struct. factors 80—6806
Co-Ni alloys, thermoelec. power and elec. resist. meas. 77—51719

electrical conductivity of liquids continued
- Co_5Ge_3, solid and liquid, physicochemical props. and structure 80—39548
- Cs, relativistic model pseudopot., appl. to elec. resist. calc. in liq. phase 78—51866
- Cs, saturation effect on thermo-EMF up to 1950°C and 140 atm. 77—51727
- Cs-Au, liq. ionic alloy, elec. props. 79—99338
- Cs-Au, liquid, metal-insulator transition, mag. susceptibility, Knight shift, theory 80—44672
- Cs-Sb(Au) liq. alloys, metal-nonmetal transition and change in electronic and mag. props. 77—51790
- Cs-Tl(Hg) alloy, elec. resist. meas. 77—51717
- $Cs_{1-x}Au_x$, liq., metal-nonmetal transition, electronic theory 78—79930
- Cu alloys, and thermal cond. 80—103661
- Cu, and thermal cond. 80—103661
- Cu, Krasko-Gurskii model potential, test of validity 80—39485
- Cu-Al(Ga)(In) alloys, temp. and conc. depend., model interpret. and alloy struct. *(Russian)* 80—88528
- Cu-Co(Cr)(Ni)(Ti), (1-1.3 at.%), elec. cond. exam. in solid and liquid phase *(Russian)* 77—62895
- Cu-Te, liq., struct. and elec. props. 80—49083
- Cu_3AsTe_4, elec. and thermal conds., thermo-EMF, solid and liq. states, temp. depends. 78—43384
- CuGa alloys with Mn impurities, liq., elec. resistivity 79—51545
- $Cu_{1-x}Ga_x$ liquid alloys, elec. resistivity 79—47073
- $CuInSe_2$-$CuInS_2$, melts, viscosity, elec. cond., density composition prop. graphs 79—14948
- Cu_3SbTe_4, elec. and thermal conds., thermo-EMF, solid and liq. states, temp. depends. 78—43384
- D-T, liq., dielectric constant and elec. cond. 80—84680
- D_2-DT-T_2 mixture, solid and liq., props. for fusion reactor applications 78—66415
- Dy, mag. susceptibility, elec. resistivity 80—20377
- Eu, electrical resistivity of solid and liquid phases, thermopower, melting temp. 80—59955
- Eu, liquid, resist. and thermoelec. power, t-matrix calc. 78—26840
- Fe, exploding wire, elec. resist. at high temp., submicrosec. pulse heating meas. 77—89747
- Fe, liquid and amorphous states, electronic states and transport 79—99474
- Fe particles in Hg, ferromagnetic liquid, resistivity 79—1591
- Fe-Ga (up to 50 at.%) alloy, 1200-1800°C *(Russian)* 78—6341
- Fe-Si alloys, liq., refractive index, absorpt. coeff., elec. cond. 78—43830
- Fe_3O_4 in kerosene, thermal and electrical cond. in mag. field *(Russian)* 78—6188
- Fr, properties from melting point to 7500K, prediction *(Russian)* 80—44296
- Ga, elec. resist. calc., 19 and 35°C, using calc. and expt. struct. factors *(Russian)* 78—56124
- Ga, interference function temp. depend. from X-ray diffr., elec. resist. calc. 77—47332
- GaAs, electrical conductivity and thermoelectric power charge due to melting 80—100490
- GaAs, liq., semicond.-metal transition at high temp. and press. 77—51784
- GaTe-SnTe, melt, temp. and composition dependence of elec. cond. and thermo EMF 79—95430
- Ga_2Te_3, liq., elec. resistivity meas. up to 30 kbar 79—38070
- Gd, liquid, electrical resistivity calc., spin disorder contrib. 80—6803
- Gd, liquid, resist. and thermoelec. power, t-matrix calc. 78—26840
- Gd, mag. susceptibility, elec. resistivity 80—20377
- Gd, thermal diffusivity, conductivity and elec. cond. 110 to 2100K 79—42516
- Ge-Te, As-Te, Ge-As-Te molten systems, metal-semicond. transition, cond. obs. *(German)* 77—1457
- $GeSe_2$-As_2Se_3-Sb_2Se_3, elec. cond. over wide range of temp. 80—88564
- H_2, liq., photoelectric determ. of conduction state energies and electron ranges 77—89487
- H_2, liq. metal, electron kinetic eqn. with exchange, elec. resist. 79—15131
- H_2O-acetic acid-silver acetate, ternary liq., elec. cond. and density 78—91464
- He, high-field carrier transport at pre-breakdown and breakdown regions 80—25305
- He, mag. susceptibility, elec. resistivity 80—20377
- Hg, electron density of states at 20 and 200°C 77—15754
- Hg, expanded, Knight shift interpretation in terms of electronic struct. and transport 77—43895
- Hg, expanded, thermodynamic and electron transport props. 79—23938
- Hg expanded liquid, simultaneous investigation of eqn. of state and elec. cond. 77—55337
- Hg, liq., elec. cond. and thermoelec. power meas. 77—59273
- Hg, liq. and dil. liq. amalgams, elec. cond. and thermoelec. power 77—55511
- Hg, melting line determ., pressures up to 1200 MPa 80—84281
- Hg, optical and elec. effects during solidification 78—47502
- Hg, resistivity from X-ray diffr. struct. at —30 to 290°C 79—46551
- Hg, supercritical, elec. cond., four electrode method 80—62685
- Hg, supercritical vap., semicond. model 77—51154
- Hg-Au(Tl)(Bi), liquid dilute amalgams, elec. cond. and thermoelec. power 78—51976
- Hg-Cd liq. amalgam, elec. cond. and thermoelec. power meas. 77—59273
- Hg-In (3 at.%), amalgam, thermodynamic and electron transport props. 79—23938
- Hg-In-Bi, liquid alloy, elec. resist. *(Russian)* 79—51544
- Hg-Na (3 at.%), amalgam, thermodynamic and electron transport props. 79—23938
- Hg-Tl, liq. alloys, struct. from elec. cond. 77—1067
- Hg-Zn(In)(Pb), dil. liq. amalgams, expanded, cond. at high temps. and press. 77—20287
- $HgCl_2$, solid and molten state, elec. conductance, relative behaviour 79—33113
- HgI_2, solid and molten state, elec. conductance, relative behaviour 79—33113
- In, liq., thermal props. at high temp. 80—75536
- In-Hg amalgam, thermal and electric cond., temp.-conc. depend. 78—43349
- In-Te alloys, transport props. interpret. using effective-medium theory 77—76806
- In-Zn binary system, melts, elec. resist., 0-700°C 80—65517

electrical conductivity of liquids continued
- InAs, electrical conductivity and thermoelectric power charge due to melting 80—100490
- InP, electrial props. at high temp. and in liquid state 77—11888
- InS(Se)(Te), fused, charge transfer nature 77—89757
- InTe-SnTe, melt temp. and composition dependence of elec. cond., and thermo EMF 79—95430
- In_2Te_3, liq., elec. resistivity meas. up to 30 kbar 79—38070
- Ir complexes with adenosine, xanthosine, prep., elec. cond., IR spectra, characterisation 78—92065
- Ir, thermophysical props. at temps. up to 7000K 80—103497
- K, liq. elec. resistivity calcs. 78—79974
- K, liquid, electrical resistivity, effect of inter-electron interactions *(Russian)* 77—24546
- K-Rb, liq., elec. resistivity, temp. depend. 78—39084
- K-Rb, liq., form factors and transport coeffs., pseudopot. perturb. theory 80—44561
- K-Rb(Cs), resistivity calc. using general model pseudopot. 77—55506
- K-Tl alloy, elec. resist. meas. 77—51717
- KH_2PO_4, aq. soln., elec. conductance in saturation region, effect of light *(Polish)* 80—10983
- KNO_3-$Cd(NO_3)_2$ molten mixtures, elec. cond. 79—90813
- KNO_3-TlBr, fused mixture, coexistence curve and elec. cond. 77—20071
- Kr, electron drift vel., mol. solute effects 77—4338
- Kr, liq., electron mobility, role of shallow traps 80—34440
- Kr, liq., excess electron mobility, Cohen-Lekner theory failure 78—19112
- La, liquid, resist. and thermoelec. power, t-matrix calc. 78—26840
- Li alloys, liq. semicond., electronic struct., resistivity and thermoelec. power 77—51753
- Li, liq., elec. resistivity and thermoelec. power, orthogonalisation hole pseudopotential calc. 80—29376
- Li, phonon frequency, liquid electrical resist. and interionic pair potential 78—10140
- Li-Au(Hg)(Tl)(Pb)(Bi), liq. semicond., electronic struct., resist. and thermoelec. power meas. 77—47712
- Li-Cd alloy, elec. resist. and Knight shift 80—75537
- Li-In, liquid alloy, elec. resist., Knight shift of ^{115}In and ^{7}Li nuclei 79—11352
- Li-Mg, liq., elec. transport props. and phase diagram 78—23070
- Li-Mg, liq. alloy, thermoelec. power and elec. meas. 77—47788
- Li-Mn liquid alloys, form factor effects, pseudopotentials, resist. calc. 80—103608
- Li-NH_3, conc. solns., elec. cond. and thermoelec. power 79—19640
- Li-Na, liq. alloy, thermoelec. power and elec. resist. 77—47788
- Li-Pb liquid alloys, elec. resistivity, negative temp. coeff. 80—88527
- LiD, soln. in liq. Li, elec. resist. 77—47786
- LiF binary binary molten salt systems with NaF, KF, CaF_2, BaF_2 *(Japanese)* 77—76588
- LiH, soln. in liq. Li, elec. resist. 77—47786
- LiN, soln. in liq. Li, elec. resist. 77—47786
- $Li_{1-x}Pb_x$, liq., metal-nonmetal transition, electronic theory 78—79930
- Lu, elec. resist. up to 1800°C, rel. to elec. struct. 78—39083
- MBBA(:TEAI), elec. drift mobility, carrier identification *(Korean)* 78—51998
- Mn-Ge (5 to 90 at.%) liquid alloy, electrical resistivity *(Russian)* 77—55509
- Mn-Sb(Sn)(In), liq., elec. resist. meas. 77—51721
- Mo, elec. resist., melting pt. to boiling pt., temp. depend. 80—96839
- Mo, liquid, thermophysical measurements up to 4300K 78—43136
- Mo, liquid and solid, thermophysical props. 78—75808
- N_2, high-field carrier transport at pre-breakdown and breakdown regions 80—25305
- N_2, liq., photoelectric determ. of conduction state energies and electron ranges 77—89487
- NH_3-metal, soln., thermophysical props., review 79—77758
- Na, electrical resist. temp. depend. calc. 77—55507
- Na, linear pot. and elec. resist., calcs. 80—65519
- Na, liq., elec. resistivity calcs. 78—79974
- Na, liquid, electrical resistivity, effect of inter-electron interactions *(Russian)* 77—24546
- Na, role of multiparticle effects *(Russian)* 79—91015
- Na-Cs, liq. alloy, thermoelec. power and elec. resist. 77—47788
- Na-Ga alloy, mag. susceptibility and elec. cond. *(Russian)* 80—29522
- Na-K(Cs), liq., form factors and transport coeffs., pseudopot. perturb. theory 80—44561
- Na-K(Rb)(Cs), resistivity calc. using general model pseudopot. 77—55506
- Na-Te, chemical pot. and resist. 77—55232
- Na-Tl alloy, elec. resist. meas. 77—51717
- NaH solution in liq. Na, elec. resist. and solubility 79—14934
- $NaNO_3$-KNO_3-$Ca(NO_3)_2.4.09H_2O$ melt, mixed alkali effect 80—34219
- $NaNO_3$-$TlNO_3$-$Ca(NO_3)_2.4.09H_2O$ melt, mixed alkali effect 80—34219
- Na_2O-SiO_2-MgO melt, elec. cond. meas., MgO behaviour *(Japanese)* 78—75857
- Na_2O-SiO_2-NaF, elec. cond. of melt, and IR absorpt. spectra of glassy phase *(Japanese)* 77—62657
- Na_2O-SiO_2-NiO melt, viscosity and elec. cond., effect of NiO conc. *(Japanese)* 79—23760
- Nb, specific elec. resistance, 200-2700K 78—39088
- Nb-K melts, thermodynamic characts., elec. resistivity, single parameter rigid sphere calcs. *(Russian)* 80—34410
- Nb_2O solution in liq. Na, elec. resist. 79—14934
- Ne, electron drift vel., mol. solute effects 77—4338
- Ni, electronic struct. and transport props. 80—29314
- Ni, exploding wire, elec. resistivity in fast RCL circuit 77—31995
- Ni, exploding wire, elec. resist. at high temp., submicrosec. pulse heating meas. 77—89747
- Ni-Ge alloys, liq., integrated emissivity, electric resistivity 78—43155
- Ni-Te, liq., struct. and elec. props. 80—49083
- Ni_5Ge_3, solid and liquid, physicochemical props. and structure 80—39548
- O_2^-, in nonpolar liqs., laser photodetachment, elec. cond. obs. 79—64057
- Pb, electrical resistivity, 300-1050K 80—24868
- Pb, electrical resistivity with spin-orbit scatt. 78—64018
- Pb, liq., elec. resist. calcs., pseudopot. depend. 80—96840
- Pb, liq., elec. resistivity, 600-860K 79—56180
- Pb, melting curve, elec. resist. determ. at high pressure 80—49337
- Pb, relativistic model pseudopot., appl. to elec. resist. and phonon spectra calc. 78—51866
- Pb, temp. depend., calc. 78—14701
- Pb-Bi alloy, liq., thermal cond. and elec. resistance up to 900°C 77—47785

electrical conductivity of liquids continued
Pb-S melt, absolute thermo-emf obs. 77—85251
PbO-PbCl$_2$-PbS, liquid system, elec. cond. meas. 78—43162
PbO-SiO$_2$ melt, behavior of MgO and NiO *(Japanese)* 79—52746
PbO-SiO$_2$ optical glass melts, resistivity rel. to viscosity 77—76589
PbO-SiO$_2$-NiO-MgO glass melt, interaction of NiO and MgO, elec. cond. and IR spectra obs. *(Japanese)* 80—24632
Pd, elec. resist., temp. depend. data 80—51967
Pd, electrical resist. calc. using muffin-tin pots. 77—69287
Pd, liq., energy bands and electronic density of states, resistivity 78—34755
Pd, liq. and solid, thermophysical props. 78—75808
Pd-Au-Si, influence of struct. on elec. resist. of glass forming alloys 80—65518
Pd-Si(—Cu), glassy, liq. and cryst., mag. and elec. props. 77—66249
Pt, thermodynamic characterisation, by isobaric expansion meas. 80—103494
Rb, electrical resist. temp. depend. calc. 77—55507
Rb, expanded liq., struct. factor, cond. calc. using NFE model 77—47335
Rb, liquid, expanded, eqn. of state, transport up to 1700°C, 400 bar 80—2136
Rb, simultaneous meas. of density, elec. cond., absolute thermopower up to 1400°C and 400 bar 77—1402
Rb, static struct. and electronic transport props., pseudopotential calc. 79—7543
Rb-Cs, liq., elec. resistivity, temp. depend. 78—39084
Rh complexes with adenosine, xanthosine, prep., elec. cond., IR spectra, characterisation 78—92065
Ru complexes with adenosine, xanthosine, prep., elec. cond., IR spectra, characterisation 78—92065
S, conductivity meas. from melting point to 900°C 78—84209
S, liq., elec. cond., 300 to 900°C 79—91050
S, single liq. droplet, optical transmission and elec. resist. changes on polymerisation 77—35460
Sb$_2$S$_3$-SnS, Sb$_s$S$_3$-As$_2$S$_3$, fused mixtures, resistivity 77—80815
Sc$_2$O$_3$, liq. and solid phase elec. cond., high temp. meas. 80—84468
Sc$_2$O$_3$, solid and liq. phases, thermophysical and electrophysical props. 80—103495
Se, electrical cond. transition at high temp. and press., Anderson localisation *(Russian)* 77—1462
Se, electronic transport props. at sub- and supercritical conditions 77—51788
Se, electronic transport props., equation of state, to 1900K and 1800 bars 80—65574
Se, liq., Anderson transition, cond., at high temp. and supercrit. press. 78—34869
Se, liq., dielectric relax. and elec. cond. 80—108150
Se liquid, pure and I doped, DC cond. and thermoelectric power *(French)* 79—56223
Se, liquid-crystal phase transition, elec. cond. changes 79—33310
Se, pure and I doped, DC cond., temp. depend. *(French)* 77—69322
Se-Na, and Se, liqs., elec. resistivity and phase separation 79—82573
Se-Te alloys, liq., electronic props., mag. susceptibility meas. 79—95567
Se-Tl-S alloys, liq., dielectric relax. and elec. cond. 80—108150
Sn, elec. resist. calcs., 232, 450 and 650°C, using calc. and expt. struct. factors *(Russian)* 78—56124
Sn, electron transfer of rare earth impurities *(Russian)* 78—95278
Sn, interference function temp. depend. from X-ray diffr., elec. resist. calc. 77—47332
Sn, Lorenz number and thermal cond. meas. 77—51716
Sn-rare earth, dil. liq., elec. resist. and mag. susceptibility 78—43350
Sn-S melt, absolute thermo-emf obs. 77—85251
Sn-Te, molten, elec. cond. and phase diagram 80—84454
Sr, elec. resist. and thermopower, meas. at melting temp. 79—99524
Sr, soln. in liq. Na., elec. resistivity, conc. depend. 78—84188
Ta, electrical resistance temp. depend. in solid and liq. states, 2200-4200K 78—10415
Ta, liquid, thermophysical measurements up to 7500K 78—43136
Tb, mag. susceptibility, elec. resistivity 80—20377
Te, elec. cond. at high temps. and press. 77—55592
Te, liq., elec. resistivity meas. up to 30 kbar 79—38070
Te, metallic cond. region, calc. using modified Ziman theory *(Russian)* 77—66149
Te, semicond.-metal transition at high temp. and press. 77—51784
Te-Co(Cr)(Au)(Ag), dil. liq. alloy, elec. cond. at high temp. and press. 78—87959
Te-Sb, liq., elec. cond. 78—84186
Te-Se liq. semicond., resist. meas. under high press. 77—51791
Te-Se mixtures, liquid, electrical conductivity and thermoelectric power, high temps. and pressures 80—39639
Te-transition metal, dilute, elec. resist., cond. electron conc. 77—15814
Te-transition metal, liq. semicond., elec. props. 80—96870
Ti, elec. resist., melting pt. to boiling pt., temp. depend. 80—96839
Ti, molten, reson. model calc. of elec. resist. 78—84189
Tl, electrical resistivity, 300-1050K 80—24868
Tl, liq., thermal props. at high temp. 80—75536
Tl-Pb, in solid and liquid state, specific electric resistance 80—103662
Tl-S melts, Hall effect 77—85239
Tl-Te, liq. alloys, mag. susceptibility rel. to elec. cond. and density of states 77—51880
Tl-Te, liquid alloy, miscibility gap 79—10952
Tl-Te liq. semicond., resist. meas. under high press. 77—51791
TlAsS$_2$(Se$_2$)(Te$_2$), elec. cond. and thermopower in solid and liquid states 77—89764
Tl$_2$Se$_3$, elec. cond. and thermoelectric power, doping effects, rel. to pseudogap model 78—2506
Tl$_2$SeAs$_2$Te$_3$, molten, temp. depend. of 10^{10} Hz elec. cond. 77—4388
TlTe, melt, elec. cond., surface tension, microhardness, influence of impurities 80—88551
Tl$_2$Te, liq., elec. resistivity meas. up to 30 kbar 79—38070
Tl$_2$Te, melt, resistivity, surface tension, microhardness, influence of impurities 80—88552
Tl$_2$Te$_3$, exam. of electrical props., density and viscosity, for solid or liquid states 79—95431
Tl$_2$Te$_3$, exam. of electrical props., in solid, liquid state 80—54686
Tl$_2$Te$_3$:Ag(Sn), effect of dopant on electrical props., density and viscosity, for solid or liquid states 79—95432
Tl$_x$Te$_{1-x}$, liq. semicond. alloy, mag. susceptibility rel. to diffusive transport 77—20541
Tl$_x$Te$_{1-x}$, rigid band behaviour, elec. cond. and thermopower 77—35845

electrical conductivity of liquids continued
Tl$_x$Te$_{1-x}$, thermodynamic evidence against large scale fluctuations in composition in heterogeneous transport models 77—28172
Tl$_2$(Te$_x$Se$_{1-x}$) mixtures, magnetic susceptibility and elec. cond. 80—88715
V, elec. resist., melting pt. to boiling pt., temp. depend. 80—96839
V, thermophysical props. at temps. up to 7000K 80—103497
V$_2$O$_5$ containing melts, activation energy of electron mobility and electronegativity 77—35971
V$_2$O$_5$ type liquid semiconductor, elec. props. control, by O$_2$ partial press. *(Russian)* 78—72142
W, density at onset of sharp fall in elec. cond. 79—33026
W, elec. resist., melting pt. to boiling pt., temp. depend. 80—96839
Xe, liq., electron mobility, role of shallow traps 80—34440
Y, electrical resistivity of solid and liquid phases, thermopower, melting temp. 80—59955
Y$_2$O$_3$, liq. and solid phase elec. cond., high temp. meas. 80—84468
Y$_2$O$_3$, specific elec. cond., m.p. to 3200K, activation energy 78—43383
Yb, liquid, resist. and thermoelec. power, t-matrix calc. 78—26840
Zn, interference function temp. depend. from X-ray diffr., elec. resist. calc. 77—47332
Zn, structure factor, 460 to 650°C, by neutron diffr., elec. resist. temp. coeff. 77—47333
Zn-Bi(Sn) alloys, specific elec. resist., temp. and conc. depend., 20-800°C 79—82571
ZnGeAs$_2$, elec. cond. in solid and liq. state 77—11912

electrical conductivity of one-dimensional systems *see one-dimensional conductivity*

electrical conductivity of plasmas *see plasma transport processes*

electrical conductivity of solids
see also electrical conductivity of amorphous metals and alloys; electrical conductivity of amorphous semiconductors and insulators; electrical conductivity of crystalline metals and alloys; electrical conductivity of crystalline semiconductors and insulators; electronic conduction in crystalline semiconductor thin films; electronic conduction in insulating thin films; electronic conduction in metallic thin films; ionic conduction in solids; recovery; superconductivity
alloy, binary, elec. resist. depend. on LRO, SRO and composition, inhomogeneous order effects 79—60781
alloy, binary, ordering, residual resist. in CPA *(Russian)* 77—24545
alloy, with off-diagonal randomness, phonon-modulated electronic transport 77—15813
alloys, disordered, temp. depend. of elec. resist., force-correlation functions 79—51542
Anderson localisation, transport props. of 2D disordered electron systems in strong mag. fields 78—95318
Anderson model, direct interaction between impurities 80—54681
Anderson model, electrical resistivity, for wide range of Coulomb coupling parameters 80—2373
Anderson model, non-orthogonal elec. resist. 80—59947
Anderson model, simple averaged DC conductivity, numerical calc. 79—99522
anisotropic percolation, square random network conductivity *(French)* 80—68142
antiferromagnet, crit. resist. below T_c 78—68004
antiferromagnet, effect of inelastic scatt. on resistive anomalies at mag. crit. points 77—55675
articulated medium, elec. and thermal cond. anisotropy, crack density tensor 77—55505
baked C mixes, anthracite, petroleum, metallurgical and pitch cokes as fillers, chracteristics study 79—57052
basalts, Indian, elec. cond. meas., 475-1100K 78—69336
basalts, oceanic, elec. resistivity meas. 80—21713
binary crystals, electrical conductivity versus interatomic bond character 80—59948
binary mixtures, near percolation threshold, expt. model *(French)* 79—1589
biological membranes as two-dimensional conductors *(Russian)* 78—23190
bipolar conductivity equations, approx. solns. 77—69336
bipolymer, electronic transport mechanisms, asymmetry role 78—6370
Bloch electrons in constant electric field, wave packet evolution 79—87073
body with large number of cracks, effective cond. taking into account capacitance and action of mech. loads 80—84242
Boltzmann eqn., phonon and electron transport in bounded systems 80—39545
bond-disordered conductance lattices, real-space renormalisation 79—7812
bond-type disorder system, electrical cond. and electron localization calcs. 78—2475
bootstrap percolation conductivity on Cayley tree 80—54743
brain tissue, dog, dielectric props. between 0.01 and 10 GHz 80—16915
Brownian motion in periodic potential, in presence of temp. and elec. potential gradients 80—4650
carbographite mats., elec. cond. temp. depend. 77—43592
casein-methylglyoxal complex, electronic props. 77—52736
CDW condensates in two and three space dimensions, nonlinear conduction mechs. 79—60807
cellulose acetate membrane, asymmetric, elec. and electroosmotic transport behaviour in dialysis-osmosis expts. 80—108745
cermet, tunnel cond., temp. depend. 77—20467
cermet film, elec. props. 77—66209
cermet film granular media, dielectric function theory, permittivity, percolation transport props. 80—88498
charge-ordered systems, cond. at const. elec. field 78—19013
chemical reaction of powdered reactants, elec. cond. var. *(German)* 80—34494
Clausius-Mossotti problem for cubic arrays of spheres 78—52422
coal, dielectric relaxation and conductive impurities 79—82921
composite, unidirectional, percolation in thin ply 79—42511
composite material, cubic arrangements of spherical particles in isotropic matrix, effective conductivities 78—55547
composite materials, phys. props. review 77—4720
composite medium, specific macroscopic conductivity, analytic props. 79—82569
conducting mixtures, percolation threshold, real-space rescaling approx. 77—40073
conductive filler polymer composites, theoretical study 79—19585

electrical conductivity of solids continued
conductive filler-polymer composite conductivity theory *(Japanese)* 78—11351
conductivity film, effect of slits on resist. 80—44740
conference on elec. transport and optical props. of inhomogeneous media, Columbus, USA (Sep. 1977) 78—56114
contact phenomena incorporation in electrodynamics eqns. 80—29374
Coulomb relaxation of electrons with oriented spins 80—6801
cracked solid, elec. cond. calc. 79—91117
critical resistivity of mag. solids 79—42213
crystal, spherical integral reps. for cond. of abruptly activated current 80—42080
crystal optics, relativistic phenomena 80—46839
crystalline films, dispersion law and struct. transition, Fermi line geometry, acoustic spectrum, resist. min. *(Russian)* 79—7764
cubic array of identical spheres, dielec. const. calc. 80—25271
cubic lattice modelling for permittivity and conductivity 77—16236
cubic lattice of spheres, cond. determ. 78—28964
cylinders, perfectly conducting arrays, transport prop. investig. 80—13011
cytochrome c anhydrous film, electrical conductivity 77—44879
DC current flow through symmetrically supplied sphere *(Polish)* 78—10414
DC electrical conductivity, microscopic fields and currents 78—56121
DC resistivity as functional of generalised dynamical susceptibilities, solid state model 79—28330
Debye solid, amorphous and disordered harmonic, struct. factors 78—9954
degenerate semiconductors and metals, cond. current and generalised Einstein rel. 77—15810
degenerate states, electron transport, rel. to Jahn-Teller effect 77—31987
dielectric, difference between electrification and resorption currents 77—62932
dielectric matrix with spherical metallic inclusions, permittivity, conductivity 78—48108
dielectrics, current injection method appl. *(Portuguese)* 80—20179
dielectrics, drift dominated conduction model, transient anal. 77—43583
dielectrics, elec. and mech. props. at increased temps., meas. equipment 77—71342
dielectrics, electric field enhanced conductivity 77—35951
dielectrics, inorganic, transfer processes, theoretical model review 80—15529
disordered alloy, quantum transport theory, CPA 77—20282
disordered alloy, soln. of generalised Kadanoff-Baym's kinetic eqns. *(Russian)* 78—43346
disordered alloys, influence of strong hybridization on elec. cond. 79—11097
disordered alloys, transport phenomena theory, coherent pot. approx. 78—87958
disordered binary substitutional alloys, elec. cond., two band model 78—14699
disordered binary substitutional alloys, elec. cond. of two-band metals 78—19014
disordered electronic system, scaling theory of localization and non-ohmic effects in two dimensions 80—44539
disordered electronic systems, spin interaction effects, loop expansion and exact relations among local gauge invariant modes 80—80221
disordered Fermi systems, in two dimensions, interaction effects 80—75655
disordered gyrotropic systems, cond. tensor, freq. depend. in presence of mag. field 80—44631
disordered material, elc. cond. and density of states, scaling relations 79—28329
disordered materials, fluctuation-induced tunnelling cond. 80—65516
disordered media, inhomogeneous transport, continuum theories 77—20283
disordered metals, conductivity electrons and elastic scatt. by static inhomogeneities *(Russian)* 80—29375
disordered solids, electronic props., numerical methods 80—44538
disordered system, AC cond. tensor in mag. field 80—92870
disordered system, conductivity and mobility edge, square and diamond lattice calc. 78—43347
disordered system, conductivity near mobility edges 78—76038
disordered system, DC cond., numerical calc. 78—23066
disordered system, particle diffusion in Anderson model 79—33273
disordered system, residual resistivity 78—87954
disordered system with n orbitals per site, n=infinity limit 79—60768
disordered system with n orbitals per site 1/n expsn. 79—90999
disordered systems, Anderson localisation theory in two dimens., real space scaling method 80—44540
disordered systems, bond-type, elec. cond., effects of fluctuations of transfer energies 77—80757
disordered systems, cluster approx. in theory of AC hopping cond. 80—2372
disordered systems, static. cond. at zero temp. and localisation of states 77—51715
disordered systems, tight binding approximation in Kubo formalism 79—60778
disordered two-phase materials, site percolation approach to transport props., effective medium theory 77—61032
dissipative conductivity, effect of collisions between current carriers *(Russian)* 78—34816
dissipative conductivity determined by carrier-carrier collisions 79—60780
dithiocarbamate complexes of Cr, Mn, Sn and Pb IR, electronic and mass spectra, mag. susceptibility, cond. meas. 80—97270
double injection in solids with traps nonuniformly distributed in energy and space theory 77—8116
dunite, elec. cond during shock compression from 12.5 to 45 GPa 78—85536
effective-medium theory appl. to resistor networks, elec. network theory 79—87074
electric current, determ. by time correlation functions force-force and force-momentum 78—95274
electric current, determ. by time correlation functions force-force and force-momentum, pseudopot. method 78—95275
electrolytes, solid oxide, elec. props., study methods *(French)* 80—22386
electron gas, interacting, elec. cond. 78—95276
electron gas, semi-infinite, nonlocal cond. tensor calc., effective optical surface region 80—20283
electron scattering due to screw dislocations 78—60101
electron transport, local electric field, appl. to electromigration 78—30896

electrical conductivity of solids continued
electron-impurity system, elec. cond. anomalous behaviour, Coulomb interactions 79—95381
electronic transport coeff., soln. between Mori-Green-Kubo formulae and Boltzmann approx. 78—79971
epoxy adhesive, A, filled, electrical cond. development by heat treatment 79—73559
epoxy polyester, PE-933, metal-filled, elec. cond., theory and expt. 80—60057
epoxy-resin, mica flake filled, thermal depolarisation currents and DC cond. studies 80—7282
fatty acid, AC and DC cond. 78—56239
fermion gas moving in strong three-dimens. random pot., conductivity 79—56130
ferromagnet, effect of inelastic scatt. on resistive anomalies at mag. crit. points 77—55675
ferromagnet, elec. resist., just below crit. temp., effect of mag.-domains 80—39557
fibre reinforced composite, single ply, thickness effect on percolation and conductivity 80—92953
fibre reinforced composites, thermal and electrical conductivities *(German)* 77—28053
film, Cottey conduction model extension 78—84183
film, inhomogeneous, galvanomagnetic props. 79—69608
film, physical interpretation of specularity parameter 78—72282
film, Ziman approx. appl. 77—59338
frequency dependence in disordered system two site model *(Russian)* 80—54666
fuel rod, simulated, for HTGR, pre- and postirradiational thermal transport and thermal expansion 79—6742
glass fibre reinforced epoxy resin composites, 2 to 290K 79—60528
grain-boundary joint, resist. calc. by pseudopot. method *(French)* 79—51539
granite core samples, methods using electrode configurations without necessity for access to sample end faces 79—67345
granular materials, thermal and elec. cond. calcs. 77—50865
graphite, intercalation compound with AsF$_5$, high elec. cond. 78—26838
graphite, intercalation compounds with AsF$_5$, elec. cond. meas. with high anisotropy 78—26837
graphite compound, metallic electronic props. and correl. with chemistry 80—44567
graphite fibre, electrical hazards 79—91111
graphite intercalates with alkali metals, basal plane elec. resist. 80—44685
graphite intercalation compounds, C$_n$K, electronic struct. and elec. props. 80—44471
graphite intercalation compounds, electronic props. review 78—30860
graphite intercalation compounds, props. and appls. 78—71711
graphite intercalation compounds struct., elec. props. 78—27446
graphite intercalation compounds with alkali metals and halogens, physical props. 78—31050
graphite intercalation compounds with K, Rb, Cs, resistivity anomalies and phase transform. 78—26839
graphite intercalation cpds., C$_n$K, de Haas-van Alphen effect, cyclotron reson., and transport props. 80—44479
graphite intercalation cpds., electronic props. 78—34744
graphite intercalation cpds., high elec. cond., engineering appl. 80—70780
graphite intercalation cpds. with AsF$_5$ and SbF$_5$, synthesis and elec. props. 80—70781
graphite nitrates, elec. props. perpendicular to layers, resistance, magnetoresistance, charge transport mechanisms 80—80268
graphite salts, $C_8^+MF_6^-$, (M=Os,Ir,As), struct. and elec. props. 80—70183
graphite-alkali metal intercalation cpds., electronic props. 80—45202
graphite-nitrate residue compounds, phys. props. 78—10199
graphite-SbCl$_5$(F$_5$) intercalation compounds, elec. resist., comp. and temp. depend. *(French)* 77—62971
graphite-SbF$_5$(Cl$_5$) intercalation compounds, compacts, elec. resistivity, C fluorination 80—34493
graphite-SbF$_5$ intercalation compounds, elec. cond. and opt. reflectance 77—62970
graphite-SbF$_5$ intercalation cpd. 77—43549
graphite-SbF$_5$/Cu intercalated composite wires, elec. cond. 80—44687
graphite/epoxy composite, single ply, elec. cond. meas. 80—92953
graphitised PAN fibre layered compounds with metal chlorides 79—91600
heat conduction, calc. via elec. analogue 77—72128
heterogeneous material, crit. behaviour of complex dielec. const. near percolation threshold 78—19012
heterogeneous matrix system, generalised conductivity and loss, tangent 80—7289
heterogeneous systems with disordered structure, generalised cond. coeffs. 79—87075
hopping conduction, master eqn. approach in presence of mag. field 80—103697
Hubbard chain, low temp. conductivity 78—47755
Hubbard model, conductivity and characteristic temp. 77—32150
Hubbard model, doubly-degenerate, elec. cond. calc. 77—20284
Hubbard model, elec. cond. in single narrow energy band 77—1400
Hubbard model, one-dimens. half-filled band Holstein-Frolich modified, transport props. 78—23237
Hubbard model, random one-body approx., higher dimens. lattices 79—37945
Hubbard model, strong-coupling non-half-filled band 78—43348
ice, thermal and electrical conductivity, 0 to −20°C 77—24450
ice DC resistivity and recrystallisation of glacier ice 80—36348
impurity effects on electron-hole pairing, thermodynamic and kinetic props. *(Russian)* 77—69318
impurity scattering in quantised mag. field *(Russian)* 78—47752
inclusions, formation, role of const. elec. current, elec. field distrib. *(Russian)* 77—55504
inflowing structure, Anderson localisation, elec. cond. temp. depend. *(Russian)* 80—103639
inhomogeneous conductors, cond. anisotropy and Hall effect near percolation threshold 80—107755
inhomogeneous conductors, cond. exponents, dimensionality depend. scaling relations 80—49684
inhomogeneous conductors, resistor networks, cooperative phenomena 78—56118

electrical conductivity of solids continued
- inhomogeneous materials, effective medium theory with dipole-dipole interactions 79−4544
- inhomogeneous media, elec. transport, optical props., exact theory 78−56119
- inhomogeneous media, electrical cond., review 78−56115
- inhomogeneous media with macroscopic inclusions, var. estimate 80−49685
- inhomogeneous mixtures, theory *(German)* 79−51538
- insulating and conducting particles mixture, percolation problem 78−60097
- insulator, radiation induced cond., analytic solns. 77−80781
- insulator-conductor mixed system, percolation theory of conduction 77−20285
- intercalation compounds, props., review *(Japanese)* 80−49838
- intercalation compounds 78−26836
- isothermal method in transport processes 80−29373
- isotopically disordered vibr. crystal quantum transport eqn., electron-phonon coupling 78−39081
- Israel Physical Society 1980 annual meeting, Rehovot, Israel (April 1980) 80−94909
- jointed granite in situ, resistivity and elastic props. 77−66909
- lamellar synthetic metals, low scatter conduction of electric charges 78−23068
- lattices of spheres, elec. cond. calcs., BCC, FCC, disordered array 78−72126
- layered compounds, book 77−39757
- layered materials and intercalates, International Conference, Nijmegen, Netherlands (Aug. 1979) 80−36771
- layered structures, intercalation, crack propag. theory 80−97559
- LF electromagnetic wave meas. method, soil resistivity appl. *(French)* 78−24394
- light scattering in solids, general theory 79−61324
- linear chain of oscillators, disordered, physical props., Monte Carlo approach 77−4177
- linear defects, local phonon modes and structural instability *(Russian)* 79−73275
- linear response theory and area preserving mappings, review 78−62174
- Lloyd's disorder model in one dimension, elec. cond. 79−60779
- localised states, transport eqn. determ. *(French)* 77−72845
- lossy dielectric material containing short randomly distributed metal fibres 80−20584
- magnetic semiconductors, critical behaviour of electronic properties, theory 80−96861
- magnetic systems, anomalous resistivity maxima 78−79977
- magnetic systems, crit. behaviour 78−87955
- many-valley semiconductor, electron-electron scatt., memory function 80−10967
- materials containing partial melts, simple cond. model from Archie's law 79−100810
- metal, isotropic Fermi surface, cond. tensor calc., cyclotron waves 79−42528
- metal fibre filled polymer, mech. and cond. props. 79−91808
- metal particle, 9 Å, in zeolite matrix, melting temp. 77−59103
- metal powders, compressed, elec. sintering processes *(German)* 80−25598
- metal-polymer films formed by electron-beam polymerisation, cond. control 78−48331
- metallic fibre reinforced composite materials 80−100450
- metallopolymer composite with var. elec. cond. 77−43676
- metals, Bloch theory agreement and limitations 79−28332
- mobility edge, classical solns. and crit. exponents 80−10936
- mobility edge problem, continuous symmetry 80−10939
- molecular solid, electronic polaron, excess electron transport, polarisation dynamical self consistency depend. 79−47030
- Mott's formula for thermopower and for Wiedemann-Franz law 80−84462
- Mott magnetic semiconductor, freq. depend. elec. cond. 77−11907
- multicomponent percolation, conduction 80−92871
- multilayer assembly, freq. depend. cond., electron transitions between localised states 77−43699
- multiphase material, average bulk props. calc., bounds 77−16237
- narrow-band solids, elec. cond. and thermoelec. power, evaluation from effective one-electron representation 79−56112
- neutron irradiated cellulose acetate rel. to personnel dosimetry 77−40776
- nonuniform systems, effective conductivity from percolation and conduction theory 80−62597
- one dimensional disordered system, cond. and electron localisation 80−103658
- one-dimensional electron system, distorted, dynamical elec. cond. calc. 80−59962
- open electron-phonon system, statistical electron transport theory 79−11096
- organic free-radical solid conductors and semiconductors, electronic structure 79−35496
- paper, non-impregnated, non-destructive breakdowns 80−55035
- Peierls systems with dil. impurities, microscopic theory of pinning effect 77−15837
- percolation application to mixture of conducting and insulating spheres 78−47753
- percolation backbone problem, large cell renormalisation group 79−69481
- percolation conduction anisotropy 78−39082
- percolation conductivity, continuous, numerical simulation 77−24544
- percolation conductivity exponents, distrib.-induced non-universality 79−82570
- percolation conductivity in anisotropic systems, infinite cluster struct. 79−93063
- percolation in square lattice, temp. depend., effective medium theory 80−96837
- percolation lattice, diffusion, random walk method, Monte Carlo method 78−60098
- percolation model, three component, reactive, conductivity calc., $Na_x(NH_3)_{1-x}$ appl. 78−68003
- percolation network samples, cond. near crit. point 80−105578
- percolation problem, recursion eqn. *(Russian)* 79−38038
- percolation problem, two-dimens., crit. indexes of cond. 77−62964
- percolation threshold, computer generated pictures of infinite clusters 78−56117
- phonon inelastic interband scatt. in transport effects 77−43552
- phonon-free DC conductivity, disordered systems *(Russian)* 77−89745

electrical conductivity of solids continued
- phosphate glass-Al alloy seals, elec. and mech. props., glass transition 80−81018
- photodielectric layer, Laplace transform of small-charge current, trapping level parameters 77−69337
- plasma, nondegenerate, dense, electron transport *(Russian)* 79−98865
- polyacetylene, doped film, elec. cond. 80−24921
- polyacetylene-I_2, highly conducting, Raman, XPS and X-ray diffr. obs. 78−80454
- polyaromatics, elec. cond. correl. with chem. struct. and synthesis, charge transfer complexes *(German)* 80−15514
- polycrystalline film gauge factor linearisation 79−78209
- polycrystalline materials, macroscopic elec. cond. determ. 79−99521
- polycrystals, statistically isotropic, bounds of conductivity 77−24541
- polymer, metal-filled, elec. cond., theory and expt. 80−60057
- polymer, predominant carrier species determ. using galvanic cell 77−69384
- polymer/metal powder compacts, cond. threshold, particle size ratio effect 80−80337
- polymeric compositions containing elec. cond. filler, struct. effect on elec. props., review *(Russian)* 79−33317
- polymeric conductors and graphite intercalation cpds., struct. and phys. props., symposium, San Jose, USA (March 1979) 80−62379
- polyphenylene derivs., temp. hysteresis in elec. cond. *(Russian)* 77−47803
- polysulphur nitride, elec. cond. at microwave freq. 80−24922
- polysulphur nitride, pure and brominated, electronic model for high cond. 80−24923
- porous bodies, exam. of conductivity 79−4543
- powder, apparatus for exam. sintering, electrical resistance 80−16217
- powder behaviour in vibrating field from cond. obs. *(Japanese)* 78−95711
- powder consisting of anisotropic grains, effective thermal and elec. cond. 77−89601
- projection operator formalism appl. to cyclotron reson. on semicond. surfaces 80−88524
- proteins, self-consistent continued fraction theory of cond. in disordred materials 79−69482
- PVC-C composite, fluctuation-induced tunnelling cond. 80−65516
- PVC-Cu composite, annealing effects on elec. resist. 78−68060
- PVC-Cu composites, elec. resistivity rel. to compacting pressure 80−34495
- PVC-Cu composites with chemically deposited ultrafine copper particles 80−93534
- pyrographite, elec. resist., during electrochem. insertion of H_2SO_4 *(French)* 80−2437
- pyrographite, Si-containing, high-temp. treatment effects 77−40429
- pyroxene, containing trivalent cations, lab. meas. of elec. cond., rel. to lunar temp. profile 80−31033
- quantum mechanical theory, uncertainty principle 78−84182
- quasi-one-dimensional solids, nomadic polarisation 77−63357
- quasi-two dimensional conductor, galvanomagnetic props., optical analogy *(Russian)* 80−60108
- random conductance lattices, conduct., renormalisation group approach 78−60100
- random metal alloy, electron-phonon dynamics and resistivity anomalies 80−10958
- random planar conductance network, rigorous results 78−30897
- random resistor lattice, bicritical macroscopic cond. exponent in dimensionalities two, three and infinity 79−33272
- random resistor lattice conductivity, crit. exponents 77−76786
- random resistor network, $6-\varepsilon$ dimensions, renormalisation group treatment 78−51956
- random resistor network, mean field theory and crit. exponents 78−79973
- random resistor network, renormalisation group approach 78−34815
- random resistor networks, critical behaviour near percolation threshold 78−87956
- random resistor tree in applied field, macroscopic cond. 77−85185
- random trees theory, appl. to conductance networks 80−65515
- random-phase model, electrical conductivity of bond-type disordered system 78−51952
- random-site honecomb lattice, effective-medium theory 79−56178
- resistivity formula rel. to Boltzmann eqn. 77−47784
- resistor lattice conductivity exponent, position space renormalisation, decimation, dimensionality depend. 78−60099
- resistor network, percolation conductivity, critical exponents 78−10413
- rock, apparent resistivity changes under uniaxial compression *(Chinese)* 80−3995
- rocks, conductivity of cylindrical cores, porosity effects 78−61401
- rubber, C-black loaded SBR, elec. cond., effect of milling and thermal-oxidative ageing 77−55529
- scaling theory of localization: absence of quantum diffusion in two dimensions 79−38037
- semiconductor, field depend. meas. by coaxial line method *(Russian)* 77−85206
- semiconductor, nonlinear equation, asymptotics of spectral boundary-value problem 80−6851
- semiconductor, partly disordered, with mobility threshold, transport props. and thermoelec. parameters 80−34449
- semiconductor, wide-gap, extrinsic, injection currents, theory 78−19052
- semiconductors, non-parabolic, average energy of conducting electrons 77−55521
- semiconductors, temp. rise due to nonlinear heat generation 78−87983
- serum albumin, bovine, hydrated, dielec. and elec. props. 80−97854
- single-impurity Kondo system, fluctuation conductivity 78−76064
- site percolation, infinitesimal renormalisation group transform. 80−88525
- site percolation threshold in random networks 80−80241
- site random conductance networks, cluster approx. in effective medium model 78−19011
- site-diluted resistor networks, renormalisation group approach 79−15128
- solid state physics, book 80−101676
- solid-state theory, introduction, book 79−33215
- spin glasses, elec. resist., thermal resist. and thermopower 80−65542
- strong correlated system, single particle Green's function calc. of elec. cond. 80−20142
- substitutionally disordered system, derivation of cluster approx. 78−84184
- substitutionally disordered systems, MCPA and Monte Carlo calc. 78−84185

electrical conductivity of solids continued

- superconductors, granular, percolation model, specific heat, elec. resistance 80–93025
- surface charge decay due to time dependent bulk cond. 78–23397
- TCNQ, elastomeric complexes, doped with pure TCNQ, elec. conductivity 78–84220
- ternary alloy, disordered DC elec. cond. calc. 77–15812
- ternary alloys, disordered, elec. cond. and density of states, CPA calc. *(Russian)* 79–47072
- thermal fluctuations of current density, EM fields and charge density, inhomogeneous anisotropic cond. medium 78–23067
- thermally stimulated relaxation in solids, transport phenomena, book 80–77553
- thermoelectromagnetic waves in conductors in a mag. field *(Russian)* 80–49695
- thin films, ion-bombarded, simple model of dose depend. of resist. 79–42669
- three-dimensional disordered lattice, numerical simulation of diffusion 79–78092
- tight-binding model, non half-filled, Peierls transition props. in commensurate phase 77–31933
- time inversion symmetry and transport props. 77–89744
- titanomagnetite sand from New Zealand, density, elec. and mag. prop 80–98311
- transient and AC steady-state response of solid with recombining space charge 77–51737
- transition metal alloys, disordered, elec. resist., force-force correlation function approach 79–51541
- transition metals, liq., multiple scatt. calcs. of resist. 78–76039
- transparent conductors, figure of merit 77–1741
- tremolite asbestos, fibrous. elec. anisotropy 78–80273
- TTF-TCNQ, anisotropic cond., X-ray effects 80–96855
- TTF-TCNQ complex, trans-diethyl-dimethyl TTF-TCNQ, one-dimens. cond. 80–96853
- two-dimensional binary mixture, effective medium theroy of cond. and Hall effect 79–95380
- two-dimensional conductor-insulator networks with controllable anisotropy, percolation threshold and crit. exponents 80–24863
- two-dimensional disordered systems, effects of interactions on non-metallic behaviour 80–92869
- ultramafic rocks, elec. cond. meas., 670-1820K 78–69335
- valence bond theory of narrow band conductors 80–24777
- vitamin A alcohol and acetate, compensation effect 79–51573
- wax-graphite composite, electrical cond. 79–24044
- Wigner crystal on liq. He surface, cond. *(Russian)* 80–6594
- wire, quantum size effect, theory 77–35907
- wustite solid solns., props. connected with localised electron state 80–107734
- zeolite interface, ionic conduction bands 77–35745
- Ag particles embedded in dielec. KCl medium, search for maximum metallic resist. 80–107756
- Ag-polystyrene powder mixture, hot-pressed 77–32556
- Ag-SiO_2 film, elect. and struct. props., ion beam sputtering 78–80071
- Al smelting cathodes, comp. and props. 77–28740
- Al-paramagnet mixture, film, nonlinear elec. props. *(Russian)* 77–24624
- AlH_3, elec. cond. meas., V/I characts. *(Russian)* 77–51752
- $Al_{2+x}O_3$, sintered, elec. cond. temp. and comp. depend., thermoelec. power 80–2438
- Al_2O_3-Cr(Re)(Nb)(Ta)(Ti)(V) heterophase films, elec. props. rel. to Al_2O_3 content 77–15969
- Al_2O_3-Fe cermet, microstruct. and physical props. 79–42279
- Al_2O_3-Nb, cermet thin film, electrical transport and thermoelectric power 77–20462
- Ar, condensed, electron drift, Davydov electron energy distribution function, diffusion *(Russian)* 80–80339
- AsF_5 intercalation with graphite and benzenoid systems, EPR, NMR and X-ray diffr. obs. 80–19775
- Au-WO_3, electrochromic cermet, optical and electrical props. 79–33674
- Au-WO_3 electrochromic cermets, resist. and optical density meas. 79–8201
- B and borides, conference, Varna, Bulgaria (Oct. 1978) 80–12842
- BaO-BaX_2-P_2O_5 glass, X=F, Cl, Br, conductivity 78–67862
- $BaPO_3F$-Al_2O_3-B_2O_3 glasses, phys. props. 78–63676
- $Ba_2TiGe_2O_8$-$Ba_2TiSi_2O_8$, pseudobinary system, pyroelectricity and related props. 78–95553
- Bi-SiO_2 cermet films, elec. and optical props. 79–78775
- C, baked mix, optimum binder content estimation 77–73253
- C, baked mixes, use of coal tar and petroleum pitches as binders 78–80483
- C fibre reinforced Cu, specific elec. resistivity, 77 to 550K *(Russian)* 77–72895
- C fibre reinforced CuO-H_3PO_4 effect of C fibre on props. 79–43192
- C fibre reinforced epoxy resin, eddy current methods of exam. 77–12760
- C fibre reinforced epoxy resin composites, 2 to 290K 79–60528
- C fibre reinforced plastic, moisture content effect on elec. resist. 79–38992
- C films with high conductivity, prep. and props. 80–80983
- C-C composite material, syntactic-foam type properties 78–44169
- C-PVC composite, fluctuation induced tunnelling conduction 78–52044
- $C_{12}Cl$ and $C_{16}Cl$ intercalation compound form., elec. resist. decrease *(French)* 80–40674
- $C_{12}{}^{2+}PtF_6{}^{-}$, struct. and elec. props. 80–70183
- $C_{24}Rb$, graphite intercalated, de Haas-van Alphen effect, cyclotron reson., and transport props. 80–44479
- CaB_6-SmB_6 system complex borides, prep. and props. 78–52703
- CaO-Al_2O_3-SiO_2 based glasses, kinetic parameters of glass ceramic form. determ. 77–24385
- CdTe thick films, prep. by sintering and elec. props. 80–29451
- $Co_2Ga_{2-x}M_x$ (M=V, Cr, Mn, Fe), mag. props. and order 77–12093
- CoS_2, change in resist. by Fe impurity 79–7990
- Cr-SiO cermet thin films, thickness effect on density, resist., adhesion and annealing coeff. 77–69432
- Cr-SiO film, elec. props., effect of P^+ and Ar^+ implantation 79–11239
- Cr-SiO film, RF sputtered, substrate bias effect obs. 78–60573
- Cr-SiO_2 cermet film, deposition by RF sputtering of powder target, elec. resist. and TCR 79–78890
- $Cr_{3\pm x}Se_4$, struct., elec. and mag. props. 80–107160
- $CsSn_2I_5$, surface props., Auger study, elec. cond. meas., photochem. study 80–66339

electrical conductivity of solids continued

- Cu alloys, dispersion type, with low temp. gradient of resist. 80–49686
- Cu powder, sp. ht. cond. and sp. elec. cond. meas., Wiedemann Franz Lorenz law *(German)* 80–92872
- Cu powder under press., behaviour *(German)* 79–69485
- Cu-Al_2O_3, composite coatings, prep. by precip., props. 78–23841
- Cu-Al_2O_3 cermet films, temp. depend. of AC and DC cond. 79–87166
- Cu-Cd-Se system, Cu-CdSe cross section and props. of cpds. formed 78–27491
- Cu-plated C fabric, plasma sputtering influence on strength and elec. cond. *(Russian)* 80–21008
- $Cu_xMo_6S_8$, thin films, low temp. normal state, resist., temp. depend. 78–91783
- D_2-DT-T_2 mixture, solid and liq., props. for fusion reactor applications 78–66415
- $ErFe(CN)_6.5H_2O$, powder, elec. transport props. obs. 80–70701
- Fe, carbonyl powder, specific elec. conductivity, 5 to 200 MPa *(German)* 80–70664
- Fe-Al_2O_3 granular films, superparamagnetism and relax. effects 80–71118
- Fe-Cu-glass ternary multiphase composite, microstruct. and props. *(German)* 77–90314
- Fe-Fe_3O_4, sintered two-phase soft mag. material, prep. and props. 77–63813
- p-GaAs, low-temp. resist. thermometers, R(1/T) curve 78–223
- Ge bicrystal, conductive layer form. at boundary *(Russian)* 77–39983
- Ge-Al(Cu), alloying effects on elec. transport props. of amorphous and crystalline Ge films 79–51689
- $Hf_xTa_{1-x}C$, thermal cond. and diffusivity, 1000-2200°C, elec. cond. 78–91491
- Hg-Xe system, metal-insulator transition temp.-coeff. of cond. 77–66188
- $HgCl_2$, solid and molten state, elec. conductance, relative behaviour 79–33113
- HgI_2, solid and molten state, elec. conductance, relative behaviour 79–33113
- $HoFe(CN)_6.5H_2O$, powder, elec. transport props. obs. 80–70701
- I, metallic, mol. and monatomic phase, elec. resist. at high press. and low temp. 80–65638
- In, resistivity measurement by eddy current decay method *(Korean)* 80–27275
- In_2O_3, transparent electrode deposition on PLZT ceramic, elec. and opt. props. 78–74848
- $In_{2-x}Sn_xO_{3-y}$ thin films, optical transmission and elec. resist. 77–69926
- IrO_2 film, A-C response 80–107926
- $KClO_4$, AC electrical conductivity meas. between temp. range 25-325°C, automated technique 80–59699
- $KClO_4$:$CrO_4{}^{2-}$($SO_4{}^{2-}$), AC electrical conductivity meas. between temp. range 25-325°C, automated technique 80–59699
- $K_xCr(Mn)(Co)O_2$, layer struct., elec. cond. behaviour *(French)* 78–26542
- $K_{1+x}Fe_{11}O_{17}$, elec. and ionic cond. meas. 77–47618
- $LaRu_xFe_{1-x}O_3$ perovskites, cryst. struct., elec., mag. and Mossbauer behaviour 77–55274
- Li-pyrographite intercalation cpds., synthesis and elec. resist. 79–91601
- $LiFe_5O_8$, elec. props. 77–80641
- MgO/Ni-Cr (80, 20 wt.%) cermets, sintered, elec. resist. temp. effect 80–3206
- Mn-MgF, cermet film, evaporated, variation of elec. resist. with prep. conditions 77–43746
- Mn-MgF, cermet film, variation of resist. with deposition rate 77–43747
- Mn-SiO, annealed cermet films, elec. resist., composition depend. 80–97007
- Mn-SiO cermet films, DC and AC resist. 80–54804
- Mn-SiO cermet films, elec. resist., annealing behaviour 80–54803
- $Mn0_2$ powders with admixed fine materials, density and conductivity under pressure 80–54682
- $MoSi_2$ refractory formation by As^+ ion beam bombardment 80–107286
- Na-NH_3 solid mixture, cond., three component reactive percolation model 78–68003
- Na-zeolite, matrix, Te cluster superlattices, N and S type volt-ampere characts., elec. cond. *(Russian)* 80–70665
- $Na_xCr(Mn)(Co)O_2$, layer struct., elec. cond. behaviour *(French)* 78–26542
- Na_2O-NaF-B_2O_3 glass, nature of conductivity 78–63876
- Nb-S system, phase relations at high temp., elec. and mag. props. 80–29932
- $Nb(OR)_2Cl_3.L$, halo-alkoxide complex, prep. and props. 78–18605
- $NbSe_2$, 2H polytype, layered cpd., thermal props. at CDW transitions 77–47750
- $NbSe_3$, incommensurate CDW, X-ray scatt. and elec. field studies 79–42471
- $NbSe_2$(2H), I-free, anomalous resist. 77–51732
- Ne, solid, elec. cond. obs., insulating up to 500 GPa 78–95315
- Ni-Eu_2O_3, specific resistivity and emissivity, 1000 to 1500K 77–43675
- Ni-Si-B powder, oxidation at 850°C, SEM, ESCA, and elec. cond. meas. 80–7717
- Ni-SiO cermet film, elec. resist., percolation effects 77–76954
- $PbMo_6S_8$, thin films, low temp. normal state, resist., temp. depend. 78–91783
- Pt-SiO_2 cermet films, struct. and props. 80–96956
- Pt-WO_3, electrochromic cermet, optical and electrical props. 79–33674
- $ReSi_2$, atomic volume deviations and supercond. T_c and elec. cond. 80–75203
- $(SN)_x$ films, electrical properties 78–91782
- $(SN)_x$, fluctuation induced cond. and dimensionality 77–28167
- $(SN)_x$, thermopower from 0.15 to 4.2K 80–34427
- Si:P, ion implanted, selective annealing of amorphous layers by Nd^{3+}:YAG laser irrad. 79–14823
- SmB_6 films, crystn., struct. and elec. resist. 77–63559
- SmB_6, mixed valent, DC transport props., metallic or insulating props. 78–68029
- SmS, mixed valent, DC transport props., metallic or insulating props. 78–68029
- SnO_2, reactor irrad. induced changes in elec. props. 77–28267
- SnO_2, transparent electrode deposition on PLZT ceramic, elec. and opt. props. 78–74848
- TaB_2-ZnS:Ag(Ag,Ni)-glass binder, thermally stable, comp. 77–63617
- $Ta(OR)_2Cl_3.L$, halo-alkoxide complex, prep. and props. 78–18605
- TaS_2 (1T), CDW-transition temp., press. depend. 77–51730
- TaS_2 (1T), low temp. elec. props. 77–85205
- TaS_2 (2H), sp. ht. and resist. near CDW phase transitions 78–34786

electrical conductivity of solids continued

- TaS_2, non-linear conduction in two-dimensional CDW 78−91685
- $TaS_{2-x}Se_x$ (1T), transport props. 80−103710
- $TaS_2(Se_2)$, 2H and 4Hb polytypes, layered cpd., thermal props. at CDW transitions 77−47750
- $TaS_2(4H_b)$, electrical cond. and CDW transitions under press., rel. to supercond. 77−43574
- $TaSi_2$ refractory formation by As^+ ion beam bombardment 80−107286
- TeO_2-MoO_3-V_2C_5, phase comp. determ. using X-ray diffr., electron microscopy and DTA *(German)* 80−88046
- (Ti, Cr)B_2-based alloys, densification of powder mixtures by hot-pressing, elec. and mech. props. 80−20812
- Ti-Al_2O_3 system mixed films, prep., phase comp., struct. and elec. props. 79−37930
- TiC, vapour deposited coatings, elec. resist., mag. susceptibility and adhesion meas. 77−44395
- TiC-VC(Nbc)(YaC), comp. depend. 77−28772
- TiC-VC(ZrC) carbide alloys, thermophys. props., temp. depend., specific elec. resist. 79−86908
- $Ti_{1-x}Fe_x$ alloys, $(0<x\leq 0.2)$, nonmetallic resistivity and simultaneous superconductivity *(Russian)* 77−36005
- TiN-MnN, solid solns., electrophys. props. 77−35914
- TiN-Nb(Ta)N, microcomposite film prod. for radio resistors 78−3052
- $Tl_xV_6S_8$, prep., struct., props. 77−19935
- $Tm_{1-x}Y_xTe$, $(0\leq x\leq 1)$, single cryst. growth and characts. 78−23603
- UC, UC_2, U_2C_3, and UC+UC_2, elec. resist., 4 to 1900K 80−59953
- β-UD_3, electronic props., metallic character 80−6693
- VN-Mn, solid solns., electrophys. props. 77−35914
- VSe_2, 1T polytype, layer cpd., thermal props. at CDW transition 77−47750
- W-Al_2O_3 cermet films, oxide evaporation deposited on Mo, Ti, Al_2O_3 substrates, struct., props. 80−25581
- W-SiO_2 cermet film, deposition by RF sputtering of powder target, elec. resist. and TCR 79−78890
- WC, sputter deposited coatings, elec. resist., mag. susceptibility and adhesion meas. 77−44395
- WO_3, thin films, electrochem. coloration, optical and elec. props. 77−85345
- WSi_2 refractory formation by As^+ ion beam bombardment 80−107286
- YIG:Ca eddy current damping 80−39876
- $YbFe(CN)_6.5H_2O$, powder, elec. transport props. obs. 80−70701
- ZnO ceramic varistors, trapping by localized states, effect on dielec. and elec. props. *(Russian)* 79−28671
- ZnO powders, direct meas. of intrinsic cond., using emulsion 79−99595
- ZnO-ZnS powder mixtures, elec. cond. and Hall effect meas., percolation effects 79−7828
- ZnO-ZnS powder mixtures, Hall effect and elec. cond. 79−51607
- ZrB_2-ZnS:Ag(Ag,Ni)-glass binder, thermally stable, comp. 77−63617
- ZrC-C composite system, electrical resist. meas., percolation theory anal. 78−84269
- ZrC-ZrN system, solid solns., elec. resist., thermo EMF, thermal cond., expansion coeffs. 78−60176
- ZrN-Mo, cermet, sintering reaction thermodynamics 80−2989
- ZrO_2 stabilised with lime at high temp. *(Rumanian)* 80−65575
- ZrO_2-CaO-Y_2O_3, formation, stability and elec. props. of fluorite-like solid solutions 77−16550
- ZrO_2-Sc_2O_3 system, high-temp. phase transitions, elec. cond., thermal props. 77−16573

electrical conductivity transitions

see also metal-insulator transition

- alkali fluoantimonates, dielectric props. and structural phase transitions *(German)* 80−25274
- alkali metal film, inert gas impurities, metal-insulator transition, optical absorption and cond. 77−24598
- alkali metal-ammonia solns., elec.-cond. and thermopower 77−1370
- alkali metal-NH_3 solution, Hall effect and cond. at metal-nonmetal transition 78−2530
- alkali metal-NH_2 solutions, metal-nonmetal transition Hall mobility, electrodeless meas. 78−56194
- alkali metal-V_2O_5 bronzes, single cryst., elec. cond., 300 to 900K 77−20369
- alloys, binary narrow-band, metal-dielectric transition, off-diagonal disorder *(Russian)* 79−4512
- amorphous films, characteristics of monostable switching 77−80817
- amorphous films, threshold switching theory 80−2433
- amorphous inorganic semiconductor, elec. switching, aggregated electrons emulsion inversion as possible mechanism 79−38139
- amorphous semiconductor, current fluctuations and switching 79−87133
- amorphous semiconductor, investigation into characts. *(Croatian)* 77−39771
- amorphous semiconductor, switching effect, anomalous temp. depend. 78−26927
- amorphous semiconductor, threshold switching, Mott model 80−29447
- amorphous semiconductors, conference, Balatonfured, Hungary (Sept. 1976) 77−76802
- anomalous frequency-dependent conductivity in disordered one-dimensional systems 79−46834
- anthracene film, switching and memory phenomena 77−12031
- anthracene thin films, high field effects and switching, local centres importance 79−73548
- bootstrap percolation conductivity on Cayley tree 80−54743
- dl-2,3-camphanedione, elec. cond., brittle-to-plastic region, cond. jump 78−39169
- dl-camphor oxime, elec. cond., brittle-to-plastic region, cond. jump 78−39169
- dl-camphoric anhydride, elec. cond., brittle-to-plastic region, cond. jump 78−39169
- carboxylic acid metallic salts, laminated cpds., nature of cond. *(Russian)* 79−42512
- cetyl alcohol with dipoles, switching and negative resist. phenomenon, quantitative model 78−14769
- chalcogenide film, threshold switching mechanism, review 78−76122
- chalcogenide glass, radiative emission during threshold ON-state 78−76119
- chalcogenide glass, threshold switch, high resist. state 77−15924
- chalcogenide glass device developments and future trends 77−69386
- chalcogenide glass film, monostable switching obs. 77−8157
- chalcogenide glass film, switching field calc. 78−14775
- chalcogenide glass film, switching phenomena 77−39976

electrical conductivity transitions continued

- chalcogenide glass films, electrothermal switching and current filament form., cond. model 77−76886
- chalcogenide glass films, high field, short pulse cond. expt. 80−49751
- chalcogenide glass films, threshold switching 80−96950
- chalcogenide glass-GaAs(InP) p-n junction, fabrication, characterization, switching 80−49892
- chalcogenide glasses, field effect, localised states and electronic transport 77−66187
- chalcogenide glasses, memory effect, local doping, switching 80−107873
- chalcogenide switch, relaxation processes in memory and threshold switches 78−60172
- chalcogenide switching device, on-state behaviour and degradation effects 77−11967
- cholesterol film with dipoles, switching and negative resist. phenomenon, quantitative model 78−14769
- current filamentation on switching, analytical theory 77−15922
- current fluctuations, low freq. in system with semicond.-metal transition 77−66189
- disordered system, props. of mobility edge 77−4330
- films, amorphous, prep., struct., props., review, book contrib. 78−48321
- graphite intercalation cpds. with H_2SO_4 and sulphuric oleums, elec. resist. evolution 80−45518
- graphite-AsF_5 intercalation compounds, resist. and magnetoresist. 79−99590
- inhomogeneous materials, effective medium theory with dipole-dipole interactions 79−4544
- inhomogeneous materials, electronic props., metal-nonmetal transitions, review 78−56073
- inhomogeneous thin amorphous chalcogenide films, reversible switching, thermal stability criteria 80−70856
- insulator-metal transition, electron-phonon interaction, electronic transport props. 77−89702
- insulators, prebreakdown phenomena, freq. dependent dielectric losses 80−45006
- inversion layer, threshold conduction 78−43450
- lead phthalocyanine film, switching effects 79−28384
- maximum metallic resistance, in two dimensions as 30000 ohms 78−95335
- maximum metallic resistivity, approx. expressions 78−14773
- melanin, wet, elec. switching, aggregated electrons emulsion inversion as possible mechanism 79−38139
- metal-filled epoxy resin, temp. variation, current interruption appl. 78−76124
- metal-NH_3 solutions, metal-nonmetal transition 77−51789
- metal-semi-insulating-n-p^+ Si devices, switching expts. 78−26965
- metal-semi-insulator-n-p^+ Si device, switching theory 78−26964
- MIM, thin film, use as non-heated source of electrons, review 80−84516
- MIM sandwich structures with anomalous props., review 77−59337
- MIM structure, new switching effect at atmos. press. 78−80067
- MIS diode, thin-insulator, switching phenomena, current-control-type negative resist. characts. 80−107915
- MOS capacitor, direct current/voltage relns. as function of oxide doping 80−88635
- N-type switching, thermal mechanism 77−85273
- one-dimensional conductors, conductivity peaks, Peierls transitions *(Russian)* 80−49700
- oxide glasses with Bi or Se granules, elec. props. and microstructure 78−2490
- oxide thin film electroforming, threshold switching and memory effects 77−76940
- [p-]quinquaphenyl film between metal electrodes, memory switching 80−2484
- photodiode, switching process and plasma effects, theory 80−65667
- phthalocyanine layers, metal-free, between Ag and Al electrodes, switching effects 80−65706
- PMMA, threshold switching effects 78−84270
- poly-N-vinylcarbazole, thin films, impedance states switching 77−20461
- polyacetylene: Br(Cl)(I)(AsF_5) electrical conductivity, metal-to-insulator transition 78−10525
- polyacetylene:AsF_5, heavily doped, transport props., evidence for metallic state 79−87121
- polyacetylene:AsF_5, thermopower and transport props. 80−65611
- polyacetylene:I, semiconductor-metal transition, thermoelec. power meas. 79−56271
- polyacetylene:SbF_5, elec. cond. meas. 80−60055
- polyacetylene, doped, elec. cond. and thermopower 80−96951
- polyacetylene, doped, fluctuation-induced tunnelling cond. in metallic regime 80−65516
- polyacetylene films, doping effect on elec. cond., chem. and optical props. 80−65572
- polyacrylonitrile, pyrolyzed, elec. cond. and dielec. const. in AC regime 78−60173
- polymer films, threshold switching, statistical aspects 79−33315
- polyvinylidene fluoride, crystn. process and elec. cond., differential scanning calorimetry 79−24024
- potassium acetylacetonate, polycryst., elec. cond., pyroelectricity, phase transition, UV spectrum 78−76392
- PVC in metal sandwich struct., switching props., voltage- and current-controlled negative resist. 80−103767
- pyrite type dichalcogenides, ^{57}Fe isomer shift, quadrupole splitting, Mossbauer study 80−15832
- p-quaterphenyl layers, thermally induced switching 77−43673
- random resistor network, elec. cond., renormalisation group approach 78−34815
- semiconductor, molten, V-I characts. in strong elec. field 77−87787
- semiconductor, switching under impact ionisation 78−72215
- semiconductor, thermal switching phenomenon 77−39904
- semiconductor sandwich, thermal switching and current-voltage characts., necessary conditions 77−4451
- semiconductor thin films, glassy-crystalline, with switching channel, electrothermal instability 80−15576
- semiconductors, n-type, metal-insulator transition and negative resist. effects 79−24026
- semiconductors with impurities, electron cond. temp. and freq. depend., two band model *(Russian)* 80−75564
- semimetal-exciton phase transition, microwave cond. 80−29430
- silicate glasses containing iron, switching and memory effects 77−8155
- sulphide group minerals, using four point probe technique, metallic to semicond. 78−64045
- switching initiation, Anderson model 78−10524

electrical conductivity transitions continued
TCNQ complex formed from cation (methyl-l-N-ethyl benzimidazolium)$^+$ conductivity transition 80—10954
TCNQ salt, $(N(CH_3)_3H)(I)(TCNQ)$, elastic props., semicond. transitions 79—95072
TCNQ salt, $(NMe_3H)(I)(TCNQ)$, one-dimens. semicond. with metal-like cond. 80—24909
TCNQ salt, Cu-TCNQ thin film between Cu and Al electrodes, elec. switching and memory phenomena 79—65562
TCNQ salt, dibenzo-TTF-$TCNQCl_2$, one-dimens. mag. semicond., mag. and elec. props. 80—88601
TCNQ salt, $MEM(TCNQ)_2$, dielec. const. obs., DC and microwave cond. obs. 80—59963
TCNQ salt, $MEM(TCNQ)_2$, phase transition electronic struct. interpretation 80—24781
TCNQ salt, $MEM(TCNQ)_2$, phase transitions, elec. cond., ESR, mag. susceptibility study 80—24981
TCNQ salt, N-propyl-quinolinium$(TCNQ)_2$, defect conc. depend. phase transition 80—44577
TCNQ salt., $NMeQn(TCNQ)_2$, role of solvent in phase transition, thermal anal. and transport props. 79—33312
TCNQ salt, NPQn $(TCNQ)_2$, neutron irrad. induced defect concentration depend. phase transition 80—29449
TCNQ salt, TEA $(TCNQ)_2$, anomalous conductivity, conductivity transitions 80—15508
TCNQ-HMTTF, metallic state stabilisation at low temp. under press. 78—30911
thermal mechanism for bias-induced switching effects in inhomogeneous thin films 80—11057
thermal switching, resist.-temp. charact. 78—64071
thin wire, max. metallic resist. 78—14663
threshold switching as a generation-recombination induced non-equilibrium transition 79—33314
threshold switching in non-cryst. semiconds. by computer simulation 78—88002
$(TMTSF)_2PF_6$ (AsF_6), linear-chain conductor, semicond.-metal transition in small elec. field 80—103730
TMTSF-DMTCNQ, metallic state, transport props. 80—24974
transition metal compounds, minimum conductivity and electron localisation near metal-insulator transition 78—30960
TTF-DETCNQ, metal-insulator transition, struct., elect. cond. and sp. ht. expts. 78—14662
TTF-SCN, quasi one-dimens. conductor, CDW phase transform., X-ray scatt. study 80—24594
TTF-TCNQ, cond. in phase transition region 80—24979
TTF-TCNQ, elec. cond., role of librations 79—19580
TTF-TCNQ, phase transitions and CDW state, induced defect depend., transport and mag. studies 80—24980
TTF-TCNQ, spin susceptibility below 53K, compared with elec. cond. data 77—43865
TTT_2I_3, quasi one-dimens. organic metal, elec. cond. and thermoelec. power 80—24899
Fe_2O_3-Bi_2O_3 sintered material, elec. switching effects due to thermal ionic breakdown *(Korean)* 80—70776
Ag-BN-Si-Al sandwich, humidity sensitive threshold switching 78—88046
Ag-SiO-Ag sandwich structures, elec. props. and nonvolatile memory effect 79—87164
Ag_3AsS_3, proustite, residual conductivity and low-temp. phase transitions 78—91729
n-Ag_8GeSe_6, elec. cond. and photoelec. props. 77—69380
$Ag_{26}I_{18}W_4O_{16}$, solid electrolyte, anisotropic elec. cond., low temp. phase transitions 80—65289
Ag_2O-P_2O_5, amorphous metaphosphate, memory cell with low switching fields *(German)* 79—19641
Ag_2S, metal-nonmetal transition, crystallographic, optical, mag. and transport props. 78—6418
Ag_2S, nonlinear V-I characts. obs. at low temp. *(Japanese)* 78—34866
$Ag_2S(Se)(Te)$, changes in elec. cond. and thermoelec. power at melting point 79—15147
Ag_2Se, metal-nonmetal transition, crystallographic, optical, mag. and transport props. 78—6418
Ag_2Se thin film, switching and Ag movement, point contact technique 80—60107
Ag_2Te film, Ag movements, switching and memory effects 79—78239
Al-Se-Ag switching elements, role of Ag in switching effect 78—19163
Al-SiO_x-Al structure with evap. amorphous films, threshold and memory switching 77—76945
AlB_{12}, α- and β-forms, elec. props. at high temps. and in strong elec. fields, thermistor appls. 80—92903
As, amorphous, effect of high press. on elec. props. 77—59309
As, elec. cond. and density meas., crit. parameters 77—47562
As, liq., Anderson transition, cond., at high temp. and supercrit. press. 78—34869
As-Sb-S-I system glasses, vitrification and volt-ampere characts. 77—31756
As-Se system glasses, structural and electronic transitions 77—76890
As-Te-Ge system glasses, thin films, effect of S, Se, Sb, Bi, Tl on volt-ampere characts. 77—15976
As-Te-Ge-Si, amorphous semiconductor thin film, high-speed switching mechanism 77—8153
As-Te-Ge-Si sandwich type amorphous films with metal electrodes, space-charge-limited switching, pre-breakdown characts. *(Japanese)* 77—69385
As-Te-metal amorphous film, switching, memory effects 80—44677
$As_{10}Ge_{15}Te_{75}$, glass, cond. and switching characts. 77—32054
$As_{10}Ge_{15}Te_{75}Ag_x$ glass, elec. and dielec. props., Ag additions effect 80—65558
As_2S_3 film, evaporated, switching effects 80—96952
AsSe, molten semicond., pseudogap, elec. cond. and optical absorption meas. 77—8160
$AsSe_x$ amorphous films, high field behaviour 79—87172
As_2Se_3, chalcogenide glass threshold switches, turnon state, maintenance mechanism *(Russian)* 77—85271
As_2Se_3, liq., semicond.-metal transition at high temp. and press. 77—51784
As_2Se_3, molten semicond., pseudogap, elec. cond. and optical absorption meas. 77—8160
As_2Se_3-As_2Te_3, molten semicond., thermoelec. power and elec. cond. near metallic cond. transition 78—10486
As_2Se_3-Sb_2S_3 glass, threshold and memory switching, expt. data 78—39170

electrical conductivity transitions continued
As_2Te_3, amorphous, press.-induced semicond.-metal and supercond. transitions 77—43671
As_2Te_3, molten semicond., thermoelec. power and elec. cond. near metallic cond. transition 78—10486
As_2Te_3, phase transitions and elec. cond. 78—10440
$As_{50}Te_{50}$, amorphous films, metal and semicond. contacts, threshold switching, IR emission 80—49831
$As_{50}Te_{45}I_5$, glass, semicond., elec. switching, high press. effects 78—72212
Au island films, forming process, I-V characts., and switching 79—11242
AuI, elec. cond. 79—42302
B, β-rhombohedral, elec. props. at high temps. and in strong elec. fields, thermistor appls. 80—92903
BN films, humidity sensitive elec. props. and switching characts. 80—107938
$B_{14}Si$, switching and high field effects, cond. mechanism 78—64048
BaF_2, powder, elec. cond. transition under high press. *(Russian)* 77—20370
$Ba_xLa_{1-x}CoO_3$, x=0 to 0.5, structural, elec. and mag. props., Zener double exchange and Goodenough's model 79—65663
BaO-CaO, amorphous film, Cu-electrodes, electrical props. 77—35997
$BaSi_2$, semicond.-metal transition, high-press. and temp. 78—43299
$BaVS_3$, elec. resist., mag. susceptibility, structural transition amd Mossbauer effect meas. 77—84923
Bi-$BiBr_3$ liquid system, miscibility gap, elec. cond. meas. 79—90790
Bi-Sb, semiconductor-semimetal transition under pressure 78—34870
Bi-Sb, single cryst., semimetal-semicond. transition. cond. 77—1459
Bi-Sb-S-I system glasses, vitrification and volt-ampere characts. 77—31756
$Bi_{0.91}Sb_{0.09}$, magnetoresistance anisotropy in strong magnetic field 79—82613
$Bi_{0.925}Sb_{0.075}$, semiconductor-semimetal transition under tensile strain, Shubnikov-de Haas oscills. obs. 80—44678
$Bi_{1-x}Sb_x$, semicond.-semimetal transition, temp. and press. depend. of transport props. 78—76120
C film, amorphous, elec. transport props. and atomic comp. 78—6457
C films with high conductivity, prep. and props. 80—80983
CaF_2, powder, elec. cond. transition under high press. *(Russian)* 77—20370
$CaFeO_3$, preparation, cryst. struct., mag. and elec. props. 78—44066
$CaV_{12}O_{30}$, phase transitions, elec. cond., susceptibility and sp. ht. meas. 78—14776
$Cd_3B_7O_{13}X$, X=Cl or Br, highly insulative, switching obs. 77—51785
$CdCr_2S_4$:In(Ga), resist. and magnetoresist. meas., effect of donor impurities 79—19608
$CdCr_2Se_4$, mag. semicond., threshold and mag. memory switching in single crysts. 77—43672
$CdCr_2Se_4$:Cu, elec. props., temp. depend. *(Russian)* 78—72181
$CdCr_2Se_4$:In(Ga), temp. driven metal-semiconductor transition, temp. and mag. field depend. *(Russian)* 78—88003
CdF_2:Mn, Y, deconversion due to vacuum heat treatment, elec. resist. and electron probe meas. 79—24025
$Cd_{0.96}Ga_2Te_{4.1}$, amorphous film crystallisation and conductivity switching 77—4459
$Cd_{0.96}Ga_2Te_{4.1}$ film, switching effect 77—43753
$Cd_{23}Ge_{12}As_{65}$, amorphous, threshold switching, expt. 80—49830
$CdGe(P_xAs_{1-x})_2$, glass, static current-voltage characteristics *(Russian)* 77—15925
n-$Cd_xHg_{1-x}Te$, conductivity inversion under laser radiation *(Russian)* 79—15198
CdS, press. quenched, mag. moment, semicond.-conducting transition 80—15683
$CdS_{0.5}Se_{0.5}$, picosecond optoelectronic switching 80—54734
CdSe, electrical cond. near metal-insulator transition 79—73550
CdSe:Au impurity light absorpt. for current control in negative resistance region 80—11052
$CdSeTl_x$—$As_2Se_3Tl_x$ thin layer system, charge transport 77—76985
CdTe films, switching obs. in sandwich structures 77—43752
CdTe single-crystal film, switching and memory effects 78—76174
$CeAl_2$, electronic transition under pressure, resist. meas. 79—33311
Co-Si interface, metal-semiconductor transition, rel. to first compound nucleation 80—24771
$Co_{3-x}Ni_xO_4$, $0 \leq x \leq 1.1$, struct., semicond.-semimetal transition, Seebeck coeff. 78—87972
$Cr_{1-x}Fe_xS$, metal-dielec. transition, X-ray, thermal anal., elec. cond. temp. depend. 78—67942
CrS-FeS, sulphorspinel, struct. and elec. props. 80—49834
CrS(Se), high press. semiconductor to metal transitions 78—26924
Cs-Au, liq. ionic alloy, elec. props. 79—99338
Cs-NH_3 solution, metal-nonmetal transition, cond. density and Hall coeff. meas. 77—51789
Cs-Sb(Au) liq. alloys, metal-nonmetal transition and change in electronic and mag. props. 77—51790
Cu-CdP_2-Cu diode structure, switching effect obs. 77—4452
Cu-Sb-S-I amorphous film formation and stimulated crystallisation, electrophysial props. *(Russian)* 78—30838
Cu-Xe film, metal-nonmetal transition, optical and resist. meas. 77—89818
CuB_{24}, elec. props. at high temps. and in strong elec. fields, thermistor appls. 80—92903
CuCl, high press. phases and anomalous props. 79—7689
CuCl, optical microscopic, X-ray diffr. and elec. resist. studies at high press. 80—11051
CuCl powder compacts, DC voltage depend. resist. under press. 80—80334
CuO-CaO-P_2O_5 glass devices, memory switching 78—56192
CuO-V_2O_5-P_2O_5 glass, elec. cond. and switching *(Japanese)* 80—34492
Cu_2O, cond. filament props. and bistable switching effect *(German)* 78—2532
Cu_2O, switching channel electron probe microanalysis, switching cycle number (life) 77—32056
Cu_2O, thermal breakdown mechanism of switching process, expt. obs. *(German)* 77—28225
Cu_xO film, growth by anodisation, switching characts. 77—55898
CuSe, lattice expansion, elec. cond. and sp. ht. at 326K transition 77—51491
$Cu_{1.8}Se$, I-V characts., switching effects, nonstoichiometry effects *(Russian)* 78—84266
$Cu_{2-X}Se$, X=0-0.23, cond. transition to superionic state, crit. conc. 79—55924

electrical conductivity transitions continued
$Cu_{1.7}Te$, and Cu_2Te, I-V characts., switching effects, nonstoichiometry effects *(Russian)* 78—84266
$Cu_{0.75}VS_2$, cryst. struct. and phys. props. *(French)* 78—14328
$Eu_{1-x}{}^{2+}Eu_x{}^{3+}N_xO_{1-x}$, resist., pressure depend., semicond.-metal transition obs. 79—78104
$Eu_{1-x}{}^{2+}Nd_x{}^{3+}N_xO_{1-x}$, resist., pressure depend., semicond.-metal transition obs. 79—78104
EuO, anomalies in transport props. under hydrostatic press. due to bound mag. polaron 77—20372
$EuO_{1-x}N_x$, ferromag. semicond., elec. and mag. props. *(French)* 78—79993
EuS-metal contact, electrical switching exam. 78—68085
α-Fe_2O_3, elec. resist. and phase transition under shock compression 80—72496
Fe_2O_3-Bi_2O_3 sintered material, elec. switching effects for temp. range 700-850°C *(Korean)* 80—70775
Fe_3O_4, finely dispersed, electronic phase transition, cond. and DTA meas. 78—91736
Fe_3O_4, finely dispersed powder, volt-ampere characts. *(Russian)* 77—62967
Fe_3O_4, low temp. phase, effect of residual stresses on Verwey temp. 77—59308
Fe_3O_4, photocond. 70-130K, temp. range including metal-semicond. transition *(Russian)* 78—56178
$FeSi_2$ films, structural and Anderson transitions, cond. and IR reflectance meas. 79—15200
Ga-NaX zeolite system, press. depend. of metal-insulator transition 78—88005
Ga-Xe film, metal-nonmetal transition, optical and resist. meas. 77—89818
GaAs, amorphous, switching obs. 79—11190
GaAs diode, reverse-biased, current-controlled negative resist., switching investig. 77—69410
GaAs, electrical conductivity and thermoelectric power charge due to melting 80—100490
GaAs ion-irradiated layers switching conduction 78—34868
GaAs, liq., semicond.-metal transition at high temp. and press. 77—51784
n-GaAs, metal-insulator transition in impurity band induced by mag. field and loss of dimens. 78—52042
n-GaAs, switching time in low-temp. impurity breakdown 77—15923
GaAs:Fe, p-π-ν-n struct., photoelec. props. 80—107862
GaAs:Fe reverse biased π-ν-n struct., switching effect 80—88628
GaAs:O, electrolum., photolum., negative differential resist. rel. to recomb. processes 80—66304
GaAs:Si, film, conversion of type of conduction stimulated by ion bombardment 77—4457
GaAs(P), semiconductor-metal transition, press. calibration above 100 kbars fixed points 80—77808
GaP meas. of transition press. to conducting phase 79—54150
n-GaP:S, elastic moduli and mode gammas 79—73242
Ga_2Se_3, single cryst., bistable cond. switching effect 77—51783
GaTe film, amorphous and polycryst., memory effects 77—20368
$Ga_{0.25}Te_{0.75}$ amorphous film, time evolution of nanosecond switching 80—6921
$Ga_{0.25}Te_{0.75}$ amorphous film, nanosecond switching, resist. fluctuations in low-resist. state 80—44676
$Ga_{0.25}Te_{0.75}$, amorphous film, off-state recovery after nonosecond switching 80—44681
Ga_2Te_3 single crystals, switching effect., carrier trapping 80—6919
$Ga_xV_{1-x}O_2$, resistivity, EPR, enthalpy and entropy meas., rel. to semicond.-metal transition 78—88004
GdB_6 single crystals, mag. behaviour and structure change at low temp. 80—71018
Gd_2S_3 with excess Gd, magnetoresist. meas. 80—49777
$Gd_xSm_{1-x}S$ K X-rays chem. shifts, electronic phase transition, semicond.-metal transition 77—28116
Ge bicrystal, two-dimensional electronic phenomena at He temp. *(Russian)* 79—56273
n-Ge, compensated, switching effect, injection mechanism of hot holes 77—69387
Ge film, amorphous, thermally induced reversible switching, effect of change in thermal resist. 77—20371
Ge:Sb, 2.5 MeV electron irradiated, cond. switching effect 77—89820
Ge-As-Te, thin chalcogenide glass film, high-field switching effects 77—32052
Ge-S-Ga amorphous thin film, memory switching effects 80—88605
Ge-S-In, chalcogenide glass, determ. of glass phases, phys. props. meas. 79—23526
Ge-Se-Ga thin film, elec. cond., switching phenomena *(Polish)* 80—11120
Ge-Te, As-Te, Ge-As-Te molten systems, metal-semicond. transition, cond. obs. *(German)* 77—1457
Ge-Te film, electrical switching 77—4411
$Ge_{33}As_{27}S_{15}Te_{25}$ glass, switching, microstructural changes 79—65523
$Ge_{10}As_{40}Te_{40}I_{10}$, chalcogenide glass film, switching delay time 78—26926
$Ge_{20}Bi_xSe_{80-x}$, semicond. glass, resist., thermoelec. power, optical absorpt. 80—88555
$Ge_{20}Bi_xSe_{70-x}Te_{10}$, semicond. glass, resist., thermoelec. power, optical absorpt. 80—88555
GeO_2 films, memory switching phenomena 79—82650
GeSe, galvanomag. meas., anisotropy, metal to semiconductor transition 80—6847
$Ge_{0.08}Se_{0.92}$, molten semicond., pseudogap, elec. cond. and optical absorption meas. 77—8160
$Ge_{1-x}Sn_xTe$ film, amorphous, elec. cond. 80—93016
$Ge_xTe_{10-x-y}E_y$, E=impurity, glass-crystn. transition, memory effect 77—47870
H_2, isentropically compressed, elec. cond. at Mbar press. 78—95315
H_xWO_3, amorphous, Anderson transition, disorder depend. and optical detection 78—47840
$HfSe_{2-x}Te_x$, elec. resist. and mag. suscept. studies 80—44599
HfV_2, C15 supercond., dielec. transitions, temp. depend. of resist. and mag. susceptibility, 4.2-300K 79—38136
HfV_2, dielectric phase transition, elec. resist. temp. depend. 79—65525
Hg expanded liquid, simultaneous investigation of eqn. of state and elec. cond. 77—55337
Hg, thermal switching at solid-liquid transition 77—8154
Hg-Ar quench condensed system, annealing effects on elec. cond. 79—60880

electrical conductivity transitions continued
Hg-Xe film, random mixtures, superconducting transition temp. and metal-nonmetal transition 80—29498
Hg-Xe system, metal-insulator transition temp.-coeff. of cond. 77—66188
Hg-Xe vapour deposited films, cond. transitions, effect of disorder on supercond. 80—88659
HgCdTe, zero gap, unusual high electron mobility and related phenomena 79—82601
n-$Hg_{0.8}Cd_{0.2}Te$, microwave bolometer heterodyne receiver based on magnetic field induced phase transition 80—13135
I, metallic, mol. and monatomic phase, elec. resist. at high press. and low temp. 80—65638
In-Ar mixture, metal-insulator transition, resistivity meas. 77—76883
InAs, electrical conductivity and thermoelectric power charge due to melting 80—100490
InAs, two dimensional accumulation layer, Anderson localisation 80—107871
InAs-GaSb superlattice energy struct. and semiconductor-semimetal transition 79—23893
InAs-GaSb superlattice, semiconductor-semimetal transition obs. 80—44710
InAs-GaSb superlattices, semicond.-semimental transition obs. 80—49882
InAs-GaSb superlattices, mag. field induced semimetal-semicond. transition 80—65656
$InAs_{1-x}P_x$, deep levels and semicond.-semimetal transition at high press. 80—11056
In_2O_3 film, evaporated, on ferroelec. ceramic, switching characts. 78—19107
InP, electrial props. at high temp. and in liquid state 77—11888
n-InP, impurity and minimum metallic cond. in mag. field 80—103731
In_6S_7, single crystal, switching effect and memory *(Russian)* 80—70774
InSb, high-purity, electron irradiation effects on transport props., evidence for semicond.-metal transition 79—23650
$InSb_{1-x}Bi_x$, multitarget RF sputtering, metastable phase, conductivity transition 80—76178
$In_{0.25}Te_{0.75}$ amorphous film, time evolution of nanosecond switching 80—6921
$In_{0.25}Te_{0.75}$ amorphous film, nanosecond switching, resist. fluctuations in low-resist. state 80—44676
$In_{0.25}Te_{0.75}$, amorphous film, off-state recovery after nonosecond switching 80—44681
K solution, in KBr, conc. fluctuations, neutron small-angle scatt. study in electrolyte-metal transition range 79—14668
KCl, polymorphic transition press. at high temp., elec. resist. meas. 78—38837
$KNbO_3$, elec. and thermoelec. singularities due to small polaron hopping motion cond. transition 79—42565
$K_{1.75}Pt(CN)_4 . 1.5H_2O$, quasi 1D metals, electric conductivity meas., semiconductor-metal transition 79—99538
$K_2Pt(CN)_4Br_{0.3}.3H_2O$, one-dimens. cond. transition, spin suscept. and DC cond. temp. depends. 78—84198
$KTa_{0.7}Nb_{0.3}O_3$, pressure-induced resistance and colour change obs. 80—75608
$K_{1.75}[Pt(CN)_4]1.5H_20$, elec. cond. studies, Peierls transition 80—24901
La_2CuO_4, high pressure phase transformation, small polaron cond. to semicond. transition 78—6156
$La_{0.71}Pb_{0.29}MnO_3$, metal-semicond. transition at Curie point, transport props. obs. 79—73554
$La_{1-x}Sr_xVO_3$, high-temp. transport meas. 77—11917
$La_{1-x}Sr_xVO_3$, semiconductor-metal transition, Anderson localisation, Hall mobility and 1/f noise meas. 79—78142
Li-NH_3, conc. solns., elec. cond. and thermoelec. power 79—19640
LiAl, anomalous elec. resistivity near critical composition 80—103673
$LiNH_4SO_4$, DC elec. cond. 80—88603
$LiNbO_3$-$3(Li_2O).Nb_2O_5$ eutectic, anomaly in elec. resist. 78—68030
$Mg_xFe_{3\ x}O_4$, polycryst., Verwey type transition, resist., magnetisation, Mossbauer effect and permeability obs. 80—75764
$MoSe_2$:Nb(Re), layered, elec. props., semicond.-metal transition 77—11922
$MoTe_{2-x}$, thermal switching mechanism 77—15920
NH_4SbF_5, dielectric props. and structural phase transitions *(German)* 80—25274
Na-Ar film, metal-nonmetal transition 77—62966
Na-NH_3 film, quench-condensed, anomalous elec. cond. obs. 77—32057
Na_2O-B_2O_3-Bi_2O_3, glass with metallic Bi granules, elec. cond. 80—84493
$Na_3Sc_2P_3O_{12}$, fast-ion conductor, struct. phase transition 80—88362
$Na_xTa_yW_{1-y}O_3$, substitution of W with Ta, Anderson type transition *(French)* 79—60879
$Na_{1.9}V_{12}O_{29.7}$, phase transitions, elec. cond., susceptibility and sp. ht. meas. 78—14776
$Na_{1.9}V_{12}O_{29.7}$, press. depend. of elec. cond., semicond.-metal phase transition obs. 78—64072
NbO_2, high-speed high-current field switching 77—80816
NbO_2, on-state decay rel. to recomb. and nonlinear props. 80—84492
NbO_2, sustaining and decaying of the high conductance on state 79—95454
NbO_2, threshold switching recovery curve, distribution trapped carrier lifetime 80—20258
Nb_2O_5 amorphous films, switching phenomena and dielec. breakdown 77—24594
Nb_2O_5, partially reduced, electrical conductivity 77—15918
Nb_2O_5, polycryst. film, switching processes, dielec. breakdown 77—39981
$NbSe_3$ and $Nb_{1-x}Ta_xSe_3$, thermoelec. power meas., 10-300K 80—20177
$NbSe_3$, non-ohmic transport props. near phase tranistions 78—72213
$NbSe_3$, quasi one-dimens. conductor, CDW phase transform., X-ray scatt. study 80—24594
$Nd_{1-x}Ca_xVO_3$, solid solutions, elec. props. 80—96866
$Nd_xSm_{1-x}S(Se)$, K X-rays chem. shifts, electronic phase transition, semicond.-metal transition 77—28116
$Nd_{1-x}Sr_xCoO_3$, Anderson transition, elec. cond. meas. 77—51786
$Ni(As_xS_{1-x})_2$, mag. elec. and structural props. meas. 77—85447
$Ni_{1-x}Co_xS_2$, elec. transport and semicond.-metal transition 80—10985
NiS, semiconductor-metal transition, UPS and XPS 79—23896
$Ni_{0.991}S$, sublattice magnetisation temp. var., neutron diffr. 77—40077
$NiS_{2-X}Se_X$, elec. resistivity temp. depend., pressure depend., paramagnetic-antiferromagnetic transition 78—10690
Pb-Xe mixture, metal-insulator transition, resistivity meas. 77—76883
PbAr, metal-insulator transition, resistivity meas. 78—80028
$PbCl_2$, evidence for diffuse transition, elec. cond. and Raman spectra meas. 79—73552
PbI polytypes, phase transforms. and electrical behaviour 78—47839

electrical conductivity transitions continued
PbO-B$_2$O$_3$-Bi$_2$O$_3$-Bi$_2$O$_3$, glass with metallic Bi granules, elec. cond. 80−84493
PbS, phase transitions under action of high press., elec. cond. meas. 77−4196
n-PbSe, pressure induced transition to gapless state 78−2533
Pb$_{1-x}$Sn$_x$Ge:In, press.-induced transition to gapless state, galvanomag. effects 78−19108
Pb$_{0.59}$Sn$_{0.41}$Se, struct. phase transition, temp and hydrostatic press. influence, Hall effect, resistivity *(Russian)* 78−51675
Pb$_{1-x}$Sn$_x$Te:In, energy spectra modifications due to comp. changes and press. appl. 80−10915
Pb$_{1-x}$Sn$_x$Te:In, semiconductor-metal-semiconductor transitions under press. 80−34491
Pd$_2$F$_6$, evidence of an electronic transition under high press. *(French)* 79−42596
Pr, localised 4f shell breakdown under press. 80−70411
Pr$_{1-x}$Sr$_x$CoO$_3$, Anderson transition, elec. cond. meas. 77−51786
Pt$_6$(NH$_3$)$_{10}$Cl$_{10}$(HSO$_4$)$_4$, chain struct. and elec. cond. 78−2469
RbAg$_4$I$_5$ superionic films, elec. cond. and optical absorpt. studies 79−99355
Rb$_{1.75}$Pt(CN)$_4$. 1.5H$_2$O, quasi 1D metals, electric conductivity meas., semiconductor-metal transition 79−99538
Ru$_{1-x}$Ti$_x$O$_2$ solid solns., metal-nonmetal transition 78−91735
S, dielectric to metal transition at ultrahigh dynamic press. *(Russian)* 79−60881
S, electrical conductivity under shock compression *(Japanese)* 78−26923
S, metallic state, elec. resist., press. effects up to 600 kbar 78−26920
S, shock wave method observation of transition to highly conducting state 80−4738
S, transition to cond. phase 79−54150
S, transition to conducting phase 77−35972
S-Ni-Fe system containing monosulphide solid soln., elec. and struct. relations 80−90038
S-Se amorphous alloys, crystn. kinetics, elec. cond. meas. 78−34441
(SN)$_x$ and S$_4$N$_4$, high press. study 78−52782
SSe$_{20}$, crystalline phase growth in amorphous solid and liquid samples 78−43107
SSe$_{22.5}$, amorphous, photo-effect on crystn. kinetics, elec. cond. obs. 79−77522
SSe$_{40}$, amorphous alloy, crystn., elec. cond. meas. 78−34440
SSe$_x$ (x=10, 15, 40), amorphous crystal transition, appl. of Kolmogorov-Avrami equation 78−67649
Sb amorphous film, elect. resist. 78−95390
Sb electrodeposit, amorphous, explosive crystn., semicond-semimetal transition and IR absorpt. 78−51849
Sb-Au amorphous film, elec. resist. 78−95390
p-Sb$_2$S$_3$, bistable switching 79−73553
Sb$_2$S$_3$, defect drift in elec. fields and bistable switching 80−92947
Sb$_2$S$_3$, hopping cond. in cryst. subjected to strong elec. fields 79−95456
Sb$_2$S$_3$, switching mechanism 77−15921
Sb$_2$S$_3$, vitreous, prep. elec., opt. and struct. props. 77−76889
Sb$_2$Se$_3$, monostable switching effect *(Russian)* 79−33316
Sc$_{2/3}\square_{1/3-y}$Sc$_y$S, elec. props. variation at high temps. *(French)* 79−82649
Se, amorphous, conducting channel temp., time depend., under monostable switching conditions 78−19109
Se, amorphous, memory and threshold switching effects 78−14774
Se, amorphous, monostable switching, current noise 80−44682
Se, amorphous, struct. and elec. cond. transitions under high press. 79−42237
Se, amorphous film, between metal electrodes, switching mechanism 78−39172
Se amorphous film, threshold and memory switching 79−82651
Se, amorphous thin film, elec. noise, monostable switching 80−44684
Se, elec. cond., 0-500 kbar 79−99589
Se film, metal ion diffusion during memory switching 78−26976
Se, film, switching characts. under pulsed bias 77−39979
Se, liq., Anderson transition, cond., at high temp. and supercrit. press. 78−34869
Se, liq., electronic transport props. at sub- and supercritical conditions 77−51788
Se, liquid, correlation between switching and struct. 77−69388
Se, liquid, electrical cond. transition at high temp. and press., Anderson localisation *(Russian)* 77−1462
Se, liquid-crystal phase transition, elec. cond. changes 79−33310
Se, metallic state, press. induced, elec. cond. meas. 80−96949
Se powder compacts, sintered, electrical cond. 80−70693
Se:Te(Ag), amorphous film, elec. cond., 300 to 350K, transition 77−4454
Se-Ag$_2$Se, heterojunction with memory, transient switching characteristics 80−44718
Se-Te-Ge, amorphous, off-state thermal switching 79−65524
Si, amorphous film, in Ti-Si-Ti struct., elec. cond. processes and threshold switching 79−78207
Si, amorphous films, RF sputtering prep. at high Ar press., props. obs. 80−80418
Si amorphous films, switching, electrothermal model 80−80407
Si diodes, p$^+$-i-n$^+$ struct., double-injection switching, effect of surface recomb. 78−88025
Si, dislocation free, C and O impurity clouds, heat treatment influence on light scatt. 80−6427
p-Si, elec. resist., shock wave compression effects 80−80265
n-Si, electron irradiated, elec. props. 77−8041
Si film, amorphous, hopping cond. control by ion bombard. induced struct. modification 80−92898
Si, heavily doped, doping density striation effects in metal-nonmetal transitions studies 79−28383
Si, metallic state, press. induced, elec. cond. meas. 80−96949
Si polycrystalline CVD films, non-volatile memory switching 80−54814
Si, static compression in [100] and [111] directions, elec. resist. obs. 80−65637
Si/In$_2$O$_3$-SnO$_2$ thin film junctions, polarity dependent memory switching effects 80−70814
Si-Au amorphous film, metal-nonmetal transition, elec. cond., thermoelectric power meas. 79−47132
Si-Ge-Te system glasses, structural and electronic transitions 77−76890
Si-liquid N$_2$ system, kinetics of switching effect and electrothermal memory 79−51641
Si-SiO$_2$-SnO$_2$ structure, switching props. 78−76138

electrical conductivity transitions continued
Si-transition metal metastable films as temp. independent resistors 78−68097
SiC diodes, S-type, high-voltage switching 77−20421
SiC, thermal S-N switching 79−24027
Si$_{1-x}$Co$_x$ film, metastable impurity band, conductivity meas., semiconductor-metal transition 77−76884
Si$_{12}$Ge$_{10}$As$_{30}$Te$_{48}$, amorphous, energy controlled switching obs. *(Japanese)* 78−34867
Si$_{12}$Ge$_{10}$As$_{30}$Te$_{48}$, chalcogenide glasses, direct obs. of switching filaments 77−24595
Si$_{12}$Ge$_{10}$As$_{30}$Te$_{48}$, chalcogenide glass threshold switches, turn-on state, maintenance mechanism *(Russian)* 77−85271
Si$_{12}$Ge$_{10}$As$_{30}$Te$_{48}$, chalcogenide glass film, switching delay time 78−26926
Si$_{12}$Ge$_{10}$As$_{30}$Te$_{48}$ chalcogenide glass threshold switch conductivity in high ohmic state *(Russian)* 78−43502
Si$_{12}$Ge$_{10}$As$_{30}$Te$_{48}$ chalcogenide glass, switching in thin layers with semicond. electrodes 79−4586
Si$_{12}$Ge$_{10}$As$_{30}$Te$_{48}$, conducting filaments and switching phenomena 79−87134
Si$_{12}$Ge$_{10}$As$_{30}$Te$_{48}$, energy-controlled switching obs. 77−35973
Si$_{12}$Ge$_{10}$As$_{30}$Te$_{48}$ glass, thermally stimulated depolarization current meas. *(Japanese)* 78−34875
Si$_{12}$Ge$_{10}$As$_{30}$Te$_{48}$ surface, heat treatment and electron bombard. effects. SEM obs., rel. to switching filament form. 77−47700
Si$_{1-x}$Ni$_x$ film, metastable impurity band, conductivity meas., semiconductor-metal transition 77−76884
Si$_{12}$Te$_{48}$As$_{30}$Ge$_{10}$ film, temp.-depend. of non-ohmic current and switching characts. 77−8158
Si$_{12}$Te$_{48}$As$_{30}$Ge$_{10}$ film, amorphous, transient cond. characts. in preswitching regime 77−32055
Si$_{10}$Te$_{40}$As$_{30}$P$_{20}$, amorphous films, optically assisted mono-stable switching 77−11968
Sm monochalcogenides, semicond.-metal phase transition 79−47017
Sm$_4$Bi$_3$, press. induced valence instability, elec. resist. transition 78−95317
Sm$_4$Bi$_3$, press.-induced valence instability 80−20261
Sm$_{1-x}$Gd$_x$S, press. induced electronic transitions 78−68058
(Sm$_{1-x}$Gd$_x$)$_3$S$_4$, mixed valence compound, elec. cond. transition 80−70777
Sm$_{1-x}$M$_x$S, M=Eu,Ca,Yb, valence transition under high press. 79−73551
Sm$_{1-x}$Nd$_x$Se, Nd substitution effect on lattice const., resist., and colour 79−56763
Sm$_{1-x}$R$_x$$^{3+}$S, (R is rare earth metal), semicond.-metal phase transition 79−47017
SmS, and Sm$_{0.8}$Tb$_{0.2}$S, resistivity and thermopower 80−20260
SmS, crit. point for isostructural black to metallic phase transition, thermoelec. power meas. 78−60174
SmS, first-order transition from semiconducting to metallic state 78−52040
SmS, Hall effect near semicond.-metal transition 77−62968
SmS, press. effect on lattice parameter, mag. susceptibility, and reflectivity 79−56272
SmS, semicond.-metal transition, phase struct. determ. 78−91618
SmS:P, neutron irrad., semiconductor-metal transition 80−24975
SmSe, pressure-induced reflectivity changes and semiconductor-metal transition 79−56763
SnO$_2$, O chemisorption, elec. cond. and EPR meas. correlation 80−84369
SnO$_2$-VO$_x$-PdO ceramic, switching and oscill. phenomena 78−6417
Sr-Te-O system, amorphous thin film, vacuum deposited, elec. cond., current cut-off *(Japanese)* 77−24625
SrCl$_2$, fast ion cond., specific heat anomaly, mol. dynamics study 80−65283
SrCl$_2$, ionic cond., self-diffusion, rel. to defect motion, mol. dynamics study 80−65282
SrF$_2$, powder, elec. cond. transition under high press. *(Russian)* 77−20370
Sr$_{1.1}$V$_{12}$O$_{29.9}$, phase transitions, elec. cond., susceptibility and sp. ht. meas. 78−14776
(TSeT)$_2$Cl, high press. metallic phase *(Russian)* 78−95316
TaS$_2$ (1T), Hall effect 79−38103
TaS$_2$ (1T) electron irradiated, lattice contraction 80−59520
TaS$_3$, one-dimensional compound, phase anal., X-ray and elec. meas. 79−51086
TaS$_3$, Raman spectra, CDW induced metal-semicond. transition 80−11404
TaS$_2$(1T) pure and doped, electrical, structural and mag. props. 79−78141
TaS$_2$(1T) pure and doped, Mott and Anderson localisation, commensurate phase transition 80−39641
Ta$_x$Ti$_{1-x}$Se$_2$, cryst. struct. and elec. props. 79−47133
Te, elec. cond., 0-500 kbar 79−99589
Te, liq., elec. cond. at high temps. and press. 77−55592
Te, liq., semicond.-metal transition at high temp. and press. 77−51784
Te, metallic state, press. induced, elec. cond. meas. 80−96949
Te-Ge-As-Si amoprhous film, voltage controlled negative resistance type characts. 79−69614
Te-Se liquid semicond., resist. meas. under high press. 77−51791
Te$_{40}$As$_{35}$Ge$_7$S$_{18}$ film, threshold switching in relax. oscill. mode 77−69389
Te$_{40}$As$_{35}$Ge$_7$Si$_{18}$ with pyrolytic graphite electrodes, threshold switching characts. 77−24593
Te$_{40}$As$_{35}$Ge$_7$Si$_8$, amorphous, threshold switching, expt. 80−49830
Te$_{48}$As$_{18}$Ge$_6$Si$_{28}$ amorphous film, I-V curve, memory switching 79−69615
TeSe$_{12.5}$, amorphous alloy, thermal and elec. cond. during devitrification 78−26922
Te$_{43}$Se$_{30}$Sn$_7$ in MSM struct., switching effects 78−19164
Te$_{50-x}$Se$_{50}$Sn$_x$, thin films, elec. cond. and thermoelectric power meas. *(French)* 80−80335
(Ti$_{1-x}$ V$_x$)$_2$O$_3$ spin glass, mag. props., metallic antiferromagnetism 79−82791
TiO$_2$, anatase single crystals, switching, coloration and memory effect 78−72216
TiO$_2$, elec. cond., temp. depend. resistivity meas. at 77 to 600K, unwsitched samples 80−20262
TiO$_2$, polycryst. film, threshold switching 78−14771
Ti$_2$O$_3$, 3d-T$_{2g}$ band optical transitions near conductivity transitions, temp. depend. 79−19900

electrical conductivity transitions continued
- Ti_2O_3, piezoresistivity and semiconductor-semimetal transition 79−42595
- Ti_3O_5-V; semicond.-metal transition, resist., enthalpy and mag. susceptibility changes obs. 77−62965
- Ti_4O_7 and $(Ti_{1-x}V_x)_4O_7$, metal-insulator transitions, EPR, elec. and mag. props. 80−2336
- Ti_5O_9, phase transitions, elec. cond., mag. susceptibility, sp. ht., EPR and struct. aspects 78−10526
- $(Ti_{1-x}V_x)_2O_3$ solid soln., struct. changes comp. depend. 77−55275
- $(Ti_{1-x}V_x)_4O_7$, metal-insulator transition investig. by resist., sp. ht. and X-ray diffr. 77−43497
- Tl-Se, liquid mixtures, press. effect on two-phase region 80−75347
- Tl-Te liquid semicond., resist. meas. under high press. 77−51791
- $TlInSe_2$-$TlPrSe_2$ system, struct., elec. cond., and thermoelec. props. 79−87119
- $TlSbS_2$, phase transitions under action of high press., elec. cond. meas. 77−4196
- $Tl_2Se.As_2Te_3$, vitreous, thermal switching process in high electric fields 80−2432
- TlTe, melt, elec. cond., surface tension, microhardness, influence of impurities 80−88551
- U_3O_{8-x}, phase transition to U_8O_{21+x}, study by elec. cond. meas. 80−100489
- V foil, air-oxidised, reversible switching, mechanism determ. 79−28387
- $V_{1-x}Cr_xO_2$, VPE and characterisation 78−3053
- $(V_{1-x}Cr_x)_2O_3$, single cryst. obtained by chemical transport method, elec. cond. transition *(French)* 77−24940
- VO_2, amorphous thin films, phase transition, resistivity and opt. transmission discontinuities 77−47871
- VO_2, cylindrical specimen, thermal switching 80−44679
- VO_2, doped, morphology, structure and props. *(German)* 78−59823
- VO_2, elec. cond. and dielec. props. 79−11379
- VO_2, film, optical consts. and electrical props. near phase transition *(Russian)* 77−59631
- VO_2, film, semicond.-metal transition, carrier density, mobility and Hall meas. 77−43751
- VO_2 films, elec. cond. near metal-semicond. phase transition 77−1503
- VO_2 interference film, colour and elec. resist. changes at phase transition temp. *(German)* 78−56533
- VO_2, metal-insulator transition, resist. meas. 78−14770
- VO_2 metal-insulator transition, technical appls. possibilities *(German)* 79−99587
- VO_2 needles, switching, voltage oscills. 79−15199
- VO_2 pyrolytic film, phase transition and electrical cond. 77−89890
- VO_2, reactively sputtered film, influence of manufacturing parameters on film struct. and props. *(French)* 77−81218
- VO_2, semiconductor-metal transition, effect of ^{18}O substitution 78−84268
- VO_2 single cryst., noise in presence of current filament 80−92952
- VO_2 single cryst., switching, visual obs. of metallic and semicond. domains 78−52041
- VO_2 single cryst. film, ion-irrad., ‘splitting’ of semicond.-metal transition 80−11053
- VO_2 single crystal, elec. switching 80−92946
- VO_2, single crystal, fluctuations of current and switching time 79−38137
- VO_2, single crystal and polycrystalline, synthesis and resist. near metal-semicond. phase-transition 80−44680
- VO_2, sputtered, switching effects in four-electrode structures 78−2596
- VO_2, switching effect, temp. depend. 80−20259
- VO_2, thermal mechanism of switching effect 77−15919
- VO_2, VPE and characterisation 78−3053
- VO_2:Ga, Mo, temp. variation with impurity content 78−76121
- VO_2:Ga(Al)(Fe), phase transforms., influence of nonstoichiometry 77−85274
- VO_2-α-Fe_2O_3-Si, transverse elec. field effect on switching V-I characts. *(Russian)* 77−55591
- VO_x, minimum conductivity and electron localisation near metal-insulator transition 78−30960
- VO_x, switching effect in V oxidised in air during laser irradiation *(Russian)* 80−24977
- V_2O_3, impurity doping effects, elec. props. obs. 80−75609
- V_2O_3, semiconductor-metal transition, effect of ^{18}O substitution 78−84268
- V_2O_3, single cryst. obtained by chemical transparent method, elec. cond. transition *(French)* 77−24940
- V_2O_{3+x}, $0 \leq x \leq 0.08$, mag. and elec. props. 80−49833
- V_2O_5 crystal, photoinduced threshold switching in VO_2 channel 80−29450
- V_2O_5, switching mech. 78−60175
- V_2O_5-GeO_2-PbO glasses, memory and threshold switching 78−23142
- V_2O_5-$NaPO_3$-P_2O_5 threshold switches, elec. props. 77−35974
- V_2O_5-P_2O_5 glass, switching and memory behaviour, Pt point contact effects 77−11970
- V_2O_5-P_2O_5 glasses, threshold and memory switching 77−76887
- V_2O_5-P_2O_5-Nb_2O_5 glasses, switching 80−88604
- V_3O_5, cond. transition at 154°C, effect on props. *(German)* 79−42594
- V_3O_5, electrical, thermodynamic and mag. props. at metal-semicond. transition, homogeneity range 77−4413
- V_3O_5, high-temp. phase transition, resistivity, valence photoelectron spectra 80−49357
- V_3O_5, insulator-metal phase trnasition at 450K, properties 78−39023
- V_3O_5, metal-semicond. transition, pressure-temp. phase diagrams anal. 79−87132
- V_3O_5, Mo,Ti, and Ga doping effects on conductivity transition 77−11971
- V_3O_5, resistivity switching due to phase transition, 154°C 79−19642
- V_3O_5, semiconductor-metal transition, effect of ^{18}O substitution 78−84268
- V_3O_5, steady-state elec. switching characts., simple thermistor model 77−8159
- V_3O_5, struct. and electronic aspects of cond. transition 78−15078
- V_xO_y film, prep. by thermal decomp. of vanadium naphthenate, and elec. props. *(Japanese)* 78−88425
- $V_{1-x}Re_xO_2$ $(0 \leq x \leq 0.15)$, insulator-metal transition, DTA, X-ray, mag. and elec. meas. 78−10353
- $V_{1-x}Ti_xO_2$, metal-insulator transition, resist. meas. 78−14770
- $V_xTi_{1-x}Se_2$, cryst. struct. and elec. props. 79−47133
- WO_3 amoprhous film, sublimed under different conditions, elec. transport props. 80−7015
- WO_3 films on Si, sapphire, glass and metal substrates, colour intensity dependence obs. *(Russian)* 80−2430

electrical conductivity transitions continued
- WO_3, semiconductor-metal transition, structural phase transition 80−107870
- WO_3-MnO-P_2O_5 system, glass form. and memory effects 77−76888
- Xe, metallic state at static press., elec. cond. meas. 79−33313
- Y_2S_3, p-n transition, elec. cond. and thermoelectric power *(French)* 78−84264
- Yb, resistivity at high temps., semimetal-semiconductor transition 78−14727
- Yb, semimetal-semicond. transition at high press., Seebeck coeff. meas. 77−62956
- Yb, shock compressed, elec. cond. behaviour and transitions, up to 220 kbar *(Russian)* 77−80761
- $Zn_xHg_{1-x}Se$, band struct. from Shubnikov de Haas effect and hydrostatic press. meas. 80−49599
- $ZnIn_2S_4$ crystals, switching effect, electric field distribution 80−107872
- $ZnIn_2S_4$, S-type negative resist. and switching effects 80−65581
- $ZnIn_2S_4$ switching investigation, negative resistance state instability, resistivity transitions 80−6920
- ZnS film, evaporated amorphous, mechanism of memory phenomena *(Japanese)* 78−23140
- $ZnS_{1-x}Se_x$:Cu,Br ceramic, current oscills. and electrolum. under high elec. fields 79−38677
- ZnSe, high-resistance layers, effect of electrode materials on switching 79−65549
- ZnSe:Al, current switching mechanism *(German)* 79−28385
- ZnSe:Cu, I, ceramic, electroluminesc., electric field induced switching effect under illum. 77−1460
- ZnSe-CdTl, epitaxial film, cond. transition, laser switched memory *(Russian)* 77−8182
- p-ZnTe film, current-voltage characts. 77−66214
- ZnTe thin film, model for off-on transition 80−54742
- ZnTe(S), semiconductor-metal transition, press. calibration above 100 kbars fixed points 80−77808
- ZrC-C composite system, electrical resist. meas., percolation theory anal. 78−84269
- ZrV_2, C15 supercond., dielec. transitions, temp. depend. of resist. and mag. susceptibility, 4.2-300K 79−38136
- ZrV_2, dielectric phase transition, elec. resist. temp. depend. 79−65525

electrical contacts
- *see also contact potential; contact resistance; ohmic contacts; point contacts*
- air pollution effects on reliability of contacts of telephone exchanges *(Polish)* 79−74573
- biomedical implantable power sources, radioisotope thermoelectric generators appl., high reliability contacts using local heat pulses 79−52952
- bridge transfer on electrodes with fibre struct. of heat-proof component 77−59325
- ceramet Ag based contacts, Brinell and Vickers hardness number comparison 79−38978
- coating layer build-up on contact materials *(German)* 80−7852
- contact resistance probing and Auger analysis of contaminants, combined technique 80−39662
- electrode, evaporation rate from cathode spot in vac. arcs. 80−49024
- electrometric circuit switching by magnetically controlled contact 77−79108
- erosion and aggregate condition near discharge, cellular structure effects *(Russian)* 79−37557
- gentle accelerated corrosion test 79−61814
- hardness and ductility 79−87025
- hole diameter meas. with universal microscope and electronic contact indicator 77−79055
- hot filament connection 79−63273
- Josephson contact microwave detector sensitivity and cutoff frequency rel. to capacitance 78−49902
- light-duty electrical contact, reliability assessment methods 78−29219
- low temperature resist. characts. 78−68072
- LV switchgear contacts, AgMgO properties *(Slovak)* 78−56603
- material transfer in contact electrification 78−6432
- metal interface of unlike metals, secondary ion-ion emission 78−11050
- metal-insulator contacts, model of charge injection 78−68088
- metal-metal contacts, use as prevention H escape from metals 80−24595
- metallic, directional effects of heat flow, thermal rectification 77−58532
- metallic, rough surfaces, anisotropic, light scatt. 79−60606
- metallic bridge, conductivity, nonlinear effects *(Russian)* 77−59326
- microwave power meter using contact between metallic probe and Ge crystal 77−37986
- molten metal bridge transfer of opening contacts, theoretical anal. 77−11987
- noble metal contact, substrate material diffusion and corrosion film formation, model 80−2312
- polymers, contract electrification, analogue model 79−51655
- pulsed high currents in Tokamak device, design and testing 80−70029
- relays, measurement of thermoelectric voltage across contacts for different metals *(German)* 79−26040
- resistance analyser system 79−99605
- RF contact for superconducting resonators 77−26923
- rotating systems, temp. meas., minimisation of contact drop error 78−73991
- self-diffusion at low-temperatures in coated contacts *(German)* 80−6538
- sintered composite material, corrosion under tropical marine climate 78−11366
- sintered materials appls. 80−29902
- skin tissue C tattoo for generation of permanent dry elec. contacts 78−77122
- slip ring circuits for strain gauge meas. 79−67291
- solid moving contacts, in versatile multicontact thin-film superconducting switch 78−4661
- steel, contact rapid meas. tech. for electrical contact resistance applied to lubricant additive studies 77−16698
- superconducting contacts, influence on magnetoresist. meas. 78−21184
- superconducting quantum magnetometer with two-contact sensor, asymptotic characteristics 79−6155
- surface damage caused by closing voltages, field-ion microscopic studies 78−64098
- surface film, method of obs. of contact area and mech. breakdown 79−37939
- thermistor bolometer with $Mn_xCo_yNi_zO_4$ spinel ceramic current noise 77−51793

electrical contacts continued
- tree root potential meas. electrode earthing method *(Russian)* 80−26420
- TSC and isothermal decay currents, influence of blocking contacts 77−28182
- tuning forks, electrically driven, Melde's experiment apparatus 80−42022
- ultrahigh vacuum and cryogenic feedthrough, with 48 pins 79−97399
- Van der Pauw method, meas. of resistivity and Hall constant 77−67467
- welding resistance of contacts in switching equipment, meas. apparatus 77−57353
- Ag contacts on InP, TEM obs. of struct. 77−62765
- Ag, electrical contact material with liquid lubricant, prod. and appl. 78−10559
- Ag electrode, evaporation rate from cathode spot in vac. arcs. 80−49024
- Ag in H_2S atmospheres, formation of contaminating layers *(German)* 80−71811
- Ag, MgO disperse particles strengthened *(Slovak)* 78−31544
- $Ag/Na_2SO_4(WO_4)$, and $Ag/Ag_2SO_4(WO_4)$ solid cell systems interface form., intergrain contact growth 77−16827
- Ag-In, asymmetric and symmetric contacts, cond. of $TlInS_2(Se_2)$, crysts. 80−6835
- Ag-Pd-Cu, contact-spring props., fatigue and spring limit *(Japanese)* 79−29117
- Ag-Pd-Cu alloys, contact-spring props. and age hardening 78−88473
- Ag-Zn, internally oxidized, elec. contact characts., alloying additions effect *(Japanese)* 80−88619
- AgCdO, powder metallurgy production, for switchgear in power engineering 80−104094
- Al/NiSi/Si system, high temp. interaction study, elec. and struct. characts. 79−24075
- $Al/SiO_x/p$-Si contacts for IMS solar cells, high temp. lifetesting 79−87988
- Al-Au bimetal thin film interdiffusion zone, intermetallic phase form kinetics, 70-160°C 78−75891
- Al-Au couple, electroformed, nonohmic characts. and electron emission 80−60066
- Al-Cr, thin film metal contact, sheet resistance changes 80−80356
- Al-Si contacts, electromigration and diffusion of Cu in Al film 79−77820
- β-$Al_2O_3.Na_2O$ cryst. or sintered disc, Au electrode interface impedance rel. to roughness 77−4437
- Au alloy electrodeposits, for electronics industry, characts. 78−52695
- Au, Co hardened, mech. film breakdown and ESCA of film, expt. 77−4436
- Au coated, Cu diffusion under high temperature obs., effects on mech. and elec. props. *(Czech)* 78−91486
- Au coating on Sn-Ni alloy electrodeposits, corrosion resist., appl. as elec. contact material 77−77633
- Au electrode, evaporation rate from cathode spot in vac. arcs. 80−49024
- Au electroplate on Cu, water vap. adsorption 77−69168
- Au, Ni and Cu diffusion, relative rates 77−80652
- Au surface, lubrication by plasma-deposited thin films of fluorocarbon polymer 80−89157
- Au tab on glass, evap. method 77−1887
- Au wire-semiconductor, spark welding method for elec. meas. applications *(German)* 79−49215
- Au-Ag, electron interferometric meas. of contact PD 77−32069
- Au-As_2Se_3 contact, model of charge injection 78−68088
- Au-$Cd_xHg_{1-x}Te(CdTe)$ contacts, photo-effect in the 77-300K range, barrier height estimation 80−107850
- Au-Co electrodeposits, heating effect on microstruct. and surface topography 77−43456
- Au-Ge-Si structure, O distrib. profile in Ge, from emitted α-particle energy anal. of $^{16}O(\alpha,\alpha)$ 79−5213
- Au-Si structure, O distrib. profile in Au, from emitted α-particle energy anal. of $^{16}O(\alpha,\alpha)$ 79−5213
- Bi microcontact, resistivity at low temp. *(Russian)* 78−80054
- Bi_2Te_3, surface prep. by etching for electroplating elec. contacts 80−108647
- CoO film, as on thermally aged Co-hardened Au electroplate, breakdown props. 77−85364
- Cu contact tarnishing and Cu-Au interdiffusion obs. 78−7098
- Cu H_2S atmospheres, formation of contaminating layers *(German)* 80−71811
- Cu, slip ring, elemental surface composition as function of temp. 80−66901
- Cu_2O and CuO powders, contact resistance, temp. and pressure dependence, obs. *(German)* 79−4555
- Cu_xS-CdS solar cells, front contacts 78−39822
- GaAs, minority carrier diffusion lengths, contact metal effects 78−72260
- GaN-In(Sn)(Sb)(Te), using GaN made by oxidation and subsequent nitridation of GaAs, I-V characts. 77−20436
- Ge film, AC cond., up to 200 kHz, 100-300K, role of contacts 77−76970
- Ge high purity planar detectors, contacts made by ion implantation 79−97949
- Ge radiation detectors, high-purity, ion implanted n-type contact 77−54416
- n-$Hg_{1-x}Cd_xTe$, photoconductor, contact noise at 77K 78−88028
- HgSe, highly-electronegative stable metallic contact for semicond. devices 77−24617
- In-$Cd_xHg_{1-x}Te(CdTe)$ contacts, photo-effect in the 77-300K range, barrier height estimation 80−107850
- InP, Gunn oscillator magnetoresist. meas. of mobility and noise, contact effects 77−62948
- InP ohmic contacts 79−28406
- Ir electrode, evaporation rate from cathode spot in vac. arcs. 80−49024
- IrSi on Si, Schottky barrier height meas. 79−47160
- Na-K-Cs alloys, liquid contact material, phase diagram calcs. 78−6145
- Pd electrode, evaporation rate from cathode spot in vac. arcs. 80−49024
- Pd-Ag in H_2S atmospheres, formation of contaminating layers *(German)* 80−71811
- Pt-GaAs contacts, sintered, eval. of W, Ti, Mo and Hf barrier metals 77−8193
- Pt-Ir, Au covered, spectral characts. of VLF noise, allowing for logarithmic creep *(Russian)* 77−85301
- resistor, improved thermal contacts 78−37015
- Rh electrode, evaporation rate from cathode spot in vac. arcs. 80−49024
- Si detector electrical contact at He temp. to evaporated Au film 78−37019

electrical contacts continued
- Si device metallisation, TiN and TaN as diffusion barriers 80−65304
- Si, radiation detector, barrier heights, electron and hole currents, Schottky contact effects 79−33293
- Si solar cells, low cost, Ni contacts 80−94017
- Si/Pd-W, contact reactions, backscattering, X-ray diffr. meas. 80−20040
- n-Si-Ni, Schottky-barrier, I-V characts. of elec. contact 79−19662
- Sn-Ni electrodeposit, contact resist. corrosion effect 78−47847
- Sn-Ni electroplated alloy, etch rates using quartz cryst. microbalance, contact resist. 77−59981
- W-Cu-Co(Ni), electrical contact material, comparison of Co and Ni effects *(Korean)* 78−10539
- Zn- and ZnO-electrolyte, current-potential characts. 77−1482

electrical contracting
- Li-FeS_2 battery development, for electric vehicles and stationary energy storage devices ANL program with industrial participation 79−48113

electrical engineering
- *see also high-voltage engineering*
- atomic power engineering development in CMEA countries *(Polish)* 77−65344
- Bell Laboratories, origin of solid-state research 77−41449
- climatic conditions of equipment in Rumania, classification *(Rumanian)* 79−44242
- education, energy option for undergraduates 80−31447
- electrical and electronic engineering undergraduate courses, engineering design importance 80−67972
- electronics, undergraduate laboratory course 80−105478
- electronics technology development, teaching 80−31470
- electronics unit for physics students, systems analysis approach 77−45625
- electrooptics for electrical engineers, undergraduate curriculum 79−11
- engineering education, perspective and some current problems 79−10
- MIDCON conference, Dallas, USA, Dec. 1978 79−87939
- power, laser thermonuclear fusion future prospects 77−38401
- power industry, need for continuing education 77−45633
- students in electronics and physics, examination, reliability 77−26103
- superconducting materials, research and elec. engineering appl., European trends *(German)* 77−55649
- superconductors, physical properties and appl. *(German)* 77−55648
- teaching electromagnetism, to undergraduates, showing practical appls. 78−20922

electrical engineering applications of computing *see electrical engineering computing*

electrical engineering computing
- *see also computerised control; computerised instrumentation; electric machine analysis computing; electric machine CAD; power system analysis computing; power system CAD*
- circuit-breaker induction calc. using standard finite element software 79−41906
- compressed magnetic field power supplies, characts. of helically wound generators, using a 2-d MHD computational model 78−17838
- cylindrically symmetric arcs, radial radiative energy flux distrib. 79−14623
- DEGRA, radioisotope thermoelectric generators, power degradation predictions 80−40879
- dry etched line edge profiles 80−71780
- electric and magnetic field problems, book 78−37787
- electric field computation using SCOFF program *(German)* 80−78740
- electric- and mag.-fields with open boundaries, two-dimensional 78−22064
- electrostatic field solution, two-dimensional, using Sander's function 79−878
- energy planning in Arab world 80−26122
- ferromagnetic cylinders with field intensity-dependent permeability, eddy current anal. *(German)* 77−40088
- fluid dielectrics impurity particle field-enhanced motion 77−43932
- fusion reactor, TNS, electrical design costing 78−55014
- fusion reactor, Tokamak, commercial, plasma driving system requirements 78−54954
- fusion reactor coil design codes 78−66367
- hysteresis modelling and digital simulation, using cubic spline functions *(German)* 79−4706
- ion milling, string segment motion algorithm 80−71779
- LF fields in linear media, two-dimensional finite element analysis 79−41297
- magnetic field, three dimensional finite element program 77−38769
- magnetic fields of eddy currents, in conducting plate, soln. using ODRA 1204 computer *(Polish)* 78−29878
- magnetisation and electrification curve approximation *(German)* 77−8338
- MHD steam power plant, coal-fired, economic optimisation 79−52942
- MHD/steam combined-cycle plant, combustion air temperature variations reduction 79−52943
- NETHAN, thermoelectric coolers with high current pulse and finite cold junction, fast transient behaviour 80−27290
- permittivity meas. through ponderomotive forces determ., computer-aided field analysis 79−215
- pole pieces with cavities, correction effect modelling *(Czech)* 79−45879
- radioisotope thermoelec. generators, design optimisation program 80−40880
- RF cavities with cylindrical symm., evaluation by computer program SUPERFISH 77−18714
- SAW resonator, distributed-feedback, computer model *(Flemish)* 80−5899
- solar energy DC-AC inverter design, effect of meterological conditions, computer simulation 80−61373
- solar total energy system evaluation program 80−30402
- static field and eddy current problems, computational methods for soln. via Fredholm eqns. 79−68344
- STESEP, solat total energy system eval. program 80−30402
- toroidal field coils, EM parameters calcs. of current paths in homogeneous media *(Japanese)* 80−106155
- transformer oil diagnosis *(Czech)* 80−97744
- two dimensional electrostatic field shape investigation *(Czech)* 79−27126
- $Ga_{1-x}Al_xAs$-GaAs solar cells, computer anal. of cell characts. incl. band gap variation 80−55866
- Nd:glass mode locked ring laser, unidirectional travelling wave operation 77−88812

electrical engineering computing continued
- SF_6, compressed in space-charge stabilised nonuniform fields, corona threshold computation 79−19118
- Si epitaxial wafer, impurity profile meas. by multilayer spreading resist. anal. 77−76449

electrical fault location *see fault location*

electrical faults
- *see also accidents; discharges (electric); electric distortion; fault currents; fault location; flashover; insulation; losses; overvoltage; protection; testing; transients*
- analogue safety data link, for Princeton Large Torus control room 78−54938
- components, mathematical simulation of life *(Spanish)* 79−21532
- fast nuclear reactors, electrical supplies and Na pumping system 80−52723
- X-ray apparatus electrical circuit fault classification 77−21604
- PbSnTe-PbTe heterostructs., effect of electrical grounding on electron irrad. 78−60194

electrical forming *see electroforming*

electrical insulation *see insulation*

electrical noise *see noise*

electrical power systems *see power systems*

electrical properties of substances
- *see also dielectric properties of substances; discharges (electric); electrical conductivity; flexoelectricity; thermoelectricity*
- dielectric thin films 78−2802
- layered compounds, book 77−39757
- materials, electronic, optical, magnetic and thermal props., rel. to energy technology 78−88412
- natural clay permafrost, electrical props. 77−44967
- random heterogeneous materials, statistical theory of effective elec. thermal and mag. props. 77−48118
- rocks and minerals, conf., Newcastle, England (April 1974) 77−37194
- steels, constructional and tool, heat treatment effects on elec., mag. and mech. props. expt. 77−77719
- Si_3N_4:Si amorphous film 77−76987

electrical resistance measurement *see electric resistance measurement*

electrical transport processes *see electrical conductivity*

electricity
- *see also atmospheric electricity; electric charge; electric current; electrical properties of substances; electromagnetism; terrestrial electricity*
- David Ausubel learning theory as reference system for content organisation in physics 80−22172
- dimensional analysis in electricity and mechanics, teaching 79−97165
- energy efficiency, problems and solns. 78−81762
- Franklin, Benjamin, exptl. philosopher, theory of electricity, for teaching 78−24630
- nuclear power, electricity generation and use in energy conversion 79−9921
- Priestley's mind, synoptic nature, electrical thought 79−84930
- SUPERCHARGE game for student visualis. of equipot. surfaces 79−30179
- teaching undergraduates EM theory 77−71167
- theory of, book 80−86051

electricity supply industry
- advanced electric power utilisation technology, review 79−24884
- advanced energy conversion and storage, electric utility appls. 80−16793
- advanced reactor and fuel cycle systems, potentials and limitations for United States utilities 80−106106
- biological risk involved in power production 80−98209
- coal-fired power stations, financial impact of air pollution control costs 80−3497
- demands fulfilment and ensuring full employment *(German)* 80−36831
- economic assessment of renewable sources, for UK conditions 79−48043
- effects of world energy resources on economy *(German)* 80−89583
- electric utility load management, thermal storage systems appls. 80−16845
- fast neutron reactor development, European electricty producers cooperation, Creys-Malville plant *(French)* 80−47689
- FBR, electric power generation, research, development and demonstration, risk and timing 80−57837
- flywheel energy storage system for electric utilities, study 79−96486
- fuel cell power plant, cost effectiveness 79−57424
- interfuel substitution, effects on electric power industry, in United States 79−87942
- nuclear power industry status, national and international recognition problems 79−93810
- nuclear waste disposal problems, present and future trends 78−66350
- offshore energy conversion (OTEC) plant design, technology considerations 79−5507
- real-time urban power dispatch with ambient air quality constraints 79−57542
- Redox flow cells, electrochem. energy storage for utility appls. 80−30456
- solar energy utilization, direct and indirect *(German)* 80−3489
- solar test systems, elec. utility demonstration projects 80−3488
- storage of off-peak power, thermal, high efficiency 79−48188
- thermal energy storage, US DOE research program for aquifer waste heat utilisation 80−97808
- thermal management of battery systems for electric vehicles and utility load leveling 80−30458
- thermionic conversion appl., Department of Energy (USA) development program 79−48154
- tidal power stations, technical details and operating experience 80−72009
- underground pressurised saturated hot water storage for peak lopping appls. 80−76653
- United States' Pacific Northwest Electric Utility, strategic solar energy planning program 79−48101
- wind energy conversion systems, value to electric utility, economic model 80−61257

electro-optical devices
- *see also electrochromic devices; liquid crystal devices; optical modulation; Q-switching*
- 2 Gbit/s electro-optic modulator for visible lasers 79−86262
- 4-bit digitally driven integrated optical amplitude modulator for data processing 80−53476
- A/C convertor using channel waveguide modulators, design and analysis 79−55249

electro-optical devices continued
- A/D conversion using channel waveguide modulators 78−66898
- A/D convertor, high-speed guided wave 80−33234
- active optical devices, seminar, San Diego, CA, USA (August 1979) 80−101664
- active Y-junction switching devices in Ti diffused $LiNbO_3$ optical waveguides 79−23091
- aerial photographic analysis and stereographic mapping with electro-optical pattern recognition 77−19186
- analogue-digital conversion, using channel waveguide modulators 78−38051
- anisotropic waveguide, guided-radiation mode interaction, appl. to direct-intensity modulators 79−76839
- array processor for complex signals 78−94428
- atmospheric degradation of electro-optical system performance 79−66805
- atmospheric degradation of electrooptical system performance 79−34940
- atmospheric effects prediction for electro-optical sensors use 79−53522
- balanced-bridge switch modified config. with two straight waveguides 79−98506
- beam deflector construction principles and efficiency characteristics *(Russian)* 79−94342
- birefringent Fabry-Perot etalon tuner for dye lasers 77−75500
- bistable devices, optical regenerative oscill. and monostable pulse generation 80−106612
- bistable mirrorless device, monostable pulse generation and optical regenerative oscill. 80−96002
- bistable optical device development from integrated two-arm interferometer, appls. *(French)* 80−69555
- bistable optical devices, overshoot switching 80−58776
- bistable optical devices 78−46763
- bistable optical devices for integrated optics and fibre optics appls. 79−55175
- bistable optical systems based on Pockels cell 79−59827
- bistable switch, based on waveguide coupler, exam. 78−38086
- Bragg deflection modulators in corrugated waveguides 79−59844
- Bragg reflector electro-optical Q-switching of semicond. lasers 77−19345
- Bragg switch, thin film 78−38088
- Bragg switch for optical channel waveguides 78−75002
- broadband travelling wave modulator, expt. design principle 78−94438
- cameras, subpicosecond resolution, progress report 77−5951
- cardiac sound and vibration recording, electro-optical sensor 77−21648
- ceramics, transparent ferroelectric, composition selection for appl. in light modulators *(Russian)* 80−91869
- channel waveguide double-pole double-throw switch/coupler, using total internal refl. 78−71233
- channel waveguide electro-optic switch, low crosstalk operation 80−38126
- channel waveguide interferometric modulator for EM field detection 80−74498
- channel waveguide switch for computer communication bus 80−9987
- coaxial Kerr cell built on coaxial 50 Ω transmission line, He-Ne laser 79−72606
- compound optical crosspoint with low crosstalk, using $LiTaO_3$ 78−33915
- conference, laser and electrooptical systems, San Diego, CA, USA (Feb. 1978) 78−42340
- conference, Minneapolis, MN, USA (June 1979) 80−77535
- conference, Utrecht, Netherlands (Oct. 1978) 80−31420
- coupled-waveguide optical modulators with Schottky contacts, embedded-and rib-waveguide configurations 79−23093
- curriculum in electrooptics for electrical engineers 79−11
- cylindrical waveguide optical modulator efficiency in thermal mode *(Russian)* 79−94345
- cylindrical waveguide wideband modulator, parameter optimisation *(Russian)* 79−94344
- DC voltmeter, direct reading, with high input resist. 78−245
- deflector, light beam streaking by induced travelling lens 79−46045
- deflector of blazed grating type, multistage system 80−106625
- deflector with cylindrical electrodes, controlling field distortion 79−98493
- deflectors, boundary effects, pot. distrib. *(Russian)* 78−71228
- deflectors, end effects rel. to operating quality 79−55223
- deflectors for laser beam scanning 78−79060
- deflectors using electro-optically controlled interference 79−1007
- device fabrication by MBE 79−43154
- dielectric resonator, trapped mode, coupling and tuning for laser beam modulation 78−55389
- differential electro-optic shutter with ns pulse operation 78−74994
- diffraction grating, electrically controllable reflection type, effects of electrode config. on voltage depend. diffr. pattern *(Japanese)* 79−94347
- diffraction grating, polarisation refl. 77−3660
- diffraction grating, refl. type elec. controllable, for intracavity laser modulation 77−58357
- diffraction modulator, large-aperture 80−33179
- digital light deflector with KD_2PO_4 polarisation switches 77−39049
- directional coupler, elec. controlled, fluoresc. visualisation 78−38049
- directional coupler, phase tuning by photostructural effect of chalcogenide glass film 77−83963
- directional coupler switch, electrooptic, used as amplitude modulator, exam. 78−42467
- directional coupler switch, polarisation independ., using weighted coupling 80−28352
- directional optical coupler, phase tuning 77−75680
- discharge gap characts., laser-radiation-triggered, influence of discharge medium, electrooptic switch control appls. 80−64818
- dispersive modulator using Stark effect system, for optical pulse compression 77−54793
- displacement meas. by interferometers with electro-optical modulators *(Russian)* 78−12667
- display structure based on reversible electrodeposition 79−15435
- distance measurement device, appl. to water levels obs. *(German)* 78−69280
- distance measuring instruments, Zeiss ELDI 2 type, error anal. *(German)* 79−21081
- distributed Bragg reflection modulators for integrated optics 77−27388
- dye CW laser, electrooptically tuned, optical switching and bistability 79−59708
- dye laser, double-wavelength electro-optically tuned synchronously pumped mode-locked CW 79−89924
- dye laser tuning by birefringent Fabry-Perot etalons *(Japanese)* 77−7125

electro-optical devices continued
dynamic electro-biased laser Q-switch with SCRs *(Chinese)* 79—45977
efficient intensity modulator 78—22190
electric and refractive index distribs., guided wave devices 77—72068
electric field intensity meas., electro-optical sensor with fibre transmission line 80—69509
electrical resistivity meas. method, using electrooptic cryst. voltage-induced birefr. 80—73386
electro-optic waveguide modulators, capacitance of electrode system rel. to modulation efficiency *(Russian)* 80—1359
electroabsorptive devices, material requirements 79—3754
electron beam spatial modulator using KH_2PO_4 77—72077
electrostatic field distribution calc. *(Russian)* 80—87514
eye refractive error, meas. using modified Foucault knife-edge test 77—4999
Fabry Perot resonator containing electrooptical element, light processing appls. 78—38001
Fabry Perot wide-band electrooptic type modulator, modulation sensitivity 79—3724
Fabry-Perot bistable devices, as optical switch, limiter or memory element 77—88931
Fabry-Perot electro-optic type wide-band modulator sensitivity, surface error influence 79—50392
Fabry-Perot nonlinear electro-optic device, using refl. light feedback 78—55457
Fabry-Perot resonator, bistable, use as optical switch, limiter or memory element 77—39024
fact directional coupler switch/modulators, novel ps optical pulse sampling method 80—58784
fail-safe fibre optics data bus using active electrooptic mirror terminals 79—23053
fast Pockel cell and GaAs switch for active pulse shaping in ps domain 80—28257
fast streak or frame camera appl. to plasma dynamics in plasma focus device 79—68950
ferroelectric ceramic, optical modulation by electrostriction during electron beam charging, spatial characts. 79—7224
ferroelectric ceramic-photoconductor structure, as optically controlled transparency 80—28343
ferroelectrics, photoelectretic states in real time spatial light modulators, photorefractive effect 80—80676
film production, highly-oriented, m-nitroaniline type 77—19463
frequency modulator with rot. elec. field, appl. to laser Doppler velocimeters 77—42620
frustrated total internal reflection switches and modulators 77—39066
GaAs homojunction rib waveguide directional coupler switch 80—69554
gate, for ruby laser ns pulse train generation *(Russian)* 77—79871
gate for nonpolarised emission *(Russian)* 78—59132
gated optical multichannel analyzer for tune resolved spectroscopy 77—74516
guided wave, for logic and computation 78—66946
heterostructure planar waveguides guided-to-radiation mode conversion and appl. to light modulation 80—87557
high-speed shaping device, for address control of laser beam deviation 78—5554
hologram electronic heterodyne recording and self-interference term rejection 80—91756
holographic data storage and processing, photosensitive electro-optical materials *(French)* 77—31077
holographic mass memories using vol. holograms 77—7041
holographic memories, interfaces between optics and electronics 77—7042
holographic one-tube goggle system engineering 80—78988
holographic phase distributions, linear and nonlinear, determ. using electro-optical system 78—58954
holographic recording materials and devices, book contrib. 78—25838
holographic storage, electro-optic crystals *(German)* 79—27198
hybrid bistable optical devices, transient response 79—59803
II-VI semiconductor Franz-Keldysh effect modulators for laser radiation *(Russian)* 77—88813
image detail enhancement system with PROM, for photographic recording 78—58086
image digitiser system design 80—48441
image evaluation, subjective effects of electronic and turbulent noise 78—65023
imagery, 2-D sampled, aliasing and blurring effects 80—99635
injection diode modulated laser pulse generator and digital control cct. *(Russian)* 80—14372
integrated bistable optical multivibrator using electro-optically controlled directional coupler switches 80—19111
integrated directional coupler switches, modulators and filters using $\Delta\beta$ reversal techniques, review 80—38132
integrated electro-optic modulators, review 79—37058
integrated electro-optical A/D convertor, using branching waveguide modulator channels 78—42474
integrated interferometric reflector with elec. control for laser reflector 77—58490
integrated optic modulator, 12GHz continuous tuning of CO_2 laser lines 77—83907
integrated optical device used as switch, amplifier, limiter and memory logic element 79—32090
integrated optical logic circuits, using electrooptic switches and modulators 78—38089
integrated optical switch, optically controlled two channel, based on directional coupler 78—83116
integrated optical switch for fibre data transmission system 77—27384
integrated optics, electro-optical active components for guided light 78—42470
integrated optics, electrooptical channel waveguide matrix switch using total internal reflection 80—58810
integrated optics modulator, anal. 77—39108
integrated optics planar technology, future *(Czech)* 77—46820
integrated optics sub-ps gate 80—58809
integrated two arm interferometer, optical bistability expts. 79—76883
integrated waveguide-hologram memory design approach 80—32940
interference polarisation filter, Q-switching ruby laser with high-frequency control of lasing conditions 80—74363
ion detector, electro-optical, for spark source mass spectrometry 80—42246
ion detector, using fibre optics, for mass spectrometer 77—45915
IR electrooptic waveguide for CO_2 laser modulation 77—27349
IR source, tunable, 2.75 GHz using CO_2 laser 77—14786

electro-optical devices continued
Josephson optical modulator with weak-link diffraction grating 79—98486
Kerr, high-speed cell, high power switching with picosecond precision 78—1327
Kerr cell driven by light-controlled Si switch 78—26925
Kerr cell for anal. of very short laser impulses *(Italian)* 78—54477
Kerr shutters, for Q-switching and radiation pulse shaping in Nd-glass lasers 79—3729
large-aperture Pockels cell design 77—19438
laser and electro-optical systems, conf., San Diego, USA (May 1976) 77—19278
laser beam deflecting, use of Kerr cell and birefringent calcite prism 77—7103
laser beam deflector, guided wave electro-optical beam deflector *(German)* 77—19417
laser beam modulation appl., comparison with acousto-optical devices 80—43380
laser impulse shape regulation, electro-optic deflectors *(Russian)* 77—19354
laser intracavity phase lock control system 79—76718
laser intracavity phase modulator, for dye laser freq. stabilisation 77—88802
laser modulator, 1 Gb/s 77—79965
laser modulator for optical coherent transient generation 80—102776
laser pulse display and shaping, subnanosecond, electro-optic technique 77—19270
laser pulse generation and modulation devices 78—25899
laser pulse shaping on multiple rot. lines, using electro-optical cryst. modulator 80—78879
laser pump, active medium and interference coating effect, temp. profile, electro-optical characts. 77—19275
laser scanner, background signals anal. 77—19425
laser sensing system for elec. and mag. fields in power transmission 77—45870
laser shutter, piezo-opt. effect on dynamics and spectral characts. *(Russian)* 77—83912
laser technique for probing coherent and incoherent decay processes 77—75338
laser triggered Krytron-Blumlein electro-optic switch 78—9450
laser unequal path interferometer with electro-optical camera and minicomputer, fabrication/test appl. 80—77847
laser wideband ring modulator, for CO_2 laser 77—88803
light beam choppers, electromechanical, review 77—27346
light beam deflector, electrooptic phased array, application to analogue-digital conversion 78—38052
light modulation by electro-optical device with feedback 79—41448
light modulator, phase matched 78—83089
light modulator with small nonactive losses 80—78981
light shutter array, large area electronically controllable, using polyvinylidene fluoride bimorph vanes 80—58696
light valve, photoconductor controlled 77—7214
linear interferometric modulator for electromagnetic field detection 80—58782
liquid crystal electro-optic switch, four-port, for unpolarized fibre light 80—58715
liquid crystal electro-optical modulators for two-dimensional data processing 78—79141
Mach-Zehnder interferometer, switch, integrated optical format 78—38084
Mach-Zehnder interferometric switch for integrated optical multivibrators 80—53479
Mach-Zehnder interferometric waveguide modulator, polarization-independent operation 79—18552
Mach-Zehnder type modulator, RF modulation characts. meas. method 80—74480
Mach-Zehnder waveguide modulators in Ti-diffused $LiNbO_3$ 80—33203
marine propag. conditions for system performance anal., weather to propag. data conversion 79—58094
matched holographic filters with Pockels readout optical modulators 80—53456
materials and applications *(Italian)* 77—42626
meter for rotation angle meas. 79—88908
Michelson interferometer, active stabilization by electrooptically tuned laser 80—86386
microchannel spatial light modulator, for real-time optical data processing 79—18534
microchannel spatial light modulator as storage medium 80—43479
microchannel spatial light modulator development, for real-time optical data processing 79—72714
microoptical switch, Mach Zehnder interferometer, for use with optical fibre transmission lines, exam. 78—38085
microwave modulator, broadband electronically tunable, for CO_2 lasers 79—64256
microwave optical radiation modulator using $LiNbO_3$ crystal resonator 77—27353
mirrorless electrooptic device with feedback, optical multistable operations 79—32051
mirrorless electrooptic nonlinear devices with two feed signals, operation characts. 80—14441
modular crystal length reduction by protruding electrodes 79—76860
modulation phase nonuniformity over light beam cross-section, rel. to phase rangefinder 79—50400
modulator, asymmetrical, electric field config. anal. *(Russian)* 80—91885
modulator, complex-internal-refl. config. 79—50384
modulator, coupled waveguide with pn-junction, strip loaded channel waveguide, design 78—46843
modulator, large bandwidth, using mm-wave drivers 78—87164
modulator, lecture on optoelectronic devices 78—25990
modulator, servo controlled, for CW laser power stabilisation and control 80—19060
modulator, thin-film, for fibre optical communication system 79—10407
modulator freq. response calibration, signal level control appl. 78—33833
modulator switch, balanced bridge, using Ti-diffused $LiNbO_3$ strip waveguides 78—63201
modulator use in or outside cavity for laser freq. shifting or stabilisation 78—5512
modulator using electro-optic phase shifter pair with optical waveguide couplers 78—66952

electro-optical devices continued
modulator-based instrument, for polarisation dependent light scatt. meas. 78—58010
modulators, switches and deflectors, physical principles and Czechoslovak developments *(Czech)* 80—19090
modulators and shutters, areas of appl. 79—94359
modulators on flat waveguides, theory *(Russian)* 79—50411
Moire contour lining system, using reference plane orientation 77—2636
moire technique for image alignment, focus and scaling 77—27362
multi-functional electro-optical device with feedback 79—32055
multi-gigahertz modulation concepts, for CO_2 laser communications 77—3681
multicavity IR electro-optical tunable filter 80—102831
multichannel detector for rapid acquisition of XPS data 79—93263
multilayer electro-optic space/time modulator resolution *(Russian)* 79—94343
multimode electro-optic guiding for single fibre data links, system design 78—38065
multimode fibre bussing, active fail-safe terminal 78—55438
multimode fibre optic switching devices, computational approach to predict optical behaviour 79—59845
multimode optical switching 79—76882
multimode time division multiplex device 77—79958
multimode waveguide modulator/switch 79—10383
multiplexer for large-numerical-aperture low-loss fibres 77—83993
multiplexer system for multimode fibre data communications 79—18510
multivibrator operation, in optical bistable device 80—58674
nephelometer, integrating, characterisation of nonspherical atm. aerosol particles 80—77106
nonlinear Fabry Perot devices, integrated optic format 78—38087
nonlinear Fabry-Perot resonator, for optical signal processing 78—42460
optical modulator, coupled-waveguide with pn junction 78—71235
optical modulator, space-time, based on $Bi_{12}GeO_{20}$ and $Bi_{12}SiO_{20}$ monocrystals *(Russian)* 77—1652
optical preprocessor, use in Earth-resources satellites 80—67430
optical switching device using leaky surface wave, controlled by electro-optic effect 79—23090
optical waveguide 4×4 switching network 77—3683
optical waveguide modulator, using electrooptic crystals, coupled mode analysis 77—42612
optical waveguide switch, 3×3, for optical switching system 78—55470
optoacoustic detection using Stark modulation 79—94325
oscillator design using integrated cutoff modulator 80—48424
passive ground-based electro-optical detection of artificial Earth satellites 79—62717
$Pb_3M_gNb_2O_9$ crystals for optical radiation control 79—81554
phase contrast microscope attachment for weak phase object visibility 80—86396
phase modulator and antiresonant ring for laser cavity dumping 78—17980
phase modulator for single-mode laser freq. modulation 78—13737
phase modulator in antiresonant ring laser, for cavity dumping 77—88792
photo-optical polarising optical system as elec. signal generator 79—1000
photoelectronic phase and frequency modulation 78—79131
photometric device for arterial thrombosis investigations 78—85456
photopolarimeter, electrooptic four-modulator, for Mueller matrix meas. 80—73417
Phototitus, image intensifier and convertor for electron microscope 77—45918
Phototitus spatial-temporal light modulators, image formation kinetics 79—50397
picosecond optical sampling, cascade of waveguide interferometers driven by microwaves 80—99849
planar electrodes, distributed capacitance, optic and SAW device appls. 77—27387
PLZT ceramic modulator for 1064nm laser Q-switching 77—38964
PLZT ceramics as electro-optic shutter material for IR appls. 79—72679
Pockels cell, for electro-optic gating of radiant emission from laser-produced plasmas 78—22561
Pockels cell, for laser sub ns pulse generation 77—19357
Pockels cell, variable length subnanosecond laser pulse prod. 78—94405
Pockels cell, variable pulse width generation for CO_2 lasers 78—46691
Pockels cell drive pulser in multiarm laser 79—14001
Pockels cell driven by light-controlled Si switch 78—26925
Pockels cell driver of fast rise time and high repetition rate using thyratron 80—69537
Pockels cell for subns. pulse prod. 77—83904
Pockels cell modulator, max. depth of light modulation 80—102819
Pockels cell system, with 2.25 cm^2 aperture, for IR pulsed radiation production 80—5806
Pockels cells, optically timed, electrooptic prepulse suppression for fusion laser systems 80—102743
Pockels double shutter in ruby laser with active phasing of spectrum *(Russian)* 79—98419
Pockels effect relay applications to optical data processing 79—72513
Pockels effect switch for HF laser 77—38910
Pockels readout optical modulator, acoustooptic snapshot, optical, signal spectrum analyser 78—90494
Pockels readout optical modulator, current status and appls. 77—72085
pockels readout optical modulator, for optical/digital processing systems 78—79125
Pockels readout optical modulator, image and signal processing appls. 78—79123
Pockels readout optical modulator, optical processing appls. 78—83100
Pockels switching system producing single and double variable length pulses 77—724
polarimeter, digital lock-in technique using electro-optic cryst. 78—273
polarisation insensitive integrated optical switch, electrode design 77—79967
polarisation switch for multimode fibres 77—27335
polarisation-conversion wavelength-selective fibre switches 80—58736
probe, for liquids refraction index sensing *(German)* 77—5889
profile meas., automated equipment appl. 79—21701
PROM, diffr. efficiency 80—14467
pulsed electric field meas. using electro-optical device 78—4644
pulsed light source with thin-film modulator, fabrication and characts. 80—43467
pyrometer single-pulse calibration flash tube 78—12702
Q-switch for pulse-periodic Nd^{3+}:YAG laser 79—45975

electro-optical devices continued
Q-switch pulsed modulation to produce dye laser nanosecond duration pulses 79—41403
real-time spatial modulators for optical/digital processing systems 78—63025
reflector, controlled, temp. fields, thermal distortions 80—96021
remote sensing multichannel data sets, integrated optical comparator 80—64213
rib waveguide switches with MOS electrooptic control, monolithic integrated optics in GaAs-$Al_xGa_{1-x}As$ 78—87168
ruby laser with electrooptical shutter, emission spectrum narrowing and single freq. giant pulse lasing 80—78877
semiconductor band-narrowing electro-optical deflector 79—98483
semiconductor iso-index coupled-wave electrooptic filter 80—1324
semiconductor laser, electrooptically tuned external-cavity CW, FM optical communication appl. 80—14351
semiconductor ridged waveguides for electrooptic radiation modulators 80—91925
semiconductor sheet, free carrier confinement for IR modulation 78—25969
semiconductor waveguide switches, and modulators, review of development progress 78—38045
shutter, for CO_2 laser pulse prod. 78—37926
shutter, passive closing for ruby laser radiation self-modulation 79—64258
shutter, passive switching to produce ruby laser picosecond pulse generation 79—36942
shutter for laser pulse shaping, Pockels cell with programmable transmission control 80—64162
signal processing activities of United States Army 80—48172
solid-state image sensors for electro-optical systems 77—39104
space qualification of optical instruments, using long duration exposure facility 78—85826
space testing and qualification, using NASA Long Duration Exposure Facility 79—5725
space-time light modulator 80—69526
space-time light modulator for laser radiation control 80—48310
spatial light modulator, for optical data processing, 1978 state of art and development trends 79—7201
spatial light modulator, using KD_2PO_4 and Se photoconductor, optical processing appl. 80—9988
spatial light modulator resolution, stored point charge effects 80—106616
spatial light modulator with CCD address 80—48445
spatial light modulators for coherent optical computing, performance evaluation 79—89989
spatial phase modulators, resolution, meas. techniques 77—79959
Stark cell appl to CO_2 laser communication 77—19444
stereoradiology, single monitor systems using PLZT electro-optic shutters 77—60247
streak camera using electrooptical beam deflector theory 79—58809
streak camera with electro-optical deflector, for picosecond laser pulse diagnostics 78—33909
surface prism laser deflector, for field destructive interference 80—87492
surface waveguide electrooptical deflector, high-resolution, prism model 80—48454
switch, bistable, multimode integrated 78—79145
switch fabrication in $LiNbO_3$ waveguide, using Ti diffusion layer 78—33834
switch/modulator, optically activated, using photoconductor and two channel waveguides 78—1437
switches, thin film periodic waveguide switches and amplitude modulators anal. 78—22215
system aspects of electro-optics, seminar, Huntsville, AL, USA (May 1979) 80—94921
system manufacture, test and process control changes 80—96044
systems analysis using two-dimensional FFT algorithm 80—78986
systems integration and optical design, conference, Reston, VA, USA (Apr. 1977) 78—50783
tacheometer, electrooptical, EOT 2000, design parameters, performance figures 78—77858
terminated crossbar matrix 77—19386
thermoplastic light modulators, status and prospects 78—79138
thin film electrooptic deflector using induced grating with variable blaze angle 80—99862
three-dimensional topographic mensuration, laser electro-optic system 80—99784
total internal reflection modulator, small glancing angles 78—74987
transmission light gate, using bistable electrets 77—50750
transverse light modulator, improvement of permissible incident angle 80—5843
travelling wave optical modulator using a directional coupler $LiNbO_3$ waveguide 80—96035
travelling-wave electro-optic element, CW laser freq. shifting for subnanosecond FID 80—38075
tunable coupler filter, composed of coupled nonidentical $LiNbO_3$ strip waveguides, description 78—38083
tunable filters, programmable 80—102830
tunable filters and polarisation conversion devices 80—102829
tunable optical waveguide directional coupler filter 78—79144
tuning element, for spectrometer wavelength modulation, using CW dye laser 78—61083
turbidity meter, multichannel 80—67423
ultralinear bistable electro-optic polarization modulator based on Pockels cell 78—83077
VHF resonator radiant energy meas. *(Russian)* 78—77944
video signal conversion device for SEM 80—57423
voltage dividers, capacitor type, current meas. appl. *(Italian)* 77—26339
waveguide, multimode, optical modulator or switch 80—23783
waveguide 3×3 switch, tuning and control theory 79—41458
waveguide array deflectors, performance criteria and limitations 80—5821
waveguide deflector performance characteristics 80—33213
waveguide modulator for fibre transmission systems, temperature stabilized *(Japanese)* 79—27391
waveguide modulator for single-mode optical fibre transmission system, temp. stabilized 79—41450
wideband thin film modulators and switches, for optical communication 78—63206
wideband UHF standing-wave light modulators 79—72689
X-ray topographic images, direct display systems, review 77—68899

electro-optical devices continued
$Al_yGa_{1-y}As$-$Al_xGa_{1-x}As$, electrooptic rib waveguide modulators and switches 78—38046
$Al_yGa_{1-y}As_{1-x}Sb_x/GaAs_{1-x'}Sb_{x'}$, buried heterojunction electroabsorption modulator, report of operation 78—38044
$Al_yGa_{1-y}As_{1-x}Sb_x$-$Ga_{1-z}Sb_z$ buried heterojunction electroabsorption modulation 78—55439
Au-Si_3N_4-GaAs-GaP structures, as elec. controlled optical transparencies, optical processing use 77—85339
$Bi_{12}GeO_{20}$, spatial-temporal electrooptic modulator, UV image conversion 77—3680
$Bi_{12}GeO_{20}$:Ga,Ca, photocond. suppression by simultaneous Ga and Ca doping, and appl. to electro-optic light valve 79—78134
$Bi_{12}SiO_{20}$ crystal, for programmable optical guided-wave device 79—23069
$Bi_{12}SiO_{20}$, optical information recording, PROM device resolution 79—41443
$Bi_{12}SiO_{20}$, optically controlled multimode planar switch 78—42476
$Bi_{12}SiO_{20}$ PROM device, image recording and erasure mechanism 80—74490
$Bi_{12}SiO_{20}$ photoelectret, in optical processing and X, γ ray imaging 80—23764
$Bi_{12}SiO_{20}$, use in incoherent-to-coherent optical image convertor of transmission type 79—94340
$Bi_{22}SiO_{20}$, Pockels readout modulation struct., information registration *(Russian)* 77—10990
CO_2 waveguide laser, electrooptically Q-switched 79—98416
CS_2 travelling wave Kerr cell, ultrafast pulse shaping and picosecond rise time elec. pulses 80—33152
CdS spatial modulator, 16×18 bit, page composer 77—39050
CdTe acousto-optic and electro-optic waveguide modulators 77—42624
CdTe crystal Pockels modulator, PCM of CO_2 TEA laser pulse 80—102742
CdTe electro-optical modulator for CO_2 lasers 77—19443
CdTe, H^+ ion implanted, optical waveguiding and electrooptic modulation 77—75679
CdTe, IR phase modulator, phase and freq. characts. 77—54805
CdTe intracavity electrooptic modulator, for high pulse repetition freq. CO_2 oscillator 77—88801
$Cd_{1-x}Zn_xS$, electro-optical multilayer film, for data storage and display 78—71176
$Ga_{1-x}Al_x$ As, metal-gap channel waveguides, intensity modulation 78—66899
GaAlAs light intensity modulators using p-n junctions 80—99871
$Ga_{1-x}Al_xAs$ Schottky directional coupler switch, construction and operation 78—25960
GaAs 400 MHz TW laser modulator 80—87541
GaAs directional couplers and electrooptic switches, wavelength depend. 78—79143
GaAs, directional-coupler switch with stepped $\Delta\beta$ reversal 77—79968
GaAs directional-coupler switch with stepped $\Delta\beta$ reversal 77—88962
GaAs electro-optic rib waveguide directional-coupler switch with stepped $\Delta\beta$ Schottky electrodes 79—98507
GaAs, electroabsorpt. avalanche photodiode waveguide detectors 78—65965
GaAs, electroabsorpt. avalanche photodiode waveguide detector, freq. demultiplexing 79—17486
GaAs, Franz-Keldysh effect modulator parameters for integrated optics systems 80—106624
GaAs layer grown by MBE, direction coupler switch 79—76878
GaAs, p^+-n^--n^+ directional-coupler switch 77—7217
GaAs rib-waveguide directional-coupler switch with Schottky barriers 78—63204
GaAs Schottky barrier modulator, strain induced optical waveguiding 79—27388
GaAs-$Al_xGa_{1-x}As$, single-mode rib waveguide switches electro-optical modulation 78—46839
GaAs-$Al_xGa_{1-x}As$ electro-optic modulator, highly sensitive, with distributed Bragg-reflectors 77—75682
GaAs-$Al_xGa_{1-x}As$ electro-optic frequency- and polarisation-modulated injection laser 80—91810
GaAsP epitaxial waveguide, electro-optic phase modulation of laser radiation 79—10417
GaP-$Al_xGa_{1-x}P$, DH electrooptical strip modulator *(Russian)* 78—1344
GaP-AlGaP, stripe-geometry electrooptical modulator 80—23798
p-Ge sheet, free carrier confinement for IR modulation 78—25969
In_2O_3-SnO_2 electro-optical film, for data storage and display 78—71176
KD_2PO_4 crystal, electro-optical extraction of Nd:YAG laser pulses *(German)* 80—87416
KD_2PO_4 crystal electron-beam spatial light modulator, resolution 80—74503
KD_2PO_4, electron beam addressed light valve, optical processing appl. 78—83099
KD_2PO_4 electrooptic modulator, field of view extension 78—94429
KD_2PO_4 light valves for optical information processing 77—72080
KD_2PO_4 light valves 77—83992
KD_2PO_4, optically addressed light valve, optical processing appl. 78—83101
KD_2PO_4 photo-spatial light modulator, optical data processing 80—102839
KD_2PO_4, ultrafast electro-optical modulator design and application 77—19432
KD_2PO4 transmission line Pockels cells, optical rise time meas. 78—46778
KH_2PO_4 crystal electro-optic reflection deflector 79—76861
KH_2PO_4 electro-optic modulator crysts., piezoelec. induced acoustic transients 80—70316
$K^2H_2PO_4$ electro-optic shutter natural birefringence compensation by β-$LiIO_3$ monocrystal 79—55247
$LiNbO_3$, acoustically tuned optical filter, electrostatic field effect 77—58443
$LiNbO_3$, anisotropic multilayer waveguide for electro-optical modulator, propag. characts. *(Italian)* 78—50904
$LiNbO_3$ balanced bridge modulator/switch with ion-etched slot 79—89993
$LiNbO_3$ blazed grating electro-optic deflector development 77—42627
$LiNbO_3$ corrugated optical waveguide, electrooptic scanning of coupled light 78—38050
$LiNbO_3$ crystal two-stage electrooptic deflector 80—106625
$LiNbO_3$ deflector, use in streak camera of approx. 100 ps resolution 79—18533

electro-optical devices continued
$LiNbO_3$, diffused waveguide as Bragg electro-optic modulator 77—34955
$LiNbO_3$ electro-optical total internal reflection diffraction industrial modulators and deflectors 77—19436
$LiNbO_3$ electro-optic phase modulator for unpolarised laser beam 79—50403
$LiNbO_3$ electro-optic deflector based streak camera, 20 ps resolution 79—85189
$LiNbO_3$ electrooptic light modulator 78—1349
$LiNbO_3$ electrooptic switches used in Nd^{3+}:YAG lasers, contrast and configs. 80—33012
$LiNbO_3$ fast-response broad-band electrooptic elements for laser beam control systems 79—89944
$LiNbO_3$, interdigitally electroded, acoustic reson. 80—19097
$LiNbO_3$, light modulator with interdigital electrodes, operating characts. 78—90511
$LiNbO_3$ microwave laser beam electro-optic modulators using rectangular waveguides, 1.0 to 10 GHz 80—43381
$LiNbO_3$, modulator/switch, switched directional coupler principle 77—7191
$LiNbO_3$ optical waveguides, electrooptic modulation and switching, recent progress 78—50945
$LiNbO_3$ phase modulator, axial mode locking of CW Nd^{3+}:YAG ring laser 78—50835
$LiNbO_3$ phase modulator, freq. shift device for optical range 78—59147
$LiNbO_3$ planar waveguide, light beam switching and modulation using built-in dielectric channel 77—88967
$LiNbO_3$ planar waveguide, light beam switching and modulation using built-in dielec. channel 78—46840
$LiNbO_3$ TE-TEM light mode convertor using acousto-optic interaction, expt. 78—46794
$LiNbO_3$, thin-film electrooptic modulator, optimal characts. 79—10405
$LiNbO_3$, Ti diffused, optical waveguide isolator using electrooptic branching waveguide 79—18532
$LiNbO_3$, Ti diffused optical waveguide, ferrolectric domain inversion 79—94338
$LiNbO_3$ Ti-diffused waveguide for cutoff modulator 80—9991
$LiNbO_3$ total internal reflection diffraction modulator/deflector performance 77—42628
$LiNbO_3$ travelling wave optical waveguide modulator, 10 GHz bandwidth 78—59134
$LiNbO_3$ waveguide, corrugated, electro-optic scanning of light diffr. from grating output coupler 78—63172
$LiNbO_3$ waveguide, planar electro-optic prism array beam splitter 80—64209
$LiNbO_3$, waveguide, single-mode planar and rigid type electro-optic waveguide modulators, design 77—11029
$LiNbO_3$, waveguide and modulator form. by ion implantation 80—48469
$LiNbO_3$ waveguide modulators and switches, Ti-diffused, fabrication on directional coupler principle 80—83678
$LiNbO_3$:Cu, holographic grating, for electro-optical laser beam modulation 77—3672
$LiNbO_3$:Fe, electrically accessible Lippmann hologram memory 77—88663
$LiNbO_3$:Fe photosensitive electro-optical crystals for image storage display and processing 77—19215
$LiNbO_3$:Ti, broad-band travelling wave waveguide modulator 77—39036
$LiNbO_3$:Ti, coupled waveguided TE/TM mode splitter 80—64142
$LiNbO_3$:Ti, electro-optic waveguide modulator, temp. stabilisation 78—50926
$LiNbO_3$:Ti, electrooptical modulator and switch *(French)* 78—30074
$LiNbO_3$:Ti, integrated bistable optical device using Mach-Zehnder interferometric optical waveguide 79—59843
$LiNbO_3$:Ti, multichannel waveguide deflector 77—42607
$LiNbO_3$:Ti, planar optical waveguides, processing and props. 80—78965
$LiNbO_3$:Ti, two mode waveguide coupler electrooptical switch 77—83961
$LiNbO_3$:Ti, Y-cut thin film waveguide, acousto-optical deflector, electro-optical modulator *(Russian)* 77—39115
$LiNbO_3$:Ti active branching waveguide modulator 77—19392
$LiNbO_3$:Ti branched waveguide amplitude modulator 77—39037
$LiNbO_3$:Ti channel waveguide high-speed cutoff modulator 80—64195
$LiNbO_3$:Ti diffused optical waveguide, guided light scatt. sources 80—78966
$LiNbO_3$:Ti diffused optical waveguide, efficient tapered gap prism coupling 80—78967
$LiNbO_3$:Ti digitally driven integrated optics amplitude modulator 80—58808
$LiNbO_3$:Ti electro-optic TE-TM mode convertor structure 80—64215
$LiNbO_3$:Ti narrow ridge optical waveguides and electro-optical, ion-bombardment-enhanced etching 80—38133
$LiNbO_3$:Ti optical branching waveguide, characts. 80—83681
$LiNbO_3$:Ti optical waveguide electrooptic devices polarisation independ. directional coupler switch and wavelength filters 80—58783
$LiNbO_3$:Ti phase-matched waveguide electro-optic TE⇄TM mode convertor 80—58749
$LiNbO_3$:Ti single mode electrooptic waveguide modulator, high-speed operation 80—91915
$LiNbO_3$:Ti waveguide directional coupler type modulator 78—66951
$LiNbO_3$:Ti waveguide thin film electrooptic Bragg modulator, bistable optical element 80—10034
$LiNbO_3$:Ti waveguide electro-optic TE⇄TM mode converter-wavelength filter 80—64210
$LiNbO_3$/CdS integrated optical half adder circuit 79—76877
$LiTaO_3$ electro-optical total internal reflection diffraction industrial modulators and deflectors 77—19436
$LiTaO_3$ fast electro-optic deflector, arbitrarily shaped optical pulsed generation 80—53421
$LiTaO_3$ modulator, temperature compensation by feedback control 77—42611
$LiTaO_3$, multimode electro-optical 2×2 crossbar switch 78—55473
$LiTaO_3$ platelet, tunable filter, birefr. electro-optic cryst., light energy coupling 79—59804
$LiTaO_3$, Ti diffused, electrooptic diffraction modulation 79—10381
$LiTaO_3$ total internal reflection diffraction modulator/deflector performance 77—42628
$LiTaO_3$, waveguide, single-mode planar and rigid type electro-optic waveguide modulators design 77—11029
$LiTaO_3$ zig-zag reflection interferometric light modulator 78—90527
$LiTaO_3$:Cu, waveguide with periodic electrodes, mode conversion 78—33840

electro-optical devices continued
$LiTaO_3$:Cu waveguide, electro-optic control of radiation loss in off-axial propagation 80—23789
$LiTaO_3$:Ti waveguide modulator structs., high optical power capabilities 77—39023
N_2 laser, pulsed, interfacing with higher freq. electro-optic instrumentation 77—50698
NH_3 Stark cell for wideband modulation of CO_2 laser R(18) line 77—23704
NH_2D Stark active mol., cavity dumping for CO_2 laser pulse generation 77—88800
$NH_4H_2PO_4$ total internal reflection intercavity laser switch 77—38955
$NH_4H_2PO_4$, total internal refl. diffr.-type modulator as laser cavity switch 78—5511
Nd^{3+}:YAG electrooptically Q-switched laser pulse duration increase by intracavity SHG 79—94255
Nd^{3+}:YAG laser, high repetition rate electrooptic Q-switching, birefringence 80—69430
PLZT ceramic, modulator for optical communication 80—78964
PLZT ceramic, possible construction of matrix-addressable controlled transparency 78—71222
PLZT ceramic, transverse electro-optical effect, matrix-addressable transparency 79—27431
PLZT ceramics, optical recording *(French)* 77—31078
PLZT ceramics, optical information storage and spatial light modulation 78—83097
PLZT colour cell for real time two colour incoherent to coherent image convertor 78—38039
PLZT electro-optic shutter stereoscopic display applications 80—90826
PLZT optical ceramic, as high speed shutter 77—79187
PLZT real time 2 colour incoherent to coherent image convertor 79—3805
PLZT shutters as thermal/flash protective devices 77—46808
PLZT spatial light modulator for a 1-D hologram memory 80—37963
PLZT transparent ceramic laser modulator *(German)* 78—5553
PLZT/TFPD thermal/flash protective lens assembly, polarised delamination investigation 80—78929
PZT paraelectric ceramic one-dimensional spatial light modulator 79—55240
$Pb_3MgNb_2O_9$ crystal electro-optic deflector design and adjustment 79—72690
$Pb_3MgNb_2O_9$-CdS, electro-optical space-time light modulation 78—18056
Si_3N_4 waveguide layer, as electro-optic phase modulator 79—23081
ZnS leaky waveguide electro-optic modulator limitations 78—22218
ZnSe, absorpt. modulation of light, and its appl. to page composer *(Japanese)* 78—83083

electro-optical effects
see also electroabsorption; electrochromism; electroluminescence; electroreflectance; Kerr electro-optical effect; photorefractive effect; Pockels effect; Stark effect
4-octyl-4-cyano-biphenyl, nematic to smectic A phase transition texture changes, thermoelectrooptic effect 80—49098
adsorbed diatomic on electrode, reson. Raman scatt. 79—51421
air, light flash excited by γ-ray source, electric field effect 79—14514
air pollutants spatial conc. estimation, new proposal for those which absorb optical energy 79—57533
aligned chiral liquid crystal structure-property relationships 77—76304
p-n-alkoxybenzoic acic series, nematic liq. crysts., electrooptical props. 79—15438
alkoxybenzylidenaminobenzonitriles, elec. field and press. induced transitions, transparency and texture 77—43317
p-alkoxybenzylidene-p,n-butylanilines, IR absorpt. spectra, elec. field effects, orientational order parameter determ. by IR dichroism 80—80778
p-alkoxybenzylidene-p-aminocyanoanilines, IR absorpt. spectra, elec. field effect, orientational order parameter determ. by IR dichroism 80—80777
5-alkyl-2-(4′-cyanophenyl)-1,3-dioxanes, nematic liq. cryst., synthesis and electro-optical characts. 80—88029
alternating electric field generation in nonlinear cryst. on light irradiation *(Russian)* 77—83920
alternating electric field light scattering by photon counting and signal averaging 80—95794
anisaldazine, colloidal particles in water, elec. polarisability anisotropy 79—39208
anisotropic crystal, induced birefringence, systematic errors elimination 79—99848
anisotropic saddle point, electro-optical signal *(Japanese)* 77—43968
anisotropy in plane of light wavefront 79—8121
anisylidenebenzidine, particle size distrib. function, electrooptical diffusion method for determ. 80—8956
anthracene:tetracene (pentacene), effect of elec. field on fluoresc. *(Russian)* 78—56521
4-(9-anthryl)-N,N-dimethylaniline, fluoresc., dipole moments and polarisabilities 80—1019
atomic spectra, Rydberg states, simultaneous strong elec. and mag. fields 78—78663
bacteria E.coli strains in aq. suspension, polarisability anisotropy and aminoglycoside antibiotic effects 80—85441
bacteriorhodopsin reorientation due to elec. field 77—66789
benzene derivatives, carbon tetrachloride dil. soln., electrooptical quantities, ellipsoidal cavity model *(French)* 78—35114
benzenes, para-disubstituted, liq., 2nd order hyperpolarisabilities, regularities, intramol. charge transfer 79—10353
biopolymers, electro-optical changes, chem. and rotational contribs. 80—85352
biphenyl mixtures with cholesteryl chloride, static and dynamic electro-optical props., cholesteric-nematic transition 80—100646
birefringence in electrically excited Z sections 80—55067
4-butoxybenzylidene-4′-alkylaniline, EHD instabilities in nematic and smectic A phases 79—90530
carbon tetrachloride dil. solns., ellipsoidal cavity model, electro-optical quantities *(French)* 78—35114
cartilage proteoglycan, association with hyaluronic acid, elec. birefringence obs. 80—85332
chiral substances, electro-optical responses, Jones matrix, meas. sytem for rot. anisotropy 80—84723
chloroethanes, electro-optical parameters, Raman spectra absolute intensities and depolaris. 77—10678

electro-optical effects continued
chloromethane gas, linear electro-optical effect 80—87843
cholesteric helix surface, elec. field-induced high-order ref. 78—35115
cholesteric liquid crystal, anisotropy fluctuations suppression by elec. field *(Russian)* 79—32900
cholesteric liquid crystal, elec. field instability threshold and deform. period *(Russian)* 80—28914
cholesteric liquid crystal, incident angle dependence calc. 78—43834
cholesteric liquid crystal mixtures, appl. to information storage *(Rumanian)* 79—78657
cholesteric liquid crystal mixtures, storage effects 77—43972
cholesteric liquid crystals, planar texture, field-induced square grid perturbation 79—90531
cholesteric textures, confocal, optical and electro-optical props. *(Russian)* 77—80419
cholesteric-nematic liq. cryst. mixtures, electro-optic charact., light scatt. modes *(Japanese)* 78—79527
cholesteric-nematic phase change, threshold voltage for electro-optic effect 79—91405
cholesteric-nematic transition, and memory effect *(Russian)* 77—84911
cholesteryl chloride-cholesteryl crotonate, polarised light transmission, DC elec. field effect 77—77173
collagen, polarisation, contribution of permanent and induced dipole moments, elec. birefringence 80—85351
colloid, dichroism in homogeneous elec. field 79—8122
colloid, electro-optical characterisation methods 77—24821
colloid, particle size distribution function, electrooptical diffusion method for determ. 80—8956
colloidal crystal latex, nonlinear electro-optical props. 79—61337
colloidal photochromic dyes, quasi-crystals produced in applied electric field 80—85225
colloids, electric polarisability, stability 80—85222
colloids, rigid, size distributions, transient electric birefringence 80—85223
conference, ferroelectric materials and their applications, Kyoto, Japan, Nov. 17-19, 1977 79—19846
critical point symmetry, use of electromodulation as probe, sensitivity 77—66477
crystal of symmetry class $\bar{4}2m$, electro-optical effect anisotropy 80—2729
crystal point groups, electric and magnetic field-induced Raman tensors, effective charges 78—43848
crystalline optical material props., symmetries and tensorial relationships 80—108174
cubic crystals, electro-optical effect rel. to spatial dispersion of permittivity 80—66151
curriculum in electrooptics for electrical engineers 79—11
p-cyanophenol mixtures, p-alkylbenzoates twisted nematic effect 79—82947
cyclohexane-methanol, crit. opalescence, AC elec. field effect 78—35159
cyclohexane-methanol, crit. opalescence, elec. field effect 79—28775
L-p-decyloxybenzylidene-p′-amino-2-methylbutyl-cinnamate, ferroelec. smectic liq. cryst., electro-optical effect 78—39527
diamond, colloidal particles in water, elec. polarisability anisotropy 79—39208
diamond, suspension, particle size distrib. function electrooptical diffusion method for determ. 80—8956
diatomic crystals, quantitative calc. of electro-optic coeffs. 80—40086
dicalcium strontium, propionate, thermodynamics of props. 78—76426
dichroic colloidal particles, size distrib. determ. by electro-optical method 79—6087
9,10-dicyanoanthracene, exciplexes, electronic struct. by electro-optical expts. 78—25581
dielectric liquid nonlinear third-order polarisation, transient effects elucidating molecular props. 80—15955
dielectrics, electric, optical and acoustic interactions from Lagrangian representation, book 80—2715
trans-4-dimethylamino-4′-nitrostilbene, mol. hyperpolarisability in soln., UV dispersion of charge transfer contrib. 79—31986
disperse system, use of two-phase Rc field 79—55060
disperse systems, electro-optical phenomena, induced dichroism rel. to elec. field calc. 78—50699
distributed Bragg reflector lasers, tunability using electro-optic effect 77—38938
DNA, calf-thymus and superhelical PM2 aq. solns., electro-optic obs. of γ-irrad. damage 80—85452
DNA, dye labelled elec. dichroism and birefringence, comparison with mol. props. from polarised fluoresc. 80—84785
DNA, Hg (II) and Ag (I) complexes in soln., theoret. interpret. of elec. dichroism obs. 80—85347
DNA solution, elec. birefringence, stabilised induced dipole behaviour 80—85349
DOBAMBC, polarized Raman scatt. and elec. field effects in aligned smectic phases 79—94873
DOBAMBC, smectic liquid crystal, ferroelectric, colour switching in elec. field 80—29719
Doppler free intermodulated optogalvanic spectroscopy, technique description and sensitivity 80—52333
EBBA, IR absorpt. spectra, elec. field effects, orientational order parameter determ. by IR dichroism, bend elastic consts. 80—80778
EBBA, nematic, dielec. permittivity and transmitted light intensity, in DC field 77—12296
electric circular dichroism in optically active fluid 79—19862
electric current and voltage meas. using laser light *(Japanese)* 80—86342
electric dichroism measurement instrument with digital processing 80—82800
electro-optic crystals, hologram formation arbitrary transport length anal., photovoltaic effects 80—78802
electro-optics/laser international conference, Brighton (1976) 77—38800
electrogyration rel. to birefr. 78—27190
electron donor-acceptor complexes, excited state dipole moments, electro-optical expts. 77—46586
N-p-ethoxybenzylidene-p′-cyanoaniline, nematic, mol. reorientation in DC elec. field, IR ATR spectra study 80—45064
exciplex fluoresc. decay, elec. field depend., quantum theoretical model 79—98133
exciplexes, electronic struct. by electro-optical expts. 78—25581
fast insulator surface flashover in vacuum, mechanism, electro-optical investig. 80—103206
ferroelectric mats., conf., Novosibirsk, USSR (Sep. 1976) 78—76393

electro-optical effects continued
ferroelectric oxide crystals for electrooptics and nonlinear optics, optical inhomogeneities, review *(Japanese)* 77—65613
ferroelectric semiconductors, appl. to optical storage *(Russian)* 80—80749
ferroelectric smectic single C liquid cryst., electric field induced bend undulation instability 80—24351
ferroelectric solid solns., perovskite struct., physical props., review *(Russian)* 77—48134
ferroelectric theory and dynamics, optical, acoustic electro-optical props., Brillouin zone struct. 80—11347
field induced twisted structure with quasihomeotropic boundary conditions, electro-optic behaviour 78—60424
fluid, rarefied, symmetries of static elec. field induced opt. effects 78—55713
fluids, polarisation state of light scatt. in elec. and mag. fields, symmetry indications 80—29751
1-formyl 2(4-nitrophenyl) hydrazine, preparation, optical and electro-optical props. 77—36201
Franz-Keldysh, optically enhanced for n^+-p-n^+ phototransistor struct. 78—60423
gas in applied elec. field, IR transmission modulation *(French)* 78—50912
glow discharges, high-pressure, electro-optical meas. of current and voltage 78—37033
graded index planar lightguide, electrooptical diffraction 80—78995
graphite, suspension, particle size distrib. function electrooptical diffusion method for determ. 80—8956
helical wormlike chain, dipole moment, elec. birefringence, elec. dichroism, statistical mech. calcs. 80—14262
p,n-hepthyloxybenzoic acid, smectic C liq. cryst., coherent light diffr. 78—1999
HF high voltage meas. 78—86301
history of electro-optics (1665-1979) *(German)* 80—15
HOBA, smectic C liq. cryst., EHD instabilities 78—91238
HOBA, smectic liq. cryst., two dimensional diffr. grating due to AC electric field, pulsating diffr. 78—15148
hologram writing by photorefractive effect, Gaussian beam at const. voltage 77—3552
holographic grating recording, pyroelectric mechanism 78—42300
holographic parameters, set up for meas. on electro-optic crystals 78—87031
holographic recording in electrooptic crysts., photogalvanic effect mechanism of nonlinear wave interaction 80—102672
holographic storage of information using birefringent electrooptic crystals 79—98322
HV measurement using quartz electrogyration effect 77—41656
hydroscopic particle humidification process, electrooptic scatt. meas. 80—77107
improper ferroelectrics, thermodynamics of props. 78—76426
indandione-1,3 derivative, layer, electrooptical effect *(Russian)* 79—73900
induced elliptic double refraction, separation into linear and circular components *(German)* 77—24817
ionic grouping theory of electro-optical and nonlinear optical effects of crystals *(Chinese)* 78—27183
large-molecule system, field-induced birefringence theory 78—76421
laser beam propagating in liquid, polarization, DC elec. field influence 80—91828
level crossing effect 78—37608
light scattering, space-time symmetry rel. to light scatt. in elec. and mag. fields 80—29750
liquid, electro-optical parameter meas. agreement with calc. values using exact local field expression and ellipsoidal model *(French)* 77—8545
liquid, new optical effects, elec. analogue of Faraday effect 77—81085
liquid, optically induced birefringence in elec. field 79—78648
liquid crystal, dichroic dyes for guest-host interactions 77—59554
liquid crystal, ferroelectric, review of props. 77—85667
liquid crystal, hybrid aligned nematic elec. field induced deform., birefr. 77—4624
liquid crystal, isotropic phase, statistical props. of scattered light 78—27189
liquid crystal, lecture on optical props. 78—35118
liquid crystal, nematic and smectic, potential of phase matched elec. field induced SHG 79—86214
liquid crystal, smectic, anisotropy of carrier mobility and electro-optical effects *(Japanese)* 77—43605
liquid crystal, smectic, elec. reversible memory effect *(Russian)* 78—31174
liquid crystal alignment films prod. by RF plasma beam technique 80—76198
liquid crystal cell, dynamic scatt. effect 77—1080
liquid crystal cholesteric layer-semiconductor layer systems, auto-oscill. behaviour *(Russian)* 77—43971
liquid crystal dyes, field-induced colour changes 80—25340
liquid crystal electrothermo-optic effects, display appls. 77—11469
liquid crystal ferroelec. phases, mag. material analogy 77—11467
liquid crystal layer, twisted nematic, transmission characts. 77—1653
liquid crystal twisted nematic displays, electro-optical props., solute effects 77—1072
liquid crystals, domain instabilities in elec. and mag. fields 79—94875
liquid crystals, effects and appls., review *(Chinese)* 79—32905
liquid crystals, electro-optical effects, charact. wave number, boundary effect of flow *(Japanese)* 77—20828
liquid insulator, linear electrooptic effect 77—16283
liquids, DC elec. field induced optical rectification and SHG 79—46005
liquids, Raman spectra, inverse electro-optical problem 78—2845
liquids, transparent isotropic, electro-optical and magneto-optical effects, review 78—84553
macromolecular, electrically induced fluorescence depolarisation 77—27210
macromolecular, solutions, Rayleigh scatt., elec. induced variations, spectral width and intensity meas., review 78—48187
macromolecular soln., electro-optical characterisation methods 77—24821
macromolecular solution, alternating elec. field light scatt., low angle approx. 80—84721
macromolecular solution, dynamic light scatt. by flexible macromols. in fluctuating elec. field 80—84722
macromolecular solution, light scatt. in AC electric field 79—47468
macromolecular solution, rot. diffusion coeff. calc. method w.r.t. mol. struct., elec. birefringence relax. time data interpret. 80—85331

electro-optical effects continued
macromolecular solution, transient elec. birefringence in reversing fields of arbitrary strength and duration 80—84719
macromolecular solutions, orient. in laser beam elec. field, anisotropic light scatt. 79—1768
macromolecule monodisperse solns., macromol. length rel. to anisotropic light scatt. in elec. field 77—32391
macromolecules, dumbbell-shaped, alternating electric field light scatt. 80—1130
macromolecules, polydispersity in nonlinear electric methods, nonlinear dielec. effect formulas derived 78—59730
macromolecules, scatt. methods, conf., Prague, Czechoslovakia, (July 1976) 79—1764
macromolecules and colloids, conf., Uxbridge, England (Apr. 1978) 80—82577
macromolecules in dilute soln., electrically induced fluorescence polarised component change meas. 80—32863
macromolecules in soln., Rayleigh scatt., elec. reorient. rel. to spectral line rot. broadening 79—1774
materials for modulator, display, and storage appls., review 80—74450
matrix theory fundamentals of active electrooptic and magnetooptic media *(Russian)* 78—63005
MBBA, annihilation of disclinations with Frank index $m=+2$ 77—58955
MBBA, doping effect on cond. anisotropy and dynamic scatt. 77—40208
MBBA, elec. field effect on optical indicatrix orientation 77—36202
MBBA, IR absorpt. spectra, elec. field effects, orientational order parameter determ. by IR dichroism, bend elastic consts. 80—80778
MBBA, liq. cryst., electrohydrodynamic instability, fluctuation of light transmission meas. 77—11468
MBBA, liq. cryst., flexoelectricity and surface polarisation 77—89376
MBBA, liq. cryst., light scatt. and birefr. 78—22646
MBBA, liq. crystal, morphological changes and electro-optical characts. appl. laser light modulation 77—20826
MBBA, nematic, dielec. permittivity and transmitted light intensity, in DC field 77—12296
MBBA, nematic liq. crys., refractive index distrib. and mol. alignment in electro-optical effect *(Japanese)* 80—20613
MBBA, nematic liq. cryst., dynamic scatt. mode due to electrohydrodynamic instability *(Japanese)* 77—43133
MBBA, nematic liq. cryst., transverse electrooptic effect 79—94897
MBBA, nematic liq. crysts., AC excited, dynamic light scatt., orient. fluctuations 79—1769
MBBA, nematic phase, elec. field induced biaxiality, PMR study 79—90532
MBBA, nematic phase, high freq. EHD instabilities, temp. depend. 79—94879
MBBA, nematic twist cells, bi-dimensional struct. in cond. region 79—90542
MBBA, positive space charge influence on texture, domain form. factor, polarised light study 80—88037
MBBA, secondary light scatt. in low frequency field, in dielectric state 78—48147
MBBA, viewed in transverse elec. field, voltage-freq. thresholds 77—7661
MBBA, Williams patterns, transverse obs. 77—19869
MBBA film, optical study of second dynamic scatt. regime *(Italian)* 78—15146
MBBA-BBCA mixture, field-induced distortion of mol. orientation 79—99060
MBBA-cholesteryl oleate mixture, memory effect characts., crit. freq. rel. to erase voltage 78—94993
MBBA-CPB nematic complex, dielec., elastic and electro-optical props. 77—32350
MBBA-EBBA, controllable liq. cryst. transparency, electrooptical characts. 80—78996
MBBA-EBBA mixture, behaviour in alternating elec. field 78—26440
MBBA-EBBA mixture, secondary light scatt. in low frequency field, in dielectric state 78—48147
MBBA-EBBA mixture, transverse electro-optic effect 77—59556
MBBA-EBBA mixtures, quinone and hydroquinone doped, dynamic scatt., elec., electro-optical props. 79—37616
MBBA-PCB (41 wt.%)+pleochroic dye, electrothermo-optic effect, optical storage device appl. 78—87611
metal-chalcogenide glass-metal structures, elec. field influence on opt. parameters, electrostimulated chem. transforms. 77—76950
methane, Raman intensity from electro-optical parameters 79—36645
methane ($-d_1,d_2,d_3,d_4$) Raman electro-optical parameters, overlay least squares calcs. 78—42105
p-methoxybenzilidenebutylaniline, nematic, domain pattern changes in electric field 77—1079
MIS photosensitive high resolution struct., spatial light modulation with liq. cryst. 80—96026
mixed oxide crystals, anionic co-ordination polyhedron model 79—99854
molecular electro-optical emission, for excited state dipole moment determ. 78—62230
molecular IR absorpt. intensities, symmetry considerations on electro-optical parameters 77—75225
multiplexed twisted nematic displays, liq. cryst. material design 79—90533
nematic layers, optical phase difference and capacitance, elec. and mag. field depend. 80—28911
nematic layers, positive dielec. anisotropy, EHD instability at DC excitation 79—94877
nematic liq., cryst. cell, with asymmetrically treated electrodes, electrooptic characts. 79—55658
nematic liq. crystal, dielectric anisotropy, IR spectra, effect of AC elec. field 78—64355
nematic liquid cryst., ZhK-440, transparency, electrooptical characts. 80—78996
nematic liquid cryst. display devices, with twisted and tilted arrangements, guest-host interactions 80—34891
nematic liquid cryst. mixture, ZLI-207, nonideally oriented layers, Freedericksz transition dynamics 80—100163
nematic liquid crystal, colour effects using birefringent films and pleochroic dyes 80—24353
nematic liquid crystal, DC dynamic scatt., flow direction rel. to dopant electrochem. props. 77—90130
nematic liquid crystal, dye-mixed DPM-4, flow speed AC appl. field effect 77—39532
nematic liquid crystal, dynamic light scatt., model 80—2730

electro-optical effects continued
nematic liquid crystal, dynamic scattering, material flow due to external electric fields 78—18543
nematic liquid crystal, elec. field suppression of fluctuations, laser speckle picture 77—7660
nematic liquid crystal, elect. conduct. based on injection-contact phenomena theory *(Russian)* 80—107807
nematic liquid crystal, hexagonal arrays 77—11478
nematic liquid crystal, orientational electrooptic effects, time characts. 78—27191
nematic liquid crystal, S-effect, growth and decay times 78—2824
nematic liquid crystal, threshold flexoelectric effect 79—94878
nematic liquid crystal, with negative dielec. anisotropy, transverse electro-optic effect 77—59556
nematic liquid crystal, ZhK-440, new type of electrohydrodynamic instability 79—14677
nematic liquid crystal, ZLI-207, electro-opt. props. *(Russian)* 77—43967
nematic liquid crystal cell, with pretilt angle, electro-optical properties *(Japanese)* 78—43837
nematic liquid crystal DC dynamic scatt. microscopic structure and role of dopants 77—77179
nematic liquid crystal display, capacitative anal. 77—43969
nematic liquid crystal matrix display, scanning capability improvement 77—55770
nematic liquid crystal mixture, for low voltage dynamic scatt. display 78—27184
nematic liquid crystal transducers, dynamic scatt., pre-excitation 80—88021
nematic liquid crystal twisted layer, light transmission 78—68476
nematic liquid crystals, field-dependent light scatt. 77—4040
nematic liquid crystals, light scattering centre dimensions, elec. field effect *(Russian)* 78—38619
nematic liquid crystals, light transmission exam., positive and negative dielectric anisotropy 77—43141
nematic liquid crystals, temp. dependent props., twisted nematic displays 79—32901
nematic liquid crysts., behaviour in inhomogeneous elec. fields 80—44118
nematic product dynamic scatt. characteristics in mag. field 77—77177
nematic-cholesteric mixture, with positive dielec. anisotropy, light scatt. in elec. field 77—72548
nematic-cholesteric mixture with positive dielectric anisotropy, light scatt. characts. 78—75537
nematic-liquid crystal, space charge freezing, electro-optic effect meas. 78—34436
p-nitroaniline, mol. hyperpolarisability in soln., UV dispersion of charge transfer contrib. 79—31986
nitrobenzene, DC elec. field induced optical rectification 77—38980
nitrobenzene, linear electrooptic effect 77—16283
nonlinear fourth-order electro-optical effect, calc. of sixth-rank tensor 79—24291
nonlinear optical phenomena induced in perovskite-type crystals, expt. *(Japanese)* 77—38990
nonlinear processes in crysts., power stabilisation by electro-, piezo-optical tuning 77—88856
nonlinear second-order crystal processes, electro-optic, piezo-optic tuning 78—46718
p-n-nonyloxybenzoic acid, smectic C phase, electro-optical effect *(Russian)* 80—92458
nucleosomes and nucleosomal DNA, electro-optical props., relax. times and chain struct. 80—85350
OCR by spatial filtering with light beam deflection 78—1370
4-n-octyl-4′-cyanobiphenyl, smectic A phase, stimulation of EHD instability 79—78656
4-n-octyl-4′cyanobiphenyl/4-n-decyl-4′cyanobiphenyl mixture, dynamic characts. of electrooptical effect with memory 80—108183
p-n-octyl-p′-cyanobiphenyl, thermally addressed liq. cryst. display, light scatt. and contrast 80—34892
trans-p-n-octyloxy-α-methyl-p′-cyanophenyl cinnamate, mag. and elec. birefr. in isotropic phase 80—80744
optical data storage material requirements and possibilities *(German)* 78—25937
optical directional coupler, phase tuning 77—10999
optical flashes from double wire explosion, photographic appl. 80—1865
optical recording media, review 78—71172
organic compounds, for possible electro-optic appl., cryst. growth in glass capillary 77—44150
organic photoconductor, electric field-induced fluoresc. quenching 80—34967
PAA, nematic, adjustable domain struct. in inhomogeneous elec. field, electro-optic props. obs. 80—10494
parametric effects anal., in optics 80—102619
parametric transformation of light polarisation in crystals 78—1153
p-n-pentyl-p′-cyanobiphenyl, nematic ordering, electric field induced second harmonic generation 79—60263
perovskite and tungsten bronze cryst. struct. types, ionic grouping theory, electrooptical, nonlinear optical effects *(Chinese)* 78—52472
phase shifting at 94 GHz using bulk crystals, microwave electro-optic coeffs. determ. 80—71382
phase transitions, ferroelectric and structural, refractive indices and electro-optics 79—19850
phenyl benzoate liq. cryst., doping effect on cond. anisotropy and dynamic scatt. 77—40208
phenyl benzoate nematic liq. cryst., dynamic scatt., alignment effects 77—40207
phenylcyclohexanes, nematic, low melting liq. crysts. with positive dielec. anisotropy, phys. props. 77—43148
photo-induced electron and hole transport in electro-optic crystals, holographic method for determ. 79—28375
photorefractive crystals with arbitrary electron transport lengths, holographic grating form. 80—1151
phthalocyanine, X-metal-free in polyvinylacetate. elec. field induced fluoresc. quenching, carrier photogeneration 78—48207
piezoelectric cryst., excitation and energy flux of acoustic harmonic, amplitude depend. on electro-optic nonlinearity 79—15404
piezoelectric crystals, surface modes, acoustic wave propagation 80—20026
planar lipid bilayers as light guides, elec. field induced scatt. 80—48148
pleochroic dyes, dissolved in nematic liq. crysts., guest-host interactions, appl. to electrooptic displays 80—44113
PLZT coarse-grained solid solutions, electro-optical processes induced by longitudinal electric field *(Russian)* 80—80750

electro-optical effects continued
PLZT electrooptic ceramic, electron beam surface charging, rel. to optical modulation 80—6952
Poincare sphere analysis 77—85690
polarimeter, electro-optical effect meas., appl. to ferroelec. crysts. *(Japanese)* 78—37045
polarised light in chemistry, electro-optic and photoelastic modulators 77—45896
polarised light in materials research, birefr., electro-, magneto-, elasto- and acousto-optics 77—48143
poly-4-vinylpyridine, electro-optic study of conformational changes induced by heavy metal ions 80—84725
poly-γ-benzyl-L-glutamate, preliq. cryst. mol. alignment, space charge effect, electro-optical obs. 77—40206
poly-γ-benzyl-L-glutamate-dichloroethane in conc. soln., mol. assoc., electro-opt. investig. 78—1973
polyarylenealkyls, colour, EPR, electron density delocalisation degree determ. *(Russian)* 80—7152
polydisperse dilute suspensions, of rod-like particles, anisotropy of electric polarisability 80—85224
polydisperse discs, particle size distrib., transient elec. birefr. data, two-parameter distrib. functions 78—40083
polydisperse ellipsoids, particle size distrib., transient elec. birefr. data, two-parameter distrib. functions 78—40084
polydisperse system, rotatory diffusion const., electro- optic decay curve, size distrib. 78—20079
polyelectrolytes, saturation of induced dipole moment, orientation mechanism and electro-optical effects 80—84785
polyethylene:NaCl, internal field strength, Raman spectra obs. 80—40061
polymethacrylic acid, dye-tagged, electrically oriented solns., fluoresc. polaris. changes 78—76523
polynucleotide solution, elec. birefringence, stabilised induced dipole behaviour 80—85349
polynucleotide solution, elec. field induced orientation and effects 80—85348
polypeptide in conc. soln., mol. assoc., electro-opt. investig. 78—1973
polypeptides, ionic and non-ionic, electro-optical studies of conformation 80—71379
polyribonucleotides, dye tagged, aqueous solns., elec. induced fluoresc. changes 80—85346
polythylene, and perdeuteropolyethylene, crysts., IR and Raman intensities, factor group splittings 79—65851
polyvinylidene fluoride, birefr. change induced by elec. field 80—55065
polyvinylidene fluoride, electro-optic and elasto- optic effects 80—80754
polyvinylidene fluoride, thermodynamic model and appl. 80—75955
pretilted nematic structure, colour control by elec. field 77—73127
N-p-propoxybenzylidene-p-pentylaniline, Williams domains, interference study 80—44114
purple membrane fragment suspensions, elec. dichroism obs., trimer model interpret. 80—89728
pyridazine, elec. field induced spectrum, 0_0^0 band near 3752Å 78—17700
quartz, electro-optical props. near phase transition 80—80756
quartz, electrogyration effect, electric field depend. of optical activity 77—32352
quartz, induced elliptic double refraction, separation into liner and circular components *(German)* 77—24817
quartz, natural, virgin (γ-irradiated), polarisation effect on thermolum. sensitivity 80—11483
racemic liq. soln., mirror isomeric mol. separation by RF rot. polarisation elec. field 78—80317
Raman scattering of light by polaritons, reviews 80—34928
Raman spectra intensity analysis, electrooptical parameters transferability 78—29820
relaxation distribution function, approx. methods and num. inversion of Laplace transform. 80—84720
relaxation times for formation and break-up of Williams domains 78—34423
resonance Raman scattering, in strong elec. field 77—16305
Rochelle salt, electrogyration during phase transitions 79—19859
Rochelle salt, refractive index, dispersion and temp. depend. 77—16275
ruby ring laser with forced mode locking 80—95915
salts, aq. solns., mechanical and electro-optical anharmonicity *(Ukrainian)* 78—2830
scintillation detector, in SEM 80—52819
semiconductor, elec. field induced optical SHG theory, Brillouin zone integral 80—69457
semiconductor, electro-optic effects anisotropy and hot electron cond., free carrier-impurity scatt. 77—4626
semiconductor, exciton absorption, electric field effect *(Russian)* 78—43902
semiconductor, IR transmission, cond. variations effects 79—15158
semiconductor, nonparabolic generalised Franz-Keldysh effect in high freq. elec. field 77—59555
semiconductor, optical absorption of diamagnetic excitons in crossed mag. and elec. fields 78—10874
semiconductor, optical generation of carriers under Franz-Keldysh effect conditions, instability 79—24017
semiconductor, piezoelectric, modulational instability of far IR laser, in presence of DC field 79—47117
semiconductor diamagnetic excitons in strong elec. field, optical absorpt. line intensities 79—38002
semiconductors, Benard effect, influence of extreme elec. field *(Russian)* 79—1750
semiconductors, EM wave absorption in quantising electric field 80—108182
semiconductors, role of excitons in dispersion effects, band gap determ. 79—65393
semiconductors, two-photon light absorption by excitons in static elec. field 80—11364
sepiolite, electric polarisability, anisotropy, length depend. of ionic contrib. 80—85224
sepiolite, size distributions, transient electric birefringence 80—85223
signal representation by implicit sampling 79—76620
simple liquids, Raman spectroscopy, electric field induced changes *(German)* 79—28715
single laser mode switching, probe of phase memory and radiationless relax. 77—10698
single-mode fibres, electro-optical polarisation control 80—91899
smectic A phase, dynamic characts. of electrooptical effect with memory 80—108183

electro-optical effects continued
smectic A phase, variable tilt, electro-optic effect giving stored colours 78−51415
smectic C liquid crystals, ferroelec., fundamentals and display appl. 80−79676
smectic C phase, mol. director behaviour at domain EHD instability 80−15000
smectic C phase, tilt angle determ. by field-induced Freedericksz transitions and X-ray meas. 79−94884
smectic liquid crystal, chiral, optics and electro-optics, kinematical diffr. theory 80−92461
smectic liquid crystal, ferroelec., linear electrooptic effect 80−11365
smectic liquid crystal, light propag. in chiral and cholesteric phases *(French)* 78−43836
smectic liquid crystals, electro-optic effects 77−69801
smectic liquid crystals, ferroelec., submicrosecond bistable electro-optic switching 80−84051
smectic mesophases, viscoelastic properties and field instabilities 79−27904
sodium bentonite, Wyoming, suspension, comparison of optico-optical scattering and birefringence 80−85226
sodium polystyrene sulphonate, dye-tagged, electrically oriented solns., fluoresc. polaris. changes 78−76523
solutions and suspensions, polarised fluoresc. in elec. field, mol. props. deriv. 80−84785
spiropyrans, photochromic transformation by electro-optical chronography 79−57264
submillimetre monochromatic spectroscopic determination of dielec. props. of electro-opt. materials 78−76428
submillimetre travelling-wave interferometer for crystal electrooptical props. study 78−21209
suspension of absorbing particles, simultaneous meas. of dichroism and birefringence in elec. field., photocurrent signal obs. 80−82801
suspension of rod-like molecular particles, rot. diffusion coeff. from decay rate of birefr. 79−38520
symmetric-top molecules, dilute gas, non-reson. microwave absorpt., kinetic theory 79−68901
tanane, crit. behaviour near ferroelec.-ferroelastic transition 78−52459
Tanane, dielec. and electrooptic meas. near ferroelec. transition 79−33587
tetracene, fluorescence, effect of weak external electric field *(Russian)* 78−80416
tetracene surface states, electric field effects, exciton-charge carrier interactions *(Russian)* 80−24989
1,2,3,4-tetrachloro-7,8-diphenylcalicene, excited states, moments anal. of electro-optical spectra 79−22698
N,N,N′,N′-tetramethylparaphenylenediamine, recomb. fluoresc., elec. field quenching 78−92107
TGS:α-alanine, electro-optic props. *(Russian)* 79−78654
TGS, electrogyration during phase transitions 79−19859
TGS, electrooptic switching anomalies 78−52473
TGS, ferroelec. transition, electrooptical hysteresis and crit. behaviour of electrooptical props. 78−2817
TGSe, ferroelec. transition, electrooptical hysteresis and crit. behaviour of electrooptical props. 78−2817
thin films, lens formation, alternating elec. field effect 80−12060
TMPD, 2,2,4-trimethylpentane, fluoresc. quenching by elec. field, above photoionis. threshold 78−33539
tobacco mosaic virus, solutions, Rayleigh scatt., elec. induced variations, spectral width and intensity meas. 78−48187
toluene, linear electrooptic effect 77−16283
transparent ceramics and ferroelec. glasses *(Japanese)* 79−65840
trichloromethane(-d$_1$), electrooptical parameters and Raman intensities obs., bond polaris. calcs., vibr. force field 77−50441
triglycine fluoroberyllate, ferroelec. transition, electrooptical hysteresis and crit. behaviour of electrooptical props. 78−2817
trigonal crystals, anisotropy of linear electrooptic effect 80−34894
trisarcosine calcium chloride crystals, ferroelec., electrooptic and ferroelastic props. 80−34865
tunable single-sideband generation in IR 80−78876
twisted nematic liquid crystal cell, off-ninety degree, electro-optical colour effect 77−77172
two-level system in sinusoidal elec. field *(Russian)* 78−58966
uniaxial crystals, local field influence on electron contribution to linear electro-optical effect *(Russian)* 80−88968
uniaxial noncentrosymmetric crysts. with intersecting dispersion curves, external actions effect 78−84552
urea, electro-optical coeffs. meas., rel. to nonlinear optics calcs. 80−34889
viologen films, on transparent oxide electrodes, morphology, electro-optical obs. 80−100703
viscosity and electrooptical characts. 79−86682
volume holograms in electrooptic birefr. crysts., light diffr. 79−55084
water, linear electrooptic effect 77−16283
ABO$_3$-type crystal, electro-opt. effect, theoretical treatment 78−76427
ADP-type crystals, electrooptic effect in ultraviolet region 78−76431
Ag, adsorption of O, dielec. perm., plasma surface vibr., modulation spectroscopy 77−48198
Al$_x$Ga$_{1-x}$As, modified-strip buried-heterostructure lasers, CW electro-optical properties 80−74359
Ar, opto-galvanic effect 79−98013
Ba(NO$_2$)$_2$.H$_2$O, hexagonal, piezoelec., electro-optic, dielec., elastic, thermoelastic props., space groups 78−76388
Ba$_2$Na(Nb,Ti)$_5$O$_{15}$, prep. and electro-opt. props. 78−76432
Ba$_2$NaNb$_5$O$_{15}$ crystal domains, amplitude modulation of light by diffr. 79−59832
Ba$_2$NaNb$_5$O$_{15}$, electrooptic coeffs. and refractive indices 79−33673
Ba$_2$NaNb$_5$O$_{15}$, electrooptical diffr. by periodic domain struct. 80−40090
Ba$_2$NaNb$_5$O$_{15}$, Raman spectra in elec. field 79−1763
Ba$_{0.725}$Sr$_{1.775}$Li$_x$Nb$_{5-x}$Ti$_x$O$_{15}$, solid soln., prep., struct., dielec. props. *(French)* 77−69782
Ba$_{0.25}$Sr$_{0.75}$Nb$_2$O$_6$, spontaneous electroopticabsorption effect 78−19443
Ba$_{0.39}$Sr$_{0.61}$Nb$_2$O$_6$, electro-optical props. 80−2728
Ba$_{0.54}$Sr$_{0.46}$Nb$_2$O$_6$:Y(La)(Tm), dielectric and electrooptic props. 78−68466
BaTiO$_3$, dielec. and optical props. using shell model 79−33654
BaTiO$_3$, electro-opt. effect, theoretical treatment 78−76427
BaTiO$_3$, paraelec. cryst., electro-optical absorpt. near Curie temp. 77−1657
BaTiO$_3$, quadratic electro-optic effect, incident light wavelength depend. 80−16010

electro-optical effects continued
BaTiO$_3$, Raman intensity analysis, symmetry coords., optical modes, electro-opt. consts. 79−95740
BaTiO$_3$, vacuum UV spectra and electro-optical prop. *(Japanese)* 79−65900
BaTiO$_3$:Mn^{2+}, electrooptical effect, charge transfer mechanism, defect. pair form. 79−38519
Ba$_2$TiSi$_2$O$_8$, fresnoite, Czochralski growth and phys. props. 78−3026
Bi$_{40}$Ga$_2$O$_{63}$ electro-optic and electrogyratory coefficient meas. 77−43974
Bi$_{12}$GeO$_{20}$, electron beam recording 79−32075
Bi$_{12}$GeO$_{20}$, light polarisation, elec. field effect *(Russian)* 77−66480
Bi$_{12}$GeO$_{20}$, mechanism of creation of internal fields and photoelectret effect 80−25290
Bi$_{12}$GeO$_{20}$, single cryst., electro-optical and photocond. props., image recording *(Russian)* 77−73129
Bi$_{12}$SiO$_{20}$ crystal, real-time holographic recording 79−72540
Bi$_{12}$SiO$_{20}$ electrooptic crystals, vol. phase holograms, light diffr. and nonlinear image processing 80−37972
Bi$_{12}$SiO$_{20}$, electrooptic photorefractive crysts. for optical information processing 80−74313
Bi$_{12}$SiO$_{20}$, image recording possibility 79−27432
Bi$_{12}$SiO$_{20}$ in insulator-semicond.-insulator struct., induced birefr., influence of kinetics of transient processes 79−24294
Bi$_{12}$SiO$_{20}$, light polarisation, elec. field effect *(Russian)* 77−66480
Bi$_{12}$SiO$_{20}$, mechanism of creation of internal fields and photoelectret effect 80−25290
Bi$_{12}$SiO$_{20}$, optical sensor for measurement of high electric field intensity 80−69509
Bi$_{12}$SiO$_{20}$, volume hologram polarisation props. and appls. 78−74859
Bi$_{12}$TiO$_{20}$ electro-optic and electrogyratory coefficient meas. 77−43974
CO$_2$, electro-optical parameters determ. from IR absorpt. 79−98128
CO$_2$, electrooptic constants, IR absorption spectrum in $2\nu_3$ vibration band 79−3442
CO$_2$ laser line, electro-optic frequency shift *(Chinese)* 80−43379
CO$_2$, Π_u symmetry transition probabilities, dipole moment and electro-optical consts. calc. 80−43115
CaF$_2$:Co^{2+}, elec. field effect on spectra induced by odd vibrs. 79−73973
CaF$_2$:Co^{2+}, parity-forbidden transitions, elec. field effect on electronic-vibr. spectrum 79−65905
CaF$_2$:R^{3+}, dichroism, elec. field effects *(Russian)* 77−24823
CaWO$_4$, centrosymmetric cryst., linear electrogyration study 80−60540
CdF$_2$:Co^{2+}, parity-forbidden transitions, elec. field effect on electronic-vibr. spectrum 79−65905
CdS, collision controlled light scatt. by electrons, influence of elec. field *(Russian)* 78−64375
CdS, domain elec. instabilities, elec. field and temp. distribs., optical meas. 79−11405
CdS, equivalent gap alteration by light scatt. by acoustic domains 77−85687
CdS, photoexcitation, effect of elec. field *(Russian)* 79−1751
CdS, strain- and electro-gyration, polarised light dispersion curve pseudocrossing 77−36196
CdS-ZnS(CdSe), film, light transmittance spectra, comparison with Schott GG 495 glass filter 78−33838
CdTe crystal in square waveguide, single sideband generation at 10.6 μm 79−55179
CdTe linear electro-optic translation of IR laser wavelengths 80−78878
CdTe optical applications, review 77−42580
CdTe single cryst., linear electro-optical props., temp. depend. 80−71376
CdTe, tunable high efficiency microwave freq. shifting of IR laser 78−71126
CdTe:H$^+$, ion-implanted, optical waveguiding and electrooptic modulation 77−7197
Cd$_{1-x}$Zn$_x$S, RF sputtered electro-optical film for data storage and display 78−83047
Co$_2$, electrooptical consts., $2\nu_3$ band induced component 80−78626
copper phthalocyanine, size distributions, transient electric birefringence 80−85223
Cr$_2$O$_3$/γ-Fe$_2$O$_3$/Pt electrode, two layer oxide surface film anal. by modulation spectroscopy *(Japanese)* 80−11491
CsCuCl$_3$, optical props. rel. to IR electro-optical modulator appl. 78−42393
CsCuCl$_3$, phase transition, refr. index, electrooptic coeff., pyroelec. signal, and NQR meas. 80−70386
CsD$_2$AsO$_4$, SHG, electro-optic and piezo-optic tuning 78−46718
CsH$_2$PO$_4$, ferroelec. transition, electrooptic 80−76005
Cs$_2$S$_2$O$_6$, hexagonal, piezoelec., electro-optic, dielec., elastic, thermoelastic props., space groups 78−76388
CuCl, electrooptic props. below absorpt. edge 77−28548
CuI single cryst., linear electro-optical props., temp. depend. 80−71376
D, Lamb shift, from elec. field quenching radiation anisotropy 78−66502
F$_2$O, absorpt. band freq. and intensities, electro-optical parameters, pot. energy, IR spectra 80−37812
Fe$_3$B$_7$O$_{13}$I, thermodynamics of props. 78−76426
GaAs DH lasers, external electro-optic modulation 77−58446
GaAs, hot electrons and exciton-electron collision under external elec. field 78−43928
n-GaAs, IR transmission, cond. variations effects 79−15158
GaAs MOS and Schottky systems, electromodulated reabsorption of luminesc. 79−15524
GaAs, nonlinear electro-optical susceptibility, coupled anharmonic oscill. model 80−2723
GaAs, nonlinear optical susceptibility and dispersion, electro-optic meas. 77−23707
GaAs, photoluminescence, electron gas coding influence in ion-bombarded layers 80−108272
GaAs, polariton scattering, free carrier effects 78−34783
GaAs single cryst., linear electro-optical props., temp. depend. 80−71376
GaAs:Cr, photoluminescence in strong electric fields 80−108270
GaAs:O, field depend. of radiative recomb. 80−20700
GaAs-Al$_x$Ga$_{1-x}$As DH laser, MBE grown, CW electro-optical props. 80−102725
GaP, nonlinear optical susceptibility and dispersion, electro-optic meas. 77−23707
n-GaSb, fundamental absorpt. and energy relax., elec. field induced changes 77−1688
GaSe(Te)-SnO$_2$ spray heterojunction, electro-optical props. 78−64102
Gd, optical conductivity, direct interband transitions 80−15488
Gd$_2$(MoO$_4$)$_3$ 78−88281
Gd$_2$(MoO$_4$)$_3$, spontaneous electrooptic effect, role of induced birefringence 78−68480

electro-optical effects continued
$Gd_2(MoO_4)_3$, spontaneous rot. of plane of polarisation of light in external field 80-93282
$Gd_2(MoO_4)_3$, thermodynamics of props. 78-76426
Ge, biexciton and trion existence, photolum. *(Russian)* 80-16088
n-Ge, IR absorption by hot carrier 80-40087
α-HIO_3, electrogyration coeff. meas. 79-19859
H_2O molecule, electro-optical parameters determ. *(Russian)* 77-14466
InGaAs-GaSbAs periodic structures, with controlled emission 79-7880
In_2O_3-SnO_2, magnetron RF sputtered electro-optical film for data storage and display 78-83047
n-InSb, Landau emission spectra, influence of bakcground radiation 78-43935
InSb, Landau level struct., magneto-electroreflectance 80-25349
n-InSb, photoluminesc. in crossed EM fields *(Russian)* 77-24892
n-InSb submillimetric-wave free-carrier Faraday effect in strong longitudinal elec. field 80-66164
n-InSb, transparency, DC field induced enhancement 79-91407
$In_{2-x}Sn_xO_{3-y}$-ZnS:Mn thin film structure, surface morphology and electro-optical props. *(Russian)* 80-49554
KCl single crystals, F-band absorpt. and thermolum. under DC field and X-ray irrad. 79-65910
KDP-type crystals, electrooptic effect in ultraviolet region 78-76431
KDP-type crystals, phase transitions, quadratic electrooptical coeff., electrostriction 78-76430
KD_2PO_4, nonlinear electrooptic coeffs. near Curie temp. 80-11366
$KH_{2(1-x)}D_{2x}PO_4$, photoelasticity and electrooptic effects at forbidden deform. *(Russian)* 78-35117
KH_2PO_4, electro-optic props. near ferroelec. transition 78-19445
KH_2PO_4, electro-optic modulators, transient acoustic waves 79-59809
KH_2PO_4, electrogyration near transition pt. in nonenantiomorphic cryst. 79-61339
KH_2PO_4, KD_2 PO_4 crystals used for laser control, acoustic vibr. suppression 78-1363
KH_2PO_4, light scatt. in elec. field, ferroelec.-paraelec. transition 80-2707
KH_2PO_4, Pockels' const., linear electro-optic consts., sign of piezoelectric const. 78-60425
KH_2PO_4, spontaneous electrooptic effect in far IR 79-95734
KH_2PO_4, vacuum UV spectra and electro-optical prop. *(Japanese)* 79-65900
KH_2PPO_4, KD_2PO_4, nonlinear electrooptic effects 80-29721
$KI{:}Eu^{2+}(Sr^{2+})(Mn^{2+})$, elec. field effect on mech. of recomb. 78-80397
$K_3Li_2Nb_5O_{15}$ films for optical waveguides epitaxial growth and characterisation 80-79016
$KNbO_3$, dielec. and optical props. using shell model 79-33654
$KNbO_3$ half-wave voltage, electro-optic and polarisation-optic coefficients 77-40211
$KNbO_3$:Fe, optically induced refractive index changes 77-4612
$K(Ta,Nb)O_3$ ceramic, prep. and electro-optical props. 80-25620
$KTa_{1-x}Nb_xO_3$, local polarisability in quantum paraelec. and quantum ferroelec. phases 78-64325
$KTaO_3$, crit. dielec. and optical props. and storage, 4K 77-24805
$KTaO_3$, SHG and quadratic electrooptic effect 78-76429
$kH_{2(1-x)}D_{2x}PO_4$, monoclinic, electro-optical props. 79-82951
$La_xPb_{1-x}Zr_yTa_{1-y}O_3$, ferroelec. with diffuse phase transition, electrostriction-optical props. 78-68457
$LiClO_4.3D_2O$, hexagonal, piezoelec., electro-optic, dielec., elastic, thermoelastic props., space groups 78-76388
$LiClO_4.3H_2O$, hexagonal, piezoelec., electro-optic, dielec., elastic, thermoelastic props., space groups 78-76388
LiF:Mg, light scatt., effect of electrostatic field 78-2823
LiH, finite-field method calcs., dipole moment gradients, polarisability gradients and elec. field effects 77-88589
α-$LiIO_3$, DC effects on transmitted light *(Chinese)* 78-10869
$LiIO_3$, electrogyration coeff. meas. 79-19859
α-$LiIO_3$, light diffr. intensity, freezing effect in electrostatic effect *(Chinese)* 79-91404
$LiIO_3$, second harmonic optical coeffs. based on highly deformed oxygen-octahedra model of $(IO_3)^{-1}$ *(Chinese)* 77-75608
α-$LiIO_3$, single crysts., light diffr. under DC field 80-11367
$LiNH_4SO_4$, $LiNH_4SeO_4$, nonlinear opt. props. including SHG 78-76396
$LiNH_4SO_4$, phase transitions and phys. props. 78-76399
$LiNbO_3$, chemical, struct. and physical props., book contrib. 79-69783
$LiNbO_3$, cleaved, crystallographic and electrooptic props. 80-59575
$LiNbO_3$ crystal, different interdigital electrode struct., electric field distrib. obs. 78-76433
$LiNbO_3$ crystal, elec. cond., optical quality, impurity depend., space charge pyroelectric field compensation 79-64295
$LiNbO_3$, electric-field induced microscopic struct. changes, modulated X-ray diffr. detect. 78-47296
$LiNbO_3$, electro-optical modulator, principal refr. indices and electrooptical coeffs. 79-42947
$LiNbO_3$, electrooptic photorefractive crysts. for optical information processing 80-74313
$LiNbO_3$, laser induced optical inhomogeneity in external electric field 79-95730
$LiNbO_3$, $LiNbO_3$:Fe, amplification of laser beams by ferroelectrics 78-90393
$LiNbO_3$, $LiNbO_3$-Fe, photorefraction in ferroelectrics rel. to electro-opt. effects 78-92048
$LiNbO_3$, $LiTaO_3$, transition metal doped, photovoltaic and photorefractive effects, origin 77-20364
$LiNbO_3$, light diffr., elec. field effects, spatial hologram appls. *(Russian)* 77-23635
$LiNbO_3$, light diffraction from volume phase holograms 79-36860
$LiNbO_3$, mechanism of hologram writing, expt. 77-19212
$LiNbO_3$, optical damage induced by X-irradiation 77-20814
$LiNbO_3$, optical waveguides by ion implantation 80-106622
$LiNbO_3$, photoelasticity tensor, including piezoelectrooptic interaction correction, Brillouin scatt. 77-24820
$LiNbO_3$ photorefractive reversible optical memory *(Russian)* 78-58943
$LiNbO_3$, pure and Fe doped, photorefraction, effect of external elec. field and light intensity *(Russian)* 79-56766
$LiNbO_3$, transition metal doped, photovoltaic effects, spectroscopic investigation 77-20365
$LiNbO_3$ transparency with vacuum-deposited electrodes *(Russian)* 78-60422
$LiNbO_3$, trigonal crysts., anisotropy of linear electrooptic effect 80-34894

electro-optical effects continued
$LiNbO_3$, Y-cut, waveguide form. by Ti diffusion, refr. index and electrooptic coeffs. 79-14114
$LiNbO_3$:Fe, phase hologram storage and fixing, review 77-19210
$LiNbO_3$:Fe, photorefractive effects under external elec. field 77-23723
$LiNbO_3$:Fe, two different phase holographic recording processes, expt. 77-19211
$LiNbO_3{:}Fe^{3+}$, electrooptical effect, charge transfer mechanism, defect. pair form. 79-38519
$LiNbO_3$:Fe(Cu), photorefractive centres, optical absorption, EPR and Mossbauer spectra meas. 77-32403
$LiNbO_3$:Ti optical waveguides, elec. field tuning of SHG, phase-matching condition 79-41412
$LiTaO_3$ platelet, tunable filter, birefr. electro-optic cryst., light energy coupling 79-59804
$LiTaO_3$, trigonal crysts., anisotropy of linear electrooptic effect 80-34894
$MNbO_3$, tetragonal, electronic struct., optical anisotropy 80-70599
$(NH_4)_2BeF_4$ crystals, incommensurate-commensurate phase transitions, optical props. 79-95733
NH_4Cl, electro-optical props. near order-disorder transition 78-31173
NH_4Cl, order parameter, electro-optic measurement 78-88280
NH_4Cl, order-disorder phase transform., effect of plastic deform. and electrooptic effect 79-33672
NH_4IO_3, static electrooptic coeffs., temp. depend. 77-28547
$NaBi(MoO_4)_2$, electrically induced optical activity 79-82942
NaBr(:I), exciton ionisation and decay, photoluminesc. in elec. field 77-44046
$NaBrO_3$, light polarisation, elec. field effect *(Russian)* 77-66480
$NaClO_3$, electrogyration and piezogyration meas. 79-28716
$NaNH_4SO_4.2H_2O$, $NaNH_4SeO_4.2H_2O$, nonlinear opt. props. including SHG 78-76396
$NaNO_2$, Raman and IR spectra, destructive Fermi reson. 77-16309
$NaNO_2$, vacuum UV spectra and electro-optical prop. *(Japanese)* 79-65900
Ne, gas discharge, laser irrad. and voltage changes 78-63606
Ne, glow discharge, voltage change due to laser irrad., 572-654 nm 78-63605
Ne, opto-galvanic effect 79-98013
PLZT ceramic, optical gate, dielec., optical props., electro-optical effect meas. 78-42418
PLZT ceramic birefringence props., transverse electro-optical meas. 78-72487
PLZT ceramic with memory, domain reorientation, alternating elec. field effect 79-47405
PLZT ceramics, electro-optic characts., w.r.t. future instrument applics. *(German)* 78-33792
PLZT ceramics, electro-optical props. *(Korean)* 79-11406
PLZT ceramics, physical, elec. and optical props. and fabrication *(Polish)* 78-56458
PLZT, controlled light scatt. 78-10909
PLZT, electrically polarised, size and conc. of light scatt. centres 77-28549
PLZT, electrooptic systems *(Japanese)* 79-65840
PLZT ferroelectric display electro-optical props. *(Russian)* 79-9211
PLZT film, electro-optic effects 78-6799
PLZT, light scatt., time depend., switching, memory modes 77-12362
PLZT, light scatt. under switching conditions, time characts. 77-52045
PLZT, phase transitions, permittivity, birefr. and light scatt. meas. 77-81074
PLZT, RF sputtered thin film, ferroelectric props. 79-69780
PLZT slim-loop and linear ceramics, longit. electrooptic effects, display appl. 80-80751
PLZT transparent ceramics, electro-optical anisotropy due to hot pressing 77-12720
PLZT, transparent ferroelec., RF sputtering and film characterisation 78-72727
PLZT type ceramics, variation of light scatt. during field induced AF→F transition *(French)* 77-90158
PLZT, with broad phase transition, birefr., electro-optic and dielec. props. 77-16280
$(Pb,La)(Zr,Ti)O_3$, ferroelec. ceramic, polarisation distrib. obs. using electro-optic effect 80-25278
$(Pb_xBa_{1-x})_5Ge_3O_{11}$, electrogyration, and dielectric props. 78-19444
$(Pb_{1-y}Ba_y)_{1-x}La_xNb_{2-x/5}O_6$, transparent ferroelec. ceramic, optical transmittance, electrooptic props. and Curie temp. 77-32395
$(Pb_{1-x}Bi_x)_5Ge_3O_{11}$, spontaneous and induced electrogyration 79-42946
$Pb_5Ge_3O_{11}$, electrogyration during phase transitions 79-19859
$xPb_5GeO_4(VO_4)_2$, $(1\text{-}x)Pb_5SiO_4(VO_4)_2$, solid solution of centrosymmetric crystals, electrically induced optical activity 80-108180
$Pb_5GeO_4(VO_4)_2$, centrosymmetric crysts., induced linear electrogyration 80-45039
$PbHPO_4$, optical props. near ferroelec. transition 79-33663
$PbMg_{1/3}Nb_{2/3}O_3$, electro-opt., elasto-opt., opt. and photo-induced props. 78-95560
$PbMg_{1/3}Nb_{2/3}O_3$, photoinduced phenomena at diffuse phase transition 78-43814
$PbMg_{1/3}Nb_{2/3}O_3$ single cryst., electro-optical hysteresis curves and phase transitions *(German)* 79-28717
$PbMg_xNb_{1-x}O_3$, ferroelec. with diffuse phase transition, electrostriction-optical props. 78-68457
$Pb_3MgNb_2O_9$, birefringence, pulse response of electro-optical effect 79-87417
$Pb_3MgNb_2O_9$, crystal growth procedure, meas. electro-optic and dielectric props. 78-88418
$PbMg_2Ta_2O_9$, crystal growth procedure, meas. electro-optic and dielectric props. 78-88418
$PbMoO_4$, centrosymmetric cryst., linear electrogyration study 80-60540
$PbMoO_4$, electrogyration coeff. meas. 79-19859
$Pb_5SiO_4(VO_4)_2$, centrosymmetric crysts., induced linear electrogyration 80-45039
$Pb(Zn_{1/3}Nb_{2/3})O_3$, diffuse phase transition, electro-optical and dielec. obs. 79-82933
$PbZn_{1/3}Nb_{2/3}O_3$, electro-opt., elasto-opt., opt. and photo-induced props. 78-95560
$Pb(Zr,Ti)O_3$, electrooptic ceramic *(Japanese)* 79-65840
$Pb(Zr,Ti)O_3$:La(Cd,W) electro-optical ferroelec. ceramic, secondary electron emission yield 79-91546
RbH_2PO_4, electro-optic props. near ferroelec. transition 78-19445
SbSI, absorption edge, elec. field effect rel. to ferroelec. props. 80-97240

electro-optical effects continued
SbSI, paraelectric phase, nonlinear optical props. 78—10870
SbSI, photoinduced birefringence, effect of elec. field 77—52037
Si (100), surface space charge layer, inter-subband optical transitions 77—15931
Si (100) surface, intersubband optical absorption in space-charge layers 77—35984
Si ion-implanted structure annealing, defect behaviour obs. *(Russian)* 80—49281
SiH_4, ν_4 fundamental, laser sideband direct freq. reading IR spectra, electro-optical, press. broadening 78—21920
α-SiO_2, trigonal crysts., anisotropy of linear electrooptic effect 80—34894
Si_2Te_3, fundamental absorption and Franz-Keldysh effect meas. 77—1694
$SnCl_3^-$, harmonic approx., force consts., electro-optical parameters and normal vibrs 78—62790
SnI_3^-, harmonic approx., force consts., electro-optical parameters and normal vibrs 78—62790
SnO_2-ZnS:Mn thin film structure, surface morphology and electro-optical props. *(Russian)* 80—49554
$Sr_{0.25}Ba_{0.75}Nb_2O_6$ film, growth and electrophys. props. 79—42928
$Sr_{0.75}Ba_{0.25}Nb_2O_6$ single cryst., electro-optical hysteresis curves and phase transitions *(German)* 79—28717
$Sr_xBa_{1-x}Nb_2O_6$, domain struct. influence on electrooptical props. 80—93283
SrClF, cryst., Raman intensity anal., normal coord. anal. 78—72493
SrF_2:Nd^{3+}, linear dichroism induced by electric field orientation kinetics of Nd^{3+} centres 79—69868
$SrMoO_4$, centrosymmetric cryst., linear electrogyration study 80—60540
$Sr_4NaLiNb_{10}O_{30}$, electro-optic, pyroelec., dielec. and piezoelec. props. *(Chinese)* 79—69810
$SrTiO_3$, crit. dielec. and optical props. and storage, 4K 77—24805
$SrTiO_3$, electrooptic coeffs. 79—33673
$SrTiO_3$, monodomain, O-D and O-H stretching vibrs., IR spectra 80—71449
$SrTiO_3$, SHG and quadratic electrooptic effect 78—76429
TE, current induced optical activity, polarisation plane rotation rate *(Russian)* 79—65830
Te, acoustoelec. domain induced transparency at 11 μm 78—27182
Te, acoustoelectric domain induced transparency near 11 micron 77—85727
TlBr, electromodulation spectroscopy of excitons 79—73444
TlCl, electromodulation spectroscopy of excitons 79—73444
$TlGaSe_2$, electrooptic effect and refr. index anisotropy 77—16281
V_2O_5-B_2O_3-ZnO semiconductivity glasses, optical and modulated absorpt. spectra in band gap region 77—48189
WO_x, anodic oxide films, quadratic electro-optic and electrostrictive effects, ellipsometry 80—108184
YAG:Ce^{3+}, scintillation detector in SEM 80—52819
ZnS, linear electrooptic coeff. dispersion 80—71380
ZnS, refr. index oscills, in strong. elec. field 79—28720
ZnS single cryst., linear electro-optical props., temp. depend. 80—71376
ZnS:Mn film, spectral and electro-optical props. 77—1736
ZnS-Na_3AlF_6 multilayer films, thermally evaporated, dispersion characts. 77—59629
ZnSe in insulator-semicond.-insulator struct., induced birefr., influence of kinetics of transient processes 79—24294
ZnSe, linear electro-optic coeff. dispersion, relation to reson. Raman scatt. 78—56459
ZnSe, parasitic birefringence dispersion induced by lattice plane defects 77—4617
ZnSe single cryst., linear electro-optical props., temp. depend. 80—71376
ZnSe single crystals, birefringence due to native defects and electro-optic effect *(French)* 79—24293
ZnSe, twinning effect on electro-optical props. 78—68478
ZnTe, electro-optic suscept. dispersion curve 77—3620

electroabsorption
alkali halide:NH_2^-, paraelectric alignment, UV electroabsorpt. and Kerr effect 77—12413
alkenes, IR absorpt. curves calc. using standard fragments computer library 80—982
anthracene crystals, and thin films, electroabsorption in disordered solids 78—95590
anthracene film, electroabsorption spectra obs. 80—50301
anthracene Langmuir film, lightly substituted, electrolum., photolum. and electroabsorption 80—20726
chalcogenide glass, Urbach tail, rel. to Mott-Street model 77—47771
cubic crystals, electrooptic absorption of anisotropic Jahn-Teller centres 78—27188
deep excitons and electrically induced light absorption 77—43973
diamond:B, epitaxial layer, charge transfer and acceptor state 78—19169
diamond:B, photoconductivity and electroabsorpt. spectra 77—4647
finite crystal, red shift rel. to band gap, pot. difference effect 77—1654
hydroxygallium phthalocyanine, exciton electroabsorpt., optical density spectra 77—85746
impurity absorption in solids, and negative ion photodestruction in elec. field 77—20897
impurity centres, quadratic Stark effect in crysts. with wideband absorption spectra, semiclassical approx. 77—66526
impurity centres in crystals, quadratic Stark effect, Jahn-Teller effect 78—68536
Jahn-Teller impurity centre, electroabsorption moments 77—48205
layered compounds, book contrib. 77—40267
merocyanine-oxazolone dye optical probe for simultaneous recording from several neurones 77—66880
microspecimens, absorpt. spectra under conditions of light diffr. in elec. field, meas. methods *(Russian)* 77—36203
oxide semiconductor crystals, with forbidden energy gap, review of spectroscopic props. 78—2876
PAA, nematic liq., cryst., light transmission in high elec. field grad. 79—19150
piezoelectric semiconductor, polaron optical absorpt., external static elec. field depend. 77—85158
polydiacetylene, single crystal, electroreflectance and electroabsorption spectra, π-electron system and excitonic transitions 79—78653
semiconductor, cubic, noncentrosymmetric, electrooptic effect 79—69812
semiconductor, disordered, electroabsorption, contact excitons influence 80—10882
semiconductor, induced birefr. in presence of electroabsorpt. 77—32351

electroabsorption continued
semiconductor, many-phonon impurity absorpt. in external elec. field 77—52144
semiconductor, photo-field ionisation of deep centres allowing for Coulomb action *(Russian)* 78—27376
semiconductor, quasi-one-dimensional, light absorpt. and Raman scatt., large exciton form. 77—16272
semiconductor with complex valence band, polarisation props. of interband electroabsorption 80—66152
semiconductor with nonspherical bands, absorpt. in crossed elec. and mag. fields 77—40264
semiconductor with nonspherical bands, diamag. excitons and Franz-Keldysh effect 78—72554
semiconductors, impurity electro- and magnetoabsorpt. coeffs., deep levels 79—24340
semiconductors, two-photon absorption in crossed elec. and mag. fields 77—85693
semiconductors with narrow band gap, multiphoton magneto-absorption and electro-absorpt. *(Russian)* 79—19867
solids, physical principles underlying electroabsorptive phenomena, optical system appl. 79—3754
vanadyl phthalocyanine, exciton electroabsorpt., optical density spectra 77—85746
$AgGaS_2$, elec. field influence on absorpt. spectrum, exciton parameters and energy of impurity levels *(Russian)* 77—69860
Al/tetracene/nesatron cell, electroabsorption and electrorefl., interfacial elec. fields 79—65548
Al-fuchsin-SnO_2 MSM structure, field depend. of electroabsorption spectra 77—40263
$Al_yGa_{1-y}As_{1-x}Sb_x/GaAs_{1-x'}Sb_{x'}$, buried heterojunction electroabsorption modulator, report of operation 78—38044
$Al_yGa_{1-y}As_{1-x}Sb_x$-$Ga_{1-z}Sb_z$ buried heterojunction electroabsorption modulation 78—55439
As_2Se_3, cryst., electroabsorption on indirect gap 80—80812
$(As_2Se_3)_{1-x}(As_2Te_3)_x$ amorphous films, changes in optical props. under elec. fields and optical excitation 79—61455
$Cd(Ca)F_2$:Co^{2+}, Jahn-Teller split $^4A_{2g}\rightarrow{}^4T_{1g}(P)$ absorption band, elec. field effect 78—15202
CdS, substitutional Ti^{2+} centres, linear electroabsorpt. 77—66525
CdSe epitaxial layers, on GaP-CdS substrates, absorption and electroabsorption 80—40178
CdTe and CdTe:Cl, semi-insulating, electroabsorpt. by impurities and defects, dichroism 77—40270
CuCl, Urbach rule at excitonic absorpt. edge, theoretical model tests 80—50299
GaAs, birefringence in presence of electroabsorpt. 77—32351
GaAs, degenerate, nonequilib. electron distrib. functions 77—63394
GaAs, electroabsorpt. avalanche photodiode, waveguide detector for 1.06 μm 78—16842
GaAs, electroabsorpt. avalanche photodiode waveguide detectors 78—65965
GaAs, electroabsorpt. avalanche photodiode waveguide detector, freq. demultiplexing 79—17486
GaAs, electroabsorption spectra obs. 80—50301
GaAs electroabsorption signal, depend. on elec. field 80—103942
GaAs, high resist., linear electroabsorpt., characts., valence band splitting 77—44018
GaAs, noncentrosymmetric cubic cryst., electrooptic effect 79—69812
GaAs, optical modulation spectra, proton damage effect 78—76487
GaAs, two-photon electroabsorption by excitons 79—42944
GaAs:Cr, optical modulation study of proton bombardment 78—6720
GaAs:Cr, optical modulation spectra affected by 150 keV proton beam 78—10871
GaAs:O, Fe, temp. depend. of ionisation energies of O and Fe levels, electroabsorption meas. 78—47736
$GaAs_{1-x}Sb_x$ epitaxial n-n heterostructures, gap energies and interface pots., modulation electroabsorpt. meas. 79—11201
GaInAsP, electroabsorption 79—78652
GaP, obs. of Γ-L indirect transition, phonon struct. 78—48194
GaP:S, shallow donor states, Stark effect and inversion splitting, electroabsorption spectral obs. 80—50385
GaS, electrolum. and electroabsorpt., 77K 77—48247
GaSe, absorpt. and electroabsorpt. near indirect edge 77—20827
GaSe thin films, electroabsorpt. spectra, exciton line splitting 80—107716
$GaSe_xS_{1-x}$, layered semicond., electroabsorpt. in fundamental absorpt. edge region 77—52043
GaTe, single cryst. prep. and electroabsorpt. spectra investig. 80—103968
GaTe:Sn, electroabsorption spectra 79—19901
$Ge_{1-x}Si_x$, with Si implanted ions, optical and photoelec. props. 79—24014
n-InAs, heated electron gas, longitudinal optical phonon form., IR absorpt. modulation 80—45079
InP, electroabsorption spectra obs. 80—50301
InP, p-i-ν diode, Franz-Keldysh effect 77—55790
InSb n^+-p junctions, photocurrent spectrum near long wavelength edge of fundamental absorption band 80—100483
p-InSb, shift of fundamental absorpt. edge in crossed elec. and mag. fields 80—76034
KCl-Tl^+,Ca^{2+}(Sr^{2+}), electrolytic colouring, colour centre form., optical absorpt. spectra 79—15497
LiF, M-centre vibronic absorpt. spectra, elec. field, method of moments 78—27186
MoS_2(2H), electro-absorpt. edge spectra, cryst. thermal modulation, exciton state field ionisation 79—61395
NaCl, thermoluminesc. and optical absorpt., simultaneous DC field and X-irrad. 79—99956
NaCl:V^{2+}, elec. field effect on Z-like centres spectrum 80—2802
NaF, M-centre vibronic absorpt. spectra, elec. field, method of moments 78—27186
SiC:B, electroabsorption, 0.35-0.45 eV, under UV illumination 79—4831
TlCl, Urbach rule at excitonic absorpt. edge, theoretical model tests 80—50299
$TlInS_2$ single crysts., three-dimensional exciton destruction, electroabsorpt. and transmission spectra 77—55803
WO_3-B_2O_3-ZnO semiconducting glasses, DC cond. and optical absorpt. 80—107783
ZnS, two-photon absorption in crossed elec. and mag. fields 77—85693
ZnS:Cl, single cryst., deep centre study by impurity electroabsorpt., photocond. meas. 77—12411
ZnS:Ga(Cl), deep traps, impurity electroabsorpt. and photocond. meas. 78—6707

electroabsorption continued
ZnS:In, polarisation of deep centre electroabsorpt., effect of random electric fields 77—48148
ZnSe, absorpt. modulation of light, and its appl. to page composer 77—40258
ZnSe, exciton-impurity complex, electroabsorption meas. 79—15484
ZnSe:Cu, discovery of bound exciton, electroabsorption 80—45038
ZnTe:In(Al), pure and doped, Zn vacancy energy levels, elec. and optical props. 79—4827

electroacoustic effects *see acoustoelectric effects*

electroacoustic generators *see acoustic generators*

electrocaloric effects *see pyroelectricity*

electrocardiogram *see electrocardiography*

electrocardiography
see also bioelectric potentials; biomagnetism; cardiology
A/D conversion, meas. changes caused by precision level 77—40865
abdominal foetal ECG and VCG recording/processing systems 78—31947
absolute ECG and clinical map curve experiences 79—39556
acceleration sensor for heart implantation, heart attack warning *(German)* 79—57802
action potential, cond. and propag., equiv. cct. 78—31791
activity models for computer simulation *(Spanish)* 78—11758
acute myocardial infarction, electrophysiological aspects 79—43858
ambulatory, computer processing system 80—89897
ambulatory arrhythmia monitoring, automated family classification 79—66566
ambulatory arrhythmia quantification by correl. technique 78—81020
ambulatory ECG computer anal., YALECG 79—70661
ambulatory ECG monitoring problems 78—11763
ambulatory EKG recording using several computers in parallel 79—62389
ambulatory monitoring, adaptive algorithm for noise rejection 79—66571
ambulatory monitoring, detect. algorithm for multiform premature ventricular contractions 79—66572
ambulatory noninvasive monitoring of physiological data, recording systolic time intervals 79—66574
amplifier with automatic lead switching 78—28106
amplifiers, instruments and maintenance, review 78—69232
anaesthesia stage indicator, signal divider 80—3858
analogue and digital transmission 79—39564
analogue cct. for fast-response frequency measurement, used for foetal heart rate 79—21708
analogue trigger device for automatic arrhythmia detection systems, P, QRS waves 77—86696
analysis program modification allowing for correlated constitutional variables 78—40385
analysis program testing 79—25146
analysis programs, diagnostic statement reproducibility 78—7495
analysis system, long term recordings, quantitative evaluation of rhythm disturbances *(German)* 80—76847
analysis system oriented toward polarcardiology 78—85447
analysis using special purpose hybrid computers 77—40842
aortic and mitral regurgitation patient surgery and vectorcardiogram changes 79—44050
Argus algorithm development 79—70680
Argus ECG monitoring system reappraisal 78—7479
arrhythmia ambulatory anal. in real-time with minicomputer 80—85523
arrhythmia analysis, dual-processor computer 79—66569
arrhythmia analysis, using non-invasive His-ECG *(Hungarian)* 78—35981
arrhythmia and conduction disturbance diagnosis from His bundle electrogram 79—44032
arrhythmia classification in context, extension of single-beat algorithm 78—85426
arrhythmia classification using R-R interval and difference histograms 77—40843
arrhythmia data base of American Heart Association 79—62391
arrhythmia detection, edit and recall system, microprocessor-based 80—89891
arrhythmia detection and classification, statistical approach 77—21644
arrhythmia detection and efficient data compression in long-term ECGs 79—70678
arrhythmia detection by RR-interval comparison *(Bulgarian)* 78—15919
arrhythmia detection program comparison data bank 78—15921
arrhythmia detection using a low-power, CMOS processor 78—73276
arrhythmia detection with a multi-microprocessor system for distributed and parallel processing 80—85524
arrhythmia detector evaluation, ECG database development 78—81018
arrhythmia identification and verification by 3-channel eval. of long-term ECG records 80—85518
arrhythmia incidence and cardiac freq., ECG recording during athletes' sleep 79—43860
arrhythmia monitor, solid state delay unit 79—25126
arrhythmia monitoring, 15-channel analogue selector 77—40898
arrhythmia monitoring, ARGUS/RT microcomputer system 78—81014
arrhythmia monitoring, joint interval histogram and correlation coeff. scatter diagram techniques 77—25572
arrhythmia monitoring, multimorphology computerised system 79—70676
arrhythmia monitoring, single scan algorithm for QRS-detect. and feature extraction 80—85520
arrhythmia monitoring systems evaluation criteria 78—11765
arrhythmia monitoring using interactive computer system, clinical evaluation 78—81028
arrhythmia monitors, review 78—69233
arrhythmia quantification, template matching algorithm evaluation 80—85519
arrhythmia simulation device 78—44636
arrhythmia simulator, cct. description 77—73608
arrhythmia simulator for monitor testing 78—61270
arrhythmia sorting, oesophageal electrode for atrial electrogram 79—39574
arrhythmia studies, interactive graphics system for quantitative data extraction 78—81027
arrhythmias, comparison of incidence and prevalence in acute myocardial infarction 79—39380
arrhythmias high speed pattern recognition 78—36004
arrhythmias in ambulatory persons, review of 1000 recordings 80—36184
arrhythmias management, automated feedback control of drug therapy 80—41307

electrocardiography continued
artifact in referential EEG recordings, minimisation by computer subtract 80—94390
atrial electrical activity, recording from esophagus 80—30916
atrial electrical activity, triaxicardiometric analysis 79—39585
atrial electrical activity evaluation, external method 79—44030
atrial electrogram, use in computer detect. and classification of cardiac arrhythmias 77—40867
atrial electrogram monitoring for diagnosis of complex cardiac dysrhythmias 79—39567
atrial overload ECG computer analysis 78—7504
atrial septal defect differential diagnosis by vectorcardiogram and computer 79—44040
atrial tracking pacer, artificial conduction system 77—25608
atrioventricular and His bundle conduction disorders in noncoronarogenic diseases 79—43848
atrioventricular block prod. by ligation of septal arteries, His bundle electrogram, dog 77—81631
atrioventricular conduction disturbances with permanent pacemakers 77—81672
atrioventricular sequential demand pacemaker, R-wave sensing methods *(Japanese)* 79—5406
atrioventricular transmission intervals, automatic recording and processing 77—25568
automated Holter anal., shape oriented system 79—70662
automated monitoring, new electrode system 80—89898
automatic ambulatory rhythm monitoring 78—85431
automatic analysis, myocardial infarction appl. 77—25577
automatic analysis of 24 hr recordings, optimum ECG morphology and quality 79—70664
automatic analysis of cardiac rhythm, histograph *(German)* 78—28114
automatic analysis on minicomputer-based system, 24 hr ECG 80—89889
automatic comparative program for ECG analysis 78—7488
automatic evaluation of ECG signals using analogue circuits *(German)* 78—92717
automatic mass ECG analysing computer 77—81600
automatic system for mass medical examination, cardiovascular desease, USSR 77—25576
avian ECG, radiotelemetry system 80—98202
avian heart rate meas. using autocorrel. techniques 78—31989
baseline estimation and removal using cubic splines and state-space computation 77—44808
baseline noise estimation and removal using cubic splines and state space computation techniques 78—11755
beat counter, versatile digital SAMI 80—85510
biological precision rate calibrator 79—20731
biopotential distribution laws rel. to functional state 78—65142
biopotential recording interference and motion artifact sources and suppression 77—81634
bipolar suction electrode catheter for intracavitary ECG 79—44018
blood pool, dynamic radio-isotopic images, time-motion display 79—5347
body control mechanism, human, investigation using analysis of body's period signals 79—66576
body surface and epicardial activity, computer-aided meas. system 79—39551
body surface ECG potential mapping, data acquisition system 79—29653
body surface mapping of cardiac field, computer-aided pattern recognition 79—39553
body surface potential distribution map recording and processing 78—57116
body surface potential image recording and processing methods 79—20704
body surface potential map estimation, limited lead selection 78—57111
body surface potential mapping, automated acquisition and processing system 78—81033
body surface potential mapping, exptl. study of isochaemia in dogs 78—44750
body surface potential mapping, improved diagnostic technique 80—26409
body surface potential mapping, microcomputer processing system *(Japanese)* 80—72347
body surface potential mapping, quantitative descriptors 77—44807
body surface potential mapping data acquisition system 77—40861
body surface potential mapping project 80—104794
cable continuity tester 77—77997
calibrator for ECG/respiration monitor 80—98159
capacitive electrodes for burn appls. 80—41279
cardiac activity continuous monitoring on commercial pilots using portable cassette recorder 77—86659
cardiac arrhythmia monitoring, Aztec replacement by correl. for VPB detect. 79—62388
cardiac arrhythmias, automatic detection in long term ECG monitoring 80—3850
cardiac arrhythmias diagnosis, online real-time pattern recognition *(Italian)* 78—85439
cardiac cell membrane electrogenesis, selective adaption 79—57617
cardiac conduction system, noninvasive external recording of activity 79—39548
cardiac contraction kinetics recording method 79—12025
cardiac event sequence following mental loading, spectral anal. 79—29516
cardiac output determ. using Kubicek formula and integration method *(German)* 78—92720
cardiac probe, microprocessor-based, for gated equilib. and beat-by-beat left ventricle function 79—62396
cardiac resuscitator, automatic, emergency treatment of cardiac arrest 79—88147
cardiac rhythms, computer diagnosis of abnormalities using P-wave detector for interval measurement 78—44663
cardiac scintigraphic cineangiography with ECG gating 77—9255
Cardiac Surveillance Unit experience with Argus ECG monitoring system 78—11762
cardioelectrical field, human, intraindividual variability obs. 79—39404
cardiopulmonary analysis, computerised data reduction 77—44814
cardiopulmonary stress testing in children 80—30911
cardiotachometer, digital device using sliding averages 77—56503
cardiotachometer histogram indicator, prototype 80—41268
cardiotachometers, comparison of 4 designs 79—92412
cardiotachygram, anal. of recurring beat sequences *(German)* 78—88753
cardiotopological data reduction 79—39392

electrocardiography continued
cardiovascular data of animal telemetering, implantable multichannel inductively powered system 77—86662
cardiovascular emergency clinical assessment, use of ECG telemetry 78—44677
cardiovascular neurography: cardiac-rhythm based neurosignal distribution display 80—41351
cardiovascular response to dynamic/static exercise monitoring, four-channel radiotelemetry 78—3633
cassette recording and automatic processing microprocessor system 78—36021
cell electric potentials, ECG, EEG and EMG differences in signal types, propag. and meas. methods 80—40995
cineangiography, physiological event marking using ECG R-wave triggering 77—52873
clinical decision support systems, automated medical signal anal. 79—34685
clinical ECG interpretation system experience 78—7486
clinical ECG laboratory methods and difficulties 78—7482
clinical ECG real-time telephone transmission usefulness and reliability 78—57108
clinical electrophysiolgy laboratory automatic control system 78—57110
clinical usefulness analysis based on Bayes theorem, ^{201}Tl myocardial imaging and ECG 79—88170
clinician and computer ECG diagnostic accuracy 78—7494
complex ECG and triaxicardiometric recording and analogue processing 79—44023
compression by prediction or interpolation and entropy encoding 80—8199
computer analysis 78—48917
computer analysis of electrocardiogram *(Chinese)* 79—57787
computer analysis of intracardiac electrograms 80—21553
computer analysis program capable of serial comparison, 1976 IBM program description and performance 78—57086
computer application programs in theoretical ECG *(Spanish)* 78—20165
computer assisted interpretation, critical appraisal 80—17151
computer based instrument complex using SK-2 cylindrical coordinator *(Russian)* 80—76856
computer display of serial changes in hypertensive cardiovascular disease 78—81047
computer processing, measurement error determ. 80—94401
computer program performance in separating normals from non-normals 78—81046
computer programs, differences in meas. results 78—81048
computer system of automatic analysis of vectorcardiograms 78—20302
computer-aided ECG analysis, state of art 78—11767
computer-aided ECG and vectorcardiogram interpretation, modular software system 77—9288
computer-assisted ECG anal. system as part of regional cardiovascular information system 78—81049
computer-assisted interpretation, routine automated quality control 78—40394
computer-evaluated ECG parameter correlation with constitutional variables in infants and children 79—39406
computer-processed ECG trends, conference, Amsterdam (1976) 78—7477
computerised acquisition, compression, and retrieval 78—36019
computerised ECG analysis system, application to hypoxic rat ECGs 78—57088
computerised ECG monitoring, state of art 78—11766
computerised ECG monitoring system, features *(Swedish)* 79—44005
computerised ECG ventricualr arrhythmia monitor, performance standards and trends 78—7478
computerised Holter tape processing systems for drug testing, validation technique 78—81017
computerised interpretation, automatic protection against diagnostic errors due to wrong electrode placement 78—81052
computerised interpretation system in ambulatory health service 79—79669
computerised measurement, evaluation of results *(Japanese)* 78—24165
computerised pacemaker centre and follow-up network 77—81691
computerised quantitative evaluation of cardiac arrhythmias 78—85435
computerised systems, current status and future trends *(Japanese)* 79—44013
computerised technique to record new components of His-Purkinje ECG 77—44801
computerised tomography, ECG synchronised, time cutting methods using special X-ray generator 79—66538
computerised tomography, ECG-gated, motion phantom 80—98115
computerized ECG diagnostic system validity experiences 79—39571
congenital cardiac disease VCG processing, right ventricular hypertrophy criteria 79—39575
contour analysis system utilising decision tables, real-time, microprocessor-based 80—89880
contour map production for electrophysiology 80—72340
cordless, and heart rate meter *(Japanese)* 78—80984
coronary artery disease, ^{201}Tl perfusion scintigrams compared to ECG 79—25069
coronary artery disease, clinical value of ^{201}Tl stress test compared to ECG 79—29595
coronary artery disease, early detect. by nonlinear anal. of ECG 80—26410
coronary artery disease, preclinical, detect. in male subjects using the omnigram 80—81767
coronary artery disease, serial VCG and ventriculogram sensitivity to infarct size 79—44044
coronary artery disease detection measurements optimisation 78—11756
coronary artery disease diagnosis, exercise ECG, VCG and body surface mapping 79—44046
coronary care unit interactive ECG monitoring 78—7481
coronary intensive care unit, computerised monitoring system 77—21656
CRT display, reading by pages for long period signals 77—25580
data analysis by computer, advantages *(Swedish)* 78—24163
data analysis for data compression 79—100766
data compression, quantisation, linear prediction, peak detect. and slope change detect. 77—40862
data compression technique for ECG/VCG storage and transmission 77—44796
data compression techniques, quantisation studies 80—26396
data interactive display system 78—53550
data processing development, status, and trends 79—39558

electrocardiography continued
data reduction using a microcomputer *(German)* 80—81748
data-acquisition module, low-power, for microprocessor systems 80—41292
defibrillation, anal. and simulation of ECG recovery 77—40910
development progress 78—3646
diagnosis improvement by nonlinear feature extraction methods 80—85530
diagnostic, classification in terms of spectral characts. 80—56264
diagnostic efficiency improvement by cardiovascular system model dynamic optimisation 79—39569
diagnostic information from HF notches 79—39570
diagnostic interactive minicomputer system 78—36022
diagnostical functions of ECG signals, effect of random noise *(Croatian)* 80—98169
diagnostics automation problems 79—39577
digital ECG systems testing 80—81756
digital filter for the QRS complex detection 80—36166
digital filters, implemented on microprocessor 78—85428
digital pulse counter for cardiovascular monitoring 78—35978
digital recording by mobile cart with microprocessor and DC 300 cartridge recorder 78—85427
digital simulator, for test appl. *(Spanish)* 78—40359
digital storage and analogue distortion 78—44674
digital voltmeter with output to punched tape 77—21646
dipole crosstalk in inverse cardiac generator 78—92615
direct coupled, design *(Japanese)* 78—24166
direct-writing recorder, ST segment distortion assessment, coronary heart disease screening appl. *(German)* 77—90945
distributed microprocessor system for cardiac arrhythmias detection and diagnostic 79—25142
documented patient file concept and implementation 78—7498
Dutch development of medical physics *(Dutch)* 80—3877
dysrhythmia anal., automated systems, review of difficulties 80—17164
eccentric spheres model for geometry and inhomogeneities study 79—70540
ECG analysis automation, advantages 78—7493
ECG classification by linear multiple regression analysis 77—13027
ECG-VCG multivariate classification by linear regression, influence of populations 77—44789
ECG/vector cardiogram interpretation modular system 78—7484
echocardiography, high-resolution, computerised US signal processing 80—76814
Einthoven, Willem, (1861-1927), electrocardiological work 79—35514
EK1T Malyshch equipment, operational errors 80—61717
electric field probabilistic model 79—39387
electrical contact generation by tattooing C into skin tissue 78—77122
electrical generator, integral characts. meas. by automatic cylindrical coordinator 79—29646
electrical generator integral characts. in normal humans 78—69244
electrical sources in a 2D anisotropic activation model 80—40994
electrocardiodynamic continuous monitoring method 80—8195
electrocardiographs, portable, Phillips Cardiopan 531, clinical/electronic evaluation 78—11757
electrocardiology 4th International Congress, Balatonfured, Hungary (Sept. 1977) 79—39384
electrocardioscopes, appl. and designs 80—41304
electrode, 4-contact, flat 79—92404
electrode impedance and offset pot. 77—40874
electrode motion artifact reduction, electronic method 77—40872
electrode-to-skin contact area and amplifier input impedance selection *(German)* 79—88205
electrodes, ECG, EEG, interfering signals arising by cable motion 80—41296
electrophonocardiographic systolic time intervals, influences on 79—34681
EM field computation, method of secondary sources 79—39391
emission computerised tomography, ECG-gated, cardiac blood pool 80—98117
endocardial electrogram and pacemaker sensing 77—81720
engineering in medicine and biology, conf. Atlanta, USA (Oct. 1978) 79—39332
epicardial activation sequence rel. to body surface maps, right bundle branch block induced in dogs 79—39402
epicardial and body surface pot. meas. in intact dog, transfer coeffs. calc. 78—92614
epicardial and body surface potential distributions related by geometric transfer coeffs. 77—21671
epicardial and torso pots., relating by multipoles 80—30917
epicardial excitation pattern spherical double layer model, using human multipole data 78—27928
epicardial excitation spread, method for registration *(German)* 80—76845
epicardial mapping, computerised display system *(Japanese)* 80—101279
epicardial mapping of ventricular arrhythmia onset by digital computer 79—70672
epicardial mapping with clock electrode array 78—28109
epicardial potential derivation from torso skin potential obs. 77—64148
epicardial signal recording probe, hand-held 80—12286
epidemiological use of rest ECG 78—7505
equilibrium left ventricular ejection fraction determ., background noise estimation 80—94365
ergometric test, computer interpretation of heart-rate var., anal. of cardiac control in exercise 78—85430
esophageal multiprobe for temp. ECG and heart and lung sounds meas. 79—57791
exercise ECG, reproducibility of computer processing 79—70667
exercise ECG anal. using microcomputer 79—70683
exercise ECG analysis, noise-impervious pattern recognition approach 78—7515
exercise ECG analysis methods and requirements 78—7509
exercise ECG automated anal., clinical experience 78—81050
exercise ECG computer analysis 78—7516
exercise ECG computer processing expts. 78—7510
exercise ECG computer-assisted anal., implementation and clinical anal. 78—81051
exercise ECG examinations, two channel storage cardioscope and multitrack video tape recorder appl. 77—70561
exercise ECG processing, influence of heart rate and coronary artery disease 78—7512
exercise ECG processing, value of orthogonal lead system 78—7514

electrocardiography continued
exercise ECG processing principles and multivariate analysis results 78—7511
exercise ECG processing reproducibility rel. to waveform recognition and lead system 78—7513
exercise ECG quantitative analysis system *(Japanese)* 79—29652
exercise ECG repolarisation phase, T-wave amplification obs. 79—43845
exercise ECG testing in diagnosis of coronary lesions of left anterior descending artery 79—70692
exercise rehabilitation of cardiac defect patients, QRS complex affinity assay 79—43854
exercise stress testing with continuous noninvasive cardiac monitoring 78—36000
exercise vectorcardiogram, spatial velocity and magnitude ECG correlation 79—43846
exercise vectorcardiogram changes rel. to left ventricular function at rest 79—43859
extrasystole monitor using FIFO 80—72360
fault-tolerant computer analysis systems 77—44811
filtering and sampling for electrocardiographic data processing 78—24162
filtering characteristics of pacemaker electrodes 77—81744
fine structure analysis by noise reduction *(German)* 78—73268
finger-tip transducer for meas. digital vol. pulse, skin-resist. response and ECG 77—86729
fish surgery, low-cost audible heart rate monitor 77—70575
foetal ECG adaptive real-time noninvasive extraction using near-orthogonal functions 78—28110
foetal ECG detection, real-time system using near-orthogonal basis functions 77—21638
foetal heart and uterus diagnostic monitoring and functional mechanics 78—36009
foetal heart rate non-invasive registration by transabdominal ECG *(German)* 78—85418
foetal heart rate recording, interference due to infusion pump *(German)* 78—85414
foetal heart rate variability anal. using spectral anal. 78—28111
foetus diagnostics appl. *(Spanish)* 78—11759
forward and inverse problems soln. using cardiac and torso digital computer models 77—40837
forward problem, relationships among Green's theorem, Helmholtz theorem and integral eqn. methods 78—57090
Frank ECG correlates of left ventricular ejection fraction 79—39405
Frank xyz signal interpretation by unmodified 12-lead computer system 80—94400
freely moving animals, cardiac frequency regulation by means of telestimulation and biotelemetry 77—44859
frequency spectrum anal., clinical usefulness 79—25147
frequency-domain analysis 80—85521
fuzzy diagnostics from ECG/VCG analysis programs 78—7499
gamma-camera adaptive gating device for heart synchronisation 78—31898
gated acquisition cardiac imaging, quantification of left ventricular function 79—70638
gated blood pool scan, radioisotope evaluation of ventricular performance 80—85483
gated cardiac blood pool imaging using multiformat imager 77—40737
gated radiography system for increased information and dose reduction 80—26344
gated radionuclide cardiac imaging system 79—70639
gated scintigrams, reliability in detect. of left-ventricular aneurysms 80—30856
gated scintigraphy, real-time system for multi-image cardiac studies 77—21611
gated scintillation probe meas. of left ventricular vol. 78—31891
gating nuclear ventriculograms, processing and display, scintigraphic data 77—86627
Glasgow Royal Infirmary ECG interpretation program 78—7483
Graphic Interactive System for Processing of Electrocardiographic Maps 79—39552
grounded, resistance to coherent mains interference, exptl. evaluation 78—85419
grounded, standardisation of resist. to external cophasal power line interference for isolated patients 78—57085
haemodynamic status evaluation with heart synchronized gamma-camera gating 79—53232
Hannover EKG system HES, description 78—7485
heart activity characteristics in terms of membrane potentials *(Dutch)* 80—8034
heart block computer detect. by correl. of surface and endocardiac ECG 80—94410
heart conduction system modelling 79—83741
heart electrical and mechanical monitoring on extensometer 80—45944
heart frequency monitor in microprocessor technology *(German)* 78—92718
heart rate analyser for long-term continuous recordings *(German)* 78—3649
heart rate and sinus arrhythmia obs. during health-resort treatment 79—43855
heart rate measurement system using phaselock loop device 77—52906
heart rate on-line statistical anal., using special-purpose computer 78—35984
heart rate radio telemetry for rats, nonobtrusive system 77—90964
heart rate recorder 80—41288
heart-rate store, PLL circuit, portable *(German)* 78—65139
heart-rate variability meas., integral pulse freq. modulator spectral props. 77—90951
Hewlett-Packard ECG analysis program 78—7490
HF, primary signal, noise, and interference sources, origin and characterisation 77—44797
HF ECG compared with ballistocardiogram 78—77123
HG ECG, computer methods for anal. 80—72352
His bundle actinvity, nonivasive detection 77—81622
His bundle activity online noninvasive recording 77—13023
His bundle analysis in human heart, meas. device *(German)* 77—40831
His bundle ECG pattern recognition program for drug evaluation 78—35999
His-bundle activity detect., theoretical anal. of error during signal averaging 80—94392
His-Purkinje system pots., effects of filtering 79—48355
Holter analysis, appls. of Dyna-Gram IIIB system 78—81019

electrocardiography continued
Holter ECG high-speed anal. 79—66568
Holter recording anal. using Argus/2H 79—70679
Holter recording processing, computer system 78—81015
Holter recordings, low cost arrhythmia analyser, GRETA 80—94403
Holter tape dual-channel anal. system, ARGUS/2H 78—81016
Holter tape high speed digital anal. with full editing capability 80—89896
Holter tape processing, 60× computer system 79—66567
homomorphic anal. and modeling 79—74768
hypertensive left ventricular hypertrophy, orthogonal ECG multivariate analysis 79—39579
hypertrophy criteria in VCG of children with Fallot's tetralogy 78—7503
IBM program for ECG analysis 78—11769
impedance cardiogram integration method for cardiac output automatic determ. 78—92719
implantable heart rate module with AGC, for animal use 78—44753
implanted pacemaker patient long-term surveillance unit 77—81722
industrial health service automated ECG analysis results 79—39563
infant heart rate determ., clinical evaluation of miniature dry surface electrode 77—56505
information content improved by turning reference axes by 20°, Frank system processing *(German)* 78—92713
initial QRS vector displacement in healthy young adults 79—43856
injury potentials, inadequacy of solid angle formulation 77—44633
instrumentation for meas. and processing *(Croatian)* 78—44665
instrumentation requirements, examination methods, recording, computer interface unit 80—41303
intensive care unit ECG protection against defibrillator pulse 77—25586
interactive analysis techniques with Random Access Mass Storage ECG Analysis System 78—81034
interpretation system evaluation results 78—7497
interpretation sytems, user's experiences 78—7496
intra-atrial conduction block vectorcardiogram diagnosis 79—44036
intra-auricular P wave monitor, experience, performance evaluation 78—11764
intracardiac ECG trends 79—44031
intracardiac electrogram, effects of width, slewrate and biphasicness on magnitude spectrum 77—44812
intrahisian block detection, endocavitary exploration classification 77—81623
inverse electrocardiology regularisation method, isolated canine heart expt. 79—39393
inverse problem solving method using finite element method *(Japanese)* 80—41272
ischaemia index using peak diastolic dV/dt of heart chambers from ECG-gated radiocardiogram 78—44602
ischaemic and infarctive ECG simulation during ventricular activation and recovery 78—36018
ischaemic cardiac disease determ., heartbeat interval analysis and questionnaire evaluation 79—39580
ischaemic episode, computerised continuous beat by beat anal. and rational plots 79—62394
ischaemic heart disease, conventional and orthogonal-lead ECG comparison by coronary angiogram discriminance analysis 79—44043
ischaemic heart disease determ. by heart beat interval anal. and medical questionnaire evaluation 78—65145
ischaemic heart disease diagnosis using respiratory sinus arrhythmia 78—65147
ischaemic myocardial reactions, triaxicardiometric obs. 79—43844
ischaemic myocardium ST segment electrical alternans obs. 79—43857
ischaemic triaxicardiographic changes induced by exercise 79—39407
isopotential surface map data reduction 79—39557
juvenile T-wave pattern incidence rel. to age and QRS transition zones 79—43849
Karhunen-Loeve expansion, automatic phase alignment 79—48356
latent cardiac arrhythmia detection, His bundle electrogram and long-term ECG methods 79—44033
lead CAD 80—85526
lead system information content *(German)* 78—69226
leads $X+20^{0}H^{0}$ and $Z+20^{0}H^{0}$, additional information 79—44037
left septal fascicular block, conduction disturbance obs. 79—43851
left ventricular aneurysm, triaxicardiometric criteria 79—39586
left ventricular function evaluation using ECG synchronised scintillation camera 78—65110
left ventricular hypertrophy and bundle branch block, vectorcardiogram interpretation 79—44028
left ventricular hypertrophy study in borderline hypertensive young men 80—109050
left ventricular hypertrophy with bundle branch block, ECG/VCG and echocardiogram correlation 79—44035
left ventricular performance parameters rel. to max. dZ/dt 80—101159
left ventricular potential quantitative assessment rel. to echocardiographic meas. 79—44042
left ventricular volume rel. to QRS voltage and Frank vectorcardiogram 79—44029
LF direct meas. cct. for heart beat disturbances anal. *(German)* 79—96671
linear filtering artifacts 77—44810
long term ECG in ambulatory clinical practice 77—81627
long-term, flexible data presentation in DCG processing 79—70681
long-term continuous ECG recorder *(Japanese)* 77—66871
long-term ECG recording and analysis system, Siretape C 79—92407
long-term recording on mag. tape 80—56243
long-term recordings, comparison of techniques for exam. 80—72349
long-term recordings, rapid computer analysis system Argus/H 78—36002
Lyon ECG interpretation program 78—7487
magnetocardiogram recording on normal subjects, morphological and multipole analysis 79—39426
magnetocardiography in hospital environment, normal aspects 79—39550
magnetocardiography recording, props. of ideal system, appl. of ECG theory 80—104700
manual electrode 79—57801
map reconstruction computer system 79—39561
mean electrical axis tracing on CRT, electronic technique, teaching aid 77—13022
medical electronics, new forms and techniques 80—3856
microcomputer based real-time recognition system for intra-aortic balloon pump control 78—36067
microcomputer based signal averaging system 80—36159

electrocardiography continued
microcomputer low cost system for digitising and preprocessing analogue signals 77—40881
microcomputer-based evaluation system, improving diagnostic capabilities 78—88761
microcomputer-controlled cardiogram cart 78—31942
microprocessor based ambulatory monitor 77—48918
microprocessor based system for ECG analysis, design and development 78—73287
microprocessor detection of R-waves 79—96685
microprocessor signal averaging for recording μV activity from cond. system of heart 77—44820
microprocessor use for routine cardiac assessment 79—83962
microprocessor-based body surface isopotential and topological maps 80—72361
microprocessor-based data compression and transmission 79—83989
microprocessor-based evaluation system for conventional leads 80—89894
minicomputer digitising and preprocessing system 77—40863
minicomputer-aided ECG diagnostic system 79—44024
Minnesota code ECG classification program 78—7506
Minnesota code ECG program validation 78—7507
model of body with heart as active elec. source, using harmonic polyphase generator volts. 77—60278
models solving direct and inverse problems, systems approach 78—28121
monitor, heart rate meter and alarm eval., proposed standard test tapes 80—89899
Monitor DKS4T-01 system, surveillance of severely ill patients 79—34679
monitor interference from patient call systems 79—74776
monitor testing using pacemaker patient simulator 80—41322
monitoring, anal. of 24 hr recording, operator-controlled computer system 80—89888
monitoring, long-term, with contourographic signal representation *(German)* 78—92714
monitoring, R-R interval prediction models compared 78—35996
monitoring, time correct. and two channel recording in 24 hour anal. 79—70658
monitoring abnormal QRS events, sequential improvements in on-line algorithm 78—81026
monitoring by contour comparison, QRS triggering with real-time correlator *(German)* 78—92715
monitoring by telephone, pacemaker, cardiac arrhythmias appl. 77—52903
monitoring cart, self-diagnosing microcomputer-based design 78—31943
monitoring in ambulatory patients 78—20309
monitoring system for rhythm diagnosis of ECG 78—40392
monitoring technique in late pregnancy toxaemia 77—81602
multichannel recording using TDM 80—101283
multiform PVC detect. using time-domain and freq.-domain anal. 79—70674
multiform ventricular complex identification, 2-dimens. clustering technique 79—66570
multiparameter clinical diagnostic miniature transducers, colloquium, London, England (May 1979) 79—100776
multiple dipole heart generator location optimisation in simple torso model 80—41277
multiple dipole heart generators, optimisation procedure for fixing locations 77—44809
multiple-electrode measurement system for ECG evaluation of acute myocardial infarction *(German)* 80—26386
multipolar content of human ECG 77—52761
multipole moments rel. to activated parts of epicardium and endocardium 79—100588
multiterminal ECG processing system experiences 79—39573
multivariate and conventional ECG analysis programs compared 78—7492
muocardial infarction ECG diagnosis in patients with transvenous ventricular pacemakers 77—81624
mutli-channel use, low cost modification 77—44813
myocardial contractility, real time meas. by analogue computer with digital displays *(Japanese)* 79—44015
myocardial electrical activity modelling, dialogue mode *(Russian)* 79—2021
myocardial imaging using ^{201}Tl, characterization of ECG-synchronized images 79—39473
myocardial infarct sizing, comparison of noninvasive methods, dog expt. 77—66869
myocardial infarction, antiarrhythmic drug and hyperkalaemia effects on ventricular electrogram 77—81667
myocardial infarction, perioperative, comparison of ECG, scintigraphy and enzyme diagnosis 80—30855
myocardial infarction, topographic relation between myocardial ^{201}Tl uptake and left ventricular kinetics 78—61243
myocardial infarction diagnosis in endocardially paced patients 77—81625
myocardial ischaemia and necrosis monitoring in acute myocardial infarction 80—85525
myocardial perfusion index calculator for prediction of subendocardial ischaemia in cardiac surgery 77—40915
non-fade monitor, battery-powered, emergency/surgery appl. 78—7528
noninvasive His bundle and sinoatrial node activity recording system 79—39560
nuclear angiocardiography, computerised, ECG-gated, automatically generated LV regions of interest 79—70626
nuclear cardiology, beat-by-beat validation of ECG gating [nuclear medicine] 80—98071
nuclear cardiology, performance characts. of a commercial ECG gate 80—98073
numerical encoding and transmission, microprocessor appl. 77—44798
oesophageal multiprobe for temp., ECG and heart and lung sound meas. 78—77146
oesophageal temperature probe position verification by ECG 80—56250
on-line body surface potential mapping of cardiac fields and its clinical application 79—83992
online cardiograph processing and display *(Italian)* 79—25135
online vectorcardiographic analysis microprocessors and instrumentation 78—36020
optimal 9-lead ECG system design 78—7500
optimisation, conf., Halifax, Nova Scotia, Canada (Jan. '79) 80—76850
optimum data processing and storage design 78—57118

electrocardiography continued
orthotics parameter assessment based on telemetric heart rate monitoring, paediatric patient appl. 78—31974
overlapping-cell clustering algorithm, biomedical appls. 80—30926
P wave detection and identification using statistical signal analysis 80—8202
P-R segment non-invasive information, clinical pot. of elec. and mag. methods 80—36182
P-wave, a new method of detect. in electrocardiograms 79—48360
P-wave detection in noise, consecutive vectorcardiogram external product technique 77—9289
P-wave recognition, using adaptive correlating filter *(Japanese)* 78—28119
pacemaker implantation, therapy/measuring combined unit *(German)* 78—7519
pacemaker implantation surgery, intracardiac ECG derivation during electrocoagulation 78—40397
pacemaker leads, time and freq. domain comparison of unipolar and bipolar electrograms 78—44726
pacemaker malfunction diagnosis, ECG before and after thoracic wall stimulation 77—81707
pacemaker patient routine monitoring using telephone-telemetry system 77—90957
pacemaker patient surveillance by automatic pacemaker function analyser 78—3679
pacemaker surveillance by telephone photoanalysis 77—81699
pacemaker therapy, importance of R-vector direction 79—44049
pacemaker tracking system based on microprocessor, hardware considerations 78—36070
pacemaker transmembrane potential generation in fish heart sinoatrial cells 79—39395
pacemaker-induced T-wave inversion obs. 79—44063
paroxysmal ischaemia, vectorcardiogram and rheokinetocardiogram relationship 79—44047
partitioned Karhunen-Loeve expansion scheme for ECG/VCG data compression 79—79506
patient monitoring during bath therapy using immersed electrodes 78—3665
patient safety using opto-electronic appls. 79—44016
pattern classification from complete computer descriptions 80—56265
pattern recognition program for continuous ECG processing in accelerated time 78—92725
phase invariant signature algorithm (PISA) processing of ECG and phonocardiogram for cardiac anomaly detect. 78—40395
phonothyreogram and phonocardiogram frequency spectrum analysis by minicomputer, ECG reference time signal 79—83966
physiological basis and biomedical apparatus *(German)* 79—100757
piecewise-linear approximated ECG waveform recognition 78—57119
pill electrode for cardiac arrhythmia study 79—39566
Pipberger program QRS onset and offset determ. algorithm parametrisation 79—39559
polarcardiography, triaxicardiometry and other displays 79—39581
polygraph for simultaneous recording of diagnostic parameters 78—36011
posterior myocardial infarction, right ventricular hypertrophy, and normal variation differentiation 79—44045
posterodiaphragmatic myocardial infarction diagnosis, Frank lead Y reliability 79—44038
potential distribution mapping instrumentation 80—21561
power spectra, effect of random freq. modulation 79—48237
preauricular O wave, embryonic origin 79—39390
precardial lead belt, general-purpose ECG 79—48361
precision requirements for computer anal., statistical approach 77—81607
precision testing technique for intensive care instrumentation 79—70687
premature ventricular beats detect. scheme 79—70657
premature ventricular contraction monitoring and detection is heart beats 77—78022
pressure-induced changes in cardiac conduction, action pot. correls. 80—81572
primary T-wave determ., spatial ventricular gradient change factors 79—43850
probability levels variation, computer-aided diagnosis 78—44664
processing A/D convertor control by microprocessor *(Bulgarian)* 79—25123
prototype waveforms generation by piecewise correlational averaging 80—109053
psychophysical stress from long term recording, hardware evaluation of parameters *(German)* 80—26388
psychophysiological techniques applied to aircraft design and other operational problems 80—26384
pulse/phono pick-up appls. in ambulant cardiological practice 78—40377
QRS automatic meas. in children's ECG and VCG, wave recognition algorithms *(German)* 78—69225
QRS detection accuracy rel. to anal. of HF components 80—17158
QRS detector/delineator devel. and eval. 80—89892
QRS-onset and offset in children, detection using parametrised templates 78—85438
quasiperiodical signal changes evaluation, automatic *(Czech)* 78—40371
R and T waves in ECG and magnetocardiography 80—104699
R-R interval measurement by statistical-difference conversion 80—56232
R-R interval prediction models, comparison of 79—39549
R-wave detection with intramyocardial electrodes 78—44713
R-wave enhancement for heart rate determ., abdominal-lead fetal ECG 80—67264
R-wave identification by derivative amplitude meas. *(Bulgarian)* 79—96536
radioisotope cardiac scan computer-aided anal., using ECG gate 78—40328
radionuclide cardiac motion study, computer-processed, ECG gating device 78—73210
radionuclide kymography, assessment of regional myocardial wall motion 79—39478
random access mass storage anal., RAMSES, for quantitative anal. of long-term ECGs 79—70663
random noise influence on signals, quantitative assessment of program accuracy *(Slovenian)* 79—25143
rate-dependent left bundle branch block patients, atrial pacing expts. 79—44019
ratemeter based on analogue divider, heart rate determ. from ECG and arterial press. curve 78—40368
real time data compression, realisation techniques *(Italian)* 79—5389

electrocardiography continued
real time phaseless filter with delay circuit, ECG appl. *(Japanese)* 80—56253
real-time analyser with digital readout, portable device 80—56234
real-time ECG contour anal. program using microprocessor system 78—73288
recorder, with statistical pulse train interval digital analyser *(German)* 77—78007
recorder and printer with fixed writing heads 80—3854
recording on tape, correction of timing errors due to tape speed variation 80—72354
recording system simplification *(Russian)* 78—40379
remote computer analysis via telephone network, data terminal with voice indication, general practitioner use 77—81613
rest ECG computer interpretation 78—7508
RF powered cage system for implanted biotelemetry 79—20737
RF powered telemetry system 79—48358
rhythm analysis, long-term ECG data storage and multipass scanning 79—39578
rhythm analysis, syntactic approach 80—89900
rhythm diagnosis, statistical approach 77—44802
rhythm diagnosis using statistical signal anal., identification of persistent rhythms, ECG/VCG 78—77141
rhythm diagnosis using statistical signal anal., identification of transient rhythms, ECG/VCG 78—77142
right bundle branch block, cardiac and noncardiac patient vectorcardiograms 79—43853
right bundle branch block aetiology, morphological and clinical aspects diagnosis 79—43852
right bundle branch block patterns during permanent right ventricular pacing 77—81704
ROM based ECG monitor 80—26401
S-T segment elevation meas. instrument, programmable 78—31956
scintigraphy, ECG-gated, appl. to studies of heart 78—7440
second-generation ECG monitoring system development 78—7480
semiconductor disc memory, high speed, for storing body surface pot. maps 77—78014
sequential ECG comparison system design 78—7501
serial ECG processing computer techniques 78—7502
servicing techniques for ECG 79—96677
sick sinus syndrome 24-hour Holter ECG monitoring 79—39562
Siemens program for ECG analysis 78—7489
signal distortion reduction by statistical deconvolution 78—28118
signal parameter trend anal. 78—15920
signal processing, digital filtering and data compression appl. *(Italian)* 79—96670
signal processing of ECG waveforms, automatic, using syntactic methods 79—62386
signal quality assessment during acquisition 79—70666
signal recognition and anal. *(Slovenian)* 79—83958
signal shape parameter automatic meas. *(Russian)* 79—25134
signal-averaging system, flexible, computerised 80—67270
simulation, adjustment of electronic machine *(French)* 79—83968
simulation using a microprocessor 80—61726
simulator, ECG and EEG *(French)* 79—57786
simultaneous telephone transmission of four ECG/EEG signals *(Spanish)* 79—62399
single myocardial fibre model, source-field relationships 79—39385
single-channel electrocardiograph with telephone transmission attachment 78—88760
singular value decomposition, electrical heart activity observability 79—11913
sinoatrial node activity, intracardiac recording by prememorised averaging 77—81621
sinus node autonomic control in man, quantitative assessment 79—70684
sinus rhythm, diagnosis by IBM ECG anal. program *(Japanese)* 80—67278
skin artifact reduction by skin puncture method 78—44672
skin impedance simulation w.r.t. Cole-Cole circular arc law 77—5101
skin potential motion artifact reduction by skin abrasion 78—40361
skin-electrode processes obs. 77—40828
slew rates in adult and infant ECG 78—53544
slow wave real-time anal., hardware implementation of selective Bouilland transform. 80—56233
solid angle interpretation, myocardial fibre orientation implications 79—39397
spatial modulus and velocity ECG variation with age 79—43847
spectral analysis in contusive myocardial injury 79—43997
spherocardiogram applicability of vectorcardiographic and polarcardiographic infarct criteria 79—39582
SQUID, appl. to cardiac recording, phase and amplitude relationships of elec. and mag. events 80—104695
SQUID, medical application *(Japanese)* 80—12290
ST-segment response in exercise ECG, accurate automatic measurements 78—77140
statistical pattern recognition for early diagnosis of heart attacks 77—25584
strain gauge transducer for myocardial stimulation and recording 79—48357
stress/duress automated detect. system 80—76852
supraventricular arrhythmia rapid anal. from long-term oesophageal recordings, drug assessment 80—89904
supraventricular tachycardia, diagnosis and management, instrumentation and therapeutic techniques, review 79—39598
surface electrode potential recording apparatus 79—83987
surface isopotential and gradient maps, image processing 79—70670
surface mapping, gradient and potential data acquisition system 79—39555
surface mapping, interpolation methods in FORTRAN 80—81750
surface mapping recordings registered at rest and during exercise, diagnostic value 78—81044
surface potential distributions, equiv. dipole recovery in presence of noise 79—70671
surface potential map reconstruction from limited no. of leads 78—57117
surface potential recording electrodes 79—100779
systolic time interval processing system, STIPS 78—81029
systolic time intervals during $+G_z$ accel., appl. to cardiovascular function estimation 77—5087
systolic time intervals during exercise 79—70668
systolic time intervals from surgical patients, continuous real-time computation and display 77—37098

electrocardiography continued
T-wave location by computer, R-T interval 80—76854
T-wave rise time rel. to heart rate, exercise vector cardiograms study 78—85434
T-waves in exercise ECG, location and occurrence 80—8200
tachometer, instantaneous cardiac, with extendable range 79—20700
technology development, analogue instrumentation and digital signal processing *(Italian)* 79—25136
Telemed programme for serial comparison fo ECGs 80—26395
TELEMED system user support organisation and program library 78—7491
telemetry, diving duck monitoring by implantable transmitter 77—44858
telemetry, totally implantable multichannel system 78—44746
telemetry apparatus, single-channel, PLL demodulator appl. *(German)* 78—57097
telemetry system, implantable, single-freq., long term monitoring 77—86688
telemetry system, inductively powered, for animal monitoring 79—74796
telemetry system Telecare *(Spanish)* 77—9296
telemetry systems for chronically instrumented animal model for electrophysiological research 80—26323
telephone transmission, analogue and digital, errors and noise 80—94398
thoracic electrical impedance, cardiac-associated changes in man 79—25128
thoracic surface, human, heart potentials distrib. with left bundle branch blocks 79—39403
three-dimensional ECG recording technique 80—41274
time series analysis on R-R intervals of electrocardiogram using autoregressive model 79—83972
time-selective filtering using computer 80—89895
torso model for potential distrib. from VCG data 79—39401
torso surface isopotential simulation using simple conduction-elec. field model with Neumann boundary 80—89706
transient cardiac arrhythmia detection, 24-hour ECG recording 79—44020
transmission over Post Office telephone network, 3-lead, central computer analysis appl. 77—86698
triaxicardiometric system polarcoordinate sensitivity 79—39587
triaxicardiometry, clinical use 79—39584
trigger circuits, QRS, reliability and precision tests using synthetic ECG *(German)* 78—92716
triggered scintigraphy of intracardiac space 78—28033
two-electrode recording 78—28107
U-wave correlation with repolarisation of Purkinje system 78—28122
ungulate cardiac electrical activity peculiarities and evaluation methods 79—39394
USA Veterans Administration ECH computer analysis system 78—11768
vectocardiogram analysis program for children, with multivariate diagnostic classification 78—81045
vector and isopotential maps, convertibility and comparison 79—39554
vector cardiographic assessment of implanted cardiac pacemakers, computer system 78—11771
vector ECG meas., bandwidth limitation effects 78—36001
vectorcardiogram, computer treated, discrimination between normals, LBBB with and LBBB without myocardial infarction 78—85448
vectorcardiogram, genetically determined variation study, computerised procedure 77—25579
vectorcardiogram, human, computer dialog modelling 79—39389
vectorcardiogram and ECG correlation with angiocardiographic left ventricular mass 79—44027
vectorcardiogram and ECG correlation with coronary arteriorgram and left ventriculogram 79—44041
vectorcardiogram computer interpretation method, prototype system 77—90954
vectorcardiogram computer system for anal., display and storage 78—85437
vectorcardiogram diagnostic algorithm improvement by outlier elimination 79—39572
vectorcardiogram information enhancement, automatic pre-processing 80—94402
vectorcardiogram parameter sensitivity to digital filtering 79—39576
vectorcardiographic discrimination of left bundle branch block, descriptive statistical methods 79—44026
vectorcardiographic microprocessor system *(Bulgarian)* 80—61722
vectorcardiographic P loop correlation with left atrial volume echocardiogram 79—44025
vectorcardiographic systems compared, Akulinitchev and McFee 79—44039
vectorcardiography, 3-dimens. 80—94405
vectorcardiography, computerised meas. and display system 77—40864
vectorcardiography, microcomputer system 79—70669
vectorcardiography display and rate analysis,, minicomputer system 78—92738
ventrical, left, ejection fraction from gated images count rate 79—29605
ventricle excitation spread, computer simulation *(Japanese)* 80—3847
ventricular arrhythmia model 80—89893
ventricular arrhythmia on-line study, computer system 78—81060
ventricular arrhythmia quantification, minicomputer system 79—70677
ventricular arrhythmias, intraoperative mapping system 80—56242
ventricular ectopic activity, semiautomated data reduction 79—66573
ventricular ectopic beat detect. in rapid Holter scanners, prematurity and height as criteria 79—66575
ventricular fibrillation detect. by computer 79—70675
ventricular fibrillation recognition using ECG power spectrum 78—81032
ventricular fibrillation signal anal. 80—85522
ventricular hypertrophy diagnosis, three-orthogonal-lead ECG criteria 79—44034
ventricular myocardial excitation, elec. field theory and integral topogram analysis 79—39386
ventricular pressure and ECG continuous monitoring during angina attacks, computer anal. 78—85436
ventricular surface excitation wave spread and collision obs. in dog 79—39398
veterinary science, use in 79—83969
video-sync mixer for cassette videotape recording of computer images 79—29604
volume conductor effects on apparent orientation of known cardiac dipole 78—28108
wave recognition method, automatic *(Japanese)* 79—57794
waveform, statistical algorithm and struct. anal. 80—72341
waveform automatic processing using syntactic methods 79—44006

electrocardiography continued
waveform recognition and representation by finite Haar transform 78−3654
Woodward polarcardiographic service for ECG diagnosis improvement 79−39583
zero-line connection, methods *(Bulgarian)* 79−79666

electrocataphoresis *see electrophoresis*

electrochemical analysis
see also electrochemistry; polarography; voltammetry (chemical analysis)
absorption spectroelectrochemistry at Pt electrode 79−74395
air pollutants determination methods *(German)* 80−26187
air pollution instrumentation using porous electrode sensors 77−17261
amperometric titration, Ag, Hg (II) and Pb determ., using thioxanthate 79−57326
application to liquid chromatography 80−50906
austenitic solid solution, chem. evaluation of B and its correlations with hardenability and hardness *(German)* 79−39230
automated controlled-current system, for coulometric, potentiometric and galvanostatic meas. 77−70353
automated electrodic potentiometry of respiratory components in E. coli membrane fragments 78−35736
autopotentiometric, developing-fixing solution concentration analysis *(Russian)* 77−54009
auxiliary unit, for a.c. voltammetric meas. on conventional d.c. polarograph 77−4954
bases, mixtures, potentiometric titrations, computer-calc. curves, learning machine appl. 80−3426
blood gas microanalyser, calomel electrode efficiency restoration 77−25575
blood serum analysis, ion-selective electrodes 78−3645
boiler feedwater redox potential meas. by Pt thin-layer electrodes 80−89578
C U determination by constant current coulometric titration in 5 to 20 mg range 80−78381
carboxyhaemoglobin, redox investig. using reson. Raman, visible absorption and electrochem. methods 78−76832
cellular protein two-dimensional analytical electrophoresis 79−96528
chalcopyrite oxidation, in acidic chloride medium electrochem. study 78−95817
chlormerodrin-203, radiochem. purity determ., electrophoretic method 77−56283
chronopotentiometry with programmed current 80−26066
computers and optimisation, conf., Amsterdam, Netherlands (April, 1978) 79−52791
conductometer to record rapidly varying electrical conductivity 80−61184
conductometric instruments metrological monitoring, for environmental contaminants control 80−55973
continuous monitoring by ion-sensitive FET *(Spanish)* 79−83986
corrosion processes, polarisation resistances method of study 77−28930
coulometer with solid electrolyte *(Japanese)* 77−36827
coulometric acid-base analyser using pH-stat 77−36801
coulometric analysers with controlled potential, review 79−39244
coulometric data unit, oxygen, long lifetime 79−39243
coulopotentiography, new method 79−34391
coulostatic impulse technique, review 78−73048
current injector for Coulomb titration of chloride 79−29684
cytochrome c, redox investig. using reson. Raman, visible absorption and electrochem. methods 78−76832
data interpolation, fast Fourier transform method 79−16061
derivative neopolarograms, shapes, theory 78−53289
differential pulse chronoamperometry 78−73111
digital computer applications, review 77−81451
digital timer for electroadsorption studies 77−90670
double potential step electrochemical mechanisms, simplex fitting and finite difference simulation anal. 78−44381
dropping Hg electrodes, drop times determ. using digital drop timer 78−3394
electroanalytical chemistry, 1952-1977, review 78−92567
electrode, rotated disc, for membrane mass transport evaluation 80−26069
electrode-electrolyte interface, solid film props., review of expt. techniques 77−77780
electrodes in modern laboratory, brief review 77−4964
electrodic potentiometry system, automated, for chem. anal. 78−35735
electrolyte-solid interface, electrochemistry of surface 78−80798
electrophoresis technique, data acquisition system *(German)* 77−52692
enzymatic activity meas., electrical method 77−12863
faradaic admittance, rapid drop time on-line FFT meas. 78−92544
faradaic admittance, SYDAGES system for on-line FFT meas. 78−20090
FET transducer research and development for biomedical appl. 78−44640
finite current detectors, for high performance liq. chromatography 77−70347
first-ordr electrochemical analysis, reversible pot. and rate const., chronoamperometric determ. 78−61086
flow cell for use with O_2 membrane electrode, glucose, glucose oxidase determ. appl. 80−61736
flow coulometry, with ring-disk electrode 80−71966
flue gas, in 200 MW plant, trial operation with Westinghouse O_2 probe *(Czech)* 80−89562
galvanic dissolved O_2 sensor, improved, activated sludge aeration appl. 77−70364
gas sensing electrodes for chem. anal., development 77−4963
gas trace determ. methods, precision 80−16753
gas trace monitor with ion sensitive electrodes, continuous and highly responsive *(German)* 79−24878
gases, concentration meas. in gas-phase systems, using potentiometric electrodes *(French)* 78−7269
gases in metals, detection by vacuum spark technique, appl. to Al wire 78−61094
glass microelectrodes, Na^+ and K^+ selective, electrochemical props. 79−91957
glue in Cu refinery electrolyte 79−48021
heterogeneous charge transfer kinetic effects, deconvolution by FFT faradaic admittance meas. 78−20091
high pressure liquid chromatography, electrochem. detectors 77−36811
immunoglobulin G, enzyme immunoassay, electrochem. determ. with antibody-bound membrane 79−53293

electrochemical analysis continued
intravascular O_2 continuous monitoring, electrochem. sensor 80−56238
ion concentration meas. with instrument using ion-selective electrode technology and LSI technology 80−1116
ion potentiometric continuous analysis, calibration method for minimizing errors 78−35748
ion selective electrodes, coated wire design 77−25344
ion selective electrodes, recent developments 77−4962
ion selective electrodes, review 78−85165
ion sensitive FET, ion selectivity and temp. depend. 79−34409
ion-selective electrode, flowing systems meas. 78−92527
ion-selective electrode, solid-state, using microcircuit prod. technique 77−16872
ion-selective electrode analysis use of microprocessor-based millivoltmeter 80−16752
ion-selective electrodes, interpret. of non-ideal calibrations 77−90661
ion-selective electrodes, liq. membrane, free and supported, ion transport, bulk elec. props. 79−83534
ion-selective electrodes, liq. membrane, free and supported, ion transport, interfacial kinetics, time depend. phenomena 79−83535
ion-selective electrodes, solid-state, for potentiometric determ. of phosphate 79−92044
ion-selective electrodes applic. in anal. chem. *(French)* 78−40093
ion-selective electrodes in titrations using tetraphenylborate 79−83530
ion-selective liquid chloride electrodes, solvent effects *(Russian)* 79−91972
ion-selective membrane electrodes, Na ions selectivity *(Russian)* 79−96337
ion-selective membrane electrodes, selectivity, statistical calcs. 78−92549
ion-sensitive membrane electrode function, linearity domain limit 77−29058
ion-sensitive membrane electrode function, nonlinear domain detection limit 77−29059
ionselective multi-disc electrode, biomedical appl. *(German)* 78−3687
isotachophoresis, appl. to practical samples *(Japanese)* 80−26092
isotachophoresis, capillary tube method *(Japanese)* 77−73451
isotachophoresis, principles and appls. 78−31738
isotachophoretic analysis, development of data processing system *(Japanese)* 79−24873
Kalousek electromechanical switch, for potentiostatic conditions 80−85236
kinetic parameters and double layer capacity, simultaneous meas. instrument 80−40704
lactate concentration meas., enzymatic and electrochem. methods *(German)* 79−2169
liquid chromatography, electrochem. detect. and fraction collection system 78−35749
LKB Multiphor, universal system for electrofocusing, electrophoresis, immunoelectrophoresis and isotachophoresis 80−7888
measurement transducers, actual distribution of errors 80−45605
mechanicochemical testing of metals, electrochemical cell for mechanicochem. behaviour determ. 78−60905
metal samples potential scanning electrochemical reactions *(Dutch)* 77−66785
metal surface , electrochemical exam. of multiple states of chemisorbed atoms 77−44512
metals, biamperometric iodometric determ. using Pt-graphite electrode system 77−70359
methylhydrazine, electrochem. oxidation on Au, appl. to gas monitoring 79−39248
microcomputer-controlled instrument for electrochemical studies 78−73128
MIS structures, review of applications, ion sensitive techniques 79−33353
MOSFET, Pd gate, to monitor H_2, H_2S and NH_3 78−44645
multiple analyser for flowing liquids and gases, features *(German)* 78−27846
nickel calcine, reactivity, contact I-V meas. 77−85975
nitroglycerine, in waste water, monitoring continuous electrochem. analyser 77−60147
on-stream analysers development, w.r.t. speed and reliability 77−66778
operational amplifiers, use in electrochemical analysis 80−21335
oxygen monitoring in process gas streams, sensor 80−52181
ozonesonde, conc. cell, performance characts., atm. appl. 79−21039
pH meter construction, standardisation, and use 77−63995
photographic emulsion, redox potential evolution during development, potentiometric anal. 78−16865
physiological monitoring, by integrated FET micro ion sensor 78−44641
polarisation studies, electrode design 80−93761
polyelectrolyte solution, thermodynamic props. determ. from Donnon equil. obs. 80−7846
polymer lattices, purification 78−7243
polymer mixture, metal fraction contents and properties meas. method *(Russian)* 80−76571
potentiometric analyser, automated, with selective electrodes, microcomputer control 80−40773
potentiometric analysis with ion-selective electrodes, computer automation 80−3424
potentiometric determination of some valence forms of Mn 77−32849
potentiometric gas sensing probes, micro-size, for ammonia, CO_2 78−61071
potentiometric sensor, for biomedical appl. 78−44644
potentiometric stripping analysis, micro-computer system 79−52793
potentiometric titration apparatus, microprocessor controlled, for equilib. studies 80−89579
potentiometric titration system, microcomputer controlled, for soln. equilib. obs. 78−92522
potentiometric titrations, PbO_2-Ag electrode system, semi-auto titrator, student experiment 79−84918
potentiometric titrations with ion-selective electrodes, automated, equivalence pt. determ. method 78−3391
potentiostat, P-04, for electrochem. meas. 80−61185
programmable charge transfer analyser 78−3406
PTFE-C black composite form. monitoring by electrochem. method 77−36446
radiolytic product detection by Pt electrode rest potential 80−11973
recording coulometer, for controlled atmosphere reactions of metals in molten salts 78−3344
reference electrode arrangement, high temp. polarisation study 78−64845

electrochemical analysis continued
reference ion sensitive FET for compensation, biomedical appl. 78—44642
review of developments over last 25 years 77—70368
review of instrumentation and dynamic techniques over past 4 years 78—85215
review of progress 79—43661
Rochelle salt, Cu and Zn plating appl., cyanide copper baths analysis *(German)* 77—25328
semiconductor gas sensors, selectivity to CO and CH_4 79—34407
semidifferential electroanalysis, derivative neopolarogram peak shapes 78—7256
serum automated electroanal. using ion-selective disc electrodes with neutral cation-carriers *(German)* 78—73269
single crystal surface, electrochemistry, surface struct., superlattice struct. 80—76519
solid electrolyte galvanic cell for gas sensing, response speed 77—60149
solid electrolyte gas sensor developments 80—61217
solid electrolytes appl. *(Czech)* 77—77779
starch-gel electrophoresis, improved vertical apparatus 77—4961
steel, C, corrosion inhibition by 2-ethylamino-ethanol in aerated 3% NaCl soln., pH effect 80—21160
steel, ferritic stainless, Cr-Mo (12,1wt.%) microstructure influence on localised corrosion behaviour 80—61018
steel, stainless, Cr, Mo effects on passivation AES and electrochemical anal. 79—74292
steel, W-Co-Mo-Cr-V-C (8.5, 8.1, 4.5, 3.5, 2.2, 1.02 wt.%), phase composition, struct. and props. 80—104163
stripping analysis, Kalousek polarography appls. 78—53290
surface water continuous analysis by NH_4^+-sensitive plastic membrane electrode 80—89701
terms, symbols and definitions 80—21348
thin-layer cell, detect. appls. for liq. chromatography 77—25327
titration using automatic conductometer, exam. 78—56933
titrimetric analyser with ammeter pick-up *(Russian)* 80—71984
toxic compounds, enzymatic sensor for continuous determ. *(French)* 78—73099
variable-potential coulometer analyser integration error analysis 80—93831
voltage supply, integrated triangular-wave generator appl. *(German)* 77—52724
water, T conc. meas. with electrolytic enrichment cell and reduction system 78—20128
water pollutants analysis using potentiostatic meas. *(German)* 80—26185
water pollution, analytical methods comparison 77—90685
water pollution by metals monitoring, instrument survey 79—74580
water quality monitoring, modular system *(German)* 80—26186
Ag concentration in electroplating solution, in presence of cyanide ions 77—1965
Al, molten, determination of H content, using electrochemical probe 79—11843
$Al-SiO_2$, film system, kinetics of interaction 77—44459
Al_2O_3, concentration determ. in electrolyte of Al cells, semicontinuous 77—48713
As_2Se_3, and $As_2(Se,Te)_3$ glasses, as ion-selective materials for solid-state electrochem. sensors 80—50897
Au concentration in electroplating solution, in presence of cyanide ions 77—1965
C paste electrode with electrolytic pasting liq. and insoluble electroactive cpds., quantitative aspects *(French)* 79—79260
CO-air streams, selective oxidation of H_2 before CO electrochem. anal. 77—63978
CO_2, content of atmosphere, continuous automatic monitoring by coulometric method 79—53537
PCO_2, continuous transcutaneous meas., electrochem. sensor 77—13020
CO_2 electrode, dynamic response 79—92025
CO_2 partial pressure in blood, meas. by rapid response electrode system *(German)* 78—85409
Cd, deposition, on metal substrate, pot. sweep, potentiostatic and optical microscopic obs. 77—59967
CdS:I single cryst., I detection by argentometric titration DEP 77—16875
Cd_xS, electrochemical characterisation and comp. modification at 25°C 77—25272
Cl, residual, in saline cooling waters, determ. via modified amperometric membrane probes 80—82112
Cl^- ion selective electrodes, appl. to biological materials 77—90974
Cl^- ions in nuclear reactor water coolant, determination by flow-type porous metallic Ag electrode 80—89577
Cl^-, trace determ. by rate controlled coulometric titration 78—11576
Co^{3+} complex ions, diffusion coeffs. meas., computer-assisted technique using Cottrell eqn. 80—3425
$Co_{1-x}Mg_xO$ ceramics as O_2 sensors, phase stability, elec. cond. and thermoelec. power meas. 78—3420
Cr^{3+} complex ions, diffusion coeffs. meas., computer-assisted technique using Cottrell eqn. 80—3425
CrFeCN epoxy resin-based membrane studies, Ag sensitive electrode 80—16726
Cu binary alloy, polarisation studies, electrode design 80—93761
Cu, chem. aspects of corrosion inhibition by benztriazole 80—16545
Cu concentration in electroplating solution, in presence of cyanide ions 77—1965
Cu corrosion inhibition, by mercaptobenzothiazole, spectro-electrochem. studies 80—30138
Cu II, determ. by ion selective electrode, ligand interference preventive buffer appls. 78—20099
Cu, refinery electrolyte containing thiourea, electrochemical method of meas. active glue conc. 77—4966
Cu-Ni alloy, in 0.1 M NaCl, electric pot. and pH meas., crevice corrosion 78—31564
Cu-Ni(10 (30) wt.%), seawater corrosion rate meas., electrochem. method validity 80—45426
Cu_xS-CdS solar cells, cu_xS growth kinetics and composition analysis by absorbance transient and galvanic electrochemical measurements 80—92797
Fe, annealed, Hz permeation, 230 to 300K *(Japanese)* 78—84004
Fe, intergranular corrosion in NO_3 solns., electrochem. and AES study 80—50751
Fe-Cr, grain-boundary segregation of carbon, electrochemical study 79—100147

electrochemical analysis continued
Fe-Cr (25wt.%) alloy, surface comp. rel. to passivation phenomena *(French)* 79—43479
Fe-Cr alloys, in acid and neutral solns., thickness and optical constants of passive and transpassive films 80—66698
Fe-Ni-Cr (40, 20 wt.%), Kh20N40 alloys, phase composition after quenching, tempering 78—60650
H electrode, construction 77—25329
H^+ analysis using integrated micro multi-ion sensor employing IGFET 78—40439
H_2 conc. in Na and cover gas in LMFBR 79—97787
HCl, determ. in ambient air at ppbv level 79—74579
HCl, gas monitoring ion-selective electrode analyser 77—60146
Hg^{2+} selective liquid-state electrode, construction and basic characts. 77—90705
K determ. in seawater using selective membrane electrode 79—53368
$K_3Fe(CN)_6$, automated electrodic potentiometry of solns. 78—35736
$Li/TiS_2(TiSe_2)(Ti_{1.1}S_2)$, electrochem. obs. of Li intercalation 80—61216
Li-B alloys, Li extraction and determ. using potentiometric titration 79—48016
Li^+-amide, assoc. in aq. soln., potentiometric obs. 77—29005
LiCl-KCl molten eutectic mixture, PbS solubility product and Li_2S solubility 80—54387
LiCl-LiF molten eutectic mixture, PbS solubility product and Li_2S solubility 80—54387
$Li_{2.33}Si$, cryst. struct. and electrochem. anal. *(German)* 80—88132
Mn (II), determ. in industrial wastes 78—61105
Mo-Re alloys Re determ., electrochem. method 79—16073
N_2H_4, electrochem. oxidation on Au, appl. to gas monitoring 79—39248
NO_3^- determination, construction and operation of electrode *(German)* 78—31643
Na, determ. in molten Al and Al-Si using β-Al_2O_3 probe 77—48714
Na^+ analysis using integrated micro multi-ion sensor employing IGFET 78—40439
Na-selective electrodes in marine geochemical studies 79—12312
NaCl stratified solutions, conc. determ. by elec. cond. meas. instrument 77—52718
NiOOH, sintered plate electrodes, residual capacity cause expts. 80—55745
O_2 activity meas. in liquid Na, development of electrolytic probes 80—18550
O_2 analysis, electrochemical sensors 80—93816
O_2 conc. in Na and cover gas in LMFBR 79—97787
O_2 content in gas-atmospheric medium under high pressure method *(Russian)* 77—44559
O_2, determ. by solid electrolyte sensor with internal reference 78—20092
O_2 electrochem. fugacity meas. rel. to geothermometry 77—2256
O_2 electrode amplifier, use of university biochem. spectrophotometer/fluorimeter 77—33807
O_2 meter calibration in 10^{-7} bar range 78—80812
O_2 meter for O_2 meas. in liquid Na 78—58337
O_2 partial pressure determ. in biological fluids, electrochem. cell 78—85420
O_2 probe, applic. to steelmaking 77—21050
O_2 sensors, solid electrolyte, noncatalytic electrodes 80—76573
PbTe-PbSe system, thermodynamic props. 80—11635
Pd MOS structure, surface chem. reactions, H_2 detection 77—73470
Pd-Si Schottky barrier chemical sensor, for H_2 detect. 78—44646
PdO-Pd miniature pH electrode description and use 80—89886
Pu, determ. by automated coulometric method, apparatus 79—16114
Pu safeguarding, computer-assisted controlled potential coulometric determ. 80—78384
S, probe for coal gasification systems 78—76947
S^- ion-selective electrode, sensitivity, surface heterogeneity effects 78—92526
SO_2, in air, potentiometric determ. using solid state detector 78—16151
SO_2, in O_2-variable gases, potentiometric determ. using solid state detector 78—20505
Si enriched SiO_2 layer in MOS structure, electrochemical identification 78—2381
Ti, corrosion inhibition in acid medium, electrochem., Auger investigs. *(French)* 78—44430
Ti-Al-Mo-Cr-Fe, distrib. of Sn, Zr between phases, temp effect. 80—55357
TiH_x film electrode, oxidation, electrochem. and surface analytical characterisation 79—39034
Ti_yO_x on Ti film electrodes, AES, XPS and electrochem. characterisation 78—7086
U, determ. by computer-controlled titration system, evaluation 79—16113
W alloys, phase anal., electrochem. separation of carbides 78—60651
W, anodisation in acidic chloride solns., formation and breakup of anodic oxide films 77—16719
W-Re alloys, Re determ., electrochem. method 79—16073
WO_3 electrode, surface growth of ternary compds., in electrolyte containing redox couples 78—61016
ZnO, single crystal, excess Zn atom conc. and elec. cond. determ. 78—3435
$ZnSO_4.7H_2O$, electrolytic soln., impurity meas. digital instrument appl. *(Polish)* 78—31653
ZrO_2 based solid electrolyte, use for study of O_2 solubility and diffusivity in liq. metals 80—59669
ZrO_2, elec. cond.-nonstoichiometry relationship, direct determ. 78—76079
ZrO_2, electrochemical cells for O_2 sensing, EMF oscills. 79—47999
ZrO_2-CaO thin film O_2 sensor, ionic transference number, cell design 77—70360

electrochemical batteries *see cells (electric)*

electrochemical electrodes
see also electrochemistry
acid oxygen carbon electrodes, electrochemical measurements and surface studies, ESCA method appl. 78—31651
adsorption isotherm equation, thermodynamic form 79—69369
air cathode, sea water activatel Al-air cell 80—26128
alkali and alkaline earth metal electrodes, in nonaqueous secondary cells, electrochem. behaviour 80—35665
alkaline accumulators parameters improvements, use of combined Cd/Zn electrodes *(Czech)* 79—70447
alternating current electrode processes, review 80—61107
anion selective electrodes, using liquid ion exchangers 78—40060
anode behaviour in cyanide-Ag baths *(German)* 80—61103

electrochemical electrodes continued

- anode dissolution by pulsed current, in electrochemical and electroerosion machining *(Russian)* 78—27652
- antibody-selective membrane electrodes 79—84058
- applications in modern laboratory, brief review 77—4964
- arterial pO_2 intravascular monitoring using catheter-tip polarographic electrode *(German)* 78—85408
- Au, adsorption of pyridine, angle-resolved Raman spectroscopy 80—52991
- batteries with gaseous electrodes, research and development, state of the art review *(Czech)* 79—39292
- battery positive electrode, operating in halide-aluminate media, experimental study 79—52923
- bioelectrochemical sensor using immobilised enzyme electrodes *(Japanese)* 80—109071
- biomedical ion sensitive FET micro pH sensor 78—44643
- blood gas microanalyser, calomel electrode efficiency restoration 77—25575
- blood pO_2 meas. polarographic technique 79—100782
- boiler feedwater redox potential meas. by Pt thin-layer electrodes 80—89578
- capacity measurements, double layer, Pt, dropping Hg electrode results 77—53933
- catecholamines, HPLC and continuous flow anal. using flow cell based on rotating disk electrode 80—66894
- catheter tip device incorporating CO_2 and O_2 sensors 79—100783
- catheter tip pH electrodes for continuous intravascular recording 80—81755
- catheter-tip electrode for continuous pO_2 and pCO_2 meas. 79—34693
- cathode, current microdistribution during electrolysis under nonstationary diffusion conditions 78—3350
- cathode with honeycomb arrangement of drain apertures *(Russian)* 79—96164
- cathodic diffusion boundary layer, free convective flow obs. with shadow Schlieren method 78—68894
- cathodic protection for small plant using Ti electrodes *(German)* 80—100943
- chlorophyll *a*-lecithin mixed monolayer coated electrodes, highly efficient quantum conversion, solar energy appl. 79—39314
- chronopotentiometry, programmed current, electrode process followed by chem. reaction 80—35595
- circular interacting microelectrodes, collection factor calcs. *(French)* 77—27759
- concentration polarisation, convectionless steady state, interferometric investig. 78—68896
- continuous moving sheet electrode, characterisation, expt. 77—21398
- continuous moving sheet electrode, current distrib. 77—60077
- convertors, electrochem., conc. type, for elec. signals, diffusion theory of conc. networks 78—61026
- corroding electrode, impedance and polaris. resistance 79—83466
- corrosion rate measurement, with dual electrodes 80—85180
- Cu-Mn alloys, thermodynamics, suitability as electrodes 79—66339
- current distribution, network-type equivalent cct. investig. 78—35705
- cylindrical, diffusion, Cottrell eqn. corrections calcs. 78—48658
- cylindrical, metals heating by electrolytic plasma, temperature distribution obs. *(Russian)* 79—1045
- diffusion between electrodes spaced on cylinder oscillating in electrolyte *(French)* 78—64849
- disc, electrode reaction, number of electrons involved determ. method 80—35596
- disc type, current distrib., analogue model investig. 79—34321
- dispersed, three-dimensional, hydro-metallurgy appl. *(French)* 80—71919
- dispersed, Zn, for primary and secondary cells, electric vehicles appl. *(French)* 80—72023
- double layer in dil. electrolyte solns., model 80—45520
- double layers, image forces influencing capacitance and interaction 79—29367
- double-layer capacitance freq. dispersion 79—20379
- dropping Hg electrode, synchronisation in natural drop expts., high speed device 80—37049
- dropping Hg electrodes, drop times determ. using digital drop timer 78—3394
- ECG manual electrode 79—57801
- ECG surface potential recording electrodes 79—100779
- effective area determination 78—73045
- electric double layer, dense part, model, adsorbed mols. 77—25282
- electrocatalysis, surfaces modified by metal adatoms, review 80—61110
- electrocatalysts, reversible poisoning by CO, air pollution detection appl. 77—37363
- electrochemical impedance, by rapid methods, transient Faraday process 78—27782
- electrochemical reactors with three-dimensional electrodes, characterisation using electrochemical tracer method 80—76520
- electrochemically formed layers, ageing effects, kinetic and structural consequences 80—61109
- electrocrystallisation, galvanostatic transients, crystn. overvoltage 78—76867
- electrode, interpretation of selective etching, electrochem. props 80—7703
- electrode materials, for photoelectrolysis of water 79—29478
- electrode-solution interfaces, role of water 78—40058
- electroluminescence of PVC, influence of cell electrodes 79—74005
- electrolyte conductivity rel. to electrode current density *(Russian)* 78—64847
- electrolyte dropping electrode, electrolysis, appls. 77—25279
- electron transfer to redox system time-depend. perturbation theory 78—61027
- electrophoretic force along equipot. electrode 78—61024
- electropolymerisation, on electrodes, book contribs. 80—50854
- endogastric probe for telemetric pH meas. *(German)* 78—85452
- fast electrode processes, kinetics from transitional sections of polarisation curves 77—25283
- fast ion transport in solids, conf., Lake Geneva, USA (May 1979) 80—57006
- fast ion transport in solids, conf., Lake Geneva, USA (May 1979) 80—105427
- FET transducer research and development for biomedical appl. 78—44640
- film-covered electrodes, electron transfer reactions, mechanisms, theory 78—20023
- film-covered metal electrodes, electron transfer reactions 78—20024

electrochemical electrodes continued

- fixed-bed, three-dimensional, porous, mass and charge transfer *(French)* 80—71920
- flow porous electrodes, axial dispersion determination 78—31650
- fluidised bed, appl. in electrodeposition of Cu at high current density 79—100063
- fluidised bed, appl. in electrodeposition of metals, math. model 79—100062
- fluidised bed cathodes, for electrowinning of metals, const. current density operation 79—24456
- fluidised bed cathodes, for electrowinning of metals 79—24455
- fluidised bed electrode, elec. cond. 77—48652
- fluidised-bed, H_2 evolving, mass transfer behaviour obs. 79—57243
- formamide oxidation at Pt alloy catalytic electrodes 79—57245
- fuel cell electrocatalytic O_2 reduction mechanism with metal chelate coating 78—23951
- galvanic electrode, tissue O_2 tension meas. in rabbits 77—13040
- gas discharge between coaxial electrodes with dielectric layer 78—75476
- gas evolving, mass transfer mechanism 78—48659
- gas evolving electrodes, heat transfer concept 79—34314
- gas evolving electrodes, mass transfer data correl. model 79—79258
- gas sensing electrodes for chem. anal., development 77—4963
- gas sparged, mass transport anal. 80—24004
- gas-evolving electrodes, mass transfer, superposition of hydrodynamic flow 78—73047
- gas-porous electrode, mass exchange in transport zones 77—32801
- glass microelectrodes, Na^+ and K^+ selective, electrochemical props. 79—91957
- glass-electrolyte solution interface chemistry 79—79256
- glassy C electrodes for photogalvanovoltaic and photovoltaic cells 80—89630
- graphite charged polyethylene membrane electrode, electron transfer *(French)* 78—27778
- graphite fibres, polymer coating by electropolymerisation 79—15644
- graphite fluorides, $(CF)_n$ and $(C_2F)_n$, prep., struct., discharge characts., electrode props. 80—89502
- n-heptylviologen salt soln., electrochemical props. 77—77788
- heterogeneous, current and pot. distrib., surface section equilib. pot. 78—53221
- holder for electrochem. stress corrosion expts. at high temp. and press. 80—61102
- hydrodynamic electrochemiluminescence cell 80—45506
- impedence measurement, accuracy of electrode props. determ. 80—61108
- inclined circular disc electrode, ionic mass transport by free convection 78—26117
- integrated micro multi-ion sensor using IGFET 78—40439
- intercalation compound, NMR investigs., review 80—60432
- intercalation compound, thermodynamic and transport props. 80—66963
- interelectrode gaps in Hg-electrolyte capillary cell, capacitive control 77—90610
- interface, electrode-solution, use of specular reflection methods 77—63926
- interface with electrolyte, orient. models for solvent 78—61017
- interfaces, electrified, theory, differential capacitances 77—48649
- interfaces processes at electrode systems of second kind, quantum mech. relations 79—100398
- interference compensation in chemotronic flowmeter for electrically conducting liquids 77—19650
- inversion voltamperometry with alternating current 79—70333
- ion adsorption parameters, zero charge pot. conc. depend. 80—40706
- ion exchange membrane electrode, for ionic activities in aq. soln. meas. 79—74392
- ion selective electrochemical electrode with MOSFET 79—34411
- ion selective electrodes, coated wire design 77—25344
- ion selective electrodes, for ion potentiometric continuous analysis, calibration method for minimizing errors 78—35748
- ion selective electrodes, recent developments 77—4962
- ion selective electrodes, standard addition method study *(Chinese)* 79—83467
- ion selective electrodes, standard addition method study *(Chinese)* 79—83468
- ion selective electrodes for dissolved gas detection *(French)* 79—100472
- ion selective membrane, polarisation at high current densities, Nernst model 79—91962
- ion-exchange membrane, all-round electrochem. investig. equipment 79—91970
- ion-selective, automated potentiometric titrations, equivalence pt. determ. method 78—3391
- ion-selective, for blood serum anal. 78—3645
- ion-selective, interpret. of non-ideal calibrations 77—90661
- ion-selective, solid-state for potentiometric determ. of phosphate 79—92044
- ion-selective disc electrodes with neutral cation-carriers for automated electroanal. of serum *(German)* 78—73269
- ion-selective electrode, flowing systems meas. 78—92527
- ion-selective electrode, solid-state, using microcircuit prod. technique 77—16872
- ion-selective electrode analysis use of microprocessor-based millivoltmeter 80—16752
- ion-selective electrodes, liq. membrane, free and supported, ion transport, bulk elec. props. 79—83534
- ion-selective electrodes, liq. membrane, free and supported, ion transport, interfacial kinetics, time depend. phenomena 79—83535
- ion-selective electrodes applic. in anal. chem. *(French)* 78—40093
- ion-selective electrodes for determination of urine-electrolytes *(German)* 80—94384
- ion-selective electrodes in titrations using tetraphenylborate 79—83530
- ion-selective liquid chloride electrodes, solvent effects *(Russian)* 79—91972
- ion-selective membrane, Ag^+ and F^- based ceramic materials appl. *(Japanese)* 80—61203
- ion-selective membrane, neutral complexing agents basis, limiting step of ionic transport using conc. cells method *(Russian)* 79—96367
- ion-selective membrane electrodes, Na ions selectivity *(Russian)* 79—96337
- ion-selective membrane electrodes, selectivity, statistical calcs. 78—92549
- ion-sensitive membrane electrode function, linearity domain limit 77—29058
- ion-sensitive membrane electrode function, nonlinear domain detection limit 77—29059

electrochemical electrodes continued
ion-sensitive solid-state-membrane electrodes—properties and applications *(German)* 79—1954
ion-specific electrode output volt. linearisation 78—35991
ionselective multi-disc electrode, biomedical appl. *(German)* 78—3687
iron phthalocyanine cathode, performance in fuel cells with H_2SO_4 electrolyte 80—21293
isolated discharge electroerosion craters, interelectrode surfactant effect *(Russian)* 79—83462
Kel-F-graphite composition electrode, voltammetric appls. 78—92489
layer and tunnel compounds, fast ion transport and electrochem. storage 80—61324
leakproof rotating disc electrode design 78—7211
linearly polarised, electrolyte stationary electric field calc. *(Russian)* 80—21289
liquid chromatography, electrochem. detect. and fraction collection system 78—35749
liquid metal electrode, polarographic max. current theory, electrochem. and hydrodynamic instability 79—24750
liquid metal electrode, polarographic max. current theory, hydrodynamic instability 79—24749
mass transfer of dissolved species, to planar electrode, combined effects 78—23949
McInnes glass electrode, use for determ. of CO_2 diffusion coeffs. through polymer membranes 78—20067
membrane-covered rotated disc electrode 80—26069
metal, absolute half-cell EMFs and single ion free energy of solvation 77—73449
metal, interaction with solvent rel. to elec. double layer struct., adsorpt. 78—61023
metal, plasma-type electroreflection, mechanisms 77—1659
metal AC anodic dissolution rate, effect of H^+ evolution *(Russian)* 80—16693
metal electrode, in liq. NH_3, photoelectron emission 79—60868
metal electrodes in molten salts, recording coulometer for controlled-atmosphere reactions 78—3344
metal-electrolyte boundary, elec. refl. and photoemission relationship 80—45211
metal-electrolyte boundary, electrodynamics in visible and near UV range, microscopic effects 80—45521
metal-electrolyte boundary, photoemission effect on elec. refl. 80—45212
metal-polymer splices, adhesive bond destruction and strength w.r.t. electrochem. interaction 79—20339
microelectrodes, Na-selective liquid ion-exchanger, for intracellular meas. 80—3888
miniature pH-sensitive polymer membrane electrode 79—100781
molten carbonate fuel cell, electrolyte comp. effect on electrode kinetics 80—101092
multi-step electrodes near equilib., linear response theory *(German)* 79—61863
multiparameter clinical diagnostic miniature transducers, colloquium, London, England (May 1979) 79—100776
n-type semiconductor anode, illum., charge transfer modes, digital simulation 80—2464
nervous system electrostimulation, stainless steel electrode corrosion control 78—7464
optically transparent electrodes, form. from reticulated vitreous carbon 78—3341
organic fluid charge carrier generation, role of molecular electroinduction effects *(Russian)* 79—96321
organic semiconductor photoelectrode processes and effects *(German)* 80—26145
oxide electrodes, electron transfer reactions, tunnelling through a space charge barrier 78—80050
oxide semiconductors in photoelectrochemical conversion of solar energy, use as cell anodes 80—101120
oxide-covered metal electrodes, direct elastic electron tunnelling, calcs. 78—52085
oxide-electrolyte interface, transition layer model 78—68895
pacemaker electrode electrochemical structure and possible improvements 77—81745
perovskite type compounds, electrode catalysts for cathodic reduction of O_2 79—29371
pH meas. instruments and appls. *(Dutch)* 79—29435
1-phenylpyrazolidin-3-one adsorption on metal electrodes, obs. 79—100391
photocell using covalently-bound dyes on semiconductor surfaces 77—4393
photoelectrochemical cells, metal, electrodes in contact with fluoresent dye solns., photovoltage generation, comprehensive model 80—40871
photoelectrochemical cells for H prod., using sunlight, semiconductor electrode stability, materials and configuration 80—45774
photoelectrochemical cells with semiconductor electrodes for solar energy conversion and storage *(French)* 80—61386
photoelectrochemistry, laser sources use for solar energy conversion 80—40873
photoelectrolysis cells, props. of oxide-based heterostruct. photoelectrodes 80—12023
photosynthetic reaction centre from bacteria working on SnO_2 electrode 80—94092
pipe wall electrode, for diffusion coeff. meas. of electrochem. solns. 79—14947
plane vertical cathode, electrodeposition of Cu, distrib. of local current densities 79—70338
polarisation studies, electrode design 80—93761
polarographic sensor for pN_2O and pO_2 anal. in blood and gas 79—62412
polyethylene capillary dropping mercury electrodes, for corrosive media appls., prep. 78—61090
polymer film coated steel, Pt and glassy C electrodes, prep., characts., stability 78—76866
polypropylene-covered galvanic cell, O_2 consumption anal. 78—31923
porous, capillary equil. and percolation theory 79—91971
porous, contained electrolyte elec. cond. meas. 77—63927
porous cathodes, flow-through, performance eval. for Cu electrodeposition 77—16514
porous electrode diffusion controlled operation, mass transport with memory 80—21298
porous electrode sensors for using porous electrode sensors 77—17261
porous electrode type cells, electrochem. and capillary characts. 79—91967

electrochemical electrodes continued
porous electrodes, flow-through, math. modelling 77—16832
porous electrodes, relative elec. cond. of soln. and matrix phases 79—52679
porous flow-through electrode, for Ag^+ removal from photographic fixing soln. 77—60076
porous flow-through electrodes, mass and charge transfer and cell design *(French)* 80—16697
porous Ti-MnO_2 anodes for matrix-type electrochemical cell 77—81414
potentiometric electrodes, for gas conc. meas. in gas phase *(French)* 78—7269
preparation techniques, in solid electrolytes *(Japanese)* 80—24658
quinone electrochemical reduction at packed, fluidised bed electrodes, kinetic behaviour 79—57235
radiolytic product detection by Pt electrode rest potential 80—11973
Raman spectroscopy at electrode-electrolyte interfaces 77—77777
reaction rate in presence of surface-active substances on electrodes 79—43597
redox reactions obs., using electrodes with covalently attached monolayers 80—45512
reference electrode for automated in situ hydrochemical meas. *(Russian)* 78—65430
reference electrode liquid junction, press.- and flow-insensitive 77—4906
reference electrodes for in vivo meas. 79—52687
resistance, effect on current density and electrode pot., rel. to cell design 77—60070
resistive electrode current density distribution 80—21302
reticulate, three-dimensional, mass transfer characts. obs. 79—1958
review, ion selective electrodes 78—85165
ring electrode shielding at rot. ring-disc electrode for micromolar voltammetric analysis 79—92018
ring-disc electrodes, collection efficiency for high freq. AC 78—64853
ring-disk electrode, in flow coulometry 80—71966
rotating, for DC cond. meas. of solns. 77—70362
rotating disc electrode, with optically transparent ring, digital simulation 78—53210
rotating disc electrode mass transfer, appl. of pulsed voltage and pulsed current 80—21292
rotating metal disc electrode, mass transfer under turbulent conditions, suspended particle effects 78—27772
rotating ring-disc electrode with pyrolytic graphite end-plane sections 78—92488
rotating thin-ring electrode, bubble nucleation 78—48664
rotating two-ring electrode, constant current effects, digital simulation *(French)* 78—7212
semiconducting oxide, O_2 reduction kinetics improvements 78—20029
semiconducting oxides, interband transitions determined from photoelectrolysis spectra 79—65378
semiconductor, charge injection, space charge region, digital simulation 77—15949
semiconductor, n-type, thermodynamic pot. for anodic dissolution, rel. to photoelectrochem. cell efficiency 78—26948
semiconductor, open-circuit photopotential, simulation 77—15950
semiconductor, photogenerated free carriers and photocurrent relax., simulation 77—15951
semiconductor electrode, electrolum. due to hole injection from electrolyte 77—20926
semiconductor electrode, surface state charge transfer in photoelectrolysis of water 79—28405
semiconductor electrodes, charge distrib. and chemisorpt. processes *(German)* 79—52689
semiconductor electrodes, photosensitivity props., correl. with electronegativity 77—44482
semiconductor electrodes for photoelectrolysis of water, appl. to solar energy conversion 79—29477
semiconductor liquid junction, for solar energy conversion, efficiency, electrochemical stability and surface preparation 78—14817
semiconductor oxide O_2 electrode characts. 79—24073
semiconductor photoanodes, corrosion stability 80—21130
semiconductor photoelectrode, appl. in reproducible photoelectrochem. imaging 80—14446
semiconductor-electrolyte boundary impedance measurement, ohmic drop correction *(French)* 79—70332
semiconductors for photoelectrolysis, book contrib. 79—65547
semitransparent rotating disc electrode, photochem. and electrochem. surface reactions 78—40056
single crystal surface, electrochemistry, surface struct., superlattice struct. 80—76519
solar energy direct photoelectrochem. conversion and storage 79—62015
solid, behaviour in normal and differential pulse voltammetry 78—73055
solid film, electrolyte systems, materials characts. and appls., review 77—77781
solid solution cathodes for electrochem. power sources, dynamic aspects 80—3508
solid state electrodes, for high energy batteries 80—55836
spectrographic determ. enhancement using alumina cup electrode *(Japanese)* 77—86418
spherical, diffusion, Cottrell eqn. corrections calcs. 78—48658
static mercury drop, voltametry appls. 80—97740
statistical mechanics of ideally polarisable electrode 79—96330
steel:Si alloy formation kinetics at solid cathodes, metal electrodeposition from molten salt electrolytes 80—26028
steel, C, rotating disc electrode in 3 wt.% NaCl solution, corrosion rate meas. *(French)* 79—43470
steel, cold-rolled, corrosion resistance in 1M $LiAsF_6$/THF, suitability for organic electrolyte Li secondary batteries 79—100387
steel electrodes, pitting corrosion currents rel. to conc. of inhibitive and corrosive anions under corrosion conditions 80—85181
surface, anisotropy of optical props. 80—60534
surface, covalently bound molecules, redox reactions, steric effects 78—73077
surface, partially covered, eqns. for chronopotentiometry 78—85236
surface water continuous analysis by NH_4^+-sensitive plastic membrane electrode 80—89701
thin layer, for differential pulse anodic stripping voltammetry 78—20089
thionine coated electrode, for photogalvanic cells 80—35696
thionine-coated electrode for photogalvanic cells, electrochem. and XPS anal. 80—72071
three-dimensional, with loose support, principles and appl. *(French)* 80—71918

electrochemical electrodes continued

- three-dimensional gauze in new cell design, mass transfer enhancement by counter-electrode gases 79–43590
- three-dimensional reactors, dimensioning, w.r.t. mass transfer phenomena *(French)* 80–71921
- tissue microelectrode design for skin pH meas. 79–100780
- transition metal chalcogenides, reversible electrodes appls. 80–61112
- transition metal dioxides, electronically conducting with rutile struct., electrode material behaviour 78–31656
- tube, radical species generation, laminar flow through EPR cavity, convective diffusion 77–24746
- vitreous C electrodes, potentiostatic growth of PbO_2 79–43596
- weakly polarised, faradaic impedance, elec. double layer effects 79–70351
- wetproofed electrode, pore filling degree with electrolyte and liq. reactant 80–40702
- Ag, adsorbed pyridine, ang. resolved Raman spectra 80–16017
- Ag, adsorbed rhodamine B, anisotropy of optical props. 80–60534
- Ag covered Ti electrodes for cathodic protection for small plant *(German)* 80–100943
- Ag, electric double layer of polycrysts. in NaF soln., diffuse capacitance minimum 79–91969
- Ag electrode, intense Raman spectra in presence of Cl^- and pyridine 80–55076
- Ag, electrode pot. effects on surface plasmon excitation 78–15149
- Ag, emersed, electrorefl. spectra 79–28788
- Ag, metal ion adsorption, kinetics, surface struct. 78–79873
- Ag, monomolecular films of Pb, anisotropy of optical props. 80–60534
- Ag, photoemission-into-electrolyte 79–74390
- Ag porous metallic electrode, for determ. of Cl^- ions in nuclear reactor water coolant 80–89577
- Ag, preparation by sintering and by chemical method, performances comparison 79–87851
- Ag, roughened, Raman band intensity of adsorbed pyridine 78–48160
- Ag sintered electrode production for concentrating cell *(Portuguese)* 78–88637
- Ag, surface, adsorption of pyridine on graphitic C overlayer, Raman spectra obs. 80–103954
- Ag/AgCl, properties, production, problems in biomedical appl. 77–40959
- Ag/AgCl highly stable electrode 78–35989
- Ag-AgCl reference electrode for high temp. eqn. environments, construction and performance 77–12803
- Ag-AgCl reference electrode, construction and thermodynamic props., high temp. aq. environment appl. 80–21288
- Ag-electrolyte interface, enhanced Raman scatt. of adsorbed molecules, background continuum obs. 79–73926
- $AgBr-SiO_2$, field effect potentiometric sensors 78–35691
- AgCl covered Ti electrodes for cathodic protection for small plant *(German)* 80–100943
- AgCl crystal plate supersensitisation, photoelectrochemical obs. 79–83486
- Ag_2SeO_4, for Li based primary cells, performance determination 79–52918
- Ag_2TeO_4, for Li based primary cells, performance determination 79–52918
- $Ag(s)/Ag_2SO_4+Na_2SO_4(l)$ high temp. ref. electrode, study 80–76622
- Al alloy electrode, corroding, acoustic emission 80–60997
- Al alloys, pit propagation, influence of anions in halide solution 78–72917
- Al disc porous electrode, prep. by powder metallurgy, performance in $LiAl/FeS_x$ cell 80–26130
- Al electrochemical electrode, oxide film growth accompanied by luminesc. 79–57236
- Al reduction cell, C cathode intercalation props. 79–43559
- Al-(Mn), effects of Mn on electrode or free corrosion potentials 80–100942
- $Al-Al_2O_3$-electrolyte, electroluminesc., nondestructive electronic avalanche 78–68563
- Al-Mg (7 wt.%), bare surface reaction rates in aq. solns. 80–101022
- Al_2O_3, anodic, passified, inhibition of reaction with water 80–89390
- As_2Se_3, and $As_2(Se,Te)_3$ glasses, as ion-selective materials for solid-state electrochem. sensors 80–50897
- Au, adsorbed Br_2, anisotropy of optical props. 80–60534
- Au anode, chem. dissolution in aq. alkaline cyanide, electron stoichiometry 80–40697
- Au, chemisorption of H(O), volume of adsorbed species, temp. and press. effects 78–84060
- Au, corrosion in H_2SO_4 solutions, effect of pH 79–70344
- Au electrode, electrochem. oxidation of alcohols using alkaline electrolytes *(German)* 78–15681
- Au, electrode pot. effects on surface plasmon excitation 78–15149
- Au electrodes, adsorpt. of Br^-, specular reflect. investig. 78–61047
- Au, emersed, electrorefl. spectra 79–28788
- Au film electrode, electrochem. adsorpt. of O_2, elec. resist. obs. *(French)* 79–29372
- Au in electrolyte, photoemission-into-electrolyte 79–74390
- Au, metal ion adsorption, kinetics, surface struct. 78–79873
- Au, single cryst., (100), solid and thin-layer, differential-pot. capacity curve with NaF aq. soln. *(French)* 79–47932
- $Ba_{0.5}FeS_2$ cathodes for nonaqueous Li batteries 80–3506
- $BaTiO_3$ electrodes, photocurrent efficiency, photo-oxidation of water 77–12000
- $BaTiO_3$, surface comp. changes during photoelectrolysis, XPS obs. 79–7894
- C cathode, intercalation props. in Al reduction cell 79–43559
- C, glassy, electrolytic durability 80–66809
- C paste electrode with electrolytic pasting liq. and insoluble electroactive cpds., quantitative aspects *(French)* 79–79260
- C, pyrolytic film electrode, fabrication, electrochem. characterisation 78–92487
- CO_2 electrode, dynamic response 79–92025
- CO_2 partial pressure in blood, meas. by rapid response electrode system *(German)* 78–85409
- Ca^+, ion-selective electrode design 79–70404
- Ca-selective membrane electrodes, asymmetric, potentiometric meas. 77–77785
- Cd plastic bonded, for Ni-Cd accumulators, production methods 80–45659
- Cd-Sn-Pb composite amalgam electrodes for standard cells 77–5871

electrochemical electrodes continued

- n-CdS electrode, photoelectrochemical behaviour in acetonitrile solns. 78–31644
- CdS electrode, photoexcited, charge transfer in electrolyte with Na_2S additive 79–99618
- CdS, in aq. soln., flatband potential, effects of dissolved Cd^{2+} and S^{2-} ions 77–51815
- n-CdS in DMF solns., electrochem., photoelectrochem., redox. pot. determ. 79–96322
- CdS, photoanode, flat band pot., depend. on surface ion effects 79–62013
- CdS photoanode, for photovoltaic cells, prep. and characts. 78–14818
- n-CdS, photoanodic behaviour in acetonitrile-iodide solns. 78–47868
- CdS, single cryst. surfaces, diffr. gratings, electrochem. recording of holograms 80–32934
- CdS-GaAs n-n voltage-enhanced photoanode, solar cell efficiency 78–14810
- CdS(Se) photoanodes, effect of S(Se) substitution, photoelectron spectroscopy obs. 80–2463
- n-CdS(Se)(Te) semicond. liq. junction solar cells, photocurrent spectra, carrier recombination 78–76142
- CdSe, chemically sprayed thin films as photoanode in photoelectrochem. cells, power charact. meas. 80–85293
- CdSe electrochem. photovoltaic cells, effect of thin film electrode prep. and conc. on efficiency 80–55847
- CdSe film photoanodes for electrochem. photovoltaic cells, fabrication and evaluation 80–76641
- CdSe photoanode improved efficiency by photoelectrochem. etching 80–104512
- CdSe photoelectrode, polycrystalline, for solar energy conversion 78–19147
- Cd_2SnO_4 and Cd_2SnO_4:CdO, thin film electrodes in H_2SO_4 electrolytes, reduction, AES and SEM 80–65674
- n-CdTe, semiconductor electrode, electrochem. behaviour in nonaqueous media *(French)* 80–66808
- Cl^- ion selective electrodes, appl. to biological materials 77–90974
- Co oxide-based electrode, air hydrophobically treated, electrochem. characts. 79–61876
- Co/CoO, relative chemical potential of oxygen *(German)* 78–31642
- CoO, Co_3O_4, free enthalpy of formation, solid oxide electrolyte galvanic cell method 78–23959
- Co_3O_4 anode, wear-resistant, use in applied electrochem. 80–40701
- Cr/Cr_2O_3, relative chemical potential of oxygen *(German)* 78–31642
- $Cr_2O_3/\gamma-Fe_2O_3/Pt$ electrode, two layer oxide surface film anal. by modulation spectroscopy *(Japanese)* 80–11491
- Cu, adsorption of pyridine, angle-resolved Raman spectroscopy 80–52991
- Cu anode, passivating behaviour and illum. effects in alkaline soln. 80–104449
- Cu, anodic oxidation in LiOH at room temp. 79–61865
- Cu binary alloy, polarisation studies, electrode design 80–93761
- Cu cathode, electrolytic deposition of Cu-Cd alloys on (100) and (110) surfaces *(Polish)* 80–44435
- Cu, cyclable solid-state cell based on intercalated electrodes 79–100511
- Cu electrocrystallisation from $CuSO_4$ solns., current density/overvoltage curves *(Russian)* 79–8236
- Cu electrocrystallisation from $CuSO_4$ solns., exptl. methods *(Russian)* 79–8235
- Cu, electrodeposition from nitrate solns., cathode polarisation obs. *(Russian)* 79–47937
- Cu, electroplated surface roughness and brightness rel. to periodic reverse current 79–96201
- Cu, flat electrode, ionic mass transfer coeffs. determ. in open channels 80–59110
- Cu II ion selective electrode, ligand interference preventive buffer appls. 78–20099
- Cu, photopotentials, rel. to corrosion 79–24648
- Cu phthalocyanine thin film electrodes, near IR photoelectrochemical responses 80–93766
- Cu:Be, alloy formation kinetics at solid cathodes, metal electrodeposition from molten salt electrolytes 80–26028
- Cu/Cu_2O, relative chemical potential of oxygen *(German)* 78–31642
- $Cu-H_3PO_4$ system, instability and oscillations *(French)* 78–64850
- Cu-Hg amalgam electrode, standard pot. 78–76874
- Cu-Ni(Al) alloys, photopotentials, rel. to corrosion 79–24648
- $CuFeS_2$, chalcopyrite, electrode surface reduction kinetics 78–56897
- Fe and Fe-C(1.54 wt.%) alloy, electrocapillary curves in liq. sodium tetraborate 79–91968
- Fe, corrosion and passivation in LiCl soln., peripheral velocity effect 80–61000
- Fe electrode, electrochem. behaviour in liq. NH_4 solns., effects of added impurities 80–50857
- Fe, kinetics, explanation 79–74103
- Fe oxide films, semicond. electrode props. 79–91093
- Fe, passive layer, semiconductor model, appl. to electrochem. reactions, review 80–26022
- Fe plating cathode current distrib. influences *(Russian)* 79–96197
- Fe, porous, discharge capacity, importance of physical struct. 80–26123
- Fe, rotating disc, partially passivated, pot. and current distrib. calcs. 80–35545
- Fe/'FeO', relative chemical potential of oxygen *(German)* 78–31642
- Fe-air batteries, bifunctional air electrode 80–72028
- Fe_2O_3, electrochem. doping 77–76430
- n-Fe_2O_3 electrodes, characterisation and behaviour in acetonitrile solns. 80–25004
- n-Fe_2O_3, enhanced photoeffects by electrocatalysis and peroxide effects 80–16815
- $\alpha-Fe_2O_3$, pure and TiO_2 doped, electrode, photooxidation of H_2O appl. 78–76886
- Fe_2O_3 semiconductor electrodes, photoassisted electrolysis of water 77–77771
- n-Fe_2O_3, sintered and flame-oxidised, photoelectrochemical props. 79–70355
- Fe_2O_3, sintered semicond. electrode, photoeffects 79–51669
- $\alpha-Fe_2O_3:TiO_2$, water photooxidation appl. 78–15684
- Fe_xO_y, semicond., prep. by Fe samples heating, photoassisted water electrolysis appl. 78–15683
- $FeTiO_3$, Fe_2TiO_4, Fe_2TiO_5, prep. and Czochralski cryst. growth 77–21017
- $FeTiO_3$, Fe_2TiO_4, and Fe_2TiO_5 anodes, appl. to photoelectrolysis of water 77–63920

electrochemical electrodes continued
Ga, electrode, crystallite interfacial impurities, electrochem. effects, microprobe anal. 77—44569
Ga, work function, electrochem. determ., rel. to In-Ga alloys 77—44489
$Ga_{1-x}Al_xAs$, interface capacitance meas., flatband pot., conduction and valence band boundaries *(French)* 79—33339
p-GaAs electrode, flatband pot. determ. from differential stress meas. 80—75638
p-GaAs, electrode, photoemission into electrolyte solns. 77—24616
n-GaAs electrodes in acetonitrile solns., liq. junction photovolt. cell 79—99617
GaAs in acetonitrile solns., photoelectrochem. behaviour 79—4600
GaAs photoanode, using n/n^+ struct., power conversion efficiency 80—50990
n-GaAs photoanodes for water photoelectrolysis 77—77789
n-GaAs semicond. liq. junction solar cells, photocurrent spectra, carrier recombination 78—76142
n-GaAs-electrolyte interface, surface pretreatment rel. to photocurrent, spectral response 80—3204
n-GaAs(P) in DMF solns., electrochem., photoelectrochem., redox. pot. determ. 79—96322
$Ga(As_{1-x}P_x)$ electrode, equilib. establishment kinetics *(French)* 79—79259
$GaAs_{1-x}P_x$, interface capacitance meas., flatband pot., conduction and valence band boundaries *(French)* 79—33339
$Ga_xIn_{1-x}P$, flat band pot., impedance meas. and photoelectrochemistry *(French)* 80—49894
n-GaP, Au-coated semicond. electrode, photoelectrochem. behaviour in water 77—21399
p-GaP, cathode of photoelectrochemical cell 78—10552
p-GaP electrode, for solar cell, differential capacitance meas. for flatband potential determ. 78—72256
n-GaP electrode, photoanodic dissolution rate, effect on surface electronic band energies 80—103748
n-GaP electrode, photoelectrochemical behaviour in acetonitrile solns. 78—31644
p-GaP electrode, photoelectrochemical effect 80—55673
p-GaP electrodes with metal adatoms, surface states form. due to impregnated H 80—54778
GaP, n-, p-type, electrode, impedance in alkaline medium *(French)* 79—43586
GaP photoelectrode, role of Au overlayers 78—14812
n-GaP, potential of Au overlayer, I-V curves 77—89848
p-GaP semiconducting photoelectrode 80—101119
GaP, single cryst. electrode, impedance, effect of freq., voltage and electrolyte comp. 78—19146
$GaP-NH_3$ electrolyte interface, photo-assisted electron injection 79—87152
Ge electrode, cathodic characts. rel. to halide ions 79—57238
Ge, electrodes, photoemission into electrolyte solns. 77—24616
p-Ge in DMF solns., electrochem., photoelectrochem., redox. pot. determ. 79—96322
H^+ concentration meas. *(German)* 79—16083
H_2, impedance, relationship with structure and flow *(French)* 78—27766
HCl, gas monitoring ion-selective electrode analyser 77—60146
Hf electrode, surface oxide film, impedance and pot. behaviour 80—61001
Hg coated graphite, anodic stripping voltammetry, environmental sample analysis appl. 79—11836
Hg, dropping electrode, for square wave voltammetry, theory 78—35733
Hg, dropping electrode, for square wave voltammetry, exptl. appls. 78—35734
Hg dropping electrode, photoemission into electrolyte solns. 77—24620
Hg electrode, adsorption of n-butanol, diffusion layer theory, exptl. test 78—35701
Hg electrode, electroreflection spectra calc., electromodulation mechanisms 77—1658
Hg electrode, membrane coated, continuous voltammetric anal., appls. 77—25341
Hg, photoemission, into electrolyte soln., five-halves law 77—44132
Hg, rotating thin film electrodes, staircase voltammetric stripping anal. 77—12843
Hg^{2+} selective liquid-state electrode, construction and basic characts. 77—90705
Hg-Au, minigrid optically transparent thin-layer electrode 77—70305
Hg-C optically transparent electrodes, prep., props. 78—7210
I_2 electrode, in $RbAg_4I_5$ electrolyte, thermodynamcis and electrochem. behaviour 79—70348
In-Ga, eutectic alloy, zero point determ. from uncharged surface pot. 77—90611
In-Ga, work function, electrochem. determ. rel. to Ga 77—44489
$In_{1.9}As_{0.1}Se_3$, growth by chem. vap. transport, characterisation as photoelectrode 78—43994
In_2O_3 semiconductor electrode, sensitised photocurrent by energy and electron transfer in dye monolayers 79—38119
InP in acetonitrile solns., photoelectrochem. behaviour 79—4600
InP, N- and p-type electrodes in acetonitrile solns., photoelectrochemical behaviour 79—99616
n-InP photoelectrode, stabilisation to photoanodic dissolution, in aqueous solutions of Te^{2-}/Te_2^{2-} 78—14814
n-InP photoelectrode, stabilisation to photoanodic dissolution in solns. containing Te^{2-} and Te_2^{2-} 78—19144
InSb, electrodes, anodic and cathodic processes 77—44487
IrO_x anodic film electrochromic cell, fabrication and display device use 80—61320
IrO_x anodic films, electrochromism and ionic cond., model 80—59706
$KFeS_2$, cathodes for nonaqueous Li batteries 80—3506
Li, anodic behaviour in aq. LiOH solns. 78—39941
Li, corrosion in alkaline soln. 77—73367
Li, electrochemical behaviour, in propylene carbonate, SEM study *(French)* 78—56899
Li electrode, cycling behaviour in $LiAsF_6$-methyl acetate solns. 78—27769
Li, electron microscopy, photoelectron spectroscopy, surface anal. *(French)* 80—50859
Li incorporated transition metal oxides, topochem. reactions, chem. prep. and characterisation 80—61115
Li, passivation layer, in $LiClO_4$-propylene carbonate solution, composition *(French)* 80—11899
Li-Al alloy electrode performance, effects of metal additives 78—23953

electrochemical electrodes continued
Li-Al electrode performance In and Mg surface additives effect 80—40698
Li-Al-Mg alloy electrodes, polarisation behaviour and struct. 79—43588
Li-Sb(Bi), thermodynamic props., 355-600°C 78—34634
Li-Si, electrode pot., Li utilisation determ. 80—81427
Li-Si alloys eval. as negative electrodes for $Li-FeS_2$ cells, thermodynamic props. 77—16547
$Li-TiS_2$ storage batteries *(German)* 80—12001
LiAl/FeS, battery system research developments at ANL 80—61323
$LiAl-NaAlCl_4-MoCl_5$ thermal battery evaluation and optimisation 79—29458
Li_5AlO_4, ionic conduction, environment effects 77—76600
Li_xCoO_2, cathode material for batteries of high energy density 80—101089
$LiFe_5O_8$, elec. props. 77—80641
Li_xFeS_2 $(0<x\leq2)$ cathodic system, chem. and electrochem. studies 80—85188
$LiNO_3$ solution cathodic gas evolution rate rel. to electrode material *(Russian)* 80—26020
$Li_2O-GeO_2-Ga_2O_3$, glass, electrode props., dissolution kinetics 80—89387
LiOH, ionic conduction, environment effects 77—76600
Li_3Sb, mixed conducting electrodes, kinetic parameters determ. 78—14772
$Li_3Sb(Bi)$, evaluation as electrode material, electrochem. expts., 360-600°C 78—11526
Li_2SiO_3 glass pH meter electrode performance *(German)* 80—40695
Li_xTaS_2 and Li_xTiS_2, chem. diffusivity of Li at 30°C 80—59737
Li_xTiS_2, $(0\leq x\leq3)$, intercalation in TiS_2, possible electrochem. cathode 80—19772
$Li_xV_{1-y}Fe_yS_2$, intercalated battery cathode material, Mossbauer studies 80—44984
Mn/MnO, relative chemical potential of oxygen *(German)* 78—31642
MnO_2 anode coating for enhanced O_2 evolution in seawater electrolysis 80—30435
γ-MnO_2 electrode, impedance in alkaline solns. 79—70350
Mo, anodic solution kinetics, in KOH, for high current densities *(Russian)* 78—11523
MoS_2, amorphous, cathode, electrochem. props. rel. to secondary Li battery 80—40851
MoS_2, layer cryst. surface, for solar energy assisted electrochem. splitting of H_2O 77—90612
$MoSe_2$ layer-type electrochem. solar cells, electrode material performance, doping effect 79—74532
n-Si, Fe_xO_y-coated, heterostruct. photoanode for photoelectrolysis of water 80—61384
NH_4NO_3 solution cathodic gas evolution rate rel. to electrode material *(Russian)* 80—26020
NO_3^- determination, construction and operation of electrode *(German)* 78—31643
NO_3^- selective electrode used in surface and effluent water analysis 79—100476
Na-S accumulator, electrical energy storage *(French)* 80—55835
Na-S cells, S electrode potential distrib. model 79—96435
Na-S cells, S electrode resistance calc. 80—35667
Na-selective electrodes in marine geochemical studies 79—12312
$NaNO_3$ solution cathodic gas evolution rate rel. to electrode material *(Russian)* 80—26020
Na_2SiO_3 glass pH meter electrode performance *(German)* 80—40695
Nb, surface changes induced by strong cathodic polarisation 79—100388
Nb_2O_5 electrodes, in aq. and acetonitrile solns., electrochromism 80—50298
Ni, appl. in rotating multipolar wiper-blade cell 79—43751
Ni, cathodic polarisation in alakaline earth metal salt solns., surface changes 79—61869
Ni, corrosion resistance in 1M $LiAsF_6$/THF, suitability for organic electrolyte Li secondary batteries 79—100387
Ni electrodeposition cathode polarisation, influence of unsaturated sulphates *(Russian)* 79—91963
Ni electrodeposition from alkaline citrate electrolytes, cathodic process rate *(Russian)* 79—8440
Ni oxide, plastic bonded, for Ni-Cd accumulators, basic electrochemical parameters 80—50951
Ni, oxide growth, effect on breakdown voltage and efficiency 79—4766
Ni oxide-based electrode, air hydrophobically treated, electrochem. characts. 79—61876
Ni, smooth electrode, potentiodynamic investig. 77—21395
Ni/NiO, relative chemical potential of oxygen *(German)* 78—31642
Ni-Cd accumulators, plastic bonded electrodes, active layer composition influence on galvanostatic and potentiostatic discharge curves 80—55834
Ni-Cd accumulators, sintered negative electrodes props. evaluation, impregnation method influence 79—57422
Ni-Cd sealed battery electrode performance meas. 80—66962
$Ni-ZrO_2$ compact cermet cathode for high temp. water vapour electrolysis *(French)* 79—74399
$NiCo_2O_4$ Teflon bonded porous electrodes, O_2 evolution 80—30247
$NiLa_2O_4$ electrodes, kinetics of O_2 evolution, appl. to electrolytic H energy prod. 80—30430
NiO electrode for photolysis 80—40696
NiO electrodes, effect of $Co(OH)_2$ on self-discharge, IR spectra obs. 80—21295
$Ni(OH)_2$ electrodes, charged, reversible potentials meas. 80—55669
$Ni(OH_2)$ electrodes, charged, thermodynamic considerations of reversible potentials 80—55670
NiOOH, sintered plate, residual capacity cause expts. 80—55745
Ni_3S_2, heazlewoodite, dissolution in acidic ferric chloride soln. at 25°C 79—95172
O electrode, reaction in alkaline soln. on transition metal oxides prepared by thermal decompositions 79—61864
O_2 activity meas. in liquid Na, development of electrolytic probes 80—18550
O_2 electrode, membrane-covered catheter-tip system, construction and performance 78—81003
O_2 molecule reduction flow probe for cerebrospinal fluid 79—100777
O_2 partial pressure determ. in biological fluids, electrochem. cell 78—85420
O_2 partial pressure measurement with thin-layer polarographic probe, intracortical appl. *(German)* 78—85410
O_2 sensing electrode stability 77—60268

electrochemical electrodes continued
O_2/C gas diffusion electrodes, electrochemical performance in acid solutions, electrolyte content effects 79—52926
Pb battery anode reverse polarisation corrosion test method *(Bulgarian)* 80—50950
Pb electrode, combined electroreflectance and double layer effects 77—85692
Pb electrode, in situ surface phase study by laser Raman spectroscopy 80—103542
Pb, electrode, potential effect on surface struct. in H_2SO_4 in anodic region 80—16592
Pb, passivation in H_2SO_4 soln. 78—76871
Pb, porous, H_2SO_4 solutions, oxidation mechanism obs. 79—100514
Pb porous electrode oxidation in H_2SO_4, potential step expts. 79—96438
Pb, surface reactions during electrolysis 77—77784
Pb/$PbCl_2$ electrode, in chloride media, low temp. props. 78—68899
Pb-acid battery, electrodes structure obs. 79—100516
Pb-acid battery charge determ. from internal impedance 79—96436
Pb-Ca-Sn alloys for battery grids, proposed phase diagram, grain struct. development, corrosion phenomena 77—16546
Pb-H_2SO_4 battery negative plates, impedance, theory 78—27771
Pb-H_2SO_4 cells, Sb alloying effect on solid Pb electrochemical properties 80—55668
Pb-PbO_2, bielectrodes, anodic polarisation 77—44483
Pb-Sn-Ca alloy sheet, continuously cast, for battery grids, ageing behaviour 77—16603
PbO_2, cyclic voltammetry for accelerated corrosion life tests 78—31582
PbO_2-Ag electrode system for potentiometric titrations, semi-auto titrator, student experiment 79—84918
PbO_2(Pb) electrode, anodic impedance during suspension-electrolysis leaching of β-ZnS in 1N H_2SO_4 soln. *(Japanese)* 79—43594
Pd, cathodic polarisation in alakaline earth metal salt solns., surface changes 79—61869
Pd, for electrolytic H prod., reaction kinetics 80—30434
PdH_2 internally-charged electrode stability rel. to charging current density 79—57251
PdO-Pd miniature pH electrode description and use 80—89886
Pt, adsorption of H, dynamic impedance meas. 79—74393
Pt black anode of implantable fuel cells, effect of O_2 77—60309
Pt, cathodic polarisation in alakaline earth metal salt solns., surface changes 79—61869
Pt, chemisorption of H, entropy, temp. and press. effects 78—84059
Pt, chemisorption of H(O), volume of adsorbed species, temp. and press. effects 78—84060
Pt, compact layer struct., absorpt., EHT calcs. 77—16828
Pt electrode, in liq. NH_3, photoelectron emission 79—60868
Pt electrode, in Na_2SO_4-NaCl melt, polarisation meas., reactions 78—68898
Pt electrode, multilayer oxides, electrochem. reduction mechanism, kinetics 78—61019
Pt, electrode, rotating, appl. to fast reaction kinetics obs. 77—16821
Pt electrode, underpotential deposition of Ag or Cu, XPS 77—59672
Pt, electrode, unroughened, I_2, I_3^- adsorbed from H_2SO_4-KI, Raman spectra 78—31689
Pt electrode (100), (111), polycryst. surfaces, comparison of electrochem. activity 78—61015
Pt electrode O_2 reduction kinetics in conc. H_3PO_4, H_2SO_4 and $HClO_4$ 78—23952
Pt electrode stimulation of nervous system, electrochem. safety aspects 77—21659
Pt electrodes, chemisorbed H, anion effects on multiple states, reflection spectra obs. 79—43634
Pt electrodes, platinised, adsorpt. of Au in aq. HCl 78—56914
Pt electrodes, polymeric surface film form. by electrooxidation of phenolic cpds., ellipsometric study 80—104450
Pt, film, Ag electrodeposition, interface struct. 77—16512
Pt microcell, for radioiodination of polypeptide hormones 79—48340
Pt, on C electrode, surface area loss in H_3PO_4 80—101091
Pt, oxide layers on electrode surface anisotropy of optical props. 80—60534
Pt, powdered, aggregation in disperse system 79—11830
Pt, spectrophotometry during electrolysis 79—74395
Pt surface, anodically polarised, ^{147}Pm deposition 78—27424
Pt, surface stress curves, electrocapillarity type curves 79—61866
Pt/ZrO_2 porous electrode/solid electrolyte system, interface polarisation effects 80—61114
Pt-electrolyte interface, electron states, photoemission studies 78—85171
Pt-electrolyte interface laser speckle movements related to electrode pot., H_2 adsorb. 78—40052
Pt-graphite, for biamperometric iodometric determ. of metals 77—70359
Pt-Mn(III)-porphyrin electrode for possible wet solar cell 79—100529
Pt-Ti bielectrode use as insoluble anode in electroplating 77—44490
ReO_4^-, liquid electrode, anal. appl. 79—16073
rotating Ni cylinder, mass transfer investigation 79—43589
Ru electrodes, adsorption and surface reactions, cyclic voltammetry and X-ray emission spectrometry 78—61018
RuO_2 anodic coating on Ti, struct., electrochem. props. *(French)* 79—83385
RuO_2 porous powder electrodes, proton diffusion meas. 80—54436
RuO_2-based anodes, electrochem. props 79—96332
RuO_2-TiO_2 anode, wear-resistant, use in applied electrochem. 80—40701
RuO_x, catalyst at anode of solid polymer electrolyte cell, corrosion 79—20376
RuO_x working electrodes in nonaqueous solvents, props. 79—91960
S, dynamic, in Na-S cell, electrical characts. obs. 79—100515
S electrode performance in Na-S battery 79—29463
S, miniature electrode, recharging characts. in two liquid phase region 80—26127
S^- ion-selective electrode, sensitivity, surface heterogeneity effects 78—92526
Sb thin film, pH sensitivity and electrode potential *(Japanese)* 79—39159
Sb-Sb_2O_3 pH electrode improvement 79—53270
Sb-SbO_x electrode sensor for continuous transcutaneous meas. of PCO_2 77—13020
Se, amorphous, anomalous currents during electrodeposition 77—44486
Si, carrier conc. determ., electrochem. method 78—60200
Si, ion implanted, in HF electrolyte, characterization by electrolytic reverse current 78—6078
n-Si, passive, complete activation initiation by local photoactivation 79—100403

electrochemical electrodes continued
Si:H, amorphous, photoelectrochem. behaviour 80—81480
Si-NH_3 electrolyte interface, photo-assisted electron injection 79—87152
Si-SiO_2 electrode, electronic cond., luminesc obs. 80—61111
Si-SiO_2 interface props., electrolyte anode polarisation effect 77—80849
SiC, electrode and container material in Na/S cell 80—35355
Sn, potentiostatic polarisation in NaOH soln., XPS 77—90608
Sn/Te/electrolyte system, interface processes 77—63923
SnO_2, effect of DC on corrosion in lead glass melt 80—85075
SnO_2 electrodes, dye-modified, erythrosin, attachment, X-ray photoelectron, photocond. investigs. 79—43600
SnO_2, of totally illuminated thin-layer Fe-thionine photogalvanic cell, electrodic phenomena 79—20374
$Sr_{0.5}FeS_2$ cathodes for nonaqueous Li batteries 80—3506
$SrTiO_3$, appl. to H_2 using solar energy and TiO_2 electrode *(Czech)* 77—29014
n-$SrTiO_3$ electrode, flatband pot. determ. from differential stress meas. 80—75638
$SrTiO_3$, electrode, photoelectrolysis of H_2O, solar energy conversion 79—52959
$SrTiO_3$, photoanode water photoelectrolysis at high current density 78—15679
$SrTiO_3$, photoelectrolytic, defect surface states obs. 78—14815
$SrTiO_3$ semicond. electrode, electrochem., photoelectrochem. props. 80—3352
$SrTiO_3$ semicond. electrodes, electroreduction process kinetics, cathodic dark current meas. 80—66807
$SrTiO_3$, transition metal doped anodes for water photoelectrolysis, response to visible and UV 79—74531
Ta, corrosion resistance in 1M $LiAsF_6$/THF, suitability for organic electrolyte Li secondary batteries 79—100387
Ta electrode, anodised, meas. of electrochem. reactions, appl. to time stimulation 78—95931
Ta-Pt, electrospark alloying for obtaining stable effective electrodes *(Russian)* 79—39157
Ti anode, with RuO_2-TiO_2 active film, Cl overvoltage, γ-irrad. effects 79—16005
Ti anodic dissolution in electrolytic machining *(Russian)* 79—83463
Ti, corrosion resistance in 1M $LiAsF_6$/THF, suitability for organic electrolyte Li secondary batteries 79—100387
Ti film electrode, oxidation, electrochem. and surface analytical characterisation 79—39034
Ti in acidic chloride solns., anodic dissolution and passivation 80—35541
Ti/RuO_2/MnO_2 electrode, anode characts. 78—68897
Ti-Pt, electrospark alloying for obtaining stable effective electrodes *(Russian)* 79—39157
Ti-RuO_2 anode; electrochem. stability 79—70346
TiH_x film electrode, oxidation, electrochem. and surface analytical characterisation 79—39034
TiO_2 (rutile) photoanode, corrosion suppression by high-energy redox reactions 78—23163
TiO_2 anodes, corrosion suppression by high energy redox reactions 77—77599
TiO_2, appl. to H_2 using solar energy and TiO_2 electrode *(Czech)* 77—29014
TiO_2 doped polycrystalline electrodes, for photo-assisted electrolysis of water, spectral response 79—29370
TiO_2, doping processes, influence on photoelectrochem behaviour 80—79822
TiO_2, electrochem. doping 77—76430
TiO_2 electrode, chem. modification for dye sensitisation, rel. to H_2O oxidation 79—91964
TiO_2 electrode, doping density dependent attachment of rhodamine B 80—54777
n-TiO_2 electrode, flatband pot. determ. from differential stress meas. 80—75638
n-TiO_2 electrode, near UV photon efficiency, H_2 prod. from solar energy 77—11956
n-TiO_2 electrode, photo-oxidation of acetate and iodide 80—81331
TiO_2 electrode, photoelectrolysis of H_2O, solar energy conversion 79—52959
n-TiO_2 electrode in $AlCl_3$-NaCl melt, electrochem. and photoelec. props. 80—81328
n-TiO_2 electrode in photoelectrochem. cell, anomalous photoresponse 77—11998
TiO_2 electrodes, chemically modified, nature of surface states 80—107905
TiO_2 electrodes, in aq. electrolytes, surface states, photocurrent obs. 80—49895
TiO_2 electrodes in photoelectrochem. cell, photothermal effect 80—7947
TiO_2 films as solar photocatalysts, preparation 79—74530
TiO_2 photoanode, water photoelectrolysis at high current density 78—15679
n-TiO_2 photoanodes, corrosion suppression mechanism 80—2462
TiO_2, reduced anodes, photoelec. props. 79—28371
TiO_2 semicond. films for water photoelectrolysis 80—26146
TiO_2, sensitised, photoelectrolysis of water in sunlight 78—19143
TiO_2, silanisation effects on semicond. props. 79—96364
TiO_2, solar energy conversion, photocatalytic prod. of H_2 77—1932
TiO_2, transition metal doped anodes for water photoelectrolysis, response to visible and UV 79—74531
TiO_2:Al(Y), polycrystalline photoanode, improved solar efficiency 79—96479
n-TiO_2:Be electrodes, photoassisted oxidation of water 80—30502
TiO_2:H photoanodes, diffusion and surface chemistry 80—35546
TiO_2:Nb semicond. electrodes, electroreduction process kinetics, cathodic dark current meas. 80—66807
TiO_2:Si(Fe)(Ni)(Mn)(Cr), anodes, performance in photoelectrolysis of water 79—74407
TiO_2-NH_3 electrolyte interface, photo-assisted electron injection 79—87152
TiO_2-RuO_2 anode, wear-resistant, use in applied electrochem. 80—40701
TiO_2-Si solar cell hybrid electrodes for photoelectrochem. H prod. 80—45775
TiS_x, cathodes in secondary Li batteries, operating characts. 77—86320
$Ti0_2$ electrodes, effect of processing variables on photoelectrochem. props 80—6975
$Ti0_2$ electrodes, room temp. diffusions, capacitance, spectral response and volt-ampere characts. 80—15294
U_3O_8-Y_2O_3(Sc_2O_3), solid soln. electrode, high temp. electrochem. appl. 80—6828

electrochemical electrodes continued
- V_2O_5 cathode, used in Li-V_2O_5 reserve cells, microstruct. optical reflectance, elec. cond. meas., chem. anal., SEM obs. 79−43752
- V_2O_5 electrode, anodic dissolution in aq. acid soln. *(German)* 79−91826
- V_6O_{13}, cathode materials for secondary Li cells 79−92073
- WC anode, performance in fuel cells with H_2SO_4 electrolyte 80−21293
- WC gas diffusion H_2 electrodes, activity composition influence 79−52925
- WO_3 anode, props. and appl. to photoelectrolysis of water 77−66757
- WO_3, electrochem. and photoelectrochem. behaviour 78−26949
- WO_3 electrode, surface growth of ternary compds., in electrolyte containing redox couples 78−61016
- WO_3 electrodes, electrochromic processes, digital simulation model 80−76518
- WO_3 layers, semiconductor electrodes, electrochromism and photoelectrochemistry 80−35544
- WO_3, semicond., influence of surface states, impedance meas. *(French)* 77−1468
- WO_3, vacuum evaporation and anodic oxidation prep., electrochromic process kinetics 79−100390
- WSe_2 d-band semicond., photoelectrochem. props., electrochem. solar cell appl. 79−66411
- $YFeO_3$ photoanode for photoelectrolysis of water 77−81409
- Y_2O_3, film, anodic glow in Y-Y_2O_3-electrolyte system 77−12447
- Zn, concentration changes during cycling 80−35666
- Zn electrode, passive film form. by chrono-ellipsometry *(Japanese)* 78−68900
- Zn, electrode, single crystal, fracture surface charge density effect 78−68787
- Zn, electrode in alkaline soln., exam. of surface state by potentiodynamic voltammetry 80−85187
- Zn electrodeposition, inhibited, electrode kinetics and deposit morphology 79−56089
- Zn, shape change resulting from cell cycling, quantitative study 79−43591
- Zn/$ZnSO_4$/Zn system, laser interferometric study of corrosion of coated and uncoated metals, technique standardisation 79−35815
- Zn-AgO cell, Zn electrode slurry-paste fabrication optimisation 79−96430
- Zn-Cl_2 battery, half-cell overpotential measurements 80−21393
- Zn-pore electrodes and cells, operation 80−26126
- Zn-tetraphenylporphine/metal electrode, photocurrent generation mechanism 78−76868
- ZnO electrode, in aq. soln., phototransition at 380 nm, anodic photocurrent obs. 78−19145
- n-ZnO electrode, photoelectrochemical behaviour in acetonitrile solns. 78−31644
- ZnO electrode, reson. Raman spectra of adsorbed rose bengal 78−76446
- ZnO electrode, role of triplet states in xanthene dye sensitisation 78−76869
- ZnO electrode surface, dye sensitisation mechanism, from reson. Raman spectrum obs. 78−42066
- ZnO, single cryst., adsorption of rhodamine B 78−31645
- ZnO surface, photocell, enhancement of photoelec. effect by organic additives 79−57437
- ZnSe electrode, electrochem. behaviour *(French)* 79−52676
- ZnTe single crystal electrodes, non-intentionally doped, electrochem. props. *(French)* 79−96326

electrochemical machining *see electrolytic machining*

electrochemical polishing *see electrolytic polishing*

electrochemistry
- *see also Debye-Huckel theory; electrical conductivity of electrolytic liquids; electrochemical analysis; electrochemical electrodes; electrolysis; electrolytic devices; electrophoresis*
- absolute electrode potentials, determ., concepts and theory 79−5161
- absolute electrode potentials, determ., theory 79−5160
- acetate, aq. soln. current-potential curve, influence of NO_3^-, SO_4^{2-}, PO_4^{3-} and Cl^-, obs. *(Japanese)* 78−85172
- acid, weak, ionisation in aq. soln., rate const. meas., elec. field jump method errors 79−43611
- acousto-electrochemical effect 79−96331
- adhesive joint failure, adhesive/electronically conducting substrate, exam. of electrochemical aspects 78−60979
- adsorbed molecule, Raman scattering 80−60563
- alcohols, electrochem. oxidation, kinetic isotope effect *(German)* 78−15681
- alkali metal-molten salt mixtures, thermal EMF calcs., Rice and Pitzer models 78−20057
- N-alkylpyridinium salts, electrochem. reduction, radical form., INDO calcs., EPR obs. 77−71821
- bacterial flagella rotation rel. to ion transport down electrochem. gradient 77−73515
- bacteriochlorophyll *b* and pheophytin pair redox potential obs. 79−39338
- bilayer membranes, elec. surface props., asymm. charge effects 77−32805
- binary liquid alloys, electrode pot., rel. to intermetallic compound content 78−9940
- bioelectrochemistry and bioenergetics (book) 80−8749
- bipolar cell stacks. leakage currents, simulation program 80−76526
- bipolar trickle reactors, electric current versus potential plots 80−76521
- bipolar trickle reactors, flow models for hydrodynamic characts. and reaction rate constants, 80−76522
- bipolar trickle reactors, study using electrochemical tracer method 80−76523
- bone healing, use of anodised Ta electrode, meas. of electrochem. reactions 78−95931
- book, undergraduate level, for teachers 78−8196
- calculations, programmable microprocessor-linked calculator appl. 79−43592
- carboxylate, aq. soln. current-potential curve, influence of NO_3^- and SO_4^{2-}, obs. *(Japanese)* 78−85173
- cathodic materials in I_2-Ag current source, compatibility with solid electrolyte $RbAg_4I_5$ 77−40555
- cathodic protection for small plant, economic method *(German)* 80−100943
- cathodic protection of pipeline systems, spline function method for polarisation effect calc. *(Russian)* 78−31566
- cathodic reaction during localised corrosion, theoretical model of location 79−70337

electrochemistry continued
- cation-exchange membranes, electrochem. props. rel. to interfacial polarization during electrodialysis 79−16038
- cell, AC component effect on convective diff. processes, characts. 77−63929
- cell processes, geometrical and spatial orientational effects, computer calcs. 77−32804
- cells, electrochemical, photovoltaic phenomena and mechanisms 78−8198
- chalcopyrite, NH_3-oxidation leaching, reaction kinetics 77−52639
- chalcopyrite, NH_3-oxidation leaching, surface deposit effects 77−48643
- chalcopyrites, acidic fermic sulphate leaching, reaction mechanism 79−83511
- charge transfer reactions in biological systems, mech. of coupling 80−76889
- charged, surface pressure, electrostatic contrib. of divalent ions 79−24752
- charged plates interaction in electrolyte soln. 79−43595
- chemical wave equation for ionic system reactions 78−15653
- chemical waves, multiple, induced by electric field 79−92047
- chlorophyll, adsorption films, electrochem. behaviour 78−31778
- chlorophyll in aqueous solns., electrochem. behaviour, cathodic reduction 79−29373
- chlorophyll monolayer electrodes, light energy conversion, photosynthesis electrochem. simulation 79−43833
- cholesteryl caprylate solns. in decane, crystn., electrogravitational effect 77−62496
- chronopotentiometry, convolution procedures for faradaic information extraction, fluorenone reduction appl. 77−25278
- coal, anodic reaction for metal electrowinning energy consumption reduction 79−91965
- cobalt phthalocyanine, electrochromism and oxidation 80−93768
- concentration-cell electrochemical convertors for seismic registering device, data readout 77−2287
- condensed adsorption layers, effect on electrode reaction rates 80−93769
- conference, Electrochem. Society fall meeting, Las Vegas, USA (Oct. 1976) 77−16831
- conference, electrochem. society fall meeting, Las Vegas, USA (Oct. 1976) 77−77787
- copper phthalocyanine film, photoelectrochem. behaviour on SnO_2 electrodes 80−15626
- coronene trimer radical cation, spin densities in CH_3Cl_2-CH_3NO_2 solvent mixture, −100°C 80−5565
- corrosion, kinetics anal. 79−96335
- corrosion, potentiostat meas. appls. 79−96237
- corrosion of metals and alloys, corrosion conditions simulation in crack-like defects using electrochemical cell *(Russian)* 79−52445
- corrosion pit, convective diffusion 80−40601
- corrosion rate measurement, with dual electrodes 80−85180
- corrosion studies, electrochemical methods, appl. and limitations *(Japanese)* 80−45465
- corrosion system, linear polarisation equation 78−48661
- corrosion theory, rel. to protective coatings 78−19918
- coulometry, potential scanning, chem. react. appls. 77−25281
- coulostatic impulse technique, review 78−73048
- coupled fluxes, concentration distributions near electrodialysis membranes 79−47974
- coupled homogeneous chemical react., kinetics, modified double pulse technique 77−25280
- crystal-electrolyte interface, pot. drop effects on surface at. electronic levels 78−19123
- current and potential distrib. calcs. 77−21394
- current distribution cell for qualitatively predicting differences in barrel plating performance of electroplating solutions 80−71917
- current source, exergetic efficiency 77−44488
- current-pot. curves discontinuities in solid electrolyte systems 80−24660
- cyanine dye monolayer/p-chloranil crystal, charge carrier injection rate const. determ., energy transfer vs. charge transfer method 79−83031
- data interpolation, fast Fourier transform method 79−16061
- diffuse charge region in thin layer cells 78−40054
- diffusion, boundary value problems, orthogonal collocation calcs. 78−40053
- diffusion, to spherical and cylindrical electrodes, Cottrell eqn. corrections calcs. 78−48658
- diffusion coefficient and number of electrons taking part in reaction, separate determ. 77−25284
- diffusion coefficients, determ. using pipe wall electrode 79−14947
- diffusion controlled electrochemical processes, mass transfer rate, drag reducing additives effects 79−43593
- diffusion layer theory, exptl. test 78−35701
- discontinuous systems, general inequality for irreversible processes 80−55676
- discrete stochastic electric double layer, electrostatic props. 79−96318
- discreteness-of-charge effects, and ion distrib. near interface 79−100399
- discreteness-of-charge effects, in inhomogeneous dielectrics 79−100400
- displacement reactions, electron microscope obs. of nucleation and growth, comparison of Cu/Fe and Cu/Al cementation systems 79−47939
- dissolution of metal rotating disc, in concentrated solns. *(Russian)* 77−56232
- double potential step electrochemical mechanisms, simplex fitting and finite difference simulation anal. 78−44381
- double-layer structure, electrohydrodynamical determination 78−95960
- duroquinone, soln., electrochem. props. obs. *(French)* 79−66301
- dye laser, broadband tuning using electrochem. reactions 78−9397
- dye laser tuning range extension using electrochem. reaction products 79−31895
- education, chemical, osmotic and electrochemical equilibrium, principle of virtual work 77−33767
- electric cells, metal/β-alumina/metal, complex admittance diagrams, grain boundary effect *(French)* 80−45653
- electric double layer, primitive models, pot. difference and charge density 80−76515
- electric double layer capacitance meas., potentiostatic method 78−85169
- electric double layer capacity, chronopotentiometric meas., reversible electrochem. reaction effects 78−80753
- electric double layer theory, modified Poisson-Boltzmann eqn., numerical soln. 80−3356
- electrical double layer, ion adsorpt. and discrete charge effects, self-consistent calcs. 80−76516
- electrical double layer, props., nonlinear AC methods obs. 78−3345
- electrical double layer theory, through Born-Green-Yvon eqn. 80−35539

electrochemistry continued
- electrical double layers, repulsive electrostatic interaction, statistical mech. theory 80−92432
- electrocapillary acceleration meters, electrolyte composition selection 80−73331
- electrocapillary acceleration meters with electrolyte in gel form 80−73330
- electrocapillary curves, automatic meas. eqpt. 78−40061
- electrocatalysis, radiotracer method investig. appls. 80−70525
- electrocatalytic O_2 evolution on reactively sputtered electrochromic IrO films 80−26125
- electrochemical mass transfer, drag-reducing polymers, effects, comparative study 80−76528
- electrochemical overpotential phenomena, appls. 78−64846
- electrochemical processes with free convection, numerical simulation 79−52681
- electrochemical reactor characterisation, marker pulse method improvements 80−76524
- electrochemical reactors with three-dimensional electrodes, characterisation using electrochemical tracer method 80−76520
- Electrochemical Society Meeting, Boston, USA, (May, 1979) 79−91959
- Electrochemical Society Spring Meeting, Philadelphia, USA (1977) 78−6837
- electrochemiluminescence reactions, background electrolyte effects *(Russian)* 78−7209
- electrochromic cell using solid proton conductor electrolyte, $HUO_2PO_4.4H_2O$ 80−89497
- electrocrystallisation, twinning nucleation, mechanism 77−62495
- electrode and spectroscopic processes correlation 79−96329
- electrode potential, meas., optimum capillary, tip-electrode distance 78−20028
- electrode potentials 79−43599
- electrode process research instruments, electrochemical appls. 78−21174
- electrode processes possessing charge transfer mechanism, overvoltage theory, in book, for teachers 78−8204
- electrode reaction kinetic parameters, programs for computer retrieval, in FORTRAN 78−31654
- electrode reactions, quantum mech. calcs., electrode surface struct. 77−16828
- electrode systems, nonequilib. polaris. states props. overvoltage theory, in book, for teachers 78−8205
- electrode-binary electrolyte systems, transient processes, equivalent cct. calcs. 79−70347
- electrode-electrolyte interface, solid film props., review of expt. techniques 77−77780
- electrode-electrolyte interfacial phenomena, solid electrolyte 77−77782
- electrodes in solution, electron transfer, review, in book, for teachers 78−8203
- electrodialysis polarisation, rotating disc studies 79−47933
- electrodiffusion problem solution for arbitrary system of singly charged ions 80−21300
- electrogenerated chromophores, electrochemical conc. profiles, mass transfer, charge transfer, laser absorpt. spectroelectrochem. obs. 80−40765
- electrolyte-vapour-solid system, equilib. calcs. *(French)* 80−3360
- electrolytic capacitors effect of electrical parameters of Al foil capacitors *(Polish)* 80−30245
- electrosorption valency, partial charge transfer coeff. 79−96334
- ellipsometry of electrochem. surface layers 78−56874
- energy considerations 78−88643
- energy conversion analysis *(Dutch)* 80−72019
- energy use optimisation *(Dutch)* 80−72020
- equilibrium and nonequilibrium states, electron transfer and multiple electrode problems *(French)* 78−27777
- excited electronic state, photoelectrochemistry 78−76872
- Faradaic impedance expt. meas. anal. prog. 80−11894
- fast electrode reactions, kinetics meas., galvanostatic double-pulse method 77−25268
- fast ionic conductors, review, device appls. 78−51724
- fast processes, use of high speed electronic memory for data acquisition *(Italian)* 77−9088
- first order reaction, reversible pot. and rate const., chronoamperometric determ. 78−61086
- fixed-bed electrodes, three-dimensional, mass and charge transfer *(French)* 80−71920
- fluorenone derivatives as electron transport materials, electron affinity and electrochemistry, rel. to photocond. 79−38127
- flux equations, solns. with variable diffusion coeff. and transference number 78−48666
- free convection mass transfer from horizontal surface, electrochemical and holographic interferometric obs. 78−87344
- fused salt systems, solid films and interfaces, review 77−77783
- galvanic corrosion control, new methods 80−40598
- galvanic current meas. instrumentation, function of velocity of metal electrolyte 77−10040
- gas evolving electrodes, mass transfer data correl. model 79−79258
- gas-electrolyte dispersions, void fraction meas. using conductivity method 80−76525
- gas-liquid interface, mass transfer, ultramicroprobe method obs. 78−63901
- generalised surface-layer model calculations, refinements 78−3348
- glass, molten, reactions with conducting materials 80−85186
- glass-electrolyte solution interface chemistry 79−79256
- glycerol monooleate bilayers, photoinitiated mediated transport of OH^- and H_3O^+ 79−88059
- graphite, electrochemical insertion of $BF_3(C_2H_5)_2O$ *(French)* 78−27438
- graphite+O_2 reaction, standard Gibbs free energy change, electrochemical determ. 77−29041
- graphite $AlCl_3$ intercalation compound, electrochem. characterisation method 80−55666
- graphite intercalation cpds. with H_2SO_4 and sulphuric oleums, elec. resist. evolution 80−45518
- heat and mass transfer rates at high Pr, electrochemical modelling 78−83383
- heat transfer, between cylinder and rising two-phase flow, electrochem. method 77−55076
- Helmholtz layer model diffuse layer, discreteness of charge effect calcs. 80−26030
- heterogeneous catalysis, conference, Varna, Bulgaria (Oct. 1979) 80−82578
- 1-hexene-water(-D_2O), field-induced surface reactions, field ionis. mass spectra obs. 78−95949

electrochemistry continued
- HPLC detection systems, review 78−48733
- hydroquinone, oxidation of centre of photographic development, electrochem. kinetics *(Russian)* 80−3367
- III-V semiconductor, anodic oxide film formation, current flow mechanism 77−90479
- III-V semiconductors, electroliquid epitaxy, role of electrotransport 79−56095
- impedance meas. method, automatic, computerised data anal. 77−70307
- impedance meter, high-speed, for electrochem. system obs 79−30490
- impedance parameters for electrochemical systems exhibiting pseudoinductance 79−66303
- impedance simulation, by AC ladder networks 77−12806
- impurity ion adsorpt. process on reactant transfer processes 80−45519
- indifferent salts, acid conc. aq. solns., H evolution at Hg electrode 78−53215
- individual ionic activity coefficients, determination, theory 78−20059
- instrumentation 80−71916
- interfacial impedance of graphite electrode/graphite-βZnS mixture electrode in acidic aq. soln. *(Japanese)* 77−52648
- interfacial tension, electrochem. data numerical differentiation by Fourier transformation 78−41139
- internal reflection method in visible region applic. to electrochem. reactions investig. 77−60069
- iodide, charge transfer to solvent spectra, spectral shift data, Madelung const. determ. 80−85204
- ion distribution in diffuse part of double layer, discreteness of charge effects 80−21301
- ion electrostatic interaction at electrode surface, ion field penetration 80−81333
- ion exchange membrane selectivity w.r.t. dialysis prospects 80−45560
- ion implantation, chemical and electrochem. aspects, review 80−100271
- ionic mass transport, cathodic gas evolution influence 79−34323
- ionic surfactants, conductance stopped flow study of micellar equilibria 79−43642
- irreversible chemical process, in elec. field, heat and mass transfer 78−11545
- kinetic model for renewal of the elements of a set leading to stable space segregation 79−20373
- kinetic parameter meas. *(German)* 79−52690
- kinetic parameters and double-layer capacity, simultaneous meas. instrument 80−40704
- kinetics in systems without supporting electrolyte, at interface with space charge layer, appls. *(German)* 77−32807
- laser-induced photoelectrochem., photoemission related currents depend. on laser characts. 79−20390
- latent and sublatent images, alternation of electrochemical props. 79−20405
- layer of symmetrical spherical dipoles, Poisson-Boltzmann treatment of capacitance 78−64844
- Leclanche cell, impedance spectrum of an undischarged cell 80−89604
- liquid crystal, nematic, electrode reactions control using dopants, Kerr meas. *(French)* 80−11898
- liquid crystal/metal interface, elec. double layer, statistical equilib. state 80−40708
- liquid metal electrode, polarographic max. current theory, electrochem. and hydrodynamic instability 79−24750
- liquid metal electrode, polarographic max. current theory, hydrodynamic instability 79−24749
- magenta pyrozolone azomethine dye, electrochemistry of fading mechanism 79−24761
- magnetite electrochemical polarisation in surfactant solns. *(Russian)* 79−83465
- matrix electrolyte cell, electrode-compressed diaphragm contact, props. 77−32802
- measurement system using phase-sensitive detector, control circuit *(Spanish)* 80−55671
- measurements and surface studies on acid oxygen carbon electrodes, ESCA method appl. 78−31651
- mechanisms studied by parameter sensitivity functions and zone diagrams *(French)* 78−88638
- membrane potentials measurements 80−3411
- membranes, cation exchange, voltage against current curves 79−96365
- membranes, ion flow, step pot. change, conc., current responses 79−5177
- metal, electrochemical reaction on surface in aq. soln. 79−83387
- metal, surface layer dissolution, effect of rate on softening during plastic strain 78−39957
- metal dioxides, pure and mixed, conductivity meas. by new method 80−45517
- metal ion electroreduction, ion-induced adsorpt. 80−21297
- metal ultrathin foils, laser monitored electrothinner *(German)* 79−34219
- metal-cellulose-metal sandwich system, spontaneous elec. current induced by heating 80−40700
- metal-inactive electrolyte interface, double layer capacity 79−43598
- metal-ionic crystal-Cl^- system, charge transfer mechanism 78−11527
- metal-polymer deposit, simultaneous electrophoretic deposition and electrochemical precipitation 79−56938
- metal-water systems at elevated temps., thermodynamic props. 78−76898
- metallic binary alloys or compounds, cathodic deposition and characterisation 79−69998
- metallic films, vapour deposited on polymer, ageing, adhesion, elec. cond., electrochem. pot. *(Russian)* 79−33362
- metallic oxides used as battery cathodes or electrocatalysts, electrochemical behaviour 80−45516
- metals, electrochemical surface treatment method for reducing H_2 absorption *(Russian)* 79−15858
- metals, electrocrystallisation and passivation kinetics, multiple stationary states and dissipative structs. theory *(French)* 80−7804
- metals, scaling, theory, electrochem. transport model 78−64761
- metals in molten salts, recording coulometer for controlled-atmosphere reactions 78−3344
- methods for determ. of kinetic props. of solids, book contrib. 79−65251
- methyl methacrylate natural rubber latex copolymer, electrochemical initiation 77−55936
- MHD phenomena in electrolytes, heterogeneous processes kinetics control *(Russian)* 78−27768
- migration currents description method, Heyrovsky method analysis 79−100404
- mixed electrolytes, conductance, relax. terms 78−67840
- multicomponent impedance diagrams, resolution technique 80−66959

- **electrochemistry** continued
  - multicomponent systems, phase diagrams and thermodynamic data, electrochem. determ. 80—71922
  - multifunctional chronopotentiometer for electrochemical studies 77—81413
  - multiply connected region, iteration process for calc. of elec. fields 77—81412
  - nematic liquid crystal, DC dynamic scatt., flow direction rel. to dopant electrochem. props. 77—90130
  - nematic liquid crystal DC dynamic scatt. microscopic structure and role of dopants 77—77179
  - nerves, electrochem. theory, steady and transient pots., in book, for teaching 78—8202
  - nervous system stimulation with Pt electrodes electrochem. reactions, safety 77—21659
  - nonisothermal, conf. Zurich, Switzerland (Sept. 1976) 78—20021
  - nonisothermal system, thermal diffusion, thermodynamic theory 78—20056
  - nonisothermal systems, individual activity coeffs., electrochem. meas. method 78—20058
  - nonpolar molecules, ionis. by alkali ion attachment at electrolyte surface 78—65998
  - nontransition metals, electronegativity parameters of theory of heats of alloy form. 79—74412
  - nuclear track emulsions, electrochemical etching of fast neutron induced recoil tracks in cellulose triacetate 80—91406
  - ohmic potential drop, rel. to crit. pitting and protection pots. 78—72900
  - optical experimental methods 78—20022
  - organic electrochemistry, progress, 1952-77, review 77—60078
  - organic ionic melts, novel class of liquids 77—35463
  - organic laser dyes, electrochemiluminescence, electrochem. oxidation, reduction 77—70304
  - organic surfactant molecules reorientation on electrode surface, electrochem. kinetics 80—45522
  - oscillations, of voltage and current, spontaneous, maths. anal. of mechanisms, in book, for teaching 78—8201
  - overvoltage theory, nonequilib. thermodynamics appls. 77—40550
  - passivating film formation, stability and breakdown 78—19937
  - passive layer, on Fe electrode, semiconductor model, appl. to electrochem. reactions, review 80—26022
  - PDK potentiostat for electrochemical investigations 79—70345
  - pentyl-cyano-biphenyl, nematic phase, transport props. of dissolved ionic species, electrochem. meas. *(French)* 79—90811
  - percolation problem for lattices of bonds, sites, perforation points, graphical technique 77—63954
  - phenomenological equations of electrokinetic processes, effect of electrochem. processes 79—70330
  - photocell using covalently-bound dyes on semiconductor surfaces 77—4393
  - photochemical diode using p-n heterojunction or Schottky barrier immersed in electrolyte 77—66201
  - photoelectrochemistry, laser sources use for solar energy conversion 80—40873
  - photoelectrophoretic imaging, mechanisms 79—24758
  - photoemission-into-electrolyte, for Au and Ag surfaces 79—74390
  - photographic developer activity, rel. to difference of electrochem. and redox potentials *(Russian)* 78—62243
  - photographic development, electrochem. models 79—52697
  - photographic development rate, effect of developer ion charge 79—24753
  - photographic fixing solution, Ag^+ ion electrochem. removal using porous flow-through electrode 77—60076
  - phthoralocyanin porous films, Becquerel photovoltaic effect 77—16907
  - Physarum polycephalum, true slime mold, surface membrane simulation using liquid ion-exchange membrane *(Japanese)* 78—31781
  - pit growth, convective diffusion in pits, ionic components conc. calc. 80—45409
  - plastic foils for neutron dosimeters, electrochem. etching prep. techniques 79—76298
  - polar liquid, electric double layer at surface 78—53212
  - polar solvent molecule interactions in the adsorbed state 80—21299
  - polarisation curve-fitting by computer modelling 79—96316
  - polarisation resistance meas. for accurate rate determ. 78—31562
  - polycarbonate foil electrochemical etching for dosimetry, bulk etching rate evaluation 78—78506
  - polydicarboxylic acids, electrophoretic and viscometric props. 80—66811
  - polyelectrolyte ion binding, Poisson-Boltzmann eqn. 80—45511
  - polyethylene membrane (graphite charged) electrode, electron transfer *(French)* 78—27778
  - polymer film coatings on metal electrodes, through electroinitiated polymerisation 77—77632
  - polymer solutions, turbulent, mass transfer rate, frictional force *(French)* 79—37357
  - polypyrrole films, electrochemical prep., chem. and phys. characterisation 80—70708
  - polystyrene sulphonic acid, charged membrane, electroosmosis and streaming potential *(Japanese)* 78—31696
  - porous electrode diffusion controlled operation, mass transport with memory 80—21298
  - porous electrodes with poorly soluble reactants, process distrib. 79—61870
  - porphyrin-water interface, photoinduced charge separation 77—81408
  - potential-pH diagram, improved algorithms for computer generation, max. constriction method 80—26019
  - potentiostat, electronic instrument for electrochemical kinetic measurements 80—105675
  - potentiostat, microprocessor controlled, for electrochem. meas. 79—85133
  - potentiostat, rapid response, construction, operation and evaluation 79—52678
  - potentiostatic etching method for intercrystallite corrosion testing of stainless steel 78—7113
  - potentiostatic measurements, automatic resist. polarisation compensator 77—21393
  - Pourbaix's thermodynamic diagrams, redox pot. 79—96336
  - power production and storage, future needs, and developments 78—8197
  - power sources and energy science 80—101023
  - primary cell systems without liq. junction, use of central connectors 78—8199
  - production by Westinghouse electrochem./thermochem. S-cycle process 80—45808
  - PTFE, anisotropic electrochemical attack 79—39004

- **electrochemistry** continued
  - PTFE/graphite bond in H_3PO_4 environment, electrochemical exam. of joint failure 78—60979
  - quantum mechanical kinetics problems, averaging principle, degenerate states and reson. effects 78—19996
  - quantum mechanical kinetics problems, averaging principle appls. 78—19995
  - quinoline derivative, interaction with coenzyme Q_{10} 79—91948
  - reaction intermediates, at rot. disc. electrodes, spectroscopic obs. 78—53210
  - reaction kinetics, discreteness-of-charge effect, electroreduction in double layer 77—32803
  - reaction kinetics, in presence of surface-active substances, eqn. selection 79—34322
  - reaction sequences, criteria for selective path promotion 80—26018
  - reactors, dimensioning, with three-dimensional electrodes, mass transfer phenomena *(French)* 80—71921
  - recovery of metal ions from dil. solns., design geometries for fixed flow-through packed beds 77—16833
  - redox reactions, Franck-Condon approx. 77—1929
  - reduced Ni oxide, H absorption 80—76529
  - reference electrode arrangement, high temp. polarisation study 78—64845
  - refractory oxide layer growth by high-temp. electrochemical vapour deposition 78—23627
  - resistive electrode current density distribution 80—21302
  - retardation of electrolytic mass transport in collinear electric-magnetic fields 80—104443
  - reverse pulsed polarography, reversibility characterisation, electrode reaction product determ. 80—66889
  - reversible galvanic cell, thermodynamics, EMF rel. to temp. 77—1935
  - rhodamine B, adsorption on ZnO single crystal, photooxidation, electrochem. meas. 78—31645
  - rose bengal, electron transfer to TiO_2 electrodes, photoelectrochem. meas. 77—66758
  - rotating body in Ostwald fluid, rate distrib. near wall, electrochem. methods *(French)* 77—42847
  - rotating disc electrode mass transfer, appl. of pulsed voltage and pulsed current 80—21292
  - rotating disc-ring electrode equipment, automated, appls. 78—95933
  - seawater, electrochemical potential of pure metals *(Chinese)* 80—31062
  - seawater deaeration procedure for conducting electrochemical expt. 79—29366
  - secondary cells, membrane appls. *(French)*· 78—3374
  - secondary cells, Ni-Cd, plastic-bonded electrodes positive active layer study 80—101088
  - secondary cells, Zn-Br, performance anal. in electric vehicle and utility applications 80—101086
  - secondary cells with C-air electrodes in alkaline electrolytes, ageing mechanism study 80—101087
  - self-organising neural net coherent electrochemical emission model *(Russian)* 78—27879
  - semiconductor electrodes, photoelectrode kinetics of H_2 evolution reaction 78—44388
  - semiconductor electrodes, photoinduced electrogenerated chemiluminesc. 79—91510
  - semiconductor p-n junction, conversion of chem. energy into elec. power thermodynamic props. 79—11219
  - semiconductor-electrolyte boundary, current flow, study of semicond. using electrochem. techniques 78—95356
  - semiconductor-electrolyte interface, photoelectrochem. processes, hologram recording utilisation 77—88667
  - semiconductor-liquid junctions, differential capacitance measurement by desk calculator controlled system 79—78170
  - semiconductors, binary, cathodic deposition and characterisation 79—69998
  - semitransparent rotating disc electrode, photochem. and electrochem. surface reactions 78—40056
  - sensitised photocurrents, temp. depend., electrochem. meas. 78—72205
  - sensors, species-selective, use of semi-permeable membranes, in book, for teachers 78—8200
  - single crystal surface, electrochemistry, surface struct., superlattice struct. 80—76519
  - slag-metal interface determination using electrochem. conc. element 78—7114
  - Smoluchowski equation, with Coulomb pot., appl. to fluoresc. quenching 78—73051
  - Smoluchowski equation with Coulomb pot., time-depend., soln. 78—73050
  - smouldering discharge at O_3 liq. surface in N_2, thin solid pellicle formation of N_2O_5 80—38827
  - sodium polyaluminate, impedance parameters in electrochemical cell, Mn ions effect 80—21296
  - sodium tetraphenylborate soln., electrolyte, steady state electrochemiluminesc. 79—57250
  - solid electrolyte cell using pt. electrodes, activity meas. in binary alloys *(French)* 79—61868
  - solid electrolyte cell using pt. electrodes, enthalpy of oxidation meas. *(French)* 79—61867
  - solid electrolyte electrochem. cells, V(I) characts. 78—35704
  - solid state, teaching approach 78—93498
  - solid state cells with $RbAg_4I_5$ electrolyte, contact between electrode and electrolyte, electrochemical investigation 80—76527
  - solid state chemistry of batteries, electrodes, and electrolytes, conference, Miami Beach, Florida, USA (Sept. 1978) 79—100393
  - solid state storage batteries, investigation 79—43754
  - solution-solid system, weak constant electric field influence obs. *(Russian)* 78—11522
  - solvated electron electrochemistry 77—16829
  - spectroelectrochemistry, light absorption at Pt electrode 79—74395
  - steady-state conversion rate rel. to surface reaction process, catastrophe theory 80—108717
  - steel, alloy, hardened, electrochem. characts. and stress corrosion cracking, ageing and cold treatment effects 80—108639
  - steel, austenitic stainless, AISI 304, stress corrosion cracking and electrochem. behaviour in $(NH_4)_2SO_4$-Cl^- solns. 80—55566
  - steel, austenitic stainless, Cr-Ni-(Mo), intercrystalline corrosion sensitivity, electrochemical determ. *(Czech)* 77—59989
  - steel, austenitic stainless, electrochemical behaviour in Ringer's soln., composition effects, SCC 77—90485

electrochemistry continued
  steel, austenitic stainless, stress corrosion crack growth, electrochem. aspects 80—97620
  steel, austenitic stainless, types 304L and 316L, work-hardened, electrochem. and corrosion behaviour in acid solns. 80—50757
  steel, C, potentiodynamic behaviour, in conc. NaOH, cyclic voltammetric obs. 79—16006
  steel, C, rotating disc electrode in 3 wt.% NaCl solution, corrosion rate meas. *(French)* 79—43470
  steel, Cr, ferritic, corrosion morphology, electrochem. pot. and Mo additions effect *(French)* 80—45439
  steel, high-strength 12KhN3A, anode and cathode processes in corrosive environment, fatigue *(Russian)* 78—35573
  steel, hydrogenation by cathode polarisation, controlling factors 77—52645
  steel, low-alloy, feasibility of electrochem. corrosion protection 79—70220
  steel, mild, adsorbed H distrib. rel. to electrochemical treatment in pure alkali 80—16589
  steel, mild, corrosion in complex aq. environment, linear polarisation investig. 78—76782
  steel, mild, cyclic strain enhanced dissolution in NH_4NO_3, corrosion fatigue props. 80—85083
  steel, notched specimens in sea water, endurance limit enhancement, specimen size, freq. effects 80—93678
  steel, passivation by sulphochromic soln. *(French)* 78—23869
  steel, stainless, 1Kh18N10T, solution annealed effect of cyclic stresses on corrosion rate in acid environments *(Russian)* 78—31577
  steel, stainless, austenitic, surface films grown in Cl^- solns., ellipsometric investig. 79—20261
  steel, stainless, cavitation-erosion in fresh water, electron microscope and electrochem. study 80—55580
  steel, stainless, ferritic, corrosion in formic acid at 70°C, effect of Mo additions 78—35551
  steel, stainless, pitting corrosion in chloride media, electrochem. aspects 80—61007
  steel, stainless 304L, stress corrosion morphology in H_2SO_4/NaCl soln. at room temp., electrochemical potential effect 78—15596
  steel, stainless intercrystalline corrosion, electrochemical testing method 80—55611
  steel, welded joints of tube 10G2SD, corrosion fatigue *(Russian)* 78—35574
  steel 45-antifrictional alloys friction pairs, electrochem.-mech. investigation *(Russian)* 80—76367
  steel electrodes, pitting corrosion currents rel. to conc. of inhibitive and corrosive anions under corrosion conditions 80—85181
  structural electrochemical series of standard potentials of elements in aqueous soln. *(French)* 77—32797
  sulphide ores, disseminated, electrochemical model of induced-polarisation phenomena 79—92526
  surface diffusion flux in Newtonian or nonNewtonian fluid, laminar flow, double pulse meas. *(French)* 78—40055
  surface processes, kinetics simulation 79—16004
  surface reacts. driven by linear pot. sweep, sequential reactions, kinetics 77—25276
  surface thermodynamics, Lippmann relation, electrocapillary theory 78—61048
  surfactant adsorption on metal surface, effect on electrochem. reaction kinetics 80—40703
  surfactant inhibition of electrochem. reaction rate, random error effect on characteristic parameters 80—40705
  symmetrical electrolytes, conductance, relax. terms 78—67840
  synthetic membrane cells, elec. relax., time-independ. rectification 77—90731
  terylene film, electret state prod. using electrochem. injection, adsorbed states, frozen field 79—91344
  tetrabutylammonium iodide/I solid/liquid electrolyte interface, impedance study 80—26031
  thermal battery, react. prods., electron probe anal. 79—43601
  thermal battery cells using molten nitrates as electrolyte and oxidiser 80—76624
  thin-layer cell, concentration impedance, unequal diffusion coeffs. and 2nd-order reactions effects *(French)* 78—53214
  thin-layer cell, concentration impedance reactive and nonreactive diffusion effects *(French)* 78—53213
  thin-layer cell, fast reaction, kinetic consts., diffusion and conc. impedance 78—73053
  three dimensional gauze electrode in new cell design, mass transfer enhancement by counter-electrode gases 79—43590
  track etching in plastic foils, for charged particle detect. 78—17521
  transition metal complex ion in aqn. soln. HCl, temp. effect on electrophoretic behaviour 79—24757
  transuranium cpds. in aq. soln., electrochem. 77—29040
  trifluoromethanesulphonic acid, and salts, electrochem. characts. in nonaqueous solvents 80—89499
  TSeF salts, mol. props., one-dimens. cond. salts form. 78—6363
  turbulent mass transfer in viscous sublayer by electrochemical method, expt. 78—83368
  turbulent pipe flow, mass transfer, electrochem. meas. 78—5830
  two-dimensional nucleation and growth, double potentiostatic step response, perturbation effects calcs. 78—51841
  two-layer baths, dynamic rectification effect calcs. 78—95934
  unsymmetrical electrolytes, conductance, relax. terms 78—67840
  valve metal oxide-semicond. oxide, electron injection, interface reactions 77—76936
  velocity sensor, freq. characts. calcs. 80—96675
  vitamin B_{12}, electrochemical reduction of methylcobalamin and methylcobinamide, one electron intermediates 78—85286
  voltage indicators, electrochemical, preparation, parameters 77—1936
  zinc phthalocyanine, electrochromism and oxidation 80—93768
  Ag, adsorption of O, dielec. perm., plasma surface vibr., modulation spectroscopy 77—48198
  Ag cluster growth on AgBr microcrystals after X-ray and low-temp. light exposure 79—83485
  Ag, electrochem. behaviour in nucl. reactor radiation field 77—52650
  Ag, single crystal, electrochem. grooving, gross linear defect obs. 78—67894
  Ag/AgCl photogalvanic cells for solar energy conversion, basic electrochemistry 80—45715
  Ag/CN, coverage meas. using surface enhanced Raman scatt. and radioisotope meas., electrochemical treatments 80—29260

electrochemistry continued
  Ag-AgCl reference electrode for high temp. and high press. electrochemistry 78—35693
  Ag-Sn alloys and amalgams, electrochem. considerations, corrosion in physiological soln. 80—93760
  AgCl electrode, electrochem. dye spectral sensitization, gelatin addition *(Japanese)* 79—57262
  AgI, interfacial electrochem., review 78—80748
  AgI-Ag oxosalt systems, solid electrolytes with glass-like struct., thermodynamic and electrochem. props. 79—10978
  AgI-$Ag_2O.B_2O_3$ system, ionic cond., struct., electrochem. prop. in galvanic cell 78—95181
  $Ag_xV_2O_5$, thermodynamic, elec. and electrochem. props. 78—84265
  Ag(s)/$Ag_2SO_4+Na_2SO_4$(l) high temp. ref. electrode, study 80—76622
  Al alloy, age-hardenable, extraction of precips., electrochem. method 77—32735
  Al, anodic behaviour in NO_3^-/Cl^- solns., electrochemical and XPS meas. 80—16694
  Al electrodeposition, cyclic reaction mechanism 79—83143
  Al, reactive electro-erosion under pulse electric discharge 79—52686
  Al, sacrificial anode dissolution, Hg effect study using ion implantation 79—39016
  Al-As_2Se_3-Al, photographic process based on electrochem. reactions *(Russian)* 79—6213
  Al-As_2Se_3-Al layers, photoelectrochem. process 77—76953
  Al-Sn, Sn effect on electrochemical behaviour in acetate buffer 78—19927
  Al-Zn-Hg alloy, cathodic protection characts., surface free energy, lattice struct. 79—29281
  Al-Zn-Mg-Cu, alloy 7075-T6, corrosion in halide solutions, exam. of anion dependency 78—60867
  $Al_xGa_{1-x}As$, solid soln., controlled electrochemical and selective etching, integrated optics appl. 77—14814
  $Al_xGa_{1-x}Sb$ solid soln., electrochem. deposition of Ni and Pd 80—93505
  AlH_3, photographic processes, thermo- and electrochemical transformations 78—89576
  Al_2O_3, anodic oxide films, luminesc., breakdown and colouring 78—19528
  Al_2O_3, porous, anodic, growth, physical model 78—48662
  Al_2O_3, porous, anodic, growth, ionic cond. 78—48663
  Au, anodic dissolution in aqueous alkaline cyanide 79—20375
  Au, electrochem. behaviour in nucl. reactor radiation field 77—52650
  Au^-, electrochemical generation, oxidation, standard pot., in liq. NH_3 79—100386
  $Au(CN)_2^-$, electrochemical reduction kinetics 78—73052
  B fibre reinforced Al composites, corrosion, electrochem. behaviour 79—20225
  Ba_3WO_6, Ba_2WO_5, and $BaWO_4$, chem. thermodynamics, galvanic cell study 80—21315
  BeF_2-LiF molten mixtures, mass transport, chronopotentiometry 77—21391
  Bi, liq., in fused alkali chloride binary mixtures, electrocapillary phenomena 77—40553
  Bi, liq., in fused KCl-KBr mixtures, electrocapillary phenomena 77—40554
  Bi-Sb alloys, electron work function determ., contact pot. difference method 77—39920
  δ-Bi_2O_3, thermoelectric power, heat of transport of O^{2-} ions 80—92713
  C gas-diffusion O_2 electrode in acid, electrochem. performance 78—31652
  CO_2, electrochem. reduction for use in energy storage 78—92490
  CO_2 electrochemical reduction for H storage 80—7934
  Ca, study using solid-state galvanic cell *(Japanese)* 77—56151
  CaF_2 solid electrolyte, meas. of O chem. pot. 80—3359
  CaO-ZrO_2 solid soln., thermodynamic investig., by EMF method 77—36485
  Cd, electrodeposition on solid Cd or CdHg amalgam, rate, impedance meas. 78—52693
  Cd-Bi alloys, electron work function determ., contact pot. difference method 77—39920
  CdS, semicond. film, contoured anodic photodissolution 79—74277
  Cd_xS, electrochemical characterisation and comp. modification at 25°C 77—25272
  Cd_2SnO_4 and Cd_2SnO_4:CdO, thin film electrodes in H_2SO_4 electrolytes, reduction, AES and SEM 80—65674
  Co, electrochemically prod. emitters, field ionis. props. 77—90254
  Co/CoO, relative chemical potential of oxygen *(German)* 78—31642
  Co_3O_4 film anode, electrochem. and corrosion processes in $HClO_4$ 79—61875
  γ-CoSe, d-electron deficit model, electrochem. meas. of free enthalpy *(French)* 78—30605
  Cr, electrochemical behaviour, in molten V_2O_5 *(Japanese)* 80—89498
  Cr/Cr_2O_3, relative chemical potential of oxygen *(German)* 78—31642
  Cr_2O_3-Al_2O_3, solid soln., effect of Cr on point of zero charge 78—61021
  Cr_2O_3-Al_2O_3 solid solution, electrochemical determ. of activity 78—44391
  Cu, amalgam, anodic oxidation in LiOH at room temp. 79—61865
  Cu, coadsorption of H_2O and Br, on (100) face, Helmholtz layer model system 80—92777
  Cu, corrosion, noble metal additions effect, Auger spectra 78—35579
  Cu deposits, morphology, polymer codeposition effects 79—74102
  Cu, electrochem. dissolution and deposition kinetics, in aq. SO_4^{2-} soln. 78—27773
  Cu, electrochem. nucleation and growth on Te and Al, TEM 80—104451
  Cu, electrodissolution kinetics in acidic chloride solns. 80—16695
  Cu, electrowinning from solvent extraction acid strip soln. using Pb-Sb anodes 77—48653
  Cu, friction under electrolyte immersion condition 78—64738
  Cu^+ formation during contact of Cu with Cu^{2+} aq. soln., rot. disk-ring electrode mechanism 79—61872
  Cu^+, in LiCl-KCl fused eutectic, diffusion and surface effects, chronopotentiometry *(French)* 78—11524
  Cu/Cu_2O, relative chemical potential of oxygen *(German)* 78—31642
  Cu-Be-Ni-Zr, anodic behaviour of intermetallic phase 78—72895
  Cu-H_3PO_4 system, instability and oscillations *(French)* 78—64850
  Cu-Sn alloy, thermodynamics of Cu and Sn solns. using copper β-alumina solid electrolyte, 800-1100K 80—107502
  $CuFeS_2$, chalcopyrite, electrode surface reduction kinetics 78—56897
  $Cu_{2-\delta}S$, Cu chem. diffusion, and nonstoichiometry, 400°C, electrochem. determ. 79—28132

electrochemistry continued
- D_2O, liq., ionisation const., thermodynamic props. determ., 298-523K 77—32821
- $Dy^{3+}+O_3(SO_5{}^{2-})(SO_2)$, in H_2SO_4 soln., electrochemiluminesc. emitters quenching by electrolysis products 79—1794
- DyF_3, thermodynamic props., galvanic cell meas. 80—21316
- ErF_3, thermodynamic props., galvanic cell meas. 80—21316
- Fe {211} surface, electrochemical dissolution, steps and kinks, quantitative anal. 79—74103
- Fe, anodic behaviour, in acidic solns. of liq. NH_3 78—27671
- Fe, corrosion and electrochem. behaviour in NaOH soln. containing $ClO_3{}^-$ *(Japanese)* 78—72928
- Fe corrosion in aq. H_2S, FeS polymorph form. 80—81231
- Fe, electrochemical behaviour, in molten V_2O_5 *(Japanese)* 80—89498
- Fe electrode, electrochem. behaviour in liq. NH_4 solns., effects of added impurities 80—50857
- Fe, film growth under organic coatings, qualitative ellipsometric-electrochem. approach 80—104344
- Fe, pitting in Na_2SO_4-NaCl solns. *(Japanese)* 78—85042
- Fe/'FeO', relative chemical potential of oxygen *(German)* 78—31642
- Fe-Co alloy, electrodeposited, comp. and struct. effects on H_2 diffusion and evolution overpot. 77—43377
- Fe-Cr alloys, feasibility of electrochem. corrosion protection 79—70220
- Fe-Cr(Ni), use of electrochemistry in understanding $\alpha\rightleftarrows\gamma$ transform., interstitials role *(French)* 77—63662
- Fe-graphite, intercalate, prod. by slow electrochemical reduction *(French)* 78—27437
- Fe-Ni, liq. alloy, electrochem. meas. of O, thermodynamic props. at 1873K 80—30244
- Fe-thionine photogalvanic, cells 80—35696
- $Fe(CN)_6{}^{3-}$, mass transfer rates at spheres, moving on circular path 77—3890
- $Fe(CN)_6{}^{3-}$, transfer characteristics at conical surfaces under axisymmetric impinging jets 77—3889
- $Fe(CN)_6{}^{3-}$-$[Fe(CN)_6]^{4-}$, electrochem. behaviour on $La_{1-x}Sr_xCoO_{3-y}$ rot. disk electrodes 79—79257
- Fe_2O_3, electrochem. doping 77—76430
- Fe_2O_3, semicond. anode in aq. electrolyte, electrolum. and electrochem. 80—76080
- n-Fe_2O_3, sintered and flame-oxidised, photoelectrochemical props. 79—70355
- Fe_2O_3-Al_2O_3, solid solns., effect on Fe on point of zero charge 78—61021
- $Fe_{80}P_{13}C_7$, amorphous and crystalline, electrochemical and semicond. behaviour *(Russian)* 80—101021
- $Fe_{1-x}Pd_x$ film, vac. deposited, oxidation and corrosion, AES, XPS and STEM obs. 79—100286
- FeV_2O_4, free energies of form., 1400-1750K, electrochem. method determ. 79—43613
- Ga, electron work function meas., dynamic capacitor method 77—39919
- Ga, liq., surface tension, low-temp. H_2 plasma influence, elec. double layer form. 79—33160
- GaAs anodic oxide, states, electrochemical meas. 80—80176
- GaAs, defect revealing etchant, electrochem. process in NH_4OH:H_2O 78—6060
- GaAs, epitaxial layer, controlled electrochemical and selective etching, integrated optics appl. 77—14814
- n-GaAs, preferential photoelectrochemical dissolution in Fe(III) based etches 78—7066
- Ge dissolution by oxidation and solvation, hole injection effect 80—26051
- GeO_2, standard Gibbs energy of formation, meas. by electrochemical method *(Japanese)* 79—83499
- H, extraction from LiF-LiCl-LiBr melt, appls. to fusion reactor blanket processing 78—53217
- H photoelectrochemical prod., solar beam-assisted electrolyser applied to Yokohama marks 5 and 6 [system for hydrogen production] systems 80—45768
- H production using hybrid electrochem./thermochem. cycles, search for electrochem. reactions 80—45807
- H^+ transfer reaction tunnelling probability 80—26032
- H-Cl electrochemically regenerative fuel cell, electrode kinetics and cell perform. 80—89610
- H-O electrochemical matrix-type cells, transport effects study 80—26027
- H_2, in molten alkali acetates, fuel cells technology appl. 79—57244
- H_2 photoelectrochem. prod., ZnTe and CdTe as photocathodes, characteristics 77—70311
- H_2, prod. from coal, water and electrons 79—61962
- H_2, sorption on Os cryst. in H_2SO_4 soln. 79—61873
- H_2 thermochemical production using H_2SO_4-SO_2 cycle, electrochem. aspects 80—97812
- HCl automatic control in air by electrochem. methods 79—96491
- H_xMoO_3, thermochemistry and electrochemical behaviour 79—100427
- H_2O, decomp., H prod. by thermochemical and thermoelectrochemical cycles 80—26029
- H_2O, photoelectrochemical evolution of O_2 using manganese chlorophyll electrode 79—83719
- H_2S oxidation by active C, electrochem. model *(German)* 78—35717
- Hg drop fall detector, circuit, design appls. 77—63924
- Hg/electrolyte interface, adsorpt. of ethylammonium bromide, from H_2O, D_2O solns., solvent props. 79—83459
- Hg-aqueous electrolyte interface, double layer charge relax., thermal jump meas. 78—53216
- Hg-Cd cell, EMF rel. to temp., thermodynamics 77—12805
- Hg-electrolyte interface, with imposed temporal and spatial periodicity, double-layer transduction 78—88639
- Hg-electrolyte interface, polarizable, dynamics of double layer 79—24756
- Hg-gas interface, electrocapillary effects, CH_2Cl_2 adsorption in CF_4 77—32798
- HoF_3, thermodynamic props., galvanic cell meas. 80—21316
- In, liq., surface tension, low-temp. H_2 plasma influence, elec. double layer form. 79—33160
- In_2O_3, standard Gibbs energy of formation, meas. by electrochemical method *(Japanese)* 79—83499
- IrO_x, anodic films, electrochem. characts., electrochromic system 78—80316
- KCl, aqueous film on Hg, secondary electrocapillary effects, interfacial tension and entropy 77—55420
- K_2TiF_6 in LiCl-KCl eutectic mixture, analysis of reduction waves of Ti ion in chronopotentiometry *(Japanese)* 78—20025
- $LaCuO_2$, enthalpy of formation and high temp. stability from EMF of galvanic cell 80—11942

electrochemistry continued
- La_2CuO_4, enthalpy of formation and high temp. stability from EMF of galvanic cell 80—11942
- $LaNi_5$ alloys, aspects of electrochem. storage of H 79—24917
- La_2NiO_4, free energy of formation 77—1240
- Li cells, electrochemical charact. of VSe_2 79—1959
- Li electrode, in lithium perchlorate-propylene carbonate solution, surface anal. *(French)* 80—50859
- $Li/Li^+/M_yV_{1-y}S_2$ cells (M=Fe, Cr), effect of metal substitution of Li intercalation 79—100395
- $Li/SOCl_2$ primary cells, $SOCl_2$ reduction mech. in supporting electrolyte 80—108792
- Li-Al system, Li solubility and chem. diffusion in Al, electrochem. study 80—107432
- Li-Te alloys, liq., electrochem. investig. of thermodynamic props. 77—1244
- Li-TiS_2 nonaqueous batteries, mechanism of Li intercalation, optical and X-ray studies 79—100394
- Li+$KFeS_2$, electrochemical reaction, in situ Mossbauer spectra study 79—100397
- Li+transition metal compounds topochemical reactions in high energy batteries, solid state electrode materials 80—55836
- LiCl-KCl:Ln^{n+}, fused eutectic, electrolytic behaviour *(Japanese)* 79—16009
- Li_xFeS_2 $(0<x\leq2)$ cathodic system, chem. and electrochem. studies 80—85188
- LiI complexes, ionic cond., electrochem. props. 77—60072
- $Li_{1-y}Ti_{1+y}S_2$, intercalation chemistry and electrochemical energy storage 79—100541
- $Li_xUO_2F_2$, $0\leq x\leq2$, use in electrochemical batteries 80—50858
- β-$Li_xV_2O_5$ bronze, thermodynamics of ordering 80—84302
- β-$Li_xV_2O_{5-y}$ bronzes, thermodynamic props. by coulometric titration 80—34209
- Li_xVSe_2, intercalation cpds., electron chem., ionicity 80—89501
- Li_xWO_3, electrochem. and chem. Li incorporation, cryst. struct. 80—88131
- Mg-AgCl seawater battery, performance and EMF at great ocean depths 80—76623
- Mg-Al-Tl(Pb) systems, phase diags., electrode pots. *(Russian)* 78—80516
- Mg-Ga-In(Tl) and Mg-In-Tl, phase diagrams and electrochem. props. *(Russian)* 80—40330
- Mg-Zn-Zr-Cd-Nd alloys, Lawes phase separation using acetate electrolyte 79—70237
- $MgSO_4.7H_2O$, thermo-electrochemical H_2 prod. using solar energy *(French)* 79—24918
- Mg_2SnO_4, Gibbs' free energy of form., electrochem. determ. 78—11548
- Mn/MnO, relative chemical potential of oxygen *(German)* 78—31642
- MnO_2, doped, dry cell depolariser, hydrazine reduction kinetics 80—89603
- MnO_2, preparation and characterisation of doped samples for appl. as dry-battery depolarisers 80—89602
- Mo complexes, oxo- and sulphido-bridged, binuclear, in aprotic media, electrochem. and redox mechanisms 77—86324
- Mo_2C, corrosion and electrochem. props. in aq. H_2SO_4, HCl, HNO_3 and KOH solns. 80—11813
- Mo_4O_{11}, anodic dissolution, periodic phenomena 77—16735
- n-$MoSe_2$ based liq. junction solar cell, nonaqueous electrolyte system employing Cl_2/Cl^- couple 80—81432
- $MoSe_2$, layer cryst., electrochem. solar cell, electron transfer mechanism 78—52077
- N compounds, electroionisation synthesis 78—23937
- NO, electrocatalytic decomp. on electrochem. reduced zirconia surface 80—61113
- Na conductive glass-Na amalgam interface, electrochem. obs. 78—76870
- Na-S batteries, load levelling and motive power appls. 77—86321
- Na-Te system, liq., electrochem. determ. of thermodynamic props. rel. to temp. 77—1245
- NaCl-graphite interface, elec. cond. 78—52060
- $Na_x{}^+(H_2O)_y[CrS_2]^{x-}$, form. and reactions 79—91961
- Na_xMS_2 (M=Ta,Ti), Na chem. pot. and free energy of intercalation, electrochemical meas. 79—100396
- Na_2O-Al_2O_3 (CaO)-SiO_2 glass, surface charge in aqueous electrolyte soln. 79—29245
- Na_2O-P_2O_5 and Li_2O-Na_2O-P_2O_5 glasses with oxide additions, eval. as membranes for chem. sources of current *(Russian)* 79—96338
- Na_2O-SiO_2(-CaO) glass, molten, metal ion diffusion and redox behaviour, electrochemical studies 80—81332
- Na_xWO_3 films, chem. pot. variation of Na, free electron gas model 80—16698
- Ni, electrochemical behaviour, in molten V_2O_5 *(Japanese)* 80—89498
- Ni, electrochemically prod. emitters, field ionis. props. 77—90254
- Ni electrocrystallisation, inhibiting factors study 79—74105
- Ni electrodes, electrochem.-ellipsometric studies of oxide films formed during O_2 evolution 79—16007
- Ni, Flade potential as thermodynamically reversible pot. 79—5159
- Ni rotating cylinder electrodes, mass transfer investigation 79—43589
- Ni/NiO, relative chemical potential of oxygen *(German)* 78—31642
- Ni/Ni(II) electrode reaction in LiCl-KCl eutectic melt, impedance meas. *(Japanese)* 79—100392
- Ni-Cd, with plastic bonded Ni oxide electrodes, basic electrochemical parameters 80—50951
- Ni-Co-Mo-Al-Cr, melt, effect of Al, Cr on O_2 activity, electrochemical determ. 79—11556
- Ni-Cr, corrosion resistance of dental casting alloys 78—31561
- Ni-hypophosphite developer, physical development as function of pH 79—24760
- $Ni_{36}Fe_{32}Cr_{14}P_{12}B_6$, amorphous, electrochem. corrosion in chloride solns. 80—50763
- $NiLa_2O_4$ electrodes, kinetics of O_2 evolution, appl. to electrolytic H energy prod. 80—30430
- NiO and lithiated NiO, thermally grown, electrochemical capacitance variations 80—29475
- NiO films, on Ni (100) electrodes, oxide defect sites role in breakdown 79—43587
- NiO, interface for xerographic Se photoreceptor on flexible Ni foils 78—29184
- β-NiSe, d-electron deficit model, electrochem. meas. of free enthalpy *(French)* 78—30605
- O electrode, reaction in alkaline soln. on transition metal oxides prepared by thermal decompositions 79—61864

electrochemistry continued
O^{2-} low partial press., thermogalvanic meas. using O^{2-} ion conductors 80—73389
O_2, adsorption on Ni and Ag electrodes in KOH soln. 79—61871
O_2 evolution on Teflon bonded $NiCo_2O_4$ porous electrodes 80—30247
O_2, sorption on Os cryst. in H_2SO_4 soln. 79—61873
Pb, liquid, O_2 activity from electrochem. meas. 80—55695
Pb-acid cells, PbO_2 formation on Pb and antimonial Pb alloy 80—76628
Pb-H_2SO_4 cells, Sb alloying effect on solid Pb electrochemical properties 80—55668
PbO_2 powder, electronic conductivity, separation of particle core and surface resistance 80—104442
$4PbO.PbSO_4$, oxidation to PbO_2 in positive plate of Pb-acid battery 79—70336
Pd-Al alloys, Fermi level position rel. to mixing behaviour, Al activity, thermodynamic props. *(German)* 78—75835
PdH_x layer, galvanostatic desorption of hydrogen, quantitative theory 80—40694
PdO, free energy of form. using impedance dispersion analysis 80—108728
Pt, adsorption of H_2, electrolyte environment and crystallite size effects 78—27774
Pt and Pt/Ru electrocatalysts for methanol oxidisation in acid electrolyte with improved steady state activity for fuel cell appls. 80—76629
Pt coating on Ti, true surface area determ. by cathodic charging in H_2SO_4 79—61877
Pt, electrochem. behaviour in nucl. reactor radiation field 77—52650
Pt, electrochemical adsorpt. of H_2, adsorpt. states, tensiodynamic meas. 77—20196
Pt electrode, in Na_2SO_4-NaCl melt, polarisation meas., reactions 78—68898
Pt electrode, multilayer oxides, electrochem. reduction mechanism, kinetics 78—61019
Pt low index surface, adsorption of H in dilute acid electrolyte 79—70342
Pt, low index surface, struct. sensitivity of O_2 reduction in acid electrolyte 79—70343
Pt surface, adsorption of H_2, rel. to electrocatalysis 78—38935
Pt surfaces, oxidation by electrosorpt., of H_2, effect of soluble prods. *(German)* 80—55717
Pt/ZrO_2-Y_2O_3 interface, electrode kinetics, complex impedance dispersion anal. 79—96325
Rb-Hg liquid amalgams, thermodynamic props. determ. from conc. cell EMFs 77—1246
$RbAg_4I_5$-metal interface, photocurrents, photoelectrochem. effects 78—34897
SF_6, arc discharge, decomposition products for SF_6 with H_2O and organic gas contaminants 79—10743
SO_2 automatic control in air by electrochem. methods 79—96491
Sb, liquid, O_2 activity from electrochem. meas. 80—55695
Sb_2O_3, standard Gibbs energy of formation, meas. by electrochemical method *(Japanese)* 79—83499
Si, doped and intrinsic, chemomech. effect 78—64751
Si film, porous, form. and oxidation by anodic reaction 79—28966
n-Si, neutron irradiated, annealing behaviour characterisation by electrochem. meas. 80—19847
n-Si, passivation, photoactivation kinetics in conc. alkali, ellipsometric investig. 77—1885
Si, porous, form. during anodic treatment in aq. HF 80—35369
Si:As, electrochemical doping 79—90684
Si:As, electrochemical doping profiles 79—90685
Si/SiO_2-electrolyte interface, electron exchange at surface of thermally grown SiO_2 80—16696
Si-SiO_2 interface, trapping props. from electrochemical current-voltage behaviour 79—69597
SiO_2, fused, surface charge in aqueous electrolyte soln. 79—29245
SiO_2-Na_2O-CaO, electrochemically coloured, chemical composition and structure of surface layers 78—84758
SiO_2-Na_2O-CaO-MgO-Al_2O_3, toughening by electrochemical treatment in Sn melt 80—11800
SiO_2-NaO-K_2O-CaO-MgO-Al_2O_3 melt, anodic dissolution of Co and Ni in melt 78—88582
Sn reactions in aqueous electrolytic solutions, review 77—86337
Sn-Pb alloys, electron work function determ., contact pot. difference method 77—39920
SnO_2, electrochem. determ. of free energy 79—82360
SnO_2, electrochemical determination of free energy of formation 79—11797
$SrTiO_3$, semicond. anode in aq. electrolyte, electrolum. and electrochem. 80—76080
$SrTiO_3$ semicond. electrodes, electroreduction process kinetics, cathodic dark current meas. 80—66807
T, metal and alloys, mechanical props., electrochemistry, oxidation and corrosion resist., conference, Nantes, France (Nov. 1978) 80—41932
Ta_xO_y on Ta, anodic film, electrochem. reactions by tunnel current 77—81340
TaS_2(2H), Li intercalation, electrochemical studies 80—39048
$Ta_yTi_{1-y}S_2$, Li intercalation, electrochemical studies 80—39048
$Tb^{3+}+O_3(SO_5^{2-})(SO_2)$, in H_2SO_4 soln., electrochemiluminesc. emitters quenching by electrolysis products 79—1794
Te-$TeBr_4$ system, Gibbs free energy of reaction, electrochem. e.m.f. expts. 79—91991
Te-$TeCl_4$ system, Gibbs free energy of reaction, electrochem. e.m.f. expts. 79—91991
Te-TeI_4 system, Gibbs free energy of reaction, electrochem. e.m.f. expts. 79—91991
Ti alloy AT-3, crack development in air, H_2, aq. H_2SO_4, electrochem. charact. *(Russian)* 77—70209
Ti alloys, hot salt stress corrosion cracking, electrochemical model 78—7078
Ti, behaviour close to corrosion potential in aerated sulphuric solution *(French)* 78—23862
Ti electrochemical machining, electrolytes development, electrochem. in static solns. 80—85182
Ti electrochemical machining, electrolytes development, electrochem. studies in flowing solns. 80—85183
Ti, oxide layer form. in acid soln., electrochem. and optical props. 78—48560
Ti, reactive electro-erosion under pulse electric discharge 79—52686
Ti:Pd, ion implanted, corrosion behaviour and Rutherford backscatt. anal. 80—71792

electrochemistry continued
Ti-Cu alloys, in acidic media, electrochemical behaviour *(French)* 78—23863
Ti-Cu dissolution mechanisms, photoelectron spectra study *(French)* 80—45198
Ti-Pd, dil., ion implanted, corrosion rate and electrochemical props. 79—43467
$TiCl_4$, electrochemical behaviour in alkali chloride baths 80—30243
TiO_2, anodically formed layers, film instability obs. 78—72916
n-TiO_2, crystal, in aqueous soln., electrochemistry and electrolum. meas. 78—48665
TiO_2 doped polycrystalline electrodes, for photo-assisted electrolysis of water, spectral response 79—29370
TiO_2, electrochem. doping 77—76430
TiO_2, semicond. anode in aq. electrolyte, electrolum. and electrochem. 80—76080
TiO_2:Nb semicond. electrodes, electroreduction process kinetics, cathodic dark current meas. 80—66807
TmF_3, thermodynamic props., galvanic cell meas. 80—21316
V_2S_5, amorphous, electrochemistry in Li cells 80—76626
W, anodic dissolution macrokinetics in alkaline solns. *(Russian)* 77—12804
W, oxidation, WO_3 amorphous anodic film growth in acidic soln. 80—81232
W, whisker fabrication, AC and DC electrochem. etching 78—43278
WO_3 electrochromic film in liq. electrolyte, chem. and electrochem. stability 78—73054
WO_3, film, electrochem. injection kinetics of Li, LF AC meas. 80—57339
WO_3, semicond. anode in aq. electrolyte, electrolum. and electrochem. 80—76080
Y-Fe-O, phase equilib. and thermodynamics, solid state high temp. electrochem. obs. 79—56967
Zn, corrosion in de-aerated 0.1 M NaCl, pH range 1.6 to 13.3 78—19921
Zn, corrosion rate, electrochem. meas. using differential pulse polarograph 77—59980
Zn electrode, passive film form. by chrono-ellipsometry *(Japanese)* 78—68900
$ZnCl_2$ in methanol-water mixtures, thermodynamic props. from EMF meas. 79—52735
ZnO particulates, Dember effect 79—20380
$ZnSO_4$ electrolytes containing Ge and Co, polarisation charact., exam. by cyclic voltammetry 80—104444

electrochromic devices
anthraquinoide, electrochromism, display devices, multiplexing 80—45037
ATR prism modulator 80—43440
cell using solid proton conductor electrolyte, $HUO_2PO_4.4H_2O$ 80—89497
cell with anodic IrO_x film electrodes 80—7329
displays, technical aspects 78—65917
electrooptical processor, iterative colour-multiplexed 80—23792
image convertor, liq., cryst., with memory effect 79—23711
information display technology, symposium, San Francisco (1978) 79—9209
modulator using dyes 77—7185
picture taking parameters display in amateur cameras, review 78—89578
short circuit memory in electrochromic displays 80—97238
viologen display, mechanism of electrochromism *(Japanese)* 80—34893
p-GaAs/heptyl viologen system, appl. in photoelectrochemical cells and photoelectrochromic displays 80—76640
$H_3PO_4(MoO_3)_{12}.29H_2O$, electrochromic solid-state cells 80—2724
$H_3PO_4(WO_3)_{12}$ electrochemichromic cells 79—15436
$(H_3PO_4)(WO_3)_{12}29H_2O$, electrochromic solid-state cells 80—2724
$HUO_2PO_4.4H_2O$, film fabrication and appl. as solid electrolyte in electrochromic displays 80—70462
IrO_2, anodic films, new electrochromic for nonemissive displays 79—99851
IrO_2 heat-treated anodic films, pH depend. of electrochromism 79—8120
IrO_x anodic film electrochromic cell, fabrication and display device use 80—61320
IrO_x anodic films, electrochromic props. and device uses 80—61319
IrO_x film, anodic, electrochromism, pH effects on corrosion stability, coloration and bleaching mech. 80—2726
WO_3 amorphous films, colouring and bleaching, expt. and anal. 77—20829
WO_3 film electrochemical colouration for displays 77—77170
WO_3, solid state electrochromism and electrochromic cell deterioration 79—78655
a-WO_3-Cr_2O_3, electrochromic layer device, characts. 79—90009
WO_3-electrolyte electrochromic cells, proton injection phenomena 80—71448
WO_3-LiF(MgF_2), electrochromic display struct., efficiency and humidity depend. 79—81540
WO_3-LiI, solid-state electrochromic cell, fabrication and characts. *(Japanese)* 80—84717

electrochromism
aniline, gas phase electrochromism studies in vacuum UV 77—50562
benzene, excited state props., by electrochromism in polymer matrix 79—22737
benzyl viologen, mechanism of electrochromism *(Japanese)* 80—34893
cholesteryl chloride+cholesteryl laurate, binary compensated, rhodamine 6G guest, electro-optical colour effect 80—71378
cobalt phthalocyanine, electrochromism and oxidation 80—93768
cyclic ketones, electrochromism and electric dichroism for studying transitions to second excited singlet 80—63692
display system application *(Japanese)* 77—1656
dye in polymer matrices, electrochromic props. and use as probe of matrix softening around T_g 80—84724
dyes in polymer matrices, intramol. charge transfer, electrochromism 79—73901
education, electrochromism in WO_3, advanced lab. expt., colour centres, proton diffusion 80—17738
electrolytic double layer, light absorpt., electrochromic changes 78—84551
excited state props., by electrochromism in polymer matrix 79—22737
formaldehyde, electrochromism of 1749 Å band, electric dipole moment and polarisability 78—66572
glass film compositions, electrochromism *(Russian)* 79—28721
graphite, reversible electrochromic effect 80—29718
graphite-alkali metal intercalation cpds., electronic props. 80—45202

electrochromism continued
- n-heptylviologen salt soln., electrochemical props. 77—77788
- merocyanine dye monolayer on p-chloranil cryst. in sandwich cell, electrochromic detection of internal charges 78—11549
- photosynthetic membrane, optical and electrochromic props., chloroplast chlorophyll orientation 77—48763
- polymer-modified electrodes, electrochromic characts. 80—66149
- polymers, network, low freq. mol. mobility, quadratic electrochromism method *(Russian)* 78—71688
- PTA-ZnCdS, electrochromic material mixed with photosensitive powder, photoinduced coloration and electrochemical bleaching 77—81082
- pyridinium salt solns., visible absorpt. spectra, 100 V/cm 77—77244
- pyrylium salt solns., visible absorpt. spectra, 100 V/cm 77—77244
- Rydberg transitions, field effects in vacuum UV region 78—66561
- short circuit memory in electrochromic displays 80—97238
- tetraphenylporphyrin, free base in PVC matrix, excited state props., electrochromism obs. 80—37815
- triphenylene, excited state polarisabilities, electrochromism and pot. energy curves 79—7034
- viologens, solutions for display appl., oxidant impurities elimination 80—78922
- zinc phthalocyanine, electrochromism and oxidation 80—93768
- Au-WO_3, cermet, optical and electrical props. 79—33674
- Au-WO_3 cermets, electrochromism 77—90129
- Au-WO_3 electrochromic cermets, resist. and optical density meas. 79—8201
- Er-diphthalocyanine complex, thin film *(Japanese)* 80—20611
- Fe complex, $FeCl_3$-tetraphenylporphyrin in PVC matrix, excited state props., electrochromism obs. 80—37815
- H_xWO_3, electrochromic characts. 78—6653
- H_xWO_y film, effect of struct. on optical and electrical props. 78—84671
- IrO_2 anodic amorphous film, electrochromism isotherms, internal entropy 80—50300
- IrO_2 anodic films, electrochromium, on transparent substrates 79—19861
- IrO_2 anodic films, electrochromism, anion mechanism 80—100647
- IrO_2, electrochromic film, prep. by reactive sputtering 80—29876
- IrO_2 film, A-C response 80—107926
- IrO_2 heat-treated anodic films, pH depend. of electrochromism 79—8120
- IrO_x anodic film electrochromics in nonaqueous acid soln. 80—2722
- IrO_x, anodic films, electrochem. characts., electrochromic system 78—80316
- IrO_x anodic films, electrochromism and ionic cond., model 80—59706
- IrO_x anodic films, electrochromic props. and device uses 80—61319
- IrO_x anodically grown film as electrochromic material 80—71377
- IrO_x, electrochromic, oxidation state changes and struct. 80—100950
- IrO_x film, anodic, electrochromism, pH effects on corrosion stability, coloration and bleaching mech. 80—2726
- $Li_2B_4O_7$, ferroelectric glass, phase transition, permittivity, electrochromism, photochromism 80—80719
- Li_2O-B_2O_3-WO_3 glass, photochromic and electrochromic props. 79—28787
- Li_xWO_3, electrochromic characteristics 78—6653
- Li_xWO_3, electrochromism, potentiostatic and galvanostatic meas. 78—43835
- MoO_3 film, electrochromism, X-ray electron spectra 78—48146
- MoO_3 film, evaporated, electrochromism *(Japanese)* 79—38686
- Nb_2O_5 electrodes, in aq. and acetonitrile solns., electrochromism 80—50298
- Pt-WO_3, cermet, optical and electrical props. 79—33674
- Rh oxide film, anodic, two-colour electrochromic system 80—66150
- $SrTiO_3$-Ni, electrochromism, optical and elec. meas. 79—95732
- TeO_2, ferroelectric glass, phase transition, permittivity, electrochromism, photochromism 80—80719
- V_2O_5 electrochromism obs. and mechanism, thin film growth *(Russian)* 77—77249
- V_2O_5 film, electrochromism, X-ray electron spectra 78—48146
- $W_9Nb_8O_{47-x}$ polycrystalline film as electrochromic material 79—65949
- WO_3 amoprhous film, sublimed under different conditions, elec. transport props. 80—7015
- WO_3 amorphous films, colouring and bleaching, expt. and anal. 77—20829
- WO_3 amorphous layers, electrochromic absorpt. depend. on crystallinity and electron localisation 77—59589
- WO_3 electrochromic absorption dependence on crystallinity 77—77314
- WO_3 electrochromic cell, deposited Cr_2O_3 as barrier 78—15147
- WO_3 electrochromic elements, prod. by electrolytic anodisation of W, and characterisation 80—25921
- WO_3 electrochromic film in liq. electrolyte, chem. and electrochem. stability 78—73054
- WO_3 electrochromic films, bleaching by electric fields 79—99852
- WO_3 electrochromic reaction kinetics 77—77176
- WO_3 electrochromics in nonaqueous acid soln. 80—2722
- WO_3 electrodes, electrochromic processes, digital simulation model 80—76518
- WO_3 electrodes, vac. evaporation and anodic oxidation prep., electrochromic process kinetics 79—100390
- WO_3 evaporated film composition and chem. structure rel. to electrocoloration 77—77175
- WO_3 film, amorphous, electrochromism and local order 77—59553
- WO_3 film, anodically formed, electrochromism 79—1752
- WO_3 film, Au surface layer effect on electrochromic behaviour 80—76004
- WO_3 film, electrochromism, X-ray electron spectra 78—48146
- WO_3 film, evaporated, electrochromism *(Japanese)* 79—38686
- WO_3 film, evaporated, mech. of elec. cond. 80—44747
- WO_3 film electrochemical colouration for displays 77—77170
- WO_3 films, ESR study after colouring by H_2 injection and after bleaching in air 80—39867
- WO_3 films, electron struct. changes during electrocoloration, XPS obs. 80—40217
- WO_3 layers, semiconductor electrodes, electrochromism and photoelectrochemistry 80—35544
- WO_3, on glass substrate, electrochromism of glass film compositions 80—29720
- WO_3, polar, electrochromic absorpt. bands, small polaron theory 78—39528
- WO_3, solid state electrochromism and electrochromic cell deterioration 79—78655
- WO_3, thin films, electrochem. coloration, optical and elec. props. 77—85345

electrochromism continued
- WO_3-BaO film, electrochromic coloration and decoloration, BaO additive effects 78—72620
- WO_3-LiF system, on glass substrate, electrochromism of glass film compositions 80—29720
- WO_3-MoO_3, film, evaporated, electrochromism *(Japanese)* 79—38686
- WO_3-MoO_3 film, amorphous, electrochromic optical absorpt., expt. results and model 78—27341
- WO_3-MoO_3 system, on glass substrate, electrochromism of glass film compositions 80—29720
- WO_3-P_2O_5 alkali glasses, electrochromic, electron-ion processes 80—25341
- WO_3-P_2O_5 glasses, electrochromic effect 79—95735
- WO_{3-y} thin films, charge storage and types of colour centre, expt. 77—20830
- $WO_{2.7}H_y$ film, colouring, comp. depend. 78—15239
- $WO_3(WO_3$-UF$)(WO_3$-$MoO_3)$ glass film compositions, electrochromism *(Russian)* 79—28721

electrodeposited coatings *see electrodeposits*

electrodeposited films *see electrodeposits*

electrodeposited layers *see electrodeposits*

electrodeposition
- *see also electrodeposits; electroplating*
- alloy, selective stripe, electrodeposition and hot flow techniques, metallurgical characteristics 80—50567
- alloy, theory review 80—11581
- alloy powders, production using electrodeposition and heating in reducing atm. 79—100079
- alpha activity electrodeposition onto Au foil, use in Si surface barrier detector 78—82565
- anodic film form., electrode pot. variation rel. to nucleation, growth 78—68634
- binary alloys, recent developments, review 77—81233
- binary alloys, thin layer deposition 78—3067
- black nickel film on Cu substrate, optical constants determ. by ellipsometry study 77—74488
- bronze powders preparation from normal salt baths of Cu, Sn, porous components fabrication appl. 78—20026
- cermet, effect of electrolyte in charge carried by suspended ceramic particle 78—68665
- coating props., review 79—91596
- composite material deposition by electrolysis *(French)* 77—73375
- conference, Electrochem. Society fall meeting, Las Vegas, USA (Oct. 1976) 77—16831
- conference, electrochem. society fall meeting, Las Vegas, USA (Oct. 1976) 77—77787
- continuous moving sheet electrode, characterisation, expt. 77—21398
- crystal face, growth behaviour in presence of screw dislocations 80—103276
- crystal growth, highly conducting inorganic complexes 77—8739
- dendritic metal crystals, electrolytic growth, CCTV obs. 78—51863
- development at electrolytic coating methods, ionic evaporation, paints, organic coatings *(French)* 80—30127
- diamond containing electroless Ni coatings, fabrication and props. 79—47795
- electrochemical phase formation 80—55309
- electrocrystallisation, galvanostatic transients, crystn. overvoltage 78—76867
- electrocrystallisation, impedance frequency dependence, in the case of DC superposition 78—51844
- electrocrystallisation, nucleation, phase form., symposium, Southampton, England (Dec. 1977) 80—51942
- electrocrystallisation, nucleation and growth mechanism, ohmic overpotential effects, simulation 78—51842
- electrocrystallisation, nucleation and growth mechanism, ohmic overpotential effects determ. 78—51843
- electrocrystallisation, recent progress in electrochem. and physical methods *(French)* 80—7510
- electrocrystallisation noise, phenomenological model 78—51845
- electrolytic crystal growth, role of screw dislocations 80—54540
- electrolytic nucleation at high supersaturation 78—61025
- electropolymerisation, on electrodes, book contrib. 80—50854
- electropolymerisation, polymer film coating in aq. medium, book contrib. 80—50778
- electrospark coating formation factors *(Russian)* 78—19908
- electrowinning, using fluidised bed cathodes, const. current density operation 79—24456
- electrowinning, using fluidised bed cathodes 79—24455
- epoxy laminate, surface prep. to promote electroless Cu bonding 77—21300
- ferromagnetic films, electrodeposition, thickness control, magnetisation meas. 78—23306
- film growth kinetics and mechanism 79—52685
- n-heptylviologen radical cation films, cathodic, growth, for alphanumeric display appl. 79—69999
- latex polymer, electrodeposition on metal 78—53015
- metal, coulostatic deposition at underpot., pot. relax., chem. effects 78—48335
- metal, coulostatic deposition at underpot., pot. relax. 78—48334
- metal, electrocatalysis, surfaces modified by metal adatoms, review 80—61110
- metal, electrodeposited from molten salts, faceting rel. to texture axis direction 79—28969
- metal, ion mass transfer migration effect 79—61523
- metal chalcogenides, using nonaqueous solvents 80—76200
- metal cluster growth and props., photography and catalysis appl., conf., Villeurbanne, France (Sep. '79) 80—105431
- metal coating of optical fibres, for strengthening and surface protection 78—30103
- metal electrodeposition fundamentals 77—36413
- metal electrodeposition protrusion growth and inhibitor action model and meas. 79—96314
- metal electrospark deposition mechanism regularities *(Russian)* 78—19932
- metal films, electrocrystallisation, soln. component interaction 80—20055
- metal foils, for X-ray filters 79—95947
- metal ion adsorption, nucleation effects *(German)* 78—68635
- metal layers, underpot. deposition, mechanisms, phase transitions, nucleation 78—60590

electrodeposition continued
- metal-polymer deposit, simultaneous electrophoretic deposition and electrochemical precipitation 79—56938
- metallic binary alloys or compounds, cathodic deposition and characterisation 79—69998
- metallic surface alloying methods *(Russian)* 78—19931
- metallurgical coatings, conf., San Francisco, USA (Apr 76) 77—31918
- metals, crystal growth, electrochem. Czochralski method, growth rate limitations 78—88433
- metals, electrochemical nucleation, potentiostatic obs. 79—15038
- metals, electrodeposition, chemical factors 80—16207
- metals, using fluidised bed electrodes, math. model 79—100062
- molten salt transport reactions, isothermal system *(German)* 77—63568
- molten salt transport reactions, isothermal system *(German)* 77—63569
- morphological stability of plane interface, electrocrystallisation from molten salts 77—35497
- multicomponent systems, electroepitaxy, theoretical model 80—65396
- noble metal surface single crystal planes, kinetic investig. of structural changes and desorption, Au (111)/Bi^{3+} appl. 80—54500
- Permalloy, electrodeposition, mag. props. *(French)* 78—64488
- Permalloy film, electrodeposition with zero magnetostriction composition, technological control 79—33955
- Permalloy film, for cylindrical magnetometer sensor 77—82576
- polar solvent molecule interactions in the adsorbed state 80—21299
- polymer graphite fibre electrodes, coating by electropolymerisation, adhesion to epoxy matrix 79—15644
- polymers, electric phenomena, book 80—46746
- polyphenylene oxide thin films, electrochem. prep., impurity effects on cond., electroforming 80—88655
- progress in electrodeposition and related processes, (1952-1977) 78—27420
- pulsed electrodeposition, time parameter correction by electrochem. response 79—70006
- quartz, electrodeposition mech., onto metal electrodeposit, cermet prop. 79—33992
- refractory metal on liq. cathode, duty ratio 77—24975
- resistive layer above pit, stabilisation 80—93506
- review 79—43162
- seawater deposition, scale control, appl. 79—66302
- selective coating electrodeposition on Al substrates for solar collectors 79—62079
- semiconductors, binary, cathodic deposition and characterisation 79—69998
- steel:Si alloy formation kinetics at solid cathodes, metal electrodeposition from molten salt electrolytes 80—26028
- steel, boriding, electrolytic, effect of iron oxides 79—39042
- steel cylinder, electrodeposition internal stress meas. using X-rays 78—27693
- steel surface corrosion protection, propargyl alcohol film growth, ellipsometric obs. *(Rumanian)* 80—60996
- stress measurement, of sphere by X-ray in depositing method 77—36409
- surface protrusion growth rate, automation of real-time optical meas. of small structures 79—85115
- surface reacts. driven by linear pot. sweep, kinetics, model one-electron react. 77—25275
- tetramethylammonium silver iodide superionic film, electrocodeposition, electrochem. cells 80—107478
- thin films electrocrystallisation under potentiostatic conditions 79—95955
- two-dimensional nucleation and growth, double potentiostatic step response, perturbation effects calcs. 78—51841
- AG, electrodeposited, role of stacking fault energy 77—29016
- Ag cathode, underpotential deposition of Pb 78—52692
- Ag, electrocrystallisation, in pulse electrolysis, expt. 78—64489
- Ag, electrocrystn., screw dislocation free (100) face growth kinetics 78—30557
- Ag, electrodeposition, influence of specific adsorpt. of S 79—20001
- Ag electrodeposition, on (100) face of single crystal Ag in presence of sulphadiazine 80—89161
- Ag filaments, cryst., electrolytic growth in Teflon capillaries, differential-capacity meas. 77—40552
- Ag film, on semicond. substrates 77—77425
- Ag, on (111) face, habit modification caused by Cl^- 80—71600
- Ag on Pt film electrode, interface struct. 77—16512
- Ag recovery from laboratory wastes, teaching appl. 79—84912
- Ag, single crystal, adsorption of metal ions on (111) and (100) surfaces *(German)* 78—68636
- Ag underpotential deposition, on Pt substrate, XPS 77—59672
- Ag-Sb alloy, reflectivity, effect of electrodeposition conditions 78—13784
- Ag-Zn alloy, controlled-potential, spontaneous transformations obs. 78—51853
- $Ag_7I_4PO_4$ film formation from electrolysis of $HI-H_3PO_4$ soln., electrocodepositional method 80—55315
- Al electrochemical electrode, oxide film growth accompanied by luminesc. 79—57236
- Al, electrodeposition, chemical factors 80—16207
- Al electrodeposition, cyclic reaction mechanism 79—83143
- Al_2O_3, anodic oxide film, behaviour of emulsion particles during electrodeposition 80—104357
- Au anodic electrodeposition from liq. NH_3 solns. 79—28957
- Au, by electrochemical reduction of dicyanoaurate, reaction kinetics 78—73052
- Au, electrodeposit, struct., texture, influence of As on brightness *(Bulgarian)* 78—79862
- Au, electroless plating on GaAs for fast characterisation of epitaxial layers 79—33347
- Au film electrodeposition, substrate effects on film props. 80—81329
- Au, heavy metal ion induced depolarisation effects 77—16511
- Au, plating assessment for printed circuits 79—43163
- Au, surface prep. of Be-Cu 78—7100
- Au-In, electrodeposited from acid cyanide electrolyte, exam. of wear and corrosion resistance 78—80482
- Bi powders, fine, precipitation on passivated electrodes 80—2977
- Bi surface, anodic oxide film, nucleation and growth 77—59966
- C fibre reinforced Ni, hot pressed and electrodeposited, strength 79—38898
- CaB_6, electrodeposition from molten salt baths, cathodic behaviour 79—11529
- Cd, deposition, on metal substrate, pot. sweep, potentiostatic and optical microscopic obs. 77—59967
- Cd, electrocrystallisation, in pulse electrolysis, expt. 78—64489

electrodeposition continued
- Cd, electrocrystn. on Cu single cryst., snowflake dendritic growth, AC effect 78—10292
- Cd, electrodeposition on solid Cd or CdHg amalgam, rate, impedance meas. 78—52693
- Cd, on Cu electrode, conditions for granular growth 80—55310
- Cd-Fe powders, predetermined comp., electrodeposition 79—70014
- CdS, electrocrystallisation of films on Cd 78—72014
- CdS film, growth by chem. bath deposition, photocond. props. 77—59703
- CdS/Cu_2S solar cell fabrication, performance rel. to Cu_2S mats. props. 77—77426
- CdS-PbS, film production, electrochem. method 77—44180
- CdSe film, soln. growth 80—66437
- CdSe film deposition, and reaction sequence of H_2SeO_3 reduction 80—71603
- CdTe cathodic deposition from aqueous electrolytes 78—64484
- CdTe thin film polycrystalline solar cells prepared by electrodeposition 80—93948
- ^{144}Ce, anodic deposition on Pt anode, electrochem. separation 79—91958
- Co, Co alloy, HCP films, chem. reduced, electrodeposition on Cu, Ni FCC crysts., struct. 79—11527
- Co, electrodeposition for solar selective surface *(French)* 79—52133
- Co-Cu, electrodeposited alloy, struct. and physicochem. props. 78—35327
- Co-Ni, electrodeposition, mag. props. *(French)* 78—64488
- Co-Ni alloy, electrodeposition of cylindrical thin films 80—29886
- Co-Ni-P, film, props. independent of mag. hysteretic and anhysteretic remanences *(French)* 80—2604
- Co-Pt alloy films, electrolytic deposition conditions over large comp. range *(French)* 80—45242
- Co-W alloy electrodeposition, influence of $MgSO_4$ and gum arabic additives *(Russian)* 80—80991
- CoNiP film, amorphous electrolytic, prep. and magnetic props. *(Slovak)* 79—51823
- Cr, electrodeposition mechanism 79—60648
- Cr film, trivalent, cathodic deposition, as bonding interface between Cu and polyethylene 80—76201
- Cr, high purity 78—84724
- Cr, high purity 80—16248
- Cr isotope target foil preparation by electrolysis 78—21110
- Cr-Cr_2O_3, black, electrolytic deposited, characterisation and thermal stability *(French)* 80—55898
- CrB_2, electrodeposition mech., onto metal electrodeposit, cermet prop. 79—33992
- Cs, pure, vac. prep. by electrolysis of glass 77—8773
- Cu, by pulsating overpotential electrolysis, digital simulation 77—81410
- Cu, cementation on Fe *(Japanese)* 79—70002
- Cu dendrites, electrodeposited, growth kinetics, cathode surface effects 79—70007
- Cu, deposits on Cu (110) electrode, morphology and crystal growth 79—47644
- Cu diffusion layer cathodic deposition and anodic dissolution rates 80—93503
- Cu, electrochem. dissolution and deposition kinetics, in aq. SO_4^{2-} soln. 78—27773
- Cu electrocrystallisation, multiple twin form. 77—39750
- Cu, electrocrystallisation, in pulse electrolysis, expt. 78—64489
- Cu, electrocrystallisation in chloride aq. soln. 77—73241
- Cu electrocrystallisation from $CuSO_4$ solns., current density/overvoltage curves *(Russian)* 79—8236
- Cu electrocrystallisation from $CuSO_4$ solns., current density under stationary surface diffusion *(Russian)* 79—8237
- Cu electrocrystallisation from $CuSO_4$ solns., exptl. methods *(Russian)* 79—8235
- Cu electrocrystallisation from $CuSO_4$ solns., expt. and slow surface diffusion theory *(Russian)* 79—11505
- Cu electrocrystallisation on graphite electrodes, nucleation 80—93504
- Cu, electrodeposited, struct, physical and mech. props. *(Russian)* 79—56939
- Cu, electrodeposition, chemical factors 80—16207
- Cu, electrodeposition, influence of specific adsorpt. of S, Cl 79—20001
- Cu electrodeposition, on a Cu single cryst. (110) face in presence of sulphaguanidine 80—76203
- Cu electrodeposition, on Cu single cryst. (111) plane in presence of sulphaguanidine 80—76204
- Cu, electrodeposition and formation of crystallised layers on Ni(111) surface, twinning 77—24495
- Cu, electrodeposition from nitrate solns., cathode polarisation obs. *(Russian)* 79—47937
- Cu, electrodeposition from cyanide solns., interaction with 2-butynediol-1,4, obs. *(Russian)* 79—47936
- Cu, electrodeposition on Cu single crystal (100) face, in presence of Br ions 78—84723
- Cu, electrodeposition on Cu single crystal (100) face and Cu polycrystal surface in presence of sulphaguanidine 80—16210
- Cu electrodeposition potential and electrolyte composition effects on surface morphology *(Russian)* 78—48337
- Cu electrodeposits obtained under influence of asymmetric AC, microscopic characts. 79—70003
- Cu, electroless bath, electrochem. control system 80—71601
- Cu, electroless deposition, pH effect, computer study 78—39709
- Cu, electroless deposition, electrochemistry 79—61520
- Cu, electrolyte development based on tripolyphosphate complexes of copper 80—45246
- Cu, electrolytic deposition from $CuSO_4$ solns. 78—61022
- Cu, electrolytic deposition, adsorption of substances used as brighteners 79—66220
- Cu, epitaxial electrocrystallisation, substrate imperfections effect 78—18921
- Cu, epitaxial nucleation and growth, on (111)Ag 80—104081
- Cu, H_2 evolution effect on current distrib. at vertical electrodes 80—35543
- Cu, in acid $CuSO_4$, ridge growth on (110) face 77—11807
- Cu, in flow-through electrodes 77—16514
- Cu, layer growth form. rate on (100) face, anions effect 80—35540
- Cu on anodised Al, pretreatment process *(German)* 80—45243
- Cu, on Au electrode in underpotential region, RHEED investig. 80—54539
- Cu, on plane vertical cathode, distrib. of local current densities 79—70338
- Cu on Su, failure anal. methods 78—24901
- Cu powder, electrodeposition prep. conditions, statistical anal. 80—20828

electrodeposition continued
- Cu powder, mathematical model for current efficiency and electric power consumption 80—20831
- Cu powder formation by constant and pulsating overpotential 77—81234
- Cu powder with homogeneous dispersion of Al_2O_3 particles 78—84743
- Cu, underpotential deposition, on Pt substrate, XPS 77—59672
- Cu, using fluidised bed electrodes, at high current density 79—100063
- Cu:Be, alloy formation kinetics at solid cathodes, metal electrodeposition from molten salt electrolytes 80—26028
- Cu-Sn alloy chemical deposition process *(Russian)* 79—47642
- Cu_2O, electroless deposition 78—27419
- Cu_xO film, growth by anodisation, switching characts. 77—55898
- Fe {211} surface, electrochemical dissolution, steps and kinks, quantitative anal. 79—74103
- Fe, cathodic electrodeposition, electrolyte acidity effect 79—61522
- Fe, in molten LiF-BeF_2-ThF_4 at electrode, voltammetric and chronopotentiometric exam. 77—1930
- Fe, powdered compacts and Armco, electrolytic boriding 79—39044
- Fe-base wear resistant dispersion hardened electrolytic coating, annealed and sintered 78—35593
- Fe-Cr-Pd, electrospark coating on alloys, corrosion resist. increase *(Russian)* 78—27669
- Fe-Ni, electrodeposition, mag. props. *(French)* 78—64488
- Fe-Ni powder, Ni clad Fe grains, exam. of electrochemical formation process 79—33974
- Fe-Ni-Cr alloy electrodeposition from sulphate electrolyte with cystine and Na citrate additives *(Russian)* 78—48336
- Fe-Ni-Cr coating, electrodeposited, exam. of passivity 78—80655
- ^{67}Ga metallic, prep. and appl. to tracer diffusion studies in liq. Ga 80—24629
- GaAs, synthesis by molten salt electrolysis 78—64486
- GaP epitaxial layers, stable growth conditions, by molten salt electrodeposition on Si and GaP substrates 79—20000
- Gd, purification by electrorefining, exam. 78—52721
- Ge powder, from fused salts 80—2979
- Ge powder electrodeposition, from molten fluoride mixtures 80—60797
- ^{166}Ho electrosorption on anodically polarised Pt surface 79—52684
- In from acid sulphate solns., electrode reactions 78—88436
- In, on Si from glycerine soln., rapid method 77—32534
- In, review 79—83144
- In-Tl, electrodeposition from aq. sulphate soln., X-ray struct. 78—84722
- InP, solvent systems, low melting point comps. in alkali metal metaphosphate/fluoride systems 79—28079
- LaB_6 electrodeposition, cathodic behaviour 79—20378
- $Li,Na/PO_3,F$ and $Li,K/PO_3,F$ systems, low melting-point comps. for electrodeposition appl. 79—43662
- γ-Mn electrodeposition influence of Cu, Ag, and Be impurities *(Russian)* 79—47938
- Mn, high-purity, from low temp. chloride electrolyte 77—4908
- MnO_2, electrodeposited from hot acidic solns., preferred cryst. growth 77—81232
- Mo alloys with Fe group metals, induced codeposition from aqn. soln. *(Japanese)* 79—4924
- Mo, electrocrystallisation from fused salts, growth rate, and struct. 77—77438
- Mo-iron group metal, binary and ternary alloys, induced codeposition from aq. soln. 79—95954
- Mo_6S_8 Chevrel phases with group IIIa metals, Nb, Hg, Pb and Cu, synthesis, stability and characts. 80—71608
- Mo_3Si, layer growth, effect of DC density, temp. 79—43160
- Mo_5Si_3, layer growth, effect of DC density, temp. 79—43160
- $Na,K/PO_3F$ system, low melting-point comps. for electrodeposition appl. 79—43662
- $Na_xLa_{1-x}B_6$, electrodeposition 79—47643
- NbO_2 hollow needles, and continuous coatings of crystallite NbO, electrodeposition from molten fluorides, SEM study 79—24423
- Nb_3Sn, high critical temperature and high sensitivity ratio on quartz 77—24502
- ^{147}Nd, anodic deposition on Pt anode, electrochem. separation 79—91958
- Ni *(Spanish)* 78—92486
- Ni, electrocrystallisation, reaction mechanism, appl. of impedance meas. *(French)* 80—103597
- Ni, electrodeposited, role of stacking fault energy 77—29016
- Ni, electrodeposition, chemical factors 80—16207
- Ni, electrodeposition from alkaline citric electrolytes, cathodic processes *(Russian)* 78—48338
- Ni electrodeposition from alkaline citrate electrolytes, cathodic process rate *(Russian)* 79—8440
- Ni electrodeposition from alkaline citrate electrolytes, coating impurity quantities and props. *(Russian)* 79—8252
- Ni electrodeposition from alkaline citrate electrolytes, Ni/electrolyte interaction *(Russian)* 79—11796
- Ni electrodeposits, influence of Ni sulphamate operating parameters on impurity content and props. 79—28971
- Ni, electroless deposition, appl. 77—70290
- Ni epitaxial electrodeposition, surface-stress phenomena at start 80—35542
- Ni films, electrodeposition, current modulation, pulse freq. rel. to struct., props. *(German)* 79—11528
- Ni, fluid bed electrolysis, deposition 80—55672
- Ni, ohmic contacts on B 77—44177
- Ni, on to $Al_xGa_{1-x}Sb$ solid soln. 80—93505
- Ni-base wear resistant dispersion hardened electrolytic coating, annealed and sintered 78—35593
- Ni-Co-Cd alloys, electrodeposition from acetate bath 78—68637
- Ni-Co-Mo alloys, electrodeposition, struct. 79—28970
- Ni-Co-W, electrodeposition, surface morphology and cryst. struct. 80—71602
- Ni-Fe alloy, continuous electrodeposition 80—16208
- Ni-Fe alloy, role of buffers and anions 80—25583
- Ni-Fe alloy film electrodeposition, modification of soln. composition 80—16209
- Ni-Fe-Cd, ternary alloy, electrodeposition from acetate bath 79—95950
- Ni-Fe-W alloy, electrodeposition, SEM and optical obs. 79—66018
- Ni-P amorphous alloys, electrodeposited and melt-quenched atomic and electronic structures 80—88062
- Ni-P coating, electroless, ultra-black surface production by chemical treatment 80—76647
- Ni-P-Al_2O_3 (SiC), composite deposit electrodeposition *(Russian)* 78—35326
- Ni-Zn alloy electrodeposition from acetate bath 77—52257

electrodeposition continued
- Pb, cathodic deposition on Ag (111) and (100) surfaces, potentiostatic obs. *(German)* 79—15616
- Pb film, on semicond. substrates 77—77425
- Pb, passivation in H_2SO_4 soln. 78—76871
- Pb, underpotential adsorption, cathodic deposition, on Ag(111) and (100) *(German)* 80—108363
- Pb, underpotential deposition on Cu substrate, phase formation 80—54538
- PbO_2 potentiostatic growth on vitreous C electrodes 79—43596
- PbSe film, soln. growth 80—66437
- Pd, electrospark coating on alloys, corrosion resist. increase *(Russian)* 78—27669
- Pd film, on semicond. substrates 77—77425
- Pd, ohmic contacts on B 77—44177
- Pd, on to $Al_xGa_{1-x}Sb$ solid soln. 80—93505
- PdH_x, preparation by low temp. electrolysis *(French)* 79—78910
- ^{147}Pm, deposition on anodically polarised Pt surface 78—27424
- ^{210}Po, galvanic deposition at rotating Ni disk electrode 80—55314
- ^{143}Pr, anodic deposition on Pt anode, electrochem. separation 79—91958
- Pt, electrodeposition, from chloride-sulphate soln., galvanostatic transients *(Russian)* 78—31655
- Pt-Fe alloy foils prep. by electrodeposition of Fe 80—35113
- Re, electrodeposited from fused salts, $(10\bar{1}1)$ texture *(Russian)* 80—92791
- RuO_2 anodic coating on Ti, struct., electrochem. props. *(French)* 79—83385
- Sb, epitaxial growth, of electrodeposits on oriented single cryst. surfaces of CU, electron diffr. study 79—66016
- Se, amorphous, anomalous currents during electrodeposition 77—44486
- Si, electrodeposited film, appl. in solar cell fabrication 78—76611
- Si, porous film, form. by anodic reaction in HF soln., struct. props. 77—24971
- Si preparation by electrolysis of fluorosilicate solns. in molten alkali halide mixtures *(French)* 78—64491
- n-Si-Cu Schottky contacts, electrochem. deposition, barrier height and ideality factor 80—75641
- SiC, electrodeposition mech., onto metal electrodeposit, cermet prop. 79—33992
- Sn fine powders, electrodeposition, effect of cathodic current density on structure 80—16238
- Sn powders, fine, electrodeposition from chloride-fluoride electrolytes 80—11598
- Sn-Bi fine alloy powder, electrodeposition, electrolyte comp. effect 80—7519
- Sn-Ni electrodeposits, worn, and Au coated, corrosion resist. 77—77633
- Sn-Pb alloys, inhibited electrocrystn. *(German)* 79—38753
- Sn-Sb alloys electrodeposition 80—25586
- Ta powder, cathodic electrodeposit, effect of electrolyte composition and process parameters, on particle size distribution 80—16233
- Te film, electrodeposition on Sn in Sn/Te/electrolyte system, interface processes 77—63923
- Te, film deposition on Cu substrate 77—48355
- Th, electroreduction from $Ca(NO_3)_2.4H_2O$ soln. 77—77772
- Ti anode, surface deposit from NaCl electrolysis, elemental anal. 78—73117
- Ti, crystallisation, effect of SO_4^{2-} radical *(Chinese)* 79—51440
- Ti, electrodeposition from $TiCl_4$ nonaqueous solns. *(Russian)* 78—48339
- TiC-Ni composite coatings, form. and wear resistant props. 77—63602
- Tl, cathodic deposition on Ag (111) and (100) surfaces, potentiostatic obs. *(German)* 79—15616
- Tl, underpotential adsorption, cathodic deposition, on Ag(111) and (100) *(German)* 80—108363
- V cathodic deposition, from crude V, V_2C and VC, hardness meas. *(Japanese)* 79—78908
- W, heteroepitaxial deposits with (110) orientation by molten salt electrolysis 78—47683
- ^{90}Y electrosorption on anodically polarised Pt surface 79—52684
- ^{169,175}Yb electrosorption on anodically polarised Pt surface 79—52684
- Zn, electrocrystallisation, reaction mechanism, appl. of impedance meas. *(French)* 80—103597
- Zn, electrodeposition, on Ni surface, nondendritic granular deposit form. 77—59968
- Zn electrodeposition, on Zn and Al single crysts., from H_2SO_4 bath, SEM obs. *(Japanese)* 80—93502
- Zn, fine powder, electrodeposition 80—60802
- Zn, from high purity industrial acid sulphate electrolyte, effects of Cd on deposit structures 79—56091
- Zn, from high purity synthetic and industrial acid sulphate electrolytes, Pb effect on deposit structures 79—56090
- Zn hot galvanisation, production components, installation and power supply *(French)* 80—66686
- Zn, inhibited, electrode kinetics and deposit morphology 79—56089
- Zn, on Cu single cryst. planes, electrocrystn. under influence of asymm. AC 77—28731
- Zn on polished Fe, reaction rate in solid state *(Japanese)* 78—15322
- Zn, on Pt single crystal spheres, critical overvoltage 80—104080
- Zn-Ag-Cu alloy powder, brazing solder, production using electrodeposition and heating in reducing atm. 79—100079

electrodeposits
- *see also electroplated coatings*
- adhesion after strain hardening, test device 80—71837
- coating props., review 79—91596
- electrocoating from molten salts 79—83394
- electrolytic Fe based composite metal-powder coating structure *(Russian)* 79—83170
- metal, electrodeposited from molten salts, faceting rel. to texture axis direction 79—28969
- metallic system, thermodynamically unstable, produced by spark discharge *(Russian)* 78—19933
- metals, electrolytic cell for making standard samples 80—85106
- microporosity induced by nucleation and growth, TEM expts. 78—10303
- multi-layer, thicknesses meas. circuit, using decade counter *(Czech)* 80—95071
- multilayer, thicknesses meas. instrument, based on destructive coulombmetric method *(Czech)* 80—8980
- multilayer Ni deposits, simultaneous thickness and electrochemical potential determination for individual layers 80—71813
- Permalloy film, electrodeposition with zero magnetostriction composition, technological control 79—33955

electrodeposits continued
Phosphate conversion coatings on steel 78—3251
polyacetonitrile film, in Pt/polymer/metal capacitors, electroforming and elec. cond. 80—54800
polymer film on Pt, energy losses, secondary electron spectra, AES, and EELS 79—99997
polytetrahydrofuran film, in Pt/polymer/metal capacitors, electroforming and elec. cond. 80—54800
spectrally selective surfaces for photothermal conversion of solar energy 80—101125
steel:Si alloy formation kinetics at solid cathodes, metal electrodeposition from molten salt electrolytes 80—26028
stereomicroscopic method for obs. of organic molecule incorporation 80—2288
stress meas. in plate, X-ray methods 79—29298
tensile testing device 80—100988
thickness determination by profilography 80—85095
thickness measurement, methods and instruments *(German)* 78—32787
underpotential deposition on Pt electrodes, XPS and AES 77—77770
Cr, hardness estimation by X-ray diffraction method 77—36708
Ag, dendritic growth inhibition by tartaric acid and tartrates *(French)* 78—87894
Ag films, electrodeposited and vac. deposited, AES depth profiling anal. 77—59232
Ag on Pt electrode, underpotential deposition, XPS and AES 77—77770
Ag-Sb alloy, reflectivity, effect of electrodeposition conditions 78—13784
Ag-Zn alloy, deposited under controlled potential, spontaneous transformations obs. 78—51853
Al on brass from $AlCl_3$/NaCl melt 77—77434
Al powder thin foil, prep. for TEM study 80—42310
$Al_xGa_{1-x}Sb$-Pd contacts, struct., preparation elec. props. 80—65684
Au alloys for electronics industry, characts. 78—52695
Au, Co-hardened, characterisation by Mossbauer spectroscopy, Co precip. formation 80—80108
Au, Co-hardened state of Co in as-deposited material, Mossbauer obs. 80—15397
Au coating, Cu diffusion process obs., under high temperature *(Czech)* 78—91486
Au, electrodeposit, struct., texture, influence of substrate *(Bulgarian)* 78—79863
Au, hard, hardening mechanisms, grain size effect 80—35302
Au surface decoration, by chemical polishing and electrodeposits on Ag (111) *(French)* 80—44445
Au-Co, characterisation by ^{57}Co-^{57}Fe Mossbauer spectroscopy 80—39989
Au-Co, Mossbauer meas. of Co chem. state 80—39990
Au-Co electrodeposit, struct. and hardness characts. 79—28245
Au-Co electrodeposits, Co hardened, chemical state of Co, Mossbauer emission spectra 79—90897
Au-Co electrodeposits, Co hardened, high temp. film formation 79—91848
C fibre reinforced Cu, electrodeposited, tensile strength *(Japanese)* 79—43333
Cd, electrocrystn. on Cu single cryst., snowflake dendritic growth, AC effect 78—10292
CdS, film electrolytically deposited, surface and bulk photocond. props. 78—60154
CdSe film, electrodeposited, for photoelectrochemical cell for solar energy conversion 80—94093
Co, and Co alloy, HCP films, chem. reduced, electrodeposition on Cu, Ni FCC crysts., struct. 79—11527
Co, electrodeposited, influence of soln. pH on microstruct. 80—65399
Co, electrodeposited coating, struct. and magnetic props. 79—46985
Co, electrodeposited film, saturation magnetisation and perpendicular anisotropy meas. 78—76277
Co-Mo alloy electrodeposits, codeposited impurities rel. to H_2 permeation, props. 79—19493
Co-Ni alloys, electrodeposited, struct., internal stress, and mag. props. 78—95471
Co-Ni-P electrolytic layers, partial anhysteretic remanent magnetisation, additivity prop. *(French)* 80—44882
Co-P, amorphous electrodeposited foils, struct. characterisation by X-ray scatt. 79—77932
Co-P, electrodeposited alloys, heat-induced structural changes *(Japanese)* 80—89263
Co-P, electrodeposited amorphous alloys with high permeability, thermal treatment with and without field 80—89372
Co-P amorphous alloy, ferromagnetic reson. exam. 79—28620
Co-P amorphous alloys, electrodeposited, magnetic anisotropy 79—28568
Co-P amorphous alloys, mag. anisotropy 80—15713
Co-P films, electrodeposited, magnetic recording media *(Japanese)* 80—29587
Co-P films with various preferred orientations, mag. props. 80—100604
Co-Pt film, saturation mag. induction, mag. anisotropy and coercive field meas. *(French)* 80—2610
CoNiP film, amorphous electrolytic, prep. and magnetic props. *(Slovak)* 79—51823
CoP, and CoNiP, cylindrical amorphous electrodeposited layers, mag. props., torsion influence 80—88848
$Co_{82}P_{18}$, amorphous alloys, electronic struct., γ-ray Compton scatt. study *(Japanese)* 80—84422
$CoPt_3$, electrolytic films, saturation mag. induction, coercive fields, thickness depend. *(French)* 80—44883
Cr, BCC, electrodeposits on {100} Cu substrates, {211} twins obs. 77—47698
Cr black films, electrodeposited, visible and IR reflectance 77—81168
Cr electrodeposit on steel, stress meas., X-ray methods 79—29298
Cr, electrodeposits, relation between preferred orientation and microstructure *(Korean)* 77—28733
Cr, formation of axial texture (111) [hkl], math. model *(Russian)* 78—84082
Cr, internal friction and bending modulus, −200 to 800°C *(Russian)* 77—39626
Cr-Cr_2O_3, black chrome electrolytic coatings for solar collectors 80—94100
Cr_2O_3 films, black, microstruct. depend. of optical props., SEM, XPS, and sputter depth-profiling 79—43049
Cr_2O_3-Cr black, on Ni, defects and their effect on props. 80—39474
Cr_2O_3-Cr black, solar collector coating, microstruct., FIM and SEM obs. 80—26166
Cr_2O_3-Cr film, optical degradation rel. to surface morphology, SEM and AES obs. 79—79401

electrodeposits continued
Cu, annealing effect on struct. and microhardness *(Russian)* 78—76668
Cu, bright galvanic coatings, crystallite size determ. 79—66221
Cu cementation on W substrate, field ion microscopy of cementation vs. substrate dissolution, pH effect 80—16206
Cu, collagen and chloride additions effects obs., on morphology and crystal orientation 78—51852
Cu deposits, morphology, polymer codeposition effects 79—74102
Cu, electrodeposit on (111) Cu substrate in presence of halo-compd. of acetic acid 80—15413
Cu, electrodeposited, struct, physical and mech. props. *(Russian)* 79—56939
Cu electrodeposition potential and electrolyte composition effects on surface morphology *(Russian)* 78—48337
Cu, electrolytic coating, brighness and adsorption of surface-active additives 80—100963
Cu electrolytic form. by electrodeposition, structural defects 77—39749
Cu electrolytically deposited on Al, annealing, ring-like pattern *(Japanese)* 78—44139
Cu film, electrodeposited, recrystallisation kinetics, X-ray scatt. *(Russian)* 78—60045
Cu film, on W substrate, cementation, vac. deposition, and electroplating, growth characts. 79—95291
Cu, layer growth form. rate on (100) face, anions effect 80—35540
Cu, obtained under influence of asymmetric AC, microscopic characts. 79—70003
Cu, on Al and Fe, defects and their effect on props. 80—39474
Cu single crystal film, electrodeposited, fatigue cracks *(Japanese)* 78—84975
Cu surface barrier influence on C diffusion in stainless steel type 1Kh18N9T *(Russian)* 80—54434
Cu, US agitation effect on hardness, porosity and grain size, work-hardening 77—60075
Cu, work function, heating temp. influence 79—33331
Cu:Be, alloy formation kinetics at solid cathodes, metal electrodeposition from molten salt electrolytes 80—26028
Cu-Al_2O_3 composite coating, electrodeposited, exam. of particle-cathode adhesion during formation 79—33954
Cu-Al_2O_3 electrodeposits, dispersion hardened, props. 79—28258
Cu-Cd, structure, electrolytic deposition on monocrystalline Cu cathodes *(Polish)* 80—44435
Cu-Cd alloy electro deposits on Cu substrate, struct. *(Polish)* 79—51437
Cu-Cd alloys obtained by electrolysis, struct. 78—91552
Cu-Cd electrodeposit on Cu, corrosion and its inhibition 79—74287
Cu-containing films, room temp. oxidation 77—48572
Fe, cast, noise reduction by electrolytic coating 78—80681
Fe coated medium C steel, distrib. of bounded fatigue limits 80—81198
Fe coatings, microhardness, Ha_5 design appl. 79—39069
Fe foil, electrodeposited, phys. and mag. props. 79—91275
Fe foils, microstruct., internal stress and mech. props. 80—20807
Fe-Co, electrodeposit, struct. *(Russian)* 79—56079
Fe-Co alloy, electrodeposited, comp. and struct. effects on H_2 diffusion and evolution overpot. 77—43377
Fe-Ni, coercive force depend. on electroplating conditions *(French)* 77—55691
Fe-Ni, sectional analyses and impurities *(Japanese)* 80—21350
Fe-Ni alloys, electrodeposit on Cu, texture investig. 77—11818
Fe-Ni electrodeposited coatings, packing defects 79—60662
Fe-P amorphous alloys, mag. anisotropy 80—15713
Fe-P electrodeposited foil, amorphous, mag. domains 80—75821
Fe-Zn, galvanization study *(French)* 80—66447
Fe-Zn, stable and metastable alloys, order-disorder, mag. interactions and corrosion behaviour 78—68422
GE, X-ray, electrochem., and electrorefl. characterisation 78—14624
KAg_4I_5, superionic solid films, preparation and elec. cond. 79—82380
Mg-Ni-S, electroforming, mech. props. rel. to heat treatment 80—35133
MnO_2 from hot acidic solutions, preferred crystal growth 77—81232
$NH_4Ag_4I_5$, superionic solid film, prep. and elec. cond. 80—54431
Ni, appl. of stereomicroscopic method for obs. of organic molecule incorporation 80—2288
Ni, crystallite morphology *(French)* 77—32535
Ni, electrodeposit, linear defect obs., TEM study 79—4304
Ni, electrodeposit structure, rel. to electrochem. noise 78—67916
Ni, electrodeposited, oxidation 78—64756
Ni, electrodeposited film, saturation magnetisation and perpendicular anisotropy meas. 78—76277
Ni, electrodeposited film, thermal anal., occlusion of gases rel. to mag. props. 80—59823
Ni, electrodeposited in sulphamate bath, cyclic stress, meas. appl. 80—19295
Ni electrodeposition from alkaline citrate electrolytes, coating impurity quantities and props. *(Russian)* 79—8252
Ni electrodeposition from alkaline citrate electrolytes, Ni/electrolyte interaction *(Russian)* 79—11796
Ni electrodeposition on Cu (001), three-dimens. epitaxial crystallites, TEM image contrast 80—88457
Ni electrodeposits, fibre textures before and after thermal treatment 79—91693
Ni electrodeposits, influence of Ni sulphamate operating parameters on impurity content and props. 79—28971
Ni electrodeposits on (001)Cu films, growth and mag. anisotropy 79—42810
Ni, electroless, on stainless steel, internal stress meas. by proximity method, features 79—64611
Ni film, electrodeposited, recrystallisation kinetics, X-ray scatt. *(Russian)* 78—60045
Ni films, electrodeposition, current modulation, pulse freq. rel. to struct., props. *(German)* 79—11528
Ni, mag. domain struct., neutron depolarisation 78—2716
Ni monocrystals, struct., effect of stress applied during electrodeposition 78—26777
Ni, on Cu, defects and their effect on props. 80—39474
Ni, on Cu, growth and microstruct. 77—11823
Ni solar collector coating, microstruct., FIM and SEM obs. 80—26166
Ni solar selective black coatings, electrochem. deposition on Zn surfaces 80—29885
Ni, textured galvanic layers, grain size determ., matrix and twinning orientations *(Russian)* 77—43461
Ni-Al_2O_3, composite coating, electrodeposited, exam. of particle-cathode adhesion during formation 79—33954
Ni-Co, strength, heat treatment and comp. var. effects 77—32660

electrodeposits continued
Ni-Co-Mo alloys, electrodeposition, struct. 79−28970
Ni-Co-P, ferromag. film, amorphous to cryst. transition, diffr. and resistivity meas. 78−60587
Ni-Fe alloys, electrodeposited, electron microscope investig. *(Russian)* 77−43442
Ni-Mo alloy electrodeposits, codeposited impurities rel. to H_2 permeation, props. 79−19493
Ni-P, electrodeposited films, amorphous and crystalline, electron microscopy, in-situ crystallisation 79−11043
Ni-P, electrodeposited film, thermal anal., occlusion of gases rel. to mag. props. 80−59823
Ni-P, magnetisation coercivity and magnetostriction 78−68338
Ni-P alloy, electrodeposited, heat induced struct. changes *(Japanese)* 78−15433
Ni-Pd surfaces, electrochem. passive film form. and comp. determ. by SEM, SIMS, XPS 80−39401
Ni-S, electrodeposited film, thermal anal., occlusion of gases rel. to mag. props. 80−59823
Ni-SiC, electrodeposited, oxidation 78−64756
Ni-SiC composite coatings, phase composition calc., wear resistance *(Russian)* 79−11709
$Ni_{1-x}P_x$, electrodeposited, amorphous, mag. and transport props. 78−52106
$Ni_{81}P_{19}$, amorphous alloys, electronic struct., γ-ray Compton scatt. study *(Japanese)* 80−84422
NiS film, mag. props., S content influence 80−44884
Pb-Bi alloy, fine powder electrodeposition and X-ray struct. obs. 78−11163
PdH_x, preparation by low temp. electrolysis *(French)* 79−78910
Pt coating on Ti, true surface area determ. by cathodic charging in H_2SO_4 79−61877
Re film, electrodeposition on Cu, packing defects, X-ray diffr. 77−1333
Sb, amorphous, explosive crystn., semicond-semimetal transition and IR absorpt. 78−51849
Si/In(-Cd), Si/Cd Schottky contacts, electrochemically deposited 80−88633
Sn-Ni, contact resist. corrosion effect 78−47847
Sn-Ni, Mossbauer meas. 80−39990
Sn-Ni alloys, electrodeposited Mossbauer spectroscopy 79−61269
Sn-Ni electrodeposit, metastable, transform. kinetics, X-ray and SEM meas. 78−38979
Sn-Ni electrodeposited equatonic alloy, cryst. struct., X-ray, electron diffr. anal. 80−79748
Sn-Ni electrodeposits, metastable, transform. kinetics 78−43262
Sn-Ni equiatomic electrodeposited alloy, surface comp. 78−47649
Tc film, supercond. transition, AC susceptibility meas. 79−95539
Ti_xO_y, oxides on Ti film electrodes, AES, XPS and electrochem. characterisation 78−7086
V cathodic deposition, from crude V, V_2C and VC, hardness meas. *(Japanese)* 79−78908
W, heteroepitaxial deposits with (110) orientation by molten salt electrolysis 78−47683
W-Ni, surface barrier influence on C diffusion in stainless steel type 1Kh18N9T *(Russian)* 80−54434
Zn coatings on steel, adhesion strength determination by centrifugal method 77−56149
Zn electrodeposit dendritic growth control using impedance meas. 78−84721
Zn, electrodeposit structure, rel. to electrochem. noise 78−67916
Zn electrodeposition, on Zn and Al single crysts., from H_2SO_4 bath, SEM obs. *(Japanese)* 80−93502
Zn, formation from various electrolytes structure dependence on cathode potential 79−57242
Zn, from high purity industrial acid sulphate electrolyte, effects of Cd contamination on deposit structures obs. 79−56091
Zn, from high purity synthetic and industrial acid sulphate electrolytes, Pb effect on deposit structures 79−56090
Zn, inhibited, electrode kinetics and deposit morphology 79−56089
Zn, on steel with Cu cladding, bond strength through intermediate Zn layer *(Korean)* 79−66213
Zn, wear resistant coating, effect of surface-active substances in electrodeposition on props. *(Russian)* 78−11359

electrodes
see also anodes; cathodes; earth electrodes; electrochemical electrodes; electron tube components; microelectrodes; welding electrodes
acoustoelectric wave excitation in piezoelec. crystals by narrow metallic electrodes 79−69777
adsorbed diatomic on electrode, reson. Raman scatt. 79−51421
air high-current pulse discharge, near-electrode process dynamics 78−71602
Al, electrodes, use of soluble corrosion inhibitors to suppress electrode dissolution 78−88565
algae, living electrode for biophotolysis of water, long-lived photoconvertor 80−104510
alkali metal seeded plasma, calc. of thermal nonequilib. near-electrode region 77−55186
alloy, high-β electron emission sites 79−61502
anodal spots form. on hot electrodes in plasma stream 78−42842
arbitrarily electroded piezoelec. plate acoustic spatial response determ. 80−99910
arc, heat exchanges obs., dependence on electrode material and cooling conditions *(French)* 80−19655
arc electrode processes thermodynamic approach *(Russian)* 77−27755
arc plasma flow-cold electrode gap, electric breakdown *(Russian)* 78−34280
array of 4 electrodes, spatial resolution, appl. to brain impedance meas. 79−84033
arterial O tension servocontrol in preterm infants 80−17183
artifact-free electrodes for recording biopotentials in strong EM fields 78−40452
atomic emission spectroscopy, discharge localisation with oxidised electrodes *(Russian)* 77−52728
atrial electrode placement, transmediastinal retrocardiac and transvenous endocardial methods 77−81685
atrial fixation permanent transvenous corkscrew electrode 77−81751
atrial-triggered cardiac pacing method and long-term results 77−81690
bacterial growth detection by impedance meas., electrode characts. 77−60325
bio-selective membrane electrode using tissue slices 79−48387

electrodes continued
biochemical sensor devices, review *(Japanese)* 79−12050
bioelectric signal recording using surface electrodes, methods of reducing movement interference *(German)* 78−85405
bioelectrode, self-correcting spherical design 77−32960
bioelectrode motion artefact model and artefact reduction by amplifier input stage design 80−56261
biological sensors of Medicor Works 79−100769
biomedical amplifier-electrode hybrid module for surface EMG pots. meas. 80−41294
biomedical electrode with SiO_2 film *(Japanese)* 80−3848
bipotential measuring, motion artifact, minimisation by skin abrasion 77−40802
blade, electrical and magnetic circuits calc. *(Czech)* 78−55273
blocking electrode, statics and dynamics of space charge regions, numerical anal. 79−51670
blood glucose sensor for implantable artificial β-cell 79−83973
boundary conditions for space charge surface layer at electrode plasma boundary, particle flux *(Russian)* 78−55736
brass, in high repetition rate spark switches, surface ageing 80−106997
breakdown dynamics, parallel electrode expts. on liquid hydrocarbons 80−15962
Bruce electrode, surface elec. field 77−75359
capacitance-dynamic electrode for bioelectric potentials 79−57782
capacitive dispersion field transducers for granular material exam. 78−85078
cardiac electrodes, safe voltage limits 79−16344
cardiac impedance during elec. stimulation, depend. on electrode, pulse duration and acid-base balance 78−27929
cardiac pacemaker electrode threshold current and optimal design *(Japanese)* 78−53569
cardiac pacing, low-threshold endocardial electrode 77−81748
cardiac pacing, signal source impedance of implanted electrodes 80−56275
cardiac R-wave detection with intramyocardial electrodes 78−44713
catalyst for water photolysis, I-V model 80−108721
catheter-tip selective electrode for measuring K in blood 77−90935
ceramic electrode in compact high-voltage vacuum feedthrough 77−26315
ceramic-based, in MHD channel, temp. distrib. 78−59258
Chang electrode profile elec. field distrib., CO_2 laser theory 79−3675
chronic sphenoidal electrodes, material improvement 79−16328
circuit breaking arcs, electrode energy balance *(French)* 80−28864
coaxial cylindrical discs, radial heat flow 78−75032
combustion product plasma, discharge on cooled Cu electrodes, rel. to erosion damage in MHD channels 78−1925
complex profiled surface alloying, automatic electrode feeding *(Russian)* 78−19936
concentric disc electrode for bladder urine vol. determ. *(Japanese)* 78−31921
conditioned metal, cohesion effects on vacuum gap electric strength 77−7618
conductivity meter for in situ ocean meas., development, testing and calibration 79−5671
conductor-two plane systems, homopolar corona volt-ampere charact. calc. *(Russian)* 78−26353
corona in SF_6 gas, electrode surface roughness effects obs., on initial corona voltage *(Croatian)* 80−54074
corona inception study on three-electrode systems, test *(German)* 77−7611
corrosion rate of basal layers, cathodic protection meas. methods *(Dutch)* 78−3297
crystal resonator electrode deposition from nozzle beam type metal vapour source 77−40376
crystallographic orientation, effect on iodide ion adsorption on Au surface 79−15020
current flow between concentric spheres at pot. up to 15 MV 77−79726
cyclic voltammograms at spherical electrodes, switching pot., drop size effects, digital simulation technique 80−40766
cylindrical electrode under corona discharge, elec. field intensity meas. 79−23473
DC corona discharges in coaxial cylinder electrode 80−33837
DC defibrillator discharge, contrib. of paddle electrode area and edge length to transthoracic impedance 80−3860
defibrillator electrode gel testing, meas. of impedance to transthoracic DC discharge 78−57056
defibrillator permanent implantable system, transvenous catheter and subcutaneous plate electrodes 79−39599
deterioration, by conc. heat fluxes in pulse discharge 77−51251
diagonal-type nonequilibrium plasma MHD generator, electrode internal and external connection effects 78−91165
diagonal-type nonequilibrium plasma MHD generator, resistive electrode and mag. flux distrib. effects 79−41884
diathermy indifferent electrodes, performance electrodes. 80−72367
dielectric constant and dissipation factor meas. in 1-200 MHz range 78−49864
dielectric space charge distrib., carrier mobility and interface injection mechanism identification 80−15974
dielectrophoresis of microscopic particles 80−50860
difibrillator electrodes, recovery curves for different materials 80−67283
ECG, 4-contact flat electrode 79−92404
ECG, EEG, interfering signals arising by cable motion 80−41296
ECG, two-electrode recording 78−28107
ECG automated monitoring, new electrode system 80−89898
ECG capacitive electrodes for burn appls. 80−41279
ECG electrode impedance and offset pot. 77−40874
ECG electrode motion artifact reduction, electronic method 77−40872
ECG surface electrode potential recording apparatus 79−83987
EEG, subdermal, orientation w.r.t. amplitude asymmetries avoidance 77−60272
EEG montage standardisation, math. logic design 77−86685
EEG sphenoidal electrode assembly for long-term monitoring of ictal or interictal EEG 77−48907
electric breakdown voltage hysteresis, electrode coating effects in air and SF_6 78−87553
electric discharge sintering, metal powder+punch electrode reactions 78−11148
electric field between two spherical electrodes with equal radii *(Japanese)* 80−28138
electrical breakdown of air gaps, 1 to 9 cm, with heated electrodes, investigation *(German)* 80−107010

electrodes continued
electro-optic modular crystal length reduction by protruding electrodes 79—76860
electro-optic waveguide modulators, capacitance of electrode system rel. to modulation efficiency *(Russian)* 80—1359
electrochemical electron transfer at electrodes in soln., review, in book, for teaching 78—8203
electrodes, laminated, for nerve biopotential recording 78—92760
electromyographic electrodes, small-size, meas. of uptake area 79—74799
electron current driven ion wave instability, excitation, electrode type effects 80—38603
electron transfer mechanism, overvoltage theory, in book, for teaching 78—8204
electrophoresis, laser Doppler, high current-density electrodes 80—89500
electroretinography improved electrode, design and standardisation 79—92401
electrosurgical dispersive electrodes, thermal performance evaluation method 79—74735
electrosurgical dispersive electrodes metal-foil, dry thermal props., skin temp. rises 80—98171
electrosurgical return electrode capable of steam sterilisation and reuse 77—40911
ellipsoidal, embedded in conductor, spreading resist. and 1/f cond. fluctuations 80—2435
EM flowmeter theory and application 80—96328
EM flowmeters with large-area electrodes, performance anal. of three models 80—1706
EMG, vector, of motor units with short, inclined and curved muscle fibres 77—86689
EMG potential sensing electrodes, types, selection criteria 77—90953
EMG surface electrode, for motor unit action potential duration meas. 78—81039
EMG surface power density spectral bandwidth rel. to electrode parameters 79—29517
endocardial electrode sensing characts. for optimal pacemaker system design 78—36072
endocardial electrogram and pacemaker sensing 77—81720
epicardial and body surface potential distributions related by geometric transfer coeffs. 77—21671
epicardial mapping with clock electrode array 78—28109
equipotential, plane meridional field analysis *(Russian)* 79—45880
erosion, under pulse discharge for various materials *(Russian)* 77—51255
erosion and aggregate condition near discharge, cellular structure effects *(Russian)* 79—37557
erosion in pulse discharge breakdown of multiple medium *(Russian)* 79—95707
evaporated interdigital electrodes, masks fabrication 78—24775
excimer laser electrodes, surface prep. metallisation techniques 80—19048
extraction electrode of ion source, cooling in long-pulse operation 80—52360
Faraday type MHD duct, lead wire position along resistive electrode, effect on current distrib. 77—76214
fibrillation threshold for intracardiac catheter as function of 60 Hz current duration and electrode area 77—86675
filters as selective electrodes for synthetic penetrating ions 80—104821
finger electrode system, tetrapolar elec. impedance plethysmography meas. 77—81608
finger-tip transducer for meas. digital vol. pulse, skin-resist. response and ECG 77—86729
flashover voltage, space charge effects *(Japanese)* 79—50917
focusing electrodes shape calculation for wedge-shaped electron-ion beam 80—53202
free-burning arc continuous radiation rel. to electrode erosion 78—71578
fuel cell electrodes, galvanostatic switching curve shapes 80—66965
fuel cell O_2 electrodes, galvanostatic transients, curve shape, 0 to 5 msec. 80—93868
fusion reactor, long pulse high current ion source electrode cooling 80—91360
gaseous electrode effect on MHD channel performance 77—84543
gastroelectric surface signal analysis, phase-lock system design 79—34687
gastroelectric surface signal analysis, phase-lock system performance 79—34688
general reciprocity theorem for conducting media 79—31770
geometrically-developed electrode-plasma boundary, electron refl. kinetic coeff. 80—24182
geometries for various dielectrophoretic force laws 78—88640
geophysical arrays for induced polarisation (IP) sounding, effects of EM coupling over uniform half-space 80—101324
glass, Mg-meso-tetraphenylporphine-coated, in photogalvanovoltaic cell *(Chinese)* 80—40865
glass-electrodes, glow discharge tube 80—33834
glassy, meas. in saline for physiological measuring and stimulating electrodes appl. 77—81764
glassy-C, elec. props. 80—17157
graphite electrode open channel config. for N_2 laser 78—55379
graphite powdered, for electrolum. anthracene diode 77—69917
heat injection into liquid, new technique 78—5637
high current diffuse vac. arc, stable mode with ring array rod electrodes 78—9894
high press. gas discharge prebreakdown processes, electrode surface inhomogeneity effects 79—14628
high pressure, discharge, in H_2 (D_2)(inert gas), props., electrode influence, spectroscopic obs. 80—38806
high-current arc electrode vapour influence and estimation 80—70070
high-current electron-optical systems, asymptotic synthesis 79—7067
high-current photomultiplier with disc electrode leads 78—58032
hot gas conductivity meas. method 80—13104
HV electrodes, epoxy resin insulation, effect on dielec. breakdown voltage of polymer sheets 80—60502
HV heavy-current arc gap 78—87514
hypodermic needle Po_2 electrode 80—98156
implantable, for recording nerve signals in awake animals 77—5119
implantable Ag electrode, for chronic recording of EEG activity in conscious dogs 77—13042
implantable stimulation electrode, standardisation problems 77—64151
implantable stress-resist. design for biotelemetry 78—44629
implanted cardiostimulator pulse recording 77—78041
inelastic electron tunnelling structure, cover electrode metal effects 78—19127

electrodes continued
instruments for use in electrode process research, review 78—21174
insulated glass electrodes, in AC display discharge, charge modes *(German)* 77—43087
intense electric fields in needle/cylinder electrodes, distribution *(Rumanian)* 80—63885
interdigital, for arrival time detection in drift mobility meas. 77—11954
interdigital transducer design with spectral weighting frequency response 77—27454
ion electrostatic interaction at electrode surface, ion field penetration 80—81333
ion extractor electrode CAD *(Japanese)* 78—86680
ion selective electrodes, appl. 79—44022
ion sensitive FET theory based on membrane electrodes 80—41280
ion-to-electron conversion dynodes, prep. by plasma anodisation 77—1887
ionic crystal, space charge polarisation involving electrode reaction with surface adsorption 77—12019
IR point-contact diode tunnelling and rectification rel. to electrode geometry 80—57378
isolated, AC discharges, gas temp. depend. 80—38800
JG ionisation gauge, effect of electrode voltages on elec. field distrib. 77—49737
Kelvin method contact PD meas. manipulator 78—57979
liquid and spherical particle permittivity meas. by dielectrophoretic levitation 79—17447
liquid crystal cell, for uniform colour generation by optical birefringence 77—68911
low press. discharge, attractive forces on electrodes 80—49041
low temp. dense plasma electrode phenomena, review 80—33743
magnetite, electrode, polycrystn., differential capacitance 80—66136
mass transfer to continuous moving surface 80—69821
membrane, chalcogenide ceramic, Cu-selective electrode *(Chinese)* 80—81357
metal, approx. soln. for damage by pulsed discharge 77—39500
metal-dielectric system, gas cavity initiation-discharges phenomena *(Polish)* 80—19660
MHD channel, with one pair of electrodes, current distrib. 77—39475
MHD convertor, current concentration due to Hall effect, elimination by variable resistive electrodes 77—80378
MHD generator, compressible laminar boundary layer separation from segmented electrode wall 77—27598
MHD generator, diagonal electrode config., nonuniform conductivity in boundary layer, effect on local characts. 77—39471
MHD generator, electrode fabrication by plasma deposition 77—39474
MHD generator, Faraday type, current profile optimisation, electrode cond. profile 78—94939
MHD generator, plasma interelectrode breakdown, model 79—55572
MHD generator channel, current distrib. 77—43084
MHD generator channel, metal electrodes erosion 80—24260
MHD generator channel electrode surface temp. selection, effect of working body props. 79—55573
MHD generator metallic electrodes, arc discharge of near-cathode region 79—1346
micro-organism electroretention effectiveness rel. to electrode type *(Russian)* 80—26419
minerals, electrodes and paste specimens for emission spectrographic anal. *(French)* 78—92563
miniature dry surface electrode for infant heart rate determ., clinical evaluation 77—56505
mirror-antisymmetric two-dimensional compound region electrode current density *(Japanese)* 79—89842
multichannel functional electrostimulator design for paretic gait correction 79—57810
multielectrode for intracortical recordings prod. by thin-film technology 77—48959
multipoint electrode for biological pot. recording 80—104784
needle electrodes, spark voltage effects *(Korean)* 78—1931
negative glow plasma, contact electrode charging time meas. 78—67525
neurological coaxial depth electrode development 79—29687
Nikrothal LX wire, 50 μm, implantable, for telemetric registration of electroureterograms 77—86668
noncatalytic, for solid-electrolyte O_2 sensors 80—76573
nonequilibrium MHD duct with resistive electrodes, computer simulation, performance characts. calc. 77—72509
nonequilibrium polarisation states props. of electrode systems, overvoltage theory, in book, for teachers 78—8205
oesophageal pacing in infants, conductive rubber electrode 77—81741
organic liquid conductivity and bulk charge determ. cell *(Russian)* 80—57328
oxide film on metal electrode, nonadiabatic theory of electron transfer 77—28237
pacemaker, endocardial screw electrode stability enhancement 77—81746
pacemaker electrode effects on pacing thresholds 78—36071
pacemaker electrode filtering characts. rel. to electrogram 77—81744
pacemaker electrode geometry rel. to pacing threshold and R-wave sensing 77—25611
pacemaker electrode insertion via cephalic vein, thrombosis obs. 77—81714
pacemaker electrode orientation, simulation of vol. conductor effects on cardiac dipole 78—28108
pacemaker electrode stimulating and sensing characteristics 77—81743
pacemaker epicardial electrode implantation 77—81703
pacemaker lead failure type discrimination 78—53570
pacemaker myocardial and endocardial screw-in electrode expts. 77—81747
pacemaker time constant variations with normal and malfunctioning electrodes 77—81724
pacemakers, bipolar sensing for demand pacing, effect of interelectrode distance 78—40418
pacing electrode longevity analysis 77—81750
pacing electrode material evaluation 77—81742
pacing threshold and sensed signals, influence of electrode positions 77—81729
partial discharge inception voltage, determ. from field distrib. of electrode arrangement *(German)* 79—94829
pasteless electrode for clinical use 79—92413
PDX neutral beam injector, multi-aperture ion accel. electrodes thermal anal. 80—102371
percutaneous electrode system development 77—5106
periodic electrode struct., elec. field, analytic method of solving simultaneous eqns. 77—75362

electrodes continued
pH, rapid response, cardiac output and ventricular residual fraction determ. 77—40860
pH measurement, continuous, enamel electrode design *(German)* 79—34413
pH measurements using polarizable electrodes 80—76514
pH monitoring instrument research, designs 77—81438
pH monitoring systems, limitations due to electrodes 80—3421
piezoelectric plates with rectangular electrodes, two-dimensional energy trapping 77—27458
pill electrode for cardiac arrhythmia study 79—39566
planar electrodes, distributed capacitance, optic and SAW device appls. 77—27387
plasma electrode, electric field compression 80—64736
plasma-electrode contact processes, microplasma diagnostics 80—59325
plasma-electrode interface, geom. extended electrode, charged particle and energy fluxes 78—79442
plastic bounded, for emission spectrometric anal. of nonconducting powders 78—48714
point to plane electrodes, corona current experimental equations *(Japanese)* 79—50918
point-plane systems, short, breakdown phenomena critical survey 79—4206
polarisation noise effect on flow transducers in electromagnetic flowmeters 79—7426
polarographic sensor with microwire indicator electrode, exam. of design 80—21340
polyethylene charge carrier injection, contactless electrode expt. 80—15540
polyethylene life test needle electrode selection 80—15969
polyethylene terephthalate charge transfer from metallic electrodes 80—15605
polymer-modified electrodes, electrochromic characts. 80—66149
polymers, elec. capacity calc. strip electrodes system for dielec. props. study 80—25327
porous electrodes, effect of porosity 80—66815
porous sintered battery material *(German)* 80—21394
positive corona electrode, negative ion counterflow, elec. field strength meas. 80—38817
precardial lead belt, general-purpose ECG 79—48361
pressurised field distortion spark gaps, arc voltage waveforms, electrode material effects 78—87549
PVF$_2$ charge injection from metallic electrode, obs. 80—15947
quartz, electroded doubly-rotated thickness-mode resonators, temp.-induced frequency 79—55298
quartz rectangular AT-cut plates with patch electrodes, vibration modes 79—55295
rare earth chromite based electrode material development for MHD generators 80—84893
rectangular electrode and array dimensioning on AT-cut quartz crystals 77—39169
RF discharge, electrode sheath 80—44052
rheographic electrode system for thyroid gland 79—57783
rheography, integral method and electrode for exertion function tests 77—77995
rotating electrode, for improved reproducibility in spark source mass spectrometry 78—93781
safety models, evoked pots. recorded from cat cerebral cortex 78—31797
SAW scattering in piezoelectric material, by metallic electrodes anal. 78—83157
scala tympani electrode for auditory prostheses, 8 channel 80—36194
screening, discharge phenomena with UHV positive and negative lightning and switching pulses for dimensioning *(German)* 80—87963
secondary cells, Ni-Cd, plastic-bonded electrodes positive active layer study 80—101088
semiconductor coated dielectric, for triggered vac. gap 77—47286
shallow bulk acoustic wave generation by interdigital transducers 79—51411
shaping electrodes for circular, conical charged-particle beam, exact anal. 77—19155
skin conductivity measurement, electrode materials *(German)* 78—85406
skin-electrode processes obs., during medical electrography 77—40828
solid solution electrodes, characterisation and performance, secondary battery appl. 80—72033
spark gap electrodes, erosion characts. 80—103204
spark gaps with parallel plane electrodes, erosion characts. 80—70076
spark-gap, electrodes, acoustic phenomena in erosion 80—64796
sputter electrode preparation for multiply charged heavy ion sources 78—66009
stainless steel, cathodic protection against corrosion, biomedical appl. 77—90923
steel, erosion resist. influence of C and carbide-forming elements *(Russian)* 78—11389
steel, for discharge sintering of metal powders, effect of diffusion coatings 77—63598
stimulating electrodes of different materials implanted in cat skeletal muscles, threshold meas. 80—101297
stress corrosion crack, electrode pot. distrib. 77—90506
superionic-electronic solid solution electrodes, partial cond. meas. technique 80—44360
supraventricular arrhythmia rapid anal. from long-term oesophageal recordings, drug assessment 80—89904
surface and coating effect on DC breakdown voltages in SF$_6$ 78—87557
surface EMG bipolar recording, influences of electrode geometry 79—53269
surface finish backscattered electron intensity meas. *(Japanese)* 77—66081
surface plasma source, H$^-$ ion form. and secondary electrons *(Russian)* 78—71503
surface potential distribution meas. by vibrating electrode 79—67340
surface potential meas., guarded electrode design which has small gap between electrode and guard ring 80—68215
surface roughness, effect on electric breakdown in air 80—84018
surface roughness effect on breakdown in N$_2$-SF$_6$ mixtures 77—39490
surface with adsorbed molecule, enhanced Raman scatt. 79—95767
suspension of charged sphere, electrode geometry choice *(Russian)* 79—10240
sweat test equipment safety improvement 79—29649
teflon, C-loaded, for chronic EEG recordings in microwave research 80—67305

electrodes continued
thermionic, cermet electrode development for flame heated thermionic convertors 80—40891
thermoelectrode material nonuniformity data analysis 77—61065
transcutaneous electrical neurostimulation serial/parallel interface system 79—92321
transparent conducting coatings, book contrib. 78—10587
transparent conductors, figure of merit 77—1741
transparent electrode deposition on PLZT ceramic, elec. and opt. props. 78—74848
transport of atoms in arc electrode channel *(Russian)* 77—52725
vacuum arc, high current, novel electrode geometry 78—1933
vacuum gap, microscopic obs. 77—84554
vacuum gap breakdown initiation by microparticle impact 80—96413
vacuum gap electrode surface sorption, mass spectroscopic obs. 78—75466
vacuum gaps, thermal press. effect on elec. strength 78—42843
vacuum tunnelling electrodes, gap control via thermal drive apparatus 77—8175
variable cross-section electrodes for miniature thermocouples, construction method 78—24788
ventricular fibrillation detection in animals appl. *(German)* 78—3461
ventricular muscle excitation threshold current rel. to electrode area, volume effect 77—81670
on vibrating sphere, mass transfer 80—61106
vibratory processes at metal-electrolyte interface, apparatus 77—39732
water, electrical breakdown in μs regime with Cu, brass, steel and Al electrodes 80—103917
wire-plane electrodes, breakdown voltage, effect of vacuum conditions 80—64798
wire/plane electrode air discharges in strong nonuniform field *(Rumanian)* 79—68964
X-ray streak camera electrode design using a plasma simulation code 79—30632
Z-pinch, noncylindrical, electrode domain, mag. field penetration *(Russian)* 77—11382
Ag, adsorbed cyanopyridine isomers Raman scatt., orientational specificity 79—69822
Ag, enhanced Raman effect from adsorbed cyanide 80—50348
Ag-AgCl reference electrode for high temp. and high press. electrochemistry 78—35693
Al, charge effects on insulating films obs., PET and SiO$_2$ 80—75625
Al electrode, cathodic luminesc. of oxide covering in electrolyte soln. 77—69915
Al, in high repetition rate spark switches, surface ageing 80—106997
Ar magnetic helical arc electrode, for MHD generator, visible, RF and probe diagnostics 78—9867
Au, diffusion into polymer film 79—77821
Au-Si-Al structure electrode mass transfer and switching with memory 78—95389
C electrode breakdown voltage dependence on adsorbed gases 78—75465
C electrode damage in arc, and current densities 79—23468
C, used in emission spectrography, isotopic labelling study, plasma appl. *(Hungarian)* 80—106976
C-fibre, elec. props. and EEG appls. 80—72355
CdO-SnO$_2$ film, DC reactively sputtered, transparent electrode props., optimum sputtering conditions 80—11116
CdTe electrode, redox reaction due to complex M(CN)$_6^{3-/4-}$ *(French)* 80—89482
CoO, evaporation curve struct. from AC arc electrodes *(Russian)* 78—3051
Cr electrodes, arcing and breakdown meas. in vacuum 77—24238
Cu, degradation in coaxial plasmatron by thermal shock, microscopic shock formation 79—14629
Cu, erosion due to high-current pulses, effect of media 79—10735
Cu, H$_2$ evolution effect on current distrib. at vertical electrodes 80—35543
Cu, with Al$_2$O$_3$ inclusions, breakdown and emission props., effect of inclusions 79—87389
Cu-BN composite electromachining tools, dynamic hot pressing 80—84889
Cu-Ni alloy, in 0.1 M NaCl, electric pot. and pH meas., crevice corrosion 78—31564
Cu-selective electrode, chalcogenide ceramic membrane *(Chinese)* 80—81357
Fe alloy electrodes, rolled from powders, sintering problems 80—25608
Fe, corrosion and passivation in presence of halide ions in aq. solns. 80—50758
Fe, pure circular disc electrodes in (Na, H)ClO$_4$ solns., complex formation meas. 80—55569
Fe, rotating disc electrode, corrosion in acidic chloride soln. O$_2$ and benzotriazole effects 78—35564
FeO-Fe$_2$O$_3$, evaporation curve struct. from AC arc electrodes *(Russian)* 78—3051
α-Fe$_2$O$_3$, polycryst., pure and TiO$_2$ doped, flatband potentials, donor densities, photocurrent meas. 78—76089
GaAs electrodes, n- and p-type, freq. depend. of impedance 77—12001
GaAs electrodes in aqueous electrolytes, localised avalanche breakdown 79—4599
GaAs:Cu electrode photographic device, CO$_2$ pulsed laser output high-speed meas. 79—14008
Gd small ion-getter pump 78—89487
H, construction 77—25329
Hg drop electrod in MOS struct., Na-induced work function shift 79—42652
In film, evaporated, resist., Hall effect and light transmittance, use as semitransparent electrode 77—39966
In$_{2-x}$Sn$_x$O$_{3-y}$ film, deposited from organometallic composition, transparent cond. appl. 78—91793
Li plasma, electrode pot. layer characts., surface ionisation and Schottky effects 77—15260
LiNbO$_3$ blazed grating electro-optic deflector development 77—42627
Mo electrode, corrosion rate in molten glass *(Chinese)* 80—66687
Mo electrodes, in glow discharge, H penetration and diffusion 77—7629
Mo, low-temperature thermionic converter with an expanded-area collector 80—70045
Mo$_2$B$_5$-based alloys, mech. props., rel. to appl. as electrodes in electrospark machining 80—21174
Nb-NbO$_x$-PbIn tunnel junctions with ultra-thin Nb electrodes 79—56398
Ni alloy, thermionic electron emission into Cs vapour, for thermionic convertors 78—60540

electrodes continued
  Ni, electrochem.-ellipsometric studies of oxide films formed during O_2 evolution 79−16007
  NiO, evaporation curve struct. from AC arc electrodes *(Russian)* 78−3051
  Pb-acid battery, effect of H_3PO_4 on positve electrode, constant pot. corrosion studies 79−92071
  Pb-acid battery positive, cyclic corrosion 79−92072
  Pb-Bi counterelectrode Pb alloy Josephson junctions 80−65743
  PbIn oxidised electrodes, symm. and asymmetric supercond. tunnel junctions, subharmonic gap struct. study 79−60981
  PbS, nonstoichiometric, increase of rest pot. with p-type semicond. character 78−56170
  $Pb(Zr,Ti)O_3$, internally electroded with Pt, resonance behaviour 80−84701
  Pd, enhanced arcing as function of organic exposure and arc current 80−38778
  Pd, in H_2O/D_2O electrolysis, H/D isotopes separation factors 79−50149
  Pd/Ag, enhanced arcing as function of organic exposure and arc current 80−38778
  Pt, elec. props., impedance meas. and time-domain anal. 78−40360
  Pt, for elec. stimulation, exposed electrode area determ. 77−86704
  Pt, for elec. stimulation, max. surface redox limits estimation 77−86705
  Pt, nonlinear AC and DC polarisation obs. 80−56247
  Pt, polished, linear AC electrode polarisation impedance anal. 77−40806
  Ru electrodes, reversibility and growth behaviour of surface oxide films 79−20263
  SF_6, compressed, influence of electrode macroscopic curvature upon surface roughness effects 80−40693
  SF_6 high-current arc props., influence of electrode material 78−71592
  Si solar cells, semiconductor thick film cell contacts, all metal 80−30489
  SiO_2, CVD film, hydration props., ellipsometry meas. 78−22986
  SiO_2 charge transfer from metallic electrodes 80−15605
  SnO_2 electrodes, dye-modified, erythrosin, attachment, X-ray photoelectron, photocond. investigs. 79−43600
  SnO_2 transparent electrodes, effect of Sb doping on elec. and optical props. *(Korean)* 77−1749
  SnO_2, VUV transparent electrode formation by chemical deposition and vacuum sputtering 79−56929
  Ta electrode, cathodic luminesc. of oxide covering in electrolyte soln. 77−69915
  Ti electrodes, RuO_2 coated, corrosion during O evolution rel. to electrode prep. *(French)* 80−76420
  TiO_2, rutile, thin film CVD 77−77409
  W electrodes, C segregation and arc damage 80−64795
  W, method for sealing into quartz 79−71463
  W_2B_5-based alloys, mech. props., rel. to appl. as electrodes in electrospark machining 80−21174
  WC-Co, conditioned metal electrode, effect on electrical strength of vacuum gap 79−90489
  WCs, preparation method effects on catalytic activity for H_2 evolution 80−101024
  Zn, intergranular dissolution of sacrifical anode in seawater at elev. temps. 79−96181
  ZnO binder electrophotography, tone reproduction and copy quality *(German)* 78−62259
  ZnTe electrode, redox reaction due to complex $M(CN)_6^{3-/4-}$ *(French)* 80−89482
  p-ZnTe, interface impedance in KOH electrolyte soln. *(French)* 77−51814
  ZrD, electrodes with externally ignited vacuum arc source of D^+ ions 80−33845
  ZrO_2-Y_2O_3-Nd_2O_3, high-temp. thermophys. props., MHD generator electrode mat. 78−26663

electrodynamics
  see also electron beams; electron optics; electron tubes; ion beams; ion optics; ion sources; quantum electrodynamics
  Abelian Higgs model relation to spontaneously broken massless scalar electrodynamics 77−54057
  Abraham-Lorentz, equation, nonrelativistic energy integral 78−17849
  AC forces acting on conductors of bifilar lead *(German)* 79−41281
  AC repulsion, Elihu Thomson expt. 79−62980
  accelerated point charge, bound and emitted four-momentum, retarded integration 78−66738
  accelerators, circular, transverse coupling impedance meas. 79−36446
  action-at-a-distance theory of electrodynamics with Dirac's monopoles 79−63059
  adiabatic hypothesis, old quantum theory, rel. to classical electrodynamics, zero-point EM radiation 79−2661
  adiabatic invariant motion, charged particle in space periodic wave, variable length pendulum *(Russian)* 79−2623
  adiabatic invariant of charged particle spiralling in longit. mag. field 78−58892
  algebras for external EM interaction with relativistic fields 77−2722
  angular momentum conservation, interaction of elec. and mag. charges 78−8253
  angular momentum radiated by classical point particles 79−97220
  anisotropic artificial dielectrics, dispersion props, investigation, electrodynamic method 80−88903
  anisotropic relativistic and dissipative fluid model *(French)* 77−67357
  arc discharge, electrodynamic anomalies, ion electron mutual action, torque 77−84549
  aspects of electrophotography *(Japanese)* 80−13170
  astrophysics, electrodynamic and gravit. effects of Proca stresses 78−93098
  asymmetric Maxwell theory, additional universal inverse square forces 80−27149
  atmosphere electrodynamic state, horizontal mag. field component influence *(Russian)* 78−73556
  atom, many-electron, in external mag. field, Hamiltonian and classical electrodynamics 77−79576
  atom interaction with pair of conducting plates 79−97990
  bag model for hadrons, classical interpretation, solns. of Maxwell eqns. 78−37183
  beam multiple scatt. displacement by parallel mag. field 79−81110
  binding energy of electron in elec. dipole field 79−98220
  birefringence in moving anisotropic media 79−80432
  bodies at rest including quadrupoles, theory *(German)* 78−81858
  Boltzmann distrib. for relativistic free particles and Rayleigh-Jeans thermal radiation law, inconsistency 79−49036

electrodynamics continued
  Born-Infeld theory, review *(Polish)* 79−35576
  boundary conditions for media with spatial dispersion and transition layers *(German)* 80−78742
  boundary problem solution for complex shape regions 80−69300
  boundary problems, method for solving 80−95773
  bounded motion, low initial vel. electron in logarithmic elec. field 79−68358
  bremsstrahlung, quasiclassical limit 77−67606
  bremsstrahlung from electron high-energy collisions, mag. field effects *(Russian)* 77−61906
  Caldirola equations, generalised, for classically radiating electron 77−82401
  cause and effect relationship 78−54108
  charge bunch radiation losses in pill-box resonator, time domain numerical computations of EM fields 79−31781
  charge creation, advanced pot. *(Russian)* 78−12580
  charge depend. on velocity 78−28965
  charge moving along elliptical orbit, spectral radn. distrib. 77−19148
  charge radiation in waveguide with transversally moving walls, anal. *(Russian)* 79−888
  charged elastic fluid sphere, interior soln. in general relativity 77−9929
  charged liquid, SCF equation, partial soln. *(Russian)* 78−74823
  charged magneton, eqns. of motion, covariant form *(Russian)* 78−13650
  charged particle, gyrating, adiabatic invariants 80−83544
  charged particle, in external EM field, invariance operator groups 77−71912
  charged particle, mag. moment vac. on nonadiabatic motion in dipole field *(Russian)* 77−42476
  charged particle beam dynamics, moment method 78−33655
  charged particle confinement in superposed cylindrical cusp field and biconical cusp field 78−18435
  charged particle crossing boundary between dielectric media, synchrotron radiation *(Russian)* 77−61903
  charged particle dynamics in quasimonochromatic wave in presence of strong mag. field *(Russian)* 77−27232
  charged particle ensemble, motion in electric field of plane electrodes *(Russian)* 77−3527
  charged particle in field of amplitude-modulated plane wave, motion and radiation 80−18976
  charged particle in field of quantised plane wave *(Russian)* 79−890
  charged particle in gravit. wave field, EM wave propagation *(French)* 77−67353
  charged particle in homogeneous magnetic field, Cartesian and polar wave functions 80−68061
  charged particle in plane waves, accuracy of adiabatic invariant conservation 80−37946
  charged particle in quasimonochromatic wave, drift theory of motion *(Russian)* 79−891
  charged particle motion at vac.-medium interface, transient radiation emission spectral distrib. 80−63901
  charged particle motion in alternating elec. fields, scaling conditions 80−63903
  charged particle motion in dipolar axially symmetric field 77−68155
  charged particle motion in homogeneous rot. mag. field *(Russian)* 77−23602
  charged particle motion in medium along EM wave 79−55037
  charged particle orbits in helical magnetic fields 80−99613
  charged particle self-reson. motion in EM wave with varying propag. vel. 77−75399
  charged particle trapped in mag. field, bounce motion 79−67150
  charged particles, classical field model 78−12807
  charged particles, equilibrium space distrib. *(Russian)* 79−22887
  charged particles, HF pot. and decay in rapidly oscill. irregular field *(Russian)* 77−6986
  charged particles in external fields, classical Dirac, Klein-Gordon eqns. 77−49829
  charged particles in plane waves, hamiltonian formalism *(Russian)* 79−98268
  charged particles in single wave fields, adiabatic and stochastic motion 80−9795
  charged particles interacting with EM field, line-integral Lagrangian 79−81346
  charged scalar particle in field of running electric wave *(Russian)* 79−889
  charged scalar solitons, electrodynamics 80−42078
  charges of finite extension, generally covariant formulation 78−77731
  Cherenkov losses of relativistic neutron in conducting medium 78−5410
  classical charged particles with spin 78−65790
  classical electrodynamics, nonlinear gauge approach, charged particle solns. 78−32695
  classical electrodynamics of point particles, energy tensor struct. 79−21566
  classical field electrodynamics, conservation principle, history, review *(Russian)* 78−36849
  classical massless scalar electrodynamics, charge confinement by classical instabilities 79−58933
  classical motion of extended charges, eqn. of motion energy balance determ. 79−10250
  classical predictive dynamics of two charges with radiation 79−88817
  classical predictive electrodynamics, energy and 3-momentum balance and scatt. cross sections 79−88818
  classical radiation reaction theory, 1-dimens. Coulomb force problem 77−74235
  classical recombination cross section 79−25876
  classical spinor field, indefinite charge 77−71221
  classical stochastic electrodynamics, positive temp. random EM field 79−40382
  coherent EM radiation intensity, produced by modulated electron/ion beams in gas 78−50686
  coherent excitations interacting in dispersive medium, envelope-soliton propagation 79−2639
  coherent radiation, from electron bunch, electron distrib. effects 78−66734
  cold black holes, fields and particles surrounding hole, motion in elec. field 78−20850
  colloids, interfacial electric polarisability, and interactions 80−108751
  comets type I tails, ray struct. and electrodynamical forces *(Russian)* 79−101119

electrodynamics continued
Compton scatt. by interfering EM fields from independ. sources 80−43241
conducting mag. top, fast rot. in inhomogeneous alternating mag. field 79−41264
conducting solid, motion near fixed point in mag. field *(Russian)* 78−13651
conductor, magnetodielectric material-coated, finite-length relativistic charge interaction 80−5666
conductor, solid, contact phenomena incorporation in electrodynamics eqns. 80−29374
conference, nonlinear problems in theoretical physics, Jaca, Gain 1978 80−4478
conformal electrodynamics in Einstein spacetime 80−31644
conservation laws for the classical Maxwell-Dirac and Klein-Gordon-Dirac equations 79−49066
contactless suspension of objects in elec. and mag. fields, oscill. field stabilising effect 77−68150
conventionality of simultaneity without one-way velocity assumptions 79−12594
cosmic electrodynamics, photon rest mass as test of Maxwell's eqns. 77−45708
cosmic ray path tracking in time independ. mag. field, helix predictor corrector method 79−62692
Coulomb centres at small separation when (Z_2-Z_1) is large *(Russian)* 78−12583
Coulomb interaction, spatial energy distrib. 79−88820
Coulomb interaction of electrons by virtual photons exchange, quasiclassical interpretation 78−41523
Coulombic scatt. of charged particle by random distrib. as two-body process 77−38789
covariant electrodynamics in a medium, formulation 79−70
crystal accelerator, radiative energy loss 80−23611
cyclotron radiation from oppositely directed electron beams 78−78874
cylindrically symmetric electrovac universes satisfying vacuum field eqns. 79−17303
Debye screening in dilute classical Coulomb systems 78−41170
definite integrals of generalized functions 79−50200
deflecting magnet for external beam of 150 keV accelerator, influence of magnetic fringing field 78−46195
deformable bodies of finite extent 77−65560
deformable bodies with electric and magnetic quadrupoles 80−62492
deformable media, electrodynamics, nonrelativistic classical field eqns. 78−49679
deformable media, electrodynamics, relativistic field equations 78−49678
dielectric, isotropic elastic thin shells, nonlinear electrodynamics 77−88626
dielectric crystal, cubic, accel. of charged particles, wave-induced reson. *(Russian)* 78−25784
dielectric isotropic nonlinear elastic shells, electrodynamics, eqns. of motion 77−88627
dielectric isotropic nonlinear elastic shells, electrodynamics, constitutive eqns. 77−88628
dielectric solids, molecular optics model, electrodynamic eqns. derivation 78−27151
dielectric sphere, motion in travelling elec. field 78−50685
differential geometrical methods in electrodynamics, space-time manifold 78−45471
diffraction radiation generators electron flow study by changes in generator heat characts. *(Russian)* 78−37796
dipole field, charged particle motion, forbidden zone 78−46501
dipole particle dyanmics, integrable problems 80−18980
dipole particles in axisymmetric electrostatic and magnetostatic fields, meridional trajectories 80−78750
Dirac equation, iterated second-order, derivation for inhomogeneous media *(German)* 79−81349
Dirac particle, in EM field, Hermitian interaction terms 77−33752
direct action theory and magnetic monopoles 78−28963
discharges in condensed media, electrodynamics problems, theoretical investigation *(Russian)* 80−75116
discrete space-time, geometric formulation of electrodynamics and general relativity 77−26184
dispersive, absorptive medium, energy density and evolved heat 77−13621
Doppler-shifted photons, origin of increased energy explained by mechanics of source, teaching 78−28897
double bremsstrahlung of soft photons *(Russian)* 77−31052
dynamical and kinematical charges in classical nonlinear scalar field 78−54208
dyon field, extended Yang-Mills formalism, Mandelstam's path depend. formalism 78−62288
eddy currents in conducting slab, electrodynamic forces on coil, anal. *(German)* 77−58226
education, Brewster angle in semi-infinite dielectric moving perpendicularly to interface 80−57034
education, charge hyperbolic motion and radiation 78−49587
education, EM field multipole expansions, spin-weighted spherical harmonics 77−33766
education, EM plane wave accel. of free electron 77−78917
education, Lienard-Wiechert field expression, circulating charge in static mag. field 78−69933
education, Lorentz theory for classical radiation reaction of accel. charged particle, dumbell model 78−49592
education, Lorentz-Dirac eqn. for classical charged particle, mass renormalisation 78−62007
education, point charge system, pot. energy of equilib. config. 77−87602
education, relativistic line of charge over ideal conductor, net force 78−36762
education, Rutherford scatt., electron deflection, inverse 1st, 2nd and 3rd power field, program 77−87594
Einstein-de Sitter universe, classical predictive electrodynamics 80−86175
Einstein-Hopf model approximations, random electrodynamics 79−80453
elastic dipole, in periodic struct., free oscills. 79−27145
elastic media, dissipative, relativistic electrodynamics 80−73219
elastic scattering and bremsstrahlung theory of fast charged particles in crystals *(Russian)* 79−28853
electric charge conservation *(Russian)* 78−77739
electrically conducting body, forces in mag. field using hydrodynamic analogy 80−34551

electrodynamics continued
electrodynamics, Coulomb law, extension to 4-dimens., confining potentials 79−36012
electrodynamics, Ritz's theory based on particle interactions, review of original paper of 1908 80−47
electrodynamics of superconductors as a consequence of local gauge invariance *(German)* 80−103778
electromagnetic quadripotential for the pure-radiation field generated by a classical charged point-particle 79−63058
electron, motion in canted hyperbolic elec. field and homogeneous mag. field 79−27146
electron acceleration by inhomogeneous electrostatic RF field 78−82538
electron acceleration in EM field, new field theory appl. *(Chinese)* 80−62494
electron autoreson. motion, effect of longitudinal wave field *(Russian)* 79−7063
electron band structure, optically induced in external plane wave field 80−106432
electron beam, Cherenkov modulation 78−5408
electron beam energy spread on result of Cherenkov diffr. 78−5407
electron beam explosive instability in helical resonator, RF emission 79−55520
electron beams, electrodynamic principles of rotating relativistic types 78−71019
electron bremsstrahlung spectrum in point Coulomb field, classical and nonrelativistic quantum theory 78−65792
electron classical motion in wave of slowly varying amplitude 80−28658
electron currents in vac. relativistic generalisation of Child/Langmuirs laws *(German)* 78−36843
electron gas, layered, with random inhomogeneities, plasma wave damping 77−51689
electron in Coulomb field, operator Green's function 78−46500
electron in magnetic field, induced angular momentum, classical and quantum calcs. 78−86060
electron in random pot., partition function 78−29040
electron in standing laser field, classical motion 78−17851
electron motion in combined magnetic and electric fields 77−27237
electron motion in elec. and mag. fields, student lab. and computing studies 80−27076
electron moving in field of two plane waves and mag. field, theory of emitted radiation *(Russian)* 77−79733
electron radiation in field of 2 plane noncollinear EM waves *(Russian)* 77−10825
electron relativistic self-field interaction, particle-like solns. 78−16666
electron scattering in LF laser field, sum rule and classical limit 80−18978
electron spin magnetic moment relativistic mass correction, classical reinterpretation 77−57213
electron theory, Grossman-Peres model, canonic formalism and relativistic invariance *(Russian)* 78−12833
electron trajectories, in homogeneous elec. fields, relativistic and classical 77−41436
electron-dipole system, semiclassical quantisation, for teaching 79−25799
electron-photon cascade production and transport is externally applied EM field, appls. 77−68157
electrons, random motion in dielectric media, energy loss, anal. calcs. 78−29888
electrons, runaway solutions and finite size 77−45710
electroslag welding, electromechanical and thermal flow phenomena 79−11758
ellipsoidal charged particle bunch, self-consistent motion, approx. soln. 79−13881
EM field calc. using integral equation method 79−64157
EM field characteristics *(German)* 77−42457
EM field energy-momentum tensor in phenomenological electrodynamics *(Czech)* 80−27146
EM radiation on change of state of radiating system 80−32894
EM radiation recoil, enhanced 77−33876
EM radiation-charged particle stimulated interaction, classical and quantum theory study *(Russian)* 78−86431
EM tachyon, prep. of three-dimens. superluminal light spot in vacuum 80−42058
EM vector potential, interpretation, for teaching 79−25809
EM wave scatt. by ideally conducting bodies in rectangular waveguide 79−81336
embedding classical fields in QFT, electrodynamics, Yang-Mills theories, gravit. appls. 78−54223
energy density convexity and hyperbolicity of partial differential eqns. in nonlinear electrodynamics *(French)* 80−62491
energy exchange between free electrons and EM waves in vacuum, anal. 80−18975
energy tensor definition for system of charged particles and EM fields 78−77734
energy-momentum tensors in theory of EM fields admitting electric and mag. charge distribs. 77−74294
equation of motion, first order iteration of Lorentz-Dirac eqn. 77−30023
equation of motion for radiating charged particle 80−57110
equilibrium states of charged particles in wave propagating along mag. field *(Russian)* 77−23601
equivalence principle, virtual quanta method as probe 78−36913
extended charged particles, radiationless internal vibr. in const. mag. field 77−88631
extended charges, motion, radiation reaction effects 77−33748
Feshbach-Villars transformation, bosons, fermions 77−87647
fields and electrons, fundamentals *(German)* 77−585
fields generated by charged particle in vac., zero vel. limit, electrostatics solns. 78−82881
finite self-interaction of classical EM field 77−49612
fluctuation EM field of infinite medium with spherical inhomogeneity, finite temp. Green's functions 78−1126
fluids, polarisable and magnetisable, thermodynamic theory in electromag. EM fields 77−57291
Fourier transform, fractional order, appl. to quantum mechanics and electron motion in magnetic field 80−82665
free electron in external field, wavefunctions, nonrelativistic treatment 80−99611
free electron laser, saturation effects, classical theory 80−95864
free relativistic electron in external field 80−99612
free-electron momentum modulation, limited interaction length with light 78−62995
fringing field effects in a cylindrical condenser 80−52821

electrodynamics continued
general relativity, charged fluid sphere, soln. for interior metric 77−2571
geometrodynamics, e.m. and gravitational fields combination *(German)* 77−76
Green's function, moving lossy media, transformation of wave eqaution 77−82398
gyrating charged particle in EM field, adiabatic invariance of mag. moment 78−78873
Hamiltonian expectation values for time-depend. Foldy-Wouthuysen transformations 77−49633
Hamiltonian guiding centre problem 80−31533
Hamiltonians, stochastic character effect on particle accelerator design 78−93606
harmonic oscillator in random EM field radiative corrections stochastic electrodynamic treatment 77−45736
heterogenous gyrotropic media electrodynamics, antisymmetric repciprocity principle conditions fulfilment *(Russian)* 80−74287
HF fields, charged particles relativistic motion *(Russian)* 78−62996
hidden variables, quantum mechanics, and stochastic electrodynamics *(French)* 78−62107
high energy electron diffusion, in elec. field 78−25783
high-energy electrons traversing matter, emitted radiation ang., spectral and polarisation props. *(Russian)* 77−68160
homogeneous conducting medium, transformed eqn. *(Russian)* 78−81866
Huygens' principle electrodynamic formulation for scatt. in nonuniform medium 77−79729
inertia of nonradiating particle, soln. of Abraham-Lorentz eqn. 77−57206
inertial mass and potential energy 77−26225
integral transport theory for charged particles in electric and magnetic fields 79−26006
interfacial EHD instability in normal electric field 77−72363
interplanetary submicron grain orbits, gravit. attraction, radiation press. and electrodynamics 79−8879
inverse square law forces, problem soln. using 'unit radius' 77−60923
ion acceleration in quasi-static field of electron beam 77−71915
ion resonance acceleration, in attenuating mag. field *(Russian)* 79−22885
ionosphere, global scale electrodynamic coupling of auroral and equatorial dynamo regions 79−44297
ionosphere, solar tides and electrodynamic effects, polarisation elec. field 78−36391
ionosphere, transitional electrodynamic processes rel. to geomag. disturbances 77−60515
ionosphere plasma, long metallic tethers electrodynamics 78−69652
ions, trajectory in const. mag. field plus orthogonal sinusoidal elec. field 78−50687
IR dynamics, classical current models 77−60947
Jupiter-Io electrodynamic interaction, theory 78−81583
Kepler problem, anisotropic, Bernoulli sequences and trajectories 77−49609
Klein-Gordon equation, identical motion in relativistic quantum and classical mechanics 77−61177
Lagrange-Maxwell eqns., derivation and unified form *(Russian)* 79−84975
Lagrangian for a system of charged particles to higher-order terms 79−97219
laser amplifier, free-electron type, exact classical electron dynamics 79−41362
laser-electron beam scattering, intensity differential cross-section 77−71914
Lie algebras associated with classical relativistic planar motion in axisymmetric EM fields 79−49064
Lienard-Wiechert eqns., rel. to electron mass *(Spanish)* 80−82654
light propagation in nonlinear electrodynamics in generalised gravitational theory 77−5727
lightning stepped leader, electrodynamics, anal. *(French)* 78−28255
longitudinally inhomogeneous travelling waves in nonlinear electrodynamics 79−10348
loop diagrams calculation in strong mag. field *(Russian)* 78−25786
Lorentz-Dirac eqn. constraints 78−77736
Lorentz-Dirac equation, causality violation and nonlocal generalisation 77−41497
Lorentz-Dirac equation, nonlocal generalisation, initial value problem 77−13622
Lorentz-Dirac equation 80−12921
Lorenz-Lorentz relation, series expansion 77−40199
Love waves, in stratified magnetoelastic solid with material boundary 78−32015
low frequency field calc., iterative method 78−29876
macroscopic electrodynamics, forces and energy-momentum tensor 77−5675
magnetic field, homogeneous, nonadiabatically varying, charged particle motion 80−32895
magnetic field motion of charged particle 80−90690
magnetic monopole, gauge transformation and vector pot. 78−4494
magnetic monopole and gauge-invariant Hamiltonian formulation of classical electrodynamics 78−45489
magnetisable and polarisable media, mech. and EM effects *(Russian)* 77−49611
marine electrodynamics, magnetostatics problems and appl. to water masses movement *(Russian)* 78−77259
massive electrodynamics with magnetic charges, duality covariant form of Maxwell's eqns. 78−4495
Maxwell equations covariance, comparison of electrodynamic systems 77−87680
Maxwell field, stochastic mechanics in Euclidean formulation 80−42081
Maxwellian electrodynamic theory, history from eqn. discovery to mag. monopoles *(German)* 78−65791
mean-field electrodynamics, and dynamo theory of Earth's mag. field 77−73636
Meissner effect explicable in terms of classical electrodynamics 80−11134
metal, electrodynamics at boundary, including plasma waves 77−59317
metric free, with electric and mag. charges, field eqn. general solns. 78−69994
MHD accelerators, electrodynamic characts. 80−64788
Minkowski force from Frenet-Serret eqns. for curve in Riemann space 80−22208

electrodynamics continued
Minkowski formulation, moving media, total energy-momentum tensor 77−78992
Mo-Papas theory, e.m. foundation 77−55
momentum of particle moving in axially symm. mag. field 78−21806
momentum transfer from waves to particles 80−18977
monopole, accelerated, field strength determ. *(Chinese)* 78−77740
monopole+charge interaction, direct action 77−13619
monopole magnetic field, particle motion by classical theory for teachers 79−97139
monopoles 't, Hooft type, time depend.-generalizations, gauge theory solns. 77−6023
moving bodies, equivalence of proposed formulations 79−35574
moving bodies, nonequivalency of 'right' and 'left' 79−25841
moving current interaction with thin conducting plate 77−19151
moving matter, EM field objectivity in Galilean approx. *(French)* 80−42079
moving media, extension of Maxwell's theory 78−12578
moving media in noninertial coord. system, ring cavity appl. 79−53990
moving sources in conducting medium, multipole expansion 80−106417
multi-spiral electron current, interaction with EM wave, nonlinear anal. *(Russian)* 79−22886
multidimensional two particle problem with noncentral pot. 78−54174
multilayer structures, algorithm for diffraction in circular cylinder or sphere *(Russian)* 79−68354
mutually interacting charge fields, gauge theoretical formulations of elementary particle processes 78−58122
nematic liquid cryst., 3D convective instability in AC field 77−62475
nematic liquid crystal, traversing weak EM wave in static mag. field, electrodynamics 79−14680
neutron stars, electrodynamics in curved space 80−90465
neutron stars, electrodynamics of disk acrretion, magnetic field structure 80−85973
neutron-proton mass difference, classical electrodynamic model 77−6123
nonadiabatic collision processes, electronic degrees of freedom, classical analogue, appl. to mol. system 79−64063
nonadiabatic losses of particles in a dipole trap *(Russian)* 78−87002
noninertial reference system, electrodynamics eqns. *(Russian)* 78−81895
nonlinear, three-dimensional soliton solution *(Russian)* 79−22884
nonlinear approach to electrodynamics spin and stability props. anal. 78−49682
nonlinear Dirac field free soln., classical electrodynamics 79−80752
nonlinear electrodynamics, Birkhoff's theorem analogue *(Russian)* 78−54273
nonlinear electrodynamics, new variant *(Russian)* 79−5990
nonlinear electrodynamics, testability using present day instrumentation 79−71675
nonlinear eqns., exact solns. 77−30021
nonlinear inverse bremsstrahlung and heated-electron distributions 80−48927
nonlocal constitutive eqns. props. of field determ. 78−20981
nonlocal spinor field theory of matter 79−49141
nonlocal stochastic equation of motion with damping in electrodynamics 80−17872
nonradiating stochastic current distributions 80−46838
nonrelativistic, surface quantities and jump conditions anal. *(German)* 78−36844
nonrelativistic electron wave diffraction by cylindrical capacitor 79−72473
nonrelativistic quantum mechanics and anomalous part of g-factor 77−74238
nonstationary, class of nonlinear media 79−21567
null infinity, full canonical formalism, Fourier transforms, Maxwell field theory 78−12581
ondulatory radiation sources, theory and appl. 80−37947
oscillating conducting sphere in mag. field, forces calc. 78−25771
paradox concerning appearance of infinitely fast signals 77−30024
paradox of a Lorentz invariant current and charge quantization 79−80451
particle 3-dimens. simulation code 77−27230
particle accelerator, nonidentical resonators with narrow coupling slits, dispersion and field distrib. characts. 79−41047
particle diffusion across mag. fields, stable profile for nonlinear diffusion eqns. 78−22456
particle in EM wave, varying freq., averaged velocity 78−18414
particle interacting with laser field, energy momentum increase by radiation reaction 79−55038
particle motion delocalisation in non-uniform HF field with finite correl. time 80−58450
particle motion in cyclotron near reson., nonlinear behaviour *(Chinese)* 79−63828
particle motion in EM field at relativistic speeds *(German)* 78−90350
particle-classical field interaction, appl. to linearised gravitation and symmetric electrodynamics 79−5992
path-dependent Lagrangians in relativistic electrodynamics 80−90670
Pauli exclusion principle proof from self consistent field theory of electrodynamics 78−49683
perturbation theory for particle in EM field, group formulation *(Russian)* 78−12627
phase free AC accleration, proof of second order effect 77−6984
plasma, fluctuation-dissipative relation in nonlinear electrodynamics *(Russian)* 78−79410
plasma spin polarisation in mag. field *(Russian)* 80−33744
plasma theta-pinch description form classical electrodynamics 79−90436
point charge moving in arbitrary way, superposition of two fields *(Russian)* 80−22251
point electric and mag. charge, nonAbelian gauge invariant classical Lagrangian formalism 79−12627
polarisation effects in penetration of barrier with applied mag. field, relativistic corrections 79−78852
polarised nonconducting dielectric fluid, anal. of force exerted on immersed elec. charge 78−78872
polarised superhigh energy electron prod. in magagauss mag. field *(Russian)* 78−42270
ponderomotive force, relativistic corrections, plasma heating by lasers 77−65897
positive-ion distribution in a strong electric field, steady state kinetic eqn. 80−33844
positivity conditions on correlation functions that imply Debye screening 79−71350
preacceleration and retrocausation 77−19150

electrodynamics continued
- Proca generalisation, rel. to charged universe cosmology 79—25766
- projection methods, applicability limit 80—91734
- quantisation, gauge invariance and mass without spontaneous symmetry breaking 79—89088
- quantisation of matter without quantising related fields 80—105525
- quaternionic EM wave equation and dual charge-filled space 77—57209
- quaternionic notation for classical electrodynamics extension, Lagrangian formulation and canonical formalism 78—81863
- radiating electron, stability of motion 78—65789
- radiating electron, stationary states in attractive pot. 77—60950
- radiating electron in strong monochromatic wave at open waveguide 79—55039
- radiating electron in waveguide, self-reson. radiation 79—55040
- radiating point charge, energy and ang. momentum splitting 78—69996
- radiation characteristics of electron flow over grating of cylinders with longit. slots *(Russian)* 77—68156
- radiation damping on anharmonic oscill. 77—50596
- radiation during classical charge annihilation *(Russian)* 77—14655
- radiation from change moving in spiral in cylindrical waveguide *(Russian)* 77—88629
- radiation from charge moving in randomly inhomogeneous media, fluctuation effects *(Russian)* 78—71017
- radiation generated by charged beam near plane flanged waveguide 79—13880
- radiation generation by relativistic electron clusters passing through air separated dielec. plates, expt. *(Russian)* 77—75396
- radiation intensity, expansion into (a/λ) power series 77—71911
- radiation reaction, covariant theory 77—54
- radiation reaction terms in classical electrodynamics 80—48126
- reflection and catching of electrons in field of opposite EM waves 77—10824
- relativistic, electromagnetic waves dispersion equations in moving media 80—57089
- relativistic channelling particle, spontaneous γ quanta emission 77—63481
- relativistic charged particle in arbitrary EM field, radiation, accel. 78—42269
- relativistic charged particle in nonuniform mag. field *(Russian)* 78—78876
- relativistic charged particles, in field of EM plane waves 77—71913
- relativistic classical, numerical solns., bound positronium 77—61904
- relativistic classical and quantum dynamics 80—22192
- relativistic electron, near conductor surface mag. insulation effects *(Russian)* 77—6985
- relativistic electron beam, 'peeling' on entering mag. field 78—66741
- relativistic electron beam, crit. current in mag. field in vacuum channel *(Russian)* 78—71016
- relativistic electron beam, in mag. field, reson. radiation 78—17852
- relativistic electron beam in mag. field, microwave radn. 77—79735
- relativistic electron beam interacting with EM wave, dielec. filled channel 79—59622
- relativistic electron beam-vacuum interface, EM surface waves 77—79734
- relativistic electron Coulomb scatt., approx. to $\cos\gamma$ 78—28962
- relativistic electron oscillator stream in EM field, explosive instability 80—53197
- relativistic electron ring azimuthal oscillations in resonator with stabilising medium *(Russian)* 78—29889
- relativistic electron ring train behaviour under longitudinal compression 79—7065
- relativistic free particle, in thermal radiation within classical electrodynamics, equilib. distrib. 80—8935
- relativistic invariance as gauge invariance, high intensity Compton scatt. 78—41201
- relativistic mechanics of mag. monopoles and electric charges 78—28967
- relativistic motion of charged particle in plane EM wave with arbitrary amplitude 77—3528
- relativistic particle in field of waves with non-zero proper mass *(Russian)* 78—21365
- relativistic particles in EM field, conservation of angular momentum 80—48129
- relativistic transformations, Newtonian force and EM field, for teaching 78—49601
- relativistic two-body electrodynamics 78—54112
- relativistic two-body interaction with radiation damping 77—30022
- relativistic vector formulation, of electric and mag. fields *(Italian)* 78—12448
- relativity, special, two combined first-order effects, test by measuring electric field inside rotating electric screen 80—46796
- resonant antenna system, anomalous radiation and electrodynamic characts. 80—69302
- resonant electron motion in polarised EM plane wave, spontaneous phase focusing 79—68357
- resonant medium, coherent radiation generation by relativistic charged particle 79—33857
- resonant wave-particle interaction, at half-integer cyclotron harmonics 78—78871
- resonator, marginally stable, gain effect on electrodynamics 80—53339
- retarded self-interaction of classical point electron, divergences anal. 77—13620
- retrocausation and formal assimilation of classical electrodynamics to Newtonian mechanics 79—97175
- retrocausation in classical electrodynamics 79—97174
- rheometric structure theory, convective differentiation and continuum electrodynamics 80—86087
- Riemannian metric description, of gravit. and EM interactions 78—36904
- Ritz's theory based on particle interactions, review of original paper of 1908 80—47
- rotary ether drag, Coriolis contribution 80—4556
- rotating body magnetic field effects and properties 78—17837
- rotating conducting sphere in mag. field, ideal conductor approx. 79—18324
- rotating dielectric column, EM scatt., relativistic soln. 78—50681
- rotating electrically conducting sphere behaviour in time-independ. homogeneous external mag. field, lab. approx. *(German)* 78—37785
- rotating relativistic electron beam, theory 78—9309
- rotational diffusion, special functions 79—72471
- Rutherford scattering, positively charged particles interaction calc. 77—27468

electrodynamics continued
- Rutherford scattering with radiation reaction, Lorentz-Dirac eqn. soln. for opposite point charges 78—55289
- scalar, asymptotic estimates of higher approx. *(Russian)* 78—12584
- scalar electrodynamic pot., convolutional functional *(Polish)* 79—50205
- scalar field theory with massive scalar field, spontaneous symmetry breaking 77—61214
- scalar QED, bound states, lump solns. of classical eqns. 77—53
- Schott term, 4/3 problem, reliability of Lorentz-Dirac eqn. 77—13623
- Schrodinger eqn., model of stochastic origins 80—81
- Schwarzschild electrodynamics, rel. to black holes and neutron stars 78—77480
- Schwarzschild sphere and classical electron self-energy 78—49681
- self-force of charged particle in EM field 77—34801
- self-resonant electron motion in monochromatic wave 78—66737
- semiclassical stochastic radiation theory 78—21010
- shell, rotating, conducting, in mag. field, forces and moments 78—37786
- shields, thin, boundary conditions, electrodynamic soln., monochromatic external field 77—54647
- shock adiabatic, given surface charge, appl. charged grid explosion *(Russian)* 77—65812
- shortwave coherent undulator radiation, classical theory 80—23195
- singularities, use of polar coords. for improper integrals 77—67301
- singularity problems in electrodynamics and gravitational theory, soln. 80—8534
- slowly moving classical point particle in two-dimens. mag. field 79—86117
- Smith-Purcell radiation generated by electron beam, non-redundant spectral tunnelling 78—78906
- solid sphere dynamics in alternating EM field *(Russian)* 77—88618
- solid surface, theory, book 80—36787
- solids, polarisable and magnetisable, theory of in electromag. fields 77—57291
- solitary waves in Born-Infeld electrodynamics 80—4554
- solution stability in truncation method calculations *(Ukrainian)* 80—31532
- space-time deformations of an elastic medium and the electrodynamic equations *(Russian)* 80—52028
- special relativistic theory with locally anisotropic space-time 77—67279
- Spencer-Lewis collision operator for small angle collisions 80—165
- spherical electrostatic spectrum., props. of Keplerian orbits in inverse-square field 79—13581
- spherical particles beam, focusing by axisymmetric mag. fields 80—78755
- spheroid turn in conducting media, EM field calc. *(Russian)* 78—46481
- spin-orbit effect in classical two-body Hamiltonian 77—68386
- spinless charged particle with external time-depend. field, quantum theory and gauge transforms 77—5680
- spinning magnetic field inducing elec. field, moving and non-moving force line hypotheses 78—9296
- spinning magnets, Jehle model of electron 78—28966
- spiral electron beam devices, generation conditions calc. *(Russian)* 78—25785
- stability of the longitudinal oscillations of a bunched beam propagating in a vacuum chamber with reactive impedance 79—85849
- static conductivity of 1-D disordered systems 77—49697
- stationary levels of electron in field of polarised neutral particle *(Russian)* 78—66733
- steady state Universe using stochastic electrodynamics, cosmic background radiation and red shift 78—77631
- Stern-Gerlach quantum-like behaviour of a classical charged particle 79—85913
- stiffness of conducting bodies config. in time-varying mag. field 80—43230
- stimulated effects upon electron jarring in external EM field 77—79737
- stochastic, and quantum mechanics *(French)* 77—50
- stochastic, coupled harmonic oscillators 79—75373
- stochastic acceleration of particle in random pot., renormalised canonical perturbation theory 77—27233
- stochastic electrodynamics, alternative to quantum mechs., path integrals 78—9307
- stochastic electrodynamics, derivation of quantum mechanics 78—36801
- stochastic physics and Abraham-Lorentz eqn. 78—20985
- stochastic theory of cosmic ray particle acceleration by background radiation 79—21117
- storage rings, interaction effects of EM fields on particle beams 80—37643
- Stormer problem, effect of perturbation on periodic solns. 78—20582
- Stormer problem, totality of periodic motions in meridian plane of mag. dipole 78—12052
- SU(2) harmonic analysis as basis for quantisation 80—9116
- successive canonical transformation in model two-body electrodynamics 79—86120
- symmetric two-body problem in one dimension 77—2546
- synchrotron radiation field, statistical states 78—66736
- tachyon + bradyon interactions, superluminal and subluminal EM fields 80—12902
- tachyons, charged, Cherenkov radiation in vac. 77—57210
- tachyons, monopoles and related topics, book 79—44718
- tensor spherical harmonics on S^2 and S^3 as eigenvalue problems 79—17324
- thermo-piezoelectric material, time depend. harmonically changing plane wave propag. anal. 80—15977
- thermoelastic solids, field-matter interactions, book 79—30270
- Thomas precession, geometrical kinematical origin 79—6
- Thomson scatt. from thermal plasma, intensity depend. frequency shift 78—42770
- three component medium with shock waves, unidimens. flow *(Russian)* 77—35250
- time-symmetric, charged point particle fields 77—71220
- trajectory of electron in electron beam source for vaporisation *(Russian)* 78—33657
- transducers, US wave generation, materials testing *(German)* 78—44294
- transition radiation, classical theory 78—82896
- transition radiation and transition scatt., review 79—27143
- transparent medium, energy-momentum and ang. momentum emission rates of moving charge, covariant electrodynamics 80—57108
- transport eqn., with random impurities 78—33654
- tubing, testing and failure localisation by electrodynamic method 77—63847

electrodynamics continued
two charged particles problem, Lagrangian and Hamiltonian up to fourth-order terms 80—91736
two electron half retarded half advanced interactions, existence and uniqueness theorem 79—49035
two-body problem, initial segment problem forward and backward extensions 79—71241
two-body problem, Lienard-Wiechert pot., existence and uniqueness theorem 78—8252
two-potential formulation, internal symm. *(Russian)* 78—4492
ultrarelativistic electron bunch in free space, lateral spreading 80—53196
unstable particles in electric field, Zel'dovich dipole moment 77—74627
vacuum, transition radiation and scatt. in strong EM field *(Russian)* 78—58895
van der Waals force in cond. media, fluctuating electrodynamics 78—30876
variational methods for solution of electrodynamic and electrostatic problems 80—1105
vector product formulation of special relativity and electromagnetism 80—105496
vortex motion, integrals of hydrodynamic equations, Helmholtz 1858 paper 79—9072
Weber's law, operational arguments, occurrence in history of physics *(German)* 78—12527
Wheeler-Feynman electrodynamics, advanced wave emergence in steady state universe 80—17816
Wigner elementary particle in external homogeneous field 77—37756
WKBJ approx. for classical particles with spin in external field 78—32692
X-ray scattering by free and bound electrons in strong laser field 78—58148
Hg films, superconducting, far-IR and electrodynamic props. meas. 80—103957

electrodynamometers *see dynamometers*

electroencephalograms *see electroencephalography*

electroencephalography
see also bioelectric potentials; biomagnetism; brain
21-channel EEG monitor with real-time result colour display 80—72364
acoustically evoked potential, age depend. 80—12163
adaptive matched filters for the measurement of acoustically evoked potentials in the EEG *(German)* 78—88755
alpha activity detection, above-threshold *(Czech)* 77—5124
alpha and non-alpha intervals alternation, queueing theory model 78—96040
alpha detection and meas. method 80—21552
alpha frequency rel. to head size, implications for brain wave model 78—69035
alpha rhythm, human, feedback control from central area 80—40988
alpha rhythm, result of corneal-retinal potential modulation obs. 79—34535
alpha rhythm blocking, absence in visuobehavioural deprivation 78—27944
alpha wave amplitude and frequency control, feedback learning system *(Japanese)* 77—44626
alpha wave asymmetry in coherence and power, effects of task and gender 79—39378
alpha-contingent visual stimulation, detect. of cerebral lateralisation of function 80—94190
alpha-detection system, feedback stimulation and data analysis system 79—29642
alpha-rhythm, neural vet model 80—76719
alternations, power spectral analysis 80—30924
amygdaloid kindling phenomenon extended first approx. model 78—53378
anaesthesia level control system 79—83974
anaesthesia stage indicator, signal divider 80—3858
analogue multiplexer for FM tape recording 79—34691
analyser-integrator model ANIEG-8 for frequency analysis, EEG signals 80—41295
analysis, Fourier-Haar transform 77—44823
analysis, using short epoch Fourier transforms, automated system 77—44824
analysis by all-pole model 80—41287
analysis methods and activation techniques *(Croatian)* 78—44666
analysis of electroencephalogram *(Japanese)* 80—41305
analysis using special purpose hybrid computers 77—40842
artifact automatic detect. during sleep 79—100759
artifact detection technique for automated anal. 78—31941
artifact from 2 respirators of different design 80—46075
artifact rejection, on-line computer method 77—40833
audiological diagnosis, use of click-evoked elec. brainstem responses 79—92237
audiometry, objective anal. 79—100632
audiometry using electric response *(Japanese)* 80—51183
auditory, visual, and somatosensory evoked potentials in pediatric diagnosis 80—26407
auditory averaged EEG response, middle components, contralateral noise effect 79—96576
auditory averaged EEG response, stimulus freq. and intensity rel. to middle components 77—52804
auditory brain stem responses, cat, effects of lesions 80—85407
auditory brain stem responses, cat, intracranial and extracranial recordings 80—85406
auditory brain stem responses in patients with acoustic neuromas 79—92235
auditory brainstem frequency, response to waveform envelope periodicity 80—61590
auditory electrophysiology, spectral analysis of cochlear and brain stem evoked potentials 80—16957
auditory event related pot. differences to ambiguous word, principal component anal. 80—8070
auditory event related potentials due to single stimuli, recognition by discriminant functions 77—9305
auditory evoked brain stem pot., sex differences in amplitudes and latencies 80—89767
auditory evoked brain stem pots., effects of analogue and digital filtering 80—89878
auditory evoked brain stem response, cochlear processes affecting wave V latency 80—16958
electroencephalography continued
auditory evoked freq. following pots. in man, evaluation, masking and clinical studies 79—70553
auditory evoked potentials, averaging and FM 79—34574
auditory evoked potentials, event-related obs. in schizophrenics 80—85405
auditory evoked potentials, freq. following responses in primary auditory and reticular formation structs. 80—12154
auditory evoked potentials during natural and drug induced sleep 80—35903
auditory evoked potentials in the brain stem, anal. method 80—41297
auditory evoked pots., differential changes, mouse obs. 79—100624
auditory evoked pots., technique for separating endogenous from exogenous pots. 79—100794
auditory evoked resonances, comparison of narcoleptics, primary insomniacs and normal controls 80—61579
auditory evoked response to LF tone-burst stimuli, determ. of freq. following response 79—83796
auditory evoked sustained potentials, nature of response 79—34572
auditory evoked sustained potentials, stimulus relationships 79—34573
auditory nervous system activity analysis 80—30921
auditory-evoked response methodology in animals 80—46103
automated monitoring of long-term implanted electrodes in human brain *(Russian)* 80—76857
automated parameter anal. as prognostic indicator in stroke 77—86699
automatic analysis using adaptive segmentation of EEG records 77—25581
automatic classification, Kullback-Leibler nearest neighbour rules 80—46079
automatic classification, Kullbeck Leibler nearest neighbour approach 79—83975
automatic EEG classification, parametric ARMA time series models 77—90944
automatic interpretation, background activity anal. 80—85503
automatic nocturnal sleep sampling 78—31916
automatic pattern recognition of EEG of patients under general anaesthesia during operations 80—17154
automatic recognition of inter-ictal epileptic activity in prolonged recordings 80—3838
automatic segmentation based on autocorrelation function 79—96673
automatic sleep staging detectors 78—53551
autoregressive analysis, a method for detect. of EEG changes in newborns to tones 80—108982
autoregressive models usefulness for EEG segments classification 78—80989
Bereitschaftspotential, rels. to late component of contingent negative variation 79—100589
Bereitschaftspotential during skilled motor task acquisition 79—62224
biofeedback conditioning, signal detection methodologies 79—29656
biofeedback of slow cortical pots., time series anal. 80—89736
in biomedical electronics developments, review 77—13017
biopotential recording interference and motion artifact sources and suppression 77—81634
bispectra computation computer program, in FORTRAN 78—92727
brain abscess, electroencephalographic computerised tomographic correls. 79—83899
brain activity anal. using Parcor coeffs. 78—35822
brain activity patterns detection and anal. using deconvolution and power spectral density 78—40386
brain functioning in health and neurological disease rel. to elec. response 80—40998
brain potential comparison, average evoked, on spectral and coherency function basis 77—2072
brain stem auditory evoked potentials and blink reflex in quiescent multiple sclerosis 80—67091
brain stem electric response audiometry and middle ear effusion 80—56151
brain stem transmission time and auditory nerve response 80—45917
brain unit and slow-wave field activity, telemetry with FM pulse subcarrier 77—25625
brainstem auditory evoked potentials, human, freq. comp. 80—16956
brainstem auditory evoked pots., influence of nonpathologic factors 79—88079
brainstem auditory evoked responses, polarity of acoustic click stimuli, proposed standard 80—45986
brainstem auditory on- and off-potentials in humans 80—16954
brainstem potentials, microwave-evoked, auditory responses, in cats 80—56061
breach rhythm, EEG rel. to skull defects 80—35862
cable telemetry seizure-monitoring system 78—3640
cassette recording system, portable four-channel 77—56498
cat, computed unit-EEG correls. and laminar profiles of spindle waves 78—11625
cat brain subdural structure resonance phenomena 77—16923
cell electric potentials, ECG, EEG and EMG differences in signal types, propag. and meas. methods 80—40995
centro-occipital power and asymmetry, preprocessing by factor anal. 79—43996
cerebellum chronic stimulation and EEG, the utility of artifact 79—96643
cerebral abnormality localisation, multivariate pattern recognition techniques 79—16327
cerebral activity monitor, using biofeedback rhythms inducing cct. *(Spanish)* 80—72359
cerebral cortex rabbit, contribs. of each layer to EEG 79—57618
cerebral hemispheres, right and left, EEG activity comparison during language, non-language tasks 80—45922
cerebral potential impulse response *(Japanese)* 78—3661
cerebral potential sources location for visual field impairment assessment in humans 80—30922
children, 24 hr, 4 channel recording using miniature tape recorder and computer anal. 79—34697
chronic recording in conscious dogs using implantable Ag electrode 77—13042
chronic sphenoidal electrodes, material improvement 79—16328
classification, automatic, decision rules comparison 80—109054
clinical seizure, long term time-lapse video monitoring system, synchronised with EEG 79—39461
cluster separation by nonlinear decision boundaries and linear filtering 77—56509

electroencephalography continued
coherence estimates, significance in determ. of central α and μ activities 80—61720
computer display system, brain lesion localisation *(Japanese)* 77—5100
computer peripheral system for acquisition and processing of EEG data 80—41270
computer rejection of artifact, contamination by drowsiness 77—90932
computerised analytical method *(Slovenian)* 78—28113
computerised clinical EEG in perspective 79—70655
computerised signal averager, flexible and low cost 79—43998
computerised statistical monitoring 77—40917
conditioning EEG activity, computerised laboratory 80—30912
conference, Courchevel, France (Feb. 1978) 80—31403
constant value curve tracing technique, minicomputer 77—70510
contingent negative variation rebound effect, visual and auditory simuli 80—3648
cortical slow negative waves following non-paired auditory and visual stimuli 80—3650
cortical slow negative waves following non-paired auditory stimuli 79—62266
current dipole model, central nervous system disease diagnosis applications 79—48238
data compression via computer-generated evoked response to sensory stimuli 78—36016
data processing, discrete Fourier transformation 80—26385
decision P350, waveform and neural mechanism, auditory click and elec. finger stimuli 80—61528
deconvolution procedure for information extraction from average evoked response signals 80—61724
delta rhythm during sleep, computerised anal. system 80—12285
development in rat, power spectral analysis 79—83742
diagnosis of subacute sclerosing panencephalitis, techniques with two children 78—20301
digital filtering, high efficiency freq. anal. and data compression 78—31939
discriminant analysis based scoring system 80—81766
discriminant function classification from renal patients, methods 78—28115
distortion by volume conduction, compensation by spatial deconvolution 80—94391
dolorimetry, cerebral response to noxious CO_2 laser stimulation 78—31882
dominant frequency, correl. with cerebral O_2 uptake and blood flow 77—5095
dominant hemisphere, changes during memorising and reasoning 77—70444
dorsal hippocampus curvature effect on elec. field generated by it 79—57619
dot-density topogram, simple, computer-generated 80—94407
dynamic evolutionary spectral analysis 78—57102
dyslexia, detect. by computerised brain mapping 80—36185
ECG artifact in referential EEG recordings, minimisation by computer subtract 80—94390
EEG-EPograms, simultaneously recorded from various parts of brains of sleeping cats 80—16951
EEG-EPograms simultaneously recorded in various parts of the cat brain 80—12153
elderly patient EEGs, technical and other considerations 80—98150
electrical contact generation by tattooing C into skin tissue 78—77122
electrocorticography, clinically effective spike recognition program 79—44000
electrode, C-fibre, elec. props. and EEG appls. 80—72355
electrodes, C-loaded teflon, for chronic EEG recordings in microwave research 80—67305
electrodes, ECG, EEG, interfering signals arising by cable motion 80—41296
electrodes orientation, subdermal amplitude asymmetries avoidance 77—60272
electrogenesis, models methodology and wavefront reconstruction 77—44627
electronic recording and display systems *(French)* 77—13025
engineering in medicine and biology, conf. Atlanta, USA (Oct. 1978) 79—39332
epilepsy, photosensitive, role of pattern in TV viewing 80—26214
epilepsy diagnostics, EEG trace coding *(French)* 80—67277
epilepsy of late onset, visual and computer-assisted assessment 80—12294
epileptic patient 24-hour monitoring using 4-channel cassette recorder 78—3639
epileptic seizures, operant conditioning of central nervous system activity 79—83881
epileptic spike morphology, quantitative obs. 80—98153
epileptic spike pattern determ. by point spectrum 77—9294
epileptic transient detect., pattern recognition techniques 78—53542
epileptic transients and background activities differentiation, nonlinear boundaries 77—40838
epileptics, EEG feedback training 79—70696
equipment for measuring potentials *(French)* 80—85516
event-related cortical desynchronisation detected by power meas. of scalp EEG 77—81494
event-related desynchronisation, graphical display and statistical evaluation 78—24192
event-related EEG sequential freq. anal., hybrid method 77—81759
event-related potential changes in chronic alcoholics 80—67076
event-related potential changes in healthy aged females 79—79500
event-related variations, dynamic computer anal. *(German)* 78—85400
evoked frequency response polygons, computer anal. technique 77—40961
evoked frequency stabilisation in cat brain electrical activity 79—34533
evoked potential, theoretical investigations and clinical appl. 80—26234
evoked potential amplitude and contingent negative variation as function of inspired N_2O concs. 80—45916
evoked potential analysis, on-line signal optimisation using minicomputer 77—5112
evoked potential averaging, cross correlation and latency-corrected averaging comparison 79—53268
evoked potential estimation, effectiveness of Wiener filtering 80—61723
evoked potential multi-channel data acquisition system, microprocessor controlled 78—11750
evoked potential on-line statistical detect., appl. to audiometry 78—69245
evoked potential records, comparative freq. anal. 80—67269
evoked potentials, appl. in brain mechanism studies and diagnosis *(German)* 80—61535

electroencephalography continued
evoked potentials, average, microprocessor-based system for studying 80—56150
evoked potentials, event-related, in normal, mentally retarded and autistic children 80—85388
evoked potentials, math. model for source localisation, somatosensory stimulation 80—89774
evoked potentials, processing, computer techniques 78—92728
evoked potentials, recording and evaluation procedure for neurophysiology and medical diagnostics *(German)* 80—26404
evoked potentials and EEG freq. in patients undergoing haemodialysis and kidney transplantation 78—61160
evoked potentials rel. to short-term memory storage in human brain 79—79503
evoked responses, peripheral versus foveal, multiple sclerosis early diagnosis appl. 80—67276
evoked responses, statistical detect., evaluation of Woody's adaptive filter 77—81757
evoked responses, Wiener filtration vs. averaging 78—3689
evoked-response data acquisition system, specification and design 80—56165
EVOQ: a system configurable for automatic simulation and recording of mean evoked potentials on a minicomputer *(French)* 80—85507
eye movement artefact, removal by correlation methods 77—44826
eye movement artifacts, spectral method for removal 79—16184
eye movement tracking and regulation test station *(German)* 79—16321
features extraction by adaptive segmentation 77—44794
feedback, posterior EEG response to complex visual stimuli 77—21645
feedback training, techniques and clinical appls. 78—36043
field plotting method for isopotential maps 79—39542
FM detector appl., digital, multichannel *(Danish)* 78—35980
focal interictal epileptiform discharges rel. to spinal field pots., rat 80—94191
focal slow waves localisation 80—94406
free-moving mouse EEG recording and drug infusion technique 79—57831
frequency analyser, real-time, microprocessor monitored 78—57092
frequency analyzed EEG, relation to monitoring behaviour 80—35863
frequency spectral analysis, physiological aspects 77—25627
frequency-domain numerical analysis 77—9292
Gaussian amplitude distrib., new test for EEG-like data 80—30915
gustatory stimuli, differential arousal response in the awake rabbit 80—12166
haemodialysis rel. to EEG, spectral anal., Hjorth's descriptors, blood variables and psychological data 78—31968
head trauma, conf., Omaha, USA (May 1978) 80—41929
head trauma and the EEG, review 80—46076
hemi-retina evoked average multichannel EEG pot. fields, latency differences between upper and lower hemi-retina 78—24067
hemispheric differential activation during complex visuomotor performance 79—16183
hierarchical modelling of EEG signals 80—109052
higher cortical functions, EEG correlates 79—100591
hippocampal theta in urethane anesthetized rats, generators and phase relations 80—40990
histological marking with multiple thin-film electrode probe for intracortical recording 80—67297
human brain electrical signals systems analysis 77—21504
human sleep EEG, spindle pattern recognition by real time anal. *(Japanese)* 80—89903
IC four-channel EEG amplifier 79—39535
identification of isolated events, automatic system 79—5400
impulse responses of cat brain obs. 79—79502
in-phase brain activities during arousal and sleep in freely moving cats 80—40991
infant, ordinary and partial coherences of bipolar and quasi-unipolar derivations 77—44828
inferotemporal cortex, role in visual selective attention, monkey obs. 79—100616
instrumentation for meas. and processing *(Croatian)* 78—44665
intellectual activity, classification of normal and anomalous forms, quantised-wave theory of coherent brain appl. *(Russian)* 80—76722
intellectual activity, psychoheuristic relationship of psychotism structs. and giftedness structs. introduction, quantised wave theory of coherent brain appl. *(Russian)* 80—76723
interference suppression during open heart surgery 79—100784
interhemispheric synchrony in full-term newborns 79—62226
interictal epileptic activity, comparison of traditional reading and automatic recognition 78—48913
interictal epileptic EEG transient morphological discrimination algorithm 79—100758
interictal spiking, spontaneous, awake kindled rat 80—67058
intermittent transient pattern detect. for diagnosis 78—31958
intracerebral currents, contribs. to EEG and evoked potentials 78—92611
intracortical EEG relationship model *(German)* 79—16180
intracortical recording of field pots., 16-fold semi-microelectrode 80—67298
ipsilateral vibrissae in adult rodents, projections on cortical somatic I barrel subfield 80—8074
jet aeroplane noise, effects on facial expression, EEG and manual responses, human subjects 80—98006
Kalman estimator anal. of EEG signals with changing spectra 78—24167
Kullback Leibler-nearest neighbour rule classification, population 80—85504
laterality preference, electrophysiology and the brain 80—3619
LED true checkerboard pattern reversal stimulator for visually evoked pots. study 80—61658
limbic spindles, cerebral activity or artifact 78—48778
linear filter appl. to evoked pot. data 79—84032
M-wave and CNV obs. in squirrel monkey 79—83805
magnetoencephalogram and electroencephalogram, comparison of spatial response 80—26245
meaningful information extraction, comment on previous article with authors' reply 79—11911
medical electronics, appl. to otology *(Japanese)* 80—67268
memory retrieval task, event related potentials in young and old adults 80—40992
memory testing, activity of human hippocampal formation and amygdala neurons 79—62225
microcomputer based digital filter for electroencephalogram processing 78—73278

electroencephalography continued
- microcomputer system for on-line analysis of electroencephalographic data 78−73277
- microcomputer-based brain function monitoring system 77−73611
- microcomputer-based period and amplitude anal. system 80−72353
- microcomputer-controlled visual stimulator for eye movement and visual evoked pots. study 80−41350
- microprocessor-based EEG spike detection and quantification 80−36173
- microprocessor-based for epileptics biofeedback training 79−62403
- model with thin meninges, theory of EEG pot. 80−51283
- monitor using Walsh transform on standard microprocessor 80−26399
- monitoring system for stroke patients 80−26394
- montage standardisation, math. logic design 77−86685
- montages, in common clinical use, review 77−81599
- montages for optimal pattern display 77−78004
- mouse head immobilisation apparatus 80−41352
- mu rhythm detect. from human scalp, functional topography 78−48777
- multi-channel EEG wave analyser, design and development 80−56254
- multichannel radiotelemetry for epileptogenic focus localisation 78−3653
- multichannel telemetering, FM/PWM, from unrestrained psychiatric patients 78−3636
- multielectrode biotelemetry, for remote monitoring and stimulation of ambulatory subject 79−5386
- multiple sclerosis diagnosis using cerebral evoked response and optokinetics 80−36183
- multivariate analysis, parametric time series models 77−40830
- multivariate EEG automatic classification 77−73607
- muscle artifact filtering 79−100764
- nervous system, EEG device in equipment system used for complex examination 80−41302
- neural basis of EEG waves 80−108868
- neural populations, simplified model eqns. and envelope eqns. 78−31798
- neurological disorders, closed EEG feedback system 79−34703
- neurological intensive care facility requirements 79−92420
- neuronal activity and focal blood flow coupling in experimental seizures 80−40989
- neuronal template-matching mechanism for sensory search with olfactory bulb, anal. 80−56069
- neurostimulation automatic triggering as function of several EEG parameters, apparatus 80−98203
- neurosurgical intensive care, non-invasive monitoring techniques 80−81757
- newborns, healthy, right mid-temporal sharp transients 80−94192
- noise averaging and improving signal to noise ratio 77−81609
- non-convulsive response induced by intermittent photic stimulation, clinical usefulness 78−69246
- nonstationary, anal. by approx. canonical expansion method 78−53555
- nonstationary data, dynamic spectral comparisons 77−44827
- nonstationary point automatic detect. *(French)* 78−57112
- NREM sleep, period and amplitude anal., young adults 80−85376
- occipital EEG, feedback delay, amplitude threshold and control 80−21465
- olfactory bulb, caiman, computer anal. of EEG activity 77−81513
- olfactory bulb and cortex, spatial props. 79−16223
- olfactory bulb elec. responses to general and hunger arousal, rat. 79−79565
- olfactory perception, neurophysiological correlates rel. to amygdalotomy 79−100637
- online real time analysis, computerised system features 79−100773
- operant conditioning of brain steady potential shifts in man 80−21466
- optical scan system for encoding and tabulation of visually scored sleep data 80−8197
- optokinetic responses in brain lesions, EEG and electro-oculographic correlative study 80−8055
- paediatric EEG reactivity, spectral and temporal analysis 77−9293
- paradoxical sleep, occipital spikes and eye movement activity, visually defective children 79−16185
- parametric pattern recognition model 79−79665
- parastriate cortex, cat, rabbit, selective response of single units 79−74624
- pathological delta waves, cortical electromicrophysiology, cat 78−11626
- pattern classification using logic windows in time domain *(Japanese)* 77−70563
- pattern reversal generator for visually evoked responses studies 80−46004
- pattern visual evoked pots., age-dependent latency change obs. 80−85390
- patterns during cognitive tasks, controlled tasks anal. 80−67059
- patterns during cognitive tasks, methodology and complex behaviours anal. 80−61531
- peak-detection algorithm for anal. 79−74772
- period analysis using minicomputer 77−13024
- pesticide exposure effects on deep brain structures, filtered EEG spike obs. 77−44806
- petit mal epilepsy, portable detect. device 79−83984
- petit mal epilepsy treatment, unobtrusive wearable device 77−25592
- phase-locked loop spindle detect. system, human and automatic validation 80−98154
- phasic event detection by microprocessor 78−57091
- photic flash response, quantitative approach 80−30923
- photic one-second stimulation, on/off effects in background EEG activity 78−69047
- physiological data teletransmission system 77−86687
- piezoelectric earphones, usefulness in recording brain stem auditory evoked pots. 80−94389
- point processes, time-connectivity patterns quantification 80−21564
- polygraph for simultaneous recording of diagnostic parameters 78−36011
- polygraphic sleep recordings, computerised scoring method 80−109049
- polysomnographic recording techniques, sleep disorder diagnosis 79−34696
- ponto-geniculo-occipital waves, correlative evidence for neuronal generation 79−24975
- postpuerperal maternal α-rhythm increase obs. 79−96534
- potential in model of thin cerebral membranes, tangentially orientated dipoles 78−15818
- potential in model of thin cerebral meninges, radial dipoles and double layers 77−86476
- potential model with thin meninges, multilayer flat cable model 77−36903
- potential source in model with thin meninges 77−56359
- power spectra parameter estimation using Gaussian functions 77−21635

electroencephalography continued
- power spectral analysis to determine stage of anaesthesia in normal dogs and cats 77−37066
- preamplifier for surgical appls. 77−40916
- primary auditory cortex of awake cats, single unit activity vs. amplitude of epidural evoked potential 80−35904
- psychophysiological techniques applied to aircraft design and other operational problems 80−26384
- pulse-time-coded, freq. anal. *(Russian)* 80−72357
- quiet wakefulness, individual differences in human EEGs 80−12072
- rat EEG activity depression by 2.45 GHz whole-body irradiation 80−3720
- real time online data processing system for EEG and body movement, mouse 79−92443
- real-time analysis of EEG using Walsh transforms 79−12020
- real-time detection of brain events, expt. 77−44793
- real-time detection using two-component wave model 80−104788
- real-time display of 2-dimens. fields 78−44651
- real-time programming system 79−100767
- recording system, portable pulse-interval modulation telemetry/multiplexing system, home use 80−67261
- recording variability, quantification method based on power spectrum anal. 79−8561
- reduced spline representations 77−44803
- renal insufficiency assessment by EEG quantification 77−73609
- renal patients, compressed spectra array data matrix anal. 77−40882
- resonance phenomena in the electrical activity of the brain 79−74627
- respirometer, noncommercial respiratory transducer for EEG laboratory 78−65138
- RF and microwave effects, low power, on human EEG and behaviour 79−96616
- RF modulated energy effect on EEG of mammalian brains, acute and chronic irradiations 79−79603
- RF modulated energy irradiation effects, mammalian brains 79−100665
- rhythmic activity generation models *(Dutch)* 78−73150
- scalp potentials, dipole layer model 78−77035
- scalp potentials in model of thin membranes of brain, multilayered spherical cable model 77−25408
- scalp recorded potentials, intracranial sources, 3D localisation, quantitative evaluation 78−92613
- scotomata, effect on responses to pattern reversal in one half visual field 79−39417
- segment classification, usefulness of autoregressive models 80−30908
- segmentation techniques for electroencephalographic records 79−8562
- seizure monitoring, cable telemetry computer system 77−5090
- sensory evoked potential rel. to sensory discrimination task 80−3645
- sensory evoked potentials, use in monitoring residual function of injured spinal cords 80−81747
- sentence information processing, EEG evoked response and CNV obs. 79−57626
- serial quantitative EEG 80−61728
- signal averaging, S/N relationships 79−83977
- signal modelling and recognition, system identification approach 80−51286
- signal processing, computerised system *(French)* 77−37112
- signal processing, digital filtering and data compression appl. *(Italian)* 79−96670
- signal processing, frequency domain and time domain anal. 79−34676
- signal processing, frequency-domain instrumentation 79−83743
- signal processing and telemetry, digital bandpass analysis 78−57107
- signal stationarity anal., human 78−7461
- simulator, ECG and EEG *(French)* 79−57786
- simultaneous telephone transmission of four ECG/EEG signals *(Spanish)* 79−62399
- skin potential motion artifact reduction by skin abrasion 78−40361
- skin-electrode processes obs. 77−40828
- sleep, neurological diagnosis appl. 77−60271
- sleep, small spike obs. during rapid eye movements stage in man 80−101155
- sleep EEG, digital filtering for estimation of alpha-delta 78−44652
- sleep EEG activity and hormonal change correlation 77−9314
- sleep EEG ambulatory monitoring and anal. 78−44650
- sleep EEG automatic K-complex detector 78−53557
- sleep EEG data classification by autoregressive model 79−57628
- sleep pattern feature extraction and recognition by real-time anal. *(Japanese)* 78−73271
- sleep research, computerised anal. 79−62377
- sleep state analysis, automatic real-time practical method, computerised 80−67263
- sleep telemetry in rat, automatic identification and recording of vigilance states 78−48948
- sleep telemetry in rat, miniaturised FM-AM transmitter for EEG and EMG 78−48947
- sleep-waking process, role of anterior raphe and area postrema 77−36906
- slope descriptor computation, time and frequency domain comparison 78−57115
- slow potential shifts and decision P350 interactions, auditory and elec. stimuli 80−61529
- somato-parietal fast rhythms during combined focal attention and immobility 79−83729
- somatosensory cerebral evoked potential changes under constant mag. field 79−39383
- somatosensory evoked potential, extended sources assessment method 80−26244
- somatosensory evoked potential early components in monkey 79−96533
- somatosensory evoked potentials, abnormalities due to brainstem lesions 80−56070
- somatosensory evoked potentials, in man, cerebral, subcortical, spinal and peripheral nerve pots. 80−16961
- somatosensory evoked potentials, recovery function of short latency components, cat 79−34534
- somatosensory evoked potentials, reduction during movement, cat extralemniscal pathways recordings 80−85421
- somatosensory evoked potentials, short latency, stimulus intensity effect 80−35924
- somatosensory evoked potentials obs., human and monkey 79−43842
- somatosensory evoked pots. in humans, short latency obs. 80−8039
- source derivation or spatial filtering technique, a new method 77−44785
- source derivations, clinico-diagnostic experience 77−44786
- spatial organisation in normal and schizophrenic subjects 80−3843

electroencephalography continued
spectral analysis, normal children 6-16 yrs. 79—70653
spectral analysis, review of methods 80—21560
spectral band analysis, contrib. to attentional processes study *(French)* 80—61721
spectral estimates of auditory brainstem responses 80—30913
spectral parameter analysis operating system 77—9291
spectrum analysis, absolute value of amplitude, hold facility 77—44792
spectrum analysis, LF activity isolation by autoregressive filter 79—96672
spike detection using combined inverse and matched filter techniques 78—61267
spike-wave and focal motor seizures in mice with inherited epilepsy 79—83736
spike-wave EEG patterns, quantification method clinical evaluation 78—11754
spinal reflexes, monosynaptic, elicited at various phases of EEG α cycle 80—12073
spontaneous activity, stationarity and Gaussianity modelling 77—40839
spontaneous and induced wakefulness states, topological distribution of power and coherence spectra *(French)* 77—32961
SQUID, medical application *(Japanese)* 80—12290
standard montages recommendation 77—86686
standardised classification, sequential epoch method 78—57101
stationarity and normality of EEG data during sleep stages 78—92610
stimulus artifact suppression, sample and hold amplifier system 78—77163
stroke patients, quantification of computer analysed serial EEGs 77—5096
stroke prognosis, appl. of digital computer period anal. 77—37096
subcortical spiking frequency, power spectral density estimates 79—24972
syntactic anal. method 79—96697
syntactic anal. software system 80—104787
TDM telemetry unit for fifteen scalp electrodes 77—40822
techniques and practical points, for ABRET oral examination, review 78—20298
technology, conf., Atlanta, USA (Sept. 1979) 80—90601
telemetered activity data from isolated olfactory bulb of rabbits 77—86516
telemetry, including PWM multichannel system 78—31914
telemetry, micropowered multichannel PAM/FM system for brain research 77—25618
telemetry system for monitoring olfactory bulb of salmon 77—86718
telemetry techniques for studies of brain elec. activity recorded from microelectrodes 77—60310
telemetry time-multiplex unit, ambulatory patients 79—44007
theta rhythm, dipole-like neuronal sources, anesthetized rat obs. 80—61527
time code cct., automatic writing on EEG paper, 10 sec. intervals 77—29219
time-domain EEG quantification in normal children 79—96532
topographical display of epileptiform transients based on a statistical approach 80—108833
tracing processing system, software development *(Japanese)* 80—94409
transient detection by matched inverse digital filtering 80—85506
video biofeedback for alpha monitoring of brain activity 78—20299
visual contrast evoked potential, invariance with retinal illuminance changes 80—51085
visual cortex, cat, tuning of receptive fields 79—57646
visual cortical evoked potentials by dynamic random-dot stereograms 79—43876
visual event related potentials of the late positive complex in visual discrimination tasks 79—39416
visual evoked cortical potential meas., signal optimisation using Kalman filter *(Japanese)* 80—72348
visual evoked cortical potentials in men during compression and saturation in He-O$_2$ 78—61173
visual evoked human-scalp EEG data monitoring, processing and displaying system 77—90936
visual evoked potential, man, early oscillatory pots. 79—70549
visual evoked potential, N1-P2 correls. of reaction time at the single trial level 80—85389
visual evoked potential to search in short-term memory, late components 78—61172
visual evoked potentials, and nerve conduction vel. in family with adrenoleucodystrophy 80—45875
visual evoked potentials, changes in P3 waves with event repetition 79—70550
visual evoked potentials, during hypothermia, prolonged circulatory arrest 79—16204
visual evoked potentials, n-hexane induced changes, ERG of industrial workers 80—45886
visual evoked potentials, single-trial classification using stepwise discriminant anal. 80—85387
visual evoked potentials, size-specific information channels and selective attention 79—62246
visual evoked potentials, transient, real-time filtering 78—31940
visual evoked potentials in monkeys 80—45885
visual evoked potentials in neurological disorders 79—24981
visual evoked response, diagnostic tool in demyelinating diseases 79—20538
visual evoked response, provoked visual impairment in multiple sclerosis 79—16202
visual evoked response meas. using computerised rapid random flash 79—83776
visual pattern evoked pots., implicit time in infants, spatial vision maturation index 80—16928
visual pattern stimulated pots., dipole localisation 80—26235
visually evoked cortical response obs., infants and adults 79—43873
visually evoked cortical responses, monocular study 80—3640
visually evoked elec. and mag. response simultaneous recording for diagnosis 78—53558
visually evoked electrocortical response rel. to microwave-induced hyperthermia, guinea pig 80—61627
visually evoked nonstationary EEG, anal. using max. entropy method 80—26397
visually evoked potential, microsecond sensitivity of human system to irregular flicker 80—81586
visually evoked potential amplitude and coloured pattern displacement 79—79546
visually evoked potential analysis *(Japanese)* 80—12090

electroencephalography continued
visually evoked potential and psychophysical obs. of light adaption 80—16939
visually evoked potentials, amplitude and degree of event-related desynchronisation 80—12087
visually evoked potentials, speed methods for vision assessment, normal and amblyopic eyes 80—61661
visually evoked potentials, steady-state, effects of meridional variation 80—56033
visually evoked potentials, use in intracranial pressure estimation 80—26398
visually evoked potentials, visual anomalies in human ocular albinos 79—43875
visually evoked potentials and sensory dimensions 80—61548
visually evoked potentials to electronic pattern reversal, latency variations 80—94202
visually evoked pots., polarity inversion obs. 79—100602
visually evoked response, multiplexing system for multichannel signal averaging 80—36165
visually evoked response, simultaneous recording to flashes at different retinal locations. 80—72279
visually evoked response test goggle system using liquid crystal shutters 79—79676
visually evoked response to bar gratings, linear extrapolation to threshold, visual acuity assessment 80—67080
visually evoked response to sinusoidal gratings, latency obs. 80—16933
visually evoked responses in children, intermittent photic stimulation *(French)* 79—16201
visually evoked scalp pot., random within-set design for sampling 80—3842
volume conduction and EEG meas. in brain, influence of elec. spread on linear relationship of activity 77—90933
volume conductor principles in scalp EEG recordings, montage design 77—78003
voluntary movement evoked cortical pots., comparative study, man and monkey 80—94189
voluntary selfpaced movement, event-related desynchronisation evaluation 79—96531
Walsh power spectra estimation for EEG signals 77—40823
Walsh spectral estimates with appls. to classification of EEG signals 80—104789
wave duration anal., microcomputer implementation 80—21558
waveform detection by microprocessor 77—73610
wrist actigraphic measures of sleep and rhythms 79—16315

electroendosmosis *see electrophoresis*

electroerosive machining *see spark machining*

electrofluidynamics *see electrohydrodynamics*

electrofluorescence *see electroluminescence*

electroforming
brass, study of process variables in the electromagnetic bulging of tubes 78—80582
metal sheet, circular, impulsive press. by underwater wire explosions, dynamic plastic deform. 80—84866
oxide thin film electroforming, threshold switching and memory effects 77—76940
polyacetonitrile film, in Pt/polymer/metal capacitors, electroforming and elec. cond. 80—54800
polyphenylene oxide thin films, electrochem. prep., impurity effects on cond., electroforming 80—88655
polypropylene film, in MIM struct. 80—25019
polytetrahydrofuran film, in Pt/polymer/metal capacitors, electroforming and elec. cond. 80—54800
prebreakdown phenomena in tap water during electrohydraulic forming *(Japanese)* 77—24977
progress in electrodeposition and related processes, (1952-1977) 78—27420
Al alloy, study of process variables in the electromagnetic bulging of tubes 78—80582
Al-SiO$_x$-Au, MIM struct., electroformed, struct. and elec. props., 4-300K 79—78206
BN films, humidity sensitive elec. props. and switching characts. 80—107938
Cu, study of process variables in the electromagnetic bulging of tubes 78—80582
Cu-GeO$_2$/BaO-Cu thin film, amorphous, effect of electroforming on conductance and capacitance 80—34537
Cu-SiO/B$_2$O$_3$-Cu thin film, amorphous, conductance and capacitance, effect of electroforming 80—34537
Mg-Ni-S, electroforming, mech. props. rel. to heat treatment 80—35133
Pt-polymer-Au capacitor, electroforming, negative resist., electron emission 80—80406
Te-Se-Cd rectifying sandwich structs., elec. forming action, Schottky junction form. 80—80371
Y$_2$O$_3$ film in Y-Y$_2$O$_3$-metal junction, electroforming and conduction 78—26969
Y$_2$O$_3$ film in Y-Y$_2$O$_3$-Au junction, defect struct. and local conduction 78—26970

electrogasdynamics *see electrohydrodynamics*

electrohydrodynamics
aerosol, β-active, emission electrification in external field 78—83497
aerosol, charged spray, evaporation in elec. field *(French)* 77—29054
aerosol, electrostatically charged, particle deposition in hollow cast of human larynx-tracheobronchial tree 79—43953
aerosols, charging migration and EHD transport 78—88660
anthracene, liq., EHD transit flow 78—75895
asymmetric stress tensor fluid, polarised, ponderomotive force 80—19520
baking, EHD augmented, corona wind impingement effects 78—87235
Bernoulli integral and conservation of velocity circulation in polarizing or magnetizing fluid 79—90341
boundary layer of dilute suspension during application of elec. field *(Russian)* 78—63503
bubbling electrofluidised bed, heat transfer rates 78—87242
bulk-coupled normal field interfacial instability 78—87407
4-butoxybenzylidene-4′-alkylaniline, EHD instabilities in nematic and smectic A phases 79—90530
cable oil, EHD pumping 78—87414
charged droplets evaporation and motion in electric field 78—42669
charged particle extraction by hydrodynamic flow, electrical charging of bodies 79—64783

electrohydrodynamics continued
cholesteric liquid crystal, EHD instability with isotropic mechanism *(Russian)* 78—87617
cholesteric liquid crystal with anisotropic dielec. permeab., transient electrodynamic instability *(Russian)* 78—51418
cholesteric liquid crystals, with course-pitch spirals, stable textures and EHD instability 79—90550
cholesteric liquid crysts., continuum theory 80—6356
cholesterics, shear flow induced propagating domains 80—54131
cholestryl nonanoate-MBBA mixture, anomalous behaviour of electrical dissipative power 79—4237
colloidal cylinders, charged, electrophoresis in salt solns., in transverse elec. field 79—1955
compressible liquid, bubble deformation in electric field 80—64618
conducting drop, in conducting fluid, induced motion and drop deformation in elec. field 79—7415
conducting fluid, laminar rot. in cylindrical vessel, elec. and mag. field effects *(Russian)* 78—75222
conducting fluid, run-off is elec. field, undamped waves 79—90271
conducting liquid, eddy current induced pumping, longit. current in corrugated tube *(Russian)* 78—75216
conducting liquid, flow through d.c. electromagnetic pump *(Rumanian)* 80—28574
conducting liquid, plane-parallel shear flow, elec. current and mag. field effects *(Russian)* 78—75221
conducting liquid in crossed electric and mag. fields, instability *(Russian)* 78—26211
conducting liquid in rot. pipe 77—42925
contacts, asperity interactions 79—20215
convective instability in dielectric fluid between two coaxial cylinders 80—74994
convertor or nozzle for jet printer, output parameter exact solns. *(Russian)* 78—75230
corona wind between wire and plate electrodes 78—71561
corona wind cooling of flat surface, convective heat transfer coeffs. 78—87234
Coulomb fluid, hydrodynamic instabilities in applied thermal and pot. gradients 77—31397
current induced flow past a cone *(Russian)* 77—24030
cylindrical Couette flow, perturbation by Coulomb force induced secondary flow, electroviscous effect *(French)* 80—24100
DHAB, nematic, ordering change due to external DC elec. field, permittivity obs. 78—94990
di-1′,4″-octyloxybenzylidene-1,4-diaminochlorobenzene, nematic with some smectic ordering, EHD instabilities 77—84640
dielectric, slightly conducting, forces acting in electric field *(Russian)* 77—51123
dielectric drop in electric field, low Peclet number heat and mass transfer 80—6050
dielectric fluid, flow and heat transfer in annular channel, electric field effect 80—103077
dielectric fluid, space charge transfer by slow flow, in strong nonuniform elec. field *(Russian)* 78—75223
dielectric fluid, stream flow from pulsed HV electrode *(Russian)* 77—3880
dielectric fluid-fluid interface, stability in elec. and gravit. *(Russian)* 77—27617
dielectric fluid-fluid interface, stability in elec. field *(Russian)* 77—27616
dielectric fluids, evaluation of electrofluidic pumps and generators, appls. *(German)* 79—94724
dielectric liquid, cond. effect on electroviscosity 78—1751
dielectric liquid, EHD coupled minimum film boiling 77—42921
dielectric liquid, elec. dispersion in different gaseous environments 78—88254
dielectric liquid, elec. stressed, motion due to Coulomb, electromech. forces, schlieren image obs. 80—100037
dielectric liquid, film condensation, heat transfer enhancement in elec. field 78—55551
dielectric liquid, stationary EHD instability, charge carrier mobility temp. induced variations effects 79—77269
dielectric liquid flow, Coulomb electrocond. force component in elec. field *(Russian)* 77—65814
dielectric liquid in electric field, two-dimensional vel. field stochastic charact. *(Russian)* 78—75208
dielectric liquids, boiling process in narrow horizontal channels due to action of elec. field *(Russian)* 80—74707
dielectric liquids, electrical convection and jet flow 80—1692
dielectric organic liquid, concentric annuli, heat and momentum transfer, electric field effects 80—96315
dielectric plate in const. current flow, appl. sea elec. field meas. *(Russian)* 77—65813
dielectric polar liq., electroviscosity rel. to cond. process, EHD model 78—1750
dielectric viscous fluids, electrohydrodynamic stability in rigid cylinder 78—59497
diffusion in porous system in crossed electric and mag. fields 78—34202
diffusive instabilities in rotating elec. conducting compressible layers 80—38379
dilute aqueous solutions, EHD liquid motion, interference with second Wien effect 79—94735
dilute suspension of ellipsoidal particles flowing in channel, elec. field effects *(Russian)* 77—68696
dipolar conducting liquids, mag. transport props. at ambient temp. 79—91258
dipolar dumbbells in a viscoelastic Oldroyd liquid, dilute soln., electric field effect on rheological behaviour 80—6009
discharge, flow patterns, rot. forces, numerical anal. 78—34380
discontinuous solutions, closed boundary condition systems 77—67286
disperse system in EM field, hydrodynamics *(Russian)* 77—80222
double injection with recombination, EHD linear and nonlinear stability 78—87412
double-layer structure, electrohydrodynamical determination 78—95960
drop, in electric field, transient heat and mass transfer 77—80226
drop, two dimens., in presence of electric field, fluid circulation, equilib. geometry 77—58797
drop motion and dissolution in current-carrying liquid 77—11275
droplet, EHD produced, specific charge and size 79—32696
droplet motion in electrically conducting fluid, EM field effects *(Russian)* 77—3878

electrohydrodynamics continued
drops, direct contact heat transfer with intermittent electric field 80—74869
drops, EHD flow, with small Reynolds number, resulting deformation 80—59126
dynamo action associated with random waves in a rotating stratified fluid 80—33687
electrically conducting fluid, laminar flow mass transfer at high Peclet numbers 80—43784
electrically conducting media with nonlinear heat release, turbulence props. 80—103024
electrically driven jet, charge distrib. and forces 79—77268
electrification of fluids, rel. to fluid dynamics 78—26200
electroconvection in weakly conducting liquids 78—18297
electroconvective instabilities overstable 79—27706
electrogasdynamic supersonic flow over wedge in presence of charged massive particles 80—33685
electrokinetic flow in a narrow cylindrical capillary 80—92233
electrolyte in nonpolar solvent, cond., field-enhanced dissoc. and EHD instabilities *(French)* 77—62655
electrolyte layer, convection onset condition 79—14492
electrolyte-gas interface motion in electric field 77—35248
electrorheological suspension flow, vibr. effect *(Russian)* 80—53877
electrostatic spraying of liquids 78—67274
electroviscous effect, AC characteristics, pressure-drop fluctuations 80—107457
electrovortic flow, in discharge between hyperboloidal electrodes *(Russian)* 78—75217
electrovortical flow in corrugated tube *(Russian)* 78—26205
EM energy-momentum tensor and the properties of material media 79—55020
film condensation of vapour in elec. field, heat exchange intensification 79—86331
flame, laminar long wave stability, EHD problem anal. 80—53866
flame gases, effect of EHD boundary layer on heat transfer 77—80228
flat plate in electrostatic field, flow pattern, induction curtains, heat dissipation *(Korean)* 77—27619
flow induced by spheroid in fluid with uniform electric current 77—75984
flow of dielectric media, meas., by electrohydrodynamic means *(Russian)* 78—26216
flow regime alteration, by corona discharge, use in automatic systems *(Russian)* 77—11269
flow visualisation by laser light scatt. from PMMA latex particles 78—75236
fluid flow in hemispherical container, distrib. current source-induced 78—26198
forced convection in HF EM fields 77—39354
Freon electrohydrodynamic flow, jet dynamic pressure obs. *(Russian)* 80—59117
Freon-113, pure and mixed with methanol, EHD coupled minimum film boiling, surface wave model 78—87240
fundamental equations and elem. phenomena, book contrib. *(French)* 77—84338
gas and dust electrocond. flow in elec. and mag. fields *(Russian)* 77—39358
gas-particle flow, contact charging 79—81987
gas-solid dispersions, heat exchange in uniform elec. field 77—11273
heat pipe designs, performance characts. 78—87241
heat pipes, electric field effects on characts. 80—83728
heat transfer in liquids by dielectrophoresis 78—94874
n-hexane, subjected to charge injection, low stress mobility, induced motion effects 79—91063
high conductivity in mean field electrodynamics 77—949
HOBA, smectic C liq. cryst., EHD instabilities 78—91238
HOBA, smectic liq. cryst., two dimensional diffr. grating due to AC electric field, pulsating diffr. 78—15148
hydrocarbons flowing through circular pipe, streaming currents developed in laminar and turbulent flows 78—87413
ideal electrically conducting gas, weak discontinuities in singular surface theory 80—43736
impact charging of an isolated cylinder with skewed field and flow 78—87404
induction flow-meas. theory for poorly conducting fluids 78—38429
instabilities of nematics, successive transitions 79—77287
insulating liquid subject to unipolar injection, EHD stability, nonlinear phenomena 78—87411
insulating liquids, electroconvection, uni- and bi-polar injection 78—87405
insulating oil, Senftleben effect, under uniform DC elec. stress 77—31395
insulating oils, co-field motion, effect of dissolved gases, organic additives and field configuration 79—37407
integration of electrodynamic equations by direct methods 80—92235
interface, miscible fluids, internal electrohydrodynamic instability in collinear field-cond. gradients 78—26199
interfacial EHD instability, viscous dominated in polar geometry 80—38501
interpenetrating EM structural continua, constitutive eqns. *(Russian)* 77—65805
inversely normalised frequency, rel. to Prandtl number 79—23369
jet, numerical anal. of two unipolar jet interaction *(Russian)* 77—39352
jets of weakly conducting dielectric liquid, nonuniform field 79—77275
laminar boundary layer, on permeable surface, in crossed elec. and mag. fields *(Russian)* 78—75118
laminar flow through porous media, electrokinetic effects, analysis *(Russian)* 78—1748
laser Doppler anemometry on transparent turbulent electromagnetically driven flow 80—103090
lifting surface theory, high elec. cond. fluids 79—27695
linear induction MHD pump, cylindrical, electrodynamic forces *(Russian)* 78—94843
liquid, cloudy bubble formation in strong nonuniform elec. field 80—53842
liquid charged, parametric surface wave excitation by AC field 79—23375
liquid convective stability in electrostatic field *(Russian)* 77—27601
liquid crystal, dissipative structures in turbulent movement *(Russian)* 78—55808
liquid crystal, EHD instabilities, director relax. time depend. on wave number near WD pt. *(Japanese)* 79—32700

electrohydrodynamics continued
liquid crystal, EHD instabilities, electric Nusselt no. *(Japanese)* 78—18356
liquid crystal, isotropic and nematic, with positive dielec. anisotropy, EHD instability *(Russian)* 77—31594
liquid crystal, with tilted orientation, EHD instabilities 77—27826
liquid crystal electro-optical props. and applications 77—77174
liquid crystal splay mode near Williams domain point *(Japanese)* 78—9952
liquid crystal twist cell, flow patterns 80—49094
liquid crystal with negative dielectric anisotropy, cholesteric planar texture EHD distortion 78—42894
liquid crystals, bubble domains, generated by electrohydrodynamic turbulence *(Japanese)* 78—22413
liquid crystals, domain instabilities in elec. and mag. fields 79—94875
liquid crystals, EHD instabilities, principle of conservation of moment of momentum study 79—46566
liquid crystals, subcritical region, vortex penetration length, cct. behaviour 79—55662
liquid dielectric, intensity of elec. field and space charge 80—11339
liquid dielectrics between charged coaxial cylinders, separation boundary equilib. 79—64781
liquid dielectrics in electric field between two cylinders *(Russian)* 78—26208
liquid dielectrics interface equilib. and instability, curved wall effects *(Russian)* 78—5807
liquid film, free, stabilised with ionic surfactants, EHD 78—87403
liquid film, surface wave propag. under charge flow *(French)* 77—31849
liquid film, thin, free, stabilised with ionic surfactants, dynamics 78—87416
liquid flow, incompressible, electro-hydrodynamic analogy, design 77—27627
liquid insulants, elec. stressed, bulk electroconvection 80—87814
liquid insulants, electrically stressed, bulk electroconvection, preliminary obs. 80—53873
liquid jets, behaviour in electric and mag. fields 80—43783
liquid metal, in elec. field, new surface instability 79—64634
liquid metal film in elec. field, instability 79—64780
liquid metal film in electric field, instability *(Russian)* 77—89203
liquid metal mixing and refining in EM chute 79—77284
liquid metals, electromagnetic confining, centering and guiding *(French)* 80—24103
liquid mixing across diaphragm in normal electric field 79—10615
low conductivity liquid flowing through metal pipe, electrification mechanism 80—48813
low-conductivity liquid, electroconvective stability 80—48814
low-density plasma, deionisation between electrodes, pot. difference effects 77—51162
low-voltage liq. conductivity effect on EHD flow intensity and efficiency 80—33699
lubricating layer *(Russian)* 78—47061
magnetohydroelectric waves in fluid dielectric 79—27703
mass exchange between dissolving sphere and elec. current carrying liq. 77—11274
mass spectrometry, EHD ionisation, instrumentation, mechanisms and appls., review 78—86378
Maxwell stress, deformable surface, general case 78—59501
MBBA, anomalous behaviour of electrical dissipative power 79—4237
MBBA, electrohydrodynamic instabilities, flow patterns and phase diagrams 77—68915
MBBA, electrohydrodynamic instabilities, power spectra and autocorrel. in flow transitions 77—68914
MBBA, HF electrohydrodynamic instability in NLC *(Russian)* 80—54130
MBBA, homeotropic nematic layer, torsional shear flow in normal elec. field 79—82155
MBBA, liq. cryst., electrohydrodynamic instability, fluctuation of light transmission meas. 77—11468
MBBA, nematic, EHD flow patterns, analogy of instabilities with classical fluid behaviour 77—84335
MBBA, nematic, EHD instabilities, director-fluctuation autocorrelation and power spectrum 79—41944
MBBA, nematic, EHD instabilities, director-fluctuation second moment 79—41943
MBBA, nematic, EHD transitions, white noise effects 80—6159
MBBA, nematic film, with two free surfaces, EHD flow 79—98817
MBBA, nematic liq. cryst., dynamic scatt. mode due to electrohydrodynamic instability *(Japanese)* 77—43133
MBBA, nematic liq. cryst., dynamically excited, transversal EHD instabilities and umbilics 78—94983
MBBA, nematic liq. cryst., electroviscous effect, electrohydrodynamic investigation 78—87804
MBBA, nematic liq. cryst., secondary dynamic scatt. mode, light transmission and microscopic obs. 79—4246
MBBA, nematic liq. cryst., temp. depend. of EHD instability 78—1998
MBBA, nematic phase, high freq. EHD instabilities, temp. depend. 79—94879
MBBA, Williams mode in EHD, applied voltage depend. 79—37620
MBBA nematic crystal, EHD instability, damped oscill. of current and flow patterns 79—46562
MBBA-CN mixed liquid crystal, dissipative structs. caused by EHD instability 77—80416
MBBA-EBBA mixture, nematic liquid cryst., anisotropic effects in dielec. cond. of thick samples 79—10795
MBBA/CC mixtures, cholesteric phase, torsional shear flow in elec. and mag. fields 79—86697
metals, liq., infiltration in medium with interconnected pores, during passage of elec. current 80—100033
metals in metallic containers, thermoelectric MHD 79—64787
microstructural EHD model of continuous medium, appl. to liquid crystals 77—42731
mixing and instability induced by colinear fields and conductivity gradients 77—72362
mixtures, flowing, motion in EM field *(Russian)* 79—32686
naphthalene, liq., EHD transit flow 78—75895
natural convection in dielectric fluid, nonuniform alternating field influence *(Japanese)* 78—5805
nematic cell, EHD instability limits under action of sinusoidal electric fields 77—47342
nematic director in dielec. regime, dynamical behaviour, EHD instabilities *(Japanese)* 80—59387

electrohydrodynamics continued
nematic layers, positive dielec. anisotropy, EHD instability at DC excitation 79—94877
nematic liq., cryst. cell, with asymmetrically treated electrodes, electrooptic characts. 79—55658
nematic liquid crystal, current density in EHD instability 77—80415
nematic liquid crystal, DC dynamic scatt., flow direction rel. to dopant electrochem. props. 77—90130
nematic liquid crystal, dye-mixed DPM-4, flow speed AC appl. field effect 77—39532
nematic liquid crystal, dynamic scattering, material flow due to external electric fields 78—18543
nematic liquid crystal, EHD flow patterns, squint, nonlinear feature 79—94876
nematic liquid crystal, EHD instability in dielec. regime 77—27812
nematic liquid crystal, electroconvective flow, vel. and orientation deform. angles *(Russian)* 79—37621
nematic liquid crystal, microstructural EHD model, constitutive eqns. 79—10791
nematic liquid crystal, nonlinear EHD effects 77—84642
nematic liquid crystal, temp. depend. of EHD instability 78—1998
nematic liquid crystal, Williams domain mode, non-linear analysis 77—62472
nematic liquid crystal, ZhK-440, new type of electrohydrodynamic instability 79—14677
nematic liquid crystal in contact with photoconductor EHD instability, nematic liquid crystal in contact with photoconductor 80—79695
nematic liquid crystals, electrohydrodynamic effect in alternating elec. field 79—14676
nematic liquid crystals, LF dielec. relax., Freedericksz transition technique meas. 78—1987
nematic liquid crystals, shear flow in presence of electric AC field, elastic and viscous const. determ. 77—43144
nematic liquid crytals, in nonuniform elec. fields, mag.-field stabilisation 79—94901
nematic liquid of positive dielec. anisotropy, electrohydrodynamic instability 77—7659
nematic mixtures, Merck 5 and 7a, EHD, ion mobility 79—33104
nematic-cholesteric binary mixture, EHD instability, phase diagram 78—1980
nematics, EHD instabilities, white noise effect 80—70115
nematics, nonlinear effects above electrohydrodynamic instability threshold *(Russian)* 78—75551
nitrobenzene, liquid, electrohydrodynamic convection, laser light scatt. exam. 78—14094
nitrobenzene, steady state electroconvection, self beating laser spectroscopy 78—87408
NLC, high frequency electrohydrodynamic instability, permittivity, elec. cond. *(Russian)* 80—49099
non-Newtonian liquids, one-dimens. steady-state EHD flows 77—7464
nonstationary flows with charge diffusion, nonlinear and linear wave processes 80—59124
4-n-octyl-4′-cyanobiphenyl, smectic A phase, stimulation of EHD instability 79—78656
organic fluids, natural convection and boiling heat transfer, electric field freq. effects 80—1560
organic liquids, electrohydrodynamic ionisation, solvated ion mass spectroscopy, anal. appl. 78—73102
partially ionised medium in elec. field, forces 79—86522
pentyl-cyano-biphenyl, nematic, hydrodynamic parameters meas. with and without applied elec. field 80—100297
plane electrogasdynamic jet, approx. calc. *(Russian)* 77—19641
plane stagnation point flow in the presence of transverse magnetic field 79—32702
plasma, charge-separated, EM wave dispersion relations, rel. pulsar magnetosphere 77—7549
PNAOBA, type C smectic liq. crysts., electrohydrodynamic instability 80—1927
polydisperse droplets, produced by EHD method, charge-to-mass ratio 78—76931
polyethylenoxide, flow rate increase by electric field 78—75210
polymer solution, drag reduction, elec. field effects 77—72334
power generator, performance characts. 80—40877
power-law liquid, dil. suspensions of dipole dumbbells, rheological eqns. of state and shear flow in elec. field 79—86473
pump, expt. investigation *(Russian)* 79—37405
pumps, in attraction mode, efficiency 80—52187
rectangular MHD channels, nonuniform conducting flow calcs. *(Russian)* 77—27613
relativistic electromagnetic fluids and Ricci collineations 79—35605
relativistic EM fluid flows, geometry 79—58601
return currents in electrogasdynamic flow 79—86521
reverse elec. currents in EHD flows *(Russian)* 78—47045
rubrene, electrochemilum. by DC, highly organised EHD convection obs. 80—71499
secondary flow, electrically induced, and cylindrical Couette flow, superposition 80—28575
self-similar shock and rarefaction waves in polarizable continuous media 78—47047
shock and detonation wave propagation in channel in nonuniform EM field *(Russian)* 77—58798
shock wave struct., anal. with complete charged component impulse eqn. *(Russian)* 78—42674
small bubble formation by using strong nonuniform electric field 80—48796
smectic A liquid crystal, EHD instability and elec. cond. anisotropy *(Russian)* 78—59753
smectic C liquid crystal, storage effect, memorisation of oriented picture of EHD instability 79—37615
smectic C phase, mol. director behaviour at domain EHD instability 80—15000
smectic mesophases, viscoelastic properties and field instabilities 79—27904
solid aerosol collection in spouted bed, electric field effect 78—91019
solid dielectric particle dilute suspension in flat duct, electric field effect 80—53868
solid spacer influence on liq. motion induced by unipolar injection 78—87406
sonoluminescence, visible, due to collapse of cavity in liquid 80—45158
sound emission by ionised inhomogeneity in nonuniform flow 78—30365
spectral anemometer, electrogasdynamic 78—87422

- **electrohydrodynamics** continued
  - sphere, conducting, proous in uniformly conducting fluid flow 78−34204
  - sphere in current carrying liq., convection mass transfer, num. anal. 80−83851
  - spherical conducting fluid system, press. distrib. in crossed elec. and mag. fields *(Russian)* 77−47109
  - subsonic grid turbulence, diffusion processes of small spots of electrostatically charged mols. 78−87410
  - superluminal flow, EM wave refl. 79−27138
  - surface wave propagation, nonlinear effects 78−67278
  - surface waves, nonlinear stability 79−50810
  - suspension, dielectric, convective heat transfer, rheodynamics, in horizontal coaxial cylindrical channel 78−59494
  - suspension of dielectric particles in plane channel, flow with perpendicular elec. field *(Russian)* 77−62305
  - suspensions, deposition in channel entrance, combined influence of diffusion, electricity and gravity 80−1674
  - Symposium, Colorado, USA (Jan. 1978) 78−87402
  - Taylor, G.I., contrib. to EHD 78−86099
  - Taylor instability of two fluids in EM field *(Russian)* 77−27602
  - thermoelectric MHD, pipe end problem, boundary layers and rotation 80−69942
  - transducer, transient characts. anal. *(Russian)* 77−24031
  - transformer oil electrohydrodynamic flow, jet dynamic pressure obs. *(Russian)* 80−59117
  - transformer oils, under 60 Hz stress elec. stress induced motion 79−90346
  - tube flow, charged particle suspension deposition 79−37416
  - turbulent boundary layer, at permeable surface, in crossed elec. and mag. fields *(Russian)* 78−94836
  - turbulent channel flow, conducting fluid in external elec. and mag. field *(Russian)* 77−3875
  - turbulent flow of charged liq., transverse charge distrib. calc. 77−84334
  - viscoelastic liquid layer, electrohydrodynamic instability 80−14832
  - vortex convertor, power jet distrib. stage anal. calcs. *(Russian)* 77−7470
  - water viscosity changes effect on electrokinetic phenomena in capillaries 80−53867
  - xylene liq. jets induced by electrostatic field, disintegration and convergence 79−81986
  - Au, EHD emitted ions, energy distrib. 79−61503
  - Cu spheres, electrically augmented pneumatic transport at low particle and duct Reynolds numbers 78−87409
  - H_2O vapour under point corona discharge, microprocessor control for vapour generator and EHD phenomena 80−106852
  - He, liq., surface, macroscopic electron lattice formation 79−77861
  - He superfluid film, very thick, electrohydrodynamic instability 79−51382
  - Hg-electrolyte interface, with imposed temporal and spatial periodicity, double-layer transduction 78−88639

- **electrojets**
  - *see also ionosphere*
  - Alaska oil pipeline, elec. current induced by electrojet 80−61756
  - auroral, acoustic gravity wave spectra 78−4033
  - auroral, altitude differences for eastward and westward currents 77−87163
  - auroral, Chatanika radar meas. compared with Anchorage VHF backscatt. obs. 78−12048
  - auroral, combination freq. radiation generation *(Russian)* 77−41268
  - auroral, geomag. dipole tilt angle influence on development 79−16744
  - auroral, gravity waves and infrasound generation, Joule heating and Lorentz force 79−66866
  - auroral, infrasonic waves emission, multiplicity of wave forms 77−29534
  - auroral, magnetostatic model 77−13163
  - auroral, parameters from mag. vars. along meridian 79−25395
  - auroral, solar flare effects 78−49198
  - auroral, spectral struct. estimate of elec. field 78−40732
  - auroral activity in midnight sector, electrojet and precip. particle characts. 78−12039
  - auroral and equatorial two-stream irregularities, nonlinear states 78−28403
  - auroral current system oscillations, Earth induction effects on Pc 5 pulsations vertical polarisation 79−12355
  - auroral currents, magnetometer array and radar backscatt. joint obs., N.Scandinavia 78−85768
  - auroral electrojet, curvature rel. to interpretation of azimuth-scan radar Doppler data 77−41266
  - auroral electrojet, empirical relations to interplanetary parameters 80−105118
  - auroral electrojet, nonpotential waves 77−49212
  - auroral electrojet activity, rel. to LF/MF transmissions non-linear demodulation and ELF signals generation 80−94639
  - auroral electrojet and auroral infrasonic waves 79−35023
  - auroral electrojet and diffuse radio aurora, radar obs. 80−41623
  - auroral electrojet as infrasonic wave source *(Japanese)* 80−17434
  - auroral electrojet during isolated substorm event 80−105132
  - auroral electrojet events, simultaneous magnetosphere dynamics from energetic electron obs. at synchronous orbit 79−66882
  - auroral electrojet in morning sector, rel. to field-aligned currents 77−29573
  - auroral electrojet intensity influenced by interplanetary mag. field 80−51602
  - auroral electrojet near dusk, current flow from inversion techniques 79−58164
  - auroral electrojets, current conc. rel. to asymmetry in infrasound generation 77−87152
  - auroral electrojets, development during double substorm in midnight sector 77−53330
  - auroral electrojets, movements during high-latit. substorms 80−109315
  - auroral electrojets, rel. to thermal plasma enhancements in topside ionosphere 77−9617
  - auroral electrojets in evening sector, relationship with radar and visual aurora 77−25810
  - auroral radio backscatter at 42 MHz, amplitude rel. to Doppler shift 80−61955
  - auroral region, elec. fields and mag. effects of solar flares 78−69576
  - auroral westward electrojet, rel. to Pc 5 activity in morning sector 78−61685
  - auroral zone currents, obs. in morning sector pass 80−98510
  - boundary definitions using energetic electron spectra and magnetometer data 79−75026

- **electrojets** continued
  - contributions to daily geomagnetic vars. at S.American geomagnetic equator 79−75021
  - counter electrojet and f_0F_2 diurnal var. at equatorial latits. 79−48600
  - counter electrojet caused by vertical wind, equator region 80−85795
  - counter-electrojet afternoon events over India 78−12044
  - counterelectrojet, search for correl. with interplanetary mag. field 78−88983
  - Doppler spectra of current-driven plasma instabilities 79−58163
  - E-region and F-region drifts over Tiruchirapalli, India, daily variations 79−84580
  - eastward electrojet and field-aligned current flow at dusk meridian 79−80076
  - eastward electrojet over auroral arc, rocket obs. of N.edge 80−101481
  - eastward electrojet position rel. to energetic electrons trapping boundary and aurora 77−25822
  - equatorial, blanketing E_s-layers, VHF radar obs. of assoc. gradient instabilities 77−29577
  - equatorial, characts. over Ethiopia 78−16229
  - equatorial, crossfield and two-stream instability spectral characts., rocket borne obs. 77−87180
  - equatorial, effect of interplanetary mag. field B_Z component fluctuations 79−53697
  - equatorial, effects of cond. channel between India and Sri Lanka 79−25189
  - equatorial, effects on total electron content over Indian subcontinent 77−64523
  - equatorial, electrodynamic effects of solar tides 77−9611
  - equatorial, equivalent circuit anal. of neutral wind effects 78−57392
  - equatorial, fading records near edge of jet over Tiruchirapalli, full correl. anal. 80−101473
  - equatorial, HF oblique radar obs. of plasma instabilities over Africa 78−49205
  - equatorial, India, internal induction field from surface and satellite geomag. obs. 77−60535
  - equatorial, neutral wind obs. 77−45210
  - equatorial, neutral winds and phase vel. of instabilities 78−57388
  - equatorial, nonlinear two-stream instability 79−53640
  - equatorial, physical process and associated plasma instabilities, review 79−8750
  - equatorial, plasma instability and electron density irregularities, HF radar obs. 80−105112
  - equatorial, radar obs. of two dimens. turbulence, nighttime type 1 waves 79−35038
  - equatorial, radar profiles over Africa 77−21976
  - equatorial, theory 78−69607
  - equatorial, three metre irregularities depend. on Zenith angle, radar obs. 80−105109
  - equatorial, two-stream irregularities, neutral atm. motions effects 79−16742
  - equatorial, type II gradient drift irregularities, numerical simulations 77−70926
  - equatorial, type II gradient drift irregularities, power spectrum studies 79−75016
  - equatorial, type II irregularities, nonlinear theory 80−61958
  - equatorial, vars. rel. to interplanetary mag. field vars. 79−84572
  - equatorial and auroral, instabilities and fine struct. 80−21869
  - equatorial anomaly, counter electrojet assoc. changes, upward drifts reversal 80−109292
  - equatorial anomaly, counter electrojet assoc. changes, upward drift reversal obs. 80−109297
  - equatorial counter-electrojet, afternoon events occurrence characts. in Indian region 80−56672
  - equatorial counter-electrojet, electron drift vel., radar obs. 80−82126
  - equatorial counter-electrojet, geomag. aspects review 78−36367
  - equatorial counter-electrojet, two-stream instability, HF radar meas. 80−26671
  - equatorial electrojet, changes during mag. storm correlated with interplanetary mag. field 78−85766
  - equatorial electrojet, effect on struct. of topside and bottomside equatorial F-region 78−36373
  - equatorial electrojet, effects of gravity wave winds and wind shears 77−5388
  - equatorial electrojet, electron density profile changes 77−45234
  - equatorial electrojet, ionospheric cond. and drifts 78−36366
  - equatorial electrojet, irregularity drift vels. observed by close-spaced antenna technique and Doppler radar 78−36365
  - equatorial electrojet, multifreq. HF radar studies of plasma instabilities in Africa 78−36370
  - equatorial electrojet, radar obs. rel. to auroral and equatorial dynamos global scale coupling 79−44297
  - equatorial electrojet, storm-time obs. 77−33276
  - equatorial electrojet, strength rel. to SSC magnitudes equatorial enhancement 80−31174
  - equatorial electrojet, type 1 radar echoes with double-peaked Doppler spectra 80−67458
  - equatorial electrojet, vars. during geomag. storms rel. to ionosphere elec. fields 77−78578
  - equatorial electrojet, vars. rel. to interplanetary mag. field vars. 78−77413
  - equatorial electrojet, westward, emergence 80−26663
  - equatorial electrojet and ionospheric drifts, review 78−36364
  - equatorial electrojet axis in India, position variability 79−35046
  - equatorial electrojet control of ionospheric total electron content 79−88539
  - equatorial electrojet induction effects in solid Earth 77−32992
  - equatorial electrojet irregularities, parallel wave propag. effects 77−2302
  - equatorial electrojet longitudinal differences, radar studies review 78−36371
  - equatorial electrojet models, comparison 78−36372
  - equatorial electrojet strength, rel. to ionospheric 80−82129
  - equatorial irregularities, VHF backscatt. near mag. equator 77−33248
  - evening sector eastward electrojet, ground-based magnetometer data 80−46341
  - field-aligned current closure and Joule heating near Harang discontinuity 80−72682
  - geomagnetic field variations during quiet conditions electrojet effects on spectral characts. 77−87179
  - gravity waves from auroral electrojet, Joule heating and Lorentz force effects 78−28393
  - ionosphere moving current systems, EM induction in Earth 79−16370

electrojets continued
- ionosphere total electron content, equatorial electrojet control 80—56673
- irregularities and daytime VHF scintillations 78—28406
- lunar tide influence on equatorial electrojet 80—61937
- magnetic field, of partially magnetospheric current systems *(German)* 80—51609
- magnetic field variations due to quiet-time electrojets 80—30985
- magnetic var. of auroral electrojets during Geomagnetic Meridian Project 79—29936
- model involving field-aligned currents 77—9600
- polar, in magnetically conjugate regions 78—28384
- polar, modulation by powerful HF waves 77—70929
- polar substorms, equatorial-auroral ionosphere coupling 78—32291
- polarisation field, model with allowance for field aligned currents 77—21974
- pressure and rel. fluctuations caused by auroral electrojet 80—82118
- Ps 6 pulsation assoc. with magnetospheric substorm, obs. polarization, two-snake model 79—66887
- radar echoes from E-region, height shift around morning and evening electrojet reversals 79—66871
- reverse currents rel. to positive bays in auroral zone *(Russian)* 78—4037
- reverse equatorial electrojet events, mag. vars. at other latits. 78—36368
- substorm intensified eastward electrojet, 3-D current flow 80—85796
- substorms, ground magnetogram timing of onset, rel. to westward electrojet intensification 79—88553
- westward electrojet north of Cambridge Bay, influence on AE index 79—75054

electrokinetic effects
- *see also electrodynamics; electrophoresis*
- biological materials separation in space environment, electrokinetic phenomena and electrophoresis 79—48351
- biological particle surface, elec. double layer phenomena *(Rumanian)* 80—94144
- capillaries of different geometries, electrokinetic parameters 77—48650
- capillary surface, zeta potential determ. method using oscillating laminar flow streaming pot. meas. 78—76873
- cation-exchange membranes, electrochem. props. rel. to interfacial polarization during electrodialysis 79—16038
- colloidal solution, two-component, differential surface coagulation 79—79303
- colloids, electrokinetic pot. determ., streaming pot. meas. 77—16868
- dimethylketone, streaming current and cross-coeff. meas. in electrokinetic processes 80—76531
- disperse hydrocarbon system electrokinetic and polarisation phenomena *(Russian)* 79—83514
- electroosmotic permeability coefficient in charged membrane model 80—108749
- electrorheological suspensions, spontaneous rotation of dielectric rotor 77—15130
- estuarine environment, natural suspended matter flocculation and electro-kinetic pot. *(French)* 80—61817
- flat plate streaming potential investigations: hydroynamics and electrokinetic equivalency 80—106777
- flow in narrow cylindrical capillary 80—92233
- interfaces, with two types of ionising group, electrokinetic and surface pots. 78—76136
- isotachophoresis process 79—25784
- laminar flow through porous media, analysis *(Russian)* 78—1748
- lubricated load-bearing surfaces, pitting mechanism 79—87761
- multiparticle systems, electrokinetic phenomena, sedimentation pot. 77—9090
- phenomenological equations, fluxes and forces 77—5779
- phenomenological equations of electrokinetic processes, effect of electrochem. processes 79—70330
- poly (N$^{\alpha}$,N$^{\epsilon}$-terephthaloyl-L-lysine) membrane for artificial red blood cells, interaction with serum proteins *(Japanese)* 80—12061
- porous materials, thermal diffusion based on electrokinetic effect, coefficient determ., calc. and obs. *(Russian)* 78—90641
- Pyrex glass, sedimentation pot. meas. device and ζ pot. determ. *(Spanish)* 77—70236
- pyrex-H_2O(aq. KCl) systems, electrokinetic coeff. determ. from sedimentation pot. 80—3365
- quartz, electrokinetic behaviour in solns. of inorganic electrolytes *(Spanish)* 77—70306
- quartz glass-water suspensions, electrolytes effect on viscosity, pH and zeta pot. props. 79—34365
- resistive pulse technique for electrokinetic meas. with submicron particles and pores 77—86384
- rheological electrokinetic phenomena in rectangular capillary, numerical simulation 80—26023
- small particles, book contrib. 77—48654
- Streaming potential and noncreeping flow in porous beds 77—84317
- surfactant adsorpt., electrokinetic investig., appls. to AgI, latex particles 80—3363
- suspension of charged particles in ionic solutions, elec. cond. 80—7866
- toner dispersions, positively charged, electrokinetic props., electrostatic image development 79—80713
- tree root potential meas. electrode earthing method *(Russian)* 80—26420
- water in single capillary, electrokinetic and rheological parameters 80—10220
- water quality control, appl. of information transducing sensor using electrokinetic effects 79—70349
- water viscosity changes effect on electrokinetic phenomena in capillaries 80—53867
- zeta potential meas. on single crysts. 77—60112
- β-Al_2O_3, suspension, mobility and zeta potential meas. in various solvents 77—36761
- Cr electrolytic oxidation in SO_2 atmosphere, CrO_3 ionic defect effects *(Ukrainian)* 78—92504
- KCl solution, streaming current and cross-coeff. meas. in electrokinetic processes 80—76531
- Na-bentonite, electrokinetic pot. determ., electrophoresis meas. 77—16868
- Rn decay products, influence of elec. charge and humidity on diffusion coeff. 80—6192
- Si, doped and intrinsic, chemomech. effect 78—64751

electroluminescence
- *see also phosphors*
- alkaline earth oxide:Cu phosphors, electroluminesc. 77—32440

electroluminescence continued
- anthracene:2-chloroanthracene, electrolum., voltage- and freq.-brightness characts., dopant conc. depend. 78—2916
- anthracene:9-vinylanthracene, electroluminesc. at room temp. 79—15532
- anthracene: 1-chloroanthracene, electrolum. meas. 78—84659
- anthracene:acridine, electroluminesc. exam. 77—63463
- anthracene Langmuir film, lightly substituted, electrolum., photolum. and electroabsorption 80—20726
- anthracene with powdered graphite electrodes, electrolum., ambient gas effects 77—69917
- 9-anthracene-$(CH_2)_n$-N,N-dimethylaniline, electrogenerated chemiluminesc., intramol. exciplex form. 78—11503
- basic processes, materials and devices, book 77—73171
- bisphenol-A-diglycidyl epoxy, light emission under high elec. field, compared with photolum. 80—25465
- chalcopyrites, for electrolum. device appl., props. and technology, book contrib. 77—73175
- chemiluminescence, electrogenerated, analytical treatment of diffusion and electron transfer in step expts. 78—27763
- 2-chloroanthracene:acridine, electrolum. at 300K 79—15531
- diamond, electroluminescence, thermoluminesc., photocurrents 79—38675
- diamond, electroluminescence at high temp. 80—45145
- diamond, ion implanted, p-i-n structure, double injection of carriers 79—11214
- p-diamond, obs. using Ag electrodes 78—15229
- diamond, synthetic, doped electroluminescence exam. 78—6783
- diamond, synthetic, electroluminescence excitation mechanism, role of defects 78—52581
- diode, laser measurement, of semiconductor materials and devices *(Rumanian)* 78—52035
- diphenyl styryl pyrazoline-active electrolyte system, electrochemiluminesc. spectral shift 77—20929
- 9,10-diphenylanthracene, electrogenerated chemiluminescence, T_2 state emission 78—60524
- discontinuous metal film, comparison with MIM struct. 78—23533
- electrochemiluminescence, excimer-monomer emission ratio 78—31640
- electrochemiluminescence reactions, background electrolyte effects *(Russian)* 78—7209
- electrochemiluminescent organic dyes and new type of laser 77—678
- electron irrad. effect on electrolum., defects form. and quenching obs. 80—55194
- electrostatic intensity appl. *(Russian)* 78—77934
- epoxy resin, electroluminesc. 78—56522
- film, electrolum. device appl., book contrib. 77—73176
- films, activating impurity diffusion coeff. *(Russian)* 77—84995
- fluorene, electroluminesc. *(Russian)* 78—92129
- fluorene, single cryst., dielec. matrix suspension, electroluminesc. 80—2862
- fluorocarbon liquid prebreakdown light emission obs. 80—15963
- gas-filled electroluminescent detector for soft X-rays, constr. and characts. 80—32569
- hot electron distribution functions, expts., review 78—27231
- hydrodynamic electrochemiluminescence cell 80—45506
- II-VI semiconductors, injection electrolum., review, book contrib. 77—73174
- III-V nitride semiconductors, physical properties and appls. in integrated optics *(Czech)* 80—28355
- III-V semiconductors, electrolum. and related props., book contrib. 77—73173
- information display technology, symposium, San Francisco (1978) 79—9209
- infrared electroluminescence as a diagnostic tool for polycrystalline GaAs solar cells 80—93885
- insulating material monitoring by electroluminescent screens, defect imaging 78—53083
- introduction, book contrib. 77—73172
- LEDs using II-VI semiconductor with wide energy gap materials *(Polish)* 79—91501
- low voltage excitation materials *(Japanese)* 77—73169
- metal cathode, electrically stressed surface elec. phenomena, electrolum. and breakdown with medium gap spacings 80—20710
- metal film, electroluminescence mechanism *(Russian)* 79—47523
- metal film, luminescence, electron beam excited *(Russian)* 79—47526
- metallic cathodes, electroluminescent impurities causing vacuum breakdown, obs. 78—84660
- metallic particle tunnel junctions, light emission 78—80066
- MIM cathode, local electron emission and electroluminescence patterns obs. 80—108327
- MIM sandwich structures with anomalous props., review 77—59337
- m.i.m. structure, light emission, by inelastic electron tunnelling 77—1734
- MIM tunnel junctions, enhancement of light emission 77—51824
- MIS tunnel junction, light emission via inelastic tunnelling effect 79—24076
- multiphonon tunnel processes in homogeneous elec. field *(Russian)* 78—39607
- neuron inhibition simulation in electrochemiluminescence cell *(Russian)* 78—27925
- nonlinear acoustoelectro-luminescence excited by SAW 80—45143
- nucleoside anion + hydrocarbon cation, electrochemiluminescent electron transfer reaction 79—88046
- nucleotide anion + hydrocarbon cation, electrochemiluminescent electron transfer reaction 79—88046
- octaethylporphin in Al-Ag sandwich cell, electroluminesc. 77—59615
- organic compounds, electrochemiluminesc. excitation via generator producing bipolar voltage pulses 77—28629
- organic laser dyes, electrochemiluminescence, electrochem. oxidation, reduction 77—70304
- organic molecules in solution 78—31260
- organic substances, electrochemiluminescence as possible source of coherent radiation, and role in biological processes *(Russian)* 80—76093
- oxalic acid dihydrate, pulsed excitation of luminesc. 78—27326
- phosphor, EL-455s, commercial, temp. depend. of electroluminescence intensity 80—45146
- phosphor, EL-590 M type, electroluminesc. excitation by SAW, nonlinear effects 80—16104
- photoconductive image intensifier parameters *(Russian)* 78—42421
- polyethylene, γ-irrad., 77K 77—32442
- polyethylene, space charge effect on local electric breakdown 77—69773
- polyethylene, space charge injected from electrode at low temps., luminesc. obs. 80—25464

electroluminescence continued
polyethylene, treeing at 77K, with needle plane electrodes, expt. 77−24792
polyethylene terephthalate, TSC and thermolum. due to electron detrapping by local mol. motions 80−96898
polyethylene-terephthalate, field-controlled photogeneration and carrier trapping 80−25285
polymers, space charge behaviour and luminescence at 77K 79−99947
pre-breakdown luminescence in dielectrics, intensification of underexposed photographs 77−24793
principles and appls. 77−40288
PVC, constant electric field effects 77−81154
PVC, electroluminescence, influence of cell electrodes 79−74005
pyrene, emission from triplet state in electrochemical at low temps. 77−77307
radiation crack detection, use of luminescent convertors 78−53125
refractories, luminescence characteristics of pure surfaces acted on by flux of field emission electrons 80−100695
rubrene, electrochemilum. by DC, highly organised EHD convection obs. 80−71499
rubrene, soln. in benzonitrite, electrochem. luminesc. 77−77776
semiconductor, luminescence emitted from excited acceptor-donor complexes subject to external electric field 77−66544
semiconductor, quenching of luminesc. by charged defects 78−23531
semiconductor electrode, electrolum. due to hole injection from electrolyte 77−20926
semiconductor lasers, single mode, spontaneous emission spectrum dip observation, generation saturation *(Russian)* 79−76691
semiconductor struct. with separate appl. to GaAlAs 80−50427
semiconductor structures, s-type switching at high current densities 77−20417
semiconductors, exciton and domain luminesc., book 80−82588
sodium tetraphenylborate solns., stationary electrochemiluminesc. *(Russian)* 78−48243
tandem solar cells, detailed balance limit of efficiency 80−72056
p-terphenyl, cryst., double injection and electrolum. 80−97342
tetracene, spatial distrib. of electrolum. and recomb. process 79−19938
tetracene, thin cryst., electrolum. detection and determ. of spatial distrib. 79−19937
tetracene anion+tetracene cation, electron transfer reaction, singlet fission 78−11502
TGS, switching induced electrolum. 79−38669
thin organic crystals, electrolum., detection and determ. of spatial distrib. 79−19937
triboinduced luminescence 78−19581
tunnel junction, small-particle type, light emission, local plasmon modes 79−19676
tunnelling during excitation of electroluminescence 78−43936
wide-gap semiconductors, population inversion of distant donor-acceptor pairs 79−99944
ZnS:Mn,Cu, thin-film phosphors, LV DC electroluminescence 79−11472
$AgGaS_2$, electroluminesc., mechanism *(Russian)* 77−69918
(Al,Ga)As injection lasers, pulsations and adsorbing defects 79−94234
Al electrochemical electrode, oxide film growth accompanied by luminesc. 79−57236
Al-Al_2O_3:Mn-electrolyte, yellow electrolum. during anodisation of Al-Mn (1 wt.%) 77−63464
Al-Al_2O_3-electrolyte, electroluminesc., nondestructive electronic avalanche 78−68563
Al-Al_2O_3-electrolyte system, electrolum. theory, thickness depend. 80−3358
Al-oxide-electrolyte system, luminesc. spectra *(Russian)* 78−76539
Al-SiO_2-Au, thin layer struct., electroluminesc. *(French)* 78−76531
Al-ZnS:Mn-SnO_2 electroluminescent capacitors, voltage-brightness curve, effect of film structs. 79−56092
AlAs-GaAs, heterostructure electroluminesc. characts., active region electron density depend. 77−12446
AlGaAs DH stripe geometry lasers, spontaneous radiation, carrier conc., and threshold current, luminesc. meas. 79−36898
AlGaAs electroluminescent heterostructures, LPE, appl. to LED fabrication 80−55308
AlGaAs heterojunction photocell with luminesc. wavelength converter 80−108800
$Al_xGa_{1-x}As$, hetero junction light-emitting diode, construction and performance characts. *(Russian)* 77−85808
$Al_xGa_{1-x}As$:N, luminescent material, appl. in optically pumped lasers and electrolum. diodes *(Japanese)* 77−44069
$Al_xGa_{1-x}As$-GaAs, quantum-well MO-CVD heterostructure lasers, band-filling props., electrolum. spectra 79−22954
p-$Al_xGa_{1-x}As$-n-$Al_yGa_{1-y}As$ junction, electrolum. spectra at high press. 77−48246
$Al_yGa_{1-y}As_{1-x}Sb_x$ heterostructure, electroluminesc., appl. to LED's 77−8663
$Al_xGa_{1-x}P$, LPE, crystallographic obs. and electrolum. 80−88445
$Al_xGa_{1-x}P$(:Zn), solution-grown single crysts., photo- and electrolum. at 77K 79−52004
$Al_xGa_{1-x}Sb$, LED, 1.54 μm efficient emission at 300K reproducible fabrication 79−42636
AlGaSbAs heterostructures and LED's luminesc. props. in 1-2 micron band 78−10988
AlN:O, energy spectrum of deep impurity 79−83035
AlN:O, UV spectra of deep impurity centres, radiative recombination 79−87490
Al_2O_3 anode film, galvanoluminesc. during pulsed excitation 79−74006
Al_2O_3, anodic oxide films, luminesc., breakdown and colouring 78−19528
Al_2O_3, cathodic luminesc. of oxide covering on Al electrode in electrolyte soln. 77−69915
Al_2O_3 film, anodic, luminesc. during growth on high purity Al 77−48589
Au, discontinous films, electroluminescence obs. 80−103998
Au, electron tunnelling from particle, polarised light emission and plasmons 79−51685
Au film, electron emission and electroluminesc. 77−90257
Au/ZnSe:Mn/n-GaAs low threshold thin film DC electrolum. cell, pulse-excited characts. 80−76081
Au-ZnO-In metal-semicond. diode, electrolum. spectra 79−99948
Au-ZnS electrolum. Schottky barrier diode, S^+-implanted, blue emission 80−76082
BaF_2, barrier instability in strong elec. fields 79−69522
BaS:Cu phosphor, photo- and electro-luminescence 79−43030

electroluminescence continued
$BaTiO_3$, light emission during repolarisation 77−36299
$BaTiO_3$, pure and Fe doped, ferroelec., switching and electrolum. 80−76079
$BaTiO_3$, single cryst., dielec. breakdown and electroluminesc. 78−2917
CaF_2, barrier instability in strong elec. fields 79−69522
CaO:Ag (Au), electroluminesc. meas. 80−40162
CaS:Bi^{3+}, Pd^{2+}, phosphor, electroluminesc., brightness and mechanism 77−48248
CaS:Nd, Cu, phosphor, electroluminesc., spectral characts. 79−19936
CaS:Pd phosphors, trap and luminescent centre location, photo-, thermo- and electroluminescence studies 80−71482
CdF_2, MnF_2 or rare earth fluoride doped, elec. cond. and electroluminesc. 79−87508
CdF_2, pure, thin powder layers 79−56865
CdF_2, rare earth doped, multicoloured electroluminesc. 79−78755
CdF_2:Eu^{3+}, electroluminescence spectra from 400 to 700 nm *(Russian)* 77−69916
CdF_2:Eu(Gd), impurity and intrinsic electrolum. 77−36298
CdF_2:Mn,Y, in MIS struct., blue-green electrolum. 79−52025
CdF_2:Mn films, electroluminesc. meas. *(French)* 79−11471
CdF_2:NaF thin films, electroluminescence obs. at 77K *(French)* 80−80866
CdS:Ag phosphor, mechanism of trap ionisation by elec. field, Gudden-Pohl flashes 79−74007
CdS-InP n-p heterodiodes, junction props. using injection electroluminescence 79−82667
p-CdSb, photoconductivity and absorpt. in submm region, electroluminesc. 77−32046
CdSe, polar semiconductor, collisions between hot excitons and hot electrons 80−7415
$CdSnAs_2$-InP, n-p heterojunction, elec. props., electroluminesc., band struct. 80−75632
CdTe optical applications, review 77−42580
n-CdTe-electrolyte solar cells, interface changes during operation, AES, electrolum. and electroreflectance meas. 79−100525
Cu cathode, electrically stressed, broad area, surface elec. phenomena, electrolum. K-spot radiation identification with electron emission 80−20711
Cu cathode, electroluminesc. from semicond. impurities on surface 77−90200
Cu cathodes, broad area type, electrolum. regions, current-voltage characts. 80−84019
p-$CuGaSe_2$, electrolum. obs. 77−32444
Cu_2O single cryst. diodes, IR electroluminesc. 79−83034
p-Cu_2Sn-n-ZnS heterojunction, I-V characts., photocond. and electrolum. 78−72251
$Dy^{3+}+O_3(SO_5{}^{2-})(SO_2)$, in H_2SO_4 soln., electrochemiluminesc. emitters quenching by electrolysis products 79−1794
Fe_2O_3, semicond. anode in aq. electrolyte, electrolum. and electrochem. 80−76080
GaAlAs DH lasers, proton-bombard., nonradiative recomb., luminesc. time-response meas. 79−98371
GaAlAs DH lasers, self-sustained pulsation suppression, effect of SiO_2 facet coating films 80−95894
GaAlAs p-n heterostructures, current-flow mechanisms, luminesc. spectra 80−20298
$Ga_{1-x}Al_xAs$, degraded DH LED, defect struct. by electrolum. topography and TEM obs. 79−60369
$Ga_{1-x}Al_xAs$, electrolum. study using high-gain image intensifier 80−55193
$Ga_{1-x}Al_xAs$ n-p_3-p_2-p_1-p_0 struct., degradation electrolum. 80−50428
$Ga_{1-x}Al_xAs$:Si p-n junction, reemission effects 78−15230
$Ga_{1-x}Al_xAs$:Si p-n junction, doping in LPE, elec. and luminesc. props. *(Czech)* 78−47851
$Ga_{1-x}Al_xP$, LPE grown, green electroluminescence 78−19571
$Ga_{1-x}Al_xSb$ p-n structure, variable-gap, elec., photoelec. and electrolum. props. 77−11996
$Ga_{1-x}Al_xSb$ p-n structure, variable-gap, electroluminescence 78−52582
GaAs amorphous film/GaAs crystal junction, optical and elec. props. 79−99611
GaAs, Auger recombination, luminesc. meas. 77−85850
GaAs, carrier lifetime, radiation induced changes, edge luminesc. spectra 77−8664
GaAs diode, quantum efficiency and nonequilibrium carrier lifetime 77−12442
GaAs, electroluminescent study of irrad. induced struct. damage, athermal annealing 80−108280
GaAs excited by HV pulses, stimulated emission and luminesc. obs. 79−59704
GaAs homojunction LED, mechanical stress induced degradation 80−2860
n-GaAs, IR luminesc. emitted by travelling acoustoelec. domains 78−27329
GaAs luminesc. emitted as a result of carrier heating 77−52185
GaAs, luminescence during streamer discharge *(Russian)* 77−55835
GaAs p^+-n diode, radiative hot carrier recomb., photoluminesc. and electroluminesc. meas. 79−38676
GaAs, polar semiconductor, collisions between hot excitons and hot electrons 80−7415
GaAs:O, electrolum., photolum., negative differential resist. rel. to recomb. processes 80−66304
GaAs:Si LED p-n structures, speed *(Russian)* 79−43044
GaAs:Si p-n junction, electrolum. power, injection current and temp. depend. *(Russian)* 77−16401
GaAs:Si p-n junction LED, electroluminesc. efficiency 80−71491
GaAs:Si p-n light-emitting structs., soln. of general minority carrier transport eqn. 80−15597
GaAs:Si p-n structure, radiative recombination region 78−52071
GaAs/(Ga,Al)As, DH laser diode, electroluminescence near 1 eV 80−60682
GaAs-AlAs multilayer heterostructure laser, power and photoelectroluminescence characts. 80−53297
GaAs-AlGaAs photoelectroluminescent diodes, characts., radiant power 80−6972
GaAs-$Ga_{1-x}Al_xAs$, n^+-i-n heterojunction, radiative recombination under double injection *(Russian)* 77−77298
GaAs-$Ga_{1-x}Al_xAs$ red LED, 4% quantum yield *(Russian)* 77−85809
GaAs-$Ga_{1-x}Al_xAs$-$Ga_{1-y}Al_yAs$ n^+-i-n heterostructure, electroluminesc. characts., 80 to 330K *(Russian)* 79−28404

electroluminescence continued
GaAs-GaAlAs DH LEDs, with thin active layer, Burrus type, internal interference in emission spectrum 78—27325
GaAs-InSe p-n junctions, 'optical' contacts, elec. props. 78—56222
GaAs-ZnS p-n heterojunction, struct., multibeam electron microscopy obs. 79—11031
GaAs$_{0.6}$P$_{0.4}$ LED, luminesc. investig. of degradation, deep-level form. at dislocations 77—40287
GaAs$_{1-x}$P$_x$ epitaxial layers, prep. *(Czech)* 78—48233
GaAs$_{1-x}$P$_x$ LED, effect of band filling on emission spectra shape 78—48236
GaAs$_{1-x}$P$_x$:N, LED, external quantum efficiency, press. effect 77—8655
GaAs$_{1-x}$P$_x$:N, photolum. and electrolum. study of N isoelectronic traps 80—89061
GaAs$_{1-x}$P$_x$:N, upper branch of N isoelectronic trap., photo- and electrolum. expts. 77—63462
GaAs$_{1-x}$P$_x$:N heterojunction, N$_x$ and N$_\Gamma$ bound states, high-press. effects on electroluminesc. meas. 77—11870
GaAs$_x$P$_{1-x}$, liquid phase epitaxial growth on GaP, growth and properties 79—47641
GaAs$_x$Sb$_{1-x}$, epitaxial layer, struct. defects rel. to luminesc. 78—72040
p-Ga$_x$In$_{1-x}$As, Auger recomb., theory and luminesc. expts. 78—56518
Ga$_x$In$_{1-x}$As p-n junction, growth and electrolum. spectra 77—20420
Ga$_x$In$_{1-x}$As:Ge LED, by LPE, radiation emitted at 1.02 μm 78—48235
Ga$_x$In$_{1-x}$As$_y$Sb$_{1-y}$, epitaxial film and DH, efficiency 77—686
GaInPAs heterostructures and LED's, luminescent props. in 1-2 micron band 78—10988
GaN, luminesc. centres 80—93405
GaN, polarised electroluminescence emission, microstructure investigations 80—97344
GaN, pure and Zn-doped epitaxial layers 78—10955
GaN:Zn, LED, blue, yellow and green emission, temp. depend. 77—8658
GaN:Zn, low voltage LED, epitaxial layer, growth and electrolum. *(Russian)* 77—77297
GaN:Zn, n-i struct., anomalous luminesc. 80—80865
GaN:Zn, polarised electroluminescence, mag. field intensity depend. *(Russian)* 79—91502
GaN:Zn, temp. and press. depends., electrolum. 78—19567
GaN:Zn LED, electrolum. centres, rel. to growth morphology, Zn conc. and etch patterns 77—1733
GaP, electrolum. study using high-gain image intensifier 80—55193
GaP electroluminescent diode struct. prep. by SSD and Czochralski methods, dynamic props. *(Czech)* 80—97425
GaP LED degradation, effect of γ-irradiation 78—95610
GaP LED with S-shaped characteristic, negative resist. and red electroluminesc., expt. 78—48237
GaP, LPE, cathodo- and electrolum., residual impurity and struct. defect effects 78—19570
GaP, LPE, LED fabrication and electroluminesc. characts. 77—28632
GaP, p-i-n LED, I-V characts., electrolum., and photocond. meas. 77—20930
GaP p-n junction, capacitance-freq. dispersion and electroluminescence efficiency 78—64101
GaP, powder, electroluminesc. excitation by SAW, nonlinear effects 80—16104
GaP, red LED degradation, diffusion model 77—8657
GaP, VPE cryst., electrolum. characts. 77—28631
GaP:Bi,N, photoluminesc., electroluminesc., 4.2 to 300K, excitons and hole traps 80—108275
GaP:Fe, current-voltage characteristics, p-i-n diodes, luminescence, absorpt. double injection methods 79—65407
GaP:H/GaAs, amorphous film/crystal junction, optical and elec. props. 79—99611
GaP:N, phonon satellite intensity distrib. in luminesc. spectrum 77—55832
GaP:N p-n structure yellow light emitting source 77—69412
GaP:N VPE LED, deep level centres, DLTS studies 79—42493
GaP:N(N,O) epitaxial struct., luminesc. study of degradation during heat treatment 80—45139
GaP:Si p-n struct., on n-Ga$_{1-x}$Al$_x$P and n-GaP substrates, electrolum. spectra 79—24368
GaP:Zn, growth, I-V characts., electroluminesc. *(Korean)* 78—52653
GaP:Zn,O, degradation in LEDs 77—81156
GaP:Zn,O, epitaxial p-n junction, IR electroluminesc. exam. *(Russian)* 78—35207
GaP:Zn,O, photodiodes, high temp. emission spectra *(Russian)* 77—66545
GaP:Zn,O LED, 76K electrolum, spectrum, γ-irrad, and forward bias effects 79—78756
p-GaP:Zn,O-n-GaP:Te,N diode struct., radiative recomb. 80—7419
plGaP:Zn-electrolyte interface, electrochemical LED, luminescence obs. 80—84507
GaP:ZnO, LED, degradation, temp. and current depend. 79—87144
GaP-GaAs, amorphous film/crystal junction, optical and elec. props. 79—99611
GaS, electrolum. and electroabsorpt., 77K 77—48247
GaSb, Auger recombination, luminesc. meas. 77—85850
GaSb, photolum., electrolum. meas. in p-n junction, temp. influence 78—72594
GaSb:Sn, p-n junction, electroluminesc. and photoluminesc. 80—66306
GaSb-Ga$_{1-x}$In$_x$Sb p-n heterojunction, electrolum. spectra and elec. props. 77—12444
GaSe, additional IR electrolum. band obs. at 77K 78—72607
GaSe, exciton-phonon quasibound states, photocond. and luminesc. study 80—96800
GaSe-SnO$_2$ heterojunction, elec. props. and electrolum. spectra 77—59328
GaSe(Te)-SnO$_2$ spray heterojunction, electro-optical props. 78—64102
Ge-Sb, far IR emission stimulation by impact ionisation 80—66301
n-Ge-ZnSe:Mn^{2+}-In$_{2-x}$Sn$_x$O$_{3-y}$ thin film electrolum. cell with low-threshold voltage 80—84786
n-Hg$_{1-x}$Cd$_x$Te, far IR recomb. radiation in elec. field, acceptor states 77—16399
n-Hg$_{1-x}$Cd$_x$Te, far IR recomb. radiation with applied elec. field 78—27324
In-ZnO-Al metal-semicond. diode, electrolum. and photoluminesc. spectra 79—99948
In-ZnSe:Al-In, MSM structure, mechanism of current flow *(Russian)* 79—78208
InAs and solid solutions, recombination mechanisms of excess carriers, luminesc. obs. 80—97337

electroluminescence continued
p-InAs, Auger recomb., theory and luminesc. expts. 78—56518
InGa-GaSe interface, microplasma electrolum. at 300K 79—11469
InGaAs-In$_{1-x}$Ga$_x$As$_y$P$_{1-y}$ DH laser, LPE fabrication, electroluminesc., lasing characts. 79—3709
In$_x$Ga$_{1-x}$As p-n homojunction, MBE grown, electrolum. meas. 78—84328
In$_x$Ga$_{1-x}$As, thick LPE growth, electrolum. obs. 78—60589
In$_x$Ga$_{1-x}$As:Si p-n structs., electrolum. spectra, 77 to 300K 80—93408
InGaAsP, injection heterojunction laser at 1.3-1.5 μm 79—89910
InGaAsP-InP, anomalous luminesc., near heterojunction interface 79—65932
InGaAsP-InP DH LED, high temp. aged, dark-spot defects, TEM obs. 80—66300
In$_{1-x}$Ga$_x$P luminesc. props. from cathodoluminesc. and electroluminesc. meas. 80—2281
In$_{1-x}$Ga$_x$P:Te,Zn, photolum. and electrolum., direct transition region 77—8659
In$_{1-x}$Ga$_x$P$_{1-z}$As$_z$ luminesc. props. from cathodoluminesc. and electroluminesc. meas. 80—2281
In$_{1-x}$Ga$_x$P$_{1-z}$As$_z$ well in InP, tunnel injection into confined particle states 78—19130
InGaSbAs heterostructures and LED's luminesc. props. in 1-2 micron band 78—10988
InP, luminesc. emitted as a result of carrier heating 77—52185
InP, polar semiconductor, collisions between hot excitons and hot electrons 80—7415
InP:Fe, deep levels 79—56166
InP-CdS heterojunction, injection electrolum. 78—23153
InP-Ga$_x$In$_{1-x}$As$_{1-y}$P$_y$ heterojunctions, energy band diagram 77—16400
InSB, impact ionisation, influence of external mag. field on recomb. radiation and I-V characts. 79—56864
n- InSb, hot electron energy relax. in quantizing mag. fields 78—31259
n-InSb, Landau emission spectra, influence of bakcground radiation 78—43935
InSb, overheating luminescence, carrier generation-recomb. equilib. shift in elec. field 77—44068
InSb-oxide-electrolyte interface, electroluminesc. in anodic oxidation *(Russian)* 77—90201
In$_2$Se-InSe p-n junctions, 'optical' contacts, elec. props. 78—56222
InTe-InSe p-n junctions, 'optical' contacts, elec. props. 78—56222
KBr, barrier instability in strong elec. fields 79—69522
KBr:Tl, electroluminescence, spectra and quantum yield activator conc. depend., cond. changes 80—89070
KCl, undoped, or In- or Eu-doped, injection electrolum., fields up to 10^4 V cm^{-1} 77—12445
KCl:Tl, electroluminescence, spectra and quantum yield activator conc. depend., cond. changes 80—89070
KCl:Tl (0.003 to 0.27 mol.%), electrolum. 80—71490
KH$_2$PO$_4$, electrophotoluminescence obs. 79—47521
KNO$_3$, and KNO$_2$, fused, electrolum. 79—99945
KNbO$_3$, single cryst., dielec. breakdown and electroluminesc. 78—2917
La$_2$O$_3$:Eu(Tb)(Tm), powder layer, electrolum., comparison with Y$_2$O$_3$ and Y$_2$O$_2$S 77—20927
LiF:Si, injection electrolum., fields up to 10^4 V cm^{-1} 77—12445
LiN$_3$, evidence for N$_3^-$ from static and dynamic props. 78—60465
LiNbO$_3$:phosphor, piezoelec., interaction with SAW, excitation of electrolum. 79—60615
Mg-MgO-Ag junction, stable room temp. light emission 78—31257
Mo (111), electroluminescence in 200 to 630 nm range 80—103997
NH$_4$NO$_3$, intrinsic electroluminescence obs. 78—80420
(NH$_4$)$_2$SO$_4$, intrinsic electroluminescence obs. 78—80420
NaCl, absorpt. spectra, influence of elec. field 80—2794
NaCl, barrier instability in strong elec. fields 79—69522
NaCl:Ag, absorpt. spectra, influence of elec. field 80—2794
NaCl:Ag, electroluminescence spectra 78—2918
NaZnGeO$_4$:Mn, electrolum., ionisation domains 80—84787
Pb$_5$Ge$_3$O$_{11}$ crystal, ferroelec., luminesc. under pulse polarisation switching conditions 77—1735
PbO single crystals, current-voltage characts., electrolum. *(Russian)* 80—2863
PbS$_{0.1}$Se$_{0.9}$ 4.6 μm LED, room temp., band gap and electrolum. 80—66302
PbTiO$_3$ single crystals, electroluminesc., elec. field, freq. and temp. depend. 78—80422
Si, amorphous, luminesc. of diode structures 77—8656
Si inversion layers, cyclotron and subband emission 78—64128
Si, inversion layers, far IR emission from hot electrons 78—30995
Si, luminesc. emitted as a result of carrier heating 77—52185
Si MOSFET, far IR emission on high index surfaces 78—48232
Si, MOSFET, voltage tunable far IR emission from inversion layers 77—12440
Si p-n junction, reverse bias high voltage, secondary surface breakdown 80—70813
Si:Al, localised exciton bound to isoelectronic trap 80—66283
Si:H, amorphous, luminesc., band tail states and thermalization 80—25455
Si-SiO$_2$ electrode, electronic cond., luminesc obs. 80—61111
SiC, 6H polytype, LPE growth by dipping technique, electroluminesc. meas. 77—8769
SiC (6H), blue-emitting diodes by CVD 80—97439
SiC LED, defect luminesc. 80—89069
SiC LEDs prepared by overcompensation method, photon assisted tunnelling 80—97341
SiC p-n junction, electroluminesc. 80—97343
SiC p-n junction, epitaxial, grown by sublimation, elec. and struct. props. *(Chinese)* 80—60067
SiC p-n junctions, electrolum. spectra and kinetics 80—66305
SiC, phys. props. and crystal growth, rel. to appl. in electrolum. devices, book contrib. 77—77299
SiC polytypes, electrolum. in anodic oxidation, band model *(Russian)* 80—50429
SiC, power, electroluminesc. excitation by SAW, nonlinear effects 80—16104
SiC reverse biased p-n junctions, prebreakdown violet luminesc. 80—7420
SiC, surface luminesc. in presence of anodisation 78—52579
B-SiC:Al, ion implanted, elec. props. and luminesc. meas. 77—12443
α-SiC:Al diodes, ion implanted, transient characts. of electrolum. 79—24369
SiC:Al(Ga)(B) (6H) LEDs, fabrication by rotation dipping technique, electrolum. mechanisms 80—50426

electroluminescence continued
β-SiC:B p-n junction, IR electroluminesc. spectrum 77−44067
SnO_2-copper phthalocyanine-Ag systems, elec. and electroluminescent behaviour 80−80864
SnO_2-Cu_xS-ZnS:Mn,Cu-Al_2O_3-Al, light-emitting struct., cond. and electrolum., heat treatment 80−97345
SrS:Cu, phosphor electroluminescence characts. 79−33838
$SrTiO_3$, semicond. anode in aq. electrolyte, electrolum. and electrochem. 80−76080
2-(stilbenyl-4)-5-phenyloxazole derivatives, electrolytic effects of substs. on electrochemiluminesc. intensity *(Russian)* 77−55834
Ta (111), electroluminescence in 200 to 630 nm range 80−103997
Ta-Ta_2O_5-ZnS:TbF_3-Au thin films, MIS struct., DC electrolum. obs., Poole-Frenkel effect 78−88038
Ta_2O_3, cathodic luminesc. of oxide covering on Ta electrode in electrolyte soln. 77−69915
$Tb^{3+}+O_3(SO_5^{2-})(SO_2)$, in H_2SO_4 soln., electrochemiluminesc. emitters quenching by electrolysis products 79−1794
$Te_{39}As_{36}Si_{17}Ge_7P_1$ amorphous film, electroluminescence from on state 79−8188
n-TiO_2, crystal, in aqueous soln., electrochemistry and electrolum. meas. 78−48665
TiO_2, semicond. anode in aq. electrolyte, electrolum. and electrochem. 80−76080
n-TiO_2-electrolyte interface, electrolum. obs. 79−47520
$Tl_2Cl_2Br_2$, excitation of luminesc. by AC elec. field 79−38670
W, surface adsorption processes following electron excitation, cathodeluminescence studies 80−100390
WO_3, semicond. anode in aq. electrolyte, electrolum. and electrochem. 80−76080
Xe electroluminescence, electron resonance trapping, temp. effects 78−14130
Y_2O_3, film, anodic glow in Y-Y_2O_3-electrolyte system 77−12447
Y_2O_3:Eu sintered slice, DC electroluminesc., impact excitation 79−47522
Y_2O_3:Eu_2O_3 based sputtered ternary metal oxides, DC electrolum. obs. 77−77300
Y_2O_3:Eu(Tb)(Tm), powder layer, electrolum., comparison with La_2O_3 and Y_2O_2S 77−20927
Y_2O_2S:Eu(Tb)(Tm), powder layer, electrolum., comparison with La_2O_3 and Y_2O_3 77−20927
(Zn, Cd, Hg)S:Cu,In, electroluminesc. temp. depend. 77−1732
(Zn,Cd,Hg)S:Cu,In, electroluminesc., brightness waves 77−59616
(Zn, Hg)S:Cu, Cl, effect of superposition of two sinusoidal fields and freq. on electroluminesc. 78−39606
Zn-CdS:Mg, electroluminescent storage screens for X-ray flaw detection, expt. 77−77722
ZnF_2:Mn, thin films, electroluminescence, brightness voltage characts. hysteresis 80−20709
$Zn_{1-x}Mg_xTe$ undoped alloys, electroluminesc. and elec. props. 80−2813
ZnO, pure and rare earth doped, photo- and electroluminesc. 79−28803
ZnO:Ce(Sm) phosphors, electrolum. 79−99946
ZnO:Ce(Tb) phosphors, electrolum. brightness, voltage and freq. depend. 80−60681
ZnO:Dy(Nd)(Sm), phosphor, electroluminesc., photoluminesc. spectra 78−80421
ZnO:Dy(Yb)(Nd)(Sm)(Pr)(Gd)(La)(Er), electrolum. brightness, field strength and freq. depend. 80−100696
ZnO:Er, phosphors, photo- and electroluminesc. 77−12428
ZnO:Er(Ag), photoluminescence and electroluminescence 78−27327
ZnO:La phosphor, electrolum. brightness waves, −168 to +85°C 78−52580
ZnO:Nd, electrolum. brightness waves, 93 to 363K 79−33839
ZnO:Pr(Gd)(Er), phosphors, photoluminesc. and electroluminesc. spectra 79−11457
ZnO:Yb(Nd)(Pr)(Sm), electro- and photoluminesc. 79−83024
ZnO-PbO electroluminesc. phosphors, AC field excitation green and yellow emission 77−59617
(ZnO-ZnS)Cu:I, double band electroluminophors, form., props. 78−19568
ZnS crystals in electrolyte, electrolum. and elec. props. 80−93407
ZnS, current and refractive index oscills. in electric fields due to barrier instability 79−91372
ZnS, electrolum. phosphors, surface phenomena occurring during ageing *(Russian)* 79−33842
ZnS, electroluminesc. and photoluminesc. spectra, fine struct. *(Russian)* 78−84661
ZnS electroluminescent films, low energy Mn implantation system 78−30658
ZnS, electroluminescent emission, UV excitation after effects 80−45144
ZnS, electroluminophor, ageing rate, voltage effects *(Russian)* 78−84662
ZnS electroluminophors, ageing effects *(Russian)* 78−15231
ZnS, excited phosphor, IR stimulation and quenching of luminesc., review *(Russian)* 80−11455
ZnS film, Joule heating, I-V characts. 78−2599
ZnS films, electrolum., bistable excitation 80−93406
ZnS, metal-semiconductor LED, injection electroluminescence 77−62992
ZnS, phosphor, voltage and temp. dependence of pre-breakdown electroluminescence 80−45147
ZnS, phosphor, voltage depend. of electrolum. brightness 80−45148
ZnS phosphors, Gudden-Pohl effect, temp. depend. and decay rate 77−44070
ZnS phosphors, Gudden-Pohl effect, field ionis. of trapping centres 77−73170
ZnS, post field recomb. in pulsed electrolum. 80−71488
ZnS powder phosphors electroluminescent cells, AC electrolum. characts. *(Japanese)* 80−71489
ZnS, prebreakdown electrolum., domain form. and negative resist. effects 80−84788
ZnS Schottky-barrier diodes, blue light emission 79−38671
ZnS, single crysts. excited by laser beam and elec. field, streamer luminesc. and photolum. obs. 80−34986
ZnS thin films, effect of fabrication parameters on electroluminescence and related props. *(Japanese)* 80−76083
ZnS:(Cu, Cl), electroluminesc., voltage effect on ageing rate 79−95848
ZnS:Ag, electroluminesc., surface barriers *(Russian)* 78−2919
ZnS:Ag, single crystal, ionisation mechanism of field trapping centres 80−45156
ZnS:Ag,Cl, embedded in HBO_3-glass matrix, blue electrolum. 80−55195
ZnS:Cu, Br based electroluminesc. cells, light, const. field effects on electroluminesc. 78−84658

electroluminescence continued
ZnS:Cu, Cl, Mn film, AC electrolum. 80−60680
ZnS:Cu, effect of elec. field on photoluminescence, model of luminogen centre 78−76522
ZnS:Cu, electroluminesc. spectra fine struct. 79−95847
ZnS:Cu, Gudden-Pohl effect, flash kinetics 79−24367
ZnS:Cu, H, double band phosphor, electrolum., −100 to +100°C 78−10987
ZnS:Cu, halogen, electroluminescent cells, visible light and DC voltage effects on ageing 77−69914
ZnS:Cu, Mn DC electroluminescent powder panels, bulk and junction effects 80−89068
ZnS:Cu, polycryst. electret, electroluminesc. light flash character *(Russian)* 77−55833
ZnS:Cu, polycryst. phosphor, excitation storage, recombination barrier participation 78−27316
ZnS:Cu,Cl, electrolum. brightness wave, effect of square pulses 77−52184
ZnS:Cu,Cl, electrolum. voltmeter design, accurate high-voltage meas. 78−24813
ZnS:Cu,Cl phosphor, effect of charged imperfections on electrolum. 77−32443
ZnS:Cu,Er,Cl film, ageing and forming, DC electroluminesc., impact excitation 79−47522
ZnS:Cu,Pb film, sublimated, pulse electrolum. meas. *(Russian)* 77−85806
ZnS:Cu AC electroluminescent patterns and polytypic transformations 78−6784
ZnS:Cu(Cl), electroluminesc. and photoluminesc. spectra, fine struct. *(Russian)* 78−84661
ZnS:Cu(Pb), phosphor, photocapacitive effect, Gudden-Pohl effect 79−65520
ZnS:Er diodes, electrolum. 79−33840
ZnS:Mn, AC thin film electroluminesc., filamentary emission and memory effect 79−38672
ZnS:Mn, AC thin-film electrolum. devices, electrolum. efficiency profiles 79−65931
ZnS:Mn, Cu, Cl films, AC electrolum. 80−60679
ZnS:Mn, Cu powder devices, DC electroluminesc. 79−38674
ZnS:Mn, electrolum. film, direct impact excitation of Mn centres 77−24900
ZnS:Mn, electrolum. films, activating impurity diffusion coeff. *(Russian)* 77−84995
ZnS:Mn AC thin film devices, domain electrolum. 80−66303
ZnS:Mn AC thin film electrolum. device, filament behaviour 80−20712
ZnS:Mn co-deposited electrolum. thin film device, phys. and elec. characterisation 80−20713
ZnS:Mn electroluminescent films, amplification factor during electric field excitation, population inversion *(Russian)* 79−78757
ZnS:Mn film, AC electrolum., memory effect 78−15228
ZnS:Mn film, AC electrolum., memory effects 79−38673
ZnS:Mn film, current conduction and light emission, physical mechanism 78−14840
ZnS:Mn film, electroluminescence theory 79−11470
ZnS:Mn film, emission centres of DC electrolum. 78−68564
ZnS:Mn film, luminesc. of highly efficient DC diodes 77−8630
ZnS:Mn film, spectral and electro-optical props. 77−1736
ZnS:Mn film device, laser modulation of electrolum. 78−52576
ZnS:Mn film in SnO_2-ZnS-Cu_xS-ZnS:Mn-Al_2O_3-Al struct., electrolum. 79−33837
ZnS:Mn films, photoluminesc. and electroluminesc., excitation mechanism of luminesc. centres 79−11459
ZnS:Mn on SnO_2/glass transparent conductive base, surface morphology effects on electroluminesc. *(Russian)* 78−48238
ZnS:Mn Schottky diodes, reverse-biased, electroluminescence, hot electron impact excitations 80−25005
ZnS:Pb, temperature dependence of brightness 77−48249
ZnS:Pb phosphor, ionisation mechanism of field trapping centres 80−45156
ZnS:Pb phosphor mech. of elec. field liberation of electrons from traps 78−72616
ZnS:RF_3 film, AC electrolum., memory effects 79−38673
ZnS:RF_3 in Ta-Ta_2O_5-ZnS:RF_3-Au struct., electrolum. and cathodolum. meas. *(French)* 77−16398
ZnS:Tb, Cu(Ag) phosphors, luminesc. props. 80−100690
ZnS:Tb^{3+}, NdF_3 film, vac. deposited, electrolum. energy transfer 80−2861
ZnS:Tb^{3+}, sputtered film, DC electroluminesc. and host-excited photoluminesc., Tb^{3+} content depend. 77−85807
ZnS:TbF_3, photoelectroluminescence, effect of electron-hole pairs 78−27328
ZnS:TbF_3 film between semicond. Y_2O_3 layers, bright green electrolum. 80−2859
ZnS-BiOCl, electroluminesc. heterojunction phys. props. 77−66198
ZnS-Cu, comet shaped electroluminesc. lines 78−52578
ZnS-Cu, polycryst., influence of alternating elec. field and UV light on struct. defects, electrolum. expts. 79−43041
ZnS-$CuGaS_2$ heterodiodes, LPE, emission spectra 79−33335
ZnS-Mn sublimated phosphor films, annealing effects *(Russian)* 78−43949
ZnS-ZnSe mixed powders, hot-pressed polycrystalline, photolum. and electrolum. 77−32426
(ZnS-ZnSe):Cu, H systems, electrolum. 77−4690
ZnSSe:Cu, Br, SCL currents and electrolum. via rad. recomb. 77−44065
$ZnS_{1-x}Se_x$, electroluminescence with In and Au contacts, comp. depend. 77−59618
$ZnS_{1-x}Se_x$:Cu,Br ceramic, current oscills. and electrolum. under high elec. fields 79−38677
ZnSe, electroluminesc. exam. high voltage pulses 79−15533
ZnSe electroluminescent diode, ageing effects 77−8660
ZnSe film, rare earth fluoride doped, electrolum. meas. 77−16397
ZnSe, Gudden-Pohl effect, release of electrons from traps 80−45149
ZnSe, hot-pressed powder LED fabrication and characts. 78−23639
ZnSe, impact ionisation electroluminesc. 77−44066
ZnSe LED, p-n and MOS structs., blue electrolum. 77−32441
ZnSe, low resist. single crysts., radiative recomb. mechanism, photolum. and electrolum. 78−6744
ZnSe, low resistance ohmic contacts using In-Ga liquid alloy, LED fabrication appl. 80−70823
ZnSe MIS diode, blue electrolum., heat treatment effects 78−19569
ZnSe MIS diode, forward-bias electrolum. 78−23532

electroluminescence continued
ZnSe MOS diodes, injection type electrolum. 77—59614
ZnSe MOS diodes, injection luminesc., edge emission 79—28842
ZnSe, photolum. and blue electrolum. in MIS structs. 77—20928
ZnSe surface barrier diode, hot charge carriers, elec., photoelec., and electroluminesc. props. *(Russian)* 79—33841
ZnSe:Cu, I, ceramic, electroluminesc., electric field induced switching effect under illum. 77—1460
ZnSe:Cu, I ceramic, injection electroluminesc. of p-n microjunctions 80—40163
ZnSe:Li diodes, expt. *(Japanese)* 77—28633
ZnSe:Mn thin film, AC electrolum. 79—47519
ZnSe:Mn-n-GaAs, single cryst. substrate low threshold DC electrolum. 77—63465
ZnSe:Mn(Al)(I), Schottky diode, direct impact excitation of luminescent centres 79—7900
ZnSe:N, ion implanted cond. type conversion on annealing *(Korean)* 78—18668
ZnSe-BiOCl, electroluminesc. heterojunction phys. props. 77—66198
ZnSe-CdTe heterojunction, radiative recomb., electrolum. obs. 77—32445
ZnSe-CdTe(ZnTe) heterojunction, cathodolum. and electrolum. 78—6782
ZnSe-GaAs thin film DE electroluminescent cell with 20 V threshold voltage 78—76141
ZnSe-ZnTe heterojunction, prep. and props. 79—95483
ZnSeCu, double comet shaped electroluminesc. 78—52577
$ZnSiP_2$ Schottky diode, electrolum. under forward and reverse bias conditions 77—63466
ZnTe, electro- and cathodoluminesc., impurity segregation 79—43042
ZnTe, low voltage green LED, struct. double diffusion procedure 80—100697
ZnTe-CdS(Se)(S_xSe_{1-x}) heterojunctions, prep. and electrolum. characts. 77—24610
ZnTe-CdSe heterojunction, radiative recomb., electrolum. obs. 77—32445
p-ZnTe-n-GaN, electroluminescent hetero-junctions, memory effect, I-V characts. *(Russian)* 77—40289

electrolysis
see also anodisation; electrical conductivity of electrolytic liquids; electrodeposition; electroforming; electrolytic dissociation; electrolytic ion mobility; electrolytic machining; electrolytic polishing
acetate aqueous soln., polarisation curve anal., Pt electrode *(Japanese)* 79—34319
ageing effects, kinetic and structural consequences 80—61109
alkali halide crystals, defect state change during electrolysis 78—95057
alkaline electrolysis, technology development for high efficiency H prod. 80—30601
alternating current electrode processes, review 80—61107
alumina reduction cells electrolytic, instabilities of metal surface, computer simulation 78—39720
annulus flow, solenoidal mag. field effect on ionic mass transport 80—26021
anodic dissolution of metal turbulent stream of electrolyte, laws *(Russian)* 79—39156
anodic electrolysis of radioactive isotopes *(Hungarian)* 80—93765
anodic oxidation, anodic oxidation, of ethyl alcohol and acetaldehyde, voltammetric meas. 79—57247
anomalous potential and temp. grads. in electrolytes in W-tube 77—60073
aqueous solutions, electrode effects, high-speed camera obs. *(French)* 79—24751
brine, application of wind energy to a system with an inherent energy storage medium 80—30368
bubble growth rate, during electrolysis in supersaturated liq. 80—61104
cathodes, phosphate pickled mild steel, behaviour during deep electrolytical water enrichment, T meas. 80—93764
cathodic diffusion boundary layer, free convective flow obs. with shadow Schlieren method 78—68894
cells, high current density, high press. advanced cells for H_2 production 80—61441
chemical industry, electrolytic hydrogen production, raw material of the future *(French)* 79—96328
concentration polarisation at electrode, convectionless steady state, interferometric investig. 78—68896
continuous moving sheet electrode, characterisation, expt. 77—21398
Cu-Mn alloys, thermodynamics, suitability as electrodes 79—66339
database, energy properties of solns. 80—3368
diaphragm type cells, voltage calcs. using adaptive algorithms 78—35700
diaphragm-type electrolysis cells, current yields of alkali 79—100402
diminished electrolyte, semi-integral electrolysis using voltammetry 79—70339
electrochemical electrodes linearly polarised, electrolyte stationary electric field calc. *(Russian)* 80—21289
electrodialysis polarisation, rotating disc studies 79—47933
electrolyser, low cost hydrogen production *(French)* 80—7803
electrolyte flocculation of stabilised potassium 79—43638
electrolytic heating use in high-pressure chamber 80—17958
electrolytic method of mass transfer meas., advantages and disadvantages 79—68827
electrolytic method of mass transfer meas., appl. in oscill. and pulsating tube flows 79—68828
electronic device dendritic growth mechanisms 78—56058
ferricyanide bleach regeneration, simplified electrolytic method 78—74090
ferrous material fractured surface exam., oxide scale removal 78—95886
fluidised bed electrode system, extractive metallurgy appl. 79—57249
free convective mass transfer, hydrodynamic model 77—81407
gas evolution, hydrodynamic instabilities 78—48660
glass containing Cs_2O, vac. prep. of pure Cs 77—8773
glow discharge, power supply unit, current regulator 77—39489
H production testing aqueous caustic electrolyzers at high temperatures 80—45655
high-density current passage through electrolyte *(Russian)* 79—83461
hydrogenating under continuous static loading, accurate electrolytic method 78—23854
hydroxyapatites, elec. cond., charge carrier identification 78—67855
industrial organic chemicals production, electrical power applications development *(French)* 79—96327
ion discharge, periodic 80—66813
ion separation, by ion exchange membranes 78—53247
lamellar eutectic, specimen thinning for TEM *(German, English)* 78—95885

electrolysis continued
limiting current density, water-splitting, ion fluxes 79—47974
limiting currents as function of base-electrolyte conc. 80—26026
magnetoelectrolysis in steady Hartmann flow cells, hydrodynamics, mass transport 77—36759
mass exchange in flat channel during electrochemical reaction 79—74394
mass transfer to stacked net electrode 80—11896
melt electrolysis, transistorised potentiostat appl. 77—86326
metal AC anodic dissolution rate, effect of H^+ evolution *(Russian)* 80—16693
metal electrowinning, energy consumption reduction via anodic coal reaction 79—91965
metal samples potential scanning electrochemical reactions *(Dutch)* 77—66785
metallic coatings, thickness meas., coulometric thickness gauge based on electrolysis laws 77—71293
metals, anodic dissolution, ionic mass exchange effects on hydrodynamic conditions 78—3349
mobile electrolytic hydrogen generators 80—45805
non-Faradaic electrolysis 79—96333
nonaqueous solution cell, heat transfer through diaphragm 78—73049
nonstationary diffusion conditions, cathode current microdistrib. 78—3350
organic substances, electrochemiluminescence as possible source of coherent radiation, and role in biological processes *(Russian)* 80—76093
Pb electrodes, surface reactions 77—77784
pH-static, instrumentation, appls. to electrosynthesis, electrode react. stoichiometry meas. 77—63928
photoelectrolysis, basic electrode processes and appls. to H prod. from H_2O 80—51016
photoelectrolysis, semiconductor electrodes properties influence 78—14816
photoelectrolysis cell for solar energy conversion 77—20423
photoelectrolysis cells, props. of oxide-based heterostruct. photoelectrodes 80—12023
photoelectrolysis irreversibilities 78—23161
photoelectrolysis of water using semiconductor electrode, surface state charge transfer 79—28405
photoelectrolysis of water with semicond. surface, review *(Japanese)* 78—6440
photoelectrolytic decomposition of water by visible irrad. of p-GaP 77—77778
polarisation of solid surfaces, to control deform. and fracture *(Russian)* 78—11356
polymer film coated steel, Pt and glassy C electrodes, prep., characts., stability 78—76866
polymer solutions, diffusion of ionic species, meas. by diffusion controlled electrolysys 80—74920
polystyrene lattices, electro-flotation, collection efficiency 80—74946
power rectifier circuit description *(Dutch)* 77—63925
pulse electrolysis, theoretical aspects 80—85191
pulsed electrodeposition, time parameter correction by electrochem. response 79—70006
pyrographite, elec. resist., during electrochem. insertion of H_2SO_4 *(French)* 80—2437
quartz, electrokinetic behaviour in solns. of inorganic electrolytes *(Spanish)* 77—70306
quartz crystal, impurity content and lattice consts., electrolysis influence 77—35580
rare earth metals, preparation methods and properties, review 79—69969
reactions, in conc. solns., ionic mass transport rates calc. method 79—70352
reduction of aromatic nitro compounds, using $Ti(SO_4)_2$ addition 79—57248
reticulate electrodes appl., three-dimensional, mass transfer characts. obs. 79—1958
ring-disc electrodes, collection efficiency for high freq. AC 78—64853
rotating electrolyser, flow field 79—52682
rubrene radical cation reduction at n-ZnO electrode, triplet state formation, luminesc. 77—16825
seawater, electrical energy tapping 79—5504
seawater, electrolytic dissociation, utilisation of ocean hydropower systems for H prod. 80—30374
seawater, for H_2 and O_2 prod. 80—30435
solid-liquid mass transfer, meas. by holographic interferometry 79—87852
solvent transport by ions, kinetic hydration and viscosity mechanisms 78—3347
specific adsorption of ions, differential capacity meas. in binary electrolyte solns. 80—26025
stainless steel, colouring processes 77—8981
steam, supercritical, isotopic separation of metals 77—63922
steam electrolysis at high temp. for H_2 production 80—61440
steel, MnCr (16, 5 wt.%), bending fatigue behaviour improvement by surface treatment *(German)* 78—84957
steel, Ni-Cr, anodic dissoln. in NaCl solns. at high current densities *(Russian)* 80—76396
steels, obs. and anal. of sulphides, using non-aqueous electrolyte-potentiostatic etching method *(Japanese)* 80—89433
theoretical efficiency limit of water electrolysis and practical means to approach it 80—45656
transition metal foil-electrolyte interface, optical and elec. expts. 78—88644
tubular electrode under laminar flow, current distrib., one electrode reaction 77—77773
ultrapure water electrolytic conductivity meas. 79—24755
urea, electrochem. removal, basis for a regenerative dialysis system 80—26417
waste fixing solutions, investigation using volt-ampere curves *(Russian)* 79—29374
water, CW and flash photoelectrolysis using ferroelectric photoanodes 80—81339
water, decomposition by fusion energy, H_2 prod., synthetic fuel 78—50335
water, development of medium temp. high press. concept. for H_2 prod. 79—74398
water, limiting conditions for use of nuclear reactor heat in thermoelectrochemical cycle *(Russian)* 78—46183
water, non-Faraday electrolysis, at low current density 79—70340
water, photoassisted, Fe_xO_y electrodes prep. and characts. 78—15683
water, photoassisted electrolysis, EPR of $VO_{aq}{}^{2+}$ ions 78—11540

electrolysis continued
- water, photoassisted electrolysis using Fe_2O_3 semicond. electrolyte 77—77771
- water, photoassisted oxidation at TiO_2:Be electrodes 80—30502
- water, photoassisted using semicond. oxide anode 77—69413
- water, photoelectrolysis, appl. of semiconductor interface system *(French)* 80—6935
- water, photoelectrolysis, suitability of $FeTiO_3$, Fe_2TiO_4 and Fe_2TiO_5 anodes 77—63920
- water, photoelectrolysis, using Fe_xO_y-coated n-Si heterostruct. photoanode 80—61384
- water, photoelectrolysis, using n-GaAs photoanodes 77—77789
- water, photoelectrolysis, WO_3 electrode behaviour 77—66757
- water, photoelectrolysis by irradiation of platinized n-type semicond. $SrTiO_3$ and $KTaO_3$ 77—86332
- water, photoelectrolysis in sunlight, using sensitised TiO_2 electrodes 78—19143
- water, photoelectrolysis using TiO_2 electrodes 79—74407
- water, photoelectrolysis using $YFeO_3$ photoanode 77—81409
- water, photoelectrolysis with TiO_2 catalyst 80—60755
- water, photoelectrolysis with TiO_2-covered solar-cell electrodes 77—1928
- water, photooxidation, at α-Fe_2O_3:TiO_2 electrodes 78—15684
- water, S cycle H prod. process, laboratory prod. model and electrolyser development 80—30602
- water, teaching demonstration 77—9843
- water, vapour, high temp., using ZrO_2 solid electrolyte cell *(French)* 79—74399
- of water as basis of future H_2 based economy *(German)* 79—79410
- water photoelectrolysis, rel. to charge transfer via surface states of semicond. 80—75636
- water photoelectrolysis with transition metal doped TiO_2, $SrTiO_3$ anodes 79—74531
- weightlessness expts., ERNO space research, with vertical Skylark rocket *(German)* 79—19980
- wound healing, similarities between animals and plants 79—92316
- Ag/α-Ag_2S, interface, electrochemical transfer across phase boundaries 78—73046
- Ag/Na_2WO_4/Ag cell, Ag^+ ion diffusion/electromigration in solid Na_2WO_4 77—1255
- AgN_3, dielec. breakdown by elec. induced chem. decomposition 80—20586
- Al alloy anodic dissolution in $NaClO_3$ and NaCl solutions compared *(Russian)* 80—21290
- Al electrolysis units, air washing tests *(French)* 79—29493
- Al lithographic sheet, AC etching 80—35547
- Al plants electrolytic baths, power consumption limitation method *(Russian)* 80—3366
- Al smelting cathodes, comp. and props. 77—28740
- Al-air, seawater activated secondary cell 80—26128
- Al-Al_3Ni, electrolytic prep. of Al_3Ni fibres, SEM and anodic polarisation studies 80—100817
- B compounds, prep. of amorphous B, review, book contrib. 78—48358
- C, prod. from solid-state reduction of carbonate ions, X-ray diffr. 78—56594
- CO_2, aqueous solution, photoelectrochemical reduction on p-type GaP in liq. junction solar cells 78—88649
- CO_2, photoelectrocatalytic reduction in aq. suspensions of semicond. powders 79—39141
- Cd_2GeO_4 anode for H_2O photoelectrolysis 80—108716
- $CdIn_2O_4$ anode for H_2O photoelectrolysis 80—108716
- CdS(Se)-based photoelectrochem. cells, characts. 77—25287
- Cd_2SnO_4 anode for H_2O photoelectrolysis 80—108716
- Cl cells, diaphragms action 80—21294
- Co, fine powder, magnetic props., effects of electrolysis conditions in prep. 77—40091
- Co_xZrS_2, ($0<x\leq0.50$), intercalation compounds, ordered phases obs. 80—33962
- Cr-W, anodic dissoln. at high current densities *(Russian)* 80—76395
- Cu, electrocrystallisation in chloride aq. soln. 77—73241
- Cu electrorefining process, quantitative evaluation of Ag transfer 80—30246
- Cu, impurities removal using high-current-rectifier 77—9089
- Cu melts, induction stirred, electrochemical deoxidation 78—39718
- Cu, powders, prep. of spherical starting particles, for suspension electrolysis 78—60689
- Cu, suspension electrolysis 79—61542
- Cu_xMS_2, ($0<x\leq0.50$) (M=Zr, Hf), intercalation compounds, ordered phases obs. 80—33962
- $CuSO_4$ soln., electrochemical analogue of Benard instability, isothermal and potentiostatic conditions 80—76530
- $CuSO_4$-H_2SO_4, electrodeposition of Cu on plane vertical cathode, distrib. of local current densities 79—70338
- D_xTaS_2, struct., form. by cathodic reduction, neutron diffr. obs. 79—73150
- Fe based binary and ternary alloys, intercrystalline internal adsorption exam. by electrolytic dissolution *(Russian)* 78—35390
- Fe, cast, anodic polarisation in slag melt *(Russian)* 80—45513
- Fe, strengthening in H_2S04, H_2 hardening rel. to struct., anodic behaviour *(Russian)* 79—15855
- Fe-Ni-C, quenched martensite, annealing during cathodic hydrogenation, 200°C *(French)* 80—93573
- Fe_xZrS_2, ($0<x\leq0.50$), intercalation compounds, ordered phases obs. 80—33962
- n-GaP, Au-coated semicond. electrode, photoelectrochem. behaviour in water 77—21399
- H diffusion in electrolytic Ni, coeff. determ. *(Russian)* 79—8441
- H, electro-/thermochemical prod. from H_2O by Westinghouse sulphur cycle 80—55940
- H electrochemical prod., solid polymer electrolyte water electrolysis status for large scale hydrogen production 80—30605
- H, electrolytic prod. by inorganic-membrane-electrolyte H_2O electrolysis 80—45804
- H electrolytic production *(Spanish)* 80—35766
- H production, thermochemical or hybrid cycles of hydrogen production techno-economical comparison with water electrolysis 80—45796
- H production from fusion reactors coupled with high temp. electrolysis 80—45771
- H storage, electrolysis-based technology R and D at BNL, review 80—40920
- H synfuel prod. by high temp. electrolysis using fusion energy 80—35792
- H, thermoelectrochemical prod. using NaCl 80—55946

electrolysis continued
- H-O electrochemical matrix-type cells, transport effects study 80—26027
- H_2 photocatalytic prod., TiO_2 electrodes, solar energy conversion 77—1932
- H_2, photoelectrochemical generation at p-semiconds. 77—89844
- H_2 production, (Conf. Brussels, Belgium. Oct 1978) 79—74511
- H_2 production, from high temperature electrolysis and fusion reactor 79—52915
- H_2 production by water electrolysis, economics and technology *(French)* 79—100543
- H_2 production from falling water, 1978 overview and prospects in USA 79—52958
- HBr, appl. to H prod. 80—35777
- HBr electrolysis for H_2 production 80—97816
- H_xNbS_2, struct., form. by cathodic reduction, neutron diffr. obs. 79—73150
- H_2O alkaline electrolysis, chrysotile asbestos corrosion in KOH, effect of SiO_3^{2-} on electrode overvoltages 80—30433
- H_2O, alkaline electrolysis using inorganic-membrane-electrolyte for H_2 prod. 80—72092
- H_2O, decomp., H prod. by thermochemical and thermoelectrochemical cycles 80—26029
- H_2O decomposition in acid molten electrolytes at 220 to 320°C for H prod. 80—45769
- H_2O, design and operation of advanced H_2O electrolysers for H_2 prod., review 80—61449
- H_2O, electrochem. splitting, solar energy assisted, on MoS_2 layer cryst. surface 77—90612
- H_2O electrolysis in fused NaOH for H_2 prod. 80—76660
- H_2O, exam. of H production kinetics using Pd electrodes 80—30434
- H_2O, for H prod., review 80—30429
- H_2O, H thermoelectrochemical prod. using H_2SO_4-SO_2 cycle, electrochem. aspects 80—35776
- H_2O, H_2 production, module design, geometry, capacity, operating temps., pressures, electrode types 80—72098
- H_2O, high temperature electrolysis of steam H_2 production, fusion reactors, synfuel production 80—72099
- H_2O, nucleate boiling, vapour bubble behaviour, heat and mass diffusion 80—67013
- H_2O photoelectrolysis, H_2/hydrocarbon fuel prod. via biomass conversion wastes 80—89653
- H_2O photoelectrolysis, stable cells prod. 77—44484
- H_2O photoelectrolysis at high current density, using TiO_2 and $SrTiO_3$ photoanodes 78—15679
- H_2O, photoelectrolysis using TiO_2 and $SrTiO_3$ electrodes, solar energy conversion 79—52959
- H_2O photoelectrolysis with semicond. materials 78—2562
- H_2O, production of H_2, on-site, for electric generator cooling 80—72097
- H_2O vapour, high temp. electrolysis for H prod. 80—30439
- H_2O, with solid polymer electrolyte, for H_2 production 80—61442
- H_2O/D_2O electrolysis, Pd electrodes, H/D isotope separation factors, and exchange efficiency 79—50149
- $H_2O(D_2O)$, at Hg cathode, $H^+(D^+)$ discharge activation energies 80—40707
- ^{125}I microelectrolytic labelling of polypeptide hormones 80—12255
- K, determ. in seawater using selective membrane electrode 79—53368
- KOH, electrolysis for H_2 prod., materials, geometry and characts. of electrolyser cell 79—74397
- LaB_6 rods, chem. and electrolytic reaction in HNO_3 aq. soln. 79—87850
- Li, electrochemical behaviour, in propylene carbonate, SEM study *(French)* 78—56899
- LiCl in water+tetrabutylammonium tetraphenylborate in nitrobenzene systems, electrolyte dropping electrode investig. 77—25279
- LiF, thermocyclic stress effects in corrosive-media, electrochem. polarization applic. *(Russian)* 78—11356
- $LiNO_3$ solution cathodic gas evolution rate rel. to electrode material *(Russian)* 80—26020
- Li_2O-SiO_2 glass, protonated, field-driven guest proton redistrib. 80—107474
- $MgCl_2$ in water+tetrabutylammonium dicarbollyl cobaltate in nitrobenzene systems, electrolyte dropping electrode investig. 77—25279
- Mo foils, device for electrolytic thinning from wire, for electron microscopy 80—85105
- $NH_4H_2AsO_4$, protonic conduction and electrolysis investig. 77—35749
- NH_4NO_3 solution cathodic gas evolution rate rel. to electrode material *(Russian)* 80—26020
- Na_3AlF_6, molten *(French)* 77—51297
- NaCl, soln., electrolysis, surface deposit on Ti anode anal. 78—73117
- NaCl:Mn^{2+} crysts., electrolysis, dendrite form., mechanism 77—1934
- $NaNO_3$ solution cathodic gas evolution rate rel. to electrode material *(Russian)* 80—26020
- Na_2O-CaO-SiO_2 molten glass, electrolysis reactions 80—89496
- Ni alloy, oxide film isolation and obs. method 77—52563
- Ni, powders, prep. of spherical starting particles, for suspension electrolysis 78—60689
- Ni-Cr, anodic dissoln. in NaCl solns. at high current densities *(Russian)* 80—76396
- Ni-Cr alloy, heat-resistant, conc. of hardening γ'-phase, effect on electrochem. shaping *(Russian)* 77—8979
- NiH_x formation, electrolytical charging of pure Ni 80—71626
- $Ni(OH)_2$, electrolytic precipitation, prep. of Ni-Cd battery plates *(Chinese)* 79—57237
- Ni_xZrS_2, ($0<x\leq0.50$), intercalation compounds, ordered phases obs. 80—33962
- P reduction in sewage effluent by electrochemical process 80—104445
- Pb, electrolytic refining, adhesion of anode slime on anode surface 78—44047
- Pb powder prod. by electrolysis of fused salts 78—19690
- Pb, powders, prep. of spherical starting particles, for suspension electrolysis 78—60689
- Pb-acid negative battery plate, form., physicochem. processes 77—4907
- Pt anode, impedance behaviour study in β-ZnS suspension-electrolysis leaching in 1N H_2SO_4 soln. *(Japanese)* 79—24754
- Pt microcell, for radioiodination of polypeptide hormones 79—48340
- Pt microelectrodes for O_2 sensing, operation 79—84043
- Pt surface, electrochem. oxidation and reduction, XPS obs. 78—95653
- Ru(II) complex, tri-biphenyl, electrochem. electron transfer reactions at SnO-H_2O interface 79—52675
- Si, anodic oxidation for abrading thin layers from wafers *(German)* 77—25176
- Si, surface, controlled stripping, automated system 78—31557

electrolysis continued
Si surface barrier detectors, dE/dx thin detector technology, n^+ layer electrolytic removal *(Russian)* 77—57823
SiF_4, thermocyclic stress effects in corrosive-media, electrochem. polarization applic. *(Russian)* 78—11356
2-(stilbenyl-4)-5-phenyloxazole derivatives, electrolytic effects of substs. on electrochemiluminesc. intensity *(Russian)* 77—55834
T enrichment in environmental samples, using controlled power supply 78—21173
T enrichment in water by electrolysis for low-level T activity meas. 78—17536
$TiCl_4$, electrolytic reduction *(French)* 78—23644
TiO_2 doped polycrystalline electrodes, for photo-assisted electrolysis of water, spectral response 79—29370
TiO_2 electrode, illuminated, Hg deposit from Hg(II) solns. *(French)* 79—52696
U from sea-water by interfacial electrolysis *(Japanese)* 77—1931
UHg prep. from uranyl ion using two-compartment electrolyser 80—802
$^{235}UO_2$ single crystals, electrochemical prep. 78—37478
$VO_{(0.67 \text{ to } 0.44)}C_{(0.20 \text{ to } 0.70)}$, extraction of V 78—40049
Zn, electrowinning, use of organic additives, eval. 78—44048
$Zn/ZnSO_4/Zn$ system, laser interferometric study of corrosion of coated and uncoated metals, technique standardisation 79—35815
$ZnCl_2$-KCl-NaCl, molten system, containing Ni^{2+} ions, appl. to electrorefining, polarographic study 80—66810
β-ZnS, suspension-electrolysis leaching in 1N H_2SO_4 soln., anodic impedance of PbO_2(Pb) electrode *(Japanese)* 79—43594
ZrO_2, cell electrolysis of H_2O at 800° to 1000°C *(French)* 80—26024
ZrO_2, cubic, anion vacancy form. during electrolysis, density change 77—80648
ZrO_2, elec. cond.-nonstoichiometry relationship, direct determ. 78—76079
ZrO_2-Y_2O_3, Faradaic reaction kinetics, impedance dispersion anal., electrode/electrolyte interface process 79—11798

electrolytes
for solid electrolytes see superionic conducting materials
see also electrolysis; superionic conducting materials
1:2 electrolytes, conc. solns., vel. correls. calcs., diffusion, cond. and transference props. 78—85166
acetate, for Lawes phase separation in Mg-Zn-Zr-Cd-Nd alloys 79—70237
acetonitrile, electrolyte solns., IR and Raman spectra interpretation, CN-stretching region 79—73941
acetonitrile-water mixture, electrolyte transfer, thermodynamic props. 80—3395
acrylonitrile methallylsulphonate copolymers in DMF, polyelectrolyte behaviour 79—66351
acrylonitrile Na methallylsulphonate copolymer electrolytes in dimethylformamide, gel permeation chromatography appl. 80—21345
adsorption, specific, electrical double layer, interface excess activity coeff. 80—49523
adsorption isotherm and solute activities from spreading pressure-surface charge data 78—14576
aerosol OT-n-heptane-water, reversed micellar solution; addition of electrolyte, neutron small angle scattering 80—104468
alkali halides aq. solns., interionic forces and thermodynamics *(German)* 79—52688
alkali metal chlorides, thermal diffusion in H_2O, D_2O, potentiometric calcs. 78—18807
alkali polymethacrylates in alkali bromide soln., ion mobilities 79—96323
alkaline, W monocryst. anode soln., surface orientation and anode current effects *(Russian)* 80—75360
alkaline cell, creepage rate of electrolytes 79—61967
alkaline citrate, Ni electrodeposition, cathodic process rate *(Russian)* 79—8440
alkaline electrolytes, electrochem. oxidation of alcohols at electrode *(German)* 78—15681
S-alkyl-isothiouronium iodides in methanol-water mixtures, conductance at 25°C, solute-solvent interaction 79—95194
annulus with non-Newtonian fluids, mass transfer to inner wall, Leveque soln. adaptation 80—10267
aqueous electrolyte solution, activity coeff. at 298.15K 77—60074
aqueous electrolyte solution, Monte Carlo calcs. of ion pair region boundary 77—36760
aqueous electrolyte solutions, thermal diffusion, Soret coeffs. meas. 78—18811
aqueous electrolyte solutions, vel. correls., improved representation 80—59360
aqueous media, ion-pairing, hard sphere model 80—96428
aqueous solns., IR librational bands, struct. making and breaking 78—56476
aqueous solns., water struct., differential IR spectral investig. 77—52651
aqueous solution, field-induced ion evap. from liq. surface at atm. press. 80—29859
aqueous solution, US study of apparent molar compressibility 78—10125
aqueous solutions, ion-solvent interactions, transport props. *(German)* 78—79790
aqueous solutions, naturally recurring, activity coeffs. rel. to ionic diffusion 78—57224
aqueous solutions, primitive model, mean spherical approx. 78—35694
aqueous solutions, refr. index, Tamman-Tait-Gibson model 78—10863
aqueous solutions, self-diffusion of H_2O, NMR spin-echo obs. 78—80243
aqueous solutions, wetting angle of quartz meniscus movement depend. 79—37899
aqueous solutions, X-ray, neutron diffr. data, termination errors, Fourier anal. 77—47299
asymmetric electrolytes, mean spherical model, chem. pot. of ions 78—27781
basic electrolyte for low-level decontamination of radioactive waste 80—37528
binary aqueous electrolyte solutions, thermal props. 79—100429
binary electrolyte solns. thermodynamics using US props. 78—73946
binary electrolytes, pair distrib., osmotic coeff. in conc. up to 1 mol/l 80—61148
binary solns., nonideality, thermodynamics 79—39155
Blum's theory, derived conclusions involving Helmholtz free energy, correlation functions 77—48651
boiling aq. solns., heat transfer coeff. 78—9532
bolaform, conform. at air water interface 80—26050
breakdown, magnetic field influence obs. *(Russian)* 78—11521
bright plating, from zincate electrolytes, progress 80—66442

electrolytes continued
Brownian dynamics 77—63921
Brownian dynamics approx., time evolution and transport props. 79—37604
caffeine in aq. electrolyte, adsorpt. isotherm and solute activities from spreading pressure-surface charge data 78—14576
capillary rise, wetting angle rel. to rate of meniscus movement 79—65292
cardiac pacemaker battery, neutron radiography investigation, USA National Bureau of Standards 80—56179
cathodic diffusion layer of electrolyte containing $CuSO_4$ and H_2SO_4, refractive index profile 77—77774
cermet electrodeposition, effect of electrolyte in charge carried by suspended ceramic particle 78—68665
cetyltrimethylammonium bromide, micellar soln., internal elec. fields, linear dichroism obs. 77—86325
charge fluctuations, two-component ionic conductor, collective dynamics 78—67841
charged hard spheres, distrib. function, mean spherical approx. 79—4222
charged hard spheres, pair correlation function, mean spherical approx. 79—4223
charged hard spheres in neutralising background, radial distrib. function 77—33936
charged hard-sphere fluid, electrified interface pot., extended mean spherical approx. calcs. 80—84502
chloride, for high-purity Mn electrodeposition 77—4908
chloride-fluoride, for fine Sn powders electrodeposition 80—11598
concentrated aqueous electrolyte solutions, transport props. *(German)* 78—80750
concentrated electrolyte solution, cond. model 77—84957
concentrated solutions, viscosity, mixture law 78—18818
concentration, effect on aperiodic electrodiffusiophoretic drift of charged particle 79—96319
concentration meas. instrum. using laser diode, optimisation of parameters 79—20488
conductance equation, compatibility with Onsager's reciprocal relation 78—31647
conductance equation, generalized, for strong electrolytes 78—31646
continuum dielectric approx. relax., Poisson-Boltzmann thermodynamics 77—36762
Coulomb interaction, screened, range in electrolytes, and double layer problems 78—27765
Coulomb systems, equilib. distrib. functions expansion in power of density 80—64681
Coulombic fluid, correlation function critical behaviour Ornstein-Zernike theory 79—1957
Coulombic system, statistical mechs., eqn. of state in restricted primitive model 77—7644
Coulombic systems, HNC and RHNC eqns. for restricted primitive model 78—67630
crystalline stoichiometric hydrates, struct., Raman spectra, H-bond interactions *(German)* 80—80804
Debye screening length, solvent effect in diffuse double layer problem 78—53211
Debye-Huckel ionic atmosphere, number density of ions 79—29369
debye-Huckel theory of model polyelectrolytes 79—5162
dielectric dispersion and friction, viscous momentum transport and relax., ion mobility 78—27775
diffuse double layer, modified nonlinearised Poisson-Boltzmann equation 79—79305
diffusion coefficient, correlation between experimental and theoretical values 77—24421
diffusion potential, concept. rel. to Maxwell's eqns. and irreversible thermodynamics 79—63171
diffusion thermodynamic coefficients in presence of mag. induction *(French)* 77—51533
diffusion through gelatin sheets 78—32910
diffusivities of CO_2 in aq. mixed electrolyte solns. 79—95190
dilute, Hall effect 77—20337
dilute solutions, Hall const., ion solvation and dynamics *(French)* 77—4910
dilute systems of dipoles and dipolar charged particles, Mayer resummation method 78—83710
diminished electrolyte, semi-integral electrolysis using voltammetry 79—70339
diphilic polyelectrolytes, surface tension of aqueous solns, Wilhelm method 80—10745
dipolar hard sphere solvent with charged hard spheres, hypernetted chain approx. 80—61130
discharge, radiation and equilib. composition 78—5975
DNA, calf thymus, flexible polyelectrolyte, elec. birefr. meas. 79—16126
double layer, aqueous, at charged plane interface, theories comparison 79—34317
double layer, dense part, model, adsorbed mols. 77—25282
double layer in dil. electrolyte solns., model 80—45520
double layer potential change meas., transistor method 77—85298
double layers, electrostatic and steric repulsion effects in thin aqueous layers between solid surfaces 79—29375
electric double layer, primitive models, pot. difference and charge density 80—76515
electric double layer mean electrostatic pot., mean spherical approx. 79—74391
electrical conductivity meas., voltage amp. for temp. compensation *(German)* 78—54399
electrical double layer, Gouy-Chapman-Stern theory, Monte Carlo calc. 79—96315
electrical double layer around charged sphere, shear flow, bulk stresses 78—48669
electrical double layer theory, generalised Poisson-Boltzmann eqn., numerical method for soln. 78—48667
electrical double layer theory, Poisson-Boltzmann eqn. including hydration forces 78—48668
electrical force between permeable charged sheets, in electrolyte soln. 79—43605
electrocapillary acceleration meters, electrolyte composition selection 80—73331
electrocapillary acceleration meters with electrolyte in gel form 80—73330
electrochemical electrodes linearly polarised, electrolyte stationary electric field calc. *(Russian)* 80—21289

electrolytes continued
electrochemical electron transfer at electrodes in soln., review, in book, for teaching 78−8203
electrochemical reaction sequences, criteria for selective path promotion 80−26018
electrochemiluminescence reactions, background electrolyte effects *(Russian)* 78−7209
electrode systems, nonequilib. polaris. states props. overvoltage theory, in book, for teachers 78−8205
electrode-electrolyte interfaces, theory, differential capacitances 77−48649
electrohydrodynamic ionisation, solvated ion mass spectroscopy, anal. appl. 78−73102
electrolyte, binary, cryst. growth kinetics during precipitation 80−49149
electrophoretic force along equipot. electrodes 78−61024
electroplating, rack parts or bulk goods, in GTL-barrel units, Zn coating using acid electrolyte *(German)* 80−84862
electrostatic boundary layer in stationary liqs. 78−15682
electrostatic interactions and the structure of water, conf. Brussels, Belgium (1972) 78−26413
N-ethylcarbazole, soln., laser induced ionic photodissoc., transient polyelectrolyte form. 80−53068
excitation quenching, Coulomb repulsive pot. 79−63927
excitation quenching in Coulomb attraction pot. 79−72351
flow measurement, transducer-electrode freq.-ampl. characts. 77−76001
flowing, interface with metal, mag. field effects on electrochemical reactions 77−73369
fluid systems, thermodynamic props., activity expansions 78−76901
fluoride mixtures, molten, for Ge powder electrodeposition 80−60797
forces between dissimilar colloidal plates for various surface conditions 77−60135
formamide, partly deuterated, in electrolytic soln., IR spectra, anion-solvent H-bonding 78−84558
formic acid solvent system, behaviour of electrolytes 79−57239
free energy, charged hard sphere system, restricted primitive model 79−27890
free energy, hard core pot. effects for charged particles in continuous dielec. medium 79−37600
free energy, of electrolyte, due to Coulombian and hard core pots. 79−23748
free energy due to Coulomb and hard-core pots., activity coeffs. 80−45537
fused salt, semiempirical analytic theory for pair correlation function 77−27800
gas cavitation nuclei, physical props. of surrounding nonionic surfactants 79−100444
gas-electrolyte dispersions, void fraction meas. using conductivity method 80−76525
gas-electrolyte interface motion in electric field 77−35248
generalised polymer problems, Flory exponents 80−107039
glass interface with anodic electrolyte solution, simultaneous transfer of different cations in elec. fields 78−30800
glass-electrolyte solution interface chemistry 79−79256
high energy primary cell electrolytes *(German)* 78−80751
hydration number of electrolyte, determ. by vapour press. meas. 79−87868
hydration numbers, US determ. 78−20027
hydrothermal stability, thermochromism 79−39187
impurities, $Pb/HBF_4/PbO_2$ electrochemical system, effects on performance 79−52927
inorganic ion exchange membranes for electrolytic H prod. 80−45804
inorganic membrane electrolyte for alkaline water electrolysis cells 79−74396
inorganic-membrane electrolytes for H_2 prod. by H_2O alkaline electrolysis 80−72092
interface with electrode, orient. models for solvent 78−61017
interionic radial distrib. function approx. scheme 77−32796
internal electric field study by linear dichroism probes 77−86325
ion distribution near phase boundary *(German)* 78−56901
ion solvation in electrolyte solutions, stat. theory 79−91966
ion-dipole mixed system, dipole-dipole distrib. function for electrolytic soln. *(Russian)* 77−35459
ion-pairs in electrolyte solns., interaction energy 77−567
ion-water interactions, survey of diffr. studies 80−24347
ionic activities meas. using ion exchange membrane electrode 79−74392
ionic and multipolar liq., thermodynamic perturbation theory 77−47316
ionic conductivity, phenomenological theory 78−83994
ionic crystals, galvanotensometric effect 77−44485
ionic drift from 50 Hz supply, pulse echo technique 80−70314
ionic fluid, equilib. props. using corresponding states concepts 79−27889
ionic mass transfer in narrow rectangular conduits 80−61105
ionic mass transport, cathodic gas evolution influence 79−34323
ionic melts, thermal diffusion, thermoelectric power meas. 78−18810
ionic solute hydration, thermodynamic and transport props., review 78−27815
ionic solution, charged square well model, virial osmotic coeffs. 79−4217
ionic solution in molecular polar solvent, stat. mech. 78−30527
ionic solutions, elec. field statistics 78−87601
ionic solvation, spectroscopic data comparison for methanolic and aqueous solns. 80−26099
ionic systems, weakly screened, evaluation of convolution integrals appearing in integral eqn. describing pair correlations 80−84044
ionic-polar mixture, equilib. props., generalised electrostatic model 79−68995
layer, convection onset condition 79−14492
light scattering, hydrodynamic theory 78−6692
light scattering and conc. fluctuations in electrolyte solns. *(Russian)* 77−1758
liquid ionic salt, Monte Carlo simulation using multipole series *(Russian)* 77−62339
liquid-air interface, dipole layer, electrolyte effect 78−51796
liquid-liquid interface, adsorbed monolayer mol. orientation, electrolyte effects, reson. Raman obs. 78−60430
lithium salt electrolyte submillimetric absorption obs. 80−60611
macroion solutions, theory of effect of small ions on electrical admittance 80−71914
macromolecule, charged, in external elec. field, spherical case 80−75145
macromolecules, scatt. methods, conf., Prague, Czechoslovakia, (July 1976) 79−1764
maleic acid-styrene copolymer, aq. soln., conform. transition 78−75526

electrolytes continued
mass transfer, ionic, in open channels, electrolyte probe determ. 80−59110
mean spherical approx. for arbitrary hard ions and dipoles, soln. for electrolytes 79−1380
metal-electrolyte boundary, elec. refl. and photoemission relationship 80−45211
metal-electrolyte boundary, electrodynamics in visible and near UV range, microscopic effects 80−45521
metal-electrolyte boundary, photoemission effect on elec. refl. 80−45212
metal-electrolyte double layer, dual capacitor model 77−60071
metal-electrolyte double layer theory 78−23948
metal-electrolyte interface, differential capacity, thermodynamic interpretation 78−27770
metal-electrolyte interface, optical methods of study *(French)* 80−7318
methacrylic acid-N,N'-ethylenedimethacrylamide crosslinked copolymer soln., 3-dimens. struct. peculiarities *(Russian)* 79−55678
microporous solid, electrical double layer on surface 80−11955
mineral ore/pore electrolyte phase boundary layer, excess voltage time depend. *(German)* 79−84233
mixed salt solution approximating seawater composition, dielec. and radiation characts. 80−97184
mixed strong electrolytes, relax. effects in limiting law region, integral representation 77−86322
mixtures, in aq. soln., viscosity, individual electrolyte effects *(German)* 78−22881
mixtures in aq. soln., viscosity contrib. coeffs. *(German)* 80−15287
model of strong electrolytes lattice-like network of ions thermodynamic quantities 78−35699
molecular dynamics simulation 80−54097
molecular spectroscopy book 80−27052
molten binary mixtures, in thermocell, Soret coeff., thermoelec. power 77−15614
molten salt, hydrodynamic correlation functions 77−31577
molten salt, Pt, Ir and Pt-Ir alloy electrodeposition 79−24640
Monte Carlo grand canonical ensemble method, appl. to electrolyte soln. 80−54092
multi-ion system, strong electrolytes, phase diagrams and solubilities calcs. 80−25665
multicomponent solutions, thermodynamic and transport props. 79−16008
multicomponent systems, velocity correl. coeffs. 78−85167
N-N dimethylformamide based, for aluminium foil electrolyte capacitors *(Slovene)* 78−31641
nonaqueous electrolyte solutions, thermal diffusion, Soret coeffs. meas. 78−18811
nonaqueous solutions, ionic nuclei, quadrupolar interaction, mag. relax., infinite dilution limit 78−35692
nonionic surfactants, stabilisation of bubble nuclei in agarose gels 80−76562
nonlinear wave processes, in dispersive media, MHD stimulation 77−7473
nuclear relax. of spin 1/2 nuclei of heavy atoms 77−24758
organic solution, NMR relaxation of ^1H, ^2D, ^{23}Na *(Russian)* 78−15053
osmotic coeffs., mean spherical approx. refined model 79−1965
outer-sphere electron transfer in polar solvents, Debye theory 80−93762
overlapping electrical double layers, repulsive interface forces 78−44382
oxide, solid, rapid method for control of conductance 77−52647
oxide, solid electrolytes, thermal and mech. props. at steelmaking temps., review *(German)* 78−15418
paired ion model, conductance-conc. function 79−37603
particles suspended in electrolytes, in crossed elec. and mag. fields, trajectories, rel. to organisms' sensitivity to fields 78−48657
Poisson-Boltzmann theory, spherical, nonlinear, Debye-Huckel linearisation 80−35538
polar fluid, long range and short range dipole correls., separation 79−1376
polar liquid, solvated electron optical props. and thermodynamic characts., polaron model 78−85170
polarisable dielectric spheres model, struct. around ions in soln. rel. to ionic solvation and activity coeff. 79−29368
polarisable fluid containing charged particles, mol. dynamics theory 78−91214
polarisable spheres model 78−56898
poly N-vinylcarbazole, soln., laser induced ionic photodissoc., transient polyelectrolyte form. 80−53068
poly-1,4-phenylene terephthalamide, in H_2SO_4, dilute soln. viscosity 78−75524
polybrene, catalysis of $Co(NH_3)_5Br^{2+}$ alkaline hydrolysis, high pressure, effect 80−55657
polyelectrolyte, 1-1 soln., excluded vol. theory, Khun statistical segment basis 78−83716
polyelectrolyte, anionic, catalyst for spontaneous aquation of $CO(NH_3)_5Br^{2+}$ volume of activation 79−39206
polyelectrolyte, coil configuration, neutron scatt. under different constraints 79−10778
polyelectrolyte, cross-linked, dimensions of disperse forms, protein precipitants and flocculants 80−11957
polyelectrolyte, non-Newtonian effects *(French)* 78−22311
polyelectrolyte, plasticised, effect of ion placement and struct. on props. 79−7679
polyelectrolyte+physiologically active substance complexation, stability, kinetics *(Russian)* 80−8006
polyelectrolyte 'catalysis' of chem. reactions 79−57217
polyelectrolyte aqueous salt soln., inelastic light scatt. obs., conformational changes 78−60474
polyelectrolyte chain in D dimensions, conformation props. 77−31034
polyelectrolyte complexes, nonstoichiometric, solubility in water *(Russian)* 80−55674
polyelectrolyte complexes, nonstoichiometric water-soluble structure *(Russian)* 80−54112
polyelectrolyte conformation, electrostatic interaction effects at varying conc. 77−35461
polyelectrolyte in solution, variation of contrast, neutron forward scatt. calc. *(French)* 80−54104
polyelectrolyte ion binding, Poisson-Boltzmann eqn. 80−45511
polyelectrolyte soln., counterion condensate around line charge as δ-function, nonlinear Poisson-Boltzmann theory 80−85184
polyelectrolyte soln., small ion self-diffusion, Manning's limiting law derivation 80−54416
polyelectrolyte soln., small ion self-diffusion coeffs., cell model 79−19385

electrolytes continued
- polyelectrolyte solution, neutron scatt. 79—77484
- polyelectrolyte solution, polyion-polyion interaction effects, computer simulation 80—35817
- polyelectrolyte solution, thermodynamic props. determ. from Donnon equil. obs. 80—7846
- polyelectrolyte solutions, activity coeffs. and osmotic coeff., higher-order limiting laws 79—29387
- polyelectrolyte solutions, apparent ionic charge 78—76875
- polyelectrolyte solutions, colligative props., chain flexibility influence 78—94962
- polyelectrolyte solutions, counterion nucl. mag. relax., quadrupolar mechanism 80—2659
- polyelectrolyte-counterion affinity, theory of Coulombic reactions 77—48648
- polyelectrolytes, appl. of Poisson-Boltzmann eqn. 79—77483
- polyelectrolytes, diffusion pots., rel. to biological electrochemical phenomena 77—4978
- polyelectrolytes, electric transport 78—31648
- polyelectrolytes, saturation of induced dipole moment, orientation mechanism and electro-optical effects 80—84785
- polyelectrolytes, translating, electrolyte friction theory 80—29194
- polyelectrolytes, weakly charged, collapse in poor salt free soln. 80—44091
- polyelectrolytes in soln., conform., small-angle neutron scatt. investigs., review 79—873
- polyelectrolytes in soln., electrostatic persistence length rel. to unified theory 78—95932
- polymer electrolytes, solid, H_2O electrolysis, H_2 technology 80—67012
- polymer solution, partially deuterated, osmotic compressibility from elastic neutron scatt., general formulation 79—90517
- polymethacrylic acid, colloidal cylinders in solns., electrophoresis, random orient. in elec. field 79—1956
- polymethacrylic acid semi dilute solutions, conformation and organisation, small-angle neutron scatt. 79—10782
- polymethacrylic acid stabilised aq. paraffin oil emulsion, mech. props. 79—39223
- polystyrene, sulphonated, polyelectrolyte solution, correlations and dynamics 80—104446
- polyvalent electrolyte apparent molal adiabatic compressibility and US vel. obs. 78—61028
- pore filling of wetproofed electrode 80—40702
- porous cellulose acetate membranes for mixed uni-valent electrolytes in aqueous solns. reverse osmosis predictability 78—53250
- potassium oxyacid salts, aq. electrolytes, apparent molar heat capacities and vols. 79—23744
- primitive model, using modified BBGY integral eqn. 79—99049
- primitive model electrolytes, grand canonical Monte Carlo calculations 80—92427
- primitive model electrolytes, symmetrical, canonical Monte Carlo calcs. 80—92428
- primitive-model electrolyte, extended mean spherical approx. 77—36763
- propylene carbonate, SEM study of electrochem. behaviour of Li *(French)* 78—56899
- Rayleigh anisotropic light scatt. *(Russian)* 79—91459
- rechargeable fuel cell battery output power stabilisation theory 80—35674
- refractory oxide electrolytes, elec. props. at steelmaking temps. *(German)* 77—90605
- reverse osmosis transport processes at membranes *(German)* 78—95946
- salt solutions in porous media, dielectric meas. *(French)* 79—52677
- sea water activatel Al-air cell 80—26128
- seawater, electrolytes partial molal vol. estimation, specific interaction model 77—60429
- second moment condition of Stillinger and Lovett 77—90609
- sodium oxyacid salts, aq. electrolytes, apparent molar heat capacities and vols. 79—23744
- sodium polyethylene sulphonate, catalysis of $Co(NH_3)_5Br^{2+}$ alkaline hydrolysis, high pressure, effect 80—55657
- sodium polyethylene sulphonate, catalysis of $Co(NH\%d3)_5Fr^{2+}$ aquation reactions, high pressure effect 80—55656
- sodium polystyrene sulphonate, catalysis of $Co(NH\%d3)_5Fr^{2+}$ aquation reactions, high pressure effect 80—55656
- sodium polystyrene sulphonate in aq. soln., quasi-elastic light scatt. 80—100661
- solid, applications survey *(Czech)* 77—77779
- solid, direct current in cell with unipolar ionic cond. 78—35703
- solid, materials, characts. and appl. *(Japanese)* 77—70308
- solid electrolyte cells, inductive effects and AC meas. 78—6623
- solid electrolytes, phase transitions and thermodynamic states 77—84975
- solid film electrolyte systems, materials characts. and appls., review 77—77781
- solid oxide, elec. props., study methods *(French)* 80—22386
- solid polymer electrolyte H_2O electrolysis, appl. to H_2 prod. 80—61442
- solid polymer electrolyte water electrolysis development status 80—30438
- solid polymer electrolyte water electrolysis status for large scale hydrogen production 80—30605
- solid-polymer-electrolyte electrolyser for H prod., development 80—30437
- solubility in non-ion-exchange polymers *(Russian)* 80—54391
- solution, radial distrib. functions, symm., in pot. theory 78—34410
- solution, stimulated Brillouin scatt. gain 77—75618
- solution, streaming at neg. polarographic maximum 78—61020
- solution, struct. factors and thermodynamic props. 78—18533
- solution, thermodynamics and correlation functions 80—24132
- solution, tracer and mutual diffusion, open-end capillary method 79—28119
- solution, two-dimens., theory 77—86323
- solution containing spherical particles, appln. of hypernetted chain approximation to particle interaction 80—85185
- solutions, 1-1 and 1-2, extended mean spherical approxs. 79—4216
- solutions, apparent ionic charge 78—76875
- solutions, aqueous, apparent molal isochoric heater capacities at 25°C 80—59671
- solutions, dielec. dispersion and dielec. friction 78—52436
- solutions, diffraction expts. and theory *(German)* 78—95935
- solutions, diffusion coeffs. meas., conductometric method 79—23753
- solutions, electron energy 80—66812
- solutions, in ethylene carbonate viscosity and conductance meas. at 40°C 79—28122
- solutions, ion motion due to elec. field, units, nomenclature, teaching appl. 77—14

electrolytes continued
- solutions, mixed, electrical transport 80—3354
- solutions, photoemission from dropping Hg electrode 77—24620
- solutions, precipitation processes, study by particle site anal. 80—50883
- solutions, preferential solvation, NMR obs. 78—95919
- solutions, preferential solvation and mol. motion, NMR obs. 78—95920
- solutions, rel. viscosities, extended Jones-Dole eqn. 78—10208
- solutions, thermodynamics, transport props., semi-phenomenological approach including short range forces 80—3353
- solutions, van der Waals forces, force density 78—42877
- solutions in alcohols, ultrasonic vel. and density meas. used to calc. compressibility, intermol. free length and salvation no. 80—96150
- solvation effects and Gurney cosphere overlaps, conductimetric approach 80—21354
- spectrographic, and electric discharge characteristics, in narrow channel *(Russian)* 77—52726
- spherical polyelectrolytes, highly charged hard sphere model, HNC approx. 78—23969
- stepwise-dissociating acids, bases, salts, high field conductance 77—40551
- strong, conc. solns., thermodynamic props. of mixed electrolytes and Harned rule basis 79—90506
- strong electrolyte, Debye-Huckel theory, polar solvent struct. 77—21397
- strong electrolyte solutions, at high concs., collective vibrational modes 77—81105
- strong II-I electrolytes, aq. soln., Raman spectrum, local order 78—84563
- strong solutions, fluctuations rel. to acoustic relaxation and light scatt. 77—15497
- structure of conc. aq. soln. from pulsed NMR 78—38605
- structure of electrolyte solns., (1952-1977) 78—26417
- surface discharge development and influence on model reactions *(Russian)* 79—96320
- surface structure, single ion hydration energies 78—26752
- surface tension of concentrated aqueous solutions of 1.1-electrolytes measured by means of Wilhelmy and laser light scattering methods 77—72745
- symmetric electrolytes, charged surface electrostatic repulsion, numerical procedure 80—104441
- symmetrical electrolytes, conductance and model for ions in soln. 80—29197
- ternary electrolytes, viscosity and ion-solvent interactions in dioxane-water mixtures 78—18817
- tetrabutylammonium iodide/I solid/liquid electrolyte interface, impedance study 80—26031
- tetraphersylanonium-tetraphenylborate assumption for single ion thermodynamics in amphiprotic and dipolar-aprotic solvents 80—55675
- thermal battery cells using molten nitrates as electrolyte and oxidiser 80—76624
- thermodynamics, kinetics of crystn. from soln. and activities 77—76340
- transition metal foil-electrolyte interface, optical and elec. expts. 78—88644
- trifluoromethanesulphonic acid, and salts, electrochem. characts. in nonaqueous solvents 80—89499
- trifluoromethanesulphonic acid monohydrate, electrochemical props. and use as fuel cell 79—61969
- unsymmetrical, highly charged hard sphere model, HNC approx. 78—23969
- uphill diffusion associated with a flux of extrinsic vacancies 79—65229
- uracil in aq. electrolyte, adsorpt. isotherm and solute activities from spreading pressure-surface charge data 78—14576
- US velocity, ionic drift depend. in aq. soln. 79—19327
- velocity correlation coeffs., particle-particle interactions 78—64852
- viscosity of conc. solns., conc. depend. 77—55378
- viscosity of conc. solns., temp. depend. 78—80749
- water, struct. changes due to hydration of monat. ions, in stoichiometric mixtures, thermodynamic props. 78—7225
- weak electrolytes, Wien dissoc., perturbation soln. 78—23950
- weak volatile, multicomponent aqueous solns., vapour liquid equilibria 79—51243
- weakly conducting fluid, separation by thermal diffusion in elec. field *(Russian)* 79—16117
- weakly-ionised, three-component, ionis. equilib. instability 80—10877
- Wien dissociation, Gauss's divergence theorem in Onsager's theory 79—47934
- Wien effect in mixed strong electrolytes 78—75856
- zeolite A, synthetic, with salt inclusions, elec. and thermal props. 79—55925
- Ag/AgI/Te thin film galvanic cell, shelf life determ. 78—35702
- Ag-Sb alloy coating deposition *(Bulgarian)* 80—93763
- AgI-Ag oxysalt, for solid state cells, investigation 77—4909
- AgI-HgI_2, solid electrolyte, ionic and electronic cond., phase composition determ. 78—2296
- $AgNO_3$, solution, sono-conductance rel. to temp. 77—15496
- Al anodisation in CrO_3 solns, film colour/structure relationship *(Russian)* 79—91851
- Al electrolytes, X-ray determ. of cryolite ratio 78—3417
- Al-Al_2O_3:Mn-electrolyte, yellow electrolum. during anodisation of Al-Mn (1 wt.%) 77—63464
- $AlCl_3$, aq. solns., order phenomena, X-ray diffr. obs. 80—1915
- $AlCl_3$/NaCl melt, Al plate on brass appl. 77—77434
- β-Al_2O_3-Li_2O-Na_2O, solid electrolytes, elec. props., stability 77—84978
- β-Al_2O_3-Na_2O, solid electrolyte, battery appl. *(Polish)* 80—12005
- Al_2O_3-Na_2O-Li_2O, phase transformations during firing 80—3036
- As electroplating conditions of operation and quality of coatings, expt. *(Bulgarian)* 77—4744
- $BaCl_2$, conc. solns., vel. correls. calcs., diffusion, cond. and transference props. 78—85166
- BeF_2-LiF molten mixtures, mass transport, chronopotentiometry 77—21391
- Bi_2O_3/Bi^+/electrolyte system, field and temp. depend. of electronic current 80—66814
- CaCl, aq., mean activity and osmotic coeffs., free energy, 298.15K, review 77—81411
- $CaCl_2$ conc. solns., vel. correls. calcs., diffusion, cond. and transference props. 78—85166
- $CaCl_2$, correlation between experimental and theoretical diffusion coeffs. 77—24421
- CaF_2, elec. cond. at high temp. 78—72159
- CaF_2, molten, struct., electrolyte 'general primitive model' prediction test 80—28902

electrolytes continued
- $Ca(NO_3)_2$, apparent molar heat capacity and volume, of 298.15K 79−65208
- $CdCl_2$, aq. solns., sound absorpt. and relax. phenomena 80−49311
- Co bi-univalent cpds., soln., activity coeffs., osmotic coeffs., water activity, Gibbs energy, molality depend. 80−51963
- Co(II)-containing aq. electrolyte soln., nucl. mag. relax., hydration shell *(Russian)* 80−54966
- $Co(NO_3)_2$, apparent molar heat capacity and volume, of 298.15K 79−65208
- CsCl, activation coefficients and solvation numbers in mixed methanol solvents 80−81334
- CsCl, CsCl+KCl mixtures, osmotic coeffs. at 298.15K 78−92509
- CsCl+KCl mixtures, osmotic coeffs. at 298.15K 78−92509
- Cu bi-univalent cpds., soln., activity and osmotic coeffs., H_2O activity, Gibbs energy, molality depend. 80−51964
- Cu refinery electrolyte, glue determ., electrochem. method 79−48021
- Cu tripolyphosphate complexes, electrolyte development for direct deposition of Cu 80−45246
- $CuBr_2(Cl_2)$, aq. soln., structural transition, neutron diffr. study 80−64872
- $CuCl_2(Br_2)$, aq. solns., EXAFS meas. 80−60714
- $Cu(NO_3)_2$, apparent molar heat capacity and volume, of 298.15K 79−65208
- $CuSO_4$, aq. soln., Soret coeff. and heat of transport 78−18809
- $CuSO_4$, solution, activity coeff. determ. 78−76874
- $CuSO_4/H_2SO_4$ electrolytes, densities, elec. cond., viscosities 80−107455
- $FeCl_2$, soln., activity coeffs., osmotic coeffs., water activity, Gibbs energy, molality depend. 80−51963
- $Fe(NO_3)_3$, aq. soln., Fe (III) hydration shells, X-ray diffr. 79−29337
- HCl aqueous soln., H^+ mobility, 15, 25, 40°C, up to 5000 atm 78−10207
- HCl aqueous solutions, diffusion coeffs. at 298K, conductimetric obs. 80−24628
- Hg/aqueous solution interface, elec. double layer in presence of adsorbed ions 79−83469
- Hg/electrolyte contacts, adsorption model for double layer capacitance 80−44706
- $Hg/Na_2B_4O_7.10H_2O$ contacts, double-layer capacitance, temp. depend. 80−44707
- Hg-electrolyte interface, with imposed temporal and spatial periodicity, double-layer transduction 78−88639
- Hg-electrolyte interface, polarizable, dynamics of double layer 79−24756
- KBr, activation coefficients and solvation numbers in mixed methanol solvents 80−81334
- KCl, activation coefficients and solvation numbers in mixed methanol solvents 80−81334
- KF, correlation between experimental and theoretical diffusion coeffs. 77−24421
- $K_3(Fe(CN)_6)$ with NaCl in aq. soln., for porosity determ. of Cu platings on C steel filaments 79−70239
- KI-Hg interface, specific adsorption of I ions, electrical double layer, interface excess activity coeff. 80−49523
- KNO_3, activation coefficients and solvation numbers in mixed methanol solvents 80−81334
- KNO_3, aq. solns., laser induced breakdown 79−87530
- KOH, aq. solns., laser induced breakdown 79−87530
- KOH, with Mo disc electrode, anodic solution kinetics *(Russian)* 78−11523
- K_2SO_4 aqueous solutions, differential diffusion coeffs. determ. diaphragm cell method 79−95193
- Li closoboranes as electrolytes in Li solid cathode cells 80−108794
- Li ionic conductors, review 77−84979
- Li salt based solid electrolyte, synthesis and characterisation, secondary cell appl. *(French)* 80−72034
- Li solid electrolytes, review 77−84980
- $Li-I_2$ pacemaker battery electrolyte exam. by neutron radiography 80−30940
- $LiAl-NaAlCl_4-MoCl_5$ thermal battery evaluation and optimisation 79−29458
- $LiAlCl_4$, solid and liq., ionic cond., 25-180°C 77−20114
- $LiAlCl_4$, solid and molten electrolyte, thermodynamic stability 80−107447
- LiCl aqueous solns., dynamical props. by ultrasonic propag. meas. 80−76517
- LiCl electrolyte influence of lasing props. of rhodamine G solutions 80−91788
- $LiNO_3$ in N,N-dimethylacetamide, Raman, IR and US relaxation studies 80−50315
- Li_2O-SiO_2, cation interdiffusivity, electrochem. determ., 1100-1350°C 78−47544
- LiSCN in N,N-dimethylacetamide, Raman, IR and US relaxation studies 80−50315
- $Mg(NO_3)_2$, apparent molar heat capacity and volume, of 298.15K 79−65208
- $Mg(NO_3)_2$, aq. soln., ionic coordination by X-ray diffr. 79−29338
- $Mg(NO_3)_2$, correlation between experimental and theoretical diffusion coeffs. 77−24421
- Mn bi-univalent cpds., soln., activity and osmotic coeffs., H_2O activity, Gibbs energy, molality depend. 80−51964
- $Mn(NO_3)_2$, apparent molar heat capacities and volumes 79−65208
- NH_3 solutions, electrochem. behaviour of Fe electrodes, impurities effect 80−50857
- NH_4Cl, activation coefficients and solvation numbers in mixed methanol solvents 80−81334
- NO_3^- in aqueous electrolyte solution, vibr. relax. theory 79−94862
- Na-S cell, solid electrolytes, appls. *(German)* 79−29460
- $Na_3AlF_6-LiF-CaF_2-AlF_3-Al_2O_3$, electrolyte, exam. of phase equilibria, review 79−11590
- Na_2CO_3, silent discharges elec. characts., expt. *(Korean)* 78−40057
- NaCl, activation coefficients and solvation numbers in mixed methanol solvents 80−81334
- NaCl, monoelectrolyte, highly mineralised salt soln., dielec. and radiation characts. 80−97184
- NaCl, solution, droplet evaporation in laminar gaseous stream *(French)* 77−51102
- NaCl solution, ionic hydration for cations 77−62460
- NaCl with $K_3(Fe(CN)_6)$ in aq. soln., for porosity determ. of Cu platings on C steel filaments 79−70239
- $NaCl-CaCl_2$, electrolyte mixture, evaporation from multi-component droplets, in stream of air 77−56255

electrolytes continued
- NaCl-KCl, aq. solns., isopiestic studies, 383 to 474K 80−21320
- NaCl-KCl electrolyte mixtures, in aq. soln., viscosity, individual electrolyte effects *(German)* 78−22881
- NaCl(l), aq. solns., laser induced breakdown 79−87530
- $NaClO_4$ electrolyte influence on lasing props. of rhodamine G solutions 80−91788
- $NaNO_2$ aqueous solutions, differential diffusion coeffs. determ. diaphragm cell method 79−95193
- $NaNO_2$, correlation between experimental and theoretical diffusion coeffs. 77−24421
- $NaNO_3$ in N,N-dimethylacetamide, Raman, IR and US relaxation studies 80−50315
- NaSCN in N,N-dimethylacetamide, Raman, IR and US relaxation studies 80−50315
- Ni bi-univalent cpds., soln., activity coeffs., osmotic coeffs., water activity, Gibbs energy, molality depend. 80−51963
- Ni coating hardness rel. to sulphamate electrolyte selection *(Bulgarian)* 78−88552
- Ni electrodeposition from alkaline citrate electrolytes, Ni/electrolyte interaction *(Russian)* 79−11796
- $Ni-P-Al_2O_3$ (SiC), composite deposit electrodeposition *(Russian)* 78−35326
- $NiCl_2$, aq. soln., partial struct. factors in long wavelength limit 78−47231
- $NiCl_2$, aq. soln., structural transition, neutron diffr. study 80−64872
- $NiCl_2$, aq. soln., viscosity meas., struct. props. 78−75863
- $NiCl_2$ solution, ionic hydration for cation 77−62460
- $NiCl_2-D_2O$ solution, hard-sphere model 77−62461
- $NiCl_2(Br_2)$, aq. solns., EXAFS meas. 80−60714
- $Ni(NO_3)_2$, apparent molar heat capacities and volumes 79−65208
- O_2/C gas diffusion electrodes, electrochemical performance in acid solutions, content effects 79−52926
- Pb bi-univalent cpds., soln., activity and osmotic coeffs., H_2O activity, Gibbs energy, molality depend. 80−51964
- Pt anode, impedance behaviour study in β-ZnS suspension-electrolysis leaching in 1N H_2SO_4 soln. *(Japanese)* 79−24754
- $RbAg_4I_5$, solid electrolyte, Rayleigh-Brillouin and low-frequency Raman spectra 79−33720
- RuO_x, catalyst at anode of solid polymer electrolyte cell, corrosion 79−20376
- S ion conducting *(German)* 77−90606
- $Si-SiO_2$ interface props., electrolyte anode polarisation effect 77−80849
- $SrBr_2$, aq. solns., EXAFS meas. 80−60714
- $SrCl_2$, molten, struct., electrolyte 'general primitive model' prediction test 80−28902
- $SrCl_2$:KCl, polycryst., ionic cond. 78−2292
- ThO_2-CaO, mixed and ionic cond. regions 77−8156
- ThO_x:Y_2O_3 solid electrolyte high-temp. vaporisation obs. 78−14456
- Ti electrochemical machining, electrolytes development, electrochem. in static solns. 80−85182
- Ti electrochemical machining, electrolytes development, electrochem. studies in flowing solns. 80−85183
- Zn electrodeposits from alkaline zincate, pyrophosphate, cyanide, acid sulphate baths 79−57242
- Zn plating electrolyte, ion-exchange chromatography of Zn, Cd and Al salts 77−16890
- Zn secondary batteries, props. of alternate electrolytes 80−104502
- Zn sulphate, cathodic current meas. 78−35707
- Zn sulphate purity determ. 78−35706
- $ZnBr_2$, aq. solns., EXAFS meas. 80−60714
- $ZnCl_2$, aq. soln., structural transition, neutron diffr. study 80−64872
- $ZnCl_2$-KCl-NaCl, molten system, containing Ni^{2+} ions, appl. to electrorefining, polarographic study 80−66810
- $Zn(NO_3)_2$, apparent molar heat capacities and volumes 79−65208
- $ZnSO_4$, electrolyte evaluation by cyclic voltammetry and SEM 77−29076
- $ZnSO_4$ electrolytes containing Ge and Co, polarisation charact., exam. by cyclic voltammetry 80−104444

electrolytes, solid *see superionic conducting materials*

electrolytic capacitors
- Al foil anodes, effect of AC compound in electrochemical etching process on specific capacitance *(Polish)* 80−35420
- aluminium foil construction, liquid electrolyte based on N-N dimethylformamide *(Slovene)* 78−31641
- capacitance meter, series connection behaviour principle 77−53949
- etching process, effect of electrical parameters of Al foil capacitors *(Polish)* 80−30245
- meter for 0 to 10000 μF, six-range 80−27319
- power, dielectric liquids flammability and degradation 80−88944
- valve metal oxide-semicond. oxide, electron injection, interface reactions 77−76936
- Al solid, pit etching method for improving freq. and temp. characts. 80−100944
- Al-Cu (0.5 to 4.6 wt.%), cathode foil for electrolytic capacitors, relationship between comp., struct., and etchability 79−74314
- Al_2O_3 composite film props., form. by water reaction and anodic oxidation 78−15606
- Al_2O_3 thin anodised film conduction and internal field obs. 80−15639
- Ta powder for volume-porous anodes, particle shape effect on parameters 79−61539
- Ta solid dielectric capacitor, props. of dielec. Ta_2O_5 *(Spanish)* 78−19405
- Ta_2O_5 films, Poole-Frenkel effect and cond., effect of heat treatment in oxygen and in vacuum 80−39693

electrolytic conductivity of liquids *see electrical conductivity of electrolytic liquids*

electrolytic deposition *see electrodeposition*

electrolytic devices
- alkaline electrolyser, sintered Ni porous diaphragm for large scale H prod. 80−30432
- alkaline electrolyzer, technological development, review 80−30431
- alkaline H_2O electrolysis cell, development and operation of high current density, high pressure advanced cell 80−45654
- alkaline water electrolysis cells, development of inorganic membrane electrolyte 79−74396
- cathodic device for electropolishing and etching metallographic sections, in situ 79−39067
- cell for gas composition and halogen concentration determ. *(Russian)* 77−40609

electrolytic devices continued
- cell for meas. optical props of semiconds. 79—93199
- concentration cell, 1/f noise theory 79—47940
- diaphragm for high temp. water electrolysis 79—74398
- electrochemical convertors, conc. type, for elec. signals, diffusion theory of conc. networks 78—61026
- HTGR, electrolytic feed adjustment for separation of Np, Pu *(German)* 79—3229
- modelling of thermal contacts behaviour *(Italian)* 77—24504
- photoelectrolytic decomposition of water by visible irrad. of p-GaP 77—77778
- resistor, 1/f noise theory 79—47940
- solid polymer electrolyte water electrolysis development status 80—30438
- solid-polymer-electrolyte electrolyser for H prod., development 80—30437
- unipolar water electrolysers for H prod. 80—30436
- H_2 production by KOH electrolysis, materials, geometry and characts. of electrolyser cell 79—74397
- S probe, coal gasification systems appl. 78—76947
- ZrO_2 solid electrolyte cell for high temp. water vapour electrolysis *(French)* 79—74399

electrolytic dissociation
- *see also electrolytic ions*
- ball lightning explanation by water electrolysis and combustion 78—69436
- conduction regimes, field-enhanced dissoc. and EHD instabilities *(French)* 77—62655
- electroviscous effect, AC characteristics, pressure-drop fluctuations 80—107457
- heavy water, prep. of D_2 using self-controlled cell 78—80752
- ion trajectories in weak electrolytes, dissociation and recomb. of ions 80—85189
- Mathematics of Wien dissociation for weak electrolytes 78—3343
- semiconductor-electrolyte contact, electrolytic decomposition and photodecomposition 78—95357
- stepwise-dissociating acids, bases, salts, high field conductance 77—40551
- stretched dipoles, in applied elec. field, distrib. function 78—64851
- water, H_2 production using solar energy and TiO_2 electrode *(Czech)* 77—29014
- water, photoelectrolytic decomposition by visible irrad. of p-GaP electrode 77—77778
- Fe anodic dissolution, electrochem. noise generation, interference, stochastic behaviour 77—25277
- GeO_2-Na_2O, Na^+ partial dissociation investigated by elec. meas. 80—92716
- H prod. by high temp. electrolysis using fusion heat 80—51012
- H_2O, H_2 prod. by fusion reactor-high temperature electrolysis system 79—18041
- H_2O photoelectrolysis, using semiconductor electrodes, electronegativity effects 77—44482
- H_2S, dissociation in seawater 78—3816
- TiO_2 doped polycrystalline electrodes, for photo-assisted electrolysis of water, spectral response 79—29370

electrolytic ion mobility
- *see also electrophoresis*
- bimolecular lipid membranes, electrophoretic mobility 79—79479
- binary molten salt mixture, ionic and mol. mobilities, inter-diffusion and self-diffusion *(German)* 77—11720
- complex ions, mobility and stability consts., counter-current ion migration determ. *(German)* 78—56900
- diagram expansions for systems with Coulomb interaction, removal of divergences 78—73056
- dielectric dispersion and friction, viscous momentum transport and relax., ion mobility 78—27775
- electrical double layer, ionic mass transport, discreteness-of-charge effect 77—32800
- electrolyte, and polyelectrolyte solns., apparent ionic charge 78—76875
- gas-porous electrode, mass exchange in transport zones 77—32801
- glass, relaxation effect on ion migration during ion exchange by electrolysis 77—66759
- Helmholtz eqn. soln. for interactions between particles of arbitrary shape 79—100453
- hot matter, conductive opacities and free-free Gaunt factors 80—3361
- isotachophoresis process 79—25784
- membranes, ion flow, step pot. change, conc., current responses 79—5177
- molten salts, ion mobilities, group vel. correl. function calcs. 77—89561
- parallel-plate channel wall solution in electrolyte laminar flow *(Russian)* 78—64848
- polar liquids in double layer capacitors, RF conduction, ion diffusion effect 80—107883
- solutions, ion motion due to elec. field, units, nomenclature, teaching appl. 77—14
- solvated ion dynamics, kinetic dielectric decrement, microscopic theory 80—7801
- solvated ion dynamics, mol. theory, fluid struct. and ionic mobility 80—7800
- solvated ion dynamics, mol. theory 78—35695
- solvation effects and Gurney cosphere overlaps, conductimetric approach 80—21354
- spectrin-actin monolayer, adsorbed at Hg-H_2O interface, ionic permeability 80—12064
- symmetrical electrolytes, conductance and model for ions in soln. 80—29197
- water, MHD motion meas. by microfluxmeter 78—79384
- AgBr, far IR spectra, cond., cation local motion 79—1754
- $Ag_{0.85}Cu_{0.15}Br$, far IR spectra, cond., cation local motion 79—1754
- Al-Nb superimposed metallic layers, ionic movements during anodization, Rutherford backscatt. and nuclear microanal. 80—71913
- γ-Al_2O_3 interface with electrolyte solns, adsorption of ions, surface conductance, ion mobility and surface pot. 80—75622
- At^-, in KNO_3 soln., ion vel., carrier free 79—34318
- AtO_3^-, in KNO_3 soln., ion vel., carrier free 79—34318
- AtO_4^-, in KNO_3 soln., ion vel., carrier free 79—34318
- $Ca(NO_3)_2$ hydrous melts, proton spin relax. and mobility 77—77118
- β-CuBr, far IR spectra, cond., cation local motion 79—1754
- HCl aqueous soln., H^+ mobility, 15, 25, 40°C, up to 5000 atm 78—10207
- $MgSO_4$, aq. soln., electrolytic conduct. affected by US waves 79—23997
- $MgSO_4$, soln., electrolytic cond. dispersion, 1-6 MHz, caused by US propag. 80—44343

electrolytic ion mobility continued
- $NaNO_3$-$AgNO_3$, molten salt mixture, ionic and mol. mobilities, inter-diffusion and self-diffusion *(German)* 77—11720
- Nb-Al superimposed metallic layers, ionic movements during anodization, Rutherford backscatt. and nuclear microanal. 80—71913
- Nb-Ta superimposed metallic layers, ionic movements during anodization, Rutherford backscatt. and nuclear microanal. 80—71913
- Ta-Nb superimposed metallic layers, ionic movements during anodization, Rutherford backscatt. and nuclear microanal. 80—71913
- UO_2^{2+}, aq. soln., ionic mobility meas., conductivity method 77—31791
- UO_2^{2+}, n-propanol soln., ionic mobility and assoc. consts. 77—31792
- ZrF_4-based glasses, elec. transport props. 80—79983
- ZrO_2-Y_2O_3, solid electrolyte, cond. maximum 78—47577

electrolytic ions
- *see also electrical conductivity of electrolytic liquids; electrolytic dissociation; electrolytic ion mobility*
- acetate, aq. soln. current-potential curve, influence of NO_3^-, SO_4^{2-}, PO_4^{3-} and Cl^-, obs. *(Japanese)* 78—85172
- carboxylate, aq. soln. current-potential curve, influence of NO_3^- and SO_4^{2-}, obs. *(Japanese)* 78—85173
- complex formation with carboxylic acids in aqueous soln., thermodynamic parameters *(Italian)* 77—48669
- counterion condensation, soln. of Poisson-Boltzmann eqn. for two parallel charged plates 79—87849
- dipolar solvent, ionic mean force, pot. anal. 77—56234
- electrodialysis and its applications 80—55702
- polyelectrolyte-counterion affinity, theory of Coulombic reactions 77—48648
- solvent struct. around ions as hard spheres, mean spherical approx. 79—70335
- stretched dipoles, in applied elec. field, distrib. function 78—64851
- trajectories in weak electrolytes, dissociation and recomb. of ions 80—85189

electrolytic machining
- *see also electrolytic polishing*
- anode dissolution by pulsed current *(Russian)* 78—27652
- epilayer anodic thinning below avalanche breakdown potential 78—10309
- metal, electroerosion and electrochemical treatments compared *(Russian)* 79—15846
- metallic foil, continuous electrochemical perforation *(Russian)* 78—20020
- metals heating by electrolytic plasma, temperature distribution obs. *(Russian)* 79—1045
- quasi-steady model, approx. method for solving problems 78—44241
- steel, Ni-Cr, anodic dissoln. in NaCl solns. at high current densities *(Russian)* 80—76396
- tools, Cu-BN composite, dynamic hot pressing 80—84889
- Ag, single crystal, electrochem. grooving, gross linear defect obs. 78—67894
- Al foil electrolytic perforation, surface film phase composition obs. *(Russian)* 80—61004
- Cr-W, anodic dissoln. at high current densities *(Russian)* 80—76395
- Fe-Ni-Al-Co-Cu-Ti magnetic alloy electrolytic treatment with programmed pulse current *(Russian)* 79—100282
- Mo electrolytic dissolution at high anodic potentials, surface quality *(Russian)* 79—39025
- Mo foil electrolytic perforation, surface film phase composition obs. *(Russian)* 80—61004
- Ni foil electrolytic perforation, surface film phase composition obs. *(Russian)* 80—61004
- Ni-Cr, anodic dissoln. in NaCl solns. at high current densities *(Russian)* 80—76396
- Ti alloy, hydrogenation during electrochemical treatment *(Russian)* 79—39024
- Ti alloy creep strength rel. to diamond electrochem. cutting conditions *(Russian)* 79—96081
- Ti alloys, electrochemical working, film form. and surface roughness *(Russian)* 80—76397
- Ti, anodic dissolution *(Russian)* 79—83463
- Ti electrochemical machining, electrolytes development, electrochem. in static solns. 80—85182
- Ti electrochemical machining, electrolytes development, electrochem. studies in flowing solns. 80—85183
- Ti foil electrolytic perforation, surface film phase composition obs. *(Russian)* 80—61004
- W electrochemical treatment, current distrib. and metal throughput *(Russian)* 79—15849
- WC, electrochemical grinding, effect of mag. field 77—86214

electrolytic polishing
- *see also electrolytic machining*
- cathode polishing effect, nanosecond discharge in vac. 80—79599
- deep etching 78—31604
- electropolishing equipment, radioactive samples for TEM 79—87766
- ferrographite, sintered, porous, electrolytic prep. 79—52530
- Incoloy 800, steam oxidised, oxide coating anal. 80—89399
- kinetics, using horizontal Cu electrodes, role of natural convection mass transfer 79—57143
- metal, high melting point, electrolytic polishing and etching to reveal struct. *(German, English)* 80—89417
- metal, polarisation curves in polishing solns. 78—56851
- metal, solution of problems rel. to current distrib. in narrow electrode space 79—91855
- metal capillary tubes, bore polishing 80—35422
- metal removal rate during electropolishing, holographic interferometry obs. 77—8985
- metal spheres, electromechanical polishing and etching 80—68188
- metal surface replica production, nondestructive mech. and electrolytic grinding and polishing *(German, English)* 77—48607
- metallic surfaces, radioactive waste electrodecontamination using a basic electrolyte 80—37529
- metallographic sections, in situ, cathodic device 79—39067
- metalloids electromechanical polishing 79—61824
- metals, AC current influence obs. *(Russian)* 79—1922
- microcell, for TEM specimens 79—96248
- mischmetal-cobalt alloy, $MMCo_5$, polished, domain wall grooving, optical microscopy and SEM obs. 77—8334
- procedures for electrolytic polishing of a number of special materials *(German, English)* 80—89382
- radioactive samples for TEM, jet equipment 79—87766

electrolytic polishing continued
rectifier for electropolishing, thyristor current control, quick-acting electronic protection from short circuits 77—74377
single crystal surfaces, grinding and electropolishing using simple goniometer 78—4604
sintered materials, porous, electrolytic preparation 79—52530
steel, Cr, exam. of surface layer after electrochemical treatment, effect on mech. props. *(Russian)* 80—7727
steel, martensitic, dendritic structure assessment with Elypovist electropolisher 77—52565
steel, Mn (16 to 20 wt.%) metallographic analysis method 80—50791
steel, stainless, 316, surface finish effect on low-cycle fatigue at 400°C 79—29277
steel, stainless, Cr-Ni-Mo, surface, scraping, mech. (electrolytic) polishing, ion etching, effects on ESCA 78—53037
steel, stainless, martensitically ageing, techniques for revealing microstruct. characts. 79—70241
steel, stainless, Ni free acid mixture electrolyte, for electrochemical polishing 80—25902
steel, stainless, stress corrosion cracking in high temp. water, surface prep. effect 79—5088
steel, tool, low alloy, methods of revealing austenitic grain 80—25949
steel medium C, type 45, electroerosion, white-layer structures detection method 79—52485
surface evaluation 78—35627
thin foils, electropolishing technique for transmission electron microscope specimen preparation 78—57919
transition metals and compounds, electromechanical polishing method 78—53073
Wagners theory of electropolishing, validity 80—3213
Ag and alloy electron microscope specimens, noncyanide electropolishing method 80—100967
Ag, electropolishing, cyanide-free solution 78—88603
Al alloys, specimen preparation for electron microscopy 80—40636
Al, chemical polishing, electrochem. props. of soln. 79—29282
Al, polishing, electrolytic and chemical, SEM exam. of gassing defects 79—34206
Al-Fe (0.02 wt.%), Mossbauer spectrum of ^{57}Fe associated with vacancies 77—85636
Au, Au-rich alloys, electropolishing for electron microscopic examination 78—35589
Au, thin disc prep. and electropolishing for TEM 78—88601
Au-Zn(Cu) alloys, electrolytic thinning for use in transmission electron microscopy 78—57918
Be bronze, using cylindrical stationary electrode 78—64783
Be bronze, using cylindrical electrode moving forwards 78—64784
Be-Cu strip surface quality and preparation 80—50779
Co, Co-Ni alloys, in alcoholic soln. of H_2SO_4 77—16718
Cu, electropolishing behaviour rel. to polarisation charact. 79—83386
Cu, horizontal cylinder, electropolishing in phosphoric acid 79—47835
Cu, in alcoholic soln. of H_2SO_4 77—16718
Cu, single cryst., deform. process, effect of surface layer 79—8315
Cu-H_3PO_4 system, instability and oscillations *(French)* 78—64850
Fe, Fe-Ni alloys, in alcoholic soln. of H_2SO_4 77—16718
$Fe_{80}B_{20}$, amorphous, crystallization 78—42917
Mg cast iron, microstruct. of spheroidal graphite, rel. to polishing and annealing treatments 77—56160
Mo, electropolishing soln., comp. and evaluation 78—15576
Mo, in alcoholic soln. of H_2SO_4 77—16718
Nb superconducting cavities, prep., AES depth profile meas. on oxide layer 77—8984
Ni, Fe-Ni alloys, Co-Ni alloys, in alcoholic soln. of H_2SO_4 77—16718
Ni, oxide film form. by electropolishing or anodising, open circuit breakdown 77—90495
Ni-Cr alloys, method of etching in Br-methanol reagent 77—90516
Pb, high purity microstructural investigation by etching with aqueous $HClO_4$ 77—56205
Pu in acidic electrolyte soln., Monte-Carlo anal. of in situ array 80—37524
Si film, porous, form. and oxidation by anodic reaction 79—28966
SiO_2 film, local defects detection by electrolytic decoration *(Bulgarian)* 78—60896
$SmCo_5$, polished, domain wall grooving, optical microscopy and SEM obs. 77—8334
$SmCo_5$ single crystals subjected to shock waves, magnetisation, creation of high-coercivity state *(Russian)* 77—66384
Ta and Ta alloys, use of pure FSO_4H 78—85094
Ti alloys VT23 and VT15, etching as a function of struct. *(Russian)* 78—15568
Ti, in perchloric acid-acetic acid soln., AES study of anodic films 79—5072
Ti, in perchloric acid-acetic and soln., polarisation behaviour, stoichiometry 79—5073
Ti, metallographic specimen prep. for chem., mech. electrolytic polishing 78—80705
Ti, optical props. from 1.8 to 3 eV 80—85088
Ti-Al-Mo-(Cr), etching as a function of struct. *(Russian)* 78—15568
α-β Ti-Mn alloys, etching and electropolishing to reveal α and β-grain size 78—3254
β-Ti-Mo alloys, thinning transformation 77—44438
V, blister form and stress build-up, under the bombardment, surface prep. effects 78—95094
V, electropolishing for TEM obs. 78—31605
W, polishing technique as prep. for TEM 80—71851
Zr base alloys, formation of phases precipitated from β solid solutions *(Russian)* 79—1869
α-Zr, electrolytic polishing optimal condition determ. from anodic impedance meas. *(French)* 80—3250

electrolytic rectifiers
thyristor current control, quick-acting electronic protection from short circuits 77—74377

electrolytic tanks
heat conduction of metallic joints determ., for single spot and conical constrictions 78—83207
liquid flow, incompressible, electro-hydrodynamic analogy, design 77—27627

electromagnetic absorption *see electromagnetic wave absorption*

electromagnetic compatibility
see also frequency allocation
antenna coupling with biological body, proximity effects 78—3548

electromagnetic compatibility continued
automobile ignition RFI suppression at distributor rotor gap 79—55586
biomedical telemetry, transmission and reception with embedded antennae 78—77125
cardiac pacemaker responses to power frequency signals 78—88771
channeltrons and channel plates, influence of radiations, review 77—26933
civilian standards and regulations 79—31777
controlled fusion expt. shielding and earth loop elimination using fibre optics 80—74007
EM pulse measurement both inside and away from nuclear source regions 78—21773
EM wave scattering by conducting cylinder arrays interspaced by inhomogeneous dielec. 78—78862
EMP radiation, nuclear explosion 77—54366
exploding-wire photon testing of Skynet satellite 79—25433
fibre optics data link, radiation testing, degradation, transient outage time performance 77—19405
fission reactor neutron flux instrumentation commissioning, EM compatibility 79—89466
GEOS booms and mechanisms 78—85825
HF ECG, primary signal, noise, and interference sources, origin and characterisation 77—44797
IEEE International EMC Symposium, Atlanta (1978) 78—82876
international calibration cycles of field intensity and power density, measurements 80—82752
Jupiter Voyager electrostatic discharge protection 78—89042
LF EM shielding props. of arbitrary cross-section conducting cylindrical shells 78—55283
lighning return stroke channel, transmission line model, computer soln. 78—85644
logic latches, mag. approach to upset prediction 77—18710
microcontroller, radiation tolerant, design, elec. and radiation tests, performance 77—18709
nuclear and space radiation effects, conf., Albuquerque, USA (Jul. 78) 79—19276
nuclear explosions EM pulse, anal. 78—21771
nuclear explosions EMP, system generated by photoelectron emission current, anal. 78—21772
nuclear reactor instrumentation, protection against EM interference 79—89465
op amp, type 108, radiation hardening by modified processing, failure anal. 77—18751
optical fibre data bus systems, on board appls. electrical control *(German)* 78—25968
pacemaker interference simulation by models 78—81069
SEASAT-A satellite intersystem interference minimisation 78—49294
shielded cables, nonlinearities and multiple exposure anomalies at CASINO, MCCABE code verification 78—58502
shielding theory of metallic enclosures with apertures 78—55282
Skynet system-generated EM pulse response, spontaneous discharges, electron charging effect 79—25432
Solar Maximum Mission GSTDN/TDRSS compatible RF system 78—45198
standard for medical electronic devices 77—81597
system-generated EM pulse boundary layer, time-dependent, scaling behaviour 79—23641
TEM lines used in EMC tests 80—83536
thermometry considerations in localised hyperthermia, review 78—53561
Si transistors, fast burst reactor neutrons, Pb, paraffin shields 77—23172

electromagnetic corrections
"electromagnetic corrections" is distinguished in use from "radiative corrections" by application to elementary particle and nuclear interactions
see also radiative corrections
baryon resonance photoexcitation amplitudes, relativistic corrections, harmonic oscillator quark model 77—13935
charge asymmetry and charge dependence of two nucleon scattering 78—4899
charged pseudoscalar meson leptonic decay 77—38162
Coulomb corrections in pp scatt., phase shift contrib. 78—70391
deep inelastic scatt. and e^+e^- annihilation, EM corrections to asymptotic freedom predictions 78—62403
dynamical masses and p-n mass difference problem 78—12912
electron in magnetic field, quantum corrections, rotator approx. of wave function *(Russian)* 77—30032
electron moving in strong EM field, radiational corrections to mass and mag. moment *(Russian)* 77—61226
EM shift of energy levels due to confinement, bag model 80—13287
fermion scattering, comment on radiative corrections in large Higgs mass limit 79—67557
grand unified field theories, two-loop corrections to mixing angle and lifetime of proton 80—13249
grand unified model, Yukawa coupling radiative corrections, lepton and quark masses 79—97555
hadron backward scatt. at high energy *(Russian)* 79—3028
hadron charge exchange at high energy *(Russian)* 79—3028
hadron interactions, high energy, radiative corrections and vacuum pole exchange *(Russian)* 79—58964
hadron scatt., calc. by general dispersion reln. method 79—9378
heavy quark semileptonic decay, gluon radiative corrections 79—75743
Higgs boson decay, QED and QCD radiative corrections 80—95275
nuclear β-decay, elementary particle approach 77—2946
nuclear decays as test of elementary particle theory, review 78—21361
photon propagation in mag. field, radiative correction to polarisation operator *(Russian)* 78—8567
positronium energy levels, radiative corrections 80—32100
QED, electron anomaly, radiative corrections, vac. polarisation insertions, ladder graphs 79—2959
QED, one-loop effective pot., radiative corrections to electron propagator 77—45996
QED, supersymmetric, absence of radiative corrections to axial current anomaly 80—13242
radiative corrections in charge-exchange and backward hadron scattering 79—17727
radiative corrections in gauge theories, QCD current algebra formulation, weak interaction universality 78—93883
radiative corrections to β and μ decays in $SU(2)_L \times U(1)$ models involving 2n flavors 79—40778

- **electromagnetic corrections** continued
  - radiative corrections to motion of e^- in non-monochromatic EM field *(Russian)* 79−22002
  - radiative corrections to parity violation in atoms in $SU(3)\times U(1)$ gauge theory 78−62402
  - radiative effects in field of EM wave with allowance for action of stationary mag. field *(Russian)* 77−2782
  - scalar electrodynamics, IR divergences, rearranged perturbation expansion 77−67601
  - soft photon emission, and electron form factors in two-dimens. QED *(Russian)* 77−46003
  - soft-photon emission effects and radiative corrections for electromagnetic processes at very high energies 79−71752
  - soliton solutions, radiative corrections in infinite volume 77−13865
  - spin-$^1/_2$ particle, energy in constant coloured mag. field 79−80742
  - $SU(2)_L\times U(1)$ theory, radiative corrections, simple renormalisation framework 80−101973
  - $SU(2)\times U(1)$ Weinberg-Salam model, weak mixing angle, grand unified gauge theories 79−89093
  - two nucleon interaction, charge asymmetry, radiative corrections 79−89161
  - vector boson masses, weak and EM radiative corrections 80−52513
  - vertex form factor radiative corrections in 2 dimensional QED approx. *(Russian)* 80−418
  - weak and EM radiative corrections to low-energy processes 80−95274
  - weak interaction second threshold related to Higgs mechanism 77−57483
  - 50-250 GeV EM corrections, *(Russian)* 78−25048
  - e^-+nucleus parity violating neutral current interaction, gauge theory predictions, radiative corrections 78−86436
  - $e^+e^-\to e^+e^-$, Bhabha scatt. one loop radiative corrections in Weinberg model 80−13310
  - $e^+e^-\to e^+e^-(\mu^+\mu^-)(\pi^+\pi^-)$, radiative corrections to cross sections, valid in α^3-approx. 79−17726
  - $e^+e^-\to\mu^+\mu^-$, 40-200 GeV, cross section, one loop corrections in Weinberg model 80−18139
  - $e^+e^-\to\mu^+\mu^-$, radiative corrections around Z^0, Weinberg-Salam model 80−99103
  - $e^+e^-\to\mu^+\mu^-$ or e^+e^-, EM corrections for μ pair prod. and Bhabha scatt., QED processes 77−18259
  - e^+e^- photoprod., radiative corrections calc. 78−45823
  - $e^+e^-\to\psi X$, EM corrections, low energy theorem, unitarity, dispersion relations *(Russian)* 77−49982
  - $e^+e^-\to\psi\pi\pi$, radiative corrections, model estimates 77−10271
  - $e^+e^-\to\rho\pi\pi$, radiative corrections, model estimates 77−10271
  - $e^+e^-\to W^+W^-$, radiative, corrections in Weinberg model 80−52512
  - ep interactions, polarised beam and target, deep inelastic scatt. asymmetry and radiative corrections 79−63483
  - $\gamma\gamma$ collision radiative corrections from $e^\pm e^\pm$ processes 79−40777
  - $K\to 3\pi$, radiative correction amplitudes from Ke_4 decay anal. 78−86451
  - $K\to\pi e\nu$, radiative correction amplitudes from Ke_4 decay anal. 78−86451
  - $K\to\pi\pi e\nu$, Ke_4 decay, radiative correction amplitudes 78−86451
  - $L^\mp\to e^\mp\nu_e\nu_L$, $\mu^\mp\nu_\mu\nu_L$, radiative corrections to charged heavy leptons decay 78−33050
  - $l^\pm N$, deep inelastic scatt., EM corrections to hadronic and neutral currents, systematic effects *(Russian)* 79−49526
  - μ decay, inner bremsstrahlung effects and radiative corrections at start of electronic spectrum *(Russian)* 80−37273
  - $\mu\to e\nu\bar{\nu}$, full electron polarisation vector radiative corrections 79−36055
  - μ-e universality, radiative corrections in gauge theory of $\pi^\pm$ decay 77−10244
  - μp deep inelastic scatt., approx. calc. of EM corrections *(Russian)* 79−67558
  - μp deep inelastic scatt., inclusive cross section, lepton pair EM prod. contrib. *(Russian)* 80−105904
  - NN interaction,, neutral scalar, pseudoscalar and neutral vector boson radiative corrections, explicit formulae 78−70372
  - ν interactions at high energy, leading log approx. 79−80818
  - $\nu_\mu e$ (and $\bar{\nu}_\mu e$) scatt., log. order α electromag. corrections 79−63467
  - $\nu_\mu e\to\nu_\mu e$, weak and EM radiative corrections, sensitivity test 80−105880
  - νN, deep-inelastic, electromagnetic radiative corrections 80−22602
  - $\nu_l N$ deep inelastic scatt., radiative correction inaccuracies, quark-parton and Weinberg-Salam theories *(Russian)* 79−93403
  - pp scatt., low energy *(Japanese)* 78−17023
  - π, form factor, resonant space and time like, radiative correction, ρ resonance interference 79−54341
  - $\pi^0\to\gamma Ps$, Ps=orthopositronium, π^0 lifetime, $O(\alpha)$ EM correction *(Russian)* 79−45089
  - $\pi+$nucleus elastic scatt., radiative corrections 77−67772
  - $\pi^- d\to\pi^+X^-$, 2.6 GeV/c, d proton screening correction and Glauber parameter 80−9175
  - πN coupling constant from simultaneous anal. of all invariant amplitudes using rational series 78−58199
  - πN interaction, Coulomb corrections, phase shift anal., S-matrix theory, below 300 MeV 79−85325
  - πN scatt., EM effects at high energies 78−93906
  - $\pi^\pm n$ backward elastic scatt. 20-40 GeV, Regge theory description, angular distrib., radiative corrections 78−62461
  - $\pi^- p\to\pi^+X^-$, 2.6 GeV/c, d proton screening correction and Glauber parameter 80−9175
  - $\pi^\pm p$ elastic and charge exchange, scatt., dispersion relation method 77−38195
  - $Q\bar{Q}$ annihilations in QCD, strong radiative corrections 79−80809
  - Υ', lepton heavy width QCD radiative corrections 79−49515
  - β-decay lifetimes, spectra, ang. distrib. 77−38249

- **electromagnetic decays**
  - σ SU(3) model, quark-loop contrib., low-energy meson dynamics 78−12869
  - baryon charm changing radiative weak decays in AFS model 80−47285
  - baryon form factor predictions and Melosh transformations 77−54105
  - baryon resonances, EM transitions, multipole moments in single quark transition model 80−62985
  - baryon resonances, radiative decay in relativistic harmonic oscillator model 79−85277
  - charmed baryon decays, EM and weak, U- and V-spin generalisations 80−47284
  - charmonium, C-even, decay sum rules in QCD 77−54081
  - charmonium atomic physics, ψ, ψ', η_c, η_c' masses and $\psi\to\eta_c\gamma$ decay 79−40740
  - charmonium electromagnetic decay, relativistic eval. 80−68459

- **electromagnetic decays** continued
  - charmonium narrow states, hadronic and EM decays 78−70343
  - charmonium state decay, nonrelativistic and relativistic theory 78−58221
  - chiral $SU(4)\times SU(4)$ breaking scheme, vector mesons radiative decays 79−22099
  - extended PCAC+Veneziano type model, Goldberger Treiman relations, $\eta\to\gamma\gamma$or $\pi^+\pi^-\gamma$ 78−21354
  - fermion radiative decay and photon mass 78−41456
  - flavour changing weak radiative decays, short and long distance effects 80−73712
  - gluonic bound states, masses and decay widths, X(2.8) as possible candidate, $\gamma\gamma$ decay 79−93364
  - hadron electromag. and weak form factors, SU(6) scheme of relativistic quark model 78−41500
  - hadron mag. moments, colour mag. moments and transition M1-moments, quark mass parameter 79−97596
  - hadron resonance, EM decay and excitation, review, book contrib. 80−47300
  - hard-photon theorems 77−38175
  - hyperon weak EM decays, 27th Hamiltonian component contribution 79−22101
  - $K_L^0\to\pi^+\pi^-\gamma$, branching ratios and γ-energy spectrum 80−47280
  - light meson radiative decay, Zweig law *(Russian)* 80−102051
  - M1 radiative meson decays, QCD corrections 79−17718
  - massive neutrinos, radiative decay rel. to cosmic element abundances 79−92668
  - massive unstable neutrinos, cosmological implications of decay modes 78−45437
  - meson decay, contact terms 79−63481
  - meson P-wave radial mixing, effect on E1 radiative decays, charmonium mass 80−37271
  - meson photocoupling in quark model 80−82954
  - meson radiative decay, decay widths, relativistic quark models anal. 79−13118
  - meson radiative decays, higher order effects 79−13131
  - meson resonances, EM decays and props. of stratons *(Chinese)* 78−29336
  - meson resonances, strong and EM decays, particle mixing and meson pole dominance 80−18127
  - meson weak and EM decays, relativistic confined quarks, MIT bag model 80−47277
  - meson-antimeson hadronic molecules, spectrum, leptonic and radiative decays *(Russian)* 80−57602
  - mesons, low-lying positive-parity, radiative transitions, VMD and single-quark selection rules 77−18279
  - mesons, radiative transitions and gluon-exchange contributions in QCD 79−45074
  - neutrino radiative lifetimes, limits from supernovae 79−16785
  - nonmonochromatic EM wave field, quantum effect probability *(Russian)* 77−41799
  - OZI rule, pseudo-dimension rule and $\psi(3770)$ decay 79−40724
  - $P\to 2\gamma$, EM decays of vector and pseudoscalar mesons, dispersion theoretic approach 79−93423
  - positronium decay, in strong mag. fields, 10^{12} Gauss 79−88578
  - pseudoscalar and vector meson decays, triangular quark diagram anomalies, ψ, η and η' appl. *(Russian)* 80−42455
  - $Q\bar{Q}$ states, P wave decays, jet ang. distrib. and kinematics 79−75737
  - quark mass differences, magnetic moments and radiative decay widths 79−71724
  - quark mass effects as isospin and SU(3) violations in radiative decays of vector mesons 79−22091
  - quarkonia, spectra, decays, levels, jets, sum rules 80−18112
  - quarkonium radiative transition amplitudes, QCD dispersion sum rules 80−52511
  - radially excited states, photon and hadron interactions 78−82170
  - $SU_3\times U_1$ calibrating theory, weak and EM interactions appl. *(Russian)* 79−35964
  - $SU(2)\otimes U(1)$ gauge model, strange baryon weak radiative decays and CP violation 79−6260
  - SU(3) quark sectors, weak hadronic and radiative decays of nonstrange charmed baryons 79−22092
  - SU(4) six-quark models, meson masses and EM decays 77−38129
  - tensor meson radiative decay in $SU(6)\times O(3)$ broken symmetry quark model 80−73710
  - tensor mesons, EM decay possible source of photons and leptons 79−13130
  - two photon decay, time correlation 80−27506
  - two-photonic decays, weak, Hamiltonian derived in model with right-handed currents *(Russian)* 78−66119
  - unified formulae for EM decays, electroprod., e^+e^- hadron pair prod. for arbitrary spin 77−57535
  - $V\to e^+e^-$, EM decays of vector and pseudoscalar mesons, dispersion theoretic approach 79−93423
  - $V\to P\gamma$, EM decays of vector and pseudoscalar mesons, dispersion theoretic approach 79−93423
  - vector meson mass spectrum, radiative decay, QCD nonrelativistic potential model 79−36046
  - vector meson radiative decay, $\delta(980)$ scalar meson contributions 79−36083
  - vector meson radiative decay, off-shell factors in vector dominance model 79−22084
  - vector meson radiative decay evaluation in spectrum generating SU_4 scheme 79−54342
  - vector meson radiative decays, SU(3) symmetry viewpoint 80−95273
  - vector meson radiative decays, vector dominance model in broken SU(3) 80−73711
  - vector meson radiative width determ. from Primakoff effect meas. 79−89157
  - vector mesons, EM decay in broken SU(3) 80−82976
  - vector mesons, leptonic and radiative decays, Schwinger model with U(3) symm. breaking 79−379
  - vector mesons, radiative decay, single parameter scheme 80−86720
  - $B\to B'\pi\gamma$, contribs. of $B\to B'\gamma$ process 80−78066
  - $\chi\to 2\gamma$, invariant mass spectrum in π^-p interactions *(Russian)* 78−45963
  - $\chi(3.45)$, radiative M1 transitions with charmonium model 79−13132
  - $\chi\to\gamma\gamma$, radiative width calc. 77−71508
  - $\chi\to\psi\gamma$, charmonium E1 radiative transitions and quark mag. moments 80−86721
  - χ_c radiative decay, ψ and ψ' prod., straton coupling constants *(Chinese)* 80−42467

electromagnetic decays continued

- $\chi_J \rightarrow \gamma\psi$, charmonium states radiative and hadronic widths, gluon spin 80−4998
- $D_{15} \rightarrow \rho\gamma$, SU(6) selection rule violation from quark hyperfine interactions 79−6329
- D**, charmed tensor meson, strong and EM decay modes 80−68451
- D_tO^*, D_t^{+*}, weak decay modes, annihilation contribs. 79−93410
- $\delta(980) \rightarrow \gamma\gamma$ decay rate implying δ is four-quark state 79−93422
- $\Delta^+ \rightarrow p+\gamma$, radiative decay in the MIT bag model 78−66110
- $\Delta^+ \rightarrow P\gamma$, ground and radially excited states, broken symmetry treatment 80−9174
- $e^+ + e^- \rightarrow \nu_H$ possibility of production and detection 79−49501
- $e^+e^- \rightarrow 3\gamma$, 3.6 GeV and ψ' reson., comparison with QED 77−46066
- $e^+e^- \rightarrow F^*\bar{F}^* \rightarrow F\gamma_1\bar{F}\gamma_2$, photon ang. correlations and prod. amplitudes 80−47319
- $e^+e^- \rightarrow \gamma\gamma$, 9.4-31.6 GeV, differential cross section, $\Upsilon \rightarrow \gamma\gamma$ decay limits 80−91073
- e^+e^- initiated $\gamma\gamma$ processes, charged pair prod., $f^0 \rightarrow \gamma\gamma$ width 80−91123
- $e^+e^- \rightarrow \psi \rightarrow 2\gamma(3\gamma)$, charmonium model calcs. 77−30387
- $\varepsilon \rightarrow \gamma\gamma$, sum rules for $\gamma\gamma$ scatt. 77−6128
- $\eta \rightarrow 2\gamma$, η-problem of meson masses, quark charges, colour model 77−57542
- $\eta \rightarrow 2\gamma(\pi\pi\gamma)$, nonet mixing and gluon effects in current quark framework 79−80799
- $\eta(\eta') \rightarrow \gamma\gamma$, quark model tests 80−78067
- $\eta \rightarrow \gamma\gamma$, radiative widths, δ and S* background, SU(3) and VDM anal. 80−419
- $\eta \rightarrow \gamma\gamma(\pi^+\pi^-\gamma)$, chiral quark model anal. *(Russian)* 80−105900
- $\eta \rightarrow \mu^+\mu^-\gamma$, branching ratio and η EM form factor 80−105899
- $\eta \rightarrow \mu^+\mu^-\gamma$, mass spectrum 79−9367
- $\eta \rightarrow \pi^0\gamma\gamma$ decay width and processes in chiral QFT *(Russian)* 80−32099
- $\eta \rightarrow \pi^+\pi^-\pi^0$, anal. based on u_3-term of $(3,\bar{3})+(\bar{3},3)$ model 77−67657
- $\eta \rightarrow \pi^0\gamma\gamma$ decay rate 77−10270
- $\eta \rightarrow \pi\pi\gamma$, quark loop model, SU(3) splitting of quark masses 80−62990
- $\eta \rightarrow \rho\gamma(\gamma\gamma)$, C-even meson radiative decay, SU(3), and VDM anals. *(Russian)* 80−68460
- η-η' mixing angle and relative radiative decay rates $\Gamma(\psi \rightarrow \eta\gamma)/\Gamma(\psi \rightarrow \eta'\gamma)$ 80−9173
- $\eta^0 \rightarrow \gamma+(e^+e^-)$, EM bound states, approx. Bethe-Salpeter wave function *(Chinese)* 80−42448
- $\eta^0 \rightarrow \gamma+(\mu^+\mu^-)$, EM bound states, approx. Bethe-Salpeter wave function *(Chinese)* 80−42448
- $\eta^0 \rightarrow \gamma\gamma(\pi^0\gamma\gamma)(\pi^0\pi^0\pi^0)$, neutral decay channels, possible $3\pi^0$ system *(Russian)* 80−42454
- η_c, production cross sections in e^+e^- colliding beams, two-photon processes 79−36089
- $\eta' \rightarrow 2\gamma(\pi\pi\gamma)$, nonet mixing and gluon effects in current quark framework 79−80799
- $\eta'(958) \rightarrow \gamma\gamma$, decay rate, axial-vector current divergences 80−9172
- $\eta'(958) \rightarrow \gamma\gamma$, total width meas. using known $\gamma\gamma$ branching ratio 79−54343
- η' EM decay, η-η' mixing and gluons 80−62981
- $\eta' \rightarrow \gamma\gamma(\pi^+\pi^-\gamma)$, chiral quark model anal. *(Russian)* 80−105900
- $\eta' \rightarrow \pi^+\pi^-\gamma(\gamma\gamma)$, quark model descript. 80−62970
- $\eta' \rightarrow \pi^+\pi^-\gamma\gamma(\pi^+\pi^-\pi^+\pi^-\gamma\gamma)$, rare decay modes near production threshold from $\pi^-p \rightarrow \eta'n$ reaction 80−9171
- $\eta' \rightarrow \rho\gamma$, radiative widths, δ and S* background, SU(3) and VDM anal. 80−419
- $f \rightarrow \gamma\gamma$, sum rules for $\gamma\gamma$ scatt. 77−6128
- $f^0 \rightarrow \gamma\gamma$, covariant polarisation density matrix analysis *(Russian)* 78−454
- $F_1 \rightarrow F_2\gamma$, nondiagonal transition amplitude for arbitrary fermion charges *(Russian)* 80−86722
- $f_c(3.55)$ absolute γ-decay rates from tensor meson dominance and QCD pots. 79−9377
- F**, charmed tensor meson, strong and EM decay modes 80−68451
- from π^-p mass spectrum 80−27498
- $\gamma \rightarrow \nu\bar{\nu}$, in strong mag. field, rel. to pulsars and neutron stars *(Russian)* 77−17360
- J/Ψ, EM transition rates, geometrodynamical quark model 80−47295
- J/ψ, radiative M1 transitions with charmonium model 79−13132
- J/ψ decay, gluon source, search for scalar gluonium, QCD 80−47296
- $J/\psi \rightarrow \eta(\eta')\gamma$ decay rate, QCD sum rules 80−52497
- K_L, weak radiative decays in chiral theory using virtual π^0 and η pole diagrams *(Russian)* 78−78172
- $K_L \rightarrow 2\gamma$, limit on mass of charm quark 77−57491
- $K_L \rightarrow 2\gamma$, Weinberg-Salam model, weak radiative decays, large dist. contribs. *(Russian)* 77−82740
- $K_L \rightarrow 2\gamma$, Weinberg-Salam model, weak radiative decays 78−41541
- $K_L \rightarrow 2\gamma$ decay, contribution of Hamiltonian derived for weak two-photonic decays *(Russian)* 78−66119
- $K_L^0 \rightarrow e^+e^-(\mu^+\mu^-)\gamma$, Dalitz decay modes, branching ratios 80−47276
- $K_L^0 \rightarrow \gamma\gamma$, $(\pi^+\pi^-\gamma)$, chiral quark model anal. *(Russian)* 80−105900
- $K_{l4} \rightarrow \pi\pi\gamma$, form factors in chiral quantum field theory *(Russian)* 79−67550
- $K^* \rightarrow K+\gamma$, radiative decay in the MIT bag model 78−66110
- $K^* \rightarrow K\gamma$, quark loop model, SU(3) splitting of quark masses 80−62990
- $K^{*0} \rightarrow K^0\gamma$, quark anomalous mag. moments 79−17693
- $K^{*0} \rightarrow K^0\gamma$, SU(3) and isospin symmetry breaking effects 80−95272
- $K_5^{0*} \rightarrow K_5^0\gamma$ and Primakoff conversion of K_L^0 to K_5^* 80−73695
- $l\bar{l} \rightarrow$ meson $\rightarrow \gamma\gamma$, CP nonconservation 79−58899
- $\mu \rightarrow e\gamma$, decay ang. distribs. and polarisation effects 77−41835
- $\mu \rightarrow e\gamma$ decay rate in P-symmetric gauge theory 77−49941
- $\mu^+ \rightarrow e^+\gamma$, upper limit for branching ratio 80−78051
- N,N* resonances, radiative decays, static quark bag model *(Russian)* 80−47299
- $\nu \rightarrow 3\Pi$, broken nonlinear chiral SU(3)×SU(3) dynamics *(Russian)* 77−65117
- $\nu \rightarrow \gamma\nu$, in strong mag. field, rel. to pulsars and neutron stars *(Russian)* 77−17360
- ν radiative decay lifetime limits 78−448
- $\omega \rightarrow \eta\pi\gamma$, three body decay width 79−36083
- $\omega \rightarrow \pi^0\gamma$, differential cross sections 79−93464
- $\omega \rightarrow \pi^0\mu^+\mu^-$, branching ratio determ., dis. in π^-p collisions 79−67556
- $\omega \rightarrow \pi+\gamma$, radiative decay in the MIT bag model 78−66110
- $\omega \rightarrow \pi\gamma$, nonet symmetry scheme 79−63480
- $P \rightarrow \gamma\gamma$, relativistic quark pair creation model for reduced decays and enhanced EM tadpoles 79−67555
- $P \rightarrow \gamma l^+l^-$, EM characts. for pseudoscalar meson decay in nonlocal quark model *(Russian)* 80−102050
- pn mass difference, effects of EM mixing, $\Lambda \rightleftharpoons \Sigma^0$, $\eta \rightleftharpoons \pi^0$, $\omega \rightleftharpoons \rho^0$ *(Russian)* 78−74255

electromagnetic decays continued

- pp bremsstrahlung, Δ isobar excitation and radiative decay 79−67586
- $\phi \rightarrow \eta\gamma$, quark loop model, SU(3) splitting of quark masses 80−62990
- $\phi \rightarrow \eta\pi\gamma$, three body decay width 79−36083
- $\phi \rightarrow KK\gamma$, three body decay width 79−36083
- $\phi \rightarrow \pi\gamma$, nonet symmetry scheme 79−63480
- π decays and π electromag. form factor, σ-model with quarks 79−22100
- $\pi \rightarrow e\nu_e\gamma$, isospin-breaking, chiral limit, conserved-vector-current violation, σ model 80−62988
- $\pi \rightarrow e\nu\gamma$, isospin violation in form factor, induced by current quark mass 80−32069
- $\pi \rightarrow e\nu\gamma$, modified quark loop model, form factors, struct. functions, radiative decay 80−91088
- $\pi \rightarrow e\nu\gamma$, vector form factor, quark masses and isospin breaking 79−13111
- $\pi \rightarrow e\nu\gamma$ and SU(3)×SU(3) σ-model 80−78054
- π radiative decay amplitude, low-energy expansion, currents, sum rules 80−52509
- $\pi^0 \rightarrow 2\gamma$, decay width as signal for nuclear matter phase transition, Primakoff effect 80−86842
- $\pi^0 \rightarrow 2\gamma$, Han-Nambu and SUB quark models, modified 80−22562
- $\pi^0 \rightarrow 2\gamma$, tensor-trace and triangle anomalies 80−73709
- $\pi^0 \rightarrow 2\gamma$ in reaction $\pi^-p \rightarrow \omega n$, $\omega \rightarrow \pi^0\gamma$, $\pi^0 \rightarrow 2\gamma$, differential cross sections 79−93464
- $\pi^0 \rightarrow 3\gamma$, C-noninvariant decay, branching ratio upper limit 80−47297
- $\pi^0 \rightarrow 4\gamma$, upper limit to branching ratio 78−93882
- $\pi^0 \rightarrow 4\gamma$ allowed decay search, branching ratio upper limit 80−47298
- π^0 decay, Compton electron scatt., 0.1 to 5.0 GeV 79−397
- $\pi^0 \rightarrow \gamma Ps$, Ps=orthopositronium, π^0 lifetime, O(α) EM correction *(Russian)* 79−45089
- $\pi^0 \rightarrow \gamma\gamma$, μe universality and μ number nonconservation in rare decays 80−42445
- $\pi^0 \rightarrow \gamma\gamma$, u-d quark mass difference effects, form factors 79−89159
- $\pi^0 \rightarrow \gamma\gamma(\pi^+\pi^-\gamma)$, chiral quark model anal. *(Russian)* 80−105900
- $\pi^0 \rightarrow x\gamma$, in 2x-dimensional space time 80−52510
- $\pi^+ \rightarrow e^+\nu\gamma$, u-d quark mass difference effects, form factors 79−89159
- π^-N, 217 GeV, dimuon prod., prod. of γ associated with $\chi \rightarrow \psi\gamma$ 79−36081
- $\pi^-p \rightarrow \eta(\eta')n$, 8.45 GeV/c, differential cross section ratio, η' decay branching 80−78094
- ψ, radiative decay, gluonic bound state O^- width 80−37272
- ψ, strong and radiative decays, $SU(3)' \times SU(3)''$ scheme of three triplet model 77−30371
- $\psi(3684)$ radiative decays, energy correlation 80−13307
- $\psi \rightarrow 3\gamma$, dispersion sum rule charmonium theory, decay probability lower bound *(Russian)* 78−89716
- $\psi \rightarrow 3\gamma$, dispersion theory of charmonium, self consistency test, decay probability *(Russian)* 78−89717
- $\psi \rightarrow 3\gamma$, heavy narrow state search, η' and η_c branching ratios 80−57600
- ψ (3100) decay, inclusive γ and π^0 momentum spectra, direct γ prod. at large x 80−42466
- ψ decay, high energy direct photons, γ, π^0 momentum distribs., QCD calcs. 80−32098
- $\psi \rightarrow \eta'(958)+\gamma$, width upper limit 77−38173
- $\Psi \rightarrow \eta'\gamma$, QCD, width, exclusive OZI violating radiative decay 80−68458
- $\psi \rightarrow \eta'\gamma$, vector dominance model of radiative decays 79−26330
- $\psi \rightarrow \eta(\eta')\gamma$, quark model tests 80−78067
- $\psi \rightarrow \eta(\eta')\gamma$, SU_3 violation, symmetry breaking and decay amplitudes 80−52499
- $\psi \rightarrow \eta(\eta')\gamma$, Ward identity anal., η,η' quark-glue struct. 80−42449
- $\psi \rightarrow \eta\gamma$, conflict with single parameter scheme for radiative decays of vector mesons 80−86720
- $\psi \rightarrow \eta\gamma$, pseudoscalar meson mixing and M1 radiative decays 77−30329
- $\psi \rightarrow \eta\gamma$, vector dominance model of radiative decays 79−26330
- Ψ family, EM decays, relativistic corrections in potential model 79−49522
- $\psi \rightarrow f\gamma$, $f'\gamma$, $\pi\pi\gamma$, $KK\gamma$, meas. using DASP detector at DORIS 78−45922
- $\psi \rightarrow f\gamma$, form factor depend. in relativistic harmonic oscill. model 79−89156
- ψ meson, phenomenology and quark confinement 78−29308
- ψ meson, radiative decays, charmonium model 77−38174
- ψ neutral decays, identification of $\psi \rightarrow \gamma\eta \rightarrow 3\gamma$ and $\psi \rightarrow \gamma\eta' \rightarrow 3\gamma$ modes 77−49968
- ψ particles, off-mass-shell coupling consts. and radiative decays in VDM 78−70371
- ψ radiative decay obs. in $e^+e^- \rightarrow 3\gamma$ 77−46065
- ψ radiative decay width from glueball model 80−62941
- ψ/J (3100) and ψ' (3700) decays results from DASP collaboration/DORIS 77−61282
- Ψ', neutral radiative decay, possible intermediate states 77−241
- ψ', ψ decay branching ratios, isospin and flavour symmetry breaking 80−95264
- ψ', radiative M1 transitions with charmonium model 79−13132
- $\psi'(3684) \rightarrow \gamma\gamma J/\psi(3093)$, cascade decays, evidence for new C=+ intermediate state 79−13115
- $\psi'(3685) \rightarrow \gamma P_c/\chi \rightarrow \gamma\gamma J/\psi(\gamma\pi^+\pi^-)(\gamma K^+K^-)$, investig. of $\gamma\gamma\mu^+\mu^-$ final state 80−18132
- ψ' and ψ decay ratios, composite particle matrix elements 80−95266
- $\psi' \rightarrow \chi\gamma$, charmonium E1 radiative transitions and quark mag. moments 80−86721
- $\psi' \rightarrow \eta J/\psi(\pi^0 J/\psi)$, investig. of $\gamma\gamma\mu^+\mu^-$ final state 80−18132
- $\psi' \rightarrow \psi\gamma\gamma$, $\psi\gamma\gamma$ final state meas., $\psi' \rightarrow \gamma\chi$, $\chi \rightarrow \gamma\psi$ branching ratios 80−57601
- $\Psi''(3772)$, radiative decay nonoccurrence 80−4997
- $(\bar{q}q) \rightarrow (\bar{q}'q')\gamma$, width, exclusive OZI violating radiative decay 80−68458
- $q\bar{q}$ resonance energy spectrum, leptonic and radiative decay widths, QCD pot. calcs. 80−52491
- $\rho \rightarrow \eta\pi\gamma$, three body decay width 79−36083
- $\rho \rightarrow \pi+\gamma$, radiative decay in the MIT bag model 78−66110
- $\rho \rightarrow \pi\gamma$, EM decay rates, spectrum generating SU(4) approach 79−26334
- $\rho \rightarrow \pi\gamma$, quark anomalous mag. moments 79−17693
- ρ/ω amplitude ratio for radiative decay, sea quark γ emission 79−63440
- $\rho^- \rightarrow \pi^-\gamma$, nonet symmetry scheme 79−63480
- $\rho^- \rightarrow \pi^-\gamma$, radiative decay width from pion excitation anal. 80−57599
- $\sigma \rightarrow 2\gamma$, Higgs meson decay amplitude, low energy theorems *(Russian)* 80−13309
- $\sigma \rightarrow 2\gamma$, tensor-trace and triangle anomalies 80−73709
- $\Sigma^0 \rightarrow \Lambda\gamma$, weak effects, small P violating E1 component in M1 EM decay 79−89160
- $\Sigma^+ \rightarrow p\gamma$, $1/2^-$ resonance poles to parity-violating amplitude, two-quark weak transitions 80−78062

electromagnetic decays continued
- $\Sigma^+ \to p\gamma$, radiative weak decays of baryons as single-quark transitions 79−40776
- $\Sigma^+ \to p\gamma$, sum rules, branching fractions and asymmetry parameters 80−410
- $T(\bar{t}t)$ decay into Higgs scalar and photon 79−36082
- $\tau^- \nu_\tau \pi^- \gamma$, π form factors, axial-vector and structure dependent, vector meson dominance model 80−62989
- Υ, EM decays, relativistic corrections in potential model 79−49522
- $\Upsilon \to 3\gamma_s$, IR and collinear divergences, cancellation in one-loop corrections to QCD cross sections 79−40730
- $\Upsilon(9.5,\bar{b}b)$, decay into Higgs scalar and photon 79−36082
- Υ (9.5) props., $SU(4)\times S_3^\alpha$ scheme in straton model *(Chinese)* 79−9347
- Υ family, EM transition rates, geometrodynamical quark model 80−47295
- $\Upsilon' \to \gamma 2^{++}(\bar{b}b)$, photonic decay widths in tensor meson dominance 79−75754
- $V \to \gamma h$, use of QCD in OZI-violating radiative decays 79−26302
- $V \to P\gamma$, relativistic quark pair creation model for reduced decays and enhanced EM tadpoles 79−67555
- X(2.83), radiative M1 transitions with charmonium model 79−13132
- $X(2.85) \to 2\gamma$, obs. in charge-exchange reaction $\pi^- p \to Xn$ 78−25047
- $X^0 \to \gamma\gamma$, prod. in $\pi^- p \to X^0 n$, four-momentum transfer region 0.38-0.79 $(GeV/c)^2$ 77−67656
- $\Xi^- \to \Sigma^- \gamma$, decay rate, sum rules, branching fractions and asymmetry parameters 80−410
- $Z^- \to \Sigma^- \gamma$, radiative weak decays of baryons as single-quark transitions 79−40776
- $\bar{b}b2^{++} \to \gamma\Upsilon$, photonic decay widths in tensor meson dominance 79−75754
- F_t^{+*}, weak decay modes, annihilation contribs. 79−93410
- $^1H(\pi^-,\gamma\gamma)n$, off-mass shell πN amplitude, $\pi^0 \to \gamma\gamma$ amplitude, chiral Lagrangian model 79−93669
- $K_s \to \gamma\gamma$, decay rate, vector-meson exchange contribs. 79−49523
- $\psi' \to \chi_0\gamma$, radiational decays in charmonium *(Russian)* 80−13308

electromagnetic energy *see electromagnetic waves*

electromagnetic field theory
- *see also electromagnetic waves; electromagnetism*
- 3D nonlinear EM field anal. using computer program TOSCA 80−95765
- adiabatic hypothesis, old quantum theory, rel. to classical electrodynamics, zero-point EM radiation 79−2661
- advanced potential solution, status anal. 79−17248
- Aharanov-Bohm effect, possible nonexistence 80−27434
- anisotropic solids with magnetic symm., unified dynamic theory 78−77713
- antenna radiation field, soln. as initial value problem *(Chinese)* 78−9294
- antenna-potential approx. of EM field 80−68060
- asymmetric Maxwell theory, additional universal inverse square forces 80−27149
- bar magnets, torque theory 77−13527
- beam mode function series approximating beam field *(Japanese)* 77−22427
- black body radiation, photon occupation numbers 79−88869
- black holes, magnetosphere, charge particle trapping 78−57573
- black-hole evaporation unified gravit. and electromag. field theory 78−53979
- book 80−5656
- Born-Infeld type nonlinear theories, uniform mag. field, stability of spherical symmetry soln. *(French)* 78−29879
- bound state, two charged media interaction, self-consistent field theory 78−16667
- boundary coupling of gravitational wave and EM radiation in cavity 78−54267
- boundary-value problems, approx. method for numerical studies 80−5658
- Brans-Dicke Maxwell fields, static Weyl solutions 79−85033
- Brans-Dicke theory, EM solns. 78−57841
- Brans-Dicke theory, generalised static EM fields 80−12972
- by Lorentz transform 78−32696
- canonical formulation of the classical electromagnetic field 80−86095
- Casimir effect, EM waves near perfect conductors 78−55278
- causal independence in local relativistic free quantum fields 79−21894
- causality and relativity 78−81901
- cavities, EM conservative fields, canonical formulation 78−33310
- cavity with cylindrical hole in wall of infinite thickness, elec. and mag. polarisabilities determ. 78−71004
- characteristic impedance of double line in front of dielec. wedge *(German)* 78−78855
- charged extended body interaction with mag. field 79−13879
- charged fluid, orthonormal tetrads in general relativity 78−54269
- charged particle config., stability 80−57109
- charged particle interaction with linearly polarised MHD plane wave, first adiabatic invariant approximations 77−78580
- charged particles interacting with EM field, line-integral Lagrangian 79−81346
- Cherenekov and Doppler effects, quantum theory paradoxes 78−45824
- Cherenkov radiation, momentum-energy Minkowski and Abraham tensors 78−45825
- chiral (γ_5) symmetry of massless fields, neutrino theory of photons 78−411
- circular bundle of relativistic particles *(Czech)* 78−66711
- classical and modern theory, appls., book 80−1101
- classical electrodynamics of point particles, energy tensor struct. 79−21566
- classical Lagrangian theory with radiative reaction, Rohrlich two field formalism extension to include monopoles 78−45488
- classical reaction force density meas. in material media at LF 79−64141
- Clebsch pots. in theory with elec. and mag. charges 77−26182
- Clifford algebra and Maxwell eqns., vector formulation 77−67302
- closed ellipsoid, short-wave asymptotic form 78−1125
- combined field integral equation formulation, singularity expansion method appl. 80−18963
- complementary variational principles for Maxwell's equations 80−32876
- complex reciprocity theorem for multiregions with piezoelectic media and surface impedance 79−61307
- compressible media, reciprocity thereom 78−8254
- conducting medium, inhomogeneous, anisotropic, thermal fluctuations of current density, EM fields, and charge density 78−23067
- conducting rectangular bar transmission gratings 78−62993

electromagnetic field theory continued
- conducting sphere in quiescent slightly ionised plasma, exact solution 79−86564
- conductivity of simple cubic lattice of spheres 78−28964
- conductor in time-varying electrically active medium, quasistationary effects 79−64148
- conformal electrodynamics in Einstein spacetime 80−31644
- conformal field equations 80−46881
- continuity equations, for transverse multipole amplitudes, EM and gravitational fields 79−58609
- corner diffraction coeff. anal., Albertsen's formulae 78−62978
- Coulomb-like quantization of the electromagnetic field on spacelike hyperboloids 79−306
- coupled EM and scalar fields, in cylindrically symm. space-time 79−85035
- coupled-bar problems, conformal transformations combined with numerical techniques 80−83538
- coupling, between two short circuited flat dipoles *(French)* 79−81320
- coupling through azimuthally symmetric apertures in bodies of revolution 78−62984
- covariant representation of microscopic charge and current densities in terms of polarisation and magnetisation fields 79−71
- crystal, spherical integral reps. for cond. of abruptly activated current 80−42080
- crystal optics, relativistic phenomena 80−46839
- current flow between concentric spheres at pot. up to 15 MV 77−79726
- current induced on crossed cylinders excited by plane EM pulse 79−13873
- D-type nondiverging and nontwisting electrovac soln. with λ 80−115
- Debye pot., scalar factorisation for Maxwells eqns. 78−77732
- deformable bodies of finite extent 77−65560
- deformable media, electrodynamics, nonrelativistic classical field eqns. 78−49679
- deformable media, electrodynamics, relativistic field equations 78−49678
- density matrix, semiclassical representation 77−61234
- dielectric, damped integrodifferential eqns., asymptotic bounds to system of solns. 80−62493
- dielectric, isotropic elastic thin shells, nonlinear electrodynamics 77−88626
- dielectric comprising several molecular species, field eqns. 77−5668
- dielectric scattering alternative surface current formulation 78−62991
- diffraction convex, smooth, ideally conducting and electrically large surfaces 78−94363
- dimensions and symmetry considerations, duality transformations 80−28139
- dipole-equivalent defect in conducting half-space *(Russian)* 77−71904
- Dirac's veto, classical Lagrangian theory of Dirac's monopole 79−40383
- Dirac equation as basis for unified treatment of electromagnetic and gravitational theory 78−8314
- discontinuous surface in EM field *(Italian)* 78−50676
- dispersive media, energy-momentum tensors by EM waves 78−17842
- dispersive media 80−36883
- displacement currents and magnetic fields in empty space, theory 77−22347
- distributions theory and EM radiation fields using Fourier transforms 77−6974
- Doppler and Cherenkov effects, quantum theory paradoxes 78−45824
- dual representation with circuit theory, Poynting's theorem 80−94963
- duality rotated Maxwell field props. 79−84974
- duals of gauge field tensors, representations 79−89057
- dyadic Green's function of EM field in unstable medium with use of random current source 79−94129
- dyon field, extended Yang-Mills formalism, Mandelstam's path depend. formalism 78−62288
- eddy currents, induced, time const. determ. *(German)* 77−19130
- education, classical mechanics gauge invariance, derivation of Maxwell's eqns. 80−73131
- education, Dirac delta function, appl. elec. current and mag. multipole distribs. 80−17740
- education, elec. electric energy density in dissipative medium by cct. analogue 78−36759
- education, EM field multipole expansions, spin-weighted spherical harmonics 77−33766
- education, EM vector pot. and its physical reality 78−61974
- education, homogeneous ellipsoidal inclusions, general theorems, Poisson theorem, dielectric polarisation, conduction and elasticity 78−61979
- education, Maxwell's eqns., Lorentz and conformal covariance, normal transformation rules 78−49589
- education, simplified relativistic force transformation equation 79−25791
- effective electric field in an inhomogeneous medium 79−13869
- effective photon hypothesis, expt. test 77−46709
- eigensolutions of field strength operator, nonlinear and linear processes *(German)* 78−83028
- Einstein's nonsymmetric unified field theory extension, geom. props. 79−44833
- Einstein Universe, with source-free EM field 79−85036
- Einstein zero mass meson field solution 77−54646
- Einstein-Maxwell, field theory with teleparallelism and Dirac electron *(German)* 79−9168
- Einstein-Maxwell eqns. for non null EM fields, general solns. 77−2569
- Einstein-Maxwell equations, charged solution, type-G 80−46904
- Einstein-Maxwell field equations in vacuo, consideration of axially symm. metric 79−85034
- Einstein-Maxwell fields in asymptotically null-spherical coords., news functions 78−12631
- Einstein-Maxwell fields with cosmological constant, null strings 78−21033
- Einstein-Maxwell generalised eqns., Birkhoff's theorem and mag. monopole solns. 78−45535
- electric dipole at centre of spherical shell, EM radiation in general relativity *(French)* 77−5709
- electric dipole radiation interactions, implications of gauge invariance 79−30268
- electric dyadic Green's functions derivation, report 78−86169
- electro-gravitational induction, relativistic theory 79−85040
- electromagnetic and gravitational Hertz potentials 79−2680
- electromagnetic quadripotential for the pure-radiation field generated by a classical charged point-particle 79−63058
- electromagnetism without monopoles, in nontrivial U(1) fibre bundles 80−12920

electromagnetic field theory continued
electron classical model based on Penney's balanced field eqns. 78—21031
electron relativistic self-field interaction, particle-like solns. 78—16666
electrovac solns., axially symm., source of gravit. and EM fields 77—60987
ellipsoidal charged particle bunch, self-consistent motion, approx. soln. 79—13881
EM field penetration through gaskets and seams, simple model 77—42464
EM instruments for use in liquid sodium, theoretical anal. 78—54857
EM radiation near black holes and neutron stars 78—53978
EM resonator eigen-oscillations, variational treatment *(Russian)* 77—79730
EM scattering from corrugated conducting surfaces with inhomogeneous surface impedance, anal. 78—62987
EM systems, parity and time inversion symmetries 79—67169
EM two-body interaction theory 78—49739
EM wave reflection on periodic corrugated solid media, anal. 79—13875
EM/acoustic waves variational expressions systematic derivation 78—93536
energy flow vector of EM field 80—83537
energy-momentum tensor, heuristic formulation *(German)* 77—60946
energy-momentum tensor vac. expectation values, depend. on manifold geom. and topology 80—355
energy-momentum tensors in theory of EM fields admitting electric and mag. charge distribs. 77—74294
equilibrium equations and duality 79—879
external physical fields of sources investigation, modelling devices construction 80—17817
field intensity computation method 80—32881
field penetration into thick, finitely conducting shell, anal. 78—62990
field problem with a non-linear condition 79—18326
field problems in multilayer composites, produced by line charge, Fourier type anal. 78—29875
field radiation by mag. dipole on smooth convex surfaces 78—62977
field sources on conducting concentric sphere, dipole approx. *(Russian)* 78—86991
fields and electrons, fundamentals *(German)* 77—585
finite antenna, EM radiation calcs. 77—68149
finite element method equations derivation, using integral forms of EM field laws 80—18961
finite element method for unbounded field problems 80—23600
finite-difference method, for crossed (doubly-periodic) gratings 79—1002
Finslerian space-time with absolute parallelism, scalar and EM fields 79—40436
fluctuation EM field of infinite medium with spherical inhomogeneity, finite temp. Green's functions 78—1126
forward scattering anomaly in hollow penetrable body 78—62986
free partical in classical electron theory with zero point radiation, diamagnetism 80—42082
Friedmann universe, photon gas 78—4543
Galilei covariant theory, minimal EM coupling 80—77634
gauge field of mag. monopoles 77—64950
gauge field operator quantisation rules 78—41405
gauge invariance, EM four pot., transformation properties 80—91002
gauge theory in Hamiltonian classical mechanics, EM and gravitational fields 80—13202
gauge transformation, distribution of fields and sources of singular vector potential 80—73190
gauge transforms and quantum theory 77—5681
Gaussian version of Amperes law 78—36848
general reciprocity theorem based on Onsager relations 79—59614
general relativistic Dirac-Pauli particle, underlying classical model 77—45743
general relativity, EM polarisation tensors, calc. by Fokker's method *(French)* 78—24695
generalised Coulomb gauges for free photon field 77—26466
generalised Einstein eqn., field eqn. for EM field and Yang-Mills instantons 80—8872
generalised uniaxial anisotropic medium, wave potential of Miyamoto and Wolf 80—37930
generalised vector field equations, symmetry group *(Russian)* 77—79206
geometric unification of classical gravitational and EM interactions 80—57165
graded-index fibres, evanescent field theory, propag. consts. of guided modes 79—98464
gravitation and electromagnetism field equations, metric-affine gravit. framework 78—45547
gravitational and EM field in flat space time, relationship, hierarchy hypothesis 77—5732
gravitational and EM field interactions 78—41219
Green tensor expansions for harmonic vector wave eqn. in spheroidal coord. systems 78—41171
H-field, E-field, and combined-field solns. for conducting bodies of revolution 78—55275
high frequency gravitational and electromagnetic wave coupling 78—8304
Hopf fibrings, associated with solns. of Yang-Mills and Maxwell eqns. 78—37129
Huygens' principle and equivalence principles 80—1106
infinite charged filament, Kasner-type naked singularities *(Russian)* 79—58557
infinite conservation laws for EM and asymptotic gravitational fields 79—21613
injection lasers, theoretical spontaneous emission factor in the rate eqn. using classical EM theory 78—9383
instruction, dynamic electric and magnetic field evolutions, visualisation using computer graphics display 80—46776
integral transport theory for charged particles in electric and magnetic fields 79—26006
interaction of electron beams with microwave-frequency field, of planar gap 80—106431
intrinsic coupling between gravitational wave and quantised EM radiation 78—54268
irregular boundaries problems, direct noniterative numerical soln. using network analogues 80—95766
Kerr metric, charge accretion *(French)* 77—71257
Kerr metric, stationary axisymmetry EM fields 79—58603
Kerr-Tomimatsu-Sato generalised metric, infinite red shift surfaces 79—58602

electromagnetic field theory continued
Killing horizon as event horizon, a necessary condition in general relativity 78—8295
leader channel temp. rise, initial stage, elec. field strength determ. *(Russian)* 77—35411
LF EM shielding props. of arbitrary cross-section conducting cylindrical shells 78—55283
LF fields in linear media, two-dimensional finite element analysis 79—41297
light beam of variable flux, gravitational influence 78—21037
linac cavities, field theoretical approach to stabilisation 78—33309
local von Neumann algebras 78—45778
localised solns. of nonlinear field from Born-Infeld Lagrangian 77—60949
Lorentz invariant current paradox, soln. 77—51
lossy anisotropic inhomogeneous media, variational formulation of EM problems 79—13866
lossy anisotropic inhomogeneous media, variational solns. of EM problems 78—77735
magnetic, interior force field, for teaching 78—54123
magnetic field meas., precision, using Ampere's law 79—21720
magnetic oblique rotator production of EM field, lowest order solns. 79—21176
magnetic shielding barrier LF field penetration 78—82886
magneto-dipole configurations in general relativity 80—67539
magnetoelastic force convertor operation anal. *(Russian)* 78—70166
marine electrical prospecting, EM field buildup by immersed dipole 77—70595
massless scalar and EM field equations interacting with gravit. field, particle-like solns. 79—54290
Maxwell's eqn. soln. for any static axisymmetric vac. space time 79—25874
Maxwell's eqns., homogeneous initial boundary value problem 79—75372
Maxwell's eqns., propagation of finite local disturbances 79—92961
Maxwell's eqns. in electromech., numerical resolution by finite element anal., eddy current effects *(French)* 79—30269
Maxwell's eqns. in expanding universe 78—4493
Maxwell's eqns. with mag. charges, conformal invariance 79—44756
Maxwell's equations, form of distributions *(French)* 79—97221
Maxwell's equations, O(3,1) approach 78—36846
Maxwell's equations, variational principles 79—2641
Maxwell's equations as conservation laws, electromagnetism in non-Riemannian space 78—77737
Maxwell's equations as one quaternion eqn., appl. to wave propag., for teaching 78—54133
Maxwell's vacuum field eqns., initial value problem 77—57208
Maxwell eqns., null solns., generalised to Yang-Mills theory 80—27388
Maxwell eqns. for six-component fields, discretisation method *(German)* 77—53790
Maxwell eqns. in inhomogeneous medium, transform into eqn. on rotation group 80—74
Maxwell equation integration in laminar media 80—68059
Maxwell field, quantisation and Poincare group extensions of zero mass representations 79—30685
Maxwell theory, quantised, rosette of rosettes of Hilbert spaces 80—32043
measuring units system, electromagnetic phenomena, relativistic aspects *(Rumanian)* 79—17382
metric-torsion gravitational theories, charge conservation 78—45544
microstrip antennas, asymptotic expansion for Sommerfeld integrals 80—14272
Minkowski formulation, interaction with moving media, total energy-momentum tensor 77—78992
mode decomposition of EM field of a homogeneous sphere in an infinite medium 78—81864
molecular interaction with EM fields, classical theory 80—95686
monochromatic wave energy density in nonabsorbent medium with freq. and space dispersion *(Russian)* 78—74818
motional EMF, rel. to animal navigation 77—60879
multiply charged periodic classical systems and random EM radiation, statistical equilib. 79—2621
multipole anal., time-depend. relativistic, definition of multipole moments 77—65087
multipole expansion, concentrated current source representation 78—5390
multipole fields in finite, spherically symmetric region 80—36881
multipole matrix elements from classical field with sources 79—9504
multipole radiation, elementary sources 79—17249
nematic liquid crystals subject to EM fields, continuum theory 80—33876
net cohomology over Minkowski space 78—93561
neutrino as axial EM field source, symm. P-invariant broadened Maxwell eqns. *(Russian)* 78—58141
non-empty space-times, conformal EM fields 79—30331
non-Lorentzian electromagnetic quadripotentials for the field of a classical point particle 79—71263
noncompletely reducible representations of the Poincare group associated with the generalised Lorentz gauge 78—70249
nonlinear classical EM theory 79—5991
nonlocal constitutive eqns. props. of field determ. 78—20981
nonradiating primary planar sources of finite extent, question of existence 79—10247
nonrelativistic transformations giving invariant Maxwell's EM theory laws 78—77738
nonsinusoidal, periodic, penetration into conducting half-space 80—18960
nonstationary and inhomogeneous, time-space-dependent power spectrum 80—77635
nonsymmetric unified field theory, physical interpretation and light propag. 79—21618
null field, embedding class one 78—36914
numerical techniques for conformal transformation 78—74816
observability differences between classical EM and gravitational gauge fields 80—36925
observable phase factors and symmetry of electric and magnetic charges 78—86428
one-dimensional medium with space-time inhomogeneities, spectral-correlation characts. evolution *(Russian)* 79—2634
one-mode fields, greatest lower bounds for degree of coherence of higher order 78—71068
parity and time inversion symmetries 77—45721
penetration and shield performance calc. 78—82885

electromagnetic field theory continued
- penetration into conducting region, soln. of reverse problem by Fredholm integral eqn. 78−94357
- penetration into conductive spherical cavity 78−86990
- penetration into conductor, mean time constants calc. *(German)* 79−3613
- perihelion precession rate in system of two charged masses 78−73897
- permanent magnet and current-carrying conductor fields, Fe filing pictures, theory *(German)* 80−28145
- permeability of vac. and light-cone structure 80−36879
- photon rest frames and null geodesics 77−57207
- physical optics method in electromagnetic scattering 80−46840
- planar nonstationary EM field in conducting medium, transient state anal. *(Polish)* 78−71000
- plane wave, moving along mag. field, radiative effects 78−29283
- plane wave scattering by semi-infinite dielectric slab 80−9790
- plane-symmetric null EM field 78−36847
- Poincare subsymmetry, associated invariant EM field *(French)* 77−61209
- point charge resting in uniformly rot. or uniformly accelerated framer of reference *(German)* 77−9891
- polarised light beams in gravitational fields, Dirac-spinor form of Maxwell's eqns. 78−50696
- polygonal obstacles, neighbourhood field computation using diffr. theory 79−89844
- ponderomotive forces, past controversies, discussion 79−41263
- presymplectic manifolds and the Dirac-Bergmann theory of constraints 79−2652
- principles and appls., book 80−32866
- QED, electron-positron field 78−41445
- quantification of EM field, half-space bounded by perfect mirror *(French)* 77−78994
- quantisation of EM field, C*-algebra formalism 77−49827
- quantum field theory, appl. to weak, EM and strong interactions, historical notes 78−28904
- quantum field theory of electrostatic potential in gravitational field 78−54270
- quasistationary time-varying field, diffusion into spherical shell 79−13870
- radiant cavity, one dimens., nonlinear field mode interaction, statistical props. 78−16668
- radiant flux through apertures, rectangular apertures 80−46836
- radiant flux through apertures, rectangular grid 80−46837
- radiating cylinder, gravitational field anal. 79−30332
- radiating Kerr-Newman metric 79−63107
- radiation from accelerated charge 80−31497
- radiation with spin, minimum size using special relativistic centroid theorem 78−69995
- radiative energy and momentum transfer, free EM field, exact eqns. 77−42462
- randomly inhomogeneous medium, mean EM field *(Russian)* 80−32882
- reactance theorem for linear, passive, time-invariant system 77−9892
- real eigenfunction expansion for symmetric complex operators 77−71906
- reciprocity and conservation theorems, for fields with general time dependence 79−80452
- Reissner Nordstrom singularity, spherically symmetric clusters of charged particles 79−12672
- Reissner-Nordstrom black hole, stationary interacting fields 78−24710
- relativisitic eqns. for massless particles, new ivariance algebras 79−58909
- relativistic field theory of electron 77−2779
- relativistic transformations, Newtonian force and EM field, for teaching 78−49601
- RF cavities with cylindrical symm., evaluation by computer program SUPERFISH 77−18714
- riemannian-Maxwellian invertible structures in general relativity 80−4618
- Robinson's theorem, shear free condition 78−93586
- rotating permanently magnetised sphere, EM field in inertial and comoving reference frames 79−71316
- rotating plane-fronted waves and their Poincare-invariant differential geometry 80−332
- rotational coords., vector Helmholtz eqn. 77−45709
- scalar and EM fields struct. in tangent bundle of spacetime with absolute parallelism *(Russian)* 78−49741
- scalar and EM wave eqn. solns. in gravit. and EM waves metric 78−8307
- scatterer surface current density, calc. using numerical technique 80−78747
- scattering by corrugated periodic trapezoidal conducting surface, TE/TM polarisation 78−62994
- scattering by irregularly shaped perfectly conducting or dielectric cylinders 79−13878
- scattering by multiple rectangular cylinders, numerical anal. 78−62992
- scattering current/aperture coupling relationship for thin finite cylinders 78−62988
- scattering from thin and finite dielec. fibres 78−62972
- self-force of charged particle in EM field 77−34801
- shielding theory of metallic enclosures with apertures 78−55282
- simultaneously radiating elec. and mag. sources, generalised EM field props. *(Russian)* 79−27131
- singular spin harmonics 79−97529
- sphere, method of variation of consts. appl. to excitation by elec. and mag. currents 78−86989
- sphere between two planes, field distrib., substitute diagram synthesis *(Polish)* 79−3611
- spin-1 particles, elec. and mag. fields and charges 77−60948
- spinless particle interaction with electromag. field, path integrals, Klein-Gordon eqn. 78−58144
- spinor eqn. of pure EM field 78−86429
- spinor Helmholtz eqn. 78−32694
- spinor representation of Maxwell's eqns., algebraic props. 80−86097
- spinor representation of Maxwell's eqns. 80−86096
- stationary, anal. by Trefftz's method, using quasiharmonic polynomials *(German)* 79−27128
- stationary rotationally symm. field representation by superimposing circular aperture and ring fields *(German)* 78−55277
- Stokes' theorem in non-orientable manifolds, relation between charge and topology anal. 77−45776
- Stokes theorem, for fields with surface discontinuities *(Italian)* 77−50589

electromagnetic field theory continued
- superconductivity, general relativistic phenomenological theory 80−2518
- suppression of diffracted waves by corrugated cylinder 79−81342
- surface integral calc. in numerical investigation of 3D fields *(Russian)* 79−64143
- suspension field calc. using computer *(Russian)* 79−59616
- teaching, moment methods, for undergraduates 78−28886
- test coil on permeable spheroid in field of coaxial line currents *(German)* 80−37928
- tetrad formalism of Maxwell equations with effect of gravitation. II 78−77784
- time asymmetries and classical and quantum physics 80−22216
- time dependent Maxwell fields, in stationary geometry 78−8308
- time domain reflection from inhomogeneous and dispersive slabs 78−62985
- tired light effects, nonexistence in Lorentz and gauge invariant EM theories 79−71261
- torsion, effect on gauge invariance, semi-minimal coupling principle 80−77675
- transfer flux macroscopic Poynting vector, transfer from fields to network *(Italian)* 79−68349
- transfinite ordinals as axiom no. symbols for unification of quantum and EM wave functions 77−5688
- transversal field configuration, in conducting plates *(Polish)* 79−3612
- transverse mag. dipole field diffraction on sphere with circular hole *(Ukrainian)* 79−31761
- unification of Maxwell, Dirac and Yang-Mills eqns., octave algebra 79−2967
- unification of various representations *(Czech)* 80−37931
- unified gauge theory of gravit., e.m., mag. monopole fields 77−57263
- uniform asymptotic theory and uniforms geometrical theory of diffraction, comparison 79−13872
- vacuum polarisation in Fock space 78−41446
- variational expressions for EM fields, derivation using unified approach 78−9295
- variational principles derivation 79−76549
- variational principles for Maxwell's equations 80−78744
- vector field decomposition by scalar potentials 79−12625
- vector multipole field transformation props. under coord. translation 77−61894
- vector product formulation of special relativity and electromagnetism 80−105496
- vector wave equation, depolarisation term anal. 80−8814
- wave character, energy transport, current and field displacement *(German)* 77−42457
- wave diffraction calc. generalised shift operator *(Russian)* 78−78868
- wire excitation, through an aperture perforated conducting screen 78−5393
- Yang-Mills, dyon solns. and symmetry, elec. and mag. charge conservation 77−26183
- zero-rest-mass fields, boundary conditions at past null infinity 78−24661

electromagnetic fields
- 200 kV Blumlein transmission line for Tokamak plasma heating, calc. and obs. 79−55521
- algebraic-topological interpretation 77−79723
- analysis and computation, computer appl. book 78−37787
- angular spectrum of EM field, elec. network equivalent 78−78867
- anisotropic and multidielectric edges, field behaviour 77−58233
- anisotropic cylindrical shell within solenoid, EM response 79−13867
- anisotropic media, calc. *(Russian)* 79−7054
- anisotropic medium, dipole located above 77−10812
- anomalous EM fields from different sources over polarized sections *(Russian)* 77−86776
- anomalous penetration along phase division boundary *(Russian)* 79−41284
- arbitrary moving magnetic dipole, EM field calc. *(Russian)* 80−9772
- axially symmetric linear homogeneous media, modal EM field solns. 78−78857
- Babinet's principle, extensions inc. concepts of resistive and conductive sheets 77−54651
- ball lightning as EM energy 77−5307
- bandlimiting in conflict with spatial bounding of radiative sources 77−83781
- behaviour of magnetodielectric edges with appl. to design of elect. and electronic devices *(German)* 79−45885
- biological effect, of HV-power line and switchgear environments 77−5028
- biological effects, state of research *(German)* 78−88728
- biological tissue, induced, arbitrary cylinder, anal. 77−12957
- biomolecular effects of 50 Hz EM fields, mechanism of effect *(Russian)* 80−51158
- biosphere and active solar processes link, role of Earth's natural electromag. field 78−61211
- blackbody radiation in cavities with walls of finite conductivity, autocorrelation functions 77−31047
- bone pyrogenic infection treatment by non-invasive EM technique 78−48854
- bone stimulation, EM fields in capacitative and inductive devices 78−40283
- book 80−5656
- Casimir forces, appl. of analytic regularisation 78−81887
- cavity resonators used in charged-particle accelerators 80−37641
- cell culture exposure under controlled temp. and field strength conditions 78−40449
- channel waveguide interferometric modulator for EM field detection 80−74498
- charge bunch radiation losses in pill-box resonator, time domain numerical computations of EM fields 79−31781
- charge moving along elliptical orbit, spectral radn. distrib. 77−19148
- charged particle in mag. field superimposed by EM wave, parametric cyclotron resonance 77−27234
- charged particle motion, perturbation effect on periodic solns. of Stormer problem 78−20582
- charged particles interacting with EM field, line-integral Lagrangian 79−81346
- charged particles motion, Lagrangian and Hamiltonian up to fourth-order terms 80−91736
- circular coil carrying AC in plane anisotropic cond. plates *(Rumanian)* 79−72456

electromagnetic fields continued
circumferential stress in large high field magnet coils, thick-thin cylinder approach 80−95761
coal seam, gasified, refl. EM fields modelling 77−41212
coaxial cable structure, with longitudinal inhomogeneity in conducting layer *(Russian)* 80−37936
coil above ferromagnetic half space, expressions for nonstationary electromagnetic field 78−74817
computation by numerical methods for undergraduate teaching 77−10803
concentric line with helical inner conductor, EM field and phase constants 79−86112
conducting cylinder in harmonically variable transverse mag. field, EM wave penetration 79−81328
conducting half space, EM field formation method *(Russian)* 79−84110
conducting liquid, in cylindrical induction furnace, velocity and EM field distrib. calcs. *(Russian)* 77−47106
conducting spherical shell, approx. static EM field penetration 80−28146
conductor, with AC or DC current, moving parallel to infinite conducting slab 80−18959
contactless method of measuring components of complex shape, gap transducer appl. 78−93648
continuous heterogeneous media, anal. *(Polish)* 78−37788
cosmic EM fields, effects of photon rest mass on current and energy densities 77−45708
crater form. at tip of crack, under powerful local electromagnetic field *(Russian)* 77−70149
crystalline slab, EM field in 80−96463
crystalline slab, EM pot. 79−77547
current on sphere surface arbitrarily distributed, anal. *(Russian)* 77−31045
cylindrical conductor, AC excited, with circumferential electrodes, boundary-value problem 79−7055
cylindrical conductor, exact surface-impedance matrix expression 79−98266
DC contactor magnet coil, electromagnetic field, transient states *(Polish)* 80−18962
DC loop near two highly permeable spheres, analysis *(German)* 78−37783
De Rham currents, field and mag. monopoles extended singularities 78−4810
detection of HF EM fields by nerve cell membranes, possibility discussion *(Russian)* 80−76785
dielectric wedge, review of thery of EM field behaviour 78−66712
dielectric wedges, Meixner's edge condition 78−13644
dipole antenna buried in stratified anisotropic media 79−94128
dipole approx., source on sphere concentric with ideally conductive globe 79−64147
dipole in boundary between two half-spaces *(Russian)* 78−78858
dipole in metal cased borehole 77−46672
Dirac-EM field interaction, localised soln. radius 77−79212
disordered EM radiation with planar symmetry, exact relativistic soln. 77−87676
dispersing medium, conservation laws of energy, pulse and pulse moment *(Russian)* 77−27221
Earth, boundary conditions for EM field above two-dimensional inhomogeneous struct. 80−85595
Earth, diffr. of EM field of infinitely long cable over wedge-shaped conducting media *(Russian)* 78−40484
Earth, EM field subsurface propag. from horizontal elec. dipoles 80−98229
Earth, EM waves and antennas above and below surface 79−66620
Earth, freq. and transient responses of EM fields created by currents in confined conductors 79−29702
Earth, harmonic and transient EM fields behaviour on surface of two-layer medium 79−92478
Earth, natural EM field short period vars. anal. for wave type and direction determ. *(Russian)* 78−85474
Earth crust, nonparallel stratified models, scattered EM radiation field 78−44773
Earth crust, nonparallel stratified models, scattered surface wave 78−40489
Earth EM field sounding, appl. of composite obs. patterns in near field *(Russian)* 79−44270
Earth scattered EM fields from buried wires 79−16369
Earth surface fields, topographic effect in three-dimensional cond. model 77−25639
eddy current problems, numerical soln. *(Japanese)* 79−81324
education, electromagnetic radiation fields: a simple approach via field lines 80−51991
effects on man and environment 77−44719
Einstein-Maxwell fields, equilib. and global integrability conditions 77−30070
Einstein-Maxwell space-times, infinitesimal holonomy group structure, Lie algebra 80−12976
elastic dielectric, crack tip stresses, EM field distrib. 79−68641
elastic dielectric, crack tip stresses generated by EM field 79−68642
electric field strength measurement, broadband antenna probes *(Polish)* 79−21722
electric machine active parts electrodynamic equations general solutions using orthotropic modelling *(Russian)* 80−99601
electrically and mag. polarised matter in waveguide, EM field, Green's function method 78−1123
electron band structure, optically induced in external plane wave field 80−106432
electron optical devices, static multipole fields, numerical calc. 77−588
ELF field strength meas. in Connecticut in 1975, summary 79−48557
elliptically polarised EM field, meas. by phase switched correl. polarimeter, D-region appls. 77−87169
energy calc., using surface integral 78−5394
energy propag. of EM field of dipole source on conducting halfspace 77−9330
energy-momentum tensor in phenomenological electrodynamics *(Czech)* 80−27146
entomological experiments on teratogenic effects of EM fields 80−85446
excitation in cavity in conducting shell by penetrating radiation 80−87263
ferrite, sphere, small anisotropic, excitation by pot. field 77−43890
ferromagnetic conductor, cylindrical, acoustic wave propag., EM field behaviour 80−88857

electromagnetic fields continued
ferromagnetic materials, EM field penetration, perturbation calc. *(Russian)* 79−59617
ferromagnetic screened half-space, impedance and power loss 77−23595
ferromagnets, EM field arbitrary discontinuity disintegration 80−28141
field calculation by successive overrelaxation (SOR) method 79−92964
finite crystals, EM field 79−77546
flowmeter with moving field, fluid flow and moving field equations *(Rumanian)* 80−64663
Fourier analysis to calculate fields around bodies of complex form *(Russian)* 78−46486
freely gravitating charge, radiation, in field of weak plane gravitational wave *(Russian)* 78−89381
Friedman imperfect fluid cosmology, local EM field propagation 79−84872
fusion reactor design, dynamic analysis of electromagnetomechanical field by finite element method *(Japanese)* 78−8967
fusion reactor magnetic coil systems, EM field, force and inductance calc. by EFFI code 78−62648
gamma source, unsteady, EM field amplitude 77−88619
generation by long-narrow slit, EM field estimation using geometric optics 78−46494
generation of fields in rapidly rotating insulators 78−46487
health effects regulation from AC transmission line electromagnetic fields 80−94286
heat front in weak mag. field, EM field perturbation *(Russian)* 78−94835
helical electron beam in resonator of gyro device with uniform EM field, nonlinear eqns. soln. 79−81348
Hertzian dipole, evanescent waves asymptotic field 77−61897
HF discharge, in inductor of finite size, field distrib. calc. *(Russian)* 77−19783
HF mag. pulse train diffusion into extended conductors, power calc. 77−27219
HF surface fields excited by point source on concave perfectly conducting cylindrical boundary 79−64146
high elec. current meas. instrum., using Faraday rotation effect 77−2669
homogeneous conducting cylinder, dynamic EM response for symmetric excitation 79−94125
homogeneous mag. materials with constant mag. permeability, anal. *(Russian)* 77−68151
horizontal electric dipole, quasi-static subsurface-to-subsurface and subsurface-to-air 78−73375
horizontal electric wire source of arbitrary length, EM fields 79−27130
induced electromagnetic fields inside human bodies, study 78−24140
induced in biological bodies, experimental and theoretical studies, comment 77−56420
induction in vacuum by US wave in magnetostrictive conductive half space, anal. 77−73415
induction MHD pump channel, EM field and longit. boundary effect, 2-dimens. theory *(Russian)* 78−47188
induction on a prolate spheroid, current and charge densities, missile guidance appl. 77−83782
inductor-screen-ingot systems, EM fields calcs. *(Russian)* 77−46671
inhomogeneous anisotropic media, static and stationary calc., variational method 78−17840
inhomogeneous axially symmetric media, coupled azimuthal potentials 77−54650
integral equation method for calc. 79−64157
intensity distribution, in focal region of wide-angular annular lens amd mirror systems 78−90485
inverse diffraction problems, solvability 79−64159
ion storage in vacuum by EM fields *(French)* 78−1106
ionosphere, spherically symmetric, representation of EM wave field 77−13152
Kerr black hole, EM fields of stationary sources in vicinity 77−49424
Kerr black hole, weak EM field of point charge on symm. axis 77−53624
Lagrangian function for intense field, dispersional representation *(Russian)* 78−94361
LF, problem of conducting ellipsoid 80−58444
LF seabed sounding *(Russian)* 80−67431
lightning, EM fields in transmission line model with general vels. 77−33156
lightning return stroke, EM fields radiation, Maxwell eqns. exact soln. appl. 78−73442
lightning return strokes, EM radiation simulation, tortuosity effects 79−8672
linear induction motor, fluid flow induced in liquid metals, investigation 80−43800
liquid crystals, thermooptical effects used to visualise EM fields 80−62723
liquid metals, electromagnetic confining, centering and guiding *(French)* 80−24103
localised RF fields, duct propag. along inhomogeneous magnetoplasma column 79−46453
Lorentz transform law for EM field, fluxoid motion example 80−67954
low frequency electromagnetic fields, biological effects *(German)* 77−86529
low frequency field calc., iterative method 78−29876
lunar surface, variable EM field calc. 77−82135
macroscopic theory of Van der Waals forces between dielectrics 78−15139
magnet airgap, uniformity correction *(Russian)* 77−53959
magnetic oblique rotator, EM field prod., exact vacuum soln. 80−58442
magnetosphere boundary layer, EM fluctuations excitation by field-aligned currents 80−67473
Maxwell's equations in anisotropic space 79−44758
metal surface, semiclassical infinite barrier model 78−64079
metal surface exposed to external radiation, solns. of Maxwell's eqns. 78−52054
Mezen' Bay (White Sea), marine tides EM fields 78−73378
MHD duct with compensating bars, EM field distrib. *(Russian)* 78−26344
MHD flow due to current between parallel electrodes *(Russian)* 78−26345
MHD laminar flow, longitudinal dynamic effects determination for Na, Al, Sn and Hg *(Rumanian)* 80−64792
MHD linear induction pump, cylindrical with inclined coils, electrodynamic force calc. 79−77281

electromagnetic fields continued

- MHD machines, external electromagnetic fields, dipolar approx. accuracy *(Russian)* 78—47192
- microwave induced hyperthermia and neurochemical correlates, orientation effects 78—24098
- momentum of EM field very close to plane interface 79—13936
- multipole expansions, using Debye potentials, for teaching 78—41116
- near field power density meas. *(Polish)* 79—21721
- nerve excitable membrane, EM wave effect on surface charge density 78—85334
- neutron star, rotating, with strong mag. field, EM field and electron cap shape 78—12265
- neutron stars, electrodynamics in curved space 80—90465
- neutron stars, EM multipole fields 80—26896
- nonlinear electrodynamics, three-dimensional soliton solution *(Russian)* 79—22884
- nonperiodic bandlimited fields in lossless nonlinear media, energy and power 79—89828
- nonradiating linear combination of quasihomogeneous current correlations 79—18327
- nonsinusoidal, nondestructive materials testing appl. *(Czech)* 79—20311
- nonstationary marine currents, theory of EM field 78—44833
- ocean, EM field of wide current for arbitrary direction of permanent mag. field 79—57946
- ocean, magnetostatics problems in electrodynamics of sea *(Russian)* 78—77259
- ocean current of finite width, EM field 79—53351
- open oscillating circuit, resonance characts., effect of spatial inhomogeneity of medium 79—41283
- open resonator, MM and sub MM wavelengths, imaging using thermoluminophorous sensor 79—93168
- oscillating circuit, broken, physical model 79—50187
- outside solid conducting cylinder surrounded by coil with current, nonsteady field 79—96273
- parallel conductors with one-sided Fe shield, EM field calc. *(Polish)* 77—31046
- particle creation in generic external fields, particle definition 78—8498
- penetration through small apertures, first order correction 79—64156
- permeable nonuniformly conducting cylinder, EM transient response 77—10810
- plate-conductors system, multiparallel, losses calc. 80—78743
- point charge field asymptotic, above high-cond. layerlike anisotropic medium 77—75361
- point charge moving in arbitrary way, superposition of two fields *(Russian)* 80—22251
- polarised matter in co-axial waveguide, general cross-section, EM field 78—1124
- precision meas., conf., Ottawa, Canada 1978 78—89462
- pulsar magnetospheres, stellar-wind model for plasma-EM fields 80—22031
- pulsed EM radiation, from line source in two-media configuration 79—64153
- quantification near plane mirror *(French)* 77—34854
- quasi-optical open resonators, phase struct. of field, meas. method *(Russian)* 78—29925
- radially symmetric reradiating scatterers in EM fields, formulae for simple treatment *(German)* 80—87270
- radiation fields by parabolic cylinder in anisotropic medium *(Japanese)* 77—54657
- radiation from vertical electric vibrator, located on axis of ideally conducting disc 80—106418
- radio waves, atmospheric, field intensity vertical pattern on one-hop path 79—58156
- radiowave propagation over curved anisotropic surfaces, fields for horizontal and vertical dipole excitations *(Japanese)* 78—42266
- range 3-30 MHz, exposure, maximum permissible intensity and duration, physiological effects *(German)* 80—12179
- rectangular conductor with AC above ferromagnetic plate, forces acting *(Polish)* 77—65554
- resonant energy transfer from electrons to a slow electromagnetic wave 80—83545
- RF, transverse linearly polarised, effect on parametric resonator line characts. *(Russian)* 78—82883
- RF plasma torch, one dimensional analysis using finite element method 80—24264
- rotating dielectric sphere in LF field 80—23602
- rotating electrically conducting sphere behaviour in time-independ. homogeneous external mag. field, lab. approx. *(German)* 78—37785
- rotating perfectly conducting sphere, EM field, boundary value soln. 77—23597
- scalar Hertz potentials for gyrotropic media 80—23598
- scale modelling, derivation of absolute units 77—14639
- scattering by cylindrical inhomogeneity in homogeneous medium, time harmonic computation 79—41286
- Schwarzschild black hole, stationary source fields, general solns. 77—29864
- sea surface, ULF/ELF EM fields generated by submerged vertical harmonic mag. dipole 79—48400
- sea surface ULF/ELF fields generated by submerged magnetic dipoles 77—6973
- sea waves, cause of EM field vars. 78—44834
- semiconductor, inductively heated, computer simulation of temperature and EM fields 78—55961
- single particle trajectories in axisymmetrical EM fields 77—80342
- slender void, in homogeneous cond. wire rope, NDT applic. 78—74813
- solar wind, EM field in Earth magnetosphere 78—28419
- spatial spectra in millimetre and submillimetre wave ranges *(Ukrainian)* 78—90344
- spatially homogeneous cosmologies with EM field 80—51924
- sphere, elec. cond., uniformly rotating in temporally periodic homogeneous external mag. field *(German)* 79—86107
- sphere, ideally cond., charged, rotating, arbitrarily time-depend. ang. vel. *(Russian)* 78—29882
- spherical, reproduction by real meas. devices, from combined radiating sources *(Russian)* 78—85729
- spheroid turn in conducting media, calc. *(Russian)* 78—46481
- spin angular momentum of field interacting with plane interface 79—81399
- static, angular momentum 80—46771
- static and stationary, determ. using variation calculus *(Hungarian)* 80—87259

electromagnetic fields continued

- static EM multipole fields *(Chinese)* 79—72472
- statistical properties, from unshifted reson. scatt. line shape of strong quasimonochromatic field *(Russian)* 77—61934
- Stormer problem, equilib. points in planar mag. binary problem 80—82178
- stratified media, due to dipoles 77—58227
- surface currents induced by perpendicularly incident point charges, anal. *(German)* 77—42461
- surface magnetostatic wave meas. 77—41658
- symmetries of generalised electromagnetic fields 78—86988
- tachyon + bradyon interactions, superluminal and subluminal EM fields 80—12902
- teaching undergraduates EM theory 77—71167
- TEM lines, EMC tests 80—83536
- theory of gravitation and electromagnetism from Bohm-Aharonov expt. 79—85028
- theta-pinch coil Em field calc. *(Japanese)* 78—9817
- thin-wire, resonant. anomalous behaviour of near fields calculated by method of moments 79—89829
- three-dimensional fields without axial symmetry, calc. by charge simulation *(Japanese)* 77—50592
- time averaged electric energy density, near wide angular lens and mirror systems 77—72051
- Tokamak magnets, EM forces, TORMAC computer program 78—62647
- toroidal resonator, successive approxs. for reson freqs. 78—17841
- transducer, straight-through screened circular primary, between multilayer cylinder and tube, EM field 80—71856
- transient, steady-state solns. in cylindrical enclosure 80—83535
- transient field processes analysis, Bubnof-Galerkin method appl. *(Polish)* 77—54643
- transient response of solenoid driven conducting cylinder 80—23599
- transverse electrical dipole on sphere with hole field diffraction *(Ukrainian)* 79—94126
- Umov vector, electrodynamic and electrotechnical importance *(Russian)* 77—50591
- undergraduate teaching, numerical method computer programs 77—10804
- uniaxial anisotropic medium, Kottler formulation by Larmor-Lorentz principle for EM field 77—83780
- uniaxial media, EM field soln. by scaling fields in isotropic media 77—570
- variational expression derivation, unified approach 77—6970
- variational methods for stationary fields 79—36815
- vector potential pf parallel conductors between metallic half-spaces, Fourier integral transform appl. *(Polish)* 77—54645
- vertical magnetic dipole on two-layer Earth 80—76906
- vertical magnetic dipole over vertically inhomogeneous Earth, EM fields components 79—34736
- VHF electromagnetic fields and power deposition in body-of-revolution models of man 79—53189
- waveguide radiated, rectangular, in dielectric medium *(Russian)* 78—82884
- weak fields around black hole, point charge on symmetry axis 78—20852
- welding arc, EM forces effect on plasma flows, calc. 80—83912
- Zeeman effect, linear, relativistic correction, Coulomb field 80—102484

electromagnetic induction

see also inductance

- acoustic and electromagnetic excitation of superradiative state in crystals with paraelectric impurities 78—66872
- Alaska oil pipeline, elec. current induced by electrojet 80—61756
- Alaska pipeline, auroral zone elec. currents induction 79—39645
- S.American geomagnetic equator, EM induction from ionospheric current meas. 79—75021
- analogue model expts. for elongated structures *(German)* 79—25199
- asteroids primordial metamorphism via elec. induction in T Tauri-like solar wind 78—69728
- Backus' necessary condition for dynamo action in a conducting sphere 78—28195
- ball bearing electric motor, for teachers 79—21488
- bimodal induction in nonuniform thin sheets, N.Pyrenean induction anomaly appl. 78—11805
- British Isles region, EM induction by analogue model 80—56368
- circuit-breaker induction calc. using standard finite element software 79—41906
- circular bundle of relativistic particles, EM field *(Czech)* 78—66711
- coal layer, thickness meas., EM technique 78—53740
- coal seam thickness meas. using resonant loop as EM sensor 78—57366
- conducting body of revolution covered with thin layer of dielectric, axisymmetrical excitation 79—81327
- conducting cylinder and solenoid in relative motion, EM interaction, wire rope NDT appl. 79—98261
- conducting cylinder motion in solenoid field, contactless elec. cond. meas. *(Russian)* 79—214
- conducting cylinder with transverse mag. field, eddy current induction 78—74815
- conducting ellipsoid in LF EM field, induced elec. and mag. moments 80—58444
- conducting plate surface element models 79—41290
- conducting slab response to source fields, EM analogue model and finite difference calcs. 78—61329
- conducting sphere, rot. in mag. field relativistic, co-rot. frame 79—53714
- conducting sphere, rotation in homogeneous periodic mag. field, isotropic frictional coupling *(German)* 80—37932
- conducting sphere in quiescent slightly ionised plasma, exact solution 79—86564
- conducting sphere rotating in time independ. homogeneous mag. field, unipolar induction *(German)* 78—17836
- conducting stratified medium, numerical analysis 79—34740
- conducting tubes in polarized plane wave fields, surface currents and charges 78—42256
- conductive fluids local induced voltage velometry *(German)* 79—86517
- conductive piston retardation in mag. field, electromech. energy conversion *(Russian)* 79—64145
- conductors in steady motion, solution in theory of eddy currents and forces 78—62970
- cross-borehole EM probing, location of high-contrast anomaly 80—72639
- cryogenic rings, current induction and decay 80—106972
- current distributions calc. in presence of ferromagnetic bodies, integral equations solution 80—18958

electromagnetic induction continued
- current induced on crossed cylinders excited by plane EM pulse 79—13873
- current-carrying coil, moving above conducting plate, forces and moments 80—87264
- cylinders, crossed electrically thick, in plane wave field, surface currents and charges 78—42257
- cylinders, tubular, in normally incident plane wave, currents and charges 78—42258
- data tablet for signature verification 80—7048
- diamagnetic sphere supported by field from annular current 78—66714
- displacement current, historical study 79—27132
- drill-rod telemetry, calcs. for toroidal coil source 78—85710
- E-polarisation, numerical soln., improved geomagnetic boundary conditions 78—77182
- Earth, alternating EM field perturbs. by cond. inhomogeneities 79—39653
- Earth, boundary conditions for EM field above two-dimensional inhomogeneous struct. 80—85595
- Earth, electrical conductivity anomalies 79—53303
- Earth, EM induction by moving ionospheric current systems 79—16370
- Earth, freq. and transient responses of EM fields created by currents in confined conductors 79—29702
- Earth, geomag. induction vectors local time var. 78—85477
- Earth, low resistivity, polarisable, EM transients formulae *(Russian)* 79—39644
- Earth, model refinement for one-dimensional EM induction problem 79—44096
- Earth, scale model results for inductive logging near single and multiple conductive bodies 79—16696
- Earth, transient EM response from irregular surface models 78—57165
- Earth, two-dimension induction in thin surface sheet of variable integrated cond. 79—16372
- Earth, VLF response of laterally inhomogeneous anisotropic ground 80—85754
- Earth and Moon, workshop proc. (Murnau, W.Germany, 1978 September 7-13) 79—79741
- Earth conductivity anomaly, response to inducing source fields, lab. model 78—36100
- Earth conductivity model and source fields, perturb. and induction arrows calc. 79—20751
- Earth EM fields of horizontal electric dipole on polarisable half-space surface 78—69283
- Earth EM induction, source field effects on transfer functions at mid-latits. 79—74831
- Earth EM sounding, induced polarisation data inversion 79—16695
- Earth induction, effects on vertical polarisation of Pc 5 pulsations recorded in auroral regions 79—12355
- Earth surface impedance, N-layered half space theory 80—76909
- eddy current field in screened transducer field, dynamic anal. *(German)* 80—95763
- eddy current induction in thin curved sheets, calc. 79—41299
- eddy current losses, in ferromagnetic plate, due to currents in parallel conductors *(Polish)* 78—29877
- eddy currents, levitation, metal detectors and induction heating 78—61967
- eddy currents in cylindrical core of induction coil considering winding helix *(German)* 80—95764
- eddy field sources determination using magnetic scalar potential method 79—81326
- eddy-currents in thin conducting plate moving in mag field, calc. using scalar pots. *(Polish)* 80—32874
- eddy-currents induced within a metal cylinder by parallel ACs, numerical anal. *(Polish)* 78—78856
- Einstein's unified field theory 79—2696
- electric generator, wave activated, design 79—20866
- electrical conductivity of solid cylinder, contactless meas. method in current ring 79—75554
- electrically conducting body, forces in mag. field using hydrodynamic analogy 80—34551
- electrode arrays for Earth induced polarisation (IP) sounding, effects of EM coupling over uniform half-space 80—101324
- electron beam, relativistic, fields excited near plane magnetoedielectric slab 80—18986
- electronic circuits implanted in freely moving animals, wireless power supply 79—29682
- EM angular momentum, experienced by magnetite cylinder 79—55027
- EM methods with distant source, terrain relief effects 79—79735
- exterior regions containing moving conductors, finite element models 79—41291
- Faraday's law of induction general formulation 79—64144
- Faraday's law problem, including nonlinear term, rel. to perturbation theory, for teaching 79—35470
- Faraday generator, one piece, paradoxical expt. from 1851 78—73813
- Faraday induction in Einstein's unified field theory 80—117
- ferrite ring, 2000 NN type, self-accel. caused by high-current electron beam interruption 80—4809
- ferromagnetic plates eddy current phenomena numerical computation method *(German)* 80—65952
- ferromagnetic solid plate, EM field induced by local lateral magnetic flux *(Polish)* 79—98259
- field distribution, induced by current in conducting sphere between two planes, substitute diagram synthesis *(Polish)* 79—3611
- finite element modelling of EM NDT phenomena 80—40633
- flowmeter with moving field, fluid flow and moving field equations *(Rumanian)* 80—64663
- Frechet derivative for one dimensional EM induction problem 77—48996
- fusion reactor eddy current analysis, finite element circuit method 78—66373
- fusion reactor eddy currents, 3-dimens., perturbation-polynomial expansion calcs. 78—66372
- fusion reactor mechanical diagnostics, techniques in fluctuating mag. fields 78—54946
- Galilean satellites, interaction with Jupiter mag. field rel. to volcanism 80—31247
- general reciprocity theorem for conducting media 79—31770
- geoelectric, EM induction in thin sheet conductivity anomalies at Earth's surface 80—76907
- geoelectric sounding of buried axial conductor, time-domain response 80—105059

electromagnetic induction continued
- geoelectric sounding of conductive circular cylinder, expt. and theoretical results 80—105058
- geoelectricity, inversion problem 78—7567
- geomagnetic disturbances, relationship between external and internal parts 80—41610
- geomagnetic field secular variation, Bashkiriya, current anomaly 77—91004
- geomagnetic induction in central Australia, meas. 80—72424
- geomagnetic induction relationship, sufficient conditions 79—79739
- geomagnetic influences on man-made systems 80—12887
- geomagnetic transfer functions at pulsation periods 80—72417
- geophysical, model of E. coast region of N.America 80—98235
- geophysical interpretation methods *(German)* 79—35001
- geophysical sounding of dipping half plane embedded in conducting rock 80—90236
- geophysical surveying, transient time-domain EM method 80—98227
- geothermal energy resources in Oregon, USA, elec. and EM sounding obs. 80—97761
- gravitational analogue to Foucault current *(Russian)* 79—21609
- ground subsurface, EM transient response 78—57166
- gyrating conducting sphere, in mag. field 79—10241
- H-polarisation induction problem soln. by wavenumber integral eqn approach 77—44913
- H-polarization induction in two thin half-sheets 79—34737
- history of Arago's, Babbage and Herschel's and Faraday's experiment 80—68013
- history of EM induction discovery, teaching 79—44682
- hollow rotational ellipsoid, distrib. of induced mag. pot. in external space *(Polish)* 80—32875
- homopolar disc dynamo system, magnetic instability 80—81808
- impulsive field build-up, current skin-layer thickness anal. *(Russian)* 79—41285
- India and Sri lanka coastline config. effects on induced field at short period 80—12337
- induced polarisation meas. using discharge transient recorder 78—65398
- induction furnaces, cylindrical charge equivalent diameter *(Czech)* 79—50188
- induction MHD pump channel, EM field and longit. boundary effect, 2-dimens. theory *(Russian)* 78—47188
- infinitely conducting oceans of arbitrary shape 78—61318
- ionosphere, thin two dimensional anisotropic, EM induction theory *(German)* 77—70917
- island-continent ocean channels, analogue model 77—9336
- island-continent ocean channels, analogue model of EM induction for H polarisation 77—81795
- law of induction from view point of relativistic mechanics *(German)* 79—41287
- layered Earth with surface loop inductor, transient response, theory 80—72410
- lightning transient anal. for aircraft, flux induced voltage transients on low-loss transmission lines 79—36814
- lunar EM induction studies, effects of magnetometer data errors 79—96932
- magnetic field calc. from current distrib., finite element techniques 78—94358
- magnetic fields, quasi-stationary, finite element anal. 78—94356
- magnetic induction, large-scale demonstration 80—101699
- magnetic MG field generation by EM flux-compression, computer simulation 79—50189
- magnetic shielding barrier LF field penetration 78—82886
- magnetic stirrer, Lenz's law and induced current expts. 78—12485
- magnetic wheel unipolar machine, for teachers 78—12499
- magnetosphere, potential and inductive elec. fields during auroras 80—21878
- magnetospheric substorms, three dimensional current systems modelling 77—56793
- magnetotelluric and magnetic variational sounding, 3-dim. modelling 78—7563
- magnetotelluric and magnetovariational study of the Gregory Rift Valley, Kenys 77—91000
- magnetotelluric apparent resistivity, effect of localised source 80—72429
- magnetotelluric investigations, induction effects detect. methods appl. in Sakhalin and Yakutia *(Russian)* 79—39642
- magnetotelluric sounding, affected by resistivity freq.-dispersion 80—41368
- mangetic AC field incident on surfaces of conducting bodies *(French)* 79—68350
- massive object with one pole of electromagnetic, magnetisation 79—50190
- mean field electrodynamics, high conductivity limit 77—949
- metallic thin film, EM wave induced voltage 79—56330
- MHD, moving conducting fluid inductive interaction with external main windings, config. effects *(Russian)* 78—75225
- MHD channel, EM field eqns. averaging, at finite mag. Reynolds no. 79—77282
- MHD generator, simplest physical model 78—71548
- MHD generators, coaxial, magnetic field distrib. *(French)* 78—55758
- MHD induction pump with side bars, thrust-flow characts. at large Re_m *(Russian)* 78—75231
- MHD pump, direct-current uncompensated conduction-type, exptl. characts. 79—77283
- microwave induced DC voltage phenomenon *(Chinese)* 78—50677
- mines, boreholes, HF induction profiling *(Polish)* 80—51547
- minor planets, EM heating in early solar system 80—36555
- Moon, forcing by diamagnetic cacity 77—87288
- Moon, modelling, solar wind parameters limitations 78—36415
- Moon, response to solar wind mag. fluctuations 78—12113
- Moon, variable EM field calc. 77—82135
- moving conducting ribbon, interaction with ferromag. inductor field *(Russian)* 78—94359
- NDT by external induction and field selective display 78—15618
- Newfoundland, geomag. sounding near northern termination of Appalachian System 78—61314
- non-uniform thin sheet at surface of uniformly conducting Earth, three dimens. induction 80—30983
- nonharmonic EM induction in two-layer spherical Earth 79—100812
- nonhomogeneous conducting sphere, secondary electromagnetic field analysis *(Russian)* 79—45887
- nonmagnetic conductors, three-dimensional eddy current calc. *(French)* 80—14270

electromagnetic induction continued
nonperiodic, in conducting Earth 78−44761
nonsteady mag. field induction meas. by prerecorded tape signal attenuation 79−67355
ocean, baseless method of electric field meas. *(Russian)* 79−39900
ocean coast effects 80−76908
ocean current induced EM fields, theory 80−61805
ocean currents velocity profiler based on geomag. induction principles 78−61569
ocean edge, H-polarisation induction 77−44912
ocean edge coupled to mantle by conducting crust, H-polarisation induction 77−48994
ocean electric current induced by Sq, around land masses 80−72413
ocean EM induction affecting Sq during IGY 80−72428
ocean floor, EM fluctuations induced by wind waves 78−40561
ocean wave motion, assoc. electrokinetic phenomena 78−69351
ocean-coast model, EM response to E-polarisation induction 78−61321
oceanic induced electric fields, coastal edge corrections calc. 79−25253
oceanic induction and spectrum shifting method 78−20353
oceans, arbitrarily shaped, of finite conductivity, EM induction solns. 79−16371
planar nonstationary EM field in conducting medium, transient state anal. *(Polish)* 78−71000
plane eddy current problems, power dissipation and inductance calc. *(German)* 78−58881
plate fixed in air-gap between salient poles *(German)* 79−86106
point charge near cond. plane, force acting, for teaching 78−49605
polarisable half-space, current pulses, transient EM field 78−96130
power transmission lines, elec. currents induced by auroral activity 79−62640
principle of equivalence, expt. test *(Russian)* 78−77795
Procopiu effect EMF in ferromag. material under torsion *(Rumanian)* 78−86986
pump for LMFBR appls. 78−17291
pumps, iterative numerical solution of laminar fluid flow 79−32699
radio wave action on rod, current, voltage generation EM to ampere energy conversion *(Russian)* 79−76548
RF energy coupling into cylindrical enclosure 78−87000
RF fields, transverse linearly polarised, effect on parametric resonator line characts. *(Russian)* 78−82883
rotating conducting sphere in mag. field, ideal conductor approx. 79−18324
rotating conductive Earth, EM induction 78−44764
scatterer surface current density, calc. using numerical technique 80−78747
scattering by irregularly shaped perfectly conducting or dielectric cylinders 79−13878
scattering current and small hole coupling for thin finite cylinders 79−18325
sea-floor coast effect in H-polarisation, model 77−2104
sheet conductor, induced eddy currents, IR meas. 80−37933
shell, rotating, conducting, in mag. field, forces and moments 78−37786
shielding effectiveness of soft mag. materials for EM pulses 80−28143
Sierra Nevada batholith, elec. conductivity of crust 80−72411
singularity expansion method applied to perpendicular crossed wires over a perfectly conducting ground plane 79−36813
solenoid deceleration in conducting tube 78−50678
solenoid experiments, for teachers 79−71204
solid cylinder fixed in air gap, eddy currents induced *(German)* 79−89827
sounding of layered structure of Earth, time domain anal. 80−72641
sphere, method of variation of consts. appl. to excitation by elec. and mag. currents 78−86989
spinning magnetic fields, unipolar induction and moving and nonmoving hypotheses 79−55026
statistical theory of electromagnetic induction in thin sheets 77−86769
steel, Cr-Ni-Mo-V, magnetic induction, struct. dependence *(Czech)* 80−50141
steel, nitrided layer depth, electroinduction meas. method 80−104379
steel surface HF inductive pulse hardening *(German)* 78−27687
stiffness of conducting bodies config. in time-varying mag. field 80−43230
strong magnetic field induction metrology 78−37040
sulphide ores, disseminated, electrochemical model of induced-polarisation phenomena 79−92526
sulphide prospect in California copper belt, broadband EM study 80−72503
superconducting solenoids fields meas., automatic, using NMR 80−57344
superconductor, quasiparticle charge imbalance induced by supercurrent with thermal gradient 80−34546
surface charge measurement by electrostatic induction 78−49807
temperature-compensated induction extensometer 79−17394
terrestrial EM induction in three-dimens. struct. for various source fields 79−66609
test coil on permeable spheroid in field of coaxial line currents *(German)* 80−37928
Tokamak machines, eddy currents, numerical and exptl. anal. 78−66374
transmission along drill rod in conducting rock 79−59618
transversal field configuration, in conducting plates *(Polish)* 79−3612
tubular cylinders, electrically thin conducting, current induced by normally incident plane electromag. wave 79−89830
two dimensional induction problems, finite difference soln. 77−2101
underground quarries, EM detection *(French)* 78−96306
underground quarries, EM transmission meas. 78−57365
Vancouver Island region, analogue model study of EM induction 80−56356
Vancouver Island region, electromagnetic induction model 80−56367
Vancouver Island region, terrestrial EM induction 80−104879
Venus magnetic tail, unipolar induction effects 80−62060
VHF radiowave induction heating of biological tissue from portable transmitter, expt. 78−57039
wave diffraction in radial array of nonintersecting 1/2-planes 80−28147
Wiegand effect voltage pulse generation 79−81322
wire rope NDT, EM field perturbation by internal void in conducting cylinder 79−34213
Fe alloys, amorphous, room-temp. saturation induction 78−95476
Fe, high purity, mag. viscosity mechanism 78−19282
Fe-Nb (3.1 wt.%), semihard mag. alloy, Recalloy, mag. props., elec. cond. *(Japanese)* 78−10723

electromagnetic induction continued
$MgM^{3+}{}_xFe_{2-x}O_4$, M=In,Al,Cr,Sc, comp. effects on ferrite characts. 78−52305
Nb-Ti, Helmholtz coils, optimisation, critical current rel. to mag. induction 79−67353
ReO_3, open orbits in cryst., EM induction meas. 79−73421

electromagnetic interference
see also radiofrequency interference; telephone interference; television interference
aerial electroprospecting, transducer interference analysis *(Russian)* 77−56766
angular scattering of water drops and ice particles [electromagnetic interference], frequencies above 10 GHz appl. 80−109183
atmospherics noise variation with sunspot number during 1600-2000 hours at Delhi 78−49083
AURORA machine studies of air chem., cond. and boundary layer 78−32144
cardiac pacemakers, diathermy interference, simulation models 79−84007
conducting screen, excitation of object through aperture 79−13871
digital signal interfaces, causes and elimination methods 77−42666
discharges for sputter deposition and sputter etching, RFI/EMI 78−71566
eCG monitor interference from patient call systems 79−74776
EEG, interference suppression during open heart surgery 79−100784
electric equipment testing laboratory, movable, type ETL-35, design *(Russian)* 80−95088
EM wave absorber with good reflection characts. at both normal and oblique incidence, synthesis 80−32891
EMP radiation, electronic systems, protection, book 77−54366
heart pacemakers, interference due to amateur radio installations, cars, domestic appliances 79−25155
HF ECG, origin and characts. 77−44797
IEEE International EMC Symposium, Atlanta (1978) 78−82876
LF interference current therapeutic apparatus *(Bulgarian)* 80−26314
lightning strokes to Earth per km^2 per year, CIGRE count (since 1962) *(German)* 78−40606
microwaves appl. in biological medical therapy/diagnosis, bio-clutter interference effects 79−11992
near-field radiation hazard and EMI meas. 77−44757
nuclear power plant equipment electromagnetic interference and RFI effects 80−57880
ocean electric fields measurement, EM phenomena accompanying movement of current fairing *(Russian)* 78−77361
optical fibre communication, A-7 ALOFT economic analysis, EM interf. and pulse tests 78−42448
pacemaker implantation surgery, intracardiac ECG derivation during electrocoagulation 78−40397
pacemaker interference, 60 Hz field and current effects 78−88769
pacemaker interference, body potentials and currents from ELF elec. fields and househould appliances 78−88770
pacemakers, implanted, galvanic coupled interference effects 77−81753
patient's virtual earth and electrical interference monitor, electrophysiological signal degradation reduction 79−57800
power line radiation effects on magnetosphere, transmitter simulation 79−12348
power station fibre-optic system installation 79−37028
quark recombination mechanism in multi-hadron production 80−18114
radiated signal, principles and expts. *(German)* 77−61900
radiation pattern meas. of microwaves in presence of biological specimens 78−48828
radiotherapy machine ionising radiation and EM interf. effects on cardiac pacemakers 79−62406
RF radiation hazards to personnel, mobile and portable transmitters, US Citizen Band Service 77−40795
shielding of electronic systems, secondary neutron polarization via penetration through a ferromagnetic shielding wall 80−47742
spacecraft charging by magnetospheric plasmas, effects, counter measures 77−22035
statistical-physical modelling, classification 77−83789
TEM cell for interference investigations, large, measurement standard 80−238
ventricular synchronous demand cardiac pacemaker advances 78−77152
weights and measures, conference, Washington (1978) 80−27260
X-ray image intensifier *(German)* 80−105761

electromagnetic lenses *see magnetic lenses*

electromagnetic oscillations
see also cavity resonators; lasers; masers; ring lasers
astrophysical nonlinear dynamos, multiple period dynamo wave oscills. and solar cycle modulations 79−16813
asymptotics of spectrum of elliptic boundary-value problems *(Russian)* 77−5673
cavity eigenfrequency density oscills. and lattice sums 77−65556
cavity with cylindrical hole in wall of infinite thickness, elec. and mag. polarisabilities determ. 78−71004
dielectric layer, natural EM oscillations excitation by stream of electrons or EM field 80−34378
diffusion approximation for mutual coherence function, anal. *(Russian)* 77−10814
Fabry-Perot resonator cavity, dielectric film effect on characts. 79−94134
ferrite spheres, magnetisation, resonance oscillation freq. determ. 80−71106
Gyrocon, efficient relativistic high power VHF generator 80−13990
insulator, modulation oscills. of travelling EM wave 80−24962
liquid crystals, four modes per freq., evanescence waves 78−14276
semiconductor, generation in LF electric field 78−64068
semiconductor, natural EM oscillations excitation by stream of electrons or EM field 80−34378
semiconductor plasma, longitudinal oscillations 80−88583
toroidal resonator, successive approxs. for reson freqs. 78−17841
wind generator oscillation modes in large power systems 79−29446
Ag-MgF_2-Ag layered system bounding dielec., ATR ang. spectra, assoc. reson. EM oscills. 79−15541
NH_3 molecular beam maser with semi-confocal cavity, output power spectral distrib. 80−43311

electromagnetic radiation *see electromagnetic waves*

electromagnetic theory of light
Gaussian beam scattering characts. at dielec. media interface 78−42275

electromagnetic theory of light continued
isotropic-anisotropic media boundary, light refl. and refr., Maxwell theory *(German)* 78−87007
losslessness of optical systems in a vectorial treatment 80−83558

electromagnetic wave absorption
see also electromagnetic wave propagation in plasma; gamma-ray absorption; light absorption; spectra; X-ray absorption
140 GHz atmospheric attenuation by rain, obs. 78−3914
absorber with good reflection characts. at both normal and oblique incidence, synthesis 80−32891
aerosol, thin flat, EM wave scatt. and absorpt. 80−91723
altitude profile determ., at 2.53 mm by zenith brightness radiometry 77−81979
antenna temp. and horizontal path attenuation due to 320 GHz water vapour absorption line, calc. 77−41139
Arctic drift ice, microwave dielec. const. and absorpt. coeff. anisotropy 78−49037
atmosphere, amplitude spectrum rel. to fluctuation frequency in absorption region 77−21878
atmosphere, meas., O_2 band, at 5.6 mm *(Russian)* 77−91210
atmosphere, propag. of microwaves, refr. and absorpt. coeffs., optimal orthogonal expansion props. 80−98414
atmosphere, radiances in absorpt. bands, calc. methods including multiple scatt. 78−61554
atmosphere, solar radiation absorpt. by H_2O vapour, including multiple scatt. 78−61553
atmosphere ELF attenuation, effects of elec. cond. of atmosphere and lower ionosphere 80−31099
atmospheric amplitude spectra in absorption region 78−44920
atmospheric attenuation of 230 GHz, meas. 78−73425
atmospheric water vapour, 10 cm-0.27 mm wavelengths, temp. dependence 77−2235
aurora, small scale absorpt. events assoc. with substorms 77−56791
auroral radio absorption, spike events 80−12589
bacterial cell microwave absorption at spectral singularities 77−40712
biological, EM power absorption, long-wavelength, by ellipsoidal models of man and animals 77−12956
biological cylindrical tissue models excited by loop antenna 79−39446
biological effects, conf., Amherst, USA (Oct. 1976) 78−40243
biological effects and meas. methods 77−16954
biological models, induction of focal hyperthermia by RF radiation and EM fields 78−40244
biostructure prolate spheroidal models, EM wave absorpt. and scatt. 77−77941
black hole, Reissner-Nordstrom, coupled gravitational and EM perturbs., scatt. matrix, energy conversion, quasi-normal modes 80−67775
bolometric laser emission convertors, thin wire, thermal processes *(Russian)* 77−18094
cloudy atm., long distance meas. by radiometry 80−90196
conducting cylinder in harmonically variable transverse mag. field, EM wave penetration 79−81328
cosmic radio noise absorpt. events meas. on riometers, due to backscatt. by E-region irregularities 77−25831
crystalline slab of point molecules, dielec. theory 80−97222
curvature radiation, absorpt. theory rel. to pulsar radio emission 79−75090
D-region, lower, Faraday rot. and absorpt. calcs. rel. to electron density meas. 80−31162
D-region, mid-latit., energetic particles precip. during baylike absorpt. disturbance 79−12333
D-region, radio wave absorpt. diurnal vars. during storm after-effect 78−65451
D-region, radiowave absorpt. results during Western European Winter Anomaly Campaign (1975/76) 78−45123
D-region absorption, effect on forward scatter radiometeor amplitude distrib. index 78−65552
degenerate semiconductor, depend. on external quantising mag. field 78−95308
dielectric cylindrical tissue models in presence of refl. surface, arm and thigh sizes 80−26258
dielectric fluid, Debye absorption at crit. liq.-vapour transition 80−100322
diffraction by strip under mixed boundary conditions 80−87268
diffraction gratings, crossed, theory of diffraction and absorption 79−18337
diffraction of absorbing cylinders suspended in outside absorbing media 77−79728
dispersion and attenuation of linear pulse propag. 77−574
dispersive medium, energy density of arbitrary EM field and dissipation 78−9304
dissipative structures, formation and stability 80−108950
E-region, radiowave absorpt. correl. with O I green line airglow emission 78−45075
E-region, solar X-rays attenuation meas. by rocket-borne proportional counters 78−45072
Earth-space communication links, rain attenuation rel. to path diversity 78−69424
Earth-space paths, tropical rain attenuation at 11 GHz, radiometric meas. in Australia 77−33165
ELF normal mode reflection and absorption, nighttime ionosphere effects 79−8754
ELF waves, attenuation in Earth-ionosphere transmission line rel. to ionospheric profiles 78−36234
EM absorbing wall with resistive sheets, circular freq. locus 80−106428
EM power deposition in prolate spheroid models of man and animals at resonance 78−31905
energy deposition in animals and human models, grounding and reflector effects 78−40346
energy deposition in inhomogeneous block model of man for near-field irradiation conditions 80−89788
ferroelectric with orientational transition, coupled elastic, EM and polarisation oscill. spectrum 79−8103
ferromagnets and antiferromagnets, EM and acoustic energy attenuation in many-domain magnets 80−7140
gas microwave absorption Fourier spectrometer for 300 GHz to 1.2 THz 77−5935
gas mixtures, IR absorpt. theory using hard sphere model *(Russian)* 80−14879
gyrosynchrotron emission from quasi-thermal electrons, gyromag. absorpt. coeff. and appl. to solar flares 80−36602

electromagnetic wave absorption continued
gyrotropic sphere, EM wave scatt. and absorpt. 79−41305
HF radiowave absorption variation in ionosphere *(Spanish)* 79−16735
holographic unslanted transmission and reflection gratings, modal theory, EM wave propag. 80−83673
human ellipsoidal model, analysis of long-wave absorption 77−9219
human head EM induced field and power absorption, ellipsoidal model 80−3724
human model, multilayered, whole-body power absorpt. 79−70580
human model near a ground plane, approx. calc. of SAR for planewave irradiation 79−100660
hydrometeors, extinction and scattering in 0.25-15 μm range 79−53501
induced electromagnetic fields inside human bodies, study 78−24140
inhomogeneous plasmas, resonant microwave absorption, nonlinear effects 79−94793
intergalactic medium rel. to pregalactic fluctuations visibility, upper limit on q_0 80−8717
intergalactic radiation field, absorpt. due to pyrolitic graphite whiskers rel. to microwave background 80−94866
ionosphere, A1 absorption measurements at 2.4 and 5.6 MHz 80−82132
ionosphere, absorpt. events at high latits. 77−21987
ionosphere, daytime absorpt. surges rel. to substorm phase and interplanetary mag. field direction 78−73575
ionosphere, diurnal radiowave absorption variation asymmetry, seasonal variation 77−87175
ionosphere, equatorial, seasonal var. of radio waves absorpt. 78−85762
ionosphere, errors in attenuation determ. for signals with small arrival angles 79−58155
ionosphere, global absorpt. meas. on board ships 80−98500
ionosphere, LF absorpt. at midlatit., interplanetary mag. field sector struct. effects 77−29546
ionosphere, lower, long-distance mid-latit. VLF transmission anomalous absorpt. 80−8485
ionosphere, lower, nighttime, mid-latit., absorpt. correl. with interplanetary mag. field 79−58151
ionosphere, lower, shortcomings in understanding revealed by radiowave absorpt. meas. 78−81492
ionosphere, MF absorpt. nocturnal var. and nighttime E-region 77−29563
ionosphere, mid-latit. absorpt. rel. to zero and maximal vel. contours in equatorial ionosphere 80−12597
ionosphere, modulation trough of anomalous absorpt. and aspect scatt. 79−58159
ionosphere, radiowave absorpt. meas. rel. to vars. of effective electron collision freq. 77−91347
ionosphere, radiowave absorpt. obs. at mag. equator using A_1-technique 79−21099
ionosphere, radiowave absorption, general formulae 79−58166
ionosphere, radiowaves attenuation rel. to oblique-incidence sporadic-E propag. 78−73578
ionosphere, riometer meas. of high latit. radio wave absorpt. 80−8488
ionosphere, sudden commencement absorpt. events at S. pole rel. to lower cleft boundary latit. 78−77437
ionosphere, waves signal vars. over sunspot cycle 77−78560
ionosphere, winter absorpt. obs., 1975/76, at about 52°N, 9°E 78−45124
ionosphere absorption, vars. rel. to geomag. influence on atmospheric press. geopotential 80−4067
ionosphere absorption near 100 km height, travelling (wave) disturbances 79−25392
ionosphere E-region, deviative radio wave absorpt. rel. to effective electron collision frequency 79−58153
ionosphere polar cap absorption, recording using ULF meas. 79−53620
ionosphere polar cap absorption event, August 1972, optical aurora diagnostics 77−29567
ionosphere radio wave absorption, morphological features of winter absorpt. anomaly at middle latits. 80−67459
ionosphere radio wave absorption, riometer meas. 78−85763
ionosphere vertical incidence absorption during winter anomaly, calcs. using electron density profiles 79−21098
ionosphere winter absorption anomaly, implications of eddy diffusion models for mesosphere and lower thermosphere 80−109198
ionosphere winter absorption anomaly, influences of NO conc. and H_2O dissoc. 79−58152
ionospheric absorption studies by riometer technique at magnetic equator 77−53275
ionospheric HF radio wave absorpt. temporal variations 77−53305
ionospheric radiowave absorpt. freq. var. in model D- and E-regions 77−13169
ionospheric radiowave absorpt. meas. at Waltair, India, D- and E-region models 77−13173
ionospheric radiowave absorpt. vars. at 2.5 MHz at Ahmedabad, India 77−13165
ionospheric radiowave absorption, Gauhati, India 77−41261
IR attenuation by atm. H_2O, lab. study of role of mol. and aerosol contribs. *(Russian)* 79−34945
Kane semiconductor, many photon electron spin orientation, EM wave absorption 80−44506
leaf radiation stochastic model 77−32880
long-path light absorption cell meas., automation, optical alignment 79−17491
magnetosphere, auroral absorpt. substorm onset obs. 78−96362
magnetosphere, morning sector, eastward movement of auroral radio absorption events 77−56792
many-valley semicond. film, electric field absorpt. coeff., self-consistent film pot. 79−69612
Mars, microwave absorption in atmosphere 77−71045
Mauna Kea, atmospheric absorpt. between 4 and 30 cm^{-1} 78−3888
metal, surface region, absorption of EM radiation 78−43456
metallic particles, low-freq. EM absorption, particle size depend. 78−88311
metallic thin film, EM wave induced voltage 79−56330
microwave, rain attenuation study on terrestrial link, weather radar appl. 77−41130
microwave absorbed dose rate distrib. in phantom heads irrad. by aperture source 77−73581
microwave absorbing ferrite-dielectric composite 77−7880
microwave absorption coefficient and refractive index, optimal orthogonal functions 80−36379
microwave absorption in atmosphere of giant planets induced by collisions of H molecules 80−90350

- **electromagnetic wave absorption** continued
  - microwave attenuation at 36.8 GHz in sea ice, freshwater ice and snow, meas. *(Russian)* 77—5209
  - microwave attenuation by atmospheric water vapour at 0.869 mm *(Russian)* 77—5277
  - microwave attenuation from rainfall rates, 10-40 GHz 78—40607
  - microwave irradiated breast tumour thermal pattern calc. *(French)* 80—3759
  - microwave power absorption differences between normal and malignant tissue 80—104640
  - microwave slant-path attenuation prediction from rainfall rate meas. 77—70741
  - microwave whole-body dosimetry in small animals, effect of body mass and exposure geometry 78—40348
  - microwaves, meas. of energy absorbed by biological systems by anal. of heating and cooling data 78—40343
  - microwaves, meas. of energy absorbed by biological systems by Dewar-flask calorimetry 78—40344
  - microwaves, whole-body biological dosimeter using drug-induced ectothermia in small mammals 78—40350
  - microwaves at 11 GHz, rain outage performance of tandem and route diversity systems 77—41131
  - MM wave propag. in 100-1000 GHz range 79—92578
  - monochromatic radiation in gas media, near resonance nonlinear propagation 79—76748
  - neutron stars, magnetic, photons free-free absorpt. rel. to radiative heat transfer in surface layers 80—94826
  - NGC 1499, H II region, decametre wavelength absorpt. obs. rel. to nebula parameters *(Ukrainian)* 79—40243
  - nonspherical dielectric objects, biological models 78—40241
  - nonspherical extinction and absorption efficiencies 79—7074
  - paramagnetic crystal, quantum amplification and absorpt. of EM wave in moderating structure 80—87361
  - particles, small, spherical, reformulation of radiation laws 78—87246
  - plane waves, oblique incidence on circular conductor, integral energy characts. 78—46491
  - planetary nebulae, He II Ly α photons absorpt. rel. to forbidden lines intensities 80—67833
  - plasma, nonlinear isotropic, abnormal linear EM wave absorpt. *(Russian)* 77—11353
  - plasma, thermal, finite density, absorpt. around electron cyclotron freq. 79—64874
  - plasma (fluid), hydrogenic, transverse dielec. function, excitation spectrum 78—67311
  - plasma density structures, spatially periodic, interaction of EM radiation, attenuation meas 80—48893
  - pulsar radiation, electron absorpt. rel. to spectra low-freq. dropoff 80—17602
  - radar, attenuation by rain at 3.2 cm and 5.4 cm rel. to surface precip. meas. *(German)* 77—82038
  - radio wave absorpt. by water vapour in atmosphere, 0.8-20 mm range 80—4086
  - radio waves, rain attenuation on terrestrial and Earth-space propag. paths 78—73490
  - radio waves anomalous absorpt. during sudden ionospheric distrubances rel. to solar X-ray radiation intensity 79—96857
  - radiowave, in tissue prolate spheroids, calc. by point matching method 78—44612
  - radiowave absorption in D-region, winter anomaly 79—58176
  - radiowaves, ionospheric equatorial absorption, lunar tides 79—44286
  - radiowaves in ionosphere, absorpt. azimuthal patterns of circumterrestrial signals 77—49222
  - radiowaves in ionosphere, seasonal pattern of freq. depend. 77—49221
  - rain attenuation, radiometric determ. at millimetre wavelengths, multiple-scatt. effects metric determ. at millimetre wavelengths, multiple-scatt. effect 80—90260
  - rain attenuation at 11 GHz *(French)* 78—77292
  - rain attenuation at 13 GHz on Earth-space paths, depend. on elevation angle 77—70742
  - rain attenuation calc. 78—44919
  - rain attenuation meas. on Earth-space paths at 37 GHz by passive radiometry 77—41109
  - rain attenuation prediction using radar and in situ meas., 28 GHz Comstar beacon signal 79—70839
  - rain rate statistics, approx. method for use in signal attenuation estimating 79—70840
  - ray equations for absorbing media, uniqueness of solns. 77—3521
  - resonant energy transfer from electrons to a slow electromagnetic wave 80—83545
  - RF, average specific absorpt. rate in ellipsoidal conductor and dielec. models of humans and monkeys 78—40349
  - RF energy absorpt. of simulated body material using portable transmitters 78—44614
  - RF power absorption in biological specimens, meas., 10-100 MHz 77—90916
  - RF radiation dosimetry handbook, descriptive summary 78—40347
  - sandy and clay soils microwave absorption *(Russian)* 78—81162
  - satellite communication systems, rain effects on propag. 77—41126
  - sea ice, initial forms, microwave refr. index and absorpt. 78—49036
  - semiconductor, absorption of strong EM waves, weak electric field effects 79—95400
  - semiconductor, degenerate, absorpt. due to electron-phonon collisions in quantising mag. field 79—7795
  - semiconductor, disordered, with soft Coulombic aperture, screening and absorpt. of long EM waves *(Russian)* 78—23001
  - semiconductor, nonlinear intense EM wave absorpt. *(Russian)* 80—29425
  - semiconductor, three-band, absorpt. of weak EM wave in presence of intensive one 79—61325
  - semiconductor film, size-quantised, EM wave absorpt. coeff. in coherent hypersonic wave field 80—29819
  - semiconductor thin film conductivity monitoring by microwave resonator absorption *(Russian)* 78—23182
  - semiconductor with superlattice in quantising electric field 80—108182
  - semiconductors, electron-phonon interactions, combined phonon resonance *(Russian)* 80—75321
  - small-radius scatterers, cyclotron resonance harmonics 80—71183
  - solar radiation absorpt. by terrestrial atm., effects of gases, aerosols and clouds 77—37407
  - solar radiation absorpt. by terrestrial atm., radiation balance 77—33183

- **electromagnetic wave absorption** continued
  - solid surface response to high-power incident flux, with temperature dependent absorptivity 78—51038
  - specific absorpt. rate over freq. range of prolate spheroidal models of humans and animals 79—100658
  - sublimation drying in UHF EM field 78—83936
  - superconductor, EM wave nonlinear absorpt. near one-photon threshold 80—60142
  - superconductor, long thin, resistive domain of small cross section in microwave EM field 79—28446
  - thermal microwave emission from random inhomogeneous layer over homogeneous medium 77—42726
  - thin absorbing films, plane-wave interaction 80—95767
  - thin finite dielectric cylinder, scattering and absorption of EM waves 80—74281
  - tissue induced EM power distribution in closed environment 80—3725
  - troposphere, attenuation statistics at 15 and 35 GHz for very low elevation angles 79—8674
  - troposphere ducting environments, radio waves path losses in beyond-horizon propag. 77—41132
  - tropospheric waveguide, numerical comparison of ray method and normal wave method 80—21858
  - turbulent absorbing medium with smooth space-time fluctuations, statistical characts. 79—81339
  - two coupled oscillators, decaying in the same bath, absorpt. line shape 79—10088
  - Venus atmosphere, microwave absorption in 21-117 GHz range 77—71040
  - vertical profiles of rain rates rel. to Earth-satellite radio attenuation modelling 79—70841
  - Al, anodised, cryogenic material, IR reflectance 79—71458
  - Ar-Xe mixture, microwave absorption, collision-induced 79—22626
  - Bi, EM wave dispersion and damping, Voigt configuration, non-local calcs. 80—100475
  - Cr, antiferromag., EM absorpt. 79—51925
  - GdTb, ferromag., magnetisation and microwave absorpt. 80—65816
  - H_2O vapour, atmospheric, microwave meas. of absolute values of absorpt. 79—66773
  - H_2O vapour laser 118.6 μm radiation absorption by H_2O vapour, temp. and press. effects meas. 78—75255
  - He I 584 Å transfer in quasars and gaseous nebulae, photon destruction efficiency 80—67550
  - n-InSb, degenerate plasma, Coulomb collision photon absorpt. dynamic screening *(Russian)* 80—92924
  - KCl, 10.6 microns absorption, calorimeter round robin meas. 79—35748
  - Ne-Xe mixture, microwave absorption, collision-induced 79—22626

- **electromagnetic wave attenuation** *see electromagnetic wave absorption; electromagnetic wave scattering*

- **electromagnetic wave diffraction**
  - *see also electromagnetic wave propagation in plasma; gamma-ray diffraction; light diffraction; X-ray diffraction*
  - γ-ray diffractometry, extinction correction 77—19850
  - absorbing cylinders suspended in outside absorbing media, diffr. props. 77—79728
  - anisotropic media, EM wave diffraction, threshold effects (Wood anomalies) 80—99608
  - antenna boundary value problems, null field approach, computational method 79—13877
  - antenna potential method *(Russian)* 80—63899
  - aperture in planar conducting screen separating partitioned half-spaces, EM diffr. 78—33651
  - arbitrary complex aperture in conductive screen 79—45893
  - axisymmetric bodies with surface fractures, diffraction field and scatt. calc. 80—43236
  - biaxial periodic surface, general integral formulation 79—98267
  - black hole, plane EM wave diffraction by spherical gravit. lens, Poynting vector calc. 79—25945
  - boundary diffraction formulation 78—9301
  - boundary wave caustic, geometrical theory modification 77—6981
  - cascaded rectangular regions in thick conducting screen 80—32885
  - circular cylinder with longitudinal slot *(Ukrainian)* 78—90345
  - circular cylinders with longitudinal slots, rigorous solution of excitation problem *(Russian)* 79—18340
  - circular discs and rectangular plates, shadow-side field meas. 77—79731
  - complex body of revolution, asymptotic method for diffr. field determ. 79—64158
  - complex shape target modelling, geometrical theory based method *(French)* 78—5395
  - concave bodies of rotation, asymptotic field determination method *(Russian)* 78—82888
  - conducting plates, nonintersecting, integral Fredholm eqns. 79—10248
  - conducting rectangular bar transmission gratings 78—62993
  - convex, smooth, ideally conducting and electrically large surface 78—94363
  - convex conducting surface, three-dimensional vectorial problem 77—75382
  - corner diffraction coeff. anal., Albertsen's formulae 78—62978
  - corrugated gratings, TE polarisation, anal. by Rayleigh hypothesis, num. evaln. 77—3520
  - creeping wave, by discontinuity of tangent plane *(French)* 78—5397
  - creeping wave scattering, by surface discontinuity *(French)* 78—5396
  - crossed lamellar transmission grating, exam. of diffr. props. 78—59139
  - curved edge, caustics and caustic corrections 77—38775
  - curved surface, wave propag. 78—37793
  - curvilinear surfaces with inhomogeneous admittance 80—69296
  - cylinder, uniform asymptotic theory of diffraction 80—28150
  - cylindrical obstacle, high freq. two-dimens. diffr. of incident anisotropic cylindrical wave 80—95770
  - cylindrical pulse, diffraction by half plane under mixed boundary conditions 79—98265
  - cylindrical pulse diffr. by metallic half plane, boundary value problem, direct transform technique 80—69573
  - cylindrical strip, in phase interface of Z semiinfinite media, EM wave diffr., spectral theory 79—94132
  - cylindrical surfaces, ribbed, EM wave diffr. 80—106424
  - cylindrical wave, diffr. from slit, above interface, paired integral eqn. calcs. 77—50613
  - cylindrical wave diffr. by cylindrical obstacle with arbitrary cross-section, asymptotic series solns. 80—99609

electromagnetic wave diffraction continued
cylindrical wave diffracted by half-plane, field in vicinity of light-shadow boundary 77−10823
cylindrically truncated planar surface, diffraction coeff. 80−9782
dense comb, plane wave diffraction 77−10820
dielectric wedge, diffracted near field 77−88624
dielectric-loaded trough, in conducting plane 77−54655
diffraction by strip under mixed boundary conditions 80−87268
diffraction grating props., theoretical model 80−91732
diffraction gratings, crossed, theory of diffraction and absorption 79−18337
dipole field diffraction by perfectly conducting thick half-plate 78−46488
double knife-edge diffraction for curved screens, Cassegrain reflector antennas appl. 80−14273
edge, in perfectly conducting surface, uniform geometrical theory 77−54654
edge diffraction, path integral technique 78−62975
edge diffraction, uniform asymptotic theory and Ufimtsev's theory, comparison 77−19132
edge diffraction with reflections in diffracted ray path 78−37792
edge-type reflection gratings, anal. algorithms 78−86998
elastic dielectric, EM wave effect on displacement field of crack 78−30231
elastic isotropic dielectric medium with crack, EM wave diffr. 78−26084
electrodynamic boundary problem solution for complex shape regions 80−69300
elliptic cylinder of finite conductivity *(Russian)* 78−17844
evanescent plane wave diffraction by a half plane 79−50197
extended path with single obstacle, attenuation factor calc. 80−95775
far field diffraction by variable thickness semi-infinite plane, parallel polarisation 79−50194
ferroelectric, EM wave diffr. at domain wall *(Russian)* 77−90118
field radiation by mag. dipole on smooth convex surfaces 78−62977
filament moving near metal band *(Ukrainian)* 78−66709
Fraunhofer diffraction, transcendental eqns., numerical soln. method 77−33750
Fresnel integral, approx. 79−64150
gamma-ray diffraction meas. on mosaic struct. of RbI in metastable press. region 77−20065
generalised natural oscillation method 77−31051
generalised shift operator *(Russian)* 78−78868
geometrical theorem and Keller's diffr. coeff. *(French)* 79−41307
geometrical theory, book 77−3524
geometrical theory, modified, for near zone calc. of circular aperture *(French)* 78−5399
geometrical theory, near-zone field of circular aperture calc. *(French)* 78−5398
geometrical theory, recent developments *(Japanese)* 79−72463
geometrical theory of diffraction for EM waves, book 80−73121
grating EM theoretical developments 80−106633
gratings, plane metallic, anal. 79−10245
gravitational diffraction of plane wave by large star 77−5724
gravitational lens effect, EM wave diffr. in Schwarzschild space-time 80−90750
Green's function moment method for solution of two Pocklington type integral equations 78−55279
guiding properties of a smoothly inhomogeneous layer and diffraction excitation of ionospheric waveguides 80−36449
gyrotropic objects, excitation diffraction coeff. calc. *(Russian)* 77−75370
H-polarised EM wave, diffr. by semiconductor strip 80−91730
half-plane diffraction under mixed boundary conditions 79−86116
by half-plane in gyrotropic medium, Wiener-Hopf method 77−2547
half-plane perpendicular to general gyrotropic medium distinguished axis 77−27222
Helmholtz equation, direct quadrature soln., three-dimens. problems 80−74285
Hertzian waves, reflection and diffraction by moving layers *(German)* 80−87266
HF, GTD soln. for radiation from sources on perfectly-conducting convex surface 80−9792
HF diffraction of arbitrary incident field by half plane, asymptotic techniques 78−42264
HF diffraction of line-source field by half-plane, ray technique solns. 77−19133
HF diffraction phenomena, spectral domain interpretation 77−83788
HF radiation from impedance surface on conducting circular cylinder 77−75380
HF scatt. from multiple-edge diffraction at shadow boundaries 77−38781
HF scattering by conic frustum 79−76552
hologram grating, boundary conditions for diffracted EM fields 79−3660
hologram grating, dephasing measure in plane wave diffr. 79−3659
holographic gratings under grazing incidence in X-ray and XUV region, EM theory 80−90962
homogeneous medium, moving areas, EM wave diffr. and scatt. *(Russian)* 79−27141
hybrid diffraction coefficients for first and second order discontinuities of two-dimensional scatterers 78−82892
impedance wedge, refl. coeff. at diffraction of plane wave, anal. *(Russian)* 77−6976
impedance wedge edge, uniform diffr. coeffs., anal. 77−75366
inclined dividing boundary between dielectric materials in rectangular waveguide 79−885
infinite multilayered grating, near-field pattern 79−86256
infinite strip with obliquely incident wave 78−46495
by infinitely long perfectly conducting screens of finite width and thickness *(German)* 80−91724
inhomogeneous media, lattice method using approximate boundary conditions *(Russian)* 78−1159
inhomogeneous media, rigorous method of analysis *(Russian)* 80−53187
inhomogeneous medium, EM wave propagation, phase function method 80−69295
integral equations from nonhomogeneous anisotropic bodies 80−18972
interference and diffraction principles and expts. *(German)* 77−61900
interference theorems of scattering theory in vector problems of low-frequency diffraction 79−86115
inverse diffraction problem of determining inhomogeneity parameters, solvability *(Russian)* 78−82889
inverse diffraction problems, solvability 79−64159

electromagnetic wave diffraction continued
inverse theory of scalar diffr., eigenvalue formulation 80−102613
ionosphere, diffr. from discrete and homogeneously structured irregularities 79−48612
ionosphere, mid-latit., geostationary satellite signals scintillation at 137 MHz 79−25388
ionosphere, spatial dependencies of props. of wavelike inhomogeneities, anal. of diffraction patterns 80−36448
line-source field by conducting half-plane 77−34811
locally deformed flat boundary, numerical soln. 77−42480
longitudinal slits, in circular cylinders in open lattice, long wavelength diffraction effects *(Russian)* 77−42470
magnetic field diffr. meas. on axes of disks and apertures, Babinet principle, complex spirals 80−102599
matrix methods in potential theory and EM scatt. 79−94133
Maxwell eqns., asymptotic soln. near caustic edge *(Russian)* 78−58882
metal grating, at dielec.-semicond. interface, plane EM wave diffr. 79−27139
MF sky wave, combined terrestrial diffraction/ionospheric reflection effects 78−28410
microstrip waveguide, theory of radiated waves using asymptotic wave diffr. theory 79−18339
microwave, 3.2 cm, circular scanning indicator *(Russian)* 77−26328
microwave diffr. by various shaped conducting objects 78−29885
microwave diffraction around Earth, bilinear model of troposphere *(Russian)* 77−64367
microwave transmission characts. *(Norwegian)* 79−29834
microwave wavelength diffr. ellipsometry, polarisation and refl. coeff. 79−55034
microwaves, near-field diffr. on the axes of disks 78−33652
modulated energy flux, wave props. 77−65559
mountain ridge snow cover effect on ultrashort wave diffraction field 77−64395
multilayer structures, algorithm for diffraction in circular cylinder or sphere *(Russian)* 79−68354
non-linear wave diffraction, similitude theory 78−46710
nonlinear Schrodinger equation, exact solution, localised wavefield evolution 80−53191
nonorthogonal series method in EM wave diffr. problems 80−69299
nonorthogonal series method of numerical investigation *(Russian)* 77−58237
numerical anal. of reverse case of diffraction on impedance loaded cylinder *(Russian)* 79−31778
open cylindrical surfaces, numerical soln. 78−58890
paraboloidal reflector backward diffraction suppression by corrugated cylinder 77−75383
pattern approximation by laser simulation 78−55287
perfectly conducting biaxial periodic surface, simplified theory of diffr. 79−41303
periodic grating of cylinders, orthogonalisation method 77−10821
periodic metal surfaces, sinusoidal height profiles, Fourier series analysis 78−1128
periodic structure of conducting semiplanes of finite structure *(Russian)* 77−31049
by periodic waveguide gratings, reson. effects *(Russian)* 79−887
periodically rough water surface, thermal radiation critical phenomena *(Russian)* 78−81188
planar, asymptotic theory of diffraction by ideally conducting solid of revolution 78−86994
planar arrays of perfectly conducting strips, analysis using physical optics approximation 80−53186
planar wave diffr., soln. from knife-edge grid with complex period struct. 79−72467
planar wave diffraction on plate with variable surface impedance 78−9323
plane δ-function pulse, diffraction at a half plane, boundary pulse effects 78−12460
plane angular sector, geometrical theory 79−45896
plane H-polarised EM wave at circ. cylinder with longitudinal slit, analogue of Helmholtz resonator 78−29887
plane stationary diffraction of E-pol. EM waves by curvilinear screens *(Ukrainian)* 80−69294
plane wave, diffr. by flanged parallel-plate waveguide and slit in thick screen 79−45891
plane wave by ferrite sphere with magnetic anisotropy, anal. *(Russian)* 77−75373
plane wave by perfectly conducting circular cylinder with narrow slit 80−28149
plane wave diffr. by half-planes and wedges 77−19163
plane wave diffraction by circular transmission grating: finite-difference approach 79−68352
plane wave diffraction by half-plane in gyrotropic medium 77−27229
plane wave diffraction by periodic surface *(French)* 80−37939
plane wave diffraction by thin dielectric half-plane 79−89833
plane wave spectrum formulations, for near fields of circular and strip apertures 78−9298
plane waves, by staggered parallel plates, spectral diffr. coeff. in Fourier transform domain 78−22071
planetary atmosphere HF radio occultation meas., phase screen concept 80−56735
plasma-dielectric boundary, diffr. of EM surface wave by boundary inhomogeneity 77−24075
plate with an even number of symmetrically placed slits 77−27227
ponderomotive effect, props. for power meas. appl. 78−71014
projection method, properties of parametric system of basic functions 80−87269
projection methods, applicability limit 80−91734
pulsed field, due to electric dipole and perfectly conducting wedge 77−54652
quartz, piezoelec. and gamma-ray diffr. props. 77−20801
radial array of nonintersecting 1/2-planes 80−28147
radiation fields in biaxially anisotropic media 78−66723
radio signals diffr. by isolated ionosphere irregularities 79−35049
radio source radiation in presence of smooth convex bodies, diffr. geometrical theory 79−64151
radiowaves from Cassiopeia A by artificial ionospheric irregularities *(Russian)* 77−29552
ray optical anal. of scattering from dielectric coated conducting cylinder 80−83542
Rayleigh diffraction of plane wave, by sphere with circular aperture 79−64161

electromagnetic wave diffraction continued
Rayleigh hypothesis in theory of diffraction by cylindrical obstacle 79−89832
Rayleigh theory for diffraction at sinusoidal surface *(French)* 80−18964
Rayleigh-Sommerfeld diffraction theory and Lambert's law 80−48125
reciprocity theorem for corrugated surfaces used in conical diffraction mountings 80−1333
reflection grating with perfect blazing at $n=-1$, design dimensions 77−65555
rough surfaces, general theory and small roughness limit 77−75423
scalar diffraction problems, related non-self-conjugate operators 77−19140
scalar diffraction theory, near-field, Fourier transform appls. 80−31455
scalar wave scattering by periodic surfaces, general modal theory 80−87271
scattering pattern calc., diffr. on slit and on strip, asymptotic methods 78−86993
Schwarzschild black hole, plane EM wave diffraction, Poynting vector near horizon 80−22250
semi-infinite complex structures, modified geometrical theory/moment method 77−75379
semi-infinite cone, transient and time harmonic diffr., Green's function representation 78−5392
semi-infinite parallel-plane waveguide in anisotropic plasma 78−1845
by semiplane of plane wave, anal. *(Russian)* 77−27223
shadow boundaries and transition regions, spectral domain formulation 77−75381
SHF two-layer asymmetrical grating, characts. *(Russian)* 77−54649
single strip diffr., Kirchhoff, geometrical theories and Maxwell eqn. exact soln. 77−6975
sinusoidal ring current EM wave, diffr. by cond. cone 79−27140
slots in plane waveguide walls *(Russian)* 78−29884
small apertures, first-order correction for EM field penetration 79−64156
small apertures in conducting screen, EM coupling 77−19134
by small apertures in conducting surfaces 78−82893
small apertures in perfectly conducting wall, polarisability 77−19136
small-aperture diffraction polarisability coefficients rel. to wall thickness 79−68355
solar radiowaves diffraction and refl. from lunar limb during solar eclipses *(Russian)* 78−65586
Sommerfeld's half-plane diffraction problem, simple solution 78−9303
source dimension estimation from diffraction image using Chebyshev approx. *(Russian)* 78−82903
spatially dispersive crystal, reflectivity and transmittivity 80−99604
sphere with circular opening, radiation form, diffr. field *(Russian)* 77−58238
sphere with circular opening, vector problem soln. 78−82891
spherical wide angle mirror under oblique illumination, diffraction in focal region 80−1108
stationary problem in non-homogeneous media 80−68
strips illuminated at grazing incidence, uniform geometrical theory of diffr. soln. 80−58447
surface impedance behaviour in vicinity of gratings, EM theory 77−65557
synchronous nonlinear interaction between waves on Bragg diffr. in media with periodic struct. *(Russian)* 80−14399
thin periodic slab, classical EM wave diffraction, rigorous approach using Green's function 78−82890
thin phase grating diffr. eqn. solns. 78−54198
three-dimensional diffraction problems, theoretical and numerical study *(French)* 78−29883
time-harmonic EM wave two-dimens. diffraction by open circular-cylindrical surface 80−43233
total reflection by small slotted capacitive cylinder 80−5662
transient response of currents and charges induced on wedges and strips 80−18974
transparent dielectric boundary, anomalous diffr. of glancing EM waves *(Russian)* 77−83793
transparent structures, soln. suing integral equations method *(Russian)* 77−68154
two parallel conducting plates, exact soln. 78−25780
two parallel dielectric cylinders, anal. *(Russian)* 78−33650
two-dimensional diffraction by parallel-plane waveguide in anisotropic plasma 78−5880
two-dimensional wave beam diffraction by stripline grid 80−87273
two-element array of bars, re-expansion method, for vigorous soln. *(Russian)* 78−17848
ultrashort-wave diffraction field in shadow of ridge-crests, simulation using dielectric prism 78−86995
unidirectionally cond. strip, electromag. wave diffr., Wiener-Hopf technique 78−58883
uniform geometrical theory of diffraction close to 90° wedge 79−89835
at waveguide corner with mirror *(Russian)* 77−19396
waveguide diffraction application of minimum autonomous block method 79−68362
waveguide fields, diffraction by small disks and apertures located at nodes 79−55036
wedge with multilayer absorbing covering, EM wave diffraction *(Russian)* 77−61899
wide-angle spherical mirror under oblique illum., EM diffr. in focal region 78−58888
wide-angle spherical mirror under oblique illum., EM diffr. integral formal expansion 79−72464
XUV gratings, classical and ionical mountings, EM diffraction 78−63188
KH_2PO_4, ferroelastic cryst., appl. of γ-ray diffractometry 77−8533

electromagnetic wave diffusion *see electromagnetic wave scattering*

electromagnetic wave interference
see also atmospherics; electromagnetic wave interferometers; electromagnetic wave interferometry; electromagnetic wave propagation in plasma; light interference; Moire fringes
Compton scatt. by interfering EM fields from independ. sources 80−43241
diffraction fields of convex bodies of revolution calc. using asymptotic method 79−64158
ELF radio waves nocturnal sporadic-E layer rel. to interference and propag. vars. 78−36392
epitaxial magnetic film thickness meas., interferometric method 79−35675

electromagnetic wave interference continued
ground screening factor evaluation to protect systems from interference *(French)* 78−49071
IR spectra, interference fringe elimination, computer method 79−12872
microwave, 3.2 cm, circular scanning indicator *(Russian)* 77−26328
modulated energy flux, wave props. 77−65559
monochromatic wave energy density in nonabsorbent medium with freq. and space dispersion *(Russian)* 78−74818
multichannel reflector radiotelescope, factors affecting noise interference, anal. *(Russian)* 77−22067
oscillator ensemble with embedded impurity oscillator, absorption spectrum windows 79−6045
radiowave propagation, tropospheric and precipitation scatter, rel. importance in interference and coordination calcs. 78−73423
radiowave propagation along lunar surface, anal. 79−5768
rain attenuation, Earth to satellite radio links statistical study *(Japanese)* 79−5555
satellite communication systems, rain effects on propag. 77−41126
site diversity effect on Earth to satellite radio links, statistical study *(Japanese)* 79−5555
superposition paradox, explanation, teaching approach 80−41999
sweeper activity in the HF and VHF bands, relation to magnetospheric phenomena 77−56689
synchronous nonlinear interaction between waves on Bragg diffr. in media with periodic struct. *(Russian)* 80−14399
vibrointerference *(Russian)* 77−163
whistler-mode waves focusing and interference in spatially varying mag. field 78−65465
whistlers, quasi-periodic struct. caused by time-shifted signals interference 77−53316

electromagnetic wave interferometers
see also electromagnetic wave interferometry; light interferometers
30 GHz Lecher wire interferometer for meas. of ion acoustic test waves in magnetized plasma 78−1903
aerial pairs, directional ionosonde appl. 77−29496
astronomical, Table Mountain 8 mm wavelength interferometer 80−26741
cardiopulmonary noninvasive noncontacting monitor using coherent microwave interferometer 78−40290
correlator interferometer, theory, radiotelescopes appl. 80−12670
digital interferometer, 2 mm wave, for Tokamak discharges in upgraded DIVA 78−75417
dispersion interferometer, with coherent response for multifreq. interrogation of interplanetary plasma 77−22038
Fabry-Perot prefilter for Raman spectroscopy 79−71532
Fabry-Perot spherical mirror interferometer for wind velocity meas. *(Chinese)* 79−77308
far IR, digital processing using microcomputer 77−2689
far IR laser interferometer, for low temp. plasma diagnostic techniques 77−58895
fast IR laser interferometry, electronic density fluctuation meas. 80−49000
incoherent energy and coherent time of depolarised microwaves meas. 78−96277
inhomogeneous Fabry-Perot, dielectric loading and general phase-frame shaping, analysis 80−13197
IR interferometer, 11 μm heterodyne system *(French)* 80−46397
IR interferometer diamond anvil cell interface with beam condenser 80−86384
IR spatial interferometer, space-borne, exposure time 79−35131
Jodrell Bank radio-link interferometer, sources phase stability, ang. struct. and position meas. 77−5452
K-band interferometer for measuring the magneto-microwave Kerr effect in semiconductors and ferrites 80−52263
maser, multiple-beam interferometric, construction and exptl. results *(French)* 79−45919
maser with 8 NH_3 beams, behaviour study using Fabry-Perot resonator *(French)* 78−42315
mica windows for interferometric vessels 77−41675
Michelson interferometer on Canberra aircraft for stratospheric studies at sub-mm. wavelengths 77−87132
Michelson interferometer with time resolved IR Fourier transform spectroscopy, practical aspects 80−86464
microwave, electron density meas. on T-II plasma device 78−55754
microwave, for biomedical appl., physiological movements meas. 79−25137
microwave interferometer, for meas. of small phase shifts with high spatial resolution 77−3994
microwave interferometer, freq. stabilized, laser prod. plasma density decay meas. 77−84524
microwave Michelson interferometer for respiration monitoring 79−8557
microwave Michelson interferometer improvement operating at 140 GHz 80−31854
microwave plasma diagnostic interferometer with fourfold signal passage 78−87487
miniature radio interferometer terminals, for Earth surveying 79−100805
multielement radio interferometer, baseline coordinate vector measurement maximum-likelihood method 80−26753
nonlinear Fabry Perot interferometer, dynamic behaviour 79−54183
off balance interferometric bridge, using heterodyne detection for recording vibratory phenomena 78−70119
optical fibre ring interferometer, Sagnac effect *(Russian)* 80−101835
polarisation interferometer, appl. to ballistic expt. 79−55435
polarising submillimetric Fourier interferometer with achromatic internal modulation 78−65959
radio astronomy, interference-excising correlating interferometer 79−75110
radio interferometer system for microwave band coherent transition radiation study 79−85181
radio interferometer with long baseline, classical response 78−61733
radio interferometers oscillator stability in interplanetary plasma meas. by satellite to Earth signals 77−60571
radio telescope, amateur, interferometer design 78−85849
radioastronomical, multifunctional broad-band recording system *(Russian)* 77−29650
radiotelescope, mm wavelength aperture synthesis interferometer 77−73950
radiotelescope, principles, effect of atmospheric disturbances *(Dutch)* 77−67041

electromagnetic wave interferometers continued
  radiowave correlation interferometers rel. to binaural perception and resolving power of bats *(French)* 78—80883
  SQUID, with RF bias, fluctuation characts. 79—9229
  submillimetre travelling-wave interferometer for crystal electrooptical props. study 78—21209
  submillimetric wire grid array Fabry-Perot interferometers 77—37974
  subMM compensation-type, accuracy independent of meas. channel loss and radiation power fluctuations 80—54037
  Toyokawa λ 8-cm radioheliograph, new local oscillator system phase stability new local oscillator system phase stability 79—101073
  troposphere random inhomogeneities, effect on operation, statistical anal. 77—13111
  two-channel, based on prismatic dividers, model of coupled multi-terminal networks *(Russian)* 80—52302
  two-element radiointerferometer, arc meas. procedure optimisation *(Russian)* 79—101082
  two-frequency dispersion interferometers for space plasma nonuniformity 79—70964
  waveguide interferometer, for precise determ. of very low dielectric losses at 9 and 29 GHz 77—8503
  Wharton and Gardner microwave interferometer for plasma density meas. 80—87948
  X-ray Fabry-Perot-type interferometer 79—86653
  X-ray interferometer, LLL type, interfering beam phase rels. 80—90973
  X-ray interferometer, three beam *(German)* 78—8483
  X-ray interferometer for meas. of K-edge dispersion anomalies in Se 80—90956
  X-ray interferometer with divergent polychromatic beams 79—27867
  X-ray interferometers in quartz crystal *(Russian)* 79—44995
  X-ray three beam interferometer, total refl. using Bragg diffr. 77—47302
  X-ray two block types, effect of deformation due to heating on diffraction focusing *(Russian)* 77—41743
  Ar plasma density meas. by Langmuir probe and microwave interferometer 80—28819

electromagnetic wave interferometry
  see also light interferometry; Moire fringes
  ALSEP-quasar differential very long baseline interferometry, for lunar position meas. 78—45245
  aperture synthesis radioastronomy *(French)* 80—46410
  astronomy, tropospheric limitations of coordinate measurements using phase and fringe freq. 79—44375
  Australian synthesis telescope, design, array config. 78—69690
  ballistic device, hypersonic wake, anomalous dispersion meas. 79—82014
  3C 119, 286, 345, 454.3, quasars, 5 milliarcsecond resolution maps at 1.67 GHz 80—82531
  3C 147, 3C 286, quasars, VLBI obs. at 329 MHz 80—67898
  3C 147, 3C 380, quasars, milli-arcsecond struct. determined by hybrid mapping with five-station array 80—46694
  3C 147, quasar, radio struct. determ. by multi-element very long baseline interferometry 78—4391
  3C 345, quasar, VLBI obs. at 1.67 GHz 80—94885
  coal, bituminous, elec. props. meas. as function of freq., polarisation, EM wave direction and temp. 79—12113
  compound conductors, impulse heating, Cu vapour conc. determ. 80—75346
  Crimea-Haystack VLBI instrument operation *(Russian)* 78—69693
  CTA 102, quasar, 5 milliarcsecond resolution maps at 1.67 GHz 80—82531
  CW phase comparison technique for determ. of remote layer thickness 79—35662
  dosimetry, interferometry and holographic interferometry appls. 80—42871
  Earth surveying 79—100805
  education, homodyne microwave Doppler velocimetry, accel. meas. 77—78920
  Fabry-Perot interferometer transients, for ultrashort laser pulse generation 78—58019
  far IR interference filters 77—22592
  far IR two-dimensional plasma interferometry with evaporographic and pyroelec. recording 77—39468
  far IR waveguides for interferometers measuring electron density in Tokamak plasma 79—73034
  Fourier transform methods, imperfect blackbody sources effects 77—38032
  fringe fractions, meas. by means of time intervals method 79—17478
  fusion reactors, interferometric phase detection system, using high speed digital techniques 78—62629
  gas mixture production method, composition control 78—1765
  gravitational wave interferometer, quantum mechanical radiation press. fluctuations 80—90770
  heterodyne interferometers, quasilinear filtration theory appl. to signal processing *(Russian)* 80—82807
  impedance matched grazing incidence films, appls. 79—93267
  impulse spark study using two-wavelength interferometry 80—86391
  interferometry techniques for high β-plasma density meas., holographic and coupled cavity laser methods 80—49006
  interstellar dark clouds, radio continuum interferometric search for newly formed H II regions 80—98699
  interstellar dark clouds, radio continuum interferometry rel. to newly formed H II regions physical props. 80—105301
  ionospheric irregularities effects on HF and VHF radio waves, ray tracing study 77—91362
  IR scanning heterodyne interferometry for pulsed fusion reactors 77—84525
  K-band microwave interferometry for measurements of high surface vels. 80—77761
  laser interferometer, optoelectronic modulation for electron density variation meas. in IR 80—4762
  liquid dielectric, pulsed breakdown, interferomatic obs. 80—80696
  M82, M104, VLBI obs. of galactic nuclei at 18 centimetres 80—22078
  microwave ferrite structures, interference effects 77—160
  microwave for biological movements *(French)* 78—53469
  microwave spectroscopy, modern aspects, book contrib. 80—52330
  Mossbauer data calibration using laser interferometer 77—88326
  NGC 1052, 4278, VLBI obs. of galactic nuclei at 18 centimetres 80—22078
  NGC 1275, Seyfert galaxy, radio interferometer study of nucleus struct. *(Russian)* 80—62288
  NGC 6251, radio galaxy, radio jets misalignment, VLBI obs. 80—27001

electromagnetic wave interferometry continued
  optical measurements on plasma initiated by a relativistic electron beam *(Japanese)* 80—48914
  Orion methanol masers, interferometric and multitransitional study 80—67891
  Pioneer Venus Differential Long Baseline Interferometry expt. 80—67578
  radar, linear phase detect. *(Italian)* 78—85855
  radio astrometry, influence of troposphere on radio-interferometric meas. of coordinates 80—67581
  radio astrometry using interferometers *(Danish)* 77—22087
  radio astronomical interferometric meas., atm. turbulence effects *(French)* 80—46402
  radio astronomy, arc meas. procedure optimisation using radiointerferometer *(Russian)* 79—101082
  radio interferometer techniques, appl. to oceanographic meas. 79—53559
  radio interferometry and aperture synthesis, review 77—9671
  radio interferometry obs. of Haystack-Westford base line vector, comparison with geodetic obs. 80—89929
  radio phase path corrections for very long baseline interferometry, atmospheric modelling techniques 77—78637
  radio sources, compact, in bright galaxies, very long baseline interferometry 79—48943
  radio sources, compact, mapping from VLBI data 78—89266
  radio sources astrometry, precise positions meas. on 35 km baseline 78—16551
  radio sources in clusters of galaxies, interferometric obs. 77—53693
  radio sources in Zwicky galaxy clusters, detailed interferometer obs. and anal. 80—22099
  radioastrometric technique, for meas. of parallaxes of objects at cosmological distances 78—53796
  radioastrometry, tropospheric limitations on meas. accuracy *(Russian)* 77—22092
  radioastrometry, Z *(French)* 80—46411
  radioastrometry for rotating sources, VLBI response freq. technique *(Russian)* 77—22093
  radioastrometry using differential VLBI, accuracy estimation *(Russian)* 77—22091
  radioastronomial, multi-freq., effect of noise on coordinate accuracy *(Russian)* 77—78644
  radioastronomical equipment, techniques and observations, review *(German)* 77—56827
  radioastronomical interferometric obs., data storage requirements 77—78651
  radioastronomy, aperture synthesis meas. processing, tangent-plane aberration, new transform 79—8847
  radioastronomy, aperture synthesis using long baseline 80—46414
  radioastronomy, atmospheric delay fluctuations with scale sizes >1 km 79—8675
  radioastronomy, interferometry theory and appl. 80—12676
  radioastronomy, phaseless aperture synthesis technique 78—32353
  radioastronomy, real-time very-long-baseline interferometry, using communications satellite 78—24469
  radioastronomy, Very Large Array, Plains of San Augustin, New Mexico, construction progress 77—17373
  radiointerferometric frequency and coordinate meas. accuracy, tropospheric fluctuation constraints 79—8848
  radiointerferometric phase meas. ambiguity detection, recurrence relationship *(Russian)* 79—25513
  radiointerferometry, Mandel'shtam's research 80—105488
  radiosource mapping with uncalibrated visibility data 80—77295
  radiotelescope aperture synthesis, electronic technique for two dimensional Fourier transformation *(Dutch)* 77—67042
  radiowave, frequency-scanning interferometry for fast-proceeding solar phenomena investigation *(Russian)* 77—22094
  radiowave, J^2 supersynthesis of circular aperture 78—40835
  radiowave propag. through turbulent atmosphere, phase difference and derivative fluctuations 78—92951
  radiowave source mapping by fixed base interferometry *(Russian)* 80—17499
  resolution improvements for a phase switching interferometer *(Italian)* 79—58271
  Satellite Emission Radio Interferometric Earth surveying (SERIES), GPS geodetic system 79—100804
  Saturn and its rings, interferometric obs. at 3.71 cm wavelength 79—96962
  schlieren method, axisymmetric, quantitative appls. 77—41677
  signal processing by acoustooptic correlation devices, radio astronomy applications 80—8543
  sonic venturi nozzle, for volume or mass flow, differential interferometric meas. 79—68872
  speckle, partially-coherent source imaging appl. 80—9032
  spinor, phase factor obs. by NMR spectroscopy 79—4731
  SS 433, change in radio struct., 1980 January to June, from VLBI obs. 80—109557
  SS 433, VLBI detect. and ang. struct. 80—31304
  stellar speckle interferometry in near IR 79—53734
  Sun, quiet, interferometric obs at 8 millimetre wavelength 79—40149
  superheterodyne tracking cct. for mm-wave measurements 80—59288
  thin films thickness meas. using X-ray interferometer based on small-angle scattering apparatus 80—27271
  three dimensional spatial autocorrelation function meas. rel. to sky brightness 80—67576
  Tidbinbilla two-element interferometer system design 78—69692
  tracking correlation receiver with feedback for radioastronomical interferometry 78—57445
  transatlantic long base line interferometry at 10680 MHz 79—48390
  Venus microrelief irregularites mean height, determination from radio transillumination data 80—72807
  Venus wind velocities, vector determ. by radio interferometry 79—48722
  very long base line, data recording and processing system *(Russian)* 77—5449
  Very Long Baseline Interferometry (VLBI), foundations and geodetic appl. *(German)* 78—45036
  very long baseline interferometry appl. to geodesy and geodynamics 77—56767
  very-long-baseline interferometry for synchronization of H-maser clocks 79—88920
  VHF interferometry for lightning source direction determ. 79—79939
  VLBI, appl. to astrometry *(Japanese)* 80—21930
  VLBI, appl. to determ. of 3C 345 and NRAO 512 relative position to submilliarcsecond accuracy 80—22097

electromagnetic wave interferometry continued
  VLBI, appl. to relative proper motion of radioemitting QSO pair 1038+528 A,D 80—51902
  VLBI, appls. to geodetic meausrement and crustal deformation monitoring *(Japanese)* 80—21929
  VLBI, clock synchronisation, influence of relativity theory *(Russian)* 77—5664
  VLBI, correction for effects of troposphere, ionosphere and Earth crustal tide *(Japanese)* 80—21926
  VLBI, first expt. in Japan during 1977 80—4268
  VLBI, general considerations of international systems *(Japanese)* 80—17501
  VLBI, improvement of freq. stability of local oscillators *(Japanese)* 80—17504
  VLBI, Japanese domestic system, general aspects *(Japanese)* 80—17502
  VLBI, Japanese domestic system, receiver and local oscillator *(Japanese)* 80—21923
  VLBI, Japanese domestic system, recording signal generator *(Japanese)* 80—21924
  VLBI, Japanese domestic system, selection of radio sources and experimental procedure *(Japanese)* 80—21922
  VLBI, mapping of planetary radio sources *(Japanese)* 80—21927
  VLBI, orbit determination of geosynchronous satellites using computer program *(Japanese)* 80—21925
  VLBI, principles of measurement *(Japanese)* 80—21921
  VLBI, resolution of celestial radio sources *(Japanese)* 80—26754
  VLBI, results of observations of radio source QSO 3C273 *(Japanese)* 80—17503
  VLBI, time synchronization *(Japanese)* 80—26755
  VLBI appl. to geodesy, Earth rot. and network geometry optimisation 78—92996
  VLBI between geostationary satellites for hectometric observations of radio stars *(Japanese)* 80—21928
  VLBI expt. with mobile equipment, 5 GHz operation 80—31217
  VLBI measurements, implications for N.American intra-plate crustal deformation 80—51379
  VLBI observations, of compact components in extended radio sources 80—17680
  VLBI techniques *(Italian)* 78—12095
  VLBI using geostationary satellite link 79—29968
  water, cooled, radiation stratified, temperature structure *(German)* 79—41687
  X-ray, impedance matched grazing incidence films, pure nuclear reflections, reson. filtering of synchrotron radiation 80—37141
  X-ray, principles, techniques and appls., book contrib. 78—42862
  X-ray, section topography as single-cryst. interferometry 78—47208
  X-ray interferometer, temp. gradient influence on fringe pattern 80—1896
  X-ray interferometry in multiwave case *(Russian)* 77—1041
  X-ray interferometry preliminary results for crystallography, Si lattice constant 79—7522
  X-ray interferometry with divergent polychromatic beams 79—27867
  Ag, thin film, thickness meas., Hall effect and interferometric methods 77—5802
  $BaTiO_3$, ferroelectric mechanisms, anharmonic couplings by scanning IR interferometry 80—75978
  H, n=2 state, lamb shift determ., atomic interferometer method 80—23324
  $MoCl_5$, dissoc, in pulsed discharge, interference method obs. 77—58186
  N_2, translational energy transfer rate, after pulsed discharge, interferometric obs. *(Russian)* 78—26322

electromagnetic wave propagation
  see also atmospheric electromagnetic wave propagation; atmospheric light propagation; backscatter; electromagnetic wave absorption; electromagnetic wave diffraction; electromagnetic wave interference; electromagnetic wave propagation in plasma; electromagnetic wave reflection; electromagnetic wave refraction; electromagnetic wave scattering; guided electromagnetic wave propagation; light propagation; light transmission; radiowave propagation
  3 GHz surface and lateral EM wave meas. 80—103742
  absorbing medium, with multiple discontinuities, inverse problem 79—31780
  absorbing medium having dispersion relations with repeated solns., quasioptical approx. 77—75377
  absorption in medium with smooth space-time fluctuations, statistical characts. 79—81339
  accelerated dielectric medium, relativistic study 78—81862
  active medium, contour integral 77—54658
  air-dielectric interface, EM wave reflection and transmission in terms of polarisation, education 80—105458
  analysis, wave-kinetic method, phase-space path integrals 78—62088
  analytical and numerical methods, book 79—72469
  anisotropic layered media, 4×4 matrix algebra 80—106445
  anisotropic medium and its appl. to transform. from anisotropic to isotropic problems 80—9776
  antenna theory, doubly orthogonal function construction 80—32888
  antennas and propagation, symposium, Amherst (1976) 77—14633
  antennas and propagation, symposium, Stanford (1977) 77—75378
  antiferromagnet, magnon-photon interaction for EM wave vector perpendicular to sublattice magnetisation 79—69662
  averaged Maxwell equations in severe random nonuniformities 80—69298
  azimuthally gyrotropic medium, EM wave spectrum, theory 80—91735
  birefringence in moving anisotropic media 79—80432
  birefringence medium, geometrical optics approx. *(Russian)* 77—68167
  birefringent layered media 79—76582
  blackbody radiation from incipient black hole 77—9767
  book *(French)* 78—13640
  book 79—50198
  boost required for zero flux, gravit. and EM compared 78—29027
  boundary waves on perfect conductors, Maxwell eqn. solns. 79—44757
  Bragg interactions, in active medium, Floquet theory, index modulation effects 77—58231
  cascaded rectangular regions in thick conducting screen 80—32885
  charged black hole interaction with EM waves, decoupled eqns. for Debye potentials 77—22261
  chiral media, macroscopic objects embedded in dielectric 79—31775
  circumsolar plasma, Venera 10 radio signal spectral meas. 80—109326
  coal, microwave propag. expts. rel. to anisotropic elec. props. 80—98312
  coherent propagation through sparse particle conc. 80—91729
  composite media, air and three-layered earth 78—22076

electromagnetic wave propagation continued
  composite media, EM wave propagation, self-consistent theory 78—56442
  compression by anisotropic crystal giving zero reflection coefficient *(Russian)* 79—883
  conducting medium in const. mag. field, two EM waves secondary field generation 79—36828
  conference on electromagnetic wave scattering in radiocommunication, Cambridge, MA, USA (Oct. 1977) 79—29836
  continuous heterogeneous media, anal. *(Polish)* 78—37788
  corrugated cylindrical waveguide, propagation characts. *(Italian)* 79—17235
  cubic crystals, paramagnetic nonlinear Faraday effect, EM wave propagation *(Russian)* 80—80761
  depth sounding interpretation, master tables, book 80—86043
  dielectric inhomogeneous medium, perturbation theory approach 78—17847
  dielectric interface, EM wave tunnelling 79—41306
  dielectric layers, computational formulas verification 78—1130
  dielectric slab, reflection and transmission coefficients with sinusoidal permittivity variation 78—71011
  dielectric surface, evanescent wave quantisation, field momentum 80—43231
  dielectric-ferrite interface, physics of microwave reflection, Renard analysis of lateral shift 79—76557
  diffusion approximation for mutual coherence function, anal. *(Russian)* 77—10814
  discontinuous or layer media, unidimensional propag. of transient signals 80—87265
  discrete random medium, statistical approach, computer simulation 77—75391
  dispersion and attenuation of linear pulse propag. 77—574
  dispersion equations near combined resonance 79—99772
  dispersive effects 79—58486
  dispersive media, energy-momentum tensors by EM waves 78—17842
  dispersive medium, calc. *(Italian)* 79—27133
  dispersive medium, energy density of arbitrary EM field and dissipation 77—27226
  dispersive medium, energy density of arbitrary EM field and dissipation 78—9304
  dispersive metals, propagation of plasmons and EM waves 80—15549
  dispersive phenomena on propag. of radiation in media with slowtime-varying refr. indexes *(Russian)* 80—28152
  doped conducting media, low-freq. props., EM wave reflection 80—103715
  Doppler freq. shift of wave in time-varying inhomogeneous anisotropic medium 79—40016
  Doppler frequency shift by fast moving boundary *(Japanese)* 80—18967
  double ray refraction, in moving anisotropic media *(Russian)* 79—18329
  Earth, comprehensive study of subsurface propag. from horizontal elec. dipoles 80—98229
  Earth, EM waves and antennas above and below surface 79—66620
  Earth, wave type and propag. direction from EM field short-period vars. anal. *(Russian)* 78—85474
  Earth interior, ferroelectric phase transitions rel. to EM wave attenuation 77—53045
  Earth lithosphere, lateral-wave propag. of EM waves 79—92482
  Earth surface layer, EM wave refl. and transmission coeffs., linear ramp model 80—61759
  education, Brewster angle in semi-infinite dielectric moving perpendicularly to interface 80—57034
  Einsteinian vel. addition and phase vel. 78—16665
  electron resonant motion in polarised EM plane wave, spontaneous phase focusing 79—68357
  elliptic beam in cylindrical conducting pipe of circular cross section, space charge potential and field *(French)* 78—42261
  EM radiation in media with spatial dispersion, spatial coherence formation and polarisation increase 80—106442
  EM response of conductive inhomogeneity in layered Earth 77—40976
  energy flux, in isotropic medium in mag. field 77—83791
  energy flux for trains of inhomogeneous plane waves 80—46817
  energy flux limitation of TE mode in medium with ionization nonlinearity 79—81338
  energy-absorbent media, wave theory generalisation *(Russian)* 78—77725
  energy-momentum tensor, heuristic formulation *(German)* 77—60946
  evanescent EM wave behaviour under Lorentz transformation 79—22880
  expanding universe, high freq. EM field propag., with Dirac coupling 79—58913
  exponential amplification in gravitational field of ultrarelativistic rotating body 78—93594
  Faraday effect, EM wave propagation in isotropic medium with nonstationary mag. gyrotropy *(Russian)* 77—28555
  in ferrite, transversly magnetised, anal. *(Russian)* 78—37791
  ferrite sheet, magnetised, excitation of surface EM waves 78—10747
  ferrite-semiconductor structure, EM wave excitation and amplification 80—6891
  ferroelectric. surface EM wave propag. along domain boundaries 77—40195
  ferromagnet, EM wave propagation, nonlinear waves and discontinuities 79—81330
  ferromagnetic material, nonlinear waves and strong discontinuities *(Russian)* 78—74819
  ferromagnetic medium, magnetised, unattenuated refracted wave propag., optical modulation appl. *(Russian)* 78—25774
  ferromagnetic medium, penetration depth calc. *(Bulgarian)* 78—50679
  ferromagnetic-semiconductor-dielectric multilayer struct., convective surface wave instability 77—24732
  ferromagnets with conduction electron spin, EM wave propagation with discrete spectrum 80—92923
  field estimation using geometric optics of slit generated waves 78—46494
  field penetration into thick, finitely conducting shell, anal. 78—62990
  field penetration through small apertures, first order correction 79—64156
  fluctuating medium, mean energy flux calc., by perturbation method *(Russian)* 77—88622
  focusing media with random-axis misalignments, second and higher order moments 79—17236
  focusing of waves in anisotropic plane-layered medium, analytical solns. of Maxwell's eqns. 80—32890
  Fourier transform appl. 77—58235

electromagnetic wave propagation continued
- free electron Compton scatt. of spectrally narrow radiation flux 80—20731
- fuzzy ball, motion in free space 77—74622
- Gaussian beam at normal incidence on dielectric sandwich slab 79—7062
- gaussian beams in transversely magnetized ferrite media 80—37943
- generalized WKB method, sufficient conditions for rapid convergence of iterations 80—53195
- good conducting media, matched electromagnetic pulse transmission 79—36823
- gravitational focusing effect, short-wave limit imposed by lens star gravity field asphericity 79—58604
- Green's function methods 77—19139
- Green tensor expansions for harmonic vector wave eqn. in spheroidal coord. systems 78—41171
- ground wave propagation, normal mode approach 80—9780
- group velocity analysis *(Hungarian)* 78—5400
- gyromagnetic media, energy-flow eqns. for bandlimited signals *(German)* 80—91725
- gyrotropic crystals, behavior of Poynting vector of EM waves in optically active crysts. 79—56758
- gyrotropic media, EM waves polarisation *(Russian)* 79—81333
- gyrotropic medium, Green's function and field of moving charges 80—58445
- half-space random medium, nonlinear approx. for mean Green's dyadic 79—81331
- harmonic plane EM wave propag. in dielec. with one-dimens. random nonuniformities, multiple scatt. 80—43232
- Helmholtz eqn. within wedge, Green's functions 79—9130
- heterogeneous media, long-wavelength EM propag. 80—63892
- HF propavation along concave surfaces, multiple reflections analysis 80—5664
- holographic gratings, sharp boundaries, modal theory, EM wave propag. 80—83672
- holographic unslanted transmission and reflection gratings, modal theory, EM wave propag. 80—83673
- homogeneous electrically anisotropic medium, dispersion equations *(Czech)* 80—37938
- homogeneous layer, transmission and refl. coeffs., integral eqn. *(German)* 78—82907
- horizontal electric dipole antenna, quasi-static range propag. within conducting slab 79—48515
- hydrodynamically responsive medium, model pulse propag., closed form soln. 79—17237
- infinite elastic dielectric with Griffith crack, EM wave propag., Voigt-Toupin model 80—1469
- information encoding and propagation in scattered fields by complex zeros 79—50238
- inhomogeneous anisotropic medium, linear wave transformation, geometrical optics approx. *(Russian)* 77—3518
- inhomogeneous dielectric, EM wave scatt. and propag., Born approx. 79—41308
- inhomogeneous lossless dielectric slab, permittivity profile reconstruct. from reflection coeff. spectral anal. 79—36819
- inhomogeneous media, computation method of inhomogeneous basic modes *(Hungarian)* 77—75367
- inhomogeneous media, horizontally polarized wave transmission and trapped waveguide modes 78—9297
- inhomogeneous media, polarisation rotation analysis by modified ray tracing 79—89831
- in inhomogeneous media, strong and weak inhomogeneities 79—31774
- inhomogeneous media, weak and strong inhomogeneities *(Hungarian)* 77—54648
- inhomogeneous medium, EM wave propagation, phase function method 80—69295
- inhomogeneous medium, random, frequency correlation *(Russian)* 77—88623
- inhomogeneous medium with large-scale random inhomogeneities statistical characts. *(Russian)* 79—882
- inhomogeneous multi-mode medium, first-order coupled equations 77—23600
- inhomogeneous parabolic layer, ray and caustic pattern peculiarities *(Russian)* 78—22066
- inhomogeneous plasma, polarised radiation transfer 80—99607
- inhomogeneous three-dimens. anisotropic media, anal. using geometric optics method 80—43235
- interface plane wave reflection and refraction, positron polarisation effects *(Russian)* 80—79431
- IR surface wave propag. distances on Ni, Pd, Pt and W metal surfaces 77—28641
- irradiance distribution function in turbulent media, theoretical review 79—64155
- isotropy in space, possible expt. 77—13228
- Jupiter decametric radio emission, extraordinary mode, nonlinear phase bunching effects 77—2366
- lake ice, microwave propag. rel. to radar and radiometry remote sensing meas. 80—85691
- laminated composites, bonding material influence 80—91726
- laminated media with helical structure *(Russian)* 77—42469
- laser, nonlinear stratified system, plane wave propagation 80—43343
- layer decomposition method for radiation propag. anal. *(French)* 80—95772
- linear wave growth in periodic structures, instabilities, amplification and stop bands 80—87276
- local energy density distributions, Wigner distribution functions appl. 80—9781
- log-amplitude and phase time fluctuations, turbulence spectrum parameters influence *(Czech)* 80—9774
- longitudinally magnetised gyrotropic ferrites *(Russian)* 80—23607
- magnetoelectric medium, standing wave pattern form. when magnetoelec. constant is nondiagonal tensor 79—27135
- massless scalar field in a de Sitter universe and its thermal flux 79—127
- Maxwell's equations as one quaternion eqn., appl. to wave propag., for teaching 78—54133
- Maxwell equations, exact soln., with Gaussian beam as limiting case *(German)* 77—71907
- mean field attenuation, dispersion medium characts. relation *(Russian)* 77—75369
- metal, EM waves near cyclotron reson. in inclined mag. field *(Russian)* 80—29625
- metal, granular, EM wave propag., self-consistent approach 78—51920

electromagnetic wave propagation continued
- metal, superconducting and normal, attenuation, EM generation and detection of US shear waves 78—39261
- metal-metal interface, plasmon polaritons, computer simulation 78—84276
- metallic conductor, hollow, image field produced by uniform or nonuniform beam 77—14638
- metallic rod, uniformly corrugated, E_{01} mode-excited, equiv. dielec. const., simulation 78—78864
- microscopically inhomogeneous material, theory of optical and microwave props. 77—77161
- microwave beam, X-band, transmission through dielec. thin slab, displacement 80—1107
- microwave radiation, kinetic theory of interaction with diatomic gas, $j=0$, $j=1$ transitions 78—9750
- microwave radiation, kinetic theory of interaction with polyatomic gas 78—9749
- microwave scatter and sea state estimation, ocean wave models 78—77244
- minimum autonomous blocks method for propagation of radiation in nonlinear medium 80—87274
- moment method solution, cell size limitations 78—5404
- monochromatic radiation in gas media, near resonance nonlinear propagation 79—76748
- Monte-Carlo simulation of photon transport in a heterogeneous phantom 80—26257
- in moving dielectrics, contradiction with Einsteinian addition of velocities, geometric resolution 78—24673
- moving media, monochromatic radiation absorpt., effects calcs. 77—76101
- moving media, plane waves and refl. from moving interfaces 80—63890
- multi-terminal networks, coupled, two-channel interferometer modelling *(Russian)* 80—52302
- multifrequency *n*th order coherence function, path integral approach 79—89836
- multilayer interference absorber, wave propag. anal. using impedance characts. method 80—18966
- multilayered structure, noise calculations by flow graph anal. 78—22069
- multiple forward scattering method, randomly inhomogeneous media 80—18969
- multiple freq. mutual coherence functions for beams in random media 78—66720
- nematic liq. crystal, EM wave nonlinear interaction 80—19698
- nematic liquid cryst., orientational fluctuations effect on evanescent modes of transmitted EM wave 80—64889
- nematic liquid crystal, traversing weak EM wave in static mag. field, electrodynamics 79—14680
- non-Minkowskian spacetime, polarisation plane rot. 79—35115
- nonhomogeneous media, Fuchsian differential equation aspects 78—9302
- nonlinear anisotropic dielectrics, nondispersive waves, EM disturbance propag. and reflection 80—106429
- nonlinear dielectric media, linearly polarised plane EM pulse propagation 77—75365
- nonlinear dissipative media, circularly polarised EM waves 80—63891
- nonlinear EM wave propagation, in strong mag. fields, second harmonic generation 80—77988
- nonlinear material, periodic propag., uniqueness theorems on new boundary-value problem *(French)* 77—38777
- nonlinear media, integral eqns. 77—58375
- nonlinear moving media, ray tracing 77—14644
- nonlinear wave in turbulent medium, with random inhomogeneities *(Russian)* 79—27134
- nonlinear waves in dielectric and electronic media, computation using random argument functions 77—19141
- nonlinear waves in periodic structures 77—10819
- nonuniform dielectric regions, remote probing wave impedances 77—13781
- nonuniqueness of 'real ray' eqns. when ray direction is complex 78—25776
- null point source intensity in stationary spherically symmetric space-time 78—57839
- one-dimensional medium, propagation in periodic structs., theory 79—45892
- one-dimensional medium with space-time inhomogeneities, spectral-correlation characts. evolution *(Russian)* 79—2634
- one-dimensional propagation, calc. of refl. and transmission coeffs. 77—23599
- paraxial beams, in vacuum, theory 79—55035
- peculiar heterogeneous wave propag., partial derivatives eqn. soln. *(French)* 77—6977
- penetration through aperture into cylindrical cavity with central dielectric rod 80—5661
- perfect crystals, propag. of EM signals generated by localised EM current distribs. 79—36817
- periodic medium, fourth-order Bragg interaction 78—58889
- periodic stratified medium, birefr., phase matching, X-ray lasers 77—65566
- periodic stratified medium, general theory 77—65565
- phase velocity, in three-dimensional infinite array of dipoles 77—54659
- piezoelectric crystal, acoustic activity and other effects due to spatial dispersion 78—2808
- piezoelectric hexagonal crystal, acousto-EM modes *(Spanish)* 77—4602
- piezoelectric rods, hexagonal crystal symmetry, wave propagation 78—56429
- plane, waves obliquely incident on moving media, radiation press. 78—71007
- plane monochromatic waves, propagation through polarised interface *(French)* 79—7057
- plane wave at skew incidence on right-angled impedance wedge 78—90346
- plane wave pulses, random media propagation 78—9324
- plane waves, relativistic invariance of complex phase 77—37764
- plane waves through lamella 80—43240
- planetary atmospheres, turbulent, effects of inhomogeneous background on radiation propag. 78—69679
- planetary nebulae, EUV radiation transmission rel. to central stars temps. determ. 80—67724
- point source in one-dimensional, randomly inhomogeneous medium, with specularly reflecting walls 80—105514
- polarisation, description by irreducible tensorial sets 77—68152

electromagnetic wave propagation continued
polarisation rotation analysis, modified ray tracing technique appl. 80−48119
polarisation state of waves, theory 80−56525
polarisation under frame dragging, dispersive rot., Mach's principle 77−26217
polarization effects in cosmological models with anisotropic curvature 80−94903
Poynting vector and energy flux in moving dispersive dielectric 77−42474
Poynting vector behaviour in lossy media near a half space 77−6979
probability distrib. at large depth in extended random medium 78−28959
problems connected with special source structs., review 80−87272
projection methods, applicability limit 80−91734
pulsar magnetosphere, quasi-transverse propag. theory rel. to individual pulse-polarisation patterns 80−46591
pulsar radio emission, propagation effects on polarisation 79−75235
pulsars scintillation, mathematical anal. of physically thin screen 78−28501
pulse dispersion in conducting medium *(Russian)* 77−38780
pulse propag. in random media 78−66715
pulse propagation, narrow-band high-freq. in homogeneous medium, review 77−6982
pulse propagation and two-frequency mutual coherence function in random medium 77−10818
pulsed radiation from line source in two-media configuration refl. and transm-tted waves 79−64153
quantification of EM field, half-space bounded by perfect mirror *(French)* 77−78994
quantum mechanics for propagator derivation 78−73886
quantum system induced radiation in time-periodic EM field 77−38109
quasi-optical parabolic aprox., in randomly inhomogeneous media, validity analysis 80−106422
quasi-static potential fluctuations, kinetic eqn. for quantum wave packet *(Russian)* 77−75371
quasimonochromatic radiation propag. in static gravit. field *(Russian)* 77−70992
quasimonochromatic radiation propag. in stationary gravit. field *(Russian)* 77−70993
radar vertical probing of glaciers, signal depolarisation 77−9557
radiating system, EM wave transformation directionality diagrams 80−87275
radiation fields in biaxially anisotropic media 78−66723
radiation from charge moving in randomly inhomogeneous media, fluctuation effects *(Russian)* 78−71017
radio waves in ionospheres of Jupiter and Saturn, spectral broadening meas. by Pioneers 10 and (11) 80−109391
radiowaves, troposcatter aperture-medium coupling loss 79−29840
random freq. modulation wave propagation in dispersive medium, statistical props. 80−32889
random inhomogeneous Poisson type medium, EM propag. *(Russian)* 77−68153
random layered media, thermal radio emission, appl. to Antarctic glaciers *(Russian)* 77−33106
random media, coupled EM and elastic waves 79−28579
in random media, degeneracy and inhomogeneity in transport theory 78−62982
random media, operator and diagram techniques for intensity moment eqns., appl. to strong scatt. 79−64154
random media, theory and appl. of wave propag. and scatt., review 77−75376
random media causing pulse spreading and wandering 80−37942
random medium with finite inhomogeneity correl. range, EM wave fluctuations *(Russian)* 78−78870
random slab problem of wave propag. through random medium 79−36827
random stratified media, statistical theory *(Russian)* 78−1157
randomly distributed dielectric scatterers, dispersion relations, coherent wave phase velocity and attenuation 79−72466
randomly inhomogeneous media, strong intensity fluctuations of EM waves *(Russian)* 77−79758
randomly inhomogeneous medium, plane wave propag., spatial correlation of wave field *(Russian)* 77−61898
ray equations for absorbing media, uniqueness of solns. 77−3521
ray surface equation and Fermat's principle, in moving anisotropic media 80−106425
real ray tracing when ray direction is complex 79−9126
reciprocity theorem for propag. in circ. cylinder, Green's function *(French)* 78−42260
of regular refraction inhomogeneities, fluctuation characts. anal. *(Russian)* 77−578
Reissner-Nordstrom black hole, reflection and absorpt. of EM and gravit. waves 79−44820
relativistic electron-positron gas, polarisation in strong mag. field, EM wave propag. 80−4896
relativistic magneto thermo viscoelastic medium, effect of mag. and thermal fields on plane wave propag. 79−2637
remote sensing of continuous inhomogeneous media, extended Rytov approximation 77−19145
resonant e.m. pulse freq. modulation 77−734
sand, moisture content, microwave optics determ. 77−37684
scalar Hertz potentials for gyrotropic media 80−23598
scattering stratified medium, varying refraction index *(French)* 79−81334
sea water, review 77−49082
semiconductor, temperature waves in nonequilib. conditions 77−43397
semiconductor plasma, unstable EM wave propagation, hot carriers, Hall effect, calc. 80−39620
semiconductor with superlattice, EM wave propag., mag. field effect 80−70745
semiconductor with superlattice, EM wave propagation, solitons *(Russian)* 78−79999
semiconductors, EM wave interaction in weakly nonlinear medium with superlattice 80−93257
slab geometry problem, approximate solns. based on Bremmer series concepts 79−64152
slow EM wave theory in conducting jets 80−91731
slow leaky waves, props. 78−78863
small convex aperture, symmetrization appl. 78−17843

electromagnetic wave propagation continued
solar metre-wave emission, wave ducting rel. to fundamental/harmonic source coincidence 80−21978
solar system, relativistic effects verification, comparison of obs. results with theoretical data *(Russian)* 79−80209
solar wind turbulent plasma, radio wave propag. meas. using three satellites 80−101518
solid, phase and group vels. determ. for dispersive waves 78−81848
source bandwidth and receiver response time effect on scintillation index in random media 77−42473
space-time anal. of propag. through turbulent medium 77−42472
space-time periodic medium, asymptotic theory of mode coupling, stable interactions 77−75375
space-time periodic medium, asymptotic theory of mode coupling, unstable interactions 78−22070
spectral domain approach to soln. of scatt. and radiation problems, review 80−5663
stochastic parametric resonance 80−18970
stochastic waves. temporal moments, mutual coherence function 78−20979
stochastically stratified medium, transmission coeff. 80−32887
stratified composite medium, surface EM waves, wave phase velocity *(Russian)* 79−45889
stratified medium optical props. determ., via matrix method *(French)* 78−30070
submillimetric wave propagation meas. techniques 77−38007
subsurface radar using video pulse for deep probing in Earth, pulse propag. in lossy media using LF window 80−74282
superconductor, surface EM waves 78−88072
superluminal flow, EM wave refl. 79−27138
surface wave, normal mode propag. at drift vel. tangential discontinuity 77−24076
surface wave propag. on rectangular bonded wire mesh over lossy ground 79−7060
surface wave propagation through gap between oppositely magnetised ferrite substrates 78−50680
surface waves at relativistic electron beam-vac. interface 77−79734
SW radio noise level variation obs., as function of ionospheric perturbations *(Russian)* 77−91359
tensorial permeability and conductivity medium, EM wave propag., ferromag. resonance, spin waves *(French)* 78−74820
thick weakly anisotropic layer with random irregularities, EM wave polarisation 77−10822
through plane layers 80−53194
time variability of random medium inhomogeneities, influence on field correlation function and wave spectrum *(Russian)* 77−88621
time-harmonic wave propag. in random media problems 78−62980
transient analysis of two-dimensional Maxwell's equations by Bergeron's method 80−1112
transient wave transverse propagation in non-homogeneous half-space 77−75374
transmission along drill rod in conducting rock 79−59618
transport equations for waves in random media 78−62981
transversely inhomogeneous slab, modal wave propag. with gain or loss variations 80−48122
turbulent media, depend. of amplitude and phasetime fluctuations spectra on turbulence spectra *(Slovak)* 79−55029
turbulent medium, joint Gaussian statistical props. 78−42265
turbulent medium with smooth space-time fluctuations, absorpt. effects on statistical characts. *(Russian)* 79−18330
two interacting intensities, evolution in space and time 78−18005
two-dimensionally inhomogeneous media, Maxwell eqns. decoupling 79−41302
uniaxial anisotropic media, duality principle 78−46493
uniaxial plasma or dielec. half-space, EM radiation from line source, theory 80−99605
vector wave equation, depolarisation term anal. 80−8814
vertically polarized waves in inhomogeneous media, full wave solns. 77−6980
water surface EM wave excitation 79−13893
wave coupling in an anisotropic medium 79−55514
wave packets, 2 dimensional in fluids, radiation pressure effects 77−17828
wave tilt sounding of a linearly inhomogeneous layered half-space 79−68353
Al, electromagnetic wave propagation, demonstration 80−73149
Bi, EM wave dispersion and damping, Voigt configuration, non-local calcs. 80−100475
Bi, EM wave excitation *(Russian)* 77−32093
Bi-Sb, semiconduct., e.m. wave propag. perpendicular to mag. field 79−82517
$Bi_{1-x}Sb_x$, EM wave propag. for rot. of mag. field from Faraday to Voigt config. 80−84419
$Bi_{1-x}Sb_x$, semicond. alloy, EM wave propag. in direction perpendicular to mag. field 79−60687
Cu film, optical consts. deduced from surface EM wave propag. 80−60697
MnF_2, ATR spectra and surface EM wave dispersion anisotropic case 77−77215
MnF_2, magnon-photon interaction for EM wave vector perpendicular to sublattice magnetisation 79−69662
MnFe ferrites, reson., effect of EM propagation 78−64277
SiO_2 film on Cu substrate, surface EM wave absorpt., optical consts. *(Russian)* 80−108216

electromagnetic wave propagation in plasma
see also ionospheric electromagnetic wave propagation; light propagation in plasma; magnetospheric electromagnetic wave propagation
10.6 μ radiation, refl. from laser plasma *(Russian)* 80−1796
abnormal linear EM wave absorpt. *(Russian)* 77−11353
absolute two plasmon parametric decay 77−76091
absorption above lower hybrid freq. 78−26296
absorption and dual propagation in warm, plasma half-space, density and temp. depend. 80−75048
absorption and refl. in magnetoactive isotropic nonhomogeneous plasma *(Russian)* 77−72453
absorption and transformation in inhomogeneous plasma 79−23424
absorption at electron cyclotron freq. 80−79457
absorption by collisionless plasma with random inhomogeneities *(Russian)* 78−22507
absorption in quantising mag. field *(Russian)* 77−47211

electromagnetic wave propagation in plasma continued
absorption in randomly inhomogeneous collisionless plasma at resonance frequencies *(Russian)* 78−59598
absorption near electron cyclotron freq. 78−55723
absorption of axially asymmetric EM waves, in inhomogeneous plasma 77−55156
absorption of HF waves in magnetoplasma 78−14171
absorption of monochromatic EM pulse, collision process effects 78−9791
acceleration of plasma in EM wave of varying freq., changing plasma conc. 78−18414
air plasma, radiowave interaction, electron velocity, collision cross-section depend. 80−103155
Alcator Tokamak submillimetric-wave emission obs. 79−32816
Alfven-ion-cyclotron instability for axially bounded plasma 80−1788
AM/FM radio signal diffraction in homogeneous dispersive medium, space time geometric theory 79−4149
amplification in waveguide following electron beam-plasma interaction *(Russian)* 77−68801
amplified scattering of EM waves, in presence of singular point, exptl. obs. *(Russian)* 78−79439
amplitude modulation anal. 78−75346
anisotropic collisional plasma half space, interaction of penetrating EM waves 78−55724
anisotropic plasma, plasma resonance of second-order wave for finite amplitude EM waves 77−84444
anisotropic warm magnetoplasma, modified wave equations 77−65876
anomalous absorption, hot electron prod. 77−68833
anomalous absorption of UHF radiation in electron cyclotron resonance range *(Russian)* 80−1807
anomalous interaction of high intensity laser beams with plasma, scaling laws *(Japanese)* 79−82070
anomalous skin effect *(Russian)* 77−51195
anomalous skin effect in bounded plasma 79−19043
anomalous skin effect in plasma column *(Russian)* 77−3942
anomalously resistive phase, spiky density fluctuations and relax oscill., microwave scatt. obs. 80−38547
antenna in plasma, detect. of natural noises 80−24181
antenna probe, circular aperture, induced HF thermal noise calc. 78−87496
antenna radiation patterns in laboratory plasma in whistler wave regime 77−27685
antenna system, dual integral eqn. method 78−75361
antenna system, multilayered, electronically scannable, for space communication 79−4151
backscatter from metallic sphere in radially inhomogeneous plasma sheath, anal. *(Russian)* 77−7558
backscattering across mag. field in bounded plasma 79−90415
barrier penetration, in inhomogeneous magnetised plasma 79−19030
beam generation of EM waves in plasma *(Russian)* 78−75364
beam-plasma system, instability due to whistler mode EM waves 79−14564
beam-plasma system, unstable, whistler wave propag. along reson. cone, diagnostics 77−31484
beam-plasma system in waveguide, EM models excitation 78−1844
boundary conditions for two plasma media 77−994
boundary conditions for wave-plasma interaction, refl. coeffs. 77−24094
bounded cold plasma stream, polarisation current and moving dielec. modes 77−19722
bounded inhomogeneous isotropic media, generalized charact. functions appl. to propag. 79−72462
bounded medium, nonlinear parametric reson., limit cycle solns. 80−19071
bounded slab medium moving relativistically along normal to interface, EM interaction 77−55151
bragg effects in microwave transmission through stationary plasma structures 80−83944
bremsstrahlung, by relativistic electrons in strong mag. field *(Russian)* 77−62393
Brewster angle for E-polarised wave interacting with moving half space 77−38776
Brillouin amplification, convective, in homogeneous plasma slab 77−24089
Brillouin backscatt., nonlinear three-wave interaction 78−75356
Brillouin sidescatter threshold, non-resonant EM pump field modification 78−67362
caviton, dissipative three-dimens. Langmuir soliton, formation *(Russian)* 80−83943
cavitons in laser irradiated fusion plasmas, EM wave propag., supersonic density humps 80−24178
Cerenkov interaction between obliquely propagating whistler wave and electron beam, computer simulation 80−43937
charge-separated plasma, EM wave dispersion relations, rel. pulsar magnetosphere 77−7549
charged particle in plane waves, accuracy of adiabatic invariant conservation 80−37946
Cherenkov adsorption of azimuthal EM travelling waves, magnetoactive heating and containment *(Russian)* 80−38675
circumsolar plasma, radio signal spectral lines formation 80−92330
Clemmow-Mullaly-Allis diagram, modified for large amplitude EM waves 77−15196
coaxial plasma waveguide system, (m=1), EM wave propag. and absorpt. 77−89263
coherent four-wave scatt., appl. to plasma diagnostics 80−28681
coherent parametric instabilities excited by two or more pump waves, theory 78−57381
cold collisional plasma, current distrib. and input impedance of antenna of revolution 77−24096
cold inhomogeneous electron plasma, relativistic effects 78−26295
cold lossless plasma half-space, transient response in presence of transverse static mag. field 78−67361
cold lossy plasma half-space in transverse mag. field, transient response 79−77388
cold magnetised plasma, radiation pressure forces 78−79437
cold magnetoplasma, Fuchsian differential eqns. 78−9302
cold plasma half-space in transverse static mag. field, transient response 77−31472
cold plasma layer, EM wave propag. in absence of collisions *(Italian)* 77−47202
collective oscills. in toroidal plasma, microwave scatt. diagnostic technique, review 80−48863

electromagnetic wave propagation in plasma continued
collisional plasma, nonlinear energy pump between radio waves *(Russian)* 77−62365
collisionless absorpt. in inhomogeneous plasma 77−47210
collisionless magnetoplasma, EM wave conversion to extraordinary wave 80−79451
collisionless plasma, microwave electron acceleration, waveguide obs. 80−43932
collisonal effects on low-freq. EM wave propag. 78−75349
column rot. and particle transport, travelling EM wave and neutral beam heating *(Russian)* 79−27798
combustion bomb microwave cavity, electrically loaded with propagating flame front electron plasma, theory and expt. 79−20369
complex nonlinear impedance of flat antenna 80−103130
complex ray analysis for plasmas 80−83902
compressible fully ionised warm plasma with collisions and an external magnetic field 77−992
Compton scattering, stimulated, wave spectrum and electron temp. evolution 77−62347
continuous transverse EM waves, in weakly dissipative plasma, nonlinear effects 79−10672
Cotton-Mouton effect in Jupiter ionosphere and magnetosphere, rel. to decametre radio emission modulation 80−67643
coupling of EM waves in neutral current sheet of plasma *(Russian)* 77−80313
covariant theory of short waves in gas in gravitational field *(Russian)* 77−62370
cross focusing of coaxial Gaussian beams in magnetoplasma, plasma wave generation 79−32779
current generation by RF travelling waves in tokamaks, numerical anal. 80−1800
current loop radiation pattern in inhomogeneous plasma column 77−76102
current susta-ning by RF travelling field in collisional toroidal plasma 78−47094
curvature radiation, from laser heated dense plasma, spectrum 79−41834
cyclotron absorption at first harmonic within quasi-transverse propag. *(Russian)* 77−39425
cyclotron absorption in plasma-filled waveguide in nonuniform mag. field 78−51315
cyclotron harmonic damping in stimulated Raman scattering from an intense relativistic electron beam 79−68946
cyclotron instability, effect of plasma drift 79−60150
cyclotron instability in plasma with relativistic particles 80−21912
cyclotron maser, high-current and plasma filled, theory 78−17890
cyclotron radiation transport in plasmas by neutron transport techniques 80−38660
cylindrical plasma, excitation with ring of magnetic currents 78−75347
cylindrical plasma, wave tracing and short-wave diagnostics 77−76100
cylindrically confined cold plasma, overdense and steep density, plane EM wave scattering 80−70005
DC arc plasma, alterations in spectral line intensities due to external mag. fields 80−79621
Debye screening modifications in ponderomotive effects 80−33777
decay instability in magnetoactive plasma *(Russian)* 78−14175
decay into two plasmons in nonhomogeneous plasma *(Russian)* 78−26290
decay processes in inhomogeneous nonstationary and 2-dimens. inhomogeneous plasmas *(Russian)* 80−10386
decimetre radiowaves in circumsolar plasma during flight of Venera-10 spacecraft 80−21886
delay line simulation, wave propag. in dispersive and attenuating media 80−82606
dense pinch, electron-positron pair production in EM field *(Russian)* 80−100092
dense plasma clarification by strong EM wave self-action 78−75360
dense relativistic electron gas, EM response in strong mag. fields, particle polarisation, mode struct. 80−43963
density cavities and localised electric fields generation 77−76092
density discontinuity in plasma, s-polarised wave absorpt. 79−23425
density fluctuations, microwave scatt. obs. 80−48851
density profile steepening at reson. absorpt., hydrodynamic model 79−46434
depolarisation, in turbulent cosmic plasma 77−17358
depolarisation in plasma with MHD turbulence *(Russian)* 80−103154
dielectric rod waveguide in magnetoplasma, TM mode propag. 78−51314
diffraction by semi-infinite parallel-plane waveguide in anisotropic plasma 78−1845
diffraction from plasma cylinder, numerical soln. *(Russian)* 77−31481
diffraction radiation characts. of an open conducting periodic struct., temp. and elect. conc. determ. *(Ukrainian)* 80−70004
diffuse boundary plasma, ordinary wave excitation under anomalous skin effect conditions 77−15204
dipole antenna in magnetoactive plasma EM field distrib. 80−100079
dipole antenna in warm isotropic plasma, boundary-value problem, multiple water bag model 78−91115
dipole excitation of ion waves 77−3950
dipole radiation of longitudinal waves in infinite plasma 79−4153
discrete modes of a system subject to an inhomogeneous, high-frequency force 80−43237
dispersion, of plasma waves propagating along mag. field in strongly anisotropic relativistic plasma 80−67542
dispersion relation, quantum field theoretical approach 77−80292
dispersive wave, energy-momentum tensors 78−17842
dye laser emission, from laser spark, nonlinear absorpt. meas. 79−64922
dynamic response to laser modulations, in CW laser prod. Cs plasma 80−14920
E-polarized waves, transmission and reflection in isotropic moving plasma 78−22513
echo of longitudinal waves in plasma layer under mirror reflection conditions *(Russian)* 77−11330
echo oscillations, generated by distributed sources, rel. to exciting field type *(Russian)* 78−71485
echo oscillations in relativistic plasma *(Russian)* 80−53990
echo surface wave propagation in confined plasma *(Russian)* 77−7520
ECR as a diagnostic for mirror trap plasma 80−38709
education, dispersion eqn., long wavelength approx., appl. EM wave in plasma 80−17735
education, plasma-laser beam self focusing using paint stripper flame 79−9066

electromagnetic wave propagation in plasma continued
education, Slinky as model for transverse waves in plasma 80—17741
effective Compton cross sections of hot plasma 79—37501
effective cross section and space charge, preionised gas laser induced breakdown 80—48930
eigenmode scattering relations for plane-stratified gyrotropic media 79—72459
electric and diffusion current generation by EM field, moving media 77—76097
electric current generation by EM radiation 78—71492
electric field fluctuations spectrum, laser fluoresc. spectroscopy meas. 80—87946
electrodynamics, role of parametric effects *(Russian)* 77—76089
electromagnetic fields of non-equilibrium plasmas 80—6210
electromagnetic waves incident on magnetoactive plasma layer, field amplification anal. *(Russian)* 78—22506
electron beam, intense, relativistic, stimulated Raman radiation spectral props. 79—64163
electron beam, relativistic, unmagnetised, stimulated scatt. anal. of HF incident pump wave 79—77345
electron beam, relativistic mirror feature, perp. temp. effects 80—78749
electron beam interaction, nonrelativistic, modulated, fast EM wave conversion, in waveguide 77—84455
electron beam interaction with EM wave, stochastic oscill. *(Russian)* 79—46460
electron beam produced inert gas plasmas, UV to near IR laser lines 80—92334
electron beam-whistler soliton interaction in external mag. field, appl. solar wind 77—11360
electron beams, relativistic intense solid, cyclotron maser instability 79—55494
electron cyclotron absorption of the ordinary wave at normal incidence 80—19570
electron cyclotron frequency, absorpt. in thermal plasma of finite density 79—64874
electron cyclotron harmonic waves excitation, lab. expt., rel. to topside ionosphere RF sounder expt. 78—93042
electron cyclotron heating in Elmo bumpy torus, review 80—28750
electron cyclotron maser interaction in cavity 79—19045
electron cyclotron resonance, emission, from Princeton Large Tokamak, diagnostic appls. 77—80280
electron density fluctuations excited by EM waves in semi-infinite anisotropic plasma 78—14173
electron density meas. by EM wave propag. in magnetised plasma column 80—43974
electron electrostatic wave, EM pump wave parametric decay, simulation 77—19683
electron energy distribution, in r.f. elec. field 78—67363
electron energy spectrum control 78—47135
electron gyroresonance cyclotron oscillation propagation obs. in nonuniform mag. field 78—75351
electron in monochromatic wave, self-reson. motion 78—66737
electron magnetised plasma, stability in circularly polarised EM wave field 80—87897
electron plasma, parametric instability excitation by high-freq. EM waves 79—19031
electron plasma, strongly turbulent, EM scattering 77—55150
electron plasma, war, isotropic, drifting, waveguide modes, relativistic electrodynamical study 79—77393
electron plasma externally launched diocotron mode-induced transport across mag. field 78—9758
electron plasma wave excitation in mag. field, transverse flux constraint 77—68771
electron wave, transform. into ion wave in multicomponent plasma during quasilongit. propag. 78—73572
electron-cyclotron resonance, wave propag. at angle to non-uniform mag. field *(Russian)* 78—71487
electron-ion oscillating discharge, excitation of EM oscill. in plasma zone 77—55188
electron-ion plasma, stimulated bremsstrahlung light absorption *(Russian)* 78—87438
electrostatic pulse generation by two electromagnetic pulses 80—92295
EM excitation of plasma wave by two coaxial Gaussian beams 79—55511
EM field modification meas. in turbulent plasma 77—42987
EM instabilities in plasma with anisotropic press. *(Russian)* 78—22503
EM instability in counterstreaming plasmas in mag. field 78—22508
EM radiation from nonlinear coupling between longitudinal excitation 77—11334
EM resonant properties of laser-prod. plasmas 80—43928
EM soliton propagation in nonequilibrium dispersive media *(Russian)* 80—106933
EM wave penetration into plasma, permittivity sign changes *(Russian)* 80—100477
EM wave resonant absorption, due to DC mag. field parallel to density gradient 80—19563
EM wave self action during modulation instability *(Russian)* 80—14905
EM wave self-action during thermal modulation instability of high hybrid oscills. *(Russian)* 80—53980
emission, absorption and transfer of waves in astrophysical diffuse magnetised plasmas, book 80—105446
emissivity near the electron cyclotron frequency from a thermal plasma of finite density 80—1801
energy conversion, transverse EM wave to longit. acoustic wave, in inhomogeneous plasma 77—68800
energy transport from 1.06 μm and 0.53 μm laser plasmas interactions at 10^{15} W cm^{-2} 80—92261
enhanced line radiation from active molecular plasmas due to electron collision induced instability 78—71491
entrainment of weakly-ionised plasma by rot. EM field *(Russian)* 77—19679
envelope solitons of relativistically strong electromagnetic waves *(Russian)* 79—37503
excitation of coherent EM radiation by relativistic beam in plasma surrounded by wall 78—67370
excited by modulated hollow beam, in semi-infinite plasma cylinder 77—39433
extraordinary mode nonlinear propag. in hot magnetoplasma 79—60148
extraordinary mode nonlinear propag. in magnetoplasma 79—14555
extraordinary mode radiation induced gyroresonant emission 77—55143

electromagnetic wave propagation in plasma continued
F-region irregularities from plasma reson. phenomena obs. by rocket-borne relax. sounding expt. 79—8767
Faraday rot. meas. in high-β fusion expts., plasma electron density and mag. field determ. 80—49008
Faraday tarotion, effects of pulsewidth 78—71540
fast electron beam, suppression in plasma in strong EM wave field *(Russian)* 80—53998
filament formation, by coupled EM wave and ion fluctuation 77—15200
filamentation, nonlinear development 79—60151
filamentation instability, spatial growth in collisionless magnetoplasma 77—80311
filamentation instability, temporal growth, EM beam of freq. up to plasma reson. freq. 78—51304
filamentation instability growth 78—1841
filamentation instability in magnetoplasma, spatial growth 78—51311
filamentation instability of extraordinary and ordinary modes in a magnetoplasma 78—83575
filamentation instability of laser beam in inhomogeneous plasma, preferential heating 80—19568
finite amplitude wave, regeneration beyond opacity barrier *(Russian)* 80—10387
finite amplitude whistler wave solitons and filaments, properties and propagation 79—41836
finite inhomogeneous plasma, EM pump wave decay, normal modes 79—68929
finite Larmor radius effects in absorpt. of EM waves near electron cyclotron freq. 79—94800
flame plasma with presence of current, EM radiation obs. *(Russian)* 80—103126
fluctuations of localised plasmons under action of EM pumping wave *(Russian)* 77—76078
fluid-ion cyclotron instability, pulsed CO$_2$ radiation scatt. obs., theory 77—31461
frequency shift of TM$_{omo}$ mode due to anisotropic temp. effect 77—84517
Gaussian beam excitation of upper hybrid waves 79—60149
Gaussian ripple growth on uniform-plane EM wave front 80—19583
Gaussian ripple on uniform EM beam, growth on magnetoplasma 79—19041
geometric optics in space and time varying plasma, internal sources 77—31479
Goos Haenchen negative shifts 78—78865
gravitational field effect on EM radiation propag., instability *(Russian)* 77—3946
gravitational field effect on EM radiation propag., relativistic anal. *(Russian)* 77—3945
gyrosynchrotron emissivity peak freq. of weakly relativistic electrons in isotropic plasma 77—64633
H-polarised EM wave by isotropic moving plasma, transient response 80—64731
heating, nonlinear conversion of EM radiation to ion-acoustic waves, near plasma reson. *(Russian)* 78—5859
heating by EM wave transmission in mag. field *(Russian)* 80—103167
heating by microwave absorption, expt. 78—75383
heating by shortwave laser pulses, electron thermal conduct. effect 77—1005
heavy-particle acceleration by charge-density waves in vacuum and in plasma 80—70044
helical antenna in compressible electron plasma, radiation resistance 78—38503
heterogeneous medium, interactions of laser radiation 80—28765
HF discharge, ionisation overheat instability in EM wave field *(Russian)* 80—106990
HF discharge plasma, resonantly sustained, by Tonks-Dattner resonance 79—4142
HF potential effect on s-polarised wave refl. from plasma layer 77—55153
high density plasma interaction with a strong EM wave, Green's function method calcs. 80—48885
high freq. rad. field in turbulent plasma 80—38648
high power level plasma waveguide mode excitation 79—41839
high power microwave pulse interaction with thermally ionised laboratory plasma 80—10409
high-frequency heating of inhomogeneous plasma in $\omega \geq \omega_{Hi}$ freq. range *(Russian)* 80—106946
high-frequency wave propag. in strongly magnetised plasma 80—103158
high-pressure atomic and molecular impurities, preionisation by UV irrad. of surface discharge 80—38847
hot collisional plasma filled waveguide, wave propag. 80—92331
hot collisional uniaxial plasma, guided waves, TM mode dispersion rel. 80—53995
hydrogenic ion lines, red shift in plasma 80—103128
hydrogenic plasmas and fluids, transverse dielec. function, excitation spectrum 78—67311
ICRF heating in TFR, preliminary obs. and further development prospects 80—28741
impulse response of Lorentz medium 80—59242
incoherent propag. due to electron density fluctuation in plasma slab 77—11348
incoherent scattering cross-section, electrostatic electron wave influence 78—34311
incoherent Thomson scattering techniques 80—48999
induced Mandelshtam-Brillouin scattering in plasma with supersonic particle drift *(Russian)* 80—14899
induced Thomson scatt., wave conversion 78—14169
inert gas discharge, reson. radiation imprisonment model 80—38756
inhomogeneous magnetoactive plasma, EM waves linear interaction 80—96364
inhomogeneous overdense plasma, nonlinear penetration of strong EM waves 78—75355
inhomogeneous plasma, EM wave field behaviour near ϵ_{xx} singularity *(Russian)* 78—34331
inhomogeneous plasma, parametric trapping of EM waves *(Russian)* 78—9780
inhomogeneous plasma, self-induced reson. absorption of intense EM wave 78—51306
inhomogeneous plasma stimulated Raman scatt. spectrum 79—7449
inhomogeneous plasmas, resonant microwave absorption, nonlinear effects 79—94793

electromagnetic wave propagation in plasma continued
  inhomogeneous semiconductor plasma filled rectangular waveguide propagation 79—68928
  inhomogeneous stationary laser plasma, stimulated Raman spectra 78—83578
  instabilities, $k_{\parallel}B_0$, second order theory 78—38483
  instability threshold in mag. neutral sheet 78—14160
  instability threshold in mag. neutral sheet 78—38500
  interaction of photons with electrons in dielectric media *(German)* 80—103117
  interaction of plasma with strong EM wave, efficient transformation of radiation frequency 80—106931
  interaction with compressible plasma column 80—38656
  interferometry techniques for high β-plasma density meas., holographic and coupled cavity laser methods 80—49006
  interplanetary plasma meas. by modulation method, amplifiers sensitivity increase 79—92676
  inverse magnetic bremsstrahlung around the electron-cyclotron frequency 79—27781
  ion cyclotron heating by azimuthally rotating RF fields, in toroidal plasma 80—28721
  ion sound wave parametrically excited in T-D reson., azimuthal angle of T-D mode induced scatt. 78—9790
  ion-acoustic fluctuations, CO_2 laser study 80—83946
  ion-acoustic instability supression by microwave field 78—71466
  ion-acoustic nonlinear waves, parametric excitation due to EM wave decomposition *(Russian)* 78—47104
  ion-acoustic oscillations, in inhomogeneous plasma layer, high freq. radiation excitation *(Russian)* 78—26270
  ion-acoustic oscillations in intense EM field *(Russian)* 79—55483
  ion-acoustic pulse generation by 2 EM pulses at difference freqs. in collisionless plasma 80—79475
  ion-acoustic solitons in electromagnetically irrad. magnetoplasma 78—22485
  ionisation nonlinearity medium, TE wave energy flux limitation effect and regime transitions *(Russian)* 79—1315
  ionisational instabilities of EM wave in homogeneous high-freq. discharge *(Russian)* 78—34382
  ionising surface electromagnetic wave propagation 77—76099
  ionosphere, decametric freq. shift of magnetoionic component 80—105104
  ionosphere, heating due to parametrically excited Langmuir waves, short-scale field-aligned density striations form. 79—8766
  isotropic homogeneous plasma layer, reflection and transform. coeffs. *(Russian)* 77—62364
  isotropic inhomogeneous moving plasma column, cross polarisation of scatt. EM waves 79—98917
  kilometric radiation in Jupiter magnetosphere, ray tracing 80—72866
  kinetic equation, for plasma in strong high freq. EM field 80—38540
  Korteweg-de Vries, complex modified eqn., dispersion, self-propagation in anisotropic medium 79—75371
  Langmuir oscills., modulational instability, in EM wave field 80—38618
  Langmuir soliton EM wave scatt., theory *(Russian)* 80—38564
  Langmuir soliton weak EM wave scatt., Doppler shift and reflection coeff. calc. *(Russian)* 79—7467
  Langmuir system, kinetic theory of mag. field generation 80—69974
  Langmuir turbulence meas., forbidden transition satellites 80—38714
  Langmuir wave decay, two-plasmon parametric instability, numerical anal. 78—14152
  Langmuir wave excitation by two pumping waves, convective instability *(Russian)* 80—14904
  large-scale localised distribution of EM waves, nonlinear dynamics 79—73008
  laser absorption by high density degenerate plasma, reflectivity of metal surface 80—1805
  laser beam interaction, weakly nonlinear systems, props., discussion 78—93535
  laser electron accelerator, mechanism 79—81103
  laser fusion, interaction and transport processes, continuous pulse shaping 80—28766
  laser fusion implications of resonance absorption and associated electrostatic field pressure 80—24176
  laser fusion plasma, HF EM wave swelling effect near crit. density 77—84443
  laser light parametric absorpt., convective parametric instability 80—100073
  laser light reflection enhancement from expanding laser prod. plasma, Brillouin scatt. 77—3963
  laser light scattering for plasma diagnostics *(German)* 77—7599
  laser plasmas, wave absorpt. and superreflectivity due to EM struct. resonances 80—24177
  laser pulse amplifier using induced Raman or Brillouin processes 80—1279
  laser radiation absorption polarisation and ang. depend., reson. absorpt. process obs. 77—76094
  laser radiation propagation, scatt., third harmonic freq. radiation flux density 80—87901
  laser spark absorpt. and laser pulse contraction meas. using dye lasers 80—48988
  laser transmittance in high-Z thin plasma, energy transport 77—80333
  laser-plasma interaction and ablative acceleration of thin foils at 10^{12}-10^{15} W/cm^2 80—83963
  layer produced by moving ionis. source *(Russian)* 78—1836
  layered plasma, use of Fuchsian differential eqns. 80—75060
  LF wave propag. in relativistic electron gas, rel. to Crab Nebula *(Chinese)* 78—67356
  limit polarisation of EM waves escaping inhomogeneous layer of magnetoactive layer *(Russian)* 78—83570
  limiting polarization of electromagnetic waves escaping from a nonuniform layer of magnetoactive plasma 79—64875
  line source in moving magnetoplasma sheath, saddle point approx. 77—51189
  line source interacting with moving magnetoplasma half space, EM radiation 77—11354
  linear conversion, plasma wave absorption 77—11337
  linear coupling between waves in mag. field *(Russian)* 79—94803
  linear interaction of EM waves in inhomogeneous magnetoactive plasma 79—94802
  linear resonant absorpt., analytic theory 78—51310
  linear transformations, in inhomogeneous isotropic plasma layers *(Russian)* 78—18415

electromagnetic wave propagation in plasma continued
  linearised plasma nonstationary signal transition 78—71493
  linearly polarised waves, parametric instabilities rel. to Crab nebula 78—45220
  local absorption in dense plasma, geometrical optics approx. 77—5396
  localised RF fields, duct propag. along inhomogeneous magnetoplasma column 79—46453
  longitudinal to EM wave conversion, WKB approx. 78—18389
  longitudinal wave excitation in semibounded plasma by obliquely incident EM waves 79—82067
  longitudinal waves excitation by obliquely incident EM waves in semi-limited plasma *(Russian)* 79—1314
  lossy magnetoplasma half space, incident impulsive plane wave 78—5877
  lossy plasma half-space, transient refl. for TM polarisation 79—98916
  low Z plasma, 1.06 μm low pulse reson. absorption 80—87903
  low-frequency radiation, from elec. dipole in isotropic plasma 79—46436
  lower hybrid wave excitation, by periodic slow E waves, appl. RF heating 77—62360
  lower hybrid wave propag. and parametric decay in WEGA Tokamak 80—28725
  lower hybrid waves, quasi-optical beam self-action in magnetoplasma 80—38657
  Lyman-α Stark profile, Stark broadening theory, in dense equilib. plasma 77—84505
  magnetic field generation due to ponderomotive force 77—31475
  magnetic plasma layer, echo propag. *(Russian)* 78—75345
  magnetically confined plasma, EM wave penetration, anomalous skin-effect 79—64873
  magnetised plasma, backscatt. of laser beam from electrostatic waves 80—33779
  magnetised plasma, circularly polarised wave effect, dispersion relation 77—27681
  magnetised plasma, in open plane periodic waveguide, reson. emission 78—26299
  magnetised plasma, propagation of high-frequency EM waves in curved space-time 80—48894
  magneto plasma half space, reflected pulse, cyclotron and upper hybrid resonance freq. 78—63569
  magneto-active plasma, parametric instabilities set up by EM radiation *(Russian)* 80—106889
  magnetoactive, EM wave reson. absorpt., small scale struct. *(Russian)* 77—47204
  magnetoactive collisional plasma, nonlinear energy repump *(Russian)* 78—34319
  magnetoactive collisional plasma half-space, EM wave penetration and refl. 80—33778
  magnetoactive plasma, propag. at freqs. comparable to plasma resonance, geometric optics method 80—43235
  magnetoactive plasma, radiation field, appl. to cyclotron and multipole radn. 77—51190
  magnetoactive plasma, total absorpt. of EM wave *(Russian)* 80—106944
  magnetoactive plasma parametric instability in HF wave generated field *(Russian)* 78—59566
  magnetoionic plasma, hyperbolic eqn. system, inverse problem 78—75354
  magnetoparametric instabilities, appl. to Crab Nebula 78—61727
  magnetoparametric instabilities, appl. to Crab nebula 79—8829
  magnetoplasma, conversion from ordinary to extraordinary EM beam 79—64872
  magnetoplasma, hot collisionless, resonant excitation of upper hybrid wave by two EM beams 79—77384
  magnetoplasma, inhomogeneous, wave trapping phenomena 77—15195
  magnetoplasma, intense EM wave absorption, numerical results 80—43890
  magnetoplasma, interaction of amplitude modulated microwave, plasma waves excitation 77—3947
  magnetoplasma, interpretation of 6-component measurements of wave field 80—83921
  magnetoplasma, modulation instability of whistler waves 77—72450
  magnetoplasma, plasma wave generation and SHG by Gaussian EM beam 79—37479
  magnetoplasma, refr. index profiles in layered media, extraordinary mode 80—77223
  magnetoplasma column in waveguide, wave packet bifurcation 77—7556
  magnetoplasma wave coupling in an anisotropic medium 79—55514
  magnetosphere, EM wave excitation rel. to plasma instabilities *(Russian)* 78—12053
  magnetosphere, gyroharmonic emissions due to energetic electrons in plasmas 79—80086
  Mandel'stam-Brillouin scatt., instability threshold *(Russian)* 78—22505
  Mars entry probe, communication black-out due to shock induced plasma flow 77—5413
  maser emission, by plasma produced electrons orbiting a positively charged wire 80—92272
  mass renormalization in stochastic acceleration of particles *(Russian)* 80—100066
  microwave, AM, LF wave excitation 77—62366
  microwave, filamentation instability 77—31473
  microwave absorption, large amplitude, intermediate freqs. 78—9794
  microwave antenna in plasma, radn. patterns *(Russian)* 78—38504
  microwave beam, reson. interaction, mag. field self-generation, probes obs. 77—35353
  microwave beam interaction, intense, with low temp. plasma flow, space distrib. 80—38578
  microwave beams in plasma diagnostics, nonlinear interaction of two beams 79—73044
  microwave bundle transmission, plasma column, dielectric const. and r depend. *(Russian)* 77—3983
  microwave dynamic interaction, probe diagnostics 80—19584
  microwave emission, near geometric mean plasma frequency, mechanism 79—82066
  microwave emission from transformed electrostatic oscills. 77—76209
  microwave excitation, upper hybrid reson. region, appl. heating *(Russian)* 77—3943
  microwave excitation by electron beam in plasma-filled waveguide 77—47224
  microwave field power transfer efficiency under electron cyclotron reson. condition 78—9789
  microwave generation by negative-mass instability in ultrarelativistic plasma 78—51289
  microwave generation during strong electron beam-plasma interaction in mag. mirror field *(Russian)* 77—11355

electromagnetic wave propagation in plasma continued
- microwave harmonic generation in plasma-filled waveguide 80—1798
- microwave heating in ELMO Bumpy Torus, anal. 80—28829
- microwave heating of plasma in EM trap *(Russian)* 80—10400
- microwave high-power absorption localisation, cold cylindrical plasma column 78—51319
- microwave interaction with isotropic collision-free plasma *(Russian)* 80—14901
- microwave irrad., anisotropic fast electron emission 77—84503
- microwave modulation, due to random fluctuations of pulse discharge plasma parameters 77—42988
- microwave plasma diagnostic interferometer with fourfold signal passage 78—87487
- microwave plasma interaction, reson. and thermoelec. mag. fields obs. 77—27678
- microwave plasma source, helical slow-down structs., electron density 78—18424
- microwave propagation constant in temperate plasma, determ. by slab line technique 80—53992
- microwave propagation effects in randomly ionized plasma, experimental system 79—27784
- microwave propagation through modulated air plasma 80—10388
- microwave pulse interaction with strongly inhomogeneous plasma, accelerated electron prod. and distrib. *(Russian)* 80—14900
- microwave radiation, energy transfer and transmission coeffs. in metallic chamber *(Russian)* 79—98915
- microwave radiation from turbulently heated plasmas 77—43080
- microwave surface wave plasma at atmospheric press. 79—50868
- microwave trajectory and electron cyclotron heating, toroidal plasma 78—59628
- microwaves, critical surface phenomena 78—51313
- microwaves, enhanced scatt. at upper hybrid freq. 77—7548
- microwaves, in overdense magnetised plasma, numerical calc. 80—28685
- microwaves and transverse pseudowaves, skin effect 78—26297
- mode conversion and collisionless absorption, electrostatic plasma wave growth and damping 77—80308
- mode coupling in inhomogeneous magnetised plasma, normal incidence case 77—84435
- mode coupling in inhomogeneous magnetized plasma, oblique incidence 77—84437
- modulation instability and plasma electrodynamic characteristics 80—38621
- modulation instability saturation, narrow beam of radio waves in magnetised plasma *(Russian)* 77—47203
- modulational instability of elliptically polarised EM waves 78—14167
- modulational instability of nonlinear wave propagation in relativistic plasmas 80—106911
- monochromatic EM wave excitation by relativistic charge particle beam in magnetoactive plasma *(Russian)* 78—87464
- monochromatic plane EM wave reflexion at plasma slab 80—24174
- monochromatic wave, turbulence spectrum modification 77—19706
- monochromatic whistler wave, nonlinear evolution in nonuniform mag. 80—43912
- moving electron plasma, interaction of large-amplitude plasma waves 79—98899
- moving gas-ionisation front, reflections and refractions of EM waves 80—19586
- moving lossy plasma, power reflection coeff. and surface impedance calc. 77—84445
- moving media, monochromatic radiation absorpt., effects calcs. 77—76101
- moving plasma, total refl. of EM waves 79—37458
- moving plasma half space, EM power refl. and transmission 77—39426
- moving randomly-inhomogeneous medium, freq. fluctuations statistical characts. *(Russian)* 77—7545
- multicomponent magnetoactive plasma, angular anisotropy of energy flux *(Russian)* 78—18416
- multiple pump ionospheric heating expt. plasma instabilities obs. 78—57382
- multiple-laser-beam expts., Compton-induced refl. 77—993
- negative absorption in anisotropic plasma 77—7554
- neutral atoms in plasma background, strong EM radiation effects 80—103157
- neutral radiant gas, kinetic eqns. with allowance for radiation polarisation 79—23399
- non-linear theory of collective processes in laser-pellet interaction and soliton generation 80—24199
- non-magnetised plasma, EM wave propag. anal. using Bergeron's method 80—43931
- non-planar dipole antenna in weakly ionised plasma, radiation pattern 77—3944
- non-stationary resonant reflectivity of plasmas, model calcs. 80—14903
- nonequilibrium plasma, kinetic eqn. for waves and wave scatt. *(Russian)* 78—14174
- nonhomogeneous plasma in radiating field, absolute dissipative instability *(Russian)* 77—19681
- nonlinear absorption in moving plasma, dynamics *(Russian)* 78—91111
- nonlinear bleaching effect in plasma layer, EM freq. below plasma freq. *(Russian)* 78—71488
- nonlinear dielectric perturbation, wave and particle interactions 80—38593
- nonlinear distortion of amplitude-modulated microwave in plasma-filled waveguide 80—28683
- nonlinear effects in propagation of lower hybrid waves in a plasma 80—10380
- nonlinear EM wave scattering 77—11350
- nonlinear EM waves, in relativistic plasma, Vlasov eqn. calcs. 77—47209
- nonlinear estimates of Brillouin scatter in plasma 80—87895
- nonlinear interaction, electron collision freq., self-consistent eqn. *(Russian)* 80—75055
- nonlinear interaction between three ordinary EM modes 77—31476
- nonlinear interaction of surface waves at plasma boundary 77—55152
- nonlinear interaction with relativistically strong EM waves 79—1316
- nonlinear ion-sound waves excitation, by whistlers and Alfven waves *(Russian)* 79—27783
- nonlinear mixing as a plasma density probe 78—77406
- nonlinear ordinary mode propag. in magnetoplasma 78—22509
- nonlinear penetration of powerful EM radiation in parametrically absorbing plasma 78—83577
- nonlinear propag. and refl. at oblique incidence on plasma layer *(Russian)* 78—26288

electromagnetic wave propagation in plasma continued
- nonlinear propag. in semi-bounded plasma *(Russian)* 78—1835
- nonlinear propag. of EM wave, modulational instability 79—19047
- nonlinear propag. of intense circularly polarised waves 77—84442
- nonlinear quasioptics in DC mag. field *(Russian)* 79—98914
- nonlinear refl. from inhomogeneous plasma bodies 80—1806
- nonlinear reflection *(Russian)* 78—26289
- nonlinear scattering of upper hybrid laser radiation by electron Bernstein modes in a plasma 80—64720
- nonlinear self-distortion in magnetoplasma 79—40031
- nonlinear self-precession and wavenumber shift under reson. and of Alfven waves 80—10389
- nonlinear subharmonic wave generation in nonuniform plasmas 80—106912
- nonlinear theory of propag. in turbulent plasma *(Russian)* 78—14165
- nonlinear transfer in turbulent plasma, emission lines broadening and displacement *(Russian)* 77—91418
- nonlinear transmission and reflection, plasma layer in longitudinal field *(Russian)* 79—19040
- nonlinear transmission and reflection of an electromagnetic wave incident on a plasma layer located in a longitudinal electric field 79—82069
- nonlinear transparency due to modulation instability *(Russian)* 78—59604
- nonlinear transparency of dense plasma layer 78—87454
- nonlinear wave packet interactions, freq. shift 79—90414
- nonlinear wave phenomena, collisional and weakly collisional cases 77—11346
- nonreflecting resonance absorption of EM waves by nonuniform isotropic plasma *(Russian)* 79—55507
- nonresonant wave spatial effects, kinetic perturbation theory and ponderomotive force 78—18417
- nonstationary plasma, anomalous radiation intensity 80—87898
- nonstationary thermal self-focusing of EM waves in low temp. plasma *(Russian)* 77—76086
- nonuniform plasma, full reson. absorpt. of EM radiation *(Russian)* 77—55154
- nonuniform plasma, reson. absorpt. of EM wave of TM type *(Russian)* 77—55155
- nonuniform Vlasov plasma, wave propagation theory 80—79508
- oblique incidence of waves on an inhomogeneous plasma with spatial dispersion *(Russian)* 79—37498
- optical absorption wave propagation in gases, struct., propag., effects 79—10629
- optical props. of thin plasma layer, parametric turbulence effects *(Russian)* 77—58864
- ordinary mode nonlinear propag., hot magnetoplasma 77—68803
- ordinary mode stability to electron heat flux, solar wind appl. 79—30049
- orthonormal decomposition in anisotropic media, duality and complex vector space 80—28620
- overdense plasma layer, jumps in nonlinear reflectivity 77—62367
- p-polarised EM wave struct. near point of reflection *(Russian)* 80—103118
- parametric absorption in magnetised plasma *(Russian)* 80—28684
- parametric absorption in plasma turbulence, instability effects *(Russian)* 77—7551
- parametric absorption of EHF radiation in magnetoactive plasma *(Russian)* 79—32790
- parametric absorption of strong EM waves appl. to extended extragalactic radio sources 78—24561
- parametric decay into two plasmons, nonlinear saturation mechanism efficiency *(Russian)* 77—11349
- parametric excitation of purely growing instabilities by EM wave 77—47188
- parametric excitation of standing waves along plasma boundary *(Russian)* 79—41856
- parametric instability damping by high power elec. field pumping *(Russian)* 77—7553
- parametric reson. between EM waves and electron surface modes *(Russian)* 78—34320
- parametric scatt. of intense EM wave, ultrarelativistic plasma 77—84489
- parametric turbulence, due to EM wave decay 77—31470
- parametrically excited surface waves, phase mismatch 80—24165
- paraxial self focusing theory 79—94304
- partially filled plasma waveguide, dipolar modes, field and power density distributions 77—7555
- particle dynamics in low freq. EM waves, magnetosphere particle flux in inhomogeneous plasma 80—1804
- penetration in collisional plasma half-space with diffuse reflection 79—19039
- penetration into magnetoactive wave 79—23420
- penetration of outer plasma layer, slow TM mode excitation by antenna waveguides *(Russian)* 77—47227
- perfectly conducting cylinder in compressible plasma, scattering *(Korean)* 78—38497
- photodetonation and supersonic radiation wave propag. in Xe plasma *(Russian)* 80—10385
- photon interaction with a turbulent medium 79—82068
- pinched discharges, runaway electron model for X-ray emission 79—46497
- plane parallel plasma layer, EM field penetration, reflective index, absorpt. coeff. *(Russian)* 79—14551
- plane wave propagation in radiative plasma, elec. props. anisotropy effects 79—14522
- plane-parallel plasma waveguide iris admittance 77—84447
- plasma accelerator, microwave generation, discharge voltage depend. 77—7538
- plasma column, overdense, reson. microwave absorpt. 80—64732
- plasma density effects on EM emission around plasma freq. induced by relativistic runaway electrons 79—82065
- plasma instability in strong circularly polarised EM wave field, anal. *(Russian)* 77—7544
- plasma sounding with finite-radiation-pattern source *(Russian)* 78—59606
- plasma-beam interaction radiation in presence of DC field, beam-wave energy conversion 79—68932
- polarisation of picosecond excited continuous X-ray radiation *(Russian)* 80—59190
- polarisation transfer eqn. in inhomogeneous magnetised plasma 77—84436
- polarisation transfer in inhomogeneous magnetised plasma, inclusion of non-orthogonality props. 79—84662

electromagnetic wave propagation in plasma continued
polarised radiation, transfer through rarefied magnetoactive plasma 79—92669
polarised radiation enhancement by Coulomb collisions of electron beam in mag. field *(Russian)* 80—54002
polarization transfer eqn. in inhomogeneous magnetized plasma, solns. 78—28506
ponderomotive craters, in phased waveguide array plasma, form. by microwave irrad. 80—83885
ponderomotive force of h.f. e.m. field *(Russian)* 77—3948
ponderomotive laser effects in collisional plasma transport 80—38562
population inversion, soft X-ray transitions in cooling plasma, H-like ions 78—87437
power reflection, transmission and absorption coefficients for a moving plasma slab in a rectangular waveguide 80—106925
Poynting's theorem for moving media, Lerche's relativistic theory 79—48660
precessional rotation and nonlinear effects due to standing waves and two-wave reson. interactions in mag. plasma 80—48892
propane-air laminar flame plasmas interaction with microwave TM_{010} mode in combustion bomb cavity 80—53939
pulse propagation, in weakly nonlinear plasma, numerical calc. 77—58863
pulse reflection, from moving inhomogeneous plasma 77—51188
pulsed reson. cone, plasma ringing with localised antenna 77—58866
pulsed RF-trapped particle interaction stochastic effects in tokamak 80—59245
pump wave, elec., HF, near lower hybrid reson., LF drift oscill. spectra modification *(Russian)* 80—1767
pump wave, finite amplitude, parametric instability, general quasi-linear theory 79—60130
pumped electron-ion plasma modulational instabilities due to relativistic electron mass variations 79—77363
quasi-static potential oscillations of thin conductor, instability 80—87900
quasilongitudinal and quasitransverse propagation in magnetically confined plasma 79—55453
quasioptics and anisotropic and dispersive media 80—38567
radar scattering from turbulent cylindrical plasma, model 78—22512
radar signal reflection from Sun, efficiency of four-plasmon interactions 80—101582
radiation fields and losses below upper hybrid freq. *(Russian)* 78—4024
radiation from mag. line source on perfectly conducting plane 78—9788
radiation of EM waves by electron beam in isotropic plasma 80—19591
radiation pattern excitation in plasma column by ring source of elec. and mag. currents 77—27677
radiation pattern of open ended waveguide in air core surrounded by annular plasma column 78—67366
radiation pressure induced nonlinear perturbations of magnetised plasma 79—86570
radiation scattering by high-temp. relativistic plasma, polarising props. calcs. *(Russian)* 80—53937
radiation scattering due to cylindrical plasmas excited by ring of elec. currents 78—67357
radiative interaction of electron gas in mag. field, distrib. function 79—60116
radiative plasma with anisotropic permittivity, developing wavefronts 80—43896
radiative power loss, from plasmas in steady state ionisation balance 79—82063
radio emission, from intense EM beam-plasma system 79—84663
radio emission from pulsars, propag. effects on polarisation 79—75235
radio emissions from plasma waves and type III solar bursts 79—44454
radio waves, backscatter from scatt. cells located in random medium 77—39428
radio waves interaction in ionospheric plasma, nonstationary processes *(Russian)* 78—93028
radio waves self action in ionospheric plasma, nonstationary theory *(Russian)* 79—48604
radiowave dispersion by plasma ejected from BL Lacertae objects 80—82516
radiowave propag. in turbulent shearing plasma, pulsar microstructure 80—94822
radiowave scattering by plasma cylinder, numerical anal. *(Russian)* 77—39424
radiowaves interaction, thermic excitation of parametric instability, controlled 80—24164
raman side-scatter instability in nonuniform plasma 79—32751
random EM wave field, anal. by maximum entropy method *(French)* 79—68926
random EM wave field in magnetoplasma, anal. of six component meas. 79—27782
randomly inhomogeneous collisionless magnetoactive plasma, anomalous EM absorption *(Russian)* 77—27683
ray and wave optics of integrable and stochastic systems, WKB method 80—59244
ray phase determ., probing radiation transmittivity modulus for plasma column 80—38658
ray tracing in nonlinear moving media 77—14644
ray tracing in the electron-cyclotron frequency range 79—1317
ray tracing near electron cyclotron reson., finite temp. effect 80—53994
ray velocity surface, CMA diagram 78—1839
rectangular plasma filled waveguide, nonlinear mixing of microwaves 79—77394
reflection, from blurred ionization-wave front 80—19587
reflection, kinetic theory 77—27682
reflection, nonlinear, parametric instability at surface *(Russian)* 78—34318
reflection by ionised region with increasing charged particle density, anal. *(Russian)* 78—38494
reflection coeff. of plasma layer *(German)* 78—34317
reflection from front of relativistic electron beam 78—34329
reflection from lossy plasma half-space 79—23422
reflection from moving ionis. front in const. mag. field *(Russian)* 80—106927
reflection from moving ionisation front 77—39430
reflection of impulsive plane wave by plasma half-space moving perpendicular to incident plane 78—67360
reflection of p-polarized waves on a plane-parallel plasma layer 77—65875
reflection of resonance cone and plasma-filled waveguide modes 78—67365

electromagnetic wave propagation in plasma continued
reflection off metallic bodies, physical optics method 77—65877
reflection process from nonhomogeneous plane stratified plasma 78—87453
refraction in randomly inhomogeneous plasma, diagnostics using geometric-optical approx. calcs. 78—9843
relativistic amplitude circ.-polarised wave damping 80—48896
relativistic effects near cyclotron resonances 80—59243
relativistic electron beam, intense, subjected to rippled elec. field, stimulated Raman scatt. 79—98439
relativistic electron beam, short pulsewidth, plasma heating, microwave emission 78—5884
relativistic electron beam, stimulated coherent EM wave scatt. by longitudinal electron waves *(Russian)* 77—7542
relativistic electron beam-EM wave interaction under autoresonance conditions *(Russian)* 80—54001
relativistic electron beams in plasma-filled waveguide, microwave radn. generation *(Russian)* 79—14566
relativistic magnetised plasma, negative absorpt. and energy distrib. function of hot electrons 79—4143
relativistic moving plane ionisation front, Doppler shift, reflected pulse duration 78—34328
relativistic nonlinear EM waves, in cold plasma, propag. modes and effects 80—79507
relativistic plasma, cyclotron radiation absorpt. coeff., computer model 78—30478
relativistic plasma, EM wave dispersion relations from hydrodynamical eqns. 80—79559
relativistic plasma, nonlinear dispersion relation for transverse wave 80—87939
resonance absorpt., mode conversion, relativistic effects 77—11391
resonance absorpt. and optimum focusing of axisymmetrically polarised laser beam, spherical plasma *(Russian)* 78—1863
resonance absorption, in laser-produced plasma, X-ray bremsstrahlung emission obs. 78—59559
resonance absorption, mag. field generation, renormalized theory 78—47126
resonance absorption, self-consistent density profiles for obliquely incident light 80—64758
resonance absorption in non-planar plasmas 79—98919
resonance cones near lower hybrid freq. 79—46487
resonance reflection and absorption of electromagnetic waves incident on a magnetoactive plasma layer *(Russian)* 79—37499
resonant absorption, electron acceleration 77—76142
resonant absorption, theory and expt. 78—75353
resonant absorption 77—72452
resonant absorption in Ar plasma at thermal equilib. 80—1799
resonant absorption of laser light, by magnetised plasma 78—51309
resonant Balmer line irrad. of H plasma, theory and laser spectrosc. meas. 80—75099
resonant EM wave absorpt. in inhomogeneous plasma 77—68804
resonant high-frequency dissipation, temp. anomaly 79—73016
resonant interaction with inhomogeneous magnetoactive plasma stream *(Russian)* 78—1837
resonant particle acceleration at EM wavefront in weakly inhomogeneous plasma 78—38501
resonant wave-particle interaction at ion gyroharmonic freq. 78—83574
RF anomalous penetration in collisionless plasma 80—64730
RF coupling, resonant behaviour, near lower hybrid freq., mirror config. effects 77—15202
RF driven currents in steady state Tokamak reactors 80—28687
RF electric fields in ion cyclotron excitation of multispecies plasma 80—1803
RF emission, in electron beam-plasma and beam-beam interactions 78—45137
RF energy absorption by hot ion-electron plasma *(Japanese)* 79—77404
RF field noncollisional losses in inhomogeneous plasma 77—51191
RF flux control of toroidal plasma 80—38582
RF focused resonance cone fields, nonlinear interactions 77—39427
RF heated Tokamak plasma, waveguide array excited lower hybrid fields 78—42773
RF heating, slow waves launched into overdense plasma by phased waveguide 79—64882
RF localised field, refl. near electron plasma freq. layer 79—19044
RF plasma heating, stochasticity role 80—28752
RF plugging, nonadiabatic, in cusped field, ion heating effect 78—59656
RF preionisation, electron cyclotron frequency sub-harmonic effect on wave absorpt. 80—28686
RF travelling field, collisional toroidal plasma, current sustaining 78—30414
RF wave heating of 26 keV ion beam trapped in Tokamak 78—59627
RF wave interaction, mag. field generation in collisionless plasma 79—7466
RF waves, in enhanced electron temp. plasma, linear coupling *(German)* 77—15201
RF waves, in enhanced electron temp. plasma, nonlinear coupling *(German)* 77—15203
RF waves, transverse-longitudinal, parametric stimulation of longitudinal oscills. *(Russian)* 78—5876
RF-generated magnetoplasma, wire antenna resonance near lower hybrid freq. 79—55516
right-handed Gaussian EM beam excitation of plasma wave 79—55495
ring aperture antenna in plasma, input admittance anal. 78—38542
satellite signals, phase shifts due to plasma shock waves and solitons 77—45273
scattering and transformation by heavy charged particles *(Russian)* 77—76087
scattering and wave transformation in fluctuating plasma *(Russian)* 77—19712
scattering by moving plasma column, cross-polarisation analysis 78—75352
scattering in plasma with strong Langmuir turbulence, anal. *(Russian)* 77—76088
scattering spectra from weakly ionised plasmas calc. *(German)* 79—77347
scattering spectrum, spectral intensity and profile 78—18418
Schrodinger equation with exponential nonlinearity, soln. in time independent case 78—14168
scintillations, fourth-order moment eqn., astrophys. appl. 80—46381
scintillations of phase and quadrature components 79—80077
second harmonic generation by Gaussian beam 78—91112

electromagnetic wave propagation in plasma continued
second harmonic generation of e.m. wave, from plasma reson. region *(Russian)* 77—995
second harmonic generation suppression effect *(Russian)* 80—87899
second helicon branch, relativistic electron motion, circularly polarised EM wave propag. *(Russian)* 77—47205
second-harmonic emission at resonance absorption 79—77391
second-harmonic generation of upper-hybrid radiation in a plasma 80—79506
secondary beam production by two EM beams interaction, appl. heating and diagnostics 77—11352
self magnetic field generation by interaction with intense microwave radiation 79—27788
self precession and freq. shift of EM wave in dissipative medium 80—79504
self-focusing, harmonic generation, axially inhomogeneous plasma 77—19714
self-focusing, limitation 78—1840
self-focusing, plasma flowing transverse to EM beam, kinetic approach 78—59602
self-focusing 78—75357
self-focusing due to relativistic electron mass variation 78—1838
self-focusing in opaque plasma layer, expt. *(Russian)* 77—3949
self-focusing of an electromagnetic wave propagating along a conductor in a plasma 79—19048
self-focusing of EM beams on short-time-scale in magnetoplasma 79—55512
self-reflection of intense EM waves in plasmas 77—84439
self-trapped cylindrical laser beams, radial intensity profile and nonlinear wavenumber shift 80—1802
self-trapping of intense optical beams in plasmas 80—92329
selflocalised EM fields in dense plasma 78—75350
semi-bounded electron-ion plasma, EM wave scatt. and incoherent reflection *(Russian)* 77—72449
semi-bounded plasma, decay interaction, anal. *(Russian)* 77—7543
semibounded magnetoactive plasma, spatial echo *(Russian)* 77—15199
semiconductor plasma column, cylindrical, dielectric coated, with ring source of magnetic current radiation pattern calc. 77—3951
semiconfined electron plasma, ballistic theory of echoes *(Russian)* 77—7521
shearing field-force plasma, propag. effects rel. to pulsar microstruct. 80—17483
SHG in magnetoactive plasma by internal source *(Russian)* 77—58868
short-wave plasma diagnostics, EM diffr. on cylindrical column 77—80376
skin effect of microwaves and transverse pseudowaves 78—59600
skin-effect, anomalous, in bounded plasmas 80—24173
slab-shaped magnetoplasma excitation by magnetic current line sources 78—55717
slow wave excitation, by relativistic beam, in waveguide 77—11364
small amplitude wave propagation, stratified media, mathematical model 79—60147
solar plasma, observations using Mars-2 and Mars-7 probes 78—49345
space plasma front parameter determ. by noncoherent response 77—45274
spectral line level shift, quantum scatt. theory 80—6257
spherical antenna covered with isotropic plasma layer, radiation characts. 80—14907
spiral electromagnetic waves, Landau and Cerenkov damping in mag. plasma, theory *(Russian)* 78—71486
spiral electron beam-EM wave interaction, plasma effects *(Russian)* 77—76125
spontaneous generation of EM waves in plasmas with electron thermal flux 77—84418
stable pulses in natural radio emission, occurrence probability 78—42737
static magnetic field of arbitrary direction, effect on wave propag. 79—68927
statistically inhomogeneous plasma, diagnostics by modulated EM wave *(Russian)* 78—38544
steady-state Tokamak reactors with RF driven currents 80—27818
stimulated backscatt. from electrostatic waves in magnetised plasma 79—90413
stimulated backscatt. from ion cyclotron waves 78—38495
stimulated backscattering in bounded dissipative plasma, nonlinear theory 77—7547
stimulated backscattering of electromagnetic ordinary waves from extraordinary waves below the upper hybrid frequency 79—32748
stimulated Brillouin backscatt. in inhomogeneous plasma 79—19046
stimulated Brillouin backscatter saturation for long CO_2 laser pulses 80—19582
stimulated Brillouin rescattering 80—87896
stimulated Brillouin scatt. from resonance layer 77—19713
stimulated Brillouin scattering, from CO_2 laser produced magnetoplasma 79—60162
stimulated Brillouin scattering initiated by ponderomotive force density fluctuations 80—103129
stimulated combinational scatt. and particle trapping 78—75358
stimulated Compton scatt., Bose condensation and onset of final equilib. state 77—51193
stimulated Compton scatt. from plasma ion bunches 77—51192
stimulated incoherent EM wave scattering on enhanced fluctuations in bounded plasmas 78—83576
stimulated light scattering by ion modes, space time evolution in homogeneous plasma 79—68930
stimulated Mandelstam-Brillouin scattering, in expanding laser plasma *(Russian)* 78—38502
stimulated radiation, leaking normal mode spectra, cold plasma cylinder 77—89231
stimulated Raman and Brillouin backscattering along mag. field 80—69983
stimulated Raman and Brillouin scatt., static mag. field effects 80—6258
stimulated Raman and Thomson scatt., beat wave electron trapping 78—51308
stimulated Raman backscatt. 78—34323
stimulated Raman backscatt. of circ. polarised EM wave 78—91113
stimulated Raman backscattering from preformed underdense plasma 78—71490
stimulated Raman backscattering of circ. polarised EM waves propagating along mag. field 79—37465
stimulated Raman scattering, by relativistic electron beam, parametric mode coupling 77—89272

electromagnetic wave propagation in plasma continued
stimulated Raman scattering, of finite length EM waves *(Russian)* 78—83571
stimulated Raman scattering of EM wave, finite-wavelength, dielectric tensor determination 79—64876
stimulated scattering, polarisation effects *(Russian)* 78—79440
stimulated scattering of relativistically strong circ. polarised pump wave, magnetised plasma 78—34330
stimulated scattering processes, saturation by electrostatic daughter waves nonlinear decay 80—79509
stimulated Thomson scattering 79—94801
stochastic heating, relativistic electron generation *(Russian)* 80—83952
stochastic photon diffusion in unstable, turbulent magnetoplasma 79—48662
stratified plasma, obliquely propag. extraordinary microwave Budden tunnelling 80—48895
strong EM wave propagation in cold electron plasma 79—4147
strong EM waves in collisionless homogeneous plasma, waveform, polarisation and nonlinear effects 78—53809
strong radio waves in ionosphere, effects of induced and combination scatt. 77—91345
strong waves in collisionless homogeneous plasma, waveform, polarisation and nonlinear effects 78—53809
sum-frequency excitation of electron plasma waves, energy transfer efficiency 78—38496
supersonic-subsonic flow transition, shock formation, enhancement by microwaves 77—65845
surface EM wave, propag. allowing for electron heating *(Russian)* 78—34321
surface EM wave interaction with relativistic electron beam 79—60153
surface modes, degenerate, at plasma-vacuum interface 77—15198
surface wave, normal mode propag. at drift. vel. tangential discontinuity 77—24076
surface wave attenuation in unmagnetised RF plasma column 77—42986
surface wave diffr. by inhomogeneity in plasma-dielectric boundary 77—24075
surface wave propagation along lossy cylindrical plasma column 78—75315
surface wave spectrum, surface impedance with specular-diffuse particle scattering 77—24058
surface waves, form. by EM waves incident on magnetoactive plasma slab 77—3931
temperate multi-species plasma around ion cyclotron freq. range, plane wave propagation 80—75050
temporal development and properties, of microwave produced overdense plasma in coaxial discharge 79—55565
temporal growth of filamentation instability of a Gaussian laser beam in a plasma 79—50865
thermal modulational instability and stratification 78—75332
third harmonic generation by Gaussian EM beam in magnetoplasma 78—83572
third order secondary echo and the non-linear transmission of electromagnetic waves across a plasma layer *(Russian)* 79—55508
Thomson scattering of EM pulses by random fluctuations, self-focusing effects 78—83573
Thomson spectrum distortion, small scatt. vols. *(Russian)* 77—19676
THOR device, wave propag. and absorpt. near electron cyclotron layer 79—98921
time varying medium, transmission and refl. of EM wave 79—81341
time-varying medium, EM wave reflection anal. 79—25385
TM modes in lossy plasma filled waveguides 79—23423
TM modes propag. in parallel plane waveguide filled with moving collisional plasma 79—82072
Tokamak, JFT-2, parametric heating by RF near lowr hybrid freq. 80—70023
Tokamak, Vlasov plasmas, geometrical optics approach to electron-cyclotron frequency heating 80—14917
Tokamak machines, Vlasov plasmas, geometrical optics approach, Tokamak appl. 80—14902
Tokamak microwave discharges, refraction losses, from measured plasma density profiles 78—22549
toroidal cavity partially filled with anisotropic dissipative plasma, wave excitation from antenna 77—24097
toroidal plasma, magnetised, steady current generation by RF travelling field 77—11313
total absorption, of p-polarized EM wave, in dense inhomogeneous plasma 77—68802
transformation into nonlinear plasma waves in hybrid reson. region *(Russian)* 77—62369
transient EM wave reflection by lossy magnetised plasma half-space 77—84446
transient scattering, time domain method 80—38655
transient setting of ponderomotive nonlinearity, self-focusing and plasma-wave excitation 79—77387
transition radiation emitted due to the presence of intense EM beam 79—86586
transmission and reflection of polarised waves, incident at an angle *(Russian)* 78—22504
transmission through regular plasma density structures 80—48893
transparency changes of plasma burst in intense optical radiation, direct meas. 78—9807
transparency increase in electron cyclotron absorpt. range, in mag. field *(Russian)* 79—4150
transverse FM waves interaction with free electrons 77—19717
travelling wave arc antenna in a warm plasma 79—82071
trifurcated parallel-plane plasma waveguide 77—84448
triode distributed coupling cable propagation 79—55515
turbulence induced by relativistic electron beam in mag. field *(Russian)* 77—62378
turbulent plasma, dispersion eqn. 79—14553
turbulent plasma, nonlinear interaction of intense HF EM field with Langmuir waves 80—53988
turbulent plasma jet, radiowave interaction and electron density fluctuation 77—989
two dimens. supersonic plasma frontwave propag., intense laser on gas 78—87470
two Langmuir wave parametric decay instability, self-trapped EM pump wave effects 80—96357
two-dimensional diffraction by parallel-plane waveguide in anisotropic plasma 78—5880

electromagnetic wave propagation in plasma continued
two-plasmon decay, profile modification, produced by 10.6 micron radiation, at $^1/_4$-crit. density 79—19061
UHF pulse heating and brightening of weakly ionised lab . plasma *(Russian)* 77—39437
UHF waves, circ. polaris., parametric phonon-turbulence *(German)* 78—34316
uniaxial plasma or dielec. half-space, EM radiation from line source, theory 80—99605
unmagnetised plasma column, anomalous skin effect, finite element calc. 79—14552
upper-hybrid reson. absorpt. of laser in plasma focus, backscatter 80—28621
vacuum polarisation by mag. field *(Russian)* 79—77392
vacuum polarization effects on radiative opacities in a strong magnetic field 79—85032
variational method for magnetoplasma 77—80310
Vlasov theory for magnetised plasma, coherent state approach 80—64675
VLF heating methods, thermonuclear prospects, review 80—28738
VLF hiss in plasma penetrated by electron beam 78—26293
VLF wave packet, cyclotron interaction with reson. electrons beam 79—53652
warm moving plasma in plane parallel waveguide, TE modes 77—80314
wave distribution in inhomogeneous plasma containing random irregularities 80—38633
wave excitation by fast electron cloud, simulation of type III solar radio bursts 79—44455
wave packet propag. across plasma-vacuum boundary 77—17828
wave packet propagation through infinite homogeneous plasma, dispersion relations 80—38653
wave packet self focusing in medium with striction nonlinearity, numerical simulation 78—83042
wave penetration into half-space collisional plasma 80—106928
wave radiation by oscillating electric dipole in moving warm plasma 80—87868
wavebreaking amplitudes in inhomogeneous plasma, temp. depend. 79—68915
waveform distortion by microwave scatt. 79—50859
waveguide, confinement by high power excitation 77—31497
waveguide, cylindrical, plasma-filled, nonlinear EM wave propag. 77—991
waveguide, plasma, parallel-plate, excitation analysis 77—62371
waveguide, plasma-filled, propag. and attenuation characts. 78—67367
waveguide, rectangular, filled with uniaxial anisotropic relativistic warm plasma, EM wave propag. and attenuation 80—59246
waveguides, effect of inhomogeneities 80—19585
weak resonance radiation, collisional redistrib. function 79—794
whistler, parametric decay, nonlinear wave interactions 77—19716
whistler, prod. by electrostatic wave decay near lower hybrid freq. 77—977
whistler, wave trapping in narrow density trough 79—64870
whistler mode radiation, generation by parametric decay of Berstein waves 77—76095
whistler mode waves, instability in anisotropic loss-cone plasma 77—87185
whistler mode waves, temp. anisotropy and beam type instabilities 77—3937
whistler propagation in magnetospheric plasma 80—90294
whistler pulse, self-distortion in plasma 79—46456
whistler range, wave radiation in plasma *(Russian)* 78—36400
whistler wave, filamentation instability due to ponderomotive force 79—14538
whistler wave ducting caused by antenna actions 78—59586
whistler wave self-channelling 77—47208
whistler wave-electron beam nonlinear interaction, computer simulation 77—3938
whistler waves, parametric excitation of kinetic Alfven waves 77—27668
whistler waves in finite plasma, dispersion and attenuation 78—63570
whistler-electron nonresonant interaction 78—9792
whistler-mode waves focusing and interference in spatially varying mag. field 78—65465
whistlers, group vel. in two-ion plasma 78—87452
whistlers, propag. in directions near reson. cone, appl. to magnetosphere electron temp. 77—82086
whistlers, scattering, nonlinear, by lower hybrid and ion Bernstein modes 80—43929
whistlers, self-focusing and filamentation 77—47206
whistlers, supersonic large amplitude electron whistler-wave-ion density perturbation coupling, solitons 77—58854
wire antenna impedance in magnetoplasma transmission line theory 77—39429
XUV gain calculation, in cylindrical C VI plasma 79—72995
Z-pinch, dense, strong optical attenuation of ruby laser 77—84520
Z-pinch high density plasma, EM radiation transmission intensity depend. 79—60145
Ar, dense plasma, complex refractive index 79—23397
Ar low temp. plasma flow, interaction with intense microwave beam 80—38654
Ar plasma, electron density, microwave refl. meas. 78—59674
Ar plasma, microwave absorption at singularity, parametric satellite excitation obs. 77—51194
Ar plasma, reflection of high power pulsed microwave 77—31474
Ar plasma, skin depth effect on EM wave penetration 79—86584
Ar plasma parameters, microwave scanning technique 80—64773
CO_2 laser-plasma interaction, stimulated Brillouin backscatter saturation 80—24175
Cs(Ar-Cs) plasmas, electron momentum transfer cross section, cyclotron reson., temp., cond., and vel. meas. 80—106930
He discharge, EM fields near antenna, probe diagnostics 77—24095
N plasma, absorpt. of energy from large amplitude electromag. pulse 79—90412
Na arc plasma, dense, high-temp., near-reson. light scatt., collision-induced fluoresc. 77—1019
Nd:glass laser irradiated fusion targets, time and space resolved harmonic emission 79—82095
Ne afterglow, recombination processes, microwave quenching 79—14624
Ne discharge, wavenumber spectra of turbulent ionisation waves 78—71541
Ne-He and Ne negative afterglows, microwave quenching and recombination processes, Ne spectral emission 77—80307

electromagnetic wave propagation in plasma continued
O (O$^+$) (O^{2+}), Rayleigh and Compton X-ray scatt. cross sections in plasma 80—43884
SiO_2, high temp. plasma, emissivity and opacity, photon group means 77—7573
Xe discharge, HF, with propag. EM wave, isotope distrib. *(Russian)* 77—76235
Xe, plasma, ruby laser radiation effects *(Russian)* 78—22514
Xe rarefied plasma, emission characts. 80—103122

electromagnetic wave reflection
see also electromagnetic wave propagation in plasma; light reflection; X-ray reflection
4-port, transmission charact. utilizing total reflection, wave transmission matrix *(Czech)* 80—37937
absorbers, direct meas. method of standing waves at oblique incidence 79—81343
absorbing medium surface, EM plane wave refl. with 0 or π phase shift 79—59619
accelerated dielectric medium, relativistic study 78—81862
air-dielectric interface, EM wave reflection and transmission in terms of polarisation, education 80—105458
anisotropic media interface, arbitrary wave refl. and refr. 77—68170
anomalous reflectivity in bounded dissipative plasma, stimulated backscattering nonlinear theory 77—7547
ATS-6 radio beacon experiment, ground refls. effects 77—53144
auroral D-region, unusually strong partial refls. obs. during absorpt. event 78—36388
beam-wave at curved interface, 'total' internal reflection *(French)* 77—58228
biological substances, dielectric props. meas. at RF and microwave freq. by coaxial line reflection methods 80—109065
black hole, Reissner-Nordstrom, coupled gravitational and EM perturbs., scatt. matrix, energy conversion, quasi-normal modes 80—67775
blurred ionization-wave front, EM wave reflection 80—19587
bounded microwave beam, total internal refl., displacements 78—13648
cholesteric liquid crystals, Bragg reflection *(Russian)* 79—4235
coal seam, EM modelling of refls. in in situ gasified section 77—41212
compression of EM waves by anisotropic media, nonreflecting crystal model, two media matching 79—81335
converting linearly polarised incidence waves to circular polarisation 79—76551
corrugated planes surface reactance, rigorous soln. 80—9775
corrugated reflector model for one-hop oblique propagation 79—35041
D-region, partial reflections, sensitivity to irregularity comp. 78—81495
D-region partial reflection experiment, appl. phase switched correlation polarimeter, 77—87169
dielectric, wave reflection by smooth variations in refractive index anal. 78—25777
dielectric slab, 3 cm microwave refl., longit. displacement 78—62973
dielectric slab, reflection and transmission coefficients with sinusoidal permittivity variation 78—71011
dielectric-ferrite interface, physics of microwave reflection, Renard analysis of lateral shift 79—76557
diffuse radiation emerging from semi-infinite medium, intensity accounting for inner refl. *(Russian)* 79—8637
doped conducting media, low-freq. props., EM wave reflection 80—103715
Doppler freq., quasi-specular beam effect of Earth's surface elec. props. *(Russian)* 79—45890
Doppler frequency shift by fast moving boundary *(Japanese)* 80—18967
E_s-layer, oblique incidence propag. and ionospheric attenuation 78—73578
E-region, appl. of group and phase height meas. to electron density profile distortion meas. 80—109299
Earth surface layer, EM wave refl. and transmission coeffs., linear ramp model 80—61759
Earth-ionosphere waveguide, VLF radio signal refl. from day-night transition region 79—96859
electrodynamic boundary problems, method for solving 80—95773
electron beam, relativistic mirror feature, perp. temp. effects 80—78749
ELF normal mode reflection and absorption, nighttime ionosphere effects 79—8754
ELF radio waves, refl. from sporadic-E layer rel. to nocturnal propag. vars. 78—36392
external dielectric reflection, beam sideways displacement 77—61896
F_2-layer, vars. of multiple rays on short radio waves 77—21972
F-region, nighttime, mid-latit., refl. min. freqs. correl. with interplanetary mag. field 79—58151
Faraday effect for Mossbauer radiation at oblique incidence 80—50236
ferrite, magnetised, nonreciprocal refl. of EM waves 78—71006
ferrites, mag. permeability meas. method, UHF wave total internal reflect. 78—57994
Gaussian beam at normal incidence on dielectric sandwich slab 79—7062
Gaussian beam wave refl. by inhomogeneous slab with permitt. perturbation 80—63897
Gaussian envelope pulse reflection from moving inhomogeneous medium 80—9777
Goos Haenchen negative shifts 78—78865
grating reflection theory, Rayleigh hypothesis validity conditions 79—50195
ground reflectances, atmospheric effects in space meas. 80—17373
H-polarised EM wave by isotropic moving plasma, transient response 80—64731
Hertzian waves, reflection and diffraction by moving layers *(German)* 80—87266
HF and VHF refl. from E_s-layer on 1050 km path, M factor determ. 77—17281
HF fading ionospheric reflection channel, delay and Doppler power spectra 79—8765
HF propagation along concave surfaces, analysis 80—5664
HF signal reflection obliquely from ionosphere, trajectories 77—21996
HF waves reflected from ionosphere, freq. var. *(Chinese)* 80—56665
homogeneous layer, transmission and refl. coeffs., integral eqn. *(German)* 78—82907
impedance wedge, refl. coeff. at diffraction of plane wave, anal. *(Russian)* 77—6976
in plasma, off metallic bodies, physical optics method 77—65877
incremental reflection coeff. at permittivity profile inflection, generalised WKB and Katsenelenbaum's methods comparison 80—91728

electromagnetic wave reflection continued
- inhomogeneous anisotropic ionosphere, refl. of $10\text{-}10^3$ Hz and 15-80 kHz normally incident waves 78—28375
- from inhomogeneous layer, asymptotic soln. 77—83794
- inhomogeneous lossless dielectric slab, permittivity profile reconstruct. from reflection coeff. spectral anal. 79—36819
- inhomogeneous media, conductivity profile determ. by time domain reflectometry 79—36820
- inhomogeneous medium with large-scale random inhomogeneities statistical characts. *(Russian)* 79—882
- inhomogeneous medium with permitt. perturbation 78—86996
- interface between relatively moving media, total refl. 79—55032
- interface plane wave reflection and refraction, positron polarisation effects *(Russian)* 80—79431
- ionosphere, effect of gravity waves on 100 kHz Loran-C signals 80—109304
- ionosphere, equatorial, theoretical model of spread-F echoes in HF and VHF bands 78—85764
- ionosphere, evidence for reflecting layer below classical D-region 80—98508
- ionosphere, ionisation profiles rel. to ELF refl. 78—36234
- ionosphere, LF field strength meas. on single-hop path 77—29547
- ionosphere, LF refl. coeff. determ. via modulation method 78—45114
- ionosphere, limited height resolution effect in differential-phase partial-refl. expt. 77—21991
- ionosphere, man-made whistler-mode signals obs. near electron gyrofrequency by spacecraft 78—28418
- ionosphere, nonlinear effects during partial radio wave refls. 77—60516
- ionosphere, O-mode HF wave refl. rel. to plasma instabilities and electron temps. 78—40756
- ionosphere, partially reflected radio signals *(Russian)* 79—48603
- ionosphere, perturbation of collisional plasma by opposing EM wave, anal. *(Russian)* 77—9605
- ionosphere, plasma disturbance by extraordinary wave 77—29542
- ionosphere, polarisation of reflected SW radio waves on slant path 78—73573
- ionosphere, radio waves oblique refl. at horizontal electron density gradient, ionogram simulation 77—78559
- ionosphere, radiowaves partial refl. expt., quasi-longit. approx. to generalized magnetoionic formula 77—13170
- ionosphere, randomly dispersive and absorbing, HF pulse reflection 79—84568
- ionosphere, reflection drift data, internal consistency analyses 79—53539
- ionosphere D-region, partial refls. ang. and temporal characts. 79—66858
- ionosphere E_s-layer, meteors propag. 77—25837
- ionosphere E-region, reflected radio waves arrival direction 79—25387
- ionosphere HF signal, group path variations from modulation envelope measurements 80—51597
- ionosphere reflected radio signals, effect of travelling disturbances on statistical characts. 78—45092
- ionosphere reflected signal, sum phase random props. investigation 79—53615
- ionosphere sudden frequency deviations (SFD), appl. as detectors of solar flares EUV radiation 80—8484
- ionosphere VLF refl. coeffs., appl. to electron density profile parameters estimation 79—53614
- ionospheric reflection of radiowaves, multimode signal operation, propag. direction fluctuations 77—53309
- ionospheric reflections, meas. of fluctuations in angle of arrival and amplitude 80—17439
- isotropically scattering semi-infinite medium, diffusely reflected radiation intensity *(Russian)* 79—34948
- lakes, ice-covered (North Slope, Alaska), radar return differences 79—2298
- layered anisotropic media, construction of input wave impedances by direct tensor method 79—94136
- layered continuously inhomogeneous anisotropic media 79—72465
- leaf radiation stochastic model 77—32880
- localised RF fields, duct propag. along inhomogeneous magnetoplasma column 79—46453
- lossy plasma half-space, transient refl. for TM polarisation 79—98916
- low latitude whistlers, lower and upper freq. cut-off explanation 80—82131
- magnetoelectric medium boundary, semi-infinite, power refl. ratio and transmission coeff. 79—31776
- magnetosphere, man-made whistler-mode signals obs. near electron gyrofrequency by spacecraft 78—28418
- materials, submillimetre wave surface reflectivity 77—36191
- Maxwell equations, time-harmonic, exterior boundary-value problem of EM reflection 80—28148
- medium with sinusoidally modulated permittivity, EM wave reflection from boundary 78—25778
- mesosphere, high-resolution VHF radar refl. rel. to turbulence structs. obs. 79—100895
- metallic cylinder, elliptic, reflection coeff. obs. 77—88620
- metallic thin film, EM wave induced voltage 79—56330
- meteor trail radar refl., maximum ionization height detect. method 80—8487
- meteors, train refl. point motion rel. to radar echo drift deceleration 78—36538
- MF sky wave, combined terrestrial diffraction/ionospheric reflection effects 78—28410
- microwave transmission characts. *(Norwegian)* 79—29834
- microwave wavelength diffr. ellipsometry, polarisation and refl. coeff. 79—55034
- microwaves reflection from air-water interface, appl. to absorpt. and spreading films detect. 79—5690
- moving dielectric medium, Brewster angle for E-polarised wave 77—38776
- moving interfaces, influence of transition layer thicknesses *(Russian)* 78—46490
- from moving ionisation front 77—39430
- moving media, plane waves and refl. from moving interfaces 80—63890
- nearly layered randomly inhomogeneous medium, reflection coefficient 80—18968
- nomogram for reflection coefficients for plane waves against flat surfaces 79—18338
- nonlinear, incident to plasma layer, in longitudinal field *(Russian)* 79—19040
- nonlinear absorbing medium, plane wave reflection *(Russian)* 79—984

electromagnetic wave reflection continued
- nonlinear anisotropic dielectrics, nondispersive waves, EM disturbance propag. and reflection 80—106429
- nonlinear medium, beam reflection and refraction 79—86206
- nonlinear medium, EM wave reflection coeff., discontinuity 80—28151
- nonlinear medium, incident radiation parameters dependence *(Russian)* 79—18328
- nonlinear medium, plane boundary, simple wave theory appl. 78—78866
- nonlinear medium with one-dimensional random nonuniformities, statistical analysis 80—106421
- nonuniform helical delay system anal. *(Russian)* 79—18336
- one-dimensional propagation, calc. of refl. and transmission coeffs. 77—23599
- opal glass, spectral reflection coeff. and luminanance factor absolute meas. *(German)* 77—87802
- perfect elastic conductor, mag. field effect *(French)* 78—25772
- on periodic corrugated solid media, reflected wave anal. 79—13875
- periodic structure with varying permittivity 79—86109
- plane and cylindrical jet streams, e.m. reflectivity and scatt., anal. 77—579
- plane heterogeneous waves, energetic balance energetic balance for a transparent incidence medium *(French)* 78—33653
- plane interface, refl. and refr. of arbitrary e.m. wave 77—580
- plane wave, vertically polarized, from periodic rough surface 78—22073
- plane wave reflection from nonlinear absorbing medium 79—81478
- plasma, EM pulse reflection, from moving inhomogeneous plasma 77—51188
- probabilistic model for the reflection of waves from a rough surface 79—40380
- pseudo Brewster angle, vertical polarization reflection coeffs., between two media 78—5403
- pulsed EM wave, from inhomogeneous layers 78—1131
- pulsed EM wave refl. by nonuniform moving conducting medium 80—43234
- pulsed radiation from line source in two-media configuration refl. and transm-tted waves 79—64153
- radar, differential reflectivity and differential phase shift 78—57270
- radar impulse reflection from nonlinear random sea 80—12416
- radar reflection from lunar surface, Luna 23 meas. at 3.1 cm wavelength 80—8560
- radar reflections in rock salt 78—96215
- radar reflectivity calibration using ground return targets 79—53471
- radar reflectivity of ground-level hail in Colorado hailstorms 79—53470
- radar reflectivity profile classified by rain types 80—101420
- radar reflectivity variations with height due to wind shear on rain cells *(French)* 78—53682
- radar reflectivity/rainfall rate relation, effect of vertical air motions 77—45098
- radar reflectivity/rainfall rate relation for seeded and nonseeded clouds 77—45099
- radar signal reflection from sea surface, spatial intensity fluctuations 80—109170
- radar signal reflection from Sun, efficiency of four-plasmon interactions 80—101582
- radiation fields in biaxially anisotropic media 78—66723
- radiative transfer with anisotropic scatt. in planar medium with collimated radiation 79—55319
- radio pulse reflection from ionospheric model, distortion, compression, approximate theoretical solution 77—21969
- radiowave refl. from ionosphere, large-scale screen speed determ. 77—9602
- radiowave scattering from uneven surface and law of conservation of energy 78—46492
- radiowaves, tropospheric reflection of differently polarized transient signals 79—29839
- rain reflectivity meas. by radar and disdrometer, comparison 79—53546
- random layered media, multiple refl. rel. to thermal-radio emission, Antarctic glaciers appls. *(Russian)* 77—33106
- randomly inhomogeneous medium with reflecting boundary, wave intensity fluctuations 80—42075
- reflection coeff. meas., computer controlled network analyser calibration 78—89463
- reflection coefficient discontinuity in total internal refl. from inverted population region *(Russian)* 78—58891
- reflection gratings, perfectly blazed with rectangular grooves, EM reflection characts. 79—10246
- relativistic Doppler frequency conversion, on relativistic electron beam front, exptl. obs. 77—34799
- relativistic electron bunch, freq. conversion efficiency 78—1143
- rough surface, asymptotic soln. for reflectivity 80—53189
- rough surface, energy conservation for refl. and transmissivity 80—53188
- rough surface, Fresnel's integrals, field calc. *(Russian)* 77—75372
- rough surface, reflection coefficients for horizontal and vertical polarization *(Japanese)* 79—94135
- scattering cross section of radiowaves reflected from planet with spherically symmetrical atmosphere 80—21935
- Schwarzschild black hole, focusing gravit. mirror effect 80—46602
- semi-infinite solid-state phase grating, optical props. 78—87155
- short-wave echo azimuthal variation obs. over 2300 km *(Russian)* 78—4027
- soil, ultrashort radio waves reflectance rel. to moisture content determ. 78—16075
- solar radiation diffusive reflection by plane parallel planetary atmosphere 77—5471
- solar radiowaves diffraction and refl. from lunar limb during solar eclipses *(Russian)* 78—65586
- Sommerfeld integral, range of applicability of Van der Pol's evaluation 79—36822
- spatially dispersive crystal, reflectivity and transmittivity 80—99604
- sporadic-E layer radiowave reflection, full-wave anal. 77—87176
- statistical analysis, wave reflected from randomly inhomogeneous layer description, by series satisfying causality condition 80—106420
- strong radio waves in ionosphere, self-focusing instability near caustic 78—45107
- submillimetre wave generation, upshifted reflection, from moving ionisation front 77—34796
- superluminal flow, EM wave refl. 79—27138
- surface wave travelling along duct, scatt. by cond. sphere, refl. and transmission consts. 78—17846
- surface waves at absorbing/amplifying media interface 80—43239

electromagnetic wave reflection continued
- time domain reflection from inhomogeneous and dispersive slabs 78−62985
- time varying medium, transmission and refl. of EM wave 79−81341
- time-varying medium, EM wave reflection anal. 79−25385
- total reflection by small slotted capacitive cylinder 80−5662
- transform-pair relationship between incident and scatt. fields from arbitrary reflector 79−7058
- tropopause, VHF radar partial specular refl. rel. to detect. 80−8411
- troposphere VHF radar echoes, appl. to velocities and irregularities study 79−16701
- VHF radar obs. of stratosphere, specular reflection 79−39822
- VHF radar signals, partial refl. and scatt. from clear atmosphere 78−81278
- VHF radar signals partial refl. from troposphere 78−85656
- VLF propagation in Earth-ionosphere waveguide, mode refl. and transmission coeffs. 77−53143
- volume phase grating, reflection, Mathieu functions theory 79−14113
- waveguide impedance meter verification scheme 78−37035
- γ-ray albedo from surface of reflecting barrier 78−1154
- Si, surface, selectively roughened, polarimetry of specular and nonmultiple scatt. EM radiation 79−13904

electromagnetic wave refraction
- *see also electromagnetic wave propagation in plasma; light refraction*
- anisotropic media interface, arbitrary wave refl. and refr. 77−68170
- atmosphere, microwave refraction coeff. rel. to humidity 78−69398
- atmosphere, propag. of microwaves, refr. and absorpt. coeffs., optimal orthogonal expansion props. 80−98414
- atmosphere, radio refr. index struct. parameter height distrib. with lower boundary spatial transition 78−73491
- atmosphere, refr. index struct. parameter from refractivity and amplitude scintillation meas. at 36 GHz 78−81316
- atmosphere, refraction of MM-wave radio noise from cosmic sources near horizon, meas. 80−21813
- atmospheric boundary layer, radio and optical waves expt. investigation 80−36400
- atmospheric radiowave refractive index meas. using digital refractometer 78−86321
- biotelemetry antenna and propagation requirements for appl. for fresh water fish 77−78074
- dielectric interface, EM wave tunnelling 79−41306
- double ray refraction, in moving anisotropic media *(Russian)* 79−18329
- Earth interior, refr. index distrib. image reconstruction via iterative ray tracing between boreholes 80−98466
- EHF clear air refractivity calc. procedure 78−57266
- electrodynamic boundary problems, method for solving 80−95773
- EMF air refractivity, variability w.r.t. temp. pressure and freq. 77−41112
- ferromagnetic medium, magnetised, unattenuated refracted wave propag., optical modulation appl. *(Russian)* 78−25774
- HF signals, magnetospheric propag. by wave refr. on electron density gradients 80−4196
- homogeneous wave energy flux under conical refraction and induced gyrotropy 78−17861
- inhomogeneous and weakly anisotropic medium, tangential conic refr. *(Russian)* 79−98291
- inhomogeneous stratified atmosphere, normal-wave soln. 78−53710
- interface plane wave reflection and refraction, positron polarisation effects *(Russian)* 80−79431
- invariant molecular tensors, definition in origin change, refraction and Faraday, effect 80−53363
- ionosphere, man-made whistler-mode signals obs. near electron gyrofrequency by spacecraft 78−28418
- ionosphere, refr. scatt. as explanation for SHF scintillations 79−48615
- ionosphere refraction, effect on mean field height determ. from Faraday fading records 80−8482
- IR lidar, atmospheric refractive effects at 10.6 μm wavelength 80−36392
- Jupiter magnetosphere, kilometric radiation refr. by Io plasma torus 80−72866
- magnetosphere, man-made whistler-mode signals obs. near electron gyrofrequency by spacecraft 78−28418
- methane, ground state, dipole oscill. strength distrib., rel. to molar refractivity and dispersion energy 77−71835
- microwave beam, X-band, transmission through dielec. thin slab, displacement 80−1107
- microwave birefringence at gyrotropic boundary by inclined plane wave *(Slovak)* 78−55281
- microwave propagation in standard atmosphere, ducting, subrefraction effects, radio links appl. *(Norwegian)* 79−29835
- microwave transmission characts. *(Norwegian)* 79−29834
- moving dielectric medium, Brewster angle for E-polarised wave 77−38776
- nonlinear medium, beam reflection and refraction 79−86206
- nonlinear medium, incident radiation parameters dependence *(Russian)* 79−18328
- nonlinear medium, plane boundary, simple wave theory appl. 78−78866
- nonstandard atmosphere, arrival angle and echo delay meas. 77−64397
- plane interface, refl. and refr. of arbitrary e.m. wave 77−580
- plane wave reflection from nonlinear absorbing medium 79−81478
- planetary atm., refraction attenuation of radio waves 80−4280
- planetary atmospheres, radiowave propag. under superrefraction, complex geometrical optics *(Russian)* 78−49353
- radar propagation, anomalous, Bass Strait, Australia 77−49131
- radar return from radar-acoustic sounding system, refractive turbulence effect 79−39821
- radiation fields in biaxially anisotropic media 78−66723
- radio refractivity diurnal variation up to 3 km over India 78−40627
- radio refractivity gradient analysis over S.E.Asia 77−91244
- radiowave propagation research, using radiosonde data 79−2350
- radiowave refraction corrections for exponential atmosphere, real-time computational method 80−98432
- radiowave refraction during transillumination of planetary atmospheres 78−96413
- ray paths in refractive scattering medium 77−68175
- ray statistics, in medium with ellipsoidal inhomogeneities and regular refr. 78−25773
- of regular refraction inhomogeneities, fluctuation characts. anal. *(Russian)* 77−578

electromagnetic wave refraction continued
- transhorizon radiocommunication by short-wave ionospheric refraction 79−84567
- troposphere, radiowaves refr. rel. to oblique-incidence sporadic-E propag. 78−73578
- troposphere, refr. index variance and its height distrib. in different air masses 77−41133
- troposphere, refr. theories of radio wave propag., review 78−69425
- troposphere, refraction effects on satellite range meas. 78−73609
- troposphere, refractive index gradients study, new approach 79−25322
- troposphere, refractive struct. using Rake probing 77−91231
- tropospheric range correction algorithm 78−61591
- VHF refraction in atmospheres of giant planets 80−98608

electromagnetic wave scattering
- *see also backscatter; electromagnetic wave propagation in plasma; gamma-ray scattering; light scattering; X-ray scattering*
- 3 mm wavelength scattering and emission characteristics of natural media 78−3770
- 11 GHz forward scattering due to rain, 9 km line of sight link 77−86995
- acoustical formations of atmosphere in field of moving point source of sound 78−32210
- active objects, negative and zero extinction cross-sections 79−13874
- aerosol, thin flat, EM wave scatt. and absorpt. 80−91723
- angular scattering of water drops and ice particles [electromagnetic interference], freq. above 10 GHz appl. 80−109183
- anisotropic scatt. in one-dimens. system, radiative transfer parametric anal. 80−5920
- antenna and scattering problems of complicated structures, mathematical methods *(German)* 79−76559
- arbitrarily shaped dielectric body inside waveguide, three-dimensional anal. 78−71005
- Arctic Ocean ice characteristics meas. by microwave scatterometry 79−84298
- array of conducting cylinders, finite difference technique 77−54656
- atmosphere, pulse propagation, scatt. and diffusion in scatterers and turbulence 79−66775
- atmosphere, radiances in absorpt. bands, calc. methods including multiple scatt. 78−61554
- atmosphere, solar radiation absorpt. by H_2O vapour, including multiple scatt. 78−61553
- atmosphere, wave scatt. by turbulent flows in wake of artificial satellites 79−8730
- atmospheric amplitude spectra in absorption region 78−44920
- attenuation caused by rain above 10 GHz freq. *(French)* 78−53686
- axially incident plane wave scattering by body of revolution 80−74284
- axisymmetric bodies with surface fractures, diffraction field and scatt. calc. 80−43236
- axisymmetric dielectric, or perfect conductors imbedded in an axisymmetric dielectric 77−58234
- axisymmetric obstacles in axisymmetric dielectrics, method of moments soln. 79−72460
- axisymmetric scattering by conical bodies 80−18971
- azimuthal angle of T-D mode induced scatt. from parametric ion-acoustic wave 78−75322
- background slab affecting scatt., profile reconstruction algorithm 80−94644
- backscatter cross-section, precision meas. as function of freq. 77−18014
- backscatter from conducting rectangular corrugations, radar appls. 79−18332
- backscatter from metallic sphere in radially inhomogeneous plasma sheath, anal. *(Russian)* 77−7558
- backscatter matrix of dielectric spheroids 78−66716
- backscatter of large rotating conducting cylinder of arbitrary cross section 79−18331
- backscattered field, from random media, spatial correlation function 78−25779
- backscattering, multiple, from randomly fluctuating media 77−50593
- backscattering effects due to diffusion by the Earth's surface *(French)* 78−24289
- biostructure prolate spheroidal models, EM wave absorpt. and scatt. 77−77941
- bistatic radar signals, scattering by planetary surfaces 80−41743
- black hole, Reissner-Nordstrom, coupled gravitational and EM perturbs., scatt. matrix, energy conversion, quasi-normal modes 80−67775
- book 79−72470
- boundary element calculation method 78−90347
- buried inhomogeneities, general three-dimens. formalism 80−95769
- charged particle shock accel. by EM wave 77−54661
- charged particles internal forces, moving faster than light in a medium 80−78751
- charged sphere, homogeneous, isotropic, EM wave scatt., surface charge effects 78−13646
- circumstellar dust shells, polarisation by Mie scatt., Monte Carlo anal. 80−98650
- circumstellar envelopes scatt., radiation linear polarisation spectrum rel. to mag. field determ. *(Russian)* 80−90344
- classical system, stimulated emission and absorpt., appl. to free electron laser 78−63047
- cloud or rain layer, microwave thermal emission, scattering effect 77−91211
- cluster of spheres, scatt. problem, soln. using Debye potentials 79−31800
- coherent EM waves in pair-correlated random distribs. of aligned scatterers 78−33676
- coherent function of radiation source field in unbounded scattering medium *(Russian)* 78−1160
- coherent scattering from relativistic electron beams, submillimetre wave generation 77−34798
- complex bodies, effective scattering area, computer aided method *(Russian)* 78−13647
- concentric finite circular cylinders, TM plane wave scatt. 77−75389
- conducting boundary multiple scatt. expansions and mode distribs. 77−42465
- conducting cylinder arrays interspaced by inhomogeneous dielec. 78−78862
- conducting half plane below stratified overburden 78−57167
- conducting screen, excitation of object through aperture 79−13871
- conference on electromagnetic wave scattering in radiocommunication, Cambridge, MA, USA (Oct. 1977) 79−29836
- corrugated conducting surface obliquely incident plane waves 77−3519

electromagnetic wave scattering continued
corrugated conducting surfaces, approx. anal. by surface impedance modelling 77—79725
from corrugated conducting surfaces with inhomogeneous surface impedance, anal. 78—62987
corrugated gratings, TE polarisation, anal. by Rayleigh hypothesis, num. evaln. 77—3520
by corrugated periodic trapezoidal conducting surface, TE/TM polarisation 78—62994
corrugated structures, invest. using impedance boundary conditions 78—37790
current source-function technique soln. for EM scattering from half plane 78—37795
cylinder, direct and inverse scatt. problems, Dirichlet boundary conditions 80—95774
cylinder, infinite tilted, linearly polarised incidence at arbitrary angle 80—58457
cylinder, inverse scattering problem, determ. of shape from far field data 80—83543
cylinder loaded by active continuously variable surface impedance 78—22068
cylinder of finite conductivity, symmetry group and natural resonances 79—45888
cylinders in translational motion, Fourier spectrum evaluation 78—9300
cylinders of finite geometry, singularity expansions 79—7056
cylindrical conductor, exact surface-impedance matrix expression 79—98266
cylindrical vector waves expansion in terms of spherical vector waves, EM scatt. appl. 77—10817
D-region, negative ions effect on Thomson scatt. in presence of electron heating 79—16739
D-region, southern hemisphere, radio wave scatt. obs. 78—36363
degenerate TM mode scattered by impedance step 79—64160
dielectric and absorbing nonspherical particles, scatt. and polarisation props. 77—34823
dielectric body, long EM wave scatt. 80—74283
dielectric circular cylinders, elimination of resonant solns. of integral eqns. 80—63896
dielectric cube, dipole moments 77—58236
dielectric cylinder, new Green's functions and integral eqns. 80—48123
dielectric cylinder, resonant scattering 77—23598
dielectric cylinder scattering, extension of boundary condition 79—18333
dielectric cylinders, surface integral representations 78—42263
dielectric discs in rectangular waveguides *(Russian)* 77—18050
dielectric grating, numerical anal. 79—886
dielectric infinite cylinder embedded into another 79—59620
from dielectric infinite cylinders, numerical results 77—31050
dielectric plate, determ. of index profile from scatt. data 79—49067
dielectric scatterers, near-field display and processing 79—76560
dielectric scattering alternative surface current formulation 78—62991
dielectric sphere, eccentrically stratified, scatt. theory 80—14275
dielectric sphere, EM scatt. in diverging radiation field 77—83792
dielectric spheroids, forward and backward scatt. 79—13876
dielectric spheroids and ellipsoids, Fredholm integral eqn. 77—19142
dielectric spheroids and ellipsoids, integral eqn. soln. 78—85622
dielectric surfaces, rough, interaction of EM waves 77—43688
dielectric wedge, numerical soln. 77—58232
dielectric-loaded trough, in conducting plane 77—54655
differential attenuation at 13 GHz and 20 GHz on 53 km link *(French)* 78—53684
diffraction on slit and on strip, scatt. pattern calc., asymptotic methods 78—86993
diffuse radiation emerging from semi-infinite medium, intensity accounting for inner refl. *(Russian)* 79—8637
diffusion equation derived from space-time transport equation 80—78772
dipole scattering of EM waves propagating through rain medium 80—36388
direct scattering from one-dimensional inhomogeneous media, anal. 79—10244
distortion characterisation of tropospherical channel for digital transmission *(French)* 79—58065
by E-region anisotropic inhomogeneities oriented along geomag. field 78—53771
Earth crust, nonparallel stratified models, scattered EM radiation field 78—44773
Earth crust, nonparallel stratified models, scattered surface wave 78—40489
Earth EM scattering from buried wires 79—16369
echelette grating scatt., smoothing process for mode-matching soln. 78—1134
echo cross-section of longitudinally slotted cylinder, method of moments anal. 78—86992
echo width meas. 79—3614
echoes scattered by random fluctuating surface, statistical model *(French)* 77—11066
edge conditions, moment method solutions 78—1127
effective electric field in an inhomogeneous medium 79—13869
effective scattering area of objects, average-value estimation in real-time *(Russian)* 77—83790
eigenmode scattering relations for plane-stratified gyrotropic media 79—72459
electron beam, axially moving cylindrical, surrounded by dielectric cylinder, EM wave scatt. 77—14645
electron scattering, calc. methods for spectral line broadening *(Russian)* 77—17347
EM wave rain induced attenuation and cross-polarization calcs. *(French)* 78—53677
energy conservation relation, scatt. from obstacles with impedance boundary condition *(French)* 77—577
evanescent waves, elastic scatt. 79—98264
Ewald-Oseen extinction theorem, Maxwell's eqns., boundary-value problem 78—62974
exosphere, global model using optical and incoherent scatter meas. 78—36343
exterior scattering from spheroidal composite objects, soln. 80—87267
extinction cross section for single particles at 100 GHz 80—82116
F-region, HF backscatter curtains rel. to plasmapause location 79—58165
F-region, nighttime, incoherent scatt. obs. rel. to neutral atmosphere parameters var. *(Portuguese)* 80—41584

electromagnetic wave scattering continued
Fermi liquid, two-component, degenerate, charged, scatt. cross-section *(Russian)* 77—7928
field problems, Green function selection and effects on matrix condition 80—14271
field theory appl. of plane wave scattering by semi-infinite dielectric slab 80—9790
fin corrugated periodic surface, TM polarised EM scatt. 77—27224
finite cylindrical scatterer near imperfectly conducting ground 78—71003
finite wedge with linearly varying surface impedance, anal. 77—61901
finned cylinder, space-time integral eqn. 77—75390
foam structures, UHF radiation scatt. *(Russian)* 77—6978
forward and backward scatt., from active spheres and fibres, calc. 78—37789
forward scatt. approx. by circular cylinder 78—32689
forward scattering anomaly in hollow penetrable body 78—62986
forward scattering in random media, path integral approach 78—62979
forward/backward scattering from liquid/solid hydrometeors, Rayleigh approx. 79—25321
Fourier transform appl. 77—58235
Fourier transform technique applied to high freq. scattering problems 80—23605
frequency selective surfaces, EM wave scatt. from periodic screens, waveguide and optics appls. 80—87278
Gaussian beam, from perfectly conducting column 77—88625
Gaussian beam wave by two semicylindrical bosses on infinite perfectly cond. plane 80—63898
Gaussian beam wave scatt. from perfectly conducting column 78—1135
grating of parallel conductors scattering anal. 78—50682
gravitational scatt. of zero rest mass plane waves 78—4542
Green's function moment method for solution of two Pocklington type integral equations 78—55279
grid of parallel cylindrical wires with finite cond., Green function method 80—53190
Gulf of Alaska SeaSat Experiment 14.6 GHz scatterometer surface wind obs. 80—46200
gyrotropic media, artificial, EM scattering 80—106423
gyrotropic media, plane-stratified, scatt. theorem 79—72461
gyrotropic sphere, EM wave scatt. and absorpt. 79—41305
harmonic, generation, plane EM wave interaction 80—48120
harmonic plane EM wave propag. in dielec. with one-dimens. random nonuniformities, multiple scatt. 80—43232
HF radiowave forecasting scattering by induced ionospheric irregularities, expt. *(Russian)* 77—29553
HF scatt. from multiple-edge diffraction at shadow boundaries 77—38781
HF scattering by conic frustum 79—76552
HF wave propagation with lateral deflection from great circle arc, investigation 78—45096
hole in surface of conducting body, rigorous and approx. methods *(French)* 79—76550
holographic gratings, sharp boundaries, modal theory, EM wave propag. 80—83672
holographic unslanted transmission and reflection gratings, modal theory, EM wave propag. 80—83673
homogeneous electrically anisotropic medium, dispersion equations *(Czech)* 80—37938
by homogeneous material body of revolution 79—36818
homogeneous medium, moving areas, EM wave diffr. and scatt. *(Russian)* 79—27141
Huygens' principle electrodynamic formulation for scatt. in nonuniform medium 77—79729
hybrid computation by Unimoment/Monte Carlo technique 77—14646
hydrometeors, extinction and scattering in 0.25-15 μm range 79—53501
ice, forward scatter, crosspolarisation 78—3853
by ideally conducting bodies in rectangular waveguide *(Russian)* 79—884
ideally conducting bodies in rectangular waveguide 79—81336
immersed object EM signature determ., modified physical optics technique 77—5372
incoherent backscatter from rough surfaces, two-scale model re-examined 78—71013
incoherent scatter radar, correlation function meas. 77—73888
incoherent scatter results for co-ordinated special intervals at St. Santin (France) 79—2416
infinitely long circular cylinder, backscatter of arbitrarily polarised EM wave 80—9778
infinitely long cylinder, plane wave scattering, numerical investigation 78—1129
information encoding and propagation in scattered fields by complex zeros 79—50238
inhomogeneous composite bodies of arbitrary shape 77—19143
inhomogeneous dielectric, EM wave scatt. and propag., Born approx. 79—41308
inhomogeneous media, characterisation via space-variant transfer functions 78—71012
inhomogeneous nonlinear medium and time-varying medium, decay interaction of wave packets 80—14386
inhomogeneous nonspherical object scattering 79—64179
inhomogeneous sphere, system of p-tuple series eqns., iterative soln. 78—62976
integral eqn. and HF asymptotic techniques combination for problem soln. 77—19135
integral eqn. resonant solution elimination 79—45895
integral formulation for randomly rough surfaces *(French)* 80—53193
interface, with uniform relativistic accel. 80—4891
intergalactic medium, Thomson scatt. rel. to pregalactic fluctuations visibility, upper limit on q_0 80—8717
interplanetary medium, weak scatt. approximation appl. to anal. of RF scintillation 77—9706
interplanetary scattering angle, anisotropy rel. to plasma inhomogeneities *(Russian)* 80—36468
inverse electrodynamic scattering problem, general prop. of field with passive scatterers 80—63893
inverse problems with causality between sources and field 80—9783
inverse scatt. problem of lossy dielectrics, exact soln. 77—79732
inverse scattering, linear delay integral equations 79—55033
inverse scattering methods 77—31048
inverse scattering problem, discrete sampling approach 77—75395
inverse scattering theory, n-dimensional FFT tomography appl. 80—9784

electromagnetic wave scattering continued
  ionosphere, Arctic, European Incoherent Scatter (EISCAT) project *(French)* 79—2437
  ionosphere, artificial quasiperiodic inhomogeneities formation due to powerful radiowave 79—84585
  ionosphere, artificial small scale irregularities, field aligned scattering *(Russian)* 78—32274
  ionosphere, asymptotic distrib. law of scatt. field amplitude and phase 77—29548
  ionosphere, auroral, field-normal plasma-line scatt. detect. expt. 78—73580
  ionosphere, backscatter echo spectral analysis and radio transmission forecasts *(French)* 79—29912
  ionosphere, effects of induced and combination scatt. on propag. of strong radio waves 77—91345
  ionosphere, foreshortened radiowave scatt. by auroral inhomogeneities *(Russian)* 77—64519
  ionosphere, H_E scatter signals power calc. 77—60520
  ionosphere, incoherent scatter radar meas. at Arecibo Observatory 78—81488
  ionosphere, incoherent scattering, total cross section 80—72690
  ionosphere, incoherent scattering of radio waves by whistler mode oscills. 78—45135
  ionosphere, intersatellite whistler-mode pulses scatt. 78—69605
  ionosphere, limited beam diffusion due to scatt. on random inhomogeneities 77—91349
  ionosphere, limited height resolution effect in differential-phase partial-refl. expt. 77—21991
  ionosphere, metallic ions of meteor origin effect in VHF forward scattering, contribution to sporadic-E formation 80—67461
  ionosphere, nonlinear scatt. of microwaves from solar power satellite, theoretical anal. *(Japanese)* 80—94634
  ionosphere, plasma parameters, incoherent scatt. of EM waves, EISCAT project *(French)* 80—82142
  ionosphere, pulse time dispersion, Earth's mag. field effects 78—45116
  ionosphere, refr. scatt. as explanation for SHF scintillations 79—48615
  ionosphere, scattering in linear layers with ellipsoidal inhomogeneities 79—62662
  ionosphere, scintillation, power law phase screen model, strong scatt. 80—61962
  ionosphere, scintillation, power law phase screen model, weak scatt. 80—61961
  ionosphere, singly scatt. wavefields, angle depend. 77—87174
  ionosphere, spatial dependencies of props. of wavelike inhomogeneities, anal. of diffraction patterns 80—36448
  ionosphere, stimulated Brillouin scatt. detect. by Jicamarca radar 78—77412
  ionosphere, whispering-gallery type mode scattering 80—98514
  ionosphere, Z-mode MF wave scatt. in propag. expts. between two satellites 79—53646
  ionosphere D-region, partial refls. ang. and temporal characts. 79—66858
  ionosphere HF signal, group path variations from modulation envelope measurements 80—51597
  ionosphere incoherent scatter measurement complex, Kharkov Poly. Inst. 77—9555
  ionosphere small-scale plasma scatt. intensity, modulation trough 79—58159
  ionospheric backscatter sounding method using spatial and spectral sampling, for investigation of plasma inhomogeneities *(French)* 79—29911
  ionospheric effects on radio communication and ranging pulses 80—26667
  irregular shape dielectric bodies, scatt. cross sections 79—76555
  isotropic scattering medium, two dimens., source function, radiative flux, intensity 77—50595
  Kirchhoff approximation in horizontally polarized backscatt. from random surface 79—7061
  Langmuir soliton EM wave scatt., theory *(Russian)* 80—38564
  large conductive cylinders, moment method/mapping function technique 77—71909
  layered media, radiative transfer theory for scatt. 79—76553
  LF EM rad. scatt. by dielec. body, variational principles 79—89837
  long thin wire scattering widths, meas. using open resonator 78—46489
  lossy dielectric bodies of revolution, arbitrarily shaped, scatt. props. 78—22072
  lossy dielectric wedge, numerical soln. 77—19144
  low frequency field calc., iterative method 78—29876
  low frequency scattering, by slit in infinite impedance plane 79—86110
  matrix methods in potential theory and EM scatt. 79—94133
  medium scale broadcasting satellite for experimental purposes, rain-scatter interference 79—8668
  medium-particle correlation effects in single scattering from particles in fluctuating medium 80—32917
  mesosphere, VHF radar scatt. and vertical vels. meas. at temp. latits. 79—16572
  mesosphere incoherent scatter spectrum, ion component meas. in 60 to 90 km region over Arecibo 79—16569
  microwave attenuation due to rainfall, rain fine structure meas. *(French)* 78—53680
  microwave backscatter modulation by shoaling ocean waves 78—57212
  microwave by sea waves, meas. at 8 mm and 30 mm *(Russian)* 77—5210
  microwave coherent scatt. from relativistic electron beams 77—42477
  microwave cosmic background, scattering in clusters of galaxies, 9 mm obs. 80—105366
  microwave cosmic background radiation, scattering in clusters of galaxies 80—105367
  microwave cross-polarization due to precipitation in atmosphere *(French)* 78—53674
  microwave exposure of animals, perturbation by dielectric restraining materials 77—21665
  microwave field distribution, phase modulated scattering method appl. *(Japanese)* 79—85151
  microwave magnetic-field distribution meas. using new resonant scatterer 79—49211
  microwave scatterometer, backscatter optimisation using complex charact. polarisation concept 79—100966
  microwave solar radiation, forward scattering from water surface 78—44872
  microwaves in plasma, enhanced scatt. at upper hybrid freq. 77—7548
  Mie scattering improved algorithms 80—78771
  Mie series solution for sphere, computer program 78—66721

electromagnetic wave scattering continued
  mm wave scattering from precipitation particles, calcs. 79—22882
  mode-matching method for two-dimens. scatt., smoothing process 78—58886
  modulated energy flux, wave props. 77—65559
  moment method solution, cell size limitations 78—5404
  moment-method solutions, convergence improvement using interpolants 79—18335
  monostatic inverse scattering model based on polarisation utilisation 77—3517
  Moon, radar scatter data rel. to surface parameters from images 79—40100
  moving scattering-absorbing layer, energy and momentum conservation laws 78—25775
  moving surface scattering, evaluation using reformulated current method 79—89834
  moving surfaces, reformulated current approach 77—75393
  multilayered lossy periodic strips on artificial dielecs. 78—42262
  multilayered spherically symmetric medium, scatt. problem 79—81329
  multiple, point source in one-dimensional, randomly inhomogeneous medium, with specularly reflecting walls 80—105514
  multiple forward scattering method, randomly inhomogeneous media 80—18969
  multiple parallel strips, infinite array, modified residue calculus technique 80—9789
  by multiple rectangular cylinders, numerical anal. 78—62992
  multiple scatt. by randomly distributed and oriented dielec. scatt. 80—53192
  multiple scatt. of waves from lattice, theory 78—16697
  multiple scattering by random distribs. of discrete scatterers with coherent pot. and quantum mech. formulism 80—95768
  multiple scattering effect on backscattering from random medium 77—19137
  multiple scattering of classical EM waves by fixed dielectric obstacles, Fredholm's method 78—71008
  multiple scattering of two-dimensional Gaussian beam wave by two parallel cylinders 80—32892
  multiple scattering of waves by particle ensembles, radiation transport 77—95
  N sphere assembly in Rayleigh approx., scatt. properties 79—41304
  negative absorption objects, resonances in EM scatt. 79—64178
  noise field scatt. by large cylinder of finite length *(Russian)* 78—55284
  non-spherical hydrometeors scattering properties *(French)* 78—53676
  noncrystalline state structure determ. techniques, phase retrieval methods 78—22656
  nonhomogeneous layer above reflecting surface, scattering of waves 80—58449
  nonlinear interaction in plasma 77—11350
  nonlinear medium with one-dimensional random nonuniformities, statistical analysis 80—106421
  nonlinear theory of stimulated coherent scatt. of EM wave by relativistic electron beams *(Russian)* 80—102601
  nonrectangular patch model, elec. field formulation using a Galerkin solution 79—81332
  nonspherical dielectric and absorbing particles, scatt. functions versus Mie theory 77—58229
  nonspherical dielectric objects, biological models 78—40241
  nonspherical extinction and absorption efficiencies 79—7074
  nonstationary radiative transfer in variable scatt. medium, statistical theory *(Russian)* 77—75368
  ocean surface, radar backscatter rel. to wind speed and fetch 78—77247
  ocean surface wind obs., SeaSat scatterometer/scanning radiometer/altimeter comparison 80—46249
  ocean wave scattering theories, review 78—77243
  offset two-dimensional Gaussian beam wave by cylinder, anal. 78—86997
  one-dimensional direct and inverse scattering in causal space 80—102600
  optical theorem and reciprocity for obliquely incident wave 78—9305
  parallel dielectric coated conducting cylinders, obliquely incident, over plane conductor 78—22074
  partially redistributed resonance radiation, ang. depend. 77—42285
  particles, small, spherical, reformulation of radiation laws 78—87246
  penetrable inhomogeneous scatterer, numerical comp. of scatt. 78—66719
  perfectly conducting cone, transient and time-harmonic dyadic Green's functions 79—18334
  perfectly conducting spherical shell with circular aperture 78—71015
  periodic deformed cylinder scattering, smoothing process on mode-matching method 79—36825
  periodic dielectric struct., appl. of unimoment method 78—66725
  periodic metal surfaces, sinusoidal height profiles, Fourier series analysis 78—1128
  periodic surface, uniqueness theorems for scattering *(Russian)* 78—49677
  periodically loaded wire grid, theory 77—42467
  perpendicular wire grids over conducting half space, e.m. scatt. 77—582
  phase problem, zeroes of entire functions 78—29900
  physical model and profile reconstruction, for inhomogeneous ionised regions 80—1109
  physical optics method in electromagnetic scattering 80—46840
  planar arrays of perfectly conducting strips, analysis using physical optics approximation 80—53186
  planar wave diffraction on plate with variable surface impedance 78—9323
  plane and cylindrical jet streams, e.m. reflectivity and scatt., anal. 77—579
  plane EM scattering by conducting rectangular cylinder 80—106427
  plane EM wave two-dimens. multiple scatt. by N slits array, asymptotic formula 80—99610
  plane grating in homogeneous medium, point matching method 78—1132
  plane grating with reflector, point matching soln. 79—45894
  plane wave, by conducting rectangular cylinder, E polarised wave case 79—31779
  plane wave, by metal cone, near its symmetry axis 80—106426
  plane wave, vertically polarized, from periodic rough surface 78—22073
  plane wave scatt. from dielectric cylinders 79—55057
  plane wave scattering in inhomogeneous turbulence 79—39857
  plane waves, oblique incidence on circular conductor, integral energy characts. 78—46491
  plane waves with arbitrary polarization and incidence angle, scatt. by cond. prolate spheroid 77—42471
  polarisation of scattered radiation, in medium with internal energy sources 80—67541

electromagnetic wave scattering continued
- polariton Fermi-resonance, EM wave dispersion 80—2344
- projection method, properties of parametric system of basic functions 80—87269
- prolate spheroid, EM plane wave scatt. 80—53185
- prolate spheroid, perfectly conducting, polarisation utilisation in profile inversion 77—50594
- prolate spheroid and half prolate spheroid on plane, EM wave scatt. with axial incidence *(French)* 80—91727
- prolate spheroids, EM vs acoustic backscattering 78—46854
- pulsar pulse scattering in interstellar medium, resulting pulse shape *(Russian)* 77—78855
- pulsar signal scattering by turbulent interstellar plasma 79—5854
- quasidipole radiation of two circular cylinders with longitudinal slits 79—72468
- radar, parallel-polarised and cross-polarised radar returns from rough sea surface 80—51408
- radar backscatter from ocean surface, friction vel. depend. 78—77246
- radar remote sensing of Earth's surface, techniques, review 79—12294
- radar scattering from turbulent cylindrical plasma, model 78—22512
- radar scatterometer discrimination of sea ice types 77—41198
- radially symmetric reradiating scatterers in EM fields, formulae for simple treatment *(German)* 80—87270
- radiation and scatt. from wires and surfaces, free space impedance functions 78—86999
- radiative transfer with anisotropic scatt. in planar medium with collimated radiation 79—55319
- radio sources, superluminal, inverse Compton scatt. in mag. dipole model 80—56959
- radio sources variable at low freqs., radiowaves scatt. rel. to microarcsecond struct. 78—16550
- radio wave scattering from artificial plasma inhomogeneities, ionospheric electron density meas. appl. 79—75074
- radio waves, envelope distrib. functions and phase of periodically nonstationary process 80—4173
- radio waves, transionospheric, scintillation time struct. under weak and strong scatt. conditions 80—90281
- radio waves scattered by meteor trails, trapping by ionospheric ducts 80—4172
- radiotelescope, chromatism due to blocking and feed scatt. 78—73630
- radiowave, broadband communication, tropospheric scatt. mechanisms and channel characterization 79—29837
- radiowave ducting by stratified troposphere 79—29842
- radiowave from acoustic atmospheric formations 79—92579
- radiowave from semi-infinite plate, linear algebraic eqns. infinite system soln. 78—55286
- radiowave from uneven surface and law of conservation of energy 78—46492
- radiowave incoherent scattering by plasma, Nyquist theorem appl. 79—75024
- radiowave propag., angular depend. of rain scatt. at freqs. below 30 GHz 80—8416
- radiowave propag., scattering amplitudes and crosspolarisation of spheroidal ice particles, calc. 77—70740
- radiowave propagation, tropospheric and precipitation scatter, rel. importance in interference and coordination calcs. 78—73423
- radiowave scatt. theory appl. to radio meteor obs. in upper atm. 79—5696
- radiowave scatter communications, review 79—34935
- radiowave signal processing in ionosphere, incoherent, computerised spectral analysis *(Russian)* 79—5621
- radiowave studies of ionosphere, incoherent scatter technique development, review 78—81503
- radiowaves, multiple scattering, iterative treatment method 79—8709
- radiowaves, pulse delay and distortion by random scattering in ionosphere 79—29934
- radiowaves, trans-ionosphere, due to equatorial F-region irregularities 79—29933
- radiowaves, troposcatter aperture-medium coupling loss 79—29840
- radiowaves, troposcatter channels and appls. of adaptive equalization techniques, statistical anal. 79—29841
- radiowaves reflected from planet with spherically symmetrical atmosphere 80—21935
- rain, multiple-scatt. effect on radiometric determ. of radiowave attenuation at millimetre wavelengths 80—90260
- rain, SHF scatt. props. of Pruppacher-Pitter form drops and cross polarisation, 11 to 34.8 GHz 77—41129
- rain attenuation and depolarization of Earth-satellite transmissions at freq. greater than 10 GHz *(French)* 78—53689
- rain attenuation distribution estimation *(French)* 78—53688
- rain depolarization statistical distribution for microwave signal propag. *(French)* 78—53673
- rain induced attenuation and cross-polarization calcs. *(French)* 78—53677
- rain induced signal fluctuations, incoherent effects investigation *(French)* 78—53679
- rain scattering of microwaves, drop-size and temp. effects on forward and backward scattering 80—17317
- rain-induced polarization, theoretical model of wind gust effects *(French)* 78—53678
- raindrop induced forward and backward scattering amplitudes, tabulations 79—34884
- random media, theory and appl. of wave propag. and scatt., review 77—75376
- random media, wave propag. and weak scatt. 78—66722
- random media causing pulse spreading and wandering 80—37942
- random media strong scatt., operator and diagram techniques for intensity moment eqns. 79—64154
- random rough-surface model, comparison of variational, perturbational and exact solns. 78—66724
- ray optical anal. of scattering from dielectric coated conducting cylinder 80—83542
- ray paths in refractive scattering medium 77—68175
- ray statistics, in medium with ellipsoidal inhomogeneities and regular refr. 78—25773
- Rayleigh hypothesis in theory of diffraction by cylindrical obstacle 79—89832
- reciprocity identity for periodic surface scattering 79—36821
- rectangular dielectric cylinders, resonant mode data 78—9299
- rectangular dielectric particles, low freq. scatt. 77—42466
- rectangular slot estimation 80—18965

electromagnetic wave scattering continued
- refractive index profile and target reconstruction using time and spectral domain integral equation approach 80—9786
- regular polygonal conducting cylinder, method of overlapping regions 77—575
- relativistic electron beam in waveguide 79—10249
- remote sensing of two-layer media, microwave radiative transfer models 77—21908
- resistive strips scattering E- and H-polarised waves 80—37941
- resonance ponderomotive effects in EM wave scatt. and emission 80—69301
- response of anisotropic conducting cylinder to external source 79—7059
- rotating cylinder, amplification of reflected waves, calc. *(Russian)* 77—3523
- rotating dielectric column, EM scatt., relativistic soln. 78—50681
- rough dielectric surface, EM wave scatt. 78—58885
- rough semi-infinite dielectric plane 78—58884
- rough surface, average impulse response, satellite radioaltimeter appl. 77—25791
- rough surface, EM surface and bulk wave coupling, scatt. indicatrix *(German)* 80—32884
- rough surface, EM surface and bulk waves *(German)* 80—32883
- rough surface, energy conservation for refl. and transmissivity 80—53188
- rough surface, Fresnel's integrals, field calc. *(Russian)* 77—75372
- rough surface, reflection coefficients for horizontal and vertical polarization *(Japanese)* 79—94135
- rough surfaces, full wave and physical optics solns. 78—66717
- rough surfaces, variational principle 77—79724
- rough surfaces with arbitrary slope and freq., full wave solns. for scattered radiation fields 80—48121
- scalar wave scattering by periodic surfaces, general modal theory 80—87271
- scattered wave focusing in periodically inhomogeneous layers *(Russian)* 78—1158
- scattering by irregularly shaped perfectly conducting or dielectric cylinders 79—13878
- scattering current/aperture coupling relationship for thin finite cylinders 78—62988
- scintillation, thin screen theory for spherical wave 78—13645
- sea ice, scattering from slightly rough boundary 78—77266
- sea return backscattering CW dual-freq. X-band radar studies 77—25687
- sea roughness radio measurement at Ukrainian Academy of Sciences 77—29313
- sea surface, oil contaminations effect on radar signal scatt. *(Russian)* 77—49089
- sea surface, radar scatt. coeff. meas. via SEASAT-A satellite scatterometer (SASS) 79—5680
- sea surface scattering theory for large incident angles 77—86911
- SEASAT-A satellite microwave scatterometer for wind sensing 77—5417
- semi-infinite dielectric slabs, plane EM wave scatt. anal. using Helmholtz eqn. 80—63895
- sinusoidal surfaces, scatt. patterns 80—58448
- slab waveguide guided modes, scattering and mode conversions by circular cylinder 80—9791
- small overdense plasma particle Thomson-like RF scatt., linear perturbation theory 80—48858
- smooth convex surface HF scatt., transform-domain Galerkin soln. 77—38783
- smooth convex surfaces, high frequency, based on Galerkin procedure 78—5401
- smooth perfectly reflecting objects in smoothly inhomogeneous medium, anal. *(Russian)* 77—38774
- soft particles, Mie series appl. 79—36824
- solar corona, effects of scatt. on quiet Sun emission at freqs. <200 MHz 78—4183
- solar corona, efficiency of four-plasmon interactions in radar signal refl. from Sun 80—101582
- solar H Lyman α reson. backscatter by hot interstellar H, comparison with intervening absorpt. 80—31185
- solar resonance radiation, multiple scatt. in nearby interstellar medium 80—41874
- solar wind, radial depend. of props. from Helios 1/2 and Pioneer 10/11 scatt. expts. 78—28595
- solar wind radio scattering, meas. of spacecraft signals 78—49277
- space structure of directed radiation field in scatt. media, Monte Carlo calc. *(Russian)* 77—14643
- spectral domain approach to soln. of scatt. and radiation problems, review 80—5663
- spherical mirror scatt. theory *(Chinese)* 79—10243
- by spherical shell with arbitrarily located circular aperture, anal. 78—62989
- spherical vector wave function expansions, approximation props. 80—9788
- statistical analysis, wave reflected from randomly inhomogeneous layer description, by series satisfying causality condition 80—106420
- statistical theory, modified Bessel function distribs. 78—37794
- statistically rough surface, wave scatt., book 80—73116
- stellar opacity, electron scatt. in strong mag. field, approx. formulae 79—92662
- stimulated EM shock radiation, intense submillimetre wave generation 77—38787
- stratified inhomogeneous media, review of one-dimensional inverse scattering problem 80—46346
- stratified media, spectral domain probing 77—19138
- stratosphere and mesosphere, UHF radar echoes, for wind and turbulence obs. 77—33135
- subsurface line conductor, multiple EM scatt. 78—61317
- successive approximation method appl. for scattering from round dielectric cylinder *(Russian)* 80—63889
- surface current density calculation by mode-matching method with smoothing procedure, algorithm 80—9773
- surface current distributions, boundary conditions, described by Dirac's impulse first derivative 78—5402
- surface scatt., electric field integral eqn. formulation 77—38784
- surface scattering from piecewise planar surfaces, algorithm 78—62983
- surface wave, by metallic strip on reactive surface, reflection and transmission coeff. determ. 77—75394
- surface wave electromagnetic scattering from notches in ground plane covered by dielectric slab 80—87277
- surface wave scatt. by circular or elliptic cylinders 77—10816

electromagnetic wave scattering continued
- surface wave travelling along duct, scatt. by cond. sphere, refl. and transmission consts. 78—17846
- SW radiowaves, periodic artificial ionospheric irregularities, transient processes *(Russian)* 78—32276
- symmetric cylindrical conductor, mode-matching method calc., smoothing process 78—58887
- symmetry analysis of scattering and antenna pattern problems 77—75388
- theory, using vibrator with nonlinear contact 80—1110
- thermal microwave emission from random inhomogeneous layer over homogeneous medium 77—42726
- thermosphere, incoherent scatter meas. of props. 79—53597
- thin finite dielectric cylinder, scattering and absorption of EM waves 80—74281
- thin finite dielectric fibres, scatt. analysis 78—62972
- Thomson scattering, collision-dominated, negative ions effect, ionospheric D-region appl. 78—45118
- Thomson scattering in strong mag. field, vacuum polarisation effects 80—86632
- three-dimensional radiation and scatt., surface-type integral eqn. approach 77—38782
- time depend., boundary value formulation, integro-differential eqns. 78—66726
- time domain inverse scattering, rotationally symmetric conducting targets with oblique incidence appl. 80—9785
- transform-pair relationship between incident and scatt. fields from arbitrary reflector 79—7058
- tree-covered surface scattered radio signal spectral density obs. 77—87049
- triangular aperture, EM field scattering 79—50192
- trilateral surface cell modelling of conducting scatterers 79—36826
- troposphere, attenuation statistics at 15 and 35 GHz for very low elevation angles 79—8674
- troposphere, refractive struct. using Rake probing 77—91231
- troposphere scatter path loss, new formulas 79—48556
- tropospheric long-distance propag., multiple scatt. effect 80—109229
- two-dimensional higher-order Hermite-Gaussian beam scatt. by offset cylinder 79—55056
- two-dimensional transient scattering, new space-time integral eqn. 78—78861
- UHF/SHF tropospheric scatter radio links, scanning beams 78—81276
- uniform asymptotic theory and uniforms geometrical theory of diffraction, comparison 79—13872
- upper atmosphere, incoherent scattering, physical processes *(Portuguese)* 79—2417
- vacuum, transition radiation and scatt. in strong EM field *(Russian)* 78—58895
- variational principle for random rough surface scattering 78—55285
- vector wave equations for scattering by inhomogeneous spherical particles 79—27137
- vegetation, first-order renormalization method appl. to scattering 77—87099
- VHF ionospheric forward scattering, effect of meteors *(Japanese)* 78—81504
- VHF radar signals, partial refl. and scatt. from clear atmosphere 78—81278
- VHF waveguide dielectric scatt. model for pulse-probe data interpretation *(Russian)* 80—62682
- Voyager 2 radio signals, ang. and spectral broadening during coronal occultation, 1979 August 80—51639
- Waterman's extended boundary condition, generalised extinction theorem 77—581
- wave packets, time dependent elastic scatt. in one dimens. 78—12461
- waveform distortion by microwave scatt. 79—50859
- wedge, 90°, calculation of scattering of plane incident wave using uniform geometrical theory of diffraction 79—89835
- Wiener-Hopf matrix factorisation for problems solvable with Hurd's method 78—66718
- wire cross, plane wave incident at an angle, induced currents 78—5391

electromagnetic waves
- *see also bremsstrahlung; Cherenkov radiation; electromagnetic field theory; electromagnetism; gamma-rays; heat radiation; light; microwaves; radiofrequency cosmic radiation; solar radiofrequency radiation; sunlight; synchrotron radiation; transition radiation; undulator radiation; whistlers; X-rays*
- amplification and generation based on Doppler-effect, nonlinear theory 80—63902
- amplitude modulated, confinement of relativistic charged particles 78—38524
- anisotropic moving media, polarisation relations and dispersion eqns. to EM waves 80—9779
- automotive distributor, arc initiating processes, EM radiation reduction 80—19665
- azimuthally magnetised bigyrotropic medium, natural waves 80—37944
- bandlimiting, at variance with strong radiation condition 77—38779
- bio-electromagnetic research, reviews 80—85444
- biological effects, state of research *(German)* 78—88728
- biological effects of EM waves, interdisciplinary and international contribs. 79—48288
- biological response to non-ionising EM radiation, research perspectives 79—48289
- black body radiation, sound scattering analogue, outdoor sound propagation and reflection from ground and buildings 80—69579
- black hole, charged, EM and gravit. waves propag. 77—87470
- black-body radiation and thermal equilibrium in static gravitational field 79—67238
- cavity, integral eqn. *(French)* 78—42259
- channelled particles in cryst., EM wave emission *(Russian)* 78—14394
- channelled relativistic particles, possible resonance radiation *(Russian)* 79—23661
- charged particle beam interaction, localised disturbances development *(Russian)* 78—88377
- charged particle in plane waves, accuracy of adiabatic invariant conservation 80—37946
- charged particle self-reson. motion in EM wave with varying propag. vel. 77—75399
- classical and modern theory, appls., book 80—1101
- closed region problems, singularity extraction in kernel functions 78—66728

electromagnetic waves continued
- collisions involving gravit. and neutrino waves in general relativity 77—17886
- compression of EM waves by anisotropic media, nonreflecting crystal model, two media matching 79—81335
- conversion of gravitational waves into electromagnetic waves by a moving charge 78—93584
- cyclotron radiation from oppositely directed electron beams 78—78874
- defective dielectrics, EM heating with time depend. param., WKB calcs. 80—71367
- dielectric cylinder, nonlinear EM wave excitation by relativistic magnetised electron beam 77—19129
- dielectric materials, electromagnetic radiation in crack formation process, exam. 78—76771
- effects on man and environment 77—44719
- Einstein's nonrelativistic work *(Czech)* 80—27095
- Einstein-Maxwell equations, EM and gravitational wave spacetimes, similarity solutions 80—57154
- electric dipole at centre of spherical shell, EM radiation in general relativity *(French)* 77—5709
- electron beam explosive instability in helical resonator, RF emission 79—55520
- electron beam generated, meas. of broad spectral EM wave energy 77—38786
- electron channelling, photon prod. 80—79846
- electron radiating in waveguide, self-reson. radiation 79—55040
- electron wavelength measurability 77—71406
- EM field penetration through gaskets and seams, simple model 77—42464
- emission by charged particle in gravit. wave field *(French)* 77—67353
- emission from source moving at arbitrary angle to cryst. optical axis 77—57923
- ferromagnetic medium with variable permeability and hysteresis loss, plane EM wave *(Polish)* 77—79722
- field calculation using integral eqn. method *(Russian)* 78—82887
- field structure spatial spectra in millimetre and submillimetre wave ranges *(Ukrainian)* 78—90344
- field three-dimensional energy distrib. 78—71009
- field vector measurement, determ. of four phase quadrature components *(Russian)* 78—22067
- general physics and heat, book 79—25814
- glass, silicate, EM pulse radiation, under symmetrical bending 80—45350
- gravitational lens effect, rel. to 3C 303, QSO group in cluster 77—78878
- gravitational waves interaction, general relativity soln. *(Russian)* 79—21605
- group theoretical approach to radiation statistics 79—86129
- group velocity, four-dimensional, electromagnetic waves in electrically and magnetically anisotropic media 80—17814
- HF discharge, EM wave ionisation instability model 78—67512
- induction on a prolate spheroid, current and charge densities, missile guidance appl. 77—83782
- interaction between plane strong EM wave and weak gravit. wave *(Russian)* 77—45774
- intrinsic waves in azimuthally magnetised bigyrotropic medium 80—91733
- inverse source problem of scalar waves, acoustic and EM examples 77—30015
- Josephson vortex in inhomogeneous junction, EM radiation due to vortex motion 79—73642
- Jupiter magnetosphere, kilometric radiation spatial and temporal studies 80—77328
- large field problem soln. by extended Kinzel sectioning method 77—27228
- line sources, elec. and mag., interaction with moving magnetoplasma slab, EM radiation 80—67537
- line sources interacting with moving uniaxial dielectric or plasma half-space, EM radiation 79—92661
- linear travelling wave induction, long cond. cylinder, EM fields 78—46484
- living tissues, simulated, temp. distrib. in EM irrad. 80—85354
- low-temperature blackbody source 80—73355
- magnetically ordered crysts., absorbent, EM waves polarisation 80—108189
- magneto-gravitational effect *(Russian)* 77—9935
- medium with uniaxial elec. anisotropy, EM radiation conditions 77—34795
- microwave and HF thawing, of cryogenically preserved canine kidneys 77—5059
- monocrystals, EM radiation of relativistic positrons and electrons during axial and planar channelling 80—79845
- multi-spiral electron current, interaction with EM wave, nonlinear anal. *(Russian)* 79—22886
- multifrequency N-th order coherence functions, path integral approach 80—95771
- noiselike radiation, noncoherent polarimetry anal. 80—1111
- non-channelling ultrarelativistic particles in crystal planes, EM radiation *(Russian)* 80—45163
- non-ionising EM radiation standardisation 77—38013
- nonlinear medium nondegenerated wave interaction with amplification, stochasticity occurrence *(Russian)* 78—83027
- nonradiating primary planar sources of finite extent, question of existence 79—10247
- occupational exposure standards for non-ionizing EM radiation 78—44558
- ondulatory radiation sources, theory and appl. 80—37947
- open resonator, complex source point theory 79—50196
- particle falling into Kerr black hole, high-freq. gravit. and EM radiation 78—16452
- particle in EM wave, varying freq., averaged velocity 78—18414
- Planck's const. time variation on cosmological scales 77—57113
- polarisation, rot. induced by non-Minkowskian spacetime 79—35115
- polarised radiation, gravit. deflection, improved upper limits 77—2596
- ponderomotive forces of EM radn. in sphere 79—76556
- positron channelling in Si, 56 MeV, producing radiation 79—51176
- Poynting vector theory, light beam shifts, total internal refl. 80—78764
- pulsed EM radiation, from line source in two-media configuration 79—64153
- pulsed RF radiation produced by scratching dielectrics *(Russian)* 78—19607
- quasimonochromatic self-oscillations, phase self-stabilisation 80—18973

electromagnetic waves continued
  radiant-energy exchange by small objects using continuum fields 78—82894
  radiating electron in strong monochromatic wave at open waveguide 79—55039
  radiation fields by parabolic cylinder in anisotropic medium *(Japanese)* 77—54657
  radiation fields in biaxially anisotropic media 78—66723
  radiation generated by charged beam near plane flanged waveguide 79—13880
  radiation on change of state of radiating system 80—32894
  radiation pressure, object experiencing force perpendicular to EM wave direction 79—22881
  recoil of radiating source, Einstein-Maxwell eqn. 77—57244
  Reissner-Nordstrom gravitational field, electric dipole *(Russian)* 79—21611
  related fast processes measurement, present methods in USSR, future prospects 80—57271
  remote sensing physical principles 77—56731
  resonant antenna system, anomalous radiation and electrodynamic characts. 80—69302
  RF radiation from portable and mobile telecommunication transmitters 77—40795
  RF radiation levels in urban areas 78—40351
  ripple radiation in extragalactic compact radio sources, rel. to low-freq. variability 79—21450
  shock wave generation of EM waves, compression waves in weak mag. field 79—77292
  shock waves in general relativity, detection 77—5710
  slowly varying medium, wave equation, multiple timescale method 78—8248
  Smith-Purcell radiation generated by electron beam, non-redundant spectral tunnelling 78—78906
  spectral density, time-depend. perturbation theory calcs. 77—13525
  spectrum at low freqs., theory 79—44350
  spherical, reproduction by real meas. devices, from combined radiating sources *(Russian)* 78—85729
  spherically symmetric electrostatic field superposed with EM wave, gravitational radiation emission *(French)* 77—57257
  stars, relativistic collapsing, radiation, linearized even-parity EM and gravit. radiation 79—75228
  stimulated EM shock radiation, book contrib. 79—27149
  stimulated EM shock radiation, by EM wave-fast electron interaction, freq. dispersive media 77—83796
  symmetry analysis applic. to wave theory 77—75387
  time-domain electromagnetics and its appl. 78—71010
  total pulse, nature of extracted signal 78—42268
  transcendental equations for freq. spectra of standing spherical waves, roots 78—29886
  transmission and propag., book 79—50198
  volume holography, coupled-wave theory generalisations 80—106495

electromagnetism
  see also electric fields; electrodynamics; electromagnetic field theory; electromagnetic induction; electromagnetic oscillations; electromagnetic waves; magnetic fields; magnetism
  acceleration through random classical radiation, thermal effects 80—73191
  averaged Maxwell equations in severe random nonuniformities 80—69298
  bifilar electric line, cranked symmetry, mag. field lines *(French)* 78—42255
  Biot Savar law, quantum mechanical generalisation, mag. field from current of assigned geometry 78—70997
  book *(French)* 78—13640
  boundary value problems, decomposition approach 80—4557
  boundary waves on perfect conductors, Maxwell eqn. solns. 79—44757
  capacitor, mag. field between discharging plates, Ampere's law, for teachers 79—21490
  CGS to SI conversion for electromagnetism 78—16592
  charged homogeneous cosmologies, theory 79—25767
  charged particle relativistic dynamics, symmetries 77—45742
  classical field theory in reference frames space, Einstein's gravit. theory, Maxwell's EM theory appls. 78—41173
  classical Lagrangian theory with radiative reaction, monopoles and positrons in Rohrlich formalism 79—72
  closed region problems, singularity extraction in kernel functions 78—66728
  complementary variational principles for Maxwell's equations 80—99603
  concentric EM resonator, gravitational wave radiation *(Russian)* 77—45772
  conducting media, eddy current phenomena, neglect of displacement current 79—13868
  conducting sphere, rot. in mag. field relativistic, co-rot. frame 79—53714
  conformal phase group and electromagnetism 77—67360
  corrosion damage in nonmagnetic parts electromagnetic determ. of degree, apparatus *(Russian)* 77—70207
  Coulomb's law in moving medium, Maxwell's eqns. and Dirac function, for teachers 78—61987
  Coulomb law and relativity theory, Horak method approach *(Polish)* 78—13639
  current magnetic structure, stability rel. to external helical perturbations *(Russian)* 77—14632
  current-carrying twin conductor, elec. and mag. forces between wires *(Russian)* 78—13638
  degenerate spacetime class, props. 78—36902
  destructive materials testing anal. *(German)* 78—23909
  diffraction gratings, theoretical method, numerical appl., Maxwell eqns. in curvilinear coords. 80—95786
  diffraction theory for transmission phase with deep rectangular grooves, Maxwell's eqns. method 79—10257
  diffusion potential, concept. rel. to Maxwell's eqns. and irreversible thermodynamics 79—63171
  dipole near and parallel to conducting plane *(French)* 80—18954
  Dirac-guage in Maxwell's theory 80—90687
  dispersive media, geometrical optics derived from Maxwell's eqns. 77—61917
  education, computer graphics and electromagnetic fields 77—33781
  education, exterior algebra and exterior differential forms for electromagnetic problems 80—57037
  Einstein-Maxwell, plane symmetric fields, comments on other solns. 77—30062

electromagnetism continued
  Einstein-Maxwell eqn. parametric type-D solns. in left-degenerate representation 77—67346
  Einstein-Maxwell equations, coupled, general soln., Ernst-Maxwell eqn. depend. on arbitrary harmonic function 77—74
  Einstein-Maxwell fields, SU(2,1) symmetry 77—53821
  Einstein-Maxwell scalar fields, stationary axially symmetric solns. 77—67361
  Einstein-Maxwell theory, energy-momentum tensor, invariance transforms. 78—21036
  electric circuit, flattened rhombus shape, mag. field lines calcs. *(French)* 77—571
  electrodynamic boundary conditions for media with spatial dispersion and transition layers *(German)* 80—78742
  electromagnetic vacuum, isotropy, testing 77—87254
  electron wavelength measurability 77—71406
  EM energy-momentum tensor and the properties of material media 79—55020
  EM response of electron gas and vacuum in strong mag. field 77—13641
  energy flow lines, Maxwell eqns., interpretation of diffr. and interf. 77—34806
  equivalence principles in electromagnetism 77—30083
  ferrofluid, nonlinear surface waves, bifurcation theory approach 80—58439
  ferromagnetic coaxial semi-infinite cylinders fitted on each other, mag. conducting capacity anal. *(Bulgarian)* 77—61891
  ferromagnetic medium, nonlinear, EM energy distribution, between orthogonal loops *(Russian)* 80—37934
  field theory development 80—16
  focusing of waves in anisotropic plane-layered medium, analytical solns. of Maxwell's eqns. 80—32890
  force between current carrying conductors, arbitrary shape, error anal. *(Slovak)* 78—22065
  free Klein Gordon fields, conservation laws 80—340
  Fresnel equations, improved treatment 79—27136
  gauge invariance and quantisation 77—61176
  gravitation, in plane space, equivalence, massive bodies of electromag. struct. *(Russian)* 79—21610
  in gravitational metric, stress-tensor trace anomaly 77—64983
  half-space, singularities in elementary soln. of boundary value problems for Maxwell's system *(French)* 77—71218
  Helmholtz equation, soln. in neighbourhood of corner 78—90335
  Helmholtz homogeneous equation, numerical soln. methods *(German)* 78—90337
  Hertz vector potentials, instructional appls. 78—12490
  interacting EM waves in general relativity exact solns. of Einstein-Maxwell eqns. 77—60985
  interfaces of two bulk phases, non-equilibrium thermodynamics including EM effects 80—13021
  interfacial EM props. using singular fields, charge density and currents 80—90691
  isotropic-anisotropic media boundary, light refl. and refr., Maxwell theory *(German)* 78—87007
  Kerr space-time, EM quadripotential of point change at rest on symmetry axis *(French)* 78—45541
  Kottler-Cartan-van Dantzig and noninertial systems for Maxwell eqns. 79—84973
  light, intrinsic angular momentum 79—58483
  lightning return stroke, EM fields radiation, Maxwell eqns. exact soln. appl. 78—73442
  llaxwell's equations, for teachers 79—21487
  local conserved currents in unified field theory 79—17307
  magentic cct. theory by analogy with electric ccts. 79—27123
  magnetic and electric charges, string and non-string Hamiltonian formulation 77—22429
  magnetic and electric charges in two-pot. approach, comments 77—67304
  magnetic dipoles, caused by circulating electric currents, a discussion 78—28969
  magnetic dynamic susceptibility and refractive index under change of origin *(French)* 77—61890
  magnetic field calc., two-dimens., boundary integral eqn. method 78—94355
  magnetic shielding by superconducting shell, theory 79—68351
  magnetothermoleastic waves, propag. in initially stressed conducting layer 79—63
  massive electrodynamics with magnetic charges, duality covariant form of Maxwell's eqns. 78—4495
  massive photons and tachyon monopoles 78—20986
  mathematical principles, classical to relativistic evolution, book 80—22162
  Maxwell, discoveries relevant to wireless and colour reconstruction 80—27093
  Maxwell, diversity of interest across phys. sciences 80—27092
  Maxwell, James Clerk, (1831-79) 80—27090
  Maxwell, J.C., scientific contribs. and upbringing role 80—27091
  Maxwell's eqns., boundary-value problem, Ewald-Oseen extinction theorem 78—62974
  Maxwell's eqns. and Clifford algebra, space-time formulation 77—71219
  Maxwell's eqns. boundary value problem with boundary condition $n.\varepsilon E=n.\mu H=0$ *(German)* 77—57205
  Maxwell's eqns. for free fields on compact Lie group manifold 77—49608
  Maxwell's eqns. in matter, covariant formulation 78—57798
  Maxwell's equation, critical view 80—43224
  Maxwell's equations, derivation from local gauge invariance 78—54109
  Maxwell's equations, energy description of propagation of monochromatic radiation along multimodal fibre 80—38116
  Maxwell's equations, exact soln. for isotropic nonlinear medium *(Russian)* 78—62971
  Maxwell's equations, form of distributions *(French)* 79—97221
  Maxwell's equations, inside and outside of source, vector spherical harmonics, for teachers 78—81747
  Maxwell's equations, numerical soln. by transmission line and lumped network models 80—27147
  Maxwell's equations, variational principles 79—2641
  Maxwell's equations derivation, in general relativity space, based on principle of minimum paths 77—53791
  Maxwell's equations in ferromagnetic materials, asymptotic solns. *(Italian)* 78—78860
  Maxwell's equations in non-inertial reference frames *(German)* 77—45720

electromagnetism continued
Maxwell's theory, Faraday induction term and Galilei invariance, teaching approach 80—41995
Maxwell's time depend. eqns., solns. by successive overrelaxation (SOR) method 79—92963
Maxwell achievements 77—572
Maxwell eqn. finite difference soln., perfect conductor simulation 77—74236
Maxwell eqn. invariance algebra 80—82923
Maxwell equations, boundary value approx. using finite element anal. *(German)* 80—91718
Maxwell equations, equivalence with inhomogeneous wave eqns., for teachers 79—97138
Maxwell equations, new invariance group 79—35575
Maxwell equations, time-harmonic, exterior boundary-value problem of EM reflection 80—28148
Maxwell equations, time-invariant, theory in arbitrary dimensional fields *(German)* 78—90336
Maxwell equations covariance, comparison of electrodynamic systems 77—87680
Maxwell equations reformulation of weakly guiding optical fibre propag. 80—78974
Maxwell-Einstein theory, local supersymmetry 77—2582
Maxwells's equations, photon rest mass as cosmic test 77—45708
Maxwells eqn. integration, implicit scheme, space and time discretisation 80—90688
metal, semi-infinite, nonlinear interaction of oppositely travelling surface plasmons 79—28393
metal surface, mol. vibr. energy transfer, classical EM theory 80—96806
method of virtual power, electromag. continua appl., coupled fields 80—58438
micropolar current and heat conducting magnetically-saturated solid, field eqns. 78—36845
microtron electromagnet, mag. field distrib. using mag. scalar pot. 80—102597
Minkowski covariance of Maxwell eqns. in Kerr-Schild metric 77—64977
monopoles, elec. and mag., without strings, heuristic pot. theory, teaching approach 79—5931
moon, EM sounding data for lithosphere 78—24474
motion of charged particle in uniform magnetic field motion of charged particle 80—90690
nonlinear medium, mag. field calc. by differential grid method *(Ukrainian)* 80—4555
null-plane analysis of electromagnetism with magnetic charges 79—31767
H.C. Oersted, first spark of electrotechnology, biography *(French)* 78—69955
photoelastic stress anal., relationship between optical theories 78—63302
photon variable mass across anisotropic medium *(French)* 77—13624
physical interpretation of EM vector pot. 80—46772
ponderomotive forces in dielectrics, validity of accepted expression 79—881
potential theory, use of non-orthogonal system of coordinates *(French)* 77—58245
Poynting vector introduction at elem. stage of physics courses 80—12865
PT asymmetry and four-fold EM degeneracy lifting, appl. to ring laser mode splitting 80—23606
quantisation of EM potential two degrees of freedom for any gauge 77—22670
quantum theory, rel. to structural information theory of sound 77—14822
radiating electron, time-delay eqn. 77—23603
radiowave propag., Maxwell's eqns. explained 79—76558
Rayleigh waves, magnetothermoelastic, with thermal relaxation, theory 79—62
relations with gravitation 78—46487
resistance variation with temperature 80—77575
response of conducting cylinder inside conducting shell 77—64198
rotating charged dust, Newtonian and general relativistic treatments 78—73908
six dimensional space time formalism of electromagnetism, mag. monopole behaviour of electrically charged tachyons 78—54182
solar wind/magnetosphere interaction, EM power flux rel. to Akasofu substorm parameter 79—75053
solenoid experiments, for teachers 79—71204
spherical laser plasma, classical optics and light press. 78—59601
spinning disc of radially inhomogeneous piezoelectric material, transient voltages and stresses 80—55039
static EM angular momentum, in vacuo obs. 80—73631
stationary boundary value problems, finite element analysis *(Polish)* 79—98258
Stormer problem, numerical determ. of asymmetric periodic solns. 77—49270
Stormer problem, periodic motions in mag. dipole meridian plane 78—85841
Stormer problem, periodic motions in mag. dipole meridian plane 78—89053
surface EM force on $BaTiO_3$ disc in axial mag. and radial elec. fields 77—26185
symmetries and vacuum Maxwell's equations 80—86178
tachyon, EM analogue, production by reflected ultrashort laser pulse *(Russian)* 77—46680
teaching, developing countries, course content 78—3
teaching, underdeveloped countries, factors against learning 78—4
teaching at University of Iowa undergraduate course, computer-managed instruction technique 77—9835
teaching undergraduates EM theory 77—71167
tensors, metric and Ricci, for D-type spacetime class 78—36903
theory and applications, book 80—86052
theory of electricity, book 80—86051
toroidal resonators for EM waves, Maxwell eqns. for toroidal geometry 80—102598
transient EM fields, two-layer polarizable Earth 77—64199
transient EM response of sphere, conductive overburden effect 77—64197
two-phase conducting diamagnetic system, coeff. of EM ejection of particles *(Russian)* 78—94364
ultrahigh acceleration of conducting rings, pulsed mag. field, approx, eqns. 78—5386
undergraduate teaching, for elec. engineering 78—20922
vacuum stresses induced by accel. of infinite plane cond. for massless scalar and EM fields 77—30071
variational principles for Maxwell's equations 80—78744
vector fields, Debye pot. representation 78—73797

electromagnetism continued
VLF-EM modelling of conductors 79—79736
vortex motion, integrals of hydrodynamic equations, Helmholtz 1858 paper 79—9072
welding arcs, gas velocity fields modelling 80—75039

electromagnets
see also coils; superconducting magnets
18 GeV electron-positron storage main ring magnet system 79—31267
30 T pulsed solenoid construction and life tests 79—31297
34MW 120MJ pulsed DC supply for Divertor & Injection Tokamak Expt. 79—31214
accelerator coils, use of Al strips instead of Cu 79—72126
accelerator magnet systems, piggy back power supplies advantages 77—83365
acoustic wave transducer, periodic magnet noncontact transducer theory and application 79—46150
Adone storage ring transverse wiggler magnet design 79—41054
air gap field configuration rel. to pole piece geometry and material inhomogeneity 79—30500
artillery projectile inspection by noncontact EM transducers 79—47872
attachable electromagnets of ferroprobe coercimeters, use of pole shoes 78—45662
AVF cyclotron, electromagnet 77—3198
bending magnet for energy doubler, prototype test 77—83366
betatron electromagnet pulsed power supply 78—82546
Bitter coils, axial compression of a coreless mag. coil by fibreglass cylindrical housing 78—93741
Bitter magnets, use in low temp. high field Mossbauer spectrom. 79—51888
bone healing electrostimulation, clinical aspects 79—83879
bubble chamber, SKAT, main parameters and magnetic field meas. 80—69022
CAD, GFUN program with interactive graphics 77—18053
CAD module, for fusion reactor system 77—23261
CERN Proton Synchrotron focus control, pole face winding design and field correction 79—31299
CERN Super Proton Synchrotron beam-splitting steel septum magnets 79—31295
CERN Super Proton Synchrotron extraction channel septum magnets 79—31296
CESR electron storage ring, ultra fast pulsed magnets for beam manipulation 77—83239
circumferential stress in large high field magnet coils, thick-thin cylinder approach 80—95761
coercimeter, electromagnetic, magnetising current amplitude and turn off speed effect 78—39997
coercimeter, with cylindrical attachable electromagnet, exam. of design 78—76809
coil for Tokamak magnet, finite element calc. 77—18058
colliding ring solenoidal detector magnetic system design and fabrication 79—31298
constant-current and AC, commercial units characts. and appl. *(German)* 80—9011
CPS continuous transfer, modulated fast bump 77—83240
cyclotron separated sector type, model magnet *(Japanese)* 80—874
DC and AC, design and operation *(German)* 79—93171
DC dynamic behaviour, proposed dynamic charact. field criteria *(German)* 78—24828
deflecting septum magnet for cyclic accelerator 78—78525
development and appls. 80—27320
differentiated-effect shims for medium field levels and saturation 77—6595
distributed computing system THESEUS for mag. field analysis 79—41293
eddy-current problems, including moving Fe parts, numerical soln. 78—90340
Fermilab booster accelerator, mag. system modification, increased energy 77—83222
Fermilab energy doubler correction magnets, construction 79—68042
Fermilab phase controlled pulsed power supplies, characts. of inversion operation 77—83223
ferromagnetic parts, magnetisation by use of applied electromagnets 78—72999
field control system 77—37950
fusion reactor, compact ignition test reactor, engineering design using Bitter type magnet 80—102310
fusion reactor, Heliotron E, helical coil design, mag. field perturbations 80—99300
fusion reactor, JET, inner poloidal field coil mechanical design 78—50387
fusion reactor, JT-60, poloidal field coil internal voltage oscills. 78—50386
fusion reactor, PDX canned poloidal coils, design, fabrication and mag. alignment 78—50385
fusion reactor, PDX poloidal field coil power tests 78—50384
fusion reactor, RFC-XX, coil system, design, fabrication, testing 78—55007
fusion reactor, TEXT toroidal field coil stress anal. 78—50381
fusion reactor, TFTR poloidal field coils design details 78—50383
fusion reactor, three-dimens. solid finite element anal. for simulating composite windings 78—55003
fusion reactor, TMX, magnets, mech. design 78—58494
fusion reactor, toroidal device with nonplanar mag. axis, magnet and coil engineering 78—55009
fusion reactor anisotropic B_T-coil two-dimens. finite element anal. of laminate sliding 78—50382
fusion reactor B_T-coil stress anal., constraint finite element anal. for contact problem 78—55004
fusion reactor coil design, cost anal., for neutral beam magnets 78—55005
fusion reactor coil design codes 78—66367
fusion reactor coil insulation and winding techniques 79—31210
fusion reactor field coils, fabrication effects on structural behaviour 80—9406
fusion reactor magnet coil, 125 kG, 1 m, design, fabrication 78—55008
fusion reactor toroidal field coil stress anal., cost effective procedures for TFTR 78—50379
GANIL separated sector cyclotron, magnet description 79—54641
geometric distortion by eddy currents in cylindrical conductors 77—50584

electromagnets continued
geometrical design expressions, for electromag. used in NDT equipment 78—85102
gradient septum magnet, effect of pole gradient 78—25369
guiding-field magnet in proton storage ring, supply ccts. current stabilisation 77—65363
helical electrostatic quadrupole, line charge system 78—25363
HEPI accelerator, active filter of annular electromagnet 78—33338
high field facilities at Francis Bitter National Magnet Lab. 79—71497
high field magnet laboratory of Grenoble, facilities and utilisation 79—71495
high magnetic field generation in Grenoble and appls., review 80—13110
high magnetic field installation at Univ. of Nijmegen 79—71496
high-resolution NMR spectrometer field homogeneity rel. to pole tip edge saturation 79—30522
high-resolution nuclear spectrograph magnet developments 79—31317
historical review of development, mech. strength, performance limits 77—10073
inhomogeneous magnetic field from electromagnet produced by parallel shift of central axis of one pole 78—55276
insulation systems, features 78—89506
intersecting storage ring, power supplies, types 77—42197
ion optic precision magnet homogenising surface coils 79—41329
KEK main ring, prototype multipole magnets, design, field uniformity 77—83220
laboratory, design cirteria *(Czech)* 79—88985
LAMPF line-D fast deflector system 77—83157
LAMPF mineral-insulated magnet experience 79—31248
LEP storage ring, C-shaped laminated magnets, implication of low field levels 79—72051
magnetic α spectrograph performance 79—31316
magnetic diverters for experimental Tokamaks and fusion reactors 80—18621
magnetic field configuration recovery, in interpolar gap 78—5070
magnetic field distribution rapid meas. using NMR 80—27322
magnetic field inhomogeneities anal. 78—29881
magnetic field inhomogeneity prod. by pole state inclination from parallel state 77—27217
magnetic induction stabilised source 78—94360
magnetic spectrograph for very heavy ions 79—31315
magnetically enhanced cylindrical sputtering system 77—73232
massive object with one pole of electromagnetic, magnetisation 79—50190
megagauss field production by Cnare effect 78—93739
MHD research, transverse-field water-cooled electromagnet 77—84528
microtron electromagnet, mag. field distrib. using mag. scalar pot. 80—102597
microtron electromagnet optimum shape, computer numerical anal. 77—18718
miniature, liquid N_2 cooled, features 78—74036
Mossbauer spectrom. with 2-4 T electromagnet 78—847
multipole DC electromagnet, working gap field analysis *(Russian)* 80—28142
National Synchrotron light source magnetic component system 79—68038
Nijmegen installation, Bitter magnets, research into high mag. fields *(Dutch)* 78—252
nMR gaussmeter for measuring field distributions of electromagnets 79—2797
NMR radiospectrometer electromagnet field uniformity rel. to pole piece shape and material 78—86309
NMR spectrometer, electromagnet current stabiliser 77—87800
noncontact EM transducer design improvement 79—46151
normal and stray flux flow dividing line definition *(Bulgarian)* 77—61094
optimal magnetic multipole for Na beam polarisation 77—30684
optimum dimensions of circular current shims for field homogeneity 78—45650
PDX toroidal field coil mag. force distrib. anal. 78—50380
PEP magnet power supply systems 77—83216
permanent magnet and coil combination for large dia. ion source 80—74066
PETRA magnets, results of field meas. 79—68040
phasotron, electron ring, const. guide field induction, acceleration, magnet system 77—83181
planar explosion mag. generator with resistive load, work performance optimisation 79—6156
plasma cluster accelerator, external mag. field influence 80—6287
polarity reversing control current magnet power supply with triangular waveform 79—12827
pole face inclination effect on mag. field distrib. 77—71352
pole-piece design, air gap field computation 79—41295
poloidal field coils for Tokamak 78—62645
Proton-Electron Tandem Ring Accelerator magnet field meas. 79—31271
pulse, mechanical characts. meas. method *(Polish)* 77—67478
pulsed high field magnet construction *(Japanese)* 79—17456
pulsed multipole mag. field with zero skin depth, anal. method, nonstandard electrode optimization 79—13863
pulsed multipole magnet field anal., including diffusion into conductors 80—5660
pulsed septum coaxial magnet, field characts. 77—53961
pulsed septum magnet for extraction from Fermilab booster synchrotron 77—83219
quadrupole gradient-length product meas. device 79—76232
quasistatic magnetic field generation using prototype switching system 80—42244
resonant cantilevered fibre-optic scanner 80—53428
ring magnet power supply, for 500 MeV synchrotron 79—18068
SATURNE II proton synchrotron, magnet design and meas. 77—83241
SAW EM transducer harmonic operation 79—46152
scanning microprobe electron instrument deflection system based on electromagnet 79—2878
for scientific research, main types, review *(Italian)* 80—17963
sectorial, mag. field inhomogeneities along central ray 79—31768
semiautomatic digital coercimeter, exam. of design 78—76817
shell-type, with supersaturated polepieces, field topography 78—74033
shimming, using computer routine 80—245
spherical multipole electromagnet development 79—31208
SPS magnet system, nonlinear fields and their compensation 77—83268
steel, mag. anisotropy, magnetostatic fields, numerical simulation 77—27220

electromagnets continued
storage ring magnet of third muon (g—2) expt. at CERN 79—22504
strong and ultrastrong pulsed mag. field generation 79—71494
strong field Fe cored, estimation of field produced by vol. mag. charge 78—16820
structural vibration testing, using electromag. forcing device, use of feedback to reduce harmonics 79—20298
synchrotron, passive filter for annular electromagnet 78—5074
synchrotron, Sirius, shaping of highly stable flat top in excitation current pulse of electromagnet 78—5075
synchrotron magnets for spallation neutron source 79—68039
Synchrotron Radiation Source booster magnet power supply 79—31272
Synchrotron Radiation Source booster synchrotron combined-function magnets 79—31269
Synchrotron Radiation Source storage ring multipole magnet prototype 79—31268
temperature distrib. in conductor in pulsed mag. field, influence of surface layer 79—31773
Tokamak fusion, Impurity Study Experiment, mag. field calcs. using GFUN-3D programme 78—66368
toroidal field coils for JET, manufacture and testing 80—5334
toroidal field ripple for Tokamaks, magnetics design 78—62643
vacuum-tight electromagnet, for moving specimens in MKh1303 mass spectrometer 78—315
wiggler magnets to control low-energy characteristics of electron storage rings 77—6585
winding supply, current regulator based on industrial thyristor convertors 77—37921
windings with constant current density, maximum permissible mag. field 78—57990
ZGS beam transport for transverse and longitudinally polarised protons 78—55074
zoom lens quadrupole magnets for Colorado Univ. energy-loss spectrograph 77—83410
Cs beam frequency standards, quadrupole and hexapole magnet combination 77—5813
Fe pole pieces, in electromagnets, mag. anisotropy effect on mag. field homogeneity *(Japanese)* 80—93111

electromechanical effects
articular cartilage, electromechanical props. during compression and stress relaxation 78—92667
bar-shaped resonators excited electromechanically in flexural vibration, equiv. electric circuit 77—42677
cholesteric liquid crystal, shear electricity, symmetry considerations 78—60394
conductor, MHD kink instability 80—6307
deformable dielectric with memory, shock and acceleration waves 77—1170
dielectric liquid, elec. stressed, motion due to Coulomb, electromech. forces, schlieren image obs. 80—100037
dielectric material, self-consistent elec. field produced during fracture *(Russian)* 77—63369
elastic dielectric, many-body theory, appl. to NaCl-structure 78—38805
elastic dielectrics, Voigt's intramolecular force balance 77—60936
electroelasticity problems, numerical soln. 80—80707
electron inertial effect, shock loaded rod, meas. of strain produced 78—51139
electronic-micromechanical interactions, conference, Lausanne (1976) 77—30140
electroplasticity, skin effect 80—21046
ferroelectric ceramics, with external inductive-resistive load, linear electromechanical responses 79—51909
flexoelectricity of liquid crystals, microscopic interpretation 77—32339
general electromechanical reciprocity relations applied to the calculation of elastic wave scattering coefficients 79—56729
ionic crystals, galvanotensometric effect 77—44485
lipid bilayers made from monolayers, volt.-depend. capacitance 78—27903
liquid film, surface deformation under charge *(French)* 77—31848
Maxwell's eqns. in electromech., numerical resolution by finite element anal., eddy current effects *(French)* 79—30269
MBBA, liq. cryst., flexoelectricity and surface polarisation 77—89376
mechanical forces, due to crossed elec. and mag. fields 78—23401
mechanical metal-semiconductor contacts, I-V characts., press. effects 78—2564
metal, electron state effect on mech. props. and electroplasticity 78—14725
metal, electroplastic deform. 78—3200
metal, electroplastic effect 79—24589
metals, electromechanical forces, theory *(Russian)* 77—81063
metals, electroplastic deform. *(Russian)* 77—86108
nematic liquid crystal, domains, of 2nd kind, form. with positive dielec. anisotropy *(Russian)* 78—18550
nematic liquid crystal, flexoelectric domains in thin layers *(Russian)* 78—18549
nematic liquid crystals, flexoelec. polar deform. and second order elasticity 78—1979
nematic liquid crystals, flexoelectric bending, e_{1z}/e_{3x} meas. 77—72555
nematogen, flexoelectricity in isotropic phases 78—63672
noncentrosymmetric crystals, effect of electric field on elastic wave propag. rate *(Russian)* 77—85654
one dimensional dynamic electromechanical constitutive relations of ferroelectric materials 79—56738
PMMA, shock-wave compressed, dielectric props. 78—80281
PMMA glass, electron bombard. induced elec. discharge, electromech. effects *(Russian)* 77—32324
polychloroprene, polar dielectric, mech. polarisation *(Russian)* 77—40174
polyethylene, electrical capacitance under high DC elec. field 80—54705
polymer film, viscoelastic props., capacitance change meas. *(Japanese)* 78—23752
polyvinylidene fluoride X-ray diffr. pattern changes due to corona charging 78—14285
protein membrane, double layer mediated energy conversion using imposed freq. and wavelength 78—88695
SAW vel. and electromech. coupling factor 80—75422
solenoid windings, nonlinear eqn. for equal loading 79—55028
steel, austenitic, tensile strength, elec. current impulse effect down to 4.2K 80—81131
steel, plastic working of wires, high-density current appl. 79—57002

electromechanical effects continued
  strain gauge, vacuum deposited, constantan alloy-film/ceramic steel system, electromech. behaviour 78—6634
  surface deformation under charge flux *(French)* 77—31847
  TBK-3, ferroelectric ceramic, 90° electric domain processes, mech. stress, X-ray diffr. 78—72478
  TGS, ferroelec. single crystal, low freq. nonlinear effects 80—84490
  thermal stress, high-current pulse in conducting rod 79—7287
  tourmaline, resonator, electroelastic constants, elec. field induced freq. shift study 80—20597
  TsTS-23, ferroelectric ceramic, 90° electric domain processes, mech. stress, X-ray diffr. 78—72478
  water-nitrobenzene interface, mechanoelectrical energy conversion using interfacial tension changes 79—14982
  AlN, epitaxial film growth by MBE, physical and optical props. 80—2293
  Al_2O_3-loaded epoxy, shock-wave compressed, dielectric props. 78—80281
  Al_2O_3-P_2O_5 glass, electron bombard. induced elec. discharge, electromech. effects *(Russian)* 77—32324
  BaO whiskers, electromech. effect 79—65800
  $Ba_2Si_2TiO_8$ fresnoite, characts. for SAW devices 79—82430
  $BaTiO_3$, 90° electric domain processes, mech. stress, X-ray diffr. 78—72478
  $BaTiO_3$ polydomain crystals, dielec. props. 78—43827
  Cd, electroplastic deform., stress relax. meas. *(Russian)* 79—38894
  $CdInGaS_4$ plate in elec. field, photostimulated ocills. 79—65799
  CdS, semicond. piezoelec. crysts., electromechanical coupling coeffs., US determ. 77—1456
  Cu, elec. resist. under torsional deform., impurities and tensile strain 78—30898
  Cu, plastic working of wires, high-density current appl. 79—57002
  Cu wire, drawn through diamond die, deformation zone EMF *(Russian)* 77—81327
  Fe, Armco low-cycle fatigue, electric field effects 77—1868
  GaSe plate in elec. field, photostimulated ocills. 79—65799
  KCl, elec. field effect on flow stress, charged-dislocation model 77—27935
  $KTaO_3$, light-sensitive surface-barrier generation of acoustic vol. waves 78—63252
  $(Li, Na)NbO_3$ ceramic, dielectric and electromechanical props. 77—40183
  LiF crystal, plastically deformed, elec. field distrib. on surface meas. 77—31716
  $LiTaO_2$ and $SiO_2/LiTaO_3$ struct., Rayleigh waves, piezoelectric leaky surface waves, temp. depend. 79—46905
  $NH_4H_2PO_4$, Z-cut, SAW props. 80—84358
  $(Na,Li)NbO_3$ ceramic, optimum prep. conditions and characterisation 78—3079
  NaCl single crystal, plasticity, effect of alternating electric field 78—15481
  NaCl whiskers, plastification in elec. field *(Russian)* 80—21010
  $NaCl(:Mn^{2+})$, influence of elec. field on flow stress 79—51193
  $NaH_3(SeO_3)_2$, ferroelectric, electromechanical props. near Curie point 80—29690
  Pb, electroplastic deform., stress relax. meas. *(Russian)* 79—38894
  $Pb_2KNb_5O_{15}$, strong electromechanical coupling of SAW 78—63919
  $Pb_{0.95}Sr_{0.5}(Zr_{0.53}Ti_{0.47})O_3+Nb_2O_5$, optimum comp. for soft ferroelectric ceramic 77—43938
  $Pb(Zr,Ti)O_3$:Fe(Nb) ceramic, elec. and electromechanical props., depend. on dopants 80—81212
  $PbZr_{0.95}Ti_{0.05}O_3$, impact loading, mech. and elec. response, elec. state effect 78—64317
  $RbHSO_4$, ferroelec., dielec. dispersion 80—97179
  $SbS_xSe_{1-x}I$ layer elec. and ferroelec. props., mech. stress effects *(Russian)* 80—50279
  $Sr_2Nb_2O_7$, phase transition at 215°C, physical props. obs. 79—56744
  Ti, effects of strain rate, temp. interstitial contact on electroplastic effect 79—83279
  TiNi, shape memory effect, spontaneous EMF generation 77—32637
  V_3Si, supercond. structure and properties *(German)* 80—93631
  W, plastic working of wires, high-density current appl. 79—57002
  WC, catalytic activity for hydrogen oxidation in acid obs., effect of starting material 79—100500
  Zn, electroplastic deform., stress relax. meas. *(Russian)* 79—38894
  ZnSe, mech. of electroplastic effect 79—28035

electromechanical filters
  elastic wave oscillator and filter design 77—19470
  fibre optic sectional filter 78—13874
  flexural-mode mechanical filter resonances 77—27435
  interdigital transducer transverse electrostatic end effects 77—27453
  α-quartz SAW temp. depend. 78—51813
  resonators, props. of materials used *(Czech)* 80—76318
  SAW filter design for nonlinear phase response, building-block method 77—27433
  SAW filter triple transit suppression by mech. and regeneration reflection cancellation 77—23829
  SAW inverse filter for NDT 77—28970
  SAW resonator cavities with unidirectional transducers 77—23849
  SAW resonator coupling and multimode filter design 77—23824
  SAW resonator reflector and transducer characteristic effects 77—39168
  SAW thin film filters *(Japanese)* 77—73116
  torsional mode transducer analysis 77—27436
  Tl_3VS_4 single-crystal substrate SAW filter performance 77—31186

electrometers
  see also charge measurement
  amplifiers, errors and nonlinearity in low-current meas. 79—6142
  analogue simulation, apparent power meas. *(Czech)* 77—5859
  auto-zero electrometer for analytical electron beam instruments 78—12721
  capacitors, PTFE film, temp. effects on potential difference 79—6141
  DC amplifier using MOS transistor, features 78—77933
  DC source (10^{-16} to 10^{-6} A) for electrometer testing 77—79112
  dosimeter, remote-reading operational amplifier type, elec. constancy checking 78—3613
  electrometer/ratiometer of high sensitivity and precision 78—70154
  electrometric circuit switching by magnetically controlled contact 77—79108
  electrometric equipment metrological provisions 77—79113
  electrometric instrument test results analysed 77—74450
  electrometric voltmeter input capacitance absorption meas. 77—79107

electrometers continued
  electrophotographic films, surface charge meter using electrostatic induction *(Japanese)* 80—77886
  electrostatic force acting on attracted disc of electrometer *(Japanese)* 78—17834
  fast response electrometer for pulse reactor experiments 78—70157
  feedback levitation electrometer for meas. of electric neutrality of matter 77—57579
  ferroelectric modulator temperature stabilisation 77—82550
  ferroelectric second-harmonic modulator design 77—82549
  fixed-capacitor and resistive methods compared 80—90866
  fluid insulator used in gas phase ions investigation 80—57336
  general-purpose electrometric set for scientific research 79—75546
  high-sensitivity, with modem amplifier 77—74447
  high-speed general-purpose, features 77—74448
  high-speed instrument for measuring small currents 79—75547
  integrating, with time-pulse signal 77—74443
  ionisation current sources for electrometer calibration 77—79111
  Keithley model 642 portable electrometer, critical input design 80—68209
  laser sensing system for elec. and mag. fields in power transmission 77—45870
  Lippmann electrometer, for interfacial tension meas., capillary wear effects 78—26751
  logarithmic, fast response, for pulse-reactor expts. 78—86291
  measuring unit and component requirements 77—74445
  modern electrometer techniques, review 80—37052
  MOS transistor electrometer, current noise meas. 78—54398
  MOSFET electrometer amplifier, characts. 77—74446
  MOSFET electrometer amplifier type MDM 77—79106
  negative-feedback charge-sensitive electrometer, for atm. ice particles elec. charge meas. 79—70895
  operation in ionizing photon radiation fields by compensation method 77—79110
  Regional Calibration Laboratory at the M.D. Anderson Hospital, Texas, USA 80—8189
  self-checking meter for reproducing small DC currents 79—75545
  solid dielectric specific resistance meas. instrument 77—79109
  surface potential microprofile meas. for electrophotographic films 77—45913
  temperature control of electrometer varactor-bridge amplifiers 79—9219
  vibrating-capacitor electrometer, current noise meas. 78—54398
  vibrating-reed, using flexing cantilever, for contact-charging phenomena 79—80585
  Po collector, reductive effect, determ. from leakage current 78—37036

electrometry *see electrometers*

electromigration
  aerosols, highly dispersed, with elec., acoustic fields, collision rates 79—47986
  amorphous thin film chalcogenide semicond. *(French)* 77—72710
  ballistic electron wind theory, quantum mech. generalisation 80—75379
  binary alloys, liq., calc. of electromigration forces and resistivities 79—82572
  concentration profiles produced by thermo- and electrotransport, calc. *(German)* 78—83995
  crystal growth by solid state techniques review 77—85935
  Das-Peierls electromigration theorem, geometry and boundary conditions 78—30776
  defected stripe, current crowding and flux divergence 78—71885
  dipole translation between crystallographic sites, absence of direct force 78—83993
  driving force, bootstrap arguments 77—20107
  driving force, weak charge solutions 79—55917
  electrolyte-membrane-electrolyte, freq. depend. of capacitance and cond., model 77—21488
  electron diffusion by positive ion, waveguide theory *(French)* 77—74240
  electron wind 79—69277
  excited atomic states in EM field, ionisation by electron diffusion *(Russian)* 78—86798
  failure under pulsed condition, model 80—49404
  Feynman-Hellmann theorem and oscillator strengths, force on atom in electrostatic field 80—65275
  film, grain boundary electromigration, low temp. theory 77—31799
  glass, electromigration in ion bombardment 78—26601
  glass interface with anodic electrolyte solution, simultaneous transfer of different cations in elec. fields 78—30800
  grain-boundary electromigration, anal., composition profiles from steepest descent methods 78—67849
  III-V semiconductors, point defects and deep traps, thermodynamic history, model 80—59908
  inclusions, formation, role of const. elec. current, elec. field distrib. *(Russian)* 77—55504
  ion exchange membrane, unstirred layer effects on pot. difference calcs. 77—48680
  ion motion in electrolyte solns. due to elec. field, teaching appl. 77—14
  ionic impurity, drift mobility in electric field, computer simulation 79—82388
  jellium, driving force, strong-coupling theory 80—65300
  lifetime, log normal distrib. theory 79—99348
  liquid alloys, driving force expression 78—51714
  liquid alloys, electromigration, driving force, pseudopot. calc. 77—55373
  liquid alloys, reversal of electromigration direction 77—55374
  liquid metals, diffusion electrotransport and thermotransport 77—55371
  liquid metals, linear-response theory of electromigration driving forces 77—55372
  membranes, ion flow, step pot. change, conc., current responses 79—5177
  metal, isotope enrichment by combined elec. migration and zone melting 78—76600
  metal films, electrocrystallisation, soln. component interaction 80—20055
  metal-chalcogenide glass-metal structures, elec. field influence on opt. parameters, electrostimulated chem. transforms. 77—76950
  metal-H system, electro- and thermotransport of H, book contrib. 80—24644
  metal-H system, permeation technique for electron transport studies 77—7904
  metal-H system, permeation technique for electrotransport studies 77—7903
  metallic thin films, book contrib. 79—1521
  metallic thin films, electromigration, and diffusion, new examination technique 78—67852

electromigration continued
- metallisation stripe, cracked, temp. gradient and current crowding, electromigration 77−51828
- metals, bulk and thin film samples, electromigration, generalized theory 77−24423
- metals, dielectric function approach using equivalence theorem 77−11733
- multicomponent systems, rel. to electroepitaxy, theoretical model 80−65396
- nearly-free-electron metals, electromigration of weak scatt. impurity in Bloch electron gas 78−6183
- proton transport in solids 80−79974
- quartz, synthetic, deuterisation, EPR and IR absorpt. characterisation 80−92721
- rare earth metals, electrotransport of solutes 77−51548
- refractory metal, surface geometry and emission parameters, changes during directional mass transport 78−2344
- resin particles, dispersed, precipitation on cellulose fibre in elec. field 78−53262
- Schottky-barrier metal-semiconductor junction carrier migration and equivalent cct. analysis *(Russian)* 78−84294
- semiconducting electrodes, defect doped, ageing effects 79−69592
- semiconductor, amorphous, diffusion phenomena, mechanisms and meas. 77−76608
- semiconductor, enhanced electrodiffusion purification in mag. field, GaAs epitaxial film appl. 80−66409
- simple cubic lattice, drift mobility correlation of interacting ions 79−37868
- soda lime glass gradient index variation by ion exchange and migration 80−14412
- solid electrolyte with structural disorder, current flow mechanism 80−19982
- solid-state diffusion in elec. field, Monte Carlo demonstration 80−27072
- substitutional impurity, driving force for electromigration 77−76618
- thin film conductor, mass transport and assoc. failures 80−59694
- transition metals electrical transfer of O, N, exam., using heat transfer of interstitial atoms *(Russian)* 79−55931
- two-phase system, field-induced vol. diffusion 79−77802
- velocity sensor, freq. characts. calcs. 80−96675
- Ag alloys, purification of solid metals by electrotransport *(German)* 78−51745
- Ag wire, ultrapure, cryst. forms of hillocks and voids formed by electromigration 77−31811
- Al and Al-alloy films, struct. induced electromigration failure, Monte Carlo calcs. 80−49405
- Al, deposited metallic thin films, H incorporation effects on stress and electromigration 80−80139
- Al film, electromigration, AC and DC studies 77−24424
- Al film, electromigration under pulsed current conditions, calc. 77−1495
- Al film, meas. of stress gradients generated by electromigration, X-ray topography and SEM 77−51541
- Al films on Si substrates, electromigration and diffusion of Cu 79−77820
- Al, of Cu, apparent effective charge, 325-500°C 77−39695
- Al, sputtered and electron gun evaporated films, grain size and orientation obs. 78−10308
- Al thin film stripes, electromigration lifetimes width depend. 80−92799
- Al-Cu (0.5 wt.%), evaporated layers, electromigration, linewidth depend. 80−65277
- Al-Cu thin films, microstruct. rel. to electromigration 80−44355
- Al-Zn, liq., physical props. study by electrodiffusion method *(Czech)* 77−84956
- Al-Zn melt, electrotransfer *(Russian)* 77−66034
- As_2S_3, amorphous, electrodiffusion profile meas. of Ag migration 78−87822
- As_2S_3, glassy, diffusion, elec. transport and first group impurities effect on elec. and opt. props. 77−76623
- As_2Se_3:Cu, amorphous, diffusion, electrodiffusion profile determ., Fickian diffusion behaviour 78−6185
- As_3Se_3:Cu, glassy, broadening of electrodiffusion profiles at high elec. fields 79−55939
- Au, epitaxial film, on NaCl substrate, electrotransport inferred from void growth rate *(German)* 80−10699
- Au film, effect of high DC density stressing on pre-existing voids 80−24770
- Au, film, grain boundary electromigration, tracer meas. 77−31802
- Au film, threshold current density and incubation time to electromigration 78−14643
- Au film, void growth in early stages of ageing and electromigration 78−38991
- Au film, whisker growth due to high current densities 77−69191
- Au, of ^{57}Co, profile shift and steady state methods at different temps. 78−71881
- Au, pure, electromigration and deform. 78−2286
- Au thin film, electromigration, adhesion layer effects 80−96685
- Au, thin film, electrotransport-induced failure site, minor constituents effects 79−23763
- Au wire, ultrapure, cryst. forms of hillocks and voids formed by electromigration 77−31811
- Au-Y_2O_3-Y junctions, migration of Au rel. to voltage-controlled negative resist., SIMS obs. 79−91157
- BaO-P_2O_5 glasses, Cu^+ ion electromigration at 400°C, luminesc. meas. 77−76610
- BeF_2-LiF molten mixtures, mass transport, chronopotentiometry 77−21391
- CdS:Cu(Ag), charge and transport mechanism of impurities, electrodiffusion doping 80−59725
- CdS:Li, subjected to elec. fields, drift of defects 80−6558
- CdS:Li(Cu), pure and doped, electrodiffusion of shallow donors, photocurrent, TSC, and exciton luminesc. meas. 80−79992
- Co film, electromigration exam. from structural changes and resistance increases 77−20213
- Co films, towards anode at 530°C, correl. to sign of normal Hall coeff. 77−62664
- Co, thermomigration and electromigration in high-purity samples 79−55919
- CoO, electrotransport 80−2196
- Cs-Au, liq. alloys, ionic conductance 77−1251
- Cu, Ag impurity diffusion coeff., 759 to 1081°C 79−10982
- Cu alloys purification of solid metals by electrotransport *(German)* 78−51745

electromigration continued
- Cu and Cu alloys, diffusion in systems involving group VA elements, review 77−39697
- Cu, electromigration of ^{113}Sn 80−6557
- Cu thin film, electromigration, adhesion layer effects 80−96685
- α-Fe, C drift velocity for electromigration temp. depend. in paramag., ferromag. phases 78−18835
- α-Fe, of C, current density and temp. effects 77−59145
- Fe-C, dil., Hall-field electrotransport of C, effective valence numbers 79−28148
- Fe-C (0.52 wt.%), FCC structure, exam. of electromigration of C by steady state method 78−75865
- γ-Fe-Ni-C, Fe-Cr-C, Fe-C, electromigration of C, effect of Ni and Cr addition 78−6184
- Fe-Si (3.1 wt.%), anisotropy of electromigration of substructure of polygonisation *(French)* 77−28047
- Ga, liq., electrodiffusion conc. of impurities 80−54414
- Ga, liq., electron transfer of rare earth metal impurities *(Russian)* 77−59132
- $Ga_{1-x}Al_xAs$, Peltier LPE, absence of electromigration of As and Al 77−81230
- GaAs layers and p-n junctions grown by current-controlled LPE, elec. characts. 78−6436
- GaAs, liquid-phase electroepitaxial growth kinetics, Peltier effect and solute electromigration 79−42401
- GaAs, melted zone displacement by current *(Russian)* 78−26727
- GaAs, migration of liquid inclusions, effect of DC current and temp. 77−7910
- GaAs, multiple insulator layers studied by Auger anal. 79−83345
- GaAs, Peltier LPE, absence of electromigration of As and Al 77−81230
- GaAs:Sn, dopant segregation during liq. phase electroepitaxy 80−54384
- GaP:Au, diffusion, solubility, and electrotransport of Au 78−91489
- GaSb, migration of liq. inclusions, effect of DC current and temp. 77−7910
- Ge, heavily-doped single cryst., macroinclusions, annealing in elec. field 77−47474
- Ge:Cu, displacement of Ge-Cu inclusions in const. elec. field, 700-850°C *(Russian)* 77−15634
- β-Hf, electrotransport and diffusion of Ta impurities *(German)* 78−87826
- α-Hf, electrotransport of O impurities *(German)* 78−87826
- $Hg_{1\ x}Cd_xTe$, LPE current controlled 80−40272
- In, electrodiffusive conc. of impurities for analysis 78−22752
- In, liq., electrodiffusion conc. of impurities 80−54414
- InAs, migration of liq. inclusions, DC current and temp. effects 77−7910
- KBr bicrystal, Ag^+ injection transport and grain boundary mobility, electrodecoration obs. 80−2214
- KNO_3-$RbNO_3$, liq., electromigration cation and mobility and isotope effect 80−10691
- K_2O-SiO_2, glass, influence of electric charge phenomena on AES *(French)* 80−50478
- K_2O-SiO_2 glass, AES obs. of K^+ electromigration to surface under electron bombardment *(French)* 79−33869
- La, electrotransport of C, N_2 and O_2 80−24674
- $LiNbO_3$, electromigration in ion bombardment 78−26601
- Mo, pure, 1100-1300°C *(Russian)* 77−47613
- Mo-Ni (40 at.%), exam. of ion transfer *(Russian)* 79−28127
- Mo_5Si_3, of Si 80−92708
- NH_4NO_3, molten, countercurrent electromigration cell, isotope separation appl. 78−47547
- Na-K, liq. alloys, electromigration driving force expression 78−51714
- Na-Rb, liq. alloys, electromigration driving force expression 78−51714
- Na_2WO_4, solid electrolyte, diffusion, electromigration of Ag^+ ions in Ag/Na_2WO_4/Ag cell 77−1255
- Nb, electrotransport of H(D) at high H concs. 80−34246
- Nb, of grain boundaries *(Russian)* 77−7909
- Nb, of H, D, electromigration measured by resistance method 79−23783
- Nd, single crystal prep. by solid state electrotransport 78−84709
- Ni, of H_2, effective valency effects *(French)* 79−23781
- P-Se glass, effect of Ag electrodiffusion on volt-ampere characteristics 79−7869
- Pb, electromigration of fast diffuser 78−47594
- Pb, of ^{64}Cu, investigation by steady state method 78−71882
- Pb, of Au, 165 to 270°C 80−29221
- Pb, of Au and Ag 77−69116
- Pb, of Cu, isothermal conditions, steady state method 78−84003
- Pb, of Ni, steady-state method 78−87820
- Pr, single crystal prep. by solid state electrotransport 78−84709
- α-quartz:Ge,Ag^+, Ag-compensated Ge centre, EPR meas. 77−77098
- Sb-Sn melt, electrotransfer *(Russian)* 77−66034
- Sc, electrotransport behaviour of C, N_2 and O_2 77−11738
- Se, of Ag, role of Ag in switching effect in amorphous Se 78−19163
- Se, photosensitive particle migration, electrophotographic film structure and process 80−101863
- Si, annealing in elec. field behaviour of second phase inclusions *(Russian)* 79−23779
- Si device technology, thin film interaction effects, book contrib. 79−1620
- Si, heavily doped films, electromigration obs. 80−65295
- Si-Al interface in semiconductors, electronic parts, electromigration aspects 80−39355
- SiO_2-Al_2O_3-CaO-MgO-Na_2O, ion exchange and electrodiffusion of Li ions in surface layer 79−20227
- Sn, liq., diffusion and electrotransport of impurities meas. 77−51535
- Sn, liq., electrodiffusion conc. of impurities 80−54414
- Sn-In dil. liq. alloy, electrodiffusion and electroconvection, effective diffusion coeff., apparent effective valence 78−87802
- Sn-Sb dil. liq. alloy, electrodiffusion and electroconvection, effective diffusion coeff., apparent effective valence 78−87802
- SnO_2:Sb film, amorphous, electrotransport phenomena obs., under DC electric field 80−59840
- Ta, electrotransport of H(D) at high H concs. 80−34246
- Ta, H mobility in elec. field, temp. depend., 20-250°C *(Russian)* 78−47587
- Ta, of H, temp. depend. *(Russian)* 77−84986
- Te, liq., electrotransfer of Se 77−11716
- Th, diffusion and electrotransport of Fe, Co and Ni, 965-1625°C 79−90828
- Th, electrotransport purification under low press. 80−15303
- Th metal, diffusion and electrotransport of Th metal 78−86611
- Th, of V, Nb and Ta, 1370-1665°C 78−59979

electromigration continued
ThO$_2$-based ceramic impurity diffusion, electrotransport method 78—67869
Ti, ^{3}H electromigration effective charge, H conc. depend. 77—51545
Ti, of H(D) 80—34247
Ti:T, temp. depend. of effective electromigration charge 79—90826
TiO$_2$, rutile ceramic, ageing in strong elec. field *(Polish)* 78—52869
V, electro- and thermo-self-transport, 1480-1822°C 79—42297
V, electro- and thermotransport of O and N 77—28040
V, electrotransport of H(D) at high H concs. 80—34246
V, of H, D, electromigration measured by resistance method 79—23783
Zn, dislocation mobility under action of current pulses, selective etching meas. 79—19259
Zn, electromigration, electron wind force calc. 78—6183
Zr, ^{3}H electromigration effective charge, H conc. depend. 77—51545

electromotive force *see electric potential*

electron absorption
see also beta-ray absorption
barium stearate film, low energy electron range meas. using radioisotope Auger electrons 80—70257
cathodic protection using lightning conductors connected with diodes, for metals and concrete reinforcements 79—52418
cosmic rays, radial distrib. for inhomogeneous absorbers 77—61669
metals, electron absorpt. and transmission characts., 5 to 30 keV, film-massive block method 78—88387
polymer electret, absorpt. and relax. of charge 80—6942
semiconductors, electron absorpt. and transmission characts., 5 to 30 keV, film-massive block method 78—88387
water, distrib. in water, Al, Fe and Pb, 22 MeV electron bombardment 78—59840
Al, 22 MeV electron bombardment, bremsstrahlung distrib. 78—59840
Al, massive target, electron absorption and transmission characts. 77—65990
Fe, 22 MeV electron bombardment, bremsstrahlung distrib. 78—59840
Pb, 22 MeV electron bombardment, bremsstrahlung distrib. 78—59840
SiO$_2$ massive dielectric target, 5-25 keV electrons penetration characts. 80—70260

electron accelerators
see also betatrons; electron ring accelerators; microtrons
2 MeV injector for pulsed betatron 78—824
5 MeV electron accelerator modulator charging system 79—13563
5 MeV linear accelerator, modulator charging system upgrade 80—23182
20 GeV linear accelerator, intercomparison of high-energy accelerator field dosimetry 78—25331
45 kW power, industrial applics. 77—59795
100 GW beam generator 78—5087
100-1000 kW power, and applics. 77—59793
200 keV accelerator with specimen transport system for plastic surface irradiation 77—57776
ALFA, electron pulse stretcher to increase Frascati Linac duty factor, feasibility study 80—23237
Amsterdam 500 MeV high duty factor electron scatt. facility, status report 80—23191
anode for an accelerator with an inductive energy accumulator 79—26785
ARAKS expt., accelerator for electron beam injection 79—21141
autoaccelerator concept at NRL 79—72021
autoaccelerator for intense relativistic electron beams 77—83287
average electron energy measurement in atmosphere, 0.3 to 1.0 MeV 79—97956
Bates Linac, projects and improvements 80—23192
beam interaction with slow waves over impedance-loaded surface *(Russian)* 77—31055
beam parameters in adherer during compression, meas. via two-coil pickup 77—65393
beam spot measurements and beam divergence for 400 keV accelerator 80—877
biomedical electron accelerators, energy calibration method based on Cherenkov effect in gases 80—18721
Bonn 2.5 GeV synchrotron, acceleration of polarised electrons, and subsequent depolarisation 79—68002
Bonn synchrotron, polarised electron accel., and possible depolarisation 79—63826
bremsstrahlung spatial distribution in water and water-iron by 22 MeV electron bombardment, meas. with activation detectors 77—57754
bremsstrahlung yield produced by 4 MeV linear electron accelerator calc. rel. to hazard in radiolysis 79—76181
bunch widening as due to self-bunching, computer simulation 77—83333
carcinotron, relativistic millimetre, electron beam in high current accelerator 79—68359
cavity resonator, self-acceleration of electron bunches, emission spectra 78—33331
CESR, characts., points of interest 79—72038
CESR, e$^+$e$^-$ storage ring, vac. system 77—83247
CESR injection linac, electron beam modulator, design, performance 77—83374
charged particle beam, short pulse detect. by reverse-current method 79—63856
charged transmission line for pulsed high current accelerators, energy transfer 78—78519
chromaticity correction in large storage rings 77—83206
circular, with strong mag. field, metrological props. 79—6779
circular electron accelerators, beam stability calc. 79—72099
closely-coupled cavity chain, unit cell reson. freq. meas. method 77—83179
coaxial Marx generator, electron beam fusion appl. 79—76177
collective acceleration methods based on high-current relativistic electron beams 79—18063
collective acceleration using laser beam 79—76166
collective effect linear accel. in presence of strong axial mag. field 77—83165
collective field accelerator, vac. diode with relativistic electron beam operation 77—24201
collective ion accel. in travelling virtual cathode 77—83166
colliding e$^+$e$^-$ beams accelerator expts., 100 GeV, particle prod., weak currents, etc. *(Russian)* 78—58194
Columbia Research Corporation 3 MeV, 45 kW accelerator, industrial, commercial and research applications 79—54215
combined-function storage rings 77—83331

electron accelerators continued
compact standing-wave electron linac with RF drive system using 3 dB hybrid junction 79—72030
computerised pulse radiolysis system 78—64862
conference on nuclear physics with EM interactions, Mainz, Germany (June 1979) 80—22145
coupled Marx-Tesla circuit for production of intense relativistic electron beams 79—17558
cryogenic equipment for point defects in solids research *(French)* 77—132
current density meas. method for electron acceleration 80—102366
current source, dialable, with ovenless construction, stability 77—50320
cyclotron, azimuthally varying electric field, isochronous uniform mag. field 77—50317
Darmstadt linear accelerator, detector system and performance of elec. scatt. system 78—70680
Darmstadt linear accelerator electron scatt. facility, beam transport and spectrom. 78—70679
Darmstadt linear accelerator electron scatt. facility, data processing 78—70681
Darmstadt linear accelerator high resolution scatt. facility 78—70653
DCI double ring facility, status report 77—83326
diode, repetitively pulsed 79—76164
diode accelerator, electron beam power increase by inductive accumulator 78—33339
diode type, with large-beam cross section 78—78517
distributed sputter-ion pumps for use in low magnetic fields, electron storage ring appl. 79—67325
dose and shielding parameters of electron-photon stray radiation 77—57755
Dynamitron system, DC, 100-1000 kW power, and applics. 77—59793
electrically conducting surface coating, of linear induction accelerator tube, beam losses and coating inhomogeneity 78—5066
electron and positron depolarisation suppression in storage rings and cyclic accelerators 80—42882
electron current density distribution, approx. formula *(Japanese)* 80—14032
electron guns, high-current, laminar beam formation 78—74516
electron injector in HV terminal, control and protection system 80—27836
electron-proton facility in CERN SPS 77—83203
electron-proton project TRISTAN, design features 77—83204
ELV-1 accelerator for industrial use 77—30679
EM interactions, high duty cycle accelerators and experimental possibilities 80—23187
energy spectrum monitoring of electron beam 80—68994
ETA gun, beam dynamics calc. with EBQ code 79—72023
ETL linear accelerator, energy increased up to 40 MeV by improvement of klystron efficiency *(Japanese)* 78—78515
Experimental Test Accelerator, off-resonance transformer charging for 250-kV water Blumlein 80—23183
ferrite accelerating structure, self acceleration of strong beam 77—23609
ferrite ring, 2000 NN type, self-accel. caused by high-current electron beam interruption 80—4809
field-emission type, heavy-current, anode foil changing system 78—9005
fissile and fertile material, non-destructive testing 77—74917
foilless diodes, hollow relativistic electron beam generation 79—76170
Frascati linac positron beam, monochromatic gamma beam facility 79—72034
fusion pulsed accelerators development review 78—5046
future technologies in high-energy physics, collective accelerators, laser accelerators, single-pass collecters 80—78466
gas laser excitation of 600 kV accelerator, design 78—13720
gas lasers pumping appl., design principles 78—5483
GELINA, electron linac, neutron time of flight meas. appl. 78—90002
Gyrocon, efficient relativistic high power VHF generator 80—13990
hadronic and nuclear EM probe system using electron accelerator and storage ring 80—23200
Hall accelerator, azimuthal drift current, induction meas. method 79—23465
Harwell, 136 MeV electron linac 80—863
Harwell 136 MeV electron linac, slow neutron production, optimisation calcs. 79—41048
heavy current electron beams prod., survey 78—33337
heavy electron scattering expts. from intermediate energy linear accelerators *(Dutch)* 79—22502
high current, with rectangular cold cathode, for laser excitation 78—25358
high current diode, mag. insulation and parasitic current, contraction instability *(Russian)* 77—58906
high current electron beam of TONUS accelerator, time struct. *(Russian)* 78—66434
high current relativistic electron beam, X-ray emission, pulsed dosimetry 79—81099
high energy low running cost linac, proposed design *(Japanese)* 78—78516
high power, low energy electron linac, radiation processing appl. 79—45472
high power beam generation, review 80—13988
high-current, for optical pumping of gases 80—32544
high-current, high pulse, inductive energy storage 78—46189
high-current, Impuls, design and testing 78—37470
high-current pulsed nanosecond electron accelerator 78—5065
high-voltage subnanosecond electron beam generator 78—4733
hydraulic surge damping with high-power water-filled shaping line 80—27837
induction linac, high power 79—49878
induction type accelerator with steady focusing field, mag. system simulation 77—42198
inductive energy storage, high-perveance electron optic system with electron-energy recuperation 77—23322
industrial accelerators, research at Siberian Institute of Physics 79—72032
industrial electron accelerators, beam energies above 150 keV, problem review 79—31243
industrial radiation safety programme for accelerators 77—83115
inertial confinement fusion, Angara 5 features and design principles 80—63384
injection system of Elektronika linear accelerator, triode gun anode modulation 79—67978
INS 1.3 GeV synchrotron, polarised electron acceleration 80—37660

electron accelerators continued
- ionising radiation produced during operation, dosage and shielding *(Czech)* 79—89505
- irradiation facility for industrial research, appl. *(German)* 77—70244
- ISABELLE closed orbit correction system 77—83336
- Japanese accelerator facilities, current status and KEK 12 GeV synchrotron 79—72041
- Kal'mar-1 pulsed electron accelerator, relativistic electron beam for fusion 80—32543
- Kharkov linear electron accelerator for obtaining beam of quasichromatic linearly polarized photons, 2-crystal goniometric setup 80—68976
- laser accelerator 79—93847
- laser electron accelerator, mechanism 79—81103
- laser-beam focus accel. of electrons 77—10574
- leakage radiation meas., effective energy determ. 78—28089
- LEP, scenarios for high energy physics 79—93848
- LEP 100 GeV e^+e^- storage ring, synchrotron injector design 77—67913
- linac, 600 MeV, Saclay, 40000 hrs. of operation, recent improvements *(French)* 79—688
- linac, low cost RF struct. 77—88293
- linac design for pion radiotherapy 77—83138
- linac for pulse radiolysis, correl. between radiation absorbed dose and elec. parameters 77—34482
- linac transient operation 77—83163
- LINAC-ESR spectrometer, modification for irrad. food component anal. 79—52699
- linear, 2 GeV, monochromatic annihilation γ-ray beam prod. 77—50322
- linear, activities at Amsterdam 77—82918
- linear, development and present status, review *(Chinese)* 79—54625
- linear, equipment and methods *(Russian)* 79—13562
- linear, freq. control methods *(Chinese)* 79—54619
- linear, high current relativistic beams, transient behaviour 80—32541
- linear, high-current injector 78—70655
- linear, high-duty cycle, 500 MeV, electron scatt. facilities 79—72036
- linear, intense electron beam transient radial motion 80—9434
- linear, irrad. system for photon activation anal. 77—63992
- linear, klystron self excited oscillator with short time delay microwave pulse 77—6578
- linear, multisection, freq. characts. calc. method 79—13560
- linear, pion production and appls. *(Japanese)* 78—78533
- linear, prebuncher design calcs. 79—54624
- linear, precise control for pulsed X-ray radiography *(Japanese)* 78—35944
- linear, radioisotope production, review *(Japanese)* 78—78534
- linear, regulations, standards, and guidelines for use in medical radiation therapy 79—53258
- linear, status, uses, 500 MeV 100 kW linac design *(Japanese)* 78—78514
- linear, superconducting, acceleration characts. 77—83178
- linear, two-section, two-component beam energy distrib. 80—9435
- linear, USSR Radiotechnical Institute developments 77—38448
- linear, [conference, Ontario, Canada (Sept. 1976)] 77—38445
- linear 35 MeV accelerator at Univ. of Tokyo *(Japanese)* 79—26786
- linear 40 MeV accelerator, therapeutic and research applications 79—57752
- linear acceleration two-conductor struct., moving EM wave refl. 79—26788
- linear accelerator, 35 MeV, Tokyo Univ. *(Japanese)* 79—54620
- linear accelerator, asymmetric focusing coils, beam dynamics by 3-D model 78—17450
- linear accelerator, computer prediction and diagnosis of failures of systems 79—693
- linear accelerator, dose monitoring system 78—92710
- linear accelerator, efficiency of calorimetric method 79—6778
- linear accelerator, reduction in energy spread of nanosec. relativistic beam 80—5397
- linear accelerator powered by laser beam, parameter estimates 77—83167
- linear accelerator with S-band subharmonic prebuncher for picosecond single electron pulse *(Japanese)* 80—78460
- linear accelerators, health physics aspects of 20 to 40 MeV operations 79—45482
- linear ALIN accelerator, waveguide system *(French)* 79—9925
- linear electron accelerator for 1-mA average current, 10 μsec duration 80—68978
- linear highfrequency electron accelerator, hazard factors and conditions for safe operation *(Czech)* 80—52794
- linear ns high current pulsed, with inductive forming element *(Russian)* 78—829
- linear supercond. 3 MeV electron accel., design and status 79—72009
- long duration pulsed electron beams, development 80—68980
- long pulse electron beam accelerator, appl. gas lasers 77—23321
- low impedance relativistic electron diode, behaviour in converging mag. gradient 77—370
- low-energy, dosimetry by calc. 80—844
- magnetic compression and electrostatic refl. of high v/γ electron beams 77—83398
- magnetic field quality requirements for PEP 77—83205
- magnetised beam, longitudinal stability, in periodic metal-dielectric system 77—65563
- Mainz 300 MeV linear accelerator, energy loss system of electron scatt. facility 78—58524
- MAX, a continuous electron accelerator system 80—23189
- microtron, race track, beam blowup anal. 79—76217
- microwave deflector for cryogenic phase selector of electrons 80—27845
- MIT Bates Linac, progress report 77—14278
- MITE, long self-magnetically insulated power transport expts. 79—90471
- multi-cavity prebunching systems 77—83119
- multipacting, elimination in supercond. struct. for electron accelerators 78—9004
- N-100 storage ring, vacuum ultraviolet-radiation extraction channels 78—5071
- nanosecond accelerator, Fitch oscillator operation 78—828
- nanosecond beam dynamics in linear electron accelerator 80—86996
- nanosecond electron beam, particle dynamics in linear accelerator 79—26787
- nanosecond pulse electron and bremsstrahlung generator 78—21308
- nanosecond pulse generators, wave processes 77—18730
- nanosecond-pulsed, 600 keV, using pulsed-charging of storage capacitors 79—691
- National Synchrotron Light Source, vac. system 79—81106

electron accelerators continued
- NDT appl. 78—40009
- neutron production by electron linear accelerator beam *(Japanese)* 78—78532
- neutron yield calcs., electron beam incidence, radiation protection implications for accelerators 78—95622
- optical reflector for energy extraction for electron synchrotron 80—78467
- para- and orthopositronium prod. by electron accelerators *(Russian)* 79—13846
- PEP, characts., points of interest 79—72038
- PETRA, 19 GeV e^+e^- storage ring 79—72037
- PETRA, damping of coherent transverse bunch oscills. 79—72142
- PETRA, physical plant 77—83335
- picosecond pulse electron linac, design and manufacturing *(Japanese)* 80—5395
- pion conversion target for Saclay electron linear accelerator 77—54384
- polarised electron gun at SLAC, operating experience 77—83396
- positron-electron 18 GeV facility at SLAC, design and status 77—83320
- positron-electron colliding beam at Cornell, design status 77—83323
- positron-electron storage ring PETRA, plans and status 77—83321
- prebuncher design calculations for 150 MeV electron linac 79—68075
- pulse electron accelerator for CO_2 laser preionization 77—88780
- pulse generator, repetitively pulsed electron beam system using cold-cathode electron gun 80—68981
- pulse radiolysis electron source, Febetron 708 type 77—88319
- pulse-power particle beam sources as fusion drivers, review 79—18066
- pulsed, of radial transmission lines 77—46425
- pulsed electron accelerator current density distrib. multichannel recorder 78—58520
- pulsed ELIT-B, design, construction and basic parameters 77—46427
- pulsed giving 20 ps 300 A electron pulses, radiation chem. appls. *(Japanese)* 78—80754
- pulsed high current 1 MeV electron accelerator *(Chinese)* 79—72033
- pulsed high current 60 keV electron accelerators 79—26784
- pulsed high current nanosecond accelerator 78—826
- pulsed high-current, pulsed, for stimulation of compressed gases 79—692
- quantum lifetime in storage rings 77—83334
- radially converging beam type for gas laser excitation 78—9391
- radiation processing appl. 77—54370
- radiation processing applications, shielding and safety 77—67904
- radiation sterilization of medical products using electron accelerators and gamma sources 79—49870
- radiotherapeutic linear electron accelerator NEPTUN-10p 78—88744
- radiotherapy, electron, X-ray, Soviet medical requirements, review 77—37032
- radiotherapy, photoneutron prod., survey of European meas. 80—51241
- radiotherapy electron accelerator neutron production, conf., Gaithersburg, USA (Apr. 1979) 80—46730
- radiotherapy linear accelerator 5.5 MeV Neptune, phys. characts. of beam *(French)* 77—29196
- REBLE accelerator for gas-laser excitation 79—94239
- reflexotron, 25 MeV, tested in medical therapy config. 77—83139
- relativistic electron beam accelerator, FX-75, 1-D coaxial transmission line model, FXPULSE program 78—58506
- relativistic electron beam destruction and equilibrium in mag. guide 79—76171
- relativistic electron beams simulation 79—26789
- relativistic electron storage device, phase free cavity resonator+mag. mirrors 77—83172
- relativistic electron storage device, phase-free cavity resonator with two mag. mirrors 77—10504
- relativistic high current nanosecond beam, transverse instability in linear accelerator 77—83180
- ring and accelerator lattices, linear and nonlinear, interactive computer program 77—83332
- Saclay 600 MeV electron linac, present and future operation 80—23190
- Saclay 600 MeV linac, (e,e′p) coincidence expts. 79—72035
- Saclay linac, 500 MeV intense positron source 79—72171
- self-acceleration expts., regulation of magnetization of ferrite 80—63425
- self-acceleration of intense beam, at trailing edge excitation of exciting system 77—75407
- self-magnetic insulation in vacuum for coaxial geometry 78—78520
- SEM with electron energies up to 5 MeV 79—80728
- Sendai 1.5 GeV linac electron accelerator with pulse-beam stretcher ring 80—23188
- shielding for high energy neutron dose 79—54609
- SPEAR, synchrotron radiation source 77—83186
- spiral electron beam devices, generation conditions calc. *(Russian)* 78—25785
- split microtron injector for Pakhra synchrotron 77—83136
- standing wave high gradient accelerator struct. 77—83143
- standing wave linear high gradient structure, design concept 78—50423
- standing wave triperiodic structure for 10 MeV medical accelerator 77—10498
- Stanford, 2 mile linac, electron source for injection gun 79—76242
- Stanford superconducting linac recyclotron, initial performance 77—83145
- STEM, accelerator system for 78—340
- superconducting bar-loaded resonator for electron accelerator application 79—36434
- superconducting recyclotron for 130 MeV electrons, proposed design 80—23198
- synchrotron, 50 MeV, with cyclotron preaccel., VUV source 77—61641
- synchrotron, beam lifetime increase using pulsed mag. field 79—3265
- synchrotron, electron beam spot, photographic obs., rel. to amplitude of betatron oscillation 78—55059
- synchrotron, weakly focusing, polarised electron accel. *(Russian)* 77—75012
- synchrotron radiation formation, role of betatron vibrs. *(Russian)* 78—50684
- synchrotron with cyclotron preaccel., beam intensity 77—61642
- synchrotrons, circularly polarised photon beam prod. by imperfection resonance methods 77—38512
- Tesla transformer accelerator, electron beam prod. 78—326
- test accelerator, computer control of beam transport system 78—25359
- Therac 6 linear accelerator, computer controlled evaluation for X-ray therapy 79—5363
- Therac 6 linear accelerator, field elongation effects on depth-dose curves, central-axis output of X-rays 79—5361
- TOF pulsed neutron diffraction of liquids using electron linac, CCl_4 appl. 78—18504

electron accelerators continued
Tohoku 300 MeV LInac, energy compressing system 78−74515
Tomsk synchrotron, system of tagged photons 78−833
Tonus, relativistic electron beam instability, passage through dense gas, energy spectrum *(Russian)* 77−3529
Tonus 2M accelerator, high-voltage pulse generator of stored energy 135Kj 78−5067
Torus multichannel commutator, HV spark gap investigation 77−71708
transmission line, charged internally switched configurations for electron acceleration 79−72024
tube for acceleration to 500 keV with 2 ns pulse duration 80−23185
undulator linac, electron dynamics, coherent radiation source 78−82539
undulator radiation, beam parameters effect on spectrum and polaris. characts. 77−75400
undulators, spin effects during electron movement *(Russian)* 78−13652
Van de Graaff, digital beam-intensity meter and fluence programmer 77−54378
vertical beam size due to orbit and alignment errors 77−83207
wiggler, helical synchrotron radiation source, orbits and fields 77−79203
wiggler with short period helical path as synchrotron radiation source 77−79202
e^+-e^- storage ring, 100 GeV facility, design concept 77−83325
e^+e^- CERN 100 GeV ring design, LEP injection 77−83135
ep colliding beams 78−78531
Al foil in quartz dust, electrical explosion for accelerator application 80−6314
H_2O, dielectric insulation for electron accelerators and impulse current generators *(Russian)* 78−75430

electron affinity
alkali atom + methane derivative, collisional ionisation, nitromethane, perfluoromethyl bromide (iodide) electron affinities 78−66639
alkali metal atoms and anions, electron affinity, model pot. SCF and CI calcs. 77−38609
alkaline earth chalcogenides, atomis. energy, electron affinity, mean amplitude of vibr. *(German)* 79−51045
atomic, optimum pot. model used to generate numerical pot., energies and electron affinities determ. 80−99534
atomic electronegativity scale rel. to work function 78−64096
atoms, ionisation pots., electron affinities, Rayleigh-Schrodinger and Green's function calcs. 77−75075
band gap narrowing, physical mechanisms 80−15478
benzenes, substituted, gaseous, negative ion states, electron transmission spectra 77−31007
benzyl radicals, monomtheyl- and dimethyl-substituted, electronic spectra and electron affinity 80−63618
bromanil, electron affinity, bound and excited negative ion states, lifetimes, electron and alkali metal collisions 79−869
carbenes, bond angles, inversion barriers, singlet-triplet energy differences, struct. fragments method 77−10782
carbenes, unrestricted HF calcs. of electronic structure 77−6683
chloranil, electron affinity, bound and excited negative ion states, lifetimes, electron and alkali metal collisions 79−869
chlorofluoromethane negative ion products, in 0-10 eV near-monoenergetic electron impact 79−41245
chlorofluoromethanes, MS $X\alpha$ calcs., ionis. pots., electron affinities 77−79540
conjugated heteroatomic molecules, ionisation pot. and electron affinities, semiempirical MO theory 79−6843
conjugated system, potentials of twofold ionization and electron affinity calcs. 77−3287
cyanomethane$^-$, ab initio calcs., electron affinity, stability 77−42239
cyclopentadiene, HAM/3 calc. of ionis. and excitation energy and electron affinity 79−26894
cyclopentadienyl ion, electron affinity and Jahn-Teller effect, laser photoelectron spectra 77−88499
data collection 77−27194
diatomic hydrides of first and second row elements, PNO-CI and CEPA calc. 79−768
diatomic molecules, containing elements from Li to F and Na to Cl, calc. from mol. dissoc. energies 78−62943
diatomic negative hydrides, photodetachment 0.5 to 3.0 eV, electron affinities *(German)* 77−61812
dioxane liquid scintillators, scintillation yield, chloroform and carbon tetrachloride quenching effects *(French)* 77−3217
doublet state, ionis. pots., electron affinities, using electron propagator, appl. to Li, Na, and BeH 79−63933
equations of motion Green's function methods, higher order terms, ionisation pots., CI comparison 80−52892
ethylene, and perfluoro derivatives, negative ion states, electron affinities, ionisation pots., overlapping spheres $X\alpha$ calc. 79−26885
ethylene, electron affinities, pi* anion, bond lengths, electron transmission spectroscopy study 80−18925
ethynylradical, photodetachment, parturbation theory calcs., ICR spectroscopy obs 79−98166
exciplexes and excited aromatic molecules, donor-acceptor props., comparison of fluorescence quenching 80−69174
first row elements, electron affinity, semiempirical predictions 80−63555
first-row hydrides, correl. energy difference models 77−10600
fluoranil, electron affinity, bound and excited negative ion states, lifetimes, electron and alkali metal collisions 79−869
fluorenone derivatives as electron transport materials, electron affinity and electrochemistry, rel. to photocond. 79−38127
fluorobenzenes, negative ion states and π-electron affinity 79−10206
fluoroethylenes, electron affinities, pi* anions, bond lengths, electron transmission spectroscopy study 80−18925
formaldehyde, and cation, vertical proton affinity in singlet and triplet states 78−90079
formaldehyde, proton affinity determ. from chem. reaction equilib. consts. 78−85189
formamide, valence ionisation energy and electron affinity, HAM/3 calc. and photoelectron, UV spectra 79−50081
Freon 13-B1 and mixtures with Xe and Kr, saturation curve 1 to 8 atm., for ionography ionisation chambers 77−12997
furan, HAM/3 calc. of ionis. and excitation energy and electron affinity 79−26894
glyoxal, electron affinity at centrosymm. trans geometry 80−87225
halogen mols., electron dissociative attachment 80−91694
HAM/3 semiempirical MO theory, unoccupied orbitals, excitation energies and electron affinities calcs. 78−13415

electron affinity continued
heavy metal halides, atomis. energy, electron affinity, mean amplitude of vibr. *(German)* 79−51045
hexafluorides, MF_6, M = S,Se,Te,Mo,W,Re,Ir,Pt ionisation 78−55226
hexafluorides, MS $X\alpha$ calc. 77−30778
hydrocarbons, cyclic, ionis. pot., electron affinity, semiempirical MO theory 77−50365
hydronaphthyl radicals embedded in naphthalene cryst., optical transition energies and ionisation energies 80−78595
insulator, rel. to secondary electron escape probabilities 78−72651
ions, ionisation potentials, electron affinities, perturbation theory-CI calcs. 78−9084
$(Li^+,-)$ model calcs., correl. between electron affinity and dipole moments 77−57857
mass spectrometer-energy analyser obs. 77−9149
metallic and nonmetallic solids, Fermi energies 80−2451
methoxide-$d_0(-d_3)$ anion, electron affinity, vibr. struct., photodetachment electron spectra 78−94282
methyl glyoxal, electron affinity at centrosymm. trans geometry 80−87225
methyl radical and anion, electron affinity determ., ab initio SCF and CI calcs. 78−5149
methylamine, affinities for $H^+(Li^+)(K^+)(CH_3{}^+)$, ab initio SCF calculations 80−102443
methylene, electron affinity, $^1A_1$-$^3B_1$ T_0-value, ab initio MRD-CI method calcs. 78−50478
methylene anion, electron affinity, $^1A_1$-$^3B_1$ T_0-value, ab initio MRD-CI method calcs. 78−50478
MNDO semi-empirical SCF-MO calcs. for atoms, mols., negative ions 78−74578
molecular electron affinities, qualitative molecular orbital theory 78−5122
molecular ions, negative, polar, thermally stable 79−7033
molecule, polar, anion, ab initio ground state pot. energy surfaces, electron affinity 79−49958
molecule, polar, anion ab initio ground state pot. energy surfaces calc. 80−47923
molecules, ionisation potentials, electron affinities, perturbation theory-CI calcs. 78−9084
molecules, ionisation pots., electron affinities, Rayleigh-Schrodinger and Green's function calcs. 77−75075
molecules containing C, N, O and H atoms, electron affinities and ionisation pot., semiempirical calcs. 80−78535
naphthalene anions, electron affinities, transition energy, comparison for gaseous liquid and solid 80−29731
naphthalene vapour, resonant scatt. of slow electrons 77−58182
negative electron affinity devices, semiconductors *(Japanese)* 79−38710
negative ions, form. processes and props., review *(Japanese)* 80−53127
negative ions of second and third period 77−3279
p-nitroacetophenone charge transfer reaction with triplet state of guanine for radiosensitisation 79−92146
nitrofuranes, substituted, electron affinity, HAM/3 calc. 79−27109
nitroimidazoles, substituted, electron affinity, HAM/3 calc. 79−27109
open shell systems, coupled cluster approach 78−58595
parabenzoquinone, and perfluoro derivatives, negative ion states, electron affinities, ionisation pots., overlapping spheres $X\alpha$ calc. 79−26885
photocathodes exhibiting negative electron affinity, model and GaAs expt. *(French)* 77−8724
polar molecules, electron affinities, ab initio calcs., dipole moments 79−89623
polar molecules, electron affinities, Born-Oppenheimer calcs. 77−75333
positronium halides, $[X^-;e^+]$, electronic struct., annihilation characts., HF calc. 77−50567
positronium nitrate, $[NO_3{}^-;e^+]$, existence, Hartree-Fock-Roothaan calcs. 80−83254
positronium nitrite, $[NO_2{}^-;e^+]$, existence, Hartree-Fock-Roothaan calcs. 80−83254
pyridine-N-oxides, substituted, absolute energy levels in gas and condensed media, ionis. energy, electron affinity 77−67995
pyrrole, HAM/3 calc. of ionis. and excitation energy and electron affinity 79−26894
rare earth metals, semi-empirical calcs. 77−6955
Rydberg formula, modified 77−26957
second row elements, electron affinity, semiempirical predictions 80−63555
second-row hydrides, correl. energy difference models 77−10600
semiconductor-electrolyte interfaces, prediction of flatband pots. from atomic electronegativities 78−40068
semiconductors with position-dependent band gap and electron affinity, current densities 77−85210
styrene anions, electron affinities, transition energy, comparison for gaseous liquid and solid 80−29731
$TCNQ^-$, electron affinity, compound states 77−65530
tetracyanoethylene molecule with high electronegativity on field polarisation 79−27111
thiomethoxide anion, electron affinity, vibr. struct., photodetachment electron spectra 78−94282
thiomethoxyl anion, and deuterate, electron photodetachment, affinities, vibr. freq. and spin-orbit splitting 80−53063
transition metal atoms and ions, electron affinities and ionis. pots. MS $X\alpha$ calcs. 79−10031
water, proton affinity, many-body Rayleigh-Schrodinger perturbation theory 78−92497
Ag cluster 78−33646
Ag_3SbS_3, pyrargyrite, thermoelec. and photoelec. work functions, Fermi level and electron affinity *(Russian)* 77−15939
Al^-, metastable, electron affinity calcs. 79−31439
$Ar+M \rightarrow Ar^+ + M + e^-$ or $+M^-$, ($M = O_2$, NO, NO_2, N_2, CO), keV energies, translational spectroscopy 78−5339
As_4S_4, electronic struct. and vertical electron affinities, INDO-type ASMO SCF calcs. 79−31402
$As_4S_4{}^-$, electronic struct. and vertical electron affinities, INDO-type ASMO SCF calcs. 79−31402
As_4Se_4, electronic struct. and vertical electron affinities, INDO-type ASMO SCF calcs. 79−31402
$As_4Se_4{}^-$, electronic struct. and vertical electron affinities, INDO-type ASMO SCF calcs. 79−31402
B, electron affinity, modified variational approx. 78−66679
B, excited in single gas collisions, high-resolution Auger spectra 80−9717
B^-, metastable, electron affinity calcs. 79−31439

electron affinity continued

BaO, single cryst. on Ir, electron affinity, conduction band edge position, low energy electron reflection spectra 78—14790
BaO, surface pot. meas., cond. band edge, electron affinity, LEER 77—24606
Be, excited in single gas collisions, high-resolution Auger spectra 80—9717
Be_n^- (n=2,3,4), electronic struct., ab initio calcs. 78—17560
BeF_2^-, electron binding, extended basis SCF calc. 79—49944
BeF_2^-, ground state, conform., electron affinity, extended basis SCF calcs. 79—72253
BeO(BeO^-), electron affinity and dipole moment, ab initio calc. 78—41938
BrO^-, electron affinity, formed in $Br^- + O_2$ reaction 77—63902
C, electron affinity, modified variational approx. 78—66679
C, excited in single gas collisions, high-resolution Auger spectra 80—9717
C^-, near-threshold photodetachment, IR meas. 77—42290
C_2, electron affinity, vibr. struct. in radiative electron attachment spectra 77—88592
C_2^-, bound electronic states and electron affinity, IC calc. 79—76349
$C_2(C_2^-)$ pot. energy curves calc. using SCF, MCSCF and CI methods, dissoc. energies, bond lengths, electron affinity 80—95523
CH_3, experimental determ. of the geometry and electron affinity 78—82860
$CH_3(CH_3^+)(CH_3^-)$, HF, GVB and CI calcs. 77—75063
CN, CN^-, HF electron affinity, SCF calcs. 77—67979
CN, free radical, electron affinity 77—47375
CN, radical, adiabatic electron affinity, CI calcs. 79—68197
CN radical, electron affinity calc. 77—1092
CN^-, electron propagator theory, mol. electron affinities calcs. 80—83521
CN^-, enthalpy of formation and electron affinity 77—35506
$(CN^-;e^+)$ complex, ab initio LCAO SCF calc., positron affinity and excitation energy 79—49945
$(CO_2)_2^-$, struct., stability, electron affinity of neutral dimer, Hartree Fock calc. 79—63912
CO_3, lower limit determ. 78—7193
CO_3, photodissociation cross-section 77—6870
Cd, electron scatt., negative ion form., shape resonances, electron affinity 77—14581
CdF_2-metal Schottky diode, photoemission, capacitance and I-V meas. barrier heights 78—26950
Cl, variation-perturbation approach 77—54513
Cl_2^-, electron propagator theory, mol. electron affinities calcs. 80—83521
ClO^-, electron affinity, formed in $Cl^- + O_2$ reaction 77—63902
Co^-, photoelectron spectra, electron affinity and fine-struct. interval 79—68212
$Cs+I_2$, ion-pair formation, energy transfer and differential scatt. 77—75272
$CsH^-CsH^+(CsH)$, ab initio ground-state pot. energy curves, electron affinities 78—41946
F compounds, ground states, mol. parameters, MINDO calcs. 78—41955
F, electron affinity, modified variational approx. 78—66679
F, variation-perturbation approach 77—54513
$(F^-;e^+)$ complex, ab initio LCAO SCF calc., positron affinity and excitation energy 79—49945
Fe^-, electron affinity, nonstatistical fine-struct. detachment intensities at 488 nm, laser electron spectra 79—41144
FeO, electron affinity, ground state vibr., new assignment 77—75212
GaAs epitaxial thin films with neg. electron affinity, photoelectron energy distrib. 80—100755
GaAs, photocathodes exhibiting negative electron affinity *(French)* 77—8724
GaAs-Cs-O photoemitter, negative electron affinity, fabrication and characts. 78—2979
GaInAs, photocathode with negative electron affinity, photoemission, influence of strong elec. field 79—8227
GaP:Cs-O simultaneous adsorption, oxidation interface chemical struct. 80—103584
GeH_3^-, electronic struct., electron affinity, inversion barrier, ab initio SCF Gaussian basis calc. 80—63552
GeX_{2-3}, (X=Cl,Br), electron impact dissoc., low-energy reson. capture 78—9263
H, electron affinity, semiempirical predictions 80—63555
H^-, electron affinity, calc. of ion lifetime in elec. field 79—54986
H^-, metastable, electron affinity calcs. 79—31439
H^{2-}, metastable, electron affinity calcs. 79—31439
H_2, electron dissociative attachment 80—91694
HC_2, ground state energy surface, ab initio SCF calc. 78—33446
HC_2 radical, electron affinity, ab initio SCF and CI calcs. 78—50468
HC_2^-, ground state energy surface, ab initio SCF calc. 78—33446
HCN, proton affinity determ. from chem. reaction equilib. consts. 78—85189
HCN^-, ab initio calcs., electron affinity, stability 77—42239
HCN^-, SCF ab initio ground state pot. energy surface, geometry, rel. to HCN 78—78646
HF^- and $(HF)_2^-$, ab initio calcs., electron affinity, stability 77—42239
H_3NO^-, ab initio calcs., electron affinity, stability 77—42239
(H_2O), electron affinity, ab initio SCF calcs. 79—76343
H_2O, electron affinity, mol. geom. effects calcs. 78—82618
H_2O, many-body Green's function, electronic mol. props. 78—25417
H_2O^-, ab initio calcs., electron affinity, stability 77—42239
H_2O^-, electron affinity, mol. geom. effects calcs. 78—82618
H_2S, proton affinity determ. from chem. reaction equilib. consts. 78—85189
He, electron affinity, semiempirical predictions 80—63555
He, electron affinity of $(1s2s)^3S$ state, CI calc. 79—59591
He^-, binding energy of metastable 1s2s2p $^4P^0$ state 80—9524
He^-, metastable, electron affinity calc. 79—31439
Hg, electron scatt., negative ion form., shape resonances, electron affinity 77—14581
$I^- + CO$, endoergic ion-molecule reaction 77—25262
$I_2(I_2^+)(I_2^-)$, HF and SCF calcs., pot. curves, electron affinity and quadrupole moment determ. 80—95527
IO^-, electron affinity formed in $I^- + O_2$ reaction 77—63902
In, meas. by dissoc. ionisation of InBr, InI *(French)* 80—63849
InAs, oriented single crysts., photoemissive props., photoelec. thresholds 77—59666

electron affinity continued

In_2O_3-Si(Ge)(GaAs)(InP) heterostructure solar cells, photovoltaic and rectifying props., electron affinity determ. 79—1618
K+halogenated methane, negative ion form., electron affinities, bond dissoc. energies 78—82827
$K+I_2$, ion-pair formation, energy transfer and differential scatt. 77—75272
Li, electron affinity, variation-perturbation approach 77—54513
Li H^-, mol. orbital calcs., diffuse functions for basis sets, electron affinity 78—25436
Li_2, ab initio calc. 77—34553
LiF(LiF^-), electron affinity and dipole moment, ab initio calc. 78—41938
LiH, LiH^-, pot. energy curves, electron affinity, spectroscopic consts. 78—5129
LiH, many-body Green's function, electronic mol. props. 78—25417
LiH, positron affinity, ab initio LCAO MO SCF calc. 78—82870
LiH^-(LiH), ab initio ground-state pot. energy curves, electron affinities 78—41946
$LiNbO_3$, thermionic emission characts. 80—104034
Mg, electron scatt., negative ion form., shape resonances, electron affinity 77—14581
MgF_2^-, ground state, conform., electron affinity, extended basis SCF calcs. 79—72253
MgO(MgO^-), electron affinity and dipole moment, ab initio calc. 78—41938
MoF_6+alkali atom(dimer), ionis. reactions, electron affinity 77—81398
N, electron affinity, modified variational approx. 78—66679
NH, electron affinity and intercombination separation 77—18970
NH_2 radical, heat of form., a diabatic electron affinity, from proton affinity meas. 79—91987
NH_3, affinities for $H^+(Li^+)(K^+)(CH_3^+)$, ab initio SCF calculations 80—102443
NO, ionis. pot. and electron affinity, overlapping sphere MS Xα calc. 78—41948
N_2O, ground state pot. energy surfaces 77—27175
$NO_2(NO_2^-)$, ionis. pot. and electron affinity, overlapping sphere MS Xα calc. 78—41948
$NO_3(NO_3^-)$, ionis. pot. and electron affinity, overlapping sphere MS Xα calc. 78—41948
Na, electron affinity, variation-perturbation approach 77—54513
$Na+I_2$, ion-pair formation, energy transfer and differential scatt. 77—75272
$NaCl^-$, mol. orbital calcs., diffuse functions for basis sets, electron affinity 78—25436
NaF(NaF^-), electron affinity and dipole moment, ab initio calc. 78—41938
NaH , mol. orbital calcs., diffuse functions for basis sets, electron affinity 78—25436
NaH^-(NaH), ab initio ground-state pot. energy curves, electron affinities 78—41946
Ne isoelectronic series, second order correl. energy, Z depend. of irreducible-pair energies 80—91417
Ni clusters, electronic props. and implications for chemisorption 79—23886
Ni^-, photoelectron spectra, electron affinity and fine-struct. interval 79—68212
O, electron affinity, modified variational approx. 78—66679
O, two electrons, from alkali and alkaline earth oxides cohesive energies 78—25736
O_3, lower limit determ. 78—7193
O_3, radiative electron attachment spectra, vibr. stretching, electron affinity, theory 77—54617
O_3^-, photoelectron, photodetachment and photodestruction spectra 79—64042
O_3^-+molecule reactions, thermochemistry, electron affinity and rate consts. 78—40040
OH, electron affinity, variation-perturbation approach 77—54513
OH_n, ab initio LCAO SCF calcs. of ionisation pot., electron, proton, H and hydride affinities 77—88387
$O^-(O_2^-)$, optimum pot. model used to generate numerical pot., energies and electron affinities determ. 80—99534
P^-, metastable, electron affinity calcs. 79—31439
P_2, electron affinity, vibr. struct. in radiative electron attachment spectra 77—88592
$P^-(^3P_{2,1,0})+h\nu$, P electron affinity, P^- fine struct. interval 77—79590
Rb^-, photodetachment, electron affinity 78—90132
Rb-tetrahydrofuran soln., photolysis, photoelectron emissive EPR signal, scavenger electron affinity reactivity 78—53224
Rb_2Te film electron affinity and photoelectron work function obs. 79—69959
SF_6, MS Xα calc. 77—30778
$SF_6+X^- \rightarrow SF_5^- + F + X$ (X=O, S, F, Br, I), electron affinity of SF_5 radical 80—45495
S_4N_4, electronic struct. and vertical electron affinities, INDO-type ASMO SCF calcs. 79—31402
S_4N_4 , electronic struct. and vertical electron affinities, INDO-type ASMO SCF calcs. 79—31402
SO_2, radiative electron attachment spectra, vibr. stretching, electron affinity, theory 77—54617
SO_3, photoelectron spectrum assignment, ionisation pot. and electron affinity, Green's function method 77—54576
SeF_6, MS Xα calc. 77—30778
Si (111) surface, relax. of surface atoms, Si_4H_9 clusters 77—8171
p-Si photoemitter, achievement of negative electron affinity 78—2980
p-Si-As_2S_3 isotype crystalline-amorphous heterojunctions, electrophysical props. 79—24063
SiH_2, electron affinity, theoretical exam. 78—29863
SiX_{2-3}, (X=Cl,Br), electron impact dissoc. of $SiCl_4(Br_4)$ 78—9263
$SnX_3^{\ominus}(SnX_2^{\ominus})$(X=Br,Cl,I), structs., electron affinities, formed by electron impact 77—61865
TeF_6, MS Xα calc. 77—30778
$Te^-(^2P_{1/2,3/2})+h\nu$, Te electron affinity, Te^- fine struct. interval 77—79590
Tl, meas. by dissoc. ionisation of TlBr, TlI *(French)* 80—63849
UF_4-MF (M=Na or K), ion-molecule equilibria, heat of form. and dissoc. and electron affinities determ. 80—104480
UF_6, electronic struct., ab initio calcs. using relativistic core pots. 79—97987
UF_6, MS Xα calc. 77—30778
UF_6+alkali atom(dimer), ionis. reactions, electron affinity 77—81398

electron affinity continued
UF_6+e^-(K)(Na)(Cs), positive and negative ion formation, electron affinity, bond dissoc. energy 77—75314
WF_5, dissoc. electron capture, electron impact mass spectra, electron affinities 77—88579
WF_6, dissoc. electron capture, electron impact mass spectra, electron affinities 77—88579
WF_6, electron and fluoride affinities, ICR spectra 79—39130
WF_6+alkali atom(dimer), ionis. reactions, electron affinity 77—81398
WF_6+Na(K) electron transfer, WF_6^- form., dissoc. energies, electron affinity 77—19071
WOF_4, dissoc. electron capture, electron impact mass spectra, electron affinities 77—88579
Xe-MF_6, M=W, Mo, U, Re, Ir, charge transfer interactions, VUV and IR obs. 78—50664
Zn, electron scatt., negative ion form., shape resonances, electron affinity 77—14581
ZnO surfaces, work function, band bending, and electron affinity 79—47145
ZrO_2 films on Zr alloys, exoelectronic emission props. and energy-band parameters 79—91571

electron annihilation *see electron-positron interactions*

electron attachment
air, dry, O_2 electron attachment coeff. meas., O_2 partial press. depend. *(German)* 79—13821
air, negative corona current O_3 density depend., 46-87 kPa 80—1852
air wake, hypersonic, ionised, free electron attachment coeff. meas. 79—27835
aliphatic chlorocarbons, electron impact dissoc., $\lesssim$10 eV, negative ion prod. 78—5359
aliphatic perfluorocarbons, electron attachment, fragmentation 0-12 eV 80—5618
aromatic heterocyclics, (N- and S-), electron attachment, mass spectroscopic obs. *(German)* 77—64001
aromatic hydrocarbons, electron attachment, mass spectroscopic obs. *(German)* 77—64001
atom, radiative attachment coeffs., 10-10^4K *(Japanese)* 77—42415
atomic electron scatt., correlation effects 78—58842
atomic electron scattering, reson. laser induced negative ion production 79—64104
benzyl halides, in matrix, UV-, γ-irrad., benzyl radical-halide ion form., charge transfer bands 77—16854
bromanil, electron affinity, bound and excited negative ion states, lifetimes, electron and alkali metal collisions 79—869
N-bromosuccinimide, X-irrad., ESR study of Br and σ^* radical 80—66037
cis-butene-2, high density vapour thermal electron attachment density depend. 79—90369
chloranil, electron affinity, bound and excited negative ion states, lifetimes, electron and alkali metal collisions 79—869
chlorofluoromethanes, electron attachment, electron swarm method 80—69245
chlorofluoromethanes, negative ion form. by 0.10 eV near-monoenergetic electron impact 79—41245
diatomic molecule, dissoc. electron attachment, adiabatic approx. *(Russian)* 79—94052
diatomic molecules, electron impact, vibs. excitation and dissoc. attachment, R-matrix calcs. 79—72228
dibromotetrafluoroethane, plasma quench reactions, electron attachment 77—90586
dichlorodifluoromethane, total ionis. and electron attachment cross sections by electron impact 79—59586
electronegative gases, sparking pots. and ionisation coeffs. 78—42705
fast electron ionisation or attachment transition probabilities, extended statistical law 77—54613
flames, kinetics of electron attachment to O_2 and H_2O 80—3349
fluoranil, electron affinity, bound and excited negative ion states, lifetimes, electron and alkali metal collisions 79—869
freon-N_2 low-pressure mixture prebreakdown current obs. 79—18995
gas, weakly ionised, ionis. and attachment effects on electron swarm parameters 78—5845
halogen mols., electron dissociative attachment 80—91694
halomethane mols., electron scavenging studied by electron cyclotron reson. 79—50143
hexafluorobenzene, slow electron attachment obs., π-orbital calcs. 77—6948
high temperature processes, chemical modelling 80—18937
inert gas-halide lasers, halide mol. negative ion prod. rates 80—18938
ion-ion collisions, crossed beam expts. 78—58843
molecular electron dissociative capture, vibr. struct. of resonances 77—34770
molecular electron scatt., dissoc. attachment, resonant states 78—58851
molecular electron scatt., dissoc. attachment 78—58849
molecular electron scatt., dissoc. attachment 78—58850
molecule, dissociative attachment of electrons 78—62931
molecule and mol. clusters, electron attachment electron-mol. collision, Rydberg electron exchange 80—63843
multiplet ratios for photoionisation and electron attachment, shell-model, LS coupling and correl. 78—17636
negative ions, form. by dissoc. attachment, ang. distrib. 79—81288
nitro compounds in cyclohexane, electron attachment reaction rates from pulse radiolysis 78—31663
perfluoro-1,2-dimethylcyclobutane, electron attachment, elec. field and energy depends. 79—36759
perfluoro-1,3-butadiene, electron attachment, press.-reduced elec. field and energy depends. 79—36758
perfluoro-1,3-dimethylcyclohexane, electron attachment, elec. field and energy depends. 79—36759
perfluoro-2-butene, electron attachment, press.-reduced elec. field and energy depends. 79—36758
perfluoro-2-butyne, electron attachment, press.-reduced elec. field and energy depends. 79—36758
perfluorobenzene, electron attachment, radiative and dissoc., negative ion lifetimes, ion cyclotron reson. spectra 80—74251
perfluorocyclobutane, electron attachment, press.-reduced elec. field and energy depends. 79—36758
perfluorocyclobutane, electron attachment, radiative and dissoc., negative ion lifetimes, ion cyclotron reson. spectra 80—74251
perfluorocyclobutene, electron attachment, press.-reduced elec. field and energy depends. 79—36758

electron attachment continued
perfluorocyclohexene, electron attachment, elec. field and energy depends. 79—36759
perfluorocyclopentane, electron attachment, elec. field and energy depends. 79—36759
perfluoromethylcyclohexane, electron attachment, $\lesssim$3 eV, rel. to perfluoro-1-heptene 79—36755
perfluoromethylcyclohexane, electron attachment, radiative and dissoc., negative ion lifetimes, ion cyclotron reson. spectra 80—74251
perfluorotoluene, electron attachment, elec. field and energy depends. 79—36759
perfluorotoluene, electron attachment, radiative and dissoc., negative ion lifetimes, ion cyclotron reson. spectra 80—74251
positive column, of electroneg. gas, transverse stability, effect of dissoc. attachment 79—23475
positive column of glow discharge of electronegative gas, molecular excitation and ionisation by electron collisions 80—49031
solvated electron reaction rates in alcohols and water 77—25259
TCNQ, negative ion form. by electron and Cs collisions, electron affinity, compound states 77—65530
tetrafluoromethane, electron impact excitation, resons. and dissoc. attachment 79—7020
tetraphenylcyclobutane, in hexamethylphosphoric triamide soln., pulse radiolysis, optical absorption decay obs. 79—16019
threshold photoelectron spectroscopy by electron attachment, high-resoln. 77—27202
trichloroethylene, interaction with thermal-energy electrons, cyclotron reson. obs. 77—19097
trichlorofluoromethane, dissoc. electron attachment, pot. curves calcs. 79—98231
trichlorofluoromethane, threshold electron attachment cross-section 79—89708
trichlorofluoromethane anion, dissoc. electron attachment, pot. curves calcs. 79—98231
trifluoromethylhalide radical anions, formation, ESR and struct. 77—32809
two-particle-hole Tamm-Dancoff approximation (2ph-TDA) equations for closed-shell atoms and molecules 78—70937
Ar, threshold photoelectron spectra by electron attachment 77—75211
Br_2, dissoc. attachment by 0-8 eV electrons 78—74776
Br_2, thermal electron dissoc. attachment rate consts., meas., in flowing afterglow 77—10773
C, pseudostate and Bethe-Goldstone approx. 77—68111
C_2, electron affinity, vibr. struct. in radiative electron attachment spectra 77—88592
CH^+, continuum electron wavefunction, electron capture width 78—78805
CO bremsstrahlung by CO^- free-free transitions continuous absorption calc. 79—63978
CO, dissociative electron attachment 77—42431
CO, $X^2\Sigma^+$, vibr. levels, UPS electron attachment obs. 80—95683
CO_2, electron swarm parameters for high E/N, Monte Carlo simulation 80—19548
CO_2, gas ionis. by nozzle expansion, negative Van der Waals polymer mols. form. 78—90307
CO_2, primary ionis. coeff., electron attachment coeff. rate coeff. 77—4900
CO_2, supersonic jet, $(CO_2)_n^-$ cluster formation and electron attachment 78—5385
CO_2-N_2-He, vol. discharge, negative ions effect 80—14956
CO_2-N_2-He-CO gas laser mixture, electron motion anal. 79—64199
$C^-(^4S^0)$, attachment energies, ab initio calc. 77—30768
CeI_3 vapour, electron irradiated, negative ion formation 77—27190
Cl_2, dissoc. attachment by 0-8 eV electrons 78—74776
Cl_2, dissoc. electron attachment, negative ion prod. rates 80—18938
Cl_2, electron dissoc. attachment peaks, 0—11.5 eV, Cl_2^- pot. energy curves 77—75312
Cl_2, electron impact total ionis. and electron attachment cross sections 79—3589
Cl_2, electron-attachment rate const., room temp. and 250°C in N_2(Ar) discharges 79—45841
Cl_2, thermal electron dissoc. attachment rate consts., meas., in flowing afterglow 77—10773
ClF_3, interaction with thermal-energy electrons, cyclotron reson. obs. 77—19097
D_2, dissociative attachment of electrons *(Russian)* 78—13621
D_2, dissociative electron attachment, Faddeev calcs. of cross sections *(Russian)* 78—70945
D_2, electron dissociative attachment rates, rot. (vibr.) excitation depend., in plasma 80—43848
DCl dissociative-attachment cross sections, fine struct. 77—71884
F_2, dissoc. attachment by 0-8 eV electrons 78—74776
F_2, dissoc. electron attachment, negative ion prod. rates 80—18938
F_2, dissociative attachment of electrons, current density meas., in controlled discharge 77—23566
F_2, electron dissociative attachment rate consts. at 300 and 500K, in discharge plasma 80—43849
F_2, electron impact, low energy, vibr. excitation and dissociative attachment 78—46453
F_2, thermal electron dissoc. attachment rate consts., meas., in flowing afterglow 77—10773
F_2-inert gas mixtures, transport and attachment processes 78—59542
F_2-N_2 mixtures, electron attachment rate to F_2, elec. cond. meas. 79—7019
$Fe(CO)_5$, gas phase collisions, negative ion form., struct. 77—6945
H^- affinity radiation, theoretical study of negative absorption 80—38001
H^{2-}, existence, alternative explanation of results, electron effects 77—19079
H^{2-}, existence, expt. evidence 77—19081
H+positronium—H^++positronium$^-$, low energy, field theoretic approach 77—10790
H_2, $c^3\Pi_u$ metastable state, dissociative electron attachment 79—89794
H_2, dissociative attachment cross sections, interference struct. around 14 eV 79—45856
H_2, dissociative electron attachment, H^- ang. distribs. 77—19099
H_2, dissociative electron attachment 77—42431
H_2, dissociative electron attachment, Faddeev calcs. of cross sections *(Russian)* 78—70945
H_2, electron dissociative attachment rates, rot. (vibr.) excitation depend., in plasma 80—43848
H_2, electron dissociative attachment 80—91694

electron attachment continued
H_2, electron impact, dissociative attachment, vibr. and rot. state depend. 79–18298
H_2, electron impact, dissociative attachment, vibr. and rot. state depend. 79–13829
H_2, HD, dissociative attachment of electrons *(Russian)* 78–13621
H_2^-, variational calcs. of resonant states 79–3571
H_3, correl., ionis. and attachment operators, diagrammatic method calcs. *(French)* 79–22607
H_3^+, correl., ionis. and attachment operators, diagrammatic method calcs. *(French)* 79–22607
HBO_2, electron attachment, rate coeff. 77–75310
HBO_2, electron attachment, rate coeff., equilib. effects 77–75311
HBr, dissociative attachment of electrons 78–62931
HBr, electron impact ionisation, vibr. excitation spectra threshold peaks, negative ion effects 80–106322
HCl, dissoc. electron attachment kinetics in flame, mass spectra obs. 78–68872
HCl, dissociative electron attachment, differential cross section, Feshbach resons. 80–83508
HCl, dissociative-attachment cross sections, fine struct. 77–71884
HCl-N_2 mixture, electron swarm, Cl^-.HCl cluster formation, dissoc. attachment, drift tube mass spectra 78–68884
HCl.H, form. by dissoc. attachment, differential cross section 79–86077
HD, dissociative electron attachment, Faddeev calcs. of cross sections *(Russian)* 78–70945
$H_2(D_2)$, dissociative electron attachment and vibr. excitation, low-energy 80–23565
HF, Feshbach resons., predissoc. investig. 80–83433
H_2O, and D_2O, Feshbach-reson. and dissoc. electron attachment 79–41246
H_2O, dissociative electron attachment 77–42431
H_2O, slow electron scatt., rigid mol. model with exchange and polarisation, vibr. excitation, dissoc. attachment 80–43194
H_2O, Van der Waals polymer mols., negative ions formed in nozzle expansion 78–90296
H_2O vapour, ionis. coeffs. and dissociative electron attachment 80–43833
H_2S, dissociative electron attachment, H^- energy and ang. distrib. 79–31710
H_2S, slow electron scatt., rigid mol. model with exchange and polarisation, vibr. excitation, dissoc. attachment 80–43194
H(1s)+Cs, differential electron attachment and elastic scatt., 30-528 eV 80–63745
He discharge, three-body electron attachment to O_2 80–24245
He, electron impact ionisation, decay modes investig. 79–72422
He, electron scatt., He^- resonances in post collision interaction 79–13820
He-$Co_2(O_2)$ volume discharge, electron recombination and attachment 77–19799
He-F_2, dissociative electron attachment, rate coeffs., appl. to lasers 78–46575
I_2, dissoc. attachment by 0-8 eV electrons 78–74776
I_2, dissoc. electron attachment, negative ion prod. rates 80–18938
I_2, dissociative attachment, thermal energy electrons 78–82850
I_2, electron attachment coeff., 35-110°C, vibr. states interpretation 79–98219
Kr-Cl_2 mixture, glow discharge positive column, electron energy distrib. and rates of inelastic processes, negative Cl ions form. 80–19632
$Kr^*(Kr^+)+NF_3$, rate consts., electron attachment coeffs., flowing afterglow 78–13578
N, pseudostate and Bethe-Goldstone approx. 77–68111
N_2, dissociative electron attachment, $N^-(^3P)$ form. 78–90308
N_2, threshold photoelectron spectra by electron attachment 77–75211
NF_3, dissoc. electron attachment, rate consts. meas. 78–3326
NF_3, dissoc. electron attachment, negative ion prod. rates 80–18938
NF_3, electron dissociative attachment rate consts. at 300 and 500K, in discharge plasma 80–43849
NF_3-N_2(Ar)(He), electron attachment coeffs. using swarm techniques 80–53915
NH_3, ionis. coeffs. and dissociative electron attachment 80–43833
NH_4^+, dissoc. electron recombination cross-sections, 0.065-2 eV 78–66671
NO, dissociative electron attachment 77–42431
NO, dissociative electron attachment, $N^-(^3P)$ form. 78–90308
NO^-, $^3\Sigma^-$ and $^1\Delta$ resonances, excitation in electron scatt. 77–31010
NO_2, electron attachment, ECR obs. *(German)* 79–10201
N_2O, dissoc. electron attachment, O^- ang. distrib. 77–75315
N_2O, gas ionis. by nozzle expansion, negative Van der Waals polymer mols. form. 78–90307
N_2O, gas phase electron attachment, temp. depend., pure, and in ethane and neopentane mixtures 79–36757
N_2O, in liq. inert gas, electron attachment, elec. field effects 77–31009
N_2O, mech. of thermal electron attachment, microwave cond. meas. 78–59536
N_2O, pure and in mixtures, electron attachment near 1 atm., microeave cond. meas. 80–1063
N_2O-CO_2(-ethane), gas phase thermal electron N_2O attachment mechanism, 5-120 torr 79–27085
N_2O-hydrocarbon mixtures, mech. of thermal electron attachment, microwave cond. meas. 78–59536
Ne, reson. free-free absorpt. by electrons in at. field, negative ion form. 77–3463
$Ni(CO)_4$, gas phase collisions, negative ion form., struct. 77–6945
O, pseudostate and Bethe-Goldstone approx. 77–68111
O_2, attachment cooling, press. depend. 80–91663
O_2 discharge plasma, metastable states role, two-step ionisation, electron densities and transition pts. 80–44019
O_2, dissociative attachment coeff. calc. 77–19100
O_2, dissociative electron attachment 77–42431
O_2, electron attachment threshold photoelectron spectra, vibr. excitation 80–83422
O_2, in discharge, non-self-maintained, three-body electron attachment to O_2, plasma decay obs. 80–43844
O_2, in liq. inert gas, electron attachment, elec. field effects 77–31009
O_2, interactions with slow electrons 79–45848
O_2, thermal electron attachment with various compounds present, microwave cavity-radiolysis 77–42422
O_2, three-body electron attachment, Boltzmann eqn. method 79–855
O_2-CO_2 (ethylene)(neopentane), thermal electron attachment meas., microwave cond., pulse radiolysis 80–28592

electron attachment continued
O_2-N_2 mixture, attachment cooling, press. depend. 80–91663
O_3, radiative electron attachment spectra, vibr. stretching, electron affinity, theory 77–54617
$O^-(^2P^0)$, attachment energies, ab initio calc. 77–30768
P, in K seeded flame, electron attachment, compound form. 79–11794
P_2, electron affinity, vibr. struct. in radiative electron attachment spectra 77–88592
SF_6, in liq. inert gas, electron attachment, elec. field effects 77–31009
SF_6, photon-enhanced dissociative electron attachment 80–9749
SF_6, photon-enhanced dissociative electron attachment, isotope selectivity 80–18939
SF_6, pure and mixtures, dielec. props., ionisation and attachment coeffs. 80–33726
SF_6, resonant single-photon dissoc. route using prelim. electron excitation 80–9662
SF_6, threshold electron attachment cross-section 79–89708
SF_6, vibr. excitation, dissociative attachment 77–3481
SF_6-N_2 mixture, electron swarm development, Boltzman eqn. anal. 80–87841
SF_6-N_2 mixtures, attachment coeffs. and ionic mobilities, 1.2-4 eV 80–96338
SF_6+Rydberg atom, reaction channels, expt. vs. theory 80–63755
SO_2, electron attachment processes investig. and mobility of negative ions 80–38518
SO_2, radiative electron attachment spectra, vibr. stretching, electron affinity, theory 77–54617
SO_2XY, (X,Y=Cl,F), positive and negative ion chemistry 78–85140
XeF_2, dissociative electron attachment, rate const., flowing afterglow obs. 77–6946
XeF_2, dissociative electron attachment, 0-20 eV 79–72430

electron avalanches
cathode initiated surface flashover, propag. vel. 78–14233
corona, positive, initiated by negative ion decay, expt. 77–55182
corona, positive, onset in atmospheric air, expt. 80–36354
corona onset voltage in nonuniform air gap, calc. methods 77–15253
dielectric solid surface breakdown in vac., desorption mechanism 78–67464
diluent in XeCl laser, performance 79–94212
discharge, luminescent, in He, electrons energy distribution function evaluation, by Monte-Carlo type simulation *(French)* 77–19795
dosimetry of impulse fluxes of ionising radiation, use of microwave methods 77–25557
electrically stressed insulator-vacuum interface, secondary electron avalanche 77–81185
electron beam self-focusing decline by gas breakdown, avalanche and plasma cond. effects 78–18420
electron swarm develop., Boltzmann eqn. anal. 78–79487
electron swarm motion parallel and perpendicular to electric field, Boltzmann eqn. anal. 78–30502
electronegative, nonlinear effect during avalanches development 77–72517
gas, distribution function of carriers in electron avalanches 77–47287
gas, high press. breakdown in strong static elec. field, plasma mechanism 80–79614
gas, self-sustained discharge form. condition, atm. press., photoionis. process 77–27770
gas breakdown, by combined laser and microwave irrad. 77–35434
gas breakdown by large amplitude EM fields, kinematic theory 80–24295
gas discharge streamer propagation mechanism based on plasma vibrs. *(Russian)* 77–84546
gas mixture electron avalanche multiplication in cylindrical elec. field 78–67557
gas under uniform electric field, simulation by Monte Carlo methods *(Japanese)* 77–39399
n-heptane, Townsend primary and secondary ionisation coeffs. and sparking voltages 80–1732
n-hexane, avalanche breakdown 79–55449
n-hexane, Townsend primary and secondary ionisation coeffs. and sparking voltages 80–1732
laser beam with retractable focus, ionis. path form. in gases 79–18992
laser spark, electron conc. limitation, electrodynamic mechanism *(Russian)* 80–59333
laser-gas interaction, neutral atom inverse bremsstrahlung, laser induced electron avalanche *(French)* 78–26309
microwave field gas ionisation, low-press., ionis. freq. spectra *(Russian)* 79–98854
multipactor microwave discharge, electron vel. distrib., homogeneous polyphase reson. anal. 77–7628
MWPC, avalanche ang. localisation 78–50434
noise, in particle flux, due to reduction and multiplication processes 79–21672
one-sided abrupt junctions, distinction between avalanche and tunnelling breakdown 78–56211
optical discharges by laser radiation, continuous equilib. plasma maintenance 80–59259
optical materials, laser induced breakdown, breakdown thresholds and multiphoton absorpt. coeffs. 79–3735
n-pentane, Townsend primary and secondary ionisation coeffs. and sparking voltages 80–1732
picosecond-probe optical breakdown, direct obs. of dynamics 78–6629
point-to-plane air gap, corona onset, breakdown voltage 78–47194
positive corona electrode, negative ion counterflow, elec. field strength meas. 80–38817
proportional counter, avalanche localisation and effects 78–46217
proportional counter, methane filled, influence of electron avalanche KE on gas amplification factor 78–50439
proportional counters, avalanche spatial distrib. 78–58543
pulsed avalanche discharge at high gas press., homogeneous form. conditions 80–49027
semiconductor, avalanche breakdown field, approx. formula 80–11025
SF_6 discharge inception voltage affected by avalanche growth space charge *(German)* 80–75109
solid, avalanche ionisation, multiphoton ionis. *(Russian)* 79–51906
solid, secondary breakdown, microplasma effect *(Russian)* 79–56722
space charge stabilised nonuniform fields, formative time-lag calc., physical model 80–49038
sphere-plane gap avalanche current pulse meas. in nonuniform fields 78–67556

electron avalanches continued
- stochastic approach to electron avalanches 77—89338
- toroidal discharge, optical meas. of primary avalanche 80—54059
- weakly ionised gas, electron energy distrib. functions under high E/N 80—53916
- Al-Al_2O_3-electrolyte, electroluminesc., nondestructive electronic avalanche 78—68563
- Ar, cathode dark space ionisation avalanche with cold cathode *(Russian)* 80—84013
- Ar, electron avalanche development, exact Boltzmann eqn. anal. 80—59318
- Ar, electron avalanches at high E/N values, Monte Carlo simulation 77—35310
- Ar, electron avalanches at high E/N values, Boltzmann eqn. anal. 77—35311
- Ar, electron avalanches parallel and perpendicular to electric field, Boltzmann eqn. anal. 78—30502
- Ar, preionised, CO_2 laser induced breakdown press. and pre-ionisation depend., cascade model 80—54010
- CO_2 self-sustained laser system, electron avalanche and electron-ion recomb. coeffs. meas. 80—102694
- H_2, Monte Carlo simulation 80—38521
- He, laser induced tunnelling, avalanche initiating electron prod. 77—39441
- He-Ne mixtures, spark channel formation 78—1936
- He-Xe-F_2 mixture, pulsed avalanche discharge at high gas press., homogeneous form. conditions 80—49027
- Hg Townsend discharge, electron swarm props. Boltzmann eqn. anal. 80—19648
- n-InSb, electron mobility at 77K in avalanche regime 79—33295
- N_2, laser induced tunnelling, avalanche initiating electron prod. 77—39441
- NaCl, laser damage, phenomenological theory 80—19836
- SF_6 avalanche breakdown as stochastic process 78—67574
- SF_6, compressed in space-charge stabilised nonuniform fields, corona threshold computation 79—19118
- SiO_2, trapping level exam. by thermally stimulated discharge of capacitor *(Russian)* 78—34845

electron beam absorption *see electron absorption*

electron beam applications
- *see also electron beam deposition; electron beam lithography; electron beam machining; electron beam welding; radiation therapy*
- adhesion determination, thin films 80—71833
- adhesives, thermosetting acrylic, electron beam curing 80—16634
- aerospace propulsion, large payloads launching into Earth orbit by relativistic electron beams 79—21135
- annealing, ion implanted Si, pulsed electron and laser beam annealing, comparison 79—52256
- ARAKS expt., accelerator for electron beam injection 79—21141
- beam-plasma parametric amplifier, nonlinear hydrodynamic amplifier 79—23462
- calorimeter, high-temperature, containerless 80—73366
- cellular repair mechanism, investigation by high dose rate electron beam 79—53195
- chemical laser initiation, coaxial HV diode 77—75562
- chemical research, appl. of electron beam pulse radiolysis 79—52730
- Cherenkov light source, intense, 60 nm to IR range 79—59784
- collective ion acceleration, by temporally modulated relativistic electron beam 78—50422
- collective ion acceleration by relativistic electron beam 77—88291
- Columbia Research Corporation 3 MeV, 45 kW accelerator, industrial, commercial and research applications 79—54215
- compact source for neutral beam production of very low vapour press. materials 78—70225
- computerised electron beam treatment planning algorithms 79—100733
- cooling of beams in heavy particle storage rings, kinetics 77—67922
- curing of coatings, beam voltage effects 77—70201
- device features review for applications 80—53198
- dosimetry for treatment planning 80—3817
- double-sided electron beam generator for KrF laser excitation, fusion appl. 80—68956
- dye gas laser, excitation by elec. discharge, electron beams, optical stimulation *(Czech)* 78—79016
- dye vapour laser pumping, inert gas mixture 77—42535
- dye vapour phase laser system, electron beam excitation 77—23672
- electric current measurement, contactless method using electron beam ring transducer 77—26334
- electron beam high resolution thermal wave microscopy 80—95158
- electron beam pumped laser, energy, time and spectral characts. 80—38005
- electron-photon cascade transport model, to lasers, fusion and X-ray source research 77—68157
- energy flux channel close-up time *(Russian)* 77—55994
- excimer laser excitation by coaxial electron beam system 80—53310
- excimer laser pumping by electron beam controlled discharge 77—10893
- film processing, electron beam scatt. and energy loss during processing 77—27930
- film recording equipment, satellite photography, automatic cartography, computer micrographics appl. 77—10120
- fission reactor fissile fuel breeding appl. 78—8992
- fluorescence diagnostic technique, meas. of vibr. level population distrib. 80—48031
- foilless anode electron-beam laser with chopper-wheel gas pulser 78—63122
- Fresnel lens film prep. by electron beam irradiated mould polymerisation 79—98515
- fusion, electron beam transport and high current density generation 77—67870
- fusion micro-explosions initiation, progress and future applicability *(French)* 78—746
- fusion reactor ignition *(Japanese)* 77—61608
- fusion reactors, electron beam-target interaction 78—755
- gas laser, electron pumped, shock wave introduction of gas 77—701
- gas laser excitation 77—711
- gas laser pumping, electron beam and discharge technologies 77—34897
- gas-chemical dosimetry, limitations of use of strong pulse electron beams 79—31231
- GEOS electron beam experiment S 329 78—93075
- heat treatment of mats., scattering of beam by target vapour *(Russian)* 77—59825

electron beam applications continued
- high-energy laser mirror thermal distortion test facility 80—14348
- high-power microwave generation by relativistic electron beams 78—5444
- high-pressure laser system, electron beam control 78—5496
- holography, appls. and theory review, background and current status 78—74866
- hypersonic turbulent flow measurements, electron beam fluoresc. method 77—35282
- inert gas halide excimer lasers, electron beam, nuclear and discharge pumped, book contrib. 79—81418
- inertial confinement fusion, light ion and electron beams appl. 80—5323
- insulators discharging, appl. to direct obs. via SEM 77—2712
- integrated grating circuit for guided-beam multiple division fabricated by electron-beam direct writing 80—91934
- integrated optics, electron beam lithography techniques 78—46844
- intense, avoidance of current limitations, fusion, ion accel. appls. 79—45898
- intense relativistic pulsed electron beam appls. in plasma phys. *(Dutch)* 78—30452
- ion acceleration, by electron beam, in gas-filled waveguide, in mag. field, theory 78—9316
- ion acceleration from turbulent plasma by electron beam 77—10137
- ion acceleration in vac., beam rot. and scanning 77—593
- ion source, high-perveance electron beam superconducting ion source 77—23333
- ionisation in electrostatic precipitators, coal processing technology appl. 78—57346
- laser, 'beats' of two coherent electron beams 79—55106
- laser, electron beam controlled, space-time evolution of cathode layer 79—10288
- laser, electron-beam-controlled, angular divergence, gasdynamic motion influence during pump pulse 79—59668
- laser electron beam excited systems, high temp. high press. vapour cell design 79—13951
- laser pumping, transmission through vac. tight Al and Ti foils, 150-400 keV 77—50604
- lasers, electron beam ionised gas, book contrib. 77—50664
- lifetime profile measurements in heavily doped emitter structures using electron beams 80—15538
- liquid vinyl monomers, ionic polymerisation and related props. at high dose rates 77—77758
- magnetosphere sounding, beam-plasma interaction expt. by JIKIKEN satellite *(Japanese)* 80—94655
- maize disinfestation by electron irrad. 77—70505
- material processing using 45 kW-power electron accelerator 77—59795
- material processing using high-power electron accelerators 77—59793
- medicine, therapy of mycosis fungoides 80—72286
- melting channel formation, electron optics model *(Russian)* 77—52336
- melting furnace, transition metals processing technology and appl. *(Hungarian)* 80—55318
- metal melting using electron beam sweeping device 78—6889
- metal surface finish meas., using backscattered electron intensity *(Japanese)* 79—4465
- metals heat treatment principle and appl. *(French)* 80—66558
- molecular excited states, prod. by electron pulse radiolysis 79—50142
- multigas electron beam pumped lasers 78—94396
- multipurpose radiation service centre, AEG, Germany 77—59796
- Nb, pure, production by carbothermic reduction-electron beam melting combination method 80—89177
- NDT, use of accelerated electrons, review 80—35480
- organic charge transfer salt process for high-density video storage 80—43269
- photochemistry, appl. of electron pulse radiolysis 79—52698
- polymer irradiation by high energy electron beams, industrial applications 80—3210
- polymer multicomponent systems, selective electron beam etching 78—45603
- polymeric, cable insulation, radiation modification using electron beams 80—66848
- POPOP dye vapour lasers, optical and electron beam pumping, review 80—48237
- projector having a thermoplastic target and operator's eye, characts. 80—96023
- pulsed electron beam annealing of ion implanted Si 79—52254
- pulsed laser electron beam sources 79—36913
- radiation curing 77—59958
- radiation processing, dosimetry and quality control 79—49871
- radiation processing 77—73281
- radiation processing on industrial scale, energy and current requirements 77—73282
- radiation sterilization of medical products using electron accelerators and gamma sources 79—49870
- radiography of thick-walled industrial equipment via stereomicrotron 77—65064
- radiotherapy with medium energy electrons, review 80—36069
- rare earth metal refining *(Russian)* 77—59687
- recording, film speed choice, TV image appl. *(Russian)* 77—38049
- relativistic beam of microsecond duration for microwave oscills. 77—38057
- relativistic electron beam Raman laser 78—74877
- residual resistivity of metals, meas. via medium temp. electron irradiation 77—54016
- retarding potential electron beam technique, for photovoltage transient meas. 77—24586
- scanned electron beams, activation of low dose Si implants in GaAs 80—75246
- SEM written diffraction gratings for integrated optics, characts. 79—68450
- semiconductor, annealing of ion-implanted defects 80—55431
- semiconductor depth profiling by electron beam induced junction current meas. 80—96977
- semiconductor DFB laser, operating in higher Bragg interaction orders, optical and electron pumping 79—89933
- semiconductor DFB laser excited by electron beam, radiation coupling out 79—90038
- semiconductor DFB laser pumped by electron beam, temporal and spectral characts. 79—94238
- semiconductor laser, electron beam pumped, use of periodic structs. with special profiles 80—95923
- semiconductor laser, electron beam pumping efficiency, coating effect 80—91795

electron beam applications continued

- semiconductor laser, longit. pumped by electron bombard., variable-gap struct. threshold characts. 79—59703
- semiconductor material research *(German)* 79—94854
- semiconductor plate cutting, beam shaping apparatus 78—21268
- semiconductor sealed scanning laser with transverse electron-beam pumping, for projection TV systems 79—89936
- seminconductor laser with electron-beam-induced stripe waveguide 80—28237
- solid-electron interactions, conf., Southampton, England (Apr. 1976) 77—44570
- spark gap, electron beam triggered, characts., investig. 80—107001
- sterilisation facilities, for medical products 77—70543
- storage device, electron beam bombard. target temp. profile, evaluation of suitable materials 77—68998
- superconducting weak link fabrication, electron beam lithography, ion implantation 78—47913
- surface hardening using electron beam gun 79—61773
- surface thickness monitoring, object accessible from one side 78—60944
- thermonuclear microexplosions, ignition with electron beams 77—27686
- thermonuclear microexplosions ignition by acceleration of magnetically insulated foils to ultrahigh vels. 78—46163
- thermoplastic light modulators, status and prospects 78—79138
- thin film formation under electron bombardment model *(Russian)* 77—55894
- transition radiation optical pulse generation for optical receiver calibration *(Russian)* 77—58409
- treatment planning, patient specific data acquisition 79—100731
- treatment planning, symposium, Cincinnati, USA (July 1977) 79—100730
- treatment planning and execution for 10 to 35 MeV electron beams 79—100732
- treatment planning for 1 to 10 MeV beams 79—100735
- treatment planning system, absorption equivalent thickness factor 79—100734
- TV signals on cine film, electron beam recording *(Russian)* 78—21251
- vaporizer with water-cooled crucible, metal vaporization rate improvement 78—21266
- vapour properties determ. above 3000K, by pulsed-electron-beam heating, appl. to Au 77—15567
- VHF resonator radiant energy meas. *(Russian)* 78—77944
- wood panel coatings, electron-beam curing 77—70200
- X-ray laser, physical props. of electron beam-sliding spark device 78—5974
- xanthene dye N-92+inert gas buffer, electron beam excited, fluoresc., energy transfer 78—25877
- zone melting by electron beam, isotope fractionation enhancement 80—45229
- zone refiner, improved emission current control 78—6844
- zone refining, single cryst. W wire fabrication 78—6845
- Al:Sb(Zn), ion implanted electron beam annealing, ion backscatt. and TEM meas. 80—59500
- Ar-N_2 mixture, electron beam pumped, lasing obs. at 337, 358, 380 and 406 nm 80—102700
- ArF*, KrF* lasers, pumped by 150 keV electrons, dominant form., quenching processes 78—33730
- As-Se-S-Ge chalcogenide amorphous film, computer-generated holograms using electron beam irrad. 80—95846
- β-B, electron beam zone refining, crucibleless, crystn. front shape 79—78871
- $Bi_{12}GeO_{20}$, electron beam recording 79—32075
- CO_2, electron beam controlled laser, with grid-controlled electron gun 78—46635
- CO_2 electron beam controlled laser, emission pulse synchronisation with plasma mirror 79—89930
- CO_2 electron-beam-controlled gas-flow laser, CW and pulse periodic lasing 79—7111
- CO_2 high-pressure Q-switched electron-beam-controlled laser characts. 79—59669
- CO_2 laser amplifier, high power large aperture electron beam controlled, development *(Japanese)* 78—66846
- CO_2 laser discharge control, beam spreading 78—5446
- CO_2, laser electron beam pulsed, sealed electron guns 78—71119
- CO_2-N_2-He laser media excitation by electron beams admitted through gasdynamic windows 80—99694
- CdS, CdS_xSe_{1-x}, scanning semiconductor laser with transverse electron-beam pumping 80—9904
- CdS, electron-beam-pumped laser, basis of scanning optical microscope 80—31864
- CdS laser, electron beam pumped, catastrophic and gradual degradation 77—61960
- CdS semiconductor laser, longitudinally pumped, electron beam scanning vel. rel. to output parameters 80—9889
- ClF-H_2 chemical laser, electron-beam initiation, energy parameters, stimulated emission from HF, HCl 79—89903
- Co, growth of single crysts. by electron-beam floating zone method 78—68624
- Fe garnet epitaxial film, thermomag. data recording by electron beam heating 78—27066
- Fe, high purity prep. by electron beam floating zone melting under ultra high vacuum 77—28751
- GaAs, electron beam pumped laser, far-field radiation pattern, optical confinement effects 79—86181
- GaAs electron-pumped uncooled laser, degradation rel. to dislocation density 80—14344
- GaInAs, electron-pumped laser, far-field radiation pattern, optical confinement effects 79—86181
- $Ga_xIn_{1-x}As_{1-y}P_y$-InP, room temp. electron-beam-pumped laser with dielec. waveguide, output characts. 80—5761
- $Ga_xIn_{1-x}As_ySb_{1-y}$ tunable electron-beam-pumped laser parameters 80—106524
- HF chemical laser initiation by relativistic electron beam 80—64005
- He_2 dimer, electron-beam pumped, anal. of feasibility of stimulated vacuum UV radiation 80—9857
- InAs, epitaxial, laser action mechanisms with electron beam excitation 80—28240
- $InAs_xSb_yP_{1-x-y}$, efficient electron-beam-pumped laser at 3.1-3.7 μm 80—5738
- N_2 electron-beam-sustained discharge stability model 78—71608
- N_2 laser, employing electron seeding technique, performance 77—71997

electron beam applications continued

- N_2, rot. temp. meas., rocketborne electron beam fluoresc. meas., reflected mol. effects 77—29519
- NO decomp. in industrial exhaust gases by electron beam irradiation 79—29490
- Pt shadowing of freeze-fractured or freeze-etched specimens using electron beam gun 78—20329
- SF_6+H_2 chemical laser, electron beam pumping 80—91784
- Si, ion beam damaged, minority carrier lifetime distribs., electron beam meas. 79—87108
- Ti-Al-V (6.4 wt.%), electron beam melting for scrap recycling 77—66604
- Xe_2 excimer laser, electron beam excitation, VUV fluoresc., lasing 80—87379
- Xe_2, simple VUV high press. laser, with coaxial electron beam pumping 79—974
- XeBr laser, electron beam excited, experimental study 79—98347
- XeCl, efficient laser output at 308 nm, electron-beam excitation 79—59678
- XeCl, electron-beam pumped excimer laser *(Japanese)* 79—64208
- XeCl laser, discharge stabilisation with 50 nsec electron beam 80—23716
- XeCl laser, electron beam, beam-stabilized discharge and fast discharge excitations 80—28204
- XeCl(B) formation in electron beam assisted Xe/HCl laser discharge 80—63988
- XeF, electron beam controlled Ne stabilised laser 79—972
- XeF laser, electron beam, beam-stabilized discharge and fast discharge excitations 80—28204
- XeF laser using Ar-Xe-NF_3 mixture, discharge stabilised by short-pulse electron beam 80—14358
- ZnSe-ZnS semiconductor waveguide laser, electron beam excited, blue emission 79—18447

electron beam deposition

- alumina deposition by activated reactive evaporation, struct. obs. 77—44176
- antireflection coatings, thickness monitoring during deposition 80—19114
- bent beam electron gun for thin film vacuum deposition 77—12534
- coating techniques, comparison between electron beam evaporation and high rate sputtering with plasmatrons 78—11110
- dielectric coatings, optical characts., effect of electric field during film condensation 80—69539
- dielectric film, electron beam produced pore form. mechanism, statistical model *(Russian)* 80—6667
- dielectric films on semiconductor devices, review of deposition techniques 78—23611
- dielectric thin films, anomalous optical absorpt. 77—20947
- dual source evaporation, rate control 80—40263
- evaporation source with integrated rate control *(Hungarian)* 80—20798
- evaporation sources, emission characts., model 79—95279
- films and coatings using conc. energy sources *(Russian)* 79—74090
- Fluorolon-3, utilisation factor determ. during electron beam sputtering *(Russian)* 79—66008
- glass films, struct. mech. and optical props. *(Czech)* 78—80469
- glass layer evaporation 78—35310
- gun, electron beam, with multi-crucible for evaporation in ultra high vac. 78—27404
- high rate, theoretical and expt. work 79—24440
- insulating film for semicond. devices, props., rel. to deposition conditions 78—23612
- interference coating production, new ideas 79—32098
- ion plating, evaporation sources, gaseous media, and transport modes 80—80984
- ion-to-electron conversion dynodes, prep. 77—1887
- ionised atom and cluster beam thin film deposition, apparatus 79—28950
- ionised-cluster beam epitaxy, film form. mechanism 79—28949
- metal film, ionised-cluster beam epitaxy, film characts. 79—28230
- metal-dielectric interference mirror coatings, high mech. strength 78—30043
- metal-polymer films, electron-beam polymerisation, cond. control 78—48331
- metal-semiconductor contact junction formation by ion evaporation 77—90285
- metal-semiconductor thin film preparation under UHV conditions 78—72733
- metallurgical coatings, vapour deposition processes in vac. 80—35430
- MIS structure, Al_2O_3 insulating layer, electron gun evaporated, HF C-V characts. and surface state density 78—84310
- multisource deposition rate control using mass spectrometer as sensing element 78—72730
- optical antireflection multiple wideband layers, production equipment *(Hungarian)* 77—3645
- optical coating production, vacuum system development, review 77—58493
- optical coatings, improved film quality, progress in vacuum generation and deposition technology 80—35101
- optical industry, UELI-1 electron beam evaporator design 78—46847
- optical multilayer coating production with continuous thickness reoptimisation 79—76890
- overlay coatings, electron beam deposition techniques 80—35100
- oxidation protective coating for Ni base TaC eutectics 77—40475
- protective coating production, principles and technology 79—24439
- rare earth compound vaporisation by cathode ray and HF ion-plasma methods 77—77380
- rare earth element sulphides, condensates, struct. and optical transmittance 80—20727
- rate automation by ion current meas. *(Hungarian)* 80—16198
- refractory coatings, deposited by electron evaporation, struct. and props. 79—23871
- refractory compound hard coating, electron beam evaporation in reactive atm. 77—44396
- refractory film evaporator with axially symmetric electron source 79—83125
- refractory metal film, electron beam evaporator for in situ deposition studies in UHV electron microscope 80—40264
- ring cathode electron gun as evaporation source, design, development 77—44168
- scale-up problems 78—72722
- scale-up problems in electron-beam evaporation and sputtering 78—95695
- secondary electron interaction with electron beam near condensing surface *(Russian)* 77—59698

electron beam deposition continued
semiconductor device contact form. by ionised-cluster beam deposition 77—32528
SOS structure, radiation dose at interface due to electron beam aluminisation 78—68089
superconducting compound film, electron beam codeposition, synthesis and props. 78—72296
Teflon-4, utilisation factor determ. during electron beam sputtering *(Russian)* 79—66008
thin film deposition process, line-edge profile simulation appl. 80—104068
thin films fabrication techniques 80—76176
vacuum, using electron beam techniques, technical problems *(German)* 80—84850
vaporisation of refractory materials, use in UVN-71R-3 installation 77—28722
wear resistant surface, review 78—72938
Al, film, ion plating deposition system using electron beam evaporation *(French)* 80—20802
Al film, vacuum deposited, rate and press. depend. of contamination 78—72732
Al film deposition on Kapton laminates by electron beam evaporation 78—76603
Al, high rate deposition on strip steel 79—24440
Al, on SiO_2 in FET, effect on electron trapping 78—80060
Al, step coverage optimisation by computer simulation and SEM 78—51838
Al, uniform film, on Kapton laminates, prep. and characterisation 78—11373
Al/Al_xO_y vacuum deposited laminates, struct. and mech. props. 79—28219
Al-Si alloy metallisation by rate controlled dual electron beam gun evaporator 79—11516
Al-Zn thin film, prep. using Sn-Zn evaporant source 80—100789
Al_2O_3 film deposition, heating of multiple layer structs. *(Russian)* 78—92192
Al_2O_3, thick vacuum condensates, electron microscopy struct. investig. *(Russian)* 78—95242
Al_2O_3-Cu composite, vapour deposition, microstruct., texture and surface topography 77—70001
As-S semiconducting glass film holographic recording media *(Russian)* 77—10864
AuAl formation by thin film interactions, identification by X-ray diffraction 79—99442
B films, amorphous, prep., struct., props., review, book contrib. 78—48321
B, preparation and purification, physical characterisation *(French)* 80—16189
B, rotatable support for ultrahigh vacuum system 79—40586
BN on Si substrate, elec. characts. of BN-Si interface, expt. 77—20459
$BaTiO_3$ on Si substrate, elec. props., expt. 77—20460
C, deposition processes, coating struct., for prosthetic devices 77—40374
CdS, grown by vac. evaporation on Si 80—25567
CdS-Si n-p heterojunction photodetector, fabrication and characts. 78—52068
CdS(Se)(Te), evap. onto electron bombarded NaCl substrates, epitaxial growth and characts. 79—28948
Co-Cr-Al based coating, electron beam evaporation of low vapour press. elements 80—40613
Co-Cr-Al-Y coated turbine airfoils, effect of electron beam deposition rate on struct. 79—23870
Cr, columnar struct. rel. to deposition conditions 78—52675
Cr films, on Al_2O_3, quartz and glass, electron-beam deposition techniques improvement 80—7496
Cu film, growth by ionised-cluster beam deposition, adhesion to substrate 77—32527
Cu-Al_2O_3 dispersed composite, struct. characterisation 77—44197
Cu-Al_2O_3 dispersed system, electron beam evaporated thick film, struct./prop. relations 77—44198
Fe, columnar struct. rel. to deposition conditions 78—52675
Fe-refractory compound, dispersion strengthened, thick vacuum condensate, control of struct. and mech. props. 80—16324
p-GaAs(P)/Au-Be ohmic contact form. by ionised-cluster beam deposition 77—32528
GaP, ionised-cluster beam epitaxial growth on GaP and Si, characts. for LED 79—28951
In_2O_3 films, electron beam evaporation, elec. and optical props. *(Japanese)* 80—60784
In_2O_3 transparent conductive coating production 80—35092
In_2O_3:Sn, glass like thin film, electron evaporated, conductive transport *(Chinese)* 80—49960
$In_{2-x}Sn_xO_{3-y}$-n-Si, electron deposited solar cell, photovoltaic props. 79—96446
Ir coating, condensation under vac. and Ar residual press. 77—44166
Kb_2S_3, condensates, struct. and optical transmittance 80—20727
LaB_6 film, prep. by electron beam evaporation, and optical and elec. props. 80—20793
Mo film, electron beam deposition on Si, X-ray obs. of silicide form., diffusion processes *(German)* 77—1341
Mo film, vacuum deposited onto SiO_2-Si substrates, elec. resist. 78—76166
Mo, on sapphire, epitaxial layer production by electron beam deposition in vacuum *(Russian)* 77—59228
Mo:N film, high T_c amorphous phase stabilisation by interstitial nitrogen 78—23622
Mo-Ni thin film junction, phys. vap. deposition parameters effect on thermoelec. power 77—39922
Mo-Re film, electron beam deposited, supercond. transition temp. conc. depend. 77—28279
Mo-Ru(-Si), amorphous superconductors, prep. by electron beam evaporation and liq. quenching, crit. temp. 80—103776
Nb, electron beam evaporated film, struct., supercond., purity *(German)* 77—52253
Nb films electron beam evaporated, struct. defects *(German)* 77—76684
Nb_3Al film, electron-beam coevaporated, prep. and characts. 80—76187
Nb_3Ge coevaporated film, high supercond. transition temp., nucleation and growth 80—76185
Nb_3Ge film, prep. and supercond. crit. temp. 78—15310
Nb_3Ge film, supercond., electron beam codeposition in O_2, Cl_2 or air, phase diagram 77—28728
Nb_3Ge superconducting film preparation and props. 79—11515

electron beam deposition continued
Nb_3Pb superconducting film, prep., vac. deposition 80—89149
Nb_3Sn film, growth morphology 77—44167
Nb_3Sn films, deposition by quasi-closed vol. method, supercond. crit. temp. 80—15645
Nb_3Sn multilayered supercond. power line conductors, elec. props. and growth morphology 77—28325
Nb_3Sn-Cu superconducting composite, electron beam co-evaporated, TEM study 79—28247
$NdAlO_3$ films, preparation, electrophys. props. in MIM structs. 77—24956
Ni-Al_2O_3(ZrO_2), dispersion strengthened, thick vacuum condensate, control of struct. and mech. props. 80—16324
Ni-Co-Cr-Al-Y coating, electron beam evap., low press. gas scatt. 77—40474
Ni-Cr thin film resistors using jumping electron beam, expt. *(Hungarian)* 77—4738
Ni-ZrO_2, dispersion-strengthened condensate, density and mech. props. 77—44196
NiCr film, evaporation, gas phase analysis *(Polish)* 79—20492
$Pb(Zr,Ti)O_3$ film, prep. by electron beam evaporation technique 77—1809
$Pb(Zr,Ti)O_3$ thin films, fabrication and characterisation 80—16188
Pd coating, condensation under vac. and Ar residual press. 77—44166
Pd deposition for Pd_2Si film form. on Si, substrate temp. effect on microstruct., TEM obs. 78—14621
PrB_6 film, prep. by electron beam evaporation, and optical and elec. props. 80—20793
Pt coating, condensation under vac. and Ar residual press. 77—44166
Si electron beam deposited film, epitaxy by pulsed laser annealing 78—56055
Si film, for solar cell appl., heat exchanges and columnar growth 79—15609
Si, film and p-n junction growth by ionised-cluster beam deposition 77—32527
Si films, electron beam evaporated, for MIS solar cells 80—93490
Si homoepitaxy in high vac., stacking fault nucleation, crit. temp. for SiC growth 78—14620
Si, polycrystalline ribbon prep. by electron bombardment *(French)* 78—64474
Si:H, evaporated amorphous film, prep. elec. cond. and photocond. 79—38201
SiC film electron beam preparation technique, diffraction pattern anal. *(German)* 80—55297
SiO_2, stoichiometric condensate form. during electron beam evaporation of quartz, electrophysical props. 77—16496
SiO_2 thin films, comparison of RI and IR spectra 80—11497
Sm, film, ion plating deposition system using electron beam evaporation *(French)* 80—20802
SmB_6 film, prep. by electron beam evaporation, and optical and elec. props. 80—20793
SmB_6 films, crystn., struct. and elec. resist. 77—63559
SnO_2-Si solar cells, fabrication, angle-of-incidence effects 79—52931
Ta, foil, periodic chemical var. effect on mech. props. 79—91590
Ta-Ta_2O_5-InP thin refractory MIS struct. deposition 80—75647
Ti films on Al_2O_3, quartz and glass substrates, electron-beam deposition techniques improvement 80—7496
Ti, high strength unsupported membrane fabrication 77—66589
TiB_2, TiB_2-ZrB_2, refractory compounds, direct evaporation deposition, struct. and props. 77—44392
TiC coating, activated reactive evaporation and sputter deposition, wear characts. 77—44394
TiC coating, activated reactive evaporation and sputter deposition, ancillary props. 77—44395
TiC, wear resistant film, activated reactive evaporation form. 77—44411
TiC-Ni composite coating, activated reactive evaporation prep., structure 77—44393
TiN, synthesis using enhanced reactive evaporation 80—2953
TiN wear resistance coatings, reactive evaporation and activated reactive evaporation *(French)* 79—57126
TiN, wear resistant film, activated reactive evaporation form. 77—44411
TiO_2 films, deposition by electron beam evap. chem. comp., refr. index, struct. *(Japanese)* 77—62777
TiO_2, metal-TiO_2-Si structure, I-V characteristics, deposition, post-deposition oxidation effects 78—80063
TiO_2 optical coatings, deposition, performance 77—88896
TiO_2/SiO_2 charge storage memory films fo IGFETs 80—11566
Tm_2O_3 film, between Al electrodes, prep. and elec. props. 80—60103
Tm_2O_3 film, electron beam deposition, elec. props., and struct. 79—87580
V epitaxial films on sapphire by electron beam evaporation *(Russian)* 77—76701
VC-TiC, high rate deposition by activated reactive evaporation, and characterisation 78—11372
W film, electron beam deposition on Si, X-ray obs. of silicide form., diffusion processes *(German)* 77—1341
W, film, ion plating deposition system using electron beam evaporation *(French)* 80—20802
W-Re film, obtained by electron beam volatilisation and vac. condensation, props. *(Russian)* 77—24490
Y, film, ion plating deposition system using electron beam evaporation *(French)* 80—20802
Y_2O5d3 films, preparation, electrophys. props. in metal-oxide-metal structs. 77—24956
ZnS 80—35096
ZnSe, evap. onto electron bombarded NaCl substrates, epitaxial growth and characts. 79—28948
ZnSe-Si heterojunctions, IR quenching of photocapacitance 80—92968
ZrB_2, refractory compounds, direct evaporation deposition, struct. and props. 77—44392
ZrC, ZrC-ZrB_2, refractory compounds, direct evaporation deposition, struct. and props. 77—44392
ZrO_2, film, refr. index and microporosity 78—90467
ZrO_2 thin film, optical props. rel. to cryst. struct. 80—97357
ZrO_2-SiO_2, protective antirefl. coatings, electron beam evaporation on glass 77—31143
ZrO_2-$ZrTiO_4$, optical film material 77—753

electron beam effects
  see also beta-ray effects; cathodochromism; cathodoluminescence; electron impact; plasma-beam interactions
  absorbed dose distrib. in thin layers rel. to electron beam incidence 80–83226
  absorbed dose for electron irradiation for polymeric part of electrical wire 79–46708
  absorbed dose of cylindrical rotating object in collimated electron beam 77–25558
  absorption curves for sinusoidally modulated beam 77–24339
  adsorbate distribution, electron-stimulated desorption ion imaging 80–103572
  AES, low beam current density, surface anal. 78–15748
  alkali halide, electron-irrad. induced fracture 77–69038
  alkali halide, irrad. stability obs. using X-ray emission meas. *(Russian)* 80–66326
  alkali halides, electron irradiated depth distrib. profiles of colour centres 79–27977
  alkali halides, influence of purity of crystals on stability of F-centres and interstitials 78–91336
  alkali halides, interstitial motion during radiation damage and sputtering processes 80–54230
  alkali halides, irradiated at room temperature, stored energy 80–79839
  alkali metal halides, F-colouring role of impurities 80–64995
  alkaline earth glasses, $45RO.5Al_2O_3.50P_2O_5$, (R=alkali earths), electron beam irrad., exam. of charge accumulation and light-sum kinetics 79–4336
  alkaline earth glasses, $45RO.5Al_2O_3.50P_2O_5$, (R=Mg,Ca,Sr,Ba), electron beam irrad., temporal change in electric field produced 79–4760
  alkaline earth glasses, RO-Al_2O_3, -P_2O_5, R=Mg, Ca, Sr, Ba, exam. of electron beam irradiation effects 79–4253
  alkaline earth oxide irrad. stability obs. using X-ray emission meas. *(Russian)* 80–66326
  alloy, solute redistrib. during in situ irrad. in HVEM 80–107324
  alloy, vapour bubble growth dynamics, electron-beam vol. heat source 77–47565
  alloys, electron irradiated, temp. depend. spall threshold 78–48504
  aluminophosphate glass, electron irrad., EM pulses during thermoexcitation 79–42107
  amino acid-quinone complexes, surface bubble form. during SEM obs. 77–15450
  amino acids, surface bubble form. during SEM obs. 77–15450
  amorphous specimens, dose minimisation as criterion for imaging mode selection in electron microscopy 77–55220
  anthracene, electron and hole generation under electron bombardment 79–73524
  anthracene, electron bombardment, field and temp. depend. of carrier yield 77–8117
  anthracene, electron irrad., creation and evolution of excited states, scintillation obs. 78–92128
  anthracene, protection against radiation damage, exciton effects 80–29055
  anthracene, pulsed electron excitation, triplet excitons, spectral and electrical investigations 80–92828
  anthracene, radiation-induced radicals, EPR and optical absorpt. obs. 77–12816
  anthracene, radiation-induced topotactic conversion from di-para-anthracene, low temp. TEM obs. 78–35710
  Artema eggs, SEM hatching obs. 80–35998
  Aspergillus niger dying spores, electron refl. and transmission SEM expts. after irrad. 80–56111
  atom displacement radiation damage, in electron microscopes 80–103394
  atomic displacement rates in collision cascade, HV microscope appl. to radiation damage studies 77–24330
  Auger scanning microprobe, approach to damage-free anal. 80–89581
  auroral electron bunching near artificial electron beam 80–98511
  barley coleoptile growth behaviour under low LET radiations 79–88122
  biological specimens, contrast and radiation damage 79–66592
  biological specimens, contrast and radiation damage conf., Nancy, France (May 1978) 79–66591
  biological specimens, electron probe analysis, effects of electron irrad. of sample 79–43969
  biological specimens, reduction of radiation damage in electron microscope exam. 79–34718
  biological specimens, structure determination, electron microscopy, optical and digital anal. *(French)* 79–66594
  bipolar transistors, emitter/collector pipes obs., use of electron-beam-induced current mode of SEM 79–82665
  bone marrow stem cells of C_3H mice, long term radiation effects 80–30787
  brain, caudate nucleus, neutotransmitter activity transient alterations after irrad., rat expts. 80–72267
  α-brass, electron irradiated, defect production and interdiffusion 78–67739
  α-brass, electron irradiated, vacancy migration props., effect on enhanced atomic mobility 79–46829
  bremsstrahlung, circularly polarised, from longit. polarised electrons in single nonmag. crysts. 78–15242
  bremsstrahlung spatial distribution in water and water-iron by 22 MeV electron bombardment, meas. with activation detectors 77–57754
  bremsstrahlung yield produced by 4 MeV linear electron accelerator calc. rel. to hazard in radiolysis 79–76181
  brittle failure of solids *(Russian)* 78–18680
  C, pyrolytic, electron induced irradiation creep, dislocation process obs. 77–47483
  cancer, electron beam therapy of lateralised lesions of oral cavity and oropharynx 80–12215
  catalase, glucose embedded, measurement and reduction of radiation damage in frozen hydrated crystalline specimens 80–89810
  catalase, solid state, electron microscopy radiation damage, amino acid composition 77–25377
  cathodoluminophor, nature of ageing 78–10994
  cavity size distrib. functions evolution, numerical study for 1 MeV electrons 80–2072
  cellular repair rates determined by split-dose and dose-rate methods, comparison 80–104680
  cellulose, degradation by high voltage electrons 80–100283
  ceramics, glassy, struct. and electron beam sensitivity 80–79841
  ceramics, glassy phase, struct. study through electron-beam induced ionisation effects, HVEM obs 80–14978

electron beam effects continued
  chalcogenide glass, refractive index increment induction, SEM written diffraction gratings for integrated optics, characts. 79–68450
  chalcogenide glass film, optical waveguide form. by laser and electron beam irrad. 77–79978
  channelling of relativistic electron and positron beams, X-ray and γ-ray emission 77–36304
  charged particle beams in liqs., elastic wave excitation, microscopic bubble acoustic emission 80–43516
  chemical effects of high-energy electrons, theory 79–52700
  chemical reaction stimulation by relativistic beam collective effects *(Russian)* 77–77763
  chemisorbed layers, electron beam damage, tunnelling spectra obs. 77–76672
  CHO cells, O_2 sensitisation at ultrahigh dose rates 80–36000
  close distrib. determ. in complex-shaped mats. 77–70263
  closed liquid Ar circuit for electron irrad. of LiH at 90K *(French)* 78–62214
  coal fly ash precipitators, improved performance by electron beam ionisation 79–44918
  coherent microwave Cherenkov radiation generation, relativistic electron beam-dielectric loaded waveguide 77–58246
  collective ion acceleration, effect of high ν/γ electron beams 77–6579
  concrete, polymer impregnated, polymerised by accelerated electrons, fabrication and strength *(Japanese)* 77–77456
  cooling of stored proton beam 77–23334
  copper hexadecachlorophthalocyanine, radiation damage 77–19987
  copper phthalocyanine, chlorinated, radiation damage mechanism 80–88000
  α'-copper phthalocyanine, struct. and susceptibility to radiation damage 79–32986
  α' copper phthalocyanine and chlorinated derivative mol. crysts., radiation damage in electron microscope 80–107328
  coronene, protection against radiation damage, exciton effects 80–29055
  covalent crystals, nanosec. electron beam effects, size depend., Ioffe effect 80–88211
  creep and growth, radiation induced, fundamental mechanisms 80–92596
  cryostats for electron irradiation of crystals 77–41619
  crystal, electron-irradiated, free radical stabilisation, filler content effects *(Russian)* 77–56241
  crystalline and organic materials, knock-on process, review 80–79840
  crystalline materials, in situ deform. by high voltage electron microscopy 80–103352
  crystals, cryostat for electron irradiation and optical study 77–37899
  curing of pressure sensitive adhesives, literature review 77–86283
  cytochrome c oxidase, macromolecular struct., electron microscopy and image anal. 80–89716
  cytosine, cryst., electron damage, electron microscope study 78–22762
  trans-decalin, liq., irrad., positive charge mobility meas. by microwave absorpt. 77–20100
  defect formation and secondary electron generation, electron energies greater than 1 MeV *(Russian)* 77–55304
  degassing metals for extreme low pressures 80–98924
  di-p-anthracene, electron beam induced monomerisation 77–12789
  diacel solid state track detector 79–750
  diamond:B, variable-range hopping cond., effect of electron irrad. induced compensating centres 77–43599
  diamond, B doped, electron irradiated, defects at low temps., elec. resist. meas. 77–11593
  diamond, B doped, electron irradiated, threshold energy for atomic displacement, elec. cond. meas. 77–11594
  diamond, defects and impurities 80–29017
  diamond, electron irradiated, photochromism 80–71454
  diamond, irradiated, MCD spectrum of GR1 line, neutral vacancy model 77–69850
  diamond, irradiated, optical study of TR12 and 3H defects 77–85772
  diamond, low-energy γ-ray anomalous yield produced by 800 MeV electrons, collimation effect 79–91521
  diamond, low-temp. electron-irrad., EPR 77–59045
  diamond, natural, rate of donor defect introduction by 2 MeV electrons, 0.348 eV absorption band 77–89477
  diamond, natural, subthreshold defect formation due to electron irrad., cathodoluminescence study *(Russian)* 80–45152
  diamond, natural semicond., isothermal annealing of electron radiation damage 77–7764
  diamond, photocurrent and Hall current, 290 and 4.2K 79–87129
  diamond, radiation-induced optical absorption spectrum, 0.4-2.0 MeV electrons 77–84798
  diamond, semicond., electron irrad., charge carrier mobility 77–11921
  diamond, synchrotron electron beam damage, study by optical, cathodoluminesc. and X-ray topography 80–39155
  diamond, thermal conductivity, high temp., electron irrad. effects 80–65318
  diamond, type Ia, electron irrad. effect on photocond., acceptor centre form. 77–47853
  diamond, type IB, electron irradiated, 2.367 eV vibronic absorpt. system, optical study 79–73975
  diamond, type Ib, electron irradiated, migration of N, optical absorption meas. 78–56505
  diamond, type IIa, electron irradiated, annealed to high temps., EPR spectrum 77–90034
  diamond, type-I, electron irrad., annealing at 800-1500°C 80–24500
  diamond, type-II_a, electron irradiated, thermal cond. reduction at low-temps. 77–47631
  diamond, type-IIa, electron irrad., EPR spectrum 80–25210
  diamond, vacancy enhanced N aggregation, electron irradiation effects IR spectra 80–70245
  diamond, visible absorpt. spectrum, vacancy charge states 77–90177
  diamonds, natural, paramagnetic centres with $S=5/2$ 79–47334
  dielectric, electron beams as virtual electrodes, review 80–6861
  dielectric, electron penetration, 20-50 keV, sandwich method meas. 80–6436
  dielectric ionization density distrib. meas. during pulsed electron beam irradiation 77–20810
  dielectric surface, charge accumulation, losses, electron-beam treatment *(Russian)* 80–75931
  dielectrics, fast electron effects, space charge build up, range reduction 77–72636
  dimethyl ether, condensed multilayers, electron bombard. effects, AES line-shape anal., XPS, and desorption meas. 80–7450

electron beam effects continued
diphenyl anthracene, 80 keV electron scatt., use for radiation damage monitoring 77—4127
discharge, volumetric, semi-self-maintaining, excited by electron beam, current maintanance in cathode layer 80—59322
dislocation damping during electron irrad. 77—35632
dislocation damping during electron irradiation, new model for peaking effect 78—87683
dislocation loop growth during HV electron microscope irrad., thin foil point defect profile 80—2018
displacement damage simulation in HVEM irrad. 80—107325
DNA, radiation induced mol. size change, electron irradiated, effect of p-nitroacetophenone 80—89807
DNA double strand breaks rel. to radiation dose, yeast cell obs. 80—72232
DNA double-strand breaks in irradiated yeast cells, survival and yield, O_2 influence 80—35992
DNA strand breaks, lymphoma cells, detected by hydroxyapatite chromatographic technique 79—43819
DNA strand breaks induced by ^{125}I in cultured human kidney cells, repair 80—12192
dose distrib. determ. on 10 MeV irrad. 77—70265
dose-rate model testing with Chlamydomonas reinhardi 80—21543
Duralumin constructional material, gas evolution obs. *(Russian)* 79—1460
dynamic and dosimetric characterisation of irrad. solids, laser and holographic interferometry obs. *(Rumanian)* 80—90886
dynamic response of materials to pulsed beam, measurement using laser interferometer 79—42102
E. coli, DNA repair in radiation resistant and radiation sensitive strains 79—34489
E. coli B_{s-1}, response to tritium-β particles rel. to 7 MeV electrons 79—57714
EBIC technique, resolution limits in determ. of diffusion lengths in semiconductors 79—21865
Ehrlich ascites carcinoma cells, effects of pions$^-$ rel. to electrons and X-rays 80—26267
n-eicosane, single cryst., electron irrad., free radical pair form., ESR 77—4913
elastic strain wave generation, high density pulse, Cu, Al, ionic crysts. *(Russian)* 77—76463
electron irrad., defects, elec. and optical props. 79—19282
electron irrad. effect on electrolum., defects form. and quenching obs. 80—55194
electron microscope, high resolution, obs. at liq. He temps., radiation damage effects 80—86517
electron microscopy, correlation analysis of radiation damage 80—100282
electron microscopy, HV, in situ radiation damage expts. 77—52605
electron microscopy, radiation damage processes and image contrast loss 78—37117
electron transport Monte Carlo calcs., orthogonal function expansion technique 77—26248
electron-matter interactions rel. to electron microscopy 80—89097
electron-sensitive materials, apparatus for measuring sensitivity and data-density 79—35893
EM wave, nonlinear excitation in dielectric cylinder by relativistic magnetised beam 77—19129
EM wave emission, from modulated electron beams, IR region *(Italian)* 77—3525
energy deposition in multilayer geometries 77—24338
energy flux channel close-up time *(Russian)* 77—55994
energy loss in electron beam lithography, Bethe and Spencer-Fano theories 78—87728
energy loss spectroscopy, tutorial 79—21872
epoxy resin, electron beam effect on struct. 77—69001
fast electron irradiated material, defect and secondary electron generation, model 78—11030
ferroelectric, polarisation switching influence of mobile point defects 78—31165
ferroelectric ceramic, optical modulation by electrostriction during electron beam charging, spatial characts. 79—7224
ferroelectric materials, repolarisation in SEM 79—15424
ferroelectric-magnetic coupled oscills., excitation by electron beam *(Russian)* 78—23257
film dosimeters, calorimeter for calibration in high intensity electron fields 78—73257
5-fluorocytosine, electron beam damage assessed by EELS 80—89809
Frenkel defects, form. and collapse, defect migration, electron irrad. effects, computer simulation 80—92523
Frenkel pair recombination radius, temp. depend. 77—89427
β-D-fructose, film, electron irrad., struct. changes, tunnelling spectra 77—10781
fusion devices, controlled, surface effects, conf., San Francisco, USA (Feb. 1976) 77—30659
$Ga_{1-x}In_xSb$, inverted diode, electron irradiation effect on props. *(Russian)* 78—14378
gas discharge, electron beam excited, space charge and inhomogeneous ionisation *(Russian)* 77—47281
gas laser operation, fast electron beam irrad. effects *(Russian)* 78—74878
generalized transport equations in quantum theory of channelling 78—10110
glass, adsorption of Au, AES study, electron bombardment effects 80—65380
glass, electron bombarded, brittle failure 77—28909
glass, electron irrad., colour centre depth distrib. 79—73217
glass electrets obs., bonded, under corona discharge and electron irradiation conditions *(Russian)* 79—4759
glutamine synthetase macromolecular struct., electron microscopy and image anal. 80—89716
glycine, electron-irrad. polycrysts., stable products obs. by ^{13}C NMR 78—15775
graphite, self focusing high current relativistic electron beam for structural and chemical transformations *(Russian)* 80—15190
graphite, synergistic effect of electrons on atomic H activity 80—106112
graphite, wall and limiter material for Tokamaks, induced desorption diffusion and gas production by 100 eV electrons and ions 79—675
graphite crystal, electron irrad., threshold energy for displacement damage 77—76461
graphites, pyrolytic, compressed, annealed, low temp. electron irrad., elastic const. meas. *(French)* 78—43050

electron beam effects continued
ham, irradiated, failure to induce genetic alterations in Drosophila 80—17009
Hastelloy B-2, corroded surface, electron bombardment effect during Auger electron anal. 80—61014
Hastelloy B-2, decomposition of metal oxide films under electron bombardment 78—19928
Hastelloy-X, electron irrad., void swelling 79—14822
heat treatment of mats., scattering of beam by target vapour *(Russian)* 77—59825
heavy particle beam cooling in an electron flux, mag. field effects 78—82557
Hela cells, recovery from sub-lethal damage when irradiated at ultra high dose rates 79—79608
heterogeneous semiconductor systems, elec. cond. and EMF relax., pulsed radiation effects 77—89842
homogeneous electron irradiation *(German)* 80—102603
HV electron microscope in situ deformation expt. limitations 79—60238
HV electron microscopy appls. in phys. metallurgy, irrad. machine, struct. obs. 77—1891
HVEM, radiation effects during obs., review 80—27379
HVEM obs. of irrad. damage 77—35589
hydrocarbons, in gas phase, chemical effects 79—43602
ice, electron-irrad., cluster-ion prod., lattice and fragmentation energies 77—4911
ice, pure and acidic, electron irrad., ESR of H atoms, motional narrowing and spin polarisation 77—20706
II-IV-V_2 phosphides, cond. compensation by electron bombardment 79—15151
II-VI compounds, electron energy radiation damage threshold meas., EPR and luminesc. 77—84799
III-V semiconductors, radiation-induced defects, review 77—80544
Inconel 675, wall and limiter material for Tokamaks, induced desorption diffusion and gas production by 100 eV electrons and ions 79—675
inertial fusion by oscillating relativistic electron beams in magnetic mirror *(French)* 79—54595
insulating materials, high energy radiation effects 80—19835
intense relativistic pulsed electron beam appls. in plasma phys. *(Dutch)* 78—30452
interstitials, mobility and interactions 78—47328
ion acceleration in vac., beam rot. and scanning 77—593
ion exchange membranes, production by electron irrad., cross linking, graft polymerisation *(Japanese)* 77—81403
ionic crystal, electron beam excited, luminesc. and cond. of nonideal degenerate electron-hole plasma 78—10488
ionic crystal, exposed to high-current electron beam pulses, min. size of excited region for crack initiation *(Russian)* 78—84961
ionic crystals, nanosec. electron beam effects, size depend., Ioffe effect 80—88211
ionisation density, spatial distrib. calc. in a material due to electron beam irradiation 80—55234
ionosphere, channel lower hybrid resonance excitation by superthermal particle streams *(Russian)* 78—4025
ionosphere, circumrocket glow spectral obs. in Zarnitsa.2 electron injection expt. *(Russian)* 80—12596
ionosphere, heating by artificially injected 40 keV electron beam 78—40746
ionosphere, MF waves generated by 8-40 keV electron beam 78—40750
IR (111) textured surface, O^+ desorption, electron stimulated, 300-1085K *(Russian)* 77—47672
irradiation effects on surface prop. of solids 80—70261
DL-leucine degradation with longitudinally polarised electrons 79—79474
lipid peroxide formation in irrad. synthetic diets, storage effects 80—101025
liquid irradiated, dosimetry by holographic interferometry *(Rumanian)* 80—9412
lymphocytes, human, chromosome aberration yields due to 15 MeV electrons 77—48843
mag. limiter plate, electron irrad. and thermal shock 78—66416
magnetosphere, high-latitude, Echo 4 beam interactions from artificial auroral streaks obs. 78—89036
magnetosphere, wave emissions prod. by JIKIKEN electron beam-plasma interaction expt. *(Japanese)* 80—94655
magnetosphere ARAKS and electron beam injection expts. 78—36405
mammalian cells, lethally damaged, proliferation obs. after irrad. by various particles 80—108971
mammalian cells irradiated at ultra-high dose rates, sublethal damage repair 80—36006
membranes in pulsed electron beam, temp. and ultimate load calcs. 79—45484
6-mercaptopurine, electron beam irrad., free radical formation at 77K 79—5165
metal, defect annealing study by positron annihilation, and elec. resistivity meas. 78—51584
metal, dynamic study of defect mobility using HVEM 78—47327
metal, irrad., elastic point defect-dislocation interactions, defect dragging model extension 80—65050
metal, irrad., selfinterstitial atomic defect interaction radii, recovery expts. and error sources 80—65049
metal, material removal by high power beam 77—81187
metal, polycryst., irrad., coherent acoustic emission *(Russian)* 77—81355
metal, refractory, BCC, free migration of self-interstitials 78—47574
metal, torsional creep under accelerator irradiation, meas. instrument 78—3262
metal crystl, anisotropy of electron radiation damage 77—84796
metal foils, electron irrad., loss of pt. defects 79—73215
metal slab, relativistic electron beam exciting Langmuir turbulence 79—10878
metal surface, electron beam impact, time-varying evaporation, metastable state lifetime 79—10943
metal surface, electron beam impact, time-varying evaporation 79—10942
metal surface-electron beam intraction, 0.4-5mA ion beam extraction 77—84456
metal-polymer films, electron irrad. controlled form., elec. props. 80—15635
metallic surface, heat treating and melting with scanning laser or electron beam 78—11406
metals, appl. of KUR LINAC to radiation damage studies 78—71760
metals, interstitial loop growth, pulsed irrad. effects 80—88210

electron beam effects continued
metals, pulsed press. created by electron beam, effect on struct. and mech. props. *(Russian)* 78−34539
metals, submicroscopic defects, influence on HVEM in-situ expts. 80−103392
metals, threshold energy for atomic displacement, bulk modulus and interatomic pot. 78−38754
metals, two and one interstitial model explanation of elec. cond. variations 80−88143
methacrylic heterocyclic ester polymers, electron beam irradiation 77−76466
methanol, condensed multilayers, electron bombard. effects, AES lineshape anal., XPS, and desorption meas. 80−7450
6-methyl-mercaptopurine, cryst., light sensitive free radical EPR after electron irrad. 80−7167
methylmethacrylate soln., aqueous, polymerisation under pulse electronic accelerator irradiation 80−66802
mica, natural, high γ- and electron-irrad. doses effect on annealing behaviour, thermal decomp. resist. 80−60897
microcircuits, radiation hardness design, SEM as diagnostic tool 79−21869
microscopy of frozen hydrated crystalline specimens, meas. and reduction of damage 80−85552
minority carrier diffusion length, Schottky barriers, electron bombard. investigation 78−68037
mirror, interference filters for improved solar radiation resistance 77−39015
MIS structure, radiation induced charge storage 80−6997
MIS structures, electron-beam irrad., RF annealing effect 79−91152
MNOS capacitors, effect of 2 MeV electrons at 80K 79−19668
MNOS devices, transient behaviour of electron-beam-induced current 79−99630
MNOS structures, electron-beam-irrad., interface defects, high temp. H_2 anneal 80−96745
modulated electron beam in inhomogeneous isotropic plasma, nonlinear wave generation 78−1852
molecular film, electron irrad., struct. changes, tunnelling spectra 77−10781
monochromatic Langmuir wave amplification by electron beam in nonlinear plasma *(Russian)* 77−76112
monocrystals, EM radiation of relativistic positrons and electrons during axial and planar channelling 80−79845
MOS capacitors, charge distribs. for large electron beam irrad. doses 80−34518
MOS capacitors, charge yield and dose effects, 80K 77−20440
MOS capacitors, dynamic model for e-beam irrad. 79−91147
MOS device, transient behaviour of electron-beam-induced current 79−99630
MOS devices with 500 Å and 700 Å thick oxides, saturation radiation effects 78−60209
MOS diodes, interface trap states due to electron beam lithography obs. *(Japanese)* 80−54787
MOS structure, electron irrad. effects, pulsed CV charact. obs. 77−76935
MOS structure, flatband shift induced by electron beam radiation, Si dopant effects 77−32085
MOS thin capacitors, electron-beam irrad., enhanced flatband voltage recovery 79−19670
MOST, effect of high-energy electrons, 15-35 MeV 78−34907
n-p junction solar cell, anal. of short circuit currents generated by electron beam 79−39308
neutral gas-electron beam interaction, mag. flux conservation test using diamag. loop 78−12734
Ni, adsorption residual C removal by electron beam irrad. and heat treatment *(Chinese)* 80−88421
Nimonic PE-16, irrad. in HVEM, void growth, vacuum environment influence 80−107323
β-nitrostyrene free anionic polymerisation during electron radiolysis, primary reactions 78−44378
nuclear emulsion, secondary ionisation, delta-ray effects 80−881
nucleation of defect clusters in crystalline solids 79−42051
oil, channels formed under electron beam action *(Russian)* 77−72353
optical fibre, low-dose radiation damage growth and decay obs. 78−1398
optical glass, radiation coloration due to fast electron irradiation 79−98452
optical materials, radiation induced transmission loss 79−94306
order-disorder transformations, electron irradiation effects on kinetics 80−34056
organic molecular crystal, phase transforms. obs. using TEM, electron beam damage 78−34621
organic molecules, radiation damage by electron diffraction 79−65119
oxidation induced by ion or electron bombardment, AES-SIMS study 80−108606
oxides, slow-electron-stimulated desorption 79−60623
p-n junction diode, electron-beam annealing of ion-implantation damage 79−77622
p-n junctions, minority carrier surface recombination velocity, lifetime, AM electron beam determ. 79−87145
pacemaker neurons, Aplysia, effects of irradiation with 20 MeV electrons 80−17013
paraffin, single crystal, STEM versus CTEM beam damage 80−103393
phosphate glass, electron irrad., elec. flield, distrib. above surface *(Russian)* 77−43763
phosphate glass, electron-irradiated, charge accumulation, comp. depend. 78−2159
phosphosilicate glass, AES quantitative anal., electron irrad. induced surface comp. changes 77−48709
phthalocyanine, cryst., electron damage, electron microscope study 78−22762
piezoelectric ceramic, excitation of acoustoelectric oscills. by ionising radiation 78−56191
piezoelectric crystal surface, periodic film form. due to SAW 78−72038
piezoelectric material with semiconducting boundary layer 78−19414
plasma, inhomogeneous, space charge wave generation 79−41845
plasma oscillations, electron beam generated, quenching by low freq. externally applied wave 80−24160
plasma production, visible and UV high intensity spectral lines 79−73012
plasma return current discharge, prod. and heating of large-volume plasmas 78−94920

electron beam effects continued
plastic fibre-optic waveguide, effect of ionising radiation on optical attenuation 78−63170
PLZT electrooptic ceramic, electron beam surface charging, rel. to optical modulation 80−6952
PMMA, optical waveguide, direct writing of gratings by electron beam 79−46091
PMMA, space radiation effects evaluation 80−70263
PMMA glass, electron bombard. induced elec. discharge, electromech. effects *(Russian)* 77−32324
point defect production, cryogenic equipment for electron acceleration *(French)* 77−132
polarised electrons, book 77−46679
poly(butadiene-co-styrene), rubber, radiation cured, dynamic phys. props. 77−69003
polybutadienes, radiation chemically cross-linked, charact. by pyrolysis gas chromatography *(German)* 80−81348
polycarbonate, impact behaviour, effects of thermal pre-treatment and mol. wt. 78−95798
polyethylene:$Br_2(I_2)$, films, electron-beam induced carrier mobility and elec. breakdown 80−80429
polyethylene, accumulated charge profile during fast electron irradiations 77−4600
polyethylene, cross linking by energy rich radiation, mech. and elec. props. *(German)* 78−20035
polyethylene, elec. props. and oxidation after electron beam irradiation and heat treatment 79−87092
polyethylene, ionising radiation effects crosslinking with accelerated electrons, ageing, SCC *(Polish)* 79−52701
polyethylene, pretreated surface, nitrobenzene contact angle, H_2O environment *(Japanese)* 78−79858
polyethylene, pristine and radiation-damaged film, electron energy loss spectra 79−81312
polyethylene, single crystal, electron microscopy study 80−103273
polyethylene, single crystal, structural changes due to electron irrad. 80−29053
polyethylene, space radiation effects evaluation 80−70263
polyethylene films, electron beam irrad., carrier mobilities 79−1600
polyethylene structural transformations under fast electron irradiation *(Russian)* 79−94987
polymer, synthetic, electron beam damage in electron microscope exam. 78−34409
polymer composite matrix materials, spacecraft, space radiation effects evaluation 80−70263
polymer films, electron irrad. controlled form., elec. props. 80−15635
polymer films, photoelectric emission and contact charging, surface states 79−33885
polymer foil, electron irradiated, charge dynamics, computer simulation 79−82915
polymer irradiation by high energy electron beams, industrial applications 80−3210
polymer spacecraft materials, electron and proton irrad. effects 80−70262
polymers, synthetic, radiative degradation, chem., phys., environmental, technological effects, review 80−40948
polymethacrylates degradation obs., for PMMA, PBMA, PMA and PMA AN 78−27795
polymethylmethacrylate, effect of accumulated charge on depth dose profile of electron beam 79−90700
polypropylene, electret, trapped injected electrons, EPR obs. 78−27093
polypropylene, electron bombarded, radical formation, piezoelectric and pyroelectric effects, ESR study 80−7169
polypropylene, electron bombarded electret, trapped charges ESR study 80−7170
polystyrene:$Br_2(I_2)$, films, electron-beam induced carrier mobility and elec. breakdown 80−80429
polystyrene, electron-beam-induced conduction 80−2397
polystyrene, inelastic interaction of electrons, mean free path, stopping power and CSDA ranges 79−23663
polystyrene-wood, polymer composite, dielec. props. at low temperature range *(Japanese)* 78−95541
polytetrafluoroethylene, degradation by electron or γ-ray bombardment in inert atmosphere *(German)* 80−19840
protamine, electron microscopic recognition rel. to radiation exposure 79−62175
protein, electron radiation damage on primary and secondary struct. level 80−89808
quartz, comparison of different radiation effects 78−26596
quartz, cultured cryst., vacuum UV transmittance before and after electron irrad. 78−83044
quartz, dislocations, electron irrad. induced vitrification 80−107252
α-quartz, electron irrad., defect struct. and radiolysis 80−107321
quartz, electron irradiated, optical and anelastic absorptions and resonator freq. 78−64385
quartz, electron irradiation effects on optical, dielec., elastic props. 80−59521
quartz, electron pulse irrad. effect on defect formation 80−15155
quartz, fused, elastic wave excitation by charged particle beam 77−89474
quartz, fused and cryst. samples, transient absorpt. on pulse electron irrad. 79−1779
quartz, OH^- impurity IR absorpt., electron irrad. effects 79−99913
quartz, synthetic, electron beam irrad., defect form., annealing and migration effects, ESR obs. 80−50180
quartz, synthetic, electron beam irrad.-induced interstitial ion mobility, ESR centres and IR spectra meas. 80−39153
quartz film, microcrack growth, electron microscope obs., electron beam induced thermal stress effects 77−69037
quartz resonator, electron irrad., optical absorpt. 77−8609
radiation damage in HVEM, simulation of neutron damage, state-of-the-art 77−51417
radiation damage problems in electron microscopy 80−59517
radiation processing, conf., Miami, FL, USA (Oct. 1978) 80−36772
radiation sterilization of medical products using electron accelerators and gamma sources 79−49870
radiative energy loss of electrons in thick layers of material, interpolation formulae 78−21829
rare earth metals, HCP, point defect production during electron irrad. at low temp. 80−49273
rare earth-transition metal amorphous films, radiation damage 77−66398

electron beam effects continued
refractory films, stability, high temp. and electron irrad. effects 77—39747
relativistic channelling radiation, energy and temp. depend. of freq. characts. 79—73236
relativistic electron and positron bremsstrahlung in crystals, theory *(Russian)* 79—61459
relativistic electron beam, submillimetric pulse production by stimulated magnetoresonant Raman scatt. 77—38846
relativistic electron beam propagation in gas 77—997
relativistic electrons, spontaneous EM emission in channel pot. 78—83848
relativistic monoenergetic electron beam in atmosphere, plasma formation and collective interaction *(Russian)* 79—77407
relativistic particle channelling in cryst., spontaneous emission of γ-quanta, new effect 78—15243
samples, electron microscopy, origin of contrast in images *(French)* 79—66593
scanning transmission microscopy, proton vs. electron, ratio of elastic to inelastic cross-sections 77—22625
sealing materials, friction and wear tests *(German)* 79—38987
seedlings, Vicia faba, effects of different radiation types on growth *(German)* 79—43961
SEM/STEM cold stage thick specimen heating model 78—61289
semi-infinite solid, electron beam heating 77—76465
semiconductor, Frenkel pair defect formation threshold energy during particle irrad. 79—90647
semiconductor, Frenkel pair formation threshold energy during particle irrad. 79—90646
semiconductor, ion implanted, pulsed laser and electron beam annealing comparison 80—92547
semiconductor, ionization and subthreshold effects in defect creation and annihilation 77—84811
semiconductor, localised defects, theory of SEM charge-collection imaging 79—1374
semiconductor, low temp. electron irrad., multipurpose cryostat 79—35755
semiconductor, threshold energy for displacement of atoms 78—47428
semiconductor substrate, work function rel. to AES, electron beam damage *(French)* 80—50479
semiconductor surface, plasma oscillation instabilities *(Ukrainian)* 79—33318
semiconductor-dielectric structure, photoresponse on electron beam scanning, video signal enhancement *(Russian)* 77—47863
semiconductor-electron beam interactions, review 80—101911
semiconductor-metal structure, electron bombarded, energy dissipation 78—87732
semiconductors, displacement defects 77—80543
semiconductors, pulsed electron beam processing 79—69159
semiconductors, Z 80—19799
p-Si, electron irrad. effect on Hall mobility temp. depend. 80—60011
silica optical fibres, large core polymer clad, radiation response 80—33171
silicate glass, space charge distrib. after 2.1 MeV electron irrad. *(Russian)* 77—69772
silicone-clad silica low-loss fibre radiation response obs. 78—1397
skew comb freq. characts., mm wave generation *(Russian)* 78—22078
skin, tumour induction and hair follicle damage rel. to electron penetration, rat 77—5052
solar corona, heating by fast electron streams 80—105228
solid, Frenkel pair formation due to passage of relativistic electrons, computer simulation *(Russian)* 80—6402
solid, high energy electron scatt., Monte Carlo calcs. 80—96422
solid, Monte Carlo simulation of energy distrib. of transmitted or backscatt. keV electrons 78—43057
solid film, passage of electrons, linear transport theory in one-velocity approx. 79—14865
solid target, electron probe penetration and energy loss characts., diffusion model 80—96585
solid-electron and X-ray interaction *(Chinese)* 80—70253
solid-electron interaction, Monte-Carlo simulation, appl. to electron probe microanal. 77—12853
solid-state plasma, coherent excitation of microwaves by electron beam 77—24579
solids, interaction with electrons and X-rays *(Chinese)* 80—80896
solute segregation, under irradiation 78—48407
spacecraft thermal control coatings, electron and proton irrad. effects 80—70262
stainless steel, ferritic SUS 410 type, coated with organometallic complexes and Ti alkoxides 80—34078
steel, austenitic 316, displacement energy determ., HVEM obs. and electron bombardment 78—6100
steel, austenitic stainless, creep dependence on electron irrad., in type SS316 steel, dislocation motion *(Russian)* 80—108495
steel, austenitic stainless, fusion reactor, first wall material, radiation damage by simultaneous accelerator microscope irrad. 79—45402
steel, austenitic stainless, HVEM irrad., point defect trapping influence on void swelling 79—23652
steel, austenitic stainless, irrad. creep of type 316 in HVEM 80—97523
steel, austenitic stainless, structure phase transitions due to high energy electron irrad. *(Russian)* 80—7553
steel, austenitic type KO 34, microstruct. changes on electron beam welding *(Hungarian)* 80—104252
steel, C martensite, electron irrad., reversible C at. redistrib. 77—65991
steel, cold worked FV548, electron irradiated, void swelling after 10 ppm He preinjection 77—19989
steel, Cr (13 wt.%), sintered, organometallic complex addition effects on mech. props. 80—25595
steel, ferritic, FV607, void swelling, theory 78—71763
steel, ferritic, FV607, void swelling in 1 MeV electron irradiation 78—71762
steel, irrad. effects at high temp., simulation by HV electron microscope 77—1153
steel, low alloy Mn-Sb(2, 0.12 wt.%), reversibility of temper embrittlement, studied by XPS and AES 77—32667
steel, low C, HF oscillations during electron beam welding *(Russian)* 80—76273
steel, low C, low alloy, electron beam heat treatment of thin bands 78—3156
steel, Si, electron irrad. in HVEM, void swelling, Si role 80—54285

electron beam effects continued
steel, stainless, electron induced irradiation creep, dislocation process obs. 77—47483
steel, stainless, electron irrad. in HVEM, radiation damage obs. 77—50233
steel, stainless, electron-bombardment surface prep. for Princeton Large Torus 77—59957
steel, stainless, radiation damage by 1 MeV electrons, dislocation struct., brittleness *(Russian)* 80—75226
steel, stainless, type 316, electron beam heating effect on extracted intermetallic precipitate 78—35394
steel, stainless, type 316, electron irradiated, void swelling 78—55891
steel, stainless, type 316, neutron irrad. damage simulation using HVEM, surface effect on void swelling 78—29572
steel, stainless, vacuum components, pre-vacuum surface finish influence on electron stimulated desorption in ultrahigh vacuum 80—57320
steel, stainless, void shrinkage during electron irrad. 78—34540
steel, stainless, void spatial regularity, impurity and temp. effects 77—47487
steel, stainless, void swelling obs., under HV electron microscope *(Japanese)* 80—54218
steel, stainless, voids, TEM, diffr. contrast 80—75218
steel, stainless, wall and limiter material for Tokamaks, induced desorption diffusion and gas production by 100 eV electrons and ions 79—675
steel, tool type M2, surface hardening and microstruct. refinement by laser melting, electron beam melting, heat treatment *(Korean)* 79—70093
steel, type FV548, 1 MeV electron irradiated, influence of pre-injected He on void nucleation and growth 80—34054
steel 45 microstruct. and hardness after electron bombardment 79—38956
steel austenitic stainless, Cr-Ni 316 type, electron irradiated, void swelling 79—42104
steel constructional material, gas evolution obs. *(Russian)* 79—1460
steels, stainless, electron irradiated, dislocation damage, HVEM study 80—103389
STEM and CTEM comparison, image contrast, radiation damage 77—49811
STEM/SEM cold storage specimens, electron beam heating temp. profiles 79—5422
stilbene, pulsed electron excitation, triplet excitons, spectral and electrical investigations 80—92828
stilbene, single cryst., free charges and excitons generated by electron pulses 78—63988
stilbene, single cryst. under pulsed electron excitation, spectral and elec. characts. 79—7838
storage rings, neutraL molecule desorption from SS(304) and Al(6061) due to particle bombardments 79—76213
superconductors, low temp. SEM appl. 80—80443
surface, rough, optical emission due to electron irrad. 78—60529
surface layer thickness-composition monitoring by high energy electron backscattering 78—53146
surface processes, interatomic forces, theories 80—107632
surface treatment, ionic deposition and electron bombardment industrial equipment, pollution control *(French)* 80—7699
Teflon, non-destructive charge release 80—24946
Teflon FEP, electron-beam-charged, population and temp. shift of TSC peaks 79—82914
Teflon FEP-A, corona and electron beam charged, TSC peak identification and surface-voltage stability 79—78614
TEM, appl. to organic solid-sate chemistry, review 79—60235
TEM, specimen damage and dehydration, struct. retrieval, instrumental limitations in biological struct. anal. 79—20735
temperature profile of target electron beam bombard. target temp. profile, evaluation of suitable materials 77—68998
thermoplastics, internal stresses revealed by artefacts produced in SEM 78—35634
thulium phthalocyanine, mol. image in high resolution electron microscopy, radiation damage effect 80—107203
toluene-9,10-diphenylanthracene, soln., electron beam pulse radiolysis, energy transfer 80—7808
5-trifluoromethyluracyl, electron beam damage assessed by EELS 80—89809
two-layer barrier, electron irrad., electron-photon flux *(Russian)* 78—48251
ultrarelativistic, energy losses in periodically inhomogeneous medium *(Russian)* 77—31705
uridine-5′-phosphate.$2Na^+$ single crysts., radiation damage, ESR obs. 80—108964
l-valine, cryst., electron damage, electron microscope study 78—22762
vinyl ester adhesive/Al lap shear specimens, electron beam curing 79—20337
void swelling, role of bulk point-defect recombination 79—42105
W, electron stimulated desorption of H^- from chemisorbed H_2 79—86999
water, condensed multilayers, electron bombard. effects, AES line-shape anal., XPS, and desorption meas. 80—7450
water, electron energy deposition model, effect of 21.4 eV plasmon 77—4135
water, electron track end effects 80—11932
water treatment by high-energy electron beams 77—70507
yeast cells, reparable and irreparable damage induced by sparsely ionising radiation 80—51167
Zener diode, breakdown voltage, electron irrad. effects 79—95472
Zircaloy, foil, dislocation loop nucleation and growth during 1 MeV electron irrad. 80—88152
Zircaloy-2, cold worked, temp. cycling effects on irradiation growth 80—2079
Zircaloy-2, electron irradiation damage, direct obs. 80—84212
Ag, Ag-Cd(In) dil. alloys, electron irrad., stage I_E recovery 77—39616
Ag, electron beam irradiation, 2.3 MeV, positron annihilation exam. of radiation defects *(Russian)* 78—34542
Ag, electron irrad., elastic moduli and internal function *(French)* 78—87703
Ag, electron irradiated, exam. of vacancy migration energies, and annealing kinetics 78—47571
Ag, electron irradiated, thermal variation of dislocation pinning by point defects 79—51150
Ag film, adhesion changes on 10 MeV electron irrad. *(Russian)* 77—43460

electron beam effects continued
α-Ag-Zn, electron irrad., atomic mobility enhancement by defects, dynamic characts. 79−37871
Ag-Zn, electron irrad. self-interstitials, migration and elimination characts. 79−37872
Ag-Zn (24 at.%), electron-irradiated, free migrating defects, rate of production *(French)* 79−10877
Ag-Zn (30 at.%), electron irrad. exam. of defect supersaturation by elasticity, and creep meas. 78−47366
Ag-Zn (30 at.%), electron irradiated, atomic mobility, elastic after-effect meas. *(French)* 78−63874
Ag-Zn (30 at.%), mobilities of self-interstitials and vacancies 77−84795
AgBr emulsion, sub-image and latent image specks form. and props. 78−21245
Al, Al-Ag(Mg) dil. alloys, electron irrad., stage I_E recovery, interstitial trapping 77−15405
Al alloy 6061 79−675
Al alloys, dil., size effect of impurity atoms rel. to trapping radii for migrating self-interstitials 78−75690
Al, creep and dislocation distribution *(Russian)* 78−95775
Al, creep and dislocation struct., electron irrad. effects 80−49268
Al disk, US wave excitation by electron beam 79−14888
Al, dislocation loops, interstitial, size distrib. for metal irradiated in high voltage electron microscope *(Russian)* 80−103335
Al, electron and neutron irrad., Doppler broadened positron annihilation meas. *(German)* 77−62563
Al, electron backscatter fractions, exptl. determ. 80−18617
Al, electron beam irradiation, 2.3 MeV, positron annihilation exam. of radiation defects *(Russian)* 78−34542
Al, electron flux depth-dose distribs., space-shielding appls. 80−39186
Al, electron irrad. induced aqueous corrosion 77−81343
Al, electron irradiated, di-interstitial formation within small defect clusters 78−26566
Al, electron-irrad., NQR, EFG around vacancies and interstitials 78−88220
Al, electron-irradiated, anelastic relax. due to single self-interstitial atoms 77−39627
Al, electron-irradiated, anelastic relax. due to clustered self-interstitial atoms 77−39628
Al film, 80 keV electron scatt., use for radiation damage monitoring 77−4127
Al film, electron transmission less than 3 keV *(French)* 78−10109
Al film, transmission, reflection, and absorp., $35 \leq E \leq 70$ keV 77−39754
Al foil, electron-irrad., interstitial trapping on impurities 79−99242
Al fracture speed during phase explosion due to electron beam irrad. *(Russian)* 80−76336
Al, interstitial clustering following electron irradiation at low temp. 79−19243
Al, interstitial loop form., effects of repeated electron irrad. 80−75220
Al, irrad., interstitial loop nucleation at impurity site *(Japanese)* 77−43247
Al, low-field galvanomag. props., Fermi surface and defect struct. effects 77−4323
Al, pure, electron irradiation damage 77−19988
Al, quenched, irradiated, anisotropic electron scatt. on defects 79−95397
Al target, C contamination, in high vacuum electron excitation X-ray tube 79−44996
Al thin foil, thin foil, electron irrad., observation of triangular loops at twin boundaries 80−34005
Al, vacancy distribution, interbonding atoms, heat peaks in scattered cascades *(Russian)* 80−39169
Al:^{111}In, electron irrad., defect trapping at impurities 78−55892
Al:Ga, pulsed electron-beam annealing, lattice site location improvement 80−107303
Al-Ag(Ge)(Mg)(Zn) alloy, dil., electron-irradiated, impurity-interstitial interaction 77−15449
Al-Co, defect structs. introduced by electron irrad., Mossbauer study 80−7239
Al-Co, dil., electron and neutron irradiation, interstititat atom clustering at ^{57}Co impurity, Mossbauer meas. 78−30607
Al-Co, electron irradiated, self-interstitials trapped at Co impurities, Mossbauer line shape anal. 78−6615
Al-Co, electron irradiated, quadrupolar relaxation effect in Mossbauer effect 78−39459
Al-Cr(Ti), electron irradiated, interstitial trapping and detrapping at undersized impurity atoms 78−47424
Al-Cr(V)(Ti), dil., electron irradiated, interaction of self interstitials with undersized solute atoms 78−63789
Al-Cu (1 wt.%), electron irradiated, dislocation damage, HVEM study 80−103389
Al-Cu (4 wt.%), enhanced precipitation under electron irradiation in HVEM 78−52818
Al-Fe, electron irradiated, interstitial-solute complexes, internal friction spectra 78−92289
Al-Ge (0.2 at.%), exam. of interstitial trapping by X-ray diffuse scatt. 78−47363
Al-gelatin-GaAs, C-V characts., irrad. effects *(Russian)* 77−51823
Al-In alloy, dilute, electron irradiation, interstitial dislocation loop obs. 78−18681
Al-Mg, dilute, dislocation loops, interstitial, size distrib. for metal irradiated in high voltage electron microscope *(Russian)* 80−103335
Al-Mg, oxidation induced stresses, dislocation network form., HVEM obs 80−14978
Al-sapphire-Si capacitor, effect of electron-beam aluminisation on Si-sapphire interface 77−89856
Al-Si alloy, dilute, electron irradiation, interstitial dislocation loop obs. 78−18681
Al-Zn (1.9 at.%), 1 MeV electron irradiated, induced homogeneous precipitation 79−77638
Al-Zn alloys, recrystallisation and superplasticity, HVEM straining 80−39207
Al-Zn-Mg alloys, H_2 bubbles in embrittlement 78−19868
$Al_xGa_{1-x}As$, defect state identification associated with Ga vacancy 77−69269
$Al_xGa_{1-x}As$, dependence of energy spectrum of levels introduced by electron irrad. on composition 79−60766
Al_2O_3, β- and β''-phases, defect struct. obs. by high resolution TEM, battery ageing relevance 80−107501
Al_2O_3, irrad. stability obs. using X-ray emission meas. *(Russian)* 80−66326

electron beam effects continued
α-Al_2O_3, radiation damage in HVEM, temp. depend. of displacement threshold 79−46706
α-Al_2O_3, radiation damage in HVEM, at high temp. and high dose 79−46707
Al_2O_3:Co, spectra, heat treatment and irrad. effects 77−4659
Al_2O_3:Cr, pure and doped, electron irrad. induced cond., TSC and EPR study 80−80277
Al_2O_3:Ti(Si), annealing, electron irrad., absorpt. spectra 77−20890
β''-Al_2O_3-Na_2O, spinel formation, TEM obs. 77−76423
β''-Al_2O_3-Na_2O-MgO, blocking defects prod. by electron beam heating 78−55879
Al_2O_3-P_2O_5 glass, electron bombard. induced elec. discharge, electromech. effects *(Russian)* 77−32324
$AlPO_4$, synthetic berlinite, electron irrad. effects, ESR, ENDOR, optical spectral study 80−80608
As, amorphous, electron irrad.-induced paramag. centres, 77K 78−88187
As film, 80 keV electron scatt., use for radiation damage monitoring 77−4127
As-S film, guided light reversible control by electron beam irrad. 78−1331
As-Se and As_2S_3 films, electron-stimulated changes in optical props. and dissolution rate 80−29709
As-Te-Ge chalcogenide films, thermally induced transformations, TEM obs. 79−94917
As_2S_3 (Se_3), electron irradiated, effects on elec., photoelec. and optical props. 80−49806
As_2S_3, glassy, optical absorption spectra after 4.5 MeV electron bombardment *(Russian)* 77−32408
As_2Se_3, amorphous, electron irrad.-induced paramag. centres, 77K 78−88187
As_2Se_3, glassy, optical absorption spectra after 4.5 MeV electron bombardment *(Russian)* 77−32408
As_3Se_2, electron irradiated, effects on elec., photoelec. and optical props. 80−49806
Au, electron and neutron irrad., quenched, Doppler broadened positron annihilation meas. *(German)* 77−62563
Au, electron irradiated, exam. of vacancy migration energies, annealing kinetics 78−47571
Au, electron irradiated, interstitials and their clusters, diffuse X-ray scatt. study 80−33997
Au, electron irradiated, low temp., Frenkel defects, diffuse X-ray scatt. study *(German)* 79−23601
Au film, transmission, reflection, and absorp., $35 \leq E \leq 70$ keV 77−39754
Au foil, heating by high-energy relativistic focused electron beam *(Russian)* 77−1154
Au foil, radiation damage, in situ study by HV electron microscopy 78−6101
Au island condensate, on LiF or NaCl, nucleation kinetics, influence of ionised atoms 77−11816
Au, thin foil, enhanced electron energy deposition heated, soft X-ray vacuum UV spectra 80−80901
Au-Ag, thin film, double layer system electron beam effects during sputter profiling AES obs. 79−65347
Au-Cu, dil., electron irradiated, interstitials and their clusters, diffuse X-ray scatt. study 80−33997
Au_4Mn, electron irrad. in electron microscope, radn. ordering 79−86818
$Au_{35}Si_{65}$, amorphous vacuum-deposited and liquid-quenched films, diffusion and crystn. 80−84094
Au_4Zn, long period ordered alloy, selective radiation damage in electron microscopy 78−10092
B and B-rich borides, protective coatings, in situ prep. for controlled nuclear fusion devices 79−3238
B film, 80 keV electron scatt., use for radiation damage monitoring 77−4127
BN, self focusing high current relativistic electron beam for structural and chemical transformations *(Russian)* 80−15190
Be film, on Pt substrate, range of primary electrons 77−4134
Bi, electron irrad., displacement threshold energy *(French)* 79−23649
BiTeI crystals, eutectic decomp. in transmission electron microscope 79−20024
C film, 80 keV electron scatt., use for radiation damage monitoring 77−4127
C foil, electron impact knock-on damage at 4K, electron microscope obs. 79−55786
CO_2 decomposition, plasma radiolysis by high current relativistic electron beam 79−91947
CO_2 laser, pulsed, elec. field distrib. in vol. discharge controlled by electron beam 80−58505
CaF_2, anion-void superlattices *(Danish)* 79−14796
CaF_2, bleaching characteristics of crystals coloured by low energy electrons 78−76497
CaF_2, electron irrad. defect aggregates, ordering, U and Th impurity effects 80−75216
CaF_2, fluorite, electron irrad., {100} faceted anion voids 79−51153
CaF_2:U(Th), and pure, electron microscopy study of lattice deformation due to electron irrad. 79−65077
CaF_2:Y, absorpt. spectra, radiation defect formation energy, F to M centre conversion kinetics 79−65079
CaF_2-NaF crysts., F_A centres, 385 and 435 nm absorpt. bands of electron irrad. crysts. 78−2889
$CaFPO_3$, colour centre form., X-ray and electron bombardment *(Russian)* 77−19948
CaO, electron irradiated, photocond. and luminesc. meas., F-centre electronic struct. determ. 78−6409
CaO, electron irradiated, symmetry assignment of new point defect 78−31261
CaO:Li, thermally quenched, generation of Li^0 centres 80−50382
CaO:OH^-, room temp. IR spectra, heat treatment and electron irrad. effects 79−51992
Cd, electron radiation damage, determ. of threshold displacement energy 78−59837
Cd, electron radiation damage in HVEM, nature of defect clusters 78−59838
Cd, faceting of interstitial loops 78−47381
Cd_3As, film, amorphous, crystallisation effects 77−35482
$CdBr_2(I_2)$, vapour growth crystals, decomposition, electron microscope study 78−92268
$CdCr_2Se_4$ film, electron irradiated, struct. 79−15032
$CdGeAs_2$, electron irradiated, change in electrical props. 79−7829
$CdGeP_2$, cond. compensation by electron bombardment 79−15151

electron beam effects continued
$Cd_xHg_{1-x}Te$, electron irradiated, elec. and recomb. characts. 78—39113
CdS, 200 keV electron induced defects, low temp. annealing 77—80796
CdS, absorpt. spectra, 400-650 nm, electron irrad. defects and absorpt. edge shift 78—64382
CdS, dislocation motion due to heating by electron beam in TEM 80—79799
CdS, electron beam induced desorption of O, AES meas. 79—77921
CdS, exciton spectra anomalies, surface state effects 78—18974
CdS, high-energy electron irrad., photoluminescence spectra, course of annealing 77—90198
CdS laser, electron beam pumped, catastrophic and gradual degradation 77—61960
CdS, neutron and fast electron irrad., local centre form., TSC and photoluminesc. meas. 78—87719
CdS, single cryst., bound excitons in surface layers, luminesc. obs. 79—28294
CdS:Cu, fast electron irradiated, isochronous annealing of IR photocond. quenching spectra 77—1450
CdS:Cu, Fermi level position, luminesc., and photosensitivity, electron irrad. effects *(Russian)* 78—14652
CdS:Cu,Pb reflectivity of Ni-salt coated powder, pre-irrad. effect on defect form. 79—27973
CdS:Cu(Cl), thin layer, electron pulse induced cond. relax. 80—2501
CdS-PbTe and CdS-Te heterojunctions, electron irrad. effect on electrophys. props., prep. conditions depend. 79—28421
CdS(Se) films, electron irrad. effect on electrophys. props., prep. conditions depend. 79—28421
CdSe, charge transport 78—84233
CdSe, electron irrad., edge emission 80—25461
p-$CdSiAs_2$, electron irrad. elec. props. annealing, lattice defects 80—100465
$CdSnAs_2$, electron induced defects, p- to n-type cond. inversion, Hall meas. 77—24557
CdTe detectors, gamma and electron irradiation effects 78—41893
CdTe, electron induced defect creation rates 78—41892
CdTe, electron-beam-controlled transmission of 10 μm radiation 79—81466
CdTe, high-resistivity, irradiation effects on carrier transport and trapping process 78—2164
CdTe metal-semicond.-metal detectors, degradation characts. due to e and γ irradiation 79—45543
CdTe, nearest-neighbour hopping cond., effect of electron irrad. induced compensating centres 77—43599
CdTe:Cl, electron irrad., defects 80—25460
Co, electron irradiated, mag. after-effect spectrum, 20-350K 77—1570
Co, low temp. electron irrad., elec. resist. recovery 77—35588
$CoFeCN.xH_2O$, electron irrad., Mossbauer spectra 80—29652
CoO-containing glass, effects of γ-rays, electron beam and neutron flux on transmissivity *(Japanese)* 77—73156
Cr, atomic displacements in electron irrad. cryst. 79—46705
Cr-SiO_x-Si MIS solar cells, photovoltaic performance and interface states, nucl. radiation effects 80—94004
Cs halides, storage layers stability under electron bombardment 78—27355
Cu (100) surface, electronically-activated N_2 chemisorption 79—66348
Cu alloys, dil., size effect of impurity atoms rel. to trapping radii for migrating self-interstitials 78—75690
Cu alloys, FCC, climb of extended dislocations due to irradiation in HVEM 80—103343
Cu, bremsstrahlung yield and distrib. of absorbed energy in electron irradiation 79—99245
Cu constructional material, gas evolution obs. *(Russian)* 79—1460
Cu, defect annealing around stage III, $\gamma\gamma$ ang. correlation expt. 79—14846
Cu, defect clusters, electron microscope exam. 78—47380
Cu, dislocation damping during electron irrad. 77—76462
Cu, dislocation damping strain amplitude depend. on 1 MeV electron irrad. and quenching 79—95023
Cu, dislocation pinning rate, neutron and electron irrad., meas. by internal friction method 80—96570
Cu, dlectron irrad. at 130K, positron lifetime investig. of stage III recovery mechanism 77—47484
Cu, elastoresistivity of Frenkel pairs, defect migration *(French)* 80—2073
Cu, electron and neutron irrad., Doppler broadened positron annihilation meas. *(German)* 77—62563
Cu, electron backscatter fractions, exptl. determ. 80—18617
Cu, electron irrad., positron lifetime exam. of annealing recovery 78—47354
Cu, electron irrad., void swelling and dislocation loops 79—99206
Cu, electron irrad. at 100K, dislocation vel. meas. etch pit technique 80—49271
Cu, electron irrad. at 100K, comparison of irrad. hardening with dislocation vel. 80—54284
Cu, electron irradiated, additional recovery around 200K 78—38755
Cu, electron irradiated, dia- and paraelastic effects 77—76482
Cu, electron irradiated, dislocation defect dragging, 4.2 to 350K 78—43027
Cu, electron irradiated, evidence for vacancy migration in stage III 78—38693
Cu, electron irradiated, exam. of vacancy migration energies, and annealing kinetics 78—47571
Cu, electron irradiated, temp. depend. of threshold energy for atom displacement 80—34055
Cu, electron irradiated, thermal variation of dislocation pinning by point defects 79—51150
Cu, electron irradiated, void nucleation, Monte Carlo simulation method *(French)* 77—59046
Cu, electron irradiation, vacancy clustering study by small angle X-ray scatt. 79—14845
Cu, electron irradiation damage, dislocation pinning investig. of crowdion model 77—69000
Cu, electron irradiation effects on He gas bubble superlattice 80—2086
Cu, electron transmission and absorption, 70 keV initial energy 78—71777
Cu, electron-irradiated, monovacancy migration during stage III annealing, NQR study 80—107576
Cu, electron-irradiated crystals, electron diffr. channelling effect on atom displacement 80—39158

electron beam effects continued
Cu, electron-irradiation internal friction behaviour, shear modulus and damping meas. 80—55444
Cu, fast electron transmission, contrib. of high-angle deflections 79—28024
Cu film, adhesion changes on 10 MeV electron irrad. *(Russian)* 77—43460
Cu film, transmission, reflection, and absorp., $35 \leq E \leq 70$ keV 77—39754
Cu foi.foil, interstitial impurity interaction investigation by stage II isochronal recovery expts. 78—47423
Cu foil, electron irradiated at low temps., annealing, form. of clusters of atomic defects 77—15416
Cu foil, electron-irrad., interstitial trapping on impurities 79—99242
Cu foils, electron-irradiated, point defect agglomerates, HVEM invest. during in-situ annealing 80—84213
Cu, formation of Frenkel pairs 79—23598
Cu fracture speed during phase explosion due to electron beam irrad. *(Russian)* 80—76336
Cu, Frenkel defects, diffuse X-ray scatt. obs. *(German)* 79—23600
Cu, Frenkel defects due to 3 MeV electron irrad. 78—47351
Cu, Frenkel pair production threshold energy, temp. depend., exam. 78—51530
Cu, irrad., elastic point defect-dislocation interactions, defect dragging model extension 80—65050
Cu, irrad., migration and thermal conversion of defects, 100 to 330K 80—59519
Cu, irrad., secondary defect formation, effect of refl. condition *(Japanese)* 77—43248
Cu, irrad., stage III recovery kinetics 78—63792
Cu, irrad. at 4.7K, recovery of Frenkel defects, defect-agglomerate effects *(German)* 77—84797
Cu, irradiation induced dislocation loops, temp. depend. 77—51410
Cu, neutron and electron irrad., interstitial formation, dislocation pinning, internal friction meas. 80—100284
Cu single crystals Au ion implanted, pulsed electron beam irrad. 80—65019
Cu, small-angle X-ray scatt. investig. of stage III recovery 77—7763
Cu, very low atom displacement threshold energy, around ⟨110⟩ directions, direct evidence 78—14379
Cu, very low atomic displacement threshold energy obs. 78—95078
Cu, yield stress of electron irrad. cryst., isochronal annealing effects 79—79037
Cu/Ni multilayer films, electron beam induced diffusion during AES depth profiling 80—19993
Cu-Ag (Au), dil., dose depend. of impurity detrapping stages after electron irradiation 78—51582
Cu-Al, dislocations, dissociated, climb mechanism, nucleated loops, Burgers vectors 80—65002
Cu-Al (2, 6.8 and 15 at.% Al), electron irrad. at 300 and 575 kV, exam. of damage rate 78—47425
Cu-Al alloy, irrad. in HVEM, climb of dissociated dislocations and point defect absorpt. 80—107257
Cu-Au(Be)(Sb), dil., electron high dosage source for residual resistance specimens and irradiation expts. *(German)* 78—21274
Cu-Be, dilute, electron irradiated, Be segregation 79—77637
Cu-Be (0.0182 at.%), radiation induced Be segregation 78—23710
Cu-Cr, vapour deposited, electron irrad., resistance behaviour *(German)* 78—47779
Cu-Fe, vapour deposited, electron irrad., resistance behaviour *(German)* 78—47779
Cu-Fe (1.5 wt.%), precipitation-effect on void formation during electron irradiation 80—84211
Cu-Fe (1.5 wt.%) alloy, void form. during irrad. in HVEM, reactor irrad. simulation and ageing effects 80—107327
Cu-Fe(2.5 wt.%), isothermally reacted austenite stability in very small particles 77—48432
Cu-Ni alloys, dislocation climb sources activated by 1 MeV electron irradiation 77—89443
Cu-Ni alloys, electron irradiated, dissociated struct. of dislocation loops with Burgers vector a⟨100⟩ 77—89444
Cu-Zn(30 at.%), electron irrad., positron annihilation, defect recovery 79—74018
Cu_5FeS_4, bornite, AES investig. of surface struct., ion sputter and electron beam effects 77—15669
$CuInS_2$, cathodolum. spectra, heat treatment and electron irrad. effects 78—10996
Cu_2O foils, electron microscope exam., Cu precipitates and CuO form. 79—1462
Cu_3Pd, electron irrad. in electron microscope, radn. ordering 79—86818
D_2, solid 0.5-3 keV electron penetration depth 78—56549
D_2O, ice cryst., electron traps, electron irrad. effects, EPR 77—1939
Dy, electron irradiated, defect annealing, recovery spectra 79—23648
Er, electron irradiated, defect annealing, recovery spectra 79—23648
Fe, appl. of KUR LINAC to radiation damage studies 78—71760
Fe, Armco, microstruct. and hardness after electron bombardment 79—38956
Fe, BCC, void nucleation following electron irrad. 80—29054
Fe, cast, hardness, wear resist. and struct., electron irrad. effects 79—96126
α-Fe, defect creation anisotropy in electron irradiated samples 77—31994
Fe, displacement energy, high voltage electron microscope obs. 77—76464
Fe, elec. resist., Frenkel pair recombination, 20K *(French)* 78—2160
α-Fe, electron irradiated, vacancy annealing 79—55785
Fe, electron-irradiated, positron lifetime meas. 80—93431
α-Fe, high purity, neutron and electron-irrad., interstitial migration at 200K 79—55920
Fe, irradiated with electrons then annealed, magnetoresistance at 20K *(French)* 80—103677
α-Fe, mag. aftereffect spectrum after low temp. electron irrad. 78—2704
Fe, pure and doped, electron irrad., mag. aftereffect 80—88838
Fe target, neutron and photon dose equivalent meas., PEP IR hall scale model 79—31227
Fe, vacancy mobility determ., HVEM expts. 80—33993
α-Fe:C, electron irrad., vacancy-C interaction, positron lifetime meas. 80—75264
Fe-Al, electron-beam-induced surface oxidation, HVEM obs. 80—14978
Fe-C, electron-irradiated, positron lifetime meas. 80—93431
Fe-Cr-Ni, electron irradiated, resistivity during annealing, 4.2-1300K 78—87962

electron beam effects continued
Fe-Cr-Ti-Mo-TiO_2 (13, 3.5, 1.5, 2 wt.%) dispersion hardened, void swelling 80—65046
Fe-N(0.013 wt.%), effect of electron irradiation on precipitation 79—52221
Fe-Ni alloy, effect of electron irradiation and deform. on martensitic transform. 77—16581
Fe-Ni alloy, martensitic transform., influence of thermal and electron irrad. treatment of austenite *(Russian)* 80—66509
Fe-Ni alloys, ordering on annealing and electron irrad., mech. props. change *(Russian)* 80—29981
Fe-Ni Invar alloy, electron irrad. effects 79—56638
Fe-Ni-Cr, pulsed HVEM irrad., effect on microstruct. evolution 80—34053
Fe-Si (3 at%), deformation and electron bombardment, influence on dislocation struct., 20-500°C *(Russian)* 80—92536
Fe-Si (3 wt.%), electron irradiated, yield strength and elongation 80—76325
$Fe_{0.5}Co_{0.5-x}Cr_x$ films, vacuum-deposited cryst. and mag. struct. *(Russian)* 80—93081
$Fe_{0.55}Mg_{0.47}SiO_3$, orthopyroxene, electron irrad. effects, Mossbauer study 80—40016
$Fe_{65}{}^{60}Ni_{35}$, electron irradiated, small angle neutron scatt. 78—52218
β-FeOOH, akaganeite, struct. changes due to radiation damage 79—28014
FeS_2, diatomic crysts. electron induced X-ray emission, channelling effects 79—56888
α-Fe(111), adsorption of water under the influence of 2.5 keV electrons 79—28199
GaAlAs-GaAs heteroface solar cells, 1 MeV electron irrad., analytical and expt. study 79—70450
GaAlAs-GaAs heterostructures, electronic excitation effects on mobility of point defects and dislocations 78—2561
$Ga_{1-x}Al_xAs$-GaAs solar cell, radiation resist., theoretical evaluation and optimisation 80—35681
GaAs, carrier lifetime, radiation induced changes, edge luminesc. spectra 77—8664
n-GaAs, conversion to p-type after 1 MeV electron irrad. 79—77636
GaAs, defect state identification associated with Ga vacancy 77—69269
GaAs, dislocation-free, point defects and rad. damage 80—88141
GaAs, electroluminescent study of irrad. induced struct. damage, athermal annealing 80—108280
n-GaAs, electron and gamma ray irradiated, introduction and annealing of defects 78—67736
GaAs, electron and neutron irrad., defect clusters 80—2077
GaAs, electron beam induced defect annealing 77—80790
GaAs, electron beam induced current, minority carrier generation distrib. 80—96900
GaAs, electron bombardment, absorption of energy 79—14847
n-GaAs, electron irrad. defects, carrier removal rate, annealing effects 80—75269
GaAs, electron irrad. induced defect levels, hydrostatic press. effect 80—92858
n-GaAs, electron irradiated, defect energy levels, influence of irrad. temp., photocond. meas. 78—2446
GaAs, electron-beam excited, efficient generation of electron-hole plasma 80—76051
GaAs, electron-irrad., deep-level defect anal. using 2γ positron annihilation and IR absorption spectra 80—16120
n-GaAs, epitaxial film, defect clusters, charge-carrier mobility temp. depend. anal. 80—54701
GaAs epitaxial layer, fast electron irrad., impurity distrib. profile obs. 77—76969
GaAs epitaxial layers, non-doped, from Ga-$AsCl_3$-H_2 system, TEM and RHEED study of micromorphology and defects 79—65340
GaAs, epitaxial layers, electron irrad. deep level trap energy depend. 80—80205
GaAs, epitaxial multilayer, electron irrad. defect study by transient capacitance 79—99241
GaAs, gamma and electron irrad. defect formation depend. on interface, luminescence study 80—34057
GaAs, laser annealing of point defects 80—107224
GaAs on $Ga_xAl_{1-x}As$, electron scatt., cathodoluminesc., loss spectra 80—104023
GaAs, primary radiation defect separation by elec. field 80—92522
GaAs, radiation defect obs. using Schottky diode characts. 78—76024
GaAs, shallow homojunction solar cell, resist. to 1 MeV electron radiation 80—50953
GaAs shallow junction solar cells damaged by electron irrad., recovery of short cct. current 79—29471
GaAs shallow-homojunction solar cells, electron radiation effects 80—97798
GaAs, solar cells, electron-irrad., annealing kinetics 80—7937
GaAs solar cells, electron and proton radiation damage 80—94034
GaAs solar cells, simultaneous radiation damage and annealing 80—94033
GaAs, struct., elec. props., effects of illumination, O_2 absorpt., electron bombard. *(French)* 78—34690
GaAs tunnel diode, electron beam bombard. induced defects, influence on excess current *(Russian)* 77—4424
GaAs VPE layers, electron irrad., electron traps 80—25026
GaAs:B, electron or neutron irradiated, low symmetry interstitial B centre 78—79605
GaAs:Cr pulsed electron beam induced recrystallisation and damage, amorphous layer formation 80—34052
GaAs:Se, pulsed electron beam annealing, doping profiles 80—6421
GaAs:Se ohmic contacts, pulsed electron beam annealing donor density, mobility 80—65678
GaAs:Se^+, implanted semi-insulating, pulsed electron and laser beam annealing effects on elec. characts. 79—73196
GaAs:Si, donor-acceptor pair defects absorpt. bands 80—16064
GaAs:Si, electron irradiated, LPE layers and Bridgman crysts., IR absorption and Hall meas. 77—16345
GaAs:Si, Li, IR absorpt., microstruct., charge compensation 80—107565
GaAs:Sn diode, LPE grown, electron irrad. effect on characts. 80—39667
n-GaAs:Te, electron-irrad., absorpt. spectra *(Russian)* 78—15200
GaAs:Te diffused LED, electron irrad. effect on characts. 80—39667
p-GaAs:Zn, optical absorpt. spectra and photocond. after 2 MeV electron irrad. *(Russian)* 77—69859
GaAs-GaAlAs wafers, defects and degradation, transmission cathodolum. evaluation 80—65395

electron beam effects continued
$GaAs_{1-x}P_x$, dependence of energy spectrum of levels introduced by electron irrad. on composition 79—60766
$GaAs_{1-x}P_x$, electron irrad., radiation defects annealing 80—29059
$GaNbO_4$ decomp. due to electron beam heating in electron microscope 78—35711
$GaNbO_4$, electron beam induced decomp., high resolution lattice imaging obs. 78—6161
GaP crystals, radiation defects, TSC obs. 80—65588
GaP, electroluminescent diode, electron irradiated, negative resistance due to impact ionisation 77—15942
GaP, electron irrad., EPR of antisite-impurity defect 80—25211
GaP, electron irrad., radiation defects annealing 80—29059
GaP, IR absorpt. spectra depend. on compensating defects and thermal treatment *(Russian)* 80—71465
GaP, O_2 adsorpt. monitoring by Auger spectroscopy 77—72777
GaP, O_2 adsorpt. monitoring by Auger spectroscopy 78—6218
GaP p-n junctions, electron beam excited carrier avalanche multiplication 79—69587
GaP:s, elec. props. following 1.7 MeV electron irradiation 78—80005
GaP:Zn, isolated Ga vacancy due to electron irrad., EPR study 78—95519
p-GaSb, electron irrad., annealing 77—51407
GaSb, inverted diode, electron irradiation effect on props. *(Russian)* 78—14378
Gd, electron irradiated, defect annealing, recovery spectra 79—23648
Gd, electron irradiated, relation of defect densities to Rayleigh parameters 77—62517
$Gd_3Fe_5O_{12}$, electron irrad., primary-ion charge compensation using SIMS 79—57322
Ge (111), oxygen adsorption, electron-beam enhanced reaction, AES meas. 77—4256
Ge, amorphous, 1 MeV electron irrad. influence on kinetics of crystallisation 77—89476
Ge, amorphous, ionisation enhanced crystallisation, elec. cond. meas. 77—35481
Ge, amorphous layer, epitaxial recrystn. by electron irrad., solar cell appl. 78—84079
n-Ge, anomaly of Hall effect after 50 MeV electron irrad. *(Russian)* 77—43619
Ge crysts., electron beam induced changes of real struct., HVEM 80—103390
Ge, defects, radiation effects 80—29016
Ge, doped, electron or neutron irradiated, vibrational absorption 78—6718
Ge, electron beam irrad., {113} faults, nature and origin 80—70258
Ge, electron beam irradiation, 2.3 MeV, positron annihilation exam. of radiation defects *(Russian)* 78—34542
p-Ge, electron bombard. at high temp., carrier lifetime and defect levels 77—55306
Ge, electron irrad., defect growth, struct. rel. to temp. 77—11591
Ge, electron irrad., light-sensitive defects 80—24498
n-Ge, electron irradiated, annealing at 6K, Watkins model explanation 78—47427
n-Ge, electron irradiated, high temp. annealing, nonequilibrium carrier lifetime and Hall effect 77—4370
n-Ge, electron irradiated, threshold energy for atomic displacement, carrier traps 80—29351
Ge, electron irradiated in HV electron microscope, defect form. and interaction with dislocation 77—19990
Ge, electron-beam-controlled transmission of 10 μm radiation 79—81466
n-Ge, energy levels 79—28316
Ge epitaxial film, ion implantation and electron beam anneal effects on carrier conc. 80—75255
Ge film, radiation damage in electron microscope 77—84794
n-Ge, Hall mobility in fast electron irradiated samples 77—55551
Ge, high-temp. irradiation effects under HVEM obs. 77—89475
Ge, irradiated and annealed, cyclotron reson. linewidth investig. of electron scatt. 77—55707
Ge, irradiation at about 6K, low temp. annealing of defect 78—2162
Ge, irradiation by 3.5 MeV electrons at high temp., carrier density and lifetime changes 77—4128
p-Ge, irradiation with fast electrons, defect distrib. with depth 80—19841
Ge, lattice images of defects and radiation damage applics. 80—107210
Ge, p-type, and n-type converted to p-type by irradiation at 77K, defect form. mechanism 79—23651
Ge, point defect formation 77—80501
p-Ge:Ag, Sb, electron beam irradiation cond. characts. 80—19842
n-Ge:As(Sb)(Bi), irradiated with fast electrons at 77K, investigation of 300K annealing stage 79—51155
Ge:Au, gamma-irradiated and electron irradiated, elec. props. meas. 77—62950
p-Ge:Au, interaction of primary radiation defects with Au atoms, after irrad. and annealing 79—51145
Ge:Au,Sb, electron irradiated, Hall effect, photocond., and photomagnetic effect meas. 77—4369
p-Ge:Au,Sb,Hg(Zn), radiation-defect form., Au influence 80—92911
p-Ge:Cd,Sb, electron irrad. at 300K, elec. props. 80—6435
n- Ge:Cu, characts. of radiation defects 78—55893
Ge:Cu, electron irrad. effects on carrier density, defect form. 80—19843
Ge:Cu(Sb), electron irradiation effects on elec. props. 78—6103
Ge:Hg, Sb, influence of electron irradiation on elec. props. 77—20318
p-Ge:Nz, Sb, influence of electron irradiation in elec. props. 77—20318
Ge:Sb, 2.5 MeV electron irradiated, cond. switching effect 77—89820
n-Ge:Sb, electron irrad., impurity photoconductivity 77—15900
n-Ge:Sb, fast electron irrad. at 77K, radiation defect changes by annealing at 220K 79—37737
Ge:Sb,Cu, photoelec. props., fast electron irrad. effects 80—60036
Ge:Sb(Ga), fast electron radiation defects, 0.52 eV absorpt. band, impurity photocond. and Hall effect meas. 78—27273
Ge-Si alloy, electron irradiation and annealing 77—55305
Ge-Te-Se/Si amorphous film-cryst. heterojunction, electron-beam-induced current 79—24060
GeO_2, radiation damaged, paramag. point defects, F-centres, ESR, absorpt. spectra 78—80213
Ge_2S_3, electron irradiated, effects on elec., photoelec. and optical props. 80—49806
H_2, solid, 0.5-3 keV electron penetration depth 78—56549
H_2, solid, electron-irrad., cluster-ion prod., lattice and fragmentation energies 77—4911

electron beam effects continued
H_2O, pulse radiolysis, hydrated electron absorbance, spur overlap 77—86328
Hg halides in aq. soln., pulse radiolysis, emission species 79—24764
Hg, X-ray microanal., quantification of losses 80—85261
HgCdTe, electron irradiated, high temp. defects 79—78122
Ho, electron irradiated, defect annealing, recovery spectra 79—23648
InAs, defect formation processes, effect on physical props. 78—2163
n-InAs, electron irrad., carrier introduction rate, annealing 80—24948
n-InAs, electron irrad., rel. to thermal and electrophysical props. *(Russian)* 80—39154
n-InAs, undoped, electron irrad., Hall coeff., elec. resistivity, optical absorption 77—89479
InAs(P), electron irrad. at 50 MeV, elec. and optical props. 77—47486
n-$In_{1-x}Ga_xP$, direct-gap semiconductor, cathodoluminesc., electron irrad. effects 80—108283
InP, defect formation processes, effect on physical props. 78—2163
InP film, electron-beam annealed, surface conduction 80—84500
n-InP, γ-ray and electron irrad., annealing of radiation point defects, elec. cond. and Hall coeff. meas. 80—65051
n-InP, room temp. electron irrad., Hall coeff. meas. 77—89478
InP:Si, pulse electron annealing, carrier activation and mobility 80—15124
InP_xAs_{1-x}, defect formation processes, effect on physical props. 78—2163
InSb, electron irrad. effects on elec. props. and recomb. 79—51584
InSb, electron irradiated, kinetics of changes in carrier density 79—56228
n-InSb film, low energy electron irrad. effect on elec. props. 80—7009
InSb, high-purity, electron irradiation effects on transport props. 79—23650
InSb, high-purity specimen irradiated at 80K, transport prop. and defect annealing 78—95307
n-InSb, high-resist., prep. using radiation compensation 80—34016
n-InSb, hole mobility temp. depend. after electron bombardment 79—33290
n-InSb, influence of electron irradiation intensity on defect formation 79—73216
InSb, irrad. real and clean surfaces, work function 78—95336
InSb, radiation defect annealing following 50 MeV electron beam irrad. 80—15154
KBr, defect accumulation under electron irrad. at 4K 80—107233
KBr, dynamic equilib. between F and F_2 centres at room temp. 79—51103
KBr, electron irrad., F-centre formation kinetics, interstitial stabilisation mechanism 79—69103
KBr, electron irrad. at 4K, role of V_K centres in equilib. among centres 78—67712
KBr, electron irradiated, defect accumulation kinetics of low temps. 80—10577
KBr, irrad., colour centres and thermolum. 77—85815
KBr, pulse radiolysis of metastable interstitial centre of high temp. 80—20658
KBr substrate, electron irrad., epitaxial growth and surface coverage of Te films 80—10825
KBr:Eu(Yb), electron-irrad., photostimulated luminesc., ionic processes 78—52561
KBr(Cl), electron irradiated, electrotransport 79—69526
KCl, brittle fracture probability distribution functions 79—86820
KCl crystal, F-H centre formation by opt. conversion of self-trapped excitons 78—91335
KCl, electron impact, colour centre distrib., channelling 79—14866
KCl, electron injection, F-centre formation efficiency 78—63790
KCl, electron irrad., F-centre absorpt., ellipsometric obs. 78—23501
KCl, electron irrad., secondary electrons and radiation defects 79—55782
KCl, electron-irrad., positron-capture centres, thermal annealing kinetics 79—95875
KCl, F-centre form. and dissociation under pulsed electron irrad. 78—18643
KCl, F-centre form. by electron irrad., efficiency penetration depth 77—51370
KCl, F-centre formation efficiency, dependence on lattice vacancy concentration 79—82203
KCl, F-centre relaxation kinetics, temp. depend. following electron irrad. 80—92527
KCl, irrad. with intense nanosecond electron beam, super-Rayleigh vel. of brittle fracture front 80—6458
KCl, single cryst., electron beam irrad. optically simulated exoelectron study 79—95908
KCl surface, electron bombard., F-centre absorpt. investigated by use of lateral light waves 78—4707
KCl, thermal and photothermal conversion of colour centres, after high-dose electronic interaction *(Russian)* 80—39156
KCl:$Fe(CN)_6^{4-}$, electron irrad., Mossbauer and ESR study 80—7238
KCl:$K_4Os^{II}(CN)_6$, electron irrad., EPR, ligand hyperfine struct. 78—60335
KCl:$SnCl_2$, action of ionising radiation on Sn aggregation processes 78—34543
KCl:Tl, F-centre formation efficiency 79—82203
KCl:Tl F-centre form. by electron irrad., efficiency penetration depth 77—51370
KCl(Br):OH^-, electron irrad., F_2^+ centre stabilisation 80—54231
KCl(I), electron range-energy relation, thermally created lattice vacancies effect 80—92574
KI:Eu, electron-irrad., photostimulated luminesc., ionic processes 78—52561
$K_2Pt(CN_4)Br_{0.3}.3H_2O$, anisotropic radiation damage in electron microscopy, diffr. spot fading rate obs. 80—107329
$KSbO_3$, cubic, K^+ ion ordering, electron microscopy 78—79550
LiCl, irrad., F-centre emission 78—60501
LiCl, radiation effects on decay time of F-centre emission 80—93381
LiF, 3 MeV electron induced, F, F_2, F_2^+, R_1, R_2 and F_2 colour centre obs., IR spectra obs. *(Russian)* 77—48210
LiF dosimeter energy response to high energy electrons <30 MeV, Monte Carlo calc. 77—86637
LiF, electron irrad., transport of valence band holes, optical absorpt. obs. 79—99188
LiF, electron irradiated, mech. characts. 78—26595
LiF TLD-100, thermolum. response to 5 to 30 keV electrons effect of annealing atm. 77—86638
LiF, thermally stimulated exoemission, radiation defects and adsorpt. centres 78—11087

electron beam effects continued
LiF, V_k-centre generation, temp. depend. 78—18644
LiF:OH^-, electron irrad., F_2^+ centre stabilisation 80—54231
$LiNO_3$, electron irrad. damage, XPS obs. 78—64444
$LiNbO_3$, optically active centres, form. by electron and γ-irrad. 78—18642
$LiNbO_3$ surfaces, ion and electron bombard., photoelectron spectroscopy and electronic props. 80—71559
$LiNbO_3$, XPS and UPS from surface defects 80—76136
$LiNbO_3$:Fe, electron irrad., photoinduced charge transfer and hologram recording 79—36859
Li_2SO_4, electron irrad. damage, XPS obs. 78—64444
Li_2WO_4, electron irrad., reduced species form., XPS 79—11498
$LiYF_4$, electron-irrad. induced defects, optical and EPR study, impurity effects 80—66238
Lu, effect of low-temp. electron irradiation 77—43249
Lu, electron irradiated, defect annealing, recovery spectra 79—23648
Lu, low-temp. electron-irradiated, recovery 78—6102
Lu-H, effect of low-temp. electron irradiation 77—43249
Mg, electron irrad. damage, dislocation loop growth, in situ obs. 78—87715
Mg, electron irrad. induced aqueous corrosion 77—81343
Mg, electron irradiation damage 77—35587
Mg, electron radiation damage, determ. of threshold displacement energy 78—59837
Mg-Ag, ion implanted, recovery stage characterisation by electron irrad. 80—107295
$MgAl_2O_4$, irrad. stability obs. using X-ray emission meas. *(Russian)* 80—66326
$MgAl_2O_4$, radiation damage, optical absorpt., F-centres 80—64994
Mg_3Cd, disordering under electron irrad. in electron microscope 78—83849
$MgCl_2$, partially hydrated powder surface, electron beam effects, XPS obs. 79—33900
MgF_2, EPR of electron irrad. induced F interstitial H- and H_A-centres 77—77099
MgF_2, M-centre, dissoc. kinetics after pulse electron irrad. 79—7601
MgF_2, optical absortion following pulsed electron irrad., 100-500K 79—8164
MgF_2, primary pair of radiation defects, energy of form., colour centre conversion rates *(Russian)* 78—6055
MgO crysts., radiation damage influence on deform. in HVEM 80—103391
MgO, dissoc. under heat and electron bombardment 80—7834
MgO, electron irrad., V^--centres, stress-induced optical dichroism, absorpt. spectra 79—61406
MgO, electron irradiation induced mobility of substitution H 77—55390
MgO, electron irradiation damage, cryst. defects 80—107320
MgO porous layers, conductivity, conditions for lag and dark current 77—20476
MgO surface, electron beam cleaved, characterisation by Au decoration 77—47657
MgO:H(D), electron irrad. induced diffusion of interstitial impurity 77—15452
MgO:Li, $[Li]^0$ defect, high temp. and ionisation induced effects 78—34509
MgO:Li, TEM studies 79—29069
MgO:OH^-, room temp. IR spectra, heat treatment and electron irrad. effects 79—51992
Mg_2SiO_4:Tb TLD, response to X-ray and electron irrad. 79—3285
MnF_2, radiation damage, optical absorpt. and luminesc. expts. 78—2161
Mo (100), adsorption sites of CO, electron stimulated desorption and LEED meas. 80—49516
Mo (100), chemisorption of O, Cs submonolayers effect on electron stimulated desorption of O^- 79—86991
Mo alloy:Re, effect of Re on mechanical props. 80—35196
Mo alloys, dil., HVEM bombarded, neutron damage simulation, defect cluster and dislocation obs. 80—107330
Mo, and oxides, AES expts., chem. shift and beam effects 79—15566
Mo, annealing in stage I, dose depend. and radiation doping defects 78—47422
Mo, BCC, void nucleation following electron irrad. 80—29054
Mo, C doped sheet, electron beam welded, low temp. ductility 79—87685
Mo, effect of microvoid size on positron annihilation and residual resistivity 77—48272
Mo, electron current density localisation and effect on damage prod. 78—22763
Mo, electron irrad., anisotropic damage prod. 80—2071
Mo, electron irrad., positron trapping in vacancies and vacancy clusters 79—52039
Mo, electron irradiated, energy and orientation depend. of at. displacement 79—99244
Mo, electron irradiated, recovery studies of pure and radiation doped crystals 79—19280
Mo, electron radiation damage and props. of point defects 77—11590
Mo, irrad. in HVEM, anisotropy of damage prod. 80—107322
Mo, point defect migration, stage III annealing 77—80548
Mo, slip geometry, HVEM straining 80—39207
Mo, Tokamak reactor, mag. limiter plate, electron irrad. and thermal shock 78—66416
Mo-C dilute alloy defect cluster nucleation and growth under 1250 keV electron microscope *(Japanese)* 78—87663
MoO_3 reduction to MoO_2 by electron beam, electron difrr., microscope investigs. *(French)* 78—95945
MoO_x, AES expts., chem. shift and beam effects 79—15566
MoS_2, lattice images of defects and radiation damage applics. 80—107210
N_2, electron beam produced, plasma, energy distribution of electrons 77—3959
N_2 gas filled chamber, passage of low current electron beam 80—38523
NH_3, cluster-ion prod. in electron-irrad. solid, lattice, and fragmentation energies 77—4911
NO, oxidation by electron beam irrad., appl. to exhaust gas treatment 78—80765
NO_2 decomposition by electron beam irradiation treatment of exhaust gases 79—79423
NO_2, reduction by electron beam irrad., appl. to exhaust gas treatment 78—80765
Na_3AlF_6 film, evaporated, electron bombard. effect on secondary electron emission, Auger peak shifts 80—2903

electron beam effects continued
$Na_4Al_3Si_3O_{12}Cl$:Br,Ge, sodalite, reflectance and luminescence obs. 79—4839
$Na_8Al_6Si_6O_{24}Cl_2$, radiolytic radiation damage, TEM obs. 79—7628
NaCl (001) substrate, preferential epitaxy of evaporated films induced by electron bombard. or elec. field 80—10824
NaCl, (111) surfaces, electron bombard. effects and subsequent Ag epitaxial growth, RHEED and AES 80—15419
NaCl crystals, formation of colour centres *(Russian)* 77—7716
NaCl crystals irrad. by high electron doses, annealing, colour centre prod. 80—2074
NaCl, defects of electron irradiated single crystals *(Russian)* 77—47488
NaCl, electron impact, colour centre distrib., channelling 79—14866
NaCl, electron irrad., secondary electrons and radiation defects 79—55782
NaCl, electron irradiated, electrotransport 79—69526
NaCl, emission of Cl atoms during V_k centre decomposition 80—10578
NaCl, exposed to high-current electron beam pulses, min. size of excited region for crack initiation *(Russian)* 78—84961
NaCl, high resolution TEM and radiation sensitivity, dislocation obs. on deformed crysts. 80—107260
NaCl, photolum. singlet from triplet self-trapped excitons, electron pulse bombardment 79—99936
NaCl:K_3IrCl_6 electron irrad., ligand field anal., EPR obs. 80—29612
NaCl:Tl, luminesc. yield, effect of fast electron channelling 78—84646
NaCl(:Ca) cryst., radiation colouring, amplitude-phase hologram appls., diffraction efficiency 77—68191
NaCl(:Ca), irrad. at room temp., stored energy rel. to thermolum. 80—10574
NaF(Cl):OH^-, electron irrad., F_2^+ centre stabilisation 80—54231
$NaMgF_3$, optical absorpt. of radiation produced defects 77—28604
Na_2O-CaO-SiO_2, Al-coated glass, electron bombarded, SIMS analysis 79—66376
Na_2O-MgO-Al_2O_3, β''''-alumina, high-resolution electron microscopy 80—75208
Na_2O-SiO_2 glass surface anal., effect of electron bombardment during AES on composition 79—83065
$NaReO_4$, EPR spectra of paramag. centres and free radicals 80—108072
Nb, adsorbed H distrib., electron-stimulated desorption ion imaging 80—103572
Nb, BCC, void nucleation following electron irrad. 80—29054
Nb, defect annealing in 7 MeV-irrad. samples, positron annihilation obs. 80—24497
Nb, effect of electron irradiation on low temp. deform., tensile stress-strain curves 79—55784
Nb, electron beam irradiation, 2.3 MeV, positron annihilation exam. of radiation defects *(Russian)* 78—34542
Nb, electron irradiated, energy and orientation depend. of at. displacement 79—99244
Nb foil, oxidized, electron irradiation damage, AES study 79—28015
Nb, high-purity, resistivity recovery following low temp. electron irrad. 77—27909
Nb, mobile interstitials after electron irrad., resistivity recovery meas. 79—55783
Nb_3Ge, low temperature electron, neutron irrad. effects on critical temp. *(French)* 80—75669
Nb_3Ge(Sn), electron irradiation at cryogenic temps., effect on T_c and transport props. 78—52122
Nb_2O_5, electron irradiation damage, AES study 79—28015
Nb_3Sn, A15 cpd., normal state, low temp. resist., disorder effects 80—107762
Nb_3Sn, gap anisotropy, electron irrad. effect on transition temp. 78—10599
Nb_3Sn, monofilaments, radiation-enhanced diffusion growth, crit. current density 80—65758
Ni (110), adsorption of CO and CO_2, electron bombard. effects, AES and electron stimulated ion desorption obs. 79—51430
Ni, electron irradiated, temp. depend. positron trapping 78—91360
Ni, electron irradiation effects on He gas bubble superlattice, He gas-bubble superlattice form. 80—2086
Ni, foil, electron bombard., impurity redistrib. during third stage of annealing, residual resist. meas. 80—6434
Ni, Frank loops, growth kinetics and 'preference factor' during electron irradiation 78—22723
Ni, HVEM obs. of irrad. damage 77—35589
Ni, irrad. in HVEM, interstitial loop growth 80—107326
Ni, oxidation, electron beam influence, disappearance potential spectroscopy obs. 77—1766
Ni, point defect-dislocation loop interaction, effect on dislocation loop growth kinetics 78—47415
Ni, pure and doped, mech., mag. relax. meas. dumb-bell self-interstitital reorientation *(German)* 78—52879
Ni surface, electron stimulated interaction of H_2O, AES obs. 77—31902
Ni-Al alloys, effects of electron irradiation in precipitation, nucleation and dislocation loop growth, TEM study 79—42106
Ni-Cr-Fe (75, 35, 12 wt.%), electron and α-particle irrad., positron annihilation and elec. resist. meas. 79—83054
Ni-Cr-Fe alloys, radiation enhanced precip. and dissolution of precipitates, point defect kinetics and dislocation obs. 80—108467
Ni-Cu, electron-irrad., neutron-scatt. studies 80—75268
Ni-Ge , defect-solute interactions and radiation-induced segregation 80—25705
Ni-S, S atom redistribution under high temp. electron irrad., residual elec. resist. reduction *(Russian)* 79—82256
Ni-Si, defect-solute interactions and radiation-induced segregation 80—25705
Ni-Si solid soln., radiation, induced precipitation dose rate effects 78—6936
Ni_3Fe, disaccommodation meas. after low temp. electron and neutron irrad. 80—88832
Ni_4Mo, electron irrad. in electron microscope, radn. ordering 79—86818
$NiSi_2$, amorphous, crystallisation by energy beam annealing 79—69012
P_2O_5-MO-Al_2O_3, (M = MgO, CaO, SrO, BaO) (45, 5 wt.%) glass, electron irradiation effect on dielec. props. 80—29056
Pb, electron irradiation at 4.7K and below 3K, annealing expts. 77—11595
Pb microbridges, supercond. breakdown under electron beam irrad. 79—56418
Pb, radiation damage and recovery processes 77—69002
Pb superconducting microbridges, two-dimens. imaging of resist. voltage changes caused by electron irrad. 80—15659

electron beam effects continued
Pb-Cu, damage and recovery processes 77—69002
Pb-Ni-Si, metallic glass, electron irrad., positron annihilation radiation, angular correlation study 78—84678
PbO-SiO_2 glasses, charge trapping and dielec. breakdown, radiation-induced, microphase separation 78—23399
PbS, photosensitive film, electron bombard. effect on elec. cond. 80—93019
$Pb_{1-y}Sn_ySe$, electron-irradiated, elec. and recomb. props. 79—56227
PbSnTe, electron irradiated, high temp. defects 79—78122
PbSnTe-PbTe heterostructs., effect of electrical grounding on electron irrad. 78—60194
$Pb_{1-x}Sn_xTe$, electron-irradiated, elec. and recomb. props. 79—56227
$Pb_{1-x}Sn_xTe$ film on BaF_2, electron beam delineation effect on MBE growth, LEED and AES obs. 79—99434
PbTe (111) epitaxial films, localised electron irrad. effects on elec. props. and O_2 sorption 80—49472
Pd, silicide formation due to laser and electron beam annealing 80—84849
Pd_4Si and Pd_2Si, amorphous, crystallisation by energy beam annealing 79—69012
Pt, electron irrad., close Frenkel pair recomb. during annealing 78—87716
Pt, electron irradiated, interstitials activation vol. 79—51154
Pt foil, quenched, 1.2 MeV electron irrad., subthreshold irrad. effects 78—51585
Pt, Frenkel defect migration and reactions, by subthreshold recoil events, exam. 78—47364
Pt, interstitial thermal conversion study by elec. cond. meas. 80—15096
Pt, radiation damage, recovery of elec. resist., interstitial migration and clustering 77—11604
Pt, radiation damage recovery curves, evidence for two self-interstitial configs. 77—7773
Pt, silicide formation due to laser and electron beam annealing 80—84849
$RbCaF_3$, optical absorpt. of radiation produced defects 77—28604
RbCl, electron bombard., colour centre photoemission, surface contamination and escape depth 80—66392
RbCl:Eu, electron-irrad., photostimulated luminesc., ionic processes 78—52561
$RbMgF_3$, irradiated, thermal conductivity 78—22909
$RbMgF_3$:Mn, low-temp. radiation damage, optical absorption meas. 78—22761
$RbMnF_3$, radiation damage, optical absorpt. and luminesc. expts. 78—2161
$RbMnF_3$:Fr, pure and doped, unirradiated and electron irrad., energy transfer 80—108254
$RbNgF_3$, radiation defect F,M,R-centre absorpt., emission, excitation spectra 79—43000
Ru (0001) surface, adsorption and desorption of NH_3, effects of electron beam 78—38955
SF_6, gas, electron beam irrad., delayed elec. breakdown 79—4200
SO_2, oxidation in moist O_2-N_2 mixture by electron irrad., appl. to exhaust gas treatment 78—80766
Sb, electron microscope irradiation effects, agglomeration of point defects, dislocation climb and loops *(French)* 80—59518
Se, amorphous, electron irrad.-induced paramag. centres, 77K 78—88187
Se, damage expts. review, defect interactions 77—84800
Si, ^{75}As implantation, scanned CW electron beam annealing 79—99225
Si, ^{75}As implanted, comparison of effects of pulsed ruby laser and pulsed electron beam annealing 79—69135
Si, 6 MeV electron bombard., radiation damage rate distrib. with depth 77—31694
Si (111), adsorpt. of O and stimulated oxidation by electron bombardment, AES 78—14599
Si, advanced material for space solar cell 80—94007
Si, amorphised by ion implant., localised states and cond., irrad. and heat treatment, doping 80—39529
Si, amorphous films, oxidised, vacuum deposited cond. change 78—10089
Si, Au diffusion enhancement by photo- and electron irrad. 77—27901
Si, channelling of electrons and positrons, correspondence between classical and quantal descriptions 78—18682
Si, channelling of relativistic electron beam, anal. of low-energy bremsstrahlung meas. 77—36304
p-Si, compensated by radiation defect centres, photoresistors 77—62961
n-Si, complex defect production rate introduced by high energy electron irradiation 77—72635
Si, damage in electron bombardment, threshold voltage 77—27910
Si, defect generation and annealing by intense subthreshold electron beam bombardment 79—51149
Si devices, dominant recomb. centres 77—72912
Si diode radiation detector, stabilisation of radiation damage 80—91377
n-Si, efficiency of radiation defect generation by electron bombardment, influence of Fermi energy 77—11596
Si, electron beam annealing, beam voltage effect modeling 80—75275
Si, electron beam irrad., {113} faults, nature and origin 80—70258
Si, electron beam irradiation, 2.3 MeV, positron annihilation exam. of radiation defects *(Russian)* 78—34542
Si, electron beam scan annealed, deep levels 80—65481
Si, electron bombardment, absorption of energy 79—14847
n-Si, electron irrad., defect energy levels, energy depend. 79—33262
p-Si, electron irrad., influence of acceptor impurity conc. and irrad. temp. on defect formation 79—19281
Si, electron irrad., limiting position of Fermi level, elec. cond. and optical absorpt. meas. 79—65484
Si, electron irrad., resistivity-fluence relation 80—54700
Si, electron irrad., rod-shaped defects, electron microscopy and IR spectra obs. 80—39159
Si, electron irrad., two-vacancy defect EPR 80—29619
Si, electron irrad. damage, capacitance meas. 80—24935
p-Si, electron irrad. induced defects, thermally stimulated capacitance 77—11933
Si, electron irrad. induced defect form., carrier density, mobility and lifetime changes 77—43250
Si, electron irrad. induced defects, bulk photo-EMF meas. 80—39160
Si, electron irradiated, EPR of C-O divacancy complex 77—69691
n-Si, electron irradiated, elec. props. 77—8041
Si, electron irradiated, high resist. surface layer, Schottky barrier meas. 78—64093
Si, electron irradiated, photolum. due to interstitial complex 77—44048
Si, electron irradiated, positron annihilation 78—87713

electron beam effects continued
- Si, electron irradiation induced corrosion 77—59960
- Si, electron irradiation induced displacement defects 77—80543
- n-Si, electron radiation defect annealing, negative stage, Hall coefficient, defect levels 79—90701
- n-Si, electron-irrad., surface defect distrib., deep-level transient spectroscopy 79—1459
- Si, electron-irradiated, {113} loops obs. 79—82225
- Si, electron-irradiated, annihilation of positrons 77—55847
- Si, electron-irradiated, positron annihilation 78—48256
- Si, energy levels and capture cross sections of defect states, capacitance transient analyses 77—80545
- p-Si, fast electron irrad., energy levels determ. by photocapacitance meas. 79—51531
- p-Si, fast electron irrad., Hall mobility, temp. depend. 78—56165
- Si, fast electron irradiated, models of luminescence centres, role of interstitials 77—81153
- n-Si, γ- and electron irradiated, influence of deform. on capture of electrons by divacancies 77—1449
- Si, heavily doped layer, electronic characts., electron beam induced current obs. 78—10473
- Si, high-resistivity layer form. during electron irrad. 80—80352
- Si, implanted amorphous, comparison of laser and thermal annealing 79—70084
- Si implanted layers, interaction of defects and impurities stimulated by induced ionisation, ESR 80—11270
- n-Si, interaction of disordered regions with point defects 79—19296
- Si, interstitials and lattice vacancies 78—10038
- Si, interstitials in radiation defect formation 77—15461
- Si, ion implanted, electron beam annealing, surface struct. study using SEM 80—70235
- Si, ion implanted, scanning electron beam annealing 80—6420
- Si ion implanted layers, pulsed electron beam annealing, TEM and particle backscatt. meas. 79—69134
- Si, ion-implantation damage, annealing using pulsed-electron-beam 79—55768
- Si, irrad., multivacancy-O complexes, EPR expt., correl. with IR absorpt. data 77—28443
- n-Si, irrad. with 1.2 GeV electrons, form. of radiation defects 79—51156
- Si, irradiated, nature of 0.97 eV A band luminesc. 77—44049
- Si, laser annealing of point defects 80—107224
- Si, lattice images of defects and radiation damage applics. 80—107210
- Si layers, ion implanted, pulsed electron beam annealing, He^+ backscatt. and TEM study 79—51152
- n-Si, lightly doped, electron irrad. induced divacancies as electron traps 77—4126
- Si, local electron irrad., Frankel pair separation, influence on photo EMF 80—44203
- p-Si, low temp. defect prod., obs. by thermally stimulated capacitance technique 77—84801
- Si MOS diode, surface state characts. obs. *(Japanese)* 79—42646
- Si, MOSFETs, Shubnikov-de Haas oscills. from electron irrad. induced two-dimens. leakage channel 79—19671
- Si materials, advanced, preliminary evaluation for space solar cells 80—94006
- Si, migration of Au, electron bombardment effects 80—100362
- Si n^+-p junction solar cells, electron irrad., DLTS spectra and defect effects 80—93999
- Si n^+p solar cells, effect of elec. bus during 1 MeV electron irrad. and isochronal annealing, elec. characts. and deep level pop. 80—94086
- Si, neutron and electron bombard., radiation defect recomb., photoelec. props. meas. 80—60039
- n-Si neutron and electron irrad., isochronous annealing influence on edge absorpt. 80—11449
- Si p-n junction, avalanche multiplication of electron beam generated carriers 77—80833
- Si p-n junction depletion layer, electron beam damage inhibition 80—70817
- Si p-n junctions, spin depend. surface recomb., electron irradiation effect 80—88627
- Si, paramagnetic defects produced by electron irrad., EPR 79—19779
- p-Si photoresistor, compensated with radiation centres, current responsivity and detectivity 79—17492
- Si, polycryst, CVD, electron beam recrystn. 80—24759
- Si processing technology, appls. of scanning CW lasers and electron beams 80—100932
- n-Si, quenched, fast electron irradiated, annealing of defects 80—89259
- Si, radiation damage effects on characts. *(Korean)* 79—60402
- p-Si, radiation defects by annealing, kinetics anal. 79—33018
- Si, radiation induced defects in high-voltage electron microscope 80—65048
- Si, radiation-stimulated vacancy diffusion, mechanisms 77—55396
- Si, radiative recomb. centre accumulation due to high temp. electron irrad. 80—93394
- Si solar cells, n^+-p, Li-counterdoped, radiation damage 80—94000
- Si solar cells, radiation damage annealing mechanisms and low temp. annealing 80—94003
- Si solar cells, ultrathin, electron and proton effects 80—94002
- Si substrate for PMMA electron sensitive layer, 400 Å linewidth electron beam lithography 80—65392
- Si, surface, pulsed electron beam processing, doping, annealing 80—75254
- Si surface electron beam deposited silicide formation using scanning CW laser beam 80—66862
- Si wafer, ion implanted, electron beam annealing, computer simulation 80—96569
- Si:Al, electron irrad. induced defects, transient capacitance study 80—59516
- Si:Al, recomb. enhanced migration of interstitial Al 79—82201
- Si:As, electron induced displacement, channelling study 80—29058
- Si:As, electron irrad. induced defect levels, annealing, deep level transient spectroscopy obs. 77—59044
- Si:As, electron irradiated, majority carrier trap prod., effect of O_2 enhanced annealing 77—1151
- Si:As, ion implanted, scanning-electron-beam annealing 79—60391
- Si:As, scanning electron beam annealing, spreading resistance, junction depth 80—75267
- Si:As high-dose implanted single crysts., pulsed electron-beam annealing 80 103373
- Si:As^+, implanted, CW laser annealing, electron-beam induced current 80—100709

electron beam effects continued
- Si:As(B), ion-implanted, scanned laser and electron beam annealing 79—73182
- Si:As(Sb), ion implant lattice location after pulsed ruby laser annealing 79—73204
- p-Si:B, defect energy levels with 1 MeV electron irrad. and annealing, transient capacitance spectra 77—62860
- Si:B, ionisation-assisted annealing 79—23628
- Si:B, p-n junction diodes, scanning-electron-beam annealing, elec. characts. 79—79128
- p-Si:B(Al), radiation defect form. and annealing study using Hall effect, cond. and carrier diffusion length 80—84214
- Si:C(O), photoluminescence spectra, radiation damage investig. 77—28620
- Si:Ga, electron irrad.-induced defects, DLTS meas. 80—24499
- p-Si:Gd, irradiated, elec. props. 79—51613
- Si:Gd, radiation defect form., effect of Gd impurities, elec. and optical meas. 78—71764
- Si:Gd, radiation defects effect on elec. props. 77—28184
- n-Si:Ge, electron induced defects, room temp. instability 80—29052
- Si:Ge, electron irrad.-induced defects, DLTS meas. 80—24499
- a-Si:H, spin defect and recombination influence on electronic transport 80—50409
- Si:H film, amorphous, bombarded, defects, luminesc. and ESR meas. 80—34977
- Si:In, electron irrad., Hall effect meas. 80—2401
- Si:Li P/N type solar cells, irradiation obs. 79—66406
- Si:O,C, electron irradiated, indirect vacancy-interstitial recomb., IR absorpt. meas. 77—43209
- Si:P, heavily doped, EPR spectra of electron irradiation induced defects 77—81008
- Si:P, implanted, pulsed electron beam annealing, Hall effect and sheet resist. meas. 80—34467
- Si:P, implanted layers, ionisation-enhanced crystallisation 79—51151
- Si:P, ion implanted, ionisation enhanced annealing, resist. changes meas. 78—30667
- n-Si:P, secondary defects produced by high-temp. electron irrad. 79—33017
- Si:P film, polycryst. pulsed electron beam annealing 80—10566
- Si:P implanted, multiscanning electron beam annealing 80—75242
- Si:P(O) p^+-n-n^+ solar cells, comparison rel. to resistance to 1.5 MeV electron irrad., majority carrier trapping 80—94087
- Si:Sb, electron irrad. damage, electron trapping centres 77—39798
- Si:Sb vacuum deposited coating, p-n junction, pulsed electron beam annealing doping, diffusion 80—75480
- n-Si:Sm,P, carrier conc. and mobility, electron irrad. effects *(Russian)* 77—66168
- Si-SiO_2, electron-beam annealing of ion-implantation damage 79—77622
- Si-SiO_2 charge accumulation during low energy electron bombardment 78—64142
- Si-SiO_2 interface, in MOS structure, effect of irrad. with low energy electrons *(French)* 77—55617
- Si-SiO_2 interface, in MOS struct., fast surface states density, electron irrad. effects 78—88042
- Si-SiO_2 interface in MOS structs. low-energy electron beam irrad., charge accumulation process anal. 80—65701
- SiC, (6H), radiation damaged, luminesc. 80—25462
- SiC, cubic, atomic displacement energy determ. by bracketing technique 80—49272
- SiC, surface defect annealing, following Ar ion and electron irrad. 80—7603
- SiC, Tokamak reactor, mag. limiter plate, electron irrad. and thermal shock 78—66416
- α-SiC(6H), electron bombardment, formation of defects on $(000\bar{1})$ surface 80—19844
- $Si_{12}Ge_{10}As_{30}Te_{48}$ glass, effect of surface, SEM obs., rel. to switching filament form. 77—47700
- Si_3N_4 film, high-speed electron irradiation effect on charge storage 77—69430
- SiO_2 coatings on SiO_2 substrate, cathodoluminescence spectra, electron irrad. 80—76085
- SiO_2, doped, fibre-optic waveguide, effect of ionising radiation on optical attenuation 78—63170
- SiO_2, electron-beam irrad., electron trapping, MOS capacitor expts. 78—72268
- SiO_2 film, electron-beam-induced cond. 80—20337
- SiO_2 film, high-speed electron irradiation effect on charge storage 77—69430
- SiO_2 film electron beam induced conductivity theory and expts. 80—15640
- SiO_2, film on Si, electron beam damage, obs. using scanning AES 80—2070
- SiO_2 films, radiation induced charge transport and build-up, low temps. 77—20478
- SiO_2 gate insulator MOS capacitors, hole transport, recovery characts. following electron beam irrad. 77—20439
- SiO_2 gate insulators in radiation-hard MOS capacitors, charge relaxation 78—60206
- SiO_2, glass, ion implanted, radiation effect on chem. stability 77—1158
- SiO_2 optical fibres, plastic-clad, short-term transient radiation effects 79—50420
- SiO_2, optical waveguide form. by low energy electron irrad. 77—7189
- SiO_2, surface electronic struct., electron irrad. effects, EELS study 80—24985
- SiO_2 surfaces, charging and dissociation, AES meas. 77—59650
- SiO_2, vitreous, compaction dependence on ionisation dose 78—67738
- SiO_2, vitreous, electron irrad., vol., refr. index and stress changes 77—47482
- SiO_2, vitreous, electron irrad. effect on sp. ht. 79—65212
- SiO_2, vitreous, low temp. thermal props. and intrinsic defects 80—29057
- SiO_2:Ge silica-core fibre-optic waveguides, effect of B, P and OH on radiation response 79—50419
- SiO_2-layers, charge transport induced by electron beam, simulation *(German)* 79—51702
- SiO_2-Si, cathodoluminesc. and AES rel. to struct. 78—43937
- SiO_2-Si, effects of processing on radiation damage 78—39223
- SiO_2-Si MOS capacitor, two-stage process for building up of radiation induced interface states 80—20313
- Sm, electron radiation damage, elec. resistivity change rates 80—59954
- Sn film, 80 keV electron scatt., use for radiation damage monitoring 77—4127

electron beam effects continued
- SnO_2-Si n-n photodiode, 5.4 MeV electron irrad. effects 77—80806
- SrO, irradiated, low temp. photocond. 77—39891
- Ta, bremsstrahlung yield and distrib. of absorbed energy in electron irradiation 79—99245
- Ta, electron irradiated, energy and orientation depend. of at. displacement 79—99244
- Ta foil, plasma production by pinched relativistic electron beam impact 79—77403
- Ta, near-threshold displacements in single crysts., electron-irrad. induced defects, resistivity meas. 79—60356
- Ta_2O_5, oxidised Ta foil, electron bombardment effects on surface composition, Auger spectroscopy, electron desorption measurements 79—77874
- TaS_2 (1T) electron irradiated, lattice contraction 80—59520
- Tb, electron irradiated, defect annealing, recovery spectra 79—23648
- Te, damage expts. review, defect interactions 77—84800
- Te, electron irrad., mobility increase due to defect prod. 80—24501
- Te, electron irradiated, dose-depend. and recovery behaviour of transport props. 78—71761
- Te, vacuum deposited film, effects of electron irradiation on surface coverage *(Japanese)* 79—82477
- Ti, electron radiation damage, determ. of threshold displacement energy 78—59837
- Ti film, on Be(Ag) substrate, range of primary electrons 77—4134
- TiC, electron irrad. damage, electron microsc. study 80—84210
- TiN-AlN, composite, erosion resist. in electron stream 78—11365
- TiO_2 powder, radiation induced defects 77—62562
- Tl-Hg, excimer band emission from electron beam initiated discharge in TlI-Hg 80—78841
- Tl-Xe, excimer band emission from electron beam initiated discharge in TlI-Xe 80—78840
- Tm, electron irradiated, defect annealing, recovery spectra 79—23648
- UC-UC_2, alloyed, electron bombarded, enhancement of U_2C_3 deposition 77—27911
- UF_4 optical interference layers, electron-beam decomposition 78—34541
- UO_2, neutron and electron irradiated, imperfect dislocation loops *(French)* 79—7606
- U_3Si, reversible twinning, in-situ obs. 80—104241
- V, electron irradiated, positron study 78—76555
- VO_2, film, metastable metallic phase due to laser and electron beam irrad., refl. spectra 79—19944
- V_2O_5, electron beam induced decomposition, appearance pot. spectroscopy 80—85203
- W (011) surface, adsorbed H_2, disordering effect of electron irradiation *(Russian)* 79—7744
- W (100), adsorbed O, electron stimulated desorption ion energy distrib. and surface struct. 78—75940
- W (110) stepped surface, electron stimulated desorption of O, atomic steps and defects influence 80—80091
- W cathodes, heating by DC electron bombardment 78—23578
- W crystal, EM showers produced by electrons, positron spectral distribution *(Russian)* 80—55218
- W, electron channelling in (111) direction, 200 to 1000 keV 78—2182
- W, electron channelling in (111) direction, 1000 to 2000 eV energy range 78—38763
- W, electron irrad., or ion irrad., stage II, point defect struct., FIM 77—80542
- W, electron irradiated, or quenched, point-defect mechanism for Stage III recovery, field ion microscope study 79—60403
- W, electron stimulated desorption of O^+ and O^- from chemisorbed O_2 79—90875
- W, Frenkel pair creation and stage I recovery of electron irrad. cryst. near threshold 79—1463
- W, single crystals, electron irradiated, recovery of resistivity, 4.5-380K *(German)* 78—87714
- W, structural defect recovery after irradiation and cold work 78—47429
- W surface, adsorbed CO, electron-stimulated desorption, photoemission, relax. energy 80—100401
- WO_3, oxidised W foil, electron bombardment effects on surface composition, Auger spectroscopy, electron desorption measurements 79—77874
- WO_3 powder, electron bombardment effects on surface composition, Auger spectroscopy, electron desorption measurements 79—77874
- WSi_2, amorphous, crystallisation by energy beam annealing 79—69012
- Y, electron radiation damage, elec. resistivity change rates 80—59954
- YAG:Nd,Ce,Cr, effect of γ-rays, fast electrons on optical props., annealing and colour centre destruction 77—8608
- YIG, electron and γ-irrad., photomagnetic effect 80—103877
- YIG, substituted, effect of electron bombardment on mag. and elec. props. 79—42103
- Y_2O_3, electron irrad., dislocations *(French)* 80—2076
- Yb, electron radiation damage, elec. resistivity change rates 80—59954
- Zn, defect recovery after low temp. electron irrad. 78—10090
- Zn, electron irradiated, diffuse X-ray scatt. exam. of self interstitials 79—73213
- Zn, electron irradiated, diffuse X-ray scatt. exam. of interstitial clustering during thermal annealing 79—73214
- Zn, electron radiation damage, determ. of threshold displacement energy 78—59837
- Zn, electron radiation damage in HVEM, nature of defect clusters 78—59838
- Zn, faceting of interstitial loops 78—47381
- Zn-Al eutectoid, superplasticity, study by electron microscopy 77—48479
- $ZnGeP_2$, cond. compensation by electron bombardment 79—15151
- $ZnGeP_2$, electron irrad., elec. and optical props. 79—33743
- ZnO, dislocation loop nucleation on prismatic faults in high voltage electron microscope 77—72620
- ZnO, electron irrad., vacancies and interstitials, EPR meas. 79—14803
- ZnO, electron irrad. damage, orientation depend. 80—2075
- ZnO, irradiation in high voltage electron microscope dislocation loops study 80—88157
- ZnO UV laser, electron-beam pumped 80—99753
- ZnO:Li, F^+ centre, photosensitivity of e.p.r. spectrum 77—1594
- ZnS, diatomic crysts. electron induced X-ray emission, channelling effects 79—56888
- ZnS, electron irrad., ESR 79—91293
- ZnS UV laser, electron-beam pumped 80—99753
- ZnS-CdS:Ag(Ni)(Co), electron-irradiated phosphors, void formation mechanism 79—55780
- ZnSe crystal, exciton reflection spectra, control of exciton-free surface layer thickness 80—7373

electron beam effects continued
- ZnSe, diatomic crysts. electron induced X-ray emission, channelling effects 79—56888
- ZnSe, electron irrad., dislocation climb, TEM obs. 79—1461
- ZnSe, electron irrad., short-lived optical absorpt. 79—51989
- ZnSe electron irradiation induced displacement defects 77—80543
- ZnSe, electron-beam-controlled transmission of 10 μm radiation 79—81466
- ZnSe, undoped and doped, pair spectra, edge emission and shallow acceptors 77—28617
- $ZnSiAs_2$, electron irrad., defects, elec. and optical props. 79—19282
- p-$ZnSiAs_2$, electron irrad. elec. props. annealing, lattice defects 80—100465
- ZnTe film, electron irrad. effect on electrophys. props., prep. conditions depend. 79—28421
- ZnTe, irradiation induced radiative centers obs. 80—66290
- Zr, dissolution of γ-ZrH, in situ study, HVEM obs. 78—55951
- Zr, electron induced irradiation creep, dislocation process obs. 77—47483
- Zr, electron irradiated, interaction of self interstitials with O_2 atoms 79—65118
- Zr, electron irradiation damage, direct obs. 80—84212
- Zr, foil, dislocation loop nucleation and growth during 1 MeV electron irrad. 80—88152
- α-Zr, vacancy recovery following 1.5 MeV electron irrad., positron annihilation meas. 77—47485
- Zr, void swelling during electron irrad., HVEM study 80—92559
- Zr-Nb(0.1, 2.5 wt.%), foil, dislocation loop nucleation and growth during 1 MeV electron irrad. 80—88152
- Zr-Sn(Fe)(Ni) (0.15 wt.%), electron irradiation damage, direct obs. 80—84212
- Zr_3Al, Ar^+ ion and electron irradiation, irradiation swelling, lattice parameter changes 79—65123
- Zr_3Al, disordering by 1 MeV electron irradiation 78—51583
- ZrN-AlN, composite, erosion resist. in electron stream 78—11365

electron beam impact *see electron impact*

electron beam lithography
- *see also electron resists*
- automatic measurements by use of a probe-forming electron-beam system 79—21868
- conference on electron, ion and proton beam technology, conf., Boston, MA, USA (29 May-1 June, 1979) 80—67927
- field emitter electron beam exposure system for semiconductor fabrication 79—30624
- flying spot scanner for conversion of SEM to lithography system 80—86512
- IC template fabrication, SEM and electron lithography optics 79—75662
- ICF targets, semiconductor process technology for mass production 80—32439
- Josephson junction fabrication by ion implantation, electron beam lithography and dry etching 80—88693
- low profile electron collector system 80—68292
- LSI, lithographic manufacturing techniques *(German)* 79—71547
- microbridge Josephson junction, fabrication 79—28457
- microfabrication for guided-wave optical devices 80—58812
- microgratings for guided-beam deflection, electron-beam direct-writing fabrication 80—102856
- microlithography, deflection and focusing system, optimization of principal parameters *(French)* 79—41319
- microstructure fabrication, using STEM and X-ray lithography and reactive ion etching, appl. 79—15844
- MOS diodes preparation, defects due to 2 to 25 keV electron beam obs. *(Japanese)* 80—54787
- MTF evaluation for optical and electron-beam lithography 80—4801
- NMOS VLSI circuits manufacture process and problems *(Norwegian)* 80—60090
- shaping by multichannel gate voltage selection 79—50204
- thin film interdigital transducers for SAW devices at GHz freqs. form. by electron beam lithography 80—4702
- toroidal deflection yokes, eddy current compensation 80—95762
- triple slit scheme for high current variable-shaped beam forming 80—68290
- two step electron beam lithography process for submicron SAW device fabrication development 79—55281
- x-ray zone plates fabricated using electron-beam and X-ray lithography 80—68335
- Nb, superconducting bridges by electron beam lithography and ion implantation Josephson effect 80—20355
- Si_3N_4 sample substrates, high resoln. electron beam fabrication using STEM 80—104104

electron beam machining
- ceramic, unfired, cavity form. by electron beam machining 78—80660
- ceramic unfired, precision e-beam machining, kinetic focusing 78—80661
- conference on electron, ion and photon beam technology, Palo Alto, CA, USA (May 1978) 78—74827
- integrated optical grating circuit fabrication by electron beam direct writing 80—64214
- micromachining, imaging conditions, illumination system 78—82899
- refractories, erosion resistance during action of highly concentrated energy fluxes 80—55562
- SAW grating electron beam erosion of Ag film on piezoelectric quartz *(Russian)* 78—18134
- semiconductor plate cutting, beam shaping apparatus 78—21268
- spatial charge and beam radius determination *(Russian)* 80—74290
- Fe_2O_3-NiO-ZnO-CoO (15.1, 17.6, 0.6 wt.%) ferrite, effect of electron beam machining on surface layer 79—34178
- TiN-AlN, composite, erosion resist. in electron stream 78—11365
- ZrN-AlN, composite, erosion resist. in electron stream 78—11365

electron beam welding
- electron beam welds, NDT by AE to detect lack of fusion *(German)* 77—56193
- fusion reactor, Heliotron E, vacuum chamber construction using electron beam welding 80—106180
- melting channel formation, electron optics model *(Russian)* 77—52336
- spatial charge and beam radius determination *(Russian)* 80—74290
- steel, austenitic, KO 34 samples, electron beam welded, Charpy test expts. *(Hungarian)* 80—104252
- steel, austenitic stainless, electron beam welding effect, on mech. props. of steels 310L, 316, 21-6-9 78—48498
- steel, ferritic-bainitic welded by electron beam, morphology and struct. of heated zone *(French)* 77—73292

electron beam welding continued
steel, stainless, N toughened, electron beam welding, fusion reactor component fabrication 80−32472
technology, principles and applications 80−82756
tetrode gun, transport of high-energy, high-power electron beams 78−89587
Al alloys, glow discharge appl. 79−73052
Mo, structure of large single crystals produced by electron beam spot welding *(Russian)* 77−44136
Ti-Al-V, VT6 alloy, butt welded joints, electron beam welding conditions effecting interstitial impurities distribution 80−39136
Ti-Mo-Zr-Sn, alloy, βIII, struct. transform. in thermally affected zones after electron beam welding 78−23919

electron beams
see also electron impact; electron optics; Schwarz-Hora effect
100 GW beam generator 78−5087
100 GW electron beam generator 77−2711
aberration averaging, image and deflection component design 78−74830
aberration elimination, electron beam scanning systems 80−78756
absolute dose rate determ. 78−74103
acceleration in laser-beam focus 77−10574
accelerator beam, parameters meas. in adherer during compression via two-coil pickup 77−65393
accelerator linear, intense electron beam transient radial motion 80−9434
accelerator pulsed electron gun systems, 1 ns pulse width 79−67977
accelerator radiation processing applications 77−54370
accelerators for long duration pulsed electron beams, development 80−68980
annular, prod. by foilless diodes 80−95779
annular electron bunches, prod. by cylindrical magnetron 77−10136
arc, low press., large cross section anode plasma with constricted channels, broad electron beam prod. 80−38840
auroral electron beam, assoc. EM radiation bursts during substorms 79−88557
auroral electron beam, electrostatic noise generation 78−85759
Auto-Resonant acceleration, computer simulation of linear and nonlinear wave growth phenomena 80−9439
autoacceleration by coaxial transmission line cavity 77−14652
autoresonant collective ion accelerator, wave amplitude var. and energy flow 79−76176
axially moving cylindrical, surrounded by dielectric cylinder, EM wave scatt. 77−14645
beam surface envelope and angular vel., propag. through gas 78−46499
beat radiation of electron waves 80−43314
betatron beam, characterisation for dosimetry calcs. 79−39519
betatron electron beam, struct. determ. via synchrotron radiation 77−65368
biological single and twin targets, low-energy interactions 80−12195
Bohm-Aharonov experiment without an electron microscope 79−894
bounded electron beam, quasilinear relaxation model *(Russian)* 78−78891
Brillouin electron beam critical current rel. to vacuum level 79−7068
broadening effects caused by discreteness of space charge 80−69309
bunch lengthening and energy spread in electron storage rings, SPEAR II data 77−83210
bunch lengthening in electron storage rings, resistive theory 77−83209
bunched beams, longitudinal instability theory 77−83208
bunching at mag. field discontinuity 80−63905
bunching at optical wavelengths; inverse Cherenkov effect 78−46497
charge decrease at transition showing hysteresis 79−64169
charge monitor, single pulse toroidal coil type 78−78036
Cherenkov modulation 78−5408
classical stimulated bremsstrahlung, electron beam bunching 80−69306
coaxial autoaccelerator, klystron instability of relativistic electron beam, stability criterion 78−82541
coaxial autoaccelerator, resonant instabilities of relativistic electron beams 78−82540
coaxial electron and atomic beams sequential multiple scatterings, random walk approach 80−99574
coherent EM radiation intensity, produced by modulated electron/ion beams in gas 78−50686
coherent radiation 77−76476
coherent radiation from modulated beam in residual gas 77−594
coherent radiation generation near cyclotron resonance 80−18979
coherent submillimetric Cherenkov radiation generated by relativistic electron beam 77−38793
coherent X-ray generation from CO_2 laser backscattered relativistic electron beam 80−53252
collection ion acceleration, power balance limit to intense relativistic electron beam front velocity 80−13997
collective accelerators, autoacceleration process for generation of high current relativistic electron beams 80−14011
collective accelerators, autoaccelerator dynamics and stability 80−14012
collective accelerators, ion burst accel. and prefocusing using rel. electron beam interactions 80−14008
collective and single-electron interactions of electron beams with EM waves and free-electron lasers 78−55330
collective field accelerator, vac. diode with relativistic electron beam operation 77−24201
collective ion acceleration, dielectric guide controlled rel. electron beam propag. 80−14001
collective ion acceleration, relativistic electron beam interaction with apertured solid dielec. anode 80−14007
collective ion acceleration and intense electron beam propagation within an evacuated dielectric guide 80−14002
collective ion acceleration and intense electron beam propag. in vacuum dielectric channels 80−14003
collective ion acceleration by intense relativistic electron beams 80−13996
collective ion acceleration controlled by a gas gradient 79−76169
collective ion acceleration from rotating relativistic electron beam injection into neutral H 79−76167
collective ion acceleration in a gas by high-current electron beam pinch 80−14000
collective ion acceleration in relativistic electron beam diode, intense slow space charge generation 78−9863
collective ion acceleration using space charge waves on electron beams 80−13995

electron beams continued
collective ionisation front accelerator using intense relativistic electron beam, experimental feasibility program 80−13998
collective particle accelerators 79−76165
collective relativistic interactions in faster than light media *(Russian)* 80−46803
collision broadening, energy spread calc. 78−42271
compact cold cathode electron beam gun, appl. CO_2 laser *(German)* 80−86501
compact source for neutral beam production of very low vapour press. materials 78−70225
compensated Pierce instability 80−102606
compression of high-current electron beam in gas, on current pulse trailing edge 78−12789
computerised dosimetry calcs., linear accelerator electron beam parametrisation 79−83945
conference on electron, ion and proton beam technology, conf., Boston, MA, USA (29 May-1 June, 1979) 80−67927
continuous fluid flow operation in an electromagnetic field, variational principle, conservation theorem 78−42267
cooling of proton beam in storage ring 77−14281
counterstreaming 10 MeV electron beam profile and position monitor 77−83403
counterstreaming electron beams, plasma form. and oscill. excitation 77−27687
coupled Marx-Tesla circuit for production of intense relativistic electron beams 79−17558
current density distribution over electron beam cross section, calc. *(Russian)* 80−14276
current meas., fast response magnetic loop current monitor 79−35791
curved electron beam system with strong deceleration at collector region, optimisation 78−74106
cyclotron maser instability, self-consistent theory for intense hollow electron beams 79−4129
cyclotron maser instability for general mag. harmonic number, appl. to electron beam propag. 79−4130
cyclotron maser instability in intense hollow electron beams, effect of energy and axial momentum spreads 80−1782
cyclotron radiation from oppositely directed electron beams 78−78874
cyclotron wave coupling, interpenetrating electron waves 78−66735
cyclotron-wave instability freq. up-shift, on a relativistic electron beam 79−22883
cylindrical diode, magnetically insulated, cathode plasma props., electron beam prod. *(Russian)* 77−74550
cylindrical-mirror electrostatic analyser for beta spectroscopy of beams 80−63446
deceleration in hollow cathode, plasma production and props. 79−27794
deceleration in longit. mag. field, energy recovery system 77−49807
deep stopping in recuperator, using transform. of beam shape 77−65562
Defelction distortion in scanning electron-beam systems 78−74835
deflected electron probe, correction of distorted spot shape using dynamic focusing and stigmator 80−57427
deflection error assessment, expt. technique 80−78757
deflection system for adjustment, scanning of electron beams 79−2878
diagnostic probe, for intense electron beams 78−12787
diamond, ultrarelativistic electron beam self acceleration probability 79−86819
dielectric, photon induced relativistic band struct. 77−32462
differential evacuation system for electron beam emission into atmosphere 79−35890
diffraction, at two-element array of bars, re-expansion method, for rigorous soln. *(Russian)* 78−17848
diffraction, stationary problem in non-homogeneous media 80−68
diffusion along mag. neutral line in quadrupole 80−6218
diffusion of electron pencil beam, one-parameter model of spatial distrib. 79−54081
diode, repetitively pulsed 79−76164
diode, space-charge limited, rigorous Poisson eqn. soln. for electron beam 77−50605
diode accelerator, electron beam power increase by inductive accumulator 78−33339
distribution function in focusing mag. field *(Russian)* 78−82898
dose and shielding parameters of electron-photon stray radiation 77−57755
dose profiles, cumulative normal distrib. model 79−88199
dosimetry, 15 to 39 MeV, cavity displacement effect and reference depths, using LiF 77−2057
dosimetry, 15 to 50 MeV, calorimetric and ionometric meas. in graphite 77−2052
drift and current flow along quadrupole mag. neutral line 80−1749
dynamic beam shaping, electron-beam lithography appl. 78−74834
dynamic deflection sensitivity in transverse magnetic field 78−86386
electron and positron depolarisation suppression in storage rings and cyclic accelerators 80−42882
electron bunching, scattering and bremsstrahlung in cryst. lattice in strong EM field 80−65113
electron guns, relativistic beam permeance *(Rumanian)* 77−46678
electron microscope beam energy broadening, Boersch effect 77−61164
electron storage ring, beam distrib. parameters using transport matrices 79−54725
electron storage ring coherent microwave emission fine struct. 78−78875
electron waves in plane periodic system, linear theory 80−48130
electron-photon cascades separation by scintillation counter system 78−78563
electrostatic deflection type electron analysers, electron refl. ghost lines, energy loss reduction 80−18050
electrostatic instability in rippled magnetic field in circ. waveguide 80−19588
EM wave emission, from modulated electron beams, IR region *(Italian)* 77−3525
EM wave scattering, from relativistic electron beam in waveguide 79−10249
energy broadening, Boersch effect 80−69308
energy broadening analysis 80−5670
energy broadening in electron-beam system, Boersch effect anal. 80−1114
energy coupling to expanding thick-shelled target 80−96365
energy exchange between free electrons and EM waves in vacuum, anal. 80−18975
energy flux density meas. using portable graphite calorimeters 80−307
energy monitoring, by in-line C and graphite monofilaments 77−61159

electron beams continued
energy spectra in plasma focus discharges 80—24262
energy spectrum analysis, electrostatic system *(Chinese)* 80—43249
energy spectrum monitoring in low-energy electron accelerators 80—68994
energy spectrum of fast beam, meas. 80—895
energy spread as result of Cherenkov diffr. 78—5407
equations of state diagrams, decompensated and partially compensated beams 80—18985
Excede 2 test, artificial auroral expt., ground-based optical meas. 78—89038
explosive instability in electron beam-plasma system 77—84454
explosive instability of electron beam in helical resonator, RF emission 79—55520
externally maintained discharge with gasdynamic window for low energy electron beam 79—32843
extraction from pulsed plasma of hollow cathode discharge 78—12790
fast, transition from non-selfmaintained volume discharge to spark discharge *(Russian)* 79—23466
fast-pulsed, energy meas. bremsstrahlung absorption spectroscopy 78—49940
Febetron 707, field emission tube, electron pulse duration reduction 77—3530
field emission electron beams, two beam interference 78—63002
field reversing E-layers, translation and compression in magnetically insulated diode 80—14017
fine-focused, current distrib. meas. method 77—83799
flare stars, fast electrons hypothesis rel. to flare emission spectrum 80—67731
focus-deflection practical system for shaped electron beams 79—76572
focusing by laser beam fields 78—74833
focusing theory, nonlinear differential eqns. *(Chinese)* 79—31783
free electron laser, operation 77—46734
free electron laser sensitivity to electron energy reduction 79—94246
fusion compression targets, fuel preconditioning studies 79—81076
Garching Pustarex accelerator 79—76162
gas neutralised, self focusing, effect of self-elec. and mag. fields 78—50692
generalised relativistic Brillouin theory, appl. to infinite vacuum transmission line 78—87004
generation in coaxial vacuum waveguide, mag. self insulation breakdown *(Russian)* 78—1145
glow discharge, high-voltage, as electron gun 77—62428
glow discharge generated high-power pulsed beams, gas dynamics diagnostics appls. 78—63515
graphite calorimeter, multisection, for energy distrib. in high current relativistic electron beam 77—46456
guiding system including automatic capture circuitry 80—99005
gun design for producing high-intensity beam with rectangular cross section 78—93785
heavy ion collective acceleration at Univ. of Maryland 79—76163
helical electron beam in resonator of gyro device with uniform EM field, nonlinear eqns. soln. 79—81348
helical electron beam shaping using synthesis of axially symmetrical systems 80—309
helical electron beams, trajectory anal. with allowance for space-charge forces 79—86127
high current, energy spectrum in neutral gas 79—12885
high current diodes, mag. cut-off 77—47276
high current electron beam of TONUS accelerator, time struct. *(Russian)* 78—66434
high current particle beam prod. by low pressure spark discharges, accelerator 79—31247
high current relativistic beam prod., duration $>10^{-5}$ sec *(Russian)* 77—10135
high energy, production using proton synchrotrons *(Russian)* 79—41058
high energy beam prod., gas amplification of filament current 77—10139
high energy deposition from pulsed electron beams 78—54500
high intensity microsecond beam formation, in gun with plasma anode *(Russian)* 78—21271
high power beam generation, review 80—13988
high power microsecond electron beam, soft X-ray prod. 80—52378
high-current, meas. of energy spectrum 77—46470
high-current electron beam stability in mag. field in waveguide 78—66742
high-perveance electron beams with Brillouin focusing 77—83802
high-voltage subnanosecond electron beam generator 78—4733
hollow beam in magnetically insulated beam, characts. 80—5398
hollow beam pot. in magnetically insulated diode 80—70046
impulsed electron beam generator with linear shaper *(Italian)* 80—52793
industrial electron accelerators, beam energies above 150 keV, problem review 79—31243
injection system of Elektronika linear accelerator, triode gun anode modulation 79—67978
inner and outer problems, curvilinear coords. soln., axis with curvature and torsion 77—592
input phase characteristic nonlinearity effect on focal spot size 80—5678
instability, rot. nonneutral beam, propag. in inhomogeneous mag. field 77—83800
intense, avoidance of current limitations, fusion, ion accel. appls. 79—45898
intense, in ultrahigh vacuum, possible method of neutralisation 80—47145
intense electron beam propagation between two plane conductors 80—91744
intense microsecond pulses, prod. from dense plasmoids 79—90476
intense pulsed ion beam meas. by nuclear activation 78—74104
intense relativistic electron beam, $\nu/\gamma \sim 1$ diode characteristics 77—15249
intense relativistic electron beam generation by foilless diodes, simulation 80—63438
intense ribbon beam dynamics in self-mag. field 80—23614
interaction with microwave-frequency field, of planar gap 80—106431
interaction with slow waves over impedance-loaded surface *(Russian)* 77—31055
interaction with target, integral eqns. *(Ukrainian)* 80—32549
intersecting storage ring, electromagnet power supplies, types 77—42197
ion acceleration by space charge plasma waves in straight-line beam 80—103166
ion cyclotron resonance spectrometer, positive ion trapping in electron beam 78—21254

electron beams continued
ion density distribution, simplified anal. 79—41318
ion neutralisation, probe beam diagnostics 79—27157
ion source electron beam modulator automatic control system 79—72173
ionosphere, electron beam injection, dynamics study 80—4179
ionosphere, Feyerverk expt. electron beam injection optical obs. 77—13160
ionosphere, VLF plasma wave excitation due to electron beam injection 80—12603
ionosphere injection expts., electric potential of rocket *(Russian)* 78—93069
iris loaded waveguide relativistic electron beam interaction, electron energy distrib. space charge effects 78—46190
iris-loaded waveguide, inhomogeneous ferrite filled, autoacceleration 78—79441
JIKIKEN satellite, electron beam emission for magnetosphere beam-plasma interaction expt. *(Japanese)* 80—94655
laminar using high-current electron guns, formation for linear accelerators 78—74516
laser, electron beam controlled, electron beam parameter optimization and choice of foil 80—48269
laser, free electron, relativistic, rippled static mag. field, simulation, waves and instability 77—54686
laser beam possible freq. conversion by electron beam 79—68413
laser pulse amplification through energy exchange with electron beam via nonlinear radiation press. effects 80—95776
laser-electron beam scattering, intensity differential cross-section 77—71914
laser-to-microwave frequency division using synchrotron radiation 79—76562
limiting current of electron in mag. field of conical electron beam 78—90348
linear accelerator production of intense ns beam, space charge and radiation field effects 78—70654
linear electron-ion beams, particle density, longit. mag. field effects 77—50597
liquid metal sources, emission mechanisms 79—85845
longitudinal stability of electron beam in channel of magneto-dielectric *(Russian)* 77—71910
low atomic number foil target, anomalous energy dissipation of tightly pinched relativistic electron beam 80—29833
magnetic compression, high current relativistic beams 77—87876
magnetic compression and electrostatic refl. of high υ/γ electron beams 77—83398
magnetic compression of relativistic electron beams, transmission through mag. mirror 77—1012
magnetic electron deflection system, high accuracy, shielding ferrite tube 80—102602
magnetically confined, counterstreaming, instability suppression by externally introduced turbulence 79—32768
magnetically confined, spatially periodic electrostatic field form. 80—5677
magnetically insulated diode, controlling hollow electron beam current with shielding beam 80—9437
magnetically insulated vacuum power transmission lines, pulse propag. 79—85765
magnetically isolated annular relativistic electron beam 78—78037
magnetised beam, longitudinal stability, in periodic metal-dielectric system 77—65563
magnetized, flowing through cavity, self-consistent potential calculation 80—91743
magnetosphere, counterstreaming electron beams at altitudes of 1 R_E over auroral zone 80—67474
magnetosphere, substorm electron beams, temp. characts. 79—101027
maser, cyclotron-type, high-current, relativistic, exptl. characts. 80—9844
merged electron-ion beam experiment, determ. overlap integral from differential-scanning meas. 80—87282
merged electron-ion beam profile scanning system 79—35891
microsecond, high-current, production in diode with mag. mirror, device characts. 77—82642
microtron, beam, extraction and transportation system 77—65061
microtron, orbit correction scheme 77—65366
microwave backscatter from intense relativistic electron beam 77—38794
microwave coherent scatt. from relativistic electron beams 77—42477
microwave generation, using sheet relativistic electron beam 77—34800
microwave generation and suppression in hollow rotating electron beam 77—83797
microwave ponderomotive effect on transverse electron beam, expt. 79—13886
mirror electron microscopy, contrast form. 80—68299
modulated electron beam, non-linear oscillation theory *(Russian)* 80—106898
modulation, by cylindrical capacitor, mechanism 77—49808
monochromatic photon beam generation by high energy electron beam *(Japanese)* 78—74821
monoenergetic, energy recuperation collector 80—87281
multiplexing electron beam patterns using single-crystal thin films 79—89041
nanosecond electron beam, particle dynamics in linear accelerator 79—26787
NBS positron annihilation in flight facility, positron beam calibration 79—31306
neutral molecule motion control by electron beams 80—99582
neutralized relativistic electron beam with current above Alfven limit 80—43248
nonlinear frequency shift, stationary waves in electron beam 80—18984
nonneutral electron beam propagation in inhomogeneous mag. field, stability 77—24175
nonperiodic bandlimited signals in three dimensional electron flow, general relations 79—68360
nonrelativistic, EM conversion in plasma filled waveguide 77—84455
nonrelativistic, injection into drift space 79—895
nonuniform elliptic, inside hollow cond. of elliptic cross-section, elec. pot. and field *(French)* 77—50582
optical frequency electron wave beat-driven free electron laser 80—43315
overlapping, use for interial confinement fusion 80—91242
parameter meas. collector plate amplifier 79—75653
parameter measurement by determining ionisation of residual gas 79—97915
particle-beam fusion experiments for fusion ignition, pellet compression and long solenoid approaches, breakeven experiments 80—47720

electron beams continued
pendulum effect influence on optical modulation of diffr. electron beam in cryst. *(Russian)* 80—55219
periodic structures excitation with electron spot *(Russian)* 78—29892
picosecond pulse electron beam longitudinal emittance analysis 77—87872
pinching from discrete cathodes, for intertially confined fusion 78—50318
planar one-dimens. magnetically insulated electron flow for arbitrary canonical-momentum distrib. 79—86125
plasma, surface oscillation cyclotron excitation, electron beam cyclotron instability *(Russian)* 80—54008
plasma electron beam for vacuum metallurgy *(Japanese)* 78—18465
plasma filled channel, stationary states of cylindrical electron beam 79—55046
point focusing through different vacuum lines 79—45499
polarisation in storage ring by laser beam interaction 79—93860
polarised by radiative separation in inhomogeneous mag. field practicality 78—82076
polarised electron beams, production methods and current status of polarisation meas. 79—63836
polarised electrons, book 77—46679
positron annihilation prod. of photon quasi monochromatic beam at 600 MeV Saclay linac 80—5425
potential changes using two-electrode plasma probe *(Russian)* 80—1841
potential theory, use of non-orthogonal system of coordinates *(French)* 77—58245
Precede, artificial auroral expt., summarised results 78—89037
production, by localised source in focused discharge 78—58093
production, by Tesla transformer accelerator 78—326
production, hollow cathode discharge as electron beam generator 80—44039
production, using HV glow discharge, electrode surface effects 79—64955
production of sinusoidally modulated electron beams of high spectral purity 78—328
propagation by Z-pinch plasma 77—87874
propagation in dielectric guide due to space charge neutralisation 80—18716
pulsar radio emission from relativistic electron beams 77—5540
pulsar radio signals spectra and microstruct., relativistic electron beam model 78—65639
pulsars, ultrarelativistic electron-positron beams rel. to radio emission 78—12257
pulse energy loss in cold dense plasma 77—19725
pulse generator, repetitively pulsed electron beam system 80—68981
pulsed, 300 keV, 0.2-0.4 ns, in vac. diode, props. obs. *(Russian)* 77—79739
pulsed, measurement of current density distrib. and energy spectrum 80—63426
pulsed, picosecond, electron beams *(Japanese)* 79—27152
pulsed electron beam gun, kinetics and spectroscopy appl. 78—5413
pulsed electron gun, plasma emitter, ≥50 kA, ≥95% transmission coeff. 77—18134
pulsed source with cold cathode and beam extraction 77—74549
quadratic grouping of electrons directed by transversely inhomogeneous magnetostatic fields *(Russian)* 78—74822
quantum modulation in field of opposite EM waves 78—74188
quasi-static field of electron beam, ion accel. 77—71915
radiation flux parameters meas. by diaphragm method 78—86387
radiation therapy, treatment planning, depth dose scaling using computerised tomography scans 80—30899
radiation therapy appl. in treating deeply situated tumors *(Chinese)* 80—56209
radiative damping effect for ultrarelativistic channelled particles 78—67758
radiative polarisation of beams in VEPP-2M storage ring 77—18719
radiative polarization at ultra-high energies for e^- and e^+ beams in storage rings 79—72127
rectangular, scaling laws 78—5416
relativistic, charge neutralisation processes, air, He and H_2 press. depend. *(Russian)* 77—19668
relativistic, coherent submillimetre Cherenkov radiation generation 77—38788
relativistic, coherent X-ray emission 80—91739
relativistic, collective ion acceleration by cyclotron or space charge waves 77—24204
relativistic, compact/tubular, in vacuum channel, max. currents *(Russian)* 77—46677
relativistic, crit. current in mag. field in vacuum channel *(Russian)* 78—71016
relativistic, critical vacuum current, virtual cathode effect 78—25790
relativistic, diocotron instability 80—27853
relativistic, Doppler freq. conversion of microwaves, exptl. obs. 77—34799
relativistic, dynamics in relativistic cyclotron maser 77—68158
relativistic, electrostatic trapping in mag. mirror 77—24120
relativistic, EM instability and stopping power of plasma 80—92289
relativistic, EM wave coherent scatt., submillimetre wave generation 77—34798
relativistic, equilibria in vacuum without mag. guide field 77—14651
relativistic, fields excited near plane magnetoedielectric slab 80—18986
relativistic, free electron laser amplification in spatially periodic transverse mag. field 80—19014
relativistic, generation in foil-less diode 77—75015
relativistic, gradB transport, bunching and focusing 80—96345
relativistic, high current, microsecond discharge, prod. and radiation damage effects 77—13823
relativistic, high current, pulse length adjustment 78—65997
relativistic, high-current, self-focused, energy dissipation at focus 80—5674
relativistic, in conical diode, self-focusing 79—89840
relativistic, in gas, exptl. stand TEREK-1R for study 80—18053
relativistic, injected into air filled waveguide, X band gigawatt microwave pulse produced *(French)* 78—25781
relativistic, insulator flashover in HV vacuum transmission line, mag. effects 77—24236
relativistic, intense, collective proton acceleration in space charge well 78—9864
relativistic, intense, guiding with axial mag. field 80—87006
relativistic, intense, ion collective acceleration, localised pinch model 78—87460

electron beams continued
relativistic, intense, meas. of broad spectral EM wave energy generated 77—38786
relativistic, intense, rot. in plasma, μs microwave radiation bursts 79—73018
relativistic, intense, stimulated Raman radiation spectral props. 79—64163
relativistic, intense, subjected to rippled elec. field, stimulated Raman scatt. 79—98439
relativistic, ion accumulation caused by ion-ion interactions 80—5417
relativistic, laminar, characts., self-mag. field effects calcs. 77—50608
relativistic, laminar flow equilib., limiting currents 77—51224
relativistic, landing on equilib. orbit in toroid 77—68850
relativistic, localisation in upper atmosphere, stabilising effects *(Russian)* 80—21868
relativistic, mag. focusing, equilib. surface ripples 79—3618
relativistic, monoenergetic, neutral, config. and current *(Russian)* 79—98269
relativistic, passage at high current through matter 80—91745
relativistic, pinched, propag., for pellet fusion 77—68163
relativistic, propag. along a wire in vacuum guide 80—74291
relativistic, propag. in vac. and low press. gases 79—76569
relativistic, radially inhomogeneous unneutralised, linear theory 79—50201
relativistic, reduction in energy spread of nanosec. relativistic beam 80—5397
relativistic, single electrode monitor, position monitoring appl. 79—6216
relativistic, slow space-charge wave propag. 80—1115
relativistic, solid, vac. propag. 79—59625
relativistic, space-charge limiting current simulation 79—59626
relativistic, stationary state in ionised gas, force-free motion 79—13887
relativistic, stimulated coherent EM wave scatt. by longitudinal electron waves *(Russian)* 77—7542
relativistic, striations in density distrib. rel. to plasma column instability 80—24154
relativistic, strong mag. field, transverse energy determ. by bremsstrahlung 77—62344
relativistic, technique for amplitude and phase vel. meas. of slow space charge wave 78—54508
relativistic, theoretical scheme for axial compression 80—96367
relativistic, theory of dissipative Cherenkov instability *(Russian)* 77—47251
relativistic, unmagnetised, stimulated scatt. anal. of HF incident pump wave 79—77345
relativistic, vac. interface, EM surface waves 77—79734
relativistic, Vlasov equilib. 77—51225
relativistic, with inhomogeneous ion density, self-consistent model 80—43247
relativistic, with variable charge neutralisation degree, equil. state 80—59249
relativistic beam, high-current, reson. ion accel., nonlinear instabilities *(Russian)* 77—11329
relativistic beam, propagating in waveguide, excitation of slow cyclotron and space-charge waves 79—86118
relativistic beam in mag. field, microwave radn. 77—79735
relativistic beam in synchrotron, ang. spread of vel. using undulator radiation 80—14021
relativistic beam injection into drift cavity, pot. profile finite size particle calc. 80—18987
relativistic beam through metallic boundary, self-consistent pot. 78—82900
relativistic beams, meas. by beam-position pickup 77—65392
relativistic beams in vacuum lines, mag. self-insulation *(Russian)* 79—27158
relativistic charged particle beams in storage rings, soliton soln., phase locked states 78—50425
relativistic electron beam, 'peeling' on entering mag. field 78—66741
relativistic electron beam, enhanced deposition, mag. and elec. fields effects calcs. 77—31491
relativistic electron beam, in mag. field, reson. radiation 78—17852
relativistic electron beam, induction auto-correl. 79—22889
relativistic electron beam, propag., Poukey-Rostoker model 78—5412
relativistic electron beam, propag. in air, exploding beam preformed plasma column 77—87875
relativistic electron beam, propag. in strong mag. field *(Japanese)* 80—91737
relativistic electron beam, propag. in vac., ion accel. from anode plasma 80—47790
relativistic electron beam, self-pinched, production and focusing of intense ion beam 77—24206
relativistic electron beam, stimulated Compton scatt. *(Russian)* 79—86122
relativistic electron beam acceleration accompanied by beam focusing, for pulsed fusion 77—34054
relativistic electron beam collective ion acceleration, localised pinch model, simulation 78—9826
relativistic electron beam deposition, field-enhanced, bremsstrahlung prod. 78—29677
relativistic electron beam destruction and equilibrium in mag. guide 79—76171
relativistic electron beam device, intense, high-power millimetre radiation generated 77—83795
relativistic electron beam diode, low impedance, pinch profile, X-ray diagnostics 77—24207
relativistic electron beam diode, medium current 77—46443
relativistic electron beam dissipative Cerenkov instability, oscill. modes, quasi-linear theory *(Russian)* 78—59564
relativistic electron beam energy spectrum, time evolution, drift tube press. effect 77—49806
relativistic electron beam focusing using axial loads 78—18464
relativistic electron beam in magnetised plasma, relax. processes, nonlinear theory, instability *(Russian)* 80—103162
relativistic electron beam in plasma, relaxation *(Russian)* 80—103161
relativistic electron beam in stimulated coherent scatt. of EM wave *(Russian)* 80—102601
relativistic electron beam injected into drift tube, limiting currents 79—10699
relativistic electron beam injection, higher energy density electron cloud form. *(Russian)* 77—3979
relativistic electron beam instability, passage through dense gas, energy spectrum *(Russian)* 77—3529

electron beams continued
- relativistic electron beam pinch formation in low impedance diodes 77—72510
- relativistic electron beam pinching and combination for inertial confinement fusion 78—50319
- relativistic electron beam propag. in circular waveguide, microwave generation 80—48128
- relativistic electron beam relaxation in dense gas, radiative energy transfer 80—69968
- relativistic electron beam ring, landing on equilib. orbit 77—35375
- relativistic electron beam transport, plasma filled channel, dissipative wall instabilities, theory 79—86123
- relativistic electron beams, appl. to large payloads launching into Earth orbit 79—21135
- relativistic electron beams simulation 79—26789
- relativistic electron beams with finite energy spread and improved emittance, development and investigation 80—91741
- relativistic electron bunch instability, in reson. storage chamber 77—54381
- relativistic electron oscillator stream in EM field, explosive instability 80—53197
- relativistic electron rings, translation and stacking 77—87877
- relativistic electron-positron counterstreaming beams plasma, radiative collapse to ultrahigh densities 79—60188
- relativistic free-electron wave generators, electrically pumped 80—91742
- relativistic high current electron beam parameters from bremsstrahlung yield meas. 79—93861
- relativistic high current nanosecond beam, transverse instability in linear accelerator 77—83180
- relativistic hollow beam within conducting coaxial screen, reduction factor calc. *(Russian)* 78—33658
- relativistic in circular waveguide, radiation efficiency in periodically inhomogeneous mag. field 77—23608
- relativistic inhomogeneous electron beam, space charge oscills. 80—78759
- relativistic intense solid beam, cyclotron maser instability 79—55494
- relativistic mirror feature, perp. temp. effects 80—78749
- relativistic polyhelical electron beam in open waveguide, diffraction radiation *(Russian)* 77—75398
- relativistic ring, facilities at Nagoya University Plasma Physics Institute 78—5919
- relativistic rotating, filamentary instabilities 77—76187
- relativistic self-focused electron beam, hose instability meas. 78—83544
- relativistic self-pinched electron beam, Bennett profile, resistive hose instability 78—83543
- relativistic sheet electron beam interaction with slow-wave structure 77—38795
- relativistic stabilised electron beam in toroidal geometry for collective accelerators 80—5401
- relativistic tightly pinched beam, obs. via X-ray streak camera 77—49818
- resonance electrons beam, cyclotron interaction with VLF wave packet 79—53652
- ribbon electron beams, equilib. and stability conditions *(Russian)* 78—70220
- rockets, payload charge neutralisation during electron beam emission, laboratory studies 80—77258
- rod pinch diodes, intense electron-beam pinch form. and propag., ion generation 79—14589
- rotating relativistic electron beams, electrodynamic principles 78—71019
- rotating relativistic theory in appl. static mag. fields 78—9309
- scanning system, variable-aperture projection, design 78—74836
- scattering of low-energy electrons on micron-size pinholes, surface pot. mapping 79—81351
- screw, synthesis of systems formation in cyclotron resonance masers *(Russian)* 78—17889
- secondary emission monitor of accelerated electron beam current 78—78033
- self acceleration in ferrite accelerating structure 77—23609
- self magnetically insulated electron flows, line voltage determination 80—69318
- self-acceleration, due to exploding conductor *(Russian)* 77—13824
- self-acceleration expts., regulation of magnetization of ferrite 80—63425
- self-acceleration of intense beam, at trailing edge excitation of exciting system 77—75407
- self-bunching in resonantly absorbing medium, radiation amplification feasibility 80—102605
- self-focused, relativistic, filamentation instability 80—74289
- self-focusing decline by gas breakdown, avalanche and plasma cond. effects 78—18420
- self-focusing in ferrodielectric channel, nonlinear eqn. anal. 77—61905
- self-focusing of pulsed high-intensity beam in low press. gas, expt. obs. 80—32899
- SEM beam splitting by HF square-wave deflection 79—75654
- SEM with electron energies up to 5 MeV 79—80728
- solar corona, electron beam dynamics in plasma 77—78759
- solar corona, electron beam injections rel. to type IV radio burst quasiperiodic struct. 80—62097
- solar corona, scatt. hypothesis for type V radio bursts 77—45378
- solar corona, three dimensional Langmuir wave instabilities rel. to type III radio bursts 77—2404
- solar flares, electron beam characts. rel to X-ray and UV emission 78—65598
- solar flares, electron beam diagnostic 80—26827
- solar flares, electron fluxes rel. to optical, X-ray and radio emission 78—89156
- solar flares, hard X-ray sources diagnostics 78—89159
- solar flares, reverse currents effects on beam dynamics and emitted X-ray bremsstrahlung 80—51711
- solar type III radio bursts, beam struct. rel. to fundamental emission 80—36603
- solar wind, electron beam energy gain due to interaction with whistler soliton 77—9649
- solar wind, nonlinear Langmuir waves during Type III radio bursts 78—93173
- space charge effects in electron probe devices 79—27154
- space charge wave propagation on rippled electron beams 77—3933
- space-charge limiting current, upper bound for annular electron beams 80—43245
- spatial charge and beam radius determination *(Russian)* 80—74290
- spatial electron beam formation, paraxial approx., electrodes in electron gun appl. *(Russian)* 78—17854
- spatial electron beam-matter interaction, model calcs. for Cu *(German)* 80—84815
- spatially modulated electron beam, parametric instability, periodic mag. field effect 80—87285
- spin-polarised electron source, features, appls. 79—17559
- spiraling beam, cyclotron-harmonic wave propag. 77—19685
- spot measurements and beam divergence 400 keV electron accelerator 80—877
- stability and current loss in magnetic insulation 79—94141
- stable extraction of intense beam from plasma, neutralisation method 77—24104
- stimulated collective EM scatt. from magnetised relativistic electron beam 77—38791
- stimulated Compton scatt., X-ray regime, growth time limitation 77—7049
- stimulated EM shock radiation for far IR and submillimetric wave generation 77—38997
- stimulated EM shock radiation with frequency up-conversion 77—38996
- stimulated scatt. with intense relativistic electron beam and zero frequency pump 77—38995
- storage rings, VEPP-2M, -3 and -4 as synchrotron radiation sources, beam characts. 78—62667
- striations, in strong current beam 79—896
- strong-current electron beam in low-press. gas, front vel. meas. 78—5415
- submillimetric magnetoresonant scatt. from relativistic electron beams 77 38792
- subpicosecond pulse generation and meas. 78—65996
- synchrotron with cyclotron preaccel., beam intensity 77—61642
- tetrode gun, transport of high-energy, high-power electron beams 78—89587
- thermal equilibrium properties of an intense relativistic electron beam 79—86126
- thermal particle motion effect on autoresonance acceleration process *(Russian)* 80—69007
- thermal sensitive paper for intense, relativistic electron beam dynamics diagnostic 78—83619
- thermionic converter, fast electron beam relax., cross sections energy depend. 80—43939
- thermionic gun with beam extraction through Al foil 77—13817
- Thompson scattering for electron beam and plasma diagnostics *(Russian)* 80—54031
- threshold temp. sensitivity of interelectrode gap determination 78—78890
- Torus accelerator, transport of high current relativistic electron beams in large vols. *(Russian)* 78—82544
- trajectory of electron in electron beam source for vaporisation *(Russian)* 78—33657
- transmission through vac. tight Al and Ti foils, 150-400 keV 77—50604
- transport through gas, high-current microsec. beam 79—22890
- triode with explosive-emission cathode, variable current density 79—72475
- turbulent perturbations, caused by crossed mag. fields 79—10252
- two counterstreaming electron beams, self-consistent computation of explosive instability 78—22494
- two-beam gain saturation in an electron-ion beam without capture of electrons 78—94919
- ultrarelativistic electron bunch in free space, lateral spreading 80—53196
- uncompensated, slipping flux instability due to transverse potential drift *(Russian)* 78—71026
- undulator radiation, beam parameters effect on spectrum and polaris. characts. 77—75400
- undulator radiation, coherence, directional pattern, wavelength spread, polaris. 79—55043
- undulator radiation theory, coherence, extension to short wavelengths 79—55042
- unneutralised intense relativistic electron beam propag. in mag. field 77—46673
- vacuum beam diodes, repetitively pulsed, lifetime and stability 80—63386
- wave amplification by spatially periodic mag. field, space charge waves 77—19158
- waveguide partially filled with dielectric, relativistic electron beam interacting with EM wave 79—59622
- waveguides, artron effect (self-reson. electron deceleration) 77—6991
- waves, Doppler shift calcs. *(German)* 80—18982
- X-ray source, high power microsecond electron beam 80—52378
- X-ray source spectral distribs., FLASH code 79—22524
- e^+e^- storage rings, expt. review of beam polarisation 79—63837
- GaAs:Zn (110), spin polarised electron production by photoemission from Cs-O overlayer 79—95903
- KD_2PO_4 crystal electron-beam spatial light modulator, resolution 80—74503
- LaB_6 cathode, directly heated, for electron beam instruments, design and optimisation 78—93783

electron bombarded semiconductor devices
- low light level performance of CCD in electron-bombarded mode 77—39092
- solid-state array and camera tube imagers compared 77—39090

electron capture
- *see also charge exchange; electron attachment*
- A^{Z+}+atom, electron capture cross section into arbitrary principal shell, approximation scheme 79—18287
- alkali atom+H^+ charge exchange, eikonal approx. 80—32830
- alkyl halide, chem. struct. determ. using electron capture response 77—21428
- atmospheric N_2O conc. meas. using electron capture-gas chromatography technique 77—9531
- atom+ion, double K-shell capture, three state, two-centre at. expansion method 79—68315
- atom+ion, electron capture, non relativistic theory and Coulomb pot. anal. 80—32804
- atom+ion collisions, continuum photon emission, radiative electron capture, mol. orbital emission 77—42401
- atom+ion collisions, electron capture, quasi-molecular binding corrections 78—90287
- atom+ion collisions, impact parameter method 78—33591
- atom+ion collisions, MO, radiative electron capture X-ray emission 77—19043
- atom+ion multielectron collisions, charge transfer at intermediate energy, atomic model 80—91652

electron capture continued
- atom-ion collisions, electron capture into arbitrary principal shells of energetic projectile ions 79—89777
- atomic and molecular collisions, book 80—27058
- atomic electron l-shell Coulomb ionization by heavy charged particles 79—94073
- atomic inner shell ionisation phenomena, conf., Freiburg, West Germany (March.-Apr. '76) 77—27040
- atomic orientation production by electron capture in beam-target interaction, semiclassical model 80—9723
- atoms and highly charged ions, charge exchange 78—62913
- bare ion+H-like atom, inner-shell electron capture, 2nd Born effects 80—48085
- bare ion+hydrogenic ion, forward electron capture, third Born approx. calcs. 78—58782
- beam-foil interaction, electron capture by protons, prod. of circular polarisation 77—3453
- benzenes, substituted, gaseous, negative ion states, electron transmission spectra 77—31007
- bound states, beam-foil excitation and decay near ionis. limit 80—9552
- charge capture to continuum, differential cross-section, cusp asymmetry 79—94082
- charge capture to continuum, differential cross-section, cusp asymmetry and second-order Born term 79—94083
- complex ions, radiative recomb. 78—17782
- continuum electron capture at high vels., non-relativistic differential cross section determ. 79—3558
- crystal lattices, atomic collisions of channelled ions, resonant coherent excitation 80—15170
- cytochrome c_3—hydrogenase, reduction kinetics, Mossbauer spectra 80—67031
- detector theoretical model 77—40620
- diatomic clusters, break-up in thin films, particle energy distrib., central peak nature 80—50490
- doubly charged negative ions, electron impact 77—31006
- education, electron-dipole system, min. dipole moment for binding, historical development 77—78926
- electron capture processes in ion-atom collisions 78—70930
- electronic and at. collisions, conference, Kyoto, Japan (Aug.-Sept. 1979) 80—62394
- fast ion+atom collisions, one electron charge transfer and capture 78—70931
- fast projectiles, electron capture into n,l excited states 80—23543
- ^{57}Fe, isomer-shift calibration by lifetime variations in electron capture decays of ^{52}Fe 80—75902
- fully ionised heavy ions, scaling of electron capture in light gas targets, low MeV energies 79—64102
- n-GaAs:Cr(Si), deep-level extrinsic photocond. response, decay at 4.2K 80—2420
- H^++Mg collisions double electron capture 78—58777
- heavy ion+at. collisions using GSI linear accelerator, X-ray production, appls. 77—19041
- heavy ion+atom, radiative electron capture, target thickness depend. 78—58778
- heavy ion beam-foil spectra, ion equilib. excitation, density effect 77—19056
- heavy ion collisions, radiative electron capture, line profiles 77—14565
- heavy ions passing through gas or solid target, electron capture effect on X-ray emission 77—27169
- highly charged atom+ion, slow collisions, one-electron capture 78—58776
- hydrocarbon, (C_nH_{2n+2}, n=1-4)+H^+, electron capture and loss cross-sections 1-20 keV *(French)* 77—38728
- hydrogenic ions, electron capture by charge particles at relativistic energies 80—102565
- inert gas atom, charge capture to continuum, differential cross-section, cusp asymmetry 79—94082
- inert gas atom +H^+, electron capture, charge-state distrib. 80—32814
- inert gases+Ar^{6+}, collisional excitation, excitation cross sections 79—98209
- inner shell capture by fully stripped ions 77—54607
- ion+atom, intermediate energy, electron capture cross-section calcs. 78—42206
- ion+ion mutual neutralisation rates, approx. scaling formula 79—72411
- ion collisions, electron capture, atomic excited state polarisation, optical detection 80—58377
- ion-atom and ion-solid collisions, continuum electron capture and loss, cusp spectroscopy of forward peak 80—14201
- ion-atom collision, electron capture, at. expansion method 79—45833
- ion-atom collision, radiative charge exchange, high energy 78—55234
- matter in nuclear statistical equilib., electron captures 79—92663
- molecular electron dissociative capture, vibr. struct. of resonances 77—34770
- molecule, polar, slow electron capture and rot. excitation 79—81287
- multicharged ion and nucleus electron capture during collisions *(Russian)* 80—87850
- multicharged ions, classical trajectory eikonal approx. 80—69233
- multielectron target+multiply charged ion, electron capture, review 80—63812
- multiplet lines emitted after beam-surface interaction, polarisation calc., time development 80—14216
- multiply charged atom+H, electron capture, unitarised distorted wave approx. 80—63814
- multiply charged ion, electron capture into different excited states in plasma 80—64679
- multiply charged ion+atom, autoionisation, electron and photon emission 80—63813
- multiply charged ion+one-electron target, electron capture, review 80—63811
- multiply charged ions+atoms (molecules), electron capture processes 77—42402
- negative ions, form. processes and props., review *(Japanese)* 80—53127
- nucleus+hydrogenic atom electron capture, ultrarelativistic limit relativistic corrections 80—14230
- orbital angular momentum transfer to nucl. spin polarisation in external mag. fields 80—14217
- plasma chromatography and electron capture detector, comparison between two techniques 80—61176
- plasma containing multiply charged ions, two-electron capture processes 80—43854

electron capture continued
- proton fast channelled continuum states, Gaussian flux peaking calcs. of electron capture, appl. to Au 79—86827
- pulsed electron capture detector measurement of ions using atm. press. ionis. mass spectrometry 79—92017
- quinones-Zn porphyrin, quinones sensitised reduction in vesicle systems 80—71897
- radiative capture anal. by ion channelling techniques 77—35350
- radiative capture and Galilean invariance 77—38730
- radiative capture by atomic ions, cross sections 77—83725
- radiative capture of an electron of a target atom by multiply charged ions 80—5617
- radiative electron capture, photon ang. distrib., retardation effects 79—41234
- radioactive decay lifetimes, influence of chemical environment, review 79—75911
- Rydberg state atom+ion, electron capture, asymptotically high impact vel. 79—54965
- second Born contribution, obs. methods for high impact vels. 78—78803
- single electron capture cross-section 79—59560
- slow atomic collision, electron detachment, energy spectrum and isotope effects *(Russian)* 77—30984
- solvated electron reaction rates in alcohols and water 77—25259
- spectroscopy, technique for surface science and ferromagnetism 80—92766
- spinel solid solutions, $A_xB_{3-x}O_4$ type, quasichemical method of cluster components, electron exchange allowance 79—51475
- l-thioproline single cryst., X-irrad., ESR and ENDOR study of radicals 80—45528
- transfer cross-section, second Born approx. 80—48080
- 2,4,6-tri-tert-butylnitrosobenzene, reactions in γ-irrad. tetrahydro-2-methylfuran glass 78—10776
- upper atmosphere, cross sections calc. 79—5693
- Ag latent image particles, electronic effects 80—82840
- Ag, radiative electron capture by channelled O ions 79—77658
- Ag(I) ions, in methyl cyanide, electron loss and capture, ESR spectra 79—33531
- Ar purification system and electronegative impurity conc. meas. instrument 80—32571
- Ar^-, electron capture expts. to search for long lived states 79—72410
- Ar+H^+, K- and L-shell electron capture, 1-15 MeV 77—54607
- Ar+multicharged ion collisions, one electron capture from inner shells 80—58376
- Ar^{2+}+Ar (Kr)(Xe), single electron capture excitation, photon emission, VUV spectroscopy 80—58379
- Ar^{2+}+Na, Ar^+ form, electron capture, Ar^+ excited states relative population distrib. 80—23544
- Ar^{2+}+Na collision, single electron capture into Ar^+ excited states, 0.2-12 eV, emission cross section 80—48071
- Ar^{2+}+Na collision, single electron capture into Ar^+ excited states, relative population distrib. 80—48072
- Ar^{2+}+Ne(Ar)(Kr) single electron capture cross-section 77—88550
- Ar^{6+}+H_2 collisions, excitation and ionisation 80—78683
- Ar^{x+}+Kr(N_2), (x=2-7), electron capture cross sections, 10-110 keV 77—6923
- B^{q+}+Ar(He)(H_2), keV electron capture cross section 80—14229
- Ba+H^+, electron capture, single and double, 1-100 keV 79—68313
- C and C^+, one-electron capture cross sections in alkali metal vapours 79—59553
- C+H^+, electron capture in foils 78—42203
- C+H^+ collision, electron capture cross section 80—63804
- C^++H(H_2), 0.1-13 keV electron capture cross-sections meas. 79—36761
- C^{2+}+H(H_2), electron capture cross-sections, 0.5-14 keV 78—42205
- $C^{3,4,5+}$+H_2, single and double electron capture cross sections, (0.3-1.2)10^8 cm s^{-1} 77—34756
- C^{6+}+Ar, bound- and continuum-state electron capture in gas, strong correlations 80—9730
- C^{6+}+Ar, electron capture to continuum states, forward ejected electron spectra 79—45831
- C^{q+}+Ar, continuum electron capture and loss, 1.6-2.8 MeV/A 78—46443
- C^{q+}+Ar, continuum electron capture, projectile vel. and Z depend. 78—55222
- C^{q+}+H(H_2), q=1-4, single electron capture cross sections 78—55233
- C^{x+}+He, electron capture, K X-ray emission ang. distrib. 77—57919
- CH^+, continuum electron wavefunction, electron capture width 78—78805
- CO, dissoc. attachment, differential cross-section meas. 77—50549
- CO_2-N_2-He-O_2 discharge mixture, three body electron attachment to O_2 80—64779
- $^{12}C^{n+}$, partially stripped, energy straggling in thin Al foil, 3-36 MeV 79—41237
- Cl, multiply-ionised, radiative electron capture on impact with Ca and Ni foils 77—6916
- Cl^{n+}+Cu, effect on projectile charact. X-rays and REC of target thickness 79—45662
- Cl^{n+}+Cu film on C foil, X-ray production, radiative electron capture 77—19063
- Cl^{q+}+Cu, K X-ray production and radiative electron capture, fluoresc. yield determ. 80—99553
- Co complex, [^{57}Co(1,10-phenanthroline)$_3$](ClO_4)$_2$.2H_2O, time differential Mossbauer spectra, aftereffects 78—27131
- $^{57}CoMn_2O_4$, after effects of orbital electron capture 79—73870
- $CoSeO_4$, electron capture and γ-radiolysis, radn. damage 80—16705
- $^{57}CoY_2O_4$, after effects of orbital electron capture 79—73870
- Cs+H^+(H), single-electron capture total cross sections 80—91656
- Cu+C^{n+}, radiative electron capture, target electron momentum distrib. 78—1075
- D^++Ar, electron capture to continuum states, forward ejected electron spectra 79—45831
- D_3^++Cs, electron capture to D_3^- and D_3^0 repulsive states 79—59563
- D^0(D^+)+Cs, D^- formation, ang. distrib., total cross sections 77—529
- ^{165}Er decay parameters and whole-body dose, for radioisotope scanning 77—70529
- F^{8+}+He, X-ray prod. cross sections resulting from electron capture and electron excitation of F^{8+} ions 79—3557
- F^{9+}+Ne, double K-shell electron capture, theory 79—68315
- F^{q+}+He, (q=1-9), X-ray prod. by electron excitation, ionisation and capture 79—76379
- F^{q+}+Ne, radiative electron capture X-ray profiles from fast collisions, calcs. 79—49975

electron capture continued
$F^{x+}+He$, electron capture, K X-ray emission ang. distrib. 77–57919
$Fe^{n+}+H(H_2)$, 50-1200 keV amu^{-1}, impact ionis. and electron capture cross-sections 78–42204
$FeSeO_4$, electron capture and γ-radiolysis, radn. damage 80–16705
GeX_4, ($X=Br,Cl$), electron impact dissoc., low-energy reson. capture 78–9263
H atom, by ions, charge depend. of cross-section, continuum distorted-wave approx. 77–68110
H like atom alignment due to electron capture in particle-atom collisions *(Russian)* 80–106379
H, one-electron capture by fast multiply charged ions, q^3 scaling 80–91658
H, positron charge exchange, positronium form., two state approx. 77–79710
H, positron scattering, positronium formation 79–89772
H^+, electron capture from Si foil, cross-section calcs. 78–95623
H^+ electron capture in gas, calc., and s-p coherence quantum beats 79–89773
H-like atom+bare ion, electron capture to continuum, cross-section cusp 78–90289
$H+{}^3He^{2+}$, electron capture at impact energies below 10 keV 78–50633
$H+{}^4He^{2+}$, electron capture and charge exchange cross sections 77–68108
$H+B^{4+}(C^{5+})(O^{7+})$, excitation distrib. following electron capture 79–36763
$H+B^{q+}(C^{q+})(N^{q+})(O^{q+})$, ($2\leq q\leq 4$, 5), cross sections at keV energies 80–78705
H+completely stripped positive ions, electron capture 77–23559
$H+H^+$, electron capture, 25 to 200 keV 77–88551
$H+H^+$, electron capture in high-energy approx. 77–42400
$H+H^+$, electron capture in 3s level, distortion approx. 80–37876
$H+H^+$, fast proton total electron capture cross section, fixed scattered approx. 79–22819
$H+H^+$, relativistic classical theory of electron capture 80–18920
$H+H^+(He^{2+})(Be^{4+})(O^{8+})$, electron capture into n, l levels, 100 keV/amu 79–22826
$H+H^{2+}$, electron capture in 3s level, distortion approx. 80–37876
H+H(inert gas), negative ion form. 77–30988
$H+He^{2+}$, electron transfer, plane-wave factor, mol. state treatment 80–63807
H+He-like ion, (of B, C, N and O), electron capture cross-sections 79–59559
H+heavy charged ion, total electron capture cross section charge depend. oscill. behaviour 78–66656
H+Li-like ion, (of B, C, N and O), electron capture cross-sections 79–59559
H+positron, charge exchange, excited positronium states form. 78–58873
H+proton, high-Rydberg state high-impact-velocity forward charge transfer as classical process 79–22824
H+slow doubly charged ions, one-electron capture 80–32828
$H+Xe^{n+}(Ar^{q+})(Fe^{q+})$, electron capture by heavy multicharged ions at low velocities total cross sections meas. 80–99548
$H+Zn^{2+}(Cd^{2+})(B^{2+})(Mg^{2+})(C^{6+})$, electron capture by slow ions, pseudo-crossing 80–43176
$H^-+{}^4He^{2+}$, electron capture cross sections 79–10198
H^-+H^+, electron capture, continuum distorted wave calcs. 78–50635
H^0+N^{3+}, electron loss cross section 80–63805
H^++alkali metal, valence and core electron capture collisions 79–94081
H^++atom, electron capture, two-state atomic expansion 78–62912
$H^++CO(CO_2)(N_2O)$, electron capture into $n=3$ states, 2.2-8.2 keV 79–50129
$H^++C(N)(O)(Ne)(Ar)$, electron capture cross sections 78–62912
H^++Cs, electron capture, H metastable fraction of $n=2$ population 77–30988
$H^++Cs \rightarrow H(2s)+Cs^+$, near reson. charge transfer, low energy 79–54964
H^++Ge collisions, electron capture cross sections 77–6922
H^++H, capture cross sections, Faddeev anal. 77–27178
H^++H, excitation and electron capture, impact parameter calc. 78–33591
H^++H, ionisation and electron capture to continuum 80–58366
H^++H_2, electron capture cross-section, anal. evaluation 79–36756
H^++H_2, electron capture into ground and excited s states 79–76509
H^++H-like ion, electron capture, Coulomb-Born approx. 79–45838
$H^++H(H_2)$, electron capture, H(2s) cross section meas. 79–72386
H^++H(He)(Ar), K-electron capture, cross section scaling, high energy 79–41236
$H^++H(1s) \rightarrow H(1s)+H^+$, electron capture at relativistic energies, scatt. amplitude 80–1061
$H^++H(1s) \rightarrow H(nl)+H^+$, cross-sections, continuum distorted-wave approx. 77–68108
H^++He, 1-1000 keV, cross-sections by charge-transfer eqns. 77–75294
H^++He, double electron capture, close-coupling approx. calcs. 77–71868
H^++He, electron capture total cross sections 78–5322
H^++He^+, ground-state electron capture cross-sections, Coulomb-Born calcs. 78–42166
$H^++He(Ar)(Kr)(O_2)(H_2)(N_2)$, 2.2-8.2 keV, $H(n=3)$ form., absolute cross sections 77–34755
$H^++He(Ar)(O_2)$, charge transfer to $H(n=2)$, mixed parity elec.-dipole oscillations 79–31678
H^++He(Xe)(Kr)(Li)(Na)(K), electron capture cross sections 79–86061
$H^++He(1s^2)$, K-shell electron capture collision, static pot. effect 80–91660
$H^++He(1s^2) \rightarrow H^*+He^+(1s)$, continuum distorted wave approx., total cross section 77–68109
H^++inert gas, binary encounter calc., cross section calc. 79–72412
H^++inert gas, charge transfer into excited states, 10-150 keV, target at. struct. depend. 79–45830
H^++Kr(Xe), electron capture into 3s state, cross-section meas. 78–42209
H^++methane, (Ne), (Ar), inner shell electron capture cross-sections 79–76510
H^++multielectron atom, fast collision, electron capture, differential cross section calcs. 78–94318
$H^++O_2(N_2)(Ne)$, K-shell capture cross-section, Auger effect 78–33602
H^++Si collisions, electron capture cross sections 77–6921
$H_2{}^+$, ion beam surface interaction, H^- formation by reson. electron capture 80–40691

electron capture continued
$H_2+{}^3He^{2+}$, electron capture at impact energies below 10 keV 78–50633
H_2+Fe^{+q} collisions, 3.4 MeV/nucleon single electron capture and loss cross sections 77–83726
H_2+H^+, electron capture probability 78–58808
H_2+He-like ion, (of B, C, N and O), electron capture cross-sections 79–59559
H_2+Li-like ion, (of B, C, N and O), electron capture cross-sections 79–59559
$H_2+O^{n+}(Fe^{n+})(Mo^{n+})(Ta^{n+})(W^{n+})(Au^{n+})$, single electron capture cross-section 79–59560
H_2+slow doubly charged ions, one-electron capture 80–32828
H_2+X^{Z+}, $Z\geq 4$, 1-20 keV, electron capture 80–37875
$H_2+Xe^{n+}(Ar^{q+})(Fe^{q+})$, electron capture by heavy multicharged ions at low velocities total cross sections meas. 80–99548
$H_2{}^++He(Kr)(Xe)$, collisional dissociation, ion-pair prod., negative ion prod., cross sections 77–14529
$H_3{}^+$, dissociative electron capture, symmetry considerations 77–46646
$H_3{}^++H_2$, 10 keV electron capture, electronically excited H_3 form. 79–41204
$H_n{}^+$ clusters with odd and even mass number 79–92840
H^+ $Ar(Xe)(Ne)(He)(Kr)(H_2)(N_2)$, electron capture, 4-20 keV, production of highly excited H atom 79–54963
$H(1s,2s)+H(H_2)$, electron capture, loss, and collisional destruction, 5-26 keV 80–5611
$H(1s)+p \rightarrow p+H(1s)$, 15-200 keV, ang. distrib., differential cross sections calc. 78–82839
$H(2s)+He(Ne)(Ar)(Kr)(H_2)(N_2)$, 5-25 keV, $H(n=3)$ excitation, Balmer α emission obs. 80–53113
H(2s)+inert gas, electron capture, H form., 4-25 keV 80–9729
He, electron impact ionis., 35 eV, triple differential cross section 79–36777
He, positron scattering, positronium formation 79–89772
He-like target+fast projectile, electron capture cross-sections 80–69231
$He+Ar^{+Z}$ ($Z=3$ to 7), electron capture into different electron states by multiply charged ions *(Russian)* 78–17788
$He+B^{3+}(C^{4+})(N^{5+})(O^{6+})$, electron transfer 78–13598
He+B(C)(N)(O)(F) bare nuclei, electron capture to excited states, X-ray cross-sections 77–71814
$He+H^+$, 25-3000 keV, continuum distorted wave approx., correl. energy 77–83727
$He+H^+$, 293 keV, electron capture differential cross sections 77–88552
$He+H^+$, double K-shell electron capture, theory 79–68315
$He+H^+$, electron capture cross sections, electron correlations 77–34758
$He+H^+$, electron capture coherent electron density distrib. oscillations 79–10200
$He+H^+$, electron capture into ground and 2s states, cross sections 77–27177
$He+He^+$, double collision spectroscopy 80–58378
$He+He^{2+}$, double K-shell electron capture, theory 79–68315
$He+He^{2+}$, single and double electron capture, high vels., independent electron approx. calc. 80–18923
He+multiply charged ions, electron capture and impact-ionis. cross sections, Monte Carlo calcs. 79–27083
$He^++Ar(H_2)(He)(Kr)(N_2)(O_2)$, metastable ion electron capture, loss and de-excitation 77–6904
$He^++Ar(N_2)(He)$, up to 70 keV, symmetric (antisymmetric) reson. charge transfer cross sections *(Korean)* 78–50636
He^++H, 35 keV to 1 MeV, electron capture, electron transfer calc., electron ionization calc., Monte Carlo method, 79–72387
$He^++H_2(He)(N_2)(O_2)(CO_2)$(methane)(ethane)(propane), 0.7-2 MeV, charge-changing collisions, electron capture 80–58372
$He^++H_2(N_2)$, 25-90 keV, fast He beam form., 2^3S population 79–31740
He^++He, electron loss cross section 79–27080
He^++inert gas, binary encounter calc., cross section calc. 79–72413
He^++Na(K), single-electron capture cross-sections 78–37737
He^++Na(K)(Cs), 5-100 keV, electron capture form. of fast metastable He 78–74760
He^{2+}+H, electron capture, impact parameter calc. 78–33591
He^{2+}+H, electron transfer, 0.1-20 keV, mol. orbital calc., convergence 78–42210
$He^{2+}+H_2(O_2)$, electron capture collisions, spin conservation 78–82837
$He^{2+}+He$, He^+ form. in various electron states *(Russian)* 78–58815
He^{2+}+He, high-energy, electron capture cross-sections, continuum distorted-wave approx. 77–83724
He^{2+}+He, K-electron capture, cross section scaling, high energy 79–41236
He^{2+}+He(Ne), electron capture collisions, spin conservation 78–82837
$He^{2+}+He(1s^2) \rightarrow He^+(\Sigma)+He^+(1s)$, continuum distorted-wave approx., cross-section 77–68109
He^{2+}+Li, electron capture, ionis. cross section, low-vel. $He^+(3l)$ production, X-ray production 79–22822
He^{2+}+methane, (Ne), (Ar), inner shell electron capture cross-sections 79–76510
$He^+(He^{2+})$+H, charge transfer and direct excitation processes 78–25696
${}^3He^{2+}$+He, many-electron systems OEDM orbitals 80–48081
$K+H^+(H)$, single-electron capture total cross sections 80–91656
Kr^-, electron capture expts. to search for long lived states 79–72410
Li+doubly charged ions, electron capture excitation, theoretical predictions in fusion plasma 80–63810
$Li+H^+ \rightarrow Li^+(X)+H(nl)$, ($X=1^1S$, 2^1S, 2^3S and $nl=1s$, 2s, 2p) continuum distorted wave method calc. 80–1062
Li+positron, positronium formation in highly excited states, first Born approx. 80–58420
Li^++Ar, up to 70 keV, symmetric (antisymmetric) reson. charge transfer cross sections *(Korean)* 78–50636
Li^++Li(Na)(Cd), electron capture cross sections 10-60 keV 80–48084
$Li^{1+}+H(H_2)$, ($q=1$-3), electron capture and loss cross sections 78–42187
Li^{3+}+methane, (Ne), (Ar), inner shell electron capture cross-sections 79–76510
${}^7Li+H_2$, electron capture collisions, 0.2 to 3 keV 77–6925
${}^{176m}Lu$, electron capture meas. *(German)* 78–33153
Mg-H^+ $2p_{3/2}$ vacancy alignment electron capture role 80–83465
$Mg+H^+$, electron capture, single and double, 1-100 keV 79–68313
$Mg+H^+$, electron capture and impact ionisation cross sections, CI calc. 80–23343
Mo^{n+} ($n\leq 42$) radiative electron capture calcs. 77–6928

electron capture continued
N^{x+}, (x=1-7), electron loss and capture in He, N_2, Ne and Ar *(Russian)* 78—13600
N^{+}+Ar(Kr)(Ne), single electron detachment cross-sections, 35 to 140 keV 77—6909
N^{+}+elements Ca to Zn, X-ray production cross section, $K\beta/K\alpha$ ratio, 0.5-2.5 MeV/amu 77—54526
N^{+}+H(H_2), 0.1-13 keV electron capture cross-sections meas. 79—36761
N^{+}+inert gas, electron capture (loss) by metastable (ground-state) ions, 2-30 keV 78—25695
N^{+}+N_2 collisions, 2.0 MeV ion energy, electron capture and loss cross section 77—34754
N^{2+}+He, electron capture, 0.2-2.4 keV, kinetic energy change 79—59558
N^{2+}+He(Ne)(Ar), electron capture, product ion energy loss spectra 79—36762
N^{2+}+inert gas target, 60-200 keV single electron capture 80—43172
N^{2+}+Ne, electron capture, 0.2-2.4 keV, kinetic energy change 79—59558
$N^{3,4,5+}$+H_2, (0.3-1.2) 10^8 cm s^{-1}, single and double electron capture cross sections 77—34756
N^{7+}+Ne, double K-shell electron capture, theory 79—68315
N^{q+}+H,(q=1 to 7), electron capture and impact ionisation cross sections 77—75290
N^{q+}+H(H_2), q=1-5, single electron capture cross sections 78—55233
N^{x+}+He, electron capture, K X-ray emission ang. distrib. 77—57919
N_2+H^{+}, electron capture and loss cross-sections, 1-20 keV *(French)* 77—38728
N_2+H^{+}(He^{+}), N_2^{+} 3914 Å emission cross sections, 0.5-34 keV 77—54598
Na+H^{+}(H), single-electron capture total cross sections 80—91656
Ne, highly-ionised, heavy ion impact, selective electron capture effects 80—14202
Ne, Li-like X-ray and Auger populations and line intensities from Cl^{13+} collisions 77—10625
Ne^{-}, electron capture expts. to search for long lived states 79—72410
Ne^{x+}, (x=1-8), electron loss and capture in He, N_2, Ne and Ar *(Russian)* 78—13600
Ne^{2+}+Ar (Kr)(Xe), single electron capture excitation, photon emission, VUV spectroscopy 80—58379
Ne^{2+}+He(Ne)(Ar)(Xe)(Kr), cross sections for electron capture, 60 to 200 keV 78—46442
Ne^{2+}+Xe, electron capture collisions, 15 to 50 keV, excitation 80—102566
Ne^{n+}+Ar(He), slow ion and electron prod., VUV radiation 78—5321
Ne^{n+}+Ar(Kr), (n=1, 2, 3, 4), energy spectra of electrons produced 79—45822
Ne^{z+}+He(H_2)(Ar), (z=1-4), electron capture into excited projectile states 77—75291
Ne^{z+}+inert gas atom (z=1-4), radiative and non-radiative deexcitation after electron capture 79—7008
O and O^{+}, one-electron capture cross sections in alkali metal vapours 79—59553
O^{q+}, electron loss, forward peak oscill. struct. 78—78796
O^{q+}-He^{2+} collisions, electron capture and impact ionisation cross sections, loss of alpha particle in Tokamak plasmas 79—68936
O^{+}+Al, Al K-vacancy cross sections, 0.15 to 91 MeV, recoil effects and mechanisms 77—19033
O^{+}+H(H_2), 0.1-13 keV electron capture cross-sections meas. 79—36761
O^{2+}+inert gas, electron transfer meas., 60-200 keV 80—83480
$O^{3,4,5+}$+H_2 single and double electron capture cross sections, (0.3-1.2) 10^8 cm s^{-1} 77—34756
O^{8+}+Ar, bound- and continuum-state electron capture in gas, strong correlations 80—9730
O^{8+}+H(1s)(He($1s^2$)), electron capture into n,l excited states 80—23543
O^{8+}+Ne, double K-shell electron capture, theory 79—68315
O^{q+}+Ar, continuum electron capture and loss, 1.6-2.8 MeV/A 78—46443
O^{q+}+Ar, continuum electron capture, projectile vel. and Z depend. 78—55222
O^{q+}+H(H_2), q=1-5, single electron capture cross sections 78—55233
O^{q+}+He, charge exchange measurements using double-tandem accelerator-decelerator source of low-energy highly-stripped O ions 80—81317
O^{q+}+He(Ar)(Ne), electron capture to continuum states, forward ejected electron spectra 79—45831
O^{x+}+He, electron capture, K X-ray emission ang. distrib. 77—57919
O_2 electron capture rate from geminate ion recombination fluoresc. data 80—74245
O_2 in liquid Xe, electron capture 80—102402
O^{7+}(O^{8+})+He, p-state alignment, X-ray emission polaris. obs. 79—50123
$Pb_{1-x}Sn_xTe$:In, tunnelling impurity self-localisation, anomalous props. nature *(Russian)* 80—59915
l-proline monohydrate single cryst., X-irrad., ESR and ENDOR study of radicals 80—45528
Rb+H^{+}(H), single-electron capture total cross sections 80—91656
S and S^{+}, one-electron capture cross sections in alkali metal vapours 79—59553
S ion+target (Z=4-40), single and double K-shell excitation, X-ray satellites, hypersatellites 77—19058
SF_6, electron capture, laser radiation influence, possible laser isotope separation appl. 79—22856
^{32}S ions+Be(C)(Ni), radiative electron capture, X-ray ang. distrib. 77—38729
Si, radiative electron capture by channelled O ions 79—77658
Si^{q+} electron loss, forward peak oscill. struct. 78—78796
Si+F^{q+}, q=3-9, Si K-shell ionis., electron transfer cross sections, solid targets 79—10192
Si^{q+}+Ar, electron capture to continuum states, forward ejected electron spectra 79—45831
SiX_4, (X=Br,Cl), electron impact dissoc., low-energy reson. capture 78—9263
$^{28}Si^{n+}$+Sc(Ti)(Cu)(Ge), K-shell ionisation, projectile charge state depend., theory 78—17786
^{28}Si+H(H_2), single electron capture cross sections 78—58812
SnX_4 (X=Br, Cl, I) electron impact dissoc.-electron capture, ionis. efficiency curves 77—61865
Ti^{2+}+H(H_2), electron capture cross-sections, 0.5-14 keV 78—42205
$^{57}CoV_2O_4$, after effects of orbital electron capture 79—73870
WF_5, dissoc. electron capture, electron impact mass spectra, electron affinities 77—88579

electron capture continued
WF_6, dissoc. electron capture, electron impact mass spectra, electron affinities 77—88579
WOF_4, dissoc. electron capture, electron impact mass spectra, electron affinities 77—88579
Xe, γ-γ PAC following nucl. electron capture, cascades perturbed by hyperfine coupling 78—37303
Xe^{-}, electron capture expts. to search for long lived states 79—72410

electron capture, nuclear *see nuclear electron capture*

electron density
see also carrier density; current density; electron density (metals); plasma density
AEROS and TAIYO satellite results 80—46340
air, electron drift velocity at 293K 80—103102
air, hypersonic wake, electron recomb. coeff., temp. depend. meas. 79—27834
air, RF discharge, electron temp. and density 78—51371
air wake, hypersonic, ionised, free electron attachment coeff. meas. 79—27835
alkali metal halides, Born-Mayer repulsive parameters, overlap parameters, free ion electronic charge densities 79—98179
alkanes, electron density, bond order, hydrogen suppressed graphs, extended Huckel theory 78—90088
Z Andromedae, atmosphere electron densities from IUE obs. 80—109450
arc, spectroscopic meas. *(French)* 77—80361
arc plasma, stabilised by N_2 injection through porous wall, thermodynamic nonequilib., plasma parameters 79—86629
arc plasma diagnostics, high-pressure, by strioscopy and IR absorption *(French)* 80—19620
at. emission obs. of plasma props. 80—19021
atmosphere, columnar electron content at Ootacamund, India, from ATS-6 satellite radio beacon meas. 79—48611
atom, quasiclassical corrections to Thomas-Fermi model, electron density eqns. of state 78—25404
atoms, electron densities and electrostatic pot. calc. 80—102430
atoms, electrostatic pot.-electronic density relationships 80—69206
ATS-6 electron content data presentation 78—61593
aurora, incoherent scatter radar meas. rel. to precipitating electrons energy distrib. 78—77390
aurora, N(^{2}D) emission and ion chemistry, satellite obs. 80—72673
aurora, pulsations of electron and ion intensity 80—61934
aurora, type A, rays, electron density rel. to O I 6300 Å emission intensification 80—4163
aurora modelling, time-depend. study 80—72672
auroral ionosphere meas. in Antarctic by sounding rockets 79—8760
auroral oval, electron density distrib. rel. to auroral arcs global form. 80—67446
azaaromatics, neutral and protonated, excited singlet and triplet states, charge densities, INDO calcs. 80—58152
Bragg cell heterodyne interferometry of fast plasma events 77—11404
breakdown, ionising wave propag. mechanisms 80—83941
Centaurus A giant radio lobes, electron density vars. from X-ray emission obs. 78—41055
chemical potential and electronegativity rel. to electron density 79—89589
combustion product plasma, electron conc. and mobility determ. by HCN laser submillimetric interferometry 78—1889
Comet Kohoutek (1973 XII) tail, electron density fluctuations 77—13285
comet plasma tails electron density deduced from refr. of occulted radiosources 79—53773
computed tomography, spectral artefact correction and determ. of electron density and at. no. 80—51231
conical laser plasma tube, electron density distrib. 78—58981
corona onset voltage in nonuniform air gap, calc. methods 77—15253
Crab pulsar, high energy electrons density and momentum distrib. 78—73727
V1016 Cygni, electron density from forbidden Fe VI emission 79—8970
V1500 Cygni (Nova 1975), shell electron temps., densities and other props. 79—30068
D- and F-regions, geomag. control and possible coupling mechanism 77—9598
D-region, and energy distrib., heating by high energy protons 77—82078
D-region, daytime solar proton event-disturbed model 78—93038
D-region, diurnal vars. during storm after-effect 78—65451
D-region, electron densities from inversion of differential absorpt. and phase integrals 77—45238
D-region, electron density distrib. at noon 77—53274
D-region, electron density diurnal var. at midlatit., from VLF meas. 77—64520
D-region, electron density meas. via payload B I rocket-borne expt. package 78—45190
D-region, electron density profiles, statistical model 80—61964
D-region, electron density profiles from gyrowave interaction expt., error anal. 79—5705
D-region, electron density variations above Urbana, Illinois 77—60536
D-region, equatorial, ion and electron densities 78—36362
D-region, gyrowave interaction expt., calc. of Fejer curves 80—36447
D-region, improved Faraday rotation expt. for electron conc. rocket meas. 77—9543
D-region, intercomparison of groundbased techniques, wave interaction and partial reflection 77—45235
D-region, ionisation effects from cosmic X-ray sources 79—35048
D-region, ionisation meas. rel. to mesosphere NO concs. 79—8651
D-region, low- and mid-latit. electron density profiles comparison 79—44302
D-region, lower, electron density meas. via Faraday rot. and absorpt. 80—31162
D-region, midlatit. winter electron density vars. 77—60532
D-region, negative ions, Thomson scatt. detect. using Arecibo radar 79—62665
D-region, nocturnal, density modulation by electrons precip. fluctuations 77—25856
D-region, partial refls. density profiles sensitivity to irregularity comp. 78—81495
D-region, polar electron density profiles during solar proton event, from VLF refl. height vars. 79—8764
D-region, positive ion chemical scheme for electron density profile 79—40007
D-region, rocket meas., rel. to winter absorpt. anomaly 77—21990

electron density continued

D-region, time vars. in winds and electron densities at Sastakoon, Canada 79—25389
D-region electron density during W.Europe 1975/6 winter anomaly 80—36440
D-region electron density during winter anomaly, temp. and NO density vars. effect 79—21087
D-region electron density variation obs. *(Russian)* 78—61652
D-region electron loss, steady state coeff., diurnal and seasonal var. 79—75023
D-region modification, density determ. via complementary cross modulation technique 77—2275
D-region plasma density measurement, rocket borne expt. 78—45126
D-region winter anomaly, recent advances 80—17437
DC arc plasma, alterations in spectral line intensities due to external mag. fields 80—79621
HR Delphini (Nova 1967), physical conditions of different regions of envelope 80—4369
diffusion to absorbing electrodes, Monte Carlo and Boltzmann calc. comparison 80—6204
dimethyl aluminium hydride dimer, electron density distrib., electrostatic mol. pot. anal. 80—52885
discharge, electron density and temp. profiles, Langmuir probe meas. *(French)* 78—30482
discharge, grazing, incomplete gas temp. and electron density diagnostics 79—55600
discharge, laser heterodyne meas. 78—30483
discharges in gases, pulsed, theoretical and expt. study 80—92416
dispersed heterogeneous system, electron conc. calc. method 78—38452
E$_s$-layer, mid-latit., effect of strong radio waves on form. 77—60514
E-layer, nighttime, electron density rel. to night sky emission *(Russian)* 77—45223
E-region, anomalous ionisation at high latits., ground based sounding obs. 77—60523
E-region, electron conc. profiles during sunrise and sunset 79—88526
E-region, electron density inhomogeneities prod. by auroral particles injection 78—45095
E-region, midlatit. nighttime model including metallic ions 77—45249
E-region, over India, turbulence obs. in electron density fluctuations 77—9609
E-region, polar electron density fluctuations, gravity wave interpretation *(French)* 80—46334
E-region, variations during geomag. disturbances 78—69567
E-region, winter anomaly as result of upper atmosphere seasonal vars. 79—53613
E-region electron density gradients from reflected radio waves arrival direction 79—25387
E-region electron density profile, distortion meas. using group and phase height meas. 80—109299
E-region f0E storm time var. at low latit. station 79—44295
electron accelerator, electron current density distribution, approx. formula *(Japanese)* 80—14032
equatorial electrojet, electron density profile changes 77—45234
equatorial spread-F, role of steepened structs. and drift waves 79—2431
erythrocyte ghost membrane, human, small-angle X-ray diffr. 77—73510
EUV spectroscopic method for electron density determ. in stellar atms. 79—16836
exosphere, night time meas., 2500 km altitude 79—16730
F$_2$ layer, mid-latit., internal gravity waves day and night effects on electron density 79—58150
F$_2$-layer, electron density long-period variation f$_0$ evidence 80—56667
F$_2$-layer, electron density vars. rel. to magnetosphere-ionosphere electrodynamic interaction 78—28372
F$_2$-layer, equatorial, vertical ionospheric soundings 77—17276
F$_2$-layer, global distrib. of electron density rel. to elec. fields in closed magnetosphere 77—64514
F$_2$-layer, hmF$_2$, NmF$_2$, high-latit. behaviour along noon-midnight meridian under quiet conditions 79—40004
F$_2$-layer, ionization balance disturbance by radiowave heating 77—17274
F$_2$-layer, mid-latitudes, mag. storm effects 80—61970
F$_2$-layer, N(h) variations at midnight 77—17275
F$_2$-layer, night-time, over Arecibo, electron density seasonal mean struct. 80—31163
F$_2$-layer, parameters at high latitude during quiet conditions 80—105106
F$_2$-layer, peak electron densities in main trough region, empirical model 78—28417
F$_2$-layer, peak electron density using servo model 80—101486
F$_2$-layer, plasma continuity eqn., comparative anal. of numerical soln. methods 78—69578
F$_2$-layer, travelling disturbances prod. by gravity waves, Hooke perturbation formula testing 79—40005
F$_2$-layer, vertical drift assoc. with polar substorm 79—53618
F$_2$-layer equatorial anomaly development, role of ambipolar diffusion 77—13168
F$_2$-layer of ionosphere, comparison of CCIR predictions with in situ meas. 78—57394
F-layer electron density inhomogeneity, thermodiffusion mechanism *(Russian)* 80—85791
F-region, cleft region perturbation during substorm 80—101483
F-region, density power spectra rel. to travelling ionospheric disturbances and assoc. gravity waves 78—28394
F-region, diffusion-recomb. parameters 77—53300
F-region, disturbances nonlinear saturation, strong radiowave effects 78—28378
F-region, electron conc. profiles during sunrise and sunset 79—88526
F-region, electron density and ion temp. profiles rel. to airglow ground-based obs. anal. 80—98496
F-region, electron density data rel. to O I 6300 Å nightglow simulation and neutral comp. vars. *(Portuguese)* 80—41584
F-region, electron density disturbances during local heating 77—29543
F-region, electron density irregularities rel. to pulse spreading and unresolved spread-F 77—78557
F-region, electron density parameters rel. to neutral atmosphere parameters at fixed height 77—91346
F-region, electron temp. models using electron density height profiles 77—60540
F-region, equatorial, irregularity patches localised origin 78—77404
F-region, equatorial anomaly, solar cycle and seasonal variation of electron content 80—41622
F-region, equatorial anomaly 80—41602

electron density continued

F-region, equatorial irregularities and electron density, radar obs. 80—77222
F-region, equatorial spread-F irregularities and electron depletion, radar obs. 80—41611
F-region, incoherent scatter radar meas. of electron density and ion vel. during isolated substorm 78—65452
F-region, midlatit., parameters diurnal behaviour in summer 79—84570
F-region, midlatitude, electron density depressions under relatively quiet geomag. conditions 78—36385
F-region, n$_2$F$_2$ annual vars. with latit. and solar activity level 78—69577
F-region, nighttime, electron content correl. with O I 6300 Å line 77—67007
F-region, nighttime ionization maintenance rel. to neutral winds 77—29555
F-region, nighttime seasonal electron density anomaly 78—69566
F-region, photoelectron fluxes, energy loss and spectral features determ. 77—45227
F-region, polar cap and auroral zone, math. model 78—65458
F-region, response to geomagnetic storms at field line L=4 80—8472
F-region, seasonal anomaly in S.America and S.Atlantic 77—17277
F-region, solar activity rel. to temp. and electron density 80—46337
F-region, VLF cross meridian refraction and electron density 80—46339
F-region, winter anomaly causes 80—85793
F-region beneath magnetospheric cusp, electron density enhancements 78—28389
F-region density max., harmonic analysis and periodicities 78—57383
F-region during mag. storm, electron content by satellite VHF signal obs. 80—101471
F-region dynamics, Sturm-Liouville problem 77—13149
F-region electron content and atmospheric gravity waves at high magnetic dip station 77—53277
F-region electron density and total electron content, latitude var. 78—36375
F-region heating, caused by powerful radiowaves, calc. *(Russian)* 78—32278
F-region height and electron content changes at midlatit. during mag. storms 77—21984
F-region irregularities and north-south aligned equatorial airglow depletions 78—45074
F-region irregularities from plasma reson. phenomena obs. by rocket-borne relax. sounding expt. 79—8767
F-region irregularity model, reconciliation with sunspot cycle vars. in spread-F occurrence 77—41262
F-region peak electron density, diurnal and solar cycle variation 80—61949
F-region polarisation field, nighttime maintenance of equatorial ionisation 80—4192
F-region striated Ba clouds, electron density struct. meas. 78—88974
F-region total electron content, geomag. activity effects 80—8480
far IR waveguides for interferometers measuring electron density in Tokamak plasma 79—73034
fluctuations excited by EM waves in semi-infinite anisotropic plasma 78—14173
free electron lasers, boundary deform. and Robinson-Liouville theorem 80—48202
free plasma column in gas at high pressure 78—75477
fusion Tokamak experiments, H(D) recycling model, influence on discharge behaviour 80—10393
galaxies active nuclei, temp. and electron density in narrow line region 80—31364
gas, distribution function of carriers in electron avalanches 77—47287
gas discharge columns with electron prod. and loss rates linear and quadratic in electron density, electron density distribs. 80—96400
gas jet target with electron beam heating, plasma density meas. 77—39457
glass, laser induced surface damage, free electron density meas. 77—40309
glow discharge, crossed-field type, electron energy distrib. diagnostics 79—27851
glow discharge, illumination effects on electron distribution functions 78—34378
glow discharge, large amplitude striations, electron conc. variation 77—89342
glow discharges, atomic and ionic spectral line excitation in cathodic region *(Russian)* 78—63611
HF second-step discharge meas. and equivalent cct. 79—7505
hollow cathode arc, plasma column parameters *(French)* 78—9885
hypersonic flow field behind blunt body, approx. calc. and electron density in wakes *(Russian)* 79—86461
IC 4329A, Seyfert galaxy, nucleus electron densities from photometry and optical spectrum 80—36706
International Reference Ionosphere, goals and status 79—5714
interplanetary dust and electrons spatial distrib. round Sun, contrib. to corona 80—46514
interplanetary integrated electron content, Mars 4-7 meas. 77—53383
interplanetary medium, electron density vars. physical form from scintillation spectra 80—72741
interplanetary medium, fluctuations rel. to RF scintillation, weak scatt. approximation anal. 77—9706
interplanetary scintillation meas. of electron density power spectrum in solar wind 78—77448
interstellar, determ. from decorrel. bandwidth of pulsar scintillation 77—78850
interstellar clouds, contrib. from assoc. ionisation of Ti and O 77—29893
interstellar clouds, electron abundances determ. method 80—41866
interstellar irregularities from pulsar scintillations freq. time struct. 80—101608
interstellar matter in front of χ Ophiuchi, optical obs. and electron density 79—25673
interstellar medium, electron densities from radio emission obs. 77—17724
interstellar medium, electron density determ. from low-latit. pulsars dispersion meas. and distances 80—101606
interstellar medium, electron density from galactic Hα background emission obs. 80—56897
interstellar medium electron density fluctuations spectra from pulsar scintillations freq. cross-correl. 80—4392
ionisation instability mode of plasma accelerator, probe method for electron distrib. function determ. 80—19612

electron density continued
- ionosphere, antenna in plasma, Debye screening and electron conc. nonuniformity 78—69563
- ionosphere, bottomside, mid-latitude trough discovery 80—109300
- ionosphere, by automatic meas. of whistler dispersion 78—93050
- ionosphere, calc. and obs. structure, AE-C satellite and incoherent scatter radar obs. 78—49203
- ionosphere, calc. technique for ground and satellite obs. 80—90275
- ionosphere, combined ground and satellite measurements, IRI model extension 80—61911
- ionosphere, cond. and electron density of reflecting layer below classical D-region 80—98508
- ionosphere, cosmic ray layer, electron density distrib., radiowave absorpt. 77—22024
- ionosphere, daily vars. at 100-200 km at middle latits. 77—64515
- ionosphere, daytime positive storm effects at middle latits., prod. by travelling atmospheric disturbances 79—25394
- ionosphere, density and recomb. coeff. profiles calc. rel. to absorpt. and rocket meas. 78—69559
- ionosphere, density depletion rel. to enhanced O I 6300 Å prod. by ionospheric modification expt. 77—33263
- ionosphere, density fluctuations from radiosource scintillations 80—36454
- ionosphere, density profile from energetic particle and spread-F obs. of E- and F-regions 78—36383
- ionosphere, density profiles calc. from ionograms via simplified inversion procedure 77—41263
- ionosphere, density response during August 1972 mag. storms 77—25858
- ionosphere, density vars. due to solar EUV flux changes, calcs. 79—44293
- ionosphere, density vars. rel. to radiowaves focusing at boundary of zone of silence 77—13158
- ionosphere, disturbed, above 100 km, approx. method for electron kinetics calc. 77—64512
- ionosphere, effect of radio wave heating on electron densities and temps. 78—77403
- ionosphere, effective recombination coeffs. for quiet conditions and solar flare occurrence 80—12595
- ionosphere, electron conc. distrib. models for quiescent atmosphere 80—41600
- ionosphere, electron conc. irregularities, Kosmos 381 meas. 78—16228
- ionosphere, electron conc. var. with height, improved model 78—49214
- ionosphere, electron concentration profile, vert. struct. 80—61936
- ionosphere, electron concentration variations rate use 80—12598
- ionosphere, electron concs. above Arecibo in E- and upper D-regions 79—101014
- ionosphere, electron content data digital processing methods 80—56629
- ionosphere, electron content determ. via galactic linear polarised radio emission obs. 77—17709
- ionosphere, electron content during storms, behaviour during positive phase 77—37480
- ionosphere, electron content quasiperiodic fluctuations during 1976 April 29 partial solar eclipse 78—24407
- ionosphere, electron content-latitude profiles at low latitudes, development and decay 78—36374
- ionosphere, electron densities and temps. from Intercosmos-10 Langmuir probe expts. *(German)* 79—2469
- ionosphere, electron density and collision rate, rocket meas. 80—41601
- ionosphere, electron density and temp. rel. to primary ion-electron prod. rates changes 80—72675
- ionosphere, electron density determ. from topside ionograms, comparison of methods 79—39978
- ionosphere, electron density disturbance spatial struct. affected by magnetosphere convection 80—41606
- ionosphere, electron density evolution, effects of O abundance increase 77—2300
- ionosphere, electron density fluctuations rel. to gravity wave spectra propag. in thermosphere 79—66848
- ionosphere, electron density in South Atlantic Anomaly region 80—12611
- ionosphere, electron density irregularities rel. to intersatellite whistler-mode pulses propag. 78—69605
- ionosphere, electron density profile analyses of ionograms, model starting heights 79—66869
- ionosphere, electron density profiles determ. from transionospheric sounding data 78—28371
- ionosphere, electron density profiles during Western European Winteranomaly Campaign 78—45125
- ionosphere, electron density profiles during winter anomaly vertical incidence absorpt. 79—21098
- ionosphere, electron density troughs and equatorial plasmapause, coincident satellite obs. 77—17291
- ionosphere, electron density vars. during 1972 August 4-5 storm 77—33269
- ionosphere, electron density vars. during solar flares rel. to sudden freq. deviations 78—28373
- ionosphere, electron density vars. rel. to sudden freq. deviations (SFD) and solar EUV radiation detect. 80—8484
- ionosphere, electron distrib. rel. to electron production and heating 80—41605
- ionosphere, electron distrib. rel. to production rate and heating 80—105103
- ionosphere, electron prod. and loss rates, satellite meas. 79—35047
- ionosphere, electron temp. and density fluctuations meas. by Aeros-B, global distrib. 79—58160
- ionosphere, electron-ion conc. and electron temp., Vertikal' 4 rocket meas. 79—84566
- ionosphere, equatorial, correl. with seasonal var. of radio waves absorpt. 78—85762
- ionosphere, equatorial, total electron content fluctuations due to atmospheric waves 78—36360
- ionosphere, equatorial electron densities, seasonal and solar cycle changes 78—36378
- ionosphere, equatorial irregularity experiment (Equion) 77—33266
- ionosphere, equatorial spread-F rel. to F-peak and bottomside electron density 79—53643
- ionosphere, field-aligned currents effect on electron density profile 79—62651
- ionosphere, general photoelectron current, meas. technique 80—12636
- ionosphere, gravity wave-induced density fluctuations and radio waves phase path changes 79—35043
- ionosphere, HF heating expt. for fluctuations of electron density 80—82140

electron density continued
- ionosphere, high-latit., electron densities rel. to aurora and particle precip. 79—40000
- ionosphere, horizontal density gradients rel. to HF transionospheric long range propag. from satellite 78—36396
- ionosphere, increase during stratospheric warming 77—91356
- ionosphere, inhomogeneities, Earth surface topography effects, airborne soundings 78—69579
- ionosphere, inverse problem solution by simplex method 80—26619
- ionosphere, irregularities, Fresnel diffraction patterns 77—9614
- ionosphere, Kosmos 381 obs. at 1000 km during calm and disturbed conditions 77—64513
- ionosphere, latit. total electron content, gradients over midlatit. stations 77—33251
- ionosphere, latit. vars. from Alouette-2 data, internal gravity waves 78—32269
- ionosphere, lower, effects of solar flares Fe XXV 1.87 Å line emission 78—65588
- ionosphere, lower, electron conc. profiles, generalised exponential model 77—67005
- ionosphere, lower, electron density and distrib. function, Boltzmann-Fokker-Planck theory 77—78564
- ionosphere, lower, electron density disturbances during Soyuz-Apollo expts. 78—45110
- ionosphere, lower, electron density profile controls from radiowave absorpt. meas. 78—81492
- ionosphere, lower, electron density profile from rocketborne meas. of VLF propagation 77—82082
- ionosphere, lower, electron density space-time vars. 77—17282
- ionosphere, lower, rocket meas. of electron density from VLF waves propag. characts. 78—49219
- ionosphere, lunar perturbations in columnar electron content, dynamo electrostatic fields interpretation 77—29570
- ionosphere, mid-latitude F_2-layer, electron density oscills. rel. to lunar tide 78—61655
- ionosphere, midlatitude, mathematical model of photoelectron fluxes 77—67009
- ionosphere, models, review 79—48617
- ionosphere, multi-region electron density profiles, fitting to analytic function of height 77—60537
- ionosphere, nocturnal, over Arecibo, electron density profiles rel. to F-region height bands 79—66863
- ionosphere, nocturnal topside, midlatit. electron density enhancements, longit. inequalities 79—16746
- ionosphere, noon and midnight mid-latit. trough obs. by Ariel 4 78—85765
- ionosphere, numerical simulation of electron content obs. rel. to thermospheric quantities determ. 77—53268
- ionosphere, O^+/electron density ratio in 140-200 km height range 80—105102
- ionosphere, over Delhi, electron density model distribs. 79—88536
- ionosphere, peak density and total electron content var. during 1973, June 30 solar eclipse 77—53302
- ionosphere, photoelec. distrib. determ. from plasma line intensity meas. 77—41259
- ionosphere, photoelectron flux calcs. 79—21103
- ionosphere, plasma bubbles spatial relationship with 1 m equatorial spread-F irregularities 80—67457
- ionosphere, polar region struct. rel. to magnetospheric convection behind plasmapause 78—40731
- ionosphere, polarisation electric field vert. distrib. in topside 80—61935
- ionosphere, quiet nighttime, electron total content and density rel. to decay rates 78—81493
- ionosphere, radar obs. of electron density revealing gravity waves 80—77182
- ionosphere, radio aurora, 398 MHz echoes, depend. on electron density and elec. field 79—66854
- ionosphere, sporadic-E and F_2 layers, electron fluctuation origins 80—101475
- ionosphere, subsonic wave-ionised plasma interaction, electron density study 80—4183
- ionosphere, substorm development in postmidnight sector, electron density vars. 77—60525
- ionosphere, temp. and electron density relaxation rel. to radiowave interaction nonstationary processes *(Russian)* 78—93028
- ionosphere, topside, electron density rel. to electron temp. models 80—67460
- ionosphere, topside, light ion and electron troughs rel. to plasmapause 77—87162
- ionosphere, topside, low density regions at high altitudes, rel. to equatorial spread-F 79—62671
- ionosphere, topside, trough morphology, occurrence freq. and diurnal, seasonal and altitude vars. 79—53645
- ionosphere, topside sounding and determination of electron profiles, review 80—56669
- ionosphere, total content meas. during 1976 Oct. 23 solar eclipse over Australia, rel. to induced gravity waves 78—49210
- ionosphere, total electron content, equatorial electrojet control 79—88539
- ionosphere, total electron content and F-region electron density distrib. near mag. equator 79—75028
- ionosphere, total electron content comparative study 80—98516
- ionosphere, total electron content determ. from Faraday rot. 77—33249
- ionosphere, total electron content determ. in transverse zone, new methods 77—33250
- ionosphere, total electron content diurnal and seasonal trends, obs. at Waltair 78—69596
- ionosphere, total electron content during 1971-4 period above Melbourne 79—5712
- ionosphere, total electron content equinoctial variations 77—60542
- ionosphere, total electron content fluctuations rel. to scintillation of VHF and GHz waves 80—109302
- ionosphere, total electron content meas. at Gauhati, using ATS-6 140 MHz transmissions 78—69598
- ionosphere, total electron content nighttime increases, ATS-6 radio beacon obs. 79—75020
- ionosphere, total electron content numerical model, corrections for satellite tracking systems 78—69587
- ionosphere, total electron content obs. at Kurukshetra, suing ATS-6 140 MHz transmissions 78—69597
- ionosphere, total electron content over Indian subcontinent, electrojet effects 77—64523

electron density continued
ionosphere, total electron content over mag. equator rel. to solar cycle during 1964-69 period 79—53636
ionosphere, total electron content rel. to balance eqn. theoretical model 78—28369
ionosphere, total electron density nighttime behaviour 78—69570
ionosphere, travelling disturbances, electron density spectra 78—77398
ionosphere, travelling disturbances characts. over Thumba 78—69590
ionosphere, travelling disturbances obs. by auroral zone incoherent scatter radar 79—48610
ionosphere, upper, perturb. assoc. with magnetospheric cleft in local summer *(French)* 78—4022
ionosphere, use of regularisation method 80—72679
ionosphere, valley problem in bottomside ionogram anal. 77—33268
ionosphere, vertical density gradients rel. to equatorial electrojet type 1 radar echoes with double-peaked Doppler spectra 80—67458
ionosphere, vertical electron density profile comp. from single magnetoionic ionogram component 77—45222
ionosphere, winter anomaly absorpt. events and E_s layer form. due to metallic ion drifts 77—9599
ionosphere, winter nighttime distortions at $L=4$ 77—87165
ionosphere baselevel trough, electron density profiles and struct. 78—28402
ionosphere D- and E-regions, electron densities, diurnal, seasonal and solar cycle vars. 77—33267
ionosphere D-region, sunrise variations of negative ions and electron conc. 80—31157
ionosphere E-region, latit., geomag. storms effect on electron density 79—44294
ionosphere electron content data, mixing freq. components identification by multiplicative homomorphic filtering 79—29929
ionosphere electron content in S.Atlantic geomag. anomaly region, east-west asymmetry 79—21097
ionosphere electron content meas. from Faraday fading records, mean field height determ. 80—8482
ionosphere electron density during winter anomaly, 70-100 km 80—36441
ionosphere electron density from ionograms, true height calc. technique 80—8486
ionosphere electron density in S hemisphere middle latits., Universal Time effect model 79—25396
ionosphere electron density of Delhi and latitudinal depend., INTASAT Faraday fading obs. 80—109293
ionosphere electron density profile parameters estimation from VLF propag. data, effectiveness 79—53614
ionosphere equatorial anomaly, dissimilar forms in E.Asia and India 80—109301
ionosphere equatorial bubbles, model computations of assoc. radio wave scintillation 80—94641
ionosphere equatorial bubbles, topside sounder obs. 79—16737
ionosphere F-region, auroral, neutral winds and particle precip. rel. to electron density 79—44296
ionosphere plasma, electron densities and temps. meas. by Injun 5 during major mag. storm 78—88987
ionosphere sporadic-E layer, midlatitude, electron density vars. during form. 77—13157
ionosphere total electron content, effect of elec. fields and vertical neutron-gas drifts 78—45089
ionosphere total electron content, lunar var. at Lunping 79—21100
ionosphere total electron content, nighttime enhancements at low latits. 80—72677
ionosphere total electron content, storm-time changes at nearby mid-latit. locations 80—31164
ionosphere total electron content at Sagamore Hill, solar cycle var. 78—81496
ionosphere total electron content during magnetic storms over Hawaii 78—16238
ionosphere travelling disturbances, wave-normal depression and disturbance amplitude height depend. 79—40006
ionosphere unstable polar cap, electron density and temp. rel. to electrostatic waves 79—29927
ionosphere VLG guide over Atlantic Ocean, obs. of shadow of mesosphere O_3 on D-region 79—58161
ionosphere-plasmasphere total electron content meas. by SHF differential phase shift method 78—36304
ionospheric, electron density profile determ. from rocket-based 40 kHz propag. obs. *(Japanese)* 78—24403
ionospheric, meas. by radio wave scattering, by artificial plasma inhomogeneities *(Russian)* 79—5636
ionospheric, meas. using radio wave scattering, from artificial plasma inhomogeneities 79—75074
ionospheric F_1-layer, electron density profiles rel. to dynamical effect 79—12340
ionospheric irregularities, characts. from Faraday fading of 40 MHz signals 77—13166
ionospheric irregularities in geomagnetic field, diffuse spread *(Russian)* 77—64518
ionospheric plasma disturbance due to earthquakes and volcanic eruptions 80—36453
ionospheric valley, electron-density inhomogeneities rel. to internal gravity waves 77—91348
ions, positive or negative, electron density, semi-statistical model 78—21850
ionsphere, topside, midlatit. trough position from ESRO 4 obs. 77—64525
ISEE electron density expt. results 79—58210
Jupiter, electron density profiles, Voyager 1 radio occultation meas. 79—96953
Jupiter, ionosphere, effect of electron precipitation, Pioneer 10 and 11 S band occultation obs. 77—56871
Jupiter ionosphere, peak electron concs. from Voyager 1 preliminary radio profiles 80—26791
Jupiter magnetosphere, electron density profile from Voyager 1 plasma wave obs. 80—26795
Jupiter magnetosphere, thermal electron density 79—40133
Jupiter magnetosphere, Voyager 1 planetary radio astronomy obs. rel. to electron density profile 80—26796
laser, free electron type, small-signal gain, space charge effect 79—920
laser, high-press. ioniser-sustainer, far IR absorpt. determ. of electron densities 77—14695

electron density continued
laser ion-source, form of ion pulses depend. on plasma characts. *(German)* 77—185
laser microplasma, electron, atom and ion density determ. *(German)* 77—7588
laser produced plasma, ultraviolet probing with picosecond pulses 78—42827
laser-heated, suprathermal electrons, 511 keV photon detect. 77—62336
laser-produced plasma, application of synchronised ultrashort Nd:glass laser pulse 78—42825
lower daytime ionosphere, model for VLF field forecasting 77—49216
lower ionosphere, density profile estimates from Hollingworth patterns in VLF range 77—64516
lower ionosphere, electron density profile from radiowave data 80—67462
magnetosphere, by automatic meas. of whistler dispersion 78—93050
magnetosphere, elec. field, plasma density and temp., field-aligned currents, S3-3 satellite obs. 80—26699
magnetosphere, electron density and temp. meas. by GEOS-1 mutual impedance expt. 79—35071
magnetosphere, electron density determ. via trigger VLF emission 78—45149
magnetosphere, electron density gradients rel. to HF signals propag. mechanism 80—4196
magnetosphere, electron density meas. via International Sun-Earth Explorers 78—85803
magnetosphere, electrostatic emissions and cold plasma densities 80—26696
magnetosphere, evidence for trapped flux limit from pulsating aurorae 80—72666
magnetosphere, local electron density and mag. field meas. via JIKIKEN (EXOS-B) satellite stimulated plasma wave expts. *(Japanese)* 80—94649
magnetosphere, lower, electron densities and temps. from Intercosmos-10 Langmuir probe expts. *(German)* 79—2469
magnetosphere, thermal electron densities and temps. in dayside cusp region 77—78574
magnetosphere, VLF cross meridian refraction and electron density 80—46339
magnetosphere, whistler duct struct. and formation 80—94659
magnetosphere electron densities determination, whistler inversion via spectral expansion 80—8495
magnetosphere electron density, small scale struct. from plasma resons. on-line tracking 79—35073
magnetosphere radiation belts, electron intensity fluctuations meas. from Cosmos 484 satellite 80—72698
mesosphere, correl. with stratospheric temp. and wind 77—9470
mesosphere, daytime midlatit., corpuscular radiation flux vars. 77—29538
metal, charge screening and Friedel oscillations of electron density *(Russian)* 78—79951
meteor trails, causes of fluctuations in effective linear electron density 78—73687
meteor wind profile comparison with electron density obs. 77—9587
meteors overdense trails, linear electron density determ. 77—13140
MHD generator, combustion-driven, boundary-layer profile meas. 77—24194
MHD generator, nonequilibrium channel, thermal diffusion of charge carriers, effect on electron density, obs. 79—68959
microwave discharge, supersonic flow in waveguide, electron densities, possible laser 80—38842
microwave induced plasma, mixed-gas low-pressure, excitation conditions 77—62422
midlatitude plasmasphere, trapped photoelectrons and secondary electrons 78—69565
molecular electron density calc., approx. differential eqn. 80—47864
molecular similarity, electron density function meas. 80—91413
molecules, electron densities and electrostatic pot. calc. 80—102430
molecules, electron distrib., ab initio anal. 80—47866
Mossbauer atoms, electron densities at nuclear centre and surface, calcs. using Dirac-Fock eqn. 80—74100
multidipole plasma, probable errors assoc. with minicomputer anal. of Langmuir probe characts. 77—24193
neurotoxin, snake venom, appl. mol. graphics to struct. determ. 78—27892
NGC 1052, elliptical galaxy, electron density and N II/$H\alpha$ line intensity ratio in nucleus 77—33642
NGC 1499, H II region, electron density from decametre wavelength obs. *(Ukrainian)* 79—40243
NGC 3516, Seyfert galaxy, optical spectrum rel. to electron density 77—26052
NGC 7027, planetary nebula, electron densities from low excitation emission spectrum 77—64823
NGC 7027, planetary nebula, electron density gradient 77—87513
nighttime ionospheric intermediate layer obs. by rocketborne impedance probe *(Japanese)* 78—61646
nonneutral plasma microstate, synchrotron radn. meas. 79—46486
Nova Delphini 1967, envelope ionisation conditions and electron densities *(French)* 77—53603
novae, spectrophotometric estimate of electron density in rapidly rot. accretion discs 79—16968
O to F type stars, Balmer lines and mean electron density 77—17564
orbitron, radial electronic charge distrib. 77—57827
outer radiation belt electron intensity rise, link with magnetosphere disturbance 80—77225
PHL 1092, narrow line quasar, Fe II emission region electron density and temp. 80—77508
physical and biological science conf., Japan (Feb. 1979) 80—12846
planetary nebulae, 10 micron props. rel. to electron density 79—48879
planetary nebulae, electron densities and evolutionary changes 77—78861
planetary nebulae, electron density and temp. from absolute flux densities for emission lines in 6000-11000 Å range 80—51857
planetary nebulae, low excitation, electron densities and temps. from spectral studies 80—17646
plasma, 60 MeV ion beam-created, electron props. diagnostics *(French)* 80—10407
plasma, adiabatic toroidal compressor, power balance anal., diagnostics 77—51219
plasma, cold, effective dielec. permeability with electron density fluctuations *(Russian)* 80—32882
plasma, collisionless, determ. by CO_2 laser 79—41879
plasma, determ. from continuum emission coeff. 77—43067
plasma, determ. using magneto-acoustic oscills. 77—80354

electron density continued
plasma, dielectron recombination, electron density effect *(Russian)* 79—98856
plasma, electronic multiplication in nonuniform elec. field 79—86559
plasma, He I and II radiation enhancement in mag. field, nonlocal thermodynamic equilib. 80—10366
plasma, HF discharge, resonantly sustained, by Tonks-Dattner resonance 79—4142
plasma, inhomogeneous, electron density profile leading edge data., algorithm 79—41880
plasma, laser heated, heat flux limitation and ion-acoustic turbulence 78—18453
plasma, laser prod., Langmuir probe meas. of parameters and expsn. 78—18456
plasma, laser prod., radiation press. effects, interferometric diagnostics 78—38540
plasma, laser-created, asymmetric electron density profile, interferometric meas. 80—75085
plasma, laser-prod., microwave diagnostics 78—9845
plasma, laser-produced, diagnostics by multicharged ion K-spectra, review 79—64908
plasma, light emission from atom beam-plasma interactions 77—72454
plasma, local high-press. regions production in vac. spark, diagnostics 79—19104
plasma, meas. in unsteady flow using Fabry-Perot laser interferometer 77—68869
plasma, meas. using three-laser intercavity interferometer 77—80357
plasma, multi-pulse ruby laser recording of temporal evolution by light scatt. 80—14938
plasma, multimillion degree, high resolution spectroscopy 77—65915
plasma, of electrons, finite-length thermal equilib. 79—32801
plasma, probe meas., ionis. rate const. 77—47143
plasma, radial electron concentration profile determ. by microwave resonator method *(German)* 79—86608
plasma, reference temp. method for determ. densities and plasma temp. 77—84510
plasma, theta-pinch, 10.6 μm interferometry and Faraday rot. meas. 77—80358
plasma, two-stream unstable, anomalous cond., electron heating 80—6219
plasma, vibration-insensitive He-Ne laser interferometer for electron density meas. 79—14610
plasma, weakly ionised, scatt. spectra calc. using two-time probability densities *(German)* 79—77347
plasma density determ. using microwave interferometers, modulated transmission and reflection types comparison 79—37546
plasma diagnostics based on coherent four-photon light scatt. by ionic sound 79—14618
plasma diagnostics using spectral line intensity ratios 78—14203
plasma diagnostics using X-ray spectrometer, high-speed, multichannel 80—57445
plasma electron density, determ. by spectral line width, at. oscill. strength effects 77—51230
plasma electron density and mag. field meas. by far IR polarimeter-interferometer 79—32817
plasma electron density display with resonance cone RF probe 77—62404
plasma electron density profile evaluation from integrated meas. 79—77418
plasma in coaxial source, optical meas. 78—1895
plasma in EM trap, density meas. *(Russian)* 78—5944
plasma jet, supersonic, ionisation in Mach disc, submillimeter laser interferometry diagnostics 80—14934
plasma oscillations, Vlasov theory, linear approx., electron distrib. initial value problem 77—84423
plasma probe, elec. highly negative, in flowing continuum plasma, ion sheath 77—72493
plasma probe, spherical, slightly ionised continuum, current-pot. curves 77—72494
plasma-wave excitation, self focusing, ponderomotive nonlinearity transient setting, carrier diffusion time 79—77387
plasmapause, electron density profile meas. stimulated plasma wave results *(Japanese)* 80—94650
plasmapause, radio sounding by geostationary satellite *(Japanese)* 78—85770
plasmasphere, 500-3500 km attitude region, electron density and temp., dawn and dusk sectors 78—32293
plasmasphere, columnar electron content 77—60533
plasmasphere, electron content and scintillations, deduced from study of ATS-6 radio beacon signals *(French)* 79—58184
plasmasphere, electron density and temp. latit. vars. 78—28383
plasmasphere, electron temp. and conc. at 3000 km altitude, ISIS-1 meas. 79—101004
plasmasphere, mid-latitude, nighttime electron content, geophysical disturbance effects, 1974 August to November 80—94642
plasmasphere, photoelectron flux buildup 78—40745
plasmasphere, slant total electron content temporal vars. rel. to ring current intensity and plasmapause 78—28404
plasmasphere, whistler duct positions 77—53301
plasmasphere electron content, magnetic storm effect 78—36403
plasmasphere electron density, whistler data on solar cycle, annual and diurnal vars. 78—88985
plasmons, wakes, and clusters, charged particle moving in medium, electron density fluctuations 79—47032
polyethylene filament, plasma prod. by staged laser heating, optical obs. 77—89321
positive column, in pulsed low-pressure Hg discharge, radial distributions 79—64920
profile inversion of simple plasmas and nonuniform regions, three-pole reflection coeff. 77—3984
protonosphere, electron conc. inhomogeneities meas. by whistler method 77—67011
protonosphere, electron content meas. from American and European sectors 78—45151
protonosphere depletion assoc. with mag. storm, and recovery 80—85784
protonosphere-ionosphere coupling, postsunset obs. with Arecibo radar 79—70915
pulsar magnetosphere, polar cap model rel. to electron energy and density *(Russian)* 79—101169
pulsar magnetospheres, power-law electron and ion distributions in a strong magnetic field 79—96908
pulsed discharge plasma, quasistationary stage props., calc. method 78—38560

electron density continued
pulsed laser discharges, interferometric meas. 80—96393
quasars, temp. and electron density in narrow line region 80—31364
radar aurora, per-unit-vol. RF scatt. cross section calc. 78—45079
radiation pressure, Thomas-Fermi eqn. of state, high temp., coupling to high-density electron plasma 77—3925
radioactive decay lifetimes, influence of chemical environment, review 79—75911
relativistic electron beams, striations in density distrib. rel. to plasma column instability 80—24154
RF discharge, electron heating and ionisation, rate eqns. 77—24237
RF discharge in mag. field, plasma rate equation 78—67455
Rosette Nebula (NGC 2237/2246), electron density and temp. from 6.5 GHz obs. 80—4414
S187, H109α recomb. line obs., core envelope type struct. 79—8965
sarcoplasmic reticulum hydrated oriented multilayers, lamellar X-ray diffr. 78—11614
Saturn, ionosphere, chem. and phys. props., model calcs. 80—26801
Saturn, ionosphere electron density from Pioneer II radio occultations 80—94751
scaling laws, width-luminosity correls., Wilson-Bappu effect 79—40177
semiconductors, electron-electron collision effect on current voltage characts. in quantising mag. field 80—103705
solar active region and flare plasmas, electron density from Fe IX lines intensity ratio 78—20771
solar atmosphere, C III 1909 Å and Si III 1892 Å emission lines, echelle obs. 80—31277
solar atmosphere, density depend. of O I like ions emission lines 79—40165
solar atmosphere, density modulation rel. to centimetre and millimetre wavelengths emission oscills. 77—22175
solar chromosphere-corona transition region, interpretation of C III and O V emission line ratios 78—28598
solar corona, density determ. from Fe IX lines 79—44429
solar corona, density distrib. models rel. to shock wave propag. 78—16375
solar corona, density from Fe XII lines intensities 77—17458
solar corona, density model for N.polar hole at 1973 June 30 eclipse 80—98627
solar corona, electron densities from Abel-inverted intensities of EUV emission lines 77—13299
solar corona, electron densities from line ratios in N I isoelectronic sequence 79—16906
solar corona, electron density depletion from Fe XIV transient obs. (1976, April 20) 78—28617
solar corona, electron density distrib. rel. to temps., temp. gradients and comps. 77—53525
solar corona, electron density in 1973, June 30 trans-polar coronal hole 77—53526
solar corona, Fe IX forbidden transitions, density depend. 79—66986
solar corona, long distance arches density from centimetric quiet Sun reinterpretation 78—28597
solar corona, meas. from Faraday rot. of Crab Nebula during occultations 77—45593
solar corona, plasma radiowave fluctuations and turbulence, Venus 10 radio transmission expt. 79—80295
solar corona, rel. to photosphere mag. field strength 80—85913
solar corona and interplanetary medium electron density profile from Mariner 6 and 7 time delay meas. 77—33435
solar corona interconnecting loops, temps. and densities during transient brightenings 80—21972
solar coronal and chromospheric spikes obs. during 1973 June 30 eclipse, photometric anal. 77—17520
solar coronal hole, physical parameters defining changing struct. 78—20770
solar coronal holes, radio and EUV meas. *(Russian)* 78—16378
solar coronal holes, thermally conductive flows rel. to electron densities 78—28614
solar coronal streamers, electrons from K-coronameter meas. 78—4182
solar coronal structure overlying type III burst producing active region, electron density 80—21976
solar emission lines of NeV, MgVII, SiIX, SXI, population levels as function of electron density and temp. 80—21963
solar filaments, electron densities in filament-cavity model from centimetre obs. 78—28602
solar flar spectra, high dielectronic satellite lines analysis for plasma props. calc. 80—12728
solar flare plasma, electron density from X-ray and XUV emission 78—12175
solar flares, determ. from X-ray spectra 80—82326
solar flares, electron densities from Ca XVII line ratios 77—87358
solar flares, electron density enhancement rel. to O I 1355.6 Å and C I 1355.8 Å lines obs. 80—90381
solar flares, XUV electron density diagnostics 79—88633
solar inner corona density distrib. from Fe XIV 5303 Å line intensity obs. 78—61843
solar limb above active regions, Skylab obs. of H Balmer lines 77—33441
solar limb above quiet region and polar coronal hole, Skylab obs. of H Balmer lines 77—33440
solar limb active regions, electron densities from 1175 to 1940 Å emission-line spectra 78—96446
solar neighbourhood electron density determ. from pulsar distance estimates by trigonometric parallax 79—88694
solar surge prominence, 31 May 1971, electron density from continuum event obs. 77—22183
solar transition region, electron density and temp. from N IV and Ne VII emission line ratios 80—17559
solar transition zone, density diagnostics for EUV spectrum 77—60739
solar transition zone, electron density, energy balance and press. from EUV spectra 80—21957
solar transition zone, electron density determ. from O III Bowen fluoresc. meas. 78—93179
solar type III radio bursts, electron density along burst trajectory 78—20808
solar wind, electron density meas. via International Sun-Earth Explorers 78—85803
solar wind, electron density small-scale fluctuations, interplanetary scintillation obs. 78—96376
solar wind, electron density spectrum from interplanetary scintillation 78—45178

electron density continued
- solar wind, suprathermal electrons population vars. near D sheets 77—29616
- solar X-ray flares, electron density profiles 80—17561
- southern H II regions models from radio recomb. line data 77—33620
- space simulation beam-plasma discharge, plasma diffusion 79—60108
- spark discharge, electron density determ. from Stark broadening of spectral lines *(Russian)* 80—28859
- spatial distrib. in nighttime polar ionosphere 78—73570
- sporadic-E layer, electron density explained by wind shear acting on metallic ions 80—46338
- SS 433, emitting region dia. and electron density from IR energy distrib. 80—31312
- Stephenson-Sanduleak 433, 1.2-2.5 μm spectroscopy, photometry and polarimetry 80—41838
- subauroral zone, electron content and f_0F_2 latit. var. 77—13164
- Sun, chromosphere above sunspot umbrae, temperature and electron density 78—53908
- Sun, electron density at 10^5K from O IV intersystem line obs. in EUV 78—53903
- Sun, quiescent prominences in He and Na emission regions *(Russian)* 78—20784
- Sun, quiet regions and polar coronal holes, electron density from EUV line intensity ratios 79—21245
- Sun, XUV flare kernels, electron density meas. 79—16913
- TEA laser discharges, inhomogeneities 77—14687
- thermionic advanced convertor with auxiliary ionisation, microwave heating 77—24216
- thermionic diode, uniformly heated, non-Boltzmann distrib. of free electrons, high space charge conditions 77—84390
- thermosphere, electron density and ion comp. meas., X-ray and EUV solar flux estimation 77—87145
- thermosphere, electron temp. and density relationship in daytime at solar minimum, model 78—61638
- tissue, Compton scatter imaging of transverse sections, corrections for multiple scatt. and attenuations 77—40742
- tissue, Compton scatter meas., calc. of single and multiple scatter photon fluences 78—28048
- tissue, determ. by computed tomography 77—81553
- tissue inhomogeneity corrections to absorbed dose calc. 78—3610
- Tokamak electron density meas., non-interferometric FIR scheme 80—14936
- topside ionosphere, electron density, comp., temps. and electron loss coeff. over Arecibo 78—36386
- topside ionosphere profile determ. by single meas. 77—56739
- total electron content at low latitudes 79—16749
- total electron content over Hawaii, secondary maxima 77—70925
- trapping region, quasiperiodic electron density pulsations, satellite detection 80—4198
- universal variational functionals of electron densities, first-order density matrices, and natural spin-orbitals and solution of the ν-representability problem 80—95516
- UV galaxies, double nuclei, visible spectra obs. *(Russian)* 80—77495
- UV photoplasma, electron density, microwave meas. 80—75097
- vacuum spark, electron density, interferometric meas. 78—5962
- Venus, nightside ionosphere, electron temp. and density models 80—46442
- Venus, polar ionosphere, Pioneer orbiter radio occultations, electron density 79—48706
- Venus daytime ionosphere, density profile from two-freq. radioscopy by (Venera 9 and 10) 78—4129
- Venus daytime ionosphere, Veneras 9 to 10 dual-freq. radio occultation expts. studies 79—96939
- Venus ionosphere, plasma diagnostics meas. by Venus Orbiter *(German)* 79—96941
- Venus nighttime ionosphere, density profiles from two-freq. radioscopy by (Venera 9 and 10) 77—91454
- W51, electron density from recomb. line impact broadening 78—28741
- wake, hypersonic, free electron distrib., RF method 79—27833
- waveform distortion by microwave scatt. 79—50859
- Wolf-Rayet stars, electron density in emission-line region 78—93263
- X-ray elastic scatt., electron density and ionisation pots., Thomas-Fermi and Hartree Fock anal. 79—52041
- Al XII, electron density meas. using Stark profiles 79—81181
- Ar arc plasma, transition probabilities, continuum emission coeffs., electron density 77—51228
- Ar ion laser, collisional radiative model and expt. 78—55338
- Ar, ionising boundary layer in shock-tube side-wall flow 79—60144
- Ar, optical breakdown at 10.6 μm near plasma layer boundary 79—60165
- Ar plasma, ion confinement and heating, by negative plasma potentials produced by supplemental electron emission 79—41861
- Ar plasma, radial distrib. of excited atoms prod. by surface wave *(French)* 80—96349
- Ar plasma, shock-compressed, thermophysical and gasdynamic characts. 77—43016
- Ar plasma radiation obs., line and continuous spectra *(French)* 80—19619
- Ar, positive column, contracted, electron density, temp., elec. field, line emission 80—6311
- Ar, positive column, contracted, balance equations anal. 80—6312
- Ar, precursor shock waves, electron density and assoc. ionisation 78—67217
- Ar, UHF discharge theory *(Russian)* 77—62430
- Ar-H plasma, electron density meas. rel. to AR I 3949 Å Stark width 79—63954
- Ar-H_2, elec. breakdown, time and space resolved spectra 78—18470
- C foil+$H^+(C^+)(N^+)(O^+)(Na^+)(Mg^+)(S^+)(Kr^+)$, charge-state distrib. effect on photon emission, 100-400 keV 79—22814
- CO CW gas lasers, effect of Xe addition on room temp. operation 79—18407
- CO-N_2-^{3}He, nucl. reactor active zone, plasma and sustained discharge props. 80—5729
- CO_2, laser discharges, determ. of recombination coeff. 78—90407
- CO_2 self-sustained laser system, electron avalanche and electron-ion recomb. coeffs. meas. 80—102694
- CO_2 TEA laser, laser output depend. on initial photoelectron density 80—43320
- CO_2 TEA lasers, one-step photoionisation, preionisation discharge effect on electron density 80—53256

electron density continued
- Cl^- free-bound continuum radiation threshold broadening obs. in plasma 78—71579
- Cs-He plasma, steady-state discharge, role of inelastic collisions, spectroscopic diagnostics 78—42709
- Cu laser, time depend. of electron density, resist. and interferometric meas. 78—25864
- Cu/CuCl double pulsed laser, extrema by electron density and output pulse energy 79—10283
- D plasma, high current pulse discharge investig. *(Russian)* 78—47171
- F_2-layer, low latitude, electron density eqn. of continuity soln. 80—101472
- Fe XXI as electron density diagnostic in solar flares 79—44435
- GaSb:Te,Zn(Te,Mn), prep. and electrophys. props. 79—87116
- H II regions, electron density errors from radio emission improper anal. 78—54000
- H spark, laser-triggered, electron densities meas. 80—106975
- H spark gap arc discharges, laser-triggered, electron density meas. 80—64822
- H-like ions, emission spectrum, depend. on electron density in laser plasma 79—27248
- H_2^+, mol. electron density distrib., binding/antibinding anal. 80—95534
- He plasma, electron density, determ. by emission coeff. and Stark broadening *(German)* 77—58903
- He plasma, in low-press. discharge, He I and He_2 line struct. 79—14523
- He, spark prod. by short laser pulses, spectroscopic meas. of temp. and electron density 77—43086
- He-Co_2-Xe plasma discharge electron conc. and temp., optical diagnostics method 79—41871
- He-Eu pulsed laser, pumping rate and electron density meas. 80—9868
- He-I^+ laser discharge, positive column, particle densities 80—103215
- He-Kr^+ laser, microwave-pulse-excited, internal plasma parameters, time variation 77—38858
- He-metal vapour lasers, positive column electron densities, experimental study *(Japanese)* 80—69376
- He-Ne laser plasma, metastable at. and electron density diagnostics 77—84499
- He-Sr pulsed laser, pumping rate and electron density meas. 80—9868
- He-Zn hollow cathode laser, electron density, excited ions radial profiles 78—29937
- Hg plasma, continuous spectra at series limit 6p′ $^3P_2$ *(French)* 77—88413
- Hg vapour, electron drift velocity at 573K 80—103103
- Hg-He(Ar), modulated discharge, elec. and optical props. 77—7627
- Kr glow discharge, electron energy distrib. function, electrical characts. investig. 80—24279
- Kr plasma, shock-heated, continuum radiation emission coefficient meas. 79—64835
- Kr(-He) arc, wall-stabilised, atm. press. 79—46503
- Li wire high energy density exploding plasma, holographic interferometry, self pinching, charge density 79—77436
- Mg break arc, LV, low current, electron density, temp., local thermodynamic equilib. 78—9878
- Mg vapour, electron momentum transfer cross section, from 0.1-5 eV 80—103104
- N_2 afterglow, chem. reactions rel. to plasma props, appl. to toluene polymerisation 80—3346
- N_2, correlated electron density using AHF GTO wavefunctions 80—23313
- N_2, electrical and optical discharge parameters at moderate press. 80—6300
- N_2-methane, rapidly developing discharge, streak camera records interpretation 80—59280
- N_2-SF_6 pulsed discharge laser with CW X-ray preionisation 80—95910
- Na vapour, electron and ion beam transportation channel form., reson. saturation based laser ionis. 79—77410
- Na-Xe, excimer lasers, high-power discharges, models 80—69373
- Ne plasma, generated by 200 MeV protons, electron density and electron temp. 78—22568
- O II and S II forbidden lines as determinant of reddening and electron density, astron. appl. 79—30114
- O_2 discharge plasma, metastable states role, two-step ionisation, electron densities and transition pts. 80—44019
- O_2, low energy electron drift velocity at 293K 80—103101
- $Pb_{0.78}Sn_{0.22}$Te:In, low current carrier conc., Hall effect, lattice constant 79—82603
- Ru complex, HF calc., electron densities and Mossbauer isomer shift, chemical binding 78—50470
- SF_6 plasma column, in Maecker type arc, diagnostics and model *(French)* 80—19652
- Si MOSFET, n-type inverted surface channel, reproducibility of electronic props. 79—99628
- Xe plasma, shock-compressed, thermophysical and gasdynamic characts. 77—43016
- Xe, pulsed high frequency discharge, energy spectrum and electron density meas. *(Russian)* 78—26354

electron density (crystallography) *see crystallography*

electron density (metals)
- alkali metals, partial pressure contributions to equation of state 80—107401
- alkali metals, vacancy formation energy calcs., electron density functional method 80—19801
- alloy, binary, surface segregation prediction using bulk alloy variables 79—65300
- colloidal particles, interaction force, calc. of electronic component 79—11829
- ferromagnetic film, influence of electron density on mag. moment 79—69700
- Hall mobility and carrier conc. in metal-like phases *(Ukrainian)* 79—95386
- hot electron distrib. at low temp. *(Russian)* 77—12056
- interatomic potentials of Na, K, Al, Cu, Fe from phonon spectra 80—19744
- liquid metal, surface ion density, nonmonotone, perturbative discrete ion introduction into jellium 78—72222
- liquid metals, charge density fluctuations in surface layer *(Russian)* 80—15580
- local density functional for kinetic energy near defect, metal surface 80—20105
- metal, electron density behaviour near impurity charge 80—75518

electron density continued
metal hydrides for H storage, effect of interstitial hole size and electron conc. 80−45789
metal surface, electron density depend. on modulation, adsorption, diffusion 80−54526
metallic film, carrier density, evaluation from transverse elec. field and cond. meas. *(French)* 80−39682
metallic film, electron density and potential, variational calc. 79−78218
metals, ground state of solids, spin density functional method, binding energy, compressibility 80−65477
metals, liq., charge density fluctuations in surface layer *(Russian)* 80−15580
nontransition metals, electron density, bulk and surface props. relation 80−103609
nontransition metals, electronegativity parameters of theory of heats of alloy form. 79−74412
point contacts, metallic, elec. cond., spectroscopy of phonons, impurities *(Russian)* 78−38797
surface, self-consistent electron theory, review 80−88616
surface electronic barrier, elec. field effect in presence of adsorbate, Thomas-Fermi model 80−49864
transition metal group VIII aluminide, NMR near equiatomic composition *(Russian)* 80−20479
unidimensional metals, plasmon freq., effect of nonuniform electron density profile *(Russian)* 80−59896
valency electron density and total energy, weak pseudopotential calc. *(German)* 77−59241
Ag clusters, charge distrib., density of states, CNDO calcs. 78−70995
Ag-Ge alloy system, atomic struct. and electronic props. *(Russian)* 77−20289
Al, surface electron density crimping, Ashcroft potential, density functional calcs. *(Russian)* 79−82653
Al-Cu films, deposition rate, mol. beam incidence angle influence on struct., film props. *(Russian)* 79−60646
Au-transition metal alloys, ^{197}Au Mossbauer isomer shift cellular atomic model 80−84673
Be metal, electron distribution and momentum density, Compton scatt. 80−11502
BiSb (>20 wt.%), electronic band struct. 80−107698
Co(GaTiV) alloys, ferromag. onset, electron conc. depend. 80−60203
Co$_3$Ti, electron energy spectrum calcs. by supplementary plane wave method 80−6711
Cr-Fe, elastic moduli, electron conc., pulse echo overlap meas. 80−59550
Cr-Ni, high temp. strength, interatomic bonds ionic component correlation *(Russian)* 79−15761
Cu crystal, cohesion and vacancy form., electron statistical model 80−54169
Cu-Ge(Sb) alloy systems, atomic struct. and electronic props. *(Russian)* 77−20289
Fe-Al, electron density distrib. vs. at. order 79−60309
Fe-Ni alloy, optical and electronic characts., 20-1750°C, comp. depend. *(Russian)* 78−84601
Fe-Si, electron density distrib. vs. at. order 79−60309
Fe$_3$Al, order-disorder transform. effect on optical and elec. props. *(Russian)* 77−39820
Ga film, monoclinic, elec. cond., classical size effect 77−89881
B-Ga, metastable, elec. props. in normal and supercond. states *(Russian)* 80−65520
Hg electrode, electroreflection spectra calc., electromodulation mechanisms 77−1658
In film, evaporated, resist., Hall effect and light transmittance, use as semitransparent electrode 77−39966
Ir, surface electron density crimping, Ashcroft potential, density functional calcs. *(Russian)* 79−82653
Nb (001) ideal surface, self-consistent pseudopot. calcs. 77−76894
Ni, defect electronic struct., strength characteristics relation by positron annihilation 79−91526
Ni films, electronic struct. calc., effects of chemisorption; contact pot. and surface magnetisation 80−103734
Ni-Fe, electronic struct. calc., effects of chemisorption; contact pot. and surface magnetisation 80−103734
Ni-Ge alloys, liq., integrated emissivity, electric resistivity 78−43155
Ni$_5$Ge$_3$, amorphous-crystalline transition, opt. and elec. characts. *(Russian)* 77−85191
Pb, dislocation electron drag coeff. temp. depend., internal friction method, superconducting state 80−29031
Pt, surface electron density crimping, Ashcroft potential, density functional calcs. *(Russian)* 79−82653
Re, surface electron density crimping, Ashcroft potential, density functional calcs. *(Russian)* 79−82653
SmS, metallic, thermal modulation of reflectivity, 1.2-3.8 eV 79−99909
Te-transition metal, liquid, dil., elec. resist., cond. electron conc. 77−15814
Ti-V, elastic moduli, electron conc., pulse echo overlap meas. 80−59550
W, surface electron density crimping, Ashcroft potential, density functional calcs. *(Russian)* 79−82653
Yb, film, amorphous and cryst., transport props. rel. to band struct. *(Russian)* 77−12026

electron density of states *see electronic density of states*

electron density of states (condensed matter) *see electronic density of states*

electron detachment
acetophenone, enolate anion, electron photodetachment cross-section resons. 78−5298
acetophenone enolate anion radicals, substituted, electron photodetachment cross sections, reson. states 80−1030
alkali metal anions, photodetachment cross-sections and multipole polarisabilities, extended asymptotic model 78−42028
atmospheric negative ions, electron detachment rates, time lags to breakdown 78−87564
atmospheric negative ions, photodissoc. and photodetachment 78−66609
atom, photoabsorption, correlation effects 77−42299
atom+ion collision, slow, electron detachment *(Russian)* 77−30985
atom+negative ion, rainbows, interference, and diffr. effects *(Dutch)* 79−50110
atom-negative ion collisions, linear approx. in generalised zero-range pot. model *(Russian)* 79−94076
atomic negative ions, photodetachment, zero core contribution model 79−93961
benzyl anion, IR multiphoton electron detachment 79−94043

electron detachment continued
cyclopentadienyl ion, electron affinity and Jahn-Teller effect, laser photoelectron spectra 77−88499
diatomic negative hydrides, photodetachment 0.5 to 3.0 eV, electron affinities *(German)* 77−61812
electron-ion collisions, crossed beam expts. 78−58843
elementary atomic processes, threshold behaviour 80−23546
ethynylradical, photodetachment, parturbation theory calcs., ICR spectroscopy obs 79−98166
excited atom ionisation due to collisions in their own gas *(Russian)* 80−91654
glow discharge, non self-sustained, detachment process effects 78−59713
halogens, negative ions, electron spin polarisation in photodetachment 78−25495
inner shell excitation processes in heavy ion-atom collisions, review 80−37874
ion electron impact detachment, ionisation, excitation, dissociation and recombination 80−63832
ionosphere D-region, sunrise variations of negative ions and electron conc. 80−31157
methoxide-d$_0$(−d$_3$) anion, electron affinity, vibr. struct., photodetachment electron spectra 78−94282
negative ion+atom, electron detachment, zero range Fermi approach 80−63798
negative ion+molecule, electron detachment *(Russian)* 79−59566
negative ion+molecule (atom), negative ion stripping, at. beam form. 77−6926
negative ion photodestruction in elec. field 77−20897
negative ions, at. and mol. collisions electron detachment for energies near threshold 80−63797
negative ions, autodetachment, spectroscopy 80−23385
negative ions, electron impact detachment cross sections, classical scaling theory appls. 80−83492
negative ions, photoabsorption spectra, long-range field effect 80−91521
negative ions, photodetachment 79−52715
open shell systems, coupled cluster approach 78−58595
positive column of glow discharge of electronegative gas, molecular excitation and ionisation by electron collisions 80−49031
resonance partial widths and partial photodetachment rate using the rotated-coordinate method 80−91428
slow atomic collision, electron detachment, energy spectrum and isotope effects *(Russian)* 77−30984
thiomethoxide anion, electron affinity, vibr. struct., photodetachment electron spectra 78−94282
thiomethoxyl anion, and deuterate, electron photodetachment, affinities, vibr. freq. and spin-orbit splitting 80−53063
total to K-shell photoelectric cross section ratios, variation with atomic number and photon energy 77−54545
Ag(I) ions, in methyl cyanide, electron loss and capture, ESR spectra 79−33531
Ar+Ar$^+$(Ar^{2+})(Ar^{3+}), electron stripping cross-sections meas. 80−83477
Ar+H$^-$, collisional electron detachment, complete ang. distrib. 78−66650
Ar+H$^-$, low-energy total electron detachment cross-sections, approximation 79−72405
As$^-$, photodetachment cross-section meas., crossed beam expt. 77−61723
As$_2^-$, photodetachment cross section, 0.5 to 3.0 eV photon energy *(German)* 77−65518
Be$_n^-$ (n=2,3,4), electronic struct., ab initio calcs. 78−17560
Bi$^-$, photodetachment cross-section meas., crossed beam expt. 77−61723
Br$^-$, electron photodetachment cross-section determ., from CsBr dissoc. 77−3330
Br$^-$+H$_2$(D$_2$)(O$_2$)(N$_2$)(CO)(CO$_2$)(methane), total electron detachment cross sections for energies around threshold 80−99550
Br$^-$+He, electron detachment, SCF calcs., BrHe$^-$ and BrHe pots. 80−23503
Br$^-$+He(Ne)(Ar)(Kr), total electron detachment cross sections, near threshold energies 79−3555
BrCl$_2^-$, photodissoc. and photodetachment, pot. curves. 79−64060
C$^-$, electron impact detachment, cross-section, 10-1000 eV 79−31702
C$^-$, electron impact detachment cross sections 79−89787
C$^-$, near-threshold photodetachment, IR meas. 77−42290
C$^-$+CO(Mg)(N$_2$), electron detachment cross-sections, 20-150 keV 78−25690
CH$_2^-$, photodetachment cross section, 0.5 to 3.0 eV photon energy *(German)* 77−65518
CH$_3^-$, photodetachment cross section, 0.5 to 3.0 eV photon energy *(German)* 77−65518
CO$_2^-$, dissoc., $^2\Sigma_g^+$ state, Wall Porter pot. surface, autodetachment and vibr. level population inversion 80−21275
CO$_2^-$, hydrated anion stable gas phase heteronuclear clusters, mass spectra, autodetachment rates 80−14266
CO$_2$-H$_2$O-O$_2$, gas mixture, photodetachment and photodissoc., mass spectra meas. 77−500
CO$_2$-O$_2$-H$_2$O, mixture, mol. negative ions, photodissoc. and photodetachment cross section 77−27129
CO$_2$-O$_2$-H$_2$O, photodissoc. and photodetachment of negative ions 80−14182
CO$_3^-$, thermally relaxed, photodetachment cross-section and solar detachment rate determ. 77−58094
Cl$^-$, electron photodetachment cross-section determ., from CsCl dissoc. 77−3330
Cl$^-$ radiative detachment threshold effect of plasma microfield 78−71580
Cl$^-$+Ar, detachment energy threshold from ArCl pot. energy curve 78−62745
Cl$^-$+Ar→Cl+Ar+e, rate const., absolute total cross section, expt. results discrepancy 77−513
Cl$^-$+Ar→Cl+Ar+e, rate const., expt. discrepancy 77−514
Cl$^-$+H$_2$(D$_2$)(O$_2$)(N$_2$)(CO)(CO$_2$)(methane), total electron detachment cross sections for energies around threshold 80−99550
Cl$^-$+He(Ne)(Ar)(Kr), total electron detachment cross sections, near threshold energies 79−3555
Cl$^-$+inert gas atom, electron detachment and inelastic processes 78−42208
Cl^{4+}+Xe(Ar)(N$_2$), 20 MeV, electron loss cross sections, pot. model data anal. 79−27082
Cl$_2^-$, photodissoc. and photodetachment, pot. curves. 79−64060
Cl$_3^-$, photodissoc. and photodetachment, pot. curves. 79−64060
ClO$^-$, photodissoc. and photodetachment, pot. curves. 79−64060
Cr$^-$, photodetachment cross-section meas., crossed beam expt. 77−61723

electron detachment continued
- Cs$^-$, multichannel photodetachment 78−42027
- F$^-$, electron impact detachment cross sections, test of classical scaling theory 79−31693
- F$^-$, near threshold electron detachment cross section, effect of resons. 77−42403
- F$^-$, photodetachment cross section, Stieltjes imaging method 78−55149
- Fe$^-$, electron affinity, nonstatistical fine-struct. detachment intensities at 488 nm, laser electron spectra 79−41144
- Fe^{4+}+N$_2$(Ar)(Kr)(Xe)(SF$_6$), 20 MeV, gaseous targets, electron loss, charge state yields 79−54957
- H$^-$, bound-free photodetachment cross-section calcs. 80−9567
- H$^-$, density meas. by photodetachment 80−48976
- H$^-$, electron detachment by electron impact, 1s state product, Born approx. 78−78816
- H$^-$, electron loss in passing through inert gases 79−13805
- H$^-$, in solar atmosphere, bound-free electron transitions, review 78−33563
- H$^-$, ion beam diagnostics using laser beam 80−95497
- H$^-$, photoabsorption spectra, long-range field effect 80−91521
- H$^-$, photodetachment, Feshbach and shape resons. 77−23480
- H$^-$, photodetachment, measurement of density in plasma 79−73045
- H$^-$, photodetachment cross sections, one and two electrons, multichannel J-matrix calc. 77−18860
- H$^-$, photodetachment cross section, dynamic polarisability calc., sum rules, basis set depend. 78−17635
- H$^-$, photodetachment cross section, Feshbach and shape reson. elec. field depend. 78−37614
- H$^-$, photodetachment cross section, perturbation-variation method 79−6921
- H$^-$ photodetachment cross section, narrow resonances near n=3 threshold 80−27988
- H$^-$, two-electon photodetachment threshold, blackbody radiation effects 80−91524
- H^{2-}, existence, alternative explanation of results, electron effects 77−19079
- H+Ar, detachment energy threshold from ArH pot. energy curve 78−62745
- H+H$^-$, electron loss by 1-300 keV H$^-$ ions 80−37857
- H+H$^-$→H+H+e, electron detachment from H$^-$ 80−37855
- H$^-$+Ar, electron detachment, 0.5 to 1.0 MeV 78−22021
- H$^-$+Ar(H$_2$)(He)(N$_2$)(Ne), collisional detachment cross-sections, high-energy obs. 77−3442
- H$^-$+H, electron detachment cross-sections, 100 keV-10 MeV 79−59561
- H$^-$+H$_2$, electron detachment cross-sections, 100 keV-10 MeV 79−59561
- H$^-$+H$_2$(He)(Ar), electron detachment, Born cross sections, Pade approximants 78−17742
- H$^-$+H$^+$, electron detachment cross sections 79−13818
- H$^-$+H(He), electron detachment cross sections 78−90265
- H$^-$+H(He), electron detachment in adiabatic regime, mechanisms 80−63800
- H$^-$+He, detachment energy threshold from HeH pot. energy curve 78−62745
- H$^-$+He, electron detachment, theoretical obs. 80−63799
- H$^-$+He, electron detachment cross-sections, 100 keV-10 MeV 79−59561
- H$^-$+He, electron detachment cross-section, target distortion calcs., 100 keV-100 MeV 79−59562
- H$^-$+He, electron detachment collision 80−23536
- H$^-$+He(Ar), electron detachment cross sections 78−58810
- H$^-$+He(Ne)(Ar), differential scatt. cross-sections, time of flight spectra 78−42161
- H$^-$+inert gas, negative ion detachment cross section determ. 80−63796
- H$^-$+N$_2$ (inert gas), charge transfer, ejected electron spectra 79−45828
- H$^+$+H$^-$, electron detachment cross-section, crossed beam meas. 77−10728
- H$_2$+H$^-$, electron loss by 1-300 keV H$^-$ ions 80−37857
- H$^-$(D$^-$)+He, collisionally induced electron detachment, 0.5 MeV, target effect 80−37858
- H(1s,2s)+H(H$_2$), electron capture, loss, and collisional destruction, 5-26 keV 80−5611
- He$^-$, electron loss in passing through inert gases 79−13805
- He+H$^-$, low-energy total electron detachment cross-sections, approximation 79−72405
- He$^-$+Ar(H$_2$)(He)(N$_2$)(Ne), collisional detachment cross-sections, high-energy obs. 77−3442
- I$^-$+Ne, electron detachment collision, 1-3 keV, differential cross-section 79−72403
- I^{5+}+Xe(Ar)(N$_2$), 20 MeV, electron loss cross sections, pot. model data anal. 79−27082
- K$^-$, multichannel photodetachment 78−42027
- K$^-$, photodetachment and at. polarisability 80−91522
- NH$_2^-$, photodetachment energy calcs. 77−27123
- NH$_2^-$, photodetachment energy, eqn. of motion method 78−5301
- NO$^-$ destruction in collisions with excited molecules 80−14189
- NO$_2^-$, electron detachment energy, equations of motion method calcs. 77−50478
- NO$_2^-$, NO$_2^-$.H$_2$O, and peroxy isomers, photodissoc. and photodetachment 3500-8250 Å, rel. to ionosphere 80−35554
- NO$_2^-$+O$_2$(CO$_2$)(NO$_2$), photodetachment and de-excitation rates 77−75236
- NO$_3^-$, NO$_3^-$.H$_2$O, and peroxy isomers, photodissoc. and photodetachment 3500-8250 Å, rel. to ionosphere 80−35554
- NaCl$^-$, NaBr$^-$, NaI$^-$, photodetachment cross section resons., 2-2.3 eV 79−54922
- Ne+H$^-$(D$^-$), electron detachment, dynamical phenomenon 80−106305
- Ni$^-$, photodetachment cross-section meas., crossed beam expt. 77−61723
- O$^-$, electron impact detachment, cross-section, 10-1000 eV 79−31702
- O$^-$, electron impact detachment cross sections 79−89787
- O$^-$, photodetachment, fine struct. transitions, photoelectron spectra 78−55151
- O$^-$, photodissoc. and photodetachment in O$_2$/CH$_4$/H$_2$O mixtures, 3500-8600 Å 79−45776
- O$^-$+CO(Mg)(N$_2$), electron detachment cross-sections, 20-150 keV 78−25690
- O$^-$+N$_2$, electron detachment, collision with vibr. excited mols. 79−54961
- O$^-$+N$_2$→N$_2$O+e, rate studies 78−40036
- O$^-$+Ne(Ar)(Kr), 0.2-1 keV, elastic and inelastic reduced differential cross-sections 80−32829

electron detachment continued
- O$^-$+O$_2$, electron detachment, collision with vibr. excited mols. 79−54961
- O$_2$ discharge plasma, metastable states role, two-step ionisation, electron densities and transition pts. 80−44019
- O$_2$, interactions with slow electrons 79−45848
- O$_2^-$, in nonpolar liqs., laser photodetachment, elec. cond. obs. 79−64057
- O$_2^-$, photodissoc. and photodetachment in O$_2$/CH$_4$/H$_2$O mixtures, 3500-8600 Å 79−45776
- O$_2^-$+N$_2$, electron detachment, collision with vibr. excited mols. 79−54961
- O$_2^-$+O$_2$, electron detachment, collision with vibr. excited mols. 79−54961
- O$_3$, (O$_3^-$.H$_2$O), photodetachment and photodissoc. cross-sections meas. 79−98170
- O$_3^-$, photodissoc. and photodetachment in O$_2$/CH$_4$/H$_2$O mixtures, 3500-8600 Å 79−45776
- O$_3^-$, photoelectron, photodetachment and photodestruction spectra 79−64042
- O$_3$+O$^-$(OH$^-$)(S$^-$)(SH$^-$), associative detachment, rate coeffs. 78−3325
- O$_4^-$, photodissoc. and photodetachment in O$_2$/CH$_4$/H$_2$O mixtures, 3500-8600 Å 79−45776
- OH$^-$, and OD$^-$, photodissoc. and photodetachment in O$_2$/CH$_4$/H$_2$O mixtures, 3500-8600 Å 79−45776
- O$_{2-3}^-$.H$_2$O, photodissoc. and photodetachment in O$_2$/CH$_4$/H$_2$O mixtures, 3500-8600 Å 79−45776
- O$_3^-$.H$_2$O and O$_3^-$.2H$_2$O, photodissoc, and photodetachment 79−833
- P , photodetachment cross-section meas., crossed beam expt. 77−61723
- P$_2^-$, photodetachment cross section, 0.5 to 3.0 eV photon energy *(German)* 77−65518
- P$^-$(^{3}P$_{2,1,0}$)+hν, P electron affinity, P$^-$ fine struct. interval 77−79590
- Rb$^-$, photodetachment, electron affinity 78−90132
- S , photodetachment, fine struct. transitions, photoelectron spectra 78−55151
- S$^-$, photodetachment cross section mag. field depend. struct., obs. 78−55148
- S , photodetachment in mag. field 79−41143
- S$_3^-$, photodetachment cross section, 0.5 to 3.0 eV photonenergy *(German)* 77−65518
- Sb$^-$, photodetachment cross-section meas., crossed beam expt. 77−61723
- Si$^-$, ground state, photodetachment cross section calc., low energy 79−63970
- Te$^-$, photodetachment cross-section meas., crossed beam expt. 77−61723
- Te$^-$(^{2}P$_{1/2,3/2}$)+hν, Te electron affinity, Te$^-$ fine struct. interval 77−79590

electron detection and measurement
- absorbed dose in water, absolute meas. using total absorpt. type calorimeter and dose detectors *(Japanese)* 78−78501
- accelerated electron beam current monitor using secondary emission detection 78−78033
- accelerator with scanned beam, measurement of average energy of electrons in atmosphere, 0.3 to 1.0 MeV 79−97956
- Akenon Air Shower project, e and μ obs., core energy flow, device description 79−72184
- anthracene, scintillation decay time determ. using low energy spectra 79 9964
- atmospheric electrons, MeV range registration instrument 79−5645
- avalanche multistep chamber 79−9965
- backscattered electron detector, multi-purpose 80−102404
- backscattered electron detector, small solid angle, cryst. orientation contrast and contrast reversal in SEM 79−17579
- backscattered electrons in SEM by conversion to secondary electrons 80−62804
- balloon born cosmic ray electron detectors, curious random counting statistics, electric circuit 78−17540
- beam dosimetry for treatment planning 80−3817
- beam parameter meas. collector plate amplifier 79−75653
- bubble chamber electromagnetic shower photographs, for teachers 78−65737
- cascade shower, 350 MeV, angular distrib. meas. by streamer chamber 79−6802
- channel plate electron multipliers, single electron detection and timing 80−9458
- constant fraction timing discriminator for channel plate electron multipliers 79−59316
- conversion electron spectroscopy following (HI,xn) reacts., kinematic Doppler correction method 79−54739
- delay line for position readout in wire chambers 80−18757
- differential calorimeter for electron radiation 79−6795
- dose distrib. in radiation processing 79−49872
- dose-rate conversion factors for external exposure to photons and electrons, modifications to DOSFACTER code 80−104775
- dosimetry standardisation in Germany 80−5353
- double focusing Fe core electron spectrometer BILL for (n,e$^-$) meas. 78−82566
- double proportional counter for measurement of radioisotope Auger electrons and X-rays 79−81129
- drift chamber in strong mag. field, electron drift angle meas. 79−3299
- electron and γ interaction ranges, Monte Carlo calc. *(Russian)* 79−12370
- electron multipliers with discrete and continuous dynodes, detection of 5-50% keV electrons *(German)* 79−97946
- electron-matter interactions rel. to electron microscopy 80−89097
- electron-photon cascades separation by scintillation counter system 78−78563
- EM shower sampling counters, characteristics of plastic scintillator and radiator layers 78−58530
- ESP detector for 300-2000 eV electron, optimum conditions theory *(Japanese)* 78−66693
- fast electron f(z) meas. using short accelerator pulses 80−12275
- film photon and electron absorbed-dose detector 80−91379
- gas proportional counter, relativistic electron ionisation loss, transition radiation effect 78−25389
- high density proportional counter, medical imaging of e$^+$ radioisotope distrib. 79−5399
- high rate 4π β-γ coincidence counting system 79−45588
- high resolution spectrometers for electron scattering 79−68129
- high-vacuum gas-discharge electron counter 79−18086
- internal conversion electron measurement following the decay of ^{152}Eu 79−36460

- **electron detection and measurement** continued
  - internal pair formation high resolution in-beam studies with magnetic+Si(Li) spectrom. 79—18073
  - Johnston electron multiplier, low energy ion counting efficiency 80—63479
  - linear accelerator facility, detection system of proportional chambers, scintillation and Cerenkov counters 80—52809
  - liquid acoustic dosimetry for ionizing radiation 79—18060
  - liquid Ar calorimeters, props. of EM and hadronic showers 79—45599
  - liquid scintillation spectrom. meas. of internal conversion electrons 79—89520
  - liquid scintillation system ^{32}P Cherenkov effect detect. efficiency meas. using ^{60}Co external source 78—25387
  - liquid xenon proportional scintillation counter, detection of ^{207}Bi conversion electrons 79—45563
  - medium-energy electron-streams, cathodoluminescence/photoresistor composite detect. characts. *(Russian)* 79—41080
  - mica dosimeters, for visualisation of electron isodose curves in a medium 80—99349
  - microchannel plate based detector for a heavy ion beam spectrometer 80—58018
  - mini-orange spectrometers, conversion electron spectroscopy 79—93864
  - modular electron calorimeter, relative and absolute calibration 78—78578
  - Mossbauer conversion electron spectroscopy at high temp., proportional 80—27886
  - MWPC positron camera, two detector, appl. medical imaging 79—5398
  - MWPC with analogue read-out, high energy e$^-$/γ detection 79—13593
  - p-i-n photodiode, time resolution 79—14608
  - phosphate glass channel multiplier efficiency 78—41898
  - photoelectrons, phase-sensitive vidicon detector for angle-resolved electron spectroscopy 80—90933
  - positron camera, cylindrical, multilayer hybrid computed tomographic system, Bi$_4$Ge$_3$O$_{12}$ scintillation crysts. 78—48876
  - positron tomography, evaluation of semiconductor detectors 79—53221
  - proportional counter, energy loss of relativistc electrons and its fluctuation 78—94171
  - relativistic electron energy loss distribs. in thin gas layers of proportional counters 80—99429
  - relativistic electrons, 0.1 to 6.0 GeV superheated superconducting colloid shower detector 80—91398
  - scintillator detector, detection efficiency and performance estimation, of HV STEM 80—101899
  - scintillator Pb-acrylic shower detector, meas. of electron and pion cascades 79—81124
  - secondary emission monitors at the Bevatron-BEVALAC 79—72186
  - secondary-electron time pickoff for pulsed charged-particle beams 79—97957
  - single isolated electron measuring technique, resource letter for teachers 78—81776
  - spark chamber, electron-photon shower recording, single-particle background suppressing method 78—78573
  - spectroscopy, appl. in fundamental research and practice *(Hungarian)* 80—18046
  - STEM, quadrant detector, appls. 80—77914
  - STEM multichannel detector system 80—68331
  - subnanosecond plastic scintillators, 100 keV electron detection 80—69037
  - synchrotron-Cherenkov detectors 80—884
  - Voyager Cosmic Ray Experiment, telescopes, electron energy meas., pulse height analysers 79—48643
  - wide-angle electron detector 79—21144
  - Zener diode, breakdown voltage, electron irrad. effects 79—95472
  - (e,e′p) coincidence expts. at Saclay 600 MeV electron linac ALS 79—72035
  - Ar, liquid, calorimeter, electron and proton response 80—47832
  - CaF$_2$:Eu, scintillation detector, in STEM 80—101897
  - FeSO$_4$ dosimetry for electrons, a re-evaluation 80—68963
  - In$_2$Te$_3$ type semiconductors, basis of ionising radiation detectors 78—86743
  - In$_2$Te$_3$-type semicond. radiation-resistant fast-electron detectors 78—78559
  - MgO coated detector for SEM backscatter to secondary electron conversion 80—68332
  - Mg$_2$SiO$_4$:Tb, TLD response to e$^-$ irrad. 79—13536
  - Mg$_2$SiO$_4$:Tb TLD, response to high energy electrons *(Japanese)* 78—78502
  - Mg$_2$SiO$_4$:Tb TLD, response to X-ray and electron irrad. 79—3285
  - Mg$_2$SiO$_4$:Tb TLD, supralinearity of response to electrons and X-rays *(Japanese)* 78—78503
  - NaI position sensitive detector, test results 79—76288
  - NaI(Tl) scintillator, electron detection efficiency for electrons and gamma-rays > few keV 79—36461
  - Ne flash tube chambers for electron and photon detection 78—58552
  - Pb-scintillation counter, modular EM shower detector for CERN ISR 79—76275
  - Pb-scintillator calorimeter, electron energy and positron measurement 79—76273
  - Pb-scintillator sandwich EM shower detector, perform. characts. 80—102385
  - Si semiconductor counters, response to relativistic pions, electrons and protons 79—13597
  - Si-Li surface-barrier detectors for electron and soft X-ray spectrometry 80—882
  - Si(Li)-emulsion shower counter for cosmic ray electron obs. 80—58033
- **electron device manufacture**
  - *see also electron tube manufacture; integrated circuit manufacture; semiconductor device manufacture*
  - component and material improvement, ion implantation techniques *(French)* 78—18667
  - crystal resonator, quartz, stable exciting electrode preparation, by ion plating of Ag film on AT-cut quartz crystal 80—2280
  - cylindrical ceramics-metal laminated components, X-radiography 79—5123
  - glass microelectrode puller for reproducibility 77—48967
  - resistors, Cr-Si coatings deposition, by flash evaporation, residual gas atmosphere analysis *(German)* 80—6681
  - waste treatment facility 77—73780
  - Zn-AgO cell, Zn electrode slurry-paste fabrication optimisation 79—96430
- **electron device noise**
  - 1/f current noise, random walk model 77—8162
- **electron device noise** continued
  - 1/f noise, amplitude distribution 79—24042
  - 1/f noise, theoretical analysis *(Polish)* 78—91737
  - amplifier noise in radioastronomical receivers *(Italian)* 78—45234
  - avalanche photodiodes, reach-through, excess noise factor 79—95482
  - backscattered electron detector, solid state, operating at TV scan rates in scanning electron microscope 79—18089
  - burst noise, physical sources 79—24033
  - C-CD, surface channel, interface trapping noise calc. 80—11058
  - carrier multiplication and noise in avalanche devices 80—15579
  - charge injection device as stellar tracking sensor 80—85861
  - conference, Bad Nauheim, West Germany (Mar. 1978) 79—24031
  - convertor, electron-optical, S/N ratio rel. to threshold characts. 77—31134
  - cosmic ray induced noise in photomultipliers, Cherenkov radiation 77—18735
  - CRM-monotron, low-frequency fluctuations calc. *(Russian)* 77—88684
  - cryogenically cooled C-band p-i-n diode integrated switch matrix for radio astronomy applications 78—96392
  - cyclic queue models of semiconductor noise and vehicle fleet operations 80—80336
  - DC SQUID, ultra-low-noise tunnel junction, design, fabrication and noise props. 80—29506
  - detector array spatial noise reduction, controlled lateral shifts 80—53436
  - digital thermocouples, study 77—22544
  - diode laser, active mode locking, effect of noise 80—19030
  - dual resistance wire wavestaff system for laboratory and coastline 80—46324
  - electronics for the physicist with applications, book 80—62403
  - forward biased junctions, excess noise sources due to defects 79—38154
  - Fourier transform spectroscopy, photon and detector noise quantitative limit, definition *(German)* 80—9049
  - gamma ray semiconductor detectors, S/N ratio optimisation *(German)* 77—10534
  - gravitation radiation detection, active resonant antennas, sensitivity and noise 79—30346
  - HgCdTe/CdTe, limited diffusion volume photodiode, characterisation 80—75627
  - image convertors, solid state, with integrated fixed-pattern noise suppression 80—14458
  - injection laser, noise props. due to reflected waves 79—36897
  - injection laser quantum noise in optical fibre communication systems 80—48259
  - inplatron, sensitivity and resolution, LF noise fluctuation 77—19779
  - IR charge transfer device imaging arrays 78—77990
  - IR photodetector, microwave biased, module construction 80—9038
  - J-FET noise model for photodiode amplifier in optical fibre receivers 78—37997
  - JFETs, generation-recombination noise at 77K 79—60883
  - Josephson microwave source, short term emission fluctuations 79—15263
  - Josephson mixer receiver, at millimetre and long submillimetre wavelengths 77—34027
  - Josephson self-oscillator mixer, submillimetre and far IR detector 77—34026
  - junction devices, generation recombination current, noise reduction, SRH centres in space-charge layer 77—76905
  - laser diode characterisation, for multichannel applic. 78—87165
  - laser diodes in optical transmitters, switching dynamics and noise *(German)* 79—89919
  - low-contrast optoelectronic primary information processing system, energy efficiency 79—76617
  - metal-oxide-metal photodetector, noise, ultimate sensitivity 77—5915
  - microbridge SUPARAMPs, phase instability noise in Josephson junctions 79—26124
  - MM-wave and sub MM-wave receiver elements, Schottky-barrier resistive mixer devices 80—11558
  - model for 1/f noise 80—98945
  - MOS transistor electrometer, current noise meas. 78—54398
  - MOSFET, flicker noise theory 80—11100
  - multilevel generation-recomb. noise spectra, appl. of equivalent network methods 77—43674
  - n$^+$-p-π-p$^+$, epitaxial Si diode for optical fibre communication at 800 to 900 nm 77—79961
  - one-electron dissector, S/N ratio rel. to image contrast 79—50407
  - optical heterodyning, additive noise component reduction 79—50239
  - optoelectronic device S/N ratio optimisation 79—26133
  - optoelectronic devices and optical imaging techniques, book 80—27059
  - p-n diode, 1/f noise calc., free carrier mobility interpretation 80—54774
  - p-n junction, noise diagnostics *(Czech)* 78—10544
  - p-n junction diode, surface flicker noise at high injection level 77—47892
  - p-n junctions, 1/f noise 79—82666
  - p-n junctions, inhomogeneous, theory of LF noise 78—2559
  - p-n junctions, microplasma noise, stochastic model, breakdown voltage of microplasma 78—47854
  - passive thermostat for electronic noise meas. 77—2654
  - photoconductive IR detectors, microwave-biased, noise performance 80—9037
  - photodetector, channelled, with charge storage, S/N ratio *(Russian)* 77—53978
  - photodiodes, wide-bandwidth in heterodyne and background-limited operation, anomalous noise behaviour 79—69568
  - photomultiplier, cosmic ray induced noise from Cherenkov radiation 77—33308
  - photomultiplier afterpulses effect in coincidence systems 77—82583
  - photomultipliers noise figure, secondary electron emission model 78—86336
  - photoreceiver system, photodiode-FET, achievable threshold limit calc. 79—49292
  - piezoelectric transducer, tangentially polarized cylindrical, intrinsic noise 79—94441
  - pulse duration methods threshold sensitivity anal. *(Russian)* 78—45593
  - quantum noise at low temperature 80—103733
  - retarding field energy analyser in electron spectrometry, noise meas. 80—27377
  - S/N ratio with optimal filtering, noise stability for pulsed signals 77—31072
  - scanning optoelectronic systems, optical and electrical filter simultaneous optimisation 79—72696
  - Schottky barriers, 1/f noise 79—82666
  - SCLC diode, hot carrier effects on thermal noise 79—24036

electron device noise continued
semiconductor, drift mobility determ. from photoresistor noise meas. 77—4414
semiconductor, physical aspects of electrical noise *(French)* 78—19111
semiconductor generation-recombination noise 79—24032
semiconductor laser intrinsic noise in optical communication systems 80—69394
semiconductor lasers 80—58538
single injection diodes, 1/f noise 78—60204
SQUID, DC, noise limitations 79—21784
SQUID, DC, voltmeter and magnetometer circuits optimisation 80—12056
strain-dependent resistors, in force meas., noise limitations 78—16771
superconducting tunnel junctions, quantum noise effects in 0-1 mV bias range 80—80449
thermal TV camera, noise, synchronisation, spatial resolution and lifetime characts. 79—35833
thermistor bolometer with $Mn_xCo_yNi_zO_4$ spinel ceramic current noise 77—51793
two-dimensional isotropic conductor, transverse and longitudinal noise 79—51642
undergraduate laboratory solid-state noise thermometry apparatus 79—62959
vibrating-capacitor electrometer, current noise meas. 78—54398
CdSe, photodetector, limiting sensitivity 79—63309
Fe^{3+}:TiO_2 86-88 GHz low-noise TW maser 80—69354
(GaAl)As-GaAs narrow stripe laser, improved optical communication system performance 80—102733
GaAs FET, ion implantation, trends 80—39132
GaAs, Gunn oscillator, magnetoresist. meas. of mobility and noise 77—62948
GaAs injection lasers, direct modulation enhancement effect of HF noise 80—83608
GaAs MESFET, epilayer hot carrier noise 79—24035
GaAs, p-i-n avalanche photodiode, excess noise factor 79—35835
GaAs-$Al_xGa_{1-x}As$ heterojunction, avalanche phototransistors, detectivity and noise 78—2558
Ge avalanche photodiode, cryst. orientation depend. of multiplication noise 79—80680
Ge, p-i-n avalanche photodiode, excess noise factor 79—35835
p^+-n Ge shallow junction avalanche photo diodes, noise and quantum efficiency 79—87143
H maser, field-operable design improvements 79—55099
He-Zn, hollow cathode laser tube, with direct current excitation *(Japanese)* 79—76704
HgCdTe, 0.1 eV photodetector performance background dependence 77—32038
HgCdTe, 0.1 eV photodetector performance 77—32039
HgCdTe, 0.1 eV photodetector performance, geometrical enhancement 77—32040
HgCdTe reverse-biased photodiodes for wideband appls., excess noise 80—107876
$Hg_xCd_{1-x}Te$, photodiode, anomalous noise behaviour in heterodyne and background limited operation 79—69568
InAs avalanche diode, noise meas. 77—4431
$InAs_{1-x}Sb_x$, epitaxial heterojunction photodiodes, IR detector appls. 77—79155
$In_xGa_{1-x}As$ avalanche diode, noise meas. 77—4431
InGaAsP avalanche photodiode, 1.3 μm, noise performance, −190°C 80—57370
InP, far IR LPE photodetector performance 79—30546
InP, Gunn oscillator magnetoresist. meas. of mobility and noise, contact effects 77—62948
$Mn_xCo_yNi_zO_4$, spinel ceramic, current noise in thermistor bolometer 77—51793
$NbSe_3$, Frohlich sliding mode, nonlinear resist. and noise 79—60808
Pb salt semiconductor laser, low freq. noise characts. 79—59698
Si diffused junction photodiode performance characteristics 80—80367
Si extrinsic photoconductive IR detectors, VLF behaviour 78—81542
Si p-i-n avalanche photodiode, excess noise factor 79—35835
Si:B, low noise avalanche photodiode fabrication by channelling implantation 79—35827
Si(Li) high resolution spectrometer, with thermoelectric cooling 79—26813
$TlInSe_2$, monocrystal, photoelec. props. *(Russian)* 80—70752
VO_2, switch, fluctuations of current and switching time 79—38137
n-ZnSe—p-GaAs heterojunction high-detectivity threshold photodetectors 79—6181

electron device testing
see also electron tube testing; integrated circuit testing; semiconductor device testing
14th Annual Reliability Physics Symposium, Las Vegas (1976) 77—40514
acoustic emission transducer calibration temperature sensitivity checking technique 78—18144
capacitor loss-angle and capacitance checking cct. 77—61085
capacitors, ceramic, using scanning laser acoustic microscopes, comparison with SEM and optical microscopy results 80—58875
circuit component LF noise meas. arrangement 77—13776
deflection system performance using resolution test specimen 80—69311
EHV choke coil measuring bridge *(German)* 77—18047
fast-response photocell time characteristics meas. 77—5913
laser diode life testing, with constant light output current 80—1215
microstructure analysis by SEM 79—80723
neutron sensor performance testing, automatic counting channel and analysis system 79—13612
pacemaker battery microcalorimetric testing 80—30933
photodetector metrological certification, using acoustooptical modulators 80—23727
photodetectors, highspeed, performance testing, optical communication appl. 79—26129
pyroelectric detector of transmitted power, coordinate-sensitive, for laser beam displacement determ. 79—75599
quartz resonator surface patterns obs., using SEM 80—71323
resistive and potentiometric transducer connection line checking *(Bulgarian)* 79—93120
SAW voltage contrast obs., using SEM 80—69618
solar arrays, for Intelsat V appl. 79—48135
solar cell arrays, telecommunication satellites appl. 79—48137

electron device testing continued
space radiation environment for electronic components, laboratory simulation 80—94689
Symphonie communications satellite components, NDT *(German)* 77—1899
CdS piezoelectric thin film transducers, testing via light diffr. by acoustic waves 77—23840
$Li-I_2$ power cell accelerated discharge test for battery longevity model 80—30938
Pt resistance thermometer response time testing in situ 79—13484

electron diffraction
see also electron diffraction crystallography; electron diffraction examination of materials; gas phase electron diffraction; high energy electron diffraction; low energy electron diffraction
Aharonov-Bohm effect revisited 80—32040
computer method for analysing TEM diffr. patterns 77—47309
conference, London, England (Sept. 1977) 78—83657
dynamical theory of electron scattering *(Hungarian)* 79—55616
Fraunhofer diffraction symmetry, series expansion of Fourier transform 79—50212
generalised nonlinear Schrodinger eqn. 77—14650
historical account covering 50 years 78—18505
history, electron diffraction, 50 years ago, lives, work of Davisson and Germer 78—30519
interference effects, Lande approach experimental contradictions 79—49081
kinematic photographing of static diffraction patterns 77—18113
kinematical theory of electron diffraction *(Hungarian)* 79—55615
microscope resolving power limitations 80—86528
microscopic diffraction patterns, direct phase determ. *(German)* 77—2713
multislice method for high-energy electron scatt., computing technique 77—84594
relativistic electron wave diffraction by cylindrical capacitor 80—5671
Schrodinger equation separation in electron diffr. and channelling, case of systematic refls. 79—46522
Smith-Purcell radiation from small gratings 77—19156
STEM of thin specimens, intensity distribs. using phase object approx. 77—55218
supersonic stream flow in vacuum meas., instrument 78—75235
wavelength measurability 77—71406
Ar, clusters in supersonic beam, electron diffr. study 80—5655
Si(111) surface, Auger spectra intensity var. due to diffr. 77—85849

electron diffraction crystallography
see also crystal atomic structure; Debye-Waller factors
3-beam elastic intensities, inversion for scalar scattering by centrosymmetric cryst. 80—107023
advances in electron physics, book 80—8742
algebraic approaches to N-beam theory 78—83663
amorphous and gaseous states, philosophical problems in struct. determ. 78—50665
amorphous solids, atomic scale determ., direct methods, review 79—37623
anomalous absorption, effect of certain intraband transitions *(French)* 77—35446
atom images under dark field, STEM and TEM comparison 78—83696
atomic aggregates, symmetry aspects in electron diffr. patterns and optical transforms using computer simulation 79—7525
axial channelling, Kossel patterns for Si and Nb 78—42869
backscattering patterns, in field emission gun SEM 80—100142
BCC materials, small dislocation loop images 78—83823
beam intensity dependence on accelerating voltage 78—5990
bent molecular organic crystals, electron diffr. intensities 80—100132
bicrystal, electron diffr. from near coincidence twist boundaries 79—7526
bicrystals, theory 80—75122
Bloch wave channelling as electron diffr. 78—83860
bonding charge densities, determ. 80—75125
Bravais lattice and reduced cells determ., programs for electron diffraction pattern indexing *(Chinese)* 78—67625
centrosymmetric cryst., inversion of 3-beam intensities for scalar scattering 80—107023
cluster model for transition state, electron diffr. study 78—10168
coincidence grain boundary, lattice displacement, electron images 77—80516
computer aided indexing, of transmission electron diffr. patterns 78—38595
computer analysis of electron diffraction patterns 77—1049
computer indexing of diffr. spots, appl. to bicryst. *(French)* 78—75507
computer indexing of point diffraction patterns 80—100136
computer simulation for one-dimens. studies *(French)* 80—1902
conference, London, England (Sept. 1977) 78—83657
contrast in non-symmetric Laue case 78—83666
convergent beam, development and appls. 80—75124
convergent beam diffraction appl. to thin MoO_3 cryst. 78—38670
convergent beam electron diffraction, determ. of crystal point groups and space groups *(Japanese)* 79—77461
convergent beam electron diffraction 80—103220
convergent-beam diffraction camera, contamination suppression 78—14252
convergent-beam diffraction patterns obtained by beam-rocking method, signal processing 80—70085
cross grating orientation, patterns in axial direction, dispersion surfaces 78—83660
crystal defects, electron microscope diffr. contrast 78—83700
crystal defects and disorders, dynamical theory for electron scattering 79—23505
crystal orientation determ., Kikuchi line intersection 78—5992
crystallographic struct. factor phases from electron-microscope dark-field moire patterns 78—51396
cubic crystal, image contrast of dislocation loops, elastic anisotropy depend. 80—103349
defect imaging, analytical contrast calcs. in two-beam case 80—100134
defect Kikuchi band from thin cryst. 78—83668
defect symmetry, electron diffr. contrast, theory 80—96418
defect symmetry and diffr. contrast 80—79778
diffraction and imaging techniques, in material science, electron microscopy [book] 79—67439
diffraction patterns, extinction problem, automatic indexing program *(Chinese)* 78—91204

electron diffraction crystallography continued
digenite-type disordered crystal, diffr. pattern, kinematical theory 80—28886
digenite-type disordered crystals, diffr. pattern, cluster theory 80—75123
digital scanning electron diffractometer, appl. to radiation sensitive materials 78—87596
direct lattice resolution *(Hungarian)* 79—55617
dislocation dipoles, high density, numerical eval. 78—71645
dislocation imaging, in anticlassical scattering region, dislocation axis contrast 80—38877
divergent beam diffr. phenomena, computer generation of identification 78—30520
double crystal interferometer, dynamical theory 80—100135
double crystal interferometer 78—83687
dynamic theory of scattering, crystal with equidistantly bent reflecting planes *(Russian)* 80—70078
dynamical diffraction from periodic arrays of dislocations 78—83669
dynamical theory, approximations 80—87997
dynamical theory, of electron diffr. 79—68981
dynamical theory, perturbation calcs. 78—83665
dynamical theory 78—83658
dynamically forbidden lines obs. in 2-D and 3-D diffr. 78—83675
elastic scattering amplitudes, for high energy electron scattering, by ionised atoms, numerical calcs. 80—49057
electron collimation, coupled-state model and weak coupling approx. 80—10588
electron density distribution, and other densities in crysts., problems of resolution and bias in experimental determ. 79—23490
electron density maps, extrapolative filtering, resolution maximisation 78—75506
electron diffraction symmetries 80—100138
electron holography appl. to micro-area electron diffr. 80—49055
electron microscopic diffr. contrast, without column approx., calc. using perturbation method *(German)* 79—50960
electron object interaction, multislice approach 78—26394
electron-plasmon and electron-phonon interactions in bulk and near surface, Kikuchi patterns 78—26759
electronometric method of meas. intensities, efficiency 79—27881
enantiomorphic crystals, electron microscopy 77—84602
enantiomorphic space group identification 78—9917
enantiomorphously related space groups, identification by electron diffr. 77—19848
experimental limitations on cryst. struct. determ. 78—83678
fast electron scattering, review 80—14969
FCC crystal, electron diffr. anal. of twin and HCP phase *(Chinese)* 79—10763
FCC matrix, electron diff. anal. of thin twin or HCP plates 77—59020
FCC metal films on NaCl, electron diffr. pattern interpretation, appl. to Ag 77—1332
film, influence of dynamic effects on height of pot. peaks 77—39517
film, partly oriented, dynamic effects 77—7996
film production device, in situ hydride, oxide, nitride prod. 77—65937
film structure, X-ray and electron diffr. methods comparison *(Czech)* 77—47696
frozen hydrated crystalline specimens, meas. and reduction of damage 80—85552
gas phase, use of rotating sector for electron intensities obs. 77—55214
gas-phase guide for publication of expt. data for struct. determ. 77—1048
glass structure, review 77—65954
graphite, zone-axis pattern maps 80—100137
HCP metals, systematic electron diffr., main beam transmission 78—63643
heavy atom discrimination using single-sideband techniques 80—6321
high energy electron diffraction, theory 79—68985
high lattice defect density, specimens, statistical theory 78—14250
high resolution electron microscopy, cryst. struct. determ. *(Chinese)* 78—1960
history, electron diffraction, 50 years ago, lives, work of Davisson and Germer 78—30519
image computation for high-resolution TEM 78—71653
imaging and diffraction techniques, (book) 79—67441
inclusions, misfitting, precipitated close together on dislocation, diffr. contrast of equiv. cylinder 77—27886
indexing of selected area diffr. pattern, graphical technique, for teaching 78—54132
industrial camera, type EMR-100 79—2842
industrial electron diffraction camera EMR-100, description 79—50963
inelastic electron scattering in crystals, extension of Yoshioka theory 80—103219
inelastic scattering, dynamical diffraction and generalised dielec. response function 80—75120
inelastic scattering background correction, automated procedure 77—27782
inelastic scattering probabilities for fast electrons in single cryst., orientation depend. 80—2905
instrumentation, review 78—83683
interferometer, modified Marton type 78—37111
interferometer diffraction pattern, amplitude modulated beam 78—63641
intergranular orientation relationships by Kikuchi electron diffr. 80—15116
interplanar spacings, precision determ., by means of reflection electron diffr. 79—64961
Kikuchi bands of backscattered and transmitted electron diffr. patterns, contrast reversals 78—34396
Kikuchi electron diffraction, and appl. tutorial 79—68984
Kikuchi electron diffraction patterns, of Si, lines of deficiency with black-white contrast 79—55614
Kikuchi lines, forbidden, formation mechanism 80—44081
Kikuchi pattern, analytical determ. of exact primary beam direction 78—5991
Kikuchi pattern indexing and geometrical analysis 77—65935
Kikuchi patterns due to plasmon and phonon excitations 77—76264
Kikuchi pseudoline pattern, obs. in objective lens *(French)* 78—18506
Kikuchi structures, energy analysis by intensity profiles *(German)* 79—7528
kinematical theory, of electron diffr., tutorial 79—68980
kinematically forbidden diffr. spots, dynamical theory *(French)* 79—90498
Kossel pattern anal. 78—83676
lattice defects, characterisation 80—103320

electron diffraction crystallography continued
lattice defects, high resolution microscope images, calc. and interpretation 79—73075
lattice fringe imaging theory 80—103225
lattice image calculations for imperfect crysts., superlattice approach 80—107030
lattice image formation, many-beam theory, TEM 80—38879
lattice images, effect of absorpt. 79—90497
lattice images of defects, computer simulation of high resolution images 80—107208
lattice parameter determination using high order Laue zone effects in elec. diffr. 77—43120
Laue spot diffusion 79—73073
Laue zones, higher-order, electron diffr. 78—26389
LEED intensity measurement using modified CCTV system 80—31946
LEED surface crystallography, past and present 78—14253
LEED surface struct. determ., multiple scatt. theory based FORTRAN computer programs, book 79—86971
LEED system, vidicon-based, instrument response functions 79—90500
line diffraction patterns, scattering model *(French)* 78—51397
liquids, expt. developments 78—83686
low-angle boundaries, misorientation, meas. 79—82237
macromolecules, graphics model building and refinement system 78—75505
manipulator for electron diffraction camera 77—19844
many-beam dynamical theory in symm. Laue case, group theoretical method 77—15290
many-beam lattice images from thicker crystals 80—88004
martensitic transformations, electron microscopy and diffr. studies 79—68989
medium energy, theory and appl. 78—83682
metal, electron wave flux distrib. fine struct. near Bragg refl. 78—83670
metal cluster generator for gas-phase electron diffr., variation of microcryst. with size 78—63645
metal-insulator transition study *(French)* 78—26815
metallic film, struct. of small particles, review 77—89671
method for indexing diffr. patterns *(Chinese)* 79—90499
microdiffraction, book contrib. 80—10464
microdiffraction methods, comparison, using STEM 79—19129
microdiffraction patterns, point group symmetry from dislocation cores 80—100140
micrograph observation in electron diffraction apparatus, use of electrostatic lens 79—80727
microscope modification to convergent-beam camera and shadow microscope 77—55215
microscopy, structure image high-speed calc. methods 79—55622
microsurfaces, obs. using thermal desorption spectroscopy combined with TEM and transmission electron diffr. 79—90888
minicomputer appl. *(Chinese)* 77—72528
Mollenstedt filter images, correction by auxiliary lenses, appl. to bend contour obs. for Al 77—39520
mosaic single crystals, electron diffr. reflection intensities, precision meas. 79—94851
multilayer close-packed structures, identification possibilities, X-ray and electron diffr. patterns 78—94951
multiple inelastic electron scatt., from cryst. specimens 80—28885
multiple inelastic scattering and dynamical diffraction 78—83667
multiple inelastic scattering in thick crysts., Monte Carlo simulation 77—7637
multiple scattering by infinite lattice plane 77—73198
multislice and many beam calculations comparison 78—83664
multislice method for calcs. of electron diffr. intensities 77—84595
nucleation models, computer simulation of microdiffr. patterns *(French)* 77—62449
omega phase, roles of electron microscopy and electron diffraction *(French)* 78—27524
optical frequency modulation depth, Pendellosung effect 80—33859
optical selected-area diffr. patterns of high-resolution electron-microscopic images for cryst. anal. 78—55789
optimal iterative phase retrieval from image and diffr. intensities 77—72531
organic crystals, direct phasing of electron diffr. data, effect of n-beam dynamical scattering 80—10465
organic crystals, quantitative validity domains of single scattering approximations 80—28888
organic molecular crystals, topochem. conversions and phase transitions 78—83680
orientation and position accuracy 78—22606
overgrowth of small crystals on single cryst. substrate, diffr. pattern intensity calc. 78—42868
pattern overlapping from two crysts. with simple orientation relationship *(Chinese)* 79—50958
patterns from multicomponent systems, indexing method 77—24250
Patterson function method, structure of ordered Ag_3Mg alloy kinematical vs. dynamical diffraction calc. 80—10530
pendulum radiation, quantum mechanical calcs. *(Russian)* 80—49054
perfect crystal, distrib. of phonon scattered electrons 77—19846
periodic misfit-dislocation networks 78—59815
phase determination, superposed diffraction patterns 80—100141
photographic emulsion response to electrons in gas-phase electron diffraction expts. 78—54482
planar interfaces, study by electron microscopy 79—68982
polar molecule, fast electron elastic scatt. intensity calcs. 77—3459
polymer single cryst., mosaic model for electron diffr., bend distortion 80—44080
protein structure determination, crystal bending, electron-diffraction data 78—53325
pseudo-Kikuchi patterns in refl. expts. during scanning of single cryst. by intermediate energy electrons 78—1964
radial distrib. anal., computer program 80—28875
radiation sensitive materials, diffr. pattern recording on luminescent radiographic screen 77—27791
reciprocal lattice plane fundamental data, extinction problems in automatic calc. *(Chinese)* 79—73072
reflection electron diffraction, medium and low energy, Laue-case Kikuchi pattern 78—1963
reflection intensities, precision meas. on electron diffraction patterns from textures and mosaic single crystals 77—43119
rotating sector use in electron scatt. intensity meas. 77—43118
sample rotating device for improved intensity meas. in texture determ. 77—65936

electron diffraction crystallography continued
sector device for electron diffraction studies on liquids 78—55788
shadow electron microscope, selected area diffraction 77—11444
single-scattering approximations, quantitative validity domains for organic crysts. 80—28888
slow electron diffraction, from thin crystal struct., theory *(Russian)* 80—64843
spherically symmetrical coherency strain contrasts, S-matrix theory calcs. 80—100133
spot broadening, resolution, X-ray and electron beam diffr. patterns *(German)* 80—84033
STEM, image contrast *(German)* 77—24251
STEM, phase determination, of inner dynamical reflections 79—14660
STEM application, two-dimens. diffr. patterns obs. and recording system 80—79650
STEM lattice imaging 78—34398
STEM microdiffraction patterns, effect of cryst. defects 78—22610
string integrals rel. to BC and CB zone axis patterns 78—83681
structure determination approaches 78—34397
structure factor and symm. determ. 78—83673
substitution order-disorder, study by X-ray and electron diffr., book contrib. 79—68983
superlattice fringe images of ordered alloys, computer simulation 80—103296
superlattices, one- and two-dimens., possibility of X-ray and electron diffr. struct. determ. 80—54560
superstructure involving inversion domains, large scale incommensurate structs. 79—95174
surface crystallography, reliability of LEED 79—37910
TEM application 77—58929
textured materials, diffraction broadening studies, coherent domain size and microstrain 79—73060
textures, reflection sphere curvature influence on reflection location geometry 80—87996
theory *(Chinese)* 80—44072
transition metal chalcogenides, diffuse intensity contours, electron diffraction patterns 79—23504
transmission electron microscopy, book 80—17726
twin interfaces, contrast using weak beam technique 79—46524
twin reflection indexing in four-axis hexagonal reciprocal lattice 80—14970
twinned crystal, diffracted electron beams, equality of intensities 78—79506
twinned crystal, multibeam dynamical theory appl. 77—19847
two beam case, use of Riemann integration method, using Bloch wave excitation powers transformation *(German)* 79—50959
two-phase cryst. structures, orientational electron microdiffr. anal. with aid of OMEGA program 80—103218
validity of assuming symm. Laue diffr. conditions in diffr. contrast 79—50961
weak-beam contrast calculation for spherical coherent precipitates *(French)* 77—35450
Ag, spherical crystal, Bragg case, Kikuchi patterns 77—84599
Al, massive target, electron absorption and transmission characts. 77—65990
Al-Cu, anal. of electron diffr. micrographs using Patterson function *(French)* 79—20044
Au, multiray calc. of cryst. lattice projection in ⟨111⟩ direction, from electron microscope image 79—94855
Bi, intervalley scattering processes, surface struct., transverse electron focusing study *(Russian)* 80—84352
Co_3Pd epitaxial films, multiray dynamic theory of diffr. contrast to explain defects nature 79—64962
c-Dy_2O_3, transmitted intensity depend. on thickness, incident beam parallel to crystallographic axis 78—63644
MgO, dynamical effects for cryst. struct. determ. 78—83679
MgO, LEED, Kikuchi pattern intensity, angular and temp. depend. 78—2349
Mo extinction length ζ_{200} meas., electron energy influence 80—90935
Si, cryst. struct. factors determ. by intersecting Kikuchi-line method 80—14971
Si crystal, contrast depend. of Kikuchi patterns on primary electron beam energy *(Russian)* 80—64844
Si, Kikuchi structures, phonon scatt. and thermal diffuse scatt., transmission electron diffraction study *(German)* 80—44082
Si, single cryst. films, temp. depend. of electron Kikuchi diagram 80—1904
Si, unindexable and forbidden lines in Kikuchi electron patterns 79—94850
Te, breakdown of Friedel's law in Kikuchi patterns as obs. in TEM 79—69046

electron diffraction examination of materials
see also gas phase electron diffraction; high energy electron diffraction; low energy electron diffraction; reflection high energy electron diffraction
adsorbate vibrations, large-angle inelastic electron scatt., theory 80—75427
adsorbed layers, photoelectron diffr. aximuthal patterns, struct. sensitivity 80—107644
afghanite, stacking variation, TEM study 79—99219
Al-Zn-Mg (5,1 wt.%), decomp. process, TEM study 80—71660
alkali halide, brittle fracture of single crysts. and active struct. of cleavage surfaces 79—28039
alkali metal titanates, $(A_2Ti_6O_{13})_n.A'Ti_4O_9$, $(A=Na, K, Rb)(A'=Ba, Pb, Sr)$, intergrowth in tunnel structures 80—28995
alkanes, thin plate microcrystals, transmission electron diffraction intensities 78—83821
alloy, internally oxidised, orientational relationships of precip. oxide phase 77—4783
alloy, with correlated system of second phase particles, X-ray and electron scatt. *(Russian)* 77—59738
alloy steel, martensite structural singularities during tempering, electron diffr. study *(Russian)* 79—100177
alloys, high resoln. diffr. and imaging characterisation 80—104050
alloys, phase transition premonitory phenomena, exam. by electron diffr. and microscopy *(French)* 80—59651
amethyst quartz, α-β phase transition, interaction of Dauphine and Brazil twins 77—62641
amorphous alloy, and metastable phases, cryst. kinetics, review *(Japanese)* 80—38912

electron diffraction examination of materials continued
amorphous materials, microdiffraction patterns from the Finney model 78—63642
amorphous materials, small area struct. studies 80—44087
amorphous metals, geometric struct. models and diffraction exam. techniques 80—79700
amorphous sample, struct. from inelastic and elastic electron scatt. *(French)* 79—90554
anthanthrene, mol. cryst. images in electron diffr. patterns 80—103315
anthracene, electron diffr. of topochem. conversion and phase transition 78—83680
astrophyllite, electron diffr. characts. of polytypic forms 77—39573
austenite, hot-worked, struct., post-deform. ht. treatment effects *(Russian)* 77—8859
austenitic steel, 45G17Yu3, structure and loss of strength after hot deform. by rolling *(Russian)* 78—39794
$Bi_7Ni_4NbO_{21}$, crystal point group determ. by high resolution electron microscope image 79—51036
bicrystals, near-coincidence twist boundaries, electron diffr. obs. 79—90675
bicyclo(4,2,0)octane, cis and trans isomers, struct. mol. mechanics and electron diffr. 77—54608
Bloch wave model for ECP contrast in Si, Cu, Ag, Au 80—96419
borozirconia glazes, low-melting, struct. and liq.-phase separation 79—60282
α-brass, 70:30, cold-worked, recrystallised grains nucleation on heating 80—29998
brass, 70:30, rolled, nucleation and annealing texture development 80—45320
brass, γ-phase region, X-ray and electron diffr. obs. 79—61562
brass, B_2, nonradial diffuse streaks and complex diffuse scatt. patterns of electrons 79—7527
β-brass, spinodal decomposition, electron microscope and diffr. study 79—78930
γ- brass type alloys, superstructures and defect obs. 80—107284
n-butane, vibr. shrinkages, mol. struct., electron diffr. obs. 77—50535
carbon tetrachloride, mol. characts. from fast low-angle scatt. 77—50537
carbon tetrafluoride+SiC(Si), reaction, metastable C phase prod. 79—29393
catalase, electron microscope exam. of new cryst. form, Fourier transform. method 77—11447
catalase, glucose embedded, measurement and reduction of radiation damage in frozen hydrated crystalline specimens 80—89810
cellulose, degradation by high voltage electrons 80—100283
cellulose II, preparation and crystal growth, electron diffr. obs. 78—91285
ceramics, high resoln. diffr. and imaging characterisation 80—104050
cermet film, as solar selective absorbers, production, struct. and optical props. 79—29485
chaoite, a new allotropic form of carbon, produced by shock compression 80—80997
composite reciprocal lattice unit cells for cubic twins *(Chinese)* 79—99213
computer assisted indexing 78—9918
convergent beam electron microscopy, appl. in materials science 80—107028
copper phthalocyanine, on graphite, epitaxial growth of new polymorph 77—80712
α'-copper phthalocyanine, struct. and susceptibility to radiation damage 79—32986
crystalline materials, struct. of grain boundaries using diffr. techniques 80—59478
cubic system, electron diffr. patterns of twins *(Chinese)* 79—99214
1,2,6-cyclononatriene, mol. struct. and conformation, gas phase electron diffr. 80—106400
cytosine, cryst., electron damage, electron microscope study 78—22762
diacetylene monocarboxylic acids, multilayers, struct. phase transitions and polymerisability 80—80129
diamond, identification by electron refl. *(German)* 80—54080
diamond, ion implantation, heteroatom size and reactivity effect 80—44226
diamond, lattice potential, high energy electron diffr. and refr. study 80—54165
diamond, synthesis and characterisation 80—50580
diamond, synthesis on nondiamond substrate, electron diffr. and luminesc. exam. 77—76344
diamond, ultradisperse, obtained by high temp. synthesis in explosion, struct. 79—29003
diamond particles, finely dispersed, in active C shock wave produced powder, electron diffr. identification 80—1903
diamond-graphite epitaxial film deposition on diamond substrate 77—4271
dichloro(dimethyl)germane, mol. struct. determ. by vap. phase electron diffr. 77—54621
dichlorodinitromethane, mol. struct., electron diffr. investig. 78—86950
dielectric materials, amorphous high permittivity *(Japanese)* 79—73876
1,1-difluoroethane, mol. struct., gas phase electron diffr. obs. 80—58385
1,1 difluoroethylene, -d_1, -d_2, mol. struct., rot. consts., gas phase electron diffr., microwave data 77—65542
dislocation core, symmetry of dynamical electron microdiffraction patterns 80—100140
disordered alloys, short range order diffuse electron scatt. 78—87595
DNA helix destabilising protein cryst. 80—85338
dolomites, low temp., microstruct. 79—62487
electron microscopy, application in modern science, review 79—26182
electron sensitive materials 78—83701
electronograph cryogenic trap construction 80—31766
epitaxial growth, role of lattice fitting 78—34728
faulted dipoles, formation and props. 77—72615
Fe-N system, fine particles growth, prep. by reactive gas evaporation technique, lattice consts. and habit study 79—56919
ferrogarnet crystal, surface layer damage thickness meas. 79—5106
ferromagnet, electron scatt. in presence of mag. surface reconstruction 79—1705
film, domain size and internal strain, studied by electron diffraction line broadening 78—30840
film adsorbed on graphite, two-dimensional phase transitions 80—107653
film defect growth and nucleation, electron microscopy and diffraction exam. *(French)* 80—59824
films, metal-semicond. and metal metal studies in ultra high vacuum scatt. chamber 79—2780

electron diffraction examination of materials continued
fluorite ceramics, doped, short range order anal. by electron diffr. 78−83672
foil, recrystn. during heating in column of electron microscope *(Russian)* 78−48421
franzinite, stacking variation, TEM study 79−99219
free jet, homogeneous nucleation of clusters, noncryst. struct. *(French)* 78−79760
gas, high-temp. review 80−52237
gas molecule images by electron holography, optical spatial domain filter theory 80−10016
gas molecules, image reconstruction by electron holography 79−68367
gas moleculues, image reconstruction by electron holography 79−68366
glasses and ceramics, characterisation with analytical electron microscope 80−84068
graphite, intercalation compounds with alkali metals and halogens, intralayer crystal struct. and order-disorder transform., electron diffr. 78−26540
graphite, zone-axis pattern maps 80−100137
graphite formation on C-Ni(No)(Fe) solid solns., high-temp. metallography investig. 79−29306
graphite intercalation cpds., struct. and order-disorder transforms. 78−71710
graphite-Rb, intercalation cpd., superlattice struct., electron diffr. study 80−75214
HCP metals, critical voltages, using n-beam dynamical theory 78−71644
n-hexatriacontane film, vacuum deposited on alkali halide crystals, structure and heat treatment 80−103600
II-VI semiconductors, thin epitaxial layer, direct synthesis *(German)* 80−104070
illite, vacancy ordering, transition state cluster model, electron diffr. 77−47547
2-iodoacetamide, mol. struct., electron diffr. obs. 80−63819
ion-water interactions, survey of diffr. studies 80−24347
ionic conductor, quasielastic scatt. of light, neutrons and electrons, Debye-Huckel eqn. *(Chinese)* 78−68521
Kevlar 49 fibre, macromol. struct., electron diffr. and dark-field electron microscope obs. 78−34446
Kevlar 49 high modulus polyaromatic fibre, supramolecular struct. 78−55819
laser evaporated film, morphological features struct. defects 78−67926
layered materials, struct. changes rel. to CDW, TEM, electron diffr., dichalcogenides appl. 80−39042
layered transition metal dichalcogenide, diffuse intensity contours in electron diffr. patterns, struct. interpretation 80−38878
liquid metallic thin film, supercooling, electron diffraction study *(French)* 79−7676
liquids, expt. developments 78−83686
liquids, single beam microdensitometer 80−86370
lonsdalite→graphite phase transform. mechanism, electron diffr. expts. 79−28099
martensite crystals, orientation relationship definition, anal. method 78−60670
martensitic transformations, electron microscope study of cryst. geometry *(Russian)* 80−108441
materials problems and basic research needs rel. to energy resources and storage 78−86703
metal, FCC, He ion irrad., He gas bubble lattice obs. 79−14858
metal crystallites, polyhedral, growth in inactive gas, review 79−27934
metal films, on alkali halide substrates, nucleation and growth, surface study techniques, review 80−10809
metal foils, polycryst. and amorphous, most probable transmitted scatt. angle calc. *(French)* 77−68901
metal oxide smoke particles prepared by gas evap., morphology and coalescence growth 80−97738
metal surface, adsorbed molecules, inelastic scatt. of slow electrons 78−9916
metal-insulator transition study *(French)* 78−26815
2-methoxacyclobutane, mol. struct., electron diffr. obs. 80−1065
mineral particulates, identification by selected area electron diffraction 77−90970
minicomputer appl. to electron diffr. study of indexing patterns of single crystals unknown lattices *(Chinese)* 78−14249
molecule characts. from fast scatt. 77−50536
naphthalene derivatives, film struct., electron microscope and diffr. obs. 79−11029
nonstoichiometry and structural disorder in some families of inorganic cpds. 79−51091
octadecylacrylamide films, oriented ultrathin, radiation-induced solid state polymerisation 80−80128
ordered alloys, long period antiphase structs. 79−95027
organic molecules, radiation damage by electron diffraction 79−65119
paraffinic multilayer crystal, slightly bent, electron diffraction intensities, Patterson function 78−5993
paragonite, 2M$_1$, cryst. struct. refinement by HV electron diffr. 78−67696
paragonite, 3T, cryst. struct., oblique texture electron diffr. 78−67697
pattern analysis design and development of projection system, for a negative viewer 80−22476
$PbO-Nb_2O_5$ system, X-ray and electron microscopic phase and struct. determ. *(French)* 80−92508
perfluoroneopentane, geom. struct. of mol., gas phase electron diffr. 78−78810
Permalloy film, implanted with C ions, HCP struct. formation, electron diffr. study *(Russian)* 79−82469
phthalocyanine, cryst., electron damage, electron microscope study 78−22762
phthalocyanines, metal free, mol. cryst. images in electron diffr. patterns 80−103315
poly(4-methylpentene-1), permanganic etchant for TEM obs. 80−21132
poly(p-phenylene terephthalamide), quiescent and strain induced crystallization from H_2SO_4 soln. 79−90571
poly 2,3-dichlorobutadiene, struct., morphology; polymorphism 79−65008
poly-γ-methyl-D-glutamate, α-helical form, annealing effect, morphology 79−14702
poly-N-vinylcarbazole, struct. model, using NMR and diffr. data 78−83750
poly-p-phenylene terephthalate, high modulus fibre, struct. obs. 78−75564
polyacrylonitrile, single cryst. formation, during soln. polymerisation, struct. determ. 80−38938

electron diffraction examination of materials continued
polydiacetylene, extended-chain crysts., struct. and morphology 79−82165
polyethylene, cross-linked crysts., deform. mechanism 78−15469
polyethylene, crystallisation of thick film from glassy state by annealing 80−54151
polyethylene, lamellar stacks, screw dislocations 80−19728
polyethylene, linear, quenching of thin films to amorphous state 80−28929
polyethylene, liq., radial distrib. functions 77−4032
polyethylene, single cryst. and spherulites, microstruct., deform. micromechanisms 78−83758
polyethylene, ultraquenched, electron diffr., morphology and thermal anal. 79−15640
polyethylene film, melt-cast, deform. in equatorial region of spherulites, electron diffr. 77−25115
polyethylene single crystals, microarea diffraction patterns by STEM 79−55620
polyethylene spherulites, STEM and microdiffr. obs. of micromorphology 78−34444
polyethylene spherulites, thin melt-cast films, high density, deform. process in non-equatorial regions 80−81124
polyethylene sulphide, cryst. struct. by electron diffr. 78−51441
polymer, amorphous, bulk, structure models and exptl. methods, review 78−22671
polymer, amorphous, domain struct. determ. by electron microscopy and electron diffr. 77−84667
polymer, amorphous state struct., conf., Atlantic City, USA (Sept. 1974) 77−76327
polymer, molten or amorphous, chain conform. determ. by diffr. 77−80429
polymer, soln.-grown cryst., diffr. line-broadening, bending contrib. 78−75574
polymer glasses and melts, struct., review of expt. results 79−37636
polymethylene, continuous diffuse electron scatt., correl. chain motion 78−6020
polymethylene compounds, continuous diffuse electron scattering, oblique layer cryst. 78−95004
polyoma virion and capsid crystal structures 80−8011
polyoxymethylene, epitaxial growth on KBr single crystal *(Japanese)* 78−56054
polyphenylene terephthalamide, fibril form. from nascent spherulite formed during polymerisation in hexamethylphosphorictriamide *(Japanese)* 78−56893
polypropylene, isotactic, epitaxial crystn. on alkali halide surface 78−26787
polypropylene, permanganic etchant for TEM obs. 80−21132
polystyrene, crazed, orientation and struct., electron diffr. meas. 80−30122
polystyrene, lamellar stacks, screw dislocations 80−19728
polytrimethylene terephthalate single crystals, X-ray and electron diffr. obs. of cryst. struct., packing analysis 79−94924
protein, cryst. struct. analysis by electron diffr., single scatt. approx., domains of validity 80−101150
protein crystal, wet, low dose electron diffr. 80−85550
quartz, handedness determination for electron diffr. convergent beam patterns 78−34498
rare earth oxide film, short-range order to long-range order transition 78−10288
rare earth oxide film, struct., electron microscope and diffr. obs. 79−11028
rare earth trialuminides, long period polytypes, electron diffr., high resolution imaging 78−83781
rare earth-transition metal alloys amorphous thin films, anisotropic mag. and microstruct. props. 78−95487
rare-earth dihydride epitaxial films, growth and struct. 79−37936
reflection electron diffraction, generalised Bethe pot. 77−62451
refractory coatings, deposited by electron evaporation, struct. and props. 79−23871
refractory metal films, evaporated, optical props., rel. to struct. 80−55211
semiconductor films, structure, influence of laser beam 79−7761
single crystal, anomaly in electron and photon emission and scattering *(Japanese)* 79−37581
solid solutions, cubic, at. mean sq. displacement and critical voltage effect 79−60236
solid state chemistry problems, appl. of electron microscopy and diffr. 79−46527
solid-electron interactions, conf., Southampton, England (Apr. 1976) 77−44570
spinel, space group, electron diffr. pattern anal. 79−7594
steel, 12KhN3A, case-hardened, friction austenite obs. *(Russian)* 77−21286
steel, Al, relax. twins in martensite, electron diffr. and electron microscopy *(Russian)* 78−47391
steel, alloy and C, ion nitrided and ion-softnitrided, comparison of compound layers *(Japanese)* 79−8386
steel, austenitic Mn, existence of carbide M_5C_2 phase, electron microdiffr. analysis *(Russian)* 78−23727
steel, austenitic stainless, Ni-alloyed, Cr_2N precipitation, interface struct. and morphology 80−11644
steel, austenitic stainless, unlubricated, friction, wear and microstruct. of types 304, 316 and Nitronic 60 80−108589
steel, austenitic stainless, welded explosively, induced martensites morphology 80−104153
steel, C, tempered martensite embrittlement, and retained austenite, exam. 78−56754
steel, Cr, high C, in situ transform. of cementite to M_7C_3 and internal defects of M_7C_3 by tempering 78−31412
steel, Cr-Mo (2.25, 1 wt.%), decarburization, carbide effects in high temp. Na *(Japanese)* 78−15403
steel, Cr-Ni-Mo-Cu, ε phase particle precipitation from martensite, local internal stress relaxation *(Russian)* 79−78969
steel, electron microdiffr. determ. of orientational correls. between ferrite and cementite 77−52584
steel, high Si dual-phase, mech. props and microstruct. anal. 80−40444
steel, high-C, type U12, U15, U17, cementite precipitation cryst. geometry singularities during decomposition of martensite *(Russian)* 80−7577
steel, high-C martensite, struct. transforms. during low temp. tempering *(Russian)* 77−59737

electron diffraction examination of materials continued
steel, hypoeutectoid, singularities of cryst. geometry of pearlite *(Russian)* 77—21093
steel, low alloy, crack form. during stress relief in heated zones *(German)* 79—74242
steel, low alloy, low C grain boundary proeutectoid ferrite formation, direct obs. method 80—3074
steel, low C, quenched, interphase precipitates obs. *(Russian)* 80—29957
steel, machining, adhesion mechanism of built-up edge and layer on rake face of cutting tool 79—47784
steel, maraging, 18Ni300, ageing, electron diffr. and microscope obs. *(Polish)* 79—34070
steel, medium-C, singularities in low temp. α-martensite decomp. *(Russian)* 77—8814
steel, mild, AISI 1009 and 1018, corrosion incipient processes in hypersaline geothermal brine at 90°C 80—50753
steel, mild, Al-Zn alloy coated, interface struct. 79—52466
steel, Ni-Co-Mo-Ti, maraging, electron diffr. obs. of second phase *(Chinese)* 80—11655
steel, quenching to form martensite, morphology and struct., electron microscope and electron diffr. study *(French)* 77—73291
steel, Si, metallography of bainitic transform., carbide precipitation 78—27527
steel, stainless, 18-8, stress corrosion cracking, in H_2SO_4-NaCl soln. *(Japanese)* 77—21315
steel, stainless, amorphous film, sputtered, prep. and characterisation 78—43266
steel, stainless, Cr-Ni, maraging, effect of Mo, Co additions on hardening 78—84835
steel, stainless, Cr-Ni (18, 9 wt.%), cold rolled, struct. 79—83214
steel, stainless, duplex, lattice-imaging technique 79—64965
steel, stainless type 316, neutron irradiated, or themally aged diamond-cubic η phase formation, TEM study 79—99249
steel, tool, type M2, laser melting and heat treatment, microstruct. charact. 79—100188
steel, tool type M2, surface hardening and microstruct. refinement by laser melting, electron beam melting, heat treatment *(Korean)* 79—70093
steel, U15 and 130 Gz, upper bainite, relation between cementite and ferrite lattice orientations *(Russian)* 78—23663
steel, V- or Cr- or Mn-, tempering, initial stages of carbide form., electron diffr. *(Russian)* 78—19760
steel austenite to martensite transformation, orientation relationships 79—78964
steel-polymer wear mechanism during fretting corrosion 78—35522
stilpnomelane, complex layer silicate, struct. of long-period polytypes 77—64266
substitutionally disordered system in transition state, cluster model, electron diffr. patterns 77—20046
substitutionally disordered system in transition state, cluster model, electron diffr. patterns 77—47547
sunlight absorber, struct. and thermal efficiency 77—125
surface films on solids, TEM study method 80—65409
surface quality estimation after polishing, Kikuchi reflection obs. *(German)* 77—86208
tetrafluoro-p-benzoquinone, mol. struct., gas phase electron diffr. obs. 80—58386
1,1,2,2-tetrafluoroethane, anti- and gauche-rotamers, struct., spectra, electron diffr. 77—50439
tetraglycidyl 4,4′ diaminodiphenyl methane epoxy, diaminodiphenyl sulphone cured, struct., deform. mode, failure 79—29141
tetramethyl-p-benzoquinone, mol. struct., gas phase electron diffr. obs. 80—58386
toluene, mol. geometry, electron diffraction obs. 78—9270
toluene, mol. struct., electron diffr. obs. 77—88559
transition metal complexes, dimethylglyoxymate films, prep. and physical props. 79—90923
transition metal dichalcogenide, stacking layer study, appl. of convergent beam electron diffr. 80—39116
transition metal dichalcogenides, octahedral intercalate ordering study by electron diffr. 80—15076
transition metal dichalcogenides, zone axis electron diffr. patterns 78—34497
trichloro(methyl)germane, mol. struct. determ. by vap. phase electron diffr. 77—54621
trifluoroethene-d_0,d_1, mol. struct., microwave and electron diffr. obs. 80—58384
trimethylamine, and analogues, struc. struct. and vibr. force fields, electron diffr. and microwave spectra 77—54609
tris(trimethylstannyl)amine, gas phase electron diffraction 80—106401
tveitite, X-ray powder and single cryst. electron diffr. study *(German)* 79—99160
vacuum deposited film, orientation axis tilt rel. to vapour angle of incidence 80—88456
l-valine, cryst., electron damage, electron microscope study 78—22762
vinyl stearate multilayers, struct. determ. 79—4469
VPE on sapphire, highly oriented film prod. 77—66097
wear study, analytical surface tool, review 78—64718
Zircaloy-2, hydride precipitation and growth at crack tips, electron optical obs. 80—108449
β'-NiAl, Ni rich, electron diffr. pattern anomalies, rel. to martensitic transform. and short range ordering 78—6926
3PbO.GeO_2, X-ray and electron diffr. exam. *(German)* 80—11632
Ag, (211)[$\bar{1}$11] single crysts., shear band effects on rolling deformation 80—50651
Ag, adsorption of O_2 , catalytic oxidation mechanism 78—61046
Ag, cold rolled, weak beam method appl. to dislocation obs. *(German)* 77—84757
Ag, dynamic theory of electron diffr. including inelastic scatt. *(German)* 79—23921
Ag film, ion plated on AT-cut quartz crystal 80—2280
Ag film, vacuum deposited on NaCl, microstructure and orientation, surface condition influence 79—82486
Ag on W (001), geom. factors of FCC-BCC epitaxy 78—60041
Ag, small particles prep. by evaporation in clean Ar atm., cryst. morphology 77—62494
Ag, vac. deposition of oriented coating on doped alkali halide substrate 80—2303
Ag-Al, short-range order, X-ray and electron diffr. study 80—54173
Ag-Al (26 at.%), massive transform, $\beta \to \zeta$, crystallography and morphology 80—97475

electron diffraction examination of materials continued
Ag-Cd (45 at.%), morphology and crystal struct. of stress-induced martensites 78—68693
Ag-Cd (47 at.%), crystal struct. and internal defects of thermoelastic martensite 77—48438
Ag-liquid Ga interface, γ-phase interlayer growth, two-dimens. electron diffr. 79—19487
α-Ag-Mg, disordered, shaft range order diffuse scatt., electron diffr., interpretation 77—84596
Ag-Zn (38 at.%), morphological and struct. studies of thermoelastic martensites 77—63669
$AgBiS(Se)_2$, polymorphism and defects, electron microscopy 78—2254
AgI aerosol particle size, struct. rel. to ice forming activity 80—61164
Ag_3Mg, long-period alloy, ordered struct. 79—27949
Ag_3Mg, ordered, rational and irrational long period struct. 79—95175
Ag_3Mg, structure of ordered alloy, electron diffraction, kinematical vs. dynamical diffraction calc. 80—10530
Ag_2S film, tetragonal to cubic phase transform. kinetics, kinematic electron diffr. 77—4269
Ag_xTiS_2, intercalation cpd., Raman scatt. and electron diffr. meas. 79—24321
Al, (110) and (100) surfaces, MEED intensity calc. using chain method 77—20169
Al alloys, rapid quenching 80—76244
Al, boundary dislocations gliding, on coincidence boundaries, TEM study 79—82224
Al, cold rolled, weak beam method appl. to dislocation obs. *(German)* 77—84757
Al, compressed, nucleation and recrystallisation study by electron microscopy and Kikuchi diffr. 79—52236
Al, deformed, nucleation and recrystallisation at second phase particles 78—6941
Al, dislocation substructure formation under hydrostatic extrusion 78—56696
Al film, He^+ irrad., overpressurised bubble obs. 79—51165
Al film, vacuum deposited, structural changes during annealing at temp. near melting point 78—84096
Al, film integral radiation ability determ. by electron diffr. *(Russian)* 80—54413
Al films, $N_2{}^+$ and $O_2{}^+$ ion bombardment, structural and phase changes 80—2094
Al films, on calcite, electron diffr. using TEM, grain boundary scattering 79—65096
Al foil, electron diffr. effects and images from inclined grain boundaries 79—82241
Al, liq. film 78—83721
Al, MEED, multilayer scatt. effects 78—83682
Al, small particles prep. by evaporation in clean Ar atm., cryst. morphology 77—62494
Al, vacuum deposited, structural singularities and porosity *(Russian)* 78—75950
Al/GaAlAs, film, epitaxial growth on (100) GaAs by hot vac. deposition and characterisation 79—56085
Al-(Mg)(Fe), pure (dilute), large wire drawing plastic deform. 80—108508
Al-Ag alloy, ageing exam. by X-ray electron spectroscopy and electron diffr. exam. *(Russian)* 78—60685
Al-Ag alloy, second ageing stage, diffuse electron and X-ray scatt. *(Russian)* 78—68711
Al-Cu, anal. of electron diffr. micrographs using Patterson function *(French)* 79—20044
Al-Cu, dil. alloy, quench condensed thin films, supercond. and struct. from electron diffr. patterns 78—47901
Al-Cu, superconducting amorphous films of high stability 80—70889
Al-Cu (4 wt.%), naturally aged, early stages of G.P. zone form. 77—90355
Al-Cu (4 wt.%), reversion charact. *(Japanese)* 77—21150
Al-Cu (4 wt.%) alloy, reversion characts. *(Japanese)* 79—56989
Al-Cu-Ni, vacancy ordering, electron microscope and electron diffr. obs. 79—27954
Al-Cu-Zn alloy, ageing, X-ray and electron diffr. meas. *(Russian)* 78—39806
Al-Fe-Si(0.5, 0.2 wt.%), cast, phase determ. 77—70032
Al-Mg, oxidation control study, electron opt. techniques eval. 80—85089
Al-Mg/Al_2O_3 composites, interface phase, Auger and electron diffr. study 80—25646
Al-Mg_2Si, ageing sequence study by electron microdiffr. 80—81068
Al-Mg-Si, precipitation of cube-shaped phases, electron diffr. study using TEM *(Japanese)* 79—43251
Al-Ni (3.6 at.%) alloy, quenched from melt, distortion of matrix caused by coherent precipitates, electron diffr. meas. 77—59791
Al-Ni (63.6 at.%), elastic softening and electron diffr. anomalies prior to martensitic transform. 77—86078
Al-Pd, rapidly solidified, new ordered phase, electron microscope obs. 79—11645
Al-Pd (6 at.%), metastable Al_2Pd phase formed by rapid quenching, electron diffr. obs. 79—51054
Al-Pt (2 at.%), splat cooled, $AlPt_2$ phase, electron diffr. obs. 79—15657
Al-Si, deformed, local lattice rotations at second phase particles 80—25709
Al-Zn-Cu (22, 0-3 at.%) alloys, coherent spinodal curve 79—87605
Al-Zn-Mg powder, selected-area electron diffr. ring patterns 80—50642
(Al+Si)-Si thin films, struct. transitions and phase comp. 80—49537
$AlBr_3.NH_3$, mol. struct., vap. phase electron diffr. obs. 77—65541
$Al_{45}Mn_{55}$, pure and C doped, phase transforms. 79—96022
AlN film on Si and Ge, growth, struct. and props. 77—55468
AlN foil, thickness determ. by TEM using diffr. and energy loss anal. 78—29088
AlN, inelastic scattering probabilities for fast electrons in single cryst., orientation depend. 80—2905
Al_2O_3 amorphous films, struct., electron diffr. investigation 80—20046
Al_2O_3 films, DC reactively sputtered, struct. 80—96764
Al_2O_3, grain boundary thickness obs. using electron diffr. techniques 80—79811
α-Al_2O_3, radiation damage in HVEM, at high temp. and high dose 79—46707
Al_2O_3, sputter deposited, struct. and heat treatment charact. 78—15307
Al_2O_3/CuO, thin film interaction, $CuAl_2O_4$ form. *(Russian)* 78—52697
β-Al_2O_3-H_3O^+ protonic cond., struct. investig. 79—19213
β-Al_2O_3-$NH_4{}^+$, protonic cond., struct. investig. 79—19213
γ- AlOOH, boehmite, dehydration to γ-Al_2O_3 80—21277

electron diffraction examination of materials continued
Ar, FCC cluster, 40 kV electron scatt. dynamic effects 77—79721
As_2S_3, amorphous, struct. determ. by electron diffr. 77—11485
As_2Se_3, amorphous, laser radiation induced struct. changes, electron microdiffr. obs. 79—10874
As_2Se_3, amorphous, struct. determ. by electron diffr. 77—11485
As_2Te_3, amorphous, struct. determ. by electron diffr. 77—11485
Au, bicrystalline, electron diffraction on networks of grain-boundary and interphase dislocations *(Russian)* 79—73168
Au bicrystals, periodic ⟨111⟩ twist grain boundary structs., electron diffr. obs. 79—65100
Au, electron diffraction phenomena, rocking curves 78—14251
Au, epitaxial growth and nucleation on NaCl during ion bombardment 79—11024
Au, FCC cluster, 40 kV electron scatt. dynamic effects 77—79721
Au film, on corundum, with intermediate Cu and Cr layers, struct. obs. 77—28084
Au film, on Si and CaF_2 substrates, interphase coincidence boundaries 79—1560
Au film, on Si or CaF_2, oriented crystn., formation of coincidence orientations on interphase boundary 79—90922
Au films, condensation on alkali halides, growth, struct., stability *(French)* 78—38989
Au films, vac. condensed at oblique vapour incidence, oriented cryst. growth, electron diffr. study 80—97432
Au, grain boundary struct. anal. by HVEM *(Japanese)* 80—15109
Au, grain boundary thickness obs. using electron diffr. techniques 80—79811
Au, multiray calc. of cryst. lattice projection in ⟨111⟩ direction, from electron microscope image 79—94855
Au on W (001), geom. factors of FCC-BCC epitaxy 78—60041
Au particle, micro-area electron diffr. using electron holography 80—49055
Au particles condensed on NaCl surface, electron diffr. pattern interpretation, computer simulation *(French)* 77—76700
Au, pentagonal symmetry, icosahedral struct. *(French)* 80—79729
Au, small particles, size-effect modifications of Debye-Waller factor 77—84877
Au, thin film bicrystal, diffraction effects from inclined grain boundaries 80—103362
Au thin films, electron diffr. investigation of Debye temp. 80—88420
Au, twinned crystals, epitaxial growth on KCl crystals, electron microscopic study of microstructure 78—91566
Au vacuum deposited layer on KI, nucleation and growth 79—61516
Au, vacuum deposition, on (100) surfaces of KBr, KCl and NaCl substrates with colloidal centres *(Rumanian)* 78—60579
Au/AuPd, bicrysts., in situ relax. of interphase interfaces 80—39455
Au/Pd, bicrysts., in situ relax. of interphase interfaces 80—39455
Au/Pt interface, diffr. studies of conc. variations 79—42322
Au-Cd (47.5 at.%), modified 2H and 9R martensites 78—14366
Au-Cu (50% at.), pretransitional fluctuations *(French)* 80—2160
Au-Cu-Ag dental alloy, age-hardened, struct. and morphology 78—92272
Au-Cu-Ag-Pd (35.4, 17.8, 9.7 at.%), dental alloy, age-hardenable, TEM obs. 77—21156
Au-Ge (27 at.%), metastable phase struct. determ. by electron diffr. 78—83780
Au-Mg, high resolution electron microscope and electron diffr. investigation, obs. of $Au_{15}Mg_4$ monoclinic phase 80—1968
Au-Mg alloys, long-period superstructures, electron diffr. obs. 79—94959
Au-Mn, orthorhombic struct., electron diffra. and electron microscopy obs. 80—15052
Au-Mn system, AABB struct., experimental evidence for occurrence 78—63698
Au-Ni (30 at.%), singularities of struct. state, diffuse electron and X-ray scatt. *(Russian)* 79—4945
Au-Pd(Zn), disordered, shaft range order diffuse scatt., electron diffr., interpretation 77—84596
Au-Si film, elec. resist. decay and struct. change on exposure to air 77—72924
Au-Si system, transition layer struct. form. and heat treatment influence, amorphisation obs. 80—54529
Au-Si thin film double layer, silicide form., electron diffr. study 80—80005
Au_3Cd, sputtered epitaxial films, order-disorder reaction obs. 78—84092
AuCu II, periodic antiphase struct. *(French)* 79—14937
AuCu II, rational and irrational long period struct. 79—95175
$Au_{11}Mn_4$, electron diffraction and microscopy obs. 78—75512
$Au_{11}Mn_4$ ordered phase formation, electron diffr. and microscopy study 80—107418
$Au_{11}Mn_4$, ordering obs. 78—71707
Au_3Mn thin film study 80—92793
Au_4Mn, high resolution dark field electron microscopy exam. of ordering 79—7615
Au_xSi_{1-x} amorphous films, phys. studies 80—75476
Au_4Zn, long period superstructure study 78—10059
Au_4Zn, ordered alloy, long-period antiphase boundary struct., growth mechanism 79—19262
B dispersed fractionated powder, struct. obs. 80—19703
B fibre reinforced Al, thermal degradation of tensile strength, due to fibre strength degradation 78—39861
B films, amorphous, prep., struct., props., review, book contrib. 78—48321
B_2F_4, molecular structure, barrier to internal rotation, temperature effects 78—13625
BN fibres, prep., struct., thermal, mech. and elec. props., appls., book contrib. 78—48360
BN, graphite-like, twinning and shear 77—4114
BP wafers, epitaxial growth by thermal decomp. of $B_2H_6+PH_3$, struct. imperfections 77—62774
$B_{0\,65}Ru_{2.7}Cr_{1.3}O_8$, short axis tripling, X-ray and electron diffr. study 79—77576
Ba, plasmon excitation by oblique incidence of primary electron beam of medium energy 78—18987
$BaCuO_2$, prep. and props. *(French)* 77—43201
$BaFe_2O_4$ amorphous film, prep. by RF sputtering, crystallisation 80—76183
$Ba_{1+x}Fe_2S_4$, electron diffr. study, orientation anomaly 80—107152
$Ba_3Nb_6Si_4O_{26}$-$Ba_3Nb_4Ti_4O_{21}$, intergrowth, nonstoichiometry, struct. obs. *(French)* 77—19932
$(Ba_3Nb_6Si_4O_{26})_n.Ba_3Nb_4Ti_4O_{21}$, multiple intergrowth and microdomains obs. by electron diffr. and microscopy *(French)* 78—95160

electron diffraction examination of materials continued
BaO thin films, on (110) face of W, struct. study by LEED 79—60659
BaO-Fe_2O_3 system, splat cooled phases struct., magnetisation and susceptibility 300-1100K *(French)* 77—48017
BaO-Fe_2O_3-B_2O_3 glass, splat cooled, low temp. micromagnetism 80—34660
BaO-SiO_2 glass-ceramic, crystallisation mechanism 79—90559
$BaO.2SiO_2$, glass, spherulitic growth and recrystallisation 77—4046
$(Ba_xSb_{1-x})TiO_3$, ferroelectric films, dielectric and semicond. props. 79—91388
$Ba_{0.7}Sn_{2.6}Cr_{1.4}O_8$, short axis tripling, X-ray and electron diffr. study 79—77576
$BaTiO_3$ ceramics, PTC-type, grain boundary study using TEM 80—107267
$BaTiO_3$, epitaxial vacuum condensates struct. 79—95290
$BaTiO_3$, vacuum condensates, epitaxial growth on $SrTiO_3$ crysts., electron diffr. and TEM anal. 79—15051
Ba_2YbF_7 single crystals, electron diffr. cryst. struct. anal. *(French)* 80—92507
Be-bronze BrB2, struct. and phase transform. during mechano-thermal treatment *(Russian)* 80—11667
Be_3N_2-$BeSiN_2$ system, crystallography and phase relationships, TEM and electron diffr. study 80—92502
Bi epitaxial film, twinning, electron diffr. 77—35838
Bi film, structure and electronic props. 80—70562
Bi film, supercooling, exam. by electron diffr. and electron microscopy *(French)* 78—14636
Bi island films, effect of surface press. on lattice spacings 79—11045
Bi oxide film, struct. by electron diffr. and TEM obs. 80—6678
Bi thin film, structural evolution 8 to 573K, supercooling effects *(French)* 79—90921
Bi-MnBi directionally solidified eutectic alloys, struct. and mag. props. 79—51815
$Bi_2Mo_2O_9$, thermal decomp. rel. to catalytic oxidation, electron diffr. study 80—35520
Bi_2O_3, thin film, struct. and dielec. meas. 79—78622
$Bi_{0.9}Sb_{0.1}$, epitaxial film, defect struct. and galvanomagnetic props. 77—89889
Bi_2Se_3 film, partly oriented, electron diffr. dynamic effects 77—7996
$BiVO_4$, ferroelastic domains, electron microscopy and electron diffr. obs. 80—100254
C, amorphous, diffraction intensities, chem. bonding effects 77—72557
C, amorphous, X-ray and electron diffr. intensities, model struct. 78—26441
C fibre, prep. from benzene, struct. changes with stepwise heat treatment up to 3000°C 77—12649
C fibre structure, recent advances 80—81069
C fibres, PAN-based type I, II and III, TEM study of structural heterogeneity 79—77465
C, filamentous catalytic, rel. crystallographic orientations of C and metal 80—89240
C film, amorphous, bonding obs. 77—20474
C film, amorphous, struct. and semicond. props. and heterojunction form. with single cryst. Si 80—25002
C film, diamond-like, ion-plated, electron energy loss spectra characterisation 80—2308
C film, vac. condensed, graphitisation, electron microscopy 80—40265
C foil, ion irrad., crystallographic transform. 79—55794
C, thin foil, irradiation with 1.2 MeV Ar^+, electron diffraction study 80—103397
C, vacuum condensed film, SRO from radial-distrib. curve analysis 77—89662
C, vapour-deposited, transparent and hard insulating layer, struct. and props. 80—10830
C_6Li, intercalate ordering in first stage graphite-Li 80—6380
Ca, plasmon excitation by oblique incidence of primary electron beam of medium energy 78—18987
Ca-Nb-O perovskites, struct. characterisation *(French)* 78—10021
$Ca_2(Al,Fe,Cr)O_5$ solid soln., planar interfaces, TEM obs. 80—65008
CaF_2, thin insulating film, lattice parameter meas. by electron microscope 77—65940
$(Ca_{0.15}Mn_{0.8}Fe_{0.05})SiO_3$, rhodonite lattice imaging of struct. defects 80—49240
$Ca_5OH(PO_4)_5$, powder, precise study of electron diffr. patterns, diffr. interpretation at high tension *(French)* 79—37594
$Ca_6Si_6O_{17}(OH)_2$, xonotlite, polytype identification 80—72519
$(Ca_{1-x}Sr_x)(Ca_{1/3}Nb_{2/3})O_3$ perovskites, cryst. struct. *(French)* 79—65044
Cd film, HCP, crystal struct. changes on ion bombard. 77—69018
Cd_3As_2 films, nucleation processes, on NaCl substrates 80—59813
$CdCr_2Se_4$ film, electron irradiated, struct. 79—15032
$(CdGeAs_2)_{1-x}D_x$ amorphous films, property control in common target sputtering, elec. cond. 80—7494
CdI_2, hexagonal-rhombohedral polytypic transformation, electron diffr. and X-ray diffr. obs. 80—49163
CdI_2 polytypes, vapour growth mechanism 80—84124
CdI_2, sublimed films, preparation, struct. 77—24491
$CdIn_2Se_4$, high resolution electron microscopic study of polytypism 80—88119
CdS, defect struct., dark-field microscopy, anal. of decoration patterns 79—23506
CdS, epitaxial growth and nucleation, on monocrystn. ZnS, substrate real struct. influence 80—88455
CdS, epitaxial layers on Cd single crystal, direct synthesis and struct. 78—68628
CdS epitaxial layers on sapphire, exciton struct. of absorpt., photoluminesc. and photocond. spectra 80—89027
CdS film, on Si, structural and transport props. 78—6463
CdS film, polycrystalline, photosensitive, struct., pseudoreplica method, using electron microscopy and microdiffr. 79—15030
CdS layers, struct. investigation by electron and X-ray diffr., and electron microscopy, growth mechanism 79—56094
CdS(Se)(Te), evap. onto electron bombarded NaCl substrates, epitaxial growth and characts. 79—28948
CdSe film, vac. deposited, elec. resist. and surface changes by laser annealing 80—2491
CdSe film, vacuum deposited, struct., resist. and Hall mobility 77—76974
CdSe films, growth kinetics and cryst. struct. during vacuum condensation 80—2305
CdTe, film grown in quasi-closed volume, struct. *(Russian)* 78—75952
CdTe films, structural imperfections depend. on crystn. temp. 79—90661

electron diffraction examination of materials continued
$Cd_{1-x}Zn_xS$, film, technical data, for low cost solar cell 79−48127
$(Ce,Ta)Ta_6O_{19}$, disordered struct., convergent-beam electron diffr. symmetry 80−54178
Ce_2O_5-P_2O_5 glass, crystallisation 77−51326
$Cl_3SiOSiCl_3$, normal vibs. and force field, calcs. using electron diffr. struct. determ. *(Russian)* 78−46317
$(Co,Fe)_{0.75}B_{0.25}$ metallic glasses, annealed, equilib. crystalline phases 80−3019
Co ferrite, growth on fine acicular γ-Fe_2O_3 particles 80−29871
Co ferrite film prep. by vac. evaporation and annealing 77−85939
Co film, HCP, crystal struct. changes on ion bombard. 77−69018
Co, HCP, relationship of effects of systematic reflections to the crit. voltage 79−41916
Co-Ar film, struct., electron diffr. meas., rel. to metal-nonmetal transition 77−51626
Co-Cr-Ni superalloy Mar-M509 standard and Mo modified, phase anal. 77−63675
Co-Fe, transformation matrices, electron diffraction patterns 77−59779
Co-Ni-Cr-Nb FCC alloy, electron microscope obs. of deform. twins 79−60380
Co-P, electrodeposited alloys, heat-induced structural changes *(Japanese)* 80−89263
Co-P alloys, geometric struct. models and diffraction exam. techniques 80−79700
Co-Se, P-T diagram and structural study 78−56622
Co-Si-B-Fe alloy magnet, Al_2O_3 particle embedded surface, amorphous mag. anal. using electron diffr. 79−56568
Co-Si-B-Fe amorphous alloy, electron diffr., mag. anal. *(German)* 79−61182
Co-Ti-Fe (3, 1 to 2 wt.%), spinodal decomposition 80−100839
Co-X-Co (X=Cr,Mo,W) systems, crystn. temp. and hardness, as quenched structures 79−77529
$CoCO_3$-LiCl-H_2O system, complexing during cryst. growth, of spherocobaltite, electron diffr., neutron diffr. and spectroscopic obs. 77−44144
Co_5Ge_3 amorphous film, elec. resist., microstruct. and annealing 77−85188
$Co_{3-x}Mo_xO_4$ films, prep., struct. and elec. characteris. 80−108353
$Co_{0.32}NbS_2$ intercalation compound, struct. and photoemission meas. 77−16453
$CoOOH \rightarrow Co_3O_4$, morphology, topotaxy, comparison with $Co(OH)_2 \rightarrow CoOOH$ 77−16817
Co_3Pd epitaxial films, multiray dynamic theory of diffr. contrast to explain defects nature 79−64962
Co_xZrS_2, $(0<x\leq 0.50)$, intercalation compounds, ordered phases obs. 80−33962
Cr, BCC, electrodeposits on {100} Cu substrates, {211} twins obs. 77−47698
Cr, deformation waves and spin density waves, electron diffr. obs. *(Russian)* 79−19721
Cr film, obtained by thermo ionic precipitation, phase composition, lattice parameters *(Russian)* 80−96756
Cr film, size effects on spin density waves, struct. and elec. props. 77−80973
Cr film, vacuum evaporated, particularities in growth on alkali halides with Pb colloids and F-centres 79−82496
Cr film, vacuum-evaporated, with A-15 struct., prep. and characterisation 77−62768
Cr film, vapour deposited on low temp. KCl substrates, struct. obs. 80−10826
Cr, oxidation kinetics, 300 to 600°C, struct. and morphology of oxide film 77−59982
Cr-C(N) coating, deposited by hollow cathode discharge, characterisation 78−11371
Cr-Ge liquid and amorphous alloys, struct. props., cond., viscosity, surface tension *(Russian)* 80−54119
Cr-$NdAlO_3$, dielectric films, phase composition and structure 80−39464
Cr-Si, amorphous sputtered film, material for kilo-ohm sheet resistances, prep. and props 79−78227
$Cr_{11}Ge_8$, CrGe, and $Cr_{11}Ge_{19}$ amorphous films, short-range order, electron diffr. obs. *(Russian)* 78−56050
Cr_3Ge amorphous films, short range order struct. *(Russian)* 78−30841
Cr_5Ge_3, amorphous film, short-range-order struct., electron diffr. meas. 79−15047
CrO_2 and CrO(OH), fine particle obs. of cryst. morphology and topotaxy 80−65969
CrO_2, ferromag. films, epitaxial growth in air, electron diffr. and SEM obs. 79−42410
$Cr_3Si_2(C_2)$, sputtered films, microstruct. and wear props. 78−64733
$Cr_{2.8}V_{0.7}Fe_{3.4}C_3$, stacking fault study, morphology, comp. and struct. 80−84190
$CsBO_2$, mean geometrical config., vapour phase electron diffr. 77−50554
$CsTi_2NbO_7$, layer struct., X-ray and electron diffr. study 80−79753
Cs_xVF_3 (x=0.25,0.19), cryst. struct. examination by electron diffr. using TEM 79−23583
Cu and Cu-Cr (0.6 wt.%), electron microscope obs. of shear bands *(German)* 77−48454
Cu, corrosion inhibition, chem. nature and struct. of protective films 77−60001
Cu, cryst. pot. in electron diffr. and band theory 78−83677
Cu, dislocation substructure formation under hydrostatic extrusion 78−56696
Cu, electron-irradiated crystals, electron diffr. channelling effect on atom displacement 80−39158
Cu, epitaxial, on (111) Au, periodic arrays of misfit dislocations, electron diffr. 78−51857
Cu films, vac. condensed at oblique vapour incidence, oriented cryst. growth, electron diffr. study 80−97432
Cu foil, determ. of oxides on surface 77−90682
Cu, foil recrystallisation during annealing in high voltage electron microscope, grain growth *(Russian)* 79−100159
Cu, grain boundaries, intrinsic struct., electron diffr. anal. 80−84186
Cu on W (001), geom. factors of FCC-BCC epitaxy 78−60041
Cu, oxidation, electron scattering study 79−83377
Cu, thin film, oxidation, RMEED/SEM studies 80−100968
Cu, thin single cryst. films, growth from vapour, electron diffr. examination 79−33932
Cu/Ni interface, diffr. studies of conc. variations 79−42322
Cu-Ag-Ge, Hume-Rothery glass form. 80−96449
α_2 Cu-Al, antiphase period and tetragonality 78−15374

electron diffraction examination of materials continued
α-Cu-Al, short range ordered, struct. and new superlattice phase 78−52756
Cu-Al alloys, α_2 phase, config. of periodic antiphase boundaries 79−95029
Cu-Al composites, laminar, polycryst., electron diffr. proportional anal. 77−44444
Cu-Al_2O_3 thin film cermets, TEM study of composition and struct. 79−99437
β_1-Cu-Al-Ni (14.2, 4.3 wt.%), quenched, metastable 2H type phase characts., TEM and electron diffr. study 79−74149
Cu-Al-Ni (14.5, 3 wt.%), fatigued, polycrystn., pseudoelastic, dislocation and martensite substructs. 79−82223
Cu-Al-Sn system, coexistence of different and brass like phases 80−89206
Cu-Al-Zn, structural phenomena preceding martensitic transform. 77−12624
Cu-Bi, grain boundary thickness obs. using electron diffr. techniques 80−79811
Cu-Bi foil, electron diffr. effects and images from inclined grain boundaries 79−82241
Cu-Ga alloys, massive phase ζ tempering, kinetics, order-disorder transform. *(French)* 78−44118
Cu-Mn alloys, Cu-rich, heat treated, segregation obs. *(Russian)* 78−27517
Cu-Ni, initial oxidation study by microprobe-AES method *(Japanese)* 79−15867
Cu-Ni-Al (5, 2.5 at.%), precip. hardening *(Japanese)* 80−71663
Cu-Ni-Cr (28, 2.8 wt.%), spinodal alloy, microstruct. and tensile props. 78−39858
Cu-Ni-Sn (10, 6 wt.%), spinodal decomposition, X-ray and electron diffr. study 80−81063
Cu-Ni-Sn (9, 6 wt.%), decomposition, initial stages, TEM study 80−2992
Cu-Pd alloy, singularities of physical props. and ordering *(Russian)* 78−76643
Cu-Pd(Pt), disordered, shaft range order diffuse scatt., electron diffr., reinterpretation 77−84596
Cu-S, thin film, phase formation conditions *(Russian)* 79−56078
Cu-Si alloy, correl. of periodicities in diffr. patterns and images from grain boundary 78−14362
Cu-SiO_2, deformed, lattice rotations at second phase particles 80−25709
Cu-Sn alloy system, long period superlattice obs. and impurity effects 80−103297
Cu-Sn(-Al), quenched and aged, struct. of phases *(Russian)* 80−49184
Cu-Ti, and Cu-Ti-Si(Fe), struct. and coalesc. of oxide particles during internal oxidation *(Russian)* 79−90781
Cu-Ti (5.7 at.%), dil., β-phase struct. 79−55700
β-Cu-Zn-Al, diffr. effects., obs. and interpretation of extra maxima 80−44173
β-Cu-Zn-Al (27.5, 4.0 wt.%), strain induced martensite, exam. of structure, microstructure 80−7648
Cu-Zn-Be, precipitation hardening 77−16599
Cu-Zn-Ga alloy, configs. of martensite variants, shape deform. matrices 77−12620
$Cu_3As_2S_3I$, space group, determ. by convergent-beam electron diffr. 80−49154
Cu_2AuPd, struct., TEM and electron diffr. meas. 78−38666
Cu_2FeS_3, pseudocubic mineral, twinning obs. in point electron-diffr. photographs 77−43225
Cu_5FeS_4, bornite, superstructuring, vacancy clustering, high-resolution electron microscopy 78−42981
Cu_3Ga, interpretation of diffuse contours in electron diffr. *(French)* 79−19377
$CuGaSe_2$ thin film, surface morphology study using RHEED 79−65564
$CuInS_2$ films, RF sputtered, growth and props. 80−80124
$CuIn_5S_8$, sulphospinel, electron microscopy study 80−88080
$CuInS_2(Se_2)(Te_2)$, film, electron and X-ray diffr. 77−11819
$CuInSe_2$ epitaxial growth on GaAs 78−84104
$CuInSe_2$, growth on CdS (0001) surface using MBE 79−56936
$Cu_{0.5}In_{2.5}Se_4$, transition state and domain struct. by electron microscopy and diffr. studies 80−15095
Cu_xMS_2, $(0<x\leq 0.50)$ (M=Zr, Hf), intercalation compounds, ordered phases obs. 80−33962
$Cu_{2+x}Mn_{1-x}Al$, omega phase, roles of electron microscopy and electron diffraction *(French)* 78−27524
$Cu_{0.5}NbS_2$ and $Cu_{0.5}TaS_2$, order-disorder and displacive transforms., domain-type microstruct. 77−4195
Cu_xNbS_2, $0.8<x<1$, order-disorder transitions and incommensurate superstruct. 77−15587
Cu_xNbS_2 and Cu_xTaS_2, electron diffuse scatt., microstruct., of transition state 77−31771
$Cu_{40}Nb_{30}X_{30}$ (X=Ti, Zr, Hf), superconductors with metastable ordered structs. 80−108484
CuO-CaO-P_2O_5 glass devices, memory switching 78−56192
Cu_2O film, reactively-sputtered, phase comp., resist. and optical consts. 79−95534
Cu_2O, laminar growth on (111) Cu single cryst. surface, microstruct. 78−72025
$Cu_{1.8}S$-Cu_2S thin films, phase transforms kinematic electron diffr. study 80−29295
$Cu_{2-x}S$, digenite, epitaxial layer 77−85117
$Cu_{2-x}S$, digenite related phases, electron microscope study 79−10840
$Cu_{2-x}S$ film, evaporated, ordering process, electron diffr. study 80−39477
Cu_9S_5, digenite, superstructuring, vacancy clustering, high-resolution electron microscopy 78−42981
Cu_xS layer, on CdS, electron diffr. obs. of phases 78−51847
Cu_3Sb, formed by saturation of Cu grains with Sb, electron diffraction exam. of diffusion layer *(Russian)* 79−33119
CuSe film, phase transforms. and decomp., electron diffr. obs. 79−42418
η-Cu_3Si precipitates in Si, cryst. struct. 78−91304
Cu_3Sn, one-dimens. long period superstructs. with Zn and Ni additions 78−83777
CuTe, Cu_2Te and $Cu_{2-x}Te$ alloys, struct., electron diffraction investigation 79−51066
$Cu_{3-x}Te_2$, non-stoichiometric phases, electron microscopic and electron diffraction studies 80−64977
CuZn, omega phase, roles of electron microscopy and electron diffraction *(French)* 78−27524

electron diffraction examination of materials continued
D_2O, atom pair correlation functions, X-ray, electron and neutron diffr. data 77–80406
D_2O, atom-atom and mol. correlation functions, electron diffr. 77–80405
$DyAl_3$, polytypism, high resolution microscopy and electron diffr. obs. *(French)* 77–11503
Dy_2O_3 film, phase transforms. on annealing 79–95285
Dy_2O_3, influence of upper Laue areas on fine struct. of bend contours near high symmetry axis 78–38596
Dy_2O_3, lattice conservating twin, bend contours due to upper Laue zones 80–15113
ErO, vac. deposited films, struct. changes due to annealing 79–77741
$Eu_{0.14}Si_{0.31}O_{0.55}$ glass, optical, magnetic, and magneto-optical props., chemical clustering 79–42951
Fe alloy, corrosion inhibition, chem. nature and struct. of protective films 77–60001
Fe alloy type G18, martensitic $\gamma\rightleftharpoons\varepsilon$ transformation, dislocation pile-ups, ε phase nucleation *(Russian)* 80–55396
Fe, cast, high Mg content (0.33%), exam. of phase composition characts. 78–84780
Fe, compressed, recrystallisation, transmission Kossel study of struct. 78–19776
Fe epitaxial growth on Au single crystals, substrate temp. effect on morphology 78–26798
Fe, film, implanted with C ions, HCP struct. formation, electron diffr. study *(Russian)* 79–82469
Fe film, thermally evaporated, contamination effects obs. 80–49545
Fe, granular film, microstructure using X-ray, electron diffr. and TEM 79–65344
Fe, oxidation, scanning electron diffr. appl. 77–25178
Fe, pure, initial grain boundaries effect on cold-rolling and annealing textures *(Japanese)* 80–35205
Fe sputtered film, amorphous, Mossbauer study and electron diffr. obs. 80–75897
α-Fe, struct. after polymorphic transform. under press. *(Russian)* 80–29946
Fe, triboelectric charging, effects of fluorinated compounds 78–60188
Fe ultrafine particles prepared by vacuum evaporation, mag. props. 78–35007
Fe vacuum deposits on Ni(Cu)(Ag) (111) FCC substrates, orientation relationships 80–59836
Fe, wear sliding track, deformation 77–12707
Fe, whiskers, high strength, polycrystalline, microstruct. obs. 79–33214
α-Fe whiskers, pure, ductile fracture, microscopic obs. of initiation mechanism 80–85044
Fe-Al-C steel, singularities of struct., electron microscope and electron diffr. analysis *(Russian)* 77–77476
Fe-As (0.22 to 1.68 wt.%), martensitic transform., struct. features 77–36499
Fe-Au (111) interface, nature of interaction layer 79–99433
β-Fe-Be, pseudotwinning and pseudoelasticity 79–96056
Fe-Be (16.5 or 19.5 at.%), four-phase model of struct. in initial ageing stages *(Russian)* 78–48430
Fe-C, oxidation at 700°C, electron diffr. obs. 79–61790
Fe-C martensite, crystal struct. and morphology of ordered phase 79–42011
Fe-C solid solution, martensite, carbide decomposition, electron microscopy and X-ray diffr. obs., review *(Russian)* 79–33998
Fe-C-(Si), splat quenched, electron diffr. and Mossbauer study of retained ε-phase 77–52354
Fe-Co-Si-B sputtered amorphous thin film, coercivity, galvanomagnetic props., resistivity 80–29578
Fe-Co-V, Vicalloy 1, γ-phase morphology and structural inheritance depend. on heating rate *(Russian)* 79–70059
Fe-Co-V alloys, effect of V on struct., electron diffr. and Mossbauer meas. *(Russian)* 77–77507
Fe-Cr-Al-Y, oxidation resistance, heat treatment and Al^+ ion implantation 80–71785
Fe-Cr-Mn, influence of alloying with Ni, Mo, N on defect conc. energy *(Russian)* 80–54241
Fe-Cr-N (5.9, 0.5 wt.%), martensitic, tempered, fine struct. 77–25079
Fe-Fe_2O_3 composite films, structural props., microhardness, 250 to 700K 78–84095
Fe-Ge amorphous alloys, radial distrib. funct., electron diffr. exam. 77–68922
Fe-Mn-C, $\gamma\rightarrow\varepsilon\rightarrow\alpha'$ martensitic transform. 79–24523
Fe-Mn-Ni base maraging alloys, age hardening 79–74170
Fe-Ni, martensitic transform. dynamic, quasi-static atomic displacements, NGR, X-ray and electron scatt. meas. *(Russian)* 78–68688
α-Fe-Ni, struct. after polymorphic transform. under press. *(Russian)* 80–29946
Fe-Ni (31%) alloy, deformed by slip, misaligned zones in $\{259\}_A$-martensite crysts. *(Russian)* 77–59850
Fe-Ni (32.86, 30.65 wt.%), characts. of quenched struct. formed in textured sheets, TEM and optical microscopy study 79–34084
Fe-Ni alloys, struct. of γ and α-phases near martensitic transform. point *(Russian)* 78–64541
Fe-Ni two-phase films, alloy component redistrib. during annealing, electron diffr. anal. *(Russian)* 79–20053
Fe-Ni-Al-Ti alloy, N27Yu2T2, aged austenite, diffuse electron scatt. distrib. during martensitic deform. *(Russian)* 78–60669
Fe-Ni-C (19 to 30, 0.04 to 0.8 wt.%) alloys, transformation of martensite in austenite, optical and electron microscopic exam. *(Russian)* 78–35382
Fe-Ni-C alloys, obs. of banded struct. formed by deformation 79–79050
Fe-Ni-Cr, Elinvar, struct. and mag. props., singularities during tempering *(Russian)* 80–50627
Fe-Ni-Cr-C, effect of austenite yield strength, stacking fault energy, on martensite morphology 78–80546
Fe-Ni-Mn, martensitic transforms. electron diffr. studies of γ solid soln. *(French)* 78–84803
Fe-Ni-Mn (20, 5 wt.%), rel. orientation between adjacent martensite laths 80–76254
Fe-Ni-Mn martensitic alloy, precipitation 77–12630
Fe-Ni-(Cr)(Ti)(Al) austenite, high N content, cryst. struct. electron diffr and electron miscroscope anal. *(Russian)* 79–24490
Fe-P film, amorphous, ion implanted, struct. and domain struct. obs. 79–91272
Fe-Pd (50 at.%) alloy, structural changes during ordering *(Russian)* 77–77471

electron diffraction examination of materials continued
Fe-Si (3 wt.%), exam. of plastic deformation, slip band dislocation, under hydrostatic pressure 78–56695
Fe-Si (3wt.%), grain-oriented, secondary recryst., grain growth inhibition 80–89245
Fe-Si-Al (5,10 wt.%) struct. anal. *(Chinese)* 79–11618
α-Fe-Ti, ion-implanted and annealed, microstruct. evolution 80–15132
Fe-X-C (X=Cr, Mo, W), quenched rapidly from melts, nonequilib. phases *(Japanese)* 80–71630
Fe-Zn intermetallides, initial stages of form. *(Russian)* 80–20889
Fe_3Al, ordered alloys, atomic order parameters from topology of electron-microscope diffr. contrast from antiphase boundaries, quantitative determ. 78–95016
$Fe_x(C,N)$, obtained by ion bombardment thermochemical treatment of Armco Fe *(French)* 77–86229
$Fe_{65.4}Cr_{20.5}Al_{10.7}V_{3.4}$, effect of Al and V on form. of $L2_1$ superstructure and stratification 77–77474
Fe_3Ge amorphous films, short-range struct. 77–24267
Fe_5Ge_3, amorphous film, elec. resist., microstruct. and annealing 77–85188
Fe_5Ge_3 film, electron diffr. study of struct. and microheterogeneity 77–85108
$Fe_{0.33}NbS_2$, intercalation compound, struct. and photoemission meas. 77–16453
$Fe_{40}Ni_{38}Mo_4B_{18}$, amorphous, crystallization, heat treatment and irradiation effects *(French)* 79–90558
$Fe_{1-x}O$, quenched, decomposition and ordering, electron diffr. and microscopy 77–31635
$Fe_{1-x}O$, wustite decomposition, coherent magnetite precipitation, electron diffraction study *(Russian)* 80–16318
α-Fe_2O_3 film, prep. by reactive condensation and mag. props. 78–64241
Fe_2O_3, powder, preparation conditions rel. to morphology 77–8777
Fe_2O_3-TiO_2 system, high temp. intergrowth struct., metal atom ordering in intergrowth boundaries 78–79573
Fe_3O_4 film, prep. by reactive condensation and mag. props. 78–64241
Fe_3O_4 film prep. and form. by Fe naphthenate thermal decomposition *(Japanese)* 77–32519
Fe_3O_4 magnetite, low temp. phase transition, diffuse electron scattering *(Japanese)* 80–24591
Fe_3O_4, spherulitic film growth, elec. and mag. props. 78–68627
Fe_3O_4-Fe_2O_3 thin film on passivated Fe, electron diffr. study *(German, English)* 80–89418
Fe_xO_y film, thermally evaporated, contamination effects obs. 80–49545
$Fe_{80}P_{16}C_3B_1$ amorphous filament, produced by glass coated melt spinning, mech. props. 78–15483
$Fe_{25}Pd_{50}Au_{25}$, atomic ordering influence on mag. props. and elec. resistance *(Russian)* 80–7551
Fe_3Pt, premartensitic phenomena *(French)* 79–8297
FeS_2 (pyrite), glide elements study by electron microscopy and electron diffr. 78–83817
FeSb alloy films, vapour-deposited, formation of metastable phase 80–44437
$Fe_{1-x}Se$, phase relation 79–14926
$FeSi_2$ films, structural and Anderson transitions, cond. and IR reflectance meas. 79–15200
Fe_xSi_{1-x}, amorphous, struct. and mag. props., giant moment form. at mag. ordering 78–68192
Fe_xSi_{1-x}, struct. exam. by electron diffr. and resist. meas. 77–89409
Fe_xSn_{1-x}, amorphous alloy stability, comp. and temp. depend. 79–19156
Fe_xSn_{1-x}, amorphous film, struct. and mag. props. 80–65972
Fe_xTaS_2, vacancy ordering, transition state cluster model, electron diffr. 77–47547
FeTi-D(H), γ-phase, neutron and electron diffr. 80–84156
FeTi-H system, TEM study 79–58850
Fe_xZrS_2, $(0<x\leq0.50)$, intercalation compounds, ordered phases obs. 80–33962
Ga, film, polymorphism, electron diffr. obs. *(French)* 78–18922
GaAs (100), VPE, role of Cl, LEED, RHEED, and AES obs. 77–1327
GaAs, anodic oxide for device application, crystallisation dynamics 79–66190
GaAs, dislocation-free, point defects and rad. damage 80–88141
GaAs, ion implantation, disordered layer physical props. 79–77624
GaAs, MBE, undoped, growth and characterisation 80–10836
GaAs oxide films, anodically and thermally grown, XPS study 80–16141
GaAs, photoelectric memory effect, effect of metallic island struct. on surface 77–55570
GaAs surface, during vapour phase epitaxial growth, characterisation techniques and meas. *(French)* 77–1817
GaAs:Au, back surface gettering 80–10758
p-GaAs:Be, ion implanted, annealing characts., defect cond. profiling, electron diffr. obs. 79–4318
GaAs-AlAs layered films, MBE prep., struct., rel. to optical props. 79–77950
GaAs-SiO_2 interface local props. *(Russian)* 78–10567
$GaAs_{1-x}Sb_x$, MBE grown, surface struct. exam. by MEED 78–87847
$GaBr_3.NH_3$, mol. struct., vap. phase electron diffr. obs. 77–65541
$GaNbO_4$, electron beam induced decomp., high resolution lattice imaging obs. 78–6161
GaP_xAs_{1-x}-GaAs one dimens. superlattice, possibility of X-ray and electron diffr. struct. determ. 80–54560
GaS, space group, determ. by convergent-beam electron diffr. 80–49154
GaSb films, amorphous and cryst., vac. evaporated, Elec. cond. thermoelec. power and optical absorpt. 80–2504
Ga_2Se_3, vapour phase deposited films, struct. 78–2383
$Ga_{1-x}Te_x$ amorphous films, elec. cond., optical absorpt. and transparency, band gap energy 79–56335
Ga_2Te_3, vapour phase deposited films, struct. 78–2383
Gd film, vac. deposited and VPE, deposition parameters effects on struct. 79–90912
Gd-Co, amorphous, sputtered very thin film struct. 77–15707
Gd-Co alloy, sputtered film, mag. props. determ. *(Chinese)* 78–2714
Gd-Co amorphous films, annealed, short-range order and perpendicular mag. anisotropy 80–15765
Gd-Co amorphous films, correlation between struct. and mag. props. *(Chinese)* 80–54532
Gd-Co amorphous films, mag. struct., mag. bubbles, electron diffr. study *(Chinese)* 80–71126
Gd-Co amorphous thin films, crystn. process and domain struct. *(Chinese)* 80–54533
Gd-Co film, amorphous, Ar sputtered, struct. 78–63946

electron diffraction examination of materials continued
- Gd-Co film, amorphous, phase separation as source of perpendicular anisotropy 78—64244
- Gd-Co film, evaporated and sputtered, struct. and mag. anistoropy 79—56578
- Gd-Co film, vapour quenched, amorphous, struct., electron diffr. meas. 77—28086
- Gd-Co-Mo film, amorphous, Ar sputtered, struct. 78—63946
- Gd-Fe film, amorphous, in-situ ion beam sputtered, microstruct. and Lorentz mag. struct. 78—63947
- Gd_2O_3, 'monoxide' film reidentified as sesquioxide formed by oxidation by hydride 79—19474
- Ge amorphous film, effects of ion implantation on structure 78—55881
- Ge amorphous films, structural relaxation and crystallisation 80—100170
- Ge, crystal struct. factor, at. scatt. factor, electron diffr. determ. 77—15291
- Ge, epitaxial film, ion sputtering, growth mechanism, struct., props. 77—31917
- Ge particles, grown in Ar gas, cryst. struct. and habit, electron microscope study 79—74071
- Ge particles, homogeneously nucleated, production and props. 77—56252
- Ge, stacking fault width determ. from 224 reflections with g.b=0 78—59722
- Ge:O, Cu, amorphous thin film, impurity effects on struct. 80—107054
- Ge-Ag, exam. of structure using electron microscope *(Russian)* 79—14738
- Ge-Cu (0, 23, 40 at.%), amorphous film struct. *(German)* 78—95391
- Ge-metal film, polycryst., struct. props. determ. 79—4494
- Ge-metal films codeposited, amorphous and polycryst., struct. and elec. props. 80—24766
- Ge-S glasses, Cu doped, thermal, structural and dielectric props. 79—60283
- Ge-Te alloy films, amorphous, semicond. props., refr. index, struct. study 78—26978
- GeP, thin films, vacuum-deposited, struct. characterisation 77—47691
- GeS, film on Ge, evaporation, thermogravimetric, electron microscopy investigs. 77—15715
- GeTe film, amorphous and crystalline, electron diffr. meas. 77—39748
- GeTe, film, local order, electron diffraction study 79—77485
- H_2 ($^1\Sigma_g^+$), charge density, X-ray scatt. factors, gas phase electron diffr. 78—930
- H_2-D_2 vacuum deposited solid films, struct. study transmission electron diffr. obs. *(Russian)* 79—11035
- H_2O, atom-atom and mol. correlation functions, electron diffr. 77—80405
- H_2O, inelastic electron scatt., geometrical parameters determ. 77—88585
- Hf, oxidation, microstructural study *(French)* 80—45436
- Hf-Nb (30 to 50 at.%) exam. of beta phase decomposition processes 78—76674
- HfF_4, mol. struct. and vibr. freqs., gaseous electron diffr. obs. 80—32836
- α-HgS films, sputter-deposited in Hg vapour, growth and props. 80—75467
- HgS, RF sputtering on NaCl, growth and struct., electron diffr. and TEM obs. 77—90271
- Ho-Co film, evaporated, struct. and mag. anistoropy 79—56578
- Ho-Co film, vapour quenched, amorphous, struct., electron diffr. meas. 77—28086
- In particles, grown in ultra-high vac. on KCl substrates, struct. and orientation 80—10814
- In, recrystallisation of films prep. by vacuum evap. 79—4488
- In submonolayer growth on Si(111)7 surface, superstruct. 79—77930
- In-Cd, shape memory *(Japanese)* 79—43243
- In-S system, vac. deposited films, form., reacts. 78—43259
- InAs epitaxial layers, on GaAs substrate, electron diffr. and SEM exam., electronic props. 79—1552
- InN film, specular reflection spectra, lattice parameters 80—7428
- In_2O_3:Sn, thin films, prep. by pyrolitic method, charact. by SEM, electron diffr. and SIMS, solar energy appl. 79—43143
- InP single crystals, uniaxial compression deform. characts. 80—84991
- InSb, prep. of thin films by ionised-cluster beam deposition *(Japanese)* 80—25576
- InSb thin layers, directed crystn. on sapphire, struct. 80—35112
- InSe luminescent film, production and characterisation *(Russian)* 78—39581
- InTe thin films, flash evaporation, electrical props. 80—65722
- $In_{1-x}Te_x$ amorphous films, elec. cond., optical absorpt. and transparency, band gap energy 79—56335
- KBr, single cryst., lattice structure distortion on freshly formed surface, electrification 77—51582
- KCl:Ba, defect struct., dark-field microscopy, anal. of decoration patterns 79—23506
- $K(Fe_{1.5}Mg_{0.5}Si_4O_{10})(OH)_2$, cryst. struct. refinement 78—26545
- $KNiCl_3$, disorder as observed by electron diffr. 80—75213
- $K_2Pt(CN_4)Br_{0.3}.3H_2O$, anisotropic radiation damage in electron microscopy, diffr. spot fading rate obs. 80—107329
- K_xVF_3 (x=0.25,0.19), cryst. struct. examination by electron diffr. using TEM 79—23583
- $K_{0.27}WO_{(3+y)}$, struct. analysis 77—11510
- Kb_2S_3, condensates, struct. and optical transmittance 80—20727
- Kr monolayer, on graphite, misfit dislocations and lattice parameters, model, diffr. data interpretation 78—34708
- La-Al amorphous alloys, internal friction, relaxation process 80—92607
- LaF_3 single cryst., electron diffr., superlattice struct. 78—42993
- $LaNbO_4$ crystals, ferroelastic, w′ walls, temp. depend. 80—10560
- $LaNbO_4$, room temp. form., symmetry determ. by convergent beam electron diffr. 80—79723
- La_2O_3, cryst. struct., X-ray powder diffr. and electron diffr. study 80—107161
- La_2O_3-CeO_2, microstruct. of La_2O_3 rich crystallites, electron microscopy and diffr. *(French)* 78—35374
- $LaSi_2$, thin film, exam. of phase transitions during vacuum annealing 79—95281
- La_5Si_3 thin film, exam. of phase transitions during vacuum annealing 79—95281
- LiF, mosaic single-cryst. film, electron diffr. reflection intensities, precision meas. 79—94851
- LiF, thin insulating film, lattice parameter meas. by electron microscope 77—65940
- $LiFeO_2$, ion ordering, transition state cluster model, electron diffr. 77—47547

electron diffraction examination of materials continued
- $LiNbO_3$, amorphous ribbons, prep., electron and X-ray diffr. obs., dielec. const. temp. depend. 79—50993
- $Li_x(NbO)_4Nb_{30}O_{90}$, struct. and ionic cond. 79—65246
- Li_2O-(Al_2O_3)-SiO_2 glass-ceramic, crystallisation mechanism 79—90559
- $LiTaO_3$, crystallographic features and domain struct. 78—34498
- $LiTbS_2$, long and short range order 78—38667
- $Li_x(WO)_4W_{30}O_{90}$, struct. and ionic cond. 79—65246
- $LuCl_3$, pyramidal struct. and force field coeffs., electron diffr. obs. 78—9250
- Mg, grain boundary struct., Kikuchi electron diffr. obs. 80—15116
- $MgAl_2O_4$ spinel, kinetics of form. from oxides in thin films *(Russian)* 79—52144
- $MgAl_2O_4$, spinel, space group 80—28937
- $MgAl_2O_4$, structural phase transition obs. by electron diffr. 77—66020
- $MgCa(CO_3)_2$, dolomite, partial thermal decomp. into MgO and $CaCO_3$, product cryst. growth 80—108706
- MgIn, atmospheric corrosion, SEM, electron diffraction and electron probe obs. 79—24681
- MgO, critical voltage effect, effect of temp. *(French)* 80—10463
- MgO, dynamical effects for cryst. struct. determ. 78—83679
- MgO, melt-grown cryst., direct evidence for brucite precip. 77—28712
- MgO, X-ray and electron diffr. crystallite size determ. *(Polish)* 79—100153
- Mn thin films, vacuum deposited in elec. field, resist., struct. 80—103761
- Mn-Al alloy, vacuum codeposited, disorder of $MnAl_6$ phase in recovery process 78—51854
- Mn-Bi film, amorphous, form. and crystn. 79—28923
- Mn-Ge amorphous films, short-range order, electron diffr. obs. 80—39473
- Mn-Zn ferrite, single crystal, surface damaged layer study *(Japanese)* 77—86260
- Mn-Zn ferrite single crystals, mech. polishing effect on mag. props. *(Japanese)* 80—16569
- Mn_3Ga, formation of DO_{22} superstruct. and para-antiferromag. transition 79—19737
- Mn_6N_5 film, cryst. struct. and phase transform. exam. by electron diffr. 78—10189
- $Mn_{0.25}NbS_2$, mag. anomaly rel. to struct. disordering 78—43557
- $Mn_{0.26}NbS_2$ intercalation compound, struct. and photoemission meas. 77—16453
- MnZn ferrites, abrasive wear measurement appl. *(Japanese)* 78—39917
- MnZn polished ferrite worked layer magnetic characts. changes meas. *(Japanese)* 78—10742
- MnZn-ferroferrites, sintered, microstruct., TEM study *(Dutch)* 80—2036
- Mo (110), oxidation of adsorbed C, electron diffr., contact pot. difference, and AES obs. *(Russian)* 79—52430
- Mo cathode, H_2 glow discharge, FCC surface layer form., electron diffr. obs. 77—55311
- Mo, electron current density localisation and effect on damage prod. 78—22763
- Mo film, carbonisation and oxidation, electron diffr. exam. *(Russian)* 77—44399
- Mo film deposited by low temp. carbonyl pyrolysis, struct. 78—72039
- Mo, He ion irradiated, TEM 77—19994
- Mo, macroscopic heterogeneity of plastic deform., metallographic examination *(Russian)* 79—100210
- Mo, surface machined, struct., electron diffr., TEM *(German)* 77—73371
- Mo-Ni film system, diffusion reaction, phase form. 77—84999
- Mo-O crystals, electron microscopy study 80—28889
- Mo-Ti (up to 5.48 wt.%), internal nitriding, hardness, nitride type, precipitation *(Japanese)* 79—79157
- Mo_2C, Mo_2N, synthesis by ion bombard. of Mo film 78—48357
- MoO_3, film, colour centre studies, optical absorpt. spectra 78—71724
- MoO_3, reduced crystals, planes of crystallographic shear, TEM study 79—46683
- MoO_3 reduction to MoO_2 by electron beam, electron difrr., microscope investigs. *(French)* 78—95945
- MoO_3, thin cryst. obs. by convergent beam electron diffr. 78—38670
- $(Mo_{1-x}Ru_x)_{80}P_{20}$, amorphous alloys, superconductivity, mag. susceptibility and electronic props., liq. quenching 78—88057
- MoS_2 film, sputtered, solid lubricant, morphological growth 77—35825
- $MoSe_2$ and other layer structs. containing hohlstellen, electron diffr. 77—80397
- $MoSi_2$, sputtered films, microstruct. and wear props. 78—64733
- β-$MoTe_2$, domain struct., dislocation fine struct., phase transitions 79—82332
- β-$MoTe_2$, layer cryst., dislocations and domain struct. 80—39102
- N_2 ($^1\Sigma_g^+$), charge density, X-ray scatt. factors, gas phase electron diffr. 78—930
- α-N_2 twinning, electron microscope and diffr. exam. 77—35574
- $Na_8Al_6Ge_6O_{24}.CO_3.2H_2$, cryst. struct. 78—83805
- $Na_{0.91}Al_2(Si_{3.09}Al_{0.91})O_{10}(OH)_2$, paragonite 1M, cryst. struct. determ., electron diffr. 78—26547
- $Na_{0.5}Ca_{0.5}Al_{1.5}Si_{2.5}O_8$, labradorite feldspars, lattice parameter determ. of exosolution structs. 77—84704
- NaCl dimer. electron diffr. study of mol. struct. 80—28951
- NaCl, single cryst., lattice structure distortion on freshly formed surface, electrification 77—51582
- NaCl-gas reactions, atmospheric, in situ TEM studies 80—104544
- NaF, thin insulating film, lattice parameter meas. by electron microscope 77—65940
- $Na_2Ti_9O_{19}$, cryst. struct. anal. by 1 MV high-resolution electron microscopy 79—73137
- Nb, electron diffraction axial channelling Kossel patterns, Bloch wave model, obs. 78—42869
- Nb film, sputtered, comparison with X-ray diffr. and AES *(Czech)* 79—51448
- Nb, H_2 embrittlement, microscopic obs. at low temps. 77—32666
- Nb on sapphire, highly oriented film prod. 77—66097
- Nb-Al (20 at.%), diffuse scatt. before Nb_3Al phase form., unstable phase *(Russian)* 78—3131
- Nb-Ge film, phase transformations due to annealing, electron diffr. study 80—54551
- Nb-Ge film, supercond., TEM expts., correl. of struct. and elec. props. 78—14628
- Nb-Ge film, supercond., two-phase, tetragonal Nb_5Ge_3 phase identification by electron diffr. 77—89665
- Nb-Zr-Al superconducting alloy, struct. determ. *(Russian)* 77—16628

electron diffraction examination of materials continued
  NbD_x, λ-phase struct., neutron and electron diffr. meas. 79—94962
  $Nb_{40}Fe_{40}P_{14}B_6$, metallic glass, explosive compaction, mech. props. 80—89176
  Nb_3Ge, RF and DC sputtered films comparison, O content effect 78—72022
  Nb_3Ge, sputtered on Cu, film-substrate interface obs. by electron microscopy 80—65398
  Nb_3Ge superconducting film, struct. 77—32123
  NbH, internal friction 78—6962
  NbH(D), ordered, TEM obs. of anisotropic lattice distortions 79—7579
  $4NbO_{0.76}$ thin film, FCC cell struct. investigation 80—92796
  NbO_2, vapour phase molecular struct., high temp. electron diffr. 79—68330
  Nb_2O_5-TiO_2, splat cooled, crystallization and ordering 77—68953
  $3Nb_2O_2.8WO_3$, circular diffuse scattering studied by 1 MV high resolution electron microscopy 80—59350
  NbS_2, intercalation compounds, octahedral, microstructural study 77—84729
  $NbS_3(Se_3)$, Peierls distortion, electron diffr. obs. 80—39503
  $NbSe_3$, CDW form., direct electron diffr. 78—30877
  $NbSe_3$, satellite electron diffr. below 59K, Fermi surface features 78—84136
  $NbSe_2Cu_x$, ordering study using electron diffr. and microscopy 80—39043
  Nb_3Sn diffusion layer material, characterisation 79—38213
  $NbTe_2$, layer cryst., dislocations and domain struct. 80—39102
  $Nb_{0.87}V_{0.13}Se_2(4Hb)$, stacking layer study, appl. of convergent beam electron diffr. 80—39116
  $NdAlO_3$, dielectric films, phase composition and structure 80—39464
  $NdNbO_4$, room temp. form., symmetry determ. by convergent beam electron diffr. 80—79723
  Nd_2O_3, cryst. struct., X-ray powder diffr. and electron diffr. study 80—107161
  Ni, C precipitation 80—29958
  Ni, dislocation substructure formation under hydrostatic extrusion 78—56696
  Ni film, implanted with C ions, HCP struct. formation, electron diffr. study *(Russian)* 79—82469
  Ni on W (001), geom. factors of FCC-BCC epitaxy 78—60041
  Ni, sputtered, on Si, annealing effects on transmission electron diffr. patterns, silicide form. 78—91562
  Ni sputtered films, hexagonal and amorphous, O incorporation, ESCA and electron diffr. meas. 79—11046
  Ni, thin film, growth on Au (001) substrates *(French)* 80—44446
  β_1-Ni-Al, elastic softening and electron diffr. anomalies prior to martensitic transform. 77—8825
  Ni-Al film, co-evaporated, comp.-depend. struct. and morphological changes 79—87020
  Ni-Al film, high-temp. condensed, electron diffr. and elec. resist. *(Russian)* 79—4485
  Ni-Al solid solutions, Ni-rich, phase transforms. during quenching 77—32577
  Ni-Al-Mo (12.7, 21.6 wt.%), directionally solidified eutectic composite, precipitation 80—108454
  Ni-Co-P, ferromag. film, amorphous to cryst. transition, diffr. and resistivity meas. 78—60587
  Ni-Cr film, long range order 79—60657
  Ni-Cu-Si (38,5 at.%), changes in modulated struct. during ageing early stages *(Japanese)* 79—100183
  Ni-Cu-X (X=Sn, Nb, Ti), spinodal decomp. alloys, linear expansion coeff. influence on morphological anisotropy *(Japanese)* 80—70431
  β-Ni-Cu-Zn, electron microscopy of premartensitic state 79—66059
  Ni-Fe (20%) film, prepared by low temp. condensation, struct. 77—59222
  Ni-Fe-Nb (Mo), magnetic alloy, TEM and X-ray obs. *(Chinese)* 80—24401
  Ni-Mo, and Ni-Mo-V alloys, struct. changes on annealing *(Russian)* 77—21145
  Ni-Mo, short range order considerations and development of long range order 77—16574
  Ni-Mo (5.8-24 at.%) solid soln. struct. and strength characts. *(German)* 79—4975
  Ni-P, amorphous electrodeposited alloys, phase-separation *(Japanese)* 80—54140
  Ni-P amorphous alloy prep. by ion implantation 78—22748
  Ni-p film, amorphous, ion implanted, struct. and domain struct. obs. 79—91272
  Ni-Pd-H, film, struct. and phases formed, when Ni, Pd are sputtered in H 80—29289
  Ni-S, defect control by heat-treatment in S atmos. 79—43293
  β-Ni-Ti, struct. changes during annealing, TEM and selected area diffr. 79—34081
  Ni-Ti alloy, near equiatomic, pretransform. lattice instability, TEM and electron diffr. 79—11616
  Ni-Zn, γ-phase region, X-ray and electron diffr. obs. 79—61562
  $Ni_{1-x}Al$ solid solution, vacancy ordering exam. by electron diffr. after annealing 78—3123
  Ni_3Al-Ni_3Nb eutectic alloy, ^{63}Ni diffusion rate rel. to struct. defects *(Russian)* 78—2288
  Ni_3C films, form. by carburisation, characterisation 80—34337
  NiGe, and Ni_2Ge, amorphous film, electron diffr. exam. of struct. 77—35828
  Ni_3Ge, amorphous film, electron diffr. exam. of struct. 77—35827
  Ni_5Ge_3, amorphous film, elec. resist., microstruct. and annealing 77—85188
  Ni_2H, hexagonal type, cryst. struct. determ. by electron diffr. 79—55724
  Ni_4Mo alloy, high temp. oxidation, oxide layer growth, struct., mech. behaviour 78—44269
  Ni_4Mo, antiphase domains growth kinetics, TEM and electron diffr. *(Russian)* 77—32557
  Ni_4Mo, quenched, short-range order, electron diffraction study 77—39560
  $Ni_{0.34}NbS_2$, intercalation compound, struct. and photoemission meas. 77—16453
  Ni_xNbS_2 vacancy ordering, transition state cluster model, electron diffr. 77—47547
  NiO, lattice parameters, microstrains, non-stoichiometry, comparison between mosaic microcrysts. and quasi-perfect single microcrysts. 80—24414
  NiO_2 single crystals, welding, optical and SEM study 79—65097

electron diffraction examination of materials continued
  NiPt, short-range order, effect of plastic deform., electron diffr. anal. *(Russian)* 80—24403
  $Ni_{3\pm x}Te_2$, long period superstructs. rel. to partial ordering 79—51056
  NiTiCu, shape memory alloys, electron microscope and X-ray diffr. study of struct. 79—82179
  Ni_xZrS_2, $(0<x\leq0.50)$, intercalation compounds, ordered phases obs. 80—33962
  O_2 $(^3\Sigma_g^-)$, charge density, X-ray scatt. factors, gas phase electron diffr. 78—930
  $OPBr_3$, mol. struct., electron diffr. and spectroscopic vibr. amplitude 80—58387
  $P_xH_yH_z$, synthesis and struct. 80—54201
  PLZT ferroelectric thin films, epitaxial growth and optical props. 80—70543
  PLZT film, epitaxial growth by RF sputtering, and characterisation 77—85937
  PLZT, thin film epitaxial growth and characteris. 79—28918
  Pb film, oxide form. on (111) surface, orthorhombic PbO 77—63835
  Pb, film, ultra-thin, hexagonal phase, struct. 78—38982
  β-Pb hydride, electron diffr. investigation 79—65062
  Pb, liq. film 78—83721
  Pb-Ar (Xe) film, struct., electron diffr. meas., rel. to metal-nonmetal transition 77—51626
  Pb-Ar films, atomic arrangements, high energy electron energy diffractogram study, Ar conc. depend. 79—99444
  $Pb_3Ge_2O_7$, dielectric thin film, obtained by sedimentation, exam. of dielectric props. and structure 80—2282
  $Pb_{1-x}Hg_xS$ epitaxial films, electroless deposition and struct. props. 79—90915
  $Pb_{1-x}Hg_xS$ film, solution-grown, struct., lattice parameters and optical band gap var. 77—69201
  $PbMg_{1/3}Nb_{2/3}O_3$, short-range ordering, electron microscope and diffr. study 80—10469
  PbO thin layers on PbO-SiO_2 glass, reaction behaviour 78—34660
  PbS, epitaxial layer, structural nonuniformities and dislocation struct. 79—23852
  PbSe film, partly oriented, electron diffr. dynamic effects 77—7996
  $Pb_{1-x}Sn_xTe$, epitaxial growth on $LiNbO_3$, electron diffr. and microscopy exam. 77—1331
  $Pb_{1-x}Sn_xTe$-PbTe heterostructures, MBE produced on mica and $LiNbO_3$, elec. props. study 80—88629
  PbTe film, epitaxial, patterns of diffuse bands on electron diffr. patterns 79—11021
  PbTe film, on NaCl and TGS substrates, photo-EMF investig. of induced elec. inhomogeneity 77—15909
  $PbTiO_3$, $(PbTiO_3)_{0.9}(B_2O_3)_{0.1}$ amorphous ribbons, prep., electron and X-ray diffr. obs., dielec. const. temp. depend. 79—50993
  $Pb_3(VO_4)_2$, ferroelastic, phase transitions, boundary walls 80—107419
  Pd, epitaxial, on (111) Au, periodic arrays of misfit dislocations, electron diffr. 78—51857
  Pd particles formed by evaporation on alkali halide crystals, orientation and struct. 78—84108
  Pd-Mn system, superstructure, electron diffr. and X-ray powder diffr. study 79—94958
  Pd-Sb film, rhombohedral phase, cryst. struct., electron diffr. determ. 80—39008
  Pd-Se, thin layers, phase identification and struct., electron diffr. 77—51615
  Pd-Zn, γ-phase region, X-ray and electron diffr. obs. 79—61562
  $PdH_{1.18}$, $PdH_{1.20}$, prep., cryst. struct., chem. comp. determ. by thermal decomp. 80—34334
  $Pd_{60}Ni_{20}Si_{20}$, amorphous, struct., high resolution electron microscopy 80—1969
  Pd_2Si layer, on Si, ion implantation damage, confirmation of channelling results 78—30676
  $Pd_{80}Si_{20}$, amorphous alloy, partial struct. functions, X-ray, electron and neutron diff. studies *(Japanese)* 80—88050
  polyethylene, permanganic etchant for TEM obs. 80—21132
  Pt small particles deposited on NaCl and mica substrates, struct. and orientation *(French)* 77—43458
  Pt-Au bimetallic films, electron diffraction on networks of grain-boundary and interphase dislocations *(Russian)* 79—73168
  Pt-Si contact, silicide layer struct., sputter etching and annealing ambient effects 77—62991
  PtO, existence 78—18923
  PuO_2-UO_2-Na aerosol, from LMFBR HCDA conditions, characterisation 78—94104
  $RbBO_2$, mean geometrical config., vapour phase electron diffr. 77—46651
  RbCl/KCl interface, diffr. studies of conc. variations 79—42322
  $Rb_{0.25}VF_3$, cryst. struct. examination by electron diffr. using TEM 79—23583
  ReO_3, absorpt. of H_2, electron diffr. obs. of H_xReO_3 phase 79—60513
  ReS_2, layer cryst., dislocations and domain struct. 80—39102
  $ReSe_2$, layer cryst., dislocations and domain struct. 80—39102
  Rh, film, annealing effect on struct., TEM, electron diffr. study 78—76682
  Rh, resistive film, electron diffr. structure obs., heat treatment effects 77—51620
  $(SN)_x$, fibrous struct. study by electron diffr. using TEM 79—65004
  $(SN)_x$, halogenated, struct. behaviour, TEM obs. 80—70126
  $SPBr_3$, mol. struct., electron diffr. and spectroscopic vibr. amplitude 80—58387
  Sb, epitaxial growth, of electrodeposits on oriented single cryst. surfaces of CU, electron diffr. study 79—66016
  Sb, epitaxial growth of electrodeposits on oriented single crystal Au and Ag 78—43267
  Sb, film growth mechanism, action of residual gases rel. to deposition conditions 79—23850
  Sb, liquid-quenched, stabilisation and transformation kinetics of metastable phases 80—3022
  Sb:Te vapour saturation, diffusion zone struct. crystallisation orientation *(Russian)* 80—54438
  Sb-Au amorphous film, quench condensed, struct. and stability 79—99459
  $Sb_{0.2(0.4)}MoO_{3.1}$, synthesis, struct. and oxidation state *(French)* 80—64971
  Sb_2S_3, vacuum deposited films, struct. and photoelec. props. 77—85092
  $Sb_2S_3(Se_3)$, IR spectra rel. to bonding, amorphous film and cryst. 77—16410

electron diffraction examination of materials continued
ScF_3, pyramidal struct. and force field coeffs., electron diffr. obs. 78—9250
ScH_2, electron diffr. investigation 80—107112
Si (111), MEED, secondary electron emission under surface state reson. 78—84688
Si, (111) cleavage, Kikuchi pattern, 40 keV incident electrons, electron energy loss spectra *(French)* 78—87594
Si, amorphisation by bombardment with O ions, electron diffr. and EPR meas. 78—10098
Si, amorphisation due to irradiation with heavy ions 77—11606
Si amorphous, diffraction intensities, chem. bonding effects 77—72557
Si, ang. distrib. of electrons, beyond single cryst., diffr. patterns 78—1962
Si electron diffraction axial channelling Kossel patterns, Bloch wave model, obs. 78—42869
Si, electron diffraction on single-cryst. slabs at 2.27 MeV 79—50962
Si, epitaxial regrowth and grain struct. of Al metallisation on ⟨100⟩Si 78—79901
Si film, amorphous, formed by CVD, crystallisation 77—39746
Si film, amorphous, structural comparison of evaporated and glow discharge samples 77—62778
Si film, CVD or evaporated, covered with Al layer, solid-phase crystn. obs. 77—85100
Si film, polycrystalline, struct. thickness relationships 77—62779
Si films, polycryst., glow discharge deposited below 250°C, struct. and morphology 80—49535
Si, forbidden 200 diffr. spots 78—47214
Si, formation mechanism of electron diffr. Kikuchi lines 80—44081
Si, implanted annealed layers, amorphised structure formation mechanism and crystallographic nature 80—29091
Si, ion bombardment induced defect distrib., IR and electron diffr. study 80—65074
Si, ion-implanted layers, radiation defect prod., refl. electron diffr. obs. 78—87696
Si, Kikuchi structures, energy analysis by intensity profiles *(German)* 79—7528
Si MOS device, electron optical identification of precipitations 80—16309
Si, monocryst. dynamic theory of electron diffr. including inelastic scatt. *(German)* 79—23921
Si, obs. of lines of difficiency with black-white contrast in Kikuchi diffr. patterns 79—55614
Si on sapphire, laser annealing dynamics epitaxial regrowth, optical reflectivity 80—29285
Si, oxide scale microstruct. of oxidised single cryst. 80—108613
Si particles, grown in Ar gas, cryst. struct. and habit, electron microscope study 79—74071
Si polycrystalline films, texture formation study 79—87662
Si, post-annealed amorphous layer, twinning struct. by transmission electron diffr. 77—76685
Si, pseudo-Kikuchi patterns in refl. expts. during scanning of single cryst. by intermediate energy electrons 78—1964
Si, single cryst. films, temp. depend. of electron Kikuchi diagram 80—1904
Si, unindexable and forbidden lines in Kikuchi electron patterns 79—94850
Si whiskers, polytypism and amorphousness 78—26801
$Si{:}B_2O_3$, analytic study of Si-B phase formed 79—19269
Si:B(P), ion implanted, polycryst. annealing characts. 77—24324
Si:N wafers, Si_3N_4 layer growth by high dose implantation and annealing, elec. props. 80—70227
Si:Ne(Ar)(Kr), ion implantation damage, annealing, comparative study 79—10867
Si:P, heavily doped, glow-discharge-produced, elec. and optical props 80—2497
Si:P spherical defect cluster and dislocation loop analysis 78—14356
$Si{:}P^+$, highly implanted, two step annealing effect on crystallinity 77—31683
β′-Si-Al-O-N, Mg-containing phases, crystn. 80—39297
Si-Al-O-N polytypes, hot-pressed, microstruct. 80—3023
Si-Al-O-N sintered ceramic, microstruct., phase composition and transformation mech., mech. props. 80—40309
Si-Au(Cr)(Pd), contact reactions between amorphous Si and metallic films, TEM, transmission electron diffr. obs. 79—23846
$Si\text{-}CoSi_2Si$, double heteroepitaxy, solid phase and MBE 80—104063
Si-Ge heteroepitaxial system, imperfections and morphology, electron microscope and electron diffr. obs. 79—42420
SiC, epitaxial layers on diamond, electron diffr. patterns 77—15720
SiC, HVEM obs. of various polytypes 80—76248
β-SiC, heteroepitaxial growth on Si substrate using $SiCl_4\text{-}C_3H_8\text{-}H_2$ system, reflection electron diffr. anal. 79—24445
SiC, one dimensional disorder 78—51492
SiC, oxide scale microstruct. of oxidised single cryst. 80—108613
SiC, polymorphism, electron diffr. and optical simulation *(French)* 77—39519
SiC polytypes, lattice imaging studies on intergrowth structs. 80—107025
SiC polytypes, stacking sequences by high resolution electron microscopy 80—15054
SiC, polytypic forms determ. from Kikuchi electron diffr. patterns 77—31566
SiC, polytypism, reflection electron diffr. 78—83694
SiC, reaction bonded, microstruct. characterisation 78—48353
SiC, sputtered, comp. and struct. props., effect of target materials 80—54549
SiC, surface defect annealing, following Ar ion and electron irrad. 80—7603
SiC, surface defects due to Ar ion bombardment, 100-1000 eV 80—6445
$\alpha\text{-}Si_3N_4$, effect of excess Si under ionic implantation of N 79—86809
Si_3N_4, films, ion-beam synthesis, IR spectra, struct., crystallisation on annealing 77—16705
Si_3N_4, reaction-bonded, microstructural analyses 77—8782
SiO_2, amorphous film, form. by thermal oxidation of Si, struct., mechanism 77—12725
SiO_2, condensed sol, electron microscopy and diffraction studies 77—29049
SiO_2 film, Ge substrate, structure investigation 78—10297
SiO_2 film, on Si, structure determ. by electron diffr. anal. 79—15050
SiO_2 films, amorphous to cryst. transform. induced by diethyl ether vapour 79—55667

electron diffraction examination of materials continued
SiO_2 layers, anodic oxidation growth on p-Si, transmission electron diffr. obs. 79—28241
SiO_2 layers, crystallisation, structural props. rel. to annealing 78—34724
SiO_2, stoichiometric condensate form. during electron beam evaporation of quartz, electrophysical props. 77—16496
SiO_x amorphous films, high energy electron diffr. study 80—38911
Sm_2O_3, 'monoxide' film reidentified as sesquioxide formed by oxidation by hydride 79—19474
$C\text{-}Sm_2O_3$, cryst. struct., electron diffr. 77—31650
Sn film, polycrystn., grain boundary scattering rel. to annealing temp., TEM study 79—65560
Sn film, vacuum deposited, substrate and substrate temp. effects on struct. 80—107677
Sn polycrystalline films, elec. props. and crystallite size, 4.2K to room temp. *(Russian)* 80—93011
Sn-plate passivation films, TEM struct. obs. 80—45416
SnO_2, catalyst particles, converger beam electron diffr. 78—83685
SnO_2 layers, study using Mossbauer effect 78—31124
SnO_2 thin films, analytical characterisation 80—20053
$SnO_2{:}F$, thin films, prep. by pyrolitic method, charact. by SEM, electron diffr. and SIMS, solar energy appl. 79—43143
SnS(Se), electron diffr. struct. anal. 80—44449
SnSe, single crysts., growth by Bridgeman technique, electron diffr. anal., lattice consts., carrier conc. 79—47616
SnTe-PbSe mixed system layers, struct. and props. *(Russian)* 77—28082
Sr, plasmon excitation by oblique incidence of primary electron beam of medium energy 78—18987
$Sr(Ca_{1/3-x}Sr_xNb_{2/3})O_3$, perovskite, X-ray and electron diffr. study *(French)* 79—99161
$Sr_2Nb_2O_7$, normal-incommensurate phase transition, electron microscopy and diffraction study 80—39277
$Sr_2Ta_2O_7$, structural phase transition to superlattice, electron microscopy and diffraction study 80—39277
$SrTiO_{3-x}$, X-ray and electron diffr. obs. of anion deficiency 78—22708
steel, Cr-Ni, ferrite precip. *(Japanese)* 80—35187
Ta epitaxial layers, formation conditions influence on struct. *(Russian)* 80—20045
Ta-N (0.6 to 6.5 at.%), supersaturated solid soln., precipitation 79—96028
Ta-O solid soln., interstitial ordering and precipitation at 100 to 270°C, exam. 78—52813
$TaBr_5$, gaseous, electron diffr. obs. of vibr. assignment, mol. struct. and barrier to pseudorot. 79—81293
$\beta\text{-}Ta_2H$, ordered alloy, electron microscope study of lattice distortions 77—11507
Ta_3N_5, polycryst. film, cryst. struct. *(French)* 77—76677
$2Ta_2O_3$ thin film, FCC cell struct. investigation 80—92796
Ta_2O_5, with hexagonal lattice in thin layers, atomic struct., electron diffr. 80—84160
Ta_xO_y deficient $Ta_{10}O_{18}$ struct., monoclinic, cryst. struct. by electron diffr. 77—39570
TaS_2, 1T polytype, intercalated with Li(Na)(K)(Eu), CDW's and superlattice patterns 77—47746
TaS_2, $1T_\beta$ to $1T_\alpha$ phase transform., cinematographical obs. 77—84925
TaS_2, intercalation compounds, octahedral, microstructural study 77—84729
TaS_2, Peierls transit transition 77—66119
TaS_2, polytypes, charge density waves and superlattice effects, intercalation with hydrazine 78—39043
TaS_3, electron diffr. evidence for one-dimens. Peierls distortion 78—10024
$TaSe_2(6R)$, stacking layer study, appl. of convergent beam electron diffr. 80—39116
Te, breakdown of Friedel's law in Kikuchi patterns as obs. in TEM 79—69046
Te film, evaporated, predeposited Ag, Sn, Bi, Al and Se nucleation centres effect on grain growth 77—4739
Te film, growth on (111) KBr films deposited on mica, TEM and electron diffr. obs. *(Japanese)* 78—64473
Te film, on electron irrad. KBr, epitaxial growth and surface coverage 80—10825
Te, Kikuchi patterns, of non-centrosymmetrical crystal 80—100202
Te/Ag double films, interdiffusion and struct. modifications *(French)* 77—62682
Ti alloys, twinned hexagonal α phase crystals, electron diffr. pattern analysis 78—56647
Ti anodic oxide film growth kinetics *(French)* 78—23864
Ti, exam. of oxidation kinetics, and oxide film structure 78—56822
Ti film, effect of surface and bulk oxidation on charact. electron energy loss spectra *(French)* 78—39641
Ti, oxide film form. during thermal treatment, morphological and struct. study *(French)* 80—50766
Ti:N surface, ion nitriding by a DC glow discharge method, surface anal. 78—80672
Ti-Al film, struct. and elec. props. 80—7002
$Ti\text{-}Al_2O_3$ system mixed films, prep., phase comp., struct. and elec. props. 79—37930
α-Ti-Al-Sn, alloy Ti-679, electron diffr. anal. of Ti_3Si phase *(Chinese)* 80—64845
Ti-Al-Zr alloy, TA6Zr5D, structural evolution during continuous cooling at different rates *(French)* 80—45300
Ti-Mn, fine cryst. struct. by diffuse X-ray and electron scatt. *(Russian)* 79—99329
Ti-Mo, fine cryst. struct. by diffuse X-ray and electron scatt. *(Russian)* 79—99329
Ti-Mo alloys, structural stability under high-pressure soaking 80—104151
Ti-Mo-Zr-Sn (11.5, 6.0, 4.5 wt.%) alloy, struct. as affected by processing history 80—84972
Ti-Mo-Zr-Sn-Fe-C-Si alloy, β-III, cold deform. and annealing, effect on struct. and mech. props. *(Russian)* 79—24533
Ti-Nb-Al, decomposition during isothermal annealing 80—25653
Ti-Nb-Ge foils, β phase decomposition, electron microscopy struct. investigation *(Russian)* 79—83172
Ti-Nb-Ta-Ge (40,20,0.8 wt.%) foil, dispersion hardening, TEM and electron diffr. obs. *(Russian)* 79—1873
Ti-Nb-V-Zr struct. determ. by optical microscopy and electron diffraction *(Russian)* 77—16628
Ti-O, anodic film structure, intensiostatically formed, pH and current density influence, TEM study *(French)* 79—66217

electron diffraction examination of materials continued
Ti-Si amorphous alloy, melt-quenched, transform. studies and mech. props. 80—100838
Ti-V (10 at.%), $\alpha \rightarrow \omega$ transformation, electron diffr. evidence of intermediate BCC phase 80—81051
Ti-V-Mo alloy system, phase equilibria and interstitial effects, TEM and X-ray diffr. study 79—43204
Ti-V-Si, equlibrium silicide, X-ray and electron diffr. obs. 78—27483
Ti-W/Au, metallisation on Al, temp. stability, barrier props., TEM obs. 79—23868
α_m-Ti-X (X=Ag, Au, Si), precipitation mechanisms and Meyrick theory of cellular reaction initiation 79—74163
TiC, oxidation at various O_2 pressures 79—96172
TiN_2, ultrafine synthesis in RF plasma, X-ray diffr. chem. and electron microscopy anal. 79—70026
TiN_x, cryst. and internal structs., electron diffr. and microscopy 77—27861
$Ti_{55}Nb_{45}$, supercond., anomalous phonon thermal resist. 77—69451
$Ti_{50}Ni_{47}Fe_3$, premartensitic phases, neutron scatt., sp. ht. and electron microscopy obs. 79—96025
TiO_2 anodic film, optical indices as function of crystallisation 77—66552
TiO_2 film, electron diffr. exam. 78—79906
TiO_2, rutile, electron diffr. patterns and extinction distances 77—76363
TiO_2:Cu, anodic, effect of Cu on optical props., rel. to possible appl. in solar energy conversion 80—16115
TiO_2-ZrO_2, submicron powders, vapour phase production from $TiCl_4$-$ZrCl_4$-O_2 system 80—40301
TiO_x, vacancy ordering, transition state cluster model, electron diffr. 77—47547
$TiO_{1.95}$iFe, quenched near melting point, transverse composition waves 79—99220
$TiS_{1.46}$, $(4H)_2$-4C type superstruct., high resolution electron microscopy determ. 79—69060
$TiS_{1.5}$, $(4H)_3$-6C-type superstruct. revealed by high resolution microscopy 80—19755
$Ti_{1+x}S_2$, short-range ordering, electron and X-ray diffuse scatt. 77—19936
$Ti_{1+x}S_2$, vacancy ordering, transition state cluster model, electron diffr. 77—47547
$Ti_{1+x}Se_2$, superlattice form., phase transform., electron and X-ray diffr. meas. 77—15383
$TiSe_2(S_2)$ (1T), electronic and vibronic struct. 80—44500
$Ti_{1-x}V_xSe_2$ $(0 \leq x \leq 0.1)$, elec. resist. and Hall effect 80—2386
Tl, α and β-phase stability range and supercooling, electron diffr. obs. *(French)* 77—84924
$TlRO_3$ (Ln=La, Nd, Sm, Eu, Gd), determ. of lattice parameters *(French)* 78—95031
$Tl_{0.25}VF_3$, cryst. struct. examination by electron diffr. using TEM 79—23583
Tl_2X_2(X=F,Cl), mol. force field and const. constraints from electron diffr. data 77—27197
TmSe, nonstoichiometry, high temp. chem. and valence instability *(German)* 79—23743
V film, supercond. crit. temp., crit. field, resist. and struct. *(Russian)* 77—4475
V-H(D), phase diagrams, struct. studies 80—66491
V-O alloys, quenched, local ordering of O, electron microscopy and diffr. 80—59453
V-Ti-C, high temp. carbide form., electron microscopy study 80—89228
V_4As_3, defect struct. 77—4112
VC_x, VN_x, vacancy ordering, transition state cluster model, electron diffr. 77—47547
V_2MoO_8, planar defects, electron microscopy and electron diffraction meas. 77—15430
VN_{1-x}, vacancy ordered structure in cubic mononitride phase, transition entropy determ. 78—43011
$(V_{1-x}Nb_x)_2$ C, C ordering formation of varieties 80—38968
$VO_{1.23}$, electron diffr. study of diffuse scattering due to atomic displacements 79—99327
$VO_{1.30}$, ordered, electron diffr. patterns of defect struct. 79—99177
VO_2, metal-insulator transition and electronic struct., ion bombard. effects 80—92948
VO_2, V_2O_3 and V_3O_5, film prep. under equil. conditions, struct. and elec. props. 80—108352
VO_x, defect ordering, electron diffr. obs. 79—23595
VO_x, defect struct., local ionic arrangements in disordered phase 80—10532
V_2O_3, low temp. crystallographic struct. domains 78—83765
V_2O_5, amorphous semicond., solubility and fibrous texture 80—75162
V_6O_{11}, metallic Magneli phase, electron state 79—94946
V_7O_{13}, metallic Magneli phase, electron state 79—94946
V_xO_y film, prep. by thermal decomp. of vanadium naphthenate, and elec. props. *(Japanese)* 78—88425
V_xO_y, film, preparation by calcining vanadium naphthenate, formation process exam. *(Japanese)* 78—30849
$VSbO_4$, catalyst particles, converger beam electron diffr. 78—83685
VSe_2 (1T), deform. modulated superstruct., electron diffr. expts. 78—51515
V_3Si, supercond. structure and properties *(German)* 80—93631
$(V_{1-x}Ta_x)_2$ C, C ordering formation of varieties 80—38968
W {100}, anisotropy of inelastic electron refl., energy loss effects 80—79642
W film, carbonisation and oxidation, electron diffr. exam. *(Russian)* 77—44399
W film deposited by low temp. carbonyl pyrolysis, struct. 78—72039
W foil, electron diffr. effects and images from inclined grain boundaries 79—82241
W, SEM expts., anomalous patterns *(Chinese)* 80—59349
W, texture and grain boundary struct., primary misorientation function, expt. deform. 79—1876
WO_3, amorphous film, vac. deposited, struct. and crystn., TEM obs. 80—2291
WO_3, hexagonal form, struct. study, X-ray powder diffr., electron diffr., and electron microscopy meas. 79—99157
WS_2, single crysts., growth by direct vapour transport method, X-ray and electron diffr. study 79—28904
Xe monolayer, on graphite, misfit dislocations and lattice parameters, model, diffr. data interpretation 78—34708
Y film, struct. and elec. resist., electron diffr. meas. 78—87888
Y-H film, rel. to temp., thickness and comp. depend. of elec. resist. 79—78221

electron diffraction examination of materials continued
YFe_2O_4, extra electron relfections 80—100139
YIG, thermomag. anal. by electron diffr. 80—108035
Y_2O_3-Al_2O_3, thin film, electron diffraction exam. of phase transformations *(Russian)* 79—34025
YSeF, direct lattice imaging of polytypes 77—4087
$YbFe_2O_4$, extra electron relfections 80—100139
$Yb_2Fe_3O_7$, extra electron relfections 80—100139
$Yb_3Fe_4O_{10}$, extra electron relfections 80—100139
Yb_2O_3, merohedral twins, many beam diffr. contrast 78—83829
Zn film deposition on Al, TEM and electron diffr. obs. 80—75460
Zn film growth, HEED and projection microscope obs., surface orientation depend. on deposition parameters 77—32523
Zn-Al, dislocation slip peculiarities during superplastic deform. 79—20102
$Zn_xCd_{1-x}S$ solid soln. films, reactive cosputtering, struct., comp. and opt. absorpt. edge *(French)* 78—6237
ZnO, crystallising in double HCP lattice, microstruct. 77—31655
ZnO, epitaxial layers, influence of deposition conditions on luminescence, electrical props. 79—99924
ZnO epitaxial layers, rel. between elec. and photoluminesc. props. and their deposition conditions 79—95530
ZnO, film, reactively RF sputtered, anal. of texture 78—67921
ZnS, defect struct., dark-field microscopy, anal. of decoration patterns 79—23506
ZnS ion beam etching, topographic changes, amorphisation, luminescence study 80—76078
ZnS:Mn on SnO_2/glass transparent conductive base, surface morphology effects on electroluminesc. *(Russian)* 78—48238
ZnS-MgF_2 alloy films, struct. and optical props. 79—90910
ZnSe epitaxial layers, organometallic CVD prop., growth kinetics and luminescent props. 79—51458
ZnSe, evap. onto electron bombarded NaCl substrates, epitaxial growth and characts. 79—28948
ZnSe:I, I vapour transport prep., conductive and photolum. cryst. 79—100035
ZnTe:Cu, voltage depend. on precip. contrast 79—1433
Zr base alloys, formation of phases precipitated from β solid solutions *(Russian)* 79—1869
Zr, electron extinction distances for twenty two lowest order reflections 78—47213
Zr, hydride precipitation and growth at crack tips, electron optical obs. 80—108449
Zr:N surface, ion nitriding by a DC glow discharge method, surface anal. 78—80672
Zr-Al martensite, DO_{19} phase formation, selected area diffr. obs. 78—84779
Zr-Nb, singularities of $\beta \rightarrow \omega$ transform. in alloy, with high content of β-stabiliser *(Russian)* 78—76644
Zr-Nb (2.5 wt.%), hydride precipitation and growth at crack tips, electron optical obs. 80—108449
Zr-Nb-Ge, singularities of $\beta \rightarrow \omega$ transform. in alloy, with high content of β-stabiliser *(Russian)* 78—76644
Zr-Nb-V-Si superconducting alloy, struct. determ. *(Russian)* 77—16628
ZrO_2 crystalline particles, TEM and electron diffr. meas. 77—21350
ZrO_2 foils, production for TEM, preferred grain orientation 79—74087
ZrO_2, hydrous, prep. from $ZrOCl_2$ soln. and cryst. texture determ. *(Japanese)* 77—89398
ZrO_2, hydrous particles, crystal texture *(Japanese)* 77—25002
ZrO_2-CaO (15 mol.%), precipitation and ordering 80—100837
ZrO_2-CaO(MgO)($YO_{1.5}$), partially stabilised, growth morphology of tetragonal phase 79—4968
ZrO_2-UF_4, orthorhombic struct., X-ray and electron diffr. study *(French)* 78—67689
ZrO_2-Y_2O_3 (9 mol.%), precipitation and ordering 80—100837
ZrO_2-Y_2O_3-Nd_2O_3(CeO_2), solid solns., form. by coprecipitation, struct., X-ray, electron diffr. anal. 77—12583
$Zr_{1-x}S$, short- and long-range ordering of vacancies, rel. to supercond. transition temp. 77—19945

electron-electron double resonance *see ELDOR*

electron-electron interactions
see also electron-electron scattering
bremsstrahlung from electron high-energy collisions, mag. field effects *(Russian)* 77—61906
colliding beams, effect of external field on bremsstrahlung 77—74670
Coulomb interaction of electrons by virtual photons exchange, quasiclassical interpretation 78—41523
Hubbard chain, half-filled band, strong coupling, low temp. absorpt. lineshape 77—59546
itinerant electron ferromagnetism at zero temp. 78—56285
jets, rel. to ψ particle expts. (1975, 1976) *(Czech)* 79—26288
neutral weak currents and parity nonconservation in two-electron atoms and ions *(Russian)* 77—46037
relativistic barriers for two spin-1/2 particles, from Breit eqn. 78—62339
transition metal alloy, electronic structure, mag. props. 78—95254
$ee \rightarrow ee\mu^+\mu^-$, virtual photon-photon collisions, equivalent photon approx. validity 80—5033
$e^-e^- \rightarrow \mu^-\mu^-$, reaction rate in vectorlike gauge model 77—61237
$e^+e^- \rightarrow \gamma\gamma$ at 6.2-7.4 GeV CM, comparison with QED predictions 77—49942
$e^+e^- \rightarrow \tau^+\tau^-$, neutral-current effects on ψ-like resonance 78—74239
$e^+e^+ \rightarrow e^+e^+(l^+l^-)$, meas. of lepton pair prod. 79—67529
$\gamma\gamma$ collision radiative corrections from $e^\pm e^\pm$ processes 79—40777
He, contact interactions, parity-violating and parity-conserving, new evaluation techniques 79—26872

electron-electron scattering
see also electron-electron interactions
elastic scatt., possible weak interaction effects, Weinberg-Salam model estimates 79—75755
energy dependent scale dimension in QED 77—79239
low energy crossed beam scattering, 90°, 300 eV 77—46004
parity violating asymmetries in polarized electron scattering 80—9111
polarised beams, properties of cross sections 79—372
resonant electron-electron bremsstrahlung in EM wave field *(Russian)* 80—52488
storage ring internal electron scatt., polarisation effects 79—85843
weak lepton interaction influence, weak, EM and interference ratio *(Russian)* 79—6333
He, contact interactions, parity-violating and parity-conserving, new evaluation techniques 79—26872

electron-electron scattering continued
Mo hole ellipsoid scatt. rate temp. dependence, magnetoacoustic obs. 79—51472
Nb hole ellipsoid scatt. rate temp. dependence, magnetoacoustic obs. 79—51472
W hole ellipsoid scatt. rate temp. dependence, magnetoacoustic obs. 79—51472

electron emission
see also cathodes; electron field emission; exoelectron emission; photoemission; secondary electron emission; spin polarised electron emission; thermionic electron emission; work function
adhesive bonds breaking under high vacuum, light and electron emission, spectral comp. obs. 80—55190
alkali halide, electron-ion emission due to ionisation of surface atoms 77—16474
angular distribution, cosine law theory 78—35233
atomic screening model for solid-state effects 77—73194
cathode plasma explosive emission surface processes 78—71569
cathode workshop, conf., Washington, DC, USA (Jan.-Feb. 1978) 79—43068
conference, Leningrad, USSR, (Jan. 1979) 80—98754
conference on surface physics, Tagow, Poland (June 1976) 78—26747
cylindrical hollow cathode negative glow, fast electron angular distrib. obs. 78—67529
electrostatic electron emission into a gaseous medium from alpha-particle tracks in liquid isooctane 79—54747
explosive, effect of press. on cathode 80—49034
ferroelectric electron emitter with negative electron affinity 80—100762
film, kinetic electron emission, intermediate energy ion effects 77—28675
heavy ion induced collective electron emission 80—80926
ion-to-electron conversion dynodes, prep. by plasma anodisation 77—1887
mechanoelectron emission mechanism following cleavage 80—7482
metallic islet film, cond. currents and electron emission, electron heating effect 78—10581
metals, laser and nuclear radiation induced emission anomalies, current sources *(Russian)* 80—25536
mica, emission of high-energy electrons during cleavage 79—56917
MIM system, electron emission modelling *(Czech)* 80—2479
polycaprolactam, stretched sheets, electron emission 78—88411
polyethylene, stretched sheets, electron emission 78—88411
review of recent advances in electron and ion emitters *(Japanese)* 77—63492
semiconducting point cathodes, explosive electron emission 77—59678
semiconductor, electron emission from surface subband, reduced work function 80—60757
spectroscopy, transmission props. of cylindrical mirror analyser viewed in energy-angle space 78—15745
steel, type 40 Kh, electron emission depend. on surface mechanical treatment *(Russian)* 80—100945
surface, charged-particle emission caused by laser beam scanning 80—11518
and surface physics, review *(Japanese)* 77—63493
Ti-Ni, electron emission and shape memory effect 80—50687
Tokamak fusion reactor, electron emission effect at divertor target 79—660
triboelectrification process in vacuum, high-energy electron emission phenomena 79—11197
Al, laser irrad., charged particle emission from back side of target 78—2949
Ar, electron transmission factor numerical determination 80—10350
Ar, electrostatic free electron emission near triple point *(Russian)* 77—24933
Cu, ang. distrib., final state effects 77—66580
Cu cathode with oxide film, emitting site lifetimes and current densities, meas. 77—27761
Cu, cryst., ion-electron emission yield, ang. depend., atomic order effects 77—85877
Cu, electron emission depend. on surface mechanical treatment *(Russian)* 80—100945
Cu, low energy He$^+$ ion bombardment, origin of autoionisation electron emission 77—20973
Cu, point cathodes, explosive electron emission 77—55873
Cu points, operation in explosive electron emission 77—18144
Cu, with Al_2O_3 inclusions, breakdown and emission props., effect of inclusions 79—87389
Cu_2O films arc cathode emission study 78—23583
D_2, electron surface barriers for dense phases 78—91754
H_2, electron surface barriers for dense phases 78—91754
H_2, solid, self-induced electron emission at o-p transition 77—12506
He, electron transmission factor numerical determination 80—10350
LiF, crystal, electron emission under uniaxial compresssion 80—7483
LiF, ion and electron emission following ion impact 80—100729
LiF, laser-irrad., emitted electrons and positive ions delay 80—29830
MgO, crystal, electron emission under uniaxial compresssion 80—7483
Mo, cryst., ion-electron emission yield, ang. depend., atomic order effects 77—85877
N_2, liquefied, prebreakdown mechanism, intermittent electron emission obs. 77—32325
NaCl, crystal, electron emission under uniaxial compresssion 80—7483
NaCl, ion and electron emission following ion impact 80—100729
Pb-Sn, eutectic, electron emission avalanche obs., during isothermal superplastic deform., *(Russian)* 77—48324
Si, ion and electron emission following ion impact 80—100729
W, laser irrad., charged particle emission from back side of target 78—2949
Zn, electron emission depend. on surface mechanical treatment *(Russian)* 80—100945

electron energy bands *see band structure*

electron energy loss spectra
A15-superconductor, surface characterisation by energy loss spectra, AES and HEED 77—24635
acetic acid, chemisorbed on Cu(100), acetate species struct. obs. 79—98232
acetonitrile, mol.excitation by electron impact, 500 and 25-70 eV, expt. and HAM/3 79—72434
acetylene, adsorbed on Ni (111), vibr. spectra from electron energy loss *(French)* 78—34696
acetylene, C K-shell excitation by electron impact, electron energy loss spectra 77—31014

electron energy loss spectra continued
acetylene, chemisorbed on Ni (111), ind. vibrs., high resolution electron energy-loss meas. 79—90877
acetylene, chemisorbed on W(110), rehybridization 78—31289
acetylene, chemisorption on Pt (111), ethylidyne group form., LEED and ELS obs. 78—73075
acetylene, condensed, electron energy loss spectra meas. 77—59652
acetylene, electron energy loss spectra, C K-shell excitation, vibr. struct. 79—22851
acetylene, higher excited states, electron energy loss spectra 80—91664
acetylene, inner shell electron energy loss obs. 79—45853
acetylene, on Pt surface 78—15701
acetylene, triplet states, electron impact energy-loss spectra 77—68128
acrolein, excitation, ionisation and electron affinity, expts., HAM/3 calcs. 80—18790
actinides and their fluorides, interband, collective and atomic (p,d) excitations, Z-160 eV, fast EELS 80—93443
adsorbed molecule, angle-resolved and variable impact energy electron vibr. excitation spectroscopy 80—76119
adsorbed molecule vibration excitation on metal surface 78—18910
adsorbed molecules, EELS selection rule 80—49495
adsorbed molecules, electron-impact vibr. excitation, specular selection rule 80—80051
adsorbed molecules, on metal surface, inelastic scattering of slow electrons 80—50485
AES, electron energy loss struct. 79—47559
alkaline earth metals 79—28310
amorphous materials, small area struct. studies 80—44087
anal. appl., processing requirements 79—43692
analytical electron microscopy 77—25346
analytical tool, data handling and processing 80—81407
apparatus for meas., cylindrical electrostatic analyser *(French)* 77—55856
atomic ions, electron impact, 1 to 100 keV, bremsstrahlung emission, theory 78—22005
atoms, near threshold struct. in K-shell spectra, photoionisation or fast charged particle ionisation 80—87064
benzene, 50000 cm^{-1} band, electron impact study 79—86075
benzene, C K-shell excitation by electron impact, electron energy loss spectra 77—31014
benzene, elec. dipole forbidden states, high resolution electron impact obs. 80—43195
benzene, variable angle electron impact energy loss spectra 79—68321
benzene adsorbed on Pt(111) and Ni(111) surfaces, vibr. loss spectra 79—23838
benzene on Ni(100) and (111), chemisorpt., LEED and high resoln. electron energy loss spectra 78—6224
benzenes, substituted, gaseous, negative ion states, electron transmission spectra 77—31007
biological materials, electron energy loss spectroscopy anal. appl. 79—39269
biological thin section quantitative analysis and mapping 79—74820
biomembrane architecture obs. 79—25177
bremsstrahlung, 1 to 2000 keV, neutral atoms Z=2 to 92 78—62920
bulk solids, transmission and absorpt. of 5 to 30 keV electrons 77—89491
1,3-butadiene, condensed, electron energy loss spectra meas. 77—59652
trans-1,3-butadiene, electron impact energy loss spectra, energy levels 79—68323
1,3-butadiene, excited singlet states, vibronic struct., electron impact energy loss spectra, 35-90 eV 78—62932
n-butane, condensed, electron energy loss spectra meas. 77—59652
butenes, electron energy loss spectra, 0-90°, 20-150 eV impact 79—68322
1-butyne, and propyne, electron impact spectra, comparison with acetylene 79—3585
cathode workshop, conf., Washington, DC, USA (Jan.-Feb. 1978) 79—43068
chemical analysis, filtered images 80—101062
chemisorbed molecules, electronic excitations, selection rule effects, EELS 78—76566
chlorofluoromethanes, electron energy loss spectra, oscill. strengths 78—58846
conference on solid-vacuum interface, Amsterdam, Netherlands (June 78) 79—42342
copper phthalocyanine, autoionisation in electron energy loss spectra 78—35232
coronene polycrystals, electron scatt. 77—32478
cross section, comparison with IR reflection spectroscopy cross section 77—85729
1,3,5-cycloheptatriene, singlet→singlet (triplet) excitation, electron impact energy loss spectra 78—46451
1,3,5,7-cyclooctatetraene, electron impact energy loss spectrum 79—10214
diamond, inelastic scatt. differential cross-sections 77—76652
diamond, total secondary electron emission spectrum 77—72759
differentiated spectroscopy in STEM 78—35786
p-difluorobenzene, electron impact singlet-singlet transition generalised oscill. strength 78—66668
direct elemental analysis 80—71998
dislocations and microplasma sites, STEBIC/STEM/EELS correlation 80—96528
dose distributions from plane infinite oblique electron sources, Monte Carlo calcs. 77—65339
electron microscope, analytical 80—86521
energy losses due to diffraction radiation *(Ukrainian)* 80—75278
ethane, C K-shell excitation by electron impact, electron energy loss spectra 77—31014
ethane, condensed, electron energy loss spectra meas. 77—59652
ethane, liq., photoelectric determ. of conduction state energies and electron ranges 77—89487
ethylene, $\pi\to\pi^*$, electron energy loss spectroscopy 79—72432
ethylene, adsorbed on Ni (111), vibr. spectra from electron energy loss *(French)* 78—34696
ethylene, C K-shell excitation by electron impact, electron energy loss spectra 77—31014
ethylene, chemisorption on Pt (111), ethylidyne group form., LEED and ELS obs. 78—73075
ethylene, electron energy loss spectra, 0-90°, 20-150 eV impact 79—68322

electron energy loss spectra continued
ethylene, electron energy loss spectra, C K-shell excitation, vibr. struct. 79—22851
ethylene, electron energy loss spectrum, intensity distrib. 79—64110
ethylene, on Pt surface 78—15701
ethylene($-d_4$), Rydberg states assignments, electron energy loss specta 80—53153
ethylene condensed, electron energy loss spectra meas. 77—59652
ethyne, electron energy loss spectra, excited states investig., electron impact spectrometer 78—25756
extremely anisotropic crystals, free excitons and exciton-impurity complexes, generation, theory 80—39509
fast electron energy loss distrib., in thin absorbers 78—29070
fluorobenzene, variable angle electron impact energy loss spectra 79—68321
fluorobenzenes, negative ion states and π-electron affinity 79—10206
5-fluorocytosine, electron beam damage assessed by EELS 80—89809
foil, surface guided modes, excitation by electrons 77—59310
foil chemical mapping with high spatial resolution 79—61934
graphite, C K-absorpt. edge, EELS meas. 78—56551
graphite, cond. electron excitation 78—39642
graphite, K-shell cross section for 80 kV electrons 79—55798
graphite, model of collective modes in layer cpds., appl. to electron energy loss data 77—47754
graphite, sintered powder, energy losses, secondary electron spectra, AES, and EELS 79—99997
graphite, wave-vector depend. of electron energy losses 77—51688
graphite film, secondary electron emission and EELS rel. to plasmons 80—50481
graphite foil, thickness determ. by TEM using diffr. and energy loss anal. 78—29088
graphite intercalation compounds, charact. by electron inelastic scatt. anal. 79—95055
graphite intercalation compounds, characterisation by electron energy loss spectra 79—95054
graphite-FeCl$_3$ intercalation cpd., electronic excitation spectrum, high resolution EELS meas. 80—45182
graphite-K intercalation compound, dielec. function, EELS study 80—45183
halomethanes, 2.5 keV electron impact energy loss spectra, inner shell excitation 78—42232
halomethanes, C K-shell electron energy loss spectra, assignments 79—89797
1,3,5-hexatriene, electron scatt. at low-energy, vibronic struct. of triplet state 79—3574
hydrocarbon liquid, model for thermalisation of quasifree electrons rel. to electron mobility 77—40316
hydrocarbons on Pt and Ni, C-H stretch vibration, broadened and softened, dehydrogenation 78—47666
incoherent multiple scattering, uniqueness and inversion problem 80—7455
inelastic electron scatt. data anal., appl. to Cu 77—73199
inelastic electron scattering: surface vibrational spectroscopy 80—107347
inelastic electron scattering as analytical tool, review 78—24010
inelastic electron-matter interactions 80—104024
inelastic scattering in thin films, keV, rel. to transition radiation, calcs. *(German)* 77—90213
inelastic scattering probabilities for fast electrons in single cryst., orientation depend. 80—2905
inert gas, liq., photoelectric determ. of conduction state energies and electron ranges 77—89487
inert gas solids, collective excitations and EELS, calc. 80—92842
inert gases, liq., model for thermalisation of quasifree electrons rel. to electron mobility 77—40316
inner-shell electron impact excitation, developments in electron energy loss spectroscopy 80—63842
intercalation compounds, characterisation by electron energy loss spectra 79—95054
light element microanalysis 79—61935
light element microanalysis by K-shell excitation EELS 79—74480
lineshape determ. by numerical integration background subtraction 79—74469
low atomic number foil target, anomalous energy dissipation of tightly pinched relativistic electron beam 80—29833
magnetic spectrometer, corrected second-order aberrations 80—87013
magnetic spectrometer for TEM energy analysis 79—26190
materials science, high resolution microanal. using electron energy loss measurements, review 77—56190
metal, electron energy loss spectra, threshold potentials and X-ray absorption, band struct. determ. *(Russian)* 78—39009
metal, K- and L-emission bandwidths from characteristic electron energy loss values 79—83057
metal, plasmon dispersion effect in (e,2e) process with atomic electron knockout 80—2904
metal adsorbed molecules, low-energy electron inelastic scatt. 79—46526
metal surface, adsorbed mole. low energy electron scatt., appl. to Ni-CO 79—56896
metal surface, chemisorption, vac. UV photoelectron spectrometer for study *(Japanese)* 78—62264
metal surface, vibr. motion of adsorbed molecules, inelastic scatt. of electrons, model 78—34718
metal-semiconductor thin film preparation under UHV conditions 78—72733
metallic thin films, electron backscattering, empirical study 80—108310
metallic thin films, Everhart theory extension of backscattered electron energy spectra 80—108309
metallic thin films, fast electron scatt. with core electron excitation, plasmon satellite 79—33873
metals, chemisorption of gases, book 79—69370
methane, and -d$_4$, electron impact K-shell excitation spectra, isotope effects 77—71879
methane, Compton profiles, high energy electrons impact spectroscopy 77—27188
methane, electron energy loss spectra, C K-shell excitation, vibr. struct. 79—22851
methane, electron transmission function and mean energy per ion pair, obs. 80—23566
methane, liquid, photoelectric determ. of conduction state energies and electron ranges 77—89487
methane, low-energy electron scatt., total 0.16 eV cross sections, vibr. excitation 79—86076

electron energy loss spectra continued
methylisonitrile, mol.excitation by electron impact, 500 and 25-70 eV, expt. and HAM/3 79—72434
microanalysis, instrumentation developments, review 78—35783
microanalysis, quantitative approach to inner shell losses 80—101059
microanalysis by energy loss spectrometry *(Japanese)* 78—85244
microanalysis of light elements by electron energy loss spectrometry 78—80441
microanalysis. operating parameter selection 79—24879
microanalysis use 78—35784
microanalysis use and errors involved 78—35785
microanalysis uses of high resolution STEM system 78—24012
microanalysis using field emission STEM 78—53286
microbeam anal., conf., Ann Arbor, MI, USA (June 1978) 79—39258
microspectrometry, using energy loss electrons in electron microscopes, review 80—104025
molecular liquid, electron energy loss processes at subelectronic excitation energies 77—89486
molecules, chemisorbed on metal surface, spectrosc., electron gas effects 80—54504
molecules, energy loss spectra, state-to-state rot. transition cross sections 80—91665
monohalobenzenes, inner shell excitation and ionis., electron energy loss spectra, XPS, assignments 78—62934
multiple Coulomb scattering and energy degradation of electrons in semi-infinite material layers *(Rumanian)* 80—29100
nitromethane, low lying electronic states, electron energy loss spectra, singlet→triplet excitation 79—27093
nitromethane, variable angle electron-impact excitation, transitions in 7-12 eV energy-loss range 80—69244
oriented molecules, inelastic low energy electron scatt. 78—72653
particle mass determination using STEM 78—21294
pentacene polycrystals, electron scatt. 77—32478
photoabsorpt. spectra, band struct., at. ionisation mechanisms, electron energy loss spectra 77—24909
photon and electron transport simulation, deceleration photons prod. using linear accelerator *(French)* 80—12282
plasmons and interband transitions, electron excitation, book 80—77555
PMMA, electron energy loss spectra, optical props. 79—10887
PMMA film, Monte Carlo simulation of electron penetration 79—23659
poly(vinyl cinnamate), excited state, low-energy EELS and INDO/S calcs. 80—106407
poly-2-vinylpyridine, core excitons and dielec. response function, 1-400 eV 79—15569
polyacetylene:AsF$_5$(I), pure and doped, electronic excitations, momentum depend., EELS study 80—76121
polyethylene, pristine and radiation-damaged film, electron energy loss spectra 79—81312
polyethylene film, soln.-cast, low energy electron scatt. obs. of band struct. 80—16131
polymer film on Pt, energy losses, secondary electron spectra, AES, and EELS 79—99997
polymer films, mech. of charact. electron energy loss spectra 77—81188
polystyrene, core excitons and dielec. response function, 1-400 eV 79—15569
polystyrene, momentum-depend. dielectric response 79—69160
POPOP vapour, triplet population, rel. to lasing 78—29947
propylene, condensed, electron energy loss spectra meas. 77—59652
propylene, electron energy loss spectra, 0-90°, 20-150 eV impact 79—68322
propyne, and 1-butyne, electron impact spectra, comparison with acetylene 79—3585
quantitation methods, recent progress 80—73542
quantitative energy-loss spectroscopy, treatment of inner-shell electron energy losses 79—12905
radiation damage, meas. of loss of gaseous elements from thin samples 80—96568
rare earth oxides, segregation study by electron energy-loss spectroscopy 80—79953
rare earths and their oxides and fluorides, interband, collective and atomic (p,d) excitations, Z-160 eV, fast EELS 80—93443
resolution optimisation, wing electron lenses between TEM specimen and electron spectrometer 80—101886
review, electron spectroscopy appls. *(Japanese)* 79—40645
saturated liquid polydielectrics, secondary electron emission and energy loss spectra 80—55239
SEM technique exam., ultra-high vacuum, secondary electron emission dependence on electron beam density dose 80—61209
semiconductor, electron spectroscopy techniques, review *(Japanese)* 80—49061
semiconductor surface electron states, optical methods of detection 77—66191
semiconductor surface electronic structure determ. by low energy electron loss spectroscopy *(Japanese)* 78—88007
simple metals, plasmon dispersion anal. from electron gas dielectric response 80—6761
small particles, characterisation and microanal. by STEM combined with other techniques 80—50901
solid, polycrystalline, backscatt. energy distrib. spectrometer *(German)* 79—95882
solid-electron interactions, conf., Southampton, England (Apr. 1976) 77—44570
specimen contamination problems 79—71577
spectrometer for surface studies, including energy loss meas. of electronic excitations 79—58849
steel, Cr-Mo (9, 1 wt.%) appl. of electron energy loss spectrometry to precipitate morphology 78—48414
STEM, appl. to materials science 80—103228
STEM, detect. limit improvement using coincidence techniques 77—25345
STEM, multi-channel averaging 80—101061
STEM, spectrograph, recording of energy loss spectra 80—86525
STEM, structural and chemical analysis, appls. 80—88003
surface analysis, AES and ESCA combined with SEM *(French)* 80—47154
surface analysis, atomic beam scatt., SIMS, and vibr. spectra, book contrib. 79—42357
surface analysis, spectroscopic methods, review *(Chinese)* 79—34414
surface characterisation, physical methods, review *(French)* 80—7889
surface chemical bonding, electron spectroscopy, book contrib. 80—24992
surface excitation by low energy spectroscopy *(Japanese)* 79—52057

electron energy loss spectra continued
surface reactions analysis, surface vibrs., spectroscopy 78—15701
surface roughness effect on image potential electron energy loss, plasmon electron scatt. 80—54748
surface studies, energy loss spectroscopy, book contrib. 77—63509
surface vibrational studies using high resolution electron energy loss spectrometer 80—2260
surfaces, electron spectroscopy, review 78—92169
TCNQ, elect. struct. determ., CNDO parametrisation and UPS data 77—1350
TCNQ film, energy loss spectra of low energy electrons 78—19116
TCNQ salt, decamethylferrocenium, monomeric and dimeric, optical and EELS study 80—100660
TEM, image contrast from single-electron excitation 80—59353
TEM, standard, implanted Si 80—99017
TEM, theory and instrum. 80—81405
TEM energy anal. appl., K-loss struct. determ. 77—44100
TEM energy loss spectra, direct display using Si self scanned photodiode array 78—45753
TEM image and electron energy loss spectrum display by self-scanned linear Si photodiode arrays 80—68330
p-terphenyl vapour, triplet population, rel. to lasing 78—29947
tetrafluoromethane, electron energy loss spectra, C K-shell excitation, vibr. struct. 79—22851
tetramethylethylene, electron energy loss spectra, 0-90°, 20-150 eV impact 79—68322
thin crystal foil, large angle electron scattering by dependent Bloch wave model 79—99257
thin film analysis and characterisation, conf., Les Arcs, France (Jan. 1978) *(French)* 79—8466
thin films, chem. anal. by energy loss spectroscopy 80—104493
thin foil, quantitative microanalysis, by energy loss spectroscopy *(French)* 80—50900
thin foils, chem. anal. by electron microscopy *(French)* 80—50899
thin specimen sections, electron microscopic chemical analysis, review *(French)* 79—8469
thiophosgene, triplet state, detected by electron energy-loss spectra 78—78808
tissue equivalent gas electron transmission function and mean energy per ion pair, obs. 80—23566
total inelastic scatt. cross section, detector solid angle depend., approx. bounds 78—17798
trajectory simulation, in material media *(Rumanian)* 80—24520
transition metal, 3d, localised moments, detection by electron energy loss spectra 77—69949
3d transition metal films, EELS, anomalous L_3/L_2 white-line ratios 80—93444
transition metal oxides, energy loss spectra, ion polarisability 78—68585
transition metals, 3d electron struct. plasmons 79—77996
transmission, microanalysis of precipitates in Ni-base superalloy 80—104492
transmitted electrons, localised chemical characterisation *(French)* 77—77850
5-trifluoromethyluracyl, electron beam damage assessed by EELS 80—89809
trimethylethylene, electron energy loss spectra, 0-90°, 20-150 eV impact 79—68322
TTF film, energy loss spectra of low energy electrons 78—19116
TTF-TCNQ, core exciton exam. by inelastic electron scatt. 77—4296
TTF-TCNQ film, energy loss spectra of low energy electrons 78—19116
uniaxial crystal foil, electron energy loss probability at oblique incidence 80—25506
water, chemisorbed on Pt (111), EELS spectra, vibr. freqs. 80—80920
water, degraded 1 keV electron energy spectra 80—9474
water, X- and γ-irrad., electron slowing-down spectra and photon RBE 80—12197
water vapour electron stopping power and energy degradation 80—23276
XPS from core levels, electron energy loss spectra, intrinsic and extrinsic plasmons 77—63532
Ag, adsorbed on Si (111), electronic and cryst. struct., Schottky barrier form. obs. 78—84091
Ag discontinuous film on (001) MgO, low energy electron spectrum 77—48288
Ag film, energy losses of 20-40 keV electrons 78—92153
Ag, photoionisation cross sections, electron-impact inverse mean free paths, and stopping powers for each subshell 80—69113
Ag, plasmon dispersion, d→f fine structure 77—11863
Ag, plasmons, influence of cryst. orientation on intensity, electron energy loss meas. *(German)* 79—23921
Ag, single cryst. film, cryst. orientation effect on EELS 78—80442
Ag, thin targets, electron transmission below 3 keV *(French)* 80—60725
Al (001), 100-2000 eV electron backscatt., surface and bulk plasmon losses 77—32480
Al, bulk and surface plasmon loss intensities in XPS, Auger and electron energy loss spectra 79—38012
Al, characteristic energy losses on C contaminated surfaces, secondary electron spectra, AES, and EELS 79—99997
Al, clean and oxidised surfaces, secondary electron spectrum, EELS and AES, comparison 80—55237
Al, dielectric function, wave-vector and freq. dependence, energy loss spectra 77—1385
Al, direct nonvertical interband transitions at large wave vectors 78—34759
Al, electron energy loss spectra, microanal. appl. 77—44099
Al, electron energy loss spectra 78—34560
Al film, electron transmission, ang. aspects *(French)* 80—49284
Al film, energy losses of 20-40 keV electrons 78—92153
Al film, initial oxidation, electron energy loss spectra 78—7088
Al film, mean free path for plasmon excitation, 1.5 to 10.9 keV 78—51915
Al film, wavelength depend. fine struct. 77—11609
Al foil, straggling of relativistic electrons, 0-4000 eV 78—14393
Al, L-shell ionisation by 80 keV electrons, transmission electron energy loss spectrometry 80—60721
Al, mean free path of electrons needed to form surface plasmons 77—51800
Al, plasmon and phonon excitation 78—72682
Al, polycrystalline, multiple plasmon excitation, in energy loss spectrum 79—4872
Al, secondary-electron energy distribution in high-energy photoemission 77—48305

electron energy loss spectra continued
Al, small spheres, bulk plasmons damping 80—75561
Al, spatial absorbed-dose distrib. for 25 MeV beam 77—88289
Al, surface plasmon dispersion, high-energy electron loss spectroscopy obs. 77—20390
AlN foil, thickness determ. by TEM using diffr. and energy loss anal. 78—29088
AlN, inelastic scattering probabilities for fast electrons in single cryst., orientation depend. 80—2905
AlN, K-shell cross section for 80 kV electrons 79—55798
Al_2O_2-SiO_2, mullite 2:1 cryst., dielectric tensor components 77—48142
α-Al_2O_3, colour centres, AES, electron energy loss, and optical spectroscopy obs. 78—35176
β-Al_2O_3-Na_2O, colour centers, AES, electron energy loss, and optical spectroscopy obs. 78—35176
Ar electron energy loss spectra, Compton defect characterised by shift and asymmetry parameters 80—95723
Ar, electron scatt., in laser radiation field, free-free cross sections meas. 78—74762
Ar, electron scatt and ejection, electron energy loss spectra 80—58394
Ar, electron scatt. in intense IR field, multiphoton free-free transitions 79—81289
Ar, electron scatt. in laser radiation field, free-free cross sections, reson. struct. 78—74763
Ar, electron transmission function and mean energy per ion pair, obs. 80—23566
Ar, energetic electron degradation spectra and initial yields 80—95724
Ar, gas phase, 1 keV electron energy loss spectrum, Mollenstedt velocity analyser appl. 79—80721
Ar L-shell ionisation, post-collision interaction, electron impact, energy loss meas. 77—19093
Ar-high energy electron spectroscopy techniques 80—62740
Au (100), characterisation of reordered and normal surfaces by LEED, AES and EELS 78—34687
Au, AES and characteristic energy loss spectra, expt. and interpretation 78—27354
Au, adsorption of Xe and CO on (100) 77—15691
Au, core-electron excitation edges 80—66345
Au electron transmission and absorption at 0.6 to 4 keV, obs. 77—84818
Au film, energy losses of 20-40 keV electrons 78—92153
Au small particles, size effects studied by electron energy loss anal. 79—47567
Au-Si interface, critical Au-film thickness obs. for room temp. interfacial reaction 80—75390
Au-Si interface, electron energy loss and AES meas. 80—89096
Au(III) and polycrystalline surfaces, O_2 adsorption, LEED, AES and energy loss spectra 80—34310
$Au_{1-x}Si$ amorphous metallic films, optical props. as function of composition 79—95865
Au(100), adsorbed Br, EELS obs. 80—50483
BN, electron energy loss spectra, core edges, orientation depend. 79—61478
BN, wave-vector depend. of electron energy losses 77—51688
Ba, ang. depend. of characteristic energy loss, surface plasmon excitation 78—2962
Ba, electron scatt., elastic and inelastic (5^1D, 6^1P) cross sections, 20-100 eV 78—74769
Ba film, monatomic, conc. depend. 77—15938
Ba monoatomic film on W (110), characteristic electron energy loss 80—100720
Ba, plasmon excitation by oblique incidence of primary electron beam of medium energy 78—18987
BaO, electron energy loss and secondary emission mechanisms, plasmon losses 78—76565
$BaTiO_3$, 0.02-2 eV, vibr. states 78—39642
$BaTiO_3$, phonon spectroscopy, amorphous versus crystalline material 78—83898
Be adsorbed layers on W(110) and (100), work function and loss spectra meas. 80—6638
Be film, on W (110), growth mode, work function, thermal desorption, and struct. 80—75477
Be, inelastic electron scattering near K-edge 78—52606
BeO film, amorphous or polycryst., dielec. function, refl., from electron energy loss meas. 78—43947
Bi (0001), chemisorption of O_2, LEED, AES and electron loss meas. 79—77908
Bi, and Bi_2O_3, AES and characteristic energy loss spectra, expt. and interpretation 78—27354
C, amorphous, diamond-like 3-fold coord. 80—50323
C, amorphous, inelastic electron scatt., valence electron contrib. 80—55240
C, amorphous and graphite, extended fine struct. in K-ionis. edge 79—47566
C, electron energy loss spectra, microanal. appl. 77—44099
C film, amorphous, surface plasmon dispersion, electron energy loss spectra meas. *(French)* 77—63504
C film, diamond-like, ion-plated, electron energy loss spectra characterisation 80—2308
C foil, degraded 1 keV electron energy spectra 80—9474
C foil, energy loss spectra of transmitted electrons, straggling and plasmon excitation 79—95058
C, transmission electron energy-loss spectroscopy, energy-differential cross-section functional form 79—100000
CF_2, energy deposition and primary current 80—39184
C_2N_2, valence excitation energy, HAM/3 calc., energy loss spectra 78—25454
CO, adsorbed on Cu (100), vibr. excitation cross-sections 80—75441
CO adsorbed on Ni, energy depend. of vibr. excitation, electron energy loss spectra 79—28201
CO, adsorbed on Pt, low temp. vibr. mode, site occupation, electron energy loss spectra 80—29263
CO adsorbed on Pt (100) 77—15688
CO and NO, coadsorbed on Ru(001), adsite symmetry by electron energy loss 79—99412
CO chemisorbed on Cu (001) surface, vibr. spectrum 79—69347
CO, chemisorbed on Ni(111), vibr. spectra from electron energy loss spectra *(French)* 78—22951
CO, chemisorbed on Ni(111), adsorption sites and long range order, vibr. spectra 79—46946
CO, chemisorobed on Ni(111), surface optical excitations, reflectance spectra, electron energy loss meas. 78—84064

electron energy loss spectra continued
CO, electron energy loss spectra, C K-shell excitation, vibr. struct. 79—22851
CO, electron impact, energy loss spectra, electronic transitions obs. 78—17805
CO, K-shell, excitation and ionisation, vibr. struct., electron energy loss spectra obs. 80—18943
CO, oscill. strengths for shape resonances near K edges 77—75224
CO_2, electron energy loss spectra, C K-shell excitation, vibr. struct. 79—22851
CO_2, electron impact, energy loss spectra, electronic transitions obs. 78—17805
CO_2, electron impact spectra, 35 keV electrons, Bethe surface and Compton profile 79—27091
CO_2, electron transmission function and mean energy per ion pair, obs. 80—23566
CO_2, low-lying and triplet states 78—46454
CO_2, reson. electron impact vibr. excitation, 3-5 eV 78—25726
CO_2, valence shell ionic photofragmentation, oscill. strengths, EELS and electron-ion coincidence meas. 80—37879
COS, electron energy loss spectra, C K-shell excitation, vibr. struct. 79—22851
COS, low-lying and triplet states 78—46454
CS_2, low-lying and triplet states 78—46454
Ca, plasmon excitation by oblique incidence of primary electron beam of medium energy 78—18987
Cd, oxidation, chemisorption and oxide regimes, UPS and EELS study 80—81236
CdI_2, ang. depend. electron energy loss meas. 79—95884
$CdI_2(Br_2)(Cl_2)$, dielec. function and band struct., EELS meas. 80—40195
CdS-metal interface, chemical reactions and local charge redistrib. 79—19661
CdS(Se)-Al function formation, coupled interface plasmons, low energy electron energy loss spectra 77—24621
CdS(Se)-metal Schottky barrier form., transition with chemical reactivity 78—30986
CdSe-metal interface, chemical reactions and local charge redistrib. 79—19661
CdTe, clean and oxidised surfaces, surface states, low-energy EELS study 80—11522
Co film, texture and adsorption of CO *(German)* 77—24485
Co, orientated mol., (e,2e) spectra, electron momentum density 79—98236
CoO (100), electron energy loss spectra exam. 78—72652
Cr, anal. of surface and volume losses 79—91547
Cs monolayer on Cu(111), dilution of electron gas by O adsorption, plasmon energy losses 79—47036
Cu (100), adsorbed formate and acetate species, EELS study 80—76120
Cu (100), chemisorption and decomp. of formic acid, EELS study 80—16729
Cu (100), chemisorption of CO, vibr. excitations and struct., EELS and LEED study 80—39437
Cu (100) reaction with ethanol and methanol, EELS study 80—16728
Cu (100) surface, interaction with O_2, AES, EELS, LEED and work function studies 80—24731
Cu (110), adsorption of CO, electron energy loss vibr. spectra and LEED obs. 79—77902
Cu (111), chemisorpt. of CO on differently prepared surfaces 78—6223
Cu (311), 30-300 eV, CO or Xe adsorption effects 77—63507
Cu, core-electron excitation edges 80—66345
Cu, electron energy loss spectra, microanal. appl. 77—44099
Cu electron transmission and absorption at 0.6 to 4 keV, obs. 77—84818
Cu film, electron energy loss spectra meas., optical functions calc. 78—19618
Cu film, energy losses of 20-40 keV electrons 78—92153
Cu, inelastic electron scatt. data anal. 77—73199
Cu, thin targets, electron transmission below 3 keV *(French)* 80—60725
Cu-Al film, electron energy loss spectra meas., optical functions calc. 78—19618
CuO film, electron energy loss spectra meas., optical functions calc. 78—19618
CuO, on Cu, identification by electron spectroscopic methods 80—60747
Cu_2O film, electron energy loss spectra meas., optical functions calc. 78—19618
Cu_2O, on Cu, identification by electron spectroscopic methods 80—60747
D_2, electron Compton profiles from energy loss spectra 79—7013
D_2, electron scatt., isotope effects 77—58188
Dy, low energy fine struct. and surface electron states 77—85860
EuO (100), disordered, LEED and electron spectroscopy 79—28178
EuO (100), EELS, Eu valence in surface region and high energy giant reson. 80—84816
F_2, electron energy loss spectra, 0-17 eV, 5-140°, repulsive valence states excitation 80—32844
Fe, elastic and magnon-inelastic spin polarised low energy electron scatt. 78—34970
Fe-Ge, characteristic energy losses and optical props. 80—29834
$FeCl_3$-graphite, intercalation compound, Fermi level lowering and core exciton spectrum, EELS study 79—74036
$FeCl_3$-graphite intercalation compound, dielec. function, band struct. EELS study 80—49643
$FeCl_3$-intercalated graphite, plasmon spectra 79—38011
$FeGe_2$, Fe_2Ge, optical consts., electron energy loss spectra meas. 77—90121
Fe_xO_y films, electron microscopy and energy-loss spectroscopy 80—80137
FeS_2, ionisation loss spectra, density of unoccupied states 80—55241
GaAs (110), adsorption of In, N, P, and As, UPS and EELS study, tight-binding calcs. 80—49496
GaAs (110) surface, chemisorption of O_2, electronic struct. theory, oxidation, electron spectra interpretation 79—42376
GaAs, (110) surface, electronic struct. of clean and O_2 covered surface 77—43685
GaAs, adsorption of Sb_2, surface state exam. by energy loss spectra 77—15935
GaAs, electronic surface structure Cs(Rb)(Na) adsorpt. processes, AES, LEED, EELS, study 79—68068
GaAs, epitaxial film, amorphous and polycrystalline, vol. plasmon energy and linewidth, electron scatt. obs. 80—50482
GaAs film, electron scatt., cathodoluminesc. meas., energy depend. of electron deposition depth determ. 80—104023

electron energy loss spectra continued
GaAs surface, electronic props., interaction with Au and O adsorbate layers 77—20385
GaAs, surface studies during MBE growth 79—90899
$GaAs:Ba^+$, Auger electron and charact. electron energy loss spectra 80—55235
GaAs:Sb (100) surface, Sb-induced surface states 78—10529
GaP(As)(Sb), surface states, contact pot. difference, photoemission, and low energy loss spectra expts. 77—85285
GaSb (100) surface, Sb-induced surface states 78—10529
$GaSb_{1-y}As_y$ alloy surface states obs. 79—15202
GaSe, plasmon and phonon excitation 78—72682
Gd, low energy fine struct. and surface electron states 77—85860
Ge (111), CO adsorption on cleaved surface, electron energy loss spectra 78—79885
Ge electron transmission and absorption at 0.6 to 4 keV, obs. 77—84818
Ge, film, epitaxial growth on Si, interdiffusion, plasmon energy loss anal. 77—31916
Ge film, volume plasmons, EELS, line shape 79—90984
Ge, oxidation of clean cleaved (111) surfaces, EELS and AES 80—3230
Ge, volume plasmon, cryst. orientation influence 80—80921
Ge-Na interfaces, interdiffusion, electron states, EELS study 80—50484
GeS (001), density of empty states, core-level EELS and photoemission spectra meas. 79—78145
GeS (001) surface, electronic struct., Auger and electron energy loss spectra meas. 77—59314
GeS(Se), dielec. function, optical and electron energy loss spectroscopy 78—15189
GeSe (001), density of empty states, core-level EELS and photoemission spectra meas. 79—78145
Ge(111), surface electronic struct., atomic geometry effects 77—85283
H, adsorbed on Pt (111), vibr. modes, EELS study 80—15377
H_2 chemisorbed on W, vibr. states 77—31877
H_2, Compton defect, high energy electron impact spectroscopy 77—71876
H_2, electron energy loss spectra, $B^2H_u{}^+$ state cross sections, Franck-Condon factors 78—13616
H_2, electron energy-loss spectra in afterglow, ground state vibr. conc. 77—31012
H_2, electron scatt., energy deposition and energy degradation, 2, 10 and 30 keV 79—31709
H_2, electron scatt., isotope effects 77—58188
H_2, electron scatt. in intense IR field, multiphoton free-free transitions 79—81289
H_2, liq., photoelectric determ. of conduction state energies and electron ranges 77—89487
HBr, electron impact ionisation, vibr. excitation spectra threshold peaks, negative ion effects 80—106322
HCN, inner shell electron energy loss obs. 79—45853
HCN, K-shell excitation by electron energy loss spectroscopy 79—31712
HCl and HBr, low-lying reson. states in 0.25-1.15 eV electron scatt. 79—45844
HF, valence orbitals momentum distribs., (e, 2e) binding energy spectra 80—14237
H_2O, electron spatial absorbed-dose distrib. for 25 MeV beam 77—88289
H_2O, Monte Carlo calcs. of spectra and yields, bioligical implications 79—7641
H_2O, spatial absorbed-dose distrib. for 25 MeV beam 77—88289
He, Compton defect, high energy electron impact spectroscopy 77—71876
He, electron scatt., interaction with electrons ejected from impact excited autoionis. states 78—42221
He gas, electron energy loss function in range 50 eV to 1 keV 77—61859
He, positron inelastic scatt. at intermediate energies, time of flight spectra 80—18932
^3He liquid, electron spectra of localised electrons above surface *(Russian)* 80—29241
Hf, electronic excitations, charact. energy loss meas. up to 50 eV 80—60723
HfO_2, electronic excitations, charact. energy loss meas. up to 50 eV 80—60723
Ho, low energy fine struct. and surface electron states 77—85860
In film, vol. plasmon dispersion and damping, electron energy loss spectra 79—7797
In, surface plasmon dispersion, high-energy electron loss spectroscopy obs. 77—20390
In ultrathin films on TbTe and Te, prep. and characterisation 77—7995
In-GaAs(Ge)(Si) Schottky barrier interface, covalent bonding of metal atoms 77—20429
In-In_xO_y-Pb tunnel-junction barriers, evidence for chemical annealing effects 79—42701
InAs:Sb (100) surface, Sb-induced surface states 78—10529
$In_{1-x}Ga_xAs$, alloy surface states obs. 79—15202
InN, thin film, characterisation using XPS electron energy loss spectra 79—87561
In_2O_3, thin film, characterisation using XPS electron energy loss spectra 79—87561
InO_xN_y, thin film, characterisation using XPS electron energy loss spectra 79—87561
InP(As), surface states, contact pot. difference, photoemission, and low energy loss spectra expts. 77—85285
InSb, electronic surface struct., Cs(Rb)(Na) absorpt., AES, LEED, EELS study 78—68068
InSb, epitaxial film, amorphous and polycrystalline, vol. plasmon energy and linewidth, electron scatt. obs. 80—50482
InSe, band structure, spin-orbit splitting and electron loss struct. of In 4d core level 77—47727
Ir (111), of benzene and pyridine, electronic transitions sensitivity to molecule-surface orientation, energy loss spectra 80—45184
$Ir_4(CO)_{12}$ EELS, AES, comparison with XPS and UV absorpt. spectra obs. 80—35021
K film, adsorbed on Ni (100), plasmon losses in electron energy loss spectra 79—61480
K-intercalated graphite (stage-1), electron energy loss expts. and band struct. theory 79—100001
KAg_4I_5, superionic film, elec. ionic cond. and electron spectra 80—6543
KOH, beam, formed at 300-800°C, electron elastic scatt. obs., species identification 80—14231
Kr, electron impact excitation, rel. differential cross-section meas., 15 to 100 eV *(French)* 78—13602

electron energy loss spectra continued
La, X-ray reson. emission, appearance pot. and charact. electron energy loss spectra 80−16126
LaB_6:C, AES, LEED and energy-loss spectra study of C layer on (100) surface 77−62715
Li, electron impact excitation, 15-190 eV, generalised oscill. strengths, differential cross sections 80−23556
Li, X-ray threshold, improved compatibility relations 77−8684
LiF dosimeter energy response to high energy electrons <30 MeV, Monte Carlo calc. 77−86637
LiF, film, characteristic energy loss and secondary electron spectra *(Japanese)* 78−15266
LiF film, guided wave excitation by fast electrons 79−24384
LiF film, surface phonons and thickness variation, EELS meas. 80−92774
LiF films, polycrystalline and single-cryst., comparative study of phonons by electron spectroscopy 80−25505
$LiNbO_3$, XPS core line intensities, electron escape depth 79−100025
Lu, crystal surface study from refl. electron energy loss spectra obs. 80−20742
Mg (0001) face, incipient oxidation, EELS and LEED studies 80−81237
Mg, ang. depend. of characteristic energy loss, surface plasmon excitation 78−2962
Mg film, electrom energy loss spectrum in excitation of volume plasmons 78−11043
Mg, plasmon-loss intensities in XPS, EELS and Auger spectra 80−10902
MnO, electron energy loss spectra exam. 78−72652
Mo (100) surface, clean and O_2 covered electron energy loss spectra meas. 77−16440
Mo, AES and characteristic energy loss spectra, expt. and interpretation 78−27354
Mo, anal. of surface and volume losses 79−91547
Mo film, polycryst., energy loss function, Kramers-Kronig anal., reflectivity, optical props., EELS 80−40194
Mo, foil, electron energy loss spectra 80−7452
Mo, plasmon and phonon excitation 78−72682
Mo, slow electron inelastic scatt., vol. and surface plasmon excitation 77−52207
MoS_2, angular loss studies on natural surfaces by low-energy electron spectroscopy, surface cleavage influence *(French)* 79−56898
$MoS_2(Se_2)$, 2H polytype, low energy electron energy loss spectra 79−95885
Mo(100) single crystals, anisotropic ionisation loss of electrons, orientational effects 79−69935
N_2, continuum, energy loss cross sections for 300, 400 and 500 eV electrons 79−94090
N_2, dipole-forbidden states 79−59588
N_2 electron impact, spatial yield spectra, microplume model 79−98235
N_2, electron impact dissoc., EELS, N^- autoionisation 80−106397
N_2 gas, electron energy degradation, Monte Carlo study 80−69969
N_2, K-shell, excitation and ionisation, vibr. struct., electron energy loss spectra obs. 80−18943
N_2, liq., photoelectric determ. of conduction state energies and electron ranges 77−89487
N_2, N K-shell excitation, high-resolution electron energy loss spectra 80−53152
N_2, orientated mol., (e,2e) spectra, electron momentum density 79−98236
N_2, oscill. strengths for shape resonances near K edges 77−75224
N_2, rot. excitation by electron impact 1-4 eV 78−55248
NH_3, Compton defect for 35 keV electrons 79−27092
NH_3, dipole oscill. strengths for excitation, ionisation and fragmentation by 5-60 eV electrons 77−68129
NH_3, lowest triplet excitation, electron energy loss spectra 77−71880
NO, adsorbed on Ru (001), inelastic electron scatt. dissoc. energies adsorbed state depend. 78−95956
NO, adsorbed on Ru (001), EELS obs. 80−20741
NO, chemisorbed on Pt(100), vibr. spectra, electron energy loss, LEED and Auger investig. 79−90866
NO, doublet-quartet transitions, 5-7.4 eV, electron-impact spectroscopy, 5-80° 78−37754
NO, doublet-quartet transitions, low energy variable-ang. electron scatt. obs. 78−62933
NO, electron impact, energy loss spectra, electronic transitions obs. 78−17805
NO, N K-shell excitation, high-resolution electron energy loss spectra 80−53152
N_2O, electron impact, energy loss spectra, electronic transitions obs. 78−17805
N_2O, N K-shell excitation, high-resolution electron energy loss spectra 80−53152
N_2O, optically forbidden electronic transitions 77−31015
N_2O, valence shell ionic photofragmentation, oscill. strengths, EELS and electron-ion coincidence meas. 80−37879
Na film, adsorbed on Ni (100), plasmon losses in electron energy loss spectra 79−61480
Na, high resolution inelastic electron scatt. at zero angle, oscillator strengths 78−9255
Na_xWO_3, intra- and interband plasmons, inelastic electron scatt. exam. 78−72098
Nb (110) and (750), interaction with O_2, LEED, AES, SIMS, and EELS obs. 80−44408
Nb, electron energy losses due to H, obs. by scanning TEM 80−79850
Nb, foil, electron energy loss spectra 80−7452
NbN, optical props. and charact. electron energy loss spectra 79−52056
Nd_2O_3, EELS, low loss peak due to plasmon 80−79953
Nd_2O_3-Y_2O_3 film, segregation obs. by EELS 80−79953
Ne, electron energy loss spectra, Compton defect characterised by shift and asymmetry parameters 80−95723
Ne, electron impact excitation of $2s2p^63s$ and $2s2p^63p$ configs., energy loss obs. 80−91685
Ne, electron impact K-shell excitation, EELS 80−106396
Ne, inner-shell contribs. 77−3474
Ni (100), adsorption of CO, EELS and concomitant surface anal. 80−7453
Ni (100), chemisorption of $H_2(D_2)(HD)$, vibr. excitation and struct., electron energy loss spectra 78−47660
Ni (100), dissociative chemisorption and mol. adsorption of NO 80−65373

electron energy loss spectra continued
Ni (100), initial oxidation, electron energy loss spectra, LEED, AES, and work function meas. 79−61795
Ni (100), O and S chemisorption, surface vibrs., electron energy loss spectra 79−33173
Ni (100) face, O-Ni system vibrs. rel. to struct. during oxidation 77−66089
Ni (100) surface, clean and gas-covered, electron energy loss spectra 79−47570
Ni, (100)p(2×2)O and (100)c(2×2)O surfaces, struct. and vibrs. of adsorbed CO 78−2375
Ni (110), chemisorption of O_2 and initial oxidation, AES, EELS, and work function meas. 80−54523
Ni (110), interaction with O_2, electron energy loss spectra and AES obs. 79−47826
Ni (111), adsorbed H, angle-resolved and variable impact energy electron vibr. excitation spectroscopy 80−76119
Ni (111), adsorption and decomp. of hydrocarbons, high resolution EELS study 80−40739
Ni (111), adsorption of acetylene, identification of CH species by electron energy loss spectra 79−15022
Ni (111), coadsorption of CO and hydrocarbons $C\equiv O$ bond weakening 79−90863
Ni (111), with submonolayer of O, H or C_2H_2, surface phonons obs. by EELS 80−39403
Ni (111) and (100), chemisorption of benzene, vibr. EELS study 80−39436
Ni (111) face, adsorbed CO, CO stretching vibr., high resolution electron loss spectroscopy 78−14605
Ni, adsorption of ethylene at room temp., surface complex vibr. from electron energy loss spectroscopy 79−73404
Ni alloy, STEM microanalytical techniques comparison for precip. comp. determ. 78−35790
Ni, CO adsorbed mols. on (100), bonding struct., vibr. excitations 77−15687
Ni, core-electron excitation edges 80−66345
Ni, dielectric matrix, analytic model 80−75512
Ni, elastic and magnon-inelastic spin polarised low energy electron scatt. 78−34970
Ni, electronic structure and optical consts. by inelastic electron scatt. 80−7451
Ni film, inelastic electron scattering 78−92155
Ni film, inelastic electron scatt. 79−15570
Ni film, interaction with O_2, AES, EELS, work function, and gravimetric meas. 80−75433
Ni stepped surface, adsorbed CO vibrs., electron energy loss spectra 79−73406
Ni superalloy, STEM microanal. of precipitates and their nuclei 80−81067
Ni surface with adsorbed CO, vibr. modes, anal. of electron-energy loss data 79−82461
Ni-Si, intergranular segregation of Si, electron energy loss spectrometers, X-ray anal. *(French)* 79−8388
NiO (100), electron energy loss spectra exam. 78−72652
NiO (100) surface, electronic states, electronic energy loss spectroscopy 78−6426
Ni(100), adsorbed CO vibr. EELS, large-ang. defl. 80−44405
Ni(111), adsorption of acetylene, evolution of adsorber species, rel. to vibr. spectra 78−95952
Ni(111), chemisorption of methanol., methoxy species, electron energy-loss spectra 79−29391
Ni(111), coadsorption of CO and H_2, surface carbide influence, vibr. electron energy loss obs. 79−52772
Nz, electron transmission function and mean energy per ion pair, obs. 80−23566
O, inelastic electron scatt., 100-500 eV, ${}^3P \rightarrow {}^3S^0$ oscill. strength 79−81282
O_2, 7 to 10 eV energy loss spectra, Rydberg states excitations 77−27193
O_2, electron impact, energy loss spectra, electronic transitions obs. 78−17805
O_2, K-shell, excitation and ionisation, vibr. struct., electron energy loss spectra obs. 80−18943
OH adsorbed on Ni, energy depend. of vibr. excitation, electron energy loss spectra 79−28201
Pb ultrathin films on PbTe and Te, prep. and characterisation 77−7995
PbS, anisotropy of vol. plasmon dispersion, electron energy loss meas. 77−35878
PbS, wave-vector depend. of electron energy losses 78−11041
PbSe, wave-vector depend. of electron energy losses 78−11041
PbTe, wave-vector depend. of electron energy losses 78−11041
Pd (100), adsorption struct. of CO, LEED and high-resolution EELS study 80−20037
Pd (111), interaction with O_2, EELS, AES and LEED obs. 79−86985
Pd, catalyst, Z-contrast, in STEM 79−46530
Pd surface, segregated S state, AES, EELS, UPS and XPS study 80−93452
Pd-Cu-Si metallic glass, energy loss spectra and Auger spectra 78−23563
Pd-Ni-P metallic glass, energy loss spectra and Auger spectra 78−23563
PdH(D), energy loss spectra and Auger spectra 78−23563
Pd(001), adsorpt. of CO, LEED, electron energy loss spectra study, surface struct. effect on weak chemisorpt. bonding 78−71987
Pt, 5d band structure effects on line shapes and intensities of core electron excitations 78−92177
Pt (100), adsorbed H_2O, bonding, electron energy loss spectra 80−34311
Pt (100), cyanogen adsorbed layers 78−14592
Pt (111), adsorption of NO, EELS, thermal desorption, LEED, and AES study 80−80086
Pt (111), adsorption sites of CO, surface vibr. modes, electron energy loss meas. 77−43422
Pt (111), at. steps role in H interaction 77−15690
Pt (111), chemisorption of mol. O_2, XPS, UPS, EELS, and work function meas. 80−76139
Pt (111), coadsorption of CO and hydrocarbons, $C\equiv O$ bond weakening 79−90863
Pt (111), surface reaction with acetylene ethylene, and H_2, EELS 78−71947
Pt (111) adsorption state of acetylene on surface vibrs. meas. 77−76657
Pt, (111) surface, characteristic loss of electrons *(German)* 78−52605
Pt, adsorbed CO, adsorbate induced electron losses 79−46959
Pt, adsorbed layers of H_2, energy loss spectra *(French)* 79−83069

- **electron energy loss spectra** continued
  - Pt, adsorption of O_2, surface struct. depend., LEED, AES, and electron energy loss spectra 79—46934
  - Pt, CO adsorption, study of surface vibrs. 77—69160
  - Pt, catalyst, Z-contrast, in STEM 79—46530
  - Pt, chemisorption of acetylene, characteristic loss spectrum and AES 77—55458
  - Pt, core-electron excitation edges 80—66345
  - Pt stepped surface, adsorbed H, adsorption sites study by EELS 80—49521
  - Pt, surface, (111), O_2 interactions, UPS, EELS and thermal desorption study 80—100409
  - Pt, surfaces (111) and 6(111)×(111), CO adsorption, EELS and thermal desorption spectroscopy 78—91547
  - Pt-$SrTiO_3$ (100) interface, struct. and electronic props., AES, LEED, EELS, and UPS study 80—24986
  - Pt(III), electronic struct. of adsorbed Na 78—19117
  - Pt(111), adsorbed ethylene and benzene, electronic energy losses 79—46931
  - Pt(111), adsorption of NO, anal. of adsorption processes and surface reactions, vibration spectroscopy 78—87868
  - Rb film, adsorbed on Ni (100), plasmon losses in electron energy loss spectra 79—61480
  - ReO_3, intra- and interband plasmons, inelastic electron scatt. exam. 78—72098
  - Rh (111), chemisorption of CO and CO_2, high resolution EELS, thermal desorption, and LEED study 80—44419
  - Rh (111), chemisorption of acetylene and ethylene, EELS, LEED and thermal desorption mass spectrometry 80—80057
  - Rh (111), dissociative chemisorption of CO_2, EELS and thermal desorption spectra meas. 80—6656
  - Ru (001) surface, chemisorbed O_2, high resolution electron scatt. spectra 79—11013
  - Ru (001) surface, clean and $CO(O_2)$ adsorbate covered, characteristic slow electron energy loss meas. 79—47562
  - Ru(001) surface, chemisorbed $CO+O_2$, and surface reaction 79—46924
  - $SCVO_4$, primary excitation processes in cathodolum. 79—11490
  - SF_6 electron scatt., total absolute cross sections, 0.5-100 eV, incl. reson. struct. 79—45843
  - $(SN)_x$, epitaxial, optical props. and plasmon dispersion, from electron energy loss spectra 77—35882
  - Sb, Sb_2O_3 and Sb_2S_3, AES and characteristic energy loss spectra, expt. and interpretation 78—27354
  - Sc and Sc_2O_3, photoabsorpt. spectra, at. ionisation, band struct. mechanisms, electron energy loss investig. 77—24909
  - Sc, crystal surface, N and O adsorption, refl. electron energy loss spectra obs. 80—20742
  - Sc, electronic excitations, charact. energy loss meas. up to 50 eV 80—60723
  - Sc, interband, collective and atomic (p,d) excitations, Z-160 eV, fast EELS 80—93443
  - Sc_2O_3, electronic excitations, charact. energy loss meas. up to 50 eV 80—60723
  - Sc_2O_3, interband, collective and atomic (p,d) excitations, Z-160 eV, fast EELS 80—93443
  - Si (100), oxides formed in Cs-O adsorbed films, ionisation loss spectra, Auger spectra 79—69365
  - Si (100) surface, slow electron elastic scatt. threshold effects 79—100002
  - Si (111), adsorption of C_2H_2 and O_2, low-energy electron loss spectroscopy obs. 77—1303
  - Si (111), adsorption of $H_2S(H_20)(0_2)$, electron energy loss spectra exam. 77—39736
  - Si (111), CO adsorption on cleaved surface, electron energy loss spectra 78—79885
  - Si, (111) 7×7 surface, adsorption of Al, electron energy loss spectroscopy and LEED 77—43432
  - Si (111) 7×7 surface, chemisorption of H_2O, AES, EELS and UPS 80—10792
  - Si (111) 7×7 surface, giant core-exciton effects, electron energy loss spectra and XPS 77—24600
  - Si (111) 7×7 surface states, low-energy electron loss spectroscopy 79—60891
  - Si, (111) cleavage, Kikuchi pattern, 40 keV incident electrons, electron energy loss spectra *(French)* 78—87594
  - Si, (111) surface, Cu phthalocyanine dye deposition, low energy electron optically modulated transmission increase 79—78133
  - Si, (111) surface, oxide formation, AES and EELS meas. 80—3232
  - Si (111) surfaces, electron energy loss spectroscopy of NO, O_2 and NH_3 78—2374
  - Si (111)-Cl(7×7), angle resolved secondary emission and electron energy loss study of electronic struct. 79—61477
  - Si, adsorption of gases, study of surface vibrs. 77—69160
  - Si, amorphous, clean and O_2 adsorbed, light sensitive electron laser meas. 79—24396
  - Si, amorphous, scanning TEM studies of cryst. inclusions 80—79699
  - Si, amorphous film, EELS microanalysis 80—100722
  - Si, annealed crystal, oxide precipitates identification by electron loss spectra 78—83952
  - Si, annealing, impurity film form., energy loss anal. 77—31916
  - Si, bulk plasmon dispersion, electron energy loss spectra meas. 80—59899
  - Si, direct nonvertical interband transitions 77—85856
  - Si, electron energy losses, anisotropy of excitation probability 78—15265
  - Si, electron scattering energy distrib., channelling effect *(Russian)* 78—2183
  - Si film, epitaxial growth on Si, impurities, plasmon energy loss anal. 77—31916
  - Si film, volume plasmons, EELS, line shape 79—90984
  - Si, identification of oxide precipitates 80—100723
  - Si, L-shell ionisation by 80 keV electrons, transmission electron energy loss spectrometry 80—60721
  - Si, optical properties of monocrystal by electron energy loss meas. *(German)* 79—24283
  - Si, phonon spectroscopy, amorphous versus crystalline material 78—83898
  - Si, plasmons, influence of cryst. orientation on intensity, electron energy loss meas. *(German)* 79—23921
  - Si, single-electron excitations, image contrast from delocalised excitations 79—46529
  - Si, surface, (111) 2×1, cleaved, O_2 adsorption, low-energy electron loss spectra 79—15840
- **electron energy loss spectra** continued
  - Si, volume plasmon dispersion at large wave vectors, EELS 78—56094
  - Si-Al(Ga)(In) interface, electron energy loss spectra of Schottky barrier states 77—48290
  - Si-Au, interface study using EELS 80—97391
  - Si-Ge heterojunction form., microscopic aspects, EELS meas. 80—80368
  - Si-SiO_2, angular-dependent X-ray photoelectron spectra 77—12485
  - Si-SiO_2 interface, electronic struct., EELS study 79—99596
  - Si-SiO_2-Si_3N_4 MNOS structure, chem. comp. and electronic states, Auger and energy loss spectra obs. 80—92999
  - Si(Li) detectors, electron counting, appl. to electron energy loss spectra, by high voltage electron microscopy *(French)* 78—54511
  - Si_3N_4 amorphous films, CVD, core and valence electron excitations, low energy electron loss spectroscopy and AES 80—2365
  - Si_3N_4 film, amorphous, AES and EELS characterisation 79—90905
  - Si_3N_4, Si(LVV) Auger spectra, ion bombardment, electron energy loss spectra 80—80911
  - SiO_2, 0.02-2 eV, vibr. states 78—39642
  - SiO_2 amorphous film, Si(LVV) Auger spectra, ion bombardment, electron energy loss spectra 80—80911
  - SiO_2 amorphous film, thermal, core and valence electron excitations, low energy electron loss spectroscopy and AES 80—2365
  - SiO_2, electronic struct., review of spectroscopic and theoretical data 77—76749
  - SiO_2, phonon spectroscopy, amorphous versus crystalline material 78—83898
  - SiO_2, surface electronic struct., electron irrad. effects, EELS study 80—24985
  - SiO_x film, amorphous, AES and EELS characterisation 79—90905
  - SiO_x, phase comp., electron spectroscopy obs. 78—60042
  - Si(111), adsorption of HBr(Cl), AES, electron energy loss spectra and electron impact desorption exam. 78—43243
  - Si(111) surface, adsorbed O, UHV cleaved, electronic transitions 78—39183
  - Si(111), surface electronic struct., atomic geometry effects 77—85283
  - Si(111), water vap. and O_2 interactions, EELS 78—14571
  - Sn, chemisorption of O_2, AES and EELS study 79—46917
  - Sn, clean and oxidised, electron energy loss spectra at low primary beam energies 79—65963
  - SnS(Se), dielec. function, optical and electron energy loss spectroscopy 78—15189
  - Sr, plasmon excitation by oblique incidence of primary electron beam of medium energy 78—18987
  - $SrTiO_3$ (100) surface, struct. and electronic props., AES, LEED, EELS, and UPS study 80—24986
  - $SrTiO_3$ (111), surface struct., electronic props., LEED, AES, UPS study, photoelectrochem. cell anode appl. 78—84035
  - $SrTiO_3$, adsorption of O_2, electron energy-loss spectra obs. 80—89521
  - $SrTiO_3$, surface defects, electronic struct., LEED, AES, UPS study 78—84273
  - Ta, adsorbed layers of H_2, energy loss spectra *(French)* 79—83069
  - Ta, foil, electron energy loss spectra 80—7452
  - TaC surface, effect of C oxidation on work function, 1250-2000K, AES 79—24054
  - Tb, low energy fine struct. and surface electron states 77—85860
  - Te, film, AES, LEED, XPS, energy loss spectra studies oxidation effects 78—73086
  - TeO_2, film, AES, LEED, XPS, energy loss spectra studies 78—73086
  - Th, absorption coefficients, near O_{IV} O_V thresholds, 5d cross sections calc. 78—90134
  - $ThNi_5$, methanation catalyst, AES and characteristic energy loss spectra 78—56915
  - Ti, electronic structure, appl. of Auger and characteristic loss spectroscopies 77—77331
  - Ti film, effect of surface and bulk oxidation on charact. electron energy loss spectra *(French)* 78—39641
  - TiH_x and $TiD_{0.9}$, surface characts., AES, EELS, SIMS, and XPS study 80—65343
  - TiO, electronic excitations, electron energy loss spectra in 3 to 60 eV range *(French)* 78—80440
  - TiO_2, 0.02-2 eV, vibr. stats 78—39642
  - TiO_2 (100), chemisorption of H_2, O_2, and H_2O, electron spectroscopy, evidence for Ti^{3+} photogeneration 78—38940
  - TiO_2, (110) and (100) surfaces, LEED and electron spectra 77—72757
  - TiO_2, chemisorption of O_2 and H_2O, electron stimulated desorption, AES and charact. loss spectra 78—22963
  - TiO_2, cluster surface states, LCAO calc., electron energy loss peak interpretation 77—43686
  - TiO_2, electronic excitations, electron energy loss spectra in 3 to 60 eV range *(French)* 78—80440
  - TiO_2, electronic structure, appl. of Auger and characteristic loss spectroscopies 77—77331
  - TiO_2, H species characterisation by electron-stimulated desorption 80—34305
  - TiO_2, phonon spectroscopy, amorphous versus crystalline material 78—83898
  - TiS_2, dielectric function, reflectivity and absorption coefficient 79—69937
  - TmSe, electron energy loss spectroscopy and UV photoemission meas. 78—31305
  - U, AES and loss spectra, changes on oxidation 77—20965
  - U, absorption coefficients, near O_{IV} O_V thresholds, 5d cross sections calc. 78—90134
  - UF_4, AES and loss spectra 77—20965
  - UF_6, excitation spectra after electron impact, 30-75 eV impact energy 79—45854
  - UIr_3, (100) surface reconstruction, LEED, AES, electron energy loss spectra study 78—75918
  - UO_2, and U_3O_8, AES and loss spectra 77—20965
  - V, electron energy losses due to H, obs. by scanning TEM 80—79850
  - V, foil, electron energy loss spectra 80—7452
  - V-Ti-C, elemental anal. by EELS 80—101069
  - V-Ti-C, high temp. carbide form., electron microscopy study 80—89228
  - VN, optical props. and charact. electron energy loss spectra 79—52056
  - W (001), atomic nature of H adsorption, surface vibr. detect. 77—76664
  - W (001) surface, electron loss spectra 79—33872
  - W (100), adsorbed H, angle-resolved and variable impact energy electron vibr. excitation spectroscopy 80—76119
  - W (100), adsorbed H-induced lattice reconstruction, surface vibr. obs. 79—19445
  - W (100), adsorpt. of acetylene, room temp., electron spectroscopy obs. 79—7749

electron energy loss spectra continued
  W (100), adsorption of O_2, surface struct. and thermally stimulated reaction 77−55451
  W (100), chemisorption of H, struct. determ. by surface vibr. modes anal., EELS obs. 80−39435
  W (100), H adsorbate low energy electron vibrational excitation 80−84375
  W (100) surface, adsorption of Co, electron energy loss spectra 78−71999
  W (100) surface, energy loss mechanisms in low energy electron scatt., use as surface sensitive spectroscopy 77−85859
  W (100) with adsorbed CO, surface vibrs. 77−62745
  W (110), codeposition of Cs and O, Cs_2O form. 80−44425
  W {100}, anisotropy of inelastic electron refl., energy loss effects 80−79642
  W, anal. of surface and volume losses 79−91547
  W, CO adsorption, study of surface vibrs. 77−69160
  W, chemisorbed CO and acetylene, IR vibration spectroscopy using refl. inelastic electron scatt. 78−14603
  W, chemisorbed H_2, vibr. spectra characts., adsorption sites 80−70535
  W, LEED and electron microscopic investigs., review *(Hungarian)* 77−47654
  W, slow electron inelastic scatt., vol. and surface plasmon excitation 77−52207
  W, vibr. states of H_2, D_2 and C_2H_2 adsorbates 77−66090
  WF_6, excitation spectra after electron impact, 30-75 eV impact energy 79−45854
  WO_3 film, intra- and interband plasmons, inelastic electron scatt. exam. 78−72098
  WO_5 film, amorphous, band structure and colour-centre band, fast electron energy loss spectrum 77−55478
  W(001), momentum transfer effects 77−85858
  W(100), adsorbed H, nondipole electron impact vibr. excitations obs. 78−63922
  W(100), chemical effects in electron loss spectrum 77−4705
  W(100), chemisorbed H, vibr. excitation of hydrogenic modes, angle dependent electron energy loss meas. 79−46914
  W(100) surface, chemisorption of CO and N_2, AES and electron energy loss spectra 77−1313
  W(211), adsorption of Be, work function changes and scatt. electron energy losses 79−46947
  Xe, transition oscill. strengths, electron spectrometric obs. 77−10769
  XeF_6 molecules with Jahn-Teller pseudo-effect, ang. depend. of inelastic scatt. of electrons 80−69246
  Y, and Y_2O_3, photoabsorpt. spectra, at. ionisation, band struct. mechanisms, electron energy loss investig. 77−24909
  Y, electronic excitations, charact. energy loss meas. up to 50 eV 80−60723
  Y, interband, collective and atomic (p,d) excitations, Z-160 eV, fast EELS 80−93443
  Y_2O_3, electronic excitations, charact. energy loss meas. up to 50 eV 80−60723
  Y_2O_3, interband, collective and atomic (p,d) excitations, Z-160 eV, fast EELS 80−93443
  Zn I,II, excited state lifetimes, electron-photon delayed coincidence meas. 78−25478
  ZnO, (0001) surface, clean and O adsorbed, AES and refl. electron energy loss spectra 79−46927
  ZnO $(000\bar{1})$ surface, surface and bulk excitations, reflection electron energy loss spectroscopy 77−20389
  ZnO, bulk and surface plasmons, single and multiple excitation 77−12474
  ZnO, electronic surface and bulk transitions exam. by electron energy loss spectra 78−30964
  ZnO, nonpolar surface, interaction with CO and CO_2, thermal desorption, AES, EELS and LEED obs. 79−65321
  ZnO on Zn (0001), oxide film growth, at. and electronic struct. 78−15587
  ZnO, polar surface, clean (O_2-H-exposed), reflection energy loss spectra, 2-30 eV 78−64434
  ZnO polar surfaces, H and O_2 exposed, ion irrad., and heat treated, cond., EELS study 80−71525
  ZnO, prismatic surface, O_2 interaction obs. 77−31899
  ZnO surface, adsorption of O_2 and CO, electron energy loss spectra meas. 78−14601
  ZnO, Zn 3d core-level transition in electron energy loss spectra, rel. to ZnSe (111) surface 78−68584
  ZnSe (100) surfaces, surface states meas. by LEED, AES and EELS *(Japanese)* 79−99599
  ZnSe (110), LEED intensity anal. and electron spectroscopy 77−43678
  ZnSe (110) surfaces, obs., by low-energy-electron loss spectroscopy *(Japanese)* 79−83071
  ZnSe (111), low-energy electron loss spectra, bulk and surface transitions 78−11042
  ZnSe(Te), clean and oxidised surfaces, surface states, low-energy EELS study 80−11522
  ZnTe (110) and (111) surfaces, O_2 adsorption, electron energy loss and Auger spectra 79−47568
  ZnTe (110) and (111) surfaces, electron energy loss spectra, bulk and surface losses 79−43080
  Zr, electronic excitations, charact. energy loss meas. up to 50 eV 80−60723
  ZrN, optical props. and charact. electron energy loss spectra 79−52056
  $ZrNi_5$, methanation catalyst, AES and characteristic energy loss spectra 78−56915
  ZrO_2, electronic excitations, charact. energy loss meas. up to 50 eV 80−60723

electron energy states (condensed matter)
  see also band structure; band theory models and calculation methods; deep levels; defect electron energy states; dopplerons; electron energy states of amorphous solids; electron energy states of liquid metals; electron energy states of liquid semiconductors; electron gas; electron traps; electronic density of states; exchange interactions (electron); excitons; Fermi level; Fermi surface; field interactions (condensed matter); helicons; hole traps; impurity electron states; Landau levels; localised electron states; magnetic breakdown; magnons; metal-insulator transition; metal theory; plasmons; polar semiconductors; polarons; positron states; ripplons; spin-orbit interactions; spin-phonon interactions; surface electron states; triplet state
  ab initio LCAO-HF-concentrated GO crystal-orbital program 77−55471

electron energy states continued
  actinides, conf. Wroclaw, Poland (Sept. 1976) 77−85124
  actinides, electronic structure, conf., Grenoble, France (30 Aug-1 Sept. 1978) 80−6685
  actinides, XPS, many-electron effects, comparison with rare earths 80−7466
  adiabatic potential energy, perturbation expansions *(Japanese)* 77−69205
  alkali dithioferrates (III), electronic struct. and hyperfine interactions, $X\alpha$ calcs. 80−100448
  alkali fluoride crysts., modified electronic charge density 77−62502
  alloy, disordered, binary decoupling schemes for many site correlation functions 78−18984
  alloy, disordered, spectral functions, augmented space formalism 78−84126
  anisotropic Green function method *(Russian)* 78−38998
  atomic chain, discreteness, effect on electron dechannelling 80−6448
  atomic scattering form factors, calc. energy spectrum of electrons in crystals 80−6688
  binary alloy, disordered, effective periodic pot. 78−10325
  binary alloys, disordered, electronic struct. 77−15755
  binary substitutional alloy, with long range order, electron energy spectrum *(Russian)* 78−84121
  binary substitutional alloy with long range order, electron energy spectra *(Russian)* 78−75974
  Bloch electrons, behaviour in mag. field, rationality non dependence 78−79914
  Bloch electrons, dynamics in constant elec. fields 80−88463
  Bloch electrons in mag. field, transfer-matrix study 77−55472
  Bloch electrons in magnetic field, quantum numbers 80−96768
  Bloch electrons in rational and irrational mag. fields, energy levels and wave functions 77−1344
  Bloch functions, by projection technique 79−15060
  Bloch generalised density matrix approx. solns., free and lattice electrons 77−31923
  Bloch waves, periodic variations in shape 77−31926
  Bloch waves, semiclassical wave propagation matrix method 79−101
  Bogolyubov's method in quantum theory of crystal with many-particle interaction 77−31928
  charge and orbital ordering in crystals 78−34738
  charge ordered state of quasi-one dimens. and finite cyclic system, ab initio LCAO-MO method 77−1343
  coherent states and Bloch functions 80−36941
  coherent states in solids using Bravais lattice operator 80−75490
  collective excitation, SBO Green's function eqns. 79−99492
  compressed atom model, energy level shifts for changed boundary conditions 77−43473
  Compton profiles *(Japanese)* 77−36306
  conduction electrons, thermodynamic method for quantitative anal. 80−59946
  correlation holes, number-sum rules and infinite system 79−23916
  Coulomb gas in d-dimensions, roughening transition 77−89718
  coupled linear chain system solitons 77−43463
  cubic crystal, perfect, non-Bloch electron states, incompletely symmetric 79−23877
  diamond, effective supersystem cryst. simulation method, geometrical parameters, bulk moduli, impurity levels calcs. *(French)* 80−15430
  diatomic one dimens. lattice with δ potentials, electron energy spectrum *(Russian)* 79−19497
  p-dichlorobenzene-p-dibromobenzene, mol. cryst., intermol. mixing of electronic states 77−85768
  dipole density wave state in electron-hole junction system, existence 78−76009
  Dirac eqn., quasistationary levels in lower continuum, WKB approx. *(Russian)* 78−45826
  discrete states, interaction with many continua 77−47707
  disordered alloy, electron correl. in Hubbard model, and spin susceptibility 77−76762
  disordered assembly, partition function 77−9957
  disordered system, electronic props. by analytic continuation from renormalisation group theory 77−8003
  disordered system, linear model, electronic energy spectrum 78−10316
  disordered system, scaling near mobility edge 77−11835
  disordered system with n orbitals per site 1/n expsn. 79−90999
  disordered system with short range order, elementary excitations 77−47709
  disordered systems, systematic approach, averaged Green functions calc. 80−80150
  disordered systems as quantum field theories 79−65354
  disordered systems with correlations, variational treatment 77−69208
  disordered transition alloys, generalized perturbation calcs. of ordering energies 77−4282
  effective electron-electron interaction in a group-theoretical diagram technique 79−28303
  electron in field of small-radius pot. well and attractive Coulomb pot., energy spectrum 78−56059
  electron momentum densities, expt. determ., review 77−76776
  electron momentum densities, theory, review 77−75039
  electron motion in one-dimens. periodic pot. under influence of uniform elec. and mag. fields 78−75972
  electron theory, empirical, for solids and molecules *(Chinese)* 79−15061
  electron-hole pairing, suppression by impurities, thermodynamic and kinetic props. *(Russian)* 77−69318
  electronic charge distribs., theory, review 77−75040
  elementary excitations, dispersion relations, with damping 78−14687
  elements with $Z\leq30$, core electron binding energies in free and standard state 77−43168
  energy band structure for one-dimensional case *(Russian)* 80−59851
  energy density functional approach, kinetic energy model 79−31357
  extended systems, Hartree-Fock orbital and total energies 79−4498
  FCC lattice, density of dynamical observables, incompletely symm. non-Bloch states 79−23879
  film, electron energy spectrum allowing for arbitrary one-dimens. internal field *(Russian)* 77−69212
  fluids, conf., Banff, Alberta, Canada, (5-11 Sept. 1976) 77−89680
  Frohlich Hamiltonian without cut-off, self-adjointness and other properties 78−38995
  heavy elements, photoemission characts. *(Dutch)* 79−1811
  Hubbard model, one-dimensional, half-filled, ground-state energy calc. 80−39488

electron energy states continued
- III-V semiconductors, electronic dielec. const., interionic separation d-core effect 78—60046
- incoherent resonance decay and coherent optical ringing from coherently prepared electronic states 77—10698
- insulator, renormalisation theory of charged particles, effective mass approx. 77—51630
- interacting electron system, time-dependent density-functional formalism 79—28306
- ionic crystal, Compton profile interpretation to give ionic deform. and bonding 77—40301
- Jahn-Teller effect in trigonal symmetry 79—82563
- KKR method, structure constants, electronic struct. 80—80152
- layered and chain crystals, electron energy spectrum in mag. field *(Russian)* 77—20220
- lectures on interaction of radiation with condensed matter, Trieste, Italy (Jan.-March 1976) 78—27172
- local density kinetic energy expressions for electronic struct. calc. 80—65473
- mathematical models of disordered systems, book 80—1878
- metal, d-electrons, electron density model 78—91580
- metal, electron correl. Gutzwiller, theory at finite temp. 77—43527
- metal cluster, electronic spectrum fluctuations, appl. to Ni and Ti 79—19501
- metal clusters, electronic states and mag. props., MO calc. 77—20219
- metallic clusters, small, extension of moment development method *(French)* 77—31925
- metallic particles, effective interactions due to irregular surface 79—99470
- mixed crystal or alloy, graded, effective Hamiltonian theory 80—34344
- mobility edge problem, continuous symmetry 80—10939
- model potential for positive ions 77—35844
- molecular crystals, PCILO calculations 77—34571
- multicentre multielectron system, wave function construction 78—893
- multiple scattering in condensed media, calc. of density of states for non-crystn. Cu and Fe 78—91578
- multiple scattering in condensed media, embedding field and effective medium 78—51867
- one-dimensional finite chain, boundary states and vibrs., tight-binding approx. 80—2317
- one-dimensional pot. arrays, ordered and disordered, electron states, one-electron density matrix, Fourier-transformed Compton profile 79—69385
- one-dimensional system, correl. functions, limiting relationships 77—62790
- operator recursion analysis, electronic struct. determ. 78—14644
- orbital calcs., deformation density transferable integrals 80—54581
- organic free-radical solid conductors and semiconductors, electronic structure 79—35496
- organic semiconductor, alternate mol. orbital method 79—65353
- periodic potential with slowly varying envelope, effective Hamiltonian theory 79—23880
- phase integral approximations, advantages over JWKB approx. 80—87027
- Pippard networks of Dingle functions and coherent states 77—20218
- plasma, nondegenerate, dense, electron transport *(Russian)* 79—98865
- Poisson's equation integration for complex system with arbitrary geometry 77—47705
- polyethylene, displacement of electronic spectrum during stretching, LCAO calc. 80—5481
- polymer crystals, electron problems by SCF method, HF matrix 77—79718
- properties of solids and electronic struct., chemical bond physics, book 80—86044
- pseudopotentials, reliability criteria 80—49563
- pyridine-N-oxides, substituted, absolute energy levels in gas and condensed media, ionis. energy, electron affinity 77—67995
- random low-density correlated medium, multiple s-scatt. 77—1355
- rare earth orthovanadates, covalency, chemical bonding and opt. spectra 77—80442
- S^2 approximation, spin orbital overlap integrals 77—43467
- screening potential, asymptotic behaviour at finite temps. 78—14685
- semiconductor, Benard effect *(Russian)* 78—84122
- semiconductor, electron excitation spectra in field of two travelling waves 80—65514
- semiconductor, electron-runaway and quasi-stationary states in electric field 77—4359
- semiconductor, hot electron energy tails, Monte-Carlo calcs. 77—62931
- semiconductor physics, conf., Edinburgh, Scotland (Sept. 1978) 79—95303
- semiconductor solid solution, compositional disorder, free carrier absorpt. 78—64387
- semiconductor superlattice, geometrical and physical props. of constant-energy surface 77—69213
- semiconductors, Benard effect, influence of external elec. field *(Russian)* 79—1750
- small metal particles, thermodynamic props. of electrons 80—59844
- solid solution, vol., electron correl. effect 77—28133
- solid-state, atomic and molecular theory, conf., Flagler Beach, Florida, USA (Mar. 1978) 79—31356
- solid-state theory, introduction, book 79—33215
- solids, electronic struct., book 77—11832
- solids, large unit cell calc. in CNDO approximation 77—28089
- solitons in condensed matter physics, theory 80—50122
- spectroscopy using synchrotron radiation 77—20882
- spin density functional method, and ground state of solid bodies *(Russian)* 78—14645
- spin susceptibility, inter- and intra-atomic electron interactions 77—62789
- structurally disordered materials, CPA theory of excitations, lattice model 79—87030
- superconductor, theory of tunnel injection *(Russian)* 79—47198
- Swiss Physical Society, autumn sessions 78—72053
- symposium, Florida, USA (March 1979) 80—51946
- TCNQ, elect. struct. determ., CNDO parametrisation and UPS data 77—1350
- TCNQ salt, n-methyl-n-ethylmorpholinium, unpaired electron states, IR refl. study 80—75491
- TCNQ salts, $Qn(TCNQ)_2$ and $NMeAd(TCNQ)_2$, rel. to dielec. const. and elec. cond. 78—60116

electron energy states continued
- TCNQ salts with asymmetric donors, rel. to mag. susceptibility 78—60264
- TCNQ-NMP, reduced Coulomb repulsion, intrachain and interchain polarisation 77—85162
- TEM, image contrast from single-electron excitation 80—59353
- term data of energy levels as derived from superimposed flow curves 79—56108
- Thomas-Fermi model, review 77—84
- transfer integral method, three dimens., appl. to harmonic cryst. 78—84161
- transition metal alloys and cpds., sp. ht. and electronic structure *(French)* 77—28400
- transition metal compound refractories, electron and phonon behaviour 80—54624
- transition metal-Al, X-ray spectra, electronic structure 79—78793
- transuranic compounds, 5f electrons delocalisation, crystal and mag. props. *(French)* 77—27857
- TTT-$I_{1.6}$, dimensionality and disorder 77—66160
- two dimensional system of electrons in uniform neutralizing positive background, absence of cryst. order 80—103610
- universal variational functionals of electron densities, first-order density matrices, and natural spin-orbitals and solution of the ν-representability problem 80—95516
- Wigner crystal, two dimens., phase diagram in mag. field *(Russian)* 77—62849
- AgPd, dil. alloys, electronic states, virtual bound states model test *(French)* 77—62809
- $Al_2O_3:Co^{3+}$, corundum, Jahn-Teller effect in trigonal symmetry 79—82563
- Au-Pd dil. alloys, electronic states, virtual bound states model *(French)* 77—62809
- B and borides, conference, Varna, Bulgaria (Oct. 1978) 80—12842
- $CdS-NiCl_2$ interface, elec. props. using SAW techniques 79—56302
- Cu adsorbed atoms on Pt electrode, optical props., electronic struct. 77—69855
- Cu-Pd dil. alloys, electronic states, virtual bound states model test *(French)* 77—62809
- Cu_3 Zn clusters, electronic structures, SCF-Xα-SW method 80—88468
- Cu_4 clusters, electronic structures, SCF-Xα-SW method 80—88468
- $Cu_xMo_3S_4$, superconductivity, lattice transforms., electronic instabilities 77—39990
- Fe complex, iron $4,7-(CH_3)_2-(1,10\text{-phenanthroline})_2(NCS)_2$, spin state transition, X-ray and Mossbauer obs. 80—7195
- Fe F2 (Fe F3), electronic struct., binding energy, X-ray emission and photoelectron spectra obs. 80—35008
- Fe-Ni alloy, optical and electronic characts., 20-1750°C, comp. depend. *(Russian)* 78—84601
- Fe_3O_4, doped, electron correls. above and below Verwey transition, Green function theory 77—51687
- H-like systems in arbitrary mag. field, excited states, variational approach 79—77973
- H_2, metallic, liq., ground state energy at zero temp. 79—38006
- $LaLi_{0.5}Ir_{0.5}O_3$, perovskite, prep. and mag. study 80—80486
- Mg-Bi alloys, liq., far IR reflectivity meas. 77—52105
- Mo complexs. bis(η-cyclopentadienyl) Mo halides, electronic struct., photoelectron spectra 77—75214
- Na particle, consisting of ats., metallic Na, model, electronic levels 78—50673
- NbC crystals, electron energy spectra 80—49568
- $Ni_{13}(O_h)$ cluster, electronic states and X-ray spectra in Xα approx. of multiple scatt. theory 77—28645
- PO_4 electron structure rel. to synthesis and utilisation of ATP 80—40955
- Pa, 5f electron character rel. to superconducting props. 80—44756
- Pu and other actinides, conf., Baden-Baden, Germany (Sept. 1975) 77—19807
- $(SN)_x$, polymeric, electronic structure, semi-empirical pseudopotential calc. 77—72812
- Si, effective supersystem cryst. simulation method, geometrical parameters, bulk moduli, impurity levels calcs. *(French)* 80—15430
- $(Si_2O_7)^{6-}$ bitetrahedra, in silicates, total energy surface, ab initio calc. 78—23056
- UF_4 matrix with ^{235m}U isomer, conversion process electron role in valence band *(Russian)* 80—13416
- $(U_xTh_{1-}x)S(Te)$ solid solns., electronic struct., mag. susceptibility and elec. resist. obs. 77—20551
- WO_3 films, electron struct. changes during electrocoloration, XPS obs. 80—40217
- Zn_4 clusters, electronic structures, SCF-Xα-SW method 80—88468
- ZrC crystals, electron energy spectra 80—49568

electron energy states of amorphous solids
see also Anderson model
- actinides and alloys, metallurgical props. rel. to electronic struct., energies calc. method 77—20221
- alkali borate glass networks, π-electron distrib. SCF INDO LCAO-MO calc., O basicity 78—79924
- all-trans-polyene, ground state props., ab initio studies 79—47002
- alloy, amorphous, electronic struct. 78—72062
- alloys, disordered, charge density function calculation method 79—42433
- alloys, random binary, electronic struct., Mott-Anderson model 80—49671
- amorphous and liquid semiconductors, conference, Cambridge, MA, USA (Aug. 1979) 80—41933
- amorphous film junction, I-V and C-V characts. 77—85307
- amorphous semiconductor, stereochemistry, shape of disorder 79—64994
- amorphous semiconductor, tetrahedrally bonded, effects of quantitative disorder on electronic struct. 79—47003
- amorphous semiconductor film, density of localised band tail states, transient photoconductivity 77—15898
- amorphous semiconductors, covalent, localised electronic states, Hubbard model calcs. 77—89732
- Anderson transition, electron localisation in disordered systems 80—29361
- Anderson transition, numerical methods 79—60767
- band theory, rel. to appls. of amorphous materials 80—107693
- Cayley trees to study excitations 79—65373
- chalcogenide glass, charged dangling bond model reassessment 77—72813
- chalcogenide glass, elec. cond. mechanism, review of developments 78—26854
- chalcogenide glass, localised gap states, Mott-street model 79—37968

electron energy states of amorphous solids continued
chalcogenide glass, optical transitions and electronic struct., review 77—76741
chalcogenide glass, Urbach tail, rel. to Mott-Street model 77—47771
chalcogenide semiconductors, optical and elec. props., comparison with SiO_2 78—6721
cluster effective lattice method, mag. and electron props. 77—66242
covalent amorphous semiconductors, local struct., bonding and electronic props. 78—51882
disordered alloy, short range order effect on electron states 77—15732
disordered alloys, ensemble averaged Green function, analytic approx. 77—11842
disordered and amorphous semiconductors, band conduction mech. 79—95414
disordered and binary alloys, Hubbard III approx. numerical results 77—51874
disordered chains, electronic props. 80—2363
disordered semicond., random field effect on carrier conc. *(Russian)* 77—51762
disordered system with correls., density of states at band tail 80—80154
disordered system with short range order, elementary excitations 77—47709
disordered systems as quantum field theories 79—65354
elementary excitations, amorphons, density of states 80—39494
energy band model, electron physics of vitreous materials *(French)* 79—33225
ethanol glass, trapped and solvated electrons produced in presence of applied electric field 80—7379
fragment method, nonempirical, electronic struct. determ. 77—89684
gap states electronic behaviour 79—87098
glass, conduction and valence bands props., review 77—66106
glass systems, electronic props. 79—42495
glasses, elec. props. 78—2479
glasses and amorphous semiconductors, band struct. and forbidden gap, review 78—75987
group V semiconductor, defect states 79—87057
II-VI amorphous semiconductors, electronic states, sublattice one-band Hamiltonian transform. 80—59861
III-V amorphous semiconductors, electronic states, sublattice one-band Hamiltonian transform. 80—59861
Ising chain, finite, thermodynamic behaviour 79—61028
itinerant ferromagnetism and density of states, off-diagonal disorder effects 77—28360
laser irradiated amorphous materials, electronic struct., one-electron approx. 80—70576
liquid and amorphous metals, electronic states, optical theorem, multiple scatt. theory 80—49578
localisation domain size in disordered systems 77—15787
low-energy excitations of phonons, magnons, electrons rel. to struct. factor 80—44488
metal, electronic states calc. 79—69399
metal, muffin-tin model, s-phase-shift model 80—88473
metal, resistivity, anomalous temp. coeff. at high temp. 78—2458
metal, tight-binding model, effective medium approx. 77—15756
metal film, disordered and amorphous, quench-condensed, optical cond. and band struct. 77—1746
metallic glass, prep. and phys. props. development 80—81003
metallic glasses, conduction electron and tunnelling level interaction 79—60817
metallic glasses, electronic structure, neutron scatt., elec. resist., Hall coeff., mag. susceptibility and XPS 78—23013
metallic glasses, electronic structure rel. to elec. cond., supercond. and mag. props. 80—65429
metallic glasses, ferromag., Mossbauer investigation of electronic struct. 78—92009
metals, amorphous and liquid, electronic states, average spectrum 80—49579
model amorphous semiconductor struct., electronic props. 79—65974
molecular crystal, exciton density of states, effect of struct. disorder 79—28288
Mott's contribution to theory of electronic processes in glass *(Slovak)* 80—6686
noncrystalline materials, personal review by Sir Nevill Mott 78—55811
one-dimensional system, energy and charge transport theory *(German)* 80—15506
optical absorption in semiconductors and insulators 77—90167
optical absorption tail, shape 80—34946
optical properties, lecture 78—31219
optical properties rel. to electron states, lecture 78—27263
phosphate glass, electron-irradiated, charge accumulation, comp. depend. 78—2159
polyacetylene:I, electronic structure, XPS and UPS meas. 80—66385
polyacetylene, band struct. 79—51477
polyacetylene, electronic energy states and charge density contours studied muffin tin orbitals technique 80—80164
polyacetylene, trans- and cis-isomer, electronic struct. calcs. 80—24788
polyacetylenes, fluorinated, electronic struct., tight-binding LCAO-SCF-MO calcs., prep. 80—70591
polydiacetylene crystals, electronic spectra and struct. 79—73923
polyenes, long chain, electronic struct. in Peierls-PPP model 80—84423
polyethylene, band structure, linear combination of localised orbitals calc. 77—62808
polyethylene, electronic band struct., tight-binding approx. with MNDO 77—89691
polyethylene, electronic energy states and charge density contours studied muffin tin orbitals technique 80—80164
polyethylene, solid liq., secondary electron emission spectroscopy 80—80916
polyethylene disordered chains, electron localisation 78—87945
polyethylene film, soln.-cast, low energy electron scatt. obs. of band struct. 80—16131
polymer, conjugated and saturated chain, electronic struct., review 80—59860
polymer, excess charges, band gap levels and elec. props. 78—23053
polymer primary structures ESCA and EHCO methods 78—52630
polymeric conjugated hydrocarbons, energy gap estimation, graph-theoretical approach 80—24789
p-polyphenyls, band struct., mol. struct. effects calcs. *(German)* 77—47722
polysulphur nitride, pure and brominated, electronic model for high cond. 80—24923

electron energy states of amorphous solids continued
PTFE, electronic energy states and charge density contours studied muffin tin orbitals technique 80—80164
pyramidally bonded solid, electronic and phonon densities of states 77—8001
random field parameters and pseudopotential, amorphous, liquid and glassy semiconductors 80—29316
random Hamiltonian eigenvalues by tridiagonalisation, density of states 80—39493
review of structural and electronic props. 80—64901
Schrodinger equation with random pot. 79—65414
semiconductor, amorphous, electronic states, effect of local rearrangement modes 78—47696
semiconductor, amorphous or disordered, cond. mechanisms, model of medium-range comp. disorder 78—79994
semiconductor, bonding and transport properties 79—90950
semiconductor, density of states determ. from field effect data 80—107688
semiconductor, disordered, absorption edges, temp. depend. 77—77160
semiconductor, electronic structure, chem. bond approach 79—65374
semiconductor, light irradiation, nonequilib. electron distrib. function in forbidden gap *(Russian)* 78—75988
semiconductor, local order as determined by electronic and vibrational spectroscopy 79—37627
semiconductor, local rearrangement mode model for pair and single particle localised states 77—76773
semiconductor, non-polar, mobility gap temp. variation calcs. 78—10339
semiconductor, optical absorpt. edge shape, band edge fluctuations 77—20880
semiconductor, tetrahedrally bonded, electronic density of states cluster calc. 77—8002
semiconductor, thermoelectric power and transport models 78—10482
semiconductor heterojunction, amorphous/cryst., energy band diagram construction 77—55602
semiconductors, amorphous, electronic transport mechanisms and coeffs. 80—80282
semiconductors, amorphous, optical absorption, theory 80—80818
semiconductors, defects, band gap states 80—80215
semiconductors, doped, electronic props. 80—80283
semiconductors, elec. and optical props. *(Japanese)* 79—23979
semiconductors, electronic states, theoretical methods 80—80167
semiconductors, low-temp., elementary excitations, struct. 80—49577
semiconductors, luminescence and absorption spectra calcs. 79—99938
semiconductors, photoelectron spectra and band struct., book contrib. 80—16155
silicate glass, dangling bond states 80—24846
tetrahedrally bonded solid, theory of fluctuations and localised states 78—10405
tetrahedrally-bonded solid, electronic struct., theoretical approach 80—29315
transition metal glasses and amorphous films, supercond. and electronic props. 79—73612
3d-transition metal-metalloid cryst. and glassy alloys, electronic struct. from magnetisation and Mossbauer meas. 80—29363
transition metals, density of electronic states, effect of struct. variation due to interatomic pot. softness 80—54597
transition metals and alloys, metallurgical props. rel. to electronic struct., energies calc. method 77—20221
trap-controlled transient current injection theory 77—47772
two-band model, Thorpe-Weaire type, localisation near band edges 78—23050
$AgAsS_2$, $AgSbS_2$ and $AgBiS_2$, cryst. and vitreous, refl. spectra, energy spectrum 77—8596
$AgAsS_2$, band struct. photoemission and refl. spectra obs. 77—66581
Al_2O_3, energy level schemes, Fermi level-electrochemical potential level coincidence, quantum yield spectrum 79—69400
As, amorphous, bonding coord. defects, Cayley trees appl. 79—65373
As, amorphous, electron and phonon density of states calcs., comp. to XPS 78—56066
As, amorphous, electronic struct. of defects using cluster-Bethe-lattice method 79—73471
As, amorphous, low-temp., elementary excitations, struct. 80—49577
As film, sputtered, density of valence states by XPS and UPS 77—24926
a-As, opt. and elec. props. 77—39894
As, phonon density of states compared to electronic density of states 78—55924
As-S amorphous chalcogenide thin film, transient photoinduced phenomena 80—80884
As-Se amorphous film, density of upper valence band states, annealing effects, UPS obs. 80—29845
As-Se:^{197}Au, glassy, Au impurity influence, elec. cond., optical absorpt. and Mossbauer meas. 77—24558
As-Se(Te)-Ge, fabrication of amorphous semicond. thin films with graded band struct. *(Japanese)* 77—55623
As_2S_3, amorphous, band-to-band luminesc., electronic band states 79—61432
As_2S_3, amorphous, temp. below 1K, props., tunnelling 80—49576
As_2S_3, amorphous, XPS, electronic struct. calcs. using scattered wave method 79—11502
As_2S_3, amorphous semicond., photo-induced optical and structural changes *(Japanese)* 78—47244
As_2S_3 and As_4S_4 vapour-deposited films, valence states, thermal and photo-induced changes UPS study 80—93459
As_2S_3, density of valence states, XPS and UPS obs. 77—48308
As_2S_3, glass, band gap, trap levels 77—4337
As_2S_3 layered crystal and amorphous analogues, XPS valence band spectra, electronic struct. 77—52218
As_xS_{100-x}, chalcogenide glass thin films, absorption in range of large optical densities *(Russian)* 80—11428
$As_2S_3(Se_3)(Te_3)$ glass, calc. by extended Hickel theory 78—23012
$As_2(Se,Te)_3$ glasses, X-ray absorption and photoelectron spectroscopy study 80—7463
$As_{1-x}Se_x$, ave. energy gap, optical freq. dielec. const. and refr. index 77—76739
As_2Se_3, effect of impurities on paramagnetic gap states 80—24848
$As_xTe_{90-x}Ge_{10}$, $As_{35}Te_{55}Ge_{10-x}Si_x$ glasses, elec. and optical props., comp. depend. 77—24555
B, evaporated, electronic struct., XPS, SXS and isochromat investig. 80—76143
Bi-Sb alloy film, rel. to amorphous nature, AC and DC cond. and Hall coeff. obs. 80—11114

electron energy states of amorphous solids continued
$Bi_4Si_3O_{12}$, eulytine, change in band structure on transition to amorphous state 79—15081
C, amorphous, elec. cond. and Hall effect, temp. depend. 78—60141
C film, elec., struct. and optical props. 77—20474
C, glassy, Compton profiles, momentum densities, comparison with graphite 80—2895
$Ca(PO_3)_2$:Eu^{3+}, amorphous, phonon-assisted site-to-site electronic energy transfer, fluoresc. line narrowing obs. 77—81140
$CdAs_2$ glasses, covalently bonded, energy gap correl. with average atomisation enthalpy 77—76740
Cd_3As_2, film, transmission spectra. 0.6-15 μm, and band struct. 78—11013
$Co_{82}P_{18}$, amorphous alloys, electronic struct., γ-ray Compton scatt. study *(Japanese)* 80—84422
$Co_{78}P_{14}B_8$, amorphous, photoemission and electronic struct. 80—2926
Cu, noncrystalline, electronic density of states, multiple scatt. calcs. 78—91578
Fe, electronic density of states, dense random packing model 79—51476
Fe, noncrystalline, electronic density of states, multiple scatt. calcs. 78—91578
Fe-B amorphous alloys, valence band spectrum, XPS study 80—50534
$Fe_{80}B_{20}$, METGLAS 2605, mag. anisotropy and electronic struct., Mossbauer meas. 77—28384
$Fe_{80}B_{20}$, metallic glass, high-resolution XPS study, electronic state struct. 80—29846
$Fe_{32}Ni_{36}Cr_{14}P_{12}B_6$, metallic glass, high-resolution XPS study, electronic state struct. 80—29846
$Fe_{40}Ni_{40}P_{14}B_6$, metallic glass, high-resolution XPS study, electronic state struct. 80—29846
$Fe_{1-x}(P,B)_x$, amorphous and crystalline, photoemission and band structure 80—60754
$Fe_{76}P_{24}$, amorphous alloy, electronic struct., KKR calc. 80—96775
$Fe_{79}P_{13}B_8$ amorphous alloys, splat cooled, Mn, Cr and V substituted, mag. and transport props. 80—84593
Ge, amorphous, electronic struct., far infrared absorption 80—45051
Ge, amorphous, molecular liquid model and electronic structure 80—54133
Ge, electronic density of states, mol. liq. model 80—49581
Ge, film, electronic struct. charge on ordering, double beam photoemission 78—19634
Ge film, evap., structural aspects in electronic transport data interpret. 77—76977
Ge, ideal network struct., electronic struct., tight-binding model 80—44485
Ge, lightly doped, heavily compensated by fast neutrons, electrical props. 77—89766
Ge:H amorphous films, photoemission spectra 80—50517
Ge-Te-As-In quaternary compounds, elec. props., Hall effect *(Spanish)* 77—69344
Ge-Te-As-In quaternary compounds, thin sheets elec. props., thermoelec. power *(Spanish)* 77—69358
GeAsS, X-ray photoelectron spectra, valence electrons density of states *(Russian)* 79—15583
GeS, amorphous, UPS and XPS, valence band struct. 77—90247
GeSe, amorphous, UPS and XPS, valence band struct. 77—90247
GeSe amorphous films, photoconductivity measurements, recombination model 78—64061
$Ge_{1-x}Se_x$, ave. energy gap, optical freq. dielec. const. and refr. index 77—76739
GeTe, amorphous, UPS and XPS, valence band struct. 77—90247
K_2O-B_2O_3:Cu II, glass, O basicity, ESR study 78—80199
K_2SO_4-$ZnSO_4$:Cu II, glass, O basicity, ESR study 78—80199
LiCl-D_2O, aq. 10 M glass, optical absorpt. spectra after X-irrad., electron scavenging efficiency 79—83476
Li_2O-BaO-Al_2O_3-SiO_2-xTiO_2 glass, X-ray spectra, Ti ion electron config. *(Russian)* 77—8674
MgO-CaO-FeO(Fe_2O_3)-Al_2O_3-SiO_2 glass, X-ray spectra, Fe ion electron config. *(Russian)* 77—8674
$(Mo_{1-x}Ru_x)_{80}P_{20}$, supercond., mag. susceptibility 78—88057
MoS_3, amorphous struct., X-ray radial distrib. anal. and XPS 80—49115
Na_2O-CaO-SiO_2 glass, electronic struct. and optical props. 80—2790
Na_2O-P_2O_5:Cu II, glass, O basicity, ESR study 78—80199
Na_2O-SiO_2 glass, electronic struct. and optical props. 80—2790
Na_2O-SiO_2 glasses, elementary electronic excitations, refl., luminesc., and photoemission meas. 80—84778
Nb-Ni glass, photoemission spectra meas. 77—55867
Ni-P alloys, amorphous, electrical transport, appl. of extended Ziman theory 77—47787
Ni-P amorphous alloys, electrodeposited and melt-quenched atomic and electronic structures 80—88062
Ni-Pd-P, Ni-Pt-P, amorphous and electronic structs., NMR Knight shifts and linewidths meas. 78—68400
$Ni_{81}P_{19}$, amorphous alloys, electronic struct., γ-ray Compton scatt. study *(Japanese)* 80—84422
PbO-SiO_2 glass, electronic struct. and optical props. 80—2791
Pd-Si, metallic glasses, XPS and UPS studies 79—74062
Pd-Si glasses, changes in density of states with alloys comp., UPS obs. 80—50531
Pd-Si(-Cu), amorphous, Hall effect meas. and electronic struct. 80—75551
Pd-Si(-Cu) amorphous ribbons, low temp. sp. ht., density of states trends 80—79957
$Pd_{80}Si_{20}$, electronic struct. calcs. 79—87032
$Pd_{80}Si_{20}$ metallic glass, high-resolution XPS study, electronic state struct. 80—29846
$Pd_{18}Si_{14}Cu_6$, glass, changes in density of states with alloys comp. UPS obs. 80—50531
$Pd_{80}Si_{17}Cu_3$, glass, changes in density of states with alloys comp., UPS obs. 80—50531
Sb_2S_3, density of valence states, XPS and UPS obs. 77—48308
Se, amorphous, defect states, SCF pseudopot. and tight-binding calc. 79—65415
Se, amorphous, electronic struct. and optical props., pseudopot. calc. 80—65428
Se, amorphous, O impurity addition rel. to elec. cond. 79—38067
Se, Compton profile, charge and momentum density 80—55220
Se film, band gap determ. from photocond. props. *(French)* 77—72886
Se, layer, localised states in band gap 80—59928
Se, photoelectronic behaviour, in glass transition region 80—60045
Se, trigonal and amorphous, Compton profiles 77—32464

electron energy states of amorphous solids continued
Se, trigonal and amorphous, electronic struct. and nonempirical calc. of struct. props. 80—59866
Se, X-ray K-shell absorpt. discontinuity 79—61467
Se-As, photoelectronic behaviour, in glass transition region 80—60045
Se-Ge, amorphous, Raman spectra and average band gap 80—50327
Se-Te-Sb glasses, electronic transport 80—88579
Si, amorphous, electronic struct. and optical dielec. function, LCAO calc. 79—42478
Si, amorphous, electronic struct., far infrared absorption 80—45051
Si, amorphous, hydrogenated, H configs., Cayley trees appl. 79—65373
Si, amorphous, hydrogenated, electronic struct., SCF Xα calc. 80—49580
Si, amorphous, molecular liquid model and electronic struct. 80—54133
Si, amorphous and cryst., electronic and optic props. 78—39013
Si, amorphous and cryst. K X-ray spectra of band struct. 79—87525
Si, amorphous film, Fermi energy shift with substitutional doping 79—46998
Si, elec. props., ion implantation effects 80—79828
Si, electron-beam-evaporated amorphous thin films, noise meas. 79—24091
Si, electronic density of states, mol. liq. model 80—49581
Si film, evap., structural aspects in electronic data interpret. 77—76977
Si, glow discharge deposited, mobility edge calc. 80—80220
Si, ideal network struct., electronic struct., tight-binding model 80—44485
Si, position of Fermi level, spectroscopic and transport determ. 80—6706
Si, random-network model, charge-density variation 80—80165
Si, structural disorder rel. to electronic props. 78—34756
Si, transport results, interpretation 80—80260
Si:F(,H), electronic struct., orthogonalised LCAO calc. 80—44486
Si:H, amorphous, Auger electron spectrosc. obs. 80—76112
Si:H, amorphous, electronic states of hydrogenated Si, theory 79—42494
Si:H, amorphous thin film, ion plating, IR absorpt. meas. 80—84857
a-Si:H, electronic states and bonding config. 80—64900
Si:H, electronic struct. calc., rel. to UPS data 80—39527
Si:H, mobility edge position using continuous random network model for struct. 80—44544
Si:H, model for variable gap intrinsic semiconductor 80—10988
Si-H, amorphous, energy gap negative-U states, Si-H-Si three centre bond model 78—91606
$Si_xGe_{1-x}O_2$, amorphous, electronic struct. 80—80166
$Si_xGe_{1-x}O_2$, electronic struct. in Bethe lattice approx. 80—44487
Si_3N_4 amorphous film, CVD, core and valence electron excitations, low energy electron loss spectroscopy and AES 80—2365
Si_3N_4, electronic struct., LCAO calc. 80—96776
Si_3N_4 film, amorphous, optical props., band gap and surface roughness 77—32396
Si_3N_4, Si(LVV) Auger spectra, ion bombardment, electron energy loss spectra 80—80911
SiO_2, amorphous, effect of second nearest neighbour forces on vibr. 78—59915
SiO_2, amorphous, optical and elec. props., comparison with chalcogenide semiconds. 78—6721
SiO_2, amorphous, temp. below 1K, props., tunnelling 80—49576
SiO_2, amorphous and α-cristobalite cryst., band struct., photoelectron and X-ray spectra interpret. 80—24787
SiO_2, amorphous and cryst., XPS electronic band struct. interpret. 77—16454
SiO_2 amorphous film, Si(LVV) Auger spectra, ion bombardment, electron energy loss spectra 80—80911
SiO_2 amorphous film, thermal, core and valence electron excitations, low energy electron loss spectroscopy and AES 80—2365
SiO_2, crystalline and amorphous density of states, bulk electronic struct., tight binding calcs. 80—44502
SiO_2, dangling bond states 80—24846
SiO_2, elec. cond. mechanism, review of developments 78—26854
SiO_2, energy level schemes, Fermi level-electrochemical potential level coincidence, quantum yield spectrum 79—69400
SiO_2 glass, electronic struct. and optical props. 80—2790
SiO_2, vitreous, existence of gap in low-energy density of states 79—60769
SiO_2, vitreous, semi-empirical mol. orbital model, appl. to radiation compaction 79—73433
SiO_2, vitreous, Suprasil-W, thermal diffusivity, 16 mK-2.3K 79—60563
$(Si_2O_7)^{6-}$ bitetrahedra, in silicates, total energy surface, ab initio calc. 78—23056
Te, amorphous, electronic struct. and optical props., pseudopot. calc. 80—65428
Te, Compton profile, charge and momentum density 80—55220
Te, film, electronic struct. charge on ordering, double beam photoemission 78—19634
Te, trigonal and amorphous, electronic struct. and nonempirical calc. of struct. props. 80—59866
Tl_xTe_{1-x}, bonding and electrical conduction 79—90951
$Tl_2Te.As_2Te_3$, vitreous, temp. depend. of cond. and thermopower, electron energy spectrum 77—76831
V_2O_5-B_2O_3-ZnO semiconductivity glasses, optical and modulated absorpt. spectra in band gap region 77—48189
V_2O_5-ZnO-B_2O_3 glass, sputtered, optical absorpt., band gap and Urbach tail 77—8597
WO_3, band struct., XPS meas. 77—59667
WO_3 films, electron struct. changes during electrocoloration, XPS obs. 80—40217
WO_5 film, amorphous, band structure and colour-centre band, fast electron energy loss spectrum 77—55478
WS_3, amorphous struct., X-ray radial distrib. anal. and XPS 80—49115
ZnO on Zn (0001), oxide film growth, at. and electronic struct. 78—15587
a-ZnSe, elec. and optical meas., Mott-type model for amorphous semicond. 78—2414
Zr-Co, amorphous and crystalline, d-band struct., alloying effects 80—59862
Zr-Ni, amorphous and crystalline, d-band struct., alloying effects 80—59862

electron energy states of glassy solids *see electron energy states of amorphous solids*

electron energy states of liquid metals
alkali metals, liq., Fermi energy, density of states, electronic props., exchange and correl. effects 80—96774
Ashcroft and Schaich, and Gyorffy theories equivalence 79—60693
book 78—51406

electron energy states of liquid metals continued
  density of states in K excitation spectra of solid and liq. phases 78−19601
  electronic theory of thermodynamics and struct., summer school lecture series 80−6353
  Hall effect sign, cond. and thermoelec. power calcs., tight binding model 77−47798
  lattice model, metal-insulator transition 77−69220
  liquid and amorphous metals, electronic states, optical theorem, multiple scatt. theory 80−49578
  liquid metal, electronic structure in muffin-tin model 77−69219
  localisation and mobility of electrons, disorder effects 77−89682
  rel. to magnetic susceptibility 77−1536
  metallic glasses, formation, model based on nearly-free-electron approx. 77−52316
  metals, amorphous and liquid, electronic states, average spectrum 80−49579
  muffin-tin model, s-phase-shift model 80−88473
  non-simple metals, electronic props. 77−47721
  one-dimensional correlated liq. metal, self-consistent approx. 77−62807
  perturbation theory, extension to dense partially ionised plasmas 80−75500
  photoelectron spectra of liq. metals and alloys 77−48321
  physical chemistry of liq. metals, conf., Konigstein, Germany (Mar. 1976) 77−1059
  rare earths, trivalent, varying d-band occupancy 78−39083
  resistivity, anomalous temp. coeff. at high temp. 78−2458
  review of optical and magnetic props. 78−2882
  structure factor shoulders and interatomic pot. rel. to electron theory 77−7658
  structured medium approximation 80−84421
  surface ion density, nonmonotone, perturbative discrete ion introduction into jellium 78−72222
  tight binding model, similarity to spin wave excitations in amorphous ferromag. 77−12109
  tight-binding model, effective medium approx. 77−15756
  transition metal, 3d, density of states of d-band, heat of vaporisation 78−95253
  transition metal, electronic states densities from struct. and entropy data 77−1347
  transition metal, quasipolycryst. approx. 79−77975
  transition metals, 3d, d-band density of states and thermodynamic props. 77−76539
  transition metals, d band, effect of nonorthogonality 77−59243
  transition metals, electronic struct. and transport props. 80−29314
  transition metals and their alloys, electronic struct. and elec. resist. 77−51647
  Al, electron momentum density, correlations and ionic potentials 78−60052
  Al, Fermi momentum, for solid and liq. phases, temp. variation, Compton scatt. obs. 80−50451
  Al, model pseudopotential 78−91582
  Al, radial distrib. function calc., pseudopot. method *(Russian)* 79−19138
  Al-Zn, physical props. study by electrodiffusion method *(Czech)* 77−84956
  Bi, solid and liq., valence band structure, XPS meas. 77−32504
  Cd, electron energy states calc. *(Russian)* 79−4506
  Co, density of states of d-band, heat of vaporisation 78−95253
  Co, liquid, Hall effect, band struct. and exchange scatt. 80−80250
  Cs-Au(Sb), liq. alloys., mag. susceptibility and electronic struct. 77−1537
  Cu, electronic spectrum 77−51646
  Cu, liq., 3d bandwidths, photoelectron spectrum 77−4286
  Cu, liq., electronic structure, structured medium approx. 80−84421
  Cu$_{0.85}$Ni$_{0.15}$, liq., 3d bandwidths, photoelectron spectrum 77−4286
  Fe, CPA theory of excitations, lattice model 79−87030
  Fe, electronic density of states, dense random packing model 79−51476
  Fe, liq., dissolution mechanism of C, rel. to electronic struct. *(Russian)* 79−51264
  Fe, liquid, Hall effect, band struct. and exchange scatt. 80−80250
  Fe, liquid, N solubility depend. on added elements, mechanism *(Russian)* 80−65223
  Fe-V-C melts, electron struct., mag. susceptibility meas. *(Russian)* 78−47729
  Ga, liq. optical density of states, low-energy photoemission meas. 77−77341
  Hg, electron energy states calc. *(Russian)* 79−4506
  Hg, expanded, Knight shift interpretation in terms of electronic struct. and transport 77−43895
  Hg, expanded liq., band model for electronic struct. 77−89690
  Hg, expanded liq., electronic props. 77−55477
  Hg, expanded liquid, electron density of states calc. using effective medium approx. 79−99468
  Hg, reflection spectra, electronic density of states, calc. 80−66229
  Hg, surface plasmon dispersion 77−62978
  Li, electron energy states calc. *(Russian)* 79−4506
  Li, liq. and solid states, γ-ray Compton profiles 77−48269
  Lu, elec. resist. up to 1800°C, rel. to elec. struct. 78−39083
  Na, liq. and solid states, γ-ray Compton profiles 77−48269
  Na-Li, liq., Knight shift calc. by multiple scatt. Xα method 80−54961
  Ni, electronic struct. and transport props. 80−29314
  Ni, liquid, Hall effect, band struct. and exchange scatt. 80−80250
  Pd, liq., energy bands and electronic density of states, resistivity 78−34755
  Sn, electron energy states calc. *(Russian)* 79−4506
  Sn, electron transfer of rare earth impurities *(Russian)* 78−95278
  Ti, density of states of d-band, heat of vaporisation 78−95253
  Tl-Te, liq. alloys, mag. susceptibility rel. to elec. cond. and density of states 77−51880
  U, liquid, electronic density of states, shock vaporization technique 80−29300
  Zn, electron energy states calc. *(Russian)* 79−4506

electron energy states of liquid semiconductors
  alkali metal-based liquid semiconductor alloys, struct. and electronic props. 78−2403
  bonding and transport properties in amorphous semiconductor alloys 79−90950
  chalcogen-based liquid semiconductor alloys, struct. and electronic props. 78−2403

electron energy states of liquid semiconductors continued
  density of states at band tail 80−80154
  localisation and mobility of electrons, disorder effects 77−89682
  metal-nonmetal transition model 77−1368
  with pseudogap, mag. susceptibility 77−1536
  random field parameters and pseudopotential, amorphous, liquid and glassy semiconductors 80−29316
  reflectance data and model densities of states 80−50364
  self-localised electron states *(Russian)* 80−2366
  tetrahedrally bonded, quasipolycryst. approx. 79−77975
  Ag-S(Se)(Te), liq., mag. susceptibility meas., electron localisation and chem. bonding 80−60178
  AgTlSe$_2$ and AgTlSe, elec. cond. and thermoelectric power, doping effects, rel. to pseudogap model 78−2506
  Au-Cs, liq. alloy, mag. susceptibility rel. to ionic charact. 77−1536
  Cs-Au(Sb), liq. alloys., mag. susceptibility and electronic struct. 77−1537
  In-Se(Te), liq., mag. susceptibility meas., electron localisation and chem. bonding 80−60178
  Li alloys, liq. semicond., electronic struct., resistivity and thermoelec. power 77−51753
  Li-Au(Hg)(Tl)(Pb)(Bi), liq. semicond., electronic struct., resist. and thermoelec. power meas. 77−47712
  Sn-Se(Te), liq., mag. susceptibility meas., electron localisation and chem. bonding 80−60178
  Te-transition metal, liq. semicond., elec. props. 80−96870
  Tl$_2$Se$_3$, elec. cond. and thermoelectric power, doping effects, rel. to pseudogap model 78−2506
  Tl$_x$Te$_{1-x}$, liq., rigid band behaviour, elec. cond. and thermopower 77−35845
  Tl$_x$Te$_{1-x}$, liq. semicond. alloy, mag. susceptibility rel. to diffusive transport 77−20541

electron field emission
  4π proportional counters, spurious Malter pulses 77−54452
  accelerator, field-emission type, heavy-current, anode foil changing system 78−9005
  adatom lattice instability and fluctuation of field emission current 79−15024
  adsorption effects, theory 78−2996
  AES in SEM, high resolution, electron sources comparison 77−25330
  air, discharge, high-current, nanosecond, explosive cathode processes and contraction 80−10449
  alkaline earth electron thermoemission and tunnelling emission *(Russian)* 77−44113
  alloy electrodes, high-β electron emission sites 79−61502
  arc discharge 78−1943
  array of metallic pins in insulator, optimisation 77−81199
  atom, polarisability meas. using field electron microscope *(French)* 77−543
  atomically clean surface environment, confirmation using field electron emission 80−52250
  axisymmetric emitter, field-induced stresses, numerical analysis 78−35274
  borosilicate glass, field-induced electron emission into ultra-high vacuum 80−104048
  cathode, film, with Mo cones, phys. props. 77−24931
  cathode, high-current, transient electron emission 78−3001
  cathode, oxygen processing method 78−64448
  cathode energy conditions in explosive electron emission 79−19111
  cathode peak field emission current, size effect 80−29863
  cathode prebreakdown field emission transition to vacuum breakdown 78−75462
  cathode sheath, ion field effect on field emission characts. 77−66582
  chemisorption on metals appl. 78−35255
  cryogenic liquid, ionic mobility measurement, pulsed spacecharge technique 77−74420
  crystal lattice electron energy spectrum depend. on external electric field *(Russian)* 80−34498
  current density from ultrasharp field emitters 78−35264
  current density maximum, rel. to cathode geometry and kinetic props. 78−72704
  current fluctuation, power spectral density *(Japanese)* 78−88407
  elliptic emission functions used in calc. of electron emission from surfaces 80−89124
  energy distrib., extended range field emission spectroscopy 78−39669
  energy distribution meas., analyser system 78−89605
  energy distribution of field emitted electrons, effects of band struct. 77−24932
  energy distributions of electrons from a field emission electron gun *(German)* 80−20773
  exploding wires, electron emission 79−50914
  explosive electron emission, drop fraction of Cu cathode erosion 80−44063
  explosive emission regime, quasiplane cathode processes 78−75460
  ferromagnet, 3d metal, electron spin polarisation in field emission, state-of-the-art 77−69972
  field at the surface of a field-emission cathode 80−100757
  field emission electron source, current instability *(Japanese)* 78−43989
  field emission medium energy diode, electron flow, HF oscills. 80−79582
  field emitter, trajectory analysis of ions formed in inter-electrode region 77−85873
  field emitter vacuum breakdown, external mag. field effects, transition period 80−38824
  film-transition layer-substrate, theorem of electrical images *(Rumanian)* 79−74064
  final states in photoemission and field emission 78−15299
  geometry of field electron source determ. by computer assisted shadowgraph technique 77−87882
  gun brightness meas. *(German)* 78−8471
  gun for electron microscope *(French)* 77−26442
  gun lenses props. calc. and obs., electrostatic 80−62809
  n-hexane, field emission into liq., 275-334K 78−88406
  hexane vapour, electric breakdown strength, effect of cathode field emission 77−47285
  high-index crystallographic faces, scatt. approach to electron field emission 77−48323
  inelastic electron interactions in liq. dielec. obs. using FEM and energy analyser 79−91369
  insulator films, porous, field-enhanced SEE coeff., nature of fine struct. 77−20970

electron field emission continued
ion effects on emission 79—69963
liquid cathode arc, cathode sheath model, liquid K in Ar *(French)* 77—1032
magnetic materials, spin polarised electron emission, review 77—73215
magnetically insulated foils, accel. to ultrahigh vels. using electron beam 78—46163
metal, creep-electron emission relation 78—6994
metal, effect of adsorption on field emission 78—35259
metal, field emission through semiconductor and dielectric layers 77—12501
metal, field emitted electrons, effect of model hybridized energy bands 77—77349
metal, photofield emission, vol. effect 77—32494
metal, total energy distrib. calc., Green function technique 77—1788
metal cathode, electrically stressed surface elec. phenomena, electrolum. and breakdown with medium gap spacings 80—20710
metal cathodes subjected to pulsed electric fields, electron field emission charact. 80—71580
metal surface, clean, spin polarised electron field emission 80—45221
metal surface, thermionic-field emission anal. 78—19642
metal surface with incident microwave radiation, secondary emission discharge 77—1026
metal whisker diode, thermal field emission, nonlinearity, response time and polarity reversal 78—2579
metal whisker diode, with thermally enhanced field emission, elec. fields, calc. by antenna theory 77—47889
metallic glass, bulk and surface properties, review 80—44147
metallic multi-point field emission source, prep. by cathodic growth 80—100758
metallic thin films, absolute work function meas. by field-emission retarding-pot. device 77—59322
metals, electron microscope study *(Polish)* 80—35063
micro Auger analysis, using field emission source 80—104020
micropoint field emitters, location, nanosecond UHV discharges 78—332
microscopic metal points, explosive emission characts. 77—7624
microscopic metal points, explosive emission characts. 77—7625
MIM, thin film, use as non-heated source of electrons, review 80—84516
MIM cathode, hot electron emission 78—2997
MIM cathode, local electron emission and electroluminescence patterns obs. 80—108327
MIM cathode, radial temp. distrib. *(Russian)* 78—6833
MIM cathodes, LF noise sources and reduction 80—108328
MIM cold cathode emission density improvement, pinhole and compound insulator methods *(German)* 78—39670
MIM sandwich structures with anomalous props., review 77—59337
MIM structure, electron emission mechanism, and electron propag. in metal electrode *(French)* 77—76944
MIM structure, emission current density in second intermediate region of Christov 79—33360
nanosecond pulse duration investigations, construction of expt. arrangement 80—105750
needle emitters, appl. to in situ determ. of nanosecond desorpt. pulse shape 77—12502
needle field emitter, ion bombardment effects, field emission microscope obs. 77—55869
nonpolar organic liquids 78—88406
Nottingham effect, region of localisation increase at low temp. 80—100756
numerical field calc. in field emission devices 79—97478
p-n junction, thermally associated field emission near precipitates 78—14801
p-n junctions, thermally assisted field emission near precipitates 78—14809
photo-induced field emission, total energy distrib. meas. 79—74068
photostimulated field emission, triangular barrier pot. model 80—100759
plasma diode, field-emission type, Thomson-scatt. diagnostics 80—43988
polarisation effects in penetration of barrier with applied mag. field, relativistic corrections 79—78852
polarisation effects in penetration of nonrelativistic electrons through potential barrier with appl. mag. field 78—11084
polymer film, in MSM struct., thermionic field emission from metal 79—1629
polymeric materials, high-energy electron emission, in breaking adhesive contact 79—65981
rare earth metal, ferromag., spin polarisation of field-emitted electrons 77—40337
relativistic electron beams, striations in density distrib. rel. to plasma column instability 80—24154
Schottky, non-degenerate diode, current-voltage characts., analytical approx. 79—95494
SEM field emission sources, review 78—21299
semiconducting point cathodes, explosive electron emission 77—59678
semiconductor, n-type, microwave induced emission of hot electrons, secondary emission study 79—69964
semiconductor, p-type, field emission theory, surface states and recomb. processes 77—85901
semiconductor junctions, electric field effect on thermal emission of traps 80—11073
semiconductor of simple geometries, field penetration and band bending in high elec. fields 79—87106
semiconductor photofield emission cathode, potential distrib. and model 78—2977
single electron field emission non-destructive SEM method 78—88410
single-point cathode, limiting current 77—8729
source, differentially pumped *(German)* 77—87886
spin polarised electrons, expt. techniques and apparatus, book contrib. 77—81198
statistics in high vacuum 77—40335
steel, stainless, electrode material, annealing temp. cycle which improves emission props. 78—95858
steel, stainless unpolished, electron field emission sites 77—21008
STEM with field emission gun, X-ray analysis of metals and ceramics inhomogeneities 80—59354
superconductors, critical parameters during field emission of electrons 80—88682
surface studies, by field emission 79—67444
T-F emitted electrons, energy spread *(Japanese)* 79—56916
temperature-field emission region, simplified current density formula 78—27384
tetramethylsilane, field emission into liq., 275-334K 78—88406

electron field emission continued
thermal field, use of W(100), TiC whisker, Re, ThW and Zr 80—66403
thermal field emission source for high resolution, high current e-beam microprobes 80—68297
total energy distributions at high current density 79—74066
transition metals, field emission and field ionisation, role in heterogeneous activation of gas molecules 78—35271
transition metals, field emission spectroscopy 78—35257
2,2,4-trimethylpentane, field emission into liq., 275-334K 78—88406
two beam interference with field emission electron beams 78—63002
ultrahigh vacuum discharge cathode erosion minimum conditions 78—75461
unified theory of electron emission, appl. 78—35256
vacuum arc cathode spot dynamic models 78—75481
vacuum breakdown initiation, 4.2K, critical field emission currents 78—75459
vacuum conductivity in high voltage gaps, emission mechs. 79—41905
vacuum gauge, to indicate surface gas coverage 79—71476
W emitter, Te adsorption effect 77—69177
whisker cathode, single crystal, activation efficiency improvement 78—27377
whiskers, atomic resolution of field electron emission microscope 78—32929
work function, absolute determ. method for metals and semiconductors 77—28697
Ag/p-In$_{0.77}$Ga$_{0.23}$As photocathode, field assisted photoemission to 2.1 microns 80—76130
Al-Al$_2$O$_3$-Au thin-film cathode anomalous electron emission 79—8232
Al-Au couple, electroformed, nonohmic characts. and electron emission 80—60066
Al-Si$_3$N$_4$-Al cathode, fluctuation noise 78—2998
Al-SiO$_x$-Au cathode, emitted electron energy distrib. 78—52645
Ar, liq., emission coeff. of cond. electrons, depend. on elec. field intensity *(Russian)* 79—78855
Au film, electron emission and electroluminesc. 77—90257
Au film, nonohmic characts. and electron emission 80—60066
Au film, quantum size effect, field emission study 80—70849
Au-SiO$_2$-Si structures, electron and ion emission from MOS field cathodes *(German)* 77—12499
Au-SiO$_x$-Au diode and triode struct., angular distrib. of emitted electrons 77—69429
BaB$_6$, work function, thermionic and field emission retarding pot. meas. 77—90233
BaB$_6$, work functions from thermionic and field emission retarding pot. methods 79—65537
BaO-CaO, amorphous film, Cu-electrodes, electrical props. 77—35997
C fibres, energy distrib. of post-accelerated field emitted electrons 77—16468
C, glass tip, field emission current stability 80—11544
C, tip, field emission characts. 80—11543
Cd$_x$Hg$_{1-x}$Te-metal contact, transport mechanism, thermionic and field emission processes 77—20425
CeB$_6$, work functions from thermionic and field emission retarding pot. methods 79—65537
CeBr$_6$, work function, thermionic and field emission retarding pot. meas. 77—90233
CeO$_2$, single cryst. whiskers, electron field emission 78—27378
Co, electrochemically prod. emitters, field ionis. props. 77—90254
Co, spin polarisation of field-emitted electrons 77—40337
Cr whisker cryst., growth incorporated with field electron emission 80—44458
Cr$_x$C, cathodic needle growth, at lower electric fields from Cr(CO)$_6$ vapour 80—76161
Cu (001) and (110), electronic wave functions by spherical wave method, vel. to field emission 79—42604
Cu, broad area electrode, high-β emission sites, energy spectra 78—35253
Cu cathode, electrically stressed, broad area, surface elec. phenomena, electrolum. K-spot radiation identification with electron emission 80—20711
Cu, cathode, ns voltage pulse breakdown of emitting sites, field emission microscopy obs. *(German)* 77—63547
Cu coaxial electrodes, I-V characts. at low H$_2$ press. 77—28702
Cu electrodes, static voltage breakdown of vac. in mag. field, pretreatment effects 77—19781
Cu, point cathodes, explosive electron emission 77—55873
Cu upper electrode effect on MIM cathode emission 77—85344
Eu chalcogenides, cond. band spin struct. 80—71577
EuO(S), spin polarisation of field-emitted electrons 77—40337
EuS, ferromag., on W, electron field emission 79—8230
EuS, spin polarised tunnelling and mixed spin states in conduction band 79—52085
EuS-W emitter junction, energy loss of field emitted electrons 77—81201
Fe (100), (111), (110), spin polarised field emitted electrons 78—60553
Fe, electron spin polarisation surface magnetism 78—68607
Fe, field-emitted electron spin polarisation by tunnelling through surface pot. 80—29861
Fe, spin polarisation of field-emitted electrons 77—40337
Ga-In liq. alloy, repetitive pulses electron emission 79—24416
p-GaAs, field electron emission current-voltage characts. 80—45219
GaAs, phonon assisted tunnel emission of electrons from deep levels 80—25532
GaAs, photo-field cathode, ageing and surface state effects *(Russian)* 77—28703
p-GaAs, role of surface electron states 78—2993
p-GaP, field electron emission current-voltage characts. 80—45219
Ge, field-emission current-voltage characts., effect of earlier measurements 80—71579
Ge, photo-field cathode, ageing and surface state effects *(Russian)* 77—28703
Ge photocathodes, Au absorbed photofield emission current spectral investigation 80—29856
He, liq., optimal positioning of field emitters for ion injection 80—24700
He Townsend discharge field emission by higher-order ion clusters 78—67550
Hf electron field emitter, temp. drop meas., allotropic transform. temp. 80—2931
InGaP/InGaAs struct. for transferred electron photocathodes, VPE growth and characterisation 80—76193
In$_2$O$_3$-SnO$_2$, patterned thin films, strong electron emission obs. 77—8731

electron field emission continued
InP/InGaAs/InP field assisted photocathode, minority carrier electron transport across p-p heterojunction 78—95651
InP-$In_xGa_{1-x}As$ alloy photocathodes, semiconductor photoemitters, field-assisted, 1-2 μm range 80—97396
Ir (111) surface, step effects on total energy distrib. 79—100026
Ir, adsorption of H_2, influence of surface steps and clusters, field emission investig. 77—28698
Ir, adsorption of N_2, field emission exam. of effect of steps on surface potential 78—30829
Ir, chemisorption levels of CO and O on (100) and (110) faces 78—84704
Ir, clean and adsorbate covered surfaces, field emission energy distrib. spectra 80—25535
Ir, field emission spectrosc. from (111) flat and stepped planes 80—76157
Ir, weak adsorption of N_2 and Xe 77—24479
Ir-Ce (0.4 wt.%), field emission characts., crystallography and heat treatment effects 78—2994
K, adsorbed layers on W (112) planes, flicker noise field emission obs. 78—26774
K adsorbed on W(112) planes, temp. depend. of noise spectral density functions 78—2992
K single crystals on W tips, field emission from individual planes 78—27385
KBr, porous insulator films, field enhanced secondary emission, energy spectrum 77—20969
KCl film, porous, injection mechanism for transmission secondary electron emission 78—19643
KCl, porous insulator films, field enhanced secondary emission, energy spectrum 77—20969
LaB_6, field emission and FIM expts. 77—90255
LaB_6, field emission patterns and emission characts. *(Japanese)* 77—85900
LaB_6 single crystal needles, thermal field emitted electron total energy distribution spread 80—45218
LaB_6, thermal field emitted electrons, total energy distrib. spread 77—52227
LaB_6, work function, thermionic and field emission retarding pot. meas. 77—90233
LaB_6, work functions from thermionic and field emission retarding pot. methods 79—65537
$LiNbO_3$, ferroelectric transitions, thermally stimulated electron emission meas. 80—25534
$LiNbO_3$:Fe, unipolar Malter emission under pyroelectric effect conditions 80—29862
Mo (100), effect of metallic adsorbates on surface reson., field emission energy distrib. studies 79—65983
Mo (100), surface resonances, photoemission and field emission meas. 79—4593
Mo (100) face, surface reson. 78—72226
Mo (100) plane, surface reson., field emission energy distrib., LCAO calc. 77—32507
Mo, adsorption of K, work function, field emission microscope obs. 77—11788
Mo cathode, ns voltage pulse breakdown of emitting sites, field emission microscopy obs. *(German)* 77—63547
Mo, electron field emission energy distrib. from surface oxide clusters 77—63548
Mo emitter, Te adsorption effect 77—69177
Mo, field emission anomalies in mag. field *(Russian)* 80—93462
Mo field emitter, adsorption of Se, field emission meas. 77—31889
Mo field emitter, adsorption of Te on single cryst. faces 78—34714
Mo fine tip cathode, field emission stability, rel. to passivation 80—100760
Mo islet films, effect of external elec. field on electron emission 80—80952
Mo single cryst., oxidation, effect of high elec. fields, 1000-1200K, field emission and TEM obs. 77—90258
Mo whisker cryst., growth incorporated with field electron emission 80—44458
Mo_xC, cathodic needle growth, at lower electric fields from $Mo(CO)_6$ vapour 80—76161
NaCl, thin single-crystal film, hot electron emission 79—15244
Nb, field emission anomalies in mag. field *(Russian)* 80—93462
Nb-Zr-Ti, needle field emitter, ion bombardment effects, field emission microscope obs. 77—55869
Ni (100), electron field emission, positive spin polarisation and band model of magnetism 77—52226
Ni, (100) and (111) planes, electron field emission, energy distribution, effect of adsorption of CO 79—8231
Ni (110) surface, positive spin polarisation in field emission and demagnetisation by H_2 adsorption 78—52646
Ni, absorption of H_2, demagnetisation of surface due to absorption 77—80990
Ni, electrochemically prod. emitters, field ionis. props. 77—90254
Ni, electron spin polarisation surface magnetism 78—68607
Ni, field-emitted electron spin polarisation by tunnelling through surface pot. 80—29861
Ni, spin polarisation, positive sign 77—73220
Ni, spin polarisation of field emitted electrons 77—32508
Ni, spin polarisation of field-emitted electrons 77—40337
Ni, spin polarisation of field-emitted electrons, theory 77—44134
Ni, wire, pulsed heating in ultrahigh vacuum, anomalous electron emission 79—55598
Pb, electron field emission, temp. effect 80—60756
Pd film, quantum size effect, field emission study 80—70849
Pd-Si-Cu metallic glass tips, appl. as electron field emission source 79—8229
PrB_6, field emission patterns and emission characts. *(Japanese)* 77—85900
Pt surface, H chemisorption obs. 77—24477
Pt tips, glass-coated, field emission microscopy Fowler-Nordheim emission regime and periodic current oscills. 79—95907
Pt, weak adsorption of N_2 and Xe 77—24479
Re tip, condensation remoulding, field emission microscopy 78—2995
Ru field emitter, adsorption of H_2, field-induced redistrib. processes 79—78854
p-Si, emission statistics 77—1791
Si field emission photocathodes, emission current noise characts. 80—100746

electron field emission continued
Si, moderately doped, ohmic contact electron emission, quantum calc. 78—68087
Si multiple tip field emission photocathode, photokinetics 80—100480
Si, photo-field cathode, ageing and surface state effects *(Russian)* 77—28703
Si photofield cathode, BaO adsorbed layer, work function and emission props. *(Russian)* 78—68608
Si, role of surface electron states 78—2993
Si, single-tip and multitip cathodes, fabrication, and photofield emission characts. 78—2976
Si, surface, photon excited field emission 79—78851
Si, whisker, amorphous, growth method for field desorption mass spectrometry 79—28262
Si-Ni Schottky barriers, thermionic field emission at room temp. 78—6445
Si_xGe_{1-x} multitip photofield emission cathode, fabricated by crystn. from vapour, emission characts. 78—2975
SmB_6, field emission patterns and emission characts. *(Japanese)* 77—85900
SmB_6, work function, thermionic and field emission retarding pot. meas. 77—90233
SmB_6, work functions from thermionic and field emission retarding pot. methods 79—65537
Ta, adsorption of K, work function, field emission microscope obs. 77—11788
Ta autocathode, influence of electric field and heating on work 80—7478
Ta, photo field emission characteristics, band struct. influence 78—27373
Ta, photo field emission spectroscopy of band structure by He-Ne laser irrad. 80—55276
Ta, photofield emission spectroscopy of band struct. 78—35261
TiC, single cryst., energy distrib. of field-emitted electrons, 77 and 290K 77—32510
TiC single crystal, work function, field emission characts. *(Japanese)* 78—19641
W (100), surface resonances, photoemission and field emission meas. 79—4593
W (100) effect of metallic adsorbates on surface reson., field emission energy distrib. studies 79—65983
W (100) face, surface reson. 78—72226
W (100) surface, with adsorbed Au, Cu layers, unmasked surface reson. 79—15595
W (110), dipole moments of single 5d metal adatoms field emission meas. 77—47674
W (110), mobility of adsorbed O, 300 to 800K, field emission current meas. 79—33187
W (110) mobility and two-dimens. compressibility of adsorbed Xe, field emission current fluctuation method 80—80089
W (110) plane, tunnelling of H in surface diffusion, field emission fluctuation method meas. 80—75416
W (310), field emission current instability induced by migrating atoms 78—35254
W [310] tip, prep. from rolled sheet 80—97447
W, adsorbate covered, field emission energy distrib., overlayer geometry effects 77—8730
W, adsorbed K, field emission flicker noise, coverage depend. 78—35262
W, adsorption of Dy, Ho, Er, field emission electron study 80—100393
W, adsorption of Fe *(Japanese)* 78—91536
W, adsorption of Gd in field ion microscope *(Russian)* 77—47662
W, adsorption of Ni, effect on surface self-diffusion FEM characts. *(French)* 77—1296
W, covered with Ga, In and Sn, tip stability, alloy form. 77—12500
W, emission statistics 77—1791
W, energy distrib., surface density of states, surface pot. effects 77—16471
W, field emission, mag. field effects 80—93463
W, field emission anomalies in mag. field *(Russian)* 80—93462
W field emission current instability, freq. spectrum, effect of H_2 and CO adsorption 77—32509
W, field emission currents, modified by external mag. fields 78—88408
W, field emitter, adsorption of Se, field emission meas. 77—31889
W field emitter, adsorption of Cu, field emission energy distribs. 77—59677
W field emitter, adsorption of Te on single cryst. faces 78—34714
W field emitter, current fluctuations from cryst. faces 78—35263
W field emitter, effect of Au adsorption on (110) and (211) planes 77—12503
W field emitter, periodic field-dependent photocurrent 78—35260
W field emitter, strong polarisation effect in photoinduced field emission 78—95684
W field emitter, surface migration and overgrowth of LaB_6 77—85902
W film, adsorbed Th layer, work function, temp. depend. 77—28701
W fine tip cathode, field emission stability, rel. to passivation 80—100760
W, fine tip microcrystal, microscopic protuberance form., crit. remoulding obs. 78—27380
W, fine tip microcrystal, thermal smoothing after critical remoulding 78—27381
W, fine tip microcrystal, vertex remoulding, effects on field emission 78—27379
W, low-index planes, adsorption of Pb, probe-hole field emission microscopy obs. 77—47677
W microneedles, field electron emission, suitability for electron source investigation 78—52644
W, needle field emitter, ion bombardment effects, field emission microscope obs. 77—55869
W, photo field emission spectra of optical transitions, band struct. 77—16467
W, photo field-emission, periodic current deviation, wavelength depend. *(German)* 78—23579
W point, energy spectrum of field-emitted electrons from microprojections 77—1789
W, point target, temp. depend. of electron emission caused by laser illumination 79—43107
W points, micro-size, change in shape and electron field emission 79—74067
W, pure and Ba covered, photo-stimulated field emission, effect of light polarisation *(French)* 80—7480
W, spin filter effect of EuS 80—45221
W, surface pot. barrier effect on photofield emission 78—60551

electron field emission continued

- W, thermal field cathode emitters, end form changes, electron microscope obs. 77—4718
- W, thin wires, electron emission into gases under strong elec. fields 79—83108
- W tip, (310)-oriented with high brightness appls. 78—27382
- W tip, condensation remoulding, field emission microscopy 78—2995
- W tip, EuS covered, field emission of monoenergetic spin-polarised electrons 77—85899
- W whisker, energy spread meas. of thermal field-emitted electron flow 78—92168
- W whisker cryst., growth incorporated with field electron emission 80—44458
- W, wire, pulsed heating in ultrahigh vacuum, anomalous electron emission 79—55598
- W, with adsorbed Pd, field emission obs. of adsorpt., diffusion and self-diffusion 78—38945
- W, work function, field emission meas., Te and Cs surface film effects 78—19645
- W, work function determ. for Bi and Bi_2S_3 78—6834
- W, work function meas., V adsorption effect 77—51607
- W/EuS field emitters, electron emission current depend. on annealing temp., mag. props. 80—16160
- W-EuS, amorphous, memory effect in field emission 80—89126
- W-EuS interface, electron spin polarisation in field emission 78—35265
- W-Zr field emitter, time-of-flight atom-probe study 80—80949
- W(110), field emission, absolute tunnelling current density 79—38724
- W{100}, adsorption of N_2, surface disorder effects on work function change 77—20192
- Xe, liq. and solid, emission coeff. of cond. electrons, depend. on elec. field intensity *(Russian)* 79—78855
- Y_2O_3 film in Y-Y_2O_3-Au junction, defect struct. and local conduction 78—26970
- ZnO, field emission energy distrib., surface state emission obs. 78—35258
- ZnO, polar surfaces (0001), (000$\bar{1}$) specificity, field emission, H adsorption 77—21009
- ZnO surface layers, high-field electrolysis during field emission 79—52084
- Zr-O-W (100) thermal field emitters, operational experience 80—71576

electron gas

see also cathode ray tubes; electron optics

- adiabatic de Haas-van Alphen effect at low temp., Fermi fluid interaction and chem. pot. effects *(Russian)* 80—84442
- adsorption system surface properties variational calcs., binding energy, Lang model 80—29279
- alkali ion+inert gas, interaction pots., gaseous ion mobilities 77—54584
- alkali metal, electron-electron scatt. in terms of dielec. and vertex functions 79—95351
- alkali metals, electron-electron scatt., thermal and elec. resistivity 80—59956
- alkali metals, phonon dispersion and electron gas pressure, theory 78—2208
- Anderson model, orthogonality catastrophe due to local electron correlation 78—43320
- Anderson transition, elementary approach 79—28279
- angular correlation in positron annihilation 80—24821
- antiparallel spin correlations 77—4307
- atom, SCF electron-gas local-spin-density model including correlation, appl. to He through Ar 80—9488
- band-discontinuity surface, temp. of electron gas induced by passage of electron currents 78—14793
- Bloch wave effects in density response function 78—56092
- Boltzmann electron gas in Gaussian random potential, mean field approach 80—107721
- bound electron gas, static semiclassical response 78—56089
- bound state of two plasmon excitations 78—39048
- CDW instability of electron gas in a strong magnetic field 78—79950
- channelled heavy ions, electron pick-up from free electron gas in thin solid film 80—107349
- charge carrier with anisotropic energy spectrum, cond. oscills. in quantised mag. field *(Russian)* 80—6886
- charge screening in electron gas of arbitrary degeneracy 77—76763
- charged particle in free-electron gas, Lindhard theory of stopping power, numerical evaluation 80—893
- charged two-dimensional isotropic Fermi liq., static and dynamical props. 79—19532
- charged-particle systems, strongly correlated, theory 77—68797
- chemisorption, image charge effects, surface plasmons 80—84381
- chemisorption, image charge effects on adsorbate valence spectra, perturbational study 80—84380
- classical diamagnetism, Gibbs method *(Russian)* 78—73918
- classical electron gas theory 79—17335
- classical electron surface layer, dynamic struct. factor 79—40443
- collective modes, ground state energy 77—66134
- Compton scatt., bound and free electron Compton scatt. in coherent EM field 78—94225
- Compton scattering, induced, relax. processes during propag. of radiation flux *(Russian)* 77—27231
- condensed matter, SCF theory, orbital and pot. functions calc., eq. of state 80—44463
- condensed matter physics, dynamic correlations, book 80—86046
- conductivity of fermion gas moving in strong three-dimens. random pot. 79—56130
- conductivity of interacting electrons 77—20351
- consistency relation for electron liquid 77—20254
- core hole relaxation energies 78—80439
- correlation energy, appl. of coupled cluster approx. 78—72102
- correlation energy, short-range 77—74320
- correlation energy and Fermi momentum of two dimens. electrons 77—79028
- correlation energy by RPA and mean component approx. calc. 80—24824
- correlation function, high density expansion 77—1386
- correlation holes, number-sum rules and infinite system 79—23916
- correlations in solids, local approach 80—29344
- Coulomb gas, classical, two-dimens., screening props. from sine-Gordon eqn. 79—4524
- Coulomb gas, correlation functions, dielectric function 79—85071

electron gas continued

- Coulomb gas in strong mag. field analogy with electron gas with backward scatt. 80—24817
- Coulomb vector gas in two-dimens., melting 79—69449
- coupled-cluster expansion, inclusion of ring and exchange effects 77—76764
- crystallisation, zero-order, Bethe-Fermi homework potential 80—63117
- cyclotron resonances, Coulomb interaction effects in 2-dimens. 78—60073
- de Haas-van Alphen effect, quasiparticle approach 80—10897
- degenerate, distrib. function in periodic external field 79—23914
- degenerate, in metal or semicond. slabs, surface plasmon damping 80—88501
- degenerate, response functions, memory function kinetic eqn. approach 79—49159
- degenerate, static density response function calc. by QHNC 80—49633
- degenerate, with elastic scatt., form of memory function 80—101753
- degenerate Anderson model, Fermi liq. theory 79—19715
- degenerate electron liquid, skipping orbit cyclotron resonance, surface state transitions 80—103889
- degenerate relativistic electron gas, electron collisions, thermal conductivity 80—109355
- degenerate semiconductor, entropy production and choice of heat flux 77—15778
- degenerate semiconductor, intervalley phonon scatt., energy loss rate and momentum relax. time 79—15139
- degenerate semiconductors, transverse magnetoresistance in strong mag. fields 79—99565
- delta function fermion gas, solitons and HF solns. 78—49755
- dense electron gas response at any degeneracy, RPA calcs., plasma modes, screening 78—36930
- dense electron gas response at any degeneracy 77—71269
- dense high-temperature, classical modelization of symmetry effects 78—65869
- dense relativistic electron gas, EM response in strong mag. fields, particle polarisation, mode struct. 80—43963
- density fluctuations induced by ions moving in condensed matter 80—24518
- density functional approach to electron and positron states 79—56107
- density functional theory, proof that $\partial E/\partial n_i = \varepsilon_i$ 79—42474
- diamagnetism and surface currents 80—88496
- dielectric constant, local-field correction, review 80—107731
- dielectric function, degenerate electron gas at metallic densities, nonlocal interactions, compressibility and dispersion 80—107730
- dielectric function, dynamical exchange decoupling, plasmon dispersion, SDW and CDW 80—59900
- dielectric function, dynamical exchange effects 80—54629
- dielectric function, freq. depend. non-RPA contribs. 77—51686
- dielectric function, freq. dependent exchange correction 77—35880
- dielectric function, time-dependent Hartree-Fock formalism 79—69448
- dielectric function at low electronic densities 78—23038
- dielectric function calc. for electron liquid 77—80749
- dielectric polarisation and Kohn effect in strong mag. field 77—4279
- dielectric response of solids, approxs. for treatment of local field effects 79—47033
- dielectric transition temp. in strong mag. field 80—24813
- Dirac-Fock relativistic free-electron gas, relativistic exchange pots. 77—13628
- dislocations rel. to electron gas thermodynamics at $2^1/_2$th order transition *(Russian)* 78—51910
- disordered conduction, dielectric function, phenomenological derivation 80—77692
- disordered Fermi systems, in two dimensions, interaction effects 80—75655
- disordered solids, light scatt. from configurational fluctuations, appl. to free electron gas with fluctuating density 79—11428
- disordered system, props. of mobility edge 77—4330
- dissociative recombination in ambient electron gas 80—36940
- drift velocity of gas in field, second-order theory 77—58240
- dynamical local field corrections in dielectric function 80—88500
- effective ion-ion interaction, third-order contrib., ang. forces, tetrahedral solids 78—67970
- elastic ion lattice-electron gas binary mixture, continuum theory 79—51503
- electrical conductivity of an interacting electron gas 78—95276
- electron dielectric function, second-order RPA 78—49753
- electron interaction with optical phonon directional flux 80—59893
- electron liquid, collective description, positron annihilation 80—4632
- electron-hole plasma current layering, electron cooling length, momentum scatt. 80—6890
- electron-positron gas in external mag. field, polaris. tensor *(Russian)* 79—35982
- ellipsoid model, two-band Cain model, band structure *(Russian)* 80—24783
- EM response of electron gas and vacuum in strong mag. field 77—13641
- energy loss of correlated charges 78—87729
- EXAFS in molecules and crystals, method for calc. of atomic phase shifts 77—48276
- exchange and correlation effects, self consistent theory 77—85161
- exchange-correlation energy, gradient correction at metal surface 77—43691
- excited states, energy density functional formalism 80—29341
- fast charged particle traversing ferromag., dynamic mag. field, RPA 79—73230
- fast ion in solid, oscillatory wake, trapped electron binding energy, RPA calc. 80—96575
- Fermi gas, one dimensional with backward scatt., gap renormalisation 80—24818
- Fermi gas quadratic response, building-up of covalent bonding in zinc-blende semiconductor 77—28132
- Fermi hypernetted chain equations, optimal correl. function 79—40870
- fermion hypernetted chain approx., optimal correlation functions 80—24822
- ferromagnet, excitonic, zero-sound excitations, Fermi liq. model 80—93101
- ferromagnetic, short-ranged correlations 79—7798
- ferromagnetic response functions, lattice effects 80—10898
- ferromagnetic semiconductor, phase transition and instability of homogeneous state 77—28398
- ferromagnetic semiconductors with hot electrons, instability of coupled spin-helical waves 80—107841

electron gas continued
- free, inverse Faraday effect and cyclotron freq. radiation shift *(Russian)* 77—8033
- free electron Compton scatt. of spectrally narrow radiation flux 80—20731
- free electron gas, n-dimens., eqn. of state *(Spanish)* 80—82718
- free lattice electron gas with nearest and second nearest neighbour hopping 78—51873
- free-electron gas, n-dimens., specific heat and density of states 78—12466
- galvanomagnetic effects in spatially inhomogeneous system *(Russian)* 78—72129
- Gaussian trial distribution functions and thermodynamic functions 77—57273
- generator coordinate method 78—60077
- grand partition function, first order term temp. depend. anomaly 79—21656
- ground state, functional spin-density method *(Russian)* 78—51914
- ground state, spin-charge density functional method *(Russian)* 79—1574
- ground state, stochastic method calcs. 80—95031
- ground-state energy of free-electron gas, transcorrelated method 80—34373
- heating, electron conc. analysis near special Van Hove pts. *(Russian)* 78—26835
- heating, model, collisions between hot excitons and hot electrons 80—7415
- hexagonal lattice equilibrium, electron gas model with noncentral forces, Tl, Zn, lattice dynamics 78—95123
- Hohenberg Kohn theorem, extension to excited states 80—80197
- Hohenberg-Kohn theorem, alternative proof 78—23035
- Hohenberg-Kohn theorem for non-local potentials 77—45793
- homogeneous, dielectric response, pair correl. function 77—72832
- Hubbard model at low temp., mag. props. *(Russian)* 78—43550
- ideal Fermi gas, analytic approx. for Fermi energy 77—85159
- inelastic positron scatt. in electron gas, plasmon excitation 80—92843
- inhomogeneous, density functional approach 79—44854
- inhomogeneous, exchange energy *(Russian)* 77—72830
- inhomogeneous, kinetic energy *(Russian)* 77—85160
- inhomogeneous, nonlocal approx. to exchange energy 78—138
- inhomogeneous, nonlocal approximation to exchange potential and kinetic energy 78—72096
- inhomogeneous, virial and Hellmann-Feynman theorems 80—88494
- inhomogeneous electron gas, exchange effects and nonzero temps. 80—84444
- inhomogeneous electron gas at jellium surface, exchange energy 80—10901
- inhomogeneous electron system, exchange and correlation 78—18985
- inhomogeneous electron system, gradient expansion in density-functional approach 77—89721
- inhomogeneous electron systems, exchange and correlation effects calc. 80—20104
- inhomogeneous relativistic electron gas 79—28304
- inhomogeneous system, electron gas model, exchange pot. charge density depend. 80—54626
- interacting electron system, dielectric permeability theory *(Russian)* 80—6762
- interacting electron system, orthogonality catastrophe 80—6757
- interacting gas in mag. field, parquet eqns. 79—90980
- interacting gas in mag. field, Schulz-Keiter model 79—90981
- intermediate density region of 2D system 79—60110
- intermediate valency compounds, conduction processes, metal-insulator transition 80—96787
- intermolecular forces model, self-exchange corrected 77—46608
- ion motion in crystal, effect of polarisation field 80—103406
- ion-ion interaction, third-order contribution, total energy calc. 78—63998
- ionic solids, lattice and defect props., modified electron gas approx. 79—42054
- ions and atoms, slow, energy loss to electronic excitation 77—84817
- jellium, two- and three-dimens., CDW, appl. to liq. He surface and semiconductors 80—65476
- jellium metal surface densities, electronic density, variational calc. 79—15205
- kinetic equation for electron gas in strong fields and inhomogeneities 79—72986
- layered compounds, effect of exchange on CDWs 78—60078
- light scattering, inelastic, photon-electron interactions 78—80368
- Lindhard dielectric function for degenerate electron gas, exchange contrib. 77—51685
- Lindhard dielectric tensor, branch cuts in complex-wavenumber plane 80—34377
- liquid metal, classical fluid model, neutralising negative background density 78—22621
- liquid surface electron layer, parametric excitation of collective modes 77—15928
- long thin superconductor, resistive domain of small cross section in microwave EM field 79—28446
- long-range order Hartree-Fock states with different magnetic properties 79—42476
- Lorentz electron gas, long time behaviour in const. uniform elec. field 80—42140
- magnetic electron gas induced by van Vleck ion, spin polarisation 79—56176
- magnetic moment in ultraquantum limit of strong mag. field *(Russian)* 77—28361
- magnetic semiconductor, sound-like plasma oscillations in electron gas *(Russian)* 78—23125
- magnetic susceptibility, temp. depend. 78—23224
- magnetic susceptibility 77—31965
- magnetised, confinement effects 79—28494
- many-electron systems, self-interaction corrected approach, beyond local spin density approx. 80—92844
- mean free path of low energy electrons, influence of damping 78—10385
- metal, damping of excited molecules located above surface 78—92160
- metal, electron density behaviour near impurity charge 80—75518
- metal, electron free energy virial expansions *(Russian)* 78—10380
- metal, electron gas, correlation effects on polarisation 80—54628
- metal, electron state effect on mech. props. and electroplasticity 78—14725
- metal, entropy production and choice of heat flux 77—15778
- metal, eqn. of state from statistical electronic free energy 79—99495

electron gas continued
- metal, excitation by fast electrons of surface plasmons on spherical voids 77—11975
- metal, in mag. field, phonon spectrum, nonadiabatic effects *(Russian)* 78—19106
- metal, local density functional for kinetic energy near defect, metal surface 80—20105
- metal, normal and magnetic, temp. depend. of plasma freq. 78—56100
- metal, quantum kinetic equation for electrons 78—91686
- metal, simple, electronic struct. of H impurity 78—67978
- metal, surface energy of electron gas, virial theorem 77—69398
- metal crystal with and without surfaces, asymptotic displaced charge round impurities 79—95364
- metal lattice heating by radiation, plasma effects, degenerate electron gas calcs. 80—70742
- metal surface, Nonlinear mixing of oppositely travelling surface plasmons 79—95460
- metal surface, SHG, hydrodynamic theory of electron gas 80—87437
- metal surface, vector potential calc., semi-infinite electron gas approximation 77—32063
- metal surface-ultrashort coherent IR pulse interaction, inertialess radiation *(Russian)* 79—95879
- metal surfaces, SHG, non-linear response to optical fields 80—83645
- metal-insulator transition, model Hamiltonian 80—34361
- metal-insulator-mseiconductor structure, magnetooptic absorpt. with participation of optical phonons 79—99858
- metallic, van der Waals pair potential between two ions 78—47723
- metallic densities, dynamical dielectric function and paramagnetic spin susceptibility 80—39514
- metallic surface, self-consistent electron theory, review 80—88616
- metallic thin films, density response function and dynamic struct. factor, nonlocal effects 79—69447
- metals, compressiblities, general pseudopotential approach 80—54631
- metals, cubic, cohesion and Cauchy discrepancy 80—54170
- metals, cubic, vol. depend. contrib. to elastic consts., pseudo-pot. theory 77—72646
- metals, degenerate electron gas, collective props. using electron knock-out processes 80—6758
- metals, electron gas model for lattice vibrations 79—14894
- metals, ground state of solids, spin density functional method, binding energy, compressibility 80—65477
- metals, polar states and free electron gas *(Russian)* 80—84415
- metals, positron annihilation, real-space approach 79—95874
- metals, simple, quasiparticle props., density functional approx., electron gas calc. 80—96808
- metals separated by dielectric, electronic component of metal-metal interaction force, calc. 78—52056
- MIS, magnetooptic absorption by electron gas, optical phonon effects 80—97248
- MIS device, polar-optical phonon interaction with two-dimens. electron gas 79—82434
- MIS structure, optical phonon-electron gas interaction, high freq. cond. 80—6888
- molecules, chemisorbed on metal surface, spectrosc., electron gas effects 80—54504
- momentum distribution function, perturbation theory calcs. 77—13693
- MOS structure, 2D electron gas, far IR Faraday rotation 80—80389
- MOS structure, two-dimens. Wigner crystallisation induced by strong mag. field 77—28253
- MOS two-dimens. systems under strong mag. field, many-body effect on level broadening and cyclotron resonance 79—78195
- MOSFET, two-dimens. electron gas, determ. of fine struct. const. based on quantised Hall resist. 80—96997
- multiphoton laser absorption of heated oxide cathode electrons 80—6224
- multiple-band systems, dielec. function in generalised relax.-time approx. 80—103637
- multipole surface plasmons, bulk-selvedge coupling theory 79—28394
- neutrally charged with surface, props. 79—38144
- neutrino bremsstrahlung in an intense magnetic field 79—30055
- neutronization kinetics in superdense matter with frozen-in mag. field *(Russian)* 78—46019
- noble metal, van der Waals forces and their contrib. to vacancy form. energy and phonon dispersion 78—91635
- non-interacting electron system, of finite number of particles, pressure at zero temp. 79—97301
- non-linear dynamical response 79—69441
- nondegenerate, gas to solid transition, in superstrong mag. field, bifurcation theory approach 80—4640
- nondegenerate electron gas, classical fluctuation theory, existence of an infinity 80—31666
- nondegenerate electron solids bifurcation domain 80—34374
- nonequilibrium electron gas, fluctuation theory, reviews 79—54043
- nonlinear electronic system, series expansions calcs. 77—39814
- nonlinear theory of sound wave propag. *(Russian)* 79—76904
- nonlocal exchange-correlation pot. for inhomogeneous electron gas and quantum fields 78—65870
- nonrelativistic electron in const. parallel elec. and mag. fields, thermodynamic characteristics 80—90777
- nonuniform, energy loss of charged particles 79—37748
- one dimensional, dynamic interaction screening, spin and charge density wave instabilities 80—24819
- one dimensional conductors, Fermi gas model, reviews 79—78083
- one- and two-dimensional, anal. using hydrodynamic eqns. of motion 77—69260
- one-component plasma ground state, two and three dimens. Monte Carlo study 79—33248
- one-dimensional, bosonisation without bosons 79—54041
- one-dimensional, correl. functions, classical calc. 78—34790
- one-dimensional, interacting, ground-state energy in mean field approx. and instabilities 80—88493
- one-dimensional, transverse susceptibility, bandwidth and momentum-transfer cutoffs, comments 77—62847
- one-dimensional, two-dimensional Coulomb gas, and two-dimensional epitaxial monolayer problems, family of mappings 80—34346
- one-dimensional, with backward scatt., excitation spectrum 77—39793
- one-dimensional, with backward scatt., soliton Green's functions 78—10386
- one-dimensional conductor, quantum solitons 77—39792
- one-dimensional conductors, Fermi gas model, review 79—47090
- one-dimensional conductors, quantum solitons 78—6285

electron gas continued
one-dimensional electron gas with backward scatt., scale invariant characteristic energy 77−31927
one-dimensional electron system with attractive interaction in mag. field, paramag. transition 80−7072
one-dimensional Fermi gas, cut-off procedures 77−20253
one-dimensional Fermi gas, energy gap, boundary conditions for renormalisation-group eqns. 78−10317
one-dimensional Fermi gas, metal-dielec. transition, correlation functions 77−15780
one-dimensional Fermi system, mag. susceptibility, and dielec. function and two-dimensional Coulomb gas 78−10387
one-dimensional Hubbard model, Friedel oscills. around a nonmagnetic impurity 80−25073
one-dimensional systems, exchange effects in plasmon dispersion 79−60741
one-dimensional Tomonaga model with impurities, localisation versus delocalisation 78−6311
optical properties in generalised HF approximation 80−24825
orbital magnetic susceptibility 78−6312
orthogonality catastrophe due to local electron interaction 79−1566
p-wave electronic recoil spectra in perturbed electron gas 80−107724
pair correlation function, consistency relations 80−49640
pair correlation function and correlation energy using Tripathy-Mandal dielec. function 79−19536
pair correlation functions in classical and quantal electron gases 78−41228
paramagnetic and diamag. susceptibilities, density depend., ring diagram contrib. 79−95571
paramagnetism, closed-shell many-electron systems 77−20539
partition function of the hydrogen system in the metallic state 79−73458
permittivity of crystal in strong EM field, light absorpt. and emission effect 80−15938
photoemission, many-body effects, book contrib. 78−95667
photoemission theory, Drude energy absorpt. 77−63534
plasma, ionic, dynamics, electronic screening of ionic motions 80−64678
plasma impurity screening effects in intermediate degeneracy region 80−14882
plasma wave damping in layered electron gas, random inhomogeneities of the conductivity 77−51689
plasma wave stability 80−6240
plasmon dispersion 78−56099
plasmon spectrum and damping, collisionless absorpt. threshold nonlinear phenomena *(Russian)* 80−49646
polarisability, many-body correction 78−60071
positron correlation energy, annihilation rate 78−92142
positron momentum distribution 79−56146
proton in interacting electron gas, electron liq. in collective description 80−10895
quadratic electronic polarizability of interacting electron gas 78−6310
quadratic response of Fermi gas, electronic charge density of valence electrons 77−1094
quantised in mag. field plasma oscill., light scatt. 77−28134
quasi-one-dimensional, pair correl. function and plasmon dispersion curve 77−62851
quasi-one-dimensional chain, inhomogeneity effects, eval. of exchange hole and exchange pot. 79−65397
quasi-one-dimensional electron gas with strong on-site interaction 78−67966
quasi-one-dimensional with strong on site interactions 77−4306
quasi-two dimensional conductor, galvanomagnetic props., optical analogy *(Russian)* 80−60108
radial distribution function, derivation from exptl. Compton profiles 78−15244
radial distribution function, noniterative calc. 77−33937
radiative interaction, with mag. field, distrib. function 79−60116
relativistic, spin-polarised, Bloch theory 80−15465
relativistic degenerate electron plasma, dielec. response function 78−71529
relativistic degenerate in strong mag. field, transport props., covariant relaxation-time model 77−41531
relativistic density functional formalism 80−10848
relativistic electron gas, ground-state energy 78−8536
relativistic electron-positron gas, polarisation in strong mag. field, EM wave propag. 80−4896
renormalised collision integral *(Russian)* 79−1575
resonance absorption of sound by electrons in quantising mag. field 78−10522
Ruderman-Kittel interaction at finite temp. *(Russian)* 80−96835
scaling and multiplicative renormalising in solid state physics *(Hungarian)* 79−11289
SCF calcs., electron exchange and correlation phenomena, effect of local electron speed 79−95356
screening energies in photoelectron spectroscopy of localised electron levels 77−1781
screening in classical 2-dimens. Coulomb gas, and 1-dimens. fermion problem 77−47745
screening of positive particle, contribs. of different partial waves 77−11878
screening of proton, Anderson model calc. 80−59895
screening of proton 77−1382
self consistent screening and approximate residual Landau interaction functions 79−19537
self-diffusion, of two-dimens. classical electron gas 80−141
self-diffusion (spin diffusion) coeff., proper connected diagram expansion 78−21067
semi-infinite, nonlocal cond. tensor calc., effective optical surface region 80−20283
semiconductor, film or wire, intraband light absorpt. by degenerate electron gas *(Russian)* 77−44077
semiconductor, heavily doped, scatt. mech., resist. and Hall effect maxima 80−75586
semiconductor, hot electrons, photoexcited in quantizing mag. field, energy distrib. calcs. 79−42586
semiconductor, nonlinear current density, theory 78−56149
semiconductor sheieding in magnetic field 80−107727
semiconductor solid solution, compositional disorder, free carrier absorpt. 78−64387
semiconductor with superlattice, Coulomb screening 78−14684
semiconductors, degenerate, energy band structure effect on transverse magnetoresistance 80−88580

electron gas continued
semiconductors, narrow-gap, plasmon-phonon interaction effect on optical phonon dispersion 80−103435
semiconductors with neutral impurity, transverse cond. in quantising mag. fields, finite radius scatterers *(Russian)* 80−29400
semimetal, phase transitions in strong mag. field, HF approx. 78−23028
semimetallic film, Wigner crystal in high magnetic field 79−73456
shielding of electric fields by surface electron states in an ionic lattice 78−52059
short range correlations 78−84156
short range order, many electron effects, pseudopotential method 78−79954
simple metals, plasmon dispersion anal. from electron gas dielectric response 80−6761
solid-state theory, introduction, book 79−33215
sound velocity variation under de Haas-van Alphen conditions 79−60681
specific heat of two-dimens. electron gas, exchange interaction contrib., calc. 80−44331
spherical electron gas, equations of motion, electron density function for Sn^{4+} 80−6763
spin density functional theory, linear response functions 78−67965
spin polarised, correlation energies for local spin density calcs. 80−107725
spin polarised, exchange and correl. energy 77−85163
spin polarised, model for conduction electrons of simple metal in mag. field and ferromag. Gd 77−8034
spin susceptibility of a many electron system 77−69465
spin-density gradient expansion for kinetic energy of electron gas, variational calc. 79−93917
spin-polarised, self-consistent screening of positive muon 78−47714
static electron gas dielectric function, simple useful anal. form 78−79953
statistical thermodynamics of quasi relativistic electron gas, pathway integral application *(Russian)* 80−22277
stopping power for slow neutrons, damping effects 80−65098
strongly degenerate plasma, double injection, vol. controlled current regime 79−51658
strongly inhomogeneous, exchange energy 77−80746
structure factor, complex dynamic, theory 79−56152
structure factor, integral eqns. 78−47720
structure factor, static, short-range correl. and Wigner crystn. 77−39795
substitutional impurity, driving force for electromigration 77−76618
superconductor, electron gas propagation, normal phase, in long superconductors of small cross-section 79−78274
superconductor, magnetic, Fermi surface nesting effect on mag. instability 80−54831
superlattice and layered cryst., statistical and thermodynamic props. *(Russian)* 79−87051
surface, He atom scattering pot., surface electron density depend. 80−104027
surface, positron-electron correlations, RPA calc. 80−40181
surface conductivity, mean free path in incidental impurity field *(Russian)* 80−44702
surface magnetic props. of Bloch electron gas in opposing elec. and mag. fields at 0K 78−63992
surface photoemission of model system, book contrib. 78−95665
surface states, Green function theory, exchange and correlation effects 77−8164
surface wave spectrum, particle beam excitation, dispersion relations 77−84434
symmetry groups basis for many-electron interaction in crystals 77−51682
thermal cond. in partially degenerate electron gas 77−71266
thermal desorption and dissociation catalyzed by a solid surface 80−108734
thermodynamic potential of electron-positron system in mag. field 78−8341
thermodynamic properties, weak field expansions, in uniform mag. field at T=0K 79−85066
three-body interatomic forces, electron gas model and SCF calcs. 78−33564
three-dimensional Wigner crystal in magnetic field, vibr. freq. 79−73457
Tomonaga fermions and three-dimens. Dirac eqn. 79−58633
Tomonaga model, one-dimens., impurity effect, electron localization and delocalization 79−73455
Tomonaga model, response function calc. method 80−22279
transport coeffs. of relativistic degenerate electron gas in strong mag. field 77−80346
two dimensional, classical, hypernetted chain solns. 78−67963
two dimensional, collective excitations and electrodynamic behaviour in three layer structure 78−60079
two dimensional, correlations 78−63996
two dimensional, ferromagnetism 78−60258
two dimensional, ground state energy 77−24506
two dimensional, in strong mag. field, Wigner solidification 78−60005
two dimensional, mag. props. 78−56095
two dimensional periodic lattice, electron ordering, CDW-disordered state transition, Hubbard model *(Russian)* 80−6754
two-dimens. electron gas high-freq. cond. determ. 79−40463
two-dimensional, correl. functions, exact short distance limit 80−24820
two-dimensional, Hartree-Fock soln. of CDW in mag. field 79−28302
two-dimensional, in mag. field, polarisability 80−107888
two-dimensional, in strong mag. field, phase diagram properties 79−78024
two-dimensional, internal energy, specific heat effective mass, temp. depend. 80−75513
two-dimensional, longit. and transverse dielec. function including exchange correls. 77−66133
two-dimensional, nonequilibrium statistical mechanics 79−33137
two-dimensional, pair correlation function 77−35877
two-dimensional, polarised, correl. energy, para- and ferromag. states 77−47757
two-dimensional, reson. excitations using IR spectroscopy, review 79−60889
two-dimensional, study in intermediate mag. field 79−60743
two-dimensional, study in weak mag. field 79−60742
two-dimensional, two-component, high-freq. cond. 80−29428
two-dimensional, variational approach to ground state, CDW instability 80−39517
two-dimensional classical plasma, on dielectric film, collective excitations *(Russian)* 78−34788

electron gas continued
two-dimensional electron fluid, collective modes, dynamic struct. factor 79—4523
two-dimensional electron fluid, collective modes 77—80661
two-dimensional electron fluid, second order exchange energy, correlation energy 80—107729
two-dimensional electron system, high- and low-density limits 77—76761
two-dimensional electron-impurity system in strong mag. field, electron spectrum and cond. *(Russian)* 78—88016
two-dimensional on liquid He surface, cyclotron reson. 79—60566
two-dimensional quantum plasma in mag. field, exchange energy 77—72904
uniaxial crystal foil, electron energy loss probability at oblique incidence 80—25506
uniform, electronic props. of H and He impurities 80—96807
vacancy formation energies and volumes, exam. of models 78—47349
Vlasovs equation with mollified density for electron gas with external mag. field 80—1756
voids, spherical, X-ray excitation of surface plasmons 77—11974
wake potential of swift ions in solids 77—20257
Wigner crystal, two-dimensional, possible re-evaporation at extremely low densities 78—56085
Wigner distribution for cylindrically symmetric system 80—65475
Wigner transition, bifurcation theory 79—97297
e^+e^- pairs and equilib. radiation in quantising mag. fields *(Russian)* 78—49990
Ag, electron inelastic mean free paths and energy losses, electron gas statisitcal model 79—46733
Al, collective properties of degenerate electron gas, (e, 2e) technique *(Russian)* 79—56149
Al, electron inelastic mean free paths and energy losses, electron gas statisitcal model 79—46733
Al, electron inelastic mean free paths and energy losses, electron gas model 79—46732
Al, liquid, momentum density of electron 78—6309
Al, plasmon dispersion, dynamical exchange effects 79—51509
Au, electron inelastic mean free paths and energy losses, electron gas statisitcal model 79—46733
Bi, electron gas heating at low temp. 78—60133
Bi, film, size effect of carrier heating, surface scatt. *(Russian)* 80—100474
Bi, stationary I-U curve, falling portion under phonon generation conditions 79—15195
CO+Ar(He)(Ne)(Kr)(Xe), intermol. pot. energy surfaces from electron gas model, ang., distance, and vibr. depend. 79—3520
CaO, modified electron gas theory, high press. effect 77—19899
$Cd_xHg_{1-x}Te$, strong elec. field effect on galvanomagnetic effects, degenerate electron gas heating 79—11159
Cs, extreme UV absorpt spectra, threshold singularities of p-shell absorpt. 77—36261
Cs monolayer on Cu(111), dilution of electron gas by O adsorption, plasmon energy losses 79—47036
Cu, electron inelastic mean free paths and energy losses, electron gas statisitcal model 79—46733
EuO:La, metallic, photothreshold, correl. and exchange energy of electron gas 77—62852
Fe_3O_4, magnetite, charge carriers, optical props. 80—34874
GaAs, compensated, influence of electron gas heating on negative magnetoresist. 77—89778
n-GaAs, coupled plasmon-LO phonon modes and Lindhard-Mermin dielec. function 79—82540
GaAs, photoluminescence, electron gas coding influence in ion-bombarded layers 80—108272
GaAs-Al_xGa_{1-x}As differentially doped heterojunction interface, two-dimens. electron gas obs. 80—49886
GaAs-AlGaAs heterojunction superlattices, inelastic light scatt. by two-dimens. electron gas 80—93360
GaAs-AlGaAs:Si heterojunction interface, two-dimens. electron gas, Hall effect and cyclotron reson. meas. 79—65530
Ge, cyclotron reson. in strong elec. fields, classical theory 80—7172
H_2, metal phase, state eqn., correlation energy of uniform electron gas *(Hungarian)* 79—1573
H_2, metallic, solubility of He, Gibbs energy, fluid state model, He conc. in giant planets 79—60602
H_2, metallic liquid, struct. and forces 78—22636
He film, sound modes of two-dimensional electron gas 77—69145
He, liq., effect of short-wave surface excitations on damping in two-dimens. electron gas *(Russian)* 79—10995
He, liq., electron gas struct. formed in image-pot. induced surface states 79—65400
He, liquid, short-wave surface excitation study using electron gas nonlinear I-V characts. *(Russian)* 80—10717
He, liquid surface quasi-one dimensional electron chain instability, string-zig zag transition *(Russian)* 80—65335
He_3 three-body interatomic forces, electron gas model and SCF calcs. 78—33564
^{4}He, liq., HF cond. of electrons trapped at surface 78—10238
n-InSb, electron gas degeneration in strong mag. field 77—66173
K, extreme UV absorpt. spectra, threshold singularities of p-shell absorpt. 77—36261
K, liquid, interionic interaction theory, pseudopotential calcs. *(Russian)* 80—79675
MgO, modified electron gas theory, high press. effect 77—19899
Mn ferrites, Fe-excess, charge carriers, optical props. 80—34874
Na liquid, interionic interaction theory, pseudopotential calcs. *(Russian)* 80—79675
Na_xWO_3, degenerate electron gas, Friedman effect, review 77—20242
Na_xWO_3 films, chem. pot. variation of Na, free electron gas model 80—16698
$Ne^-+Na^+(K^+)(Li^+)$, electron gas model pots. and collision integrals *(French)* 78—42169
Ni, electron inelastic mean free paths and energy losses, electron gas statisitcal model 79—46733
O_2 discharge, electron gas, transport coeff. and energy distrib. function calcs. 77—68742
PbSe, electron gas magnetisation, energy band parameters determ., use of Faraday effect 80—45047
PbSe, Faraday effect and electron gas magnetisation, Kane two band model calcs. *(Russian)* 80—34899
$Pb_{1-x}Sn_xTe$, Faraday effect and electron gas magnetisation, Kane two band model calcs. *(Russian)* 80—34899

electron gas continued
Rb, extreme UV absorpt. spectra, threshold singularities of p-shell absorpt. 77—36261
$(SN)_2$, theory of plasmon excitations 77—69266
Si, (100) inversion layer, electromigration in two dimensional electron gas, driving force 80—84441
Si, doped, basis functions for studying intervalley effects 79—69442
Si, electron inelastic mean free paths and energy losses, electron gas statisitcal model 79—46733
Si, high index surface, natural orientational superlattice in 2D electron gas 79—99598
Si, influence of one-dimensional superlattice on two-dimensional electron gas 77—43683
Si inversion layer, cyclotron resonance in extreme quantum limit, collective ground state 80—50191
n-Si inversion layer, electron mag. suscept. 78—52009
Si inversion layer, influence of natural superlattice on 2-dimens. electron gas spectrum *(Russian)* 78—68064
Si inversion layer in MOS struct., carrier-phonon interaction, nonohmic transport 80—49943
Si, screening of donor ions by delocalised electrons 79—69466
Si, screening of ions, band struct. calcs. with screening variants 78—67938
Si surface, MOS struct. band structure, minigaps, magnetoresistance, cond., space charge layers 80—92980
Si:P, heavily doped, degenerate electron gas, Friedman effect, review 77—20242
Si:P, heavily doped, electronic sp. ht. meas., rel. to metal-nonmetal transition 78—6162
Si(100) inversion layers, two-dimensional electron fluid, spin density, valley density waves 77—69400
Te, liquid, classical fluid model, neutralising negative background density 78—22621
Ti (III) halides, bonding, struct., ligand field splitting, electron gas calcs. 78—17557
Zn, electromigration, electron wind force calc. 78—6183

electron guns
accelerator radiation processing applications 77—54370
AES of O_2 adsorpt. on GaP, O_2 adsorpt. in electron gun 77—72777
AES of O_2 adsorpt. on GaP, O_2 adsorpt. in electron gun 78—6218
annular cathode gun for in-line injection in racetrack microtron 77—3193
beam current control for improved stability 80—84814
beam deceleration, in longit. mag. field, energy recovery system 77—49807
beam focusing by small perturbation anal. 77—50602
bent beam electron gun for thin film vacuum deposition 77—12534
Boersch effect, energy broadening 80—69313
brightness improvement by ZrC coating on W filament 79—67438
Brillouin electron beam critical current rel. to vacuum level 79—7068
centrifugal electrostatic shaping of high intensity electron beams 80—13183
coaxial, electron flux formation in strong mag. field *(Russian)* 79—98998
coaxial diode electron beam system for excimer laser excitation 80—86509
cold cathode electron gun, in compact high-press. laser system 78—5496
cold cathode gun coupled to pulsed blowdown apparatus, for low-temp. and high-pressure supersonic flow electronic transition lasers 79—59723
collision broadening in electron beam, energy spread calc. 78—42271
compact cold cathode electron beam gun, appl. CO_2 laser *(German)* 80—86501
crossed-field, pot. min. determ. 80—95188
cylindrical relativistic diode, space charge limited, voltage distrib. and current calc. 80—63437
design for producing high-intensity beam with rectangular cross section 78—93785
diffraction radiation generator, starting currents, dynamic and static electron shiftings influence, theory and expt. *(Russian)* 79—3617
electron beam focal spot size, input phase characteristic nonlinearity effect 80—5678
electron gun, for computer driven STEM, image registration 80—104838
electron injector, high perveance, LaB_6 cathode, 1650 to 2000 deg C range, microwave device, plasma-beam experiments appl. *(Russian)* 77—38535
electron injector in HV terminal, control and protection system 80—27836
electrostatic accelerators, laminar beam injection, experimental 500 kV electron gun 80—47788
electrostatic and electromagnetic lenses 80—99007
electrostatic einzel lenses, reduced spherical aberration field emission guns appl. 78—74831
emission instability, grid aperture contamination in guns using directly heated LaB_6 sources 79—12907
energy broadening in electron-beam system, Boersch effect anal. 80—1114
ETA gun, beam dynamics calc. with EBQ code 79—72023
evaporated layer production in ultra high vac., electron beam gun 78—27404
field electron source geometry determination by computer assisted shadowgraph technique 77—87882
field emission, appl. to TEM 77—54023
field emission, comparison of cold and thermal types used in the same electron microscope 80—101890
field emission, energy distrib. of electrons *(German)* 80—20773
field emission, for Lorentz microscope obs. of mag. domains 77—63228
field emission, for TEM, advantages in high resolution and in-line Fraunhofer holography *(French)* 77—34057
field emission, noise and energy broadening 80—101889
field emission, off-axis electron holography 80—101905
field emission, Philips EM 400 TEM/STEM performance 80—57441
field emission, SEM appls. *(Czech)* 79—6240
field emission, STEM appl., X-ray analysis of metals and ceramics inhomogeneities 80—59354
field emission electron gun *(Japanese)* 77—61162
field emission electron microscope *(Japanese)* 80—47146
field emission electron tube, pump for compact IR semiconductor laser 79—59725
field emission gun, electron optical characteristics *(German)* 79—893
field emission gun brightness meas. *(German)* 78—8471

electron guns continued
field emission gun for sub-angstrom resolution TEM 80—82851
field emission gun SEM column electron-optical performance obs. and model 80—68328
field emission gun use in TEM, phase contrast transfer improvement due to low energy spread 77—10145
field emission instability effects on SEM display, electronic removal device 78—21279
for field emission microscope *(French)* 77—26442
for field emission microscope with energy dispersive spectrometer *(French)* 77—26443
field emission source, differentially pumped *(German)* 77—87886
field emission systems, using single-pole magnetic lenses 79—31784
field-emission source, theoretical investigation of rotationally symmetric gun 80—99006
glow discharge, cold-cathode, for pulsed ionisation of high-pressure CO_2 laser 79—27269
glow discharge, high voltage, in electron gun regime 79—86638
glow discharge, high-voltage, as electron gun 77—62428
glow discharge electron gun, with plane-frustrum cold cathode, characts. 79—7495
glow discharge generated high-power pulsed beams, gas dynamics diagnostics appls. 78—63515
glow discharge lamp, use as electron gun for Auger spectroscopy 77—31027
grid-controlled, for electron beam controlled CO_2 laser 78—46635
helical electron beams, extended and intense with space-charge forces, trajectory anal. *(Russian)* 79—918
high current density, axially symmetric, synthesis 78—55063
high energy, gas amplification of filament current 77—10139
high intensity microsecond electron beam formation, in gun with plasma anode *(Russian)* 78—21271
high-current, laminar beam formation for linear accelerators 78—74516
high-power long-pulse thyratron modulator with small off-duty factor 78—86380
hot cathode electron gun brightness at high emission densities 79—71566
HV electron gun power supply protection 79—44989
HV pulsed discharge, electron beam production 80—9072
impulsed electron beam generator with linear shaper *(Italian)* 80—52793
injector for LLL induction linac ETA 79—76157
intensity regulator for 5 to 50 keV electron guns *(French)* 78—54499
ionospheric rocket expt. high-power electron gun *(Japanese)* 78—61566
large-area cold-cathode grid-controlled for Antares CO_2 laser amplifier 80—68955
lenses props. calc. and obs., electrostatic, for high-brightness field emitters 80—62809
long pulse high current, for e-beam sustained excimer laser 77—88733
long-pulse, high-current, for e-beam sustained excimer lasers 78—29967
low energy anticontamination, for surface originating contamination elimination in electron microscopes 79—30622
low energy gun, appl. to direct obs. of insulators via SEM 77—2712
mass spectrometer three-dimens. quadrupole electron gun, compact tube assembly poisoning resistant 78—54493
microscope Cambridge University 600 kV high resolution, engineering performance 80—82849
microscopes, electron source size in field-emission gun 79—71575
microtron, electron injection and capture processes, digital simulation 77—18717
miniatured, for measurement of work function variations by method of retarding potential in axial magnetic field 79—80719
modulator/repetitively pulsed field emission electron beam gun interface for CO_2 laser 78—5482
photocathode with pulsed illumination, for electron beam controlled laser 77—50678
plasma cathode and built-in gas generator 80—106947
plasma emitter, electron optical system simulation 78—67442
plasma production modified magnetron discharge facility 78—75380
point cathode type, electron-optical props. *(German)* 78—82901
polarised electron gun at SLAC, operating experience 77—83396
portable, containing source, monochromator, counters, for particle detector calibration 78—78539
pulse generator, repetitively pulsed electron beam system using cold-cathode electron gun 80—68981
pulsed, four-electrode, with emission of stream of large cross-section 79—35889
pulsed desorption slot, cathode, operating stability 80—87002
pulsed electron beam gun, kinetics and spectroscopy appl. 78—5413
pulsed electron gun, plasma emitter, ≥ 50 kA, $\geq 95\%$ transmission coeff. 77—18134
pulsed electron gun systems, 1 ns pulse width 79—67977
pulsed electron gun with Ta cathode, for linear accelerator *(Russian)* 79—9924
pulsed laser electron beam sources 79—36913
relativistic beam permeance, high voltage electron gun appls. *(Rumanian)* 77—46678
repetitively pulsed CO_2 lasers, electron gun operation 79—31943
ring cathode electron gun as evaporation source, design, development 77—44168
scanning electron microsope appl. *(German)* 77—5965
screw electron beams, systems form. synthesis *(Russian)* 78—17889
SEM, Broers type LaB_6 gun design 78—21283
SEM, electron gun evaluation unit for electron optical parameters meas. 78—21285
SEM, photographic recording system 80—101903
single-pole magnetic lens as condenser for field emission electron gun 80—68325
solid-electron interactions, conf., Southampton, England (Apr. 1976) 77—44570
source imaging detector 78—21284
spatial electron beam formation, paraxial approx. *(Russian)* 78—17854
with spherical diode with plasma anode 77—591
sputtering evaporation chamber LV electron guns with longitudinal compression *(Russian)* 80—50551
STEM, computer driven, image registration 80—104838
STEM, thermal cathode illumination system, for round beam electron probe systems 80—57436
STEM optical system, practical considerations, review 78—21301
STEM with field-emission gun, for microanalysis use 78—32948
student apparatus for electron motion obs. in elec. and mag. fields 80—27076

electron guns continued
surface AES with secondary emission imaging 78—11475
surface change method, computer anal. of characteristics 80—101891
tetrode gun, transport of high-energy, high-power electron beams 78—89587
thermionic emission source coherence props. 77—22622
thermionic gun with beam extraction through Al foil 77—13817
thoriated W hairpin filament electron source for high brightness appl. 78—341
triode and diode guns, electron optics numerical determ. of beam profile 80—106435
triode keV anode-controlled telefocus electron gun, focusing props. 78—342
triode with explosive-emission cathode, variable current density 79—72475
vacuum gap breakdown strength, 200-500 kV pulses, anode grid 78—5980
voltage supply pulse transformer, for a linear induction accelerator 77—75007
X-ray tube, microfocus, electron source with single-pole mag. lens and novel focusing system 78—32964
LaB_6 cathode electron gun, current beam intensity and brightness meas. *(French)* 77—590
LaB_6 cathode gun from transmission electron microscope appls. 80—18048
LaB_6 gun, 100 kV, combined CTEM and STEM 80—86516
LaB_6, optimum brightness problem 78—21298
LaB_6 three-electrode 250 A pulsed electron gun 78—82553
W, impregnated cathode, mechanism of operation, life-tests 79—78821
W tip, use of focused laser beam for cathode heating *(German)* 78—89591
Zr-O-W (100) thermal field emitters, operational experience 80—71576

electron-hole avalanches *see impact ionisation*

electron-hole drops
antiferromagnet, existence of states with superfluid flow, Ginzburg-Landau theory *(Russian)* 78—72085
antiferromagnet, itinerant electron, dynamic magnetisation as internal Josephson effect 78—47931
Bose condensate of electron-hole pairs, superfluidity *(Russian)* 77—31957
bulk compressibility and surface energy of electron-hole liquids 80—65465
condensation and liquefaction in strong mag. field, RPA and variational calcs. 78—63984
condensation effects of excitons, review 78—2427
condensation of droplets, phase transition in open system 79—37993
conference, Tomakomai, Japan (Sept. 1975) 77—43510
crystal surface-electron-hole drop interactions, interaction energy 80—29335
damping of movement of drop with vel. close to that of sound *(Russian)* 79—19529
deformation in mag. field *(Russian)* 78—10371
diamond, semiconducting, electron-hole liquid formation conditions and parameters 79—78013
direct gap semiconductor, final state interactions in gain and absorpt. spectra 78—43305
direct gap semiconductors, electron-hole droplet condensation 80—103630
electron-hole binding and exciton formation *(Russian)* 80—65468
electron-hole drops, surface struct. 78—60058
energy condensation, comparison with ball lightning *(Russian)* 80—107712
equilibrium form, cryst. lattice effect *(Russian)* 77—72824
exchange interaction, singlet charge density formulation 80—20094
excited semiconductor, extended phase diagrams, review 80—44521
exciton condensation in electron-hole drops *(Russian)* 79—19522
exciton drops, effect of repulsion on formation 78—23029
exciton physics, review, book contrib. 80—44517
far IR radiation from electron-hole drops *(Russian)* 78—72600
Fermi liquid, two component, with electron-hole pairing, microscopic theory *(Russian)* 78—51905
gamma-drop, orientational depend. of shape in mag. field 77—66121
Ge, large uniaxial stress, effect of non parabolicity of valence band 78—47703
ground state energy of small electron-hole drops 79—47024
hydrodynamic model for electron-hole droplets 78—43309
indirect band gap semiconductor, Auger recomb. of electron-hole drops 78—39600
inhomogeneous electron hole system, plasma oscills. 79—99496
instability and motion, recombination flow, exciton gas *(Russian)* 80—15458
interaction with ballistic phonons in heat pulses, effect of phonon wind 78—6279
isotropic semiconductor, shape of moving electron-hole drop 80—20093
kinetic theory for electron hole condensation 77—85151
layered electron-hole liquid, ground-state energy 77—51672
low-dimensional crystals, excitonic superfluidity 78—6359
metallic crystals, low-dimensional, excitonic 'superfluidity' 77—20248
mobility, effect of fluctuation pairing 78—2434
mobility *(Chinese)* 80—65466
motion damping, deform. pot. scatt. 78—67950
motion damping, impurity and piezoelec. scatt. 78—67951
non-radiative recombination by phonon-assisted Auger recomb. 79—60716
noncrystalline system, continuous and discontinuous metal insulator transitions 78—56076
nonuniform electron-hole liq., props. in high density limit 77—43505
nucleation, Fokker Planck treatment 80—6732
nucleation theories for exciton condensation 79—33239
phase diagrams for electron-hole droplet condensation in semiconductors 79—38001
phase transition during formation of exciton condensate *(Russian)* 78—60060
phonon wind, electron-hole droplet theory 80—107707
plasma, created by pulse, hydrodynamics 79—65389
plasma nucleation, time evolution 80—49616
polar semiconductor, electron-hole liquid, electron-phonon interactions 80—6739
polar semiconductor, phase diagram 77—89706
polar semiconductor, strongly anisotropic, electron-hole liq. in mag. field 80—59890

electron-hole drops continued
polar semiconductor, theory of excitons bound to neutral impurities 79—73441
polar semiconductors, electron-hole system, interaction with phonons 80—6738
quasi two dimensional in strong mag. fields *(Russian)* 78—34781
quasi-two-dimensional semiconductor, electron-hole liq. ground state energy 77—1376
resonance radiation at plasma freq., surface plasmon radiative decay *(Russian)* 77—62841
semiconductor, acoustic studies progress *(Japanese)* 80—49310
semiconductor, appl. of density profiles and surface tension of charged fluids 80—44689
semiconductor, collective excitations of electrons and holes in strong EM field and absorpt. of light *(Russian)* 78—79945
semiconductor, crit. points for electron-hole system 80—44511
semiconductor, dielec. electron-hole liquid, ground state energy and excitation spectrum 77—89713
semiconductor, dielectric electric-hole liquid form. 77—43508
semiconductor, direct and indirect gap, electron-hole plasma phase transition 80—24803
semiconductor, electron-hole drop in rapid motion *(Russian)* 79—60727
semiconductor, electron-hole drop mobility, effect of Coulomb interaction 79—15096
semiconductor, electron-hole droplet nucleation and stability, hydrodynamic approach 78—72080
semiconductor, electron-hole drops under microwave radiation, kinetics of instabilities 78—60059
semiconductor, electron-hole liq., equilib. props., review *(Russian)* 78—34773
semiconductor, electron-hole liquid, ‘neutrality’ question of impurities 80—92822
semiconductor, electron-hole liquid, prod. and props. at low temp. 79—82527
semiconductor, exciton condensation, microwave cond., book contrib. 80—11043
semiconductor, highly excited excitation induced optical absorption 77—44025
semiconductor, layered, electron-hole liq. and metal-dielec. transition *(Russian)* 78—2425
semiconductor, layered, electron-hole liquid exam. 78—18975
semiconductor, optical props. under intense laser fields 78—72513
semiconductor, spin-polarised electron-hole liq., theory 78—43307
semiconductor, temp. of moving electron hole drop *(Russian)* 78—67953
semiconductor, thermodynamics of electron-hole system 78—43304
semiconductor, two-dimensional electron-hole systems in high mag. fields, phase transitions 80—49608
semiconductor, US absorption 77—89814
semiconductor and semimetal, strongly anisotropic, electron-hole fluid energy calc. *(Russian)* 77—1379
semiconductor electron-hole-droplet condensation, scaling relations 79—99484
semiconductor layer structure, laser-induced photolum. and collective effects *(Russian)* 79—95830
semiconductor physics, conf., Edinburgh, Scotland (Sept. 1978) 79—95303
semiconductor with complex band structure, two-component electron-hole liquid 79—15099
semiconductor-metal interface, electeon-hole liq., binding energy 78—30985
semiconductor-metal transition, electron-hole fluid 77—43500
semiconductors, basic principles *(Russian)* 78—72081
semiconductors, electron-hole drop formation, phonon wind influence *(Russian)* 80—92825
semiconductors, electron-hole liquid theory, generalised RPA 78—87914
semiconductors, exciton condensation and electron hole liquids, state-of-the-art 80—49625
semiconductors, particle complexes, $N=1$ to ∞, book contrib. 80—80194
semiconductors, recombination, conference, Southampton, England (Aug.-Sept. 1978) 79—38087
semiconductors, RPA calcs. 80—6743
semimetal, excitonic and gas-liquid type transition of electron-hole system in strong mag. field 79—60718
semimetal in strong mag. field, metal-dielectric transition of electron-hole fluid *(Russian)* 77—80731
shape in mag. field and strain induced potential well 79—23903
shape in mag. fields *(Russian)* 79—90964
shape in magnetic fields, anal. 78—67954
size effects, work function determ. 78—72077
spectrum of electron-hole system in one-dimensional infinitely deep potential well *(Russian)* 78—67944
stability of spherical form *(Russian)* 79—42464
supercooling in adiabatic spraying *(Russian)* 78—43306
surface tension coefficient and binding energy, exciton condensation kinetics 78—10370
thermalisation phonons, role in producing electron-hole droplet cloud 80—49617
thermodynamics of electron-hole liq. superstrong mag. field 78—43310
two-dimensional dielectric electron-hole liquid, feasibility 78—87917
two-dimensional electron-hole liquid in strong mag. field 77—80739
two-dimensional electron-hole metallic liquid, RPA calc. 77—47743
two-dimensional system, phase diagram for electron-hole plasma to liq. transition 79—95342
AgBr, electron-hole liq. and biexciton pocket, luminesc. obs. 78—15216
AgBr, time resolved luminesc. spectra at high excitation density 79—78751
CdS, condensation of optically excited carriers, electron-hole-liquid phase diagram 77—31950
CdS, electron-hole condensate, luminesc. obs. *(Russian)* 78—19552
CdS, electron-hole liq., effect of excited electron states lifetime on gain spectra 77—85748
CdS, electron-hole liquid, non-equilib. transmission spectroscopy meas. 77—20883
CdS, electron-hole pairs behaviour in energetic ion tracks 80—65457
CdS, exciton condensation effects on refr. index 77—20818
CdS, exciton-contrib. to reflection spectrum at high excitation intensities 78—43900
CdS, gain spectroscopy and plasma recomb. 78—88327
CdS, highly excited semicond., linear optical response, electron-hole liq. 79—51980

electron-hole drops continued
CdS, noninteracting droplet fluctuation model for condensation 78—10367
CdS, pure and Cl doped, stimulated emission due to indirect band-band transitions 80—7376
CdS, spatial diffusion of excitons under intense excitation 77—44061
CdS, spin-polarised electron-hole liquid, theory 78—43307
CdS, spontaneous and stimulated emission from electron-hole plasmas 77—69241
CdS, Wannier exciton and Wannier-exciton-ionised-donor complex, binding energies of lowest excited states 80—34363
CdS$_{1-x}$Se$_x$, mixed cryst., electron-hole drops and plasma, luminesc. obs. *(Russian)* 78—92119
CdS$_x$Te$_{1-x}$, emission spectra at high excitation levels *(Russian)* 79—74004
CdSe, highly photo-excited, time-resolved luminesc. spectra, 1.8K 78—35197
n-CdSe, laser excited stimulated emission, optical gain spectrum 80—76050
CdSe, optical gain spectra, exciton collision processes and electron-hole plasma 79—28814
CdTe, electron-hole liquid formation in pure and doped crystals, luminesc. study *(Russian)* 80—55184
CdTe:In, pure and heavily doped, electron-hole liq. form., luminesc. spectra 80—10884
CuCl, electron-hole pairs behaviour in energetic ion tracks 80—65457
GaAs, electron-hole drop transition to metallic condensed state, Hartree-Fock theory 79—56136
GaAs, electron-hole liquid form., luminesc. 79—33804
GaAs, final state interactions in gain and absorpt. spectra 78—43305
GaAs, long-wavelength wing in absorpt. spectra due to electron-hole pair excitation 79—69857
GaP, camel’s back excitons, rel. to band structure 78—47707
GaP, camel’s back induced stabilisation of electron-hole liquids 79—19524
GaP, electron-hole drop, luminesc. 79—33812
GaP, electron-hole drops, self-consistent surface calculation 80—65464
GaP, electron-hole liq., cathodolum. spectra meas., 4.2-20K 77—63470
GaP, electron-hole liquid obs. by luminesc. spectra 77—51668
GaP, electron-hole liquid exam. 78—2430
GaP, electron-hole liquid, emission band from time-resolved spectra 78—43938
GaP, electron-hole liquid props., luminescence at high excitation intensity 79—69882
GaP, electron-hole plasma photolum. obs. 78—52559
GaP, electron-hole plasma luminesc. 79—38651
GaP, luminesc. emission band, electron-hole liquid 77—69245
GaP, luminesc. from electron-hole drops, 2 to 77K 79—11454
GaP, motion damping, impurity and piezoelec. scatt. 78—67951
GaP, stabilisation of electron-hole liquid by camel’s back 80—6740
GaP:N, electron-hole liq., luminesc. obs. 80—25438
GaP:N, luminesc. from electron-hole drop 79—33813
GaP:N, radiative recomb. from electron-hole drops, impurity induced transition 78—19547
GaP:N, radiative recomb. of electron-hole liq. 79—73442
GaSe exciton absorpt., change under a pulsed dye laser 78—92088
Ge, acoustic phonon propag. and interaction with electron-hole drops *(Russian)* 80—29336
Ge, Auger recomb., luminesc. meas. 77—48240
Ge, binding energy, optical threshold studies 79—38652
Ge, carrier density in electron-hole drops, plasma reson. determ. 77—24522
Ge, carrier relaxation rate temp. depend. and pair density in large electron-hole drop 80—75509
Ge, compressed electron hole plasma, luminesc. 78—72592
Ge, condensation of electron-hole drops in supersaturated gas of free excitons 77—69242
Ge, cyclotron reson., exciton and electron-hole drop diffusion coeffs. 77—48055
Ge, cyclotron resonance and radiative recomb. with laser excitation, book contrib. 80—11472
Ge, cyclotron resonance peaks under high excitation 77—48056
Ge damping of motion of electron-hole drops by mag. field 77—69244
Ge, deform. of laser induced electron-hole drops under high magnetic fields *(German)* 78—23027
Ge, determ. of nonradiative decay rate in electron-hole drops at 1.6K 77—8143
Ge, direct gap recombination, at high excitation level and low temp. 79—38650
Ge, direct transition absorpt. coeff. modulation by electron-hole drops 77—90153
Ge, doped, electron-hole drops, low-temp. photolum. spectra obs. 77—69900
Ge, droplet decay kinetics, microwave expts. 77—43517
Ge, droplet shape under uniaxial stress 77—43518
Ge, electron hole drop diffusion const., hysteresis effect determ. 79—23902
Ge, electron hole drop recombination spectrum, low energy tail 77—59612
Ge, electron-hole correlation density depend., in electron-hole liq., under uniaxial stress 79—15090
Ge, electron-hole drop and exciton atmosphere 80—6748
Ge, electron-hole drop deform., accel. and luminesc. under influence of radiation press. 77—47739
Ge, electron-hole drop dispersion under strong optical stimulation, phonon interaction effects *(Russian)* 77—1723
Ge, electron-hole drop drag by ultrasound *(Russian)* 80—100437
Ge, electron-hole drop drag, interaction with thermal pulses 80—103631
Ge, electron-hole drop ejection from continuously generated electron hole liquid 79—78017
Ge, electron-hole drop emission kinetics, effect of nonequilib. phonons, 4.2K 78—14674
Ge, electron-hole drop formation, nucleation phenomena 79—33240
Ge, electron-hole drop freq. depend. damping 80—88482
Ge, electron-hole drop interaction in stationary and alternating mag. field *(Russian)* 77—62845
Ge, electron-hole drop luminescence at high mag. fields 79—65390
Ge, electron-hole drop luminesc., phonon wind induced anomalous depend. at low mag. fields 80—34980
Ge, electron-hole drop magnetostruction 78—87912
Ge, electron-hole drop magnetoplasma resonance 79—60722

electron-hole drops continued
- Ge, electron-hole drop magnetoplasmas, radius-independent elec. and mag. reson. 79—73446
- Ge, electron-hole drop motion recorded by microwave probe meas. 77—76755
- Ge, electron-hole drop motion 80—6744
- Ge, electron-hole drop motion, phonon wind 80—10887
- Ge, electron-hole drop net negative charge, giant fluctuating photocurrent obs. 77—35963
- Ge, electron-hole drop phase separation due to uniaxial stressing 78—84145
- Ge, electron-hole drop radius temp. depend. 77—76753
- Ge, electron-hole drop recombination radiation due to heat pulse action *(Russian)* 80—16087
- Ge, electron-hole drop transition to metallic condensed state, Hartree-Fock theory 79—56136
- Ge, electron-hole drop velocities as probe of phonons 78—68517
- Ge, electron-hole drop velocities, excitation wavelength depend. 78—88358
- Ge, electron-hole droplet, effect of nonlocal contributions to energy 77—69246
- Ge, electron-hole droplet, attachment to donor 78—87916
- Ge, electron-hole droplet condensation model, phase diagram and surface tension 80—6734
- Ge, electron-hole droplet cloud form., phonon wind, luminesc. obs. 80—45136
- Ge, electron-hole droplet condensation, crit. point 80—49612
- Ge, electron-hole droplet cloud kinetics, thermalisation phonons 80—88483
- Ge, electron-hole droplet magnetoresistance 78—14744
- Ge, electron-hole droplet scattering of acoustic phonons, total scatt. rate and anisotropy 79—33241
- Ge, electron-hole droplets, capillary-wave reson. investig. by US attenuation 77—8027
- Ge, electron-hole droplets, conc. in mag. field, magnetoplasma absorpt. spectra meas. *(Russian)* 77—24854
- Ge, electron-hole droplets, magnetoplasma reson. with submillimetre circularly polarised waves 77—89712
- Ge, electron-hole droplets, reson. scatt. of free carriers 78—2500
- Ge, electron-hole droplets, surface props., SCF calc. 78—51904
- Ge, electron-hole droplets, transient photoluminesc. intensities 78—88353
- Ge, electron-hole droplets, variation of α_3 electron density at constant stress 79—47025
- Ge, electron-hole droplets, luminesc. and absorpt. lineshapes, RPA theory 80—49613
- Ge, electron-hole droplets, percolation theory of cond., expt. 80—92896
- Ge, electron-hole droplets in high stress limit 78—10369
- Ge, electron-hole droplets distrib., and phonon wind 80—103629
- Ge, electron-hole drops, accel. by IR radiation field 78—95264
- Ge, electron-hole drops, appearance of plasma at high excitation rates 78—26821
- Ge, electron-hole drops, far IR absorption 78—56467
- Ge, electron-hole drops, far IR magneto-optical effects 78—84565
- Ge, electron-hole drops, IR absorpt. spectra 79—87423
- Ge, electron-hole drops, IR magnetoplasma absorptions 80—6728
- Ge, electron-hole drops, inflammation radiation under action of ultrasound *(Russian)* 79—7788
- Ge, electron-hole drops, kinetics of spatial distrib. *(Russian)* 78—43312
- Ge, electron-hole drops, laser Doppler velocimetry 77—43504
- Ge, electron-hole drops, motion in low mag. fields 79—23904
- Ge, electron-hole drops, non-isothermal nucleation 80—44514
- Ge, electron-hole drops, photoluminesc. kinetics 78—23524
- Ge, electron-hole drops, phonon lifetime and acoustic attenuation due to phonon-assisted Auger recomb. 80—34462
- Ge, electron-hole drops, resonant power absorpt., Alfven wave anal. 79—42569
- Ge, electron-hole drops, repulsive interaction and spatial distrib. 79—99488
- Ge, electron-hole drops, size distrib., light scatt. meas. 79—28292
- Ge, electron-hole drops, spatial distrib., time and spatially resolved absorption at 3.4 μm 78—92075
- Ge, electron-hole drops, surface struct. 78—60058
- Ge, electron-hole drops at high mag. fields 79—60721
- Ge, electron-hole drops interaction with phonons 80—6747
- Ge, electron-hole Fermi liquid, in ⟨111⟩-stressed Ge, unusual phase diagrams 79—63137
- Ge, electron-hole fluid drift in crossed electric and mag. fields, photocurrent dynamics *(Russian)* 79—99487
- Ge, electron-hole gas and liq. coexistence 78—14668
- Ge, electron-hole liq. thermalisation between mag. field split valleys 80—25444
- Ge, electron-hole liquid, ground state props. under ⟨111⟩ uniaxial stress 79—69428
- Ge, electron-hole liquid, luminesc. under infinite uniaxial compression 78—87915
- Ge, electron-hole liquid, MHD effects 80—80190
- Ge, electron-hole liquid, pinch effect 78—87993
- Ge, electron-hole liquid, range of energetic Auger electrons 79—90970
- Ge, electron-hole liquid, strain-confined 78—10355
- Ge, electron-hole liquid, strain-confined 80—6745
- Ge, electron-hole liquid in magnetic fields, expt. and theoretical investigations, review 79—60720
- Ge, electron-hole luminesc. replicas, ground-state Fermi energy from recomb. mechanisms 79—60728
- Ge, electron-hole two component liq. phase diagrams under stress 80—29332
- Ge, electron-hole-droplet cloud, photoluminesc. of laser excited surface, phonon wind 78—84146
- Ge exciton and electron-hole drop decay, far IR magnetoabsorption obs. 77—40252
- Ge, exciton and electron-hole drop entrainment by nonequilib. phonons 80—6751
- Ge, exciton condensate and electron-hole droplet, metastable state, effect of illumination and high-frequency heating 79—15097
- Ge, exciton condensation, electron-hole drop investigation in UHF field, nucleation *(Russian)* 80—80193
- Ge, exciton condensation, light scatt. by electron-hole drops 80—84435
- Ge, exciton condensation, microwave cond., book contrib. 80—11040
- Ge, exciton condensation, microwave breakdown, luminesc., book contrib. 80—11471

electron-hole drops continued
- Ge, exciton drops nucleation centres under conditions of inhomogeneous strain *(Russian)* 78—2429
- Ge, exciton microwave breakdown, electron-hole drops, book contrib. 80—11041
- Ge, excitons, influence of temp. on high freq. breakdown in presence of electron-hole drops 78—26820
- Ge, explosive instabilities in electron-hole drops under microwave radiation 77—31951
- Ge, far IR absorpt., damping and size effects, Mie theory 79—78685
- Ge, far IR magnetoabsorption, excitons, electron-hole drops and impurities 78—6664
- Ge, Foucault currents in electron-hole drops *(Russian)* 77—8030
- Ge, γ-electron-hole drop formation, time delay 77—31952
- Ge, HF breakdown of excitons effect on kinetic of electron hole droplets *(Russian)* 77—59260
- Ge, high density electron-hole plasma, infrared absorpt. at low temp. 78—92078
- Ge, highly degenerate multicomponent plasma thermodynamic props., electron-hole drop transition 80—33739
- Ge, highly excited, theory of electron-hole plasma 78—10363
- Ge, highly excited luminesc. and transport props. 77—48241
- Ge, IR absorption and scatt. by electron-hole drops 78—51903
- Ge, in superfluid He, threshold phenomena *(Russian)* 79—42462
- Ge, inhomogeneous stressed, electron-hole drop light scatt. and absorption 80—108212
- Ge, inhomogeneously stressed, giant electron-hole drop investig. by IR absorpt. 77—39785
- Ge, inter-valence-band absorption in electron-hole droplets 79—4515
- Ge, interaction of electron-hole drop with crystal surface 78—79941
- Ge, intervalence band absorption 80—6742
- Ge, kinetic theory for electron-hole condensation 77—85151
- Ge, luminescence circular polarisation in mag. field, Landau levels paramag. splitting 77—32435
- Ge, luminescence kinetics and electron-hole drop motion 77—77288
- Ge, luminescence line shape of free exciton, electron-hole droplet binding energy 77—44041
- Ge, mag. field luminesc. lifetime, quantum oscills., phonon wind effects 80—93385
- Ge magnetoacoustic effects in the drag of electron-hole drops by phonons 78—68057
- Ge, magnetodipole reson., 0.6 to 1.35 mm wavelength *(Russian)* 77—80736
- Ge, magnetoluminescence of electron-hole liq. 80—29790
- Ge, magnetoplasma reson. spectra, electron-hole drop shape effects 79—1712
- Ge, magnetoplasma resonance *(Russian)* 78—79944
- Ge, magnetoplasma resonance, at arbitrary crystallogrphic orientation in mag. field 79—78018
- Ge, magnetoresistance of electron-hole liq., percolation model 80—96920
- Ge, magnetostriction, drop distortion 77—85540
- Ge, microwave exciton breakdown and luminesc., under one- and two-photon excitation 77—31955
- Ge, microwave exciton discharge, collision frequency, hot carrier temp. determ. *(Russian)* 79—65507
- Ge, motion at low exciton densities 77—47865
- Ge, motion damping, impurity and piezoelec. scatt. 78—67951
- Ge, Mott distortion of the electron-hole fluid phase diagram, luminesc. meas. 79—42457
- Ge, Mott transition of exciton gas in equilib. with electron-hole droplets 77—4298
- Ge, movement under action of force of mutual repulsion *(Russian)* 77—89710
- Ge, nonequilibrium charge carrier-mag. field interaction electron-hole drops, recombination *(Russian)* 80—75511
- Ge, nonuniformly deformed, electron-hole drop density depend. on size *(Russian)* 80—20092
- Ge, nucleation anal. of electron-hole drops 77—69243
- Ge, ODMR using luminescence of electron-hole drops *(Russian)* 77—90072
- Ge, optically stimulated, electron-hole drops and appearance of dense plasma *(Russian)* 77—4688
- Ge, oscillatory exciton breakdown, microwave cond. 80—103716
- Ge, periodic explosions under light and microwave heating 77—11950
- Ge, phase diagram of electron-hole fluid in low temp. photoexcited semicond. 77—69237
- Ge, phonon damping of electron-hole droplet motion 77—85152
- Ge, phonon drag of electron-hole drops in longit. quantizing mag. field *(Russian)* 78—64070
- Ge, photocurrent magneto-oscillations 80—6911
- Ge, photocurrent oscillations in mag. field, intense excitation *(Russian)* 78—26915
- Ge, photoluminesc. decay from electron-hole drops 77—66532
- Ge, pure, electron hole size distribution at pulse optical excitation 80—59883
- Ge, pure, large, electron hole drops, microwave heating and evaporation 79—28287
- Ge, pure, magnetic phase transition between electron-hole drops and free-excitons 78—6278
- Ge, pure and doped, electron-hole drops net charge, photocond. and photoluminesc. 79—38589
- Ge, recombination luminesc. spectra from hot and cold carriers in electron-hole drops 79—38608
- Ge, rest friction of electron-hole drops *(Russian)* 79—42463
- Ge, sign reversals of charge, calc. of surface props. 77—89711
- Ge, size effect on far IR absorption and scatt. *(Russian)* 78—10903
- Ge, size effects in small electron-hole drops 79—82530
- Ge, strain-confined electron-hole liq. 77—47738
- Ge, strain-confined electron-hole liquid, density variation 78—34779
- Ge, strain-confined electron-hole liquid, lifetime and radiative efficiency vs density 79—38000
- Ge strain-confined large electron-hole drop characteristics 80—65469
- Ge, strained, crit.-point for electron-hole droplets 79—4516
- Ge, stressed, α_1 and α_3 electron-hole droplet luminesc. 79—28820
- Ge, stressed, metal-insulator transition, luminesc. 80—20695
- Ge, stressed, recombination luminescence from hot carriers in electron-hole droplets 78—6754
- Ge, stressed cryst., props. of strain-confined electron-hole liquid 79—7787
- Ge, strong microwave field effects, luminescence kinetics 79—87047
- Ge, surface energy calcs. 77—47741
- Ge, surface energy effect on electon-hole drop luminesc. 77—48239

electron-hole drops continued
Ge, transport props. of high density electron-hole plasma at low temp. 77−47864
Ge, US wave absorpt. under optical excitation, recomb. radiation 77−31954
Ge, ultra-pure drop condensation, nucleation phenomena 77−47744
Ge, uniaxially deform., electron-hole drop flight, photolum. max. press. depend. 78−10977
Ge, uniformly deformed, free carrier cyclotron resonance, electron-hole drops *(Russian)* 80−71182
Ge, uniformly stressed, density and binding energy of electron-hole droplets, photolum. meas. 78−60062
Ge, unstrained, electron-hole drop shape in mag. field 79−42458
n-Ge:As, heavily doped, luminesc. from electron-hole drops 77−81144
n-Ge:As(Sb), moderately heavily doped, electron-hole drops photoluminesc. 80−7417
Ge:In (Sb) and pure cryst., kinetics of strain-confined large electron-hole drop and its clinging exciton system 80−75508
Ge:Sb, electron-hole drop lifetime, quenching temp. influence 80−59889
Ge-Sb, meas. of electron-hole drop size by light scatt. 80−44515
He, liquid, first and second sound generation by immersed Ge cryst. optical pumping 80−6581
MgO, electronic excitations and luminescence, review *(Russian)* 78−72575
NH$_4$Br:Tl, and pure crystals, luminesc., VUV irradiated at 80K *(Russian)* 80−84763
PbI$_2$ crystals, exciton condensation, excitation and luminesc. study 80−55182
PbI$_2$ direct gap polar semicond., electron hole liquid phase diagram *(Russian)* 80−93314
PbI$_2$ direct gap semiconductor, exciton lifetime and condensation threshold, luminescence spectra 80−34981
PbI$_2$, exciton spectra depend. on strong excitation, crystal transmission 79−69433
PbI$_2$, temp. depend. of electron-hole drop emission *(Russian)* 77−16394
Pd, phonon linewidths and electronic mass enhancement, electron-phonon contrib. 79−95099
Si, Auger recomb., luminesc. meas. 77−48240
Si, Auger recombination, localized and free carrier comparison 79−38090
Si, deformed, recomb. radiation from electron-hole drops and free excitons 77−8641
Si, electron-hole drop luminescence, hysteresis effect and surface energy 78−2907
Si, electron-hole drop transition to metallic condensed state, Hartree-Fock theory 79−56136
Si, electron-hole droplet, effect of nonlocal contributions to energy 77−69246
Si, electron-hole droplet condensation, phase diagram and surface tension 79−19521
Si, electron-hole droplet condensation model, phase diagram and surface tension 80−6734
Si, electron-hole droplet condensation, crit. point 80−49612
Si, electron-hole droplet luminesc., laser excitation threshold meas. 79−33821
Si, electron-hole droplet spatial distrib., luminesc. obs. 80−49615
Si, electron-hole droplets nucleation at swirl defects 79−15095
Si, electron-hole drops, far IR absorpt. spectrum 78−47706
Si, electron-hole drops, nonequilib. paramagnetism 80−6749
Si, electron-hole drops, nucleation, time resolved luminesc. spectroscopy 78−6280
Si, electron-hole drops, nucleation, luminesc. threshold obs. 79−33822
Si, electron-hole drops, thermodynamical parameter determ. from luminescence data 80−2845
Si, electron-hole drops radius, luminesc. meas. 80−50415
Si, electron-hole liquid, free excitons, biexciton gas, luminesc. 80−6750
Si, electron-hole liquid, spatial condensation of strain-confined excitons and excitonic mols. 78−39592
Si, electron-hole liquid and exciton and biexciton gas in elastically deformed cryst. *(Russian)* 78−34782
Si, exciton-plasma Mott transition, luminescence spectra 77−62836
Si, excitons and electron-hole drops, phonon assisted luminescence lineshape 79−99942
Si, excitons and electron-hole liquid, luminesc. 80−6746
Si, high purity, exciton lifetime, temp. depend., photoluminesc. meas. 80−44508
Si, highly excited, theory of electron-hole plasma 78−10363
Si, intrinsic, phonon replicas of electron-hole liq. luminesc. line 79−28831
Si, large uniaxial stress, effect of non parabolicity of valence band 78−47703
Si, luminesc., simultaneous kinetics of drops and excitons during drop formation 77−48222
Si, near and far IR emission spectra 77−48242
Si, non-equilib. orientation of electrons in electron-hole droplets in mag. field *(Russian)* 77−36294
Si, nonequilib. electron-hole system, gas-liq. phase diagram *(Russian)* 77−43509
Si, p-i-n structures, pinch effect expt. obs. 79−90971
Si, photoluminescence of electron-hole drops under uniaxial stress 79−91491
Si, strained, crit.-point for electron-hole droplets 79−4516
Si, stressed, one- and two-component electron-hole liq. at T=0 80−80189
Si:B, photolum. of heavily doped p- and n-type 80−20708
Si:B(P), uniaxially stressed, impurity-assisted intervalley scatt., photoluminesc. obs. 80−34979
Si:P, heavily doped, electron-hole droplets, photolum. obs. 1.5 to 80K 77−36289
Si:P heavily-doped, photoluminescence 78−72572
n-Si:P(B), elec. cond. oscills., electron instability effects due to dislocations 80−103704
SiC (15 R), polytype, many valleyed polar semicond., electron-hole-liquid, obs. from excitation and time delayed spectra 79−28289
SiC, cubic, electron-hole liq., luminesc. obs. 78−31239
SiC, cubic, electron-hole liq., ground state props. calc. 79−69429
SiC, luminesc., electron-hole drop 79−38606
Si$_3$N$_4$-GaAs, layer struct., electron-hole liq. at interface 79−69434
Si$_3$N$_4$-GaAs structure, photoluminesc. and collective effects 78−6727
ZnO, electron-hole liq., optical gain meas. 77−85794

electron-hole drops continued
ZnO, multiparticle exciton complexes, luminesc. spectra *(Russian)* 80−16090
ZnO, reflection spectra, exciton reflection at high excitation levels 77−69853
ZnSe, single cryst., electron-hole drops, boundary luminesc. *(Russian)* 78−80412
ZnTe, reson. secondary radiation 79−99886
ZnTe, single cryst., electron-hole drop conc. *(Russian)* 79−11460

electron-hole recombination
see also carrier mobility
AC response, influence of states in gap and generation-recomb. effects 77−4362
alkali halide: monovalent cation, recomb. luminesc. $(V_K+e)_A$-type emission 77−28615
alkali halide, hole capture kinetics, influence of autolocalised and zone holes *(Russian)* 80−54714
ambipolar diffusion meas. using nonlinear transient gratings 78−80000
amorphous semiconductors, photogeneration of charge carriers and recomb. 77−81147
anthracene, electron bombardment, field and temp. depend. of carrier yield 77−8117
anthracene, field depend. of photocond. 79−99578
anthracene, photo-oxidised, current oscills. due to recomb. instability in high field domain 77−4353
anthracene, single crystal, photoconductivity quantum yield, experimental validation of fund. theory 80−6909
anthracene thin films, high field effects and switching, local centres importance 79−73548
Auger recombination of carriers bound to centres involving phonons 80−107805
bipolar conductivity equations, approx. solns. 77−69336
bipolar semiconductor, strong EM wave propagation, effect of generation-recombination processes *(Russian)* 79−78115
bisphenol-A-polycarbonate:N-isopropylcarbazole, hole photogeneration efficiency 79−56243
bulk trapping processes and trap occupancy 77−39876
capture probabilities of two deep impurity levels, photoconductivity decay analysis 77−89808
carrier effective lifetime modulation, surface recomb. and mag. field effects 77−28193
carrier photogeneration efficiency, Onsager theory of geminate recomb. 79−56242
CdS, green edge luminescence spectrum, temp. depend. 80−108274
chalcogenide glass, mech. for electron-hole recomb. 78−72196
chalcogenide glasses, non-radiative recombination of electron-hole pairs 78−6759
chalcogenide glasses, radiative recomb. obs. as efficient luminesc. 78−2914
conference, luminescence, Paris (July 1978) 79−33755
current instabilities in semiconductors, theory and expts. *(Hungarian)* 77−39857
decay kinetics in diffusion approx. in presence of particles pair correlation 78−80398
deep centres, ODMR *(French)* 80−60461
degenerate semiconductor, phonon-assisted Auger recomb. 77−59292
degenerate semiconductor, recombination-generation currents derivation 78−52007
DH devices, interface recomb. effects on transient response 77−88722
diamond, role of electron-hole interaction in optical spectra, review 80−45113
dielectrics containing impurities, carrier distribs. and currents, numerical simulation *(French)* 80−70718
diffusion length and lifetime meas. and assessment by SEM 80−96902
diffusion length and surface recomb. vel. determ., light excitation 78−91725
disordered semiconductors, recomb. radiation spectrum *(Russian)* 79−4855
donors with excited states, kinetics of electron transitions 80−39600
electrode and volume controlled photocurrents 80−6908
electron-beam-induced current, minority carrier generation vol. influence 80−84475
electron-hole drop shape in mag. field and strain induced potential well 79−23903
electron-hole drops, non-radiative recombination by phonon-assisted Auger recomb. 79−60716
electron-hole transitions, nonstationary processes, numerical anal. *(Ukrainian)* 78−84229
ferromagnet-semiconductor contact, spin-depend. recomb. and scatt. on electron injection 80−65654
finite systems containing traps, Hall effect, two-carrier one-dimens. transport anal. 80−44614
frozen-in conductivity, nature of recomb. barriers 79−56245
n-GaP, quasidirect radiative recombination of free holes at neutral shallow donors 78−64410
halides, vacancy-interstitial pair prod. by electron-hole recomb. 79−4530
heterostructure laser, elec. characterisation 78−79020
HgCdTe/CdTe, limited diffusion volume photodiode, characterisation 80−75627
high-resistivity semiconductors, theory and expt. *(Japanese)* 80−6850
homojunction direct gap solar cells, theoretical limit efficiency 80−97795
III-V compound heterojunctions, recomb. vel., appl. to Al$_x$Ga$_{1-x}$As-GaAs$_{1-y}$Sb$_y$ solar cells *(Korean)* 80−54771
III-V semiconductor, acceptor levels, anisotropy of Zeeman splitting and polarization of luminesc. in mag. field 79−24365
III-V semiconductors, Auger coeffs. calc. 79−15160
III-V semiconductors, electrolum. and related props., book contrib. 77−73173
III-V semiconductors, props. and optoelectronic device appls. 79−74088
III-V semiconductors, radiative recomb., optical evaluation review 80−60647
n-InSb, surface recomb. vel., repeated cyclic surface treatment effects 77−32065
insulated crystal, primary photocurrent kinetics for simultaneous trapping and recomb. 80−6899
insulator, charge carrier injection, Onsager model 78−80001
insulators, transient radiation induced ionisation effects 77−80788
JFETs, generation-recombination noise at 77K 79−60883
junction devices, generation recombination current, noise reduction, SRH centres in space-charge layer 77−76905

electron-hole recombination continued
kinetics, many-particles correlation 79—47502
kinetics, subject to allowance for correl. between particles 80—80858
laser, single heterostruct., spatial distrib. of radiative recomb. rate, time delays and Q-switching 79—22953
latent image formation, influence of recombination 77—5945
LED, DH, output power and response time, thickness depend. 79—95479
lifetime measurement using pulsed MOS capacitor 80—25012
luminescence, debye-Edwards electron recombination kinetics 79—87495
metal surface, with adsorbed molecules, giant Raman scatt. mechanisms 79—51960
minority carrier recombination 80—65591
minority carrier recombination at surfaces, dislocations and microdefects, luminesc. evaluation 78—6769
MIS structures, surface recombination and photoeffect, statistics *(Russian)* 78—39221
MOS capacitor, Au-doped, bulk and interfacial prop. determ. using quasiequilibrium and linear voltage ramp techniques 79—95501
MOS capacitors, electron injection studies of radiation induced positive charge 77—20441
MOS pulsed capacitor, minority carrier lifetime meas. influence of Si-wafer surface state density 80—60098
MOS structures with external p-n junction, linear gate volt., impulse-current behaviour *(German)* 79—56319
MOSFET, recomb. lifetime determ. 80—62683
multilevel generation-recomb. noise spectra, appl. of equivalent network methods 77—43674
narrow gap semiconductor, plasmon emission 78—39046
narrow gap semiconductors, recombination mechanisms, review 80—96905
narrow-gap semiconductor, recomb. instability of electron-hole plasma 80—39621
negative differential cond. of hot electrons in mag. field due to carrier density nonlinearity 77—55540
octaethylporphin in Al-Ag sandwich cell, electroluminesc. 77—59615
Onsager model, time-depend. quantum efficiency 79—11194
p$^+$-i-n$^+$ structure, double-injection negative differential resist. problem, surface recomb. effects 78—88024
p-i-n structure, forward biased, with band to band Auger recombination, numerical simulation 79—7879
p-i-p structure, two-dimensional carrier transport at high injection rate 79—15213
p-n junction, current-voltage charact. effect of generation-recombination *(Rumanian)* 78—2553
p-n junction, diffused, space-charge recombination current 80—88623
p-n junction solar cells, determ. of lifetime and recombination currents 80—89637
p-n junctions, minority carrier surface recombination velocity, lifetime, AM electron beam determ. 79—87145
p-n junctions, variable gap, recombination currents in space charge layer 80—20303
pair correlation of particles under decay conditions, recomb. kinetics in diffusion approximation 78—91702
pentamethinium cyanine dye, single cryst., depend. of photocurrent on recomb. 79—51626
phonon-assisted nonradiative recombination phenomena in semiconds. *(Polish)* 77—69339
photochromic glasses, electron-hole separation, influence on recombination probability 80—11445
photoconductivity, rate and continuity equations solution, for time region before excited carriers recomb. *(Japanese)* 79—4584
photoconductors, possibility of observing ambipolar photoconductivity and its optical quenching 78—14764
photodielectric, stationary recombination equations, analytical solutions in source limiting cases 80—44662
photoexcited hot electrons in high mag. field, mean energy 78—30955
photogalvanic effect under electron-hole interaction conditions 80—88591
photogeneration and fluoresc. quenching theory, appl. to x-metal-free phthalocyanine 79—65513
photovoltaic effect, impurity centre models *(Russian)* 78—60153
planar diode, heavily doped, collection efficiency and surface recomb. vel. modulation 80—20291
polar semiconductor crystalline thin films, surface vibr. states, IR absorpt. spectra obs. *(Russian)* 80—60606
polydiacetylene bis-(toluenesulphonate), single cryst., charge carrier mobility and recomb. 77—8132
polydiacetylene-bis(toluenesulphonate), transient photocond. meas. 78—30951
polydiacetylene-toluenesulphonate, photocond. meas., 0.62-3.1 eV 80—70757
pyridine, adsorbed on Ag, giant Raman scatt. 79—95768
quartz, crystalline, thermolum. sensitivity, proton and gamma induced 77—90205
radiationless Auger-recombination of electrons on three centres *(Russian)* 79—78114
radiative and nonradiative recomb. at metal ions, core struct. effects, review 79—4834
radiative spectra from hot photocarriers 78—31249
resonance radiation of electron-hole droplets, surface plasmon radiative decay *(Russian)* 77—62841
rhodamine B adsorbed on anthracene, electron-hole pair in external elec. field 79—73558
ruby, induced absorpt., radioluminesc., thermoluminesc., Cr^{3+} conc. depend. *(Russian)* 77—90206
Schottky barrier, real and ideal, photosensitivity losses 80—2452
Schottky barrier solar cells, back-illuminated, theoretical performance 80—61345
SEM meas. of diffusion const., lifetime and surface recomb. vel. 78—91701
semi-infinite direct-gap semiconductor optically generated minority carriers 78—95312
semicondctor diffusion length and surface recombination velocity determ. by intensity modulated SEM 78—10472
semiconductor, adiabatic approx. in transient donor recomb. 80—49761
semiconductor, ambipolar hot-carrier size effect kinetics 80—107799
semiconductor, Auger recombination, carrier density depend. 79—38089
semiconductor, Auger recombination cross sections associated with deep centres 78—47810
semiconductor, Auger recombination rate, nonequilib. carrier distrib. 80—65578
semiconductor, biexcitons, one-photon radiative recomb. 80—70621

electron-hole recombination continued
semiconductor, dimaond-like narrow-gap, Auger recomb. calc. 78—63978
semiconductor, disordered, electroabsorption, contact excitons influence 80—10882
semiconductor, donor-acceptor pair in elec. field, anomalous Stark shift of ground state energy 79—19564
semiconductor, drift mobility temp. depend. in presence of trap-recombination centres *(Russian)* 78—26880
semiconductor, elec. parameters determ. by electron probe method 79—9259
semiconductor, electric field induced nonequilib. phase transitions 80—10879
semiconductor, electron relaxation, electron-hole interaction effect 78—10437
semiconductor, electron-donor recombination, Monte Carlo studies of transitions between excited donor states 79—38093
semiconductor, graded-gap, internal photo-effects, excess carrier distribs. 80—107847
semiconductor, highly excited, photomagnetoelectric effect under Auger recombination 80—44664
semiconductor, hot electrons, photoexcited in quantizing mag. field, energy distrib. calcs. 79—42586
semiconductor, impurity interaction and donor-acceptor recombination 80—16094
semiconductor, indirect band gap, Auger recomb. of electron-hole drops 78—39600
semiconductor, inhomogeneous, theory of residual cond. 78—14739
semiconductor, ionization and subthreshold effects in defect creation and annihilation 77—84811
semiconductor, lifetime of carriers recombining in disordered regions, injection depend. 78—14742
semiconductor, magnetoconcentration effect, use of Boltzmann formalism *(French)* 77—32025
semiconductor, magnetodiode and magnetoconcentration effects, influence of field effect 80—107903
semiconductor, multiphonon electron-hole recomb. processes 78—6750
semiconductor, multiphonon recombination processes 79—38643
semiconductor, narrow gap, mag. quantum oscills. of Auger transition rate 77—69340
semiconductor, ODMR appl. to recombination processes 79—42871
semiconductor, optical parameters in strong EM field, effects of finite wavelength of light 77—44050
semiconductor, p-type, field emission theory, surface states and recomb. processes 77—85901
semiconductor, phonon-assisted Auger recomb., scatt. mechanisms 77—85804
semiconductor, phonon-assisted Auger recomb. transition probability 77—44064
semiconductor, photoluminescence, deep level recombination temp. depend. 79—47497
semiconductor, photomagnetoelectric effect, injection-level dependent lifetime 80—80319
semiconductor, polycryst., electronic processes at grain boundaries under optical illum. 77—55561
semiconductor, radiative and nonradiative recomb., spontaneous and stimulated emission *(Polish)* 80—53293
semiconductor, radiative recomb. at donor-acceptor pairs, majority impurity config. average calcs. 80—40154
semiconductor, recomb. centre distrib., scanning photocurrent microscopy 79—35822
semiconductor, recomb.-enhanced defect reactions 77—51377
semiconductor, recombination and generation mechanisms, band-type models exhibiting phase transitions 79—47049
semiconductor, recombination at deep traps, review 79—38100
semiconductor, recombination enhanced defect reactions 79—38094
semiconductor, recombination of nonequilib. carriers in presence of dislocations 79—82607
semiconductor, recombination radiation mag. depolaris., spin level quadrupole splitting of lattice nuclei *(Russian)* 79—38666
semiconductor, recombination radiation transfer effect on diffusion of nonequilibrium charge carriers 77—76843
semiconductor, spin dependent recomb., theory 80—103708
semiconductor, spin-depend. recomb. effect 78—34841
semiconductor, stationary recombination equations, analytical solutions in source limiting cases 80—44662
semiconductor, with high quantum yield and recomb.-radiation reabsorpt., induced-current, in SEM 79—11140
semiconductor bicrystal, charge carrier interface recomb., photocond. meas. method 79—99431
semiconductor depth profiling by electron beam induced junction current meas. 80—96977
semiconductor detector with alternating bias, energy resolution 77—10553
semiconductor device, surface recombination, effect on steady-state relationships 78—39191
semiconductor device, surface recombination effect 79—82664
semiconductor electrode, electrolum. due to hole injection from electrolyte 77—20926
semiconductor film, carrier temperature and density self-oscills. near instability threshold 80—11118
semiconductor generation-recombination noise 79—24032
semiconductor laser, atom displacement as result of nonradiative recomb., defect form. mechanism 79—10308
semiconductor laser, stimulated emission threshold, surface recombination influence 79—10311
semiconductor laser crystals, defect-forming resonance electron capture, theory 80—14341
semiconductor models for non-equilibrium phase transitions due to impact ionisation from traps 79—51520
semiconductor plate edge, effect of surface recomb. on excess charge carrier distrib. and base current 77—39866
semiconductor stable electron-hole plasma, diffusion in magnetic field 79—24001
semiconductor surface, macroscopic recomb. centres 80—6933
semiconductor under illumination, simple model of generation and recombination processes 79—69523
semiconductor with position depend. composition, carrier generation, recomb., trapping and transport 77—43613
semiconductor-electrolyte functions, photocharacts. 78—91764
semiconductors, Auger recombination processes 79—38091
semiconductors, Auger recombination with traps 80—49763

electron-hole recombination continued
- semiconductors, generalised transport equations 79—95398
- semiconductors, heavily doped, compensated, long wavelength recomb. radiation 80—7403
- semiconductors, high density excitons and biexcitons, recomb. radiation bands profiles, time depend. 80—45140
- semiconductors, interimpurity radiative recombination, intermediate exciton state *(Russian)* 80—49621
- semiconductors, multiphonon electron-hole recomb. processes 78—6751
- semiconductors, narrow-gap, recomb. instability under crossed elec. and mag. fields 80—70712
- semiconductors, nonradiative recombination, combination of Auger and many-phonon processes 79—87111
- semiconductors, optical saturation for high carrier recomb. freq. *(Russian)* 80—88585
- semiconductors, p-n junction area *(Polish)* 80—53294
- semiconductors, p-type, mag. oscills. of momentum distribution of hot photoexcited electrons *(Russian)* 80—2854
- semiconductors, phonon assisted electron impact ionisation and Auger recombination, theory 80—39591
- semiconductors, photocond., photoelec. effects, book contrib. 80—84488
- semiconductors, radiative recomb., book contrib. 80—84784
- semiconductors, radiative two-electron transitions 79—43026
- semiconductors, recombination, conference, Southampton, England (Aug.-Sept. 1978) 79—38087
- semiconductors, recombination processes, review 79—38088
- semiconductors, recombination wave instability threshold, external load, boundary condition depend. 78—19053
- semiconductors, recombination wave modes in case of several trap levels 80—39602
- semiconductors, scatt. influence on Auger transition, depend. of impact ionisation on electron energy 80—44608
- semiconductors and insulators, role of electron-hole interaction in optical spectra, review 80—45113
- n-Si, recombination centres and carrier lifetimes after γ-irrad. 80—60004
- small signal electrical response theory, generation-recomb. and trapping kinetics 77—89772
- solar cell, absolute efficiency meas., effect of recombination-centre saturation 79—83597
- solar cell, Auger recombination limit on efficiency at high level of illumination 80—108797
- solar cell, p-n junction, polycryst., grain boundary influence on recomb. 80—93913
- solar cells, $Cu_{2-x}S$-CdS, collection coefficient theoretical anal. at conjunction 80—101094
- solar cells, polycryst., recomb. at grain boundaries, effect on photoresponse 80—108796
- solar cells, surface recombination velocity and diffusion length meas. 80—93965
- SOS films, carrier recomb. props., magnetosensitive method 79—38186
- SOS films, surface recomb. profile and transport parameters 79—33357
- surface trapping phenomena rel. to surface states 77—39916
- p-terphenyl, cryst., double injection and electrolum. 80—97342
- tetracene, spatial distrib. of electrolum. and recomb. process 79—19938
- N,N,N′,N′-tetramethyl-p-phenylenediamine, TMPD, glassy soln., photoionisation, recombination isothermal luminesc. *(French)* 77—16404
- threshold switching as a generation-recombination induced non-equilibrium transition 79—33314
- trapping parameters for thermally stimulated luminesc. and cond. 77—52190
- triphenylamine in 3-methylpentane and ethanol glasses, γ-radiolysis, IR spectra, trapped electron 77—16842
- TSC, with participation of two trapping levels 79—56244
- TSC and thermoluminescence correlation, simultaneous meas. 77—81160
- TTT, dark injection current, sign inversion of low mag. field *(Russian)* 79—73602
- variable gap semiconductor, photolum. emission and excitation spectra 78—76526
- xerographic photoconductor, bimol. recomb., reciprocity 77—51775
- zircon, natural and synthetic crysts. Hf and Tb activated, capture centres and luminescence mechanism *(Russian)* 77—28626
- γ-rays from pair recombination in travelling wave struct., stimulated emission 78—37863
- AgBr, electron-hole kinetics 79—24005
- AgBr, photoexcited electrons and holes in latest image form., review 80—73496
- AgBr, recombination process in photolysis 79—24789
- AgBr(I), emulsion coating, hydrogen hypersensitisation to diminish recomb. and increase quantum efficiency 77—5942
- AgCl, cryst. luminesc. and photovoltaic effect kinetics 78—64391
- AgCl, luminescence fatigue, adsorbed Ag atoms 80—66281
- AgCl, optically detected EPR of excited states rel. to luminesc. 77—12256
- AgCl:Ni, optically detected double resonance, radiative recombination electron traps 80—20518
- $AgGaS_2$, electroluminesc., mechanism *(Russian)* 77—69918
- (Al,Ga)As DH injection lasers, sustained oscills. depend. on DC current bias 79—68392
- Al-Al_2O_3-InSb MIS structures, recomb. processes and carrier lifetimes 79—38177
- Al-SiO_2-Si Schottky barrier solar cells, recomb. effects 79—39310
- AlGaAs heterojunctions, nonradiative recomb. vel. estimate from edge luminesc. props. 80—65668
- AlGaAs-GaAs proton irradiated solar cells, deep level defects and recombination parameters 80—94032
- n-$Al_xGa_{1-x}As$, epitaxial, photolum. emission and excitation spectra 78—76526
- $Al_xGa_{1-x}As$ p-n junction, photolum. and current, interface recomb. effects 78—95346
- $Al_xGa_{1-x}As$:Cu, variable-gap semicond., impurity props., carrier recomb. 80—96907
- $Al_xGa_{1-x}As$-GaAs, p-n heterostruct. laser, tunnel injection and phonon-assisted recomb. 80—5733
- $Al_xGa_{1-x}As$-GaAs heterostructure photoluminesc., origin of large dark spots 77—85763
- $Al_xGa_{1-x}As$-GaAs heterostructure, nonradiative large dark spots rel. to minority carrier transport 78—9378
- $Al_xGa_{1-x}As$-GaAs quantum-well heterostructures, phonon-assisted recomb. and stimulated emission 80—74358
- $Al_xGa_{1-x}As$-GaAs quantum-well heterostruct., exciton in recomb. 80—103990

electron-hole recombination continued
- $Al_xGa_{1-x}As$-$GaAs_{1-y}Sb_y$ solar cells, appl. of recomb. vel. at III-V cpd. heterojunctions *(Korean)* 80—54771
- α-Al_2O_3 recombination luminescence excitation by synchrotron radiation 79—95841
- α-Al_2O_3, recombination luminescence mechanism 80—71477
- Al_2O_3:Cr, pure and doped, electron irrad. induced cond., TSC and EPR study 80—80277
- Al_2O_3:Mg, pure and doped, recombination luminesc. spectra 79—83021
- As_2S_3 and As_2S_3-Sb_2S_3 system glasses, long-term photocond. relax. 77—76874
- Au-GaAs, photosensitivity losses, field and spectral depend. 80—2452
- Au-n-Si Schottky barrier solar cells, recombination in space charge region 80—61351
- BaFCl crystals, F-centres, X- and γ-irradiation, thermoluminescence and optical absorption spectra 80—45155
- $Ba_3(PO_4)_2$, recomb. luminesc. mechanisms 80—2874
- Bi, intervalley scatt. influence on mobilities, thermopower calc. 78—26866
- CN^-, adsorbed on Ag, giant Raman scatt. 79—95768
- CaF_2:Co, X-irrad., luminesc. spectra 79—28801
- CaO, doped, thermal stability of hole centres and hole recombination luminescence *(Russian)* 78—72614
- CaO, undoped and Cl-, F- or Al-doped, X-ray and UV luminesc., electron-hole recombination processes *(Russian)* 78—76528
- CaO:F(Cl)(Al), phosphon, luminesc., electron-hole recombination processes 79—65919
- CaS, phosphors, hole recombination luminescence *(Russian)* 78—72576
- $CaSO_4$:Dy, thermolum. origin, test of model on $CaSO_4$:Eu 77—85813
- $CaWO_4$, type selfactivated luminophors, nature of optically active centres 77—69880
- $CdGaS_2$, single crysts., peculiarities of photocond. in strong elec. field 80—54736
- Cd_xHg_{1-x} Te, photodetectors, recomb. processes, photoconductive decay obs. 79—38129
- n-$Cd_{0.3}Hg_{0.7}Te$, recomb. levels 79—91076
- n-$Cd_xHg_{1-x}Te$ crystals, carrier recomb. in extrinsic conduction range 80—70722
- $Cd_xHg_{1-x}Te$, inhomogeneous composition effect on carrier lifetime and photosensitivity *(Russian)* 79—73526
- $Cd_xHg_{1-x}Te$, photoelectric props. at high temp. 77—4403
- CdI_2 (Br_2), cathodoluminescence, 300 and 80K *(Russian)* 79—78760
- CdS, Auger effects in donor acceptor pair spectra 80—20707
- CdS, charged impurity centres, drift during passage of photocurrent 80—70767
- CdS, defects formed by laser radiation of subthreshold intensity, bulk photo-EMF investigation 79—91098
- CdS, drift mobility in presence of trapping-recomb. centres 78—19054
- CdS, exciton luminescence, surface recombination, space-charge-layer effects 78—80410
- CdS films, amorphous and polycrystalline, microinclusion distrib. of high resist. phase and residual cond. 80—7008
- CdS, highly excited, stimulated emission processes, electron-hole plasma recomb. 80—97307
- CdS, laser thresholds and stimulated emission, intrinsic recomb. processes 79—15489
- CdS, localised level anal. from generation-recomb. noise spectra 78—14777
- CdS pulsed optically detected resonance, time depend. recomb. processor study 79—38411
- CdS, quasimonopolar semicond., recombination in near surface space charge region *(Russian)* 80—88574
- CdS, recomb. radiation of electron-hole liq., quantum oscills. *(Russian)* 77—36293
- CdS, recombination electric domains, production mechanism 80—29433
- CdS, stress-induced photolum. bands, photocond., rel. to dislocation electron states 80—25447
- CdS:Cu, dye-sensitised, photocond. and photocurrent decay time obs. 80—6893
- CdS:Cu, photocond. under high excitation intensity 78—52033
- CdS:Cu(Cl), thin layer, electron pulse induced cond. relax. 80—2501
- CdS:Li, TSC and optical photocurrent quenching spectra, Auger excitation of recomb. centres 79—33294
- CdS:Ni, nonradiative recomb., photocond. spectra 80—70764
- CdS:Ni, recomb. parameters, photocond. spectra meas. *(Russian)* 80—49820
- CdS-Cu_2S heterojunction, influence of surface recomb. on photoelec. props. 77—43711
- CdS-$CuInSe_2$ solar cells, grain boundary and interface recomb. effects 79—39311
- n-CdS(Se)(Te) semicond. liq. junction solar cells, photocurrent spectra, carrier recombination 78—76142
- CdSe, charge transport 78—84233
- n-CdSe, laser excited stimulated emission, optical gain spectrum 80—76050
- CdSe, recombination mechanism at dislocations, photoluminescence 80—103993
- $CdSiP_2$:Na(Bi), single crystal, photocond. under laser excitation 80—44661
- CdTe diode, generation-recomb. and ionisation processes, temp. depend. *(Russian)* 77—39942
- n-CdTe films, uniform trap distrib., transient photocond. effects 79—28423
- CdTe p-n homojunction, elec. and photovoltaic props. rel. to solar energy conversion 79—51668
- CdTe p-n junction, short-circuited, estimation of surface recomb. rates, electron-probe meas. 77—43713
- p-CdTe:Cl, mech. of electron recomb. 79—11176
- CdTe:Cr, impurity photoionisation transitions, EPR meas. 80—39857
- CdTe-metal, diode contact, elec. characts., generation-recombination space charge region *(Russian)* 78—39214
- CsI:Na, tunnelling recomb. of electron-hole pair, optical detection of ESR and circ. dichroism 79—47360
- CsI(Br)(Cl):Tl, $[X_2^-]$ centre dynamic props. 79—65730
- Cu cathode, electroluminesc. from semicond. impurities on surface 77—90200
- Cu, hot cathodoluminescence study, electron-hole recombination 80—93410
- CuCl, donor-acceptor recomb. spectra 80—45131
- $CuGaSe_2$, photoluminesc. spectra at 76K 79—38655

electron-hole recombination continued
Cu_2S-CdS solar cells, interface recombination phenomena and tunnel effect 80—66978
Cu_xS-CdS solar cells, space charge region recombination, SEM meas. 80—16808
D_2O ice, crystalline, irrad., temp. depend. of trapped electrons, 77 to 6K 79—83474
(Ga,Al)As:Si(Ge), epitaxial layers, radiative recomb., compensation, cathodolum. study 80—66307
GaAS, photoluminescence in polycrystalline samples at 5K, possible solar cell material 79—99929
GaAlAs DH laser, optimum p-n junction depth, photoluminesc. method 79—4598
GaAlAs DH lasers, electron-hole recomb. effects 79—45944
GaAlAs DH lasers, proton-bombard., nonradiative recomb., luminesc. time-response meas. 79—98371
GaAlAs-GaAs double heterostructure, interfacial recomb. velocity, photolum. meas. 78—68075
GaAlAs-GaAs heterostructures, electronic excitation effects on mobility of point defects and dislocations 78—2561
$Ga_{0.5}Al_{0.5}As$-GaAs, DH, interfacial recomb., photolum. time decay meas. 78—95347
$Ga_{1-x}Al_xAs_{1-y}P_y$ epitaxial film, nonradiative recomb. at dislocations 80—44213
$Ga_{1-x}Al_xAs_{1-y}P_y$ epitaxial layer heterojunction, nonradiative recombination at misfit dislocations 80—96901
GaAs, acceptor bound exciton Auger and radiative transition rates, radiative recomb. 80—6733
GaAs amorphous film/GaAs crystal junction, optical and elec. props. 79—99611
GaAs, electron-beam excited, efficient generation of electron-hole plasma 80—76051
GaAs, electron-spin relaxation and recomb. kinetics, time-resolved luminesc. study 80—108074
GaAs epitaxial film recombination props. *(Russian)* 80—49812
GaAs epitaxial layers, photocond. high field effects on carrier capture and recomb. 77—43646
GaAs epitaxial layers, undoped, recomb. of non-equilib. carriers, steady-state photocond. 77—85357
p-GaAs, Fe-compensated, photocond. under strong excitation 77—15904
GaAs, film, radiative relax. time, nonequilibrium carriers 78—84657
GaAs, Gunn effect, carrier generation-recomb. processes 79—38080
GaAs, γ- and electron irradiation, influence on recomb. characts. near surface 80—71478
GaAs, H ion bombard., carrier removal effects 80—92542
GaAs heterojunction laser, origin of dislocation climb during laser operation 77—51380
GaAs, illuminated, carrier lifetime profile, depth depend. 78—68036
n-GaAs, impurity interaction and donor-acceptor recombination 80—16094
GaAs LED, optimum p-n junction depth, photoluminesc. method 79—4598
GaAs, LPE layers, outdiffusion of recomb. centres from substrate during growth 80—39466
GaAs, luminesc. emitted by deep centres, illumination-induced change in internal quantum efficiency 79—91495
GaAs, minority carrier diffusion length, reabsorbed radiation effect 77—28191
GaAs p^+-n diode, radiative hot carrier recomb., photoluminesc. and electroluminesc. meas. 79—38676
GaAs, p^+-n^0-n^+ struct., control of modulation of base resist. 79—91133
GaAs p-n junction, short-circuited, estimation of surface recomb. rates, electron-probe meas. 77—43713
GaAs, photoluminescence intensity rel. to heat treatment in S vapour *(Russian)* 78—48216
GaAs, photon transfer of excitation of nonequilib. carriers, conc. profile and relax. time 77—69907
GaAs, plastically deform., photocond., spectral response and decay process 80—29435
GaAs, point defect generation by electron-hole recombination at dislocations 79—37699
GaAs, proton irradiated, low energy, deep level defects and hole diffusion length meas. 80—60000
GaAs pure and Se-doped, photoluminescence at dislocations, band gap electronic levels 79—99926
GaAs, recombination radiation, anomalous temp. depend. 80—2847
n-GaAs, recombination scheme for $h\nu_m \approx 1.0$, 1.2 and 1.3 eV luminesc. bands 77—69906
GaAs, spin-depend. recomb., photoluminesc. obs. 80—60666
n-GaAs, surface recomb. vel. meas., diffr. from transient optical grating 79—1604
GaAs, surface recomb. vel., psec. optical techniques 80—70784
GaAs, surface recombination velocity, diffr. from picosecond transient free carrier gratings 79—47109
GaAs, surface recombination rate reduction by Ru chemisorption 80—49866
GaAs, thermalisation of electron-hole plasma 79—95439
GaAs: Si(Te), radiative recomb. *(Russian)* 79—91499
GaAs:C, Zeeman effect of effective mass acceptor, polarised luminesc. 79—4541
GaAs:Cr, semi-insulating, TSC, carrier recomb. and trapping 77—32014
GaAs:Cr, semiinsulating, hole recomb. domains, Hall mobility and photocond. 77—15867
GaAs:Cr, strong quenching of thermally stimulated conductivity by elec. field *(Russian)* 77—1434
GaAs:Cr, surface and bulk recombination parameter determ. from photoluminesc. spectra 77—55820
GaAs:Ge, stress depend. of donor-acceptor recomb. energy 79—15113
GaAs:Mg, photoluminesc. temp. depend., 4.2-293K 77—69878
GaAs:Mg ion implanted, photoluminesc. and annealing characts. 77—16361
GaAs:O, electrolum., photolum., negative differential resist. rel. to recomb. processes 80—66304
GaAs:Si, influence of stoichiometry on recomb. processes 80—93396
GaAs:Si p-n structs., effect of growing conditions on distrib. of recomb. parameters 80—39668
n-GaAs:Te, heavily doped, interband luminesc. intensity, heat treatment effect 78—72593
GaAs:Te, recombination barrier, dark cond., photocond., and Hall mobility meas. 80—15559

electron-hole recombination continued
n-GaAs:Te, vibr. props. of 1.0, 1.2 and 1.3 eV luminesc. centres 77—55823
GaAs:Zn-$Al_{0.5}Ga_{0.5}As$ p-n junction, surface layer effect on surface recombination current 79—69585
GaAs/AlGaAs, DH laser, degradation under Ar laser irrad. 79—98375
GaAs-$Al_xGa_{1-x}As$ double heterojunctions, dark-line defects and recomb. centres, scanning photocurrent microscopy 79—35822
GaAs-AlAs heterojunction, recombination currents 78—14806
n-GaAs-electrolyte interface, surface pretreatment rel. to photocurrent, spectral response 80—3204
$GaAs_{1-x}P_x$:S, deep level, photoconductivity, carrier nonradiative recombination 80—20112
p-$Ga_xIn_{1-x}As$, Auger recomb., theory and luminesc. expts. 78—56518
$Ga_xIn_{1-x}As$ p-n junction, growth and electrolum. spectra 77—20420
$Ga_{1-x}In_xSb$:Zn(Te), photolum. and stimulated emission obs. 78—72595
GaN:Zn, cathodolum. obs., recomb. model 79—11474
β-Ga_2O_3, intrinsic UV emission obs. 78—80396
GaP, electrical recomb. behaviour at dislocations 79—82606
GaP, electron-hole liquid, emission band from time-resolved spectra 78—43938
GaP, electron-hole liquid props., luminescence at high excitation intensity 79—69882
GaP, electron-hole plasma luminesc. 79—38651
GaP, epitaxial layer, carrier recomb. at dislocations 77—20932
GaP, frozen-in pt. defects annihilation 79—99949
n-GaP, interface-recomb.-controlled minority carrier lifetime obs. 77—12027
GaP LED, surface treatment effect on surface recomb. vel. and leakage current 77—20410
GaP, overlap integrals and Auger recomb. coeff. direct calc. 79—69524
GaP, polar semicond., radiative recomb., electron-phonon interaction effects, calc. 80—49631
GaP, stabilisation of electron-hole liquid by camel's back 80—6740
GaP:H/GaAs, amorphous film/crystal junction, optical and elec. props. 79—99611
GaP:N, Cd(Zn),(C), interimpurity recomb., acceptor binding energies 78—34796
GaP:N, photoluminesc., temp. depend., exciton recombination mechanism 78—88355
GaP:N, spin dependent exciton recombination at N_2 isoelectronic traps 77—69734
GaP:Ni, via deep state 79—99560
GaP:S(Se), donor bound exciton excited states 80—66284
GaP-GaAs, amorphous film/crystal junction, optical and elec. props. 79—99611
GaSb, photolum., electrolum. meas. in p-n junction, temp. influence 78—72594
p-GaSb:Te, effective radiative recombination centre nature, photoluminescence spectra 79—90998
n-GaSb:Te, heavily doped, photoluminesc. spectra 78—84644
n-GaSb:Te, heavily doped, spontaneous radiative recomb. vel., photoluminesc. spectra 79—11458
$GaSb_{1-x}As_x$, disorder-enhanced Auger recomb. 79—43014
GaSe, electron beam excited free exciton luminesc., rel. to band struct. 79—19940
GaSe, exciton luminesc. kinetics, intermediate electron-hole states 80—93389
GaSe, highly excited, polarisation of luminesc. spectra and electron-hole plasma radiation 77—52169
n-GaSe, photomagnetoelec. and photocond. current spectral distrib. 79—42585
n-GaSe, photomagnetoelectric effect, photocond., in presence of traps 80—39631
GaSe, photovoltaic spectra 80—20240
p-GaSe, single cryst., negative photocond. induced by elec. field 79—19623
GaSe:Cu(Cd, Sb), photovoltaic spectra 80—20240
GaSe:Sn, single crystal, transient photoconductivity *(Russian)* 79—11171
Ge (111), adsorption of polar molecules, surface recomb. centre neutralization 79—38147
Ge, adsorption of water, neutralization of surface recomb. and fast capture centre 79—33184
Ge, ambipolar hot-carrier size effect kinetics 80—107799
Ge, amorphous, ionisation enhanced crystallisation, elec. cond. meas. 77—35481
Ge, Auger recombination probability calc. for degenerate carriers 80—24944
Ge, cyclotron resonance and radiative recomb. with laser excitation, book contrib. 80—11472
Ge, dislocation energy band width, carrier lifetime anal. 77—11874
Ge, electron-hole drop recombination radiation due to heat pulse action *(Russian)* 80—16087
Ge, electron-hole drops, Auger recomb. 77—48240
Ge, electron-hole drops, phonon lifetime and acoustic attenuation due to phonon-assisted Auger recomb. 80—34462
Ge, electron-hole-liquid, recomb. induced dynamic paramagnetism 79—60720
Ge, energy-gap narrowing and state filling under laser irrad. 79—42441
n-Ge, γ-irrad., nonlinear steady-state recomb., nonequilib. carrier lifetime and density 80—20215
Ge, homopolar semiconductor, quantum efficiency 80—20254
n-Ge, impact ionisation at 4-9.5K 80—10994
Ge, indirect recomb. mechanisms 79—60728
Ge, low temp. recombination into shallow donors, transient case 79—38092
Ge, magnetic field influence on 1/f noise, surface origin evidence 79—99592
Ge microconductor mag. field transducer, cast, galvanomag. recomb. effect 79—19609
Ge, near intrinsic, negative differential cond., ambipolar size effect due to hot carriers 78—72185
Ge, nonequilibrium charge carrier-mag. field interaction electron-hole drops, recombination *(Russian)* 80—75511
Ge, optical pulse transmission, pulsewidth depend., phonons and plasmons role 78—31198
Ge, phonon assisted Auger recomb. in indirect gap semiconductors 78—39126
Ge, photomagnetic effect, space inhomogeneous nonequilibrium carrier lifetimes *(Russian)* 80—71152

electron-hole recombination continued
Ge, pressure tuning of picosecond pulse transmission, plasmon-assisted recomb. model 77—88871
Ge, recombination at dislocations 79—38023
Ge recombination characteristics used in design of semicond. devices *(Russian)* 79—42557
Ge, size effects in small electron-hole drops 79—82530
Ge, solid-state plasma, ultrafast transient response, theory and expt. 77—80748
Ge, strain-confined electron-hole liquid, lifetime and radiative efficiency vs density 79—38000
Ge, stressed cryst., props. of strain-confined electron-hole liquid 79—7787
Ge, surface recomb. before and after laser annealing, 10-μm transmission meas. 80—1247
Ge surface states, recomb. centres, regularities, electrolyte contact effects *(Russian)* 80—65652
Ge, surface states, recombination centre formation *(Russian)* 80—29459
Ge:As(Bi), donor bound exciton luminesc. and absorpt. 80—29777
Ge:Ba, Ca, recomb. props. 78—56156
p-Ge:Ga, dislocation density effect on carrier lifetime and deep recomb. centres 79—51598
Ge:Mn, impedance characts., near threshold of excitation of recomb. waves 77—69342
Ge:Mn, Sb, recombination waves, convective instability development 80—70721
n-Ge:Ni, recombination of hot electrons on Ni impurity centres 80—44612
n-Ge:Ni,Sb, transient response at 4K, nonequilib. carrier recomb. 77—43659
Ge:P(Sb)(Bi), γ-irrad., carrier trapping and recomb. at point radiation defects 80—107810
Ge:Sb, electron-hole drop lifetime, quenching temp. influence 80—59889
Ge:Sb, Ni(Mn), recombination wave spectrum, two-level traps 80—96906
Ge-GaAs heterojunction, elec. and recomb. props., interface defect effects 80—80365
Ge-Se, amorphous, photocond., photo-induced ESR, optical edge shift 80—49809
GeS orthorhombic layer crystals, photolum. spectra, long wavelength band rel. to carrier recomb. 80—2851
GeSe amorphous films, photoconductivity measurements, recombination model 78—64061
GeSe$_2$, amorphous film, photocond., photo-induced ESR, optical edge shift 80—49809
GeSe$_2$, glassy, powdered and bulk, fatigue of photolum. 80—80855
HgCdTe, radiation effects on low-temp. carrier recombination lifetimes, photocond. meas. 78—6400
HgCdTe, recomb. effects, mag. quantum oscills. in Auger transition rate 79—82610
HgCdTe-CdTe photodiode, 1.33 μm, grown by LPE, phys. props. 80—107892
Hg$_{1-x}$Cd$_x$Te, acceptor bound exciton Auger and radiative transition rates, radiative recomb. 80—6733
Hg$_{1-x}$Cd$_x$Te, long-term Hall-type conversion by vacancy diffusion at room temp. 79—65498
Hg$_{1-x}$Cd$_x$Te, recombination processes using impact ionization capture cross sections 80—75577
nHg$_{1-x}$Cd$_x$Te, single-phonon and plasmon recomb. lifetime effect, with magnetically tuned bandgap 79—38098
Hg$_{a-x}$Cd$_x$Te, single-LO-phonon and -plasmon recombination channels narrow-bandgaps 78—91728
n-Hg$_x$Cd$_{1-x}$Te, narrow band gap, Auger effect under high mag. fields 79—82609
HgI$_2$, phonon-assisted recomb. of free electron-hole pair 78—23521
HgTe, gapless semicond., magnetophonon conc. oscills. *(Russian)* 77—11943
III-V alloys, disorder-enhanced Auger recomb. 79—43014
p-InAs, Auger recomb., theory and luminesc. expts. 78—56518
n-InAs, heated electron gas, longitudinal optical phonon form., IR absorpt. modulation 80—45079
n-InAs, recomb. of nonequil. charge carriers at high photoexcitation levels 77—44053
InAs$_{1-x}$Sb, disorder-enhanced Auger recomb. 79—43014
In$_{0.53}$Ga$_{0.47}$As photodiodes with dark current limited by generation-recombination and tunneling 80—107893
InGaAsP DH, luminesc., quantum efficiency determ. 80—108273
p-InGaAsP, on InP surface, diffusion coeff. and surface recombination velocity 80—39598
InGaAsP/InP DH lasers, temp. depend. characts. 80—58541
InGaAsP-InP DH lasers, interfacial recomb., influence on oscill. characts. 80—87393
InGaAsP-InP DH laser, threshold current, temp. depend. 80—106521
In$_{0.5}$Ga$_{0.5}$P-GaAs heterojunction, interfacial recomb. vel. determ. 77—51809
n-In$_{1-x}$Ga$_x$P, direct-gap semiconductor, cathodoluminesc., electron irrad. effects 80—108283
In$_{1-x}$Ga$_x$P, epitaxial film, cathodolum. obs., recomb. mechanisms 78—72613
In$_x$Ga$_{1-x}$P-GaAs heterojunction, interface recomb. velocity determ. 77—89838
In$_x$Ga$_{1-x}$P-GaAs lattice mismatched heterojunction, recomb. props. 78—13707
In$_{1-x}$Ga$_x$P$_{1-z}$As$_z$ well in InP, tunnel injection into confined particle states 78—19130
In$_{1-x}$Ga$_x$P$_{1-z}$As$_z$-In$_{1-x}$Ga$_x$P$_{1-z}$As$_z$ visible spectrum multiple-quantum-well heterostruct. lasers 80—106537
InP, n- and p-type, surface recomb. vel. meas., diffr. from transient optical grating 79—1604
n-InP, photolum., evidence for low surface recomb. vel. rel. to n-GaAs 77—40272
InP, surface recomb. vel., psec. optical techniques 80—70784
InP, surface recombination velocity, diffr. from picosecond transient free carrier gratings 79—47109
InP:Bi, uniaxial stress effect on free and Bi-bound excitons 79—56854
InP-In$_{1-x}$Ga$_x$P$_{1-z}$As$_z$ laser, phonon-assisted recombination 79—89906
InSb, Auger-governed decay of laser-induced plasma, optical probing 80—76105
InSb, electron irrad. effects on elec. props. and recomb. 79—51584
n-InSb, electron recombination between Landau-levels 79—38096
n-InSb, high-resist., recomb. of carriers at 77K 77—51761
InSb, high-resistivity p-type or crystals of n-type, recombination processes, photocond. and photomag. effect meas. *(Russian)* 80—88567

electron-hole recombination continued
InSb, impact ionisation, influence of external mag. field on recomb. radiation and I-V characts. 79—56864
InSb, intrinsic, photoinjected electron hole pairs, Auger lifetime, photoconductive decay obs. 80—39629
InSb, magnetoconcentration effect, nonlinear current carrier recomb. 79—33298
n-InSb, n-type, photoconductivity with different surface treatment 78—2517
n-InSb, optically pumped stimulated recomb. radn. in mag. fields 79—94284
InSb, overheating luminescence, carrier generation-recomb. equilib. shift in elec. field 77—44068
n-InSb, photoconductive lifetime, surface pot. effects 80—11029
n-InSb, photoconductivity, recombination processes 80—11030
InSb, reabsorbed radiative recomb. and photon recycling 80—76076
n-InSb, recomb. of hot electrons, photoelectromag. and dynamic photocond. meas. 79—38081
InSb, recombination processes using impact ionization capture cross sections 80—75577
InSb, stimulated spin-flip Raman scatt. and stimulated recomb. radn. 79—72623
InSb, surface carrier accumulation in crossed elec. and mag. fields 80—20205
InSb:Cr(Zn)(Mn)(Ge), recombination of nonequilibrium carriers 79—65496
InSb-anodic oxide MIS struct., electrophys. props. *(Russian)* 77—39961
K halide, Yb^{2+} activated, X-ray and intracentre luminesc. 78—6737
KBr:Eu(Yb), electron-irrad., photostimulated luminesc., ionic processes 78—52561
KBr(I), photostimulated recomb., electron spin polarisation 80—60673
KCl:AgCl, tunnelling-recombination luminesc. 78—88354
KCl:Eu^{2+}, γ-irrad., photostimulated low temp. recomb. luminesc. 80—11435
KCl:SnCl$_2$, photostimulated hole recombination luminesc. *(Russian)* 80—80833
KCl:Tl, hole capture kinetics, influence of autolocalised and zone holes *(Russian)* 80—54714
KClO$_4$, X-irrad. induced paramag. defects, ESR study 80—24493
KI, recomb. luminesc. of H-centre and F-centre electrons *(Russian)* 78—80402
KI:Eu, electron-irrad., photostimulated luminesc., ionic processes 78—52561
KI:Eu^{2+}(Sr^{2+})(Mn^{2+}), elec. field effect on mech. of recomb. 78—80397
KI:Tl, electron-hole and V$_k$-Tl recomb., TSC and thermolum. study *(French)* 80—34461
KNO$_3$-Ca(NO$_3$)$_2$ glasses, radiation products and recombination 79—57261
LiNbO$_3$:Fe, photorefr., surface recombination 79—56759
LiNbO$_3$:Fe, X-ray and γ-ray irradiation effects on Fe charge state, Mossbauer study 80—40013
MgO, cryst. short-wave luminesc. V-centre electron recomb., impurity effects *(Russian)* 77—20921
MgO, doped, thermal stability of hole centres and hole recombination luminescence *(Russian)* 78—72614
MgO doped powder phosphors, photo- and thermostimulated luminesc. obs. *(Russian)* 80—66263
MgO, electron irradiated, luminescence, radiative recombination kinetics 80—7421
MgO, pure and doped crysts., X-ray stimulated luminesc. 79—28802
MgO, single crystal, thermal and optical stimulation processes of V-centres *(Japanese)* 80—11485
MgO-Al$_2$O$_3$-SiO$_2$:Ce^{3+} glass scintillator, energy transfer, luminesc. efficiency under UV and charged-particle excitation 79—95821
NH$_3$, cryst., radiolysis yield, temp. effects, Arrhenius depend. 77—48662
NaCl:Cu, X-irrad., thermoluminesc., F-centres 79—33849
NaCl:Tl$^+$, γ-irrad., aquoluminesc. obs. 80—2856
NaI:Cu$^+$, luminesc. of iolated V$_K$-centres 78—84641
NbO$_2$, on-state decay rel. to recomb. and nonlinear props. 80—84492
p-n junction space charge region, thermally stimulated current, impurity centre parameters 77—85237
Pb chalcogenides, Auger recomb., theory 80—65586
Pb$_{1-x}$Sn$_x$Se epitaxial layers, radiative and nonradiative recomb. processes 80—60670
Pb$_{1-y}$Sn$_y$Se, electron-irradiated, elec. and recomb. props. 79—56227
PbSnTe-like semicond., Auger recomb., nonparabolic approx. 79—15161
Pb$_{0.83}$Sn$_{0.17}$Te, recomb. at high levels of optical excitation 78—10503
Pb$_{0.86}$Sn$_{0.14}$Te/PbTe, interface recomb. velocity in DH laser diodes 79—64222
Pb$_{1-x}$Sn$_x$Te, electron-irradiated, elec. and recomb. props. 79—56227
Pb$_{1-x}$Sn$_x$Te, epitaxial layers, carrier lifetime meas. 79—42559
Pb$_{1-x}$Sn$_x$Te, photoconduct., photoelectromag. effect, laser intensity depend., carrier lifetimes 77—15896
Pb$_{1-x}$Sn$_x$Te, photomagnetic effect at low temps. 77—62960
Pb$_{1-x}$Sn$_x$Te, small-gap, recomb. mech. 79—38099
Pb$_{1-x}$Sn$_x$Te:Cd, photocond., photomag. effect, carrier lifetimes 80—44658
Pb$_{1-x}$Sn$_x$Te:Cd, photoelec. props., surface recomb. effect 80—44659
PbTe, Auger recomb., photocond. decay time expts. 77—72879
PbTe epitaxial film, stimulated emission, absorption spectra and recombination 78—80409
PbTe epitaxial films, carrier recomb. and deep levels, photocond., Hall effect, and luminesc. meas. 79—38024
PbTe, epitaxial layers, carrier lifetime meas. 79—42559
PbTe p-n junction, minority carrier lifetime, step pulse recovery 77—11995
PbTe photovoltaic detector, detectivity limits 80—105709
PbTe, spin orientation under two-photon pumping 79—74000
RbCl:Eu, electron-irrad., photostimulated luminesc., ionic processes 78—52561
RbI, photostimulated recomb., electron spin polarisation 80—60673
Se, amorphous, photoconductivity quantum yield, experimental validation of fund. theory 80—6909
Si, amorphous, EPR and spin-dependent effects 80—80592
Si, amorphous, electron-hole recombination, mech. 78—72196
Si, amorphous, mag. field depend. of luminesc. 79—43034
Si, amorphous, photoluminesc. spectra from 77K to room temp. 77—20916
Si, amorphous, photoluminescence, fast radiationless recombination 79—99939
Si, amorphous, radiative recomb. obs. as efficient luminesc. 78—2914

electron-hole recombination continued
- Si, amorphous, spin depend. recomb., luminesc. and light induced ESR 80—50393
- Si, amorphous, spin-depend. photocond. 77—59302
- Si, amorphous and crystalline, heating by Q-switched laser radiation 80—84963
- Si, amorphous hydrogenated solar cells, field depend. quantum efficiency, electron-hole recombination 80—66971
- Si, Auger band-to-band recomb. temp. depend. 80—29416
- Si, Auger recomb. coeff. meas. using laser excitation 79—38654
- Si, Auger recombination, localized and free carrier comparison 79—38090
- Si, Auger recombination 78—26883
- Si bars, generation-recombination noise at 77K 79—60883
- Si based MOS device irradiation with γ-rays, minority carrier generation, CV characts. 80—88637
- n-Si, bipolar ohmic contact with macroscopic recomb. centres. 80—80379
- Si, carrier capture at amphoteric deep level defects 80—88569
- P-Si, conductivity and carrier lifetime, high injection effects 80—70719
- Si, deformed, recomb. radiation from electron-hole drops and free excitons 77—8641
- Si, dense plasma dynamics during pulsed laser annealing, carrier density, recombination 80—84479
- Si, diamagnetism of excitons and biexcitons, recomb. spectra *(Russian)* 80—7412
- Si diode, Auger recombination coefficient at very high injection rates 78—47863
- Si diode, transient switching duration, linear carrier lifetime, emitter efficiency and Auger recomb. coeff. determ. 79—11207
- n-Si, edge dislocation and stacking fault defect electrical recombination efficiency 80—15106
- Si, electrical recomb. behaviour at dislocations 79—82606
- n-Si, electron recombination, role of intervalley scatt. *(Russian)* 79—19605
- Si, electron-hole drops, Auger recomb. 77—48240
- n-Si, γ-irrad, (E_{max}=100 MeV), carrier recomb. 78—56158
- Si, heat treated, spin-depend. recomb. at dislocations 79—47122
- Si, heavily doped, carrier recomb. through shallow donor and acceptor states 80—15535
- Si, heavily doped layer, electronic characts., electron beam induced current obs. 78—10473
- Si, high purity, exciton lifetime, temp. depend., photoluminesc. meas. 80—44508
- Si, highly doped and highly exerted, Auger coeffs., radiative band to band recomb. lifetime meas. 77—85764
- Si, hole localisation, solid solubility, excitonic Auger lifetime of acceptors 80—20216
- Si, hole-hole-electron Auger recombination 80—70720
- Si, homopolar semiconductor, quantum efficiency 80—20254
- n-Si, hot carrier noise and generation-recomb. noise 79—38140
- Si, influence of surface recombination rate and carrier diffusion on photocond. 80—44660
- n-Si, interaction of disordered regions with point defects 79—19296
- Si, interstitials and lattice vacancies 78—10038
- Si, intrinsic, radiative recombination probability *(German)* 79—61441
- Si, intrinsic semiconductor, radiative recombination probability *(German)* 78—95608
- n-Si, ionisation of low donor levels and recomb. of hot electrons at low temp. 79—51596
- Si, laser induced dense plasma, dynamics 80—65612
- Si MOS capacitors, pulse response anal., lateral depletion region around gate area 79—38187
- n-Si, meas. of recomb. rates of non-equilib. carriers, absorption modulation method 77—55575
- Si, minority carrier lifetime and surface recombination velocity meas. by photocurrent 78—10515
- Si, nonradiative recombination and luminesc. 79—33770
- Si p^+-i-n^+ diodes, double-injection switching, effect of surface recomb. 78—88025
- Si p-n junction, avalanche multiplication factor and reverse current 77—11991
- Si p-n junction, charge carrier recomb. at dislocations, combined SEM and TEM study 80—15105
- Si p-n junction I-V reln. calc. 77—43704
- Si, p-n junctions, current-voltage relation 79—42632
- Si p-n junctions, depletion layer recombination theory 77—80828
- Si, phonon assisted Auger recomb. in indirect gap semiconductors 78—39126
- Si polycrystalline solar cells, recombination, electron-beam-induced current characterisation 80—81470
- Si, recomb. centre study by spin-depend. photocond. 80—49805
- Si, recombination at dislocations 79—38023
- Si recombination characteristics used in design of semicond. devices *(Russian)* 79—42557
- Si, recombination luminescence, electron-hole drop, excitons orientation in mag. field 78—88362
- a-Si, resonant and non-resonant photoconductivity changes 80—49814
- a-Si, resonant and non-resonant luminesc. changes theory 80—50410
- Si, role of electron-hole interaction in optical spectra, review 80—45113
- Si solar cells, minimisation of recombination at illuminated surface 80—12017
- Si solar cells, polycrystalline p-n junctions, recombination currents, physical models 80—93892
- Si, spin dependent effects, theory 78—23342
- Si, spin dependent recomb. at dislocations, EPR and photocond. 79—38095
- Si, spin effects in electron transitions via dislocation states 79—82642
- Si, spin-depend. recomb. at exchange-coupled dislocation centres 77—89725
- Si surface, metal doped, recomb. of nonequilib. carriers at high excitation rates 79—7835
- Si, surface, spin-depend. carrier recomb., photocond. expt. 78—19096
- Si, temp. depend. of Auger recomb. coeff. 80—24942
- Si:Al, recomb. enhanced migration of interstitial Al 79—82201
- Si:B, antiferromagnetic ordering of holes, recombination radiation polarisation *(Russian)* 80—45121
- Si:B, bound multiexciton luminesc., recomb. kinetics 79—38591
- Si:B, hot-carrier scatt. and recomb. characts. 79—91069
- Si:B, photolum. of heavily doped p- and n-type 80—20708
- Si:B(Li)(P), piezospectroscopic studies of bound multiexciton complexes 80—16006

electron-hole recombination continued
- n-Si:Cs, ion implanted, minority carrier lifetime and defect struct., annealing effect 78—6395
- Si:F,H, amorphous efficient carrier generation for solar photovoltaic energy conversion 80—92906
- Si:H, amorphous, defect photoluminesc. meas. 80—97334
- Si:H, amorphous, excess carrier thermalisation and recomb., luminesc. decay and photocond. 80—50397
- Si:H, amorphous, geminate recombination model for photoluminescence decay 80—71481
- Si:H, amorphous, optical studies of excess carrier recomb., evidence for dispersive diffusion 80—76059
- Si:H, amorphous, radiative recomb. by diffusion and tunnelling, photocond. quantum efficiency 80—50394
- Si:H, amorphous, solar cells, carrier generation, recombination, and transport 80—55844
- Si:H amorphous, plasma-deposited, luminesc. decay 79—73989
- Si:H film, amorphous, reactively sputtered, H content effect on props. 80—49714
- Si:Li, photolum. of bound exciton and bound multiexciton complex, Zeeman effect 80—108265
- Si:O, carrier recomb. processes, role of vacancy-O complexes 80—65592
- Si:O, heat treated, excess carrier recomb. rate, defect levels 80—75579
- Si:P, heavily doped, origin of photoluminesc. 79—56856
- n-Si:P(B), elec. cond. oscills., electron instability effects due to dislocations 80—103704
- Si:Zn, recombination waves threshold parameters in microwave field 77—28206
- Si:Zn, reson. characts. of impedance near excitation threshold of recomb. waves 80—20301
- n-Si:Zn,P, local deform. of cryst. lattice, charact. parameters or recomb. waves 77—4386
- Si:Zn (Mn) (In), surface characterised by negative electrochemical pot., electronic props. 80—44695
- Si:Zn p-n junctions, I-V characts. using exact DC circuit model 79—95476
- Si-H, amorphous, sputtered, photolum. obs. 80—80856
- Si-P, excess carrier recomb., photocond. 79—65495
- Si-SiO_2 interface of MIS structure, generation-recomb. characts., effect of γ-irradiation *(Russian)* 77—76938
- α-SiC, short-wavelength photocond. and capacitance photo-EMF meas. 78—26906
- 4H-SiC:Ga(Al), photoluminesc. spectra 77—66530
- Si_xGe_{1-x}-GaAs, heterojunction, elec. and recomb. props., interface defect effects 80—80365
- SiO, doped, thermal stability of hole centres and hole recombination luminescence *(Russian)* 78—72614
- SiO_2, amorphous, high-field transport of excess electrons and holes 77—89767
- SiO_2, dielectric breakdown, impact ionisation-recombination model 78—6633
- n-SnO_2, high resist., photoelectronic processes 78—60157
- SrO, luminesc. band edge, 4-6.5 eV, optical absorpt., photoluminesc., cathodoluminescence, photocond. obs. 80—50411
- Te, carrier recombination at high optical excitation 77—72884
- Te, magnetoacoustic effect 77—62963
- TiO_2 treated with quinoline, effect of inorganic redox couples on recomb. 79—66352
- $TiSe_2$, UPS, excitonic instability indicated from study of band struct. 78—56069
- TlCl, role of electron-hole interaction in optical spectra, review 80—45113
- $TlGaSe_2$, monocrystal, processes of recombination and trapping levels, photocond. meas. *(Russian)* 80—70751
- V_2O_5 layer, photocond. investig. using V_2O_5-n-Si system 77—76875
- Y_2O_3, electron and hole migration distances determ. 78—19526
- Y_2O_2S:Tb, cathodoluminesc., nonlinear depend. on activator concs. 79—8190
- $ZnIn_2S_4$, recomb. process of photoexcited carriers 77—44042
- ZnO, electron-hole recombination emission, temp. depend. and phonon repetitions *(Russian)* 79—15521
- ZnO epitaxial film on Al_2O_3 substrate, recombination radiation in intense single photon excitation 80—7410
- ZnO, laser thresholds and stimulated emission, intrinsic recomb. processes 79—15489
- ZnO, luminescent, phonon detection by shallow electronic trap states 79—14902
- ZnO, negative photocond. by excitation of exciton-impurity complexes, recomb. mechanism *(Russian)* 79—28379
- ZnO:Pr(Gd)(Er), phosphors, photoluminesc. and electroluminesc. spectra 79—11457
- α-ZnP_2, local centre parameters, photoelectron transition scheme, recomb. process anal. 80—44654
- Zn_3P_2-metal contacts, photoelectric props. 80—92930
- ZnS, high-level photocurrent excitation and carrier recombination expt. *(Russian)* 79—95446
- ZnS, pulsed optically detected resonance, time depend. recomb. processor study 79—38411
- ZnS, time resolved ODMR, electron-hole recombination 79—42872
- ZnS:Ag, photon counting statistics of cathodoluminesc. light emission 79—24371
- ZnS:Al(Te) phosphors, luminesc. excitation spectra and exciton struct. 80—55165
- ZnS:Cu, Al phosphors, mechanism of IR stimulated and quenching 77—69881
- ZnS:Cu, polycryst. phosphor, excitation storage, recombination barrier participation 78—27316
- ZnS:Ga, self-activated emission, A-centre ODMR 79—95685
- ZnSe and ZnSe:Sb, photoconduction under Nd laser irrad., local level distrib. 77—55580
- ZnSe, near band edge photoluminescence, electron-hole recombination 80—80835
- ZnSe, polar semicond., radiative recomb., electron-phonon interaction effects, calc. 80—49631
- ZnSe, residual cond., recomb. of photoexcited carriers, Hall coeff. 80—75605
- ZnSe:Al single crysts., photoluminescence spectra *(Russian)* 77—28627
- p-$ZnSiAs_2$:Au(Tl)(S), photoluminesc., radiative recombination 77—24883
- p-$ZnSiP_2$, single cryst., recomb. processes, photoelec. props. *(Russian)* 78—68053

electron-hole recombination continued
  p-ZnTe, doped and pure, photoluminesc. and photocond. spectra 77—55826
  ZnTe, electron-phonon coupling, donor-acceptor pairs selective excitation 80—11475
  ZnTe, laser thresholds and stimulated emission, intrinsic recomb. processes 79—15489
  ZnTe:As(Li), donor-acceptor pair excitation and recomb., photoluminesc. obs. 80—20691
  ZnTe-In Schottky diodes, photocapacitance determ. of electron-hole recomb. *(French)* 79—47119

electron impact
  see also atomic electron impact excitation; atomic electron impact ionisation; molecular electron impact dissociation; molecular electron impact excitation; molecular electron impact ionisation; secondary electron emission
  adsorption, electron beam induced, enhanced adsorpt. due to ion beam 77—11778
  adsorption, kinetic eqn. under electron bombard. conditions *(Russian)* 79—77893
  alkali halides, electron sputtered atoms, energy distrib., time of flight method 78—48263
  alkali halides, electron stimulated dissoc. 80—34301
  alkali halides, exciton mechanisms of electron sputtering process 77—55857
  alkali halides, sputtering of molecules, low-energy electron bombardment 80—35026
  atom, resonant potential scattering in a low-frequency laser field 80—23545
  atomic and surface physics, conf., Salzburg, Austria (Feb. 1980) 80—57010
  atomic metastable states, props., energy transfer mechanisms, exptl. techniques 80—27921
  bremsstrahlung from tightly pinched relativistic electron beam, X-ray streak camera obs. 77—49818
  bulk plasmon excitation due to electron scatt. from single crystals 78—87933
  CdS thin films, slow electron mean free path 79—99998
  computer program, SANDYL, for electron and photon transport, statistical accuracy, optimisation 77—8675
  Coulomb electron atom scatt. in laser field, asymptotic dynamics 79—94084
  crystal, fast electron reson. scatt. *(Russian)* 79—47569
  desorption, electron stimulated, surface bonding determ. 77—62746
  desorption, electron-impact, of CO, isotope effects 77—55460
  desorption, electron-stimulated, ion ang. distrib. and three-dimens. model 78—26770
  desorption due to electrons or photons, mechanisms 80—34301
  dielectric, energy struct. determ. by electron absorpt. spectra 78—11040
  dielectric, irrad. by electron beams, effect of bulk and surface cond. on pot. 80—2446
  dielectric materials, spacecraft, charging and discharging 80—71315
  dielectrics, radiation induced charging and discharging, analytic solution 79—78612
  doubly truncated spherical electrostatic energy analyser for (e, 2e) expts. 78—58872
  dynamic response of materials to pulsed beam, measurement using laser interferometer 79—42102
  elastic and inelastic slow electron scatt. in solids 79—90857
  elastic reflection of electrons from solid surface, Boltzmann eqn. 79—43078
  electron probe analysis, spatial distrib. of electrons in homogeneous, isotropic target 79—43687
  electron reflection from metal surfaces, surface roughness, IR absorpt. 80—71526
  electron resist failure, energy deposition functions, Monte Carlo simulation of electron scatt. 79—56897
  electron scattering, in the scanning electron microscope 79—21880
  electron-matter interactions rel. to electron microscopy 80—89097
  electrostatic deflection type electron analysers, electron refl. ghost lines, energy loss reduction 80—18050
  focused electron beam as probe of solid state, review *(Czech)* 77—24915
  foil, electron scatt., appl. of Monte Carlo type calc. *(French)* 77—7636
  fusion devices, controlled, surface effects, conf., San Francisco, USA (Feb. 1976) 77—30659
  fusion pellet-target system, optimum material and design for relativistic electron beam 78—17416
  gas, ionisation, ion density calc. partial differential eqn. *(Russian)* 77—11306
  graphite, electron elastic reflection angular characts., low primary energy 80—29835
  graphite, slow electron elastic reflection characts. 80—25507
  graphite film, relativistic excitations by inelastic electron scatt. 77—1463
  grazing scattering of fast electrons from polycryst. solid surface 77—32481
  hydrocarbon, long chain single cryst., carrier transport meas. 80—6874
  hydrocarbon liquid, model for thermalisation of quasifree electrons rel. to electron mobility 77—40316
  inelastic electron scattering: surface vibrational spectroscopy 80—107347
  inelastic electron-matter interactions 80—104024
  inert gases, liq., model for thermalisation of quasifree electrons rel. to electron mobility 77—40316
  ion analysis, conference, Paris, France, (May 1977) 77—86406
  ion desorption by core hole Auger decay 78—48262
  ionisation in Nier-type electron impact ion source, repeller curve interpretation 80—57421
  ionisation spatial distrib. for 0.5 to 500 keV electron bombarded solids, empirical eqns. 79—19956
  Kinetic theory description of electron stimulated desorption 78—14613
  LEED system, electron-stimulated desorption 78—14567
  low atomic number foil target, anomalous energy dissipation of tightly pinched relativistic electron beam 80—29833
  low-energy electron impact excitation, electron gun for Auger spectroscopy 77—31027
  metal, electron-surface-plasmon scatt. using parabolic nontouching trajectory 77—28228
  metal, excitation by fast electrons of surface plasmons on spherical voids 77—11975
  metal, plasmon dispersion effect in (e,2e) process with atomic electron knockout 80—2904

electron impact continued
  metal ion source using high power density electron impact 78—54497
  metal oxides, electron stimulated dissoc. 80—34301
  metal surface, image force for fast particle 77—69939
  metal surface, oxide covered, primary electron beam effect on secondary emission coeff. *(French)* 79—47563
  metal surface, soot covered, refl. of slow electrons 77—36327
  metals, degenerate electron gas, collective props. using electron knock-out processes 80—6758
  metals, electron penetration and energy transfer in solid metal targets, film bulk method 78—2963
  molecular metastable states, props., energy transfer mechanisms, exptl. techniques 80—27921
  molecular solid, film, 0-15 eV electron transmission spectra 80—35023
  molecular solids, interaction with 0-15 eV electrons, formation of charged excitonic complexes 80—107708
  molecule, momentum distrib. calcs. using FSGO 77—30933
  MOS structures, electron bombardment effects on instantaneous characts. *(French)* 77—55616
  multicomponent target, medium energy electrons inelastic scatt. *(Russian)* 79—91548
  multiple Coulomb scattering and energy degradation of electrons in semi-infinite material layers *(Rumanian)* 80—29100
  multiple scattering by infinite lattice plane 77—73198
  negative resist, electron depth distrib., expt. test of Bethe-Bloch model 80—16132
  neutron yield calcs., on C, Al, Fe, Ni, Cu, Ag, Ba, Ta, W, Au, Pb, U 78—95622
  photographic sensitive material, short time exposure, expt. technique 80—86477
  polymer electret, absorpt. and relax. of charge 80—6942
  polymer film, carrier transport meas. 80—6874
  polymethyl methacrylate, direct obs. of zero field surface 80—16133
  polymethyl methacrylate resist, electron depth distrib., expt. test of Bethe-Bloch model 80—16132
  PVC, Cu evaporated film, electron-induced metallochromic reaction for metal image formation 80—86476
  range for transmitted, reflected, and absorbed ions and electrons, phenomenological description 79—68173
  reflection and transmission secondary emission *(Japanese)* 80—45180
  reflection and transmission through surface pot. barrier, Schrodinger eqn. 80—87998
  refractory metals, vaporisation by electron bombardment in UVN-71R-3 installation 77—28722
  scattering by atomic planes in single crysts., and band struct. with intrinsic values of transverse energy *(Russian)* 78—39639
  secondary electron kinetic emission from electron and ion bombardment 80—66342
  semiconductor glasses, scattered electrons emission angle and energy distribution 79—91545
  slow electron elastic reflection characts. of solids 80—25507
  solid, compression wave interaction, pulsed electron beam initiation 80—79877
  solid, polycrystalline, backscatt. energy distrib. spectrometer *(German)* 79—95882
  solid layers, conversion electron scatt. processes anal. 80—45181
  spatial electron beam-matter interaction, model calcs. for Cu *(German)* 80—84815
  spectrometer, using axial magnetic field for collimation 79—49334
  spectrometry, high energy resolution using hemispherical electrostatic energy selector 77—23577
  spectroscopy, theory, techniques, and appl., book 80—8748
  spectroscopy, total current, study of surface regions and bulk physics 80—31952
  spectroscopy of molecular excitation functions, trapped electron restrictions 80—69184
  steel, stainless, exoelectron emission, effect of gas press. and sample temp. during slow electron excitation 79—61505
  steel, stainless, type 304, electron stimulated desorption rel. to CTR first wall appl. 78—51818
  stereoselective rearrangement reaction, electron impact induced, temp. depend. 77—25288
  supernovae, Type I, electron energy deposition rel. to interpretation of spectra 78—49467
  surface, (e,2e) reactions, theory 78—39640
  surface acoustic and electrostatic wave excitation by electron beam 77—24473
  surface bombardment, by electrons, protons and heavy ions, characterisation of materials 79—96406
  surface physics, conf., Eindhoven, Netherlands (June 1976) 77—62708
  surface roughness meter using backscattered electron intensity *(Japanese)* 79—93131
  target, for neutron production, by electron accelerator 3 to 10 MeV *(Rumanian)* 79—63855
  target exposed to intense pulsed electron beam, kinetic temp. meas. method 77—82524
  thin films, thickness determination, using backscattered electrons as tool 79—21704
  total current spectroscopy, review 80—45185
  transition metals, 3d, electron impact excited soft X-ray spectra, resonances and many body effects 80—50468
  transmission and backscatt. in solid layers, energy loss, 10 to 30 keV 77—59653
  TTF-TCNQ, electron-electron interaction strength, electron scatt. and spin-lattice relax. data 78—30878
  two-layer target, moderate energy electron interactions, direct statistical modelling *(Russian)* 77—66561
  vacuum breakdown mechanisms, electron-beam bombarded anode 78—18476
  W values and backscatt. coeffs. for slow electrons in air, dosimetry appls. 80—19551
  wavefunctions for electron+atom or electron+ion system, coupled integro-differential equations 80—18924
  WO_3, (100) and (111) layers, electron stimulated desorption of O^+, LEED obs. 79—23840
  X-ray microanalysis, spatial resolution in thin foils 80—101065
  (e,2e) reaction, possibility for solids, expt. conditions 77—90225
  Ag (100) and (111) surfaces, positronium form. due to slow positron trapping 80—107748
  Ag (331), adsorpt.-desorpt. props., coadsorpt. and surface struct. chem. of O_2 and Cl_2 78—34711

electron impact continued
  Ag, electron backscatt. by bulk target, theoretical model *(French)* 80−60722
  Al alloy, 6061, vacuum material, desorpt. of neutral mols. by electron and ion bombardment 78−95229
  Al, beta-ray backscattering variation with target thickness, self-absorpt. coeff., Z depend. 79−78801
  Al, electron backscatt. by bulk target, theoretical model *(French)* 80−60722
  Al, electron backscatter fractions, exptl. determ. 80−18617
  Al film, (e, 2e) reaction, ang. correlation functions, plasmon satellites 79−19955
  Al film, electron transmission, calc. 80−60724
  Al film, simulation of transmission of 1 keV electrons 77−12475
  Al, high-current electron beam refl. coeffs. *(Russian)* 78−84690
  Al, propane adsorption SIMS and EID obs. 77−69167
  Al, thin foil, Monte Carlo calcs. of electron transmission 77−80555
  Al/Pb two-layer target, moderate energy electron interactions, direct statistical modelling *(Russian)* 77−66561
  Au film, electron transmission, calc. 80−60724
  Au film, simulation of transmission of 1 keV electrons 77−12475
  Au films, (111), sputtering in high voltage electron microscope 80−35027
  Au, surface proton and electron channelling on reflection 80−39193
  C film, backscattered electron intensities, ang. depend 77−40317
  C, low energy electron backscattering, 0.5-10 keV 77−52206
  C, sputtering by fast electrons 77−90226
  CO on Rh (110), electron-impact props. 78−6225
  CdS surfce, slow electron refl., 0-6 eV 78−11039
  Cl_2, electron dissoc. attachment peaks, 0−11.5 eV, Cl_2^- pot. energy curves 77−75312
  Cr, oxidation, combined AES and threshold potential spectroscopy 78−11026
  Cr_2O_3, fine struct. in elastic-electron-yield spectra at transition-metal core energies 79−69938
  Cu (111) surface, positronium form. due to slow positron trapping 80−107748
  Cu, beta-ray backscattering variation with target thickness, self-absorpt. coeff., Z depend. 79−78801
  Cu, electron backscatt. by bulk target, theoretical model *(French)* 80−60722
  Cu, electron backscatter fractions, exptl. determ. 80−18617
  Cu film, electron transmission, calc. 80−60724
  Cu film, simulation of transmission of 1 keV electrons 77−12475
  Cu, fine struct. in elastic-electron-yield spectra at transition-metal core energies 79−69938
  Cu, high-current electron beam refl. coeffs. *(Russian)*. 78−84690
  Cu, surface, electron stimulated desorption, glow discharge treatment 79−65964
  Fe, elastic and magnon-inelastic spin polarised low energy electron scatt. 78−34970
  Fe, sputtering by fast electrons 77−90226
  GaAs, adsorption enhancement by electron beam excitation of gas mols. 78−43238
  GaAs-Cs-O, negative electron affinity, refl. of slow electrons, 0.4-3 eV 78−11038
  GaAs-O_2 system, electron beam induced adsorption, ion beam effects 77−11778
  GaP, surface sensitivity, low energy electron transmission optical modulation 78−76567
  Ge, electron and positron bremsstrahlung spectra *(Russian)* 79−91522
  He-like three-electron atoms and ions, inelastic-reson. quasiprojection operators 79−3581
  n-InSb, Gunn effect, influence of impact ionisation 80−44609
  KBr(I), sputtering, depend. on beam energy and target temp. 79−1804
  La, electron impact excited soft X-ray spectra, resonances and many body effects 80−50468
  LiF (TLD-100), thermoluminescent response to 0.1-5 keV electrons 79−95852
  MgO-Au cermet film, high intensity electron bombard. effect on secondary electron yield 77−81184
  Mo, (100) surface, O-covered, electron-stimulated desorption of O^+ and O^- ions 79−82444
  Mo, chemisorption of CO, low energy SIMS and electron impact desorption expts. 78−38941
  Mo, electron backscatter fractions 78−87717
  Mo, electron stimulated desorption of negative ions from adsorbed gases 78−91549
  Mo, electron-surface-plasmon scatt. using parabolic nontouching trajectory 77−28228
  Mo surface, anisotropy of elastic refl. of electrons from single cryst. 79−28870
  Mo, surface, electron-stimulated desorption of negative ions, work function 78−72654
  Mo-Rh, secondary electron emission and inelastic refl. coeffs. 78−15264
  MoS_2 (2H), refl. of electrons from surface, total current spectroscopy 79−61479
  N_2, solid, interaction of 1-3 keV electron beam, range and secondary emission 79−15568
  NaCl, energy struct. determ. by electron absorpt. spectra 78−11040
  NaCl, sputtering of atoms by 540 eV electrons, delay times 80−35025
  Ni, elastic and magnon-inelastic spin polarised low energy electron scatt. 78−34970
  Ni:K^+(Ba^+), ion implantation, effect on inelastic refl. and energy losses of fast primary electrons 78−55900
  Ni/Au film on silicon vacuum deposited, electron impact mass spectrometric exam. of surface contaminants 78−75957
  NiO, fine struct. in elastic-electron-yield spectra at transition-metal core energies 79−69938
  Pb, beta-ray backscattering variation with target thickness, self-absorpt. coeff., Z depend. 79−78801
  Pb, high-current electron beam refl. coeffs. *(Russian)* 78−84690
  PbO-SiO_2 reduced glass, electron backscattering 77−85855
  Pd (100) surface with adsorbed O, obs. of O^- and O^+ during electron bombardment 79−95883
  Pt (100), CO or C_2N_2 adsorpt. induced backscatt. enhancement 77−90227
  RbBr, sputtering of atoms by 540 eV electrons, delay times 80−35025
  RbBr(I), sputtering, depend. on beam energy and target temp. 79−1804
  RbI, sputtering of atoms by 540 eV electrons, delay times 80−35025
  Re, desorption of O_2 *(French)* 77−85853

electron impact continued
  Ru (001), chemisorption of CO, electron stimulated desorption ion ang. distribs. bonding geometry and bending vibrs. 79−33189
  Ru(001), chemisorpt. of H_2O, conformation, electron stimulated desorption ion ang. distribs. 77−89637
  Si (100) surface, slow electron elastic scatt. threshold effects 79−100002
  Si (111), (e,2e) reactions, theory 78−39640
  Si coated with copper phthalocyanine dye, optical modulation of low energy electron transmission 79−69939
  Si, electron scattering energy distrib., channelling effect *(Russian)* 78−2183
  Si, oxidation induced by ion or electron bombardment, AES-SIMS study 80−108606
  Si, surface, optical modulation of low energy electron reflection and transmission 78−88388
  Si thin crystal, electron backscatt. in electron microscope 78−75510
  Si/Al-Si systeym, vacuum deposition, rate controlling and composition anal. by electron impact emission spectroscopy 79−91591
  Si_3N_3, film growth by reactive sputtering, influence of electron-ion bombard. *(Russian)* 77−28717
  SiO_2, surface charge, effect of doping with P+B, differing vacuum deposition conditions *(French)* 77−85286
  Si(111), adsorption of HBr(Cl), AES, electron energy loss spectra and electron impact desorption exam. 78−43243
  Sn, beta-ray backscattering variation with target thickness, self-absorpt. coeff., Z depend. 79−78801
  Ta (110), electron-stimulated desorpt. of O 78−2363
  Ta, (111) surface, 100 eV electron bombardment, adsorbed mol. luminesc., coherent bremsstrahlung *(Russian)* 78−31290
  Ta, electron-stimulated desorption of O_2 bound state obs., 300K 77−85082
  Ti, Tokamak plasma, atomic struct., highly ionized states 80−75086
  V surface interaction with O_2, H_2, H_2+O_2 and H_2O, SIMS, EID 77−62753
  V{100}, Au(Au) layer growth, total current spectroscopy 77−36329
  W (100), electron and photon-stimulated desorption of CO 79−99414
  W (100), electron-stimulated desorpt. of O 78−2363
  W, (100) and (110) faces, electron stimulated desorption of O_2, CO, and H_2, threshold behaviour 77−47678
  W (100) and (111), O_2 electron stimulated desorption patterns, computer simulations 80−75443
  W (110), electron impact desorption of CO and O_2, isotope effects 77−76658
  W (110) and (111) surfaces, KCl adsorption-desorption behaviour 80−75442
  W, desorption of O_2 *(French)* 77−85853
  W, desorption of O^+ and O, electron stimulated, cross-section temp. depend. 77−31908
  W, electron backscatter fractions 78−87717
  W, electron stimulated desorption of F and Ba from polycryst. ribbon 77−11793
  W, electron stimulated H^+ desorption, (100) face 77−66091
  W, O_2 adsorption on (110), electron impact and thermal desorption at high temp. 78−30821
  W ribbon, with adsorbed CO, CO_2, or methane electron beam induced C deposition, AES obs. 77−89651
  W surface, (100), photon and electron stimulated desorpt. of O 80−100397
  W surface, elastic refl. of slow electrons 79−28869
  W, viscoelastic wave propagation model at near-melt conditions, electron-photon impact energy deposition 79−77002
  ZnO powder, CO_2 desorption during electron irrad. and interaction with atomic H 77−89638
  ZnO powders, electron-beam-induced desorption, phase-sensitive detection 80−54502
  ZnSe surface states, electron interaction characterisation, by low energy electron transmission photovoltaic modulation 79−60896

electron interactions *see elastic scattering of electrons by atoms and molecules; electron attachment; electron beam effects; electron beams; electron-electron interactions; electron-electron scattering; electron impact; electron-nucleon interactions; electron-nucleon scattering; electron-nucleus reactions; electron-nucleus scattering; electron-positron interactions; electron-positron scattering; electron spectra; hadron electroproduction; neutrino-electron interactions; neutrino-electron scattering; secondary emission*

electron ionisation *see electron impact*

electron lenses
  see also aberrations; electron microscopes; electron optics; electrostatic lenses; magnetic lenses
  aberration coeffs., computer calc. using CAMAL 77−38798
  aberration correction, round lenses 80−78758
  aberrations, reduction by optimisation techniques 80−87290
  achromator using three elec.-mag. quadrupoles *(German)* 77−61166
  anastigmatic electron deflection system between beam-shaping lens and probe target 79−27155
  beta-spectrometer, double tube electron optics, slow electron preliminary accel. 77−23356
  cathode lens having a quasispherical field 80−95782
  cathode lenses, with combined elec. and mag. fields, third order aberration theory 79−41317
  centrifugal electrostatic shaping of high intensity electron beams 80−13183
  charged particle trajectory calc. in electrostatic field, teaching 80−90635
  chromatic aberrations, third-order aberrations of cathode lenses 79−81352
  chromatically corrected objective lens, of electron microscope, test *(German)* 79−892
  collimated electron trajectory in nonuniform transverse mag. field 80−53201
  combined focusing and deflection systems, electron trajectory aberration formulae 78−45756
  computer algebra, unconventional electron lens calcs. 77−67542
  condenser objective, single field, advantages and limitation for min.-exposure 80−87292
  condenser-objective, combined CTEM and STEM 80−86516
  crossed lenses, theoretical and expt. study 80−95780
  double focus electron probe, lens for STEM 80−9074
  einzel lens, depend. of aberration consts. on magnification 77−75404
  einzel lenses, symmetric, with thick central electrode, axial potential 80−18983
  electron gun, with electrostatic and electromagnetic lenses 80−99007

electron lenses continued
- electron-beam focusing optimisation with specified image parameters 78—86385
- electrostatic crossed lens, for electron microscopic devices 80—87289
- electrostatic double cylinder lenses, spherical aberration coeffs. and focal props. 79—86124
- energy broadening in electron-beam system, Boersch effect anal. 80—1114
- energy-loss spectral resolution optimisation wing electron lenses between TEM specimen and electron spectrometer 80—101886
- field solution convergence in nonlinear environment by network method *(Czech)* 79—81350
- focal properties and geometries of electron-lens systems used in low-energy electron or ion scattering 79—50202
- foil lens, spherically corrected, for electron phase microscopy *(German)* 80—83546
- gun, electrostatic, for field emission 80—62809
- hexapole spherical aberration corrector 79—76571
- HICOREX, for low magnification TEM with wide field, features 79—17564
- image reconstruction, computerized, fragment size choice 80—78785
- image tube lens, MTF 78—9428
- isoplanar nonaxisymmetric system, frequency contrast characts. 78—17855
- Johansson three-electrode objective, appl. to surface struct. studies *(French)* 80—47152
- magnetic lens spherical aberration correction with foil lens 77—67537
- magnetic spectrometer, corrected second-order aberrations 80—87013
- microscope, chromatic field aberration compensation with additional imaging lens *(German)* 77—10149
- microscope electrostatic lens *(German)* 79—49339
- microscope objective lens focus and spherical aberration meas. 77—54024
- moving objective lens, for deflective aberration free system 77—61908
- moving objective lens and Fraunhofer condition for predeflection 79—41316
- multi-element electrostatic cylinder lenses, computer program for calc. of electron trajectories 80—87283
- objective, with compensated axial chromatic aberration, for electron microscope 80—87293
- objective lens aberrations in HV electron microscope *(Japanese)* 80—52364
- one and two-lens electron-optical system parameter comparison 80—87284
- optical parameter formulae, of mag. electron lenses *(Chinese)* 77—88633
- optical properties and aberrations, lenses with electron-transparent foils 77—10828
- parallel plate retarder in electrostatic zoom lens 78—329
- pinhole image potentials, low-energy electron deflection, electron lens 80—53199
- probe forming systems, optimisation with respect to aberrations and vertical beam landing 80—68291
- quadrupole lens for beam shape transform., rel. to deep stopping in recuperator 77—65562
- rotationally symmetric, with curved charged transparent foils, third order spherical and axial chromatic aberrations *(German)* 77—10827
- scanning beam system, moving objective lens design 78—74829
- Scherzer's formula and the correction of spiral distortion in the electron microscope 77—71407
- Scherzer theorem and ideal lenses 77—67547
- SEM, photographic recording system 80—101903
- SEM lens system design, snorkel or condenser-objective 80—57438
- SEM objective lens, spherical and chromatic aberration coeffs., meas. method 78—21286
- SEM with electron energies up to 5 MeV 79—80728
- single-pole electron lens finite element analysis 80—69315
- spherical aberration, design of electron lenses consisting of two double cylinders, calcs. 80—23613
- spherical aberration, new correction system 80—5676
- spherical aberration correction by holography 79—85203
- spherically corrected apochromatic electron lens *(German)* 77—22620
- STEM, post-specimen optics, lens-spectrometer system optimisation 77—22621
- STEM, single atom microscopy, instrumental aspects 80—86522
- superconducting, for imaging organic materials in electron microscope 80—73553
- superconducting electron microscope lenses, construction of cryostat for testing 77—22627
- superconducting lenses applic. to electron microscopy 77—71408
- TEM, high resolution, 600 kV Cambridge Univ., condenser-objective lens design and construction 78—32938
- TEM, spiral distortion correction 78—32942
- TEM, viewing arrangement improvements 78—32941
- TEM lens system with eucentric goniometer for ferromag. material obs. 77—72530
- TEM multilens imaging system design for minimum distortion at low magnifications 79—12897
- triple slit scheme for high current variable-shaped beam forming 80—68290
- triplets of 2-electrode astigmatic tubular lenses, spherical aberration 79—50203
- tube-aperture lens for ang. depend. spectrometry 77—79200
- twin, Philips EM 400 TEM/STEM performance 80—57441
- unipotential, focal and aberration props. calc. 77—68162
- wave aberration from superposition diffractograms 77—71411

electron lifetime (metals) *see electron relaxation time (metals)*

electron mean free path (metals)
- A15 superconductors, elec. resist., phenomenological model 77—43775
- alloy, binary, elec. resist. depend. on LRO, SRO and composition, inhomogeneous order effects 79—60781
- bulk, rel. to interrelation of thermoelec. power and TCR in film 77—76957
- complex metals, RF size effect, mean free path depend. of reson. strength 79—56202
- diffusion thermpower, boundary scatt. effect 80—6817
- disordered and spinodally decomposed alloy, residual elec. resist. 79—19569
- disordered metals, incipient Anderson localisation role in resistivity 80—49687
- dynamic screening of core hole, semiclassical model 79—69445

electron mean free path continued
- electron gas, mean free path of low energy electrons, influence of damping 78—10385
- EM to acoustic energy conversion, temp. depend. 77—51780
- Fermi surface, electron-phonon and electron-impurity collision frequencies, RF size effect method 77—20227
- ferromagnetic metal slab, transmission of 24 GHz radiation, effect of diffuse surface scatt. of carriers, calc. 80—34780
- film, calc. 78—72283
- film, grain boundary electron scatt. in total film cond. model 80—7004
- film, grain boundary scattering model 79—15234
- film, Hall coeff. in mean free path model 79—11240
- film, homogeneous, elec. cond. determ. 77—15973
- film, Mayadas-Shatzkes conduction model, treated as Fuchs-Sondheimer model 77—80855
- granular materials, size effects in cond. and supercond. 80—77581
- liquid metal, electrical resistivity in short mean free path regime 79—56184
- metal, superconducting and normal, attenuation, EM generation and detection of US shear waves 78—39261
- metal, theory of electronic transport of sound packets in parallel mag. field *(Russian)* 78—84261
- metal wires, DC resistance, size effect correction 78—91679
- metallic film, grain boundary electron scattering by effective mean free path 78—84320
- metals, acoustoelectric current for conductivity electron arbitrary dispersion law *(Russian)* 80—49829
- metals, ferromagnetic, point contact spectroscopy, electron-magnon interactions *(Russian)* 80—54766
- metals, sound pulse spike like transport near acoustic cyclotron resonance *(Russian)* 80—100617
- polycrystalline metals, elec. cond., statistical model for grain boundary effects 80—6814
- polycrystalline-thin metal films, thermoelectric power, mean free path model 80—107770
- single electron excitation damping, conduction electron scatt. *(Russian)* 80—15510
- spin glass, generalised mean field theory with spin correls. 78—2691
- superconducting transition temperature, influence of electron mean free path 79—82702
- thin metallic plate in strong mag. field, electron scatt. elec. cond. theory *(Russian)* 80—59974
- transition metals, HCP, electrical resistivity high-temp. anisotropy 79—65429
- wire, cylindrical, elec. resist., scatt. processes, Monte Carlo calc. 80—75560
- Ag, Fermi surface and thermoelec. power, de Haas-van Alphen calc. 79—4503
- Ag film, defect density, thickness depend., elec. resist. obs. 80—70568
- Ag film, in situ resistivity meas. 80—97008
- Ag film, size effect in thermoelec. power, MFP and Fermi surface 77—69433
- Al, film, photoelectron-grain boundary scatt. in Al-SiO$_2$-Si struct. 78—64120
- Al film, rel. to TCR calc. 77—76960
- Al foil, electrical conduction, electron mean free path, surface scatt. 80—88535
- Al, low-field galvanomag. props., Fermi surface and defect struct. effects 77—4323
- Al, mean free path of electrons needed to form surface plasmons 77—51800
- Al, Sondheimer size effect, phonon-limited mean path, 1.8-12K 80—49698
- Al superconducting film, 2 GHz SAW attenuation meas. of mean free path 77—39999
- Al superconducting film, cylindrical, granular, crit. currents and electron mean free paths 80—7057
- Al-Cu, dil., anisotropic scattering of conduction electrons on dilute Cu impurities 79—47082
- Au, electron inelastic scatt. MFP, 60-140 eV 77—62909
- Au, Fermi surface and thermoelec. power, de Haas-van Alphen calc. 79—4503
- Au, thin film, self-sustaining, electron mean free path meas. 80—92883
- Au-Ag film, thermoelectric power and resist. meas., MFP and Fermi surface meas. 77—51826
- Au-Cu-Fe spin glass alloys, impurity mag. resist. meas. 80—59972
- Au-Fe, spin glass, quench-condensed film, reduced MFP influence on elec. resist. 77—69306
- Au-Fe film spin glass, low temp. resistivity, mean free path effects 78—80163
- AuFe alloy films, mag. susceptibility, Fe concentration and annealing depend. 79—61119
- Be wires and strips, elec. resist. at 77K, size factor *(Russian)* 80—24867
- Cd film, elec. cond., classical size effect 77—89881
- Cd film, surface RF impedance in strong mag. fields *(Russian)* 80—92920
- Cd foil, monocrystalline, anisotropy of size effect 79—38048
- Cd, surface impedance, Gantmakher-Kaner oscills. *(French)* 77—66195
- CeCu$_2$Si$_2$, transport anomalies 80—20148
- Cu (111) surface, high resolution photoemission spectra 79—52082
- Cu, Fermi surface and thermoelec. power, de Haas-van Alphen calc. 79—4503
- Cu film, elec. resist. temp. coefficient 77—89883
- Cu$_2$Mo$_6$S$_8$, normal state and superconducting property measurements 78—91660
- Fe whiskers, galvanomag. size effects 78—14709
- Ga film, monoclinic, elec. cond., classical size effect 77—89881
- B-Ga, metastable, elec. props. in normal and supercond. states *(Russian)* 80—65520
- Ga, supercond. thin film, tunnelling meas. in high mag. field 78—68120
- Ga, ultra-pure, bulk residual resist. 80—10950
- Gd, spin wave temp. depend., exchange coupling role 78—68199
- Gd, thermoelectric power anisotropy at high temp. 79—23952
- Gd-Al(C)(Cu)(Ga)(Ni)(Pd)(Rh) alloys, amorphous, mag. and elec. props. 80—80499
- Hf, rel. to high temperature thermophysical properties 78—91404
- In, electron MFP, conduction electrons injected from ferromag. 79—15135
- In, thin films, elec. props. effect of thickness and temp. 80—44742

electron mean free path continued
Mg film, Fuchs Sondheimer theory, size effect, elec. cond., Fermi surfaces 79−99637
Mo, US attenuation meas. of mean free path temp. dependence 77−39825
Nb, high temp. elec. resist., supposed failure of Boltzmann eqn. 77−72849
$Nb_3Ge(Al)$, anomalous resistivity, insight from band theory 78−60106
$(Nb_{0.99}Ti_{0.01})_{1-x}Ge_x$, high T_c, resist. meas. 80−88531
Ni, effects of grain size on resist. anomaly near Curie point *(French)* 77−4318
Ni-V, magnetocryst. temp. and conc. depends., rel. to resistivity 77−40052
$PbMo_6S_8$, normal state and superconducting property measurements 78−91660
Pd film, elec. resist. 80−93013
Pd thin film, temp. coeff. of resist. meas. 80−107930
PdGdH, diagram of state elec. props., indirect exchange interaction, EPR study *(Russian)* 80−50179
Rh, thin films, polycryst., resistivity and temp. coeff. of resistivity 80−88648
Sm film, electrical resistivity in 77 to 300K range 77−59339
Sn film, evaporated on cooled substrate, electron mean free path for 100-370K 79−65561
Ta film, oxidation in ambient conditions, resist. and ellipsometric meas. 79−34209
Tb, thermoelectric power anisotropy at high temp. 79−23952
Ti, electrical resistivity high-temp. anisotropy 79−65429
Ti, rel. to high temperature thermophysical properties 78−91404
Tl film, Fuchs Sondheimer theory, size effect, elec. cond., Fermi surfaces 79−99637
V, superconducting vacuum-deposited film, electrophys. props. *(Russian)* 77−59345
W film, surface RF impedance in strong mag. fields *(Russian)* 80−92920
W, low temp. transport props., phonon and impurity scatt. 78−10418
W, RF size effect signal, anomalous behaviour 77−89788
W, US attenuation meas. of mean free path temp. dependence 77−39825
Y, thermoelectric power anisotropy at high temp. 79−23952
Yb, film, amorphous and cryst., transport props. rel. to band struct. *(Russian)* 77−12026
Zn, bicrystals, galvanomagnetic phenomena at common boundary, electric field potential distribution *(Russian)* 80−29388
Zr, rel. to high temperature thermophysical properties 78−91404

electron micrographs *see electron microscope examination of materials; electron microscopy*

electron microprobe analysers *see electron probe analysis*

electron microprobes *see electron probes*

electron microscope applications
see also electron microscope examination of materials; scanning electron microscope applications
analytical electron microscopy, book 79−97479
atom, polarisability meas. using field electron microscope *(French)* 77−543
autoradiography of serial sections, method for holding electron microscope grids 78−20331
backscattered electron images of biological specimens 80−104827
biological application, quarter-micron serial sectioning and stereoscopy 80−72384
biological data processing and synthesis 79−25180
biological specimen exam., conf., Nancy, France, 1978, May 79−66591
cathodoluminescence high-resolution anal. system 77−13806
cell membrane particles diameter meas. via picture processing 79−84065
contaminant identification by energetic beams 79−39250
convergent beam diffraction in HV electron microscope 78−83674
crystal potential, electronic microscopy, real and imaginary terms *(French)* 77−84697
Earth sciences, use of electron microscopy 80−105091
education, electron interference using standard electron microscope and electron biprism as interferometer 78−62005
electron diffraction instrumentation 78−83683
electron emitter integral emission characts. determ. 79−9263
energy analyser/electron microscope combination, microanal. accuracy improvement 78−15737
ferromagnetic film thickness meas. by diffraction electron microscopy 78−86392
field emitter electron beam exposure system for semiconductor fabrication 79−30624
film thickness meas., backscattered electron intensities, ang. depend. 77−40317
film thickness measurement, of amorphous and crystalline thin films 79−26186
gas-solid interactions study by controlled atmosphere electron microscopy 77−29042
HV, displacement rates in collision cascade, radiation damage studies 77−24330
HV, in-situ elec. resistivity meas. 80−101893
industrial atmosphere submicroscopic asbestos fibre evaluation 79−74585
interaction energy, procedure for precision meas. of condensed bodies under various physicochem. conditions 79−21736
isotope separation using electron microscope, and electron spectroscopy, rotating ion-collectors 80−32850
Lorentz microscopy, thin film and bulk specimen, recent advances 78−35002
Lorentz microscopy using STEM for domain wall profiles determ. 78−35003
medical diagnosis using clinical pathology liver and kidney samples, computer assisted 80−85485
microfield measurement on solid surface using raster electron microscope 80−31790
multiplexing electron beam patterns using single-crystal thin films 79−89041
n-p junctions, determ. of transport parameters of minority carriers using electron microscope 80−65665
p-n junction, thinned, TEM image interpretation 77−20414
pattern writing, mol. struct. template form. 77−30217
photomicrography of marine microorganisms on submerged surfaces 78−85454

electron microscope applications continued
plant root transport studies using ion localisation, freeze substitution method 80−85569
review, TEM, STEM, and SEM: microscopy to microfabrication 78−32936
roughness measurement of supersmooth surfaces, using electron mirror interference microscope 79−93260
semiconductor, TEM/SEM observations comparing diffr., elec. and luminesc. contrast from dislocations 78−38714
semiconductor device characterisation using STEM 78−34893
semiconductor surface potential distrib. meas. using mirror electron microscope 79−35784
size determination of sonicated vesicles, spray freezing method 80−98188
solid-electron interactions, conf., Southampton, England (Apr. 1976) 77−44570
STEM, use for cathodoluminescence analysis 78−32950
stylus examination, roughness meas. of engineering surfaces *(German)* 80−68182
thick-section parallel membrane separation estimation 79−70718
two-dimensional mag. microfield electron microscopy 79−6239
ultrahigh vacuum, in situ meas. of thermal EMP 79−26184
Si_3N_4 sample substrates, high resoln. electron beam fabrication using STEM 80−104104

electron microscope examination of materials
see also electron microscope applications; electron microscopy; scanning electron microscope examination of materials; scanning-transmission electron microscope examination of materials; transmission electron microscope examination of materials
adenovirus hexon, three dimensional structure from electron microscopy, computer modelling 80−35833
β''-Al_2O_3, Mg- and Li-stabilized, high electron microscopy images of defects 79−73135
Al-Cu(4wt.%), θ' precipitation, effect on Young's modulus, electron microscope obs. *(French)* 79−47689
alkali halide, crystal, irradiation-induced defects 80−107316
alkali halide, morphology of growth and evaporation surface 78−79544
alkali metal titanates, $(A_2Ti_6O_{13})_n.A'Ti_4O_9$, (A=Na, K, Rb)(A'=Ba, Pb, Sr), intergrowth in tunnel structures 80−28995
alkaline earth hexaborides, electron fractography 77−8906
alkaline silicate glass, surface layers, plasticity and microcrack formation, electron microscopy *(German)* 80−40469
alloy, solute redistrib. during in situ irrad. in HVEM 80−107324
alloy structural steel, electron fractographic pattern of fatigue fracture under cyclic loading 77−56094
alloys, high resoln. diffr. and imaging characterisation 80−104050
alloys, phase transition premonitory phenomena, exam. by electron diffr. and microscopy *(French)* 80−59651
almandine-pyrope-grossular garnet, exsolution obs. 78−32074
amethyst quartz, α-β phase transition, interaction of Dauphine and Brazil twins 77−62641
amorphous alloy, and metastable phases, cryst. kinetics, review *(Japanese)* 80−38912
amorphous material, electron scattering, 1.2 to 3 MeV, Monte-Carlo method *(French)* 79−99037
amorphous material, high resolution dark-field images 78−26398
amorphous materials, high resolution imaging 79−99039
amorphous solids, inorganic, struct., review 80−15004
amphiboles, high-resolution electron microscopy 80−75241
animal plasma membranes, study using freeze-fracture technique 80−104842
anodic film, behaviour of emulsion particles during electrodeposition 80−104357
Antarctic aerosols particle anal., comp. 80−77091
anthanthrene, mol. imaging by high resolution electron microscopy 78−79600
anthracene thin films, struct. rel. to substrate temp., thickness, condensation rate 78−30845
asbestos fibre, identification techniques 77−60018
asbestos fibres concentration meas., in air and liquid, analytical methods review 80−72120
asbestos fibres identification, electron microscope techniques comparison 78−66012
austenite, hot-worked, subgrain struct., X-ray diffr. and electron microscope obs. *(Russian)* 79−15698
austenite, lattice stability loss near $\gamma \rightarrow \alpha$ and $\gamma \rightleftarrows \varepsilon$ transitions *(Russian)* 79−61584
bacterial cell wall, surface charge and morphogenesis of regular arrays of macromols. 80−85366
bacteriophage DD6, contracted tail, three dimensional struct. 78−11608
bacteriophage FI-5, struct. in intact state 79−70513
BCC crystal, electron microscope image contrast, theoretical predictions for non-edge dislocation loops 80−24326
BCC crystal, electron microscope image contrast from edge dislocation loops 77−76409
benzonitrile, anodic polymer growths during electrical breakdown conditions, TEM study *(French)* 78−75960
bimetal, failure during fatigue testing, electron microscope obs. *(Russian)* 78−23808
biological materials, high-resolution imaging, radiation damage, review 79−5331
biological membranes and proteins, plastic deformation during freeze-cleavage, review 78−14400
biological samples, origin of contrast in images *(French)* 79−66593
biological specimens, reduction of radiation damage by superconducting lens system 79−34718
biological specimens, structure determination, electron microscopy, optical and digital anal. *(French)* 79−66594
biomacromolecules, image analysis *(Czech)* 78−31983
biomembrane ultrastructure rel. to function, review 78−15785
Birbeck granule-containing cells of mice, occurrence of cored tubule 79−34515
Bloch wave model for ECP contrast in Si, Cu, Ag, Au 80−96419
blood, transport of catecholamines from adrenomedullary cells 79−66464
blood cells, red, human, frozen section prep. for electron probe anal., fracturing or cutting 79−39625
blood proteinpolymer interfacial behaviour, influence of hydrophilic-hydrophobic type of microphase separated struct. *(Japanese)* 80−12051

electron microscope examination of materials continued
- borosilicate photochromic glasses, photosensitivity rel. to AgCl particle shape 78—31223
- brass, 70:30, rolled, nucleation and annealing texture development 80—45320
- α-brass, dislocation struct., deform. *(Polish)* 80—24454
- brass, FCC rolling texture origin with rolling plane parallel to {111} 79—91674
- β-brass, spinodal decomposition, electron microscope and diffr. study 79—78930
- β_1 brass containing α-precipitates, reversible shape memory effect *(Japanese)* 78—60711
- breast tissue exam. using neutron activation and electron microscopy 80—21536
- butadiene, styrene, 4-vinylpyridine terpolymer, cross-linked by coordination with Fe (III) chloride, ion clustering 78—83748
- n-butanol, microemulsion, dynamical and structural props., by chem. physics method 79—79308
- butyl rubber dispersion, electron-microscopic investigation 78—53268
- butyl rubber ethylene propylene ternary copolymer mixture, permeability, diffusion of gases and solvents 79—95217
- carbide crystals, high resolution dark-field images 78—26398
- carbon tetrafluoride+SiC(Si), reaction, metastable C phase prod. 79—29393
- carboxyl terminated butadiene nitride-diglycidyl ether of bisphenol A epoxy resin, struct. and mech. props. 78—52901
- cast steel, heat treatment, effects of explosive loads, radiographic anal. 77—25072
- catalase, electron microscope exam. of new cryst. form, Fourier transform. method 77—11447
- catalase crystal lattice stability 77—25380
- cell, surface photoelectron micrographs and quantum yields 78—61148
- cell average size and shape meas. light scatt. photometry compared with microscopy 79—84030
- cell cultures, Halobacterium halobium membrane microstruct. 77—25386
- cell wall struct., Bacillus subtilis, S/N enhancement by interactive computation 79—5427
- cellulose, comparison of conclusions from small-angle X-ray scattering and electron microscope obs. 79—86717
- cellulose, degradation by high voltage electrons 80—100283
- ceramic compact, morphological investigations significance 79—33988
- ceramic powders, electron microscope determination of particulate sizes *(German)* 78—57891
- ceramics, glassy, struct. and electron beam sensitivity 80—79841
- ceramics, glassy phase, struct. study through electron-beam induced ionisation effects, HVEM obs 80—14978
- ceramics, high resoln. diffr. and imaging characterisation 80—104050
- ceramics nonoxide, high resolution electron microscopy 79—90501
- cermet film, as solar selective absorbers, production, struct. and optical props. 79—29485
- chalcedonies, structural disorder by IR spectroscopy 79—87450
- chloritoid intergrown polytype identification by electron multiple scatt. 80—70184
- chromatin, DNA-protein complexes, electron microscope visualisation, book contrib. 79—5434
- chromindur, origin of coercivity, Lorentz microscopy, magnetisation and Mossbauer effect 78—64219
- chromites high-resolution observations 80—75241
- clay minerals, appl. of high resolution electron microscopy *(French)* 78—26396
- coke, anisotropic spheres obtained during needle coke form., struct. obs. 77—63573
- collagen fibril cross-striation, thermodeform., electron microscopy and X-ray diffr. 77—86438
- collagen/synthetic polymer laminar copolymers, tissue compatibility 77—60289
- colloidal photochromic dyes, quasi-crystals produced in applied electric field 80—85225
- composition and structure of engineering and industrial materials, instrumentation 77—4882
- compound eye of worker honey bee, cell junctions 80—85383
- conducting and semiconducting materials, surface study using Johansson three-electrode objective *(French)* 80—47152
- conference, Nancy, France (May 1978) *(French)* 79—41915
- conference of Electron Microscopy Society of Southern Africa, Port Elizabeth, S.Africa (Feb. 1980) 80—73099
- controlled pore glass, pore struct., determ. by electron microscopy and Hg penetration 78—43165
- convergent beam electron microscopy for materials science 80—107028
- copper hexadecachlorophthalocyanine, radiation damage 77—19987
- copper phthalocyanine, chlorinated, radiation damage mechanism 80—88000
- copper phthalocyanine, chlorinated, stacking disorder 78—34622
- copper phthalocyanine, on graphite, epitaxial growth of new polymorph 77—80712
- copper phthalocyanine, simulated mol. images, point models and kinematical struct. amplitudes 80—103223
- α′-copper phthalocyanine, struct. and susceptibility to radiation damage 79—32986
- coronene, minimal exposure high resolution electron microscopy 80—79653
- corundum, derived from dehydration of diaspore (α-AlOOH), periodic regular texture 79—99328
- cowpea chlorotic mottle virus packing in crystalline monolayers 80—89922
- crack tip strain meas. by electron micrograph stereoscopy 80—69752
- crystal analysis, optical selected-area diffr. patterns of high-resolution electron-microscopic images 78—55789
- crystal orientation, grain boundary characterisation, zone axis method *(French)* 80—44215
- crystalline materials, semiconductors, developments in high resolution imaging 80—99001
- Cu-Al, FCC, study of dipoles using weak-beam electron microscopy 78—22724
- cup and cone fatigue fracture, electron fractographic obs. *(Japanese)* 78—72838
- cytochrome c oxidase, macromolecular struct., electron microscopy and image anal. 80—89716
- cytosine, cryst., electron damage, electron microscope study 78—22762
- defect imaging, approx. for dynamical calc. of microdiffraction patterns 78—26393

electron microscope examination of materials continued
- defects which exhibit no generalised cross section, identification using computed electron micrographs 77—51383
- devitrificates, quantitative charact. of microstruct., electron microscope study *(Polish)* 79—100311
- devitrificates, quantitative charact. of microstruct. *(Polish)* 79—91889
- diamond, Fresnel diffraction at platelets, defect struct. anal. by 3 Å phase-contrast microscopy 78—87701
- diamond, platelets, giant, on cube planes, electron microscopy 77—84765
- diamond, thermal cond. at low temp., correl. with IR absorpt. features 80—49435
- diamond crystals, synthetic, etch-pit formation on cube faces 80—75232
- diamond-Si heterostructure, Auger spectra electron microscopy study 80—34340
- direct observations of H entrapment 78—48585
- dislocation core geometry, electron microscopy *(French)* 79—42072
- dislocation generation from grain boundary, in situ obs. 78—51547
- dislocation loop growth during HV electron microscope irrad., thin foil point defect profile 80—2018
- dislocation loops in cubic media, black-white contrast 80—75234
- dislocation mobility, core struct. by electron microscopy *(French)* 79—42071
- dislocation velocity, thermal activation exam. of applied stress and temp. depend., expt. methods *(French)* 80—59474
- dislocations, collective behaviour, velocity of slip band and mobile dislocation densities, HVEM study *(French)* 80—65006
- dislocations, dissociated, weak-beam technique, appl. to quartz, Al_2MgO_4 *(French)* 79—42070
- DNA, spreading of large associations, dark field electron microscopy 80—85563
- DNA and chromatin molecule preparation for electron microscopy 79—25171
- DNA entrapment mechanism at air-water interface 77—60181
- DNA kinetoplast, ultrastruct., interpretation of dark field electron microscopy images of isolated purified networks 80—85369
- DNA occluded in epitaxial single cryst. Au film, electron microscope contrast 79—57568
- DNA structure, meas. by several techniques 79—24948
- electrical discharge machining, workpiece craters, electron microscopic study 80—30157
- electron sensitive materials 78—83701
- enantiomorphic crystals, electron microscopy 77—84602
- enzymes, molecular struct. reconstruction from electron microscopy images 80—89715
- epoxy resin, plastic deform. effect on crack propag. 80—97563
- ethylene-tetrafluoroethylene copolymer, chem. etching of fission tracks 80—896
- ethylene-vinyl acetate emulsion, morphology 77—48692
- failure analysis, fault tree technique and electron fractography 78—53071
- fatty acid synthetase, from yeast, three-dimens. electron microscopy, struct. and image reconstruction 77—12883
- Fe, Armco, electron microscope object prep. method 80—50789
- Fe-Cr-Co-Si-Mo, plastic deform. influence on structure and mag. props. *(Russian)* 79—70176
- Fe-N system, fine particles growth, prep. by reactive gas evaporation technique, lattice consts. and habit study 79—56919
- feldpsar in porcelain, melting behaviour *(German)* 79—90758
- feldspar, dislocation image contrast in electron microscopy and X-ray topography 78—26573
- ferrite bubble film struct., EM and RHEED, Mn and Mn-Cu ferrites 77—11801
- ferrite powder grain size meas., sample prep. *(German)* 78—56833
- ferritic alloy, reinforced by dispersed oxide, mech. props., modification by recovery heat treatment *(French)* 77—59837
- ferritin particles, BeO supporting films in high resolution electron microscopy 78—12792
- ferroelectric domains, surface pot. meas. 78—15132
- ferroelectric substances, electron microscopy investigations, review *(Japanese)* 80—71366
- ferrofluid, particle size distrib. parameters 79—1687
- ferromagnetic film, domain wall width meas. with electron microscope, astigmatism effects 79—19753
- ferromagnetic ordered structures, domain structure, effect of defects, electron microscopy 78—64214
- fibre, inorganic, refractory behaviour testing 77—25204
- film, epitaxial crystal growth, electron microscope obs. *(Japanese)* 78—91568
- film, evaporated at oblique incidence, columnar grains inclination angle 80—75468
- film defect growth and nucleation, electron microscopy and diffraction exam. *(French)* 80—59824
- fluorophlogopite mica, glass-ceramic, thermal diffusivity, crystallisation effects 78—6190
- fluorophosphate optical glass melt, disintegration of vitreous C 78—30101
- foil, dislocation loop nucleation and growth during 1 MeV electron irrad. 80—88152
- fracture mechanics parameters, applicability to creep, fatigue crack propag., at evalated temp., exam. using various materials *(Japanese)* 78—52962
- free cells, preparation technique for electron microscopy using conical glass tube for centrifugation 79—34711
- freeze-fracture techniques and appls. in struct. anal. of mammalian plasma membranes, book contrib. 80—30960
- frozen liquids, cold-stage microscopy system 79—71573
- gamma-irradiated cells, conference, Tokyo, Japan (Apr. 1979) 80—27034
- garnets, concentrational inhomogeneities, appl. of vacuum decoration method 79—14835
- geometrical and chemical knowledge at high resolution, electron microscopy and inner shell excitations 80—79646
- glass, ancient samples, trace element anal. by neutron activation, rel. to corrosion and devitrification 78—12801
- glass, phase separation 78—2015
- glass, two-phase, struct. and texture, electron microscope 79—64999
- glass chip, reducing agent effect on crystn. 78—46736
- glass tip, surface and crystallographic struct. using field-ion and electron microscopy 80—10767
- glial smooth endoplasmic reticulum acid phosphatase transport into damaged axons, role of microtubules 80—85381

electron microscope examination of materials continued
gliovascular interphase in irrad. brain tissue, horseradish peroxidase transport 80—41119
gliovascular interphase in irrad. brain tissue, phosphatases location 80—41120
glomerular permeability in foetal rabbit 80—85372
glutamine synthetase macromolecular struct., electron microscopy and image anal. 80—89716
glutamine synthetase reconstruction from electron micrographs using computer averaging 79—92452
glycoproteins in lipid bilayers, freeze-fracture technique 78—48764
grain boundaries, high angle, plane matching secondary relaxations 80—103363
graphite, phase contrast electron microscopy of holes and steps 77—38063
graphite catalytic gasification using Pt, Ir, Pt-Ir, small bimetallic particle identification by controlled atm. electron microscopy 79—83502
graphite crystal, electron irrad., threshold energy for displacement damage 77—76461
graphite $FeCl_3$ intercalate, interpenetration of 'stages' direct imaging 80—84037
graphite foil, thickness determ. by TEM using diffr. and energy loss anal. 78—29088
graphite-$FeCl_3$ intercalation compounds, form. kinetics and microstruct. *(German)* 79—43560
graphitic carbon, electron microscope imaging of isolated individual sheets 79—2890
graphitisation of bulk mesophases, electron microscope obs. 78—44035
haematite, reduction to magnetite, HVEM 78—6892
haemocyanin of Limulus polyphemus, quaternary struct. 80—85337
haemoglobin, sickle cells, 3-dimens. reconstruction of fibres 78—44452
herpesvirus of turkey, image reconstruction of core 79—97477
hexadecachlorophthalocyanato-copper discrimination of individual atoms in mol. images 80—100226
hexaphenylene mercury, bright-field imaging of single heavy atoms in an electron microscope with superconducting lens system 80—10472
histidine decarboxylase quarternary struct. 79—92129
histology, small object processing device 80—3887
HVEM obs. of irrad. damage 77—35589
II-VI semiconductors, thin epitaxial layer, direct synthesis *(German)* 80—104070
III-V compounds, stacking fault energy and ionicity 78—30651
Inconel 718, low cycle fatigue at 298 and 823K 77—86151
insulation layers of magnetic laminations, FeO, Fe_2O_3, and Fe_2O_4 *(Polish)* 77—12743
insulators, direct obs. via SEM 77—2712
intrinsic boundary dislocation spacing meas. from electron micrographs 78—30632
island films, diffusive mass transfer, review 80—20054
isotropic crystals, ang. glissile dislocations, method of moments theory and electron microscope obs. *(Russian)* 80—24449
jimthompsonite and anthophyllite from Swiss Alps, disordered intermediate minerals imaging 80—72518
Kevlar 49 fibre, macromol. struct., electron diffr. and dark-field electron microscope obs. 78—34446
Kevlar 49 high modulus polyaromatic fibre, supramolecular struct. 78—55819
L-cells, γ-irrad. effect on chromatin struct., mouse 80—30793
lattice imaging, direct obs. of plane matching 78—6072
lattice imaging, ultramicrostructs. 79—77467
leucine aminopeptidase crystalline aggregates, interpretation of electron microscope images 78—68988
leucocytes, differential counts, comparison between light and electron microscopic results 79—5429
lipid bodies, saturated, in organ pipe cactus visualisation by cytochem. technique 80—76873
liquid crystals, defects, struct., optical, electron microscopy *(French)* 79—46567
liver, rat, ion movements during energy-linked mitochondrial structural changes 80—12065
LMFBR, Na test of bellows expansion joints, metallographic study *(Japanese)* 79—67850
lunar anorthosite from Luna 20 landing site, petrography and electron microscopy 77—60631
lung, rapidly frozen under controlled physiological conditions, prep. technique 79—39619
magnetic domain wall observation device for use with 1 MeV electron microscope 80—101882
magnetic thin film, magnetisation changes during main stage of nonuniform rot. *(Russian)* 77—32224
martensite, shape memory, crystallographic similarities 79—66102
martensitic transformations, electron microscope study of cryst. geometry *(Russian)* 80—108441
material wear, electron metallography using SEM, TEM 80—76455
mercury acetate, direct observation of Hg atoms in make-up of heteroorganic compound 79—35898
metal, BCC, fine particles formed by gas-evap. technique, cryst. struct. and habit 79—27935
metal, dynamic study of defect mobility using HVEM 78—47327
metal, friction pair, seizure centres on contacting surface *(Russian)* 77—70185
metal, hardening due to increased subgrain boundary stability 78—52934
metal, load-bearing surfaces, secondary structures obs. by electron microscopy, specimen thinning method 79—52484
metal, oxidation of high temp. material, lattice vacancy effect 77—70203
metal, very thin foils, crack propag., electron microscope obs. 77—63792
metal crystallites, polyhedral, growth in inactive gas, review 79—27934
metal systems, high voltage electron microscopy of dislocation dynamics *(Japanese)* 77—47458
metal ultrafine crystallites, form. by gas evaporation technique, crystal habit 77—52239
metal-insulator transition study *(French)* 78—26815
metal-metalloid amorphous systems, thermal instability, crystn. characts. 77—4044
metallic surface, mirror electron microscopy for total electron refl. coeff. determ. 78—5994
metallic thin film, vacuum deposition, early stage obs. using microbalance technique and electron microscopy *(Japanese)* 80—54554
metallography, feasibility and methodology of in situ experimentation *(French)* 80—68301

electron microscope examination of materials continued
Cd-metallothionein, test object for dark field electron microscopy of protein struct. 78—11610
metals, abrasive finishing with refractory carbide micropowders, surface struct. 80—11842
metals, BCC, dislocation processes, straining expts., electron microscope obs. 80—29025
metals, FCC, atomic defects, computed electron microscope images 78—26392
metals, FCC, deformed single crysts., struct. evolution at heating 80—103337
metals, submicroscopic defects, influence on HVEM in-situ expts. 80—103392
metals, submicroscopic surface relief after finishing 79—29276
metals and alloys, close-packed, temp. depend. of stacking fault energy 79—19266
metals research, steel microstructure determ. *(German)* 80—15089
metamorphic plagioclases from Japan, modulated microstructure 79—96760
meteorites, stony, mineral grain substructs. study 77—87349
methacrylic acid-N,N'-ethylenedimethacrylamide crosslinked copolymer soln., 3-dimens. struct. peculiarities *(Russian)* 79—55678
N-methacryloil-ω-aminolauric acid cholesterol ester, liq. cryst. polymers, copolymers, structuring *(Russian)* 79—55665
mica, metamorphic white, surface microtopography 80—54493
microcrystals on C foil, size distrib. from electron micrograph obs., UV absorpt. spectra obs. 80—55121
microemulsion, freeze fractured, electron microscopy examination of micellar and lamellar struct. *(French)* 78—15714
micrograph, computer simulation for crystal defect identification 78—30525
micrograph images, determ. of structs. relative orientation 79—70714
microtubules in optic nerves of temperature acclimated goldfish, electron microscopy 80—85395
milk fat globule membrane, cryst. struct. 80—85364
mineral dusts, environmental monitoring 77—81877
mitchondrial complex III membranes preps., cryst. struct. 80—85365
mitochondrial inner membrane, ribbon struct. 78—11618
mixed-chain silicates, new ordering schemes 79—99142
modulated structure phenomena, survey 79—95033
mullite-corundum ceramics, electron microscopy of damaged surface 80—88413
muscle fibre, skeletal, helicoids in T system and striations, HV electron microscopy 78—53356
muscovite, natural cryst., submicroblock struct., electron microscopy 79—14816
myelin, frog nerve, comments on the paracrystalline nature 79—16161
myelin, paracrystalline nature 77—52748
myelin sheath, thickness irregularities distrib., paracryst. struct. 77—12892
myelin structure, of sciatic nerve from bull frog, melamine resin as embedding medium 78—92764
NaCl crystals, air cleaved, anisotropy of round evaporation spirals, electron microscopy study 79—73300
naphthalene crystal nucleation on anthracene microcrystals suspended in vapour-gas stream 80—76165
naphthalene derivatives, film struct., electron microscope and diffr. obs. 79—11029
nephrite jade, struct. irregularities, electron microscope obs. 77—19969
neutron-bombarded, diffuse X-ray scattering *(Russian)* 80—92560
Ni-Cr-Mo and Ni-Cr, impact strength, effect of modified ausforming *(Japanese)* 79—11692
Nimonic 80A superalloy, contrast from cavities in HVEM 80—79780
Nimonic PE-16, irrad. in HVEM, void growth, vacuum environment influence 80—107323
noncrystalline solids, models and exptl. methods, review 78—22655
nuclear reactor pressure vessel/cladding interface, residual gas analysis *(German)* 77—40603
nucleic acid molecules, preprocessing of electron micrographs for automatic computer anal. 79—70711
nucleic acids, electron microscopy using basic protein film method 80—104844
Nucleopore membrane, pore struct., determ. by electron microscopy and Hg penetration 78—43165
nucleosome core particles of chromatin, struct. 77—86440
Nylon 6, solution crystallization 79—86719
Nylon 6 gut yarn, fine struct. change in twisting, annealing and untwisting, X-ray and electron microscopy obs. 80—84904
nylon-11, folded-chain crystal, pressure-induced crystallisation from melt, annealing 77—84671
nylon-12, folded-chain crystal, pressure-induced crystallisation from melt, annealing 77—84672
Nylon-6, shish-kebab struct., obtained from quiescent soln. by self seeding 80—15017
nylon-6 pressure-crystallised, annealing under pressure 77—84670
omega phase, roles of electron microscopy and electron diffraction *(French)* 78—27524
oocyte paracrystalline structs., mouse, Mus cervicolor poppaeus 80—89731
opal, ordered arrangements of SiO_2 spheres of two different sizes 78—87658
optic tectum, goldfish, fine struct. 80—85396
optical glass, laser induced pre-threshold changes 78—29999
ordered alloys, long period antiphase structs. 79—95027
organic solids, electron microscopic approach to struct. and reactivities 79—73077
ovalene, minimal exposure high resolution electron microscopy 80—79653
ovarian cortex effect of daily prenatal gamma irrad. in beagle pups 80—85453
oxide glasses with Bi or Se granules, elec. props. and microstructure 78—2490
paraffin wax, elec. cond., 33-55°C and 1-2 kV cm^{-1} 79—99555
Parlodion coating of highly fragile freeze-fracture replicas 80—8231
$Pb_3(PO_4)_2$, ferroelastic props., domain struct. *(French)* 80—44216
periodic grain boundary struct., interaction with lattice dislocations 79—51117
periodic regular texture 79—99328
perlite, low temp., processes occurring during firing 80—11607
perlite, water content obs. *(Russian)* 77—66908
Permalloy film, mag. microstruct. obs. in nonlinear ripple magnetis. case *(Russian)* 80—65971

- **electron microscope examination of materials** continued
  - Permalloy film, magnetic leakage fields above stripe domains 77—77077
  - Permalloy film, submicroscopical magnetisation structs. induced by fields normal to film plane 79—1697
  - Permalloy film, two-layer, with magnetostatic coupling, creep of domain boundaries *(Russian)* 77—43857
  - Permalloy-Co film, domain walls, magnetisation ripple *(Russian)* 79—47314
  - phospholipid smectic phases, defect struct., freeze-fracture electron microscopy 77—21473
  - photographic emulsion, solarization, elimination by adding halogen acceptors, electron microscopy investigation 79—24790
  - photographic emulsion grains, latent image distrib., etching and recrystn. effects of solns. 80—77890
  - photosynthetic membrane 80—26210
  - photosynthetic membranes, supramolecular organisation model based on freeze-fracture electron microscopy 77—29106
  - phthalocyanine, cryst., electron damage, electron microscope study 78—22762
  - phthalocyanine, metal-free, molecular imaging and phase transformations using electric microscopy 79—33198
  - pigeonite, inverted, from SW Norway, precipitation temp. estimation 80—72500
  - plagioclase feldspars, modulated structs., X-ray diffr. and electron microscopy obs. 79—95031
  - planar defects, exptl. and calc. images at high resolution 77—35575
  - plastic, load-bearing surfaces, secondary structures obs. by electron microscopy, specimen thinning method 79—52484
  - PMMA, amorphous, electron microscope and small angle X-ray studies 77—84666
  - PMMA, destructive mech. cracks, electron microscope exam. of generation centres 78—68782
  - PMMA, electron beam scattering, Monte Carlo simulation 80—100148
  - PMMA-PVC mixtures, dielec. relax. and struct. rel. to formation *(Russian)* 77—20073
  - PMMA-styrene acronitrile system, selective electron beam etching 78—45603
  - point defects, small, possible source of error in determ. of defect type 77—65941
  - poly(p-phenylene terephthalamide), crystallised during polymerisation, morphology *(Japanese)* 77—51328
  - poly 2,3-dichlorobutadiene, struct., morphology, polymorphism 79—65008
  - poly-m-toluenylsilsesquioxane mesomorphic struct., form. during polymerisation *(Russian)* 80—61095
  - poly-p-phenylene terephthalate, high modulus fibre, struct. obs. 78—75564
  - poly-p-xylylene, α-β phase transition, electron microscopy study 79—69241
  - polyacetylene films, stretch-aligned, prep. and morphology 80—66471
  - polyacrylic acid film, structurisation and mech. props., EM obs. *(Russian)* 80—59406
  - polyacrylonitrile, single cryst. formation, during soln. polymerisation, struct. determ. 80—38938
  - polyalkane imides, crystallisability, supermol. and crystalline structures 80—84100
  - polyamide, aromatic, fibre, high modulus, mol. and supramol. struct. 80—79710
  - polyamide 6, reinforced and unreinforced, fatigue fracture types under circular flexural loading *(German)* 79—70170
  - polyamide single crysts., struct. *(Russian)* 77—43158
  - polyamide-Cu system, antifrictional props., struct. 80—40552
  - polyaromatic molecule, high resolution dark-field images 78—26398
  - polyarylate organosiloxane polyblock copolymer, struct., props., phase conversion *(Russian)* 79—65010
  - polybutadiene-poly-α-methylstyrene copolymers, struct. obs., prep. *(French)* 80—59401
  - polybutene-1 film, tubular-extruded, light scatt. from crystn. superstruct. 77—55796
  - polycarbonate, amorphous, electron microscope and small angle X-ray studies 77—84666
  - polycarbonate, craze thickening mechanism during craze growth 79—91823
  - polycarbonate, struct. 79—55675
  - polycarbonate styrene-acrylonitrile copolymer mixture, determ. of phase structure 80—103272
  - polyconjugate system, interrelation between physicochem. props. and microstruct. 78—55816
  - polyethylene, adhesion to Cu, reactions of CuO with Cu or polymer 79—39118
  - polyethylene, cross-linked crysts., deform. mechanism 78—15469
  - polyethylene, crystallisation of thick film from glassy state by annealing 80—54151
  - polyethylene, crysts., subject to fold-surface tensile stress, elastic deform. 78—76712
  - polyethylene, electron microscopy with chlorosulphonation aid 77—89351
  - polyethylene, high density, film, melt growth, cryst. superstruct., small angle light scatt. 77—31602
  - polyethylene, high density, oriented extended chain crystals, transparency *(Japanese)* 80—38955
  - polyethylene, high-density, semicryst., fold-surface morphology effect on deform. processes 78—34447
  - polyethylene, high-density oriented, lamellar struct. obs. 77—55244
  - polyethylene, lamellar stacks, screw dislocations 80—19728
  - polyethylene, linear, melt-crystallised sharp fraction, lamellar morphology 80—84099
  - polyethylene, linear, quenching of thin films to amorphous state 80—28929
  - polyethylene, microstruct. obs., variation during drawing and annealing, electron microscopy *(German)* 80—38944
  - polyethylene, nascent, electron microscope study 80—38940
  - polyethylene, pyramidal crysts., soln.-grown, collapse mechanics 78—76713
  - polyethylene, shish-kebab crystals, core struct. 80—38945
  - polyethylene, single crystal, electron microscopy study 80—103273
  - polyethylene, stress cracking in aqueous detergent 77—12727
  - polyethylene, stress crystallised, melting behaviour 77—47554
  - polyethylene, structural changes induced by high elec. field *(Japanese)* 79—23532
  - polyethylene, structure change on uniaxial compression *(Russian)* 79—34119

- **electron microscope examination of materials** continued
  - polyethylene, supermolecular structure, polymerisation at low pressure *(Russian)* 79—64126
  - polyethylene, terephthalate, amorphous, electron microscope and small angle X-ray studies 77—84666
  - polyethylene, ultradrawn, electron microscope exam. of struct. after annealing 80—11662
  - polyethylene fibres, electron microscope investig. of internal struct. 80—28926
  - polyethylene films, hard elastic, deform. mechanism 77—32652
  - polyethylene single crystals, fold domain boundaries, diffr. contrast 77—15428
  - polyethylene terephthalate, struct. 79—55675
  - polyethylene/ethylene vinyl acetate copolymer mixture, rel. between hypermol. struct. and stability *(German)* 80—64929
  - polyethyleneterephthalate, crystallised from thin layer melts, temp. depend. of morphology 80—54149
  - polyhexamethylene terephthalate/polyoxytetramethylene block copolymers, supramolecular texture 78—91261
  - polymer, amorphous, domain struct. determ. by electron microscopy and electron diffr. 77—84667
  - polymer, multicomponent, homopolymer blends, macroscopic phase separation 80—45289
  - polymer, porous, prep., appl. as stationary phase in gas chromatography *(German)* 79—29434
  - polymer, synthetic, electron beam damage in electron microscope exam. 78—34409
  - polymer blend morphology, methods for study and specimen prep. 78—75580
  - polymer crystallisation in strained melts 78—26450
  - polymer electrophoretic coating, effect of silicone additive on electrophys. props. *(Russian)* 79—15615
  - polymer film, micropore localisation 80—103271
  - polymer film, supermolecular structure and mech. stress distrib. among chem. bonds 78—75562
  - polymer interfaces, visualisation by phase contrast electron microscopy 78—14295
  - polymeric cryoprotectants in preservation of biological ultrastruct., aq. soln. low temp. states 78—65157
  - polymers, crystalline, bulk, lamellar struct. and plasticity mechanisms 77—65957
  - polymers, HVEM in-situ deform. 80—104215
  - polymers, morphological study, using C replicas, wide angle electron scatt. *(Russian)* 79—32923
  - polymers, plastic deformation during freeze-cleavage, review 78—14400
  - polyoxymethylene, epitaxial growth on KBr single crystal *(Japanese)* 78—56054
  - polyoxymethylene, nascent, morphology, optical and electron microscopic obs. 80—59403
  - polyoxymethylene-copolyamide melts, flow, fibrillation, mechanism 77—4765
  - polypropylene, cold-drawn isotactic bars and thin films, microstruct. and annealing 78—95760
  - polypropylene, monofilaments, drawing behaviour, melt-induced orientation effects 78—84922
  - polypropylene, structure change on uniaxial compression *(Russian)* 79—34119
  - polypropylene nonfilaments, highly drawn, plastic deform. 78—44174
  - polypropylene systems, elastomeric impact modifiers rel. to morphology 79—66154
  - polysiloxane dizwitterionomers, morphology, ionic aggregation 80—49130
  - polystyrene, isotactic, morphology and growth of chain struct. *(German)* 78—75597
  - polystyrene, lamellar stacks, screw dislocations 80—19728
  - polystyrene, Millar interpenetrating network, viscoelasticity and phase domain form. 78—83749
  - polystyrene, struct. 79—55675
  - polystyrene in tetrachloroxylene and tetrachlorobenzene, morphology of crystallized additives 79—99082
  - polystyrene latex, particle size determ. by electron microscopy 79—21698
  - polystyrene latex particle size by electron microscopy and light scattering 79—66365
  - polystyrene-polyethylene/propylene block copolymer, micelle form. in lubricating oil 80—61171
  - polyurethane adhesives, modified, struct. *(German)* 79—100333
  - polyurethaneurylenes, segmented, structural features *(Russian)* 77—47356
  - polyvinyl alcohol, crystallisation from dil. soln. by stirring *(Japanese)* 77—89388
  - polyvinyl chloride, struct. 79—55675
  - polyvinylidene fluoride vinyl fluoride copolymer, epitaxial crystallization 79—65005
  - Porphyra osmoregulation, struct. aspects 80—85370
  - protamine, electron microscopic recognition rel. to radiation exposure 79—62175
  - protein molecule, simulation of single mol. images combining computer and electron micrograph analysis 78—37781
  - protein supramolecular structure, ordered, electron micrographs, image processing 80—89923
  - PTFE fibres, US effects on structure *(Polish)* 78—68702
  - purple membrane particles, freeze-fractured, protein content 77—90735
  - PVC:Fe(Cu) film, struct. and optical props., soln. growth technique 78—51837
  - PVC, filled with SiC particles, abrasion resistance *(Japanese)* 78—7055
  - PVC, mechanochemical degradation in primary struct., mech. vibration effects, IR spectra *(German)* 78—19769
  - PVC, plasticised, processing-morphology-mech. props. relation 79—8264
  - PVC, rigid, tensile fracture morphology, rel. to mol. props. 77—59883
  - PVC, rubber-modified, stress whitening and yield mechanism 79—8324
  - PVC, suspensions, melts, rheological props. rel. to struct. 79—3983
  - PVC block copolymers, physical props. and morphology 79—82166
  - PVC mixture with processing aids, mech. props. and morphology 79—57047
  - PVC-g-butyl rubber grafted copolymer, tensile strength increased by S_2Cl_2 curing 79—95993
  - pyrocarbon, low temp., isotropic, permeability study *(French)* 79—7549
  - pyroceramic plate surface quality obs. after mechanical polishing 79—72732
  - quartz, amorphous layer on mech. treated single crysts. electron microscope and RHEED obs. 80—24721
  - quartz, ion-etching of grooves for SAW devices 78—95822

electron microscope examination of materials continued
quartz, microtopographical obs. of 2nd order prism faces, hydrothermally-grown crysts. 80—54481
quartz, synthetic, annealed, light scatt. centres 77—11586
quartz, synthetic, growth spirals on prism faces, electron and optical microscope obs. 77—7723
quartz dislocation fine structure under electron irrad. 80—70213
quartz film, microcrack growth 77—69037
quartz grains, from coastal plain of Rio Grande do Sul, Brazil, coaxial crescentic marks *(Spanish)* 78—92816
quartz natural microcrystals, elementary growth layers on faces 78—14634
quaterrylene, minimal exposure high resolution electron microscopy 80—79653
quenched-in vacancy defects behaviour, electron microscopy study 77—1120
radiation-damage artefacts in biological electron microscopy, technique for visualisation 79—20726
radioactive waste, solidified, composition, structure and properties of final product obs. *(Czech)* 78—66353
rare earth fluorides, as antirefl. coatings, evaluation 77—61963
rare earth hexaborides, electron fractography 77—8906
rare earth metal oxide films, crystallisation, electron microscope obs. 79—15034
rare earth oxide film, struct., electron microscope and diffr. obs. 79—11028
rare earth oxyphosphates, x Ln_2O_3.y P_2O_5, synthesis, characterisation and thermal stability 80—16256
rare earth $Zr_{1-x}O_{2-x/2}$ growth from skull melting, directional solidification 78—60567
rare earth-transition metal amorphous films, radiation damage 77—66398
rare-earth dihydride epitaxial films, growth and struct. 79—37936
red cell ghosts active transport, cytoplasmic contamination obs. 80—45874
refractory composites, fibre reinforced, directionally solidified tensile tests, in HVEM, deform. and fracture *(French)* 78—68785
refractory metal, vapour-phase epitaxial growth *(Russian)* 77—59227
refractory metal film, electron beam evaporator for in situ deposition studies in UHV electron microscope 80—40264
refractory metals, technique for investigation of nonmetallic inclusions 77—52587
Rene 80, dislocation behaviour during plastic deform. *(Japanese)* 80—108504
retina, rat, rod and cone-type photoreceptors in post-equatorial region 80—85384
Rhacopholus embryo yolk platelets, freeze fracture study of crystalline struct. 80—104552
ribosomal particles, electron microscopic investigation using tilting technique 79—34514
ribulose bisphosphate carboxylase, two-layered square-shaped mol. 77—56336
ribulosebisphosphate carboxylane, electron microscopy of 79—70515
Rochelle salt, ferroelec. thin crysts., struct. investig. 79—27962
rock magnetism, domain structure obs. by Lorentz electron microscopy 80—72502
ruby, concentrational inhomogeneities, appl. of vacuum decoration method 79—14835
S glass-Ni sphere composite, exam. of crack shape and fracture toughness 78—72886
sapphire, concentrational inhomogeneities, appl. of vacuum decoration method 79—14835
semiconductor, dislocation struct. and elec. props. 80—70201
semiconductor, dislocations studied by weak beam electron microscopy 79—82216
semiconductor, ion-implanted, post annealing meas. using optical and electron microscopy 79—69121
semiconductor, recomb.-enhanced defect reactions 77—51377
semiconductor defects, SEM in EBIC mode vs. HVEM images 78—9923
semiconductor epitaxial and diffusional interfaces, obs. of individual misfit dislocations 79—82222
semiconductor materials, microcharacterisation 80—101911
semiconductor thin sample etching for electron microscope exam. 80—86272
semiconductors, appl. of analytical techniques to crystal growth and defects 80—73546
semiconductors, conf., Oxford, England (April 1979) 80—67928
semithin large epoxy sections resectioning for electron microscopy 80—8233
shape memory alloy, martensite boundaries, lattice imaging study 80—107359
short range order classification by electron microscopy 78—38623
Si whiskers, shadow electron microscopy study of steps of {112} faces 79—60666
Sialon, high resolution electron microscopy 79—90501
silica gel, microporous amorphous toroidal, spectroscopic and thermal analysis, adsorption properties 79—57305
silicate glass, low voltage electron microscopy of heated surfaces using C replica technique 80—25974
silicate HV high-resolution electron microscopy 80—70096
silicate mineral, identification and asbestiform varieties, election optical and X-ray techniques 80—8446
silicate minerals, lattice imaging 78—30522
silver thioamides, precip., electron microscope and potentiometric studies, growth of photosensitive crysts. 80—33107
single crysts., fatigued age-hardenable, dislocation structure *(German)* 80—54247
small protein struct. anal. by electron microscopy, valinomycin, bacitracin, LMW-CSA N and B 79—92453
sodalite, hydrothermal growth on seed crysts. covered with boundary layers, growth mechanism 78—30571
sodium dodecyl sulphate, microemulsion, dynamical and structural props., by chem. physics method 79—79308
sodium octanoate-decanol-water system, liq. cryst. C phase, struct. determ. using electron microscopy 77—47341
solid solutions, cubic, at. mean sq. displacement and critical voltage effect 79—60236
solid state chemistry problems, appl. of electron microscopy and diffr. 79—46527
β-spodumene-mica glass ceramics, phase evolution and TiO_2, MgF_2 additive effects, exam. 78—44089

electron microscope examination of materials continued
sputtered coatings, metallurgical characterisation 79—15056
stacking fault, antiphase boundary energies, investig. methods, review, appls. to FCC metals *(French)* 79—42080
stacking faults, inelastic scattering effect, electron microscopy obs. *(French)* 79—60388
stearic acid, evaporating cryst. surfaces in vacuum 79—77740
stearic acid, microscopic obs. of cleaved surface 79—95248
stearic acid, single cryst. growth mechanism 78—30562
stearic acid cryst., etch pit obs. of dislocations 78—87676
steel, 0.7% C, welded zone, fatigue strength and microstruct. *(Japanese)* 80—89339
steel, 35NiCr18, bainite transformation, study with aid of hot stage microscope 80—76253
steel, 37Kh12N8G8MFT, precipitation hardening, hardness meas. and electron microscope exam. *(Russian)* 79—38843
steel, 45G17Yu3, deformed, influence of hot rolling on struct. *(Russian)* 77—25073
steel, 50N29 type, self-consistent junctions and spatial relative organisation 80—19750
steel, Al, relax. twins in martensite, electron diffr. and electron microscopy *(Russian)* 78—47391
steel, alloy, Cr-C (12, 0.2 wt.%) growth of grain boundary ferrite allotriomorphs, photoemission electron microscope exam. 78—88468
steel, alloy, Fe-C-Zn (0.45, 1.56 wt.%), pearlite transformation during continuous cooling 78—80538
steel, alloy, Fe-Cr-Ni-Mo-Al, (13, 8, 2, 1, wt.%), H_2 effects on fracture, exam. 78—60809
steel, alloy, Mn (Ni), Mossbauer, X-ray and electron microscope studies of martensite 78—56621
steel, alloy type, photoemission electron microscope obs. of high temp. precip. behaviour 80—108456
steel, and alloy, austenitic transformation, temp.-conc. range of product formation 79—100135
steel, austenite form. from ferrite-cementite mixtures, HVEM obs. 77—66639
steel, austenitic, 16H2NMB, struct., texture and mech. props. of product of transform. 78—92273
steel, austenitic, cold worked 10Kh11N23T3MR, structural transformations, aging effect, electron microscope obs. 80—40402
steel, austenitic, Cr-Mn, Kh4G18F, microstruct. and mech. props. during tensile deform. *(Russian)* 79—20114
steel, austenitic, Cr-Ni-Mo (25, 28, 20 wt.%), containing N_2, electron microscope obs. of Cr_2N precipitates *(Japanese)* 78—15404
steel, austenitic, dislocation struct. formed by interstitial diffusion of C 77—4223
steel, austenitic, dislocation structural changes on hot rolling *(Russian)* 77—59805
steel, austenitic, martensitic transform. effect on hardening kinetics and fracture resist. of friction surface of 45Kh12G8 and 110G13 *(Russian)* 80—50727
steel, austenitic, metallography study of high temp. decomposition 79—61559
steel, austenitic, Ni alloy, stacking fault energy of austenite, high resolution electron microscopy *(Russian)* 80—44219
steel, austenitic, substructure change in hot deform. process *(Russian)* 77—16617
steel, austenitic, supercooled, decomposition by heat treatment, carbide particle morphology *(Russian)* 77—70076
steel, austenitic, type 70, cold brittleness structural depend., fracture mechanisms *(Russian)* 80—97571
steel, austenitic, wire rod, austenite transform. kinetics accompanying interrupted cyclic cooling *(Russian)* 79—70064
steel, austenitic 316, displacement energy determ., HVEM obs. and electron bombardment 78—6100
steel, austenitic stainless, deformed plate, X-ray line profile anal. *(Japanese)* 78—7144
steel, austenitic stainless, fatigue under static and cyclic heating fractographic peculiarities, electron microscope obs. *(Russian)* 77—52465
steel, austenitic stainless, ferritic, single phase ferritic solidification in welds, exam. 80—7546
steel, austenitic stainless, grain boundary as dislocation source during high temp. deform. *(Russian)* 78—15453
steel, austenitic stainless, irrad. creep of type 316 in HVEM 80—97523
steel, austenitic stainless, partial dislocation separation and dislocation substructure, effect of applied stress 78—22727
steel, austenitic stainless, precipitation of $M_{23}C_6$ type carbide on twin boundaries 80—89226
steel, austenitic stainless, stacking fault energy measurement, by weak beam electron microscopy 78—18661
steel, austenitic stainless, structural inhomogeneity, electron and optical microscope exam. 78—72827
steel, austenitic stainless, welds, exam. of austenitic solidification mode 80—7545
steel, austenito-martensitic, struct. changes during plastic deform., mutual influence of phases *(Russian)* 80—30015
steel, ball bearing, martensitic decay during rolling contact fatigue 77—32682
steel, C, decomposition of supercooled austenite, exam. of carbide formation *(Russian)* 78—35388
steel, C, fatigue crack features, in S 35 C and SK 5, anal. by precision matching method *(Japanese)* 78—52955
steel, C, fatigue crack propag., crack closure, dislocation struct., electron microscopy obs. *(Japanese)* 80—25845
steel, C, fatigue crack propag. and fractography under periodic overstressing, exam. *(Japanese)* 78—52958
steel, C, ferritic-pearlitic transform., struct. study by optical and electron microscopy *(French)* 78—68685
steel, C, machined, microdefects on surface 80—16607
steel, C, non-propagating microcrack, opening and closing behaviour in rotating bending and torsional fatigue *(Japanese)* 80—25846
steel, C, rubbed surface, continuous hard layer *(Japanese)* 77—52501
steel, C, second stage of tempering 79—61627
steel, C, spheroidised, fracture toughness, cementite particle effects, optic and electron obs. 78—60785
steel, C, tempered martensite embrittlement, and retained austenite, exam. 78—56754
steel, C, U8A, struct. after low-temp. thermomech. treatment 79—79008
steel, C, wear charact. of worn surface layer under lubrication *(Japanese)* 78—35526

electron microscope examination of materials continued
steel, C (0.54 wt.%), torsional fatigue process, obs. by electron microscope *(Japanese)* 77—12690
steel, C-Mn-(Cr), structural changes during stress cycling after heat treatment and cold rolling *(Russian)* 78—19787
steel, carbide phases formation during annealing, of lower bainite *(Russian)* 78—6930
steel, case-carburized, low alloy, rolling contact fatigue 78—35518
steel, CC Cr-Mo-V (1,1,.25 wt.%), Mo_2C-V_4C_3 precipitation, creep rupture test *(Japanese)* 79—70070
steel, Ce, Nb, addition effects on hot plasticity *(Russian)* 77—66680
steel, cleaning corroded surfaces for electron microscope exam. by cathodic polarisation 79—70242
steel, Co-Si-Cr-Mo, alloying additions effect on pearlite interlamellar spacing *(German)* 80—40327
steel, complex alloy, ε-carbide precip. in bainite *(Russian)* 77—66647
steel, complex alloy, exam. of temper brittleness 78—44209
steel, Cr, and Cr-Mo-Ni, austenite decomposition, deform. effects, ferrite reaction 79—1842
steel, Cr (12 wt.%), thermomechanical treatment, high temperature, effect on props. and struct. *(Czechoslovakian)* 77—32603
steel, Cr and Ni-Cr, cyclic re-austenitizing 80—35222
steel, Cr-C (13, 0.15 wt.%), bainitic transform. *(German)* 78—11218
steel, Cr-Mn eutectoid, pearlite growth kinetics and partitioning 80—29963
steel, Cr-Mo, creep resistant, creep, effect of carbide precipitation *(German)* 77—52398
steel, Cr-Mo (2.25, 1 wt.%), decarburization, carbide effects in high temp. Na *(Japanese)* 78—15403
steel, Cr-Mo-V, heat treated, mech. props. *(German)* 80—25724
steel, Cr-Ni-Mo-Cu, ε phase particle precipitation from martensite, local internal stress relaxation *(Russian)* 79—78969
steel, CrMoV, creep resistant, cast, creep rupture and creep *(German)* 77—70098
steel, En 24, Cr, V, deform. effect on decomp. of austenite, carbide precipitation 80—84938
steel, eutectoid, partitioning of Si during pearlite growth, electron microscopy study 79—83201
steel, eutectoid, Si partitioning during pearlite transform., analytical electron microscopy applic. 80—108458
steel, Fe-Al-C alloy, redistribution of C during tempering *(Russian)* 77—90371
steel, Fe-Cr-C, austenitizing temp. effect on microstruct. and mech. props. 80—16341
steel, Fe-Mn-(Cr)-C, intermediate phase form. during martensite form. 77—12626
steel, Fe-Mn-C austenitic, deform. twinning and mech. props. 77—59868
steel, heat resistant, explosive loading effects on struct. and mech. props. *(Russian)* 78—39787
steel, high strength, 33Kh35NMVFA, low cycle fatigue fractures, electron microscope exam. *(Russian)* 78—31512
steel, high strength, fatigue crack propag. and fractography under periodic overstressing, exam. *(Japanese)* 78—52958
steel, high strength, hypereutectoid, low alloy, microcrack frequency and fracture toughness rel. to martensitic struct. *(Czech)* 77—70163
steel, high strength, weld cold cracking, anal. of fracture morphology, using SEM *(Japanese)* 78—52960
steel, high tensile strength, base plate and welded joints, exam. of fatigue crack growth rate *(Japanese)* 78—52956
steel, high V-W-Mo, high speed, phase composition and struct. of atomized powders 77—90323
steel, high-speed, shiny nonfusion rings in friction welding, origin 78—23872
steel, high-strength maraging, N18K9M5T, nitriding effect on fracture resist. 80—21092
steel, hypoeutectoid, C22, recrystn., influence of carbides distrib., electron microscope exam. *(German)* 79—38850
steel, hypoeutectoid, singularities of cryst. geometry of pearlite *(Russian)* 77—21093
steel, hypoeutectoid Widmanstatten struct. form., contrib. to the laws *(Slovenian)* 78—84817
steel, inclusions, SiO_2 Al_2O_3, FeS, effect of high temp. heating on size, number and distrib. 78—44145
steel, irrad. effects at high temp., simulation by HV electron microscope 77—1153
steel, low alloy, low C grain boundary proeutectoid ferrite formation, direct obs. method 80—3074
steel, low alloy, over-heating embrittlement, fracture surface examination *(Japanese)* 79—79088
steel, low alloy and C, bainite morphology 78—68682
steel, low alloy composite, ferrite-carbide struct., cold plastic deform. 77—90408
steel, low alloy type 12Kh1MF, effect of thermal cycling on life under creep conds. 79—57075
steel, low C, 10Kh2G3M, development of plastic deform., slip and dislocation struct. *(Russian)* 79—15722
steel, low C, austenite transform., TTT diagrams 77—70031
steel, low C, fatigue, low cycle, cyclic stress-strain curve eval. 77—44347
steel, low C, fatigue crack tip, observation of crack closure phenomena, by electron microscopy 78—68794
steel, low C, fractographic study of stage 1 cracking, endurance limit *(Japanese)* 77—8936
steel, low C, gas nitrocarburized, cyclic stressing 79—57098
steel, low C, high C, bainite transform. heat treatment effects *(Czech)* 77—63661
steel, low C, hot rolling effects on struct. *(Russian)* 78—19793
steel, low C, Mn, strain hardening parameters, electron microscope obs. 77—63690
steel, low C, packet martensite struct. and localisation of residual austenite, electron microscope obs. *(Russian)* 80—25695
steel, low Si, martensite struct. and mech. props. *(Korean)* 80—93614
steel, low-alloy 12GN2MFAYu, heat treated, testing temp. influence on fatigue strength *(Russian)* 80—40501
steel, low-C, coherent precip. of VC 78—35392
steel, low-C, ferritic, deform. microstruct., electron microscopy *(German)* 78—64589
steel, maraging, 18Ni300, ageing, electron diffr. and microscope obs. *(Polish)* 79—34070
steel, maraging, ageing kinetics and struct. of N12K7M5TYu, effect of high temp. deform. of austenite *(Russian)* 80—84960

electron microscope examination of materials continued
steel, maraging, hardening mechanism of quenched samples, tempering *(Czech)* 79—78989
steel, maraging low-Ni, isothermal martensitic transformations *(Russian)* 78—88465
steel, martensitic, ageing, thermal recovery 77—56011
steel, martensitic, high-C, formed from hot-worked austenite, struct. obs., electron microscopy *(Russian)* 78—6950
steel, martensitic, modulated struct. form. by tempering, high resolution electron microscopy obs. 79—96042
steel, medium C, fatigue crack propagation under repeated two-step loadings above and below threshold condition *(Japanese)* 79—38945
steel, mild, cold-deformed, struct. changes during annealing, electron microscope obs. *(Russian)* 78—23722
steel, mild, fatigue crack initiation, fractographic exam. *(Japanese)* 78—52957
steel, mild, impact velocity effect on fracture surface *(Japanese)* 79—96118
steel, mild and HSLA, mech. behaviour, deform. rapidity influence *(French)* 79—57056
steel, Mn-C, formation of filamentary V(C,N) precipitates during diffusional $\gamma \rightarrow \alpha$ transform *(Russian)* 79—1865
steel, Mn-Cr-V, structural changes during solution annealing *(Czech)* 78—84864
steel, Mn-Cr-V, tool, quenched and tempered, fracture toughness *(German)* 80—25726
steel, Mn-Mo-Nb-C, transform. charact. and struct. during continuous cooling 79—29057
steel, Mo-Cr (3 wt.%), CrC formation in isochronal tempering, electron microscope study 80—7584
steel, N32, $\alpha \rightarrow \gamma$ transform., struct., texture conc. var. depend. on plastic deform. *(Russian)* 79—66050
steel, N-Cr-Mn, influence of nitride phase on corrosion behaviour *(Bulgarian)* 79—61798
steel, Nb, controlled-rolled into ferrite temp. range, soln. temp. and rolling effects 80—11678
steel, Ni and W, recrystallisation mech. during laser treatment 80—50658
steel, Ni-Cr, temper embrittled, electron microscope and X-ray microstruct. obs. 79—38870
steel, pearlitic, struct. variations under plastic strain and subsequent heating, cementite decomp. *(Russian)* 80—84954
steel, pearlitic, temp. relationship of failure charact. 78—3158
steel, pearlitic or spheroidal plastic deform. and fracture *(French)* 78—35448
steel, plain C, eutectoid, alloying additions effect on pearlite interlamellar spacing *(German)* 80—40327
steel, plain C, quench ageing avoidance, critical cooling rate *(German)* 79—52244
steel, quenching to form martensite, morphology and struct., electron microscope and electron diffr. study *(French)* 77—73291
steel, reinforcing wires, high strength, microstruct. obs. *(Czech)* 79—43342
steel, Si, electron irrad. in HVEM, void swelling, Si role 80—54285
steel, stainless, 12Kh13 and 15Kh11MF, austenite transform. kinetics 79—87612
steel, stainless, 304, annealed and 9% prestrained, cyclic hardening and softening, room temp. 77—52483
steel, stainless, ε-martensite, direct obs. of reverse transform. 77—55967
steel, stainless, austenitic, precipitation hardening and N_2 effects obs. *(Rumanian)* 77—55973
steel, stainless, C-Cr-Ni-Mn-V , non mag., aged, struct. and mech. props. *(Russian)* 78—56666
steel, stainless, cavitation-erosion in fresh water, electron microscope and electrochem. study 80—55580
steel, stainless, Cr-Ni (18, 9 wt.%), cold rolled, struct. 79—83214
steel, stainless, dislocation structure, of $\Sigma=9$ related coincidence boundary 79—27994
steel, stainless, electrohydraulic effect and struct. changes *(Russian)* 78—23783
steel, stainless, electron irrad. in HVEM, radiation damage obs. 77—50233
steel, stainless, ferritic, electron microscope obs. of precipitation hardening *(French)* 79—34049
steel, stainless, fracture micromechanism when kept isothermally in sulphur pulp 80—76355
steel, stainless, grain boundaries, electron microscope obs. *(Russian)* 79—4311
steel, stainless, He ion bombard., in situ electron microscope examination 80—34094
steel, stainless, in-pile irrad. effect simulation by Ni ion bombardment, dislocation density, swelling 77—347
steel, stainless, martensite nucleation, in situ electron microscope obs. 80—7572
steel, stainless, martensite nucleation and growth, expt. study 78—3125
steel, stainless, precipitate crystallography using electron microscopy 78—83698
steel, stainless, radiation damage by 1 MeV electrons, dislocation struct., brittleness *(Russian)* 80—75226
steel, stainless, single crystals, shear cracks, electron microscope study 80—40522
steel, stainless, type 316, electron beam heating effect on extracted intermetallic precipitate 78—35394
steel, stainless, type 316, neutron irrad. damage simulation using HVEM, surface effect on void swelling 78—29572
steel, stainless, type Kh17N13M2T, strengthening by plastic deformation and cold working *(Russian)* 78—52839
steel, stainless, used as reactor cladding material, void swelling obs. by HV electron microscope *(Japanese)* 79—42108
steel, stainless, void shrinkage during electron irrad. in electron microscope in situ obs. 78—34540
steel, stainless 304, crack propagation under fatigue-creep conditions and fractography *(Japanese)* 80—104267
steel, stainless 304, recrystallisation, effect of dislocation structure 77—32595
steel, structural, austenite form. during heating *(Russian)* 77—32572
steel, structural, supercooled austenite, structural characts. of decomposition 80—60870
steel, structural recrystallisation, phase and struct. transformations during heating 77—55990

electron microscope examination of materials continued
- steel, tempering effect on struct. and mech. props. of types 70, U8, and U12 *(Russian)* 80−50655
- steel, Ti (0.1 to 0.55 wt.%), strengthening by carbide precipitation 77−25062
- steel, tool, blanking punch, chipping behaviour *(Japanese)* 79−100250
- steel, tool, NC6, carbide lattice, kinetics of its destruction *(Polish)* 78−92280
- steel, transformers, inhibitory phase *(Russian)* 78−3139
- steel, type 1Kh18N9T, neutron irradiated, microstruct. and mech. props. *(Russian)* 80−24503
- steel, type 304, faceted fracture surfaces, selected area channelling patterns 77−77565
- steel, type 33Kh3SNMVFA, failure surface study using electron microscopy *(Russian)* 79−70152
- steel, types 10G2 and 18G2F, formation of transform. microtwins in ferrite *(Russian)* 79−1866
- steel, unhardened, grinding by Si_3N_4-based abrasive material 78−35529
- steel, W and Mo, quantitative anal. of carbides formed during tempering 78−64571
- steel, W-Co-Mo-Cr-V-C (8.5, 8.1, 4.5, 3.5, 2.2, 1.02 wt.%), phase composition, struct. and props. 80−104163
- steel, W-Cr (3 wt.%), CrC formation in isochronal tempering, electron microscope study 80−7584
- steel, white layers forming at high rates of friction, struct. props. *(Russian)* 79−15800
- steel, X5CrNiTi26.6, ferrite-austenitic struct., optical and electron microscopy 78−84848
- steel, Zi, high permeability grain-oriented, AlN precip. study 79−83337
- steel, Zn coated, cold rolling influence on struct. and deform. of diffusional layer *(Russian)* 80−55465
- steel, Zn coated strips, plastic deform. influence on struct. and quality *(Russian)* 80−40377
- steel 0Kh16N15M3B, neutron irradiated, kinetics of nucleation and growth of vacancy pores and dislocation loops *(Russian)* 77−51408
- steel 120Kh3G3, lattice defects during $\gamma \to \alpha \to \gamma$ transform., electron microscopy obs. *(Russian)* 79−47681
- steel 12Kh1MF, fine struct., effect of isothermal transform. temp. 77−21137
- steel 15G2AFDps, brittle fracture of Fe quantitative electron fractography 77−63804
- steel ball bearing, fatigued, phase changes, nomenclature 80−89198
- steel Kh18N9T, fractographic features of rupture, rel. to struct. changes 77−63801
- steel nitride phase hardening, precipitation and solution kinetics after heat treatment 78−95756
- steel turbine casings, residual life determ. 80−93585
- steel-Babbitt bimetal, exam. of structure of transition layer 79−100293
- steel-Cu M3 bimetal, eutectic alloy, crack development, failure energy capacity *(Russian)* 80−40480
- steels, 110G13 and 40Kh10G10, hardening and structural transformations during friction *(Russian)* 77−52527
- steels, C, cold worked and recrystallised, attenuation behaviour *(German)* 78−48445
- steels, C, quenched and tempered, struct.-prop. relationships 80−7599
- steels, high-purity and commercially based, containing 10 wt.%W or 5 wt.%Mo, tempering behaviour 80−7600
- steels, hypereutectoid, 120G4 and U15 type, with initially pearlitic struct., mechanism of structural inheritance *(Russian)* 77−52329
- steels, stainless, electron irradiated, dislocation damage, HVEM study 80−103389
- stilpnomelane, complex layer silicate, struct. of long-period polytypes 77−64266
- styli of electrical surface roughness meas. instrums., examination of wear *(German)* 80−101782
- styrene-butadiene block polymers, multiphase systems, struct., props. 77−31600
- styrene-diene block copolymers, pressure sensitive adhesives, morphology and viscoelastic behaviour 77−52419
- sublayer, influence on stability and photographic characteristics of AgBr evaporated layers *(Bulgarian)* 80−42281
- sytrene-tetrahydrofuran block copolymer, H_2O contact angle and surface struct. *(Japanese)* 78−79861
- TCNQ salt, Ag.TCNQ, cryst. struct. 80−70186
- 2,3,4,5-tetraacetoxymercurithiophene, dark-field imaging, computer simulation 80−100151
- tetraglycidyl 4,4′ diaminodiphenyl methane epoxy, diaminodiphenyl sulphone cured, struct., deform. mode, failure 79−29141
- TGS, ferroelec. cleavage surface microscopic struct. by electron microscopy 79−51403
- TGS, interaction of γ-irrad., induced defect electron microscope expts. 79−10876
- thermoplastics, structural changes during deformation, rel. to impact resistance 80−25800
- thin film bicrystals, dislocation interaction, with grain boundaries during plastic deform. 80−54281
- thin film fabrication for photothermal solar convertors 80−11573
- thin foil, X-ray microanalysis in electron microscope *(French)* 80−61191
- thin foils, chem. anal. by electron microscopy *(French)* 80−50899
- Ti alloy, VT22, hot deform., microstruct. form. and mech. props. *(Russian)* 77−28830
- Ticonal with magnetic texture, struct. damages during ageing 77−16626
- Tishomingo Fe meteorite, microstructural study 79−16898
- tissue, Sephadex spheres used for localising specific regions 79−5428
- toluene, microemulsion, dynamical and structural props., by chem. physics method 79−79308
- transition metal complexes, dimethylglyoxymate films, prep. and physical props. 79−90923
- transition metal dichalcogenides, zone axis electron diffr. patterns 78−34497
- transition metal oxide catalysts, reduction, cryst. defects influence, in-situ electron microscopy 80−81322
- transition metal-W-O system, phase relations in dioxide-trioxide region, 1373K 78−11212
- triacetoxymercuraurine, direct observation of Hg atoms in make-up of heteroorganic compounds 79−35898
- twin boundaries, electron microscope images, contrast mechanism 78−30640
- twin boundaries, electron microscope images 77−11568

electron microscope examination of materials continued
- uterus, mouse, US irradiation at therapeutic intensities in standing wave fields 80−41112
- V-VI-VII ferroelectric semiconductor film growth, effect of artificial nucleation centres 79−11032
- l-valine, cryst., electron damage, electron microscope study 78−22762
- valinomycin-cholesterol (stearic acid) monolayers, struct., area and compressibility determ. 78−44461
- vinylidenechloride-vinylchloride latex copolymers grafted on to elastomers, film struct. and props. *(Russian)* 77−21090
- viral infections diagnosis, contrib. of electron microscopy *(Italian)* 80−109024
- viroid RNA, covalently closed circular mols., conform. states 80−85340
- water-in-oil-in-water emulsions, electron micrography 78−7245
- wear debris anal., quantitative methods 78−64912
- wire conductors, explosion, investigation of resulting particles *(Russian)* 79−37558
- wustite, intrinsic rates of reduction and mechanism 79−83153
- zinc oxalate, isothermal crystallisation from soln. 80−108336
- Zircaloy-4, cyclic nature of corrosion in 633K water, optical and electron microscope study 79−66207
- Zircaloy-4, polytype struct. of intermetallic precipitates, electron microscope obs. 79−43250
- α-Zr, crystalline anisotropy in α-phase, charact. by thin oxide film form. *(French)* 79−20269
- Ag, (111) surface electron microscopy 80−103556
- Ag and alloy electron microscope specimens, noncyanide electropolishing method 80−100967
- Ag, colloidal, lattice defects, X-ray diffr. and electron microscopy exam. 78−51567
- Ag, electrodeposit, on (111) face, habit modification caused by Cl^- 80−71600
- Ag epitaxial films, grain boundary struct. evolution during recrystn., interface energy effect *(Russian)* 80−15387
- Ag expitaxial film, twin boundaries of recrystn. type, electron microscope obs. *(Russian)* 79−4484
- Ag, FCC, dislocations, elastic instability 79−82235
- Ag film, in situ struct. determ. by internal stress meas. 80−54569
- Ag film, on MgF_2 and SiO substrates, internal stresses correl. with struct. 79−87026
- Ag film, on mica, microstruct. changes 78−72013
- Ag film, substrate surface structure effects on absorptance 78−19585
- Ag film, twin boundary faceted struct., struct. coarsening due to dislocations *(Russian)* 79−99215
- Ag films, on mica, graphite, and Si, early growth by ion-beam sputtering 77−44158
- Ag films, UV photostimulated oxidation *(Russian)* 78−95850
- Ag, fine particles prep. by vacuum evap. onto running oil substrate 79−28925
- Ag, granules and colloidal particles on Cs_2O film in Ag-O-Cs photocathode *(Chinese)* 80−2279
- Ag, multiply twinned particles, internal and surface struct. by electron microscopy 80−84189
- Ag on W (001), geom. factors of FCC-BCC epitaxy 78−60041
- Ag particles on graphite, particle motion rel. to heating in gaseous environments 78−34695
- Ag powder, ultrafine, sintering, coalescence growth stage 80−89174
- Ag, pure, temp. depend. of stacking fault energy 78−51565
- Ag, recrystallisation texture development after plane-strain deform. 77−48448
- Ag, rolled, dislocation struct. and recovery during annealing *(Russian)* 79−29084
- Ag, scatt. cross sections, 300 to 1200 keV 78−9922
- Ag ultra-thin film, deposited on MgF_2 and SiO substrates, struct. and internal stress 78−91572
- Ag, vac. deposition of oriented coating on doped alkali halide substrate 80−2303
- Ag, vacuum deposition, on evaporated AgBr layers, growth mechanism 80−35095
- Ag:He, implanted films, solid solutions radiation induced polymorphism 79−86810
- Ag-AgI film, electron microscopy and photoinduced dichroism *(Russian)* 77−1743
- Ag-AgI island granular film, Weigert effect, anomalous dichroism 77−12455
- Ag-Al, dislocation interactions with migrating interphase boundary electron microscope obs. 77−55963
- Ag-Cd (45 at.%), morphology and crystal struct. of stress-induced martensites 78−68693
- Ag-Cd (47 at.%), crystal struct. and internal defects of thermoelastic martensite 77−48438
- Ag-CdO cermets, coprecipitated carbonates and hydroxides, physicomech. props. 80−25706
- Ag-Cu (8 wt.%), plastic deform. effect on discontinuous precipitation 80−3053
- Ag-Ge eutectic alloys, unidirectional solidification, electron microscope study of twinning 79−61574
- Ag-Pd-Cu-Au dental alloy, age-hardening characts. 79−87646
- Ag-Sn alloys containing Au, splat cooled ribbons, electron microscope exam. 78−39987
- Ag-Sn-Cu-Hg, constitution of quaternary amalgam at 37°C *(German)* 77−81250
- Ag-Zn (38 at.%), morphological and struct. studies of thermoelastic martensites 77−63669
- $AgBiS(Se)_2$, polymorphism and defects, electron microscopy 78−2254
- AgBr, Herschel effect, latent image centre struct. changes under laser irrad. 80−77900
- AgBr layer, sensitised, topography of developed centres 80−73491
- AgCl film, on complementary cleavage planes of TGS, morphology, electron microscope obs. 79−15031
- AgCl, surface crystallisation, due to colloid adsorption 80−54544
- AgI hydrosols, kinetics and mechanics of colloid systems formation 80−101045
- AgI nascent hydrosol absorption spectra and microcrystal growth 79−100449
- AgI-Ag oxysalt high cond. glasses, struct. obs. 79−32908
- Ag_3Mg, long-period ordered, struct., high resolution electron microscopy obs. 79−94960
- Ag_3Mg, periodic antiphase boundaries, electron microscopy study *(French)* 80−59481
- Ag_2S film, vacuum deposition and struct. 77−73233

electron microscope examination of materials continued
Al, [111] single crystal, in situ deform., HVEM obs. 78−52886
Al, Al ion irradiated, void swelling and annealing of voids, electron microscopy study 80−88216
Al alloy, fatigue crack propag. and fractography under periodic overstressing, exam. *(Japanese)* 78−52958
Al alloy, fatigue crack propagation under repeated two-step loadings above and below threshold condition *(Japanese)* 79−38945
Al alloy D16, supersaturated solid soln., decomp. process, electron microscope obs. and acoustic anal. *(Russian)* 79−15650
Al alloys, dil., quenched, foreign element effects on dislocation loop form. 80−54239
Al alloys, specimen preparation for electron microscopy 80−40636
Al, alloys, thermomechanical working effect on mech. props. *(Russian)* 77−21181
Al and Al-Mg alloy N4, irradiation with 100 and 400 keV Al ions, obs. and analysis of damage struct. 77−4133
Al and Al-Mn (1 wt.%), subgrain growth during annealing after cold work 78−56656
Al, anodic film, formed in H_2SO_4, electron microscopy 78−68843
Al, bend contour electron microscopic images, n-slice approx., calc. of inelastic scatt. effect 77−62455
Al, bend contours, obs. using correction of Mollenstedt filter images by auxiliary lenses 77−39520
Al binary alloys, exam. of dislocation structure, using diffraction electron microscopy *(Russian)* 79−10857
Al, compressed, nucleation and recrystallisation study by electron microscopy and Kikuchi diffr. 79−52236
Al, creep and rupture, in torsion, mech. *(Russian)* 79−5030
Al, creep at intermediate temps., in situ study of cell boundary evolution, HVEM 78−48480
Al, deformed, nucleation and recrystallisation at second phase particles 78−6941
Al, dislocation activation, using UHV electron microscope const.-load tensile device 78−11462
Al, dislocation behaviour at melting, HV electron microscope in-situ obs. *(Japanese)* 77−43216
Al, dislocation generation from grain boundary, in situ obs. 78−51547
Al, dislocation loops, interstitial, size distrib. for metal irradiated in high voltage electron microscope *(Russian)* 80−103335
Al, dislocation loops and pores due to 23 MeV proton irrad. *(Russian)* 80−54235
Al, electron irrad., interstitial loop nucleation at impurity site *(Japanese)* 77−43247
Al epitaxial films, grain boundary struct. evolution during recrystn., interface energy effect *(Russian)* 80−15387
Al film, dislocation observation by electron microscope using convergent beam *(French)* 80−96532
Al film, nucleation and growth on C layers, adsorption energy and surface diffusion 79−99451
Al film, vacuum deposited, structural changes during annealing at temp. near melting point 78−84096
Al film, vacuum deposited, O_2 contamination effect on form. 79−82487
Al films, N_2^+ and O_2^+ ion bombardment, structural and phase changes 80−2094
Al, high purity, development of rolling and recrystallisation textures 77−25070
Al, interstitial loop form., effects of repeated electron irrad. 80−75220
Al, laser strengthening, struct., hardness and dislocation density *(Russian)* 80−76399
Al, low vacuum condensates, struct., IR refl. obs. *(Russian)* 78−30850
Al, low-order Fourier coeff. of pot., modified thickness fringe method 80−75130
Al, plastically deformed, spreading of extrinsic grain boundary dislocations 78−43023
Al, polycrystalline, movement of 3-fold nodes of boundaries in high temp. creep 80−89317
Al, polycrystn., HVEM in-situ investigation of creep mechanism 80−104214
Al, porous anodic film, ion beam thinned, electron microscopy 78−92390
Al, prismatic dislocation loops, (g.b)s product sign determ. *(Russian)* 78−38705
Al, prismatic displacement rings, plane normals determ. *(German)* 77−86118
Al, quenched, vacancy annihilation at surface and dislocation loops 79−60351
Al, recovery annealing, exam. using in situ high voltage electron microscopy 80−7596
Al, recrystallised, substructure strengthened, long-term strength 77−21173
Al, scatt. cross sections, 300 to 1200 keV 78−9922
Al, single crystal, superplasticity 79−1901
Al, superplastic deformation depend. on subgrain struct. electron microscope study *(Russian)* 79−83257
Al, thin foil, adhesion and friction, rel. to observed dislocation density 78−64706
Al, vacuum deposited, structural singularities and porosity *(Russian)* 78−75950
Al, with He-bubbles, TEM obs. 77−4132
Al/Pb two-layer target, moderate energy electron interactions, direct statistical modelling *(Russian)* 77−66561
Al-Ag, struct. of two-layer film 79−23851
Al-Ag, type-II superconductor, torque oscillations in mag. field *(Russian)* 80−103800
γ'-Al-Ag (15 wt.%), dislocation splitting mechanism, cessation above critical temp. 78−26572
Al-Ag (up to 40 at.%), exam. of anelastic phenomena and structural state 78−76693
Al-Al_3Fe, anodic film struct. and stability 78−48564
Al-Al_3Ni directionally solidified eutectic, microstructural degradation in temp. gradient 78−3145
Al-Al_3Ni eutectic, cryst. struct., orientation, electron microscopy, computer calcs. *(German)* 77−72582
Al-alloy type 2124 T351, crack tip closure assessment by electron fractography 80−19875
Al-Cr, rapidly solidified, crystalline and amorphous structures 77−44274
Al-Cu, splat quenched, amorphous regions 77−4047
Al-Cu, splat quenched, amorphous regions, comment 77−4048
Al-Cu (1 wt.%), electron irradiated, dislocation damage, HVEM study 80−103389

electron microscope examination of materials continued
Al-Cu (2-5 wt.%), precipitation total surface influence on resistivity *(French)* 80−71650
Al-Cu (4 wt.%), elastic accommodation of semicoherent θ' 78−64543
Al-Cu (4 wt.%), size distrib. and form. mechanism of GP zones *(Japanese)* 77−25054
Al-Cu (4 wt.%) alloy, θ' precipitate growth kinetics, electron microscope obs. *(French)* 77−44253
Al-Cu alloy, vacuum deposited thin film, abnormal grain growth before melting transition and subsequent struct. change 79−60663
Al-Cu thin films, microstruct. rel. to electromigration 80−44355
Al-Cu-Mg (1.3, 1.3 at.%) alloy, natural ageing, meas. of quenching vacancy dislocation loops 79−15704
Al-Cu-Mg-Mn-Fe-Si, alloy D16, effect of mechanisothermal treatment on mech. props. 78−56674
Al-Cu-Ni, vacancy ordering, electron microscope and electron diffr. obs. 79−27954
Al-$CuAl_2$, directionally solidified eutectic, structural changes during strength tests *(Russian)* 80−7543
Al-Fe-Si(0.5, 0.2 wt.%), cast, phase determ. 77−70032
Al-Fe-X-Si (X=transition metal), struct. and comp. by electron microscopy 80−88093
Al-In alloy, dilute, electron irradiation, interstitial dislocation loop obs. 78−18681
Al-Li (1.3 wt.%), prismatic dislocation loop rows due to precipitation *(Japanese)* 79−52220
Al-Mg, dilute, dislocation loops, interstitial, size distrib. for metal irradiated in high voltage electron microscope *(Russian)* 80−103335
Al-Mg, oxidation control study, electron opt. techniques eval. 80−85089
Al-Mg, oxidation induced stresses, dislocation network form., HVEM obs 80−14978
Al-Mg (0.3 wt.%) single cryst., dislocations obs. by high voltage electron microsc. 80−79796
Al-Mg (33 at.%), liquisol quenched, decomposition 79−61622
Al-Mg (4.4 wt.%), Burgers' vector of boundary dislocation, electron microscope obs. 78−43025
Al-Mg (5 wt.%), recovered dislocation substruct. during plastic flow 79−83273
Al-Mg cold drawn wires with FCC lattice, texture and structure 77−70067
Al-Mg supersaturated solid soln., spinodal decomposition at 20°C *(French)* 77−85987
Al-Mg-Ag, age effect on age hardening *(Japanese)* 78−52831
Al-Mg-Si, heavily rolled, electron microscope obs. of cube oriented region, rolling texture 79−29093
Al-Mg-Zn alloys, evaporation effect of alloying elements Mg and Zn in in-situ EM studies 80−103388
Al-Ni (63.6 at.%), elastic softening and electron diffr. anomalies prior to martensitic transform. 77−86078
Al-Ni foil, vapour deposited, multiply twinned particles, electron microscopy 77−28083
Al-Pt (2 wt.%), rapidly solidified alloy, metastable phase formation and decomposition 79−52194
Al-Si (9 wt.%), precipitation hardening during isothermal ageing 80−29969
Al-Si alloy, dilute, electron irradiation, interstitial dislocation loop obs. 78−18681
Al-$Si_xN_yO_z$-Al structure, electron microscope obs. of irreversible changes *(Russian)* 77−85342
Al-Sn, (<0.28 wt.%) corrosion behaviour in 16% HCl 78−85054
Al-Ti alloy spark alloying, cathode weight change and hardened layer obs. *(Russian)* 80−61005
Al-Ti-B alloys, segregation of Ti, electron microscope exam. 78−52820
Al-Zn, grain boundary reaction sites, determ. of struct. aspects 80−103359
Al-Zn, plastic deform. effect on struct. transform. at elev. temp. *(Czech)* 79−79044
Al-Zn (30 wt.%), metastable phases, transformation kinetics, quenching rate effects meas. 77−55960
Al-Zn (30 wt.%), precipitation ageing plastic deform. effects 77−66645
Al-Zn (3.9 wt.%), single crysts., fatigued age-hardenable, dislocation structure *(German)* 80−54247
Al-Zn (40 wt.%), plastic deform. effect on discontinuous precipitation 80−3053
Al-Zn (6.8 at.%), decomposition, electron microscope study *(French)* 77−40422
Al-Zn (70, 30 wt.%), decomp. study, 25-160°C *(Czech)* 80−89225
Al-Zn eutectoid, superplastic, fracture, electron microscope obs. 78−31533
Al-Zn-Mg, fractographic stage I fatigue facets 77−16680
Al-Zn-Mg, plastic deform. influence on structural transform. and mechanical props. *(Russian)* 80−7623
Al-Zn-Mg, precipitation of η' phase, heat treatment, electron microscope obs. 78−68699
Al-Zn-Mg, stress corrosion cracking, grain boundary precipitate size and distrib. electron microscopy study *(Japanese)* 79−79159
Al-Zn-Mg (3.6, 1.95 wt.%), ageing and plastic deform., effect on structure, electron microsc. and X-ray diffr. study *(Russian)* 80−81108
Al-Zn-Mg (4.5, 2 to 3 at.%) solid state reactions by interrupted continuous heating 80−25737
Al-Zn-Mg (91, 6, 3, wt.%), H embrittlement and trapping, HVEM obs. 80−76364
Al-Zn-Mg alloy, Ag addition and pre-precipitation treatment, influence on GP zone growth 80−71658
Al-Zn-Mg alloy, microstruct. obs. by optical and electron microscopy *(German, English)* 77−52601
Al-Zn(11 wt.%), dynamic recovery during and after steady state deform. 77−1842
Al_4Ca, phase transformation, struct. and orientation relationships 79−78963
AlCu, electron microscope spot prep. of deform. bands 79−15922
Al_4Cu_9, rhombohedral γ-brass, direct imaging of struct. and structural defects 80−15115
$Al_xGa_{1-x}As$ epitaxial films, microanal. in photoemissive electron microscope 79−16068
Al_3Mg_2, diffusionless phase transformation 80−104150
Al_8Mn_5, rhombohedral γ-brass, direct imaging of struct. and structural defects 80−15115
AlN powder, synthesis in low-temp. plasma 80−16257
Al_2O_3, anodic film transient pitting during film growth 78−56817

electron microscope examination of materials continued
Al_2O_3, corundum, impurity striation, light scatt., optical and electron microscopy meas. 78—22757
Al_2O_3, derived from boehmite, phase transformations and microstruct. 80—60857
α-Al_2O_3, grain boundary segregation 80—103361
Al_2O_3, grain boundary thickness obs. using electron diffr. techniques 80—79811
Al_2O_3, layer, obtained by reactive evap., surface struct. and morphology *(Polish)* 79—28242
β-Al_2O_3, long-period structs., electron microscope obs. 80—92501
β''-Al_2O_3, Mg- and Li-stabilised, high-resoln. electron microscopy images 80—107277
Al_2O_3, thick vacuum condensates, struct. *(Russian)* 78—95242
β-Al_2O_3-MgO ceramic, formation and structure of atomic scale cracks 80—45395
β-Al_2O_3-Na_2O-SiO_2, solid electrolytes, exam. of microstruct. ionic resistivity 78—80566
Al_2O_3-SiO_2-P_2O_5, refractory glasses, exam. of liquid immiscibility and crystallisation 78—55814
γ- AlOOH, boehmite, dehydration to γ-Al_2O_3 80—21277
Al-AlOOH, disapore, superstructure form. on dehydration, electron microscopy obs. 80—3327
Al_xVO_2, reduced, microstruct., crystallographic shear planes, electron microscope obs. 79—1443
As_2S_3-PbS glasses, structural props. 79—27925
Au (111) film, sputtered, surface struct., HV electron microscopy and theoretical model 78—22981
Au, (111) surface electron microscopy 80—103556
Au, atomic cluster, on W support film, computer simulation of phase contrast 80—100150
Au, Au-rich alloys, electropolishing for electron microscopic examination 78—35589
Au bicrystals, interaction of lattice dislocations with grain boundaries, electron microscope obs. 78—51579
Au, coherent twin boundary, electron microscopy obs. *(Japanese)* 79—82130
Au, colloidal, particle conc. determ. technique 79—87883
Au, condensation kinetics on KCl substrate, evolution of size distrib. function 79—28243
Au crystallites, formation in flowing Ar system, density, size distrib. and size dispersion 78—88415
Au, effect of intermittent deposition on nucleus formation and growth on alkali halide substrates 79—23853
Au epitaxial films, grain boundary struct. evolution during recrystn., interface energy effect *(Russian)* 80—15387
Au epitaxial growth, cluster mobilities, in-situ electron microscopes obs. 80—15407
Au, epitaxial growth and nucleation on NaCl during ion bombardment 79—11024
Au epitaxial layer, grain boundaries obs. 79—11025
Au epitaxial particles, high resolution dark field electron microscopy 77—85111
Au film, detection of faceting on (h,k,0) surfaces by diffr. in electron microscope at 100 kV 78—43273
Au, film, discontinuous, morphology and size distribs. of islands 77—62766
Au film, early growth stages on amorphous C, cluster migration obs. 79—77964
Au film, epitaxial growth, whisker form. 77—76713
Au film, integrated condensation coeff. on NaCl cleavage faces, Rutherford ion backscatt. obs. and electron microscopy 80—59827
Au film, modifications of optical and elec. props. as function of struct. during deposition 79—78777
Au, film, on C/Ag system, epitaxial growth in ultra high vacuum 77—1336
Au film, on complementary cleavage planes of TGS, morphology, electron microscope obs. 79—15031
Au film, on MgF_2 and SiO substrates, internal stresses correl. with struct. 79—87026
Au film, on Si, coincidence site phase boundaries 78—67927
Au film, on Si, early growth by ion-beam sputtering 77—44158
Au, film growth on mica substrate, surface defects and heterogeneous nucleation 78—47684
Au films, (111), sputtering in high voltage electron microscope 80—35027
Au films, condensation on alkali halides, growth, struct., stability *(French)* 78—38989
Au foil, radiation damage, in situ study by HV electron microscopy 78—6101
Au foil, sputtering in a high voltage electron microscope 77—36328
Au, grain boundary structure, high resolution HVEM 80—103360
Au, grain boundary thickness obs. using electron diffr. techniques 80—79811
Au, interstitial, calc. images and diffraction patterns 80—100152
Au island film real structure and electrical conductivity obs. 79—77948
Au island films, forming process, I-V characts., and switching 79—11242
Au, multiply twinned particles, internal and surface struct. by electron microscopy 80—84189
Au, multiray calc. of cryst. lattice projection in ⟨111⟩ direction, from electron microscope image 79—94855
Au, nucleation on NaCl from new vapour source, temporal and electron micrograph obs. 79—77954
Au, nuclei on KCl, growth mechanism and kinetics 77—62780
Au on W (001), geom. factors of FCC-BCC epitaxy 78—60041
Au, pentagonal symmetry, icosahedral struct. *(French)* 80—79729
Au powder, ultrafine, sintering, coalescence growth stage 80—89174
Au, pure metal and Au-Sn dil. alloy, vacancy clusters, quenching and ageing 78—76671
Au, scatt. cross sections, 300 to 1200 keV 78—9922
Au single cryst., nearly aberration-free lattice images in HV microscopy 79—32865
Au single particles, high resolution electron microscopy using BeO specimen supporting films 77—27793
Au, thin film bicrystal, annealing twin form. by boundary dissociation 79—47729
Au, thin foil, growth of stacking fault tetrahedra 80—19815
Au, tilt boundary, $\Sigma = 11$, simulated and observed struct., vibr. of individual atoms at grain boundary 80—88167
Au, VPE on NaCl, role of surface steps 78—79902

electron microscope examination of materials continued
Au, vacuum deposition, on (100) surfaces of KBr, KCl and NaCl substrates with colloidal centres *(Rumanian)* 78—60579
Au vacuum deposition on dielectric substrates, ellipsometric and electron microscopic meas. 79—74011
Au/Fe/Au superimposed layers, influence of O_2 on interdiffusion, controlled-atmosphere electron microscopy 77—51552
Au-Ag-Cd, martensitic transformation, preceding struct. anomaly 78—68692
Au-Cd (47.5 at.%), modified 2H and 9R martensites 78—14366
Au-Mg, high resolution electron microscope and electron diffr. investigation, obs. of $Au_{15}Mg_4$ monoclinic phase 80—1968
Au-Mn, orthorhombic struct., electron diffra. and electron microscopy obs. 80—15052
Au-Mn system, AABB struct., experimental evidence for occurrence 78—63698
Au-Ni alloy, modulated struct. form. by spinodal decomp., lattice imaging electron microscopy obs. 79—95996
Au-Pt epitaxial film system, mismatch dislocations obs., electron microscopy 77—4268
Au-SiO_x-Ge, sandwich structure, exam. of image structure using mirror electron microscopy *(German)* 79—11019
AuCu II, periodic antiphase struct. *(French)* 79—14937
AuMn alloy, ordered, vacuum deposited epitaxial films, orientation control by external stress 80—100426
$Au_{11}Mn_4$ ordered phase formation, electron diffr. and microscopy study 80—107418
Au_4Mn, electron irrad. in electron microscope, radn. ordering 79—86818
Au_4Mn, fully ordered, microstruct., high resolution electron microscopy 79—1439
Au_4Mn, high resolution dark field electron microscopy exam. of ordering 79—7615
Au_5Mn_2, electron microscope exam. of ordering 78—63697
Au_5Mn_2, monoclinic, ordering, high resolution electron microscopy 79—43290
$Au_{35}Si_{65}$, amorphous vacuum-deposited and liquid-quenched films, diffusion and crystn. 80—84094
Au_xSi_{1-x} amorphous films, phys. studies 80—75476
Au_4Zn, long period ordered alloy, selective radiation damage in electron microscopy 78—10092
Au_4Zn, long period superstructure study 78—10059
Au_4Zn, ordered alloy, long-period antiphase boundary struct., growth mechanism 79—19262
B film growth by phys. vapour deposition 80—16200
BN, graphite-like, twinning and shear 77—4114
BN, high pressure synthesis, exam. of relationship between synthesis condition, and crystal shape, size *(Japanese)* 79—20018
BN prep. by water solvent, electron microscope charact. 78—47253
BN structure after high temp. shock compression 80—39220
BN, wurtzite type, phase and struct. changes at high temps. 77—12618
BN wurtzite-sphalerite phase transition, stacking fault role 80—6418
BPO_4-$AlPO_4$, non-equil. phase diagram, electron microscope obs. 79—43225
BPO_4-SiO_2 system, new data to prevent B_2O_3 or P_2O_5 loss at elevated temp. 80—20914
Ba ferrites, lattice imaging 78—30522
Ba film, structure effects on work function, electron micrographs and photoemission meas. 79—83107
$BaFeO_{2.79}$, 6H polytype, perovskite related phase, electron microscope obs. 77—51391
$Ba_{1+x}Fe_2S_4$, electron diffr. study, orientation anomaly 80—107152
$BaMgTi_7O_{16}$, hollandite struct. electron-optical imaging at 3 Å resolution 77—65939
$Ba_5Nb_4O_{15}$, 5H polytype, perovskite related phase, electron microscope obs. 77—51391
$Ba_3Nb_6Si_4O_{26}$-$Ba_3Nb_4Ti_4O_{21}$, intergrowth, nonstoichiometry, struct. obs. *(French)* 77—19932
$(Ba_3Nb_6Si_4O_{26})_n.Ba_3Nb_4Ti_4O_{11}$, n=3/2 to 29/2, intergrowth series, electron microscope obs. *(French)* 78—83762
$(Ba_3Nb_6Si_4O_{26})_n.Ba_3Nb_4Ti_4O_{21}$, multiple intergrowth and microdomains obs. by electron diffr. and microscopy *(French)* 78—95160
BaO film on W surface, struct. of crit. nuclei in heterogeneous crystn., LEED and FEM 77—11817
BaO films on Ir, thermionic props., Auger, LEED, and emission microscopy 79—43089
BaO-Fe_2O_3 system, splat cooled phases struct., magnetisation and susceptibility 300-1100K *(French)* 77—48017
$BaO.2SiO_2$, glass, spherulitic growth and recrystallisation 77—4046
$BaPO_3F$-Al_2O_3-B_2O_3 system, liq. phase separation, IR spectra, microstruct. 80—29940
$Ba_{0.1}Sr_{0.9}MnO_{2.96}$, 4H polytype, perovskite related phase, electron microscope obs. 77—51391
$BaTiO_3$, donor doped, exam. of heterogeneous microstructure *(German)* 79—24632
$BaTiO_3$, electron microscopy investigs. of ferroelec. substances, review *(Japanese)* 80—71366
$BaTiO_3$, epitaxial ferroelectric, appl. of electron microprobe methods 80—44443
$BaTiO_3$, ferroelectric, polarisation reversal, electric field induced phase transform. 80—103925
$BaTiO_3$, single crysts., electron microscope study of domain and defect structs. 79—15425
$BaTiO_3$, unipolar cryst., topography of defect. and thermodepolarisation currents 77—43954
Ba_xWO_3, (0.01<x<0.33) series form. 79—65046
Be bronze BrB2, quenched deformed, substruct. and props., effect of prerecrystallisation annealing *(Russian)* 78—60677
Be, hot-extruded, fracture in impact, static tensile and fatigue tests *(Russian)* 77—52458
Be, phase struct. *(Russian)* 78—15401
Be, ultra fine-grained, recrystn. after deform. 79—52239
Be-bronze BrB2, struct. and phase transform. during mechano-thermal treatment *(Russian)* 80—11667
BeO powder, sinterable and unsinterable, sintering processes, electron microscope exam. 79—33986
BeO_2-Al_2O_3-SiO_2-MF_2 (MF) glasses, M=Mg, Ca, Sr, Ba, Li, Na, fluoride ion role during crystn. 79—65176
BeSiN ceramics, glass free grain boundary 79—90671
Bi, epitaxial films, grain boundary struct., electron microscopy obs. *(Russian)* 79—46671
Bi, epitaxial growth, decoration of Sb surface 79—28227

electron microscope examination of materials continued
Bi film, supercooling, exam. by electron diffr. and electron microscopy *(French)* 78—14636
Bi film, surface defects and struct., electron microscopy and elec. props. *(French)* 80—15415
Bi film, vap. deposited, effect on deposition parameters and substrate condition on crystallinity 78—10290
Bi film deposition by vacuum evaporation on $NaNO_3$ single cryst. cleavage 80—35091
Bi, spheres mean inner pot., elec. diprism and interf. electron microscopy 80—49063
Bi thin film, structural evolution 8 to 573K, supercooling effects *(French)* 79—90921
Bi-MnBi, mag. props. singularities, electron microscope exam. *(Russian)* 78—39363
Bi-Sb, bicrystal rearrangement of grid of nonconformity dislocations on (111) interface during heating 79—28215
$Bi_2CaNa_{n-2}Nb_nO_{3n+3}$, intergrowth, IMV high-resolution electron microscopy 80—107436
Bi_2O_3, thin film, struct. and dielec. meas. 79—78622
$Bi_{1-x}Sb_x$ film, evaporated, cross-sectional struct., electron microscopy and replica technique study *(German)* 78—22977
$Bi_7Ti_4NbO_{21}$, mixed-layer cryst. struct. determ. by super-high-resolution electron microscopy 77—84703
$BiVO_4$, ferroelastic domains, electron microscopy and electron diffr. obs. 80—100254
$Bi_2W_2O_9$, layered struct., 1 MV high-resolution electron microscopy obs. 79—27955
C, adsorption of Ag and U, scanning-transmission electron microscope obs. 77—51597
C fibre structure, recent advances 80—81069
C fibres, PAN based, structural parameters obtained by electron microscopy and X-ray diffr., comparison 77—47353
C fibres, surface treatment with tetra-(octadecyl) titanate, X-ray and electron microscope study *(Japanese)* 79—74280
C film, diamond-like, ion-plated, electron energy loss spectra characterisation 80—2308
C, film, image contrast rel. to inelastic scattering 80—100154
C film, vac. condensed, graphitisation, electron microscopy 80—40265
C foil, electron impact knock-on damage at 4K, electron microscope obs. 79—55786
C, glassy, struct. evolution due to thermal treatment at 1000 to 2700°C, tridimens. config. 77—68924
C graphitic, imperfectly ordered ultramicrostruct. characts. direct imaging feasibility by high resolution electron microscopy 79—77463
C, graphitisation, cooperative accelerating effect of $CaCo_3$ and N_2 80—55429
C, hard, heat-treated under pressure, characterisation of carbon phase by electron microscope 80—60855
C, nongraphitizable, catalytic graphitization by Cr_2O_3, MnO_2 80—97440
C particle formation,C_2+C_3 as possible first step 78—68876
C, pyrolysis mechanism, electron microscopy, DTA, IR, ESR obs. 78—56593
C, texture change on ht. treatment under press. 78—60687
C, thin film, high resolution dark-field images 78—26398
C, vapour-deposited, transparent and hard insulating layer, struct. and props. 80—10830
C_8 crystalline diamond-like form, cryst. struct. *(Russian)* 79—99114
Ca film, structure effects on work function, electron micrographs and photoemission meas. 79—83107
Ca-Nb-O perovskites, struct. characterisation *(French)* 78—10021
CaF_2:U(Th), and pure, electron microscopy study of lattice deformation due to electron irrad. 79—65077
$Ca_3Ga_2Ge_3O_{12}$, substrate, electron examination of microstruct. and microsegregation 78—67919
CaO-Al_2O_3-SiO_2-ZnO, continuous unidirectional crystn. of fibrous metasilicates from melt 78—95739
CaO-MgO-Al_2O_3-SiO_2-ZnO, continuous unidirectional crystn. of fibrous metasilicates from melt 78—95739
CaO-SiO_2 glass, solid reactions, study by hot stage electron microscope *(Japanese)* 78—12798
$3CaO.Al_2O_3+CaSO_4.2H_2O$, effects of prehydration on liq. hydration 79—100354
$Ca_{10}(PO_4)_6(OH)_2$, synthesis and characterisation in dense polycryst. form 77—4749
$CaSiO_3$ (wollastonite), individual silicate chains obs. by high resolution electron microscopy 79—100829
$(Ca_{1-x}Sr_x)(Ca_{1/3}Nb_{2/3})O_3$ perovskites, cryst. struct., twinning phenomena obs. *(French)* 79—65044
$Ca_4YFe_5O_{13}$, cryst. struct., electron microscopy and X-ray diffr. study 80—88116
Cd, electron radiation damage in HVEM, nature of defect clusters 78—59838
Cd_3As_2 film on NaCl substrate, vacuum deposition, growth morphology, microstructure 80—75479
CdI_2 polytypes, defect struct., electron microscopy 79—14809
$CdIn_2Se_4$, high resolution electron microscopic study of polytypism 80—88119
$Cd(OH)_2$, highly dispersed precipitate, microstruct. and exchange props. 77—36793
CdS, chemically sprayed film, prod. by centrifugal disk atomizer, struct. 79—65343
CdS, electron micrograph equal thickness fringes, phase angles and absolute struct. pot. 77—76383
CdS, epitaxial layers on Cd single crystal, direct synthesis and struct. 78—68628
CdS film, inhomogeneities responsible for residual cond., microinclusions 77—28269
CdS film, polycrystalline, photosensitive, struct., pseudoreplica method, using electron microscopy and microdiffr. 79—15030
CdS film, precipitation from solns., form. characts. 79—11524
CdS layers, struct. investigation by electron and X-ray diffr., and electron microscopy, growth mechanism 79—56094
CdS, polycrystn. layers on CdS substrate, electron microscope study of surface struct. 78—22940
CdSe films, growth kinetics and cryst. struct. during vacuum condensation 80—2305
CdTe films, structural imperfections depend. on crystn. temp. 79—90661
CeO_2 coating of laser optical components, electron microscope obs. 80—43342

electron microscope examination of materials continued
Co, deformed, microstruct. singularities in pre-transform. temp. range *(Russian)* 80—45347
Co, FCC, ferromag. domains of fine particles, Lorentz electron microscopy obs. 78—27053
Co film, evaporated, columnar struct. depend. on degree of texture 80—54567
Co film, evaporated, texture and columnar struct. 80—54566
Co film, magnetic domain wall width, shadow and interf. electron microscope exam. 79—11330
Co, foil, wall struct., bubble, plate domains, 1 MeV electron microscope study 78—84463
Co, HCP, relationship of effects of systematic reflections to the crit. voltage 79—41916
Co, HCP-FCC transition, mag. domain behaviour, Lorentz electron microscopy 77—80958
Co intercalation compound, electron microscopy 80—84164
Co-Cr-C alloys, $M_{23}C_6$ precip. mechanism 78—44130
Co-Cr(VC)((Ti,V)C)-(Al), eutectic alloy, unidirectional solidification, oxidation and tensile tests 78—52790
Co-Fe-Nb (12, 3 wt.%), semihard magnetic alloy, relationship between precipitation and coercivity 77—8839
Co-Fe-Si-B, decomp. of amorphous state during annealing below recryst. temp. *(Russian)* 80—75164
Co-Gd(Ho) film, amorphous, stripe domains and mag. anisotropy by Lorentz microscopy 77—63243
Co-Mo oxidic precursory state, supported on SiO_2 and γ-Al_2O_3 hydrotreating catalysts 79—61898
Co-Ni-Cr-Nb, effect of Fe addition on precipitation behaviour 80—29962
Co-Ni-Cr-Nb FCC alloy, electron microscope obs. of deform. twins 79—60380
Co-Ti-C, secondary precipitation and allotropic transform., TEM obs. 80—108453
Co-V alloy system, Co rich, low temp. phase, electron microscopy 77—84766
Co_5Ge_3 amorphous film, elec. resist., microstruct. and annealing 77—85188
$CoOOH \rightarrow Co_3O_4$, morphology, topotaxy, comparison with $Co(OH)_2 \rightarrow CoOOH$ 77—16817
$Co_2Ti_{2-2x}Fe_{2x}O_{6-x}$ solid solution, extended defect model, X-ray diffr. and electron microscopy *(French)* 77—47446
Cr film, effect of substrate temp. on formation, electron microscope obs. 80—39469
Cr, film, vac. deposition onto low temp. substrate, cryostat *(Japanese)* 78—27403
Cr film, vacuum evaporated, particularities in growth on alkali halides with Pb colloids and F-centres 79—82496
Cr island film real structure and electrical conductivity obs. 79—77948
Cr, oxidation kinetics, 300 to 600°C, struct. and morphology of oxide film 77—59982
Cr, pure, oxidation, electron microscope study *(Japanese)* 77—48577
Cr-Fe-Ni alloys, cryst. struct. and defects, high resolution electron microscopy obs. 79—94961
Cr-Ge amorphous films, annealing effect on elec. resistance and struct. 80—54667
Cr-$NdAlO_3$, dielectric films, phase composition and structure 80—39464
Cr-Ni VKh-4 alloy, deformation and fracture mechanism investigation *(Russian)* 80—11738
Cr-Ni-Mo steel, low-cycle fatigue in sea water, mechanism *(Russian)* 77—59970
$CrBr_2$, ferromag. domains, using liq. He mag. specimen stage 80—103855
CrC-Ni-(P), hard alloys, sintered, fracture props., P addition effects 78—60610
CrO_2, synthesis and morphology 79—24481
$Cr_2O_3.SH_2O$, heat-treated, narrow particle size distrib., surface props. 78—85210
$CrSi_2$ film, kinetics of growth 77—43454
CsI:Na, crystal, kinetics of decay of surface solid soln. 79—23810
CsI:Tl, precipitation of Tl solid solns. 80—70419
Cu, (111) surface electron microscopy 80—103556
Cu, alloy, stacking fault energies, weak beam method of electron microscopy 77—19971
Cu alloys, jog formation and glide on dissociated dislocations, direct obs. 77—68977
Cu and Cu-Cr (0.6 wt.%), electron microscope obs. of shear bands *(German)* 77—48454
Cu, cold-rolled, microstruct. 79—83216
Cu complex, hexadecachlorophthalocyanatocopper (II), atomic resolution by computer image processing from electron micrographs 80—100149
Cu, corrosion inhibition, chem. nature and struct. of protective films 77—60001
Cu, cracks in fatigue early stages, direct obs. of substruct. by electron microscope *(Japanese)* 78—7028
Cu, cubic crystals, anisotropic, dislocation loops, electron microscope image contrast 80—39101
Cu, defect clusters, electron microscope exam. 78—47380
Cu, deformed by hydrostatic extrusion, drawing or drawing under press., dislocation struct. obs. *(Russian)* 77—21213
Cu, deposits on Cu (110) electrode, morphology and crystal growth 79—47644
Cu, dislocation etch pit obs. on {111} surfaces 79—10861
Cu, electron irrad., secondary defect formation, effect of refl. condition *(Japanese)* 77—43248
Cu, electron irrad., void swelling and dislocation loops 79—99206
Cu, electron irradiated, temp. depend. of threshold energy for atom displacement 80—34055
Cu, electron-irradiated crystals, electron diffr. channelling effect on atom displacement 80—39158
Cu, FCC, dislocations, elastic instability 79—82235
Cu, fatigued, early stage crack tip dislocation morphology, electron microscope obs. 78—27628
Cu fatigued polycrystals, point defect cluster rel. with yield stress temp. depend. 78—6989
Cu film, in situ struct. determ. by internal stress meas. 80—54569
Cu film, on (001) Ag, FCC and BCC metal-on-metal epitaxy, geometric factors, electron microscopy 78—22980
Cu film, on Ni, recrystallisation and interdiffusion, electron microscope obs., 450-600°C 80—39363
Cu film growth on amorphous C, energy characts., in situ electron microscope determ. 79—11027

electron microscope examination of materials continued
Cu film on Mo substrates, film stability on reinforced fibre substrates *(Russian)* 80—39462
Cu foil, electron irradiated at low temps., annealing, form. of clusters of atomic defects 77—15416
Cu foils, electron-irradiated, point defect agglomerates, HVEM invest. during in-situ annealing 80—84213
Cu, foils, faulted defect formation by moving boundaries 80—107281
Cu, fragmentation and dynamic recrystallisation after heavy and very heavy deform. *(Russian)* 78—39793
Cu, Frenkel pair production threshold energy, temp. depend., exam. 78—51530
Cu, HVEM determ. of true segment length and interforest spacings of recovered dislocation arrays 78—30631
Cu, heavily rolled, electron microscope obs. of cube oriented region, rolling texture 79—29093
Cu, irradiated, small edge dislocation loops, electron microscope image contrast, Burger's vector determ. 77—76410
Cu on W (001), geom. factors of FCC-BCC epitaxy 78—60041
Cu phthalocyanine, grain boundary struct., crystallographic planes 80—103366
Cu, polycrystn., strain localisation during hot deform. 80—104195
Cu, prismatic dislocation loops, (g.b)s product sign determ. *(Russian)* 78—38705
Cu, rolled, dislocation struct. and recovery during annealing *(Russian)* 79—29084
Cu, scatt. cross sections, 300 to 1200 keV 78—9922
Cu, single cryst., deform. process, effect of surface layer 79—8315
Cu, single crysts., ⟨110⟩ oriented, tensile deformed, HVEM of recrystn., recrystallised state 80—89256
Cu, single-crystal thin foil, determination of struct. potentials from Kossel Mollenstedt diagrams 80—6324
Cu, tensile deformed ⟨110⟩ orientated single cryst., recrystn., high voltage electron microscopy study 80—84958
Cu thin foils, intrinsic struct. in grain boundaries and boundary mobility 80—103368
Cu, very low atom displacement threshold energy, around ⟨110⟩ directions, direct evidence 78—14379
Cu-Ag, deformed, recrystallization nucleation at second phase particles, electron microscope obs. 79—34059
Cu-Ag (8 wt.%), plastic deform. effect on discontinuous precipitation 80—3053
α_2-Cu-Al, antiphase period and tetragonality 78—15374
Cu-Al, α_2 phase form. process 77—48464
Cu-Al, dislocation core cut-off parameter, estimation from stacking fault nodes 80—103370
Cu-Al, dislocations, dissociated, climb mechanism, nucleated loops, Burgers vectors 80—65002
Cu-Al, faulted dipoles, geometry and form. 78—59809
Cu-Al, intrinsic temp. depend. of stacking-fault energy 78—51564
α-Cu-Al, short range ordered, struct. and new superlattice phase 78—52756
Cu-Al (10.5 at.%), dislocation generation and displacement in single crystal in bending 79—60368
Cu-Al (11 at.%) single cryst., dislocation reactions during deform. twinning 80—79795
Cu-Al (15 at.%), FCC, dislocations, elastic instability 79—82235
Cu-Al (15.8 at.%), extension of jogs on dissociated dislocations, electron microscopy obs. 79—95017
Cu-Al (2, 6.8 and 15 at.% Al), electron irrad. at 300 and 575 kV, exam. of damage rate 78—47425
Cu-Al (21 at.%) transition state, tempered and quenched alloy *(French)* 80—55392
Cu-Al (5.8 at.%) dislocation multipoles, weak-beam electron microscope obs. 79—73171
Cu-Al (8 at.%), coplanar slip, related with specimen size and axis *(Japanese)* 78—34518
Cu-Al alloy, ordered, superlattice fringe images, computer simulation 80—103296
Cu-Al alloys, α_2 phase, config. of periodic antiphase boundaries 79—95029
Cu-Al dil. alloy crystal, dislocation etch pits on {111} surfaces *(Japanese)* 77—62536
Cu-Al-Ni alloys, deformed, fine struct. of martensite *(Russian)* 78—6923
Cu-Al-Ni-Fe, (10, 5, 5 wt.%), cast microstruct. 78—80535
Cu-Al-Zn, structural phenomena preceding martensitic transform. 77—12624
Cu-Al(Au), critical voltage effect *(Japanese)* 78—91206
Cu-Al(Au) alloys, HV electron microscopy, crit. voltages depend. on comp., temp. and short-range order 80—100146
Cu-Be (0.99 wt.%), direct obs. of small Guinier-Preston zones 78—72776
Cu-Be-Co, cuboid (Co, Cu, Ni, Fe)Be inclusions, metallography, ageing effects 80—11645
Cu-Be(30 at.%), eutectoid decomp., elastic interaction between precip. phase particles *(Russian)* 77—8833
Cu-Bi, grain boundary thickness obs. using electron diffr. techniques 80—79811
Cu-Bi alloys, grain boundaries, electron microscopy 77—12694
Cu-Cd-Cl stretched photochromic glass, polorisation effects 79—95729
Cu-Co (2 wt.%), single crysts., fatigued age-hardenable, dislocation structure *(German)* 80—54247
Cu-Fe (1.5 wt.%), precipitation-effect on void formation during electron irradiation 80—84211
Cu-Fe (1.5 wt.%) alloy, void form. during irrad. in HVEM, reactor irrad. simulation and ageing effects 80—107327
Cu-Fe(2.5 wt.%), isothermally reacted austenite stability in very small particles 77—48432
Cu-Mn alloys, Cu-rich, heat treated, segregation obs. *(Russian)* 78—27517
Cu-Ni alloy, dislocation density during deform., comparison of electron microscopy and X-ray diffr. *(Russian)* 79—5002
Cu-Ni alloys, electron irradiated, dissociated struct. of dislocation loops with Burgers vector a⟨100⟩ 77—89444
Cu-Ni bimetallic film, Moire patterns, interdiffusion effects 77—51621
Cu-Ni-Al, grain boundary reaction under isothermal ageing at 623 to 973K *(Japanese)* 79—70090
Cu-Ni-Be (30, 0.5 wt.%), grain boundary reaction after ageing and quenching, obs. *(Japanese)* 79—70089
Cu-Ni-Be-(Al) (30,0.5,(0.2-2) wt.%), Al addition effect on grain boundary reaction *(Japanese)* 80—54254

electron microscope examination of materials continued
Cu-Ni-Cr, microstruct. behaviour and mechanical hardening 78—47281
Cu-Ni-Cr system, coarsening in the $(\gamma_1+\gamma_2)$ region, metallographic study 78—84762
Cu-Ni-Fe (26,8 wt.%), microduplex struct. form., hardness meas., optical and electron microscopy *(Japanese)* 78—76659
Cu-Pd, disordered, antiphase domain boundaries, high resolution electron microscopy obs. 79—95030
Cu-phthalocyanine, chlorinated effects of dynamical scattering on mol. images, in high resolution electron microscopy 78—14255
Cu-Pt alloy, quenched, SRO, microdiffr. obs. 77—76360
Cu-Sb-S-I amorphous film formation and stimulated crystallisation, electrophysial props. *(Russian)* 78—30838
Cu-Si (6.5 at.%), plastic deformation, HVEM study *(French)* 80—66605
Cu-Si (8 wt.%), intrinsic struct. in grain boundaries and boundary mobility 80—103368
Cu-Si alloy, correl. of periodicities in diffr. patterns and images from grain boundary 78—14362
Cu-SiO_2, dispersion hardened, surface plasticity effect 78—52832
Cu-SiO_2 single crystals, dispersion hardened, exam. of yield stress between 77 to 1200K 78—76720
Cu-Sn, deformed, martensitic transformation *(Russian)* 79—15668
Cu-Sn, ε and η phases, surface struct. changes due to sputtering 77—73206
Cu-Sn (25 wt.%), struct. after ultrahigh-speed quenching *(Russian)* 78—80563
Cu-Ti, deform. effect on precipitation and recrystallisation, electron microscope study 77—70115
Cu-Ti, internally oxidised, morphology, struct., particle precipitation singularities *(Russian)* 79—70067
Cu-Ti, liquid phase sintering, metallographic electron beam microanalytical investigation 78—95888
Cu-Ti, Zr effects on cellular precipitation 77—16587
Cu-Ti (Zr), strength improvement by thermomechanical treatment *(Japanese)* 78—48426
Cu-Ti (5.7 at.%), dil., β-phase struct. 79—55700
Cu-Ti alloys (0.5 to 4.0 wt%) ageing charact. determ. 79—20089
Cu-Ti-Cr(Fe), internally oxidised, morphology, struct., particle precipitation singularities *(Russian)* 79—70067
Cu-W composite powder, prod. by H_2 reduction of $CuWO_4$ 79—20006
Cu-Zn, interface sliding of FCC and BCC boundaries 80—104240
Cu-Zn (30 wt.%), rolled, electron microscope exam. of recrystallisation 78—76663
Cu-Zn-Al, β_1' martensite crystal crossing rel. to reversible shape memory effect *(Japanese)* 80—108499
β-Cu-Zn-Al, diffr. effects., obs. and interpretation of extra maxima 80—44173
β-Cu-Zn-Al, electron microscope exam. of premartensitic state 78—72801
Cu-Zn-Al, pseudoelastic alloy, exam. of fatigue props. 78—76744
β-Cu-Zn-Al (27.5, 4.0 wt.%), strain induced martensite, exam. of structure, microstructure 80—7648
Cu-Zn-Be, precipitation hardening 77—16599
β-Cu-Zn-Si, premartensitic instability 77—12625
Cu-Zr, vapour quenching prod. (thermal evaporation and r.f. sputtering), amorphous film for electron microscopy 78—6851
Cu-Zr alloys, isothermal transformation diagram 80—20902
CuAu alloy, ordered, vacuum deposited epitaxial films, orientation control by external stress 80—100426
CuAu, exam. of streaming due to intrinsic fluctuations 79—11602
Cu_3Au, alloys, superlattice-fringe imaging theory, images formed from two beams 80—79649
Cu_3Au, long-range order parameter from electron micrograph thickness fringes 77—65938
Cu_5FeS_4, bornite, superstructuring, vacancy clustering, high-resolution electron microscopy 78—42981
CuI, film, prep. on NaCl by reactive sputtering, struct. and composition investigation 79—90900
$CuIn_5S_8$ sulphospinel electron diffr. study 80—88080
$Cu_{0.5}In_{2.5}Se_4$, transition state and domain struct. by electron microscopy and diffr. studies 80—15095
Cu_2MnAl, dislocation structure, antiphase boundary energies, deformation behaviour prediction *(Russian)* 79—65085
Cu_2MnAl, plastically deformed, domain struct., X-ray diffr. and electron microscope obs. *(Russian)* 79—20110
$Cu_{2+x}Mn_{1-x}Al$, omega phase, roles of electron microscopy and electron diffraction *(French)* 78—27524
$Cu_{0.5}NbS_2$ and $Cu_{0.5}TaS_2$, order-disorder and displacive transforms., domain-type microstruct. 77—4195
Cu_2O polycrysts., dislocation obs. by elecron microscope *(Spanish)* 80—75230
Cu_2O, radiation damage 77—84809
Cu_3Pd, electron irrad. in electron microscope, radn. ordering 79—86818
Cu_3Pd, periodic antiphase boundaries, electron microscopy study *(French)* 80—59481
CuPt, quenched, state of local order 79—47722
$Cu_{2-x}S$, digenite related phases, electron microscope study 79—10840
Cu_7S_4, alternative transform. behaviour, direct obs. by TEM 77—1227
Cu_9S_5, digenite, superstructuring, vacancy clustering, high-resolution electron microscopy 78—42981
Cu_3Sn, one-dimens. long period superstructs. with Zn and Ni additions 78—83777
$Cu_{3-x}Te_2$, non-stoichiometric phases, electron microscopic and electron diffraction studies 80—64977
CuZn, omega phase, roles of electron microscopy and electron diffraction *(French)* 78—27524
Dy, magnetoplastic deform., 70-90 kOe, 4.2K 77—8376
$DyAl_3$, polytypism, high resolution microscopy and electron diffr. obs. *(French)* 77—11503
Dy_2O_3, contrast near bend contours of upper Laue areas 79—55621
Dy_2O_3, influence of upper Laue areas on fine struct. of bend contours near high symmetry axis 78—38596
ErO, vac. deposited films, struct. changes due to annealing 79—77741
ErO_x, nonstoichiometric film, short-range order characts. and its effect on elec. behaviour 79—99435
Eu_2O_3-Gd_2O_3-Ta_2O_5 system at 25, 50 and 75 mole.% Ta_2O_5, cross section investig. 77—12607
Eu_2O_3-R_2O_3-Ta_2O_5, R=La, Gd, Y, quasibinary cross sections 77—90333
Fe alloy, corrosion inhibition, chem. nature and struct. of protective films 77—60001

electron microscope examination of materials continued

- Fe, Armco, fatigue micromechanism *(Russian)* 78—23818
- Fe, Armco, flat-rolled and annealed, dislocation struct. and mech. props. *(Russian)* 79—20062
- Fe based alloy, amorphous, liq. quenched, struct., thermal stability and mech. props. 80—88059
- Fe, bonding of Al, growth of intermediate phases, effect of O and N impurities 78—27680
- Fe, cast, Mg micro distrib., microprobe anal., electron fractography 77—70373
- Fe, cast, modified with Al and S, nonmetallic inclusion effects, electron microscope obs. *(Russian)* 77—65987
- Fe, degree of charging of surfaces polished by TiC and synthetic diamond micropowders 78—60880
- Fe, dislocation struct. round fatigue cracks 78—48519
- Fe, displacement energy, high voltage electron microscope obs. 77—76464
- Fe, epitaxy on Au, growth processes, ultra high vac. in situ electron microscopy 78—30842
- α-Fe, exam. of structural defects due to shock waves, and induced hardness 78—48427
- Fe, fatigue crack propag., crack closure, dislocation struct., electron microscopy obs. *(Japanese)* 80—25845
- Fe film, columnar grain struct. 77—11808
- Fe film, domain wall struct. obs. by Lorentz electron microscopy 77—85527
- Fe film, evaporated at oblique incidence, columnar and textural struct. *(Japanese)* 77—62776
- Fe films, evaporated at oblique incidence, columnar struct. and texture 79—77967
- Fe, foil, fatigue crack, low growth rate, microstruct. round top 77—16674
- Fe foil, ferromag. domain-wall width, anisotropy depend. 78—19269
- Fe, fracture mechanism in various temperature and stress intervals *(Russian)* 79—24600
- Fe, grain boundaries, electron microscope obs. *(Russian)* 79—4311
- Fe intercalation compound, electron microscopy 80—84164
- Fe ore, water bearing mineral effects on X-ray fluorescence analysis 77—12866
- Fe, oxidation and domain structure, electron microscope exam. *(Russian)* 79—1437
- Fe, plastic deform. and fracture, H_2 effect, studied by electron microscopy and Auger spectrography *(French)* 77—77545
- Fe polycrystals, grain misalignment, electron microscope determ. *(Russian)* 80—103358
- α-Fe, single crystal, Sb diffusion induced dislocations 78—30798
- Fe, single crysts., effect of hydrostatic pressure on plastic flow props., dislocation distribs. 79—38887
- Fe, sintered, fracture mechanics *(German)* 77—8948
- Fe, stray mag. fields above stripe domains, electron microscope and μ^*-tensor determ. 80—71089
- α-Fe, struct. after polymorphic transform. under press. *(Russian)* 80—29946
- Fe, vacancy mobility determ., HVEM expts. 80—33993
- Fe, wear of surface due to friction, surface hardening 78—44227
- α-Fe whiskers, pure, ductile fracture, microscopic obs. of initiation mechanism 80—85044
- Fe-Al, electron-beam-induced surface oxidation, HVEM obs. 80—14978
- Fe-Al, single crystals, deform. at high temps. 80—81125
- Fe-Al (25 at.%), long-range ordered, compression induced mag. anisotropy 77—69546
- Fe-Al alloy, ordered, superlattice fringe images, computer simulation 80—103296
- Fe-Al-C steel, singularities of struct., electron microscope and electron diffr. analysis *(Russian)* 77—77476
- Fe-Al-(Nb), fatigue deform. 77—44350
- Fe-Al(Cr)(V)(Ti), hardness after nitriding, metallographic, electron microscopic and microprobe anal. 78—51608
- Fe-Al(25 at.%), mag. anisotropy induced by plastic deform., dislocations, long-range order 77—4544
- Fe-Au (111) bicrystal films, misfit dislocations obs., for 500°C substrate temp. 77—51624
- Fe-Au bimetal epitaxial films, examination of interaction at temps. ≥600°C 80—75482
- Fe-B, rapidly quenched, metastable phases 80—76234
- Fe-B, rapidly solidified, metastable phases *(German)* 79—29045
- Fe-B_4C powder mixtures, phase changes and struct. of sintered materials *(Russian)* 78—6872
- Fe-B_4C sintered material, mech. props. and struct. characts. 79—100084
- Fe-C, dil. alloys, softening, conventional and in situ expt. 79—47744
- Fe-C, dilute alloys, softening, conventional and in situ expt., HVEM obs. 79—47743
- α-Fe-C (0.03 wt.%), structural singularities of transition from thermally activated to force-induced fracture *(Russian)* 78—56731
- Fe-C martensite, crystal struct. and morphology of ordered phase 79—42011
- Fe-C-Mn-V, austenite microstruct. memory *(German)* 80—84977
- Fe-C-Mo, dynamics of transform. interface, ferrite-austenite interface 78—52795
- Fe-C-Mo, dynamics of transform. interface, at intermediate temps. 78—52796
- Fe-C-Si, struct. and constitution on quenching from liquid state *(Russian)* 77—52309
- Fe-Co (33 wt.%), oxidation and domain structure, electron microscope exam. *(Russian)* 79—1437
- Fe-Co-Cr, Cr effect on struct. of ordering 78—35407
- Fe-Co-Ni-W alloy, 45KKhVN, plastic deform., electron microscope obs. *(Russian)* 78—80584
- Fe-Co-Ta for semipermanent magnets *(French)* 79—47675
- Fe-Co-V(-Ni), annealing effect on microstruct. rel. to mag. and mech. props. 80—89267
- Fe-Cr, high-temp. oxidation, borate inhibitors 80—66705
- Fe-Cr, role of C in transform. by heating in $(\alpha+\gamma)$ phase *(French)* 78—52798
- Fe-Cr (9 wt.%), extrinsic grain boundary dislocations, low C content influence 80—107273
- Fe-Cr-Co permanent magnet system, miscibility gap, microstruct. and mag. props. obs. 80—76228
- Fe-Cr-N (5.9, 0.5 wt.%), martensitic, tempered, fine struct. 77—25079
- Fe-Cr-Ni, foil, in situ oxidation in HVEM 80—104354

electron microscope examination of materials continued

- Fe-Cr-Ni (18,14 wt.%), γ to ε to α martensitic transform., external stress effect, double tensile deform. exam. 80—108438
- Fe-Cr-Ti-Mo-TiO_2 (13, 3.5, 1.5, 2 wt.%) dispersion hardened, void swelling 80—65046
- Fe-Cr(6 to 9 wt.%), transform. study during $(\alpha+\gamma)$ region reversion *(French)* 77—59780
- Fe-Cu, modulated microstruct., continuous cooling effect, hardness and electron microscope obs. 79—87665
- Fe-Cu (4.54 wt.%) alloy, scaling behaviour, 700-1000°C, 1 atm. O_2 80—93679
- Fe-Cu-Ni (2, 5 wt.%), interphase precipitation obs. in assoc. with Widmanstatten ferrite lateral growth 80—40365
- Fe-Ga (25 at.%), precipitation *(French)* 77—70057
- Fe-Gd films, crystallisation, electron microscope obs. 79—15034
- Fe-Mg, Burgers vector determ., crystal defect observation by weak beam image *(Japanese)* 79—82130
- Fe-Mn, mechanical twinning of close-packed hexagonal ε-phase during plastic deform. *(Russian)* 80—60909
- Fe-Mn, stacking fault energy, Mn conc. depend. *(Russian)* 77—1836
- Fe-Mn-C, $\gamma\rightarrow\varepsilon\rightarrow\alpha'$ martensitic transform. 79—24523
- Fe-Mn-C, variation of martensite morphology with Mn and C composition 80—50635
- Fe-Mn-Ni base maraging alloys, age hardening 79—74170
- Fe-Mn-Ni-C, age hardenable, struct. and strength 77—8844
- Fe-Mn(Ni), fracture mechanism in various temperature and stress intervals *(Russian)* 79—24600
- Fe-Mo alloys, cryst. struct. and defects, high resolution electron microscopy obs. 79—94961
- Fe-Mo quenched alloy, electron microscope exam. of planar defects 79—79000
- Fe-N, nucleation and precipitation growth on dislocations, electron microscope studies 80—3064
- Fe-N(0.013 wt.%), effect of electron irradiation on precipitation 79—52221
- Fe-Ni, $\alpha\rightarrow\gamma$ conversion, electron microscope and X-ray spectral microanal. 79—78966
- α-Fe-Ni, struct. after polymorphic transform. under press. *(Russian)* 80—29946
- Fe-Ni (31%) alloy, deformed by slip, misaligned zones in $\{259\}_A$-martensite crysts. *(Russian)* 77—59850
- Fe-Ni (32 wt.%), electrohydraulic effect and struct. changes *(Russian)* 78—23783
- Fe-Ni (4 wt.%), extrinsic grain boundary dislocations, low C content influence 80—107273
- Fe-Ni alloy, α to γ slow transformation mechanism, Ni content influence *(Russian)* 80—7569
- Fe-Ni austenite, $\alpha\rightarrow\gamma$ transform and stabilisation, Mossbauer and electron microscopy obs. *(Russian)* 78—23703
- Fe-Ni-Al, struct. of aged austenite *(Russian)* 77—52357
- Fe-Ni-Al (18.2 wt.%) aged, fracture toughness and mode, grain size depend. 77—12700
- Fe-Ni-Al (30, 4wt.%), ageing, peculiarities of struct. state *(Russian)* 79—57008
- Fe-Ni-C, HVEM study of strain induced martensite 79—20047
- Fe-Ni-C (30, 0.5 wt.%) single cryst., stress induced martensitic transform. 80—60860
- Fe-Ni-Co-W(Mo) (18.65, 8.99, 4.87 wt.%), ageing characts., 380-530°C 80—60876
- Fe-Ni-Cr coating, electrodeposited, exam. of passivity 78—80655
- Fe-Ni-Cr-Ti-Mn-Mo, (25.8, 14.04, 2.17, 1.27, 1.30 wt.%), superalloy A-286, precipitation hardening, exam. of fracture toughness and mech. props. 78—92355
- Fe-Ni-Mn martensitic alloy, precipitation 77—12630
- Fe-Ni-Mo, martensitic transformation, annealing, influence on struct. of austenite *(Russian)* 80—81057
- Fe-Ni-Mo, small angle X-ray scatt. study, pre-precipitation phenomenon obs. *(French)* 78—19757
- Fe-Ni-Mo (16.4, 8.1 wt.%), effect of substituting Mo by W during ageing 80—29991
- Fe-Ni-Ti (30, 6 wt.%), austenitic, discontinuous coarsening of lamellar cellular precipitates, morphology 79—78967
- Fe-Ni-Ti (30, 6 wt.%), austenitic, discontinuous coarsening of lamellar cellular precipitates, growth kinetics 79—78968
- Fe-Ni-Ti-Al-Nb, struct. mechanism for inverse $\alpha\rightarrow\gamma$ transform. *(Russian)* 80—40351
- Fe-Ni-V, nitrided austenitic alloys, modulated substitutional interstitial solute atom clustering 79—74160
- Fe-Ni-V alloy, ageing of martensite *(Russian)* 78—39808
- Fe-Ni-(Cr)(Ti)(Al) austenite, high N content, cryst. struct. electron diffr. and electron miscroscope anal. *(Russian)* 79—24490
- Fe-Pd (50 at.%) alloy, structural changes during ordering *(Russian)* 77—77471
- Fe-Si, dislocation struct. of plastic relax. zone at tip of brittle crack 77—77582
- Fe-Si, domain struct., influence of insulating coating, high voltage SEM obs. 77—1565
- Fe-Si, domain struct. obs. by high voltage SEM 77—1564
- Fe-Si (2.5%), mag. stray fields above stripe domains, electron optic meas. 80—15755
- Fe-Si (3 wt.%), (110)[001] oriented single crystal, form. of rolling and annealing texture 77—16608
- Fe-Si (3 wt.%), grain oriented, MnS precipitate distribution, electron microscope observation *(Chinese)* 78—95751
- Fe-Si (3 wt.%) high-permeability grain-oriented steel, quenching effect on primary recrystn. texture development 80—84956
- Fe-Si (3 wt.%) layers, with ceramic coating, interface struct., electron microscopy and Mossbauer obs. *(Russian)* 79—28216
- Fe-Si (3.25 wt.%), Burgers vector identification from electron microscope images 80—2030
- Fe-Si alloy, deformed by slip, polygonal boundary form. *(Russian)* 79—24534
- Fe-Si amorphous film, struct. and crystallisation, Mossbauer study 80—11300
- Fe-Si-Al alloy, cryst. lattice deform. at antiphase boundaries, theoretical electron images exam. 77—11448
- Fe-Si-N alloy, BCC→FCC transform., martensitic character obs. *(Russian)* 78—48397
- Fe-$SiO_2(Al_2O_3)(ZrO_2)$ granular films, superparamag., Mossbauer effect 80—7131
- Fe-V(Nb)-N, precipitation study, 550 to 600°C *(German)* 77—90350

electron microscope examination of materials continued
Fe-W(Ni), recrystallisation under laser irradiation *(Russian)* 78−35396
Fe-Zn, quenched, martensite struct. and hardness, electron microscope exam. *(Russian)* 80−66619
FeAl, order parameter, atomic scattering factor, thickness fringes in electron micrographs 79−10832
Fe_3Al, alloys, superlattice-fringe imaging theory, images formed from two beams 80−79649
Fe_3Al, long-range order parameter from electron micrograph thickness fringes 77−65938
Fe_3Al, ordered alloys, atomic order parameters from topology of electron-microscope diffr. contrast from antiphase boundaries, quantitative determ. 78−95016
Fe_3Al, phase separation 77−63664
Fe_3Al-M, ternary ordered solid solns. with M=Ti, Mn, Ni, Cu, Ge substituent 77−43177
$Fe_{80}B_{20}$, amorphous, crystallization 78−42917
$Fe_x(C,N)$, obtained by ion bombardment thermochemical treatment of Armco Fe *(French)* 77−86229
$Fe_{50}Co_{50}$, disordering by laser irradiation, Mossbauer transmission spectroscopy and electron microscopy study *(French)* 79−23639
Fe_5Ge_3, amorphous film, elec. resist., microstruct. and annealing 77−85188
Fe_xGe_{1-x}, amorphous alloy, short range order anal. 77−80423
$(Fe_{1-x}M_x)_2O_3$, yH_2O, M=Cr,Cu,Ni, crystal growth, characterisation by Mossbauer spectroscopy, mag. meas. and electron microscopy *(French)* 80−80655
Fe_2MnAl, dislocation structure, antiphase boundary energies, deformation behaviour prediction *(Russian)* 79−65085
Fe_2MnAl, plastically deformed, domain struct., X-ray diffr. and electron microscope obs. *(Russian)* 79−20110
Fe_xNi_{1-x}, amorphous films, crystallisation, effect of codeposited O_2, N_2 or Kr gases 80−10807
$Fe_{40}Ni_{38}Mo_4B_{18}$, amorphous, crystallization, heat treatment and irradiation effects *(French)* 79−90558
$Fe_{1-x}O$, quenched, decomposition and ordering, electron diffr. and microscopy 77−31635
α- Fe_2O_3, mutual orientations and morphology obs. *(French)* 79−37647
α-Fe_2O_3, prep. by evaporative decomposition of $Fe(NO_3)_3.6H_2O$ soln. 79−20011
γ-Fe_2O_3, prep. from thermal decomp. of $[Fe_3(HCOO)_6(OH)_2]HCOO.4H_2O$ and characterisation 78−80741
α-Fe_2O_3, prod. by α-FeOOH dehydration, mosaic struct. and twin form. 79−86802
γ-Fe_2O_3 recording tapes, orientation, Mossbauer, X-ray and electron microscope meas. 77−16219
Fe_2O_3, twinning dislocations, electron microscopy obs. 79−99218
Fe_2O_3 ultrafine particles in PTFE matrix, EPR and Mossbauer study 80−100625
γ- Fe_2O_3:Co powder, increased coercivity by epitaxial doping 79−82833
xFe_2O_3-$(1-x)PbO$-$3B_2O_3$ glass, Mossbauer study of Fe cations 79−91325
Fe_2O_3-PbO-B_2O_3 glass, X-ray and electron microscope studies, mag. and Mossbauer effect meas. 80−28919
Fe_2O_3-TiO_2 system, high temp. intergrowth struct., metal atom ordering in intergrowth boundaries 78−79573
Fe_3O_4, Co modified, synthesis with autoclave in H_2 atm. 80−35117
Fe_3O_4, effect of Al ion on formation and structure *(Japanese)* 77−59727
Fe_3O_4 ferrofluid suspension, mag. props., stability 79−87293
Fe_xO_y films, electron microscopy and energy-loss spectroscopy 80−80137
β-FeOOH, akaganeite, struct. changes due to radiation damage 79−28014
FeOOH, crystal growth in $FeSO_4$ solution with NaOH or NH_4OH as precipitant, phase diagrams *(Chinese)* 80−44158
FeOOH crysts., prep. by hydrolysis, struct. and reactions with silica 78−35678
β-FeOOH, dehydration 80−79767
α-FeOOh, goethite, superstructure form. on dehydration, electron microscopy obs. 80−3327
$20Fe_2O_3.80[3B_2O_3.(1-x)PbO.xGeO_2]$ glass, phys. props. 80−49119
$Fe_{75}P_{15}O_{10}$, amorphous, ferromag. domain-wall width, anisotropy depend. 78−19269
Fe_3Pt, atomic thermal vibr. anisotropy, martensitic transform. model *(French)* 80−70355
FeS_2 (pyrite), glide elements study by electron microscopy and electron diffr. 78−83817
FeS_2, pyrite, high-resolution electron micrograph of twin boundary 77−65983
$Fe_{1-x}S$, NC-type, wave distrib. of vacancies 79−99178
Fe_3Si, ordering energy, electron micrography determ. 78−14353
Fe_xSn_{1-x}, amorphous alloy stability, comp. and temp. depend. 79−19156
Fe_xVO_2, reduced, microstruct., crystallographic shear planes, electron microscope obs. 79−1443
Ga-As-Se, exam. of phase diagram, rel. to LPE of GaAs:Se 79−1849
GaAs, annealing rel. to stoichiometry deviation, Hall effect, electron microscope meas. 77−24410
GaAs, dissociation of dislocations 79−46665
GaAs, layer structures revealed by decoration method and electron microscopy 77−27902
GaAs layers, from gas phase, impurity influence on growth micromechanism 80−45237
GaAs, photoelectric memory effect, effect of metallic island struct. on surface 77−55570
GaAs, semi-insulating, optical and electron microscopy exam., line dislocation precipitates 80−70205
GaAs, surface chem. changes on annealing, optical and electron microscopy study 79−73383
GaAs, VPE layer on Ge, antiphase domain structures 77−69193
GaAs:Si, Cr, carrier concs. from Hall effect, microscopy, localised vibrational modes absorption meas. 78−56104
GaAs-AlAs, epitaxial struct. with alternate layer comp. modulation, fabrication and characterisation 77−1322
n-GaAs-n-GaN, diffusion growth kinetics, morphology and electrical properties 80−20294
$GaAs_{1-x}P_x$, structural defects, optical props. effect 80−55208
$GaAs_xSb_{1-x}$ solid solution epitaxial layer, morphology and defect structure 77−1330
$Ga_{1-x}In_xAs$-GaAs low-misfit epitaxial interface, electron microscope contrast 79−73416

electron microscope examination of materials continued
$GaNbO_4$ decomp. due to electron beam heating in electron microscope 78−35711
GaP epitaxial layer, crystal defects influence on luminesc. obs. 79−87511
GaP, VPE layer on Si or Ge, antiphase domain structures 77−69193
GaP:S LEC grown crystals, HVEM investig. of defects 79−60376
Ga_xVO_2, reduced, microstruct., crystallographic shear planes, electron microscope obs. 79−1443
Gd clusters in faujasite type zeolites, mag. suscept. temp. depend. 78−14925
Gd, mag. domains, Lorentz microscopy obs. 78−84448
Gd-Co amorphous film, sputtered, perpendicular anisotropy exam. 79−73707
Gd-Co amorphous thin films, crystn. process and domain struct. *(Chinese)* 80−54533
Gd-Co film, amorphous, Ar sputtered, struct. 78−63946
Gd-Co film, amorphous, phase separation as source of perpendicular anisotropy 78−64244
Gd-Co-Au amorphous magnetic films, domain wall obs. by Lorentz electron microscopy 77−80979
Gd-Co-Mo film, amorphous, Ar sputtered, struct. 78−63946
Gd-Fe film, amorphous, in-situ ion beam sputtered, microstruct. and Lorentz mag. struct. 78−63947
a-GdCoAu(Mo) films, perpendicular anisotropy temp. depend., Lorentz microscopy 77−28419
$Gd_3Ga_5O_{12}$, substrate, electron examination of microstruct. and microsegregation 78−67919
$Gd_2(MoO_4)_3$, electron microscope exam. of ferroelec. and ferroelastic props., domain walls and cryst. defects 77−69786
$Gd_2(MoO_4)_3$, ferroelec. and ferroelastic, electron microscopic study 77−85675
$Gd_2(MoO_4)_3$, ferroelec. ferroelastic, antiphase boundary image anal. phase transformation obs. 78−15134
$Gd_2(MoO_4)_3$, ferroelectric, polarisation reversal, electric field induced phase transform. 80−103925
GdO film, new reduced variant due to annealing 77−89660
Gd_2O_3-Al_2O_3 glasses, crystallization 79−50998
Gd_2SiO_5, atomic positions, high resolution electron microscopy 80−100220
Ge alloy, amorphous film, formation and stability criteria 79−10799
Ge alloys, amorphous film, crystn. transform. kinetics 78−22653
Ge, amorphous, in situ meas. of thermal EMP, by ultrahigh vacuum electron microscopy 79−26184
Ge amorphous evaporated film, to metal contact resist. diffusion and microstruct. 77−89880
Ge amorphous film, bright-field hollow cone images 80−75136
Ge amorphous films, structural relaxation and crystallisation 80−100170
Ge, bicrystal, dislocation core structure *(French)* 78−26571
Ge bicrystals, low angle [011] tilt boundary 79−82239
Ge, dislocation electron image filtering in electron microscopy 80−75129
Ge, dislocation mobility 77−76413
Ge, dislocations, lattice images 79−82215
Ge, electron beam irrad., {113} faults, nature and origin 80−70258
Ge, electron irrad., defect growth, struct. rel. to temp. 77−11591
Ge, electron irradiated in HV electron microscope, defect form. and interaction with dislocation 77−19990
Ge, electron microscope obs. of nonequilibrium walls *(Russian)* 78−14347
Ge, epitaxial film, ion sputtering, growth mechanism, struct., props. 77−31917
Ge, epitaxial growth of very thin electron microscopy specimens 80−100793
Ge epitaxial layers, on GaAs substrate, misfit dislocation multiplication mechanism 78−87673
Ge, evaporated film, lattice parameters and phase transition temp., surface influence of glass substrates 78−94996
Ge film, amorphous, ^{74}Ge ion implanted, defect struct. obs. 78−51848
Ge film, amorphous, high resolution electron microscopy, digital processing use 78−37116
Ge film, amorphous, thermoelec. power and structural investigs. using in-situ electron microscopy 77−76983
Ge film, radiation damage in electron microscope 77−84794
Ge, film, vac. deposition onto low temp. substrate, cryostat *(Japanese)* 78−27403
Ge, grain boundary, lattice imaging in electron microscope 78−6069
Ge, high resolution electron microscopy, dislocation and grain boundary struct. 3-4 Å resolution 78−38707
Ge, multi-beam lattice images in (011) orientation 77−24252
Ge particles, homogeneously nucleated, production and props. 77−56252
Ge, polycrystalline epitaxial film, exam. of growth kinetics and props. 80−55304
Ge, second-phase inclusions after O_2 treatment, electron microscope obs. 77−43238
Ge, stacking faults of dislocations, constrictions obs. using weak-beam electron microscopy 77−35576
Ge:O, Cu, amorphous thin film, impurity effects on struct. 80−107054
Ge-Ag, exam. of structure using electron microscope *(Russian)* 79−14738
Ge-GaAs, heteroepitaxial systems, misfit dislocations obs. using HV electron microscopy 80−100242
Ge-S-In, chalcogenide glass, determ. of glass phases, phys. props. meas. 79−23526
GeTe, low temp. alloys, microstruct. obs. *(Russian)* 78−19768
Hf, polymorphic transition, emission images obs. in temp. range 1800-2100°K 80−100836
HfB_2, oxidation in O_2 atmosphere, exam. 80−11814
Hg, atom, on C support film, signal-to-noise enhancement by incoherent superposition 80−101906
Hg, condensation, two-dimensional, on W 80−107666
Hg film, melting and crystallisation kinetics, electron microscopy 77−15725
$Hg_{1-x}Fe_xTe$, struct. invest. using X-ray diffr. and electron microscopy 80−75365
HgSe film, anomalous photocond., electron microscope study 80−65623
In epitaxial growth, cluster mobilities, in-situ electron microscopes obs. 80−15407
In, film, vac. deposited, influence of ion bombardment during condensation 79−82483
In-Sn alloy crystals, phase changes and shape memory effect *(Japanese)* 80−108502

electron microscope examination of materials continued
  InN film, specular reflection spectra, lattice parameters 80—7428
  InP:S^+(Se^+), ion-implanted VPE layers, laser annealing, elec. and struct. anal. 79—73199
  InSb, single crystal, chem. and ion etching, surface changes *(French)* 80—108614
  $(In_{1-x}Sn_x)_2O_{3-y}$, pyrolytic selective coating, Sn additions effect 78—43499
  IrO_x, electrochromic, oxidation state changes and struct. 80—100950
  KBr, single crystal, preirradiation and radiation defects, electron microscopic estimation *(Russian)* 78—75695
  KCl, additively coloured, colloid size distrib., replica microscopy, absorpt. spectra 77—47449
  KCl crystal, surface elementary steps interaction with Au particles 80—39400
  KCl, single crystal, preirradiation and radiation defects, electron microscopic estimation *(Russian)* 78—75695
  KCl:Ba^{2+}, precipitation kinetics, supersaturation effects, geometry of formed heterophase struct. *(Russian)* 78—84824
  KCl:Pb, solid solution, electron microscope exam. of decomposition, of naturally aged specimens 79—96030
  KCl:Pb crystal surfaces, Au decoration, electron microscope study 80—15144
  KCl:Pb exam. of simultaneous effect of heat treatment, Pb concentration on state, phase diagram construction 79—96008
  KCl:Sr, single crystal, thermally stimulated topochemical reactions 79—28011
  KH_2PO_4, ferroelec. thin crysts., struct. investig. 79—27962
  KNO_3, ferroelec. thin crysts., struct. investig. 79—27962
  $KNbO_3$, layer growth, optical and electron microscopy 77—59021
  K_2O-Ta_2O_5 mixed oxides, cryst. struct., electron microscopy study 78—91309
  K_2O-Ta_2O_5 mixed oxides, cryst. struct., electron microscopy study 78—91310
  $K_2Pt(CN_4)Br_{0.3}.3H_2O$, anisotropic radiation damage in electron microscopy, diffr. spot fading rate obs. 80—107329
  $KSbO_3$, cubic, K^+ ion ordering, electron microscopy 78—79550
  $LIFe_5O_8$, absolute struct. and space group determ. by electron microscopy 77—62454
  LaB_6, high temp. interaction with 0_2, AES and mass desorption expts. 80—7698
  La_2O_3-CeO_2, microstruct. of La_2O_3 rich crystallites, electron microscopy and diffr. *(French)* 78—35374
  $LaSi_2$, thin film, exam. of phase transitions during vacuum annealing 79—95281
  La_5Si_3 thin film, exam. of phase transitions during vacuum annealing 79—95281
  Li aggregated deposits, optical props., 1-6 eV 77—66549
  LiF, deformed, influence of surface on density of edge components of dislocations 77—31670
  LiF, electron irradiated, defects, selective etching and electron microscopy *(Russian)* 77—47488
  LiF single crystals, exam. of void morphology effects on their disappearance kinetics 79—10843
  LiF:Co^{2+}, solid soln. decomp., precip. of new phase, electron microscope expt. 79—11619
  LiF:Co^{2+}, X-ray and electron microscope obs. of CoF_2 precip. morphology 77—31777
  $LiFe_5O_8$, material loss and high-temp. phase transition 78—64534
  $LiFe_5O_8$, microstruct. and magnetic props., electron microscope obs. 79—87290
  $Li_{0.5}Fe_{2.5}O_4$-$Bi_2O_3(V_2O_5)$ systems, phase diagrams, sintering conditions 78—35366
  $(Li_{0.5}Fe_{2.5}O_4)_{0.8}(CuFe_2O_4)_{0.2}$, struct., magnetic props., rectangular hysteresis loop 77—20645
  Li_2O-SiO_2 glass, water content effect on crystal nucleation and growth 79—55670
  $Li_{x+2}P_xO_{3x+1}$, polyphosphate, melting and crystallisation 80—70376
  $Li_2Si_2O_5$ glass, steady state crystal nucleation rate 79—90565
  $LiTaO_3$, crystallographic features and domain struct. 78—34498
  $LiTaO_3$-SiO_2-Al_2O_3, transparency in relation to microstruct. 78—53005
  $LiTbS_2$, long and short range order 78—38667
  Mg alloy MA12, thermally strengthened, fatigue cracking in air and vacuum *(Russian)* 78—35481
  Mg, dislocation struct. after US deform. *(Russian)* 80—29027
  Mg, electron irrad. damage, dislocation loop growth, in situ obs. 78—87715
  Mg, hydrogenation kinetics, electron microscope expts. 77—52553
  Mg rough deposits, surface struct. autocorrelation function, electron microphotographs 78—26756
  Mg-Ga, metastable cryst. and glassy phases, X-ray struct. anal. and electron microscopy *(German)* 79—46601
  Mg-Mn-Ce alloy, superplastic deform., role of grain boundaries 78—19843
  Mg-Nd-Zn dilute alloy, metallography and precip. kinetics 80—71655
  Mg_3Cd, disordering under electron irrad. in electron microscope 78—83849
  $Mg(Cu_{1-x}Al_x)$ with $x=0.465$, Friauf-Laves phase, electron microscope obs. 77—19908
  MgO bicrystal, fracture mechanism obs. 77—44339
  MgO, crack propagation during in-situ deform., plastic zone formation 80—16468
  MgO crysts., geometrical-statistical parameters of dislocation interactions with point obstacles 80—103341
  MgO crysts., radiation damage influence on deform. in HVEM 80—103391
  MgO, dislocation motion 79—4309
  MgO, dissolution, surface roughening effects and mechanism distinction 79—47975
  MgO, electron diffr., dynamical effects for cryst. struct. determ. 78—83679
  MgO, high temperature prestrain effect on plastic props., dislocation struct. 80—79866
  MgO, multiple-beam dynamic effects, in Kikuchi patterns 79—46528
  MgO, point-obstacle distance distrib. during motion of screw dislocations 77—11744
  MgO, precipitation on dislocations, ultramicroscopy and chem. etching 78—67720
  MgO, residual image contrast of dislocation loops 78—47382
  MgO, single crystals, deform., dislocation motion and multiplication in HV electron microscope 77—84754

electron microscope examination of materials continued
  MgO single crystals, surface atomic steps obs. by electron microscopy, dark- and bright-field techniques 80—84040
  MgO single crysts., dislocation processes, obs. by HVEM in-situ deform. 80—103340
  MgO, slip line struct. using replica electron microscope technique 79—7605
  MgO, X-ray and electron diffr. crystallite size determ. *(Polish)* 79—100153
  MgO-Al_2O_3-SiO_2, metastable liq. phase separation region, electron microscope exam. 78—88451
  MgO-CaO-Al_2O_3-SiO2(-TiO_2) systems, glass-ceramics, crystn. kinetics *(Russian)* 79—37626
  MgO-CdO, interface, coincidence-site-lattice relations 80—103588
  Mg_2SiO_4, single cryst., (010) cleavages, etch patterns and dislocations, interferometric obs. 78—2127
  Mg0 bicrystals, electron microscope exam. of secondary grain boundary dislocations in high angle twist boundaries 80—6415
  Mn thin films, vacuum deposited in elec. field, resist., struct. 80—103761
  Mn-Al alloy, domain struct., cryst. defect effects 77—69609
  MnAlGe film, mag. domains and amorphous to cryst. phase transition, electron microscopy obs. 80—71129
  Mn_3Ga, formation of DO_{22} superstruct. and para-antiferromag. transition 79—19737
  MnGaGe film, mag. domains and amorphous to cryst. phase transition, electron microscopy obs. 80—71129
  $Mn_3(PO_4)_2$ coating on steel, wear resistant appl. 80—16609
  MnS-Y_2S_3, chem. twinning, electron microscopic study 79—46678
  MnZn ferrites, abrasive wear measurement appl. *(Japanese)* 78—39917
  Mo, adsorption of K, work function, field emission microscope obs. 77—11788
  Mo alloys, dil., HVEM bombarded, neutron damage simulation, defect cluster and dislocation obs. 80—107330
  Mo, cellular structure, initial stages of formation in rolled single crystals 79—23611
  Mo, deformed, dislocation-free channels prod. by heat pulses, electron microscope obs. and hardness meas. *(Russian)* 79—52251
  Mo dislocation a ⟨100⟩ stability, plastic deform. at high-press. 78—43030
  Mo, dislocation structure inhomogeneity in electromachining crater zone *(Russian)* 80—16326
  Mo, dislocation structure of diffusional welding zone *(Russian)* 80—96531
  Mo, electron irradiated, energy and orientation depend. of at. displacement 79—99244
  Mo, electron radiation damage and props. of point defects 77—11590
  Mo extinction length ζ_{200} meas., electron energy influence 80—90935
  Mo, foil dislocation struct. of rolling texture *(Russian)* 78—59810
  Mo, grain boundaries, electron microscope obs. *(Russian)* 79—4311
  Mo, He ion irradiated, ordered arrangement of micropores on dislocations 77—19943
  Mo, irrad. in HVEM, anisotropy of damage prod. 80—107322
  Mo, irradiated, small edge dislocation loops, electron microscope image contrast, Burger's vector determ. 77—76410
  Mo, neutron bombard., radiation damage, electron microscopy obs. *(Russian)* 80—44235
  Mo, plastic deform. by rolling at 293K, dislocation struct. *(Russian)* 77—48481
  Mo polycrystals, grain misalignment, electron microscope determ. *(Russian)* 80—103358
  Mo, self-ion damage, influence of material purity and irradiation temp., electron microscope exam. 77—35562
  Mo, single and polycrysts., struct. change during work softening, HVEM 80—103336
  Mo, slip rosettes and dislocation struct. formed by microindentations 78—14349
  Mo, strain localisation and fatigue, glide plane shearing stress 80—7683
  Mo, stress-to-rupture strength at high temps., struct. effect 77—70175
  Mo-C dilute alloy defect cluster nucleation and growth under 1250 keV electron microscope *(Japanese)* 78—87663
  Mo-Co-Si alloys, cryst. struct. and defects, high resolution electron microscopy obs. 79—94961
  Mo-Re alloy MR47-VP, dislocation struct. and fatigue damage during room temp. deform. *(Russian)* 79—20111
  Mo-Zr, nitride form. in N_2 atmos. *(Russian)* 78—19938
  Mo-Zr-C (0.63, 0.06 wt.%), quenched and deformed, structural changes during heating to ageing temp. *(Russian)* 79—1879
  Mo-Zr-C-B, dilute, electron microscope obs. of planar defect diffr. contrast patterns 77—43227
  Mo-Zr-Nb-C and Mo-Zr-C, carbide precip. hardening kinetics, ageing singularities *(Russian)* 77—25059
  Mo-ZrC, internal oxidation, struct. formation law, microstruct. examination 78—84836
  Mo_2C, Mo_2N, synthesis by ion bombard. of Mo film 78—48357
  MoO_3, reduction at low temps., surface defects obs. in HV electron microscope 77—35564
  MoO_3, reduction at low temp., role of defects, electron microscope obs. 77—77755
  MoO_3 reduction to MoO_2 by electron beam, electron difrr., microscope investigs. *(French)* 78—95945
  MoO_3, ultrafine crystals, exam. of reduction using electron microscopy *(Russian)* 79—29394
  MoS_2, molybdenite crystal, direct imaging of atom configuration projected onto the basal plane 80—64847
  MoS_2, poorly crystalline 'rag' struct. 80—6391
  β-$MoTe_2$, domain struct., dislocation fine struct., phase transitions 79—82332
  α-N_2 twinning, electron microscope and diffr. exam. 77—35574
  $NH_4H_2PO_4$, dislocation obs. using electron microscopy and replica method 77—59013
  Na-A zeolite, struct. obs. by high-resolution electron microscopy 80—84175
  Na_3AlF_6 film, cryolite, struct., electron microscopy 77—59226
  NaCl, (100), (110) and (111) surfaces annealed in vac. 400-800°C, evap. struct. 77—15572
  NaCl bicrystal, grain boundary segregation, Au decoration obs. 77—68982
  NaCl, cleavage faces, evaporation pattern determ. by decoration method in electron microscopy *(German)* 80—107626
  NaCl, cleavage of single crystals, investigation of fast electrical processes 79—24045

electron microscope examination of materials continued
- NaCl cleaved surface structure, electron microscope 79−7735
- NaCl crystal surface struct., effect of ionic bombardment *(German)* 80−24507
- NaCl crystals irrad. by high electron doses, annealing, colour centre prod. 80−2074
- NaCl, deformed, influence of surface on density of edge components of dislocations 77−31670
- NaCl, electron irradiated, defects, selective etching and electron microscopy *(Russian)* 77−47488
- NaCl, evaporating surface, step motion obs. and simulation 78−26766
- NaCl, impurity precipitation and grain boundary diffusion 80−107567
- NaCl, monatomic step struct., decoration technique 80−103554
- NaCl, prep. of fine crysts. demonstrated by electron microscopy 78−48302
- NaCl, single crystal, surface markings, left by unsteady cleavage crack propag. 79−46746
- NaCl, with dispersed Au particles, age hardening of surface, double decoration obs. 79−11634
- $NaCl:Eu^{2+}$, oriented growth and cryst. struct. of precipitated phases 80−24303
- NaCl:Fe(Mn), nucleation of Au, surface imperfection effects 77−15699
- $NaCl:OH^-$, additively coloured, form. and decay of defect clusters and elec. double layers, Au decoration obs. 79−10850
- $NaCl\text{-}O^{2-}$ X-ray irrad., defect generation during radiolysis 80−7831
- NaF, deformed, influence of surface on density of edge components of dislocations 77−31670
- $Na_2Mg_6Si_8O_{22}F_2$, fluoramphibole, fibrous, crystn. from gas phase, mechanism 78−34451
- $NaNO_2$, ferroelec. thin crysts., struct. investig. 79−27962
- $NaO\text{-}B_2O_3\text{-}SiO_2$, phase separated glass, viscosity and microstruct., heat treatment effect 79−99343
- $Na_2O\text{-}B_2O_3\text{-}Bi_2O_3$, glass with metallic Bi granules, elec. cond. 80−84493
- $Na_2O\text{-}B_2O_3\text{-}SiO_2$ glass, phase separated, HCl leaching rate and microstruct. 79−29242
- $Na_2O\text{-}CaO\text{-}Al_2O_3\text{-}SiO_2\text{-}F\text{-}B_2O_3\text{-}ZrO_2$ glaze, crystallisation, MgO, ZnO, BaO and SrO effects 79−60279
- $Na_2O\text{-}CaO\text{-}Al_2O_3\text{-}SiO_2$ glass, crystn. for the purpose of obtaining vitroceramics *(French)* 80−75163
- $Na_2O\text{-}CaO\text{-}SiO_2$, foil, exam. of surface plasticity, and cracks, by electron microscopy 78−68733
- $Na_2O\text{-}CaO\text{-}SiO_2$ glass, water content effect on crystal nucleation and growth 79−55670
- $Na_2O\text{-}CaO\text{-}SiO_2$ glass foils, HVEM in-situ straining expts. 80−104216
- $Na_2O\text{-}MgO\text{-}Al_2O_3$, β''''-alumina, high-resolution electron microscopy 80−75208
- $Na_2S_2O_3$, breakdown on Ag halide grains, electron microscopy 78−21237
- $NaSbSe_2$ films, struct., photoelec. and opt. props. 78−51834
- $Na_2Ti_9O_{19}$, orthorhombic, unit-cell twinning of monoclinic $Na_2Ti_9O_{19}$, cryst. struct. 80−107155
- $(Na_2Ti_6O_{13})_n.(BaTi_4O_9)_m$, tunnel struct. intergrowth, electron, microscopy investigations 80−100218
- Nb, cubic crystals, anisotropic, dislocation loops, electron microscope image contrast 80−39101
- Nb, deformation at 77-158K, slip and dislocation struct. 79−83277
- Nb, dislocation struct. after tensile creep test under reactor radiation conditions *(Russian)* 80−45348
- Nb, electron irradiated, energy and orientation depend. of at. displacement 79−99244
- Nb, low temp. annealing effect, precip. of Nb_2O_5 *(Russian)* 77−52456
- Nb, neutron bombarded, defect size distrib. influence on hardening *(Russian)* 80−10580
- Nb, superconducting, torque anisotropy due to defects flux line pinning 77−20509
- Nb-H(D), H ordering, review 80−60850
- Nb-Ni-Al alloys, cryst. struct. and defects, high resolution electron microscopy obs. 79−94961
- Nb-Ti(Zr)(Hf)-N, exam. of phase equilibrium using electron microscopy and X-ray analysis *(Russian)* 79−15654
- Nb_3Al, obs. of shear struct., electron microscopy *(Russian)* 78−6938
- $NbFe_{2-x}Si_x$, crystalline struct., electron microscopy determ. *(French)* 80−54174
- Nb_3Ge, RF and DC sputtered films comparison, O content effect 78−72022
- NbO_2, slightly substoichiometric, microstructure 77−47584
- $Nb_{12}O_{29}$, high resolution lattice image, by HV electron microscope 77−15292
- $Nb_2O_5\text{-}TiO_2$, splat cooled, crystallization and ordering 77−68953
- $Nb_2O_5\text{-}WO_3$, solid-state reactions, electron microscopic obs. 77−16818
- Nb_xO_y, lattice imaging 78−30522
- $3Nb_2O_2.8WO_3$, circular diffuse scattering studied by 1 MV high resolution electron microscopy 80−59350
- NbS_2, intercalation compounds, octahedral, microstructural study 77−84729
- $NbSe_2Cu_x$, ordering study using electron diffr. and microscopy 80−39043
- $(Nb_{1-x}Ta_x)_2C$, modulated structs., periodic antiphase domains 79−94969
- Nd-Co film, amorphous, exam. of domain struct. 78−68336
- $NdAlO_3$, dielectric films, phase composition and structure 80−39464
- $Nd_xPr_ySm_zCo_5$ permanent magnets, coercive force, low-temp. annealing influence *(Russian)* 80−39812
- $Nd_{1-x}S$, grown-in defect exam. 78−43014
- $Nd_2Zr_2O_7\text{-}Nd_2Hf_2O_7$, struct., elec. cond. and melting point 80−54197
- Ni (110), adsorption of O_2, obs. by electron microscopy, AES and LEED *(French)* 77−62732
- Ni alloy 718, fatigue crack growth at 298 and 823K, frequency and wave form effects 78−64636
- Ni alloy powder, crystallised by supercooling methods, struct. props. *(Russian)* 80−54483
- Ni alloys, plasticity, heat treatment effect 80−76277
- Ni base heat resistant casting alloy, fatigue resistance, microstruct. obs. 79−66159
- Ni base superalloy Nimonic 80A, microstruct. anal. by high-resolution electron microscopy 80−76459
- Ni based alloy, amorphous, liq. quenched, struct., thermal stability and mech. props. 80−88059
- Ni, C precipitation 80−29958
- Ni, creep, struct. and activation characts., effective stress, electron microscopy and resistometric obs. *(Russian)* 80−40427

electron microscope examination of materials continued
- Ni, cubic crystals, anisotropic, dislocation loops, electron microscope image contrast 80−39101
- Ni, defect cluster evolution, ion implanter adaption on 100 kV electron microscope 79−2888
- Ni, deformed, struct. form. during annealing, Ni_3Al type ordered phase precipitation *(Russian)* 80−45325
- Ni, deformed, work-hardening, dislocation and mosaic struct., X-ray and electron microscopy 77−35625
- Ni, deformed by hydrostatic extrusion, drawing or drawing under press., dislocation struct. obs. *(Russian)* 77−21213
- Ni, dislocation struct formed by C diffusion in single crystals, electron microscope obs. *(Japanese)* 78−10053
- Ni, dislocation structure evolution after hydroextrusion *(Russian)* 80−96530
- Ni electrodeposit, crystallitemorphology *(French)* 77−32535
- Ni electrodeposit on Cu, growth and microstruct. 77−11823
- Ni electrodeposits, fibre textures before and after thermal treatment 79−91693
- Ni electrodeposits on (001)Cu films, growth and mag. anisotropy 79−42810
- Ni, electrolessly deposited, structural comparison with electroplated films 79−23869
- Ni, electron irrad. in HVEM, interstitial loop growth 80−107326
- Ni film, effect of He ion implantation on domain struct., Lorentz electron microscopy 77−20654
- Ni film, hexagonal phase identification *(Russian)* 77−15711
- Ni film, on (001) Ag, FCC and BCC metal-on-metal epitaxy, geometric factors, electron microscopy 78−22980
- Ni, form. of vacancy micropores during bombardment by 300 keV Ni ions 78−2172
- Ni, Frank loops, growth kinetics and ‘preference factor’ during electron irradiation 78−22723
- Ni, HVEM obs. of irrad. damage 77−35589
- Ni intercalation compound, electron microscopy 80−84164
- Ni, mag. domains, μ^*-tensor method, temp. and surface orientation depend. 77−16098
- Ni, microscopic elastic limit, effect of preliminary plastic strain *(Russian)* 77−76485
- Ni on W (001), geom. factors of FCC-BCC epitaxy 78−60041
- Ni, point defect-dislocation loop interaction, effect on dislocation loop growth kinetics 78−47415
- Ni, polygonisation, high press. grain growth, dislocation struct., electron microscopic obs. 77−16613
- Ni, pure, fatigue crack propagation, quantitative stereoscopic fractography study 79−74238
- Ni, rolled, dislocation struct. and recovery during annealing *(Russian)* 79−29084
- Ni sheet, surface, adsorbed ^3H, ethylene-^{14}C determ., autoradiography method 77−63989
- Ni, single cryst., cyclically deformed, HVEM in-situ deform. study 80−103339
- Ni single crystal, stretched, electron microscope exam. of deformation cell structure during polygonization *(German)* 80−7651
- Ni, splat quenched, gaseous impurities effect on struct. 77−4042
- Ni, stacking fault energy, by electron microscope obs. of dissoc. edge dislocations and faulted dipoles 77−72627
- Ni, stray mag. fields above stripe domains, electron microscope and μ^*-tensor determ. 80−71089
- Ni superalloy powder, thinning technique for microstruct. obs. using analytical electron microscopy 78−48587
- Ni, thin film, growth on Au (001) substrates *(French)* 80−44446
- Ni, US deform., electron microscope exam. *(Russian)* 78−35447
- Ni, US induced mag. reversals, stroboscopic electron microscope obs. 77−48026
- $Ni/Ni_3Al\text{-}Ni_3Nb$ eutectic, directionally solidified, plastic deformation *(Russian)* 78−39843
- Ni-A-Ti (6,1 wt.%), γ' phase precip., deform. effects *(Russian)* 78−48404
- Ni-Al (14 at.%), two stage ageing effect on spatial distrib. of γ'-phase particles *(Russian)* 78−39805
- Ni-Al (6.05 wt.%), prediction and meas. of precipitate number density 78−19756
- Ni-Al (6.35 wt.%) foil, radiation-induced precipitate redistrib. 78−30681
- Ni-based alloys, binary, ternary, complex, TiC additions, effects 78−92305
- Ni-Be alloy, annealed under load, spatial distrib. of precips. *(Russian)* 77−59790
- Ni-ceramic coating structure, influence of micropowder inclusion *(Russian)* 80−59820
- Ni-Co-Al (1, 35.2 at.%), tempered martensite, new ordered phase 79−11560
- Ni-Co-Cr superalloy, powder produced, necklace struct. development 80−40395
- Ni-Cr, (30 wt.%), collective dislocation movements, in situ study 80−100243
- Ni-Cr, deformed, struct. form. during annealing, Ni_3Al type ordered phase precipitation *(Russian)* 80−45325
- Ni-Cr, dispersion strengthening, prep. from powder, mech. props. 79−91658
- Ni-Cr, high temp. thermomech. treatment effect on tensile diagrams of KhN77TYuR *(Russian)* 80−60884
- Ni-Cr (Mo), solid soln., US deform., electron microscope exam. *(Russian)* 78−35447
- Ni-Cr (33 at.%), plastic deformation, HVEM study *(French)* 80−66605
- Ni-Cr alloy KhN70VMTYu, heat resistant, explosive loading effect on struct. and mech. props. *(Russian)* 78−39787
- Ni-Cr film, long range order 79−60657
- Ni-Cr-Mg alloy, KhN70VMTYu, Mg effect on grain boundary struct., props. 79−19261
- Ni-Cr-Ti-Al-Fe-Co (19.65, 2.40, 1.37, 0.78, 0.52 wt.%), strength of γ' hardened alloy, ageing exam. 78−88501
- Ni-Cu-Si (38,5 at.%), changes in modulated struct. during ageing early stages *(Japanese)* 79−100183
- β-Ni-Cu-Zn, electron microscopy of premartensitic state 79−66059
- Ni-Fe films, in state of undersaturation in perpendicular fields, micromagnetic struct. *(Russian)* 79−61193
- Ni-Fe oxidised films, easy-axis switching 79−91266
- Ni-Fe-Co-Ti, electron microscopy and mag. meas. 80−71097
- Ni-In, FCC, cellular precipitation kinetics 78−52823

electron microscope examination of materials continued
- Ni-Mo, and Ni-Mo-V alloys, struct. changes on annealing *(Russian)* 77–21145
- Ni-Mo, short range order considerations and development of long range order 77–16574
- Ni-Mo (20.8 wt.%), order, heat treatment effects 80–40406
- Ni-P, electrodeposited films, amorphous and crystalline, electron microscopy, in-situ crystallisation 79–11043
- Ni-P amorphous alloy prep. by ion implantation 78–22748
- Ni-Ti (48 at.%), annealed and rolled electron microscope and probe analysis of structure 79–100189
- β-Ni-Zn, eutectoid decomposition kinetics *(German)* 77–8819
- γ'-$Ni_3(Al,Ti)$, single crystal, dislocation movement, HVEM obs. *(Japanese)* 80–108503
- Ni_3Al-Ni_3Nb, eutectic alloy, crack development, failure energy capacity *(Russian)* 80–40480
- $Ni_{66}B_{34}$, morphological, structural and phys. props. *(French)* 80–44444
- $Ni_{62}Co_4Al_{34}$, fine struct. of martensite, electron microscopy obs. *(Russian)* 79–46672
- $NiCo_2O_4$, ferrimagnetic spinel, neutron diffr. study 79–99681
- NiFe, single and multilayer thin films, strip domains, inplane magnetisation 80–103866
- NiFe, US induced mag. reversals, stroboscopic electron microscope obs. 77–48026
- $Ni_{0.83}Fe_{0.17}$ films, reson. oscills. of mag. domain walls and Bloch lines, stroboscopic electron microscopy 80–54931
- Ni_3Fe, compression induced mag. anisotropy and superlattice dislocations, annealing effect 78–31067
- Ni_3Fe, superlattice dislocations, compression induced mag. anisotropy 77–85443
- $NiFe_2O_4$, microstruct. and magnetic props., electron microscope obs. 79–87290
- NiFr, mag. film, pulse switching at low temp. 80–103868
- Ni_3GA single crystals, anomalous temp. depend. of strength, dislocation struct., optical and TEM 79–74228
- Ni_3Ga, stacking fault form. in situ obs. by stretching thin foils in electron microscope 77–62547
- Ni_5Ge_3, amorphous film, elec. resist., microstruct. and annealing 77–85188
- Ni_4Mo, electron irrad. in electron microscope, radn. ordering 79–86818
- Ni_4Mo, stoichiometric and quenched, short range order and order-disorder transform. 79–78955
- NiO, lattice parameters, microstrains, non-stoichiometry, comparison between mosaic microcrysts. and quasi-perfect single microcrysts. 80–24414
- NiPt, quenched, ordering kinetics and domain struct. form. during isothermal tempering *(Russian)* 80–66502
- Ni_3S_2, initial growth on Ni single crystal, electron microscope obs. *(Japanese)* 77–52670
- Ni_7S_6, alternative transform, behaviour, direct obs. by TEM 77–1227
- $Ni_{3\pm x}Te_2$, long period superstruct., electron microscopy 79–86761
- NiTi, reversible martensitic transformations 78–27516
- NiTi, stacking faults prod. by martensite transition, lattice imaging electron microscopy obs. 79–96026
- NiTiCu, shape memory alloys, electron microscope and X-ray diffr. study of struct. 79–82179
- Ni_3V, dissociation of $^1/_2\langle112\rangle$ perfect dislocations and nature of slip dislocations 78–43022
- Ni_3V, ordered, domain size effect on mech. props. 79–79027
- Ni_3V, stacking faults, twinning deform., electron microscopy obs. 78–6070
- P, amorphous, struct. by electron microscopy 80–84065
- Pb foil, type I supercond., crit. current density, pinning force density, shadow electron microscopy obs. 80–88696
- Pb, melting, changes in electron image contrast 80–100147
- Pb, splat quench in vacuum 79–52268
- Pb, splat-cooled and vapour-deposited, metastable structs. 79–87018
- Pb, superconducting film, intermediate state, shadow electron microscopy 79–11276
- $Pb_3Ge_2O_7$, dielectric thin film, obtained by sedimentation, exam. of dielectric props. and structure 80–2282
- $Pb_{1-x}Hg_xS$ epitaxial films, electroless deposition and struct. props. 79–90915
- $PbMg_{1/3}Nb_{2/3}O_3$, short-range ordering, electron microscope and diffr. study 80–10469
- PbO formed on (111) surrace of Pb, electron microscope anal. 78–23878
- PbO-B_2O_3-Bi_2O_3, glass with metallic Bi granules, elec. cond. 80–84493
- PbO-B_2O_3-SiO_2, glass enamel, heat treated, exam. of microstructure and chemical durability 79–29254
- $Pb_3(PO_4)_2$, ferroelastic phase, structure domains, electron microscope obs. 79–42078
- PbS, colloidal, light scatt. and electron microscopy 78–3379
- PbS epitaxial film, struct., optical and elec. props. 78–19583
- PbS, epitaxial layer, structural nonuniformities and dislocation struct. 79–23852
- PbS epitaxial layers, ion bombardment effects on struct., and annealing 79–10882
- PbS, film condensation on amorphous substrate, struct. and growth 78–38981
- PbS islands, vacuum deposited, electron microscope obs. 80–103601
- PbS, oxidation, $PbSO_4$ distrib. in products *(Polish)* 80–25883
- PbS, vap. deposited film, island growth obs. by optical diffr. from electron micrograph 78–10291
- PbSe, epitaxial growth, cluster mobilities, in-situ electron microscopes obs. 80–15407
- PbSe-PbS(Te) and PbS-PbTe epitaxial layers, electron microscope contrast of misfit dislocations 77–85113
- $Pb_{1+x}Sn_xTe$, epitaxial growth on $LiNbO_3$, electron diffr. and microscopy exam. 77–1331
- $Pb_{1-x}Sn_xTe$ single crystals, selection using travelling solvent method *(German)* 80–2936
- PbTe film, struct. anal. and sensitisation 78–22982
- PbTe, VPE, on $LiNbO_3$, struct. and morphology obs. 80–54561
- $Pb_3(VO_4)_2$, ferroelastic, phase transitions, boundary walls 80–107419
- $Pb(Zr,Ti)O_3$-$Pb_3Ge_5O_{11}$ ceramic, sintering conditions rel. to piezoelec., dielec. props., microstruct. 77–16252
- Pd, (111) surface electron microscopy 80–103556
- Pd, catalyst hollow cone dark field microscopy on γ-alumina substrates 78–61049

electron microscope examination of materials continued
- Pd crystallite morphology, surface struct., electron microscopy obs. 80–29257
- Pd particle array, on amorphous SIO_2 substrate, model catalyst, electron microscopy and UPS expts. 79–4899
- Pd particles formed by evaporation on alkali halide crystals, orientation and struct. 78–84108
- Pd-H alloys, in situ electron microscope obs. of precipitation 79–61589
- Pd-Si amorphous alloy, neutron irradiation effects *(Japanese)* 77–84806
- Pd-Si metallic glass, high-resolution electron microscopy 80–84097
- Pd_3Fe foil, $L1_2$ superstructure, antiphase boundary orientation and energy 80–39112
- Pd_3Fe, X-ray and electron microscope obs. of antiphase domains and superdislocations *(Russian)* 77–86017
- $Pd_{60}Ni_{20}Si_{20}$, amorphous, struct., high resolution electron microscopy 80–1969
- $Pr_{24}O_{44}$, beta phase, high resolution cryst. struct. images 78–42991
- Pr_7O_{12}, n-beam struct. images, expt. observations and computer calc. 78–38593
- Pt, adsorption of H, face specificity, field emission probe-hole microscope obs. 77–11783
- Pt complex, $[2, 2', 2''$-terpyridine $PtCl]^+$, motion of Pt atoms, electron microscopy obs. 80–103314
- Pt crystallite morphology, surface struct., electron microscopy obs. 80–29257
- Pt, electrochemical adsorpt. of H_2, adsorpt. states, tensiodynamic meas. 77–20196
- Pt intercalation compound, electron microscopy 80–84164
- Pt small particles, on graphite substrate, crystallographic struct., electron microscopy study 79–99465
- Pt small particles deposited on NaCl and mica substrates, struct. and orientation *(French)* 77–43458
- Pt-Co, magnetically hard, struct. and morphology, electron microscope study 79–82171
- Rb_2O-Nb_2O_5 mixed oxides, cryst. struct., electron microscopy study 78–91309
- Rb_2O-Nb_2O_5 mixed oxides, cryst. struct., electron microscopy study 78–91310
- Rb_2O-Ta_2O_5 mixed oxides, cryst. struct., electron microscopy study 78–91310
- Re vicinal faces, adsorption of O_2, mirror electron microscopy, LEED and AES obs. 79–65323
- RuO_x, catalyst at anode of solid polymer electrolyte cell, corrosion 79–20376
- Sb, cleavage faces, evaporation pattern determ. by decoration method in electron microscopy *(German)* 80–107626
- Sb, dislocations, contrast simulation *(French)* 79–60374
- Sb, epitaxial growth on Bi substrate 78–95246
- Sb, film, microrelief, electron microscope obs., grain size and condensation rate 77–55469
- Sb, film growth mechanism, action of residual gases rel. to deposition conditions 79–23850
- Sb, splat-cooled and vapour-deposited, metastable structs. 79–87018
- Sb, thin film, electron microscopy identification criteria of dislocations *(French)* 77–76411
- Sb, thin layer, amorphous to crystalline phase transition *(German)* 77–69196
- Sb_2S_3, film, defect struct., electron microscope mode 79–28224
- Sb_2S_3, lattice resoln. anal., of coincident-site boundaries of electron microscope images 80–33861
- Sb_2S_3, vacuum deposited films, struct. and photoelec. props. 77–85092
- Sb_2Te_3, cleavage faces, evaporation pattern determ. by decoration method in electron microscopy *(German)* 80–107626
- Se, amorphous, vac. deposition on polymer substrates, use of temp. gradient vac. coating device 80–35099
- Se, amorphous evaporated layers, struct. inhomogeneities due to prep. technology fluctuations 77–76710
- Se electrophotographic films, ageing effects on structure and properties 77–47699
- Se film, amorphous, block formation during crystn., electron microscope obs. 79–11030
- Se, undeformed rhombohedral, dislocations, electron microscope obs. *(French)* 78–51548
- $(Se)_x$, crystn. and melting 80–40241
- Si, (110) oriented, electron optical conditions for struct. image form. 80–75131
- Si, amorphous, hydrogenated film, struct. determ. using electron microscopy 80–10806
- Si, chemisorption of H_2, magnetic-sector atom-probe field ion microscopy exam. of hydride form. 77–80699
- Si cryst., images of atoms projected onto (110) plane using high resolution techniques 79–32866
- Si, crystal structure images of diamond structure 78–14256
- Si crysts., dynamic processes associated with stacking faults and deform. twins, HVEM in-situ obs. 80–103369
- Si crysts., in-situ HVEM obs. of dislocation processes during high temp. deform. 80–103342
- Si, deformed crystal, faulted dipoles 78–59814
- Si, dislocation mobility 77–76413
- Si, electron beam irrad., {113} faults, nature and origin 80–70258
- Si, electron irrad., rod-shaped defects, electron microscopy and IR spectra obs. 80–39159
- Si, electron-irradiated, {113} loops obs. 79–82225
- Si epitaxial layer, minority carrier lifetime obs. *(Russian)* 80–49765
- Si, extended glide dislocations, motion obs. by high voltage electron microscopy 80–10555
- Si film, amorphous, high resolution electron microscopy, digital processing use 78–37116
- Si film, amorphous, structural comparison of evaporated and glow discharge samples 77–62778
- Si film, deposited on quartz and MgO substrates, by double cathode sputtering system *(Japanese)* 77–55889
- Si film, on graphite, early growth by ion-beam sputtering 77–44158
- Si film, polycryst., electron microscopic investigation of initial stage of growth 79–23849
- Si film, polycryst., substruct. 79–23848
- Si, forbidden 200 diffr. spots 78–47214
- Si, HVEM struct. images of extended 60° and screw dislocations 80–59466

electron microscope examination of materials continued
Si, heavily damaged ion implanted (100) and (111), development of secondary defects 79—51166
Si, ion implantation of noble gases, high fluence retention 79—23627
Si, ion implanted, laser annealing, periodic regrowth phenomena 78—67724
Si, ion implanted, voids, electron microscopy 78—67757
Si, ion-implanted, secondary defects development, three-stage model 78—87725
Si, ion-implanted amorphous, laser epitaxial recrystallisation threshold energy 80—70571
Si, laser annealing of SiO_2 layers 80—97505
Si, MBE growth for semiconductor devices 79—83141
Si, prismatic dislocation loops, (g.b)s product sign determ. *(Russian)* 78—38705
Si, radiation induced defects in high-voltage electron microscope 80—65048
Si, solid-phase-epitaxial, deposited above 380°C, defects obs. 78—63942
Si, thermal oxidation, mechanism of appearance of surface roughness and surface defects 77—7956
Si thin autoepitaxial layers low temp. growth mechanism in $SiCl_4$-H_2 system 80—20795
Si thin crystal, electron backscatt. in electron microscope 78—75510
Si wafer, thin surface layers, amorphous to cryst. transform., obs. technique 80—107288
Si:Au(P)(B) whiskers, impurity inhomogeneity 80—39145
Si:O, annealed, precipitates, dislocation and stacking fault loops, TEM characterisation 77—4111
Si:P, depth of melting produced by pulsed-laser irrad. 79—55756
n-Si:P, secondary defects produced by high-temp. electron irrad. 79—33017
$Si:P^+$, misfit dislocation formation mechanism, effect of implantation temp. 78—38708
Si-Al-O-N polytypes, direct lattice resolution using high resolution electron microscopy 78—38682
Si-Ge heteroepitaxial system, imperfections and morphology, electron microscope and electron diffr. obs. 79—42420
Si-SiO_2 interface, high-resolution electron microscopy study 78—56046
Si-SiO_2 layer formation by O_2^+ ion implantation, interface struct. and C-V characts. 77—1142
Si-SiO_2-Mg-Cu powder compact, nitridation to form Si_2ON_2 whiskers *(Japanese)* 80—93674
Si_5-Al-O-N_7, hot pressed, exam. of fracture mechanisms 78—72879
SiC, 126R polytype, struct. determ., use of lattice imaging in electron microscope 78—26498
SiC coatings for first-wall candidate materials by RF sputtering 80—25563
SiC, electron microscopical fractography *(Russian)* 77—25146
SiC polytypes, lattice imaging studies on intergrowth structs. 80—107025
SiC polytypes, stacking sequences by high resolution electron microscopy 80—15054
SiC, reaction sintered, microstruct. *(Japanese)* 77—1825
SiC, reaction sintered transform. interface morphology 78—31364
SiC, sintered, high resolution electron microscopy 79—90501
β-SiC, twinned crystals, fracture characts. 80—3193
β-SiC whisker, failure and defects 79—96145
SiC-B eutectic alloys, struct. of crystallising graphite 79—38829
SiC-B_4C (B+1 wt.% C), sintering 77—36432
Si_3N_4, α to β transform., TEM and electron diffr. obs. 78—27507
Si_3N_4, films, ion-beam synthesis, IR spectra, struct., crystallisation on annealing 77—16705
Si_3N_4, hot press, high resolution electron microscopy 79—90501
Si_3N_4, MgO-fluxed, hot pressed, grain boundary phases 78—27464
Si_3N_4, reaction-bonded, struct., form. mechanisms and kinetics 77—4760
Si_3N_4, struct. of slow crack interface, light and electron microscope obs. 78—68770
Si_3N_4, thin intergranular phase, imaging by high-resolution electron microscopy 79—90895
Si_3N_4:C film struct., oxidation, defects 79—51455
$Si_3N_4.Y_2O_3$ prepared by hot press, cryst. struct. 80—10534
SiO_2, condensed sol, electron microscopy and diffraction studies 77—29049
SiO_2, crystobalite form. in evacuated silica ampoules, cryst.-amorphous transform. 77—68933
SiO_2 gel, steam treatment, struct. changes 80—35579
SiO_2 glass, electron microscopic determ. of struct. 79—90561
SiO_2-based glass, with thin surface metal film surface struct. and topography 77—1285
SiO_2-CaO-ZnO-B_2O_3-Na_2O-S, SrO effect on crystallisation 80—54135
SiO_2-Li_2O-K_2O-ZnO glass ceramic, prep., phase transformations and physical props. 80—45299
SiO_2-Na_2CO_3, sodium Erevanit-25, sintering, struct. 79—43284
SiO_2-TiO_2-Al_2O_3-SrO(BaO), glasses, ceramic form. rel. to Al_2O_3 content 77—25005
SiO_x ultrathin oxide on Si, struct. obs. by high-resolution electron microscopy 80—103592
$SiTe_2$, dislocations and stacking fault energy 78—47378
$Sm(Co,Cu)_z$, precip.-hardened, mag. and metallographic props. 77—8339
$SmCo_5$ based alloys, dissociation process *(Russian)* 78—27542
$SmCo_5$, mag. domain structure rel. to crystal defects 80—103856
$SmCo_5$ sintered magnets, periodic struct. and coercive force *(Russian)* 79—28554
$SmCo_5$ sintered magnets, eutectoid decomp. 80—89219
SmO film, new reduced variant due to annealing 77—89660
$Sm_{0.5}Pr_{0.5}Co_5$ sintered magnets, periodic struct. and coercive force *(Russian)* 79—28554
Sn, extremely fine crysts., surface melting 77—62622
Sn film, melting and crystallisation kinetics, electron microscopy 77—15725
Sn, film, vac. deposited, influence of ion bombardment during condensation 79—82483
Sn island film, melting and crystn. kinetics, dark field electron microscopy 79—11026
Sn-O system, amorphous, characterisation by appl. of Mossbauer effect 79—61283
SnO_2:Sb, and pure cryst., microstruct., X-ray diffr., optical and electron microscope studies 78—79619
SnO_2:Sb, transparent cond. film prep. by thermal decomp. of Sn salt of organic acid *(Japanese)* 77—90269
SnTe-PbSe mixed system layers, struct. and props. *(Russian)* 77—28082

electron microscope examination of materials continued
SnTe-Sn epitaxial system, electron microscope contrast of misfit dislocations 77—85113
Sr film, structure effects on work function, electron micrographs and photoemission meas. 79—83107
Sr-Ti-O system, perovskite oxides, nonstoichiometry rel. to dielectric const. 77—80628
$SrFe_{12}O_{19}$, microstruct. and magnetic props., electron microscope obs. 79—87290
$Sr_2Nb_2O_7$, normal-incommensurate phase transition, electron microscopy and diffraction study 80—39277
$SrSO_4$, surface crystn., on $BaSO_4$, isotope exchange and electron microscopy study 80—34332
$Sr_2Ta_2O_7$, structural phase transition to superlattice, electron microscopy and diffraction study 80—39277
$SrTiO_3$, ferroelectric, polarisation reversal, electric field induced phase transform. 80—103925
steel, 36NKhTYu, aged, rate of discontinuous precipitation of γ'-phase, short high-temp. treatments *(Russian)* 78—11226
steel, C, eutectic, YU8, effect of segregating structurally free ferrite *(Russian)* 79—15677
Ta, adsorption of K, work function, field emission microscope obs. 77—11788
Ta, electron irradiated, energy and orientation depend. of at. displacement 79—99244
Ta epitaxial layers, formation conditions influence on struct. *(Russian)* 80—20045
Ta, neutron irradiated, microstruct. and swelling 77—69006
Ta-H(D), H ordering, review 80—60850
β-Ta_2H, ordered alloy, electron microscope study of lattice distortions 77—11507
Ta_2O_5, ion-bombarded cryst., structural and compositional changes 79—46724
TaS_2, intercalation compounds, octahedral, microstructural study 77—84729
TaS_2, polytypes, charge density waves and superlattice effects, intercalation with hydrazine 78—39043
Tb, mag. domains, Lorentz microscopy obs. 78—84448
Tb-Fe amorphous magnetic films, domain wall obs. by Lorentz electron microscopy 77—80979
$TbAl_3$, polytypism occurrence 80—44164
Te, c-slip, asymmetry and orientation depend. 77—27888
Te film, evaporated, crystallinity and electronic props., annealing effect 77—85107
Te/Ag double films, interdiffusion and struct. modifications *(French)* 77—62682
TeO_2-GeO_2 system, phase diagram, X-ray phase analysis, DTA and electron microscopy 77—15545
TeO_2-MoO_3-V_2C_5, phase comp. determ. using X-ray diffr., electron microscopy and DTA *(German)* 80—88046
TeO_2-P_2O_5, electron microscope exam. of phase equilib. and immiscibility 78—52779
Ti alloys, grinding, effect on surface struct. 80—25878
Ti anodic film, growth kinetics, determ. *(French)* 78—76788
α-Ti, crack growth under tensile loading, in-situ obs. *(Chinese)* 79—96121
Ti, degree of charging of surfaces polished by TiC and synthetic diamond micropowders 78—60880
α-Ti, electron fractography 77—63778
Ti, electron microscope specimen prep. technique for dynamic straining expt. 78—88602
Ti, fatigue cracking, initial stage under bending and torsion *(Japanese)* 79—20165
Ti, fatigue fracture surface microstruct., electron microscope obs. 78—60834
Ti, industrial grade structural changes during polygonization *(Russian)* 78—19779
Ti, oxide film form. during thermal treatment, morphological and struct. study *(French)* 80—50766
α-Ti, plastically deformed by rolling, optical and electron microscope obs. 79—91666
α-Ti, primary recrystallization study by three dimensional anal. of textures and annealing, HVEM obs. 79—91677
Ti thin sheet, texture and mechanism of primary recrystallisation 78—23721
Ti-Al, elec. spark Al doping of VT-18, surface struct. and props. *(Russian)* 80—76398
Ti-Al, structural and phase changes due to annealing *(Russian)* 80—55440
Ti-Al-Cr-Mo-V alloy VT-22, effect of heating rate on phase recrystallisation *(Russian)* 79—34077
Ti-Al-Mo, type BT22, phase transformations under step-by-step heat treatment *(Russian)* 80—108436
Ti-Al-Mo-Sn-Si (2.25, 4, 11, 0.25 wt.%), type IMI 680, internal friction study of martensitic transformations 80—7573
Ti-Al-Mo-Sn-Si (2.25, 4, 11, 0.25 wt.%), type IMI 680, stability of martensitic phases 80—7574
Ti-Al-Mo-Sn-Si (4, 4, 4, 1/2 wt.%), type IMI 551, internal friction study of martensitic transformations 80—7573
Ti-Al-Mo-Sn-Si (4, 4, 4, 1/2 wt.%), type IMI 551, stability of martensitic phases 80—7574
Ti-Al-Mo-Sn-Si (4,4,2,0.5 wt.%), fracture toughness and crack propagation 78—39892
Ti-Al-Sn (5, 2.5 wt.%), electron microscope and X-ray diffr. exam., of basal and near basal hydrides 78—80550
Ti-Al-V (6, 4 wt.%), type IMI 318, internal friction study of martensitic transformations 80—7573
Ti-Al-V (6, 4 wt.%), type IMI 318, stability of martensitic phases 80—7574
α-Ti-Al-Zr (6.16, 5.23 wt.%), alloy IMI 685, electron microscope observations of strain induced hydrides 78—72828
Ti-Al-Zr-Mo-Si (6,5,0.5,0.25 wt.%) fracture toughness and crack propag. 78—39892
Ti-Cr (15 at.%), aged omega phase, electron microscope exam. 78—72783
Ti-Mo, structure associated with BCC to omega transform. *(Russian)* 80—108432
Ti-Mo-Fe (3, 0.13 at.%), metastable phases, Mossbauer study 80—7243
Ti-Mo-V (8 wt.%, 8 wt.%), FCC phase, decay of β-solid soln., electron microdiffr. 79—15670

electron microscope examination of materials continued
Ti-Mo-Zr-Sn-Fe-C-Si alloy, β-III, cold deform. and annealing, effect on struct. and mech. props. *(Russian)* 79−24533
β-Ti-Mo-Zr-Sn(11.5, 6, 4.5 wt.%), metastable phase III, microstruct. and age hardening response 80−84945
Ti-Mo(Nb)(Ta), BCC struct., tetragonal phase form. by cold deform. *(Russian)* 78−88462
Ti-Nb superconducting composite in Cu matrix low temp. fracture exam. 79−57119
Ti-Nb-Al, decomposition during isothermal annealing 80−25653
Ti-Nb-Mo(V)(Ta)(Al)(Zr), BCC struct., tetragonal phase form. by cold deform. *(Russian)* 78−88462
Ti-Si amorphous alloy, melt-quenched, transform. studies and mech. props. 80−100838
Ti-V-Si, Si effects on precipitation and strengthening 77−55970
TiB_2, crystal growth by chem. vapour transport 80−16164
TiC, electron irrad. damage, electron microsc. study 80−84210
TiC single crystal, deformation behaviour, operative slip systems 79−100211
TiC single crystal, vapour deposited on Mo and W wires, electron microscope study 77−1795
TiC-Ni-Mo sintered hard alloy TN-20, fracture surfaces 80−7684
TiC_x, fused material, microstruct. 78−44115
$TiC_{1-x}N_x$ formation in high temp. N flow, ultra disperse powder, thermodynamic anal. *(Russian)* 80−55325
TiC_xN_y, fused material, microstruct. 78−44115
TiN, gaseous phase, crystallisation, effect of temp., vapour-gas mixture conc., and deposition time 79−33910
TiN_x, cryst. and internal structs., electron diffr. and microscopy 77−27861
Ti_3N_4 plasma condensation on steel and carbide *(Russian)* 80−20796
$Ti_{50}Ni_{47}Fe_3$, premartensitic phases, neutron scatt., sp. ht. and electron microscopy obs. 79−96025
$TiO_{0.3-0.5}$, O atom ordering, electron microscopy obs. 79−99150
TiO_2, anodically formed layers, film instability obs. 78−72916
TiO_2, sintering, hardness, density, elec. cond. and colour *(Japanese)* 78−68659
TiO_2:Mg, high-resolution reflex images of crystal defects 78−6073
TiO_2-Ga_2O_3, crystallographic shear planes and defect pair splitting, electron microscopy 77−76425
TiO_2-Ga_2O_3 system, phase relations and microstructs. 78−3107
TiO_2-P_2O_5 reduced glasses, prep., elec. transport, chem. anal., DC, AC cond., seebeck coeff. 78−30924
TiO_2-Ti_2O_3-P_2O_5, glass form., struct. and elec. props. 80−44592
TiO_2-ZrO_2, submicron powders, vapour phase production from $TiCl_4$-$ZrCl_4$-O_2 system 80−40301
TiO_x evaporated films, epitaxial growth on NaCl, electron microscopy obs. 80−10822
TiO_x film, growth and struct. determ. 78−48328
Ti_6O_{11}, electron-optical imaging, at 1.6 Å point-to-point resolution 79−46531
Tm_2O_3 film, electron beam deposition, elec. props., and struct. 79−87580
U core fuel elements, of A-1 reactor, volume growth *(Czech)* 80−27745
UO_2, commercial fuel pin, irradiation induced volume changes, comparison with model 78−78465
UO_2 epitaxial films, epitaxial, channelling studies 79−49683
UO_2 fracture strength meas. of sintered specimens by diametral compression testing, effect of temp. and deformation rate 79−79074
UO_2, neutron and electron irradiated, imperfect dislocation loops *(French)* 79−7606
UO_{2+x}, sintering mechanism 77−21071
U_3Si for heavy-water-cooled reactor, arc melting and hydrogenation methods comparison *(Chinese)* 79−85721
V,V-Zr (2 wt.%), internally oxidised, neutron irradiated, annealing effect on mech. props., elec. cond. and electron microscope obs. *(Japanese)* 79−15701
V, annealing after irradiation with 210 keV He at 625°C at high fluences 78−67751
V, different grain sizes, room temp. microstrain *(German)* 77−36614
V, film, vac. deposited, influence of ion bombardment during condensation 79−82483
V foil, air-oxidised, reversible switching, mechanism determ. 79−28387
V, polycryst., struct. changes during deform. *(Russian)* 78−48447
V, structural changes in single crystal under single electric impulse discharge *(Russian)* 79−65086
V-H(D), hydrogen ordering, review 80−60850
V-Mn, equiatomic, ordering kinetics and antiphase domain coarsening 80−7559
V-O alloys, quenched, local ordering of O, electron microscopy and diffr. 80−59453
V-Ti-C, high temp. carbide form., electron microscopy study 80−89228
V_4As_3, defect struct. 77−4112
$(V_{1-x}Cr_x)_2O_3$, vapour phase transport, single cryst. growth *(French)* 77−24940
V_2MoO_8, planar defects, electron microscopy and electron diffraction meas. 77−15430
VN_{1-x}, vacancy ordered structure in cubic mononitride phase, transition entropy determ. 78−43011
$(V_{1-x}Nb_x)_2C$, modulated structs., periodic antiphase domains 79−94969
VO_2, reduced, microstruct., crystallographic shear planes, electron microscope obs. 79−1443
V_2O_3, crystallographic structure changes due to phase transition, electron microscope study *(French)* 79−7688
V_2O_3, low temp. crystallographic struct. domains 78−83765
V_2O_3, vapour phase transport, single cryst. growth *(French)* 77−24940
V_2O_4, struct. from electron microscopy of Tyep F-2 fibre 78−2087
V_2O_5 amorphous films, CVD prep., structural characts. 80−49114
V_2O_5 and lower oxides, defect structures and related props. 80−59454
V_2O_5-Fe_2O_3-LiO_2 system, physical properties 78−84503
W (100), laser induced desorption, mirror electron microscopy 78−84067
W, adsorption of CO, adsorption state at 300 to 80K *(Japanese)* 77−85057
W, anode, dendritic growths during prebreakdown conditions in organic residual gas, electron microscope obs. 78−44383
W, doped wire, secondary recrystallisation temp., bubble parameter effects 77−32596
W, electron channelling in (111) direction, 200 to 1000 keV 78−2182
W, fine tip microcrystal, microscopic protuberance form., crit. remoulding obs. 78−27380

electron microscope examination of materials continued
W, fine tip microcrystal, thermal smoothing after critical remoulding 78−27381
W, fine tip microcrystal, vertex remoulding, effects on field emission 78−27379
W, LEED and electron microscopic investigs., review *(Hungarian)* 77−47654
W, signal-to-noise enhancement by superposition of bright-field images obtained under different illumination tilts 80−6329
W, thermal field cathode emitters, end form changes, electron microscope obs. 77−4718
W, whisker fabrication, AC and DC electrochem. etching 78−43278
W wire, cold drawn, dislocation processes occurring during tensile testing *(Hungarian)* 77−48450
WC-Co, rupture of bending specimens, use of quantitative metallography and stereology *(French)* 77−28899
WC-Co powder, prep. by direct carburisation of WO_3 in presence of Co_3O_4 80−50573
WO_3 film, amorphous, struct. and crystallisation, high resolution electron microscopy 78−43268
WO_3, hexagonal form, struct. study, X-ray powder diffr., electron diffr., and electron microscopy meas. 79−99157
WO_3, reduction, defect role, in situ HVEM obs. 80−81323
WO_3 reduction in hydrogen, electron microscopic obs. of solid phases formed *(Hungarian)* 77−48635
Y-H film, rel. to temp., thickness and comp. depend. of elec. resist. 79−78221
YAG, high-resolution many beam lattice image anal. 80−14979
YAG, interrelationship between mech. props. and elec. relief on surface layer 79−23821
YAG, simulated mol. images, point models and kinematical struct. amplitudes 80−103223
$Y_3Al_5O_{12}$, laser cryst., struct. inhomogeneity obs. by vac. decoration 77−35701
$Y_3Al_5O_{12}$, layer structuresrevealed by decoration method and electron microscopy 77−27902
Y_2O_3, dislocation and plasticity dissociation 80−107247
Y_2O_3, electron irrad., dislocations *(French)* 80−2076
Y_2O_3, plastically deformed monocryst., HV electron microscopy obs. of dislocation config. *(French)* 79−55747
Y_2O_3 sintered body, luminous pipe of high press. Na discharge lamp, corrosion resistivity *(Japanese)* 78−19915
Y_2O_3-Nb_2O_5, solid state reactions, 1275 to 1350°C, electron microscopy, EPMA, X-ray diffr., dilometry *(Japanese)* 78−63883
$Y_2Ti_2O_7$, precipitation from oxalates, carbonates, exam. 80−55641
Zn, coating on steel strip, plastic deform. 77−90368
Zn, electron radiation damage in HVEM, nature of defect clusters 78−59838
Zn, single crystal, crack growth in contact with liq. Hg and Ga 79−87757
Zn-Al (0.4 wt.%), intergranular slip during in situ superplastic deform. 80−96538
Zn-Al (1.1 wt.%) superplastic alloy, grain size determ. *(Czech)* 80−81118
Zn-Al (22 wt.%), superplastic deform. mechanism, electron microscope obs. 78−3167
Zn-Al eutectoid, superplasticity, study by electron microscopy 77−48479
ZnO, dislocation loop nucleation on prismatic faults in high voltage electron microscope 77−72620
ZnO, electron irrad. damage, orientation depend. 80−2075
ZnO-Al_2O_3-SiO_2 glass, crystalline phase precipitation, crystallisation *(Japanese)* 79−32916
ZnO-Bi_2O_3-Sb_2O_3-Co_2O_3-MnO_2-Cr_2O_3, nonohmic ceramic, microstruct. exam. 78−47292
ZnS, crystal, layered struct. microscopic observations *(Japanese)* 78−38725
ZnS film, struct. electron microscopy 77−59226
ZnS, film, vac. sputtering deposition by CW CO_2 laser beam *(Russian)* 77−21024
ZnS:Mn on SnO_2/glass transparent conductive base, surface morphology effects on electroluminesc. *(Russian)* 78−48238
ZnS-Na_3AlF_6 multilayer dielectric optical filter, irreversible thermal effect 77−7195
ZnS(Se)(Te) film, on semicond. substrates, early stages of growth, electron microscope obs. *(Russian)* 78−38976
ZnTe, epitaxial film growth initial stages 77−80707
ZnTe film, prepared by single-source vacuum deposition method *(Japanese)* 80−6664
ZnTe:Cu, precipitates, electron microscopic investigation 80−45312
ZnTe:Cu, voltage depend. on precip. contrast 79−1433
Zr, creep, optical and electron metallographic anal., 473 to 873K 78−39986
Zr, deformed at 77K, effect of fast-neutron irradiation on deformation twinning, TEM and optical microscopy obs. 79−37741
Zr, dissolution of γ-ZrH, in situ study, HVEM obs. 78−55951
Zr, foil, dislocation loop nucleation and growth during 1 MeV electron irrad. 80−88152
Zr, microstructure exam. by electron microscopy, oxide film appl. 79−70243
Zr, void swelling during electron irrad., HVEM study 80−92559
Zr-H alloy, precip. of γ-ZrH, shear mechanism 80−104170
Zr-Nb (0.1, 2.5 wt.%), foil, dislocation loop nucleation and growth during 1 MeV electron irrad. 80−88152
Zr-Nb (2.5 wt.%), effect of irradiation on stability of precipitates 77−69007
Zr-Nb (2.5 wt.%) alloys, microstruct investigation by electron microscopy using oxide films 79−70243
Zr-Nb solid solutions, BCC, direct imaging of linear defect using diffuse scatt. 78−22726
Zr-Nb-V-Al (Fe) alloys, decomp. of β solid soln., metastable and equilib. phases 79−11632
Zr-Nb-V-Fe (12 wt.%, 6 wt.%, 4 wt.%), struct. changer during decay of BCC β solid soln. 79−15669
ZrB_2, oxidation in O_2 atmosphere, exam. 80−11814
γ-ZrH, precipitation in Zr, exam. of precipitation mechanism due to shears, electron microscope exam. 78−84809
ZrO_2, hydrous, prep. from $ZrOCl_2$ soln. and cryst. texture determ. *(Japanese)* 77−89398
ZrO_2, hydrous particles, crystal texture *(Japanese)* 77−25002
ZrO_2, neutron irrad., monoclinic to cubic transform. 78−87720
ZrO_2, partially stabilised, toughening mechanism 77−56084

electron microscope examination of materials continued
α-ZrO_2, structure factor determ. using crit. voltage effect, comments 77—1102
ZrO_2-Al_2O_3-SiO_2, subsolidus equilibria and stabilization of tetragonal ZrO_2 78—27497
ZrO_2-CaO, microstruct., ordering, elec. props. 77—15374
ZrO_2-CaO, stabilised microspheres, structure, mechanical props. *(Russian)* 80—100379
ZrO_2-CaO(MgO)($YO_{1.5}$), partially stabilised, growth morphology of tetragonal phase 79—4968
ZrO_2-Y_2O_3, stabilised microspheres, structure, mechanical props. *(Russian)* 80—100379
$Zr_3Sc_4O_{12}$, n-beam struct. images, expt. observations and computer calc. 78—38593
Zr_xWO_3, perovskite-type, stability in ZO_2-WO_2-WO_3 phase diagram 77—15582

electron microscopes
see also electron microscopy; field emission electron microscopes; scanning electron microscopes; scanning-transmission electron microscopes; transmission electron microscopes
200 kV, type H-700, by Hitachi, Japan 77—53877
200 kV electron microscope with resolution limit less than 0.25 nm 80—101881
600-kV electron microscope, atomic resolution 79—97475
achromator using three elec.-mag. quadrupoles *(German)* 77—61166
AEI 801, binocular mount of improved design, specimen rod-holder 77—87881
air-lock system for reactive sample transfer to Philips 300S electron microscope 78—41382
analytical, for electron energy loss anal. 80—86521
analytical electron microscopy, book 79—97479
ANL HVEM-TANDEM accelerator facilities 80—101896
aperture stops, production using vac. deposited metallic film 79—85202
applications in biological and materials science fields 80—53198
beam energy broadening, Boersch effect 77—61164
calibrating using grating replica 79—2893
calibration by photogrammetric technique 78—336
Cambridge University 600 kV high resolution, engineering performance 80—82849
camera, electromech. arresting mechanism 77—74560
chromatic field aberration compensation with additional imaging lens *(German)* 77—10149
chromatically corrected objective lens, of electron microscope, test *(German)* 79—892
coherence in bright field microscopy of weak objects 78—32955
column of EM-300 electron microscope, power supply system 79—12888
components, RF sputtering apparatus for cleaning 77—54022
conference, Glasgow, Scotland (Sept. 1977) 78—32934
conference, Tashkent, USSR (Oct. 1976) 79—6219
conference, Toronto, Canada (Aug. 1978) 80—82579
construction, operation and special types, review 80—86529
contamination by surface diffusion of adsorbed hydrocarbon mols., theory 80—99013
contamination due to surface diffusion of hydrocarbons and elimination method 80—73545
contrast transfer for tilted and conical bright field illumination 78—37115
cooling stage, high-resolution double-tilt, for 1.2 MV HVEM 80—68322
cryostat for 400 kV superconducting electron microscope *(French)* 77—192
curved axis electron optics of 3-dimens. imaging microscope *(German)* 79—13889
data acquisition technique, minicomputer, method and experimental detail *(French)* 77—34056
diffraction patterns, direct phase determ. *(German)* 77—2713
digital scanning and recording system for spot electron diffr. patterns 77—13825
electric power supply for an electron-optical corrector *(German)* 80—42308
electron image processing, and improvement 78—24890
electrostatic decelerator, resolution *(German)* 79—49346
electrostatic decelerator *(German)* 79—30620
electrostatic lens *(German)* 79—49339
electrostatic lens design 79—35894
energy filter, correction of second order aberrations *(German)* 77—22624
energy filter, for HV microscopy 77—79198
environmental cell for 3MV-class microscope, and its appl. to metallurgical problems 77—10141
exoelectron microscope, appl. to study of damaged metal surface *(Japanese)* 78—74108
field solution convergence in nonlinear environment by network method *(Czech)* 79—81350
foil lens characts. for spherical aberration correction of strongly excited magnetic lens 79—71567
goniometer, for use in high resolution objective lens pole-pieces 79—58844
goniometer, high resolution, for EM 10 electron microscope 77—74561
heating stage, double tilt design for structural anal. of metals 77—57430
high resolution, 600 kV electronic mechanical and electron-optical engineering design features 80—86518
high resolution, developments in imaging crystalline materials 80—99001
high resolution, EM 400, chromatic aberration effects compensation and thick specimen imaging 77—41738
high resolution, obs. at liq. He temps. 80—86517
high resolution 600 kV microscope, principles and performance 80—42309
high resolution JEOL 200CX, performance eval. and appls. 80—82850
high voltage, Si(Li) detector, electron counting, appl. to electron energy loss spectra *(French)* 78—54511
high voltage electron microscope, constructed for high resolution crystal struct. images obs. 78—89600
high voltage electron microscope and its characteristics *(Chinese)* 79—54236
high voltage with supercond. microwave lenses, development prospects w.r.t. mol. imaging 77—10147
high-voltage supplies, capacitive meas. of slow fluctuations 77—13826
historical development 80—68320
hot stage, usable up to 2000°C *(Japanese)* 78—12798
human factor considerations in design 77—13828

electron microscopes continued
HV, accurate stigmating using optical diffr. pattern of micrograph 78—49941
HV, design features of photographic film 78—8478
HV, EM-300, design characts. 79—6220
HV, high resolution image of $Nb_{12}O_{29}$ 77—15292
HV, objective lens aberrations *(Japanese)* 80—52364
HV, specimen chamber with side entry config. 78—32943
HV 3 MV type, mech. vibr. sources and effects *(French)* 80—82848
illumination system for 600 kV high resolution microscope with condensor-objective lens 77—38064
image convertors, for HVEM 80—104839
image formation, partial coherence and inelastic scatt. 78—46505
image formation, partial coherence and inelastic scatt. 78—58897
image formation in partially coherent illumination including inelastic scatt. 78—32956
image interpretation, instrumental, environmental conditions *(Polish)* 79—30623
imaging mechanism, 1 MV high-resolution microscope, crystal struct. anal. *(Japanese)* 78—74113
introduction to operating principles 79—35899
ion detection using cellulose nitrate 78—45755
ion implanter adaption on 100 kV electron microscope for in situ expts. 79—2888
lenses, superconducting, construction of cryostat for testing 77—22627
low temperature specimen stage and transfer system for JEOL JEM 100C 78—32945
magnetic condenser-objective lens, for high resolution microscope, optical characts. 78—25788
magnetic energy filter, for error-free image, second order approx. *(German)* 77—191
magnetic filter 1 MV, second order image abberations 77—61165
magnetic lens spherical aberration correction with foil lens 77—67537
magnetic shielding of corrected microscope *(German)* 78—24895
magnetic specimen stage, liq. He, investigation of ferromag. domains in $CrBr_3$ 80—103855
magnetic spectrometer, corrected second-order aberrations 80—87013
microprobe instrument evolution, SEM and STEM 78—70233
mirror electron microscope, microprocessor system 80—62798
modified specimen airlock for Siemens electron microscope EM-101 *(German)* 80—9076
new developments, instruments, image processing, review 77—41732
objective lens focus and spherical aberration meas. 77—54024
objective lens using solid-state props. of dielectrics 79—2886
optical diffractometer analogue 80—69494
with optical diffractometer for immediate image analysis 79—6225
optical model, design and use 80—86534
photoemissive, electrostatic retarding-field energy analyzer 79—12890
photographic system, external 80—101902
power supply instability, theory and expt. estimate 79—6230
raster electron microscope in secondary electron emission regime, interaction between probe and object material 79—93259
raster electron microscope test object 78—86393
raster type, improved sweep block for video monitoring device 78—8470
resolution power, influence on estimation of basic method spatial struct. parameters 79—52543
resolving power limitations 80—86528
sample holder, Be, EDS spectral contamination 80—101907
sensitivity of films used in high-voltage electron microscopy 80—22474
shadow type, stereo images form. 80—95195
Siemens Elmiskop 102, optimised energy dispersive X-ray microanalysis 80—4811
single-polepiece lenses, magnetised iron sphere model 78—32940
single-polepiece objective and projector lenses 80—68326
solid surface characterisation, combined SEM-XPS-micro AES methods 79—30625
specimen devices, for in-situ experiments 80—101910
specimen holders, Philips, in high-resolution stage, restoration of damage 78—62265
spiral distortion correction double-lens system 80—68327
stabilisers, Hg-Zn battery as reference voltage source 79—9262
stage design, electron microscope, and applications 80—37127
stroboscopic subnanosec. illumination for thin film magnetic reversal obs. 77—18138
superconducting lens system for 500 kV electron microscope 80—68321
superconducting lens system for radiation damage reduction 79—34718
surface originating contamination elimination, using low energy anticontamination electron gun 79—30622
thermionic emission sources, coherence props. 77—22622
UHV, const.-load tensile device and appls. to materials science 78—11462
ultrahigh temperature, functional features 77—45923
vacuum pump, high-performance oil-free design 80—99011
vacuum system backing pressure automatic regulation device 79—49241
video monitor with colour-coded CRT display 79—80729
water leak detector for water cooled electron microscope 78—21277
X-ray leakage from conventional and HV microscopes 77—38066
X-ray microanalysis facility, electron microscope 79—12887
LaB_6 cathodes, mounting methods and operating characts. 80—57437
LaB_6 cathodes, single crystal, of <100> and <110> orientations, brightness meas. from 1500 to 1950K 80—62808

electron microscopy
see also electron microscope applications; electron microscope examination of materials; electron microscopes; field emission electron microscopy; metallography; scanning electron microscopy; scanning-transmission electron microscopy; specimen preparation; transmission electron microscopy
aberration correction 80—86531
accurate fan-beam reconstruction 78—78931
amorphous materials, thin, dark field speckle patterns in high resolution electron microscopy 78—34402
analytical, book 79—97479
analytical, reduction of contamination *(Japanese)* 80—11978
analytical electron microscope optimization of X-ray microanalysis, instrum. problems 80—73540
analytical microscopy at 200 keV 80—73547
atom displacement radiation damage, in electron microscopes 80—103394
atom resolution, in mol. images 80—100226
atomic resolution, with 600-kV electron microscope 79—97475
atomic structure of cryst., direct obs. 77—43122

electron microscopy continued
Auger electron microscopy, instrumental capabilities 78—70227
Auger spectrometer, gridless cylindrical mirror analyser for electron energy meas. 79—71563
automatic investigation of electron microscope images 80—92425
autoradiograms of serial sections, preparation for electron microscopy 80—67312
autoradiographs, iterative anal., sample sizes and confidence limits 79—35896
autoradiographs, iterative anal. method 79—35895
autoradiography, direct deposition method, radioactivity detect. 78—77167
autoradiography of diffusible intracellular constituent using freeze-dried frozen sections of mammalian intestinal epithelium 79—84039
autoradiography of isolated mols. 80—85564
autotutorial methods utilizing sound-on-slide presentations 80—73534
baceteriophages, freeze drying method for electron microscopy 80—104826
beam scattering, in organic specimen, Monte Carlo simulation 80—100148
biological autoradiography, soln. of reverse problem 80—94419
biological macromolecule, high resolution struct. determ. by electron microscopy 80—89717
biological macromolecules, 3D struct., electron microscopical anal. 80—35836
biological material, electron microscope autoradiography and X-ray microanalysis of diffusable substances using ultrathin frozen sections 77—60314
biological objects, 3-dimens. image, computer simulation 77—13046
biological photoelectron microscopy of surfaces power requirements for high magnification 77—40963
biological research, electron microscopy, megavolt, advantages 77—70580
biological specimen replication at −150°C with improved freeze-fracture apparatus 80—85560
biological specimens, electron exposure-dependent contrast transfer 80—104837
biological specimens, parameters affecting bright field electron micrographs 77—73621
biological specimens, structure determination, electron microscopy, optical and digital anal. *(French)* 79—66594
biological structure electron micrograph processing computer programs 79—57835
biological tissue blocks, LKB Pyramitome and Target Marker modifications 77—60313
biological tissue embedding in low viscosity epoxy resin Quetol 651 for electron microscopy, rapid method 78—20322
biological X-ray microanalysis, principles 80—73566
biomembrane thin sectioning development 79—74819
bone biopsies, undecalcified human bone prep. for electron microscopic investigation 78—20332
book, advances in optical and electron microscopy, vol.7 80—31437
bright field images, signal-to-noise enhancement by incoherent superposition 80—101906
bright- and dark-field iterative algorithms in single side band holography 77—7640
bright-field hollow cone illumination 80—75136
bright-field imaging of single heavy atoms in an electron microscope with superconducting lens system 80—10472
carbonaceous material, image contrast, comparison of theory and expt. 77—10142
cartilage proteoglycan simultaneous localisation by light and electron microscopy 80—85571
cell marking and relocating method 79—74808
cell membrane particle diameters meas. by computer from electron micrographs 80—101307
cell ultrastructure, computer anal. 80—85555
charged particle detection by photographic recording systems, appls. 78—17527
chloroplast membranes, electron optical artifacts 78—15934
chromosome model reconstruction from electron microscopic projections 80—8235
cluster anal. for characterization of particle distribs. by stereological methods 79—71569
coating, thin, on bulk materials, electron backscatt. w.r.t. thickness determ. *(German)* 77—10146
coherence, partial 77—71410
coherence in bright field microscopy of weak objects 78—32955
cold-stage system for fast-frozen liquids 79—71573
colloid preparation by freeze-fracture 78—337
combined scanning microdensitometer and diffractometer 80—73529
composition and structure of engineering and industrial materials, instrumentation 77—4882
computed electron micrographs, use in defect identification 79—69101
computer image processing, atomic resolution from 500 kV electron micrographs 80—100149
computer indexing of diffr. spots, appl. to bicryst. *(French)* 78—75507
computer simulation of phase contrast of W support film 78—334
computer-aided analysis of micrographs 80—4813
computerised picture processing, electron micrographs, error sensitivity, resolution limit 79—71570
conference, electron microscopy and analysis, Brighton, England (Sept. 1979) 80—67936
conference, Glasgow, Scotland (Sept. 1977) 78—32934
conference, Johannesburg, S.Africa (Dec., 1976) 77—49814
conference, Melbourne, Australia (Feb. 1980) 80—82572
conference, Nice, France (May 1977) 78—24889
conference, Pretoria, South Africa (Dec. 1978) 79—71576
conference, Reston, VA., USA (Apr. 1977) 78—45683
conference, Tashkent, USSR (Oct. 1976) 79—6219
conference, Toledo, USA (Sep 1978) 79—100796
conference, Toronto, Canada (Aug. 1978) 80—82579
conference, vacuum science, Jerusalem, Israel (April 1978) 79—67322
conference of Electron Microscopy Society of Southern Africa, Port Elizabeth, S.Africa (Feb. 1980) 80—73099
conically tilted projections, 3-D reconstruction 80—99618
contrast enhancement of negatively stained macromols. and biomembranes by single sideband phase contrast interference 77—45920
contrast near bend contours of upper Laue areas with beam nearly parallel to cryst. axis 79—55621
contrast transfer for tilted and conical bright field illumination 78—37115

electron microscopy continued
controlled atmosphere, gas-solid interaction study 77—29042
convergent beam electron diffraction 80—103220
convergent beam electron microscopy, appl. in materials science 80—107028
critical point dryer, low-cost, with continuous flow dehydration attachment 78—53595
cryo-ultramicrotomy and myofibrillar fine struct., review 78—53592
crystal defect observation *(Japanese)* 79—82130
crystal orientation determ. from selected area channelling patterns 80—70092
crystal structure image, influence of inelastic electron scatt. by plasmons *(French)* 77—76269
crystal structure images periodicity, variation with cryst. thickness 78—30524
crystal structures and cryst. defects, electron microscope imaging 80—88006
crystal surface, in-situ cleaning by ion sputtering 80—101895
crystalline materials, high resolution imaging techniques 80—99001
crystalline materials, in situ deform. by high voltage electron microscopy 80—103352
crystallographic aspects, review 80—14969
crystallographic struct. factor phases from electron-microscope dark-field moire patterns 78—51396
current trends 78—32935
dark field image calcualtion 80—75137
dark field image of weak phase objects *(German)* 77—10150
dark-field imaging, computer simulation 80—100151
decoration, of Sb surface, with epitaxial Bi condensates 79—28227
decoration method, rel. to crystal growth *(German)* 80—103222
decoration technique, surface step struct. determ. 80—103554
defect imaging, analytical contrast calcs. in two-beam case 80—100134
defect symmetry, electron diffr. contrast, theory 80—96418
defocus spread and illumination aperture effect, in brightfield electron microscopy 79—231
defocusing depend. of lattice plane image contrast *(German)* 78—38594
defocusing of dark-field electron micrographs, crystal point defect accumulations investigation 79—99036
density reconstruction using arbitrary ray-sampling schemes 78—80954
dielectric surface, electron-charged, microscopy using electrostatic field *(German)* 78—82081
differential sensitivity of neurosecretory and non- neurosecretory neurones of an aphid 80—98195
diffraction and imaging techniques, in material science, electron microscopy [book] 79—67439
diffraction contrast, without column approx., calc. using perturbation method *(German)* 79—50960
diffraction pattern orientation rel. to electron micrograph determ. method 77—49809
diffractometer for analysis and correction of electron microscope images 78—21275
digital image restoration simulation in electron microscopy 77—57431
direct observation of Hg atoms in make-up of heteroorganic compound 79—35898
dislocation, Burgers vector determ. by weak-beam image in HVEM *(Japanese)* 80—70199
dislocation, calc. of electron microscope images and Burgers vector sign determ. 77—59017
dislocation configurations, jog and dipole, computer simulation of electron microscopic diffr. contrast 77—84750
dislocation core structure, conditions for obs. by multibeam interference *(French)* 78—26571
dislocation core studies in high resolution microscopy, image calc. methods 80—96535
dislocation image contrast, calc., foil surface stress relax. effect 77—31665
dislocation image contrast, elastic anisotropy influence, appl. to feldspars 78—26573
dislocation imaging, high-resolution, additional image peak interpretation 77—68978
dislocation imaging, in anticlassical scattering region, dislocation axis contrast 80—38877
dislocation interaction, with grain boundaries during plastic deform. 80—54281
dislocation loops, direction of black-white contrast 77—15423
dislocation pile-ups, plane, electron microscope contrast 79—27986
displacement damage simulation in HVEM irrad. 80—107325
DNA electron microscopic preparation on uncharged C films 80—12320
Doppler shift of electron waves, illustration using electron mirror interference microscope 80—95783
dynamic phenomena, in situ appl. of DC electric field 80—103925
dynamical image contrast, small lattice defects 77—15422
einzel lenses, symmetric, with thick central electrode, axial potential 80—18983
elastically-anisotropic cubic crystals, image contrast of inclined dislocations 79—27991
electrical relief, on crystal surface during cleavage 79—24045
electrocyte stacks of torpedine ray, assembly for quick-freezing tissues 80—67316
electron excitation and optical pot. in electron microscopy 77—80399
electron gun, with electrostatic and electromagnetic lenses 80—99007
electron image processing, and improvement 78—24890
electron microscope, fluoro-autoradiography, improvement of efficiency 78—65162
electron object interaction, multislice approach 78—26394
electron optics, developments at the Cavendish Laboratory 80—37948
electron-matter interactions rel. to electron microscopy 80—89097
electron-sensitive materials, apparatus for measuring sensitivity and data-density 79—35893
electrostatic crossed lens, for electron microscopic devices 80—87289
Electrotitus, detective quantum efficiency 80—42307
EM, electron exposure-dependent contrast transfer 80—104837
embedding with GMA and Quetol 523 for electron microscopic obs. on semi-thin sections for light microscopy 78—53588
energy loss microanalysis system with high collection efficiency 80—86508
energy loss spectroscopy, contrib. to anal. microscopy 77—25346
environmental cell for 3MV-class microscope, and its appl. to metallurgical problems 77—10141
epitaxial growth process at UHV 78—55790
failure analysis tools comparison and selection 80—71865

electron microscopy continued
- fast convolution of large arrays, using number theoretic transforms 78—22092
- ferromagnetic film, domain wall width meas. with electron microscope, astigmatism effects 79—19753
- fibre sizing using Fraunhofer diffraction 79—171
- filament measurement, micrometer clamp 79—21700
- film, small voids obs. technique 78—34403
- film casting method for electron microscopy samples, particularly elastomers 78—29213
- film grain noise, spectral density estimation *(French)* 80—9075
- film thickness determination, electron backscatt. method 77—47703
- fixative, using formaldehyde- and formaldehyde glutaraldehyde-OsO_4 mixtures 79—17404
- focused image production through visible-optics convection of defocusing and spherical aberration 79—6231
- foil lens, spherically corrected, for electron phase microscopy *(German)* 80—83546
- freeze etching and related techniques, resist. monitor for automatic film thickness regulation 78—49810
- freeze fracture, size determination of sonicated vesicles, spray freezing method 80—98188
- freeze fracture autoradiography, red blood cell plasma membrane 80—98192
- freeze-drying apparatus, appl. to adenovirus particles 80—21578
- freeze-drying technique for prep. biological tissue without chem. fixation 78—65164
- freeze-drying technique using modified freeze-etching device, for viruses and phages 77—70572
- freeze-etching improvement using evaporated film 80—85558
- freeze-fracture electron microscopy freezing method evaluation by low temp. X-ray diff. 78—57145
- freeze-fracture image enhancement by reversal processing of sheet film 78—62267
- freeze-fracture specimen temp. changes during rapid quenching in liq. coolants 78—57140
- freeze-fracture technique, appl. to study of animal plasma membranes 80—104842
- FREINT, an integration routine calculating Fresnel diffraction 79—30612
- Fresnel diffraction effects on high-resolution images, spherical aberration effect 79—27153
- Fresnel diffraction images, at edge of screen, inelastic diffusion contrib. to formation *(French)* 80—18045
- Fresnel fringe on high resolution electron microscope under partially coherent illumination *(Chinese)* 79—94142
- frozen hydrated crystalline specimens, meas. and reduction of damage 80—85552
- frozen hydrated specimens, mass loss and etching by the electron beam 80—47147
- Gabor holography, twin image and quadratic term error correction *(French)* 77—42510
- gas analysis, combined photoemission/mass spectrometry technique *(German)* 77—40603
- GMA-Quetol 523, ultraviolet polymerisation in embedding procedure for semithin sections prod. 78—92767
- grain boundary dislocation interactions, electron microscopic obs. 78—34517
- grain boundary dislocations, Burgers vector identification from electron microscopic images 80—19807
- grain boundary reaction sites, determ. of struct. aspects 80—103359
- graphite, thin support films, 2 nm, prep. for high resoln. electron microscopy 77—87880
- grid handling, of semi-thin sections of GMA-Quetol 523 embedded tissue, with reference to O_5O_4 78—92766
- guinea pig keratinocytes and melanocytes in tissue culture, influence of observational techniques on results 80—21583
- heavy atom discrimination using single-sideband techniques 80—6321
- HEED, critical voltage effect, zone axis, interpret. using atomic string approx. 80—96421
- helical structure reconstruction from projections, phage tail appl. 80—8237
- high resolution, appl. of Fraunhofer holography 80—99016
- high resolution, appl. to clay minerals investigation *(French)* 78—26396
- high resolution, dark field, technique for obs. of small metal particles 77—85111
- high resolution, digital processing use for image assessment and restoration 78—37116
- high resolution, for studies of local variations of struct. in crystals 79—94853
- high resolution, mol. struct. determ. 80—21595
- high resolution, solids fine struct. appls., advances 79—50965
- high resolution dark-field images 78—26398
- high resolution electron micrographs *(Chinese)* 79—80732
- high resolution electron microscopy, cryst. struct. determ. *(Chinese)* 78—1960
- high resolution imaging of isolated individual sheets of graphitic carbon 79—2890
- high resolution shadowing by sputter deposition 77—55219
- high voltage, materials testing in situ experiments, feasibility and methodology *(French)* 80—68301
- high voltage, New York State Dept. of Health facility 79—44986
- high voltage, quantitative anal. of in situ straining experiments, strong frictional force 80—100244
- high voltage, recent applications to biology 80—41347
- high voltage electron microscope autoradiography, HeLa cells 78—36077
- high voltage electron microscopy review 77—41737
- holey film preparation by ion-etching method 80—105751
- hollow cone illumination, transfer functions in electron microscopy *(French)* 79—63327
- holographic filter, for electron micrography image improvement 80—99680
- holographic image processing, resolution improvement and three-dimens. reconstruction 77—10862
- homogeneous electron irradiation *(German)* 80—102603
- HV, in situ obs. techniques and applics., review *(Japanese)* 80—59351
- HV, in situ oxidation of Fe-Cr-Ni foils 80—104354
- HV, materials science appl. 77—52605
- h.v., push-pull straining device for in-situ foil deform. expt. 77—4875
- HV, simulation of neutron damage, state-of-the-art 77—51417
- HV electron microscope in situ deformation expt. limitations 79—60238

electron microscopy continued
- HV electron microscopy, total scatt. cross-section obs. 79—21859
- HVEM, in-situ techniques for condensed matter studies 80—14977
- HVEM, radiation effects during obs., review 80—27379
- hybrid image processing for feature extraction and constant variance enhancement 80—53224
- hydrocarbon molecules, strongly adsorbed, contamination rate reduction 79—1550
- illumination divergence determ. method 78—4737
- image accumulation, digital storage and processing system 80—101901
- image analysis, problems and approaches 79—80725
- image analysis in electron microscopy 80—31947
- image calculation system, interactive 80—24325
- image contrast, crystallographic structure changes due to phase transition, of V_2O_3 *(French)* 79—7688
- image contrast, of cluster atoms, rel. to inelastic scattering 80—100154
- image contrast and localized signal selection techniques 80—37126
- image contrast of small dislocation loops and stacking fault tetrahedra 80—6326
- image correction methods, exptl. anal. 79—12889
- image correction using phase-shift holographic filters 77—18139
- image deconvolution using Sayre's eqn. *(Chinese)* 79—67430
- image enhancement, digital processing method *(German)* 78—89599
- image formation, propag. problems connected with special source structs. 80—87272
- image formation in partially coherent illumination including inelastic scatt. 78—32956
- image formation using hollow-cone illumination, S/N considerations 80—4815
- image processing, biological molecules, optical diffraction and filtering, fast Fourier transforms 80—30956
- image processing, man-machine interactive digital, of HV electron micrograph images 79—17568
- image processing, optical vs. computerised 77—67541
- image processing 79—30613
- image processing by linear integration technique, periodic structures obs. *(Japanese)* 80—52363
- image processing of micrographs of deformed filaments 77—57428
- image processing system for micrographs based on minicomputer 80—73549
- image processing systems, appl. to random noise removal 78—12791
- image processing techniques, electron micrograph quantitative interpretation 79—82128
- image reconstruction, 3-dimens., electron noise effects 77—13829
- image reconstruction, 3-dimens. with Fourier method *(Japanese)* 78—78048
- image reconstruction, three dimensional, and spatial filtering 79—97477
- image reconstruction and holographic methods 77—65062
- image reconstruction from hollow and truncated projections, theory 78—24912
- image reconstruction from projections, blurring due to object movement 80—78784
- image reconstruction of low and high dose micrographs of neg. stained glutamine synthetase 80—85551
- image reconstruction problems 79—75661
- image recording system, detection quantum efficiency 80—99009
- image restoration of weak phase objects, digital technique 78—58098
- image reversal process for films 79—2892
- image simulation, defect displacement field construction from angular dislocation segments 80—6325
- image synthesis from electron micrographs taken at different defocus 79—54234
- image two-dimensional reconstruction algorithms 77—82379
- image wavefunction asymptotic approx., extension to biprism edges 80—95193
- images of coincidence grain boundaries 78—30639
- images reconstruction using Wiener filters 79—71572
- imaging, at 1.6 Å point-to-point resolution 79—46531
- imaging and diffraction, from localised defects and disorder 80—100152
- imaging and diffraction techniques, (book) 79—67441
- imaging characts., third order aberration theory exam. *(German)* 78—32926
- imaging magnetic energy filters free of second-order aberrations, optimization 80—4816
- imaging methods, non standard 77—71409
- imaging of thin phase objects, tilted and extended 80—99617
- immunoelectronmicroscopy in detect. of antibodies to rabies virus 80—85567
- improvement of cross-correlation peaks by image filtering 79—76610
- inelastic electron scattering as analytical tool, review 78—24010
- inelastic electron-matter interactions 80—104024
- interface, for elec. field distrib. meas. 79—17567
- interfacial dislocations, Burgers vector determ. using electron microscopy 78—34720
- interference method for particle shape determ. in films, inner pot. determ. and external field determ. *(Russian)* 78—29209
- intergranular thin film detect. by high resolution electron microscopy 80—4824
- interplanar spacings, precision determ., by means of reflection electron diffr. 79—64961
- inverse pole figure construction using electron microscope *(Russian)* 77—60012
- ion beam sputtering, application to high resolution electron microscopy 78—32925
- ion techniques for specimen prep. 78—32947
- isolated atoms visualisation *(French)* 78—24892
- isoplanatic imaging, complex degree of coherence determ. 77—2691
- Johansson three-electrode objective, appl. to surface struct. studies *(French)* 80—47152
- Kikuchi pattern, analytical determ. of exact primary beam direction 78—5991
- Kikuchi patterns, multiple-beam dynamic effects 79—46528
- laboratory floor vibration detection by record-player cartridge 79—54233
- lattice defects, high resolution microscope images, calc. and interpretation 79—73075
- lattice fringe imaging applications 80—88005
- lattice fringe imaging theory 80—103225
- lattice image calculations for imperfect crysts., superlattice approach 80—107030
- lattice images of zeolite cryst., phase contrast components determ. 77—11446

electron microscopy continued
  lattice imaging, introductory paper 78—79508
  lattice imaging 78—30522
  lattice imaging theory *(French)* 77—19845
  lattice imaging use in cryst. struct. analysis 78—34404
  lattice resolution analysis, of coincident-site boundaries of electron microscope images 80—33861
  light microscope attachment for isolating small specific areas from slide embedded monolayers 78—53596
  light optical diffractometer, for electron microscope images operating on line 80—101900
  linewidth correction procedure for electron image meas. 77—35449
  liver acinus anal. using double embedding technique 80—3885
  long-range order parameter from thickness fringes, high-accuracy method 77—65938
  LV, localisation of inelastic scatt. events, biological objects 77—37118
  LV, practical appls. 79—6223
  macromolecules, high-resolution metal replication 77—25621
  magnetic bubbles, electron microscope obs., review 77—28417
  magnetic domain wall observation device for use with 1 MeV electron microscope 80—101882
  magnetic domain walls, off-axis electron microholography 78—82080
  magnetic field distrib. mapping of thin mag. foils by holographic processing 79—89868
  magnetic film, magnetization amplitude and direction var., electron-microscope obs. procedure 78—6548
  many-beam lattice images from thicker crystals 80—88004
  many-beam structure images, optimal comput. techniques 80—95203
  mass thickness of biological sections, determ. from electron micrographs 77—70573
  membrane preparatory procedures, for electron microscopic anal., at mol. level resoln. 80—104843
  metal shadowed objects, low cost internegative prod. 78—74109
  metal-insulator transition study *(French)* 78—26815
  metallic film, struct. of small particles, review 77—89671
  metallographic sample preparation, procedures 80—57272
  microchannel intensity amplifier for electron microscope images during X-ray spectral anal. of light elements 77—12848
  microdensitometer—computer correlation analysis of ultrastructural periodicity 80—85553
  microdiffraction obs. of SRO, applic. to quenched Cu-Pt alloy 77—76360
  microfractography *(Japanese)* 80—71841
  micrograph observation in electron diffraction apparatus, use of electrostatic lens 79—80727
  microgrid preparation as specimen support for high resoln. electron microscopy 77—87879
  micropositioning stage, piezoelec. driven, 50 micron range, subnanometer resolution 79—17407
  microthermometry, technique for local specimen temp. meas. in electron microscope 79—67297
  microtome modification for improved ultra-thin sectioning 80—17207
  mineral particulates, identification by selected area electron diffraction 77—90970
  minimal exposure high resolution, organic materials 80—79653
  mirror electron microscopy, contrast form. 80—68299
  mirror electron microscopy, theory and appl. 79—67443
  mirror microscopy, with monochromatic electron beams *(German)* 78—89598
  mirror technique for total electron refl. coeff. determ. at metallic surface 78—5994
  molecular biology, detection and resolution of atom images *(French)* 79—66595
  molecular image, effects of dynamical scattering, in high resolution electron microscopy 78—14255
  molecular imaging, photographic averaging technique 78—79600
  molecule images, simulation by point models and kinematical struct. amplitudes 80—103223
  Mollenstedt filter images, correction by auxiliary lenses, appl. to bend contour obs. for Al 77—39520
  motif detect. in quantum noise limited electron micrographs by cross correl. 77—67546
  multi-beam, general extinction criteria for extended defects 77—72532
  multilayer heterostructures, prep. and ion etching of thin foils for electron microscopy 79—12779
  multiple inelastic scattering in thick crysts., Monte Carlo simulation 77—7637
  negative print production, electron micrographs of metal shadowed materials 80—18051
  neurons, section embedding technique for sequential light and electron microscopic exam. 80—67317
  nonperiodic objects, reconstruction from electron micrographs using correlation methods 80—86527
  numerical aperture and f-stop utilisation 80—105753
  oblique illumination stereoscopy, using shadow electron microscopy 79—21862
  optical and digital spatial freq. filtering of electron micrographs, expt. results 78—82079
  optical Fourier transformation of two-dimens. image signals *(German)* 78—32932
  optimal iterative phase retrieval from image and diffr. intensities 77—72531
  oral epithelium, rat, ultrastruct. effects of X-irrad. 77—56434
  ordered alloys, atomic order parameters from topology of electron-microscope diffr. contrast from antiphase boundaries, quantitative determ. 78—95016
  organic materials, imaging with superconducting lenses 80—73553
  orientation and position accuracy of electron diffr. 78—22606
  oxides, fluorite and ReO_3, n-beam struct. images, expt. observations and computer calc. 78—38593
  perfusion fixation of animals, press. controlled device 77—44866
  phase contrast, appl. to holes and steps on graphite 77—38063
  phase contrast of support films, simulation 80—4812
  phase contrast simulation, of Au cluster atoms on W support film 80—100150
  phase evaluation by electron diffr. by electron interfs. *(German)* 78—74112
  phase problem, in electron microscopy, review 80—33862
  phase problem, partial coherent illumination influence 80—62800
  phase problem, rel. to holography 80—99681
  phase problems, image recovery from Fourier transform modulus 78—82918

electron microscopy continued
  phase problems 78—70230
  phase reconstruction problem 78—25811
  phase retrieval algorithms for semi-weak objects, from noisy electron micrographs 78—78047
  phase retrieval from image and diffr. pattern, algorithm 77—18140
  phase retrieval from image and diffr. pattern, uniqueness and stability of soln. 77—10144
  phase retrieval from image and diffr. patterns, algorithm development 77—10148
  phase retrieval from intensity meas., uniqueness question 79—13915
  phase transformations, electron microscopy, quantitative analytic studies 80—2998
  phase-grating calculations of high resoln. images of thin crystals 77—19851
  phosphorylase A crystals, automated struct. determ., from micrographs 80—92425
  photoelectron microscopy, bacteriochlorophyll monolayer quantum yield and image contrast 78—44453
  photoemission, principles and appls. 80—89424
  photoemission electron microscopy, use in phase transformation continuous obs. 80—2999
  photoemission in high vacuum region, influence of residual atm. and other parameters on image brightness and contrast 78—55791
  photographic exposure meter for electron microscopy 77—26435
  photographic exposure timer applic. 77—41730
  Phototitus, image intensifier and convertor for electron microscope 77—45918
  physical metallurgy, appls. of HV electron microscopy irrad. machine, struct. obs. 77—1891
  physiological sample, fusion progression during rapid freezing for electron microscopy 80—3884
  planar defect ‘on edge’, electron wave function in vicinity 80—88002
  planar interfaces, study by electron microscopy 79—68982
  polyacetal, exam. of fatigue crack propag. 78—48497
  polymer, microscopic images quantification *(Polish)* 79—49347
  polymer multicomponent systems, selective electron beam etching 78—45603
  polymers, partially cryst., struct. anal., soln. and melt-grown films as model specimens 78—30523
  pore-channel marking, electron microscopy of polymer films 80—103271
  postcontamination avoidance using room with controlled microclimate 78—54350
  practical methods, staining and X-ray microanal., book 78—4739
  precipitates, effect of diffuse scatt. on dark field contrast 78—67627
  precision electrical meas. using superconductivity *(German)* 77—79124
  preparation of structural fragile cell-biological specimens, exchange method 80—98190
  prevention of losses and damage during X-ray microanalysis 80—73567
  protein film method, basic, in electron microscopy of nucleic acids 80—104844
  protein structural differences evaluation from electron micrographs 79—53040
  protein supramolecular structure, ordered, electron micrographs, image processing 80—89923
  proteins, solid state, radiation damage, amino acid composition of catalase 77—25377
  protozoan cell specimen preparation, freeze-drying technique 79—20724
  quantitative electron mirror microscopy 78—15132
  quantitative metallography with automated electron microscope-microprobe systems 78—35631
  radiation damage, correl. anal. 80—100282
  radiation damage problems in electron microscopy 80—59517
  radiation damage processes and image contrast loss 78—37117
  radiation sensitive materials, diffr. pattern recording on luminescent radiographic screen 77—27791
  radiation-damage artefacts in biological electron microscopy, technique for visualisation 79—20726
  real-space filtering of images from optical autocorrel. patterns 78—8479
  recording densitometer for electron micrographs 79—49343
  refrigerated moving-object technique and accessories *(French)* 77—29235
  relative humidity indirect meas. in electron microscope side entry environmental stage 78—8480
  replica technique, glue films for detaching single-stage C replicas 80—61038
  replica techniques appl. to steel separations estimation, use of X-ray microanalysis *(Bulgarian)* 78—40012
  resolution, prospects for extending limit 80—37128
  resolution estimation in electron microscopy 80—77911
  resolution improvement for crystal structure imaging and atomic movement dynamic obs. 80—70090
  resolution improvement to 3 Å using low beam divergence and minimising thermal spread 77—65939
  review, 1976-77 78—82077
  review, possibilities and limits *(German)* 77—82652
  review of developments of last 25 years 77—67540
  ribosome subparticle fine struct. investigation by optical filtration of electron microscope images 80—81779
  sample preparation, rapid cooling characterisation by pyroelectric polymer films *(German)* 80—13185
  sample preparation effects on decoration patterns 79—86658
  samples, geometric stability *(Ukrainian)* 77—67536
  scanning electron probe microanalyser, development of x-ray microanalysis 80—37139
  Scherzer’s formula and the correction of spiral distortion in the electron microscope 77—71407
  Schrodinger equation separation in electron diffr. and channelling, HV, case of systematic refls. 79—46522
  screening effect by dielectric support film 80—86504
  secretory granule membrane, particle clustering induced by centrifugation, freeze-fracture anal. 80—85559
  self-shadowed replicas, controlled sputtering 77—26434
  SEM, voltage meas. via new electron energy analyser 77—54019
  semiconductor applications of electron microscopy, advances 80—101911
  shadow electron microscope, selected area diffraction 77—11444
  shadow microscopy, electron interference 77—18141
  sighting preparation method 77—49810
  signal-to-noise enhancement by superposition of bright-field images obtained under different illumination tilts 80—6329

electron microscopy continued
silicate mineral, identification and asbestiform varieties, election optical and X-ray techniques 80—8446
single-scattering approximations, quantitative validity domains for organic crysts. 80—28888
small angle diffraction in electron microscopes, review 79—50966
spatial coherence in axial high resolution microscopy 77—82654
spatial frequency filtering by optical and digital means 78—70231
spatial measurement using images corres. to different reflexes 77—55216
specimen contamination, small probes 77—18143
specimen deposition and fabrication by ion beam sputtering 80—82855
specimen supports, single cryst., method of prep., H_2O_2 exfoliation of vermiculite 77—38061
specimen temp. meas. using opt. pyrometer, controlled atmosphere 78—93690
specimen thickness, determ. by continuum integration 80—31713
splat quenched specimen prep., comment 77—4755
splat quenched specimen prep. 77—4754
stacking fault width determ. from 224 reflections with g.b=0 78—59722
stereo electron micrographs restitution, approximate soln. 79—26189
stereo imaging in shadow microscope 80—95195
stereology, quadrat choice for geometrical struct. determ. of two-phase specimen 78—12793
stochastic image restoration procedure 77—10858
structure and space group determ., dynamical theory 77—62454
structure determination approaches 78—34397
superconducting lens, electron microscope appl. 80—86530
superconducting lenses applic. 77—71408
superconductivity applications in electron microscopy 77—38059
support film phase contrast, Fourier spectrum analysis 80—95199
surface bombardment, by electrons, protons and heavy ions, characterisation of materials 79—96406
symposium, Toledo, Ohio, USA (Aug. 1979) 80—82571
tail structure of temperate phage no.1 of Bacillus megaterium, 3-D reconstruction 80—35831
thin film, thickness determ., by electron backscattering 80—101904
thin film studies by interference electron microscopy 80—6328
three dimensional, minimal dose technique 80—86526
three dimensional high resoln., for non-periodic structs. 77—71893
three-dimensional computer graphics, computational morphology appl. 78—28132
tilted beam imaging mode, phase contrast transfer, effective aperture representation 78—24894
tilted illumination imaging, contrast transfer functions 80—95198
tissue section electron microscope image texture discrimination and automated meas. 78—57099
tissue section lifting for electron microscopy 79—74823
tissue surfaces cryofixation for electron microscopy 79—53294
transfer functions for partially coherent axial illumination and chromatic defocus spread 77—87883
transfer functions in closed form with tilted illumination 80—52368
transmission electron type, image improvement, problems 77—30218
two-layer target, moderate energy electron interactions, direct statistical modelling *(Russian)* 77—66561
UHV microscope, electron beam evaporator for in situ deposition studies of refractory metal thin films 80—40264
ultrahigh temperature, functional features *(Japanese)* 77—45919
ultramicroscopy in scanning microscopes 80—95137
ultrathin frozen section supported by polyethylene glycol 78—20337
ultrathin serial section transfer and orientation, accessory equipment 78—73976
uses, differences from optical microscope 80—13186
vacuum pipette for processing groups of specimens 80—18052
vacuum station (VUP-2K) for specimen preparation, improvement of 77—38058
very high resolution, in biology *(French)* 78—28144
virus negative staining technique, applications in electron microscopy 80—41348
wave aberration, sign conventions 77—589
wavelength measurability 77—71406
weak beam calculations, effects of column approximation 79—32863
weak-beam contrast calculation for spherical coherent precipitates *(French)* 77—35450
weak-beam images of dislocation dipoles and multipoles, calc. 80—75231
weak-beam method, of electron microscopy 79—67440
wet technique for study of living materials 80—12317
wide-field, appls. in biology and medicine 77—56553
work function variations, mirror electron microscopy meas. 80—86505
Al alloys, use of electrospark cutting for preparing thin foils for electron microscope exam. 77—52590
Al_2O_3 supermicrogrid for high resolution electron microscopy 79—17563
Al_2O_3 supermicrogrid preparation and props. for use as support film in high resolution electron microscopy 80—99010
Al_xO_y supporting film prep. by Al evaporation 77—67538
BeO specimen supporting films for high resolution electron microscopy of single Au particles 77—27793
Ge, dislocation electron image filtering in electron microscopy 80—75129
Pb stain artefacts, technique for minimizing occurrence 79—84040
Si thin crystal, electron backscatt. in electron microscope 78—75510
U stain artefacts, technique for minimizing occurrence 79—84040
ZnO, hexagonal spot pattern production with light source and electron beam 77—69148

electron mobility
see also carrier mobility; electron mobility (metals)
air, dry, electron lateral diffusion to mobility ratio 80—6203
air, electron drift velocity at 293K 80—103102
air, electron radial diff. coeff. to mobility ratio 77—19666
benzene, gaseous, critical and liquid, electron transport 80—64673
biological systems, advantage to low mobility 79—39346
butane, gas, electron drift vel., Ramsauer-Townsend minima in electron scatt. 78—87427
butane liquid, high-field electronic conduction obs. 79—4587
butene isomers, gaseous, density and temp. effects 80—33725
CO, electron drift velocity and longit. diffusion coeff. time of flight meas. 77—80264
cyclohexane, gaseous, crit. and liq., density and temp. effects on electron mobilities 79—27739
cyclopentane, gaseous, crit. and liq., density and temp. effects on electron mobilities 79—27739
dense gas, electron drift velocity 78—1785

electron mobility continued
dense gases, electrons and positrons, review 80—103106
dielectric liquids, cond. and breakdown, conf., Mont-Saint-Aignan, France (July 1978) 79—91354
diffusion theory and Monte Carlo calcs. of electron transport, depend. on initial ang. distrib. of injected electrons 80—53136
diffusion to absorbing electrodes, Monte Carlo and Boltzmann calc. comparison 80—6204
2,2-dimethylbutane, fluid phases, electron mobility, density effects meas. 77—7619
dipolar molecule plasma, in elec. field, electron mobility and electron atom collisions 77—76029
drift and diffusion in neutral gas in electrostatic field 80—10349
drift velocity in counter gas mixtures 80—28590
drift velocity of gas in field, second-order theory 77—58240
electron swarms diffusion to mobility ratio, pulse meas. technique 79—55448
ethane, gas, electron drift vel., Ramsauer-Townsend minima in electron scatt. 78—87427
ethane, gas, liq., and crit., electron mobility, density and temp. effects 80—92246
ethane, liq., excess electron mobility, elec. field depend. 78—72218
ethane, liq., excess electron mobility, field and temp. depend., −50 to +26°C 79—91115
ethane, Ramsauer-Townsend minimum in electron scatt. cross section 77—89821
ethane, supercritical, electron mobility as function of density and temp. 80—59163
ethane, thermal electron mobility at high density, electron quasilocalisation 79—27740
flame, electron-neutral energy exchange in AC field 77—42519
freon-N_2 low-pressure mixture prebreakdown current obs. 79—18995
gas, Boltzmann eqn. soln. two-term approx., validity 77—35309
gas, drift velocity, density dependence, high press., quantum mech. theory 79—1285
gas, electron collision and vel. distrib. in elec. field, Boltzmann eqn. 77—30115
gas, electron diffusion to anode, Monte Carlo and Boltzmann calcs. comparison 80—38519
gas, electron swarm with anisotropic vel. distrib. function 80—38520
gas, field-dependent mobility at drift vels. near sound vel. 80—43840
gas, swarm motion, monte carlo simulation 77—84392
gas, weakly ionised, ionis. and attachment effects on electron swarm parameters 78—5845
gas discharge positive column plasma, absolute and convective instability of helical wave, depend. on anisotropy of electron mobility *(Russian)* 79—37478
gas discharge streamer propagation mechanism based on plasma vibrs. *(Russian)* 77—84546
gas mixtures, drift velocities as function of elec. and mag. variables 78—71424
gases, multiple scatt. effect 80—58383
n-hexane, gaseous, crit. and liq., density and temp. effects on electron mobilities 79—27739
hydrocarbon liquid, model for thermalisation of quasifree electrons rel. to electron mobility 77—40316
hydrocarbons, gas phase, thermal electron interactions, drift vel. meas. 78—62919
hydrocarbons, liq., mobility of localised and quasi-free excess electrons 79—4589
hydrocarbons, localised and quasifree excess electron mobility, cond. state energy and temp. depend. 79—4588
hydrocarbons, pulsed irrad. electron mobilities and reaction rate consts. for electron-solute reactions 79—91112
hydrocarbons, saturated open-chain, transport behaviour of excess electrons and props. 80—39643
hydrocarbons liq., geminate pair of charges, neutralisation escape with field depend. electron mobility 78—26865
ice, excess electron yield and mobility after nanosecond pulse ionization 78—39176
inert gas, liquid, Ramsauer-Townsend minimum in electron scatt. cross section 77—89821
inert gas mixture, electron drift vel., Monte Carlo simulations 80—48843
inert gases, liq., model for thermalisation of quasifree electrons rel. to electron mobility 77—40316
inert gases, liquid, effect of nonelectronegative molecules on excess electron mobility 78—2534
ionised gas, collision-dominated, drift eqn. and Ohm's law 77—47140
liquid, field depend. mobility, probability of escaping neutralization 77—8105
liquid ionisation chambers, current status of electron mobility and free-ion yield in high mobility liquids 79—45531
methane, compressed, drift velocity of excess electrons 79—91113
methane, dense gas, electron drift velocity 78—1785
methane, electron radial diff. coeff. to mobility ratio 77—19666
methane, excess electrons, zero-field mobility in dense gas 78—22452
methane, fluid, electron mobility, density and temp. effects 80—10351
methane, gas, electron drift vel., Ramsauer-Townsend minima in electron scatt. 78—87427
methane, liq., drift vel. of excess electrons 80—54744
methane, liquid, Ramsauer-Townsend minimum in electron scatt. cross section 77—89821
methane, thermal electron mobility at high density, electron quasilocalisation 79—27740
methane liq., high field electronic conduction obs. 79—4587
methane-d_0(-d_4), electron drift and diffusion, elec. field effects 78—63531
methane-ethane liquid mixture, field-depend. excess electron mobility 77—89822
methylpentanes, electron mobilities and penetration ranges in liq. and crit. regions 78—72220
neopentane, critical, electron mobility, gravity effect 78—91738
neopentane, gas, electron drift vel., Ramsauer-Townsend minima in electron scatt. 78—87427
neopentane, liq., excess electron mobility, elec. field depend., parity and differentiability restrictions 79—38141
neopentane, liq., field depend. electron mobility, probability of escaping neutralization 77—8105
neopentane, photoinjected electrons, escape probability, field depend. mobility effect 78—72219

electron mobility continued
neopentane, solid and liq., effect of n-butane impurity on electron mobility and electron-ion recomb. 80—24984
neopentane liq., high-field electronic conduction obs. 79—4587
neutralisation escape probability, field depend. mobility effects 78—14737
nonpolar fluid, excessive electrons near crit. points 80—92836
one-component molecular solution, excess electron diffusion 78—52043
pentane, isomers, gas and liq. phases, electron transport, density and temp. depend. 79—91114
pentane isomeric vapours, electon transport mechanisms, density induced transition 80—24122
pentane isomers, vapour and liq., electron mobility 79—72984
plasma in pulsed EM accelerator, time distrib. *(Russian)* 77—47267
positron mobility in uniform elec. field 80—9793
propane, gas, electron drift vel., Ramsauer-Townsend minima in electron scatt. 78—87427
propane, Ramsauer-Townsend minimum in electron scatt. cross section 77—89821
swarm transport coefficients, iterative method calcs. 80—96336
tetramethylsilane, liquid, effect of nonelectronegative molecules on excess electron mobility 78—2534
tetramethylsilane liq., high-field electronic conduction obs. 79—4587
thermionic convertors, effect of electron thermal conductivity, theory 80—40892
toluene, gaseous, critical and liquid, electron transport 80—64673
trajectory curvature effect in strong elec. field 78—83517
transport properties of electrons with narrowly defined bands at low temp. *(Russian)* 80—103656
two-component molecular solution, excess electron diffusion 78—52043
Ar, back diffusion of electrons, in the presence of an electric field 78—75251
Ar, compressed gas, electron drift vel., density depend. 78—63534
Ar, dense gas, electron drift velocity 78—1785
Ar, electron avalanche development, exact Boltzmann eqn. anal. 80—59318
Ar, electron drift and diffusion, Monte Carlo simulation 79—7441
Ar, electron mobility and lateral diffusion coeff. 77—35307
Ar, electron momentum transfer cross-sections 0.4 eV 77—35308
Ar, electron radial diff. coeff. to mobility ratio 77—19666
Ar, fluid, dense, excess electron drift vel., hopping model 80—43838
Ar, liq., compressed, excess electron mobility theory 80—80338
Ar, liq., drift vel. of excess electrons 80—54744
Ar, liq., electron drift vel., mol. solute effects 77—4338
Ar, liq., electron mobility, role of shallow traps 80—34440
Ar, liq., electron mobility/diffusion coeff. 80—44593
Ar, liq., high-field electronic conduction obs. 79—4587
Ar, liq., mobility of excess electrons, deform. pot. theory 80—24982
Ar, low-energy electron drift vel. at 293 and 90K 77—35306
Ar-hydrocarbon mixtures, electron drift velocity meas. 79—41079
Ar-methane, liq., drift vel. of excess electrons 80—54744
Ar-methane liquid mixtures, excess electrons drift vel. 77—59288
CO, electron swarm motion simulation for high E/N 77—19667
CO, ratio of lateral diffusion coeff. to mobility for electrons 79—50840
CO_2 electron drift velocity and longit. diffusion coeff. time-of-flight meas. 77—80264
CO_2, electron drift vels., time-of-flight meas. 80—28855
CO_2, electron swarm parameters for high E/N, Monte Carlo simulation 80—19548
CO_2 gas, electron mobility to lateral diffusion coeff. ratio 80—43836
CO_2, ratio of lateral diffusion coeff. to mobility for electrons 79—50840
CO_2, ratio of lateral diffusion to mobility for electrons at moderate E/N 80—59160
CO_2-N_2-He laser mixtures, electron swarm parameters, Boltzmann eqn. anal. 79—18396
CO_2-N_2-He-CO gas laser mixture, electron motion anal. 79—64199
Cs vapour, electron drift vel. and momentum transfer cross section 79—82032
H_2, dense gas, electron drift velocity 78—1785
H_2, electron avalanche, Monte Carlo simulation 80—38521
H_2, electron drift velocity and longit. diffusion coeff. time of flight meas. 77—80264
H_2, electron swarm motion simulation for high E/N 77—19667
H_2, electron swarms, motion, Monte Carlo simulation 77—39398
H_2, gas, electron swarms, anisotropic scatt. model 78—91059
H_2, lateral diffusion to electron mobility ratio 79—1284
He, electron radial diff. coeff. to mobility ratio 77—19666
He, gas, electron mobility, anomalous density and temp. depend. at low temp. 78—75253
He, gas, electron thermalisation, theory 80—53914
He, gaseous, positron mobility edge 80—83880
He, liq., hot electrons on surface *(Russian)* 78—87832
He, liq., surface electron mobility due to electron-ripplon interaction *(Russian)* 77—35770
He, liq., surface electron mobility, 0.02 to 1K 79—55985
He, liquid, short-wave surface excitation study using electron gas nonlinear I-V characts. *(Russian)* 80—10717
He, liquid, solid, and dense gaseous, mobility of charges 78—2324
^{4}He, liq., electron mobility at surface, 1.17-2.7K 77—39712
Hg, electron drift vel., expt. 78—30403
Hg Townsend discharge, electron swarm props. Boltzmann eqn. anal. 80—19648
Hg vapour, electron drift vel., momentum cross-section, theory 78—30404
Hg vapour, electron drift velocity at 573K 80—103103
Kr, liq., electron drift vel., mol. solute effects 77—4338
Kr, liq., electron mobility, role of shallow traps 80—34440
Kr, liq., excess electron mobility, Cohen-Lekner theory failure 78—19112
Kr, liq., high-field electronic conduction obs. 79—4587
Mg vapour, electron momentum transfer cross section, from 0.1-5 eV 80—103104
$(Mo_{1-x}Ru_x)_{80}P_{20}$, amorphous alloys, superconductivity, mag. susceptibility and electronic props., liq. quenching 78—88057
N_2, dense vapour, electron localisation 80—87840
N_2, electron drift velocity and longit. diffusion coeff. time of flight meas. 77—80264
N_2, electron drift vels., time-of-flight meas. 80—28855
N_2, electron swarm parameters for high E/N, Monte Carlo simulation 80—19548
N_2, lateral diffusion to electron mobility ratio 79—1284
N_2-CO_2 laser mixture, electron drift vels., time-of-flight meas. 80—28855

electron mobility continued
NH_3, compressed gas, electron drift vel., density depend. 78—63534
NH_3, dense vapour, electron localisation 80—44558
NH_3 vapour, supercrit. and subcrit. 80—59162
NO, electron radial diff. coeff. to mobility ratio 77—19666
Na, electron drift vel., expt. 78—30403
Na vapour, electron drift vel., momentum cross-section, theory 78—30404
Ne discharge, Boltzmann eqn., numerical study 77—35424
Ne, discharge streamer propagation mechanism based on plasma vibrs. *(Russian)* 77—84546
Ne, electron swarm with anisotropic vel. distrib. function 80—38520
Ne, liq., electron drift vel., mol. solute effects 77—4338
O_2, electron lateral diffusion to mobility ratio 80—6203
O_2 gas, electron mobility to lateral diffusion coeff. ratio 80—43836
O_2, low energy electron drift velocity at 293K 80—103101
S_n, liq., mobility variations of photoinjected charge carriers 79—91065
SF_6, electron swarm development, Boltzmann eqn. anal. 80—6205
Tl, electron drift vel., expt. 78—30403
Tl vapour, electron drift vel., momentum cross-section, theory 78—30404
Xe, electron mobilities in various phases, density, elec. field and temp. effects, quasilocalisation 78—59535
Xe, liq., electron mobility, role of shallow traps 80—34440
Xe, liq., high-field electronic conduction obs. 79—4587

electron mobility (metals)
asymmetric electron scatt., anomalous Hall effect in ferromags. *(Slovak)* 78—79986
conductivity in random pot., diffusive mode existence 79—65421
ferromagnet, metallic, thermopower near crit. point, inelastic scatt. processes 77—15836
foils, surface scatt. data table 79—60907
Hall mobility and carrier conc. in metal-like phases *(Ukrainian)* 79—95386
noncommensurate charge density wave dynamics in K-like metals 78—30913
one-dimensional conductor, phenomenological eqns. of motion for electrons, phonons and librons 80—10955
spin-fluctuation resistivity, low-temp., effect of pot. scatt. 77—15840
transition metals and alloys, d electrons as current carriers and electron scatterers 78—91689
Au film, ultrathin evaporated, acoustoelectric meas. of electron mobility and diffusion 80—65707
Bi, film, size effect of carrier heating, surface scatt. *(Russian)* 80—100474
Co, amorphous and liquid states, electronic states and transport 79—99474
Cu film, electron transport props., struct. defects role 77—40117
Cu-Al(Ge)(Sn) alloy films, electron transport props. 77—76955
Fe, liquid and amorphous states, electronic states and transport 79—99474
B-Ga, metastable, elec. props. in normal and supercond. states *(Russian)* 80—65520
In film, evaporated, resist., Hall effect and light transmittance, use as semitransparent electrode 77—39966
K, elec. resist., temp. depend., low temp. limit 77—11892
Ni, amorphous and liquid states, electronic states and transport 79—99474
Pb-Sn(Ag), dil. alloys, dislocation motion and electron-dislocation interactions 77—7728
$Pd_{95}Rh_5$, low-temp. spin-fluctuation resist., effect of pot. scatt., effect of Ni addition 77—15840
V_3Si single crysts., elec. resist. and Hall coeff., temp. depend., 17-300K *(Russian)* 77—69292
Yb, film, amorphous and cryst., transport props. rel. to band struct. *(Russian)* 77—12026
Zn, monocryst., electron motion, Hall effect and Fermi surface 77—47793

electron multipliers
Bendix layer, channel electron multiplier, secondary electron emission yield, energy depend. 77—54471
CEM, addition to Varian movable Faraday cup assembly for photoemission obs. 77—44130
ceramic channel electron multiplier, detect. efficiency in vacuum UV 78—12759
channel, high count rate, exponential decay and recovery of model gains 80—87022
channel, measurement of efficiency using photoemission electron source 79—100016
channel, phosphate glass, absolute efficiency for tritium radiation 77—67945
channel, secondary-electron time pickoff for pulsed charged-particle beams 79—97957
channel electron multiplier, fully-screened high-voltage vacuum feedthrough 78—24814
channel electron multiplier appl. to gas electron diffr. 78—83684
channel electron multiplier for ion mass discrimination, operation 78—5375
channel electron multiplier role in picosecond resolution time vacuum tubes 77—54429
channel electron multipliers, characts. and operating principles 79—93248
channel electron multipliers, microchannel plates, props., development, appls. 78—46221
channel plate, constant fraction timing discriminator 79—59316
channel plate, direct detection of minimum ionising charged particles 77—54447
channel plate electron multiplier, gain, detection dynamics *(French)* 78—46229
channel plate electron multipliers, detection of hard X-rays (10-140 keV) 77—88322
channel plate electron multipliers, single electron detection and timing 80—9458
channel plate in image tube, MTF 80—19108
channel plate multiplier as emissive mode detector for SEM 78—339
channel type, gain fatigue mechanism 80—9077
continuous channel multiplier, wall current and charge distrib. in range 20-100°C *(French)* 77—79516
count rate effect on channel electron multiplier 77—6623
counting characts. dependance of secondary-electron multipliers on residual gas pressure 80—106239

electron multipliers continued
detection efficiency of phosphate glass channel multiplier 78−41898
discharge, multiplier-assisted, new type of cold cathode 79−55591
electron detection using electron multipliers with discrete and continuous dynodes *(German)* 79−97946
Faraday cup for simultaneous ion-beam current obs. and meas. 78−49865
funnel type channel multipliers, sensitivity characts. *(German)* 77−88330
high gain, mass spectrometric positive ion detect. 78−74095
high-conductivity channel electron multipliers, performance characts. 78−86334
ion counting with CEM on double focusing mass spectrometer 77−79194
ion source, self-triggered channel type, operating characts. 79−17562
Johnston, low energy ion counting efficiency 80−63479
magneto-electrostatic electron multipliers, long-term efficiency changes *(German)* 80−5448
mass spectrometer electron multiplier three-state time delay switch 80−37116
mass spectroscopy, electron multiplier gains determ. for various ions by pulse counting method 80−57418
microchannel plate detectors 79−72200
microchannel plates, elec. props. during and after high-temp. vacuum bakeout 79−97935
microchannel plates, high gain, performance characteristics 78−37526
microdensitometer system for use in TEM 80−95197
movable dynode multiplier for radioactive ion detector in on-line mass spectrom. 79−716
multi-anode microchannel array detector tube, effects of 1 MeV gamma-rays 79−71582
narrow energy distribution of output electrons from modified single channel electron multiplier 80−57337
neutral particle detection, channel electron multiplier characteristics 78−58554
open microchannel multiplier secondary electron multiplication efficiency and nonlinearity 77−79513
parallel plate electron multipliers, multidetector array 79−31334
parallel-plate electron multiplier, theoretical and meas. anal. 79−36466
particle counting system, proton and H atoms detect. efficiency 77−10552
particle multiplier gain factors for singly charged alkali ions 77−30215
proton detection, low energy, helical channel electron multiplier, characts. *(Russian)* 79−3324
pulse counter, high-speed DC coupled, sensitivity and performance 79−89524
pulse counting measurement systems, optimum parameters determ. 79−89523
scintillator detector-electron multiplier system, for positive/negative ions pulse counting, mass spectrometer appl. 78−89583
secondary electron open-type, for X-ray spectroscopy and electron microprobe anal. 80−99027
semiconducting channel ion sorce, secondary emission and ion feedback 80−31936
single channel electron multiplier, energy distrib. of output electrons 79−35789
soft X-ray analysers for pulsed-source emissions 80−31957
UV-valence electron spectroscopy, multichannel detector system 77−23520
X-ray detection in 60-190 Å range using secondary-electron multipliers 77−21446
Be-Cu surface, secondary electron yield, for electron multiplier ion detector 78−74094
CsI, potential and limitations as dynode materials 78−23566
CuBe, electron emission following ion bombardment of electron multiplier dynode 78−23576
Pb glass, secondary electron emission yield, reducing and heat treatment conditions, electron multiplier appl. *(German)* 79−56894

electron nuclear double resonance *see ENDOR*

electron-nucleon interactions
see also electron-nucleon scattering; electron-proton interactions
baryon resonance electroproduction, review of expt. information 77−22745
Bjorken scaling violation, dynamical approach, N struct. functions 77−49976
Bjorken scaling violations in large angle electroprod. 77−87980
deep inelastic, review of parton model 77−57498
deep inelastic eN scatt., EM corrections to asymptotic freedom predictions 78−62403
deep inelastic polarised scatt., QCD corrections 80−52517
deep inelastic scatt., heavy lepton mixings, Weinberg-Salam model 80−62992
deep inelastic scatt., polarisation meas., struct. function anal. 79−67566
deep inelastic scatt., quark model, field-theoretic, quark indistinguishability, nucleon structure function 80−62993
deep inelastic scatt. and rising $\sigma(\bar{\nu})/\sigma(\nu)$ ratio, neutron-proton structure function difference 77−49978
deep inelastic scattering asymmetries, gauge theory predictions 79−22104
deep inelstic pp, πN, eN scatt., lepton-hadron relation, multiparticle prod. phenomena, average multiplicities 78−37247
deep-inelastic leptoproduction off nucleons, struct. function model in asymptotically free gauge models 79−40786
exclusive meson electroprod. on nucleon, cross section asymptotics, scaling functions *(Russian)* 79−22111
hadronic final states in deep inelastic scatt., vector meson prod. 78−78184
jet analysis, QCD calcs. and phenomenological models 80−52523
meson electropod. in deep inelast. scatt. from polarised targets 78−25053
nucleon Fermi motion in deuteron, smearing effects, (West β correction), on expt. results. 80−32107
odd-parity interactions, electron and quark anapole moments *(Russian)* 79−45093
parton model anal. of deep inelastic scatt. 78−62405
physical pion low energy electro- and photoprod., Ward identity, chiral symmetry breaking struct. 80−5003
physical pion low energy photo- and electroprod., photoprod. phenomenology, quark mass 80−5004
projection operator method and electron-nucleus nonintegrated sum rules 77−2967
QCD and short range nuclear phenomena 80−91060

electron-nucleon interactions continued
relativistic theory of P violation in many-electron atoms 80−91042
residual proton production in deep inelastic electron scatt. 78−70381
scaling deviations in νN, eN, μN inelastic scatt., energy depend. 77−49948
scaling violation, Callan-Gross relation, colour excitation in electroproduction 77−65159
scaling violation patterns in eN scatt., p-n mass difference 77−57536
scaling violations in electromagnetic and neutrino charged-current interactions 79−17713
target mass effects in polarized electroproduction 80−78072
weak, indications given by optical activity of heavy metal vapours *(Russian)* 77−10618
weak, parity nonconservation effects in atoms 77−13890
weak interactions, optical experiments as a means of verification 79−6313
weak neutral currents, parity non-conservation in e-N, μ-N forces 77−57484
eD, 19.4 to 22.2 GeV, unpolarised target, parity violation in inelastic scatt. of polarised electrons 79−63482
ed, 2.3 GeV, inclusive electroprod. cross sections for final state nucleons 77−34159
ed, charged pion forward electroprod. at $Q^2=1.0(\mathrm{GeV}/c)^2$, $\pi^{\pm}$ cross section ratio 79−93434
ed, deep inelastic scatt., nucleon struct. function moments anal., asymptotic freedom critical tests 79−54344
ed, $K^{\pm}/\pi^{\pm}$ ratio and symmetry props. of quark- parton model, fragmentation functions 78−93888
ed deep inelast. scatt., struct. function, dispersion anal. of deuteron 77−2795
ed deep inelastic scatt., p-violating asymmetries, neutral current couplings, sea quark contrib. 79−97630
ed deep inelastic scatt. at 19.4 GeV, polarised electrons, search for P violation 77−34156
ed deep inelastic scattering, phenomenological determ. of electroprod. struct. functions 79−63478
ed$\rightarrow$eX, polarised deep inelastic scatt., test of Weinberg-Salam model 79−22006
ed$\rightarrow$e$'$+X, polarised e, parity non-conservation in inelastic scatt. 78−89719
ed$\rightarrow$e$'$+X, polarised electrons, asymmetric inelastic scatt., effect of odd-parity components of deuteron 79−89166
ed$\rightarrow$e$'$p$_s$pπ^-, 0.70 and 1.35 GeV^2, cross section 77−10264
ed$\rightarrow$hadrons, inclusive distrib. of hadrons from deep inelastic scatt. 79−89167
eN, 50, 100, 300 GeV, in emulsion, cascade showers 3-dimens. development 80−86724
eN, deep inelastic scattering and asymptotic freedom 80−27511
eN, pion production, vector-like theories *(Russian)* 78−37221
eN deep inelastic scatt., QCD anal. 80−95276
eN deep inelastic scattering, scaling prediction and prod. struct. functions 79−17738
eN$\rightarrow$e meson boson, nature of gluons, spin, helicity struct. of amplitudes 77−18293
eN$\rightarrow$eDC$_1$, charm particle electroproduction near threshold *(Russian)* 78−8675
eN$\rightarrow$eX, form factors and structure functions, review, book contrib. 80−47294
eN$\rightarrow$eX, generalised vector meson dominance model, sum rules 78−45810
eN$\rightarrow$eX, quark structure functions for hadrons, Drell-Yan model anal. 78−21476
eN$\rightarrow$eX, $SU(2)_L \times U(1)$ gauge theory distinguished from $SU(2)_L \times SU(2)_R \times U(1)$, neutral currents, z-bosons 80−62908
eN$\rightarrow$e$'$pX longitudinal-transverse separation 77−49977
eN$\rightarrow$e$'\pi^{\pm}$X, longitudinal-transverse separation 77−49977
eN$\rightarrow$e+hadrons, E<2 GeV, formalism, review, book contrib. 80−47312
en$\rightarrow$enπ, pol. e, P-odd asymmetry and cross sections, SU(2)xU(1), SU(3)xU(1) calcs. *(Russian)* 80−62998
eN$\rightarrow$eπ_s+X, test of soft-pion theorem in inclusive pion electroprod. 79−17739
eN$\rightarrow$e$\pi^{\pm}$X, ^{1}H, ^{2}H targets, π^+/π^+ ratio, Q^2 to 4 GeV^2 77−74693
en$\rightarrow$e$\pi^{\pm}$X, π^+/π^- ratio meas. 77−18295
eN$\rightarrow$e$\pi\Delta$, low energy, ΔN axial form factors soft-pion theory 78−70380
eN$\rightarrow$eπN, π form factor determ. 78−66128
eN$\rightarrow$hadrons+anything, scale invariant limit on average transverse momentum 77−67659
eN interactions, parity nonconservation, $SU(2)_L \times SU(2)_R \times U(1)$ gauge model anal., Z boson decay widths 80−47302
eN$\rightarrow$pX, ^{1}H, ^{2}H targets, forward protons to $Q^2=9.5$ GeV^2 77−74690
e$^-$N, inclusive pion production due to $\gamma q \rightarrow \pi q'$ process, quark-parton model *(Russian)* 80−78073
e$^-$N$\rightarrow$e$^-\Delta$(3/2, 3/2), P-odd asymmetry, P nonconserving neutral current interaction 80−57611
e$^-$N$\rightarrow$e$^-$Nπ, electromag. and weak process from weak neutral current interaction *(Russian)* 78−45928
e$^-$N$\rightarrow$e$^-$X, parity violating asymmetry, constraint on right-handed electron weak charge 79−17734
e$^-$N$\rightarrow$e$^-\pi$X, high Q^2 cross-section meas. 78−21439
ep$\rightarrow$eΛX, electroprod. of forward Λ baryon near/along virtual photon direction 79−22116
e$^-$p, deep inelastic scatt., EM corrections to hadronic and neutral currents, systematic effects *(Russian)* 79−49526
e$^+$p, deep inelastic scatt., EM corrections to hadronic and neutral currents, systematic effects *(Russian)* 79−49526
eZ$\rightarrow$Z$\mu\bar{\nu}_\mu\nu_e$, muon spectra V-A theory 77−65148
ne scattering length, expt. determ. and degree of precision, review 79−58961
π electroprod. at low energy, and hadron form factors, book 79−85306
^{209}Bi, P violating eN pot., determ. of effects by optical rotation meas. 79−26277
^{209}Bi, transitions, parity nonconservation due to neutral weak currents 77−13913
^{205}Tl, transitions, parity nonconservation due to neutral weak currents 77−13913

electron-nucleon scattering
see also electron-nucleon interactions; electron-proton scattering
asymmetry predictions for deep inelastic and elastic scatt. and Δ electroproduction 78−58193
charged spin-1 gluons, integer charged quarks, e- and ν- prod. 77−49894

electron-nucleon scattering continued
- deep inelastic $F_2^n(x)/F_2^p(x)$ near $x=1$, chirality 77—10258
- deep inelastic n charge radius and quark parton model 77—71488
- deep inelastic processes and SU(4) symmetry 77—22741
- deep inelastic scatt., N_2 struct., nuclear forces in quark model *(Russian)* 77—61299
- deep inelastic struct. function for rest frame, quark-parton model 77—87942
- deep inelastic struct. function higher order asymptotic freedom corrections for e, M, γ scatt. 79—93426
- EM probes of nucleons, photo- and electro-excitation, quark model anal. of nucleon struct. 79—49520
- gauge model of weak and electromag. interactions, polarised lepton scatt. 78—45901
- Han-Nambu and SUB quark models, modified, appl. to deep. inelastic electron-nucleon scatt. 80—22562
- light-cone field-theory and the parton model, book contrib. 78—82220
- nucleon polarisabilities α,β and deep inelastic e-N scatt. 77—49966
- P-odd asymmetry in l-N scatt., unified model *(Russian)* 77—61300
- pion electroproduction, quark-parton model consistency 77—79254
- polarisation effects, C- and T-invariance perturbation *(Russian)* 77—10256
- polarised e scattering, elastic and deep inelastic covariant formulation 80—78069
- polarised scatt., P-violation, test of unified gauge theories 79—17732
- quark-parton model inconsistency with $\bar{\nu}N(\nu N)$ CERN data *(Russian)* 77—49951
- structure function moment asymptotic behaviour and light cone singularities 78—4804
- $SU(2)_L \times (T_3)_R \times U_V(1)$ gauge unified model, neutral current interactions, ed and ν scatt. 80—18107
- unified formulae for EM decays, electroprod., e^+e^- hadron pair prod. for arbitrary spin 77—57535
- e d polarised elastic scatt., parity violation 79—36085
- ed, elast. scatt., polarisation meas. and percentage D state of deuteron 80—420
- ed, parity nonconservation, $SU(2)\otimes U(1)\otimes U'(1)$ gauge anal. 79—17731
- ed, parity violating asymmetries in polarized electron scattering 80—9111
- ed, polarised e, elastic scatt. asymmetries in $SU(2)\times U(1)$ gauge theory 79—40781
- ed, polarized scatt., parity violation Weinberg-Salam model without parton model 79—40787
- ed, quasi-elastic scatt. and form factor of n 78—82210
- ed deep inelastic scatt., parity nonconservation 79—75776
- ed elastic scatt., d form factors and struct. functions, charge and struct. radius *(Russian)* 79—40841
- ed elastic scatt., P-odd effects due to neutral weak currents, cross sections *(Russian)* 80—13312
- ed elastic scatt., recoil d vector polarisation, p-violation 79—398
- ed elastic scattering, neutral weak currents *(Russian)* 78—21434
- ed inelastic scatt., electrodisintegration at high energy and momentum transfer, exchange currents 79—6342
- ed large angle elastic scatt., deuteron mag. struct. function meas. at 1.0 $(GeV/c)^2$ 77—57537
- ed quasi-elastic scatt., en coincidence, n electric form factor 79—67563
- ed scat., d disintegration, polarised e, neutral weak currents, right-left asymmetry 79—80787
- ed scatt., energy weighted sum rules, almost realistic NN pot. anal. *(Russian)* 80—13465
- ed scatt., meson exchange currents for deuteron form factor 77—18290
- ed scatt., P-violation calc. in weak interaction theory 80—42469
- ed tensor polarisation and d wave function short range behaviour 79—67564
- en, polarised e, elastic scatt. asymmetries in $SU(2)\times U(1)$ gauge theory 79—40781
- $eN \rightarrow e+$anything, 2.3 to 13.6 GeV electrons in nuclear emulsion, cross sections, μ comparison 77—46161
- eN elastic scatt., pol. e, nucleon form factors, P violating symmetry, Weinberg-Salam calcs. 80—68461
- eN elastic scatt. in nuclei, P violating asymmetry due to weak neutral currents 80—73713
- e^-N elastic scatt., weak interaction model independent anal., e-q neutral current 79—71753
- ep(d) scatt., nucleon struct. function moments, asymptotic freedom critical test 79—85300

electron-nucleus reactions
- *for inelastic electron-nucleus scattering, see "electron-nucleus scattering"*
- *see also electron-nucleon interactions; nuclear electron capture*
- actinide nuclei, photo- and electro-fission cross sections and yields, giant resonances 80—5187
- CERN School of Physics, Austerlitz-Zeist, Holland (June 1978) 79—30857
- conference on nuclear interactions, Canberra, Australia (Aug.-Sep. 1978) 80—4476
- cosmic rays, cascade build up, Landau-Pomeranchuk effect 77—64558
- cross-sections, 5 to 500 MeV and nuclear research bibliography 78—29338
- deep inelastic hadron leptoproduction on nuclei, inclusive hadron final states 78—54741
- deep inelastic scatt., $\Delta(1232)$ production 80—57772
- electro- and photonuclear EM sum rules 80—22810
- electrofission of light nuclei, recent obs. 79—3185
- electrofragmentation of p-shell nuclei *(Russian)* 79—67746
- electropion prod., deep inelastic scatt. and struct. from electron coincidence expts. at Stanford 80—22821
- electroproduction above pion threshold, EM interactions and mag. sum rules 80—42639
- electroproduction of light fragments on nuclei, quasielastic knockout by electrons, general theory *(Russian)* 79—13276
- excitation, giant monopole, energy-weighted isoscalar sum rules 80—63174
- few body systems and EM interactions, conference, Frascati, Italy (March 1978) 79—71804
- few nucleon systems, intermediate energies 77—79363
- few-nucleon systems studied with electromagnetic probes, future prospects 79—71809
- GeV-electron accelerator physics in nuclei 80—42645
- H=3 nucleus complete electrodisintegration, interaction role in final state *(Russian)* 77—74835
- hadron electroproduction from nuclei 78—66267

electron-nucleus reactions continued
- heavy nucleus, coherent and inclusive prod. of hadrons with low P_T, Coulomb excitation and decay of projectile 80—83100
- high energy particle-nucleus interactions, discussion 79—30858
- hole states, continuum shell model approach for (p,2p) and (e,e′p) reactions 79—22162
- inner shell core struct. of nuclei from high energy electron elastic scatt. and knockout reactions 78—54739
- low level excitation, inelastic electron scatt. *(Russian)* 78—58265
- meson exchange currents, effect in electron inelastic scatt., book contrib. 80—480
- mesonic and relativistic effects in the nuclear electromagnetic interaction 80—22818
- momentum wave function determ. in atomic, molecular and nuclear systems 77—88556
- nucleon Fermi motion in deuteron, smearing effects, (West β correction), on expt. results. 80—32107
- nucleon motion in nuclei, determ. using high energy electron induced knock-out reactions *(French)* 79—445
- nucleonic mass distrib. using mag. spectrometer *(French)* 79—449
- parity violating neutral current interaction, gauge theory predictions, radiative corrections 78—86436
- phenomenological model for nuclear leptoproduction 79—63660
- photoneutron yields released by incident electrons, improved calc. 80—27630
- photonuclear reacts., conf., International school, Erice, Italy, 1976 77—88111
- pion electroproduction from the nucleon near threshold 80—68651
- pion production thresholds, pseudoscalar and pseudovector Lagrangian densities 78—29449
- positron energy spectra and ang. distrib., 0.2-2 GeV electron conversion on W targets 78—86713
- QCD and short range nuclear phenomena 80—91060
- quasielastic scatt., nucleon emission and meson exchange flux *(German)* 80—47468
- reaction mechanism at asymptotically high impact vel. 79—97700
- relativistic theory of P violation in many-electron atoms 80—91042
- shadowing in electroproduction, geometrical origin, virtual photon generation 77—82913
- spallation reaction and its appls. *(Japanese)* 78—74345
- spherical nuclei, dipole states, transition densities and electroexcitation, GDR form factors *(Russian)* 80—52611
- synchrotron radiation spectrum, electron prod., high energy struct. from $^{12}C(\gamma,\gamma)$ scatt. 78—13062
- three-nucleon systems, EM processes, electrodisintegration 79—71806
- threshold pion electroproduction, nuclear response surface 78—93989
- two-nucleon system EM processes, baryon resonances 77—79364
- virtual photon description, Weizsacker-Williams method, Moller potential 77—79361
- (e,α), $Z=29\text{-}79$, direct and statistical effects, cross sections and ang. distribs. 79—530
- $(e^-,\alpha\nu)$ on heavy nuclei, peripheral model 80—37369
- (e,e′), on ^{40}Ca, ^{48}Ca, ^{90}Zr, and ^{208}Pb, (in)elastic scatt., self-consistent calcs. of nuclear density *(Russian)* 79—80928
- (e,e′d), cross sections, short range correls. in nuclei, two body density 78—54743
- (e,e′N) reaction, energy depend. optical potential calc. *(Russian)* 78—41706
- (e, e′p), eN interaction in quasifree scatt., nonrelativistic Hamiltonian through 2nd order 80—52663
- (e,e′p), heavy nuclei, isospin effect 79—80926
- (e,e′p), optical potential variation effects 77—41955
- (e,e′p), wave function orthogonality, bound state to continuum transitions 78—78335
- (e,e′p) coincidence expts. at Saclay 600 MeV electron linac ALS 79—72035
- $(e,e'\pi^{\pm})$, threshold production 79—85452
- (e,e’p) quasi-free scatt., spectral function, sum rule discrepancy, shell model deviation 80—42641
- $(e,e'\pi)$, π electromag. processes, theoretical aspects 80—22822
- $(e,e'\pi^{\pm})$, near threshold, reactions on ^3He, ^6Li, ^{11}B, ^{12}C and ^{16}O 77—10388
- (e,X) 4.5 GeV heavy particle production semicond. telescopic detection setup *(Russian)* 80—63461
- $eZ \rightarrow Z\mu\bar{\nu}_\mu\nu_e$, muon spectra V-A theory 77—65148
- (γ,d), odd-Z light nuclei, from (e,e′d), cross section, E2 transistors giant resonance and clusters 80—63169
- π electroproduction, closure approx. improvement applied 78—16680
- $^{45}Sc(e,e'p)$ cross-sections meas., (γ,p) cross-sections calc. 77—26666
- $^{102}Ag(e,\gamma)^{102}Pd$, 1592 keV E0 transition, half life measurement 80—22762
- ^{107}Ag, comparison of absolute cross sections for electron and photon induced reactions, DWBA calc. test 77—41958
- $^{107}Ag(e,\alpha)$, 100 MeV, energy spectra, cross sections 77—18529
- Al+e, 800 MeV, multicharged particle emission during nucleus disintegration 78—41702
- $^{27}Al\ (e,\alpha)$, 120 MeV, preequilibrium α-emission, α energy spectra 79—85459
- $^{27}Al(e,e'p)$ 77—10389
- $^{27}Al(e,e'\pi^+)$, 130 to 580 MeV, cross sections, impulse approx., multipole decomp. 77—54206
- $^{27}Al(e,e'\pi^+)$, energy and ang. distribs. of πs, low lying residual states 78—54740
- $^{27}Al(e,x)$, electrodisintegration charged particle yield, α to t cross section ratio *(Russian)* 80—86902
- $^{27}Al(\gamma,p)$, cross sections and proton energy spectra from (e,e′p) 80—13461
- $^{197}Au\ (e,\alpha)$, 120 MeV, preequilibrium α-emission, α energy spectra 79—85459
- $^{197}Au(e,xn)$, 37 to 147 MeV, cross sections, giant dipole reson. 79—89296
- $^{10}B(e,e'p)$, 700 MeV, proton spectral functions, momentum distribs., DWIA anal. 78—41701
- ^9Be, π^+ electroprod., distorted wave impulse approx. anal. 79—17894
- $^9Be(e,X)$, transverse and longit. form factors for electrodisintegration, small momentum transfer *(Russian)* 79—80927
- $^9Be(e,e'p)$, 700 MeV, proton spectral functions, momentum distribs., DWIA anal. 78—41701
- $^9Be(e,e'p)$, single hole state momentum and energy distribs. 80—22674
- $^9Be(e,e'\pi^+)$, energy and ang. distribs. of πs, low lying residual states 78—54740

electron-nucleus reactions continued
^{9}Be(e,π^{+}), 1848 MeV, virtual photon spectrum, virtual photon theory test 80−102183
^{9}Be(e,$\pi^{\pm}$), 10 MeV π, of PWIA calcs. 79−93607
^{9}Be(γ,X), charged particle emission in (e,e′x) reaction, virtual phonon theory 80−13460
^{209}Bi(e,f), 110 MeV electrons, mass and kinetic energy distribs. 79−93672
^{12}C, comparison of absolute cross sections for electron and photon induced reactions, DWBA calc. test 77−41958
^{12}C, excitation cross sections induced by 1 GeV protons and electrons, Glauber theory *(Russian)* 78−41684
^{12}C, π^{+} electroprod., distorted wave impulse approx. anal. 79−17894
^{12}C(e, e′p), eN interaction in quasifree scatt., nonrelativistic Hamiltonian through 4th order 80−47469
^{12}C(e, e′p), quasifree scatt., spin-orbit distortion of emerging nucleon 80−52664
^{12}C(e, $\pi^{\pm}$), 17 and 29 MeV 79−63659
^{12}C(e,e′N), energy and ang. distribs. diffraction approx. for final state interaction *(Russian)* 77−18531
^{12}C(e,e′P)^{11}B, nonorthogonality of initial and final nucl. states *(Russian)* 78−66265
^{12}C(e,e′), role of two-particle scatt. *(Russian)* 80−91178
^{12}C(e,e′d), deuteron knock-out yield, contrib. to inelastic scatt. cross section *(Russian)* 80−27621
^{12}C(e,e′p), 700 MeV, DWIA anal. proton spectral function 77−6353
^{12}C(e,e′p), cross sections from DWIA, optical, and shell model calcs. *(Russian)* 80−32270
^{12}C(e,e′p), p-shell nucleon momentum distrib. determ. 78−17182
^{12}C(e,e′p)^{11}B, cross section calc. based on shell model with residual interaction *(Russian)* 77−311
^{12}C(e,e′p)^{11}B, energy spectra calc. in terms of dynamic collective model *(Russian)* 78−8804
^{12}C(e,e′p)^{11}B, recoil momentum distribs., optical potential variation effects, HF calcs. 77−41955
^{12}C(e,e′p)^{11}B, validity of the factorised DWIA 79−59054
^{12}C(e,e′π^{+}), ^{12}B analogue states at 4.5 MeV giant resonance region, strong spin-isospin mode 80−78250
^{12}C(e,e′π^{+}), energy and ang. distribs. of πs, low lying residual states 78−54740
^{12}C(e,e′π^{+})^{12}B, near threshold, equivalent photon approx., Kroll-Ruderman term 78−13065
^{12}C(e,eπ), total cross section from square reaction matrix element *(Russian)* 80−32271
^{12}C(e,n)^{11}C, 30 MeV, cross section absolute meas., corresponding (γ,n) cross section 78−66270
^{12}C(e,$\pi^{\pm}$), 10 MeV π, of PWIA calcs. 79−93607
^{12}C(e,π), charged π electroprod. near threshold, data anal. 78−66266
^{12}C(ee′d), electroproduction cross section, Born approx. *(Russian)* 79−26427
^{40}C, π, electroproduction, near threshold, inelastic response functions 78−33172
^{40}Ca(e,X), deep-inelastic electron scatt. in the transverse region, 150, 200, 250 MeV 79−17895
^{40}Ca(e,e′p), multiparticle approach to expt. data anal. 77−88112
^{40}Ca(e,e′p) 77−10389
^{44}Ca(e,e′p) cross-sections meas., (γ,p) cross-sections calc. 77−26666
^{111}Cd, 1330 keV level excitation cross section from positron annihilation 80−68583
^{140}Ce(e,e′), giant dipole resonance, E1 form factor and breathing mode existence 79−3125
^{59}Co(e,e′p), isospin effects in GDR region 78−78344
^{52}Cr(e,p_0(p_1)), differential cross section in giant dipole resonance region 79−63655
^{63}Cu, comparison of absolute cross sections for electron and photon induced reactions, DWBA calc. test 77−41958
^{63}Cu(e,α), 100 MeV, energy spectra, ang. distribs. 77−18529
D(e,e′n)H, Princeton Large Tokamak, D electrodisintegration neutron spectrum 77−84521
D(e,e′p)n, 160 to 300 MeV/c neutron-spectator impulse region *(Russian)* 77−50118
D(e,e′p)n, 500 MeV, coincidence cross section and deuteron momentum distrib. 79−67747
^{56}Fe(e,α), E2 isoscalar resonance sum rule, DWBA anal. 80−68621
^{56}Fe(e,e′α), 60 and 120 MeV, evidence for α-clusters 79−6569
^{2}H, elastic and inelastic electron scatt., quarks and dimensional scaling 77−6132
^{2}H electrodisintegration, study of e.m. processes in nuclei 79−71797
^{2}H photodisintegration and electrodisintegration, weak interaction and P nonconservation 78−89849
^{2}H, weak and EM lepton reactions, exchange currents, isobaric excitations and form factors *(German)* 79−93523
^{2}H(e, ep)n, spectator momentum distrib., quasielastic knockout mechanism *(Russian)* 79−30817
^{2}H(e,e′)NΔ, electroproduction cross section for reson. $\Delta_{3/2}$ *(Russian)* 77−67737
^{2}H(e,e′p), consistent nonrelativistic treatment including meson exchange currents and isobar configurations 79−40905
^{2}H(e,e′p), single hole state momentum distrib. 80−22674
^{2}H(e,e′p) 1180 MeV electrons, proton distribution, neutron momentum distribution *(Russian)* 80−68652
^{2}H(e,e′p)n, cross-section, neutron electric form factor 79−3138
^{2}H(e,e′p)n, recent developments in lepton scattering 79−80929
^{2}H(e,eπ), total cross section from square reaction matrix element *(Russian)* 80−32271
^{2}H(e,n)p EM sum rules, exchange currents and isobar configurations 79−93526
^{2}H(e,ne)^{1}H, meson exchange effects at quasi-elastic peak 77−30556
^{2}H(e,np), dispersion approach *(Russian)* 77−22737
^{3}H electrodisintegration, quasi-elastic region, realistic interactions 79−71850
^{3}H, influence of structure on cross-section of complete electrosplitting *(Russian)* 79−22272
^{3}H(e,e′)nd, three-body calc. 78−33170
^{3}H(e,e′p)2n, realistic NN interactions, three body variational wave functions, spectral functions 80−47470
^{3}H(e,e′X), X=p or n, coincidence reactions, electrodisintegration cross sections 80−22823
^{3}H(e,np), disintegration and Coulomb excitation cross sections in channelled nuclei 80−59539

electron-nucleus reactions continued
He, contact interactions, parity-violating and parity-conserving, new evaluation techniques 79−26872
^{3}He, influence of structure on cross-section of complete electrosplitting *(Russian)* 79−22272
^{3}He(e, e′p) electrodisintegration by 1200 MeV electrons *(Russian)* 80−37370
^{3}He(e, e), charge formfactors, second Born approx. and pole model 80−18155
^{3}He(e,e′)pd, three-body calc. 78−33170
^{3}He(e,e′p), cross-section, Fadeev technique, nucleon-nucleon interaction *(Russian)* 80−73842
^{3}He(e,e′p)^{2}H, 1.2 GeV, p angular distrib., recoil nucleus momentum distrib. *(Russian)* 79−9550
^{3}He(e,e′X), X=p or n, coincidence reactions, electrodisintegration cross sections 80−22823
^{3}He(e,π^{+})^{3}H, cross section from t recoil cross section meas. 79−6574
^{3}He(e,π^{+})e′t, (e,t)e′π^{+} cross-sections and ang. distribs. calc. 78−21545
^{4}He (e,e′pp) reaction cross-section and ground state shell model calcs. *(Russian)* 80−78283
^{4}He(e,^{3}H), ^{4}He 2^{+} resonance evidence at 40 MeV 80−86880
^{4}He(e,e′p)^{3}H, 1186 MeV, recoil nucleus momentum distrib. *(Russian)* 78−54748
^{165}Ho(e,α), 100 MeV, energy spectra, cross sections 77−18529
^{139}La(e,e′p), $f_{7/2}$ ground isobaric analogue resonance, proton decay mode 78−29450
^{139}La(e,p), 15-25 MeV, T_0+1 giant dipole resonance and characteristic decay mode 80−78247
^{6}Li breakup by electrons, quasifree scatt., d-α vertex const. calc. 77−6354
^{6}Li(e,d)e′^{4}He, meas. and anal. based on α-d cluster model, ^{6}Li(γ,d)^{4}He cross-sections extracted 77−6355
^{6}Li(e,e′d)^{4}He, ^{6}Li(e,e′τ)^{3}H, d-α cluster model anal. 77−26673
^{6}Li(e,e′d)^{4}He, p-shell nuclei electrofragmentation, Born approx. *(Russian)* 79−67746
^{6}Li(e,p), 16 MeV, nonexistence of 16.1 MeV state in (γ,p) cross section 79−45174
^{7}Li(e,^{3}H)^{4}He,e′, 6-15 MeV, cross sections 77−26672
^{7}Li(e,X), X=^{6}He,^{6}Li, 108-198 MeV, ang. distribs. and cross sections 80−42647
^{A}Li, A=6,7, π^{+} electroprod., distorted wave impulse approx. anal. 79−17894
Li(e,e′p), A=6,7, 700 MeV, proton spectral functions, momentum distribs., DWIA anal. 78−41701
Li(e,e′π^{+}), A=6,7, energy and ang. distribs. of πs, low lying residual states 78−54740
^{24}Mg+e, 21 to 32 MeV, E0 and E2 excitations, fission into two ^{12}Cg.s. nuclei 78−54744
^{24}Mg(γ,p), cross sections and proton energy spectra from (e,e′p) 80−13461
^{A}Mo (e,α), A=92, 94, 120 MeV, preequilibrium α-emission, α energy spectra 79−85459
^{15}N(e,t_0), 20-25 MeV, photodisintegration and electrodisintegration 79−80922
^{142}Nd(e,e′p), spectra and ang. distribs. meas., $T_{>}$ giant reson. anal. 78−13069
^{20}Ne(e,e′α), EM induced α emission, α spectroscopic amplitudes, anal. solvable model 80−32267
Ni (e,α), 120 MeV, preequilibrium α-emission, α energy spectra 79−85459
^{A}Ni(e,α), A=60,62, 16 to 50 MeV, cross sections, giant reson. decay modes 79−17877
^{A}Ni(e,p), A=60,62, 16 to 50 MeV, cross sections, giant reson. decay modes 79−17877
^{A}Ni(e,p),(e,α), A=58, 60, 62, electrodisintegration cross sections, E1, E2 absorption, DWBA anal. 80−106052
^{58}Ni(e,α), 16 to 50 MeV, cross sections, giant reson. decay modes 79−17877
^{58}Ni(e,e′α), electric quadrupole giant resonance α-decay *(Russian)* 79−85434
^{58}Ni(e,e′p), electric quadrupole giant reson. decay *(Russian)* 79−85434
^{58}Ni(e,p), 16 to 50 MeV, cross sections, giant reson. decay modes 79−17877
^{60}Ni(e,α)e′X, alpha particle spectra, statistical model calc., direct reaction component 78−41704
Ni(e,α), E2 strength in resonance regions statistical decay 80−91146
^{237}Np(e,e′f), 20-120 MeV, electrofission cross section, E1, E2 strengths 78−13174
^{237}Np(e,f), 10-34 MeV, electrofission cross section, E2 transition mode and giant resonances 80−106084
^{237}Np(e,f), 110 MeV electrons, mass and kinetic energy distribs. 79−93672
^{16}O, π, electroproduction, near threshold, inelastic response functions 78−33172
^{16}O, π^{+} electroprod., distorted wave impulse approx. anal. 79−17894
^{16}O(e,e′p), polarisation effect on quasi-free electron scatt. 77−71607
^{16}O(e,e′p), single hole state momentum and energy distribs. 80−22674
^{16}O(e,e′π^{+}), energy and ang. distribs. of πs, low lying residual states 78−54740
^{16}O(e,π^{+}), 180.4 MeV, virtual photon spectrum, virtual photon theory test 80−102183
^{16}O(e,$\pi^{\pm}$), 10 MeV π, of PWIA calcs. 79−93607
^{16}O(e,π), charged π electroprod. near threshold data anal. 78−66266
^{141}PR(e,e′p), $f_{7/2}$ ground isobaric analogue resonance, proton decay mode 78−29450
Pb+e^{+}, 0.5-3.5 GeV positron initiated showers, test of cosmic ray shower calcs. 78−37332
Pb(e,e′f), 28-44 MeV, anomalous reson. struct. obs. 77−82972
^{141}Pr(e,p), 15-25 MeV, T_0+1 giant dipole resonance and characteristic decay mode 80−78247
^{294}Pu, muonic atom direct electroprod., finite nuclear size effects *(Russian)* 80−69272
^{28}Si (e,f), K=2 symmetry intermediate state 80−47514
^{28}Si electrofission, decay to ^{12}C($2_1{}^{+}$)+^{16}O($0_1{}^{+}$) fragments 78−41793
^{28}Si(e,e′^{16}O)^{12}C^{2+}, 23-34 MeV, ^{12}C yields and ang. distrib. meas. 77−61466
^{28}Si(e,f), alpha cluster model approach, intermediate state to ^{12}C+^{16}O 79−40972
^{181}Ta(e,α), 100 MeV, energy spectra, cross sections 77−18529
^{159}Tb(e,α), 100 MeV, energy spectra, cross sections 77−18529

electron-nucleus reactions continued
^{232}Th (e, f), 7-65 MeV, absolute electrofission cross sections, fragment ang. distribs. 80−5185
^{232}Th(e,e′f), 20-120 MeV, electrofission cross section, E1, E2 strengths 78−13174
^{232}Th(e,f), 110 MeV electrons, mass and kinetic energy distribs. 79−93672
^{46}Ti(e,e′p) cross-section meas., (γ,p) cross-section calc. 77−26666
^{169}Tm(e,α), 100 MeV, energy spectra, ang. distribs. 77−18529
^{A}U, A=237,238, nuclear excitation rate for low lying states, e and γ induced transitions 79−17856
^{235}U(e,f), 110 MeV electrons, mass and kinetic energy distribs. 79−93672
^{236}U, giant E2 isoscalar resonance determ. 80−27607
^{238}U (e, f), 7-65 MeV, absolute electrofission cross sections, fragment ang. distribs. 80−5185
^{238}U electrofission, 6-60 MeV, relative E1 contrib. 77−6471
^{238}U(e,α)e′^{234}Th, cross section, α-spectra, γ-spectra of ^{234}Th decay 78−58262
^{238}U(e,e′α), 13.1 MeV, cross section in giant quadrupole resonance region 79−6573
^{238}U(e,e′f), 20-120 MeV, electrofission cross section, E1, E2 strengths 78−13174
^{238}U(e,e′n)^{237}U, 6-25 MeV, transition multipolarities 78−590
^{238}U(e,e′f), 5.5-9 MeV, fission fragment ang. distribs. DWBA anal., low lying fissioning levels 80−42713
^{238}U(e,f), 110 MeV electrons, mass and kinetic energy distribs. 79−93672
^{238}U(e,n), 20, 120 MeV, 80−22757
^{238}U(e,p), 40 MeV, p spectra, deduced ternary fission cross section 79−9549
^{51}V(e,e′p), isospin effects in GDR region 78−78344
^{51}V(e,e′p) 77−10389
^{51}V(e,e′$\pi^{\pm}$), 130 to 580 MeV, cross sections, impulse approx., multipole decomp. 77−54206
^{51}V(e,p$_0$), 15-26 MeV, differential cross section in giant dipole resonance region 79−63655
W, photo- to electrodisintegration yield ratios *(Russian)* 77−50112
^{A}W(e,f), A=182,184,186, 35-55 MeV, fission barriers, pairing strength deformation depend., stat. anal. 80−57810
^{89}Y(e,e′π^{+}), energy and ang. distribs. of πs, low lying residual states 78−54740
^{64}Zn, electroexcitation of giant multipole reson. *(Russian)* 78−58264
^{90}Zr(e,α), 135-66.5 MeV, (γ,α) statistical and pre-equilibrium cross sections and multipolarities 80−68646

electron-nucleus scattering
see also electron-nucleon scattering
^{3}He(e,e′p) coincidence expt. at Saclay 600 MeV linac 79−71849
A=40-100, charge distrib. from (e,e) and muonic X-ray meas. 78−54679
A dependence of photoabsorpt. processes, from inelastic electron and muon scatt. studies 77−82911
activities at Amsterdam 77−82918
bremsstrahlung, inverse, for $\gamma+e_1^-+Ze \to e_2^-+Ze$, Born approx. *(Russian)* 78−13064
bremsstrahlung of relativistic electrons in screened Coulomb potential effect *(Russian)* 78−46050
charge and density distribs., scatt. of fast particles *(Russian)* 78−25161
collective excitations from high-q electron scatt., RPA AND ATDMF calcs. 80−22673
collective props. of nuclei deduced from electron scatt., deformed nuclei, review 78−50064
conference on high energy physics and nuclear struct. Vancouver, Canada (Aug. 1979) 80−41936
conference on interacting bosons in nuclear physics, Erice, Italy (June '78) 80−27042
conference on nuclear physics with EM interactions, Mainz, Germany (June 1979) 80−22145
deep inelast. electron scatt., nucleon polarisabilities 77−82919
deep inelastic, meson exchange currents from Fermi gas model 78−66268
deep inelastic Coulomb corrections 79−89299
deep inelastic scatt., N$_2$ struct., nuclear forces in quark model *(Russian)* 77−61299
deformed nuclei, electron scatt., elastic differential cross section calc. 77−82912
deformed nuclei, transition densities for electroexcitation 78−17183
Dirac-Coulomb functions, asymptotic expansions of radial integrals 79−308
double bremsstrahlung in e-nucleus Coulomb scatt. *(Russian)* 77−50117
(e,e), elastic and inelastic A=12-40, 22 79−63571
eikonal anal. of high energy scatt. *(Russian)* 77−22908
eikonal approx., electron-oriented nucleus scatt., polarisation of e$^-$, nuclei and emitted γ rays 78−37331
eikonal approx. of electron scatt. by spherically symmetric nuclei 78−37330
elastic, three body correlations, influence on charge form factor of closed shell nuclei 79−6571
elastic electron scatt. and atom parity nonconservation caused by nuclear parity violation 80−27427
elastic electron scattering; n-p interaction effect on cross section by dipole giant resonance positioning 77−82914
elastic electron scattering at large momentum transfer, review 80−22820
electron scatt. results at MIT using 200 MeV linac 77−82916
electron scatt. theory, EM struct. from DWBA and other models 80−5133
electropion prod., deep inelastic scatt. and struct. from electron coincidence expts. at Stanford 80−22821
EM interactions, high duty cycle accelerators and experimental possibilities 80−23187
EM sum rules for (γ,γ), (e,e), transitions and giant resonances 80−5090
exchange current affairs 79−71846
few body systems and EM interactions, conference, Frascati, Italy (March 1978) 79−71804
few-nucleon systems, energy-weighted longit. sum rule for electron-nucleus scatt. and nuclear forces 78−58238
few-nucleon systems studied with electromagnetic probes, future prospects 79−71809
form factors, relativistic quantum field theory calc. 77−74765

electron-nucleus scattering continued
GeV-electron accelerator physics in nuclei 80−42645
giant reson. and quasielastic excit. in electron scatt. and muon capture 77−57651
giant resonance electroexcitation 77−82897
heavy electron scattering expts. from intermediate energy linear accelerators *(Dutch)* 79−22502
high energy elastic scatt., prediction from nucleon density distrib. 78−54738
inelastic, magnetic dipole excitation 77−30560
inelastic, results obtained with Darmstadt electron Linac 77−83183
inelastic electron scatt., nuclear charge and current spatial struct. 80−5134
inelastic electron scattering charge distribs. expansions for model independent anals. 77−50114
inelastic electroproduction, review 77−34289
inelastic scattering, evidence for giant resonances 79−17883
interacting boson model, electron scatt. data anal., Sm-Nd region 78−62522
inverse bremsstrahlung, high energy, nucl. mag. contribs. 78−74350
isoelastic processes, one-body density matrix formalism 77−18528
isoscalar dipole strength excitation in GQR region by inelastic electron and hadron scatt. 80−47448
isovector M6 excitations, open shell RPA calcs., appl. to electron scatt. form factors 78−50112
Lauricella function, analytic continuations 79−17645
light nuclei correlation struct. 77−18532
linear accelerator, high-duty cycle, 500 MeV, electron scatt. facilities 79−72036
low-energy transport, validity of extended transport cross-section correction 79−71843
magnetic dipole and quadrupole state excitation, inelastic electron scatt., various nuclei 78−50154
Majorana exchange forces contrib. to scatt. by light nuclei *(Russian)* 77−312
meson exchange currents in scatt. from light nuclei 77−10390
multipolar sum rules *(Russian)* 78−21548
nuclear shell model, globally self-consistent, magic nuclei and spherical nuclei calculations 79−59020
odd-A deformed nuclei, EM and electron scatt. form factors, selection rules 79−9458
one-photon-exchange approx., higher order EM corrections 77−2946
parity nonconservation in elastic scatt. with $0^+ \to 0^-$ transition *(Russian)* 77−61402
photonuclear reacts., conf., International school, Erice, Italy, 1976 77−88111
quadrupole transition densities and electron scatt. in the interacting boson model 80−27598
quasielastic cross section calc., using momentum depend. pot. in Fermi gas model 78−21546
quasielastic scatt., Δ(1232) contrib. 77−79366
relativistic electron scattering, expt. techniques for excited nuclei studies 77−30701
research at Saclay 77−82917
semileptonic weak and EM interactions, (e,e) P-vibrations and state abnormal P admixtures 79−75977
semileptonic weak and EM interactions, multipole operators, HO single particle matrix elements 80−73840
semileptonic weak and EM interactions, nuclear current operators 79−6515
shadowing measurements in low $|Q^2|$ inelastic electron scatt. expts. 79−59053
spherical nuclei, elastic scatt. of high-energy electrons, differential cross section calc. 78−17181
sum rules electron scatt., giant reson. 77−14114
teaching, from Compton effect to quarks, at., proton, and nucl. struct. 78−24596
thin foils, electron scatt., Monte Carlo study 79−67745
two-nucleon system EM processes, baryon resonances 77−79364
virtual photon spectra calc. by matrix differential eqn. 77−88115
weak neutral currents, P-violation in nuclear EM and semi-leptonic interactions 77−71479
(e,e), 25-302 MeV, nucleon density distribution in nucleus 79−75831
(e,e), A=2, 3, 4, scaling laws in relativistic impulse approx. model, spin effects 80−52662
(e,e), A=60 region, nuclear radius, core polarisation and isotone shifts, muonic X-rays 80−22685
(e,e), c.m. motion effects in oscillator shell model 80−106050
(e,e), finite dimension nuclei, differential cross section static correction, shell model 79−75976
(e,e), form factors, magnetisation density, mag. moments and valence nucleon orbits 80−22690
(e,e), high momentum and energy transfer coincidence expts. with GeV electron beams 80−42646
(e,e), low-q, A=14 nuclei, isospin T=2, 1 and 0 collective resonances, shell model 80−510
(e,e), on ^{40}Ca, ^{48}Ca, ^{90}Zr, and ^{208}Pb, (in)elastic scatt., self-consistent calcs. of nuclear density *(Russian)* 79−80928
(e,e), proton and neutron densities 80−22684
(e,e), relativistic e, helicity representation 80−5132
(e,e), virtual photon intensity and finite nuclear size effects, PWBA calcs. 79−26424
(e,e) determination of valence nucleon radial distrib., exchange current role 79−40878
(e,e) elastic mag. scatt., valence neutron radial distrib. determ. 77−57652
(e,e) elastic scatt., spectroscopic information and form factors 80−9260
(e,e) on nuclei with quadrupole moment, differential cross section static correction 79−6570
(e,e′), 1p nuclei M2 giant resonance calcs. 80−22784
(e,e′), 70 MeV, 1p shell nuclei, shell model cross sections, giant M2, transversal E1 resonances 80−63143
(e,e′), A=12, 24, 28, isovector M1 excitations, current and spin contribs. 80−68582
(e,e′), cross section near quasielastic maximum, shell and optical models *(Russian)* 80−91179
(e,e′), light and medium nuclei, high energy approx. anal., transition densities and probabilities *(Russian)* 80−63129
(e,e′), radial integrals with finite energy loss for Dirac-Coulomb functions 77−23000
(e,e′), shift of quasielastic peak 79−6572

electron-nucleus scattering continued

- (e,e′), transition strengths, unnatural parity state excitation of stretched configs., NN forces 79−63626
- (e,e′), transverse excitation of rotational states, cranking model velocity fields 77−10342
- (e,e′) and (p,p′) scattering, microscopic models, core polarisation, transitions, cross sections, form factors 78−604
- (e,e′) in giant resonance region, review 79−93585
- (e,e′) polarised low energy scatt., test for weak interaction theories 77−74836
- (e,e+axion), bremsstrahlung mechanism for axion prod. *(Russian)* 79−54431
- eN→e+anything, 2.3 to 13.6 GeV electrons in nuclear emulsion, cross sections, μ comparison 77−46161
- eN high-energy scattering, eikonal approx. corrections, bremsstrahlung 77−215
- N EM struct. effect on elastic cross-section *(Russian)* 77−25676
- ^{207}(e,e′), transverse scatt. amplitude suppression, form factors, neutron hole states 80−91129
- ^{27}Al, inelastic electron scatt., charge distrib., Coriolis band mixing calc., C2 form factors 79−529
- ^{27}Al(e,e′), 62 to 112 MeV, form factors, ^{27}Al energy spectrum, transition probabilities 77−34288
- ^{27}Al(e,e′), 70-340 MeV, odd parity state electroexcitation, form factors, transition probabs. 80−78208
- ^{27}Al(e,e′), cross sections, shadowing effect at small four momentum transfer 80−63176
- ^{27}Al(e,e′), transition widths, multipolarity assignment DWBA calc. 78−13068
- ^{27}Al(e,e′), internuclear nucleon effective mass in quasielastic scatt. *(Russian)* 79−3076
- ^{27}Al(e,e) multipole operators in semileptonic weak and electromagnetic interactions 80−73840
- ^{27}Al(e$^-$,e$^{-\prime}$), comparison of inelastic electron and positron scatt. cross sections 79−49621
- ^{27}Al(e$^+$,e$^{+\prime}$), comparison of inelastic electron and positron scatt. cross sections 79−49621
- ^{36}Ar(e,e′) 65-115 MeV, charge distrib. 77−18527
- ^{40}Ar(e,e′) 65-115 MeV, charge distrib. 77−18527
- Ar(e,e′), A=36, 40, 65 to 115 MeV, low lying level struct., lifetimes 78−8798
- Au, eikonal approx. of electron scatt. by spherically symmetric nuclei 78−37330
- ^{10}B(e,e′), 67-194 MeV, form factors, transitions and ground state radiative width 79−75898
- ^{10}B(e,e′)^{10}B, 40-61 MeV, multipolarities, transition widths 77−10356
- ^{10}B(e,e), 140 MeV, resonances in e spectra *(Russian)* 78−78367
- ^{11}B (e,e′) 120-250 MeV, excited state form factors, shell and diagram model anal. *(Russian)* 79−40852
- ^{11}B(e,e^1), E1 transitions to unnatural parity states 80−22758
- ^{11}B(e,e′) non-normal parity state electroexcit. calcs., E1, M2 giant reson. 77−57643
- B(e,e), A=10, 11, form factors, Hartree Fock calcs. 78−58263
- ^{9}Be, molecular model, charge form factors for electron scatt. 78−46015
- ^{9}Be, quasielastic elec. scatt., final state interaction effects *(Russian)* 78−41708
- ^{9}Be(e,e′), internuclear nucleon effective mass in quasielastic scatt. *(Russian)* 79−3076
- ^{9}Be(e,e′p), suppression factor, final-state interaction and cross-sections in shell model *(Russian)* 77−61401
- ^{9}Be(e,e), longitudinal form factor for $1/2^+$ resonance 80−22682
- ^{209}Bi, charge distrib. from elastic electron scatt. and muonic X-ray data anal. 78−54681
- ^{209}Bi/^{208}Pb isotone pair, charge distrib. polarisation from e$^-$ scatt. and muonic X-ray data consistency 77−22873
- ^{12}C, α-cluster deformation, elastic form factors of electron scatt. 79−17829
- ^{12}C, elastic and inelastic scatt., resonating group method calc. of form factors 78−50108
- ^{12}C, high energy scatt., deformed translationally invariant model 79−58996
- ^{12}C, radial depend. of transition current density from ground to 15-1 MeV state 77−30560
- ^{12}C(e,e′), 1^+(T=1, 15.1 MeV) state excitational pionic modes, M1 form factor 80−78195
- ^{12}C(e,e′), 12.71 MeV 0^+ to 1^+ transition, axial isoscalar neutral current, polarisation asymmetry 79−26425
- ^{12}C(e,e′), 500 KeV inclusive scatt., plane wave impulse approx. 78−50214
- ^{12}C(e,e′), allowed weak and EM transitions, improved impulse approx. treatment 78−41662
- ^{12}C(e,e′), cross sections, shadowing effect at small four momentum transfer 80−63176
- ^{12}C(e,e′), deep inelastic 60-130°, 160-520 MeV response function 79−13284
- ^{12}C(e,e′), E2 transitions, convection currents and spin magnetisation 79−13244
- ^{12}C(e,e′), internuclear nucleon effective mass in quasielastic scatt. *(Russian)* 79−3076
- ^{12}C(e,e′) excitation of 2^+ T=1 state at 16.11 MeV, radiative width, magnetisation density 78−25176
- ^{12}C(e,e′)^{12}C*, 4.4 MeV, transverse excitation of first excited state 77−10342
- ^{12}C(e,e′π^+)^{12}B, 195 MeV, photopion cross-section determ. 78−13066
- ^{12}C(e,e′πs) threshold prod. at 280 MeV, π^+/π^- ratio 77−41957
- ^{12}C(e,e’) 57-215 MeV, 2^+ (4.43 MeV) state, transition DWA anal., electron scatt. form factors 79−67704
- ^{12}C(e,e’) nuclear struct. anal., depend. of meson exchange currents, high momentum transfer data 79−13283
- ^{12}C(e,e), 180° scatt., transverse inelastic form factors and spectra, collective 2^+ state 80−9261
- ^{12}C(e,e), 25-115 MeV, ground state charge distrib. and RMS charge radius 80−57672
- ^{12}C(e,e), electroexcitation cross sections, incoherent superposition of single nucleon processes 80−32269
- ^{12}C(e,e) , 12.71 and 15.11 MeV level struct. and isospin mixing from form factors 80−32186
- ^{12}C(e,e) 140 MeV, resonances in e spectra *(Russian)* 78−78367
- ^{12}C(e$^-$,e$^{-\prime}$), comparison of inelastic electron and positron scatt. cross sections 79−49621

electron-nucleus scattering continued

- ^{12}C(e$^+$,e$^{+\prime}$), comparison of inelastic electron and positron scatt. cross sections 79−49621
- ^{14}C(e,e′), 37, 50.5, 60.5 MeV, 180° scatt. cross sections, excited states, spin parity 77−30557
- ^{22}C, electroexcitation of collective M1 resonances, RPA calcs. 77−46104
- ^{A}Ca(e,e′), backward scatt., A=40, 42, 44, 48, mag. dipole ground state transition search 80−106009
- ^{A}Ca(e,e), A=40,42,44,48, elastic and inelastic scatt. cross-sections from Hartree-Fock densities *(Russian)* 79−13287
- ^{A}Ca(e,e), A=40,48, static and transition densities, self consistent RPA theory test in fast scatt. *(Russian)* 79−49604
- ^{14}Ca, A=40,42,44,48, E0 matrix elements determ. from (e,e′) scatt. 78−33141
- ^{40}Ca, 1^-, T=0 state at 6.95 MeV, isospin forbidden electroexcitation 78−25177
- ^{40}Ca(e,e′), microscopic model of isovector multipole giant resonances *(Russian)* 78−54747
- ^{40}Ca(e,e′), quasi-elastic scatt., scaling law test, knockout process contribution 79−22274
- ^{40}Ca(e,e′), strong mag. dipole transition, coherent spin flip transitions, ground state correlations 79−71817
- ^{40}Ca(e,e), 757.5 MeV, cross-sections meas. 78−8801
- ^{40}Ca(e,e), cross sections, model independ. charge density 80−27548
- ^{40}Ca(e,e), high energy differential cross sections, nucleon density distrib. 78−54738
- ^{48}Ca(e,e), 757.5 MeV, elastic cross section 80−63175
- Ca(e,e′), A=40, 4, at 250 MeV, coupled-channel partial wave anal. 77−74837
- ^{114}Cd(e,e′), 40-110 MeV, vibr. nuclei, branching ratios 77−6356
- Cd(e,e′) for even-mass isotopes, 68, 112 MeV, B(E2) and Q($2_1{}^+$) 77−71585
- ^{140}Ce(e,e′), 50-92 MeV, E0, E1, E2, E3 and E4 giant resonances, cross section, shell model anal. 79−54423
- ^{A}Cl(e, e′), 116, 194 MeV, A=35, 37, charge distrib. and RMS charge radius 80−102109
- ^{59}Co, electron elast. scatt. cross sections, phase shift anal. and HF calcs. *(Russian)* 78−41707
- ^{59}Co(e,e), mag. elastic scatt., radial distrib. of $1f_{7/2}$ proton orbit using cross sections 78−13067
- ^{59}Co(e,e), magnetic e scatt., exchange current effects, plane wave Born approx. 80−78282
- ^{59}Co(e,e), valence nucleon orbit determ. 78−54669
- ^{A}Cr(e,e), A=50,52,53,54, 226.7 MeV, charge density distrib. *(Russian)* 78−86473
- ^{50}Cr(e,e), 227 MeV, differential cross sections, Fermi charge density distribs. *(Russian)* 78−89785
- ^{52}Cr(e,e′), 40-110 MeV, vibr. nuclei, branching ratios 77−6356
- ^{52}Cr(e,e′), 90-226 MeV, excitation of low-lying states *(Russian)* 78−54746
- ^{53}Cr(e,e′), 90-226 MeV, excitation of low-lying states *(Russian)* 78−54746
- Cu, A=63, 65, electron elast. scatt. cross sections, phase shift anal. and HF calcs. *(Russian)* 78−41707
- ^{65}Cu(e,e′)^{65}Cu, 120 MeV, low-lying level struct. *(Russian)* 77−74838
- D+e scattering, neutron struct. function extraction, space-time descript. 78−62404
- (e,e′), giant multipole resonance width, momentum transfer dependence 79−54420
- ^{166}Er(e,e′), 35-350 MeV, coupled channels anal., rot. band excited states, charge densities 79−3139
- ^{18}F (e,e′), polarised e, parity mixing and form factors from elementary particle theory anal. 79−89233
- ^{19}F, electroexcitation of ground state rotational band 78−66191
- ^{A}Fe(e,e), 100-275 MeV, A=54,56,57, cross sections and muonic X-ray meas., charge distrib. systematics 80−86801
- ^{A}Fe(e,e), A=54,56, 226.7 MeV, charge density distrib. *(Russian)* 78−86473
- ^{56}Fe(e,e′), 0.1-14 GeV, deep inelastic inclusive scatt. response functions and momentum distrib. 80−42640
- ^{56}Fe(e,e′), Coulomb form factor for $O^+\rightarrow 4^+$ transition, collective 4^+ states, shell model 80−57664
- ^{56}Fe(e,e′), longitudinal and transverse inelastic response functions and cross sections 80−57771
- ^{1}H(e,e)^{1}H elastic scatt. cross section, study of nucleon struct. and N′N interaction 79−71797
- ^{2}H electrodisintegration, meson exchange current and isobar config. effects 79−71840
- ^{2}H, quasi-elastic scatt., deuteron structure aspects 79−71847
- ^{2}H, weak and EM lepton reactions, exchange currents, isobaric excitations and form factors *(German)* 79−93523
- ^{2}H(e, e′) d bag, nuclear bag states containing quarks, detection 78−70465
- ^{2}H(e, e)pn, polarised e, neutral weak currents, right-left asymmetry 79−80787
- ^{2}H(e,e′), 19.4 GeV, polarized electrons, parity violation 79−13286
- ^{2}H(e,e′), 56.4 MeV, cross sections, form factors, meson exchange current contrib. 80−68649
- ^{2}H(e,e′), electrodisintegration at high energy and momentum transfer 79−6342
- ^{2}H(e,e), charge and structure radius, form factor and structure function *(Russian)* 79−40841
- ^{2}H(e,e), deep inelastic scatt., P nonconservation 79−75776
- ^{2}H(e,e), EM form factors, relativistic formulae, moment corrections 80−63075
- ^{2}H(e,e), EM interactions and mag. sum rules 80−42639
- ^{2}H(e,e), elastic and deep inelastic, nuclear matter density at large momentum transfers *(Russian)* 78−86529
- ^{2}H(e,e), electric and mag. scatt., tensor polarisation, mesonic exchange current effects 79−85374
- ^{2}H(e,e), energy weighted sum rules, almost realistic NN pot. anal. *(Russian)* 80−13465
- ^{2}H(e,e), form factors, tensor pol., and two-nucleon force calcs. 80−106045
- ^{2}H(e,e), parity nonconservation, SU(2)⊗U(1)⊗U′(1) gauge anal. 79−17731
- ^{2}H(e,e), quasi-elastic scatt., en coincidence, n electric form factor 79−67563
- ^{2}H(e,e), tensor polarisation and d wave function short range behaviour 79−40900

electron-nucleus scattering continued
^{2}H(e,e), tensor polarisation and d wave function short range behaviour 79-67564
^{2}H(e,e)^{2}H elastic scatt. cross section, study of nucleon struct. and NN′ interaction 79-71797
^{3}H(e,e), many-body exchange effects, charge form factors calc. 78-33169
H(e^{+},e^{+})H, s-wave scatt., effective range expansion 80-47467
He, contact interactions, parity-violating and parity-conserving, new evaluation techniques 79-26872
^{2}He(e,e) energy weighted sum rules *(Russian)* 80-86900
^{3}He, elastic electron scatt. data, comparison with charge form factor calcs. 79-71848
^{3}He(e,e′), 0.1-14 GeV, deep inelastic inclusive scatt. response functions and momentum distrib. 80-42640
^{3}He(e,e′), nuclear high momentum components and y scaling 80-106051
^{3}He(e,e′) 1000-1100 MeV, differential cross section for quasi-elastic scatt. *(Russian)* 78-86528
^{3}He(e,e′)pd, Faddeev calc., scatt. cross-sections 77-18530
^{3}He(e,e′p)d, Faddeev calc., scatt. cross-sections 77-18530
^{3}He(e,e), 29-95 MeV, RMS charge radius and charge form factor 77-57653
^{3}He(e,e), 3-15 GeV, inclusive scatt. 80-13464
^{3}He(e,e), charge density distrib., charge form factor, of ^{3}He 78-29453
^{3}He(e,e), charge formfactors, second Born approx. and pole model 80-78133
^{3}He(e,e), elastic and inelastic cross sections 40-60 Mev, possible 10 MeV state 79-40908
^{3}He(e,e), form factors and dimensional scaling quark model 78-93991
^{3}He(e,e), model depend. of charge densities 78-78248
^{3}He(e,e), relationship to ^{3}He(π^{-},π^{-}) 80-78323
^{3}He(e,e) 170 to 750 MeV, EM structure, form factors and distribs. 77-54208
^{4}He, struct. effects on α-decay of superheavy nuclei 78-17158
^{4}He(e,e), cross section anal., nuclear charge form factor, short range correl. 78-8746
^{4}He(e,e), form factors and dimensional scaling quark model 78-93991
^{4}He(e,e) 170 to 750 MeV, EM structure, form factors and distribs. 77-54208
He(e,e), A=3,4, many-body exchange effects, charge form factors calc. 78-33169
He(e,e), A=3 and 4, high momentum transfer, elastic struct. functions 78-62521
He(e^{+},e^{+})He, s-wave scatt., effective range expansion 80-47467
^{165}Ho, electron-oriented nucleus scatt., eikonal approx. calc. 78-37331
^{165}Ho(e,e), polarised target, as possible test for charge density waves in finite nuclei 77-54144
^{115}In, K-shell positron annihilation, excitation of nucleus *(Russian)* 78-33171
^{39}K(e,e′), mag. dipole and quadrupole state excitation 78-50154
^{6}Li, Coulomb energy determ. from electron scatt. spectrum *(Russian)* 77-30479
^{6}Li, electron excitation cross sections, short-range correlations *(Russian)* 79-36169
^{6}Li, quasielastic elec. scatt., final state interaction effects *(Russian)* 78-41708
^{6}Li(e, e), charge formfactors, second Born approx. and pole model 80-18155
^{6}Li(e,e′), 102, 123 MeV, excitation form factor, ^{3}H-^{3}He cluster model 80-78190
^{6}Li(e,e′), 140-330 MeV, 3.65 MeV 0^{+} state form factor at high momentum transfer 80-495
^{6}Li(e,e′), 76-141 MeV, form factors, appl. to (π^{-},γ), phenomenological model 80-83068
^{6}Li(e,e′)^{6}Li at 40.5 and 50.5 MeV, ^{6}Li 5.36 MeV excitation form factor 77-54177
^{6}Li(e,e), charge formfactors, second Born approx. and pole model 80-78133
^{6}Li(e,e), elastic and inelastic charge form factors from shell model wave functions 80-68523
^{6}Li(e,e), electroexcitation cross sections, incoherent superposition of single nucleon processes 80-32269
^{7}Li, electron excitation cross sections, short-range correlations *(Russian)* 79-36169
^{7}Li, quasielastic elec. scatt., final state interaction effects *(Russian)* 78-41708
^{7}Li(e,e′) at first πN resonance, cross section longitudinal and transverse components *(Russian)* 80-86901
^{6,7}Li(e,e′p), suppression factor, final-state interaction and cross-sections in shell model *(Russian)* 77-61401
^{24}Mg, 6 MeV 4^{+} state, configuration anal., electron scatt. form factors 78-25115
^{24}Mg(e,e′), 6^{-}, T=1 reson. discovery at 15 MeV 77-41940
^{24}Mg(e,e), 4$_{1}$$^{+}$4.12 MeV and 2$_{2}$$^{+}$4.24 MeV level resolution, E2 and E4 form factor meas. 79-17811
^{24}Mg(e,e) form factor calc., test of 1s-0d shell effective interactions 77-61400
^{25}Mg (e,e) 80-215 MeV, magnetic moment form factors, M1, M3, M5 transitions 79-40844
^{25}Mg(e,e), 180° scatt., magnetisation distrib., mag. multipole moments 80-9228
^{25}Mg(e,e), 40-260 MeV, cross sections, Coulomb multipole moments and magnetic form factor 78-25178
^{14}N (e,e′), 40-60 MeV, at 180°, M1 transitions and transition widths 79-49598
^{14}N(e,e′), internuclear nucleon effective mass in quasielastic scatt. *(Russian)* 79-3076
^{14}N(e,e) in storage ring, elastic form factor 80-22819
^{15}N(e,e′), 52-195.3 MeV, giant resonance electroexcitation, C1, C2 strength distribs. 79-510
^{15}N(e,e′), excitation of energy levels 9.7 to 14.7 MeV, 60-194 MeV, EM form factor meas. 78-25175
^{15}N(e,e′), form factors meas., obs. of low-lying states 78-12976
^{93}Nb (e,e), 80-215 MeV, magnetic moment form factors, M1, M3, M5 transitions 79-40844
^{93}Nb(e,e), 180° scatt., magnetisation distrib., mag. multipole moments 80-9228
^{93}Nb(e,e), magnetic e scatt., exchange current effects, plane wave Born approx. 80-78282
^{93}Nb(e,e), valence nucleon orbit determ. 78-54669

electron-nucleus scattering continued
^{150}Nd(e,e′), possible K$^{\pi}$=0^{-} octupole band, e scatt. form factors 79-9447
^{20}Ne, α-cluster deformation, elastic form factors of electron scatt. 79-17829
^{20}Ne quadrupole transitions, electron scatt. form factors, shell model calcs. 78-62523
^{20}Ne(e,e′), E1 and E2 giant resonances excitation at 60-120 MeV 78-50144
^{20}Ne(e,e′) data anal., 0g orbit mixing 78-493
^{22}Ne(e,e′), 60 to 110 MeV, spin, parity, form factor, reduced transition prob. determ. 79-63661
Ni giant resonances using virtual and real photons 80-22791
^{A}Ni(e, α) A=58, 60, 62, 50 MeV electroproduction and decay of giant resonances 79-26413
^{A}Ni(e,e′), 102 MeV, A=58,60, E1-E4 giant multipole resonance comparison, shell model anal. 80-42614
^{A}Ni(e,e), 100-275 MeV, A=58,60,62,64, cross sections and muonic X-ray meas., charge distrib. systematics 80-86801
^{14}Ni(e,e′), mag. dipole and quadrupole state excitation 78-50154
^{58}Ni, charge density, HF calcs. from (e,e) data 79-89260
^{58}Ni, comparison with proton scatt., large momentum transfer 77-38262
^{58}Ni(e,e′), 120-264 MeV, J$^{\pi}$=6^{+}, 5.125 MeV state isoscalar character, form factors, transition strengths 80-9262
^{58}Ni(e,e′), 153-264 MeV, fragmentation of isovector M8 strength 78-37305
^{58}Ni(e,e′), 40 to 75 MeV, excitation of T$_{0}$+1 giant M1 resonance 77-14118
^{58}Ni(e,e′), mag. dipole and quadrupole state excitation 78-50154
^{58}Ni(e,e′) 5.125 MeV J$^{\pi}$=6^{+} state excitation, isoscalar character 79-22227
^{60}Ni, electron elast. scatt. cross sections, phase shift anal. and HF calcs. *(Russian)* 78-41707
^{60}Ni(e,e′), 40 to 60 MeV, excitation of T$_{0}$+1 giant M1 resonance 77-14118
Ni(e,e′) A=58, 60, 64, isospin splitting of giant dipole resonance *(Russian)* 77-50116
^{16}O, α-cluster deformation, elastic form factors of electron scatt. 79-17829
^{16}O(e,e′), 799, 996, 1178 MeV, cross sections *(Russian)* 80-68653
^{16}O(e,e′πs) threshold prod. at 280 MeV, π^{+}/π^{-} ratio 77-41957
^{16}O(e,e′), internuclear nucleon effective mass in quasielastic scatt. *(Russian)* 79-3076
^{16}O(e,e), high energy differential cross sections, nucleon density distrib. 78-54738
^{16}O(e,e), spectroscopic amplitude determ. 80-5127
^{16}O(e,e), T=1 level form factors, Helm model, pion photoprod. and muon capture appls. 80-52553
^{17}O, charge distrib. differences between A=16, 17, and 18 isotopes 79-63583
^{17}O(e,e′), 65-168 MeV, giant resonance excitation 78-4930
^{17}O(e,e), elastic and inelastic, cross sections, excited states, charge radii 78-46049
^{17}O(e,e), mag scatt., form factors, HF calcs., core polarisation effects 80-42579
^{17}O(e,e), transverse form factor, ground state mag. distrib. 79-63658
^{18}O(e,e′), 80-165.7 MeV, giant dipole and quadrupole resonances, form factors 80-102168
^{18}O(e,e′), isovector mag. dipole and quadrupole transitions, analogues, (π^{-} γ) relation 80-106010
^{189}Os(e,e′), 72-100 keV, nucl. excitation by electron transition 78-41703
Pb, A=204-208, charge distrib. from elastic electron scatt. and muonic X-ray data anal. 78-54681
^{A}Pb(e,e′), A=204, 206-208, levels and inelastic cross sections 80-22698
^{207}Pb+e, high resolution inelastic scatt. cross sections, induced charge of neutron, form factors 78-78366
^{207}Pb(e,e), magnetisation distrib. from elastic mag. form factors, core polarisation, exchange currents 80-47372
^{208}Pb (e,e′), 2^{-} giant resonance twist mode excitation, B(M2) values, form factors 80-78246
^{208}Pb (e,e), 502 MeV, high-momentum-transfer, charge-density distrib. anal. 77-38258
^{208}Pb, charge distrib. polarisation from e^{-} scatt. and muonic X-ray data consistency 77-22873
^{208}Pb core with valence nucleon or hole, mag. props., exchange currents, electron scatt. 80-22689
^{208}Pb, eikonal anal. of high energy proton and electron scatt. *(Russian)* 77-22908
^{208}Pb, eikonal approx. of electron scatt. by spherically symmetric nuclei 78-37330
^{208}Pb, high-spin states, form factors for electroexcitation 77-14116
^{208}Pb(e,e′), E2 transitions of fragmented isoscalar quadrupole giant resonance 80-22758
^{208}Pb(e,e′), 50 and 63.5 MeV, mag. quadrupole strength fragmentation 78-41705
^{208}Pb(e,e′), 50 to 335 MeV, 12^{-} mag. spin state excitations 78-50155
^{208}Pb(e,e′), 50-335 MeV, J$^{\pi}$=12^{-}, 14^{-} high spin states, DWBA anal. 79-93490
^{208}Pb(e,e′), 60 MeV, backward scatt., 2$\hbar\omega$ M1 excitation search 80-32234
^{208}Pb(e,e′), 70-335 MeV, natural parity high spin state excitation 80-63060
^{208}Pb(e,e′), cross section calc. using microscopic wave functions 78-50142
^{208}Pb(e,e′), Ex<100 MeV, giant multipole reson. electroexcitation 77-34279
^{208}Pb(e,e′), giant multipole resonance excitation, particle-hole interaction 80-22789
^{208}Pb(e,e′), isospin fine struct., 8-12 MeV, multipole assignment of 8.9 MeV reson. 78-13071
^{208}Pb(e,e′), M2 giant resonance excitation, spin-magnetism mass depend. quenching, M1 strength reduction 78-86521
^{208}Pb(e,e′), mag. dipole and quadrupole state excitation 78-50154
^{208}Pb(e,e′), RPA calcs., existence of breathing mode 78-25163
^{208}Pb(e,e′), form factors of states with spin up to J=10 obs. 77-310
^{208}Pb(e,e), 502 MeV, charge density distrib. variations 79-75830
^{208}Pb(e,e), elastic and inelastic, static and transition densities, self consistent RPA theory test *(Russian)* 79-49604
^{108}Pd, vibr. states study, elastic and inelastic electron scatt., anharmonic vibrator model 78-62520
^{110}Pd(e,e′), 40-110 MeV, vibr. nuclei, branching ratios 77-6356

electron-nucleus scattering continued
^{103}Rh(e,e′), 350-800 keV, isomer Coulomb excitation cross sections 80−22659
^{32}S, eikonal approx. of electron scatt. by spherically symmetric nuclei 78−37330
^{32}S(e,e) form factor calc., test of 1s-0d shell effective interactions 77−61400
^{87}SR(e,e) elastic mag. scatt., 175 to 300 MeV, 1g$_{9/2}$ neutron radial distrib. 77−57652
^{A}Si(e,e'), 126-293 MeV, A=28,29, levels and form factors, particle-phonon coupling anal. 80−105977
^{28}Si(e,e′), 38.7-57.5 MeV, energy levels, isovector M1 strength, DWBA anal. 79−75847
^{28}Si(e,e′), 6^- T=1 resonance form factor, mag. strength quenching, meson exchange currents 80−86882
^{28}Si(e,e′), 92 MeV, E2 strength distrib., giant quadrupole 79−36192
^{28}Si(e,e′), M2 giant resonance excitation, spin-magnetism mass depend. quenching, M1 strength reduction 78−86521
^{28}Si(e,e′), mag. dipole and quadrupole state excitation 78−50154
^{29}Si(e,e′), 63-112 MeV, ground state transitions props. and transition radii of excited levels 77−50115
Si(e,e′), A=28, 29, 30, 18.5-117.1 MeV, ground, excited state charge distribs. 77−54142
^{152}Sm, giant resonance excitation by (e,e′) at 60-105 MeV, DWBA analysis *(Russian)* 78−41686
^{152}Sm(e,e′), 251.5 MeV exciting ground-state rot. band 77−30475
^{152}Sm(e,e′), 35-350 MeV, coupled channels anal., rot. band excited states, charge densities 79−3139
^{A}Sn(e,e′) A=116, 120, 124, electric moment distrib., lowest lying quadrupole states excitation 79−6392
^{116}Sn(e,e′), 40-110 MeV, vibr. nuclei, branching ratios 77−6356
^{124}Sn, electron excitation of giant multipolar resonances *(Russian)* 78−8802
^{124}Sn(e,e) ^{150,225}MeV giant multipole resonances, positions and half widths *(Russian)* 78−78349
^{87}Sr(e,e), magnetic e scatt., exchange current effects, plane wave Born approx. 80−78282
^{87}Sr(e,e), valence nucleon orbit determ. 78−54669
^{88}Sr(e,e), 400 MeV, charge density distrib. variations 79−75830
^{181}Ta, deformed nuclei, electron scatt., elastic differential cross section calc. 77−82912
^{181}Ta, ground state rotational band, electroexcitation 78−33168
^{181}Ta(e,e′), 79-119 MeV, DWBA anal., giant multipole resonance parameters 77−30558
^{181}Ta(e,e′), giant monopole and quadrupole resonances excitation 78−17184
^{46}Ti eikonal approx. of electron scatt. by spherically symmetric nuclei 78−37330
^{48}Ti eikonal approx. of electron scatt. by spherically symmetric nuclei 78−37330
^{48}Ti(e,e), 227 MeV, differential cross sections, Fermi charge density distribs. *(Russian)* 78−89785
^{48}Ti(e,e), elastic and inelastic scatt. cross-sections from Hartree-Fock densities *(Russian)* 79−13287
^{49}Ti(e,e), cross section, 1f$_{1/2}$ neutron orbit radial distrib. 79−93541
^{49}Ti(e,e), magnetic e scatt., exchange current effects, plane wave Born approx. 80−78282
Tl, A=205,203, charge distrib. from elastic electron scatt. and muonic X-ray data anal. 78−54681
^{235}U, K-shell positron annihilation, excitation of nucleus *(Russian)* 78−33171
^{235}U($1/2^+$; 73 eV) isomer *(Russian)* 79−9511
^{238}U(e,e′), 87.5 MeV, deformed fissionable nucleus, giant multipole resonances and isovector states 80−42612
^{238}U(e,e′) scatt. from octupole band, model for nuclear surface vibrations 78−37333
^{238}U(e,e′f), 5.5-28.3 MeV, E2 isoscalar giant resonance in photofission cross section 79−512
^{51}V(e,e′), shell model calcs., effective charges 77−26674
^{51}V(e,e), mag. elastic scatt., radial distrib. of 1f$_{7/2}$ proton orbit using cross sections 78−13067
^{51}V(e,e), magnetic e scatt., exchange current effects, plane wave Born approx. 80−78282
^{51}V(e,e), valence nucleon orbit determ. 78−54669
^{89}Y(e,e′), 92.5 MeV, giant reson. and bound collective states 78−13070
^{A}Zn(e,e), 100-275 MeV, A=64,66,68,70, cross sections and muonic X-ray meas., charge distrib. systematics 80−86801
^{64}Zn, electron excitation of giant multipolar resonances *(Russian)* 78−8802
Zn(e,e′) A=64, 66, 68′ 100-275 MeV, levels, transition charge density 77−50077
^{90}Zr, giant resonance levels, study by proton and electron scatt. *(Russian)* 79−3127
^{90}Zr(e,e′), 2^- giant resonance twist mode excitation, B(M2) values, form factors 80−78246
^{90}Zr(e,e′), M2 giant resonance excitation, spin-magnetism mass depend. quenching, M1 strength reduction 78−86521
^{90}Zr(e,e′), mag. dipole and quadrupole state excitation 78−50154
^{90}Zr(e,e), elastic and inelastic, static and transition densities, self consistent RPA theory test *(Russian)* 79−49604

electron optics
see also beta-ray spectrometers; electron beams; electrostatic lenses; ion optics; magnetic lenses; particle optics
3-electrode axisymmetric lens, cardinal elements 77−30221
600-kV electron microscope, electron-optical performance and atomic resolution 79−97475
aberration, spherical, for teaching 78−54135
aberration correction, mag. deflection systs. 78−66740
aberration elimination, electron beam scanning systems 80−78756
aberrations, algorithm computation using Chebyshev polynomials 79−27156
aberrations, reduction by optimisation techniques 80−87290
anode for an accelerator with an inductive energy accumulator 79−26785
axisymmetric beam in elec. field with two spatial scales 77−54665
beam coasting off axis, electrostatic potential and field 77−38796
beam deceleration, in longit. mag. field, energy recovery system 77−49807
beam deflection error assessment, expt. technique 80−78757

electron optics continued
beam dynamic deflection sensitivity in transverse magnetic field 78−86386
beam envelopes in quadrupole lens and sector magnet containing systems 79−64168
beam focusing theory, nonlinear differential eqns. *(Chinese)* 79−31783
beam in plasma filled channel, stationary states of cylindrical electron beam 79−55046
beam limiter system, current density distrib. 78−5414
beam modulation, by cylindrical capacitor, mechanism 77−49808
beam shaping by multichannel gate voltage selection 79−50204
beam transport through gas, high-current microsec. beam 79−22890
beta-ray coinc. spectrom. with reduced spherical aberration 77−10529
biplanar electron-optical image converter as a circuit element 80−78994
Boersch's electron optical bench, modifications 80−87286
Boersch effect, energy broadening 80−69313
Boersch effect in electron-optical instruments 80−69308
bright field TEM, partially coherent attenuation envelope shape 80−101885
bright-field image contrast and resolution in STEM and conventional TEM 80−95200
bunching, in linear accelerator, optimum phase energy distrib. determ. 77−379
Busch method for determ. of specific charge on electron, errors in textbook treatment *(Russian)* 78−9311
carbonaceous material, image contrast, comparison of theory and expt. 77−10142
cardinal elements, partial fractions expansion 77−67543
cathode electron optical system, optimisation, influence functions 79−76575
cathode lens, transient processes, finite-particle method 77−61909
cathode lens having a quasispherical field 80−95782
cathode lenses, with combined elec. and mag. fields, third order aberration theory 79−41317
centrifugal electrostatic shaping of high intensity electron beams 80−13183
charged particle trajectory calc. in electrostatic field, teaching 80−90635
circular electron accelerators, beam stability calc. 79−72099
coaxial cone electrostatic velocity analyser 80−22480
coherence, in electron optics, review 80−32900
collective field accelerator, vac. diode with relativistic electron beam operation 77−24201
collimated electron trajectory in nonuniform transverse mag. field 80−53201
combined system of electrostatic round lens and mag. deflector, electron-optical characteristics *(Chinese)* 78−82897
compression of beam by mag. mirror, high current density generation for fusion 77−67870
compression of high-current electron beam in gas, on current pulse trailing edge 78−12789
computer image processing, atomic resolution of 500 kV electron micrograph 80−100149
condenser lens for electron beam *(Japanese)* 80−53200
condenser objective, single field, advantages and limitation for min.-exposure 80−87292
conference on electron, ion and photon beam technology, Palo Alto, CA, USA (May 1978) 78−74827
conference on electron, ion and proton beam technology, conf., Boston, MA, USA (29 May-1 June, 1979) 80−67927
conically tilted projections, 3-D reconstruction 80−99618
crossed lenses, electron optical characts., trajectory anal., aberrations from axial pot. profile 80−63909
crossed lenses, theoretical and expt. study 80−95780
crossed-field energy analyser, stigmatic, focusing and dispersing props. 78−74832
crystal structures and cryst. defects, electron microscope imaging 80−88006
CTEM, on-line electron-optical correlation computing 80−99008
curved electron beam system with strong deceleration at collector region, optimisation 78−74106
cylindrical-mirror electrostatic analyser for beta spectroscopy of beams 80−63446
deflection and focusing system design *(French)* 79−41319
deflection multiplication in electron lens system 80−5673
deflection system performance using resolution test specimen 80−69311
deflection systems combined with mag. lenses, optical props. 80−31938
deflective aberration free system using moving objective lens 77−61908
defocus spread and illumination aperture effect, in brightfield electron microscopy 79−231
developments at the Cavendish Laboratory 80−37948
device with spherical diode with plasma anode 77−591
diamond, ultrarelativistic electron beam self acceleration probability 79−86819
diffraction radiation generator, starting currents, dynamic and static electron shiftings influence, theory and expt. *(Russian)* 79−3617
diffraction radiation generators, echelette use, electron flow *(Russian)* 80−69314
distortion correction and deflection calibration by laser interferometry in exposure system 80−69310
Doppler shift of electron waves, illustration using electron mirror interference microscope 80−95783
education, electron and ion optical bench 77−45641
education, electron interference using standard electron microscope and electron biprism as interferometer 78−62005
einzel lens, depend. of aberration consts. on magnification 77−75404
electric power supply for an electron-optical corrector *(German)* 80−42308
electric quadrupole lens, fringing field, conformal mapping method 79−41315
electric-magnetic focusing deflection system, relativistic aberrations formulae 78−13653
electrographic image detectors, development, and applications in UV astronomy and scientific research 80−43465
electron beam welding and processing, model for melting channel formation *(Russian)* 77−52336
electron brightness meas. by 2-limiter method, accuracy calc. 79−6234
electron bunch in magnetodielectric channel, elec. field 79−64166
electron gun, with electrostatic and electromagnetic lenses 80−99007
electron gun, with point cathode, electron-optical props. *(German)* 78−82901

electron optics continued
electron guns, high-current, laminar beam formation for linear accelerators 78—74516
electron impact spectrometer using concentric hemispheres, appls. *(French)* 78—41380
electron microscope, 3-dimens. imaging, curved axis electron optics *(German)* 79—13889
electron microscope contrast enhancement of negatively stained macromols. and biomembranes by single sideband phase contrast interference 77—45920
electron microscopy, focused image production through visible-optics correction of defocusing and spherical aberration 79—6231
electron motion in elec. and mag. fields, student lab. and computing studies 80—27076
electron probe, compensation of aberrations, dynamical focusing with stigmator 80—87291
electron waves in plane periodic system, linear theory 80—48130
electron-beam focusing optimisation with specified image parameters 78—86385
electron-lens systems used in low-energy electron or ion scattering, geometries and focal props. 79—50202
electrostatic analyser, spherical, focusing using supplementary electrodes 77—9155
electrostatic crossed lens, for electron microscopic devices 80—87289
electrostatic decelerator for electron microscope *(German)* 79—30620
electrostatic energy filter, telescopic, with cylindrical mirror analysers 80—87296
electrostatic field in complex periodic structures, computer-aided anal. *(Russian)* 78—33648
electrostatic lens, six electrode crossed doublet, stigmatic operation 79—13888
electrostatic lenses for control of ion or electron beams 80—32897
electrostatic mirror, two-electrode, transaxial, aberrations, gap depend. 77—27242
electrostatic mirror, two-electrode, transaxial, cardinal elements, aberrations 77—27241
electrostatic one-foil lenses, round, electron optical properties, charges induced on foil 80—53203
electrostatic prism, electron optics for Auger spectrometer 79—29437
electrostatic prism spectrometer, aberration coeffs. and spectral window 79—40647
electrostatic telescope, zero spherical aberration, ang. aberration calcs. 77—75406
electrostatic telescope, zero spherical aberration, paraxial props. 77—75405
Electrotitus, detective quantum efficiency 80—42307
element computation by finite element method 79—31785
energy analyser, electrostatic, appls. 79—44990
energy analyzer, two-stage with cylindrical mirrors, aberration reduction 79—40640
energy loss spectroscopy, spectrometer design, electron optical props. 79—12903
ESCA spectrometer operation, using monochromated UV discharge lamp with XPS spectrometer 78—89601
field emission gun, electron optical characteristics *(German)* 79—893
field emission gun SEM column electron-optical performance obs. and model 80—68328
field solution convergence in nonlinear environment by network method *(Czech)* 79—81350
filtered diffr. patterns and images, direct prod. 80—31950
focus-deflection practical system for shaped electron beams 79—76572
focusing electrodes shape calculation for wedge-shaped electron-ion beam 80—53202
focusing of beam from electron gun by small perturbation anal. 77—50602
focusing of high-current beam, in vac. chamber with dielec. walls *(Russian)* 77—83801
focusing with strong magnetic field in image convertor 78—5556
foil lens, correction of spherical aberration, appl. to STEM 80—87294
foil lens, spherically corrected, for electron phase microscopy *(German)* 80—83546
Fourier images theory, appl. of self imaging anal. *(German)* 79—89839
Fresnel diffraction effects on high-resolution images, spherical aberration effect 79—27153
Fresnel fringe on high resolution electron microscope under partially coherent illumination *(Chinese)* 79—94142
gun lenses, electrostatic for high-brightness field emitters 80—62809
helical electron beams, extended and intense with space-charge forces, trajectory anal. *(Russian)* 79—918
hemispherical electrostatic 180° deflector, optimisation *(French)* 78—21269
hexapole spherical aberration corrector 79—76571
high-current electron-optical systems, asymptotic synthesis 79—7067
high-perveance system with electron-energy recuperation 77—23322
IC template fabrication, SEM and electron lithography optics 79—75662
image deflection system, crossed elec. and mag. field, intensity modulation 78—89592
image formation, partial coherence and inelastic scatt. 78—46505
image formation, partial coherence and inelastic scatt. 78—58897
image formation, partially coherent, two dimens., computer simulation 80—106434
image formation in electron microscopy using hollow cone illumination, S/N considerations 80—4815
image formation in scanning microscopes with partially coherent source and detector 78—58923
image processing, biological molecules, optical diffraction and filtering, fast Fourier transforms 80—30956
image reconstruction, 3-dimens., electron noise effects 77—13829
image reconstruction, computerized, fragment size choice 80—78785
image tube designs, examination using electron optical demountable system 79—81575
imaging of relatively strong objects in partially coherent illum., linear transfer theory 78—22091
imaging of thin phase objects, tilted and extended 80—99617
incoherent illumination method with conventional electron microscope, granular noise elimination 80—95201
interference electron microscopy using electron holography and Mach-Zehnder interferometry 79—54231
interference microscopy, image wavefunction asymptotic approx., extension to biprism edges 80—95193
interferometer, modified Marton type 78—37111

electron optics continued
interferometry, appl. to Au-Ag contact PD meas. 77—32069
inverse interior Dirichlet problem 79—98270
inverse problem uniqueness, scatt. object reconstruction, book contrib. 79—31824
inverse source problems in optics, book 79—31821
isoplanatic image formation, photometry and partial coherence 78—9312
isoplanatic imaging, complex degree of coherence determ. 77—2691
lattice image formation, many-beam theory, TEM 80—38879
lattice images, effect of absorpt. 79—90497
LEED apparatus, using high-tension source, construction 78—38591
lens, three-electrode , crossed, electron focusing, spherical aberration 78—33659
lens aberration coeffs., computer calc. using CAMAL 77—38798
lens system for optimum deflection sensitivity 80—23615
lenses, crossed, electron optical image position, ang. magnification aberration 78—50691
linear accelerator, asymmetric focusing coils, beam dynamics by 3-D model 78—17450
low energy crossed beam scattering, 90°, 300 eV 77—46004
low profile electron collector system 80—68292
magnetic domain walls, off-axis electron microholography 78—82080
magnetic energy filter, without second-order aberrations 80—86524
magnetic field distrib. mapping of thin mag. foils by holographic processing 79—89868
magnetic field distribs. with min. spherical aberration, dynamic programming 78—9313
magnetic filter 1 MV, second order image abberations 77—61165
magnetic imaging filter, electron optical experiments 80—87295
magnetic insulation wave, propag. in vacuum coaxial line 79—27144
magnetic lens and deflection system, electron-optic props. and aberrations *(Chinese)* 77—58244
magnetic prism, design, for TEM energy filter 80—86523
magnetic spectrometer, corrected second-order aberrations 80—87013
magnetic spectrometer design with corrected second-order aberrations, theory 78—89604
magnetic spectrometers, approx. and ideal design, appl. to STEM 78—8475
micromachining, imaging conditions, illumination system 78—82899
microprobe instrument, spherical aberration correction, using zone plates 79—45899
microscope, high resolution, 600 kV, electronic mechanical and electron-optical engineering design features 80—86518
microscope, mag. energy filter, for error-free image, second order approx. *(German)* 77—191
microscope energy filter, correction of second order aberrations *(German)* 77—22624
microscope image interpretation, instrumental, environmental conditions *(Polish)* 79—30623
microscope resolving power limitations 80—86528
microscopes, electron source size in field-emission gun 79—71575
microscopic diffraction patterns, direct phase determ. *(German)* 77—2713
microscopic images quantification *(Polish)* 79—49347
microscopy, high resolution, appl. of Fraunhofer holography 80—99016
microscopy, phase contrast transfer with different imaging modes 78—70232
microscopy, phase problem, partial coherent illumination influence 80—62800
microtron, cathode focusing and drift apertures, hybrid computer calc. 78—21796
minimal exposure high resolution, electron microscopy, organic materials 80—79653
mirror, electrostatic, two-electrode transaxial, for large incidence ang. electron beam 78—37797
monochromator, telescopic, in CTEM, with cylindrical mirror analysers 80—87296
multielement system, with third-order aberration, trajectories 79—41321
nonperiodic objects, reconstruction from electron micrographs using correlation methods 80—86527
nonrelativistic electron wave diffraction by cylindrical capacitor 79—72473
objective lens, with compensated axial chromatic aberration, for electron microscope 80—87293
off-axis image electron holography, proposal 77—10151
one and two-lens electron-optical system parameter comparison 80—87284
optimisation of electron optical systems using orthogonal functions 80—63908
optimisation using dynamic programming 77—61907
p-n junctions, TEM, defocused images, stationary field approx. 78—67628
paraxial eqn. asymptotic solns., singular perturbation theory, chromatic aberrations of cathode electron optics 79—41320
partially coherent sources, radiometric quantities 77—38797
phase reconstruction problem for wave amplitudes and coherence functions, book contrib. 79—31823
phase retrieval in electron microscopy from image and diffr. pattern, uniqueness and stability of soln. 77—10144
pico-femtosecond electron-optical photography 79—18342
plane electron-optical system, electrostatic field anal. with integral eqns. of first kind 77—19157
plane-symmetric optical systems, equilib. and stability conditions *(Russian)* 78—70220
plasma emitter, electron optical system simulation 78—67442
point characteristic function determ. method, system with straight optical axis 80—5672
potential in system of rotational symm., integral method 77—587
potential in system of rotational symm., numerical calc. 77—586
potential solution V(x,y,z) for symmetric rectangular stepwise constant-potential boundaries at $y = \pm Y$ 78—46506
prism, cone-shaped, combined elec./mag. fields, relativistic particle optics 78—50690
prism, exact non-relativistic eqns. for charged particle trajectories 77—23607
prism, wedge-shaped, combined elec./mag. fields, relativistic particle optics 78—50689
probe forming systems, optimisation with respect to aberrations and vertical beam landing 80—68291
protein supramolecular structure, ordered, electron micrographs, image processing 80—89923

electron optics continued
  pulsed electron beam, in Ar, He, and O_2, self-focusing, polyatomic additives effects 77−68164
  quadrupole lens for beam shape transform., rel. to deep stopping in recuperator 77−65562
  quantum phenomena in dense electron beams, soln. of Schrodinger eqn. 79−76568
  radiation flux parameters meas. by diaphragm method 78−86387
  relativistic, laminar, characts., self-mag. field effects calcs. 77−50608
  relativistic electron beam, diode compression 77−24197
  relativistic electron beam, focusing and energy transfer on to target 77−42186
  relativistic electron beam, focusing limitations in low-press. gas 79−41322
  relativistic electron beam, in conical diode, self-focusing 79−89840
  relativistic electron beam, induction auto-correl. 79−22889
  relativistic electron beam diode, annular cathode, pinching rot. and reflexing in axial mag. field 78−9860
  relativistic electron beam in plasma, coherently radiating, radiation press. at surface 78−9314
  relativistic electron bunch, phase distrib. in reson. storage chamber 77−380
  relativistic electron wave diffraction by cylindrical capacitor 80−5671
  relativistic hollow beam within conducting coaxial screen, reduction factor calc. *(Russian)* 78−33658
  rotation-free mag. lens for transmission electron microscope 78−78042
  scanning electron probe voltage contrast, device ground level floatation 80−73527
  scanning system, for 5 MeV STEM 79−12913
  SEM, photographic recording system 80−101903
  SEM, REM-200, design and operating characts. 79−6221
  SEM fiducial grid prep. by electron resist. technique 77−25230
  SEM lens system design, snorkel or condenser-objective 80−57438
  SEM selected area channelling patterns, optimum instrumental procedures 78−34408
  sextupole corrector limitations 80−102604
  sextupole system for spherical aberration correction 80−43246
  shadow microscopy, electron interference 77−18141
  single beam collective phenomena 78−78893
  single-particle dynamics, electron motion 78−78892
  single-polepiece lenses, magnetised iron sphere model 78−32940
  slow electron spectrometer, electron-optical system 77−41733
  slow-wave system, phase motion of particles in beam-excited self consistent field 79−10253
  spatial electron beam formation, paraxial approx., electrodes in electron gun appl. *(Russian)* 78−17854
  spectrometer with double focusing, adjustment with nonuniform mag. field 77−6606
  spherical aberration, new correction system 80−5676
  sputtering evaporation chamber LV electron guns with longitudinal compression *(Russian)* 80−50551
  static EM multipole fields *(Chinese)* 79−72472
  static multipole fields, numerical calc. 77−588
  STEM, differential phase contrast role 80−95202
  STEM, image formation, 2-D computer simulation of heavy atom model compounds 80−75135
  STEM, images, matching illum. to specimen struct. 80−73551
  STEM, multi-signal detection and processing 80−73552
  STEM, partially coherent image form. 77−190
  STEM, post-specimen optics, lens-spectrometer system optimisation 77−22621
  STEM object wave reconstruction, off-axis holograms 79−54230
  STEM optical system, practical considerations, review 78−21301
  stimulated diffr. effects on aperture in non-transparent screen *(Russian)* 78−71018
  stroboscopic SEM, picosecond pulse, electron optical design 79−21870
  support film phase contrast in electron microscopy, Fourier spectrum analysis 80−95199
  synchrotron radiation source, X-ray monochromatisation, phase space analysis 78−62276
  telescope system, 3 electrode with mirror, spherical aberration elimination 77−50606
  TEM, magnetic energy filter optics 78−32944
  TEM, object reconstruction from real part of scatt. wave 79−93262
  TEM, spiral distortion correction 78−32942
  TEM, universal magnification curve 79−49340
  TEM, viewing arrangement improvements 78−32941
  TEM coma-free alignment using optical diffractograms 79−21860
  tilted illumination imaging in electron microscopy, contrast transfer functions 80−95198
  trajectory analysis of electron optical system, cubic spline approx. 77−50603
  transverse focusing at large emitter currents *(Russian)* 80−87280
  triode and diode guns, electron optics numerical determ. of beam profile 80−106435
  triple slit scheme for high current variable-shaped beam forming 80−68290
  two-electrode electron optical systems, electrostatic field of disc cathode 79−64167
  two-lens projection systems, reduction of third-order distortion 80−48134
  undulator radiation, irregularity effects 80−99614
  use of light optical diffractometer 80−101900
  variable-shaped beam systems, adjustment accuracy requirements for submicron pattern prod. 80−69312
  wave aberration, sign conventions 77−589
  wave aberration sign, addendum 77−61910
  wave aberration sign 77−22623
  wavelength measurability 77−71406
  waves, Doppler shift calcs. *(German)* 80−18982
  X-ray tube, microfocus, electron source with single pole mag. lens and novel focusing system 78−32964
  Young-Fresnel double-mirror interference experiment with electrons *(German)* 78−90351
  zone-plate coded imaging on microscopic scale 77−54673
  e^+e^- storage rings, beam-beam interactions 78−78894
  $Gd_2(MoO_4)_3$, ferroelec. temp. depend. of spontaneous biref. and electrooptic reponse 79−33662
  KD_2PO_4 monocrystal, electrooptical props. in paraelectric phase *(Polish)* 80−11368
  LaB_6 cathodes for Kohler illum. and brightness meas. 80−68296

electron optics continued
  Si, (110) oriented, electron optical conditions for struct. image form. 80−75131
  Si, electron beam annealing, beam voltage effect modeling 80−75275
  Si:As, scanning electron beam annealing, spreading resistance, junction depth 80−75267
  W support film for high resoln. electron microscopy, phase contrast, computer modelling 78−1144

electron pair annihilation *see electron-positron interactions*

electron pair production
  γ-ray internal pair conversion, form. of monoenergetic e^+ 79−6502
  astrophysical transrelativistic plasmas, photon pair prod. 78−20632
  asymmetry of prod. by circularly polarised protons *(Russian)* 78−29286
  axion$\rightarrow e^+e^-$ after emission from ^{12}C excited state 80−32235
  black holes, electron-positron pair production in hot unsaturated Compton accretion models 80−36658
  black holes, evaporating, observational consequences of positron prod. 80−46599
  black holes, primordial, electron-positron radiation, spectrum rel. to galactic radio spectrum 80−62179
  bone mineral content meas. using gamma-ray attenuation by pair prod. 77−44740
  compact extragalactic radio sources, electron-positron pair prod. rel. to Faraday rot. 78−73770
  cosmology, appls. of pair prod. in intense mag. fields 77−13505
  Coulomb correction to electron pair prod. by intermediate energy photons 78−13060
  creation of e^+e^- from vacuum induced by variable elec. field *(German)* 77−82695
  cross section calc. on nuclei in range $1 \leq Z \leq 92$ 80−503
  crystal nuclei, e^+e^- and e^- bremsstrahlung photoprod. cross sections, longitudinal polarisations 79−75969
  dense pinch, electron-positron pair production in EM field *(Russian)* 80−100092
  Drell-Yan contrib. to lepton pair prod., incident hadron $q\bar{q}$ correlation function 78−89668
  e^+e^- angular distribution of e^+e^- pairs produced by linearly polarized photons *(Russian)* 79−40904
  early cascade development of energetic electrons in emulsions 79−89158
  electron-photon cascades, Monte Carlo simulation of cascade development 79−44322
  electron-positron pair, and photon, formation from photon in nuclear field *(Russian)* 79−22267
  EM wave field, nonmonochromatic, quantum field probability *(Russian)* 77−41799
  exploding black hole, radio pulse spectrum calc. 78−12271
  external field, quantum processes in strong EM field *(Russian)* 77−13902
  Friedmann cosmological models, fermion pair creation by gravit. field and singularity *(Russian)* 78−93493
  Furry procedure for quantum processes in strong EM field *(Russian)* 77−13901
  gamma-ray pulsars, curvature radiation-pair prod. model 79−5852
  gamma-ray-detector, form of high energy interaction, effect on spectral peak centroid determ. 79−36468
  hadron-hadron, e^+e^- pair prod. calc., high energy internal conversion of bremsstrahlung photons 79−420
  hadronic collisions, inclusive lepton pair prod., invariated helicity struct. funcions anal. 79−13172
  heavy ion collisions, e^+e^- spontaneous creation, charged vacuum existence *(German)* 77−67607
  heavy ion collisions, positron prod. 78−50198
  heavy ion collisions, positron prod. meas. 78−50197
  heavy ion molecular collisions, QED test in strong elec. fields, pair creation 78−45829
  heavy ion quasimol. collisions, electron pair prod., vacuum polaris. shakeoff 77−30945
  heavy-ion scatt., critical dist. for electron two-centre problem 77−71553
  heavy-ion sub-Coulomb collisions, e^+-e^- pair creation as probe for strong Coulomb fields 78−12962
  hot accretion disks in galactic nuclei, pair production and gamma-ray luminosities 80−56930
  identical photons in nuclear field, Born approx. perturbation theory *(Russian)* 77−30290
  internal pair formation following heavy ion collisions, conversion coeff. calcs. 78−50135
  internal pair production in alpha decay, probability 79−71821
  J particle discovery, review *(Hungarian)* 79−17778
  laser radiation pressure for e^+e^- pair prod. 79−40700
  longitudinal electric wave field, e^+e^- prod. *(Russian)* 79−6300
  near threshold screening effects, partial wave calc., energy shift screening theory 80−57768
  neutrino absorption in Coulomb field of nuclei in strong mag. fields, radiation loss by pair prod. 77−14115
  neutron star, plasma interface, physical processes in strong gravit. field, electron-positron pair prod., γ-ray emission *(Russian)* 79−80333
  neutron stars, pair formation and electric field boundary conditions at magnetic poles 80−101613
  nonstationary gravitational field, creation of fermion pairs *(Russian)* 77−74635
  nuclear excitation and target recoil effects *(Russian)* 77−26677
  nuclear field, pair form. from two photons *(Russian)* 78−45819
  nuclear pair production in field of bichromatic plane EM wave *(Russian)* 79−6299
  nucleus$+\gamma$, screening corrections for intermediate, high energies, using relativistic form factors 78−93986
  pair opening angles, determ. using nucl. emulsion plates opening angles of pairs, meas. in nuclear emulsion, photon spectra prediction 77−46035
  Penrose pair production, in massive extreme Kerr black holes 79−21322
  Penrose pair production in black holes in Centaurus A, 3C 273 and NGC 4151, rel. to gamma-ray emission 80−56925
  Penrose pair production in massive Kerr black hole, power source for active nuclei 79−44352
  photon elastic scatt. in intense field, pair and photon photoproduction *(Russian)* 77−22673
  photon induced, intermediate energy, Coulomb correction to total cross section 78−21540
  photon propagator and pair production in steady electric field *(Russian)* 79−9320

electron pair production continued
photon scattering by intense EM wave in homogeneous mag. field *(Russian)* 80—47227
photon-atom sections, 100 eV to 100 GeV 77—54536
photon-photon scatt. in strong mag. field 78—4816
photons, ultrahigh energy, traversing cosmic blackbody photon gas, effective penetration distance 79—5742
by photons in constant electromagnetic field in general relativity 78—8568
photoprod. of e^+e^-, radiative corrections calc. 78—45823
photoproduced in crystals by circularly polarised γ-quanta 78—17005
photoproduction, at nucleus, in field of plane EM wave *(Russian)* 77—61225
photoproduction, in field of bichromatic plane EM wave *(Russian)* 77—30291
photoproduction of lepton pairs in thick target, Monte Carlo simulation 78—21432
photoproduction of relativistic parapositronium, and muonium perturbation expansion *(Chinese)* 79—49432
photoproduction on nuclei, 1-10 GeV, total cross section meas. 80—78280
pion-quark scattering model for lepton pair production from $q\bar{q}$ annihilation 79—13056
plasma, relativistic particles, Compton effect and pair production *(Russian)* 77—24052
point-Coulomb calc., analytic continuation to tip of positron spectrum 77—26475
polarisation, lepton and photon nuclear interactions, bremsstrahlung, pair production *(Russian)* 77—88104
polarised e^- and e^+ prod. at ultrahigh energies, use of mag. convertors 77—87963
polarised positron, electron production by colliding photon beams in storage ring 80—5426
positronium production in nucl. monopole transitions 77—54635
prompt electron yield from hadron interactions anal. 77—26517
pulsar magnetosphere pair prod. 79—44515
pulsar polar cap, pair prod. rel. to inhomogeneous struct. and radiation processes 79—25623
pulsar polar caps, pair form. and struct. of low altitude accel. zone 79—92790
pulsar polar caps, pair prod. discharges 77—53618
pulsars, hadronic photoabsorpt. and pair production 78—12261
pulsars, pair creation model rel. to source of coherent radio emission 80—82403
pulsars, radio pulses production mechanism 77—13372
QED, strong and supercritical fields, book contrib. 78—74193
QED in an external gravitational field, S-matrix evaluation, pair prod. 78—82131
QED of pair creation in strong EM field *(Russian)* 77—30288
quantized magnetic field influence, equilib. *(Russian)* 78—4812
quasars, gamma-ray sources rel. to pair prod. and radio components 79—25747
radial integrals for electron pair production in a point-Coulomb potential 80—22598
radio galaxies, gamma-ray sources rel. to pair prod. and radio components 79—25747
scintillation counter NE213, organic liquid, Monte Carlo calcs. of electron energy loss spectrum for incident gamma-rays 77—6613
screening corrections in electron pair production by intermediate- and low-energy photons 79—30686
spontaneous creation in inhomogeneous mag. fields 80—22540
supercritical nuclear composites, spontaneous vacuum decay 78—25235
superdense magnetised astrophysical objects, electron-positron pair prod. 80—17603
superheavy ion collisions, slow, spontaneous positron creation 79—9603
superheavy quasi-molecules, positron creation from K-shell vacancy 77—58220
total cross-section near threshold determ. *(French)* 78—455
vacuum, e^+e^- pair creation by free EM field *(Russian)* 77—71467
vacuum-to-vacuum transition probability, in QED with pair-producing external field *(Russian)* 78—12842
vector meson production, 6 GeV, anomalous interaction mediator, e^+e^- prod. data anal. *(Chinese)* 77—67664
α-decay, e^+e^- pair production probability determ. 78—50133
α-decay, pair production probability estimate 78—13036
χ production properties from inclusive electron pair and J/ψ prod. at CERN ISR 79—36113
$^3D_1$-charmonium decay into $e\bar{e}$ and relativistic effects of constituent quarks 79—3017
e/π ratio at low p_T in high energy hadronic collisions, possible $Q\bar{Q}\to e^+e^-X$ mechanism 79—71687
e^+ production by Coulomb centre in homogeneous mag. field *(Russian)* 77—41798
e^+e^- annihilation, spin-0 electron or muon pair prod., cross section supersymmetry predictions 80—32092
$e^+e^-\to e^+e^-$, 400 GeV, search for narrow reson. states near 6 GeV 77—74699
$e^+e^-\to e^+e^-X$, $X=e^+e^-$, $\mu^+\mu^-$, $\pi^+\pi^-$, η', photon-photon interactions, QED test 79—93425
$e^+e^-\to e^+e^-(\mu^+\mu^-)$ EM processes, vector resons. cross sections *(Russian)* 77—57517
$e^+e^-\to l^+l^-$, $l=3$, μ, τ, charged lepton universality test 80—32091
$\gamma\to e^-e^+$ generalised conservation laws of physics, electron energy spectra theory 79—85246
$\gamma\to e^-e^+$ generalised conservation laws of physics, electron energy spectra theory 79—85247
γ-rays in liquid Xe, cross section, 25 to 1750 MeV *(Russian)* 77—6188
$\gamma\gamma$-scattering using focused laser beam, spontaneous pair prod. 77—87962
$\gamma\gamma\gamma\to e^+e^-$, reaction probability *(Russian)* 78—45820
$\gamma p\to e^+e^-p$, reson. struct. obs. background process *(Russian)* 78—89722
μ+atom, e^+e^- pair prod., energy spectrum, screening effects *(Russian)* 78—55250
$N+\mu$, e^+e^- pair production cross-section, transferred momentum depend. *(Russian)* 79—54432
NN collisions, lepton pair prod., $\gamma\gamma$ background of Drell-Yan process 79—13057
$p+Ne\to e^+e^-$, 300 GeV/c, comparison with QED theory 78—8569
pp, 53, 63 GeV, massive electron pair prod., Υ ang. decay, scaling function 80—68495
pp, 53, 63 GeV, Υ and ψ prod., dielectron decay angles 80—68496
pp, 62.4 GeV, e^+e^- massive pair prod., continuum and Υ resonance cross sections 80—18153
$\bar{p}p$ annihilation, low energy, prompt e^+e^-, ω^0 and η^0 prod., inclusive prod. rates 80—42506
$\bar{p}p\to e^+e^-$ annihilation, weak neutral current effects *(Russian)* 80—105837
$pp\to e^+e^-X$, 52, 63 GeV, cross section, ψ' prod. cross section, continuum cross section 79—425
$pp\to e^+e^-X$, 53 and 63 GeV, prod. of high transverse momentum low mass e^-e^+ pairs 79—54365
$pp\to e^+e^-X$, J/ψ prod. at $\sqrt{s}=52$ GeV 77—65181
$pp\to e^+e^-X$, large p_T, reference to $\Upsilon(9.5)$, $\xi(3.5)$ and direct γ-prod. 78—89749
$pp\to e^+e^-X$, limits on prod. of large transverse momentum direct photons 79—9418
$pp\to e^+e^-X$, review of CERN-Columbia-Rockefeller-Saclay expt. 77—263
$pp\to e^+e^-$+anything, 23-62 GeV, meas. 77—2877
pp interactions, 12 GeV/c, direct e^+e^- prod. 78—78221
pp interactions, e^+e^-, cross section, and Υ(9.5 GeV) prod. 78—25085
pp→virtual gamma+hadrons soft bremsstrahlung, external emission dominance model 78—62430
$\pi^0\to e^+e^-$, branching ratio meas. 78—41538
$\pi^0\to e^+e^-$, form factor slope meas. 78—41537
$\pi^+N\to e^+e^-$, 830 MeV/c, comparison with recent data 77—87996
π^-p, 360 GeV/c, direct e^+e—pair prod. in liquid H, comparison with QED calcs. 77—10285
$\pi^-p\to e^+e^-n$, S and D-wave resonances parameters in quasi-threshold kinematic config. 79—63516
$\pi^-p\to ne^+e^-$, virtual photon polarisation, PCAC anal. 78—12930
$\pi^+p\to e^+e^-$, 4.0 GeV/c, direct and via ρ^0, ω^0 decay 77—26542
$\pi^\pm p\to e^+e^-$, 18 GeV, direct pair prod. meas. 79—427
$\pi^\pm p\to e^+e^-+X$, direct and indirect pair production 79—9419
$\Upsilon\to e^+e^-$, widths and b-quark interpretation of peaks 79—63435
^{241}Am, α-decay, e^+e^- pair production probability determ. 78—50133
Be+p, 12 GeV/c, direct e^+e^- prod. 78—78221
Fe+μ, 2 to 800 GeV, EM interactions of cosmic ray muons, e^+e^- prod. and knock-on e^- prod. 79—66902
Ge, photon induced electron pair prod. cross section *(French)* 79—524
Ge, total pair prod. cross section near threshold, meas. using variable energy source *(French)* 79—85866
Ge(γ,e^+e^-), cross section near threshold, atomic electron screening effects 80—78279
Ge(γ,e^+e^-), near threshold, variable energy source, total cross section *(French)* 80—37367
H, photon interactions, total pair prod. cross-sections for hydrogen in range 330-910 MeV 77—2783
He(-Ne), electron pair production cross sections, 2.614 MeV, triplet events 77—57580
^{32}P, β^- decay, energy spectra of positron pairs 79—6506
U, absolute pair prod. cross sections 79—63973
W(α,$\alpha'e^+e^-$), 1.0-2.5 MeV, e^+e^- pair prod. search 80—27637
W(p,p$'e^+e^-$), 1.0-2.5 MeV, e^+e^- pair prod. search 80—27637
^{136}Xe+Th(Au)(Al), 624 MeV, internal pair conversion positron spectra 77—67769

electron pairs
see also electron pair production; positronium
ferromagnetism in one dimens. 79—61020
free electron pair, possible ferromagnetism of triplet state 79—30272
internal pair formation high resolution in-beam studies with magnetic+Si(Li) spectrom. 79—18073
pair conversion particles, angular distribs. 79—6498
Weinberg-Salam theory 78—82194

electron paramagnetic resonance *see paramagnetic resonance*

electron-phonon interactions
see also phonon drag; strong-coupling superconductors; tunnelling spectra; tunnelling spectroscopy; Umklapp process
1/f noise, originating from lattice scatt., expts. on p-Ge and n-GaAs 78—64074
A15 compounds, mode softening and high supercond. crit. temp. 78—14851
A15 compounds, new aspect of superconductivity, Fermi level rel. to electron-phonon interaction 79—7927
A15 compounds as Jahn-Teller systems, multiple band electron-phonon transport theory 80—24902
A15 superconductors, supercond. and phonon softening in unstable systems 79—65587
A 15 type superconductors, acoustic phonon spectra, electronic density of state function *(French)* 80—80444
A-15 compound, V_3X and Nb_3X, (X=Al, Ga, Si, Ge, Sn), electronic struct., electron-phonon interactions, and low temp. anomalies 79—60701
A-15 compounds, supercond. props., band struct. calcs. 79—33388
A-15 high-T_c supercond., apparent T^2-depend. of normal-state resist. and lattice sp. ht. 77—47921
acoustic waves, parametric excitation in presence of electron currents *(Russian)* 80—80328
acoustoelectric effect, electron drag by coherent Lamb phonons in quantising magnetic field 80—80330
actinide, transport props. and sp. ht., role of optical and acoustic phonons 77—15821
actinides, lattice vibrs. role in transport props. determ. 77—28158
adsorbate vibrations, large-angle inelastic electron scatt., theory 80—75427
adsorbed layer, electronic transforms, near boundary separating mag. and nonmag. states 80—92961
adsorbed layer, nonuniform charge distribution, phase transitions, Hartree-Fock calcs. 80—54525
adsorbed layer, struct. and electron alterations, electron-phonon interaction effects *(Russian)* 78—87880
Ag, anisotropy of electron-phonon collision frequency on Fermi surface, RF size effect 77—15750
alkali halide, avalanche impact ionisation, in optical breakdown 79—42895
alkali halides, relaxed excited state of F-centre, vibronic theory of Stark effects 77—85691
alkali halides, resonance Raman scattering, electron-phonon interaction for F centres 78—68519
alkali halides, review 78—63991

electron-phonon interactions continued

- alkali halides, spectra of O_2^-, S_2^- and NO_2^- mol. ions, electron-phonon interaction 77−52174
- alkali metal, crossing of dispersion curves in $(\zeta 00)$ direction 78−38795
- alkali metal, low-temperature elec. resist., empirical expressions, validity 79−23945
- alkali metal halides, F-centre coupling to lattice modes 79−77596
- alkali metals, electron relax. time energy depend., electron-phonon resist. 79−60805
- alkali metals, ideal thermal resist. and Lorenz number due to conduction electron-phonon scatt. 80−29377
- alkali metals, point contacts, current-voltage characts. at liq. He temps. 80−39663
- alkali metals, thermopower and elec. cond., relationship at low temps. *(Russian)* 80−92882
- alloy, dil., thermoelectric coeff., vertex and other electron-phonon corrections to impurity scatt. 79−95390
- alloy, dil., thermoelectric effects 79−38054
- alloy, dilute, sp. ht., electronic, mass renormalisation and band density of states influences 78−43137
- alloy, dilute, thermoelectric effects, near cancellation of electron-phonon corrections 79−33283
- alloy, disordered, DC conductivity temp. depend. meas. in off-diagonal CPA 77−28153
- alloy, with off-diagonal randomness, phonon-modulated electronic transport 77−15813
- alloys, binary, supercond. transition temp. lowering by nonmagnetic impurities 80−100546
- alloys, dil., of polyvalent and noble metals, deviations from Matthiessen rule 80−65525
- alloys, disordered, temp. depend. of elec. resist., force-correlation functions 79−51542
- alloys, thermoelectric props., effect of electron-impurity and electron-phonon interactions 79−33282
- amorphous metals, electron-phonon coupling const. and Eliashberg function 80−39567
- amorphous metals, electron-phonon interaction effect on thermopower 80−29393
- amorphous metals, superconducting properties rel. to ordering 80−65735
- amorphous semiconductor, mobility gap temp. derivative calc., polar contrib. 78−26861
- amorphous semiconductor, non-polar, mobility gap temp. variation calcs. 78−10339
- amorphous semiconductors, mobility gap, phononless hopping 77−55527
- amorphous solids, electron-phonon interactions, fluoresc. line broadening and spectral diffusion 78−84655
- amorphous superconductor, ratio of energy to transition temp. 78−10619
- amplification of HF phonons in field of intrinsic EM wave 77−69060
- antiferromagnet, superexchange, charge transfer light absorpt. 78−34975
- anisotropic superconductor, functional derivative of critical temp. with electron phonon spectral density 80−49971
- anomalous EM fluctuations, quantum theory 78−14679
- anthracene, hole mobility mechanism interpretation of cyclotron reson. results 78−10438
- anthracene, phonon-assisted mobility due to intermol. vibrs. 78−6383
- anthracene, temp.-independent mobilities, phonon-induced electron hopping 79−28347
- anthracene-PMDA, charge transfer cryst., 2K, zero-phonon lines, singlet spectra 78−23484
- anthracene-trinitrobenzene complex, neat and mixed cryst. and glass opt. spectra 77−40274
- antiresonant electron-phonon system, in strong-coupling limit, moments and absorption line shape 77−24875
- antiresonant system, closed form canonical transformation calcs. 77−31741
- Auger recombination of carriers bound to centres involving phonons 80−107805
- benzene, deuterated mixed crysts., phonon assisted trap-trap triplet energy migration, 0K limit, phosphoresc. obs. 77−48218
- benzene, mol. cryst. $S_0 \rightleftharpoons S_1$ transition, non-Born-Oppenheimer phonon coupling 77−15523
- benzene-d_6:benzene-d_0, phonon side bands of specular optical transitions 78−26649
- benzened_0:phenol, phonon side bands of specular optical transitions 78−26649
- 1,12-benzoperylene in n-alkane, zero-phonon lines in luminesc. spectra 78−56512
- p-benzoquinone, mixed crysts., PMDR and thermal modulation spectroscopy, electron-phonon interaction 77−32297
- 2-benzoylpyridine crystals, optical spectra of lowest triplet state 80−16081
- 1, 12-benzperylene, in alkane matrices, zero-phonon lines, press. shifts *(Russian)* 78−76502
- biexciton binding energy, influence of lattice polarisation 77−8028
- binary alloys, random, specific heat enhancement and electron-phonon interaction 80−65242
- binary compound, Kohn anomaly in optical phonon branch 80−92626
- Boltzmann eqn., solution for electron-LO phonon scatt. in a static elec. field 79−19586
- boson linear coupling systems, general props. 80−2124
- bound polaron, exciton states 77−69256
- bound polaron, non-perturbative variational method 80−88485
- boundary condition for the distribution function of electrons interacting with phonons *(Russian)* 79−60458
- brass, lattice thermal cond. component, 4.2 to 30K, microscopic mechanisms 80−107757
- CDW, impurity effects on long-range order in incommensurate phase 77−51678
- CDW commensurate-incommensurate phase transition, 1-D electron-phonon system 78−14682
- CDW distorted linear chain, electronic response and longit. phonons 79−11074
- CDW phase transition, effect of electron-phonon scattering 78−95265
- CDW transition temperature, scatt. effects 80−107720
- cerium ethylsulphate, elec. susceptibility evidence for electronically driven lattice dilation 77−76781
- chalcogenide glasses, non-radiative recombination of electron-hole pairs 78−6759
- charge ordered crystals, low lying collective electronic excitations, NQR study problems 79−78561

electron-phonon interactions continued

- charge-transfer solid, quasitone dimens., Hall effect and transverse mobility 77−4326
- chevrel phases, $A_xMo_3X_4$ (A=Cu, Pb, Zn and x=S, Se, Te), anomalous elec. resist. 79−56221
- close packed compounds, superconducting T_c, heterogeneous hybridisation *(Chinese)* 80−107940
- commensurate-incommensurate CDW phase transition in one-dimensional electron-phonon system 78−67959
- commensurate-incommensurate phase transition in nearly half-filled band 79−65384
- complete nonstationary density matrix in functional integration representation 79−55846
- Condon approximation, shape of absorpt. and fluorescence bands, effect of electron-phonon coupling *(Russian)* 77−48212
- conducting mol. crystal, electron-phonon interaction, effect on electron energy levels 79−4499
- conductors, quantum acoustic bleaching, acoustic zones 80−70324
- conference on lattice dynamics, Paris, France (Sept. 1977) 78−59869
- cooperative Jahn-Teller systems of T nature, electron-phonon excitation branches 78−63823
- coronene, in alkane matrices, zero-phonon lines, press. shifts *(Russian)* 78−76502
- coupled electron-phonon system in two dimensions and implications for inversion layers 78−6425
- covalent semiconductor, heating of charge carriers, energy dissipation 80−49755
- crystal lattice dynamics, microscopic theory 78−87746
- crystals, theory of phononless line broadening for impurity center 78−35180
- cubic crystals, electrooptic absorption of anisotropic Jahn-Teller centres 78−27188
- cubic semiconductors, bulk hot-electron props., review 79−99553
- cyclotron resonance, retarded, effect of electron-phonon coupling *(Russian)* 79−8051
- cyclotron resonance, two dimensional electrons interacting with surface and volume phonon 78−80221
- cyclotron resonance lineshape arising from electron-phonon interactions 80−97142
- cyclotron resonance lineshape for two-dimensional electron-phonon system, quantum theory 79−47336
- DC hopping conductivity, phonon-assisted, exact asymptotic formula 77−62920
- de Haas-van Alphen effect, electron-phonon scatt. calc., appl. to Hg 79−65360
- de Haas-van Alphen effect, quasiparticle approach 80−10897
- deformation potential screening by free electrons in multivalley cond. band 77−76756
- degenerate electron-phonon system, non-linear ultrasound absorption 78−87745
- degenerate polar semiconductor, asymptotic soln. to Boltzmann transport equation 77−4332
- degenerate semiconductor, intervalley phonon scatt., energy loss rate and momentum relax. time 79−15139
- degenerate semiconductor, Peierls instability in field of strong EM wave 79−15106
- degenerate semiconductor, permittivity of electrons interacting with optical phonons 77−24815
- degenerate semiconductor, phonon-assisted Auger recomb. 77−59292
- degenerate semiconductors, heavy hole-phonon bound states for valence band with degeneracy point *(Russian)* 80−15461
- degenerate semiconductors, hot electron transport in parabolic energy bands, kinetic theory, transport coeffs. 80−29412
- degenerate semiconductors, longitudinal thermo-EMF in quantising mag. field, scatt. mechanism *(Russian)* 80−24960
- degenerate semiconductors, transverse magnetoresistance in strong mag. fields 79−99565
- diamond, resonant Raman scatt., first and second order 78−60471
- diamond, resonant Raman scattering 78−48176
- p-diamond, synthetic, semicond., rel. to photoconductivity spectra 79−69550
- dielectric singularity, causing Kohn anomaly and soft modes 79−60470
- dielectric slab, electronic polarisability effect on electron-phonon interaction 77−35651
- dielectric slab, polaron self-energy 79−56144
- dielectrics, electron multiplication, phonon scatt., ionisation rate calcs., Markov processes 80−50267
- dilute alloy, Seebeck coefficient, electron-phonon enhancement 80−70685
- dilute magnetic alloys, electron sound absorpt., disordered mag. impurities, spin glasses *(Russian)* 80−80503
- direct-gap semiconductor, absorpt. coeff. of light due to indirect transitions 79−91400
- dirty superconductor limit, microjunction phonon spectroscopy *(Russian)* 79−11272
- dirty superconductors, collective excitations and electron-phonon scatt. *(Russian)* 77−85380
- disordered alloy, electronic transport, effect of thermal and off-diagonal disorder 78−30902
- disordered alloys, temp. depend. of elec. resist., elastic electron-phonon scatt., CPA calcs. 79−56185
- disordered quasi-one-dimensional materials, review 78−6361
- disordered semiconductor, DC phonon assisted hopping conduction, in mobility gap, theory, rate eqns. 79−60826
- disordered semiconductors, resonance Raman scatt. 79−11419
- disordered system, AC cond. tensor in mag. field 80−92870
- disordered system, DC Hall effect in hopping region 77−66174
- disordered system, phase transition characts. 77−51662
- disordered system, reson. Raman scatt. 80−2772
- disordered systems, hopping cond., freq. depend., two-site model 77−76825
- disordered systems, hopping Hall mobility 77−72846
- disordered systems, phononless HF cond. 77−89789
- disordered systems, theory of Hall effect in hopping region 77−47836
- dispersion self-energy of an electron in a dielectric 79−42461
- doped narrow gap semiconductor, two-channel vibronic mechanism of ferroelectric phase transitions *(Russian)* 79−56745
- durene:naphthalene, spin-lattice relax. in photo-excited triplet states, spin axes rot. on thermal excitation 78−76294
- electrical conductivity freq. depend. in disordered system two site model *(Russian)* 80−54666

electron-phonon interactions continued
- electron charge ordering, Peierls distortion, quasi one-dimensional spinless fermion model 79—87050
- electron energy loss in passage through crystal in presence of quantised mag. field *(French)* 77—11607
- electron gas, electron interaction with optical phonon directional flux 80—59893
- electron gas, one-dimens., interacting, ground-state energy in mean field approx. and instabilities 80—88493
- electron subsystem, steady-state statistical equilib. conditions, adiabatic approx. 78—87754
- electron transport, local electric field, appl. to electromigration 78—30896
- electron-hole binding accompanied by Wannier-Mott exciton form. 80—59887
- electron-hole droplet, motion damping, deform. pot. scatt. 78—67950
- electron-hole droplet, motion damping, impurity and piezoelec. scatt. 78—67951
- electron-hole drops, non-radiative recombination by phonon-assisted Auger recomb. 79—60716
- electron-hole plasma current layering, electron cooling length, momentum scatt. 80—6890
- electron-plasmon and electron-phonon interactions in bulk and near surface, Kikuchi patterns 78—26759
- electronic contrib. to electron-phonon interactions 77—15524
- electronic Raman scatt. in polaron gas 79—95753
- electronic system with two-fold degenerate band, free energy change due to electron-phonon coupling 79—42500
- elementary excitations in crystals, dielectric theory 78—60076
- Eliasberg's equations, solvability *(Russian)* 78—39250
- Eliashberg equation, solution at $T=T_c$ 78—34918
- emission spectra and phonon relax. 77—77279
- energy mismatch in multiphonon relax. 77—24371
- energy relaxation of photoexcited hot electrons at very low temperatures 78—91724
- exciton motion depend. on lattice vibr., inner potential energy, ground state, effective mass *(Chinese)* 80—54610
- exoelectrons, energy and angular distribution 77—85904
- fermi gas, one-dimens., electron-phonon interaction in adiabatic approx. for supercond. state *(Russian)* 77—47753
- ferroelectric, instability and phase transition in system with interband interaction 77—12346
- ferroelectric phase transition, by impurity carriers, electron-phonon interaction *(Russian)* 78—48134
- ferroelectric semiconductor, electronic density of states, effect of soft phonon-electron interaction *(Russian)* 77—80718
- ferroelectric semiconductor, magnetic field influence, ferroelectric transitions 80—55049
- ferroelectric semiconductors, vibronic, mag. field effect on phase transition 77—40193
- ferroelectric structural transitions, electron subsystem 78—43813
- ferroelectric transition in system with strong electron-phonon interband interaction 77—66462
- ferroelectricity, vibronic theory 79—38492
- ferroelectrics, absorption edge anomalies in phase transitions 80—2718
- ferroelectrics, vibronic, band struct. temp. depend. 80—70598
- ferroelectrics, vibronic model, fluctuations of order parameter and anharmonic interaction 77—52022
- ferromagnet, itinerant electron, magnetoresist. and anomalous Hall effect due to electron-phonon interactions 80—70680
- ferromagnetic disordered binary alloy, CPA theory of magnetoabsorption, electron scatt. mechanisms *(Russian)* 77—8549
- ferromagnetic metals, magneto-optical effects, electron scatt. 77—90133
- ferromagnetic semiconductor, carrier-assisted magnon contrib. to phonon damping 77—20018
- ferromagnetic semiconductors, free carrier absorpt. of radiation 80—97227
- ferromagnets, itinerant electron, lattice props. depend. on cond. electron magnetisation, elastic props. 79—61035
- film, bound states of electrons and optical phonons 78—39038
- film, size quantised, thermomag. effects in strong mag. field *(Russian)* 77—63002
- fluctuations in quasi-one-dimens. electron-phonon systems, Peierls transition 77—89703
- free electron metal, comparison with metallic hydrogen 77—66125
- free polaron multiphoton absorpt. spectra, electron reson. coupling via longit. optical phonons 79—95347
- Froelich Hamiltonian, perturbation theory calcs. 79—33247
- Frohlich and Bloch approaches, equivalence 79—46772
- Frohlich-Mitra modified tight-binding approx. for electron motion in deformed lattice 77—69253
- n-Ge, degenerate, Brillouin scatt. by phonon zero sound, in quantising mag. field 77—69847
- glass, trapped electrons, electron-phonon interaction 79—78697
- granulated superconductors, phase transitions, Josephson energy *(Russian)* 80—84540
- graphite, anomalous galvanomagnetic properties, in strong mag. field 79—23986
- graphite, electron-phonon interactions, rel. to elec. transport 80—34156
- graphite intercalation compounds, C_nK, electronic struct. and elec. props. 80—44471
- graphite intercalation cpds., acceptor type, elec. cond. theory 80—44686
- group IV semiconductors, acoustic deform. pot., pseudopot. calc. 77—1363
- group-V layer compounds, 2H-polytypes, origin of CDW, elec. susceptibility, electron-phonon interactions 77—51679
- heavily doped, Raman phonons, interband excitation effects 78—52501
- heavily doped compensated semiconductor, phonon drag effect in disordered media 77—24576
- heavily doped semiconductor, magnetoconductivity, effect of resonant phonon-plasmon coupling 80—24954
- homopolar cryst., anharmonic props. and nonlinear electron-lattice interaction *(Russian)* 77—51691
- hopping, phonon-assisted, due to both acoustic and optical phonon interactions 77—66146
- hopping conductivity in ordered and disordered solids, review 77—1420
- hopping promoted by electron-electron coupling 80—59987
- hopping transport, rate equations, theory 77—43590
- hot electron distribution functions, expts., review 78—27231
- hot electron quantum energy distribution function in crossed elec. and mag. fields 77—32019

electron-phonon interactions continued
- hot electron semiconductor, capture of charge carriers rel. to I-V curves, phonon heating 79—51589
- hot luminescence in F centres, nonradiative quenching 80—11467
- hot photoexcited electrons, time evolution of electron temp. in high mag. field 80—54709
- Hubbard model, electrical conductivity calc. including electron-phonon interactions 77—47804
- Hubbard model, half-filled, charge ordered solution local mag. moments, repulsion energy renormalisation 79—61034
- Hubbard model, one-dimens. half-filled band Holstein-Frolich modified, transport props. 78—23237
- hybridised conduction band, intrinsic upper limit of electron-phonon coupling *(Chinese)* 80—54589
- ice film, low-temp. diffusion of electrons, evidence for polaron bands 77—1380
- II-VI compounds, Jahn-Teller effect, average phonon energy 79—15122
- II-VI semicondcutors acoustic deform. pot., pseudopot. calc. 77—1363
- III-V semiconductors, acoustic deform. pot., pseudopot. calc. 77—1363
- III-V semiconductors, optical phonon scatt., review 79—19587
- impure metals at low temperatures, conductivity 80—103669
- impurity absorption and fluorescence spectra, quadratic electron-phonon interaction and impurity-ion band shape 78—6731
- impurity atom in solid, reson. fluoresc., transient spectrum, intensity, and intensity correl. 80—84777
- impurity centre, electron-vibr. transitions in presence of several minima of adiabatic potentials 77—81150
- impurity centres, electron-phonon coupling from structured optical spectra, review 80—89038
- induced electron tracks and structural phase changes in MCr_2O_4 type cryst. *(Dutch)* 79—1585
- inelastic electron tunnelling spectroscopy, golden rule formalism 79—94050
- inert gas crystal, bound self-localised hole states assoc. with lattice distortion 77—24530
- insulator to superconductor phase transition, possibility 79—47190
- insulator-metal transition, electron-phonon interaction, electronic transport props. 77—89702
- insulator-metal transition, role of electron-phonon interactions in narrow-energy-band solid 77—89701
- interimpurity tunnelling of electrons in solids, theory 78—88019
- intermediate valence compound, pressure-temperature phase diagram 79—28283
- intermediate valence compounds, phonon produced instabilities, periodic Anderson model 78—79964
- intermediate valence cpds., phonon effect on press.-temp. phase diagram 80—24849
- intermediately coupled localised electron-phonon system, transient reson. Raman scatt. Franck-Condon-like excitation 79—8141
- internal photoemission, phonon scatt. effects 77—85315
- inversion layers, carrier effective mass, contribs. of electron-electron and electron-phonon interactions 78—64087
- inversion layers, mag. field depend. of reson. line width 78—56380
- inversion-layer electrons, temp. depend. cyclotron reson. lineshape, theory 78—64086
- ion-electron chains, anharmonic effects, electron-phonon coupling 79—60459
- ionic compounds, electron irrad., broad band radioluminesc. 77—32446
- ionic crystals, nonradiative multiphonon transitions in impurity centres with extremely weak electron-phonon coupling 80—25436
- ionic crystals, surface polaron 78—60020
- ionic semiconductors, cyclotron resonance, elec. cond., electron-phonon interactions 80—93180
- ionic solids, surface phonon-plasmon coupling (surface plasmarons) 80—54497
- IR absorption spectrum, effect of electron-phonon interaction on vibronic peaks and phonon lines 78—43086
- IR lattice band profile, electron spin reversion in mag. field, Nf-R curve 79—28771
- isotopically disordered vibr. crystal quantum transport eqn., electron-phonon coupling 78—39081
- itinerant electron ferromagnets, elastic props. and electronic struct. 80—66001
- IV-VI compounds, phase transitions induced by electron-phonon interaction 80—10656
- IV-VI compounds, structural instabilities and transverse effective charges 77 - 27999
- IV-VI semiconductors, structural phase transitions, anomalous resist., electron-soft phonon interactions 80—108167
- Jahn-Teller centre optical band polarisation dichroism, forbidden transitions 80—55062
- Jahn-Teller cooperative phase transition, helical ordering 79—46778
- Jahn-Teller cooperative systems, low-freq. dynamics 79—82565
- Jahn-Teller cooperative $T-(e+t)$ systems, heat current operator 80—34405
- Jahn-Teller cooperative T-$(e+t)$ system, thermal cond. 80—70479
- Jahn-Teller ions, spin Hamiltonian parameters, temp. depend. 78—30891
- Jahn-Teller system, lattice relax., photo-absorpt.-luminesc. polarisation correl. 77—51708
- kinetic equation, chronological and antichronological T-products 80—70627
- kinetic equation for dynamic system *(Russian)* 80—54619
- kinetic equations for electrons and phonons in strong const. elec. field 80—34157
- large radius polaron model, soliton excitations 79—42470
- laser crystals, theoretical problems, current status *(Chinese)* 79—45948
- lattice, deformable, local and global stabilities of electron 80—54620
- lattice gas, thermoelectric power in half-filled bands 79—60859
- lattice instabilities, electronically driven, theory 78—10158
- lattice thermal resist. due to bound state electrons in doped cryst. 79—46850
- layered compound, supercond. and charge-density waves 80—34542
- layered semiconductors, high pressure effects 77—51654
- layered semiconductors, transport props., book contrib. 77—43587
- LCAO Slater-type orbital band structure calcs., computable expressions, derivation 80—24776
- light scattering, resonant and luminesc., of localised electron and weakly coupled phonons 77—12374
- light scattering by localized electrons, broad phonon wing and zero phonon line 80—7365
- linear conductor, diagrammatic calc. of IR props. 77—32374

electron-phonon interactions continued
linear conductor, IR absorption, amplitude and phase mode dynamics 77—16313
local heating, quantum transitions in coupled electron-vibr. system 79—15514
localised electron-phonon system, linearly coupled, reson. Raman scatt. polaris. effects 79—91428
localised nearly degenerate electronic states, dynamic effects 78—6338
localised system, strongly coupled, photon echo phenomenon 80—64118
localization aspect of electron phonon-coulomb system 79—7793
long-wave quasiparticle states localized at screw dislocation *(Russian)* 78—95126
magnetic field induced phonon splitting of cryst. field levels 80—13110
many valley semiconductor, rel. to nonlinear effects in US propag. 77—59305
many-band metals, elect. resistivity from force correlation function method 78—43357
many-valley semiconductors, ellipsoidal energy surface, high field magnetoresist. and magnetothermal EMF 77—43621
martensitic transformation mechanism, effect of electron-phonon system *(Russian)* 78—3127
matrix element calculation, phase transitions 78—79703
metal, adsorbate vibrational excitation by inelastic electron scatt. 77—43428
metal, BCC, elec. cond. temp. depend., anharmonic effects 78—76045
metal, closed Fermi surface, galvanomagnetic phenomena, in intermediate magnetic fields *(Russian)* 78—34822
metal, compensated, with closed Fermi surface, rel. to Hall coeff. temp. depend. 77—8074
metal, cond. electron relax. time, review *(Japanese)* 78—30910
metal, cubic, dipole-nuclear acoustic resonance, electron band struct. influence 79—19787
metal, cubic, impurity effect on electric field gradient 78—23061
metal, cubic, Sharma-Joshi model, correl. exchange effects 80—10613
metal, dirty, resist. temp. depend., causes of Matthiessen's rule deviations *(Russian)* 77—69291
metal, electron mediated nucl. spin-phonon interaction 77—1604
metal, electron-phonon and electron-impurity collision frequencies, RF size effect method 77—20227
metal, electron-phonon drag and interaction of first and second sound 77—66009
metal, electron-phonon interaction effects on spin susceptibility 80—93108
metal, exchange enhancement of electron-phonon coupling 78—47968
metal, Fermi surface topological transition, electron-phonon interaction contrib. calc. 80—6697
metal, ferromag., antiferromag., magnetoelastic coupling effect on magnetoelec. reson. 80—75837
metal, general theory for elec. resist. temp. depend. 78—47757
metal, high resistivity, supercond. transition temp., influence of electron mean free path 79—82702
metal, in mag. field, phonon spectrum, nonadiabatic effects *(Russian)* 78—19106
metal, kinetic equation, iteration soln. 77—43564
metal, low temp. impurity cond. temp. depend., kinetic eqn. *(Russian)* 79—7817
metal, low temp. phonon resist. 77—62888
metal, low-freq. longit. sound attenuation, viscous and induction mechanisms 77—8152
metal, magnetism influence 77—73040
metal, many-body effects of electron-phonon interaction on thermoelectricity 79—69499
metal, Matthiessen rule deviations, electron scatt. by dislocations, impurities and phonons 78—19026
metal, monovalent, contrib. of John Bardeen 80—57057
metal, normal, electron-phonon interaction function determ. by proximity effect *(Russian)* 77—89902
metal, one- and two-dimens., periodic lattice distortion and CDWs 79—60678
metal, one-dimensional, ideal resist. 77—32002
metal, phonon-limited resist., correction from non-Hermiticity of pseudopotential 79—7815
metal, quasi one dimensional, Peierls instability criterion *(Russian)* 77—89516
metal, rel. to thermal resist. calc. 77—62894
metal, temp. depend. of low freq. surface impedance 78—56207
metal, thermoelectricity, electron-phonon enhancement 78—56135
metal, thermoelectricity, electron-phonon mass enhancement 79—65452
metal alloy, random, electron-phonon dynamics and resistivity anomalies 80—10958
metal hydrides, anharmonicity and superconductivity 77—15988
metal RF size effect, small-angle scatt., exactly solvable models 78—47821
metal surface, adsorbed layer, structural and electronic reconstruction 78—84280
metal surface, electron-phonon coupling in image-potential bound states 80—54752
metal theory and generator coordinate method 79—28299
metal-insulator transition, anharmonism effects 78—56072
metal-insulator-mseiconductor structure, magnetooptic absorpt. with participation of optical phonons 79—99858
metal-insulator-superconductor junction, electron interactions with phonons and mag. impurities 77—16004
metal-ion point defects in solids, non-radiative relax. 78—6753
metal-liquid He interface, electron-phonon interaction, thermal boundary resistance 78—67899
metal-liquid He interface, thermal boundary resistance, determ. in transport approach 78—51815
metal-metal microbridge, electron-phonon coupling and phonon generation 77—76510
metal-semiconductor interface, photoelectron injection, quantum mech. transmission and optical phonon scatt. 80—84511
metallic alloy, highly resistive, elec. resist. calc. including Debye-Waller factor 77—66150
metallic compound, phonon spectrum renormalisation due to electron-phonon interaction 77—66008
metallic film, phonon fluorescence stimulated by laser radn. 79—87504
metallic point contacts, nonlinear resist. rel. to phonon emission and background effects 78—68074
metallic point contacts, small radius, voltage-current curves, electron-phonon interaction theory of results *(Dutch)* 77—62985

electron-phonon interactions continued
metallic system, X-ray line shapes for core levels, phonon broadening 77—12464
metallic thin film, effects of electron-phonon interaction, possible realisation of supercond. state 80—49977
metallic thin film surface wave attenuation due to electron-phonon interaction 79—55848
metals, elec. cond., band mixing generalisation 79—38060
metals, electrical and thermal resistance, influence of static atomic displacements 80—103674
metals, electron-phonon interaction and lattice thermal conductivity 79—42189
metals, frictionless heat motion at low temps. 79—69495
metals, low temp. resistivity, electron-phonon scatt. anisotropy influence 79—60818
metals, nonlinear vol. photoelectric effect, anal. 79—15593
metals, normal hexagonal, temp. depend. anisotropy of phonon scatt. resist. 78—51967
metals, phonon drag direct obs. feasibility *(Russian)* 77—85187
metals, phonon point-contact spectroscopy 79—65152
metals, polyvalent, Matthiessen's rule deviation crit. resist. 80—6811
metals, positron trapping by defects influence of positron-phonon and electron-phonon interactions *(Russian)* 80—93425
metals, RF size effect as tool for cond. electron scatt. investigations 79—23957
metals, superconductivity studied by electron-phonon and Coulombian e-e coupling strength and quasi particle mass 80—88666
metals, surface impedance, extreme anomalous limit, diffuse refl. from boundary 80—29460
metals, thermoelectric power, electron-phonon enhancement 77—72855
metals, thermoelectricity theory, electron relax. time 79—69498
metals with $Z \leq 49$, supercond. props. 77—66221
microscopic theories of lattice dynamics, developments 78—59870
MIM system, electron emission modelling *(Czech)* 80—2479
MIS device, polar-optical phonon interaction with two-dimens. electron gas 79—82434
MIS structure, optical phonon-electron gas interaction, high freq. cond. 80—6888
MIS tunnelling spectra, interaction of holes with local modes and one and two optical phonons 77—20457
mixed valence compounds, phase diagrams, lattice props., electron hole symmetry 79—91002
mixed valence compounds, structural phase transitions, effect of electron-phonon coupling 79—33265
mixed valence cpds., elec. cond., periodic Anderson model, memory function approach 80—84458
mixed valence cpds., electron-hole symmetry, phase diagrams, and lattice props., periodic Anderson model 80—15481
mixed valence systems, theory 80—70343
molecular chain, 1-D electron motion, electron-phonon interaction, acoustic solitons 80—70628
molecular crystal, charge carrier mobility temp. depend. 78—10376
molecular crystal, exciton bandwidth effects on electron-phonon coupling 77—4172
molecular crystal, polarisation energy of localised charge, appl. to anthracene and naphthalene 80—15034
molecular crystals, electronic transport theory, local linear electron phonon coupling 80—65545
molecular crystals, thermal modulation spectroscopy, electron-phonon interaction 77—32392
molecular liquid, electron energy loss processes at subelectronic excitation energies 77—89486
molybdenum ternary sulphides, Chevrel phase, synthesis and superconductivity *(German)* 80—25038
monovalent metal, electron-phonon coupling const., calc. 79—99286
monovalent metal, resistivity, 1-4K, HF phonons role 77—15828
Mott's formula for thermopower and for Wiedemann-Franz law 80—84462
Mott magnetic semiconductor, freq. depend. elec. cond. 77—11907
multi-phonon processes due to absorption at localized centres in noncond. cryst. 78—27278
Multiphonon effects in the theory of electron tunelling between deep impurity levels and the conduction band in strong electric fields 78—2447
multiphonon relax., localised electron radiationless decay, continuum and cluster modes 77—52158
multiphonon tunnel processes in homogeneous elec. field *(Russian)* 78—39607
multiple band electron-phonon transport eqn. derivation 80—100318
multiple band transport theory, generating functional approach 80—92633
naphthalene, doped, role of nonequilibrium phonons in stimulated radiation emission 80—103971
naphthalene, doped, zero-phonon lines and absorpt. spectra, temp. depend. of shift and broadening 79—69866
naphthalene, electron band hopping transition 78—39155
naphthalene, temp.-independent mobilities, phonon-induced electron hopping 79—28347
naphthalene-β-naphthol mixed mol. cryst., multiplet struct. of electron absorption spectra 77—1706
naphthalene-d_8:β-methylnaphthalene -d_{10}, phonon side bands of specular optical transitions 78—26649
naphthalene-TCPA charge transfer triplet states, electron-phonon coupling 79—38601
narrow band gap semiconductor, electron-phonon interaction, effective mass of carriers determ. 79—11058
neutron scattering obs. of phonons, book contrib. 77—89504
noble metal, rel. to temp. depend. of thermal resist., in free electron approx. 77—66152
noble metal point contacts, direct meas. of electron-phonon coupling 78—6433
noble metals, electrical resistivity, pseudoharmonic effect of phonons 80—34414
noble metals, electron relax. time energy depend., electron-phonon resist. 79—60805
noble metals, pure, low-temp. transport props. 77—8072
noble metals and their dil. alloys, electronic struct., de Haas-van Alphen studies, book contrib. 79—37967
non-radiative processes in solids, dynamic multiphonon processes 80—11463

electron-phonon interactions continued
  non-stationary density matrix, representation by function integral 78—71818
  nondegenerate semiconductor electrons in strong elec. and quantizing mag. fields 78—10457
  nonequilibrium free carrier distrib. in EM wave field, luminesc. intensity and IR scatt. cross section 79—69888
  nonequilibrium superconductor, effect of pair breaking on branch relax. 79—78257
  nonlinear impurity electron-phonon oscillations 80—49327
  nonpolar semiconductor, normalised theory of impact ionisation and vel. saturation using Markov chain 79—91067
  normal metals, low temp. resistivity, correl. with electron-phonon scatt. anisotropy 79—56190
  n-octane-3,4,6,7-dibenzpyrene impurity, fluorescence impurity spectra, phonon free line broadening *(Russian)* 80—108279
  one dimension, electron-optical phonon interaction with strong coupling via deform. potential, vibr. excitations 78—51907
  one dimensional conductors, electron-electron interactions and Kohn anomaly 80—24895
  one dimensional cryst., electrical conductivity anomalies due to two mechanisms of electron phonon interaction *(Russian)* 80—34430
  one-dimension, electron-acoustic phonon interaction via deform. potential 77—4302
  one-dimensional conductor, dispersionless phonons effect on electron kinetics *(Russian)* 77—32005
  one-dimensional conductor, incommensurate Frohlich model, displacement correl. of classical ions 78—6291
  one-dimensional conductor, lattice stability, phonon dispersion, Kohn anomaly 80—96603
  one-dimensional conductor, phonon dynamics 78—79704
  one-dimensional conductor, phonons effect on localisation and electrocond. 78—6362
  one-dimensional conductors, inorganic, modulated structs., formation and nature 79—94968
  one-dimensional conductors, quasiparticle approach 77—20305
  one-dimensional electron-phonon system, dynamics, Frohlich model 77—15781
  one-dimensional electron-phonon system, renormalisation *(Russian)* 78—43314
  one-dimensional electronic systems, instability due to electron-phonon interaction 79—99536
  one-dimensional Fermi gas, energy gap, boundary conditions for renormalisation-group eqns. 78—10317
  one-dimensional Frohlich model dynamics, Green's function anal. 80—20170
  one-dimensional metal, phonon drag and sliding CDW 80—20173
  one-dimensional system, electron-phonon interaction, soliton solns. 79—23691
  one-dimensional systems, electron trapping and transport by supersonic solitons 78—72139
  open electron-phonon system, statistical electron transport theory 79—11096
  optical absorption spectra, correl. with g-shifts 78—23485
  optical properties, temp. depend., transport eqn. 78—23421
  organic metals, transport theory, electron-phonon scatt. 80—20161
  organic molecular crystal, electron mobility, temp. independent, theory 79—69509
  p-n tunnel junctions, photoinduced transitions, theory 80—65669
  parallel spin electron-electron interaction 80—10622
  parametric excitation in solids, quantum calcs. 80—103714
  parametrized model for obtaining electron scattering rates from radio-frequency size-effect data 79—69541
  Peierls dielectric, one dimensional, selftrapped excitations in Peierls-Frohlich state *(Russian)* 80—54678
  Peierls instability in nearly free electron model with nonlinear screening 77—4304
  Peierls systems with dil. impurities, microscopic theory of pinning effect 77—15837
  Peierls transition, Frohlich model, one-dimens., CDW stability, electron-phonon coupling 80—65452
  Peierls-Frohlich system, nearly 1/3 filled band ground state, charge density waves 77—51681
  Peierls-Hubbard model, antiferromag. and lattice-distortion 77—47964
  Peierls-Hubbard model, antiferromagnetism and lattice distortion 77—55656
  Peierls-Hubbard model, quasione dimens., antiferromagnetism and Peierls distortion 78—67931
  perfect crystal, electron diffr. pattern, distrib. of phonon scattered electrons 77—19846
  periodic lattice, theory of coexistence of supercond. and magnetism, supercond. transition temp. 80—34543
  perylene in n-alkane, zero-phonon lines in luminesc. spectra 78—56512
  phase transition in electron-phonon system with deform. interaction in mag. field *(Russian)* 77—35873
  phonon assisted DC hopping conductivity, Anderson localised electronic states 77—32010
  phonon bottleneck, influence on dynamic nucl. polarisation by solid effect 80—20511
  phonon emission by metal heater film into insulating substrate, spectral distrib., model treatment 79—14896
  phonon instability in the presence of two radiation fields 79—56141
  phonon spectroscopy, spectral, spatial and temporal 78—83892
  phonon-assisted radiative electronic transitions 79—24348
  Phonon-cyclotron absorption in a transverse electric field 78—2741
  photoemission from bulk bands of solids, electron-phonon interaction effects 80—20767
  photoexcited hot electrons in high mag. field, mean energy 78—30955
  photoferroelectric phenomena, physical models derivation, electron-phonon interaction modification 79—15407
  photovoltaic effect mechanism, expt. obs. of thermal and spectral variations in the photovoltaic current in ferroelectrics 78—91719
  piezoelectric material, photovoltaic effect, phonon mechanism 79—7862
  piezoelectric semiconductor, cascade capture of carriers by attractive impurity centres, cross section 78—56157
  piezoelectric semiconductor, effect of strong doping on sound attenuation 80—2120
  piezoelectric semiconductor, optical absorpt. by free polaron 77—59547
  piezoelectric semiconductor, photocurrent in quantising magnetic field in presence of nonequilibrium photoelectrons, spectral oscill. and energy relax. by interaction with acoustic phonons 79—91100

electron-phonon interactions continued
  piezoelectric semiconductor, polaron optical absorpt., external static elec. field depend. 77—85158
  piezoelectric semiconductor, scatt. anisotropy in longit. quantizing mag. fields 78—26890
  piezoelectric semiconductor film, Rayleigh wave amplification, quantum theory approach 77—69158
  piezoelectric semiconductors, acoustic phonon-conduction electron interaction, Brillouin scatt. theory 77—40255
  piezoelectric semiconductors, acoustoelectric surface phonon-conduction electron interaction 79—42360
  piezoelectric semiconductors, surface phonon acoustoelectric interaction, elastic anisotropy effects 80—6610
  piezosemiconductor film, surface-mode acoustic wave amplification 79—46907
  point contacts, metallic, elec. cond., spectroscopy of phonons, impurities *(Russian)* 78—38797
  point contacts between identical metals, HF rectification at low temp. 80—105706
  polar amorphous dielectric, elec. breakdown 77—20333
  polar crystal, bulk photovoltaic effect due to electron-phonon coupling 77—20358
  polar crystal, bulk photovoltaic effect due to electron-phonon coupling 78—14757
  polar crystal, effective electron-hole interaction for intermediate and strong electron-phonon coupling 77—80735
  polar crystal, hot electron transport, eikonal approx. for energy loss 77—1426
  polar crystal, hot electron transport, loss to single phonon modes 77—1427
  polar crystal, polaron effective mass temp. depend., electron interaction *(Chinese)* 80—84436
  polar crystals, vibrational Raman scatt. induced by Jahn-Teller systems 79—69830
  polar semicond., secondary radiation intensity oscills., effect of high mag. field 79—19880
  polar semiconductor, effective Hamiltonian for few-particle systems 77—15776
  polar semiconductor, electron-hole liq., phase diagram 77—89706
  polar semiconductor, electron-hole liquid, electron-phonon interactions 80—6739
  polar semiconductor, electron-phonon and electron Raman scatt. in mag. field 79—91438
  polar semiconductor, high elec. field, electron momentum distrib. 77—1428
  polar semiconductor, impurity levels, influence of electron-phonon coupling 78—64007
  polar semiconductor, multiphonon cascade theory of light scatt. 78—19490
  polar semiconductor, surface inversion layers, energy loss of warm and hot carriers 77—11981
  polar semiconductor, theory of excitons bound to neutral impurities 79—73441
  polar semiconductor crystalline thin films, surface vibr. states, IR absorpt. spectra obs. *(Russian)* 80—60606
  polar semiconductors, anharmonicity influence on cond. in quantising mag. field 80—2406
  polar semiconductors, chemical shift of Zeeman masses 78—10338
  polar semiconductors, electron-hole system, interaction with phonons 80—6738
  polar semiconductors, HF mobility in longitudinal quantising mag. field 79—51619
  polar semiconductors, photoexcited, carrier and optical phonon distrib. time evolution 80—34158
  polar semiconductors, resonant magneto-Raman scatt. 79—51958
  polar semiconductors, secondary cyclotron emission giant oscillations of intensity and line shape 80—66192
  polar semiconductors HF conductivity at low temperatures, anal. *(Russian)* 77—8128
  polaron, bound, variational calc. of ground state energy 78—84152
  polaron bound to Coulomb pot., energy 80—88487
  polaron effects on excitons 80—24811
  polaron gas, interacting, ground state energy 77—76758
  polaron model, dressed electron construction, Brillouin-Wigner and Tamm-Dancoff approaches 80—49629
  polarons, Frohlich, mean field theory, phase transitions 80—34371
  polarons, generalised path integral formalism, ground state energy corrections 80—84438
  polarons in one-dimension, lower bounds to self-energy 77—72827
  polyvalent metals, electron relax. time energy depend., electron-phonon resist. 79—60805
  pseudocontinuum approach to interaction theory for impurity defects in crystal lattice 79—69214
  pyrene-PMDA complex, electron-phonon interaction, phosphoresc. 78—48208
  quantum system interacting with nonequilibrium phonons, light absorption props. 78—88340
  quasi one-dimensional conductor, phonon drag conductivity in Frohlich Peierls phase, effect of impurities 78—60114
  quasi one-dimensional metal, static cond. at finite temp. *(Russian)* 78—10428
  quasi-one dimensional metal, Peierls instability in field of strong EM wave 79—15106
  quasi-one-dimensional conductor, high temp. struct. instability, tight-binding approx. and fluctuation model 78—6292
  quasi-one-dimensional conductor, Kohn anomalies, anharmonic effects 77—1197
  quasi-one-dimensional conductor, Peierls instability and superconductivity, possibility of coexistence 78—31028
  quasi-one-dimensional electron-phonon system, electron jump effect on phase tansition *(Russian)* 80—92673
  quasi-one-dimensional metal, longitudinal cond. at finite temp. 78—2473
  quasi-two dimensional conductor, galvanomagnetic props., optical analogy *(Russian)* 80—60108
  quasi-two-dimensional semiconductor, warm carrier relax. via acoustic phonons 77—43694
  quasione dimensional compound, commensurability effect 78—72095
  quench-condensed films, superconducting transition temp., elastic stress and strain effects 80—70883
  quinzarin in alcohol glasses, electron-phonon coupling, photochemical hole burning 80—97265

electron-phonon interactions continued
Raman effect in solids, interacting elementary excitations, review 78−43846
Raman light scatt. efficiency, comparison of various crystals *(Russian)* 77−52104
Raman scattering, electron-phonon interaction effects on polarisation 80−55088
Raman spectral line shape, quantum field theoretic formulation 78−31187
Raman spectroscopy, semiconductors *(German)* 79−28729
rare earth alloys and intermetallic cpds., US attenuation, temp. and mag. field depend. 80−15195
rare earth chalcogenides, cond. mechanism and thermoelec. efficiency 79−38110
rare earth chlorides, doubly degenerate E-phonons, mag. field splitting 77−43297
rare earth compounds, spinless periodic Anderson model with phonons, appl. to mixed valence systems 78−84153
rare earth compounds, valence fluctuations, electron-phonon coupling effect 80−20134
rare earth compounds electron-phonon interaction influence on electronic phase transitions *(Russian)* 78−47743
rare earth ions in crystals, nonradiative processes, book contrib. 80−55188
rare earth metal compounds, high temp. paramagnetic-supercond. phase transitions, mag. cell symm. *(Russian)* 79−78255
rare earth metals, electrical resistivity, high temp., scatt. mechanisms 80−39553
rare earth metals, HCP, microscopic theory of lattice dynamics 77−43292
rare earth mixed valent compounds, lattice dynamics 79−73268
rare earth molybdenum chalcogenides, Chevrel phase correlation between struct. and supercond. transition temp. 80−7023
rare earth systems with valence transitions, phonons 80−96611
rare earth ternary borides, coexistence of magnetism and superconductivity 79−73630
rare earth trichlorides, magnetic phonon splitting, Raman spectra 77−52099
relativistic, oscillating rigid muffin-tins 78−47713
relaxation of nonequilib. electrons at very low temps. 78−60121
relaxation times in solid-state theory and one-dimensional molecular systems *(Russian)* 80−100640
resonance absorption of sound by electrons in quantising mag. field 78−10522
resonance Raman profile with consideration for quadratic vibronic coupling 80−55099
resonance Raman scattering in systems with localised carriers 80−7356
resonant light scatt. and luminescence in weakly coupled localised electron-phonon system 80−40100
resonant light scattering and luminescence, singular aspect in localised electron-phonon system with linear interaction 78−43919
resonant Raman scattering, intensity of electronic and vibr. contribs. 77−77186
resonant Raman scattering in systems with localised electron states, theory 79−15455
rigid muffin tin approximation used in theory of electron-phonon interaction, expt. test 79−65364
Rochelle salt, cryst., oriented intrinsic absorpt. edge shape 77−66505
ruby, high energy phonon spectroscopy 78−83893
ruby, phonon bottleneck effect, 29 cm^{-1} phonons 78−68562
ruby, resonance interaction of electronic two-level states and short-wave phonon radiation 80−24551
s-f model with electron-hole reson., antiferromag. behaviour and phonon spectrum 78−47992
saturation effects in electron transport 78−76065
second order optical processes, localised electron-phonon system, stationary response 78−43916
second order optical processes, localised electron-phonon system, transient response 78−43917
self-trapped acoustic polaron with site diagonal and off-diagonal electron-phonon interaction 80−2348
self-trapping barrier height *(Russian)* 77−69252
semiconducting crystal, opaque, inelastic dynamical light diffraction 80−25399
semiconducting crystal, phonons and localisation at impurities 80−24812
semiconductor, absorption line profile in static elec. field, effect of impurities 78−92101
semiconductor, absorption of EM and sound waves in strong coupling case, effect of acoustic superlattice 78−26630
semiconductor, absorption of strong EM waves, weak electric field effects 79−95400
semiconductor, acoustomagnetoelectric effects in inelastic scatt. of electrons by optical phonons 77−4372
semiconductor, anal. using photoacoustic cell 78−68027
semiconductor, anisotropic carrier energy spectrum, quantum cyclotron reson. line width 77−8008
semiconductor, Auger transition probability, phonon-assisted 79−15120
semiconductor, bounded samples, phonon heating influence on volt-ampere characts. 77−39863
semiconductor, bounded samples, volt-ampere characts., nonequil. phonons influence on thermal dimensional effects 77−43611
semiconductor, carrier capture cross section by attractive Coulomb centres, piezoelec. scatt. 78−72170
semiconductor, compensated, electron capture probability by Coulomb centre in case of optical phonon emission 80−20214
semiconductor, compensated, phase transition of impurity electrons interacting with lattice 77−24535
semiconductor, conduction electron scattering by vibrating impurities 78−95297
semiconductor, current-voltage characts. of hot electrons under phonon heating and recomb. conditions 79−51591
semiconductor, deep traps, nonradiative multiphonon carrier-capture cross-section, temp. depend. approx. 78−43415
semiconductor, deformation potential, possibility of screening by free carriers 77−72826
semiconductor, degenerate, electromagnetic wave absorpt. due to electron-phonon collision in quantising field 79−7795
semiconductor, degenerate, surface optical phonons 80−70520
semiconductor, degenerate electrons, relax. of spin and energy 80−10965
semiconductor, dielectric response, local field effects in phonon-induced density change 79−51510

electron-phonon interactions continued
semiconductor, doped, photoemission, calc. of escape probability of electrons *(Russian)* 79−24408
semiconductor, doped, reson. scatt. theory 78−64036
semiconductor, doped lattice thermal cond., role of electron-phonon interactions and peripheral phonons, appl. to Ge:P 78−79702
semiconductor, effect of overlap function on electron mobility in quantising mag. field 78−43374
semiconductor, elec. cond. in quantising mag. field, and electron heating, mutual electron-phonon drag 77−69355
semiconductor, electron distribution function, temp. gradient effect 78−72145
semiconductor, electron drag by photons during intraband absorption of light 79−51633
semiconductor, electron drift vel. and phonon multiplication 80−6848
semiconductor, electron heating by strong static and HF elec. fields 77−8112
semiconductor, electron multiphonon capture by edge dislocation *(Russian)* 79−86861
semiconductor, electron scattering interaction with coupled plasmon-polar-phonon modes 79−42536
semiconductor, electron temperature superlattice, nonlinear theory *(Russian)* 79−78112
semiconductor, electron trap, positively charged, hot electron capture coeff. 78−52003
semiconductor, electron-electron relax. in ultraquantum mag. fields, electron-phonon interactions 77−4371
n-semiconductor, electron-phonon drag in longit. quantising mag. field 77−76805
semiconductor, electron-phonon interactions rel. to diffraction transverse acoustoelectric effect 77−35967
semiconductor, electron-runaway and quasi-stationary states in electric field 77−4359
semiconductor, excitation spectrum and optical props. in field of standing EM wave and homogeneous field 78−91625
semiconductor, extrinsic, parametric reson. of acoustic and optical phonons at low temps. 78−10519
semiconductor, gapless, bottleneck effect at low temp., hole heating 78−10470
semiconductor, gapless, magnetophonon reson. for hot electrons and holes *(Russian)* 79−4565
semiconductor, ground state energy of shallow impurity centres 77−4314
semiconductor, high field transport, inter-valley scatt., intra-collisional field effect 80−34455
semiconductor, high intensity photoexcitation, hot electrons and phonons 78−26905
semiconductor, hot electron current voltage curves, transverse mag. field, phonon heating 78−6384
semiconductor, hot electron distrib. in strong electric and quantised mag. fields 79−95417
semiconductor, hot electron fluctuations with displaced Maxwellian distrib. 80−29418
semiconductor, hot-electron energy distrib. in strong mag. field 78−43400
semiconductor, influence of strong inelastic scatt. on electron energy relax. 79−23959
semiconductor, inhomogeneous elec. fields in oscillatory photocond. 80−2421
semiconductor, intervalley cyclotron-phonon reson., IR absorption in mag. field 78−60448
semiconductor, ionic., ionisation of doubly charged centres 79−11085
semiconductor, ionic, nonlinear intraband absorpt. and harmonic generation 78−33779
semiconductor, ionisation energy of deep centres from absorpt. spectra, electron-phonon coupling 77−4663
semiconductor, light scatt. spectra, interference effects 79−82977
semiconductor, longitudinal isothermal Nernst-Ettingshausen effect in a quantising magnetic field 79−51617
semiconductor, low-temp. photocond., effect of electron phonon interactions 77−66186
semiconductor, magnetic susceptibility of hot electrons 78−10648
semiconductor, magnetophonon resonance due to two-phonon scatt. by acoustic phonons 77−69356
semiconductor, magnetophonon resonance oscills., peak shape, theory 80−107824
semiconductor, many-photon absorption by intraband transitions in mag. field 78−27261
semiconductor, microwave absorpt. near optical phonon creation threshold 78−47823
semiconductor, multiphonon electron-hole recomb. processes 78−6750
semiconductor, n-type, nonequilibrium photoelectron distribs. and absolute negative cond. in quantising mag. fields 80−65622
semiconductor, narrow cond. bands, hypersound amplification in quantising elec. field 77−89811
semiconductor, narrow gap electron-phonon interaction constant 79−7794
semiconductor, negative cyclotron resonance of hot carriers 78−2492
semiconductor, negative electron diffusivity in high fields 78−30935
semiconductor, Nernst-Ettingshausen effect, thermopower, strong elec. field 78−23122
semiconductor, non-radiative multiphonon carrier-capture cross-sections of deep traps, high-temp. limit 77−90191
semiconductor, noncoherent interaction of a light pulse 80−106561
semiconductor, nondegenerate, band electrons at arbitrary electron-phonon coupling, transport props. 80−39592
semiconductor, nondegenerate, magnetophonon reson. in acoustic relax. of hot electron energy 78−26892
semiconductor, nondegenerate nonpolar, quantum theory of magnetophonon reson. 77−28200
semiconductor, nonparabolic, inelastic acoustic phonon scatt., in longit. quantising mag. field 77−28196
semiconductor, nonparabolic, Monte Carlo transport calcs., acoustic scatt. inelasticity effects 77−51754
semiconductor, nonradiative multiphonon carrier capture and ejection props. of deep traps 78−35190
semiconductor, optical absorption by impurities, phonon-electron interaction 78−56502
semiconductor, optical phonon amplification by EM wave field in presence of mag. field 80−65181
semiconductor, optical phonon generation on intraband absorpt. of EM radiation *(Russian)* 77−48235

electron-phonon interactions continued
  semiconductor, paramagnetic phonon resonance, theory 80−50187
  semiconductor, parametric reson. of acoustic and optical phonons at low temp. 77−51779
  semiconductor, parametric resonance of acoustic and opt. phonons 77−15915
  semiconductor, phonon fluorescence stimulated by laser radn. 79−87504
  semiconductor, phonon induced hopping between Stark levels 80−92900
  semiconductor, phonon-assisted cyclotron reson., single and two-phonon pinning, review 79−15356
  semiconductor, photoconductivity due to phonon scatt. and emission 78−10514
  semiconductor, photoexcitation phenomena, low density 78−27319
  semiconductor, photoluminescence, deep level recombination temp. depend. 79−47497
  semiconductor, piezoelec. and nonpiezoelec. cyclotron-phonon resonance due to polarisation scatt. from phonons 79−95649
  semiconductor, polar, mobility in mag. field, extreme quantum limit, iterative technique 78−2498
  semiconductor, polaron aspects of generalised Haynes' rules 78−18978
  semiconductor, polarons in degenerate-band case, weak to intermediate hole-phonon coupling 77−66126
  semiconductor, quantum electron-phonon system, theory of parametric excitation 78−10489
  semiconductor, quantum limit magnetoresist. for acoustic phonon scatt. 77−76847
  semiconductor, quantum transport theory under high elec. field 78−23099
  semiconductor, quasi-two-dimensional, electron scatt. by polar optical phonons 78−72237
  semiconductor, Raman scattering from impurities 78−56468
  semiconductor, Raman scattering from impurities 78−56469
  semiconductor, rel. to cyclotron reson. theory 79−73817
  semiconductor, scattering by light by phonon zero sound 79−56145
  semiconductor, Seebeck and Hall coeffs. Lorenz number, anisotropy, theory *(German)* 80−65608
  semiconductor, sound absorption at very low temps. 79−95089
  semiconductor, statistical theory of multiple-phonon scattering 78−67794
  semiconductor, two stage model for deep level capture 78−10396
  semiconductor, unipolar, acoustophotoelectric effect theory 77−55577
  semiconductor, weakly polar, IR absorption by optical polaron in mag. field 77−66127
  semiconductor, zero-gap props. correlated to Γ_8 symmetry, review 80−6717
  semiconductor, zincblende struct., phonon attenuation in presence of internal strains and mag. field 78−76118
  semiconductor film, electron-phonon interactions in quantizing mag. field 79−69610
  semiconductor film, phonon spectrum under one-dimens. quantisation conditions 77−66007
  semiconductor film, transverse conductivity due to scatt. by acoustic phonons in quantizing mag. field 78−2594
  semiconductor in inhomogeneous EM field, nonlinear HF cond. 77−51773
  semiconductor ionisation, kinetic approach including acoustic phonon contrib. 79−56211
  semiconductor junctions, phonon assisted current 80−24997
  semiconductor longitudinal magnetoresist. in quantising mag. field, var. calc. 77−43630
  semiconductor multilayer heterojunction struct., impurity and phonon scatt. 80−2456
  semiconductor or insulator, impurity optical spectra, p-phonon processes 80−16061
  semiconductor quantised inversion layers, hot electron microwave cond. calc. 77−43734
  semiconductor superlattice, phonon spectrum, effect of strong elec. field, parametric reson. 80−44273
  semiconductor surface, cyclotron reson., projection operator formalism 80−88524
  semiconductor thin film, polaron near-threshold spectrum 80−65471
  semiconductor thin films, ferroelectric properties, quantum size effect 80−97201
  semiconductor transport props., effect of temp. depend. band shifts 77−55522
  semiconductor with complex band struct., free carriers effect on Raman scatt. 77−44001
  semiconductor with degenerate valence band edge, hole polaron self energy 77−43519
  semiconductor with elliptical isoenergetic surface, photon drag theory 77−1443
  semiconductor with superlattice, phonon spectrum 77−47528
  semiconductors, anomalous phonon induced light transmission below plasma edge 78−80368
  semiconductors, Auger recombination processes 79−38091
  semiconductors, binding energy in exciton-impurity systems, Haynes rule 79−15112
  semiconductors, cyclotron resonance, high frequency differential cond., needle shaped distribution model 79−65509
  semiconductors, cyclotron-phonon reson., review 79−56615
  semiconductors, degenerate, energy band structure effect on transverse magnetoresistance 80−88580
  semiconductors, diamond-type, doped, US attenuation and electron-phonon scatt. in mag. field 79−46771
  semiconductors, differential conductivity with inelastic electron scatt. *(Russian)* 80−2399
  semiconductors, disordered, light induced stationary non-equilibrium distribution of electrons, balance equation 80−39528
  semiconductors, doped, IR absorpt. in Drude tail, effect of finite electron densities 79−47449
  semiconductors, drift mobility and Hall factor, nonpolar optical scatt. mechanism 79−51579
  semiconductors, elec. cond. in elec. and mag. fields, carrier scatt. mechanisms 79−65467
  semiconductors, electron multiplication, phonon scatt., ionisation rate calcs., Markov processes 80−50267
  semiconductors, electron-electron collision effect on current voltage characts. in quantising mag. field 80−103705
  semiconductors, electron-phonon interactions, combined phonon resonance *(Russian)* 80−75321
  semiconductors, free electron scattering and dynamical cond. 78−2476

electron-phonon interactions continued
  semiconductors, galvanomagnetic effects in high mag. fields, for electron scatt. by optical phonons 80−2405
  semiconductors, heat pulse absorpt. in nonquantising mag. fields 80−60054
  semiconductors, hot electron maximum mobility in longitudinal quantising mag. fields 79−69519
  semiconductors, hot electron recombination at impurity centres 80−10995
  semiconductors, hot electron transverse escape galvanomagnetic effects *(Russian)* 80−80289
  semiconductors, hot electrons in longitudinal quantising mag. fields 80−39593
  semiconductors, lattice vibration amplification in field of EM wave 77−76511
  semiconductors, magnetic, spin wave electron amplification theory 80−97083
  semiconductors, multiphonon capture rate 79−38022
  semiconductors, multiphonon electron-hole recomb. processes 78−6751
  semiconductors, nondegenerate, effect of nonparabolicity on transverse magnetoresist. 77−51763
  semiconductors, nonequilib. electron and phonon fluctuations *(Russian)* 77−80770
  semiconductors, nonradiative recombination, combination of Auger and many-phonon processes 79−87111
  semiconductors, parametric conversion of acoustic optical phonons 80−15209
  semiconductors, phonon assisted electron impact ionisation and Auger recombination, theory 80−39591
  semiconductors, photoionisation cross-sections and phonon coupling 79−51518
  semiconductors, piezoelec., degenerate, transverse magnetoresist. in strong field, quantum effect 80−80299
  semiconductors, polar, resonance electron-phonon Raman scatt., cross-section oscills. 80−60598
  semiconductors, quantum limit cyclotron resonance linewidth 80−7171
  semiconductors, scatt. influence on Auger transition, depend. of impact ionisation on electron energy 80−44608
  semiconductors, semimetals, electron heating by phonons, acoustic absorpt. and acoustoelectric current quantum oscills. *(Russian)* 79−19639
  semiconductors, thermoelectric and thermomagnetic effects, heat transfer due to quasi-particle subsystems *(Russian)* 80−24959
  semiconductors, van Hove critical point region, electron-phonon interactions, dispersion law 80−70344
  semiconductors, weakly polar, intraband magnetoabsorption theory 79−42949
  semiconductors and insulators, non-radiative processes multiphonon recomb. 78−6752
  semiconductors electron-photon mechanism of cyclotron absorpt. hysteresis 79−69726
  semiconductors with superstructure, weakly bound states of elementary excitations 79−60733
  semimetal, intrinsic, dielec. and supercond. phase transitions 77−66111
  semimetal, phonon spectrum, influence of mag. field induced quasi-local levels 78−18946
  semimetal-insulator ferroelectric phase transition due to interband electron-phonon interaction 77−8531
  shell-model crystal, electron-phonon interactions effect of F-centre on shell screening 77−72825
  silicate galss:Eu^{3+}, fluoresc. linewidth variation, electron-phonon coupling 78−19531
  singularities of the small polaron effective mass 78−63989
  SnTe film, polycrystalline, anomalous resist. at struct. phase transition 80−29488
  solid, impurity atom fluoresc. radiation, intensity correlation, low temp. limit 80−80847
  solid, phonon dispersion effects on nonradiative transitions 78−43926
  solid, pseudoatom potential, rel. to screening and lattice dynamics 79−60736
  solid-state theory, introduction, book 79−33215
  solitons in a one-dimensional modified Hubbard model 78−87895
  sound velocity, amplitude dependent, in collisionless regime *(Russian)* 78−52037
  spectral band shape, quadratic electron-phonon interaction effect 77−32342
  squared electron-phonon coupling constant, tight-binding calc. in transition metals and alloys 79−1571
  Stark-Ladder current theory 78−68035
  strongly coupled localised system, pot. curves crossing problem, Landau-Zener formula *(Japanese)* 79−87049
  strongly degenerate plasma, double injection, vol. controlled current regime 79−51658
  structural Peierls transition in quasi-one-dimensional systems with anisotropic electronic and elastic properties 79−7671
  structural phase transitions *(Japanese)* 79−4384
  structural phase transitions driven by electron-phonon interactions *(Japanese)* 79−65195
  structural phase transitions in crystals, effect of high-power visible and IR laser radiation 78−71825
  structural transitions of antiferroelectric and displacive modulated type caused by electron-phonon interactions 78−43092
  superconducting B-W type compounds, resist. characts. in normal state 78−51963
  superconducting crit. temp. prediction, theory of high T_c superconductors 79−65582
  superconducting dilute alloys, eqn. for crit. temp. 78−72300
  superconducting film, acoustic coupling and effective quasiparticle lifetime 77−20499
  superconducting films, thick, phonon damping of virtual levels 79−4626
  superconducting junction, nonequilibrium phenomena *(Russian)* 78−34934
  superconducting metal, reliability of tunnel density of states 79−28483
  superconducting microbridges, non-equilib. effects, superconductivity stimulation by RF radiation and DC current *(Russian)* 80−39714
  superconducting transition temp. enhancement by localised states, band struct., electron-phonon interaction 78−47902
  superconducting transition temperature, A15 cpds. 78−91801
  superconducting transition temperature, calc. for very large electron-phonon coupling 79−73620
  superconducting tunnel junction, involving high temp. A15 lattice type superconds., nonlinear phenomena 78−14898

electron-phonon interactions continued
- superconducting tunnel junction, nonequil. excitation distrib. and phonon generation *(Russian)* 78—23204
- superconductive tunnelling in metals, electron-phonon interaction function determ. using dispersion relation 78—34931
- superconductivity, exchange enhancement of electron-phonon coupling 79—7930
- superconductivity, high T_c, theory 78—14870
- superconductivity, phenomenological parameters, thermodynamic and quantum mech. derivation 77—12054
- superconductivity, radiation induced enhancement 78—39249
- superconductivity and lattice instability 80—88663
- superconductivity and phonons, review 80—84543
- superconductivity dispersion ratio for tunnel density of states, analytical props. *(Russian)* 77—39995
- superconductivity-ferromagnetism coexistence, transition temp., magnon freq., indirect exchange 80—44757
- superconductor, amorphous, Eliashberg function, tunnelling and crit. temp. anal. 80—80455
- superconductor, dirty, mixed state, thermal cond. anisotropy 80—7036
- superconductor, elastic tunnelling spectroscopy of single-particle excitations 78—56260
- superconductor, Frohlich model, macroscopic phonon wave function 77—51839
- superconductor, high T_c, dynamic instabilities 78—10607
- superconductor, high T_c, quasilocal excitation role 80—2508
- superconductor, kinetic eqns. for electron excitations and phonons 80—7032
- superconductor, nonequilib., hypersound enhancement *(Russian)* 80—34552
- superconductor, phonon mechanism for sound-affected energy gap *(Russian)* 77—43781
- superconductor, transition temp. for weak and strong electron-phonon coupling 77—39996
- superconductor order parameter singularities, tunnelling currents, Fermi surface calcs. *(Russian)* 80—80458
- superconductors, critical temp. correlation with electronic and phonon props. 79—69620
- superconductors, high temperature, tunnelling spectra, electron pairing anal., appl. to Nb_3Sn 79—87205
- superconductors, phonon Raman scatt. 80—100657
- superconductors, quasiparticle charge imbalance relax. 79—60960
- superconductors, relaxation processes, nonequilib. electrons and phonons 78—91807
- surface exciton energies and radii 80—92829
- surface inversion layers, energy relax. to acoustic phonons 78—26857
- TCNQ, electron- and phonon-polaron effects in valence and cond. bands 77—76757
- TCNQ salt, K-TCNQ, energy gap, electron-phonon interaction, IR spectrum 78—15167
- TCNQ salt, NMP-TCNQ, X-ray diffuse scatt. rel. to charge transfer 77—80496
- TCNQ salts, model for cond. 78—10426
- TCNQ-NMP, elec. cond. temp. depend. 77—85203
- TCNQ-TSeF, crit. behaviour at electronically driven struct., phase transition 77—80767
- $TEA(TCNQ)_2$, linear chain semicond., phase phonons, intramol. electron-phonon coupling 77—32373
- tetrabutylammonium europium yttrium isothiocyanate, conc.-depend. electron-phonon coupling, and self-quenching 80—60657
- tetradecane, with tetra-4-tert-butylphthalocyanine impurity mols., luminesc. 77—18965
- di-(tetraethylammonium)tetrahalomanganate, mag. circular and linear dichroism obs. 80—29725
- tetrahedral semiconductors, valence band degeneracy, polar electron-phonon interaction effect, exciton binding energy 79—56140
- thermal ionisation of an impurity in strong electric fields *(Russian)* 78—43410
- thermodynamics of solids, entropy, free energy, sp. ht., electron-phonon interaction corrections 80—49387
- thermomagnetic effects in strong magnetic fields 77—62954
- thermomagnetic effects in weak magnetic fields, formulation of theory 77—62953
- thin surface layer, interactions between nondegenerate electrons, effect on cyclotron resonance, mag. cond. *(Russian)* 80—15802
- tight-binding metals, electronic struct. and kinetic props. at high temp. 80—59848
- TMTTF fluoroborate, transmission spectra with electron-phonon coupling phenomenological model 79—19891
- trans-polyacetylene, intrinsic, electron-phonon coupling 80—79901
- transient resonance Raman scatt., quantum theory, appl. to strongly coupled localised electron-phonon system 78—94412
- transition metal, 4d BCC, electron-phonon interactions 79—95107
- transition metal, electron-phonon coupling, comparison of reson. and tight-binding description 77—15746
- transition metal alloy, binary, conc., superconductivity and electron-phonon interactions, theory 78—14868
- transition metal alloys, ferromagnetic, low temp. resist. calc. 80—24919
- transition metal binary alloy, amorphous and crystalline, superconducting transition temp. correlation with solute conc. 78—52139
- transition metal compound refractories, electron and phonon behaviour 80—54624
- transition metal compounds, phonon anomalies due to d-band effects, electron-phonon matrix elements 78—30720
- transition metal compounds, reduced ionisation potentials as parameters in superconducting transition temp. calcs. 80—75671
- transition metal compounds, saturating contrib. to elec. resist. from electron-phonon contrib. 80—2376
- transition metal dichalcogenides, periodic lattice distortions, charge density waves 79—82536
- transition metal dihydrides, band struct. and electronic props., electron-phonon coupling 79—47011
- transition metal hydrides, electron-phonon interaction const. calc. 79—65160
- transition metal ions in crystals, thermal broadening and shift calcs. 77—48208
- transition metal superconductors, specific heat anharmonic components, phonon freq. temp. shift *(Russian)* 79—91183
- transition metals, 4d electronic contrib. to electron-phonon mass enhancement 77—62811
- transition metals, conf., Toronto, Canada (Aug. 1977) 78—91577

electron-phonon interactions continued
- transition metals, d-band superconds., s-electron current density calc. 77—47926
- transition metals, electron-phonon coupling, electronic aspects 77—69255
- transition metals, electronic Gruneisen parameter 79—82297
- transition metals, generalisation of modified tight-binding approximation 80—88288
- transition metals, McMillan-Hopfield factor and ideal phonon limited resist. 78—64024
- transition metals, paramagnetic susceptibility, phonon instability, mixed localised-collective electron states 80—103811
- transition metals, relativistic electron-phonon interaction 79—82532
- transition metals, supercond., effect of s-, d-electron hybridisation *(Russian)* 78—39243
- transition metals, supercond. transition temp., ab initio calc. 80—25036
- transition quasilinear spectra of resonant secondary emission *(Russian)* 80—16102
- transiton metals, lattice dynamics calculations, superconductivity parameters 79—7655
- transparent dielectrics, optical break-down in const. elec. fields *(Russian)* 77—8509
- transport effects, phonon inelastic interband scatt. 77—43552
- transport equation, model, with inelastic scatt. of electrons, exact soln. 77—59272
- transport equation and photocurrent of electrons, in EM field 78—26913
- transport equation for electrons in nonmonochromatic EM field 80—10937
- transport properties of electrons with narrowly defined bands at low temp. *(Russian)* 80—103656
- TSEE from insulating layers, Monte Carlo method simulation, effect of electron-phonon interactions *(German)* 80—2932
- TSeF-TCNQ, resist., crit. behaviour anisotropy 78—10430
- TTF and derived cpds., intramolecular vibrs. and vibronic effects, IR and Raman spectra 80—25387
- TTF-TCNQ, $4k_F$ anomaly, density correlation of classical dimensional electron gas 77—80744
- TTF-TCNQ, ^{15}N, ^{2}H isotope labelled, IR, Raman spectra, mol. vibrs., electron-phonon interactions 77—69835
- TTF-TCNQ, anharmonic effects of phonons with Kohn anomalies 77—1197
- TTF-TCNQ, conductivity and dielec. permeability, freq. depend. 78—79984
- TTF-TCNQ, conductivity model 79—51557
- TTF-TCNQ, crit. behaviour at electronically driven struct. phase transition 77—80767
- TTF-TCNQ, delocalisation in organic molecular conductors 79—78086
- TTF-TCNQ, divergent mag. responses at $2k_F$ and structural phase transitions 80—20376
- TTF-TCNQ, elec. cond. and spin susceptibility, press. and temp. depend. 80—24894
- TTF-TCNQ, elec. resist., electron-phonon scatt. 80—92884
- TTF-TCNQ, electronic props., connection between theory and expt. 79—19581
- TTF-TCNQ, Kohn anomaly, electron-phonon coupling, neutron scatt. 77—7812
- TTF-TCNQ, linear CDW, melting of phase locking *(Japanese)* 77—43522
- TTF-TCNQ, metallic cond. press. depend., single particle phonon scatt. description 79—69503
- TTF-TCNQ, metallic conductivity temp. depend. 78—6357
- TTF-TCNQ, microscopic model for three low temp. phases 79—73303
- TTF-TCNQ, periodic lattice distortions, charge density waves 79—82536
- TTF-TCNQ, resist., crit. behaviour anisotropy 78—10430
- TTF-TCNQ, self-energy calcs. 79—4499
- TTF-TNCQ, mobility due to mol. optical phonon scatt. 77—85202
- tunnel self-trapping of electrons or Frenkel excitons, theory *(Russian)* 78—60192
- tunnelling, electron, in real layer structures, theory 77—66196
- tunnelling during excitation of electroluminescence 78—43936
- two band model with electron-phonon interactions for narrow-gap electron spectra 79—90961
- two-dimensional electron gas, electron-phonon interaction and cyclotron reson. 80—25014
- two-level electron system with electron-phonon interactions in field of strong EM wave 77—24524
- two-phonon Raman scattering, double reson. 77—40226
- two-phonon transitions, phonon assisted, in mag. field, four-band model 77—36260
- unfilled f-shell, elec. resist. *(Russian)* 78—72141
- Urbach's rule derived from thermal fluctuations in the band-gap energy 79—33729
- vibron ferroelectric, intrinsic anomalous photovoltaic effect *(Russian)* 80—44665
- vibronic ferroelectric semiconductor, mag. susceptibility calc. 80—2711
- vibronic splitting and Zeeman effect for $^4A_{2g} \to ^2E_g$ transition 78—60495
- vibronic theory of antiferroelec. and struct. modulated transitions, soft modes 78—79719
- vibronically coupled systems, cluster model 79—19540
- weak itinerant magnetism as inhibited superconductivity 79—51715
- weak-coupling superconductor, effect of electron-phonon renormalisation on thermodynamics 79—99655
- wurtzite structure semiconductor, transport in longit. quantizing mag. field 78—26891
- zero-gap semiconductor, ferroelec. phase transitions, effect of Coulomb interaction on RPA calc. 79—28691
- zero-point energy of electrons and phonons 78—78603
- zinc blende semiconductors, small-gap, electron scatt. and transport props. 78—95294
- zinc blende semiconductors, small-gap, electron scatt. and transport props. 78—95295
- zinc blende-type hosts, Co^{2+} impurities Huang-Rhys number rel. to props. of host lattice 79—83018
- Ag alloys, dil., transport props. 78—76046
- Ag, electrical resistivity, low temp., T^4 behaviour rel. to electron scatt. mechanisms 80—39552
- Ag, electron-phonon interaction determ. from current-voltage curve at 1.5K *(Russian)* 77—47789
- Ag, Fermi velocity from proximity effect tunnelling 78—51875
- Ag film, optical props. in intermediate region between pure Drude and interband absorption 77—81170

electron-phonon interactions continued
Ag film-Pb sandwich, supercond., effective renormalisation interactions 79—56397
Ag halides, physical props. rel. to photographic processes 79—19555
Ag halides, quadrupolar deformability theory by tight binding method 80—10614
Ag halides, review 78—63991
Ag host, impurity effect on electric field gradient 78—23061
Ag, metal and dil. alloys, electrical resistivity at low temp., ultra high resolution meas. 79—60795
Ag, phonon limited elec. resist., temp. depend. 80—24876
Ag, phonon-limited elec. and thermal resistivity 79—42517
Ag_3AsS_3, prustite ferroelectric order model in prustite type nonlinear crystals *(Russian)* 79—65807
AgBr, magneto-optics, two-phonon pinning interaction 79—91411
AgCl(Br), multivalent impurities 79—19556
$AgClO_3$, γ-irradiated, resonant Raman effect of O_3^- centres 78—48178
Ag_2Se, electronic and electrogalvanic props. in α-phase region *(French)* 80—107820
Ag_2Te, low temp. thermal cond., thermoEMF 78—43423
Al and dilute alloys with Ge and Zn, magnetoresist. depend. on temp., 4.2-70K 80—70682
Al, anisotropic Fermi vel., surface Landau level reson. 78—10333
Al, band struct. effects on electrical and thermal cond. 78—34820
Al dilute alloys, elec. resist., impurity and temp. depend. 80—65526
Al, electrical resist. and magnetoresist., 2 to 40K, Matthiessen rule deviations *(Russian)* 77—31996
Al, electrical resistivity of ultra pure samples at low temp. 79—60794
Al, electron-phonon collision frequencies, RF size effect, Fermi surface study 79—90945
Al, electron-phonon enhancement of electron-electron scatt., elec. and thermal cond. 80—49326
Al, electron-phonon scattering rates, anisotropic, meas. on Fermi surface 78—87753
Al, lattice thermal cond. at low temps., Ashcroft pseudopotential method 80—19897
Al low-temp. electron-diffusion magnetothermopower meas. 77—15834
Al, magnetoresist., linear growth in strong. mag. fields *(Russian)* 78—51972
Al, magnetoresistance, path integral method calc. 80—65537
Al, Nernst-Ettingshausen coeff., electron-phonon Umklapp scatt. 78—26848
Al, non-pair inter ion interaction through cond. electrons, inelastic neutron scatt. theory *(Russian)* 79—46773
Al, press. depend. of electron-phonon interaction rel. to normal state resist. 79—28063
Al, press. depend. rel. to supercond. transition temp. 79—95106
Al, pure and dil. alloys, diffusion thermopower, inelastic electron-phonon interaction 80—96851
Al, quasi-particle properties, anisotropic, electron-phonon interaction study 77—43480
Al, Sondheimer size effect, phonon-limited mean path, 1.8-12K 80—49698
Al, supercond., appl. of non-local extension to Gaspari-Gyorffy theory 78—80093
Al, superconducting, energy gap enhancment by tunnelling extraction 80—34564
Al superconducting film, 2 GHz SAW attenuation meas. of mean free path 77—39999
Al, superconducting transition temp., electron-phonon mass enhancement, pseudopot. calcs. 78—2604
Al, thick film, supercond., tunnelling characts., geometrical reson. in Al-Pb struct. 79—38260
Al, tunnelling characts., phonon struct. enhancement by high energy spectral weight 79—60984
Al-Ag(Mg)(Zn)(Ga)(Ge), dil., deviations from Matthiessens's rule, 4-OPW approx. calc. 79—19574
Al-Cr, Kondo alloys, spin and phonon resistivity independ. 78—47777
Al-Cu dil. alloys, elec. resist. temp. depend. 77—8068
Al-Ga, dil., low-temp. electron-diffusion magnetothermopower meas. 77—15833
Al-Ga(Mg)(Zn), electrical resist. and magnetoresist., 2 to 40K, Matthiessen rule deviations *(Russian)* 77—31996
Al-Li, Fermi surface impurity scatt. 79—56114
Al-Mn, Kondo alloys, spin and phonon resistivity independ. 78—47777
$Al_xGa_{1-x}As$-GaAs DH laser operation, phonon contrib. 80—102724
$Al_xGa_{1-x}As$-GaAs heterostructures, MO-CVD, phonon assisted recomb. and stimulated emission 80—1205
$Al_xGa_{1-x}As$-GaAs quantum-well heterostructures, phonon-assisted recomb. and stimulated emission 80—74358
$Al_xGa_{1-x}As$-GaAs-$Al_xGa_{1-x}As$ quantum well, carrier collection 79—15211
AlH_x, electronic struct. and electron-phonon interaction, hydrogenation effect, rel. to supercond. 80—107694
AlN:Mn(Eu), luminescence at high excitation levels with and without doping 77—1721
Al_2O_3, exoelectron emission, energy and ang. distrib. anal. *(German)* 78—92180
$Al_{10}V$, supercond. transition temp. determ., localised phonon modes 77—63016
Ar, liq., emission coeff. of cond. electrons, depend. on elec. field intensity *(Russian)* 79—78855
Ar, solid, lattice dynamics calc. using energy band theory 80—49320
As, electrical and thermal props. 78—14747
As, thermal resist. associated with electron-phonon scatt., temp. depend. 79—19610
As-Se-Ge(-S), photostructural change in Urbach tail 80—76021
As_2S_3, temp.-independent mobilities, phonon-induced electron hopping 79—28347
AsSe, molten semicond., pseudogap, elec. cond. and optical absorption meas. 77—8160
As_2Se_3, molten semicond., pseudogap, elec. cond. and optical absorption meas. 77—8160
Au, CESR obs., spin orbit relax. by phonons 77—24743
Au, effect of press. on resistivity 78—79978
Au, elec. resist. exam. 79—38042
Au, electron-phonon interaction determ. from current-voltage curve at 1.5K *(Russian)* 77—47789
Au, phonon limited elec. resist., temp. depend. 80—24876
Au, phonon-limited elec. and thermal resistivity 79—42517
Au-Cd alloy, α and ζ phase, low temp. sp. ht. 78—18789

electron-phonon interactions continued
Au-Ga, resist. and supercond. meas., electron-phonon interaction and Coulomb pseudopot. determ. 78—43358
$Ba(ClO_3)_2H_2O$, γ-irradiated, resonant Raman effect of O_3^- centres 78—48178
$BaTiO_3$, phonon spectroscopy, amorphous versus crystalline material 78—83898
$BaTiO_3$, undoped and Cu doped, Γ_{15} phonon freezing, electronic instability, LCAO calc. 80—25318
$BaTiO_3$, X-ray diffr. intensities, anomalous temp. depend. *(Russian)* 79—1484
Be, HCP, electron-phonon interaction, thermal effects 79—33057
Be, spin susceptibility, electronic effective mass, spin density functional calcs. 78—43291
Bi, acoustic waves, giant quantum attenuation at high mag. fields, angular depend. *(Japanese)* 79—4585
Bi, amorphous, superconductivity and the very strong electron-phonon interaction *(Japanese)* 79—95552
Bi bounded semimetals, phonon two-stage drag of electrons, thermoelectric power, scatt. mechanism 80—92919
Bi, electrical resistivity due to electron-phonon scatt. on small cylindrical Fermi surface 79—4562
Bi, hole relaxation time, temp. depend., cyclotron reson. 79—47108
Bi, intervalley scatt. influence on mobilities, thermopower calc. 78—26866
Bi, intravalley electron-phonon scatt. non parabolicity, thermoelectric power 79—99539
Bi, magneto-thermopower, weak-field, implication for scatt. mech. 80—49790
Bi, magnetoresist. under phonon generation conditions 77—11940
Bi, nonequilibrium phonons, negative differential cond., life time oscills. *(Russian)* 78—76117
Bi, nonlinear properties under sound generation conditions 79—60845
Bi, phonon generation rate, nonreciprocity of current-voltage curve *(Russian)* 77—89776
Bi, resistivity at ultralow temp., high precision meas., scatt. mechanisms 77—80776
Bi, Shubnikov-de Haas effect *(Russian)* 79—7840
Bi, thermal conductivity at ultralow temp. 79—1532
Bi, transverse magnetoresist. high-temp. oscills., rel. to Fermi surface *(Russian)* 77—24570
Bi type, semimetals, electron heating due to acoustic phonon scatt. *(Russian)* 80—10991
Bi:Te(Sn) , elec. resist., 1.8 to 77K, electron-phonon scatt. mechanism 79—15144
Bi-Pb amorphous alloys, superconductivity and the very strong electron-phonon interaction *(Japanese)* 79—95552
Bi-Tl film, superconductivity and phonon spectrum *(Russian)* 79—91190
$Bi_{1-x}Sb_x$, elec. resist., 1.8 to 77K, electron-phonon scatt. mechanism 79—15144
n-Bi_2Se_3, single cryst., new aspect of carrier scatt. 80—49707
Ca, FCC, ground-state props. 78—75989
CaF_2:Er, hydrogenated and deuterated, optical and EPR specra 79—61209
CaF_2:Sm^{2+}, pseudo-Jahn-Teller effect 79—69476
CaO:Bi^{3+}(Pb^{2+}), impurity centres vibronic spectra, lattice dynamics and electron-phonon interactions 80—7396
$Ca(PO_3)_2$:Eu^{3+}, amorphous, phonon-assisted site-to-site electronic energy transfer, fluoresc. line narrowing obs. 77—81140
Cd, Azbel'-Kaner high freq. cyclotron reson. meas. 79—11056
Cd, electron-phonon interactions, inelastic neutron scatt. meas. 79—99285
Cd, HCP anisotropic metal, cryst. dynamics 77—43289
Cd, magnetic susceptibility, temp. depend., electron-phonon interaction effects 79—61046
Cd point contacts, electron-phonon coupling, microcontact spectroscopy investig. *(Russian)* 78—38796
Cd, temp. depend. Knight shift 80—2655
Cd_3As_2, elec. resist. and HF dielec. const. calcs. *(French)* 77—59284
Cd_3As_2, thermoelectric power and transverse Nernst Ettingshausen coefficent 79—38104
$CdBr_2(I_2)$, exciton spectra, temp. and press. effects 77—20881
$CdBr_2(I_2)$, Mn activated, electron-phonon interaction, lattice vibr. effective energies *(Russian)* 78—59911
$CdCl_2$:Mn^{2+}, null points in zero-field splitting of mag. impurity levels 79—87066
p-$CdCr_2Se_4$:Ag, electrical props., 100-300K 80—54692
$Cd_xHg_{1-x}Se$, carrier mobility, 4.2 to 300K, scatt. mechanisms 79—4561
$Cd_xHg_{1-x}Se$, elec. props., 77-400K *(Russian)* 78—2485
$Cd_xHg_{1-x}Se$ mixed cryst., electron mobility and electron scatt. 78—95296
$Cd_xHg_{1-x}Te$, electron mobility and conc. near gapless state, influence of hydrostatic press. 79—65486
$Cd_xHg_{1-x}Te$, temp. shift of energy gap 77—51658
$Cd_xHg_{1-x}Te$, zero gap semiconductor, interband optical-phonon scattering 80—6846
Cd_3P_2, thermomagnetic transport effects obs. 77—15883
CdS, electron drift vel. and phonon multiplication 80—6848
CdS, parametric action of strong radiation field 78—14752
CdS, polaron cyclotron resonance freq. shifts, halfwidths, cumulant expansion method calcs. *(Russian)* 80—88880
CdS, semicond. pizeoelec. crysts., electronic attenuation of US waves 77—1456
CdS:Cu_2 US absorpt. in heavily doped piezoelec. semicond. 79—11189
CdS-Co^{2+}, IR spectrum, 4.2K, electron-phonon interaction effect on emission spectrum 78—27270
CdTe, average number of phonons emitted in optical transition 77—8614
$CeCl_3$, doubly degenerate phonon states, mag. field dependent splitting 77—16320
$Ce_xLa_{1-x}F_3$, paramag. mixed crystal, scattering of optical phonons by rare earth ions 78—68518
$Ce_xLa_{1-x}F_3$, phonon self-energy and electron-phonon interaction 79—65159
CoSi, Mn_nSi_{2n-m}, thermoelectric and optical props. 78—91714
Cr antiferromagnetic with nonmagnetic impurities, mag. susceptibility using two band model 80—2559
Cr, diffuse electron scatt. *(Russian)* 80—103438
Cr, spin density wave, Nambu-Eliashberg eqns. for k-state electron-hole pairing 80—97050
Cr_3Si, specific heat at low temps., electron density of states, Debye temp. *(Russian)* 80—54398

electron-phonon interactions continued
Cs, elec. and thermal resist. calc. using modified noncentral force model 79−91016
Cs halides, F-centres, first excited degenerate states, props. of electron-phonon interaction 78−63824
Cs-halide, optical response function from Jahn-Teller systems, F-band absorpt. band shape 79−43005
CsBr, electron-phonon interactions of F-centres, first-order Raman scatt. 78−64370
CsCl, electron-phonon interactions of F-centres, first-order Raman scatt. 78−64370
CsCl(Br)(I), photoemission, electron-phonon interaction effects, Monte-Carlo calc. and expt. 78−11071
CsF, doped with F-centres, first order Raman scatt. 78−52492
CsF, electron-phonon interactions of F-centres, first-order Raman scatt. 78−64370
$CsSiF_6:Mn^{4+}$, splitting of vibronic levels 78−60496
Cu alloys, dil., transport props. 78−76046
Cu and dilute Cu-Au alloy, magnetoresist. depend. on temp., 4.2-70K 80−70682
Cu, anisotropic electron-phonon interaction theory 79−78022
Cu, anisotropy microcontact spectroscopy *(Russian)* 78−43372
Cu, electron-phonon interaction, scatt. and transport props. 79−91037
Cu, electronic transport properties, OPW calcs. 77−43553
Cu, Fermi surface, electron-phonon enhancement factor 77−1357
Cu film, optical props. in intermediate region between pure Drude and interband absorption 77−81170
Cu, partial densities of states, electron-phonon interaction 78−51869
Cu, phonon limited elec. resist., temp. depend. 80−24876
Cu, phonon-limited elec. and thermal resistivity 79−42517
Cu-Al alloy, lattice thermal cond. meas., 0.06-2K 77−15822
Cu-Pb proximity sandwiches, tunnelling expt., barrier transmission effects 80−50002
Cu-Sn, amorphous, electron-phonon interaction effect on thermopower 80−29393
CuBr, exciton absorpt. band shape, dielectric const. real part derivatives *(Russian)* 80−25413
CuCl crystal resonant Raman scatt. and luminescence competition *(Japanese)* 80−80770
$CuCr_{2-x}Fe_xO_4$, charge transfer, Mossbauer spectroscopy 80−15836
$CuGaS_2$, reson. Raman scatt. by extraordinary phonons obs. 77−85704
n-$CuInSe_2$, single cryst., elec. props. 78−43397
Cu_2MnAl Heusler alloy, elec. resistivity 79−91020
$Cu_{1.8}Mo_6S_8$, supercond. energy gap and phonon-induced structs. in tunnelling density of states 79−51728
$Cu_{1.8}Mo_6S_8$, supercond. Chevrel phase, electron tunnelling spectroscopy expts. *(German)* 80−107966
Cu_2NiSn, Heusler alloy, elec. resist., 4.2 to 300K 80−75547
CuO_2, width of reson. Raman scatt. enhancement profiles, phenon-lifetime contrib. 79−19883
Cu_2O, exciton spectrum, effect of isotopic substitution 78−67955
Cu_2O, hole mobility, scatt. mechanisms, elec. field effect 77−80786
$CuPbSbS_3$, piezoelectric semiconductor, electron-phonon interaction, temp. depend. 77−51464
Cu_2S film, reactively sputtered, Hall effect meas., 90-300K 80−15541
D-T, solid, estimated heat capacity, enthalpy, thermal cond. and diffusivity 77−4228
o-D_2, solid, up to 150 kbar, 5K, Raman spectrum 80−50332
Dy, ferromag., rel. to magnetoresist., fields up to 75 kOe, 1-70K 77−20297
ErS, heat carrier scatt., thermal and elec. cond. from 5-400K 79−14974
Eu, monochalcogenides, multiphonon inelastic light scatt. 77−90144
Eu-alloys, mixed valence, role of phonons and Coulomb interactions 79−38032
EuSe, optical absorption exam., electron phonon interactions 78−10923
EuTe, mag. ‘Bragg’ scatt. obs. through Raman scatt. 80−66179
$Eu_{1-y}X_yS$ (X=Sr,Gd), spin-disorder-induced Raman scatt. from phonons, expt. investigation 80−20635
EuX(X=0,S,Se) 80−20635
Fe, elec. resist. between 2 and 30K, deviations from Matthiessen’s rule 80−10944
Fe, electron-phonon coupling, point contact spectroscopy obs. *(Russian)* 80−70342
Fe, highly pure, phonon contrib. to elec. resist., 1.6-298K 78−84194
Fe, partial densities of states, electron-phonon interaction 78−51869
Fe, point contacts between ferromag. metals, singularities depend. in d^2V/dI^2, phonon spectra 79−60457
Fe, purification, recrystn. temp. and elec. resistivity *(Japanese)* 80−100780
Fe-Co(Cr), electron state density and elec. resist. 80−39558
Fe-Mn(Ni), electron state density and elec. resist. 80−39558
Fe-Ni, martensitic transformation, microscopic mechanism *(Russian)* 79−34036
$FeCl_2$, electron-phonon coupling, temp. depend. Raman scatt. obs. 79−15451
FeF_2, absolute first order Raman polarisabilities 78−64369
$Fe_{1-x}Mn_xCl_2$, low-lying electronic excitations in antiferromag. and paramag. phases Raman scatt. study 80−71414
Fe_3O_4, magnetite, Verweg transition temp., isotope effect, elec. resist. and DTA meas. 80−24976
Fe_3O_4, Verwey transition, electron-phonon versus Coulomb interaction effects 80−39280
Fe_3O_4, Verwey transition, charge density-phonon condensation 80−65217
Fe_3Pt Invar alloys, elec. resist. anomalous crit. behaviour 79−78067
Ga, anomalous US penetration at low temp., effect of trajectorial electron transfer *(Russian)* 77−43670
α-GaAs, amorphous, mobility gap temp. derivative calc., polar contrib. 78−26861
n-GaAs, coupled plasmon-LO phonon modes, Raman scatt. meas. 78−60472
GaAs, electron scattering interaction with coupled plasmon-polar-phonon modes 79−42536
GaAs, forbidden Raman scatt. by LO phonons 78−64367
GaAs Gunn diodes, static domain form. 77−8111
p-GaAs, heavily doped, self energy of phonons 80−44277
n-GaAs, high temp. mobility anal. in three-valley ($\Gamma_6{}^c$-$L_6{}^c$-$X_6{}^c$) model 79−99544
n-GaAs, hot electron distrib. function with LO phonon kink, photoluminesc. 79−19925
n-GaAs, non-Maxwellian electron distribution function, from electric field-depend. photolum. spectrum 79−11450

electron-phonon interactions continued
n-GaAs, non-equilibrium acoustic phonon generation by hot electrons 80−6477
GaAs, nonradiative multiphnon carrier-capture cross sections of deep traps, intermediate-temp. depend. 78−43414
GaAs p^+-n diode, radiative hot carrier recomb., photoluminesc. and electroluminesc. meas. 79−38676
GaAs, phonon assisted tunnel emission of electrons from deep levels 80−25532
n-GaAs, piezoelectric semiconductor, influence of acoustic phonon disturbances on conductivity 78−91697
p-GaAs, piezoresistance, relax. time for heavy and light holes determ. 79−19599
GaAs, Raman scatt., electron-phonon deformation potential coupling 78−52502
GaAs, reson. Raman scatt. at indirect gap 79−73931
GaAs, resonance Raman scattering by 2 TO phonons and cond. band minima ordering 77−20854
GaAs, surface exciton energy 80−92829
n-GaAs, two stream instability 78−2509
GaAs, two-photon interband transitions, carrier drag 79−7858
n-GaAs, uncompensated, mech. of energy relax. at low temps. 77−62921
GaAs, valence band struct. obtained by magnetophonon effect 77−76748
GaAs:Cr, site symmetry of Cr ions, ground-state splitting, ballistic phonon expts. 78−95273
GaAs:Cu, electron-phonon interaction in optical transitions between deep impurity level and allowed bands 79−42591
GaAs:Cu, photoionisation spectrum of deep impurities in presence of weak electron-phonon interactions 79−51529
GaAs-$Al_xGa_{1-x}As$, heterojunction and superlattice, magnetophonon reson., polaron mass 80−44715
GaAs-$Ga_{1-x}Al_xAs$, superlattice umklapp processes in resonant Raman scattering 78−64362
GaP, donor-acceptor pair spectra, electron-phonon interactions 79−38631
GaP, electron-hole liquid exam. 78−2430
GaP, optical absorption and struct. of acceptor centres 78−48205
GaP, polar semicond., radiative recomb., electron-phonon interaction effects, calc. 80−49631
GaP, refr. index, 100 to 420K, permittivity calcs. *(Russian)* 77−90156
GaP, scatt. mech., mobility tensor 80−6826
$GaP:O^-$, two electron state, electron capture 78−39054
GaP:S, Se, Te, Si, shallow donors, excitation spectra 77−81128
GaP:S(Te), photostimulation spectra, bound electron phonon interactions *(Russian)* 77−1712
n-GaSb, galvanomagnetic effects 78−72172
p-GaSb, heavily doped, LO phonon-carrier interaction, Raman interf. lineshapes 80−93319
GaSb, reson. two phonon Raman scatt. near E_1 and $E_1+\Delta_1$ gaps 78−60470
n-GaSb:Te, elec. transport mechanism in cond. band from Hall mobility and transverse mangetoresist. meas. 79−73531
GaSe, electron-phonon interaction and optical props. 80−34942
GaSe, Hall mobility anisotropy 78−68041
GaSe MSM struct., inelastic tunnelling investigation of lattice dynamics 80−20330
GaTe, excitonic absorpt. edge, transmission and refl. meas. 80−40133
p-GaTe, scatt. by homopolar optical phonons, Hall effect meas. 77−28197
GaTe, transport anisotropy 79−23975
$Gd(OH)_3$, dynamical effects of interaction between 4f electrons and optical phonons 80−108196
Ge, amorphous, thermoelec. power in phonon-assisted hopping regime, Coulomb effects 78−76097
Ge, amorphous film, persistent photoconductivity, dangling bonds 80−84487
p-Ge, bleaching, optical heating and cooling of electrons involving intraband transitions 79−10365
n-Ge, cyclotron reson. line width in quantizing mag. field 78−10336
Ge, degenerate, scattering by light by phonon zero sound 79−56145
n-Ge, drag effects, heated electron-phonon system 78−23078
Ge, electron mobility in Δ_{1c} minima, temp. depend. 79−65473
Ge, electron-hole drop dispersion under strong optical stimulation, phonon interaction effects *(Russian)* 77−1723
Ge, electron-hole drop emission kinetics, effect of nonequilib. phonons, 4.2K 78−14674
Ge, electron-hole drop luminesc., phonon wind induced anomalous depend. at low mag. fields 80−34980
Ge, electron-hole drop motion, phonon wind 80−10887
Ge, electron-hole drop velocities as probe of phonons 78−68517
Ge, electron-hole droplet scattering of acoustic phonons, total scatt. rate and anisotropy 79−33241
Ge, electron-hole drops interaction with phonons 80−6747
Ge, exciton and electron-hole drop entrainment by nonequilib. phonons 80−6751
Ge, explosive instabilities in electron-hole drops under microwave radiation 77−31951
Ge, γ-electron-hole drop formation, time delay 77−31952
p-Ge, heavily doped, self energy of phonons 80−44277
p-Ge, highly deformed, hole scattering 77−20309
p-Ge, hole drift vel. in high field 79−95415
Ge, hole drift velocity, time-of-flight meas. 78−10444
Ge, hot hole distribution function at low densities 79−11138
Ge, hot phonon influence on energy relax. of high-density carriers 79−82608
n-Ge, impact ionisation at 4-9.5K 80−10994
Ge, impurity breakdown field increase due to strong compensation 80−20204
n-Ge, internal strain and impurity elec. field effect 78−14418
n-Ge, internal stress effect on electron-phonon interaction, thermal cond. anal. 79−42468
Ge, nonpolar semiconductor, IR free carrier absorpt., two short wavelength phonon scattering 79−78665
Ge, optical pulse transmission, pulsewidth depend., phonons and plasmons role 78−31198
Ge, phonon assisted Auger recomb. in indirect gap semiconductors 78−39126
Ge, phonon cond. correction term and electron-photon scatt. relax. rate, appl. to doped and undoped samples 80−39369
Ge, phonon scattering and dislocation effect on low temp. phonon cond. 78−51754
p-Ge, phonon thermal cond., 0.1-7K, Ziman model 77−35763

electron-phonon interactions continued
Ge, piezospectroscopic determ. of electron-phonon to hole-phonon interaction 79—95783
Ge, solid-state plasma, ultrafast transient response, theory and expt. 77—80748
Ge, valence band struct. obtained by magnetophonon effect 77—76748
Ge:Li, thermal cond., 0.4-20K, Li valley-orbit splitting 79—15111
Ge:P, lattice thermal cond., role of electron-phonon interactions and peripheral phonons 78—79702
Ge:P, lattice thermal resistivity due to electrons 78—51756
Ge:P, peripheral phonons and phonon cond. 79—14973
Ge:P, phonon drag thermoelectric power at low temp. 80—107828
Ge:P(As)Ga, lightly doped semicond., electron-phonon scatt., role of compensation 79—60456
Ge:Sb,In, lightly doped semicond., electron-phonon scatt., role of compensation 79—60456
Ge:Sb semiconductors, inhomogeneously strained, phonon resonance scatt., Kwok's theory method 79—60455
GeS, absorpt. spectra, electron-phonon interactions 80—80810
GeS, low temp. photoluminesc. 77—77287
GeSe, low temp. photoluminescence 77—77287
$Ge_{0.08}Se_{0.92}$, molten semicond., pseudogap, elec. cond. and optical absorption meas. 77—8160
GeTe, electron-phonon interactin induced phase transition 79—82338
H_2, metallic, comparison with free electron metal 77—66125
H_2, metallic, electron-phonon interaction and superconductivity, APW calcs. 78—14854
Hg, de Haas-van Alphen effect, influence of electron-phonon interaction 79—65361
Hg, de Hass-van Alphen effect, electron-phonon scatt. calc. 79—65360
Hg, single cryst., de Haas-van Alphen effect 78—84130
$Hg_{1-x}Cd_xSe$, zinc blende structure, optical and electronic properties 80—6723
$Hg_{0.86}Cd_{0.14}Te$, spin-flip electron scatt., longit. magnetoresist. obs. 77—43622
HgI_2, red, resonant Raman scatt. in B-exciton and band to band transition regions 79—61381
HgSe, dielec. function at 2, 95, and 300K, reflectivity spectra meas. 79—15458
HgTe, magnetophonon oscills. of thermoelec. power 80—49789
HgTe-type crystals, inverted band structure, influence of interband scattering on cond. *(Russian)* 79—51563
In, electron scattering rates, RF size effect meas. under multiple-turn conditions 78—14654
In, Lifshits transition, electron-phonon interaction 80—29502
In, RF size effect signals, anomalous behaviour 79—4502
In, superconducting, relaxation time determ. 77—55638
In, superconducting transition temp., electron-phonon mass enhancement, pseudopot. calcs. 78—2604
In:Sn, phonon spectrum, electron-phonon interaction *(Russian)* 78—18722
In-Cd, high temp. deviation from Mattheissens rule 77—43560
In-Sn alloy, Lifshits transition, electron-phonon interaction 80—29502
In-Sn alloy, phonon spectra and superconductivity, single-particle electron-tunnelling expts. 77—40005
InAs, second order Raman scatt., electron-two phonon deform. pots. determ. 78—60473
n-InAs, Shubnikov-de Haas oscills., conduction electron density, phonon scatt. 77—15768
n-InAs, transport props., influence of higher energy bands, calcs. 79—19598
$In_{1-x}Ga_xP_{1-z}As_z$ DH laser diode, defect and phonon assisted tunnelling 78—13708
InP, compensation ratio, electron mobility and free-carrier absorpt. 80—80261
InP, high-field transport 77—8107
InP, reson. Raman scatt., deformation pots. 78—52495
n-InSb, acoustoelectric gain coeff., nonlinear elec. field depend. 78—76115
InSb, CESR at high mag. fields, scatt. mechanisms 80—93177
p-InSb, cyclotron reson. of nonequilib. photoelectrons, distrib. function and line profile 78—60336
n-InSb, cyclotron reson. study of conduction electrons, strong mag. field 80—2639
InSb, electron mobility, low-field, Monte Carlo calc. 80—10973
n-InSb, electron recombination between Landau-levels 79—38096
InSb film, threshold singularity on quantising mag. fields 78—87904
p-InSb, heavily doped, LO phonon-carrier interaction, Raman interf. lineshapes 80—93319
n-InSb, high power helicon, interaction with semiconductor-free space interface 79—38114
InSb, hot electrons, Monte Carlo calc. of transport characts. and distrib. functions of hot electrons 80—6853
n-InSb, hot electrons relax. in quantising mag. field *(Russian)* 80—6876
n-InSb, laser induced magneto-photoconductivity, conduction band transitions 77—55566
InSb, magneto-optical anomalies of impurity electrons, two-LO-phonon region 78—72415
InSb, magnetophonon effect temp. depend., 80 to 190K 77—59293
n-InSb, magnetophonon effect, temp. depend. below 90K 79—56247
n-InSb, magnetophonon reson. under hot electron conditions 77—24568
n-InSb, magnetoresist. in strong elec. field *(Russian)* 78—19056
n-InSb, mobility in mag. field, extreme quantum limit, iterative technique 78—2498
n-InSb, optical phonon emission in intraband magneto-optical transitions, photocond. meas. 80—34481
n-InSb, phonon heating by hot electrons in quantising mag. field 77—4354
n-InSb, phonon-assisted cyclotron reson. strongly depend. on surface condition 80—70755
InSb, polar semicond., longit. magneto-Seebeck coeff., effect of polar-optical-phonon scatt. 79—56250
InSb, polar semicond., resonant magneto-Raman scatt. 79—51958
InSb, polar semiconductor, impact ionisation in crossed elec. and mag. fields 79—28355
n-InSb, propagation of high power helicons 78—19070
n-InSb, rel. to sign reversal of acoustomagnetoelec. effect 77—24592
n-InSb, transverse magnetoresist. in strong mag. fields 79—4571
n-InSb, ultrasound modulation in mag. field 79—69196
InSb, valence band struct. obtained by magnetophonon effect 77—76748

electron-phonon interactions continued
InSb-type semiconductor, inelastic scatt. of electrons by optical phonons 78—76073
InSe, exciton and polaron anisotropies, reson. Raman scatt. study 80—76033
InSe, excitonic absorpt. edge 78—88352
K, elec. resist., effect of energy depend. of electron relax. time 77—69296
K, elec. resist., temp. depend., low temp. limit 77—11892
K, electrical conductivity, Toya's theory 78—51965
K, electrical resistivity at low temp., phonon-dislocation scatt. 79—60820
K, low-temp. lattice cond., phonon drag thermopower 79—60789
K, Matthiessen's rule, low temp. deviations 78—14724
K, phonon-electron and phonon-phonon scattering relax. times, rel. to elec. resist. 77—39813
K, thermal cond. electronic contrib., 1 to 330K 77—20291
K, thermoelectric power, high-temp., first-principles calc. 78—91672
K, thermomagnetic and thermoelectric properties, phonon scatt. processes 80—29390
K, ultrasonic attenuation at low temp., spherical Fermi surface model 80—84255
KBr, doped with F-centres, Raman spectra meas. excitation in F and K bands 80—16027
$KBr:H^-$, U-centre absorpt. band shape, piezodichroism dispersion curve and electron-phonon interaction 77—24873
$KBr:Tl^+$, thermally induced absorpt. transfer between impurity bands, electron-lattice interactions 77—77257
KCl, absorption spectra of F-aggregate centres, 2K 77—48207
KCl, F-centre first excited state radiationless decay, cluster model 77—52158
KCl, F-centre first order reson. Raman spectra, line shape freq. depend. 77—32370
$KCl:Au^-$, absorption bands and MCD, electron-lattice interaction 77—55808
$KCl:Pb^{2+}$(0.005% Pb), A band fine structure, electron-phonon interaction 78—60491
$K_2CuCl_4.2H_2O$, thermal effects in mag. exchange interaction 77—16067
KI, perturbed by Jahn-Teller centres, lattice dynamics 80—107394
$KI:Tl^+$, pre-resonant enhancement of Raman scatt. 80—7354
$KMgF_3:Mn^{2+}$, exchange and spin-orbit interactions, optical spectra study 79—95817
$K_2Pt(CN)_4Br_{0.3}\times 3.2D_2O$, Kohn anomaly in longit. acoustic phonon 77—7812
$KZnF_3:Mn^{2+}$, exchange and spin-orbit interactions, optical spectra study 79—95817
La, DHCP and FCC phases, phonon density of states 78—67791
La, FCC, ground-state props. 78—75989
La, hydrostatic press. depend. in superconducting phase 78—80087
La-Al(Ge)(Au), amorphous, alloying effect on supercond. props. 79—60951
La-In alloys, cohesive and superconducting props. from electronic struct. calcs. 79—99113
$La_{1-x}Ga_x$ foils, amorphous, splat cooled, calorimetric and resistive meas. 79—33417
LaS, heat carrier scatt., thermal and elec. cond. from 5-400K 79—14974
γ-La_2S_3, indirect electron transitions, diffuse refl. and vibr. spectra 78—84576
Li, elec. and thermal resist. calc. using modified noncentral force model 79—91016
Li, electrical resistivity, non-alkali-metal behaviour 79—60793
Li MIM struct., electron-phonon interaction function investigation by microcontact spectroscopy 79—95108
Li, X-ray emission and absorpt. edges, temp. depend. 78—31282
LiF films, polycrystalline and single-cryst., comparative study of phonons by electron spectroscopy 80—25505
$LiNbO_3$, reduced, electron Hall mobility, photo-Hall meas. 77—8121
$Lu_3Al_5O_{12}:Er^{3+}(Ho^{3+})$, stimulated radn., electron-phonon interaction *(Russian)* 77—8605
Mg, spin susceptibility, electronic effective mass, spin density functional calcs. 78—43291
Mg, superconducting transition temp., electron-phonon mass enhancement, pseudopot. calcs. 78—2604
MgF_2, absolute first order Raman polarisabilities 78—64369
MgF_2, X-irradiated, radiation conductivity 79—69555
Mg_2Ge, L, electron-phonon interaction and phonon cond. at low temp. L n-type semicond. 79—14903
$MgO:Co^{2+}$, electronic and impurity-induced Raman scatt. 80—100659
$MgO:Fe^{2+}$, impurity electron-phonon reson. relax. time, thermal cond. 77—59085
Mg_2Sn, L, electron-phonon interaction and phonon cond. at low temp. L n-type semicond. 79—14903
MnF_2, absolute first order Raman polarisabilities 78—64369
Mo, diffuse electron scatt. *(Russian)* 80—103438
Mo, effective mass meas. and electron velocities 80—96773
Mo, elec. resist., quadratic contrib., 2 to 40K *(Russian)* 80—92874
Mo, electron-phonon coupling and supercond. transition temp. 79—56360
Mo, Hall effect, effect of electron-phonon scatt. anisotropy *(Russian)* 80—10947
Mo, phonon dispersion, anomalous struct., tight-binding calcs. 78—10137
Mo, scatt. rate temp. depend. from magnetoacoustic expts. 79—65522
Mo_6Se_8, Chevrel phase, supercond. isotope effect meas. *(German)* 80—25038
$Mo_5SnGa_xS_6$ heat capacity from 2 to 25K 78—43518
N_2:N, dynamically induced electronic transitions of matrix isolated atom 78—63825
$(NH_4)_2[Pt(CN)_4]Cl_{0.42}.3H_2O$ quasi one dimensional conductor, physical props., cond. freq. depend. 79—95393
NO_2^- ion in nitrite salt cryst., $^{1,3}B_1 \rightarrow ^1A_1$ transition spectra, reasons for diffuseness 80—97276
Na, electrical conductivity, Toya's theory 78—51965
Na MIM struct., electron-phonon interaction function investigation by microcontact spectroscopy 79—95108
NaCl, F-centre aggregation, initial stage study by Raman scatt. 79—56791
NaCl, laser damage, phenomenological theory 80—19836
$NaCl:H^-$, U-centre absorpt. band shape, piezodichroism dispersion curve and electron-phonon interaction 77—24873
NaF, quasimolecular struct. characts. of $NaL_{II,III}$ absorpt. edge 80—93436
NaI:F, electron-lattice coupling of F-centres, optical props. 80—60641

electron-phonon interactions continued
$NaNO_2$:Mn^{2+}, zero-field splitting, ferroelec. soft-mode contrib., phase transition, EPR obs. 79−15344
Nb alloys, supercond. and normal phases, electron scatt. and lattice thermal cond. 77−77001
Nb, calc. using APW band struct. calcs. and measured phonon spectra 78−14869
Nb, diffuse electron scatt. *(Russian)* 80−103438
Nb, effect of changes in $\alpha^2(\Omega)F(\Omega)$ on the zero-temp. energy gap 80−97025
Nb, electron-coupled phonon spectrum, effects of strain 79−7943
Nb, electron-phonon contrib. to phonon linewidth determ. 78−10146
Nb, electron-phonon interaction, relativistic, APW calc. 80−92837
Nb, electron-phonon spectral function and mass enhancement 78−26988
Nb, electronic contrib. to electron-phonon interactions 77−15524
Nb, Fermi surface, Fermi velocity, electron-phonon interaction parameter 79−7778
Nb, momentum dependence of electron-phonon interaction 79−7665
Nb, Nb-Mo alloys, phonon dispersion, anomalous struct., tight-binding calcs. 78−10137
Nb, phonon linewidths and electron-phonon interaction 79−73273
Nb, plastically deformed, changing lattice dynamics 78−67793
Nb, quasiparticle velocity, anisotropic many-body effects 79−33223
Nb, scatt. rate temp. depend. from magnetoacoustic expts. 79−65522
Nb, single cryst., superconductive tunnelling meas. 79−47203
Nb supercond., Eliashberg eqns. soln. 77−43776
Nb, superconducting, optical props. and electron-phonon interactions 80−2510
Nb, superconducting, thermodynamic props. 80−107955
Nb, superconducting critical magnetic field and crit. temp. 79−7947
Nb, superconducting phonon struct. obs. in proximity tunnelling 77−77008
Nb-Al, diffuse electron scatt. *(Russian)* 80−103438
Nb-Mo system, electron-phonon coupling const. and supercond. transition temp., average T-matrix approx. 80−39707
Nb-Ti, thermal conductivity in low temp. range 78−39259
Nb-Ti and Nb-Ti-Zr, electrical cond. at low temp. 77−28157
Nb-V(Ta) alloys, electron-phonon interaction and supercond. transition temp. *(Russian)* 79−28426
$Nb_3Al(Sn)$, electron-phonon coupling and supercond. crit. temp. 79−33379
NbC, electronic struct. of vacancies, effect on supercond. transition temp. 80−29347
NbC, superconductor, appl. of non-local extension to Gaspari-Gyorffy theory 78−80093
Nb_3Ge, amorphous and crystalline A-15 phases 78−83896
Nb_3Ge film, in supercond. proximity sandwich, energy gap struct., appl. to electron-phonon spectra 79−56401
Nb_3Ge supercond. film, of high transition temp., US attenuation 80−49991
$Nb_3Ge(Al)$, anomalous resistivity, insight from band theory 78−60106
$Nb_3Ge(Sn)$, superconducting, optical props. and electron-phonon interactions 80−2510
$Nb_{80}Mo_{20}$, $Nb_{75}Mo_{25}$, supercond., phonon cond. below 1k 78−14881
$NbMo_2Be$, predicted A15 struct. and T_c=30K 78−76182
$NbSe_2$ (2H), electronic response function including electron-phonon matrix elements 79−28300
$NbSe_2$ (2H), layered, anisotropy and electron-phonon coupling effects on sp. ht. 77−51844
$NbSe_2$, supercond. and normal state, thermal cond., temp. and mag. field depend. 78−26992
$NbSe_2$(2H), Raman spectra of soft modes at CDW transition, electron-phonon coupling 77−16301
Nb_3Si, high T_c, supercond. props. from extrapolation of sp. ht. meas. on A-15 Nb-Si 80−25045
Nb_3Sn, effect of changes in $\alpha^2(\Omega)F(\Omega)$ on the zero-temp. energy gap 80−97025
Nb_3Sn, phonon softening and T_c, strong electron-phonon coupling 78−31009
Nb_3Sn, supercond., crit. fields Pauli paramag. limiting and material parameters 79−78277
Nb_3Sn tunnel junctions, tunnelling density of states and electron-phonon spectral function 79−65618
$Nb_{80}Ta_{20}$, supercond., phonon cond. below 1k 78−14881
$Nb_{1-x}V_xSe_2$, elec. and mag. anomalies at CDW transition 80−107722
$Nd(OH)_3$, dynamical effects of interaction between 4f electrons and optical phonons 80−108196
Ne, solid, lattice dynamics calc. using energy band theory 80−49320
Ni, electron-phonon coupling, point contact spectroscopy obs. *(Russian)* 80−70342
Ni, ferromagnetic, Hall effect, anomalous, rel. to scatt. processes 80−44572
Ni, magnetoresistance anisotropy, planar Hall effect 79−23947
Ni, point contacts between ferromag. metals, singularities depend. in d^2V/dI^2, phonon spectra 79−60457
Ni-Cu, ferromagnetic, Hall effect, anomalous, rel. to scatt. processes 80−44572
Ni-Cu alloy, magnetoresistance anisotropy, planar Hall effect 79−23947
Ni-Fe, film, anomalous Hall and Nernst-Ettingshausen effect, contribution of phonon and impurity scatt. *(Russian)* 78−64145
Ni-transition metal alloys, deviation from Matthiessen's rule in elec. resist. 77−4319
$NiBr_2(Cl_2)$ two-phonon vibronic progressions, Raman obs. 80−29742
$Ni_{1-x}Co_xS_2$, elec. transport and semicond.-metal transition 80−10985
$Ni_{76}P_{24}$, cryst. and amorphous, thermopower and resist. meas. 80−20145
$NpSn_3$, itinerant f-electron antiferromag. obs. 77−8315
Os; electrical resistivity and thermal diffusivity meas. 80−15495
(Pb, Sn)Te-type semiconductors, displacive ferroelec. phase transitions, vibronic theory 80−11354
Pb and Pb-Mg, dil., resistivity, multiple plane wave calc., Fermi surface, vel. and band struct. 77−51723
Pb, band structure, and electron-phonon interaction, supercond. transition temp. determ. 79−19512
Pb chalcogenide mixed crystals, intraband absorption due to chemical disorder 79−56789
Pb, effect of changes in $\alpha^2(\Omega)F(\Omega)$ on the zero-temp. energy gap 80−97025
Pb, film, polycryst. or amorphous, thermal cond., 0.5-11K 78−39260
Pb, phonon softening, neutron scatt. at high press. 78−80091
Pb, press. depend. of electron-phonon interaction rel. to normal state resist. 79−28063

electron-phonon interactions continued
Pb, pure and dil. alloys, diffusion thermopower, inelastic electron-phonon interaction 80−96851
Pb, superconducting film, radiation induced critical temp. 79−87179
Pb, superconducting transition temp., electron-phonon mass enhancement, pseudopot. calcs. 78−2604
Pb, thermal conductivity in supercond. and normal states, press. effects 77−43779
Pb-Bi alloys, phonon-electron interaction, normal and supercond. state thermal cond. and elec. resist. meas. 79−60460
Pb-In, superconductive, electron tunnelling under hydrostatic press. 77−51850
Pb-Mn, dil., supercond. film, H_{c2} meas., mag. impurity effects, pair breaking theory 79−42708
Pb-Sn-Te, solid solution, scattering mechanism of carriers 80−49710
Pb-Tl-Bi-In, localised phonons studies by supercond. tunnelling 79−87210
Pb-Tl-In, localised phonons studies by supercond. tunnelling 79−87210
p-Pb_{1-x} Sn_xTe, carrier mobility, acoustical phonon and impurity scatt., deform. impurity const., conc. depend. 80−39570
$Pb_{1-x}Be_xTe$, anomalous resist. near ferroelec. phase transition 80−20196
$Pb_{0.98}Bi_{0.02}$-Cd, superconductor-normal-metal boundary resist., mag. field depend. 80−44772
$PbBr_2(Cl_2)$, exciton spectra, temp. and press. effects 77−20881
$Pb_{0.9}Cu_{0.1}$, film, polycryst. or amorphous, thermal cond., 0.5-11K 78−39260
$Pb_{1-x}Ge_xTe$, electron-phonon interaction effect on ferroelec. transition 78−76416
PbI_2 (2H), electronic transport and cyclotron reson. 79−28369
PbI_2, exciton absorpt. band shape, dielectric const. real part derivatives *(Russian)* 80−25413
$PbMg_{1/3}Nb_{2/3}O_3$, ferroelec., crit. electron-phonon phenomena and diffuse phase transition in elec. field 79−38497
$PbMo_{5.1}S_6$, high supercond. T_c, soft mode behaviour 78−14855
$PbMo_6S_8$, supercond. Chevrel phase, electron tunnelling spectroscopy expts. *(German)* 80−107966
$PbMo_6S_8(Se_8)(Te_8)$, Chevrel phase correlation between struct. and supercond. transition temp. 80−7023
n-PbSe, polar semicond., mag. field influence on high-freq. relaxation time 79−95438
n-$Pb_{0.83}Sn_{0.17}Se$, carrier mobility, 77-300K, scattering mechanism *(Russian)* 78−2486
n-$Pb_{1-x}Sn_xSe$, absorption spectra investigation 80−2768
$Pb_{1-x}Sn_xSe$, band inversion effect on phonon spectra 78−79699
$Pb_{1-x}Sn_xSe$, displacive transition, temp. and press. depend., elec. meas. 80−10672
$Pb_{0.82}Sn_{0.18}Te$, Hall mobility, scatt. mechanisms, temp. and carrier conc. depend. 77−55548
$Pb_{1-x}Sn_xTe$, anomalous resist. near ferroelec. phase transition 80−20196
$Pb_{1-x}Sn_xTe$, electron-phonon interaction 78−71819
p-$Pb_{1-x}Sn_xTe$, mobility meas., impurity and phonon scatt. mechanisms 78−23091
$Pb_{1-x}Sn_xTe$, Mossbauer investig. of phonon softening at semicond.-semimetal transition 77−43908
PbTe, electron scattering interaction with coupled plasmon-polar-phonon modes 79−42536
PbTe, electron-phonon interactin induced phase transition 79−82338
PbTe epitaxial layers, submillimetre spectroscopy 79−83048
n-PbTe film, transverse magnetoresistance oscillations, depend. on film thickness 79−65567
PbTe, TO phonon softening, free carriers and defects effects 78−79720
PbTe, TO-phonon mode softening, far IR Fourier transform spectroscopy 77−40248
Pd, elec. resist. and supercond. transition temp., electron-phonon contrib. 78−80085
Pd, electron-phonon coupling and supercond. transition temp. 79−56360
Pd, electron-phonon interaction, expt. test of rigid muffin tin approximation 79−65364
Pd, electron-phonon parameters and supercond. p-state pairing 80−25041
Pd, phonon linewidths and electronic mass enhancement, electron-phonon contrib. 79−95099
Pd, phonon mediated interaction for triplet pouring 79−23911
Pd-Ag alloys, elec. resist. meas., density of states and Debye temp. 77−76715
Pd-Ag-D system, instability and superconductivity 78−39248
Pd-H, optical phonons in supercond. 77−63021
Pd-H, supercond. and phonon softening in unstable systems 79−65587
Pd-H alloys, optic mode influence on the vol. depend. of electron-phonon interaction parameters 77−63026
Pd-H like compounds, supercond. T_c increase by optical phonons 77−1509
Pd-H system, instability and superconductivity 78−39248
Pd-H(D), band struct. and supercond. props., APW calc. 79−56354
Pd-H(D), superconductivity and electron-phonon interaction 80−49975
Pd-H(D) system, normal state phonon resist. and supercond. tunnelling density of states 79−56402
Pd-H(D) system, superconductivity and phonon softening 79−73626
Pd-Rh-H and Pd-Ag-H, band struct. and supercond. props., APW calc. 79−56354
Pd_cAg_{1-c}, possibility of superconductivity 80−10862
$Pd_{1-y}Ag_yH_x$, electronic struct. and supercond., APW calc. 79−95318
$Pd_{1-y}Ag_yH_x$, superconducting transition temp., APW band struct. calcs. 78−95393
$Pd_{0.91}Ag_{0.045}Rh_{0.045}H_x$, supercond. transition temp. rel. to optical phonon spectrum 79−56355
PdD, electron-phonon mass enhancement factor and supercond. crit. temp. 79−87184
PdH, electron-phonon mass enhancement factor and supercond. crit. temp. 79−87184
PdH, role of optic phonons in superconductivity 78−39251
PdH, supercond., book contrib. 80−25037
PdH_x, CPA calculations of density of states 79−23882
PdH(D), superconducting props., effect of hybridisation, band struct. determ. 79−69628
$PdH_x(D_x)$ films, electron-phonon coupling, elec. cond. obs. 80−50011
$PdH_x(D_x)$, optical mode phonons, nonadiabaticity 78−55916
$Pd_{1-y}Rh_yH_x$, electronic struct. and supercond., APW calc. 79−95318
PrS, heat carrier scatt., thermal and elec. cond. from 5-400K 79−14974
Pt complex, KCP, periodic lattice distortions, charge density waves 79−82536

electron-phonon interactions continued

- Pt, specific heat, electron-phonon effects and anharmonic contrib. 79—90795
- RbDy$(MoO_4)_2$, Dy^{3+} doublets, temp. anomaly in splitting separation due to structural phase transformation *(Russian)* 80—39274
- Re, elec. resist., quadratic contrib., 2 to 40K *(Russian)* 80—92874
- Re, electrical resistance anisotropy, temp. depend. *(Russian)* 78—76041
- Re, Fermi surface, RF size effect, temp. depend. 80—65424
- Re, plastic deform. rel. to low temp. sp. ht., supercond. *(Russian)* 78—31005
- Ru, elec. resist., quadratic contrib., 2 to 40K *(Russian)* 80—92874
- Ru, electrical resistance anisotropy, temp. depend. *(Russian)* 78—76041
- RuO_2, thermal conductivity meas., rel. to elec. cond. 80—65317
- $(SN)_x$, electrical cond. at high press., scatt., evidence for semimetallic band struct. 77—43573
- $(SN)_x$, polymeric, electronic structure, semi-empirical pseudopotential calc. 77—72812
- $(SN)_x$, thermoelec. power, 0.1 to 4.2K, phonon drag contrib. and supercond. transition 79—56356
- $(SN)_x$, thermopower from 0.15 to 4.2K 80—34427
- SO_2 phosphorescence in Xe, Kr, Ar, N_2 matrices, environmental perturbation effects *(French)* 77—3407
- Sb, ideal part of elec. resist. in terms of carrier-phonon scatt. 79—73507
- Sb, magnetoresistivity, mutual drag effect, temp. depend 78—52012
- $Sb_{35}Se_{65}$, polycrystalline, elec. cond. mech. 80—49705
- Si (100) inversion layer, hot electron drift velocity, Monte Carlo calcs. inc. 3 subbands 78—91752
- Si (111) inversion layers, CDWs, effect of four valley interaction terms 79—33324
- Si, amorphous, thermoelec. power in phonon-assisted hopping regime, Coulomb effects 78—76097
- Si, anal. using photoacoustic cell, in pulsed elec. field 78—68027
- n-Si, carrier recomb. and photoionisation via E-centre resonance state 79—60847
- n-Si, carrier scatt. anisotropy, Hall mobility calcs. 77—24552
- n-Si, electron recombination, role of intervalley scatt. *(Russian)* 79—19605
- n-Si, electron-phonon scatt. and high-field transport 79—42552
- n-Si, electron-two phonon scatt. 77—47527
- Si, excitons and electron-hole drops, phonon assisted luminescence lineshape 79—99942
- n-Si, heavily doped, self energy of phonons interacting with free electrons, Raman scatt. 78—64366
- p-Si, highly deformed, hole scattering 77—20309
- p-Si, hole drift vel. in high field 79—95415
- Si, hole mobility temp. depend., valence bandstruct. 77—80771
- Si, hot electron diffusivity, theory 77—62940
- n-Si, impurity-assoc. magnetophonon reson. 80—20221
- p-Si, interband transitions, contrib. to conductivity at submillimetre wavelengths 80—34473
- n-Si, internal strain and impurity elec. field effect 78—14418
- n-Si, internal stress effect on electron-phonon interaction 79—42468
- n-Si intervalley electron-phonon deform. pot. consts. from high-field transport props. 77—62938
- Si, inversion layer electrons, temp. depend. cyclotron reson. lineshape 78—10568
- Si inversion layer in MOS struct., carrier-phonon interaction, nonohmic transport 80—49943
- n-Si, inversion layers, many-valley electron-phonon interactions, piezoresistance, anisotropic cond., Shubnikov-de Haas oscillations 78—52096
- Si, laser induced dense plasma, dynamics 80—65612
- Si, lattice scattering mechanism in quantised inversion layers 79—78187
- Si, non thermal laser induced ordering, plasma life time, phonon interactions 80—84481
- Si, nonpolar semiconductor, IR free carrier absorpt., two short wavelength phonon scattering 79—78665
- Si, phonon assisted Auger recomb. in indirect gap semiconductors 78—39126
- Si, phonon induced intervalley transitions, violation of selection rules 78—30875
- Si, phonon spectroscopy, amorphous versus crystalline material 78—83898
- Si, phonon-mediated intervalley electron-electron interaction 78—95125
- Si, piezo—spectroscopic study of ratio of electron—TO phonon to hole—TO phonon interaction 79—24289
- Si, piezospectroscopic determ. of electron-phonon to hole-phonon interaction 79—95783
- p-Si, Raman scattering by phonons and electrons, interference effects 78—60469
- p-Si, Raman spectra, pseudopot. calc. of discrete-continuum interference 80—2747
- Si, reson. Raman scatt. at indirect gap 79—73931
- n-Si, strained cryst., role of phonon reson. scatt. in phonon cond., appl. to Si:Li 79—19407
- Si:As(B)(Ga)(In)(P)(Sb), mean square dynamic displacement of atoms, effect of electron-phonon interactions *(Russian)* 78—10145
- Si:H amorphous, plasma-deposited, luminesc. decay 79—73989
- Si:Li, electron-phonon scatt., in intermediate conc. region 80—65180
- Si:Li, thermal cond., low temp. phonon scatt., internal strain effects 80—96706
- n-Si:P, low-compensated, Hall factor, electron-phonon interactions 79—4570
- Si:P, phonon cond., electron-phonon relax. rate 79—46771
- Si:P, thermal cond., electron-phonon interaction at low temps. 80—92730
- p-Si-Ge, heavily doped, hot pressed, high temp. phonon thermal cond. *(French)* 78—43190
- n-Si-Ge, phonon thermal cond. of hot-pressed alloy, 300-1100K 78—91494
- Si-SiO_2, interface free carrier mobility in inversion layer, influence of polar phonon scatt. 79—73597
- Si-SiO_2 interface, remote polar phonon scatt. in Si inversion layers 80—80095
- Si-type, semiconductor, interimpurity radiative recomb. with phonon cooperation 77—16385
- SiC (6H), phonon drag and phonon-electron interaction *(Russian)* 78—79701
- SiC, absorption of US waves 78—72210
- SiC, cubic, electron-hole liq., luminesc. obs. 78—31239
- SiO_2, amorphous charge transport and storage 80—6864
- SiO_2, amorphous electron transport and breakdown at high elec. fields 79—78108

electron-phonon interactions continued

- SiO_2, dielectric breakdown, impact ionisation-recombination model 78—6633
- SiO_2, phonon spectroscopy, amorphous versus crystalline material 78—83898
- SmB_6, f-d hybridisation, optic phonon anomalies 78—92080
- SmS, f-d hybridisation, optic phonon anomalies 78—92080
- SmS, lattice dynamical model 80—96610
- SmS, valence fluctuation phenomena 80—24800
- $Sm_{0.25}Y_{0.75}S$, phonon anomalies and electron-lattice coupling 80—39490
- $Sm_{1-x}Y_xS$, mixed valence system, theory 80—70343
- Sn superconducting film, phonon-injection-induced destruction of supercond. 80—6956
- Sn, superconducting film, radiation induced critical temp. 79—87179
- $SnMo_5S_6$, high supercond. T_c, soft mode behaviour 78—14855
- $SnMo_6S_8(Se_8)(Te_8)$, Chevrel phase correlation between struct. and supercond. transition temp. 80—7023
- SnTe, carrier density depend. of soft TO-phonon, Raman scatt. meas. 78—6684
- SnTe, displacive transform., interband electron-phonon interactions, phase diagram 80—93252
- p-SnTe, elec. resist. anomaly in vicinity of struct. phase transform. 79—19597
- SnTe, electron-phonon interaction effect on ferroelec. transition 78—76416
- SnTe, electron-phonon interactin induced phase transition 79—82338
- SnTe, mag-props., effect of structure transition 78—6158
- SnTe, softening of TO phonon mode *(Japanese)* 78—2225
- SnTe, structural phase transition threshold instability in strong EM field 80—103477
- SnTe-PbTe-GeTe, alloy semiconductor, phase transition *(Japanese)* 78—91443
- SrF_2:Eu^{2+}, spectral, spatial and temporal phonon spectroscopy, new spectrometer 78—83892
- SrF_2:Sm^{2+}, pseudo-Jahn-Teller effect 79—69476
- SrO:Pb^{2+}(Bi^{3+}), impurity centres vibronic spectra, lattice dynamics and electron-phonon interactions 80—7396
- T, US attenuation due to electron-phonon interaction 79—77687
- TTF-TCNQ, irradiated, libron and phonon equilibration, resistivity meas. 79—42530
- Ta, calc. using APW band struct. calcs. and measured phonon spectra 78—14869
- Ta, effect of changes in $\alpha^2(\Omega)F(\Omega)$ on the zero-temp. energy gap 80—97025
- Ta, electron-phonon interaction, relativistic, APW calc. 80—92837
- Tb, ferromag., electron-magnon interaction and elec. resist., 1.5 to 50K 79—60790
- Tb, high-precision elec. resist. meas., 1-4K 77—15817
- $Tb(OH)_3$, dynamical effects of interaction between 4f electrons and optical phonons 80—108196
- TbZn, ferromag., thermoelec. power, temp. depend. and crit. behaviour 80—96852
- Tc, rel. to superconductivity and Fermi surface calcs. 80—70873
- Te, photoconductivity under pulse excitation conditions, scatt. mechanism and carrier mobility meas. 80—2425
- Th, FCC, ground-state props. 78—75989
- Th, lattice dynamics in reson. model pseudopot. theory 79—19334
- Th, superconducting transition temperature calculation 79—7928
- Th-H system, supercond., book contrib. 80—25037
- Th-U, Kondo alloys, spin and phonon resistivity independ. 78—47777
- Th_4H_{15}, superconductivity and electron-phonon interaction 80—49975
- Th_4H_{15}, ThH_2, phonon densities of states rel. to supercond. props. 77—27960
- $Th_4H_{15}(D_{15})$, normal and supercond., low-temp. sp. ht., Debye temp. and supercond. props. 77—4466
- Ti, partial densities of states, electron-phonon interaction 78—51869
- Ti-Cr, diffuse electron scatt. *(Russian)* 80—103438
- Ti-Mo, diffuse electron scatt. *(Russian)* 80—103438
- Ti-Nb, diffuse electron scatt. *(Russian)* 80—103438
- Ti-V, anomalous elec. resistivity, mag. susceptibility, soft-phonon induced structural inhomogeneities 78—60104
- TiC, high temp. thermal cond., ambipolar diffusion contrib. 78—26742
- $TiCl_3$, lattice instability, d-electron-lattice interaction 80—44276
- $TiN_{0.96}$, electronic component of thermal cond., inelastic electron-phonon scatt. 79—86937
- TiO_2, phonon spectroscopy, amorphous versus crystalline material 78—83898
- TiO_2, unambiguous assignment of fund. absorpt. edge 78—71817
- TiS_2, carrier-lattice coupling 78—63822
- TiS_2, semimetallic charact. 77—62926
- $TiSe_2$, carrier-lattice coupling 78—63822
- $TiSe_2$, mechanism for 200K transition, sp. ht. meas. 78—22853
- $TiSe_2$, semimetallic charact. 77—62926
- $Ti_{1+x}Se_2$, superlattic form., phase transform., Fermi surface instability 77—15383
- Tl films, supercond. amorphous, effective phonon spectrum and lattice sp. ht. 80—70895
- Tl-Pb-Bi alloys, supercond., electronic density of states from heat capacity meas. 79—56383
- $TmPO_4$:Gd^{3+}, EPR spectrum and Jahn-Teller induced nonuniform dynamic strains 77—85565
- US attenuation due to electron-phonon interaction 79—77687
- V, calc. using APW band struct. calcs. and measured phonon spectra 78—14869
- V, electron-phonon coupling constant calc. *(Russian)* 80—70624
- V, electronic density of states, effective mass, electron-phonon interaction, Coulomb pseudopot. *(Russian)* 78—26804
- V, electronic structure, model potential calcs. *(Russian)* 80—100431
- V, Fermi surface area, effective heat, optical masses, surface anisotropy critical temp. depend. *(Russian)* 79—90943
- V oxides, change in phonon damping due to metal-insulator transition 80—103625
- V, partial densities of states, electron-phonon interaction 78—51869
- V, thermal conductivity in ultrapure normal, mixed and supercond. states *(Russian)* 79—4617
- V-Nb-Ta, supercond., elec. resist. and electron-phonon interaction parameters 78—14862
- V-Ta alloys, electron-phonon interaction and supercond. transition temp. *(Russian)* 79—28426
- $V_3Ga(Si)$, high T_c supercond., electron-phonon coupling, effect of electronic density of states sharp struct. 78—14877

electron-phonon interactions continued
$V_3Ge(Si)$, electron-phonon coupling and supercond. crit. temp. 79−33379
VI_2, antiferromag., zone-boundary phonon Raman scattering, modulation of exchange interaction 80−11386
VI_2, mag. 'Bragg' scatt. obs. through Raman scatt. 80−66179
$V_{75-x}M_xGa_{25}$, M=Ti, Cr, Mn, Fe, Co, Ni, supercond. transition temp. and electron-phonon coupling parameter 79−60952
VN, electronic struct. of vacancies, effect on supercond. transition temp. 80−29347
$VN_{0.74}$ and $VN_{0.89}$, low-temp. specific heat and superconducting critical temp. meas., density of states 80−54835
VO_2, change in optical props. at semicond.-metal transitions 77−28597
VO_2, diffuse X-ray scatt. due to lattice instability near metal-semiconductor transition 78−56074
VO_2, magnetic susceptibility in insulating and metallic phases, electron-electron and electron-lattice interactions 80−96788
VO_2, metal-insulator transition and electronic struct., ion bombard. effects 80−92948
VO_2, semiconductor-metal transition, effect of ^{18}O substitution 78−84268
VO_2, thermal cond. meas., metal-dielectric phase transition, phonon scatt. mechanism 78−87831
V_2O_3, semiconductor-metal transition, effect of ^{18}O substitution 78−84268
V_2O_3, thermal cond. meas., metal-dielectric phase transition, phonon scatt. mechanism 78−87831
V_3O_5, semiconductor-metal transition, effect of ^{18}O substitution 78−84268
V_3O_5, thermal cond. meas., metal-dielectric phase transition, phonon scatt. mechanism 78−87831
V_3Si, channelling, at displacements and electron phonon/defect interactions 77−84815
V_3Si, E_g optical phonon, Raman scatt. meas. 79−24316
V_3Si, elec. resist. below 77K, phonon assisted interband scatt. 78−14703
V_3Si, electronic struct., electron-phonon interaction and high temp. superconductivity, APW calc. 78−14871
V_3Si, single crystals, supercond. tunnel characts. 80−7044
V_3Si single crysts., elec. resist. and Hall coeff., temp. depend., 17-300K *(Russian)* 77−69292
V_3Si, supercond., crit. fields Pauli paramag. limiting and material parameters 79−78277
V_3Si, superconducting, optical props. and electron-phonon interactions 80−2510
V_3Si thin films, Holstein processes and electron-phonon spectral function, far IR meas., 19K 79−87445
$(V_{1-x}Ti_x)Ge$, pseudobinary A15 compound, supercond. transition temp. 80−49970
W, elec. resist., quadratic contrib., 2 to 40K *(Russian)* 80−92874
W, ferromagnetic layer coating, longitudinal conduction electron spin waves, Larmor wave 79−33543
W, low temp. transport props., phonon and impurity scatt. 78−10418
W, scatt. rate temp. depend. from magnetoacoustic expts. 79−65522
WO_3 electrochromic absorption dependence on crystallinity 77−77314
Xe, liq. and solid, emission coeff. of cond. electrons, depend. on elec. field intensity *(Russian)* 79−78855
YAG:$Er^{3+}(Ho^{3+})$, stimulated radn., electron-phonon interaction *(Russian)* 77−8605
YAG:Nd^{3+}, many-phonon nonradiative transition probabilities 79−95842
$YAlO_3$:Nd^{3+}, thermal broadening and shift calcs. of Nd^{3+} energy levels 77−48208
$YAlO_3$:Yb^{3+}, absorption and luminescence spectra, electron-phonon resonances, Stark splitting *(Russian)* 80−20674
$Y(OH)_3$, dynamical effects of interaction between 4f electrons and optical phonons 80−108196
YS, electronic instability and phonon softening, APW calc. 80−29323
Yb monochalcogenides, multiphonon inelastic light scatt. 77−90144
Zn, anisotropy, microcontact spectroscopy *(Russian)* 78−43372
Zn, anisotropy and temp. depend. of electron-phonon mass enhancement 77−15745
Zn, cyclotron mass and superconducting energy gap calc. as a function of Fermi surface position 79−69625
Zn, electron-phonon interaction anisotropy, microcontact spectroscopy *(Russian)* 79−37786
Zn, Hall effect and phonon scattering in pure crystal 79−23948
Zn point contacts, electron-phonon coupling, microcontact spectroscopy investig. *(Russian)* 78−38796
Zn, superconducting transition temp., electron-phonon mass enhancement, pseudopot. calcs. 78−2604
Zn-Cr, Kondo alloys, spin and phonon resistivity independ. 78−47777
Zn-Mn, Kondo alloys, spin and phonon resistivity independ. 78−47777
Zn-Pb proximity sandwiches, tunnelling characts. 79−56396
$Zn_xCd_{1-x}Te$, resonant Brillouin scattering *(Japanese)* 79−15474
$Zn_xHg_{1-x}Se$, band struct. and scattering mechanism, determ. from transport coeffs. 77−59254
$Zn_xHg_{1-x}Se$, current carrier scattering mechanism 80−65546
$Zn_xHg_{1-x}Se$, galvanomagnetic effects, Shubnikov-de Haas oscill. determ. of band struct. 80−6884
ZnO, band gap depend. on energy of zero-point vibrs., luminesc. obs. 79−73436
n-ZnO film, highly degenerate, IR absorption by free polarons 77−4697
ZnO, surface phonon-plasmon coupling (surface plasmarons) 80−54497
ZnO:Co^{2+}, polarised optical absorpt. spectrum, crystal field transitions 77−48206
ZnS, phosphor, voltage and temp. dependence of pre-breakdown electroluminescence 80−45147
ZnS phosphors, Gudden-Pohl effect, field ionis. of trapping centres 77−73170
ZnS:Cu, current pulses stimulated by elec. field at low temp. 78−39121
ZnS:Fe^{2+}, impurity electron-phonon reson. relax. time, thermal cond. 77−59085
ZnS:Pb current pulses due to elec. field liberation of electrons from trapping centres by tunnel processes 79−28378
ZnS(Se)(Te):Cr^{2+}, Jahn-Teller coupling 78−67997
ZnSe crystals, doped and undoped, optical absorption edge 80−60626
n-ZnSe crystals, electron scatt. mechanisms, high mobility 80−34433
ZnSe, cubic monocrystal, electron-phonon interaction, low temp. luminesc. *(Russian)* 80−25451
ZnSe, multiphonon ionisation of deep point centres in a charged dislocation field *(Russian)* 80−100281
ZnSe, photoexcited hot electrons at 2K, photolum. meas. 79−78741

electron-phonon interactions continued
ZnSe, polar semicond., radiative recomb., electron-phonon interaction effects, calc. 80−49631
ZnSe:In, Li, binding energy of excitons bound to donor-acceptor pairs, electron-phonon coupling 77−4689
ZnSe/metal, dielectric phonon-metal electron interaction, effect on optical props. *(Russian)* 79−19663
n-$ZnSiP_2$, lattice limited Hall mobility, nonpolar optical scatt. mechanism 79−51579
ZnTe, electron-phonon coupling, donor-acceptor pairs selective excitation 80−11475
ZnTe, free-exciton emission band under high-intensity photoexcitation 79−73993
ZnTe, wavelength-modulated reflectance spectrum, electron-phonon and exciton-phonon interactions 79−11434
ZnTe:Li, electron-phonon interactions in Raman scatt. 80−60594
Zr, H(D) implanted, superconductivity enhancement obs. 80−70884
Zr_xBe_{1-x} noncrystalline alloy, phonon-electron scatt., superconducting temp. 80−54330
ZrC_x, x=0.99 to 0.13, elec. cond., supercond. state 78−43504
ZrS_3, quasi one-dimens. semicond., elec. transport props. 80−107790
$ZrZn_2$, phonon contrib. to Stoner enhancement factor, ferromag. and possible superconductivity 80−25070

electron-positron inclusive interactions
$\gamma\gamma$ processes, tests of QCD 80−22628
σ_L/σ_T electroprod. data, colour excitation, proposed direct inclusive leptoprod. tests 80−52514
annihilation, 12-31.6 GeV, τ production and decay branching ratios, lifetime 80−78052
annihilation, 13-31.6 GeV, charged particle multiplicity growth, cross section 80−37286
annihilation, 30 GeV, inclusive K^0 prod. $K^0K^+/\mu^+\mu^-$ prod. ratio 80−91103
annihilation, 3.6-5.2 GeV, charged π, K, N inclusive prod. 79−30743
annihilation, Λ_c charmed baryon prod., branching ratio, inclusive cross sections 80−37280
annihilation, charge current asymmetry as QCD test, neutral gluons 80−57616
annihilation, charged Higgs boson prod. signatures, Weinberg-Salam parametrisation 80−57620
annihilation, CM energies 29.90-31.46 GeV, narrow resonance search upper limit 80−63003
annihilation, energy correlations, sensitivity of QCD tests to gluon spin 79−89113
annihilation, energy correlations in perturbative QCD 79−85310
annihilation, fine energy scan for narrow states between 29.9 and 31.46 GeV 80−22627
annihilation, gg and qg coupling equality on resonance, QCD calcs., expt. tests 80−389
annihilation, gluon jets and heavy quarkonium prod., QCD test, ψ prod. 80−42479
annihilation, hadron and lepton prod., τ-lepton decay, $K^\pm$, p, $\bar{p}$ yields, quark flavours 80−73725
annihilation, hadron prod. total cross section, CM energies 1.4-2.0 GeV 80−57619
annihilation, hadronic final state charge current asymmetry, QCD test, neutral gluons 80−37289
annihilation, hard gluon bremsstrahlung from heavy quarks, jet cross section 80−32078
annihilation, heavy quark fragmentation functions from inclusive hadron spectra *(Russian)* 79−40756
annihilation, heavy quark jet ang. distribs., quark mass, QCD anal. 80−42481
annihilation, high energy, secondary hadron transverse momentum, QCD anal. 80−37285
annihilation, higher order QCD corrections 80−47316
annihilation, jet ang. distrib., QCD correction 80−42482
annihilation, jet azimuthal ang. correlations in QCD 80−9179
annihilation, narrow resonance search upper limit at PETRA, 29.90-31.46 GeV 80−57618
annihilation, polarised gluon bremsstrahlung as QCD test 80−32077
annihilation, QCD and jet acollinearity, quark-gluon coupling 80−105914
annihilation, QCD and semilocal duality (hadrons/$\mu^+\mu^-$) cross section ratio 80−78085
annihilation, quark fragmentation in field-theoretic model of composite hadrons 80−82986
annihilation, quark jet fragmentation into mesons and baryons, chain decay model 80−63001
annihilation, radiative corrections, review, book contrib. 80−47320
annihilation, sphericity like distribs., testable QCD predictions 80−37284
annihilation, spin-0 electron or muon pair prod., cross section supersymmetry predictions 80−32092
annihilation, superheavy flavour prod., weak current effects, Z^0 effects 80−57614
annihilation, three-jet analysis, minimisation of sum of squares of transverse momenta 80−63008
annihilation, two and three gluonic jet prod., perturbation theory *(Russian)* 80−52525
annihilation, vector or scalar gluon jets 80−27474
annihilation, weak neutral currents of quarks hadron prod. cross section P-odd depend. *(Russian)* 79−93445
annihilation and deep inelastic leptoproduction, structure functions, QCD and parton model 80−63010
annihilation and deep inelastic reactions, jet anal., thrust distrib., summing leading logs 80−63004
annihilation and hadron-induced events, multiplicity ratio 80−105877
annihilation by one-photon processes, review, book contrib. 80−47272
annihilation cross section, fourth-order QCD contribs. 80−82987
annihilation cross section of $e^+e^-\rightarrow$hadron near $N\bar{N}$ threshold *(Russian)* 79−85311
annihilation cross sections, operator approach, one-photon approx. 80−47315
annihilation on atoms, δ function operator method 79−94088
annihilation radiation from galactic centre, role of positron prod. by evaporating black holes 80−46599
annihilation radiation from point isotropic photon sources, numerical calc. 79−85096
anomalous muon events at 4.8 GeV, charm and heavy lepton explanations 77−247

electron-positron inclusive interactions continued
- anomalous muon signal at 7.3 GeV, $n_{ch} \leq 2$ final state multiplicity, cross sections 78—41559
- bare quark masses positivity domains 77—18309
- bremsstrahlung model of Brodsky and Gunion, comments 79—93362
- charged multiplicity distributions, comparison of $\bar{p}p$, pp, and e^+e^- interactions 77—57577
- charged-particle multiplicities in high-energy collisions 77—34194
- charm and heavy lepton prod., energy bounds 77—2810
- charm meson decay, inclusive electron spectrum 77—13970
- charm particles, review 78—17035
- charm production of pseudoscalar and vector mesons 77—2855
- charmed axial vector meson prod., nonrelativistic quark model 78—25055
- charmed axial vector meson prod. rate, non-relativistic quark model 77—38184
- charmed baryon production model 79—49530
- charmed meson produced in e^+e^- annihilation 80—91106
- charmonium model of ψ family 78—78143
- charmonium potential models, testing Q^2 duality 79—45082
- coherent state model 80—13321
- colliding beam physics, review 77—74700
- colour, jet prod., exponentiation of leading logarithmic cross sections 79—63445
- conference, LEP summer school, Les Houches, France (Sep. 1978) 79—97916
- current-induced reactions, dual unitarisation 78—74233
- D-meson decay at $\psi(3772)$, inclusive props. 78—93876
- diquark and quark jet fragmentation model, appl. to inclusive annihilation 79—2979
- $e^+e^- \rightarrow$hadrons, 9.4-10.4 GeV, three Υ states, mass spacings, lepton pair widths 80—68465
- e^+e^- annihilation, phenomenological interpretation, ψ prod. and props., multihadron events 77—67668
- electron-photon cascade simulation by Monte Carlo programs 79—54330
- fragmentation functions beyond leading order in QCD 80—13282
- fragmentation functions of heavy quarks into hadrons, ν reactions, e^+e^- annihilation appls. 79—3013
- gluon fragmentation functions from quark jets 79—49453
- gluon jet production, quark models 80—22576
- gluon observation in P-wave quarkonium decay 80—32068
- hadron, fragmentation from heavy quark partons 78—8603
- hadron decay from jet, transverse momentum 78—74268
- hadron distributions in quark jets, pion and proton form factors 79—54317
- hadron EM interactions, book 80—46749
- hadron final state props. at 13 GeV and 17 GeV 79—63491
- hadron jet production, review 80—47321
- hadron jets, test for planar events in QCD 79—40794
- hadron jets from quantum chromodynamics 78—25056
- hadron jets transverse momentum and ang. distribs. from QCD 79—40793
- hadron multiplicity at 10 to 40 GeV 80—63007
- hadron prod., molecular charmonium spectroscopy 77—30394
- hadron prod., overlapping resonances 77—2848
- hadron prod., total cross section, screened quark confinement force 77—22692
- hadron prod. cross-section struct. in 0-8 GeV range, quark models and heavy leptons 77—30392
- hadron production, inclusive study, momentum distrib., energy and multiplicity 80—57613
- hadron production, multiplicity distribution, Regge like parton model *(Russian)* 80—78100
- hadron spectrum in e^+e^- inclusive annihilation, test for prod., hadronic decay and mass of heavy leptons 77—18304
- hadronic annihilation, 22-31.6 GeV, top threshold, sphericity and thrust distrib. 80—429
- hadronic jet structs., QCD tests, max. directed momentum parameter 78—25057
- hadronic structure using parton anal. of deep inelastic scattering and rel. processes 79—80803
- hard processes, large rapidity separation of baryonic number, partons, and dual topology 80—95255
- heavy flavour prod. in e^+e^- annihilation, QCD contrib., inclusive quarkonium prod. 79—85267
- heavy lepton production and decay in e^+e^- collisions, inclusive distribs. 77—87961
- heavy lepton production in e^+e^- annihilation, QED background 79—75706
- heavy particle pair production, secondary particle distribs., τ properties 80—62960
- Higgs particle search at PETRA using Wilczek mechanism 80—105838
- high energy data from PETRA, QCD anal., QCD coupling constants 80—82985
- high energy interactions *(Chinese)* 80—78074
- inclusive hadron prod., polarisation and p nonconservation asymmetries, π, $K^{\pm}$, $D^{\pm}$ prod. 80—78084
- jet analysis, QCD calcs. and phenomenological models 80—52523
- jet angular distrib. eccentricity, technique for detecting new quark flavors 78—70383
- jet invariant mass in QCD 79—85307
- jet production, weak corrections to three-jet angular distributions 80—22629
- jet production by a gluon source in QCD 79—22056
- jet production to order α^3 and α^4 including QCD corrections 80—13322
- jet structure events at LEP energy, detector system 79—97953
- jet structures of leptons, quarks and gluons, perturbative QCD, process dependence 80—68470
- jets, colour-singlet subsystems, large rapidity gaps 80—68469
- jets, two-particle distribs. from single-particle fragmentation functions, effects of heavy quark flavours 80—68468
- Landau's hydrodynamic model, further aspects 78—82173
- leading logarithm sum for struct. functions in QCD 79—71735
- lepton energy spectra, charmed hadron decay 77—65161
- lepton pair prod. in processes with hadronic jets 80—27512
- low-momentum π,K,p inclusive prod. at CERN ISR with x=0 77—18303
- many-hadron final states, in inclusive e^+e^- annihilation 78—29339
- meson production, b-quark quantum number mesons, cross-section from equivalent photon approx. 80—68467
- multihadron production, 1.45 to 1.61 GeV, ρ^0 production across full range 79—63489

electron-positron inclusive interactions continued
- multilepton events, evidence for bottom quark 79—54319
- multiperipheral fireball model, momentum distribs. 77—67665
- multiperipheral fireball model scaling function of e^+e^- annihilation 77—87985
- multiplicities in hadronic and current induced reactions, e^+e^- annihilation, clustering 77—46070
- multiprong events, inclusive electron prod., 3.9-7.4 GeV, charmed particle decay 78—66136
- new particle searches in e^+e^- interactions at LEP energies 79—97617
- new particles observed in e^+e^- annihilation 80—95283
- parton model for e^+e^- annihilation, finite energy results 78—419
- perturbative QCD, hard hadronic processes, e^+e^- annihilation, lepton-hadron deep inelastic scatt. 80—52477
- PETRA results for fluons, nuclear forces, t-quarks and quark-lepton symmetry 80—86731
- positron annihilation ang. correl. curves anal. using ANNIH program 80—37709
- prospects at high energies 80—91074
- QCD, hard semi-inclusive processes 78—93862
- QCD, non-perturbative effects in hadronic e^+e^- annihilation 79—89173
- QCD, struct. functions, perturbation theory *(Russian)* 78—8595
- QCD jet dynamics, hadron and photon prod. at large transverse momentum 79—45077
- QCD jet simulation, cutoff choice effects 80—102015
- QCD jets from coherent states 80—13266
- $Q\bar{Q}$ bound states hadronic decay azimuthal correlations 79—93442
- quark cascade model, appl. to meson spectra in e^+e^- annihilation 78—41482
- quark cascade model, inclusive meson and baryon spectra in pp, πp, e^+e^- 77—50025
- quark decay patterns, liberated QCD and confined QCD theory 79—9328
- quark fragmentation functions in Monte Carlo quark parton model of e^+e^- annihilation 79—80791
- quark jets, transverse momentum profile 80—57621
- quark jets in e^+e^- annihilation, forward-backward asymmetries 79—97605
- quark mass differences in high energy collisions 78—45868
- resonance decays above charm prod. threshold, single channel dominance 78—66133
- scaling and cluster decay phenomena 77—2854
- scaling in bound state models 77—38181
- semi-local duality in inclusive e^+e^- annihilation, duality sum rule 77—49985
- spacelike features and asymptotic behaviour of e^+e^- annihilation 80—86630
- spin dependent photon structure functions from Drell-Yan and e^+e^- reactions 80—82973
- thermodynamical two-fireball model, rich yield of high momentum hadrons 77—30335
- total hadronic cross-section in 4 Gev region, quark model with broken colour symmetry 77—22748
- two-particle final states ang. distrib., simple quark model 77—49984
- $U(1)\times SU_L(2)\times SU(3)$ theory, integer charge quarks, lepton hadronic processes *(Russian)* 80—86653
- vector meson of mass 1.82 GeV obs. 77—65162
- weak interactions, summer school, Varenna, Italy (Jul. 1977) 80—90597
- weak selection rules, inclusive prod. of charmed particles and heavy leptons 78—8679
- $b\bar{b}$ prod. and decay in e^+e^- data at PETRA 79—63492
- $D \rightarrow K^*\mu\nu$, in e^+e^- annihilation, T-odd asymmetry in CP violation model *(Russian)* 80—105885
- D meson production in e^+e^- annihilation, c quark fragmentation function *(Russian)* 79—85312
- $e^+ + e^- \rightarrow \nu_H$ possibility of production and detection 79—49501
- e^-e^+ annihilation, >2 GeV, production of charmed particles and charged τ lepton, review 78—17006
- e^+e annihilation, 3.1-5.2 GeV, DASP results 80—42483
- e^+e^-, 27-4, 27.7 GeV/c, hadron prod./muon prod. cross section ratio, thrust distrib., average sphericity 80—426
- e^+e^-, 31.57 GeV, $(e^+e^- \rightarrow \text{hadrons})/(e^+e^- \rightarrow \mu^+\mu^-)$ cross section ratio, thrust distrib. and average spherocity 79—89175
- e^+e^-, jet cross sections and quark current-photon pointlike coupling, sum rules 80—32104
- e^+e^-, ψ/J prod., expt. results and interpretation, review *(Russian)* 77—269
- $e^+e \rightarrow$ hadron jets, 13-31.6 GeV, planar events evidence, transverse momentum and broadening 79—93441
- $e^+e^- \rightarrow$ hadrons, 1.6 GeV, total cross section, pion multiplicity 77—49983
- $e^+e^- \rightarrow$ hadrons, quark existence and theory 80—37234
- $e^+e^- \rightarrow$ hadrons, scaling and quark struct. 80—425
- $e^+e^- \rightarrow$ hadrons, string model investigation 79—58946
- $e^+e^- \rightarrow$ hadrons, two-fireball model, jet problem 77—65165
- $e^+e^- \rightarrow$ jets, in Υ and Υ' region, sphericity and charged multiplicity 80—428
- $e^+e^- \rightarrow$ jets, on-shell QCD quark form factor from two particle correlations 80—86740
- $e^+e^- \rightarrow$ jets, transversely polarised annihilation, charged gluon jets, Pati-Salam model 80—86739
- $e^+e^- \rightarrow$3 jets, integer charge quark model, gluon jets 80—91101
- $e^+e^- \rightarrow$3 jets, three gluon coupling in perturbative QCD 80—105913
- $e^+e^- \rightarrow$4 jets, differential 4-jet acoplanarity distribs., QCD predictions, heavy quark prod. 80—78083
- e^+e^- annihilation, 3.6-5.8 GeV, inclusive D and K meson prod. cross sections 79—93439
- e^+e^- annihilation, 6 GeV, η_c existence, possible $c\bar{c}c\bar{c}$ state 77—82755
- e^+e^- annihilation, expts. at LEP 79—97613
- e^+e^- annihilation, form. of forward leptons *(Russian)* 77—2811
- e^+e^- annihilation, gluon jets, multiplicity and ang. distribs. asymmetries 80—91105
- e^+e^- annihilation, hadron secondary average transverse momentum, comparison with deep inelastic scatt. 80—37281
- e^+e^- annihilation, high energy, QCD tests 80—42420
- e^+e^- annihilation, multiparticle inclusive prod., QCD high energy predictions using methods of cut vertices 79—89128
- e^+e^- annihilation, opposite side quantum number correlations 80—105863
- e^+e^- annihilation, Q^2 duality test with nonrelativistic potentials 80—102011

electron-positron inclusive interactions continued

- e^+e^- annihilation, QCD calc. of heavy flavour multiplicities at very high energies 79−75744
- e^+e^- annihilation, recent DORIS results 80−91107
- e^+e^- annihilation, sum rules for Υ-family formation, QCD anal. *(Russian)* 79−54347
- e^+e^- annihilation, tensor anal., QCD test 80−42396
- e^+e^- annihilation, zero mass limit for class of jet-related cross sections 79−71736
- e^+e^- annihilation at high energies and search for the t-quark continuum contribution 80−102012
- $e^+e^- \to b\bar{b}$, heavy quark masses and C- and P-odd asymmetries, Weinberg-Salam model *(Russian)* 80−102060
- $e^+e^- \to$charmed hadrons, quark mass effect on fragmentation functions 80−91098
- e^+e^- collisions, jet prod. and two-photon annihilation, hadron spectra 80−91121
- $e^+e^- \to D^0$, SPEAR expt. results 79−93444
- $e^+e^- \to D^+$, SPEAR expt. results 79−93444
- $e^+e^- \to \bar{D}D$, above charm threshold at energy corresponding to $\psi''(3770)$ 80−73723
- $e^+e^- \to D+$anything, 7 GeV, inclusive momentum and energy spectra 79−75780
- $e^+e^- \to D(1875)$ charmed meson semileptonic decays 78−4854
- $e^+e^- \to \Delta X$, polarisation effects in nonperturbative parton model, scaling 80−105912
- $e^+e^- \to \Delta(1232)X$, struct. functions and nucleon longitudinal polarisation *(Russian)* 79−22121
- $e^+e^- \to e^+X$, QCD predictions for deep inelastic scattering on an electron 79−63493
- $e^+e^- \to e^+e^-B\bar{B}$, cross-section from equivalent photon approx. 80−68467
- $e^+e^- \to e^+e^-X$, beam polarisation effects on cross section 77−61269
- $e^+e^- \to e^+e^-X$, virtual 2 photon processes, luminosity functions, rapidity distrib., QED factors 80−86734
- $e^+e^- \to e^+e^- + 2$ jets, $\gamma\gamma \to q\bar{q}$ contrib. to cross section, QCD corrections 80−78106
- $e^+e^- \to e^+e^-\chi_b$, cross-section from equivalent photon approx. 80−68467
- $e^+e^- \to e^+e^-\eta_b$, cross-section from equivalent photon approx. 80−68467
- $e^+e^- \to e^+e^-\eta_c$, two photon process, numerical distrib. studies 79−13142
- $e^+e^- \to e^+e^-\gamma\gamma \to e^+e^-\bar{q}q \to e^+e^-h$, 100 GeV, QCD tests 80−18141
- $e^+e^- \to e^+e^-\pi$ 79−13142
- $e^+e^- \to e^+e^-qg(q\bar{q}) +$ jet, $\gamma\gamma$ initiated 3 jet events in QCD 80−102057
- $e^+e^- \to e^\pm K^\mp +$anything, D-meson decay, K-e correl. anal. 78−78179
- $e^+e^- \to e^\pm X^\mp$, 3.1 to 7.4 GeV, threshold behaviour of $\tau^+\tau^-$ prod. 78−70351
- $e^+e^- \to e^\pm\mu^\pm +$anything by $\Psi''(4.4) \to \Omega'\bar{\Omega}'$, $\Omega' \to \Xi^0 e^-\nu_e$ or $\Xi\mu^-\nu_\mu$, anomalous lepton prod. explanation 77−41834
- $e^+e^- \to e^\pm\mu^\mp$nything, effect of transverse beam polarisation on anomalous leptons 77−6102
- $e^+e^- \to eX$, τ branching ratio and e momentum spectrum, D decay 78−89693
- $e^+e^- \to$electrons, 3.6-5.2 GeV multiplicity distrib. anal. 77−87964
- $e^+e^- \to \eta X$, $F \to \eta\pi$ F meson prod. characts. 79−26338
- $e^+e^- \to F^+$, SPEAR expt. results 79−93444
- $e^+e^- \to$gluon and quark jets 80−91100
- $e^+e^- \to \gamma X$, angular asymmetries, weak contribs. 80−101976
- $e^+e^- \to \gamma X$, obs. at DORIS 80−102058
- $e^+e^- \to \gamma +$hadrons, γ-spectra and QCD anal. 78−8678
- $e^+e^- \to \gamma +$hadrons, high energy, lepton radiation and γ struct. functions, quark parton model 80−32113
- $e^+e^- \to \gamma +$hadrons, quark-parton model predictions, sum rules, charge asymm. 77−10219
- $e^+e^- \to \gamma^* \to \gamma +$hadrons, QCD predictions 80−63009
- $e^+e^- \to \gamma^* \to$hadrons, hadron calorimetric meas., QCD predictions, gluon emission 80−91102
- $e^+e^- \to \gamma \to q\bar{q}g$, charge distrib., Sterman-Weinberg criterion, QCD test 79−71694
- $e^+e^- \to \gamma\pi^0$, inclusive production, 4.9 to 7.4 Gev, cross sections 78−89723
- $e^+e^- \to h_1h_2X$, polarised electrons, structure functions, γ^* partial widths *(Russian)* 77−61308
- $e^+e^- \to h^\pm X$, 13 and 25 GeV^2, cross sections, scaling 77−49989
- $e^+e^- \to h^\pm X$, dynamical scaling 77−6137
- $e^+e^- \to h^+X$, violation Bjorken scaling, momentum fluctuation, range of timelike photon 79−3033
- $e^+e^- \to HX$, associated production of gluonic jets and heavy mesons 78−93892
- $e^+e^- \to hX$, high energy predictions from perturbative QCD 80−42417
- $e^+e^- \to hX$, naive parton model failure in quark-gluon theory 77−67618
- $e^+e^- \to$hadron jets, 30 GeV, strong coupling constant and QCD test 80−37283
- $e^+e^- \to$hadron jets, 7.7-31.6 GeV, two particle ang. correlations 80−47318
- $e^+e^- \to$hadron jets, QCD, Monte Carlo model 80−27514
- $e^+e^- \to$hadron jets, quark helicities, neutral current vector and axial couplings 80−32114
- $e^+e^- \to$hadron jets, two fireball model anal., Monte Carlo method *(Russian)* 80−37288
- $e^+e^- \to$hadron$+X$, WKB calc., hadronic amplitudes in scaling region 78−41484
- $e^+e^- \to$hadron(p)$+X$, Callan-Symanzik eqn. for structure function moments 79−21929
- $e^+e^- \to$hadrons, 12, 30 GeV, jets, quark fragmentation and coupling constant, QCD comparison 80−105915
- $e^+e^- \to$hadrons, 12, 30 GeV, π,k,p,$\bar{p}$ production 80−105916
- $e^+e^- \to$hadrons, 13-31.6 GeV, gluon bremsstrahlung evidence, seagull effect, one sided jet broadening 80−430
- $e^+e^- \to$hadrons, 1.35 to 2.125 GeV, hadronic cross sections 79−58968
- $e^+e^- \to$hadrons, 1.42-3.09 GeV total CM energy, total cross section 79−93440
- $e^+e^- \to$hadrons, 33-35.8 GeV, new quark flavour search, cross sections and thrust 80−86736
- $e^+e^- \to$hadrons, 3.6 to 5.2 GeV, total cross sections, resonance peaks 78−62416
- $e^+e^- \to$hadrons, 400 GeV, search for narrow reson. states near 6 GeV 77−74699
- $e^+e^- \to$hadrons, 5-7.8 GeV, $D^{*+} \to D^0\pi^+$ obs., decay width, Q value 77−57531
- $e^+e^- \to$hadrons, 53 GeV^2, $\pi^\pm$ and $K^\pm$ cross sections, scaling 78−78201
- $e^+e^- \to$hadrons, asymptotically free quark model predictions in complex plane 77−71522

electron-positron inclusive interactions continued

- $e^+e^- \to$hadrons, asymptotically free QCD perturbation theory for multijet final states 78−74267
- $e^+e^- \to$hadrons, azimuthal correlations, quantum chromodynamics anal. 78−70382
- $e^+e^- \to$hadrons, below 2 GeV, comparison of QCD sum rules with expt. 79−49458
- $e^+e^- \to$hadrons, causal cascade model of quark fragmentation, charge retention in hadronic jet 78−29313
- $e^+e^- \to$hadrons, deviation from Bjorken scaling, differential dispersive anal. 77−74698
- $e^+e^- \to$hadrons, direct photon emission from excited hadronic states relativistic oscillator model 78−37208
- $e^+e^- \to$hadrons, EM corrections to asymptotic freedom predictions, gluon corrections 78−62403
- $e^+e^- \to$hadrons, energy correls. in QCD, asymptotically free perturbation theory 79−63497
- $e^+e^- \to$hadrons, finite energy sum rules, cross section, QCD calcs. 78−62413
- $e^+e^- \to$hadrons, fourth Υ state observation in annihilation events 80−86737
- $e^+e^- \to$hadrons, higher order QCD corrections 80−95280
- $e^+e^- \to$hadrons, inclusive distribs., jets, $1+1$ dimens. QCD 78−66137
- $e^+e^- \to$hadrons, jet behaviour, review 80−52524
- $e^+e^- \to$hadrons, jet struct., three-hadron-ball model 78−82224
- $e^+e^- \to$hadrons, jet struct. and statistical model 78−21440
- $e^+e^- \to$hadrons, jet struct. in the energy range 3.1-9.5 GeV 78−89725
- $e^+e^- \to$hadrons, jets from heavy quarks, QCD perturbation theory 80−63012
- $e^+e^- \to$hadrons, multiplicity, scaling, inclusive spectrum, simple hadron cascade model 78−66135
- $e^+e^- \to$hadrons, narrow resonance at 9.46 GeV 78−62415
- $e^+e^- \to$hadrons, neutral weak current effects 77−49987
- $e^+e^- \to$hadrons, new flavour search at PETRA 80−37282
- $e^+e^- \to$hadrons, non-perturbative QCD vacuum, total cross section corrections 80−86735
- $e^+e^- \to$hadrons, parton model and QCD 80−105860
- $e^+e^- \to$hadrons, planar events, gluon jet identification 80−47317
- $e^+e^- \to$hadrons, QCD perturbation theory sum rule, ρ, ω and ϕ mesons 79−85268
- $e^+e^- \to$hadrons, QCD test 80−102006
- $e^+e^- \to$hadrons, QCD theory prediction of jet structs. 78−12920
- $e^+e^- \to$hadrons, R problem, QED and QCD corrections, quarks and leptons 80−95281
- $e^+e^- \to$hadrons, reson. behaviour around 1820 MeV 77−65163
- $e^+e^- \to$hadrons, resonant states struct. 3.9-4.6 GeV, multistate formula 77−71521
- $e^+e^- \to$hadrons, search for narrow resonances in 1.45-1.92 GeV mass region 78−89724
- $e^+e^- \to$hadrons, semiinclusive hadron prod., quark fragmentation function corrections, QCD 80−63013
- $e^+e^- \to$hadrons, three-jet events and QCD test at PETRA 79−97631
- $e^+e^- \to$hadrons, total cross section, QCD higher order corrections 79−85309
- $e^+e^- \to$hadrons, total cross-section meas. from 3.1 to 4.8 GeV 77−30395
- $e^+e^- \to$hadrons, two and three point energy correlations, QCD struct. 80−102019
- $e^+e^- \to$hadrons, Υ, Υ', Υ'' states, mass differences, leptonic width ratio 80−68466
- $e^+e^- \to$hadrons, Υ''' observation at CESR, mass and leptonic width 80−86738
- $e^+e^- \to$hadrons $(\mu^+\mu^-)$, $\Upsilon(9.46)$ muonic branching ratio, total and leptonic width 80−86703
- $e^+e^- \to$hadrons reson. struct. in 1700-1950 MeV region 77−65164
- $e^+e^- \to$hadrons$+X$, structure functions in next to leading logarithm approx., ϕ^3 field theory 80−37268
- $e^+e^- \to$heavy leptons, coupling of heavy leptons to W^0 anal. 78−33051
- $e^+e^- \to H\nu\bar{\nu}$, 40-70 GeV, neutrino counting from Higgs boson production 79−97612
- $e^+e^- \to J/\psi X$, 4.0-5.0 GeV, Zweig rule violation 77−61305
- $e^+e^- \to$jets, energy cone distrib. around jet axis, QCD anal. 80−86732
- $e^+e^- \to$jets, exclusive calcs. for QCD jets, Monte Carlo approach 80−105911
- $e^+e^- \to$jets, high energy, $q\bar{q}$ pair conversion model, seagull effect 80−5007
- $e^+e^- \to$jets, jet ang. momentum, ang. distrib., oblateness and invariant mass, QCD calcs. 80−73722
- $e^+e^- \to$jets, particle ratios from quark statistical model 80−73724
- $e^+e^- \to$jets, t-quark pair prod. effects in annihilation, Kobayashi-Maskawa model 80−86733
- $e^+e^- \to$jets, two photon four jet anal. 80−27513
- $e^+e^- \to K_s^0X$, 3.6-5 GeV, prod. cross section 77−49991
- $e^+e^- \to K^+X$, 3.6 to 5 GeV, total cross section 77−49990
- $e^+e^- \to K+$anything, statistical model anal., two-parameter fit 77−6138
- $e^+e^- \to L^-L^+ \to$ pions, test for chirality of heavy-lepton current 77−18308
- $e^+e^- \to L^+L^-$, hadron spectra from heavy lepton decay *(Russian)* 78−12919
- $e^+e^- \to l^+l^-$, polarisation studies at Z^0 pole, expt. feasibility 79−97615
- $e^+e^- \to M+X$, $M=$pseudoscalar meson, forward-backward asymmetry from neutral currents 79−71759
- $e^+e^- \to$multihadrons, PETRA energies, total cross section and average multiplicity 80−22626
- $e^+e^- \to$multihadrons, planar three jet events, gluon bremsstrahlung, strong coupling constant 80−57617
- $e^+e^- \to \mu^+\mu^-X$, possible Higgs boson detection in missing mass plot 80−4977
- $e^+e^- \to \mu^+\mu^-X$, search for Higgs boson 80−27496
- $e^+e^- \to \mu^+\mu^-(\tau^+\tau^-)$, cross sections, charge asymmetry, polarisation in $SU(2)\times SU(2)\times U(1)$ models 79−97616
- $e^+e^- \to \mu^\pm +$charged particle(s), 3.8 GeV, anomalous μ prod., new particle pair prod. 78−8637
- $e^+e^- \to \mu 3\pi$, above 6 GeV, inference of τ decay 78−50042
- $e^+e^- \to \mu e+$anything, longit. polarised beam, asymmetries, props. of heavy leptons 77−10238
- e^+e^- narrow angular jets, QCD and hadron phenomenology, cones or tubes 80−13320
- $e^+e^- \to n\bar{n}$, $p\bar{p}$, simultaneous meas. of decay channels at J/ψ resonance 78−93893
- $e^+e^- \to p^-X$, charmed baryon pair prod. cross section, pole-dominated form factor 78−12922

electron-positron inclusive interactions continued
$e^+e^-\rightarrow pX$, weak neutral current, polarisation effects, asymm. parameters *(Russian)* 78—459
$e^+e^-\rightarrow\pi^+\pi^-\pi^0$, 1.45-1.875 GeV, ω behaviour at 1.55 GeV 80—82984
$e^+e^-\rightarrow\pi^+\pi^-\pi^+\pi^-$, 1.45-1.875 GeV, ρ behaviour at 1.55 GeV 80—82984
$e^+e^-\rightarrow\pi^\pm X$, weak neutral-current effects 77—13968
$e^+e^-\rightarrow\pi X$, soft π prod., PCAC hypothesis, current algebra commutator relations 78—33075
$e^+e^-\rightarrow\pi$+anything, statistical model anal., two-parameter fit 77—6138
$e^+e^-\rightarrow\psi X$, EM corrections, low energy theorem, unitarity, dispersion relations *(Russian)* 77—49982
$e^+e^-\rightarrow\psi X$, estimate of inclusive ψ and $\psi\eta_c$ prod., QCD anal. of cross section 79—85308
$e^+e^-\rightarrow\psi(3770)$, cross section, ψ mass, total width and e^+e^- partial width 80—73696
$e^+e^-\rightarrow Q\bar{Q}$, heavy quark study approach 80—105859
$e^+e^-\rightarrow q\bar{q}$, quark form factor and jet cross sections, high energy asymptotics 80—32112
$e^+e^-\rightarrow q\bar{q}$ amplitude, enhanced flavour charge in integer quark charge model 79—49457
$e^+e^-\rightarrow q\bar{q}X$, free quark existence, theoretical possibilities 79—17744
$e^+e^-\rightarrow q\bar{q}\rightarrow BX$, weak-neutral current effects 80—42480
$e^+e^-\rightarrow q\bar{q}\rightarrow 3$ gluons$\rightarrow 3$ jets, jet kinematics and observability 79—45070
$e^+e^-\rightarrow q\bar{q}g$, (3g), jet-mass spectra, perturbative QCD 80—63006
$e^+e^-\rightarrow q\bar{q}g$, cross sections and ang. distrib. 80—102061
$e^+e^-\rightarrow q\bar{q}g$, energy-momentum distrib. 79—71696
$e^+e^-\rightarrow q\bar{q}g$, gluon bremsstrahlung, neutral current and beam polarisation effects 80—99106
$e^+e^-\rightarrow q\bar{q}g$, gluon fragmentation, polarised 80—82988
$e^+e^-\rightarrow q\bar{q}g$, long. polarised beams, beam-event asymmetry, massless QCD null result 80—91104
$e^+e^-\rightarrow q\bar{q}gg$, 4-jet prod. in lowest order QCD perturbation theory 79—49459
$e^+e^-\rightarrow q\bar{q}q\rightarrow$jets, ang. energy flow in perturbative QCD 79—49455
$e^+e^-\rightarrow q\bar{q}q\bar{q}$, 4-jet prod. in lowest order QCD perturbation theory 79—49459
$e^+e^-\rightarrow$quark jet, dimensionally regularised box graphs, zero mass case 80—102005
$e^+e^-\rightarrow$quark jet, two particle correlations in QCD 80—105858
$e^+e^-\rightarrow$quarkonium state, D,F, Υ mesons, importance as experimental tool in new particle searches 80—42425
$e^+e^-\rightarrow$three jets, acoplanar angle relative to beam polarisation, vector/scalar gluons 80—63005
$e^+e^-\rightarrow\tau^+\tau^-$, inclusive distribs. of ρ^0 mesons from cascade decays of τ heavy leptons *(Russian)* 79—9390
$e^+e^-\rightarrow\tau^+\tau^-H^0$, Higgs scalar boson production, Weinberg model calcs. *(Russian)* 80—68442
$e^+e^-\rightarrow U^+U^-\rightarrow l^+(p_+)l^-(p_-)$+neutrals, cross section calcs., possible heavy lepton U 78—25029
$e^+e^-\rightarrow U^+U^-\rightarrow\mu^\pm$+hadrons+neutrinos, inclusive and exclusive anal. 77—67663
$e^+e^-\rightarrow\Upsilon(9.46)$, electronic width determ., energy spectra for hadron inclusive production 79—26339
$e^+e^-\rightarrow VX$, parton model, polarisation effects *(Russian)* 80—63002
$e^+e^-\rightarrow VX$, polarisation states and differential cross sections for πA_1 and $\rho^+\rho^-$ *(Russian)* 80—102059
$e^+e^-\rightarrow VX$, polarization states of produced vector meson *(Russian)* 78—25058
$e^+e^-\rightarrow W^\pm$+hadrons, single $W^\pm$ prod. 77—46061
$e\mu$ and μ events, anal. *(Chinese)* 77—67641
$ep\rightarrow 4\pi$ or 2π, 1.6 GeV region, spontaneously broken gauge theory model 77—2845
η prod., 4-5.2 GeV, F, F* masses determ. 77—87988
F-meson semileptonic decay modes, explanation of inclusive electron spectra 78—37202
γ spectra from $\psi(3095)$ and $\psi'(3684)$ decays in e^+e^- colliding beams 77—57549
$\gamma\gamma\rightarrow X$, equivalent-photon approx. for two-photon processes, role of dynamical cut-off 80—47314
K^0 prod. in e^+e^- annihilations, 3.4-7.6 GeV 77—87987
μ anomalous prod., heavy lepton spin, decay parameters 77—61267
μ inclusive anomalous prod., 3.9 to 7.8 GeV, heavy lepton decay 77—22722
μe anomalous prod., heavy lepton evidence, new lepton number 77—61268
pp, 62 GeV/c, multiparticle prod. mech., e^+e^- comparison in parton model 80—78103
π spectra from inclusive e^+e^- annihilation, parton fragmentation model 77—18305
ψ meson, e^+e^- expts. (1975 and 1976) 77—87991
$q\bar{q}$ decay, semiclassical model, vacuum polarisation by colour field 80—63011
$qq\bar{q}\bar{q}$ diquonium states, production in e^+e^- processes 80—57615
SU(8)×SL(3,R) colour quark model, vector states in e^+e^- annihilation at 3.9-4.5 GeV 77—41850
$\sigma(e^+e^-\rightarrow\text{hadrons})/\sigma(e^+e^-\rightarrow\mu^+\mu^-)$, asymptotic freedom predictions leading to paradox 77—49988
τ, production in e^+e^- annihilation, experimental evidence review 79—75758
τ decay involving hadronic vector current 78—66101
$\tau\rightarrow K^*\pi\nu$, in e^+e^- annihilation, T-odd asymmetry in CP violation model *(Russian)* 80—105885
Υ, narrow high mass resonance formation in e^+e^- annihilation at 9.46 GeV, heavy $q\bar{q}$ bound state 78—62414
$\upsilon(9.5)$, prod. in e^+e^- annihilation, photoprod., decay modes, quark model 78—12877
Υ' at $M(\Upsilon')=10.02$ GeV in e^+e^- annihils. using NaI lead-glass det. 78—93894
Υ' obs. at $M(\Upsilon')=10.01$ GeV in e^+e^- annihils. using DASP det. 78—93895
Z^0, prod. in e^+e^- collisions, important landmark 79—97567

electron-positron interactions
see also electron-positron inclusive interactions; electron-positron scattering; positron annihilation in liquids and solids
$\Delta S=0$ weak hadron neutral current, quark parton model, νN and e^+e interactions 78—12859
$\sigma(e^+e^-\rightarrow\text{hadrons})/\sigma(e^+e^-\rightarrow\mu^+\mu^-)$, heavy quark model explanation *(Russian)* 77—57550
amorphous state analogy 79—54370

electron-positron interactions continued
annihilation, charge asymmetry anal. 78—12898
annihilation, CP violating effects, D^0, G^0 and H^0 meson decays 79—80769
annihilation, in university science course for talented high-school students 78—89282
annihilation, is there a QCD test at available energies? 79—40748
annihilation, production of new particles, J/ψ, ψ' and τ props. 80—5008
annihilation, QCD perturbation theory test, review 79—326
annihilation, renormalisation group appls. 77—57461
annihilation energy correlations, QCD test 79—13141
annihilation event shapes, QCD perturbation theory calcs. 79—36056
annihilation experiment review, ψ spectroscopy and charmed particles D and F 79—49533
annihilation in mag. field, γ-production in neutron stars 77—10236
annihilation into boson resonance pair, multipole form factors, parametrisation of EM vertex *(Russian)* 77—74701
annihilation quanta, nonlocality and polarisation correlations 77—2563
annihilation radiation at 511 keV from galactic centre direction 79—5902
annihilation radiation measurement in activation analysis, specificity enhancement by triple coincidence 77—90687
anomalous e prod. in e^-e^+ annihilation, two charged and multi-prong events 78—78200
anomalous lepton prod., charmed mesons and heavy leptons 78—66134
asymptotic freedom and parton model appl. to leptonic processes 80—4959
baryoniums coupled directly to photon 79—17694
beam polarisation in e^+e^- storage rings, expt. review 79—63837
charge polarisation of quark jets 77—38183
charged energy fraction data, Drell ratio and second heavy lepton 79—13097
charm and heavy lepton production by e^+-e interactions recent results, review 79—26337
charm particles, general survey *(German)* 77—22729
charm particles, in debris *(Polish)* 79—54345
charm production, mass scales, in deep inelastic processes, parton model, generalised VDM 77—13930
charmed axial vector meson prod. in e^+e^- at $\sqrt{S}\simeq 4.1$ GeV 77—13969
charmed baryon pair prod., symm. quark model, $c\bar{c}$ pair creation model 77—54111
charmed hadron pair production rates based on $c\bar{c}$ dominance 77—74703
charmed meson pair prod., quark model of broken SU(8) symm. 77—38182
charmed meson prod., quark model 78—8680
charmed meson prod. and lifetime ratios 77—61307
charmed meson prod. at SPEAR 78—4865
charmed meson threshold prod. in bound-state model 77—10269
charmed particle prod. and subsequent decay, complete ang. correl. calc. 77—49986
charmed particle prod. in e^+e^- annihilation 78—78199
charmed quark d-wave $c\bar{c}$ in e^+e^- charm prod. 77—22749
charmonium spectroscopy, spin forces, obs. in $\psi'(3.68)$-$\psi''(3.77)$ struct. in e^+e annihilation 79—36047
colliding beam physics, review 77—74700
colliding beams, effect of external field on bremsstrahlung 77—74670
colliding e^+e beams accelerator expts., 100 GeV, particle prod., weak currents, etc. *(Russian)* 78—58194
conference, quarks and leptons as fundamental particles, Schlamding, Austria, (Feb.-Mar. 1978) 80—17709
conference on hadron struct. and lepton-hadron interactions, Cargese, France (July 1977) 80—4473
conference on particle physics, Honolulu, Hawaii (Aug. 1977) 79—49485
Crab pulsar, electron-positron flux at neutron star surface 77—64789
DESY e^+e^- experiments, QED checks, τ and Υ studies 80—18111
DESY-DORIS expts., $c\bar{c}$ spectroscopy, heavy lepton search *(German)* 77—41849
dimuon and other possible heavy-lepton events, short review 77—30473
dimuon events, production by heavy lepton decay, appl. to e^+e^- collisions 77—54093
discrete charm of new resonances 77—34129
duality between resonances and free quark-antiquark pairs 79—63448
$e^+e^-\rightarrow\pi^+\pi^-(\pi^0\omega)$, $\rho'(1250)$ description, EM form factors, bound states, N/D method *(Russian)* 80—42465
e^+e^- annihilation, phenomenological interpretation, ψ prod. and props., μ-e events 77—67668
eight quark model, modified left-handed currents, ν reactions and e^+e annihilations 78—16982
Einstein Podolsky Rosen nonseparability, nonlocality in Feynman's antiparticle theory, e^+e^- annihilation *(French)* 77—41498
electron type heavy neutral lepton prod., cross section and coupling const. 80—52485
electron type neutral heavy lepton, leptonic decays 80—52486
errors on ratios of small numbers of events 80—105879
exotic mesons and p-$\bar{p}(e^+$-$e^-)$ annihilation 78—21393
galactic cosmic ray positrons, annihilation and gamma radiation spectrum 79—44309
gamma ray monochromatic beam prod. at Frascati Linac 77—83438
gamma rays from annihilation of positrons produced by pulsars, 511 keV line 80—46590
gamma-ray lines observed in balloon flights at high rigidity, extraterrestrial line flux upper limit 80—21882
gluons in e^+e^- annihilation, QCD anal. of strong interaction dynamics 79—9386
hadron polarization operator insuperrenormalizable model, rainbow approx. of $(\lambda/2)\Phi^2\phi$ model 80—105821
hadron prod., parton model asymptotic freedom without non-Abelian gauge theories 77—30314
hadron prod., struct. near 4 GeV 77—248
hadron prod. constraints in asymptotically free theories with anomalous dimens. 77—30393
hadron production and new colour 77—87927
hadron production at 13, 17 GeV CMS, first observation with PLUTO detector 79—36088
hadronic cross section, hadronic effects 78—70339
hadrons and quarks in high energy collisions, review 79—49482
heavy flavoured meson decays, charged Higgs bosons 79—22014
heavy lepton, spinless meson pair prod., two photon processes at high energy 77—71524
heavy lepton pairs produced in e^+e^- annihilation leptonic decay, computer calcs. 78—21409

electron-positron interactions continued
heavy lepton prod., SU(3)×SU(1) model 78−45900
heavy lepton radiative decay modes, effect on $e\mu$ distrib. anal. 77−18263
heavy neutral lepton, right-handed, possible e^+e^- prod. 77−57518
heavy neutral lepton obs. 78−21441
heavy quark and gluon two jet prod. in e^+e^- annihilation *(Russian)* 78−89696
heavy quark fragmentation and parton transverse momentum in annihilation 78−82150
heavy quark-antiquark spectra in e^+e^- annihilation 77−26494
heavy vector meson prod. in e^+e^- annihilation, quark model estimations 77−18306
Higgs boson, bremsstrahlung prod. with heavy fermion pair in e^-e^+ collisions 78−86449
Higgs meson prod., possible signals in high energy collisions, gauge groups 78−89649
high energy annihilation, possible signature of charged Higgs particles, SU(2)×U(1) model 79−35995
hydrodynamic model, nonlinear pion+pion chiral Lagrangian, e^++e^- and p+p collisions 78−32966
inclusive baryon prod. meas. of inclusive antiproton, Λ and $\bar{\Lambda}$ prod. cross section charmed baryon prod. 78−17034
inert gas mixtures, positron annihilation, conc. and elec. field depend. 79−43062
jet struct., test of QCD and quark-confining string 78−33040
jet struct. in e^+e^- annihilation, single-cluster description 77−67666
jet structure in e^+e^- annihilation, deviation variable, QCD calc. 79−9388
left-right symmetric $SU(2)_L\times SU(2)_R\times U(1)$ theory, atomic parity, e^+e^- collisions asymm. at PETRA, PEP energies 78−12820
meson pair prod., multichannel aspects, quark confinement 77−22747
meson resonances, low energy, narrow 78−29341
methane, positron annihilation rates in applied electric field 77−27179
momentum density of electrons, two-gamma positron annihilation determ. 77−69211
multihadron annihilation anomalous behaviour, resonant K*(892) prod. 78−66132
multihadron prod., phenomenology 77−34170
narrow resonance, 2.5-3.0 GeV/c^2 mass region in e^+e^- 77−2852
narrow resonance search in 2.5-3.0 GeV mass range in e^+e^- 77−2851
narrow resonances, search in 2520-2990 MeV mass region in e^+e^- 77−2850
neutral current effects in baryon-antibaryon prod. 77−18310
neutral current model examination by diagonal lepton processes anal. 79−6310
neutral heavy leptons, search with e^+e^- annihilations at 0.5-1.5 GeV/c^2 78−4848
neutral weak current effects, gauge model anal. 77−61243
neutron-irrad., void annealing, positron annihilation obs. 77−76469
nonperturbative QCD effects at large momentum transfers, e^+e^- annihilation to hadrons 78−82226
nucleon production in quark parton model, e^+e^-, ep and large $p_\perp$ reactions 78−21391
optically stimulated electron-positron annihilation 77−57519
ortho-positronium self-trapping in dense fluid He 77−10793
pair annihilation, 1γ and 2γ, in strong mag. fields 79−17704
pair annihilation in strong mag. field *(Russian)* 79−17705
pair annihilation in superstrong magnetic fields, appl. to neutron stars 80−85847
particles and fields conference, Argonne, IL, USA (Oct. 1977) 78−78130
Pati-Salam neutral vector gluons, possible expt. search in e^+e^- collisions 80−37202
physics associated with very high energy e^+e^- colliding beams 77−38516
positron annihilation investigation apparatus, review 80−23240
positronium, hyperfine structure, order-α^4R_∞ contribs., radiative corrections calcs. 79−76538
positronium halides, [X^-; e^+], electronic struct., annihilation characts., HF calc. 77−50567
positronium halides, [X^-; e^+], electronic struct., annihilation characts., HF calc. 77−50568
pseudomesoniums, spectroscopy, prod. and decay props. 79−45058
pulsed distribution from experimental data, parameter reconstruction statistical method 78−41290
QCD, e^+e^- annihilation energy, asymptotically free perturbation theory 78−66045
QCD, three gluon jets as test 78−25001
QCD and jets in leptoproduction 79−45059
QCD predictions for e^+e^- annihilation jets, ang. correlations and asymmetries 79−9389
QCD vacuum, effects on hadronic currents, instantons, e^+e^- annihilation and precocious scaling 79−332
QED infrared singularities, Feynman diagram investigation for e^+e^- annihilation 79−71671
quark, diquark prod. thresholds, charm, colour excit. in 4-GeV region 77−79276
quark-lepton interactions and $\bar{e}$-e ($\bar{p}$-p) annihilation 77−22746
quark-parton model, direct test in e^+e^- annihilation 79−75728
R, cross section ratio, in six quark model without right handed currents 77−6081
relativistic electron pair model of nucl. particles 79−45042
resonance decay modes in Han-Nambu colour model 77−18307
resonance production above charm threshold 77−79275
resonance states below 2.2 GeV observed in e^+e^- annihilations 78−78197
resonant structure, mass 1780 MeV, obs. 77−46063
review, hadron prod., tests of QED 77−57551
review 79−80833
review of three years e^+e^- research at SPEAR 79−63490
semileptonic decay distribs. of next heavy quark 79−45066
soft π prod. in e^+e^- annihilations, nucleon pole term 79−36090
solar flares, 0.51 MeV gamma-ray line prod. 77−13292
SPEAR, synchrotron radiation source 77−83186
spin tests for charmed mesons produced in e^+e^- annihilation at $\sqrt{s}=4.028$ GeV 78−74269
Sterman-Weinberg improved jet formula 79−63447
Sterman-Weinberg jet formula corrections for e^+e^- annihilation from QCD perturbation theory 79−36086
stimulated annihilation, coherent γ-emission 79−55104

electron-positron interactions continued
$SU_L(2)\times U(1)$ and $SU_L(2)\times SU_R(2)\times U(1)$ predictions at high Q^2, neutral currents, Z-bosons 80−63029
SU(3) symmetry violation models for interactions with vector mesons, tests *(Russian)* 77−10196
sum rules, semiclassical method, bound state energy relations 78−70308
sum rules for charmonium and charmed mesons in QCD 77−30327
tachyon production branching ratio in e^+e^- annihilation, search using Michelson expt. 77−54127
tauonium: $\tau^+\tau^-$, a bound state of heavy leptons 78−37194
three-photon couplings in QED 77−71474
total annihilation cross section, new meas. F, F* discovery, inclusive particle prod. 78−78198
transverse quark polarization in large P_T reactions and e^+e^- jets 79−63410
transversely polarised annihilation, heavy lepton prod. and decay 77−18261
triplet heavy leptons, charged energy fraction, anomalous $e\mu$ events in e^+e^- annihilation 78−45897
two gluon jets in e^+e^- annihilation, scaling limit ang. distrib. 79−54314
two jet processes, asymptotic cross sections in QED *(Russian)* 77−6068
two quantum positron-K-electron annihilation *(Russian)* 77−27180
two-photon annihilation, hadron production, polarisation effects *(Russian)* 77−74702
two-photon annihilation stimulation of relativistic electrons and positrons 79−64195
unified formulae for EM decays, electroprod., e^+e^- hadron pair prod. for arbitrary spin 77−57535
universal multihadron jets, quark interactions 77−38132
vacuum polarisation, breakdown of normal threshold dispersion relation, naive quark model 77−2849
VDM approach to e^+e^-annihilation and deep inelastic scatt., vector meson+photon coupling 77−46068
vector meson production, 6 GeV, anomalous interaction mediator, e^+e^- prod. data anal. *(Chinese)* 77−67664
W^+W^- and Z^0Z^0 pair production 79−40820
weak and EM interactions at high energy [conf. Les Houches, France (July 1976)] 79−80785
weak neutral current effects, unified theories *(Hungarian)* 79−9326
weak-EM interference, neutral currents, P-violation, in polarised e-scatt. and e^+e^- interactions 79−63404
weak-EM interference effects, LEP studies 79−97614
Weinberg-Salam theory 78−82194
D(1.87) mesons semileptonic decay, multiplicity effects 77−49953
D and D* prod. from e^+e^- annihilation, form factors and free quark model 78−37222
D and D* production near 4 GeV in e^+e^- 77−82754
D meson prod. and decay in e^+e^- at 4.03 , 4.41 c.m. energy 77−87989
D meson spin anal. near 4.03 GeV 77−74697
D semileptonic branching ratio and lifetime from $e^+e^-\to e^\pm X$ 80−4983
D-meson prod. model, charmed particles 77−38124
$D\bar{D}$* production and decay, VDM, dual amplitude anal., e^+e^- annihilation 77−49992
E^0, neutral electron-type heavy lepton, and W-boson mass 78−66100
$(e^+d^-\to$-hadrons$)/(e^+e^-\to\mu^+\mu^-)$ cross sections ratio, differential dispersive anal., narrow resonances 78−37223
$e\bar{e}\to\gamma\gamma\to q\bar{q}$ 79−49531
$e^-e^-(e^+)\to e^-e^-(e^+)\gamma$, infrared divergences in QED 77−6001
$e^-e^+\to$charmed particles, contrib. of d-wave charmed quark pair 77−26534
$e^-e^+\to$hadrons, finite energy sum rules in QCD 79−40754
$e^-e^+\to\mu^-\mu^+$, high energy total cross sections, Salem-Ward-Weinberg model 79−22086
$e^-e^+\to N^*\bar{N}^*$, weak neutral current effects for polarised e^+e^- pair 80−37287
$e^-e^+\to\psi(z)$, spin correlations, spin 0, $^1/_2$, or $^3/_2$ pair prod. *(Russian)* 79−22117
$e^+e\to\pi^+\pi^-\gamma$, virtual electrons bremsstrahlung photon, Feynman diagrams, Weizsacker-Williams approx. 80−52484
$e^+e\to Z^0\gamma\to\mu^+\mu^-\gamma$, Weinberg model anal. of Z^0 decay ang. distrib. 80−47275
e^+e^-, vector and axial vector gluon prod., as signatures for axial chromodynamics 79−40729
$e^+e^-\to$ hadrons, dual unitarisation and quartz model 77−10272
$e^+e^-\to$ heavy spin-1/2 particles, form factors and decay parameters meas. 77−26536
$e^+e^-\to$-$\mu^+\mu^-\gamma$, neutral current effects and hard photon correction 79−13096
$e^+e^-\to 1^{++}$ resonance states, direct production through neutral currents 78−93891
$e^+e^-\to 3\gamma$, 3.6 GeV and ψ' reson., comparison with QED 77−46066
$e^+e^-\to 3\gamma$, ψ radiation decay and new heavy reson. obs. 77−46065
$e^+e^-\to 3\gamma$, total cross section, analytic expressions 79−6334
e^+e^- annihilation, 4 and 7 GeV, $\bar{n}$ and $\Sigma^\pm$ prod., cross sections 79−63494
e^+e^- annihilation, hadron/muon pair prod. ratio, nonasymptotic contribution to quark-parton model 77−34169
e^+e^- annihilation, meas. of gluon spin 79−30701
e^+e^- annihilation, prod. of orbitally charmed hadrons, free quark model anal. 79−22120
e^+e^- annihilation, ratio of secondary baryon and meson yields and quark combinatorics *(Russian)* 79−49532
e^+e^- annihilation, search for narrow resonances in mass region 1.4 to 1.75 GeV/c^2 79−17743
e^+e^- annihilation, single particle hadron prod. QCD high energy predictions using methods of cut vertices 79−89128
e^+e^- annihilation, weak mass mixing and CP violation with heavy quarks, V-A model anal. 79−30695
e^+e^- annihilation and other processes, event shape anal., QCD perturbation theory 79−13140
e^+e^- annihilation and quark fragmentation functions, Monte Carlo quark-parton model 79−22119
e^+e^- annihilation at SPEAR, total hadron cross section, ψ prod., μe events 77−57548
e^+e^- annihilation channel, differential dispersive theory of ψ/J 78−45933
e^+e^- annihilation in upsilon region, quark model predictions 78−54640
e^+e^- annihilation to hadrons, overlapping resonances with variable channel struct., ψ prod. 79−22118
e^+e^- annihilation with polarised beams 79−36111

electron-positron interactions continued
$e^+e^-\to$baryon-antibaryon pairs, vector meson dominance model 78-21442
$e^+e^-\to\bar{b}b$, single lepton spectra, coupling strengths 79-49461
e^+e^- collisions, many-lepton final states, heavy lepton families 78-45899
$e^+e^-\to D^0\bar{D}^0+x\pi^0+y\gamma$, mixing of neutral spinless charmed mesons, decay, CP, violation tests 77-46067
$e^+e^-\to D\bar{D}$, P-wave bound states 78-45857
$e^+e^-\to D\bar{D}(DD^*)(D^*\bar{D}^*)$, prod. ratio 77-6140
$e^+e^-\to e^+e^-$, 400 GeV, search for narrow reson. states near 6 GeV 77-74699
$e^+e^-\to e^+e^-$, $\gamma\gamma$, $\mu^+\mu^-$, 5.2 GeV, tests of QED 78-66064
$e^+e^-\to e^+e^-$, implications of light neutral gauge boson 78-58154
$e^+e^-\to e^+e^-$ or $\mu^+\mu^-$, decay products from new charged heavy lepton pair prod. 78-74238
$e^+e^-\to e^+e^-K\bar{K}$, δ and S^* meson interf., S^*-ε mixing angles, and K^+K^-, $K^0\bar{K}^0$ cross sections *(Russian)* 79-80832
$e^+e^-\to e^+e^-X$, $X=e^+e^-$, $\mu^+\mu^-$, $\pi^+\pi^-$, η', photon-photon interactions, QED test 79-93425
$e^+e^-\to e^+e^-+2$ gluon jets from $\gamma\gamma$ interactions cross section, gluon role in QCD 80-4976
$e^+e^-\to e^+e^-+$hadrons, double equivalent-photon approx. *(Russian)* 79-403
$e^+e^-\to e^+e^-(\gamma\gamma)$, 27.7-31.6 GeV, QED test, Weinberg angle 80-77995
$e^+e^-\to e^+e^-(\mu^+\mu^-)$ EM processes, vector resons. cross sections *(Russian)* 77-57517
$e^+e^-\to e^+e^-(\mu^+\mu^-)(\gamma\gamma)$, 12-31.6 GeV, QED test and Weinberg angle 80-91027
$e^+e^-\to e^+e^-(\mu^+\mu^-)(\pi^+\pi^-)$, radiative corrections to cross sections, valid in α^3-approx. 79-17726
$e^+e^-\to e^+e^-(\mu^+\mu^-)(\tau^+\tau^-)$, high energy colliding beams, Mark J detector study 80-95282
$e^+e^-\to e^+e^-\chi_c$ differential cross section, two photon exchange mechanism 77-61306
$e^+e^-\to e^+e^-e^+e^-$, $\gamma\gamma$ interactions, partial width upper limit 79-40825
$e^+e^-\to e^+e^-\eta'$ (958), radiative width in two photon interaction 79-89174
$e^+e^-\to e^+e^-\gamma$, large angle final particle emission, energy distribs., Born approx. 79-30722
$e^+e^-\to e^+e^-\gamma$, new limit for heavy electron existence 78-8640
$e^+e^-\to e^+e^-\mu^+\mu^-$, beam polarisation effects on cross section 77-61269
$e^+e^-\to e^+e^-\pi^0$, beam polarisation effects on cross section 77-61269
$e^+e^-\to e^+e^-\pi^+\pi^-$, beam polarisation effects on cross section 77-61269
$e^+e^-\to e^+e^-\rho$, bremsstrahlung production of neutral vector mesons 80-5006
$e^+e^-\to e^\pm U^\mp$ or $e^\pm$ hadron$^+$, anomalous events, heavy lepton pair prod. and decay 78-8676
$e^+e^-\to e^\pm(\mu^\pm)+1$ charged track, cross section energy depend., τ mass 78-89695
$e^+e^-\to e^\pm\mu^\mp$ anomalous prod., heavy lepton current chirality 77-74668
e^+e^- EM annihilation into quarkonium states with even charge conjugation, vector dominance 79-93438
$e^+e^-\to e\mu$ events, Higgs particle prod. 78-8644
$e^+e^-\to\eta'(X^0)\gamma$, generalised VMD theory 77-10268
$e^+e^-\to F^+F^-$ ($F^+=\mu^+$,p,π^+, etc.), polarised beams, weak neutral currents effects 77-26483
$e^+e^-\to F\bar{F}$, with polarised particles, weak asymmetries, unified gauge theory anal. 78-8636
$e^+e^-\to F\bar{F}(B\bar{B})$, $\tau\nu$ decay signature for $F^\pm$ and $B^\pm$ detection 80-91099
$e^+e^-\to F^*\bar{F}^*\to F\gamma_1\bar{F}\gamma_2$, photon ang. correlations and prod. amplitudes 80-47319
$e^+e^-\to\gamma V\to\gamma\nu\bar{\nu}$, neutral vector meson radiative prod. and decay *(Russian)* 80-52492
$e^+e^-\to\gamma\gamma$, 9.4-31.6 GeV, differential cross section, $\Upsilon\to\gamma\gamma$ decay limits 80-91073
$e^+e^-\to\gamma\gamma$, Einstein-Podolsky-Rosen nonseparability, Feynman nonlocality 77-34110
$e^+e^-\to\gamma\gamma$, weak interaction effects, QED tests, SU(2)×U(1) gauge theory 79-40767
$e^+e^-\to\gamma\gamma\gamma$, large angle final particle emission, energy distribs., Born approx. 79-30722
$e^+e^-\to\gamma\nu\bar{\nu}$, calc. of number N_ν neutrino types 79-26321
$e^+e^-\to\gamma\nu\bar{\nu}$, neutrino counting, $e^+e^-\to3\gamma$ background 80-68441
$e^+e^-\to\gamma\nu\bar{\nu}$, neutrino type counting possibilities 79-49502
$e^+e^-\to$HHZ, test of Higgs boson nature 79-63405
$e^+e^-\to$hadron+anything, test of Compton amplitude duality 77-30388
$e^+e^-\to$hadrons, appl. of moving mirror effects in hadronic reactions 79-54303
$e^+e^-\to$hadrons, D semileptonic branching ratio at $\psi''(3770)$ 78-45934
$e^+e^-\to$hadrons, generalised vector meson dominance model, sum rules 78-45810
$e^+e^-\to$hadrons, high energies, two-fireball model, jet problem *(Russian)* 77-82756
$e^+e^-\to$hadrons, manifestation of heavy leptons, decay props. *(Russian)* 77-26537
$e^+e^-\to$hadrons, neutral and weak currents anal. 77-26533
$e^+e^-\to$hadrons, perturbation theory, determ. of quark-gluon coupling constant 77-38127
$e^+e^-\to$hadrons, relative total hadronic cross section meas. 79-54346
$e^+e^-\to$hadrons, review 77-57551
$e^+e^-\to$hadrons, review of parton model 77-57498
$e^+e^-\to$hadrons, scale dependent quark mass in colour gauge theory 77-30320
$e^+e^-\to$hadrons, scaling and quark binding anal., generalised vector dominance 77-249
$e^+e^-\to$hadrons, search for narrow resonances in mass region 1.42-1.92 GeV/c^2 79-17740
$e^+e^-\to$hadrons, total cross sections, c.m. energy range 1.92 to 3.09 GeV 79-45094
$e^-e^-\to$hadrons, weak interaction effects, ang. distrib. charge asymm. baryon longitudinal polarisation *(Russian)* 77-30397
$e^+e^-\to$Higgs boson$+\gamma$ in standard SU(2)×U(1) model, resonance enhancement 79-54331
$e^+e^-\to H\mu^+\mu^-$, Higgs boson prod. 80-32111
e^+e^- inclusive hadron prod., neutral weak currents 78-50041
e^+e^- initiated $\gamma\gamma$ processes, charged pair prod., $f^0\to\gamma\gamma$ width 80-91123
$e^+e^-\to K_S^0K_L^0$, ϕ meson mass meas., $\omega\phi$ interference obs. *(Russian)* 78-45935
$e^+e^-\to K^+K^-$, 1.6 GeV, total cross-section meas., pion form factors determ. 77-46064

electron-positron interactions continued
$e^+e^-\to K^+K^-$, asymmetry, one- and two-photon terms interference 77-10270
$e^+e^-\to L^+L^-$, energy spectra of secondary leptons *(Russian)* 77-38156
$e^+e^-\to L^+L^-$, heavy lepton decay, energy spectra of secondary e or μ 77-71503
$e^+e^-\to L^+L^-$, longitudinally polarized beams collisions, energy depend. of parity asymm. 77-38154
$e^+e^-\to L^+L^-$, scalar model of weak interactions 77-18264
$e^+e^-\to L^+L^-$, test of lepton no. assignment of heavy leptons 77-18266
$e^+e^-\to L^+L^-X(X\to e^+e^-)$, possible heavy lepton spin determ. 77-2847
$e^+e^-\to L^+L^-\to(e^-\bar{\nu}_e\nu_L)+(\mu^+\nu_\mu\bar{\nu}_L)$, V-A and V+A model anal. 77-18262
$e^+e^-\to l^+l^-$, electric and weak magnetic dipole moment effects 77-46036
$e^+e^-\to l^+l^-$, l=3, μ, τ, charged lepton universality test 80-32091
$e^+e^-\to l^+l^-$, neutral current effects around vector resonances, polarisation 80-105878
$e^+e^-\to l^+l^-$ via many-vector boson exchange, cross sections from unified models 80-22597
$e^+e^-\to$multiple lepton+hadron final states, flavour changing neutral currents 77-30363
$e^+e^-\to\mu^+(\tau^+)\mu^-(\tau^-)$, neutral current couplings, lepton polarisation, p violation in SU(2)×U(1) model 80-4975
$e^+e^-\to\mu^+\mu^-$, 30 GeV, charge asymmetry, QED and weak corrections 77-61266
$e^+e^-\to\mu^+\mu^-$, 40-200 GeV, cross section, one loop corrections in Weinberg model 80-18139
$e^+e^-\to\mu^+\mu^-$, 5.8-7.4 GeV, neutral currents strength limit, pole angle asymm. 78-78157
$e^+e^-\to\mu^+\mu^-$, 9.4 GeV, QED test 80-101965
$e^+e^-\to\mu^+\mu^-$, $[SU(4)]^4$ unifying symm. for light neutral Z^0 boson, PETRA and PEP expts. 78-37154
$e^+e^-\to\mu^+\mu^-$, contribution of weak neutral currents *(Russian)* 78-62383
$e^+e^-\to\mu^+\mu^-$, contribution of weak neutral currents *(Russian)* 78-62384
$e^+e^-\to\mu^+\mu^-$, early weak gauge boson restrictions from PETRA QED cut-off 80-52487
$e^+e^-\to\mu^+\mu^-$, Higgs bosons, effects on experimental observables, and fermion mass scale 80-32061
$e^+e^-\to\mu^+\mu^-$, hypothesis test, purely diagonal single Z boson neutral currents 79-40713
$e^+e^-\to\mu^+\mu^-$, implications of light neutral gauge boson 78-58154
$e^+e^-\to\mu^+\mu^-$, neutral current anal., weak and radiative asymmetries 79-26320
$e^+e^-\to\mu^+\mu^-$, Pauli type interaction, vector meson role 80-4974
$e^+e^-\to\mu^+\mu^-$, polarised e^+,e^-, ψ/J excitation models 79-13095
$e^+e^-\to\mu^+\mu^-$, radiative corrections around Z^0, Weinberg-Salam model 80-99103
$e^+e^-\to\mu^+\mu^-$, sign of weak interaction const. from odd P asymm. *(Russian)* 77-30357
$e^+e^-\to\mu^+\mu^-$, weak neutral electron current, Lorentz struct. 79-80788
$e^+e^-\to\mu^+\mu^-$ 6.2-7.4 GeV CM, comparison with QED predictions 78-74194
$e^+e^-\to\mu^+\mu^-$ at J/ψ energy, ang. distrib. of muon pairs, asymm. parameter 77-2846
$e^+e^-\to\mu^+\mu^-$ or e^+e^-, EM corrections for μ pair prod. and Bhabha scatt., QED processes 77-18259
$e^+e^-\to\mu^+\mu^-\gamma$, large angle final particle emission, energy distribs., Born approx. 79-30722
$e^+e^-\to\mu^+\mu^-\gamma$, QED distribs. for hard photon emission 77-61265
$e^+e^-\to\mu^\pm e^\mp+$ neutrinos, heavy vector meson intermediate state 77-30396
$e^+e^-\to$neutral heavy leptons, prod. and decay mechanisms anal. 78-41524
$e^+e^-\to n\pi$, jet struct., lightlike (zero mass) quarks anal. 79-63496
$e^+e^-\to\nu_e\bar{\nu}_e\gamma$, gauge theory analysis, Weinberg-Salem model, ang. and energy distribs. 78-12894
$e^+e^-\to\nu\bar{\nu}$, in strong mag. fields, rate of energy loss 78-29326
$e^+e^-\to\nu\bar{\nu}\gamma$, formula for differential cross-section, including weak interaction and V-A interaction *(Russian)* 78-62385
$e^+e^-\to\nu\bar{\nu}\gamma$, weak current anomalous interaction with EM field *(Russian)* 77-6104
$e^+e^-\to$O particle, decay, mass, prod. from Zweig rule intermediate vector particle model *(Chinese)* 80-73697
$e^+e^-\to\omega\pi$, inelastic effect of $\omega\pi^0$ channel on pion form factor 77-46062
$e^+e^-\to p\bar{p}$, 1925-2180 MeV total energy, form factors and cross sections 80-427
$e^+e^-\to p\bar{p}$, asymm. and polarisation of p,$\bar{p}$, neutral weak currents *(Russian)* 78-58195
$e^+e^-\to p\pi^-\pi^+$, partial conservation of axial flow *(Russian)* 78-8681
$e^+e^-\to p\pi^0\pi^0$, partial conservation of axial flow *(Russian)* 78-8681
$e^+e^-\to\phi\to K^+K^-$, average mass meas. of K^+ 79-30742
$e^+e^-\to\phi\pi^0$, OZI rule violation and cryptoexotic mesons 79-71760
$e^+e^-\to\pi^0\gamma$ or $\eta\gamma$, reaction rate, weak neutral current corrections, 3γ background 77-46069
$e^+e^-\to\pi^+\pi^-$, 0.78 to 1.34 GeV, π form factor meas. 78-33076
$e^+e^-\to\pi^+\pi^-$, 400 MeV, pion form factors *(Russian)* 79-3034
$e^+e^-\to\pi^+\pi^-$, near threshold, π form factor *(Russian)* 80-4996
$e^+e^-\to\pi^+\pi^-$, π form factor, ϕ peak, unitarity and gluonic corrections 80-22615
$e^+e^-\to\pi^+\pi^-$, search for $\phi\to\pi^+\pi^-$ decay *(Russian)* 78-45915
$e^+e^-\to\pi^+\pi^-$, vector meson dominance anal. for π form factor 78-70370
$e^+e^-\to\pi^+\pi^-(K^+K^-)$, $\sqrt{s}=1.5$ GeV, EM timelike form factors for π and K 80-91089
$e^+e^-\to\pi^+\pi^-\pi^0$, 750-1100 MeV, ω and ϕ meson interference 80-105910
$e^+e^-\to\pi^+\pi^-\pi^0$, neutral current and one-photon graph interf. 77-87990
$e^+e^-\to\pi^+\pi^-\pi^0$, ϕ meson mass meas., $\omega\phi$ interference obs. *(Russian)* 78-45935
$e^+e^-\to\pi^+\pi^-\pi^0$, weak neutral current effects, asymmetries 77-6139
$e^+e^-\to\pi^+\pi^-\pi^+\pi^-$, 890-1100 MeV, cross section, πA_1 prod., ϕ branching ratio 79-36087
$e^+e^-\to\pi^+\pi^-\pi^+\pi^-$ cross section, current algebra calc., props. of hadronic axial vector current 79-17742
$e^+e^-\to\pi\bar{N}\Delta$, contact term model 79-13139
$e^+e^-\to\psi(3,1)\to e^+e^-$, leptonic creation and decay processes, radiational effects *(Russian)* 77-46060
$e^+e^-\to\psi(3772)\to D\bar{D}$, anomalous electron prod. by semileptonic D meson decay 78-37203

electron-positron interactions continued
- $e^+e^-\to\psi\to2\gamma(3\gamma)$, charmonium model calcs. 77—30387
- $e^+e^-\to\psi\to\eta'(958)+\gamma$, decay width upper limit 77—38173
- $e^+e^-\to\psi\to l^+l^-$, leptonic creation and decay processes, radiational effects *(Russian)* 77—46060
- $e^+e^-\to\psi\pi\pi$, radiative corrections, model estimates 77—10271
- $e^+e^-\to q\bar{q}$, high energy total cross sections, Salem-Ward-Weinberg model 79—22086
- $e^+e^-\to q\bar{q}$, transverse quark polaris., quantum chromodynamics test 79—17741
- $e^+e^-\to q\bar{q}$ chromoelectric-flux-tube model of particle production 79—89176
- $e^+e^-\to q\bar{q}\gamma$, IR and collinear divergences, cancellation in one-loop corrections to QCD cross sections 79—40730
- $e^+e^-\to q\bar{q}\gamma_s$, IR and collinear divergences, cancellation in one-loop corrections to QCD cross sections 79—40730
- $e^+e^-\to\rho\epsilon$, transition form factors, dispersion theory 79—63495
- $e^+e^-\to\rho\pi\pi$, radiative corrections, model estimates 77—10271
- $e^+e^-\to tt$, single lepton spectra, coupling strengths 79—49461
- $e^+e^-\to\tau^+\tau^-$, 3.9-5 GeV, τ lifetime experimental upper limit 79—40826
- $e^+e^-\to\tau^+\tau^-$, heavy leptons discovery and props., review 78—89694
- $e^+e^-\to\tau^+\tau^-$, parity violating effects measurement 79—36057
- $e^+e^-\to\tau^+\tau^-$, τ spin from two body decay energy spectra *(Chinese)* 79—49503
- $e^+e^-\to\tau^+\tau^-$, $\tau\to\nu\rho\pi$ decay mode obs. 78—29340
- $e^+e^-\to\tau^+\tau^-$, $\tau\to\rho\nu\pi$, halflife and mass determination, e^+e^- hadronic cross section 78—89765
- $e^+e^-\to\tau^+\tau^-$ near Z^0 pole, heavy lepton polarisation and radiative effects 79—22085
- $e^+e^-\to\tau^+\tau^-\to$cascade π and ρ, parity violation from weak and EM interaction interference *(Chinese)* 79—49504
- $e^+e^-\to\tau^+\tau^-\to\mu e+4\nu$, Monte Carlo method for the analysis of low statistics experiments 79—18095
- $e^+e^-\to U^+U^-\to\mu^\mp+e^\pm+$neutrinos differential cross-section anal. 77—67640
- $e^+e^-\to U^+e^-$, $SU(2)\otimes U(1)$ gauge models 77—71502
- $e^+e^-\to\Upsilon$, suggested search for gluon hadronic states in collinear gluon jets 78—89663
- $e^+e^-\to V^+V^-\to e^+\nu_e\text{-}\mu^-\bar{\nu}_\mu$, beam polarisation, anomalous events 77—74669
- $e^+e^-\to V(b\bar{q}$ or $\bar{b}q)$, $b\bar{q}$ resonance prod. below $b\bar{b}$ threshold via flavour-changing neutral currents 79—89123
- $e^+e^-\to$vector mesons, colour quark model for new reson. above 4 GeV 78—17033
- $e^+e^-\to V\pi\to\pi^+\pi^-\pi^0$, EM mixing effects, dynamics of vector meson prod. *(Russian)* 78—58191
- $e^+e^-\to W^+W^-$, charact. of μe events anal. in Weinberg model 77—71478
- $e^+e^-\to W^+W^-$, polarisation amplitudes 80—42484
- $e^+e^-\to W^+W^-$, radiative, corrections in Weinberg model 80—52512
- $e^+e^-\to W^+W^-\gamma(e^+e^-W^+W^-)$, Yang-Mills coupling 80—68443
- $e^+e^-\to W+$hadrons, from Z^0 pole to threshold 80—105917
- $e^+e^-\to X$. (X=system of hadrons) 78—82222
- $e^+e^-\to x\pi$, even G parity hadronic cross section, $\rho'(1600)$ 2π branching ratio 78—12921
- $e^+e^-\to ZZ$, polarisation amplitudes 80—42484
- $e^+e^-a\mu^+\mu^-\gamma$, virtual electrons bremsstrahlung photon, Feynman diagrams, Weizsacker-Williams approx. 80—52484
- $e\mu$ anomalies, heavy muon as possible cause 77—61241
- η_c, production cross sections in e^+e^- colliding beams, two-photon processes 79—36089
- γ polarisation correl. function 78—78158
- $\gamma^*\gamma^*\to2$ jets in e^+e^-, parton model QCD corrections for doubly deep processes 80—73758
- K_s^0e prod., charmed particle weak decay 77—2853
- μ-e events, alternative heavy-lepton model 78—66102
- μe prod., intermediate heavy-lepton pairs 77—18265
- $\mu^+\mu^-$ anomalous prod. from e^+e^- annihilation, heavy lepton prod. and decay 78—82190
- $\phi\pi$ prod. in e^+e^- annihilation and diffractive photoprod., 4 quark state signature 79—6324
- π, pair production in two-photon e^-e^+ events 77—71523
- $\pi\pi$ production via two-photon states, inelasticity effects 77—67667
- ψ, charmonium state, decay modes, prod. mechs. 77—10247
- ψ particles and charm, 1975 and 1976 expts. *(Czech)* 79—26288
- ψ to charm particles, 1975 and 1976, e^+e^- colliding beam technique *(Polish)* 78—74297
- $\psi/J(3100)$ production in storage rings expt., partial decay width for $\psi\to\eta'(958)\gamma$ 77—49956
- ρ, ω, ϕ mesons, radial excitations 78—4866
- ρ-recurrences in e^+e^- annihilation 78—8677
- $\bar{\Sigma}^\pm$ prod., 4-7 GeV e^+e^- annihilation 79—9387
- t-quark detection from associated equal sign dileptons 79—67528
- τ, charged heavy lepton, mass and leptonic branching ratios determ. 78—4849
- τ decay, large timelike Q^2, conservation of vector current and current algebra 78—78155
- τ decay dynamics, scaling prop. and Michel parameter 78—37195
- τ decay modes and mass determ. 78—29325
- τ particle properties, QCD type gauge theories, absence of $\tau^+\tau^-$ resonance in e^+e^- annihilation 78—37144
- $\tau^\pm$ heavy lepton in e^+e^- annihilation, review 79—49505
- $\tau^\pm$ production in e^+e^- annihilation 79—6336
- Υ flavoured vector mesons, production in e^+e^- annihilation at DORIS energies 78—93890
- υ prod. from duality and new quark charge 78—74224
- W boson e^+e^- prod. calcs. in Weinberg-Salam model 77—30301
- W^0 effects in e^+e^- interactions on a^- resonances 80—42386
- Ar, clustering of atoms around positron and positive ions 78—55270
- Ar gas, annihilation decay rate, positron vel. distrib. at equilib. 77—71870
- Ar, gas, slow positron annihilation and momentum transfer rates 79—22828
- Ar, momentum density of electrons, two-gamma positron annihilation determ. 77—69211
- Ar, positron annihilation decay consts., temp., elec., and mag. field depend., computer anal. 78—78809
- Ar positron scatt., elastic, diffusion and annihilation cross sections 79—36769
- Ar-Ne gas, annihilation decay rate, positron vel. distrib. at equilib. 77—71870

electron-positron interactions continued
- GaAs, positron annihilation rel. to surface treatment *(Russian)* 77—44081
- H, positron annihilation rate, p-wave contrib. 78—17790
- H, positron scatt. and annihilation, s and p pseudo-states 78—42217
- He, clustering of atoms around positron and positive ions 78—55270
- He, gas, positron and positronium decay rates at high densities 77—54636
- He, orthopositronium decay, 77K 77—39713
- He, positron annihilation decay consts., temp., elec., and mag. field depend., computer anal. 78—78809
- He, positron decay rate nonlinear density depend. 80—71509
- He-Ar mixture, positron annihilation decay consts., temp., elec., and mag. field depend., computer anal. 78—78809
- Kr, elastic positron scatt., phaseshifts and elastic, diffusion and annihilation cross section 80—53134
- N_2(-Ne), gas, 77K, positron annihilation lifetime spectra 79—10630
- Ne, clustering of atoms around positron and positive ions 78—55270
- Ne gas, annihilation decay rate, positron vel. distrib. at equilib. 77—71870
- Si, positron annihilation rel. to surface treatment *(Russian)* 77—44081
- Xe, elastic positron scatt., phaseshifts and elastic, diffusion and annihilation cross section 80—53134
- Xe, ortho-positron quenching rate critical slowing down near gas-liquid transition 77—24907

electron-positron scattering
- *see also electron-positron interactions*
- Federbush model, absence of induced counterterms e^+e^- scatt. amplitudes 78—50023
- polarised beams, properties of cross sections 79—372
- QED test at 9.4 to 31.6 GeV 80—101965
- $e^+e^-\to e^+e^-$, 13 and 17 GeV, test of QED 79—54289
- $e^+e^-\to e^+e^-$, Bhabha scatt. one loop radiative corrections in Weinberg model 80—13310
- $e^+e^-\to e^+e^-$, Coulomb interf. near Z^0 pole, Bhabha luminosity monitor 79—85289
- $e^+e^-\to e^+e^-$, $\Upsilon(9.46)$ electronic branching ratio and total width 80—86702
- $e^+e^-\to e^+e^-(\gamma\gamma)$, 27.7-31.6 GeV, QED test, Weinberg angle 80—77995
- $e^+e^-\to e^+e^-(\mu^+\mu^-)(\gamma\gamma)$, 12-31.6 GeV, QED test and Weinberg angle 80—91027
- $e^+e^-\to e^+e^-(\mu^+\mu^-)(\tau^+\tau^-)$, high energy colliding beams, Mark J detector study 80—95282
- $e^+e^-\to e^+e^-gg$, gluon jet polarisation in photon-photon scatt., QCD test 80—52550

electron probe analysers *see electron probe analysis*

electron probe analysis
- accuracy, basic relationships 79—43688
- Allende meteorite, occurrence of Fe-Ni-Cr-S-O compounds *(French)* 78—32411
- alloy, lamellar multiphase, struct. and spatial comp. variation, analytical STEM 78—24011
- alloys, with second phase precipitates, transient sputtering characteristics, glow discharge optical spectroscopy meas. 77—44156
- aluminosilicate glass, diffusion of Sn(IV) 80—49417
- analytical electron microscopy, reduction of contamination *(Japanese)* 80—11978
- applications, in mineralogy *(French)* 79—5628
- archaeometry, sampling stylus 78—70246
- asbestos, fibre identification, selected area electron diffr. patterns in analytical TEM, optimum procedure using tilted specimens 78—24009
- asbestos aerosol electron microscopy and analysis *(French)* 77—37461
- asymmetric electrostatic lens for field-emission microprobe applications 79—75656
- atomic number correction 78—20118
- Auger scanning electron microprobe, analytical techniques 79—79359
- Auger scanning microprobe, approach to damage-free anal. 80—89581
- Auger spectrometer, electron microprobe, with ultra high vac. SEM capability *(Japanese)* 78—27849
- auto-zero electrometer for analytical electron beam instruments 78—12721
- automated microprobe *(French)* 79—6237
- automated X-ray microanalysis with electron microprobe and SEM 78—27840
- automatic microprobe anal. using energy dispersive spectrometry 80—55765
- automation using microcomputer system 79—43703
- backscattering theory, using Boltzmann transport equation 80—57439
- barium mordenite, dehydrated, position of cations and molecules, electron probe anal. 78—51509
- bibliography 78—23536
- bimetallic strip, interface struct., scanning Auger microprobe study 80—34322
- biological bulk specimens electron probe analysis, ZAF-correction procedures 79—44073
- biological fluids, ultramicroanal., by energy dispersive X-ray spectrometry 78—92768
- biological frozen hydrated bulk specimens instrumentation and specimen prep. for electron beam X-ray anal. 78—57142
- biological frozen-hydrated specimens, in SEM 77—56552
- biological material, prep. for X-ray microanal. of diffusible elements, methods of drying ultrathin cryosections 78—77166
- biological material prep. for X-ray microanal. of diffusible elements, rapid freezing and ultrathin section prep. 78—77165
- biological materials, low-temp. SEM, X-ray microanal. 79—39627
- biological samples, low temperature prep. using biochamber for X-ray microanal. 79—39628
- biological samples, review 77—86730
- biological samples charging effect in electron-irrad. ice 78—57141
- biological specimen microanalyser cold stage 78—31746
- biological specimen preparation for X-ray microanalysis, review 78—24214
- biological specimens, cryosectioning for X-ray microanal. 79—39626
- biological specimens, electron probe analysis, effects of electron irrad. of sample 79—43969
- biological specimens, hydrated, bulk-frozen, prep. for X-ray microanal. 79—39629
- biological specimens, quantitative electron probe microanal., analysed spot ρX value 79—25169

electron probe analysis continued
biological specimens, X-ray micro anal., iso-atomic droplets as models 78—53598
biological thin sections, energy dispersive X-ray analysis, detection limits 78—24215
biological thin sections, quantitative microanal. methods electron probe microanalysis of biological thin sections, quantitative methods 77—25620
biological ultrathin section, electron probe microanalysis, local mass thickness meas. using STEM 79—62416
blood cell, red, Fe content anal. by electron microprobe and scanning electron microscopy 79—53065
blood cells, red, human, frozen section prep. for electron probe anal., fracturing or cutting 79—39625
bone and cartilage, calcification studies using X-ray microanalysis 80—76885
in book, practical methods in electron microscopy 78—4739
boride coatings, diffusion-deposited on WC-Co, elemental and phase comp. 80—15402
brass, inface segregation in α/β two phase bicrystal and polycrystal *(Japanese)* 79—15675
α-β brass, interface segregation 80—89231
brass, nondestructive determ. of in-depth profile 80—93836
α-brass, quenched, chemical composition in stacking fault tetrahedron 77—21183
bytownite megacrysts., study of trapped basaltic melts, petrogenetic process study 78—95688
cathodoluminescence, bibliography of papers till 1977 79—21482
cathodoluminescence in electron beam instruments, review 78—4740
ceramic materials, SEM and anal. techniques *(German)* 78—56832
chalcogenide magnetic semiconductors, spinal-type, closed tube vapour transport method *(Japanese)* 80—25539
coal particles and composition determ., computer evaluation of SEM images 80—71994
coating techniques, for SEM and X-ray microanalysis 79—12783
computer controlled beam-scanning and camera circuit 79—43706
computer operating system for X-ray diffr., fluoresc. anal. and electron microprobe anal. 80—322
computer-controlled microanalyser, CAMEBAX system, operating experience 78—35779
conference, electron microscopy and analysis, Brighton, England (Sept. 1979) 80—67936
conference, Lannion, France (June 1977) 78—41378
correction procedure, microanalysis meas., conversion to elemental weight concentrations 78—76950
correction procedure, Monte Carlo derivation of surface ionisation function 78—20119
correction procedure for quantitative microanalysis, crit. appraisal 80—85242
corrections, quantitative, effect of electron incidence angle 79—39270
cryoultramicrotomy, prep. of thin sections for electron probe anal. of calcifying cartilage 78—31988
daguerreotypes, plates and process obs. 80—68286
deconvolution of microprobe conc. profiles 77—52606
desert varnish of Sonoran Desert, comp. from optical and electron probe microanal. 79—79834
developments, and appl. to TEM specimens *(French)* 79—5244
diamond, industrial, anal. cathodoluminesc. studies in SEM 80—81410
diamond tool, metallic binder, microstruct. charact. by electron probe anal., SEM obs. *(Rumanian)* 79—74114
diffusion model for electron probe into solid target, energy depend. 78—71652
dispersion influence on spatial resolution of X-ray microanalysis in STEM 80—85257
effects due to probing electrons and sputtering 77—90706
electrically conductive coating influence on X-ray microanalysis accuracy 80—11988
electron beam positioning, computer automated 79—43704
electron microprobes and scanning electron microscopy, conf., Orsay, France, Dec. (1978) 80—11979
electron probe anal., energy dispersive/wavelength dispersive combined X-ray system, automated control 79—43705
elemental concentration, estimations, in small particles using X-ray anal. in SEM 79—16098
elemental mapping techniques in microscopic domain 78—24013
energy analyser/electron microscope combination, microanal. accuracy improvement 78—15737
energy and wavelength dispersive spectrometers, minimum detection limits comparison 78—24002
energy dispersive electron probe X-ray quantitative anal., compact procedure 80—40793
energy dispersive filtration for simultaneous energy and wavelength dispersive analysis 79—12918
energy dispersive spectrometer systems, quantitative chem. anal. 79—39260
energy dispersive X-ray analysis, stat. limitations to accuracy and spectral resolution 78—24001
energy dispersive X-ray analysis in STEM, optimum kV selection 78—24008
energy dispersive X-ray analysis in STEM, semiquantitative analysis method using ref. spectra and empirical scale factors 78—24005
energy dispersive X-ray analysis in TEM/STEM, sensitivity limits for thin specimen analysis 78—24007
energy dispersive X-ray analysis procedures for ultralight elements 78—24003
energy dispersive X-ray particle analysis system using beam blanking and digital scan-stop 78—24004
energy dispersive X-ray spectra, anal., computer techniques 79—43690
energy dispersive X-ray spectrometry, qualitative and quantitative analysis problems 80—85249
energy loss spectrometry, differentiated, in STEM 78—35786
energy loss spectrometry, use in microanalysis and errors involved 78—35785
energy loss spectrometry use in microanalysis 78—35784
energy loss spectroscopic microanalysis. operating parameter selection 79—24879
energy loss spectroscopy, contrib. to anal. microscopy 77—25346
energy loss spectroscopy and microanalysis, instrumentation developments, review 78—35783
energy-dispersive X-ray analysis, false peaks and other problems 77—52731

electron probe analysis continued
energy-dispersive X-ray microanalysis, background reduction due to backscatt. electrons 78—20121
energy-loss analysis, single crysts., in TEM, diffr. conditions influence 80—81406
energy-loss analysis, theory and instrum. 80—81405
energy-loss spectroscopy, as analytical tool, data handling and processing 80—81407
epithelium, fluid-transporting, ion distrib. 77—4991
feldspars from Mt. Rokko granites, electron probe X-ray microanalysis 80—31038
ferroelectrics, appl. to study of epitaxy 80—44443
field emission micro SEM, for UHV surface anal. 80—86519
film, binary compound, A 15-struct., electron microprobe quantitative anal. *(German)* 77—16893
films, orientation effects in quantitative X-ray microanal. 80—85259
films, thin, on substrate, thickness meas., electron probe anal. technique *(French)* 78—41276
films on substrates, charact. fluoresc. effects calc. 80—81408
fly ash particles, effect of chem. variability on cell exposure 79—16172
foil chemical mapping with high spatial resolution by electron energy loss spectroscopy 79—61934
fracture mechanics anal. and NDT/destructive test correlations 77—90526
fracture surfaces, quantitative analysis problems in energy dispersive X-ray spectrometry with Si(Li) diodes *(French)* 80—89571
frozen hydrated tissue section prep. for X-ray microanalysis using satellite vacuum coating and transfer system 78—24200
glass fibres and spheres, microscopic, production and charact. for microanal. 79—24487
glaze-porcelain system, intermediate layer investig. by electron probe microanalysis 77—8965
glaze/glass-ceramic, interface reactions, electron microprobe anal. 80—84398
graphite, spheroidal, presence of magnesium studied with electron probe microanalyser *(Ukrainian)* 80—26072
Hastelloy-X, Ni-Cr-Fe-Mo, cyclic oxidation resist. improvement by high temp. etching treatment 80—97627
heterogeneous materials, conc. inhomogeneities control, electron and ion probe testing 79—43505
high-temperature applics. in metallurgy using X-ray emission spectroscopy *(French)* 77—29074
hip replacements, total, causes of failure 77—81662
IC, pattern overlay errors, automatic meas., using EL-1 lithographic system 79—21868
II-VI semiconductors, thin foils, electron microscopic investigations 79—32864
III-V semiconductor ternary alloys, VPE growth lattice mismatch effects 79—28220
implanted ion detection by X-ray emission anal. in TEM 78—51575
in-situ gas reaction cell, for field emission SEM 80—81415
Incoloy 800, oxidation resistance, alloy depletion effect 77—8989
Inconel 617, creep, morphological changes of carbides, affect on creep props. 80—108509
Inconel 625, nitriding in N_2-H_2 glow discharge 80—16590
inelastic electron scattering as analytical tool, review 78—24010
inert gases, determ. in semiconductor sputtered layers, EPMA method 80—3443
instrumentation and techniques, review *(Chinese)* 79—34415
integrated circuit, MHz, microcomputer controlled stroboscopic SEM, to meas. signal waveform 79—21871
ionisation density, spatial distrib. calc. in a material due to electron beam irradiation 80—55234
kaolin bodies, effect of mineralizers on firing shrinkage, microstruct. and strength 80—97488
lead borosilicate glass, phase separated, components distrib. by electron probe microanal. *(Japanese)* 79—52844
light element microanalysis by electron energy loss spectrometry 79—61935
light element microanalysis by K-shell excitation EELS 79—74480
light elements, ultrasoft X-ray spectroscopy, local anal., electron-microprobe excited radiation 80—99027
LMFBR type mixed oxide fuel pins, composition of corrosion product oxide phases in pin gaps 78—70599
LSI surface analytical techniques applied to electronic components [Si LSI chip inspection] 80—81392
LWR residues of reprocessed fuel 80—5306
lyophilised solutions, electron probe anal., calibration curve linearity limits 79—44075
major element whole rock anal. using sample fusion technique with electron microprobe 77—64494
material analysis by electron beam bombardment *(Japanese)* 77—86416
materials failure and corrosion, microstructural aspects, obs. 79—52610
materials science, high resolution microanal. using electron energy loss measurements, review 77—56190
metal, microcrack, generated in oxides during high temp. oxidation, detection by slight sulphidisation 77—8999
metal, thin foil, energy dispersive X-ray meas. 77—52721
metal, thin foil, energy dispersive X-ray meas. 77—52722
metallic film thickness measurement by electron probe microanal. *(Czech)* 79—44899
metallic surfaces, adsorption of inorganic and organic molecules, mechanism and effects, exam. *(German)* 78—51828
metallic thin films, thickness meas., electron mode microanalyser 79—2744
metallurgical and mineralogical specimens, energy dispersive analysis 77—60152
metallurgy, use of combined ion-, electron-beam techniques 79—43700
meteorite, Santa Barbara, mineralogy and petrology 79—25551
meteorite, Santa-Catharina, Fe-Ni alloy detection *(French)* 79—16895
meteorite Zaisho, Japanese pallasite, mineralogical and petrographical study 80—46509
meteorites, identification of ordered FeNi 80—8604
microanalyser, computerisation development 79—11859
microanalyser, MAR-2, operation in two-channel mode with spectrum standardisation 77—52703
microanalysis of solid matter in a scanning electron microscope *(Czech)* 79—8465
microarea elemental anal. using electron energy analyser 77—63984
microbeam anal., conf., Ann Arbor, MI, USA (June 1978) 79—39258
microbeam analysis, lateral resolution 80—101064

electron probe analysis continued
microbeam analysis developments, application of Monte Carlo calc. method *(Japanese)* 78—3431
microchannel intensity amplifier for electron microscope images during X-ray spectral anal. of light elements 77—12848
microchemical environment, anal., electron and photon beam appls. 78—44434
microhomogeneity studies by electron microprobe, computer program 80—21352
microparticles, quantitative anal. with electron beam instruments 79—21866
microprobe instrument evolution, SEM and STEM 78—70233
microstructure determination of thin surface layers *(German, English)* 77—56204
mineral fibre characterisation using energy dispersive X-ray spectrometry in TEM *(French)* 80—82857
mineralogical use of energy dispersive X-ray spectrometry with Si(Li) diodes *(French)* 80—85251
mineralogy, appl. of cathodolum. microscopy and spectrometry 77—69919
minerals, anal. of C and O_2, ZAF correction procedure *(French)* 80—11983
minerals, computerised data processing, using FORTRAN IV programs 77—86878
minerals, Na and K determ., low temp. sample holder design *(French)* 80—85248
minimum depth electron probe X-ray microanalysis for determining S content of human hair surface 80—22500
Monte Carlo calculations, use in electron probe microanalysis and SEM 77—74562
multielement energy dispersive microprobe anal., procedure, program 77—56317
multielement film, on substrate, quantitative electron microprobe analysis 77—9150
Murchison carbonaceous chondrite meteorites, Si in metal grain, electron probe anal. 80—77363
muscle, frog, vacuolation and subcellular comp. in fatigue 79—24963
Nimonic 105, quantitative STEM chem. anal. using standard and standardless programs 79—17578
nuclear ceramics, quantitative image anal. using light and SEM obs. 79—12912
optical glass containing PbO, effect of Al_2O_3/Na_2O ratio on rate of ion exchange 78—44377
oxide film characterisation, using low energy electron induced X-ray spectroscopy *(French)* 78—41386
oxide layers on Ni-Cr and Fe-Ni-Cr alloys, compar. study using secondary ion emission and electron probe analysis *(French)* 77—56286
particle analysis and identification in pharmaceutical industry 78—61125
particle mass determination using STEM 78—21294
particle size anal., Monte Carlo electron trajectory simulation 79—43693
particles, new method for X-ray micro-anal., based on peak to background meas. 79—24881
particles smaller than region excited by electron beam *(German, English)* 77—77857
particulate matter characterisation 77—60139
particulates, quantitatives charact. by computerised high voltage, SEM 79—48036
peak-to-background method for quantitative anal. of single particles, development progress 80—73541
phase diagrams, electron microprobe and STEM determ. exam. of techniques 79—6241
phosphosilicate films, deposited, P conc. meas. 79—69014
plant and animal tissue, freeze-substitution, for localisation of water-soluble cpds. by electron probe microanalysis 77—37115
plasma ashing technique for energy dispersive X-ray analysis of biological specimens in SEM 78—24199
polybutadiene, adsorption behaviour, surface tension exam. *(Japanese)* 78—31690
portland cement, doped with ZnO, struct. and props. 80—60914
power plant stack emissions, trace element analysis techniques 78—3938
primary X-ray production, depth distrib. 79—79348
principles and appl. to surface anal. *(French)* 79—48034
proustites, optical props. and chem. comp. rel. to pyrargyrites 78—95566
pyrargyrites, optical props. and chem. comp. rel. to pyrargyrites 78—95566
quantitative, 4-40 keV, electron backscatt. coeff. meas. 80—35608
quantitative, correction procedure 79—43686
quantitative analysis practicality using energy dispersive spectrometer *(German, English)* 77—63994
quantitative metallography with automated electron microscope-microprobe systems 78—35631
refractory solid/liquid reaction zones applic. *(French)* 77—32848
Santa Catharina, Fe-Ni (50 wt.%) superstructure obs. 79—30024
scanning cathodoluminescence microprobe analyser 80—81409
scanning electron microscope with field emission gun for solid surface studies *(Czech)* 79—6240
scanning microanalyser design, performance and applic. in materials research 78—35780
scanning microprobe microscopy, conf., Paris, France (Oct. 1979) 80—82569
SEM bulk mode anal. 77—60140
SEM cathodoluminescence analysis of impurities, localisation and sensitivity 78—95985
SEM circle mounts for elemental anal. or morphological studies 77—45921
SEM electron probe microanal. by means of X-ray spectrometers, review 80—95194
SEM-AES-IMA combination with SIM spectrometer, Si device anal. appls. *(Japanese)* 78—85249
semiconductor minority carrier diffusion length meas. using electron microprobe 77—39867
semiconductor spectrometers for elemental anal. in electron microscope 79—11838
semiconductor wafer diagnostics, using computer automated scanning low-energy electron probe 79—4214
shielded specimen holder for X-ray microanalysis in JOEL U3 SEM 77—49816
silicate glaze, diffusion of Sn(IV) 80—49417
skeletal muscle bulk specimen, quantitative X-ray microanal. of diffusible ions 78—57143
small particle identification, review 78—48739

electron probe analysis continued
solid surface characterisation techniques, review 78—22945
solid-electron interaction, Monte-Carlo simulation, appl. to electron probe microanal. 77—12853
solid-electron interactions, conf., Southampton, England (Apr. 1976) 77—44570
solids, X-ray prod. range by 2 to 15 keV electrons, thin film and bulk targets 79—19298
spatial distrib. of electrons in homogeneous, isotropic target 79—43687
specimen contamination problems 79—71577
spectroscopic techniques, with STEM for electronic props. of defects and impurities in semiconductors 79—14812
spherical aberration correction, using zone plates 79—45899
stainless steel, quantitative STEM chem. anal. using standard and standardless programs 79—17578
steel, Al semikilled, $(Fe_xMn_{1-x})O.Al_2O_3$ inclusions, deoxidation, thermodynamic conditions 80—60830
steel, Al-Cr, $FeO.(Al_xCr_{1-x})_2O_3$ inclusions, thermodynamics 80—60831
steel, alloy, fretting corrosion, exam. of secondary structures 79—100292
steel, alloy, type 11Kh18M, eutectic carbide composition change due to heating 80—16353
steel, alloy, V-W-Mo-Cr, exam. of carbide transformation 80—16299
steel, austenitic stainless, ferritic, single phase ferritic solidification in welds, exam. 80—7546
steel, austenitic stainless, high temp. oxidation, high temp., in low O_2 press., surface anal., impurity diffusion effects 77—56142
steel, austenitic stainless, unlubricated, friction, wear and microstruct. of types 304, 316 and Nitronic 60 80—108589
steel, austenitic stainless, welds, exam. of austenitic solidification mode 80—7545
steel, austenitic type 304, sensitised, intergranular stress corrosion cracking inhibition study 80—100939
steel, ball bearing, fatigue damage, influence of dispersed phases in martensitic matrix 80—108549
steel, composition effect on carburizing 80—35432
steel, Cr (10 wt.%), precip. free ferrite form., STEM 80—84941
steel, Cr-Mo, ferritic, grain boundary segregation, X-ray microanal. by STEM 80—66740
steel, Cr-Mo, oxidised, mechanism of crack decoration of oxides by electrodeposition 80—97560
steel, eutectoid, Si partitioning during pearlite transform., analytical electron microscopy applic. 80—108458
steel, ferritic Cr-Mo type, microanalysis of precipitates using TEM 80—108688
steel, fully killed, nonmetallic inclusions, microprobe and metallographic exam. 80—30196
steel, galvanised, interface struct., scanning Auger microprobe study 80—34322
steel, high speed, annealed, carbide determ. by anodic oxidation technique *(Japanese)* 78—85040
steel, high speed, R18 and R6M5, rolled and annealed carbide phase investigation 77—90374
steel, inclusions, rapid microprobe analysis using energy dispersive spectrometer and minicomputer *(German, English)* 79—92038
steel, inclusions, SiO_2 Al_2O_3, FeS, effect of high temp. heating on size, number and distrib. 78—44145
steel, low alloy, microsegregation testing *(Croatian)* 77—36516
steel, low C, rapidly solidified laser surface alloyed, electron microprobe obs. 79—70201
steel, machining, adhesion mechanism of built-up edge and layer on rake face of cutting tool 79—47784
steel, mild, AISI 1009 and 1018, corrosion incipient processes in hypersaline geothermal brine at 90°C 80—50753
steel, mild, Al-Zn alloy coated, interface struct. 79—52466
steel, Mn, diffusion of C, Si, V, W, electron probe microanalysis *(Czech)* 77—59149
steel, Mn-Ni-Cr, diffusion of Fe, Mn, Si, V and W *(Czech)* 77—59148
steel, rusted, exam. of tannin treatment action mode 78—88564
steel, spheroidised, H_2 embrittlement, fracture characts., electron probe anal. of inclusions 79—57109
steel, stainless, alloyed with C, magnetron-sputtered, microstruct., and cryst.-amorphous transition 80—19719
steel, stainless, corrosion and grain boundary penetration on exposure to coal gasification environment 80—61003
steel, stainless, Ni-Cr-Mo, two-phase, compositional charge of ferrite and austenite *(Japanese)* 79—4948
steel, stainless type 316 welds, post weld heat treatments on struct., composition and ferrite amount 80—29992
steel, structural, supercooled austenite, structural characts. of decomposition 80—60870
steel, tool and high-speed, high freq. induction melting and centrifugal casting in instrumental anal. 80—84886
steel fibre reinforced Mg, fibre-matrix interfacial reactions 80—20043
steel foil, microanalysis by energy dispersive X-ray spectrometry *(French)* 80—85250
steel gas nitrosulphurising, S25C, wear property 80—50729
steel/SiO_2-Al_2O_3 glaze, adhesive behaviour of metallic cation glaze exchanged on acid site struct. *(Japanese)* 79—66216
steels, austenitic-C steel diffusion couple, diffusion of C, 773-1373K 79—19392
steels, stainless, surface characterisation rel. to adhesive bonding chem. etching, SEM, AES, XPS and electron probe microanal. 80—88416
STEM, chem. anal., principles, instrumentation, resolution 79—39262
STEM, high resolution, microanalysis uses 78—24012
STEM, precipitates in Ni-base superalloy 80—104492
STEM, structural and chemical analysis, appls. 80—88003
STEM 79—39261
STEM microanalysis detect. limit improvement using coincidence techniques 77—25345
STEM with field-emission gun, for microanalysis use 78—32948
superalloys, phase extraction, chemical and X-ray diffr. anal. 78—72951
surface analysis, coordinated, using SEM, electron probe microanalysis and electron spectroscopy 79—96381
surface analysis, electron probe methods, AES, electron stimulated desorpt. 77—44098
surface analysis, electron-excited core level spectroscopies, book contrib. 77—63503
surface charact., combined ion scattering spectrocopy, SIMS, SEM, energy dispersive X-ray techniques 79—43702
surface layers and thin films, thermal diffusivity of microsections, IR and X-ray electron-probe microanal. 78—2314

electron probe analysis continued
- surface microstructure determ. and microanalysis by ultrahigh vacuum field emission gun SEM 80—96423
- surface problems, in materials science and technology, conference, Gothenburg, Sweden, June 1979 80—51950
- TEM, appl. to Nb_3Sn thin films 80—104491
- TEM, contamination reduction using liq. N_2 cold trap assembly 80—101056
- TEM energy anal. appl., K-shell excitation microanal. 77—44100
- TEM foil thickness measurement for quantitative metallography 78—35632
- TEM/STEM performance, Philips EM 400, with field emission gun and twin lens 80—57441
- tephra attributed to Glacier Peak, Washington, electron microprobe data 78—24273
- tephra set W, Mount St. Helens, Washington, electron microprobe anal. of glass shards 78—24274
- thermal battery, react. prods., electron probe anal. 79—43601
- thick specimens, proton and electron induced X-ray spectrometry, detect. sensitivities 78—20087
- thin coatings, microanalysis charact. fluoresc. correction 80—7881
- thin film, and surface anal., modern methods 80—54486
- thin film analysis *(French)* 77—32856
- thin films, localised elemental anal. of microphases and inclusions 78—85261
- thin foil, energy dispersive X-ray microanal. 77—60153
- thin foil, X-ray microanalysis in electron microscope *(French)* 80—61191
- thin foil, X-ray microanalysis in scanning transmission electron microscope, limitations 78—20122
- thin foil microanalysis using XPS and STEM, surface film effects 78—35789
- thin sections, use of pure C specimen holders 77—56555
- thin specimen, precision and optimisation *(French)* 77—77849
- thin specimen, TEM attachment *(French)* 77—81445
- thin specimens, X-ray spectra characteris. in TEM 78—35788
- thin surface film detection, in depend. on substrate 80—35607
- tissue sections, electron probe anal., improvement of peak/background ratios 79—39631
- ultrasoft X-ray microanalyser detector using secondary electron multiplier 77—21446
- ultrathin tissue sections, P standards for electron probe X-ray microanalysis 80—98193
- window glass, knots and cords, EPMA characterisation 80—84085
- X-ray absorption edges, emission wavelengths, analytic expressions 78—61111
- X-ray analysis, appls., conf., Denver, USA (Aug 1975) 77—56307
- X-ray analysis in the TEM/STEM, review 78—24014
- X-ray dispersive crystal spectrometers, geometric accuracy *(Chinese)* 80—22495
- X-ray emission, fluorescent and continuous *(French)* 77—36838
- X-ray emission and critical absorpt. energies calc., evaluation of mathematical expressions 77—29065
- X-ray energy dispersive spectrometer appl., data collection, review 77—56312
- X-ray energy dispersive spectrometry, data interpretation and quantitative treatment *(French)* 77—36839
- X-ray image processing, quantitative, with SEM, surface meas. appls. *(French)* 78—41379
- X-ray interferences correction, graphical method 79—43707
- X-ray mass absorption coeff., semi-empirical law 77—32468
- X-ray microanalysis, in TEM up to 1000 kV 80—101063
- X-ray microanalysis, quantitative investigation of thin specimens 80—101068
- X-ray microanalysis, quantitative microcrystal standards and excessive background 77—36842
- X-ray microanalysis, spatial resolution in thin foils 80—101065
- X-ray microchemical analysis, optimising conditions 80—101067
- X-ray quantum counters, dead time determ., accuracy estimation 80—99022
- X-ray source size in electron microprobe 77—77861
- X-ray spatial resolution, for SEM and STEM specimens 80—101066
- X-ray standardless thin film analysis in electron microscope 78—24006
- zeolites, dehydrated Na-exchanged mordenite, cation and molecular distrib. 79—90617
- Zircaloy-2 cladding, bonding to UO_2 fuel, mechanisms determ. by SEM and EPMA 78—17317
- β-ray quantitative microautoradiograhy, by X-ray emission microanal. 78—20545
- Ag-Au, composition changes under ion bombardment, scanning Auger microprobe obs. 79—83076
- Ag-In-Sn, internal oxidation, precipitation behaviour of oxide *(Japanese)* 80—66515
- Ag-Sn alloys containing Au, splat cooled ribbons, electron microscope exam. 78—39987
- $AgInS_2(Se_2)$-$SnS_2(Se_2)$, degree of solid solubility and phases characts. 78—35377
- AgMg two phase bicrystal, growth by solid state diffusion couple method 80—60773
- Ag_2S, distrib. on sensitised AgBr emulsion grains, X-ray microanalysis 78—62248
- Ag_2S-In_2S_3-SnS_2 system quaternary and ternary sulphide spinels, solid solubility and struct. 78—35376
- Al alloy, anodic finish exam. by SEM and electron probe micro anal. obs. 79—96278
- Al alloy, fretting corrosion, exam. of secondary structures 79—100292
- Al, coating on steel by thermal decomposition of alkyls 78—15590
- Al, electron energy loss spectra, microanal. appl. 77—44099
- Al, small spheres, bulk plasmons damping 80—75561
- Al, stopping power of valence electrons, Monte Carlo calcs. 79—10886
- Al-Ag (15 wt.%), precipitate growth kinetics 77—28817
- Al-Ag alloy, thin foil, X-ray microanalysis 77—81439
- Al-Ag alloy, thin foil, X-ray microanalysis, surface film effect 78—44428
- Al-Ag_2Al, eutectic alloy, exam. of terminal solid solubility limits 78—76633
- Al-Au, interdiffusion *(Czech)* 77—62684
- Al-Cu (4 wt.%), precipitation hardened and fatigued alloys, solute loss at fracture surface, EPMA exam. 78—39893
- Al-Cu alloy, microsegregation *(Japanese)* 77—16589
- Al-Cu thin films, microstruct. rel. to electromigration 80—44355

electron probe analysis continued
- Al-Mg, homogenisation process, effect of solidification rate and alloying *(Polish)* 79—78949
- Al-Mg-Li alloy, metastable S′-phase, struct. *(Russian)* 80—103291
- Al-Mg-Si, depleted zone formation, in air and vacuum 79—57013
- Al-Mg(An), depleted zone formation, in air and vacuum 79—57013
- Al-Si (0.57 at.%), Si precipitate dissolution kinetics 80—84935
- Al-silicide-Si systems with $CoSi_2$, $Pt_xNi_{1-x}Si$, and $MoSi_2$ as silicide, diffusion, compound form., and microstructure 80—34253
- Al-vitreous C composite, microchem. inhomogeneity of transition zone 77—24985
- Al-Zn-Mg, depleted zone formation in air and vacuum 79—57013
- Al-Zn-Mg (3,1.5 wt.%), precipitation hardened and fatigued alloys, solute loss at fracture surface, EPMA exam. 78—39893
- Al-Zn-Mg alloy, welded, solute profiles at weld bead/parent metal interface 78—19942
- Al-Zn-Mg-Cu foil, STEM-microanal., specimen thickness effect on X-ray count rates 77—70374
- $Al_xGa_{1-x}As$:Zn epitaxial layers, composition and Zn carrier conc. 80—25585
- β-Al_2O_3, field assisted bonding to metals 80—45474
- Al_2O_3, sintered, electron microprobe anal. of impurity and additive distribs. 80—40359
- Al_2O_3, sintering temperature effect of titanate additions 80—60808
- Al_2O_3-glass seals, diffusion of Al, electron microprobe study 80—107577
- Al_2O_3-SiO_2 refractory, SiO_2-rich glassy phase, deconvolution of microprobe conc. profiles 77—52606
- $3.5Al_2O_3.2SiO_2$, mullite, decomposition by SiO_2 volatisation 80—61082
- Ar, determ. in Si sputtered layer EPMA method 80—3443
- Au, thin foil, spatial resolution of X-ray microanalysis 80—101065
- Au_3Si, room temp. dissociation 78—35672
- B fibre reinforced Mg, fibre-matrix interfacial reactions 80—20043
- B-C system, electron probe microanalysis and destructive chem. methods of study *(French)* 80—11982
- B-C system, region of existence of B_4C phase 78—76636
- B-Si, (0 to 14.3 at.%), phase charact., regions of existence *(French)* 80—104117
- B-Si alloys, B-rich, prep., anal. and cryst. growth *(French)* 80—104091
- B_4C, melting and phase homogeneity range 80—20911
- B_4C, quantitative electron microanalysis *(French)* 78—76948
- B_2O_3, microprobe state anal. by X-ray OK and BK emission band spectra *(Japanese)* 78—19606
- BaO-SiO_2-Fe_2O_3 permanent mag. ceramics, exam. of phase diagram, using X-ray analysis, optical microscopy, electron probe anal., and thermal analysis *(German)* 79—29012
- $Ba_{0.5}Sr_{1.5}Al_4Si_{12}O_{32}.10H_2O$, brewsterite cryst. struct. refinement 77—80471
- $BaTiO_3$ ceramics, grain boundary pot. barriers, cathodoluminesc., electron probe anal. 80—2864
- $BaTiO_3$, doped-undoped ceramic composites, sintering behaviour 79—100094
- $BaTiO_3$, epitaxial ferroelectric, appl. of electron microprobe methods 80—44443
- $(Ba_{1-x}Y_x)TiO_3$ ceramic, resistivity rel. to donor dopant content 79—65474
- Be, phase struct. *(Russian)* 78—15401
- Bi-Sb, melts, interdiffusion, long capillary method and electron probe obs. 77—89563
- $Bi_{100-x}Sb_x$, chem. microhomogeneities, topographical and electron beam microanalysis obs. 79—65206
- $Bi_{0.52}Sb_{1.48}Te_3$ thermoelec. solid soln., homogeneity, effects of prep. method 78—52698
- $Bi_2Te_{3-x}Se_x$, thermoelec. mat., prep. effects on inhomogeneities 78—51576
- C, electron energy loss spectra, microanal. appl. 77—44099
- CaO-Al_2O_3-SiO_2 diffusion triangular diagram, diffusion between lime and sintered kaolinite *(French)* 79—69296
- Ca_2SiO_4, bredigite-larnite rock from Scawt Hill, electron microprobe anal. 78—68952
- $Ca_3Y_2Ge_3O_{12}$:Eu^{3+}, garnets, prep., struct., luminesc., absorpt. spectra, Eu^{3+} localisation 77—69884
- Cd distribution in bullfrog skin, determ. by electron probe X-ray microanalyzer 79—79707
- CdF_2:Mn, Y, deconversion due to vacuum heat treatment, elec. resist. and electron probe meas. 79—24025
- $Cd_xHg_{1-x}Te$, single cryst. homogeneity and molar conc. determ. with electron microprobe *(German)* 78—2109
- $CdS_{1-x}Se_x$, chem. comp. and luminescence obs. 80—80869
- $Cd_{1-x}Zn_xS$ solar cell thin films, microprobe characterisation *(French)* 80—61349
- Ce-Ga system, phase equilib. and cryst. struct. of phases 80—35159
- $CePd_3$ single crystal Czochralski growth and characterisation 80—60767
- Co, corrosion in Ar-SO_2 atmospheres, scale struct. obs. *(Japanese)* 80—55568
- Co-Cr-Al, ternary system, interdiffusion, electron probe anal. 80—34256
- Co-Cr-Ni-Ta-Al-Y (25, 10, 5, 3, 0.5 wt%), exam. of hot corrosion 79—20251
- Co-Ga alloys, phase diagrams and cryst. struct., DTA, X-ray diffr. and microprobe anal. *(French)* 79—47660
- Co-Ga-B, phase diagram, metallographic, X-ray and electron probe anal. 78—92241
- Co-Ge binary system, phase diagram rel. to that of Ni-Ge *(French)* 80—97463
- Co-mischmetall system, phase relations, microstruct., mag. props. 80—104118
- Co-Mo oxidic precursory state, supported on SiO_2 and γ-Al_2O_3 hydrotreating catalysts 79—61898
- Co-Ni, interdiffusion coeffs. and conc. penetration curves, electron microprobe meas. 77—66047
- Co-Ni (0.45 to 7.23 wt.%) theoretical analysis of cation distrib. in (Co, Ni)O scale 77—12747
- Co-WC hard alloys, rapidly quenched struct. 80—76233
- CoB-based boride coatings on Co base alloys, microstruct. and mech. props. 78—11427
- CoF_2, antiferromag. crit. props., neutron scatt. obs. 80—88749
- Co_5Sm crystals, microstruct., homogeneous precip. and nucleation 80—104160
- $Co_{1-x}Zn_xF_2$, antiferromag. crit. props., neutron scatt. obs. 80—88749
- Cr, corrosion in SO_2, 700-1000°C 80—97642
- Cr-Fe (30 wt.%) alloys, refined fine comminution 78—60598

electron probe analysis continued
Cr-Ge system, phase diagram, thermal anal., X-ray diffr., microhardness, and electron probe anal. *(French)* 80–97462
$Cr_{2.8}V_{0.7}Fe_{3.4}C_3$, stacking fault study, morphology, comp. and struct. 80–84190
Cu adhesion to Au, surface treatments and surface impurities 77–15701
Cu alloy, fretting corrosion, exam. of secondary structures 79–100292
Cu dilute alloys, compositional changes in oxide thin films, Auger electron microanalysis *(Japanese)* 77–21319
Cu, electron energy loss spectra, microanal. appl. 77–44099
Cu rich dental amalgams, SEM and energy dispersive X-ray analysis 78–24184
Cu/Sn-Ni/Au tricouples, electrodeposited, interdiffusion obs. 80–84331
Cu-Ag interface, interdiffusion, X-ray and electron microprobe data 77–4225
Cu-Al (0.05 wt.%), dil. alloy, anisotropic oxidation, electron microprobe Auger spectroscopy 77–12748
Cu-Al-Ni, mixed powder compacts, Ni content influence in sintering behaviour *(Japanese)* 80–35130
Cu-Al-Ni-Fe, (10, 5, 5 wt.%), cast microstruct. 78–80535
Cu-Al(Sn), effect of Al and Sn on friction and wear 78–11348
Cu-Fe phase diagram, 650 to 1050°C *(German)* 78–60658
Cu-Ga, binary alloy constituent EDS anal., secondary fluorescence, SEM study *(Chinese)* 80–85231
Cu-Ni, sulphidation between 653 to 770K, exam. of scale morphologies, using X-ray diffr., and electron microprobe anal. 78–88559
Cu-Ni diffusion couple, diffusion bonding process, fracture surface exam. *(German)* 77–35762
Cu-Ni-Ti system, phase equilibria in Cu rich region and Cu-T quasi-binary constitution *(Japanese)* 80–89203
Cu-Sn, ε and η phases, surface struct. changes due to sputtering 77–73206
$CuGaSe_2$ crystals, electron probe microanal., correction procedure 80–2171
$CuInS_2(Se_2)$-$GeS_2(Se_2)$, degree of solid solubility and phases characts. 78–35377
$CuInSe_2$ crystals, electron probe microanal., correction procedure 80–2171
Cu_2O, switching channel electron probe microanalysis, switching cycle number (life) 77–32056
$ErM_3(BO_3)_4$, M=Fe,Ga, quantitative X-ray spectral analysis 79–46635
$3Er_2O_3$-Ta_2O_5 refractories, prep. and anal. 77–48384
Fe, cast, electron probe determ. of traces of modifying agents in spheroidal graphite 79–52814
Fe, cast, Mg, despheroidising effect of Bi, Sn on graphite in alloy 78–56670
Fe, cast, Mg micro distrib., microprobe anal., electron fractography 77–70373
Fe, cast, tensile strength, Al addition effects *(Korean)* 80–71736
Fe, cast, with Mn, high S, exam. of sulphide phases, cocrystallisation during solidification 78–56646
Fe, chem. diffusion coeffs. and solubility limits for Cu, 690-1050°C 77–59146
Fe, grey cast, P effect on distrib. of alloying elements 77–12634
Fe-Al(Cr)(V)(Ti), hardness after nitriding, metallographic, electron microscopic and microprobe anal. 78–51608
Fe-C, diffusion of Sn, microprobe anal. of intermediate phases *(French)* 80–50596
Fe-C, dil., Hall-field electrotransport of C, effective valence numbers 79–28148
Fe-C-Mg, cast iron, graphite phase obs. *(Russian)* 77–59744
Fe-C-Si alloy, lattice parameters of cementite after quenching 78–11198
Fe-Cr, high-C, sulphide inclusion distrib. obs. 79–74168
Fe-Cr (20 wt.%), high temperature oxidation resistance, effect of rare earth and reactive element additions *(Japanese)* 79–20271
Fe-Cr-Al, electrical heating material, SEM obs. and surface analysis of oxide films formed at high temps. 77–16738
Fe-Cr-Al-Ce, high temp. oxidation *(Japanese)* 78–11413
Fe-Cr-C system at 870°C 77–28782
Fe-Cr-Ni, analysis and synthesis of phase diagrams 79–11563
Fe-Cr-O system, phase relations at 1200°C using diffusion couple technique 80–89205
Fe-Cr-Y, Y addition effect on high temp. oxidation resistance *(Japanese)* 79–70223
Fe-Cr-(C), oxidation, grain size and growth effects *(Japanese)* 77–48583
Fe-Mn cast alloys, homogenisation annealing and chemical diffusion *(Czech)* 80–66551
Fe-Mn-Ni-C, age hardenable, struct. and strength 77–8844
Fe-Mn(Sb)(Sn), additive effect, on eutectoid transformation of Fe 78–52799
Fe-Ni, grain boundary segregation, X-ray microanal. by STEM 80–66740
Fe-Ni, segregation of inhomogeneities during crystallisation *(Russian)* 78–27521
Fe-Ni (19wt.%) alloy, oxidation in CO_2, 700 to 1000°C, thermal and metallographic anal., EPMA 78–72931
Fe-Ni (3 wt.%), grain boundary segregation of Sn and P embrittling additions, STEM microanal. 78–76654
Fe-Ni (3 wt.%), grain boundary segregation microanal. using X-ray (STEM) and AES 78–87685
Fe-Ni (3 wt.%) alloys, embrittled, microanalysis of grain boundary segregation using STEM 78–35633
Fe-Ni mixed powders, effect of Ni particle size and unequal interdiffusion, on sintering process *(Japanese)* 78–84728
Fe-Ni-Al system, multiphase diffusion at 1000°C, diffusion structs. and props. 80–19995
γ-Fe-Ni-C, Fe-Cr-C, Fe-C, electromigration of C, effect of Ni and Cr addition 78–6184
Fe-Ni-Cr (30.6, 21.3 wt.%), Alloy 800, high temp. oxidation at low O_2 press., SEM, AES and electron probe microanal. study 80–93688
Fe-Ni-Cr-Al-Y, oxidation mechanism, Y addition effect on kinetics and oxide adherence 80–97623
Fe-Ni-Cr-Mn-Al-Ti Incoloy 800, exam. of scale morphology, alloying element distrib. after oxidation 78–80677
Fe-Ni-S, exam. of liquidus surface and tie lines, using electron probe analysis 79–11557
Fe-Ni-Ti (25.9, 2.15 wt.%), exam. of effect of inhomogeneous solid soln., on martensitic transformation *(Russian)* 79–34034
Fe-Ni-(P), phase diagram determ., 700 to 300°C 80–108399
Fe-Sb system, α-phase, interdiffusion 79–73349

electron probe analysis continued
Fe-Si (3wt.%), grain-oriented, secondary recryst., grain growth inhibition 80–89245
Fe-Si(Cr)(Ni)(Mn)(C), alloy layers formed by reaction with molten Al, X-ray, EPMA anal., hardness meas. *(Japanese)* 78–72926
Fe-W-C, eta carbides at 1250°C 77–36506
Fe-W-C-Cr, eta carbides at 1250°C 77–32581
FeB_x coatings on steel, formed by B diffusion, pack cementation process, microstruct. and mech. props. 78–15592
$Fe_{32}Ni_{36}Cr_{14}P_{12}B_6$ metallic glass, crystn. kinetics by TEM 80–75186
Fe_2O_3-NiO-ZnO-CoO (15.1, 17.6, 0.6 wt.%) ferrite, effect of electron beam machining on surface layer 79–34178
FeSi-Fe_2Si_5 eutectic, $FeSi_2$ formation, annealing temp. and time effects 79–24512
ε-FeTi, Ce addition effect on H_2 absorption capacity 79–61899
Ga, electrode, crystallite interfacial impurities, electrochem. effects, microprobe anal. 77–44569
Ga-In-As-Sb quaternary system, phase equilib. and heterojunctions 79–34016
GaAS, binary alloy constituent EDS anal., secondary fluorescence, SEM study *(Chinese)* 80–85231
$Ga_{1-x}Al_xSb$, LPE growth and phase diagram *(French)* 77–24974
GaAs, anodic oxide for device application, crystallisation dynamics 79–66190
n-GaAs wafer, defect studies by ASLEEP, SEM and scanning AES 79–19256
GaAs:Cr, semi-insulating, i.r. induced modulation of cathodoluminescence, and specimen current 77–1737
GaAs:Zn epitaxial layers, composition and Zn carrier conc. 80–25585
GaP:N LED structures, local dopant conc. determ. using SEM cathodolum. spectra 80–101057
$(GaP)_x(ZnSe)_{1-x}$/GaP, epitaxial heterostructures, chem. microinhomogeneity 77–80831
GaSb film, ion bombard. effects on elemental Sb incorporation probability during sputter deposition 79–83120
Gd-Co alloy, sputtered film, mag. props. determ. *(Chinese)* 78–2714
Gd_2O_3-Ga_2O_3 system, phase diagram relationships of garnet-perovskite transform. 80–97460
graphite, intercalation compounds with $FeCl_3$ intercalation kinetics 78–31354
HF with interstitial O, quantitative TEM obs. of small agglomerates 80–107227
HfO_2 film, CVD growth, struct., elec. and optical prop. characterisation 77–55891
Hg, quantification of losses in X-ray microanal. 80–85261
Hg-Ag-Sn, dental amalgams, corrosion penetration in crevices 80–3238
n-InAs:Cr, Czochralski growth of high-resist. single crysts. 77–66587
$In_{1-x}Ga_xAs$, LPE growth on InP, electron probe anal. of etched surface 79–23862
In_2O_3:Sn, thin films, prep. by pyrolitic method, charact. by SEM, electron diffr. and SIMS, solar energy appl. 79–43143
In_2O_3:Sn films, doping profiles and elec. props., appl. to optoelectronic devices 79–38203
InP, LPE growth on GaAs, etching and electron probe anal. 79–11526
n-InP wafer, defect studies by ASLEEP, SEM and scanning AES 79–19256
InP:Fe, precipitate mixture 77–77485
InSb film, ion bombard. effects on elemental Sb incorporation probability during sputter deposition 79–83120
InSb-GaSb alloys, directionally solidified, composition variations, electron probe anal. 79–24513
$KMn_{1-x}Ni_xF_3$, antiferromag. crit. props., neutron scatt. obs. 80–88749
$K_6Ta_{10.8}O_{30}$, cryst. struct., X-ray diffr. and electron microprobe meas. 78–34489
$K(Zn,Mn,Co)F_3$, crysts., Mn, Co distrib., as function of cryst. region *(German)* 78–14375
Kr, determ. in GaAs sputtered layer, EPMA method 80–3443
$LaNi_{4.4}B_{0.6}$, H_2 absorpt. props. 80–88432
$La_4Si_2O_7N_2$ single cryst. growth by floating zone method with SiO_2-Si_3N_4 additions 80–93481
$LiNbO_3$:Ti, planar and channel optical waveguides, anisotropic diffusion expts. 80–64200
$Lu_{2-x}Si_2O_7:Eu_x$, synthesis and spectroscopic study 80–84846
Mg $(Fe,In)_2O_4$:Pb,Pt film, LPE 77–77436
Mg-Si-Al-O-N, grain boundary segregation, combined X-ray microanal. and lattice fringe imaging determ. 79–15681
MgIn, atmospheric corrosion, SEM, electron diffraction and electron probe obs. 79–24681
$MgO.Al_2O_3$-$MgO.nAl_2O_3$ spinel, coordination state of atoms, charact. X-ray emission *(Japanese)* 78–6816
Mn nodules, deep-sea, diagenetic features, X-ray spectral and SEM anal. 79–16099
MnSi-Si system, striations and cryst. struct. of matrix 80–103292
$Mn_{15}Si_{26}$, growth by Bridgman method and chemical transport, electron probe analysis 79–100043
Mo powder, influence of powder reduction processes on props. 80–89175
Mo-Mn-Fe-Si/Al_2O_3 ceramic seal, interfacial phases 78–72011
Mo-Zr-C (0.08, 0.02 wt.%), struct. and banding tendency, thermomechanical treatment effects 77–86063
MoS_2 hydrotreating catalysts, Co, Fe and Ni effects on microstruct., TEM, SEM and EPMA obs. 79–52762
$(NH_4)_{2(1-x)}Rb_{2x}SO_4$, stoichiometry defects, electron probe microanal. 80–39143
NaCl-KCl, interdiffusion and demixing, electron microprobe anal. *(French)* 80–54444
NaCl-KCl system, interdiffusion, miscibility, Kirkendall effect 80–107568
Na_2O-Al_2O_3-$SiO_2.xH_2O$, fibrous crystal growth in silica gel, X-ray, electron probe and IR spectra obs. 80–25541
Na_2O-CaO-SiO_2, corroded glasses, electron microprobe analysis 77–4956
Na_2O-CaO-SiO_2, multicomponent liq. state diffusion 78–55962
Na_2O-CaO-SiO_2 glass, microprobe anal. of corroded surface 80–7704
Na_2O-CaO-SiO_2 molten glass, electrolysis reactions 80–89496
Na_2O-NaF-CaO_xZnO_{1-x}-Al_2O_3-SiO_2, opal glasses, strength, surface composition 80–30066
Na_2O-SiO_2 melt, diffusion coeffs., electron microanal. meas. of Na and Si concs. 77–31790
Na_2O-TiO_2-SiO_2 glass, co-ordination of Ti, X-ray emission spectra study 80–84072

electron probe analysis continued
- $Na_2O(K_2O)$-P_2O_5 glasses, P K-band X-ray emission spectra, state anal. 80−40190
- β-$Na_xV_2O_5$, Bridgman and Czochralski single cryst. growth 79−47618
- Na_2.n.Al_2O_3, polycrystalline, Na^+ and Ag^+ conc. profiles, electron microprobe determ. 79−24737
- Nb based superconductors, comp. meas. 77−12852
- Nb-Ga-Fe ternary system, phase equilib. at 1000°C, supercond. transition temp. 80−35158
- Nb-Ga-Ir system, phase equilib. at 1000°C and supercond., Nb-rich portion 77−36480
- Nb-Ge system, reaction diffusion, electron probe anal. 79−28152
- Nb-Sn-Si(As), ternary A15 phase regions, solubility 77−44215
- Nb_3Al-Nb_3Ge-Nb_3Ga system, supercond. crit. temp., composition determ. 77−8218
- $NbGa_2O_x$, O stabilised cpd., struct. determ. 80−103301
- Nb_3Ge film, supercond., intercorrelations between composition, lattice parameter a_0 and T_c 77−8217
- Nb_3Sn-Cu multifilamentary composite wire, Nb_3Sn filament morphology and grain size 80−100855
- $NdM_3(BO_3)_4$, M=Fe,Ga, quantitative X-ray spectral analysis 79−46635
- $(Ni,Cr)_xPy$, layer formed on phosphidation of Ni-Cr alloy in P vapour, 700°C 80−25906
- Ni alloy, STEM microanalytical techniques comparison for precip. comp. determ. 78−35790
- Ni base alloy, precipitation identification by electron probe microanalysis *(German, English)* 77−77857
- Ni, corrosion in SO_2, high temp. 79−20281
- Ni-(Co)-Cr, aluminide coating, microstruct. and chem. 80−76189
- Ni-Al, (2 and 6 wt.%), oxidation, α-Al_2O_3 growth, microstruct., precip. 80−108626
- Ni-Al-Nb ternary system, electron microprobe analysis of nickel-rich region at 1473K 80−71631
- Ni-Co-Al alloys, continuous precip., SEM, TEM, X-ray diffr. study 80−89220
- Ni-Cr-Mg alloy, KhN70VMTYu, Mg effect on grain boundary struct., props. 79−19261
- Ni-Cr-Ta system, phase equilib. of Ni rich region at 1523 and 1273K 80−93541
- Ni-Fe_3O_4 system, interdiffusion 79−69301
- Ni-Ga alloys, phase diagrams and cryst. struct., DTA, X-ray diffr. and microprobe anal. *(French)* 79−47660
- Ni-Ge binary system, phase diagram rel. to that of Co-Ge *(French)* 80−97463
- Ni-P alloy, electrodeposited, heat induced struct. changes *(Japanese)* 78−15433
- Ni-Ta-Al system, phase equilibria and diagram, electron probe, X-ray diffr. anal. 80−29927
- Ni-Ta-C, composites of γ+TaC 77−85965
- Ni-Ti (48 at.%), annealed and rolled electron microscope and probe analysis of structure 79−100189
- $NiAl_3$, quantitative STEM chem. anal. using standard and standardless programs 79−17578
- Ni_3Al-Ni_3Nb eutectic alloy, aluminide coating microstruct. exam. 78−15593
- NiCr, sputtered, detection by electron probe microanal., substrate depend. 80−35607
- $Ni_xFe_yCr_{1-x-y}$ films, struct., mag. props., and corrosion resist. 80−34706
- Ni_4Mo alloy, high temp. oxidation, oxide layer growth, struct., mech. behaviour 78−44269
- NiO-Al_2O_3 system, concurrent meas. of vol., grain boundary and surface diffusion coeff. 77−55399
- NpO_2 single crystal growth, gas phase chemical transport method *(French)* 80−60760
- $Pb_5Ge_3O_{11}$, sputtered ferroelec. films, prep. struct. and dielec. props. 80−75452
- PbO, microprobe state anal. by X-ray OK and BK emission band spectra *(Japanese)* 78−19606
- PbO-B_2O_3-SiO_2, molten mixture, microprobe state anal. by X-ray OK and BK emission band spectra *(Japanese)* 78−19606
- PbS_xSe_{1-x}, chalcogen interdiffusion, electron microprobe obs. 79−28145
- PbTe:Bi-PbSmTe-PbTe, epitaxial laser struct., growth, p-n junction position and lasing region 79−89908
- PbTe-PbSnTe heterjunction, misfit dislocations, etch pit and electron probe study 79−77926
- Pd-amorphous Si thin film interaction, metal rich Pd-silicide formation 80−2284
- Pt film on Si, PtSi form. kinetics, AES, SIMS, EPMA 77−11800
- PtRh5 alloy, phosphate glass addition effect on high temp. strength *(German)* 80−25807
- Pu-Pt(Rh)(Pt-Rh), exam. of phases and crystal structure 78−80518
- Sc-Rh-Si system, partial phase diagram, X-ray diffr. and microprobe anal. 80−25659
- Si diode, impurity profiles, scanning electron microprobe anal. 80−79832
- Si filamentary crystals, grown from vapour, electron probe microanal. 79−77538
- Si MOS device, electron optical identification of precipitations 80−16309
- Si wafer, defect studies by ASLEEP, SEM and scanning AES 79−19256
- Si:H amorphous films, role of Ar in deposition process, IR absorpt. and photocond. meas. 80−50321
- Si:P, ion-implanted, carrier conc. reduction caused by wet O_2 oxidation 80−10565
- Si-Al-O-N ceramics, grain boundary segregation determ. by X-ray microanal. and lattice fringe imaging 79−15681
- Si-B-O film, electron probe microanal., Monte Carlo calcs. 79−83533
- Si-Ge amorphous films, effects of annealing and crystn., ESR microstruct. and elec. meas. 78−26790
- SiC fibre reinforced Ni-Cr alumina coated fibres, hot pressed, annealed, IR study 78−60623
- Si(Li) detector for energy dispersive analysis *(French)* 77−26445
- Si_3N_4, reaction bonded, creep, internal oxidation effects 78−56701
- Si_3N_4, reaction-bonded, internal oxidation processes role in high-temp. mech. props. 79−38915
- Si_3N_4, reaction-bonded, microstructural analyses 77−8782
- Si_3N_4 ultra-thin film composites of FET wafers and devices, thickness determ. by microprobe technique 77−36397
- Si_3N_4:$(MgO+Al_2O_3)(Y_2O_3)$, hot-pressed and sintered, microstruct. and impurity distrib. 80−49261

electron probe analysis continued
- Si_3N_4/Al_2O_3, powder compact, electron microprobe investigation of reactions *(French)* 80−26009
- SiO_2 gel, $SiO_2Al_2O_3$, SiO_2MgO, pore structure influence on X-ray intensity in EPMA *(Japanese)* 80−26046
- SiO_2, microprobe state anal. by X-ray OK and BK emission band spectra *(Japanese)* 78−19606
- SiO_2 ultra-thin film composites of FET wafers and devices, thickness determ. by microprobe technique 77−36397
- SiO_2-Al_2O_3 porous catalysts, EPMA quantitative anal., new correction calc. method, modified ZAF method *(Japanese)* 80−93822
- SiO_2-Al_2O_3-K_2O-Na_2O, exam. of leucite crystal growth 79−19496
- SiO_2-MgO porous catalysts, EPMA quantitative anal., new correction calc. method, modified ZAF method *(Japanese)* 80−93822
- SiO_2-Na_2O (Li_2O), phase separation detection 77−1890
- $Si_2R_2O_7$, (R=Tm, Er, Ho, Dy), flux growth, substantial impurity levels determ. by EPMA 79−52097
- $Si0_2$ film, RF sputtered, stoichiometry and atomic defects obs. 79−90904
- Si⟨111⟩Al/Si, growth kinetics of ⟨111⟩Si through Al layer, SEM and electron probe anal. 79−28236
- $SmCo_{5-x}Cu_x$ magnet alloy, metallurgical study *(Korean)* 77−8853
- Sm_2O_3-Ga_2O_3 system, garnet-perovskite transform., phase diagram relationships 80−97460
- Sn droplets, on Bi, Zn and Al, heterogeneous nucleation 80−44294
- SnO_2:F, thin films, prep. by pyrolitic method, charact. by SEM, electron diffr. and SIMS, solar energy appl. 79−43143
- SrO-SiO_2-Fe_2O_3, permanent mag. ceramics, exam. of phase diagram, using X-ray analysis, optical microscopy, electron probe anal., and thermal analysis *(German)* 79−29012
- Ta-Pd system, phase diagram exam. of composition by X-ray diffr., electron microprobe anal., and metallography 78−76632
- ThO_2, ceramic oxide, thermally stimulated depolarisation currents as probes diffused in ceramic bulk 79−65792
- ThO_x:Y_2O_3 solid electrolyte high-temp. vaporisation obs. 78−14456
- Ti-Al-V (6,4 wt.%), metallogaphically prepared, fracture surface, phase anal. by energy dispersive X-ray microanal. *(German, English)* 77−48606
- Ti-Cu (Ni), oxidation, high temp., comparative study with Ti *(French)* 79−20285
- Ti-Mo-Al, determ. of interaction parameters from EPMA data 77−63635
- Ti-Nb (4.32 wt%), high temp. oxidation kinetics under 1 bar pressure, 1255-1471K 80−89410
- Ti-Nb-Na (4 to 31, 8 to 38 at.%), with uniform distribution of refractory metal, prep. *(Russian)* 77−28747
- Ti-Ta (4.37 wt%), oxidation kinetics, 1258-1473K, and at pressure of 0.013, 0.133 and 1.0 bar 80−89411
- Ti-TiN phase system, diffusion of N_2 77−39699
- TiB_2 coatings, CVD, electron microprobe, SEM, X-ray diffr. characterisation *(French)* 78−43271
- TiB_2, erosion resistant boride coating on Ti and Ti alloys 79−20290
- TiC-Au film, prep. by activated reactive evaporation, struct. and mech. props. *(Japanese)* 78−3252
- $TiCrB_2$-Ni(Ni-Mo) systems, interphase reactions, electron probe anal., metallography and hardness exam. 80−2990
- (U,Ce), U self-diffusion 80−92711
- (U,La)C, U self-diffusion 80−92711
- (U,Pu)C, sintering, role of Ni as sintering additive 80−84892
- (U,Pu)CNO irradiated fuel, electron microprobe anal. 78−70601
- (U,Y)C, U self-diffusion 80−92711
- (U,Zr)C, U self-diffusion 80−92711
- U minerals, quantitative microprobe anal. 78−61126
- U-Y-C FBR nuclear fuels, phase anal., 1400°C 80−66485
- $(U$-$Pu)O_2$ interaction with stainless steel cladding, corrosion products 79−26524
- UC, sintering, role of Ni as sintering additive 80−84892
- UC_2 and $(8Th, 1U)O_2$ fuel kernel, experimental containing CVD ZrC coatings, irradiation behaviour 77−3103
- UO_2-$20CeO_2$ mixed powder, X-ray and microprobe exam. of homogenisation 80−25609
- UO_2-PuO_2 fuel pin, hyperstoichiometric, post irradiation examination 80−63258
- UO_2-zircaloy-4, reaction kinetics at high temps., O_2 diffusion 80−16667
- UO_{2+x}-ThO_2-MgO system, in air, phase rel., X-ray diffr., electron probe and metallography anal. 79−74137
- V foil, air-oxidised, reversible switching, mechanism determ. 79−28387
- V-Os system, equilib. phase fields, X-ray diffr., elec. resist., DTA, and EPMA meas. 79−47661
- V-Ti-C, elemental anal. of second phase carbides using electron loss spectroscopy 79−20500
- $V_{3-x}M_xGa$, M=Ti, Cr, Mn, Fe, Co, Ni, cryst. struct. and microhardness meas. 79−86740
- $VSe_{2-x}S_x$ $(0<x<2)$ solid solutions, characterisation 80−88730
- W, annealed wire, analytical determ. of K content of single bubbles 78−64909
- W fibre reinforced Ni, high temp. stability 77−48372
- W:Os coated dispenser cathode, chemical and physical process obs. 79−28885
- WC-Co DC and RF sputtered coatings, bias effect, struct., X-ray-Auger study 80−70565
- WC-Co molten Zn reaction, lamellar struct. form. 79−33964
- XE bonded fission gas, radial distrib. in mixed carbide fuel pins, electron probe anal. 79−36318
- Xe, retained in advanced nuclear fuels, meas. by microprobe anal. 79−40997
- YIG, Al- and Ga-substituted, floating zone method growth, interface shape and horizontal variations of Al and Ga contents by electron pulse anal. 79−33929
- $YM_3(BO_3)_4$, M=Fe,Ga, quantitative X-ray spectral analysis 79−46635
- $(Y_{1-x}2Co_x)Co_5$, mag. props. annealing effects, phase segregation, EPMA 78−91898
- ZnO ceramics, microstructural evaluation 79−55750
- $ZnSiP_2$, growth under nonstoichiometric conditions in gas phase, microanalytical investig. *(German)* 79−33909
- $ZnSnP_2$-$ZnSiP_2$, heterocombination simultaneous crystallisation 78−60560
- Zr diffusion in Cu, microstruct. and microanal. study of coating formed *(Rumanian)* 78−19917
- Zr-Zr_2Al_3, diffusion weldings between 1000 and 1300°C, electron microprobe anal. *(German)* 78−84011

electron probe analysis continued
  ZrC-Ni, refractory-liquid metal, interfacial reactions, C effect, electron microprobe analysis 77−12829
  ZrN, sintering in vacuum and in N_2 77−12586
electron probe microanalysis *see electron probe analysis*
electron probe microscopy *see electron probe analysis*
electron probes
  see also electron probe analysis
  aberration compensation, dynamical focusing with stigmator 80−87291
  AC corona meas. using field-filter probes 80−47082
  Auger scanning microprobe, approach to damage-free anal. 80−89581
  automated, evolution of quantitative elementary point anal. in geosciences *(French)* 78−78046
  automated microprobe *(French)* 79−6237
  beam deflection error assessment, expt. technique 80−78757
  correction of distorted spot shape using dynamic focusing and stigmator 80−57427
  deflection system for adjustment, scanning of electron beams 79−2878
  double focus, lens for STEM 80−9074
  field emission source advantages for restricted divergence probe 80−68324
  history of SEM and electron microprobe *(German)* 78−41381
  LSI circuits, appl. of electron beam meas. techniques for verification of computer simulations 79−21875
  magnetic lens third-order field geometrical aberration of single slot lenses forming electron probe 79−3619
  minicomputer driven microprobe *(French)* 78−74111
  scan-forming unit for controlling coupled beams from an electron-beam probing device 80−52366
  scanning electron probe voltage contrast, device ground level floatation 80−73527
  solid target, electron probe penetration and energy loss characts., diffusion model 80−96585
  space charge effects in electron probe devices 79−27154
  steel, austenitic stainless, electron beam welding effect, on mech. props. of steels 310L, 316, 21-6-9 78−48498
  STEM, thermal cathode illumination system, for round beam electron probe systems 80−57436
  surface electron states, electron emission spectroscopy probe 77−51798
  thermal field emission source for high resolution, high current e-beam microprobes 80−68297
  variable-shaped beam systems, adjustment accuracy requirements for submicron pattern prod. 80−69312
  LaB_6 highly stable single cryst. cathode for conventional electron microprobe instruments 78−78043
  Ti-Al(Fe) microprobe anal. of alloying addition distrib. 80−55358
electron-proton interactions
  see also electron-proton scattering
  bremsstrahlung model of Brodsky and Gunion, comments 79−93362
  CERN proton synchrotron, electron ring addition, proposal for weak interaction study 78−55062
  deep inelastic, many-photon exchange contrib. 80−9177
  deep inelastic asymmetry meas., Bjorken sum rule, p spin struct. models 78−70376
  deep inelastic ep scattering, scaling property *(Chinese)* 77−10257
  deep inelastic longitudinally polarised ep scatt., asymm., depolarisation, p struct. functions 77−6133
  deep inelastic scatt., σ_L/σ_T ratio from quark model 80−82979
  deep inelastic scatt., intro. to basic quark/parton phys., book 79−85276
  deep inelastic scatt., nucleon struct. function moments anal., asymptotic freedom critical tests 79−54344
  deep inelastic scatt., nucleon structure functions 78−50036
  deep inelastic scatt., polarisation asymm., source theory anal. 77−34160
  deep inelastic scatt., quark-parton model with logarithmic scaling violation 80−78071
  deep inelastic scatt. cross sections, quark-parton model with broken scaling *(Russian)* 80−32109
  deep inelastic scattering, appl. of quark parton model 79−30715
  deep inelastic scattering, asymm. in cross section 77−38178
  deep inelastic scattering, rest frame quark-parton model of proton, scaling 78−70374
  deep inelastic scattering, scaling deviations, parton model anal. 79−58966
  deep inelastic scattering on π-pole Regge *(Russian)* 78−12918
  inclusive cross-sections meas. at 50° and 60°, 6.5-19.5 GeV 77−2843
  inclusive interactions flavour symmetry breaking in antiquark distribs. 79−36006
  inclusive reactions, eμ event, associated charm quark pair creation 77−2841
  inelastic ep scattering, charged hadron multiplicities, inclusive π^- distribs. 78−41552
  light-cone expansions and parton model 77−54077
  microcausality, equal-time current commutators, sum rules *(Russian)* 77−74689
  nucleon production in quark parton model, e^+e^-, ep and large $p_\perp$ reactions 78−21391
  polarised beam and target, deep inelastic scatt. asymmetry and radiative corrections 79−63483
  polarised deep inelastic scatt., energy and y depend. of cross section asymm. 78−45926
  polarised deep inelastic scatt., test of Weinberg-Salam model 79−22006
  polarised deep inelastic scatt., vector meson dominance anal. 78−33073
  QCD corrections to parity-violating asymmetries 80−22618
  QCD perturbative corrections 78−74263
  quark-parton model, three photon struct, function of proton, inelastic electron scatt. data 77−46022
  structure functions in deep inelastic scatt., second-order contributions, QCD predictions 80−13314
  e^+/e^- ratio on hydrogen at 13.5 GeV 77−13966
  $e+p\to e'n+\pi^+$, σ_L, σ_U separation, π EM form factor 77−79269
  ep, 20.5 GeV, inclusive π^0 electroprod. in deep inelastic region 80−52520
  ep, deep inelastic scatt., meson spectra in forward jets, hadron cascade model anal. 80−32103
  ep, sea quark and gluon momentum distribs., perturbative vs. asymptotic freedom corrections 79−17736
  ep deep inelastic inclusive K_s^0 and Λ electroproduction, quark fragmentation 78−66123
  ep deep inelastic scatt., EM form factors asymptotic behaviour, Fourier transform singularities 79−40789
electron-proton interactions continued
  ep deep inelastic scatt., p-violating asymmetries, neutral current couplings, sea quark contrib. 79−97630
  ep deep inelastic scatt., pol. p and e, straton model, sum rule *(Chinese)* 80−42475
  ep deep inelastic scatt., scaling violations and QCD parametrisations, struct. functions *(Russian)* 80−37277
  ep deep inelastic scattering, phenomenological determ. of electroprod. struct. functions 79−63478
  $ep\to e\Delta^+$ scatt. asymmetry predictions, SU(2) gauge theory 78−58193
  $ep\to eK^+\Lambda^0$, scalar transverse separation 77−71520
  $ep\to eK^+\Sigma^0$, scalar transverse separation 77−71520
  $ep\to eK^+$+anything, invariant cross section, DESY studies 78−41553
  $ep\to eN\pi$, $\gamma^+ p\Delta^+(1231)$ vertex transition form factor *(Russian)* 80−37269
  $ep\to eX$, SLAC data anal., parton distribution functions for polarised protons 77−82747
  $ep\to e'+X$, polarised e, parity non-conservation in inelastic scatt. 78−89719
  $ep\to e'nX$, π exchange, π EM struct. functions calcs. 78−70375
  $ep\to e'n\pi^+$, 0.06-1.35 GeV^2, cross section 77−10263
  $ep\to e+hadron+x$, parton picture from QFT, structure function scaling behaviour 79−402
  $ep\to e\gamma+X$, QCD predictions for processes involving real photons 79−6330
  $ep\to epK^+\pi^+K^-\pi^-$, 1.8, 2.1, 2.5 GeV/c^2, meson resonance observ. 80−82982
  $ep\to epX$, photon fragmentation region, Regge pole expansion 77−54108
  $ep\to epX$, pion struct. function determ. *(Russian)* 79−22097
  $ep\to ep\eta$, meas. in S_{11} (1535) reson. region 78−50038
  $ep\to ep\eta$ at $S_{11}(1535)$ resonance, longit. to transverse cross sections ratio 78−78194
  $ep\to ep\omega$, prod. by virtual photons, ω prod. to ρ^0 prod. ratio 79−6344
  $ep\to epp\bar{p}$, cross sections and possible resonances in final state $p\bar{p}$ system 79−71756
  $ep\to ep\phi$, Q^2 depend. of diffractive slope, decay ang. distrib., vector dominance model 79−89169
  $ep\to ep\pi^0$, coincidence electroproduction of single neutral pions in the resonance region at $q^2=0.5\ (GeV/c)^2$ 79−89168
  $ep\to ep\pi^0$, elastic π^0 electroprod. above resonance region, cross section, direction 78−62412
  $ep\to ep\pi^0$ or $en\pi^+$, threshold cross section slope, form factors, π axial mass and radius 78−62411
  $ep\to ep\pi^+\pi^-$, exclusive ρ^0 prod. by virtual photons 79−22113
  $ep\to ep\pi^+\pi^+\pi^-\pi^-$, 1.8 GeV/c^2, meson resonance observ. 80−82982
  $ep\to ep\rho^0$ or eX, polarised beam and target, cross section asymm., vector-meson dominance model 77−6135
  $e\bar{p}\to e\pi^{-+}n$, longitudinal and transverse contribs., π^+ EM form factor 78−66126
  $ep\to e\pi^+n$, scalar transverse separation 77−18296
  $ep\to e\pi^\pm X$, π^+/π^- ratio meas. 77−18295
  $ep\to e\pi^\pm X$, quark-parton model charged π electroprod. 79−13136
  $ep\to e\pi^\pm$+anything, π^+, π^- structure function behaviour, various W and Q values 77−10262
  ep→hadrons, inclusive distrib. of hadrons from deep inelastic scatt. 79−89167
  $ep\to\omega p$, ω prod. by virtual photon, ang. distrib., cross section 77−61302
  $ep\to\pi^0X$, duality and finite energy sum rules 80−42477
  $ep\to W^+(Z^0)+X$, inclusive cross sections, quark-parton model calcs. 79−71755
  e^-p, π multiplicity and asymmetric fireballs 79−93474
  $e^-p\to e^-p$+anything, virtual photon photoprod. invariant cross section 77−46058
  $e^-p\to e^-\pi^\pm X$, comparison with $\bar{p}p\to p\pi^\pm X$, quark parton model anal. 79−63512
  $e^-p\to Wp\nu$, from Z^0 pole to threshold 80−105917
  $e^\pm p\to e^\pm\gamma+X$, deep-inelastic bremsstrahlung, quark charges, colour gluon mass 78−74216
  $\gamma_v p\to K^+X^0$, $K^+\Lambda$, or $K^+\Sigma^0$, K^+ electroprod. along virtual photon direction, cross sections 77−41848
  high-energy scatt. of polarised electrons from polarised protons 77−34157
  K electroproduction, $K^\pm/\pi^\pm$ ratio and symmetry props. of quark- parton model, fragmentation functions 78−93888
  K inclusive electroproduction, K/π and K^+/K^- prod. ratios 78−37217
  $p+e\to\pi+N$, form factor determ. *(Russian)* 79−9382
  π prod. at threshold, two-pion radius and axial mass determ. *(Russian)* 77−10267
  ϒ(9.46), prod. in e^+e^- interaction at DORIS, quark parton model agreement 79−93443
  ϒ′(10.02), prod. in e^+e^- interaction at DORIS, quark parton model agreement 79−93443
  W-boson prod. in ep and pp collisions 77−61247
  $ep\to en\pi^+$, forward π^+ electroprod. in Δ(1232) resonance region 79−22115
  ep→epX, one-pion exchange model, pion struct. function anal. *(Russian)* 80−13291

electron-proton scattering
  see also electron-proton interactions
  deep inelastic scaling, possible valence gluons 77−30310
  deep inelastic scatt., density matrix appl. to scaling props. 78−8673
  deep inelastic scatt., parton model asymptotic freedom without non-Abelian gauge theories 77−30314
  deep inelastic scatt., renormalisation group anal., parton model connections 79−40784
  deep inelastic scatt. in ω=1 region, field theory and parton model anal. *(Russian)* 78−78190
  deep inelastic scattering, Lorentz invariant generalized functions, rel. to EM form factors 78−8544
  deep-inelastic scatt. on virtual particles, π and ρ struct. functions 77−18292
  elastic scattering, VDM, p EM form factor *(Russian)* 78−17026
  leptoproduction, azimuthal depend., parton model calcs. 78−93887
  longitudinal cross section and asymmetries for jets in leptoproduction 80−32106
  longitudinally polarized ep elastic scatt., 6.5 GeV, cross section asymm., p form factors 77−6131
  polarisation phenomena *(German)* 80−27508
  polarised scattering, asymmetries, gauge models 80−62991

electron-proton scattering continued
relative differential cross section at 4.5 GeV, mean square proton elec. radius calc. *(Russian)* 79−49525
spin effects in EM interactions 80−42470
teaching, from Compton effect to quarks, at., proton, and nucl. struct. 78−24596
universal multihadron jets, quark interactions 77−38132
ep, deep inelastic scatt., higher order asymptotic freedom corrections 80−105903
ep, nucleon structure from electron scatt., EM form factors 80−42468
ep, parity violating asymmetries in polarized electron scattering 80−9111
ep(d) scatt., nucleon struct. function moments, asymptotic freedom critical test 79−85300
ep deep inelastic scatt., parity violation and neutral currents 80−22559
$Ep \to e'p\gamma$, 111 MeV, radiation tail spectrum of electrons *(Russian)* 79−30739
ep elastic scatt., absolute differential cross sections, form factors and charge radius 80−27509
$ep \to ep\pi^0$, $-k^2=0.88$ (GeV/c)^2, comparison with various models 77−18294
e^-p, polarised e, elastic scatt. asymmetries in SU(2)×U(1) gauge theory 79−40781
$e^-p \to e^-p$, elastic scatt., polarisation of final lepton *(Russian)* 77−26529
$e^+p \to e^+\gamma X/e^-p \to e^-\gamma X$, deep inelastic scatt., quark-parton model 77−41846
high-energy scatt. of polarised electrons from polarised protons 77−34157

electron radiation
axion production search in low energy electron bremsstrahlung 79−63401
bremsstrahlung, ang. distrib. of nonrelativistic intensity calcs., program 78−87001
Caldirola equations, generalised, for classically radiating electron 77−82401
channelled electrons in crystals quasi-synchrotron radiation characts. 80−92572
electrodynamics, classical, radiation reaction terms 80−48126
field of 2 plane noncollinear EM waves, total radiation anal. *(Russian)* 77−10825
induced radiation in plane wave in mag. field 80−37196
measurement standards, primary, Soviet, for 5 to 50 MeV 77−75031
planar-channelled electrons, emission spectrum 80−44240
plasma, polarisation freq. depend. of electron cyclotron emission 80−33808
QED calculation of radiation from electron in quantised field of nonmonochromatic EM wave *(Russian)* 78−82132
relativistic electron radiation in variable undulator *(Russian)* 77−75397
relativistic polyhelical electron beam in open waveguide, diffraction radiation *(Russian)* 77−75398
stimulated electron radiation due to wiggled magnetic field 80−58451
storage ring, SHF radiation, coherent synchrotron vibrs. effect *(Russian)* 78−66438
synchrotron-Cherenkov radiation, expt. aspects 77−19146
UHF nonequilibrium plasma diagnostics by atomic bremsstrahlung continuum 78−67483
Vavilov-Cherenkov effect, radiator size depend. *(Russian)* 78−5405
Ar plasma radiation obs., line and continuous spectra *(French)* 80−19619
Au+e, atomic field bremsstrahlung, absolute cross section meas. 77−50529

electron relaxation time (metals)
A15-compounds, electron lifetime affecting electronic props. 79−15134
A-15 compound, defect influence on T_c 80−20345
rel. to acoustic wave attenuation, low-freq. longit. waves, viscous and induction mechanisms 77−8152
alkali metals, elec. and thermal cond. in weak mag. fields 80−65535
alkali metals, electron relax. time energy depend., electron-phonon resist. 79−60805
alloy, disordered, energy band struct. and elec. cond., effect of short-range order 80−10860
alloys, binary, elec. resist. near crit. point 80−96847
analysis at high temp. 78−2465
de Haas-van Alphen effect, influence of long-range dislocation pots. 77−8009
degenerate free electron metal, cyclotron wave propag., finite $\omega\tau$ effect 77−20228
diffusion thermopower, boundary scatt. effect 80−6817
dilute alloys, elec. transport and deviations from Matthiessen's rule 80−65524
rel. to emissivity estimation, classical electron theory *(Russian)* 78−38859
energy dependent relax. times in electronic transport props. 79−60804
ferromagnetic metal, freq. depend. elec. cond. 77−66181
ferromagnetic metal, magnon and cond. electron relax. processes *(Russian)* 80−7102
film, monocryst., TCR, analytical expression 79−42670
film, optical determ. by surface plasmon excitation 77−1499
film, strain coeffs. of resist., deduced from effective Fuchs-Sondheimer model and relax. time model 79−78222
high-frequency props., electron relax. time and impurity scatt. amplitude *(Russian)* 77−32033
kinetic equation, iteration soln. 77−43564
liquid metal, Hall effect theory 77−47797
metallic glasses, elec. resist., anomaly in temp. depend., modified relax. time approx. 79−65424
metallic glasses, electronic lifetime, noncommutative two-level model 80−103663
multiphonon contribution to struct. factor, rel. to relax. time calc. 77−1206
noble metals, electron relax. time energy depend., electron-phonon resist. 79−60805
polyvalent metals, electron relax. time energy depend., electron-phonon resist. 79−60805
resistivity anomaly at low temp. *(Russian)* 77−35918
review *(Japanese)* 78−30910
sound absorption temp. and freq. depend. *(Russian)* 78−34827
spiral dislocation scattering, t-matrix 78−39101
thermoelectricity theory, electron-phonon interactions 79−69498

electron relaxation time continued
transition metals and alloys, BCC, electron lifetime affecting electronic props. 79−15134
waiting time paradox, graphic illustration for teaching 78−36771
Al alloy, dil., Hall coeff., calc. by 4-OPW approx. 78−76052
Al, impurity low-field galvanomag. coeffs., 4 OPW calcs. 77−69304
Al-Ag(Ga)(Ge) dil. alloys, Hall coeff., residual resist., and relax. times 79−11107
Al-Cr, Al-Mn, Al-Cr-Mn, dil. alloys, Hall coeff. and elec. resist. 77−11898
Al-Ga(Ag), dil, Hall coeff. by OPW Fermi surface model 80−6816
Cd, Fermi surface, 3rd band sheet, electron effective mass and relaxation time 79−11056
Co, optical consts. and electronic characts., 20 to 1750°C 79−38516
Cu, electronic relax. time in Sondheimer size effect, temp. depend. 79−87086
$Cu_2Mo_6S_8$, normal state and superconducting property measurements 78−91660
electrical resistivity, relax. time near order-disorder transition 78−87788
Fe, optical and electronic props., temp. depend., 20, 1400 and 1600°C 79−87412
Fe-Al (45%), ordered and disordered states, optical and elec. props. 77−85826
Fe-Ni alloy, optical and electronic characts., 20-1750°C, comp. depend. *(Russian)* 78−84601
Fe_3Al, order-disorder transform. effect on optical and elec. props. *(Russian)* 77−39820
$Fe_{68}Co_{32}$, ferromagnet, magnon heat cond. and lifetimes, 1-2 to 4.5K 77−16066
Hg electrode, electroreflection spectra calc., electromodulation mechanisms 77−1658
K, elec. resist., effect of energy depend. of electron relax. time 77−69296
K, ideally pure, anisotropy correction to elec. resist. 77−4317
Mg, pure and dil. alloys, electron lifetime anisotropy, Dingle temp. due to dislocation scatt. 79−78082
Nb_3Ge, electron-lifetime effects on props. 80−10951
Nb_3Sn, electron-lifetime effects on props. 80−10951
Ni-Ge alloys, liq., integrated emissivity, electric resistivity 78−43155
Ni_5Ge_3, amorphous-crystalline transition, opt. and elec. characts. *(Russian)* 77−85191
Ni_3Mn, elec. resist., relax. time near order-disorder transition 78−87788
Pb, plastically bent, effect of dislocations on electron relax. time, cyclotron reson. 79−24217
$PbMo_6S_8$, normal state and superconducting property measurements 78−91660
Sn, sound attenuation and velocity depend. on mag. field *(Russian)* 80−29446
Ti-V-Cr, electron-lifetime effects on props. 80−10951
W, total hemispherical emissivity 79−10973
W-Re amorphous alloys, phase-slip and localisation diffusion lengths 80−107747

electron resists
conference on electron, ion and photon beam technology, Palo Alto, CA, USA (May 1978) 78−74827
conference on electron, ion and proton beam technology, conf., Boston, MA, USA (29 May-1 June, 1979) 80−67927
energy deposition functions, Monte Carlo simulation of electron scatt. 79−56897
energy loss in electron beam lithography, Bethe and Spencer-Fano theories 78−87728
lithography, dynamic beam shaping, advantages, system design 78−74834
negative resist, electron depth distrib., expt. test of Bethe-Bloch model 80−16132
PMMA, cross-linked positive electron resist, synthesis and props. 80−76221
PMMA, molecular weight depend. of developed contours 79−87859
PMMA, use in nanostructure fabrication, dense metal patterns 79−75657
polymer, dissolution kinematics, numerical solution and expt. verification 78−26687
polymethacrylates degradation obs., for PMMA, PBMA, PMA and PMA AN 78−27795
polymethyl methacrylate resist, electron depth distrib., expt. test of Bethe-Bloch model 80−16132
positive resist, plasma etching durability, additive effects 80−66683
SEM fiducial grid prep. by electron resist. technique 77−25230
solid-electron interactions conf., Southampton, England (Apr. 1976) 77−44570
two-level process for self-aligned thin film struct. fabrication with 1000 Å resolution 80−49996
vector scan electron beam lithographic system, deflection distortion 78−74835

electron ring accelerators
acceleration of ions in electron storage rings 79−18064
Astron Accelerator, 5 MeV, 400 A, 500 MHz modulation system for beam energy 77−24202
beam-beam interactions in e-p storage rings 78−78889
collective accelerator, JINR, Dubna, plasma source of neutral particles 77−75013
collective accelerator for heavy ions *(Russian)* 77−67914
collective accelerators, current status 79−76161
collective ion accel. program at Maryland, electron ring and linear beam methods 77−83168
collective ion acceleration, book 80−865
collective ion acceleration with electron rings, book contrib. 80−867
collective methods of acceleration, conference, Irvine, CA, USA (May 1978) 80−4479
collective particle accelerators 79−76165
colliding beam accelerators, large dia. supercond. solenoid mag. spectrometers 77−26919
compression system, IPP-Japan 80−95490
data acquisition and processing on electron beam fusion accelerators 78−37469
deceleration of intense relativistic electron rings by ions, stopping length 77−14282
E layers, stability and equilib. props., determ. of holding power and focusing parameters 80−5408
E-ring formation with time varying mirror coil 79−72020

electron ring accelerators continued
- electron beam, relativistic, ion accumulation caused by ion-ion interactions 80–5417
- electron-ion instability, numerical anal. of nonlinear effects 79–54622
- EM induction conductor accelerator efficiency increase method 80–99355
- field reversing E-layers, translation and compression in magnetically insulated diode 80–14017
- Garching Pustarex accelerator 79–76162
- heavy-ion accelerator, dimensions of electron ring meas. by synchrotron radiation 80–42877
- heavy-ion collective acceleration in electron rings, 'Pustarex' expt. 77–83285
- instabilities in compensated electron ring beams *(Russian)* 78–37467
- ion acceleration in electron storage rings, conf., USSR Acad. of Science, (June 1977) 79–18062
- laser pumped ring accelerator, particle focusing with rectified light 80–42879
- longitudinal coupling impedance of an electron ring in an anisotropic conducting cylinder 80–5404
- magnetic shielding of electron ring effect on ring motion 80–13991
- magnetostatic system of the collective electron ring accelerator 80–5407
- microwave generation and suppression in hollow rotating electron beam 77–83797
- mirror system, wideband, for electron ring diagnostics, using synchrotron radiation 78–78518
- neutralised, two-stream instability 78–25357
- nonneutral electron layer trapping, using static mag. mirror system and resistive wall 80–5409
- optical diagnostics of electron rings using synchrotron radiation and light scattering meas. 80–5405
- phasotron, electron ring, const. guide field induction, acceleration, magnet system 77–83181
- Pustarex device, trapping and compression of electron rings 80–5403
- radial beam blowup in Maryland ERA, observation and suppression 77–83164
- relativistic electron ring, retarding force of image currents in resistive cylinder, stopping length 77–67918
- relativistic electron ring azimuthal oscillations in resonator with stabilising medium *(Russian)* 78–29889
- relativistic electron rings, longitudinal instability 77–67920
- relativistic particle ring, coherent oscillations, Vlasov eqn. 78–55060
- relativistic ring with discrete and continuous eigenvalue spectrum, resonance crossing 78–58507
- ring formation and trapping, using resistive walls and static mirror coils 78–45752
- synchrotron radiation, appls., review 78–9010
- UMERA system, E-ring formation with time varying mirror coil 79–72020
- e^+e^- storage ring, PETRA 78–78530
- e^+e^- storage rings, beam-beam interactions 78–78894

electron scattering *see elastic scattering of electrons by atoms and molecules; electron beam effects; electron beams; electron-electron interactions; electron-electron scattering; electron impact; electron-nucleon interactions; electron-nucleon scattering; electron-nucleus reactions; electron-nucleus scattering; electron-positron interactions; electron-positron scattering; electron spectra; hadron electroproduction; neutrino-electron interactions; neutrino-electron scattering; secondary emission*

electron solvation *see solvation*

electron spectra
- *see also Auger effect; conversion electron spectra; electron energy loss spectra; electron impact; electron spectroscopy; photoelectron spectra*
- acetophenones, di- and trisubstituted, π^*-π systems, UV electronic absorpt. spectra 80–74132
- acetophenones, mono substituted, semi empirical Π-electron calcs. 80–74131
- anthracene surface, Ar impact, Penning ionisation electron spectra and photoelectron spectra 80–66352
- astronomical synchrotron radiation component, effect of interstellar mag. field inhomogeneities 80–85849
- atom, autoionisation intersecting terms of collisions, electron spectra interference struct. *(Russian)* 78–1070
- atom, collisionally excited, electron ang. distrib. from autoionising states 80–43007
- atom+atom collision, Penning and assoc. ionisation, complex. pot. and electron spectrum 78–94310
- atomic collisions, fast particle electron emission, line shape, acceptance function effects 80–37787
- atoms, ejected electron spectra, displaced thresholds 78–5349
- atoms, electron coincidence ionisation spectra, Green's function anal. 79–31714
- atoms, excited, collisionally aligned, angular correl. of autoionisation electrons, photons 77–14385
- atoms, photoionisation, electron spectrosc. obs. using synchrotron radiation 79–31485
- auroral electrons energy distrib., incoherent scatter radar and photometric meas. comparison 78–77390
- auroral secondary electrons spectrum at low altitudes, collisionless effects 79–40008
- autoionisation-radiative emission interference of at. excited state decay 79–26945
- benzene, excited electronic states, variable angle electron impact spectroscopy 78–13612
- benzene, solid, electron transmission, 0 to 15 eV, reson. structs. 79–87536
- beta decay, K-shell internal ionisation, many electron effect, relativistic theory 77–18890
- conference, Melbourne, Australia (Aug. 1978) 79–33868
- 1,3-cycloheptadiene, electron impact, electronic spectra 79–45855
- 1,3-cyclohexadiene, electron impact, electronic spectra 79–45855
- 1,4-cyclohexadiene, excited electronic states, electron impact spectrosc. 79–45842
- cyclohexane, excited electronic states, electron impact spectrosc. 79–45842
- 1,3-cyclopentadiene, electron impact, electronic spectra 79–45855
- deconvolution, electron loss data as unit impulse response function 79–9265
- dielectric, photon induced relativistic band struct. 77–32462
- electronic and at. collisions, conference, Kyoto, Japan (Aug.-Sept. 1979) 80–62394

electron spectra continued
- ethylene, (e,2e), correlation effects, electron momentum distributions in valence orbitals 79–862
- ethylene, electron affinities, pi* anion, bond lengths, electron transmission spectroscopy study 80–18925
- F-region, energetic electrons spectra meas. by Hadamard energy spectrometer *(Japanese)* 80–94637
- fluorobenzenes, excited electronic states, variable angle electron impact spectroscopy 78–13612
- graphite fluorides, $(CF)_n$ and $(C_2F)_n$, prep., struct., discharge characts., electrode props. 80–89502
- heavy ion+at. collisions using GSI linear accelerator, X-ray production, appls. 77–19041
- heavy ion+atom, outer shell electron emission, differential cross sections 79–45817
- heavy ion+C coil collisions, electron emission, energy distribs., solid state effects 77–19062
- heterocyclic aromatic molecules, Penning election spectra and photoelection spectra, rel. intensities 80–95725
- high-current beams, meas. of energy spectrum 77–46470
- hydrocarbons, unsaturated, Penning electron and photoelectron spectra, relative intensities comparison 79–81237
- hydrogenic ion, electron impact, mutual ang. and energy distribs. near ionis. threshold 79–64108
- inert gas+diatomic (triatomic) mol., Penning ionis. process from electron spectroscopy 77–14555
- inner-shell vacancy filling detector, scintillation counter 77–18749
- ion-acoustic turbulence-plasma interactions and electron spectrum in electric fields 80–38617
- ion-atom and ion-solid collisions, continuum electron capture and loss, cusp spectroscopy of forward peak 80–14201
- ion-induced kinetic electron ejection, pot. emission, semiconductors and insulators, review 77–44109
- ionosphere, lower, displaced Maxwellian vel. distrib. rel. to continuum momentum eqns. 77–87171
- ionosphere, lower, electron distrib. function and ion concs., Boltzmann-Fokker-Planck theory 77–78564
- ionosphere, winter, thermal electrons energy distrib. obs. by S-310-5 rocket *(Japanese)* 80–94636
- magnetic thin films, substructural defect anal. by coherent methods *(Russian)* 79–61190
- magnetopause, energetic electron spectrum meas. from Prognoz 3 80–72697
- magnetosphere, International Sun Earth Explorer 1 electron spectrometer expt. 78–85809
- magnetosphere, substorm-assoc. particle fluxes and spectra at $L=6$ to 8, GEOS-1 obs. 79–35067
- magnetosphere, thermal/suprathermal plasmas electron and ion spectra obs. by GEOS-1 S-302 expt. 79–35070
- magnetosphere polar cusp, precipitating electrons spectra during 1977, September 19 to 21 mag. storm 79–35056
- metal vapour, excited by electron impact, ejected-electron spectra from autoionising levels 80–37893
- metallic surface, anisotropic contrib. to optical pot., in electron spectroscopy, theory 80–44086
- metallic surfaces covered with adsorbed species, vibrs., electron impact spectrometer appl. *(French)* 78–41380
- molecular electronic structure, investig., electron coincidence spectrometer appls. 79–30617
- molecules, electron coincidence ionisation spectra, Green's function anal. 79–31714
- molecules, electronic excitation functions by low electron impact spectroscopy, trapped electron restrictions 80–69184
- multiply charged ion+atom, autoionisation, electron and photon emission 80–63813
- norbornadiene, excited electronic states, electron impact spectrosc. 79–45842
- norbornene, excited electronic states, electron impact spectrosc. 79–45842
- one-dimensional crystal, surface pot. influence on electron refl. intensities 77–63506
- Penning ionisation processes investig. by electron spectroscopy 80–58364
- phosphine 3R hydrochloride, interaction with aliphatic acids and alcohols, IR and electron spectra *(Russian)* 78–21930
- plasma focus, 1 kJ, neutron-, ion-, and electron-energy spectra determ. 77–35404
- porphin, electron spectra, PPDP/S approx. calc. *(Russian)* 78–13435
- pyridine, solid, electron transmission, 0 to 15 eV, reson. structs. 79–87536
- quasistationary states decay, electron and photon spectra *(Russian)* 79–49969
- rare earth metal, 4f levels, obs. by bremsstrahlung isochromat and XPS spectroscopy 79–24411
- relativistic electron beam instability, passage through dense gas, energy spectrum *(Russian)* 77–3529
- resonant elastic scatt. of electrons for surface struct. meas. 77–63505
- Rydberg states, fine struct. splitting, quantum beat and double reson. spectroscopy 78–86979
- semiconductor detector active volume, determ. from gamma ray interactions, Monte Carlo method 80–63448
- solar coronal X-ray burst source, power-law electron spectrum 80–26836
- solar wind, International Sun Earth Explorer 1 electron spectrometer expt. 78–85809
- solid, electron MFP determ. by depth and ang. depend. of inelastically scatt. electron spectra 78–92154
- tetrafluoromethane, electron impact excitation, resons. and dissoc. attachment 79–7020
- TTF-TCNQ, mol. core excitons, high energy electron inelastic-scatt. spectra 77–69235
- upper atmosphere, Auger electrons fluxes and spectra 78–28376
- using cylindrical mirror spectrometer 79–63326
- (n,e^-) high precision spectroscopy, internal conversion coeffs. for nuclear struct. 80–37353
- Al, electron MFP determ. by depth and ang. depend. of inelastically scatt. electron spectra 78–92154
- Ar, high resoln. pulsed electron beam time-of-flight ejected electron spectra 77–3462
- $Ar+C^{2+}(O^{4+})(Si^{n+})$, $n=10,11,12$, intense low energy autoionisation lines 79–31674
- $Ar+H(H^-)$, 0.5 MeV $H(H^-)$ ionisation comparison 79–41230

electron spectra continued
$Ar+He^+(He^{2+})$, ionisation, differential cross-sections, 0.3 to 2 MeV 79−81271
Ar^*+H, assoc. ionis., rovibronic struct. in electron energy spectrum 80−106380
As_2Se_3:Pt, glass, effect of impurities on elec. props. 80−103699
Au, adsorbed layer comp. anal., by ion-forwarded electron spectra 77−31850
B^++methane, single collision, time delayed autoionisation spectra 78−1067
BN, electron spectra, regularisation method *(Russian)* 79−41215
BaO, epitaxial, on Ir, low energy electron spectra, electron affinity, conduction band edge position 78−14790
Be^++methane, single collision, time delayed autoionisation spectra 78−1067
^{7}Be, electron capture decay, internal ionisation 77−18892
C, secondary electron spectroscopy 77−85854
$C^{6+}+Ar$, electron capture to continuum states, forward ejected electron spectra 79−45831
$C^{q+}+Ar$, continuum electron capture and loss, 1.6-2.8 MeV/A 78−46443
CO, ejected electron spectroscopy of autoionising states using electron-electron coincidence technique 79−3587
CO, inner-shell ionisation, vibr. struct., sudden approx. calcs. 79−50002
CO^+, electronic struct., CO(e, 2e) reaction meas., CI calcs. 77−34769
CO_2, electron impact, 50-400 eV, secondary electrons double differential cross section 80−37897
CO_2, ionised states, core and valence, ab initio HF calcs. 77−79597
CO_2, valence shell ionis. spectra, theory and dipole (e-2e) spectra expts. 79−76522
^{14}C(e,e′), 37, 50.5, 60.5 MeV, 180° scatt. cross sections, excited states, spin parity 77−30557
Ca, 2 keV electron excitation and ionis., ejected electron spectra 77−3466
Ca II, electron impact excitation, identification of low energy autoionising levels 79−31703
Cd, 5^3P_1 autoionising state, 150 eV electron impact excitation, (e, 2e) ang. distrib. study 80−83495
Cd, electron impact, ejected electron spectrum of autoionis. levels 77−27185
CdS adsorption of N_2, CO, and O_2, total current spectrum interpretation 77−85857
CdS, explanation for total current spectrum 77−8693
^{60}Co isotopic γ-ray source, quantum yield of electrons from cylindrical casing 79−31289
Cr_2O_3-MoO_3, physicochem. investig. of phase struct. 77−8807
Cu, broad area electrode, high-β emission sites, energy spectra 78−35253
$D^+ +Ar$, electron capture to continuum states, forward ejected electron spectra 79−45831
D_2, Compton profile determ. by high energy electron impact spectroscopy 77−68083
D_2O, Penning ionis. electron spectra 77−42392
GaAs, doped with Group IV elements, etching, electron spectra, cathodoluminesc. study of inhomogeneities 77−11556
GaAs thin films, reactively sputtered, ESCA/XPS study 80−97430
Ge (100), chemisorption of H, expt. results compared with pairing model calcs. for Si (100) 78−34719
Ge, electron MFP determ. by depth and ang. depend of inelastically scatt. electron spectra 78−92154
H, electron coincidence ionisation spectroscopy, rel. to impulse approx. calcs. 79−31715
$H^- +N_2$ (inert gas), charge transfer, ejected electron spectra 79−45828
$H^+ +Ar$, 5-1.5 MeV, ejected-electron energy and ang. distrib., differential cross sections 77−88547
$H^+ +He$, proton energy degradation, approx. yield spectrum 79−31643
$H^+ +He(Ne)(Ar)$, ionisation, projectile energy depend., secondary electron energy distrib. 78−42211
$H^+ +N_2$ collisions, proton energy deposition and secondary electron spectra calcs. 78−74746
H_2, Compton profile determ. by high energy electron impact spectroscopy 77−68083
H_2, statistical fluctuations in ionisation yield, rel. to electron degradation spectrum 80−99581
$HBr+He(2^3S)$, Penning ionis. electron spectra, 584å photoelectron spectra 77−79687
$HCl+He(2^3S)$, Penning ionis. electron spectra, 584å photoelectron spectra 77−79687
$H^-(D^-)+He$, collisionally induced electron detachment, 0.5 MeV, target effect 80−37858
HF, Feshbach resons., predissoc. investig. 80−83433
$HF+He(2^3S)$, Penning ionis. electron spectra, 584å photoelectron spectra 77−79687
$HI+He(2^3S)$, Penning ionis. electron spectra, 584å photoelectron spectra 77−79687
H_2O, molecule, (e,2e) separation energy spectra, valence orbital electron momentum distribs. 77−38736
H_2O, Penning ionis. electron spectra 77−42392
H_2O, vapour, fast electron impact, secondary electron energy distrib. 77−58148
H_2S, Penning ionis. electron spectra 77−42392
He, Compton profile determ. by high energy electron impact spectroscopy 77−68083
He, electron impact, low energy, post collision interaction, ejected electron energy distrib. 79−72423
He, electron impact ionis., post-collision interaction anal. from ejected electron spectra 77−42416
He, electron impact ionis., 35 eV, triple differential cross section 79−36777
He, electron impact ionisation, emitted electron ang. distrib. 78−55241
He, electron scatt., interaction with electrons ejected from impact excited autoionis. states 78−42221
He, high resoln. pulsed electron beam time-of-flight ejected-electron spectra 77−3462
He+He, (2^3S) and (2^1S) metastable states, direct and assoc. ionisation rate consts. in afterglow, electron energy spectra 79−13812
$He+Li^+$, 2 to 5 keV, ejected electron profile variation with impact angle 78−37729
$He^{+,2+}+Ar$, 2 MeV, ejected electron spectra, 20-450 eV, 0-10° 77−34746
$He^+ +Ca(Ba)$, 2-1000 eV, spontaneous ionis. mechanisms 79−64090

electron spectra continued
$He^{2+}+C$ foil collisions, electron emission, energy distribs., solid state effects 77−19062
$He^{2+}+He$, 2 MeV, non-occurrence of Fadeev interference struct. in 245 eV electron spectrum peak 77−58155
$^3He^{2+}(^4He^+)+C$ foil, electron vel. distrib., nonexistence of wake bound states 78−13571
$^4He^+ +He$, electron vel. distrib., nonexistence of wake bound states 78−13571
He^*+Ar, Penning ionisation, laser modified collisional effects in electron energy spectrum 78−90278
$He(2^3S,2^1S)+H$, Penning ions. 79−64089
Hf IV, one-electron spectra energy levels and line lists 79−49953
Hg, electron elastic scatt., 4-6 eV, reson., scatt. ang. and spin polaris. spectra 78−25702
Hg, electron impact spectra, intermediate energy 78−82842
K, core thresholds, inelastic electron scatt. spectra meas. 79−95359
K I, electron impact excitation identification of low energy autoionising levels 79−31703
Li I, autoionising levels, electron impact excitation, ejected electron spectrum 78−9259
$Li^+ +He$, <5 keV, autoionised electron spectra 80−32823
$Li^+ +He$ collisions, Li-K shell excitation, autoionisation spectra meas., total cross sections 77−19053
Li^++methane, single collision, time delayed autoionisation spectra 78−1067
LiF film, electronic excitations, inelastic electron scatt. spectra 77−32479
LiI, electron-mol. beam collisions, autoionising states, electronic spectra *(Russian)* 78−22023
^{6}Li, Coulomb energy determ. from electron scatt. spectrum *(Russian)* 77−30479
Mg, 2p-electron excitation and ionisation by electron impact, autoionising states, electron spectra 77−14590
Mg I, Mg II, ejected electron spectrum from autoionis. levels after electron impact 77−75304
Mg, L-shell ionisation and excitation, electron spectra 77−10765
Mo [110], metastable He impact, secondary electron spectra 78−95642
$N_2{}^+$, 1s hole satellite spectrum, large-scale CI calc. 77−65428
N_2+He^*, Penning ionisation, ejected electron spectra obs. 80−48074
NO_2, valence shell ionis. spectra, theory and dipole (e-2e) spectra expts. 79−76522
Na, 54.4-150 eV differential cross sections, 12-140°, optical model calcs. 78−74761
Na, core thresholds, inelastic electron scatt. spectra meas. 79−95359
Na, diabatic field ionisation of highly excited at. states 80−43202
Na, ejected-electron spectrum of autoionis. levels excited by 35-400 eV electrons 77−14582
$Na+H^+(He^+)$, Na $2p^53s^2\ ^2P_{3/2}$ state alignment by 5-30 keV excitation 80−14200
Ne, autoionisation region states, differential excitation function resons. obs. 77−6939
Ne, autoionising states, scatt. electron spectra, post collision interaction effects 78−58819
Ne, K-$L_{2,3}L_{2,3}$, post-collision interaction Auger effects 79−45686
Ne^- scatt. electron spectra, distinction from neutral autoionising states 80−83482
$Ne+He^+(Li^+)(Mg^+)(Na^+)(Ne^+)$, autoionising level excitation, electron spectra 77−14554
$Ne^+ +Ba$, 2-1000 eV, spontaneous ionis. mechanisms 79−64090
$Ne^{n+}+He(Ne,Ar,Kr)$, (n=1, 2, 3, 4), energy spectra of electrons produced 79−45822
Ne^*+H, assoc. ionis., rovibronic struct. in electron energy spectrum 80−106380
Ni (100) surface, electron spectra from He metastable beam impact 77−36334
Ni sputtered films, hexagonal and amorphous, O incorporation, ESCA and electron diffr. meas. 79−11046
N(n,γ), 14 MeV neutron source, electron recoil spectra from gamma-rays anal. 77−26683
$O^{q+}+Ar$, continuum electron capture and loss, 1.6-2.8 MeV/A 78−46443
$O^{q+}+He(Ar)(Ne)$, electron capture to continuum states, forward ejected electron spectra 79−45831
O_2 electron coincidence spectrosc., valence electron momentum distrib. and binding energies 80−102583
Os VIII, one-electron spectra energy levels and line lists 79−49953
Pb-Pb quasimolecular states, inner shell ionis. spectra during form. 78−33592
^{210}Po, α-decay inner shell ionis., L-electron-alpha ang. correlation 77−34267
Pt, secondary electron spectroscopy 77−85854
^{239}Pu, e and $\bar{\nu}$ energy spectra from fission fragments *(Russian)* 77−23120
^{239}Pu(n,f), thermal n, reactor $\bar{\nu}$ and e spectra calc. 79−67791
Rb, ejected electron spectrum of autoionis. levels excited by electron impact 77−58174
Ru (001) surface, chemisorbed O_2, high resolution electron scatt. spectra 79−11013
Ru (~001) stepped surface, O_2 chemisorption, LEED and AES obs. 80−11947
SF_6, electronic props., (e,2e) spectrosc. obs. 80−5527
$SF_6+H^+\rightarrow SF_6{}^+ +e^- +H^+$, 0.3-1.8 MeV, electron energy and ang. distrib. 78−22015
SO_2, Penning ionis. electron spectra 77−42392
Si (111), surface reproducibility and impurity segregation ion neutralisation spectra and UPS obs. 78−34688
$Si^{q+}+Ar$, electron capture to continuum states, forward ejected electron spectra 79−45831
Sr, 2 keV electron excitation and ionis., ejected electron spectra 77−3466
^{182}Ta-containing Ta sheet, radioactive electron emission spectrum (exoelectrons), surface elec. field and Auger effects 78−72705
$TeF_6+H^+\rightarrow TeF_6{}^+ +e^- +H^+$, 0.3-1.8 MeV, electron energy and ang. distrib. 78−22015
U+U, K-shell ionis., classical relativistic trajectory method appl., 1, 10 GeV/n 80−43129
^{235}U, e and $\bar{\nu}$ energy spectra from fission fragments *(Russian)* 77−23120
^{235}U(n,f) thermal n, reactor $\bar{\nu}$ and e spectra calc. 79−67791

electron spectra continued
V (100), sorption investig. using total current spectroscopy of slow electrons 77—8694
V{100}, Au(Au) layer growth, total current spectroscopy 77—36329
W adsorption of N_2, CO, and O_2, total current spectrum interpretation 77—85857
W VI, one-electron spectra energy levels and line lists 79—49953
ZnO, low-energy-electron transmission, optical modulation 79—83070

electron spectrometers
see also beta-ray spectrometers
AES, electronics design 79—30615
analyser based on retarding field method for use in gas medium 80—45598
angle-resolved electron spectrometer with large-angle visual display 80—52808
anthracene, scintillation decay time determ. using low energy spectra 79—9964
ARAKS expt., spectrometers for artificially injected particles 79—21143
Auger, directional effects, review *(French)* 80—47153
Auger, microcomputer-based multiplexer for performing depth profiling 79—67435
backscattering energy distrib. spectrometer, polycryst. solids *(German)* 79—95882
coaxial cone electrostatic velocity analyser, analysis of electron optical props. 80—22480
coaxial cone electrostatic velocity analyser, construction and use in high-resolution electron scattering expts. 80—22481
cylindrical mirror, eqns. of motion of electrons theory 80—86503
cylindrical mirror electron spectrometer, for gas and metal vapour obs. 79—63326
cylindrical-mirror photoelectron energy anal., use of continuous resistive material 80—4820
dipole magnets for 180° electron scatt. 79—49891
double focusing Fe core electron spectrometer BILL for (n,e^-) meas. 78—82566
double pass, cylindrical mirror type, nuclear spectroscopy and atomic phys. appl. 79—713
doubly truncated spherical electrostatic energy analyser for (e, 2e) expts. 78—58872
electric field analyser for study of ionisation particularly near forward direction 79—93261
electron coincidence spectrometer with position sensitive detectors 79—30617
electron energy analyser used in Vacuum Generators HB5 STEM 80—73543
electrostatic cylindrical electron vel. analyser, 127°, relativistic effects 80—86506
electrostatic prism spectrometer, aberration coeffs. and spectral window 79—40647
electrostatic spectrometer, for conversion electron Mossbauer spectroscopy 78—88238
electrostatic spectrometer, in plasma analyser expt. on Pioneer Venus Orbiter 80—67498
energy analyser, electrostatic, appls. 79—44990
energy dispersive spectrometer systems, quantitative chem. anal. 79—39260
energy loss spectroscopy, spectrometer design, electron optical props. 79—12903
fringing field correction for 127° cylindrical and 180° spherical electron spectrometers 79—89042
gas-phase time-of-flight photoelectron spectrometer using synchrotron radiation 80—4818
Hadamard energy spectrometer, appl. to F-region energetic electrons spectra meas. *(Japanese)* 80—94637
high resolution electron energy loss spectrometer for surface vibrational studies 80—2260
high resolution spectrometers for electron scattering 79—68129
internal pair formation high resolution in-beam studies with magnetic+Si(Li) spectrom. 79—18073
linear accelerator facility, detection system of proportional chambers, scintillation and Cerenkov counters 80—52809
low-energy electron spectrometer using concentric hemispheres and a grid retarding field 79—12894
magnetic, corrected second-order aberrations 80—87013
magnetic, for TEM energy analysis 79—26190
magnetic, with directional sensitivity, for GEOS-1 satellite appl. 78—94161
magnetic plus Si(Li)-Si(Li) sum coinc. technique for internal pair transitions 80—18752
magnetic spectrometer design with corrected second-order aberrations, theory 78—89604
microchemical anal. electron spectrometer for 100 kV TEM 79—39251
mini-orange spectrometers, conversion electron spectroscopy 79—93864
Mollenstedt, for measurement of HV fluctuations 79—67434
Mollenstedt electron vel. analyser high-order energy loss lines removal 78—93786
Mossbauer spectroscopy, internal conversion electrons detect. 80—7202
photoelectron spectrometer, for surface studies, gas press. up to 1 Torr 80—4822
photoelectronic spectrometer, use of pulse height analyzer and D/A convertor 80—22473
position sensitive multidetector based on charge coupled imaging device 80—86502
retarding energy analyser, potential distribution of high resolution energy *(Japanese)* 80—68302
retarding potential field electron emission spectrometer 80—22479
SERBE, low-energy (1-16 keV) spectrometer 79—21145
simulated spherical, design procedure 79—89043
storage ring, part of apparatus of investigating electron scattering by atomic nuclei 79—97473
superconducting field photoelectron spectrometer, collimating and magnifying props. 80—22478
threshold-potential spectrometer based on Auger electron spectrometer 80—52365
trochoidal electron monochromator, optimization of parameters 80—86511
two-channel coincidence, 0.7 ns resolution 80—91363
vacuum dependent scientific instruments, hydrocarbon contamination 79—63259

electron spectrometers continued
vacuum UV photoelectron spectrometer for metal chemisorption studies *(Japanese)* 78—78044
versatile, for measurement of electron spectra of solid surfaces in ultrahigh vacuum 79—58849
wideband electron spectrum analyser, 10 to 275 keV electron energy 78—86719
In_2Te_3-type semicond. radiation-resistant fast-electron detectors 78—78559
NaI(Tl) scintillator, electron detection efficiency for electrons and gamma-rays > few keV 79—36461
Si-Li surface-barrier detectors for electron and soft X-ray spectrometry 80—882
Si(Li) electron spectrometer on-line with an automatic irradiation apparatus 78—90014
Si(Li), with superconducting transporting magnets 80—27376

electron spectroscopy
see also electron spectra; photoelectron spectroscopy
adhesion, surface chemistry studies, anal. appls. 80—88440
adsorbed atoms and molecules, core level spectroscopy, surface relax. energies, theory 77—89830
aerosols, urban, characterisation 77—41157
AES, chemical-state effects 78—92566
AES, convolution and deconvolution 78—52601
AES, microarea anal. system with submicron anal. capacity, performance tests 78—73106
AES, quantitative, background determ. method 77—1968
AES depth profiling, appl. of tailored modulation techniques 77—15702
AES depth profiling with N_2^+ ion sputtering 77—16889
AES in SEM, high resolution, electron sources comparison 77—25330
AES of surfaces, effects due to probing electrons and sputtering 77—90706
AES/APS self-convolution inversion, FFT and digital signal processing 79—71430
air filters, ESCA investigation 79—96383
alkali tetrachloroaluminates, vapor characterisation by photoelectron spectrosc. 80—81388
alkali tetrafluoroaluminates, vapor characterisation by photoelectron spectrosc. 80—81388
ammonium tetrachloroaluminate, vapor characterisation by photoelectron spectrosc. 80—81388
analyser for inelastically scatt. electrons from atoms 78—70936
analytical electron microscopy, book 79—97479
angle resolved Auger surface spectroscopy, for chemisorbed atoms on metal surface 77—28694
angular-dependent spectrometry, tube-aperture lens system 77—79200
applications in fundamental research and proctice *(Hungarian)* 80—18046
asbestos, elemental intensity ratio variation used to identify fibres 80—3462
atomically clean surfaces, instruments for anal. and imaging 80—105749
Auger, vacuum improvement technique 80—27381
Auger electron spectroscopy, general principles, experiments and appl. *(French)* 79—8468
Auger electron spectroscopy blanking resistive heating cct. 77—29078
Auger emission, data acquisition control using HP 9845 desktop computer 79—21726
Auger for light duty electrical contact reliability assessment 78—29219
Auger for microelectronic device bonds, glass-metal seals and weld metal failure anal. 78—24900
Auger line shape changes effect on depth profiles, correction 77—40605
Auger microprobe, microcomputer controlled 80—81414
Auger peaks, bremsstrahlung-induced, utility in spectroscopy 79—30618
Auger spectra, instrumental distortion, cylindrical energy analyzer construction 78—8469
Auger spectrometer, electron microprobe, with ultra high vac. SEM capability *(Japanese)* 78—27849
Auger spectrometer, secondary emission effects in retarding field instrument 78—23564
Auger spectroscopy, low-energy detectability enhancement 80—22477
Auger spectroscopy, quantitative, effect of electron escape depth 77—21452
Auger spectroscopy, tailored waveform modulation calc. for integral spectra 77—32860
Auger spectroscopy, use of glow discharge lamp as electron gun 77—31027
binding energy and charge density meas., electron coincidence spectroscopy 80—63817
biological thin section quantitative analysis and mapping 79—74820
biology research, impact of photoelectron spectroscopy 78—65156
book 78—16896
book series, introduction 78—16897
channel electron multiplier, fully-screened high-voltage vacuum feed-through 78—24814
for chemical anal., appls. to materials for electrophotography 78—92565
coincidence experiments, two-parameter 78—20135
coincidence spectroscopy, orbital shape, charge density, mol. struct. determ. appls. 79—27113
composition and structure of engineering and industrial materials, instrumentation 77—4882
computer controlled ESCA for nondestructive surface characterization utilizing a TV-type position sensitive detector 78—76969
computerised approach 78—86390
conference, Lyons, France (Apr. 1976) *(French)* 77—36354
conference, Melbourne, Australia (Aug. 1978) 79—33868
contaminant identification by energetic beams 79—39250
conversion electron Mossbauer spectroscopy, electron transport anal. 78—94159
conversion electron Mossbauer spectroscopy down to 4.2K, applications to thin film and surface studies 78—84504
conversion electron spectrometer, in-beam use 78—55086
corrosion science, surface analytic techniques 80—31929
cylindrical mirror analyser, transmission props. viewed in energy angle space 78—15745
cylindrical mirror analyser 78—24899
cylindrical mirror analyser system for AES, Auger electron appearance pot. spectroscopy and disappearance pot. spectroscopy 78—23986
cylindrical-mirror electrostatic analyser for beta spectroscopy of beams 80—63446

electron spectroscopy continued
Darmstadt linear accelerator, detector system and performance of elec. scatt. system 78—70680
Darmstadt linear accelerator electron scatt. facility, beam transport and spectrom. 78—70679
Darmstadt linear accelerator electron scatt. facility, data processing 78—70681
deconvolution methods, review 79—26188
deep-level trap spectroscopy, signal analyser 77—87789
depth selective Mossbauer effect spectroscopy empirical method of quantitative anal. using conversion electrons 78—20130
differential retarding field analyser characts., photoelectron and Penning ionis. spectrometry 77—41735
double focusing Fe core electron spectrometer BILL for (n,e^-) meas. 78—82566
double-focusing electron spectrometer, new effective transmission determ. from focalization props. 78—17463
electron capture spectroscopy, technique for surface science and ferromagnetism 80—92766
electron emission from nuclear accelerator targets *(Russian)* 79—49335
electron impact spectrometer using concentric hemispheres, appls. *(French)* 78—41380
electrostatic analyser, experimental data components isolation via Fourier transforms 78—36434
electrostatic cylindrical mirror analysers, response functions 78—1146
electrostatic deflection type electron analysers, electron refl. ghost lines, energy loss reduction 80—18050
electrostatic photoelectron spectrometer, analyser brightness determ. 77—25331
electrostatic retarding-field energy analyser, improvement 77—82647
electrostatic spectrometer design, energy loss and UV spectroscopy *(French)* 77—82651
EM isotope separation and in-beam electron spectroscopy, Pt target preparation 80—52812
EM shower sampling counters, characteristics of plastic scintillator and radiator layers 78—58530
energy analyser, for voltage meas. in SEM 77—54019
energy analyzer, two-stage with cylindrical mirrors, aberration reduction 79—40640
energy dispersive spectroscopy 80—27378
energy loss, measurement of radiation damage 80—96568
energy loss microanalysis system with high collection efficiency 80—86508
energy loss spectrometry, differentiated 78—35786
energy loss spectrometry, local characterisation of solids 80—31948
energy loss spectrometry, use in microanalysis and errors involved 78—35785
energy loss spectrometry, using SEM and electrostatic mirror 77—61168
energy loss spectrometry use in microanalysis 78—35784
energy loss spectroscopy, contrib. to anal. microscopy 77—25346
energy loss spectroscopy, spectrometer design, electron optical props. 79—12903
energy loss spectroscopy, tutorial 79—21872
energy loss spectroscopy and microanalysis, instrumentation developments, review 78—35783
energy-loss, as analytical tool, data handling and processing 80—81407
energy-loss analysis, theory and instrum. 80—81405
energy-loss spectral resolution optimisation wing electron lenses between TEM specimen and electron spectrometer 80—101886
energy-loss spectroscopy in context of TEM, review 80—31945
ES200B spectrometer with laterally inhomogeneous sample, ang. and spatial depend. intensity 79—74468
ESCA, AES and SIMS analysis of thin films, expt. *(Hungarian)* 77—4952
ESCA, appls. in industrial research 79—74462
ESCA, conf., Uppsala, Sweden (May 1977) 78—53297
ESCA, electrostatic quadrupole prism spectrometer characts. 77—1970
ESCA, insulator charging, line energy corrections 80—50898
ESCA, principles and appls. 78—27375
ESCA, quantitative surface anal., limitations, depth profiling, catalyst surface anal. 78—53298
ESCA, surface anal. and electronic structure *(French)* 80—7891
ESCA, X-ray type, C 1s contaminant buildup on conductors and insulators 78—95981
ESCA 36 spectrometer, advanced data anal. 77—90684
ESCA apparatus *(Dutch)* 79—1982
ESCA chemical shift, indirect evaluation of Coulombic contribution to ionis. pots. for nonbonding electrons 78—92572
ESCA chemical shifts and modified Sanderson electronegativity calcs. 77—83656
ESCA photoionisation cross section, relative intensities calcs., comparisons 78—50464
ESCA spectra automatic analysis by top down method *(Japanese)* 77—40598
ESCA spectrometer retarding lens system, computer optimisation 77—13827
ESCA using monochromated UV discharge lamp and XPS spectrometer 78—89601
ESCA-ion scatt. spectroscopy-SIMS, review, chem. appls. 79—43701
exoelectrons (chemically stimulated, photostimulated and tribostimulated), meas. apparatus for 77—90260
failure analysis tools comparison and selection 80—71865
fast projectile electron spectroscopy, autoionizing ion levels and lifetimes 77—38749
field electron emission spectrometer with hemispherical analysing element 78—37108
films, metal-semicond. and metal metal studies in ultra high vacuum scatt. chamber 79—2780
flaw detectors, sensitivity comparison 78—44322
fluoroethylenes, electron affinities, pi* anions, bond lengths, electron transmission spectroscopy study 80—18925
furnace, inductively heated, high temp., construction and operation 77—82521
gas atmosphere quantitative analysis adsorption chamber 80—85234
graphite, electron-spectroscopic analysis of neutron-irradiated pyrographite 80—63261
heavy particle collisions, electron spectroscopy 77—42397
hemispherical electrostatic 180° deflector optimisation, via electron energy distribs. calc. *(French)* 78—21269
high resolution techniques 80—62740
high sensitivity degradation, signal-to-noise ratio calc. 77—61163

electron spectroscopy continued
impact electron spectroscopy of molecular excitation functions, trapped electron restrictions 80—69184
impact spectrometry, high energy resolution using hemispherical electrostatic energy selector 77—23577
in-beam electron spectroscopy meas. of internal conversion coeff. 78—13374
inelastic electron scattering: surface vibrational spectroscopy 80—107347
inelastic mean free paths of solids, data tables 78—84686
inner-shell electron spectroscopy, for microanal. 80—68303
instrument function of cylindrical energy analyzer in raster Auger spectroscopy 80—42886
International Sun Earth Explorer 1, electron spectrometer expt. 78—85809
ionising excited atom thermal energy collisions, electron spectrometric studies 80—63788
isotope separation using electron microscope, and electron spectroscopy, rotating ion-collectors 80—32850
kaolin bodies, effect of mineralizers on firing shrinkage, microstruct. and strength 80—97488
kaolinite-mullite reaction sequence, spectroscopic anal. of Al coordination changes 78—48719
light element microanalysis by K-shell excitation EELS 79—74480
lunar regolith, secondary electron emission characts. determ. method 80—12687
magnetic prism beta spectrometer for low energies 80—99403
metal oxides, ESCA, Madelung pot. effects 80—104036
metal surfaces, clean, AES anal., contamination effects obs. 78—53293
metal-oxide system characterisation by high-resolution electron spectroscopy 77—40624
metals, electron penetration and energy transfer in solid metal targets, film bulk method 78—2963
microanalysis by energy loss spectrometry *(Japanese)* 78—85244
microfoil conversion electron detector for Mossbauer spectroscopy 78—70698
mini-orange spectrometers, wedge shaped $SmCo_5$ magnets 78—58531
molecular photoelectron spectroscopy, review 78—94283
molecule, free, ultra-soft X-ray emission spectroscopy, correl. with electron spectroscopy 78—50558
Mollenstedt electron spectrometers, new entrance slit 77—54018
momentum filter for separation of electrons and negative ions 78—78034
Mossbauer depth selective spectroscopy, low energy electrons in matter 80—15930
Mossbauer depth selective spectroscopy influence of atomic number of inert component in surface layer 80—15931
multicomponent deposition processes, monitoring and controlling techniques, review 78—11113
non-crystalline solid, surface and thin film chem. anal. techniques *(French)* 77—73495
nondestructive testing appl., of thin films and powders 78—3430
optical Be filter in He discharge lamp for photoelectron spectroscopy 78—79115
Penning ionisation electron spectroscopy, metastable He impact, electron energy distrib. 79—52060
phosphosilicate glass, AES quantitative anal., electron irrad. induced surface comp. changes 77—48709
photoelectron spectroscopy, 90° spherical deflector for spin-polarization measurements by Mott scattering 80—31951
photoemission, many-electron theory, in electron spectroscopy book 78—17714
polyethylene low density flame treatment of surface, XPES study 79—66179
polymers, struct., bonding, reactivity by ESCA 78—53299
positron spectrometer, low-background, many cryst. scintillation triple $\beta\gamma\gamma$ coincidence 77—54446
pseudobinary systems, internal calibration technique for quantitative analysis, AES 77—36834
pulsed electron beam gun, kinetics and spectroscopy appl. 78—5413
quantitative energy-loss spectroscopy, treatment of inner-shell electron energy losses 79—12905
radionuclide radiation precision spectrometry using semiconductor detectors *(Russian)* 79—31305
recoil shadow method in-beam spectroscopy of low energy conversion electrons 78—33372
relativistic electron scattering, expt. techniques for excited nuclei studies 77—30701
retardation system for Auger electron spectroscopy 78—50654
retarding field energy analyser for beam-plasma system 77—35392
retarding field energy analyser in electron spectrometry, noise meas. 80—27377
review, electron spectroscopy appls. *(Japanese)* 79—40645
RHEED-AES combined system, simultaneous struct. and comp. information 78—47216
sample manipulator and heater for ultrahigh vac. 79—44988
scanning Auger electron microscope, calc. of effects of backscattered electrons on spatial resolution 80—81412
scanning Auger microscopy, developments 80—101909
scanning Auger microscopy, resolution, quantification and sensitivity 80—81411
scanning ESCA, operation and limitations 77—36818
secondary electron emission ion detector, low noise, high voltage for polyatomic ions 77—40601
secondary electron emission spectroscopy of solid surfaces, review 77—36326
semiconductor, electron spectroscopy techniques, review *(Japanese)* 80—49061
SIMS/AES, instrumentation and appls. in Japan 79—35883
slow electron spectrometer, electron-optical system 77—41733
solid surface electron spectra in ultrahigh vacuum, measurement using versatile spectrometer 79—58849
solid surfaces, quantitative, electron inelastic mean free path 79—92041
spectrometer, double-stage retarding field type, expt. 77—82649
spectrometer, double-stage retarding field type, theory 77—82648
spin polarisation detector, experimental exam., using Hg+e scatt. 78—32927
steel, ferritic stainless, effect of Cl ions on passive layers 80—59766
steel, stainless, Cr-Ni-Mo, surface, scraping, mech. (electrolytic) polishing, ion etching, effects on ESCA 78—53037
steels, stainless, passive state, electron spectroscopy anal. 80—59765
STEM microanalysis detect. limit improvement using coincidence techniques 77—25345

electron spectroscopy continued
surface AES with secondary emission imaging 78—11475
surface anal. tools review 80—103540
surface analysis, book 77—63545
surface analysis, coordinated, using SEM, electron probe microanalysis and electron spectroscopy 79—96381
surface analysis, electron-excited core level spectroscopies, book contrib. 77—63503
surface analysis, introductory survey, book contrib. 77—63502
surface analysis, quantitative, by electron spectroscopy 78—92552
surface analysis, review of ESCA technique, instrumentation, and appl. 78—68947
surface analysis, system, modular combined ESCA, UPS, AES, and SIMS 78—73107
surface analysis spectrometer, design, book contrib. 77—61169
surface and bulk microanalysis, electron spectroscopy apparatus *(French)* 80—47151
surface characterisation, multiple technique instrument, ESCA, scanning Auger, UPS and SIMS 78—73108
surface chemical analysis, direct comparison of AES and ESCA 77—1969
surface microscopy, and microanal., electron spectroscopy 80—52367
surface sensitive analytical techniques, eval. 78—27876
surface structure analysis at high press. 78—73103
surfaces, electron spectroscopy, review 78—92169
surfaces and interfaces, analysis by combined Auger, X-ray and SEM studies 80—81413
surfaces and thin film studies by combined system of SIMS, AES and XPS 80—86536
temperature controller for use in low-energy electron spectroscopies 79—44987
thin films, chem. anal. by energy loss spectroscopy 80—104493
thin surface layers, depth and composition determ. by depth-selective photoelectron spectroscopy 79—43090
total current spectroscopy, review 80—45185
total current spectroscopy, study of surface regions and bulk physics 80—31952
ultrathin film thickness meas. by AES 79—35663
vidicon-camera parallel-detection system for angle-resolved electron spectroscopy 80—4817
X-ray conversion electron spectroscopy using modified photoelectron spectrometer 78—50557
X-ray photoelectron spectroscopy, development (1900-1960) 79—12560
X-ray photoelectron spectroscopy, quantitative, parameters, appls. 79—43697
X-ray source, Cu lines in achromatic Mg X-ray source 79—75667
XPS/SIMS combined apparatus, system for transferring samples between chambers in UHV 79—12809
Ag films, electrodeposited and vac. deposited, AES depth profiling anal. 77—59232
Al complex of glycine, XPS study of glycine binding 79—41196
Al-Mg (2.5wt.%) sheet, surface oxide state and weldability 80—59769
CdSe, thin film, total current spectrosc. investig. 80—7454
Co/γ-Al_2O_3 catalyst, ESCA and EPR meas. after hydrodesulphurization reaction *(French)* 79—52755
CoMo/γ-Al_2O_3 catalyst, ESCA and EPR meas. after hydrodesulphurization reaction *(French)* 79—52755
CoO film on thermally aged Co hardened Au, mech. film breakdown and ESCA, expt. 77—4436
Cr, oxide film form., combination anal. using ESCA, AES and SIMS 79—16092
Cu electrodeposition on Su, reliability anal. 78—24901
Fe-Cr-Al-Y, oxidation resistance, heat treatment and Al^+ ion implantation 80—71785
Fe-Ni-Cr, oxide film form., combination anal. using ESCA, AES and SIMS 79—16092
GaAs, anodic native oxide, ESCA 79—61767
GaAs oxide, plasma grown, semiquantitative chemical depth profiles, Auger spectroscopy and neutron activation anal. 78—53284
GaAs oxide films grown by anodization in electrolytes, electron spectroscopy exam. *(German)* 79—15837
GaP oxide films grown by anodization in electrolytes, electron spectroscopy exam. *(German)* 79—15837
GaSb oxide films grown by anodization in electrolytes, electron spectroscopy exam. *(German)* 79—15837
Ge, film, amorphous, contamination anal. by AES 77—36828
H_2S, valence momentum distribs., binding energies, binary (e,2e) spectrosc. meas. 79—31713
He I polarised radiation source for surface studies 78—74959
He^+, Auger deexcitation spectrosc., impact on Ni(100) with adsorbed K^+ 79—100010
n-InP, epitaxial layer, (100) surface chemistry, ESCA study 80—103552
InSb oxide films grown by anodization in electrolytes, electron spectroscopy exam. *(German)* 79—15837
Li^++Ne collisions, vel. dependence of Ne 2s and 2p, vacancy production, electron spectroscopy 80—58344
Ni (111), adsorption of acetylene, identification of CH species by electron energy loss spectra 79—15022
Ni passivation, S influence study by Auger and electron spectroscopy 80—65347
Ni-Cr resistor layers, ESCA meas., expt. *(Hungarian)* 77—4951
Si, amorphous film, RF plasma deposition from $SiCl_4$-H_2, characterisation 80—66435
Si(Li) detectors, electron counting, appl. to electron energy loss spectra, by high voltage electron microscopy *(French)* 78—54511
SiO_2, amorphous forms, surface struct. ESCA, X-ray line shift meas. *(Russian)* 77—66775
Sn-Ni, electroplated, passive layer, ESCA study 78—23867
Te compounds, electron spectroscopic studies *(French)* 80—108770
V-Ti-C, elemental anal. of second phase carbides using electron loss spectroscopy 79—20500
Zr complex of glycine, XPS study of glycine binding 79—41196

electron spin
anomalous electron mag. moment near conducting plane, non-relativistic calc. 77—61229
anomalous moments in EM field 80—37197
charge current density of Pauli eqn. using vel. operator method, nonrelativistic derivation 78—73872
Dirac equation, mechanical sphere, magnetic momentum and lines of force *(Hungarian)* 80—68344

electron spin continued
education, electron spin, nonrelativistic quantum mechanics derivation from Schrodinger eqn. 78—69942
electron spin coherence in nonphosphoresc. triplet states, optical detect. meas., TADMR and FMDR 78—25578
equations of motion in external field 80—18102
magnetic moment, relativistic mass correction, classical reinterpretation 77—57213
magneto-optical effect, influence of ESR saturation, allowance for dipole-dipole reservoir of electron spins 79—15442
neutrino-electron mixture, influence of spin and Weinberg-angle on bulk viscosity 77—61223
nonlinear effects in theory of erratic electron 78—93825
Planck's constant, origin of quantum theory 80—27179
Poynting's theorem, nonrelativistic and 2-component spin, transition probability 78—24986
spin-density gradient expansion for kinetic energy of electron gas, variational calc. 79—93917
undulators, spin effects during electron movement *(Russian)* 78—13652

electron spin-lattice relaxation
acoustic, liquids 80—97128
alkali halides, spin lattice relax. and g-shift 80—15799
alkali metal-ammonia solns., spin site exchange mechanism for electron relax. times 78—27077
anthracene in glassy matrix, triplet state spin relax. time, anisotropy *(French)* 77—65492
benzene-d_0,-d_6, phosphoresc., Boltzmann population and spin-lattice relax., decay processes 78—31230
benzil, cryst., excited triplet state spin-lattice relax. probabilities, temp. depend. *(Russian)* 80—88860
benzil, cryst., phosphoresc. kinetics rel. to spin-lattice relax. 79—87485
benzophenone, migration of triplet excitons, EPR profiles and phosphoresc. decay data 80—84641
2-benzoylpyridine crystals, lowest triplet state, optically detected EPR 80—15827
calcium copper acetate hexahydrate, and deuterated cpd., tunnelling reson. effects in nonreson. spin-lattice relax. 79—86726
carbazole, triplet state of X-traps, ODMR 79—24231
cubic crystals, calc. of spin-lattice relax., appl. of Houston method 78—2726
cyclohexane, neutron irradiation, radical distribution, ESR study *(Japanese)* 80—44920
cytochrome P-450_{cam}, Fe^{3+} zero-field splitting, Orbach relax. rates 77—21483
cytochrome P-450, anomalous T^7 temp. depend. of Raman spin-lattice relax. 77—21482
di-t-butylnitroxide radical, solid, nucl. and electron spin relax. times meas. 78—60350
diamond:N, spin-lattice relax. of Jahn-Teller N centre 77—66412
dibenzofuran, triplet state of X-traps, ODMR 79—24231
dibenzothiophene, triplet state of X-traps, ODMR 79—24231
diethylammonium manganese chloride, T_1 and T_2 meas. by LODESR 78—15064
diffusion of radical-ion pairs, spatial distrib., electron spin echo obs. 80—29622
α-diketone radical anions, spin-lattice relax. in soln. 79—22735
dilute paramagnet, mag. reson. linewidth due to two-particle interaction 77—90012
diphenylmethylene-d_0,-d_{10}, in benzophenone, ground triplet state, electron spin echo expts. 77—16144
durene:naphthalene, spin-lattice relax. in photo-excited triplet states, spin axes rot. on thermal excitation 78—76294
electric-dipole paramag. relax. due to carriers in quantising mag. fields 79—38381
ethanol-d_0, -d_1, -d_5, γ-irrad., trapped electron spin-lattice relax. 77—60089
ethylene oxide, gas, EPR rot. transitions, T_1 and T_2 relax. 80—9622
fast relaxing centres, in paramag. cryst. *(Russian)* 79—15340
ferromagnetic metals and semiconductors, electron spin-lattice relaxation *(Russian)* 80—103823
field dependence, influence of thermal cond. 78—15013
fluorene, triplet state of X-traps, ODMR 79—24231
$Ga_xAl_{1-x}As$, optically oriented electron, nuclei spin instability *(Russian)* 80—70660
glass-forming polymer, paramag. spin-lattice interactions 80—7149
glasses, echoes and elec. dipole echoes at low temps. 79—69771
glassy organic matrices, electron spin-lattice relax. of radiation-produced Ag atoms, temp. depend., tunnelling relax. 79—34331
graphite lamellar cpds. with Li, K, Rb, HNO_3 and SO_3, EPR studies 80—44902
guanidinium chromium sulphate hexahydrate, multilevel system, spin-lattice relax. from AC susceptibility 77—55702
guanidinium vanadium sulphate hexahydrate, susceptibility meas. spin-lattice relax. effects 77—66279
ice matrices, polycryst., electron spin-lattice relax. of radiation-produced Ag atoms, temp. depend., tunnelling relax. 79—34331
inhomogeneous systems, line broadening, spin-spin and spin-lattice relax. rate meas. 80—58292
insulators, spin lattice relax. and g-shift 80—15799
KCN, relax. times of F-centres meas. at 83K phase transition 77—59458
$KZnF_3$:Er excitation of 650 GHz phonons in spin-lattice relax. 78—27089
lanthanum ethyl sulphate nonahydrate: Tb^{3+}, ESR spectrum, spin lattice relax., effect of hydrostatic compression 78—88185
liquid, APR line form. induced by anisotropic spin-lattice interactions *(Russian)* 78—52338
liquid, electron spin echo phase memory decay, generalised cumulant expansions appl. 79—11334
liquid crystals, nematic and smectic, EPR and NMR relax., first-rank tensor component effects 78—14275
liquid solution, relaxation studies in magnetic resonance spectroscopy 79—73841
magnetic field-pulsed ELDOR spectroscopy for electron spin-lattice relax. time meas. 79—93188
measurement, new method for spin-lattice relax. time, inhomogeneously broadened ESR lines 79—15343
mechanical detection of EPR dispersion signals 79—30520
melanin, relax. times, saturation recovery meas. 78—96017
metals, electron bottleneck effect, impurity spin relax. and EPR linewidth 79—28589

electron spin-lattice relaxation continued
- metals, electron spin-transverse phonon interaction, spin lifetime perturbation calc. 77−12189
- methanol-H_2O matrix, 77K, electron solvation and presolvation, electron spin-lattice relax. 79−57260
- methyl radical in glassy organic matrices, electron spin-lattice relax. 78−76312
- molecular crystals, anisotropy at low temperatures and high mag. fields 79−42822
- naphthalene: quinoxaline, isolated triplet mol. direct spin-lattice relax., librational model 79−11444
- naphthalene, in durene, photoexcited triplet state spin-lattice relax., local phonons effects 78−6605
- naphthalene, mag. effects on delayed fluoresc. at high and low triplet exciton density 77−8634
- naphthalene in durene matrix, spin-lattice relax. of phosphoresc. triplet state, PMDR study 79−27012
- naphthalene-d_8, metastable triplet states, spin-lattice relax. at high mag. fields, phosphoresc. meas. 78−15063
- nitroxide free radicals in liquids, electron spin-echo obs. 80−63685
- ODMR, spin-lattice relax. and triplet-triplet. absorpt. effects 79−19807
- paramagnetic centre interaction with soft phonon modes 79−28590
- paramagnetic insulator, magnetically dil., nonlinear susceptibility in parallel mag. fields 77−59450
- paramagnetic ions in solids, review 77−69672
- paramagnetic nonresonance absorpt., kinetic eqns. 80−7151
- paramagnetic salts, field depend. of spin-lattice relax. 78−6567
- paramagnetic substance, relax. at high press. *(Russian)* 77−43868
- particles, quantum size effect obs. by CESR and NMR 77−20700
- phonon bottleneck, influence on dynamic nucl. polarisation by solid effect 80−20511
- PMMA, neutron irradiation, radical distribution, ESR study *(Japanese)* 80−44920
- polycarbonate, irrad., electron spin-lattice relax. at low temp. 78−68382
- polyethylene, neutron irradiation, radical distribution, ESR study *(Japanese)* 80−44920
- polymer, spatially cross-linked, spin-lattice relax. time meas. of free radicals 78−19331
- pyrene in glassy matrix, triplet state spin relax. time, anisotropy *(French)* 77−65492
- pyrene-d_{10}, EPR line shape of photo-excited triplet state, in cryst. and glass 79−24210
- quartz, fast neutron irradiated, spin-lattice relax., 0.1 to 4.2K 79−78519
- quasi-one-dimensional organic metals, electron spin relax., temp. depend., Peierls fluctuations, EPR meas. 79−73802
- rare earth systems, NMR, EPR, and Mossbauer effect, book contribs. 80−39883
- ruby:Cr^{3+}, high mag. field spin-lattice relax. rates in ground state of ion 79−61407
- ruby:Cr, relaxation behaviour, EPR study, environmental effects 80−66021
- ruby:Ti^{3+}(V^{3+}), cross-relax. 80−71163
- ruby, excited state spin-phonon interaction, time resolved spectroscopic exam. 78−19549
- ruby, resonant cross-relaxation to Jahn-Teller Cr^{4+} ion 79−65723
- ruby, two level spin system, second harmonic generation, time depend. 79−65719
- semiconductor, conduction electron paramag. relax., Coulomb mechanism 78−88191
- semiconductor without inversion centre, conduction electrons spin relaxation *(Russian)* 78−52355
- semiconductors and insulators, non-radiative processes multiphonon recomb. 78−6752
- semiquinones in protic solvents, saturation behaviour, ESR 77−6808
- smectic A mesophase, spin-probe longitudinal relax. 79−94871
- spectral-diffusion decay in echo experiments 79−1723
- spin diffusion and spin-lattice relaxation in paramagnetic crystals 79−33525
- spin relaxation in photo-excited triplet states via vibronic excitation: rotation of spin axes 79−78503
- spin system, optical-acoustic two-phonon relax. 80−11244
- spin-phonon interaction, dynamic screening by carriers, effect on paramag. relax. times 77−16150
- summation process, numerical soln. 79−61200
- surface relaxation in CESR, evidence of spin lattice character 79−28615
- tC $FeCr_2S_{4-x}Se_x$ chalcospinels, ESR spectrum and paramag. susceptibility 80−15789
- TCNQ alkali salt, spin-Peierls transition, 1-D antiferromag. Heisenberg model 80−29395
- 1,2,4,5 tetrachlorobenzene, triplet excitons, high. mag. field, spin-lattice relax. study 80−20517
- 1,2,4,5-tetrachlorobenzene, triplet state spin-lattice relax. in cryst. and matrix isolated mol. 79−11449
- tetramethylammonium manganese trichloride, ESR meas., evidence for two paramag. species 79−61208
- TGS X-irradiated, paramag. relax, spin-echo study 80−7168
- transient ESR line profiles, $S=I={}^1/_2$ system, calcs. 78−88170
- tris-sarcosine calcium chloride:Mn^{2+} ferroelec. dynamics, EPR and ENDOR study 80−75972
- trissarcosine calcium chloride:Mn^{2+}, ferroelec., electron spin-lattice relax. 78−80208
- TTF halides, spin-lattice relax. 78−88190
- two level spin system, second harmonic generation, time depend. 79−65719
- unordered solids, EPR spin lattice relax., dipole induced contrib. 78−80193
- uranyl phenanthraquinone radical ion complex, longitudinal spin-lattice relax. time determ. 80−108076
- vanadyl octaethylporphyrin, radical cation EPR linewidth inversion, relax. theory 77−10693
- zinc bisdiethyldithiocarbamate:Cu^{2+}, exchange interaction of Cu^{2+}-Cu^{2+} pairs, spin-lattice relax. 78−48034
- Ag, adsorption of O_2^-, catalytic oxidation mechanism 78−61046
- AgCl, paramagnetic S-centres, saturation props., ESR meas. 80−50181
- Al, with plastic surface coating, g-factor and spin relax. time of cond. electrons 77−32258
- Al_2O_3, $3d^4$ ion study by cross-relaxation 79−99755
- Al_2O_3:Cr^{3+}, new method for spin-lattice relax. time, inhomogeneously broadened ESR lines 79−15343
- β-Al_2O_3-Na_2O, colour centre ESR by localised tunnelling states 80−108073

electron spin-lattice relaxation continued
- Al_2O_3-SiO_2, glass, spin-lattice relaxation times of paramag. hole and E_1'-centres 80−39871
- Al_2SiO_5:Fe^{3+} crystals, andalusite, spin-lattice relaxation, lattice oscillator heating 78−23329
- BaF_2:Eu^{2+}, spin-lattice coeffs., meas. using uniaxial stress method 77−36129
- $BaWO_4$:Er^{3+}, spin-lattice and spin-spin relax. times, electron spin echo obs. 79−28609
- BaY_2F_8:Nd^{3+}(Ho^{3+})(Er^{3+})(Yb^{3+}), ESR spectra and spin-lattice relax. 80−11263
- $CaCO_3$:Fe^{2+}, electronic spin relax., effect of second-order spin-orbit coupling 80−10935
- CaF_2:Ce^{3+}, Kapitza limited spin-bath relax., paramag. Faraday effect meas. at liq. He temp. 79−95642
- CaF_2:Eu^{2+} single cryst., temp. depend. of second-order spin-lattice coeffs. 77−90029
- CaF_2:Gd^{3+}, cubic, strain effects on EPR by UMER method 77−1592
- $CaMoO_4$:Er^{3+}, phase relax., EPR spin echo expts. 79−99767
- $CaMoO_4$:Mo^{5+}, g-factor, ground state, line broadening, EPR obs. 80−39863
- $Ca_5(PO_4)_3F$: Cr^{5+}, spin-lattice relax. time and Debye temp., EPR obs. 79−28601
- $Ca_5(PO_4)_3F$:Yb^{3+}(Nd^{3+}), spin-lattice relax. times meas., Raman processes 77−51953
- $CdCo_3$:Fe^{2+}, electronic spin relax., effect of second-order spin-orbit coupling 80−10935
- $CdCr_2S_4$(Se_4), EPR linewidth, 100-300K 77−51942
- $CdCr_2Se_4$, crit. speeding-up of spin-relax. 78−48028
- CdS, donors, EPR and spin-lattice relax., Faraday rot. meas. 80−54939
- CdS:Mn^{2+}, spin-lattice relax. ang. depend. 79−73807
- CdS:Mn^{2+}, temp. depend. of rate of spin-lattice relax. 79−42832
- CdTe:Mn, spin-lattice coeffs. of Mn^{2+} 80−84646
- $Ce_2Mg_3(NO_3)_{12}$, spin-lattice relax., dynamic susceptibility meas., liq. He contact effects 80−66011
- $Ce_2Mg_3(NO_3)_{12}.24H_2O$, EPR of Ce^{3+} appl. of SQUID detection system 79−75560
- Co salts:M^{2+}, M=Mn,VO, spin-lattice relax. time meas., 180-380K 78−64268
- $Co(N_2H_5)_2(SO_4)_2$:Co, Mossbauer effect and paramag. relax., superparamag. behaviour of correl. spin domains 77−69756
- $Co(NH_4)_2(SO_4)_2.6H_2O$, LF relax. meas. 78−15012
- $CoSO_4.7H_2O$:Mn^{2+}, host spin-lattice relax. narrowing in single cryst. 78−27079
- $CoSiF_6.6H_2O$, paramag., nucl. and electron spin lattice relax. 78−84494
- CsBr(Cl), spin-lattice relax. of F-centres, magneto-optical meas. 77−43884
- Cs_2CoCl_4, mag. susceptibility and magnetisation curve meas. 80−11176
- Cs_3MnCl_5, multilevel system, spin-lattice relax. from AC susceptibility 77−55702
- $CsMn_{1-x}Co_xCl_3.2H_2O$, impure Heisenberg linear chain, EPR meas. 78−43634
- Cs_2NaYCl_6:Yb^{3+} electron spin-lattice relax. 77−63274
- $(Cu,Zn)Cs_2(SO_4)_26(H,D)_2O$, thermal contact between nucl. Zeeman and electron dipole-dipole interaction system 77−90065
- Cu-Mn, dil., Kondo deviations of Mn electron spin relax. and g-factor, NMR meas. 79−51747
- $CuSiF_6.6H_2O$, paramag., nucl. and electron spin lattice relax. 78−84494
- Dy^{3+}, free-radical relax. agent in biological tissues 78−81090
- emerald:Cr^{3+}, spin-lattice coupling consts. 79−99761
- $Fe(N_2H_5)_2(SO_4)_2$:Co, Mossbauer effect and paramag. relax., superparamag. behaviour of correl. spin domains 77−69756
- $Fe^{3+}(^6S)$ paramagnetisations, spin lattice relaxation Mossbauer study, dynamic spin Hamiltonian formalism 80−97173
- $FeSiF_6.6H_2O$, paramag., nucl. and electron spin lattice relax. 78−84494
- GaAs, electron-spin relaxation and recomb. kinetics, time-resolved luminesc. study 80−108074
- Gd^{3+} impurity ions, EPR spectra, linewidth narrowing due to spin-lattice relax. of lanthanide Kramers host ions 80−108061
- $Gd_xLa_{1-x}Pd_3$, ESR linewidths, g-shifts, effective electron interaction, spin-lattice relax., spin-flip scatt. 78−68372
- $Gd_xY_{1-x}Ir_2$, ESR meas., bottleneck and relax. rates 79−38369
- Ge, amorphous, ESR and DC cond. 77−48032
- H_2SO_4, glass, trapped H spin-lattice relax., modulation, saturation ESR 77−9095
- $HgCr_2Se_{4-x}S_x$, EPR linewidth, 100-300 K 77−51942
- n-InSb, spin polarisation, anisotropic size effect, effect on CESR signal 80−70743
- InSb, spin-flip Raman laser, cond. electron T_1 meas. 77−3593
- K halides, spin-lattice relax. of O_2^- centre 80−88863
- KBr, F-centre spin-lattice relax., theory and MCD meas., phonon-modulated HFS 77−43883
- KBr(Cl), F_A(Li)-centre spin-lattice relax. at 4.2K 78−91950
- $KBr(Cl)PO_2^-$, spin-lattice relax. in triplet state of PO_2^- centres, pulsed photoexcitation 79−95644
- KCl:V^{2+} 78−91941
- KCr alum, relaxation behaviour, EPR study, environmental effects 80−66021
- $KCr(SO_4)_2.12H_2O$, ESR, spin-lattice relax., ambient gas atm. thermal cond. effect 79−8046
- $K_3Fe(CN)_6$, paramag. relax., phonon bottleneck effects 78−23322
- KI:S_2^-, spin-lattice relax. rate, 1.5 to 2.2K 77−20686
- $KMgF_3$:Er^{3+}, Orbach-Aminor paramag. relax. processes, phonon bottleneck 79−28610
- $KMgF_3$:Yb^{3+}, temp. depend. of relax. time 77−51950
- $K_2Pt(CN)_4Br_{0.3}.3H_2O$, spin-lattice model for elastic anomalies 80−15179
- $KZnF_3$:Yb^{3+}, temp. depend. of relax. time 77−51950
- LaF_3:Er^{3+}, optically excited, direct-process spin-lattice relaxation 80−93378
- LaF_3:Er^{3+}, spin-lattice relax. meas. in excited $^4S_{3/2}$ state by purely optical method 79−19923
- $LaMg(NO_3)_2$:Cu^{2+}, spin-lattice recovery rate 78−10760
- $La_2Mg_3(NO_3)_{12}.24H_2O$:$Ce^{3+}$, under uniform compression 77−90028
- $LaNbO_4$:Tb^{3+}(Ho^{3+}), EPR and spin-lattice relax., Stark levels *(Russian)* 77−85563
- $LaRh_2$:Nd^{3+} cubic metallic host, spin-lattice relaxation, ESR obs. 79−1710
- Li, metallic, obs. of intrinsic spin-lattice relax. of conduction electrons 78−10774
- Li-methylamine soln., metal-nonmetal transition, electron and nucl. spin-lattice relax. 79−87306

electron spin-lattice relaxation continued
LiF:Mg(Ag), electron spin-lattice relax. of V_k-centre 78—95518
LiH, EPR line shape of Li colloids created by γ-irrad. 77—77097
$LiNbO_3$:Fe, electron spin relaxation study, Mossbauer effect, mag. and crystal field effects 80—39902
$LiNbO_3$:Fe, Mossbauer spectra quadrupole doublet asymmetry 80—44960
$LiTmF_4$ Van Vleck paramagnet, electron and nuclear spin-lattice relaxation of Er^{3+} ions 79—95643
MgO:Cr^{2+}, APR under applied stress 80—88865
MgO:Cr^{3+}, ODMR study, Cr^{3+} ions in tetragonal symm. sites 80—88892
MgO:Fe^{2+}, intrinsic spin-lattice relaxation rates, nonresonant US meas. 78—80203
MgO:Fe^{3+}, spin-lattice relax. time, meas. 80—66020
MgO:Mn^{2+}, spin-lattice relax. time, meas. 80—66020
Mn II-lecithin lipid-water system, NMR and EPR obs. 80—61168
ND_4Cl:Cu^{2+}, high-press. EPR, order-disorder transitions 78—19310
$NH_4Al(SO_4)_2.12H_2O$:Fe^{3+}, spin-lattice relax. of paramag. ions, Mossbauer effect 79—95688
NaBr(Cl), spin-lattice relax. of F-centres, magneto-optical meas. 77—43884
NaCl:V^{2+} 78—91941
Ni complex, Ni(detc)$_2$, spin-lattice relax. of Cu^{2+} 77—59453
Ni complex:Cu^{2+}, Ni(II)bis(diethyl-dithiocarbamate):Cu^{2+}, electron spin-lattice relax. 77—1589
$Ni(BF_4)_2.6H_2O$, EPR, cryst. field symmetry 79—28593
$NiSiF_6$, dilute, single-spin cross-relax. calcs. 80—97129
$NiSiF_6.6H_2O$, non-Kramers system, spin-lattice relaxation at strong fields 80—100612
$NiSiF_6.6H_2O$, paramag., nucl. and electron spin lattice relax. 78—84494
OCS, gas, EPR of rot. transitions, T_1 press. depend. 80—9621
OCS+He(Ne)(Ar)(Kr)(H_s)(0_2)($C0_2$), gas, EPR of rot. transitions, T_1 press. depend. 80—9621
$Pb_5Ge_3O_{11}$, spectral diffusion, coherent effects in ESR of Gd^{3+} 79—51852
Rb halides, spin lattice relaxation meas. of O_2^- centre 80—88863
RbCl:V^{2+} 78—91941
$RbMnF_3$:Fe^{2+}(Co^{2+}), high-temperature EPR linewidth, impurity fast relax. effects 77—85556
Si, amorphous, ESR and DC cond. 77—48032
Si, amorphous, mag. field depend. of luminesc. 79—43034
Si amorphous film, saturation meas. on ESR signals 79—33535
Si, EPR and spin-lattice relax. of dislocation spin chains *(Russian)* 79—91291
Si, spin dependent recomb. at dislocations, EPR and photocond. 79—38095
Si:As(P), Orbach spin-lattice relax. rate, uniaxial stress depend. 78—72391
Si:Cr^0($Mn^{)}$, spin-lattice relax. of Jahn-Teller centres, coexistence of minima with different symmetries 80—80602
Si:Fe^0, spin relax. rate ang. depend. for pulsed saturation of inhomogeneously broadened ESR line 79—65721
Si:O, evaporated amorphous film, effect of O_2 on props., ESR spectra 80—11265
n-Si:P, heavily depend., spin-lattice relax. at high temp. 78—39403
Si:P, optical excess charging $D^0 \rightarrow D^-$, photoelectron spin relaxation *(Russian)* 79—78572
SiO_2, disperse, EPR, O_2 vacancy relax. rel. to substrate struct., gas adsorpt. *(German)* 79—95645
SiO_2, glass, ^{29}Si hyperfine struct. of E' centre, microwave saturation props. 80—7165
SiO_2, vitreous, spin-lattice relaxation times of paramag. hole and E_1'-centres 80—39871
Sm^{3+} in cubic environment, importance of T^{-5} and T^{-7} terms in spin-lattice relax. time 80—25192
SrF_2, spectral diffusion, coherent effects in ESR of Gd^{3+} 79—51852
SrF_2:Gd^{3+}, spin-lattice relax. of Gd^{3+}, EPR line shifts meas. 78—72404
SrF_2:Tm^{2+}, modulation magnetooptic spectroscopy of cross-relaxation resonances 79—15381
SrO, electronic struct. of F-centre 78—30887
$SrWO_4$:Er^{3+}, spin-lattice and spin-spin relax. times, electron spin echo obs. 79—28609
$TbFeO_3$, ortho-ferrite, electron spin relax. time temp. depend. 77—90026
TiO_2, Mn^{3+} ion electron spin-lattice relaxation 80—108054
TiO_2:Fe^{3+}, uniaxial stress method for determ. of spin-lattice coeff. for Fe^{3+} 77—90018
TiO_2:Mn^{4+}(Cr^{3+}), rutile, temp. depend. of EPR 78—76299
$YLiF_4$:rare earth, spin-lattice relax. and nuclear polarisation *(Russian)* 79—8049
$Y(OH)_3$:Tb^{3+}, spin-lattice relax. at high gap energies using pulsed tunable dye laser 77—48047
Y_2SiO_5:Ce^{3+}(Nd^{3+})(Er^{3+})(Yb^{3+}), EPR and spin-lattice relax. 80—108063
$YbCl_3.6H_2O$:Gd^{3+}, EPR, temp. depend., spin-lattice relax. time 80—93173
zinc formatedihydrate: Co, spin lattice relax. of Co^{2+} ions 80—75847
Zn complexes, Zn(detc)$_2$ and Zn(desc)$_2$, spin-lattice relax. of Cu^{2+} 77—59453
$Zn(BF_4)_26H_2O$:Ni, phase transition study, EPR of diluted Ni^{2+}; 98-298K 80—75846
$Zn(BrO_3)_2.6H_2O$:Cu^{2+}, Jahn-Teller system, EPR and spin-lattice relax. 78—10760
$ZnCO_3$:Fe^{2+}, electronic relaxation, Mossbauer effect 78—19385
$ZnCr_2Se_4$, EPR linewidth, 100-300K 77—51942
ZnO:Cu^{2+}, electronic struct., optical absorpt. and ESR 79—87312
ZnS:Co^{2+}, spin-lattice relax., phonon heating effect *(Russian)* 78—19317
ZnS:Fe^{3+}, spin-lattice relax., expt. evidence for optical phonons 80—20451
ZnS:Mn^{2+}, spin-lattice coupling coeffs. of Mn^{2+} ions in stacking faults 77—20690
ZnS:Mn^{2+}, spin-lattice relax. time, continuous saturation expts., spin diffusion 77—36120
ZnS:Mn^{2+}, spin-lattice relaxation, EPR, optical phonons 80—39852
ZnS:Yb^{3+}(Nd^{3+}), spin-lattice relax. times meas. 78—19324
$ZnSiF_6.6H_2O$, spin-phonon interaction between Ni^{2+} ions, phonon bottleneck effects, splitting parameters *(Russian)* 80—15796
$ZnSiF_6.6H_2O$:Ni^{2+}, spin-lattice relax. at press. up to 6.5 kbar 78—48033
$ZnSiF_6.6H_2O$:V^{2+}, spin-lattice relax. at normal and high press. 80—2632
ZnTe:Mn, spin-lattice coeffs. of Mn^{2+} 80—84646

electron spin polarisation
see also CIDEP; spin polarised electron emission
actinide compounds, conduction electron polarisation, model density of states 79—37949
actinide oxides, electronic struct. and chem. bonding, spin-polarised model 79—33264
atom spin transition, nonadiabatic, in time-depend. mag. field 80—9576
atomic and electronic collisions, polarisation phenomena, review 80—83501
atomic electron scatt., optical model 78—50646
bacterial photosynthetic reaction centres, light induced electron spin polarisation 80—63681
book 77—46679
bremsstrahlung by transversely polarised electrons, azimuthal asymmetry due to spin-orbit coupling 80—60705
chemical reactions, spin polarisation analysis using intermolecular interactions theory, chemical polarisation, exchange repulsion 80—76510
chemically induced dynamic spin polarisation, orientation depend. 80—63656
detector for 300-2000 eV electron, optimum conditions theory *(Japanese)* 78—66693
electron gas, ferromagnetic response functions, lattice effects 80—10898
electron gas, spin polarised, exchange and correl. energy 77—85163
electron gas, spin polarised, model for cond. electrons of simple metal in mag. field and ferromag. Gd 77—8034
electron gas, spin polarised, self-consistent screening of μ^+ 78—47714
electron liquid with any spin polarisation, correlation energy, local exchange-correlation pot. 79—65399
electron spin density functional gradient expansion, local approx. calcs. 80—44792
Fermi gas, hard core, spin-polarised, ground state energy 78—43197
ferroelectric crystal without centre of symmetry, photo-Hall effect *(Russian)* 78—60152
ferromagnet, low-field magnetoresistance and domain drag 78—68014
ferromagnetic semiconductor, doped, electron spin polarisation and conduction band struct. 80—65449
ferromagnetic semiconductors, electronic quasiparticle spectrum 80—97051
ferromagnetic transition metals, review 78—76591
ferromagnetic transition metals, review 78—76592
ferromagnets, spin polarised LEED, calc. 79—99686
Heusler alloy, Mn-containing hyperfine field and magnetic behaviour 79—78360
Heusler alloys, ferromag. alignment rel. to conduction electron polarisation 80—60235
itinerant ferromagnet, inhomogeneity corrections to ground state props. 78—14921
Kane semiconductor, many photon electron spin orientation, EM wave absorption 80—44506
LEED, spin-polarised, symm. props. 80—96420
LEED, spin-polarized, time reversal and spatial symmetries 80—87999
magnetic electron gas induced by van Vleck ion, spin polarisation, ion mag. moment 79—56176
magnetic insulator, supertransferred hyperfine interaction, theory 77—85403
magnetic metal, spin-polarised electron liq., impurity resist. 78—84205
magnetic semiconductor, sound-like plasma 78—23125
magnetic surface props., polarised electron scatt. study 80—93160
magnetite, spin polarisation, effect of temp. and photon energy 80—45221
metal, ferromag., electron spin polarised tunnelling from superconductors 79—78263
metal, spherical solid model for muon and H in metals 79—78601
metals, electric properties calc., book 79—28274
metals, spin and charge polarisation around mag. impurities 80—75714
metastable spin-aligned crysts. decay kinetics 80—34669
Mott polarisation analyser, capable of inline meas. 79—17560
noncentrosymmetric crystal, photocurrent due to spin polarisation 79—69558
optically pumped electron spin polarised targets, polarised ion beam prod. 80—27851
perovskite-like structures, supertransferred hyperfine interaction 78—14913
phenanthrene-PMDA, spin polarization of charge-transfer excitons, EPR meas. 79—19766
photoelectrons, ang. depend. of spin polarisations 80—78652
photoemission, spin polarised, study of surface magnetism 79—52083
photoemission of spin polarised electrons, book contrib. 78—95675
plasma spin polarisation in mag. field *(Russian)* 80—33744
polarised electrons, book 77—46679
polarised LEED, symmetry 79—60233
polarised LEED using a GaAs spin polarised electron source 78—83693
rare earth, multiplet splitting of s-core levels, free-electtron-gas exchange correl. 78—10407
rare earth ferromagnets, spin polarised electron tunnelling 78—68094
rare earth intermetallic compounds, NMR anal. of indirect mag. interactions 80—71193
rare earth intermetallics, RAl_2, orbital and spin polarisations of cond. electrons 80—65791
rare earth metal, ferromagnet-simple helix transition, cond. electron spin polarisation *(Russian)* 79—7995
rare earth metals, rel. to US altenuation in applied mag. fields 77—51933
rare earth-Al_2(Zn), mag. coupling mechanism 79—4655
relativistic spin polarised band struct. calcs. 77—85128
ruby, spin dependency of optical feeding into $\bar{E}(^2E)$ metastable doublet 79—28812
secondary electron emission, theory 78—76564
semiconductor, spin polarisation induced by optical pumping 79—95681
semiconductor, spin-dependent recomb. and scatt. in presence of optical orientation of electrons 80—96908
semiconductor, spin-polarised electron-hole liq., theory 78—43307
semiconductors, doped, local spin-density-functional method, appl. to metal-insulator transition 80—96789
spin dependent phenomena in electron-atom collisions 80—63830
supercondcutors, surface relax. of conduction electron spins 79—60995
superconductive tunnelling with spin polarised electrons 79—4627
surface study appl. *(Japanese)* 79—37911
TCNQ salt, K^+TCNQ^-, spin polarised band struct., effective Coulomb repulsion 77—15734

electron spin polarisation continued
transition metal, 3d, multiplet splitting of s-core levels, free-electron-gas exchange correl. 78—10407
transition metal 3d monoxides, specific vol. and mag. moment calcs. 80—65822
transition metal-rare earth dil. alloy, hyperfine field of rare earth impurity 79—1588
two-electron systems, spin polarisation processes *(Russian)* 79—94085
Al film, supercond. crit. field, spin-polarised tunnelling meas., test of high field supercond. theory 79—87220
Am, 5f-electron delocalisation 80—70595
Au (110), electron spin polarisation in LEED 78—83692
Au (110), spin polarisation in LEED, theory and expt. 78—18508
CdS, spin-polarised electron-hole liq., theory 78—43307
Co, tunnelling electron spin polarisation rel. to band struct. 78—68095
Cr, spin density wave, CDW and strain wave, effects of spin polarisation of reservoir and imperfect nesting 78—56284
Cs, photoelectron energy distrib. curves, depend. on light polarization 79—15591
Cu-Fe, dil., NMR evidence for transferred orbital hyperfine field 78—27098
EuB_6, ferromag., spin-polarised energy band struct., APW calc. 80—96779
EuO:Gd, surface mag. props. 80—71566
$Eu_xSn_{1-x}Mo_6S_8$, Chevrel phase supercond. cond. electron polarisation by Eu^{2+}, effect on supercond. props. 79—56650
Fe, effective mag. field on ^{119}Sn, press. depend., Mossbauer obs. 78—52382
Fe, elastic and magnon inelastic differential cross sections of spin polarised low energy electrons 78—34970
Fe, ferromag., rel. to energy band calcs. 78—10343
Fe, ferromag. film, surface states, surface magnetisation and electron spin polarisation 80—65648
Fe, ferromagnetic, cluster method, environmental effects 78—95405
Fe, field emission, surface magnetism 78—68607
Fe, spin polarised electron tunnelling results 79—28417
Fe, thin film, core electron polarisation measurement 79—4756
Fe, tunnelling electron spin polarisation rel. to band struct. 78—68095
Fe-Al, hyperfine field meas. using muon-spin-rotation method 80—10933
Fe_3Si-based alloy, dil., cond. electron polarisation and moment perturbations 78—68224
Fe_3Si-based dil. alloys, conduction electron polarisation, moment perturbations 78—68225
$Fe_{3-x}V_xSi$, selective site substitution and spin polarisation 79—78583
GaAs, electron-spin relaxation and recomb. kinetics, time-resolved luminesc. study 80—108074
GaAs-$Al_xGa_{1-x}As$ multilayer, photoluminesc., electron spin orientation 80—25453
p-GaP:Zn,S, spin polarisation of donors and acceptors in mag. field, optical and microwave study 80—93393
Gd, ferromag., spin polarised electron gas model 77—8034
$GdCo_5$, spin-polarised energy band struct. 78—10342
H, spin-polarised, Bose condensation, phenomenological description 80—77699
H, spin-polarised, Bose-Einstein condensation 80—77698
^4He magnetometer, optically pumped *(Japanese)* 80—8434
Hg, electron elastic scattering, 8 to 18 eV, electron spin polaris. 80—91669
n-InSb, spin polarisation, anisotropic size effect, effect on CESR signal 80—70743
KBr(I), photostimulated recomb., electron spin polarisation 80—60673
KCl:Sr, triplet state of F_2-centres, ESR spectra 80—29616
KH_2AsO_4-KH_2PO_4, AsO_4^{4-} centre, EPR central peak dynamics 79—33523
$NH_4H_2AsO_4$-$NH_4H_2PO_4$, AsO_4^{4-} centre, EPR central peak dynamics 79—33523
Na_2+He(Ne)(Ar), collision induced dissoc. rate, vibr. distrib. depend. 79—22791
Ni alloys, spin polarised tunnelling 78—95494
Ni and Ni alloys, tunnel currents, spin polarisation, simple band theory interpretation 79—78451
Ni and Ni alloys, tunnelling electron spin polarisation rel. to band struct. 78—68095
Ni band structure, rel. to lattice const., spin polarised APW calc. 80—20073
Ni, effective mag. field on ^{119}Sn, press. depend., Mossbauer obs. 78—52382
Ni, elastic and magnon inelastic differential cross sections of spin polarised low energy electrons 78—34970
Ni, ferromag., rel. to energy band calcs. 77—39774
Ni, ferromag. film, surface states, surface magnetisation and electron spin polarisation 80—65648
Ni, ferromagnetic, electron-magnon interactions 78—68205
Ni, field emission, surface magnetism 78—68607
Ni film, ferromagnetic (100) and (110), energy bands photoelectron spin polarisation reversal 79—1630
Ni film, granular, tunnelling of spin-polarised electrons and magnetoresist., exchange effects 77—12024
Ni film (111), ferromag., energy bands and planar densities of states, LCAO calc. 79—4509
Ni, spin polarisation in LEED 77—43696
Ni_2MnSn, ferromag. Heusler alloy, electronic struct., spin polarisations, theory 80—54598
NiO (111) surfaces, antiferromag., mag. scattering by polarised LEED, spin polarisation effect in theory 80—29529
Ni(001) surface states, surface magnetisation, electron spin polarisation 80—88612
$Pb_{1-x}Sn_xTe$ films, size quantisation, optical orientation of free carriers 80—20725
Pd, metallic, positive muon Knight shift 80—71280
Pd-Fe alloys, dil., spin polarisation effect on hyperfine interactions, anal. of Mossbauer meas. *(Russian)* 79—47055
Pd_2MnSn, ferromag. Heusler alloy, electronic struct., spin polarisations, theory 80—54598
Pt, (111) and (001) faces, spin-polarised LEED 78—14556
Rb-tetrahydrofuran soln., photolysis, photoelectron emissive EPR signal, scavenger electron affinity reactivity 78—53224
RbI, photostimulated recomb., electron spin polarisation 80—60673
$SmCo_5$, spin-polarised energy band struct. 78—10342
SmS, mag. susceptibility in semicond. phase, in homogeneity region 79—28502

electron spin polarisation continued
UTe, electronic and spin struct. negative spin polarisation of photoelectrons 79—19514
UTe, photoemission energy distrib. curve and electron spin polarisation 79—52074
W,LEED and electron microscopic investigs., review *(Hungarian)* 77—47654
W (001), adsorption of N_2, effect on LEED electron spin polarisation and intensity profiles 80—65377
W (001), disordered CO and O_2 overlayer effect on electron spin polarisation in LEED 79—60632
W (001), double diffr., spin polaris. effects 79—64963
W (001), electron spin polarisation and intensity in LEED, temp. depend., 1000-300°C 79—14989
W (001), LEED intensity curves, spin-depend. features, model calc. 78—34685
W (001), ordered CO overlayer effect on electron spin polarisation in LEED 79—60633
W (001), spin polarisation in LEED, theoretical predictions 77—31855
W (100), specular scattering of polarised low energy electrons 79—60233
W crystal-atom and W(001) surface, low-energy positron diffraction, theoretical study 80—84034
W, spin polarised LEED, energy and ang. distrib. *(German)* 80—49468
W-EuS, amorphous, memory effect in field emission 80—89126
Xe, 5-300 eV elastically scattered electron polarisation, 30-120° 80—23548
Xe, electron scatt., optical model for electron spin polaris. 78—50646
YCo_5, spin-polarised energy band struct. 78—10342

electron spin relaxation *see electron spin-lattice relaxation*

electron spin resonance *see paramagnetic resonance*

electron states, impurity *see impurity electron states*

electron states, surface *see surface electron states*

electron streams *see electron beams*

electron structure of solids (crystallography) *see crystallography*

electron structure of solids and liquids (energy structure) *see electron energy states (condensed matter)*

electron theory
see also Dirac equation; quantum electrodynamics
anomalous mag. moment calc. 78—37254
anomalous magnetic moment, Pauli eqn. in crossed mag., electrostatic fields *(Russian)* 78—16962
anomalous magnetic moments, eighth order contrib. calcs., QED tests 78—45821
Bloch electrons in external electric field, evolution operator 79—49426
Caldirola equations, generalised, for classically radiating electron 77—82401
Casimir model, self-stress in dielectric and conducting balls 80—86625
charge depend. on velocity 78—28965
charged vacuum existence in supercritical fields, e^+e^- prod. in heavy ion collisions *(German)* 77—67607
chronon in quantum theory of electron, existence of heavy leptons, neutrino spectrum 78—70008
classical electron, impossibility of radiationless motion 79—17247
classical model based on Penney's balanced field eqns. 78—21031
classical radiating electron, time-delay eqn. 77—23603
classical radiation reaction theory, 1-dimens. Coulomb force problem 77—74235
classical recombination cross section 79—25876
classical theory of electron, finite difference eqns. basis 78—24925
classically radiating electron, stationary states in attractive pot. 77—60950
coherent states of an electron in a quantized electromagnetic wave 79—22000
continuum Dirac electron, Coulomb field, simple asymptotic wave function 78—41455
coupling constant singularities in QED 79—21991
covariant wave equations, Galilei group and mag. moment of electron 77—64955
current commutator anomaly, regularised dimensionally using hyperfunctions 78—12845
De Sitter symm. space, gravit. interaction and spinning electron eqn. 78—103
Dirac's extended electron model, quantum and classical theory elaboration 78—82134
Dirac's extended electron model 79—26269
Dirac electrons, moving in periodic mag. fields, one-photon emission 78—12844
Dirac eqn., Bunge-Kalnay position operator 78—36864
Dirac essentially self adjoint operator, resolvent estimator near infinity 78—49992
Dirac particle, supersymmetry and position operators 79—6305
Dirac theory, Hermitian interaction terms 77—33752
Dirac type essentially self adjoint operators 78—16957
Dyson-Schwinger equation solns. for electron propagator 78—24984
Einstein unitary field theory with tele-parallelism, Dirac's classical theory of electrons 79—12685
electric charge conservation *(Russian)* 78—77739
electric dipole moment, quantum supercond. interferometric meas. *(Russian)* 78—37158
electron internal dynamics, rel. to Lamb-Rutherford shift and microwave generation 80—13239
electron mass operator in 2-D QED approx., radiative convections 80—4900
excited-mass states of the electron, chronon 78—21004
experimental verification of special relativity 78—57777
extended charged particles, radiationless internal vibr. in const. mag. field 77—88631
extended model of Dirac electron 77—22436
external coherent EM field interaction, null-plane formulation, Volkov soln. expansion 77—13898
finite self-mass in nonperturbative iterative scheme of QED 78—89641
free electron as localised stationary state of vacuum EM polarisation *(Polish)* 77—38107
g-factor, sixth order contributions, anal. evaluation of graphs 77—6066
gauge depend. of truncated mass 80—22542
Grassmann functional Schrodinger description for fermions 79—30642
Grossman-Peres model, canonic formalism and relativistic invariance *(Russian)* 78—12833
gyromagnetic ratio in Coulomb field 80—82870

electron theory continued
  hidden-parameter theory of extended Dirac electron 77−57212
  inertial mass, asymptotic, soln. of Dirac eqn. 79−2961
  lepton wave packets produced by strong short-range potentials 78−45828
  logarithmic pots., Dirac eqn. soln. 78−41448
  logarithmic pots., Schrodinger eqn. soln. 78−41447
  Lorentz, experimental indistinguishability from special relativity 77−45695
  magnetic moment anomaly determ. using two level dual vac. polarisation model 78−54632
  magnetic monopole-electron interactions, without Dirac strings, quantum-mech. formulation 79−21994
  mass, possibility of determ. from finite QED 78−12841
  mass and Pontecorvo oscillations of neutrinos using chronon concept in electron theory 78−36879
  mass formula for charged leptons, chronon in electron theory 80−47224
  ME-EM field model of free electron, determ. of electron parameters 78−29281
  ME-EM field model of free electron state 78−29280
  ME-EM field model of free electron state 78−49988
  mixed finite difference and differential eqns., generating function, electron theory appl. 77−82371
  model using phase-locked cavity 79−63089
  models for muon and electron 78−29371
  monopole pot., wave function for electron motion *(Chinese)* 78−77768
  motion and radiation of a charge in a plane wave and a magnetic field *(Russian)* 79−21986
  negative energy electrons, explanation of inertia *(German)* 79−88842
  nonlinear effects in theory of erratic electron 78−93825
  nonlinear problems due to self-field of electron 80−4901
  Planck's constant, origin of quantum theory 80−27179
  Poincare stresses, dynamical basis 79−6303
  Poynting's theorem, nonrelativistic and 2-component spin, transition probability 78−24986
  pseudoclassical relativistic electron and supersymmetries 77−13845
  QED, electron anomalous mag. moment, dispersive approach, 6th order contrib. 79−9316
  QED, electron anomaly, radiative corrections, vac. polarisation insertions, ladder graphs 79−2959
  QED, electron-positron field 78−41445
  QED, nonlocal, relativistically invariant, bubble electron model, fundamental length and causality 79−30687
  QED of constant field, radiative effects, mass operator eigenfunctions *(Russian)* 79−17652
  QED with internal fermion excitations, $e\mu$ system 80−9130
  radiating electron, covariant semiclassical theory 77−26478
  radiationless motions of relativistically rigid classical electron 78−20983
  relativistic electron model from the introduction of the chronon 78−93827
  relativistic field theory 77−2779
  relativistic mechanics of mag. monopoles and electric charges 78−28967
  relativistic model 79−35975
  relativistic motion of charged particle in plane EM wave with arbitrary amplitude 77−3528
  relativistic self-field interaction, particle-like solns. 78−16666
  relativistic theory of the classical electron, review 80−12923
  relativistic wave eqn. of electron *(Hungarian)* 79−12928
  retarded self-interaction of classical point electron, divergences anal. 77−13620
  runaway solutions and finite size 77−45710
  Schrodinger equation, math. props. of finite difference eqn., appl. to free electron *(Italian)* 77−78993
  Schwarzschild sphere and classical electron self-energy 78−49681
  self-energy in non-local QED and correspondence principle 77−22671
  self-mass of electron, eqn. of motion calc. 78−28995
  short-time stochastic electron, modified Brownian particle, Schrodinger eqn. 78−36853
  spin, Dirac equation, mechanical sphere, magnetic momentum and lines of force *(Hungarian)* 80−68344
  spin magnetic moment, relativistic mass correction, classical reinterpretation 77−57213
  spin motion eqn. in external field, Dirac particle quasiclassical theory 80−18099
  spinning electron, quantum mech. rotor, dynamics, invariance requirements 78−70250
  spinning magnets, Jehle model of electron 78−28966
  superheavy elements, $118<Z<138$, electronic spectra, anomalous levels 77−14331
  unstable electron, lifetime, charge nonconservation, paradoxes 79−6335
  vacuum polarisation in Fock space 78−41446
  Vavilov-Cherenkov effect, radiator size depend. *(Russian)* 78−5405
  wave mechanics of electrons in Kerr geometry 78−12622
  weak charge of electron, $SU_2 \times U_1$ theories, $\bar{\nu}_\mu e$ scatt., isospin 78−16974

electron theory of metals *see metal theory*

electron traps
  see also colour centres; hole traps; impurity electron states
  AC response, influence of states in gap and generation-recomb. effects 77−4362
  activation energy determ. by different trap spectroscopy techniques 80−75582
  alchohols, glassy, spectra shift of trapped electrons, after γ-irrad. 79−78709
  alcohol glasses, X-irradiated, electron scavenging mechanism 77−56235
  alcohols, glass, electron trapping, pulse radiolysis obs. 80−30264
  alcohols, trapped electron spectral relax., random-walk model 78−60493
  alkali borate binary glass, energy storage behaviour studied by thermoluminesc. 80−50432
  alkali halide, electron trapping by alkali ion impurities 78−47809
  alkali halides, F-centre trapping of conduction electrons, photocond. study 78−56179
  alkali halides, XPS, trapped electrons at F-centres and anion defects, photoionis. cross sections 77−90249
  alkali metal-ammonia solutions containing cryptands, metal anion and trapped electrons form. by evap. 79−100340
  alkaline glass: tryptophan (tyrosine), γ-irrad., electron traps, stimulated luminesc. 78−11536
  alkaline ice, trapped electrons, photostimulated decay, time-depend. rate const. 79−52692
  alkane glass, γ-irradiated, charge trapping, isotope and mol. struct. effects 79−5164

electron traps continued
  amorphous insulator film, high-field cond. 79−56320
  amorphous material, trap-controlled transient current injection, models of trapping level 79−23984
  amorphous materials, exponential distribution, majority carrier eqn. determ. 78−14760
  amorphous semiconductor, charge transport behaviour, model 79−91048
  amorphous semiconductor, size and field variation of activation energy for drift mobility 80−49769
  amorphous semiconductor, trapping, photo-stimulated and thermally-stimulated current obs. 77−28192
  amorphous solid, anomalous transit time dispersion, Monte Carlo simulation 77−47827
  amorphous solid, photoconduction, model involving capture and escape from multiple traps 77−76863
  anisotropic semiconductor, with traps, kinetic theory of acousto-electrical effect in nonhydrodynamic collision region *(Russian)* 79−24019
  anthracene: tetracene, singlet exciton trapping mechanism, fluoresc. mag. field modulation obs. 77−77267
  anthracene, charge storage and trapping levels, TSC studies 80−6875
  anthracene, cryst., photocurrent induced by detrapping of charge carriers trapped by radicals 79−82643
  anthracene, electron and hole generation under electron bombardment 79−73524
  anthracene, electron bombardment, field and temp. depend. of carrier yield 77−8117
  anthracene, laser excited single crystal, numerical anal. for TSC results *(Japanese)* 80−34464
  anthracene, photo-oxidised, current oscills. due to recomb. instability in high field domain 77−4353
  anthracene, single cryst. with discrete shallow traps, computer simulation of TSC 79−99819
  anthracene, single crystal, contact charging and photoemission 79−47586
  anthracene, single crystal, disperse photocurrent transients rel. to multiple trapping 79−99564
  anthracene, single crystals, TSC excited by Q-switched ruby laser 80−29417
  anthracene, space-charged-limited photo-enhanced currents 79−82599
  anthracene, surface states and persistent internal polarisation via photocurrent transients 77−89825
  anthracene, thermally stimulated currents from shallow trapping centres *(Japanese)* 78−92015
  anthracene, thin surface layer, delayed fluoresc. obs., surface trap influence 77−77291
  anthracene, trapping effects on emission-limited current flow 80−29413
  anthracene, triplet exciton trapping, structural imperfections and delayed fluorescence 78−68551
  anthracene, TSC and carrier retrapping 80−39599
  anthracene, TSC meas. induced by Q-switched ruby laser 78−19087
  anthracene crystals, superficial trapping levels, pulsed photocurrent transients 78−76021
  anthracene crystals, TSC, monomolecular glow peak 77−39869
  anthracene crystals, TSC, monomolecular glow peak revealed by thermal cleaning 77−39870
  anthracene thin films, high field effects and switching, local centres importance 79−73548
  aqueous glass, γ-radiolysis, photolysis of trapped electrons, quasi-free electron IR absorpt., luminesc. 77−21401
  aqueous glasses, electron trapping reaction kinetics, non-Gaussian diffusion model 78−34843
  L(+)arabinose, irradiated single crystals, electron trapping, ESR obs. 78−88646
  arabinose, X-irradiated single crystal, intermol. electron trapping, hyperfine ESR pattern 79−39166
  benzene, deuterated mixed crysts., phonon assisted trap-trap triplet energy migration, 0K limit, phosphoresc. obs. 77−48218
  benzene, isotopic mixed crysts., triplet excitation energy transfer theory 77−28611
  2-benzoylpyridine crystals, lowest triplet state, optically detected EPR 80−15827
  biomolecules, dielectric transient response following UV-irradiation 80−51166
  bulk trap energetic distribution props., space charge limited current meas. use 80−80293
  bulk trapping processes and trap occupancy 77−39876
  n-butanol, glassy and crystalline forms, trapped electrons, conc. of mol. vacancies determ. 77−65948
  C-CD, surface channel, interface trapping noise calc. 80−11058
  capacitance methods for minority and majority carrier trap characterisation 77−51692
  capacitance transient spectroscopy, book contrib. 78−10548
  carbohydrate compounds, X-irrad., trapped electrons, ESR and ENDOR obs. 80−93161
  cellulose, thermally stimulated discharge studies 80−11329
  chalcogenide glass, charged dangling bond model reassessment 77−72813
  chalcogenide glass films, threshold switching 80−96950
  chalcogenide glasses, electronic gap states, origin, structural relax., electronic transport and trapping 80−54648
  chalcogenide glasses, trap controlled transient photocond. 80−44641
  chalcogenide semiconductors, optical and elec. props., comparison with SiO_2 78−6721
  channelling, nuclear reaction modulation for high-energy negative particles 79−77655
  chlorophyll a-n-chloranil lamellar system, heat stimulated conductivity 79−53043
  chlorophyll-a, microcryst., trapped-electron doping in photovoltaic sandwich cells 78−53334
  copper phthalocyanine, imperfect cryst., elec. transport phenomena, charge carrier conc. 77−1421
  covalent semiconductors, low temp. galvanomag. effects, shallow attractive traps 80−88575
  current jump region, I-V characts. *(Russian)* 77−39875
  cyclodextrin, trapped electrons in cryst. matrices, ESR, optical absorption spectra 78−80768
  deep fast trapping dielectric, SCL current injection 80−6862
  deep level capture, two stage model 78−10396
  deep traps, nonradiative multiphonon carrier-capture cross-section, temp. depend. approx. 78−43415
  deep-level trap spectroscopy, signal analyser 77−87789
  defect dielectrics containing electron trap centres, transient current model *(Russian)* 78−60134

electron traps continued
- degenerate semiconductor, recombination-generation currents derivation 78—52007
- diamond:B, thermoluminesc., TSC, correlation meas. 78—88369
- dibenzofuran:anthracene, cryst., prompt fluoresc., temp. depend., trap effects *(German)* 80—93400
- 1,4-dibromonaphthalene, proton spin relaxation by optically excited triplet states 79—19810
- dielectric, SCL cond., field ionisation and annihilation of traps of different elec. nature *(Russian)* 77—69330
- dielectric, solid, energetic struct. of traps, from SCL currents 80—24941
- dielectric, solid thermally stimulated characts., dipolar relaxation time, trap levels and ionic space charge polarisation 80—84685
- dielectric, trap-controlled transient photocond., numerical study 80—50285
- dielectric diode, Joule instability under space-charge-limited current conditions 80—15618
- dielectrics, thermally stimulated depolarisation as method of studying charge trapping 80—11325
- diffusion traps for divalent ions, dielectric loss and ionic thermocurrent techniques 80—6566
- dipolar centres, tunnelling to electron release 79—95420
- disordered semiconductor, hopping mechanism of dispersive transport 80—10971
- dispersion and Faraday rotation associated with point-imperfections 78—19449
- dispersive transport by hopping and transport, theory 78—14726
- DLTS, photo-excited, minority carrier trap meas. 80—96816
- double injection in solids with traps nonuniformly distributed in energy and space theory 77—8116
- dulcitol, X-irrad., 4.2K, electron traps, alkoxy hyperfine coupling, ENDOR obs. 80—50863
- dulcitol, X-irradiated single crystal, intermol. electron trapping, hyperfine ESR pattern 79—39166
- dyes, photographic emulsion spectral sensitisation, latent image form., subcond. band events 78—32905
- electrets and dielectrics, conf., Sao Carlos, Brazil, Sept. (1975) 80—7251
- electro-optical spatial light modulator resolution, stored point charge effects 80—106616
- electron trapping, donor state generation, photo I-V study 80—20210
- energetical trap distribs., first principles model, linear finite defect chain 80—59912
- ESR and ENDOR obs. 80—93161
- ethanol, semiquantitative model for electron conc.-dose depend. in glassy matrix 78—20034
- ethanol glass, trapped and solvated electrons produced in presence of applied electric field 80—7379
- ethylene glycol-water glass, γ-irrad., temp. depend. photobleaching of trapped electrons 79—66320
- ethylene-vinyl acetate copolymer, X-ray irrad., trapped carriers, TSC 77—69338
- ferrocene films, plasma-polymerised, carrier trapping, elec. cond. meas., 300 to 525K 80—100543
- finite systems containing traps, Hall effect, two-carrier one-dimens. transport anal. 80—44614
- fluorescence in prescence of traps, general theory 80—11478
- fluorphlogopite, synthetic, luminesc. props. 78—19579
- forward biased junctions, excess noise sources due to defects 79—38154
- forward-biased diode structures, numerical anal. based on direct gap semicond. 79—65542
- frozen media, electron transfer reactions and multiphonon transition theory 80—7812
- GaAs MBE growth, deep levels effect on electron and hole trap densities 80—49652
- Gaussian trap distribution in solids, theory of single and double injection 77—11935
- glass, alcoholic and aq., 4.2K, trapped electron photocond. and optical spectra following radiolysis 79—29378
- glass, trapped electrons, electron-phonon interaction 79—78697
- glassy matrix, trapped electron decay time as function of preirrad. annealing time 79—66323
- glassy polar matrix, electron trap relaxation model 80—15470
- graded and stepped energy band-gap MIS structures 80—2473
- homogeneous insulator with traps, SCLC characts. 78—39122
- hydrocarbon, long chain single cryst., carrier transport meas. 80—6874
- II-VI compounds with three deep trapping levels, theory of transient photocond. processes 77—76865
- III-V semiconductors, point defects and deep traps, thermodynamic history, model 80—59908
- impurity centre repulsive barrier, anisotropy in electon penetration 79—65497
- impurity photoconductivity, monopolar injection *(Russian)* 79—24004
- indandione-1,3 derivative, layer, electrooptical effect *(Russian)* 79—73900
- indanthrone film, SCL conduction, trapping 77—15978
- information storage in piezoelectric semiconducting single crystals 78—15101
- n-InSb, photoconductivity relax. temp. depend., carrier recomb. processes 77—4363
- insulated crystal, primary photocurrent kinetics for simultaneous trapping and recomb. 80—6899
- insulating films trap analysis, influence of spatial trap distrib. on SCLC charact. 79—56343
- insulator, arbitrarily distributed traps, SCL currents anal. 79—11132
- insulator, current carrier trapping, SCL current-voltage characts. 80—39588
- insulator, extension of theoretical description of space-charge-limited currents 78—39128
- insulator, with two sets of traps distributed in energy, SCL currents, theory and expt. test 77—89768
- insulators, noncryst., electron density captured at traps, liberated to conduction band 78—87946
- insulators, trap struct. anal. by fractional glow techique 79—11078
- ionic crystal:transition metal, excitation and trapping at impurity sites 79—33776
- ionic crystal, intrinsic electronic excitations and defects, review *(Russian)* 80—10881
- lattice migration, diffusive and percolative excitons 80—59879
- lead acetate trihydrate:Mn^{2+}, ESR, elec. cond. 80—93165
- LED, deep trapping levels energy and conc. meas. *(Polish)* 78—34797

electron traps continued
- Lexan polycarbonate, N-isopropylcarbazole and triphenylamine doped, trap-controlled dispersive hopping transport 77—15850
- magnetic semiconductor, self-trapped electrons 77—59262
- magnetoelectrets, review 80—25289
- malononitrile, plasma-polymerised, in Ag-polymer-Ag struct., SCL currents and carrier trapping 79—51687
- metal-insulator contact, electron tunnelling and its role in contact electrification 80—2453
- metals, FCC, H implantation, lattice location and trapping, ion beam anal. 79—55769
- methanol, dry-electron localisation, impurity trapping, solvated electron rate consts. 79—1990
- methylcyclohexane, trapped electron charge distribs., optical transitions 77—28139
- 3-methylpentane, γ-irradiated, isothermal luminescence in presence of aromatic solutes at 77K 78—76519
- 3-methylpentane, trapped electron charge distribs., optical transitions 77—28139
- 2-methyltetrahydrofuran-methanol mixed glasses, annealed, γ-ray produced electrons transfer from IR to bisible traps 80—11440
- MIM structure, thermal dielec. relax. 77—76941
- MIM structures, thermal dielec. relax. 79—11237
- MIM system, electron emission modelling *(Czech)* 80—2479
- MIMOS structure, charge storage props., effect of Pt particles in dual SiO$_2$ interface 77—35992
- MIS capacitors with single-level traps in semicond. region, model 77—35991
- MIS insulator charge centroid determ. by photoinjection or photodepopulation 77—85323
- MIS solar cell, effects of pinholes, oxide traps and surface states 78—80055
- MIS structure, localised states, Frenkel effect in strong elec. field, kinetics of nonequilib. processes 77—66206
- MIS structure, radiation induced charge storage 80—6997
- MIS structure, thermal generation of carriers through surface centres 79—69603
- MIS structures, dielectric layer, transient processes during charge trapping for injecting contact 80—70844
- MNOS, dharge distribs. in Si$_3$N$_4$ film exam. 79—38184
- MNOS capacitors, simple technique for charge centroid meas. 80—34521
- MNOS devices, small-signal response of bulk traps 77—39959
- MNOS devices, switching characts. at low fields 79—56311
- MNOS devices, transient charge and current distribs. calc. 77—55611
- MNOS diode, trap distribution, memory characteristics 77—85326
- MNOS structure, Au-diffused, with chem. oxidised ⟨100⟩ substrate Si-SiO$_2$ interface traps 77—62995
- MNOS structure, non-biased, charge storage by irradiation with UV light 77—43735
- MNOS structure, trap parameters determ., review of expt. techniques 77—55612
- MNOS structures, discharge behaviour 79—38174
- MNOS structures with tunnelling-thickness SiO$_2$ films, charge trapping obs. 78—95379
- molecular crystal, band structure, excitonic processes, trap distrib. 80—6720
- molecular crystal/electrolyte interface, illuminated, space charge behaviour 78—84290
- molecular crystals, shallow traps, spin triplet population temp. depend. 77—1371
- molecular crystals, trapping rates for sensitized fluoresc. 79—11455
- molecular solid, disordered, exciton migration, dynamical approach 79—65916
- MOS capacitor, nonequilib. response to linearly varying voltages 78—52091
- MOS capacitors, dynamic model for e-beam irrad. 79—91147
- MOS capacitors, electron injection studies of radiation induced positive charge 77—20441
- MOS capacitors, irradiated and avalanche injected, trapping effects 79—19669
- MOS device, nonequilibrium response to linear voltage ramp, bulk discrete traps 78—6450
- MOS devices, interfacial and bulk trap props., expt. characterization techniques 80—49950
- MOS elements in depletion, interfacial tunnel interaction anal. 78—64121
- MOS insulator, energy and spatial distrib. of electron traps, photocurrent response 77—39947
- MOS insulator trapped electron release by UV photoinjection 78—6453
- MOS interface states density, photoemission obs. using photocurrent and photocapacitance meas. 80—92990
- MOS structure, B ion implanted, form. and annealing of radiation damage 79—56321
- MOS structure, electron trapping region to improve performance 78—19150
- MOS structure, leakage effects 79—91155
- MOS structure, quench-in defects and interface states exam. by transient capacitance techniques 78—39225
- MOS structure, quenched-in bulk defects and interface states, transient capacitance spectroscopy 79—24081
- MOS structure, trapped charge location in Al implanted SiO$_2$, using photo I-V technique 79—15227
- MOS structure, with ion implanted oxide layer, optically induced charge storage 77—35994
- MOS structure under strong inversion conditions, freq. response of bulk traps. 77—39958
- MOS structures, inversion layer near electrode edge, pot. and charge density distribution 80—88642
- MOS structures, irradiated SiO$_2$ film, electron and hole trapping 80—11098
- MOS structures, quasistatic and nonequilibrium phenomena with constant gate-current bias 80—80385
- MOS system containing interface traps, equilibrium and nonequilibrium response to linear voltage ramp 79—38173
- multilevel trapping fluctuation processes spectral props. of physical processes of Markov-correlated events 79—21665
- multiple trapping theory 77—55542
- multiple-trapping model and time-dependent random walk 78—34842
- muon, diffusion in presence of traps, spin depolarisation, stochastic theory 79—28666

electron traps continued
naphthalene, cryst., photocurrent induced by detrapping of charge carriers trapped by radicals 79—82643
naphthalene, deep exponential distrib. of traps, long-time decay of surface pot. 79—47041
naphthalene, electron trapping, one-carrier TSC and SCL currents 80—70715
naphthalene, space charge transport 80—20209
naphthalene, surface pot. decay, trap modulated mobility 78—72164
naphthalene-h$_8$ and -d$_8$ mixed crystal, two-dimens. lattice, cluster-cluster interactions, model inhomogeneous distribs. 79—23922
non-polar dielectrics, TSC and carrier retrapping 80—39599
one-carrier SCL currents in solid with two sets of traps distributed in energy 78—72158
one-dimensional, semiconducting polymer, demonstration of high mobility 80—20212
one-dimensional systems, electron trapping and transport by supersonic solitons 78—72139
optical absorption spectra evolution for localisation in trapping and solvation 77—90173
organic compounds, irradiated single crystals, electron trapping, ESR obs. 78—88646
organic glass, electron-cation recombination; charge distrib. simulation and luminesc. kinetics 80—2855
organic glass, photochem. of trapped electrons 79—52722
organic insulator, space-charged-limited photo-enhanced currents 79—82599
organic semiconductor films, relax. currents, polarisation and depolarisation currents obs. 80—49764
p-n junction solar cell response to concentrated sunlight and partial illum. 79—61996
p-n junctions, TSC, impurity centre parameter determ. 78—47857
pentacene, evaporated film elec. cond. meas. for various temps., SCL 78—10584
Perspex magneto-electret, equiv. elec. field calc. from thermally stimulated discharge current 80—7259
PET, photoexcited, thermolum. and carrier detrapping mechanism 79—61445
phenanthrene:anthracene, cryst., triplet-triplet annihilation, shallow traps effect, 77-293K 79—11446
phosphor, stationary recombinatorial luminesc. without thermal transitions, model 79—8193
photocells, electron trap, for laser flux intensity meas., characts. 78—286
photochromic glasses, electron-hole separation, influence on recombination probability 80—11445
photoconductivity-controlled imaging systems, limitations on sensitivity 80—6907
photoconductor, electron trapping kinetics at broadened levels, transient behaviour 77—47826
photoconductors, noise theory and measurements for modelling electronic processes and transport phenomena 79—56264
photoconductors, possibility of observing ambipolar photoconductivity and its optical quenching 78—14764
photodielectric effect in photocond., improved model including effect of traps 77—1445
photodielectric layer, Laplace transform of small-charge current, trapping level parameters 77—69337
photographic emulsion sensitisation during latent image formation, nature of sensitivity specks 77—82637
photoluminescent crystal, minimum entropy prod. rel. to the dynamical behaviour of trapped electrons *(French)* 77—77263
photoluminescent crystal trap depths, appl. of thermodynamics of single particle *(French)* 77—77264
phthalocyanine layers, metal-free, between Ag and Al electrodes, switching effects 80—65706
phthalocyanine-dodecane interface, photostimulated charge transfer flash expt., trapping model 77—66182
piezoelectric semiconductor, cascade capture of carriers by attractive impurity centres, cross section 78—56157
piezoelectric semiconductor, rel. to stationary acoustic wave nonlinear theory 77—76878
polar fluid, improved model of long range electron solvent interaction of localised electron 77—90710
polar glasses, aq. and alcoholic systems, trapped electrons, photocond., optical spectra 77—85742
poly(n-vinylcarbazole)-trinitrofluorenone films, charge carrier trapping 78—14846
poly-α-naphthol, semicond., isothermal depolarisation currents, electron trap parameters 80—60492
poly-N-vinylcarbazole, soln., picosecond time-resolved fluoresc. by pulse radiolysis 80—28122
poly-p-xylylene films, carrier traps, X-ray induced TSC, thermolum. and dielec. loss study 80—88570
polycarbonate, and charge-transfer complex modifications, TSC 80—88572
polyethylene, γ-irradiated, effect of elec. field on TSC 79—65790
polyethylene, γ-irradiated, investigation of traps by photostimulated detrapping current analysis 77—15894
polyethylene, anomalous photodepolarisation, trapping 78—10838
polyethylene, carrier traps, photostimulated detrapping currents and TSC meas. 78—10458
polyethylene, dielectric props., investigation for morphology changes created by mechanical drawing and annealing 80—84697
polyethylene, elec. props. and oxidation after electron beam irradiation and heat treatment 79—87092
polyethylene, elongated low density film, TSC 79—47106
polyethylene, high density, carrier trapping, X-ray induced TSC 80—11005
polyethylene, high density, thermolum. and its oxidation effects 77—77305
polyethylene, high density, trapped carriers, thermally stimulated currents, influence of oxidation 77—80792
polyethylene, high density, TSC field depend. 78—76090
polyethylene, low density, γ-irrad., unixial elongation effect on elec. cond. 80—25812
polyethylene, oxidised, charge carrier, transport phenomena 80—15515
polyethylene, oxidised and gamma-irradiated, carrier traps, thermally stimulated currents 78—19050
polyethylene, relation between electrostatic capacity and electronic space charges induced by high field 79—15154

electron traps continued
polyethylene, space-charge storage under high DC voltage condition, TSC meas. *(German)* 80—75576
polyethylene, surface charge release, crossover phenomenon, thermally stimulated discharge current study 80—50255
polyethylene, X-ray irrad., trapped carriers, TSC 77—69338
polyethylene electrets, charge trapping mechanism, TSC, DTA and optical meas. 80—11322
polyethylene films, corona charged, charge trapping 80—88571
polyethylene terephthalate, anomalous photodepolarisation, trapping 78—10838
polyethylene terephthalate electrets, TSC due to injected charges, electron trapping props. 79—4566
polyethylene terephthalate photoelectret, TSC and photostimulated detrapping current obs. 78—10459
polyethylene TSC resulting from trapped carriers 78—6393
polyethylene-terephthalate, field-controlled photogeneration and carrier trapping 80—25285
polyhydroxy compounds, X-irrad., trapped electrons, ESR and ENDOR obs. 80—93161
polymer, carrier trap study by X-ray induced TSC and thermoluminescence *(Japanese)* 80—54713
polymer, dielectric breakdown, DC trees caused by space charge accumulation, carrier injection and trapping effects 80—84695
polymer electret, absorpt. and relax. of charge 80—6942
polymer electret, charge dissipation, transport mechanisms 80—7268
polymer film, carrier transport meas. 80—6874
polymer film electret, charge distrib., generalized model 80—6873
polymer films, photoelectric emission and contact charging, surface states 79—33885
polymers, pulsed photoconduction 80—24969
polymers powders, corona-charging props. 80—6946
polynaphthol film, semicond., trap depth and trapping cross section from TSC curves 79—51700
polypropylene, electret, trapped injected electrons, EPR obs. 78—27093
polypropylene, electron bombarded electret, trapped charges ESR study 80—7170
polypropylene film, vac. evaporated, electron trap depth, TSC meas. for MIM struct. 79—95535
polypyromellitimide, thermal depolarisation current 78—52429
polystyrene, atactic, bulk and surface elec. props., contact charging obs., dielec. const. 80—15615
polystyrene, electron trap depth distribs., thermolum. data 78—11002
polystyrene, pure and doped, metal contact effect on persistent internal polarisation 79—78617
polystyrene, thermoluminescence glow curves, quenching and isothermal decay plots 77—48258
polystyrene atactic carrier transport and photogeneration 80—80318
polystyrene film, in MIM struct., elec. conduction and free radicals 80—20340
polystyrene foils, breakdown-charged, surface charge densities and depths, TSC spectra 80—7260
polystyrene thin films, TSC and surface charge meas. 80—103769
polyvinylcarbazole, Coloumb trap controlled hopping mobility model tests, mobility and permittivity meas. 79—56226
polyvinylidene fluoride, X-ray induced TSC 80—75578
positron prethermalisation trapping model, appl. to Pb 77—43541
1-propanol, dry-electron localisation, impurity trapping, solvated electron rate consts. 79—1990
1-propanol, electron traps, prestabilised electron relax. model 78—27803
1propanol, glassy, electron trapping, pulse radiolysis obs. 80—30264
n-propanol, glassy and crystalline forms, trapped electrons, conc. of mol. vacancies determ. 77—65948
pyrene, band structure, excitonic processes, trap distrib. 80—6720
quartz, comparison of different radiation effects 78—26596
quartz, crystalline, thermolum. sensitivity, proton and gamma induced 77—90205
quartz, electron capture by impurity ions, cross sections eval. using thermolum. data 79—95855
quartz, impurity microdefects. electron capture cross-sections *(Russian)* 78—76025
quartz, trapping levels 78—91703
α-quartz, uncompensated Ti^{3+} centre, annealing, X-irrad., EPR meas. 79—65731
quasifree excitons and electrons, impurity trapping 80—59880
radiation-induced trapped electron yields, close effects, tunnelling processes 79—39161
relaxation semiconductor, theory of carrier transport in p$^+$-ν junction 79—60914
resonant tunnelling current for general junction pot. barrier 79—51656
rhamnose, single cryst., X-irrad. at 4.2K, trapped electrons and electron traps characts. 79—78037
ruby, induced absorpt., radioluminesc., thermoluminesc., Cr^{3+} conc. depend. *(Russian)* 77—90206
sapphire, Czochralski-grown, excess charge carriers, generation, transport and trapping 79—82646
sapphire-Al interface barrier, transport and trapping obs. 77—76921
Schiff's base, thin layer samples, mechanism of change carrier photogeneration *(Russian)* 77—32045
Schottky barrier, tunnelling current assisted by deep traps, theoretical evaluation 77—43722
Schottky diode, effect of thin oxide layer between metal and semicond. 77—20432
Schottky diode, trap refilling, depth and capture cross section determ. 78—80052
SCL current-voltage charact. of homogeneous solid, arbitrary energetic trap distrib. 78—84224
self-trapping barrier height *(Russian)* 77—69252
semiconductor, deep bound states, temp. depend. of ionisation energies 77—31975
semiconductor, deep trap activation energy, effect of non-exponential transients, DLTs method 80—20115
semiconductor, electron trap, positively charged, hot electron capture coeff. 78—52003
semiconductor, estimates of degeneracy factors, energy levels, from solubility data 78—14691
semiconductor, Faraday rotation in presence of attractive traps 78—76081
semiconductor, Faraday rotation in the presence of deep repulsive traps 80—29724

electron traps continued
- semiconductor, high resist., continuous energy distrib. of trapping centres, dynamic charact. of SCL current 78—56153
- semiconductor, impact ionization, review 80—65577
- semiconductor, impurity acoustoconduction, nonlinear theory 77—15914
- semiconductor, interpretation of thermolum. and TSC, extensions of conventional model 78—27335
- semiconductor, local level parameters from thermally stimulated excitation curves, influence of variations of rate of heating 80—6769
- semiconductor, multiphonon recombination processes 79—38643
- semiconductor, non-radiative multiphonon carrier-capture cross-sections of deep traps, high-temp. limit 77—90191
- semiconductor, nonlinear conductivity, vortex waves, carrier mobility and lifetime 80—96893
- semiconductor, nonradiative multiphonon carrier capture and ejection props. of deep traps 78—35190
- semiconductor, nonradiative multiphonon carrier capture by deep neutral traps 80—6871
- semiconductor, nonradiative multiphonon carrier capture props. of deep charged and neutral centres 77—15866
- semiconductor, photo-EMF during charge carrier trapping *(Russian)* 79—42574
- semiconductor, photocond., influence of surface space-charge layer 80—15563
- semiconductor, photoelectret state form. by IR light quenching photoelec. current *(Russian)* 79—91345
- semiconductor, photoexcitation, electron lifetime and capture by trapping centres *(Russian)* 77—32047
- semiconductor, recomb.-enhanced defect reactions 77—51377
- semiconductor, recombination at deep traps, review 79—38100
- semiconductor, spatial distrib. of traps obs. with SEM *(Russian)* 77—32449
- semiconductor, strong electron-lattice interaction, review *(Japanese)* 80—49664
- semiconductor, surface properties, investigation by laser and photovoltages *(Russian)* 78—23130
- semiconductor, techniques for detecting electrons and holes trapped at bulk and interface imperfections 77—11934
- semiconductor, transient injection currents, charge transport allowing for trapping 78—26884
- semiconductor, two-photon absorpt., free carrier storage by deep centres *(Russian)* 78—23131
- semiconductor, wide-gap, extrinsic, injection currents, theory 78—19052
- semiconductor containing traps, minority, carrier lifetime 78—60137
- semiconductor detectors of nuclear radiation, effect of trapping on response 80—5447
- semiconductor film, carrier temperature and density self-oscills. near instability threshold 80—11118
- semiconductor junctions, electric field effect on thermal emission of traps 80—11073
- semiconductor laser, self pulsing due to deep level traps 79—22950
- semiconductor lasers, triggerable, light-coupled logic appl. 80—74360
- semiconductor photosensitive element, discharge process, capture of carriers *(Russian)* 77—69343
- semiconductor surfaces, relaxation time spectrum of slow traps *(Russian)* 77—15937
- semiconductor under illumination, simple model of generation and recombination processes 79—69523
- semiconductor with arbitrary energy spectrum of trapped states, surface region of space charge 80—107811
- semiconductor with position depend. composition, carrier generation, recomb., trapping and transport 77—43613
- semiconductor-insulator boundaries, capture coeff. of neutral surface traps, influence of image forces 79—51683
- semiconductors, Auger recombination processes 79—38091
- semiconductors, Auger recombination with traps 80—49763
- semiconductors, capture of carriers by attractive centres 79—7836
- semiconductors, covalent, substitutional deep traps, theory 80—54651
- semiconductors, current instabilities, theory and expts. *(Hungarian)* 77—39857
- semiconductors, defect-density profiles, constant-capacitance DLTS meas. 79—95361
- semiconductors, II-VI and III-VI types, competition between two-photon absorption and two-stage absorption via deep traps 80—29764
- semiconductors, multiphonon capture rate 79—38022
- semiconductors, negative injection conductivity 79—69517
- semiconductors, nonradiative multiphonon carrier-capture cross section of deep traps, low temp. depend. 78—10469
- semiconductors, nonradiative recombination, combination of Auger and many-phonon processes 79—87111
- semiconductors, phonon assisted electron impact ionisation and Auger recombination, theory 80—39591
- semiconductors, photocond., photoelec. effects, book contrib. 80—84488
- semiconductors, photoelectric fatigue 77—80808
- semiconductors, polycryst., with low angle grain boundaries, residual cond. 80—15525
- semiconductors, recombination processes, review 79—38088
- semiconductors, thermally stimulated conductivity luminescence, defect levels, traps, book contribution 80—80296
- semiconductors and insulators in contact with metals, charging of bulk states 80—54781
- semiinsulator, minority carrier injection effect on TSC 78—10466
- shellac platina, elec. cond., temp. and thickness depends., mechanism 79—99645
- shielded point defect potential well calcs. using Poole-Frenkel effect 80—20122
- silastic tubular electret, mag. polarised, thermal currents 80—40037
- single-injection solid-state diodes with exponential trap distrib., elec. cond. of hot carriers 79—99556
- sisal wax, electronic conduction and persistent internal polarisation 78—80277
- small signal electrical response theory, generation-recomb. and trapping kinetics 77—89772
- solutes, trapped electron two-step tunnelling 79—96288
- solvated electrons, statistical model, distrib. function of hydrated electron energy 80—30271
- sorbitol, X-irrad., 4.2K, electron traps, alkoxy hyperfine coupling, ENDOR obs. 80—50863
- space charge limited current-voltage characts., steady state, validity of anal. eqns. 80—107800
- space charge limited I-V characts., differential method of anal. 77—69333
- sucrose, single cryst., absorption spectrum of electron traps, pulse radiolysis obs. 80—93369
- sucrose, single cryst., X-irrad. at 4.2K, trapped electrons and electron traps characts. 79—78037
- superlinear filling of traps in crystals due to competition during irradiation 79—33850
- surface avalanched p-n junctions, localised charge injection and trapping 77—76907
- surface self-trapped states, surface polarons and surface excitons *(Japanese)* 80—2445
- surface trapping phenomena rel. to surface states 77—39916
- Teflon, negatively corona charged, new model of isothermal charge transport 80—34536
- Teflon FEP, electron beam charged film, charge centroid location 78—15095
- Teflon FEP-A, corona and electron beam charged, TSC peak identification and surface-voltage stability 79—78614
- Teflon film, TSC studies of carrier trapping and mobility 80—7016
- p-terphenyl, single cryst., delayed fluoresc., mag. field depend., 130-300K 79—69879
- tetracene, amorphous film, TSC meas., carrier traps 80—2496
- tetracene, polycryst., SCL currents and trap distrib. 79—1603
- tetracene, space-charged-limited photo-enhanced currents 79—82599
- tetracene, trapping effects on emission-limited current flow 80—29413
- 1,2,4,5-tetrachlorobenzene, mol. solid, heat pulses, phonon-induced delocalisation of trapped excited triplet states 80—89053
- 1,2,4,5-tetrachlorobenzene, proton spin relaxation by optically excited triplet states 79—19810
- thermally stimulated capacitance method fitting anal. 79—47107
- thermally stimulated electron emission, dependence on heating rates, conduction electron retrapping probability *(Russian)* 80—84826
- thermally stimulated recombination, reaction order 79—95853
- thermally stimulated release of trapped carriers, trap level spectroscopy 78—10461
- thermoluminescence and TSC, evaluation of model, reliability of trap depth determ. 77—32451
- thermoluminescence dosimeter, response, nonlinear behaviour 78—33293
- thermoluminescence glow curves, reflection of electron trap distrib. activation energy 79—43047
- thermoluminescence intensity depend. on heating rate, competing deep trap model 77—73590
- thermoluminescence method for trap depth determ. 80—80211
- thermoluminescence yields, nonlinear effects 78—11007
- thermoluminescent dosimetry, TLD 700, parameters affecting overall calibration accuracy 79—63821
- thermoluminescent process, entropy production 78—23539
- thermostimulated recombination, reaction order *(Russian)* 78—76536
- thin insulator, SCL currents, effects of finite contact energy barriers and traps 79—38209
- transient current injection, trap-controlled 77—24565
- transient photoconduction, trap controlled 78—10507
- transition metal oxides, XPS, trapped electrons at F-centres and anion defects, photoionis. cross sections 77—90249
- transport via extended states with traps, space-charge hopping equivalence 79—95399
- TSC, trap depth determ., theory 80—70716
- TSC, with participation of two trapping levels 79—56244
- TSC and isothermal decay currents, influence of blocking contacts 77—28182
- TSC in MIS and polyethylene, rate-determining process 77—59290
- TSC technique, trap modulated electron and hole mobility meas. in insulators 78—10441
- TSC under monomolecular recomb. conditions, calc. method for trap parameters 77—8495
- TSC with slow retrapping, trap depth determ. 80—59998
- TSC with two trapping levels, calc. 80—60489
- TTT, dark cond. and photocond. effect of strong mag. field, at charge carrier injection *(Russian)* 79—69607
- tunnelling during excitation of electroluminescence 78—43936
- two-valley semiconductor, domain instability *(Russian)* 77—62934
- water, solvated electrons, photon-induced electron transfer transitions 79—8154
- wave hierarchy interpretation of multiple trapping model 80—6894
- wide-gap semiconductor, recomb.-trap barriers 77—8119
- xylitol, X-irrad., 4.2K, electron traps, alkoxy hyperfine coupling, ENDOR obs. 80—50863
- Ag halide emulsion grains, photographic effects of electron and positive hole traps 77—82635
- Ag speck nucleation and phase formation in latent image 80—97716
- AgBr, localisation of polarons on (100) surface, rel. to photographic sensitivity *(Russian)* 77—35983
- AgBr, pure and doped, identification of shallow electron centres 77—59267
- AgBr:Pd(II), photolysis-induced trapping behaviour, EPR study 80—54949
- AgBr(I) microcrystals, photocond. and luminesc. 78—26904
- AgCl, pure and dopded, identification of shallow electron centres 77—59267
- AgCl:Ni, optically detected double resonance, radiative recombination electron traps 80—20518
- AgCl:Pd^{2+}, EPR, role of vacancies in impurity based trapping 77—28439
- AgCl-AgI, mixed cryst., trap distrib., thermolum. 78—68568
- AgCl(Br), crossed elec. and mag. fields, hot electrons, streaming motion, population inversion 80—44649
- β-AgI:Cu, pure and doped, photoconductivity, band struct., trap nature 79—95449
- Ag_3SbS_3, pyrargyrite, US absorption, influence of illumination, photocond. and photoabsorption of sound 79—42153
- Al/Al_2O_3/Al structures with organic monomolecular layer, cond. at high elec. fields 80—80402
- Al-Al_2O_3-Al structures, elec. props. of anodic Al_2O_3 films 79—99646
- Al-Al_2O_3-Pb structure, traps in Al_2O_3 detected by tunnelling 77—8202
- Al-Al_2O_3-Si structure, study of charge trapping 80—60097
- Al-GaAs Schottky barrier diode, Richardson const. 77—20424
- Al-SiO_2-Si MOS diodes, interface trap states obs. due to electron beam lithography *(Japanese)* 80—54787
- Al-TeO_2-Al, field-assisted cond. mechanism 80—11105

electron traps continued
AlGaAs semiconductor lasers, single-mode stabilisation by traps 80—95893
n-$Al_{0.3}Ga_{0.7}As$, layer of (AlGa)As DH laser, deep levels 78—46605
$Al_xGa_{1-x}As$ triggerable semiconductor lasers made by deep proton bombardment 80—69408
$Al_xGa_{1-x}As$:Te, persistent photocond. trapping centre, donor complex model, photocapacitance meas. 79—65517
Al_2O_3 anodic films, trapping levels study using TSC 80—103768
α-Al_2O_3, crystal defects from X-ray irradiation, F-centres, X-ray luminesc. obs. 80—55176
Al_2O_3, thin films, due to neutron irradiation 80—2505
Al_2O_3, X-irrad., electron and hole traps, TSC and optical bleaching meas. 79—28356
Al_2O_3:Cr, pure and doped, electron irrad. induced cond., TSC and EPR study 80—80277
α-Al_2O_3:Er(Cr), crystal defects from X-ray irradiation, F-centres, X-ray luminesc. obs. 80—55176
Ar, liq., electron mobility, role of shallow traps 80—34440
Ar, liq., recomb. and self-trapped exciton luminesc., free electron dynamics, excited states 80—25463
As_2S_3 and As_2S_3-Sb_2S_3 system glasses, long-term photocond. relax. 77—76874
As_2S_3 glass, localised paramag. states, As_4S_6, As_4S_4 units, mol. analogue models 78—60087
As_2S_3 glass, trap levels, determ. from thermal relax. time 77—4337
As_2S_3, glassy, thermally stimulated depolarisation 77—24782
As_2S_3-Sb_2S_3, vitreous, dispersive charge transport analysis 79—95418
$AsS_{3.5}Te_{2.0}$ glass, gamma-irradiated, TSC meas. 77—66166
As_2Se_3, amorphous, defect states, exptl. study. 80—54645
As_2Se_3, amorphous, hole emission defect states 80—49759
As_2Se_3, crystalline, electron drift mobility and DC cond., trapping model 77—47815
As_2Se_3, modulated photocurrent, analysed for trap-limited case *(Japanese)* 80—60030
As_2Se_3:Al, glassy, energy spectrum of deep localized states, thermal dielectric relaxation 78—15088
a-As_2Se_3:Tl(Ga)(In)(Cu), hopping channel modifications, trap buildup due to impurity concs. 79—60846
As_2Te_3, charge screening length 79—23974
$As_{40}Te_{48}Si_{12}Ge_{10}$, charge screening length 79—23974
Au-CdS junction diodes, chemically etched CdS cryst. surfaces effect on barrier layer 80—44722
Au-GaAs Schottky barrier diode, Richardson const. 77—20424
B_2O_3-CaO-Fe_2O_3 glasses, semicond., cond. models, electronic props., 77-800K 80—54688
Ba_2CaUO_6, luminescence and energy migration 79—4837
$BaMnF_4$, luminesc., emission from localised traps 79—33777
BaS:Cu, thermoluminesc. and decay 78—80426
$BaSO_4$, with small retrapping factor, thermolum. glow curve 77—52188
$BaSO_4$, X-ray irrad., electron and holes traps, g-factors, ESR obs. 80—50183
$BaTiO_3$, melt grown, drift mobility meas. 79—19596
$BaTiO_3$, photocond. of doped single cryst., photoexcitable levels 77—4391
$BaTiO_3$, polycryst., elec. resist. anomaly in phase transition region 78—43381
$BaTiO_3$, pure and doped, photocurrent kinetics 79—42576
$BaTiO_3$, reduction inhibition by impurity ions 80—101018
$BaTiO_3$, SCL currents, carrier mobility and trapping 77—15863
$BaTiO_3$:Co, trap recomb. consts., photocurrents 78—43435
$BaWO_4$:Mo, P, thermoluminesc. traps, EPR meas. 77—90032
Be (0001) oxidised surfaces, internal electron source contrib. to TSEE trap population 80—16161
BeO, anomalous exoemission, laser irrad., electron trap ionisation *(Russian)* 77—1792
BeO, thermoelectret props. 80—7269
$Bi_{12}GeO_{20}$, photoelectret state 80—11315
$Bi_{12}GeO_{20}$ vacuum-deposited film elec. and photoelec. props. *(Russian)* 78—60237
$Bi_{12}GeO_{20}$, vol. hologram recording, charge transfer process 78—5437
Bi_2O_3 anodic films, struct. and electronic props., photoeffects 80—44749
$Bi_{12}SiO_{20}$, vol. hologram recording, charge transfer process 78—5437
Ca halophosphates, thermoluminesc., defects *(Russian)* 79—56869
$CaCO_3$, calcite, X-ray irrad., luminesc. and dielec. loss decays 77—12431
CaF_2:Dy^{3+}, thermolum., associated luminesc. centres and traps 77—28638
CaF_2:Eu, Mn, cathodoluminescence SEM appl., stroboscopic 80—70088
CaO:Ce,Gd phosphors, trap distrib., phosphoresc. decay characts. obs. 80—29773
CaO:Cu(Ag)(Au), thermoluminesc., following UV excitation, 290-500K 77—40292
CaO:Eu(Tb), phosphor, isothermal decay 80—55156
CaS:Bi,Dy phosphors, thermoluminesc. 77—69921
CaS:Pd phosphors, trap and luminescent centre location, photo-, thermo- and electroluminescence studies 80—71482
CaS:Zr, Gd phosphors, thermoluminesc., trap distrib., activator effects 78—2929
CaS-Pb,Mn, phosphors, thermoluminesc. and fluoresc. spectra 78—64396
$CaSO_4$:Dy, competing deep trap model for thermoluminescence 79—83039
$CaSO_4$:Dy phosphor powder, effect of grinding on thermoluminescent sensitivity 79—33852
$CaSo_4$:Mn trap depth, thermolum. meas. 77—36301
$CaWO_4$:Mo, P, thermoluminesc. traps, EPR meas. 77—90032
Cd, positron trapping at low temp. lifetime spectra 80—84799
$CdGa_2Se_4$, electron traps, energy spectrum, photocurrent decay, TSC temp. depend. *(Russian)* 78—64057
CdI_2, thermoluminesc. of traps *(French)* 79—4856
$CdInGaS_4$, TSC and SCL cond. investig. of electron trap parameters, 120 to 350K 77—69341
$CdIn_2S_4$, photocond. and trap. distrib. 78—39164
$CdIn_2S_4$, photocond. and electron trap distrib. 79—28373
CdS, deep level electron trap characts. 79—78036
CdS, drift mobility in presence of trapping-recomb. centres 78—19054
CdS, electron and hole trapped centres, EPR, photoluminescence, photoconductivity study 80—108071
CdS, electron traps, admittance spectra on hetero- and Schottky junctions 79—56159
CdS, electron traps, DLTS meas. 80—24949
n-CdS film, transient photoconductivity effects *(French)* 78—87994
CdS, impurity cond., temp. depend. *(Russian)* 78—47829

electron traps continued
CdS, neutron irradiated, intrinsic defects 78—51599
CdS, obtained from CdS-Cr_2O_3 system, α-Cr_2O_3 effect on props. *(Russian)* 79—65469
CdS, phase memory effect and vel. of trap-controlled high-field domains 77—47855
CdS, photocond. cryst. characterisation of electron-trap responsible for acoustic holographic echoes *(French)* 79—19544
CdS, polycrystalline evaporated layers, donor and trap densities 80—20213
CdS polycrystalline layers, electron trapping depend. on preparation conditions 79—78232
CdS, trapping level parameter determ., limiting current injection *(Russian)* 78—39129
CdS, vap. phase grown cryst., stoichiometry control, elec. cond. 79—100034
CdS, wide-gap extrinsic semicond., injection currents, theory 78—19052
CdS:Ag, induced impurity photocond. spectrum obs. 77—1447
CdS:Ag phosphor, mechanism of trap ionisation by elec. field, Gudden-Pohl flashes 79—74007
CdS:Cu, C-V curves of MIS diode used to examine trapping levels 80—65697
CdS:Cu, Cl films, photocond. growth and decay time 80—60041
CdS:$CuCl_2$($CdCl_2$) sintered layer, distrib. of energy levels of local centres 80—15568
CdS:Li, photocond. characts., electron and hole traps obs. 77—8140
CdS:Mn(Co), intensity and spectral distrib. of luminescence *(Russian)* 77—16392
CdS-Cu_2S junctions, carrier trap density, deep level defects 80—107801
CdS-Cu_2S single cryst. heterojunction, trap depths in depletion region 78—52064
CdS_xSe_{1-x}, electron traps, DLTS meas. 80—24949
CdSe, dark current relaxation 80—44613
n-CdSe, with single deep electron trap, negative photocond. 77—15905
$CdSiP_2$:Na(Bi), single crystal, photocond. under laser excitation 80—44661
n-CdTe, deep trapping levels in high resistivity films 77—72930
CdTe detectors, gamma and electron irradiation effects 78—41893
n-CdTe films, uniform trap distrib., transient photocond. effects 79—28423
CdTe, high-resistivity, carrier transport and trapping processes, growth parameter effects 77—39871
CdTe, high-resistivity, irradiation effects on carrier transport and trapping process 78—2164
CdTe, Schottky diode, trap density determ. 79—7899
CdTe sputtered films, struct., photocond., and trap distrib. 80—29489
CdTe, thermostimulated capacitor discharge, trapping levels obs. *(Russian)* 78—10842
CdTe:Cl, anomalous props., molecular centre with charge-state dependent config. 77—89728
CdTe:Cl, capacitance meas. and trapping, mol. centre model *(French)* 77—39872
CdTe:Cl, cryst., high resist., SCL currents, DC meas. 77—66170
CdTe:Cl, description of anomalous centres by non-purely electronic model 78—30886
CdTe:Cl(In), photoelectronic investig. of trap depths, TSC and SCL cond. 77—39893
CdTe:Zn, TSC, carrier traps, depth and quenching by IR radiation 78—56420
$Cd_{1-x}Zn_xS$ 10 μm film optical and electrical characterisation *(French)* 78—64153
CsCl, impurity and defect sites, elec. field gradient calc. 79—78034
β-Cu phthalocyanine electrophotographic props. rel. to particle size *(Japanese)* 80—13171
n-$CuInS_2$, mag. props., obs. 80—70939
Cu_2O, defect levels, TSC 77—66138
Cu_2O single crystals, photomemory effect, kinetics of excitation and deexcitation processes 77—85262
Cu_2S-CdS heterojunctions, electron trap characterisation by capacitance transient meas. 79—78163
D_2O, ice cryst., electron traps, electron irrad. effects, EPR 77—1939
1,6-di-(N-carbazolyl)-2,4 hexadiin, cryst. struct., luminesc., γ-ray polymerisation 78—18629
EuS, ferromag., on W, electron field emission 79—8230
GaAS, proton isolation layer, lateral spread, elec. meas. 77—80520
(GaAl)As injection lasers operating with optical fibre resonators 80—91812
$Ga_{1-x}Al_xAs$, epitaxial, radiative deep states 80—76061
$Ga_{1-x}Al_xAs$, photoluminescence, deep level trap emission capture 80—29805
GaAs bulk and epitaxial crysts., electron traps characterisation 77—39865
GaAs conducting MIS structures and metal-semicond. structures, effects of ultrathin oxides 79—1626
GaAs, deep bound states, temp. depend. of ionisation energies 77—31975
GaAs, deep centre free energy level determ. by transient capacitance technique 80—103641
GaAs, deep centres, collective thermal emission of electrons 80—10918
GaAs, deep centres, electron and hole capture cross sections 79—99510
n-GaAs, deep electron traps, determ. by time-resolved capacitance meas. 77—39797
GaAs, deep level profile anal., double correlation technique 77—80830
GaAs, deep level trap emission identification by indirect conduction minima technique 78—84163
n-GaAs, deep level traps, transient and thermally stimulated capacitance meas. *(Chinese)* 79—91072
GaAs, deep trap characts. by photocapacitance spectroscopy 78—6398
GaAs, deep trap study by free exciton refl. spectra 79—60761
GaAs, deep traps exam. by capacitive method 77—11869
n-GaAs, deform. produced deep levels, DLTS meas. 80—54634
GaAs, domain elec. instability in two-valley semiconds. 77—76842
GaAs, electrical and optical props. at low temps. 80—39636
GaAs, electron trap at E_c-0.75 eV, direct evidence for nonassignment to O 79—90988
GaAs, epitaxial film, field effect struct., elec. breakdown, negative resist. 77—12030
n-GaAs epitaxial film, pure and Cr doped, heavy electron trapping, Gunn oscills. 80—6857
GaAs epitaxial layers, photocond. high field effects on carrier capture and recomb. 77—43646

electron traps continued
GaAs epitaxial layers, undoped, recomb. of non-equilib. carriers, steady-state photocond. 77—85357
GaAs, epitaxial layers, grain boundaries, deep level transient spectroscopy study 80—49234
GaAs, epitaxy by metallorganic and chloride depositions, defect characterisation at growth interface 80—59817
GaAs grown by VPE using organometallic method, deep trap levels 80—10923
GaAs, Gunn effect, carrier generation-recomb. processes 79—38080
n-GaAs, heat treatment effect on electron traps 78—6396
GaAs, LPE, residual impurities and deep levels, FET fabrication 79—28964
GaAs LPE layers, deep levels by photocapacitance and related techniques 78—6334
n-GaAs, MBE, correl. between electron traps and growth processes 80—65387
n-GaAs, MIS structures, C-U curves, surface state densities 77—85335
GaAs MOS structure, small signal admittance study, trap distrib. 80—2478
GaAs MOS structures, leakage current for anodic oxide layers, space charge trapping effects 80—60091
GaAs, nonradiative multiphnon carrier-capture cross sections of deep traps, intermediate-temp. depend. 78—43414
GaAs, organometallic VPE, with varying As/Ga ratios, deep states 80—65480
GaAs oxidation saturation and MOS diode equivalent cct. 78—47875
GaAs oxides, appl. of selective chemical reaction concept for controlling props. 79—47790
GaAs, photoluminescence, deep level trap emission capture 80—29805
GaAs, proton irradiated, low energy, deep level defects and hole diffusion length meas. 80—60000
GaAs Schottky barrier structure, defects from proton irradiation, thermal transients and optical capacity *(French)* 80—59534
GaAs, Schottky diode, trap levels, admittance spectroscopy 79—51672
n-GaAs surface barrier diodes for nuclear radiation detection, deep trapping centres 80—92849
GaAs type FET with buffer, bias effects due to deep centres in struct. *(French)* 80—107917
n-GaAs, undoped, proton radiation defect detect. by transient capacitance spectroscopy 79—11089
GaAs, VPE, incorporation of deep levels, effects of growth conditions 80—20111
GaAs VPE layers, electron irrad., electron traps 80—25026
GaAs, VPE layers, growth conditions effect on deep levels 79—95360
GaAs:Be, deep levels 80—29358
GaAs:Be MBE films, elec. characterization 79—91168
GaAs:Cr, deep acceptor level, DLTS and optical DLTS study 80—92852
GaAs:Cr, high resist., anomalously strong elec. field induced release of carriers from traps 78—6397
GaAs:Cr, hot electron relax. process and ionization of traps *(Russian)* 79—28354
GaAs:Cr, Schottky barrier, effect of trapping processes on photocapacitance 77—76866
GaAs:Cr, semi-insulating, TSC, carrier recomb. and trapping 77—32014
n-GaAs:Cr, semi-insulating, contact effects, trapping levels 78—10465
GaAs:Cr, strong quenching of thermally stimulated conductivity by elec. field *(Russian)* 77—1434
GaAs:Cr, thermally grown, DLTS study of Cr trap density 80—96815
GaAs:O, deep traps, photocapacitance meas., complementary transition energy threshold determ. 79—19550
GaAs:O, photocond., electron traps, level-broadening, 90 to 150K 78—60158
n-GaAs:O, press. depend. of deep level associated with O, transient capacitance meas. 78—64000
GaAs:O, slow domains, origin 78—60132
GaAs:Si, positron lifetime temp. depend. 80—29826
GaAs-GaAlAs DH LED, transient current trap spectroscopy 78—80049
GaAs-GaAlAs LEDs, deep levels *(French)* 78—56218
n-GaAs-GaAs:Cr, interface elec. props., substrate effects 78—6438
n-GaAs-GaAs:Cr. semiinsulating, low freq. current pulses 77—8176
GaAs-insulator interface, processes of electron emission from traps 79—73598
GaAs-native oxide interface, electronic props. 79—73590
GaAs$_{0.6}$P$_{0.4}$, anodic oxide, negative charge traps at interface 79—61771
GaAs$_{0.6}$P$_{0.4}$, deep level profile anal., double correlation technique 77—80830
GaAs$_{0.6}$P$_{0.4}$:N, isoelectronic tape by ion implantation and CO$_2$ laser annealing 80—24464
GaAs$_{0.65}$P$_{0.35}$, gamma irradiated, deep level study using DLTS and photocapacitance methods *(Japanese)* 80—49665
GaAs$_{1-x}$P$_x$, bound exciton, luminesc. reson. excitation 79—95840
GaAs$_{1-x}$P$_x$, N trap bound state, Hall effect determ. 78—19055
GaAs$_{1-x}$P$_x$, thermal oxide, electron trapping at oxide-semiconductor interface 79—61772
GaAs$_{1-x}$P$_x$:N, LED, external quantum efficiency, press. effect 77—8655
GaAs$_{1-x}$P$_x$:N, N isoelectronic trap, model calc. of N$_\Gamma$ and N$_x$ electronic states 78—10398
GaAs$_{1-x}$P$_x$:N, photolum. and electrolum. study of N isoelectronic traps 80—89061
GaAs$_{1-x}$P$_x$:N, upper branch of N isoelectronic trap., photo- and electrolum. expts. 77—63462
GaAs$_{1-x}$P$_x$:S, deep level, photoconductivity, carrier nonradiative recombination 80—20112
Ga$_{1-x}$In$_x$As, VPE layers, main electron trap, transient capacitance spectroscopy obs. 78—34800
GaP crystals, radiation defects, TSC obs. 80—65588
n-GaP, deep state controlled minority carrier lifetime 80—20211
GaP diodes, TSCAP and admittance spectroscopy of gamma-ray induced defects 77—89472
GaP, electrical and optical props. at low temps. 80—39636
GaP, electron irrad., radiation defects annealing 80—29059
GaP, electron traps around dislocations in p-n junction and metal-semicond. structs. 80—34388
GaP, non-radiative recombination and structural defects 78—19566
GaP p-n junction, capacitance-freq. dispersion and electroluminescence efficiency 78—64101
GaP, photovoltage transients, intensity and chopping freq. depend. 77—47859
n-GaP, shallow trapping centres, electron lifetime from photocond. meas. 79—99563

electron traps continued
GaP:Bi(N), luminesc. decay kinetics 79—38646
GaP:Fe, double electron trap state, ESR identification 77—36124
GaP:Fe, photo-EPR study Fe(3d^6) centres and deep electron traps 80—44910
GaP:N, spin dependent exciton recombination at N$_2$ isoelectronic traps 77—69734
GaP:N VPE layers, thermal emission energies, trapping, and carrier lifetimes, deep level capacitance spectroscopy 79—42487
GaP:Ni, deep traps, near IR luminesc., polarised spectra meas. 80—16077
GaP:Ni, optical and EPR study of two-electron-trap state 79—73806
GaP:Ni(Fe), multivalence impurities, EPR and optical absorpt. meas. 80—75844
GaP:Zn,O, red LED, deep-level changes associated with degradation 77—1472
n-GaS, TSC, electron traps 80—11002
n-GaSe, photoconductivity and TSC investig. of trapping centres 77—20359
n-GaSe, photomagnetoelectric effect, photocond., in presence of traps 80—39631
GaSe, space-charge-limited currents at different temps. 77—43607
n-GaSe:I, SCL currents, expt. test of theory for insulator with two sets of traps distribution in energy 77—89768
GaSe:Sn, single crystal, space-charge-limited currents *(Russian)* 80—11001
Ga$_2$Te$_3$ single crystals, switching effect., carrier trapping 80—6919
Ge, adsorption of N$_2$ and CO, adsorption potentials and trapped electrons role 79—90872
Ge, donor-acceptor electron transfer at low temps., photocond. tail 78—84249
Ge, electrical and optical props. at low temps. 80—39636
Ge, electron irrad., light-sensitive defects 80—24498
n-Ge, electron irradiated, energy levels 79—28316
n-Ge, electron irradiated, threshold energy for atomic displacement, carrier traps 80—29351
Ge FET, fabrication on high purity substrate 79—45579
Ge, high purity, carrier trapping 79—47104
Ge, high purity, nature of large traps, expt. on p$^+$-n-n$^+$ struct. 78—19051
p-Ge, Li-compensated, carrier capture 77—15792
Ge, light scattering, by pure single cryst., influence of photoexcitation 79—28780
Ge p$^+$-ν-n$^+$ structures, large-scale trap characts. 80—92966
Ge p-i-n diodes, deep level transient spectroscopy 79—47105
Ge surface, optical charging meas., 120-300K 80—49817
Ge:Au, capacitance oscillations, trap recharging waves 77—43614
n-Ge:Au, electron capture by negatively charged traps, effect on hot electron enrgy energy distrib. 78—43398
Ge:Au, trap charge exchange waves *(Russian)* 78—34846
n-Ge:Ni, recombination of hot electrons on Ni impurity centres 80—44612
Ge:Ni compensated, hot electron recomb. anisotropy 78—39125
Ge:P(Sb)(Bi), γ-irrad., carrier trapping and recomb. at point radiation defects 80—107810
Ge:Sb, γ-irrad., electron capture mechanism by radiation defects 78—26885
n-Ge:Sb, γ-irradiated, trapping and recomb. coeffs. 77—43616
Ge:Sb, Ni(Mn), recombination wave spectrum, two-level traps 80—96906
Ge-GeO$_2$, optical charging memory, influence of doping GeO$_2$ with metal ions *(Russian)* 79—24077
Ge-pyrolytic SiO$_2$ system, carrier trapping, GeO$_2$ sublayer effect 78—91775
Ge-S film, amorphous, photo-induced ESR and optical absorption edge shift 78—88374
Ge-Si$_3$N$_4$ system, potential barriers determ. from photoinjection carriers trapping 80—103756
GeO$_2$, hexagonal and glassy, X and γ-irrad., thermolum. and paramag. centres 77—63472
Ge$_x$Se$_{1-x}$, amorphous semicond., elec. props. 78—84219
Ge$_x$Se$_{1-x}$ chalcogenide glasses, trap-controlled carrier mobility, time of flight meas. 79—4557
Ge$_x$Se$_{1-x}$ chalcogenide glasses, drift mobility of optically injected carriers 79—19627
H$_2$O, crystalline ice, localised excess electrons yield studied as function of dose rate 80—97712
He, liq., electron bound states on surface 79—28166
He, liq., surface with trapped electron, parallel mag. field effect on interband transition 78—87835
Hg$_{1-x}$Cd$_x$Te photodiodes, long cutoff wavelength, effect of trap tunnelling on IR detector performance 80—73451
HgI$_2$, and photomagnetoelectric and photocond. meas., carrier lifetimes 77—55562
HgI$_2$ crystals, native defect compensation, doping, mobility-lifetime and TSC meas. 77—55492
HgI$_2$, photo-EM effect and photocond., trapping effects 77—32042
HgI$_2$, photoelectronic props. 78—41897
HgI$_2$:Ag, trapping effects, TSC, photocond. and photolum. meas. 77—32023
α-HgS, trapping parameters determ. by TSC meas. 80—59997
In-GaAs:Cu-In S-type diode, role of deep trapping levels in form. of current-volt. characts. 77—76948
In$_{1-x}$Ga$_x$As$_y$P$_{1-y}$, traps in device quality n- and p-type LPE material 80—10999
In$_x$Ga$_{1-x}$As$_{1-y}$P$_y$ epitaxial layers, characterisation and relation to lattice matching 80—100540
In$_2$O$_3$-InSb system, with Al(Au) electrode interface state density and oxide charge meas. 77—8200
InP, deep level electron traps, emission and capture props. 80—29806
InP, deep trap characts. by photocapacitance spectroscopy 78—6398
InP, deep trap study by free exciton refl. spectra 79—60761
InP, deep-level traps and cond.-band struct. 79—19542
InP, electrical and optical props. at low temps. 80—39636
n-InP film, polycrystalline, elec. props. 77—76965
n-InP grown by synthesis solute-diffusion method 79—90987
n-InP, heat treatment effect on surface carrier conc. 77—11936
n-InP Schottky barriers, photocapacitance effects of deep traps 78—43325
InP:Fe, Fe acceptor charge states, photolum., absorpt. and ESR meas. 77—36123

electron traps continued
InP:Fe shallow trap thermally stimulated cond. spectroscopy, photocond. spectrum under DC conditions 80−65585
n-InP-SiO_2 capacitor, carrier generation and trapping 80−49929
In_6S_7, TSC at various cooling rates *(Russian)* 80−11000
InSb MOS structs., energy spectrum of traps in oxide layer 80−107922
n-InSb, photoconductive lifetime, surface pot. effects 80−11029
n-InSe, layered semiconductor, current-voltage characts. investig., 130 to 400K 77−4342
$KBr{:}Cl^-$, diffusion traps for divalent ions, dielectric loss and ionic thermocurrent techniques 80−6566
KCl, coloured, trap-controlled photoelectron mobility, transit-time expts. 77−72880
KCl, electron trapping by alkali ion impurities 78−47809
KCl, F-F′ conversion at room temp. 78−51539
KCl, X-ray irrad., thermoluminescence, TSC and thermal stability 79−95859
$KCl{:}Ca^{2+}$, $Cl^-(Br^-)$, diffusion traps for divalent ions, dielectric loss and ionic thermocurrent techniques 80−6566
KCl:Na, electron trapping from α_A and F_A-centres, low temp. depend. 80−11444
KCl:Tl, effective cross sections ratio of charged and neutral centres for holes and electrons *(Russian)* 79−28319
$KCl(Br){:}OH^-$, electron irrad., F_2^+ centre stabilisation 80−54231
K_2CrO_4, ice, γ-irrad., electron trap depth, ESR 79−66317
$KF{:}Pd^{2+}$, pure and doped, two-step photoionisation, laser-active F_2^+ centre form. 79−963
$K_2Fe(CN)_6$ ice, γ-irrad., electron trap depth, ESR 79−66317
$KI{:}Eu^{2+}(Sr^{2+})(Mn^{2+})$, elec. field effect on mech. of recomb. 78−80397
$KMnF_3$, luminesc., emission from localised traps 79−33777
Kr, liq., electron mobility, role of shallow traps 80−34440
Kr, liq., recomb. and self-trapped exciton luminesc., free electron dynamics, excited states 80−25463
La_2O_2S:Eu, slow phosphoresc., high press. study 80−80839
LiCl aqueous glass, X-irradiated, localised electron optical, IR and photoconductivity spectra 78−73064
LiCl, deuterated aq. glasses, pulse radiolysis, trapped electron reactions 79−24804
LiF (TLD-100), thermoluminescent glow peaks 78−35211
LiF, irradiated and plastically deformed, thermoluminesc. defect centres 77−1740
LiF TLD phosphor, residual thermoluminescence effect on sensitisation 80−108287
LiF, TLD phosphor, Z_3 centre, thermolum. and optical absorption spectra 79−24374
LiF TLD-100, thermoluminesc., kinetics and trapping parameters, dose depend. 80−2872
LiF, TLD-100, trapping centres, optical absorpt. spectra defect and thermolum. mechanism models 80−50436
LiF, thermoluminescence mechanism, extension of Mayhugh-Christy model 78−80425
LiF:Mg, X-ray irrad., trapping processes, Z-centres and dipoles, two models 80−49222
$LiF{:}OH^-$, electron irrad., F_2^+ centre stabilisation 80−54231
LiH (D), single crystals, electronic excitations, review *(Russian)* 78−72574
$LiNbO_3$, pure and Fe doped, photorefraction, temp. and light intensity depend. 80−50288
$LiNbO_3$:Fe, electron irrad., photoinduced charge transfer and hologram recording 79−36859
$LiNbO_3$:Fe, thermally activated trapping caused by small polaron formation 77−20259
$LuYScO_3{:}Er^{3+}(Tm^{3+})(Ho^{3+})$, thermolum. meas. 80−97354
MOS, photocurrent-voltage characts., insulator bulk trapped charge 78−30991
MgO doped powder phosphors, photo- and thermostimulated luminesc. obs. *(Russian)* 80−66263
MgO, electron irradiated, luminescence, radiative recombination kinetics 80−7421
MgO, γ-irrad. polycryst., isothermal luminesc., recomb. of electron from F_s^+ centres 80−34985
MgO, single crystal, thermal and optical stimulation processes of V-centres *(Japanese)* 80−11485
MgO:Be epitaxial layers, vacuum UV luminescence 80−11480
MgO-P_2O_5-Al_2O_3-$3P_2O_5$ glass, absorpt. shift, electron and hole traps, thermolum. meas. 79−65897
$MgWO_4$, luminesc. and capture centres *(Russian)* 78−52543
Mo, quenched sample, UV photoelectron spectra, exoelectron-like emission 79−15587
Mo-n-Si Schottky barrier, sputtered, freq. cond. charact. 77−20426
$NaBrO_3$, single crystals, thermolum., optical absorpt., X-ray effect 79−95858
NaCl, electron trapping by alkali ion impurities 78−47809
$NaF{:}Mn^{2+}$, two-step photoionisation, laser-active F_2^+ centre form. 79−963
$NaF(Cl){:}OH^-$, electron irrad., F_2^+ centre stabilisation 80−54231
$NaNO_3$, γ-irrad., electron trap depth, ESR 79−66317
Na_2O-Li_2O-NiO-Fe_2O_3-B_2O_3-SiO_2 glasses, thermally stimulated cond. studies of trapping centres 79−78113
Na_2O-SiO_2 glass, tunnelling recomb. luminesc. 80−2875
NaOH aqueous glassy systems, 77K, γ-irrad., struct. stabilisation 79−91976
NaOH ice, γ-irrad, ESR and absorpt. spectra of trapped electrons 79−66318
NaOH ice, γ-irrad., electron trap depth, ESR 79−66317
$NaOH{:}CrO_4^{2-}(NO_2^-)$, electron tunnelling, pulse radiolysis 80−108722
$NaOH{:}Fe(Cn)_6^{3-}$, electron tunnelling, pulse radiolysis 80−108722
Nb_2O_5, electron energy spectrum by optical and thermal methods 79−69418
PbI_2, photoelectromagnetic investigation, expt. 79−24010
$PbMg_{1/3}Nb_{2/3}O_3$, photoinduced phenomena at diffuse phase transition 78−43814
PbO-SiO_2 glasses, charge trapping and dielec. breakdown, radiation-induced, microphase separation 78−23399
3PbO.2GeO, TSC in thermoelectret state during ceramic synthesis, pyroelec. currents and energy struct. of capture centres 80−55014
PbS film surface with oxysulphate layer, photoelec. memory effect 77−55584
PbS oxide, optical excitation meas. of trap charging surface film *(Russian)* 78−76180

electron traps continued
$Pb(WO_4)_{1-x}(MoO_4)_x$ mixed crystals, X-irrad., EPR and thermoluminesc. 79−15352
S magnetoelectret, thermally stimulated discharge current 79−91341
S:P, ion implanted, defect annealing 450-800°C, deep-level transient spectroscopy 79−47042
Sb_2S_3 film, coevaporated, elec. cond. meas. 80−65726
Se, amorphous, theory of anomalous dispersion of photocurrent transients 78−6412
Se electrophotographic films, ageing effects on structure and properties 77−47699
Se, epitaxial monocrystalline film, trapping, TSC meas. 77−85349
Se layers, amorphous and partially crystallised, trap spectrum, TSC and I-V characts. 77−76981
Se, modulated photocurrent, analysed for trap-limited case *(Japanese)* 80−60030
α-Se, multiple-trapping model of anomalous transit time dispersion, transient photocurrent data 78−34860
a-$Se_{97.5}As_{2.5}$, trapping, photo-stimulated and thermally-stimulated current obs. 77−28192
$Se_{12}Te_{49}As_{29}Ge_{10}$ semiconductor amorphous films, field effect, trapping 80−84472
Si, amorphous, Schottky barrier solar cells, deep hole traps, spectral response and TSC meas. 80−50962
Si, amorphous presence of acceptor states around Fermi level 78−2445
Si, annealed, ion-implanted, in MOSFET, defect spatial distrib. 77−11973
Si, deep centres, majority carrier thermal capture cross section, TSC meas. 78−10468
Si, deep level transient spectroscopy *(French)* 79−11079
Si doping by thermal neutron irrad., annealing characts. of bulk electron traps obs. 80−49244
Si, electron emission coeffs. for electron and hole traps 79−91075
n-Si, influence of deform. on capture of electrons by divacancies 77−1449
Si inversion layers, effective mass variation 79−24050
Si, ion implanted, laser annealed, deep levels study 79−69457
Si ion implanted p-n junction, cryst. damage influence on elec. props. 78−56219
Si junction diode, diffused, with deep level traps, negative capacitance 80−96976
n-Si, lightly doped, electron irrad. induced divacancies as electron traps 77−4126
Si, MOS device, subject to linear voltage ramp, non-steady-state studies 79−78189
Si MOS diode, bulk traps and interface states determ., deep-level transient spectroscopy appl. *(Japanese)* 79−42645
Si MOS diodes, P^+ implanted, DLTS of bulk traps and interface states 79−33350
Si MOS struct., space-charge generation props. of Au 80−2475
Si MOSFET, n-type inverted surface channel, reproducibility of electronic props. 79−99628
Si MOSFET n-channel, Hall meas. on trap states at 77K 80−44732
Si, n^+-p diode, γ-radiation defects, annealing and recomb. props. 80−65045
Si n^+-p solar cells, degradation mechanisms associated with Ti impurities 80−81465
Si, neutron-produced defects, deep level transient spectroscopy 79−47047
Si, p^+-n diode, neutron irrad., defect levels, G-T and C-T curves obs. 77−62986
Si p-n junction I-V reln. calc. 77−43704
Si p-n junctions, spin depend. surface recomb., electron irradiation effect 80−88627
Si, polycryst., energy distrib. of trapping states, from impedance of MOSS struct. 80−65691
Si, polycrystalline, phenomenological model for mobility 80−65564
n-Si, Re-compensated, deep levels, electron traps, photocond. 77−15902
Si resistors, polycryst., elec. props. in nonlinear regime, grain boundary trapping model 79−38204
Si, self-implanted, defect-density profiles, constant-capacitance DLTS meas. 79−95361
Si thin film, polycryst., CVD, elec. props. 80−107934
Si, transmutation doped, deep trap level analysis 78−10471
n-Si wafer, trap centres of self-interstitials 80−75516
Si:Al, localised exciton bound to isoelectronic trap 80−66283
Si:Al, thermally induced deep levels, TSC meas. 77−31974
Si:As, electron irradiated, majority carrier trap prod., effect of O_2 enhanced annealing 77−1151
Si:Au, C-V curves of MIS diode used to examine trapping levels 80−65697
Si:Au, carrier capture cross-section at low temp. *(Rumanian)* 79−15163
Si:Au, electron capture cross section, energy level of Au acceptor centre 78−51926
Si:Au p^+-i-n^+ diode, double injection switching, effect of trapped space charge 77−1473
Si:Au(Pt), heavily doped, gradual p^+-n junctions, trap levels *(French)* 80−34392
p-Si:B, defect energy levels with 1 MeV electron irrad. and annealing, transient capacitance spectra 77−62860
Si:B effect of elec. field on carrier capture by attractive centres. 79−11145
Si:B MOS structures, implanted laser beam irrad. effects on interface electrophys. props. 79−1627
Si:Co, study of impurity states 78−76020
-Si:Fe, effect of γ-irradiation, photocapacitance meas., impurity centre conc. 78−18993
Si:Ga, electron irrad.-induced defects, DLTS meas. 80−24499
n-Si:Ge, electron induced defects, room temp. instability 80−29052
Si:Ge, electron irrad.-induced defects, DLTS meas. 80−24499
Si:H, amorphous, defect photoluminesc. meas. 80−97334
Si:H, amorphous, solar cells, trap spectroscopy using transient current techniques 80−104508
Si:H film, amorphous, bombarded, defects, luminesc. and ESR meas. 80−34977
p-$Si{:}N_2^+$ implanted, anneal behaviours of lateral photovoltaic method, trap concentrations 79−14825
Si:Ni deep impurity levels, electron capture probabilities rel. to temp. 78−2523
Si:Os, P, photoelec. props., depend. on P conc. 79−91099
Si:P, defect annealing, ionisation effects. DLTS meas. 80−24483
Si:P, doped by neutron transmutation, electron traps 78−84164

electron traps continued
Si:P, effect of annealing on charge carrier conc. on floating zoned crystals 78—47805
Si:p, film, polycrystalline, low press. CVD, resist. meas. 80—2494
Si:P, impurity doped, electron lifetime and transport in upper Hubbard band 79—95452
Si:P, neutron transmutation doped, electron trap annealing, deep level transient spectra 78—14368
Si:P, neutron transmutation doped, EPR, electron trapping 79—73179
Si:P CVD films, ion-implanted, doping effect on elec. props. 80—2495
Si:P(O) p^+-n-n^+ solar cells, comparison rel. to resistance to 1.5 MeV electron irrad., majority carrier trapping 80—94087
Si:Pt, elec. props., deep-level transient spectroscopy and thermal emission meas. 79—82542
Si:Sb, electron irrad. damage, electron trapping centres 77—39798
Si:Sc, photocapacitance and photoconductivity 80—107859
Si:Ti, deep level impurity, Hall meas. 80—6768
Si:V p-n junctions, thermal emission rates and capture cross sections of majority carriers at V centres 80—96980
Si:Zn, trapping struct., analysis of TSC meas. 77—8045
Si/SiO_2, CCD, incomplete charge transfer, fringing fields and interface states effects 77—15964
p-Si-As_2S_3 isotype crystalline-amorphous heterojunctions, electrophysical props. 79—24063
Si-insulator interface, non-avalanche charge injection, expt. study, charge trapping effects 80—60099
n-Si-Se, ion implantation studied by deep level transient spectroscopy 78—10392
Si-SiO_2, charge injection at low fields, electron trapping centres 77—39945
Si-SiO_2, effects of processing on radiation damage 78—39223
Si-SiO_2, MOS interface states density, meas. techniques and model development 80—92988
Si-SiO_2 interface, Au doping, trapping states 80—20319
Si-SiO_2 interface, avalanche injection of charge carriers, oxide current decay 77—43728
Si-SiO_2 interface, trapping props. from electrochemical current-voltage behaviour 79—69597
Si-SiO_2 interface traps energy distribution meas., in MOS devices, under non-steady-state *(Korean)* 78—64119
Si-SiO_2 MOS interface states density, transient capacitance meas. eval. 80—92989
Si-SiO_2-Mo-Si_3N_4-Al MNOS structures with metal grains, charge transport at SiO_2-Si_3N_4 interface 80—65693
Si(:Au), gamma-induced trapping levels 79—87059
SiC, electron trap depth, additional IR absorption induced by UV excitation *(Russian)* 79—78721
SiC, semi-insulating in struct. with injecting contacts, cond. in strong elec. field 78—19160
SiC, spin-flip scatt. of laser light from photoexcited excitons 80—93330
$Si_{12}Ge_{10}As_{30}Te_{48}$ chalcogenide glass threshold switch conductivity in high ohmic state *(Russian)* 78—43502
$Si_{12}Ge_{10}As_{30}Te_{48}$ glass, thermally stimulated depolarization current meas. *(Japanese)* 78—34875
Si_3N_4, amorphous insulator film, high-field cond. 79—56320
Si_3N_4 film, CVD, high-field dark currents 80—54791
Si_3N_4, low press CVD film, steady-state electron and hole space charge distrib. 80—29493
SiO_2, amorphous, high-field transport of excess electrons and holes 77—89767
SiO_2, amorphous, optical and elec. props., comparison with chalcogenide semiconds. 78—6721
SiO_2, As-implanted, electron trapping and detrapping characts. 80—65692
SiO_2, electron-beam irrad., electron trapping, MOS capacitor expts. 78—72268
SiO_2 film, Al implanted, in MOS struct., electron traps characts. obs. 79—15226
SiO_2 film, electron-beam-induced cond. 80—20337
SiO_2 film, in MIS struct., current-field characts. 79—99623
SiO_2 film, localised states, low-temp. photocurrent spectroscopy 78—19090
SiO_2 film, thermally stimulated depolaris. current, model *(Russian)* 79—56342
SiO_2 film on Si, negative bias instability 78—91773
SiO_2, glass, irrad., EPR of Al E_1' centres 80—11268
SiO_2, high field electron capture by screened Coulomb attractive centre 79—56237
SiO_2, high-field electron trapping, I-V characts. of MOS capacitor 78—6449
SiO_2 in FET, electron trapping due to electron beam deposited Al 78—80060
SiO_2, in IGFET struct., thermal reemission of trapped electrons 79—42650
SiO_2 layer used for MOSFETs, electron trapping behaviour 80—92981
SiO_2 layers on Si, ionis. thresholds of electron traps 80—92983
SiO_2 MOS capacitor, defect current obs. 80—92987
SiO_2 MOS structures, removal of electron traps by RF annealing 80—44728
SiO_2 sputtered films in thin film transistors, trapping centres 80—7014
SiO_2, thermal, elec. stressed film, dielec. breakdown 78—64322
SiO_2 thermal films, hole and electron trapping density reduction 80—2400
SiO_2 thermally-grown, highly stressed ultrathin films, cond. and trapped of electrons 77—66216
SiO_2 thin films, radiation-induced trapping centres, rel. to MOS transistor technology 80—107804
a-SiO_2, transient photocond. simulations using multiple-trap model 80—49801
SiO_2, trapping level exam. by thermally stimulated discharge of capacitor *(Russian)* 78—34845
SiO_2, vitreous, charged defect centres 80—107745
SiO_2, vitreous, paramag. centres associated with bonding defects 80—80609
SiO_2:Al film, ion-implanted, electron trapping behaviour 78—67729
SiO_2:As^+ implanted layers in MOS struct., electron trapping and detrapping characts. 80—92982
SiO_2:B, ion implanted, props. 79—65106
SiO_2:B implanted, thin films, props. *(Polish)* 80—39692
SiO_2:W film electron trapping characts., obs. by avalanche injection techniques 77—89862

electron traps continued
SiO_2-CdSe thin film transistors, slow states, trapping state densities and cross sections 80—15613
SiO_2-Si interface, hot electron capture process, expt. method for study 79—38180
Si(100)-SiO_2 interface, mobility in Si inversion layers, screening and neutral impurity effects 79—28412
n-SnO_2, high resist., photoelectronic processes 78—60157
SnO_2:Eu^{3+}, luminesc. and charge compensation 77—28618
SnO_2-ZnO-Bi_2O_3, ceramic semiconductor, injection currents 79—11141
SrFCl, thermolum. and optical absorption spectra 80—66309
SrS:Hf phosphor, activation energy and freq. factor calcs. from glow curves 77—12451
SrS:Nd, phosphorescence decay, trapping levels 80—104003
p-Te, photocond. and lifetime, surface trapping, spectral distrib. 78—34840
a-$Te_{40}As_{35}Ge_7Si_{18}$, trapping, photo-stimulated and thermally-stimulated current obs. 77—28192
TiO_2, plasma growth, photoelectronic props. 78—52662
TiO_2 sputtered film, photocond. and TSC meas. 80—15560
$TlGaSe_2$, monocrystal, processes of recombination and trapping levels, photocond. meas. *(Russian)* 80—70751
V_2O_5 single crystals, contact-limited conduction 79—95493
Xe, liq., electron mobility, role of shallow traps 80—34440
Xe, liq., recomb. and self-trapped exciton luminesc., free electron dynamics, excited states 80—25463
YAG, colour centres conceived as bound polarons 78—63990
YAG, transient colour centres caused by UV radiation 77—84744
YAG, traps, energy spectra, X-irrad. effects and thermoluminesc. *(Russian)* 77—20940
YIG, LPE film, non-Ohmic currents 78—68099
$Zn_3(BO_3)_2$:Sm^{3+}, photoluminescence obs. *(Spanish)* 79—73986
ZnO ceramics, non-Ohmic transient cond. phenomena, current-voltage overshoots 79—91057
ZnO, luminescent, phonon detection by shallow electronic trap states 79—14902
ZnO, negative photocond. by excitation of exciton-impurity complexes, recomb. mechanism *(Russian)* 79—28379
ZnO, nonhomic ceramic, current oscillation phenomena 79—69515
ZnO, photoelectret, nonisothermal relax. 77—12306
ZnO photoelectret, recomb. and trapping kinetics determ. 79—38083
ZnO varistors, cond. model 78—14736
ZnO:Cu, O, Fe(Co)(Ni) photocond., electron escape probabilities and trap depths 77—32041
ZnP_2, trapping levels, TSC and thermolum. meas. 79—15115
Zn_3P_2, thermoluminescence glow curve method for radiation induced traps 80—60689
$Zn_3(PO)_2$, thermoluminescence glow curve method for radiation induced traps 80—60689
ZnS, low-temp. trap anal. thermally stimulated luminesc. model extension 80—80877
ZnS phosphors, Gudden-Pohl effect, temp. depend. and decay rate 77—44070
ZnS phosphors, Gudden-Pohl effect, field ionis. of trapping centres 77—73170
ZnS, radiation emission, stimulation by IR light, electron traps and polaron energy determ. *(Russian)* 77—66542
ZnS, self-activated, trap distrib. and photoelectronic effect due to UV, IR and visible excitation 77—36282
ZnS, shallow traps, thermolum. glow curves obs. 79—91508
ZnS:Ag, Al(Cu), trap parameters, thermostimulated luminesc. and cond. meas. *(Russian)* 77—72868
ZnS:Ag, cryst. struct., electron traps and glow curves 79—61437
ZnS:Ag, single crystal, ionisation mechanism of field trapping centres 80—45156
ZnS:Ag, TSC and induced impurity photoconductivity, existence of two electron trapping centres 80—44655
ZnS:Cl^-, Cu^+(Ag^+), phosphor, high press. effect on thermoluminesc. 78—64419
ZnS:Cu, Co, deep traps and stationary luminescence *(Russian)* 78—48227
ZnS:Cu, current pulses stimulated by elec. field at low temp. 78—39121
ZnS:Cu, O(Fe,Co,Ni) photoconductors, killer impurities effect on electron escape probabilities and trap depths 77—4392
ZnS:Pb current pulses due to elec. field liberation of electrons from trapping centres by tunnel processes 79—28378
ZnS:Pb phosphor, ionisation mechanism of field trapping centres 80—45156
ZnS:Pb phosphor mech. of elec. field liberation of electrons from traps 78—72616
ZnS-CdS:Ag(Cu), cryst. struct., electron traps and glow curves 79—61437
ZnS_xSe_{1-x}, electron trap associated with anion vacancy, DLTS study 80—80210
ZnSe, electron trap associated with anion vacancy, DLTS study 80—80210
ZnSe, Gudden-Pohl effect, release of electrons from traps 80—45149
ZnSe, heat-treated in controlled partial press. of Zn or Se, TSC 80—59910
ZnSe, laser induced modulation of opt. absorpt. 78—88324
ZnSe:Al, current switching mechanism *(German)* 79—28385
$ZnSiP_2$, photocond. under laser excitation *(Russian)* 78—84258
ZnTe, electronic and optical parameters of O related centre 77—24534
ZnTe:Li, O, Hagemark theory, O modification isoelectronic trap 80—75517
ZnTe:O, deep centres, photocapacitance detection 79—95362
ZnTe:O, Ne or Al implantation, electronic and optical parameters of O-related centre 78—6399
$ZnWO_4$, luminesc. and capture centres *(Russian)* 78—52543
ZrO_2 films on Zr alloys, exoelectronic emission props. and energy-band parameters 79—91571
ZrO_2:Ti(Th)(U)(Nb)(Dy), thermoluminescence, traps and emission centres 79—24373
ZrS:O_4, X-irradiated, trapping and emission centres, thermolum. meas. 80—89076

electron tube components
see also electron guns
Sm-Co ring magnets for BWO, 110 to 170 GHz, design and appl. *(German)* 80—105684

electron tube diodes *see diodes*

electron tube manufacture
- ceramic-metal seal technology, history and trends 78−81992
- microchannel plate surface finishing using liquid 78−90544
- vacuum-deposited layers, stable structure formation 80−80979
- Cr film vacuum deposition on glass display panels 78−39694
- SnO$_x$:Sb,F film CVD for bistable storage CRT 77−77410

electron tube rectifiers *see rectifier tubes*

electron tube testing
- microchannel plate life tests 77−61117
- photomultiplier, ITT FW-130, linearity test 79−58255
- photoreceiver sensitivity nonlinearity determ. by high-speed raster device 77−79150
- X-ray tube kVp meas. with Si p-i-n photodiode *(German)* 79−232

electron tubes
- *see also cold-cathode tubes; diodes; electron emission; microwave tubes; nuvistors; pentodes; relativistic electron beam tubes; tetrodes; thermionic tubes; triodes; ultra-high frequency tubes; vacuum tubes; X-ray tubes*
- diffraction radiation generators electron flow study by changes in generator heat characts. *(Russian)* 78−37796
- electron beam deflection tube, for current and mag. induction meas. 78−54393
- Febetron 707, field emission tube, electron pulse duration reduction 77−3530
- II-VI semiconductor laser screens, for electron-hole tubes, stimulated emission mechanism 79−94237
- laser electron-beam tube under scanning conditions, using CdS screen 79−13983
- pulsed tube electrode working surface, temp. evaluation *(Russian)* 77−19512
- CdS, CdS$_x$Se$_{1-x}$, scanning semiconductor laser with transverse electron-beam pumping 80−9904
- CdS$_x$Se$_{1-x}$ laser electron-beam tube, possibility of acceleration voltage lowering 79−89929

electron tunnelling *see tunnelling*

electron valves *see electron tubes*

electron-wave tubes
- *see also klystrons; magnetrons; travelling-wave-tubes*
- cyclotron resonance maser tube with transverse current, theory of oscillation 79−89877
- gyroresonant electron-wave interaction without prespiralling *(Russian)* 77−31054

electronegativity
- acetaldehyde, proton affinity, geom. and basis set depend., MO calcs. 78−50461
- alkali metal bromates and chlorates, alkali and ^{17}O NQR, spin echo double reson. method, electronegativity 80−54970
- atomic electronegativity, density functional theory 80−99440
- atomic electronegativity scale rel. to work function 78−64096
- atoms, correl. of CNDO-bonding parameters 78−74577
- atoms and ions, valence region energies, electronegativity, Politzer-Parr partitioning, finite difference approx. 78−78612
- atoms in molecules, diamag. shieldings rel. to electronegativity 80−102524
- bases, K$^+$ affinities ab initio SCF calc. 78−58585
- benzaldehyde, proton affinity, MINDO/3 results compared to ICR obs. 78−1103
- binary compounds, energy gap trends, correl. with electron transfer parameters from optical spectroscopy 80−80174
- brass, liquid, thermodynamic props. *(German)* 80−66482
- carbenes, heterosubstituted, singlet-triplet splitting depend. on heteroatom electronegativity and conform. 80−63553
- cells, electrochemical, photovoltaic phenomena and mechanisms 78−8198
- chalcogenide glasses, heteropolar, coordinates of ground state and of negative U defects 80−54137
- charge distribution in ions and mols., inductive effect 80−47837
- core electron binding energy, prediction with four-parameter equation 77−30745
- density functional viewpoint 78−66485
- diatomic molecules, containing elements from Li to F and Na to Cl, calc. from mol. dissoc. energies 78−62943
- diatomic molecules, dipole moments, electronegativity and photoemission chem. shifts 79−13655
- diatomic molecules, spectrosc. consts., rel. to electronegativity 80−28007
- diatomic mols., electronegativity, bond charge and chemical pot. approach 80−91703
- dimethyl sulphoxide, form. of (CH$_3$SOCH$_3$)$_2$H$^+$ and CH$_3$.CH$_3$SOCH$_3$$^+$ in ICR mass spectrometry, proton affinity 78−3319
- effective atomic charge rel. to electronegativity and ionicity 77−24287
- electron density, calc., of electronegativity and chemical potential 79−89589
- electronegative gas plasma, negative ion ambipolar diffusion coeffs. 80−44046
- electronic distribution and electronegativity, theory 80−23283
- electrostatic pot. energy of atoms in mols., electronegativity, charge transfer and polarisation 79−63885
- ESCA chemical shifts and modified Sanderson electronegativity calcs. 77−83656
- fluorides, molten, significance of variable oxygen electronegativity in binary oxides 78−5157
- formaldehyde, proton affinity, geom. and basis set depend., MO calcs. 78−50461
- formic acid, proton affinity, geom. and basis set depend., MO calcs. 78−50461
- gas glow discharge, plasma instability boundary conditions *(Russian)* 80−38739
- grain boundary segregation, computer simulation using Mie type interatomic pot. 80−54259
- infinitesimal perturbation and energy changes 79−22574
- inorganic binary iono-covalent compounds, cryst., inorganic static effective charge calcs. *(French)* 80−2331
- ionization potential and chemical potential, fundamental difference 80−907
- IV-VI semiconductors, transverse effective charge from one dimens. band struct. calc., rel. to chem. electronegativity 80−15038
- liquid semiconductor, metal-insulator transition model 77−1368
- Lytle potential, modified, for extended fine struct. of X-ray absorpt. edge 77−85839
- metal, electrochemical reaction on surface in aq. soln. 79−83387

electronegativity continued
- metal, electronegativity scale 79−73129
- metal, surface pot. drop and contact pot. difference in terms of orbital electronegativity 78−2546
- methane, H-X bond position, correlation with electronegativity 78−9069
- 4-methylene-cyclohexadiene-2,6-one-1, proton affinity, MINDO/3 results compared to ICR obs. 78−1103
- molecular reactivities rel. to struct., Taft and Kirkwood-Westheimer eqns. 78−62738
- molecule, diatomic, hetero- or homonucl., empirical rel. for vibr. freqs. 79−81197
- Mulliken electronegativities, rel. to work function 78−9096
- nonempirical scale, ab initio FSGO wavefunction calcs. 77−26966
- nontransition metals, electronegativity parameters of theory of heats of alloy form. 79−74412
- organic compounds, electronic theory *(Chinese)* 77−26958
- organic compounds, heat of formation, dissociation energy from dynamic electronegativity *(Chinese)* 79−96351
- organic fluid charge carrier generation, role of molecular electroinduction effects *(Russian)* 79−96321
- organic ring mol., INDO finite perturbation theory, contact proton spin-spin coupling 77−50361
- oxide spinel, systematic trends in geometry, ionic radii and electronegativity 80−19778
- oxides, binary, variable electronegativity of oxygen, relevance to molten fluorides 78−5157
- positive column, of electroneg. gas, transverse stability, effect of dissoc. attachment 79−23475
- pyrite type dichalcogenides, ^{57}Fe isomer shift, quadrupole splitting, Mossbauer study 80−15832
- quartz, low, CC Si-O bond characteristics 80−84132
- representation based on LCAO and Schrodinger eqn., new scale *(Chinese)* 77−75034
- scale, determ. from effective nuclear charges and X-ray spectra 77−75037
- semiconducting cpds., average valence-⟨4⟩ X-ray K-absorpt. edge shift and electronegativity 77−16424
- semiconductor-electrolyte interfaces, prediction of flatband pots. from atomic electronegativities 78−40068
- simple bond charge model 78−9050
- simple compounds, Mulliken electronegativity scale, struct. stability 79−23562
- spark breakdown current growth gas dynamic processes, electronegative gas mixture 78−87588
- spin-orbital, and catalytic activity 78−73078
- sulphide spinel, systematic trends in geometry, ionic radii and electronegativity 80−19778
- sulphones, group electronegativities, empirically estimated from geometrical and vibr. data 79−81300
- tertiary phosphine oxide+aliphatic alcohol, pπ-dπ conjugation, electronegativity and H-bond energy 78−82863
- transition metal alloys, d-band hybridisation, electronegativities, structural stability 79−42007
- transition metal alloys, vol. corrected isomer shifts 78−39470
- transition metal compound form., Miedema's empirical theory, microscopic basis 80−45541
- transition metal dichalcogenides, of CdI$_2$-type, electronegativity diff. correlation to reduced length 79−27963
- transition metal impurities, volume corrected isomer shift, orbital electronegativity scale 77−73103
- transition metalloid atom solubility and electronegativity difference correl. with phase stability and d-electron/atom ratio 78−6914
- tropone, proton affinity, MINDO/3 results compared to ICR obs. 78−1103
- UV photoelectron spectra at high temp., interpretation 78−17718
- vinylidene fluoride-trifluorochloroethylene copolymers, ^{19}F NMR *(Russian)* 80−7181
- zinc blende-type semiconductors, interstitial PDs, electronegativity diff. and effective ionic charges 77−76766
- AgBF$_4$, ionic radii and chem. shifts, correl. with electronegativity 80−66054
- AgH, bond dissoc. energy, electronegativity pot. function pot. energy curves 77−10784
- Al chalcogenate and chalcogenite double salts, form. laws and acid-base props. 80−101070
- Ar purification system and electronegative impurity conc. meas. instrument 80−32571
- As$_2$S$_3$, glassy, build-in mechanism of impurities, electronegativity influence 77−76313
- BeO$_2$$^-$, electron binding, ab initio calc. 79−45628
- CN$^-$, proton affinity, enthalpies of form. and soln. 77−47375
- CN$^-$, proton affinity, integral Hellmann-Feynman theorem 78−70767
- CO, proton affinity, integral Hellmann-Feynman theorem 78−70767
- Ca+NH$_4$$^+$(CH$_3NH_3$$^+$)(PH$_4$$^+$), proton transfer reaction cross sections, 1-6 eV 78−20003
- CdS, photoanode, flat band pot., prediction from atomic electronegativity 79−62013
- Cl-containing molecules, hybridisation, bonding orbitals effects 79−36510
- Co complex, bis-(β-diketonato) Co(II) dihydrate, Fe chem. states, Mossbauer emission 80−15917
- CsBF$_4$, ionic radii and chem. shifts, correl. with electronegativity 80−66054
- CsI crystals, relation of struct. and bond type to slip geometry 80−88165
- Cu-M-O ternary liquid alloys, thermochem. calcs. 80−85209
- F compounds, ground states, mol. parameters, MINDO calcs. 78−41955
- Ga chalcogenate and chalcogenite double salts, form. laws and acid-base props. 80−101070
- H$_2$, electronic chemical pot., natural orbitals occupation numbers and electronegativity 80−63509
- HBr, proton affinities calcs. 78−21840
- HCl, proton affinities calcs. 78−21840
- HF, H-X bond position, correlation with electronegativity 78−9069
- HI, proton affinities calcs. 78−21840
- H$_2$O, H-X bond position, correlation with electronegativity 78−9069
- In chalcogenate and chalcogenite double salts, form. laws and acid-base props. 80−101070
- LaO molecule, potential energy curves, Rapid method by Morse function 77−26998

electronegativity continued
- LiF crystals, relation of struct. and bond type to slip geometry 80—88165
- MoO_3-M_2O_3 system, solid-state chem., rel. to trivalent metal electronegativity 77—24288
- N_2, proton affinity determ. from N_2H^+ appearance pot. from N_2H_2 78—58869
- NH_3, H-X bond position, correlation with electronegativity 78—9069
- NH_4BF_4, ionic radii and chem. shifts, correl. with electronegativity 80—66054
- Ni-Au alloy, electronegativity and core electron binding energy shifts of Au 77—15346
- OH^-, proton affinity, integral Hellmann-Feynman theorem 78—70767
- PbS, crystals, relation of struct. and bond type to slip geometry 80—88165
- Pd-Au alloy, electronegativity and core electron binding energy shifts of Au 77—15346
- Pt-Au alloy, electronegativity and core electron binding energy shifts of Au 77—15346
- SO_3, electron impact mass spectrometry, proton affinity, ion-mol. reactions 78—3415
- V_2O_5 containing melts, activation energy of electron mobility and electronegativity 77—35971
- ^{67}Zn Mossbauer spectroscopy with 93 keV reson. 80—66095

electronic calculators
for calculator applications see under relevant applications e.g. engineering computing; natural sciences computing
- airborne noise, personal calculator program for A-weighted sound pressure level and noise ratings 80—23828
- children's pocket calculators, educational pot. and teacher reactions 80—22178
- chromatography automatic evaluation systems appl. *(Hungarian)* 77—56289
- desktop calculator library module, for advanced composite materials anal. 80—77764
- diffraction grating, electronic analog 80—46753
- gamma-ray detector total efficiency calc., algorithm for small calculators 79—9938
- gamma-ray spectra evaluation, appl. of programmable calculators and minicomputers 79—9956
- hand calculator, appls. 78—12483
- heart or respiration rate calculator 78—35987
- HP-25 programmable calculator, use in power supply for multichannel analyser 77—42218
- least square fitting, pocket calculator program with variable precision 80—67976
- least squares regression analysis with confidence limits, calculator program 77—29060
- microprocessor based interface/controller for desktop programmable calculator 79—35690
- noise level digital recording using programmable calculator 79—23130
- partial radiation detector, pocket calculator as counting cct. and display *(German)* 77—14314
- physics teachers and students guide to calculator choice 80—4494
- programmable, electrochemical calc. appl. 79—43592
- programmable pocket calculator, short circuit current calc. *(German)* 80—68186
- programmable pocket calculator as physics teaching aid, numerical integration appl. 78—86083
- selection criteria 78—12506
- skew ray tracing with the TI-59, programmable calculator 80—48141
- spectral analysis, programmable calculator as alternative to minicomputer-based analyser 79—9985
- Texas Instruments programmable calculator, TLD data anal. appl. 80—36136
- TI-59, program for solving Hartmann interpolation equation 79—98451
- time measurement, using light digit, four function calculators 78—175

electronic component manufacture *see electron device manufacture*

electronic conduction in crystalline semiconductor thin films
for electronic conduction in amorphous thin films, see "electrical conductivity of amorphous semiconductors and insulators"
see also electrical conductivity of amorphous semiconductors and insulators; electrical conductivity of crystalline semiconductors and insulators; electrical conductivity transitions
- adenine film, polycryst., energy conversion processes, quantum yields, 4 to 10 eV 80—88589
- anthracene derivative, Langmuir-Blodgett multilayer film, semiconducting props., optical and elec. meas. 80—11122
- cell for measurement over wide temp. range 77—51830
- $CoCr_2S_4$ films, galvanomagnetic and thermoelec. props. 80—54717
- compensated semicond. film, jump-over cond., control by external field 78—80080
- conductivity measurement, combined four-probe method 79—67348
- conductivity monitoring by microwave resonator absorption *(Russian)* 78—23182
- copper phthalocyanine film, electroconductivity, effect of adsorption 77—85356
- coronene thin films, elec. cond. mechanism 77—28189
- diamond:B, epitaxial layer, charge transfer and acceptor state 78—19169
- diamond-like C film, plasma stream condensation with RF pot., props. 79—15612
- dimethyl stilbene chloride, organic semiconductor thin film on glass, voltampere charact. *(Rumanian)* 79—38196
- dislocation superstructures and conduction electron kinetics *(Russian)* 79—19678
- double injection in transverse mag. field, theory 80—80421
- electron spin orientation in quantum size effect conditions 78—68575
- films, elec. and galvanomag. props., microstruct. 80—70859
- germanium phthalocyanine, elec. cond. temp. depend. 80—80271
- Hall effect and magnetoresist. determ. in weak and strong mag. fields by four-probe method 79—60853
- heteroepitaxial film, electrical characterisation, book contrib. 79—82699
- indanthrone, SCL conduction, trapping 77—15978
- ion beam milling, amomalous sputter yield behaviour 80—108624
- iron phthalocyanine film, electroconductivity, effect of adsorption 77—85356
- Kane semiconductor films, thermomag. and thermoelec. effects, theory 80—70864
- multilayer spreading resistance anal., high-speed implementation and expt. evaluation 79—4324

electronic conduction in crystalline semiconductor thin films continued
- negative high-frequency conductivity of media having a nonuniform distribution of mobility in crossed E and H fields 79—82619
- one- and two-dimensional periodic superstructures, possibility of formation in thin films and semicond. surfaces 79—11044
- organic films, heating, electrode barrier presence, polarisation and depolarisation currents obs. 80—49764
- organic semiconductor films, Schrieffer effect 80—60118
- pentacene, evaporated film elec. cond. meas. for various temps., SCL 78—10584
- polycrystalline, carrier conc. depend. on crystallite size 77—85361
- polycrystalline, charge carrier effective mobility and concentration 77—28264
- polycrystalline, Hall and drift mobilities 79—95531
- polycrystalline films, barrier-limited cond. 79—95527
- polycrystalline films, cond., photocond. mechanisms 78—47891
- polycrystalline layers, modified barrier model *(German)* 80—7012
- polymer films, conf., Dublin, Eire (July 1977) 79—55012
- potential distribution, two dimensionality 77—20463
- p-quaterphenyl, polycryst. thin layer-metal sandwich, elec. cond. 80—34526
- review 78—2598
- semiconductor film, transverse conductivity due to scatt. by acoustic phonons in quantizing mag. field 78—2594
- semiconductor sheet resistance meas. by four point probe technique *(Chinese)* 80—52262
- silicon phthalocyanine, elec. cond. temp. depend. 80—80271
- solar cells, thin film polycrystalline materials, resistivity and Hall effect meas. 80—93899
- sputter-deposited materials, electrical and optical props. 79—47181
- TCNQ salt, Cu-TCNQ thin film between Cu and Al electrodes, elec. switching and memory phenomena 79—65562
- temperature coeff. of resistance of polycryst. films, linearized expressed 78—14838
- p-terphenyl, polycryst., charge carrier transport and DC cond. 80—70858
- p-terphenyl polycrystalline layers, AC cond. 80—44746
- tetracene, polycrystalline layer, carrier mobility and AC cond. 79—65569
- thymine film, polycryst., energy conversion processes, quantum yields, 4 to 10 eV 80—88589
- TTT film, hopping cond. AC and DC meas. and EPR 80—11111
- variation due to crystallisation, model and its verification for Ge 77—20475
- $AgInS_2$, and $AgIn_5S_8$, spray pyrolysis, film struct., elec. and optical props. 80—71592
- Ag_2O film, prep. and effect of O_2, Ar and H_2 gases *(French)* 78—14637
- Ag_2Re films, galvanomag. props. and quantum size effects, obs. 80—70866
- Ag_2Te film, Ag movements, switching and memory effects 79—78239
- Al-CdSe-Ag dry air stabilised struct., elec. cond. mechanism, breakdown phenomena 80—34527
- Al-GaAs-Al sandwich-type sputtered film, elec. props. 78—91780
- Al-lead stearate-Hg, transient and alternating electric currents 78—84311
- Al-TeO_2-Al, field-assisted cond. mechanism 80—11105
- $Al_xGa_{1-x}As$, compensated, electron mobility temp. depend. 80—96868
- n-$Al_xGa_{1-x}As$ epitaxial films, elec. cond. press. depend. 79—56337
- $Al_xGa_{1-x}As$, graded-gap crystal, voltage-current characteristics 79—69613
- $Al_xGa_{1-x}As$, high-resistivity film LPE growth and semi-insulating props. 77—44179
- $Al_xGa_{1-x}As$, VPE and LPE growth, electron mobility 79—91165
- $Al_xGa_{1-x}As$:Cu(Ag)(Au), LPE film, impurity levels, elec. and optical props. meas. 78—26862
- $Al_xGa_{1-x}As$:Te, epitaxial film, elec. cond. and Hall coeff. rel. to donor levels 77—24630
- AlN, reactive ion beam sputtering deposition, form. and characterisation 80—44452
- BN films, elec. resist., depend. on relative humidity 79—4609
- BN, high temp. reactive plasma deposition, struct., resist., and dielec. const. meas. 77—7988
- $(Ba_xSb_{1-x})TiO_3$, ferroelectric films, dielectric and semicond. props. 79—91388
- $Ba_{0.4}Sr_{0.6}TiO_3$ films, DC conductivity, strong microwave field effect 80—65727
- $Ba(Ti,Sn)O_3$, thin film elec. and photoconductivity 79—33366
- $BaTiO_3$ film, sputtered, elec. props. 79—42676
- $BaTiO_3$, thin film elec. and photoconductivity 79—33366
- $(Bi, Sb)_2Te_3$ solid soln., semiconductor film, oxidation, electrophysical props. 80—45407
- Bi, carrier conc. and mobility, resist., galvanomag. and thermoelec. meas. 78—52111
- Bi, elec. cond., obs. of epitaxial growth mechanism *(French)* 78—84329
- Bi film, charge carrier scatt. *(Russian)* 78—80079
- Bi, film, evaporated, elect. and elastoresistance props. 79—33367
- Bi, film, quantum size effect, electric field effect, Thomas-Fermi approx. energy surfaces, cond. 78—47890
- Bi film, quantum size effect and band struct. Bi-dielec.-metal system obs. 80—54811
- Bi, film, size effect on electrical cond. 78—84331
- Bi film, structure and elec. props. 77—1339
- Bi, Hall effect, magnetoresist., resist. and TCR 78—2589
- Bi, polycrystalline film, elec. resistivity, thickness depend., temp. coeff. 78—14839
- Bi, surface defects and struct., electron microscopy and elec. props. *(French)* 80—15415
- Bi thin film, structure and electronic props. 80—70562
- Bi-Sb alloy, elec. resist., magnetoresist., Hall coeff., 4.2K, conc. depend., anomalous size effect *(Russian)* 77—89884
- Bi_2O_3, film, resist. and current controlled negative resist. 78—39238
- $Bi_{1-x}Sb_x$ alloy films, quantum resistance oscills. at low temps., surface band distortion *(Russian)* 80—11110
- $Bi_{1-x}Sb_x$ epitaxial layers, effect of film thickness on elec. props. *(Russian)* 79—11244
- $Bi_{1-x}Sb_x$ epitaxial thin films, galvanomag. props. in semimetal and semicond. regions 79—11254
- $Bi_{1-x}Sb_x$ film, low temp. anomalies of elec. props. and quantum size oscillations 79—65571
- $Bi_{1-x}Sb_x$ thin films, elec. props., 4.2-300K *(Russian)* 79—24087
- $Bi_{2-x}Sb_xTe_3$, solid soln. film on mica substrate, effect of stresses on elec. cond. 78—51859

electronic conduction in crystalline semiconductor thin films continued
$Bi_2TE_{3-x}Se_x$, solid solution films, prep. and props. 78—44013
Bi_2Te_3-Sb_2Te_3 film, cond., galvanomag. Seebeck and Nernst-Ettingshausen effects under press., band model 77—47907
BiTeI-SbTeI, solid solns., phase diagrams, photocond., elec. props. 79—38125
$Bi_{2/3}Te_{1-x}S_x$, single cryst. film, field effect mobility, peaked struct. 77—66207
$Bi_2(Te_{1-x}S_x)_3$, quasi 2-D cryst., I-V and magnetocond. meas. 77—85360
$Bi_2(Te_{1-x}S_x)_3$, thin cryst. two-dimens. system, electronic props. 78—60181
$Bi_2Te_{3-x}Se_x$ films, surface band struct. and scatt. mechanism 80—34535
Cd-Sb thin film prep. by vacuum deposition, elec. props. 78—92194
Cd_3As_2 78—2600
n-Cd_3As_2, vacuum evaporated, Shubnikov-de Haas effect 79—99644
$Cd_xHg_{1-x}Te$, vacuum departed struct. and elec. props. 77—59344
$Cd_xHg_{1-x}Te$ films, epitaxial growth, optical, elec., and photoelec. props. 79—11512
$Cd_xHg_{1-x}Te$ graded-gap epitaxial layers, photocond. meas. 0.5 to 6 μm, detector appl. 79—60869
$Cd_xHg_{1-x}Te$ layers, epitaxial graded-gap, nonlinear elec. effects 80—100468
$Cd_xHg_{1-x}Te$ polycrystalline films, electrical props., rel. to struct. *(Polish)* 78—31002
CdO, electrophysical properties *(Russian)* 77—63008
CdO thin film conductivity, H_2O and CO adsorption effects 79—56340
CdO-SnO_2, DC reactively sputtered, transparent electrode props., optimum sputtering conditions 80—11116
CdO-SnO_2 DC reactively sputtered films, elec. and optical props. 80—103763
CdO-SnO_2 film, DC sputtering prep., visible and near IR transmission, resist. 78—88049
CdO-SnO_2 film, prep. by RF sputtering, elec. cond. and transparency 80—7492
CdS, chemically deposited, cond. depend. on thickness, grain size, annealing time *(Russian)* 77—8210
CdS, chemically sprayed, carrier conc. and mobility, thermoelec. and photothermoelectric meas. 80—2503
CdS, dark- and photo-currents, annealing time effect 79—38199
CdS, epitaxial film, conductivity control by S vacancy form., light modulation appls. 77—4455
CdS epitaxial film, with grain-boundary barriers, field characts. of elec. cond. 77—55626
CdS evaporated films, growth rate and resist. determ., in situ meas. technique 79—77940
CdS evaporated films, O chemisorpt. kinetics, effects on elec. cond. 78—6464
CdS film, chemically sprayed, elec. and photocond. props. 78—34913
CdS film, current-field characts. 80—2490
a-CdS film, DC cond. Seebeck data 77—24626
CdS film, inhomogeneities responsible for residual cond., microinclusions 77—28269
CdS film, non-ohmic elec. cond. 80—2489
CdS film, on Si, structural and transport props. 78—6463
CdS, film, residual conductivity, effect of transverse electric field 77—4458
CdS film, second harmonic generation by transverse acoustic wave 77—51782
CdS, film, surface struct. and elec. props. 80—34531
CdS film, temp. depend. of dark and residual cond. 77—55625
CdS, film, X-ray diffr. and elec. cond. 78—64149
CdS, film electrolytically deposited, surface and bulk photocond. props. 78—60154
CdS, film for solar cells, struct. and elec. props., thickness depend. 78—72289
CdS films, growth, residual cond., inclusions 78—43492
CdS films, photosensitive, growth by reactive RF sputtering, props. *(French)* 78—35308
CdS, films, photovoltaic effect in wedge shaped film 79—56331
CdS films, prep. by reactive pulverisation, chemical, crystallographic and electronic props. *(French)* 80—60112
CdS films, vac. evaporation from CdS.Cr_2O_3 system, photoelec. props. 78—80074
CdS, growth by chem. bath deposition, photocond. props. 77—59703
CdS, microinclusion distrib. of high resist. phase and residual cond. 80—7008
CdS, polycryst. films, microstruct. and X-ray cond. 79—56336
CdS polycrystalline films, high strain sensitivity 80—93017
CdS, spray pyrolysis prep., elec. transport props. 78—2590
CdS sprayed films, elect. and optical props. 78—39241
CdS thin films, growth and evaluation for fabrication of high performance photovoltaic solar cells 80—93501
CdS thin films on brass substrates, nondestructive resistivity meas. tech. 80—93898
CdS:Cu, Cl films, photocond. growth and decay time 80—60041
CdS:Cu,Cl, photocond. props., rel. to use in laser-addressed electrolum. display screen 77—51777
CdS:Cu(Cl) thin films, surface and bulk photoconc. 80—88653
CdS:In, high cond., high transmittance, growth by evaporation method, and characterisation 77—77386
CdS:In films, vacuum deposited, growth, elec. and optical props. 79—51460
CdS:Li chemically deposited filter, elec. props. 80—11113
CdS:M, M=Zn, Te, doping and solid soln. prep. during VPE 77—85353
CdS:Na, dark- and photo-currents, annealing time effect 79—38199
CdS:Na thin film, photoconducting props. 80—39623
CdS-CdSe, unactivated film, calc. of induced impurity photocond. due to donor-acceptor pairs 77—43749
CdS(Se), electron irrad. effect on electrophys. props., prep. conditions depend. 79—28421
CdS_xSe_{1-x} solid soln. film by spray pyrolysis 77—81214
CdSb, monocrystalline film, prep., elec. props. 79—43159
CdSe, conductivity instability when exposed to the atmosphere 77—15980
CdSe, epitaxial, condensation from gas phase of controlled comp., and props. 80—54562
CdSe evaporated films, elec. props. 80—2498
CdSe film, effect of growth conditions on electrophysical properties 78—44024
CdSe film, Hall voltage meas. 77—69434

electronic conduction in crystalline semiconductor thin films continued
CdSe film, laser annealing effects on surface struct. and elec. characts. 79—73605
CdSe film, resistivity rel. to vapour deposition parameters 77—12033
CdSe, film, specific resist., deposition conditions, depend. 77—85363
p-CdSe layers, ion implantation prep., elec. props. 79—51699
CdSe, polycrystalline, analogue elec. model 77—39974
CdSe, polycrystalline analogue elec. model 77—36000
CdSe, stimulated recrystn. influence on photocond. 77—43754
CdSe, structure, resist. and Hall mobility 77—76974
CdSe, vacuum deposited, stabilisation by heat treatment in vac. *(French)* 79—95532
CdSe, vacuum deposited, elec. resist. and surface changes by laser annealing 80—2491
CdSe:Cu:Cl, induced impurity photocond., 0.6 to 1.2 eV 79—24012
CdSe:In, epitaxial layer, effect of activator distribution on conductivity 78—43047
CdSe:Zn(Ga), epitaxial film, impurity distrib., current transfer features *(Russian)* 77—47908
Cd_2SnO_4 film, sputter deposition and characterisation 79—43146
Cd_2SnO_4, RF sputtered from powder targets, props. 77—43759
CdTe epitaxial layers on GaAs, cryst. struct. and phys. props. 79—33202
CdTe film, photogenerated carrier transport props. 80—88590
CdTe, films grown by hot wall epitaxy, elec. props. 79—28420
CdTe, growth by photostimulated VPE, electrophys. props. 77—40390
CdTe, low resist., prep. by multi-source evaporation method, and characterisation 80—25582
CdTe sputtered films, deposition conditions effects on struct. and props. 77—43452
CdTe thin film on ferroelectric TGS, influence of polarisation reversal on elec. cond. 80—65720
CdTe:Cl, LPE from $CdCl_2$ soln., elec. props., defects 80—39689
CdTe-Te film, prep. by combined hot-wall-flash evaporation method, and characterisation 80—55296
CdZnS thin films, growth and evaluation for fabrication of high performance photovoltaic solar cells 80—93501
$Cd_{1-x}Zn_xS$ 10 μm film optical and electrical characterisation *(French)* 78—64153
$Cd_{1-x}Zn_xS$ films, thermal evaporation prep., phys. props. 80—84410
Cds film on metal substrate, resistivity 79—95522
Cds, pure and Na doped, chemical bath deposited, photothermoelectric effect 80—6906
$Co_{3-x}Mn_xO_4$, prep., struct. and elec. characteris. 80—108353
$CuGaSe_2$ thin films, on GaAs substrates, structural and elec. props., photoluminesc. meas. 79—65564
$CuGaTe_2$ epitaxial layers, elec. props. as function of growth temp. 79—65565
$CuGaTe_2$ films deposited on GaAs substrates by flash evaporation, struct. and elec. cond. 80—24755
$CuIn_{0.7}Ga_{0.3}Se_2$ epitaxial layers, on GaAs substrates, struct. and elec. props. 80—107670
$CuInS_2$, epitaxial thin film on GaAs, exam. of growth, electrical props. 80—24754
$CuInS_2$ films, RF sputtered, growth and props. 80—80124
$CuInS_2$ films prepared by spray pyrolysis, elec., optical and struct. props. 79—73609
$CuInS_2$ films prod. by RF sputtered Cu-In films exposure to H_2S 79—95926
$CuInS_2$, photoconductivity effects 77—43662
$CuInS_2$ thin films, growth, struct., and elec. props. 79—38729
$CuInSe_2$ epitaxial growth on GaAs 78—84104
p-$CuInSe_2$ film, prep. from vac. evaporation of $CuInSe_2$, optical and elec. props. 79—82697
$CuInSe_2$, photoconductivity effects 77—43662
$CuInSe_2$ thin films for solar cells, radiofrequency sputtering technique, elec. props. 80—93487
$CuInTe_2$ epitaxial layers, on GaAs, growth and props. 80—108359
$CuInTe_2$, photoconductivity effects 77—43662
$CuInTe_2$, vac. deposited film, growth, struct. and elec. characts. 77—69995
Cu_2O, reactively-sputtered, phase comp., resist. and optical consts. 79—95534
Cu_xO, growth by anodisation, switching characts. 77—55898
$Cu_{1.8}S$ film, vacuum evaporated, props. rel. to elec. cond. 77—36001
Cu_2S epitaxial films, reactive sputtering prep. and electronic props. 79—78885
Cu_2S, film preparation for solar cells, elec., optical, struct. props. 78—76602
Cu_2S, optical and calorimetric meas. of thin films for Cu_2S-CdS solar cells 80—55863
Cu_2S, polycryst. thin films, struct., optical and elect. props. for solar energy appl. 80—10837
Cu_2S, reactively sputtered, Hall effect meas., 90-300K 80—15541
$Cu_{2-x}S$ films, vacuum deposited, electrical conduction and phase transitions 78—84332
Cu_xS, $1 \leq x \leq 2$, quantum temp. size effect and magnetism *(Russian)* 80—103764
Cu_xS films, magnetron reactive sputtering deposition and elec. props. 79—78884
Cu_xS, layers produced by reactive RF sputtering, struct., elec. and optical props. 79—90908
Er_2Te_3, films, prep., elec. props. 78—43494
EuS film, struct., elec. and opt. prop. changes during annealing in air 77—7983
EuS films, mag. and elec. props. rel. to stoichiometry and defects 80—97122
EuS, on amorphous substrate, anisotropic growth and characterisation 77—12547
Fe_xO_y film, semicond. model for electronic struct., high electronic cond. 80—2493
$Ga_{1-x}AlAs$:Zn, acceptor energy level and elec. props. 80—65482
$Ga_{1-x}Al_xAs$ epitaxial layer, elec. cond., Ha effect, band struct. 80—49964
$Ga_{1-x}Al_xAs$, LPE growth and characterisation 80—50566
GaAs and related cpds., conference, St. Louis, MO, USA (Sept. 1978) 80—8737
GaAs, CVD on W coated graphite, characterisation, and Schottky barrier solar cell characts. 79—28930
GaAs, compensated, electron mobility temp. depend. 80—96868
GaAs compensated VPE thin film, electron Hall mobilities 80—107932
n-GaAs, cond. mechanism in strong elec. field determ. 77—1430

electronic conduction in crystalline semiconductor thin films continued
- n-GaAs, epitaxial, high temp. carrier transport 80–65725
- n-GaAs, epitaxial, thermoelec. power, temp. depend. in mm wavelength range 79–23996
- n-GaAs epitaxial film, pure and Cr doped, heavy electron trapping, Gunn oscills. 80–6857
- n-GaAs epitaxial films, residual cond. meas., struct. perfection rel. to photomemory 80–7010
- GaAs, epitaxial layers, MBE grown, Hall mobilities, substrate temps. 80–20335
- GaAs epitaxial layers on polycryst. GaAs substrates, LPE growth characts. 80–75471
- GaAs, epitaxy on semiinsulating GaAs, elec. props. of transitional layers rel. to growth conditions 77–15977
- GaAs, heavily doped, strongly compensated, hopping cond. 79–47180
- GaAs, hydride VPE growth for FETs, and characterisation 78–27407
- GaAs, ion-implanted layers, close contact capless annealing, elec. props. 80–84192
- GaAs, LPE growth on O-implanted GaAs substrate, elec. props. 78–2592
- GaAs layers, electroepitaxy and thermal LPE growth, defect struct. and electronic characts. 80–2290
- GaAs, MBE, undoped, growth and characterisation 80–10836
- GaAs MBE epilayers, photoluminesc. and elec. characterisation 80–11500
- GaAs, MBE layers, H_2 effect on residual impurities, photolum. obs. and elec. characts. 79–47636
- GaAs, minority carrier diffusion lengths, contact metal effects 78–72260
- GaAs, O^+ implantation, effect on LPE growth and elec. props. 80–24477
- GaAs, plastic deform. prod. by thermocompression bonding, elec. props. 77–76807
- GaAs, VPE, electron Hall mobility meas., attempted correlation with growth parameters 78–43417
- GaAs, VPE, high purity, residual donors, photocond. expts. 77–85174
- GaAs, VPE, hole diffusion lengths, surface prep. and heat treatment effects, etchant evaluation 80–15627
- GaAs, VPE, hole diffusion lengths, effect of transition metal diffusional doping 80–15628
- GaAs VPE layers, elec. props., semi-insulating substrates effect 80–11123
- GaAs VPE layers, electron irrad., electron traps 80–25026
- n-GaAs vapour phase epitaxial film electrophysical props. rel. to growth temp. *(Russian)* 80–49961
- GaAs:Be, annealing effect during MBE 78–79898
- GaAs:Be, deep levels 80–29358
- GaAs:Co, epitaxial layers and bulk, diffusion and elec. activity of Co 79–56333
- GaAs:Cr, epitaxial layers, MBE grown, Hall mobilities, substrate temps. 80–20335
- GaAs:Cr, semiinsulating, LPE and elec. props. 77–44178
- GaAs:Cu, diffused layers, photocond. spectra, hole conc. and mobility *(Russian)* 78–14758
- GaAs:Fe, for FET, VPE and characterisation 78–19672
- GaAs:Fe LPE layers, negative resist. effects and deep acceptor model 77–72929
- GaAs:Ge, cryst. and epitaxial layers, ion-implanted, elec. props. 79–99542
- GaAs:Ge, LPE, on semi-insulating GaAs, film-substrate interface characterisation 78–72017
- GaAs:Ge film, MBE grown, heavily doped, elec. props. rel. to growth parameters 80–100537
- GaAs:Se(Zn) polycrystalline film, Hall effect, resistivity meas. 80–96911
- GaAs:Si, accelerated growth rate effect on MBE, Hall mobility and photolum. meas. 80–104067
- GaAs:Si(Mg), doped and undoped, sputtered epitaxial films, elec. props. 79–78234
- GaAs:Sn epitaxial layer, electronic props. and epilayer-substrate interface props. 77–89886
- GaAs:Te, Ge, compensated, activated cond. 77–76968
- $GaAs_{0.6}P_{0.4}$, VPE, hole diffusion lengths, surface prep. and heat treatment effects, etchant evaluation 80–15627
- $GaAs_{0.6}P_{0.4}$, VPE, hole diffusion lengths, effect of transition metal diffusional doping 80–15628
- $(GaAs)_{1-x}(ZnSe)_x$, LPE growth, resist., Hall effect and cathodoluminesc. meas. 77–28270
- GaAs;Cu, epitaxial and bulk conductivities compared *(Russian)* 78–10585
- GaInAs-InP, growth by low-pressure metalorganic CVD 80–71595
- $Ga_xIn_{1-x}As$, on ⟨111⟩B InP, LPE growth, characterisation of high purity lattice 80–104082
- $Ga_xIn_{1-x}As$-InP, MBE film growth, composition control obs. 80–84399
- GaInAsP, VPE growth and props. 80–16194
- $Ga_xIn_{1-x}As_yP_{1-y}$, conduction band and phonons, Shubnikov-de Haas effect, magnetophonon resonance, Raman scattering 80–24795
- $Ga_xIn_{1-x}As_{1-y}P_y$:Ge(Sn)(Te), epitaxial film, elec. and optical props. 79–11251
- $Ga_xIn_{1-x}Sb$, LPE, growth by vertical dipping method and elec. props. 77–85949
- GaN, plasma deposition and elec. cond. 78–60585
- GaN, thermoelec. power and Hall coeff. meas. 77–55627
- GaN, VPE growth rate influence on elec. and luminesc. props. 80–100702
- GaN:Zn epilayers, growth parameters effect on props., device struct. 78–26975
- GaN-AlN, solid solution, epitaxial growth and electrical props. 77–73236
- GaP, epitaxial growth from Sb and Bi melts 79–52131
- GaP, epitaxial layer, thickness and diffusion length, photocurrent meas. 77–32096
- n-GaP epitaxial layers, transverse magnetoresist. *(Russian)* 77–76964
- GaP film, deposited by RF sputtering *(Czech)* 78–52667
- GaP layers, LPE growth, elec. props., residual impurities 79–38202
- GaP, RF sputtering on glass and Au film substrates, struct. and elec. props. 80–2311
- GaP, vac. deposited film, structural, elec. and photoelectric props. 79–82698
- GaP:N VPE LED, deep level centres, DLTS studies 79–42493
- GaP:Sn, LPE growth from Sn soln., elec. resist. and Hall coeff. meas. 78–2593

electronic conduction in crystalline semiconductor thin films continued
- GaP:Te on GaAs, LPE growth fron Sn, exam. of impurity band conduction effects 79–11249
- GaSb, electrical cond. thermoelec. power and optical absorpt. 80–2504
- GaSb, sputtered films, on GaAs, growth, Hall effect, impurity levels 80–20334
- GaSb thin layers, directed crystn. on sapphire, props. 80–35111
- GaSe film, charge transport models *(Russian)* 78–60233
- Ga_2Se_3, film, electrical and optical props. 77–1505
- Ge, electrical resistance, long term stability rel. to ambient atmosphere changes 78–2597
- Ge epitaxial film, ion implantation and electron beam anneal effects on carrier conc. 80–75255
- Ge epitaxial film, vac. deposited on GaAs, doping effect of annealed GaAs surface 80–65718
- Ge film, elec. props., prep. by DC sputtering *(Japanese)* 79–78237
- Ge film, electrical cond. during laser-induced crystallisation 79–47175
- Ge film, polycrystalline, structural and elec. props. 78–76173
- p-Ge film on GaAs, cond., Hall effect and transverse magnetoresist., anisotropy 79–51697
- p-Ge, fragmented struct., elec. cond., Hall coeff. and magnetoresist. meas. 77–15979
- Ge heteroepitaxial film, ethanol pulsed adsorption effect on elec. cond. 80–93014
- P-Ge, heteroepitaxial film, galvanomagnetic effects, influence of mechanical stresses 79–91171
- Ge, in Al/Ge/Al sandwich struct., interdiffusion effect on film cond. 79–23788
- Ge plate, anisotropic cond. thickness depend., intervalley scatt. *(Russian)* 77–85352
- Ge, thickness depend. of resist. 77–39978
- Ge:metal, polycrystalline film, electron transport props. 79–99642
- Ge:Sb(In), film, electronic props. 78–84330
- Ge-Al, elec. resist. and IR transmission, comp. and substrate temp. depend. 78–52112
- Ge-metal films codeposited, amorphous and polycryst., struct. and elec. props. 80–24766
- Ge-Se-Ga, elec. cond., switching phenomena *(Polish)* 80–11120
- Ge-Si alloy, epitaxial growth by getter sputtering, characts. 79–28915
- Ge-Si solid solution film, elec. props. in range 4.2 to 500K 77–8214
- GeS, effective electron mass determ. from current-voltage characts. in thermionic region 77–85135
- GeTe film, elec. props. 77–51831
- GeTe films, elec. props. and struct., influence of annealing and condensation conditions 80–15388
- $Hg_{1-x}Cd_xTe$, epitaxial layers, elec. properties in the range 4.2 to 300K *(French)* 80–65721
- $Hg_{1-x}Cd_xTe$, LPE growth and characterisation 80–50565
- HgTe, vacuum deposited, elec. props., 78-420K 80–11119
- IN_2O_3:Sn, RF magnetron sputtered film, elec. and optical props. 80–104065
- InAs, epilayer, MBE growth parameters, relationship with elec. props. 80–2296
- InAs epitaxial layers, on GaAs substrate, electron diffr. and SEM exam., electronic props. 79–1552
- InAs film, DC sputtering, struct. and elec. props. 77–66567
- InAs films, MBE grown on GaAs, electron mobilities, lattice mismatch effect 80–80419
- InAs, heteroepitaxial, charge transport obs. by gate-voltage-controlled meas. on MOS struct. 77–47912
- InAs heteroepitaxial layers, VPE grown, effect of $AsCl_3$ mole fraction on elec. props. 79–11255
- n-InAs, VPE layers, on GaAs substrate, electronic profile 79–95525
- $InAs_{1-x}Sb_x$, epitaxial film, carrier recomb., elec. and optical props. 79–15164
- $In_{0.53}Ga_{0.47}As$, LPE layer on InP, electron mobility and energy gap 77–24627
- p-$In_{0.53}Ga_{0.47}As$:Zn on InP, elec. and optical props. 80–75662
- $In_{1-x}Ga_xAs_yP_{1-y}$, hole mobility over temp. range 77 to 300K 80–60111
- InO_3:Sn film, prep. by spray hydrolysis, struct., elec. and optical props. *(Japanese)* 79–42678
- In_2O_3, conductive, transparent, optimal reactive sputtering conditions for prep. 79–95295
- n-In_2O_3 film, on Pb(Zr,Ti)O_3 ceramic, ferroelec. field effect 79–47177
- n-In_2O_3 film, RF sputter grown, substrate bias effect on elec. and optical props. 78–64150
- In_2O_3, films, activated reactive evaporation technique of prep. 80–80989
- In_2O_3 films, electron beam evaporation, elec. and optical props. *(Japanese)* 80–60784
- In_2O_3 films, reactively evaporated, elec. props. 80–84521
- In_2O_3, In_2O_3-SnO_2, transparent thin films for satellite temp. control 79–80187
- In_2O_3, reactive ion plating onto insulating substrates, and elec. and optical props. 79–87588
- In_2O_3, thermally evaporated film, struct. and elec. props. 80–104066
- In_2O_3, thin film, sputter deposition form., optical and elec. props. 80–60123
- In_2O_3, transparent films, state of art *(Chinese)* 79–73610
- In_2O_3, transparent heat mirror formation by ion plating on ambient temp. substrates and props. 80–25578
- In_2O_3:Sn, coating on polyester film, elec. and optical props. 79–99959
- In_2O_3:Sn, film, HF sputtered, cond., Hall mobility, oxidation, charge carrier density 78–72287
- In_2O_3:Sn, films, activated reactive evaporation technique of prep. 80–80989
- In_2O_3:Sn, HF sputtered films, temp. depend. studies of the elec. transport props. 78–76170
- In_2O_3:Sn, sputtered film, optical and elec. props. 78–76177
- In_2O_3:Sn, transparent conducting films, prep. by $InCl_3$ thermal decomp., transmittance, resistivity 79–33944
- In_2O_3:Sn films, CVD prep. and elec. resist. meas. 79–52120
- In_2O_3:Sn films, elec. and optical props., solar energy conversion appl. 79–65945
- In_2O_3:Sn films, prep. at low deposition temps. by ion-beam sputtering, elec. and optical props. 79–66004
- In_2O_3:Sn films, pure and doped, prod. by ion plating, elec. and optical props. 80–2488
- In_2O_3:Sn films; vac. deposited, elec. props. 80–100542
- In_2O_3:Sn transparent cond. films, hydrolysis deposition, elec. and optical props. 79–43144
- In_2O_3-SnO_2, stress, and elec. and optical props. 78–51861

electronic conduction in crystalline semiconductor thin films continued
In_2O_3-SnO_2, thin films deposited on cold substrates, initial resist. effect on life stability 79—23867
In_2O_3-SnO_2 thin film, effects of heat treatment on resist. and optical absorpt. 78—43495
In_2O_3-SnO_2 thin film, Hall mobility, temp. depend., grain boundary effects 80—75658
n-InP, epitaxial, Hall effect, electron mobility and density, temp. depend. 78—72288
n-InP, epitaxial, subthreshold velocity-field charact., 77K 78—64038
InP epitaxial films, grown on heavily doped substrates, carrier mobility study, magnetoresist. meas. 80—60116
n-InP film, polycryst., deposited on Mo sheets, elec. props. obs., w.r.t. varying deposition conditions 79—4608
n-InP film, polycrystalline, elec. props. 77—76965
InP, ion-implanted layers, close contact capless annealing, elec. props. 80—84192
InP, planar reactive deposition on CdS, heterostruct. format on and elec. evaluation 78—72738
$InP:S^+(Se^+)$, ion-implanted VPE layers, laser annealing, elec. and struct. anal. 79—73199
InP:Si(Mg), ion implantation and PH_3 ambient annealing under VPE conditions 79—42085
InP:Sn, LPE growth from Sn soln., elec. props., 80 to 300K 79—11250
p-InP:Zn, vapour grown, prep. and props. 80—54268
n-InSb, degenerate, electron conc. and resist. temp. depend., band struct. 77—76971
p-InSb, excess In, polycryst. thin film, elec. transport props., non-stoichiometric effect 79—95528
p-InSb film, elec. transport props. 78—72291
n-InSb film, low energy electron irrad. effect on elec. props. 80—7009
InSb film, quantum size effects, transport props. 78—76171
InSb films on $LiNbO_3$, prep. and props. 80—35093
n-InSb, galvanomagnetic meas. of surface layer carrier conc. and mobility 77—55628
InSb, heteroepitaxial, MBE growth and elec. props. 80—2301
InSb, melt-grown, point defect effect on elec. props., 77-300K 80—2502
InSb, polycryst. film, Hall and drift mobilities 79—95531
InSb recrystallised thin films on mica substrate, elec. props. 80—70867
InSb, thin film prep. with remelting, elec. props. 77—52255
InSb, thin films, electrophysical props. obs. 80—103765
p-InSb:Cu(Zn) film, heavily doped, ionized impurity scatt., Hall effect and DC cond. meas. 79—99643
$InSb_{1-x}Bi_x$, multitarget RF sputtering, metastable phase, conductivity transition 80—76178
InSe films, residual photocond., field quenching 80—60037
$In_xSi_yO_z$, thin film, sputter deposition form., optical and elec. props. 80—60123
$(In_{1-x}Sn_x)_2O_{3-y}$, pyrolytic selective coating, Sn additions effect 78—43499
$In_{2-x}Sn_xO_{3-y}$-ZnS:Mn thin film structure, surface morphology and electro-optical props. *(Russian)* 80—49554
$In_{2-x}Sn_xO_{3-y}[SnO_2]$-CdSe-CdS:Cd,Cl sandwich photoconductor injection obs. *(Russian)* 80—54773
InTe thin films, flash evaporation, electrical props. 80—65722
In_2Te_3 film thermal deposition, transmission spectra and elec. cond. *(Russian)* 80—49555
LaB_6, prep. by electron beam evaporation, and optical and elec. props. 80—20793
$MnCo_2O_4$ DC sputtered films, struct. and elec. props. 80—54812
MnTe film, elec. props. 78—43498
NbO_2, threshold switching recovery curve, distribution trapped carrier lifetime 80—20258
NiSe, thin film phases, struct. and resist. 78—39236
$Pb_{1-x}Cd_xS$, epitaxial, resist. and Hall coeff., substrate temp., thickness and comp. depend. 78—72290
$Pb_{1-x}Cd_xS$, metastable epitaxial films, elec. props. 78—26979
$Pb_{1-x}Hg_xS$ electroless-deposited films, optical and elec. props. 80—7011
PbO:Ag film, X-ray stimulated diffusion, current-voltage characts. 77—80653
PbS, chemically deposited film, photosensitivity, effect of morphological struct. 79—82647
PbS epitaxial film, struct., optical and elec. props. 78—19583
PbS, photosensitive film, electron bombard. effect on elec. cond. 80—93019
PbS, polycryst., chem. deposition from soln. and characterisation 78—72743
PbS, thin film, photoconductivity expts. 79—78130
PbS-PbO vacuum evaporated films, elec. cond. and photocond. 80—75656
PbSe, film, photoconductivity, temp. depend. 79—38200
PbSe films, current carrier conc. and type control, elec. cond., synthesis process *(Russian)* 80—100412
PbSe, polycryst. film, low temp. illumination, residual cond. 77—43756
$Pb_{1-x}Sn_xSe(Te)$ epitaxial layers, growth, phase diagram, p-n junctions, optical, elec. props. 78—44029
$Pb_{0.78}Sn_{0.22}Te$:In epitaxial layers, dislocation density, Hall effect, conductivity, photoeffects 80—25024
$Pb_{1-x}Sn_xTe$ film, effect of mechanical strains on elec. props. 77—58621
$Pb_{1\ x}Sn_xTe$ epitaxial films, adsorption-induced accumulation layer form. on surface 80—60117
$Pb_{1\ x}Sn_xTe$, epitaxial layers, cond. *(Russian)* 77—24629
$Pb_{1-x}Sn_xTe$ film, deposition, elec. and piezoresist. props. 78—6465
$Pb_{1-x}Sn_xTe$ film, pure and Bi doped, polycryst., struct., elec., optical props. 79—42542
p-$Pb_{1-x}Sn_xTe$, LPE layer, carrier conc. and mobility 79—99639
$Pb_{1-x}Sn_xTe$, sputtered, for IR detector appl. elec. and optical props. 80—35084
$Pb_{1-x}Sn_xTe$:In, Hall const. depend. on temp., autocompensation, band gap temp. depend. explanation 79—69527
$(Pb_{1-x}Sn_x)_{1+y}Te_{1-y}$ system, VPE parameters influence on epitaxial film props. 79—28229
$Pb_xSn_{1-x}Te$, RF sputtered film IR detector, photocond. response speed improvement by annealing 79—58790
PbTe (111) epitaxial films, localised electron irrad. effects on elec. props. and O_2 sorption 80—49472
PbTe, characts. of photocond. spectra and reflectivity 77—55624
PbTe film, electronic thermal cond. and thermoelec. power 80—93018
PbTe film, residual conductivity 78—2595
PbTe film, struct. anal. and sensitisation 78—22982

electronic conduction in crystalline semiconductor thin films continued
PbTe films grown from vapour, optimum conditions and elec. characts. 79—52117
PbTe, ion-implantation-induced lattice defects 77—68985
PbTe, ion-implanted, doping profile evaluation by Hall effect and sheet resist. meas. 78—59831
n-PbTe, LPE layer, carrier conc. and mobility 79—99639
PbTe, uncontaminated films on mica sustrates, elec. props. obs. 77—76967
n-PbTe:In(Cu) epitaxial films, elec. transport props. 80—75659
$PbTe_{1-x}Se_x$, epitaxial layers synthesis, cryst. struct. perfection and elec. characts. 79—87587
PrB_6, prep. by electron beam evaporation, and optical and elec. props. 80—20793
$Ru_xTi_{1-x}O_2$ films, elec. props. and IR spectra 79—38207
Sb film, elec. cond., and struct., thickness depend. 78—26974
Sb, semimetallic film, elec. cond., grain boundary scatt. effects 80—103766
Sb, thin plates, electron conduction, 4-293K, surface reflection ang. depend. *(Russian)* 78—19170
Sb_2S_3 film, coevaporated, elec. cond. meas. 80—65726
SbSI-BiSI, solid solns., phase diagrams, photocond., elec. props. 79—38125
Sb_2Te_3 epitaxial films, growing conditions effect on elec. cond., thermo-EMF 80—39687
Se film, crystallisation using org. catalysts, struct. and elec. props. 77—51613
Se film, vacuum deposited, struct. asymmetry, reflectivity elec. cond. 79—23855
Se photoconductive layers, impedance-freq. characts. meas. *(Japanese)* 79—38120
Se photoreceptors, phthalocyanine sensitized, elec. cond., charge decay characts. 80—15630
p-Si, $^{49}BF_2$ ionised mols. obtained by implantation of 78—31003
Si, CVD films, polycryst., elec. and optical props., electronic density of states model 79—56332
n-Si channel ⟨100⟩ inversion layer MOSFET, valley splitting, conductivity 80—70840
Si, elec. props., effect of amorphous to polycryst. transition 79—28425
Si, electrodeposited film, appl. in solar cell fabrication 78—76611
Si, electron beam deposited, elec. and struct. props. 79—1632
Si, epitaxial layer deposition by ion beam methods 80—100417
Si epitaxial layer substrate junctions, carrier lifetime and abnormal conduction phenomena *(Korean)* 78—47888
Si epitaxial layers, doping the P cpds., process parameters effect on electrophys. characts. 78—38734
Si, epitaxial layers, minority carrier lifetime and diffusion length meas., photocurrent technique 78—95302
Si film, low press. CVD prep., struct., elec. and optical props. 80—70548
Si film, sputtered, physical props. 79—77938
Si films, polycrystalline, elec. props., grain size and dopant conc. influence 80—29492
n-Si films on sapphire, crystalline defects effect on elec. props. 77—20470
Si, glow discharge film decomposed from silane, on amorphous substrate, elec. cond., RHEED study 80—20044
Si, graphoepitaxy on fused SiO_2 using surface micropatterns and laser crystn. and characterisation 80—70554
Si heteroepitaxial films on sapphire, vac. deposited, struct. and elec. props. 80—15390
Si, LPE using Ga_xAl_{1-x} solvent, resist. and Hall mobility 77—36411
Si, laser annealed, elec. props. 79—69609
Si, lightly doped, cond. mechanisms, correl. with SEM examination of film 79—1634
Si, MBE, on n^+ Si, with wide range doping control 78—27402
Si MBE layer resistivity and carrier mobility obs. *(Russian)* 80—49962
p-Si, on sapphire, elastoresist. coeffs., room temp. 80—34532
Si, on sapphire, Hall mobility, carrier distrib. effects 77—51818
Si on sapphire, residual strain effect on elec. props. *(Japanese)* 80—84522
Si, P implanted low pressure CVD polycryst. films, elect. characts. 80—60114
Si, polycryst., growth, props. and MIS appl. *(Slovak)* 78—92196
Si, polycryst. CVD film electrical props. 78—6466
Si, polycryst. film doping during deposition and with diffusion 78—6088
Si polycrystalline film resistivity reduction by Nd:YAG laser annealing 80—100539
p-Si polycrystalline films on graphite substrates *(French)* 78—64154
Si, sputtered, on quartz and MgO substrates *(Japanese)* 77—55889
Si thin film, polycryst., CVD, elec. props. 80—107934
Si, thin sheet, Sb impurity profile eval. in p-n diffusion junction by anodisation and resist. meas. 79—46695
Si:Ar, ion-implanted, epitaxial regrowth by laser annealing, microstruct. 80—84404
Si:As, polycrystalline, As segregation at grain boundaries, elec. props. meas. 80—75259
Si:As(B)(P), ion-implanted polycrystalline films, laser annealing 79—73181
Si:As(P) film, polycryst. laser annealed, resistivity changes during thermal annealing 79—91163
Si:As(P)(Sb), implanted, elec. cond., sheet resist. as function of ion dose and temp. 79—78235
Si:B, highly-doped polycryst. thin film, growth kinetics and properties 78—44016
Si:B, polycryst., effect of laser annealing on struct. and elec. props. 79—11243
Si:B, polycryst., N_2 heat treated, anomalous resist. change due to Bn form. 78—2591
Si:B, sputter-deposited, elec. props., struct., SEM and TEM obs. 79—95298
Si:B(Al), (P)(As)(In), ion implanted film, elec. prop. impurity depend. 80—24467
Si:B(P), ion implanted, polycryst. annealing characts. 77—24324
Si:B(P) polycrystalline thin film, plasma annealing, effect on elec. props. 80—7005
Si:Ga(Al), MBE, growth, struct. and elec. props. 77—89458
Si:Ga(Sb), epitaxial film, doping efficiency *(Japanese)* 79—73201
Si:N wafers, Si_3N_4 layer growth by high dose implantation and annealing, elec. props. 80—70227
Si:O, O rich polycryst. film, carrier transport 78—80076

electronic conduction in crystalline semiconductor thin films continued
Si:O, polycrystalline layer on Si p-n junction, charge transport and passivation 79—38206
Si:O, semi-insulating polycryst. film, cond. through localised and extended states 77—28268
Si:p, film, polycrystalline, low press. CVD, resist. meas. 80—2494
Si:P, polycryst., CVD, elec. activation of impurities, EPR obs. 80—34774
Si:P, polycryst. films, elec. props., EPR, defect states, doping effects 80—75660
Si:P, sputter-deposited polycryst. films, resist. meas. 78—14842
Si:P CVD films, ion-implanted, doping effect on elec. props. 80—2495
Si:P film, polycryst., heavily doped, mobility and carrier conc., optical determ. 80—66314
Si:P film, polycryst. pulsed electron beam annealing 80—10566
p-Si:P implanted films, piezoresist. stress tensors, ion dose depend., −80 to 120°C 80—100538
Si:P(B), film, electronic props. 78—84330
Si-F-H:P, film, dark cond., struct., Raman scatt. 80—88588
n-SiC, 6H, epitaxial layer, saturated electron drift velocity meas. 78—19168
n-SiC, 6H polytype, expitaxially grown, electronic props. meas. 77—39975
SiC (6H), epitaxial film, electronic props. 79—60942
Si_3N_4 film deposited from SiH_2Cl_2 and NH_3, characterisation 79—11521
SiO_2 film formed by ion implantation, dielectric props. 78—35090
SmB_6, prep. by electron beam evaporation, and optical and elec. props. 80—20793
SmS film, semicond. and metallic modifications, elec. props. 77—32098
SmS, first-order transition from semiconducting to metallic state 78—52040
$Sn_{1-x}Ge_xTe$, evaporated thin films, characts. 79—60944
SnO_2, CVD, surface and bulk cond., process parameters effect 77—1502
SnO_2 CVD coating on glass, elec. resist. rel. to cryst. microstruct. 80—84520
SnO_2, CVD using $SnCl_4$-H_2O and $SnCl_4$-H_2O_2 systems, elec. and optical props. 78—52686
SnO_2 doped films for spectral-selective surfaces, refl. and elec. props. meas. 79—74013
SnO_2 film, doped, electron effective mass and elec. props., carrier density depend. 77—43750
SnO_2 film, pure and Sb doped, transparent cond., prop., characts., stability, struct. *(Japanese)* 78—47889
SnO_2, growth by DC sputtering from compressed target, cond. and optical props. 77—59690
SnO_2, reactive ion-plasma sputtered, elec. and opt. props. 79—42677
SnO_2, transparent films, state of art *(Chinese)* 79—73610
SnO_2, two-step deposition process using DC sputtering and oxidation, and characterisation 78—95691
SnO_2:As film, prep. and elec. cond. 80—2959
SnO_2:F films, elec. and optical props., solar energy conversion appl. 79—65945
SnO_2:P, CVD films, elec. props., cryst. to amorphous transition effects 80—107933
SnO_2:SB,X, X=Fe,Cu,S, CVD thin film, resist. temp. coeff. 79—38198
SnO_2:Sb, transparent cond. film prep. by thermal decomp. of Sn salt of organic acid *(Japanese)* 77—90269
SnO_2:Sb, transparent cond. films, hydrolysis deposition, elec. and optical props. 79—43144
SnO_2:Sb film, DC sputtered, substrate temp. effect on cond. 77—39971
SnO_2-Cu_xS-ZnS:Mn,Cu-Al_2O_3-Al, light-emitting struct., cond. and electrolum., heat treatment 80—97345
SnO_2-ZnS:Mn thin film structure, surface morphology and electro-optical props. *(Russian)* 80—49554
$Sn_{1-x}Pb_xTe$, epitaxial layers synthesis, cryst. struct. perfection and elec. characts. 79—87587
SnTe, film, heat treatment in air, effect on struct., props. 79—11037
SnTe, polycrystalline, anomalous resist. at struct. phase transition 80—29488
SnTe-PbSe, semicond. film, growth, phase composition, condensation temp. rel. to cond. type 77—28266
SnTe-PbSe mixed system layers, struct. and props. *(Russian)* 77—28082
$(SnTe)_{1-x}(PbSe)_x$ films on glass-ceramics, struct. and elec. props. 77—52251
$SrTiO_3$:B layers, ion implanted, conductive props. Hall mobility, defect energy levels 79—82693
TE, atm. comp. influence on elec. surface props. 78—26980
Te, annealing effect on elec. cond. and Hall effect 77—8213
Te, evaporated film epitaxial and amorphous-crystalline phase transition growth and struct. 79—51449
Te, field effect meas. 77—43757
Te film, elec. props. effect of deposition rate 78—14844
Te film, on TGS substrate, ferroelec. field effect 79—42675
Te film condensed on mica, struct. and electrophysical props. 80—39688
Te films, elec. props., 77 to 450K, thermal width of band gap 79—51698
Te, films, elect. and galvanomag. characts. 79—33365
Te, oriented films, semiconducting props., Hall coeff., band structure 80—70854
Te, photovoltaic effect in thin films, 10.6 μ, prep. methods 80—20252
Te, thermally evaporated, elec. cond., Hall voltage and thermoelec. power. 77—47913
Te, thin evaporated films, 130 Å, temp. depend. of elec. props. 79—95529
Te thin film, thermoelec. EMF, Seebeck coeff., elec. cond. structural depend. 79—78230
Te:Cu films, elec. transport props. 80—60120
$TlGaS_2(Se_2)$, elec. and photoelec. props. *(Russian)* 78—52109
$V_{1-x}Cr_xO_2$, VPE and characterisation 78—3053
VO_2, chemically deposited, chemical transition layers at interface with substrate, AES and SEM obs. 79—95533
VO_2 film, negative resist. region, applic. as oscillator element and transducer *(Russian)* 77—85359
VO_2, V_2O_3 and V_3O_5, film prep. under equil. conditions, struct. and elec. props. 80—108352
VO_2, VPE and characterisation 78—3053
VO_2(:Al,W), layers, liq. phase prep., resist.-temp. behaviour *(German)* 77—77435
W_2O_{5-x} current noise due to adsorption of water 78—6421
$(Y,Eu,Tm,Ca)_3(Fe,Ge)_5O_{12}$, Ca, Ge substituted garnet LPE films, elec. props., charge imbalance, Seebeck effect 78—68101
$(Y,Sm)_3(Fe,Ge)_5O_{12}$, Ca, Ge substituted garnet LPE films, elec. props., charge imbalance, Seebeck effect 78—68101

electronic conduction in crystalline semiconductor thin films continued
Y-H system, temp., thickness and comp. depend. of elec. resist. 79—78221
YIG, LPE film, non-Ohmic currents 78—68099
Yb_2Te_3, films, prep., elec. props. 78—43494
$Zn_{1-x}Cd_xS$, polycryst., reactively sputtered, MSM struct. obs. of dielec. props. and cond. mechanism *(French)* 78—14841
$Zn_{1-x}Cd_xS$, reactively sputtered polycryst. film, cond. mechanism and grain boundary barriers *(French)* 77—76972
$Zn_xCd_{1-x}S$ epitaxial layers, elec. resist. and luminescence obs. 78—19540
$Zn_xCd_{1-x}S$, film for heterojunction solar cell 77—8208
$Zn_xCd_{1-x}S$ films, spray pyrolysis, elec. props. 80—75657
$Zn_xCd_{1-x}S$, prep by soln. spray method, and struct., optical and elec. props. 78—52666
$Zn_xCd_{1-x}S$ solid soln. film by spray pyrolysis 77—81214
$Zn_xCd_{1-x}S$, thin solid soln. films, vapour deposited, elec. and optical characts. 80—60110
$Zn_xCd_{1-x}S$:In, low resist. film for solar cell window 78—71200
$ZnIn_2S_4$ (I), one-packed polytype, resist., photocond. and luminesc. 79—1608
ZnO CVD epitaxial layer, highly conductive layer, cond. and Hall coeff. obs. 79—51696
ZnO, CVD growth and elec. props. 77—76973
ZnO, CVD of epitaxial films on sapphire, SAW interdigital transducer fabrication 80—66430
ZnO, DC sputtered, prep. and characterisation 78—3040
ZnO epitaxial film, nonuniform cond. due to H chemisorption *(Russian)* 80—65723
ZnO film, chemisorption of H, electrical cond. exam. adsorption centres 78—67913
ZnO film, prep. by reactive ionized cluster beam deposition, and characterisation 80—10829
ZnO, film for solar cell appl. structural, optical and elec. props. 80—2294
ZnO films, RF sputtered single-cryst., on sapphire, struct. and SAW props. 80—80105
ZnO, low energy ion capture, elec. cond. increase *(Russian)* 77—12034
ZnO, sputtered, high-resist., band and hopping cond., AC cond. and capacitance meas. 77—72928
ZnO sputtered films, undoped and Ga doped, props. rel. to deposition conditions 80—107935
ZnO thin film SAW device manufacture, sputtering system and film characterisation 78—95692
ZnO-resin photoconductive layers, impedance-freq. characts. meas. *(Japanese)* 79—38120
ZnS sputtered film, interband photocond. edge *(French)* 77—8212
ZnS, vacuum-evaporated conducting films, prep. and props. 79—66007
ZnS:Cu, film effect of Cu valency on cond. 79—11246
ZnSb, epitaxial films, growing conditions effect on elec. cond., thermo-EMF 80—39687
ZnSe, electron irrad. effect on electrophys. props., prep. conditions depend. 79—28421
ZnSe, film, hopping cond. 80—2499
ZnSe film, MBE and resistivity 79—100059
ZnSe, high conductivity films appl. to p.n. heterojunctions 78—68100
ZnSe layers, cond. type determ. by pot. profiling 80—73387
ZnSe, MBE growth, elec. and optical props. 80—75462
ZnTE, MBE growth, elec. and optical props. 80—75462
ZnTe, conduction mechanisms in non-ohmic off-state 77—72932
ZnTe, epitaxial growth on GaAs by closed-tube chemical vapour transport method, elec. props. 79—99449
p-ZnTe film, current-voltage characts. 77—66214
ZnTe film, LF oscills. of dark current obs. 78—19093
ZnTe films, simple and modified Poole-Frenkel cond. 80—97017
ZnTe MBE thin film growth, elec. and optical props. 78—47887
ZnTe:Cu films, high cond., elec. and optical props. 80—88651
ZnTe:Sb, as function of growth temp. 78—76172

electronic conduction in insulating thin films
see also electrical conductivity of amorphous semiconductors and insulators; electrical conductivity of crystalline semiconductors and insulators
alkali halide thin films, high-field electron injection, ionic cond., photocond. 80—75665
amorphous insulator film, high-field cond. 79—56320
cadmium behenate in Langmuir multilayer assembly system, single layer conductance 79—51701
carbonaceous film, deposition on RF target in butane plasma 77—16507
carbonaceous film, hard, phys. props. 77—39752
chalcogenide glass films, weak field behaviour 77—36004
chlorophyll-a, microcryst., trapped-electron doping in photovoltaic sandwich cells 78—53334
dielectric film, glow polymerised, struct. and props. *(German)* 77—20799
FEP polymer foil, charge transport, injected carrier hopping model 78—19171
ferrocene films, plasma-polymerised, carrier trapping, elec. cond. meas., 300 to 525K 80—100543
fluorocarbon polymer, plasma-deposited thin films for lubrication of Au contact surfaces 80—89157
hexamethylcyclotrisilazane film, glow-discharge-polymerized, in MIM and MIS structs., elec. cond. mechanism 79—42680
Langmuir-Blodgett films, elec. and photoelec. transport props., device appl. 80—80431
lead phthalocyanine film, switching effects 79—28384
malononitrile, plasma-polymerised, in Ag-polymer-Ag struct., SCL currents and carrier trapping 79—51687
metal-polymer films, electron irrad. controlled form., elec. props. 80—15635
oxide thin film electroforming, threshold switching and memory effects 77—76940
PMMA film, in Al-PMMA-Al struct. SCL currents and cond. mechanism 79—51686
PMMA film in small area lateral MIMS device, cond., switching 80—97003
poly(N-vinylcarbazole) layers, supermol. struct. effect on elec. props. 80—44606
poly(p-xylylene), film, high field cond. 79—99647
polyacetylene films, undoped, nonlinear current-voltage charcts. 80—75574
polyacrylonitrile film, elec. cond. 80—11125

electronic conduction in insulating thin films continued
polycarbonate, and charge-transfer complex modifications, isothermal dark currents 80—88559
polyethylene film, high density, anomalous transient currents around 50-70°C 79—33368
polyethylene films, electron beam irrad., carrier mobilities 79—1600
polyethylene films, surface pot. decay, appl. of Scher-Montroll method 79—7851
polyethylene films electrical conductivity under various conditions *(French)* 80—70869
polyethylene terephthalate, elec. cond., 120-180°C, anal. of results 79—47102
polyethylene terephthalate, elec. cond. and space charge accumulation 80—10998
polyethylene terephthalate, nonlinear elec. cond. and space-charge effect 77—39980
polyethylene terephthalate charge transfer from metallic electrodes 80—15605
polyethylene terephthalate films, current peaks obs. with linearly increasing voltage 80—88654
polyethylene terephthalate films, high-temp. elec. conduction 79—51588
polyethylene terephthalate thin films, electronic mobility 80—15634
polyferrocene, in MIM sandwich, I-V and I-d characts. 78—80064
polyimide films, transient current in time range 10^{-4} to 10 s at temps. 180 to 280°C 80—65729
polymer films, conf., Dublin, Eire (July 1977) 79—55012
polymer films, electron irrad. controlled form., elec. props. 80—15635
polymer foil, charge distrib. determ., thermal pulse technique, meas. accuracy 78—80287
polymer thin films formed in RF discharge using monomer organic semicond., elec. props. obs. 80—80432
polymethylsiloxane, in MIS struct., C-V characts. and charge movements 77—85340
p-polyphenyl, thin polycryst. layer, TSC 79—60946
polyphenylene oxide thin films, electrochem. prep., impurity effects on cond., electroforming 80—88655
polypropylene, vacuum evaporated, electron trap depth, TSC meas. for MIM struct. 79—95535
polypropylene film, evaporated, elec. props. 78—84335
polypropylene thin film conduction mechanism, expt. obs. 77—28271
polystyrene:I films, thermally stimulated discharge, I conc. and polarisation temp. depend. 80—107937
polystyrene film, acrylic acid doped, elec. cond. and activation energy conc. depend. 80—15631
polystyrene film, in MIM struct., elec. conduction and free radicals 80—20340
polystyrene films, soln. grown, elec. cond. meas. 80—97020
polystyrene thin film, glow discharge formed, dark current and photocurrent obs. *(Japanese)* 80—15633
polystyrene thin films, TSC and surface charge meas. 80—103769
polytetrahydrofuran, electrochemically prepared between metal electrodes, DC elec. props. 80—39695
polytetrahydrofuran, electrochemically prepared between Pt and Au electrodes, AC elec. props. 80—40062
polyvinyl alcohol films, pure and doped, elec. cond. temp. depend. 78—88052
polyvinyl fluoride film, pure and vanadyl ion doped, elec. cond., annealing 78—26859
polyvinylacetate, in MIM struct., DC cond. phenomena 80—25020
PTFE films, plasma-polymerized, cond. mechanism, AC cond. and capacitance meas. 79—24093
PTFE grafted membranes, struct.-properties relationships *(French)* 80—61136
PVC:Cu films, electron transport and dielec. props. 79—82700
PVC, solution-grown, between Al electrodes, AC elec. props. 80—15619
PVC films, soln. grown, DC cond. mechanisms, field and temp. depend. 80—97021
PVC in metal sandwich struct., switching props., voltage- and current-controlled negative resist. 80—103767
p-quaterphenyl oriented layers, charge carrier transport, hopping model 80—2506
resistive layer above pit, stabilisation 80—93506
shellac platina, elec. cond., temp. and thickness depends., mechanism 79—99645
sputter-deposited materials, electrical and optical props. 79—47181
stearic acid, DC cond. using unconventional electrode geometry, Poole-Frenkel effect 77—55631
stearic acid film, in MIM struct., AC cond. and dielec. props., freq. depend. 80—55030
Teflon film, TSC studies of carrier trapping and mobility 80—7016
Teflon films, hole transit, trap modulated mobility and dispersive hopping discussion 79—69616
temperature coeff. of resistance of polycryst. films, linearized expressed 78—14838
p-terphenyl, polycrystalline thin film, elec. cond., temp., thickness and elec. field depend. 79—65572
tetracene, in MIM struct., depletion layer, LF capacitance meas. 79—56328
thermal mechanism for bias-induced switching effects in inhomogeneous thin films 80—11057
transient thermal emission current model *(Russian)* 77—15982
trap analysis, influence of spatial trap distrib. on SCLC charact. 79—56343
ALF_3 film, amorphous, AC elec. props. 78—2804
Al-Al_2O_3-Al junctions, Dy doped at Al_2O_3-Al interface, electron transport mechanisms and barrier height 78—91778
Al-Al_2O_3-Al structure, tunnel I-V characts., transmission coeffs. 78—80068
Al-SiO-Al structure, tunnel I-V characts., transmission coeffs. 78—80068
AlF_3 in Al-AlF_3-Al MIM thin film structures, dielec. and elec. props. *(Slovak)* 80—100536
$Al_xGa_{1-x}As$ native oxide, low leakage, MOS characterisation 78—91795
AlN, chemical and plasmachem. vapour deposition, optical and other props. 77—28727
AlN films, RF glow discharge deposited, current-voltage characts. 80—84515
Al_2O_3, amorphous film, non-thermal switching in Al-Al_2O_3-Al struct. *(Russian)* 78—80069
Al_2O_3 anodic film peak voltage rel. to ellipsometric thickness 77—77597
Al_2O_3, anodised film, in strong elec. field, pulsed V-I characteristics *(Russian)* 78—64156

electronic conduction in insulating thin films continued
Al_2O_3 composite films, elec. instability 78—68452
Al_2O_3, DC reactively sputtered, in MIS structs. optical and elec. props. 79—19486
Al_2O_3, effective electron mass determ. from current-voltage characts. in thermionic region 77—85135
Al_2O_3, elec. props. in MIM struct. 79—99646
Al_2O_3, electron trapping due to neutron irradiation 80—2505
Al_2O_3, film, CVD, props. rel. to deposition parameters 78—92197
Al_2O_3 film, dielec. props., AC and DC elec. characts. 78—68445
Al_2O_3 films, static compression to 1.2 Mbars, elec. resist. 79—55822
Al_2O_3 films for Si devices, surface and bulk elec. conduction obs. 77—43761
Al_2O_3, high temp. amorphous film, transport props., prep. conditions effect 77—12040
Al_2O_3 plasma anodised film on Si, elec. resist. 80—7722
Al_2O_3 plasma-anodised, current efficiency 78—91797
Al_2O_3, porous film, elec. cond. charact. 78—76179
Al_2O_3, RF sputtered, transient currents 78—23184
Al_2O_3, RF sputtered film, transient current meas. 78—52113
Al_2O_3 thin anodised film conduction and internal field obs. 80—15639
BN films, humidity sensitive elec. props. and switching characts. 80—107938
$BaTiO_3$, RF-sputtered tetragonal films on Si, ferroelec. and insulating props. 79—78888
BeO reactively evaporated film, elec. and optical props. 77—32512
$Bi_{12}GeO_{20}$ vacuum-deposited film elec. and photoelec. props. *(Russian)* 78—60237
Bi_2O_3, thermally grown, I-V characts., current controlled neg. resist. 80—15637
Bi_2O_3, thermally-grown capacitor-film, dielec. props. 80—2480
C film, diamond-like, produced in butane plasma, XPS anal. and elec. props. 79—82484
C, film with random struct. growth from ion impact damage in butane plasma 79—83139
C, vapour-deposited, transparent and hard insulating layer, struct. and props. 80—10830
CoO, Poole Frenkel effect and elec. breakdown props. 77—85364
Cr-SiO, sputtered, elec. and struct. props. 80—39694
Cu-GeO_2/BaO-Cu thin film, amorphous, effect of electroforming on conductance and capacitance 80—34537
Cu-SiO/B_2O_3-Cu thin film, amorphous, conductance and capacitance, effect of electroforming 80—34537
ErO_x, in MIM struct., nonstoichiometry effects on elec. cond. 79—1635
$Eu_{1-x}Gd_xS$ films, mag. and elec. props. 80—15766
FeF_3, elec. cond. mechanisms 79—99649
FeF_3, localised electronic states effect on elec. cond., MIM struct. meas. 80—20328
Fe_xO_y, prep. by reactive sputtering, struct. and props. *(Japanese)* 78—92190
GaAs anodic oxide, electrical props. 79—38170
GaAs anodic oxide, on n-GaAs, C-V and I-V characts. 77—89863
GaAs anodic oxide film, direct current-voltage characts. 78—23186
GaAs oxide, thermally grown, elec. props. 78—2601
Ga_2O_3 film, growth by reactive vapour deposition, optical and elec. props. 77—48347
GaP, anodically grown insulating layers, prep. and props. *(German)* 78—64158
Ge_3N_4 films, synthesis and principal props. 77—24960
GeS amorphous layers between Al electrodes, dielec. relax. currents, pot. distrib. 77—16250
HfO_2, CVD growth, struct., elec. and optical prop. characterisation 77—55891
$Hg_{1-x}Cd_xTe$, anodic oxide films, formation and props. 80—3212
InO_3:Sn transparent conducting films, homeotropic orientation of liquid crystals *(Russian)* 80—108181
In_2SnO_3 film, effect of ambient atmosphere during annealing, elec. props. 80—97510
$MgAl_2O_4$-Al_2O_3 powder prep., for plasma arc spraying, coating props. 77—66612
MgF_2 film, crystn., AC glec. props. 78—2804
MgO porous layers, conductivity, conditions for lag and dark current 77—20476
MgO thin film, DC conduction 78—88051
Nb-Nb_2O_5-Au thin film, conduction phenomena, drift phenomena 78—2581
Nb-Ta-N sputtered films and their anodic oxides, elec. props. of resist. and dielec. films 80—11126
Nb_2O_5 amorphous film, in Nb-Nb_2O_5-MnO_2 sandwich, elec. cond. variation during heat treatment 79—82593
NiF_2 film preparation and characterisation 80—59815
$Pb_2Nb_2O_7$, electric cond. and dielect. props. of cathodic-sputtered films *(French)* 79—33371
$Pb_{1.8}Zn_{0.15}Na_{0.05}Nb_2O_{6.95}F_{0.05}$, electric cond. and dielect. props. of cathodic-sputtered films *(French)* 79—33371
PtO_2, sputtered film, optical props. under H_2 reduction 80—20728
PtO_x films, electronic struct., reduction processes, photoemission, optical absorpt. and resist. meas. 80—80931
$(SN)_x$ polymer, elec. props. of amorphous thin film and single crystal, role of chain breaks *(Japanese)* 78—68104
Si oxides, grown in Cl-containing ambients, correl. between elec. and material props. 80—39479
Si, polycrystalline, electrode shape effects on oxide conduction 80—96890
SiN_x, plasma deposited, comp. and characterisation, optical and elec. props. 80—15401
SiN_x, plasma deposited dielectric film, elec. props. 78—68103
Si_3N_4, amorphous insulator film, high-field cond. 79—56320
Si_3N_4, CVD film, elec. cond., film formation by pyrolysis of SiH_4-NH_3 79—91176
Si_3N_4 CVD films on Si, dark currents 79—78240
Si_3N_4, cond. mechanism, double injection, trap SCL current 77—32099
Si_3N_4 film, CVD, high-field dark currents 80—54791
Si_3N_4 film, in MNOS struct., kinetics of irreversible changes in cond. 79—73600
Si_3N_4 film, in MNS structures, dark conduction and photoconduction phenomena 78—30989
Si_3N_4 film, pyrolytically deposited, AC cond. at low freq. 78—84334
Si_3N_4 films, CVD in MNOS and MNS structs., elec. resist. 80—97019
Si_3N_4 films, elec. cond. 79—95499
Si_3N_4 films for Si devices, surface and bulk elec. conduction obs. 77—43761

electronic conduction in insulating thin films continued
Si_3N_4 films grown by pyrolytic reaction between silane and ammonia, DC cond. 79—15243
Si_3N_4, highly insulating film, current cond., CV curves, and IR absorpt. 79—38208
Si_3N_4, in MNOS structure, V/I characts. determ. *(Russian)* 77—8201
Si_3N_4 layers, cond. process kinetics 77—76991
Si_3N_4, on Si, hole conduction, shallow junction diode detection 77—8215
Si_3N_4, reactive ion beam sputtering deposition, form. and characterisation 80—44452
Si_3N_4, Si rich, CVD film prep. and props. 78—76607
Si_3N_4 thin film, reactively sputtered, struct. and elec. props. 80—88656
$Si_xN_yO_z$ film, band diagram, optical props. and elec. cond. meas. 78—84333
SiO amorphous thin film capacitor, EPR, elec. cond. 78—68358
SiO-B_2O_3, amorphous composite dielec. film, AC conductivity 79—51703
SiO_2, amorphous electron transport and breakdown at high elec. fields 79—78108
SiO_2 amorphous film, dye-sensitised steady-state photocond. in Au-dye-SiO_2-Au struct. 80—107924
SiO_2 charge transfer from metallic electrodes 80—15605
SiO_2, electron-beam irrad., electron trapping, MOS capacitor expts. 78—72268
SiO_2, electron-beam-induced cond. 80—20337
SiO_2 film, plasma grown, thermally stimulated depolarisation current meas. *(Russian)* 78—80082
SiO_2 film, spin-on oxide, phys. and cond. meas. 77—43762
SiO_2 film electron beam induced conductivity theory and expts. 80—15640
SiO_2 film grown by Si oxidation in O_2-H_2-HCl mixture, elec. props. 80—40569
SiO_2 film preparation and props., Si planar technology 78—10589
SiO_2 films, electron beam induced charge buildup, 80K 77—20440
SiO_2 films, grown in presence of O_2-trichloroethylene, room temp. negative bias instability 80—60102
SiO_2 films, radiation induced charge transport and build-up, low temps. 77—20478
SiO_2 films, thickness and dielectric const., elec. cond. mech. *(Japanese)* 79—8084
SiO_2 films in poly-oxide poly Si structures, elec. cond. and charge distrib. 80—92984
SiO_2 gate insulator MOS capacitors, hole transport, recovery characts. following electron beam irrad. 77—20439
SiO_2 grown on polycrystalline Si, DC conduction obs. 77—76989
SiO_2, high temp. amorphous film, transport props., prep. conditions effect 77—12040
SiO_2, in MOS struct., charge transport, TSD obs. 77—89870
SiO_2 in MOS struct., room temp. cond., mobile Na^+ location 78—39217
SiO_2 layer anodically grown on high resistivity n-Si wafer, improved homogeneity 79—24642
SiO_2 MOS capacitor, defect current obs. 80—92987
SiO_2, pyrolytic, C-V characts., non-equilib. lowering in inversion mode 77—55630
SiO_2 pyrolytic film, conduction process determ. 77—20479
SiO_2, RF sputtered films, AC conductivity and conduction mechanisms 80—20338
SiO_2, Si rich, CVD film prep. and props. 78—76607
SiO_2, thermally grown films, LF conductance 78—80081
SiO_2 thermally-grown, highly stressed ultrathin films, cond. and trapped of electrons 77—66216
SiO_2:Cs(B) film, implanted electronic cond. mechanism in MOS struct. 77—15983
SiO_2:Na, RF sputtered, low elec. field Poole-Frenkel effects in MIM struct. 79—95536
SiO_2-layers, charge transport induced by electron beam, simulation *(German)* 79—51702
SiO_x, evaporated film, influence of electronic leakage current on meas. of ion polarisation 77—63014
SiO_x film, MIM struct., DC bias dependent dielectric dispersion props. 78—76178
SiO_x, in MIM sandwich, elec. props. 77—72933
SiO_x thin film dielec., in MIM struct., interfacial props. rel. to non-stoichiometry 80—80399
$Si_xO_yN_z$, on n-GaAs, C-V and I-V characts. 77—89863
$SiO_{2-x}Nx$ thin CVD film processing and characteristaion 77—77413
SnO_2, reactive ion plating onto insulating substrates, and elec. and optical props. 79—87588
SnO_2 sputtered film, thermal ageing, thickness dependent effects 78—6462
Ta-Al-N thin film resistors with improved elec. props. 80—100544
Ta-Ti-N, reactive sputtered film, elec. props. 78—84336
TaN, sputtered thin films, cross-sectional composition by SIMS, elec. resist. calcs. 79—77953
TaN_x, triode sputtered, struct. and elec. props. 79—78242
Ta_2N, and TaN_x, films, thermal oxidation and resist. 80—60125
Ta_2O_5 anodic film with Au counterelectrodes, conduction process 78—84312
Ta_2O_5 anodic films, elec. cond. mechanism, admittance meas. 80—70705
Ta_2O_5, defective anodic film on Ta, elec. characts. 77—12039
Ta_2O_5 films, Poole-Frenkel effect and cond., effect of heat treatment in oxygen and in vacuum 80—39693
Ta_2O_5, for MIS device, CVD and characterisation 77—4742
Ta_2O_5, reactive DC sputtering deposited films with magnetron-plasmatron, mechanical elec., optical props. 80—25566
Ta_2O_5, sputtering conditions rel. to electronic cond. 77—40365
TbF_3 thin films, AC conduction obs. 80—70868
TiN film, struct. and elec. props. 78—26788
TiN films, reactively RF sputtered, struct. and elec. props., substrate bias effects 80—96763
TiN films deposited by reactive sputtering, elec. props. 80—15638
TiN_x, reactively sputtered in Ar-N_2 atm., elec. and struct. props. 80—15636
TiO_2 film, ion plated, DC cond. study 80—100457
TiO_2, metal-TiO_2-Si structure, I-V characteristics, deposition, post-deposition oxidation effects 78—80063
TiO_2, reactive DC sputtering deposited films with magnetron-plasmatron, mechanical elec., optical props. 80—25566
Tm_2O_3, electron beam deposition, elec. props., and struct. 79—87580
Tm_2O_3 film, between Al electrodes, prep. and elec. props. 80—60103
YH_2, struct. and elec. resist., electron diffr. meas. 78—87888

electronic conduction in insulating thin films continued
Y_2O_3 film in Y-Y_2O_3-metal junction, electroforming and conduction 78—26969
Y_2O_3 film in Y-Y_2O_3-Au junction, defect struct. and local conduction 78—26970
Y_2O_3, struct. and elec. resist., electron diffr. meas. 78—87888
ZrO_2, plasma sprayed coatings, elec. cond. and gas permeability 79—82478

electronic conduction in metallic thin films
see also discontinuous metallic thin films; electrical conductivity of amorphous metals and alloys; electrical conductivity of crystalline metals and alloys
adsorbed impurities, microscopic calc. of elec. cond. at low adsorption coverage 79—15236
amorphous, structural and amorphous props. 78—84323
boundary scattering indicatrix of cond. electrons, expt. data *(Russian)* 77—39969
carrier density, evaluation from transverse elec. field and cond. meas. *(French)* 80—39682
carrier relaxation time, optical determ. by surface plasmon excitation 77—1499
conduction electron focusing by inhomogeneous mag. field *(Russian)* 80—70850
deposition by ion beam sputtering, composition and stress state 77—89674
discontinuous, field effect of electrical conductance 77—39964
discontinuous film, elec. cond. and current noise mechanism, theory 78—56244
discontinuous film, field effect of elec. cond. series-connected island model 79—78219
discontinuous film, high temp. elec. cond., model 79—78220
discontinuous film, struct., optical and electrophys. props. review 77—76698
discontinuous films, elec. props., effect of distrib. of particle size 77—66209
discontinuous layer, energy for electron transmission between two neutral islands determ. 77—80852
discontinuous metal films, resist. and strain gauge factors expressions, quantitative formulation 79—95521
discontinuous metal films, review 78—19167
disordered electronic systems, low-dimensionality, Anderson localisation, resist. 80—84491
dispersed metallic film, I-V characts., struct. changes *(Russian)* 79—38195
electron MFP calc. 78—72283
electronic props. and elec. cond. 79—78228
EM energy transformation into acoustic energy, temp. depend. 77—55619
EM wave induced voltage 79—56330
evaporated metal film, oxidation resistivity change meas. *(Japanese)* 79—11723
ferromagnetic, resistivity anisotropy theory 77—59342
field effect, series-connected islands model *(Japanese)* 80—11107
films, in situ meas. in ultrahigh vac. at low temp., optical reflectivity and transmissivity, DC resistivity, Au appl. *(French)* 78—39617
free-electron films, optical props., theory including electron surface scatt. 80—29817
gas adsorption effects on elec. resist., review *(Rumanian)* 79—82691
grain boundary and surface scatt., statistical model 80—103762
grain boundary electron scatt. in total film cond. model 80—7004
grain boundary electron scattering by effective mean free path 78—84320
grain boundary resist., three-dimens. model 80—7003
grain boundary scatt., Hall coeff., theory 80—88649
granular film, temp. depend. 77—47903
granular materials, size effects in cond. and supercond. 80—77581
granular metal films, minimum metallic cond. 78—56241
Hall coeff., temp. depend. 79—95516
Hall coeff. and cond. using Boltzmann transport eqn. 79—11240
Invar, mag. props. and elec. resist. 77—32221
island type metal condensates on insulator, elec. cond., statistical theory 78—10582
islet film, cond. currents and electron emission, electron heating effect 78—10581
Kubo formalism 79—7909
linear variations with thickness 80—103760
magnetomorphic oscillations, thin films with unlike surfaces, generalised Sondheimer model 78—56243
Mayadas-Shatzkes conduction model, treated as Fuchs-Sondheimer model 77—80855
Mayadas-Shatzkes-based model parameters rel. to RF sputtered film obs. *(French)* 78—43491
metal film, temperature coefficient of total resistance 80—70853
metal films, resistance and magnetoresistance 79—61225
metal vapour condensate, anisotropy in electric field 80—15624
metallic films, metal-dielectric boundary thermal resistance, nonlinear elec. resistance *(Russian)* 80—65530
metallic thin films, electric field distrib. and emission currents of island condensates 78—88047
metallic thin films, hot electron distribution function, nonlinear elec. resistance *(Russian)* 80—65717
metallic thin films, resistivity strain coeff. calcs. 80—100449
metallisation stripe, cracked, temp. gradient and current crowding, electromigration 77—51828
metglas type system, structural and amorphous props. 78—84323
monocrystalline, size and grain boundary effects in elec. cond. 78—76164
multicomponent alloy films, struct. form. laws and elec. prop. changes obs. during vacuum condensation 78—6850
negative temperature coefficient of resistivity for thin films and wires 79—78217
nonmetallic conduction at low temps. 80—97012
oscillation kinetic effects, boundary electron scatt. *(Russian)* 78—52104
Permalloy, film, magnetoconductivity modulation by substrate electrostriction 79—60908
Permalloy, thin film, oscillatory metallic field effect and surface magnetoelasticity 79—56282
Permalloy RF sputtered films, O effects in mag. and elec. props. 80—100603
polycrystalline film, longit. magnetoresist. 79—78224

electronic conduction in metallic thin films continued
  polycrystalline film, strain coeffs. of resist., deduced from effective Fuchs-Sondheimer model and relax. time model 79—78222
  polycrystalline film, superimposed effects of three arrays of scattering planes on electrical conductivity 80—80412
  polycrystalline film, temp. coeff. of resist. using Mayadas-Shatzkes model 77—80854
  polycrystalline film resistivity decomposition from Mathiessen's rule 80—7000
  polycrystalline films, grain boundary reflection coeff. thermal expansion effect on resistivity temp. coeff. 79—91162
  polycrystalline metal films, cond. description, Cottey model adequacy 79—95517
  polycrystalline metallic films, analytical approx. eqns. for resist. and its temp. coeff. 77—85346
  polycrystalline thin film, approx. expressions for product of resist. and its TCR 80—25022
  polycrystalline-thin metal films, thermoelectric power, mean free path model 80—107770
  polymer films, conf., Dublin, Eire (July 1977) 79—55012
  potential distribution, two dimensionality 77—20463
  rare earth, O_2 and H_2 contamination effect on elec. resist. 77—80856
  refractive index for X-rays, elec. current density influence *(Spanish)* 79—78784
  resistivity, temp. coeff. of resist., and Hall coeff. in grain boundary cond. model 80—39683
  resistivity and TCR of monocrystalline films, approx. analytical expressions 80—39685
  resistivity of monocryst. films determ. using Mayadas-Shatzkes eqns. 77—28261
  size and other transport effects, theory *(Czech)* 77—47902
  size effect, total resistance temp. coeff. 78—84318
  size effect, Umklapp processes of charge carriers and anomalous transmittance in RF range *(Russian)* 80—70851
  size effect conductivity in transverse mag. field, Hall coeff. *(French)* 78—91787
  size effects, anal. 78—76162
  size effects, resistivity derivation 78—76163
  size effects and resist., approximate expressions 80—88645
  sputtered compressive stress transition 78—10310
  strain coefficients of resistivity, general Fuchs-Sondheimer expressions 78—52107
  strain gauge factor anal., grain size depend. 78—6458
  superconducting inhomogeneous film, cond. near superconducting transition temp. 80—93031
  surface impedance oscillation effects due to one sided RF excitation *(Russian)* 80—11106
  surface scattering of conduction electrons and kinetic phenomena *(Russian)* 79—56210
  TCR of monocrystalline films, analytical expression 79—42670
  temperature coeff. of resistance of polycryst. films, linearized expressed 78—14838
  temperature coefficient of resistance, size effect 78—43489
  temperature-fluctuation noise of substrate supported films 80—92949
  thermal strains, effect of support, theory 80—88647
  thermoelectric power, deduced from Mayadas-Shatzkes model 77—47904
  thermoelectric power, Fuchs-Sondheimer eqns. for film with grain boundary scatt. 78—52108
  thermoelectric power, thermal stress effects, theory 80—65714
  thermoelectric power and TCR, interrelationship 77—76957
  thermoelectric power and temp. coeff. of resistivity 78—91788
  thickness dependence, quantum size affect *(German)* 80—86344
  thin wires, exptl. study of Anderson localisation 80—96849
  transition metal film, chemical compound formation by ion bombardment 78—30846
  transverse E-type quantum waves *(Russian)* 78—91785
  ultrathin metal film, evaporation cryostat for elec. and optical meas. under ultrahigh vac. 77—87769
  unlike surface properties, transport coeffs., diffuse surface scatt. 80—20331
  vapour deposited on polymer, ageing, adhesion, elec. cond., electrochem. pot. *(Russian)* 79—33362
  very thin films, elec. cond. calc. 77—15971
  VPE on sapphire, highly oriented film prod. 77—66097
  wave-phase dependence of elec. resist. of metallic thin films, general well pot. 80—20332
  wire, thin-film, possible explanation of nonlinear cond. 80—97011
  Ag, appl. of percolation theory 80—65712
  Ag, defect density, thickness depend., elec. resist. obs. 80—70568
  Ag, discontinuous, adsorption of alkali halide mols., effect on elec. cond. 80—2487
  Ag, energy depend. of defect production in displacement cascades 77—31700
  Ag, evaporated, chemisorption effects on reflectance and elec. resist. 80—11495
  Ag film, annealing study of elec. resist. and defect density 78—76167
  Ag film, chemisorption effects on optical reflectance and elec. resistance 79—33361
  Ag film, electronic stopping power on irrad. by He, Li, C ions, damage-rate measurements 79—77654
  Ag film, Frenkel pair prod. by light energetic ions, elec. cond., changes 77—59050
  Ag film, Ge coated, electrical resistance and ageing *(Russian)* 80—103759
  Ag film, in situ resistivity meas. 80—97008
  Ag film, polycrystalline with artificial surface roughness, electrical resistivity temp. coeff. *(Russian)* 79—82688
  Ag, film growth on C, conductance meas. 79—82495
  Ag in As_2S_3-Ag contact, resist. change meas. for photodissolution kinetics determ. 77—15955
  Ag, Maxwell stresses at charged surface from elastoresistance 80—49957
  Ag, proton irrad., radiation-annealing effects in energetic displacement cascades, film resist. meas. 78—26603
  Ag, size effect in thermoelec. power, MFP and Fermi surface 77—69433
  Ag, thermal and elec. cond., Lorenz no. 78—43487
  Ag, thin film, elec. resist., effect of annealing In electrodes 80—80416
  Ag, vacuum condensate, effect of Ge coatings on ageing kinetics *(Russian)* 77—59340
  Ag, vacuum deposited, defect density and activation energy depend. on deposition rate 80—29294
  Ag, vacuum deposited on Al substrate, recrystallisation 78—60044

electronic conduction in metallic thin films continued
  Ag:He, implanted films, solid solutions radiation induced polymorphism 79—86810
  Ag-Au thin film couples, polycrystalline, low temp. diffusion, resist. obs. 79—4435
  Ag-InP Schottky barrier, hot electron attenuation length 80—49904
  Ag-Pd, thermal treatment and comp. depend. of resist., 273 to 700K *(French)* 77—76963
  Ag-Te amorphous films, effect of annealing on elec. resist., phase transitions 79—11241
  Al, deposited metallic thin films, H incorporation effects on stress and electromigration 80—80139
  Al, electron beam evaporation, on Kapton laminates, and characterisation 78—11373
  Al epitaxial layers, elec. props. 79—42671
  Al, epitaxial resist. vs. grain diameter curves, theory and expt. 77—76961
  Al film, effect of annealing of electrode films on elec. resist. 78—23179
  Al film, electron transport, grain boundary scatt. 79—60937
  Al film, internal stress, effect of residual gas press. 77—66100
  Al film, lattice and bulk heat capacity meas. for normal and supercond. states 80—92684
  Al film, single cryst., elastoresist. effect 78—84321
  Al film, sputtered, physical props. 79—77938
  Al film, struct. and props., effect of ion implantation 79—77936
  Al, film, surface resist. freq. depend. in range 7.7 to 37 GHz 77—20468
  Al, film growth on C, conductance meas. 79—82495
  Al, film on Si(111) substrate, struct., props. depend. on vapour flow, ionisation *(Russian)* 80—75453
  Al films, Al^{2+} irrad., increase of resist. and supercond. transition temp. 80—7027
  Al films, deposited on calcite substrate, grain boundary scattering, elec. resistivity meas. 79—65096
  Al films, RF sputtered, resist. recovery obs. 77—8207
  Al films, resistance changes due to bombardment by N, C, or Ar ions 80—103670
  Al, granular, transition to localisation, elec. resist. 80—70877
  Al, ion-beam-activated vacuum deposition, struct. and props. 80—15422
  Al, Maxwell stresses at charged surface from elastoresistance 80—49957
  Al metallization of semiconductor devices by high rate magnetron/plasmatron sputtering 79—28919
  Al, nucleation grown, RF sputtered, Mayadas-Shatzkes cond. 77—1498
  Al, polycrystalline, analytical approx. eqns. for resist. and its temp. coeff. 77—85346
  Al, quench-condensed ultrathin film, two-dimensional elec. cond. 78—39233
  Al, RF sputtered, TCR, calc. and expt. 77—76960
  Al, sputtered and electron gun evaporated films, grain size and orientation obs. 78—10308
  Al, sputtered film, thermal ageing, thickness dependent effects 78—6462
  Al thin conducting film, electromigration under superimposed DC and noise powers 80—107879
  Al, thin film, elec. resist., effect of annealing In electrodes 80—80416
  Al, thin film, thermal cond. meas., size effect 80—65715
  Al, thin film resistor, rare earth alloying effects *(Russian)* 79—78211
  Al thin films, dielectric coating effect on superconductivity 80—7026
  Al, transversal magnetoresist. meas. 77—72925
  Al/Cu thin film couples, interfacial reactions, low temp. contact resist. meas. 80—44709
  Al-Cr, thin film metal contact, sheet resistance changes 80—80356
  Al-Cu, superconducting amorphous films of high stability 80—70889
  Al-Cu alloy, deposition from RF induction source, onto laminated polyimide substrates and characterisation 80—16535
  Al-Cu films, deposition rate, mol. beam incidence angle influence on struct., film props. *(Russian)* 79—60646
  Al-Ge film, random percolation, elec. resist. meas. 79—28418
  Al-Pt film sandwich, interdiffusion and intermetallic form. 77—24448
  Al-Si, DC magnetron-sputtered, residual gas influence on props. 80—80968
  ^{241}Am, elec. resist. meas., 3.6 to 300K 77—28263
  Au 79—77938
  Au, annealing curves, size effect parameter determ. from Mayadas Shatzkes theory 77—76962
  Au coating for radioactive source backing, spontaneous resistance variations 77—54386
  Au, discontinuous, high temp. elec. cond., model 79—78220
  Au, discontinuous, substrate radiation damage effect on resist. and strain gauge stability 79—95520
  Au, discontinuous, vac. evaporated on C and SiO, struct. and elec. cond. 80—39686
  Au discontinuous film, elec. cond. and current noise, temp. depend. meas. 78—56245
  Au, discontinuous film, film resistance as function of film thickness 78—6246
  Au, evaporated, 890 GHz surface resistivity meas. by pyroelectric detector 77—39915
  Au film, adatom surface diffusion at low temps., elec. resist. study *(French)* 80—65376
  Au film, electrical resistivity, influence of metallic adsorption *(French)* 79—19677
  Au film, epitaxially grown, struct., LEED, AES, resist. and X-ray diffr. analysis 77—59223
  Au, film, evaporated, DC elec. resist. 80—29487
  Au film, low temp. void growth and resistivity decay 78—10302
  Au film, quantum size effect, field emission study 80—70849
  Au film, ultrathin evaporated, acoustoelectric meas. of electron mobility and diffusion 80—65707
  Au film electrode, electrochem. adsorpt. of O_2, elec. resist. obs. *(French)* 79—29372
  Au film sandwiches, recovery kinetics and early stages of diffusion, DC resist. expts. 79—77971
  Au, films, optical props. meas. rel. to electron surface scatt. theory 80—29818
  Au, growth, optical and elec. prop. meas. during depositon *(French)* 77—70007
  Au island film real structure and electrical conductivity obs. 79—77948
  Au island films, forming process, I-V characts., and switching 79—11242
  Au, Maxwell stresses at charged surface from elastoresistance 80—49957
  Au, nonohmic characts. and electron emission 80—60066
  Au, polycryst., RF bias-diode and triode sputtered, resist. and microstruct. 78—80072

electronic conduction in metallic thin films continued
Au, proton irrad., radiation-annealing effects in energetic displacement cascades, film resist. meas. 78—26603
Au, pure, small resistivities, size correction 77—43742
Au, quench-condensed ultrathin film, two-dimensional elec. cond. 78—39233
Au, thin film, discontinuous, high resist., Hall effect meas. 80—65716
Au, thin film, elec. resist., effect of annealing In electrodes 80—80416
Au vapour deposited film, attenuation and phase vel. of SAW interacting with charge carriers 79—46136
Au/Ti thin film, temp. and humidity effect on interdiffusion 79—51317
Au/Ti thin films, effect of Cl_2 on elec. resistance, Ti atom migration and preferred orientation 80—34530
Au-Ag, thermoelectric power and resist. meas., MFP and Fermi surface area 77—51826
Au-Co, co-evaporated, struct. and ohmic behaviour 79—87021
Au-Cr bifilm, resistivity and struct. changes under heat treatment, diffusion effects 77—1497
Au-Cu film, elec. resist. and temp. coeff. of resist. 77—39968
Au-Fe, spin glass, quench-condensed film, reduced MFP influence on elec. resist. 77—69306
Au-Fe film spin glass, low temp. resistivity, mean free path effects 78—80163
Au-Ge evaporated film, effect of substrate on conductivity 79—78213
Au-Pd coating for radioactive source backing, spontaneous resistance variations 77—54386
Au-Si, elec. resist. decay and struct. change on exposure to air 77—72924
Au-$Ti_{0.3}W_{0.7}$, thermal annealing study of metallisation on Si 80—80134
Au-TiC, multilayer struct., microhardness and elec. resist. 80—2950
Au_xSi_{1-x} amorphous films, phys. studies 80—75476
Be film, vapour quneched, mech. stresses and elec. cond. 79—73414
Be, RF sputtered film, props. rel. to deposition conditions 77—39965
Bi, amorphous metal films, crystallisation with and without mag. field 80—70570
Bi film, adatom surface diffusion at low temps., elec. resist. study *(French)* 80—65376
Bi film, evaporated, lattice distortion spectrum, elec. resistance temp. variation 80—54806
Bi films, resistance changes due to bombardment by N, C, or Ar ions 80—103670
Bi, thin film, resistivity, rel. to thickness 80—107928
Cd, elec. cond., classical size effect 77—89881
Cd film, surface RF impedance in strong mag. fields *(Russian)* 80—92920
Co, amorphous, magnetoresist., in fields up to 80 kG 77—39823
Co, amorphous ferromag. film, resist. anisotropy rel. to struct. 77—72926
Co, ferromag. film, magnetoresistance parameter meas. *(Spanish)* 80—2485
Co film, electromigration exam. from structural changes and resistance increases 77—20213
Co film, texture and adsorption of CO *(German)* 77—24485
Co-Si interface, metal-semiconductor transition, rel. to first compound nucleation 80—24771
CoP metallic glasses, elec. and optical props., annealing effects 79—38565
Cr containing Cr_2O_3, film struct., oxide percentage determ. and temp. coeff. of resist. 80—103607
Cr film, size effects on spin density waves, struct. and elec. props. 77—80973
Cr island film nonlinear I-V characteristics, 20 Hz to 15 GHz 79—7910
Cr island film real structure and electrical conductivity obs. 79—77948
Cr, preparation by decomp. of bis-arene cpds., struct. and phys. props. 80—60785
Cr, thin film resistor, rare earth alloying effects *(Russian)* 79—78211
Cr-Ge amorphous films, annealing effect on elec. resistance and struct. 80—54667
Cr-Si, amorphous sputtered film, material for kilo-ohm sheet resistances, prep. and props 79—78227
Cr-Si, deposition method, for controllable comp. with given elec. props. 80—35087
Cs film, elec. props. *(Russian)* 77—47906
Cs wires, size effect and temp. depend. of resist. 79—51691
Cs wires, size effect and temp. depend. of resist. 79—51692
Cu, adsorption of CO, effect on resist., negative p-values 77—85083
Cu alloy vacuum condensed films, alloying addition influence on electrophysical props., elec. cond. *(Russian)* 80—34529
Cu, discontinuous film, ageing effect on elec. cond. 79—24084
Cu, elec. resist. temp. coefficient 77—89883
Cu, electron transport props., struct. defects role 77—40117
Cu film, annealing effect on grain size 78—72015
Cu film, complex impedance, IR transmission and refl. meas. 79—78216
Cu, film, Frenkel pair prod. by light energetic ions, elec. cond. changes 77—59050
Cu films, resistance changes due to bombardment by N, C, or Ar ions 80—103670
Cu, Maxwell stresses at charged surface from elastoresistance 80—49957
Cu, proton irrad., radiation-annealing effects in energetic displacement cascades, film resist. meas. 78—26603
Cu, quench-condensed thin film, annealing effect on resistivity 78—43488
Cu, quench-condensed ultrathin film, two-dimensional elec. cond. 78—39233
Cu sandwiches, size effect 79—73604
Cu, strain coeff. of resist., film thickness and grain size depend. 77—55620
Cu, thin film, elec. resist., effect of annealing In electrodes 80—80416
Cu, vacuum deposited on Al substrate, recrystallisation 78—60044
Cu-Ag, amorphous, resistivity, Hall coeff., thermopower and annealing kinetics 77—43744
Cu-Al alloy film, vacuum deposited, comp. struct. resistivity 78—6852
Cu-Al films, elec. cond. of vacuum condensates depend. on composition, annealing *(Russian)* 80—65709
Cu-Al(Ge)(Sn) alloy films, electron transport props. 77—76955
Cu-Au thin film system, interdiffusion coeff. from cond. and Auger anal., 25 to 250°C 77—59154
Cu-Fe, dil. alloy, quench-condensed thin film, annealing effect on resistivity 78—43488
Cu-Fe (0.04 to 0.9 at.%), resistivity temp. depend., 1.5 to 17K, impurity interactions 77—63007
Cu-Ge alloys, thin films, elec. cond., Ge influence 79—82690

electronic conduction in metallic thin films continued
Cu-Ge codeposited film, elec. resist. and thermoelec. power, rel. to struct. 79—87168
Cu-Mn alloys, vacuum deposited, electrophys. props. 77—63006
Cu-Mn-Ni, thin film, vacuum deposited, struct., elec. cond. *(Russian)* 78—19668
Cu-Ni, comp. modulated alloy films, transport props., 10 to 300K 79—95515
Cu-Ni film, struct. and mag. order effects on electron transport props. 78—6460
Cu-Ni films, thickness depend. of Curie temp., resist. meas. 78—6545
Cu-Ni thin films, ferromag., Hall effect meas. 80—80428
Cu-Ni/Au-Ni multilayer films, ohmic behaviour, use as strain gauge 80—65713
Cu-Ni/Au-Ni multilayers obtained by co-evaporation in UHV, ohmic stability and TCR 79—78226
Cu-Ti-Fe (0.7, 0.9 wt.%) film, dispersion-strengthened, form. by high rate magnetron/plasmatron sputtering, and props. 80—25715
Dy, discontinuous thin films, electronic conduction mechanism 79—87169
Dy film, elec. resist. results 78—84326
Dy film, vacuum-evaporated, thickness depend. of elec. resist. 77—39967
Dy, Hall effect meas. in para- and ferromag. regions 77—55622
Dy, thickness depend. of resist., effect of presence of dihydride 77—51829
Er film, elec. resist. results 78—84326
Er, thickness depend. of resist., effect of presence of dihydride 77—51829
Er, vacuum-evaporated, thickness depend. of resist. 77—76956
Er-H_2 system, work function changes correlated with phase changes, elec. resist. meas. 77—11828
Fe, adsorption of CO, resistance changes, work function change and thermal desorption meas. 79—19450
Fe, ferromag. film, magnetoresistance parameter meas. *(Spanish)* 80—2485
Fe film, amorphous and polycrystalline, Hall effect, resistivity and mag. moment 78—91786
Fe film, amorphous-polycrystalline resistivity transform. temp., of codeposited N_2 78—6461
Fe, Hall resist., effect of N impurity codeposition 78—64146
Fe, polycryst., heat of adsorpt. of H_2 and D_2, calorimetric and resist. expts. 78—91530
Fe-Al (30 or 45 at.%), elec. resist. and magnetoresist., atomic ordering effects *(Russian)* 77—80853
Fe-Al (45%), ordered and disordered states, optical and elec. props. 77—85826
Fe-Cr-Al, Kanthal films, vac. deposited, evaporation characts., comp., struct. and elec. props. 80—88646
Fe-Ni films, on glass substrate, thermoelec. effect 80—107769
Fe-Si amorphous film, Hall const. and magnetoresistive effect 78—52105
Fe-Si-Al, Sendust, 12 μ thick film prep. by sputtering, mag. and other props. 77—55888
Fe_3S_4, galvanomagnetic props., resist. and Hall effect meas., 4.2-300K 80—54673
Ga, amorphous metal films, crystallisation with and without mag. field 80—70570
B-Ga, metastable, elec. props. in normal and supercond. states *(Russian)* 80—65520
Ga, monoclinic, elec. cond., classical size effect 77—89881
Gd film, elec. resist. results 78—84326
Gd films, electrical props. correlation with microstructure 80—97009
$Gd_{1-x}Co_x$, film, resistivity, Hall effect, domain wall density 78—76169
$(Gd_{1-x}Co_x)_{1-y}Ar_y$ amorphous mag. film, elec. and mag. prop. depend. on Ar 80—80410
Ge alloys, amorphous film, crystn. transform. kinetics 78—22653
Ge-Al, elec. resist. and IR transmission, comp. and substrate temp. depend. 78—52112
Ge-metal films codeposited, amorphous and polycryst., struct. and elec. props. 80—24766
$HfPt_3$, corrosion resist. and elec. cond., bulk and film samples 78—72285
Hg-Xe vapour deposited films, cond. transitions, effect of disorder on supercond. 80—88659
Ho, thickness depend. of resist., effect of presence of dihydride 77—51829
In, discontinuous film, DC resist. in normal and supercond. states 79—56357
In, film growth on C, conductance meas. 79—82495
In, on Au, ultrathin, quantum size effect *(French)* 77—20466
In, resistivity, Hall effect and light transmittance, use as semitransparent electrode 77—39966
In sandwiches, size effect 79—73604
In, thin films, elec. props. effect of thickness and temp. 80—44742
In, transversal magnetoresist. meas. 77—72925
In, vacuum deposited, growth conditions effect on elec., optical, and structural props. 79—78215
In-Ge film, random percolation, elec. resist. meas. 79—28418
K wires, size effect and temp. depend. of resist. 79—51691
K wires, size effect and temp. depend. of resist. 79—51692
$LaNi_5$, H_2 absorption in thin film hydriding alloys 80—65238
Mg and Mg-Fe films, defect energy distrib., elec. resist. meas. during annealing 80—54808
Mg, deposited at 4.2K, elec. resist. meas. *(French)* 77—8206
Mg film, Fuchs Sondheimer theory, size effect, elec. cond., Fermi surfaces 79—99637
Mg-Fe, dil. alloy, single impurity Kondo behaviour in elec. resist. *(French)* 79—60815
Mn, anomalous low temp. resistivity 78—91789
Mn, anomalous low-temp. resist. 78—2583
Mn film, elec. resist., deposition rate effect 80—97010
Mn film, heat treated, lattice distortion energy, resist. meas. 79—19492
Mn film, resistivity-temperature variation 79—24085
α-Mn, low temp. resist., rel. to deposition conditions 79—78223
Mn thin film, DC resist., activation energy, thickness depend. 80—84518
Mn, vacuum deposited, in elec. field, resist., struct. 80—103761
Mn, variation of elec. resist. with deposition conditions 77—43746
Mn, variation of resist. with deposition rate 77—43747
Mn-SiO cermet thin film, DC resist., activation energy, thickness depend. 80—84518
MnBi film, electrical props., in situ annealing effect 80—65708
MnSi, amorphous, sputtered, mag., elec., struct. and thermal props., spin glass behaviour 80—50124
Mo, discontinuous film, room temp. oxidation rate consts., resist. meas. 77—32723

electronic conduction in metallic thin films continued
Mo, evaporated, annealing behaviour, SEM obs. 80—65397
Mo film, cc preparation by H_2 reactive sputtering *(Japanese)* 79—95929
Mo film, deposited by cylindrical magnetron sputtering, internal stresses, optical reflectance and elec. resist. 77—43449
Mo film, evaporated, grain size and resist. 80—88650
Mo, film, specularity coefficient of conduction electrons, angular dependence *(Russian)* 79—87167
Mo, film, vacuum deposited, elec. cond., internal stresses, surface corrosion, MOS gate appl. *(Japanese)* 78—80073
Mo film, vacuum deposited onto SiO_2-Si substrates, elec. resist. 78—76166
Mo, on SiO_2/Si substrate, effect of heat treatment after deposition on internal stress, elec. resist. obs. 78—22973
Mo, sputtered, elec. resist., annealing and struct. effects 80—60109
Mo, thin film deposition by high current ion beam sputtering, struct. and elec. props. 80—59837
Na wires, size effect and temp. depend. of resist., martensitic transform. effect 79—51691
Na wires, size effect and temp. depend. of resist. 79—51692
Na-NH_3 film, vapour deposited, elec. resistivity, metal-nonmetal transition 78—84317
Nb film, thermal and elec. cond., 9-50K 79—87078
Nb, ion bombardment with N_2^+, Ar^+, struct. changes, chemical compound formation *(Russian)* 78—95084
Nb on sapphire, highly oriented film prod. 77—66097
Nb-Ni, amorphous thin film, vapour quenched, elec. resistivity and thermoelectric power 79—33275
Ni, adsorption of CO, effect on resist., negative p-values 77—85083
Ni, amorphous film, getter sputtered at 25K, resistivity, Curie temp. 78—52673
Ni, evaporated, elec. resist. and galvanomagnetic props. 80—80411
Ni, evaporated at oblique incidence, residual stress, mag. anisotropy and elec. resist. 78—22992
Ni, ferromag. film, magnetoresistance parameter meas. *(Spanish)* 80—2485
Ni film, CO adsorption effect on galvanomagnetic and magnetic props. 78—43490
Ni film, deposited by cylindrical magnetron sputtering, internal stresses, optical reflectance and elec. resist. 77—43449
Ni film, effects of finite size on crit. phenomena, resistivity anomaly 79—38192
Ni film, evaporated, galvanomag. and mag. props., thickness depend. 78—23181
Ni film, evaporated on cold substrate, temp. depend. of elec. resist. 78—19166
Ni films, adsorption and decomp. of ethylene, coverage depend. meas. 80—96743
Ni films, CO-covered, adsorpt. of H, isotherms, resist., work function changes 78—75926
Ni foil, hydrogenated, surface states of chemisorbed H_2 and elec. cond. 77—69399
Ni, foil substrate with Ag island film, elec. props. 77—43745
Ni island film, cond. of two-layer metal systems *(Russian)* 79—51693
Ni, size depend. electronic cond., annealing effects 79—47174
Ni, thin film resistor, rare earth alloying effects *(Russian)* 79—78211
Ni, vac. deposited, field effect meas., influence of CO adsorption 80—11108
Ni, vacuum deposited on liquid-He-cooled sapphire, galvanomag. props. 79—95519
Ni-Ag, thin-film, elec. cond. depend. on substrate film thickness and condensation temp. 79—7911
Ni-Al, high-temp. condensed, electron diffr. and elec. resist. *(Russian)* 79—4485
Ni-Au, amorphous, magnetoresist., in fields up to 80 kG 77—39823
Ni-B, amorphous, electronic transport and crystn. activation energies *(French)* 80—6807
Ni-B amorphous alloy film, atomic and electronic transport *(French)* 78—84325
Ni-Co, ferromag. films, magnetoresistance effect, crystal struct. 78—68017
Ni-Co films, electron-beam evaporated, magnetoresist. anisotropy, deposition temp. effect 80—34528
Ni-Cr, electrical props. rel. to AES conc. depth profile 77—32092
Ni-Cr, RF sputtered, Seebeck coeff. 77—63004
Ni-Cr, struct. transforms. induced during annealing, resist. obs. 79—77965
Ni-Cr, vac. deposition, elec. props. and comp. struct. 79—77966
Ni-Cr, vacuum deposited, comp. and temp. coeff. of resist., AES obs. 79—91161
Ni-Cr film, resistance stabilisation by surface oxide formation 79—78214
Ni-Cr films implanted with N ions, electric properties *(Russian)* 80—107927
Ni-Fe, film, anomalous Hall and Nernst-Ettingshausen effect, contribution of phonon and impurity scatt. *(Russian)* 78—64145
Ni-H, implanted film, resistivity and TDPAC meas. 78—39229
NiFe film, sputtered, physical props. 79—77938
Ni_3Mn, anomalous behaviour of Hall effect *(Russian)* 77—28262
$Ni_{1-x}P_x$, electrodeposited, amorphous, mag. and transport props. 78—52106
PZT, ferroelec. film, elec. props., composition anal., AES 78—84530
Pb, amorphous, nucleated with Mo, supercond. and normal elec. cond. 77—24633
Pb film, conducting coating effect on supercond. transition temp. and normal-state cond. 77—16007
Pb film, monocryst., heteroepitaxial growth, struct. defects, and elec. props. *(Russian)* 80—84403
Pb film, reactive ion beam sputtering 78—19666
Pb, quench-condensed ultrathin film, two-dimensional elec. cond. 78—39233
Pb-Ar films, atomic arrangements, high energy electron energy diffractogram study, Ar conc. depend. 79—99444
Pd, discontinuous, on rocksalt, H_2 absorpt. effects 77—47905
Pd, evaporated, resist. and thermoelec. power, annealing effects 80—39684
Pd film, elec. resist. 80—93013
Pd, film, electrical resist., influence of hydrogenation 77—85348
Pd, film, on ZnO, struct., elec. props., AES, UPS study 78—76168
Pd film, quantum size effect, field emission study 80—70849

electronic conduction in metallic thin films continued
Pd, on Melinex, resistance-strain behaviour, island struct. effects 77—55621
Pd sandwiches, size effect 79—73604
Pd thin film, temp. coeff. of resist. meas. 80—107930
PdH_x film, elec. resist. meas. 78—31011
PdH_x film, elec. resist., comp. depend. 79—1631
$PdH_x(D_x)$ films, electron-phonon coupling, elec. cond. obs. 80—50011
Pd_2Si film on Si, metallic, resist. and Hall mobility meas. 78—47886
Po-Ge film, random percolation, elec. resist. meas. 79—28418
Pt, discontinuous, adsorption of alkali halide mols., effect on elec. cond. 80—2487
Pt, quantum size effect, and its temp., tunnelling obs. 79—91160
Pt, ultrathin film, elec. cond., amorphous Ge overlayer thickness depend. 78—72284
Rb film, elec. props. *(Russian)* 77—47906
Rb wires, size effect and temp. depend. of resist. 79—51691
Rb wires, size effect and temp. depend. of resist. 79—51692
Rh, thin films, polycryst., resistivity and temp. coeff. of resistivity 80—88648
$Ru_xTi_{1-x}O_2$ films, elec. props. and IR spectra 79—38207
$(SN)_x$, discontinuous film, DC resist. in normal and supercond. states 79—56357
Sb, Maxwell stresses at charged surface from elastoresistance 80—49957
Sb-Au amorphous films quench-condensed, resistivity and Hall effect meas. 79—99638
Sc thin films, obtained in vac. of 10^{-5}-10^{-6} Torr, struct. and elec. resist. 80—107931
Se, film, obliquely deposited, elec. resist. anisotropy 80—2486
Si-Au films, quenched condensed, elec. resist. and supercond. 80—54669
SiO_2-Ni granular metal films, minimum metallic cond. 78—56241
Sm, determ. of electron mean free path, Neel temp., spin-disorder resistivity 77—59339
Sm film, elec. resist. results 78—84326
Sm thin film, elec. props. 80—107929
$SmCo_5$, H_2 absorption in thin film hydriding alloys 80—65238
SmS film, semicond. and metallic modifications, elec. props. 77—32098
Sn, aggregate film, resist., temp. depend. 78—39230
Sn, elec. resistivity and temp. coeff. of resistivity 77—63005
Sn, excess conductivity above supercond. transition temp. 77—32100
Sn film, evaporated on cooled substrate, influence of annealing temp. on elec. resist. and struct. 79—65561
Sn film, polycrystn., elec. props., internal size effect rel. to annealing temp. 79—65560
Sn film, substrate dependent excess electrical conductivity above superconducting transition temp. 78—84324
Sn, on Au, ultrathin, quantum size effect *(French)* 77—20466
Sn polycrystalline films, elec. props. and crystallite size, 4.2K to room temp. *(Russian)* 80—93011
Sn, quench-condensed ultrathin film, two-dimensional elec. cond. 78—39233
Sn, superconducting, paraconductivity above transition temp. 80—54845
SnO_2 film, optical and elec. props., rel. to stoichiometric deviation and struct. 77—47701
SnO_x films, non-stoichiometric, DC reactively sputtered, elec. props. 80—80415
SnSb, metallic, defect density variation with deposition rate, annealing, elec. resist. meas. 77—21027
Ta, amorphous, UHV deposited, struct. and thermal depend. obs. 78—6233
Ta, bias ion beam sputter deposited, elec. props. and structures 79—82692
Ta, deposition by ion beam sputtering, cond. and struct. 77—73228
Ta, deposition parameters, struct., and elec. props. 77—81222
Ta film, deposited by cylindrical magnetron sputtering, internal stresses, optical reflectance and elec. resist. 77—43449
Ta film, oxidation in ambient conditions, resist. and ellipsometric meas. 79—34209
Ta film, RF sputtered, thermoelec. power, Hall coeff. and struct. props. 77—43743
Ta, film, sputtered, physical props. 79—77938
Ta, ion bombardment with N_2^+, Ar^+, struct. changes, chemical compound formation *(Russian)* 78—95084
Ta, planar-magnetron-sputtered, props. 79—82474
Ta, planar-magnetron-sputtered, phys. and elec. props. 80—6673
Ta, reactively sputtered, N content and TCR, X-ray diffr. expts. 77—76693
Ta thin film, elec. cond., strain gauge factor, ion bombardment effects 80—80417
Ta, thin film deposition by high current ion beam sputtering, struct. and elec. props. 80—59837
Ta:N, triode sputtered, struct.-related cond. props. 79—78225
Ta-Co(Ni)(N)(Ar), amorphous metal films, struct. and elec. characterisation 79—87017
Ta-Ni alloy, amorphous, UHV deposited, struct. and thermal depend. obs. 78—6233
Ti film, deposited by cylindrical magnetron sputtering, internal stresses, optical reflectance and elec. resist. 77—43449
Ti, film, elec. resist. Hall effect and absolute differential thermoEMF *(Russian)* 79—24083
Ti, film, reactive ion beam sputtering 78—19666
Ti, interaction with O_2, resist. and work function changes obs. 80—45431
Ti, ion bombardment with N_2^+, Ar^+, struct. changes, chemical compound formation *(Russian)* 78—95084
Ti, vacuum deposited, cryst. struct. and elec. props. 78—79908
Ti-Al, structure and elec. props. 80—7002
Ti-$C_x(N_x)(O_x)$, solid soln. film prep. by reactive sputtering, solubility and effect on props. 79—28231
Ti-Permalloy thin film diffusion couples, low temp. interdiffusion interdiffusion 78—71889
Ti-Pt link on dielec., laser vaporisation, resist. meas. 77—69941
Ti-Si cosputtered films, silicide form., X-ray diffr. and resist. study 80—54546
Ti-Si film thin film interaction, metallisation, X-ray diffr. and sheet resist. 80—54442
Ti-W, bias-sputtered, resist. and comp. 80—25023
Ti-W films, bias-sputtered, quantitative anal. 80—80114
Tl film, Fuchs Sondheimer theory, size effect, elec. cond., Fermi surfaces 79—99637
U film, condensed on cold substrate, electronic props. *(Russian)* 79—7912

electronic conduction in metallic thin films continued
V film, vac. evaporated, elec. props. 80—80414
V thin film-amorphous Si interface, V silicide formation, backscattering diffraction meas. 80—2285
W, film, specularity coefficient of conduction electrons, angular dependence *(Russian)* 79—87167
W film, sputtered, physical props. 79—77938
W film, surface RF impedance in strong mag. fields *(Russian)* 80—92920
W-Al_2O_3 granular film, percolation conductivity 78—84319
W-Cu(N) amorphous metal films, struct. and elec. characterisation 79—87017
W-Re, electron beam deposited, struct. and props. *(Russian)* 77—24490
W-Re films, amorphous, one-dimensional quantum localisation 80—80413
WSi_2, sputtered, props. for MOS IC appl. 80—70831
Y, and Y-H system, temp., thickness and comp. depend. of elec. resist. 79—78221
Y, struct. and elec. resist., electron diffr. meas. 78—87888
Y, thickness dependent polymorphism rel. to resistivity 78—39232
Yb, amorphous and cryst., transport props. rel. to band struct. *(Russian)* 77—12026
Yb, amorphous metal films, crystallisation with and without mag. field 80—70570
Zn film, RF sputtered, ageing processes 78—84322
Zn, film growth on C, conductance meas. 79—82495
Zn, RF sputtered, thickness 200 to 1100 Å 79—42674
Zn, sputtered film, thermal ageing, thickness dependent effects 78—6462
Zr film, reactive ion beam sputtering 78—19666
$ZrPt_3$, corrosion resist. and elec. cond., bulk and film samples 78—72285

electronic data processing *see data processing*

electronic density of states
4f substances, electronic props. at config. crossover 77—47775
A15 compound trends, self consistent band calcs. 78—79925
A15 compounds, elec. struct., 3-D k.p model 78—2405
A15 compounds, high supercond., T_c, attributed to linear chains or cubic symmetry 79—38221
A15 compounds, new aspect of superconductivity, Fermi level rel. to electron-phonon interaction 79—7927
A15 compounds, rel. to mode softening and high supercond. crit. temp. 78—14851
A15 compounds, self-consistent LMTO band calcs. 79—37954
A15 compounds, supercond. crit. temp. for model density of state using Eliashberg gap eqns. 80—93034
A15 ordered and disordered cpds., density of states calc. 79—87033
A15 superconductor, density of states broadening and its effect on T_c 79—65577
A15 superconductors, supercond. and phonon softening in unstable systems 79—65587
A15 type compound, props. and one-dimensionality 80—2530
A15-compounds, electron lifetime affecting electronic props. 79—15134
A15-superconductor, surface characterisation by energy loss spectra, AES and HEED 77—24635
A-15 compound, V_3X and Nb_3X, (X=Al, Ga, Si, Ge, Sn), electronic struct., electron-phonon interactions, and low temp. anomalies 79—60701
A-15 compounds, density of states model for lattice transforms. 80—65219
A-15 compounds, disordered, resist. and supercond. transition temp. 80—107944
A-15 compounds, disordered, T_c depression, appl. to Nb_3Ge 80—7020
A-15 compounds, effect on critical temp. for supercond. of disorder, induced by α-particles 78—47897
A-15 compounds, supercond. props., band struct. calcs. 79—33388
A-15 type superconductor, comment on new 3-dimens. $\bar{k}.\bar{p}$ model for electronic struct. 80—10865
A-15 type superconductor, reply to comment on new 3-dimens. $\bar{k}.\bar{p}$ model for electronic struct. 80—10866
actinide compounds, conduction electron polarisation, model density of states 79—37949
adatom density of states, impurity atom effects 80—92958
adatom monolayer, on model transition metal surface, densities of states, chemisorption effects 78—26769
adatom valence-level position variation on metal surface 80—88611
adsorbates, photoexcitation theory rel. to angle-resolved UPS and surface EXAFS 80—39426
adsorption of atoms on metals, Green's function formalism for studying electronic struct., local density of states calc. 80—107884
AES, obtaining density of states information from self-deconvolution of Auger band-type spectra 78—92150
alkali graphite intercalation compound, evidence for alkalilike cond. bands 80—45201
alkali graphite intercalation compounds, evidence for alkali-like conduction band, UPS study 80—45208
alkali halide film, low energy electron scatt. 78—26928
alkali halides, F-centre photoionisation, semicontinuum model 79—99509
alkali halides, U_2 centres, cluster-Bethe lattice calc. for electronic density of states 79—4531
alkali halides, U-centre, electronic struct., self-consistent model 79—65406
alkali metal alloy, cond. electron density depletion by charge transfer state 79—95372
alkali metals, adsorbed on metal substrates, electronic struct. 79—87139
alkali metals, density of states effective masses, liq. and solid phases, model pseudopot. calc. 77—76738
alkali metals, liq., Fermi energy, density of states, electronic props., exchange and correl. effects 80—96774
all-trans-polyene, ground state props., ab initio studies 79—47002
alloy, dilute, sp. ht., electronic, mass renormalisation and band density of states influences 78—43137
alloy, disordered, bulk and surface density of states, effect of surface segregation 77—15729
alloy, disordered muffin tin type, coherent pot. approx. appl. 79—15062
alloy, one-dimensional, electronic struct. 79—69391
alloy, random elementary excitations 77—4278
alloy, substitutional, analytic approximation for Herglotz property 79—37946
alloy, three-dimens., with site diagonal disorder, numerical results 78—30858

electronic density of states continued
alloy, two-band model, self-consistent cluster Bethe lattice study 80—29303
alloy, XPS, asymm. of core electron lines *(Ukrainian)* 78—2982
alloy thin film, thickness depend. of CPA electronic densities of states 80—65644
alloys, binary disordered, electronic density of states, optical theorem and multiple scatt. theory 79—4500
alloys, disordered, charge density function calculation method 79—42433
alloys, disordered, muffin-tin model, electronic struct. and density of states, theory 80—29301
alloys, dressed-cluster approx. 78—95249
alloys, local density of states and local environment 79—82509
alloys, magnetisation calc. method based on moments of density of states 80—65770
alloys, self-consistent cluster theories for diagonal and off-diagonal disorder 79—37950
alloys, substitutional, self consistent cluster theory for off diagonal disordered systems 80—84272
alloys, with off-diagonal disorder, density of states and cond., CPA calc. 80—24780
amorphous alloys, density of states of n-components 80—80153
amorphous and ordered films, adsorbed on metal surface, electron state of adsorbed atoms *(Russian)* 79—51425
amorphous film junction, I-V and C-V characts. 77—85307
amorphous materials, laser irrad., electronic struct., one-electron approx. 80—70576
amorphous metal, electronic density of states 78—51868
amorphous payramidally bonded solid, electronic and phonon densities of states 77—8001
amorphous Schottky barrier, capacitance-voltage meas., localised density of states determ. 80—49900
amorphous semicond., optical props. and densities of states *(French)* 77—72809
amorphous semiconductor, tetrahedrally bonded, effects of quantitative disorder on electronic struct. 79—47003
amorphous semiconductor, tetrahedrally bonded, gap density of states 79—19545
amorphous semiconductor or insulator, optical absorption 77—90167
amorphous semiconductors, density of states determ. from field effect data 80—107688
amorphous semiconductors, doped, electronic props. 78—19030
amorphous semiconductors, doped, electronic props. 80—80283
amorphous semiconductors, thermopower, conductivity, statistical shift, doping effects 79—69537
amorphous solids, elementary excitations, amorphons 80—39494
amorphous system, cluster effective lattice method, mag. and electron props. 77—66242
amorphous systems with dense random packed hard sphere structure, density of states and itinerant ferromagnetism 78—34950
amorphous tetrahedrally bonded solid, theory of fluctuations and localized states 78—10405
amorphous tetrahedrally-bonded solid, electronic struct., theoretical approach 80—29315
Anderson model, one dimensional site disordered lattice, AC conductivity 78—84199
Anderson model, quasiparticle lifetimes 80—44532
Anderson-localised states, intrastate and interstate interactions 80—20113
aperiodic materials, recursion method 78—34739
atoms, exchange energy as function of electron density 80—91426
Auger lineshape anal. of molecules and solids 80—76113
BCC and simple cubic lattice, density of states of tight-binding s-bands using modified-moments method 80—15431
bimetallic junctions, interface plasmon modes, theoretical anal. 80—54767
binary alloy, completely disordered, position of electronic energy bonds, CPA calc. *(French)* 78—22999
binary alloy, density of states, CPA with nonretracing paths 77—31924
binary alloy, short range order effect on density of states *(Russian)* 78—67929
binary alloy model, 2D disordered system, chain-like localisation 78—91646
binary alloys, charge transfer and transport props. in tight-binding model 79—82577
binary alloys, density of states in CPA 77—51633
binary alloys, electronic density of states, generalized cluster-Bethe-lattice approach 79—42432
binary alloys, electronic density of states in Bethe lattice, using Weaire-Thorpe Hamiltonian 78—51870
binary linear chain, electronic props., short-range order effects 80—96769
borides, hexa- and di-, electronic structs., elec. props., book contrib. 78—47701
α-brass, electronic momentum densities by two-dimensional angular correlation of annihilation radiation 78—91605
CdS film, polycryst, optical spectra, 0.5-6.5 eV 80—55212
central peak in the density of states of a disordered linear chain 80—100428
charge carrier conc., temp. depend., computer data anal., effect of band parameter errors *(Russian)* 78—52006
chemisorption on model insulator 77—85072
classical spin glass, propagating modes in 3 dimensional planar model, dynamic struct. factors 79—99703
cluster calculation, fast self-consistent, for large systems, appl. to electronic struct. of solids 79—82513
complex tight binding systems, surface density of states determ. 80—20272
Compton profile, expt., one dimens. Fourier transform 77—73187
Compton profiles, struct. depend. 78—35223
computational algorithm 80—44466
conducting mol. crystal, electron-phonon interaction, effect on electron energy levels 79—4499
CPA and CSEM methods, comparison 77—4280
crystal and infinite cluster, electron density of states 80—10850
cubic crystal, perfect, non-Bloch electron states, incompletely symmetric 79—23877
cubic crystals, non-Bloch electron states determ. 77—1352
cubic crysts., perfect, nonBloch electron state density 80—75487
d-band metals and alloys, s-d hybridisation 78—91644
dense fluid, electronic struct., cluster effects 79—95305
dense fluid, one-dimensional, Katz-Rice calc. 80—20063

electronic density of states continued
- density of states in K excitation spectra of solid and liq. phases 78—19601
- diagonal vertex approx. for Gaussian random systems 78—23003
- diamond, (100) surface states, SCF extended tight-binding method 77—47881
- diamond, valence bands, strong-coupling method 77—28679
- diamond, valence electrons, energy-depend. photoionisation probability calc. 77—16462
- diamond, valence electrons XPS spectrum, OPW calc. 77—4715
- differential areas method for cryst. symm. independ. calcs. 79—82508
- dilute alloy, perturbation expansion for the asymmetric Anderson Hamiltonian 80—80202
- dilute alloy, with off-diagonal disorder 78—34741
- dilute mag. alloy, density of energy states from sp. ht. as function of temp. 79—19741
- diluted ferromagnets, mag. excitations, appl. of recursion method 78—23223
- disorder and single electron spectrum, in linear chain *(Russian)* 78—56060
- disordered alloy, electron correls. and ferromagnetism 78—43548
- disordered alloy, self-consistent boundary site approx. in cluster theories 79—19500
- disordered alloy, short range order effect on electron states 77—15732
- disordered alloys, density of states, and their moments 77—11837
- disordered alloys, electronic density of states in muffin tin model 80—88467
- disordered alloys, electronic struct., CPA calcs., short-range order 78—63964
- disordered binary alloys, three-dimens. model, density of states calcs. 77—43469
- disordered chain, analytic behaviour of tight-binding spectrum 77—76716
- disordered chains, low energy density of states 79—60676
- disordered material, density of states in N-dimens. space 77—76718
- disordered material, elc. cond. and density of states, scaling relations 79—28329
- disordered metals, conductivity electrons and elastic scatt. by static inhomogeneities *(Russian)* 80—29375
- disordered one-dimensional lattice systems, diffusion and hopping conductivity 80—59991
- disordered one-dimensional system, electron density of states and Peierls transition *(Russian)* 80—29304
- disordered semiconductor, 1-dimensional, density of states, 2-band approx. calcs. *(Russian)* 79—7768
- disordered semiconductor, possibility of density of state determ. by tunnel spectroscopy *(Russian)* 77—47713
- disordered semiconductors, recomb. radiation spectrum *(Russian)* 79—4855
- disordered system, Coulomb gap, Monte-Carlo simulation 78—84168
- disordered system, density of states calc. by continued fraction method 77—24508
- disordered system, density of states calc. using augmented space formalism, comment 80—2322
- disordered system, elec. cond., tight binding approx. Kubo formalism 79—60778
- disordered system, electron density of states asymptote in a random field 80—44489
- disordered system, electronic states spectral density, semiclassical approach 78—2404
- disordered system, exact calc. of average density of states 78—43282
- disordered system, four dimens., electron density of states determ. 78—72057
- disordered system, four-dimensional, electrons 77—8039
- disordered system, one-dimens., density of states and wavefunction shape, periodic boundary condition influence 80—80223
- disordered system with correls., density of states at band tail 80—80154
- disordered system with short range order, elementary excitations 78—23000
- disordered systems, Coulomb gap computer simulation 79—51465
- disordered systems, density of states, variational melthod 80—49565
- disordered systems, fluctuation levels *(Russian)* 77—31981
- disordered systems, spectral density of electronic states calcs. 78—72055
- distorted one dimensional system with bond disorder, electron density of states, CPA calcs. 80—24778
- doped semiconductors, impurity states, cluster model 80—20117
- electron density, bulk and surface atoms, from ab initio model calcs. 79—4590
- electron gas, 1-dimens., with backward scatt., excitation spectrum 77—39793
- electron gas, degenerate, static density response function calc. by QHNC 80—49633
- electron gas, screening of proton, Anderson model calc. 80—59895
- electrons in disordered metals and at metallic surfaces, conf., Ghent, Belgium (Sept. 1978) 80—41946
- exponential tail in random potential 80—65423
- extended systems, HF density of states, appl. to thin films and polymers 80—6689
- Fano effect theory, electronic structure, d band metals and alloys 78—2402
- FCC lattice, incompletely symm. non-Bloch states 79—23878
- Fermi level, normal systems 78—23004
- Fermi system, quasi-one-dimensional, electronic density of states *(Russian)* 80—6755
- Fermi systems, disordered in two dimensions, interaction effects 80—75655
- Fermi-Dirac integral $\mathcal{F}_{1/2}(\eta)$ approx. 78—22997
- ferroelectric semiconductor, effect of soft phonon-electron interaction *(Russian)* 77—80718
- ferromagnetic instability in two-band Hubbard model 79—1653
- ferromagnetic metal, electron-magnon mass enhancement 77—15748
- ferromagnetic metals, spin fluctuation theory, Curie temp., mag. susceptibility 80—65937
- ferromagnetic semiconductor, two-band s-d model hybridization 80—65446
- film, surface density of states calc. within tight-binding scheme 77—55594
- finite crystal, electron density of states, rel. to infinite cryst., LCAO calcs. 77—24507
- fluoride perovskite- and tysonite-type, upper valence bands, tight binding calc. 77—80730
- fluorite-type crystals, universal density of states curve 77—35864

electronic density of states continued
- Fourier method, symmetrized for interpolating band-structure results 79—73419
- Friedel sum rule generalisation 77—62795
- n-GaAs, temp. depend. density of states, activation energy, screening, chem. pot. calcs. 79—56109
- Gaussian random potential, path-integral approach 79—69389
- graphite, electronic props., self-consistent LCAO calc. 78—51887
- graphite, electronic struct. exact exchange HF calcs. 80—65438
- graphite, H chemisorption, cryst. orbital NDO calcs. 77—7965
- graphite, heteroatom doped, electronic struct., energy spectrum, HMO LCAO calcs. 77—43539
- graphite, high energy cond. and valence band states, XPS 78—39664
- graphite, momentum density of electrons, two-gamma positron annihilation determ. 77—69211
- graphite, photoemission, C 1s core-electron line shape, excitonic effects, Fermi energy and hole density of states 80—29848
- graphite, polycryst., EPR meas. rel. to temp., crystallite orientation, paramag. suscept. 78—35023
- graphite, X-ray emission and absorption, XPS, electronic struct. 77—16431
- graphite intercalation compounds, electronic props. in dil. limit 77—47714
- graphite intercalation compounds with K and tetrahydrofuran *(French)* 78—26692
- graphite intercalation cpds., Fermi surface and transport props., LCAO model 80—80159
- graphite lamellar cpds., ^{13}C NMR studies 80—44936
- graphite lamellar cpds. with Li, K, Rb, HNO_3 and SO_3, EPR studies 80—44902
- graphite monofluoride, self-consistent semi-empirical LCAO calcs. of electronic band struct. 77—85142
- graphite-alkali metal intercalation cpds., electronic props. 80—45202
- graphite-nitrate residue compounds, phys. props. 78—10199
- Green's function and generalised phase shift for surface and interface problems, Green's function and generalised phase shift 79—60895
- Green function and electron density of states in field of randomly distributed impurities 77—8052
- heavily doped semiconductor, density of eigenvalues, localisation, general disordered system 78—56109
- heavily doped semiconductor, density of states at band tail 80—80154
- heavily doped semiconductors and devices, review 79—47039
- Heisenberg antiferromagnet, anisotropic, excitations at finite temp., CPA calcs. 79—95562
- Heisenberg antiferromagnet, dil., CPA calc. 78—68263
- Heisenberg ferromagnet, randomly diluted, 2-dimens., dynamics calcs. 77—40024
- hexagonal lattice, mag. subband struct. of electrons 79—95307
- homomorphic cluster coherent pot. approx., appl. to random systems 79—90930
- homomorphic cluster CPA analyticity 79—90929
- homopolar tetrahedral solids, Gaussian relaxation method of density of states calc., appl. to Ge 77—39760
- Hubbard bands, interaction as mechanism in metallic phase transitions 77—85148
- Hubbard model, random, coherent ladder approx. 77—62799
- Hubbard model, random one-body approx., higher dimens. lattices 79—37945
- Hubbard model, random one-body approx., one-dimens. case 79—37944
- Hume-Rothery Phases, electronic struct., main features 79—23883
- hybridised conduction band, intrinsic upper limit of electron-phonon coupling *(Chinese)* 80—54589
- ideal gas, self-trapping of electrons 79—2662
- II-IV-V_2 semiconductor, electronic struct. determ. 77—76751
- II-VI amorphous semiconductors, electronic states, sublattice one-band Hamiltonian transform. 80—59861
- III-V amorphous semiconductors, electronic states, sublattice one-band Hamiltonian transform. 80—59861
- III-V semiconductor, amorphous, electronic local density of states, cluster Bethe lattice method 77—11868
- III-V semiconductor, electronic struct. determ. 77—76751
- impact ionisation thresholds, as generalisation of van Hove singularities 77—77295
- infinite crystal, electron density of states, rel. to finite cryst., LCAO calcs. 77—24507
- insulator, disordered, charged impurity states, Lloyd model 80—29360
- insulator, in inhomogeneous elec. field, localized states in forbidden band 77—8060
- insulator-to-metal transition for half-filled Hubbard band in paramagnetic state 80—92817
- insulators, noncryst., electron density captured at traps, liberated to conduction band 78—87946
- intermediate valence compound, pressure-temperature phase diagram 79—28283
- interstitial compounds, electronic structure and useful phys. props. 77—89683
- ionic and partially ionic solids, electron-lattice interaction 77—20274
- ionic solids, variation of shellwise s-electron density at nucleus 79—42507
- itinerant antiferromag., partially disordered, electronic density of states 77—4494
- itinerant ferromagnetism and density of states, off-diagonal disorder effects 77—28360
- itinerant system of coupled diamagnetic pairs of electrons, electronic and magnetic correlations 79—61033
- KKR-CPA equations, numerical solution 80—44474
- Lenz-Jensen pot. calc. using third order approx. for electron density, in amorphous material 78—95099
- lightly doped semiconductors, impurity band struct. 79—69461
- linear Brillouin zone integration method, generalised susceptibility calcs. 80—88462
- linear chain, arbitrary number of impurities, analytic conditions 78—2443
- linearly analytical tetrahedron method calcs. *(Russian)* 79—82507
- liquid, electronic structure, structured medium approx. 80—84421
- liquid alloys, magnetic properties, review 79—51741
- liquid and amorphous metals, electronic states, optical theorem, multiple scatt. theory 80—49578
- liquid metal, electronic density of states, pseudopotential calcs. 80—70578
- liquid metal, electronic theory of thermodynamics and struct., summer school lecture series 80—6353

electronic density of states continued
liquid metal, integrated density of states, expression in Roth's effective-medium approx., generalisation of Friedel formula 79−99467
liquid metal, tight-binding model, effective medium approx. 77−15756
liquid metals, density of states and effective medium approach 77−76717
liquid metals, strong binding model, electronic density of states, Green's function calcs. *(Russian)* 80−70111
liquid semiconductor, density of states at band tail 80−80154
liquid semiconductor, metal-insulator transition model 77−1368
liquid semiconductors, normal refl. data and model densities of states 80−50364
liquid transition metal, from struct. and entropy data 77−1347
liquid-like random Kronig-Penney model, electronic density of states, CPA calc. 79−1567
Lloyd formula and muffin-tin CPA local density of states 80−70577
local density of states, cluster Bethe lattice method, appl. to amorphous III-V semiconds. 77−11868
low O_2 exposure effects on electronic surface props. 79−47146
magnetic alloy, highly concentrated, density of states of cond. electrons 79−24134
magnetic alloys, conc., density of states, Kondo effect, theory 80−65780
magnetic crystal, effect of impurity on local density of states 79−33263
magnetic semiconductors, excitation spectrum, temp. and band occupation depend. 80−49588
magnetoelectronic density of states for model cryst. 79−77978
metal, amorphous, electronic and vibr. props. 78−10151
metal, amorphous, electronic states calc. 79−69399
metal, BCC, chemisorption of monolayer of atoms, charge in density of states determ. 77−47682
metal, d-band, shake-off reduction of single particle spectrum in XPS 79−1812
metal, density matrix, using Wannier functions 77−69210
metal, dislocations rel. to electron gas thermodynamics at $2^1/_2$th order transition *(Russian)* 78−51910
metal, electron densities at muons 79−56655
metal, FCC, (100) surface, chemisorption-induced interaction between electronic levels of two-level adsorbate 80−39644
metal, H-impurity, energy and electron density of states 80−34398
metal, inhomogeneous electron system, nonlocal exchange and correlation 78−56097
metal, narrow band, quasiatomic Auger spectra 78−60536
metal, physisorbed inert atoms, polarisation due to short range interaction with substrate 80−39428
metal, quasiparticle bands, cond. electron mixing with impurity d(f) ions *(Russian)* 78−10409
metal, simple, density profile, potential for spherical voids 79−11077
metal, XPS angular depend. *(Russian)* 79−38722
metal dihydrides, synchrotron XPS obs., rel. to Peterman theory 80−55275
metal film, electronic density of states, sp. ht. and spin susceptibility 77−15730
metal films, one-dimens., electronic states 80−54758
metal particles, small, characterisation and props., book contrib. 80−84417
metal surface, narrow band, self consistent model calc. of electronic states 78−95333
metal surface, with substitutional disorder, Green's function theory 78−23145
metal surface electronic density of states, random distribution of impurity atoms 78−6424
metal surface with substitutional disorder, electronic struct. 78−23144
metal-amorphous Si barrier, electronic props. 80−11089
metal-insulator interface region, band gap closure in insulator 80−11086
metal-semimetal system, local and total density of states determ. *(Russian)* 80−54586
metal-tunnel oxide-Si junctions, processing condition depend. 80−80380
metallic disordered system, nonorthogonality effect 77−59243
metallic surface, density function theory, review 80−44698
metallic system, heterogeneous state form. due to long range interaction *(Russian)* 77−7842
metallic thin film, electronic props. and elec. cond. 79−78228
metals, amorphous and liq., s-phase-shift model 80−88473
metals, density of states and spin susceptibility, normal and giant surface effects 78−10322
metals, electric properties calc., book 79−28274
metals, positron annihilation expts., electronic struct. and Fermi surface studies 80−54594
metals and alloys, physical props., correl. with outer electron density of state *(Chinese)* 79−51466
MIS structure, capacitance-voltage characts., built-in charge fluctuation effects, negative surface state density 80−6992
mixed crystal, semi-infinite, local electronic states, CPA extension 79−65401
mixed valence compounds, periodic Anderson model self-consistent treatment, specific heat, susceptibility 79−99514
mixed valence state, electronic structure, spin-orbit interaction effects, mag. susceptibility 80−54657
mixed valence state, electronic structure 79−11092
mixed valence systems, phonons, effect of valence changes due to $f \rightleftarrows d$ electronic transitions 79−95104
MNOS p-channel transistor, memory characts., H_2 anneal effects 80−80388
MNOS structures with tunnelling-thickness SiO_2 films, charge trapping obs. 78−95379
model amorphous semiconductor struct., electronic props. 79−65974
molecular crystal, band structure, excitonic processes, trap distrib. 80−6720
molecular crystals, electronic transport theory, local linear electron phonon coupling 80−65545
molecular models of condensed systems and interfaces *(German)* 80−20062
molecule-metal interaction and surface reactions, theoretical description 80−39652
MOS, density of states mass for quantised accumulation layers from C-V characts. 78−26967
MOS inversion layer, 2-dimens. disordered electron systems in strong mag. fields 77−76930
MOS structure, use of mini-computer for rapid evaluation of C-V-plots *(Russian)* 79−28413
MOS structures, total dose effects on interface state density 77−20443

electronic density of states continued
Mott transition in the multidimensional Hubbard model *(Russian)* 79−28282
muffin-tin Hamiltonian, density of states 77−28090
muffin-tin potential cluster calculations, scattering theory 78−18940
muffin-tin potentials, arbitrary array, local density of states 80−92805
multi-Lagrangian interpolation for evaluation of density of states 78−84118
multiple scattering in condensed media, calc. of density of states for noncrystn. Cu and Fe 78−91578
multishell method, exact calc. of cluster in effective medium 78−10319
narrow band gap semiconductor, 1D with impurities, density of states calc. *(Russian)* 77−39761
noble metal alloys, disordered, bulk electronic structure 80−44467
noble metal based, disordered alloy, dil., virtual bound states, reson. model pot. theory 79−23934
noble metals, liq., muffin-tin pot. model, electronic density of states determ. 77−51645
noncrystalline materials, optical props., lecture 78−31219
nondegenerate strongly doped compensated semicond., electron props. *(Russian)* 77−11839
normal metal-superconductor double-layer, photon struct. induced into normal side by proximity effects 79−99659
one dimensional disordered cryst., density of states *(Russian)* 80−15433
one dimensional Fermi gas model in relation to spin and field theoretical models 80−24816
one-dimensional disordered system, average density of states, augmented space method 79−28265
one-dimensional disordered system, electron density distrib. for localised states *(Russian)* 77−11877
one-dimensional disordered system, numerical expt., Coulomb gap *(Russian)* 77−31932
one-dimensional disordered systems of atomic potentials, δ-functions use and limitations 78−10321
one-dimensional electron-phonon system, dynamics, Frohlich model 77−15781
one-dimensional model crysts., surface density of states, rel. to adsorbed molecule 80−107889
one-dimensional oscillator systems, density of states-frequency theorem 80−82602
one-dimensional pot. arrays, ordered and disordered, electron states, one-electron density matrix, Fourier-transformed Compton profile 79−69385
one-dimensional semiconductor, with impurities *(Russian)* 77−85127
one-dimensional superlattice, exact solns. 80−75488
one-dimensional systems with half-filled zone, singularity of electronic density of states due to impurities 78−6254
optical absorption by excitons 77−80734
optical joint density of states, oscillator strength effects 77−11838
Orbital-charge ordering in crystals 78−18988
ordered overlayers, on FCC metal surface, electronic struct. calcs. 79−60906
paramagnet, electron state density for narrow-band model with Coulomb interaction 80−10852
perovskite-structure crystals, calc. including all 14 primary valence and cond. bands 77−76720
perovskites, d-band, surface electronic props., π-bands exam. 79−38145
phase transition theory, electron density of states tail, profile in Gaussian random field 80−6691
phonon-free DC conductivity, disordered systems *(Russian)* 77−89745
polar semicond., secondary radiation intensity oscills., effect of high mag. field 79−19880
poly(2-vinyl pyridine), electronic struct., molecular-ion states and dielectric props. 79−37969
polyacetylene:AsF_5, mag. susceptibility, Fermi surface density of states, semicond.-metal transition 79−95566
polyacetylene, band struct. 79−51477
polyenes, model results for π electrons 78−55128
polyethylene, new algorithm 78−18939
polymer primary structures ESCA and EHCO methods 78−52630
polymers, self-consistent continued fraction theory of cond. 79−69482
polymethineimine, all-trans, ab initio cryst. orbital calcs. 79−77530
polyyne, linear infinite chain, ground-state props., ab initio studies 79−95306
proteins, self-consistent continued fraction theory of cond. in disordred materials 79−69482
pyrene, band structure, excitonic processes, trap distrib. 80−6720
quantum shift in a Gaussian random pot. 78−18941
α-quartz, electronic struct., local disorder influence 80−59870
α-quartz, valence electron states calc. by pseudopotential method 77−20239
α-quartz electron states, self-consistent pseudopot. calc. 77−62823
quasi-one dimensional conductor, electron density of states, influence of disorder 77−28091
quasi-one-dimensional metallic systems, crit. behaviour, Ginzburg-Landau theory 79−56147
quasi-one-dimensional organic conductor, chem. trends and stabilisation of nearly one-dimens. state, review 78−10328
quasiparticles, in anisotropic flat slab, in effective mass tensor approx. 79−28266
random alloy, optical absorption and photoemission spectra 80−45216
random alloy with short-range order, iterative calc. of energy levels 77−66104
random alloys, CPA calcs. cluster extensions, appraisal of applicability 79−15063
random binary alloy with partial order, electronic struct., self-consistent approx. 77−62796
random chain, low-energy density of states and long-time behaviour, scaling approach 79−25994
random chain of oscillators, CCPA calcs. of spectral density 79−37792
random Hamiltonian eigenvalues by tridiagonalisation, density of states 80−39493
random harmonic chain model, essential singularities of sp. ht. and density of states 77−72665
random impurity system, density of states tails, fluctuations and mobility edges 78−67983
random low-density correlated medium, multiple s-scatt. 77−1355
rare earth alloys, RM_2, (M=Fe, Co, Ni), magnetism, review 80−20365
rare earth intermetallics, cubic, direct coulombic contrib. of cond. electrons to cryst. elec. field 79−91005

electronic density of states continued
rare earth intermetallics, RCo$_2$, itinerant metamagnetism, Van Vleck model 79—78297
rare earth metal, 4f levels, obs. by bremsstrahlung isochromat and XPS spectroscopy 79—24411
rare earth metals, density of 4f states below and above Fermi level, XPS and bremsstrahlung isochromat spectroscopy 80—76140
rare earth molybdenum chalcogenides, Chevrel phase correlation between struct. and supercond. transition temp. 80—7023
rare earth tellurides, electron density distrib. from Mossbauer spectra 78—23374
rare-earth metal, semi-infinite surfaces with mag. struct., density of states calc. 80—10851
recursion method and non-orthogonal orbitals 78—43284
recursion method for the extended impurity problem 80—96814
refractory compounds, electron struct. and phys. props. 80—54585
s-d alloys, density of states calc. using coherent potential approx. *(Japanese)* 77—76721
scalar mag. field in anisotropic medium with piecewise-constant parameters, density of states calc. 79—69388
scaling critical exponents with neglect of cutoff, dimensional anal. 79—93087
Schrodinger equation with random pot. 79—65414
self consistent cluster-Bethe lattice calc. 78—67930
semiconducting alloy, two-band, electronic and optical props., multiband theory 79—37952
semiconductor, amorphous, field effect and capacitance-voltage meas. anal., localised density of states 80—103686
semiconductor, amorphous, tetrahedrally bonded, cluster calc., reduction of size effects 77—8002
semiconductor, complex energy band under optical excitation, high-frequency negative cond. and population inversion 80—107858
semiconductor, density of states of impurity bands 77—31979
semiconductor, density of Wannier-Stark states, calc. 77—11885
semiconductor, disordered, Coulomb gap in energy spectrum 78—14648
semiconductor, disordered, with soft Coulombic aperture, screening and absorpt. of long EM waves *(Russian)* 78—23001
semiconductor, doped, impurity band density in atomic limit 80—107735
semiconductor, doped, metal-insulator transition, anal. 80—88478
semiconductor, doped and strongly compensated, fluctuation pot. and density of states *(Russian)* 79—95366
semiconductor, electron excitation spectrum in resonance field of standing EM wave *(Russian)* 77—63386
semiconductor, electron states at planar and stepped surfaces 78—10531
semiconductor, electron-hole liquid, prod. and props. at low temp. 79—82527
semiconductor, heavily doped, closely compensated, density of states tail 78—47689
semiconductor, heavily doped, conductivity electrons and elastic scatt. by static inhomogeneities *(Russian)* 80—29375
semiconductor, heavily doped, perturbation potential distrib. and density of states 79—47052
semiconductor, impurity acoustoconduction, nonlinear theory 77—15914
semiconductor, impurity band, first and second moments of density of states calc. 78—6329
semiconductor, noncrystalline, mag. freeze out effect 78—43281
semiconductor, quantum oscillation amplitude, depend. on spin splitting 79—15066
semiconductor, quasilocal acceptor states, effects on band gap and electron mobility *(Russian)* 78—60082
semiconductor, with defects or impurities, local density of electron states 80—92857
semiconductor, zincblende type, building-up of covalent bonding, quadratic response of Fermi gas 77—28132
semiconductor alloys, pseudobinary, electronic density of states, cluster-Bethe-lattice method 79—90939
semiconductor in mag. and US wave fields, electronic density of states *(Russian)* 78—72056
semiconductor surface, chemisorption of mol. complexes, bond orbital model *(German)* 80—59807
semiconductor surfaces and interfaces, electronic struct. calc., scattering theoretic approach 80—6940
semiconductor/adsorbate system, local density of states calcs. *(German)* 80—60062
semiconductors, amorphous, electronic states, theoretical methods 80—80167
semiconductors, amorphous, electronic transport mechanisms and coeffs. 80—80282
semiconductors, compensated and amorphous, hopping cond. and density of localised states 77—89763
semiconductors, elementary excitations in disordered systems with localised electrons, polarons *(Russian)* 80—49632
semiconductors, grain-boundary resist., DC voltage depend. 79—82597
semiconductors, optical props. under press., book contrib. 80—84715
semiconductors, partially disordered, density of states calcs., forbidden gap energy depth *(Russian)* 80—34347
semiconductors, van Hove critical point region, electron-phonon interactions, dispersion law 80—70344
semiconductors with position-dependent band gap and electron affinity, current densities 77—85210
semiinfinite crystal with surface substitutional disorder, electronic struct. 77—72903
simple metal alloys, electronic theory for metal-non-metal transition 78—47702
simple metals, Fermi energy, density of states 77—76730
simple metals, singular struct. in density of levels 79—77997
single-particle density matrix, perturbation expansion 80—54635
solid, density of states of two interacting holes 77—1348
solid solution, density of states in forbidden band and band edge smearing 79—73418
solid solution, nondiagonal disordered system, excitation spectrum 80—15429
solids, chemical bonding studied using scattering theory concepts 80—103289
spatially disordered system, two-dimens., localisation and conductivity exam. 78—18998
spin chain impurity zone fine struct. *(Russian)* 80—6787
spin glass model Hamiltonians, zero temp. spin dynamics 77—85467
spin system, disordered, commutator and anticommutator Green's functions 79—51792

electronic density of states continued
spin-Peierls dimerised Hubbard chain, optical absorption spectrum 79—60677
stereoregular polymers, new algorithm 78—18939
structurally disordered materials, CPA theory of excitations, lattice model 79—87030
structurally disordered systems, with diagonal and off-diagonal disorder in non-orthogonal basis set, numerical study 79—69387
superconducting contact, paramag. impurity effect on tunnel characts. 77—69455
superconducting crit. temp., functional derivative with electronic density of states, Eliashberg eqns. 79—56368
superconducting film, geometrical reson. effect, electron tunnelling density of states meas., review *(French)* 78—2626
superconducting transition temperature, electronic density of states depend. 78—76186
superconducting tunnel current, paramag. impurities, singularities of second derivatives in Abrikosov-Gor'kov model 77—69456
superconducting virtual bound state alloys with resonant impurity scatt. centres theory 79—99654
superconductivity proximity effect, McMillan tunnelling model 79—73639
superconductor, effect of varying electronic density of states 80—75672
superconductor, with overlapping bands, tunnelling density of states, ultrasound attenuation 79—7934
superconductor critical temp. depend. on radiation defects, electron density of states calcs. 80—44758
superconductor-insulator phase transition in electric field 78—6481
superconductor-normal metal interface in a finite geometry 79—33404
superconductors with energy depend. electronic density of states, gap and crit. temp. 80—84538
superconductors with transition metal impurities 77—63024
superlattice, electronic band struct. in mag. fields 79—65355
surface, narrow-band, self consistent model calcs. of electronic states 77—85295
surface density of states in tight-binding formalism 78—10530
surface phase shift rule, and density of states 78—2538
surface reconstruction of two band crystal, change in density calcs. 78—14543
surface reconstruction of two band crystal, model for CsCl structure 78—14544
surface states, model calcs. using Koster-Slater type surface potential 79—7872
symmetric Wolff model, weak-coupling—long-time—zero-temp limit 77—80907
TCNQ, dimer gas model 78—87926
TCNQ salt, NMP-TCNQ, realisation of disordered Hubbard model, dielec. props. 78—79917
TCNQ salts, electron arrangement in ground state, optical spectra interpretation 78—47715
TCNQ salts, electron tunnelling 78—47769
TCNQ salts, with disorder, singularities in density of electronic states 77—8006
ternary alloys, density of states, CPA calc., off-diagonal disorder 78—22998
ternary alloys, disordered, elec. cond. and density of states, CPA calc. *(Russian)* 79—47072
tetrahedron method for evaluating spectral props. of solids 80—10855
thin disordered film, electronic energy spectrum calcs. extended Halpern Green's function technique 80—20066
thin film, 11-layered, CPA calc. of local density of electronic states 80—65643
tight binding calc., overlap and next-nearest-neighbour interaction effects 78—72059
tight-binding chains, off-diagonal disorder, density of states, localisation length 78—88247
tight-binding metals, electronic struct. and kinetic props. at high temp. 80—59848
TiO, local density of states, X-ray spectra, Hartree-Fock and $X\alpha$ calcs. discrepancies 79—77980
Tomonaga-Luttinger model, one particle temp. Green's function 80—57182
transition metal, 3d, electron and spin densities along energy axis 79—69455
transition metal, 3d, liq., density of states of d-band, heat of vaporisation 78—95253
transition metal, 3d, paramag., energy band calcs. 78—91608
transition metal, 4d, photoabsorption spectra near K-edge 78—92144
transition metal, chemisorption of ordered atomic layers, HF Green's function formalism and phase shift technique 80—24733
transition metal, d-series, density of partially delocalised d electron, calc. of equilib. distance between partial dislocations 79—14811
transition metal, disordered, multiple scattering theory, optical theorem 78—95250
transition metal, disordered, optical theorem and electronic states 77—76719
transition metal, energy band structure and X-ray emission spectra, calc. *(Russian)* 77—1763
transition metal, many-body effects, role of density of states 77—15777
transition metal, surface density of states, continued fraction method 77—20388
transition metal, surface electronic structure calculations 78—95329
transition metal, thermal and electrical conductivity at high temperature, interpretation of temp. depend. 77—35912
transition metal alloys, binary, energy of formation 77—15341
transition metal alloys, binary, state density curves, relation between short-range order and Fermi level position, CPA calculations 80—107687
transition metal alloys, density of states and complex band struct. for one-dimens. model 78—79919
transition metal alloys, disordered, bulk electronic structure 80—44467
transition metal alloys, disordered, density of states, elec. cond., extended Hubbard model 79—37948
transition metal alloys, disordered, local densities of states 77—59244
transition metal alloys, ferromag., effects of order on electronic struct. 79—90938
transition metal alloys, heats of formation, tight binding theory, moments approach 79—61891
transition metal alloys, sigma phase, from tight-binding Hamiltonian 77—59750

electronic density of states continued

- transition metal borides, narrow band types, electronic density of states, many-electron Hubbard model calcs. 80—20064
- transition metal carbides, complex phases with NaCl struct., microhardness rel. to electronic structure 77—90438
- transition metal carbides, d-metal, band struct. calc., Fermi level *(Russian)* 78—39019
- transition metal carbonitrides, carboxides and oxynitrides, electronic struct., theoretical approach 80—54584
- transition metal cluster, local densities of states and bonding props. 77—20401
- transition metal compound form., Miedema's empirical theory, microscopic basis 80—45541
- transition metal dichalcogenides, layered, electronic band struct. and bonding by atomic orbitals methods 79—15077
- transition metal dihydrides, band struct. and electronic props., electron-phonon coupling 79—47011
- d-transition metal hydride, mag. suscept. and quasirigid model *(Russian)* 78—26805
- transition metal hydrides, electronic states calc. 79—7769
- transition metal surface, electron states at steps, cluster-Bethe lattice approx. 78—52045
- transition metal surface electronic states, self-consistent model calcs. 79—42618
- transition metal surface electronic struct., influence of size and roughness 78—14785
- transition metal-H systems, energy and electron density of states, improvements to theory 80—70636
- transition metals, 3d, liquid, at Fermi level, Percus-Yevick, eqn. soln. *(Japanese)* 77—76579
- transition metals, 3d, liquid, d-band density of states and thermodynamic props. 77—76539
- transition metals, 3d electron struct. plasmons 79—77996
- transition metals, acoustic wave induced elec. field gradient 79—38034
- transition metals, amorphous, density of electronic states, effect of struct. variation due to interatomic pot. softness 80—54597
- transition metals, chemisorption of light gas atoms, on (100) surface, model calcs. 77—11797
- transition metals, core levels between surface and bulk atoms, variation of binding energy shifts 80—88615
- transition metals, d-electron surface density of states 77—85296
- transition metals, elastic constants, temp. depend. rel. to conduction electron density of states *(Russian)* 78—38769
- transition metals, ferromag., dil. H electronic struct. 80—70638
- transition metals, liq., electronic struct. and transport props. 80—29314
- transition metals, liq., muffin-tin pot. model, electronic density of states determ. 77—51645
- transition metals, local pseudopotential theory 78—30863
- transition metals and alloys, BCC, electron lifetime affecting electronic props. 79—15134
- transition-metal perovskitelike compounds, covalency effects, partial densities of p- and d-states photoelectron spectra 79—38718
- TTF-DETCNQ, heat capacity, elec. cond., cryst. struct., metal-insulator transition 77—8077
- TTF-TCNQ, band struct., Fermi surface and density of states, LCAO calc. 78—60048
- TTF-TCNQ, crit. behaviour near 53K phase transition, Ginzburg-Landau theory 79—33249
- TTF-TCNQ, divergent mag. responses at $2k_F$ and structural phase transitions 80—20376
- TTF-TCNQ, electronic struct. near Fermi level, tunnelling spectra 77—85126
- TTF-TCNQ, Madelung energy, electronic struct. *(Russian)* 78—6253
- TTF-TCNQ, self-energy calcs. 79—4499
- TTF-TCNQ salts, self-consistent continued-fraction theory of cond. 79—69482
- TTT film, hopping cond. AC and DC meas. and EPR 80—11111
- two-dimensional, Hartree-Fock soln. of CDW in mag. field 79—28302
- type II superconductor, A15 struct., electronic density of states and T_c changes with atomic ordering 78—91800
- V_2VI_3 compounds, electronic struct., X-ray emission, XPS, UPS obs. 78—52638
- valence electron distribution, in crysts., diffr. data processing 80—92418
- Van Hove singularities and continued fraction coeffs. 77—62793
- zero bias anomaly in tunnel resistance and electron-electron interaction 79—65539
- zero-component field theories, high order behaviour without $n \to 0$ limit 79—75438
- zincblende (110), surface relaxation 79—38143
- zone structure in tight binding calc., program 79—42430
- Ag clusters, charge distrib., density of states, CNDO calcs. 78—70995
- Ag, electronic density of states, cluster approx., compared with photoemission spectra 79—60675
- Ag halides, valence and cond. states, UPS, temp. depend. 77—20997
- Ag, spin-orbit projected d density-of-states 78—38999
- Ag-Cu, surface segregation, electronic theory, density of states, cluster-Bethe-lattice approx. 80—49369
- Ag_n, n=7,10,13,19, atom clusters, local density of states, Xα scattered wave calcs. 78—18989
- $AgAsS_2$, cryst. and amorphous, band struct., photoemission and refl. spectra obs. 77—66581
- AgH, electronic struct. and supercond., APW calc. 79—95318
- AgI, lattice instability, XPS 79—11500
- AgI, superionic conductor, density of valence states, photoelectron spectra meas. 80—25523
- $Ag_{1-x}Sn_{1+x}Se_{2-y}$, supercond. and normal state props. 77—36008
- Al, 3d impurities, self-consistent spin density functional calcs. 80—70635
- Al (001), density of surface states in two-dimensional Brillouin zone 79—60894
- Al, adsorption of O_2, relation between energy-band and cluster model 78—52048
- Al, Auger spectra, KLL and KLV, screening effects and plasmon gains 80—80913
- Al, band struct. and density of states, calc. using model pot. method 77—76742
- Al, electronic momentum densities by two-dimensional angular correlation of annihilation radiation 78—91605
- Al, electronic structure exam. by soft X-ray and X-ray photoelectron spectroscopy 77—85136
- Al, energy bands, densities of states and X-ray spectra, superposed self-consistent pots. 78—39010

electronic density of states continued

- Al, Fermi momentum, for solid and liq. phases, temp. variation, Compton scatt. obs. 80—50451
- Al film, supercond., meas. of effective quasiparticle recombination times, density of electronic states at Fermi level 79—38264
- Al, K X-ray absorption, K-emission spectrum, band struct. using APW method 80—97380
- Al, SCF Xα scattered wave calc. for clusters up to 43 atoms 78—10323
- Al, singular struct. in density of levels 79—77997
- Al tunnel junction, quasiparticle recomb. times and electronic density of states at Fermi level 79—56414
- Al/AlO_x/La-rare earth metal tunnel junctions, cond. meas., cryst. field effects 80—88694
- $Al-Al_2O_3-SnTe$ structure, tunnelling characts., model anal. 80—29480
- Al-Cu, disordered, electron energy struct. and X-ray emission bands, average t-matrix approx. *(Russian)* 80—24779
- $Al-SiO_2-Si$ MOS diodes, interface trap states obs. due to electron beam lithography *(Japanese)* 80—54787
- AlAs-GaAs (100) interface, tight binding calc. of electronic struct. 78—95342
- AlAs-GaAs (110) interface, self-consistent calc. of interface states and electronic struct. 78—52066
- AlB_2, band struct. and density of states, metallic behaviour 77—59249
- $Al_xGa_{1-x}As-GaAs$, quantum-well MO-CVD heterostructure lasers, band-filling props. 79—22954
- $Al_xGa_{1-x}As-GaAs$ quantum-well heterostructure laser diode, threshold current temp. depend. 80—43331
- AlH_x, electronic struct. and electron-phonon interaction, hydrogenation effect, rel. to supercond. 80—107694
- Al_2O_3, electronic struct., XPS meas. 77—73217
- Al_2O_3, valence band density of states from self-deconvolution of $L_{23}VV$ Auger spectrum 79—47561
- Al_2O_3-Al, disordered, energy diagram model 79—56110
- As, amorphous, electron and phonon density of states calcs., comp. to XPS 78—56066
- As, amorphous, electronic struct. of even-ring network model 79—23884
- As, amorphous, electronic struct. of defects using cluster-Bethe-lattice method 79—73471
- As, amorphous, optical, vibr., transport and defect-related props., review 79—51935
- As film, sputtered, density of valence states by XPS and UPS 77—24926
- As, phonon density of states compared to electronic density of states 78—55924
- As, rhombohedral, electronic struct. and optical props. var. with internal displacement parameter 79—60702
- As-Se amorphous film, density of upper valence band states, annealing effects, UPS obs. 80—29845
- AsF_5-intercalated graphite, mag. spin susceptibility, density of states at Fermi energy 79—7966
- As_2O_3, density of valence states, photoemission meas. 77—72808
- As_2S_3, amorphous, density of valence states, XPS and UPS obs. 77—48308
- $As_xS_{100-x}(Se_{100-x})$, localised states density near valence band edge *(Russian)* 80—103638
- $As_2S_3(Se_3)(Te_3)$ glass, electronic struct. calc. by extended Huckel theory 78—23012
- As_2Se_3, glass, density of optically induced localised paramagnetic states 78—52354
- Au, core level binding energy and density of states from first atomic layer, XPS meas. 79—87563
- Au, electronic density of states, cluster approx., compared with photoemission spectra 79—60675
- Au, energy band structure, X-ray emission spectra, APW calc. 80—92811
- Au, $M_{4,5}VV$ Auger spectrum, analysis 77—59649
- Au, spin-orbit projected d density-of-states 78—38999
- Au-Ag(Cu), surface segregation, electronic theory, density of states, cluster-Bethe-lattice approx. 80—49369
- Au-Mn, band profile, density of states, quantum defect-Green's function calcs. 80—54599
- Au_xAg_{1-x}, density of states and resist., CPA calc. 80—24780
- Au(Ag)(Cu)-Sn liquid, optical reflectivity spectra of virtual bound states 80—89021
- $AuCu_3$, ordered, band struct. and optical props. at 30K 79—60696
- β-B, rhombohedral, localised states charact., review, book contrib. 78—47728
- BN, electronic energy band struct., X-ray spectra, pseudopotential calcs. 79—78008
- BN, electronic struct., exact exchange HF calcs. 80—65438
- $BaCl_2$ film, UPS exam. 79—38716
- BaF_2 film, UPS exam. 79—38716
- $BaTiO_3$ (001), LEED and UPS studies 80—100747
- $BaTiO_3$, electronic props., SCF-MS-Xα calc. 80—54607
- $BaTiO_3$, electronic struct., XPS and band struct. calc. 79—38708
- $BaTiO_3$, K-edge X-ray absorpt., cond. band states 80—97382
- $BaTiO_3$, valence band UPS and partial p and d density of states 80—71560
- $BaTiO_3$, XPS, band struct., density of states, photoionisation cross sections 78—52629
- Be, charge-density from X-ray structure factors 77—19893
- Be, dielectric function from APW calcs. 79—65817
- Be, electronic struct., NMR study 80—108085
- Be, inelastic electron scattering near K-edge 78—52606
- Be, spin susceptibility, electronic effective mass, spin density functional calcs. 78—43291
- Be, XPS expt. 78—6829
- Be-Mg, two-band alloy, electronic and optical props., multiband theory 79—37952
- BeB_2, band struct. and density of states, metallic behaviour 77—59249
- BeNi, dil., electronic struct., NMR study 80—108085
- BeO, free film and Au substrate, transmission spectra and photoemission characts. 77—24925
- BeS, electronic energy bands, APW and LCAO calc. 77—20236
- BeSe, electronic energy bands, APW and LCAO calc. 77—20236
- BeTe, electronic energy bands, APW and LCAO calc. 77—20236
- Bi, film, oxidation, UPS, valence band, cond. band and 5d core states 77—20995
- Bi film, oxidation kinetics and interfacial bonding using final states 77—56127
- Bi, liquid and solid, UPS, optical densities of states 80—2924
- Bi, oxidation, charge transfer obs. from final state changes 77—51703

electronic density of states continued
Bi, Shubnikov-de Haas effect *(Russian)* 79—7840
Bi, solid and liq., core-level line shape, high-resolution XPS meas. 77—59668
BiI$_3$, octahedrally coordinated, layer cpd., electronic struct. using synchrotron-radiation photoemission spectroscopy 79—74058
Bi$_{2-x}$Sb$_x$Te$_{3-y}$Se$_y$ solid solution, density-of-states effective mass, carrier mobility temp. depend. 80—24931
C film, amorphous, elec., struct. and optical props. 77—20474
C, glassy and fibrous, density of states, magnetoresistance theory appl. 80—44620
C$_8$K, K-graphite intercalation compound, electronic struct. using semi-empirical tight-binding scheme 78—6255
CO molecular adsorbed on Mo (110) surface, electronic states, photoemission spectra 80—65363
CO$_2$, metallic, one-electron dispersion relations 77—62794
Ca films, thin and ultrathin, vac. deposited, struct. and photoemission meas. 80—11538
Ca, optical props., 2-11 eV 78—15191
CaB$_6$, electronic struct. APW and muffin-tin calcs. 80—29320
Cd, band structure, density of states and Fermi surface, APW calc. 77—20232
Cd$_3$As$_2$, electronic g-factor, effective mass and density of states 79—60691
CdF$_2$, UPS and XPS spectra, rel. to optical props. 80—66386
CdGeP$_2$, electronic struct. at cryst./vitreous transition, X-ray K-absorpt. and emission 78—15248
α-CdIn$_2$Se$_4$, defect zincblende struct., electronic props. 77—15767
CdS, surface energy struct. changes during ion cleaning and thermal annealing 80—92962
CdSe, electrical cond. near metal-insulator transition 79—73550
p-CdSnAs$_2$, Hall effect, thermo EMF, thermomagnetic effects 80—107822
n-CdSnAs$_2$, optical absorption rel. to energy spectra *(Russian)* 78—75994
n-CdSnP$_2$, Hall coeff. and elec. cond. meas., 24-900K 80—54721
CdTe, amorphous, photocond., effective density of localised states 77—28210
CdTe, Schottky diode, expt. determ. 79—7899
β-Ce, electronic energy band calcs. by KKR method 79—95317
Ce, electronic structure, 4f band *(German)* 77—55479
CeAs, evidence for valence fluctuations, ^{75}As Knight shift data 78—91966
Ce$_{3-x}$S$_4$, Ce$_{3-x}$Sm$_x$S$_4$, elec. cond. mechanism, thermoelec. power, Hall and absorpt. coeffs. 77—24559
Co, amorphous and liquid, density of electronic states 79—23881
Co, amorphous and liquid states, electronic states and transport 79—99474
Co, band model of high temp. magnetism 78—26809
Co, liq., density of states of d-band, heat of vaporisation 78—95253
Co, UPS, single cryst. and polycryst. film, electronic struct. 78—11081
Co-Al, band struct. and density of states, KKR method and X-ray meas. 80—10863
Co-M alloys, M=Si, Ge, Al, Ga, band model of high temp. magnetism 78—26809
Co-V, solid and liq., mag. susceptibility and electronic struct. 80—39738
CoAl, bonding, self-consistent energy bands 78—91610
CoAl, electronic struct., cluster calc. 77—69209
CoF$_2$, valence-electron density of states, XPS meas. 77—69963
CoMn(Cr)(V)(Ti), dil., low temp. specific heat and magnetisation 80—65925
Co$_{1-x}$Ni$_x$Al, Knight shift and mag. susceptibility study, electron struct. peculiarities *(Russian)* 80—15814
CoS$_2$, e$_g$ band, density-of-states curve 79—7990
Cr, (100) surface, clean ($\sqrt{2}\times\sqrt{2}$)R45° struct. 80—2255
Cr, band struct., X-ray emission bands, self-consistent calc. 77—28104
Cr-Al, band struct. and density of states, KKR method and X-ray meas. 80—10863
Cr-Au alloys, dil., elec. resist., 77-700K 78—64035
Cr-Fe-Si alloy, sp. ht., 1.4-4.2K 77—20079
CrH, electronic props., H alloying effects, book contrib. 79—82522
Cr$_3$Si, mag. susceptibility, 2 to 300K, rel. to electron energy spectrum 80—60185
Cr$_3$Si, specific heat at low temps., electron density of states, Debye temp. *(Russian)* 80—54398
Cs-Ag, dil., electronic struct., density functional approach 80—44492
Cs$_{1-x}$Au$_x$, liq., metal-nonmetal transition, electronic theory 78—79930
CsI, cond. band density of states, rel. to secondary electron spectra 77—12473
Cu (001) monolayer, electronic struct., self-consistent LCAO calc. 79—4606
Cu (100), electronic struct., self-consistent local-orbital calc. 80—80348
Cu (100), three-layer film, work function and density of states, self-consistent calc. 77—35978
Cu (100) film, chemisorbed N$_2$, electronic struct. 77—59315
Cu (100) monolayer, self consistent electronic struct. 80—6926
Cu (110) film, energy bands, tight binding calc. 77—15761
Cu (111) film, energy bands, tight binding calc. 77—15760
Cu atom in bulk, local density of states 79—37947
Cu, Brillouin zone integration special directions, electronic density of states calcs. application 80—49569
Cu, bulk and (001) films, extended tight-binding calcs. 80—70592
Cu, bulk d-band densities of states calc., optimisation of local orbitals 77—47711
Cu, chemisorption of H, density of states and chemisorption energy calc. 80—34315
Cu, clusters, size, geometric effects, catalysis implications 78—73131
Cu, electronic density of states, cluster approx., compared with photoemission spectra 79—60675
Cu film, electronic struct., self-consistent calc. 77—76959
Cu, lattice relaxation around μ^+ 79—56658
Cu, liq., electronic structure, structured medium approx. 80—84421
Cu, magnetic susceptibility, thermal density of states, non-local exchange-correlation effects 78—14924
Cu, multipole wave functions for photoelectrons, constant-energy-surface harmonics, s-d band appl. 79—37955
Cu, noncrystalline, multiple scatt. calcs. 78—91578
Cu on Ag (001), ultrathin film electronic states calc. 78—6318
Cu, partial densities of states, electron-phonon interaction 78—51869
Cu, powder, exam. of consolidation process based on electronic structure of solid 80—20842

electronic density of states continued
Cu surface, (001), electronic struct. of steps 78—34884
Cu, UPS, 14-45 eV, density of states function 77—90244
Cu, XPS, angle-resolved, valence band density of states distrib. 77—44123
Cu-Ni, alloys, electronic states, KKR-CPA calc. 78—84125
Cu-Ni, density of states of d-electrons, tight binding approx. calcs. 80—59863
Cu-Ni, disordered muffin tin type, coherent pot. approx. appl. 79—15062
Cu-Ni, soft X-ray emission and local densities of states 79—83059
Cu-Ni, UPS, surface and bulk density of states, comp. depend. 77—44125
Cu-Ni alloys, density of states determ. by continued fraction method 78—47690
Cu-Ni(Zn)(Ga)(Ge), dil. impurity electron struct., self-consistent Korringa-Kohn-Rostoker Green's function calc. 79—78040
CuBr, density of states of cond. band calc. 77—62819
CuBr, UPS, temp. depend., dynamic hybridisation 77—20998
CuCl, density of states of cond. band calc. 77—62819
CuCl, XPS and Auger spectroscopy, elec. struct. 80—29852
Cu$_2$MnAl, alloy, up-spin and down-spin electron density-of-states curve 79—4507
Cu$_{1-x}$Ni, disordered muffin-tin, electron momentum density in average-t-matrix approx. 79—69390
Cu$_x$Ni$_{1-x}$, bulk electronic structure, comparison of CPA and ATA techniques 80—44467
Cu$_x$Ni$_{1-x}$, disordered alloy, muffin-tin model, electronic struct. and density of states calc. 80—29302
Cu$_x$Ni$_{1-x}$, paramag., Bloch spectral functions and partially averaged local density of states 79—19502
Cu$_{2-x}$Se, elec. props. and band struct. 79—73513
Cu$_x$Zn$_{1-x}$, disordered alloy, muffin-tin model, electronic struct. and density of states calc. 80—29302
Cu$_{60}$Zr$_{40}$ glassy metal, photoemission and mag. susceptibility 79—28896
EuMo$_6$S$_8$, Chevrel phase, mag. interactions, LMTO energy band studies 80—70606
EuO(s), mag. semicond., s-f model, intermediate coupling theory 79—95326
EuS, conduction band density of states, redistrib. near ferromag. saturation 78—67939
EuS, phonon anomalies and electron-lattice coupling 80—39490
Fe (001) surface, spectral density of transfer matrix formalism 78—39185
Fe, (111), (100) and (110) surfaces, UPS obs. 79—38712
Fe, amorphous and liq., electronic struct., dense random packing model 79—51476
Fe, bulk d-band densities of states calc., optimisation of local orbitals 77—47711
Fe, density of states, photoemission expts. above and below T$_c$, rel. to magnetism model 77—20536
Fe, energy bands, tight binding calc. *(Korean)* 79—51479
γ-Fe, ferromag., Stoner theory support for two-state hypothesis 77—69477
Fe, ferromag. nonrelativistic LCAO energy band calc. 78—10343
Fe, liq., CPA theory of excitations, lattice model 79—87030
Fe, liquid and amorphous states, electronic states and transport 79—99474
Fe, noncrystalline, multiple scatt. calcs. 78—91578
Fe, partial densities of states, electron-phonon interaction 78—51869
Fe, powder, exam. of consolidation process based on electronic structure of solid 80—20842
Fe, UPS, density of states determ. 78—52623
Fe-Al, band struct. and density of states, KKR method and X-ray meas. 80—10863
Fe-Al systems, band struct. and cluster calcs. 79—51480
Fe-Co(Cr), electron state density and elec. resist. 80—39558
Fe-Mn(Ni), electron state density and elec. resist. 80—39558
Fe-Ni alloys, electronic struct. by XPS obs., proposed model density of states 79—33226
Fe-Rh alloy, nonmag. and mag., band theory 79—37973
FeAl, B2-cpd., band struct. and density of states, KKR calc. 78—63969
FeAl, bonding, self-consistent energy bands 78—91610
FeAl, electronic struct., cluster calc. 77—69209
FeAl, isomer shift, electronic charge density 78—80264
FeCo, electronic structures, order effect 79—90938
Fe$_{1-x}$Co$_x$Al, Knight shift and mag. susceptibility study, electron struct. peculiarities *(Russian)* 80—15814
FeF$_2$, valence-electron density of states, XPS meas. 77—69963
Fe$_{0.65}$Ni$_{0.35}$, UPS, density of states determ. 78—52623
Fe$_{1-x}$Ni$_x$Al, Knight shift and mag. susceptibility study, electron struct. peculiarities *(Russian)* 80—15814
(Fe$_{0.5}$Ni$_{0.5}$)$_{1-x}$Co$_x$, rel. to paramag. susceptibility, solid and liq. phases, 1000-1800°C *(Russian)* 77—16040
FeS$_2$, ionisation loss spectra, density of unoccupied states 80—55241
Ga, liquid and solid, photoemission, conduction electrons 79—87566
GaAS, O$_2$ chemisorption on (110) surface, bonding sites 78—38938
GaAs (110), steps 80—49846
GaAs (110), surface electronic struct. calcs. 80—80343
GaAs (110), valence band Auger spectra 78—35230
GaAs (110), valence band Auger spectra, from Ga and As CCV transitions 78—92149
GaAs (110) surface, chemisorption of O$_2$, electronic struct. theory, oxidation, electron spectra interpretation 79—42376
GaAs (110) surface states, surface relax. models, tight-binding calcs. 79—4594
n-GaAs, absorption tails in surface depletion layer and bulk 78—64379
GaAs, conduction band mapping by angle-resolved photoemission 79—83105
GaAs, density of states, spontaneous emission rate calcs., 120, 160, 200K 77—4292
n-GaAs, density of states tail in heavily doped closely compensated semicond. 78—47689
GaAs epitaxial layers, electronic surface props., photoluminesc. exam. 77—20901
GaAs, impurity density of states, effect of doping and injections, models and calc. method 79—73466
GaAs, LMTO self consistent band struct. calc. 80—20078
In-GaAs, MOS capacitor struct., elec. props., annealing effects 80—34519
GaAs surfaces, electronic struct., tight-binding calc. 80—54755

electronic density of states continued
GaAs-Ga$_{1-x}$Al$_x$As heterostructures, quantum size effect in superlattices, electronic props. 80—29471
GaAs-Ga$_{1-x}$Al$_x$As superlattice, sub-band dimensionality 78—63981
GaAs-oxide, electronic density of states from voltage-capacitance characts. of metal-oxide-semiconductor diode 79—66188
GaAs(110) surface, photoemission spectroscopy and tight binding calcs. 77—85888
GaS, reflectivity from 4 to 32 eV, Kramers-Kronig anal. 80—34943
GaS, XPS and valence band density of states, tight binding approx. 78—63974
GaSb films, amorphous and cryst., vac. evaporated, Elec. cond. thermoelec. power and optical absorpt. 80—2504
GaSe, band struct. and electron density of states in two-dimens. approx. 79—37987
GaSe, layer, upper valence bands using bond-orbital model 79—15078
GaSe, reflectivity from 4 to 32 eV, Kramers-Kronig anal. 80—34943
GaTe, reflectivity, 1-35 eV, electron props. determ. 77—20872
GaTe, transport properties under hydrostatic pressure 80—75589
Gd, HCP, ferromag. band struct. and Fermi surface, KKR band calcs. 77—62815
Gd in CsCl type alloys, exchange between localised 4f and cond. electrons 77—63279
Gd, magnetic crystalline anisotropy, Fermi level, electronic density of states 80—84596
Gd pnictides, band struct., semicond.-metal trend 77—28111
GdCo$_5$, spin polarised energy band struct., APW calc. 78—10342
Gd$_{1-x}$M$_x$, M=Co, Ni, Fe, temp. depend. of magnetisation 77—77043
GdMg, noncollinear mag. struct., nonlinear band behaviour 80—75706
GdRh$_4$B$_4$, magnetic and electrostatic props., NMR study 80—93195
Ge-(100), density of states, simple modelistic treatment of virtual surface states 80—103739
Ge, amorphous, ideal network struct., electronic struct., tight-binding model 80—44485
Ge, amorphous, mol. liq. model 80—49581
Ge, amorphous, substitutional doping, electronic props. 77—1418
Ge, electronic states associated with 60° edge dislocation 77—89724
Ge, exciton energy gap and LA and LO momentum-conserving phonon energies 79—90965
Ge film, amorphous, high field effects, 100-300K 77—24563
n-Ge, heavily doped, negative magnetoresistance model, spin-up spin-down electron effective mass variations 79—95423
Ge, mag. field luminesc. lifetime, quantum oscills., phonon wind effects 80—93385
Ge, stressed, α_1 and α_3 electron-hole droplet luminesc. 79—28820
Ge surface, Cl chemisorption, cluster calc. by iterative EHT 77—32062
Ge surfaces, electronic struct., tight-binding calc. 80—54755
Ge, valence electrons, XPS, LCAO and OPW calc. 77—12496
Ge, X-ray emission spectra formation, role of nonequilibrium electron density *(Russian)* 77—63490
Ge, X-ray spectra and energy band struct. 79—69407
Ge-GaAs, heterojunction, electronic structure 79—73572
Ge-GaAs (110) interface, self-consistent calc. of interface states and electronic struct. 78—52066
Ge-GaAs heterojunctions, electronic struct. 78—19138
Ge-GeO$_2$, optical charging memory, influence of doping GeO$_2$ with metal ions *(Russian)* 79—24077
Ge-SiO$_2$-p$^+$Si tunnel junctions, for determ. of AC cond. of amorphous Ge 77—24608
Ge-ZnSe, (100) interface, electronic struct. calc., scattering theoretic approach 80—6940
GeO$_2$, electronic struct. and densities of states, tight-binding calcs. 80—15447
GeS (001), density of empty states, core-level EELS and photoemission spectra meas. 79—78145
GeS, density of valence states, tight binding calc. 79—77976
GeSe (001), density of empty states, core-level EELS and photoemission spectra meas. 79—78145
GeSe, density of valence states, tight binding calc. 79—77976
Ge$_{0.8}$Si$_{0.2}$, elec. cond., density of states, impurity and temp. depend 80—65568
GeTe, density of valence states, tight binding calc. 79—77976
GeTe, effective masses for cond., density of states 80—88472
GeTe-Sb$_2$Te$_3$, solid solutions, cond., density of states 80—88472
Ge(100) surface electronic state localisation, layer density of states calcs. 80—6931
(HF)$_n$, n=1-∝, ab initio hydrogen bond and electronic parameters, phonons 77—14342
Hf, isochromat spectroscopy using SXAPS equipment 79—95877
Hf, valence band XPS, correl. to supercond. 79—65980
HfC$_x$N$_y$O$_z$, valence band XPS, correl. to supercond. 79—65980
Hg, electron density of states at 20 and 200°C 77—15754
Hg, expanded liq., band model for electronic struct., Knight shift and electronic transport 77—89690
Hg, expanded liquid, using effective medium approx. 79—99468
Hg, reflection spectra, electronic density of states, calc. 80—66229
Hg$_{1-x}$Cd$_x$Te, acceptor impurity band form. 80—20119
Hg$_{1-x}$Cd$_x$Te, acceptor levels due to local impurity potential 79—11084
Hg$_{1-x}$Cd$_x$Te, resonant acceptor level, single and multiple scatt. effect 77—47767
α-HgS, electronic energy level calcs. 80—6718
In, relativistic energy bands, density of states, and optical spectra, KKRZ calc. 79—51478
In-Au double layer, ultrathin, quantum size effect *(French)* 77—20466
InAs, longitudinal magnetoresistance in extreme quantum limit *(Russian)* 80—11008
InAs(P), electron irrad. at 50 MeV, elec. and optical props. 77—47486
In$_x$Ga$_{1-x}$As$_y$P$_{1-y}$, densities of states and self-energies, correl. with bond-energy levels 79—73435
In$_2$S$_3$, valence band densities of states, XPS meas. 79—28892
n-InSb, electron gas degeneration in strong mag. field 77—66173
n-InSb, heavily compensated, hopping cond. in mag. field 79—7842
n-InSb, longitudinal magnetoresistance in extreme quantum limit *(Russian)* 80—11008
InSb, n-type, anodic oxide film dielectric, MOS structure *(Russian)* 77—89874
InSb:Cr:Zn, cond. band, change in electron density with mag. field 79—15169
InSb-anodic oxide MIS struct., electrophys. props. *(Russian)* 77—39961
InSe, optical props. from 2-25 eV 80—29760
InSe, reflectivity from 4 to 32 eV, Kramers-Kronig anal. 80—34943

electronic density of states continued
In$_{0.69}$Tl$_{0.31}$, supercond. transition temp., specific heat, pseudopotential form factor 80—97026
Ir, energy band structure, X-ray emission spectra, APW calc. 80—92811
K, electron density redistribution on passing from atom to cryst. *(Russian)* 77—66103
KCl, cluster expansion of density matrix and crystal energy 78—87952
KI, cond. band density of states, rel. to secondary electron spectra 77—12473
KN$_3$, exptl. electron density distribs. cf. theoret. density distribs. of N$_3^-$ 77—46489
KNbO$_3$, electronic props., SCF-MS-Xα calc. 80—54607
KNbO$_3$, electronic struct., XPS and band struct. calc. 79—38708
KNbO$_3$, XPS, band struct., density of states, photoionisation cross sections 78—52629
β-K$_2$O-Al O$_3$, cation distrib. 77—80487
K$_3$Sb, optical and dielectric props., energy spectra, density of states calcs. 80—20083
KTaO$_3$, electronic props., SCF-MS-Xα calc. 80—54607
KTaO$_3$, electronic struct., XPS and band struct. calc. 79—38708
La, electronic structure, 4f band *(German)* 77—55479
La hydrides, S conduction electrons at Fermi level, depend. on H concentration 78—88217
La-Al(Ge)(Au), amorphous, alloying effect on supercond. props. 79—60951
La-In alloys, cohesive and superconducting props. from electronic struct. calcs. 79—99113
LaAg, band calcs., rel. to mag. and electronic props. and martensitic transform. 77—8014
LaAg, electronic struct., NMR relax. times meas. 79—51871
LaB$_6$, de Haas-van Alphen effect and Fermi surface 77—15743
LaB$_6$, metallic, energy bands and bonding 77—43486
LaF$_3$, quantum yield, photoelectron spectra, density of states struct. 78—68601
La$_{1-x}$Ga$_x$ foils, amorphous, splat cooled, calorimetric and resistive meas. 79—33417
La$_{1-x}$Pb$_x$MnO$_3$, spin polarised XPS and UPS, elec. struct. 77—8717
LaRh$_2$:Nd^{3+} cubic metallic host, spin-lattice relaxation, ESR obs. 79—1710
Li Al, electronic struct., mol. cluster calc. 78—14649
Li, Auger line shape KVV, energy band theory 79—43074
Li cluster, density functional calcs. 77—8031
Li, electron density redistribution on passing from atom to cryst. *(Russian)* 77—66103
Li, local orbital energy bands using Kohn-Sham and near Hartree-Fock exchange 78—30866
Li, transition density of states, AES meas. 77—36325
LiC$_6$, and LiC$_{12}$, intercalation cpds., electronic struct. calcs. 80—70613
LiC$_6$, band struct., density of states and Fermi surface props. 79—37982
LiCd$_{1-x}$Tl$_x$, intermetallic, X-ray and Knight shift meas. of ^{205}Tl and ^{113}Cd 79—42851
LiF, evaporated film, UPS, doublet struct. 77—63528
LiNbO$_3$, valence band UPS and partial p and d density of states 80—71560
LiOH, electron distrib. of OH$^-$ 78—75973
Li$_{1-x}$Pb$_x$, liq., metal-nonmetal transition, electronic theory 78—79930
Lu, band structure, influence of relativistic effects 78—75991
LuH$_2$, electronic struct., photoelectron spectra study 80—50527
LuRh$_4$B$_4$, magnetic and electrostatic props., NMR study 80—93195
MOS capacitor, photoionisation cross section and interface state density 80—92974
Mg, Auger spectra, KLL and KLV, screening effects and plasmon gains 80—80913
Mg, bandstruct. using potentials with exchange and correlation, KKR methods 79—11060
Mg, dielectric function from APW calcs. 79—65817
Mg, L$_{23}$VV Auger spectrum 78—39634
Mg, spin susceptibility, electronic effective mass, spin density functional calcs. 78—43291
Mg, XPS expt. 78—6829
MgB$_2$, band struct. and density of states, metallic behaviour 77—59249
MgB$_2$, LCAO calc. 79—90957
MgF$_2$, electronic struct. and densities of states, tight-binding calcs. 80—15447
β'-MgHg, energy bands and Fermi surface calc. 77—43481
MgO, electronic struct., XPS meas. 77—73217
MgO, free film and on Au, transmission spectra and photoemission 77—24925
β'-MgTl, energy bands and Fermi surface calc. 77—43481
MnAu$_2$, helical antiferromagnetic compound, optical props. and electronic struct., visible and IR obs. *(French)* 80—45101
MnAu$_2$, helical antiferromag., optical absorpt., density of states 80—66224
MnCl$_2$, lattice dynamics, density of states and sp. ht. calc. 80—92624
MnF$_2$, valence-electron density of states, XPS meas. 77—69963
MnP, spin polarised energy band struct., electronic specific heat, APW calcs. 80—65431
MnSi, electronic energy band struct., self-consistent APW calc. 80—65433
Mo, adsorption of CO, O$_2$, metastable He de-excitation spectroscopy and UPS study 80—34314
Mo, band struct., X-ray emission bands, self-consistent calc. 77—28104
Mo, density of states, optical mass and DC elec. resist. Slater-Koster interpolation 77—15731
Mo, electronic props., first-principles nonlocal pseudopot. approach 79—95319
Mo superconducting film, amorphous and crystalline, transition temp. exam. by UPS 79—28433
Mo, surface relaxation and electronic structure of (100) surface 79—73561
Mo-Nb solid solutions, enthalpy of soln. of H meas., rel. to density of electron states 80—2166
Mo$_6$ clusters, electronic struct., scattered wave-Xα calc. 79—11053
Mo$_3$Ge, density of states, increase with superconducting T$_c$ 79—15249
MoO$_3$, film and cryst., long range potential centres 78—30920
(Mo$_{1-x}$Ru$_x$)$_{80}$P$_{20}$, amorphous alloys, superconductivity, mag. susceptibility and electronic props., liq. quenching 78—88057
(Mo$_{1-x}$Ru$_x$)$_{80}$P$_{20}$, amorphous, liq. quenched, mag. susceptibility, supercond. and electronic props. 79—56376
Mo$_6$S$_8$, relationship between electronic struct. and supercond. transition temp. 77—85368

electronic density of states continued
- Mo_6Se_8, relationship between electronic struct. and supercond. transition temp. 77—85368
- $Mo_{1-x}V_x$, supercond., NMR and mag. susceptibility meas. 79—56388
- N_3^-, theoret. electron density distrib. cf. expt. density distribs. of NaN_3 and KN_3 77—46489
- Na, adsorbed on Al, adatom valence-level position variation 80—88611
- Na, Auger spectra, KLL and KLV, screening effects and plasmon gains 80—80913
- Na cluster, density functional calcs. 77—8031
- Na, electron density redistribution on passing from atom to cryst. *(Russian)* 77—66103
- Na, momentum density of electrons, two-gamma positron annihilation determ. 77—69211
- Na, X-ray edge shape, band struct. role 77—16425
- Na, XPS expt. 78—6829
- NaCl, photoemission exam. of Na^+-2p core excitons 78—43982
- NaN_3, exptl. electron density distribs. cf. theoret. density distribs. of N_3^- 77—46489
- Na_2O-CaO-SiO_2 glass, electronic struct. and optical props. 80—2790
- Na_2O-SiO_2 glass, electronic struct. and optical props. 80—2790
- Na_xWO_3, band struct. calcs. 77—62824
- Na_xWO_3 enhanced T_c, interband coupling 78—91804
- Na_xWO_3, optical props. 79—38515
- Nb (001) ideal surface, self-consistent pseudopot. calcs. 77—76894
- Nb, BCC lattice, optical props., energy band calc. of combined density of electron states 79—15075
- Nb, band struct., X-ray emission bands, self-consistent calc. 77—28104
- Nb chalcogenides and chalcogenide halides, geometrical struct. and metal-metal bonding 80—80172
- Nb, density of states, optical mass and DC elec. resist., Slater-Koster interpolation 77—15731
- Nb, electronic structure, APW calcs., self-consistency and exchange effects 77—66109
- Nb films, supercond. props. and electronic density of states *(Russian)* 79—28439
- Nb, optical properties and electronic props. 79—42439
- Nb/H, heat capacity and supercond. between 1.5 and 16K 80—2521
- Nb-Al_2O_3 cermet-type film, thermoelec. power and annealing effects 77—47911
- Nb-Al_2O_3 composite, semicond. films, cond. on localised states 77—24628
- Nb-Mo alloy, electronic density of states, temp. depend. of elec. resist. and mag. susceptibility 77—11891
- Nb-Mo-Tc alloys, supercond., point-group symmetry 78—64163
- Nb-Zr(Hf)(W) alloys, rel. to single cryst. elastic consts. 77-298K 78—84879
- Nb_3Al, band struct. and density of states from self-consistent pseudopotentials 79—69401
- Nb_3Al, metallic bonding, electronic states calcs. 78—79916
- $Nb_3Al_{0.8}Ge_{0.2}$, supercond., sp. ht. meas., rel. to band density of states 77—28296
- Nb_3Au, BCC, density of states, comparison with A-15 78—80095
- NbC, electronic struct. of vacancies, effect on supercond. transition temp. 80—29347
- NbC(N), critical temp. enhancement, surface effect on phonon spectrum and electronic state density *(Chinese)* 80—2507
- $Nb_{0.75}Ga_{0.25}$, A 15 phase high transition temp., sp. ht. determ. 80—60140
- Nb_3Ge, A15 superconductor, rel. between transition temp. and density of states 79—15247
- Nb_3Ge, α-particle irrad., relationship between density of states and supercond. transition temp. 79—42684
- Nb_3Ge, band struct. and density of states from self-consistent pseudopotentials 79—69401
- Nb_3Ge, density of states from critical field meas. 79—42690
- Nb_3Ge, electron-lifetime effects on props. 80—10951
- Nb_3Ge, metallic bonding, electronic states calcs. 78—79916
- Nb_3Ge, superconducting hybridisation and bonding, XPS exam. 78—2988
- Nb_3Ge(Al), anomalous resistivity, insight from band theory 78—60106
- $Nb_{1-x}Mo_xSe_2$, supercond. transition temp. and mag. susceptibility, electronic density of states determ. 77—12043
- $Nb_3Nb_{1-x}Si_x(Ge_x)$, impurity stabilised A15 supercond., transition temp., lattice consts., specific heat 80—93026
- NbO_2, electronic band struct., optical props., generalised susceptibility, struct. transition 79—95328
- NbS_2, 2H layer cpd., tight-binding fit to bond struct. 78—39000
- NbS_2, intercalation with pyridine, nucl. spin-lattice relax. meas. 80—54962
- NbS_3 and Nb_3S_4, electronic struct. and predicted cond. props. 80—92815
- $NbSe_2$, 2H layer cpd., tight-binding fit to bond struct. 78—39000
- $NbSe_2$ pure and intercalated with ethylenediamine, positron annihilation study 80—84801
- $NbSe_2$(2H) intensity vars. of angle-resolved photoemission spectra 79—83104
- Nb_3Si, high T_c, supercond. props. from extrapolation of sp. ht. meas. on A-15 Nb-Si 80—25045
- Nb_3Sn, A-15 cubic phase, band calc. using APW method 79—56120
- Nb_3Sn, α-particle irrad., relationship between density of states and supercond. transition temp. 79—42684
- Nb_3Sn, density of states from critical field meas. 79—42690
- Nb_3Sn, effect on critical temp. for supercond. of disorder, induced by α-particles 78—47897
- Nb_3Sn, electron-lifetime effects on props. 80—10951
- Nb_3Sn, supercond., crit. fields Pauli paramag. limiting and material parameters 79—78277
- Nb_3Sn(Al)(Sb), superconducting, NMR of ^{93}Nb and density of states 77—85388
- $Nb_{1-y}Ti_ySe_2$, supercond. transition temp. and mag. susceptibility, electronic density of states determ. 77—12043
- $Nb_{0.75}Zr_{0.25}$, effect of force constant, disorder on Eliashberg function 80—29504
- Ni (001) film, electronic struct. by self-consistent numerical-basis-set LCAO discrete variational method 79—60938
- Ni, (001) surface, local density of states, asphericity of pot. and charge transfer, ab initio self-consistent calcs. 79—15064
- Ni (100), electronic struct. of c(2×2) and p(2×2) O overlayers 79—47144
- Ni, amorphous and liquid states, electronic states and transport 79—99474

electronic density of states continued
- Ni, band model of high temp. magnetism 78—26809
- Ni, bound hole pairs, XPS study, satellite peaks 80—40218
- Ni, bremsstrahlung isochromat, incident electron energy and final-state symm. effects 79—69909
- Ni clusters, FCC and icosahedral structs., relax. and stability, cohesive energy minimization 79—42479
- Ni clusters local densities of states 80—88466
- Ni, density of states, photoemission expts. above and below T_c, rel. to magnetism model 77—20536
- Ni, ferromagnetic, electronic struct. by real space approach 80—65432
- Ni film, few atomic layers thick, transition from Pauli paramag. to band ferromag. 80—44885
- Ni, film (111), ferromag., energy bands and planar densities of states, LCAO calc. 79—4509
- Ni, H_2 solubility correlation, 500-1000°C *(Japanese)* 78—38845
- Ni, liq., electronic density of d-states, hard-sphere model and tight-binding approx. calc. 79—15065
- Ni, liquid, electronic struct. and transport props. 80—29314
- Ni, magnetic surface anisotropy of transition metals, model calc. 80—34625
- Ni, magneto-optical Kerr effect in UV region, electronic struct. 77—52127
- Ni, UPS, density of states determ. 78—52623
- Ni, XPS valence band spectra 77—21007
- Ni-Al, band struct. and density of states, KKR method and X-ray meas. 80—10863
- Ni-Al, electronic, mag., and cohesive props. 80—44491
- β-Ni-Al, X-ray absorpt. spectra meas., Fermi level location 80—35005
- Ni-Co(Fe)(V)(Ti), dil., optical absorpt., electronic struct. 80—108227
- Ni-Cr, H_2 solubility correlation, 500-1000°C *(Japanese)* 78—38845
- Ni-Cu, mag. anisotropy, temp. and conc. depend. 77—63172
- Ni-Cu alloy, optical absorpt. meas. 78—19518
- Ni-Fe, split bands rel. to sp. ht., g-factor and magnetostriction data 77—72977
- Ni-In(Sn), electrical cond. and magnetic susceptibility of B 8_2-compounds *(German)* 79—42520
- Ni-M, alloys, M=Si, Ge, Al, Ga, band model of high temp. magnetism 78—26809
- Ni-Mo, H_2 solubility correlation, 500-1000°C *(Japanese)* 78—38845
- Ni-Pd alloys, mag. props., average and local density of states, CPA calc. 77—59242
- Ni-Pd-P, Ni-Pt-P, amorphous and electronic structs., NMR Knight shifts and linewidths meas. 78—68400
- Ni-Pt disordered alloy, off-diagonal, T-matrix itinerant electron ferromagnetism calcs. 80—25067
- Ni-Ti, structural instability, deform. effects on electron energy spectrum 80—39284
- Ni-V, solid and liq., mag. susceptibility and electronic struct. 80—39738
- NiAl, bonding, self-consistent energy bands 78—91610
- β'-NiAl, density of states, XPS meas. 78—48284
- NiAl, electronic struct. by cluster calc., comparison with self-consistent APW method 77—69209
- β'-NiAl, self consistent embedded cluster model for Fe, Co, Ni mag. impurities 80—2549
- NiF_2, valence-electron density of states, XPS meas. 77—69963
- Ni(Fe,Cr) and Ni_3(Fe,Cr), electron states density model and mag. characts. calcs. *(Russian)* 80—92804
- NiFe, magnetic surface anisotropy of transition metals, model calc. 80—34625
- Ni_3Fe alloys, low-temperature specific heat, long and short range order effects 80—100339
- Ni_3Fe, electronic structures, order effect 79—90938
- NiH_x, electronic band struct. and interatomic bond 78—43295
- NiSb, bandstructure and density of states calc. 80—70580
- $Ni_{1-x}Si_x$, electronic states of Si NMR study 80—50216
- $NpAl_4$ clusters, band struct., variational Xα calc. 79—4508
- O, on Al (100), overlayer electronic struct. 77—85058
- Os, correlation effect of crystal pot., RAPW calcs. 78—6265
- P, amorphous, stability in air, XPS study, comparison with cryst. polymorphs 80—25517
- Pb, ab initio band struct. calcs. 80—75502
- Pb, band structure, and electron-phonon interaction, supercond. transition temp. determ. 79—19512
- Pb film, supercond., meas. of effective quasiparticle recombination times, density of electronic states at Fermi level 79—38264
- Pb, liquid and solid, UPS, optical densities of states 80—2924
- Pb, surface density of electronic states 77—20397
- Pb tunnel junction, quasiparticle recomb. times and electronic density of states at Fermi level 79—56414
- Pb-In, CPA interpretation of positron annihilation *(Russian)* 80—11507
- PbI_2, electronic struct. and exciton problem, photoelectron spectra meas. 77—63540
- PbI_2, octahedrally coordinated, layer cpd., electronic struct. using synchrotron-radiation photoemission spectroscopy 79—74058
- PbI_2, tight binding band structure using scaled parameters 78—79927
- $PbMo_6S_8$, relationship between electronic struct. and supercond. transition temp. 77—85368
- $PbMo_6S_8$:Fe, elec. cond. anomalous temp. depend., mag. moments *(Russian)* 80—92878
- $PbMo_6S_8(Se_8)(Te_8)$, Chevrel phase correlation between struct. and supercond. transition temp. 80—7023
- $PbMo_6Se_8$, relationship between electronic struct. and supercond. transition temp. 77—85368
- PbO-SiO_2 glass, electronic struct. and optical props. 80—2791
- PbO-SiO_2 glass, reduced channel-plate, variable range hopping conductivity 80—107466
- PbO_2, electronic struct. and densities of states, tight-binding calcs. 80—15447
- PbPo, electronic struct., relativistic band struct. calc. 79—4510
- $Pb_{1-x}Sn_xSe$, carrier effective mass, thermomag. effect meas. 77—24572
- $Pb_{1-x}Sn_xSe$, energy band parameter determ. from Shubnikov-de Haas effect 77—69227
- PbSnTe/PbTe inverted heterostructure mosaics, long wavelength, energy gap-Fermi level temp. depend. 79—85182
- $Pb_{0.82}Sn_{0.18}Te$, thermomagnetic, thermoelectric props., valence band struct. *(Russian)* 80—54724
- p-$Pb_{1-x}Sn_xTe$, influence of press. on density of states and Fermi energy 79—69413
- $Pb_{1-x}Sn_xTe$, photoelec. props. 30 to 4.2K, temp. depend. of electron density 80—20246

electronic density of states continued
$Pb_{1-x}Sn_xTe$:In, Hall effect and photoconductivity *(Russian)* 80—103720
Pd (111), electronic states calc. and adsorbate-induced photoemission struct. interpretation 78—60179
Pd, clusters, Hartree-Fock-Slater model calcs. 77—31930
Pd, clusters, size, geometric effects, catalysis implications 78—73131
Pd, electronic struct., effects of press. and alloying with Ru, Rh, Ag, and Rh+Ag 78—91581
Pd, liq., energy bands and electronic density of states, resistivity 78—34755
Pd on Ag (001), ultrathin film electronic states calc. 78—6318
Pd, phonon linewidths and electronic mass enhancement, electron-phonon contrib. 79—95099
Pd, recursion method 79—90937
Pd, spin-orbit projected d density-of-states 78—38999
Pd-Ag alloys, elec. resist. meas., density of states and Debye temp. 77—76715
Pd-H sytem, electronic struct. of H, mol. cluster and pseudojellium models 80—24832
Pd-H(D), band struct. and supercond. props., APW calc. 79—56354
Pd-H(D), superconducting transition temp., conc. depend. and inverse isotope effects 77—80864
Pd-Pt alloys, mag. props., average and local density of states, CPA calc. 77—59242
Pd-Rh-H and Pd-Ag-H, band struct. and supercond. props., APW calc. 79—56354
Pd-Si, metallic glasses, XPS and UPS studies 79—74062
Pd-Si glasses, changes in density of states with alloys comp., UPS obs. 80—50531
Pd-Si(-Cu) amorphous ribbons, low temp. sp. ht., density of states trends 80—79957
Pd-Si(—Cu), glassy, liq. and cryst., mag. and elec. props. 77—66249
$Pd_{1-y}Ag_yH_x$, electronic struct. and supercond., APW calc. 79—95318
$Pd_{1-y}Ag_yH_x$, superconducting transition temp., APW band struct. calcs. 78—95393
$Pd_{21}Ge_8$, cryst. struct. *(German)* 78—18586
PdH, electronic struct. and proton spin-lattice relax. calc. 78—67937
PdH, electronic struct. and supercond., APW calc. 79—95318
PdH, stoichiometric, recursion method 79—90937
PdH_x, CPA calculations of density of states 79—23882
PdH_x, electronic props., H alloying effects, book contrib. 79—82522
α-PdH_x, electronic states and Fermi surface props. 80—29310
$PdH_x(D_x)$, band struct., supercond. props., APW calcs. and neutron scatt. 78—43511
PdO, electronic struct., XPS and UPS study 80—35061
$Pd_{1-y}Rh_yH_x$, electronic struct. and supercond., APW calc. 79—95318
PdSb, electronic struct., optical transitions, Fermi surface 78—51885
$Pd_{0.81}Si_{0.19}$, amorphous, partial densities of states, XPS, UPS and AES meas. 79—95315
$Pd_{80}Si_{20}$, amorphous, electronic struct. calc. 79—87032
$Pd_{18}Si_{14}Cu_6$, glass, changes in density of states with alloys comp. UPS obs. 80—50531
$Pd_{80}Si_{17}Cu_3$, glass, changes in density of states with alloys comp., UPS obs. 80—50531
$PdTe_2$, bandstructure, Fermi surface, LMTO method 78—6264
Pt band-structure determ., angle-resolved photoemission 80—66398
Pt, energy band structure, X-ray emission spectra, APW calc. 80—92811
Pt, spin-orbit projected d density-of-states 78—38999
$Pt_3Mn_xCr_{1-x}$, electronic specific heat meas. comparison with band model calcs. 80—54400
PtO_x films, electronic struct., reduction processes, photoemission, optical absorpt. and resist. meas. 80—80931
PtTe, electronic struct., self-consistent and non-self-consistent band calcs. 80—44499
$PuAl_4$ clusters, band struct., variational Xα calc. 79—4508
PuO_2, thermal and transport props., electronic contrib. 80—15432
Rb halides, role of quantum effects in lattice dynamics, Debye temp., shell model calcs. 80—70336
Rb-halide, UPS exam., band struct. determ. 77—40330
Rb_2NiF_4, planar antiferromagnet, cluster-Bethe-lattice method 80—22306
RhH, electronic struct. and supercond., APW calc. 79—95318
Ru, electronic struct. and X-ray emission band intensities 77—20960
$(SN)_x$, electron tunnelling, absence of supercond. energy gap 78—47769
$(SN)_x$, electronic props., ab initio LCAO HF orbital calc. 77—51635
$(SN)_x$, electronic struct., X-ray and UV photoemission obs., OPW and pseudopot. calcs. 78—6832
$(SN)_x$, electronic struct. by extended tight-binding method, comparison with S_2N_2 precursor 77—76722
$(SN)_x$, energy band struct., self-consistent calc. by intersecting spheres model 79—28269
$(SN)_x$, LCAO band struct. calc. for one-dimens. chain and three-dimens. cryst. 77—76723
$(SN)_x$, lattice and electronic sp. ht. contribs. density of states 77—43344
$(SN)_x$, polymeric, electronic structure, semi-empirical pseudopotential calc. 77—72812
$(SN)_x$, temp.-depend. of elec. resist. and mag. susceptibility, density of states determ. 77—51877
$(SN)_x$, with H impurities, CPA calculations 80—44468
$(SN)_x$, XPS calc. using photoionisation cross sections 78—72697
S_2N_2, electronic struct. by extended tight-binding method, comparison with $(SN)_x$ 77—76722
$(SNH)_x$, density of states, CPA calcs., effect of H impurities 79—42431
Sb_2O_3, density of valence states, photoemission meas. 77—72808
Sb_2O_3-Na_2O-B_2O_3-SiO_2 glass, elec. cond. meas., —160 to 200°C 80—20190
Sb_2S_3, amorphous, density of valence states, XPS and UPS obs. 77—48308
Sc, band structure, density of states, absorpt. spectra, KKRZ calc. 80—70593
Sc-Zr(Mg), low-temp. heat capacity 80—75370
ScAg(Pd)(Ir)(Ru), UPS exam. 78—48276
$ScAl_2$, NMR of ^{45}Sc 77—63276
ScCl, electronic struct., self-consistent and non-self-consistent band calcs. 80—44499
ScH_2, electronic struct., band theory 79—78006
ScH_2, electronic struct., photoelectron spectra study 80—50527
ScM (M=Cu, Ag, Pd, Rh, Ir, Ru), electronic struct., NMR relax. times meas. 79—51871
ScM, (M=Ru,Rh,Pd,Ag), electronic struct., self-consistent local density functional calcs., LMTO method 79—11059

electronic density of states continued
ScP, electronic struct., self-consistent Hedin-Lundqvist and Xα APW calcs. 80—29322
Se, amorphous, electronic struct. and optical props., pseudopot. calc. 80—65428
Se, amorphous, trigonal and monoclinic, 2p photoabsorpt. spectra 78—23551
Se, amorphous layer, localised states in band gap 80—59928
Se, electronic struct. of cryst. phases and hydrostatic press. effects 80—59865
Se film, amorphous, density of localised states 78—34742
Se, photoelectronic behaviour, in glass transition region 80—60045
Se, trigonal and amorphous, electronic struct. and nonempirical calc. of struct. props. 80—59866
Se, trigonal reflectivity and density of states press. depend., self-consistent pseudopotential calc. 77—31931
Se:Te, amorphous, pure and doped, freq. depend. of elec. cond., 150 to 310K 79—42545
Se-As, photoelectronic behaviour, in glass transition region 80—60045
Si, (001) (2×1) reconstructed surface, dimer model self consistent calcs. 80—88613
Si (100), transition density of states from $L_1L_{2\ 3}V$ and $L_{2\ 3}VV$ Auger spectra 77—40314
Si (111), adsorption of Cl, electronic energy states, cluster-type calcs. 79—47149
Si (111), chemisorbed O_2 electronic struct. tight-binding calc., XPS and UPS meas. 80—49845
Si (111), with chemisorbed Al, electronic struct., self-consistent pseudopotential calc. 78—34880
Si (111), with chemisorbed Cl and F, electronic energy struct. calcs. 79—78144
Si (111) 7×7 clean surface and O chemisorbed stage valence band density of states from $L_{23}VV$ Auger spectra 80—100717
Si (111) surface, chemisorbed Al, local density of states 79—47142
Si, (111) surface, electronic density of states changes during O adsorption, AES obs. 79—65528
Si (111) surface, with Al overlayers, electronic states 80—11061
Si (111) surface with Al overlayers, electronic struct., self-consistent pseudopotential method 79—4595
Si, AES, convolution and deconvolution 78—52601
Si, amorphous, doped, density of states determ. from transport meas. 80—49720
Si, amorphous, doped, optically induced ESR, correl. effects 77—40115
Si, amorphous, doped, photoconductivity and recomb. meas. 77—89800
Si, amorphous, electrical transport and photocond. 77—85355
Si, amorphous, hydrogenated, electronic density of states determ. from Schottky diode meas. 80—49907
Si, amorphous, ideal network struct., electronic struct., tight-binding model 80—44485
Si, amorphous, mol. liq. model 80—49581
Si, amorphous, structural disorder rel. to electronic props. 78—34756
Si, amorphous, substitutional doping, electronic props. 77—1418
Si, amorphous, topological and electronic struct. 77—28102
Si, amorphous and cryst., electronic and optic props. 78—39013
Si, amorphous discharge produced, electronic density of states 79—46992
Si, amorphous film, TSC, density of localised states distrib. 80—65587
Si, amorphous films, halogenated and hydrogenated, elec. and optical props. 80—97016
Si, amorphous films, hopping conduction, dangling bond generation by high temp. annealing 80—60115
Si, amorphous films, ion implanted, elec. and photocond. props. 80—49717
Si, Auger line shape $L_{2,3}$ VV, energy band theory 79—43074
Si, Auger spectra, KLL and KLV, screening effects and plasmon gains 80—80913
Si, bicrystals, grain boundary states and varistor characts. 80—24829
Si, CVD films, polycryst., elec. and optical props., electronic density of states model 79—56332
n-Si, degenerate, density of states from elastic consts. 80—6690
Si, electron-beam-evaporated amorphous thin films, noise meas. 79—24091
Si, electron-hole drops, thermodynamical parameter determ. from luminescence data 80—2845
Si, electronic states associated with 60° edge dislocation 77—20261
Si, heavily doped, characts. of distrib. of density of states 79—15072
n-Si, heavily doped, negative magnetoresistance model, spin-up spin-down electron effective mass variations 79—95423
Si, hydrogenated amorphous, gap states, comparison of photoemission and photocond. results 80—103724
Si, ion-excited L-shell Auger spectra, characts. 79—87533
Si MOS diode characts. obs., electron irradiation damage effects *(Japanese)* 79—42646
Si, Schottky diodes on sputtered amorphous Si:H, light induced ageing effects, interpretation of photovoltaic stability 80—54780
Si surface, Cl chemisorption, cluster calc. by iterative EHT 77—32062
Si surface, local density of states method and bond orbital model calc. 77—8165
Si surface, valence band Auger line shape, corrected numerical results 78—52602
Si surfaces, electronic struct., tight-binding calc. 80—54755
Si, thermionic electron emission, from defect states at grain boundaries 79—91559
Si, valence bands, strong-coupling method 77—28679
Si, valence electrons, energy-depend. photoionisation probability calc. 77—16462
Si, valence electrons XPS spectrum, OPW calc. 77—4715
Si, X-ray emission spectra formation, role of nonequilibrium electron density *(Russian)* 77—63490
Si:As, amorphous, field effect and thermoelectric power 79—33289
Si:F,H, amorphous, elec. and optical props. 80—60031
Si:F,H, amorphous, glow discharge deposited elec. props. and device aspects 80—44744
Si:F(,H), amorphous, electronic struct., orthogonalised LCAO calc. 80—44486
n-Si:H, amorphous, bulk density of deep states, DLTS meas. 80—88518
Si:H, amorphous, density of states determ. using field effect 80—49937
Si:H, amorphous, effect of gap state density on photocond. and photolum. 79—91096
Si:H, amorphous, glow discharge deposited, laser annealing 80—49104
n-Si:H, amorphous, thickness depend. cond. 80—49724
Si:H,B, amorphous, field effect and thermoelec. power 80—96924

electronic density of states continued

Si:H,P, amorphous, heavily hydrogenated, high gap state densities 80−49803

Si:H,P, amorphous, in MOS tunnel junction, electron tunnelling characts. 79−73592

a-Si:H MIS junction, electronic struct. study by tunnelling 80−44729

a-Si:H Schottky barrier diodes, capacitance studies 80−49908

Si:Li, electron-phonon scatt., in intermediate conc. region 80−65180

Si:O, O rich polycryst. film, carrier transport 78−80076

Si:P, amorphous, CVD, defect compensation 80−54644

Si:P, CVD amorphous film, electronic density of states 79−46993

Si:P, electronic states, NMR of metallic and intermediate samples 79−4511

Si:P, heavily doped, electronic sp. ht. meas., rel. to metal-nonmetal transition 78−6162

n-Si:P, piezoresist. under strong uniaxial elastic deform. 77−15858

Si-SiO_2, intentionally contaminated interface, transient capacitance meas. 79−33349

Si-SiO_2 interface, density of states, theory 80−80395

Si-SiO_2 interface, improved characterisation, refined quasistatic and cond. methods 80−96990

Si-SiO_2 MOS interface, surface-state density and minority carrier generation rate, meas. by DLTS, hot hole effect 80−100527

$Si_{1-x}B_x$:H, amorphous films, thermopower and cond. for mixed band and broad tail state cond. 80−49786

n-SiC (6H), density of states effective mass determ., high temp. meas. of elec. props. 79−15073

$Si_xGe_{1-x}O_2$, amorphous, electronic struct. in Bethe lattice approx. 80−44487

$Si_xGe_{1-x}O_2$, amorphous, electronic struct. 80−80166

Si_5H_{12} cluster, Si valence band Auger spectrum, cluster approach, comparison with experimental spectrum 80−40191

SiO_2, amorphous and α-cristobalite cryst., band struct., photoelectron and X-ray spectra interpret. 80−24787

SiO_2, Auger line shapes, final state correlation effects 80−89095

SiO_2, calculated and measured Auger line shapes 79−83067

SiO_2, crystalline and amorphous density of states, bulk electronic struct., tight binding calcs. 80−44502

SiO_2 glass, electronic struct. and optical props. 80−2790

SiO_2, new interpretation of structure 78−84120

SiO_2, surfaces, electronic struct. calc., scattering theoretic approach 80−6940

SiO_2, valence band density of states from self-deconvolution of $L_{23}VV$ Auger spectrum 79−47561

SiO_2, vitreous, existence of gap in low-energy density of states 79−60769

SiO_2, vitreous, low temperature heat capacity enhancement model 80−75369

SiO_2, vitreous, Suprasil-W, thermal diffusivity, 16 mK-2.3K 79−60563

SiO_x system, cluster plus effective medium tight-binding study 79−33216

SiP_2, pyrite structure, density of states 77−15733

Si(111), partial monolayers of H, UV photoemission, disordering effect 77−1308

Si(111), surface density of states from soft X-ray absorpt. spectra 80−40187

$SmCo_5$, spin polarised energy band struct., APW calc. 78−10342

SmS, intermediate valence compound, pressure-temperature phase diagram 79−28283

SmS, phonon anomalies and electron-lattice coupling 80−39490

$Sm_{0.25}Y_{0.75}S$, phonon anomalies and electron-lattice coupling 80−39490

Sn, supercond., quasiparticle recomb. time and normal electronic density of states at Fermi surface from tunnel junction expts. 79−24108

Sn tunnel junction, quasiparticle recomb. times and electronic density of states at Fermi level 79−56414

Sn-Au double layer, ultrathin, quantum size effect *(French)* 77−20466

$SnMo_6S_8$, Chevrel phase, mag. interactions, LMTO energy band studies 80−70606

$SnMo_6S_8(Se_8)(Te_8)$, Chevrel phase correlation between struct. and supercond. transition temp. 80−7023

SnO_2, electronic struct. and densities of states, tight-binding calcs. 80−15447

SnS_2, conduction and valence band density of states 77−62817

SnS_2, octahedrally coordinated, layer cpd., electronic struct. using synchrotron-radiation photoemission spectroscopy 79−74058

SnS_2, refl. using Kramers-Kronig anal., optical functions 79−95798

$SnSe_2$, refl. using Kramers-Kronig anal., optical functions 79−95798

SrF_2, UPS and XPS spectra, rel. to optical props. 80−66386

SrO, electronic struct., XPS meas. 77−73217

$SrTiO_3$, (100), LEED and UPS studies 80−100747

$SrTiO_3$, calc. of matrix element effects in freq. dependent dielectric function 80−70632

$SrTiO_3$, electronic struct., XPS meas. 77−73217

$SrTiO_3$, K-edge X-ray absorpt., cond. band states 80−97382

$SrTiO_3$, non-orthogonal orbitals and recursion method 78−43284

$SrTiO_3$, valence band UPS and partial p and d density of states 80−71560

$SrTiO_3$, XPS, band struct., density of states, photoionisation cross sections, theoretical determ. 78−52629

Ta, density of states, optical mass and DC elec. resist., Slater-Koster interpolation 77−15731

Ta, density of unoccupied electronic states, UV isochromat spectra and SXAPS 79−77977

Ta, electronic structure, APW calcs., self-consistency and exchange effects 77−66109

Ta, optical properties and electronic props. 79−42439

Ta, photo field emission spectroscopy of band structure by He-Ne laser irrad. 80−55276

Ta-W alloy, electronic density of states, temp. depend. of elec. resist. and mag. susceptibility 77−11891

TaH_x, H diffusion and electronic struct., pulsed NMR obs. 80−54967

TaS_2, intercalation with pyridine, nucl. spin-lattice relax. meas. 80−54962

$TaSe_3$, effect of press. on supercond. transition temp. 79−91182

Te, amorphous, electronic struct. and optical props., pseudopot. calc. 80−65428

Te, electronic struct. of cryst. phases and hydrostatic press. effects 80−59865

Te, trigonal, electronic and optical props., press. depend., self consistent pseudopotential formalism 79−65838

Te, trigonal and amorphous, electronic struct. and nonempirical calc. of struct. props. 80−59866

electronic density of states continued

Te-transition metal, liq. semicond., elec. props. 80−96870

TeO_2, electronic struct. and densities of states, tight-binding calcs. 80−15447

Th, correlation effect of crystal pot., RAPW calcs. 78−6265

Th, photoelectron spectra study, core and valence levels 80−66394

Th, valence and 5f states, XPS and bremsstrahlung isochromat spectroscopy 80−66393

ThC_xN_y, NMR, Knight shift and spin-lattice relax. 80−100621

$Th_4H_{15}(D_{15})$ normal and supercond., low-temp. spt. ht., density of states at Fermi level 77−4466

ThN, photoelectron spectra study, core and valence levels 80−66394

ThO_2, thermal and transport props., electronic contrib. 80−15432

Ti (0001), valence band struct. and chemisorption, XPS and UPS study 80−35062

Ti alloys, Fermi sphere limiting electronic capacitance, Brillouin zones *(Russian)* 80−92808

Ti, electronic structure, appl. of Auger and characteristic loss spectroscopies 77−77331

Ti, electronic structure of omega and alpha phases, nonrelativistic APW method 79−90952

Ti, liq., density of states of d-band, heat of vaporisation 78−95253

Ti, partial densities of states, electron-phonon interaction 78−51869

Ti-V-Cr, electron-lifetime effects on props. 80−10951

$TiBe_2$, de Haas-van Alphen effect, Fermi surface, theory 80−103614

TiC, mag. suscept. rel. to temp. in homogeneity region 78−34953

TiC, TiN and VC, charge distrib. and bond ionicity 78−63961

TiC, valence X-ray photoelectron spectrum, density of states 77−81197

TiC_{1-x}, substoichiometric, electronic density of states 80−2319

$TiC_xN_{1-x}(O_{1-x})$, electronic struct., KKR-ATA method 80−65447

$Ti(Fe_{1-x}Co_x)$, density of states estimation from magnetisation and resistivity meas. 78−84119

$TiFe_{1-x}Co_x$, electronic struct. and mag. moment calcs. 80−65821

TiH_2, electronic density of states and tetragonal distortion, APW calc. 79−37986

TiH_x, temp. depend. of thermo-EMF coeff., 100 to 350K 77−11944

TiI_4, temp. depend. of thermo-EMF coeff., 100 to 350K 77−11944

TiN_{1-x}, substoichiometric, electronic density of states, CPA method calcs. 80−88464

TiN_xO_{1-x}, electronic struct., KKR-ATA method 80−65447

$Ti_{1-x}Nb_xH_{1.94}$, electronic struct. MNR meas. 80−15439

TiNi, soft X-ray spectra, electronic struct. 77−44091

TiO, energy band struct. and density of states *(Russian)* 80−44493

TiO_{1+x}, conduction band determ. 78−60055

TiO_2 (rutile), (001) and (110) surfaces, surface and bulk density of states calcs. 80−49858

TiO_2, electronic struct., XPS meas. 77−73217

TiO_2, electronic structure, appl. of Auger and characteristic loss spectroscopies 77−77331

TiO_2, rutile, K-edge X-ray absorpt., cond. band states 80−97382

TiO_x, interstitial alloy, electronic state, XPS, mag. susceptibility and elec. resist. 77−12486

TiS_2, valence density of states 80−44465

$TiS_2(Se_2)$, core states, energy bands, and valence densities of states 79−95322

$TiS_2(Se_2)$, valence density of states, Gilat-Raubenheimer method 80−88465

$TiSe_2$, structural distortion, band Jahn-Teller type mechanism 77−62875

$Ti_{1-y}V_yH_x$, electronic props., H alloying effects, book contrib. 79−82522

Tl, band struct., by LMTO method 77−39773

Tl, liquid and solid, UPS, optical densities of states 80−2924

Tl, polycryst. film, photoelectron spectra, UV incident 78−2986

Tl, relativistic Green's function theory 79−82512

Tl-Pb-Bi alloys, supercond., electronic density of states from heat capacity meas. 79−56383

TlCl, ground-state props., Wannier functions, and electronic struct., ab initio self-consistent calc. 80−80178

TlCl, UPS, valence band struct., dynamic hybridisation 77−20999

β-Tl_2O-Al_2O_3, cation distrib. 77−80487

Tl_xTe_{1-x}, amorphous, bonding and electrical conduction 79−90951

$Tl_2(Te_xSe_{1-x})$ mixtures, liq., electrical conductivity, magnetic susceptibility 80−88715

$Tl_2Te.As_2Te_3$, vitreous, temp. depend. of cond. and thermopower, electron energy spectrum 77−76831

U compounds, NaCl struct. type, relativistic energy bands, LMTO calcs. 80−65442

α-U, electronic band struct. and props. 80−10861

U, liquid, electronic density of states, shock vaporization technique 80−29300

U, photoelectron spectra study, core and valence levels 80−66394

U, valence and 5f states, XPS and bremsstrahlung isochromat spectroscopy 80−66393

UAl_4, clusters, band struct., variational Xα calc. 79−4508

UGe_3, de Haas-van Alphen effect, band struct. calc. 78−72068

UN, band struct. and density and states, PES meas. 79−42454

UN, density of states calc. 80−6715

UN, photoelectron spectra study, core and valence levels 80−66394

UO_2, electronic struct. contribs. to excess enthalpy at 3000K and in liq. phase 80−15265

UO_2, photoelectron spectra study, core and valence levels 80−66394

UO_2, thermal and transport props., electronic contrib. 80−15432

US, band struct. and density and states, PES meas. 79−42454

US, density of states calc. 80−6715

US, ferromagnet, electronic structure, reflectivity *(German)* 80−49567

US, optical props. and electronic struct. 80−25410

US(Se)(Te), electronic struct. and exchange band splitting, optical refl. meas. 80−66226

USe (s) 80−16053

USe, ferromag., spin polarisation of photoelectrons 79−78831

UTe, electronic and spin struct. negative spin polarisation of photoelectrons 79−19514

UTe_xSb_{1-x}, photoemission energy distrib. curve and density of states 79−52074

UTe_xSb_{1-x}, photoemission, densities of states 80−16147

$U_xTh_{1-x}As$ (Sb), electronic struct., relativistic KKR-averaged T-matrix approx. method 80−107702

V, band struct., X-ray emission bands, self-consistent calc. 77−28104

V, electronic density of states, effective mass, electron-phonon interaction, Coulomb pseudopot. *(Russian)* 78−26804

V, electronic structure, APW calcs., self-consistency and exchange effects 77−66109

electronic density of states continued
  V, electronic structure, model potential calcs. *(Russian)* 80—100431
  V, energy bands, calcs. using LCGO method 78—91608
  V, Fermi surface area, effective heat, optical masses, surface anisotropy critical temp. depend. *(Russian)* 79—90943
  V film, supercond. crit. temp., crit. field, resist. and struct. *(Russian)* 77—4475
  V, optical properties and electronic props. 79—42439
  V, partial densities of states, electron-phonon interaction 78—51869
  V/Al-Al_xO_y-Pb tunnel junction, superconducting transition, critical currents, Josephson effect *(Russian)* 80—29507
  V/H, heat capacity and supercond. between 1.5 and 16K 80—2521
  V-Al, band struct. and density of states, KKR method and X-ray meas. 80—10863
  V-based A15 compounds, nuclear spin-lattice relax. time, electronic density of states 77—59354
  V-Cr alloy, electronic density of states, temp. depend. of elec. resist. and mag. susceptibility 77—11891
  V-Zr-Nb alloy, rel. between density of states and martensitic and superconducting phase transition temps. 78—10594
  VC, energy band struct., chem. bonding 78—18958
  VC, TiC and TiN, charge distrib. and bond ionicity 78—63961
  $(V_{1-x}Cr_x)_3Si$, mag. susceptibility, 4.2 to 320K, density of states model 80—7035
  $V_{0.75-x}Ga_{0.25+x}$ ^{51}V, nucl. spin-lattice relax. time, annealing and neutron effects 79—82710
  V_3Ga, NMR and mag. suscept. *(Russian)* 78—39420
  V_3Ga, self-consistent APW band struct. calc. 78—47697
  V_3Ga, superconducting transition temp. and electron density of states 77—32105
  $V_3Ga(Si)$, high T_c supercond., electron-phonon coupling, effect of electronic density of states sharp struct. 78—14877
  V_3Ge, superconducting transition temp. and electron density of states 77—32105
  VH_x, electronic props., H alloying effects, book contrib. 79—82522
  $V_2(Hf,Zr)$, NMR and mag. susceptibility, density of states determ. *(Russian)* 80—66053
  $V_2Hf_{1-x}Zr_x$, normal and supercond. state, transition temps., mag. susceptibility and specific heat determ. *(Russian)* 80—60132
  VN, electronic struct. of vacancies, effect on supercond. transition temp. 80—29347
  $VN_{0.74}$ and $VN_{0.89}$, low-temp. specific heat and superconducting critical temp. meas., density of states 80—54835
  $V_{2-x}Nb_3Hf$, NMR of ^{51}V and mag. susceptibility, 20-300K *(Russian)* 80—93192
  VO, energy band struct. and density of states *(Russian)* 80—44493
  VO, surface states in unreconstructed (001) surface 77—32060
  VO_2, metallic, electronic struct., lattice instability 78—14664
  V_2O_5, energy band structure, bonding props., projected density of states anal. 80—70603
  $VS_2(SE_2)$ (1T), electronic struct. using nonspherical cryst. pot. 80—44498
  V_3Si, electron spectrum characts., mag. susceptibility depend. on resistivity ratio 79—95320
  V_3Si, magnetic susceptibility, density of states model for lattice transformation in A-15 compounds 80—65219
  V_3Si, NMR of ^{51}V above and below 21K struct. transition *(Russian)* 80—34796
  V_3Si, neutron irrad., sound velocity, magnetic susceptibility and upper critical field 78—88074
  V_3Si, neutron-irrad., ht. capacity and resistivity 78—88075
  V_3Si, supercond., crit. fields Pauli paramag. limiting and material parameters 79—78277
  $(V_{1-x}Ti_x)Ge$, pseudobinary A15 compound, supercond. transition temp. 80—49970
  W (001), chemisorption of H, HF Green's function formalism and phase shift technique 80—24733
  W (001) clean surface, spectral density of states 78—39181
  W (100) surface, adsorbed Au, Cu layers, electron field emission revealing unmasked surface reson. 79—15595
  W, field electron energy distrib., surface density of states 77—16471
  W, photoemission of spin polarised electrons 78—35248
  W, secondary electron emission spectra, angular depend. and phenomenology 79—43076
  W, secondary emission and photoemission props., effect of one-electron density of states 80—16152
  W surface, (110), chemisorpt. effects on dielec. function, refl. spectra 80—75616
  W, surface electronic structure and spectral densities 77—80824
  W, surface relaxation and electronic structure of (100) surface 79—73561
  WO_3 amorphous film, elec. cond. and dielec. const. 78—60238
  WO_3, optical props. 79—38515
  W(001), surface density of states for directional photoemission spectroscopy 77—20396
  Y, electronic struct. and X-ray emission band intensities 77—20960
  $Y_{0.7}$ $Th_{0.3}C_{1.58}$, specific heat 78—91813
  YB_6, metallic, energy bands and bonding 77—43486
  YCo_5, spin polarised energy band struct., APW calc. 78—10342
  $Y_{1-x}Co_x$, temp. depend. of magnetisation 77—77043
  $YFe_2(Co_2)(Ni_2)$, density of states, mag. props. 79—90936
  YH_2, electronic struct., band theory 79—78006
  YH_2, electronic struct., photoelectron spectra study 80—50527
  YS, phonon anomalies and electron-lattice coupling 80—39490
  Zn, band structure, density of states and Fermi surface, APW calc. 77—20232
  Zn, electronic band struct., pseudopotential calcs. 79—19510
  Zn, Fermi surface-Brillouin zone interaction, XPS obs. 79—52078
  ZnF_2, valence-electron density of states, XPS meas. 77—69963
  $ZnGeP_2$, cryst., electronic struct., X-ray K-absorpt. and emission 78—15248
  $ZnIn_2S_4$, layered semicond., reflectivity spectra 79—8155
  ZnO (0001), $(000\bar{1})$ and $(10\bar{1}0)$, UPS rel. to elec. struct. 78—15288
  ZnO, electronic struct. calc., appl. of O nonlocal ionic pseudopot. 77—51659
  ZnO, low-energy-electron transmission, optical modulation 79—83070
  ZnSe, amorphous thin film, prep. and electronic props. 77—85350
  Zr, electronic structure of omega and alpha phases, nonrelativistic APW method 79—90952
  Zr-Pd, metallic glasses, electronic props. and supercond. 79—73486
  ZrB_2, band struct. and XPS 77—90253

electronic density of states continued
  ZrB_2, self-consistent band struct., XPS, reflectance, NQR, Hall effect and density of states meas. 80—107689
  ZrBr(Cl), electronic struct., self-consistent and non-self-consistent band calcs. 80—44499
  ZrC, toothed profile of C Auger peak from density of occupied states 79—69929
  ZrC_x, x=0.99 to 0.13, elec. cond., supercond. state 78—43504
  $Zr(Fe_{1-x}Co_x)_2$, density of states estimation from magnetisation and resistivity meas. 78—84119
  $Zr_xHf_{1-x}V_2$, polycrystalline superconductor, resist. and mag. susceptibility, transition temp., temp. depend. 80—25113
  ZrS_2, valence density of states 80—44465
  $ZrS_2(Se_2)$, core states, energy bands, and valence densities of states 79—95322
  $ZrS_2(Se_2)$, valence density of states, Gilat-Raubenheimer method 80—88465
  $ZrZn_2$, de Haas-van Alphen effect, Fermi surface, theory 80—103614

electronic density of states of amorphous solids *see electron energy states of amorphous solids*

electronic density of states of liquid semiconductors *see electron energy states of liquid semiconductors*

electronic desk calculators *see electronic calculators*

electronic engineering computing
  see also circuit analysis computing; circuit CAD; computerised instrumentation; logic CAD
  antennas and propagation, symposium, Amherst (1976) 77—14633
  bevelled p-n junction in Si power device, elec. field in controlled region and blocking capabilities determ. 77—1474
  bevelled shallow junctions, spreading resistance data correction 80—80358
  capacitor charging, polymer filled, injection times obs. 80—70796
  coupled-bar problems, conformal transformations combined with numerical techniques 80—83538
  field effect transistors, computer simulation, student lab expt. 79—44673
  frequency meter simulation, LF and infra-LF, with digital positive feedback, metrological characteristics improvements *(Russian)* 78—4656
  hysteresigraph with data printout 79—58760
  inline production magnetron sputtering 78—3048
  Josephson junction, computer simulation of vortex motion, induced by phonon injection 79—73636
  Josephson junction, frequency-agile, biasing for precise freq., analogue computer study 79—28455
  kinescope spot size, relation to picture quality 77—44675
  laser amplifier gain, program for programmable calculator 79—18442
  loudspeaker driver parameters, time domain measurement implemented with digital computer 79—59901
  magnetic hysteresis, vector model, based on interacting dipoles 78—76271
  MOS structure, use of mini-computer for rapid evaluation of C-V-plots *(Russian)* 79—28413
  MOST structure modelling, using hybrid computer, Poisson partial differential equation solution *(Slovak)* 80—75643
  p-n-n^+ junctions, epitaxial planar, two-dimensional anal. of breakdown 78—80045
  parallel-plate sputtering system deposition rate model 79—87579
  Schottky-barrier solar cell sensitivity computation 79—62004
  SEM voltage state prediction 79—40644
  semiconductor charge flow analogue computation, attenuation-free upwind difference formula 77—28241
  semiconductor design using parallel computer in University research 79—54114
  semiconductor electrode, charge injection, space charge region, simulation 77—15949
  semiconductor electrode, open-circuit photopotential, simulation 77—15950
  semiconductor electrode, photogenerated free carriers and photocurrent relax., simulation 77—15951
  semiconductor wafer diagnostics, using computer automated scanning low-energy electron probe 79—4214
  semiconductors, temp. depend. of Fermi Level, calc. 80—39491
  thin film deposition process, line-edge profile simulation appl. 80—104068
  transducers error evaluation, continuous random-signals reproduction from pulse-frequency sequence 77—74386
  US transducer damping by multilayer front face 79—55301
  Si, diffused p-n junction, computer calcs. of photoresponse using Gummel-de-Mari algorithm 78—56221
  Si, impurity redistribution during single oxidation step, computer program calc. 80—2060
  Si, oxide growth, ambient water vapour trace effects 77—77618
  Si, resistivity depth profiles calcs. from spreading resist. meas. using math. algorithm 80—2393

electronic equipment manufacture
  black box electronic unknown, for undergraduate electronic laboratories, construction 77—60874
  digital measuring instrument manufacture in Rumania, frequency meters, voltmeters appl. *(Rumanian)* 77—74452
  ellipsometer measurement of thin films on wafers, real time, computer assisted 80—73418
  equivalent continuous noise levels, instrument design, electronic 77—65654
  glass fibres for optical communication, low-loss, fabrication technologies state of art 79—10420
  hermetic package water content anal. by mass spectroscopy 78—21263
  instrument design, modern circuit technologies impact 77—5861
  IR pyrometer performance parameters and applications *(German)* 80—86315
  leads, solderability of external coatings after storage at 25-400°C 78—184
  liquid crystal display, surface alignment treatment giving controlled low angle tilt 77—19871
  loudspeaker, bimorph element using piezoelectric ceramic *(Japanese)* 80—53597
  medical electronic equipment manufacture in India 79—96676
  pacemaker pulse generator design, manufacture and performance documentation for reliability 77—81715
  PC fabrication, detrimental effect of aged Sn-Pb surfaces 80—108625
  plasma spraying technique appl. *(Japanese)* 80—55558

electronic equipment manufacture continued
- PWB holes counting, wide-aperture telecentric laser scanning system design 80—1264
- Shimadzu medical equipment manufacture trend *(Japanese)* 79—88209
- solar cells, Si of Si/Cu_xS, w.r.t. optimum yield, Baude process appl. *(French)* 79—96448
- surface measurements in manufacturing processes, precise mechanical test method *(German)* 80—62624
- thin films fabrication techniques, evaporation and sputtering 80—76176
- vacuum deposition and sputtering, automation and programming of production plants *(Hungarian)* 77—4736
- wires electroplating, uniform, rotating cell design with helicoidally shaped internal surface 80—80990

electronic equipment testing
- anemometer, constant-temperature hot-wire, freq. response and electronic testing 77—58820
- Aryabhata, Indian scientific satellite, magnetic testing 78—40793
- balloon-borne slow-scan TV camera performance test *(Japanese)* 80—12635
- capacitance testing, using comparator 78—16811
- cardiac monitor, heart rate meter and alarm eval., proposed standard test tapes 80—89899
- cardiac pacemaker leak testing methods 78—57133
- cardiac pacemaker reliability technology workshop, Gaithersburg, USA (Oct. 1977) 80—27038
- cardiac pacemaker RF susceptibility tests 78—48935
- cardiostimulator, implanted, contactless rhythm indicator 79—39602
- computerised tomographic scanner acceptance testing 77—73569
- computerised tomographic scanner image quality evaluation phantom 77—73573
- computerised tomography scanner commissioning 77—73570
- conductivity meter for in situ ocean meas., development, testing and calibration 79—5671
- demand pacemaker standard test signal proposal 77—81721
- digital phase shift for meter calibration 79—44898
- digital recording system for tipping bucket raingauges, description and field testing 80—77161
- digital time-interval meter test rack 77—74373
- electro-medical servicing, quality maintenance 78—77126
- electrocardiostimulator parameter tester 77—21658
- electromanometric system frequency response visualisation device 77—48890
- electrometric equipment metrological provisions 77—79113
- electrometric instrument test results analysed 77—74450
- failure analysis of metal parts using fractography 79—61811
- ferritometer, using DC magnetic field 77—16766
- flowmeter, EM, non-flow test method *(Russian)* 77—3899
- HV power supplies, voltage testing techniques 77—74422
- large imaging CCD array development and test results 77—41316
- nuclear reactor, class 1E electronic instruments, ageing 78—8945
- oscilloscopes, microprocessor equipped, self-test facilities 79—88935
- pacemaker sensitivity testing, sine squared waveform generator 77—25612
- particle simulation unit for counter circuitry testing 78—81002
- pressure tolerant electronic systems 80—46317
- radiography equipment safety and preventative maintenance in rural community hospitals 77—40758
- raster electron microscope test object 78—86393
- reliability evaluation by neutron radiography 78—31610
- solar cell arrays, flat plate PV modules, elec. and environmental testing requirements for terrestrial appls. 80—61368
- stator end winding under short circuit, dynamic deform. and strength *(Japanese)* 78—11465
- Symphonie communications satellite components, NDT *(German)* 77—1899
- timer group testing installation 77—79083
- vacuum gauge testing and calibration for low absolute pressure 77—57341
- vibration charact. determ. by holographic interferography 78—29916
- voltmeter, digital, using linearly rising voltage *(German)* 77—5791
- voltmeter checking using UPMA-3, extension of meas. limits 80—13058
- wideband current and voltage comparators 77—57356
- wideband electronic voltmeter testing installation 77—79119

electronic music
- *see also musical acoustics; musical instruments*
- 440 Hz standard A tone generator 78—46863
- almost locked oscillator, for electronic music synthesis 77—68340
- digital waveshaping synthesis for musical sound generation 79—68526
- electro-piano, cantilever, harmonization of vibration *(Japanese)* 79—18634
- electronic music, keyboards for pure music, use of consonant chords 78—83183
- four-channel percussion synthesiser using 5700 type modules, construction details 80—106681
- metronome, accentuated beat, ETI, using 555 timers 78—46864
- microcomputers developments and appl. 78—90610
- MOS-LSI organ circuits *(German)* 77—19493
- organ Boehm Professional 2000, programmable *(German)* 79—37096
- patchable percussion synthesizer 77—68341
- percussion synthesizer, construction and operating controls 80—106682
- PMOS programmable sound generator, microprocessor-compatible, electronic music appls. *(German)* 80—79092
- portable electronic organ 80—96148
- quadrophonic, Interface 227 multiple function generator 248 appl. *(German)* 78—66993
- RE electronic piano, organ pedal cct. construction, tone cct. elements *(Dutch)* 80—99904
- synthesizer, sample and hold facility 78—46865
- tone filters for electronic organs, tone spectra and source waveforms 80—106683

electronic structure, atomic *see atomic structure*

electronic structure, molecular *see molecular electronic states*

electronic switching systems
- microelectronic appls., conf., Calcutta, India (Jul. 79) 80—96755

electronics applications of computing *see electronic engineering computing*

electrons
- *see also beta-rays; cosmic ray electrons; positrons*
- anapole moment, static parity violating coupling to EM field, unified gauge theory 80—68390

electrons continued
- anapole moments, source of odd-parity electron-nucleon interactions *(Russian)* 79—45093
- anomalous mag. moment, γ-γ scatt. contrib. 79—433
- arbitrary plane wave EM field, electron motion, radiational corrections, mass operator *(Russian)* 80—57534
- auroral E-layer, plasma lines meas. 79—25386
- band structure, optically induced in external plane wave field 80—106432
- continuous slowing down approx. ranges in metals 80—23269
- cooling experiments, mag. and vacuum system for NAP-M proton storage ring 77—65362
- correlations, effects on opacity in photon-electron scatt. 77—64634
- decay, DD $e\to\nu_e+\gamma$, lower bound of 3.5×10^{23} years *(Russian)* 79—40827
- e/m ratio measurement apparatus, power supply 77—60873
- Earth bow shock, energetic electrons meas. in upstream solar wind 80—90308
- electron-muon mass ratio in $Sp(1,Q)\otimes U(1)$ unified gauge theory 77—61236
- electron-muon symmetry of Callan-Symanzik function: two-lepton case 80—73627
- electron-positron storage ring, elementary particle physics *(Polish)* 79—76218
- extrastellar electron cloud around spherical limb-darkened star, Thomson scatt. rel. to light polarisation 79—58324
- flux quantization model, $e:\mu$ mass ratio, EM coupling const. 77—79240
- form factors in two-dimens. QED *(Russian)* 77—46003
- g-2 experiments as a test of special relativity 79—58539
- g-2 measurement for high-γ for special relativity test 79—58540
- g-factor analytic contributions in sixth order 80—22612
- gravitational interaction, QED corrections 77—30305
- gyromagnetic ratio, QED consequence 80—22548
- inertial mass, Mach's Principle 80—62538
- intrinsic magnetic moment of free electron in mag. field, meas. possibility *(Russian)* 78—86430
- ionosphere, comparison between calculated and measured photoelectron fluxes from Atmosphere Explorer C and E 78—28400
- ionosphere, effective electron collision freq. vars. from multiple-freq. mas. of radiowave absorpt. 77—91347
- ionosphere, high-latit., energy spectra and origin of 1 to 500 eV electrons 77—29568
- ionosphere, precipitating and thermal electrons rel. to elec. currents and nightside auroras 78—32267
- ionosphere photoelectrons, Coulomb-collision induced trapping by geomag. field 79—8739
- ionosphere photoelectrons flux, low-altitude plasma line anisotropy theory 78—77414
- ionospheric electron heat budget 77—53276
- Jupiter inner magnetosphere, revised Pioneer 10 absolute electron intensities 77—37563
- magnetic moment, muon effects in QED 80—62899
- magnetic moments, anomalous, QED test 80—77996
- magnetic moments of e^- and e^+ compared 77—18365
- magnetosheath, Prognoz 4 obs. of $\lesssim$2 MeV electrons and cold plasma 80—90296
- magnetosheath and magnetotail, energetic protons and electrons simultaneous meas. 79—16760
- magnetosphere, electron flux modulations rel. to geomagnetic pulsations 78—16247
- magnetosphere, energetic electrons distrib. in geomag. field 77—22006
- magnetosphere, high energy electron flux obs. and comparison with VLF emissions by EXOS-B satellite *(Japanese)* 80—94652
- magnetosphere, low energy electrons and protons obs. 78—36407
- magnetosphere, trapped electrons rel. to substorm dependences of magnetosphere ELF chorus 78—28437
- magnetosphere, vel. distrib. modification by VLF signals rel. to quiet band prod. 77—64534
- magnetosphere energetic electrons, chorus generation during substorms 78—96356
- magnetosphere energetic electrons, obs. in magnetosheath and solar wind 80—90310
- magnetosphere energetic electrons in magnetosheath and solar wind, correl. with geomag. activity 79—80095
- magnetosphere low altitude polar cusp, correlated elec. field and low-energy electron meas. 78—40770
- magnetosphere morning sector, auroral electron discontinuity location meas. by Molniya-1 satellite 79—8778
- mass, self-energy formula with grav. self-energy 79—9314
- mass calc. in terms of meas. quantities 78—66180
- mass formula, chronon in electron theory 80—47224
- mass formula of charged leptons 80—13244
- mass formulae from EM self energy *(Chinese)* 79—93416
- mass operator in plane wave field, near cyclotron reson. region *(Russian)* 78—86432
- model using phase-locked cavity 79—63089
- muon-electron mass ratio in a semi-classical model 80—91072
- neutrino-electron mixture, influence of spin and Weinberg-angle on bulk viscosity 77—61223
- plasmasphere, parameters of energetic electron distrib. function 78—4035
- polarisation radiative corrections in muon decay 79—36055
- proton/electron mass ratio, limits to past variability from quasar absorpt. line redshifts 77—61338
- QED, one loop effective potential with anomalous moment, electron Lagrangian 78—58146
- inner radiation belt, electron flux vars. near trapping zone boundary during substorms 80—67470
- outer radiation belt, maximum fluxes of electrons with $E>1$ MeV (1958-1971) 80—61968
- radiation belt electrons, struct. of atmospheric loss cone 77—33294
- radiation belts, high-energy electrons behaviour during reson. interaction with geomag. pulsations 78—28422
- radiation belts trapped electrons structure, effects of man-made VLF waves 78—45150
- radio sources, compact, electron energies and source models 78—4384
- relations between electron and other leptons *(Hungarian)* 79—13180
- relativistic electrons, synchrotron radiation oscillatory behaviour 79—26271
- rest energy, using X-ray photoelectron spectrometer, student demonstration 79—25802
- rest mass, continuous increase hypothesis *(Chinese)* 77—71209

electrons continued
- rest-mass, Compton collisions, student laboratory expt. 78−16607
- self mass in semiclassical limit 78−33008
- single isolated electron measuring technique, resource letter for teachers 78−81776
- size, lower limits in general relativity 80−22245
- solar corona, fast electrons from hard X-ray bursts rel. to type III-V radio bursts 78−89157
- specific charge determ., theory of modified Busch method *(Russian)* 77−79296
- steady state plasma, electron temp. and density meas. system 78−87490
- e-μ-τ spontaneous symmetry breaking and rare τ decays 79−9301
- e*, heavy electron, new limits for existence from $e^+e^- \rightarrow e^+e^-\gamma$ meas. 78−8640
- $e\bar{e}\nu_e\bar{\nu}_e$ mixture, covariant transport eqns., collision terms from Weinberg Salam theory 77−74315
- $e^-\mu^-\tau$ asymmetry, conserved currents *(Chinese)* 79−58904
- e^-p mass ratio, direct determ. using cyclotron resonance technique 78−70093
- $\mu \rightarrow e$ transmutation, failure to observe conversion, reasons and results 79−369
- μ-e universality, radiative corrections in gauge theory of $\pi^{\pm}$ decay 77−10244
- μe problem, mass difference, lepton number and symmetry conservation, forbidden transitions *(Chinese)* 79−13121
- μe universality breakdown of neutral weak currents in $SU_2 \times U_1$ gauge *(Russian)* 79−75712
- μe universality correction, rare decay mode calcs. 78−45898
- μe universality violation in renormalisation theory, neutral leptonic currents *(Russian)* 78−45837
- π^-p, 21 GeV, prompt e^- associated with strange particle in strong interaction, direct evidence 79−419

electrooptics *see electro-optical effects*

electroosmosis *see osmosis*

electrophoresis
- *see also electrophoretic coating techniques*
- AC cataphoresis meas. techniques and apparatus 79−8442
- agargel electrophoresis, protein transport, stochastic model 77−77769
- agarose gel immunoelectrophoretic determination of molecular weights of tubulin antigens 80−67313
- albumin, bovine serum, solutions, fluctuation transport theory 78−70057
- analytical electrophoresis, book contrib. 80−12322
- bacterial proteins, quantitation of electrophoretic profiles 79−70331
- bimolecular lipid membranes, electrophoretic mobility 79−79479
- bioelectrochemistry and bioenergetics (book) 80−8749
- biological cell electro-orientation and dielectrophoresis meas. devices *(Russian)* 80−51300
- biological cell electrophoretic mobility meas. using new automatic method 80−67322
- biological cell suspension, electrophoretic analysis, Doppler spectra line shape smoothing 79−84053
- biological cells, medical appl., Zeiss rectangular chamber cytopherometer 77−13034
- biological intracellular microelectrophoresis, contrib. of volumetric charge to mobility of nuclei 77−86710
- biological materials continuous flow electrophoretic separator, for sounding rocket expts. 78−85398
- biological materials fractionation in space by deflected lamina electrophoresis 78−85397
- biological materials separation in space environment, electrokinetic phenomena and electrophoresis 79−48351
- biological particle surface, elec. double layer phenomena *(Rumanian)* 80−94144
- biological surfaces observation using laser electrophoretic light scatt. 80−41359
- blood cell electrophoretic mobility study, semi-automatic system 80−3851
- blood cells, electrokinetic props. on exposure to phys. factors 77−70431
- capillary isotachophoresis, principle, instrumentation and appl. 77−90607
- cataphoresis laser oscillators, Al_2O_3 ceramic discharge tubes 77−75551
- cell membrane, electrophoresis and diffusion obs. 79−57599
- cell membrane, embryonic muscle, electrophoresis of concanavalin A receptors 77−29121
- cell membranes 77−25405
- cell mobility, effects of X-rays on polymorphonuclear granulocytes and FL-cells *(German)* 77−56442
- cell surface receptors, molecular movements 80−45866
- cellular protein two-dimensional analytical electrophoresis 79−96528
- charged particle, aperiodic electrodiffusiophoretic drift 79−96319
- chromaffin granule electrophoretic mobility meas. by light scatt., effect of Ca^{2+} and Mg^{2+} 78−53357
- colloid particle, spherical, dipolophoresis and electrophoresis, in presence of linear grating of cylinders 79−57234
- colloid particle, spherical, electrophoretic mobility 79−34316
- colloid particles with adsorbed polyelectrolyte, electrophoresis 79−47991
- colloidal, suspension, electrophoretic clarification 77−60127
- colloidal cylinders, charged, electrophoresis in salt solns., in transverse elec. field 79−1955
- colloidal cylinders in solns., electrophoresis, random orient. in elec. field, polyelectrolyte appls. 79−1956
- colloidal particles in gap between nonconductive fibres, electroconcentration 80−11895
- colloidal spherical particle, nonlinear polarisation of diffusion part of thin double layer 77−25315
- colloidal spherical particle, numerical method for electrophoretic mobility determ. allowing for polarisation 77−25269
- colloidal spherical particle, zeta-pot. determ. from electrophoretic mobility, double-layer polarisation 77−29015
- colloids, electrostabilisation effect in elec. field 79−39210
- colloids, field separation with hydrodynamic amplification 78−27779
- concentrated suspensions, accurate electrophoretic analysis 77−73450
- cylinder with high surface charge density, electrophoretic mobility 79−96373
- cytopherometer, reproducibility improvement 77−52954
- data acquisition system, chem. anal. appls. *(German)* 77−52692
- DC discharge, isotope enrichment by reson. trapping and cataphoresist. 77−27752
- DC glow discharge, periodically pulsed, theoretical model 79−34313
- deoxyribonucleoprotein, gamma-ray protein damage 78−53338
- deposition, industrial prospects *(French)* 79−47941

electrophoresis continued
- developers for pictorial electrophotography 79−17523
- diagnosis of malignant tumours, electrophoretic mobility test 79−79680
- dielectric fluid, electro-dielectrophoretic forces acting on spherical impurity particles, analytical evaluation 78−88641
- dielectric liquid, charge exchange mechanism between impurities and electrodes 79−91356
- dielectric liquid, DC cond. due to impurity particles, computer simulation and comparison with expt. 79−91060
- dielectric liquid, gas bubble dielectrophoresis 77−56233
- dielectric spheres, dielectrophoretic force 79−47935
- dielectrophoresis of microscopic particles 80−50860
- dielectrophoretic effect use for dielectric meas. 77−22570
- dielectrophoretic force, theory expt. 80−72403
- dielectrophoretic forces, expt. anal. 78−64892
- dielectrophoretic levitation of spheres and shells 79−81318
- disperse particles, aperiodic inertial drift, in inhomogeneous alternating fields 79−96317
- display device, for large area X-ray image receptor 80−98091
- divinyl benzene suspension, dielectrophoresis 80−3362
- electrode, equipot., electrophoretic force 78−61024
- electrode geometries for various dielectrophoretic force laws 78−88640
- electrodialysis reversal process, desalination with automatic self-cleaning facility 80−3357
- Electrokinetic measurements with submicron particles and pores by the resistive pulse technique 77−86384
- electrolyte flocculation of stabilised potassium 79−43638
- electroosmosis as distinguished from electrophoresis 80−45514
- electrophotographic images, electrophoretically developed, applicability of Siedentopf's law 79−45881
- electrophotography, latent electrostatic images and electrophoretic development 79−17522
- electrophotography, liquid immersion development 80−31920
- enamelling of domestic electric and gas cooking equipment using electrophoresis, installation and process details *(French)* 80−108719
- erythrocyte electrophoretic mobility, effect of UHF EM radiation 78−53442
- erythrocyte surface charge decrease, target of X-irrad. and dislocation of sialic acid 77−52853
- Escherichia coli, aq. colloid suspension, electrophoretic mobility and elec. polarisability 78−35813
- fission products, short-lived, rapid paper electrophoretic separation, γ-rays and half-lives determ. 77−44498
- future development potential 80−55665
- gas discharge, DC, time-depend. cataphoretic gas separation with end volumes 80−79603
- gel electrophoresis, 2-dimens., in study of somatic cell differentiation 80−46114
- glass, particle size influence on force moving particle in inhomogeneous elec. field, influence of field frequency 79−11795
- Graphon, colloidal dispersion in butanol, stability ratio 79−29413
- heat transfer in liquids by dielectrophoresis 78−94874
- n-hexane, impurity particle behaviour and cond. pulses 79−91059
- n-hexane, impurity particle motion, under DC and AC conditions, expt. results and computer simulation 78−88642
- image display, X-Y address technique, multilevel voltage select system 77−74381
- image display medium, changing mechanism identification, IR method 79−74389
- immunoelectrophoresis, fluorography of ^3H-labelled proteins 80−17220
- inert gas discharge, electrophoresis anal. using plasma kinetic eqns. 77−43100
- inert gas mixture, high-pressure arc characts. 77−19797
- insulating liquid, fields up to 3×10^7 Vm^{-1} 79−57241
- insulating particles in insulating liquids, high field electrophoresis 80−90865
- insulating particles in insulating liquids, high-field electrophoresis, basic transport mechs. 80−93767
- ion focusing for chem. anal. *(German)* 79−57334
- Ioncote coating process, using field emission systems for corrosion and abrasion protection *(German)* 80−76205
- iontophoresis circuit isolated current monitor for cell membrane studies 77−60311
- iontophoresis device for safe elec. administration of ionised drugs 78−31965
- iontophoretic isolated current monitor for cell membranes 77−25626
- isotachophoresis, capillary tube method *(Japanese)* 77−73451
- isotachophoresis, principles and appls. 78−31738
- isotachophoresis process 79−25784
- isotachophoretic analysis, development of data processing system *(Japanese)* 79−24873
- keratin, mammalian, organisation of polypeptide chains 77−4981
- laser Doppler, high current-density electrodes 80−89500
- latex sphere aggregates, dynamic shape factors determ. by sedimentation vel. meas. in capacitor 80−26063
- liquid and spherical particle permittivity meas. by dielectrophoretic levitation 79−17447
- liver cells, regenerating, specific resist. and electrophoretic mobility, effect of RNase and neuraminidase 77−25402
- living cell dynamic dielectrophoretic levitation 80−51062
- LKB Multiphor, universal system for electrofocusing, electrophoresis, immunoelectrophoresis and isotachophoresis 80−7888
- lymphocyte sensitisation meas., electrophoretic mobility test improvements 79−25138
- macromolecule, charged, in external elec. field, spherical case 80−75145
- mass transport, apparatus 78−85168
- mast cells, rat, electrophoretic mobility distrib. alteration after immunological activation 80−67047
- metal drops in electrolytes, electrocapillary motion, elec. field strength effects 78−3346
- metal-polymer deposit, simultaneous electrophoretic deposition and electrochemical precipitation 79−56938
- microelectrophoresis, AC apparatus 77−29237
- microelectrophoretic measurements using rotating prism in microscope 77−21389
- microiontophoresis apparatus, circuit to automatically supply current balance 80−41341
- microscope, PARMOQUANT, biological appl. 79−79700
- microscope, test results with PARMOQUANT 79−79701
- mobility of blood cells, measurement using wide-angle, crossed-beam laser Doppler scattering configuration 80−33011

electrophoresis continued
- motor-car corrosion protection improvement, primer paint appl. by electrocoating effect *(Dutch)* 80—71915
- nonlinear, of dielectric and conducting ideally polarisable particles 77—25270
- particles suspended in electrolytes, in crossed elec. and mag. fields, trajectories, rel. to organisms' sensitivity to fields 78—48657
- particles suspended in low-cond. liqs., field depend. of electrophoretic mobility 78—56919
- pattern analysis, FORTRAN program DIANA 2 77—40549
- percutaneous electrophoresis of amino acids and urea 78—61237
- photoelectrophoretic imaging, mechanisms 79—24758
- phthalocyanine-alkane interface, charge transfer, rel. to photoelectrophoretic image form. 80—65616
- plasma, weakly-ionised, rotating, mass separation process *(Russian)* 80—1745
- polyacrylamide gel block, instrument, biopolymer appl. 78—7549
- polydicarboxylic acids, electrophoretic and viscometric props. 80—66811
- polystyrene, colloidal dispersion in butanol, stability ratio 79—29413
- polystyrene spheres suspended in isodecane, field depend. of electrophoretic mobility 78—56919
- proteins in intercellular bridges 80—89734
- PTFE, colloidal, in butanol, electrophoretic mobility, charge origin 78—85211
- pulsed DC glow discharge, cataphoresis eqns. 78—67506
- PVC particles dispersed in vinyl chloride monomer during polymerisation 79—79250
- radio-scanning, continuous method, for ^{14}C-labelled compounds 77—70367
- radiocolloid particles, size and charge distribs. nuclear medicine appls. 80—30853
- radiotracer study of zone electrophoresis, double labelling method 79—79278
- resin particles, dispersed, precipitation on cellulose fibre in elec. field 78—53262
- retrograde cataphoresis process 78—15680
- serum-electrophoresis, quantitative, by digital picture processing *(German)* 80—94306
- solutions, fluctuation transport theory 78—70057
- starch-gel electrophoresis, improved vertical apparatus 77—4961
- suspended particles in estuarine and coastal waters, electrophoretic mobility and surface charge 80—36331
- suspension, in nonpolar dispersion media, particle size and number conc. meas. 80—9082
- suspension of charged particles in ionic solutions, elec. cond, 80—7866
- suspensions, electrophoretic mobility, mass transport method 78—35696
- synaptic vescles and synaptosomal membranes, electrokinetic props. 80—67055
- tibosomal RNA interacting sequences, expt. determ., method and results 80—3586
- tissue regeneration by electric potentials 80—41308
- transition metal complex ions, charges in HCl aq. soln. *(Japanese)* 78—35698
- transition metal complex ions, in HCl aq. soln. *(Japanese)* 78—35697
- transition metal complex ions in aq. HCl, temp. gradient chromatography *(Japanese)* 78—61120
- α-tropomyosin, specific splitting at cysteine-190, physicochem. study of fragments 80—30647
- uniformly heated fluid between vertical parallel plates, thermal convection 79—98727
- water drops, impaction and electrical effects on collisions with spherical particles 78—28272
- water-immiscible liquid, membraneless electrophoresis 79—57240
- X-ray images, self-contained instant display erasable 80—22491
- yeast cell electrophoretic mobility, X-ray effect 78—31868
- zone electrophoresis, voltage gradient, rel. to resolution 78—31649
- AgBr, photographic gelatin dispersion, cryst. habit. rel. to Br^-, cyanine absorpt. 78—32908
- AgBr, sol, electrophoresis of spectral sensitising dyes, dye layering obs. 77—56240
- β-Al_2O_3, suspension, mobility and zeta potential meas. in various solvents 77—36761
- Ar-Ne, mixture, cataphoretic segregation, spectroscopic meas. 79—79261
- $^{\wedge}$Br A=84-88, fission products, rapid electrophoretic separation technique 79—54982
- C blacks, colloidal, in butanol, electrophoretic mobility, charge origin 78—85211
- Ca^{2+} effect on rat cell electrophoretic mobility after X-irrad. 79—92293
- Cr_3C_2-Ni alloys, electrophoretic deposition from conc. suspensions for P/M prep. of hard alloys 77—63575
- Cr_2O_3-Al_2O_3, solid soln., effect of Cr on point of zero charge 78—61021
- Fe_2O_3-Al_2O_3, solid solns., effect on Fe on point of zero charge 78—61021
- He-Cd^+ laser output, effects of transverse mag. field 79—86169
- He-Na mixture, low-pressure discharge, radial cataphoresis obs. 78—67507
- He-Ne, glow discharges, AC cataphoresis meas. using light spectrometry 79—60096
- He-Ne laser, output power, unsaturated gain distrib. 78—50751
- He-Ne mixture, cataphoretic gas separation in DC glow discharge with end volumes 80—79428
- Kr-Xe, glow discharges, AC cataphoresis meas. using light spectrometry 79—60096
- Na-bentonite, electrokinetic pot. determ., electrophoresis meas. 77—16868
- Ne, isotope separation by cataphoresis in DC gas discharge 80—103213
- Ne-Ar, glow discharges, AC cataphoresis meas. using light spectrometry 79—60096
- Ne-Ar discharge, transient cataphoresis, time depend. 80—38753
- Ne-Ar mixture, cataphoretic segregation, mass spectra obs. 77—52649
- Ne-N_2 mixture, cataphoretic segregation in DC discharge, mass spectral anal. 77—32799
- ^{99m}Tc-radiopharmaceuticals, ligand determ. method 80—40699
- TiO_2, suspended in highly insulated liq., photoelectrophoretic phenomenon, direct imaging system 77—54005
- ZnF_2-He positive column discharge cataphoretic distrib. of Zn and F atoms 77—68886
- ZrO_2, isoelec. points, effect of pH on electrophoretic mobility 80—35548

electrophoretic coating techniques
- dielectric films on semiconductor devices, review of deposition techniques 78—23611
- enamelling of domestic electric and gas cooking equipment using electrophoresis, installation and process details *(French)* 80—108719
- industrial prospects *(French)* 79—47941
- Ioncote coating process, using field emission systems for corrosion and abrasion protection *(German)* 80—76205
- pigment separation and deposition, electron sensitive *(German)* 80—108365
- porcelain enamel, electrocoating, appl. 79—33947
- WC-Co particles deposition, on metal surfaces, wear resistant coatings preparation *(German)* 80—2969
- CrC electrophoretic coating, electric field strength effect on deposition rate 78—19677
- CrC_x, electrophoretic coating deposition on coaxial surfaces 78—11528
- MgO, electrophoretic deposition on stainless steel mandrel 80—11580

electrophoretic coatings
- polymer electrophoretic coating, effect of silicone additive on electrophys. props. *(Russian)* 79—15615
- waveform analysis for blood serum protein composition determ. 78—64928
- WC-Co particles deposition, on metal surfaces, wear resistant coatings preparation *(German)* 80—2969
- X-ray image intensifier output screens 78—4755
- X-ray sensitive imaging device 80—22501
- CrC electrophoretic coating, electric field strength effect on deposition rate 78—19677
- Cr_3C_2 electrophoretic alloy coatings on C steel, sintered, struct. form., Ni-P undercoat effect 80—61027
- Cr_7C_3 electrophonetic coatings on steel, sintering 80—66707
- Cu_2S-CdS thin film solar cell fabrication by electrophoresis 80—55862
- ThO_2 electrophoretic coating for poisoning resistant Ir filament electron gun 78—54493

electrophotography
- amorphous materials appls. 80—107693
- autoionography of beta-emitting radionuclides distrib. on thin-layer chromatograms 78—20126
- biological objects obs., high-frequency discharges effects *(German)* 80—17216
- bit capacity limitation, toner size and deposition 80—62762
- chalcogenide glasses, electronic props., xerographic use 80—20242
- charge transfer electroradiography, physical processes 79—17594
- charged particle electrophotography, role of radiation and system noise on granularity and DQE 79—17537
- colour slide film, process *(Japanese)* 77—71394
- conference, Rochester, USA, 1978, Aug. 79—20394
- conference, Washington, USA (Nov. 1977) 79—2849
- contact copying of microfiches and microfilms 80—47127
- contact press. in mag. brush developer 79—75633
- copier photoconductor drum cooling methods 78—62245
- corona charging devices, characterisation and modelling 79—19110
- corotron, DC two dimens., numerical modelling 79—19109
- developer, size distrib., particle charge and toner-carrier force *(German)* 80—73493
- developer neutralisation mechanisms 78—16863
- developing electrographic images using charged dielectric vapours *(Russian)* 77—67522
- development, time dependence of latent images 78—29186
- development of electrostatic image 79—17539
- development of electrostatic images, high speed 78—62249
- diagnostic imaging systems, non-silver halide, recent developments and pot. 80—41223
- document copy machine, physics *(Japanese)* 80—82842
- dry hot roll fusing technology for electrophotographic printing machines 80—37105
- dry powder toner concentration control *(Japanese)* 78—24878
- edge effect in large area imaging with ZnO binding agent layers and development electrode *(German)* 77—38045
- electret applications, book contrib. 80—80709
- electrodynamic aspects *(Japanese)* 80—13170
- electrographic image detectors, development, and applications in UV astronomy and scientific research 80—43465
- electrographic processes, increasing the effective sensitivity *(Russian)* 79—6211
- electrographical imaging of objects, in electric discharge *(Czech)* 80—37104
- electron spectroscopy for chemical anal., appls. to materials for electrophotography 78—92565
- electronic imaging hard copy methods and printing systems 80—47134
- electrophoretic developers for pictorial electrophotography 79—17523
- electrophoretically developed images, applicability of Siedentopf's law 79—45881
- electroradiographic image laser readout 80—41225
- electroradiography, image quality, charge transport random fluctuations influence 78—66015
- electrostatic aspects, review 78—25768
- electrostatic calculation of electrographic development 80—77888
- electrostatic duplication master, using organic photoconductor memory effect 79—17521
- electrostatic readout, use of powder or liquid toners 78—70212
- electrostatic recording head using indirect discharge 80—47138
- electrostatic X-ray imaging, book contrib. 80—36112
- electrostatic X-ray imaging techniques for medical and industrial appl. 79—79645
- exposure modulation during photoprinting of highly-contrasting negatives by electronic copier *(Russian)* 80—292
- film evaluation apparatus 79—93244
- films, surface charge meter using electrostatic induction *(Japanese)* 80—77886
- frosted thermoplastic images, formation and characteristics *(Russian)* 80—47133
- fused xerographic images, optical density model 79—17550
- fusing xerographic toner images against bare metal surfaces, release agent chemistry 79—17528
- fusing xerographic toner images against bare metal surfaces, release mechanisms 79—17527
- halftone noise characterisation, meas. technique using scanning microdensitometer 79—26151

electrophotography continued
- heat transfer in toner during flash fusing, study using electrical analogue networks 80—47139
- high sensitivity electrophotography 78—29187
- high-speed non-impact printer, design and principles 78—21247
- high-speed non-impact printer, optical character generation requirements 78—21246
- image development by an electrode insulated from electrophotographic layer substrate *(Russian)* 79—26170
- image granularity, multilayer model 78—21242
- image information content and noise analysis 80—101861
- imaging process efficiency and quality, electrophotographic process, electronographic cameras and image intensifiers 78—78932
- imaging system requirements interacting with copier architecture 80—77895
- ink transfer analysis 79—17516
- insulating particles in insulating liquids, high field electrophoresis 80—90865
- insulating particles in insulating liquids, high-field electrophoresis, basic transport mechs. 80—93767
- insulating webs and conducting rollers, electrostatic interaction 80—47137
- ion modulator imaging process, long-term memory 79—26158
- ionography, high-press. gas, amplification and resolution degradation 77—70532
- ionography, optimisation of design parameters 78—31888
- ionography, powder cloud development technique 77—56462
- KC film digital recording performance 78—78024
- laser recording and information handling, seminar, San Diego, CA, USA (Aug. 1979) 80—101663
- laser unconventional recording materials for He-Ne laser 80—18040
- latent and developed electrophotographic images, stat. correl. 77—71400
- latent electrostatic image transfer *(Japanese)* 80—73487
- latent electrostatic images and electrophoretic development 79—17522
- layer, electrophotographic, electrostatic force calc. *(German)* 80—42285
- light-scanned image convertor with electronic readout 79—71554
- liquid developer, permittivity and conductivity meas. *(German)* 78—62257
- liquid developer, standardisation of props., manuf. process *(Czech)* 79—30592
- liquid immersion development 80—31920
- lithographic coated polyester panchromatic plate system 80—13172
- magnetic brush development characteristics for xerography 80—4798
- magnetic brush xerographic development, image noise 79—17526
- materials sensitivity, deterioration of coloured images due to illum. in diaprojector *(Russian)* 80—62782
- metal-photosemiconductor-insulator multilayered structure, charge pattern formation during recharging 80—47129
- metal-photosemiconductor-insulator multilayered structure, optical image recording, As_2Se_3 photosensitive element 80—42286
- narrow band gap semiconductor electrophotographic processes 80—13169
- noise perception and level of graininess 80—62753
- optical data storage with transparent electrophotographic film 77—71946
- optical storage materials and methods, conf., San Diego, USA (Aug. 1977) 78—71171
- organic double-layer electrophotographic system, photoconduction mechanism 79—26161
- organic photoconductors, charge acceptance calc. 78—80020
- organic xerographic photoconductors, bimolecular recomb., reciprocity failure 80—49798
- PET-CdS photoreceptors, air space effects on electrophotographic props. *(Japanese)* 79—44962
- photo migration imaging, anal. 78—86370
- photo-response characts. of electrophotographic plates in nanosecond periods 78—62251
- photoactive pigment electrophotographic imaging system, dark charge exchange process 80—62758
- photoactive pigment electrophotography, photographic characts. 77—22605
- photoconductor, bimol. recomb., reciprocity 77—51775
- photoconductor for charge transfer electrophotography 78—65989
- photoconductor image charge transfer to electrographic film 80—101864
- photoconductor-insulator interface, carrier injection 80—24970
- photocopying appl., improvement of information content 79—21837
- photoinjection in chalcogenide semicond.-PVK systems 79—19633
- photoinsulator-air-dielectric surface charge density determ. 78—2549
- photoreceptor, insulator overcoated, electrophotographic processes 79—2858
- photoreceptor, near IR sensitive 80—48369
- photoreproduction grating with non-regular element struct., freq.-contrast characts. *(Russian)* 79—58825
- photosensitivity of electrophotographic molecular recording media during nanosecond exposures *(Russian)* 80—73516
- photosensor array, solid-state, for electronic imaging 79—21836
- photothermoplastic devices, conventional and self-developing, sensitivity and development 79—44958
- physical processes, review 79—17536
- pictorial electrographic printing, tone reproduction and screen design 80—62752
- pictorial electrophotography, image quality and development 79—17538
- plate with polyvinylcarbazole overlayer and CdS-resin layer 77—61146
- poly(N-vinyl carbazole) sensitisation with Se, purification effect on electrophotographic characts. 80—49825
- poly-n-epoxypropilcarbazole electrophotographic layers, photogeneration and drift mobility 79—19631
- poly-N-vinylcarbazole, electrophotographic film, dark discharge 78—34864
- polymer, molecularly doped, photosensitisation processes 79—2857
- polymeric double layer system, high field cond., xerographic characts. 79—95448
- polymeric electrophotographic developer, triboelec. two-step decay scheme 79—80711
- polyvinyl acetal derivatives of 9-anthraldehyde, preparation and electrophotographic props. 78—29183
- polyvinylcarbazole xerographic film, discharge kinetics 77—13810
- polyvinylidine fluoride, corona charging at 12.5 kV, obs. 78—92027
- powder-bead mixture, triboelec. charging, incremental charge-mass characterisation 78—17833
- process configuration, architectures, review 78—29188
- PVK/PVK-TNF/TNF.PMG system, electrophotographic characts. 80—62759

electrophotography continued
- pyrazoline-based carrier transport layers use in layered photocond. systems for electrophotography 77—69375
- radiography, electrophotographic imaging using high purity Al_2O_3 78—35936
- recording media, high resolution, expt. characts. 78—70208
- relief plate preparation by subtractive development 79—21831
- resolution of electrophotographic films *(Russian)* 77—49800
- review, history, present status and future potential 79—2854
- gamma-Ruticon image buffer, imaging props. 78—66915
- scientific basis of process 80—68287
- semiconductor, amorphous, photoelectric properties in ionic contact regime 77—76873
- semiconductor amorphous and organic layers, injected charge dirft and localisation *(German)* 78—91794
- sensitometry, conference, Binghamton, N.Y., USA (Sep. 1976) 77—30214
- single fine line, reproduction accuracy, direct and reversal development 78—29194
- solid area imaging response, math. model 79—2856
- solid state camera speed electrophotographic KC film 78—70211
- solid state electrophotographic imaging with ionic dielectric X-ray receptors 78—16899
- spectrographs with electronic pulse readout 79—26147
- spreading phenomenon in dry powder electrophotography 78—63904
- surface potential microprofile meas. instrument 77—45913
- thermoplastic layers with fast heating, discharge process 78—49920
- thermoplastic recording material, latent image and surface deformation *(German)* 80—42284
- toned paper reflectance 79—2855
- toner, recycled in xerographic development system, cycle distrib. 80—62760
- toner dispersions, positively charged, electrokinetic props., electrostatic image development 79—80713
- toner electric field detachment, development in xerographic system 79—17525
- toner-carrier pair, surface interaction model for triboelectrification 79—17524
- transfer of electrostatic images 79—26162
- transparent electrophotographic film for high-resolution holographic recorders 80—102671
- transparent electrophotographic films, information recording 78—70210
- transvenous xeroarteriography, peripheral blood vessel angiography *(German)* 79—2126
- triboelectrical properties of toner and carrier 80—18039
- two-component developer discharge and contact interaction *(German)* 78—62258
- vacuum deposition, from strip source, onto arbitrarily oriented rotating cylinder, for xerography appl. 78—95696
- Western Europe electrophotography developments (1974-77) 79—71556
- X-ray images, electronic recording 80—62815
- xerographic and insulator-photoconductor sandwich systems, comparison 79—17520
- xerographic cascade flow, carrier bead velocity distribution meas. probe 80—47136
- xerographic copy line profile meas. using microcomputer/microdensitometer system 78—74088
- xerographic developer, collisional dynamics of charge exchange 77—10122
- xerographic development, transfer function model 78—65991
- xerographic discharge in binder layers 80—47140
- xerographic image, measurability of structure fluctuations 77—18119
- xerographic images on paper, optical model 79—17549
- xerographic papers, electrostatic props. 78—78852
- xerographic toner, charge optimisation 77—182
- xerography, amorphous Se electronic props., defects 79—97454
- xerography and AgX photography compared *(Japanese)* 78—24876
- xeromammography, image optimisation, detailed systems-based anal. 79—39483
- xeromammography exposure timing 78—40291
- xeroradiographic imaging linearity and MTF applicability 80—4825
- xeroradiography, for teaching 78—45449
- xeroradiography for direct field control in radiotherapy 77—81551
- Al-As_2Se_3-Al layers, photoelectrochem. process 77—76953
- AlH_3, elec. cond. meas., V/I characts. *(Russian)* 77—51752
- AlH_3, localised states spectrum, photosensitivity 79—78135
- As_2S_3, amorphous film, light enhanced vaporisation, photolithographic process, photographic appls. 77—5949
- As_2Se_3, amorphous, dark discharge, relaxation current meas. *(German)* 80—49760
- As_2Se_3, amorphous, electrophotographic props., photodecomp. effect 78—49918
- As_2Se_3, film, amorphous, fatigue and recovery of electrophotographic props. 78—21253
- As_2Se_3 layers for electrophotographic use *(German)* 80—42283
- As_2Se_3 vitreous films, crystn. stimulated by org. subst. and electrophotographic parameters 77—76319
- B multidionate acceptors 79—19632
- $CdGa_2Se_4$, electrophotographic props. *(Russian)* 78—59100
- $CdInGaS_4$, pure and Cu-doped, electrophotography layers *(Russian)* 80—68282
- CdS powder layers, surface pot. dark decay, moisture sorption and heat treatment effects 80—18038
- $CdS_{1-x}Se_x$-Cu, electrophotographic props. 77—45910
- β-Cu phthalocyanine electrophotographic props. rel. to particle size *(Japanese)* 80—13171
- HgI_2:CdS binder layer photoreceptor, surface charge characts. thickness depend. 80—57409
- HgI_2-CdS binder layers, surface charge characts. for electrophotography 77—10123
- $LiNbO_3$, photovoltaic effect, latent-image formation kinetics, electrophotography appl. 78—84246
- NiO, interface for xerographic Se photoreceptor on flexible Ni foils 78—29184
- PbO, binder layer, properties of radiographic system 78—21238
- Se, amorphous, electronic props., xerographic use 80—20242
- Se, amorphous, evap. layers, electrophotographic props. depend. on thermal treatment of initial material 77—76978
- Se, amorphous, interface with poly-N-vinyl carbazole, photoinsulator-air gas-dielectric system, charges on surfaces 79—67407

electrophotography continued
Se, amorphous electrophotographic layers, resolution parameters 80—31926
Se, appl. to xerography 80—57415
Se, electrophotographic characts. of films rel. to viscosity of bulk specimens *(Russian)* 80—73505
Se electrophotographic films, ageing effects on structure and properties 77—47699
Se electrophotographic film current density/voltage characteristic rel. to substrate temp. *(German)* 77—55629
Se layer crystallinity meas., combination microwave resonator method *(Russian)* 78—22652
Se layers, latent electrophotographic image, formation mechanism *(Russian)* 79—26157
Se photoreceptors, phthalocyanine sensitized, elec. cond., charge decay characts. 80—15630
Se, photosensitive particle migration, electrophotographic film structure and process 80—101863
Se plate, sensitivity exam. for xeroradiography appls. 77—45909
Se, polycrystalline trigonal layer, freq. depend. elec. behaviour and its relationship to xerographic performance of Se particle contact photoreceptors 79—82640
Se spheres embedded in polymer matrix, electrophotographic film, optical props. 78—83055
Se, X-ray sensitivity, induced photocurrents, xeroradiographic meas., pair creation energy 80—22490
Se xeroradiography films, photosensitivity recovery from X-ray induced fatigue 77—2709
Se:As X-ray plates, electronic transport *(German)* 80—80290
Se-As alloys, appl. to xerography 80—57415
Se-Bi-I, amorphous, high sensitivity visible-near IR photoconductor development and characterisation 78—39153
Se-binding agent electrophotographic film characteristics and sensitivity *(German)* 80—4789
SeTe/Se multilayer photoreceptor, transient photoconductivity *(Japanese)* 80—75596
Si, amorphous, as photo-receptor for electrophotography 80—47126
Si:Au, impurity photocond., for IR electrophotographic system 77—24589
TiO_2, suspended in highly insulated liq., photoelectrophoretic phenomenon, direct imaging system 77—54005
ZnCdS:(Cu+Ag) binder layer for electrophotography 80—4797
ZnCdS:Cu, binders effect on electrophotographic characts. 79—80712
ZnCdS:Cu, high field photoconduction in binder layer 79—47121
ZnCdS-Ag binder layers, electrophotographic characts. eval. for use in charge transfer electrophotography 77—41714
$Zn_{0.35}Cd_{0.65}S$ binder layers, doped and undoped, xerographic characts. 79—56288
$Zn_xCd_{1-x}S$:Cu crystallophosphors, spectra of IR electrophotographic sensitivity *(Russian)* 80—50423
ZnO binder electrophotography, tone reproduction and copy quality *(German)* 78—62259
ZnO binder layers, regeneration of sensitising dyes 78—21241
ZnO, dye adsorption, contact pot. difference, appl. in electrophotography 80—27365
ZnO dye sensitisation in electrostatic photography 79—67404
ZnO, electrophotographic layer, fatigue recovery 79—63321
ZnO, fatigue of electrophotographic layers 79—63320
ZnO layers, electrophotographic processes 80—4802
ZnO, light sensitivity rel. to local internal fields *(Russian)* 78—49932
ZnO, particulate, Dember effect, rel. to electrography 78—95314
ZnO, red, electronic and opt. props., electrographic props. 77—57419
ZnO resin layer leakage current in corona charging *(Japanese)* 78—24877
ZnO sensitized photolayer, overall spectra of local electronic levels 79—23933
ZnO:Li_2O single crystal, triboelectric charge and photodischarge obs. 79—82663
ZnO-binder system, reciprocity failure, photoconductivity 78—39151
ZnO-polystyrene photoreceptors sensitised by β-Cu phthalocyanine 79—17552
ZnO-resin electrophotographic layers, light decay curve empirical eqn., reciprocity law failure *(Japanese)* 79—39158
ZnO-resin photosensitive layers, dark decay mechanism of corona charge *(Japanese)* 79—24002
ZnS:Cu crystallophosphors, spectra of IR electrophotographic sensitivity *(Russian)* 80—50423

electrophotoluminescence *see electroluminescence; photoluminescence*

electrophysiology *see bioelectric phenomena*

electroplated coatings
additive-free hard Au for electric connectors and PCB contacts 80—108718
adhesion, determ. by Jacquet peel test 80—50815
barrier layers, against diffusion 80—66444
black chrome, electroplated layer, field ion microscopy study 79—28246
black Cr and Ni electrodeposit spectral selective props. for solar absorbers 79—62036
brittle coating, ductility meas., four point bend test 78—48577
deposit-substrate systems, adhesion testing 80—50814
diamond-based, fabrication and wear resist. 80—40576
diamond-composite abrasion-resistant coatings 79—61737
electrolytes for Ag-Sb alloy coating deposition *(Bulgarian)* 80—93763
galvanic coating thickness gauge performance characteristics 77—32746
plastic, metal electroplated, durability and struct. 78—3242
residual stresses, effect of triacetylpyridine and polyethylene glycol additives to NH_4Cl electrolytes 80—21190
solar photothermal non-selective and energy control films coatings 80—26157
stresses meas., internal, effects in Ni and Zn *(German)* 78—56049
testing and control *(German)* 80—2967
thickness testers, Kocour electronic models, evaluation 79—21702
thickness tests, Indian and international standards 79—8405
tinplate, electron reemission Mossbauer spectra 79—19820
wear resistance, appl., survey 78—72913
Ag electroplated lead frames, surface struct. rel. to bonding behaviour, IC prod. *(German)* 79—11010
Ag, films, stress meas. using holographic interferometry 80—20806
Ag-Cu surface alloyed films, laser melt quenched, microstruct. 80—76423

electroplated coatings continued
Au, electrodeposited and sputtered, hard, reactive softening, X-ray diffr. studies 80—100414
Au, electroless deposition, substrate structure influence 77—8771
Au electroplated layer, dropwise steam condensation, thickness depend. 79—46791
Au, immersion plating on Al, adhesion and contact resist. 79—39033
Au, microstruct. and hardness, effect of thickness and deposition conditions 80—20057
Au on Cu, water vap. adsorption 77—69168
Au thickness measurement with beta-ray backscattering, influence of parameters *(Slovene)* 78—6860
Au, using polyphosphate, citrate-phosphate and sulphite baths, comparison w.r.t. internal stress and grain size 79—7756
Au-Co, 'polymer' inclusions, chem. identity obs. 79—37931
Au-Co electrodeposits, heating effect on microstruct. and surface topography 77—43456
Au-SnNi-Au ohmic contacts on n-GaAs 78—35319
Co, plated film, magnetisation and mag. interface anisotropy 77—85510
Co-Sn alloy, oxide films, XPS/AES expts. 79—15862
Co-W alloy electrolytic coatings, heat treatment effects on coercivity, hysteresis and structure *(Russian)* 80—60381
CoO solar absorber surface spectral selectivity rel. to temp. and UV ageing 79—62027
Cr coatings, electrodeposition, conditions rel. to H_2 conc., internal stresses 77—1933
Cr electroplated steel, laser treatment 80—21191
Cr, labelled, coating on Ni-Cr alloys, component transport numbers determ. 77—62667
Cr plated steel, factors influencing durability 80—108643
Cr-Cr_2O_3, black, electrolytic deposited, characterisation and thermal stability *(French)* 80—55898
Cr-Cr_2O_3, black chrome films, surface microstruct. rel. to optical props. in solar absorbers 79—52036
Cr-Cr_2O_3, black chrome solar selective absorber, microstruct. 79—56875
Cr-Cr_2O_3, black chrome electroplating for solar energy photothermal conversion, prep. and struct. 79—74544
Cr-Cr_2O_3, black chrome electroplating for solar energy photothermal conversion, optical props. 79—74545
Cr-Cr_2O_3 black, electroplated solar collector coatings, high temp. optical and struct. degradation 80—66995
Cr-Cr_2O_3 black solar absorber surfaces, microstruct. rel. to electroplating parameters 80—61418
Cr-Cr_2O_3 chrome black, selective surface, thermal emittance, solar absorpt., refl., and roughness 79—79406
Cr-plated Cu crystal, const. strain rate tests, yield stress 79—83276
Cr_2O_3/Cr solar-absorber surfaces, chemical and struct. anal. 79—95283
Cu electrodeposits, bright, low conc. of ions effect on internal stress 80—25909
Cu, electroplated surface roughness and brightness rel. to periodic reverse current 79—96201
Cu film, on W substrate, cementation, vac. deposition, and electroplating, growth characts. 79—95291
Cu, levelling kinetics, interferometric investigation *(Bulgarian)* 78—79864
Cu, Ni alloy protection against hydrogen embrittlement, aerospace engine appl. 80—76416
Cu-Al_2O_3 coatings, electrodeposited, dispersion hardened, exam. of props. 79—34181
Cu-Al_2O_3 composite coating, codeposition kinetics from $CuSO_4$ plating bath 78—15555
Fe, electroplated with soft Fe coating, fatigue fracture, struct. characts. 80—55524
Fe, membranes, effect of electrodeposited metals on H permeation, proposed catalytic mechanism 78—53252
GaAs, shallow-homojunction solar cell by MBE, conversion efficiency 80—30476
Ni, black, solar collector selective coatings, optical and thermal props. 79—62028
Ni, change in twin faults during growth, X-ray study 79—65334
Ni coating hardness rel. to sulphamate electrolyte selection *(Bulgarian)* 78—88552
Ni, electrochem. overgrowths, role of substrate dislocations and grain boundaries in nucleation and growth 79—51454
Ni, electroless plating, oxidation kinetics 78—95847
Ni, electrolessly deposited, structural comparison with electroplated films 79—23869
Ni, electroplated, fuchsin additive effect on low-temp. annealing characts., resist. meas. 77—32725
Ni, electroplated layer, field ion microscope study 79—28246
Ni, electroplated layers, internal friction and ΔG effect, rel. to bath comp. and annealing 78—19296
Ni epitaxial monocrystal structure rel. to externally applied stress 77—76708
Ni, labelled, coating on Ni-Cr alloys, component transport numbers determ. 77—62667
Ni, plated film, magnetisation and mag. interface anisotropy 77—85510
Ni, struct., electrolyte anions influence 80—20056
Ni-In alloy, on Kovar, vacuum seal for borosilicate glass appl. *(Italian)* 80—40621
Ni-NiO_x-NiS_y, black Ni, struct.-depend. thermal and optical props., rel. to solar thermal conversion 79—79404
Ni-P alloy, amorphous, NMR expts. and interpretation 79—8060
Ni-plated Fe, surface film softening in single slip orientation 77—32719
Ni-TiO_2 electrochem. composite coating phase composition and microhardness factors *(Russian)* 79—91598
Pd, props., deposition parameters influence *(German)* 80—20808
Pt, Schottky barrier metallisation, Au diffusion, AES obs. 79—14968
Sn/CU electroplated bimetallic films, interfacial reaction 80—96765
Sn-Ni, electroplated, passive layer, ESCA study 78—23867
Sn-Ni, equiatomic, metastable, transformation kinetics, Avrami parameters calc. method 78—92239
Sn-Ni, etch rates using quartz cryst. microbalance, contact resist. 77—59981
Sn-Ni metastable alloy, surface film comp., time depend., XPS 78—60870
SnNi electroplate, anal. by SIMS, ion scatt. spectrometry, and Rutherford backscatt. 78—95979
Ti-Cu, evaporated adhesion after electroplating 79—82475
Zn, chromated, electroplate on steel, corrosion, effect of chromate content 79—20286

electroplated coatings continued

- Zn deposition by pulse plating *(German)* 80—60792
- Zn, electrodeposited, planar stress relaxation 79—24563
- Zn, residual stress diagrams 80—16588

electroplating

- acid-Cu electrolytes, effect of periodic reverse current process on deposit props. 79—33951
- anode behaviour in cyanide-Ag baths *(German)* 80—61103
- automatic barrel line type ATS closed system, small parts electroplating, after-treatment and drying *(German)* 80—84861
- bright plating, from zincate electrolytes, progress 80—66442
- brush plating, for wear resist. appls. 80—66443
- contamination control by activated C 79—91822
- current distribution cell for qualitatively predicting differences in barrel plating performance of electroplating solutions 80—71917
- electrocoating, cell design, Fourier transform soln. of Laplace eqn. 78—76609
- electrocoating from molten salts 79—83394
- electroplating method for high-temp. stress meas., fundamentals *(Japanese)* 78—15616
- embrittlement protection of Ni alloy, by Cu electrodeposits, aerospace engine appl. 80—76416
- injection laser diode mode structure enhancement by backface plating 80—64056
- laser enhanced maskless pattern generation, convective mass transport theory 80—20803
- levelling, geometric and true, in electroplating, study using stylus methods 80—66445
- magnetostrictive pulse-producing wire plating 80—2618
- metal barrier-layer protective deposits, inorganic finish selection and appl. 80—71812
- metal distribution in electroplating systems 79—91599
- metals, for engineering components and structures 78—35587
- mirror preparation as student expt., electroless plating of Cu on treated glass 80—36817
- plating discrete microparticles for laser-fusion targets 79—15841
- progress in electrodeposition and related processes, (1952-1977) 78—27420
- pulse electrolysis, theoretical aspects 80—85191
- pulsed plating vs direct current plating, quantity of metal deposited 80—2968
- Schottky contacts, submicron, high-field pulsed electroplating technique 80—49899
- solar energy appl., 1979 prospects w.r.t. economics 80—3490
- steel, C, filaments, Cu platings porosity determ. 79—70239
- steel, Cr-Mo, oxidised, mechanism of crack decoration of oxides by electrodeposition 80—97560
- steel, electroplating and failure assoc. with H-embrittlement, in situ anal. 78—7299
- steel, mild, panels, electrodeposition painting, effect of surface pinholing 79—43493
- steel, mild wire nails, with Ni, Zn and Cu, barrel plating efficiency 80—100964
- surface finishing for protection and component build-up 78—35586
- testing and control procedures *(German)* 80—2967
- thin film prep. for solar energy utilisation 80—84847
- wires, uniform, rotating cell design with helicoidally shaped internal surface 80—80990
- Ag coil for liq. stream thermostat 78—8402
- Ag, concentration analysis in presence of cyanide, electroanalytical technique 77—1965
- Ag halide complexes on $In_{2-x}Sn_xO_{3-y}$ contacts, appl. to display struct. 79—15435
- Ag, manufacture of semiconductor diodes using electroplating 79—33952
- Al, new method 79—70228
- Al on brass from $AlCl_3/NaCl$ melt 77—77434
- ^{241}Am thin source preparation 80—18730
- As compounds, conditions of operation, expt. *(Bulgarian)* 77—4744
- As, conditions of operation and quality of coatings, expt. *(Bulgarian)* 77—4744
- Au and Sn-Pb alloys, comparison *(French)* 80—89158
- Au, concentration analysis in presence of cyanide, electroanalytical technique 77—1965
- Au, hard in 2 μm layers 79—74104
- Au, immersion plating on Al, adhesion and contact resist. 79—39033
- Au plated Ni powder for electroplating conductive pastes 79—95957
- Au, pulsed potentiostatic deposition from Au(I) sulphite solns. 78—15321
- Au, selective, on Pd-Ti conductor patterns, Si IC manufacturing appls. 79—95951
- Au thickness measurement with beta-ray backscattering, influence of parameters *(Slovene)* 78—6860
- Be, surface prep. by zincating 77—40397
- Co concentration monitoring, by automatic colorimeter 80—105691
- Co, electrodeposition using insoluble anode 77—8772
- Cr, black, plating process for solar selective absorber 79—62031
- Cr particulate layer on Cr_2O_3, high solar absorpt. characts., selective surface electroplating 78—87111
- Cr trivalent plating solns., prod. experience 80—71606
- Cr-Cr_2O_3, black chrome electroplating for solar energy photothermal conversion, prep. and struct. 79—74544
- Cu adhesive layers on ferrite substrates, prep. *(Polish)* 78—35537
- Cu and Zn, using cyanide copper baths, Rochelle salt influence and analysis *(German)* 77—25328
- Cu barrel plating C steel nails, efficiency 80—100964
- Cu, concentration analysis in presence of cyanide electroanalytical technique 77—1965
- Cu electrodeposition in cylindrical pores by pulse plating 80—81330
- Cu, electroplated surface roughness and brightness rel. to periodic reverse current 79—96201
- Cu electroplating method for sensitizing stress meas. *(Japanese)* 80—68197
- Cu, onto C fibre reinforced epoxy resin, coating props. *(Japanese)* 77—36412
- Cu powders, electroless tinning 80—25607
- Cu, raising temp. by gelatin addition to plating soln. *(Japanese)* 79—38754
- Cu-Al_2O_3 composite coating, codeposition kinetics from $CuSO_4$ plating bath 78—15555
- Cu-Ni, electrolytic plating 80—35425
- Fe plating cathode current distrib. influences *(Russian)* 79—96197

electroplating continued

- Fe powder, electrolytic Ag plating 79—66017
- Fe-Ni-Co coating electrodeposition optimum conditions *(Russian)* 79—83292
- γ-Fe_2O_3 powders, mag. props., effect of Co plating 79—69699
- In-CdS ohmic contacts, by electrolytic deposition 77—8194
- Ir coatings, from molten chloride and cyanide 79—24640
- Nb, onto W 77—59704
- Ni *(Japanese)* 78—15617
- Ni barrel plating C steel nails, efficiency 80—100964
- Ni electrocrystallisation, inhibiting factors study 79—74105
- Ni electroless plating, effect of ultrasonic irrad. 79—33953
- Ni, electroless plating, Schottky barrier solar cell fabrication 79—83591
- Ni electroless plating of Fe powder 80—61026
- Ni electroless plating process and props. for diamond turning optical surfaces 80—1375
- Ni films, self-supporting, electroplating method of prep. 80—66436
- Ni, high freq. current appl., operating param. *(Russian)* 77—55897
- Ni plating, surface props. of Ni after each step of activation process 78—95243
- Ni, structure-internal stress relationship 80—70561
- Ni-Fe-Cr soft magnetic film plating bath 79—43465
- Ni-In alloy, on Kovar, vacuum seal for borosilicate glass appl. *(Italian)* 80—40621
- Pb-(Sb)(Sn)(Ag) anodes, film behaviour for Cr electroplating 80—35115
- Pt coatings, from molten chloride and cyanide 79—24640
- Pt, on Co-Cr-Al-Y coating, composite corrosion-resist. coating formation 78—11437
- Pt-Ir alloy coatings, from molten chloride and cyanide 79—24640
- Pt-Ti bielectrode use as insoluble anode 77—44490
- Sn, autocatalytic deposition on steel, Ni, Cu, polypropylene and ABS 80—100965
- Sn plate, quality evaluation method using elasticity characts. 77—52582
- Sn-Co alloy plating from sulphate electrolyte 80—16597
- Zn barrel plating C steel nails, efficiency 80—100964
- Zn bright coating, rack parts or bulk goods, in GTL-barrel units *(German)* 80—84862
- Zn deposition by pulse plating *(German)* 80—60792
- Zn electroplating process, optimisation 79—43452
- Zn plating electrolyte, ion-exchange chromatography of Zn, Cd and Al salts 77—16890

electropolishing *see electrolytic polishing*

electroreflectance

- cholesteric liquid crystal, Bragg light reflection induced by electric field *(Russian)* 79—51932
- cholesteric liquid crystal, incident angle dependence calc. 78—43834
- electroreflection exam., short range order in surface layers 78—6703
- highly conducting material, electroreflectance by deep field penetration 79—19864
- III-V semiconductor, d core levels, electron-hole interaction 77—11880
- MBBA-Ge interface, electrorefl., IR transmission and frustrated total internal refl. 78—19513
- metal electrodes, plasma-type electroreflection, mechanisms 77—1659
- metal-electrolyte boundary, elec. refl. and photoemission relationship 80—45211
- metal-electrolyte boundary, photoemission effect on elec. refl. 80—45212
- metal-film-electrolyte system, appl. of electroreflectance 79—42945
- metals, electromodulation spectroscopy, developments, mechs. 77—66475
- narrow-gap semiconductors, externally induced band population effects on electroreflectance 77—66114
- nematic liquid crystal, spontaneous polarisation, rel. to mol. orientation, electro-reflection meas. *(Russian)* 78—55809
- polydiacetylene, single crystal, electroreflectance and electroabsorption spectra, π-electron system and excitonic transitions 79—78653
- Schottky barrier, charge carrier conc. determ. from low-field electrorefl. spectra 77—85320
- semiconductor, doping inhomogeneity, meas. by low-field electrorefl. 77—11584
- semiconductor, heavily doped, degenerate, electroreflectance and complex interband dielec. function 80—40088
- semiconductor surface evaluation *(Japanese)* 79—82949
- semiconductors, crystal termination effects, field reversal 77—69802
- semiconductors, modulation spectroscopy in far UV 77—66516
- semiconductors, ternary and binary, composition variation determ. using electrolyte electroreflectance 78—80809
- solid-liquid interface, optical methods of study *(French)* 80—7318
- zincblende-type crystals, electromodulation, piezomodulation, theory 80—93281
- Ag (110), surface state contrib. 80—80755
- Ag (111) electrodes, electroreflectance spectra meas. 77—59591
- Ag (111) surface, obs. of surface plasmon splitting by electroreflectance spectroscopy 79—61338
- Ag, bonding of CN^-, electrorefl. exam. 77—80700
- Ag electrode, emersed, electrorefl. spectra 79—28788
- Ag, electrode pot. effects on surface plasmon excitation 78—15149
- Ag, electroreflectance spectroscopy, longitudinal surface plasmons 80—40137
- Ag film, electroreflectance effects 79—43055
- Ag, single cryst. electrodes, electroreflectance obs. in aqueous solns. 80—25342
- Ag surface, (111) and (100), crystallographic anisotropy in surface plasmon decay to photoelectrons, electroreflectance meas. 79—24052
- Ag-Al_2O_3-Au structure, electrorefl. meas. *(French)* 80—50366
- Al/tetracene/nesatron cell, electroabsorption and electrorefl., interfacial elec. fields 79—65548
- n-$Al_xGa_{1-x}As$, ion implanted films, optical and luminesc. props. 80—60699
- As_2Se_3, single crysts., fine struct. of direct gap from electrorefl. spectra 80—93280
- Au (110), surface state contrib. 80—80755
- Au electrode, emersed, electrorefl. spectra 79—28788
- Au, electrode pot. effects on surface plasmon excitation 78—15149
- Au film, electroreflectance effects 79—43055
- Au, single cryst. electrodes, electroreflectance obs. in aqueous solns. 80—25342
- Au surface, electroreflectance spectra 80—55066
- Au-GaS, Schottky-barrier electroreflectance spectra under uniaxial stress 79—56767
- $Cd_xHg_{1-x}Te$, comp. determ. by electroreflection method 77—52708

electroreflectance continued
CdS, single cryst., surface treatment effects on photoluminesc., struct. and optical props. *(Russian)* 78—15224
CdS:P, implanted, photoluminesc. and electroreflection spectra *(Russian)* 78—52544
CdSe crystals, photocurrent and electrorefl. spectra, stoichiometry defects revealed by annealing *(Russian)* 77—52134
CdSe, electrorefl. and photocurrent of ground state excitons 79—99905
CdSe:Ag, In, cryst., photocurrent and electroreflection, 77 to 300K *(Russian)* 78—23136
CdSe:Ar(N)(P), implanted, electroreflection obs. 80—40089
CdSe:Fe, exciton electroreflectance spectra, impurity effects 77—16335
n-CdTe-electrolyte solar cells, interface changes during operation, AES, electrolum. and electroreflectance meas. 79—100525
Cu (110), surface state contrib. 80—80755
Cu, electroreflectance, influence of surface microtopography 79—15437
Cu monocrystals, anisotropic surface effects, electrorefl. spectra 79—8123
Cu, single cryst. electrodes, electroreflectance obs. in aqueous solns. 80—25342
CuBr, single oriented crystals., electroreflectance, exciton transitions 77—66517
$CuGaSe_2$, obs. of energy transitions from lower valence band states 78—95576
$CuGaTe_2$ and $CuInTe_2$, electroreflectance data, direct gap obs., cryst. field splitting and hybridisation degree 78—39557
$CuInTe_2$, direct energy band gap determ., electroreflectance meas. 78—2418
$CuInTe_2$, optical transitions from valence band states 79—87416
Fe passive film AC electroreflectance and impedance obs. 78—7093
Ga-group V semiconductors, electroreflectance spectroscopy using synchrotron rad. 78—10912
$Ga_{1-x}Al_xAs$, topographical stoichiometry determ. using electroreflectance 78—23483
n-GaAs anodised MOS, electrorefl. spectra 79—99901
GaAs, carrier conc. variations using electrolyte electroreflectance, topographical features 79—99562
GaAs, carrier concentration determ. using electroreflectance 78—23483
GaAs, exciton quenching, obs. at room temp. using electrolyte electroreflectance 80—60546
GaAs, exciton-polariton reflectance spectra, exciton impact ionization and illum. intensity effects 79—42943
GaAs film, electroreflectance effects 79—43055
GaAs, implantation disorder, flux and fluence depend., electrorefl. expts. 78—83833
n-GaAs, ion implanted films, optical and luminesc. props. 80—60699
GaAs, ion-bombarded, energy band struct., electrorefl. obs. 79—19517
GaAs, k-linear coupling, E_1' transitions 78—91583
GaAs, optical modulation spectra, proton damage effect 78—76487
GaAs, Schottky barrier electrorefl. under uniaxial stress, band struct. 77—48193
GaAs, Schottky barrier ellipsometric electroreflectance spectra, energy band parameters 79—99853
GaAs, Schottky barrier electrorefl. meas. by sample rotating technique 80—60544
GaAs Schottky-barrier, linear and quadratic electroreflectance, minicomputer-controlled meas. 80—97241
n-GaAs, spectra, light induced, electrolyte and Schottky barrier techniques of meas. 80—76046
GaAs:Cr, optical modulation study of proton bombardment 78—6720
GaAs:Cr, optical modulation spectra affected by 150 keV proton beam 78—10871
GaAs-electrolyte interface, surface barrier electroreflection anisotropy *(Russian)* 80—34895
$GaAs_{1-x}P_x$ epi-wafer, comp. profile of heterogeneous struct., anodisation-electrorefl. meas. 78—26782
$GaAs_{1-x}P_x$ epitaxial layers, charge carrier conc. determ. from low-field electrorefl. spectra 77—85320
$GaAs_{1-x}P_x$, heterogeneous struct. obs. by anodisation-electrorefl. technique 78—84088
$GaAs_{1-x}P_x$, solid state diffused, conc. distrib. obs., electroreflectance and tracer sectioning obs. 80—54389
GaAs(P)(Sb), fine struct. in energy derivative reflectance spectra 79—78705
n-GaP, ion implanted films, optical and luminesc. props. 80—60699
GaP, ion-bombarded, energy band struct., electrorefl. obs. 79—19517
GaP, line shape and symmetry analysis of core-level electroreflectance spectra 77—8600
GaSb, E_1 and $E_1+\Delta_1$ edges using electroreflectance, Franz-Keldysh oscills., high mag. fields 77—66518
GaSb, electrorefl. spectra from 0.6 to 26 eV 77—20825
GaSb, interband masses of E_1 and $E_1+\Delta_1$ edges 77—32353
GaSe, anisotropy effects on electroreflectance spectra at oblique incidence 77—52042
$GaSe_{1-x}Te_x$, room temp. electroreflectance meas. 77—12361
p-Ge, 2.1 to 2.3 eV, influence of light beam 77—90169
Ge, carrier conc. variations using electrolyte electroreflectance, topographical features 79—99562
Ge chalcogenides, electrorefl. spectra 77—16282
Ge, crystal struct., influence of implanted O ions, electroreflection method 77—84783
n-Ge, direct identification of $L_3'\rightarrow L_1$ transition 77—1689
Ge, E_1-optical struct. from electroreflectance spectra 78—43897
Ge, effect of surface and nonuniform fields 78—68511
Ge, electrodeposited, X-ray, electrochem., and electrorefl. characterisation 78—14624
N-Ge, electrorefl. spectra, light induced, electrolyte and Schottky barrier techniques of meas. 80—76046
Ge, electroreflectance, field reversal asymm. at direct gap 77—69802
Ge, electroreflectance spectra, meas. on $Al-SiO_2-Ge$ struct. 77—1677
Ge, electroreflectance spectra, nonparabolicity effects of bands *(Russian)* 79—4791
Ge film, electroreflectance effects 79—43055
Ge, multioscillatory electrorefl. spectra *(Russian)* 77—8590
Ge, Schottky barrier electrorefl. under uniaxial stress, band struct. 77—48193
$Ge_{1-x}Si_x$, with Si implanted ions, optical and photoelec. props. 79—24014
GeTe film, evaporated, electro-reflectance meas. 80—11496
GeTe film 79—43055
Hg electrode, electroreflection spectra calc., electromodulation mechanisms 77—1658

electroreflectance continued
$Hg_{1-x}Cd_xTe$, props. and appls., book contrib. 77—39834
$Hg_{1-x}Cd_xTe$, surface topographic stoichiometry variations, electrolyte electrorefl. obs. 78—27249
InAs, electroreflectance spectrum 78—19479
InAs(P)(Sb), fine struct. in energy derivative reflectance spectra 79—78705
InAs(Sb), in MOS struct., electrorefl., band-population effects under heavy surface accumulation 77—48167
InGaAsP, bandgap energy by electroreflectance and photoluminesc. spectra 80—107700
InGaAsP, quaternary alloy, physical props. *(Japanese)* 80—15449
$In_{0.79}Ga_{0.21}As_{0.54}P_{0.46}$, LPE layer, electroreflectance meas. 79—24290
$In_xGa_{1-x}As_yP_{1-y}$ layers on InP, LPE and opt. props. characteris. 79—28849
$In_{1-x}Ga_xP_{1-z}As_z$, lattice matched to InP, electroreflectance obs. 80—93416
In_2O_3, thermally evaporated film, struct. and elec. props. 80—104066
In_2O_3:Sn, film, optical modulation effects in electroreflectance spectra 78—6800
In_2O_3:Sn film, electroreflectance effects 79—43055
InP, Kramers-Kronig electroreflection spectra 77—4655
InP-Au, Schottky barriers, electroreflectance spectra 77—43698
InS, prep., and elec. and optical props. 77—77361
InSb, carrier conc. variations using electrolyte electroreflectance, topographical features 79—99562
InSb, film, E_0, E_1 absorption edge size quantisation, optical and electroreflectance spectra 80—34998
InSb-CdTe solid solns., electroreflectance spectra, Brillouin zone transitions 80—7330
$Mg_xCd_{1-x}Te$, electroreflection spectra, comp. depend. 80—66230
MnZn ferrite, optical refl. and electroreflection spectra obs. 78—27262
n-Si, ion implantation causing surface defects, electroreflectance 79—19274
Na_xWO_3 bronzes, electroreflectance vs. bulk dielectric behaviour, classical model 77—66479
Na_xWO_3, metallic, optical and electronic props. 80—24398
Na_xWO_3, optical props., analysis of free- and bound-electron contribs. 77—77248
Pb electrode, combined electroreflectance and double layer effects 77—85692
$Pb_{1-x}Sn_xTe$, electroreflectance, Faraday rot., elec. band struct. parameters 77—66113
$Pb(Zr,Ti)O_2$ ceramic, surface barrier electroreflectance, hysteresis, ageing 80—80752
Sb film, electroreflectance effects 79—43055
SbSI, electroreflectance exam. 78—48145
SbSI, energy band struct. from modulation spectra 78—43892
Si (2p) optical transitions, final state effects, soft X-ray electroreflectance study 77—66553
Si, amorphous, hydrogenated film, electroreflectance study 80—88967
Si, carrier conc. variations using electrolyte electroreflectance, topographical features 79—99562
Si, electro- and thermo-reflectance spectra, line-shape anal. 79—24296
Si, electroreflectance, dielec. function, ellipsometric meas. 79—4790
Si epitaxial film, correlation between electrooptical and electrical props., IR absorpt. spectra *(Russian)* 78—60453
Si film, electroreflectance spectra, 2.8 to 5.0 eV, ion bombard. effects 77—1752
Si, ion implanted films, optical and luminesc. props. 80—60699
Si, optical critical point structures, symm. anal. by low-field electroreflectance 77—66478
Si, polarisation dependent electrorefl. spectra, surface phenomena 78—68479
n-Si, surface-barrier electroreflection, polarisation anisotropy 79—24295
Si, symmetry analysis of E_2 structs., low-field electroreflectance meas. 77—40209
Si, transition layer form., band struct., electroreflectance 77—16333
Si:Ar(B), implantation doped, electroreflection spectra 79—51983
Si:H, amorphous, refr. index, temp. depend., implications for thermoreflectance and electroreflectance 80—50290
SiC, α- and β-types, electroreflection spectra of natural and low-energy ion-bombard. surfaces 79—61340
Sn chalcogenides, electrorefl. spectra 77—16282
SnTe film, electroreflectance effects 79—43055
SnTe film, evaporated, electro-reflectance meas. 80—11496
TiO_2, electronic energy levels, electrorefl. spectra 77—24870
TiO_2 films, in $Ti-TiO_2$-electrolyte system, electroreflectance response 79—42945
TiO_2 single cryst., refl. and electrorefl. spectra 78—2870
TiO_2 single cryst., refl. and electrorefl., energy levels 78—2871
V_2O_5, electronic and band struct. and spectra, CNDO CI cluster method 79—11091
ZnTe, undoped, electroreflectance of fundamental edge, exciton levels *(Japanese)* 80—20612
ZnTe:In(Al), pure and doped, Zn vacancy energy levels, elec. and optical props. 79—4827

electrospark machining *see spark machining*

electrostatic accelerators
see also Van de Graaff accelerators
12UD pelletron, Tsukuba, performance data 78—25347
14 UD Pelletron accelerator terminal, ion optics, high energy acceleration tube 78—33321
anode for an accelerator with an inductive energy accumulator 79—26785
beam aberrations in displaced quadrupole triplet charge selector 77—38443
beam transmission in electrostatic accelerators, problems during design, operation, upgrading 78—33320
belt charging system, investigation into limited belt lifetimes 78—25355
chain charging systems, present status 78—25353
charge-exchange accelerator for fast-neutron spectrometer 80—63440
coaxial Marx generator, electron beam fusion appl. 79—76177
Cockcroft Walton 860 keV preaccelerator for SIN high current injector cyclotron 79—67975
collective field acceleration of heavy ions with intense relativistic electron beam 79—50863
Columbia Research Corporation 3 MeV, 45 kW accelerator, industrial, commercial and research applications 79—54215
conductance for the gas flow of an accelerating tube 80—102359

electrostatic accelerators continued
- coupled Marx-Tesla circuit for production of intense relativistic electron beams 77−17558
- cryogenic pump for long continuous running *(French)* 78−32829
- cyclotron energy boosters 78−33306
- direct current accelerator for 14 MeV neutron prod., thermal-mech. design 78−66383
- direct voltage accelerators, Tesla transformer design 80−27838
- direct-action accelerators with inductive energy storage and exploding conductors 80−68974
- Dynamitron 4 MV accelerator, energy calibration of analysing magnet 79−54736
- dynamitron beam anal. rel. to high precision electron and positive ion operation 78−33312
- Dynamitron fault diagnosis using (p,γ) resonances 78−29671
- Dynamitron tandem, energy calibration of heavy ion beam analysing magnet 79−59287
- electron, nanosecond-pulsed, 600 keV, using pulsed-charging of storage capacitors 79−691
- electron acceleration by inhomogeneous electrostatic RF field 78−82538
- electron gun laminar beam injection in electrostatic accelerators, 500 kV design 80−47788
- electrostatic inflector and extractor for cyclic accelerators, HV expts. 78−50421
- foil strippers, remote control system 78−29670
- folded tandem, Oxford, development from vertical injector Van de Graaff 78−25345
- fusion reactor, PDX neutral beam injector, ion accel. structural anal. 80−102375
- Hall accelerator, four-lens, pure ion beam struct. 78−66441
- heavy ion 400 kV accelerator of Thomson-CSF Central Research Lab. *(French)* 78−41880
- heavy ion beam buncher control system 79−72148
- heavy ion generator, 150 keV, for sputtering 79−697
- heavy ion low and medium energy accelerators, recent design advances 79−67984
- heavy-ion accelerators, book contrib., review 78−90003
- Heidelburg postaccelerator, computer control system 79−72214
- high gradient field tandem, Kyushu Univ. 78−25341
- implantation type accelerator, 400 kV, energy resolution, stability and calib. using (p,γ) react. 79−30604
- industrial accelerators, research at Siberian Institute of Physics 79−72032
- laddertron, Daresbury, developments 78−25356
- large stripper foil mounting method 78−29664
- low cost 500 kV Mercury preaccelerator, for heavy ions 79−76155
- low energy, high current accelerator for 14 MeV neutron production 80−99353
- mass spectrometric applications, for ^{14}C dating, negative ions 78−32917
- metal-ceramic accelerator tube development at Daresbury Lab. 78−33315
- MP belt deterioration, accelerator structure, belt capability 78−25354
- MP tandem, Yale, performance, operation since upgrading 78−25349
- MP tandem at Munich, power shaft 78−33325
- MP tandem at Munich, variable circular beam apertures 78−33324
- MP tandems, European performance characteristics, operating experiences 78−25337
- MP tandems−USA, current states, operating characteristics 78−25338
- multiply charged ion prod. at low energy 78−66437
- nanosecond pulse electron and bremsstrahlung generator 78−21308
- negative heavy ion beam production by charge exchange in metal vapour, EN tandem accelerator accessory 78−33346
- neutral beam, continuously operating, convectively cooled ion accelerator, mech. design and fabrication 80−102374
- neutral beam system, 120 keV, for fusion reactor ignition 78−66377
- Orsay MP gas handling system 78−29673
- pellatron, 14UD, Rehovot, acceptance performance, terminal charge selector, sputtering ion source, chopper-buncher 78−25340
- pellatron accelerator, 14UD design developments to improve efficiency 78−25339
- Pelletron, 14 UD, subnanosecond chopper buncher 78−33322
- Pelletron at Sao Paulo, chain breakage problem 78−29665
- pulsed high current 1 MeV electron accelerator *(Chinese)* 79−72033
- pulsed high current 60 keV electron accelerators 79−26784
- pulsed proton gun, microsec. operation 79−89510
- RF ion source, modified extraction geometry 78−33349
- Scandinavian low output isotope separator, upgrading to 300 kV 78−66008
- sputter heavy ion source for tandem accelerator 78−33305
- stripper foils, energy straggling of heavy ion beams at tandem energies, C foil appl. 78−33353
- suppressed accelerator tube installations, design, performance 78−33319
- tandem, 30 MV, at Daresbury, construction 78−25350
- tandem, for heavy ions, pulsing system 78−33323
- tandem, nuclear safety facility at Daresbury, shielding methods for insulators, ICs, other components 78−33318
- tandem accelerator tubes, characts., performance 78−33314
- tandem accelerators as injectors to heavy ion boosters 78−33329
- tandem EGP-10-1, Rossendorf, physical parameters 78−25344
- tandem electrostatic 30 MV accelerator, nuclear struct. facility at Daresbury Lab. 78−55056
- tandem for sensitive C analysis, design implications of stable N$^-$ prod. in sputter ion source 78−33350
- tandem Holifield heavy-ion research facility 78−25351
- tandems, heavy ion linac boosters 78−33328
- TFTR type neutral beam system, ion accelerator design and fabrication 78−66381
- TRIUMF 100 μA beam, achievement and control 79−54699
- two-grid accelerator systems, ion beam divergence characts. 78−82074
- two-stage ion beam optics for accelerator 78−50418
- ultra-sensitive particle identification systems based upon electrostatic accelerators, review 79−72182
- ultrasensitive mass spectrometry with tandem electrostatic accelerators 80−101876
- van de Graaff, mass spectrometer appl. for ^{14}C dating 78−32916
- C stripper foil, lifetime meas. 80−23216
- C stripper foil preparation, under heavy ion bombardment 80−18717
- C stripper foils, lifetime enhancement by slackening technique 80−23186
- C$^-$ ion source for radiocarbon dating using tandem accelerators 80−94620
- ^{14}C, beam production for Munich tandem 78−90008

electrostatic accelerators continued
- ^{14}C dating of mg geological samples with electrostatic accelerators 79−25361
- SF$_6$ purification in const. temp. adsorption process, appl. to electrostatic accelerators 78−29672
- ^{32}S 96 MeV heavy ion ps pulses, rebunching of MP Tandem pulses by spiral resonator 78−33357

electrostatic coating techniques
- back discharge effects in electrostatic powder coating *(Japanese)* 77−52516
- charging characts. of some powders, deposition efficiency 80−50780
- efficiency obs., discharges in electrostatic coatings meas. 80−71593
- electron-ion technique for complex shape articles 77−48557
- enamelling by electrostatic frit powder spraying 80−97428
- integral glass covering of spacecraft solar cells by electrostatic bonding 80−93676
- involatile molecule thin films, electrospray deposition for ^{252}Cf plasma desorption obs. 80−35584
- metallic coatings, electric field atomisation from melt 80−76174
- paint and powder spray coating developments 79−83363
- painting on Al foil using Van de Graaff generator, teaching demonstration 78−54136
- powder coating, parametric study, charging, transport, deposition props. 78−80662
- terrestrial photovoltaic arrays, electrostatic bonding as encapsulation technique 80−94020

electrostatic coatings
- discharges obs., using image intensifier and laser Doppler anemometer 80−71593
- powder, particles velocity meas. by laser anemometer 78−18364
- relief plate preparation by subtractive development 79−21831

electrostatic devices
- *see also capacitors; dielectric devices; electrostatic accelerators; electrostatic generators; electrostatic lenses; electrostatic precipitators*
- aerosol particle size classifier, parallel plate electrostatic device 80−95070
- air filters, portable electrostatic devices 80−36158
- airborne conducting particles and fibrils, electronic detector system 79−62164
- airborne particle repulsion system for surgical room contamination protection 78−28125
- analyser, for energy spectra in low energy ion scatt., comparison with TOF energy spectra 79−2895
- analyser, spherical, focusing using supplementary electrodes 77−9155
- charge mobility analyser, variable freq., appl. to latex aerosols 78−77945
- chimney discharges, dust level determination, equipment charact. *(French)* 78−3948
- circular neutraliser of static electricity, field anal. *(Czech)* 78−55272
- contactless electrostatic-acoustic transducer equivalent cct. analysis 77−19507
- control system for heavy ion electrostatic analyser control system *(French)* 77−42211
- copying processes of latent electrostatic image transfer *(Japanese)* 80−73487
- corona ion generator for removing dust and aerosol particles in rooms *(Finnish)* 77−66883
- cylindrical electrostatic analyser, design procedure 79−13885
- cylindrical electrostatic mirror analyser, image line aberrational expansion, nonplanar trajectories 79−41327
- cylindrical mirror analyzers, response functions 78−1146
- decelerator for electron microscope *(German)* 79−30620
- differential spectroscopy of charged particle beams, cylindrical mirror 77−50600
- double cylindrical electrostatic sector as an ion energy analyzer 80−23208
- droplet source suitable for laser targets 77−34074
- education, electrostatic motor 77−37690
- electric quadrupole field production, electrode system 77−54012
- electro-gas dynamic technologies, corona discharge industrial applications, qualitative analysis *(Rumanian)* 80−70061
- electron oscillator design optimisation, ion source and vacuum gauge 78−74107
- electron retarding-field energy analyser, improvement 77−82647
- electrophotographic films, surface charge meter using electrostatic induction *(Japanese)* 80−77886
- electroscope, oscillating type, construction details 78−41123
- electrostatic analyser, meas. of nuclear excitation energies 77−30741
- energy analyser, in secondary ions mass and energy spectrometer 77−13814
- Faraday cup for simultaneous ion-beam current obs. and meas. 78−49865
- fast electrostatic chopper of low power consumption 79−31284
- fibre-optic switch with electrostatic deflection cantilever 80−53427
- filter, electret fibre, non-woven, high efficiency 80−76691
- filter, inverse corona elimination *(Russian)* 79−1355
- focus-deflection practical system for shaped electron beams 79−76572
- gyroscope, geometry of suspension, max. rigidity case 78−62072
- gyroscope, suspended, electrofield torque due to offset of envelope assembly *(Chinese)* 80−43225
- hemispherical electrostatic 180° deflector, optimisation *(French)* 78−21269
- HTGCR fuel, electrostatic transport system for spherical particles *(German)* 77−67847
- industrial flare flames, smoke detection and control by electric fields 78−81360
- inertial confinement fusion targets, electrostatic levitation, control and transport 80−47723
- ion analysers for laser prod. plasma detection, space charge effects 80−96392
- ion beam deflector, using two-dimensional electrostatic quadrupole field 78−5417
- ionography, closed-system, image transfer to outside chamber, for diagnostic radiology 77−9242
- Kelvin, background, teaching motivation, demonstrations 80−42025
- kilovoltmeter errors in unearthed circuits 77−13773
- Lampard type electrostatic systems, analysis of the effect of the metrological properties *(Polish)* 78−77928
- liquid dynamic surface tension meas. instrument 80−42313
- magnetoelectrostatic traps, charged particle injection *(Russian)* 78−37102

electrostatic devices continued
- mass spectrometer electrostatic analyser attachment 78—86377
- meter, Smith field mill type, for measurement of fast transient electric fields 79—21723
- microcantilever electrostatic deflection system for transmission optical modulator array 80—87512
- mirror, approx. cylindrical field, focal line correction 77—50599
- mirror, axisymmetric, two-electrode paraxial props., aberrations 78—71025
- mirror, plane electrostatic, resolution improvement method 80—78753
- mirror, second order focusing space charge effects 77—50598
- mirror, transaxial, for large-incidence ang. ion beams 78—37798
- mirror, two-electrode, transaxial, aberrations, gap depend. 77—27242
- mirror, two-electrode, transaxial, cardinal elements, aberrations 77—27241
- mirror, two-electrode, transaxial, for large incidence ang. electron beam 78—37797
- mirror for heavy ion handling 77—18136
- mirrors, Bosi's method for solving Laplace's equation 79—68347
- multichannel charge-exchange energy analyser with high time resolution, plasma energy spectrum 79—41882
- multistage cylindrical analyzer for simultaneous detection of several beams with different energies 79—22891
- neutral beam injectors, electrostatic energy recovery system 78—66400
- optical component protection in dusty environments, electrostatic techniques 80—58657
- parallel-plate analyser for ion energy selection 78—83610
- particle guide, parameter anal. using radioactive recoil ions 78—33343
- particle separator, DC, for high energy physics, voltage breakdown in vac. 77—26921
- particle separator with built in HV generators 78—29693
- piezoelectric receivers, amplitude-freq. response determ. for acoustic emission 80—87699
- plasma planar electrostatic retarding field analyser, size effect on distrib. functions meas. 79—55562
- precipitator, DC corona discharge in rarefied air, coherent ion plasma oscillations 77—76230
- precipitator, free-fall, motion of charged particles, determ. 78—71020
- printer recording head using indirect discharge 80—47138
- prism, electron optics for Auger spectrometer 79—29437
- prism, three and five electrode wedge-shaped, telescopic and dispersion conditions. 77—54664
- probe for absolute measurement of SAW amplitude 79—50543
- pulsed electrostatic probes as diagnostic for transient plasma 78—94937
- quadrupole lens, asymmetric, 3-dimens., for time of flight mass spectrometer 80—4807
- scanning multiple collector electrostatic analyzer with application to plasma potential measurement 79—73046
- SIMS detector sensitivity improvement using electrostatic energy filter 79—26172
- spherical plate electrostatic analyser, long entrance aperture effects on azimuthal response 78—89494
- telescope, zero spherical aberration, ang. aberration calcs. 77—75406
- telescope, zero spherical aberration, paraxial props. 77—75405
- transducer, for Rayleigh waves detect. 77—19498
- X-ray quantum statistics limited electrostatic imaging 78—7451
- ^{2}H-^{3}H fuel pellet electrostatic injection *(Japanese)* 80—78434

electrostatic fields *see electric fields*

electrostatic generators
- *see also Van de Graaff generators*
- 850 kV generator with conducting charge transporter 77—13769
- accelerator terminal, beam aberrations in displaced quadrupole triplet charge selector 77—38443
- computer control 78—29666
- delay line voltage multiplier 78—33326
- education, electrostatic generator from piezoelectric gas lighter 77—37689
- electret, for pocket ion chamber dosimeters 78—13382
- high voltage generator for TEM, stability improvement *(French)* 78—62268
- rotating ball pulse generator, up to 1 kV 78—49866
- terminal voltage on-line feedback stabilisation using digital computer 78—82004

electrostatic lenses
- *see also aberrations; focusing; particle beams*
- 3-electrode axisymmetric lens, cardinal elements 77—30221
- aberration in accelerating mode *(French)* 78—46504
- accelerating immersion lens with minimum spherical aberration, dynamic programming search 78—25789
- achromatic ion prism, two-dimens. for mass spectrometer 77—54015
- analyser with oblique cut plates, focusing props. 77—54667
- analysers, image aberrations rel. to electrode tolerances 77—23611
- asymmetric electrostatic lens for field-emission microprobe applications 79—75656
- axisymmetric post-deflection, third-order distortion 80—32898
- beam trajectories through einzel lens for linear accelerator ion source *(Japanese)* 80—18718
- bipotential lens, with axial pot. function $\Phi(\mu)=\mathrm{V} \exp (\mathrm{K}_0 \arccos \mu)$ 77—23606
- cathode lens, electron image anal. 80—5675
- cathode lens, transient processes, finite-particle method 77—61909
- cathode lens with spherical photocathode, accelerating pot. 77—27240
- centrifugal electrostatic shaping of high intensity electron beams 80—13183
- channel plate in image tube, MTF 80—19108
- charged-particle beam, axisymmetric, focusing in hyperbolic electrostatic field 78—50688
- coaxial, hollow charged particle beam focusing appls. 77—82640
- coaxial lens, soln. techniques 80—69307
- coaxial lenses 80—74061
- coaxial probe forming lens suitable for high-energy ion beams 79—31787
- combined system of electrostatic round lens and mag. deflector, electron-optical characteristics *(Chinese)* 78—82897
- condenser lens for electron beam *(Japanese)* 80—53200
- crossed, spherical aberration 77—54662
- crossed lenses, electron optical characts., trajectory anal., aberrations from axial pot. profile 80—63909
- crossed lenses, electron optical image position, ang. magnification aberration 78—50691

electrostatic lenses continued
- crossed six-electrode doublet, stigmatic electron optical operation 79—13888
- cylindrical, optical characts. 78—8473
- design, for electron microscope 79—35894
- developments at the Cavendish Laboratory 80—37948
- double cylinder lenses, spherical aberration coeffs. and focal props. 79—86124
- double Q lens in mass spectrometer focusing props. 78—37100
- double-aperture immersion lenses, pot. distribs. and lens parameters 80—48133
- doublet of crossed electrostatic lenses, characts. 80—99615
- Einzel lens with curved electrodes, Fourier-Bessel soln. 78—82878
- einzel lenses, reduced spherical aberration field emission guns appl. 78—74831
- ELCO lens, ion microprobe system 80—47144
- electron beam control 80—32897
- electron diffraction apparatus, observation of micrographs 79—80727
- electron field emission energy distribution meas., analyser system 78—89605
- electron lens, spherical aberration correction system 80—5676
- electron microscope with electrostatic decelerator, resolution *(German)* 79—49346
- electron microscopy lens *(German)* 79—49339
- ellipsoid of revolution, elongated, motion in vac. electrostatic fields 78—5411
- ESCA spectrometer retarding lens system, computer optimisation 77—13827
- Faraday double transmitting cup, ion optical control device 78—82556
- focusing electrodes shape calculation for wedge-shaped electron-ion beam 80—53202
- Gabor lenses, configurations and beam optical performance 79—68070
- gun, for high-brightness field emitters 80—62809
- heavy ion beam focusing, accelerating, decelerating beams 78—89588
- high-current electrostatic scanner-deflector 77—13820
- immersion crossed lens, trajectory, anal. 80—99616
- ion beam control 80—32897
- ion beam focusing for low energy heavy ion accelerator 77—14654
- ion beam focusing from quadrupole mass filter using electrostatic lens 79—229
- ion microscope aberrations and image form., study by magnetic anal. of beam from HF source 78—55293
- ISOCELE high-current on line separator development 77—26922
- lens, three-electrode , crossed, electron focusing, spherical aberration 78—33659
- lens properties and computational techniques 79—44983
- mass spectrum, second order image aberration correction by electrostatic hexapole lens 78—70216
- mass-separator beam, quadrupolar focusing lens system 80—47801
- microscope objective lens using solid-state props. of dielectrics 79—2886
- mirrors for heavy-ion manipulation and focusing 77—10520
- Mollenstedt filter images, correction by auxiliary lenses, appl. to bend contour obs. for Al 77—39520
- multielectrode immersion tubular lens, cardinal elements, approx. eqns. 77—50607
- non-rotationally symmetric systems, computer aided anal. and design 77—79740
- open electron optical system with rotational symmetry, Fourier-Bessel series soln. for pot. and field intensity 79—76570
- optical properties and aberrations, lenses with electron-transparent foils 77—10828
- parallel plate retarder in electrostatic zoom lens 78—329
- particle optics, telescope electrostatic system with removable spherical aberrations 77—6989
- particle optics, telescope electrostatic system with removable spherical aberrations 77—6990
- pinhole image potentials, low-energy electron deflection, electron lens 80—53199
- potential distrib. and focal props. of electrostatic quadrupole lenses 78—37107
- prism, exact non-relativistic eqns. for charged particle trajectories 77—23607
- prism design, for β-spectrometer, exact eqns. 77—27239
- quadrupole, plane electrodes, 3D field distrib. calc. method 77—83803
- quadrupole lens, fringing field, conformal mapping method 79—41315
- quadrupole lens, ideal soln. using many electrodes, theory 78—33660
- quadrupole lens spatial field determ. 78—55292
- quadrupole lenses, electrostatic and mag., ion orbit 5th order solns. 77—19159
- quadrupole lenses with equal excitation, particle focusing 78—25787
- quadrupole mass analyser-field ionis. source interfacing, ferrite insert, repeller electrode 77—18125
- quadrupole systems for mol. beams, spherical aberration anal. 77—50601
- quadrupole triplet, for 10 mA MeV ion beam focusing, construction and performance details 79—3621
- radial field doublet lens 79—76573
- retarding electrostatic prism, with increased transmission 78—71022
- rotationally symmetric, with curved charged transparent foils, third order spherical and axial chromatic aberrations *(German)* 77—10827
- rotationally symmetric periodic electrostatic focusing system field distrib. 79—76574
- round electrostatic one-foil lenses, electron optical properties, charges induced on foil 80—53203
- round lenses, asymptotic aberration coeffs., systematic transformations 78—74828
- scanning electron beam instrument for studying metals/alloys thermoemission props. 78—74025
- single crossed lens, first-order electron optics props. 77—27243
- space charge lens for high current ion beams 78—55075
- telescope system, 3 electrode with mirror, spherical aberration elimination 77—50606
- thick central electrode for isolated electrostatic lens, field calcs. using overlap method 80—18981
- three-electrode emission lens, appl. for secondary ion microscopy 79—41324
- three-electrode lenses, general theory based on axial potential model 78—37110
- transaxial lens, curved charged particle beam focusing, image coords. and aberrations 78—46503
- triple cylinder lenses, accurate expression for potential by Bessel function expansion 79—72474

electrostatic lenses continued
two cylinder lenses, expression for potential 79—30626
two element lens, acceleration and deceleration of high intensity ion beams 78—89595
two-electrode tubular lens, astigmatic, spherical aberrations 77—34804
two-electrode tubular lens, astigmatic, spherical aberrations, object position effects 77—34805

electrostatic microphones *see microphones*

electrostatic precipitation *see electrostatic precipitators; precipitation (physical chemistry)*

electrostatic precipitators
aerodynamic theory, gas turbulence, Deutsch law 80—53758
aerosol, electrodiffusion precipitation of charged particles onto cylindrical channel walls 79—14463
aerosol particle collection at intermediate Reynolds number 77—36799
aerosols, charging migration and EHD transport 78—88660
aerosols, Reynolds no. range 10-100 77—86388
back discharge, flashover meas., streamer or steady glow mode, dust layer effects 78—59708
back discharge, initiation condition and mode 78—16814
back discharge in electrostatic precipitator, light meas. technique 77—76232
cement kiln dust emission control by electrostatic precipitator, meas. 79—52989
charge measurement, positive and negative corona 80—96403
coal fly ash precipitators, improved performance by electron beam ionisation 79—44918
cohesive force and resistivity between electrostatically- precipitated particles 79—86102
corona, point source current distrib. in external field 79—10727
corona discharge, spherical probe, I-V characts., precipitator testing appl. 78—79467
corona discharge theory analytic developments *(Rumanian)* 80—70062
corona ion generator for removing dust and aerosol particles in rooms *(Finnish)* 77—66883
corona system, under neg. direct and pulsed voltage, characts. 79—19107
Cottrell, Frederick Gardner, biography 78—20926
DC corona discharge in rarefied air, coherent ion plasma oscillations 77—76230
deviated field construction as design improvement 80—22390
discharge in air gap, drift rel. meas. of charged particles 80—52267
dust deflection from optical components by 20 kV negative potential 79—76888
dust particles, charged, vel. meas. using laser Doppler velocimeter 80—95083
dusts, electrostatic precipitation *(German)* 80—89532
electret filters for high efficiency air cleaning 80—56569
electron beam ionisation, coal processing technology appl. 78—57346
flashover voltage meas. method principle and results *(Polish)* 77—67471
formation by heated corona wires of electrostatic precipitator 80—47081
gas flow distribution effects 80—53804
gas purification using unipolar positive corona, expt. 77—39492
hot gases purifier, air temp. influences on negative corona integral characts. *(Russian)* 79—41892
mists, electrostatic precipitation *(German)* 80—89532
needle plate electrodes electric field, current and air flow meas. 78—16819
particle diffusion in electrostatic precipitators 77—3526
particle velocity, laser Doppler anemometry study 80—59144
particulate emission from calcining of clay, removal using electrostatic precipitator 79—24925
particulate layer deposition, resistivity meas. under ionic bombardment 80—68218
precipitator, free-fall, motion of charged particles, determ. 78—71020
prediction of particle separation, statistical reliability *(German)* 79—4072
pulsed electrostatic precipitator and flame photometer for total S aerosol conc. meas. 78—95975
re-entrainment, particle trajectories and gas flow 78—13642
sinter plant air pollution control system options 77—66982
suspension deposition in entrance of a diffuser, electrostatic and gravitational effects, laminar flow 80—14785
wire-duct type, back corona effects, math. model 80—49028
Hg, atoms, collection by electrostatic precipitators 78—95964

electrostatics
see also electrets; electric charge; electric fields; electrostatic devices; static electrification; triboelectricity
aerosol particle charging in continuum regime 78—90349
aerosol particle deposition in channel due to diffusion and electric charge 78—90978
aerosol particle electrostatic collection on sphere 79—47994
aerosol particles, hot β active emission electrification in varying force fields 80—7868
aerosols, charge distrib., appl. of four-parameter distrib. model 78—85213
aerosols, submicrons, in aluminised Mylar bags, electrostatic deposition losses 79—58114
air, electrostatic forces effect on thermodynamic props. and equilibrium composition 78—55710
anisotropic media, problems, theorems development *(Spanish)* 77—71901
anisotropic medium and its appl. to transform. from anisotropic to isotropic problems 80—9776
atomisation of petrol in internal combustion engine 78—27829
auroral electron beam, assoc. EM radiation bursts during substorms 79—88557
auroral electron beam, electrostatic noise generation 78—85759
auroral plasma, electrostatic V-shocks approximate equipotentials 80—21870
auroral processes, IAGA/IAMAP symposium (Seattle, August 1977) 79—88521
auroral zone magnetic field lines, electrostatic wave measurements 79—88555
axisymmetric field system, pot., method of paired series *(Russian)* 77—6968
axisymmetric torus electrostatic problem, perturbation method soln. 78—78851
bar magnet field, analogue simulation by electrostatic field, boundary conditions 77—61892

electrostatics continued
black holes, charged, Maxwell's eqns. multipole solns., field of point test charge 77—17613
book *(French)* 78—13640
boundary layer in stationary liqs. 78—15682
boundary value problem of four strips inside grounded cylinder 79—13862
Brans-Dicke theory, charged particle field 78—65849
Brownian motion of charged particles, long and short range correlations 78—62155
canonical ensemble partition function, incorporation of long range electrostatic effects 78—21065
capacitance bounds and equivalent radius, conducting ellipsoid 77—19126
capacitive discharges, charge transfer meas. 80—52265
capacitor of staggered parallel strips in bounded space 79—7052
capacitor plate-plate electrical configuration with injected unipolar space charge *(Portuguese)* 80—28132
capacity of charged disc or sphere in concentric hole of grounded sheet 77—14635
capacity of two unequal adhering spheres 80—91719
Casimir self-stress on a perfectly conducting spherical shell 79—13859
cathode directed streamer propagation, charge sheath model 78—67459
characteristic impedance of double line in front of dielec. wedge *(German)* 78—78855
charge and multipole distrib., appl. of Dirac δ-function 77—75356
charge redistribution in system of conductors in relative motion *(Russian)* 79—41267
charge singularity at vertex of slender cone of general cross-section 78—5389
charge storage, charge transport and electrostatics conference, Kyoto, Japan (Oct. 78) 80—7252
charged conducting sphere and charged dielectric sphere in elec. field, electrostatic force 77—25749
charged dielectric spheres interaction, appl. to water droplets and ion-pairs 77—567
charged disk interactions in various dielectric media, biological cell modelling 78—66706
charged droplets metastable state *(Czech)* 78—86231
charged dust grains accretion, role of induced charges 79—8966
charged particle in box, nonlinear integrodifferential eqns. with delay, soln. existence 79—27124
charged particle interaction with electrostatic field near media interface, interaction force *(Ukrainian)* 80—9770
charged particle limited systems, generation of method of collective variables *(Russian)* 77—14637
circular membrane reflector made by surface bending due to electrostatic tension 80—91876
circular neutraliser of static electricity, field anal. *(Czech)* 78—55272
classical Yang-Mills theory, screening solns., static external source 78—62302
colloids, electrostatic interaction between spherical colloidal particles 80—55724
condensers, toroidal, approx. capacities 80—28137
conducting ribbon, ring shaped, capacitance, exact upper and lower bounds 79—36811
conducting sphere, earthed, force due to dipole layer 77—50588
conference, Oxford, England (Apr. 1979) 80—67932
conformal transformation, allowing for spatial dispersion *(Russian)* 80—53183
Congress, Grenoble, France, (Apr. 77) 78—25767
cooling effects exam., steel plate at 500°C 80—69628
coplanar parallel charged strips, electrostatic problems 79—31765
coplanar parallel strips, electrostatic problems 79—31766
corona discharge effect on spraying mode of liquid *(Japanese)* 79—5186
cosmic dust, electrostatic attraction between charged spherical grains 77—3509
Coulomb's law, simple demonstration expt. 79—5940
Coulomb energy, of uniformly charged hollow circular cylinder *(French)* 77—42460
Coulomb interactions of electrons, modifications by polarisable atoms 77—11879
cubic array of identical spheres, dielec. const. calc. 80—25271
cylinders, circular 2-D electrostatic problems, integral eqn. soln. 80—83533
cylindrical conductor, between conducting surfaces, electrostatic field 78—9293
cylindrical conductor encircled by plane, capacitance calc. 79—36812
demonstration, attraction and repulsion of metallic particles over water 77—13559
dielectric, electrostatic props., theoretical 77—63365
dielectric attenuation of substituent effects, field transmission in partially occluded cavities 78—2789
dielectric elastic half space with point charge, stress and polarisation anal. 77—83776
dielectric ellipsoid, in inhomogeneous field 79—7053
dielectric ellipsoid or elliptic cylinder, Laplace eqn. soln. to electrostatic boundary value problem 80—63884
dielectric liquid electrostatic drop formation characts. 80—37926
dielectric parabolic wedge, electrostatic edge modes 77—28231
dielectric wedge, electrostatic edge modes 77—28230
diode with sharp point cathode, elec. field distrib. 80—5657
dipole correlations in conducting media 78—62969
dipole field in charged black hole electrostatics 80—112
Dirichlet problem, Fourier transform technique for boundary condition of infinitely long strip 77—45679
discharge energy, max., of electrostatically rechargeable liquids, estimate *(German)* 80—38737
discharge energy determ., using mathematical and physical models 80—70065
discharging to earth *(Italian)* 80—43226
discrete stochastic electric double layer, electrostatic props. 79—96318
distribution of concentration of electrically-conducting particles during autovibrational movement in plane capacitor *(Russian)* 80—48117
double layers, review 78—67368
drop formation, effects of conductive liquid props. 78—1122
drop formation rel. to liquid viscosity 79—55024
drop formation using liquid, expt. 79—57302
drops, electrified, pendent, axially symmetric, equilib. profiles 78—87846
education, conditionally divergent series, rearrangement, induced charge on parallel plates 77—87599

electrostatics continued
- education, point charge in three-dielectric medium with planar interfaces, method of images 79—9055
- education, point charge system, pot. energy of equilib. config. 77—87602
- electric double layer mean electrostatic pot., mean spherical approx. 79—74391
- electric field distribution, problems with simple dielectric boundary, solution method 78—12458
- electric vaccum breakdown, electostatic forces effect 79—56724
- electrical double layer theory, through Born-Green-Yvon eqn. 80—35539
- electrically driven jet, charge distrib. and forces 79—77268
- electrification curves, computer-aided approximation *(German)* 77—8338
- electrification of objects under DC transmission lines, charge simulation calcs. 78—78853
- electro-aerosols, precipitation in the airways, effect of electrostatic scatter 80—108929
- electro-optic waveguide modulators, capacitance of electrode system rel. to modulation efficiency *(Russian)* 80—1359
- electrographic development, electrostatic calc. 80—77888
- electrohydrostatic theory of surface tension 78—43213
- electrolyte, spherical nonlinear Poisson-Boltzmann theory Debye-Huckel linearisation 80—35538
- electrolyte double layers, electrostatic and steric repulsion effects in thin aqueous layers between solid surfaces 79—29375
- electron beam, magnetized, flowing through cavity, self-consistent potential calculation 80—91743
- electron drift and diffusion in neutral gas in electrostatic field 80—10349
- electron energy spectrum analysis, electrostatic system *(Chinese)* 80—43249
- electrophotographic developer, size distrib., particle charge and toner-carrier force *(German)* 80—73493
- electrophotographic layer, electrostatic force calc. *(German)* 80—42285
- electrophotography, transfer of electrostatic images 79—26162
- electrostatic capacity of two unequal adhering spheres, Dirichlet problem solns. 79—27127
- equivalence charge concept, appl. to electrostatic energy of charges and multipoles 79—18323
- exterior Dirichlet boundary-value problem with rot. symm., Fourier-Bessel series soln. 80—1103
- Faraday's denial of electrostatic action at a distance, conceptual and expt. bases 79—17180
- field anal. in complex periodic structures, computer-aided anal. *(Russian)* 78—33648
- field between conductors, bi-cyclide coordinates 78—1121
- field mill, electrostatic field meas., school use 78—16613
- field near charged surface, integral evaluation method 80—99599
- field plane method for designing 2D electrostatic fields 79—50185
- fields generated by charged particle in vac., zero vel. limit, electrostatics solns. 78—82881
- fluid, electrification, rel. to fluid dynamics 78—26200
- force acting on attracted disc of electrometer *(Japanese)* 78—17834
- force measurement, student expt. 79—17164
- force on conducting sphere due to charge on dielectric halfspace 77—3511
- Fredholm integral equations in computational methods for solving static field and eddy current problems 79—68344
- free space capacitance calc. for a square cylinder of finite length *(Chinese)* 78—66705
- fuel cell electrodes, galvanostatic switching curve shapes 80—66965
- gas mixtures, ignition energy by capacitive discharge and through discharge of person charged with static elec. *(French)* 80—10446
- Gaussian version of Amperes law 78—36848
- general relativity, electrostatics in certain axially symmetric static space-times *(French)* 79—49112
- GEOS, booms/mechanisms for equipment protection against interference 78—4073
- gramicidin A ion channel kinetic behaviour, electrostatic calcs. 78—53368
- gravitational mass change in two point charges system, for teaching 79—35460
- gyroscope, suspended, electrofield torque due to offset of envelope assembly *(Chinese)* 80—43225
- half-space lattice sums, new inversion formula 77—58224
- Helmholtz eqn. soln. for interactions between particles of arbitrary shape 79—100453
- history, quest for charging mechanism to end of 19th century 78—12525
- human body, electrostatic volt., capacitance and energy storage characts. 77—40954
- imaging problems with plane boundaries, demonstration 80—90629
- induced potential problem in 3-D, functional analytic approach 78—58880
- inertialess charged particles, collection on circular cylinders by elec. forces and gravitation 78—44400
- inertialess charged particles, collection on elliptical and irregular cylinders by elec. forces and gravitation 78—68924
- inhomogeneous dielectric, static field calc. *(Russian)* 77—3510
- ink jet drop formation characteristics *(Japanese)* 78—25766
- insulating webs and conducting rollers, electrostatic interaction 80—47137
- interdigital transducer transverse electrostatic end effects 77—27453
- ion channel, energy and pot. profiles and interactions between ions 78—53367
- ionospheric generated large scale fields, penetration into lower atmosphere *(Russian)* 77—9606
- Jupiter magnetosphere, electrostatic waves obs. 80—72865
- Kelvin water dropper demonstration of electrostatic charges, teaching 78—28899
- Laplace equation, inhomogeneous anisotropic media, finite difference operators 77—46670
- least capacitance region, free boundary optimisation problem 79—13864
- least capacitance regions, free boundary optimisation problem 79—13865
- Lichtenberg figures 79—44693
- liquid, cloudy bubble formation in strong nonuniform elec. field 80—53842
- liquid dielectric, with free boundary, equilib. between 2 charged spheres *(Russian)* 78—46482
- lunar soil electrostatic transport, terminator configuration model 79—35157
- macromolecule adsorption on charged surface, weak electrostatic attraction 77—19118
- magnetosphere, double layers and electrostatic shocks review 80—36460

electrostatics continued
- magnetosphere, electrostatic shocks, double layers and anomalous resistivity 78—45152
- magnetosphere, electrostatic waves rel. to inverse loss cone electrons temp. anisotropy relaxation *(Russian)* 80—109314
- magnetosphere, gyroharmonic emissions due to energetic electrons in plasmas 79—80086
- magnetosphere, mode of propag. electrostatic plasma waves and radio waves determ. using stimulated plasma wave results *(Japanese)* 80—94650
- matrix methods in potential theory and EM scatt. 79—94133
- measurement and effects of electrostatic charges *(French)* 79—64140
- metal, classical cleavage energy, layer summation method 77—85287
- metallic spray theory 77—25317
- metals, HCP, electrostatic contrib. to second- and third-order inner elastic consts. for different axial ratios 79—51186
- Meteosat, electrostatic discharge phenomena obs. 80—17463
- methane, stored energy needed to ignite, by discharger from charged person 80—54063
- microstrip, static field problems of dielectric objects, moment formulation 77—3512
- mixed boundary value problems 78—42254
- mixed boundary-value problems of steady-state thermoelasticity and electrostatics 80—55
- molecular attraction of crossed fibres, depend. on air gap width 77—27216
- moment of forces on truncated rotor, edge effect *(Russian)* 80—28135
- multielement proportional counters, electrostatic problems 79—93877
- neutral periodic assembly of charged particles, electrostatic lattice sums 79—71376
- non-local electrostatics, appl. to cylindrical interface 80—18955
- noninertial particle transfer to rotating in laminar flow under external force field 80—10250
- nonlinear electrodynamics, three-dimensional soliton solution *(Russian)* 79—22884
- nonlocal electrostatic 78—82879
- normal modes at small polyhedral particles 77—58225
- organic liquid surface, charged drop formation from bubble bursting 77—14634
- paradox and resolution, teaching approach 77—75357
- parallel conductors in external field 80—28136
- parallel plate condenser, mixed boundary value problem of electrostatic field 77—58222
- particle electrification by impact on metal plates 79—50180
- planar electrostatics, teaching 80—90623
- plane electron-optical system, electrostatic field anal. with integral eqns. of first kind 77—19157
- plasma, electrostatic shear flow instability theory and appl. to magnetopause and solar wind 80—96359
- point charge as electrically invisible object, nonlinear Poisson-Boltzmann theory Coulomb singularity 80—43228
- point charge between grounded planes, conditionally convergent series, for teachers 79—71201
- point charge between infinite parallel plates, infinite series evaluation of teaching 79—25803
- point charge between parallel grounded plates, total charge on plates soln. 77—13544
- point charge electrostatic potential in Reisser-Nordstrom gravitational field 79—30335
- point charge near cond. plane, force acting, for teaching 78—49605
- point to plane electrodes, corona current experimental equations *(Japanese)* 79—50918
- point-multipole expansion, charge distrib., for teachers 78—61992
- polymer powder, pneumatic conveyance through metal pipes, charging tendency meas. 79—50186
- potential, laboratory and theoretical comparison 80—105461
- potential distribution around point charge in three dielectric media, calc. using image method 77—42459
- potential expression, influence of geometric and electric parameters of system *(French)* 80—48118
- powders, electrostatic behaviour, methods for study 80—52266
- refractory metal powder adhesion forces on metallic substrates, electrostatic eval. method 77—52564
- relativistic Lagrangian with variable mass *(French)* 77—9882
- relaxation, teaching approach, calcs. 79—58489
- rubber, C black filled, friction behaviour sliding against Al, applied voltage effects 79—74266
- rubber adhesion and friction, surface charge contribution 77—80826
- Schwarzschild space-time, electrostatics, electric fields and black holes *(French)* 79—40432
- semi-circular strip problem, Fredholm integral eqn. soln. 79—86104
- separation of particulate materials, vibrated bed electrostatic separation 80—16641
- solar wind, electrostatic fluctuations source 79—80183
- spark discharges from body, nature and incendiary behaviour obs. 80—72406
- sparks detection and characts., by radio methods 80—68217
- spheres, almost touching, temp. field or elec. pot. 79—41268
- spherical insulating particle, ionic charging 79—45882
- spherically symmetric electrostatic field superposed with EM wave, gravitational radiation emission *(French)* 77—57257
- spherically symmetric objects, electrostatic and gravitational field determ. 77—71253
- spheroidal cavity, in polarisable dielectric continuum, charge distrib. free energy 77—27215
- spraying of liquids, role of Joule heating 77—32837
- static electricity generation, dangers and safety precautions *(Italian)* 80—28131
- surface dipole layers, forces between plates 80—70793
- suspension of charged sphere, electrode geometry choice *(Russian)* 79—10240
- toroidal charge and current configurations, static fields described in terms of ring multipoles 80—78741
- torus, Kelvin transform., axisymmetric charge distrib. 79—36809
- torus and spherical sector, conducting, axisymmetric electrostatic field soln. 79—55023
- two coaxial circular discs in a free space, electrostatic pot. problem 79—76542
- two dimensional, general anal. representation 79—13863
- two dimensional electrostatic boundary-value problem for two strips and grounded cylinder 79—72452

electrostatics continued
two point charge system, electrostatic pot. energy and inertial mass change 78—54116
two-dimensional field numerical solution, using Sander's function 79—878
two-dimensional problem anal. 77—31043
two-electrode electron optical systems, electrostatic field of disc cathode 79—64167
unequal adhering spheres, electrostatic field generation 80—99598
variational methods for solution of electrodynamic and electrostatic problems 80—1105
variational technique for solving two-dimensional problems *(Hungarian)* 78—58879
water vapour condensation, electric field influence 80—14268
weakly ionised gases, in electrostatic field, Maxwell model, ion vel. distrib. and moments 78—94879
weighted SAW transducers, electrostatic neighbour and end effects 77—31200
xerographic papers, electrostatic props. 78—78852
xylene liq. jets induced by electrostatic field, disintegration and convergence 79—81986
Bi, Bernstein waves, electrostatic wave dispersion relation in mag. field 80—34471
Ge dust, n- and p-type electrification 79—56276
Li^+, hydrated, polarisation model, review 80—54115

electrostriction
see also piezoelectric materials; piezoelectricity
acoustic waves, parametric excitation in presence of electron currents *(Russian)* 80—80328
alkali halide, rocksalt-type, quadratic electrostrictive effects 77—24796
benzonitrile, hexane and CCL_4 solns., nonlinear dielec. effect 79—78602
biomembranes, role of nonlinear capacitive currents in gating currents 77—48771
Born model, electrostriction rel. to dielec. and thermoelastic props. 80—71322
capacitance type AC dilatometer for piezoelectric and electrostriction const. meas. 80—77747
composite electrostrictive resonators, finite element simulation 78—59237
cubic crystal/cubic crystal interface, transverse surface acoustoelec. wave propag., due to electrostriction 77—66082
cupric formate tetrahydrate, uniaxial stress effect on dielec. props. 78—48125
dielectric, elastic, containing 2 rigid spherical conductors, electrostrictive stress conc. 77—23883
dielectrics, heterogeneous, spherical shells, stresses 80—45011
education, light momentum density in refracting medium, electrostriction, Peierls method 77—33772
electroconvection in weakly conducting liquids 78—18297
EM energy-momentum tensor and the properties of material media 79—55020
ferroelectric, uniaxial, crit. behaviour, electrostrictive coupling role 80—71329
ferroelectric, uniaxial, electrostrictive interaction, mode damping 80—34862
ferroelectric, with anomalously high dielec. const., self-focusing of EM wave 80—14408
ferroelectric ceramic, optical modulation by electrostriction during electron beam charging, spatial characts. 79—7224
glass, optical anisotropy due to laser-induced electrostriction *(Russian)* 79—99846
highly electrostrictive ceramic capacitor 79—47390
isotropic solid, electrostrictive birefr. induced by high-intensity laser radiation 79—27340
isotropic solid, self-focusing anisotropy 77—75626
liquids, photoacoustic and photorefractive detect. of small absorpts., electrostrictive limits 80—108171
long rods, radial motion under axial mag. field 78—68456
magnetic-field trasnducer design 77—57371
Maxwell stress tensor derivation, electrostrictive effects in cryst., for teachers 77—33792
microelectrostriction in medium ionization *(Russian)* 79—19839
microwave irradiated materials, rel. to acoustic signal generation 78—24095
nitroethane, cyclohexane and benzene solns., nonlinear dielec. effect 79—78602
optical waveguide, Bragg electrostriction, power balance approach 77—75660
optical waveguide, electrostrictive mixing, acoustic surface wave generation, theory 77—19424
optical waveguides, SAW electrostrictive mixing analysis 77—27390
order-disorder type ferroelectrics, static and dynamic electrostrictive props. 77—85652
paraelectric-ferroelectric-antiferroelectric phase transitions, electrostrictive effects 80—97209
Permalloy, film, magnetoconductivity modulation by substrate electrostriction 79—60908
piezoelectric cryst., excitation and energy flux of acoustic harmonic, amplitude, depend. on electrostrictive nonlinearity 79—15404
plane-parallel absorbing layer, nonlinear optical props. 80—58631
plate with circular hole, stress distrib. under simple tension in electrostriction 78—10845
polarised nonconducting dielectric fluid, anal. of force exerted on immersed elec. charge 78—78872
polyvinylidene fluoride, film, piezoelec. relax. 79—87394
polyvinylidene fluoride films, stretched and rolled, electrostriction and piezoelectric effects *(Japanese)* 80—55041
refracting medium-vacuum boundary, ponderomotive forces of light *(Russian)* 78—22082
relaxor ferroelectrics, electrostrictive effects 80—66112
Rochelle salt, thermal expansion and spontaneous strain meas., −40 to 40°C, electrostrictive consts. 77—16262
semiconductors, electrostrictive effect of hot electrons spherical energy band model 79—69778
solid, anomalously high permitt., acoustic to EM wave conversion 78—91734
stimulated Brillouin scatt., three dimensional, for focused Gaussian beam 80—69456
stimulated scattering of ultrashort pulses, electrocaloric effect 79—10358
surface acoustoelectric waves, electrostriction-induced, at interface between media 77—16255

electrostriction continued
tetraglycine, aq. soln., density, viscosity and dielectric const., 0-60°C 78—47462
TGS, admixed with nitroanilines or L-alanine, US vel. and absorpt., ferroelec. transition 77—32333
TGS, electromech. coupling of surface acoustic waves near ferroelec. transition 78—19415
TGS, electrostrictive and dielec. coeffs., neutron diffr. study 80—75943
TGSe, cryst., US vel., crit anomaly and electromech. effects 79—55832
triglycine, aq. soln., density, viscosity and dielectric const., 0-60°C 78—47462
two-dimensional, of elastically anisotropic dielec. 77—12312
uniaxial ferroelectric, acoustic attenuation near transition point 80—11350
uniaxial ferroelectrics, static and dynamic crit. behaviour, elastic and electrostrictive consts., US attenuation 78—35103
US transducer electroacoustic efficiency and load matching 79—68541
US transducers, proposal of method for evaluation of electrostictive material for 80—38208
vapour, radiatively cooled resonant, 3rd order nonlinear optics processes 79—81477
$(Ba,Sr)TiO_3$ polycrystalline solid soln., electrostriction constants, reson.-antireson. meas. *(Russian)* 78—10849
$BaTiO_3$, based ceramics with large permittivity, electrostriction consts. 77—66457
$BaTiO_3$ ceramic, degradation under high AC elec. field 80—60499
$BaTiO_3$ ceramic, electromechanical coupling effect studied using resonance method 77—20802
$BaTiO_3$, isotropic dielectric, US vel. and longit. elec. field *(Russian)* 78—38785
$BaTiO_3$, paraelectric crystal, nonlinear props. 80—84699
$BaTiO_3$, polycrystalline, dielec. nonlinearity coeffs. difference in free and clamped specimens *(Russian)* 80—25314
$BaTiO_3$, Rayleigh wave generation by surface piezoelectricity 78—71925
$BaTiO_3$-based nonpiezoelectric ceramic, acoustic convolution in paraelectric phase 80—6467
$Cd_2(NH_4)_2(SO_4)_3$, X-ray and optical studies of ferroelec. phase transition 79—38495
CsH_2PO_4, ferroelec. transition, deuteration and press. effects 78—35101
Cu-Cl boracite, ferroelec., X-ray study on phase transition 79—33622
$Gd_2(MoO_4)_3$, piezoelectric and electrostriction coeffs. near ferroelastic transition *(French)* 77—40182
^4He, liq., phase transitions, positive and negative ion mobilities meas. 78—87833
$KD_3(SeO_3)_2$, optical and dielec. props. near ferroelastic phase transition 79—38518
$KH_3(SeO_3)_2$, optical and dielec. props. near ferroelastic phase transition 79—38518
$KNbO_3$, piezoelec. and electrostrictive coeffs. 77—85653
$KTaO_3$, Rayleigh wave generation by surface piezoelectricity 78—71925
$La_xPb_{1-x}Zr_yTa_{1-y}O_3$, ferroelec. with diffuse phase transition, electrostriction-optical props. 78—68457
N_2, liq., photoacoustic and photorefractive detect. of small absorpts., electrostrictive limits 80—108171
Na, radiatively cooled vapour, 3rd order nonlinear optics processes 79—81477
NaCl, calc. 77—36178
$NaNO_2$, electrostrictive constants, isothermal and adiabatic, in antiferroelec. transition region 77—12317
Nb, anodic oxidation, open circuit transient anal., dielec. and elec. props. of oxide film 80—3245
$PbHAsO_4$, hydrostatic press. effect on ferroelec. transition 78—35102
$PbHPO_4$, hydrostatic press. effect on ferroelec. transition 78—35102
$Pb(Mg_{1/3}Nb_{2/3})O_3$, electrostrictive effect 80—66113
$Pb(Mg_{1/3}Nb_{2/3})O_3$:$PbTiO_3$, ceramic dielectric, electrostriction, relaxation, polarisation 80—80700
$Pb(Mg_{1/3}Nb_{2/3})O_3$-$Pb(Mg_{1/2}W_{1/2})O_3$, solid soln., electrostriction, strain gauge obs. 80—55043
$PbMg_xNb_{1-x}O_3$, ferroelec. with diffuse phase transition, electrostriction-optical props. 78—68457
$Pb(Zn_{1/3}Nb_{2/3})O_3$, electrostriction investigation, strain gauge method 79—87395
$Pb(Zr,Ti)O_3$:Ba, paraelectric ceramic, giant electrostrictive effect 79—91378
$Pb(Zr,Ti)O_3$:Ba, paraelectric ceramic, electrostrictive effect 80—80701
RbH_2PO_4, electrostrictive effects, US rel. 80—75941
SiO_2 film, thermally grown or sputtered, electrostriction and piezoelectricity 77—12010
$Sr_{0.61}Ba_{0.39}Nb_2O_6$, electromechanical props., permittivity, elastic compliance, piezoelectric moduli 80—29691
$Sr_{0.75}Ba_{0.25}Nb_2O_6$, electrostriction 77—48130
W, anodic oxidation, effect of electrostriction, ellipsometry meas. 78—92394
W, anodic oxidation, open circuit transient anal., dielec. and elec. props. of oxide film 80—3245
WO_x, anodic oxide films, quadratic electro-optic and electrostrictive effects, ellipsometry 80—108184

electrosynchronisation *see synchronisation*

electroviscous effect
see also colloids; viscosity
AC characteristics, pressure-drop fluctuations 80—107457
acetone, transient pressure-drop fluctuations in electroviscous effect 80—15286
benzene:tetra-n-butylammonium bromide, electroviscous effect, AC characts. 79—99341
n-butyl acetate, electroviscous effect, AC characts. 79—99341
chloroform, electroviscous effect, AC characts. 79—99341
chloroform, electroviscous effect, AC characts. 79—99342
convective heat transfer in coaxial horizontal channel, influence of electroviscous effects 79—77100
n-hexane/acetone mixtures, electroviscous effect, AC and DC meas. 79—14949
MBBA, electroviscous effect 79—69010
MBBA, nematic liq. cryst., electroviscous effect, electrohydrodynamic investigation 78—87804
monochlorobenzene, electroviscous effect, AC characts. 79—99341
1-nitropropane, electroviscous effect, AC characts. 79—99341
nonpolar liquids, electroviscous effect 79—77796
polyvinyl alcohol, hydrocarbon suspension, temp. depend. of electroviscous effect and dielectric parameters 79—79299

electroviscous effect continued
  rheological electrokinetic phenomena in rectangular capillary, numerical simulation 80—26023
  starch, hydrocarbon suspension, temp. depend. of electroviscous effect and dielectric parameters 79—79299
  water, mechanism in DC and AC fields 79—51294
  DPM-4, electroviscous effect 79—69010
  SiO_2 gel, hydrocarbon suspension, temp. depend. of electroviscous effect and dielectric parameters 79—79299

element origin
  see also cosmic ray origin; cosmology
  antimatter model for galactic nuclei and quasars *(Chinese)* 78—73771
  big bang model, element prod. 78—8177
  big-bang model and ^{4}He abundance, review, book contrib. 78—89277
  big-bang nucleosynthesis with nonzero lepton numbers 78—16583
  bypassed elements, neutrino induced prod. 77—45408
  carbonaceous chondrite fission Xe, elimination of ^{248}Cm as possible progenitor 77—37581
  cosmic ray source material synthesis, evidence from Ne, Mg and Si isotopes meas. 80—51631
  cosmological and stellar nucleosynthesis, review 80—62359
  cosmological element formation, inhomogeneity in D prod. 79—21471
  cosmology, nucleosynthesis in charged universe 79—25766
  cosmoradiogenic ghosts in meteorites, rel. to origin of Ca-Al rich inclusions 78—12162
  Dirac cosmology, onset of galactic nucleosynthesis, and age of Universe 77—13514
  dynamical r-process, nuclei far from β-stability 77—26004
  early universe, nonlinear primordial fluctuations rel. to nucleosynthesis 79—25773
  elemental evolution and isotopic composition, teaching 78—41128
  explosive nucleosynthesis, massive star evolution preceding and during supernova, element abundances *(German)* 79—44469
  formation by β^- decay *(Russian)* 79—8818
  galactic ^{4}He and heavy elements enrichment by stellar nucleosynthesis 78—28657
  galactic cosmic ray Fe nuclei source, neutron excess from isotopic comp. 80—72729
  galactic disc chemical evolution, inflow problem 80—62279
  galaxies, irregulars and blue compacts, chemical comp. and evolution from spectrophotometry 80—36711
  galaxies, two-component, chemical evolution, analytical approach 79—25711
  Galaxy, chemical evolution, effect of stars mass loss by stellar wind 80—41814
  Galaxy, chemical evolution rel. to metals distrib. among stellar populations 78—96545
  Galaxy chemical enrichment, effect of increasing He content and disc dwarfs evolution 79—88733
  galaxy evolution and element distrib. 80—22084
  heavy and neutron-rich elements synthesis by rapid neutron capture process 78—77488
  heavy element, origin in star development supernovae and galactic matter *(German)* 79—44468
  heavy element nucleosynthesis, current astrophysical theory review 77—29644
  heavy element origin, supernova model, r- and s-processes 77—56825
  heavy elements in X-ray emitting clusters of galaxies, prod. of abundance gradients 77—91654
  heavy elements production in massive stars, effects of binary evolution 80—46534
  hot CNO nucleosynthesis, ^{18}O/^{17}O abundance ratio 77—78767
  light elements, abundances in matter-antimatter model of universe 78—45439
  light elements, form. in chaotic cosmology 77—57112
  light elements, prod. by cosmological cosmic rays 78—12436
  light elements formation, thermal cycle, isotopic abundances problem *(French)* 78—96574
  long neutron capture chains, abundances evaluation method 78—45216
  metals, explosive nucleosynthesis rel. to Al/Fe ratio in metal-poor-stars 78—57549
  n-process of neutron capture, alternative to r-process 77—2336
  p-process nuclei, neutrino-induced nucleosynthesis 77—87582
  primordial black hole evaporation rel. to D origin *(Russian)* 77—74172
  r-nuclei prod. sites in Galaxy 80—72932
  r-process, astrophysical, implications of fission mass distrib. 78—93204
  review 79—97118
  s-process studies, exact soln. for unbranched network 78—28649
  solar system abundances of nuclides and nuclear structure 77—82130
  solar system elements, influence of supernovae 80—17509
  solar system material and cosmic rays, origin of elements just beyond Fe 77—70952
  solar system s-process elements, difficulties, with ^{22}Ne as neutron source 80—72926
  stellar nucleosynthesis, cosmochronology after Allende 80—4462
  stellar spectrum, abundance distribs. and origin of elements, reln. to evolution of universe 77—26099
  universal abundances and origin *(French)* 77—26097
  vortex cosmologies, light element synthesis 77—45622
  ^{26}Al, prod. from stellar evolutionary sequence 79—5809
  ^{26}Al, synthesis in explosive H burning 80—85929
  Ar, galactic nucleosynthesis rel. to low Ar abundances in three halo planetary nebulae 80—82443
  B production by cosmic rays, evidence from interstellar B detect. in front of κ Orionis 80—51841
  ^{11}B, neutrino-induced prod. in stellar C layer 80—82337
  Ba, Y, s-process elements, abundance in old halo stars rel. to nucleosynthesis in Galaxy 78—65616
  Be, constraints on form. from abundance in α Centauri A 77—41379
  Be, origin rel. to abundance in Hyades 77—53584
  C, N and noble gases, origin and abundances in terrestrial planets and meteorites 78—28559
  CNO, isotopes origin and isotopic abundance ratios evolution 78—93201
  CNO rare isotopes, prod. in novae by explosive hot CNO-Ne cycle H burning 79—44489
  ^{14}C in groundwater, possible subsurface prod. rel. to dating 80—85690
  D, cosmological origin rel. to pair prod. in intense mag. fields 77—13505
  D formation by nonequilib. processes 77—53423
  D formation in early solar system, evidence from H and O isotope study in chondritic meteorites 80—36518

element origin continued
  D, galactic radial gradient, rel. to universe origin 79—40232
  D, obs. and interpretations 77—71160
  D, prod. by high energy particles 77—33709
  Eu, r-process element, abundance in old halo stars rel. to nucleosynthesis in Galaxy 78—65616
  Fe group elements, prod. in supernova outburst *(Russian)* 80—62167
  Fe meteorites, trace element abundances rel. to superheavy elements fission 79—48742
  Fe peak elements, nucleosynthesis rel. to lower mass limit for C detonation supernovae 77—17553
  ^{2}H, neutrino-induced nucleosynthesis 77—87582
  He and heavy elements, origin in cold early universe rel. to black hole and galaxy form. 78—16585
  He, cosmic abundance rel. to time-varying gravit. const. 79—92667
  He enrichment during galactic chemical evolution 77—22208
  He origin, evidence from subdwarfs He abundance 80—22003
  He, primordial nucleosynthesis rel. to Dirac Large Numbers Hypothesis 79—92900
  He production and universal anisotropy limits 78—36737
  He, production in Brans-Dicke and relativistic cosmologies *(Polish)* 80—27024
  ^{3}He, interstellar detect., no evidence for low-mass stars nucleosynthesis 79—25689
  ^{4}He primordial abundance, upper limit 78—45444
  ^{4}He production, nonzero neutrino rest mass effects 80—105413
  K, Ar, interstellar, supernova nucleosynthesis rel. to isotopic anomalies 78—28761
  Kr, fission, in carbonaceous chondrites, origin 79—35199
  ^{86}Kr in meteorite, s-process nucleosynthesis and s-process neutron capture time scale 80—73080
  ^{7}Li, big bang prod. and abundance rel. to universal baryon density 78—4420
  ^{7}Li, prod. in nova explosions 78—57555
  Mg, stellar nucleosynthesis rel. to isotopic abundances in G and K dwarf stars 80—51757
  N, in planetary nebula in irregular galaxy NGC 6822, abundance and nucleosynthesis 80—41867
  N, nucleosynthesis rel. to abundances in F- and G-type stars 77—91530
  N, primary nucleosynthesis rel. to galaxies ages determ. 79—25728
  ^{15}N, galactic evolution 77—87264
  O, enrichment rate in Galaxy determ. from planetary nebulae O/H ratios age depend. 80—105328
  ^{107}Pd, solar system prod. rel. to isotopically anomalous Ag in Santa Clara and Pinon Fe meteorites 80—85902
  Te isotopic composition in meteoritic and terrestrial materials 78—82856
  Xe, fission, in carbonaceous chondrites, origin 79—35199

element relative abundance
  see also isotope relative abundance
  108-76°1, new halo planetary nebula, He and O abundances 77—45510
  Abee meteorite, C rich material with high volatile element content, implications 80—85908
  absorbing material towards quasistellar object PKS 0528—250, abundance anal. 79—40288
  abundance gradients, reassessment from spectrophotometry of Perseus arm H II regions 80—22055
  AC arc, variable current, element concs. during interruption time depend. *(Russian)* 78—22597
  actinide abundance determ. for rocks using NaI detectors 79—80043
  actinides in English Channel, transfer into S.North Sea 79—48519
  actinides in stellar spectra 77—78769
  Adelaide meteorite, carbonaceous chondrite chemical anal. and Ca/Al ratio 79—2532
  Adelaide meteorite, member of new carbonaceous chondrites subgroup, comp. and mineralogy 78—65573
  aerosols, atm., instrumental anal. of light element comp. 78—69516
  aerosols, from Jungfraujoch, Switzerland, chem. comp. 77—45056
  aerosols, urban, in Nagoya area, Si and Al concs. for atmospheric soil particles characterisation 80—26581
  aerosols from coal-fired power plants, minor and trace elements emissions and particle size distribs. 79—92108
  air pollution, X-ray fluorescence spectroscopy, proton induced, trace element anal. 77—36831
  alkaline earths, cosmic abundances rel. to oxides occurrence in cool stars and sunspots 78—85933
  Allende meteorite, amoeboid olivine aggregates trace element anal. 80—17553
  Allende meteorite, metal particle comp. 77—5510
  Allende meteorite, tracer elements loss mechanism after heating to 1400°C rel. to primitive meteorites thermal metamorphism 80—109401
  Allende meteorite (C3V), tracer element loss after heating to 1400°C, rel. to primitive meteorites thermal metamorphism 80—109402
  Allende meteorite inclusions, trace element distrib. in mineral separates and genetic implications 78—49400
  Allende meteorite trace elements, results from coarse-grained inclusions 78—49401
  Am-stars, abundance indices problem *(French)* 77—29863
  analysis of asteroid surfaces, space mission goals 80—36474
  ancient Cu alloys, epithermal neutron activation anal. method 78—8490
  ancient pottery, characterisation by neutron activation anal., suitable element selection 78—8484
  ancient pottery, nondestructive neutron activation anal. 78—12802
  Ankara atmosphere aerosol, trace elements and size distribs. determ. by thermal neutron activation anal. 78—81377
  Antarctic aerosols particle anal., comp. 80—77091
  Antarctic meteorite Yamato 74123, new ureilite 79—35206
  Antarctic Peninsula igneous rocks, transverse geochemical vars. rel. to calc-alkaline magmas genesis 80—56466
  Ap stars, magnetic, anomalies of chemical comp., correls. between overabundances *(Russian)* 77—22239
  Arabian Sea, DSDP Site 220, Fe, Mn and Ti distrib. 77—73708
  Archaean precious-metal hydrothermal systems, Ontario, rare earth element and 0 isotope relations 80—12383
  astronomical, lifetime meas. astronomical applications, beam-foil method 77—41313
  astrophysical objects, oscillator strengths 80—12656
  tropical Atlantic, element charts, construction method *(Russian)* 77—60485
  atmosphere, marine, trace elements in size separated aerosols 79—20989

element relative abundance continued
atmosphere, trace element concs. in United Kingdom, 1975 survey results 77—25759
atmospheric aerosols, meas., Quillayute, Washington, (USA) 78—36270
atmospheric trace elements in UK, 1978 survey 80—90208
Azorean lavas, REE and LIL element compositions 77—25669
B2 1225+31, high-redshift QSO, abundances in $z=1.7941$ absorpt. line system 80—12826
Baltic Sea, P, N and organically bound C conc. annual vars. 77—49084
barite rare earth composition rel. to formation conditions 80—41439
basalt-seawater interaction, trace element and Sr isotopic vars. in glassy basalt 80—8286
basaltic achondrite meteorites, rare earth element abundance patterns rel. to origin 80—36581
basalts, Ce, Sm and Yb vars. rel. to open system cryst. fractionation 77—66916
basalts, deep sea, trace element distrib. pattern, neutron activation anal., rel. to genesis 78—11879
Bench Crater meteorite, member of new carbonaceous chondrites subgroup, comp. and mineralogy 78—65573
Bencubbin polymict meteoritic breccia, elements concs. rel. to form. 78—96443
Bombay Harbour sediments, elemental concs. 77—73709
α Bootis (Arcturus), O and C abundances *(Russian)* 78—16420
C2 chondrite meteorites, evidence for chemical fractionations 80—109400
C3 carbonaceous chrondrite (Ornans), noble gas component of minerals 80—51698
C, N and noble gases, origin and abundances in terrestrial planets and meteorites 78—28559
3C 120, Seyfert galaxy, assoc. nebulosity O/H and N/O ratios 80—67890
3C 286, quasar, Mg and Fe abundances in intervening matter from optical absorpt. lines 80—4454
Canadian clay, neutron activation anal. 78—8487
carbonaceous chondrites, comparison with solar Na/Ca and S/Ca ratios 77—29735
carbonaceous chondrites, ion beam analysis 80—62089
carbonaceous chondrites, spallogenic nuclides abundances rel. to parent bodies form. 80—36580
carbonaceous chondrites, type III, chem. comp. *(Russian)* 77—9718
carbonaceous chondrites of Ornans type, comp. rel. to metamorphic sequence 77—87341
E.Carpathian volcanic rocks, rare earth elements and Y, Rb, Sr, Cs, Ba, Pb, Th, U, Zr, Hf and Sn concs. 77—5151
Cassiopeia A, element abundances rel. to progenitor evolution involving supergiant mass loss 78—36623
Cassiopeia A supernova remnant, abundance inhomogeneities 80—12797
V553 Centauri, CH-type Cepheid, chemical comp. and luminosity 79—62849
α Centauri binary system, spectroscopic chemical anal. 80—62128
Chainpur meteorite, volatile elements concs. in chondrules 79—101121
charnockite gneisses with low potash and high Fe, chemistry and origin 77—86882
Chassigny meteorite, cumulate dunite, comp. of hydrous amphibole-bearing melt inclusions 79—21235
chemically peculiar (CP) stars, element underabundances rel. to planetesimal impact hypothesis 78—20834
chondritic meteorites, rare-earth abundances 79—21234
chondritic meteorites, trace element anal. 78—69756
clusters of galaxies, OSO 8 X-ray spectra rel. to intracluster gas Fe abundance 79—25734
coal 79—48015
Cocklebiddy meteorite, comp. determ. by chemical anal. scheme 79—2483
coins, ancient Greek, neutron activation and at. absorpt. anal. 78—8489
cool stars, abundance determ., molecular data uncertainty effects 77—29805
cosmic abundances, rel. to universe nonlinear primordial fluctuations 79—25773
cosmic rays, abundances of elements in $26 \leq Z \leq 30$ interval 79—40044
cosmic rays, comp. from Si to Ni meas. with nuclear emulsion 77—5404
cosmic rays, Fe, Co, Ni abundances rel. to time delay between nucleosynthesis and accel. 78—28455
cosmic rays and solar system material, origin of elements just beyond Fe 77—70952
cosmological light elements, constraint for G var., comment on errors 80—72767
Crab Nebula, photoelectric spectrophotometry of filaments, abundances 78—41006
Crab Nebula outskirts, remarkable spectra and element abundances 78—36662
Cretaceous mid-ocean ridge basalt (MORB), Nd and Sr isotopic comps. and rare earth element abundances 80—94520
Cretaceous-Tertiary boundary event, Os and Ir enrichment of sediments 80—76976
curve of growth anal. of HD 161698 Hg-Mn star 79—30070
Cygnus Loop, SNR, abundances and filament shock vel., UV obs. 80—94848
deep sea sediment cores, Au, Pd, Ir, Mn sources, neutron activation anal. 80—17247
Dhajala meteorite, unequilibrated H3 chondrite, major and minor element chemistry 78—32425
diamond, different types, trace elements conc. 79—14838
diamonds from S.Africa, elemental concs. and Pb and Sr isotopes 79—34775
DO white dwarfs, atmospheric He/H ratios and effective temps. 79—35249
30 Doradus nebular complex, chemical comp. and struct. obs. 80—62226
DSDP Leg 37 basalts, trace elements and petrogenesis 77—91076
Earth, isotopic comp. and trace elements concs. rel. to mantle and crustal reservoirs mean age 80—51359
Earth inert gas composition, origin from solar nebula 80—61785
Earth mantle, Mg/Fe ratio and mineralogy above 1000 km 77—33015
Earth mantle differentiation and crustal growth, geochem. model 80—21684
Earth mantle melting, past and present, isotope and trace element evidence 78—65238
eclipsing binaries, late-type, mass-luminosity and radius relations, chem. composition 78—28728
elemental evolution and isotopic composition, teaching 78—41128
elliptical galaxies, chemical evolution 80—67843

element relative abundance continued
elliptical galaxies, metal abundance rel. to giant stars population evolutionary synthesis 78—57626
eucrite meteorites, rare earth elements abundances rel. to parent body comp. and evolution 78—20766
eucrite parent body, chondritic comp., inference from trace elements 78—69755
evolution in galaxies 80—22084
Farmington chondrite, U-Pb abundances and Pb isotopic studies 80—56778
Fe in planetary nebulae, abundance rel. to grain condensation and nebula form. models 79—40238
ferromanganese concretions in Baltic Sea, trace metal distrib. rel. to accretion rates 77—81864
ferromanganese nodules, oriented, U-Th series nuclides rel. to growth rates and turnover times 79—29740
Floridan Aquifer rocks, Sr content rel. to dolomitisation 79—53346
fossil bone, age determination, nondestructive neutron activation anal. 78—15743
Fraser River (British Columbia) deltaic sediments, heavy metals content 77—33048
Frontenac Axis dikes, Ontario, ^{40}Ar/^{39}Ar dating and apparent Ca/K ratios 79—62466
G333.6—0.2, G298.2—0.3, compact H II regions, IR emission lines rel. to elemental abundances 78—96522
galactic centre, Ar overabundance from forbidden Ar II emission obs. 79—48922
galactic chemical evolution, He enrichment 77—22208
galactic clusters, abundances from weak lines 77—29890
galactic cosmic rays, ultraheavy $(Z>52)$ nuclei abundances 77—9641
galactic disc chemical evolution, inflow problem 80—62279
galactic stellar populations, metals distrib. rel. to Galaxy chemical evolution 78—96545
galaxies, absorption features radial gradients rel. to metallicity 79—40254
galaxies, chemical evolution, review 80—77486
galaxies, element, abundances rel. to radio continuum radiation from discs 77—13460
galaxies, elliptical and S0, absorpt.-line strengths and metallicities 80—4430
galaxies, irregulars and blue compacts, chemical comp. and evolution from spectrophotometry 80—36711
galaxies, metal abundances rel. to progression in Cepheids period-amplitude diagrams 78—53956
galaxies, N/O abundance ratios rel. to ages 79—25728
galaxies, two-component, chemical evolution, analytical approach 79—25711
Galaxy, abundance gradients derived from H II regions, spectrophotometry 78—41036
Galaxy, chemical abundance gradient determ. from open clusters H-R diagrams anal. 80—56938
Galaxy, chemical evolution, effect of stars mass loss by stellar wind 80—41814
Galaxy, disc chemical evolution and radial metallicity gradient 77—29937
Galaxy chemical enrichment, effect of increasing He content and disc dwarfs evolution 79—88733
garnet lherzolite, high-press. phase equilibria and Mg^{2+}-Fe^{2+} partitioning among constituent minerals 79—66687
garnets, Fe, Ca, Mg, Mn distrib. in zoned specimens 77—2148
gaseous nebulae, model anal. of ionisation correction formulae 78—57623
gaseous nebulae, N and O abundances 78—8093
γ Geminorum, differential abundance anal. rel. to α Lyrae standard 80—82362
geological materials, multielement trace anal., solvent extraction-flame AAS method 78—7259
geological samples, f/α particle track anal. for U, Th and isotropic disequilibria 78—7799
geological samples, multielement anal. by sequential instrumental and radiochem. neutron activation 78—7798
geological samples, multielement determ., instrumental neutron activation anal. 79—53550
geothermal vapour dominated field, Larderello, Italy, noble gas concs. 79—74919
geothermometry, chemical and isotopic techniques 78—69501
glass, ancient samples, trace element anal. by neutron activation, rel. to corrosion and devitrification 78—12801
global processes, sedimentary cycling models 78—16162
globular clusters, metallicity rel. to spatial struct. of cluster system 77—37625
globular clusters, six-colour photometry rel. to metal abundance 77—13407
globular clusters evolved stars, Fe/H ratios rel. to CN strengths and UV excesses 77—64753
globular clusters heavy element abundance rel. to Oosterhoff dichotomy 77—78837
hailstone samples, Project DUSTORM, microprobe anal., element abundances 78—73453
halogen content of ultramafic nodules, determ. by gamma-ray spectroscopy and radioactivity meas. 80—76945
halogens, 'cosmic' abundance from sample activation anal. 78—12111
HD 94028, subdwarf, Mn abundance and Mn/Fe ratio 78—45328
heavy element depletion unlikely in Orion Nebula 78—69854
heavy elements, spatial distrib. in X-ray emitting clusters of galaxies 77—91654
heavy elements in galactic halo, radial abundance gradient 79—92857
heavy elements production in massive stars, effects of binary evolution 80—46534
heavy metal levels related to wind direction, Belgian North Sea coast 79—83665
heavy metal pollution detection in estuarine sediments 78—73546
heavy metals, Belgian network meas. of atmospheric concs. 77—70833
heavy-element abundance effect on classification of G-type giant stars 77—29834
heavy-element excess in late spectral class stars 80—26854
Helix Nebula, abundance anomalies in planetary nebula 78—86001
Holbrook chondrite, vapour phase comp. from mass spectrometry 78—65568
Iceland high-temperature geothermal systems, aquifer chemistry 78—96245

element relative abundance continued
igneous lithic clasts from mesosiderites and howardites, petrography and chemistry compared with eucrites and diogenites 80−72890
Indian continental shelf, distrib. patterns of Al, Ti, Mn, Cu and Ni in sediments 79−25225
S.Indian Craton, Archaean gneiss Rb-Sr date of 3360 Myr old 80−46155
inert gases abundance patterns in granite samples, Sudbury phenomenon *(Japanese)* 77−73735
inert gases in atmospheres of Venus, Earth and Mars, abundances rel. to planetary interiors outgassing 79−48721
inert gases in meteorite serpentine, solubility 80−12712
Inman, McPherson County, Kansas, meteorite, mineralogy, petrology and comp. 79−2527
intercluster intergalactic medium, comp. 80−4426
intergalactic gas, Fe-enriched, in clusters of galaxies, origin and evolution 78−93390
interplanetary corotating energetic particle streams, H, He, C, O and Fe distrib. functions 79−70938
interplanetary dust grains collected from stratosphere, neutron activation study 80−82319
interstellar abundances in ζ Ophiuchi clouds 79−48875
interstellar Ca, Ti depletions towards Cepheus OB2 assoc., interstellar lines anal. 80−22052
interstellar contracting clouds, molecule formation 77−22294
interstellar dense molecular clouds, chem. evolution 78−28749
interstellar gas clouds, heavy element abundance rel. to initial stellar mass function 77−56907
interstellar gas near 30 Doradus, element abundances from UV absorpt. lines obs. 80−85978
interstellar gas phase depletion anomalies and ionization potentials 80−31342
interstellar heavy element depletion model, thermal sputtering in high vel. shocks 77−17662
interstellar high velocity cloud near ζ Orionis, density, temp. and comp. 77−22291
interstellar high-velocity gas clouds, abundance vars. 77−26039
interstellar matter, composition and properties, review 79−53900
interstellar matter in front of χ Ophiuchi, optical obs. and abundances 79−25673
interstellar matter toward Orion OB1 association, element depletions from Copernicus obs. 80−22050
interstellar medium, C depletion rel. to 2175 Å feature strength and origin 80−17638
interstellar medium, elemental depletions model 78−36654
interstellar medium, elements depletion from weak lines below 3400 Å in ζ Persei 77−45509
interstellar medium, elements depletion rel. to new model of interstellar dust 80−26934
interstellar medium, Fe, Mn and Mg depletion derived from S 59 obs. of 67 stars 79−2563
interstellar medium, K I and Na I column densities and depletions 78−20872
interstellar medium, metal depletions rel. to hot medium filling factor 80−17634
interstellar medium, S and Cl depletion on oxide grains 80−17635
interstellar medium contrib. of thermally pulsing high luminosity stars to element enrichment 78−40917
interstellar medium depletions, implications of RF mol. emission spectra obs. towards ζ Ophiuchi 80−26958
interstellar medium in HD 50896 sightline, Copernicus obs. rel. to atomic abundances 77−26036
interstellar radio spectrum lines, review 77−71138
interstellar Sc II in ζ Ophiuchi spectrum, abundance upper limit 80−82445
ion microprobe analysis, calibration using matrix ion species ratios, appls. 78−61070
Italian chondritic meteorites, Cu, Ir, Pt and Au content by destructive neutron activation anal. 78−12172
Jupiter atmosphere, cloud struct. and C/H ratio from methane line profiles near 1.1 μ 80−62067
Jupiter atmosphere, He/H_2 ratios from cosmic ray albedo neutron fluxes 78−45271
Jupiter magnetosphere, energetic ions comp., Voyager 1 obs. 80−26798
Jupiter magnetosphere, low-energy charged particles comp. 80−26797
K648, halo planetary nebula, spectrophotometry and element abundances 78−41011
K-type stars, abundance effects in classification 77−29833
Kakangari chondrite, elemental abundances rel. to uniqueness 77−29738
Kakangari meteorite, unique chondrite, noble gases abundances and isotopic comps. 78−65570
Kapteyn's star, M-type subdwarf, metal abundance 77−13330
Karoonda (C4) chondrite, volatile/mobile trace elements abundances 78−20768
Krymka chondrite, heating to 400-1000°C, trace element anal. 77−64710
Krymka LL-chondrite carbonaceous inclusion, noble gas and trace element anal. 80−17555
L-6 chondrite, perogenesis evidenced by mineral chemistry 80−41775
Lake Lisan-Dead Sea aragonite, element and isotropic comp. rel. to pleistocene geochemical evolution 78−49047
lanthanides in Si Ap-star HD 192913, spectral identifications and abundances 78−45345
lanthanides in titanite, relative concs. rel. to host rock type 79−62492
large impact craters melt, Ge, Ir, Ni, Os, Pd, Re abundances rel. to meteorite types 78−57208
LDS 785A (EG 153), DB white dwarf, atmospheric He/H ratio 77−45425
Lewisian gneisses, Sm-Nd systematics and implications for granulites origin 79−20777
lherzolites, comp. rel. to comp. of Earth mantle 80−76940
light element abundances, galactic evolution and universal baryon density 79−40302
light elements, abundances from prod. by cosmological cosmic rays 78−12436
light elements, abundances in matter-antimatter model of universe 78−45439
light elements cosmic abundances, effects of massive neutrinos radiative decay 79−92668
light isotopes abundances in galactic cosmic rays, rel. to interstellar gas density 80−17456

element relative abundance continued
light noble gases in chondrites, achondrites and ureilites, anal. compilation 78−65574
light rare earths in composite dike, partitioning between co-existing acidic and basic melts 79−2233
light rare gases, abundances in primary particles of Moon dust sample (61501) *(French)* 80−51674
light rare gases, abundances in solar wind 500 Myr ago *(German)* 80−51637
LIL-element enrichment rel. to $^{143}Nd/^{144}Nd$ and $^{87}Sr/^{86}Sr$ ratios in Azore basalts 79−74873
Lithuanian lake catchment area soil N and P distrib. *(Russian)* 79−96780
Lonar Crater, India, chem. study of impact glasses and basalts 79−20836
Louvem volcanogenic Cu deposit, Quebec, lithogeochem. anomalies 79−5480
Luna 24 soil samples, Co and Ni abundances of metallic phases 78−32367
Luna 24 soil samples, light noble gas comps. rel. to depositional history 79−88608
lunar basalts and regolith, anal. of var. in Al, Mg and Si abundances 78−16320
lunar crust, trace element abundances rel. to differentiation processes 77−60651
lunar drill sample, neutron activation and radiochemical anal. *(German)* 80−51673
lunar mare basalts, comparison with terrestrial mid-ocean ridge basalts 79−16424
lunar mare basalts, crystal chemistry, mineralogy and petrology 77−45334
lunar mare basalts, Fe^{2+} reduction by S loss 77−9681
lunar materials, KREEP origin 80−4279
lunar plutonic rocks, suite of materials depleted in trace siderophile elements 79−62766
lunar regolith, depletion of volatile elements 77−9680
lunar regolith, light element chemistry of Apollo 12 site 78−65515
lunar regolith samples from Luna-24, element abundance determ., neutron activation obs. 80−67597
lunar rocks, major and trace element anal. *(German)* 77−41327
lunar rocks, mineralogy and petrochemistry *(German)* 77−41326
lunar samples, Li and halogen contents 77−60638
lunar samples, major element fractionation and trace element enrichment by preferential sputtering 77−29666
lunar samples, primary matter, neutron activation anal. 78−7890
lunar soil, from mare and highland areas, element abundance anomalies 78−49349
lunar soil grains, surface comp. from Auger and X-ray photoelectron (ESCA) spectroscopy 78−32366
lunar soil samples from Luna 24, inert gas element and isotope composition 80−67593
lunar soil samples from Luna-24, N_2 abundance, neutron activation obs. 80−67594
lunar soils, exotic component rel. to global radioactive crust 77−60643
RR Lyrae stars in ω Centauri, Fe/H ratios from UBV photometry 78−73719
M32, metallicity and galaxy age from spectral synthesis 80−67842
M32-1, planetary nebula in M32, spectrophotometry rel. to chemical abundances 79−25664
M82 nucleus, Brackett-line obs. rel. to Ne abundance 79−25704
M83, H II regions spectral characts. and chemical abundances 80−56927
M87 halo globular clusters, metallicity meas. 78−89244
Magellanic Clouds, chem. comp. of H II regions, photoelec. spectrophotometry 78−77607
Magellanic Clouds, chemical composition, model nebulae anal. 80−22085
Magellanic Clouds, H II regions chem. comps. 78−93381
main sequence stars, element abundance regularities rel. to nucleosynthesis *(Russian)* 77−45431
major element whole rock anal. using sample fusion technique with electron microprobe 77−64494
Malvern howardite meteorite, petrology and chemistry 77−49346
Manych meteorite, L-3 chondrite, droplet chondrules comp. and chondrules origin 79−30014
Marda calc-alkaline suite, rare earth elements, Archean geochem. analogue of Andean-type volcanism 78−11898
Mare Crisium gabbroic and basaltic fragments, opaque mineral chemistry 78−32369
marine basalts, U conc. and distrib. and K/U ratios 77−81886
Markarian 59 , supergiant H II region in SBm galaxy NGC 4861, metal abundance from spectroscopic obs. 80−98705
Mars, chem. composition of interior, cosmochemical model 80−72813
Mars atmosphere, comp. of surface layer 78−20706
Mars Chryse Planitia sample, Viking X-ray fluorescence expt. 77−17410
metabasalts from Point Sal ophiolite, California, rare earth and trace element geochemistry 78−32092
metagabbro at bottom of Michigan Basin deep drill hole, Rb-Sr geochronologic anal. 79−39680
metal abundance determ. in late-type stars, new method 79−12405
metal concs. in soil solns. 79−34824
metal content of Hyades star cluster rel. to solar colour 80−101569
metal depletions and interstellar H_2 abundances 77−91605
metal enrichment of sediments, partitioning of metals, Ranafjord N. Norway 79−83641
metal poor stars in SMC 79−96995
metal-deficiency of NGC 2243, old open star cluster 78−93333
metal-enriched sediments from the TAG Hydrothermal Field 79−20805
metal-poor dwarf stars, abundance anals. of yellow spectra 79−92760
metallicity gradient across galactic disk 79−48905
metallicity of NGC 6635 globular star cluster 80−90483
metals in H II regions and stellar populations in bright galaxy nuclei 80−98708
metals in Walker Branch Watershed, atmospheric input and origin 77−86956
meteorite, Holbrook chondrite, chem. alterations due to terrestrial weathering 79−71007
meteorite inert gas isotope and element anomalies, He and Xe 80−56779
meteorite Springfield specimens, mass spectroscopic element and isotope anal. 77−60731

element relative abundance continued
meteorites, abundance anomalies rel. to explosive neutron processing of stellar He burning shells 79—58302
meteorites, chemical fractionation in ureilites 77—41369
meteorites, Kenna ureilite, C and S abundances 77—41365
meteorites, noble gases abundance in separated minerals 77—33429
meteorites, Poluyamki, Rakity and Markovka chondrites, composition *(Russian)* 77—9721
meteorites, ureilites, abundances rel. to genesis 77—41363
meteorites, ureilites, classification and elemental fractionation 77—41364
meteorites of British Museum (Natural History) collection, chemical anals. 78—65569
meteorites of cumulate eucrite type, Serra de Mage and Moore County 80—36587
meteorites of iron type, superheavy element fission tracks 80—26821
meteorites with gas-rich nature, volatile element trends 80—51701
meteoritic spherules in oceanic sediments, trace element concentrations 79—84755
micaceous kimberlites, micas chemistry 79—16465
micrometeorites, in stratosphere, element abundances and detect. of ^{4}He 77—56878
microtektites, chemical comparison of bottle-green and normal microtektites and tektites 77—82179
Mid-Atlantic Ridge rocks, Fe, Ni, Cu, S and Co abundances in sulphide minerals 77—91122
mid-ocean ridge basalts, comparison with lunar mare basalts 79—16424
minerals, magnetic trends on alkali-Fe-Mg diagrams 78—85551
minor metals in surface seawater particulates and organic-rich shelf sediments 78—92853
monazite sand, determ. of Th, U, and K from spectrometry of natural γ-activity 78—20408
Moon, basaltic magmatism and bulk comp., major and heat-producing elements 78—7891
Moon, Earth and eucrite parent body, bulk chemical comps. 77—60636
Moon, Mg/Fe large-scale var. from orbital gamma-ray data 78—12123
Moore County, eucrite meteorite, comp. rel. to quench temp. 78—96444
Morasko meteorite, composition and origin 80—77359
Mundrabilla, Fe meteorite, chem. obs. by neutron activation 78—12171
muscovite in medium to high grade metapelites of NW.Maine, comp. var. 79—62493
N132D, supernova remnant in LMC, O/H ratios rel. to supernova nucleosynthesis 78—93345
natural diversity of material, causes 77—71161
neutron capture elements, evaluation of abundances in long reaction chains 78—45216
NGC 1851, 6624, globular cluster, abundance gradients spectroscopic investigation 80—82437
NGC 2420, old disc cluster, chemical comps. of stars 80—46620
NGC 2768, galaxy, metal abundances rel. to optical and IR photometry 78—36683
NGC 300, NGC 1365, southern galaxies, H II regions comp. 80—4441
NGC 3115, galaxy metal abundances rel. to optical and IR photometry 78—36683
NGC 4378, anaemic spiral galaxy, extended rot. curve and evidence for metal enrichment 79—8990
NGC 6366, metal-rich globular cluster, BV photometry and metallicity 77—5462
NGC 6720 (Ring Nebula), Ne, N and S abundances from forbidden line spectrum 77—26035
NGC 6888, circumstellar nebula, He and N overabundances from forbidden N II /Hα ratio 79—8964
NGC 7027, planetary nebula, CNO elements abundances from UV spectrum 80—82459
NGC 7027, planetary nebula, low excitation emission spectrum and element abundances 77—64823
noble gas anomalies in josephinite and assoc. rocks 79—79761
noble gases, abundances and isotopic compositions in Earth mantle 78—85521
noble gases, in St. Mesmin brecciated chondrite, implications for irradiation history 78—28593
Nova Cephei 1971, He, O and N abundances in ejecta 78—12244
Nova Scotia southern plutons, Na, K, Rb and rare earths in tonalites and granites 77—49064
novae, nebular stage, abundance determ. methods 77—87279
nuclear and differentiated abundance patterns 77—9656
nuclear decay chains, abundances evaluation method 78—45216
nuclear fuels, elemental and isotopic conc. anal. using nondestructive assay 79—49691
nuclear matter with neutrinos retention, eqn. of state and chemical comp. 78—96390
nuclear oil well logging using 14 MeV neutron-excited gamma-ray spectrometry 79—48581
nuclear waste from extraterrestrial civilisations, stellar spectra 80—82230
oceanic residence times of trace metals, river discharge effects 77—78228
oceans, Cl/Br ratio rel. to origin 78—65342
Oklo natural reactor, rare earth elements behaviour 78—49019
old halo stars, chemical comp. rel. to nucleosynthesis in Galaxy 78—65616
ρ Ophiuchi dark cloud, Mg, Si and Fe depletion in S II region 78—49500
ordinary chondrites, trace element distrib. between mag. and nonmag. portions 79—35205
organic materials, nuclear backscattering using cyclotron 78—80807
Orgueil carbonaceous meteorite, Ni and S abundances correl. in phyllosilicates 78—12169
Orion nebula, C and Mg abundances from UV spectrum 80—41882
Orion Nebula, chem. comp. from emission line obs. 77—49456
Orion Nebula, Cl and Fe abundances from forbidden Cl II and Fe II near IR mapping 80—62217
Orion Nebula, spectrophotometric obs., ion abundances, and thermal balance 77—67121
Orion Nebula, temps. and abundances in outer part 79—53868
Orion Nebula peripheral regions, O/H and He$^+$/H$^+$ ratios 80—36686
p-nuclei, abundances produced by low-temp. photonuclear nucleosynthesis in degenerate H burning zones 78—57540
N.E.Pacific Ocean, deep water ^{226}Ra maximum 77—5221
palaeoatmospheric O$_2$ and element distrib. in sedimentary rocks 77—5272
pallasites, metal comp., classification, relationship with Fe meteorites 77—64709

element relative abundance continued
particulate material in stack effluent of coal-fired power plant, comp. and size distrib. 77—45136
particulate matter, conc. on membrane ultrafilters, neutron activation anal. 79—52841
partitioning in clinopyroxene-orthopyroxene pairs from spinal peridotite xenoliths 79—62488
phenocrystic minerals, Ca-Mg-Fe ratios, pyroclastic deposits correl. in S.Kyushu, Japan *(Japanese)* 77—64278
in photoelectric spectrophotometry of emission lines, abundances, from photoelectric spectrophotometry of emission lines 78—81677
plagioclase, zoned, of different magmatic environments, preliminary ion-microprobe anal. 79—34815
planet interior differentiation processes, trace elements as probes 80—98584
planetary nebula in irregular galaxy NGC 6822, spectrophotometry and He, N, O and Ne abundances 80—41867
planetary nebula NGC 7027, ionization struct. and comp. 78—28745
planetary nebulae, abundances from weak diagnostic spectral lines 80—109531
planetary nebulae, abundances of He, Ne, Ar, N, and Cl 80—109532
planetary nebulae, C abundances from C IV 1550 Å lines fluxes 79—17051
planetary nebulae, classification according to abundance, chem. kinetic and spatial props. 80—109509
planetary nebulae, CNO abundances rel. to central stars masses and Population II planetaries origin 78—85992
planetary nebulae, Fe abundances from forbidden Fe VI emission 79—8970
planetary nebulae, hot stellar wind model for refractory elements gas-phase abundances 80—109516
planetary nebulae, implications for galaxy abundance 80—109530
planetary nebulae, S and Ar abundances from 10 micron obs. 79—48879
planetary nebulae, spectrophotometry and chemical abundances 78—36663
planetary nebulae central star abundances corrections from UV flux determ. 80—72945
planetary nebulae in M31 (Andromeda galaxy) and companions, comps. rel. to nucleosynthesis and cosmic He abundance 80—109520
planetary nebulae in Magellanic Clouds, He, N and O abundances, effects of excitation class 80—109519
planetary nebulae of galactic halo, photoionisation models and chemical abundances of K 648, 49+88.1° and (108—76.1°) 80—109507
planetary nebulae truncated composite shell models, chemical comp. rel. to emission line spectra 79—25677
planetary-type rare gases in an upper mantle derived amphibole 78—96167
planets, comp. rel. to mass distrib. in solar nebula and planetary system 78—12109
PN 108-76°1, halo planetary nebula, spectrophotometry and element abundances 78—41011
PN 49+88°1, halo planetary nebula, spectrophotometry and element abundances 78—41011
polar solar wind, heavy ions abundances rel. to Saito coronal density model 77—37591
Pontlyfni, differential meteorite related to group IAB irons, chemical anal. 77—82177
potsherds, Melian, instrumental neutron activation anal. 78—8485
potsherds, S.W. African, neutron activation anal. of trace elements, characterisation 78—8486
potsherds, Turkish, neutron activation anal. 78—8487
pottery, sigillated, trace element archaeochem. using neutron activation anal. 78—8488
Precambrian basement of W.Canada, Hg and As distrib. and abundance 80—56419
precious metals, values in interflow sedimentary rocks from Kambalda (W.Australia) komatiite sequence 79—20830
primary fractionation of elements among Fe meteorites 79—35210
primordial universal abundances rel. to light element-relic radiation interaction *(Russian)* 78—4423
QSOs, element abundances from emission-line spectra 78—57677
QSOs, high redshift, metal abundances in emission line regions 79—21458
quartz sand from Lasko Polje, determ. of Th, U, and K from spectrometry of natural γ-activity 78—20408
quasi-stellar objects, C, N, O and Si abundances rel. to 1400 Å emission feature identification 80—12825
quasi-stellar objects, C/Si, Al/Si and Fe/Mg abundance ratios 78—20903
Quaternary volcanic rocks of New Hebrides, geochemistry and origin 78—20375
'r-process' elements, abundances from n-process neutron capture nucleosynthesis 77—2336
r-process elements, implications of fission mass distrib. 78—93204
radioactive ores, hazard indices rel. to nucl. high-level waste 78—15913
rainfall in Trinidad conc. determ. 80—82045
rare earth abundances in anorthosite complexes 77—78177
rare earth and trace element data, Archaean granite in Yellowknife, Northwest Territories, Canada 80—4007
rare earth and trace element geochem. of Jurassic seafloor, Point Sal, California 78—32094
rare earth composition of Icelandic basalts, Reykjanes Peninsula 80—21725
rare earth element, abundances in layered Komatiite lava flow, Ontario, Canada 79—29764
rare earth element patterns in Archean sedimentary rocks, rel. to crystal evolution 77—60374
rare earth elements, determ. in geological materials, using thermal and epithermal neutron activation 78—7797
rare earth elements, distrib. in N Atlantic Kimmeridgian black shales 79—44187
rare earth elements, geochemistry in Archaean metasedimentary rocks from Kambalda, Western Australia 80—109143
rare earth elements, partitioning between hydrous silicate melt, amphibole and garnet peridotite 79—20775
rare earth elements evidence for changing oxidation states in Precambrian Fe formations 77—64284
rare earth elements in chert, indication of form. in marine environment 77—37200
rare earth elements in Earth, Moon and achondrites, rel. to chemical history 77—60639

element relative abundance continued
- rare earth elements in sea-floor basalt, behaviour during weathering 79−57910
- rare earth elements in tholeiitic basalts, behaviour during submarine weathering 78−73369
- rare earth geochemistry and mineralogy, book contrib. 80−46157
- rare earth geochemistry of Late Cainozoic alkaline lavas from Antarctica 77−41030
- rare earth patterns, crustal evolution and Australian post-Archaean sedimentary rocks 77−41015
- rare earths, cosmic abundances rel. to oxides occurrence in cool stars and sunspots 78−85933
- rare earths in HD 187473, Si star 80−98671
- rare earths in Melrose-b howardite 80−101566
- rare gas abundances on Mars rel. to volatile outgassing on Earth and Mars 77−45342
- rare gas elemental and isotopic ratios in Luna 24 drill core soil samples 80−26760
- rare gases in Mars atmosphere, effects of regolith adsorption on relative concs. 78−49358
- rare gases in volcanic rocks, mass fractionation as indicator of gas transport to or from magma 80−98292
- red giant stars in globular clusters, abundances in M92 and (M15) 79−92759
- Red Sea brines, He/Ne ratio 77−25693
- REE mobility and fractionation during granodiorite weathering 79−62512
- refractory elements, fractionations among carbonaceous chondrite groups 80−36595
- refractory lithophile elements, condensation and fractionation 80−36517
- refractory-element-rich inclusions in CM meteorites 79−30022
- Richardton chondrite, U-Pb abundances and Pb isotopic studies 80−56778
- Ries impact crater, siderophile and volatile element anal. 80−17552
- ring sundial, imitation old scientific instrument, identification by neutron activation anal. 78−8491
- Rochechouart meteorite crater, France, projectile identification 77−33025
- rocks, element determ. in National Institute for Metallurgy (S.Africa) reference samples 79−88356
- rocks, trace element content, direct-reading spectrometer 78−85738
- rocks and minerals, multielement analysis by photon or neutron activation 78−12018
- Rogue and Galice formations, Klamath Mountains, element abundances rel. to Jurassic island arc sequence identification 79−100836
- s-process elements, abundance determ. in G- and K-type Ib supergiants 77−33482
- s-process elements, effects of unthermalised isomeric states and time-varying neutron flux on branching ratios 80−90410
- s-process elements in Ba star HR 774, Reticon spectra 79−25594
- FG Sagittae, Fe-peak and s-process elements abundance *(Russian)* 78−12253
- FG Sagittae nebula, spectrum and He, N, O, Ne and S abundances 78−49498
- Sagittarius B2, He abundance problem 78−49496
- Saguenay Fjord, suspended particulate matter geochemistry 78−92852
- Saguenay fjord sediments, distrib. and partition of Co, Ni, Cr and V 77−33100
- seawater, ^{226}Ra and Ba concs. at GEOSECS stations in Atlantic and Pacific 77−5222
- seawater, trace element estimation using radioactive ^{14}C *(Dutch)* 77−29459
- sediments, in Gulf of Kutch, element distrib. 79−48450
- Shaw meteorite, L-group chondrite, missing metal 77−5511
- Shergotty achondrite, Rb-Sr age and isochron age resetting 80−41774
- siderophile and volatile elements 78−7892
- siderophile elements, fractionation in enstatite chondrites 80−98617
- siderophile elements indigenous abundances in lunar highlands, rel. to lunar origin 79−5767
- siderophiles in lunar highlands, indigenous contents and abundance ratios 80−8562
- Sikhote-Alin meteorite, chem. comp. *(Russian)* 77−9715
- silicate rocks, multielement anal. by epithermal neutron activation, detector systems 78−20123
- silicate spherules in deep-sea sediments, extraterrestrial origin 79−48743
- snow, natural enrichment of elements 78−77303
- soil pollution elemental deposition downwind of coal-fired power plant 79−20838
- soil weathering, geochemical study and elemental redistrib. 78−7634
- soils, multielement determ. by computerised instrumental neutron activation anal. 77−44546
- solar abundance data for 67 elements 77−53542
- solar abundances of Fe group elements, from corrected absolute oscillator strengths 77−3310
- solar and stellar element abundance, atomic and mol. f-values 78−20792
- solar composition, review 78−20793
- solar corona, temps., temp. gradients and comps., evidence for H^{+} depletion 77−53525
- solar energetic particles in corotating events, comp. 79−25414
- solar Fe abundance, from 300 nm to 900 nm Fe I spectrum 77−5516
- solar flare cosmic rays, element abundance in $2 \leq Z \leq 28$ range 80−90382
- solar heavy nuclei enhancement at high energies, 1974 July 4 event 78−28641
- solar nebula, rare earth element condensation and fractionation 80−72796
- solar O, N and C abundances, new radiative lifetimes and oscill. strengths in visible and IR spectra 78−50506
- solar photosphere, abundances of elements Na to Ca 78−49411
- solar photosphere Fe abundance, curve of growth and fine anal. 77−56883
- solar quiescent prominences, He/H ratio from H and He spectra 77−13295
- solar quiet corona, O/N abundance ratio from highly ionised O and N X-ray spectrum 78−45297
- solar system, comparison with galactic halo stars *(French)* 80−72933
- solar system, continual matter accretion, elemental heterogeneities 79−2489
- solar system abundances of nuclides and nuclear structure 77−82130
- solar system chemical abundances, comparison with chemical yields from mass-losing massive stars 80−36614

element relative abundance continued
- solar system formation, re-evaporation of condensed matter, evidence from meteorite mineral content 78−85864
- solar wind, ^{3}H and ^{14}C abundances 77−5407
- solar wind, α-particle/proton abundance ratio anticorrel. with particle flux in three-fluid model 78−57418
- solar wind, He abundance long-term vars., Imp 6, 7 and 8 results 78−77452
- solar wind, plasma comp. expt. on International Sun-Earth Explorer A 78−85810
- in spiral galaxies, chemical enrichment correl. with density wave energy 80−98715
- spiral galaxies, heavy elements abundances rel. to line intensity vars. across discs 77−13459
- spiral galaxies nuclei, stellar population and metal abundance 80−56926
- stars, A0-G2 type, abundance effects in Geneva photometric system 77−29830
- stars, abundance determ. by photometric and spectroscopic methods 77−29807
- stars, abundance determ. in sequences of old open clusters 77−29888
- stars, abundance effects in classification, IAU Symposium 72 (Lausanne, Switzerland, 8-11 July 1975) 77−29802
- stars, abundance effects in spectral classification of peculiar objects 77−29859
- stars, abundance effects on atmosphere calcs. 77−29803
- stars, abundance effects on uvby photometry 77−29808
- stars, age-abundance relation 77−29813
- stars, chemically peculiar, nuclear and differentiated abundance patterns 77−17597
- stars, large-scale abundance effects 77−29812
- stars, lifetimes and abundance ratios in chemical evolution 79−53801
- stars, metal abundance and MK class. for F5-K4 type objects 77−29809
- stars, red giants, abundances in M3 and 13 globular clusters 78−93334
- stars, very cool white dwarfs, abundance change effects on spectra 77−29829
- stars in main sequence, diffusion and turbulence rel. to abundance anomalies 78−89198
- stellar He/H ratios, evidence from eclipsing binaries masses, radii and absolute magnitudes 79−44520
- stellar spectrum, abundance distribs. and origin of elements, reln. to evolution of universe 77−26099
- stone artifacts, Japanese, trace elements, neutron activation anal., rel. to archaeological provenience 78−8492
- stratification of elements in the envelopes ejected by type I supernovae 79−16997
- subdwarf stars, odd-Z and r-process elements abundances from spectroscopic anals. 80−62122
- Sun, He abundance affected by global oscills. 80−51724
- Sun, Ti abundance from recent Ti I oscillator strengths 78−45306
- superheavy element data from monazite, background re-evaluation 77−33077
- superheavy element search in Earth samples, meteorites and cosmic rays *(Russian)* 79−84277
- superheavy element search in giant-halo inclusions using synchrotron radiation 77−22925
- superheavy elements, detection by fission activity detect. *(Russian)* 79−13358
- superheavy elements in primaeval Moon 78−96412
- superheavy elements in search bulk monazite by ^{32}S ion backscattering 77−21773
- superheavy elements search in terrestrial substances *(Chinese)* 79−84281
- supernova, remnants, O, N and S abundances, optical emission from shock waves 77−49447
- supernova remnants, element abundances and shock conditions determ. from optical emission 77−64816
- supernova remnants, evidence for element depletion from far UV spectrophotometry 80−90498
- supernova remnants, H abundance rel. to H deficiency in Type I supernovae 78−53969
- symmetry theory of unit cubes in a cube of side three 79−97541
- tephra attributed to Glacier Peak, Washington, Ca, Fe and K contents 78−24273
- tephra set W, Mount St. Helens, Ca, Fe and K in glass shards 78−24274
- terrestrial sediment Ir enhancement, lunar material transfer by supernova 80−56731
- thermal fluids of Abano region, N.Italy, comp. rel. to sources and circulation paths 79−20883
- thermonuclear astrophysics, element abundances rel. to nucleosynthesis *(Italian)* 79−53715
- Thunder Bay, Lake Superior, element conc. in post-glacial sediments 77−78237
- trace element abundances in rocks, possible diffusional effects 77−41008
- trace element conc. in hot water springs in N.Spain *(Spanish)* 77−49097
- trace element distrib. in terrestrial life rel. to panspermia hypotheses 77−32968
- trace element geochemistry of Sokoman Fe Formation 77−81884
- trace element model study of Archean greenstone belts, Nyanzian System W.Kenya 77−60375
- trace elements in basalts from Nauru Basin 80−94499
- trace elements in metal, silicate and sulphide phases of chondritic meteorites 77−9711
- trace elements in shergottite meteorites: implications for the origins of planets 79−44420
- trace elements in the fluid phase of the Earth's mantle 79−34779
- trace elements in Tieschitz primitive H3 chondrite, effects of thermal metamorphism 78−20765
- trace elements partition patterns in sediments from DSDP Site 219 78−36143
- trace elements survey, 1977 results for UK air 79−20960
- trace metal distrib. in Long Island Sound sediment core, biological mixing effects 79−66672
- trace metals in Antarctic snows (1914 to 1974) 79−34867
- trace metals in coastal waters, monitoring by neutron activation analysis 77−41068
- trace metals in Saguenay fjord, rel. to runoff inputs 77−5251
- 47 Tucanae, globular cluster, chemical comps. of stars 80−46620
- Tunguska cosmic body, chemical comp. and nature 78−61810

element relative abundance continued
Tunguska cosmic body, silicate microspherules chemical comp. and cosmochemical anomaly 78—96430
Turkish clay, neutron activation anal. 78—8487
Tuscany hot springs, geochemistry rel. to geothermal areas location 77—49049
Tycho supernova remnant, Type I SNR, elemental abundances from X-ray spectrum 80—46635
Tysnes Island, meteorite, comp. of unusual Fe+FeS and silicate clast 79—2526
U, conc. and isotopic comp. in Edwards carbonate aquifer, Texas, rel. to aquifer oxidation/reduction state 80—98362
unevolved stars, abundances rel. to interstellar gas mixing *(Russian)* 79—40192
universal abundances and origin *(French)* 77—26097
urban aerosols, Boston area, multivariate anal. for element sources identification 77—37357
τ Ursae Majoris, Am star, microturbulence and metal content determ. 80—82377
Venus surface rock, radioactive element concs., Venera 9 and 10 meas. 77—78691
volatiles in chondrites and 'mysterite' as late condensate in solar nebula 78—7946
volatiles in chondritic meteorites rel. to metamorphism or nebular fractionation 79—66966
volatiles in Hawaiian tholeiitic submarine basalts 79—34795
W50, supernova remnant, N overabundance from optical spectrum 80—90557
white dwarfs, diffusion time scales rel. to element abundances 79—92761
Yamato meteorites (j), (k), (l) and (m) from Antarctica, petrology 79—2528
Z=116, possible detection expt. in marine creatures 77—3503
III Zw 77, compact galaxy with broad emission lines, Fe/Ne ratio 78—73760
β^+ nuclei, thermally induced particle emission as possible formation process 77—6340
Al dissolved in French hot spring water *(French)* 79—74913
Al in cool halo stars, implications for galaxy abundance 80—105232
Al/Fe, ratio in metal-poor stars 78—57549
^{241}Am/$^{238,239+240}$Pu, ratio in water entering N.North Sea, vars. 79—16520
Ar content of Mars atmosphere, Viking 1 X-ray fluorescence spectroscopy 77—13270
Ar degassing models of Mars 77—29700
Ar, interstellar depletion rel. to grain temps. in diffuse clouds 80—51848
Ar isotope abundances in Venus thermosphere, upper limits 80—4281
Ar/Cl in planetary nebulae rel. to galactic abundances 79—5887
Ar/H, low abundances meas. in three halo planetary nebulae 80—82443
Ar/O in planetary nebulae rel. to galactic abundances 79—5887
^{40}Ar concentrations in sialic crust and atmosphere, rel. to form. from upper mantle 79—44153
As content of Atlantic Ocean waters *(Russian)* 77—60428
B abundance determ. in rocks, soils, plants, waters and fertilisers 78—85559
B abundance in solar system 77—49318
B, concs. in carbonaceous chondrites 79—16897
B, content in bottom sediments interstitial waters on trans-Pacific profile 80—36289
B, inorganic, in St. Lawrence Estuary, determ. *(French)* 78—77274
B, interstellar abundance and depletion models 80—46630
B/Be ratio in meteorites rel. to interstellar grain synthesis 79—16894
B/H, interstellar ratio from B detect. in front of κ Orionis 80—51841
B/Na ratio in coastal N. Florida rainfall 77—21838
^{11}B, abundance from neutrino-induced prod. in stellar C layer 80—82337
Ba abundance implications in metal rich Ba II stars 79—71024
Ba conc. determ. in stony meteorites 78—65557
Ba profiles in Atlantic Ocean, GEOSECS expedition 77—81918
Be in main sequence stars 77—13332
Be in subgiant stars rel. to post-main sequence evolution 77—13333
^{9}Be/H in Population I giant stars, theoretical surface abundances 80—94796
^{214}Bi/^{214}Pb in S.California coastal air 78—49087
Br/Cl ratio in Bay of Bengal 79—25267
Br/Pb ratio for petroleum and atmospheric particulate 77—91254
Br/Pb ratios in atmospheric particulate matter over Perth, W.Australia, 1971-6 var. 79—34455
C abundance in planetary nebula IC 418, determ. from UV spectra 80—67832
C depletion in interstellar medium, from Cygnus Loop UV spectrum obs. 79—21398
C enhanced abundances in long-period variable C stars 77—33501
C I, abundances, UV grain albedos and pressures in interstellar medium 79—92818
C in Orion Nebula and IC 418 from visible and IUE obs. 80—82451
C, N, O, abundances in solar photosphere 78—24497
C, N and P particulate fluxes in upper water column of NE.Pacific 79—88368
C, N in Jupiter atmosphere, abundances deduced from absorpt. bands in refl. sunlight 80—56758
C, O abundances in planetary nebula NGC 7662, determ. from photoionisation model 80—62233
C overabundances in C star atmospheres 79—21284
C, primordial retention by terrestrial planets 79—40102
C/Fe ratio in metal-poor stars from CH features 79—16945
C/Fe ratio of K-type dwarf star 14 Herculis 78—93227
C/H, C/N in Jupiter, ratios determ. using new spectroscopic method 79—84734
C/H, in cool giant stars, from obs. and anal. of CO at 5 μm 78—36569
C/H, in Jupiter, determ. from methane-d_1 phase 78—28572
C/H in high excitation planetary nebulae, IUE satellite obs. 80—94860
C/H in Uranus atmosphere, evidence for enhancement over solar ratio from methane-spectrum 80—98609
C/H ratio, on Jupiter, from IR and visible spectrum 79—48729
C/H ratio for Jupiter from 8-9 μm IR spectrum 80—67638
C/N abundances on first giant branch of NGC 6752 globular cluster 80—67719
C/N/P ratios in ocean rel. to sedimentation rates and organic matter chemical reactions 77—64325
C/O ratio in cool C stars 77—91533
C/O ratio in Orion Nebula, determ. from long-slit spectroscopy in rocket UV 80—105297

element relative abundance continued
C/O yield of massive stars, convection and semi-convection effects 80—17579
C-poor events, IMP 8 ULET sensor meas. of solar flares 79—92739
CHNS, simultaneous determ., combustion-gas chromatographic method, data processing 80—40762
CN abundances in red giant stars in 47 Tucanae cluster 79—97000
CNO abundances, in red giants after main-sequence mixing 77—33475
CNO abundances in atmosphere of β Lyrae, IR spectra *(Russian)* 80—67794
CNO abundances in B-type stars in associations and general field 80—67702
CNO, abundances in G and K Ib supergiant stars 78—24509
CNO abundances in G- and K-type giant stars 77—5530
CNO abundances in red giant envelopes 77—29825
CNO anomalies in spectra of OB stars 77—29835
CNO, depletion in galactic dust/molecular clouds 80—26925
CNO in main-sequence stars, meas. in α Canis Minoris, 45 Tauri and HD 27561 78—93222
CNO in Population I giant stars, theoretical surface abundances 80—94796
CNO in Sun, abundances rel. to Si in different solar regions 80—46518
CNO, initial stellar abundances rel. to CN strengths and ^{12}C/^{13}C ratios in K-type giants 78—93229
CNO var. in massive binary stars, Wolf-Rayet appls. 80—94802
^{12}C/^{13}C abundance ratio in C stars 77—33494
Ca, abundances in F-type supergiants in Magellanic Clouds 80—98655
Ca, cosmic ray source abundance 78—28467
Ca excess in snow and rain samples, Japan, from calcite source 79—39766
Ca in giant stars in globular clusters 80—72940
Ca, in Sun, rel. to upper photosphere models and empirical damping parameters 77—33445
Ca, Mg, Na, K, supply from rainfall to NE.Rhodesia 79—57988
Ca/H, ratio in two extremely metal-deficient stars 78—69797
Ca/H ratio in RR Lyrae variable stars in globular clusters 79—16962
Cd, concs. in fractions of H3 chondrites Tieschitz and Brownfield correl. with isotope fractionation 80—94764
Cd, determ. in sea and fresh waters, interlaboratory comparison 78—81209
Ce depletion in Melrose-b howardite 80—101566
Cl abundance towards 10 stars, Copernicus obs. 78—36646
Cl in stratosphere rel. to O_3 diurnal var. and scattering 78—7710
Cl/O in planetary nebulae rel. to galactic abundances 79—5887
Co, interstellar abundance and depletion models 80—46630
Cr content of magnetite from Bushveld Complex upper zone, vars. rel. to magma chambers heterogeneity 80—56421
Cr in stars, Utrecht UV spectrophotometer obs. 78—69793
Cr, interstellar abundance and depletion models 80—46630
Cr, Mn, Fe, abundances in early type peculiar stars 77—78803
Cr, solar abundance from photospheric spectra and oscillator strengths 78—69757
^{137}Cs, contents in coastal sediments 79—57974
Cu, cones, in E.Atlantic Ocean, 23°N to 47°N 77—5239
Cu, geochemistry in sediments of Gulf of St. Lawrence and estuary 78—92855
Cu-Ni enriched ferromanganese nodules and crusts from Bauer Basin, mineralogy and chemistry 77—86851
D abundance in Galaxy rel. to cosmology 78—69883
D, abundance in solar atm. 79—66982
F conc. meas. in meteorites 77—87342
F content of hot spring waters, Japan *(Japanese)* 80—31074
F, contents in basalts of Iceland and Reykjanes Ridge 79—57900
F/Cl in Nasu hot spring water *(Japanese)* 79—8648
Fe Abell 1060 galaxy cluster, abundance from X-ray spectrum obs. by (HEAO A-2) 80—82518
Fe abundance in M87/Virgo cluster X-ray source, determ. form 1.1 keV line emission 79—25758
Fe abundance in solar system rel. to nucleosynthesis 77—53435
Fe abundance in X-ray galaxy clusters 79—12530
Fe abundances in gaseous nebulae, from forbidden Fe III and Fe VI lines intensities 78—53806
Fe and C gas phase abundances in planetary nebulae 78—28744
Fe conc. determ. in Vellar estuary 80—77015
Fe content determination in natural waters 79—84550
Fe group elements, relative abundances from prod. in supernova outburst *(Russian)* 80—62167
Fe group elements abundances in Sun from singly-ionised lines 78—93189
Fe in Centaurus galaxy cluster, abundance from X-ray spectrum obs. by (HEAO A-2) 80—82518
Fe, in cosmic ray flux from meteoritic hypersthene tracks 77—41276
Fe in red giant star ε Virginis, differential model atmosphere analysis 79—25604
Fe, in solar corona, determ. from XUV emission lines 78—4180
Fe in stars, Utrecht UV spectrophotometer obs. 78—69793
Fe, interstellar gaseous depletion, Fe II resonance line UV obs. 79—44584
Fe meteorites, chemical fractionations and cosmochemical history of metal phase 77—49347
Fe meteorites, condensation and comp. 79—30021
Fe meteorites, cosmic ray produced nuclides, ^{41}K/^{40}K-^{4}He/^{21}Ne exposure ages and age distribs. 79—30015
Fe meteorites, Ga, Ge and Sb concs. rel. to chemical classification and nebular condensation 80—36594
Fe meteorites, group IC, comp., mineralogy and origin 78—32414
Fe meteorites, trace element abundances rel. to superheavy elements fission 79—48742
Fe meteorites of groups IAB and IIICD, element abundances rel. to origin 80—109404
Fe meteorites with low Ga and Ge concs., comp., struct. and genetic relationships 79—21236
Fe partition patterns in recent sediments of Indian continental shelf 77—73710
Fe, solar abundance from 300 to 900 nm Fe I lines using precise oscillator strengths 79—40155
Fe, Ti, V, Ca, Ni, Co, abundances in late-type dwarf stars 77—78779
Fe/H abundance determ., catalogue for 515 stars 77—29815
Fe/H abundance in 628 stars, catalogue 80—98579
Fe/H abundance ratio in giant stars of G and K type 79—16944

element relative abundance continued
Fe/H abundances of extreme Population II stars in globular and dwarf galaxies 78—40939
Fe/H calibration of subdwarf star 37—45 colour excess 80—82363
Fe/H determ. catalogue for stellar atmospheres, comments 77—29806
Fe/H in metal-poor dwarf stars 80—51751
Fe/H of F- and G-dwarf stars, determ. using CORAVEL radial vel. scanner 80—94791
Fe/H ratio and $^{12}C/^{13}C$ ratio correl. in K-type giant stars atms. 79—48798
Fe/H ratio for metal-poor stars and globular clusters 78—53937
Fe/Ni partition, in metamorphosed olivine-sulphide assemblages from W. Australia 77—5185
Fe-group elements, oscillator strengths for V I and Co I in solar photosphere 78—40905
Ga, Ge, Cu, Sb, moderately volatile siderophiles in ordinary chondrites 80—8595
Ge/Si and Ga/Al ratios vars. along Reykjanes Ridge and Iceland 79—8617
H I/He I, ratio in local interstellar medium rel. to ionisation state 80—90502
H II regions, abundance determ., empirical method test 78—61908
H II regions, influence of chemical comp. on ionisation and temp. struct. 78—61911
H II regions, metal rich, abundance determ. errors 80—82461
H II regions near nucleus of spiral galaxy NGC 3310, metal abundance and N/O ratio 80—62235
H in anisotropic universe, mass fraction rel. to primaeval radiation polarisation 80—82552
H/D ratio in planetary atmospheres, determ. from CH_3D 9613 Å band 78—86861
H/He ratio in ν Eridani, atm. parameter determ. 80—67739
H/N ratio in H II regions *(Italian)* 79—21395
H-He fluid planets, dynamics and He distrib. 78—28555
H_2/H_2+He abundance on Saturn from Pioneer 11 IR radiometry obs. 80—82290
^2H, limits on heavy neutrino props. from primordial nucleosynthesis 78—57438
He abundance in galactic H II regions, recombination line obs. 80—98703
He abundance in H II regions in Galaxy 79—21389
He, abundance in horizontal-branch A-type stars 79—62829
He, abundance in subdwarf stars, also galactic halo rot. 80—22003
He abundance in white dwarf HZ 43, stellar struct. from soft X-ray obs. 80—72944
He abundance var. in galactic globular clusters 80—56894
He and heavy element abundance in H II region in NHC 2366, visible and radio obs. 80—77475
He content of solar models, implications for convective mixing length 80—26835
He, cosmic abundance rel. to time-varying gravit. const. 79—92667
He, cosmological abundance, rel. to number of neutrino species and Universe lepton number 80—8730
He enrichment due to He shell flashes 77—45428
He enrichment in planetary nebulae 79—21380
He in chaotic Friedmannian Universe 80—67920
He in Earth interior, incorporated from immature Sun *(Russian)* 80—81856
He in galactic globular star clusters 78—45370
He, in solar corona, abundance determ. from He^+ 304 Å radiation 77—91510
He, ionisation struct. and abundance in Orion Nebula, SHF obs. 80—105315
He, N, O abundances of planetary nebulae in Magellanic Clouds 78—4338
He, primordial nucleosynthesis rel. to Dirac Large Numbers Hypothesis 79—92900
He, production in Brans-Dicke and relativistic cosmologies *(Polish)* 80—27024
He spots caused by diapiric magma from upper mantle, Matsushiro fault zone, Japan 79—8618
He survey in S.India for structural mapping, water sample obs. 80—8261
He universal abundance 80—62356
He/Ar and N_2/Ar ratio vars. in fault zone groundwater air bubbles for earthquake prediction 78—88803
He/C, C/O ratios in C_2 white dwarf LP 145-141, rel. to strong UV absorpt. 80—67715
He/H abundance ratio in H II regions 78—86000
He/H abundance ratio in stellar atmospheres in O-associations and young clusters *(Russian)* 77—64815
He/H in Jupiter atmosphere, ratio from Voyager 1 IR obs. 80—26790
He/H in Sagittarius B2, He recombination line obs. interpretation 80—62300
He/H ratio in planetary nebulae 78—93376
He/H ratio in solar quiescent prominences, theoretical models 78—49405
He/H ratio of B-type stars in young clusters and associations 77—29887
He/H rel. to N/O in planetary nebulae 79—35326
He/M ratios in planetary nebulae 77—9781
He^+/H^+ in M8, ratio from radio recomb. line obs. at 5 and 10 GHz 79—84832
He^+/H^+ ratio in galactic centre source G 0.7—0.0, interpretation of recomb. line emission 77—17651
He^+/H^+ ratio in H II region G0.7-0.0 (Sagittarius B2) 78—45380
He-rich stars 77—37608
$^3He/^{21}Ne$, ratio in Djermaia (H) chondritic breccia rel. to preirradiation history 80—36579
$^3He^+/H^+$, interstellar abundance ratio and significance 79—25689
^4He primordial abundance for superweak particle cosmological constrains 79—84667
Hf, in stony meteorites 79—92731
Hf, solar abundance from Hf II spectral lines obs. 77—17518
Hg conc. determ. in Arabian Sea waters 79—25268
Hg determ. in sea and fresh waters, interlaboratory comparison 78—81209
Hg in Gulf Stream 80—7965
Hg levels in soil and water in Israel and Sinai 77—29337
Hg, natural conc. in Iceland 77—64244
Hg-Mn stars, chemical abundances 80—56838
Hq, abundance in Greenland Ice Sheet 78—65349
I in Yarra River estuary water 79—34855
I/Xe, IIE iron meteorites, Weekeroo Station and Netschaevo 80—77360

element relative abundance continued
K, determ. in seawater using selective membrane electrode 79—53368
K in aerosols from S.American rain forests 79—100910
K in Earth, implications of K solubility in Fe-S and silicate-K-(Fe-S) equilibria 78—11843
K/Na ratios in dew drops rel. to atmospheric aerosol comp. 77—91190
K/Rb, chondrites, CI and CM, discordant, leaching experiments, Rb-Sr studies 79—84754
k/Sr, chondrites, CI and CM, discordant, leaching experiments, Rb-Sr studies 79—84754
K/U ratio in Earth interior, evidence from differentiated He and Xe in deep-sea basalts 80—31040
La, abundance in solar photosphere from exptl. lifetime determ. 77—30827
La, solar photosphere, new lifetime meas. of La^+ 78—17618
Li, 'cosmic' abundance from sample activation anal. 78—12111
Li, abundance in atmospheres of M-type supergiants *(Russian)* 80—72950
Li, abundance in cosmic rays, balloon borne telescope meas. 78—40785
Li abundance in Luna 24 soil samples 80—67590
Li, Be, B, galactic abundances rel. to cosmic-ray nucleosynthesis and extragalactic matter infall rate 79—17084
Li, determ. in weak-G band giant stars 78—53948
Li in G and K-type giant stars, abundance meas. 80—41819
Li in Keweenawan rhyolites, anomalous abundance 79—84252
Li in stellar atmospheres *(Russian)* 77—64748
Li in tektites and impact glasses 80—61799
Li/K ratio of interstellar matter towards ζ Persei and ε Aurigae 78—49494
Li/Na ratio upper limit for novae 79—101156
^7Li, abundance as constraint on universal baryon density 78—4420
$^7Li/H$ in Population I giant stars, theoretical surface abundances 80—94796
Mg abundance gradient NGC 7027 planetary nebula 80—41875
Mg and Ne abundances in red giants and planetary nebulae, ^{22}Ne neutron source effects 78—49430
Mg index in old galaxy populations 78—41033
Mg, interstellar column density towards nearby stars from Mg II obs. 78—41023
Mg/Ca in He-rich white dwarf star Ross 640, UV spectra 80—94790
Mg/Cr ratio in achondrites and mesosiderite silicate fraction 80—51704
Mn, distrib. in Pacific Ocean 80—56494
Mn, in belemnites, as evidence of post-depositional alteration, effects on ^{18}O palaeotemps. 77—29455
Mn in Galapagos Rift from hydrothermal circulation 77—86939
Mn in Jervis Inlet, British Columbia, distrib. rel. to Mn deposition and nodule growth 78—96187
Mn in NE.Pacific water 80—101384
Mn nodules, from sea-bed, isotopic and elemental composition, U, Pa, Th, radiochem. anal. 78—77215
Mn, solar abundance, Mn^+ oscillator strengths 78—17619
$Mn/^3He$, in deep sea hydrothermal plumes, injection ratios and Mn scavenging residence time 78—32121
Mn-Hg stars, differential curve-of-growth analyses 79—16971
N abundance and isotopic comp. in stony meteorites 78—65558
N, abundance anomaly in globular cluster 47 Tucanae 79—48867
N, abundance in H II region 80—46680
N and He overabundance in PK 6-2°1 southern planetary nebula 77—78849
N, concs. in tektites and natural glasses 80—41446
N distribution and C/N ratio in lake sediments 78—28250
N, interstellar abundance from XUV absorption line obs. 79—5741
N, overabundance in nucleus of NGC 6946 spiral galaxy *(French)* 78—89257
N/C in Q0353—383, QSO abundance anomalies, UV and visible spectral obs. 80—82532
N/C ratio determination in atmospheres of C stars, peculiar red giants 80—17580
N/O in galaxies 80—8686
N/O in planetary nebulae 79—35326
N/O ratio in planetary nebulae 78—93376
N/O ratio in Venus upper atmosphere, Pioneer Venus Orbiter meas. 80—77310
N/S gradient in M33 galaxy, supernova remnant evidence 80—56929
N/S in spiral galaxy NGC 5236, radial var. of abundance ratio from emission line obs. 80—82497
Na in M13 red giants, evidence for protocluster gas inhomogeneities 80—82439
Na in nightglow from Na I D doublet excitation obs. 80—98497
Nd abundance in solar photosphere 78—9104
Nd/Sm ratio of lower continental crust, constraints from mantle Nd-Sr isotope correl. 80—94498
Ne in gas-rich samples of carbonaceous chondrite meteorites 78—65559
Ne in planetary atmospheres, interstellar cloud material contrib. 79—25698
Ne/O in planetary nebulae rel. to galactic abundances 79—5887
Ne/O of solar flare-accelerated Ne nuclei 79—92740
Ni I solar photosphere from oscillator strength obs. 80—98625
Ni in Cu alloy of Mayfield chondritic meteorite 80—67671
Ni in olivine of pallasite meteorites, ion microprobe anal. 79—58304
O, abundance in emission clumps of irregular galaxy (Markarian 325) 80—67869
O, abundance in H II region 80—46680
O, abundances in metal-poor stars 80—36610
O, conc. in lower ionosphere, fluorescence spectra 80—36434
O deficiency in Elefsis Bay, Greece 79—84299
O deficit in Earth atmosphere, consequences *(German)* 77—70799
O, Fe in globular cluster stars, influence on horizontal-branch morphology 80—67695
O in Pacific Ocean, surface distrib. and min cond. depths 77—25696
O, in supernova remnant in NGC 4449, abundance rel. to nucleosynthesis 80—56895
O, interstellar abundance toward ζ Ophiuchi 79—44583
O vertical distrib. in Atlantic and Mediterranean near Gibraltar *(Russian)* 78—16058
O/C in red giants, abundance ratio from TiO absorpt. bands 78—96480
O/H abundance ratio determ. in Galaxy from H II regions radio obs. 80—36692
O/H ratios in planetary nebulae, meas. rel. to Galaxy O enrichment 80—105328

element relative abundance continued
O/Mg abundance ratios in solar atmosphere effects of diffusion 80—4318
P abundance towards 10 stars, Copernicus obs. 78—36646
P containing particles, deposition velocity over southern Lake Huron 79—83666
P distribution control in estuary water 77—21823
P in aerosols from S.American rain forests 79—100910
P, N and organic C distrib. in sediments of Lake McIlwaine, Rhodesia 77—33114
P, uncertainty analysis of lake loading 78—81262
P/H ratio for Jupiter from 8-9 μm IR spectrum 80—67638
P/H ratio in Jupiter atmosphere, results from 10 to 13 μ spectrum 79—8876
Pb baseline in troposphere, anthropogenic sources effects 78—7757
Pb concs. rel. to 1000 mb geostrophic back trajectories at Quillayute, Washington 77—29421
Pb, geochemistry in sediments of Gulf of St. Lawrence and estuary 78—92855
Pb in environment 79—34443
Pb in hydrosphere, global and regional distrib. 79—16517
Pb in subalpine pond sediments, anthropogenic source var. 80—85315
Pb total in soil, comparative study of analysis methods 78—16221
^{210}Pb/^{226}Ra and ^{210}Po/^{210}Pb disequilibria in seawater and suspended particulate matter 77—5224
Pd, Ir, Au, abundances in mafic and ultramafic rocks from Mid-Atlantic Ridge 77—91073
^{108}Pd/^{109}Ag in Santa Clara and Pinon Fe meteorites, meteorites, rel. to isotopically anomalous Ag origin 80—85902
Pr solar abundance from Pr lines in photospheric spectrum 79—44443
Pt concentration in deep sea Mn nodules from Pacific Ocean *(German)* 79—44169
Pu, contents in coastal sediments 79—57974
^{244}Pu, existence in early solar system 77—29663
^{244}Pu/^{238}U, ratio in St. Severin chondrite 80—72889
^{226}Ra, behaviour in Pee Dee River—Winyah Bay estuary, S.Carolina 80—98360
^{226}Ra, distrib. in Antarctic Ocean 77—5220
^{226}Ra, distrib. in Atlantic Ocean 77—5219
Rb/Sr, chondrites, CI and CM, discordant, leaching experiments, Rb-Sr studies 79—84754
Rb/Sr ratio of lower continental crust, constraints from mantle Nd-Sr isotope correl. 80—94498
Rb/Sr whole-rock systems and chemical control 78—61366
Re/Os cosmochronology, nuclear correction factor 80—17485
Re-Os, rel. abundance, rel. to nuclear chronometer reliability 78—85919
^{187}Re/^{186}Os in Earth mantle, rel. to use of Os isotopes as petrogenetic and geological tracers 80—89989
^{187}Re/^{186}Os in meteorites, rel. to solar system early chronology and Galaxy age 80—41778
Rn and Rn decay products, disequilibrium ratio in the atmosphere *(Spanish)* 80—31083
Rn concentration in groundwater, continuous monitoring using ionisation chamber 79—21068
Rn concs. in geothermal reservoirs 78—69381
Rn in groundwater, continuous meas. method for earthquake prediction 77—44935
^{222}Rn in Hudson River estuary, distrib. and transport across sediment-water interface 78—16064
Ru determ. in silicate rocks, preseparation procedure for neutron activation anal. 77—44547
S and trace elements in aerosols from South American continent, conc. relationships 78—57245
S budget for sour gas plants in Alberta 77—37372
S content and acidity of soil in Alberta, SO_2 effect 77—73843
S distribution in oceanic crust layer 2, effect of low-temp. seawater-basalt interaction 80—41432
S in 20 galactic planetary nebulae, spectrophotometry 78—45375
S in aerosols from S.American rain forests 79—100910
S in lunar rocks rel. to C content 78—4123
S in Martian lithosphere, possible overabundance 80—72832
S in planetary nebulae, abundance from IR line meas. 80—82444
S in rainwater in rural areas of England and Wales 79—16562
S/Ne/A ratios in NGC 7027, planetary nebula 79—21400
Sb content of Atlantic Ocean waters *(Russian)* 77—60428
Se in estuarine water in Solent area 78—57230
Si overabundance in chemically peculiar stars and oblique rotator model 79—30067
Si/He, line ratios in Magellanic Clouds O and B0 supergiants 77—78777
Sm II, solar abundance, spectral transition probability, 3000-7000 Å 79—31453
Sm/Nd, in Earth mantle, results from isotropic investigations of Isua supracrustals 78—36129
Sm-Nd age of lunar KREEP basalt 80—12686
Sn determ. in rocks by thermal neutron activation anal. 77—44552
Sn, solar abundance from Sn I line intensity profiles 78—20772
Sr in aragonite, distrib. rel. to transform. to calcite in marine gasteropod 79—62485
Sr/Ca ratio for ocean temp. 80—12568
Tc in late-type stars, spectral analysis 80—8623
Th, in Indian Kimberlites 77—60376
Th, U, Pu, Cm in solar nebula, condensation and fractionation 79—35154
Th/U in sedimentary rocks, rel. to crustal evolution and sedimentary recycling 80—85654
Th/U ratio in Archaean granites from NE.Minnesota 78—61356
Th/U ratios for phosphates in stony meteorites 79—75162
Ti distrib. on lunar surface 80—17510
Ti, in stony meteorites 79—92731
Ti, interstellar, depletion from Ti II 3384 Å line obs. 78—57611
Ti, solar abundance from Ti I transition probabilities 77—29743
Ti, solar abundance from weak spectral lines obs. 77—29778
U and Ac series nuclides in soil, radioactive disequilib. 80—4014
U and Th abundance in Precambrian basement, W.Canada, petrologic and tectonic controls 80—17257
U and Th in rocks, determ. via fission/α technique 77—29497
U anomaly in Black Sea sediments, accumulation mechanism 77—91105
U anomaly in sediment under Galapagos hydrothermal mounds 80—56434
U distribution and evolution in oceanic lithosphere 79—84226
U, in chondritic meteorites, abundance and isotopic comp. 78—4157

element relative abundance continued
U, in Indian kimberlites 77—60376
U in marine rocks, content distrib. and meas. by neutron induced fission track method 79—79809
U in oceanic crust 80—8287
U in South Africa and South West Africa 79—84268
U in USA, genesis and exploration 79—84267
U in volcanic rocks of E.Avoca-Ballard mineralised belt 78—69346
U in world rivers, evidence for higher natural content 79—44208
U occurrences and mode of origin, N.Saskatchewan, Canada 79—84272
U-Th-Pb of Saint Severin amphoterite meteorite 78—65560
V, interstellar abundance and depletion models 80—46630
V/H ratio in early A-type stars 79—21314
W, concs. in Fe meteorites 79—35200
W, in ordinary chondrite meteorites, abundance and distrib. 78—32412
^{129}Xe, excesses in Hawaii lavas olivine phenocrysts and xenolithic dunites 79—34814
Y, Ba and rare earth elements in Ap and Am stars 77—33505
Yb, in meteorites and terrestrial samples 78—32419
Zn, geochemistry in sediments of Gulf of St. Lawrence and estuary 78—92855
Zn rel. to Si concentrations in NE.Pacific water 78—36200
Zn, solar photosphere abundance, discrepancy with meteorite abundance 80—72897
Zr, in stony meteorites 79—92731
Zr/Hf, determ. in silicate rocks, meteorites and lunar samples by neutron activation 78—20547

elemental semiconductors
adamantine family of semiconductors, props. and commercial appl. 79—42447
amorphous, crystallisation and decomposition 79—41959
amorphous, diamagnetic susceptibility enhancement 79—65640
amorphous, high field transport, impact ionisation, carrier mobility 80—80286
amorphous, local order as determined by electronic and vibrational spectroscopy 79—37627
amorphous, struct. models 79—37628
amorphous, vac. evaporated, doping, transport and optical props. 80—49715
amorphous, vibr. props., review 77—84873
amorphous group V semiconductor, defect states 79—87057
atomic diffusion in semiconductors, review 79—4423
α-B, rhombohedral, magnetic props. and ESR spectra 80—20452
band structure trends, isoelectronic series 77—89696
core excitons and inner well resonances in surface soft X-ray absorpt. spectra 80—40187
core-level photoyield exam. of empty surface states 77—55593
crystal defects in integrated circuits, review 78—88547
crystal growth aspects of electronic materials, review 80—66405
cubic many-valley type, cond. in warm electron region, phenomenological theory 77—43586
diamagnetism rel. to chem. bonds 77—59380
diamond:^{111}In, ion implanted, intrinsic limitations of doping 80—34019
diamond: B, natural, sub PPM determ. of B, identification of acceptor centre 77—59035
diamond: Li, ion implantation doped, IR photocond. 80—20249
diamond:B, B conc. and impurity-to-band activation energy 79—56165
diamond:B, epitaxial layer, charge transfer and acceptor state 78—19169
diamond:B, photoconductivity and electroabsorpt. spectra 77—4647
diamond:B, synthetic, current-voltage characteristics, temp. depend. *(Russian)* 79—7825
diamond:B, synthetic semicond., thermostimulated conductivity *(Russian)* 79—7834
diamond:B, thermoluminesc., TSC, correlation meas. 78—88369
diamond:B, variable-range hopping cond., effect of electron irrad. induced compensating centres 77—43599
diamond:B hopping conductivity in range 12 to 1300K 78—51994
diamond:Li, ion implantation, Hall effect and elec. cond. meas. 80—15526
diamond:Li, ion implantation, investigation of Li^+distrib. 79—77630
diamond:N, effect of displacement upon impurity levels, pseudopotential calc. 77—39803
diamond:N, photocond. in N2 absorpt. band 79—91102
diamond:N(B)(Si)(O), substitutional impurities 79—87056
diamond:Sb, implanted, radiation damage and annealing study 80—100263
diamond:Sb, ion implanted under channelling conditions, depth profile, distribution tail 80—2057
diamond:Xe, quadrupole interaction of implanted Xe 79—61279
diamond, (100) surface states, SCF extended tight-binding method 77—47881
diamond, (111) surface, quantum photoyield and secondary-electron distribs., stable negative-affinity emitter 79—100023
diamond, accelerator irradiation, heavy ion irradiation damage 80—100291
diamond, adiabatic bond charge model 77—69057
diamond, applications in electronics *(Czech)* 77—1414
diamond, B doped, electron irradiated, defects at low temps., elec. resist. meas. 77—11593
diamond, B doped, electron irradiated, threshold energy for atomic displacement, elec. cond. meas. 77—11594
diamond, band structure of diamond like crystals, cluster-Bethe lattice model calc. 80—6713
diamond, cathodoluminescence of defects *(French)* 80—34988
diamond, Compton profiles, X-ray struct. factors, band struct., LCAO calc. 78—51889
diamond, covalent semicond., depend. of energy gap on short-range order 78—84142
diamond, defect electronic struct. and lattice config., MO approaches 80—65495
diamond, defects and impurities 80—29017
diamond, dielectric function, optical frequency model calcs. 78—51921
diamond, dielectric polarisation calcs., microscopic local fields 80—20582
diamond, different types, trace elements conc. 79—14838
diamond, dynamic Jahn-Teller distortions at trigonal optical centres 79—87069
diamond, effective supersystem cryst. simulation method, geometrical parameters, bulk moduli, impurity levels calcs. *(French)* 80—15430
diamond, elasto-optical constants, determ. from piezobirefringence 79—73899

elemental semiconductors continued
- diamond, electroluminescence, thermoluminesc., photocurrents 79—38675
- p-diamond, electroluminescence 78—15229
- diamond, electron channelling gamma-ray spectra 80—40023
- diamond, electron irradiated, photocurrent and Hall current, 290 and 4.2K 79—87129
- diamond, electronic energy bands of diamond-type crysts., appl. of EHT method 78—87907
- diamond, electronic struct. of deep levels, LCAO, SCF method 79—82555
- diamond, elementary excitation in crystals, dielectric theory 78—60076
- diamond, energy band calcs. using intersecting spheres model 77—66110
- diamond, five-atom clusters, unrestricted Hartree-Fock calcs. 77—11866
- diamond, gamma radiation angular distribution of channelled 900 MeV electrons *(Russian)* 80—19858
- diamond, GR1 and UV band, fine struct. 80—20678
- diamond, GR 2-3 absorpt. line, uniaxial stress effects 78—72563
- diamond, GR defect, high resolution optical spectra after electron irrad. 78—56515
- diamond, ground-state, electronic properties, ground-state in local-density formalism 77—69223
- diamond, high temp. ion implantation 79—23623
- diamond, homogeneous formation in gas phase, laser beam effects *(Russian)* 80—104052
- diamond, implanted ^{129m}Xe, lattice location, combined Mossbauer and IPAC meas. 78—43733
- diamond, ion implantation, heteroatom size and reactivity effect 80—44226
- diamond, ion implantation, review 78—87698
- diamond, ion implanted, p-i-n structure, double injection of carriers 79—11214
- diamond, ion-doped with Li electron transport 80—92917
- diamond, irradiated, Hall current meas. by split electrode method 77—1435
- diamond, irradiated, optical spectrum 78—6719
- diamond, isomer shift values of implanted ^{133}Xe/^{133}Cs, Mossbauer spectra 80—7240
- diamond, Jahn-Teller coupling at ND1 and GR1 centres 78—56103
- diamond, Jahn-Teller coupling at neutral vacancy 80—71453
- diamond, large unit cell semiempirical mol. orbital approach to props. of solids 79—87036
- diamond, linewidth of GR2-8 transition 78—60488
- diamond, local field, microscopic electronic polarisation 80—25283
- diamond, low lying levels of GR 1 centre, satellite line struct. 77—20269
- diamond, magnetic field and stress splitting of GR1 line 78—60095
- diamond, momentum density, Compton profile 77—20235
- diamond, natural, anisotropy and saturation of hot carrier drift velocity 80—6867
- diamond, natural, dislocation-N$_2$ impurity interaction, photoconductivity spectra, resistivity 79—91097
- diamond, natural, elec. cond. and thermoelec. power 78—39115
- diamond, natural, electron effective mass and lattice scatt., Monte Carlo anal. 80—44484
- diamond, natural, free exciton luminesc. line shape 80—40165
- diamond, natural, high conc. of implanted Si ions, He backscatt. and IR absorption 77—89466
- diamond, natural, lattice scattering and effective mass of holes 79—60842
- diamond, natural, $N_{S(111)}$ impurity segregation on diffuse X-ray scatt. 79—95046
- diamond, natural, rate of donor defect introduction by 2 MeV electrons, 0.348 eV absorption band 77—89477
- diamond, natural, subthreshold defect formation due to electron irrad., cathodoluminescence study *(Russian)* 80—45152
- diamond, natural semicond., isothermal annealing of electron radiation damage 77—7764
- diamond, natural semicond. motor photocond. and internal photoemission 79—69546
- diamond, neutral vacancy, generalised val. bond calc. 77—55493
- diamond, nonlinear optical susceptibility, tight binding bonding orbital model 80—5784
- diamond, optical absorption and luminesc. spectra, review 80—2848
- diamond, optical surface modes calc. 77—59200
- diamond, optical transitions between E and T electronic states each coupled to e-modes, GR1 band 80—20677
- diamond, optically active centre effect on strength props. 80—40462
- diamond, phonon spectra calc. using dielectric matrix approach 79—4381
- diamond, plastically deformed, EPR of two N atom centre 78—72408
- diamond, polarisation charge density and microscopic local field induced in external elec. field 80—49645
- diamond, pseudo-Jahn-Teller effects in H3 vibronic spectrum 77—90182
- diamond, refractive index dispersion 79—24280
- diamond, relaxation about the vacancy 78—71722
- diamond, resonant Raman scattering 78—48176
- diamond, role of electron-hole interaction in optical spectra, review 80—45113
- diamond, semicond., electron irrad., charge carrier mobility 77—11921
- diamond, semicond., energy band struct., elec. and optical props., review 77—35862
- diamond, semiconducting, band gap temp. depend, dilation and vibr. contribs. determ. 80—10868
- diamond, semiconducting, electron-hole liquid formation conditions and parameters 79—78013
- diamond, semiconducting, GR1 cathodoluminescence, fine struct. 78—68566
- diamond, sound excitation orientational effect due to channelled electrons 80—84254
- diamond, state density and X-ray photoelectron spectra of valence bands calc. 77—28679
- diamond, static dielectric function, local field correction, tight-binding model 79—95355
- diamond, structure and motion of self-interstitials 79—37700
- diamond, surface electronic struct., self consistent pseudopotential calc. 78—47842
- diamond, synthetic, doped electroluminescence exam. 78—6783
- diamond, synthetic, elec. cond. 78—56144
- diamond, synthetic, electroluminescence excitation mechanism, role of defects 78—52581
- diamond, synthetic, p-n junction prod. and doping, I-V characts. 77—15943
- p-diamond, synthetic, semicond., photoconductivity spectra 79—69550

elemental semiconductors continued
- diamond, synthetic, semiconducting, X-ray exam. of inclusion 77—84788
- diamond, synthetic and natural, neutron irrad., optical and elec. props. *(Russian)* 78—59841
- diamond, synthetic semiconductor, IR spectroscopy and cathodoluminesc. *(Ukrainian)* 79—78758
- diamond, temperature field dynamics during synthesis 79—38755
- diamond, two-phonon bound state, Raman freq. 80—65179
- diamond, type Ia, electron irrad. effect on photocond., acceptor centre form. 77—47853
- diamond, type IB, electron irradiated, 2.367 eV vibronic absorpt. system, optical study 79—73975
- diamond, type IIa, electron irradiated, annealed to high temps., EPR spectrum 77—90034
- diamond, uniaxial stress splitting of E to E transitions at trigonal centres in cubic crystals 80—97312
- diamond, UV absorpt. produced by substitutional N$_2$ pairs 80—29770
- diamond, valence band calc. using many-electron theory 80—15434
- diamond, valence electrons, energy-depend. photoionisation probability calc. 77—16462
- diamond, valence electrons XPS spectrum, OPW calc. 77—4715
- diamond ceramic, elec. cond., thermal cond. rel. to temp. 79—15140
- diamond crystal, deep centres, changes in Van Hove singularities in vibronic spectra 77—8645
- diamond cubic structure, kink formation and migration, rel. to Fermi level 79—82218
- diamond detectors, elec. props. and performance for α- and β-particles 79—36481
- diamond detectors, transport props 85 to 700K 79—45542
- diamond Ge(B)(B$_4$C), doping by diffusion at high temp. and press. 79—19273
- diamond like, group IV elements, density of valence charge 78—34463
- diamond ratio of photoionisation cross-sections of valence s- and p-electrons *(Ukrainian)* 77—73211
- diamond Schottky barrier, electronic struct., pseudopot. calc. 78—95364
- diamond Schottky barrier, electronic struct., pseudopotential method, jellium model 79—38162
- diamond Schottky barriers, photocapacity meas. 78—52057
- diamond semiconductors, electronic structure, self consistent local description 80—20067
- diamond structure, plasmon line shape, local field effects 78—76011
- diamond structure semicond., lattice dynamics calc. prog. using adiabatic bond charge model 80—10599
- diamond type crystals, semicond.-metal transition 78—72072
- diamond type IIb, soft X-ray source for high resolution X-ray lithography 79—97481
- diamond type materials, lattice dynamical calc. using extended Born-von Karman scheme 78—59889
- diamond with local-field correction, dielec. const. calc. 80—11312
- diamond-like materials, electro-optic effects due to the Stark splitting of energy bands 79—82950
- diamond-Si heterostructure, Auger spectra electron microscopy study 80—34340
- diamond-type crystal, lattice dynamics from Keating's valence force field 78—79687
- diffusion of Al in open tube high vacuum system 78—91349
- dislocation electronic states, effect of hybridisation 78—51936
- dislocation mobility, effect of doping 79—82550
- displacement energy threshold, from energies of vacancy and interstitial form. and of lattice distortion 77—89430
- dose depend. in laser annealing 78—91354
- effects of junction depth and impurity conc. 80—55877
- electric susceptibility from chemical-bond approach 78—51922
- electron trapping, donor state generation, photo I-V study 80—20210
- electron-hole liquid theory, generalised RPA 78—87914
- electronic states and initial steps in oxidation 78—91534
- electronic struct. from SCF calc. using intersecting spheres model 78—51888
- electroreflectance, dielec. function, ellipsometric meas. 79—4790
- EPR of thermally induced defect 77—81005
- exoelectronic emission, mechs., sensitivity meas., surface study appls. 77—52228
- film, evaporated amorphous, hydrogenation by plasma treatment 78—91555
- films, amorphous, prep., struct., props., review, book contrib. 78—48321
- films, elec. and galvanomag. props., microstruct. 80—70859
- force variation due to charged defects 80—92634
- fundamental absorpt. spectra, direct interband transitions 78—63972
- Ge:P, radiation-accelerated diffusion 80—6559
- n-Ge, degenerate, Brillouin scatt. by phonon zero sound, in quantising mag. field 77—69847
- Ge, electron-hole droplets, large uniaxial stress 78—47703
- Ge, film growth kinetics under high adatom conc., surface diffusion parameters 77—28088
- Ge, heavily doped, dislocation vel., electronic effects 77—11547
- n-Ge, noise and hot carrier diffusion in mag. fields 79—11193
- Ge, refr. index, 95-298K, 2.5-12 μm 77—8535
- Ge electrode, electon injection in liq. NH$_3$ 80—6977
- n-Ge US attenuation due to donors and acceptors 77—28223
- graphite, band struct., calc. based on rigorous cellular method 77—15762
- graphite, carrier mobility, temp. depend. determ. from magnetoresist. expts. 80—11009
- graphite, electron elastic reflection angular characts., low primary energy 80—29835
- graphite, electron-phonon interactions, rel. to elec. transport 80—34156
- graphite, electronic props., self consistent LCAO calc., point vacancy in 2-dimens. cryst. 78—51932
- graphite, electronic props., self-consistent LCAO calc. 78—51887
- graphite, Hall coeff. in mag. field range below 1.2 kOe 77—15871
- graphite, layered, electronic band struct., direct evaluation by angle resolved photoemission 77—51652
- graphite, resistivity and magnetoresistance, 4.2 to 293K 80—100459
- graphite, slow electron elastic reflection characts. 80—25507
- graphite, thermoelec. and thermomag. props., cylindrical band model 80—39616
- graphite, thermoelectric power, low temperature, anomaly rel. to phonon drag 80—65610
- group IV, diamond type, Madelung energies, stability of high-press. phase 77—1097
- group IV, Mossbauer spectroscopy of defects, radiation damage and deep levels 80—59533

elemental semiconductors continued
  group IV, thermal expansion and MP, ionicity and bond length effects 77–47606
  Hartree-Fock energy band struct. determ. using LCAO basis 77–35848
  heterojunctions between monatomic semicond., interface spacing effect on interface states 79–95478
  impurity ion potential, in spatially varying dielec. const. semicond., variational calc. 79–7800
  ion beam milling, amomalous sputter yield behaviour 80–108624
  ion implantation, in crystals of diamond struct., computer modelling 77–43235
  ion implanted, laser-annealed, theoretical anal. of thermal and mass transport 78–91364
  ion implanted layers, complex refr. index profile, ellipsometric meas. 80–93262
  irradiated, under subthreshold irrad. conditions, defect formation ionisation mechanism possibility 80–6430
  irradiation induced crystalline to amorphous transition, Gibbs energy 80–70371
  laser annealing, optical constants, ellipsometry observation 80–34024
  laser damage, 10.6 μm CW CO_2 beam 77–63497
  lattice energy, strong orthogonality, requirement in calcs. dealing with crysts. by geminal method 78–14307
  metal-amorphous Si barrier, electronic props. 80–11089
  metal-ZnO-SiO_2-Si structures, charge injection 80–49919
  model pseudopotential, band struct. calcs., liquid semicond. resistivity calcs. 80–20075
  MOS structure, photon assisted tunnelling at Al/SiO_2 and Si/SiO_2 interfaces 77–89865
  multiple-trapping model and time-dependent random walk in α-phase 78–34842
  N-type switching, thermal mechanism 77–85273
  p-type, infrared absorption and plasma reflection 80–97284
  photon drag detector design and choice of semiconductor 80–57374
  photovoltaic technology, conf., San Diego, CA, USA (Jan. 1980) 80–86041
  point cathodes, explosive electron emission 77–59678
  polarisability of donors 78–14693
  polycrystalline, grain growth study 78–92188
  positron thermalisation, theory *(Russian)* 78–84170
  properties and use for making devices, review 78–60131
  radiation-produced vacancies and interstitials, annihilation processes 77–89432
  ribbon growth using scanned focused CO_2 laser beams 80–66417
  ribbon-to-ribbon growth method and sample characterisation Si 78–11103
  semiconductor depth profiling by electron beam induced junction current meas. 80–96977
  semiconductors, energy states under high press. *(Chinese)* 79–56128
  Si:Au, step junction, mathematical model *(Rumanian)* 79–87148
  n-Si:B, ion implanted, rapid identification of faulted loops 79–19254
  Si:B, isolated A^+ states under high compressive stress, long wavelength photocond. spectra 79–60765
  a-Si:H_x structure, effect of H-Ar plasma contact on elec. props., and optical gap 80–34533
  Si:P^+, ion-implanted, annealing characts., X-ray diffr. exam. 78–14372
  Si:P(As)(Sb)(Bi), high resolution study of group V impurities absorption 80–7388
  ρ-Si, deionisation effect on hole mobility evaluation 77–35945
  n-Si, dislocation images, electron beam induced current, charge collection process 79–17580
  n-Si, donor energy and polarisability in weak mag. field, rel. to hydrogenic atoms 79–3594
  n-Si, elec. cond. in weakly heating alternating elec. field 79–23977
  Si, electron-hole droplets, large uniaxial stress 78–47703
  Si, epitaxial film, kinetics of doping, gas-phase decomposition of SiH_4 77–16499
  p-Si, interstitial Fe and thermal defects, Hall effect and resist. meas. 79–82200
  Si, multiple bound exciton states, valley-orbit splitting 79–60725
  Si, n- and p-type, reactivity with organic nitrogen compound, rel. to polishing *(Russian)* 79–70192
  Si, single cryst. characteris. by SEM using Schottky barrier charge collection microscopy 77–4444
  Si inversion layers, prep. domain studies of intersubband optical transitions 80–20637
  Si surface, line tension induced dislocation motion 79–82212
  p-Si US attenuation due to donors and acceptors 77–28223
  Si wafer, anomalously transmitted X-ray intensity enhancement by asymmetric diffr., appl. to microstructure 79–14647
  n-Si-electrolyte junction, Schottky barrier height and reverse current 80–6979
  solar cells, minority carrier MIS diodes appl. *(Slovak)* 80–97792
  SOS, cryst. perfection rel. to MOS transistor mobility 78–75956
  SOS films, cryst. quality improvement by Si ion channelling, annealing 80–44222
  SOS MOS devices, hole mobility under residual stress, Hall meas., valence band struct. 78–88039
  SOS single crystal films, struct. and elec. props., review *(Japanese)* 77–63009
  SOS structure, radiation dose at interface due to electron beam aluminisation 78–68089
  SOS structures, high-field electron transport, drift vel. meas. 80–80387
  spatial distribution of temperature rise induced by Gaussian laser beam 79–69917
  specific heat at constant volume, leading anharmonic contribs. 77–89549
  static response, local field effects 78–76010
  superconductor-semicond. device research, future prospects 79–28467
  surface damage induced by RF-diode sputtering 77–90274
  surface dislocations, depth localization definition by HF gas-discharge plasma *(Russian)* 77–31664
  surface structure, chem. and spectroscopy, review 80–59764
  surface/adsorbate systems, local density of states calcs. *(German)* 80–60062
  p-Te, impact ionization rate of holes at 77K 80–10993
  uniaxially compressed crystal, exciton molecule radiation *(Russian)* 80–108264
  VPE growth, book contrib. 79–69997
  wafer characterisation by photonic injection+microwave meas., appl. to Si *(French)* 78–23106

elemental semiconductors continued
  web dendrites, dislocations, stacking faults, X-ray topographic study *(Chinese)* 80–88148
  X-ray scattering from small defects in very perfect crysts. 78–47395
  zincblende structure group IVA covalent crystals, Murnaghan parameter estimates from Morse pot. 78–95014
  n-Si, deep levels in p-n junctions or Schottky barriers determ., hybrid method 79–24067
  Si:P, sheet resistance of Gaussian n-type ion-implanted layers 79–87103
  a-Si:H, effect of H conc. on photovoltaic props. 79–99577
  Ag-In_2S_3-Si layered struct., Hall effect, I-V characts., surface states *(Russian)* 80–97001
  Al-amorphous Ge-nSi, photoelectric props. 80–70822
  Al-In_2S_3-Si layered struct., Hall effect, I-V characts., surface states *(Russian)* 80–97001
  Al-nSi-Al, p^+np^+ reach through structs., electronic cond. mechanism 78–64103
  Al-Si, ion plated contacts *(Rumanian)* 78–88029
  Al-Si contacts, effect of vacuum ambience 77–43718
  Al-Si contacts, electromigration and diffusion of Cu in Al film 79–77820
  Al-Si_3N_4-SiO_2Si, MNOS structures degradation under UV irradiation effect 80–107923
  Al-SiO_2-Si structure, Auger depth profiling and ion sputtering of interfaces 77–20200
  Al-SiO_x-Si minority-carrier MIS photodiodes, elec. characts. 79–51676
  Al-SiO_x-p-Si MIS solar cells with back surface fields 80–12006
  As, amorphous, AC cond. and photo-induced states 79–87128
  As, amorphous, absence of photodarkening 80–103970
  As, amorphous, defects, band gap states 80–80215
  As, amorphous, effect of high press. on elec. props. 77–59309
  As, amorphous, intermediate range order from polarised features of Raman spectrum 80–49113
  As, amorphous, photoluminescence, bulk and sputtered thin films 80–25457
  As, amorphous, refr. index meas. near absorpt. edge 78–2819
  As, amorphous, short-range order, theory and probes 80–79698
  As, amorphous, theoretical calc. of defect states 80–49657
  As, amorphous, vibr. excitations at defect sites, IR and Raman spectra calc. 80–49329
  As, amorphous, vibrational excitations of defect sites 80–49332
  As, amorphous and cryst., NQR for tunnelling modes and local struct. order 79–61261
  As amorphous films, interference enhanced Raman scatt. 80–50326
  As, black phosphorous struct., Raman vibr. spectra and bonding 80–11411
  a-As, opt. and elec. props. 77–39894
  As:Ni(Ge)(S)(Se)(Te) film, amorphous, chemical modification of props. 80–49250
  Au-Ge Schottky diode, phonon energies, barrier heights, photovoltage spectra 78–64112
  Au-n-Si-p-Si structure with wavelength depend. photocurrent sign, photodetector 79–12849
  Au-Si system, transition layer struct. form. and heat treatment influence, amorphisation obs. 80–54529
  Au-Si thin film double layer, silicide form., electron diffr. study 80–80005
  Au-SiO_2-nSi, tunnelling MIS struct. 80–92995
  B amorphous film, elec. cond. in strong elec. field 77–11928
  B amorphous film, interference enhanced Raman scatt. 80–50326
  B, β-rhombohedral, elec. props. at high temps. and in strong elec. fields, thermistor appls. 80–92903
  B, β-rhombohedral, field effect on hopping cond. 79–82589
  B, diffusion of Au, Ag and W, temp. depend. of coeffs., mechanism 77–7898
  B film, elec. field effect on struct. 80–20050
  B modifications, exam. of physical props. and electron structure 79–94954
  B, properties of α- and β-rhombohedral, and tetragonal types, review 79–42532
  B, purity evaluation by elec. meas. 78–59822
  B, residual photoconductivity in single crysts. 80–20241
  β-B, rhombohedral, AC cond. meas., 150 to 300K, hopping cond. mechanisms 80–15521
  β-B, rhombohedral, dielec. loss temp. depend., −196 to 350°C 80–20585
  β-B, rhombohedral, EPR, book contrib. 78–48041
  α-B, rhombohedral, elec. cond., thermoelec. power, and Hall coeff. 80–6843
  β-B, rhombohedral, high field elec. cond., single voltage pulse meas. 80–20201
  β-B, rhombohedral, hopping cond., book contrib. 78–47797
  β-B, rhombohedral, influence of impurities on elec. cond. 77–4345
  β-B, rhombohedral, Knoop hardness and room temp. resist., rel to purity 80–21084
  β-B, rhombohedral, localised states charact., review, book contrib. 78–47728
  β-B, rhombohedral, thermally activated hopping, 140-300K 80–20189
  β-B:C, rhombohedral, EPR meas. partly resolved absorpt. spectra 80–20449
  B:H amorphous CVD films, IR, visible, and near UV optical props. 80–50442
  Bi, magneto-thermopower, weak-field, implication for scatt. mech. 80–49790
  Bi, neutral point defect electronic struct., self consistent method 78–91641
  C, amorphous film, hopping cond., thickness depend. 77–89887
  C film, amorphous, elec. struct. and optical props. 77–20474
  C film, amorphous, elec. transport props. and atomic comp. 78–6457
  C film, amorphous, struct. and semicond. props. and heterojunction form. with single cryst. Si 80–25002
  C, film, amorphous, two-dimensional variable range hopping cond. 80–10977
  C, glassy, prep. and DC cond. at low temps. 79–95404
  C, reconstruction-induced subsurface strain, theory 78–91516
  C, vacancy, tight-binding calc. 80–24844
  C:H, film, amorphous elec. props., chem. modifications by doping 80–84523
  CdS-Ge heterojunction, grown by chemical transport, props. 77–4422
  CdS-Te, heterostructure, effect of low cond. CdTe interlayer on charact. 80–44721

elemental semiconductors continued
CdS-Te-Ge heterojunction, prep. photosensitivity, and negative cond., 77K *(German)* 77—20413
Cs-O adsorbed films on Si (100), oxide formation, ionisation loss spectra, AES 79—69365
GE, microscopic inverse dielec. matrix, local field correction and acoustic sum rule 77—84863
GE, microwave cyclotron resonance lineshape, magnetoplasma interference effect, reinterpretation of excitonic polaron 78—43287
GE, RF etch-sputtering under controlled atmosphere 77—44397
Ga-GaAs heterojunctions, electronic struct., tight-binding and pseudopot. models 79—42633
GaAs-Ge interface, abrupt, electronic struct., self-consistent calc. 77—24611
Ge, ^{57}Co implantation, Mossbauer spectra, dose depend. 79—82899
Ge, 16 μm generation from phase-matched 4-wave mixing of CO_2, NH_3 lasers 79—3745
p-Ge, 2 mm wave radiation interaction with charge carriers *(Russian)* 78—87991
Ge, (001)-(2×1) surface, reconstruction-induced mean-square displacements 80—15343
Ge (100), chemisorption of H, expt. results compared with pairing model calcs. for Si (100) 78—34719
Ge (100), dimer reconstruction, photoemission obs. 80—80939
Ge (100), surface structure and chemical state 77—15670
Ge (100) surface, electronic struct., scattering-theory formulation 79—42607
Ge (100) with Cs and $Cs+O_2$ overlayers, negative electron affinity surface, thermal stability of work fn. 78—92167
Ge (110) surface, sublimation of deposited GeS film, LEED meas., structural transitions 77—59195
Ge (111), adsorption of K and Cs, effect on surface elec. props. 79—90880
Ge (111), adsorption of polar molecules, surface recomb. centre neutralization 79—38147
Ge (111), CO adsorption on cleaved surface, electron energy loss spectra 78—79885
Ge (111), chemisorption of H_2, calc. using Anderson Hamiltonian 77—55463
Ge (111), electron struct., photoelec. props. 80—100493
Ge (111), mosaic single cryst., neutron integrated reflectivities 79—86656
Ge (111), spectroscopy of electron subbands 80—71422
Ge (111) clean surface, O_2 adsorption rate and electron work function 80—59779
Ge, (111) cleavage face, struct. changes, LEED and Auger spectroscopy study 79—95249
Ge (111) coadsorption of K and O_2, rel. to work function, K thermodesorpt. spectra 78—79874
Ge (111) surface, 500 eV Ar^+ bombard., high temp. annealing, recovery, RHEED obs. 78—87723
Ge (111) surface, annealed, atomic structure 78—75916
Ge (111) surface, chemisorption of O_2, surface-molecule model 79—90885
Ge, (111) surface, clean, double diffr. spots in RHEED patterns 79—90855
Ge, (111) surface, clean and O_2 adsorbed photoemission yield spectroscopy of electronic surface states 79—91122
Ge (111) surface, clean and CO-covered, UPS and ion-neutralisation spectroscopy 80—10785
p-Ge (111) surface, Cs adsorption, work function meas., adsorption site model 79—23839
Ge (111) surface, n-channel inversion layer, subband energies 80—11063
Ge (111)-amorphous film of SiO_2 or Si_3N_4, dislocation interactions, substrate bending and edge effects 80—39472
Ge, absorption edge, hydrostatic press. effects 77—43994
Ge, acceptor complex spectra, tunnelling H systems 80—89036
Ge, acceptor ground state, US attenuation meas. *(Japanese)* 78—19105
Ge, acceptor ground state, stress effects 80—34385
Ge, acceptor levels, ionis. energy and IR absorpt. 79—78033
Ge, acceptor spectra, interpretation 78—43332
P- Ge, acceptor wavefunctions in spherical approx. and piezoresist. 80—29405
Ge, acceptors, transitions from second excited state, photocond. meas. 79—11082
n-Ge accumulation layers, effect of low-energy Ar^+ ion bombardment on electron scatt. 77—66205
Ge, acoustic deform. pot., pseudopot. calc. 77—1363
Ge, acoustic phonon geometric propag., anisotropic continuum acoustics 77—4170
Ge, acoustic phonon propag. and interaction with electron-hole drops *(Russian)* 80—29336
Ge, acoustic phonon scattering by electron-hole drops, deform. potential 78—10360
Ge acousto-optical deflector performance at 10.6 μm 80—102835
Ge, adiabatic bond charge model 77—69057
Ge, adsorbed metal atoms effect on surface electron props. 77—55597
Ge, adsorption of Ar, Kr and Xe on (111) plane, adsorpt. pot. 78—26768
p-Ge, adsorption of Au, effect on I-V characteristics field emission study 78—67925
Ge, adsorption of N_2 and CO, adsorption potentials and trapped electrons role 79—90872
Ge, adsorption of O, enhancement by elec. field of polarity facilitating field-ion emission 79—65325
Ge, adsorption of O_2 on surface, degree of freedom of rot. and translational motion of O particles 79—23842
Ge, adsorption of water, neutralization of surface recomb. and fast capture centre 79—33184
Ge, adsorption-desorption kinetics of H_2, O_2 and other gases, catalysis 77—47684
Ge, Akhieser region, nonlinearity parameter and US attenuation coeffs., temp. depend. 79—37762
Ge, ambipolar hot-carrier size effect kinetics 80—107799
Ge, amorphons, appl. of theory of AC and DC hopping cond. 80—54698
Ge, amorphous, -metal junction, current-voltage charact., contact material effect 80—44725
Ge, amorphous, 1 MeV electron irrad. influence on kinetics of crystallisation 77—89476
Ge, amorphous, annealing effect on absorpt. edge *(Korean)* 79—15142
Ge, amorphous, anomalous magnetoresist., hopping model 78—23117

elemental semiconductors continued
Ge, amorphous, anomalous magnetoresistance 80—6877
Ge, amorphous, crystallisation study 80—33889
Ge, amorphous, defects, band gap states 80—80215
Ge, amorphous, dislocation model 80—1929
Ge, amorphous, dislocation model 80—1930
Ge, amorphous, doping, Schottky barrier and p-n junction form. by RF sputtering 77—8187
Ge, amorphous, EPR expts. 78—88167
Ge, amorphous, ESR and DC cond. 77—48032
Ge, amorphous, elastic moduli, random network model, calc. 78—6119
Ge, amorphous, elec. and opt. props., review 78—23094
Ge, amorphous, elec. cond. obs. of crystn., expt. verification of model 77—20475
Ge, amorphous, electronic density of states, mol. liq. model 80—49581
Ge, amorphous, far IR absorption 78—88306
Ge, amorphous, first order transition to metallic liquid, calc. of transition temp., enthalpy and entropy 79—69227
Ge, amorphous, growth rate of crystallisation, Raman spectroscopy study 80—44227
Ge, amorphous, IR absorpt., first-order effective charges due to at. displacements 77—48164
Ge, amorphous, ideal network struct., electronic struct., tight-binding model 80—44485
Ge, amorphous, ideal surface, definition and characts. 80—107623
Ge, amorphous, ionisation enhanced crystallisation, elec. cond. meas. 77—35481
Ge, amorphous, laser crystallisation, for production of large grained sheets for solar cells 80—93570
Ge, amorphous, laser reordering of implanted amorphous layer 79—19270
Ge, amorphous, molecular liquid model and electronic structure 80—54133
Ge, amorphous, Mott's parameters for hopping cond., effect of annealing 77—69324
Ge, amorphous, O_2^+ ion implanted, influence on electrical and optical props. 77—89891
Ge, amorphous, optical absorpt. edge shape, band edge fluctuations 77—20880
Ge, amorphous, possible ABB-type excitonic superconductor *(Chinese)* 80—7029
Ge, amorphous, pure and H doped, voids, atom probe FIM 80—49107
Ge, amorphous, pure and hydrogenated, Raman spectra 79—61358
Ge, amorphous, struct., dislocation model 78—42911
Ge, amorphous, struct. and growth kinetics, topological principles 80—49123
Ge, amorphous, substitutional doping, electronic props. 77—1418
Ge, amorphous, thermoelec. power in phonon-assisted hopping regime, Coulomb effects 78—76097
Ge, amorphous, tunnelling states simulation and sp. ht. 79—37791
Ge, amorphous, two-band model Thorpe-Weaire type, localisation near band edges 78—23050
Ge, amorphous and crystalline, hopping conduction, semiclassical theory 79—91052
Ge, amorphous and crystn. films, contamination behaviour, XPS examin. 79—1815
Ge, amorphous and polycryst. layers, sputtered, elec. cond. and thermoelec. power 78—2586
Ge amorphous film, AC conductivity, anomalous freq. depend. 77—4456
Ge amorphous film, crystn. front velocity during scanned laser crystn. 80—107662
Ge, amorphous film, DC cond., Meyer-Neldel rule 78—64152
Ge, amorphous film, DC sputter deposited, effect of trapped Ar on minimum temp. for impulse stimulated explosive crystallisation 80—100422
Ge amorphous film, disorder induced phonon absorpt. meas. using double beam Fourier spectrometer 80—105725
Ge amorphous film, effective medium theory and freq. depend of conductivity 79—24090
Ge amorphous film, effects of ion implantation on structure 78—55881
Ge, amorphous film, effects of alloying chalcogen atoms 80—49670
Ge amorphous film, evaporated, non-destructive density meas. 80—6680
Ge, amorphous film, freq. response characts. 79—56334
Ge amorphous film, high freq. phonon scatt. 80—49328
Ge, amorphous film, high freq. cond., AC loss 80—49792
Ge, amorphous film, hopping cond., thickness depend. 77—89887
Ge, amorphous film, in situ meas. of thermal EMP, by ultrahigh vacuum electron microscopy 79—26184
Ge, amorphous film, ion-implanted, regrowth 79—15043
Ge, amorphous film, large aligned grain solid-phase growth during scanned laser crystallisation 80—49100
Ge, amorphous film, laser pulse annealing 80—15006
Ge amorphous film, O depth profiling by SIMS 80—39480
Ge, amorphous film, optical consts. in near IR range *(Korean)* 79—8137
Ge, amorphous film, persistent photoconductivity, dangling bonds 80—84487
Ge, amorphous film, post nucleation growth, computer simulation 78—34729
Ge, amorphous film, temp. thermal conductivity 78—22994
Ge amorphous film, ultra high vac. prep., DC elec. cond. 80—49721
Ge, amorphous film, vac. evaporated, density meas., microcrystalline model of struct. 80—2313
Ge, amorphous film, variable range hopping 78—76176
Ge amorphous films, high elec. field cond. and magnetoresist. at 4.2K 80—49748
Ge amorphous films, self-ion bombard., electronic props. 79—28422
Ge amorphous films, structural relaxation and crystallisation 80—100170
Ge, amorphous layer, comparison of laser and electron beam pulsed annealing 79—69374
Ge, amorphous layer, epitaxial recrystn. by electron irrad., solar cell appl. 78—84079
Ge, amorphous layer, on single cryst. Si, heteroepitaxy by laser annealing 79—77952
Ge, amorphous overlayer on ultrathin Pt film, effect on cond. 78—72284
Ge amorphous solid dielectric loss meas. by submillimetric waveguide laser 79—33603
Ge, amorphous sputtered films, hydrogenated, photoinduced optical absorpt. 80—50362
Ge, amorphous thin film, fast crystn. and void precipitation in laser pulse annealing, TEM exam. 79—56086
Ge, amorphous whisker growth 78—2400

elemental semiconductors continued
Ge, amorphous/cryst. interface, supercond. mechanism 80—44783
Ge and Ge:O(Li), shallow defects, PTIS meas. 80—24971
Ge and Ge-diamond bolometers operated at 4.2, 2.0, 1.2, 0.3, 0.1K, design and construction 80—77868
Ge, anisotropic many-valley semicond., kinetic theory of impact ionisation 78—14740
Ge, anisotropic oxidation, ellipsometry meas. *(Russian)* 79—43451
n-Ge, anisotropy of thermal and convective noise, in magnetic field 78—34873
Ge, anomalous avalanche breakdown 80—80284
Ge, anomalous muonium state 79—56677
Ge, anomalous muonium states 80—34841
Ge, anomalous X-ray transmission in the presence of four-wave diffraction ($\bar{1}$11, 200, 311) 78—79494
n-Ge, anomalously enhanced plasma diffusion transverse to mag. field 80—96931
n-Ge, anomaly of Hall effect after 50 MeV electron irrad. *(Russian)* 77—43619
Ge, As impurity precipitation from solid soln., neutron irrad. effect 80—29177
Ge, Au-migration at room temp. 78—76161
Ge, Auger recomb. of electron-hole drops 78—39600
Ge, Auger recombination probability calc. for degenerate carriers 80—24944
Ge, Auger spectra, comparison with multiplet struct. calc. 78—31287
Ge, autofocusing of X-rays and γ-rays 79—12916
Ge avalanche photodiode, cryst. orientation depend. of multiplication noise 79—80680
Ge, backscattered energy spectra, charged particles energy losses 79—83086
Ge, band structure of diamond like crystals, cluster-Bethe lattice model calc. 80—6713
Ge, band structure under high stress, nonperturbative calc. 78—10344
Ge bicrystal, cond., Hall effect and Shubnikov-de Haas oscills. 80—10984
Ge, bicrystal, two-dimensional electronic phenomena at He temp. *(Russian)* 79—56273
Ge bicrystal cleavage plane, Shubnikov-de Haas oscills. *(Russian)* 78—64094
Ge bicrystals, [011] tilt boundary, grain boundary stability 79—82240
Ge bicrystals, high angle tilt boundaries, TEM *(French)* 80—70224
Ge bicrystals, low angle [011] tilt boundary 79—82239
Ge, biexciton and trion existence, photolum. *(Russian)* 80—16088
Ge, black, solar selective absorber characterisation 80—80112
p-Ge, bleaching, optical heating and cooling of electrons involving intraband transitions 79—10365
p-Ge, bleaching assoc. with intraband transitions in CO_2 laser radiation absorpt. 77—68244
Ge, bound electron states close to conduction band due to 60° dislocations 77—28141
Ge, bound exciton complexes, density functional calc. 80—10890
Ge, Bragg reflection in case of multiple X-ray scatt. 80—100127
Ge, bremsstrahlung spectra for 1 GeV electrons and positrons, planar and axial channelling *(Russian)* 77—32465
p-Ge, broadband modulation of 3 μm light by 10 μm light 78—42389
Ge, bulk hot-electron props. 79—99553
Ge, capture of carriers by attractive centres 79—7836
Ge, carrier conc. variations using electrolyte electroreflectance, topographical features 79—99562
Ge, carrier density in electron-hole drops, plasma reson. determ. 77—24522
p-Ge, carrier drag by photons, comparison with p-GaAs 79—11185
p-Ge, carrier heating by weak electric field 77—11927
n-Ge, carrier relax. time, mag. field effects, rel. to Hall effect 80—39608
Ge, carrier relaxation rate temp. depend. and pair density in large electron-hole drop 80—75509
p-Ge, carrier scatt. by ionised impurities, rel. to carrier mobility calc., 10-70K *(Russian)* 78—39103
n-Ge, cathodically treated, surface mobility of electrons 77—51801
Ge, channelling of 160 MeV protons, deuterons and α particles, stopping powers 79—86826
Ge, channelling of H^+ and He ions, backscatt. particles ang. distrib. 79—51174
Ge, charge carrier diffusion coeff. 78—84218
Ge, charge carrier scatt. and compensation effect on Hall mobility of majority carriers *(Russian)* 77—32026
Ge, charge density calc., Gaussian relaxation method 77—39760
Ge, chemical etching processes, review 78—95832
Ge, chemisorption of CO(Cl), surface photoemission, adsorption gate geometry 78—73079
Ge, chemisorption of Cl_2, photoemission polarisation effects with synchrotron radiation 78—14580
Ge, chemisorption of O_2 on (111) and (100) surfaces, CNDO calc. 77—55464
Ge, chemomagnetic effect, elec. cond. change due to surface recomb. of H atoms 77—8086
Ge, clean surface, geometrical struct. rel. to electronic props. 77—62719
Ge, cleaved in liquid He, surface elec. cond. *(Russian)* 80—15588
Ge coaxial detectors, n-type high purity, construction and performance 79—41075
Ge coaxial detectors with reverse electrode, radiation damage resistance 79—41076
Ge, coexisting phases in electron-hole plasma 77—1374
Ge, cold semiconductor, Mott transition 78—91616
n-Ge, compensated, impurity photoconductivity 78—10512
Ge, compensated, impurity photocond. relax times 80—88592
p-Ge, compensated, sub mm and mm radiation absorpt., acceptor conc. depend. 77—28664
Ge, compensated, sub mm radiation absorpt., temp. depend. 80—66331
n-Ge, compensated, switching effect, injection mechanism of hot holes 77—69387
Ge, compensated by thermal defects, Hall effect anomalies 79—69535
Ge, compensated by thermal defects, recomb. and optical props. 80—64989
Ge complanar X-ray resonator circulating beam, high symm. multiple wave configurations *(Russian)* 80—78875
Ge, composition of inclusions, single cryst. 77—15441
Ge, compressed electron hole plasma, luminesc. 78—72592
Ge, Compton profile anisotropy, pseudopot. calc. 79—28854
Ge, conductivity of cleaved surface *(Russian)* 79—51654

elemental semiconductors continued
Ge, contrib. to lattice thermal cond. due to correction term in Callaway integral 77—62693
Ge, covalent semicond., piezoresistance coeffs. of holes, temp. depend. 77—39847
Ge, crit. points in E′ region from ellipsometric data 77—80726
Ge, crystal growth, O equilib. between Ge and gas over melt 80—2938
Ge, crystal growth and segregation under zero gravity 79—43130
Ge, crystal struct. factor, at. scatt. factor, electron diffr. determ. 77—15291
Ge crystals, orientational depend. of photoacoustic effect *(Russian)* 80—65167
Ge crysts., electron beam induced changes of real struct., HVEM 80—103390
n-Ge, current carrier-dislocation interactions, resistance in UHF range *(Russian)* 80—54732
Ge, current instabilities in semiconductors, theory and expts. *(Hungarian)* 77—39857
Ge, cyclotron reson., exciton and electron-hole drop diffusion coeffs. 77—48055
Ge, cyclotron reson. in strong elec. fields, classical theory 80—7172
n-Ge, cyclotron reson. line width in quantizing mag. field 78—10336
Ge, cyclotron resonance and radiative recomb. with laser excitation, book contrib. 80—11472
n-Ge cyclotron resonance line shape at 337 μm, obs. 77—39770
Ge, cyclotron resonance peaks under high excitation 77—48056
n-Ge, D state struct. rel. to photocond. expts. 80—59924
n-Ge, D^--band conduction 77—76821
Ge, DC hopping, analytical formulae, degenerate hopping in wide bands 77—89761
Ge, damping of motion of electron-hole drops by mag. field 77—69244
Ge, deep dislocation states 80—24836
Ge, deep donor character of muons and protons 80—10911
Ge, deep impurity levels, activation energy 80—107742
Ge, defect form. under radiation-accelerated diffusion conditions 80—19854
Ge, defects, radiation effects 80—29016
n-Ge, deform. induced point defects, Hall coeff. meas. 80—19800
Ge, deform. of laser induced electron-hole drops under high magnetic fields *(German)* 78—23027
Ge, deformation, annealing characts., X-ray study 78—75713
n-Ge, deformed, 0.1 eV optical transition, interpretation using electronic states theory for Si 77—20261
n-Ge, deformed, 1/f noise, resist., mobility, and carrier density 77—8161
Ge, deformed at relatively low temps., Hall effect 79—82612
Ge, degenerate, doped with nonmag. impurities, Kondo effect 78—14746
Ge, degenerate, scattering by light by phonon zero sound 79—56145
p-Ge, depend. of saturation intensity on impurity conc. and residual absorption at 10.59 microns 80—45125
Ge detector, high purity, fast neutron damage 80—59526
Ge detector, intrinsic, for meas. of soft X-ray spectra of Tokamak plasma 77—51232
Ge detector for X-ray and gamma-ray spectroscopy, high-purity, preparation and properties 78—86723
p-Ge, detector-grade single crysts., impurity background 79—11088
Ge detector; high-purity, effect of crystal growth direction on energy resolution 79—45541
Ge, determ. of nonradiative decay rate in electron-hole drops at 1.6K 77—8143
Ge, diamagnetic excitons, fundamental absorption edge, Faraday config. 79—8144
Ge, dielectric const. associated with direct interband transitions 77—20817
Ge, dielectric polarisation calcs., microscopic local fields 80—20582
Ge, dielectric properties, mean point value calc. 78—87930
p-Ge, differential relax. times and diffusivities of hot carriers 77—62936
p-Ge, diffusion coeff. for hot holes in mag. field 80—39614
Ge, diffusion coeff. of hot holes meas. 78—6387
Ge, diffusion of Ga along dislocations 79—82385
Ge diode, influence of mechanical stresses on effective carrier diffusion length in base region 77—35987
Ge, direct gap recombination, at high excitation level and low temp. 79—38650
n-Ge, direct identification of $L_3' \rightarrow L_1$ transition, electroreflectance 77—1689
Ge, direct transition absorpt. coeff. modulation by electron-hole drops 77—90153
Ge, dislocation electron image filtering in electron microscopy 80—75129
Ge, dislocation electron states, from press. depend. of photocond. 80—96819
Ge, dislocation energy band width, carrier lifetime anal. 77—11874
Ge, dislocation energy levels, Hall effect meas. 78—6328
Ge, dislocation ensembles motion in neutron irradiated covalent crystals *(Ukrainian)* 80—10579
Ge, dislocation free single crysts., six wave diffr. of X-rays, anomalous transmission 79—14650
Ge, dislocation free single cryst., swinging fringes, six wave diffr. of X-rays 79—14649
p-Ge, dislocation microwave cond. and Hall effect meas. *(Russian)* 77—47848
Ge, dislocation motion near surface 79—82219
Ge, dislocation-induced elec. pots., appl. 79—82551
n-Ge, dislocational microwave conductance anisotropy *(Russian)* 79—91092
p-Ge, dislocations, grown-in defects, electrical props., deep level transient spect., Hall effect 80—39524
Ge, dislocations, lattice images 79—82215
Ge, dislocations under high stress, stacking fault energies, TEM study 80—70202
Ge, dispersion law of indirect excitons 80—24805
Ge, dissociated dislocations, statistics of kink formation 79—82207
Ge, dissociated dislocations, constriction correlation with jogs 80—79801
Ge, dissociation of hot excitons by long-wavelength acoustic phonons, photocond. spectra 77—4300
Ge, donor energy spectrum, mag. field effect, submm. photocond. meas. *(Russian)* 77—43666
Ge, donor ion pot., small r behaviour of nonlinear Poisson eqns. 80—54652
Ge, donor polarizability, multivalley effective mass calc. 80—96817
Ge, donor-acceptor electron transfer at low temps., photocond. tail 78—84249

elemental semiconductors continued
Ge, doped, D^- band width, influence of resonances 79—11061
n-Ge, doped, dopant distrib. from carrier drift distrib. in high elec. field 79—51140
Ge, doped, electron or neutron irradiated, vibrational absorption 78—6718
Ge, doped, electron-hole drops, low-temp. photolum. spectra obs. 77—69900
Ge, doped, polarisability of donors 78—14693
Ge, doped, semiconductor-metal transition, modified screened impurity pot. 79—99500
Ge, doping inhomogeneity, meas. by low field electrorefl. 77—11584
p-Ge, double injection characteristics under high voltages 79—51590
n-Ge, drag effects, heated electron-phonon system 78—23078
Ge, drift mobility and Hall coeff. factor of holes 78—43379
Ge, drift velocity of plasma cloud, at high elec. field 80—6887
Ge dust, n- and p-type electrification 79—56276
Ge, dynamical recovery and self-diffusion 79—82379
Ge, E_1-optical struct. from electroreflectance spectra 78—43897
Ge, EHT calcs. of energy bands and pressure dependences *(Japanese)* 78—34747
n-Ge EM wave interaction with hot electrons, in strong mag. field with Voigt config. 77—69367
Ge, EXAFS, in real space, struct. determ. 77—15273
Ge, EXAFS amplitudes, many-body effects 80—97379
Ge, EXAFS at high press. 80—97376
Ge, EXAFS in photoelectron yield spectra 80—16123
Ge, edge dislocation struct., lattice distortion and surrounding vacancy distrib. 77—19954
Ge, edge-type dislocations, energy spectrum 80—24842
n-Ge, effect of non-parabolicity in quantum mechanical treatment of cyclotron reson. 77—31937
Ge, effect of valence state on X-ray Compton line shape 77—8682
Ge, effective dielectric function calc., exchange interaction effects 79—99494
Ge, effective masses of heavy and light holes, from ohmic mobility data 80—80160
Ge, effective screening function 78—10383
Ge, elastic moduli, drag coeffs. and Keating's parameters 79—73238
n-Ge, elastically deformed, anisotropy of thermoelec. effect 78—19066
a-Ge, elastoresistive effects 79—60838
n-Ge, elec. cond., effect of shock waves *(Russian)* 78—87979
Ge, elec. conductivity tensor, warm electron range 78—39123
Ge, electric field gradient-elastic tensor components, acoustic NMR obs. 80—25229
Ge, electric field influence on exciton states, Stark effect 80—54617
Ge, electric quadrupole sum rules rel. to optical consts. 79—38036
Ge, electrical and optical props. at low temps. 80—39636
Ge electrode, cathodic characts. rel. to halide ions 79—57238
Ge, electrodeposited, X-ray, electrochem., and electrorefl. characterisation 78—14624
Ge, electrodes, photoemission into electrolyte solns. 77—24616
Ge, electron and positron bremsstrahlung spectra *(Russian)* 79—91522
Ge, electron beam irrad., {113} faults, nature and origin 80—70258
p-Ge, electron bombard. at high temp., carrier lifetime and defect levels 77—55306
Ge, electron heating by nonuniform elec. field, I-V characteristics 77—47825
Ge, electron heating in inhomogeneous elec. field 78—2494
Ge, electron hole drop, surface energy calcs. 77—47741
Ge, electron hole drop diffusion const., hysteresis effect determ. 79—23902
Ge, electron hole drop far IR absorpt., damping, size effects, Mie theory 79—78685
Ge, electron hole drop recombination spectrum, low energy tail 77—59612
Ge, electron hole droplets, intervalence band absorption 80—6742
Ge, electron interaction with many excitons 78—26823
Ge, electron irrad., light-sensitive defects 80—24498
n-Ge, electron irradiated, annealing at 6K, Watkins model explanation 78—47427
n-Ge, electron irradiated, energy levels 79—28316
n-Ge, electron irradiated, high temp. annealing, nonequilibrium carrier lifetime and Hall effect 77—4370
n-Ge, electron irradiated, threshold energy for atomic displacement, carrier traps 80—29351
Ge, electron irradiated in HV electron microscope, defect form. and interaction with dislocation 77—19990
Ge, electron microscopy, high resolution image interpretation 78—14259
Ge, electron microscopy, multi-beam lattice images in (011) orientation 77—24252
Ge, electron mobility based on dielectric function modification of Dingle pot. 79—60836
Ge, electron mobility in Δ_{1c} minima, temp. depend. 79—65473
n-Ge, electron occupancy of dislocation levels 77—15795
Ge, electron scatt. by charged impurities under cyclotron reson. conditions 77—63286
Ge, electron scattering, inelastic, 70-1400 eV, mean free path 78—84696
Ge, electron states associated with core region of 60° dislocation 78—39057
Ge, electron states associated with dislocations 79—82544
Ge, electron states below cond. band originating from dissociated 60°-dislocations, calc. using effective mass method 79—19546
Ge, electron-beam-controlled transmission of 10 μm radiation 79—81466
Ge, electron-hole correlation density depend., in electron-hole liq., under uniaxial stress 79—15090
Ge, electron-hole drop, surface props. calc. 77—89711
Ge, electron-hole drop and exciton atmosphere 80—6748
Ge, electron-hole drop binding energy, optical threshold studies 79—38652
Ge, electron-hole drop deform., accel. and luminesc. under influence of radiation press. 77—47739
Ge, electron-hole drop dispersion under strong optical stimulation, phonon interaction effects *(Russian)* 77—1723
Ge, electron-hole drop drag by ultrasound *(Russian)* 80—100437
Ge, electron-hole drop drag, interaction with thermal pulses 80—103631
Ge, electron-hole drop ejection from continuously generated electron hole liquid 79—78017
Ge, electron-hole drop emission kinetics, effect of nonequilib. phonons, 4.2K 78—14674
Ge, electron-hole drop formation, nucleation phenomena 79—33240

elemental semiconductors continued
Ge, electron-hole drop freq. depend. damping 80—88482
Ge, electron-hole drop interaction in stationary and alternating mag. field *(Russian)* 77—62845
Ge, electron-hole drop luminescence at high mag. fields 79—65390
Ge, electron-hole drop luminesc., phonon wind induced anomalous depend. at low mag. fields 80—34980
Ge, electron-hole drop magnetostruction 78—87912
Ge, electron-hole drop magnetoplasma resonance 79—60722
Ge, electron-hole drop magnetoplasmas, radius-independent elec. and mag. reson. 79—73446
Ge, electron-hole drop motion at low exciton densities 77—47865
Ge, electron-hole drop motion recorded by microwave probe meas. 77—76755
Ge, electron-hole drop motion 80—6744
Ge, electron-hole drop motion, phonon wind 80—10887
Ge, electron-hole drop movement under action of force of mutual repulsion *(Russian)* 77—89710
Ge, electron-hole drop net negative charge, giant fluctuating photocurrent obs. 77—35963
Ge, electron-hole drop phase separation, due to uniaxial stressing 78—84145
Ge, electron-hole drop radius temp. depend. 77—76753
Ge, electron-hole drop recombination radiation due to heat pulse action *(Russian)* 80—16087
Ge, electron-hole drop transition to metallic condensed state, Hartree-Fock theory 79—56136
Ge, electron-hole drop velocities as probe of phonons 78—68517
Ge, electron-hole drop velocities, excitation wavelength depend. 78—88358
Ge, electron-hole droplet, effect of nonlocal contributions to energy 77—69246
Ge, electron-hole droplet, motion damping, impurity and piezoelec. scatt. 78—67951
Ge, electron-hole droplet, attachment to donor 78—87916
Ge, electron-hole droplet condensation model, phase diagram and surface tension 80—6734
Ge, electron-hole droplet cloud form., phonon wind, luminesc. obs. 80—45136
Ge, electron-hole droplet condensation, crit. point 80—49612
Ge, electron-hole droplet cloud, role of thermalisation phonons 80—49617
Ge, electron-hole droplet cloud kinetics, thermalisation phonons 80—88483
Ge, electron-hole droplet decay kinetics, microwave expts. 77—43517
Ge, electron-hole droplet magnetoresistance 78—14744
Ge, electron-hole droplet shape under uniaxial stress 77—43518
Ge, electron-hole droplet scattering of acoustic phonons, total scatt. rate and anisotropy 79—33241
Ge, electron-hole droplets, capillary-wave reson. investig. by US attenuation 77—8027
Ge, electron-hole droplets, conc. in mag. field, magnetoplasma absorpt. spectra meas. *(Russian)* 77—24854
Ge, electron-hole droplets, magnetoplasma reson. with submillimetre circularly polarised waves 77—89712
Ge, electron-hole droplets, reson. scatt. of free carriers 78—2500
Ge, electron-hole droplets, surface props., SCF calc. 78—51904
Ge, electron-hole droplets, transient photoluminesc. intensities 78—88353
Ge, electron-hole droplets, variation of α_3 electron density at constant stress 79—47025
Ge, electron-hole droplets, luminesc. and absorpt. lineshapes, RPA theory 80—49613
Ge, electron-hole droplets, percolation theory of cond., expt. 80—92896
Ge, electron-hole droplets in high stress limit 78—10369
Ge, electron-hole droplets distrib., and phonon wind 80—103629
Ge, electron-hole drops, accel. by IR radiation field 78—95264
Ge, electron-hole drops, appearance of plasma at high excitation rates 78—26821
Ge, electron-hole drops, Auger recomb. 77—48240
Ge, electron-hole drops, far IR absorption 78—56467
Ge, electron-hole drops, far IR magneto-optical effects 78—84565
Ge, electron-hole drops, IR absorpt. spectra 79—87423
Ge, electron-hole drops, IR magnetoplasma absorptions 80—6728
Ge, electron-hole drops, inflammation radiation under action of ultrasound *(Russian)* 79—7788
Ge, electron-hole drops, in superfluid He, threshold phenomena *(Russian)* 79—42462
Ge, electron-hole drops, kinetics of spatial distrib. *(Russian)* 78—43312
Ge, electron-hole drops, laser Doppler velocimetry 77—43504
Ge, electron-hole drops, magnetoplasma resonance at arbitrary crystallographic orientation in mag. field 79—78018
Ge, electron-hole drops, motion in low mag. fields 79—23904
Ge, electron-hole drops, non-isothermal nucleation 80—44514
Ge, electron-hole drops, photoluminesc. kinetics 78—23524
Ge, electron-hole drops, phonon lifetime and acoustic attenuation due to phonon-assisted Auger recomb. 80—34462
Ge, electron-hole drops, resonant power absorpt., Alfven wave anal. 79—42569
Ge, electron-hole drops, repulsive interaction and spatial distrib. 79—99488
Ge, electron-hole drops, size distrib., light scatt. meas. 79—28292
Ge, electron-hole drops, spatial distrib., time and spatially resolved absorption at 3.4 μm 78—92075
Ge, electron-hole drops, surface struct. 78—60058
Ge, electron-hole drops, US absorpt. and recomb. radiation, 1.8 to 3.5K 77—31954
Ge, electron-hole drops at high mag. fields 79—60721
Ge, electron-hole drops formation, nucleation theories 79—33239
Ge, electron-hole drops interaction with phonons 80—6747
Ge, electron-hole drops size effect on far IR absorption and scatt. *(Russian)* 78—10903
Ge, electron-hole Fermi liquid, in ⟨111⟩-stressed Ge, unusual phase diagrams 79—63137
Ge, electron-hole fluid drift in crossed electric and mag. fields, photocurrent dynamics *(Russian)* 79—99487
Ge, electron-hole gas and liq. coexistence 78—14668
Ge, electron-hole liq. thermalisation between mag. field split valleys 80—25444
Ge, electron-hole liquid, ground state props. under ⟨111⟩ uniaxial stress 79—69428

elemental semiconductors continued
Ge, electron-hole liquid, luminesc. under infinite uniaxial compression 78—87915
Ge, electron-hole liquid, MHD effects 80—80190
Ge, electron-hole liquid, pinch effect 78—87993
Ge, electron-hole liquid, range of energetic Auger electrons 79—90970
Ge, electron-hole liquid, RPA calcs. 80—6743
Ge, electron-hole liquid, strain-confined 78—10355
Ge, electron-hole liquid, strain-confined 80—6745
Ge, electron-hole liquid in magnetic fields, expt. and theoretical investigations, review 79—60720
Ge, electron-hole luminesc. and transport props. 77—48241
Ge, electron-hole plasma, destruction of pinch channel by longit. mag. field *(Russian)* 77—80802
Ge, electron-hole plasma, helical instability excitation in strong. mag. field *(Russian)* 77—69368
Ge, electron-hole two component liq. phase diagrams under stress 80—29332
Ge, electron-hole-droplet cloud, photoluminesc. of laser excited surface, phonon wind 78—84146
n-Ge, electron-phonon interaction, internal strain and impurity elec. field effect 78—14418
Ge, electronic and struct. props., nonlocal pseudopot. calc. 80—34349
Ge, electronic charge density of valence electrons 77—1094
Ge, electronic energy bands of diamond-type crysts., appl. of EHT method 78—87907
Ge, electronic inversion channel anomalous Hall factors *(Russian)* 79—95467
Ge, electronic states associated with 60° edge dislocation 77—89724
Ge, electronic states of isolated negative donor ion, binding energy 79—65404
Ge, electronic struct. of fast donor defect, stress effects, calc. 80—54641
Ge, electronic structure, self consistent local description 80—20067
Ge, electronic subsystem heating by Dember field for ambipolar diffusion *(Russian)* 77—39898
p-Ge, electrorefl. spectra, 2.1 to 2.3 eV, influence of light beam 77—90169
N-Ge, electrorefl. spectra, light induced, electrolyte and Schottky barrier techniques of meas. 80—76046
Ge, electroreflectance, field reversal asymm. at direct gap 77—69802
Ge, electroreflectance spectra, meas. on Al-SiO_2-Ge struct. 77—1677
Ge, electroreflectance spectra, nonparabolicity effects of bands *(Russian)* 79—4791
Ge, energy band gap dilation and vibr. contrib. determ. 79—60703
Ge, energy bands and wavefunctions, localised orbital description 78—18942
Ge, energy gap, impurity conc. depend., calc. 80—80170
Ge, energy levels of Mott excitons 78—6282
Ge, energy loss spectra of C^{2+} ions 80—65114
Ge, energy spectra of dislocations 80—70637
p-Ge, energy spectrum of impurities and effect of mag. field *(Russian)* 77—47770
Ge, energy spikes due to heavy ion bombardment, semiempirical model 78—47453
Ge, energy-gap narrowing and state filling under laser irrad. 79—42441
Ge, entropy and enthalpy of vacancy form., comparison of theory with quenching expts. 77—11872
Ge, epitaxial, in situ X-ray topography, misfit dislocations 78—47671
Ge, epitaxial, on n-GaAs, with Ni overlayer, smooth and continuous ohmic contact form. by solid-state diffusion 78—68086
Ge, epitaxial, on Si, misfit, strain and dislocations, book contrib. 79—82499
Ge, epitaxial and amorphous film growth, low energy ion beam deposition 77—28729
Ge, epitaxial film, crystallographic imperfections 77—35826
Ge epitaxial film, ion implantation and electron beam anneal effects on carrier conc. 80—75255
Ge, epitaxial film, ion sputtering, growth mechanism, struct., props. 77—31917
Ge epitaxial film, misfit dislocations, determination of Burgers vector *(Russian)* 79—33207
Ge epitaxial film, ohmic contacts for GaAs devices 78—88027
Ge epitaxial film, vac. deposited on GaAs, doping effect of annealed GaAs surface 80—65718
Ge, epitaxial film growth by hydride-iodide method 77—48343
Ge epitaxial films, structural perfection rel. to deposition conditions 78—43258
Ge, epitaxial growth from monogermane at 685°C 78—51833
Ge, epitaxial growth of very thin electron microscopy specimens 80—100793
Ge, epitaxial layer deposition by vacuum pyrolysis 78—52676
Ge epitaxial layer on GaAs tetragonal distortion in heteroepitaxial layer, X-ray diffr. exam. 78—67922
Ge epitaxial layers, on GaAs substrate, misfit dislocation multiplication mechanism 78—87673
Ge, epitaxial-diffusion p-n junction, inductive props. in secondary breakdown 80—15598
Ge eqn. of state, under press. 78—75801
Ge, evaporated film, lattice parameters and phase transition temp., surface influence of glass substrates 78—94996
Ge, evidence for correlated hopping in impurity cond. at moderate impurity conc. 77—20317
Ge, excitation spectra of shallow acceptors, Zeeman effect, expt. 80—7381
Ge exciton and electron-hole drop decay, far IR magnetoabsorption obs. 77—40252
Ge, exciton and electron-hole drop entrainment by nonequilib. phonons 80—6751
Ge, exciton condensate and electron-hole droplet, metastable state, effect of illumination and high-frequency heating 79—15097
Ge, exciton condensation, electron-hole drop investigation in UHF field, nucleation *(Russian)* 80—80193
Ge, exciton condensation, light scatt. by electron-hole drops 80—84435
Ge, exciton condensation, microwave cond. below 1K, book contrib. 80—8997
Ge, exciton condensation, microwave studies, book 80—10886
Ge, exciton condensation, microwave cond., book contrib. 80—11040
Ge, exciton condensation, microwave breakdown, luminesc., book contrib. 80—11471
Ge, exciton condensation in electron-hole drops *(Russian)* 79—19522
Ge, exciton contrib. to oscillatory magnetophotocond. 79—15180

elemental semiconductors continued
Ge, exciton damping by phonons 77—1373
Ge, exciton droplets, energy condensation *(Russian)* 80—107712
Ge, exciton drops nucleation centres under conditions of inhomogeneous strain *(Russian)* 78—2429
Ge, exciton effects on intervalence band transitions 77—4297
Ge, exciton energy gap and LA and LO momentum-conserving phonon energies 79—90965
Ge, exciton gas, entropy ionisation, luminesc. meas. 78—35196
Ge, exciton gas, plasma model *(Russian)* 77—11860
Ge, exciton luminesc. polarisation in mag. field *(Russian)* 77—12436
Ge, exciton microwave breakdown, electron-hole drops, book contrib. 80—11041
Ge, exciton mol. by phonon-assisted two-photon absorpt., theory 78—48197
Ge, exciton recombination with emission of single phonon, luminesc. replicas, detect. and anal. 79—60728
Ge, excitons, influence of temp. on high freq. breakdown in presence of electron-hole drops 78—26820
Ge, explosive instabilities in electron-hole drops under microwave radiation 77—31951
Ge, far IR magneto-absorption of donor-bound excitons, pseudo-acceptor model 77—63418
Ge, far IR magnetoabsorption, excitons, electron-hole drops and impurities 78—6664
Ge, far IR magnetoabsorption of free and bound excitons 78—52474
Ge far IR photoconductive detector speed, limitation 79—30550
Ge, far IR photon drag and radiation pressure in refractive media 80—60048
Ge, far IR radiation amplification on hot hole population inversion *(Russian)* 80—16060
Ge, far-IR absorpt. spectra interpret. 77—40233
Ge, Faraday rotation and ellipticity, interband transitions, comparison with Si 77—52048
Ge, fast and slow quenching defects 78—39052
Ge, fast particle irrad., Frenkel defect formation threshold energy 80—6404
Ge, faulted dipoles, high-resolution TEM study 80—103345
Ge, Fermi level, minority carrier conc., effective intrinsic conc., Einstein relation 77—85209
Ge, field effect characts. rel. to surface inhomogeneity 78—26933
Ge, field-emission current-voltage characts., effect of earlier measurements 80—71579
Ge film, AC cond., up to 200 kHz, 100-300K, role of contacts 77—76970
Ge film, amorphous, ^{74}Ge ion implanted, defect struct. obs. 78—51848
Ge film, amorphous, crystn. kinetics, elec. cond. obs. 77—62767
Ge film, amorphous, high field effects, 100-300K 77—24563
Ge film, amorphous, high resolution electron microscopy, digital processing use 78—37116
Ge film, amorphous, influence of deposition parameters on e.p.r. 77—1586
Ge film, amorphous, LF vel. of sound for Young's modulus mode 77—35636
Ge film, amorphous, prep. conditions influence on supernetwork struct. 77—76709
Ge film, amorphous, prepared by evap. or sputtering, AC loss meas. 80—65560
Ge film, amorphous, thermally induced reversible switching, effect of change in thermal resist. 77—20371
Ge film, amorphous, thermoelec. power and structural investigs. using in-situ electron microscopy 77—76983
Ge film, amorphous, two-dimensional variable range hopping cond. 80—10977
Ge film, amorphous, vac. deposited, XPS and elec. props., evidence for polycryst. phase 77—28691
Ge film, amorphous and crystalline, optical props. 77—16412
Ge film, amorphous and crystalline, effects of Al and Cu alloying on elec. transport props. 79—51689
Ge film, amorphous evap., structural aspects in electronic transport data interpret. 77—76977
Ge film, amorphous or cryst., elec. resist., temp. depend. 77—39978
Ge film, amorphous to crystalline transform. 77—20206
Ge, film, dense electron-hole plasma, negative differential resistance 77—89794
Ge film, elec. props., prep. by DC sputtering *(Japanese)* 79—78237
Ge film, elec. resist., long term stability rel. to ambient atmosphere changes 78—2597
Ge, film, elec. resist. and struct., post-deposition heat treatment effects 79—78229
Ge film, electrical cond. during laser-induced crystallisation 79—47175
Ge, film, electronic struct. charge on ordering, double beam photoemission 78—19634
Ge film, electroreflectance effects 79—43055
Ge film, evaporated amorphous, angle of deposition effects, electron microscopy 77—43451
p-Ge film, fragmented struct., elec. cond., Hall coeff. and magnetoresist. meas. 77—15979
Ge film, growth on graphite substrate by thermal reduction 78—18934
Ge film, in Al/Ge/Al sandwich struct., interdiffusion effect on film cond. 79—23788
Ge film, polycrystalline, structural and elec. props. 78—76173
Ge film, prep. by low press. reactive deposition process 79—24449
Ge film, radiation damage in electron microscope 77—84794
p-Ge film, tranverse magnetoresist. meas. 78—72293
Ge film, volume plasmons, EELS, line shape 79—90984
Ge film amorphous, complex refractive index and reflectance 77—52121
Ge film black, solar selective absorber surface 79—29484
Ge film bolometer, radiation loss from JFT-2 Tokamak, meas. 80—95141
p-Ge film on GaAs, cond., Hall effect and transverse magnetoresist., anisotropy 79—51697
Ge film on Si, influence of fragmentary struct. on galvanomag. effects *(Ukrainian)* 78—84327
Ge, film used as absorbing surface in solar collector 78—5580
Ge films, adhesion to substrates, effect of Ar^+ ion irrad. 79—11047
Ge films, evaporated, oxide layers 77—76927
Ge films on semicondcuting substrates with diamond structure, computer model of autoepitaxial growth 79—95927
Ge foil, thinning for electron microscopy 79—49217
Ge, formation of sulphide layers in S vapour on surface 79—7757

elemental semiconductors continued
Ge, Foucault currents in electron-hole drops *(Russian)* 77—8030
Ge, four wave mixing, tunable IR generation 79—98444
Ge, four-wave X-ray diffraction, intensification of Borrmann effect 77—39501
Ge, free carrier, intervalence band indirect absorpt., at high optically created carrier densities 79—42961
n-Ge, free carrier mobility and density, four-probe magnetoresist. meas. 77—43626
Ge, free-carrier plasma edge, fast transient spectroscopy 77—8558
p-Ge, free-carrier reson., photoconductivity spectra in submillimetre wavelength 79—15353
p-Ge, freq. depend. of effective temp. of hot carriers 79—11135
Ge, galvanomagnetic-recombination field effect, theoretical model 78—43420
Ge, gamma electron-hole liq., orientational depend. of shape in mag. field 77—66121
Ge, gamma irrad. above threshold, defect formation impurity ionisation mechanism 80—6433
Ge, gamma irradiated, radiation defects, formation kinetics, successive capture of vacancies by impurities 79—10873
Ge, gamma-irradiated, number of Frenkel defects 78—14377
a-Ge, Ge-O removal in pre-crystallisation annealing 78—9957
Ge graded p-n junction, volume EMF of hot carriers 77—47895
Ge, grain boundary, lattice imaging in electron microscope 78—6069
Ge, group III acceptor impurities, oscillator strengths of dipole optical transitions 79—56823
n-Ge, group V doped, point defect form. due to γ-ray irrad., carrier density, mobility meas. 78—71759
Ge, growth from lightly doped melt, dopant distrib. 78—2039
Ge, γ-electron-hole drop formation, time delay 77—31952
n-Ge, γ-irrad., nonlinear steady-state recomb., nonequilib. carrier lifetime and density 80—20215
n-Ge, γ-irrad. and subjected to arbitrary excitation and rate, recombination 79—38101
Ge, H atom recombination at surface, elec. cond. and chemomag. effect *(Russian)* 79—91125
n-Ge, H-linear planar Hall effects of hot electrons 78—76082
Ge, HF breakdown of excitons effect on kinetic of electron hole droplets *(Russian)* 77—59260
Ge, HF field effect meas. 77—55556
n-Ge, HF plasma oscills. in external mag. field 80—54731
n-Ge, Hall coeff. and cond. mech. in intermediate conc. at He temps. 79—95422
Ge, Hall effect, influence of dislocations 79—82611
n-Ge, Hall effect, uniaxial deform. effects 80—65605
Ge, Hall effect in finite specimens of arbitrary lifetime and trap content 78—72175
Ge, Hall effect noise, theory and expt. 78—39173
n-Ge, Hall mobility in fast electron irradiated samples 77—55551
in-Ge, Hall mobility in strong elec. field, appl. of instrum. for Hall current meas. 79—35779
Ge, heat capacity and phonon dispersion, using five force schemes *(Russian)* 77—62649
p-Ge, heaviliy doped, anomalous magnetoresist. under uniaxial compression *(Russian)* 79—33302
n- Ge, heavily doped, extrinsic sp. ht. in metallic regime 78—59956
Ge, heavily doped, far IR props. of shallow impurity states 79—95786
Ge, heavily doped, microcreep breakdown 80—97549
Ge, heavily doped, multiplex AC hopping conduction 79—11122
n-Ge, heavily doped, negative magnetoresistance model, spin-up spin-down electron effective mass variations 79—95423
p-Ge, heavily doped, self energy of phonons 80—44277
Ge, heavily doped, vacuum hot-pressing thermal and electrical props. 77—40400
Ge, heavily doped, vacuum hot pressing, effect on thermal and elec. props. 80—25594
Ge, heavily doped and compensated, photoluminesc. exam. 78—2902
Ge, heavily-doped single cryst., macroinclusions, annealing in elec. field 77—47474
Ge, heavy ion impact, meas. of life-time of inner-shell vacancy in recoiled Ge atoms 77—63513
Ge, heterodiffusion due to H atom surface recombination stimulation, Cu, Zn, In coated *(Russian)* 80—59726
Ge heteroepitaxial film, ethanol pulsed adsorption effect on elec. cond. 80—93014
P-Ge, heteroepitaxial film, galvanomagnetic effects, influence of mechanical stresses 79—91171
Ge, high density electron-hole plasma, infrared absorpt. at low temp. 78—92078
Ge, high parity detectors, 6 GeV/c proton irradiation 78—37508
Ge, high purity, carrier trapping 79—47104
Ge, high purity, nature of large traps, expt. on p^+-n-n^+ struct. 78—19051
Ge, high purity, surface inversion layer electron and hole mobilities 77—76937
Ge, high purity melt, stability of oxide second phases 79—47898
Ge, high refl. phase conjugation at 10 μm, intracavity CO_2 laser techniques 80—78894
n-Ge, high-field magnetoresist. and magnetothermal EMF in many-valley semicond. 77—43621
Ge, high-purity, with Al, B and P, residual impurities, photothermal cond. 80—24965
Ge, high-purity dislocation-free, divacancy-hydrogen complexes 78—2449
Ge, high-temp. radiation effects under HVEM obs. 77—89475
p-Ge, highly deformed, hole scattering 77—20309
Ge, highly degenerate multicomponent plasma thermodynamic props., electron hole drop transition 80—33739
Ge, highly excited, theory of electron-hole plasma 78—10363
Ge, hole diffusion 78—6372
Ge, hole drag current in two-photon transitions due to EM wave momentum 79—15187
p-Ge, hole drift vel. in high field 79—95415
Ge, hole drift velocity, effect of impurity scatt. 78—60127
Ge, hole drift velocity, time-of-flight meas. 78—10444
p-Ge, hole-hole collisions, effect on carrier mobility above 80K 80—6838
n-Ge, homogeneous, avalanche ionisation and current oscills. 77—15864
Ge, homopolar semiconductor, quantum efficiency 80—20254
Ge, hopping cond. at intermediate impurity concs. 80—6840
n-Ge, hopping magnetoresistance percolation analysis 79—38106
p-Ge, hopping transport at high mag. field at uniaxial stress 79—95412

elemental semiconductors continued
Ge, hot electron diffusion coefficient anisotropy 77—76838
Ge, hot electron distrib. function, response to step changes in elec. field 80—24937
Ge, hot hole distribution function at low densities 79—11138
Ge, hot hole distribution function, effect of impurity and hole hole scatt. 79—11139
p-Ge, hot hole relax., IR saturated absorption, LO phonon emission 77—28569
Ge, hot light hole distrib. function and light absorpt. 79—60844
Ge, hot microdeformation and simultaneous X-ray topography apparatus *(French)* 80—38871
Ge, hot phonon influence on energy relax. of high-density carriers 79—82608
Ge, hot-electron diffusion, Boltzmann eqn. 77—51757
Ge, hot-electron diffusion coefficient 78—87982
p-Ge, hot-hole relax. rates by saturation spectroscopy 77—65611
Ge, hydrogen multivalent acceptor complexes 77—55491
Ge, hydrogenated amorphous and cryst., IR spectra 79—61359
Ge IGFET cryogenic temp. operation 79—69604
Ge, IR absorption and scatt. by electron-hole drops 78—51903
n-Ge, IR absorption by hot carrier 80—40087
Ge, IR absorption by laser-excited nonequilibrium holes *(Russian)* 79—95752
Ge, IR absorption coeff. by holes, temp. depend., effective mass *(Russian)* 80—50350
n-Ge, IR cyclotron reson. in field up to 200 T 77—52059
Ge, IR detector based on carrier photon drag 77—74507
p-Ge, IR light free hole absorpt., nonvertical optical transitions *(Russian)* 80—80802
Ge, ideal vacancy, electronic struct., tight-binding calc. 79—4529
Ge, illumination influence on surface cond. irreversible elec. cond. increase *(Russian)* 80—92963
Ge, immersed in liquid He, optical pumping to generate first and second sound 80—6581
n-Ge, impact ionisation at 4-9.5K 80—10994
Ge, impact ionisation by electrons and holes, threshold energy 79—38078
Ge, impact ionisation of shallow donor states, 4 to 7K 78—30936
Ge, impurity anal. by photoelectric spectroscopy, review 77—24584
n-Ge, impurity breakdown field, temp. depend. 79—24263
Ge, impurity breakdown field increase due to strong compensation 80—20204
Ge, impurity cloud form., anal. using heat treatment effects on light scatt. in pure crystals 80—15146
Ge, impurity determ. in very pure sample by photoelec. spectroscopy 77—39888
Ge, impurity levels of H and muons 79—56162
Ge, impurity modes due to point defects, comparison with IR and Raman meas. 79—4386
Ge, impurity photocond., temp. elec. field and impurity centre conc. effects 78—56190
Ge, impurity photoconductivity 79—82631
Ge, impurity spectral linewidth meas., free electron effects 80—71463
Ge, impurity-ion potential, electron-conductivity mobility, spatially variable dielectric function calcs. 79—78105
a-Ge, in Al-Al_2O_3-(a-Ge)-Al junction, press. effect on electron tunnelling 80—49938
p-Ge in DMF solns., electrochem., photoelectrochem., redox. pot. determ. 79—96322
Ge, indentation hardness and semicond.-metal transition 78—35499
Ge, indirect exciton excited states 78—30873
Ge, indirect excitons, photoexcitation spectra, 2.0-2.6 meV 77—44051
Ge, inelastic X-ray scatt. cross section accompanied by intermediate momentum transfer 79—24387
Ge, influence of dislocations on free-exciton lifetime 78—60064
p-Ge, infrared absorption and plasma reflection 80—97284
Ge, inhomogeneous mag. field effects on conductivity 77—4374
Ge, inhomogeneous stressed, electron-hole drop light scatt. and absorption 80—108212
Ge, inhomogeneously stressed, giant electron-hole drop investig. by IR absorpt. 77—39785
p-Ge injecting contact, sign of developed hot-carrier thermo-EMF 77—55606
Ge, injection current in presence of electron and hole mobility, gradients 77—69326
Ge, inter-valence-band absorption in electron-hole droplets 79—4515
Ge, interatomic force consts. from lattice vibrs. 77—20020
Ge, interface structural model between amorphous and crystalline phase 78—63941
Ge, internal photoelectric effect, spectral depend. of quantum efficiency 78—39150
Ge, internal Stark effect on impurity states, low-temp. magnet. absorption meas. 80—60636
n-Ge, internal stress effect on electron-phonon interaction, thermal cond. anal. 79—42468
p-Ge, intervalence-band transitions, saturation, theory 80—75997
Ge, intervalley diffusion of hot electrons 78—84227
Ge, intervalley electron-electron scattering effect on optical transitions 80—108267
Ge, intrinsic photodiode as IR detector, fabrication and performance 77—57388
n-Ge inversion layers, broken-symmetry ground states 77—47873
Ge, ion beam irrad., defects prod. by individual displacement cascades, TEM study 80—70265
Ge, ion bombarded, radiation defect formation, atom-atom collision cascades modelling 80—10582
Ge, ion bombardment energy distrib. of positive secondary ions and sputtered atoms 77—32485
Ge, ion bombardment-induced photon emission as function of target temp. 80—100698
Ge, ion implanted, cond. and valence bands study by X-ray bremsstrahlung and photoelectron spectra 80—2360
Ge, ion implanted, ruby laser pulse effects 79—69125
Ge, ion irrad., accumulation and annealing of struct. defects, secondary emission obs. 78—2167
Ge, ion irradiated, Auger electron spectra struct., possible surface diagnostic methods 79—69946
Ge, ion-implanted, laser pulse annealing, TEM and channelling study 80—100264
Ge, ion-implanted amorphous, epitaxial regrowth on Ge 77—35835

elemental semiconductors continued
Ge, ion-implanted amorphous layers, melting model for pulsing-laser annealing 79—56080
Ge, ionisation rates, cryst. orientation depend. 80—103700
Ge, ionised impurity scatt. limited mobility in semiconductors with spatially variable dielec. function 78—51986
Ge, irrad., cyclotron resonance 78—72416
Ge, irradiated and annealed, cyclotron reson. linewidth investig. of electron scatt. 77—55707
Ge, irradiation at about 6K, low temp. annealing of defect 78—2162
Ge, irradiation by 3.5 MeV electrons at high temp., carrier density and lifetime changes 77—4128
n-Ge, irradiation induced compensation, elec. meas. 77—85225
p-Ge, irradiation with fast electrons, defect distrib. with depth 80—19841
Ge, isomer shift values of implanted ^{133}Xe/^{133}Cs, Mossbauer spectra 80—7240
Ge, kinetic theory for electron-hole condensation 77—85151
Ge, LCAO band structure, overlap and distant neighbour effects 80—49585
Ge, LMM Auger spectra, rel. to L_{23} photoelectron spectra 77—77348
Ge, LMM Auger spectra, transition probabilities, term splittings and effective Coulomb interaction 77—44126
Ge, large shaped single cryst. prod., Stepanov method 78—3014
Ge, laser annealing, optical refl. meas. of melted layer 79—78796
Ge, laser induced elec. damage, carrier removal, mobility degradation 77—80791
Ge, laser interaction, multiple refls. contrib. to thermal runaway, heat cond. eqn. 80—33044
n-Ge, laser irrad., accumulation of defects, effect on elec. props. 80—107317
Ge, laser irrad. effect on cohesion 80—50470
Ge, laser irradiation, photoacoustic detection 80—2901
Ge, laser pulse annealing, induced nucleation, crystal growth 80—84966
p-Ge, laser radiation excited, gradient EMF anisotropy 80—75604
Ge, laser-induced bulk breakdown and free carrier generation, photocond. meas. 80—35018
Ge, lattice defects formed on γ-irrad., effect on elec. props. 80—19839
Ge, lattice disorder due to mol. and atomic ion implants 77—59056
Ge, lattice disorder influence on optical spectra in interband transition region 79—43006
Ge, lattice dynamics, inversion matrix, approx. inversion 78—71797
Ge, lattice dynamics under press 80—92627
Ge, lattice dynamics using Born-van Karman model 79—73271
Ge, lattice parameter determ. by X-ray multiple diffr. study *(Russian)* 80—10460
p-Ge, lattice scatt. identified as cause of 1/f noise 78—64074
Ge, lattice stability, pseudopotential theory and problem of covalent bonding 77—55490
Ge, lattice thermal conductivity, contrib. due to correction term, generalised Callaway integral 78—2318
Ge, lattice thermal conductivity, effect of Debye temp. var. 78—18850
Ge, lattice thermal conductivity three phonon processes 78—34662
p-Ge, Li-compensated, carrier capture 77—15792
Ge, light scattering, by pure single cryst., influence of photoexcitation 79—28780
Ge, light scattering due to microdefects 78—27248
n-Ge, lightly doped, compensated by disordered regions, conductivity and Hall mobility 80—11016
Ge, lightly doped, heavily compensated by fast neutrons, electrical props. 77—89766
Ge, lightly doped, nonohmic impurity cond. 78—14738
n-Ge, line shape cyclotron reson., 337 μm, 15-80K 78—6577
p-Ge, linear magnetoresist. in strong elec. fields 77—43632
Ge, liquid, surface tension exam., sessile drop method *(French)* 77—20162
Ge Lo-Hi junctions, avalanche injection delay and ionization rate at low electric field 79—95475
Ge, local field, microscopic electronic polarisation 80—25283
Ge, local IR transmission 80—7357
Ge, localised states, Cayley trees appl. 79—65373
Ge, localised states due to isocoric donor impurities 77—76768
Ge, localised vacancy state 79—82543
Ge, localised vibrational modes of isolated impurities, Green's function method 77—39650
n-Ge, longit. piezoresist., in strong elec. field 78—56147
Ge, longitudinal intervalley EMF due to inhomogeneities 78—19045
n-Ge, low temp. galvanomag. effects, shallow attractive traps 80—88575
Ge, low temp. recombination into shallow donors, transient case 79—38092
Ge, low-energy heavy-ion implantation damage, spike effects 77—59055
Ge, low-field study of p^+nn^+ or p^+pn^+ structs. on forward direction 80—60072
Ge, low-temp. dislocation cond. mechanism in plastically-deformed pure samples 80—15527
Ge, low-temperature bolometer, characts. 79—30561
Ge, luminescence circular polarisation in mag. field, Landau levels paramag. splitting 77—32435
Ge, luminescence kinetics and electron-hole drop motion 77—77288
Ge, luminescence line shape of free exciton, electron-hole droplet binding energy 77—44041
Ge, luminescence meas., presence of trions, molecules and excitons above Mott density 77—80737
Ge, MIS, photocurrent spectra investig. of fund. absorpt. edge 77—4397
Ge MIS photocapacitative IR detector 80—47106
Ge MIS struct., electrophysical characts. 79—82680
Ge, mag. field luminesc. lifetime, quantum oscills., phonon wind effects 80—93385
Ge, magnetic field effects on hot-hole noise 77—4415
Ge, magnetic field influence on 1/f noise, surface origin evidence 79—99592
Ge, magnetic susceptibility of light and heavy holes 79—42734
p-Ge, magneto-microwave Kerr effect, expt., scatt. mechanisms 78—39139
Ge magnetoacoustic effects in the drag of electron-hole drops by phonons 78—68057
Ge, magnetoconductivity meas. at 9.3 GHz, using three-wave interferometer *(French)* 77—47844
Ge, magnetodipole reson., 0.6 to 1.35 mm wavelength *(Russian)* 77—80736
Ge, magnetoplasma reson. spectra, electron-hole drop shape effects 79—1712

elemental semiconductors continued
Ge, magnetoplasma resonance in electron-hole drops *(Russian)* 78—79944
n-Ge, magnetoresist. anisotropy, in quantizing mag. fields, under conditions of mixed scatt;. 77—15877
Ge, magnetoresistance meas., transverse diffusion currents on source of error 79—7843
Ge, magnetoresistance of electron-hole liq., percolation model 80—96920
Ge, magnetostriction of electron-hole drop 77—85540
n-Ge, magnetothermal cond., 4.2K 80—24688
p-Ge, magnetothermal conductivity at low temp. 79—28158
n-Ge, many-valley semicond., elec. breakdown criteria 78—19046
Ge, many-valley semicond., current-voltage characts., intrinsic magnetoresistance 79—38108
n-Ge, many-valley semicond. anisotropic acoustoelectric effect, thermo-EMF anisotropy fluctuation depend. on ultrasound freq. 79—69562
Ge, matrix isolated cluster, optical absorpt. 80—16045
Ge, mean square atomic displacements, in single crysts., X-ray determ. *(German)* 78—30726
Ge mechanical strength in brittle fracture region, influence of Si and O impurities 79—87682
Ge, melt grown single crystals, preferred growth directions and perfection 79—77537
Ge, melt growth conditions and doping level influence on impurity distrib. ratio 77—12516
Ge microconductor mag. field transducer, cast, galvanomag. recomb. effect 79—19609
Ge, microdefect distrib. due to dislocation injection, selective etching 78—2122
Ge, microflaw vol. conc. determ., etching method 79—24688
Ge, microscopic mechanism of film growth from non-condensed phases, kinetic anal. 80—54565
Ge, microscopic screening of ion-ion interaction and phonon dispersion, tight-binding calc. 77—24528
Ge, microwave absorption by nonequilibrium carriers, carrier density determ. method 77—8148
Ge, microwave absorption by nonequilib. current carriers, book contrib. 80—11042
Ge, microwave exciton breakdown and luminesc., under one- and two-photon excitation 77—31955
Ge, microwave exciton discharge, collision frequency, hot carrier temp. determ. *(Russian)* 79—65507
n-Ge, microwave Faraday effect in strong mag. field 77—1662
Ge, migration energy of intrinsic point defects in different charge states 77—89582
n-Ge, minority-carrier injection and extraction 80—49767
Ge, mobility calcs. including low impurity conc. limit 77—28173
Ge mobility of screw and 60° dislocation at low stresses 77—11554
Ge, mode Gruneisen coeff. at point X, effect of lattice softening 78—38804
p-Ge modulation of 3.39 μm abs. by CO$_2$ laser irrad. *(Japanese)* 80—74410
Ge, molten zone movement under influence of Peltier effect 78—44007
Ge, momentum distrib. of electrons, anisotropy, positron annihilation *(Russian)* 78—84676
Ge, monocryst., for IR optics, prod. techniques and characts. 78—50873
Ge, Mott distortion of the electron-hole fluid phase diagram, luminesc. meas. 79—42457
n-Ge, Mott transition, dielec. enhancement and conduction electron screening 78—72073
Ge, Mott transition of exciton gas in equilib. with electron-hole droplets 77—4298
Ge, multicomponent exciton gas, composition calc. 80—49618
Ge, multioscillatory electrorefl. spectra *(Russian)* 77—8590
Ge, multiply charged impurity centers, energy spectrum 79—69469
Ge, multivalley struct., helical instability *(Russian)* 79—47101
Ge, muonium relaxation rates 80—75912
n-Ge, μ^+ depolarisation, post muonic stage *(Russian)* 77—48116
Ge, μ^+ meson polarisation, H impurity behaviour 77—20786
Ge, n- and p-type, fast neutron irrad. at low temp., resistivity, annealing characts. 77—89481
Ge, n- and p-type, magneto-impurity effect, review 79—91081
Ge, n- and p-type, photoemission into electrolyte soln., energy diagrams, Volta pots., voltage drop 77—62990
Ge, n- and p-type, solubility and diffusion of Na, vacancy mechanism 77—89592
Ge, n-type, magnetoresistance in strong UHF electric fields 77—1437
Ge, n-type, thermo-EMF, bulk differential meas. 77—4380
Ge, near intrinsic, negative differential cond., ambipolar size effect due to hot carriers 78—72185
Ge, nearest-neighbour atom mean-square relative displacements, EXAFS spectra 79—91532
p-Ge, negative magnetoresist. and Hall effect, press. and field depend. 80—70733
Ge, neutron irrad., absorpt. edge 80—93320
Ge, neutron irrad., Hall effect and magnetoresist. meas. 80—6883
Ge, neutron irrad., substitution of impurity atoms by self-interstitials, Ge(n,γ) reaction 80—39166
p-Ge, neutron irrad. quenched sample, lattice defects 79—19284
Ge, neutron irradiated, capture of positrons by radiation defects 78—38756
Ge, neutron irradiated, positron annihilation, ESR and resist. meas. 80—15160
Ge, neutron-irradiated, positron lifetime 80—97374
p-Ge, noise, energy relax. time and diffusion of hot holes 77—76839
n-Ge, noise, small signal conductivity and diffusion in strong elec. fields 79—11192
p-Ge, noise calc. in strong elec. field using Monte Carlo method 80—15578
n-Ge, noise spectra of hot carriers 78—76083
Ge, non-collinear phase matched 4-wave mixing of CO$_2$ and NH$_3$ laser radiation 79—988
Ge, nonequilibrium carrier excitation by CO$_2$ laser radiation 77—89803
Ge, nonequilibrium charge carrier-mag. field interaction electron-hole drops, recombination *(Russian)* 80—75511
n-Ge, nonlinear absorption of CO$_2$ laser radiation by nonequilib. carriers 79—32000
Ge, nonlinear acoustics, third-order elastic const. meas. 80—33292
p-Ge, nonlinear IR absorpt., theory 79—65868
Ge, nonlinear optical susceptibility, tight binding bonding orbital model 80—5784

elemental semiconductors continued
- Ge, nonlinear reflection props. rel. to thermal effects 78—42371
- Ge, nonlinear susceptibility, four-wave mixing at room temp. for tunable IR generation 80—9940
- Ge, nonlinear susceptibility, 10 μm, determ. by time resolved ellipse rotation 80—83633
- Ge, nonlocal pseudopotentials 77—11848
- Ge, nonpolar semiconductor, IR free carrier absorpt., two short wavelength phonon scattering 79—78665
- Ge, nonradiative transitions at impurity centre with participation of short-wavelength phonons 80—16099
- Ge, nonuniform electron-hole liq., props. in high density limit 77—43505
- Ge, nonuniformly deformed, electron-hole drop density depend. on size *(Russian)* 80—20092
- Ge, nucleation anal. of electron-hole drops 77—69243
- Ge, ODMR using luminescence of electron-hole drops *(Russian)* 77—90072
- p-Ge, odd magnetoresist., ionised impurity scatt., theory 78—72178
- p-Ge, odd magnetoresist. in strong elec. and mag. fields 79—51612
- p-Ge, odd magnetoresist. of warm holes 77—43628
- p-Ge, odd magnetoresist. under weak carrier heating conditions 80—96917
- Ge, optical absorpt. in samples with 60° dislocations 78—39577
- Ge, optical absorption from indirect transitions at high mag. fields 79—47441
- p-Ge, optical cooling and carrier heating, intraband photocond. meas. 79—11174
- Ge, optical excitation of dislocation states, photocond. meas. 77—69273
- Ge, optical excitation of dislocation states 77—85265
- Ge optical props. in 2.5-15 micron region 80—80775
- Ge, optical pulse transmission, pulsewidth depend., phonons and plasmons role 78—31198
- Ge, optical surface modes calc. 77—59200
- Ge optical switch, picosecond pulse generation at 10.6 μm 79—7159
- Ge, optically stimulated, electron-hole drops and appearance of dense plasma *(Russian)* 77—4688
- Ge, oscillatory exciton breakdown, microwave cond. 80—103716
- Ge oscillistor, hysteresis effects and N-shaped V-I characts. 79—33306
- Ge, oscillistor effect in strong mag. fields, ambipolar drift and breakdown 78—2511
- Ge, oxidation of clean cleaved (111) surfaces, EELS and AES 80—3230
- Ge p$^+$-n-m and m-n-m structures, current-voltage characts. 77—1476
- Ge p$^+$-n-n$^+$ and p$^+$-i-n$^+$ structures, inhomogeneous, influence of longitudinal mag. field 77—1479
- Ge p$^+$-ν-n$^+$ structures, charge transport under impurity freezeout conditions 80—92965
- Ge, p-i-n avalanche photodiode, temp. depend. characts. 79—35835
- Ge, p-n homojunction breakdown voltage for onesided abrupt junctions *(German)* 78—56210
- Ge p-n junction, current filament form., fluctuations and thermal noise 77—69411
- Ge, p-n junction, hot photocarrier and hot electron effects 78—30980
- Ge, p-n junction, I-V curve for microplasma breakdown, at. size difference effect 78—2550
- Ge, p-n junction, IR radiation modulation, light absorption by injected current carriers *(Russian)* 80—10013
- Ge p-n junction, photo-EMF generation in saturation region 80—75635
- Ge p-n junction injection characteristics in strong elec. fields 77—76913
- p-Ge, p-n junction with hot carriers in charge accumulation regime, influence of light on operation 79—51661
- Ge, p-n junction with hot carriers, current-voltage characts. 79—91135
- Ge p-n junctions, impurity photoelec. effect 79—56300
- Ge, p-type, and n-type converted to p-type by irradiation at 77K, defect form. mechanism 79—23651
- Ge, p-type, hole conductivity anisotropy 77—4360
- Ge particles, grown in Ar gas, cryst. struct. and habit, electron microscope study 79—74071
- Ge, partly dissociated excitons and impurity atoms system, collisional processes, charge transport theory 80—44581
- Ge, Pendellosung fringe shape depend. on specimen-film distance *(Russian)* 80—87994
- Ge, phase diagram of electron-hole fluid in low temp. photoexcited semicond. 77—69237
- N-Ge, phenomenological cond. relax. time, uniaxial stress and electron-electron scatt. effects 77—15862
- Ge, phonon assisted Auger recomb. in indirect gap semiconductors 78—39126
- Ge, phonon boundary scatt., reduction of lattice thermal cond. 78—55921
- Ge, phonon cond. correction term and electron-photon scatt. relax. rate, appl. to doped and undoped samples 80—39369
- n-Ge, phonon conductivity and attenuation 77—4167
- Ge, phonon damping of electron-hole droplet motion 77—85152
- Ge, phonon density of states determ. from sp. ht. 77—7809
- Ge, phonon dispersion and microscopic screening, extreme tight-binding model 80—49324
- Ge, phonon dispersion curves, appl. of deformable-ion model 78—59887
- Ge, phonon drag of electron-hole drops in longit. quantizing mag. field *(Russian)* 78—64070
- Ge, phonon energy variation under high press. band struct. changes, tunnel spectroscopy study *(Russian)* 80—2134
- Ge, phonon imaging, ballistic, low-temp., rel. to focusing theory 80—10605
- Ge, phonon scattering and dislocation effect on low temp. phonon cond. 78—51754
- p-Ge, phonon thermal cond., 0.1-7K, Ziman model 77—35763
- Ge, phonon viscosity tensor 78—34570
- Ge, phonon-assisted exciton emission, temp. depend. of relative integrated intensities 77—1375
- Ge, phonon-phonon scatt. strength, thermal cond. in low- and high-temp. regions 77—43296
- Ge, phonons, directional depend. of boundary scatt. mean free path 79—73354
- Ge, photo-field cathode, ageing and surface state effects *(Russian)* 77—28703
- Ge, photoacoustic effect, free flexural vibrs. damping 77—89813
- Ge photocathodes, Au absorbed photofield emission current spectral investigation 80—29856
- n-Ge, photocond., excited by CO_2 laser pulses, depend. on intensity 79—69548
- Ge, photocond., inversion of magneto-impurity oscills. 77—15913

elemental semiconductors continued
- Ge photoconductive IR detectors, microwave-biased, noise performance 80—9037
- Ge, photoconductivity, carrier lifetimes in excited states of impurities *(Russian)* 77—76864
- Ge, photoconductivity, magnetoimpurity oscills. 79—82626
- Ge, photoconductivity spectra of shallow impurities 79—82625
- Ge, photocurrent magneto-oscillations 80—6911
- Ge, photocurrent oscillations in mag. field, intense excitation *(Russian)* 78—26915
- Ge, photoelastic consts. determ. 78—68474
- Ge, photoelectric spectra of shallow impurities, mag. field effect 79—82624
- Ge, photoelectric spectra of impurity groups 79—82627
- Ge, photoelectric spectra of remanent impurities 79—87125
- Ge, photoemission spectroscopy of surface states and oxidation 77—55863
- p-Ge, photoexcited charge carrier capture by shallow impurity centres *(Russian)* 80—15571
- Ge, photoluminesc., high excitation intensities, direct and indirect gap transitions 77—12429
- Ge, photoluminesc. decay from electron-hole drops 77—66532
- Ge, photomag. EMF, reson. struct., energy relax. mechanisms 78—2515
- Ge, photomagnetic effect, space inhomogeneous nonequilibrium carrier lifetimes *(Russian)* 80—71152
- p-Ge, photon drag spectrum 77—32044
- p-Ge photon drage detector, performance in 2 to 33 μm range 79—35834
- Ge photon-drag detector submillimetric-wave performance 79—30547
- p-Ge, photon-drag voltage nonlinearity at high laser intensity 78—19081
- Ge, photothermal cond., low temp. depend. 80—70756
- Ge, picosecond Nd laser pulse reflectivity 79—18469
- Ge, picosecond optical absorption, at high optically created carrier densities 79—47462
- Ge, picosecond optical response, effects of parametric scatt., energy-gap narrowing and state filling 80—11424
- p-Ge, piezo Hall effect meas. 80—96883
- n-Ge, piezo-thermal cond. calc. 77—15639
- n-Ge, piezoresist. calc. 78—19036
- Ge, piezoresistance, energy and momentum relax. of charge carriers 78—47786
- n-Ge, piezoresistance under mechanical stress, rel. to cond. band minima 80—6836
- n-Ge, piezoresistance with deform. axis symm. rel. to all const. energy ellipsoids 77—55533
- Ge, piezoresistive vibrating circular membrane, reflectance light modulation 80—97232
- Ge, piezospectroscopic determ. of electron-phonon to hole-phonon interaction 79—95783
- Ge, piezospectroscopy of group V impurities 79—99915
- n-Ge, piezothermomagnetic analogue of Grabner effect 77—4378
- Ge, plasma excitation, ultrafast optical props. 78—31248
- n-Ge, plastic deformation, impurities and dislocations interaction, cond. *(Russian)* 79—47100
- n-Ge, plastically deform., dislocation state spectrum, photocond., elec. cond., and Hall const. meas. *(Russian)* 80—2362
- n-Ge, plastically deformed, elec. cond., magnetoresistance, Hall effect study *(Russian)* 79—99568
- Ge, plastically deformed, photocond. and absorpt. spectra, dislocation levels 77—28219
- Ge, plastically deformed, photocond. produced by polarised light 79—82641
- Ge, plastically deformed low temp. cond. *(Russian)* 80—6831
- Ge, plastically deformed under high temp. creep conditions, elec. props. 80—92915
- Ge plate, anisotropic cond. thickness depend., intervalley scatt. *(Russian)* 77—85352
- Ge, plates, semicond., scribing marks rel. to sclerometric microhardness 79—15891
- Ge, point defect creation by plastic deform., Hall const. electrical conductivity 78—6053
- Ge, point defects formation, electron or γ-irradiation reliable of questionable hypotheses 77—80501
- Ge, polarisation of implanted ^{12}B 78—43653
- Ge, polycrystalline epitaxial film, exam. of growth kinetics and props. 80—55304
- Ge, positron annihilation, effect of vacancies 79—24385
- Ge powder, elec. cond., temp. and press. depend. 77—8090
- Ge powder/Au electrode contact pot. difference, grain size depend. 80—44723
- N-Ge, pressure influence on photoconductivity temp. dependence 78—76109
- Ge, pressure tuning of picosecond pulse transmission, enhanced transparency 77—88871
- n-Ge, proton and γ irrad., minority carrier recombination 80—65591
- Ge, proton bombardment damage, irrad. energy depend., channelling meas. 80—24511
- Ge, pseudopotential method of band struct. anal. 78—51886
- Ge, pure, degree of compensation, capacitance meas., 4.2-150K 79—7624
- Ge, pure, electron hole size distribution at pulse optical excitation 80—59883
- Ge, pure, large, electron hole drops, microwave heating and evaporation 79—28287
- Ge, pure, magnetic phase transition between electron-hole drops and free-excitons 78—6278
- Ge, pure and doped, electron-hole drops net charge, photocond. and photoluminesc. 79—38589
- Ge, pure and n-type, US velocity and attenuation, second and third order elastic moduli 80—70325
- Ge, purification by zone refining 78—39683
- Ge, quantum cyclotron reson. linewidth 77—15752
- Ge, quenched, defect annihilation process near 100°C 79—95047
- Ge, quenched n- and p-type, intrinsic defects migrating near 100°C 77—62670
- Ge, quenching temp. effect on annealing rate of quenched-in acceptors 79—82590
- Ge, radiation piezoelec. effect, EMF generation under α-irrad. and uniaxial deform. 77—12320
- Ge, radiation pressure, photon drag effect in far-IR 80—50452
- Ge, radiative electromagnetic effect, alpha-particle irrad., Hall effect, photoelectromagnetic effect 78—10434

elemental semiconductors continued
- Ge, ratio of photoionisation cross-section of valence s- and p-electrons *(Ukrainian)* 77—73211
- Ge, reach-through avalanche photodiode, temp. depend. characts. 79—95482
- Ge, reaction with S vapour, applicability of Kossel's crystal model 79—87833
- Ge, reactor irrad., opt. props. 77—90137
- Ge read out, by SAW, optical image memory in slow surface states 77—79942
- Ge, recombination at dislocations 79—38023
- Ge recombination characteristics used in design of semicond. devices *(Russian)* 79—42557
- Ge, recombination luminesc. spectra from hot and cold carriers in electron-hole drops 79—38608
- Ge, recombination of nonequilib. carriers in presence of dislocations 79—82607
- Ge, reconstructed (001)2 x 1 surface structure, LEED intensity calcs., dimer model variations 79—77875
- Ge, reconstruction-induced subsurface strain, theory 78—91516
- Ge, reflection switch for CO_2 laser 77—3609
- Ge, reflectivity, picosec. laser pulses and electron-hole plasma 79—47463
- Ge reflectivity changes due to illumination by beams of unequal frequency 79—76749
- Ge, refr. index and refl. changes due to intense laser irrad., surface heating effect 78—42372
- Ge, refractive index dispersion 79—24280
- Ge, regrowth under laser irrad. 80—24481
- Ge, relax. time energy depend. and surface galvanomag. props. 78—43459
- p-Ge, relaxation dynamics and photoconductivity 79—51636
- n-Ge resistance thermometer material for 14 to 300K *(Russian)* 80—49731
- Ge resistive sensing devices, temp. calibration and reproducibility, high mag. field effect *(Czech)* 80—37029
- Ge, reson. Raman scatt. under uniaxial stress near E_1 gaps 79—42960
- Ge, rest friction of electron-hole drops *(Russian)* 79—42463
- Ge, review of point defect characts. *(Japanese)* 77—89428
- Ge ribbon single crysts. grown from melt, dislocation struct. form. under thermal stress 80—107082
- Ge, S-type diode, photoelec. props. 77—24614
- p-Ge, saturable absorption isolator for CO_2 laser systems 77—19284
- p-Ge, saturable absorption of picosecond CO_2 laser pulses 80—95956
- p-Ge, saturation characts. over CO_2 laser spectrum 77—88869
- Ge, saturation of transmitted intensity of CO_2 laser pulses 80—64111
- Ge, Schottky barrier, electronic struct., pseudopot. calc. 78—95364
- Ge Schottky barrier, electronic struct., pseudopotential method, jellium model 79—38162
- Ge, Schottky barrier electrorefl. under uniaxial stress, band struct. 77—48193
- Ge, screened donor impurities in many-valley semiconds., anisotropic mass effect 78—10399
- Ge, screw dislocations, effect of dislocation dissociation on localised electron and hole states 79—82546
- Ge, self- and impurity diffusion 80—29213
- Ge, self-consistent localised electronic struct. 79—42445
- Ge, self-diffusion, activation energy and entropy factors 80—88353
- Ge, self-diffusion, dynamical recovery 80—29215
- Ge, self-diffusion mechanism 79—90824
- Ge, self-interstitials, vacancies and their clusters 77—80500
- Ge, Sellmeier coeffs. temp. depend., nonlinear optics average power limit 79—50349
- Ge, semiconductor detector material, purification, cryst. growth, ion implantation 78—47674
- n-Ge sensor, resist.-temp. characts., 50-125K 77—41602
- Ge, shallow acceptors produced by quenching 79—51523
- Ge shallow hydrogenic centres, ground states, isotope shifts, photoelectric spectrosc. 78—39055
- Ge, shallow impurities, excited states, population and lifetime *(Russian)* 79—51532
- Ge shallow impurity bound states, IR spectroscopic obs. 77—39806
- p^+-n Ge shallow junction avalanche photo diodes, noise and quantum efficiency 79—87143
- Ge, shaped crystals, grown by Stepanov method, struct. perfection 78—2123
- Ge shaped single crystal, Stepanov method growth, temp. distri b. 78—2032
- p-Ge sheet, free carrier confinement for IR modulation 78—25969
- Ge, short dislocation line movement at low stresses *(Russian)* 77—47462
- Ge, single cryst., anisotropic oxidation, ellipsometric obs. 77—70194
- Ge single cryst., atomic H interaction, highly efficient electron accommodation *(Russian)* 79—78818
- Ge, single cryst., proton irradiated, defect study using X-ray diffuse scattering 79—95048
- Ge single cryst., radiation piezoelec. effect 78—19419
- Ge, single cryst. growth, supercooling needed for Czochralski and Stepanov methods 78—3015
- n-Ge, single cryst. with dislocations, UHF cond. *(Russian)* 79—78128
- Ge, single crystal, stress-induced phase change 79—23720
- Ge single crystal of circular cross section, thermoelastic stresses 78—2033
- Ge single crystals, constitutional supercooling growth conditions, structural and chem. inhomogeneities 80—93473
- Ge single crystals, photopiezoelectric effect under elastic deform. 80—107856
- Ge, size effects in small electron-hole drops 79—82530
- Ge slab, intrinsic, longit. cond., influence of surrounding gas *(French)* 78—10448
- Ge slab in waveguide, microwave absorpt. due to geometric reson. of longitudinal-section elec. surface waves 80—39874
- Ge, slow surface, states, optical excitation investigation 78—76129
- Ge slow surface states, optical image storage for $LiNbO_3$ SAW readout 77—23773
- Ge, solid-liquid interfacial tension determ., glassy sphere nucleation by rapid cooling 77—51570
- Ge, solid-phase epitaxial growth through PdGe layers, channelling and backscatt. obs. 77—85936
- Ge, solid-state plasma, ultrafast transient response, theory and expt. 77—80748
- p-Ge, spectral depend. of drag of electrons by photons 79—42590

elemental semiconductors continued
- Ge, spectral diffusion in acceptor-hole system at low temp., ultrasonic hole-burning expt. 80—92610
- Ge, spectrally selective EM wave absorber, solar energy collector material, props. *(Dutch)* 78—50872
- Ge, spectrum of photocapacitance current near fundamental absorpt. edge 77—28217
- Ge, spin Hamiltonian and anomalous muonium states 80—71286
- Ge, spreading resist. rel. to load applied to meas. probe 78—4647
- Ge, sputtered hydrogenated amorphous, steady-state and transient photocond. meas. 78—10506
- Ge, stacking fault energies 79—82205
- Ge, stacking faults of dislocations, constrictions obs. using weak-beam electron microscopy 77—35576
- Ge, static dielectric function, local field correction, tight-binding model 79—95355
- Ge, stationary creep depend. on deform. stabilisation of material struct. *(Russian)* 80—100300
- Ge, strain-confined electron-hole liq. 77—47738
- Ge, strain-confined electron-hole liquid, density variation 78—34779
- Ge, strain-confined electron-hole liquid, lifetime and radiative efficiency vs density 79—38000
- Ge strain-confined large electron-hole drop characteristics 80—65469
- Ge, strain-narrowing of luminesc. line from excitons 79—24356
- Ge, strained, crit.-point for electron-hole droplets 79—4516
- Ge, stressed, α_1 and α_3 electron-hole droplet luminesc. 79—28820
- Ge, stressed, metal-insulator transition, luminesc. 80—20695
- Ge, stressed, recombination luminescence from hot carriers in electron-hole droplets 78—6754
- Ge, stressed cryst., props. of strain-confined electron-hole liquid 79—7787
- p-Ge, stretched along ⟨111⟩ axis, bulk negative differential cond. and current oscills., 78K 79—19601
- Ge strips grown by Stepanov method, thermoelsatic stress calc. 78—2034
- Ge, strong microwave field effect on electron-hole drops, luminescence kinetics 79—87047
- p-Ge, strong uniaxial deform. at low temps., piezoresist. 78—19038
- n-Ge, subjected to high voltages, distrib. of injected carriers 79—56239
- Ge, submillimetre wave dispersive Fourier transform spectroscopy obs. 77—37915
- Ge substrate for GaAs solar cells, thin film shallow homojunction struct., quantum efficiencies 80—35677
- n-Ge, substrate for slab of GaAs, surface polaritons, hydrodynamical model 80—6752
- Ge, sum rule for intraband optical absorpt. of shallow acceptor impurities 79—28793
- Ge, supecond, friction layer formed during friction between Ge and Pb *(Russian)* 78—52143
- Ge, supercond. at high press., crit. temp. 80—60130
- Ge surface, (111), ion-bombarded and annealed, spectroscopic ellipsometry study 80—103543
- Ge surface, adatom indirect interaction, theory 80—44696
- Ge surface, atomically pure, optical consts. and temp. depends. 79—65823
- n-Ge surface, chemical channel of recombination 80—39656
- Ge surface, Cl chemisorption, cluster calc. by iterative EHT 77—32062
- Ge, surface, cluster model approach for electronic struct. 78—56205
- Ge surface, field penetration and band bending in high elec. fields 79—42613
- Ge, surface, Hall effect study, channel cond. *(Russian)* 80—92909
- Ge, surface, high freq. cond. and cyclotron reson. 80—11273
- Ge surface, line tension induced dislocation motion 79—82212
- Ge surface, nonequilib. electron effects due to chem. excitation 78—72239
- Ge surface, optical charging meas., 120-300K 80—49817
- Ge surface, self diffraction of light, mechanism, rel. to nonequilib. carrier behaviour 79—72685
- Ge surface, wetting by Sn, Pb rel. to cryst. orientation 78—43211
- Ge surface, X-irradiated, slow relaxation of surface states 77—62980
- Ge, surface (110) atomic struct. 79—69331
- Ge surface during X-irradiation, oxide hydration degree determ. 77—24605
- n-Ge, surface electron mobility, Hall effect and cond. meas. 79—56281
- Ge, surface electron states, relaxed (111), self consistent pseudopot. calc. 77—47880
- Ge surface electron states, review of optical methods of detection 77—66191
- Ge surface electron states, appl. of surface photovoltage spectroscopy 77—69391
- Ge, surface electronic props. meas. by SEM, sand-blasting effect 77—62976
- Ge, surface electronic struct., self consistent pseudopotential calc. 78—47842
- Ge, surface energy effect on electon-hole drop luminesc. 77—48239
- Ge surface Hall effect and cond., electron, hole conc. and mobility *(Russian)* 80—44619
- Ge surface ion implanted far IR composite bolometers 79—30549
- Ge surface microwave cond. observations *(Russian)* 80—2447
- Ge, surface mobility of irrad. sample, interpretation using two-layer model *(Russian)* 77—51804
- Ge, surface recombination before and after laser annealing, 10-μm transmission meas. 80—1247
- Ge, surface slow states conc. determ. by field effect meas. 77—28232
- Ge surface states, recomb. centres, regularities, electrolyte contact effects *(Russian)* 80—65652
- Ge, surface states, recombination centre formation *(Russian)* 80—29459
- Ge surface states, Tamm-like and field sustained, model studies, localisation props. 78—64092
- Ge, surface structure, LEED and spot photometric meas. 79—23811
- Ge surface with p-n junction, photovoltaic effect under conditions of surface recomb. of H atoms 77—66185
- Ge surfaces, electronic struct., tight-binding calc. 80—54755
- p-Ge, temp. depend. of noise and diffusion of hot holes 78—39174
- p-Ge, test of electronic band struct. by laser-induced reson. 78—37949
- p-Ge, theory of photon-drag effect, parabolic and anisotropic band-struct. approx. 78—47825
- Ge, thermal cond. calc. using numerical soln. of Boltzmann eqn. 80—44373
- p-Ge, thermal conductivity, effect of uniaxial stress 79—23792
- Ge, thermal conductivity, low temp. calc. for impure insulators 79—33128
- Ge, thermal conductivity at high temperature 79—55857

elemental semiconductors continued
p-Ge, thermal conductivity meas. down to 50 mK, acceptor state exam. 77—80658
Ge, thermal conductivity of semiconductors, quantum acoustical method, thermal phonon lifetimes 80—65312
Ge, thermal expansion coeff. and Gruneisen const. 77—59128
Ge, thermal expansion coeff., optical mode Gruneisen const. 79—46820
n-Ge, thermal phonon scatt., piezo-thermal cond. 80—70482
Ge, thermal rectification and negative differential cond. 79—42554
Ge, thermal relaxation time, laser heating effect at 1.3K , book contrib. 80—11519
n-Ge, thermo-EMF drag, anisotropy parameter *(Russian)* 77—80799
Ge, thermodynamic functions and normalised moments 79—51279
n-Ge, thermoelec. power in quantising mag. field, phonon-phonon interactions 80—107832
Ge thin films on glass substrates, annealing by Ar ion bombardment 80—80136
n-Ge thin plate, transverse magnetoresist. meas., size effect 78—72179
Ge, thin single crystal, (110) orientation, preparation technique 79—95930
Ge, third order elastic constant 79—51184
Ge, threshold energy for displacement of atoms 78—47428
Ge, transmission Faraday rot., due to intervalence band transitions 79—38521
Ge, transmutation doped, high field magnetoresist. of hopping transport 78—10474
Ge, transmutation-doped, impurity cond., 1.5-4.2K 77—89758
Ge, transport props. of high density electron-hole plasma at low temp. 77—47864
n-Ge, transverse magnetoresist. effects on Hall voltage meas., theory 77—72870
Ge, trapping defects, deep level transient spectroscopy 79—47045
p-Ge, tunable laser induced grating dip for sub-picosecond relax. meas. 77—75623
Ge, twin lamellas formation due to deposition of metal contacts 78—10060
Ge, two photon absorption of light with optical transitions between heavy- and light-hole states 79—11421
Ge, two-band system, acoustic scatt., appl. to hole transport props. 79—60823
Ge, two-phonon difference absorption spectra 78—76452
Ge, two-photon transitions from deep neutral impurity centres, light absorpt. and drag effect 79—91478
Ge type semiconductor, interimpurity zero-phonon radiative transitions 78—15222
n-Ge type semiconductor, thermomagnetic tensor struct. 77—62952
Ge, UHF heating of charge carriers using lumped-capacitance resonators 80—20203
Ge, US absorption, depend. on orientation 79—69197
Ge, US attenuation, temp. variation, 273K to 500K at 4 MHz *(Rumanian)* 79—77691
Ge, US attenuation and nonlinearity const., temp. depend. 78—43075
n-Ge, US attenuation by impurities 77—69047
Ge, ultimate yield strength calc. 78—43062
Ge, ultra high vac. cleaved, photolum., role of intrinsic surface states 78—52571
Ge, ultra pure, method to determ. composition and struct. of non-elemental acceptor and donor centres 78—39658
Ge, ultra-pure electron-hole drop condensation nucleation phenomena 77—47744
Ge, ultrashort optical pulse transmission, pulse-width depend. 78—55403
p-Ge, uniaxial compression influence on carrier heating by weak electric field 80—10978
Ge, uniaxially deform., electron-hole drop flight, photolum. max. press. depend. 78—10977
Ge uniaxially deformed, cyclotron resonance of RF field heated hot holes, *(Russian)* 80—44925
n-Ge, uniaxially deformed, longitudinal magnetoresist. in quantising mag. field 79—15168
p-Ge, uniaxially deformed, magneto-impurity oscills. of photocond. 78—34862
n-Ge, uniaxially stretched along [111] axis, negative differential conductance 77—51759
Ge, uniformly deformed, free carrier cyclotron resonance, electron-hole drops *(Russian)* 80—71182
Ge, uniformly stressed, density and binding energy of electron-hole droplets, photolum. meas. 78—60062
Ge, unrelaxed vacancy states appl. of local formalism 77—4313
Ge, unstrained, electron-hole drop shape in mag. field 79—42458
Ge, vacancy, tight-binding calc. 80—24844
Ge, vacancy formation and stability due to noncentral force 80—70192
Ge, vacancy paradox 78—59804
Ge, valence band effective mass strain depend. 78—51880
Ge, valence band relaxation energies during XPS 78—39657
Ge, valence band splitting in mag. field, LCAO interpolation *(German)* 77—59251
Ge, valence band struct. obtained by magnetophonon effect 77—76748
Ge, valence electron radial and momentum distribs., X-ray form factors and Compton profiles 79—65956
Ge, valence electrons, XPS, LCAO and OPW calc. 77—12496
Ge, vapour transport rate, Ge-I$_2$ equilib. 700 to 1300K *(French)* 78—64476
n-Ge, vel. component of hot charge carriers' thermoelectromotive force 80—44630
Ge, voltage-current curves, specimens of variable cross-section 77—8113
Ge, volume plasmon, cryst. orientation influence 80—80921
Ge waveguide, nonlinear third harmonic generation of submillemetre waves 80—44632
Ge, weak heating of electrons, cyclotron reson. conditions, quantising mag. field 78—39141
Ge, wedge shaped film, photovoltaic effect 77—1454
Ge, whisker growth from vapour phase 80—15426
Ge, whiskers nucleation, effect of machining support surface *(Russian)* 79—65352
Ge, work function, meas. by thermionic emission 78—19628
Ge, X-ray anomalous transmission at three-wave diffraction (220;202) *(Russian)* 78—34393
Ge, X-ray anomalous transmission at three-wave diffraction (220;202) *(Russian)* 78—34394
Ge X-ray detector, Au contact layer thickness meas. 80—62627

elemental semiconductors continued
Ge, X-ray diffraction, effect of dislocations on temp. depend. of integrated intensities 77—39513
Ge, X-ray diffraction, six-beam anomalous transmission, interpretation from eigensolns. 77—19832
Ge, X-ray emission spectra formation, role of nonequilibrium electron density *(Russian)* 77—63490
Ge, X-ray linear absorpt. coefficients, in energy range 5 to 50 keV 79—73066
Ge, X-ray six-beam anomalous transmission pattern, computer anal. 77—4021
Ge, X-ray spectra and energy band struct. 79—69407
Ge, Zeeman split acceptor levels, calc. method 79—28322
Ge^{+}, low energy mass analysed ion beam deposition on Ge and Si substrates 79—33946
n-Ge: Ga(P), uniaxial compression, 0.6-2.9 mm radn. absorpt. 79—82629
Ge:^{119m}Sn, impurity lattice dynamics, Mossbauer spectra, Debye temp. 80—84262
Ge:^{57}Co, ion-implanted, Mossbauer study, annealing effects 80—7231
p-Ge:Ag, Sb, electron beam irradiation cond. characts. 80—19842
Ge:Ag(Ni), gamma ray effects on impurity states 80—96822
Ge:Al, acceptor levels, Zeeman splitting, far IR photoconductivity spectrum 78—43444
Ge:Al, limiting solubility, rel. to charge carrier conc. 80—24596
Ge:Al, solid solns. decomp. 80—15249
Ge:Al, Zeeman effect in excitation spectra, photoelectric spectroscopy 79—82633
Ge:Al(B), uniaxially stressed, photoionisation of acceptors, impurity photocond. meas. 78—10509
Ge:Al(B)(P), impurity ground state levels from photo-thermal cond. in mag. field 77—51699
Ge:Al(Sb) film, amorphous, ion implantation, effect on cond. 78—83839
Ge:As, containing dislocation loops, dynamic scatt. of X-rays, extinction effect 78—47384
Ge:As, far IR transmission spectra, singlet-triplet optical transitions in ground states of donors 78—2887
n-Ge:As, heavily doped, luminesc. from electron-hole drops 77—81144
Ge:As, interaction of muonium with atoms 79—11373
Ge:As, many-valley semicond., donor binding energies, variational calc. 78—23041
Ge:As, NMR, conduction electrons in impurity band, metal-nonmetal transition 79—78544
Ge:As, recomb. of donor bound excitons, luminesc. intensity decay 80—25441
Ge:As, thermally induced defects properties obs. 77—63692
Ge:As, uniaxially stressed, electronic Raman scatt. from valley-orbit transitions 78—15166
n-Ge:As closely compensated, photolum. of charge carriers localised in trails of density of states 77—77294
Ge:As(Bi), donor bound exciton luminesc. and absorpt. 80—29777
Ge:As(Ga), photoconductivity oscillation with respect to applied mag. field *(Russian)* 78—80026
Ge:As(P)(Sb), impurity photocond. spectra under uniaxial compression 80—44656
Ge:As(Sb), D^{-} states in mag. fields, photocond. spectra, and far IR absorption spectra 79—95370
Ge:As(Sb), D^{-} states investigated by long wavelength photoconductivity 78—6323
n-Ge:As(Sb), far IR absorpt. spectra 79—91469
n-Ge:As(Sb), moderately heavily doped, electron-hole drops photoluminesc. 80—7417
Ge:As(Sb), phonon-bound donor resonance scatt., donor-electron radius mag. field depend. 79—77847
n-Ge:As(Sb)(Bi), irradiated with fast electrons at 77K, investigation of 300K annealing stage 79—51155
Ge:As(Se^{+}), energy spectra, multivalley effective mass calcs. 77—59266
Ge:Au, capacitance oscillations, trap recharging waves 77—43614
n-Ge:Au, current oscill. damping in weak transverse mag. field 77—4365
Ge:Au, current-voltage phase shift, impedance of subthreshold domains 77—43609
n-Ge:Au, electron capture by negatively charged traps, effect on hot electron enrgy energy distrib. 78—43398
Ge:Au, gamma-irradiated and electron irradiated, elec. props. meas. 77—62950
Ge:Au, IR detector, impurity photoconductivity *(German)* 78—82036
p-Ge:Au, interaction of primary radiation defects with Au atoms, after irrad. and annealing 79—51145
Ge:Au, moving elec. domain, impedance 77—1429
n-Ge:Au, negative photocond., field and temp. depend. 77—43660
n-Ge:Au, negative photoconductivity 78—34863
Ge:Au, p-n junction, injection amplification of photocurrent 79—51663
Ge:Au, recomb. at repulsive centres, photocond. lifetime meas. 77—43617
Ge:Au, Sb, Hall mobility, temp. dependence 80—96919
Ge:Au, Sb 79—69577
Ge:Au, trap charge exchange waves *(Russian)* 78—34846
Ge:Au, unipolar injection influence on high frequency conductance 80—34474
Ge:Au,Sb, electron irradiated, Hall effect, photocond., and photomagnetic effect meas. 77—4369
p-Ge:Au,Sb,Hg(Zn), radiation-defect form., Au influence 80—92911
Ge:Au film strain gauges, press. sensor *(Japanese)* 80—105631
n-Ge:Au piezoresistance in presence of deep levels, stress anisotropy 80—10979
Ge:Au under laser illumination, non-equilibrium conduction 80—6896
Ge:B, epitaxial film, exam. of doping during chemical deposition from gas phase 79—1446
Ge:B(Al)(Ga), shallow acceptor spectral line intensities 80—88517
Ge:B(Al)(Ga)(In)(Tl), binding energy, excited state spectra, photolum., semi-empirical short range pot. 80—44534
Ge:B(P), ion implanted, laser-induced regrowth 79—69130
Ge:Ba, Ca, recomb. props. 78—56156
Ge:Ba, heavily doped, second phase inclusions on melt growth 78—22751
Ge:Ba distrib. pattern, partition coeff., limiting solubility and energy levels 77—15444
Ge:Ba(Ca), elec. props. and effect of impurities on γ-radiation defect formation 78—10088
Ge:Be, P, absorption of radiation, 0.6-2.8 mm, 4.2 to 20K 80—66332
Ge:Be(Mg)(Ca)(Ba), positron annihilation ang. distrib 80—45165
n-Ge:Bi,O, plastically deformed, dislocation scatt. anisotropy, effect of state of O in Cottrell atm. 78—19028

elemental semiconductors continued
Ge:Cd, compensated, complex oscillatory impurity photocond. spectrum 77—43656
p-Ge:Cd,Sb, electron irrad. at 300K, elec. props. 80—6435
Ge:Cu, anelastic relax., internal friction temp. depend. meas. 79—65143
n- Ge:Cu, characts. of radiation defects 78—55893
Ge:Cu, deep-level impurities, insulating props. 78—39124
Ge:Cu, degree of Cu contamination in heat treated Ge 80—2359
Ge:Cu, displacement of Ge-Cu inclusions in const. elec. field, 700-850°C *(Russian)* 77—15634
Ge:Cu, electron irrad. effects on carrier density, defect form. 80—19843
Ge:Cu, hot photoexcited holes at low temp. 78—30954
Ge:Cu, IR detector, impurity photoconductivity *(German)* 78—82036
Ge:Cu, low frequency oscillations 77—15872
Ge:Cu, press. effect on energy spectrum of carriers, elec. cond. and Hall coeff. expts. 79—23930
Ge:Cu, quenched, energy levels of thermal acceptors, annealing effect 78—34798
Ge:Cu, quenched, interaction between shallow-level defects and Cu atoms, Hall effect meas. 78—64002
Ge:Cu, solubility and behaviour of Cu, internal friction investigations 80—92678
Ge:Cu, surface waves at static domain boundaries *(Russian)* 80—80288
Ge:Cu photodetector, I-V characts. 78—19141
Ge:Cu photoresistor, liquid H_2 cooled, detectability 78—80019
Ge:Cu short wavelength quenching of photoconductivity 78—26907
Ge:Cu(Sb), electron irradiation effects on elec. props. 78—6103
n-Ge:D^-; energy spectrum of D^- impurity band 77—51702
Ge:Fe, amorphous film or ion-implanted, comparison of ^{57}Fe Mossbauer data 77—40159
Ge:Fe, implanted, Mossbauer spectra, conversion electron, temp. dependence 80—40025
Ge:Fe, recoil implantation Mossbauer expt. in presence of external mag. field 80—44981
Ge:Ga, appl. of heat pipe to Czochralski growth, segregational behavior 79—61511
p-Ge:Ga, carrier heating by weak elec. field, hole-hole collision influence 78—72161
p-Ge:Ga, cryst. defects due to γ-irrad., annealing 79—55779
Ge:Ga, cryst. defects due to neutron irrad., elec. cond. and annealing 79—55789
p-Ge:Ga, dislocation density effect on carrier lifetime and deep recomb. centres 79—51598
Ge:Ga, effects of destabilising vertical thermal gradients on cryst. growth and segregation 78—52659
p-Ge:Ga, heavily doped, elec. resist., 40 mK to 300K 79—38071
Ge:Ga, heavily doped, structure defect evolution during heating *(Russian)* 78—43026
p-Ge:Ga, lattice defects induced by γ-irrad. 80—29051
Ge:Ga, magnetoacoustic resonance attenuation, Zeeman splitting of acceptor ground state 77—47869
Ge:Ga, resonant scattering of phonons by bound holes in temp. range 1 to 5K 80—75393
p-Ge:Ga, saturation behaviour at CO_2 laser wavelengths 78—1307
Ge:Ga, uniaxially stressed, far IR photocond. meas. 78—10496
Ge:Ga,Sb, compensated, low temp. props. rel. to appl. in bolometry 80—31867
p-Ge:Ga far IR absorption and photoconductivity obs. 77—39899
Ge:Ga photoconductor detector performance in low optical background 77—37999
Ge:Ga photoconductors in low IR backgrounds 79—63305
Ge:Ga(In), resonant phonon interaction with localised acceptor levels 80—6784
Ge:Ga(In), shallow acceptor ground state, thermal cond. meas. 77—43540
p-Ge:Ga(Sb), proton irradiated, kinetics of accumulation of radiation defects, minority carrier lifetime 79—10885
Ge:H, amorphous, H content determ. by IR absorpt., gas evolution and nuclear reaction methods 80—44130
Ge:H, interstitial impurity levels, pseudopot. calc. 80—44533
Ge:H, photoelec. spectra, acceptor and donor behaviour 80—29443
Ge:H amorphous films, photoemission spectra 80—50517
Ge:Hg, anomalous photocond. with 10.6 μm laser light *(Russian)* 77—47861
Ge:Hg, anomalous room-temp. impurity photocond. 78—39159
Ge:Hg, S-type diode, elec. props. 80—20299
Ge:Hg, Sb, influence of electron irradiation on elec. props. 77—20318
Ge:Hg photoconductive detector, laser damage thresholds calc. 78—90443
Ge:Hg S-type diodes, photoelec. props. 80—6964
p-Ge:Hg(Cu)(Cd)(Zn), deep levels, optical-phonon-assisted capture of carriers 79—51597
Ge:In, magneto-optical transitions between discrete levels of In acceptor, far-IR obs., 4.2K 78—2890
Ge:In (Sb) and pure cryst., kinetics of strain-confined large electron-hole drop and its clinging exciton system 80—75508
Ge:In(Hg), impurity characterisation from thermal carrier meas. 80—65595
Ge:inert gas, ion implantation, UV photoemission exam. 78—80457
Ge:Li, Cu p-n junctions, current stimulated LiCu complex formation, photocurrents 80—107897
Ge:Li, long wavelength photoconductivity spectrum 77—43641
Ge:Li, supersaturated solid solns., decomp., surface impurity content 78—51681
Ge:Li, thermal cond., 0.4-20K, Li valley-orbit splitting 79—15111
Ge:Li,O, EPR and piezospectroscopy 80—25338
Ge:Li-O, donor complex EPR and photoelectron piezoelectric spectra, dynamic tunnelling 79—1711
Ge:metal, polycrystalline film, electron transport props. 79—99642
Ge:Mg, diffusion and p-type cond. 80—6419
Ge:Mg, energy level behaviour, Hall coeff. and elec. cond. meas. 80—34396
Ge:Mn, amorphous, cond. increase by Mn doping 78—72155
Ge:Mn, amorphous, EPR meas. 77—85559
Ge:Mn, impedance characts., near threshold of excitation of recomb. waves 77—69342
Ge:Mn, Sb, recombination waves, convective instability development 80—70721
Ge:Na (111) surface, O_2 adsorpt., work function, surface cond. changes meas. 78—79875
n-Ge:Ni, negative differential conductance of surface channels 79—11134

elemental semiconductors continued
n-Ge:Ni, quasi-surface conduction effects on photocond. spectrum and IR quenching 77—1452
n-Ge:Ni, recomb. waves, current instabilities obs. 77—1431
n-Ge:Ni, recombination of hot electrons on Ni impurity centres 80—44612
n-Ge:Ni,Sb, transient response at 4K, nonequilib. carrier recomb. 77—43659
Ge:Ni compensated, hot electron recomb. anisotropy 78—39125
n-Ge:Ni p^+-n-n^+ structs., double-injection current-voltage characts. 80—60074
p-Ge:Nz, Sb, influence of electron irradiation in elec. props. 77—20318
Ge:O, Cu, amorphous thin film, impurity effects on struct. 80—107054
n-Ge:O, Czochralski growth, O content rel. to props., IR, Li precipitation determs. 77—15445
Ge:O, elec. props., O donor levels determ. 77—8123
Ge:O, elec. props., O interaction with point defects 79—11081
Ge:O, IR absorpt. at low temp. *(Chinese)* 80—108228
n-Ge:O, impurity-saturated, dislocation-free, anomalously high magnetoresist., vacancy effects 77—43629
Ge:O, intrinsic γ detector, deep level defect connection with O content *(Russian)* 78—43331
Ge:O, slow thermal relax. of cond. rel. to donor complexes 80—70704
Ge:O ion implanted, O localisation determ. 79—95040
Ge:P, amorphous, electronic transport and photocond. 79—60834
Ge:P, bound-exciton luminesc. and absorpt. 79—87469
Ge:P, charact. temp. and lattice thermal cond. 80—59743
Ge:P, conc. depend. of diffusion coeff. at P diffusion 78—95185
Ge:P, doping of epitaxial layers, in chloride and hydride processes 78—43036
n-Ge:P, electric dipole excitation of spin resonance 77—4551
Ge:P, lattice thermal cond., role of electron-phonon interactions and peripheral phonons 78—79702
Ge:P, lattice thermal resistivity due to electrons 78—51756
Ge:P, peripheral phonons and phonon cond. 79—14973
Ge:P., phonon drag thermoelectric power at low temp. 80—107828
Ge:P, solubility and segregation of electrically active P 77—15442
n-Ge:P,Ga, compensated, uniaxially compressed, anisotropy of mm. and submm. wave absorpt. 78—19074
n-Ge:P(As), nonlinear optical susceptibility, Raman scatt. cross-sections for impurities 77—46759
Ge:P(Sb), growth atm. effect on struct. microdefect form. 80—20779
Ge:P(Sb)(Bi), γ-irrad., carrier trapping and recomb. at point radiation defects 80—107810
Ge:Pb, ion implanted, lattice reordering, channelling and sheet resist. meas. 77—35577
Ge:Pb, ion implanted damaged layer, laser induced reorder 80—84201
Ge:Pd and pure, photoelectric props., surface states *(Russian)* 80—60043
Ge:S, photoionisation cross section of deep impurity centres 78—56510
Ge:Sb, 2.5 MeV electron irradiated, cond. switching effect 77—89820
Ge:Sb, acoustic attenuation, uniaxial stress effects 78—59863
n-Ge:Sb, adiabatic approximation in transient donor recombination 80—49761
Ge:Sb, amorphous, electronic transport props. 80—44589
Ge:Sb, annealing stages of thermal defects, elec. meas. 77—55282
Ge:Sb, bolometer element, absorpt. spectra, bias depend. 79—30553
p-Ge:Sb, cryst. defects due to γ-irrad. 79—55779
Ge:Sb, cryst. defects due to neutron irrad., elec. cond. and annealing 79—55789
Ge:Sb, Czochralski growth, orientation depend. of impurity distrib. coeff. 79—69976
n-Ge:Sb, deep levels obs., freq. depend. of capacitance of p-n junctions 77—4315
Ge:Sb, dopant distrib. rel. to direction of cryst. growth 77—51400
Ge:Sb, effect of degree of doping on surface state charact. 79—69577
n-Ge:Sb, electron irrad., impurity photoconductivity 77—15900
Ge:Sb, electron-hole drop lifetime, quenching temp. influence 80—59889
Ge:Sb, excited donor states, double optical transitions, reson. absorpt. meas. 80—93371
n-Ge:Sb, exciton absorption 78—6688
n-Ge:Sb, fast electron irrad. at 77K, radiation defect changes by annealing at 220K 79—37737
n-Ge:Sb, fast neutron irrad. effects on donor conc., and annealing 78—56107
Ge:Sb, γ-irrad., electron capture mechanism by radiation defects 78—26885
n-Ge:Sb, γ-irrad. effects on donor conc. and compensation by acceptors 78—56106
n-Ge:Sb, γ-irradiated, trapping and recomb. coeffs. 77—43616
Ge:Sb, heavily doped, anomalous magnetoresist., metallic impurity cond., down to 5 mK 79—65502
Ge:Sb, heavily doped, mass anisotropy, and multiple scattering effects 80—107802
Ge:Sb, heavily doped, scatt. of electrons 77—59283
Ge:Sb, heavily doped semicond., scatt. mechanism, resist, and Hall coeff. maxima 80—75586
n-Ge:Sb, high-field Hall effect spectroscopy 80—65600
Ge:Sb, lattice thermal resist. due to bound state electrons 79—46850
Ge:Sb, limiting solubility, rel. to charge carrier conc. 80—24596
Ge:Sb, low temp. anomaly of impurity cond. 79—95428
Ge:Sb, low-freq., low temp. dielec. behaviour below metal-insulator transition 80—50250
Ge:Sb, neutron irrad., carrier mobility theory and expt. 78—56166
Ge:Sb, neutron irradiated, hopping cond. between shallow defect levels 77—4347
n-Ge:Sb, neutron-irradiated, paramag. defects, analysis of EPR spectra 77—55703
Ge:Sb, Ni(Mn), recombination wave spectrum, two-level traps 80—96906
Ge:Sb, phonon thermal cond. calc. 78—71893
Ge:Sb, shock polarisation anisotropy in elastoplastic compression range 77—16244
Ge:Sb, solid solns. decomp. 80—15249
Ge:Sb, thermal defects, influence on radiation defect formation and annealing 77—55281
Ge:Sb, Zn(Hg), photoelec. props., 70 to 300K 80—65621
Ge:Sb,Au, photoelectronoc exam. of multilevel gold structure 77—69272
Ge:Sb,Cu, exactly compensated, impurity absorpt. and photocond. spectra 78—56189
n-Ge:Sb,Cu, exactly compensated, static photocurrent-voltage characts. 79—38131

elemental semiconductors continued

- n-Ge:Sb,Cu, exactly compensated, unipolar injection influence on photoconductivity 79—42592
- Ge:Sb,Cu, high resist. compensated, impurity of photocond., pulsed unipolar injection carriers 80—92935
- Ge:Sb,Cu, photoelec. props., fast electron irrad. effects 80—60036
- Ge:Sb,In, lightly doped semicond., electron-phonon scatt., role of compensation 79—60456
- Ge:Sb (As), isolated D^- states and D^- complexes in mag. fields 80—15473
- Ge:Sb crystals, purification by zone recrystallisation with temp. gradient 79—4916
- Ge:Sb semiconductors, inhomogeneously strained, phonon resonance scatt., Kwok's theory method 79—60455
- Ge:Sb(As), experimental data anal. 77—35933
- Ge:Sb(As)(Ga), fast-neutron irradiated, shallow radiation defect levels, electronic props. 78—23049
- Ge:Sb(As)(P), implantation doping, annealing and doping profile determ. 77—19972
- Ge:Sb(Au) cleaved surface, influence of impurities on local surface states 79—78150
- Ge:Sb(Ga), amorphous, doping effects on Fermi level, electrical meas. 79—42546
- Ge:Sb(Ga), fast electron radiation defects, 0.52 eV absorpt. band, impurity photocond. and Hall effect meas. 78—27273
- Ge:Sb(In), film, electronic props. 78—84330
- Ge:Si, impurity lattice modes due to single and paired defects 78—75780
- Ge:Si, impurity modes and IR absorption 78—76506
- Ge:Sn, ion implantation of radioactive ^{119}Sn 80—59495
- Ge:Te, ion-implanted, thermally assisted Xe-flash annealing, Rutherford backscatt. meas. 79—10881
- Ge:Te$^+$, ion implanted, alignment of irrad. induced defects, TEM obs. 80—15168
- Ge:transition metal, amorphous, impurity effects on hopping conductivity 79—65485
- Ge:Zn photoresistor, current responsivity rel. to nonequilib. hole lifetime 80—60035
- Ge:Zn$^-$, G and D lines, stress induced components 80—71447
- Ge:Zn^{II} carrier lifetime, nonequilibrium, phase method for determ. 80—65629
- Ge/Al thin film couples, accel. ageing 80—44726
- Ge/GaAs (110) heterojunction, valence band discontinuity in XPS spectra, precise determ. 80—84834
- Ge-Al (1.15 wt.%), US wave vel. meas. for anal. of solid soln. breakup 78—23887
- Ge-CdSe heterojunctions, epitaxial, azimuthal rotation 78—84085
- Ge-electrolyte contact, current-voltage characts., effect of mechanical deform. 78—68082
- Ge-Fe, laser annealing of implanted ^{57}Co sources, Mossbauer obs. 80—39139
- Ge-Ga (1.13 wt.%), US wave vel. meas. for anal. of solid soln. breakup 78—23887
- Ge-$Ga_{1-x}Al_xAs$, MBE of ultra thin film superlattices on GaAs substrates, TEM study 79—37932
- Ge-GaAs, (100) interface, electronic struct. calc. 80—49861
- Ge-GaAs, heteroepitaxial systems, misfit dislocations obs. using HV electron microscopy 80—100242
- Ge-GaAs, heterojunction, electronic structure 79—73572
- Ge-GaAs, n-n isotype heterojunctions, fixed-interface-charge model 78—56215
- Ge-GaAs, p-n heterojunctions, surface electron states 79—73578
- Ge-GaAs (100) interface, electronic struct., scattering-theoretic approach 78—95340
- Ge-GaAs (110), heterojunction chemistry, photoemission expts. 78—95244
- Ge-GaAs (110) interface, relax., self-consistent pseudopotentials 78—30981
- Ge-GaAs (110) interface, self-consistent calc. of interface states and electronic struct. 78—52066
- Ge-GaAs (110) junction, interface states and electronic struct. 77—69408
- Ge-GaAs abrupt (110) interface, electronic struct. 78—95339
- Ge-GaAs abrupt interface, electronic struct., self-consistent wave mechanical calcs. 77—89837
- Ge-GaAs abrupt interface, orientation depend. of interface dipole energies, XPS expts. 78—39196
- Ge-GaAs heteroepitaxial system, dislocation struct. in stress measurements 80—29030
- Ge-GaAs heterojunction, band discontinuities, angle-resolved UPS obs. 79—7878
- Ge-GaAs heterojunction, electrostatic dipole shifts contrib. to valence band discontinuities 79—51657
- Ge-GaAs heterojunction, elec. and recomb. props., interface defect effects 80—80365
- Ge-GaAs heterojunction, interface geometry, model 80—49879
- Ge-GaAs heterojunctions, electronic struct. 78—19138
- Ge-GaAs inter faces, heteroepitaxial, misfit dislocations, TEM obs. 79—23610
- Ge-GaAs interface, electronic struct. of Ge overlayers on (100) GaAs 80—49880
- Ge-GaAs interface, photoemission 80—25530
- Ge-GaAs interface, surface and interface states of (111) surfaces 79—15206
- Ge-GaAs interface, XPS obs. of electronic struct. 78—95341
- Ge-GaAs p-n diode, microplasma breakdown 79—91140
- Ge-GaAs p-n heterojunction, current fluctuations 79—11209
- Ge-GaAs p-n junction, microparameters determ. 79—11216
- Ge-GaAs p-nn$^+$ junction I-V characts., inverse branch, effect of dislocation defects *(Russian)* 79—15217
- Ge-GaAs structure, electronic struct., ang.-resolved photoemission obs. 80—49881
- Ge-GaAs superlattice and interface, electronic struct. 78—52065
- Ge-Ge (Sn) friction pairs, elec. cond. of Ge tribolayers at He temp. 79—87140
- Ge-GeO_2, optical charging memory, influence of doping GeO_2 with metal ions *(Russian)* 79—24077
- Ge-GeO_2 system, optical charge memory obs. 77—89871
- p-Ge-In injecting contact, sign of developed hot-carrier thermo-EMF 77—55606
- Ge-In Schottky barrier interface, covalent bonding of metal atoms 77—20429

elemental semiconductors continued

- Ge-InAs based MIS struct., avalanche carrier multiplication 80—88566
- Ge-$LiNbO_3$, layer struct., acoustoelectronic phenomena 77—55556
- Ge-MBBA interface, electrorefl., IR transmission and frustrated total internal refl. 78—19513
- Ge-metal contacts, surface electron state spectrum surface treatment effects *(Russian)* 80—34497
- Ge-metal oxide, elec. props., molecular deposition method 80—34525
- n-Ge-metal Schottky barrier contacts, IR optoelectronic props., quantum detector appls. 80—75640
- Ge-Mo amorphous semicond.-granular metal film system, elec. transport and thermopower 77—76984
- n-Ge-n-GaAs isotype heterojunctions, modelling, characts. 80—103747
- Ge-Na interfaces, interdiffusion, electron states, EELS study 80—50484
- p-Ge-nn$^+$-Si, heterojunction, γ-radiation effect on forward I-V characteristics *(Russian)* 78—72255
- Ge-$Pb_{1-x}Sn_xTe$, amorphous/crystalline heterojunction, rectification props., IR detector appl. *(Japanese)* 78—60197
- Ge-pyrolytic SiO_2 system, carrier trapping, GeO_2 sublayer effect 78—91775
- Ge-Sb, D^- complexes and band form., photocond. 78—84251
- Ge-Sb, far IR emission stimulation by impact ionisation 80—66301
- Ge-Sb, meas. of electron-hole drop size by light scatt. 80—44515
- Ge-Si, solid phase heteroepitaxy 80—6670
- a-Ge-Si crystal interface, low resist. elec. behaviour 77—89843
- Ge-Si junction, Si monocryst. and Ge film, elec. props. 79—51660
- Ge-Si n-n heterojunctions, photovoltaic response 78—14804
- Ge-Si sandwich struct., sputter profiling, combined Auger-X-ray anal. 80—66909
- Ge-Si_3N_4 system, potential barriers determ. from photoinjection carriers trapping 80—103756
- Ge-SiO_2-Al, vacuum heating effect on stability 78—64143
- Ge-SiO_2-p$^+$Si tunnel junctions, for determ. of AC cond. of amorphous Ge 77—24608
- Ge-Si(GaAs) heterodiodes, interfacial structural defects effect on avalanche breakdown 79—42644
- Ge-Sn solid solution, cooling rate effect on partition coeff. of Sn between liq. phase and crysts. 77—12510
- Ge-transition metal interfaces, planar, first phase to nucleate 77—62764
- Ge-type semiconductors, two-photon parametric excitation of phonons 80—29339
- Ge-YIG layer structure, amplification of bulk magnetostatic waves 78—34972
- Ge-YIG structure, profile and position of reson. galvanomag. effect curve 78—72242
- Ge-ZnS p-n heterojunction, epitaxial, elec. props. *(Russian)* 78—88023
- Ge-ZnSe, (100) interface, electronic struct. calc., scattering theoretic approach 80—6940
- Ge-ZnSe, (100) interface, electronic struct. calc. 80—49861
- Ge-ZnSe abrupt (110) interface, electronic struct. 78—95339
- Ge-ZnSe heterojunction, change in interfacial microstruct. on high temp. annealing 77—28242
- Ge-ZnSe heterojunction, elec. and photoelec. props. *(Russian)* 77—32070
- Ge-ZnSe interface, electronic struct., self-consistent pseudopot. calc. 78—91747
- Ge-ZnSe p-n heterojunctions, effect of interfacial condition on optoelectronic props. 79—24061
- n-Ge-ZnSe:Mn^{2+}-$In_{2-x}Sn_xO_{3-y}$ thin film electrolum. cell with low-threshold voltage 80—84786
- Ge+Br_2, surface reaction, rate-limiting step, ellipsometric and photochem. meas. 80—16730
- $Ge_{1-x}H_x$, amorphous, atomic struct., X-ray study 80—49106
- Ge(Li) commercial coaxial large-volume detectors, time characts. 78—9029
- Ge(Li) detector, fast neutron damage 80—59525
- Ge(100) surface, Ar ion bombarded, determ. of atomic steps, LEED 78—63913
- Ge(100) surface electronic state localisation, layer density of states calcs. 80—6931
- Ge(111), chemisorption of Cl, threefold co-ordinated site chemisorption, cluster model calc., extended Huckel theory 78—39178
- Ge(111), dangling-bond surface states 78—43452
- Ge(111), high resolution photoemission yield, surface states 77—69392
- Ge(111) surface, diffuse scatt. at high temp., RHEED study 80—80043
- Ge(111), surface electronic struct., atomic geometry effects, photoemission and electron energy loss spectra 77—85283
- Ge(111)2×1, oxide layer, surface states detect optical reflectivity obs. 80—50368
- Ge(111)2×1, surface electron states detected by external reflectivity 78—80036
- In-Ge:As, Schottky barrier tunnel junction, zero bias resistance, temp. depend. 78—72258
- In_2O_3-SnO_2/Si solar cells, antireflection props. of oxide film 80—3513
- $(In_{1-x}Sn_x)_2\ O_{3-y}$-Si solar cells, degradation 80—94047
- $(In_{1-x}Sn_x)_2O_2$-Si-N solar cell efficiency and elec. props. 80—35676
- $In_{2-x}Sn_xO_{3-y}$-insulator-poly-Si solar cells, photovoltaic conversion parameters 80—101093
- K X-ray prod. for Br ions 79—47547
- $LiNbO_3$-Si, acoustoelectronic memory, effect of band-bending 80—70771
- MIS solar cells, comparison of majority- and minority carrier 80—85280
- Mo-n-Si Schottky barrier, sputtered, freq. cond. charact. 77—20426
- n$^+$-n-pGe avalanche photodiode, noise factors, internal quantum efficiency 80—70803
- n-Si, (111) inversion layers, valley splitting, Shubnikov de Haas oscills. 80—65698
- n-Si, Fe_xO_y-coated, heterostruct. photoanode for photoelectrolysis of water 80—61384
- n-Si, ion implantation causing surface defects, electroreflectance 79—19274
- NaX-Se semiconductor superlattice absorpt. edge, light scatt. *(Russian)* 80—71438
- P, amorphous, red, far IR absorpt. spectra 80—34923
- P, amorphous, red, photolum. props. and band gap 80—50403
- P, amorphous, vibrational excitations of defect sites 80—49332
- P, amorphous red, Raman scattering 80—11416
- P, black phosphorous struct., Raman vibr. spectra and bonding 80—11411
- PbS-Ge heterojunction, influence of conduction band discontinuity on lux-ampere characts. 78—39200

elemental semiconductors continued
- PbS-Si heterojunction, space charge capacitance, PbSn film thickness depend. 80—88630
- PbS-Si heterojunction, PbS film growth and struct. 80—96762
- PbS-Si heterojunction detector, direct injection readout 80—4765
- Pd-Si structure, epitaxial silicide growth, LEED and AES study 80—103590
- Pt-Si:As, silicide form. during laser irrad., p-n junctions and ohmic contacts 80—84397
- S, liq., eqn. of state determ., crit. props. and mol. comp. 80—49336
- S:P, ion implanted, defect annealing 450-800°C, deep-level transient spectroscopy 79—47042
- S:Si, implanted, defect signature by thermally stimulated meas. 78—91643
- SE, Compton profile, charge density and momentum density determ. 77—63480
- Sb, amorphous, vibrational excitations of defect sites 80—49332
- Se, amorhpus and liquid state, Raman spectra, crystn. processes 80—60608
- Se, amorphous, AC cond. magnitude and variation *(French)* 79—47095
- Se, amorphous, acousto-optic props., 10.6 μm 77—43966
- Se, amorphous, bulk, DC cond. expts., cond. mechanism 78—43401
- Se, amorphous, bulk, Raman scatt. near Tg 80—60596
- Se, amorphous, bulk, reson. Raman scatt. 80—60597
- Se, amorphous, carrier lifetime and drift mobilities 78—87985
- Se, amorphous, conducting channel temp., time depend., under monostable switching conditions 78—19109
- Se, amorphous, correl. between mol. struct. and props. 77—11484
- Se, amorphous, defect states, SCF pseudopot. and tight-binding calc. 79—65415
- Se, amorphous, density of surface states 77—76897
- Se, amorphous, diffusion and electrodiffusion of Ag and its role in switching effect 78—19163
- Se, amorphous, dipolar activity at glass transition temp., AC method 77—66454
- Se, amorphous, effect of doping on mol. struct. and valence alternation states 80—49249
- Se, amorphous, elec. cond., activation energy, density, cryst. Se effect 80—65548
- Se, amorphous, elec. field effect on crystn. 77—15318
- Se, amorphous, electrical transport, activation energy 79—95406
- Se, amorphous, electronic props. rel. to xerography, defects 79—97454
- Se, amorphous, electronic struct. and optical props., pseudopot. calc. 80—65428
- Se, amorphous, hole diffusion obs. 77—76828
- Se, amorphous, influence of O_2 on phase separation 77—47354
- Se, amorphous, interface with poly-N-vinyl carbazole, photoinsulator-air gas-dielectric system, charges on surfaces 79—67407
- Se, amorphous, localised gap states, variable range hopping 77—72866
- Se, amorphous, luminescence 80—80862
- Se, amorphous, memory and threshold switching effects 78—14774
- Se, amorphous, monostable switching, current noise 80—44682
- Se, amorphous, O impurity addition rel. to elec. cond. 79—38067
- Se, amorphous, photoconductivity quantum yield, experimental validation of fund. theory 80—6909
- Se, amorphous, photoinjection of holes into triphenylamine doped bisphenol-A-polycarbonate polymer 78—72191
- Se, amorphous, press. depend. of AC cond. 77—76858
- Se, amorphous, relax of sound velocity, struct. determ. 78—38786
- Se, amorphous, sound propag. at low temps. 77—72657
- Se, amorphous, struct., DSC and X-ray diffr. expts. 78—22662
- Se, amorphous, struct. and elec. cond. transitions under high press. 79—42237
- Se, amorphous, struct. relax. effects, obs. by mech. props. *(French)* 79—51201
- Se, amorphous, TSC, dielec. relax. modes 77—90090
- Se, amorphous, theoretical calc. of defect states 80—49657
- Se, amorphous, theory of anomalous dispersion of photocurrent transients 78—6412
- Se, amorphous, thermal quenching of photocond. 78—23137
- Se, amorphous, transient electrical transport, general and unified treatment 80—59977
- Se, amorphous, trap-limited model for dispersive transport of holes 78—6378
- Se, amorphous, trigonal and monoclinic, 2p photoabsorpt. spectra 78—23551
- Se, amorphous, trigonal and α-monoclinic, positron annihilation 79—11484
- Se, amorphous, US attenuation at low temp., internal friction peak 80—65152
- Se, amorphous, US relaxation and retardation of deform. near T_g point 80—84256
- Se, amorphous, vac. deposition on polymer substrates, use of temp. gradient vac. coating device 80—35099
- Se, amorphous and cryst., X-ray K-shell absorpt. discontinuity 79—61467
- Se, amorphous and liq. states, Raman scatt. meas. 80—50328
- Se, amorphous and liq. state, mol. structure, local atomic arrangement at intrinsic bonding defects 80—59374
- Se, amorphous electrophotographic layers, resolution parameters 80—31926
- Se, amorphous evaporated layers, struct. inhomogeneities due to prep. technology fluctuations 77—76710
- Se, amorphous film, AC conductivity at radio and microwave frequencies 79—11248
- Se, amorphous film, between metal electrodes, switching mechanism 78—39172
- Se, amorphous film, crystn., thermal and photo-effects 77—47692
- Se, amorphous film, dark and photoconductivities 79—87173
- Se, amorphous film, dielec. activity obs. near glass transition temp. 80—75933
- Se, amorphous film, highly disordered, UPS study 80—76148
- Se, amorphous film, influence of wavelength on optical quenching of photoconductivity 80—60046
- Se amorphous film, interference enhanced Raman scatt. 80—50326
- Se, amorphous film, photocond., dark cond., rel. to crystn. 80—88596
- Se, amorphous film, photodeposition by Selor process, kinetics 78—75963
- Se, amorphous film, photodeposition by Selor process, struct. and kinetics 78—75964
- Se amorphous film, spherulite formation and role of stresses due to volume changes in crystallisation 77—1083

elemental semiconductors continued
- Se amorphous film, stabilisation by thermal treatment *(French)* 79—47176
- Se amorphous film, threshold and memory switching 79—82651
- Se, amorphous film, vac. evaporated, density meas., microcrystalline model of struct. 80—2313
- Se, amorphous film-metal system, contact pots. distrib. and photo-EMF, work function 77—76925
- Se, amorphous films, characts. determ., majority carrier eqn., exponential trap distribution 78—14760
- Se, amorphous films, evaporated, ageing and crystn., DTA 80—65413
- Se amorphous films, structural relax., viscosity, creep, heat capacitors, and IR spectra meas. 79—42424
- Se, amorphous layer, localised states in band gap 80—59928
- Se amorphous layer structure, influence of vacuum deposition conditions *(German)* 78—63957
- Se amorphous layers, dielectric relax. in glass transition range, ageing 79—82923
- Se amorphous layers, substrate range depend. on dielec. relax. in glass transition temp. 79—69773
- Se, amorphous thin film, elec. noise, monostable switching 80—44684
- Se, amouphous film, photodeposition by Selor process struct. 78—75962
- Se, and related materials, historical study, 1833-1919 78—57727
- Se and Te, homology of phonons, scaling formalism for phonon freqs. 80—54326
- Se, appl. to xerography 80—57415
- Se, bonding coordination defects 80—59927
- Se, charge density, self-constent OPW and pseudopot. calcs. 80—92813
- Se, Compton profile, charge and momentum density 80—55220
- Se, crystallisation kinetics correlation with molecular structure 78—94998
- Se, cubic modification prepared by shock compression 78—34494
- Se, dielectric function in trigonal phase, model calc., local-field corrections 78—39045
- Se diode surface states determ. by conductance and capacitance 77—85318
- Se, effective charge tensor, microscopic treatment 78—59879
- Se, elastic and piezoelec. consts., US phase vel. meas. 79—86834
- Se, elec. cond., 0-500 kbar 79—99589
- Se, electrical conductivity after X-ray irradiation 79—51567
- Se, electroconductivity, X-ray effects *(Russian)* 80—15519
- Se, electronic struct. of cryst. phases and hydrostatic press. effects 80—59865
- Se electrophotographic films, surface potential microprofile meas. 77—45913
- Se electrophotographic films, ageing effects on structure and properties 77—47699
- Se electrophotographic film current density/voltage characteristic rel. to substrate temp. *(German)* 77—55629
- Se, electroradiographic layer, radiographic contrast 80—12241
- Se, epitaxial monocrystalline film, trapping, TSC meas. 77—85349
- Se, evaporation kinetics from temp. programmed large area source 77—69996
- Se, exciton luminesc. in trigonal form 79—33802
- Se film, amorphous, block formation during crystn., electron microscope obs. 79—11030
- Se film, amorphous, crystallisation induced by corotron charging 77—35832
- Se film, amorphous, density of localised states 78—34742
- Se film, amorphous, photocond. props. *(French)* 77—72886
- Se film, amorphous, struct. and crystn., far IR transmission spectrum and DSC obs. 77—85106
- Se film, amorphous, thermo-crystn. obs. 77—11810
- Se film, crystallisation using org. catalysts, struct. and elec. props. 77—51613
- Se film, epitaxially grown on Te substrates, crystallinity, RHEED and SEM meas. 77—40373
- Se film, gas-evaporated, selective absorpt. characts. and emissivity 80—50998
- Se film, metal ion diffusion during memory switching 78—26976
- Se film, noncryst., ageing and crystn. obs., tentative struct. model 80—2295
- Se film, noncryst., controlled vapour deposition, crystn., and optical props. 78—39696
- p-Se film, photocond., phase-memory effect 78—91723
- Se film, resonance Raman spectrum 79—28760
- Se, film, switching characts. under pulsed bias 77—39979
- Se film, trigonal, sputtered and evaporated nucleation and growth processes 77—31920
- Se films, Ag diffusion, effect on interferometric thickness meas. 80—96695
- Se, Fourier-transformed Compton profile as microstruct. probe 77—59636
- Se, glass transition temp., enthalpy rel. to annealing, DSC 77—15561
- Se, glassy, localised electronic states, photoluminesc. and ESR studies 80—65501
- Se, glassy, pure and K-doped, photolum. and optically induced ESR 80—50398
- Se, hexagonal, resistivity depend. on applied elec. field freq. during crystn. 77—35938
- a-Se, hole form. energy, heating time and cooling rate depend. 79—41958
- Se layer crystallinity meas., combination microwave resonator method *(Russian)* 78—22652
- Se layers, amorphous, steady-state photocond. meas. 77—35961
- Se layers, amorphous and partially crystallised, trap spectrum, TSC and I-V characts. 77—76981
- Se, liq., electronic transport props. at sub- and supercritical conditions 77—51788
- Se, liq., electronic transport props., equation of state, to 1900K and 1800 bars 80—65574
- Se, liq., eqn. of state determ., crit. props. and mol. comp. 80—49336
- Se, liq., estimate of self-diffusion coeffs. from viscosity data 77—55370
- Se, liq., pure and I doped, DC cond., temp. depend. *(French)* 77—69322
- Se, liq., pure and I doped, thermopower, temp. depend. *(French)* 77—69360
- Se, liq., review of continuous metal-nonmetal transitions 77—51787
- Se, liq., US rel. temp. depend., melting effects 78—38782
- Se, liq. and amorphous, struct. by pulsed neutron diffr. using an electron LINAC 77—51307
- Se, liquid, correlation between switching and struct. 77—69388

elemental semiconductors continued
Se, liquid, electrical cond. transition to high temp. and press., Anderson localisation *(Russian)* 77—1462
Se liquid, pure and I doped, DC cond. and thermoelectric power *(French)* 79—56223
Se, liquid-crystal phase transition, elec. cond. changes 79—33310
Se, liquid-glass transition, P-V-T relations 77—24387
Se, metallic state, press. induced, elec. cond. meas. 80—96949
Se, modulated photocurrent, analysed for trap-limited case *(Japanese)* 80—60030
Se, monoclinic to trigonal transform., DTA, X-ray diffr. and optical microscopy meas. 78—14461
α-Se, multiple-trapping model of anomalous transit time dispersion, transient photocurrent data 78—34860
Se, nanosecond switching investigation 80—20263
p-Se, photocond. film, phase memory effect and deep levels 79—82556
Se, photoconductive film, field instability, Ar^+ ion irrad.-induced defects 78—87997
Se photoconductive layers, impedance-freq. characts. meas. *(Japanese)* 79—38120
Se, photoelectronic behaviour, in glass transition region 80—60045
Se photoreceptors, phthalocyanine sensitized, elec. cond., charge decay characts. 80—15630
Se physics, conf., Konigstein, Germany (May 1979) 80—51958
Se, polycryst., low-frequency coupled photocurrent and temp. oscillation 80—60044
Se, polycrystalline trigonal layer, freq. depend. elec. behaviour and its relationship to xerographic performance of Se particle contact photoreceptors 79—82640
Se, positron lifetime meas., comparison with theory 77—63483
Se powder compacts, sintered, electrical cond. 80—70693
Se, radiation damage expts. review, defect interaction 77—84800
Se, red amorphous film, textural change, thermal and photo effects 78—63951
Se, rhombohedral, IR absorpt. spectrum 80—103949
Se, SAW vel. and electromech. coupling factor 80—75422
Se, Se:Te, amorphous, negative magnetoresist., doping depend. 78—56161
Se single crystal, behaviour in strong electric field 77—62942
Se, single crystals, fast neutron irradiated, annealing expts., dark conductance, reflectivity spectra 77—85266
Se, thin film selective absorber coatings, prod. using an oblique vacuum deposition technique 80—81488
Se, trigonal semicond., electronic states, tight-binding model Hamiltonian 77—59250
Se, trigonal, acoustoelectric current saturation 80—60053
Se, trigonal, behaviour of optical gap under press. 80—80171
Se, trigonal, cryst. growth from CS_2 soln. 78—23596
Se, trigonal, dielec. matrix calcs. 80—54630
Se, trigonal, electronic props. under press. 77—31939
Se, trigonal, electronic struct., near metal transition, press. depend. 78—34758
Se, trigonal, force field calc. of phonon dispersion relations 80—54328
Se, trigonal, indirect exciton ground states, photoluminescence 79—24361
Se, trigonal, inverse dielec. tensor in static limit local field corrections 77—51690
Se, trigonal, low temp. sp. ht. and elastic consts., piezoelec. effect influence on phonons 80—54404
Se, trigonal, luminesc. identification of indirect transition 80—55189
Se, trigonal, model of lattice dynamics using long and short range interactions 78—59893
Se, trigonal, NMR chem. shift, tight-binding calc. 78—2759
Se, trigonal, normal mode calcs. 80—84259
Se, trigonal, Raman scatt. at very high press. 80—60566
Se, trigonal, state-of-the-art review of model calcs. 80—54327
Se, trigonal, surface lattice dynamics, mean square displacement spectra in long wavelength limit 80—54498
Se, trigonal, transverse magnetoresistance meas., influence of illumination 80—65607
Se, trigonal, vitreous and red amorphous, phonon density of states comparison 80—54329
Se, trigonal and amorphous, Compton profiles 77—32464
Se, trigonal and amorphous, electronic struct. and nonempirical calc. of struct. props. 80—59866
Se, trigonal and amorphous, positron lifetimes, positronium form. 80—60711
Se, trigonal and vitreous, sp. ht. and thermal cond., 3 to 300K 80—59676
Se, trigonal or amorphous, thermal expansion and Gruneisen coeffs., 10-300K 78—22870
Se, trigonal reflectivity and density of states press. depend., self-consistent pseudopotential calc. 77—31931
Se, trigonal single crystal, dark current relax., barrier cond. mech. 80—6904
Se, trigonal single crystal, peak in temp. dependence of elec. cond. 80—44663
Se, undeformed rhombohedral, dislocations, electron microscope obs. *(French)* 78—51548
Se, vitreous, crystn., optical microscope obs. 77—84659
Se, vitreous, darkened films, thermal and optical bleaching, light transmission obs. 80—50447
Se, vitreous, mech. props. at temps. <300K, uniaxial compression tests *(French)* 78—55908
Se, wedge shaped film, photovoltaic effect 77—1454
Se:As, amorphous, pure and doped, photoelectronic preps. in glass transition region 79—4583
Se:As, amorphous film, dielec. activity obs. near glass transition temp. 80—75933
Se:As X-ray plates, electronic transport *(German)* 80—80290
Se:As(Cl), trigonal, defect and impurity electron levels, surface photovoltage spectra 78—72108
Se:Cd dilute liquid, perturbed ang.-correl. meas. of motional-correl. time 79—41930
Se:Ge(Si)(Sn), vitreous, crystn. kinetics study by elec. cond. meas. 79—65526
Se:Hg amorphous film, photocond. anomaly due to HgSe layer form. 77—66183
Se:Hg film, amorphous, anomalous photocond. and residual interelectrode photo-EMF 77—69376
Se:I, vitreous, crystn. kinetics determ. *(German)* 80—79936
Se:O, amorphous, photocond. spectrum impurity effect 77—76862

elemental semiconductors continued
Se:O(Cl)(K) amorphous, elec. cond. increase on impurity addition 77—11920
Se:P, vitreous, crystn. kinetics study by elec. cond. meas. 79—64998
Se:P, vitreous, stabilisation of cond. 77—11910
Se:Ta, electrophysical meas. rel. to control of conductivity type 77—24323
Se:Te, amorphous, conductivity and activation energy depend. on dopant conc. 77—69325
Se:Te, amorphous, pure and doped, freq. depend. of elec. cond., 150 to 310K 79—42545
Se:Te(Ag), amorphous film, elec. cond., 300 to 350K, transition 77—4454
Se:Tl, hole drift mobility meas. by light pulse technique 78—19086
Se:U, cryst. and amorphous, impurity conc. and distrib., solid state nuclear track detection 79—46694
Se-Ni-Mylar multilayered struct., interfacial bonding effect on adhesion, ESCA obs. 79—95274
Se-polystyrene hexylmethacrylate, interface photocurrent studies, charge transfer mechanism 79—99627
Se_8, monoclinic, XPS and valence band struct., comparison with trigonal form and S_8 77—44124
shallow impurity bound states, IR spectroscopic obs. 77—39806
p-Si, $^{49}BF_2$ ionised mols. obtained by implantation of 78—31003
Si, ^{57}Co implantation, Mossbauer spectra, dose depend. 79—82899
Si, ^{75}As implantation, scanned CW electron beam annealing 79—99225
Si, ^{75}As implanted, comparison of effects of pulsed ruby laser and pulsed electron beam annealing 79—69135
Si, 1-10 keV H^+, He^+ irrad., role of Auger processes in electron emission 79—15579
Si, 100 keV Sb ion irradiated, disorder accumulation, saturation and sputter limitation 78—67753
Si, 2p hole core level spectra, electronic polarisation effects 80—6765
Si, 3-15 keV Ar^+ induced Auger electron emission from Si and Ar 77—59654
n-Si, 300 keV proton irrad., temp. depend. of defect prod. 78—6113
Si, 5 MeV α-particle irrad., X-ray exam. of surface layer struct. changes 78—6114
Si, 6 MeV electron bombard., radiation damage rate distrib. with depth 77—31694
Si, 60° dislocation, X-ray diffraction contrast, section topography 78—83819
n-Si, 77K hot electron repopulation and anisotropy *(Japanese)* 79—82600
Si, (001), clean, double diffr. spots in RHEED patterns 79—90855
Si, (001) (2×1) reconstructed surface, dimer model self consistent calcs. 80—88613
Si, (001) and (111), geometrical and electronic struct., review 80—80039
n-Si (001) on sapphire, galvanomag. effect for holes, valence band 79—91166
Si (001) substrate for Pd_2Si epitaxial islands 80—96748
Si (001) surface, energy gaps in inversion layer band struct., spectroscopic determ. 79—82658
Si (001) surface struct., high energy ion scatt. study 80—59772
Si (001) wafer, pyramidal hillocks, TEM obs. during chemical etching 80—70508
Si (001)-SiO_2, n-inversion layer, valley splitting without effect mass approx. 80—15586
Si, (001)-(2×1) surface, reconstruction-induced mean-square displacements 80—15343
Si (1,1,0) direction, channelled particle radiation spectra, emitted quanta angular distrib. 80—96578
Si (100), (111) substrates for rare earth metal silicide thin film formation, backscattering study 80—70542
Si (100), atomic and electronic structs., energy minimisation calcr. 80—49480
Si (100), chemisorption of H, new type of chemisorptive bond, theory 78—26930
Si (100), chemisorption of H, pairing model calcs., compared with expt. 78—34719
Si (100), dimer reconstruction, photoemission obs. 80—80939
Si (100), H adsorption, MeV ion scatt. study 80—80071
Si (100), intensity-energy spectra 77—47653
Si (100), intrinsic surface states, photoemission study 80—50514
n-Si (100), O_2 partial press. depend. of fixed surface state charge due to thermal oxidation 79—70179
Si (100), oxidation induced stacking fault retrogrowth, O_2 press. depend. 78—64747
n-Si (100), oxidation-induced stacking faults, O_2 partial press. depend. 78—39922
Si, (100), reconstruction induced subsurface strain, appl. of theory 78—63914
Si (100), reflection of high freq. phonons 79—65304
Si (100), self-ion implanted, laser annealing, channelling and TEM meas. 80—24466
Si (100), struct., LEED study, atomic arrangement model 78—71922
Si (100), surface space charge layer, inter-subband optical transitions 77—15931
Si (100), transition density of states from $L_1L_{2\,3}V$ and $L_{2\,3}VV$ Auger spectra 77—40314
Si (100), vicinal, LEED obs. of stepped surface 80—59773
Si (100) (2×1) clean surface, struct. using averaged LEED 77—59194
Si, (100) and (110), anisotropic etching for fabrication of 3-D microstructures 79—15826
Si, (100) and (110), anisotropic etching 79—15827
Si (100) inversion layer, hot electron drift velocity, Monte Carlo calcs. inc. 3 subbands 78—91752
Si, (100) inversion layer, electromigration in two dimensional electron gas, driving force 80—84441
n-Si (100) inversion layer mobility depend. on intersubband scatt. at low temps. 79—95506
Si (100) inversion layers, effective masses, Shubnikov-de Haas oscills. under mechanical stress 77—43625
p-Si (100) inversion layers, intersubband spectroscopy by photocond. and absorpt. 78—10566
Si (100) MOST, comparison of Shubnikov-de Haas effect and cyclotron reson. under uniaxial stress 80—20320
Si (100) reconstructed surface struct. study using thermal energy He diffr. 80—60731
Si (100) surface, cyclotron reson. of electrons in surface space charge layers 77—8169

elemental semiconductors continued
Si (100) surface, diffr. of He atoms obs. 78−52609
Si, (100) surface, effective mass and collision time 78−64081
Si (100) surface, electronic struct., scattering-theory formulation 79−42607
Si (100) surface, intersubband optical absorption in space-charge layers 77−35984
Si (100) surface, LEED meas. 78−60016
Si (100) surface, models of (2×1) surface struct., quasidynamical calc. of LEED intensities 78−71921
Si (100) surface, pairing model, electronic pot., charge density, Fermi energy and surface density of states 77−47875
Si (100) surface, reconstructed, atomic and electronic struct. 79−73381
Si (100) surface, slow electron elastic scatt. threshold effects 79−100002
Si (100) surface, surface cyclotron resonance, freq. depend. 77−8170
Si (100) surface accumulation layer, subband struct. and inter-subband absorption in strong mag. field 78−39177
Si, (100) surface space-charge layer, intersubband cyclotron combined resonances 79−69571
Si (100) with Cs and $Cs+O_2$ overlayers, negative electron affinity surface, thermal stability of work fn. 78−92167
Si (100)-Pd_2Si-Si system, Si epitaxy obs. by ^{31}Si tracer and Rutherford backscatt. methods 79−4431
Si (100)-SiO_2 inversion layers, exchange and correl. contribs. to subband energies 79−42654
p-Si, (100)-oriented, n-channel inversion layers, MOS field-effect devices, mag. quantisation effect on surface capacitance 80−70834
Si (110), (111) surfaces, inter-subband spectroscopy in hole space charge layers 77−32064
Si (110), chemisorption of Cl, LCAO calcs., Auger line shapes, localized density of states 78−56202
Si, (110) oriented, electron optical conditions for struct. image form. 80−75131
Si, (110) plane, quantum state observation during fast electron channelling *(Russian)* 80−59541
Si (110) surface, chemisorption of H, UPS spectra meas. 77−20186
Si (110) surface peak anal. by 100-350 keV protons 80−55247
Si (111), 2×1 reconstructed, self-consistent anal. 78−91518
Si, (111), 7×7 and 1×1, chemisorption of Cl_2, UPS obs. 78−34704
Si (111), (100) and (110) ideal surfaces, valence-band Auger lineshape theory 77−48286
Si (111), adsorpt. of Cs, LEED, work function and thermal desorpt. 78−14590
Si (111), adsorpt. of O and stimulated oxidation by electron bombardment, AES 78−14599
Si (111), adsorption of Cl, electronic energy states, cluster-type calcs. 79−47149
Si (111), adsorption of $H_2S(H_20)(0_2)$, electron energy loss spectra exam. 77−39736
Si (111), CO adsorption on cleaved surface, electron energy loss spectra 78−79885
Si (111), chemisorbed Cl layer, SCF LCAO band struct. calcs. 78−88010
Si (111), chemisorbed O_2 electronic struct. tight-binding calc., XPS and UPS meas. 80−49845
Si (111), chemisorbed O_2 bonding geometry, electron yield EXAFS meas. 80−50461
Si (111), chemisorpt. of Cl, electronic states tight-binding method appl. 80−49564
Si (111), chemisorption of $H_2(Cl)$, conduction-band surface resonance 78−52051
Si (111), chemisorption of H, localised model, ab initio HF-LCAO calc. 80−6930
Si (111), Cl_2 chemisorption, ang. resolved UPS and LEED meas. using Vidicon intensity processor 78−71972
Si (111), cleaved, geometrical struct., LEED expts. 78−91517
Si (111), desorpt. kinetics of two-dimens. phases on single cryst. substrate, Au ad Ag 78−14598
Si (111), dynamic effective charge and surface reconstruction, soft-mode theory 79−4460
Si (111), growth and etching vectors, adsorption and step reconstruction 79−23548
Si (111), impurity stabilised by Te deposition, atomic arrangement, LEED exam. 77−11770
Si (111), intermediate oxidation state, core photoelectron absorpt. vs. chemical shifts 80−81220
Si (111), ion bombard., struct. changes, AES obs. 80−79842
Si (111), low-pressure-baked, EPR study 79−82860
Si (111), nitridation, AES and LEED results 80−80041
Si, (111), struct. depend. oxidation, high resolution photoemission yield spectroscopy 77−1305
Si (111), surface reaction with acetylene and NH_3, 1225 to 1380°C 79−100441
Si (111), surface relax., mol. SCF calcs. 78−91522
Si (111), surface relax., EHT and cluster calcs. *(Chinese)* 80−59762
Si (111), surface reproducibility and impurity segregation ion neutralisation spectra and UPS obs. 78−34688
Si (111), surface states and surface struct., angle-resolved PES 79−28390
Si (111), surface structure, high temp. RHEED obs. using metal-backed fluoresc. screen 80−75126
Si (111), UHV cleaved, adsorbed O, electronic transitions 78−39183
Si (111), with and without H chemisorption, Auger surface spectroscopy 80−50472
Si (111), with chemisorbed Al, electronic struct., self-consistent pseudopotential calc. 78−34880
Si (111), with chemisorbed Cl and F, electronic energy struct. calcs. 79−78144
Si (111) 1×1, surface, chemisorption of Cl in vacancies 79−77910
Si, (111) 2×1 surface, LEED theory and expt. 79−46895
Si (111) 7×7 clean surface and O chemisorbed stage valence band density of states from $L_{23}VV$ Auger spectra 80−100717
Si, (111) 7×7 surface, adsorption of Al, electron energy loss spectroscopy and LEED 77−43432
Si (111) 7×7 surface, giant core-exciton effects, electron energy loss spectra and XPS 77−24600
Si (111) 7×7 surface, of H_2O 80−10792
Si (111) 7×7 surface, Schottky barrier formation, photoemission, exam. of filled surface states and band bending 77−28250
Si (111) 7×7 surface, secondary electron emission from surface state resonances 79−69930

elemental semiconductors continued
Si (111) 7×7 surface, structure model from anal. of RHEED patterns 80−49471
Si (111) 7×7 surface electronic struct., angle-resolved UPS study 80−50513
Si (111) 7×7 surface states, low-energy electron loss spectroscopy 79−60891
Si (111) 7×7 surface structure investigation, RHEED 80−96723
Si (111) (7×7) surface structs., LEED anal. and energy minimisation calcs. 80−49478
Si (111) clean surface, internal pot., interplanar spacing, LEED 77−89627
Si, (111) cleavage, Kikuchi pattern, 40 keV incident electrons, electron energy loss spectra *(French)* 78−87594
Si (111) covalent surface, pot. and charge distribs. and dangling-bond state 78−2537
Si (111) face, cryst. film growth, transfer of impurity during condensation of mol. beams 78 -10299
Si (111) face, surface states and photoemission 77−72900
Si (111) inversion layers, CDWs, effect of four valley interaction terms 79−33324
n-Si (111) MOS charge layer, optical spectrum of inter-subband transition 78−64133
Si (111) substrate, MBE deposition kinetics of Bi film 80−10817
Si (111) surface, 1-3 keV He^+, Ne^+, Ar^+, Xe^+ bombard., AES obs. 79−33877
Si (111) surface, 500 eV Ar^+ bombard., high temp. annealing, recovery, RHEED obs. 78−87723
Si, (111) surface, Ag interaction, AES 78−14589
Si (111) surface, Al overlayers, theoretical study 78−95366
Si (111) surface, anal. by ion-electron spectroscopy 78−72670
Si, (111) surface, ang.-resolved photoemission, matrix element effects 79−69957
Si, (111) surface, annealing of scratches 79−60609
Si (111) surface, atomic and electronic struct. 78−72223
Si (111) surface, atomic and electronic struct. 80−54746
Si (111) surface, atomically clean, diffusion of adsorbed Au 78−72037
Si (111) surface, clean, ESCA obs., Ni(Au) surface impurities 78−52640
Si (111) surface, clean, new diffr. phenomena in RHEED 78−63910
Si (111) surface, clean and O_2-chemisorbed, electron states by AES 80−54747
Si, (111) surface, Cu phthalocyanine dye deposition, low energy electron optically modulated transmission increase 79−78133
Si, (111) surface, electron inversion layers, obs. of sixfold valley degeneracy 79−38176
Si, (111) surface, electronic density of states changes during O adsorption, AES obs. 79−65528
Si (111) surface, H chemisorbed, electronic struct. 78−39182
Si, (111) surface, LEED intensity measurement by photographic method with digital image processing 79−60234
Si, (111) surface, low energy H^+ and He^{++} ion refl., computer simulation 80−11524
Si, (111) surface, low press. baked, dominant interactions and average distances between paramag. centres 80−15783
Si (111) surface, non-orthogonal tight-binding approach to surface states 80−2442
Si (111) surface, O_2 adsorption, atomic steps and residual gas effects 80−54517
Si, (111) surface, oxide formation, AES and EELS meas. 80−3232
Si (111) surface, oxidised, energy depend. of photoelectron attenuation length 78−52643
Si, (111) surface, proton dechannelling under channelling, blocking and double alignment conditions 80−88235
Si (111) surface, relax. of surface atoms, Si_4H_9 clusters 77−8171
Si (111) surface, relax. of surface atoms, Si_4H_9 clusters 77−35980
Si (111) surface, surface energy bands and atomic position of chemisorbed Cl 78−56041
Si (111) surface, with Al overlayers, electronic states 80−11061
Si (111) surface reconstruction, milk-stool model, quantum chem. ab initio calc. 80−49477
Si (111) surface states, step depend., self-consistent pseudopot. calcs. 77−20384
Si (111) surface structs., induced by Ag evaporation, RHEED obs. 79−23814
Si (111) surface structure induced by Ag evaporation, RHEED meas. 78−22942
Si, (111) surface structure phase transform, screw dislocations RHEED study 80−88153
Si, (111) surface substrate for $NiSi_2$ epitaxial film, interfacial order, backscatter, channelling study 80−65390
Si (111) surface substrate for Al film, struct., props. depend. on vapour flow *(Russian)* 80−75453
Si (111) surface with Al overlayers, electronic struct., self-consistent pseudopotential method 79−4595
Si (111) surfaces, 2×1 to 7×7 struct. transition during annealing, LEED obs. 79−42352
Si (111) surfaces, cleaved, electronic structure following Al adsorption 80−75610
Si (111) surfaces, electron energy loss spectroscopy of NO, O_2 and NH_3 78−2374
Si (111) surfaces, geometric struct., LEED obs. 80−49479
Si (111) surfaces, relax. and reconstruction using Si_4H_9 clusters, MINDO/3 calc. 79−42356
Si (111)-Au interface, chemically driven intermixing, UPS study 80−50533
Si (111)-Pd interface, microscopic Pd_2Si form., UPS obs. 80−24743
Si (111)-SiO_2 interfaces, sixth-valley state stability a priori calc. 80−49859
Si (111)-1×1, electronic struct. of surface, model pseudopot. calc. 80−65651
Si (111)7×7, dangling-bond surface states and O_2 adsorption, reflectometric study 79−99600
Si (111)7×7 surface electronic struct., angle-resolved UPS study 80−40226
Si (111)$(\sqrt{31}\times\sqrt{31})R\pm 9°$-In struct., RHEED obs. 79−60612
Si (2p) optical transitions, final state effects, soft X-ray electroreflectance study 77−66553
Si, ⟨100⟩, defect etch for evaluation 79−90657
Si, ⟨111⟩ surface, 2×1 reconstruction mechanism 77−66079
Si, A-centre, photoionisation cross section 78−39063

elemental semiconductors continued
Si, A-centre formation by vacancy-O_2 recomb., acceptor impurity conc. effect 77—43243
n-Si, A-centre ionisation energy change due to uniaxial deform. 78—71733
Si, AES, convolution and deconvolution 78—52601
Si, AES examination of Ar^+ ion retention during Ar sputtering 78—56552
Si, AES quantitative anal. of impurities *(Japanese)* 78—91356
Si, ab initio effective pots. 77—69222
Si, ab initio self consistent calcs., charge density and band struct., Wannier function scheme 79—69409
Si, absorpt. spectrum red shift, spectrum temp. depend. 79—78699
Si, acceptor levels, ionis. energy and IR absorpt. 79—78033
Si, acceptor spectra, interpretation 78—43332
Si accumualtion layers, temp. depend. of inter-subband transitions, many-body effects 79—60899
Si, accumulation layer, intersubband-cyclotron combined resonance, theory 80—20278
Si, acoustic deform. pot., pseudopot. calc. 77—1363
Si, acoustic phonon geometric propag., anisotropic continuum acoustics 77—4170
Si, adiabatic bond charge model 77—69057
Si, adsorbed metal atoms effect on surface electron states 77—55597
Si, adsorbed Pd impurity, effect on surface electronic props. *(Russian)* 79—91124
Si, adsorpt. of O, chem. shift of Si 2p core level in SiO_x, relax. contrib. 79—47141
Si, adsorption of O_2, early stages, AES, LEED, and XPS obs. 79—46937
Si, adsorption of organic solvents *(Russian)* 78—91537
Si, adsorption-desorption kinetics of H_2, O_2 and other gases, catalysis 77—47684
Si, advanced material for space solar cell 80—94007
Si, Al-coated, surface phonon Brillouin spectra 79—78694
Si, ambient effect of O precipitation, self interstitial mechanisms, IR spectra, TEM study 80—66510
Si, amorphisation by $^{31}P^+$ ion irrad. 79—51172
Si, amorphisation by bombardment with O ions 78—10098
Si, amorphisation by ion implantation energy depend. 77—7769
Si, amorphisation by ion implantation, homogeneous or heterogeneous nucleation 77—11578
Si amorphisation dependence on low-energy irrad. conditions 79—60408
Si, amorphisation due to irradiation with heavy ions 77—11606
Si, amorphised by ion implantation, EPR obs. of mag. ordering 79—24186
Si, amorphised by ion implant., localised states and cond., irrad. and heat treatment, doping 80—39529
Si, amorphous, anomalous magnetoresist., hopping model 78—23117
Si, amorphous, anomalous magnetoresistance 80—6877
Si, amorphous, as photo-receptor for electrophotography 80—47126
Si, amorphous, asymmetrical profile of ion implanted P 79—46693
Si, amorphous, CVD, retarding crystn. by alloying with C,N,B or Ge 80—44129
Si, amorphous, chemical effects on freq. of Si-H vibrations 79—51227
Si, amorphous, clean and O_2 adsorbed, light sensitive electron laser meas. 79—24396
Si, amorphous, control of dihydride bond density using RF sputtering 80—34327
Si, amorphous, Coulomb gap and hopping cond. 80—44583
Si amorphous, crystallisation study 80—33890
Si, amorphous, defects, band gap states 80—80215
Si, amorphous, diamagnetism temp. depend. 78—47940
Si, amorphous, discharge produced, reversible cond. changes 77—85256
Si, amorphous, discharge produced, optical and photocond. props. 78—39147
Si, amorphous, dissolution with Al 78—95188
Si, amorphous, doped, density of states determ. from transport meas. 80—49720
Si, amorphous, doped, drift and Hall mobility, photocond. 79—65477
Si, amorphous, doped, electronic props. 78—19030
Si, amorphous, doped, electronic props. 80—80283
Si, amorphous, doped, optically induced ESR, correl. effects 77—40115
Si, amorphous, doped, photoconductivity and recomb. meas. 77—89800
Si, amorphous, doping, Schottky barrier and p-n junction form. by RF sputtering 77—8187
Si, amorphous, doping and absorption edge 80—29042
Si, amorphous, doping effects on cond. in hopping transport regime 79—28424
Si, amorphous, EPR and spin-dependent effects 80—80592
Si, amorphous, EPR expts. 78—88167
Si, amorphous, ESR and DC cond. 77—48032
Si, amorphous, ESR linewidth, exchange interaction effect 79—61216
Si, amorphous, effective mass theory, impurity states in band gap 79—77992
Si, amorphous, elastic moduli, random network model, calc. 78—6119
Si, amorphous, elec. and opt. props., review 78—23094
Si, amorphous, elec. props., ion implantation effects 80—79828
Si, amorphous, electrical transport and photocond. 77—85355
Si, amorphous, electron and hole drift mobility meas. 78—19027
Si, amorphous, electron-hole recombination, mech. 78—72196
Si, amorphous, electronic density of states, mol. liq. model 80—49581
Si, amorphous, electronic props. and localised states, review 77—62871
Si, amorphous, electronic struct. and optical dielec. function, LCAO calc. 79—42478
Si, amorphous, electronic struct., far infrared absorption 80—45051
Si, amorphous, epitaxial regrowth by pulsed laser beam 78—91554
Si, amorphous, epitaxial regrowth, structure and impurities effect 80—84401
Si, amorphous, first order transition to metallic liquid, calc. of transition temp. 79—69227
Si, amorphous, glow discharge deposited, photolum. decay 78—72590
Si, amorphous, glow discharge, fatigue effect in luminesc., recovery by annealing 80—50416
Si, amorphous, glow discharge deposited, mobility edge calc. 80—80220
Si, amorphous, glow discharge produced, defect creation, high optical excitation 80—97327
Si, amorphous, glow-discharge deposited, ODMR spectrum, deposition temp. and annealing effects 80—50229
Si, amorphous, hopping conduction, semiclassical theory 79—91052
Si, amorphous, hopping model for activated charge transport 79—87099
Si, amorphous, hydrogenated, photolum., heating effects 78—15204

elemental semiconductors continued
Si, amorphous, hydrogenated, spin depend. photoluminesc. 78—72589
Si, amorphous, hydrogenated, diffusion of D_2, SIMS anal. 78—75877
Si, amorphous, hydrogenated, work function and Auger spectroscopy of initial oxidation 78—76132
Si, amorphous, hydrogenated, pure and B doped, annealing effect on cond. and band gap states *(Korean)* 79—15142
Si, amorphous, hydrogenated, H configs., Cayley trees appl. 79—65373
Si, amorphous, hydrogenated film, struct. determ. using electron microscopy 80—10806
Si, amorphous, hydrogenated, small angle X-ray scatt., void distrib. 80—15087
Si, amorphous, hydrogenated, soft H plasma effect, IR absorpt. *(French)* 80—45054
Si, amorphous, hydrogenated, electronic struct., SCF $X\alpha$ calc. 80—49580
Si, amorphous, hydrogenated, electronic density of states determ. from Schottky diode meas. 80—49907
Si, amorphous, hydrogenated, stacked solar cells 80—55842
Si, amorphous, hydrogenated, electron drift mobility meas. 80—75565
Si, amorphous, hydrogenated film, electroreflectance study 80—88967
Si, amorphous, hydrogenated and deuterated, struct. 80—103245
Si, amorphous, hydrogenation and density of defect states, hopping cond. 79—60757
Si, amorphous, hydrogenation using DC and HF plasma treatment 80—59497
Si, amorphous, IR absorpt., first-order effective charges due to at. displacements 77—48164
Si, amorphous, ideal network struct., electronic struct., tight-binding model 80—44485
Si, amorphous, ideal surface, definition and characts. 80—107623
Si, amorphous, implanted, recrystn. induced by scanning CW laser, reaction rates, analytical model 80—66334
Si, amorphous, implanted, struct. transition under laser irrad. 79—50992
Si, amorphous, implanted ion trajectory and spatial distrib., Monte Carlo simulation 77—11611
Si, amorphous, in contact with electrolyte, Schottky barriers at interface 79—78169
Si, amorphous, interface with V, V silicide formation, backscattering, diffraction meas. 80—2285
Si amorphous, ion bombardment, controlled hydrogenation at low temps. 79—69119
Si amorphous, ion implantation, negative magnetoresist., localised mag. states 80—70731
Si, amorphous, ion implantation method, B and P ions 80—100274
Si, amorphous, ion implanted, laser annealing, reflectivity meas. 80—29039
Si, amorphous, ion irradiated, elec. cond. 79—11127
Si, amorphous, ion-implanted, hopping parameter at natural phonon freqs. 79—15152
Si, amorphous, large vacancy cluster annealing by ion bombard, EPR investig. 77—68965
Si, amorphous, laser crystallisation, for production of large grained sheets for solar cells 80—93570
Si, amorphous, laser-induced epitaxial regrowth, substrate and doping effects 79—56082
Si, amorphous, Lifshitz constant for calc. of van der Waals force between two solids *(French)* 80—107658
Si, amorphous, luminesc. of diode structures 77—8656
Si, amorphous, luminescence 80—80862
Si, amorphous, MIS diode I-V characts. 78—43485
Si, amorphous, mag. field depend. of luminesc. 79—43034
Si, amorphous, molecular liquid model and electronic struct. 80—54133
Si, amorphous, opaque, surface phonon attenuation, Brillouin scatt. 80—80808
Si, amorphous, optical absorpt. edge shape, band edge fluctuations 77—20880
Si, amorphous, optically detected ESR obs. 78—84500
Si, amorphous, p-n junction preparation, by SiH_4 decomposition *(Czech)* 77—63560
Si, amorphous, p-n junction devices, barrier profile effect on elec. props. 80—49890
Si, amorphous, phonon interaction in luminescence 78—43927
Si, amorphous, photo-induced changes in elec. props., defect states 79—82553
Si, amorphous, photoconductivity, mag. field depend. 78—80023
Si, amorphous, photogeneration of charge carriers and recomb. 77—81147
Si, amorphous, photoluminesc. spectra from 77K to room temp. 77—20916
Si, amorphous, photoluminesc. and radiative lifetimes 79—61419
Si, amorphous, photoluminescence, fast radiationless recombination 79—99939
Si, amorphous, photostructural changes, photodarkening 80—49121
Si, amorphous, photovoltaic characts., rel. to appl. in solar cells 78—84253
Si, amorphous, photovoltaic diodes, influence of mag. field on charge transport 80—49891
Si, amorphous, photovoltaic cell, plasma deposited, horizontally multilayered struct. 80—50964
Si, amorphous, position of Fermi level, spectroscopic and transport determ. 80—6706
Si, amorphous, possible ABB-type excitonic superconductor *(Chinese)* 80—7029
Si, amorphous, prep., glow discharge decomposition method *(Japanese)* 77—81226
Si, amorphous, prep. by RF sputtering, photoconductivity determ. 77—73231
Si, amorphous, prep. by reactive RF sputtering in Ar-silane mixtures, undoped, n-type and p-type targets 80—76182
Si, amorphous, production by glow-discharge method *(Japanese)* 77—90283
Si, amorphous, pure and H doped, picosecond relax. of optically induced absorption 80—97302
Si, amorphous, pure and hydrogenated, Raman spectra 79—61358
Si, amorphous, pure and hydrogenated, far IR absorption coeff. meas. 80—108213
Si, amorphous, radiative and non-radiative tunnelling, photoluminesc. decay meas. 79—83026
Si, amorphous, radiative recomb. obs. as efficient luminesc. 78—2914
Si, amorphous, Raman spectra, vibrational properties 79—99881

elemental semiconductors continued
- Si, amorphous, random-network model, charge-density variation 80—80165
- Si, amorphous, reduced intensity functions, thermal vibr. coupling 78—42910
- Si, amorphous, scatt. intensity and radial distrib. function, random stacking model 79—27919
- Si, amorphous, Schottky barrier and p-n junction props. 79—28407
- Si, amorphous, Schottky barrier solar cell, large-area RF sputtered, contact form, scaling and optimisation 80—45679
- Si, amorphous, semiconductor technology, solar cells *(Japanese)* 79—57430
- Si, amorphous, Si implanted, substrate-orientation depend. of epitaxial regrowth rate 78—79900
- Si, amorphous, small dia. laser beam annealed, temp. distrib. and microstructure 79—73098
- Si, amorphous, solar cell appl. *(Chinese)* 80—45671
- Si, amorphous, solar cells, efficiency, transport props. 80—50961
- Si, amorphous, solar cells, and photovoltaic devices *(Japanese)* 80—50965
- Si, amorphous, solar cells, design considerations 80—85277
- Si, amorphous, solar cells, barrier props. determ. by differential I-V characts. meas. 80—94053
- Si, amorphous, spin depend. recomb., luminesc. and light induced ESR 80—50393
- Si, amorphous, spin-depend. photocond. 77—59302
- Si, amorphous, spin-pairing at defect centres, mechanism in terms of chem. bonding 79—23928
- Si, amorphous, sputter-deposited electrical and optical props. 79—47181
- Si, amorphous, sputtered, Auger surface spectroscopy 80—50472
- Si, amorphous, sputtered, resist. control by ion implantation 80—100262
- Si, amorphous, struct. and growth kinetics, topological principles 80—49123
- Si, amorphous, structural disorder rel. to electronic props. 78—34756
- Si, amorphous, structural defects EPR 80—25208
- Si, amorphous, substantially doped, electronic props., review 79—87175
- Si, amorphous, substitutional doping, electronic props. 77—1418
- Si, amorphous, substrate orientation effect on regrowth by laser pulses, channeling, backscatter 80—84409
- Si, amorphous, thermoelec. power in phonon-assisted hopping regime, Coulomb effects 78—76097
- Si, amorphous, thin film reaction with Pd, metal-rich silicide formation 80—2284
- Si, amorphous, time resolved photoluminesc. near band gap 80—25445
- Si, amorphous, time-resolved ODMR and luminesc. 80—25254
- Si, amorphous, topological and electronic struct. 77—28102
- Si, amorphous, transient electrical transport, general and unified treatment 80—59977
- Si, amorphous, transport results, interpretation 80—80260
- Si, amorphous, tunnelling states simulation and sp. ht. 79—37791
- Si, amorphous, UHV evaporated, annealing behaviour of spin density 80—93163
- Si, amorphous, undoped, photocond., continuous illum. effect 80—84486
- Si, amorphous, undoped and B doped, ESR-linewidth temp. depend. meas. 80—20459
- Si, amorphous 79—28103
- Si, amorphous and cryst., electronic and optic props. 78—39013
- Si, amorphous and cryst., optical absorpt. at $\lambda=1.06$ μm, temp. depend. 79—82939
- Si, amorphous and cryst. K X-ray spectra of band struct. 79—87525
- Si, amorphous and crystalline, hydrogenation and dehydrogenation 78—51677
- Si, amorphous and crystalline, heating by Q-switched laser radiation 80—84963
- Si, amorphous and crystalline, ion implanted, UPS meas. 80—97411
- Si, amorphous and polycryst. thin film solar cells, perform. parameters, review 80—93882
- Si, amorphous CVD fabrication for solar photothermal conversion appl. 80—7504
- Si, amorphous CVD film photodetector for picosecond pulses 80—47101
- Si, amorphous CVD films for high temp. solar photothermal conversion 80—26161
- Si, amorphous co-sputtered doped, photovoltaic material appl. 80—93488
- Si, amorphous deposited, laser induced epitaxy 79—69372
- Si, amorphous discharge produced, electronic density of states 79—46992
- Si, amorphous evaporated, picosecond optoelectronic detect., sampling and correlation meas. 80—100478
- Si amorphous evaporated film, doping 79—51127
- Si amorphous film, AC conduction 77—66213
- Si amorphous film, acoustic study using Rayleigh waves 80—75312
- Si, amorphous film, analytical techniques, review 80—80120
- Si amorphous film, anisotropic etching phenomenon, appl. as solar selective absorber surfaces 80—72054
- Si amorphous film, crystallisation kinetics and morphology, TEM obs. 78—84093
- Si amorphous film, crystn. on annealing at low temps. in contact with Al 80—24765
- Si amorphous film, dangling bond ESR, light-induced quenching 80—50162
- Si, amorphous film, drift mobility and photocond. 79—15143
- Si, amorphous film, EELS microanalysis 80—100722
- Si amorphous film, EPR rel. to elec. cond. 77—69692
- Si, amorphous film, ESR, cond. secular change on annealing *(Japanese)* 79—15238
- Si, amorphous film, electron beam evaporated, freq.-depend. dielec. behaviour 79—99549
- Si, amorphous film, epitaxial laser crystallisation 78—84078
- Si, amorphous film, Fermi energy shift with substitutional doping 79—46998
- Si amorphous film, film, glow discharge deposited, refl. spectra and dielec. function 80—50360
- Si, amorphous film, glow discharge deposition, rate enhancement by mag. field 80—65412
- Si, amorphous film, glow-discharge, optical props. *(Japanese)* 79—65946
- Si amorphous film, glow-discharge, optically detected mag. reson., annealing and substrate temp. effects 80—20519
- Si, amorphous film, heavily doped, glow discharge, AC cond. 80—49718
- Si amorphous film, heavy doping by alkali ion implantation 80—2045
- Si amorphous film, hole carrier transport 80—2500
- Si, amorphous film, hole drift mobility, temp. depend. 79—23973
- Si, amorphous film, hopping cond., thickness depend. 77—89887

elemental semiconductors continued
- Si, amorphous film, IR and Raman spectra of Si-H bonds 78—19482
- Si, amorphous film, in Ti-Si-Ti struct., elec. cond. processes and threshold switching 79—78207
- Si, amorphous film, interface charge, influence on transfer meas. 79—15237
- Si amorphous film, ion-implanted, regrowth 79—15043
- Si amorphous film, optical props., electronic states 80—25475
- Si, amorphous film, oxidised, vacuum deposited, cond. change due to electron irrad. 78—10089
- Si, amorphous film, plasma-deposited, photoluminesc. and EPR meas. 79—4864
- Si, amorphous film, RF plasma deposition from $SiCl_4$-H_2, characterisation 80—66435
- Si, amorphous film, RF-sputtered, influence of O_2 and deposition conditions, elec. cond., IR absorpt. and ESR 80—2949
- Si amorphous film, saturation meas. on ESR signals 79—33535
- Si, amorphous film, selective laser recrystn. over heavily doped lines 80—84947
- Si amorphous film, sputter-deposited, elec., optical, and photoelectronic props. 79—24433
- Si, amorphous film, sputtering by 0.5 to 5 keV Ar^+ ions 79—91550
- Si, amorphous film, TSC, density of localised states distrib. 80—65587
- Si amorphous film, vacuum deposited, microscopic voids, gas absorpt., crystn. study 80—49534
- Si, amorphous film, variable range hopping 78—76176
- Si, amorphous film deposition from silane glow discharge plasma 77—44173
- Si amorphous film effect of gas exposure on EPR signal 78—84475
- Si, amorphous film prepared from glow discharge, quantitative H anal. 77—69188
- Si, amorphous film prepared by CVD, optical props. and struct., solar absorber appl. 79—52035
- Si, amorphous films, halogenated and hydrogenated, elec. and optical props. 80—97016
- Si, amorphous films, hopping conduction, dangling bond generation by high temp. annealing 80—60115
- Si, amorphous films, ion implanted, elec. and photocond. props. 80—49717
- Si amorphous films, laser beam annealing, optical information storage possibilities 79—87515
- Si amorphous films, RF sputtered, appl. as Schottky barrier solar cells 79—34434
- Si, amorphous films, RF sputtering prep. at high Ar press., props. obs. 80—80418
- Si amorphous films, self-ion bombard., electronic props. 79—28422
- Si, amorphous foil, electronic energy straggling of light ions, at. number depend. 77—11612
- Si, amorphous heavy ion ranges, He^+ backscatt. obs. 78—63796
- Si, amorphous hydrogenated, manufacture of Schottky-barrier and MIS tunnel solar cells *(French)* 79—24897
- Si, amorphous hydrogenated, fabrication method 80—80956
- Si, amorphous hydrogenated solar cells, field depend. quantum efficiency, electron-hole recombination 80—66971
- Si, amorphous laser effects 79—69921
- Si, amorphous layer, comparison of laser and electron beam pulsed annealing 79—69374
- Si, amorphous layer, epitaxial growth by laser annealing 78—79899
- Si amorphous layer, inhomogeneity formed by ion bombardment 77—69017
- Si amorphous layer, ion-beam induced epitaxial regrowth 79—69378
- Si, amorphous layer, ion-implanted, spatially controlled cryst. regrowth by laser irradiation 78—55810
- Si amorphous layer, solar furnace annealing to induce solid-phase epitaxy 80—2277
- Si, amorphous layer crystn., effect of ^{16}O, ^{12}C, ^{14}N and inert gases 78—14623
- Si, amorphous layer prod. by ion implantation, diffusion broadening, ESR study 80—92552
- Si amorphous layer recrystallisation by laser beam 80—93566
- Si amorphous layers, glow-discharge, laser-annealed, elec. props. 80—75661
- Si, amorphous layers, laser induced As profile broadening 79—95045
- Si amorphous layers, on Si substrates, deposited and ion-implanted, laser-annealing behaviour 79—69373
- Si, amorphous layers, RF-sputtered on sapphire, crystallisation by CW ion laser annealing 80—80109
- Si, amorphous layers, recrystallisation, pulsed laser annealing 80—65404
- Si amorphous p-n junctions, high current, characts. 80—70807
- Si, amorphous presence of acceptor states around Fermi level 78—2445
- Si, amorphous Schottky barrier solar cells, deep hole traps, spectral response and TSC meas. 80—50962
- Si amorphous sputtered film, solar energy selective absorber, spectral emissivity 78—83045
- Si, amorphous sputtered film, elec. cond. and photocond. 79—87097
- Si, amorphous sputtered films, hydrogenated, photoinduced optical absorpt. 80—50362
- Si, amorphous sputtered thin film, US anomalies, 0.5-300K 80—34145
- Si, amorphous surface layer produced by ion bombardment, insulating props. of interfacial layer 77—59327
- Si, amorphous thin films, appl. in solar cells, recent developments 78—80016
- Si, amorphous ultrahigh vacuum evaporated films, ESR obs., deposition effects 79—33534
- Si, amorphous whisker growth characts. by SiH_4 thermal decomposition 80—34342
- Si, amorphous/cryst. interface, supercond. mechanism 80—44783
- Si, amorphous-implanted, laser induced struct. changes related to pulse shape 79—69123
- Si and its cpds., chemical aspects of fluorocarbon plasma etching 79—83350
- Si, and Si:H, amorphous, ps. relax., optically induced absorpt. 80—48325
- Si, and Si:H, amorphous, sputter deposited, O_2 incorporation during and after fabrication 80—49541
- Si and Si:H amorphous films, porosity and oxidation of evap., sputtered and plasma-deposited films 80—10838
- Si, and SiO_2 on Si, ranges of implanted B^+ and B^{2+} 77—31687
- Si, anisotropic etching by $CCl_4(+O_2)$ gas plasma 77—32701
- Si, anisotropic momentum densities from Compton profiles 77—48268
- n-Si, anisotropy of differential conductivity and transverse diffusion coefficient 78—76078

elemental semiconductors continued
Si, annealed, ion-implanted, in MOSFET, defect spatial distrib. 77—11973
Si, annealed, neutron-irradiated, EPR centre (S=1), characts. 80—71177
Si, annealed, photoluminesc. anal. of defects 80—80836
Si, annealed crystal, oxide precipitates identification by electron loss spectra 78—83952
Si, annealing, using laser pulses, impurity incorporation at melt-cryst. interface 80—59504
Si, annealing during Czochralski growth, influence on defect density 80—60769
Si, annealing in elec. field behaviour of second phase inclusions *(Russian)* 79—23779
Si, annealing of vacancy clusters produced by ion bombardment 77—89485
Si, annealing with 1.06 μm laser pulses 79—69913
p-Si, anodic etching for discriminating between elec. active and inactive defects 80—108605
Si, anodic oxidation, mobile ion identification, Rutherford backscatt. analysis 77—44381
Si, anodic oxidation at constant voltage, mechanism 79—70184
Si, anodic oxidation for abrading thin layers from wafers *(German)* 77—25176
Si anodic oxidation in RF induced O plasma 80—100931
Si, anodisation at low substrate temp. by low pressure O$_2$ plasma 80—104314
Si, anomalous avalanche breakdown 80—80284
Si, anomalous etch structures using ethylenediamine-pyrocatechol-water based etchants and their elimination 80—81217
Si, anomalous field evaporation 79—15596
Si anomalous muonium states, time behaviour of μ spin polarisation 79—11371
Si, anomalous muonium state, μSR 79—56674
Si, anomalous passage of positrons, expt. 79—95052
Si, anomalous sputter yields of interfacial species, cascade mixing process for interpretation 80—76122
n-Si, appearance of high-field domain in pinch channel 78—26900
Si, appl. of high throughput ion implantation systems 80—34029
Si, appl. of photoelastic stress. meas. technique 80—48656
Si, application of Pd for reducing recovery time of reverse current in pulse diodes *(Russian)* 79—99226
Si, Ar and B implantation effects on cond. 77—80779
Si, Ar bombarded, blistering effects, SEM obs. 78—67745
Si, Ar ion etching, carbide form. 80—81222
Si, As diffusion from As doped oxide film, stress effect on film roughening 78—2389
Si, As diffusion from doped polycryst., conc. depend. 78—34656
Si, As implantation *(Japanese)* 78—38738
Si, As implantation profiles, calc. comparison with expt. 78—38748
Si, As-doped, effect of elec. and struct. parameters on avalanche breakdown localisation 77—11926
Si, as-grown Czochralski crystal, multiple p-n junction structure obtained by heat treatment, appl. to solar cells 80—101099
Si, atomic displacements damped by chemical bonds, computer calc. 78—47370
Si, atomic wave functions localisation and band struct., LCAO calcs. 77—51648
Si, Au diffusion enhancement by photo- and electron irrad. 77—27901
Si, Auger band-to-band recomb, temp. depend. 80—29416
Si, Auger electron prod. by Ne$^+$ bombard. 80—7460
Si, Auger line shape $L_{2,3}$ VV, energy band theory 79—43074
Si, Auger lineshape, one-electron theory for $L_{23}VV$ and $L_1L_{23}V$ 78—72645
Si, Auger peaks, bremssrahlung-induced 80—45199
Si, Auger recomb. coeff. meas. using laser excitation 79—38654
Si, Auger recomb. of electron-hole drops 78—39600
Si, Auger recombination, localized and free carrier comparison 79—38090
Si, Auger recombination 78—26883
Si, Auger spectra, KLL and KLV, screening effects and plasmon gains 80—80913
Si, Auger spectra induced by 100 keV Ar$^+$ impact 80—84820
Si, autoepitaxy, displacement of microrelief 80—2307
Si, avalanche regime, carrier drift vel. effect on meas. ionisation coeffs. 79—69516
Si, axially channelled protons, transmission meas. using two-dimensional position-sensitive detector 79—1471
Si, B implanted, enhanced annealing behaviour, p-n junction formation 77—43233
Si, B implanted layers, damage obs. by X-ray double refl. 77—15463
Si, B ion irradiated, long-range damage to crystallinity, X-ray diffr. meas. 78—2171
Si back surface field solar cell degradation at high intensity due to base cond. modulation loss 80—94085
Si, back-wall Schottky barrier solar cell with interfacial layer 77—62993
Si, band struct., modulation spectroscopy, two-ray methods *(Russian)* 78—54469
Si, band struct. and valence charge density, self consistent pseudopot. method with Gaussian orbitals 79—90928
Si, band structure, self-consistent pseudopotential *(Japanese)* 77—43491
Si, band structure, use of two-centre approx. with Hartree-Fock eqns. 77—76726
Si, band structure of diamond like crystals, cluster-Bethe lattice model calc. 80—6713
Si, band structure selfconsistently determined with X_α potentials using MAPW method 79—33227
Si, band structure under high stress, nonperturbative calc. 78—10344
Si, bandgap narrowing model in moderately to heavily doped material 79—99477
Si bars, generation-recombination noise at 77K 79—60883
Si based alloys, amorphous, photovoltaic behaviour, solar cell appl. 80—94051
Si based MIS negative barrier contact for induced back surface field solar cell 80—101101
Si based MIS structure, photoelectric characts. carrier injection levels *(Russian)* 80—96946
Si based MOS capacitors, scanning photovoltage investigation 80—80396
Si based MOS device irradiation with γ-rays, minority carrier generation, CV characts. 80—88637
Si beam epitaxy for epitaxial film growth and p-n junction formation in high vacuum 80—16187

elemental semiconductors continued
Si, behaviour of B molecular ion implants 78—47405
Si, bent crystal, γ-radiation beam deflection due to 900 MeV channelled electrons 80—84223
Si, bent single crystal, proton beam trajectory control *(Russian)* 80—19859
Si, bicrystals, grain boundary states and varistor characts. 80—24829
Si, biexcitons, photoluminesc. spectrum exam. 78—47705
n-Si, bipolar ohmic contact with macroscopic recomb. centres. 80—80379
Si, birefringence of dislocation lines in (111) wafers 79—61332
Si, blistering due to 400 to 1800 keV ^{4}He$^+$ ions, modal range determ. 80—100289
Si, blocking effect, backscatt. method *(Chinese)* 79—90708
Si, bonding electron distribution 79—90594
Si, bonding states of adsorbed O$_2$, photoemission obs. 78—92170
Si, bound exciton lifetimes for acceptors 77—80738
n-Si, bound excitons and bound multiexciton complexes, excitation spectra 80—96792
Si, bound multiexciton complexes, luminesc. 80—10888
Si, bound-exciton spectral lines, conc. broadening at high impurity concs. 80—80826
Si, Bragg diffraction from crysts., Mo K_α radiation polarisation 80—1893
Si, Bragg-case X-ray tnin cryst. rocking curves, theory and expt. comparison 78—55785
Si, bremsstrahlung spectra for 1 GeV electrons and positrons, planar and axial channelling *(Russian)* 77—32465
Si bridging epitaxy from Si windows onto SiO$_2$, ruby laser pulse annealing 80—44441
Si, brightening and darkening wave generation by Nd:glass laser 78—18023
n-Si, bulk, high field characts. *(Japanese)* 78—34837
Si, bulk and surface equlib. props., self-consistent pseudopotential calcs. 79—60750
Si, bulk deep centres, continuous energy spectrum, isothermal capacitance relaxation method 80—107741
Si, bulk plasmon dispersion, electron energy loss spectra meas. 80—59899
Si, bulk-hot electron props. 79—99553
Si buried-grid fabrication by LPE 79—78906
Si, CC Si$_3$N$_4$ film formation by ^{14}N$_2^+$ ion implantation into Si 79—99455
Si, CCD processing, elimination of stacking faults 78—10065
Si, CF$_3^+$ ion bombardment, XPS and Auger study 79—70367
Si, CF$_3^+$ ion-surface interactions in plasma etching 77—90473
Si, CVD, characterisation and morphology 79—33938
Si, CVD, for appl. in high temp. photothermal conversion 79—79403
Si, CVD, surface anal. during growth using RHEED and Auger spectroscopy 80—66433
Si, CVD, underlying oxide layer thickness effect on in-process thickness monitoring 80—6679
Si, CVD, using CO$_2$ laser for substrate heating 78—39698
Si, CVD amorphous films, effect of surface characts. on visible and UV optical props. 80—60698
Si, CVD epitaxial film, stacking fault nucleation and growth 78—10064
Si, CVD epitaxial growth, from SiCl$_4$+H$_2$, in vertical cylinder reactor, transport processes analysis 77—48344
Si, CVD epitaxy, book contrib. 77—12544
Si, CVD film, transport props. 79—24089
Si CVD film on amorphous substrate, CW laser recryst. 79—90894
Si, CVD films, polycryst., elec. and optical props., electronic density of states model 79—56332
Si, CVD from SiH$_4$-HCl-H$_2$ system, rate-determining reactions and surface species 80—84405
Si CVD grown polycrystal recrystallisation 78—64560
Si, CVD growth, high- and low-temp. models 78—6244
Si, CVD growth and film morphology, rel. to model of mass transport 77—59233
Si, CVD growth rate, temp. and conc. effects, mass transport model 77—59234
Si, CVD growth surface, singular instabilities 77—24969
Si, CVD mechanism, book contrib. 79—69991
Si, CVD mechanism, epitaxial growth, IR obs. 79—23859
Si CVD of polycrystal on liquid Sn layer 78—64479
Si, CVD on liq. Sn layers in HCl presence, enhanced crystallinity 78—6853
Si, CVD on SiO$_2$ and Si$_3$N$_4$, SEM study *(Dutch)* 80—2960
Si, CVD on SiO$_2$ and Si$_3$N$_4$ substrates, nucleation in SiH$_4$-HCl-H$_2$ system at high temp. 80—49538
Si, CVD polycryst. film, growth texture 77—7990
Si, CVD prepared solar thermal absorber, temp. variation of absorpt. edge 80—12028
Si, CVD using CO$_2$ laser 78—56589
Si, CVD using Si-H-Cl system, theoretical anal. of equilib. adsorption layers 79—23858
Si, CW laser annealed, defect luminesc. 80—50388
n-Si, capture cross section and generation lifetime determ. of Au, MOS expts. 78—91772
Si, carrier capture at amphoteric deep level defects 80—88569
Si, carrier conc. determ., electrochem. method 78—60200
Si, carrier conc. variations using electrolyte electroreflectance, topographical features 79—99562
Si, carrier concentration distribution by scanning IR absorption 79—61356
Si, carrier generation in depletion layer, effect of stacking faults 79—23983
Si, carrier lifetime, comparison of meas. by photocond. decay and surface photovoltage 78—68038
Si, carrier lifetime and its impact on solar cell characts. 79—74521
Si, carrier lifetime degradation at room temp. 78—95301
Si, carrier lifetime depth distrib. due to Ar ion implantation 80—70232
n-Si, carrier recomb. and photoionisation via E-centre resonance state 79—60847
n-Si, carrier relax. time, mag. field effects, rel. to Hall effect 80—39608
n-Si, carrier scatt. anisotropy, Hall mobility calcs. 77—24552
Si, cast, growth structure and photovolt. props. of solar cells 80—94008
Si, cast polycryst., laser annealed for solar cells 80—93918
Si, cast polycryst. p-n junction solar cell, hydrogenation effects 80—93916
n-Si channel $\langle 100 \rangle$ inversion layer MOSFET, valley splitting, conductivity 80—70840

elemental semiconductors continued
Si, channeled B and P implantation along ⟨111⟩ and ⟨110⟩ axes 78—22739
Si, channelled and random proton stopping power, 30-1000 keV 78—67760
Si, channelled protons, energy loss to valence electrons, dielec. calc. 77—55312
Si, channelled-ion implantation of group III and group IV ions 78—75682
Si, channelling of 160 MeV protons, deuterons and α particles, stopping powers 79—86826
Si, channelling of H^+ and He ions, backscatt. particles ang. distrib. 79—51174
Si, channelling of π^- and π^+ 79—60414
Si, channelling of relativistic electron beam, anal. of low-energy bremsstrahlung meas. 77—36304
Si, channelling of relativistic protons in bent crysts., theory 80—96581
Si, characterisation and analytical techniques *(Japanese)* 77—84735
Si, characterisation by photoluminescence method *(Japanese)* 78—80404
Si, characterisation by photolum. method *(Japanese)* 79—38638
Si, characterisation techniques and trends 78—11487
Si, charge density, struct. props. electron-electron interactions 78—47725
Si, charge disturbance around neutral defect, simple new method, appl. to ideal vacancy 79—82554
Si charge transfer by SAW in ZnO 77—27415
Si, charge transport properties, review 77—39851
Si, chem. etching, comp. selection, geometry effects 77—21299
Si, chemical etching processes, review 78—95832
Si, chemical staining due to suboxide form. 78—35540
Si, chemically etched, metal contact, electron and hole currents correl. 78—91769
Si, chemisorbed Al monolayer on (111) surface, local density of states 79—47142
Si, chemisorption of CO(Cl), surface photoemission, adsorption gate geometry 78—73079
Si, chemisorption of Cl_2, photoemission polarisation effects with synchrotron radiation 78—14580
Si chemisorption of Ga on (111) surface, Ga-induced surface states 79—19644
Si, chemisorption of H on (111) 77—62743
Si, chemisorption of H_2, atom-probe FIM obs. 78—71968
Si, chemisorption of H_2, magnetic-sector atom-probe field ion microscopy exam. of hydride form. 77—80699
Si, chemisorption of XeF_2 and SiF_4, XPS and Auger spectra, surface chemistry 80—81358
Si chip manufacture for fibre alignment in lightguide cable connectors 80—64188
Si circular slices, resistivity var. meas. using automated photovoltaic systems 80—52274
Si, clean and gas (O_2 and H_2O) covered surface, appl. of UPS ultrahigh vacuum apparatus *(Japanese)* 80—37125
Si, clean SiO_2 film prep., use of poly-Si oxidation tubes 78—39924
Si, clean surface, geometrical struct. rel. to electronic props. 77—62719
Si, clean-cleaved, Schottky barrier height meas. accuracy 78—52081
Si, cleaved surface, metal contact props. and influence of intermediate adsorbed layers 80—49905
Si, coated by insulating film, dissolution and corrosion in high temp. water and moisture 77—48564
Si coated with copper phthalocyanine dye, optical modulation of low energy electron transmission 79—69939
Si coated with Pd, interference effects on irrad. with laser beam 80—66333
Si, coating of mullite ceramic substrate, for solar cell appl. 79—34432
Si, commercial, nitridation, effect of BaF_2 80—81359
Si, commercial diodes, wide range temp. sensor, mag. field depend. 78—45623
Si, comparison of interactions between sequential Ga-P and Ga-As diffusions 77—80655
p-Si, compensated by radiation defect centres, photoresistors 77—62961
Si, compensated by thermal defects, recomb. and optical props. 80—64989
Si, compensated monocrystal, IR absorption spectra, Fourier transform obs. 80—60644
n-Si, complex defect production rate introduced by high energy electron irradiation 77—72635
Si, complex doping effects on limiting electron conc. 78—22740
Si, complex permittivity and cond., microwave meas. 79—65784
Si, composition of inclusions, single cryst. 77—15441
Si, compression, effect of press. on lattice defects up to 90 kbar *(Japanese)* 77—72654
Si, Compton profile anisotropy, pseudopot. calc. 79—28854
Si concentrator cells, high efficiency, design, fabrication and meas. 80—93938
Si concentrator solar cells, new technology for fabrication 80—81457
Si concentrator solar cells, effects of nonuniform illumination 80—93942
Si concentrator solar cells, high efficiency, state-of-the-art design and processing 80—93958
n-Si, cond. in warm electron region, temp. depend. of anisotropy of nonlinearity coeff. 77—43610
Si, conductivity, study with supercond. metal contacts 80—15621
P-Si, conductivity and carrier lifetime, high injection effects 80—70719
Si, conductivity of holes at low temp., electric field depend. 77—28179
Si conductor-insulator-semicondcutor solar cells, automated production, outlook 80—94021
Si, containing stacking faults, MeV He ion irrad., TEM obs. of defect clusters 77—89483
Si continuous polycrystalline films on C substrates 78—64490
Si, continuum-exciton effect in optical spectrum 80—25416
Si, controlled dislocation formation, struct. density *(Russian)* 80—107244
Si, controlled etching in catalysed ethylenediamine-pyrocatechol-water solns. 80—3223
Si, cooling rates of large diameter crysts. 78—35291
Si, core and valence electron excitations, AES, chemical shift and line shape 80—2365
Si, core exciton binding energies 80—80188
Si, core levels, chem. shift and relaxation energy, temp. dependence 80—39520
Si, core levels, temp. depend. of conduction band and core exciton energies 80—24828
Si, core structure of glide-set 90° and 30° partial dislocations 80—96523

elemental semiconductors continued
Si, correl. between photolum. spectra and impurity conc. 78—23513
Si, covalent semiconductor, electronic response to high symmetry lattice vibr. 80—10619
Si, crack free ingots, by directional solidification using heat exchanger method 79—8242
Si, crack-tip dislocation pattern, X-ray topography *(French)* 80—107253
Si, critical resolved shear stress, 800 to 1050°C indentation dislocation rosettes 79—24577
Si, cross-slip of single dissociated screw disclocations, double etching and X-ray topography studies 80—15104
Si, crucible grown, virgin and implanted, laser irradiation effects on surface structure 80—92768
Si, crucible-free growth, zone melting in combined heating system 78—3031
Si cryst., images of atoms projected onto (110) plane using high resolution techniques 79—32866
Si, cryst. and amorphous surface layers, ruby laser pulse effects 79—69920
Si, cryst. growth, float zone, low ohmic seeds and dislocations 78—27398
Si crystal, contrast depend. of Kikuchi patterns on primary electron beam energy *(Russian)* 80—64844
Si crystal, Czochralski grown, enhanced Borrmann effect 80—70191
Si crystal, high O_2 content, Czochralski growth parameters related to epitaxial stacking faults 79—4314
Si crystal, impurities determ. and resistivity after reactor neutron irrad. 80—65563
Si crystal, obtained by local epitaxial accretion, facing and shape meas. 77—4270
Si crystal, shape stability in float zoning 77—47362
Si, crystal defect obs. by TEM *(Japanese)* 77—84752
Si, crystal defects and impurities interaction obs. by electron microscopic methods 80—65003
Si crystal growth, for electronic devices 80—66419
Si, crystal growth by floating zone melting, limitations in using KHz radio frequencies 79—19989
Si, crystal growth conditions effect, on microdefect distrib. 80—50549
Si, crystal growth from melt in vac., origin of SiC impurities 80—2940
Si crystal inclusions, microscopic, nondestructive monitoring 79—55749
Si crystal microcrack detection by ultrasonoprobe 80—66733
Si crystal production and perfection for photodetectors 78—11107
Si, crystal structure stability, P-T diagrams 78—51886
Si, crystalline, regrowth into amorphous layers 79—69040
Si, crystalline order-disorder transformation, repeatable, using intense laser beam 80—39150
Si, crystalline sheets production, low cost, crystal growth techniques comparison 80—35083
Si, crystalline struct. and lattice imperfections 80—24398
Si crystals, temp. distrib. anal. in floating-zone method 79—74082
Si, crystn. front face effect on at displacements *(Russian)* 78—67781
Si, Cs ion-bombarded, surface Cs concs., AES meas. 79—83073
n-Si, current carrier-dislocation interactions, resistance in UHF range *(Russian)* 80—54732
Si, current instabilities in semiconductors, theory and expts. *(Hungarian)* 77—39857
n-Si, current instability due to temp.-elec. domain pulsations 77—43608
n-Si, current load capacity of contacts with Au, Ni_xSi and Al *(Czech)* 77—89846
n-Si, current-volt. characts. along ⟨110⟩ 79—78111
n-Si, current-voltage characts., static high field domains 78—84223
Si, Czochralski and web crystals, transition metal doped for solar cells 78—35297
Si, Czochralski cryst., hillock etching of microdefects, TEM obs. 78—87678
Si, Czochralski cryst. growth, faceted and nonfaceted, Sb microsegregation 80—45227
Si, Czochralski crystal growth and charact., oxidation induced stacking faults 79—47621
Si, Czochralski crystal growth, low O content 80—40251
Si, Czochralski crystals, O microsegregation, swirl defect distrib., growth rate depend. meas. 80—39295
Si, Czochralski grown, dislocation free, swirl defect form., doping effect 80—92519
Si, Czochralski grown, inhomogeneous O precip. and stacking fault form. 79—14820
Si, Czochralski grown, intrinsic gettering by oxide precipitate induced dislocations 77—27903
p-Si, Czochralski grown, microdistrib. of O, SEM and spreading resist. obs. 80—79830
Si Czochralski grown, O distrib. meas. 77—11580
Si, Czochralski grown, oxide precip. homogeneous nucleation 80—65221
Si, Czochralski grown, oxide precipitates, diffusion-limited growth 80—97484
Si, Czochralski grown crystal, radial impurity distrib. improvement 77—73225
Si, Czochralski grown crystal, O precip., nucleation behaviour and dislocation loop form. *(Japanese)* 80—59664
Si, Czochralski grown crystals, swirl-type defect obs. 80—100236
Si, Czochralski growth, drop form. and crystn. rel. to dislocation struct. 78—2030
Si, Czochralski growth, equilib. of dissolved C and O with CO in ambient atm. 80—1949
Si Czochralski growth, large crystal, convection and segregation 78—6843
Si, Czochralski growth from heavily Sb doped melt, interface morphological instability 80—2939
Si, Czochralski growth with automatic diam. control 78—52658
Si Czochralski wafer intrinsic gettering by oxide precipitate induced dislocations 78—6092
Si Czochralski wafer oxidation-induced stacking faults correl. with bulk defects 77—76428
Si Czochralski wafer oxide precipitate-dislocation complex characterisation 78—14357
Si, Czochralski wafers, oxidation induced stacking fault sources 77—7737
Si Czochralski wafers, thermally oxidized, stacking fault distrib., O conc. depend. 80—2042
Si Czochralski wave, oxid. induced stacking fault, oxygen content influence 78—10062
Si, Czochralski-grown, oxide precip. form. process 80—49364
Si, Czochralski-grown cryst., swirl defect formation and defect migration 77—76405

elemental semiconductors continued
Si, Czochralski-grown crysts., thermally induced microdefects, annealing temp. and starting material effects 80—49141
Si, DC MOSFET dopant profile method 80—70244
Si DC sputtered, amorphous, dark conductivity and photocond. obs. *(French)* 78—64155
Si, damage in electron bombardment, threshold voltage 77—27910
Si, damage profile after H_3^+-ion irradiation, proton backscatt. exam 79—60410
Si, dangling bonds, EPR, localised states and unpaired electrons on microcrack surfaces 78—52351
n-Si, Debye temperature, electronic effect 78—83901
Si, dechannelling of H^+, generalised Fokker-Planck eqn. calc. 77—19999
Si, deep amorphous layer implantation, laser effects, channelling diffr. study 80—25494
Si, deep centres, majority carrier thermal capture cross section, TSC meas. 78—10468
Si, deep centres associated with plastic deform. and quenching *(French)* 77—28145
Si, deep dislocation states 80—24836
Si, deep donor character of muons and protons 80—10911
Si, deep impurity levels, activation energy 80—107742
Si, deep level defects, struct. bonding, amphoteric centres 80—88506
Si deep level determ. using deep depletion MOSFET test structure 78—10571
Si, deep level transient spectroscopy *(French)* 79—11079
Si, deep levels, detection in high power materials and devices 79—28318
Si, deep planar Ga and Al diffusion 79—69290
Si, deep-level point defects, effective-mass nature 80—59922
Si, defect annihilation depth by pulse laser annealing 80—16128
n-Si, defect charge states, complex form., gamma-ray effects 80—96564
p-Si, defect form. due to multiple N^+ and B^+ irrad. 79—90706
Si, defect form. during high press. low temp. steam oxidation 79—29238
Si, defect form. under radiation-accelerated diffusion conditions 80—19854
Si, defect formation kinetics during charged particle irrad. 80—29096
Si, defect generation and annealing by intense subthreshold electron beam bombardment 79—51149
Si, defect prod. by GeV muons, thermally stimulated current technique 78—5099
Si, defect storage kinetics during neutron irrad. 80—24505
Si, defects, divacancy and split 100 interstitial, electronic structure calc. 80—65494
Si, defects, electrically active, correl. of electrolytic etch and surface photovoltage methods 79—77929
Si defects in surface due to oxidation, exam. using double crystal back reflection topography *(German)* 79—51098
n-Si, deform. pot. shear const. determ. 77—15763
Si, deformation, annealing characts., X-ray study 78—75713
p-Si, deformed, 1/f noise, resist., mobility, and carrier density 77—8161
Si, deformed, annealed and recrystallized, struct., implications for solar cells 80—60922
Si, deformed, defect states associated with dislocations, capacitance transient spectroscopy 79—42483
Si, deformed, ENDOR of dislocation centre 78—72434
Si, deformed, faulted dipole, TEM obs. 78—38712
Si, deformed, photo-EPR of dislocations 80—11267
Si, deformed, recomb. radiation from electron-hole drops and free excitons 77—8641
n-Si, deformed, thermal treatment effect on elec. cond. and dislocation mobility 80—107265
Si, deformed surface, defect struct. rel. to elec. props. 78—72231
n-Si, degenerate, density of states from elastic consts. 80—6690
p-Si, degenerate, Raman effect, interacting elementary excitations 78—43846
Si, degenerate four wave mixing of 1.06 μm laser radiation 80—5794
p-Si, delineation of n-type ion implant 79—77619
Si, dendritic film growth on alumina, solar cell appls. 77—77432
Si dendritic web for solar cells 80—89634
Si dendritic web growth, correlation of solute and interface partition coeffs. 79—24427
Si, dendritic web growth processes for solar cells, computer modelling 79—11508
Si, dense plasma dynamics during pulsed laser annealing, carrier density, recombination 80—84479
Si deposition by SiH_4 pyrolysis at low temps. and atm. press. 79—91595
Si, deposition on rotating disc, one-dimens. model 80—75461
Si, deposition using solar furnace 80—89148
Si, destruction mechanisms by intense IR laser radiation *(Russian)* 78—39633
Si detector, α-particle dense track charge losses 77—3233
Si detector, ionisation energy for channelled 160 MeV α-particles 78—62680
Si detectors, high resistivity n-type prod. by neutron transmutation doping 79—45540
Si detectors, vac. UV performance, 500-2000 Å 77—26397
Si, device starting material, crystal defects, high voltage TEM obs. 78—10037
Si device technology, thin film interaction effects, book contrib. 79—1620
Si devices, application of epitaxy technology, deposition techniques 80—7501
Si devices, implantation damage, review 77—27899
Si devices, metallisation, TiN and TaN as diffusion barriers 80—65304
Si, diamag. and dielec. susceptibility, temp. depend. 78—10646
Si, diamagnetism of excitons and biexcitons, recomb. spectra *(Russian)* 80—7412
Si, dielectric function spectra, ellipsometric determ., many-particle effects at E_1-transition 80—93363
Si, dielectric polarisation calcs., microscopic local fields 80—20582
Si, dielectric properties, mean point value calc. 78—87930
Si, dielectric screening, microscopic theory, phonon dispersion, moment expansion calcs. 79—55839
Si, dielectric screening and zone-centre phonons 78—67785
Si, diffracted X-ray channelling by special deform. fields 80—100295
Si, diffused p-n junction, computer calcs. of photoresponse using Gummel-de-Mari algorithm 78—56221
Si, diffusion and power spectral density and correl. function of vel. fluctuation for electrons 80—65576
Si, diffusion coeff. of Se, by sheet Hall coeff. meas. 79—46843
Si, diffusion coefficient determ. from carrier conc. depth profile 80—107566

elemental semiconductors continued
Si, diffusion coeffs. for O impurity, determ. from optical absorpt. 79—69294
Si diffusion in Au-refractory thin film systems obs., by combination of scattering techniques 80—65308
Si, diffusion layers, B distrib. 77—7753
Si, diffusion mechanism of P, migration channels along vacancies and interstices 80—79996
Si, diffusion of ^{71}Ge and ^{32}P, effect of dislocation struct. on migration rate 77—51551
Si, diffusion of As, from As-doped oxide source 77—47477
Si, diffusion of B,P and Sb, implantation damage effects 78—55988
Si, diffusion of B and P, influence of dislocations 78—18840
Si, diffusion of B from CVD BN covered with Si_3N_4, appl. to master slice p-MOS IC 80—107564
Si, diffusion of B impurity, separation factor estimation 79—86926
Si, diffusion of B in oxidised atmosphere, minicomputer model *(Rumanian)* 79—82247
Si, diffusion of Ga, using open-tube system 80—19822
Si, diffusion of Ga in closed capsule, surface damage elimination 78—87691
Si, diffusion of Ga through SiO_2 layer, junction depth 78—51574
Si, diffusion of impurities accelerated by γ rays 77—55394
Si, diffusion of Na, retarding action of radiation defects 77—1140
Si, diffusion of Ni below 475°C, role of defects 79—51319
Si, diffusion of nitrogen during annealing, effects on ion implanted layers 77—24436
Si, diffusion of Os, diffusion parameters using photocapacitance and four-probe methods 79—51314
Si, diffusion of P, 900-1150°C, controlled surface conc. condition 77—7746
Si, diffusion of P, dislocations, creation conditions 79—95039
Si, diffusion of P, elastic deform. relax. and dislocation generation 80—79997
Si, diffusion of P, excess vacancy generation by E-centre dissociation 77—72720
Si, diffusion of P, oxidation effects 79—51309
Si, diffusion of P from spin-on SiO_2:P film 80—2050
Si, diffusion of Sb, along dislocations, 1165-1320°C 77—15631
Si, diffusion of self-interstitials and As, B and P, radn.-enhanced 80—29216
Si, diffusion of transition elements, anomalous behaviour 80—29044
Si, diffusion profiles, P and B diffusion determ. *(Rumanian)* 79—77615
Si, diffusion-induced lattice strain and dislocation obs. by X-ray diffraction *(Japanese)* 77—84753
Si diode, Auger recombination coefficient at very high injection rates 78—47863
Si, diode, high dislocation density effect on charact. *(German)* 79—33336
Si diode, impurity profiles, scanning electron microprobe anal. 80—79832
Si diode, thermometric characts., 15 to 300K 78—8403
Si diode, transient switching duration, linear carrier lifetime, emitter efficiency and Auger recomb. coeff. determ. 79—11207
Si diode radiation detector, stabilisation of radiation damage 80—91377
Si diode storage correlator optical imaging and memory characteristics 77—23772
n-Si, diode with Au traps, negative differential conductance 79—11221
Si dip-coated on graphite substrate, photovoltaic effects 80—29442
Si, dislocation defect states, capacitance transient spectroscopy 79—82549
Si, dislocation density, effect on C-V characts. of MOS struct. *(Russian)* 78—6447
Si, dislocation dipole lattice image, stacking fault energy 79—60375
Si, dislocation dissoc. and mobility of partial dislocations 77—68980
Si, dislocation dynamics during plastic deform., stress-strain characts. 79—27996
Si, dislocation dynamics in plastic deform., theoretical anal. 79—42077
Si, dislocation electronic states, Schottky diode meas. 79—82548
Si, dislocation energy spectrum, appl. of EPR and elec. meas. 79—82547
Si, dislocation ensembles motion in neutron irradiated covalent crystals *(Ukrainian)* 80—10579
Si, dislocation etch pits on various cryst. planes 77—24317
Si, dislocation formation, under high stress, low temp. 78—47386
Si, dislocation free, C and O impurity clouds, heat treatment influence on light scatt. 80—6427
n-Si, dislocation free, memory effect associated with appearance of prismatic dislocation loops 77—1130
Si, dislocation free, O_2 precipitation, stacking fault form. 78—38731
n-Si, dislocation free, process induced cryst. defects 80—24392
Si dislocation free, quantitative determ. of microdefect density by preferential chem. etching 80—65001
Si, dislocation free crystal growth 79—100030
Si, dislocation generation, influence of film stress and thermal oxidation 79—23609
Si, dislocation generation in local oxidation 80—107245
Si, dislocation growth during laser melting and solidification 80—2022
Si, dislocation loop, of hexagonal interstitial Frank type, dissoc. 77—35556
Si, dislocation loops, creation in region of interface, after annealing 79—82210
Si, dislocation mobility and mech. behaviour 79—82208
Si, dislocation motion from indentation rosette 80—79798
Si, dislocation motion near surface 79—82219
Si, dislocation structure, effect of induction heating *(Russian)* 77—21180
Si, dislocation study by high voltage electron microscopy and SEM 79—82217
Si, dislocation velocities as function of electronic doping 77—4117
Si, dislocation velocities meas. 79—82230
Si, dislocation-free, deep centres formed after high temp. treatment 80—96824
Si, dislocation-free, defect formation, high temp. treatment, growth-band influence *(Russian)* 79—4299
Si, dislocation-free, O_2 precip., IR and TEM obs. 80—29173
Si, dislocation-free crystal point defect condensation 78—6026
Si dislocation-free crystal O precipitation obs. 78—6095
Si, dislocation-free Czochralski-grown, detection of microamounts of O *(German)* 78—26592
Si, dislocation-free single crystals, growth microdefects, etching and X-ray expts. 78—47385

elemental semiconductors continued
Si, dislocation-free single crystals, microdefect type by anomalous X-ray transmission 79—95019
Si, dislocation-induced elec. pots., appl. 79—82551
Si, dislocationless plates, microdefect dissolving due to high temp. annealing *(Russian)* 80—54378
Si, dislocations, depth distrib. planar channelling anal. with 2 MeV He backscattering 79—7640
Si, dislocations, EPR meas. 79—82871
Si, dislocations, luminesc. spectra *(Russian)* 77—90197
Si, dislocations, stacking faults, swirl defects, production and mechanisms *(Chinese)* 79—46684
Si, disorder depth distrib. prod. by N$^+$ irrad. 79—73227
Si, disorder distrib. extraction, semiempirical method of applying dechannelling correction 78—22781
Si, disorder produced by high-dose implantation, channelling meas. 77—11573
Si, dispersion law of indirect excitons 80—24805
Si, dissociated dislocations, statistics of kink formation 79—82207
Si, dissociation of hot excitons by long-wavelength acoustic phonons, photocond. spectra 77—4300
Si, dissolved O$_2$ precipitation, homogeneous nucleation 77—11695
Si, divacancies due to proton irrad., IR absorpt., annealing effects 80—20673
Si, divacancies orientation induced by IR light, EPR spectra 80—25209
Si, divacancy, hyperfine interactions from ENDOR meas. 79—42868
Si, divacancy, positive, EHT calcs. 79—99184
Si, divacancy charge states, photoconductivity spectra 77—15899
Si, donor bound excitons and bound multiexciton complexes 77—40282
Si, donor ground state wave functions 78—87937
Si, donor ion pot., small r behaviour of nonlinear Poisson eqns. 80—54652
Si, donor polarizability, multivalley effective mass calc. 80—96817
Si, donors, dispersive screening and Bloch function interference, large binding 79—51525
Si, dopant distrib. in mono- and polycryst. samples, C-V technique 80—6425
Si, dopant segregation by pulsed-laser annealing, test case for thermal melting concept 80—24489
Si, dopant striae, SEM obs. by Schottky barrier charge collection 77—31684
Si, dopant survey for IR detector appl., 2 to 2.7 and 3 to 5 μm 77—15433
Si, doped, basis functions for studying intervalley effects 79—69442
Si, doped, many-valley semiconductor, effective mass theory of intervalley mixing 77—47763
Si, doped, polarisability of donors 78—14693
Si, doped amorphous, transport props., conductivity, thermopower, temp. depend. 79—73512
Si, doped and amorphous, L$_{2,3}$ threshold spectra 77—69934
Si, doped oxide film formation mechanism, X-ray spectral anal. 79—87008
Si, doped with metal impurities contact angle, water adhesion energy *(Russian)* 77—89620
Si, doping, low temp. radiation induced impurity diffusion 77—15439
Si doping by nuclear transmutation 77—84782
Si doping by thermal neutron irrad., annealing characts. of bulk electron traps obs. 80—49244
p-Si, doping by Ti diffusion 78—18670
Si, doping impurity distrib., during cryst. growth by Czochralski method *(Russian)* 80—100276
Si, doping process, effect of disloc. density *(Hungarian)* 77—62553
Si double polycrystalline VLSI devices, low temp. differential oxidation 80—16521
n-Si, drag thermoelec. power, anisotropy parameter determ. 80—20235
Si, drift mobility and Hall coeff. factor of holes 78—43379
Si, dry etching induced surface contamination, SIMS, AES, and XPS obs. 80—11810
Si, dynamical recovery and self-diffusion 79—82379
Si, EFG ribbon, characterisation by ion beam tech. 80—79833
Si, EHT calcs. of energy bands and pressure dependences *(Japanese)* 78—34747
Si, EMF appearance under action of thermal field pulses with high temp. gradients 79—56252
Si, EPR and spin-lattice relax. of dislocation spin chains *(Russian)* 79—91291
n-Si, EPR linewidth, Orbach relax. process, conc. depend. 80—44901
Si, EPR of quenched-in defects 80—29620
Si, EPR of radiation damage due to complete stopping of 30 MeV protons 77—65994
Si, EPR of radiation defects, temp. depend. 78—15023
Si, ESR in neutron transmutation doped samples 80—20462
Si, early oxidation stages, AES study *(French)* 79—8379
n-Si, edge dislocation and stacking fault defect electrical recombination efficiency 80—15106
Si, edge dislocation struct., lattice distortion and surrounding vacancy distrib. 77—19954
Si, edge-defined film-fed growth of controlled shape crysts. 78—31327
Si, edge-type dislocations, energy spectrum 80—24842
Si, effect of disorder on H content 80—75258
n-Si, effect of random var. in impurity conc. on Fermi level 79—51470
Si, effect of SiO$_2$ precip. on generation currents in MOS capacitor 79—78188
Si, effective dielectric function calc., exchange interaction effects 79—99494
n-Si, effective mass from intraband Faraday rot. and Hall effect 77—52049
Si, effective mass from Kramers-Kronig analysis for various doped crysts. 77—31942
Si, effective masses of heavy and light holes, from ohmic mobility data 80—80160
Si, effective supersystem cryst. simulation method, geometrical parameters, bulk moduli, impurity levels calcs. *(French)* 80—15430
n-Si, efficiency of radiation defect generation by electron bombardment, influence of Fermi energy 77—11596
Si, efficient stimulated Raman scattering using Q-switched single mode Nd:YAG laser 79—94289
Si, elastically bent cryst., intensity of diffracted beams in general case of diffr. 79—50935
Si, elasto-optic constants, real and imaginary, direct absorpt. and Raman scatt. meas. 80—97234

elemental semiconductors continued
Si, elec. cond. between 500 and 1200°C 77—11923
n-Si, elec. cond. control by hot electron intervalley transfer 80—59993
Si, elec. conductivity tensor, warm electron range 78—39123
Si, elec. props., plastic deform. and annealing temp. depend., dislocation effects *(Russian)* 77—89765
p-Si, elec. props. and thermal defects, influence of high temp. treatment 79—69531
p-Si, elec. resist., shock wave compression effects 80—80265
Si, electrical characterisation, review 78—60120
Si, electrical conduction in amorphous semiconductors, mechanisms 79—56214
Si, electrical conductivity, inertia of electron heating, expt. and theory 80—65613
Si, electrical properties of single crystal, dislocation effects *(Rumanian)* 79—73504
Si, electrical props. affected by heat treatment *(Russian)* 78—11352
Si, electrical recomb. behaviour at dislocations 79—82606
Si, electro- and thermo-reflectance spectra, line-shape anal. 79—24296
Si, electrochem. carrier conc. profiling 80—2461
Si, electrodeposited film, appl. in solar cell fabrication 78—76611
Si, electrodes in HF electrolyte, characterization by electrolytic reverse current 78—6078
Si electrolyte interface, energetic barrier height hypothesis 79—19657
Si, electron and hole effective mass, intrinsic conc., temp. depend. 80—107692
Si, electron beam annealing, beam voltage effect modeling 80—75275
Si electron beam deposited film, epitaxy by pulsed laser annealing 78—56055
Si, electron beam irrad., {113} faults, nature and origin 80—70258
Si, electron beam irrad. at 31 GeV, polarised photon emission *(Russian)* 80—29811
Si, electron beam scan annealed, deep levels 80—65481
Si, electron bombarded, capacitance transient analysis of defect states 77—80545
Si, electron bombardment, absorption of energy 79—14847
Si, electron diffraction on single-cryst. slabs at 2.27 MeV 79—50962
Si, electron drift in high elec. fields, long-time tail of autocorrelation function 80—103702
Si, electron emission coeffs. for electron and hole traps 79—91075
Si, electron energy loss spectra, direct nonvertical interband transitions 77—85856
Si, electron energy losses, anisotropy of excitation probability 78—15265
p-Si, electron field emission statistics 77—1791
n-Si, electron heating by static elec. field 80—96894
Si, electron impact ionis., direction depend. of threshold energy 79—42550
Si, electron inelastic mean free paths and energy losses, electron gas statistcal model 79—46733
Si, electron inversion layer on vicinal plane, minigaps 80—20282
n-Si, electron irrad., defect energy levels, energy depend. 79—33262
p-Si, electron irrad., influence of acceptor impurity conc. and irrad. temp. on defect formation 79—19281
Si, electron irrad., limiting position of Fermi level, elec. cond. and optical absorpt. meas. 79—65484
Si, electron irrad., resistivity-fluence relation 80—54700
Si, electron irrad., rod-shaped defects, electron microscopy and IR spectra obs. 80—39159
Si, electron irrad., two-vacancy defect EPR 80—29619
Si, electron irrad. damage, capacitance meas. 80—24935
Si, electron irrad. devices, dominant recomb. centres 77—72912
p-Si, electron irrad. effect on Hall mobility temp. depend. 80—60011
p-Si, electron irrad. induced defects, thermally stimulated capacitance 77—11933
Si, electron irrad. induced defect form., carrier density, mobility and lifetime changes 77—43250
Si, electron irrad. induced defects, bulk photo-EMF meas. 80—39160
Si, electron irradiated, EPR of C-O divacancy complex 77—69691
n-Si, electron irradiated, elec. props. 77—8041
Si, electron irradiated, high resist. surface layer, Schottky barrier meas. 78—64093
Si, electron irradiated, O-vacancy pair, EPR of optical absorption 77—16173
Si, electron irradiated, photolum. due to interstitial complex 77—44048
Si, electron irradiation induced displacement defects 77—80543
Si, electron mobilities on inverted surfaces near cond. threshold, appl. of meas. techniques 79—69602
Si, electron mobility based on dielectric function modification of Dingle pot. 79—60836
Si, electron probe determ. of pn-junction depth *(German)* 78—2552
n-Si, electron radiation defect annealing, negative stage, Hall coefficient, defect levels 79—90701
n-Si, electron recombination, role of intervalley scatt. *(Russian)* 79—19605
Si, electron states associated with core region of 60° dislocation 77—35887
Si, electron states associated with core region of 60° dislocation 78—39057
Si, electron states associated with dislocations 79—82544
Si, electron transport and ionisation at high fields 78—30933
Si, electron-beam-evaporated amorphous thin films, noise meas. 79—24091
Si, electron-exciton elastic scatt. cross sections, central field and exchange approxs. 77—62919
Si, electron-exciton inelastic collision cross sections 79—90967
Si, electron-hole drop luminescence, hysteresis effect and surface energy 78—2907
Si, electron-hole drop transition to metallic condensed state, Hartree-Fock theory 79—56136
Si, electron-hole droplet, effect of nonlocal contributions to energy 77—69246
Si, electron-hole droplet condensation, phase diagram and surface tension 79—19521
Si, electron-hole droplet condensation model, phase diagram and surface tension 80—6734
Si, electron-hole droplet condensation, crit. point 80—49612
Si, electron-hole droplet luminesc., laser excitation threshold meas. 79—33821
Si, electron-hole droplet spatial distrib., luminesc. obs. 80—49615
Si, electron-hole droplets nucleation at swirl defects 79—15095
Si, electron-hole drops, Auger recomb. 77—48240

elemental semiconductors continued

- Si, electron-hole drops, far IR absorpt. spectrum 78—47706
- Si, electron-hole drops, near and far IR emission spectra 77—48242
- Si, electron-hole drops, nonequilib. paramagnetism 80—6749
- Si, electron-hole drops, nucleation, time resolved luminesc. spectroscopy 78—6280
- Si, electron-hole drops, nucleation, luminesc. threshold obs. 79—33822
- Si, electron-hole drops, surface struct. 78—60058
- Si, electron-hole drops, thermodynamical parameter determ. from luminescence data 80—2845
- Si, electron-hole drops formation, nucleation theories 79—33239
- Si, electron-hole drops radius, luminesc. meas. 80—50415
- Si, electron-hole liquid, free excitons, biexciton gas, luminesc. 80—6750
- Si, electron-hole liquid, RPA calcs. 80—6743
- Si, electron-hole liquid, spatial condensation of strain-confined excitons and excitonic mols. 78—39592
- Si, electron-hole liquid and exciton and biexciton gas in elastically deformed cryst. *(Russian)* 78—34782
- n-Si, electron-irrad., surface defect distrib., deep-level transient spectroscopy 79—1459
- Si, electron-irradiated, {113} loops obs. 79—82225
- Si, electron-irradiated, annihilation of positrons 77—55847
- Si, electron-irradiated, positron annihilation 78—48256
- Si, electron-irradiated crystals, positron trapping, temp. depend. 80—104009
- n-Si, electron-phonon interaction, internal strain and impurity elec. field effect 78—14418
- Si, electron-phonon interaction anal. using photoacoustic cell 78—68027
- n-Si, electron-phonon scatt. and high-field transport 79—42552
- n-Si, electron-two phonon scatt. 77—47527
- Si, electronic and struct. props., nonlocal pseudopot. calc. 80—34349
- Si, electronic defect levels in self-implanted CW laser annealed samples 79—87053
- Si, electronic energy bands of diamond-type crysts., appl. of EHT method 78—87907
- Si, electronic energy levels strain depend., pseudopot. method 77—39775
- Si, electronic interface states in intrinsic stacking-faults 80—75522
- Si, electronic properties, rel. to chem. bonding and lattice dynamics 80—44169
- Si, electronic screening of lattice vibrs. 78—59875
- Si, electronic states associated with 60° edge dislocation 77—20261
- Si, electronic states of isolated negative donor ion, binding energy 79—65404
- Si, electronic states of vacancies, covalent states 79—23926
- Si, electronic struct., non-spherical local pseudopotential calcs. 80—39496
- Si, electronic struct. from SCF calc. using intersecting spheres model 78—51888
- Si, electronic structure, self consistent local description 80—20067
- Si, electronic structure at high press. near semicond.-metal transition 80—49586
- Si, electronic vacancy states by chemical pseudopot. method 79—23929
- Si, electrophysical props. of single crysts. with and without dislocations 77—47812
- Si, electrotransfer in Mo$_5$Si$_3$ 80—92708
- Si, emission spectra, excitons bound to isoelectronic trap 79—33772
- Si, emission spectra of ultrarelativistic collimated positrons 80—7434
- Si, energy band gap dilation and vibr. contrib. determ. 79—60703
- Si, energy bands and wavefunctions, localised orbital description 78—18942
- Si, energy depend. of amorphisation by ion implantation 78—2175
- Si, energy deposition in heavy-ion path using Monte Carlo transport anal. of delta rays in track 80—39185
- Si, energy gap, impurity conc. depend., calc. 80—80170
- Si, energy gap temp. depend. as thermodynamic problem *(German)* 77—43488
- Si, energy losses on C contaminated surfaces, secondary electron spectra, AES, and SEM 79—99997
- Si, energy spectra of dislocations 80—70637
- p-Si, energy spectrum and thermal stability of radiation defects 77—4406
- Si, energy spectrum of Fe group impurities 79—23932
- Si, energy spikes due to heavy ion bombardment, semiempirical model 78—47453
- Si, energy-integrated inelastic X-ray scattering cross sections, energy-integrated, separation of components 78—38587
- Si, enhanced conductivity in plasma hydrogenated films, thermionic emission 80—70692
- Si, entropy and enthalpy of vacancy form., comparison of theory with quenching expts. 77—11872
- Si, epitaxial, elec. activity of stacking faults, determ. using SEM in EBIC mode 77—43445
- Si, epitaxial, minority carrier lifetime and impurity conc. meas. *(Japanese)* 80—25025
- Si, epitaxial, on sapphire, characterisation, X-ray rocking curves 80—75458
- Si, epitaxial, on Si or sapphire, misfit, strain and dislocations, book contrib. 79—82499
- Si, epitaxial, optical constants meas. by far IR ellipsometry 78—93753
- Si, epitaxial (111) surface, etching observation of stacking faults, dislocations, S-pits, etch pits *(Chinese)* 80—70197
- Si, epitaxial and amorphous film growth, low energy ion beam deposition 77—28729
- Si epitaxial film, containing struct. defects formed during growth, positron annihilation 80—93433
- Si epitaxial film, correlation between electrooptical and electrical props., IR absorpt. spectra *(Russian)* 78—60453
- Si, epitaxial film, dopant incorporation model 79—99228
- Si, epitaxial film, dopant incorporation during growth, theory and expt. 79—99229
- Si, epitaxial film CVD growth, inelastic light scatt. as in situ probe of chem. reaction 77—40383
- Si epitaxial film concentrated inhomogeneity detection by selective etching *(Russian)* 78—10298
- Si epitaxial film deposition, vapour-phase, small-scale system design and operation 79—43151
- Si epitaxial film dopant incorporation, transient response 77—76976
- Si, epitaxial film growth by hydride-iodide method 77—48343
- Si epitaxial film growth on sapphire in SiH$_4$-H$_2$ system, optimum deposition 77—77397
- Si, epitaxial film growth on Si(111) and sapphire (1$\bar{1}$02), simultaneous RHEED/AES study 80—10833
- Si, epitaxial film on sapphire, optical absorption and interface comp. profiles 77—12459
- Si epitaxial film on sapphire, microtwins, TEM exam. 80—70555
- Si epitaxial films on Czochralski sapphire, optimisation of deposition conditions in SiH$_4$-H$_2$ system 80—75464
- Si, epitaxial growth, adsorbed layer model for autodoping mech. 80—7505
- Si, epitaxial growth, impurities incorporation kinetics *(French)* 78—22749
- Si epitaxial growth, in SiCl$_4$-HCl-H$_2$ system, model based on flow graph 79—42405
- Si, epitaxial growth, novel reactor for high volume, low cost prod. 79—24442
- Si, epitaxial growth, nucleation 77—62770
- Si, epitaxial growth, of submicrometer thickness 79—95932
- Si, epitaxial growth by partially ionized vapour deposition, low temp. 77—40389
- Si, epitaxial growth chambers cleaning, improved method using KOH solution 78—64478
- Si, epitaxial growth from vapour, dopant inclusion model *(German)* 79—42088
- Si, epitaxial growth kinetics in damp H$_2$ 77—44171
- Si, epitaxial growth kinetics, experimental verification of theoretical model 79—95278
- Si, epitaxial growth on ion-implanted Si:As 78—6243
- Si epitaxial growth on porous Si layer, struct. 79—1557
- Si, epitaxial growth on sapphire by partially ionised vapour deposition, RHEED-AES obs. 80—80985
- Si epitaxial interface migration, theory and expt. test 80—29290
- Si, epitaxial layer, growth mechanism from ion-molecular beams 80—2299
- Si, epitaxial layer, incorporation conc. depend. of P from silane-phosphine-H$_2$ mixture 80—2053
- Si epitaxial layer, large-area uniform growth through Al film by solid epitaxy 78—3033
- Si epitaxial layer, minority carrier lifetime obs. *(Russian)* 80—49765
- Si epitaxial layer, on Si ribbon substrate, dislocation density, X-ray topography obs. 77—85102
- Si, epitaxial layer CVD, appl. to Si, II-VI and III-V semiconductor growth 77—32530
- Si, epitaxial layer deposition by ion beam methods 80—100417
- Si, epitaxial layer grown by saturated Sn melt undercooling, morphology 78—22969
- Si epitaxial layer on sapphire, twin three dimens. distrib. 77—89666
- Si epitaxial layer regrowth due to laser annealing mechanism, liquid and solid phase regimes 80—100712
- Si epitaxial layer substrate junctions, carrier lifetime and abnormal conduction phenomena *(Korean)* 78—47888
- Si, epitaxial layer thickness meas. using phase correction function of substrate resistivity *(Rumanian)* 80—90812
- Si, epitaxial layers, cryst. quality improvement by ion implantation, backscatt. and TEM obs. 79—42397
- Si epitaxial layers, dechannelling by stacking faults, channelling effect technique using He$^+$ and D$^+$ ion backscatt. 79—4361
- Si epitaxial layers, development, structure and props. of stacking faults *(Russian)* 80—24461
- Si epitaxial layers, doping the P cpds., process parameters effect on electrophys. characts. 78—38734
- Si epitaxial layers, grown by sublimation in vacuum, TEM study of surface 79—46982
- Si epitaxial layers, grown in vac. at low temps. P and Sb doping 80—88189
- Si epitaxial layers, meas. of doping profiles *(Hungarian)* 80—70545
- Si, epitaxial layers, minority carrier lifetime and diffusion length meas., photocurrent technique 78—95302
- Si, epitaxial layers, stacking defect distrib. anal. using ion channelling tech. 80—100294
- Si epitaxial layers, temp. dependence of P dopant inclusion in gas phase deposition *(German)* 79—52127
- Si epitaxial layers, thickness meas. during deposition using diffraction *(German)* 79—97355
- Si epitaxial layers, vacuum deposited, conditions for impurity migration from B, P, Sb doped sources *(Russian)* 80—107570
- Si epitaxial layers, X-ray topographic study using Berg-Barrett techniques 79—28221
- Si epitaxial layers on metallurgical-grade polycryst. substrates, characteris. 79—28967
- n-Si epitaxial layers on oppositely conducting substrates, two layer Hall coeff. meas. technique 80—80297
- Si, epitaxial layers on ribbon substrates, solar cell prod. and characterisation 77—77354
- Si, epitaxial on sapphire substrates, Al conc. as a function of depth using ^{27}Al(p,α_0) reson. reaction 79—4328
- Si epitaxial p-i-n photoconvertor characteristic deterioration at high illumination 78—89536
- Si epitaxial reactor, doping system, transient steady state response, transfer function approach 79—42086
- Si, epitaxial regrowth and grain struct. of Al metallisation on ⟨100⟩Si 78—79901
- Si, epitaxial regrowth of thin amorphised layers by laser annealing, absorpt. coeff. influence 79—46968
- Si epitaxial solid-phase growth, rapid 77—21022
- Si, epitaxial stacking faults, nucleation sites 77—20201
- Si epitaxial stacking fault nucleation site identification, annihilation, and suppression 77—76705
- Si epitaxial structures, junction layer width and impurity conc. estimates *(Russian)* 80—49893
- Si epitaxial thin film growth on sapphire and spinel by MBE 80—76186
- Si epitaxial wafer, impurity profile meas. by multilayer spreading resist. anal. 77—76449
- Si, epitaxial wafer, saucer pit microdefects reduction by intrinsic gettering 80—75450
- Si epitaxial wafers, role of metallic contamination in formation of 'saucer' pit defects 77—39588
- Si epitaxy, autodoping effects 80—100259
- Si epitaxy, vapour phase deposition technology 80—75472
- Si epitaxy and oxidation, first-order process models 78—72049
- Si, epitaxy by solid phase crystn. of amorphous film 78—19663
- Si, epitaxy lateral autodoping kinetics 78—6087
- Si eqn. of state, under press. 78—75801

elemental semiconductors continued
Si, etch rate loading effect and temp. depend. in CF_4 plasma 79-34167
Si, etch rate uniformity in $CF_4+4\%$ O_2 plasma 80-40568
Si, etching by CF_4, plasma deposition reactor gas phase characts., mass spectra 80-70566
Si, etching by CF_4 plasma, mechanisms 78-72907
Si, etching by tetrafluoromethane plasma, mechanism 79-15832
Si, etching characts. using reactive ion etching with tetrafluoromethane-Cl_2 gas mixture 80-104313
Si, etching in He-F_2 plasma, etch rates, mass spectra, direct ion sampling study 80-79510
Si, etching in reactive plasmas 80-71778
Si, etching using XeF_2 vapour, adsorption/desorption process 79-43449
Si, evap. heteroepitaxial film, deep defect states obs. 78-72292
Si, exchange and correlation pot., band struct. calc. 78-56068
Si, excited by ultrashort laser pulses, self-diffr. effects 78-18022
Si, exciton and deformation pot. fine struct. 78-88301
Si, exciton ground state splitting 80-6736
Si exciton luminescence in mag. field or under uniaxial stress 78-27322
Si, exciton mol. by phonon-assisted two-photon absorpt., theory 78-48197
Si, exciton-impurity complexes, emission spectra, Zeeman splitting *(Russian)* 78-64413
Si, exciton-plasma Mott transition, luminescence spectra 77-62836
Si, exciton-plasma transitions, dense electron-hole system portrait composition *(Russian)* 80-49622
Si, excitonic molecules, thermodynamics, luminesc. 80-25442
Si, excitons, far IR absorption 78-31201
Si, excitons and electron-hole drops, phonon assisted luminescence lineshape 79-99942
Si, excitons and electron-hole liquid, luminesc. 80-6746
n-Si, exoelectron emission, effect of surface polishing rel. to defect distrib. in surface layer 80-40239
Si, extended glide dislocations, motion obs. by high voltage electron microscopy 80-10555
Si, extended Huckel theory calc. of hyperfine interactions of positive divacancy 77-89742
Si, extinction fringes and Burgers vector determ., single-crystal interferometric technique 79-95013
Si extrinsic IR detectors, As doped, low-level γ-ray irrad. effects 80-37085
Si extrinsic photoconductive IR detector, counterdoping scheme 78-49896
Si extrinsic photoconductive IR detectors, VLF behaviour 78-81542
Si, extrinsic stacking faults, core struct., TEM obs. 78-55878
Si, F-enhanced plasma growth of native layers, Auger profiles 80-93662
Si, failure in strong melt grown single crysts. 78-3205
Si, far IR impurity spectra, effects of high uniaxial stress 78-56508
Si, far IR photon drag and radiation pressure in refractive media 80-60048
n-Si, Faraday rot. temp. depend., effective mass determ. 80-71392
Si, Faraday rotation and ellipticity, interband transitions, comparison with Ge 77-52048
Si, fast electron bound states on axial channelling *(Russian)* 77-80562
Si, fast electron channelling, quantum-mechanical approx. 78-87731
p-Si, fast electron irrad., energy levels determ. by photocapacitance meas. 79-51531
p-Si, fast electron irrad., Hall mobility, temp. depend. 78-56165
Si, fast electron irradiated, models of luminescence centres, role of interstitials 77-81153
Si, fast neutron and ion irradiation, radiative recombination centres 77-81152
Si, fast particle irrad., Frenkel defect formation threshold energy 80-6404
Si, feeding-in and blocking of 2 MeV protons, simple diffusion model 78-22782
Si, Fermi level, minority carrier conc., effective intrinsic conc., Einstein relation 77-85209
Si, ferromagnetism induced by ion irrad., e.p.r. investig. *(Russian)* 77-1595
Si fibre growth and struct. 79-69970
n-Si, field and current domains, at low temp. 80-6868
Si, field effect characts. rel. to surface inhomogeneity 78-26933
Si, field penetration in FIM, band bending 79-87567
Si, filamentary, grown by chem. transport reaction method, banded struct. 80-38978
Si filamentary crystals, grown from vapour, electron probe microanal. 79-77538
Si filamentary piezoresistor for pulsed wave process meas. 78-57980
Si film, amorphous, effects of annealing of gap states 78-72115
Si film, amorphous, formed by CVD, crystallisation 77-39746
Si film, amorphous, glow discharge deposited, for low cost solar cells 80-61355
Si film, amorphous, high resolution electron microscopy, digital processing use 78-37116
Si film, amorphous, hopping cond. control by ion bombard. induced struct. modification 80-92898
Si film, amorphous, LF vel. of sound for Young's modulus mode 77-35636
Si, film, amorphous, optical absorption at high press. 78-35216
Si film, amorphous, plasma-deposited, H_2 evolution, mass spectrometry and RHEED obs. 78-72050
Si film, amorphous, prep. conditions influence on supernetwork struct. 77-76709
Si film, amorphous, structural comparison of evaporated and glow discharge samples 77-62778
Si, film, amorphous, two-dimensional variable range hopping cond. 80-10977
Si film, amorphous and crystalline, optical properties 77-24906
Si film, amorphous and polycrystallised, localised states, elec. and optical props. 78-64008
Si film, amorphous evap., structural aspects in electronic data interpret. 77-76977
Si, film, CVD, low press., struct. and stability, X-ray diffr. and TEM obs. 78-91559
Si film, CVD or evaporated, covered with Al layer, solid-phase crystn. obs. 77-85100
Si, film, chemically deposited on amorphous SiO_2, influence of substrate temp. and SiH_4 to N ratio on struct. 79-65346
Si film, critical surface tension, aligning props. of nematic MBBA mols. 79-90846

elemental semiconductors continued
Si film, crystallographic orientation using surface relief grating and laser crystn. 79-95277
Si film, electron beam deposited, elec. and struct. props. 79-1632
Si film, electron beam evaporation, for solar cell appl., heat exchanges and columnar growth 79-15609
Si film, electroreflectance spectra, 2.8 to 5.0 eV, ion bombard. effects 77-1752
n-Si film, epitaxial, electrical activity of stacking faults 77-39744
Si film, epitaxial growth by partially ionised vapour deposition, RHEED-AES-QMS study 79-83136
Si, film, focused ion beam designs for sputter deposition 79-89841
Si film, glow discharge deposition, SiH_4 discharge parameters obs. 80-44030
Si film, high electron mobility, grown on sapphire at high growth rate 77-81225
Si film, hydrogenated amorphous, Brillouin scatt. 78-72538
Si film, ion bombarded, crystalline-to-amorphous transition, defect-rich film prep. 80-65071
Si film, lightly doped, polycryst., cond. mechanisms, correl. with SEM examination of film 79-1634
Si film, low press. CVD prep., struct., elec. and optical props. 80-70548
Si film, MBE, cryst. defect props., substrate treatment effects 80-70551
Si film, on graphite, early growth by ion-beam sputtering 77-44158
Si film, on sapphire, defect struct., TEM obs. 77-47693
p-Si film, on sapphire, elastoresist. coeffs., room temp. 80-34532
Si film, on sapphire, etching method 78-7070
Si film, on sapphire, Hall mobility, carrier distrib. effects 77-51818
Si film, on W (100) struct. and work function, LEED meas. 77-66096
Si film, optical characterisation from guided wave optics 78-48245
Si film, plasma etching, role of chemisorpt. of CF_4, CF_3H, CF_3Cl, CF_2Cl_2 and CCl_4 79-11714
Si film, polariton resonance obs. from reflectivity meas. 77-69251
Si film, polycryst., electron microscopic investigation of initial stage of growth 79-23849
Si film, polycryst., ellipsometric meas. *(Polish)* 78-21095
Si, film, polycryst., for photovoltaic appl., grain size effects 78-72034
Si film, polycryst., grain struct. and surface roughness, TEM study 80-70556
Si film, polycryst., laser-induced CVD growth from $SiCl_4$ 80-84852
Si film, polycryst., substruct. 79-23848
Si film, polycryst., thinning using plasma etching *(Slovak)* 80-45405
Si film, polycrystalline, struct. thickness relationships 77-62779
Si film, porous, form. and oxidation by anodic reaction 79-28966
Si film, prep. by plasma-induced CVD from $SiCl_4$-H_2 79-83132
Si film, removal using anodic oxidation, determination of active impurity distrib. 80-40583
Si film, semi-insulating, with 40 at.% O, AES and PES study 80-107939
Si film, solid phase epitaxy, Au and O distrib. 77-66095
Si film, sputtered, physical props. 79-77938
Si film, sputtered amorphous, P and B doped, elec. cond. and thermopower meas. *(French)* 78-47403
Si film, volume plasmons, EELS, line shape 79-90984
Si, film and p-n junction growth by ionised-cluster beam deposition 77-32527
Si, film deposition, growth kinetics under low H_2 press. 78-56586
Si film deposition, on quart z and MgO substrates, using double cathode sputtering system *(Japanese)* 77-55889
Si film deposition by CO_2 laser irrad. of SiH_4 80-16190
Si film double-mesa reach-through avalanche photodiode with large gain-bandwidth product 79-12845
Si film on sapphire, electron mobility 78-91792
Si film on sapphire, quality evaluation using soft X-ray rocking curve 77-80711
Si film thickness meas. from visible refl. spectra 79-99960
Si films, CVD, amorphous and polycryst., microscopic surface roughness, effective-medium models, ellipsometric expts. 80-24756
Si films, electron beam evaporated, for MIS solar cells 80-93490
Si films, electron-beam-deposited on W substrates, growth and struct., AES and SEM obs. 79-46972
Si films, polycryst., annealing of paramag. vacancy-type defects, EPR obs. 79-10848
Si films, polycryst., glow discharge deposited below 250°C, struct. and morphology 80-49535
Si films, polycrystalline, elec. props., grain size and dopant conc. influence 80-29492
Si films, RF sputtered, Ar conc. as function of operation frequency and discharge pressure 80-65393
Si films, ribbon-against-drop process, physical and chemical characterisation 80-92798
n-Si films on sapphire, crystalline defects effect on elec. props. 77-20470
Si, fine pattern etching by RF sputtering *(Japanese)* 77-70196
Si, fine structure of lowest exciton state *(Russian)* 80-96801
Si, float zone, meas. of deep levels by photovoltage spectroscopy 80-103723
Si, float zone, process-induced effects on carrier lifetime and defects 80-81216
Si, float zone crystal, dislocation creation and elimination 80-107072
Si, float zone crysts., large diameter, growth parameters 78-31336
Si, float zone growth, maximum stable zone length 79-91582
Si, float-zone cryst. growth, shape of melt interfaces and radial P distrib. 77-24952
Si, floating zone structural perfection changes by high temp. treatment, dendrites, dislocation interactions 80-29049
Si, floatzone, P doping by thermal-neutron irradiation 78-22750
Si, fluorocarbon ion beam etching characts. 80-35363
Si, foil, thinning for electron microscopy 79-49217
Si for integrated optics high quantum efficiency waveguide coupled photodetectors 80-58805
Si, forbidden 200 diffr. spots 78-47214
Si, foreign interstitial atoms rel. to thermal intrinsic defects 80-29018
Si four-point probe meas. error factors, SEM obs. 79-71484
Si, free carrier and interband absorpt. at 1.06 μm, temp. depend. 80-2783
Si, free exciton luminesc. band, resolved splitting 79-73995
Si, free excitons, drift and diffusion, luminesc. obs. 80-84434
Si, furnace preannealed (111) ion implanted, laser irrad. 80-65015
p-Si, galvanomagnetic effects 79-33297

elemental semiconductors continued
Si, gamma radiation angular distribution of channelled 900 MeV electrons *(Russian)* 80—19858
n-Si, gamma ray irrad., impurity composition influence on recombination centre formation 80—6872
Si, gamma-irradiated, number of Frenkel defects 78—14377
Si, gas phase etching, with HCl-H_2 mixture 79—96165
Si gates ion implantation, without implanting ions into SiO_2 insulating layer 79—7619
Si, gettering by ion damage, minority carrier lifetime and backscatt. study 80—100286
Si, gettering effects, of P ions and P induced dislocations for Au impurities 78—91346
Si, gettering effects *(Japanese)* 79—83356
Si, glow discharge deposited, optical spectra, reflectance, dielectric function and oscillator strength 80—11492
Si, glow discharge film decomposed from silane, on amorphous substrate, elec. cond., RHEED study 80—20044
Si, grain boundary defects in thin semicrystalline material 80—93889
Si, grain boundary elec. props./impurity correl. using surface anal. of multigrained samples by SIMS and AES 80—79816
Si, graphoepitaxy on fused SiO_2 using surface micropatterns and laser crystn. 80—70554
Si, ground state props. in density-functional pseudopot. approach 80—92803
Si, growth, chem. transport, transfer inversion using Mo catalyst 79—11517
Si, growth and melting processes, origin of swirl defects 77—76407
Si, growth and thermal evaporation kinetics of oxide film on Si surface 78—3246
Si, growth from Al-Si-Cu melt, faceted cryst., cellular hole growth 77—4061
Si, growth from melt, temp. distrib. calc. in working zone of composite heater 78—3016
Si, growth kinetics of low-temperature SiO_2 films by oxidation of SiH_4 77—8763
Si, growth of large grain polycryst. layers on graphite substrates by CVD on liquid layers 80—55849
Si, growth processes, in-situ obs. *(Japanese)* 80—35104
n-Si, γ-irrad, (E_{max}=100 MeV), carrier recomb. 78—56158
n-Si, γ-irrad., galvanomagnetic effect anisotropy rel. to layer inhomogeneity 79—33299
n-Si, γ-irradiated, with layer inhomogeneity, quantum current oscillations 80—11010
Si, γ-ray induced elec. cond. at low temps. 78—52002
Si, H chemisorbed, relation of Si-H vibr. freq. to surface bonding geometry 80—49502
Si, H_2^+ irrad., annihilation of free excitons, inelastic scatt. by SiH_4 mols., photolum. obs. 78—19561
Si, H^+ and H_2^+ ion implantation profiles determ. by SIMS 79—4334
Si, H-related interstitial defects, vibr. electronic struct., extended Huckel theory 77—62604
Si, HCl oxidation conditions for stacking fault nuclei gettering and undesirable etching 78—68830
Si, HF field effect meas. 77—55556
n-Si, HF plasma oscills. in external mag. field 80—54731
Si, HVEM struct. images of extended 60° and screw dislocations 80—59466
Si, Hall effect, influence of dislocations 79—82611
n-Si, Hall effect appl. in coaxial power meter 78—238
Si, He impurity props. investigation by EHT calcs. 79—99183
Si, heat treated, minority carrier lifetime, effect of swirl defects 77—39868
Si, heat treated, spin-depend. recomb. at dislocations 79—47122
Si, heat-treated dislocation-free, elec. props. of stacking faults and precipitates 77—39796
Si, heavily damaged ion implanted (100) and (111), development of secondary defects 79—51166
Si, heavily disordered, fast neutron irrad., IR absorption following heat treatment 78—2448
Si, heavily doped, approx. of Einstein relation, carrier diffusivity to mobility ratio 79—65494
Si, heavily doped, bandgap narrowing and diffusion length meas. 79—7781
Si, heavily doped, bandgap narrowing 80—15479
n-Si, heavily doped, carrier conc., comparison of expt. and theory, screening effects 77—85216
Si, heavily doped, carrier diffusion coeff. 79—47099
Si, heavily doped, carrier mobility calc., 300K 79—56215
Si, heavily doped, carrier recomb. through shallow donor and acceptor states 80—15535
Si, heavily doped, characts. of distrib. of density of states 79—15072
Si, heavily doped, doping density striation effects in studies of metal-nonmetal transition 79—28383
Si, heavily doped, electronic effects on dislocation velocities 77—62531
Si, heavily doped, excess intrinsic carrier density, deionisation of impurities as explanation 80—96864
n-Si, heavily doped, extrinsic sp. ht. in metallic regime 78—59956
p-Si, heavily doped, intra- and interband Raman scatt. 79—95788
p-Si, heavily doped, intra- and interband Raman scatt. by free carriers 80—108208
n-Si, heavily doped, intraband Raman scatt. by free carriers 78—19483
n-Si, heavily doped, meas. of minority carrier transport parameters 80—15537
Si, heavily doped, microcreep breakdown 80—97549
Si, heavily doped, minority carrier injection, model 77—39874
Si, heavily doped, minority-carrier transport parameters meas. 80—80291
n-Si, heavily doped, negative magnetoresistance model, spin-up spin-down electron effective mass variations 79—95423
n-Si, heavily doped, Raman phonons, interband excitation effects 78—52501
n-Si, heavily doped, self energy of phonons interacting with free electrons, Raman scatt. 78—64366
p-Si, heavily doped contact layers on IR detectors, IR transmissivity 80—108190
Si, heavily doped energy gap 77—43489
Si, heavily doped films, electromigration obs. 80—65295
Si, heavily doped implantation layers, laser beam annealing 78—88481
Si, heavily doped layer, electronic characts., electron beam induced current obs. 78—10473

elemental semiconductors continued
Si, heavily implanted, lattice defects and strains after high temp. annealing 78—10077
Si, heavily irrad., ESR study of annealing characts. 78—10771
n-Si, heavily-doped, EPR near metal-nonmetal transition 77—28446
Si, heavy ion induced disorder in surface and at shallow depths 80—59535
Si, heteroepitaxial, prep. and props., book contrib. 79—83128
Si, heteroepitaxial early growth island morphology rel. to deposition conditions 78—6245
Si, heteroepitaxial films, photomagnetoelectric effect 77—85264
Si heteroepitaxial films on sapphire, vac. deposited, struct. and elec. props. 80—15390
Si heteroepitaxial growth using SiH_4 in He-H_2 atm. 77—77396
Si, heteroepitaxial growth using SiH_4 in H_2-He atm. 80—20049
Si, heteroepitaxial vacuum deposited films, doping *(German)* 77—84779
Si, heteroepitaxy, refractory oxides as substrates *(French)* 77—44181
Si, high capacity arc heater production for solar cell manufacture 79—11509
Si, high dislocation density crystals, photoelectret state investigation 80—97191
Si, high dose Pb^+ and Cs^+ distribs., determ. using low angle Rutherford He ion backscatt. 79—4327
Si, high dose self-irrad., spatial correl. between primary and secondary defect profiles 80—59536
Si high efficiency solar cells, laser annealing, reviews 80—93976
Si, high electronic current density in anodic oxidation 80—89386
Si, high field electron transport, effect of ionised impurities 77—28186
Si, high index surface, natural orientational superlattice in 2D electron gas 79—99598
Si, high level photogeneration, absorpt. and free carrier distrib. 79—33309
Si, high O conc., electrical and mechanical props., influence of heat treatment 77—35934
p-Si, high ohmic material, deep level investigation, vacuum growth *(Russian)* 80—54654
Si, high press. pyrogenic oxidation in the production environment 78—35547
Si, high purity, exciton lifetime, temp. depend., photoluminesc. meas. 80—44508
Si, high quality oxidation *(Chinese)* 79—52401
Si, high rate reactive ion etching 80—85070
Si, high resistivity, specific resistance depend. determ. using impedance freq. depend. *(Czech)* 80—15536
n-Si, high resistivity wafer, oxide layer anodically grown, improved homogeneity 79—24642
Si, high sensitivity depth profiling of As and P, SIMS 77—7742
Si, high-current high-dose implantation visible interf. effects 77—7743
Si, high-dose Ar implantation, X-ray topographic obs. of strains and damage 80—59496
Si, high-index surface, valley-valley splitting in inversion layers 78—39219
Si high-intensity solar cell, fabrication and AM1 efficiency 79—43760
Si, high-meniscus ribbon growth, thermal balancing via distributed inert gas streams 78—31329
Si, high-purity, preparation by H_2 reduction of trichlorosilane *(Korean)* 77—21034
Si, high-resist. diffusion layers, determ. of hole-mobility 77—66204
Si, high-resistivity, characterisation by Hall meas. 78—10480
Si, high-resistivity, local IR refraction and transmission 79—15429
p-Si, high-resistivity, TSC and photo-EMF in p-n junction, deep levels 77—72913
Si, high-resistivity layer form. during electron irrad. 80—80352
Si high-resistivity structure, photoelec. props. 78—91730
n-Si high-temp. vacuum etching, p-n junction photodetectivity 78—95355
p-Si, highly deformed, hole scattering 77—20309
P-Si, highly doped, thermoelec. coeffs. meas. at semicond. solid-metallic liq. interface 77—39887
Si, highly doped and highly exerted, Auger coeffs., radiative band to band recomb. lifetime meas. 77—85764
Si, highly excited, theory of electron-hole plasma 78—10363
Si, highly transparent semicond. crysts., multiphonon IR absorpt. 78—10885
Si, highly transparent semicond., multiphonon IR absorpt. 78—60461
Si, hole diffusivity, time-of-flight and noise meas. 79—56233
p-Si, hole drift vel. in high field 79—95415
Si, hole localisation, solid solubility, excitonic Auger lifetime of acceptors 80—20216
Si, hole mobility temp. depend., valence bandstruct. 77—80771
Si, hole-hole-electron Auger recombination 80—70720
Si, homoepitaxy, local selective, at reduced temp. using Si-I transport system 79—24444
Si homoepitaxy in high vac., stacking fault nucleation, crit. temp. for SiC growth 78—14620
Si, homogeneous epitaxial layers, production, appl. of neutron transmutation doping 78—38737
Si, homogeneous n-type doping by thermal neutrons 80—2051
Si, homogeneous plates, theory of arising longitudinal photoeffect *(Russian)* 79—19614
Si, homopolar semiconductor, quantum efficiency 80—20254
Si horizontal epitaxial reactor transport expt. and model 77—77399
Si, horizontal ribbon growth from melt, theoretical anal. 78—75604
n-Si, hot carrier noise and generation-recomb. noise 79—38140
Si, hot electron diffusivity, theory 77—62940
Si, hot electron distrib. function, response to step changes in elec. field 80—24937
n-Si, hot electron repopulation at 77K, electron-electron scatt. effect 78—10456
Si, hot hole diffusion and white noise, microscopic Monte Carlo model 78—30937
Si, hot holes, drift and diffusion 79—78110
Si, hot holes negative Hall effect 79—87118
Si, hot-electron diffusion, Boltzmann eqn. 77—51757
n-Si, hot-electron diffusion, effect of ionised impurity scatt. 78—56151
n-Si, hot-electron diffusion noise, meas. using radiometric method in X-band region 77—39905
Si, hydrogenated, amorphous, theoretical calc. of defect states 80—49657
Si, hydrogenated, discharge produced amorphous film, gap state role in carrier transport 79—73608
Si, hydrogenated amorphous, laser annealing 80—100713

elemental semiconductors continued
Si, hydrogenated amorphous, gap states, comparison of photoemission and photocond. results 80—103724
Si, hydrogenated amorphous film, XPS and UPS 78—19636
Si, hyperpure, large scale prod. and prep. *(German)* 78—95704
Si, IR absorption spectra, Si-H bonds, crystal defects *(Chinese)* 80—55073
Si, IR detector, free carrier absorpt. 78—37060
Si, IR photoresponse at 1.15 microns 79—7864
n-Si, IR spectra of surface photocond. and photo-EMF 77—76868
Si, ideal vacancy, electronic struct., tight-binding calc. 79—4529
Si, ideal vacancy, self consistent Green's function calc. 78—91640
Si, impact ionisation, threshold energies calcs. for electons and holes 77—62933
Si, implantation, microstruct., fabrication, ion channelling effects 80—70230
Si, implanted ^{16}O, lattice location of ^{16}O by α-particle backscatt. method 78—10080
Si, implanted ^{222}Rn TIPAC measurements 78—43732
Si, implanted amorphous, comparison of laser and thermal annealing 79—70084
Si, implanted annealed layers, amorphised structure formation mechanism and crystallographic nature 80—29091
Si, implanted crystal, laser induced annealing and diffusion behaviour 80—88202
Si, implanted ions, energy deposition profiles from range data, simple method for calc. 77—39619
Si, implanted layer anal. for semiconductor device processing 77—76447
Si implanted layers, interaction of defects and impurities stimulated by induced ionisation, ESR 80—11270
Si implanted layers, utilisation coefficient of impurities after laser annealing 77—76437
Si, implanted Li atoms, depth profiles and sputtering anal. by optical spectra 77—35579
Si implanted with ^{31}P, ^{75}As, ^{11}B, amorphous layer reordering 78—14622
Si, implanted with low solubility dopants, laser annealing, TEM study 80—70233
Si, impurities displacement by H$^+$ or He$^+$ irrad. 79—86824
Si, impurity anal. by photoelectric spectroscopy, review 77—24584
Si, impurity conc. from MOS DC transfer characts. 78—2155
Si, impurity content characterisation, exciton luminesc. 80—60653
Si, impurity determ. in very pure sample by photoelec. spectroscopy 77—39888
Si, impurity determination, by neutron activation analysis 78—11586
Si impurity diffusion through SiO$_2$ layer, physicochemical processes *(German)* 78—2149
Si, impurity doping influence on free-exciton absorpt. 77—69861
Si, impurity interstitials, EHT calcs. 80—24845
Si, impurity levels of H and muons 79—56162
Si, impurity penetration depth, chemical-spectral determ. 80—19830
Si, impurity redistribution during single oxidation step, computer program calc. 80—2060
Si, impurity screening, local-field effects 79—60759
Si, impurity solubility limit after laser induced melting 80—107426
Si, impurity states, localised orbital approach 80—92851
Si, impurity states and core excitons, binding energies, perturb. theory 80—49659
n-Si, impurity-assoc. magnetophonon reson. 80—20221
Si, impurity-ion potential, electron-conductivity mobility, spatially variable dielectric function calcs. 79—78105
Si, in HCl-O$_2$ gas mixture, mobile Na ion passivation 79—70187
Si in MOS structure Pt diffused, hysteresis and memory props. 80—96992
n-Si, in MOSFET inversion layer, Gunn instability 78—84305
Si, inclusion type defects removal from bulk of single cryst. by elec. fields 79—43126
Si, indentation hardness and semicond.-metal transition 78—35499
Si, indirect free exciton, ground state, magneto-optical investigation 77—51670
Si, inelastic X-ray scatt. cross section accompanied by intermediate momentum transfer 79—24387
n-Si, influence of deform. on capture of electrons by divacancies 77—1449
Si, influence of imperfections on microplasma formation in p-n junctions 77—8177
Si, influence of one-dimensional superlattice on two-dimensional electron gas 77—43683
Si, influence of surface recombination rate and carrier diffusion on photocond. 80—44660
Si ingots, polycrystn., growth and characterisation from metallurgical grade source material 79—87576
n-Si, inhomogeneous impurity distrib., elec. props., effect of γ-irradiation 77—55550
Si, initial oxidation rate 79—91817
Si, integrational etching composition and method 78—10055
n-Si, interaction of disordered regions with point defects 79—19296
Si, interactions between sequential dopant diffusions, review 77—27900
Si, interband and free carrier absorpt. consts. at high-level photoinjection 79—38514
p-Si, interband transitions, contrib. to conductivity at submillimetre wavelengths 80—34473
Si, interface structural model between amorphous and crystalline phase 78—63941
Si intermixing with Pt(Ni)(Hf) films, ion-beam induced silicide form. 79—46718
Si, internal photoelectric effect, spectral depend. of quantum efficiency 78—39150
n-Si, internal stress effect on electron-phonon interaction 79—42468
Si, interstitial swirl defect form. in dislocation free floating zone cryst. 77—7682
Si, interstitials and lattice vacancies 78—10038
Si, interstitials in radiation defect formation 77—15461
n-Si intervalley electron-phonon deform. pot. consts. from high-field transport props. 77—62938
Si, intrinsic, electronic properties, temp. depend. *(German)* 77—76822
Si, intrinsic, phonon replicas of electron-hole liq. luminesc. line 79—28831
Si, intrinsic, radiative recombination probability *(German)* 79—61441
Si, intrinsic, self-diffusion, 885-1175°C 80—10700
Si, intrinsic, two-phonon assisted free exciton recomb. radiation 78—2922

elemental semiconductors continued
Si, intrinsic semiconductor, radiative recombination probability *(German)* 78—95608
Si, introduction of defects during growth and processing 79—95925
Si, inversion layer, 1/f noise and percolation in impurity bands 79—24029
Si inversion layer, cyclotron resonance in extreme quantum limit, collective ground state 80—50191
Si, inversion layer, dynamic conductivity of electrons, temp. depend. 78—19115
Si inversion layer, elec. break-through, exactly solvable model 78—56234
Si inversion layer, elec. cond., freq. depend. 78—72270
n-Si inversion layer, electron mag. suscept. 78—52009
n-Si inversion layer, electronic bound states, theory 78—60217
n-Si inversion layer, exchange instabilities 78—52052
Si inversion layer, far IR photoresponse 77—38002
Si inversion layer, Γ and X electric breakthrough interference effect 79—47137
Si, inversion layer, Hall effect meas. 78—56199
Si inversion layer, high freq. cond., Drude relax., 2D plasmons and minigaps in surface lattice 78—60230
Si, inversion layer, impurity scatt., self-consistent calc. 79—28415
Si inversion layer, in strong mag. fields, electron localisation 78—60219
Si inversion layer, influence of natural superlattice on 2-dimens. electron gas spectrum *(Russian)* 78—68064
Si inversion layer, inter-subband optical absorpt. in mag. field 77—32375
Si, inversion layer, interacting electron system, cyclotron reson. 78—87902
Si, inversion layer, magnetoplasmon reson. lineshape theory 79—1615
Si inversion layer, negative differential resist. 78—60225
Si inversion layer, obs. of localisation ion two-dimens. systems 78—60213
Si, inversion layer, on vicinal plane, band structure 80—24994
Si inversion layer, photoconductivity meas. 78—10498
Si, inversion layer, polaron model for localisation 80—20280
Si inversion layer, press. depend. of struct. of field effect mobility 78—60216
Si inversion layer, random attractive electron-electron interactions in two-dimens. systems 78—60183
n-Si inversion layer, resist. minima in surface quantum oscills. 78—60215
p-Si, inversion layer, screening effect and quantum transport in strong mag. fields 78—19155
Si inversion layer, surface quantum oscillation under pressure 78—60228
Si, inversion layer, temp. depend. of subband energies, exchange and correlation effects 80—20281
n-Si inversion layer, thermal activation of two-dimens. Shubnikov de Haas cond. extrema 78—60218
Si inversion layer, transient response under hot electron conditions 78—60223
Si inversion layer, transient response of hot electrons, calc. 80—49747
Si inversion layer, two-dimensional magnetoplasmon 78—2440
Si inversion layer, valley splitting, effects of misorientation 79—73564
Si, inversion layer, voltage tunable far IR emission 80—25018
Si inversion layer, warm electrons 78—60222
Si inversion layer (100), wavevector, depend. of the 2D plasmon disp. relationship 78—76101
Si inversion layer electronic transitions for voltage-tunable far IR emission 77—39962
Si, inversion layer electrons, temp. depend. cyclotron reson. lineshape 78—10568
Si inversion layer in MOS struct., carrier-phonon interaction, nonohmic transport 80—49943
Si inversion layer surface cyclotron resonance, temp. and stress effects 78—60229
Si inversion layers, Anderson transition, random field origin, substrate bias effect 77—28255
n-Si inversion layers, broken symmetry states 79—15229
Si inversion layers, CDW mag. fields and stability 78—10533
Si inversion layers, cyclotron and subband emission 78—64128
Si inversion layers, discrepancies between absorption and photocond. meas. 78—6451
Si inversion layers, effective mass variation 79—24050
n-Si inversion layers, electronic g-factor, spin-split Landau levels 80—80346
Si inversion layers, far IR transmission spectra, two-dimensional plasmons 77—76931
Si, inversion layers, far IR emission from hot electrons 78—30995
Si inversion layers, far IR reson. magnetotransmission, temp. and band gap light depend. 78—64363
Si, inversion layers, far IR cyclotron emission 79—61226
Si, inversion layers, first order intervalley scatt. 80—29484
Si inversion layers, Hall effect, consistency with presence of macroscopic inhomogeneities 79—51681
Si inversion layers, harmonic generation due to hot electrons 80—65694
Si inversion layers, high field magnetocond. 77—32020
p-Si inversion layers, hot carrier effects in high mag. field, 1.25-20K 78—34908
n-Si inversion layers, in strong mag. field, quantum galvanomag. expts. 78—60214
Si, inversion layers, intervalley transitions and subband splitting 77—20455
Si inversion layers, low density, far IR resonant magnetoabsorption 77—55789
Si inversion layers, magnetocond. in ground Landau level, defect diffusion in Wigner cryst. 77—39914
Si, inversion layers, magnetic localisation of electrons 78—43481
n-Si inversion layers, many-body effects, excitation to higher subbands MOS struct. 77—62997
n-Si, inversion layers, many-valley electron-phonon interactions, piezoresistance, anisotropic cond., Shubnikov-de Haas oscillations 78—52096
Si inversion layers, mobility temp. depend., Coulomb and surface roughness scatt. 80—80390
Si inversion layers, near threshold at low temps., cond. anomalies and electronic states 77—59333
Si, inversion layers, nonmetallic cond. at low temp. 80—70833
Si inversion layers, phase diagram in strong mag. fields 80—88492
Si inversion layers, piezoresistance 77—35935
Si inversion layers, quantum magnetoresist. results, using pulsed fields up to 35 T 79—73528
Si inversion layers, random pair attractive interaction model of carrier correl., compared with expt. 78—60212
n-Si inversion layers, resist. temp. depend. at liq. He temps. 80—80391

elemental semiconductors continued
Si inversion layers, resolution of Shubnikov-de Haas paradoxes 80—39648
Si inversion layers, stress effects on electronic props. 78—43476
Si inversion layers, stress and intersubband correlation 78—60227
n-Si inversion layers, stress and temp. depend. of subband struct., plasmon-pole approx. 79—95461
Si, inversion layers, submillimeter cyclotron reson. at low electron density 79—60925
Si, inversion layers, two-subband screening and transport 78—64126
Si inversion-layer electrons, temp. depend. cyclotron reson. lineshape, theory 78—64086
n-Si, inverted MOSFET surfaces, quantum oscills., valley splitting, lineshape in state density effects 79—56318
n-Si, inverted MOSFET surface, evidence for Lande factor $g=2$, finite valley splitting 80—6989
Si, ion beam damaged, minority carrier lifetime distribs., electron beam meas. 79—87108
Si, ion beam irrad., defects prod. by individual displacement cascades, TEM study 80—70265
Si, ion bombard. effect on surface struct., RHEED and Au decoration 80—2096
Si, ion bombard. induced residual stress in amorphous implanted surface layers 77—35610
Si, ion bombarded, radiation defect formation, atom-atom collision cascades modelling 80—10582
Si, ion bombardment, anomalous surface damage from channelling-backscatt. meas. 80—84222
Si, ion bombardment, energy distrib. of positive secondary ions and sputtered atoms 77—32485
Si, ion bombardment induced buildup of disordered material, model 77—47496
Si, ion bombardment induced light emission, investig. of cpd. form. 77—48257
Si, ion bombardment induced defect distrib., IR and electron diffr. study 80—65074
Si ion damage critical gettering microstructures 78—6098
Si ion damage critical gettering doses, elec. characts. 78—10085
Si, ion damage TEM study of laser annealing 80—88215
Si, ion implantation, atomic collision theory and range-energy relations 78—71753
Si, ion implantation, channelled, through metal silicide film 80—70231
Si, ion implantation, channelling, alignment effects 80—88183
Si, ion implantation, high dose, solid phase epitaxial regrowth 80—103380
Si, ion implantation, investigation of radiation damage by pendellosung topography 79—51125
Si, ion implantation, recent progress 79—14831
Si, ion implantation, semiconductor device processing 80—34031
Si, ion implantation, TSC meas. of coupled levels 78—84165
Si, ion implantation, target heating, temp. measurement 80—34032
Si, ion implantation 77—59029
Si, ion implantation and pulsed laser annealing of group III and group V dopants, supersat. alloy form. 80—54267
Si, ion implantation by laser annealing, characterisation, solar cell applications 80—70247
Si, ion implantation damage, annealing, role of stresses 78—75679
Si, ion implantation of noble gases, high fluence retention 79—23627
Si, ion implantation radiation damage, SEM electron beam absorpt. meas. 78—75696
Si, ion implantation with Li$^+$, characts. for thin film solar cell use *(Korean)* 77—51812
Si, ion implantation-induced damage after Ar and P implantation, defect density and distrib. *(German)* 77—24337
Si, ion implanted, annealing of heavy ion cascade damage, channelling meas. 80—89255
Si, ion implanted, annealing by ion beam heating 80—103382
Si, ion implanted, CW laser annealing 80—92550
Si, ion implanted, colour generation model 77—85868
Si, ion implanted, complex annealing behaviour of amorphous layers, TEM obs. of defect struct. 80—107299
Si, ion implanted, damage profiles, Rutherford backscattering 80—100733
Si, ion implanted, damage struct. obs. using TEM and cross section specimens 80—107298
Si, ion implanted, defect struct., dislocation loops and elongated defects 80—107300
Si, ion implanted, difference between ruby and Nd:YAG laser annealing 79—37723
Si, ion implanted, dopant depend. of oxidation rate 80—89384
Si, ion implanted, dynamic behaviour of pulsed-laser annealing, time depend. optical reflectance meas. 79—60393
Si, ion implanted, EPR line shape exam. of amorphous centres 79—28587
Si, ion implanted, electron beam annealing, surface struct. study using SEM 80—70235
Si, ion implanted, extent of annealed or melted regions as function of pulsed laser irrad. energy 79—74025
Si, ion implanted, laser annealing, periodic regrowth phenomena 78—67724
Si, ion implanted, laser annealing 79—69124
Si, ion implanted, laser annealing 79—69126
Si, ion implanted, laser annealed, elec. characterization 79—69137
Si, ion implanted, laser annealed, deep levels study 79—69457
Si, ion implanted, laser annealed, elec. props. and annealing kinetics 79—69508
Si, ion implanted, laser annealed microstructure 79—74027
Si, ion implanted, mode-locked Nd:YAG laser annealing, recrystn. 80—19817
Si, ion implanted, photovoltaic effect related to annealing 78—76111
Si, ion implanted, pulsed electron beam annealing 79—52254
Si, ion implanted, pulsed electron and laser beam annealing, comparison 79—52256
Si, ion implanted, pulsed ruby laser annealing 79—52255
Si, ion implanted, pulsed-laser annealed, Raman obs. 79—73189
Si, ion implanted, radiation defect production at different temps. 80—103398
Si, ion implanted, ruby laser pulse effects 79—69125
Si, ion implanted, scanning electron beam annealing 80—6420
Si, ion implanted, scanning CW and pulsed laser annealing 80—92549

elemental semiconductors continued
Si, ion implanted, self implanted, self annealing using high ion current density treatment 80—89254
Si, ion implanted, SiO$_2$ antireflection coating effect on CW laser annealing 80—49242
Si, ion implanted, spin density effect on laser annealing 80—11517
Si, ion implanted, standard for TEM, EELS 80—99017
Si, ion implanted, structural and elec. profiles for double damage layers 78—2169
Si, ion implanted, voids, electron microscopy 78—67757
Si, ion implanted amorphous layers, free carrier plasma effects 77—73133
Si, ion implanted and laser annealed, characterisation 80—29043
Si, ion implanted by high energy C ions structural and optical props. 80—107292
Si, ion implanted films, optical and luminesc. props. 80—60699
Si, ion implanted Kr migration during anneal 78—18834
Si, ion implanted layers, laser annealing 78—67732
Si ion implanted layers, pulsed electron beam annealing, TEM and particle backscatt. meas. 79—69134
Si ion implanted p-n junction, cryst. damage influence on elec. props. 78—56219
n-Si ion implanted surface potential barriers, LiNbO$_3$ SAW obs. 77—28234
Si, ion irrad., temp. and dose depend. of defect profiles 80—29097
Si, ion irrad. by 50 keV N$^+$ and P$^+$, depth distrib. of struct. defects, secondary emission obs. 78—2168
Si, ion irrad. damage, strain effect contrib., channelling meas. 78—67752
Si, ion irradiated, Auger electron spectra struct., possible surface diagnostic methods 79—69946
Si, ion irradiated, room temp., depth distrib. of disorder 79—37745
Si, ion irradiation prod. of stable vacancy-interstitial pairs 77—27925
Si, ion penetration, computer program 80—88185
Si ion-controlled diodes, acid-base exposure effects, SiO$_2$-Si interface state density 80—96984
Si, ion-excited L-shell Auger spectra, characts. 79—87533
Si, ion-implantation damage, annealing using pulsed-electron-beam 79—55768
Si, ion-implantation gettering effects, crit. microstructure 77—43229
Si, ion-implanted, annealing using scanning CW laser system 80—100265
Si, ion-implanted, cryst. to amorphous transform., ESR expts. and composite model 78—59825
Si, ion-implanted, defect struct., SEM, TEM and X-ray topography expts. 77—51399
Si, ion-implanted, disorders, nature and annealing behaviour, review 78—83836
Si, ion-implanted, effect of free-carrier absorpt. on annealing by pulsed laser 79—55757
n-Si, ion-implanted, elec. characts. after laser annealing 80—88562
Si, ion-implanted, impurity activation monitoring by SAW techniques 80—65020
Si, ion-implanted, lapping and staining techniques, junction depth determ. 80—29468
Si, ion-implanted, laser annealing at 1.06 μm, computer simulation 79—47556
Si, ion-implanted, laser annealing dynamics 79—69121
Si, ion-implanted, laser annealing, appls. 79—73202
Si, ion-implanted, laser irrad., characterisation by X-ray topography 79—74026
Si, ion-implanted, laser pulse annealing, TEM and channelling study 80—100264
Si, ion-implanted, low-fluence, primary defects, transient capacitance spectroscopy 80—44238
Si, ion-implanted, period surface struct. in laser annealing, new expt. evidence 80—29836
Si, ion-implanted, pulsed-laser annealing, dynamic behaviour by optical reflectance meas. 79—69122
Si, ion-implanted, secondary defects development, three-stage model 78—87725
Si, ion-implanted, thermally oxidised, Rutherford backscatt. analysis 78—19910
Si, ion-implanted amorphous layers, melting model for pulsing-laser annealing 79—56080
Si, ion-implanted amorphous, laser epitaxial recrystallisation threshold energy 80—70571
Si ion-implanted dopant redistribution under laser annealing 80—70242
Si, ion-implanted drift field solar cell 77—24615
Si, ion-implanted layers, crystalline-to-amorphous transition, radiation defect prod. 78—87696
Si, ion-implanted layers, crystn. by ns laser pulses, TEM and RHEED 80—100421
Si, ion-implanted layers, epitaxial regrowth by laser beam and flash annealing 80—100420
Si, ion-implanted layers, impurity profile meas. after laser annealing 78—87702
Si, ion-implanted layers, residual defects after high temp. annealing 78—87695
Si ion-implanted layers, total X-ray reflection investig. of clustering 78—6081
Si, ion-implanted polycrystalline film, defect build-up efficiency 80—2054
Si, ion-implanted semiconductor, annealing, crystallisation, laser pulse energy depend. 78—34528
Si ion-implanted solar cells, factors controlling efficiency 80—81451
Si ion-implanted solar cells 80—81452
Si ion-implanted structure annealing, defect behaviour obs. *(Russian)* 80—49281
Si, ion-implanted surface, profiling method 78—95075
Si, ion-induced Auger electron emission, depend. on ion energy 79—78814
n-Si, ionisation of low donor levels and recomb. of hot electrons at low temp. 79—51596
Si, ionised impurity scatt. limited mobility in semiconductors with spatially variable dielec. function 78—51986
n-Si, irrad. with 1.2 GeV electrons, form. of radiation defects 79—51156
Si, irrad. with Cr$^+$, form. and annihilation, of defects, ESR investigation 79—90707
Si, irradiated, nature of 0.97 eV A band luminesc. 77—44049
n-Si, irradiated with large neutron doses, defect annealing 80—19849
Si, isolated dislocation motion, velocity determ. *(Chinese)* 80—107243
Si, isolated vacancy, electronic struct., SCF method 80—80208

elemental semiconductors continued
Si, isomer shift values of implanted ^{133}Xe/^{133}Cs, Mossbauer spectra 80—7240
Si, Jahn-Teller distorted vacancy, electronic struct. 80—10869
Si, Jahn-Teller Mn^0 centre ESR spectrum, depend. on axial press. 80—44911
Si, joining and recrystallisation using thermomigration process 80—65298
Si junction, As-diffused, ion implantation effects on leakage current 77—62555
Si junction diode, diffused, with deep level traps, negative capacitance 80—96976
Si junction diodes, fabrication by LPE on Si:B substrates, and characts. 80—80363
Si, Kikuchi structures, energy analysis by intensity profiles *(German)* 79—7528
Si, Kikuchi structures, phonon scatt. and thermal diffuse scatt., transmission electron diffraction study *(German)* 80—44082
Si, L$_{2,3}$ VV AES, local probe of atomic charge 78—48261
Si, L-shell ionisation by 80 keV electrons, transmission electron energy loss spectrometry 80—60721
Si, LO and TO phonon assisted free exciton luminesc. 79—33833
Si, LPE from Sn melt, kinetics 78—19675
Si, LPE from Sn melt by dipping 78—6871
Si, LPE growth from supersaturated Sn melt 78—56592
Si LPE layers, dopant distrib., meltback effects 79—69151
Si, LPE using Ga$_x$Al$_{1-x}$ solvent 77—36411
Si, LVV Auger spectra 79—52055
Si large grain films on metallurgical Si substrates, chem., struct., elect. and photovoltaic props. 80—61357
Si, large single crystal production, using directional solidification tech. 78—35298
Si, large unit cell semiempirical mol. orbital approach to props. of solids 79—87036
Si, laser annealed, charge collection microscopy, carrier lifetime determ. 79—69136
Si, laser annealed, EPR and cyclotron resonance 80—34773
Si, laser annealed, elec. props. 79—69609
Si laser annealed, nonequilibrium solubility and segregation 80—84296
Si, laser annealed, solubility of impurities 79—69247
Si, laser annealed ion implanted, elec. props., melting threshold 80—10969
Si, laser annealing, nonequilib. incorporation of impurities during rapid solidification 80—55286
Si, laser annealing, nonlinear dynamic transport processes 80—93437
Si, laser annealing, optical refl. meas. of melted layer 79—78796
Si, laser annealing, surface layer temp. distrib. 79—74029
Si, laser annealing, threshold energy density, amorphous-liquid-crystalline transitions 79—60390
Si, laser annealing after ion implantation, temp. distrib. 80—54265
Si, laser annealing at 1.06 μm, free carrier absorpt. role 80—24964
Si, laser annealing mechanisms, disordered overlayers, crystalln. 80—84967
Si, laser annealing of ion bombardment damage 80—25502
Si, laser annealing of semiconductors, review 80—107301
Si laser annealing of SiO$_2$ layers 80—97505
Si, laser assisted doping, ohmic contacts and p-n junction form. 78—79621
Si, laser damage statistics rel. to structural defect statistics '80—91829
Si, laser heating of lightly damaged material, carrier diffusion effect 80—84809
a-Si, laser induced crystallisation mechanism, epitaxial regrowth 80—84962
Si, laser induced damage, effect of applied electric field 77—40310
Si, laser induced dense plasma, dynamics 80—65612
Si, laser induced elec. damage, carrier removal, mobility degradation 77—80791
Si, laser induced formation of metal silicides 79—70366
Si, laser induced reactions with metal films, silicide formation 79—70365
Si, laser induced surface deforms. 79—82262
p-Si, laser irrad., accumulation of defects, effect on elec. props. 80—107317
Si, laser irrad., anisotropic melting and epitaxial regrowth, surface struct. 79—33163
Si, laser irrad. effect on cohesion 80—50470
Si, laser irradiated, positron annihilation crystal struct. imperfection monitoring 80—11506
Si, laser measurement, of semiconductor materials and devices *(Rumanian)* 78—52035
Si, laser pulse induced amorphous to cryst. transition, thickness depend. 78—47678
Si, laser pulse train shaping for polycrystal recovery in self-ion implanted samples 79—47555
Si, laser pulsed annealing, carrier diffusion role in lattice heating 80—45172
Si, laser pulsed heating, lattice temp., Raman meas. 80—80780
Si, laser-induced bulk breakdown and free carrier generation, photocond. meas. 80—35018
Si, lattice constant, press. depend., X-ray diffr. meas. effect of nonhydrostaticness of press. 77—35439
Si, lattice constants anomalous temp. depend. 79—46821
Si lattice constraints on structure of interface states 77—20379
Si, lattice damage, influence of laser annealing 79—23608
Si, lattice dynamics, inversion matrix, approx. inversion 78—71797
Si, lattice dynamics under press 80—92627
Si, lattice dynamics using Born-van Karman model 79—73271
Si, lattice energy, pseudopotential calc. 78—23002
Si, lattice parameter determ. by X-ray multiple diffr. study *(Russian)* 80—10460
Si, lattice parameters and perfection *(Japanese)* 79—4300
Si, lattice scattering mechanism in quantised inversion layers 79—78187
Si, lattice stability, pseudopotential theory and problem of covalent bonding 77—55490
Si, lattice strains induced by localized oxidation, high temp. real-time X-ray topographic studies 80—108489
Si, lattice thermal cond., 2-1400K, phonon scatt. calcs. 78—2311
n-Si, lattice vibr. excitation conditions, vol. charge redistrib. effect *(Russian)* 80—103427
Si layer, neutron activation analysis, contamination and cross-contamination 78—83837
Si layer, on buried SiO$_2$ layer formed by high-dose, O ion implantation, TEM, AES, and XPS obs. 80—88172

elemental semiconductors continued
Si layer growth by CVD on Sn-coated background *(Dutch)* 80—7502
n-Si, layer impurity distrib., γ-ray and neutron irradiated, transverse magnetoresist and Hall effect meas. 78—19058
Si layers, carrier profiling using four-point probe method 79—37732
Si layers, ion implanted, pulsed electron beam annealing, He$^+$ backscatt. and TEM study 79—51152
Si layers, solid phase epitaxial growth temp. depend. 78—10305
Si layers, solid phase epitaxial growth, crystalline qualities, ^{4}He backscatt. and TEM exam. 78—10306
Si layers amorphized by molecular ions, laser annealing 80—103379
Si, Li ion implantation, depth distrib. variation after heat treatment 79—86814
Si, lifetime control through impact sound stressing 77—85238
Si, lifetime in Ar$^+$ ion implant damage gettered, MOS voltage ramping 80—75247
Si, lifetime of free vacancies 79—10851
Si, light energy transfer by semiconductor in crossed elec. and mag. fields *(Russian)* 77—75453
Si, light reflection, effect of repeated oxidation 79—52402
Si, light scattering due to microdefects 78—27248
Si light-controlled switch, appl. to high speed Kerr and Pockels cells 78—26925
Si lightguide connector component characts. 80—69544
n-Si, lightly doped, electron irrad. induced divacancies as electron traps 77—4126
Si, liq., dissolution of quartz, effect of C, rel. to melt growth 80—70414
Si, liq., sound vel. meas. 79—77684
Si, liq. solubility in metallic solvents *(French)* 77—27978
Si, liquid, interaction with die material during edge defined film fed growth 80—104060
Si, Lo-Hi junctions, avalanche injection delay and ionization rate at low electric field 79—95475
Si, local electron irrad., Frankel pair separation, influence on photo EMF 80—44203
Si, local field, microscopic electronic polarisation 80—25283
Si, local mechanical defects, annealing and effect on autoepitaxial growth *(Russian)* 80—7701
Si, local pseudopotential, Gaussian band charge model 80—88477
Si, localised defect, self consistent Green's function calc. 80—10919
Si, localised states due to isocoric donor impurities 77—76768
Si, longitudinal intervalley EMF due to inhomogeneities 78—19045
Si, low cost production for solar cells, growth from melt 78—3028
Si, low dislocation density, plastically deformed, electron mobility anisotropy anomaly *(Russian)* 77—80777
Si, low energy Ar ion bombardment, evidence for spike-effects 79—19292
Si, low energy primary electron irrad., secondary electron emission 79—69934
n-Si, low noise ohmic contact prep., transport props. 77—43723
Si, low press. epitaxial reactor for multi-wafer growth 79—43153
p-Si, low temp. defect prod., obs. by thermally stimulated capacitance technique 77—84801
p-Si, low temp. depend. of elastic const. c$_{44}$ 77—84831
Si, low temp. relax. of local stresses, dislocation behaviour, X-ray obs. 79—69110
Si, low-energy heavy-ion implantation damage, spike effects 77—59055
Si, luminesc., simultaneous kinetics of drops and excitons during drop formation 77—48222
Si, luminesc. emitted as a result of carrier heating 77—52185
Si, luminescence of multiparticle exciton-impurity groups 79—83003
Si, MBE, cryopumped ultra high vac. system 77—67448
Si, MBE, on n$^+$ Si, with wide range doping control 78—27402
Si, MBE, state-of-the-art 79—24450
Si, MBE growth and surface struct. 80—10816
Si, MBE growth for semiconductor devices 79—83141
Si MBE layer resistivity and carrier mobility obs. *(Russian)* 80—49962
Si, MIS, photocurrent spectra investig. of fund. absorpt. edge 77—4397
Si MIS capacitors, C-V curves, outer oxide surface conditions effects 80—97000
Si MIS grating solar cells on minority carrier blocking back surface field substrates 80—94078
Si, MIS photocapacitive IR detector 78—62223
Si MIS phototransistors, photoelec. props. at high illum. intensities 80—60101
Si MIS solar cells, 655 mV open-circuit voltage 79—79391
Si MIS solar cells, spectral response and diffusion length 79—92077
Si MIS solar cells with Cr, Hf, Be, Sc and Y as barrier forming metals, expt. investigation 80—94077
Si MIS structure, Al-ZnO-SiO$_2$-Si, charge-transfer device using SAW 79—11229
Si MIS structure using LaF$_3$ insulator 79—78182
Si MIS switch diode, charge storage effects, threshold depend. on driving voltage pulse freq. 80—49939
Si MIS/inversion layer solar cells 80—94075
Si MNOS structures with tunnelling-thickness SiO$_2$ films, surface channel hole mobility obs. 78—95380
Si MOS (111) inversion layers, angular dependent negative magnetoresist. 78—80062
Si, MOS capacitor, interface state parameter determ. by DLTS 80—65642
Si MOS capacitor, minority carrier lifetime, effects of swirls and stacking faults 77—32088
Si, MOS capacitor, nondestructive of P$^+$ and He$^+$ induced damage, doping profiles 80—34087
Si, MOS charge layer n-channel (001) surface induced valley splitting 79—28414
Si, MOS device, subject to linear voltage ramp, non-steady-state studies 79—78189
Si MOS devices, SEM, electron beam induced currents, Si stacking fault investig. appl. 79—42665
Si, MOS diode, dependence of minority carrier bulk generation on HCl concentration 80—88639
Si MOS diodes, electron beam lithography induced defects, DLTS obs. *(Japanese)* 80—54787
Si MOS inversion layer, Anderson localisation and Wigner crystal form. *(Japanese)* 77—69425
Si MOS inversion layer, subband struct., many body effects 78—64131
Si, MOS inversion layers, Hall effect 78—64118
n-Si MOS inversion layers, Hall cond. meas. 80—39676
Si, MOS inversion layers, negative magnetoresist. 80—49922

elemental semiconductors continued
Si MOS structure, low leakage, determ. of surface- and bulk-generation currents 79—24055
Si, MOS structure, p-channel, effect of isotropic stress on Si valence band struct., press. transducer appl. 80—25011
Si, MOS structure with Al_2O_3 grown by molecular beam reaction under UV excitation 79—60927
Si MOS tunnel junctions, processing condition depend. of props. 80—80380
Si MOSFET, conductance oscills., source-drain limited cond. 80—20316
Si MOSFET, electron and hole drift velocities in high elec. field, Monte Carlo calc. 78—60224
p-Si MOSFET, intersubband reson. photoresponse, mechanism 79—82677
Si MOSFET, method to determine effective channel length 79—69601
Si MOSFET, n-channel, Hall meas. on trap states at 77K 80—44732
Si MOSFET, n-type inverted, surface, mag. field depend. of valley splitting 79—19650
Si MOSFET, spin orbit interaction and many body effects in surface states 78—64132
Si, MOSFET, voltage tunable far IR emission from inversion layers 77—12440
Si MOSFET fabricated on MBE Si layer 79—78179
Si MOSFET inversion layers, IR photocond. and absorption 78—64123
Si MOSFET structures, photocond. rel. to intersubband transitions 78—64127
Si, MOSFETs, Shubnikov-de Haas oscills. from electron irrad. induced two-dimens. leakage channel 79—19671
Si, mag. props. of dislocations, spin polarons 79—82531
Si, magnetic susceptibility of light and heavy holes 79—42734
Si, magnetodiode, effect of mag. field on current-voltage characts. at low temp. 79—91134
Si, magnetodiode effect, expt. *(Slovak)* 77—8186
Si, magnetodiode with polar magnetosensitivity 79—73579
n-Si, magnetoresistance, growth layer influence, effect of randomly distributed inhomogeneities 80—20229
Si, many-valley semicond., current-voltage characts., intrinsic magnetoresistance 79—38108
n-Si, many-valley semicond. anisotropic acoustoelectric effect, thermo-EMF anisotropy fluctuation depend. on ultrasound freq. 79—69562
Si, many-valley semiconductor, linear galvanomag. effects of hot electrons 79—11154
n-Si, many-valley semiconductor, relative displacement of D_1 and D_2' bands under shear deform. influence 79—15080
Si, masking effects of Sb diffusion, from doped oxide source 77—15437
Si, mass-anisotropy exciton splitting determ. 78—6685
Si material processing, point defect thermodynamics 78—6054
Si materials, advanced, preliminary evaluation for space solar cells 80—94006
Si, matrix isolated cluster, otpical absorpt. extended Huckel calcs., electron energy levels 80—16045
Si, matrix O_2 precipitation and stacking fault formation 77—76427
Si, MeV region O^+ implantation, induced luminesc. spectrum 78—6788
n-Si, meas. of recomb. rates of non-equilib. carriers, absorption modulation method 77—55575
Si, mechanical Q meas., low temps. 78—48118
Si, mechanical strength, origin of difference in Czochralski grown and float-zone-grown cryst. 80—44212
Si, mechanically damaged surfaces, EPR meas., role of microcracks 79—42836
Si, mechanically treated surface, chem. state *(Russian)* 80—11805
Si, mechanism of cryst. growth during chemical reactions in Si-H-Cl system 78—2392
Si, melt and vapour growth for integrated circuits and solar cells 79—47609
Si, melt grown crysts., impurity incorporation, calcs. 80—79718
Si, melt surface boundary, mass transfer, influence on crystal habit during growth 79—14712
Si, melting and resolidification, laser-induced, surface morphology 79—87529
Si, metal contacts to O_2 contaminated surfaces, Schottky diodes 79—56309
Si, metallic state, press. induced, elec. cond. meas. 80—96949
Si, metallisation, $CrSi_2$ formation on Pd_2Si and PtSi 78—60578
Si, metallurgical grade, impurity gettering of polycrystalline solar cells 80—81441
Si, metallurgical grade, purification and charact. 78—56573
Si, microcracks detection using US sonoprobe 80—76462
Si, microdefect distrib. due to dislocation injection, selective etching 78—2122
Si, microdefect obs., using double cryst. X-ray topography 77—4105
Si, microdefects, diffuse X-ray scatt. obs. 80—34014
Si, microdefects, X-ray topography 79—86797
Si, microscopic inverse dielec. matrix, local field correction and acoustic sum rule 77—84863
Si, microscopic mechanism of film growth from non-condensed phases, kinetic anal. 80—54565
n-Si, microwave and far IR hot carrier mobility, Monte Carlo calc. appl. to mm. transit time oscill. efficiency 78—72184
Si, microwave oxidation, negative role of fast electrons 78—64744
Si, migration energy of intrinsic point defects in different charge states 77—89582
Si, migration of Au, electron bombardment effects 80—100362
p-Si, millimetric and far IR cond., evidence for interband transitions 78—52022
p-Si, millimetric and far-IR cond., freq.-depend. carrier relax time 80—34460
Si, minority carrier diffusion length, Schottky barriers, electron bombard. investigation 78—68037
Si, minority carrier lifetime and surface recomb. vel. meas. 77—28194
Si, minority carrier lifetime profiles meas. 77—39873
Si minority carrier lifetime degradation effect of $POCl_3$ emitter diffusion 77—76917
Si, minority carrier lifetime and diffusion length meas. contactless nondestructive technique 77—80789
Si, minority carrier lifetime and surface recomb. vel. determ. 77—89771
Si, minority carrier lifetime degradation by $POCl_3$ emitter diffusion 78—2496
Si, minority carrier lifetime and surface recombination velocity meas. by photocurrent 78—10515
Si, minority carrier lifetime meas. by contactless technique 78—23102

elemental semiconductors continued
Si minority carrier lifetime meas. methods and results *(Hungarian)* 79—56241
Si, minority carrier lifetime, effect of SiO_2 coating deposited by sputtering 80—11003
Si, minority carrier lifetime in neutron doped samples 80—20218
p-Si, minority carrier lifetime, effect of low dose ion implantation *(Japanese)* 80—54715
Si, minority carrier lifetime improvement through laser damage gettering 80—65589
Si minority carrier MIS solar cells, design and expt. results 80—81445
Si minority carrier MIS solar cells, AM1 efficiencies 80—93975
Si, minority-carrier diffusion length and drift mobility determ. using a modulated SEM beam 79—19607
Si, misfit dislocations removal by laser irrad. 79—83063
n-Si, mobility and resist. as functions of dopant density and temperature 78—2487
Si, mobility of positrons, drift vel. meas. 78—6808
Si, mobility of segments of dislocation loops, model of nonconservative dislocation motion 78—18647
Si, models for irradiation effects on impurity diffusion 77—80654
Si, moderator for slow positron beams 79—71888
Si, mol. beam and solid-phase epitaxies under ultrahigh vacuum 79—28945
Si, momentum density, Compton profile 77—20235
Si, momentum distrib. of electrons, anisotropy, positron annihilation *(Russian)* 78—84676
p-Si, monocryst., diffusion of As, Henry const., temp. depend., 1448 to 1523K 79—42399
Si, monocryst. plates, purification by thermal diffusion, impurity migration anal. 80—25553
Si, monocrystal, channelling of 5 MeV protons *(Rumanian)* 79—14863
Si monocrystal peripheral fusion channelling under HF heating *(Russian)* 80—59627
Si monocrystalline rod growth from gas phase 78—64453
Si monocrystalline sheet fabrication for solar cells, CLF Czochralski furnace and enhanced slicing technology 80—93476
n-Si, Mott transition, dielec. enhancement conduction electron screening 78—72073
Si, muffin-tin phaseshift parametrization, position of energy states 77—55473
Si, multiband and multivalley effective mass theory for impurities 79—65409
Si multicrystalline solar cell material prep., fast-pulled float zone, CZ and cast ingot and foil methods 80—93483
Si, multigrained, grain boundary elec. and compositional props., surface anal. 80—76575
Si, multigrained, impurity segregation to grain boundaries, AES and SIMS obs. 80—65027
Si multilayer structure dopant distrib. and minority carrier diffusion length, SEM obs. *(Russian)* 78—10543
Si, multiple band excitons, binding-energy calc. 78—34775
Si, multiple ribbon growth by EFG 79—8245
Si, multiply charged impurity centers, energy spectrum 79—69469
Si, multivalley struct., helical instability *(Russian)* 79—47101
n-Si, multivalued Sasaki effect 80—107795
Si, multiwave Bormann effect, expt. detect. 79—14648
Si, muon depolarisation, diamag. and paramag. states obs. *(Russian)* 79—87370
Si, muon depolarisation 79—56675
Si, muon state, muon spin rot. exam. 78—60373
Si, muonium state, anomalous 79—56673
Si muonium states, form. probability meas. 79—11370
Si, μ^+ spin relaxation in longitudinal mag. fields *(Russian)* 78—88245
Si, μ^+-meson depolarisation, spin relax. *(Russian)* 78—52416
Si, μSR, spin Hamiltonian and anomalous muonium states 80—71286
Si n/n^+ epitaxial layers, anomalies of Sb distrib. 80—65035
Si, n- and p-type (100) wafers, oxidation induced stacking faults 77—32699
Si n^+ pp^+ solar cells, back illuminated, internal quantum efficiency 79—34435
Si n^+-p diffused diode, optical lifetime meas. in heavily doped diffused regions 77—80829
Si, n^+-p diode, γ-radiation defects, annealing and recomb. props. 80—65045
Si n^+-p junction, microplasma sites, SEM and TEM characterisation 77—43702
Si, n^+-p junction, surface peripheral leakage currents 78—26939
Si n^+-p junction solar cells, electron irrad., DLTS spectra and defect effects 80—93999
Si n^+-p solar cell, forward and reverse bias tunnelling 80—85274
Si n^+-p solar cells, degradation mechanisms associated with Ti impurities 80—81465
Si, n^+p junction, spin dependent recombination *(French)* 78—80047
Si n^+p solar cells, effect of elec. bus during 1 MeV electron irrad. and isochronal annealing, elec. characts. and deep level pop. 80—94086
Si n-channel (100) inversion layer, valley splitting, formulation by extended zone effective mass theory 77—85329
Si n-channel (100) inversion layer, theory of valley splitting, electric break through 77—85330
Si n-channel (100) inversion layer, valley splittings, enhancement by many-body effects 77—85331
Si, n-channel (100) inversion layers, valley splittings due to elec. break through 79—4592
Si n-channel ⟨100⟩ MOSFETS, Shubnikov-de Haas oscills. on mag. fields up to 35 T 79—91154
Si, n-channel inversion layers, multivalley effective mass theory 79—47136
p-Si, n-channel inversion layers, mag. susceptibility of electrons in presence of quantising mag. field. 80—75650
Si, n-n^+ junction, influence of internal field on its elec. props. 79—56297
Si, n-n^+ point junctions 80—44719
Si n-p junction vertical solar cells, Al-plated, photovoltaic effect variation with impurity conc. 79—100522
Si n-p planar diode, Al layer covered, laser beam produced alloy areas, characterisation 79—69594
Si, n-p-n heterojunction transistor 80—6959
Si n-type, electron irrad., positron annihilation, effect of high-temp. annealing 78—76552
Si, n-type, noise meas. on ohmic point contact 77—4443

elemental semiconductors continued

- Si, n-type, thermally oxidised, natural inversion layer, UV photodiode construction 79—30559
- Si, n-type, thermo-EMF, bulk differential meas. 77—4380
- Si, n-type, V-I response in epithermal electron range 77—4361
- Si, n-type and p-type, carrier removal rate by fission-fragment irradiation 77—51418
- Si, n-type inversion layer, theory of impurity-shifted intersubband transitions 80—20324
- Si, n-type inverted MOSFET (100) surfaces, quantitative determ. of valley splitting 79—51678
- Si, n-type with ^{11}B implanted ions, high-temp. treatment effect on distrib. profile *(Russian)* 77—89454
- Si, NMR of ^{29}Si in weak mag. fields 79—65746
- p-Si, Na impurity diffusion, ion irrad., defect form. effects *(Russian)* 77—43386
- Si, Ne ion implanted, oxidation expanded defects, effect on MOS parameters 78—19152
- Si, near (III) surface, dislocation movement at annealed scratches, X-ray topography obs. 80—2029
- Si, near (111) slices, scratches made by diamond stylus 77—12726
- n-Si, negative absolute conductance, electrothermal mechanism 79—69518
- Si, negative conductivity due to hot electrons transfer in geometric space *(German)* 78—56150
- Si, negative differential mobility and geometrical magnetoresist. calc. 77—43624
- Si, negative electron affinity, statistics of transmission secondary emission 77—48287
- Si, negative electron affinity (100) surface, electron emission 77—52215
- Si, negative electron affinity surface activation, laser beam scanning obs. 79—4890
- Si, neutral vacancy, generalised val. bond calc. 77—55493
- Si, neutral vacancy electronic struct. 77—62865
- Si, neutron and electron bombard., radiation defect recomb., photoelec. props. meas. 80—60039
- n-Si neutron and electron irrad., isochronous annealing influence on edge absorpt. 80—11449
- Si, neutron damage, displacement and ionis. fractions of fast neutron kerma 78—30669
- Si, neutron displacement cross section, radiation effects intercalibration, damage coeff. 79—23653
- Si, neutron doped, γ-irrad. influence on elec. props. 80—6845
- Si, neutron irrad., displacement damage for monoenergetic neutrons 78—30670
- Si, neutron irrad., EPR, ⟨100⟩ split di-interstitial, positive charge state 77—20698
- Si, neutron irrad., Hall effect and magnetoresist. meas. 80—6883
- Si, neutron irrad., internal friction obs. of defects 78—51597
- Si, neutron irrad., point defects photopopulation and photoionis., IR spectra meas. 80—25423
- Si, neutron irrad., residual radioactivity meas. 80—19829
- Si, neutron irrad., small angle neutron scatt. meas. 80—29073
- p-Si, neutron irrad. effects, admittance meas. of n^{+}-p diode 78—51587
- Si, neutron irrad. effects on lattice parameter and anomalous X-ray transmission 79—86821
- n-Si, neutron irradiated, annealing behaviour characterisation by electrochem. meas. 80—19847
- Si, neutron irradiated, changes in lattice period, X-ray meas. 77—7767
- Si, neutron irradiated, characts. of defect form. 78—14382
- n-Si, neutron irradiated, characts. of changes in mobility 78—39135
- Si, neutron irradiated, direct band gap transition, IR absorpt. 79—73980
- p-Si, neutron irradiated, elec. props. 78—51939
- Si, neutron irradiated, influence of defects and temp. on positron annihilation 77—4699
- Si, neutron irradiated, intrinsic defect exam. by IR spectra 78—52534
- Si, neutron irradiated, resistivity and minority carrier lifetime, radial inhomogeneity *(Russian)* 78—26881
- n-Si, neutron or γ-irrad., elec. props., in strong elec. fields 79—95416
- Si, neutron transmutation doped, zero-bias resist. of grain boundaries 78—76072
- Si, neutron transmutation doping, detect. and identification of potential impurities activated 79—42090
- Si, neutron transmutation doping, photoluminesc. characterisation 80—11453
- Si, neutron transmutation doping, impurities 80—15134
- Si, neutron transmutation doping, radioactivity form. 80—15135
- Si, neutron transmutation doping for IR detector material 80—15136
- Si, neutron transmutation doping in Harwell reactors 80—15138
- Si, neutron transmutation doping, irrad. facilities 80—15139
- Si, neutron transmutation doping, General Electric test reactor 80—15140
- Si, neutron transmutation doping, automated irrad. facility 80—15141
- Si, neutron transmutation doping, annealing, lattice damage 80—15163
- Si, neutron transmutation doped, highly compensated, resistivity fluctuations 80—15531
- Si, neutron transmutation doped, elec. props. 80—15532
- Si, neutron transmutation doping, irrad. techniques 80—19827
- Si, neutron transmutation doped, isochronal annealing of resistivity 80—19828
- Si, neutron transmutation doping, ^{31}P conc. meas. 80—19833
- Si, neutron transmutation doping, at. displacement effects 80—19852
- Si, neutron transmutation doping, annealing, deep defect levels 80—20123
- Si, neutron transmutation doping using nuclear reactor thermal neutron irrad., review 80—39161
- Si neutron-prod. defects, investigation by transcond. meas. of JFETs 77—15455
- Si, neutron-produced defects, deep level transient spectroscopy 79—47047
- Si, neutron-transmutation doped, annealing behaviour, EPR obs. 79—86804
- Si, new materials properties achievable by ion implantation doping and laser processing 79—69127
- Si, new preferential etch for defects in (100) and (111) oriented n- and p-type cryst. 77—59954
- n-Si, new small donors, energy spectra, photoionisation energy *(Russian)* 80—34391
- n-Si, new type of galvanising effect for hot electrons 77—32028
- Si, noise at high elec. fields 77—8163
- Si, non thermal laser induced ordering, plasma life time, phonon interactions 80—84481

elemental semiconductors continued

- Si, non-equilib. orientation of electrons in electron-hole droplets in mag. field *(Russian)* 77—36294
- Si noncrystalline film, struct., interatomic distances, SRO 80—107053
- Si, nondiagonally screened model potential appl. to band struct. calc. 78—14651
- Si, nonequilib. carriers generated by Nd laser, relax. rate temp. depend. 78—26911
- Si, nonequilib. electron-hole system, gas-liq. phase diagram *(Russian)* 77—43509
- Si nonequilibrium carrier excitation by CO$_2$ laser radiation 77—89803
- Si, nonequilibrium carrier density relax., lifetime determ. using light absorption 78—15170
- Si, nonideal, lifetime and diffusion length rel. to solar cell appl. 79—15192
- n-Si, nonlinear birefr. and dichroism at microwave freqs. and intervalley scatt. 79—19602
- Si, nonlinear optical susceptibility, tight binding bonding orbital model 80—5784
- Si, nonlocal pseudopotentials 77—11848
- Si, nonpolar semiconductor, IR free carrier absorpt., two short wavelength phonon scattering 79—78665
- Si, nonradiative deexcitation in O$_2$ atmos., using differential meas. of excited state lifetime 78—2920
- Si, nonradiative recombination and luminesc. 79—33770
- Si, nonsingle crystalline, solar cells, book contrib. 79—43771
- Si, nuclear spin-lattice relax. in weak mag. fields *(Russian)* 79—51879
- Si, nucleation of stacking faults at oxide precipi tate-dislocation complexes, TEM 77—19967
- Si, O content and depth profiling, ^{16}O(α, α)^{16}O reaction method obs. 79—34408
- Si, O impurity precipitation from solid soln., neutron irrad. effect 80—29177
- Si, obs. of cyclotron reson. absorptions due to excitonic ion and excitonic mol. ion 77—73082
- p-Si, odd magnetoresist. under weak carrier heating conditions 80—96917
- Si, off-axis channelling disorder anal. 77—24325
- p-Si, ohmic contact formation method 78—76137
- Si, ohmic contacts, two carrier operation 77—43716
- Si on ceramic, coating with inverted meniscus (SCIM) technique, solar cell appl. 80—89163
- Si on ceramic, growth from melt for solar cell appl. 79—11511
- Si on sapphire, deposition kinetics and interface characteris. 79—28234
- Si, on sapphire, early growth, TEM 77—24961
- Si, on sapphire, early growth, models 77—24962
- Si, on sapphire, epitaxial, crystalline quality improvement by ion implantation and furnace regrowth 80—88452
- Si on sapphire, laser annealing dynamics epitaxial regrowth, optical reflectivity 80—29285
- Si, on sapphire, MOS inversion layer, magnetoconductance oscillations 80—20325
- Si on sapphire, residual strain effect on elec. props. *(Japanese)* 80—84522
- Si, on sapphire, Schottky magnetodiode, integrated mag. sensor 80—68223
- Si on sapphire, stacking faults and twins, TEM obs. at early stage of epitaxy 79—28233
- Si on sapphire, stress-relieved regrowth by laser annealing 80—65389
- Si on sapphire film, laser annealing non-thermal theory expt. test 80—89273
- Si on sapphire in SOS technology, gettering effect by O implantation, Hall and Rutherford backscattering meas. 79—65103
- n-Si on sapphire magnetoresistance anisotropies and electronic struct. obs. 77—20471
- Si on sapphire thin film, Hall effect, magnetoresistance *(French)* 80—65601
- Si, open-tube P diffusion kinetics 79—33117
- Si, optical absorption by acoustic phonons related to shallow impurity levels 77—4665
- Si, optical constants at 5461 Å 78—92043
- Si, optical consts. by unpolarised incident radiation 80—76044
- Si, optical critical point structures, symm. anal. by low-field electroreflectance 77—66478
- Si, optical excitations, many particle effects 79—87046
- Si, optical properties of monocrystal by electron energy loss meas. *(German)* 79—24283
- Si, optical spectroscopy, absorpt. coeff., lattice vibrs. modes, band gap, acoustic approach 77—69822
- Si, optical spectrum, many particle effects, band struct. 80—89024
- Si, optical surface modes calc. 77—59200
- Si, optically pumped, distrib. of polarisation of electrons and nuclei 77—59485
- Si, optically pumped, dynamic polarisation and mag. relax. of ^{29}Si 78—48081
- Si, optically stimulated ESR, dielec. effects 77—73080
- Si, order-disorder transformation, pulsed UV laser induced 79—60400
- Si, orientation anal. of polycrystalline samples 79—1438
- Si, Overhauser effect in optically pumped compensated samples 79—73857
- Si, oxidation, AES photoelectron spectra exam. of early stages 79—74272
- Si oxidation, dopant redistrib., Cs^{+} SIMS anal. appl. 79—39265
- Si oxidation, effect of chlorinated ambients 79—100278
- Si, oxidation, film defect equilibria and growth reactions 78—11377
- Si oxidation, high press. techniques, review 79—100279
- Si, oxidation, in dry O$_2$ and H$_2$O ambients, initial oxidation regime obs. 79—29240
- Si, oxidation, masking effect of thermal oxidation rate of covering Si$_3$N$_4$ film 78—64749
- Si, oxidation, oxidation-induced lattice defects, review *(Japanese)* 78—39931
- Si, oxidation, phase comp. of SiO$_x$, electron spectroscopy obs. 78—60042
- Si, oxidation, solubility and transport behaviour of water, dissolution 80—93801
- Si, oxidation, stress in thermal SiO$_2$ during growth 79—91812
- Si, oxidation, thermal growth kinetics, SiO$_2$ profile meas. 78—88551
- Si, oxidation, thermal growth mechanisms of vitreous oxide layers 80—93675
- Si, oxidation, use of new high press. steam apparatus 77—63818

elemental semiconductors continued
Si, oxidation at 1000°C, Na contamination and furnace cleaning procedures 77—59955
Si, oxidation in HCl/O_2 ambients, phase separation and Na passivation in thermal oxides 80—3219
Si oxidation in HCl-O_2 atms., Si etching and SiO_2 bubble form. 77—63823
Si, oxidation in high-press. steam, 800 to 1000°C, rate consts. 77—48565
Si, oxidation in presence of Cl and Cl cpds. 78—53009
Si, oxidation induced by ion or electron bombardment, AES-SIMS study 80—108606
Si, oxidation induced stacking fault growth, role of point defects 78—10061
Si, oxidation induced stacking faults, wafer orientation and ion implantation effects 78—10063
Si oxidation mechanism and kinetics 78—95833
Si, oxidation of dry O_2, revised model 78—92373
Si, oxidation stacking faults and microdefects, growth behaviour during high temp. annealing 78—72901
Si, oxidation stacking faults, shrinkage and growth, bulk O_2 effects 80—96546
Si, oxidation with trichloroethylene additive to eliminate oxidation induced stacking faults 80—39118
Si, oxidation without stacking fault form. 78—7062
Si, oxidation-induced Frank sessile dislocation loops, struct. change 80—75228
Si, oxidation-induced stacking faults, refl. X-ray topography 77—84767
Si, oxidation-induced stacking fault form., by high press. steam oxidation 78—83830
Si, oxidation-induced stacking faults, control by Cl implantation 79—46682
Si, oxidation-induced stacking faults, nucleation mechanism 80—15122
Si, oxidation-induced stacking faults, influence of annealing ambient on shrinkage kinetics 80—29035
Si, oxidation-induced stacking faults, distinction between clean and decorated faults by etching 80—79818
Si, oxide film struct. determ. by electron diffr. 79—15050
Si, oxide formation in microwave discharge 79—52406
Si, oxide growth, ambient water vapour trace effects 77—77618
Si, oxide growth kinetics for SiO_2 films in low O_2 partial press. *(Japanese)* 78—27665
Si, oxide layer, electron capture by deep levels, vibration of adsorbed molecules 80—29458
Si, oxide layer form. by O^+ ion implantation, Rutherford backscatt. and IR transmission obs. 79—51141
Si, oxide scale microstruct. of oxidised single cryst. 80—108613
Si, oxidised, stacking fault generation annihilation 77—76419
Si, oxidised in trichloroethylene-O_2, Cl incorporation and elec. props. 79—91827
Si, oxidised on one side, elastically flexed, dynamic X-ray scatt. *(Russian)* 77—43115
Si, oxidised surface, irregular growths of $B(OH)_3$ 78—39926
Si, P diffused sample, stacking faults and dislocations formation from interstitials 78—95059
Si, P implanted, low temp. annealing characts. 77—11576
Si, P implanted low pressure CVD polycryst. films, elect. characts. 80—60114
Si, p- and n-type, field emission, role of surface electron states 78—2993
Si p^+-i-n^+ field induced junction solar cells, conversion efficiency limit in concentrated sunlight 80—85282
Si p^+-n contaminated junction, precip.-induced and generation-recomb. currents 78—2555
Si, p^+-n diode, neutron irrad., defect levels, G-T and C-T curves obs. 77—62986
Si, p^+-n diode under forward bias, effects of radiation-induced deep levels on admittance 78—23157
Si p^+-n high efficiency solar cell, B diffusion process 77—85302
Si, p^+-n junction, irrad. with α-particles, defect form 80—24509
Si, p^+-n junction diodes, flow fluence S implanted unequal defect densities, dynathermal obs. 80—20293
Si p^+-n-n^+ back surface field concentrator solar cells 80—93939
Si p^+-n-n^+ back-surface-field solar cells, physics underlying performance 80—85283
Si, p^+-n-n^+ high efficiency back surface field solar cells, design and fabrication 78—84283
Si p^+nn^+ reverse-bias struct. with confined space-charge region, field profile 79—73581
Si $p^+\pi pn\nu n^+$ structure form. by epitaxial growth 77—76906
Si p-channel MOS structure, stress effects on elec. props., press. transducer props. 80—100526
Si, p-i-n avalanche photodiode, temp. depend. characts. 79—35835
Si, p-i-n laser detector, wavelength and temp. depend. characts. 80—13134
Si p-i-n photodiode meas. of X-ray tube kVp *(German)* 79—232
Si p-i-n structure, ESR of conduction electrons 80—93179
Si, p-i-n structures, pinch effect expt. obs. 79—90971
Si p-n diode, 1/f noise calc., free carrier mobility interpretation 80—54774
Si p-n heterojunction, DC sputtering growth, photocond. and photovoltaic effects 79—33337
Si p-n homoepitaxial junctions, elec. and struct. characts. 80—6662
Si, p-n homojunction breakdown voltage for onesided abrupt junctions *(German)* 78—56210
Si, p-n junc. solar cell, forward bias capacitance and current meas. for lifetime and band narrowing detn. 79—7892
Si, p-n junction, alpha-particle effects, photoelec. parameters determ. *(Russian)* 77—31702
Si p-n junction, avalanche multiplication of electron beam generated carriers 77—80833
Si p-n junction, breakdown voltage drift, walk-out phenomenon, model 77—80834
Si p-n junction, charge carrier recomb. at dislocations, combined SEM and TEM study 80—15105
Si p-n junction, compressed by shock wave, rectifying props. 77—4429
Si, p-n junction, current-voltage characts., misfit dislocations, high press. effects 80—65671
Si p-n junction, DC characts. at avalanche breakdown including selfheating 79—42629
Si p-n junction, dielectric props., freq. depend. of capacitance and conductance 78—43469

elemental semiconductors continued
Si, p-n junction, dopant conc. diffusion length and lifetime variations, SEM obs. 79—82604
Si, p-n junction, ellipsometric method of temp. meas. rel. to secondary breakdown *(Russian)* 80—11074
Si p-n junction, high-voltage, microplasma characts. 77—11997
Si p-n junction, mesoplasma formation, light-emitting properties of secondary breakdown region *(Russian)* 79—91131
Si p-n junction, microplasma characts., temp. depend. 77—4430
Si p-n junction, microplasma instability, effect of space-charge field of mobile carriers 78—19140
Si p-n junction, negative annealing of γ-radiation defects 77—43246
Si p-n junction, passivation by slightly conductive chalcogenide film 78—2556
Si p-n junction, passivation by amorphous Si:H layer 79—47155
Si, p-n junction, plasmon mechanism for secondary breakdown 78—95352
Si p-n junction, reverse bias high voltage, secondary surface breakdown 80—70813
Si p-n junction, small signal equivalent circuit, finite carrier multiplication 80—65664
Si p-n junction, subnanosec. current drops in delayed breakdown 80—75633
Si p-n junction, subnanosec. current drops in delayed breakdown 80—75634
Si, p-n junction, through oxide As implantation, Ar implantation gettering 78—14802
Si p-n junction, unified approach to breakdown phenomena 79—42630
Si, p-n junction, with hot carriers, amplification 78—39203
Si p-n junction depletion layer, electron beam damage inhibition 80—70817
Si p-n junction diodes, reversed-biased, permanently induced negative resist., expt. 78—56214
Si p-n junction diodes and solar cells, minority carrier diffusion length 80—107894
Si p-n junction I-V reln. calc. 77—43704
Si p-n junction in surface region obtained by evaporation in UHV 78—39198
Si p-n junction local temp. meas. using pulsed SEM, induced-current mode 80—54775
Si p-n junction made by ruby laser pulses, characts. *(Polish)* 78—84286
Si p-n junction pressure transducer characteristics *(Polish)* 77—89832
Si p-n junction sensor for high intensity solar flux mapping 78—40720
Si p-n junction solar cells, photon degradation effects 79—92078
Si p-n junction solar cells, importance of surface recombination and energy-bandgap narrowing 79—100520
Si p-n junctions, avalanche breakdown anisotropy 80—70811
Si, p-n junctions, current-voltage relation 79—42632
Si p-n junctions, depletion layer recombination theory 77—80828
Si p-n junctions, electron emission from depletion layers 80—100509
Si p-n junctions, high-voltage, elec. props. by optical scanning 80—6969
Si, p-n junctions, neutron transmutation doping, breakdown process 80—15600
Si p-n junctions, secondary breakdown, pre-mesoplasma state expsn. *(Russian)* 79—56723
Si p-n junctions, spin depend. surface recomb., electron irradiation effect 80—88627
Si, p-n junctions, voltage-current characts., fast neutron irrad. effects *(Russian)* 80—65659
Si p-n step junctions, temp. depend. of capacitance 79—15210
Si, p-n-n^+ structure, external resistance effect on current-mode second breakdown 78—56216
Si, p-type and n-type, temp. coeff. of resist. calc. 78—91698
n-Si, *p*-type regrowth layer formed by brazing with metal support disc, diode appl. *(Japanese)* 79—15833
Si, packing defects, change in size during heat treatment 80—39079
Si, paramagnetic defects produced by electron irrad., EPR 79—19779
Si, paramagnetic state (μ^+e^-) at high temp. 79—56676
Si, partial dislocation electron states 79—60760
Si particles, grown in Ar gas, cryst. struct. and habit, electron microscope study 79—74071
n-Si, passivation, photoactivation kinetics in conc. alkali, ellipsometric investig. 77—1885
n-Si, passive, complete activation initiation by local photoactivation 79—100403
Si, Pb implantation, channelling and RHEED anals. 78—30657
Si, Pendellosung fringes in synchrotron X-ray topographs 79—32858
Si, periodic stepped structure, on vicinal planes, LEED obs. 80—24725
Si, phase gratings in semiconductors with one- and two-photon excitation 77—8546
n-Si, phenomenological energy relaxation time, temp. depend. 78—43409
Si, phonon assisted Auger recomb. in indirect gap semiconductors 78—39126
Si, phonon boundary scatt., reduction of lattice thermal cond. 78—55921
p-Si, phonon conductivity and attenuation 77—4167
Si, phonon induced intervalley transitions, violation of selection rules 78—30875
Si, phonon scattering at low-angle grain boundary 79—77708
Si, phonon spectra calc. using dielectric matrix approach 79—4381
Si, phonon viscosity tensor 78—34570
Si, phonon-assisted Auger recomb., direct calc. of overlap integrals 80—107808
Si, phonon-assisted exciton emission, temp. depend. of relative integrated intensities 77—1375
Si, phonon-mediated intervalley electron-electron interaction 78—95125
n-Si, phonon-phonon relaxation 80—96609
Si, phonon-phonon relaxation investigation for conventional and neutron doped crystals 80—96927
Si, phonons, directional depend. of boundary scatt. mean free path 79—73354
Si, photo-field cathode, ageing and surface state effects *(Russian)* 77—28703
p-Si, photoabsorpt. associated with divacancies 79—15502
Si, photoacoustic effect, free flexural vibrs. damping 77—89813
Si, photoacoustic signal changes assoc. with crystallinity, recrystallisation after laser annealing 80—16127
Si, photocapacitive MIS IR detector, spectral response, noise characts. 80—75644
Si photocathode, negative electron affinity process obs. by laser beam scanning *(Japanese)* 80—55262

elemental semiconductors continued
  Si photocell, with field-induced p-n junction, inversion layer solar convertor 77—15906
  n-Si, photocond. of negative donor ion states, for far IR detect. 77—59299
  Si photoconducting films, amorphous, undoped, I-V characts. of vacuum deposited films 80—60049
  Si, photoconductivity, extrinsic, contrib. by hopping through excited states of donors 78—6411
  Si, photoconductivity, temp. dependence, excitation with laser pulses *(Russian)* 80—11031
  Si, photoconductivity and Dember effect, theory, allowance for long-range fields of charged impurities 79—24013
  Si, photoconductivity kinetics, effect of exciting illumination *(Russian)* 80—11032
  Si photodetector, for improved short-wavelength quantum efficiency 80—31874
  Si photodetector, shallow junction type, internal quantum efficiency meas. model fits, visible quantum yield 80—267
  Si photodetector, surface-barrier 80—4771
  Si photodetector storage-mode operation 77—39075
  Si, photodiode, 1.06 μm range, neutron and γ-irrad. effects 79—97433
  Si photodiode, in combination with PbS and PbSe photocells, multicolour detectors *(Czech)* 79—26126
  Si photodiode, multidecade linearity meas. 79—75592
  Si photodiode, refl. and external quantum efficiency change after surface cleaning 79—93212
  Si, photodiode, violet and near UV sensitive, prep. and expt. study *(Chinese)* 79—49285
  Si photodiode for optical channel waveguides 80—102805
  Si photodiode imaging array design factors 77—39085
  Si, photodiode photodetector, UV enhanced responsivity 77—74499
  Si photodiode saturation at high modulation freq. 78—54453
  Si photodiodes, linear arrays, use for high-energy electrons detection, SEM assessment 78—32951
  Si, photoelectret effect, plastic strain induced dislocation relax. time enhancement *(Russian)* 79—15397
  Si photoelectric convertors, photoelectric parameters under illumination 80—40857
  Si photoelectric convertors, bilateral sensitivity, optical characts. anal. 80—40858
  Si, photoelectric spectra of remanent impurities 79—87125
  Si, photoelectron emission due to Bragg diffr. of X-rays 79—69960
  Si, photoelectron escape depths determ. from X-ray photoelectron spectra 78—27368
  Si, photoelectron yield variation under asymmetric diffr. condition of X-rays 79—65972
  Si, photoemission electron microscopy in high vacuum region, image brightness and contrast 78—55791
  Si, photoemission spectroscopy of surface states and oxidation 77—55863
  Si, photoemission study of energy depend. of bulk plasmon loss intensity 79—47035
  p-Si photoemitter, achievement of negative electron affinity 78—2980
  Si, photoexcited, highly stressed, electronic Raman scatt. and antireson. 80—29737
  Si, photoillumination effect on field ion microscopy 79—78850
  n-Si, photoionisation of doubly charged divacancies 79—51526
  Si, photoionisation of Group III acceptors, model 78—35174
  Si, photoluminescence of annealed cryst., defect anal. 79—87500
  Si, photoluminescence of electron-hole drops under uniaxial stress 79—91491
  Si, photoluminescence of thermal donors after annealing 79—87499
  p-Si, photon drag detection 78—43440
  p-Si, photon drag detector, performance in 2 to 33 μm range 79—35834
  Si, photon emission due to Ar^+ ion bombard., adsorbed and recoil-implanted O effect 80—80872
  p-Si, photopassivation kinetics in alkali soln., spectral depend. 77—1886
  p-Si photoresistor, compensated with radiation centres, current responsivity and detectivity 79—17492
  p-Si, photosensitivity of elastic moduli and surface tension 78—83864
  Si, photovoltaic and photomagnetic effects, rel. to intervalley electron transfer 80—60034
  Si, photovoltaic cell, absolute spectral sensitivity calibration, radiometry, photometry *(Chinese)* 80—86367
  Si photovoltaic low series resistance concentrator for high intensity appl. 80—93940
  Si, piezo-optical consts., Raman meas. 78—65951
  Si, piezo—spectroscopic study of ratio of electron—TO phonon to hole—TO phonon interaction 79—24289
  Si, piezobirefringence above fundamental edge, Raman scatt. meas. 79—42941
  Si, piezobirefringence in opaque region 80—60541
  n-Si, piezoresist. effect, influence of temp. and impurity conc. *(German)* 77—62924
  n-Si, piezoresist. rel. to piezothermoelec. power, electron-phonon drag region 80—70737
  Si, piezoresistance, energy and momentum relax. of charge carriers 78—47786
  Si, piezospectroscopic determ. of electron-phonon to hole-phonon interaction 79—95783
  Si, piezospectroscopic effect on zero phonon luminescence lines 80—50406
  Si, planar and O_2 etched (111) surface, CO adsorption, AES, SEM, ESD, flash desorption mass spectra 78—63934
  Si, planar bipolar devices, dislocation effects 79—82221
  n^+nn^+Si planar device, hot electron flicker noise at 78K 80—103732
  Si planar diode, Al coated, binary memory device, laser writing 79—69593
  Si planar semiconductor junctions, disruptive voltage calc., ionisation coeff. *(Rumanian)* 80—103746
  Si planar structures, Haynes-Shockley expt. for students 78—28888
  Si, planarized solid state epitaxy for Schottky barrier diodes 78—35302
  Si plasma deposited amorphous hydrogenated film, optical props., annealing effect 79—56874
  Si, plasma effects during pulsed laser annealing 80—84480
  Si, plasma etching, effect of O_2 additions to CF_4 plasmas 78—72908
  Si, plasma etching, loading effect 77—90475
  Si, plasma etching in Freon plasma, for microelectronics appls. 80—3080
  Si, plasma etching using CF_4 78—39921
  Si, plasma etching using microwave discharge 78—11361
  Si, plasmon dispersion relation, local microscopic field effects 80—20103

elemental semiconductors continued
  Si, plasmon sideband exam. by synchrotron radiation tuning of electron escape depths, UPS 77—47755
  Si, plasmons, influence of cryst. orientation on intensity, electron energy loss meas. *(German)* 79—23921
  Si, plastic properties, internal friction, dislocation motion *(Russian)* 80—54305
  n-Si, plastically deformed, donor action of dislocations, elec. props. 79—11126
  Si, plastically deformed, dislocation structure with different sample orientation 80—70207
  Si, plastically deformed, EPR spectra of point defects., temp. depend. 77—90033
  Si, plastically deformed, hot-exciton luminesc. as function of strain 78—88361
  Si, plastically deformed, spin-depend. charge transport 80—6895
  n-Si plate, effect of nonequilibrium carriers on IR transmission 79—38548
  Si plate, internal friction temp. depend. 77—15491
  n-Si plate, internal friction illumination effects, 50-250°C *(Russian)* 77—20010
  Si plate prod. by Stepanov method, stability analysis *(Russian)* 78—52655
  Si, plates, semicond., scribing marks rel. to sclerometric microhardness 79—15891
  Si, pn-product calc. as function of temp. and impurity conc. 77—35891
  Si, point charge impurity screening 80—6783
  Si, point defect clusters identification by TEM 77—43210
  Si, point defects, H passivation 80—75515
  Si, point defects, laser annealing 80—107224
  Si, point defects, multiple scatt. Xα model 80—54636
  Si, point defects, negative-U props. 80—49660
  Si, polarisation dependent electrorefl. spectra, surface phenomena 78—68479
  Si, polarisation of recombination radiation from multiparticle exciton-impurity complexes, induced by uniaxial deform. *(Russian)* 79—78754
  Si, polished plate, internal friction *(Russian)* 78—15441
  Si, poly crystalline, electronic behaviour of grain boundaries, solar cell appl. 80—92859
  Si, poly-oxide-poly struct., elec. cond., charge distrib. in SiO_2 films 80—92984
  Si, polycryst, CVD, electron beam recrystn. 80—24759
  Si, polycryst., anisotropic plasma etching 80—85069
  Si, polycryst., CVD, recrystn. on heating 80—80107
  Si, polycryst., charges at laser recrystallised poly Si/insulator interface 80—54789
  Si, polycryst., deposition as example of pyrolytic CVD process 80—84407
  Si, polycryst., edge etch process for minimum geometry windows 78—31550
  Si, polycryst., elec. and photovolt. props., grain size effects 80—49800
  Si polycryst., end point detection in plasma etching by optical emission spectroscopy 80—50733
  Si, polycryst., energy distrib. of trapping states, from impedance of MOSS struct. 80—65691
  Si, polycryst., growth, props. and MIS appl. *(Slovak)* 78—92196
  Si, polycryst., growth kinetics in low press. CVD reactor 79—91594
  Si, polycryst., lateral diffusion of B, influence on submicron MOST fabrication 78—26588
  Si, polycryst., layer structure dependence on carrier gas moisture and O_2 content *(Bulgarian)* 80—59811
  Si, polycryst., low press. CVD production processes 77—77395
  Si, polycryst., on oxide-covered single cryst. Si substrate, deform. 78—26778
  Si, polycryst., oxidation, morphological aspects 80—76388
  Si, polycryst. and amorphous, sputtering with keV Ar^+ ion, meas. and Monte Carlo calc. of sputtering yield 79—95886
  Si, polycryst. CVD film electrical props. 78—6466
  Si, polycryst. film, ion plating on Al, growth from eutectic melt 77—8765
  Si polycryst. film, ion-implanted, pulsed laser annealing 79—77612
  Si, polycryst. film doping during deposition and with diffusion 78—6088
  Si, polycryst. film from low. temp. pyrolysis of SiH_4 78—31342
  Si, polycryst. film on Si, disloc. config. under periodic stress field 78—10312
  Si, polycryst. films, transport props. and grain boundary charact. by TEM 80—50980
  Si, polycryst. layers, ribbon-against-drop pulling process 79—8241
  Si, polycryst. manufacturing methods for photovoltaic energy prod., solar cells, grain growth from melt *(Dutch)* 78—52661
  Si, polycryst. p-n junction solar cells, grain-boundary and intragrain recombination currents 80—81442
  Si, polycryst. rods, p-n junction appls. and transport props. 79—99612
  Si, polycryst. with columnar struct., crystn. using casting technique and microstruct., book contrib. 79—43137
  Si, polycryst.-single cryst. p^+-n and n^+-p junctions, elec. characts. 80—11077
  Si, polycrystalline, As segregation at grain boundaries, elec. props. meas. 80—75259
  Si, polycrystalline, electrode shape effects on oxide conduction 80—96890
  Si, polycrystalline, for efficient low cost solar cells 80—21405
  Si, polycrystalline, grain boundary effects on minority-carrier diffusion length and solar-cell efficiency 79—48124
  Si, polycrystalline, grain boundary obs. by TEM, solar cell appl. 80—72057
  Si, polycrystalline, Hall mobility 80—60006
  Si, polycrystalline, large grain size, gross defects effect on effective carrier lifetime 77—80793
  Si polycrystalline, low cost conversion into sheet by heat exchange method and fixed abrasive slicing technique 80—93479
  Si, polycrystalline, neutron transmutation doped, grain boundary zero-bias resistance 79—15153
  Si, polycrystalline, p-n junctions, solar cell appls. 78—56220
  Si, polycrystalline, passivation of grain boundaries 79—56158
  Si, polycrystalline, phenomenological model for mobility 80—65564
  Si, polycrystalline, recrystn. after plastic deform. and annealing 80—3145
  Si, polycrystalline, ribbon to ribbon, using laser scanning, solar cell appl. 78—35299
  Si, polycrystalline, solar cells, grain-boundary hydrogenation technique for improvement 80—85273
  Si, polycrystalline, thermal oxide anomalous stress 80—93661

elemental semiconductors continued
Si, polycrystalline barrier heights and passivation of grain boundaries 80—93890
Si polycrystalline CVD film optical props. 77—77315
Si polycrystalline CVD film formation and props. 77—77401
Si polycrystalline CVD films, non-volatile memory switching 80—54814
Si, polycrystalline Czochralski-grown, MIS solar cell characterisation using scanned laser response exam. 80—93884
Si polycrystalline film, effect of defects/grain boundaries on photovoltaic mech. 80—93883
Si polycrystalline film resistivity reduction by Nd:YAG laser annealing 80—100539
Si polycrystalline films, anomalous etching effects 77—77613
Si polycrystalline films, texture formation study 79—87662
Si, polycrystalline films, meas. of effective diffusion length, by surface photovoltage meas. 80—80424
p-Si polycrystalline films on graphite substrates *(French)* 78—64154
Si, polycrystalline layer, laser-induced single cryst. transition, RHEED and backscatt. obs 78—87704
Si, polycrystalline layers on C substrates, RAD process, solar cells appl. 80—89635
Si, polycrystalline multilayer support struct., control of deform. in dielec. isolated substrates 80—107681
Si polycrystalline p-n junction deposition 78—10549
Si, polycrystalline ribbon prep. by electron bombardment *(French)* 78—64474
Si, polycrystalline solar cell base material characterisation, defect states 80—50979
Si polycrystalline solar cells fabricated from refined metallurgical-grade Si, impurity gettering 80—94011
Si, polycrystalline structure stability, stacking defects, twins grain struct. *(Russian)* 80—100248
Si polycrystalline thin-film solar cells 79—57426
Si, polycrystalline-metal contacts, minority carrier injection 80—103750
Si polycrystalline-metal Schottky barrier solar cells, elec. and photovoltaic contact props. 80—93936
Si, polymorphism under high press. *(Russian)* 78—59947
Si polymorphs, optical props., orthogonalized LCAO calc. 78—10345
Si, porous, form. during anodic treatment in aq. HF 80—35369
Si, porous, formation during anodic treatment in HF aq. soln., growth kinetics and density 80—20059
Si, porous film, form. by anodic reaction in HF soln., struct. props. 77—24971
Si, porous layer, oxidation, and oxide film props. 80—55556
Si, porous layer, struct. and heat-treatment effect 79—1557
Si, porous layer form. mechanism by anodisation in HF soln. 80—71769
Si, positively charged divacancy photoionisation cross section by photocapacitance meas. 80—6901
Si, positron annihilation, mag. field effect, positronium states 77—16417
p-Si, positron annihilation, effects of applied elec. field *(German)* 78—72634
Si, positron annihilation, effect of doping 79—24385
Si, positron annihilation rel. to surface treatment *(Russian)* 77—44081
Si, positron implantation profile and mobility, elec. field effects 77—48273
Si, post-annealed amorphous layer, twinning struct. by transmission electron diffr. 77—76685
Si, postimplantation damage profiles, backscatt. meas. 78—47402
Si, postimplantation defect annealing in samples heavily damaged by 140 keV Si^{2+} ions 77—11602
Si, powder, reaction with HF and $HF+H_2SO_4$ mixture 79—11821
Si powder semicond., microwave propagation, Rayleigh limit 79—78126
Si, powdered, microwave propag. 78—56175
Si powders, laser synthesis using SiH_4 79—74119
Si, power transistor and solar cell epitaxy from SiH_2Cl_2 source 77—77402
Si, precipitation of Au, supersaturated soln., Hall effect meas. 77—89465
Si, precipitation of O, 1000°C TEM, IR absorpt. and X-ray studies 80—34194
Si, precipitation of O, 650°C, IR absorpt. and X-ray diffr. 80—76258
Si, precipitation of O, annealing, IR spectra meas. 80—24606
Si preparation, by SiO_2 reduction by C in plasma, thermodynamic anal. 77—40530
Si, preshaped single crystal prep. by pendant drop method *(French)* 78—64466
Si, process stress analysis by IR photoelastic meas. 78—11488
Si, process-induced in-plane distortion, correl. with wafer bowing 80—54579
Si, prod. of polySi vapour deposited coatings for solar cells, cost anal. 80—93495
Si production, low-cost low-energy processes 78—11126
Si, production by reduction of SiO_2 with C black in plasma reactor, feasibility 78—27426
Si production from rice husk ash for solar cells 79—62008
Si, profile anal. using anodisation and stripping, computer algorithm 77—43241
Si, proton damage 78—34556
Si, proton irrad., efficiency of form. and nature of defects, Hall meas. 80—6444
p-Si, proton irrad. magnetiodiode effect, heat treatment, photocond. spectra 79—69591
Si, proton irradiated, IR absorption 79—33742
Si, proton irradiated and annealed, hydrogen containing radiative recomb. centres 77—24896
Si, proton irradiation, energy depend. of rate of degradation of cond. 77—62944
Si, proton random and aligned stopping powers, 80 to 300 keV, backscatt. meas. 77—27931
Si, pseudopotential calculation of phonon dispersion curves 80—10620
Si, pseudopotentials for band struct. and cryst. energy calcs. 79—82514
Si, pulsed laser annealing, nonthermal, plasma annealing 80—25498
Si, pulsed laser annealing, mechanism 80—25739
Si, pure, lattice parameters, and topographic meas., using double-beam triple-cryst. X-ray spectrometer 80—77915
Si, pure and doped amorphous photolum. meas. 77—36285
Si, pure and heavily doped, 2p core levels and core exction binding energy, photoemission obs. 78—76583
Si, pure and n-type, US vel. and attenuation, evaluation using elastic moduli 80—70325
Si purification, plasma melting zone technique *(French)* 80—89141

elemental semiconductors continued
Si purification, plasma melting zone technique, optimisation *(French)* 80—89142
Si purification, using silicon fluoride as transport 78—35316
Si, purification technology for the development of low cost solar cells 80—50976
Si, pyrolytic BN wafer as diffusion source characterisation 78—91352
n-Si, quadratic piezoresistance, ang. depend. *(Russian)* 78—47782
Si quantised inversion layers, hot electron effects 77—28188
Si quantised inversion layers, hot electron microwave cond. calc. 77—43734
Si, quantitative anal. with SIMS 80—101052
Si, quantum cyclotron reson. linewidth 77—15752
n-Si, quantum magnetoresist. results, using pulsed fields up to 35 T 79—73528
Si, quasi two-dimensional, crit. conc. of hot carriers 77—35977
Si, quasi-two dimensional space charge layers, transport phenomena 79—95508
n-Si, quenched, fast electron irradiated, annealing of defects 80—89259
Si RF sputter-etched surface, cryst. damage, spectroscopic ellipsometry obs. 80—103538
Si, RF sputtered amorphous film, high temp. metal induced crystn. 77—11825
Si, RTR ribbon, impact of defects on photovoltaic potential 79—11186
Si, radiation damage effects on characts. *(Korean)* 79—60402
Si, radiation defect clusters, form. kinetics and parameters 77—11545
Si, radiation defects, influence of dislocations on accumulation, elec. props. 80—92558
p-Si, radiation defects by annealing, kinetics anal. 79—33018
p-Si radiation defects due to 30 MeV proton irrad., rel. to solar energy convertors 78—71776
Si, radiation detector, barrier heights, electron and hole currents, Schottky contact effects 79—33293
Si, radiation induced defects, IR absorpt. bands 80—25424
Si, radiation induced defects in high-voltage electron microscope 80—65048
Si, radiation pressure, photon drag effect in far-IR 80—50452
Si, radiation-doped and annealed, carrier density and mobility meas. 78—56145
Si, radiation-stimulated dissociative diffusion of Au, model 79—23785
Si, radiation-stimulated vacancy diffusion, mechanisms 77—55396
Si, radiative electron capture by channelled O ions 79—77658
Si, radiative recomb. centre accumulation due to high temp. electron irrad. 80—93394
Si, radiative recombination involving silane mols. 79—73998
Si, Raman cross section and its press. depend., theoretical study 79—91448
Si, Raman scattering absolute cross-section 80—11410
p-Si, Raman scattering by phonons and electrons, interference effects 78—60469
p-Si, Raman spectra, pseudopot. calc. of discrete-continuum interference 80—2747
Si, random and channelled energy loss for positive and negative, 2-15 GeV/c pions, kaons and protons 79—3332
Si, range distribs. of energetic protons, Monte Carlo computer simulation 78—22777
Si, range of 100 keV Pr^{2+} and Tb^{2+}, M-shell X-ray cross-sections 77—35614
Si, rapidly grown RTR sheet, props. and solar cell processing 79—100048
Si, ratio of photoionisation cross-section of valence s- and p-electrons *(Ukrainian)* 77—73211
n-Si, Re-compensated, deep levels, electron traps, photocond. 77—15902
Si, reach-through avalanche photodiode, temp. depend. characts. 79—95482
Si reach-through photodiodes, avalanche buildup time 77—15892
Si, reaction of rare earth impurities with carbon during cryst. growth 79—38733
Si, reactive close-spaced vapour transport, simplified theory 80—15396
Si, reactive ion beam etching expts., selectivity, anisotropy 80—104308
Si, reactive ion etching in CF_4 plasma, competitive mech. 79—91816
Si, reactive plasma etching with CF_4, mag. field control 80—11796
Si, reactive sputtering, current-voltage charact. 79—95888
Si, recomb. centre study by spin-depend. photocond. 80—49805
n-Si, recomb. parameters of heat treatment defects in diodes 79—56299
Si, recombination at dislocations 79—38023
n-Si, recombination centres and carrier lifetimes after γ-irrad. 80—60004
Si recombination characteristics used in design of semicond. devices *(Russian)* 79—42557
Si, recombination luminescence, electron-hole drop, excitons orientation in mag. field 78—88362
Si, reconstructed (001)2 x 1 surface structure, LEED intensity calcs., dimer model variations 79—77875
Si, reconstructed surface (111)2×1, polarization depend. of optical absorpt. spectrum 79—28396
Si, reconstructed surface physics, review 80—10766
Si, reconstruction-induced subsurface strain, theory 78—91516
Si, recording of free-carrier holograms by ultrashort pulses *(Russian)* 77—14680
Si, recrystallisation of CVD-grown polycryst. Si and influence of B, Al dopants on grain growth 80—54575
Si, reflectivity time dependence during pulsed laser annealing 80—66214
Si, refr. index, 95-298K, 2.5-12 μ 77—8535
Si, refractive index dispersion 79—24280
Si, regrowth under laser irrad. 80—24481
n-Si, relaxation of electron energy, carrier-density dependence 80—107809
Si, residual stacking-fault-type contrast after unfaulting reactions 79—82243
Si, residual stress and defects induced by scribing 80—60990
Si resistivity and carrier mobility effects of dissolved interstititial O_2 77—76824
Si, resistivity and deep impurity levels at 300K anal. 77—43591
Si, resistivity depth profiles calcs. from spreading resist. meas. using math. algorithm 80—2393
Si, resistivity meas. simplified temp. corrections 77—26338
Si resistors, polycryst., elec. props. in nonlinear regime, grain boundary trapping model 79—38204
Si, reson. Raman scatt. at indirect gap 79—73931
Si, resonance dechanneling of fast protons in axis to plane transitions 79—14861

elemental semiconductors continued
- a-Si, resonant and non-resonant photoconductivity changes 80—49814
- a-Si, resonant and non-resonant luminesc. changes theory 80—50410
- Si, resonant interaction of acceptor states with optical phonons 77—1394
- Si, resonant interaction of optical phonons with acceptor continuum states 78—35178
- Si reverse-biased p-n junction DC characteristics interpretation *(Polish)* 78—91761
- Si, review of point defect characts. *(Japanese)* 77—89428
- Si ribbon, crystal characterisation, growth with dies 78—76598
- Si ribbon, dendritic web growth, solar cell prod. and characterisation 77—77366
- Si ribbon, dendritic web growth from melt, solar cell module fabrication 80—93478
- Si ribbon, EFG, C contaminant conc. determ. by nuclear techniques and SIMS 80—59506
- Si, ribbon, edge-defined film-fed grown, orientation depend. of defect struct. 77—1134
- Si ribbon, edge-defined film-fed growth, solar cell prod. and characterisation 77—77365
- Si ribbon, edge-defined film-fed growth, melt temp. distrib. 79—52108
- Si, ribbon, impurity distrib. in EFG 78—91280
- Si ribbon, low angle sheet growth technique, direct shaping characts. 80—93480
- Si ribbon, prep. by rapid quenching 79—33957
- Si ribbon crystal evaluation for solar cells 77—76813
- Si ribbon crystal growth, 10 cm wide, temp. distrib. meas. in die 80—104059
- Si ribbon crystals, edge-defined film-fed growth technique for solar cells 80—89633
- Si ribbon grown by capillary action shaping technique, electron channelling analysis 77—76418
- Si ribbon growth, ribbon-to-ribbon process, thermal environment control 80—35116
- Si ribbon growth, Stepanov technique, recent develop. 79—11510
- Si ribbon growth, technology assessment 1978-1986, computer anal. using PECAN 79—8244
- Si, ribbon growth, via RTR technique, process update and material characterisation 78—76597
- Si ribbon growth by capillary action shaping technique 80—29888
- Si ribbon growth by EFG, thermal sensitivity and stability 80—107080
- Si, ribbon growth by edge-defined film-fed process, morphology, stability 77—24947
- Si ribbon growth from melt, monitoring device for width and thickness uniformity 80—35077
- Si ribbon parallel twinned structure development by shaped crystallisation 78—64465
- Si ribbon solar cell, EFG, diffusion length enhancement under illum. 78—14756
- Si ribbon solar cells, defect anal. using laser scanner 80—94089
- Si ribbon solar cells, var. of minority-carrier diffusion length with light intensity, heavy metal doping effects 80—93937
- Si ribbon-graphite in-situ thermocouple, calibration and meas. accuracies manufacture 79—97386
- Si ribbons, capillary action shaping tech., lifetime charact. 78—34847
- Si ribbons, edge-defined film-fed growth technique for solar cells 80—89138
- Si ribbons, roller quenching method of prep., grain sizes and carrier conc. 80—40275
- Si ribbons for solar cells, ultra high speed growth, elec. props. 80—89162
- Si ribbons grown by capillary action shaping technique, surface quality and impurity distrib. 80—108343
- Si, ribbons produced through capillary action shaping, elec. and struct. characts. 78—47804
- Si rich SiO_2-SiO_2-Si rich SiO_2 layers for dual electron injector struct. 80—96991
- Si, ring shaped stacking faults induced by oxide precipitates 78—67723
- n-Si, rod, in rectangular waveguide, microwave field distribution 80—39622
- Si, role of electron-hole interaction in optical spectra, review 80—45113
- Si, SAW meas. of surface elec. props. 77—20387
- Si, SOC (Si on ceramic) continuous coating for solar cells 80—93904
- Si scattering surface layer, optical props. *(Russian)* 80—11419
- n-Si, Schottky barrier diodes, temp. anomalies 78—14823
- Si, Schottky barrier height approaching band gap, minority carrier injection effect 77—20434
- Si Schottky barrier metallisation characteristics 77—76922
- Si Schottky barrier photovoltaic IR detector 80—9040
- Si Schottky barrier solar cell, V-I characts. and efficiency 78—14828
- Si, Schottky barrier structs., proton bombarded, defect states 80—29356
- Si, Schottky diode ageing, influence of metal electrode O diffusion coeffs. 79—99620
- Si, Schottky diodes on sputtered amorphous Si:H, light induced ageing effects, interpretation of photovoltaic stability 80—54780
- Si, screened donor impurities in many-valley semiconds., anisotropic mass effect 78—10399
- Si, screening of donor ions by delocalised electrons 79—69466
- Si, screening of ions, band struct. calcs. with screening variants 78—67938
- Si, screw and 60° dislocations velocities 79—86798
- Si, screw dislocation networks, TEM study 80—70204
- Si Seebeck effect position sensor for CO_2 laser beam alignment 80—5772
- n-Si, selective anodic oxidation after P implantation *(German)* 79—52411
- Si selective anodic oxidation in O_2 plasma 80—108610
- Si, selective etching rel. to SiO_2 by $CBrF_3$ plasma without undercutting 80—76380
- Si, selective oxidation in high press. steam, using Si_3N_4 mask 79—38997
- Si, selectivity of deposition from $SiCl_4$ 77—24958
- Si, self diffusion entropy 80—29211
- Si, self implanted, and additional impurity implanted laser induced recrystn., threshold power density 79—69131
- Si, self- and impurity diffusion 80—29213
- Si, self-consistent pseudopotential cal. of electronic states associated with reconstructed vacancy 79—73465
- Si, self-diffusion, activation energy and entropy factors 80—88353
- Si, self-diffusion, dynamical recovery 80—29215
- Si, self-diffusion, probed by (p,γ) resonance broadening method 80—24646

elemental semiconductors continued
- Si, self-diffusion and dynamical recovery at high temps., local equilibrium breakdown 79—69284
- Si, self-diffusion coeffs. between 1320K and 1660K, extended-interstitial mechanism 77—84985
- Si, self-diffusion mechanism 79—90824
- Si, self-implanted, ⟨100⟩ and ⟨111⟩, crystallised layers by laser annealing, struct. 78—47644
- Si, self-implanted, defect-density profiles, constant-capacitance DLTS meas. 79—95361
- Si, self-implanted layer, grain size, laser irrad. energy density depend. 78—72012
- p-Si, self-interstitials, influence of white light on annealing process *(German)* 79—19245
- Si, self-interstitials, vacancies and their clusters 77—80500
- Si, self-ion implanted, amorphous to polycrystalline transition induced by laser beam 77—84771
- Si, self-scanned photodiode array, evaluation for integrated optics spectrum analyser 80—58806
- Si, self-supporting polycryst. film deposited by energy beam plasma, for terrestrial solar cells 79—11523
- Si, semi-empirical APW calc. of band structure 80—84424
- Si, semi-insulating polycrystalline CVD layers, AES and XPS characterisation 80—16129
- Si, semiconductor charge densities with hard-core and soft-core pseudopotentials 79—33266
- Si, semiconductor detector material, purification, cryst. growth, ion implantation 78—47674
- Si semiconductor plates, control of quality of surface treatment, using Al spraying technique 80—60989
- Si, semicrystalline layer, deposited on stainless steel and Pyrex glass, growth conditions and props. 79—82482
- Si, semicrystalline vs. single crystal for photovoltaics 80—93917
- Si, semivacancy and pair of semivacancies calc. by CNDO/2 method 78—51537
- Si, shallow contact formation substrate temp. depend., Pd-W alloys 80—96963
- Si, shallow donor states, substitutional donors 79—65403
- Si, shallow donors, Zeeman interaction, relativistic corrections and very small g-shifts, contrib. to EPR 78—72393
- Si, shallow impurities, photolum. anal. 78—23512
- n-Si shallow impurity states for far IR heterodyne detection 77—38005
- Si shallow junction device, silicide contact 80—70819
- Si, shallow p-n junction, energy loss and escape depth of hot electrons 79—78159
- n-Si, shear deformed, Smith-Herring and mobility change piezoresistance 80—6842
- Si sheet, high speed growth, heat transport analysis 80—107669
- Si sheet casting for solar cells 80—89139
- Si sheet edge-defined film-fed growth, for photovoltaic cells 79—61982
- Si sheet-form solar cells, efficiency improvement, minority carrier diffusion length limitations 80—93925
- Si, short range order in surface layers, electroreflection exam. 78—6703
- Si, Si_3N_4 film formation by N ion implantation 79—90692
- Si, SiO_2 diffusion sources under oxidising ambient conditions, solar cell fabrication 78—2148
- Si, SiO_2 electronic energy, structure calc. using tight binding approximation 77—69215
- Si, silicide forming systems, solid phase epitaxy 78—23613
- Si, simple scheme for describing dislocation motion 79—65259
- Si, single cryst., dislocations, computer simulation methods in X-ray topography 79—23484
- Si, single cryst., electrolytic buffing using non-abrasive electrolyte *(Japanese)* 77—4862
- Si, single cryst., heterogeneities meas. *(Japanese)* 77—35549
- Si, single cryst. growth, temp. gradient meas. by photoelec. pyrometer 77—40359
- Si, single cryst. growth in clear SiO_2 crucibles, heat exchanger method 79—33919
- Si, single cryst. ribbon growth, thermal anal. 78—3029
- Si, single crystal, depth profile of radiation damage using lattice deform. study *(German)* 77—39618
- Si, single crystal, fracture under several liq. environments 80—81157
- Si single crystal, improved horizontal ribbon growth technique 80—108345
- Si, single crystal, kinetics of annealing of vacancy complexes 78—87666
- Si single crystal, planar channelling of fast electrons 78—2178
- Si single crystal growth advances 78—6842
- Si single crystal growth by heat-exchanger casting 78—11104
- Si single crystal ingot growth from metallurgical grade Si, inhomogeneities 80—59416
- Si, single crystal sheets grown from melt require no slicing or polishing 79—74079
- Si single crystal surface, ang. variations of backscatt. yield with 20 keV proton bombardment 79—4879
- Si single crystal surface, He^+ bombardment, damage production, defect diffusion 80—39181
- Si, single crystals, thermal conductivity calculation *(Hungarian)* 80—65311
- Si, single crysts., devices for resistivity meas. *(German)* 79—12824
- Si single crysts., mech. polishing with reagent, activation energy effects *(Japanese)* 80—89379
- Si, single-crystal, grown-in structural defects 79—10860
- Si single-junction magnetotransistor, characts. 79—24066
- Si, single-tip and multitip cathodes, fabrication, and photofield emission characts. 78—2976
- Si, sintered, grain boundaries, TEM obs. 80—15118
- n-Si, size-induced magnetoresist. in strong elec. fields 80—65582
- Si slice, minority carrier diffusion lengths, surface photovoltage meas. 78—72168
- Si, slice double-sided free polishing 78—11380
- Si slices, application of capacity gauges *(Polish)* 79—2784
- Si slices dislocation density determ., using ellipsometer *(Hungarian)* 79—99198
- Si, slip, room temp., TEM obs. 80—79804
- Si, slip dislocation nucleation during laser annealing 80—84179
- Si, small defects in Czochralski grown and zone-floated monocrystals, TEM identification 79—95001
- Si, small-diameter cryst. grown by pedestal technique, investigation of microdefects using X-ray topography 79—55683
- Si, Sn or Ge complex with vacancy, many-electron approach 78—67980

elemental semiconductors continued
Si, snowflake defect due to annealing in H at 1000°C, X-ray topography study *(Chinese)* 80—49227
Si, solar cell, amorphous, technological development trends for low cost energy requirements 80—26136
Si solar cell, CC Si diffused junction, n$^+$pp$^+$ or p$^+$nn$^+$, prep. using solid diffusion sources 80—35689
Si solar cell, elec. characts. of Pd$_2$Si and PtSi Schottky barriers 78—14825
Si solar cell, fabrication using zone melting of CVD Si on graphite, and performance 77—85945
Si, solar cell, minority carrier lifetime *(Korean)* 78—23103
Si, solar cell, minority carrier excess charge and time const. 78—30938
Si solar cell array with concentration, design and development 80—45700
Si solar cell arrays, fixed-base, flat panels, possible developments for more competitive power production 80—72050
Si solar cell arrays, for earth orbital and orbit transfer missions 80—94044
Si solar cell fabrication, R and D on low-cost processes, effect of impurities on cell performance 80—50978
Si solar cell fabrication from multiple ingots using melt replenishment Czochralski method, cell anal. 80—93477
Si solar cell parameters, grain size dependence 80—94049
Si solar cell processing, pulsed laser techniques for annealing ion-implantation damage 80—81453
Si solar cells, all-plate low cost contact system 80—93992
Si solar cells, analysis of short-circuit current 80—85285
Si solar cells, base resist. influence on temp. characts. 80—89618
Si solar cells, calculations of absorption coefficient 80—7944
Si solar cells, capacitance transient spectra of processing- and radiation-induced defects 80—61340
Si solar cells, carrier lifetime meas. from transient photoresponses of pulsed laser *(French)* 79—24898
Si solar cells, crystal growth, heat exchanger method, fixed abrasive slicing technique 80—35082
Si solar cells, design for limit conversion efficiency 80—93960
Si solar cells, diffusion fabrication process, low cost, highly automated 80—30487
Si solar cells, edge-illuminated p$^+$-nn$^+$, analytical model under concentrated sunlight 80—7942
Si solar cells, effects of B and P impurities on cell performance 80—55848
Si solar cells, effects of metallic impurities 80—85278
Si solar cells, experimental efficiency optimisation of n$^+$pp$^+$ and p$^+$nn$^+$ cells 80—30486
Si solar cells, fabrication using continuous or pulsed lasers *(French)* 80—61350
Si solar cells, fundamental efficiency limitations 80—93963
Si solar cells, high open circuit voltage, P implantation 80—89642
Si solar cells, inhomogeneities and their influence on cell performance 80—93967
Si solar cells, ion implanted, from EFG Si ribbons 80—30485
Si solar cells, ion implantation and annealing technology 80—93996
Si solar cells, ion implanted grating type 80—101102
Si solar cells, ion-implanted, expt. study of efficiency controlling factor 80—93997
Si solar cells, junction formation techniques using spray-on polymer dopants, cost effective, high throughput 80—94014
Si solar cells, light-enhanced diffusion length obs. by DC photocurrent meas. 79—39301
Si solar cells, limit efficiency evaluation 80—93973
Si solar cells, low cost, Ni contacts 80—94017
Si solar cells, low cost processes for fabrication 80—94013
Si solar cells, low-cost sheet fabrication structural defects, effect on electronic props. and cell performance 80—50977
Si solar cells, manufacturing cost anal. of flat plate vs. concentrator solar cells 80—93949
Si solar cells, metallurgical-grade, fabrication by epitaxial growth or direct diffusion 80—101104
Si solar cells, minority carrier lifetimes determ. from spectral and transient meas. 79—100533
Si solar cells, n$^+$-p, Li-counterdoped, radiation damage 80—94000
Si solar cells, Ni-Cu conductor system 80—93991
Si solar cells, POCl$_3$ gettering of Ti, Mo and Fe-contaminated cells 80—94010
Si solar cells, photoelectric effect and principles of operation and efficiency 80—50983
Si solar cells, photoreactance of p-n junction diodes 80—81464
Si solar cells, photovoltaic energy conversion efficiency, photoacoustic spectra 79—15178
Si solar cells, polycrystalline n$^+$/p, computer model of spectral response and photocurrent 80—55853
Si solar cells, polycrystalline p-n junctions, recombination currents, physical models 80—93892
Si solar cells, polycrystalline, from recrystallized plasma deposited thin films 80—104509
Si solar cells, preparation using laser processing 80—81454
Si solar cells, production process effect on fracture strength 80—93656
Si solar cells, proton irradiated, processing influence on elec. performance 80—94001
Si solar cells, radiation damaged, origin of reverse annealing 80—76630
Si solar cells, radiation damage annealing mechanisms and low temp. annealing 80—94003
Si solar cells, realisation by laser induced diffusion of deposited Sb 80—93998
Si solar cells, review and current developments 80—108801
Si solar cells, review of physics underlying recent improvements 80—93974
Si solar cells, semiconductor thick film cell contacts, all metal 80—30489
Si solar cells, single-crystal, HV, multijunction, parameters and characteristics 80—89615
Si solar cells, solid source diffusion process for fabrication 80—93994
Si solar cells, spray-on TiO$_2$ antireflection coatings 80—80963
Si solar cells, surface passivation by SnO$_x$ films, effect on cell transport props. and short circuit current 80—61360
Si solar cells, TiO$_2$ AR coating by spray deposition 80—104511
Si solar cells, ultrathin, electron and proton effects 80—94002
Si solar cells, unified model of fundamental limitations 80—81448
Si solar cells, updating limit efficiency 80—81447
Si, solar cells amorphous, glow discharge produced 80—12013
Si solar cells using minority carrier MISS 80—101103

elemental semiconductors continued
Si solar cells with fire through contacts printed on anti-reflection coating 80—93993
Si solar cells with screen printed diffusion and metallisation 80—94015
Si solar concentrator cell, effects of nonuniform illumination and temp. profiles under concentrated sunlight 80—93941
Si, solar grade, advances in Dow Corning process 79—8243
Si, solar grade, by SiHCl$_3$ CVD process, low cost 79—62007
Si, solar grade, by silane pyrolysis, process design and economics 79—8234
Si, solar grade, Czochralski growth, solar cell efficiency vs. metallic impurity conc. 78—31330
Si, solar grade, directionally solidified using C crucibles, TEM study 79—47617
Si, solar grade, prod., using Dow Corning process 80—29894
Si solar power cell production by capillary action shaping technique 79—34431
Si, solid phase epitaxial growth through Al film 79—24432
Si, solid phase epitaxy, Si$\langle 100\rangle$/Pd$_2$Si system, dissoc. mechanism 77—7980
Si solid phase grown, structural obs. 78—2397
Si, solid solubility of Co, 1000-1270°C, radiotracer obs. 77—51500
Si, solid-phase epitaxial growth stages in Si(crystal)-Pd$_2$Si-Si(amorphous) system 77—85114
Si, solid-phase epitaxy in Si (100)/Pd$_2$Si/Si (amorphous) system, radioactive tracer obs. 77—89663
Si, solid-phase-epitaxial, deposited above 380°C, defects obs. 78—63942
Si, solid-state epitaxial growth of amorphous layer 80—10803
Si, solubility of Au, gettering by P 78—83961
Si, solubility of group III and V elements 77—84928
Si, solute loss on laser annealing solute out diffusion 80—100840
Si source for vacuum deposition, with two independent filaments 80—76190
Si spectrochemical anal. for traces of Br and Cl using hollow cathode of special design *(Russian)* 77—29083
Si spectroscopic applications of structures produced by orientation-dependent etching 80—93668
Si, spherical effective impurity electron mass 77—24532
Si, spin dependent effects, theory 78—23342
Si, spin dependent recomb. at dislocations, EPR and photocond. 79—38095
Si, spin dependent recombination and photoconductive resonance 78—43439
Si, spin effects in electron transitions via dislocation states 79—82642
Si, spin-depend. recomb. at exchange-coupled dislocation centres 77—89725
Si, splitting of 1s excitons, derivative spectra of optical absorption 77—69249
Si, spreading resist. rel. to load applied to meas. probe 78—4647
Si, spreading resistance calibration, effect of specimen preparations 78—10450
Si, sputter cleaning using Ar$^+$ ions, temp. depend. of residual damage, 25 to 800°C 77—48558
Si sputter-machined surface, Ar$^+$ ion, lattice disordering obs. *(Japanese)* 80—3228
Si, sputtered, cluster formation, influence of HF plasma interaction 78—64441
Si, sputtered amorphous film, photocond. and electronic props., effects of annealing in plasma gas 80—44644
Si, sputtered atom ang. distribs. for keV Ar$^+$ bombard. 80—84819
Si, sputtered film, in Al-Si-Al(Mo), photovoltaic props. 77—24623
Si, sputtered layers, EPMA of Ar content 80—3443
Si, sputtering and sputter etching, thermal history 80—25562
Si, sputtering by Ar$^+$ ions, energy depend. of excitation 79—56906
Si, sputtering by low energy Ar ions, temp. depend. of sputtering coefficient 79—15578
n-Si sputtering-induced defects, elec. characts. 78—51941
Si, square single crystals, Czochralski growth 80—97422
Si, stacking fault annihilation by impurity diffusion 77—19968
Si, stacking fault energies 79—82205
Si, stacking fault energies, intrinsic and extrinsic, by TEM 80—10562
Si, stacking fault form. model during oxidation and ageing, defect clustering 77—24322
Si, stacking fault formation, elimination by preoxidation annealing in N$_2$/HCl/O$_2$ mixtures 78—88550
Si, stacking fault growth, oxidation-induced, HCl and interstitial effects 80—49241
Si, stacking faults, weak-beam contrast in TEM 80—75132
Si, stacking faults growth by Bardeen-Herring mechanism 79—99222
Si, stacking-fault nuclei gettering by trichloroethylene oxidation 77—43226
Si, state density and X-ray photoelectron spectra of valence bands calc. 77—28679
Si, static compression in [100] and [111] directions, elec. resist. obs. 80—65637
Si, static dielectric function, local field correction, tight-binding model 79—95355
Si, stationary creep depend. on deform. stabilisation of material struct. *(Russian)* 80—100300
Si, status of defect studies 77—84742
Si, steam oxidation, low temp., high press., oxide growth kinetics and props. 80—16523
Si, steam oxidation at any elevation, improved theoretical predictions 79—20230
Si, stopping power for channelled 160 MeV α particles, expt. 78—26613
Si, strain meas. by Pendellosung effect after P ion bombard. 78—55773
Si, strained, crit.-point for electron-hole droplets 79—4516
n-Si, strained cryst., role of phonon reson. scatt. in phonon cond., appl. to Si:Li 79—19407
Si, stress enhanced diffusion of B, using SiO$_2$ diffusion masks, photodiode fabrication 78—67865
Si, stressed, at high mag. field, submillimeter cyclotron res. of electrons 77—81012
Si, stressed, one- and two-component electron-hole liq. at T=0 80—80189
Si, stretched, lattice vibr. anharmonicity, influence of stress on elastic moduli, Raman spectra 80—80791
Si, strip-type crystals, growth mechanism, morphology 79—7559
Si strips, growth by Stepanov's method 79—78867
Si, struct. of L$_{2,3}$VV-Auger line, rel. to soft X-ray spectra 78—2953
Si, structural defects on (115) plane 78—87675

elemental semiconductors continued
- Si, structural props., self-consistent calc. 80-28947
- Si, structural props. using electron-ion Hamiltonian using density-fundamental methods 79-82177
- Si, structurally related bulk and surface props., self-consistent pseudopot. method 80-54632
- Si subnanosecond detector, charcts. 78-9027
- Si substitutional diffusion model 78-71884
- Si substrate, crystn. of amorphous SiO_2, Si_3N_4 and $Si_xO_yN_2$ films 79-28225
- Si substrate, for wet thermal oxide film, trap emptying kinetics 80-92983
- Si substrate, heteroepitaxy of deposited amorphous Ge layer by laser annealing 79-77952
- Si substrate, implantation effects on hardening and Si_3N_4 film stress reduction 78-71748
- Si substrate, ion induced intermixing of Pd or Pt film 80-15420
- Si substrate, low temp. migration into Au/Pt film, with interposed Cr layer 79-10981
- Si substrate, Nb thin film intermixing with substrate, ion induced silicide formation 80-34101
- Si, substrate, nucleation controlled interaction with metal film, silicide form. 80-10711
- Si substrate, reaction with Ti film, backscatt. anal. of silicides 79-69377
- Si substrate, Si_3N_4 growth using anhydrous NH_3 79-43141
- Si substrate, silicide formation with large bilayers of Pd-Pt, Pd-Ni and Pt-Ni 79-51444
- Si substrate, silicide formation in Mo-W bilayer films 79-99376
- Si substrate, stress field, induced by Si_3N_4 film edge, indentation-injected dislocation half-loops obs. 78-30839
- Si substrate, struct. stability of dielec. film 80-54564
- Si substrate, substrate, p- and n-type, establishment of inversion layer under high oxide field conditions 77-66202
- Si substrate, thermally oxidised, interface props., sputter deposition parameters effects *(German)* 80-40257
- Si, substrate for Al film, annealing effect on eutectic point *(Russian)* 80-100850
- Si substrate for Au films, use of sputtering for layer removal 79-78813
- Si substrate for epitaxial crystn. of GaP films by ns laser pulses 80-107674
- Si substrate for PMMA electron sensitive layer, 400 Å linewidth electron beam lithography 80-65392
- Si substrate for Pd and Pt, silicide formation by laser, electron beam annealing 80-84849
- Si substrate for RF sputtered ferroelectric $BaTiO_3$ films, ferroelectric props. 80-80697
- Si substrate for SiO_2 film, ellipsometric spectra, thickness determ. *(Chinese)* 80-86379
- Si, substrate for ZnS, Na_3AlF_6 films, H_2O absorpt., IR anal. 80-75446
- Si substrate package for integrated GaAs laser arrays, fabrication 79-18555
- Si substrate prep. for epitaxial solar cells, low-cost, unidirectional solidification process 80-93924
- Si substrate solar cells, upgraded metallurgical grade, epitaxial growth 80-93905
- Si, substrate temp. influence on shallow contact formation on Si, shallow contact formation substrate temp. depend., Pt-W alloys 80-96963
- Si substrate thinness, device design, solar cell processing, empirical study of interaction 80-93995
- Si substrates, appl. of silicates to detection of flaws in glassy passivation films 77-39745
- Si substrates, reactive ion etching 79-83351
- Si, substrates, review of defects 77-39597
- Si, subthreshold irrad., migration of Sn, Mossbauer obs. 77-15462
- Si, superlattice and 2-D electron gas 78-64080
- Si surface, (111), energy states, computer renormalisation-group calc. 80-75617
- Si surface, (111), metastable 2×1 reconstructed, dangling bond mediated attractive electron-electron model 78-91520
- Si, surface, (111) 2×1, cleaved, O_2 adsorption, low-energy electron loss spectra 79-15840
- Si surface, (111)7×7, electronic struct. calc. 80-24993
- Si surface, adatom indirect interaction, theory 80-44696
- Si surface, atomically pure, optical consts. and temp. depends. 79-65823
- Si, surface, Auger spectrum, high energy plasmon satellites 78-2955
- Si surface, Cl chemisorption, cluster calc. by iterative EHT 77-32062
- Si, surface, cluster model approach for electronic struct. 78-56205
- Si, surface, controlled stripping, automated system 78-31557
- Si surface, decontamination of Au impurities by etching 80-55559
- Si surface, depth profiling, optoacoustic technique 80-65337
- Si surface, electron states, surface photovoltage spectroscopy study, doping effects 80-49860
- Si surface, electronic struct. at semicond.-vacuum and semicond.-metal interfaces 77-20428
- Si, surface, energy-minimisation approach to atomic geometry 78-95213
- Si, surface, etched and heat-treated, optically stimulated ESR investigation 80-11245
- Si surface, field penetration and band bending in high elec. fields 79-42613
- Si surface, high index, theory of inversion layers 80-44697
- Si surface, ideal and 2xl chain-reconstructed, electronic struct. determ. 78-52050
- Si surface, influence of mech. treatment, charact. by ellipsometry 78-15141
- Si surface, interaction of oxygen gas discharge plasma 78-83840
- Si surface, ion bombardment enhanced mixing of Ag layers, Rutherford backscatt. meas. 80-65034
- Si surface, laser-annealed, characterisation by ellipsometry 80-103544
- Si surface, local density of states method and bond orbital model calc. 77-8165
- Si surface, MOS struct. band structure, minigaps, magnetoresistance, cond., space charge layers 80-92980
- Si surface, metal doped, recomb. of nonequilib. carriers at high excitation rates 79-7835
- Si, surface, morphology and electronic struct. 79-78194
- Si, surface, optical modulation of low energy electron reflection and transmission 78-88388
- Si surface, oxide overlayer, angular-depend. XPS exam. 77-55864
- Si, surface, photon excited field emission 79-78851
- Si surface, plasma etching as diagnostic technique 77-44385

elemental semiconductors continued
- Si, surface, plasma etching in CF_4-H_2 glow discharge, AES meas. 79-98922
- Si, surface, pulsed electron beam processing, doping, annealing 80-75254
- Si surface, reduction growth, autoepitaxy *(Russian)* 80-107672
- Si, surface, spin-depend. carrier recomb., photocond. expt. 78-19096
- Si, surface, sputter etched, damage, contamination, ion backscatt. obs. 79-33167
- Si, surface, stacking fault generation due to mech. damage, preoxidation annealing influence 80-54261
- Si, surface, stressed, n-inversion layers, Hartree calc. 78-68066
- Si surface, thermal oxidation induced defects, origin and growth *(Chinese)* 80-66681
- Si surface, valence band Auger line shape, corrected numerical results 78-52602
- Si surface, wetting by Pb, Sn, Ge in H_2+HCl 78-43210
- Si surface (100), vicinal plane surface band struct. electron inversion layers, minigaps 78-68062
- Si, surface (100)(1×1)H struct., LEED study 78-67910
- Si, surface (110) atomic struct. 79-69331
- Si, surface (111), LEED, Auger spectra, PES study, Ag monolayer electronic props. 79-77934
- Si surface (111)7, In submonolayer growth, superstruct. 79-77930
- Si, surface and films on sapphire, quality determ. using IR and UV specular reflectance meas. 80-108684
- Si surface barrier detectors, dE/dx thin detector technology, n^+ layer electrolytic removal *(Russian)* 77-57823
- Si surface barrier detector, Fano factor for protons 79-36480
- Si, surface Brillouin scatt. from acoustic phonons 80-55113
- Si, surface characterisation by Si-electrolyte interface impedance meas. 78-84291
- Si, surface characterisation using SAW 80-11069
- Si, surface charging during illumination, effect of various surface treatments 79-51651
- Si, surface cleaning by pulsed laser irrad. 80-45173
- n-Si, surface conductivity anisotropy in accumulation layers 78-10536
- Si, surface contamination during high dose ion implantation, AES obs. 79-70374
- Si surface doped channels, gate controlled, quantum galvanomagnetic effects 78-64134
- p-Si, surface elec. behaviour after chem. treatment 80-20185
- Si surface electron beam deposited silicide formation using scanning CW laser beam 80-66862
- n- Si, surface electron states, props. determ. at 77K 77-55598
- Si surface electron states, review of optical methods of detection 77-66191
- Si surface electron states, appl. of surface photovoltage spectroscopy 77-69391
- Si, surface electron states using discontinuous potential model 79-69574
- Si, surface emission of hot electrons 78-30998
- Si, surface final-state effects on core electron transition energies 78-91745
- Si surface formation during etching of thin thermally grown oxide layers, ellipsometric control *(Russian)* 80-104315
- Si surface interacting with adsorbed gases, paramag. props., EPR study 80-34772
- Si, surface inversion layers, intersubband optical absorpt., Auger-type transition 80-29741
- Si, surface layer defects, influence of multiple oxidation *(Russian)* 78-47650
- Si surface layers, impurities, elec. and photoelec. props. 80-2298
- Si, surface oxidation, after Ar^+ bombardment *(Russian)* 79-15028
- Si, surface oxidation, in wet O_2 environment 80-3410
- n-Si, surface photocond. and photo-emf spectra 79-73544
- n-Si, surface polaritons in DC current 80-34369
- Si, surface potential, influence of metal impurities, surface photo-EMF obs. 78-19122
- Si, surface potential spread rel. to chemical treatment *(Russian)* 78-11363
- Si, surface props. using SAW attenuation in adjacent $LiNbO_3$ 79-87131
- n-Si, surface quantum oscills. in inversion layers under uniaxial press. 78-88041
- Si, surface radiation damage cross sections, influence of distortions 80-6442
- Si, surface resistivity, effect of hydrofluoric acid treatment 78-10537
- Si, surface roughness evaluation by UV refl. 80-39393
- Si, surface self-diffusion, investigation by slow electron diffr. method *(Russian)* 78-51808
- Si, surface space charge layer, electron subbands, mag. field effect 77-20393
- Si surface space charge layers, cyclotron reson. of holes 77-76932
- Si, surface space charge layer, anisotropic and tilted valley systems, absorption 77-85726
- n- Si, surface space-charge layer, intersubband-cyclotron combined reson. 78-68063
- Si, surface state distrib. after treatment with HF and H_2O using photovoltage pulses 79-60888
- Si, surface structure, LEED and spot photometric meas. 79-23811
- Si, surface structure changes by laser pulses 78-14548
- Si, surface structures after pulsed laser annealing, LEED obs. 80-54494
- Si, surface topography changes due to pulsed laser annealing 80-84348
- Si, surface treatment by the low-energy ions of plasma accelerators 80-97608
- Si, surface with incomplete impurity ionisation, quantum model 78-34877
- Si surface-barrier detectors with Sn electrodes, characts. 78-5097
- Si, surface-barrier detector, impurity distrib., influence on characts. 80-18766
- n-Si, surface-barrier electroreflection, polarisation anisotropy 79-24295
- Si surfaces, amorphous, hydrogenated, and monocryst., AES and LEED, comparative study *(French)* 80-44398
- Si surfaces, electronic struct., tight-binding calc. 80-54755
- Si surfaces, influencing microstruct. deform. process by impurity type *(German)* 79-65107
- Si surfaces and contacts, O distrib. profile, from emitted α-particle energy anal. of $^{16}O(\alpha,\alpha)$ 79-5213
- Si surfaces etched in CF_4 or CF_4-O_2 plasma, morphology 80-93671
- Si, swirl defect characterisation in floating-zone cryst., comment 77-4098

elemental semiconductors continued
Si, swirl defect formation in floating-zone cryst., reply to comments 77—4099
Si, swirl defects, formation by agglomeration of self interstitials 77—80507
Si, swirl defects, gettering effects, obs. by photoluminesc. meas. 78—84623
Si, swirl type defects in float-zone and Czochralski single crysts. 79—27992
Si switch, laser-activated, high-power switching with ps. precision 80—2416
Si, symmetry analysis of E_2 structs., low-field electroreflectance meas. 77—40209
Si, TO and TA phonons, electronic and struct. energies calc. 78—59874
Si tandem junction solar cell, operation and parameters, model 79—100521
Si technology, ion implantation appls. 79—51124
Si technology, phys. and thermodynamic props. data for $SiCl_4$ 79—65218
Si, technology and physics, review 80—34353
Si, temp. depend. of Auger recomb. coeff. 80—24942
Si, temp. rise induced by laser beam, nonlinear heat cond. 79—11487
Si, temperature during CW laser heating, Raman scatt. meas. 80—76109
Si temperature field determ. under laser irradiation *(German)* 80—25496
Si, temperature variation in bulk moduli in solids 79—73237
Si, temporary trap characteristic after heat treatment *(German)* 80—34459
Si terrestrial solar cells, stress tested, contact integrity testing 80—94018
Si, testing aspherical atom refinements 79—7516
Si textured solar cell, hairline crack detect. using focused laser scanner 79—48123
Si, textured wafer, selective absorber for solar thermal conversion 80—30544
Si, thermal annealing study of Au-$Ti_{0.3}W_{0.7}$ metallisation 80—80134
Si, thermal cond. calc. using numerical soln. of Boltzmann eqn. 80—44373
Si, thermal conductivity at high temperature 79—55857
Si, thermal donor energy levels, Hall effect meas. 78—6335
Si, thermal donor generation in temp. range 600-800°C 79—11121
Si, thermal expansion coefficient and Gruneisen const. 77—59128
Si, thermal expansion coeff., optical mode Gruneisen const. 79—46820
Si, thermal expansion meas., 6 to 340K, using linear absolute dilatometer 77—47603
p-Si, thermal noise, effects of hot carriers 79—24036
Si, thermal oxidation, ^{18}O study 79—52400
Si, thermal oxidation, high resolution Rutherford backscatt., implanted ions analysis 79—87911
Si, thermal oxidation, in O_2/N_2 mixture, kinetics, 950-1100°C 77—86202
Si, thermal oxidation, in O_2-HCl mixture, Cl incorporation in SiO_2 films 79—70186
Si, thermal oxidation, in presence of oxides of group III metals 77—12722
Si, thermal oxidation, mechanism of appearance of surface roughness and surface defects 77—7956
Si, thermal oxidation, role of H_2O, ellipsometry expts. 78—27656
Si, thermal oxidation, role and effects of Cl 80—108622
Si, thermal oxidation at 1200°C, effects of trichloroethylene addition 78—27660
Si, thermal oxidation in Cl-H-O ambient, gas phase comp. considerations 77—48562
Si, thermal oxidation in O_2-H_2O and O_2-Cl_2 mixtures 78—44239
Si, thermal oxidation in O_2-trichloroethylene mixture, 900, 1000 and 1100°C 80—3221
Si, thermal oxidation in wet O_2/trichloroethylene mixtures at 1200°C 80—16522
Si, thermal oxidation kinetics in O_2/HCl mixture, rate consts. 77—59953
Si thermal oxidation kinetics in O_2/HCl mixtures 77—77617
Si, thermal oxidation kinetics in pyrogenic water and HCl-H_2O mixture 78—64748
Si, thermal oxidation kinetics, steady-state transport anal. 80—71773
Si, thermal oxidation kinetics, theoretical perspective 80—76387
Si, thermal oxidation technology, improved using 1,1,1-trichloroethane as optimised additive 79—29239
Si, thermal oxides prepared in O_2-HCl and H_2O-HCl ambients, Cl conc. profiles using SIMS 79—65110
Si, thermally induced donors due to heat treatment and Fe contamination 79—78035
Si, thermally induced microdefect form., C and O role 80—11439
Si, thermally induced microdefects, effect of C, TEM obs. *(Japanese)* 80—54244
Si, thermally oxidised surfaces, electron mobility in inversion and accumulation layers, MOS devices 80—103753
Si, thermionic electron emission, from defect states at grain boundaries 79—91559
Si thermomigrqation of molten Ga 77—69118
Si, thermoreflectance near $L_{2,3}$ soft X-ray threshold, temp. depend. 78—35224
Si thick-film growth using contiguous capillary coating on porous C substrates 80—93507
Si thin autoepitaxial layers low temp. growth mechanism in $SiCl_4$-H_2 system 80—20795
Si thin film, effect of O on thin film compositions obtained by secondary ion emission 80—26079
Si thin film, polycryst., CVD, elec. props. 80—107934
Si thin film for solar cells, thermal expansion shear separation technique 80—81439
Si thin films, selective etchant 79—86793
Si thin p-n junction solar cells, minority carrier mirrors and optical confinement for high efficiency (27%) 80—93933
Si thin ribbon grown at high speed, thermal stresses, reduced thermal buckling 80—107078
Si, thin sheet, Sb impurity profile eval. in p-n diffusion junction by anodisation and resist. meas. 79—46695
Si, thin single crystal, MeV ion scatt. and channelling obs. of interfaces 80—50492
Si, thin slabs, vibr. freq. calcs., dimens. effect 80—60585
Si, thin sub-monolayer film, Auger emission coeffs. meas. 80—55236
Si thin-film polycrystalline vacuum-deposited solar cells, TiB_2 bottom electrode, 10% efficiency 80—93489
Si, third order elastic constant 79—51184

elemental semiconductors continued
Si, three-dimensional electron-positron pair momentum density from positron annihilation meas. 79—43059
Si, threshold energy for displacement of atoms 78—47428
Si, total energy calcs. by r-space method, Wannier functions 80—88503
Si, tracer diffusion of ^{71}Ge and ^{31}Si in intrinsic and doped samples 80—29214
Si transistor, defect obs. using stroboscopic SEM 79—9261
Si transistor damage characts. by neutron displacement cross section 79—42118
Si, transition layer form., band struct., electroreflectance 77—16333
Si, transition metal deep centres, model 79—78045
Si, transmutation doped, deep trap level analysis 78—10471
Si, transmutation doped, stabilisation 78—10449
Si, transport phenomena in strong elec. fields, intervalley electron scatt. 79—56240
Si, transverse effective mass of E_1 and $E_1+\Delta_1$ transitions, rel. to band struct. 77—80725
Si, trichloroethylene and HCl grown oxides compared 77—76988
Si tube growth by EFG process 80—108344
Si, twinned, neutron diffr. topographic obs. 78—38727
Si, two dimensional impurity bands, Hall mobility 79—95509
Si, two-dimensional electrons in superlattice, HF cond. 78—64055
Si, two-dimensional inversion layer on surface, minigap and conductivities 80—20267
Si, two-photon transitions from deep neutral impurity centres, light absorpt. and drag effect 79—91478
Si two-step impurity diffusion, effect of internal elec. field 77—76624
Si, two-step photoconductivity by dislocations 78—14761
Si type semiconductor, interimpurity zero-phonon radiative transitions 78—15222
Si, UHF heating of charge carriers using lumped-capacitance resonators 80—20203
p-Si, US attenuation by impurities 77—69047
Si, ultimate yield strength calc. 78—43062
Si, ultra high vacuum epitaxy on Si substrates *(German)* 77—47702
Si, uncompensated, influence of carrier transit time on small-signal admittance of SCLC diode 77—85305
Si, under stress, density functional calc. of subband struct. 80—20321
Si, under uniaxial compression, photocond., polarisation effects appl. of exptl. technique 79—4581
Si, uniaxial stress effects and excited states for multiple bound excitons 78—6281
n-Si, uniaxially deformed, intervalley scatt., 78-300K 77—20330
Si, uniaxially deformed, photoluminesc., biexcitons *(Russian)* 77—59611
Si, uniaxially stressed, excitonic molecule emission spectra, electron valley degeneracy effects 80—60669
Si, unindexable and forbidden lines in Kikuchi electron patterns 79—94850
Si, V-grooves formed by etching, phosphosilicate glass bridge struct. 80—104312
Si, VPE, fine struct. formation *(French)* 78—43275
Si, VPE, gas-flow dynamics in horizontal CVD reactor, book contrib. 79—82498
Si, VPE, pattern shift comparison in vertical, horizontal, and cylindrical reactor geometries 78—27408
Si, VPE, state of art 79—33937
Si, VPE, stationary model, appl. to $SiCl_4$-H_2 system 78—52679
Si, VPE at reduced pressure, autodoping 77—77389
Si VPE film growth on insulators 78—48327
Si, VPE growth, in process monitoring and control of doping gas conc. 79—24443
Si, VPE growth *(French)* 77—59236
Si, VPE growth mechanisms 79—28929
Si, VPE layer props. control using boundary layer characts. 80—50561
Si, VPE tangential growth, thickness meas. 77—35836
Si, VPE via SiH_2Cl_2 in barrel reactor 78—52685
Si, vacancies and interstitials 80—29015
p-Si, vacancy, charge states, Jahn-Teller stabilisation energy 80—80209
Si vacancy, defect electronic energy levels calc., optimisation 79—28315
Si vacancy, electron states, Anderson negative-U system 80—96820
Si, vacancy, local energy levels in Wannier approx. 77—20264
Si, vacancy, possible Anderson negative-U system 80—2358
Si, vacancy, self consistent Green's function method 80—24843
Si, vacancy, self-consistent electronic states 80—29354
Si, vacancy, tight-binding calc. 80—24844
Si, vacancy cluster props., effect of natural anisotropy *(Russian)* 77—62522
Si, vacancy electronic struct., self-consistent approach 79—78043
Si, vacancy electronic struct., self-consistent Koster-Slater method 80—10920
Si, vacancy formation and stability due to noncentral force 80—70192
Si, vacancy paradox 78—59804
Si, vacancy screening, dielec. const., exchange correl. pot., Thomas-Fermi description 80—44528
Si vacuum deposited polycryst. films, p-n junctions investigation 77—28249
Si, vacuum deposition, combined with Sb ion implantation *(Japanese)* 78—88428
Si vacuum deposition combined with Sb ion implantation, neutron activation anal. 79—47631
Si, vacuum deposition of polycrystalline film on metal substrate 79—91588
Si vacuum sublimated thin film structure impurity distrib. 78—95354
Si, vacuum-crushed surface, adsorption of H_2 and Cl_2, EPR meas. 79—46957
Si, valence band model, nonlocal exchange and correl. pot. 77—43492
Si, valence band relaxation energies during XPS 78—39657
Si, valence bands, XPS excited by Zr Mζ radiation 80—40236
Si, valence bond Wannier functions calcs. 78—60053
Si, valence charge density calc. 78—34463
Si, valence electron radial and momentum distribs., X-ray form factors and Compton profiles 79—65956
Si, valence electrons, energy-depend. photoionisation probability calc. 77—16462
Si, valence electrons XPS spectrum, OPW calc. 77—4715
Si, valley-orbit interaction and effective-mass theory 78—23043
Si, van der Waals electron correlation energy 78—95013
Si, vapour epitaxy, optimum growth conditions 78—76608
a-Si, vapour species rel. to amorphous film deposition 78—14641

elemental semiconductors continued
- Si, vapour-liq.-solid growth, using Pt and Au liq. forming agents, kinetics and morphology 78−42935
- Si, vapour-liq.-solid growth, using Pt and Au liq. forming agents, struct. perfection 78−42936
- Si, variation of thermal conductivity with temperature 79−23793
- Si, vertical etching, at very high aspect ratios, review 80−50744
- Si, vicinal surface struct., LEED exam. 79−60611
- Si, voltage-current curves, specimens of variable cross-section 77−8113
- Si, volume plasmon dispersion at large wave vectors, EELS 78−56094
- Si wafer, automatic meas. system for resist. profiles 80−39574
- Si wafer, bending by thin polycrystalline Si film deposition and by film doping using B diffusion 79−95276
- Si wafer, chemically etched, surface roughness by gas adsorption techniques 80−15398
- Si wafer, colour-band generation during high dose ion implantation 79−1449
- Si wafer, colour-banded, sheet resist. variation following high dose implantation at high dose rates 78−95074
- Si wafer, Czochralski grown, interstitial O gettering 77−86196
- Si wafer, Czochralski grown, precipitation during high temp. oxidation 78−11381
- Si wafer, defect studies by ASLEEP, SEM and scanning AES 79−19256
- Si wafer, deformation *(Japanese)* 78−43064
- Si wafer, dislocation propagation and emitter edge defects, appl. to transistors 77−1128
- Si wafer, HCl etching, smooth or pitted surface struct., gas phase comp. effect 78−11360
- Si wafer, heat treatment behaviour of microdefects and residual impurities, X-ray diffr. and IR absorpt. study 80−49214
- Si wafer, high resolution SIMS 78−56929
- Si wafer, ion etching, secondary ion monitoring 79−91551
- Si wafer, ion implanted, electron beam annealing, computer simulation 80−96569
- Si wafer, migration of fine molten Al rich wires, vertical p-n function fabrication 78−68077
- Si wafer, nondestructive method for meas. of spatial distrib. of minority carrier lifetime 80−13098
- Si wafer, oxidation induced stacking faults, surface vs. bulk nucleation 77−62545
- Si, wafer, photovoltaic technique for meas. resistivity variations 79−21783
- p-Si wafer, self-interstitials form. during chemicomech. polishing *(German)* 79−34175
- Si wafer, shrinkage and annihilation of stacking faults 77−39598
- Si wafer, slotted mask, direct deposition of metal contact pattern on MIS solar cells 80−97786
- Si wafer, stress meas. in film, X-ray method 78−51860
- Si wafer, stresses generated by thermomigration of liquid inclusions 79−37875
- Si, wafer, suppression of oxidation stacking fault generation by preannealing in N_2 atm. 78−30648
- Si wafer, surface characterization by ellipsometry 79−90853
- Si wafer, surface exam. of ion-implantation using SAW convolver 77−72897
- Si wafer, thermal characts. of H_2SO_4-H_2O_2 cleaning soln. 80−3225
- Si wafer, thermal neutron irrad., charge carriers behaviour obs. *(Japanese)* 79−42484
- Si wafer, thermally oxidised, stress and strain meas. *(Russian)* 78−11375
- Si wafer, thin surface layers, amorphous to cryst. transform., obs. technique 80−107288
- n-Si wafer, trap centres of self-interstitials 80−75516
- Si wafer, trichloroethane oxidation, effect on SiO_2 and Si props. 79−70193
- Si wafer C impurity IR absorption spectrometry, thickness fringe elimination 80−55132
- Si wafer contaminated, Au redistrib. during growth of oxide or phosphosilicate glass 77−4121
- Si wafer creep testing using stress provided by deposited Si_3N_4 film 77−66000
- Si wafer diagnostics, using computer automated scanning low-energy electron probe 79−4214
- Si wafer O interstitial IR absorption spectrometry, multiple reflection correction 80−55131
- Si wafer processing, CO_2 laser heating dynamics 80−76106
- Si wafer prod., diffusion furnace temp. profile meas. systematic errors, theoretical model *(German)* 80−8989
- Si wafer stacking fault formation model 77−76426
- Si wafer stacking faults, preoxidation gettering by reverse side P diffusion-induced misfit dislocations 80−60988
- Si wafer surface sputtering, secondary postive ion mass and kinetic energy anal. 78−88391
- Si wafer thermal gradient induced slip, effect of starting cooling temp. 78−10057
- Si wafers, Au contamination during plasma etching 80−19831
- Si wafers, B predeposited, anal. by combined ion beam techniques and X-ray microanal. 79−5238
- Si wafers, Czochralski, gettering of surface and bulk impurities 78−64456
- Si wafers, Czochralski grown, crystal defects, photoluminesc. topographic obs. 79−1432
- Si wafers, Czochralski grown, minority carrier transport props., laser beam scan for homogeneity anal., photovoltaic cell appls. 80−92905
- Si wafers, Czochralski-grown, lifetime improvement by two-step annealing 80−49916
- Si wafers, deep level detect. using variable temp. apparatus 79−88951
- Si wafers, dislocation dynamics during annealing, X-ray topography system obs. 77−76261
- Si wafers, etched in HCl, exam. of bunch formation 78−68831
- Si wafers, floating-zone, etch struct. on microdefects as affected by dopants and surface treatment 80−79773
- Si, wafers, HCl etched, surface morphology, etch pit origin 79−96166
- Si wafers, microwave plasma etching, role of ions and neutral active species 80−3217
- Si wafers, N heat-treatment effects, stacking faults formation 78−85016
- Si wafers, n- and p-type (100), oxidation-induced stacking faults 77−39599
- Si wafers, preparation of preselected areas for TEM 78−24887

elemental semiconductors continued
- Si wafers, process-induced in-plane distortion and wafer bowing 79−11048
- Si wafers, saw damage reduction in lubricant environment 80−108585
- Si wafers, scribing and subsequent fracture 80−11743
- n-Si, warm-electron magnetoresist. 79−65503
- Si, wave functions and optical cross sections associated with deep centres 78−34801
- Si waveguide photodetector matrix, appl. in integrated-optics demultiplexer 79−32095
- Si, weak heating of electrons, cyclotron reson. conditions, quantising mag. field 78−39141
- Si whisker, (111) oriented, FIM and atom-probe FIM obs. 80−10473
- Si, whisker, amorphous, growth method for field desorption mass spectrometry 79−28262
- Si whisker, amorphous, meas. of Young's modulus 78−83865
- Si, whisker, growth by reduction of $SiCl_4$ in H_2 gas current 77−15726
- Si, whisker growth in amorphous state, in SiH_4-Ar atmosphere, visual obs. 78−84112
- Si whiskers, polytypism and amorphousness 78−26801
- Si, whiskers nucleation, effect of machining support surface *(Russian)* 79−65352
- Si wide ribbon, high speed edge-defined film-fed growth 80−104058
- Si, wide ribbon crystal growth apparatus 78−48307
- Si, with dislocations, noise spectrum 80−107881
- Si, with non-spherical pots. for two basis atoms, electronic struct. 78−72069
- Si with thermal defects, photocond., effect of annealing on elec. resist. 80−6837
- Si, with various dislocation densities, ang. depend. of X-ray polarisation of curve of 111 Bragg reflection 79−46509
- Si, work function and Auger spectroscopy of initial oxidation 78−76132
- Si, X-irrad., photocond. spectrum 77−15903
- p-Si, X-irrad., subthreshold defect prod., Hall meas. of carrier conc. and photocond. spectra 77−89470
- Si, X-ray, multiple diffr., Bragg. refl. theory 79−94842
- Si, X-ray absorption K-edges *(Russian)* 79−47541
- p-Si, X-ray bombard. effects on elec. resist., and carrier density, annealing effect 77−4125
- Si, X-ray channeling technique anomalous transmission, appl. to microdefects induced by heat treatment 79−19124
- Si, X-ray diffr., meas. of dynamical and kinematical components with triple cryst. diffractometer 79−50948
- Si, X-ray diffraction characterisation, highly collimated beam 78−9912
- Si, X-ray diffuse scatt. close to reciprocal lattice points, high-resolution technique 77−39511
- Si, X-ray emission spectra formation, role of nonequilibrium electron density *(Russian)* 77−63490
- Si, X-ray intensity anomalously transmitted, ε_{220} values 78−83650
- Si, X-ray K-spectra, fine struct. intensity, temp. depend. *(Ukrainian)* 77−55850
- Si, X-ray $L_{2,3}$ emission spectrum, high energy plasmon satellite 79−82538
- Si, X-ray linear absorpt. coefficients, in energy range 5 to 50 keV 79−73066
- Si, X-ray mass attenuation coeff. meas. 77−31556
- Si, X-ray resonance Raman scattering, solid target, proton bombarded 79−61465
- Si, X-ray section topography in the Bragg case 80−79637
- Si, zone melting, swirl defects A-type as source of dislocation generation on macroscopic scale 80−25554
- Si, zone refined, prep. of solar cells 78−64475
- Si: (B, P, Ge), impurity-pair diffusion, influence of elastic stresses 78−87824
- Si: As(Pb), high-dose ion implanted and annealed, implant redistribution 80−107309
- Si: Li, absorpt. and luminesc. transitions involving exciton excited hole states 79−78038
- Si:^{119m}Sn, impurity lattice dynamics, Mossbauer spectra, Debye temp. 80−84262
- Si:^{11}B, amorphous, calc. of implanted-ion range and energy-deposition distrib. 77−7748
- Si:$^{31}P^{+}$, implanted layers, characterisation by ellipsometry 79−90683
- Si:^{57}Co, ion-implanted, Mossbauer study, annealing effects 80−7231
- Si:^{57}Co/^{57}Fe, Mossbauer spectra, deep level Co impurity study 80−29666
- Si:^{57}Co(^{57} Fe), implanted, Mossbauer spectra, study of dose dependence 80−75900
- Si:^{57}Fe, electric quadrupole coupling at Fe nuclei 78−27137
- Si:^{85}Kr, ion-implanted, impurity distrib. 80−15145
- Si:0, electrical activity due to heat treatment, Hall effect meas. 80−15543
- Si:Ag, photoexcitation of electrons from ionised AG acceptors 78−2519
- Si:Ag, surface layer, ellipsometry 78−19121
- Si:Ag (Zn,Fe), diffusion mechanism of fast impurities, distrib. in surface layers 77−11735
- Si:Al, absorpt. line broadening 78−95594
- Si:Al, bound exciton and bound multiexciton complexes, electronic structure, luminesc. obs. 79−56139
- Si:Al, bound exciton and multiple bound electron luminesc., fine struct. 77−48221
- Si:Al, bound-exciton absorption 78−56507
- Si:Al, diffusion, open-tube high-vacuum method 78−6084
- p-Si:Al, diffusion and incorporation of dopant in closed system, elec. props. 77−59026
- Si:Al, electron irrad. induced defects, transient capacitance study 80−59516
- Si:Al, localised exciton bound to isoelectronic trap 80−66283
- Si:Al, P-diffused, recomb. centres, thermally stimulated capacitance meas. 77−72834
- Si:Al, polycryst. film, grain boundary diffusion, Auger sputter profiling 80−75388
- Si:Al, recomb. enhanced migration of interstitial Al 79−82201
- Si:Al, thermally induced deep levels, TSC meas. 77−31974
- Si:Al, valley-orbit splitting of bound exciton states 79−28290
- Si:Al film, low-temp. diffusion of Al 78−38878
- Si:Al p-n lamellar structures, processing by molten Al rich wire thermomigration 78−10068
- Si:Al ribbon, edge-defined film-fed growth, Al redistrib. 80−29873
- Si:Al(B)(P), bound multiexciton complexes, work function thermodynamic determ. 78−72078

elemental semiconductors continued
Si:Al(Ga), O_2 diffusion, conc. profile meas. 80—79990
Si:Al(Ga), spreading resist. calibration using Si:B 80—103690
Si:Al(In), acceptor levels, IR spectra 78—67972
Si:Al(Sb) film, amorphous, ion implantation, effect on cond. 78—83839
Si:Ar, As, ion implanted, laser annealing, doping profiles, channelling 80—97506
Si:Ar, ion implant gettering of MOS capacitors using linear voltage ramp and N^+ backscattering 79—95502
Si:Ar, ion implanted, amorphous, epitaxial regrowth 79—10868
Si:Ar, ion-implanted, epitaxial regrowth by laser annealing, microstruct. 80—84404
Si:Ar, ion-implanted, high resolution LMM Auger spectra 79—83066
Si:Ar^+(Si^+). implantation effect on carrier lifetime, damage obs. by TEM 79—65493
Si:Ar(B), implantation doped, electroreflection spectra 79—51983
Si:Ar(Ne)(O)(N), ion-implanted, defect reverse annealing, 550-650°C 80—88875
n-Si:Ar(P), single cryst., positron annihilation parameters, energy-band struct. on surface in free-electron approx. 79—15555
Si:As, 1.5 MeV H^+ and He^+ irradiations of As diffused layers 78—47447
Si:As, amorphous, appl. of EXAFS methods for struct. determ. 79—37624
Si:As, amorphous, field effect and thermoelectric power 79—33289
Si:As, annealed, dopant profile parameter contactless probing by IR spectroscopy 79—77629
Si:As, anomalous tail generation, As ion channelling 80—49246
Si:As, As implantation damage and atom location, channelling meas. 77—59032
Si:As, CVD, doping using SiH_4-H_2-AsH_3 system 80—79823
Si:As, CW laser annealing mechanism, annealed spot size, solid phase epitaxial regrowth 79—78798
Si:As, depth profile detect. limit of 3×10^{15} atom cm^{-3} using Cs^+ bombardment negative SIMS 77—65988
Si:As, diffused, laser irrad., stability study 80—65547
Si:As, diffusion model, degeneracy and partial ionisation effects 80—96693
Si:As, diffusion of implanted As induced by laser annealing 77—89590
Si:As, displacement effect beam energy depend., vacancy trapping 80—33996
Si:As, dual wavelength, laser ion implantation damage annealing 79—69117
Si:As, effects of recoil-implanted O on elec. activation of As 79—99227
Si:As, elec. activation of implanted As during low temp. anneal, Hall effect meas. 78—51571
p-Si:As, electrochem. doping, depth profile analysis 77—72630.
Si:As, electrochemical doping 79—90684
Si:As, electrochemical doping profiles 79—90685
Si:As, electron induced displacement, channelling study 80—29058
Si:As, electron irrad. induced defect levels, annealing, deep level transient spectroscopy obs. 77—59044
Si:As, electron irradiated, majority carrier trap prod., effect of O_2 enhanced annealing 77—1151
Si:As, H, amorphous system, struct. and defects, Raman and EPR meas. 80—49103
Si:As, heavily As-diffused, Hall mobility and resist. rel. to carrier conc. 80—107815
Si:As, high conc. diffusion from double-layer sources 78—10075
Si:As, high-dose implanted, irrad. time and subsequent heat treatment effects on laser annealing 80—29041
Si:As, implantation into polycryst. Si and diffusion into Si substrate 77—59025
Si:As, implanted, laser annealing reduction in defect conc. 77—62559
Si:As, implanted, residual defects after one- and two-step annealing 78—6083
Si:As, implanted, spatially varied activation during regrowth of amorphous layers, sheet resist. and backscatt. obs. 78—71749
Si:As, implanted, thermal diffusion of As 80—39352
Si:As, implanted through SiO_2 films, elec. props., defect struct. 80—54264
Si:As, ion implantation system, high current, design of end station 80—34030
Si:As, ion implanted, amorphous-cryst. transition induced by multiple-pulsed ruby laser 79—90555
Si:As, ion implanted, annealing characts., elec. props. 77—19974
Si:As, ion implanted, anomaly of elec. activation by additional Ne irradiation 78—84211
Si:As, ion implanted, anomalous diffusion of As 79—14842
Si:As, ion implanted, beam techniques 80—24474
Si:As, ion implanted, formation of As complexes 80—59511
Si:As, ion implanted, glow discharge optical spectroscopy 78—22755
Si:As, ion implanted, laser scanning apparatus for annealing 78—34526
Si:As, ion implanted, low temp. thermal annealing 80—96552
Si:As, ion implanted, pulsed ion beam annealing 80—103395
Si:As, ion implanted, pulsed laser annealing, partial solid-state regrowth 80—103591
Si:As, ion implanted, recrystallisation by free running ruby laser 79—73185
Si:As, ion implanted, scanning-electron-beam annealing 79—60391
Si:As, ion implanted, two-step annealing 78—18664
Si:As, ion implanted, two-step annealing, TEM study 79—82249
Si:As, ion implanted layers in device structures, boundary effects in laser annealing 79—73188
Si:As, ion-implanted, CW IR laser annealing 80—34022
Si:As, ion-implanted, channelling anal. of CW Ar laser annealing 79—73186
Si:As, ion-implanted, dislocation loops and etch pits, X-ray diffr. and TEM obs. 79—42068
Si:As, ion-implanted, laser annealing, channelling obs. of As cluster form. 79—69128
Si:As, ion-implanted, laser recrystallisation by freq.-doubled Nd:YAG laser 79—77613
Si:As, ion-implanted and post-annealed, dislocation loops, TEM obs. 77—84776
Si:As, ion-implanted layers, ellipsometric anal. of laser annealing 79—73190
Si:As, laser annealing, channelling, optical obs., and resist. meas. 79—1444
Si:As, laser annealing of implanted layers 77—55296
Si:As, laser induced diffusion and annealing processes 77—69943

elemental semiconductors continued
Si:As, MBE with simultaneous ion implant doping 80—66432
Si:As, melting by high power ns laser pulsing, As diffusion 78—79789
Si:As, neutron damage mechs. in IR detectors 78—30668
Si:As, p-n junction form. by laser annealing, space charge region, effects on reverse current 80—54772
Si:As, planar and axial channelling of 800 keV As 77—19995
Si:As, relation between total and electrically active As conc. produced by diffusion 79—55773
Si:As, SIMS, energy distrib. of sputtered ions 79—38706
Si:As, scanning electron beam annealing, spreading resistance, junction depth 80—75267
Si:As, segregation and desorption kinetics for evaporation of As 79—99410
Si:As, segregation and substructure, TEM obs. 77—63674
Si:As, shallow junctions by high-dose implants 80—96694
Si:As, solid solubility and thermal behaviour of metastable 80—75359
Si:As, solid solubility of As determ. by ion implantation, CW laser annealing 80—6517
Si:As, time-resolved reflectivity during laser annealing 78—92086
Si:As,Sb, amorphous, damage depend. of epitaxial regrowth during annealing 78—47679
Si:As detector, high-low junction contact at low temp. 77—39925
Si:As high-dose implanted single crysts., pulsed electron-beam annealing 80—103373
Si:As implanted emitters, oxidizing drive-in ambient deleterious effect 80—2044
Si:As ion implanted, laser induced diffusion modelling 80—24672
Si:As ion implanted layers, annealing by CO_2 laser, doping profile shift 80—84965
Si:As ion implanted shallow junction 80—70228
Si:As ion implanter system, high current, architecture and control 80—31942
Si:As laser annealing, heat and mass transport model 80—92546
Si:As photoconductive detector for IR astronomy, responsivity and system noise 80—51665
Si:As thermal diffusion retardation by inert gas ion implantation 79—77616
Si:As wafers, laser annealing, Rutherford backscatt., optical, and TEM obs. 79—1445
Si:As^+, annealing by scanning Ar ion laser, dislocation loop density comparison 78—47438
Si:As^+, implanted, CW laser annealing, electron-beam induced current 80—100709
Si:As^+ sheet resistivity rel. to isochronal annealing and defect structures 77—76443
Si:As^+(P^+) ion implanted, laser annealed, correlation of struct. and elec. props 80—70855
Si:As^+(P^+)(Sb^+), implantation damage removal by laser irrad. and its thermal stability, TEM study 79—74024
Si:As(B), heavy-doping effects and impurity segregation during high-press. oxidation 80—65014
Si:As(B), implanted CW laser annealing, elec. props., cryst. struct. and limitations 80—39131
Si:As(B), ion implanted, pulsed laser annealing appl. to device fabrication 79—73180
Si:As(B), ion-implanted, scanned laser and electron beam annealing 79—73182
Si:As(B)(Ga)(In)(P)(Sb), mean square dynamic displacement of atoms, effect of electron-phonon interactions *(Russian)* 78—10145
Si:As(B)(N)(P), conc. profiles of ions and recoiled N after implantation through Si_3N_4 films 79—55764
Si:As(B)(P), ion-implanted polycrystalline films, laser annealing 79—73181
Si:As(Li)(P), luminesc., stress effects on donor exciton satellites 77—85786
Si:As(P), ion implanted, TEM study after laser and furnace annealing 80—70234
Si:As(P), Orbach spin-lattice relax. rate, uniaxial stress depend. 78—72391
Si:As(P), oxidation-enhanced diffusion of impurities 79—46840
Si:As(P) film, polycryst. laser annealed, resistivity changes during thermal annealing 79—91163
Si:As(P)(Sb), donor-polarizability enhancement as the insulator-metal transition is approached from the insulating side 80—80184
Si:As(P)(Sb) film, implanted, elec. cond., sheet resist. as function of ion dose and temp. 79—78235
Si:As(Pb), ion-implanted, impurity redistrib. during laser irrad. 80—100280
Si:As(Sb), implanted, pulsed ruby-laser annealing, Rutherford backscatt., TEM and ion channelling study 79—86805
Si:As(Sb), ion implant lattice location after pulsed ruby laser annealing 79—73204
Si:As(Sb), ion implanted, lattice location of impurities after pulsed laser annealing 80—88196
Si:As(Sb), ion-implanted, CO_2 laser annealing 79—73183
Si:As(Sb), MBE, n-type doping techniques 80—15126
Si:As(Sb)(Bi)(P), luminescence associated with transitions from bound exciton excited states 78—23534
Si:Au, autoradiographic detection of getter effect, Ar ion implantation 78—38739
Si:Au, C-V curves of MIS diode used to examine trapping levels 80—65697
Si:Au, carrier capture cross-section at low temp. *(Rumanian)* 79—15163
Si:Au, deep impurities, book contrib. 78—10403
Si:Au, degeneracy factor of acceptor level 78—51927
Si:Au, diffusion, effect of C concentration 78—10076
Si:Au, diffusion of Au anal. 79—23786
Si:Au, EPR spectrum, strong nucl. quadrupole effect 80—93172
Si:Au, electron capture cross section, energy level of Au acceptor centre 78—51926
Si:Au, IR absorption and elec. resist. meas., impurity centres 79—38580
Si:Au, impurity diffusion and distribution obs. by neutron activation analysis *(Japanese)* 77—84787
Si:Au, impurity induced internal friction, impurity centre symmetry 79—73252
Si:Au, impurity photocond., for IR electrophotographic system 77—24589
Si:Au, influence of carrier heating on exclusion 77—8110
Si:Au, neutron irradiated, penetration of Au into Si 78—59984

elemental semiconductors continued
Si:Au, nonequilib. population of electron states and photomemory of surface pot. 78—56206
Si:Au, O(H), film, amorphous, elec. cond. meas. 80—80423
Si:Au, p$^+$-n junction, quantitative study of Au atoms by TSC method 80—2458
Si:Au, P-induced point defects influence on Au gettering mechanism 80—65030
Si:Au, precipitation of solid soln., effect of gamma irradiation 80—59515
Si:Au, thermally stimulated capacitance method fitting anal. 79—47107
Si:Au Ar ion implant gettering obs. by MOS and Rutherford backscatt. techniques 80—39119
Si:Au deep level parameter determ. by isothermal capacitance transient spectroscopy 80—88507
Si:Au donor and acceptor centre obs. using IR absorpt. and dynamic nucl. polarisation with optical pumping 80—54639
Si:Au n$^+$p diodes, deep level transient spectroscopy, system effects and data anal. 79—99501
Si:Au p$^+$-i-n$^+$ diode, double injection switching, effect of trapped space charge 77—1473
Si:Au p$^+$-i-n$^+$ diode, I-V characts., recomb. centre influence 78—19134
Si:Au p$^+$-n junction, small area, acceptor level conc., determ. from TSC curves 80—75631
Si:Au surface, electronic props. 77—66194
Si:Au use in weakly absorbed nucl. radiation detectors 77—67947
Si:Au(Hg), photomag. effect 77—4401
Si:Au(P)(B) whiskers, impurity inhomogeneity 80—39145
Si:Au(Pt), electron and hole capture, DLTS obs. 80—49661
Si:Au(Zn) deep-level impurities, insulating props. 78—39124
Si:B, annealing mechanism of radiation change and dopants in pulsed laser irrad. ion implanted layers 79—46691
Si:B, anomalous B profiles prod. by BF_2 implantation 80—75252
Si:B, antiferromagnetic ordering of holes, recombination radiation polarisation *(Russian)* 80—45121
Si:B, As, first and second order Raman scatt. by pair modes 79—65869
Si:B, autodoping during epitaxial growth from SiH_4 77—47476
Si:B, B segregation during dry, nearly dry and wet O_2 oxidation 79—66178
Si:B, bound many-exciton complexes, luminescence spectra, mag. props. 80—103994
Si:B, bound multiexciton luminesc., recomb. kinetics 79—38591
Si:B, conc. depend. of B diffusion coeff. 80—39353
Si:B, conc. profile of implanted cryst., by $^{11}B(p,\alpha)$ chem. anal., annealing *(German)* 78—83843
p-Si:B, defect energy levels with 1 MeV electron irrad. and annealing, transient capacitance spectra 77—62860
Si:B, detection of atomic plane displacement in near-surface layers, ang. depend. of photoemission during X-ray Bragg diffr. 78—47207
Si:B, diffusion for very shallow defect free p$^+$-n junc. for solar cells 79—15218
Si:B, diffusion from BN source with H_2 injection, AES study 80—19986
Si:B, diffusion length, SEM-EBIC/Schottky diode 79—82605
Si:B, diffusion of As atoms from ion implanted layers, conc. profiles 77—43376
Si:B, diffusion of B atoms and growth kinetics of oxidation induced stacking faults, correlation 79—37720
Si:B, diffusion of B from B_2H_6-CO_2 system, lower temp. limit of 775°C 77—43232
Si:B, diffusion of randomly implanted ions during high temp. processing 77—24439
Si:B, diffusion with BN, expt. *(Bulgarian)* 78—59824
Si:B, diffusional impurity redistrib., elastic stress field effect *(Russian)* 77—72719
Si:B, dislocation net form. during annealing 77—51385
Si:B, distrib. profiles, high temp. treatment effects 79—69150
Si:B, dopant density and temp. depend. of hole mobility and resistivity 79—38075
Si:B, dopant density determ. by nucl. track technique 78—55886
Si:B, ESR at zero and small external stress, interpreted in spin Hamiltonians 78—43641
Si:B, ESR at zero and small external stress, elastic strengths for point defects 79—19764
p-Si:B, Fe, 0.45 eV majority carrier trapping level after quenching 78—18990
Si:B, He$^+$ irradiation-induced diffuiion, effect on impurity distrib. 80—70470
Si:B, heat treatment centres changes, EPR obs. 80—29601
Si:B, heavily doped, annealing characteristics obs., Ne$^+$ ions implantation for damage density control *(Japanese)* 78—18666
Si:B, heavily doped, paramagnetic props., anomalous hole spin susceptibility *(Russian)* 80—54861
Si:B, heavily implanted wafers, secondary defect generation suppression by HCl oxidation 78—10069
Si:B, high conc. effects in ion implantation 80—75245
p-Si:B, high temp. treatment, effects on ion implanted impurity distrib. profile 78—79625
Si:B, highly-doped polycryst. thin film, growth kinetics and properties 78—44016
Si:B, hole mobility calc. for dopant density and temp. var., resistivity meas., effective mass calcs. 80—54703
Si:B, hole trapping by B atoms at low temps. 79—7837
Si:B, hot-carrier scatt. and recomb. characts. 79—91069
Si:B, implantation energy, rel. to dose, Szabo-Bogancs effect 78—38740
Si:B, implanted, effectiveness of charged vacancies in diffusion 80—34239
Si:B, implanted, free carrier conc. and impurity location, Raman scatt. obs. 77—55295
Si:B, implanted, laser-annealed, lattice dilatation 79—46690
Si:B, implanted, oxidation induced precipitate defects, TEM 78—31556
Si:B, implanted, oxidation-induced stacking faults, EBIC and TEM expts. 78—39923
Si:B, implanted, shrinkage of rod shaped defects 78—6061
Si:B, implemented laser annealed samples, unidirectional contraction 78—71747
Si:B, impurity conc. from photoluminesc. anal. 78—63785
Si:B, impurity excited state lifetimes 78—60083
Si:B, inhomogeneous surface layer, diffusion and implanted, X-ray rocking curves 80—6603
Si:B, interstitial Si atom formation by light ion bombardment 78—47406
Si:B, ion implantation, anal. of disordered regions in crystal with Promiss protonograph 80—19823
Si:B, ion implantation, channelling and random distrib. of B ions meas. 77—47473
Si:B, ion implantation using B_2O_3-B mixture, Auger spectra, channelling anal. 79—4317
Si:B, ion implanted, comparison of range and range straggling 77—55293
Si:B, ion implanted, depth and lateral profiles of B atoms, Monte Carlo simulation 77—55297
Si:B, ion implanted, ellipsometric study for low doses, cryst. damage parameter 79—65105
Si:B, ion implanted, laser annealing 78—34525
Si:B, ion implanted, laser and thermal annealing compared, TEM obs. 78—75681
Si:B, ion implanted, laser annealed, thermal annealing effect 79—73191
Si:B, ion implanted, laser annealed, IR and Raman spectra 79—73914
Si:B, ion implanted, laser annealed, Raman scatt., Fano interactions, lattice damage 79—78711
Si:B, ion implanted, localised defects, TEM study 78—87699
Si:B, ion implanted, radiation defect accumulation and annealing, X-ray diffr. obs. 79—37726
Si:B, ion implanted, SOS device struct., nonlinear impurity redistrib. 79—1625
Si:B, ion implanted, struct. of rod defects, TEM obs. 78—71744
Si:B, ion implanted, structure defects formation and behaviour under annealing in various ambients 80—65033
Si:B, ion-implantation doped, influence of radiation dose on diffusion processes 77—1141
Si:B, ion-implanted, annealing by incoherent light source 79—19267
Si:B, ion-implanted, dislocation climb, TEM obs. 78—6062
Si:B, ion-implanted, influence of US waves on charged particle channelling 79—23668
Si:B, ion-implanted, rod-like defects, TEM obs. 77—68975
n-Si:B, ion-implanted damage, positron annihilation and sheet resist. meas. 80—35003
Si:B, ionisation-assisted annealing 79—23628
Si:B, irrad. with fast neutrons true profiles of impurity photocond. bands from piezodichroisms 79—91103
Si:B, laser damage obs. by DLTS 78—76023
Si:B, lateral effect of oxidation on B diffusion 80—29217
Si:B, lattice location of implanted ions after laser annealing 78—30660
Si:B, layer resist. depend. on implanting and annealing conditions *(German)* 80—96551
Si:B, low conc. B diffusion using doped-oxide film 77—76431
Si:B, low noise avalanche photodiode fabrication by channelling implantation 79—35827
Si:B, many-body exciton-impurity complexes, stress depend. of photolum. meas. 79—28833
Si:B, N-implanted junction capacitance meas., appl. of dynamic lateral photovoltaic effect 77—85304
Si:B, near intrinsic ⟨100⟩ and ⟨111⟩ samples, inert and oxidising ambients, diffusion, segregation 78—75882
Si:B, P, first and second order Raman scatt. by pair modes 79—65869
Si:B, P, high temp. diffusion, effects of laser irrad. on diffused layer 79—14834
Si:B, P, long range enhancement of B diffusivity by P diffusion 80—103386
Si:B, p-n junction diodes, scanning-electron-beam annealing, elec. characts. 79—79128
Si:B, p-n junction form. by B deposition and laser-induced diffusion 78—87690
Si:B, photoconductivity, impact neutralisation of H$^-$-like centres 77—69377
Si:B, photolum. of heavily doped p- and n-type 80—20708
Si:B, piezothermoelec. power 78—56173
Si:B, polycryst., effect of laser annealing on struct. and elec. props. 79—11243
Si:B, polycryst., N_2 heat treated, anomalous resist. change due to Bn form. 78—2591
Si:B, polycryst. film, piezoresistive gauge factor 77—12029
Si:B, polycrystalline, depth profiles of implanted B atoms, meas. by secondary ion mass spec. *(Japanese)* 78—67734
Si:B, predeposition of B using BBr_3 78—55882
Si:B, proton-irrad.-enhanced diffusion 80—29227
Si:B, RF glow discharge sputtering damage centres, barrier formation 79—33329
Si:B, redistrib. of B during thermal oxidation, numerical and analytical calcs. 80—49259
p-Si:B, reduction of vibration noise, suitable orientation of element, rel. to crystallographic axes 79—11123
Si:B, resonant scattering of phonons by bound holes in temp. range 1 to 5K 80—75393
Si:B, SEM obs. of dislocations using Schottky barrier EBIC technique 78—79614
Si:B, selective etching by NaOH soln. 79—70189
Si:B, self-interstitials location by Rutherford backscatt. of channelled ions 80—2101
Si:B, solubility and precip., and supersat. resulting by thermal predeposition 78—11232
Si:B, sputtering influence on distrib. profile of ion-implanted impurities 79—42091
Si:B, TEM study of stacking fault form. and annealing 78—51566
p-Si:B, thermoelec. power, 20-300K 78—19067
p-Si:B, total piezoresist. tensor, 20 to 300K 78—19037
p-Si:B, trace determ. of U impurity by fission track method 79—79354
P-Si:B, US spectroscopy, energy splitting of acceptor ground state 79—33260
Si:B, use of BN source to achieve high surface concentration of B *(Russian)* 80—107639
Si:B, using oxidised BN dopant source, sheet resist., rel. to temp. and deposition time 77—43231
Si:B, with insulating coating, mechanical stress influence on B diffusion, strained surface layers 80—29224
Si:B,As selective area simultaneous doping 80—34015
Si:B,In, sharp line series in near-band-edge photolum. 80—16092
Si:B,P, anomalous diffusion 80—29229
Si:B,P, diffusion patterns obs., for SiO_2 deposited by means of centrifuge *(Bulgarian)* 77—76429
Si:B,P, double implanted layer, n-p-n struct., single pulse laser annealing 80—49247
Si:B,P, high conc. diffusion without disloc. generation 78—10072

elemental semiconductors continued
n-Si:B,P, radiative recombination at thermal defects, luminescence centre electron struct. 79—91496
Si:B,P, simultaneous diffusion, radioactivation techniques 77—76622
Si:B (0.2 wt.%) ion implanted, B atom displacement due to low temp. irrad. 80—88234
Si:B amorphous film, CVD prep., EPR, elec. and optical props. 79—4558
Si:B deep diffusion at solid solubility limits for p-channel MOS IC 78—10070
Si:B deposition diffusion from B_2H_6, AES analysis 78—6085
Si:B diffusion at Si-SiO_2 interface, Auger spectra, Rutherford backscattering 80—70471
Si:B doping from BN sources, impurity transfer considerations 77—76441
Si:B effect of elec. field on carrier capture by attractive centres. 79—11145
Si:B epitaxial layer, B diffusion coeff. 79—99372
p-Si:B epitaxial layer, proton-implanted, annealing characts., carrier conc. profiles 77—32097
Si:B film, sputter-deposited, elec. props., struct., SEM and TEM obs. 79—95298
Si:B high-temp. diffusion, glass layer formation obs. 78—7069
Si:B implanted wafers, ionis. assisted annealing and effects 80—100257
Si:B ion implanted, strain profiles from X-ray rocking curves 80—107290
Si:B ion implanted, X-ray topographical images at different absorption conditions 80—2052
Si:B ion implanted grating-type solar cells, var. of junction depth, collection efficiencies 80—93934
Si:B ion implanted layers, light refl. and transmission coeffs., computer program 80—66316
Si:B MOS structures, implanted laser beam irrad. effects on interface electrophys. props. 79—1627
Si:B photodiode front region collection efficiency models 80—96899
Si:B radiation damage and minority carrier lifetime, SEM-EBIC obs. 80—96573
Si:B recombination emission polarisation of bonded multiple-exciton complexes in mag. field *(Russian)* 78—2905
Si:B redistribution after oxidation, integro-differential eqn. 77—76453
Si:B sputtering by Ar^+, computer simulation of sputter broadening in impurity depth profiling 80—2908
Si:B_2O_3, analytic study of Si-B phase formed 79—19269
p-Si:B-SiO_2 interface in MOS structures, carrier mobility and impurity distrib. 78—34902
Si:B^+, ion implanted, lateral spread of B^+ ions through SiO_2 mask 79—51130
Si:B^+, TEM of lateral implantation effects near mask edges in wafers 79—37724
Si:BF_2^+, anomalous migration of F and electrical activity of B 78—34654
Si:BF_2^+, ion implantation appl. in semicond. device production 80—103383
Si:BF_2^+, ion implanted, arc annealing by flash lamp 80—44223
Si:BF_2^+, recrystallisation of implanted amorphous layers, F migration 79—55763
Si:BF_2^+ implanted, low-temp. annealing characts. 79—55759
Si:BF_2^+(Si^+,B^+), recrystallisation of implanted amorphous layers, elec. props. 79—55762
Si:B(Al), (P)(As)(In), ion implanted film, elec. prop. impurity depend. 80—24467
p-Si:B(Al), radiation defect form. and annealing study using Hall effect, cond. and carrier diffusion length 80—84214
Si:B(Al)(Ga)(In)(Tl), high resolution recomb. radiation, investigation, electron excited 78—15233
Si:B(Al)(Ga)(In)(Tl), binding energy, excited state spectra, photolum., semi-empirical short range pot. 80—44534
Si:B(As), polycrystalline, ion implanted, AES analysis 77—31690
Si:B(As)(P), doping, new paint-on diffusion source 77—4118
Si:B(BF_2), p^+-n junction form., ion implantation damage, leakage current 77—24334
Si:B(Be)(Li) ion implanted, channelling and random equivalent depth distrib. 80—100293
Si:B(Ga), heavily doped, form of occurrence of acceptor impurities 77—11581
Si:B(Ga), IR spectra of acceptor levels 80—34953
Si:B(Ga)(Sb), plastic deform. and formation of dislocation loops, effect of Au atoms 79—69184
Si:B(Li)(P), piezospectroscopic studies of bound multiexciton complexes 80—16006
Si:B(P), amorphous, photo- and dark conductivity 77—28216
Si:B(P), deformed, EPR fine struct. spectrum of dislocation 77—66422
Si:B(P), diffusion induced imperfections, laser annealing, rel. to junction characts. 78—75678
Si:B(P), dislocated crysts., DC cond., Hall effect, and energy spectrum 78—10400
Si:B(P), dislocated crystals, microwave cond., localised electron energy spectrum 78—14694
Si:B(P), dislocations under high stress, stacking fault energies, TEM study 80—70202
a-Si:B(P), Hall effect and impurity cond. 77—72871
Si:B(P), heavily diffusion-doped layers, Co diffusion 78—59982
Si:B(P), impurity-peak form. during proton-enhanced diffusion 79—55772
Si:B(P), ion implanted, polycryst. annealing characts. 77—24324
Si:B(P), ion implanted crystalline and amorphous laser annealing 80—97509
Si:B(P), ion implanted layers, carrier distrib. meas. precision 77—43603
Si:B(P), ion implanted processing parameters for diffusion redistribution 79—10871
Si:B(P), minority carrier diffusion coeffs. 79—99559
Si:B(P), photocond. spectra of H^--H^+-type complexes 79—95451
Si:B(P), positron annihilation in 100 and 111 orientation 77—44083
Si:B(P), proton enhanced diffusion, vacancies diffusion length 80—29226
Si:B(P), proton-irrad., impurity uphill diffusion, vacancy mechanism 80—92719
Si:B(P), recombination spectra of bound multiexciton complexes, Zeeman splitting *(Russian)* 79—38526
Si:B(P), single crysts., oxidation investigations, 780°-1150°C 79—5068
Si:B(P), uniaxially stressed, impurity-assisted intervalley scatt., photoluminesc. obs. 80—34979
Si:B(P) implanted layers as strain sensors 77—35098
Si:B(P) impurity conc. profile determ. by anodic oxidation 79—28010

elemental semiconductors continued
Si:B(P) polycrystalline thin film, plasma annealing, effect on elec. props. 80—7005
Si:B(P)(As), impurity diffusion from implanted layer, influence of radiation damage 77—76621
Si:B(P)(As), ion implantation, 20-2800 keV, obs. of X-rays produced 78—14367
Si:B(P)(As)(Cu)(Fe), dopant profile changes induced by laser irrad. using SIM and backscatt. meas. 79—69148
Si:B(P)(As)(Sb), ion implanted, redistrib. of dopants by pulsed laser annealing 79—7620
Si:B(P)(As)(Sb)(Cu)(Fe), ion implanted, doping profile, pulsed laser annealing effects 80—88197
Si:B(P)(Ge), strain distributions rel. to dopant conc., accurate determ. by X-ray Bragg reflection 77—19835
Si:B(P)(Sb), multiparticle impurity complexes *(Russian)* 78—72601
Si:B(Sb), deform. coeff. due to impurity diffusion 78—18671
Si:B(Sb)(P), microdefect formation depend on doping, Cu decoration, X-ray transmission topography, preferential etching 79—69120
Si:Ba, Geiger counter determ. of Ba by neutron activation 79—52816
Si:Be, ion implanted, correl. of atomic distrib. and implantation induced damage profiler 80—88199
Si:Bf_2^+ layers, ion-implanted, anomalous carrier tail generation mechanism 80—19819
Si:Bi, ion implanted, channelling obs. of pulsed Q-switched ruby laser annealing 80—59542
Si:Bi, ion-implanted, solid phase epitaxial growth during annealing, supersaturated solid soln. form. 80—103384
Si:Bi(,As), optical polarisation of ^{29}Si nuclei, nucl. relax. due to optical pumping 80—2665
Si:C, disorder profiles by proton backscattering, proton bombardment annealing 78—47449
Si:C, electron irrad., C interstitial, photo EPR 77—16175
Si:C, H^+ and He^+ beam impact phemomena, damage annealing rates 78—47450
Si:C, impurity determ. by IR absorpt. spectroscopy, room temp. and low temp. meas. comparison 80—108237
Si:C(O), photoluminescence spectra, radiation damage investig. 77—28620
Si:Cd n^+-n-n^+ structs., photoresist. props. under exclusion conditions 80—39666
Si:Cd(Zn), n^+-n-n^+ structure, photocond. lifetimes, deep level occupancy in exclusion region 78—72253
Si:Co, diffused distrib. and state of Co atoms 77—1146
Si:Co, diffusion coeff. of Co meas. 77—20126
Si:Co, diode minority carrier lifetime, Lax method meas., effect of Co diffusion 79—69525
Si:Co, high-temp. ion-implanted and diffused samples, Mossbauer spectra of ^{57}Co 79—51891
Si:Co, implanted or diffused, and annealed, localisation of Co atoms, Mossbauer obs. 80—39140
Si:Co, minority carrier lifetime investigation 80—80292
Si:Co, study of impurity states 78—76020
Si:Co, substitutional Co and Co precipitates, identification by Mossbauer spectroscopy 79—11631
Si:Cr, ion implanted, Cr conc., depth distrib. and diffusion coeff. 80—49243
Si:Cr, photoconductivity exam. 77—20361
Si:Cr, specific resistance, activation energy of deep levels, and carrier mobility *(Russian)* 78—72146
Si:Cr, spin-lattice relax. of Jahn-Teller Cr^0 centre *(Russian)* 78—72402
Si:Cr^0(Mn), spin-lattice relax. of Jahn-Teller centres, coexistence of minima with different symmetries 80—80602
Si:Cr^+ EPR spectra and spin state population inversion with unpolarised optical lighting *(Russian)* 80—44909
n-Si:Cs, ion implanted, minority carrier lifetime and defect struct., annealing effect 78—6395
p-Si:Cu, influence of Cu on diffusion of Au 77—62679
Si:Cu, interaction between vacancy emitting absorbing precipitates and dislocations, TEM obs. 78—71755
Si:Cu, parameters of Cu levels determ. by photocapacitance meas. 77—62869
Si:Cu, photocond. spectra and IR quenching 77—55568
Si:Cu, precipitate morphology, IR microscopy study *(Chinese)* 80—103539
Si:Cu, segregation effects after laser pulse melting 79—1843
Si:Cu extinction of X-ray topographic images of Cu precipitates 80—45310
Si:Cu(Au), recoil implantation from thin surface films, backscatt. obs. 78—63783
Si:D, amorphous, thermal stability, comparison with Si:F 80—49542
Si:D, ion implanted, D depth distribs., SIMS meas. 80—54279
Si:D, ion implanted, struct. of impurity centre 79—7623
Si:F, amorphous, heat resistant, prep., elec. cond., IR absorpt., annealing 80—65719
Si:F, amorphous, pure and doped, vibr. excitations at defect sites, IR and Raman spectra calc. 80—49329
Si:F, amorphous, thermal stability, comparison with Si:D 80—49542
Si:F, amorphous alloys, RF sputtering prep. in SiF_4-Ar gas mixture, spectra 80—80772
Si:F, amorphous film, effect of F on elec. cond. 80—34444
Si:F, H amorphous films, optical props., photoconductivity, photostructural changes 80—11034
Si:F,H, amorphous, elec. and optical props. 80—60031
Si:F,H, amorphous, glow discharge deposited elec. props. and device aspects 80—44744
Si:F,H, amorphous efficient carrier generation for solar photovoltaic energy conversion 80—92906
Si:Fe, anisotropic broadening of linewidth in EPR spectra of Fe^0 77—66417
Si:Fe, B, Fe reaction with ion implanted B 79—77620
Si:Fe, B thermally activated Fe interstitial, elec. and kinetics props. *(German)* 80—34035
Si:Fe, EPR and neutron activation anal. of thermal defects 78—91355
Si:Fe, ESR, cryst. field under stress, C_{11} and C_{44} meas. 77—12194
-Si:Fe, effect of γ-irradiation, photocapacitance meas., impurity centre conc. 78—18993
Si:Fe, implanted, annealing and stripping, Mossbauer expts. 80—39141
Si:Fe, implanted, Mossbauer spectra, conversion electron, temp. dependence 80—40025
Si:Fe, interstitial form., Au dopant effect 80—29611

elemental semiconductors continued

- Si:Fe, ion implanted, laser annealing studies using Mossbauer spectroscopy 80—79827
- Si:Fe, laser annealing of implanted ^{57}Co sources, Mossbauer obs. 80—39139
- Si:Fe, laser implantation, Mossbauer obs. 80—39125
- Si:Fe, photoconductivity and Hall effect 79—4579
- n-Si:Fe 79—28312
- Si:Fe group ion, energy spectrum of deep centres, ESR spectrum 77—90023
- Si:Fe^0, spin relax. rate ang. depend. for pulsed saturation of inhomogeneously broadened ESR line 79—65721
- Si:Fe^0 interstitial localisation, EPR spectrum 79—1582
- Si:Fe(Al), compensated substrates for solar cells, effects of Fe and Al 80—94009
- Si:Fe(Au)(Pt)(Ag)(Ti), photoionisation cross-sections and energy levels 79—87060
- Si:Fe(Cr), EPR line intensity and widths, temp. depend. 79—28604
- Si:Fe(Cu), impurity segregation and microstructural changes by pulsed laser irrad. 79—82254
- Si:Fe(Cu)(Pt), implant redistrib. and enhanced solubility following laser irrad. 79—69129
- Si:Ga, As, sequential diffusion, radiotracer obs. 78—10073
- Si:Ga, bound-exciton absorption 78—56507
- Si:Ga, diffusion of impurity into cryst., doping profile 79—77621
- Si:Ga, electron irrad.-induced defects, DLTS meas. 80—24499
- Si:Ga, gettering of Au and Cu during Ga diffusion 78—91350
- Si:Ga, IR absorption of dopant centres, spectral depend. on doping, impurity conc. and temp. 80—76053
- Si:Ga, LPE growth on Si substrate, melt-back approach 78—80481
- Si:Ga, LPE on Si, technique and characterisation 79—38751
- Si:Ga, luminescence fine struct. from bound exciton and multiexciton complexes 77—32430
- Si:Ga, neutron irrad., Hall effect meas. of shallow donor levels 80—20124
- p-Si:Ga, neutron transmutation counterdoped, shallow defect levels, Hall effect and photocond. obs. 79—87055
- Si:Ga, possibility of use in fabrication of fast response photodetectors 79—15184
- Si:Ga, sealed tube diffusion, Au and Cu gettering behaviour 77—76445
- Si:Ga (Al)(In) extrinsic detector material props. 77—89797
- n-Si:Ga laser doped, segregation, Rutherford backscattering 80—103483
- Si:Ga$^+$, impurity distrib. profiles using SIMS and Hall effect method 79—69152
- Si:Ga(Al), edge luminesc. spectra of acceptors, multiexciton complexes 78—56517
- Si:Ga(Al), MBE, growth, struct. and elec. props. 77—89458
- Si:Ga(As), laser-doped, impurity distrib., Rutherford backscatt. and channelling anal. 80—59507
- Si:Ga(As) 80—19824
- Si:Ga(Sb), epitaxial film, doping efficiency *(Japanese)* 79—73201
- Si:Ga(Zn), impurity ground states 79—28313
- n-Si:Gd, depth of energy levels of As and P from impurity photocond. 79—90996
- p-Si:Gd, irradiated, elec. props. 79—51613
- Si:Gd, magnetic props. and interaction of impurities 79—11286
- Si:Gd, radiation defect form., effect of Gd impurities, elec. and optical meas. 78—71764
- Si:Gd, radiation defects effect on elec. props. 77—28184
- Si:Gd(Pr), photoconductivity anomalies due to mag. impurities *(Russian)* 80—103722
- n-Si:Ge, electron induced defects, room temp. instability 80—29052
- Si:Ge, electron irrad.-induced defects, DLTS meas. 80—24499
- Si:Ge, recryst. after implantation using different temp. and energy sequences 80—84196
- Si:Ge, regrowth behaviour from backscatt. and channelling meas. 80—2300
- Si:Ge,Sn, role of interelectronic correl. in paramag. props. of impurity-vacancy complex 77—62858
- Si:Ge B, strain compensation, X-ray Bragg reflexion 80—39137
- Si:H, 50-250 keV H$^+$ irrad. damage distrib., ^{4}He$^+$ channelling obs. 78—26587
- Si:H, amorphous, 2p level shift, XPS obs. 80—97401
- Si:H, amorphous, Auger electron spectrosc. obs. 80—76112
- Si:H, amorphous, band tail absorpt., photocurrent meas. for Schottky barrier solar cell 80—60032
- Si:H, amorphous, Brillouin scattering from acoustic bulk and surface waves 80—11425
- n-Si:H, amorphous, bulk density of deep states, DLTS meas. 80—88518
- Si:H, amorphous, control and anal. of deposition, using plasma spectroscopy 80—45230
- Si:H, amorphous, defect creation and H evolution 80—50392
- Si:H, amorphous, defect photoluminesc. meas. 80—97334
- Si:H, amorphous, defect states, luminesc. and ESR obs. 80—76075
- Si:H, amorphous, density of states determ. using field effect 80—49937
- Si:H, amorphous, discharge prod., optically induced cond. changes 80—96937
- Si:H, amorphous, doped, Fermi level position, photoelectron spectra 79—47592
- Si:H, amorphous, effect of gap state density on photocond. and photolum. 79—91096
- Si:H, amorphous, electronic states of hydrogenated Si, theory 79—42494
- Si:H, amorphous, electronic struct. calc., rel. to UPS data 80—39527
- Si:H, amorphous, excess carrier thermalisation and recomb., luminesc. decay and photocond. 80—50397
- Si:H, amorphous, exodiffusion of H, EPR expts. 80—49102
- Si:H, amorphous, glow discharge deposited, thermal dehydrogenation, IR spectra 80—44442
- Si:H, amorphous, glow discharge deposited, laser annealing 80—49104
- Si:H, amorphous, H content determ. by IR absorpt., gas evolution and nuclear reaction methods 80—44130
- Si:H, amorphous, HV photovoltaic cells, design parameters 80—101105
- Si:H, amorphous, image pickup devices 80—100481
- Si:H, amorphous, in p$^+$-i-n$^+$ struct., hole diffusion length meas. 80—44712
- Si:H, amorphous, light-induced ESR and photoluminesc., dangling bonds with positive correl. energy 80—50161
- Si:H, amorphous, luminesc., band tail states and thermalization 80—25455
- Si:H, amorphous, mobility edge position using continuous random network model for struct. 80—44544
- Si:H, amorphous, model for variable gap intrinsic semiconductor 80—10988
- Si:H, amorphous, optical studies of excess carrier recomb., evidence for dispersive diffusion 80—76059
- Si:H, amorphous, p$^+$-i-n$^+$ struct. solar cells, material parameters and deposition condition optimisation study for higher efficiencies 80—45676
- Si:H, amorphous, photoelectrochem. behaviour 80—81480
- n-Si:H, amorphous, photoelectromagnetic effect 80—107845
- Si:H, amorphous, plasma deposited, cond. adsorbate and insulating layer effects 80—49749
- Si:H, amorphous, plasma-deposited, effect of DC elec. field superimposed during deposition 80—44643
- Si:H, amorphous, prod. by high temp. thermal decomp. of SiH$_4$, and photocond. 79—87585
- Si:H, amorphous, Pt film growth, AES and LEED study 80—88447
- Si:H, amorphous, RF sputtered, suitability as solar cell material 80—40864
- Si:H, amorphous, RF sputtered, Schottky barrier solar cells, photovoltaic props. and capacitance-voltage charact. 80—45678
- Si:H, amorphous, radiative recomb. by diffusion and tunnelling, photocond. quantum efficiency 80—50394
- Si:H, amorphous, radiative recomb. and luminescent processes 80—55152
- Si:H, amorphous, refr. index, temp. depend., implications for thermoreflectance and electroreflectance 80—50290
- Si:H, amorphous, rehydrogenation, photoluminesc. recovery 78—72571
- Si:H, amorphous, Schottky diode, spectral response and hole drift mobility 80—39673
- Si:H, amorphous, Schottky barrier solar cell, degradation mechanisms affecting stability and operation 80—45680
- Si:H, amorphous, Schottky barrier solar cell, deposition parameter effects on elec. props. 80—45681
- Si:H, amorphous, Schottky diodes, elec. props., light-induced effects 80—103741
- Si:H, amorphous, short-range order, theory and probes 80—79698
- Si:H, amorphous, solar cell struct., photocurrent meas., absorpt. coeff. 80—50960
- Si:H, amorphous, solar cells, carrier generation, recombination, and transport 80—55844
- Si:H, amorphous, solar cells, trap spectroscopy using transient current techniques 80—104508
- Si:H, amorphous, solar-cells, charge collection and spectral response 80—85275
- Si:H, amorphous, sputtered, Auger surface spectroscopy 80—50472
- Si:H, amorphous, sputtered on Gd$_2$(MoO$_4$)$_3$, ferroelec. domain wall motion, image scanning 80—83663
- Si:H, amorphous, sputtered Schottky barrier solar cells, conduction mechanism 80—104506
- Si:H, amorphous, stacked solar cells, development 80—94050
- Si:H, amorphous, structural model 80—49105
- Si:H, amorphous, surface activated, photoemission spectra, minority carrier diffusion length 80—40235
- Si:H, amorphous, surface states distribution using MOS tunnel junctions 80—103735
- Si:H, amorphous, temp. depend. of photolum. 80—89063
- n-Si:H, amorphous, thickness depend. cond. 80—49724
- Si:H, amorphous and crystalline, hydrogenation and dehydrogenation, luminesc. spectra 80—11477
- Si:H, amorphous defect model 80—24363
- Si:H, amorphous field induced and quenched-in excess cond. 80—24968
- Si:H, amorphous film, anal. of intrinsic photocond. spectrum 79—73541
- Si:H, amorphous film, prep. by plasma decomp. of SiH$_4$ under mag. field, and characterisation 80—45239
- Si:H, amorphous films, plasma-deposited, defect states, IR, ESR, and refractive index meas. 79—65944
- Si:H, amorphous hydrogenated film, decomp. kinetics 79—100342
- Si:H, amorphous Schottky barrier solar cells, depletion region, capacitance study 80—50963
- Si:H, amorphous Schottky solar cells, prep. and characts. of diode RF reactive cathodic sputtered films *(French)* 80—61347
- Si:H, amorphous sputtered, excitation spectra and photoluminesc. 80—50396
- Si:H, amorphous thin film, ion plating, IR absorpt. meas. 80—84857
- Si:H, amorphous thin film solar cells 80—81478
- Si:H, amorphouse film, optical and elec. props. 79—82694
- Si:H, Cl(F), amorphous, photocond., dark cond. and photoluminesc. 80—49802
- Si:H, defects in monovacancy Si cluster, semi-empirical calc. 78—43329
- α-Si:H, discharge produced, electronic props. rel. to solar cell characts. 79—15241
- Si:H, electron states 80—29355
- a-Si:H, electronic states and bonding config. 80—64900
- Si:H, evaporated amorphous film, prep. elec. cond. and photocond. 79—38201
- Si:H, H$^+$ sputtered as result of ion bombardment, ionis. mechanism 79—100009
- a-Si:H, influence of H on optical props., H conc. and H bonds 80—76098
- Si:H, interstitial electronic struct., self-consistent pseudopotential calcs. 79—73469
- Si:H, ion implanted, anal. of methods used for H profiling in materials using ion beams 79—5197
- Si:H, ion implanted Monte Carlo calcs. of profiles of H ions 78—55889
- Si:H, ion-implanted, photoluminesc. spectrum 80—45129
- Si:H, new IR absorpt. bands 79—87472
- a-Si:H, spin defect and recombination influence on electronic transport 80—50409
- a-Si:H, structural interpretation of vibr. spectra 79—69864
- Si:H,B, amorphous, field effect and thermoelec. power 80—96924
- Si:H,F,O amorphous, plasma deposited, comp. and optical props. 80—50441
- Si:H,Li, amorphous, DC electrical conductivity, absorption edge and IR meas., role of H 80—54694
- Si:H,Li, amorphous, photoluminescence obs. 80—66280
- Si:H,P, amorphous, heavily hydrogenated, high gap state densities 80—49803
- Si:H,P, amorphous, in MOS tunnel junction, electron tunnelling characts. 79—73592
- Si:H,P amorphous film, elec. cond., thickness and temp. depend. 80—65559
- Si:H alloy, amorphous, dihydride model of vibrational spectra 80—80827

elemental semiconductors continued
a-Si:H alloys, sputter deposited thin film coatings, property-comp. relationships 80—80975
Si:H amorphous, plasma-deposited, luminesc. decay 79—73989
Si:H amorphous, solar cell structure, optical absorption by gap states 80—94052
Si:H amorphous film, H quantitative depth profiling by nuclear reactions and SIMS 78—14373
Si:H amorphous film, plasma-deposited, growth morphology and defects 80—44128
Si:H amorphous film, plasma-deposited, elec. and comp. heterogeneity 80—44745
Si:H amorphous film, prep. by RF glow discharge decomp. of SiH_4, optical props. and H conc. 80—15416
Si:H amorphous film, prop. by glow discharge deposition, and plasma parameter effects on props. 80—45240
Si:H amorphous film, sputtered in Ar-SiH_4 mixtures, props. 79—87023
Si:H amorphous film, sputtered IR vibr. spectra and photolum., effects of partial evolution of H 80—44413
Si:H amorphous films, conductivity and temp. dependence of optical gap 80—100462
Si:H amorphous films, ESR, optical gap and elec. cond. meas. 80—75842
Si:H amorphous films, effects of glow-discharge prep. conditions on H content 79—46969
Si:H amorphous films, IR spectrum and struct. 80—97277
Si:H amorphous films, interference enhanced Raman scatt. 80—50326
Si:H amorphous films, optoelectronic behaviour depend. on impurity incorporation during plasma deposition 80—49804
Si:H amorphous films, photovoltaic and photocond. spectra, photoluminesc. 80—44645
Si:H amorphous films, photoinduced optical absorpt. and photocond. 80—50361
Si:H amorphous films, reactively sputtered, prep. and characterisation 80—100785
Si:H amorphous films, role of Ar in deposition process, IR absorpt. and photocond. meas. 80—50321
Si:H amorphous glow discharge film, optical absorpt., near IR region 79—87518
Si:H amorphous layer as passivant for p-n junction in crystalline Si 79—47155
Si:H amorphous layers, ion bombard., AES study, $L_1L_{23}V$ Coster-Kronig transition 79—99992
Si:H amorphous MIS solar cell, loss mechanisms and photovoltaic parameters, overview 80—93923
Si:H amorphous semiconductors, prep. from SiH_4 and characts. 78—48326
Si:H amorphous sputtered film, photoluminesc., photocond. 80—20729
Si:H amorphous sputtered films, optical gap, IR absorpt. meas. 80—50320
Si:H film, amorphous, bombarded, defects, luminesc. and ESR meas. 80—34977
Si:H film, amorphous, elec. cond., effect of adsorbed gases and illumination 78—88048
Si:H film, amorphous, H-associated disorder modes, PMR spin-lattice relax. time meas. 80—93202
Si:H film, amorphous, photocond. imaging 80—1300
Si:H film, amorphous, plasma-deposited, small angle X-ray and neutron scatt. studies 80—59826
Si:H film, amorphous, reactively sputtered, H content effect on props. 80—49714
a-Si:H film, glow discharge deposited, H profiles, doping level 80—84202
a-Si:H highly homogeneous, for low-cost solar cell fabrication 80—72053
a-Si:H MIS junction, electronic struct. study by tunnelling 80—44729
Si:H plasma deposited film, amorphous, microstruct., TEM and SEM obs. 80—10801
a-Si:H Schottky barrier diodes, capacitance studies 80—49908
a-Si:H solar cells, photoexcited carrier collection efficiency 79—100526
Si:H solar cells, photovoltage source in photocond. materials due to comp. and doping var. 80—7938
Si:H sputtered amorphous film, luminesc. and non-radiative decay 80—50395
a-Si:H sputtered films, ohmic contacts by H depletion, H diffusion 80—34511
a-Si:H/Pt, Schottky diode, influence of prep. conditions on forward bias currents 79—78171
Si:H(B)(P), amorphous, UV absorpt. spectra 80—25420
Si:H(D), amorphous films, CVD, post-hydrogenation 80—54552
Si:H(D), H-related defects, channelling and IR meas. 80—25422
Si:H(F), amorphous, Schottky barrier profiles, depletion region width 80—49871
Si:Ho(Gd)(Yb), impurities behaviour, dynamic nuclear polarisation 79—78568
Si:In, absorpt. spectra, impurity excited state lines 80—108243
Si:In, backward wave phonon spectroscopy 80—2357
Si:In, bound exciton photolum. obs. 78—95607
Si:In, bound-exciton absorption 78—56507
Si:In, C, 0.111-eV acceptor level, X-level defect conc. from IR absorpt. and Hall meas. 79—51512
Si:In, capture cross section of excitons on neutral In impurities, photoluminesc. decay 78—6760
Si:In, clustering and precipitation, time-dependent perturbed ang. correlation meas. 80—65234
Si:In, dopant energy levels, Hall meas. interpretation 80—107736
Si:In, doping conc., meas. by Hall, C-V and junction breakdown methods 79—14824
Si:In, electron irrad., Hall effect meas. 80—2401
Si:In, gradient transport soln. growth, IR monitoring, 950-1300°C 79—100040
Si:In, implanted, laser annealing 79—52050
Si:In, ion implanted, annealing behaviour, time differential PAC obs. 77—89455
p-Si:In, ion implanted, doping profiles from capacitance-voltage characts. 80—88203
Si:In, MOSFET device structure for characterising imperfection centres 79—73595
Si:In, neutron irrad. to compensate for residual B, photocond., IR focal plane array 78—67727
Si:In, new acceptor level determ. from Hall effect and photocond. meas. 77—66136
Si:In, obs. of long lifetime lines in photolum. 79—47512

elemental semiconductors continued
Si:In, photoelec. props. meas 77—89804
Si:In, photoluminesc., In acceptor excited level 79—47506
Si:In,P, photoinduced IR absorpt. and luminesc. 79—33828
Si:In amorphous films, EPR, elec. cond., and magnetoresist. 80—50160
Si:In extrinsic detectors, compensation of residual B by neutron transmutation 78—281
Si:In extrinsic IR detector material with high responsivity compensated by neutron transmutation, float-zone growth 80—75597
Si:In growth by Czochralski crystal pulling, characterisation for extrinsic IR detectors, focal-plane arrays 80—76168
Si:In(Sb), incorporation of implanted impurities during amorphous layer regrowth 79—55761
Si:Ir, Ir diffusion and solubility 77—15448
Si:Ir, magnetosensitive diodes, characts. 79—24069
Si:Ir, precipitation of solid soln., photocapacitance, electrical resistivity meas. 78—47833
Si:Ir S-type diodes, characts. 78—56224
Si:K, bound exciton luminescence in mag. field *(Russian)* 80—108278
Si:K, ion implanted, influence of doping and annealing on carriers 78—38742
Si:l, obs. of donor exciton in far IR transmission meas. 79—91477
Si:Li, amorphous, elec. cond. and thermopower 79—73537
Si:Li, amorphous, interstitial doping by in-diffusion and implantation and elec. characterisation 78—26585
Si:Li, bound exciton complexes associated with Li, photolum. meas. 79—28823
Si:Li, bound-exciton excited states, uniaxial anal. 80—71475
Si:Li, defect electronic struct. and config., semi-empirical calc. 80—107739
p-Si:Li, dislocation free, minority carrier lifetime, effects of heat treatment *(Japanese)* 79—65492
Si:Li, EPR in mechanically affected sampler 78—39385
p-Si:Li, electrolytical doping, depth-profile anal. 79—77623
Si:Li, electron-phonon scatt., in intermediate conc. region 80—65180
Si:Li, luminesc. of bound exciton and bound multiexciton complexes 79—28821
Si:Li, nonrandom strain, EPR of thermally excited donors 78—43629
Si:Li, photolum. of bound exciton and bound multiexciton complex, Zeeman effect 80—108265
Si:Li, precipitation centres, elec. cond., Hall effect meas. 78—48417
Si:Li, strongly doped, piezoresist., gas-liq. type transition 77—43600
Si:Li, thermal cond., low temp. phonon scatt., internal strain effects 80—96706
Si:Li amorphous, thermopower and cond. meas. 79—69142
Si:Li P/N type solar cells, irradiation obs. 79—66406
Si:Li radiation detector, influence of distrib. of drift temp. on props. 77—3234
Si:Li X-ray detector, escape peaks and internal fluoresc., general geometry case 77—18150
Si:Li(Na)(K)(F)(Cl), amorphous, implantation effects on elec. props. 80—49716
n-Si:Mg, energy levels and degeneracy ratios determ. by Hall effect meas. 79—90993
Si:Mg, Zeeman effect of excitation spectrum of neutral donors 77—63439
Si:Mn, amorphous, cond. increase by Mn doping 78—72155
Si:Mn, amorphous, EPR meas. 77—85559
Si:Mn, characts. of residual cond. 79—15188
p-Si:Mn, defect levels, transient capacitance spectroscopy 78—6322
p-Si:Mn, giant residual cond. 80—20250
Si:Mn, negative photoconductivity 79—38132
Si:Mn, photosensitivity, residual cond. effects 78—19099
p-Si:Mn, temp.-elec. instability, photocond. meas. 77—1448
Si:Mn,Bi, standard, doubly implanted, Rutherford backscattering meas. at MeV energies, screening corrections 80—88204
Si:Mn(Fe)(Ni) amorphous films, ESR and elec. cond. 80—50171
Si:N, amorphous, DC sputtered, enhanced, photocond. 78—56183
Si:N, amorphous, prep. by RF sputtering and props. 80—44229
Si:N, high energy ion implantation of buried insulating layers 80—88188
Si:N, implantation at high doses, annealing conditions for homogeneous buried insulating layer *(French)* 80—59498
Si:N, interstitial Si atom formation by light ion bombardment 78—47406
Si:N, ion implantation, refractive index, IR spectra, ion range and straggling meas. 80—34020
Si:N, ion implanted, oxidation characts. 80—89385
Si:N, laser-annealed, Jahn-Teller distorted donor, EPR meas. 80—84642
Si:N, struct. defects formed by 50 keV N^+ irrad., depth distrib. 78—18688
Si:N wafers, Si_3N_4 layer growth by high dose implantation and annealing, elec. props. 80—70227
p-Si:N_2^+ implanted, anneal behaviours of lateral photovoltaic method 79—14825
Si:N(P), ion implanted, IR transmission and rel. spectra study 80—108244
Si:Na, quantitative analysis of residual impurities with SIMS 78—87688
Si:Na ion implanted, Hall effect temp. depend., electron surface density and mobility 80—11018
Si:Na^+, inversion layer, far IR optical spectroscopy 80—20680
Si:Na^+, variation of cond. in two-dimensional impurity band with Fermi level position 79—95510
Si:Na(K)(Cs), amorphous, ion implanted, control of cond. 79—60835
Si:Ne, amorphous, implanted, cond. change 78—23097
Si:Ne ion implanted, channelling anal. of disorder struct., ^{4}He ions, 0.7 to 2.2 MeV 79—4321
Si:Ne(Ar)(Kr), amorphous, implanted and sputtered, epitaxial regrowth, influence of noble gas atoms 80—2289
Si:Ne(Ar)(Kr), ion implantation damage, annealing, comparative study 79—10867
Si:Ne(Kr), ion implanted, amorphous, epitaxial regrowth 79—10869
Si:Ni, capture probabilities of two deep impurity levels by photocond. decay 80—49799
Si:Ni, low temp. annealing effect on behaviour of Ni 79—10862
Si:Ni,Co,Mn, γ-irrad., interaction of deep-level impurity atoms with radiation defects 77—76457
Si:Ni,O, interaction of Ni with O, influence of heat treatment, IR absorption meas. 77—4667
Si:Ni deep impurity levels, electron capture probabilities rel. to temp. 78—2523
Si:Ni p^+n and n^+p diodes, thermally stimulated capacitance obs. of Ni acceptor levels 78—19137

elemental semiconductors continued
Si:Ni(Co)(Mn), influence of neutron irradiation as elec. props. 78—55895
Si:O, 9 μm absorpt. band attributed to dissolved O, from expts. on quartz particles 79—19914
Si:O, A centre, theoretical study 80—75521
Si:O, amorphous, sputtered, influence of O and deposition conditions 80—54693
Si:O, annealed, minority carrier lifetime 79—23985
Si:O, annealed, precipitates, dislocation and stacking fault loops, TEM characterisation 77—4111
Si:O, annealing behaviour of O donor, conc. reductions via resistivity meas. 79—51129
Si:O, C, impurity conc. profiles and process-induced defects 78—6094
Si:O, CVD layer, RHEED study of surface crystallinity, annealing effect on structure 79—69371
Si:O, carrier recomb. processes, role of vacancy-O complexes 80—65592
n- Si:O, charge carrier scattering on neutral centres 80—49762
Si:O, crit. stress of dislocation movement, determ. new method 77—80503
Si:O, cryst., annealed, struct. defects 78—75673
Si:O, cryst., donor form. during annealing, elec. resist. study 80—49653
Si:O, Czochralski crystal, oxygen striation and thermally induced microdefects 80—100275
Si:O, dislocation-free, Si-O complexes, heat treatment effects 77—62557
Si:O, EPR spectra of heat treatment centres 78—48039
Si:O, effect of interstitial O on elec. props. 77—76846
Si:O, electrial and infrared spectroscopic investigations 80—34389
Si:O, evaporated amorphous film, effect of O_2 on props., ESR spectra 80—11265
Si:O, heat treated, excess carrier recomb. rate, defect levels 80—75579
Si:O, high temp. annealing effect on impurities 78—38745
Si:O, IR absorpt. at low temp. *(Chinese)* 80—108228
Si:O, IR absorpt. spectra of Si:O complexes 78—19520
Si:O, implanted O location, channelling effect meas. 78—26593
Si:O, impurity conc. profiles, scanning IR absorpt. using semicond. laser 80—50376
Si:O, incorporation of O during pulsed-laser irrad. 80—96557
Si:O, interstitial Si atom formation by light ion bombardment 78—47406
Si:O, ion-implanted between 2 and 20 MeV, range and range straggling 80—44241
Si:O, kinetics of donor formation, under heat treatment in 450-900°C range 80—75523
Si:O, O rich polycryst. film, carrier transport 78—80076
Si:O, polycrystalline layer on Si p-n junction, charge transport and passivation 79—38206
Si:O, semi-insulating polycryst. film, cond. through localised and extended states 77—28268
Si:O, specific resist. rel. to annealing, Si-O complex form., O_2 distrib. *(German)* 77—72863
Si:O, Xe, ion implanted, Xe retention, Rutherford backscatt., comparison with SiO_2+Xe 79—4320
Si:O,C, electron irradiated, indirect vacancy-interstitial recomb., IR absorpt. meas. 77—43209
Si:O,H, amorphous plasma-deposited, electronic and struct. props. 80—50391
Si:O,H amorphous, time resolved luminesc. 80—66288
Si:O film, near IR absorption, O impurity states 78—88333
Si:O film, near IR reflectivity at high temps. 78—56532
Si:O film, thermally deposited, semi-insulating, crystallographic study 78—75954
Si:O wafer, annealed, surface- and inner-microdefects, TEM obs. 80—54236
Si:O wafer, dislocation pinning effect of O atoms 77—89437
Si:O_2^+, in-depth distrib., Cs^+ SIMS anal. appl. 79—39265
Si:O(C), implant redistribution, annealing effects, SIMS meas. 80—96561
Si:O(C) wafers, impurity meas. by Fourier transform IR spectra 80—89030
Si:O(C) wafers, impurity meas. by Fourier transform IR spectra at low temp. 80—89031
Si:Os, P, photoelec. props., depend. on P conc. 79—91099
Si:Os, photocapacitance meas. of impurity levels 77—55579
Si:P, absorpt. due to creation of bound excitons 78—23025
Si:P, acceptor bound multiexciton complex recomb., shell model, luminesc. line splitting 78—6275
Si:P, amorphised by Ne^+ implantation, high fluence P implants, plasma region obs. 79—86807
Si:P, amorphous, CVD, defect compensation 80—54644
Si:P, amorphous, CVD, substitutional doping, electronic props. 79—23923
Si:P, amorphous, elec. cond. and thermoelectric power 77—89783
Si:P, amorphous, substitutionally doped CVD, electrical props. 79—99566
Si:P, amorphous, thermoelectric power and conductivity 77—89782
Si:P, and of P diffused layers 78—38736
Si:P, annealing after ion implantation, ellipsometric study 80—65018
p-Si:P, annealing behaviour, recovery, surface carrier density and Hall mobility meas. 77—32012
Si:P, annealing characteristics at low temp., elec. props. 78—63781
Si:P, anomalous doping profiles, numerical anal. 79—73206
Si:P, As, chem. etching, thick epitaxial layers prod. for dopant conc. investigations by neutron activation anal. 79—37728
Si:P, Au, neutron irradiated, distrib. of P and Au determ. 78—79627
Si:P, BF_2^+ ion implantation, anomalous carrier profiles 80—2048
Si:P, bound exciton and multiexciton complex struct., luminesc. obs. 77—81138
Si:P, bound multiexciton complexes, shell model 77—31953
Si:P, CVD amorphous film, electronic density of states 79—46993
Si:P, carrier mobility and distrib. rel. to annealing, 400-910°C 78—79995
Si:P, characterisation by IR reflectivity 78—56501
p-Si:P, Cu, influence of Cu on diffusion of P meas. 77—1267
Si:P, Cu(Au) radiation-doped, influence of growth defects on elec. props. 79—69144
Si:P, Czochralski growth, dopant evaporation coeffs., resistivity distrib. 77—16487
Si:P, defect annealing, ionisation effects, DLTS meas. 80—24483
p-Si:P, defect energy levels, ion implantation effects, Hall coeff., sheet resist. meas. 77—85173
Si:P, defects, SEM in EBIC mode vs. HVEM images 78—9923
Si:P, depth of melting produced by pulsed-laser irrad. 79—55756

elemental semiconductors continued
Si:P, determ. of P content in high-purity Si using meas. of Mo in 12-molybdophosphoric acid by NAA and AAS 80—15148
Si:P, dielec. susceptibility meas., polarisation catastrophe at metal-insulator transition 80—59873
Si:P, diffusion eqn. numerical soln. 79—51311
Si:P, diffusion from ethylene glycol grown anodic oxide 77—76440
Si:P, diffusion of P, 900-1100°C, distrib. of excess vacancies 77—72631
Si:P, diffusion of P impurities stimulated by gas discharge Ar plasma, low temp. 80—6560
Si:P, diffusion-doped laser irradiation effects, electrical reactivation of P 80—39124
Si:P, diffusional doping, diffusion-induced strain and dislocation effects 79—42084
Si:P, diffusivity, strain-induced band gap narrowing, E-centres 80—29228
Si:P, diffusivity, versus Si oxidation rate 77—15436
Si:P, distrib. of implanted impurity after laser annealing, e.s.r. and neutron activation analysis 77—4122
Si:P, donor excited state lifetime, delayed avalanche breakdown 77—85231
Si:P, doped by neutron transmutation, electron traps 78—84164
Si:P, doped by neutron transmutation, lattice defects 80—34018
n-Si:P, doping, by zone melting using solid dopant source 78—43035
Si:P, doping by diffusion from phosphosilicate glass sheets *(German)* 77—39604
Si:P, doping by neutron transmutation, residual radioactivity 79—33009
Si:P, doping during growth from gas phase, thermodynamic analysis 80—59489
Si:P, E-centre formation mechanism 77—72614
Si:P, EPR line shift, 0.56 to 4.2K, investig. of interacting donor clusters 77—77084
Si:P, EPR of interacting donor centres, Overhauser effect and ENDOR 77—77085
Si:P, ESR-induced changes in DC resistance 78—35037
n-Si:P, edge dislocation energy level, differential capacitance meas. 79—23927
Si:P, effect of annealing on charge carrier conc. on floating zoned crystals 78—47805
Si:P, electrical conductivity oscillation, effect of dislocations 78—6388
n-Si:P, electron mobility and resist., dopant density and temp. depend. 77—76816
Si:P, electronic states, NMR of metallic and intermediate samples 79—4511
Si:P, electrostatic field on impurity atoms, heavy doping effects 78—51570
Si:P, emitter-misfit dislocation formation during P diffusion 78—91338
Si:P, epitaxial layer, vapour phase grown, temp. dependence of dopant inclusion, differential molar solution enthalpy *(German)* 79—52128
n-Si:P, etched, high sensitivity temperature sensor, 1-10K 77—13757
Si:P, excess vacancy generation by P diffusion *(Japanese)* 77—89460
Si:P, excitation density depend. of cathodoluminesc. from bound multiexciton complexes 78—72609
Si:P, excitation spectrum of P donors introduced by neutron transmutation, high resolution study 79—47460
Si:P, exciton complexes bound to impurities, resolved fine structure 77—62843
Si:P, exciton two-electron luminesc., temp. and impurity-conc. depend. 78—39585
Si:P, expt. evidence against shell model of bound multiexciton complexes 78—10368
n-Si:P, fast neutron irrad., defect clusters and defect build-up kinetics 79—33019
Si:p, film, polycrystalline, low press. CVD, resist. meas. 80—2494
Si:P, Gd, optical orientation of ^{29}Si nucleus, effect of donor level implantation depth *(Russian)* 77—8452
Si:P, Ge, simultaneous diffusion processes, elastic stress influence 77—89591
Si:P, Hall effect 78—72176
n-Si:P, heavily depend., spin-lattice relax. at high temp. 78—39403
Si:P, heavily doped, 100 GHz ESR of impurity band 79—95631
n-Si:P, heavily doped, carrier conc., Hall coeff. and elec. cond. meas. 77—8094
Si:P, heavily doped, degenerate electron gas, Friedman effect, review 77—20242
Si:P, heavily doped, diffusion of Au 77—51550
Si:P, heavily doped, EPR spectra of electron irradiation induced defects 77—81008
n-Si:P, heavily doped, elec. cond. and Hall effect meas., impurity effects 78—19032
Si:P, heavily doped, electron-hole droplets, photolum. obs. 1.5 to 80K 77—36289
Si:P, heavily doped, electronic sp. ht. meas., rel. to metal-nonmetal transition .78—6162
Si:P, heavily doped, electron mobility carrier conc. relationship 79—65470
Si:P, heavily doped, glow-discharge-produced, elec. and optical props 80—2497
Si:P, heavily doped, IR bound-exciton luminesc. spectra 78—15211
Si:P, heavily doped, influence of impurities and crystalline defects on electron mobility 79—78095
Si:P, heavily doped, mag.-field depend. of sp. ht. 80—29183
Si:P, heavily doped, metallic region, resist. decrease due to ESR 77—16178
Si:P, heavily doped, origin of photoluminesc. 79—56856
Si:P, heavily doped, paramagnetic spin susceptibility 79—78306
Si:P, heavily doped, sp. ht. near metal-nonmetal transition, generalized Matsubara-Toyozawa theory 79—73321
Si:P, heavily doped, thermal oxidation 78—56793
Si:P, heavily doped semicond., scatt. mechanism, resist, and Hall coeff. maxima 80—75586
Si:P, heavily doped wafer, anomalous bending obs. 78—10074
Si:P, heavily ion implanted, polycrystalline, grain growth 79—19477
Si:P, high dose implantation, outside dislocation generation 78—87672
Si:P, high fluence ion implantation, layer thickness and refr. indices, IR refl. meas. 79—82248
Si:P, homogeneous nuclear transmutation technique, thyristors appl. 80—70236
Si:P, IR absorpt. and D^--band 78—52533
Si:P, impact excitation of P at low temps. 78—23098
Si:P, implantation damage of channelled P ions, elec. activity recovery stages 77—59034

elemental semiconductors continued
Si:P, implantation depth distrib. meas. by neutron activation anal., SIMS, junction depth method 77—31693
Si:P, implanted, dislocations obs. by backscatt. spectrometry and TEM 79—4308
Si:P, implanted, pulsed electron beam annealing, Hall effect and sheet resist. meas. 80—34467
Si:P, implanted, SiO_2-film-covered, laser annealing behaviour 79—86808
Si:P, implanted, two-stage laser annealing of lattice disorder 79—1452
Si:P, implanted layers, ionisation-enhanced crystallisation 79—51151
Si:P, implanted low temp. annealed, elec. activation, damage depend. 80—88182
Si:P, impurity band states calc. and photoluminesc. meas. 77—8046
Si:P, impurity conc. from photoluminesc. anal. 78—63785
Si:P, impurity cond., hopping conduction and the Coulomb gap 80—44605
Si:P, impurity doped, electron lifetime and transport in upper Hubbard band 79—95452
Si:P, impurity redistrib. by Ar ion hot implantation 77—72633
Si:P, incoherent light flash annealing, elec. props., backscattering spectra 80—97504
Si:P, interstitial supersaturation near P-diffused emitter zones 79—65541
Si:P, ion implantation, effects of high dose rate 78—83835
Si:P, ion implantation defect annealing investig. by CESR 77—8404
Si:P, ion implantation doped, positron annihilation meas. 78—14380
Si:P, ion implanted, damage layer props. obs. using ellipsometric parameters *(Russian)* 77—43234
Si:P, ion implanted, ionisation enhanced annealing, resist. changes meas. 78—30667
Si:P, ion implanted, irrad. by laser of different wavelengths, annealing behaviour 79—69132
Si:P, ion implanted, laser and thermal annealing, elec. cond. and Hall effect meas. 79—69145
Si:P, ion implanted, lattice damage and electrical activation correlation 78—67726
Si:P, ion implanted, regrowth of damage structs. by laser annealing 80—107289
Si:P, ion implanted, resist. changes induced by ESR 78—68377
Si:P, ion implanted, selective annealing of amorphous layers by Nd^{3+}:YAG laser irrad. 79—14823
Si:P, ion implanted, sheet resistance variations at elevated temps. 78—43041
Si:P, ion implanted, subsurface damage, TEM and channelled Rutherford backscatt. study 80—107337
Si:P, ion implanted low temp. elec. cond. 79—56225
Si:P, ion implanted with small doses, defect annealing by nanosecond laser pulses 80—107297
Si:P, ion-implanted, carrier conc. reduction caused by wet O_2 oxidation 80—10565
Si:P, ion-implanted, damage-dependent elec. activation 79—55793
Si:P, ion-implanted, laser annealing 80—10564
Si:P, ion-implanted, optical refl. obs. of damage 78—55883
Si:P, ion-implanted and unimplanted, laser annealing, photoluminesc. study 80—2049
Si:P, ion-implanted layers, CESR meas., impurity distrib. inhomogeneity 78—2738
Si:P, low energy and high dose ion implantation, through SiO_2 film 77—15435
n-Si:P, low-compensated, Hall factor, electron-phonon interactions 79—4570
Si:P, luminesc. lines, multiexciton complexes and unaixial stress 78—92114
Si:P, luminescence circular polarisation, emission by many exciton complexes 80—93398
Si:P, many-valley semicond., donor binding energies, variational calc. 78—23041
Si:P, measurement techniques for determining P densities 80—75262
Si:P, mechanism of diffusion of P 77—7906
Si:P, metal-nonmetal transition, Anderson localisation 79—95335
Si:P, model for exciton bound to donor pair, photolum. data anal. 79—51498
Si:P, N implantation through Si_3N_4 film, depth distrib. of knock-on N, SIMS meas. 78—10066
Si:P, neutron irrad. crysts., qualitative distrib. of P using autoradiography 80—24486
Si:P, neutron irradiated, influence of growth defects on change in cond. 78—39117
Si:P, neutron transmutation doping distrib. by emitted β-radiation meas. 77—19977
Si:P, neutron transmutation doped, electron trap annealing, deep level transient spectra 78—14368
Si:P, neutron transmutation doped, radiation damage exam., elec. props. 78—95080
Si:P, neutron transmutation doped, EPR obs. of annealing behaviour 79—1453
Si:P, neutron transmutation doped, EPR, electron trapping 79—73179
Si:P, neutron transmutation doping, elec. props. rel. to neutron fluence 80—96555
Si:P, neutron transmutation doping, resist. homogeneity rel. to compensation ratio 80—96556
Si:P, optical excess charging $D^0 \rightarrow D^-$, photoelectron spin relaxation *(Russian)* 79—78572
n-Si:P, optical orientation of ^{29}Si and its depend. on pumping light intensity *(Russian)* 77—4581
Si:P, optically induced divacancy reorientation, EPR spectra 78—80216
Si:P, phonon cond., electron-phonon relax. rate 79—46771
Si:P, photodielectric effect associated with impurity excitation 79—82630
Si:P, photolum. obs. of donor pairs 79—52014
Si:P, photoluminesc. associated with impurity clusters 79—38656
n-Si:P, piezoresist. under strong uniaxial elastic deform. 77—15858
n-Si:P, piezothermoelec. power in electron-phonon drag region, anisotropy 80—70738
Si:P, polycryst., CVD, elec. activation of impurities, EPR obs. 80—34774
Si:P, polycryst., channelling of implanted P during MOS device processing 80—65017
Si:P, polycryst., growth in epitaxial reactor at 800°C, using PH_3 doping 77—1815
Si:P, polycryst., neutron transmutation doped, elec. props. 78—34836
Si:P, polycryst. etching characts. in CF_4 plasma 78—76777
Si:P, polycryst. films, elec. props., EPR, defect states, doping effects 80—75660

elemental semiconductors continued
Si:P, polycrystalline, thermal oxidation in wet O_2 78—92376
Si:P, polycrystalline laser recrystallised film on Si substrate, cryst. struct., thermal oxidation 80—65391
Si:P, quantitative model for diffusion of P and emitter dip effect 77—76611
Si:P, RF sputtered polycryst. film, MOS compatibility 78—6455
p-Si:P, random and aligned implants, Rutherford backscatt. and TEM exam. 78—47454
Si:P, satellite of bound excitons, transient decay 80—11466
n-Si:P, Sb, reson. four wave mixing, valley orbit splitting 79—89960
Si:P, secondary defect generation suppression and diffusivity restraint by HCl oxidation 79—70191
n-Si:P, secondary defects produced by high-temp. electron irrad. 79—33017
Si:P, shallow strain distrib. near cryst. surface, asymmetric X-ray Bragg reflexion 77—76252
Si:P, SiP precipitation concomitant with P predeposition 77—24326
Si:P, solid planar source for diffusional doping, with SiP_2O_7 active component 77—1139
Si:P, spin relax. time of electrons determ., dynamic polarisation of ^{29}Si nuclei 77—55730
Si:P, spin-on borosilica diffusion source, doping uniformity factors 77—76442
Si:P, sputter-deposited polycryst. films, resist. meas. 78—14842
Si:P, stacking fault and dislocation growth induced by P predeposition 77—59023
Si:P, strain-induced band-gap narrowing effect on P diffusion 79—55935
Si:P, strongly compensated, temp. depend. cond. meas. down to 1K 77—72865
Si:P, submillimetre wave study of metal-insulator transition 79—95336
Si:P, temp. depend. of anomalous struct. in wavelength-derivative absorption spectra 77—52143
Si:P, thermal cond., electron-phonon interaction at low temps. 80—92730
Si:P, thermally annealed, high dose, ion-implanted, dislocation array prevention by prior laser annealing 79—73187
Si:P, through-oxide implanted samples, anomalous residual defects after annealing 77—76432
Si:P, uniaxially deformed, multiparticle impurity complexes, luminesc. spectra *(Russian)* 79—4854
Si:P, variable range hopping conduction, in lowest temp. region 79—73511
Si:P, variable range hopping at very low temp. 80—49736
Si:P,B, amorphous, localised level density 79—56168
Si:P,B, wafer, long range enhancement of B diffusivity induced by high surface conc. P diffusion 79—46687
Si:P,Sb(Te), impurity implantation effect on CESR, spin-orbit interactions 77—36133
n-Si:P,V, degeneracy ratios and impurity levels of V, resist. and Hall effect meas. 77—20260
Si:P amorphous films, doping and annealing effects on localized states, ESR meas. 79—38380
Si:P bipolar transistors, interstitial supersaturation and misfit dislocation climb, TEM study 80—70203
Si:P bound multiexciton complexes, expt. evidence for shell model 78—39036
Si:P CVD films, ion-implanted, doping effect on elec. props. 80—2495
Si:P Czochralski crystal donor homogenisation by thermal neutron irradiation 78—6108
Si:P epitaxial layer, strain distrib. at interface with substrate, obs. by X-ray double cryst. method 79—99461
Si:P film, amorphous, unusual temp. depend. of thermoelec. power 77—59343
Si:P film, CVD polycrystalline, low press. and atmos. press., oxidation 80—3214
Si:P film, polycryst., heavily doped, mobility and carrier conc., optical determ. 80—66314
Si:P film, polycryst. pulsed electron beam annealing 80—10566
Si:P heavily-doped, photoluminescence 78—72572
Si:P implantation profiles, neutron activation anal. 78—7284
Si:P implanted, multiscanning electron beam annealing 80—75242
p-Si:P implanted films, piezoresist. stress tensors, ion dose depend., −80 to 120°C 80—100538
Si:P non-Fickian diffusion, parameter depend. on doping level and impurity gradient *(German)* 80—54440
p-Si:P p-n junctions, dislocations investig. rel. to P diffusion, SEM, X-ray topography techniques 77—76433
Si:P photochronic detector, IR detect. using delayed breakdown 79—58786
Si:P polycrystalline layer, role in lattice defect reduction assoc. with P predeposition 80—70229
p-Si:P semiconductor detector in radiometric inspection problems 80—62819
Si:P solar cell, minority carrier lifetime degradation during ion implanted processing, surface photovoltage 79—39305
Si:P solar cells, improved P diffusion using laser treatment 80—55850
Si:P spherical defect cluster and dislocation loop analysis 78—14356
Si:P^+, highly implanted, two step annealing effect on crystallinity 77—31683
Si:P^+, ions implanted through SiO_2 mask window, lateral spread 79—77627
Si:P^+, misfit dislocation formation mechanism, effect of implantation temp. 78—38708
Si:P^+, Zeeman energy transfer at surface layer 80—11247
Si:P^+ ion implanted single crysts., secondary defects development during annealing 80—44228
Si:P(As), conc. profiles of P (or As) and recoiled O atoms after ion implantation into SiO_2-Si, SIMS obs. 79—51138
Si:P(As)(B), nonequilibrium solid solutions obtained by heavy ion implantation and laser annealing 80—92544
Si:P(As)(B)-SiO_2 interface oxidation kinetics, high doping levels, experiment 80—11828
Si:P(As)(Sb) donors, polarisability binding energy in mag. field 79—1581
n-Si:P(B), elec. cond. oscills., electron instability effects due to dislocations 80—103704
Si:P(B), film, electronic props. 78—84330
Si:P(B), high temp. impurity diffusion via vacancies and self-interstitials 80—24667
Si:P(B), multiple-particle exciton-impurity complex form. *(Russian)* 78—43925

elemental semiconductors continued
Si:P(O) p$^+$-n-n$^+$ solar cells, comparison rel. to resistance to 1.5 MeV electron irrad., majority carrier trapping 80—94087
p-Si:P(P$^+$) photolytic props. in HF 80—89504
Si:P(Sb), electron-nucl. interaction under optical pumping, ^{29}Si optical polarisation meas. 79—95680
n-Si:P(Sb)(As), characts. of piezoresist. 77—51750
Si:Pb, diffusion behaviour of Pb in high dose implanted Si layers during isothermal annealing 79—1525
Si:Pb, He$^+$ Rutherford backscatt. and TEM exam., implant species effect on recrystn. 78—47452
Si:Pb, implanted, laser annealing 78—75685
Si:Pb, implanted and annealed, impurity redistrib. 78—75689
Si:Pb, ion-implanted and annealed, dose depend. of residual lattice disorder 77—43228
Si:Pb, lattice location of dopant and amorphous zones, by Rutherford backscatt. 77—68990
Si:Pb, low-solid solubility ion-implanted, pulsed and continuous laser annealing and furnace annealing comparison 79—73184
Si:Pb implanted layers, recrystn. on annealing, backscatt. and TEM obs. 77—51421
Si:Pd, deep levels, conc., activation energies, thermal emission rate 79—51524
Si:Pd, energy levels obs. 77—35890
n-Si:Pd, surface, photocond. and photo-emf spectra 79—73544
Si:Pt, deep level, exam. by thermally stimulated current and capacitance techniques 79—1579
Si:Pt, depth depend. of atomic mixing by ion beams 80—29837
Si:Pt, elec. props., deep-level transient spectroscopy and thermal emission meas. 79—82542
Si:Pt, hole capture cross-section at $E_v+0.34$ eV, capacitance meas. *(French)* 80—65493
Si:Pt, implanted and laser annealed, segregation and increased dopant solubility 80—65016
Si:Pt, photoionisation cross-sections, photocurrent and photocapacitance meas. 78—10497
Si:Re, diode, barrier capacitance and photocapacitance, uniaxial press. effect 77—20416
n-Si:Re, photon-capture cross sections of Re levels, spectral depend. 77—89726
Si:Re diode, photocapacitance and induced photocapacitance spectra 77—4404
n-Si:Re diode photocapacitance spectra, Re centre dissociation 79—90997
Si:Rh, p$^+$-n-n$^+$, n$^+$-n-n$^+$, p$^+$-n-p$^+$, structs., S- and N-type I-V characts. 77—43706
Si:Rh(Pd), Schottky diode, capacitance characts., donor and acceptor levels 77—43697
Si:Ru, photon- and carrier-capture cross sections of Ru levels 79—90995
Si:S, deep level characterisation, implantation predeposition technique 80—100444
Si:S, electron-nuclear interactions during pumping, influence of mag. field 79—95378
Si:S, existence of isotope shift for S deep level, isothermal transient capacitance meas. 78—63999
Si:S, γ-irrad. influence on elec. props. 80—6845
Si:S, i.r. photodetector, background-limited operation near 77K 77—122
Si:S, two-electron donor centre, photoionisation cross sections meas. 77—8044
Si:S diode, ionisation energies of S levels, photocapacitance meas. 77—4432
Si:S IR detectors, performance and elec. transport props. 78—45702
Si:S p$^+$-n junction, optical props., photocurrent meas. 77—4425
Si:S(Se), IR absorption and photocond., donor levels 77—55809
Si:Sb, amorphous, electronic transport props. 80—44589
n-Si:Sb, arbitrary doping profiles produced by MBE 79—7617
Si:Sb, diffusional doping by doped oxide method 80—15127
Si:Sb, dopant implantation, activation analysis errors due to isotope comp. *(German)* 80—34037
Si:Sb, dopant microsegregation rel. to crystal and crucible rotation 78—11106
Si:Sb, electron irrad. damage, electron trapping centres 77—39798
Si:Sb, epitaxial film, growth by mol. beam technique 80—2292
Si:Sb, epitaxial layers, doping profile techniques 80—44231
Si:Sb, epitaxial regrowth of amorphous layers created by high-dose Sb implantation 78—30654
Si:Sb, heavily doped, TEM obs. of impurity effects in dislocation motion 77—43220
Si:Sb, high dose implanted, orientation dependent annealing effects 78—18665
Si:Sb, high dose Sb ion implantation, buried layer appls. 80—88186
Si:Sb, implantation of Sb for buried layers appl. *(French)* 77—80527
Si:Sb, in solar cell struct., heavily doped, dopant striation, SEM 79—39312
Si:Sb, ion implanted, annealing behaviour of stress 78—63778
Si:Sb, ion implanted, Sb diffusion during oxidation, snow-plough effect 80—88366
Si:Sb, ion implanted and annealed, influence of implantation temp. on dislocation generation 80—88158
Si:Sb, laser doping, evaporation loss and diffusion of Sb, under pulsed laser irrad. 80—59508
Si:Sb, low energy ion implantation, profile determ. 80—88176
Si:Sb, low energy ion implantation Schottky barrier diodes and resistors 80—88177
Si:Sb, MBE film, doping technique 80—79821
Si:Sb, Mossbauer spectra of ^{119}Sn defect struct. 80—97174
Si:Sb, polarisability of Sb donors in mag. field 79—95368
Si:Sb, produced by ion implantation and laser annealing, Sb behaviour above solid solubility 80—88200
Si:Sb, redistribution of thin impurity layers after laser annealing, theoretical model and expt. results 79—69147
Si:Sb, vacuum deposition combined with ion implantation *(Japanese)* 79—28005
Si:Sb,As, autodoping effect of Sb-As simultaneous diffusion 77—80522
Si:Sb,P, double implants, residual defect reduction after damage anneal 80—88170
Si:Sb vacuum deposited coating, p-n junction, pulsed electron beam annealing doping, diffusion 80—75480
Si:Sb wafers, laser annealing, Rutherford backscatt., optical, and TEM obs. 79—1445
Si:Sb(As)(P), bound excitons and bound multiexciton complexes for shallow donors, luminesc. meas. 79—24363

elemental semiconductors continued
Si:Sb(Ga)(Bi)(In), dopant solubility limit, laser irrad. effects 80—84295
Si:Sb(P) (B) homoepitaxial film, interpretation of temp. depend. of partition and sticking coeffs. 77—7756
Si:Sb(P)(As), shallow donor states with strong central cell perturbation theory 78—51933
Si:Sb(P)(As), shallow donor electrons, hyperfine interactions, reply to Onffroy's calcs. 78—51934
Si:Sb(P)(B)(Ga), low angle boundary formation, in single crysts., effect of impurities on cryst. growth conditions 80—11555
Si:Sc, photocapacitance and photoconductivity 80—107859
Si:Se, detector for 3-5 μm appl. development 79—35825
Si:Se, energy levels, resistivity and Hall coeff. 79—69528
Si:Se, impurity states, A- and B-centres, electron, hole thermionic emission rates 80—96813
Si:Se,B(Ga)(Al)(In), diffusion of Se, solubility and ionization levels, Hall effect and photocond. meas. 79—42486
n-Si:Sm,P, carrier conc. and mobility, electron irrad. effects *(Russian)* 77—66168
Si:Sn, Mossbauer study of defects due to ^{119}In implantation 80—80641
Si:Sn, thermal conductivity, Hall mobility depend. on Sn conc., phonon-defect scatt. 80—29232
Si:Te, ion implanted, laser annealed, lattice location of Te 78—67725
Si:Te, laser melting, surface Te atom accumulation, profiles 80—100258
Si:Te, Mossbauer spectra of ^{119}Sn defect struct. 80—97175
Si:Te implanted, laser annealing, Mossbauer obs. 80—39127
Si:Te(Sm), implanted impurity location, Mossbauer and channelling expts. 80—39128
Si:Th, ion implanted, meas. of stopping power of channeled B ions 79—28025
Si:Ti, deep level impurity, Hall meas. 80—6768
Si:Ti substrate for epitaxial solar cells 80—61341
Si:Tl, energy level, deep level transient spectroscopy 79—19541
Si:Tl, IR excitation spectra 78—88289
Si:Tl, ion implantation, indirect doping method 80—10568
Si:Tl, optical absorption and photolum. of bound exciton 78—88359
Si:transition metal, amorphous, impurity effects on hopping conductivity 79—65485
Si:transition metal, electronic states of impurities 77—43531
Si:V p-n junctions, thermal emission rates and capture cross sections of majority carriers at V centres 80—96980
Si:Y, photoelectric props. 80—107860
Si:Zn, implanted atom diffusion during laser annealing 79—37725
Si:Zn, minority carrier lifetime investigation 80—80292
Si:Zn, P$^+$-n-n$^+$ struct., deep doubly ionized centres, impedance calc. 79—11202
Si:Zn, photoionisation of deep impurity levels 80—34386
Si:Zn, recombination waves threshold parameters in microwave field 77—28206
Si:Zn, resist. inhomogeneity effects on photoelec. props. 77—8151
Si:Zn, reson. characts. of impedance near excitation threshold of recomb. waves 80—20301
Si:Zn, trapping struct., analysis of TSC meas. 77—8045
n-Si:Zn,P, local deform. of cryst. lattice, charact. parameters or recomb. waves 77—4386
Si:Zn (Mn) (In), surface characterised by negative electrochemical pot., electronic props. 80—44695
Si:Zn p-n junction diode, computer-aided study of carrier lifetimes 80—24999
Si:Zn p-n junctions, I-V characts. using exact DC circuit model 79—95476
p-Si:Zn$^-$, deep levels, optical-phonon-assisted capture of carriers 79—51597
Si/Al and Si/Al-Si(Cu), Si regrowth minimisation through overlying Al or Al alloy film 80—70569
Si/Al interfaces, chemical bonding states, low energy AES 80—6985
Si/Al thin film couples, accel. ageing 80—44726
n-Si/As-Te-Ge film, heterojunction, elec. and photovolt. props. 80—100514
a-Si/Au barrier, capacitance and cond. 80—2469
Si/Au films, laser-irrad., phase transform. study 80—49536
a-Si/$In_{2-x}Sn_xO_{3-y}$, p-i-n heteroface solar cell, device physics and design 80—101113
n-Si/In_2O_3:Sn heterojunction solar cell, fabrication and characts. 78—15314
Si/In_2O_3-SnO_2 thin film junctions, polarity dependent memory switching effects 80—70814
Si/In(-Cd), Si/Cd Schottky contacts, electrochemically deposited 80—88633
a-Si/metal barrier, capacitance and cond. meas. interpretation 80—49909
Si/metal system, silicide form. by thin film interactions, review 80—49429
Si/NiSi/Al system, high temp. interaction study, elec. and struct. characts. 79—24075
Si/Pd interface, chem. and struct. props. during silicide form., AES and TEM obs. 80—49430
Si/Pd system, solid phase epitaxial growth control by C ion implantation 80—75466
Si/Pd-W, contact reactions, backscattering, X-ray diffr. meas. 80—20040
p-Si/rare earth metal contacts, surface pot. barrier 80—60086
Si/refractory metal-Ni(Pd)(Pt) interactions, phase separation 80—65303
Si/Si-Ge alloy, amorphous, solar cell, multijunction structure, increased conversion efficiencies, low cost 80—45677
Si/SiO_2, adsorbed methanol, light scatt. from clusters 79—33721
Si/SiO_2 interface, slow-trapping instability, kinetics 78—76151
Si/SiO_2 interface, transition region thickness, determ. by He$^+$ backscatt. 77—62762
n-Si/SiO_2 solar cells, fabrication and characterisation 79—79393
n-Si/SnO_2 spray-deposited solar cells 80—12007
Si/surface porous oxide film, impurity distrib. during P diffusion 77—39944
Si/V_2O_5-P_2O_5/SnO_2 heterojunction, static optoelectronic characts. 79—87146
n-Si-^{119}Sn resonant detector for Mossbauer spectroscopy 80—883
Si-^{3}He interface, phonon reflection 78—84043
Si-absorbing film system, ellipsometry 79—99964
Si-Ag boundary, electronic and cryst. struct. of Ag adsorbed on Si (111), Schottky barrier form. obs. 78—84091
Si-Ag interfaces, solar cell contacts 80—92973
n-Si-Ag Schottky-barrier diodes, excess current mechanism under uniaxial press. 78—91771

elemental semiconductors continued
- n-Si-Ag(Au) evaporated contact photoelectric props. *(Russian)* 78—43473
- Si-Al, contact resist. response surface of sintered Al film on Si(100) 79—78175
- p-Si-Al, ohmic contacts, Si dissoln. and recrystn. effects, computer calc. 80—103749
- p-Si-Al barrier junction form. 77—12006
- Si-Al devices, thickness meter for Al contacting layers *(Russian)* 80—36980
- Si-Al interface, ellipsometric anal. methods, correl. between optical props., thickness and surface roughness meas. *(German)* 80—55215
- Si-Al interface, solid phase epitaxial growth of Si 80—34324
- Si-Al interface in semiconductors, electronic parts, electromigration aspects 80—39355
- n^+-Si-Al ohmic contacts, metallisation structs. for very shallow n^+/p junctions 80—60084
- Si-Al Schottky barrier solar cell, using polycryst. Si, grain boundary effects on elec. behaviour 80—85279
- Si-Al Schottky diodes, with Ti contact, voltage-current characts., appl. to ignition circuits 80—11088
- Si-Al solid-phase epitaxial growth, substrate effects, SIMS and backscatt. spectra 79—42421
- Si-Al system, Si regrowth minimisation methods in Al films 80—15384
- Si-Al_2O_3, inversion layer subbands, magnetocond. oscills. 78—64124
- Si-Al_2O_3 interface, charge injection from surface depletion region 80—54797
- Si-Al_2O_3-Al structure, study of charge trapping 80—60097
- Si-Al_2O_3-SiO_3 in MIS struct., charge accumulation and spreading *(Russian)* 78—64116
- Si-Al-Al_2O_3 system, solid phase Si regrowth on sapphire 80—100413
- Si-Al-Si, isothermal version of the moving solvent method 79—1824
- Si-Al(Ga)(In) interface, electron energy loss spectra of Schottky barrier states 77—48290
- Si-$As_2Se_3Ge_4$ heterojunction, elec. props. 78—6434
- Si-As(Sb) temp. depend. of irradiation-induced displacement of impurities, backscattering meas. 78—26605
- Si-Au, interface study using EELS 80—97391
- p-Si-Au, Schottky barrier IR detector 77—37985
- Si-Au, spatial origin of electrons in internal photoemission struct. *(French)* 78—91770
- Si-Au boundary, Schottky barrier height, interfacial layer effects 78—14824
- Si-Au contact, O determ. by SIMS, nuclear reaction and Rutherford backscatt. anal. 79—4482
- Si-Au interface, critical Au-film thickness obs. for room temp. interfacial reaction 80—75390
- Si-Au Schottky barrier solar cell fabrication, doping of a-Si· 80—50969
- n-Si-Au Schottky barrier solar cells, recombination in space charge region 80—61351
- Si-Au Schottky diodes, role of O in formation mechanics 79—42639
- Si-Au Schottky-barrier, formation process anal., V-I characts. *(French)* 78—91768
- Si-Au substrate-film system, relax. effects, internal friction meas., temp. range 20 to 900°C 78—18886
- Si-Au-P system, partition coeff. of P, temp. depend. 79—43158
- Si-Au-Si, Auger line intensity, contrib. of backscattered electrons 79—65962
- Si-Au(Cr)(Pd), contact reactions between amorphous Si and metallic films, TEM, transmission electron diffr. obs. 79—23846
- Si-Au(Rh)(In), Schottky diode, X-ray effects on elec. props., irrad. induced diffusion 77—4439
- Si-B, diffusion-free annealing, use of scanning CW Kr laser 78—91345
- Si-B, exam. of two stage diffusion of B, under a gas phase oxide film 79—95044
- Si-B, P diffusion and activity after Ar ion bombardment 78—95192
- Si-based technology for hemispherical laser fusion target fabrication 79—89495
- Si-borosilicate glass, B diffusion from sputtered glass film into Si 80—29040
- Si-C interface on polycryst. Si ribbon, effect on solar cell efficiency *(French)* 80—54531
- Si-C-o-Ar, high temp. plasma, prod. quenching mol. dynamics simulation 78—39711
- Si-CdS p-n heterojunction photodetector fabrication and characts. 78—52068
- Si-CdSe n-n heterojunction, photovoltage sign reversal, energy band profile *(Korean)* 80—29469
- Si-chalcogenide cryst. amorphous heterojunction, energy band diagram construction 77—55602
- Si-Co interface metal-semiconductor transition, rel. to first compound nucleation 80—24771
- Si-$CoSi_2$Si, double heteroepitaxy, solid phase and MBE 80—104063
- n-Si-Cr, Schottky barrier IR detector 77—37985
- Si-Cr interfaces, metallurgical and electrical props. 80—60081
- Si-Cr Schottky diode, I-V characts., inverse branch, effect of dislocation defects *(Russian)* 79—15217
- Si-Cr_2O_3-Al, current-voltage characts., oxide film effects 80—70841
- Si-CsSe p-n heterojunction, vacuum deposition, photovoltaic effects *(Korean)* 77—28243
- n-Si-Cu Schottky contacts, electrochem. deposition, barrier height and ideality factor 80—75641
- n-Si-electrolyte boundary, selective anodic oxidation 78—15563
- Si-electrolyte contact, current-voltage characts., effect of mechanical deform. 78—68082
- Si-electrolyte contact, implantation profile meas. from capacitance-voltage characts. *(German)* 77—1145
- Si-F-H amorphous solar cells, DC glow discharge fabrication 80—72041
- Si-F-H:P, film, dark cond., struct., Raman scatt. 80—88588
- Si-GaP, heterojunction, photosensitivity spectrum, characts. 79—24071
- Si-GaSe n-p heterojunction, elec. characts., interface states 80—70812
- Si-Ge heteroepitaxial system, imperfections and morphology, electron microscope and electron diffr. obs. 79—42420
- Si-Ge heterojunction form., microscopic aspects, EELS meas. 80—80368
- Si-Ge junction, Si monocryst. and Ge film, elec. props. 79—51660
- Si-$Ge_{20}Te_xSe_{80-x}$ cryst.-amorphous heterojunction, elec. and photovoltaic props. 79—65546
- Si-H, amorphous, plasma-deposited, H evolution and defect creation 80—44914
- Si-H, amorphous, struct. and press. induced transition 80—44131
- Si-H, amorphous film, in situ prepared, photoemission studies 80—35060

elemental semiconductors continued
- Si-H, amorphous plasma deposited film, H content and density 79—82472
- Si-H (up to 15 at.%), amorphous, ion implanted, laser annealing obs. 79—69133
- Si-H amorphous film, reactively sputtered, prep. and props. 79—78889
- a-Si-H sputtered solar cells, temp. depend. of Schottky barrier characts. 80—45669
- Si-H:P amorphous film, dark cond., struct., Raman scatt. 80—88588
- Si-In Schottky barrier interface, covalent bonding of metal atoms 77—20429
- p-Si-In Schottky barrier structure, optical quenching of photovoltaic effect 77—55608
- p-Si-$In_{2-x}Sn_xO_{3-y}$ solar cells, thermal degradation mechanisms 80—55841
- Si-$In_{2-x}Sn_xO_{3-y}$ SIS heterostructure solar cells, spray-deposited 80—101106
- n-Si-In_2O_3:Sn, solar cell characterisation *(French)* 79—39306
- Si-In_2O_3:Sn heterojunctions, current mechanisms and barrier height 80—11083
- Si-In(Rh)(Au) Schottky diodes, X-ray irradiated, radiation-accelerated diffusion of impurities in Si 78—26952
- Si-insulator interface, non-avalanche charge injection, expt. study, charge trapping effects 80—60099
- Si-insulator structures, contact pot. meas., vibr. condensor method *(German)* 79—11232
- n-Si-$IrSi_x$, Schottky diode, rectifying barrier height meas. 79—99619
- p-Si-$LiNbO_3$, frequency doubling of the two-pulse and three-pulse echoes in surface acoustic waves 79—69335
- Si-$LiNbO_3$ layer struct., acoustoelectronic phenomena 77—55556
- Si-$LiNbO_3$ structure, acoustoelectronic interaction between SAW and transverse drift current 77—69424
- Si-Li(Au)(Cu), diffusion-induced defects, X-ray triple cryst. diffractometry 80—2213
- Si-liquid He interface, refl. of high frequency phonons, role of phonon focusing 77—80691
- Si-liquid N_2 system, kinetics of switching effect and electrothermal memory 79—51641
- Si-metal contact, transport theory of Schottky barriers 80—80372
- Si-metal contacts, analytical techniques, review 80—80120
- Si-metal interface, silicide formation, interface marker technique obs. 80—59734
- a-Si-metal Schottky barrier, I-V characts., barrier heights 77—8191
- p-Si-metal Schottky contact surface state spectra and current transport mechanism *(Russian)* 78—43472
- Si-metal systems, interfacial reaction and Schottky barrier 80—39672
- Si-metal thin film reactions, laser annealing 79—70364
- p-Si-Mn contact, barrier height 80—34510
- Si-Mo diffusion couples, $MoSi_2$ or Mo_3Si/Mo_5Si_3 form. 79—77836
- Si-Mo sputtered contacts, contact resistance 80—92970
- Si-Mo substrate-film interface, reaction on heat treatment, silicide formation 80—79999
- Si-MoO_3 photodiode, fabrication as function of O_2 partial press. 80—29464
- Si-NH_3 electrolyte interface, photo-assisted electron injection 79—87152
- Si-$NaNO_3$ aq. soln., anodic polarisation of semicond. electrode 77—11999
- n-Si-Ni, Schottky barrier, thermal annealing effect on props. 79—69596
- n-Si-Ni, Schottky-barrier, I-V characts. of elec. contact 79—19662
- Si-Ni interface, NiSi formation from Ni_2Si, Pt marker study 78—87830
- Si-Ni substrate-film interface, annealing effects on transmission electron diffr. patterns, silicide form. 78—91562
- n-Si-Ni surface barrier junction, rectifying, struct. and elec. characts., effect of low temp. annealing 78—14821
- Si-Ni surface barrier struct., surface electronic states, annealing effects *(Russian)* 78—6441
- Si-Ni wafer-thin interface, marker motion in Ni_2Si formation 77—89593
- Si-Ni(Pd)(Pt) film struct., silicide form. He^+ back scatt. and X-ray diffr. obs. 79—51442
- Si-Ni(Pt)(Al) Schottky diode, type II localised interface states, Si surface prep. effects 78—39210
- Si-O system, modern view 78—10045
- Si-on-ceramic solar cells, short-circuit current density meas. using light-beam-induced-current tech. 80—93887
- Si-on-sapphire MOS devices, effects of planar defects near Si-SiO_2 interface on elec. props. 79—11231
- Si-P, dislocation networks due to ion implantation, TEM exam. 77—35563
- Si-P, excess carrier recomb., photocond. 79—65495
- Si-P dust, electrification and cond. 79—82662
- Si-P MOS devices, time dependence of depletion region formation at cryogenic temp. 80—34522
- Si-Pb heterojunction, RHEED, Mossbauer spectroscopy and I-V characts. 80—70828
- Si-PbS heterojunction, characts. and operation, IR detector appls. 78—52075
- Si-PbS heterojunction, effect of Si substrate orientation on struct. and interface props. 80—80097
- Si-PbS heterojunction, struct. and comp. 80—54530
- Si-PbS n-p heterojunctions, AC admittance meas. 80—96979
- Si-PbS photosensitive n-p heterojunction, energy band diagram 79—95489
- n-Si-Pd diodes, chemical reduction process for fabrication 80—60082
- n-Si-Pd_2Si contact, interface struct. and Schottky barrier height, correl. obs. using TEM 80—100504
- Si-Pd_2Si heterostructure growth by solid-phase epitaxy from Si (111)-Pd-Si (amorphous) 77—51617
- Si-Pd_2Si-Si, kinetic aspects of solid phase epitaxial growth of amorphous Si 79—4491
- Si-Pd-Si structure, epitaxial growth, backscattering and transmission electron microscopy studies of layered structures 80—80123
- Si-Pd-Ti, silicide form. in evaporated films 80—80006
- Si-polymer interface states in MOS structure, capacitance and cond. meas. 77—20438
- Si-Pt contact, silicide layer struct. and elec. props., effect of processing conditions 77—62991
- Si-Pt Schottky barrier, laser formation and characts. 80—60079
- Si-PtSi interface, impurity effects 80—80037
- n-Si-Re(Os) Schottky contact barrier height meas. 80—65675
- Si-refractory metal contacts, thermally cleaned surfaces 80—100521

elemental semiconductors continued
- Si-refractory metal structs., interface modification by ion implantation 80—70475
- Si-sapphire, interface radiation induced charge trapping, rapid anneal phenomena 79—19666
- Si-sapphire interface charge trapping, effects of sapphire type and epi growth conditions 77—20447
- Si-sapphire interface in SOS ICs, elec. investigation 80—11097
- Si-sapphire interface structure, SIMS obs. 77—76675
- n-Si-Se, ion implantation studied by deep level transient spectroscopy 78—10392
- Si-Si, Van der Waals interaction, influence of optical absorpt. 79—95273
- Si-Si interface, elec. cond. rel. to interface state population 80—65672
- Si-Si_3N_4 interface, effect of F ions on props. and stability, expt. 78—64141
- Si-Si_3N_4 interface in MNS capacitors, surface state density investigation 80—60100
- Si-Si_3N_4-Al, electrical strength, effect of struct. defects in Si_3N_4 *(Russian)* 78—26955
- n-Si-SiC film junction device, elec. props. 80—15591
- Si-SiC p-n and n-n heterojunctions, prep. by ion implantation, tunnelling cond. 77—43710
- Si-SiC struct. formation on ^{12}C ion implantation in Si, optical and photoelectric props. 79—91136
- Si-SiO_2, Al-implanted, low-temp. annealing effect on charge and surface state density 77—85337
- Si-SiO_2, anodic polarisation in electrolyte containing fluoride ions, effect on oxide props. 80—39679
- Si-SiO_2, bonding at (111) interface, stoichiometry and kinetics, synchrotron radiation photoemission spectroscopy 80—24744
- Si-SiO_2, electron photoemission from Si, band struct. effects 79—19977
- Si-SiO_2, flat-band voltage due to fixed surface charge density, modified expression 79—56317
- Si-SiO_2, Fowler-Nordheim tunnel injection into SiO_2, Si surface pot. effect 79—91151
- Si-SiO_2, generation of interface states due to emission of leaky electrons 77—62972
- Si-SiO_2, impurity redistrib. during oxidation, numerical soln. including interfacial fluxes 80—25888
- Si-SiO_2, influence on frequency-temp. coeff. of SAW devices 80—79066
- Si-SiO_2, interface, doping depend. of interface states and charges 80—92992
- Si-SiO_2, interface, electronic ground state of inversion layers 77—43731
- Si-SiO_2, interface, hopping conduction, anal. in impurity bands in inversion layers 79—47171
- Si-SiO_2, interface, morphology and electronic struct. 79—78194
- Si-SiO_2, interface, props. of surface states reviewed 77—20449
- Si-SiO_2, interface, reconstructing states 80—49925
- Si-SiO_2, interface, stress meas. technique 80—84395
- Si-SiO_2, interface defect states obs. by constant capacitance DLTS 80—49924
- Si-SiO_2, interface states from capacitance-voltage term spectra anal. 77—4446
- Si-SiO_2, inversion layer, electronic ground state, stress, temp., mag. field and gate voltage depend. 78—60226
- Si-SiO_2, ion bombardment by H_2^+, D_2^+, changes in annealing behaviour 79—78185
- Si-SiO_2, ion implantation through SiO_2 film, recoil implantation of O, EPR study 80—88180
- Si-SiO_2, MOS interface states density, meas. techniques and model development 80—92988
- n-Si-SiO_2, MOS structures, radiation states 80—103758
- Si-SiO_2, oxide defect density depend. on appl. elec. field and thickness 80—19791
- Si-SiO_2, P ion implantation, elec. transport props. 80—39130
- Si-SiO_2, recoil implanted O profile after ion implantation through SiO_2 80—88198
- n-Si-SiO_2, screening of charged impurity centre localised inside oxide and at interface of inversion layer 79—73563
- Si-SiO_2, SiO_2 layer charging in UV irrad. of MISS struct., photoinjection currents *(Russian)* 80—39680
- Si-SiO_2, thermally oxidised, origin of fixed charge, Si diffusion in transition region 77—20381
- Si-SiO_2, two layer system, P^+-ion penetration tails, expt. and computer anal. 80—75249
- Si-SiO_2 (111) interfaces, sixfold valley degeneracy in electron inversion layers 80—49936
- Si-SiO_2 abrupt interface form. by very high dose O^+ ion implantation 80—75253
- Si-SiO_2 boundary, surface charge transport in valence band of Si 80—70789
- Si-SiO_2 charge accumulation during low energy electron bombardment 78—64142
- Si-SiO_2 double barriers, reson. tunnelling 77—80846
- Si-SiO_2 electrode, electronic cond., luminesc obs. 80—61111
- Si-SiO_2 in MOSFETs, inversion layer carrier mobility, theory 80—60094
- Si-SiO_2 interface, (001) vicinal planes, minigaps in inversion layers, far IR absorpt. meas. 80—107919
- Si-SiO_2 interface, amorphous, electronic states, Cayley trees appl. 79—65373
- Si-SiO_2 interface, anisotropic photoinduced ESR 78—23345
- Si-SiO_2 interface, Au doping, trapping states 80—20319
- Si-SiO_2 interface, Au surface state energy levels and Au diffusion 79—51652
- Si-SiO_2 interface, Auger-sputter profiling obs. of P pileup 78—95240
- Si-SiO_2 interface, backscattering-channelling study 80—34320
- Si-SiO_2 interface, barrier height in MOS tunnelling structures 80—88644
- Si-SiO_2 interface, chem. struct. of transitional region 78—95824
- Si-SiO_2 interface, cluster Bethe-lattice method appl. 80—49852
- Si-SiO_2 interface, continuous random network and tight-binding models 77—89866
- Si-SiO_2 interface, density of states, theory 80—80395
- Si-SiO_2 interface, ESCA and ellipsometric study 79—82678
- Si-SiO_2 interface, effect of thin transition layer on electron mobility and energy levels 77—20458
- Si-SiO_2 interface, effect of ^{11}B and ^{19}F ion implantation on charge density 79—10865
- Si-SiO_2 interface, effect of hot electron injection on interface charge density 80—49921
- Si-SiO_2 interface, elec. props., rel. to SiO_2 layer struct., 200-600°C heat treatment effects *(Russian)* 77—15967

elemental semiconductors continued
- Si-SiO_2 interface, electron injection into oxide due to mobile ion induced internal field 77—15963
- Si-SiO_2 interface, electronic struct., field depend. internal photoemission probe 77—20450
- Si-SiO_2 interface, electronic props. of n-Si inversion layers, stress and temp. depend 78—19113
- Si-SiO_2 interface, electronic states, review 78—30992
- Si-SiO_2 interface, electronic struct., EELS study 79—99596
- Si-SiO_2 interface, electrically active paramag. centres detect., photocond. reson. obs. 80—50185
- Si-SiO_2 interface, evolution of surface states density during bias temp. treatment 78—14832
- Si-SiO_2 interface, fitting stress and its effect on vacancy generation and distrib. 77—28087
- Si-SiO_2 interface, form. and struct., AES obs. 79—56314
- Si-SiO_2 interface, Hg probe *(Chinese)* 77—89857
- Si-SiO_2 interface, high-resolution electron microscopy study 78—56046
- n-Si-SiO_2 interface, hot carrier surface thermo EMF depend. on surface band bending 80—44734
- Si-SiO_2 interface, improved characterisation, refined quasistatic and cond. methods 80—96990
- Si-SiO_2 interface, impurity electron states near interface 78—95320
- Si-SiO_2 interface, in MOSFET struct., electronic props. 79—42662
- Si-SiO_2 interface, interface-state parameters near band edge, MOS conductance meas. 79—11226
- Si-SiO_2 interface, intermediate chem. state of Si during sputter profiling, Auger spectra 79—11230
- Si-SiO_2 interface, inversion layer transport, radiation hardness effects, review 79—19673
- Si-SiO_2 interface, MeV backscatt. channelling meas. of Si monolayers 79—11020
- Si-SiO_2 interface, N_2 gas reaction, elec. and structural characts. 77—39950
- Si-SiO_2 interface, Na^+ drifted, impurity bands in inversion layers 78—60211
- Si-SiO_2 interface, optical props. of CDW ground states in Si inversion layers 77—43732
- Si-SiO_2 interface, oxidation stacking faults, growth rel. to self-diffusion 80—49239
- Si-SiO_2 interface, props. variation in SiO_x region 80—49548
- Si-SiO_2 interface, rad. hardness, carrier localisation in inversion layer 77—85332
- Si-SiO_2 interface, relax. of injected charge, temp. depend. 78—72269
- Si-SiO_2 interface, remote polar phonon scatt. in Si inversion layers 80—80095
- Si-SiO_2 interface, sputter profiling, ion knock-on mixing model 79—83081
- Si-SiO_2 interface, stacking fault-free region formation by annealing 78—51561
- Si-SiO_2 interface, surface generation velocity study, gate-controlled diode structure application 80—6986
- Si-SiO_2 interface, surface states characterization, expt. techniques review 80—49949
- Si-SiO_2 interface, thermally oxidised, oxide thickness effects on electron scatt. 78—88033
- Si-SiO_2 interface, thermal SiO_2 sputter induced roughness, Auger sputter profiling study 80—75424
- Si-SiO_2 interface, thermally grown, surface pot. inhomogeneities after stress ageing 80—92993
- Si-SiO_2 interface, trapping props. from electrochemical current-voltage behaviour 79—69597
- Si-SiO_2 interface, valley degeneracy splitting in n inversion layer, effective-mass approx. 79—99629
- Si-SiO_2 interface, with Cl^- incorporated, characterisation by low temp. cond. meas. 78—60220
- Si-SiO_2 interface charge inhomogeneities effect on surface state density meas. by MOS AC cond. technique 78—14833
- Si-SiO_2 interface formation, by anodic oxidation, F^- and Cl^- ions effect obs. 79—15842
- Si-SiO_2 interface in MOS capacitors, lateral diffusion of Na^+, neutralisation 80—92986
- Si-SiO_2 interface in MOS solar cells, operational characts. and struct. 80—93901
- Si-SiO_2 interface layer characterisation by spectroscopic ellipsometry 80—50738
- Si-SiO_2 interface oxidation kinetics, high doping levels, theory 80—11827
- Si-SiO_2 interface props., electrolyte anode polarisation effect 77—80849
- Si-SiO_2 interface state density in MNOS structures 78—47873
- Si-SiO_2 interface state spectrosocpy using MOS tunnelling strucures 80—6991
- Si-SiO_2 interface state distribution, Br incorporation effects 80—11091
- Si-SiO_2 interface state density, dependence on thermal oxidation process variables 80—15607
- Si-SiO_2 interface states, effect on memory characts. of thin-oxide MNOS devices 79—82681
- Si-SiO_2 interface states, deposition of H containing layers and annealing 80—92991
- Si-SiO_2 interface struct. by cross-sectional TEM, amorphous oxide layer 77—24487
- Si-SiO_2 interface study by XPS 80—50507
- Si-SiO_2 interfaces, local atomic and electronic struct., high resolution XPS 80—49927
- Si-SiO_2 interfaces, surface state form. during bias-temp. stress aging 79—78193
- Si-SiO_2 interfacial regions obs., by XPS, ultrathin oxide films 79—15039
- Si-SiO_2 interfacial region on TCE/O_2 and CCl_4/O_2 oxidised Si, struct. and comp. 80—50741
- Si-SiO_2 interfacial transition layer thickness, XPS obs. 80—11540
- Si-SiO_2 interlayer, optical evidence 79—69800
- Si-SiO_2 inversion layer, n-channel, anomalous magnetoresist., model 80—96996
- Si-SiO_2 inversion layers, applied stresses, cyclotron masses and CDWs 77—55596
- Si-SiO_2 inversion layers, bound states at interface 79—42655
- Si-SiO_2 laminar ion-implanted systems, struct. change investig. by MSSI method *(Russian)* 80—107918
- Si-SiO_2 layer formation by O_2^+ ion implantation, interface struct. and C-V characts. 77—1142
- Si-SiO_2 layers, physics, electron and ion motion, Cl, Na and K ion effects *(Dutch)* 80—60093

elemental semiconductors continued
- Si-SiO$_2$ MIS systems, dynamic props. of switching, appl. to charge transfer devices 80—92997
- Si-SiO$_2$ MOS capacitors, relationship between trapped holes and interface states 80—70830
- Si-SiO$_2$ MOS interface states density, transient capacitance meas. eval. 80—92989
- Si-SiO$_2$ MOS struct., specific memory effect, radiation defects 79—51680
- Si-SiO$_2$ microsensor, surface conductivity effect of aliphatic alcohol molecule adsorption *(Russian)* 78—34887
- Si-SiO$_2$ structure, alkali metal ion migration and accumulation, interface struct. 80—107574
- Si-SiO$_2$ structure, oxide charge evaluation, appl. of Kelvin method 78—19157
- Si-SiO$_2$ structures, AS77 scanning analyser for electrophysical props. *(Polish)* 79—95498
- Si-SiO$_2$ structures, B ions implanted, energy spectra of shallow traps at various implantation energies 80—80392
- Si-SiO$_2$ structures, scanning analyser of electrophysical parameters of MOS transistors *(Polish)* 79—91145
- Si-SiO$_2$ surface states, influence of Φms(T) 79—99597
- p-Si-SiO$_2$ system, C-V meas. using Au/Hg probe, work function difference between probe and Si 80—2450
- Si-SiO$_2$ system, implanted with N, P, and Te ions, reflectance spectra and interference fringes 79—23629
- Si-SiO$_2$ system, structural defect formation rel. to thermal oxidation kinetics *(Russian)* 78—43478
- Si-SiO$_2$ systems, spectral characts. *(Russian)* 79—42657
- Si-SiO$_2$ transition region width, SIMS depth profiling 80—39454
- Si-SiO$_2$:B structure, AES meas. 77—39951
- Si-SiO$_2$-Al, interface barrier energies for tunnel oxides, internal photoemission meas. 80—84512
- Si-SiO$_2$-Al, internal photoemission, pot. barrier height determ. 80—65699
- Si-SiO$_2$-Al MOS surface channel influence on channel-to-contact diode charact. 80—92994
- Si-SiO$_2$-Al structure, mechanical stress at Si(111) surface 78—63921
- Si-SiO$_2$-Al structure, neutralisation of mobile ions in insulating films *(Japanese)* 79—73591
- Si-SiO$_2$-Al structures, SiO$_2$ thin dielec. film elec. props. with DC voltage *(Slovak)* 80—88634
- Si-SiO$_2$-Al with thick dielec. layer, photoelec. props. 80—92979
- Si-SiO$_2$-Au Schottky barrier solar cells, back-illuminated, theoretical performance 80—61345
- Si-SiO$_2$-Au system, oxide film 16-36 Å thick, tunnel currents 80—70842
- Si-SiO$_2$-CdS solar cell, I-V characteristics 80—89621
- Si-SiO$_2$-Si capacitor, polycryst., capacitance voltage characterisation 80—70794
- Si-SiO$_2$-Si structures, P, As depth profiles, ion microanal. *(Japanese)* 78—85251
- Si-SiO$_2$-Si thin film MOS structures, elec. props. with applied DC voltage *(Slovak)* 80—92977
- Si-SiO$_2$-Si$_3$N$_4$ MNOS structure, chem. comp. and electronic states, Auger and energy loss spectra obs. 80—92999
- Si-SiO$_2$-SI MOS structures, charge motion, TSC meas. 80—100534
- n-Si-SiO$_2$-ZnO-Al, SAW convolver in monolithic MIS struct. 77—23791
- Si-SiO$_2$-polySi thin film structures, dielectric props. *(Slovak)* 80—75934
- Si-SiO$_2$(Si$_3$N$_4$), interface layer determ. by spectroscopic ellipsometry 79—95275
- Si-SiO$_3$ interface, effect of Au recomb. centres on interfacial trapping states 79—38175
- Si-SiO$_s$ interfaces, carrier transport processes, electron states, conference, Durham, England (July 1979) 80—90612
- Si-SiO$_x$ interface, evidence for superlattices, magnetocond. expts. 77—89868
- Si-SiO$_x$ interface, localisation in inversion layer due to states in gap of oxide 77—12012
- Si-SiO$_x$-Al photodiode experimental verification of theoretical predictions 80—29485
- Si-SiO$_x$-SiO$_2$ interface, energy gap variation 79—91148
- Si-silicide-Al systems with CoSi$_2$, Pt$_x$Ni$_{1-x}$Si, and MoSi$_2$ as silicide, diffusion, compound form., and microstructure 80—34253
- Si-Sn heterojunction, RHEED, Mossbauer spectroscopy and I-V characts. 80—70828
- Si-SnO$_2$ heterojunction, barrier height meas. by HF capacitance method 77—69406
- Si-SnO$_2$ heterojunctions, complementary Schottky barriers 79—78166
- Si-SnO$_2$ heterojunctions, elec. and photovoltaic props. 80—26141
- Si-SnO$_2$ solar cell, max. theoretical efficiency 79—83598
- Si-SnO$_2$ solar cells electron-beam-deposited, fabrication, angle-of-incidence effects 79—52931
- Si-Te, laser and thermal annealing, Mossbauer resonance lines 79—99810
- Si-thermal SiO$_2$-electrolyte system, cond. in superhigh elec. field 78—52080
- Si-TiO$_2$-Al, current-voltage characts., oxide film effects 80—70841
- Si-transition metal interface, silicide formation, book contrib. 79—1530
- Si-transition metal metastable films as temp. independent resistors 78—68097
- Si-transition metal silicide Schottky barrier, effect of glassy membrane 77—85311
- Si-transition metal silicide interface, chemical state, AES expts. 78—91767
- Si-type, semiconductor, interimpurity radiative recomb. with phonon cooperation 77—16385
- Si-undoped poly Si interface, in oxidation process, defects generation 80—40571
- Si-V$_2$O$_5$ p-n heterostructure, photocond. *(Russian)* 79—42622
- n-Si-V$_2$O$_5$ system, carrier transport mechanisms 77—62999
- Si-V$_2$O$_5$-Al, current-voltage characts., oxide film effects 80—70841
- Si-ZnS n-n heterojunction, epitaxial, elec. props. *(Russian)* 78—88023
- Si-ZnSe n-n heterojunction photovoltaic effect, freq. meter in visible wavelength *(Korean)* 79—60915
- Si+Ga$^+$ ion implantation at high current density, lattice disorder, proton backscattering 80—34085
- Si+XeF$_2$(F$_2$)(Cl$_2$) plasma etching, electron or ion bombardment, Ar$^+$ enhancement 79—82073
- Si(:Au), gamma-induced trapping levels 79—87059
- Si(-H), amorphous, H atom effect on Si-Si atomic short-range order, X-ray diffr. obs. 79—64996

elemental semiconductors continued
- p$^+$-Si$_{1-x}$Ge$_x$-nSi junction diodes, lattice misfit effects on I-V characts. 80—70804
- Si$_{1-x}$H$_x$, amorphous, atomic struct., X-ray study 80—49106
- Si$_{1-x}$H$_x$, amorphous, gap states, DLTS 80—49656
- a-Si$_{1-x}$H$_x$, oxygenated thin film, sputtered, elec. cond. and optical props. 79—15239
- Si(III) inversion layers, CDW induced cyclotron reson. harmonics 78—64085
- Si(Li), 2D position sensitive detector with 100 μm resolution 79—45544
- Si(Li) X-ray detector, Au contact layer thickness meas. 80—62627
- SiO, role of O in phonon conductivity 79—42326
- SiO$_2$-Si, film-substrate, single reflection retarders for different Hg spectral lines 78—79122
- SiO$_2$-Si, low-energy neutral particle bombardment of SiO$_2$ film, degradation 80—54790
- SiO$_2$-Si boundaries, insulator charges evaluation *(German)* 79—82682
- SiO$_2$-Si:P, P pile-up at interface 78—84303
- SiO$_3$-Si, B ion implanted MOS struct., form. and annealing of radiation damage 79—56321
- Si(001)2×1 surface, struct. determ. by LEED 79—19438
- ^{29}Si, nuclear dynamic polarisation, impurity centre photoionisation, extrinsic light absorpt. *(Russian)* 79—15378
- ^{30}Si(n,β)^{31}P transmutation doping 78—6107
- ^{30}Si(n,β)^{31}P transmutation doping and electrical characterisation 78—10071
- ^{31}Si, radioactive marker in thin film silicide form. 77—62681
- Si(100) 1×1 surface, interacting with H monolayer, electronic props., self-consistent calc. 77—43690
- Si(100) (1×1)H surface structure, LEED meas. 78—14602
- Si(100) inversion and accumulation layers, effective mass and collision time of electrons, oscillatory magnetoconductance 78—34909
- Si(100), inversion layer, interaction induced transition at low density 80—15581
- Si(100) inversion layers, effects of uniaxial stress on cyclotron reson. 80—20322
- Si(100) inversion layers, magnetoelec. and piezoresist. evidence for mobility domains 77—4447
- Si(100) inversion layers, two-dimensional electron fluid, spin density, valley density waves 77—69400
- n-Si(100) inversion layers on sapphire, surface quantum oscills. 78—19158
- Si(100) surface, temp. depend. of electron intersubband reson. 78—14783
- Si(100)-SiO$_2$ interface, mobility in Si inversion layers, screening and neutral impurity effects 79—28412
- Si(111) 7×7, surface struct., LEED, theory and expt. 77—85033
- Si(111) 7×7 surface struct., LEED seventh order diffr. beams interpretation 77—62716
- Si(111), chemisorption of H, formation of monohydride and trihydride phases 79—15004
- Si(111), conduction-band surface resonance 78—52051
- Si(111), dangling-bond surface states 78—43452
- Si(111), high resolution photoemission yield, surface states 77—69392
- Si(111) ideal and relaxed surface, electronic struct. 79—60901
- Si(111), ion-bombard., O$_2$ adsorption, SIMS study 80—70522
- Si(111) reconstructed 7×7 surface superlattices, microdomain model 80—107625
- Si(111) surface, interpretation of intrinsic surface states 78—6423
- Si(111), surface electronic struct., atomic geometry effects, photoemission and electron energy loss spectra 77—85283
- p-Si(111) surface inversion layer, Cs covered, negative magnetoresist. in 2D impurity band 78—64135
- Si(111):Pb ion implanted amorphous layers, recrystallisation, impurity out-diffusion model *(Chinese)* 80—88363
- Si(111)/Pt/Ni Schottky diodes, current-voltage characts. and comp. profiles 80—84508
- Si(111)-(7×7), and impurity stabilised Si(111)-(1×1) surface, photoemission studies 80—104041
- Si(111)-$\sqrt{3}\times\sqrt{3}$-Ag structure, atomic arrangement, low energy ion scatt. spectroscopy 80—96724
- Si(111)2×1, oxide layer, surface states detec., optical reflectivity obs. 80—50368
- Si(111)2×1, surface electron states detected by external reflectivity 78—80036
- Si(111)(7×7) surface models, LEED anal. 80—75418
- Si; Ar ion bombarded, projectile energy depend. and line shape of Ar-L AEs 80—16139
- Si;O, effect of displacement upon impurity levels, pseudopotential calc. 77—39803
- Si{001}2×1 reconstructed surface, atomic struct., LEED intensity analysis 77—28068
- Si⟨111⟩/Al/Si, growth kinetics of ⟨111⟩ Si through Al layer by solid phase epitaxy 79—28236
- Sn, α- and β-phases, isomer shift in Mossbauer spectra of implanted ^{129}I 78—15067
- α-Sn, band structure of diamond like crystals, cluster-Bethe lattice model calc. 80—6713
- α-Sn, dielectric polarisation calcs., microscopic local fields 80—20582
- α-Sn, dimensions of muonium atoms, depolarisation of positive muons 79—11374
- α-Sn, electronic energy bands of diamond-type crysts., appl. of EHT method 78—87907
- α-Sn, gapless semicond., effect of nonlocal pot. on hole energy spectrum in mag. field 78—39017
- α-Sn, gapless semicond., sound propag., RPA calc. 77—31721
- α-Sn, implanted with Sn, Sb or Te, impurity-defect structs., Mossbauer expts. 80—39129
- α-Sn, lattice stability, pseudopotential theory and problem of covalent bonding 77—55490
- α-Sn, optical surface modes calc. 77—59200
- α-Sn, reson. first and second order Raman scatt. 78—35144
- α-Sn, zero-gap props. correlated to Γ_8 symmetry, review 80—6717
- SnO$_2$-Si solar cells, electron-beam deposited, struct., photovolt. props. 80—50956
- substrate, thin film of Ag or Al, work function Si *(French)* 80—80353
- T-metal, thin film contact, time evolution of photovoltaic effect 80—65687
- Te (10$\bar{1}$0) and (0001), direction effects in double beam photoemission 79—74059
- Te (1$\bar{1}$00) surface, electron-hole cyclotron resonance freq. depend. 79—69724

elemental semiconductors continued
- Te, a-edge dislocated crystals, mobility anisotropy 80—107781
- Te acousto-optic modulator, props., for IR laser beam control *(Russian)* 77—72073
- Te, acousto-optic props. at 10.6 μm 79—91401
- Te, acousto-optical props. at wavelength of 10.6 μm 80—76001
- Te, acoustoelec. domain induced transparency at 11 μm 78—27182
- Te, acoustoelectric current flow, acoustic refraction effect 79—19637
- Te, acoustoelectric domain induced transparency near 11 micron 77—85727
- Te, acoustoelectric instability of current, mag. field influence 79—73547
- Te, adsorption on single cryst. faces of Mo and W field emitters 78—34714
- Te, adsorption on W and Mo field emitters 77—69177
- Te, adsorption on Zn (0001), UPS investigation 79—91563
- Te, amorphous, electronic struct. and optical props., pseudopot. calc. 80—65428
- Te, amorphous, localised gap states, variable range hopping 77—72866
- Te, amorphous, obtained by splat cooling crystallisation 77—65949
- Te, amorphous, Rayleigh scatt. of Mossbauer radn., lattice dynamics 80—15845
- Te amorphous and liquid state, Raman spectra, crystn. processes 80—60608
- Te, amorphous film, vac. deposited, phonon-assisted hopping cond. 80—2392
- Te and Se, homology of phonons, scaling formalism for phonon freqs. 80—54326
- Te, anisotropic thermal motion of atoms, X-ray exam. 78—18730
- Te, band struct., laser-modulated photoemission expts. 77—28686
- Te, breakdown in high microwave impulse field, by impact ionisation 77—62957
- Te, carrier density nonlinearity of interacting acoustic fluxes 77—51781
- Te, carrier mobility, free, associated with dislocation strain fields 77—51738
- Te, circular photogalvanic effect in optically active crystal 79—73542
- Te coating of PbTe surfaces, struct. and junction characts. 80—50743
- Te, Compton profile, charge and momentum density 80—55220
- Te conduction band parameters, interband magnetoabsorption meas. in Faraday configuration 77—89695
- Te crystal, photo-EMF obs., depend. on sign of circular polarisation of light *(Russian)* 78—80025
- Te, crystallisation in constant electric field, thermoelectric parameters 77—44146
- Te, cyclotron reson. in pulsed high mag. fields, cond. band struct. 80—59867
- Te cyclotron resonance, transport and surface phenomena 77—40132
- Te, Czochralski growth of single crystals 79—4912
- Te, deformed and annealed cryst., elec. props., directional depend. 79—7847
- Te detector for CO_2 pulsed laser radiation, using photon drag and optical rectification 78—21216
- Te, dielectric function in trigonal phase, model calc., local-field corrections 78—39045
- Te, diffusion and cond. props., NMR investigation 79—78547
- Te, dislocations influence on galvanomag. props. 80—54722
- Te double-beam photoemission, electronic structure 77—66576
- Te, elastic and piezoelec. consts., US phase vel. meas. 79—86834
- Te, elec. cond., 0-500 kbar 79—99589
- Te, elec. props. anisotropy, influence of deform. and annealing 77—15859
- Te, electron irrad., mobility increase due to defect prod. 80—24501
- Te, electron irradiated, dose-depend. and recovery behaviour of transport props. 78—71761
- Te, electron mobility, elec. field depend., 77K 77—85233
- Te, electronic struct. of cryst. phases and hydrostatic press. effects 80—59865
- Te, energy gap, laser emission study of press. depend. 79—82521
- Te, energy gap meas. under press., photocond. and transmission spectra 77—85267
- Te, evaporated deposition, absorptivity and emissivity 80—25473
- Te, evaporated film epitaxial and amorphous-crystalline phase transition growth and struct. 79—51449
- Te evaporated film nucleation on Au oriented islands, Hall mobility meas. 78—2388
- Te facet coating, for side lobe suppression in far field of AlGaAs DH stripe laser 80—5744
- Te, Faraday-type microwave Kerr effect 79—23998
- Te, film, AES, LEED, XPS, energy loss spectra studies oxidation effects 78—73086
- Te film, annealing effect on elec. cond. and Hall effect 77—8213
- Te film, atm. comp. influence on elec. surface props. 78—26980
- Te film, deposition on Cu substrate by electrolytic method 77—48355
- Te film, elec. props. effect of deposition rate 78—14844
- Te film, electrodeposition on Sn in Sn/Te/electrolyte system, interface processes 77—63923
- Te, film, electronic struct. charge on ordering, double beam photoemission 78—19634
- Te film, evaporated, crystallinity and electronic props., annealing effect 77—85107
- Te film, evaporated, predeposited Ag, Sn, Bi, Al and Se nucleation centres effect on grain growth 77—4739
- Te film, field effect meas. 77—43757
- Te film, gas-evaporated, selective absorpt. characts. and emissivity 80—50998
- Te film, Hall consts., thickness depend. of mobility 79—87171
- Te film, interference enhanced Raman scatt. 80—42273
- Te film, on electron irrad. KBr, epitaxial growth and surface coverage 80—10825
- Te film, on TGS substrate, ferroelec. field effect 79—42675
- Te film, piezoresistance 79—95524
- Te film, polycryst., hole mobility, influence of tunnelling through barriers on grain boundaries 77—43748
- Te film, stability in moist air, rel. to information storage capability, atmospheric corrosion model 80—71774
- Te film, surface morphology depend. on vacuum deposition angle 80—103553
- Te film, thermally evaporated, elec. cond., Hall voltage and thermoelec. power 77—47913
- Te film, vacuum deposited, growth and morphology of crysts. 80—96766
- Te film and trilayer antireflection structure for optical recording 79—94329

elemental semiconductors continued
- Te film condensed on mica, struct. and electrophysical props. 80—39688
- Te film growth on KBr (111) on mica *(Japanese)* 78—79903
- Te films, elec. props., 77 to 450K, thermal width of band gap 79—51698
- Te, films, elect. and galvanomag. characts. 79—33365
- Te, galvano- and thermomagnetic effects 78—30939
- Te, galvanomagnetic props., surface layer effects reduced by etching 77—51769
- Te, growth of single crystals by Czochralski method 80—66423
- p-Te Hall effect meas. at high elec. fields 77—66175
- Te, hexagonal film vac.-evaporated at normal incidence, X-ray Fourier line shape anal. 79—99454
- Te, high efficiency SHF of 12.8 μm laser radiation 78—25923
- Te, high pressure metallic phase, cryst. struct. 80—49161
- Te, hole cyclotron reson. with B⊥c 78—10777
- Te, hole mobility anisotropy in edge dislocated cryst. 80—24936
- Te, hole susceptibility anisotropy, spin contrib. and total 77—85413
- Te, IR cyclotron reson. in field up to 200 T 77—52059
- Te, imperfect pure cryst., thermomag. effects, dislocation effects and Auth model 77—85248
- Te, impurity spectroscopy 80—65499
- Te in MIS structure, impurity photocond. 78—72203
- Te, induced acceptor levels and free-carrier mobility due to c̄-screw dislocations 77—89730
- Te, interband photocond. at up to 10 kbar, 1.6-200K 77—47850
- Te, intervalence band absorption, press. and defects influence 80—55149
- Te intrinsic, intermediate IR optical absorpt., 5-20 μm 78—84562
- Te, inversion layer, surface quantum levels, calc. from Shubnikov de Haas meas. and triangular surface pot. well 79—15207
- Te inversion layers, surface quantum oscillations 77—89777
- Te inversion layers, surface quantum transport 78—64088
- Te inversion layers in mag. fields 80—44690
- Te, isomer shift values of implanted ^{133}Xe/^{133}Cs, Mossbauer spectra 80—7240
- Te, laser induced EMF, photon drag, optical rectification and spurious signals 78—19083
- Te, lightly doped, galvanomagnetic props. in fields up to 140 kOe 78—91707
- Te, liq., elec. cond. at high temps. and press. 77—55592
- Te, liq., elec. resistivity meas. up to 30 kbar 79—38070
- Te, liq., estimate of self-diffusion coeffs. from viscosity data 77—55370
- Te, liq., semicond.-metal transition at high temp. and press. 77—51784
- Te, liq., US rel. temp. depend., melting effects 78—38782
- Te MIS structure, photosensitivity spectrum 78—14834
- Te, mag. inversion of Hall effect *(Russian)* 77—4376
- p-Te, magneto-impurity effect, review 79—91081
- Te, magnetoacoustic effect 77—62963
- Te, metallic state, press. induced, elec. cond. meas. 80—96949
- Te, NMR spectrum, electron paramagnetism and atomic self-diffusion mechanism 78—72426
- Te, natural optical activity and features of struct. of electronic energy spectrum 79—8110
- Te, negative photoconductivity, intraband absorpt. *(Russian)* 80—107854
- Te, opt. props. under high press., band struct. transform. 80—55112
- Te, optical activity, de Haas-van Alphen oscillations and cond. band parameters 80—54605
- Te, optical activity rel. to band struct., 4 to 300K 77—77165
- Te, optical bleaching near fundamental absorpt. edge at 80K 80—28287
- Te, optically active crystals, circular photogalvanic effect 80—54739
- Te, oriented films, semiconducting props., Hall coeff., band structure 80—70854
- Te, paramagnetic state (μ^+e^-) at high temp. 79—56676
- Te, photo-excited carriers, far IR magneto-spectroscopy 80—50343
- p-Te, photocond., 1.6-4.2K, spectral features 77—24591
- Te, photoconductivity in strong mag. fields, doping effects, impurity levels 80—75602
- Te, photoconductivity spectrum in 1.6-4.2K band, nonequilibrium electron mobility *(Russian)* 77—11960
- Te, photoconductivity under pulse excitation conditions 80—2425
- Te, photocurrent generated by polarised light, direction depend. on polarisation *(Russian)* 78—64065
- Te, photon drag effect 77—1443
- Te, photon drag effect theory 78—19084
- p-Te photon-drag detectors for CO_2 lasers 77—5911
- Te, photovoltaic effect in thin films, 10.6 μ, prep. methods 80—20252
- Te physics, conf., Konigstein, Germany (May 1979) 80—51958
- Te, piezo-Hall effect from 4.2 to 77K 77—76848
- Te, piezoelec. semicond., photoelasticity and acousto-optic diffr. 80—29715
- Te, piezoelectrical free-carrier scatt. by screw dislocations, Hall effect and cond. meas. 80—24926
- Te, pure and Sb doped, impurity state and impurity cond., press. effect 80—54723
- Te, radiation damage expts. review, defect interactions 77—84800
- Te, SHG, optical modulation 79—86212
- Te, SHG in cryst., IR irrad. *(German)* 79—50345
- Te, SHG of ps pulses 79—45995
- Te, SHG under two-photon reson. conditions 80—99803
- Te, screw dislocation substruct. studied by torsion expt. 79—10859
- Te, screw-dislocation-induced scatt. and acceptor states, galvanomag. and optical expts. 77—28142
- Te, self-defocusing of CO_2 laser radiation under phase matched SHG conditions 78—83043
- Te, single cryst. growth by hydrothermal method *(French)* 78—11096
- Te, single crysts., Czochralski growth, etch pit orientation study 79—43133
- Te, stimulated Brillouin scattering of CO_2 laser radiation 79—47469
- Te, strained and unstrained, SHG and propag. of CO_2 laser radiation 80—58641
- Te, surface cyclotron resonance, freq. depend. 78—64084
- Te, synthetic, optical props. in visible spectrum and microhardness meas. *(French)* 77—28590
- Te textured thin films, prep., high solar absorptivity by multiples refl. 80—11568
- Te, thin evaporated films, 130 Å, temp. depend. of elec. props. 79—95529
- Te thin film, thermoelec. EMF, Seebeck coeff., elec. cond. structural depend. 79—78230
- Te, thin film selective absorber coatings, prod. using an oblique vacuum deposition technique 80—81488

elemental semiconductors continued
p-Te, transverse and longit. Nernst-Ettingshausen effect, theory and expt. 78−76095
Te, trigonal, ^{129}I Mossbauer obs. at high press. 80−55005
Te, trigonal, dielec. matrix calcs. 80−54630
Te, trigonal, electronic and optical props., press. depend., self consistent pseudopotential formalism 79−65838
Te, trigonal, electronic struct., near metal transition, press. depend. 78−34758
Te, trigonal, model of lattice dynamics using long and short range interactions 78−59893
Te, trigonal, NMR chem. shift, tight-binding calc. 78−2759
Te, trigonal, Raman scatt. at very high press. 80−60566
Te, trigonal, self-consistent ground state, X_α calcs. 80−54604
Te, trigonal, state-of-the-art review of model calcs. 80−54327
Te, trigonal, surface lattice dynamics, mean square displacement spectra in long wavelength limit 80−54498
Te, trigonal and amorphous, electronic struct. and nonempirical calc. of struct. props. 80−59866
Te, trigonal semicond., electronic states, tight-binding model Hamiltonian 77−59250
Te, two types of carriers 80−60013
Te, undoped, elec. cond., magnetoresist. and Hall meas., hydrostatic press. effect 77−47830
Te, uniaxially stressed, cyclotron resonance 79−87319
Te, uniaxially stressed, submm. cyclotron reson., deform. pots. and k.p coeffs. 80−54606
Te, vacuum deposited film, effects of electron irradiation on surface coverage *(Japanese)* 79−82477
Te, valence band struct., hydrostatic press. effect 77−47724
Te, valence band struct. under press., spin-orbit splitting, intraband absorpt. spectra 80−2330
Te, valence-band X-ray emission spectrum 78−84682
Te, warm hole conductivity 78−72160
Te, weakly doped, impurity spectroscopy, magnetoresist. meas. under nonohmic conditions 78−30942
Te:Cu films, elec. transport props. 80−60120
Te:I, semicond., elec. efficiency *(German)* 78−84166
Te:Sb, 96 to 500K, cond. Hall const., hole mobility, conc., dislocation effects *(Russian)* 78−64039
Te:Sb, impurity states and impurity conduction, hydrostatic pressure 80−39521
Te:Sb, surface carrier effects on Hall mobility at low temp. 77−80794
Te:Ta, quadrupole interaction at ^{181}Ta, TDPAC meas. 80−20521
Te/Ag double films, interdiffusion and struct. modifications *(French)* 77−62682
Te-Ag thin film system, stress-relief appearance conditions 80−65416
Te-Au thin film interface, evolution, switching effects *(French)* 80−6660
Te-Bi multilayer thin film struct. thermoelec. props. 80−92964
Te-Bi thin film system, stress-relief appearance conditions 80−65416
Te-Se-Cd, sandwich structure, fabrication and characteristics 80−60089
Te-transition metal, liq. semicond., elec. props. 80−96870
YIG-Ge layered struct., anisotropy of EMF under nonlinear ferromag. reson. conditions 77−8417

elementary particle coupling constants
$\lambda\rho^4/N$ theory, vac. stability, quark confinement 77−82677
Adler-Weisberger relation and quark model 78−45849
Adler-Weisberger sum rule and the σ-commutator for the kaon-proton system 80−101956
Adler-Weisberger sum rule and the σ-commutator for the kaon-neutron system 80−101957
analytic pole extrapolations, accurate tests 78−24976
asymptotic catastrophe, temporary freedom in lepton and quark interactions 79−85253
asymptotic energy scale factors for pseudoscalar meson scatt. and charmed meson couplings 78−8620
asymptotically free gauge theory, higher-order effects for coupling const. 77−34095
baryon mesonic couplings and EM props. in SU(4) 77−22663
baryon resonance photocoupling anal. in relativistic quark model 78−66086
baryon resonance photocouplings, using mixed nucleon and even-wave harmonic oscillator theory of baryonic states 77−82752
baryon resonances and electromagnetic couplings 79−9384
baryons and baryonium, SU_6 symmetry, duality and unitarity 78−8622
bound triquark nucleon model, mag. moment and weak interaction coupling constant ratios 79−67517
C_V'/C_V and C_A'/C_A via ^{3}H β-polarisation 77−10369
channel coupling effects and resonance phenomena in pp interactions, N/D eqn. study 79−71765
charmed meson coupling, asymptotic scale factors 77−38202
charmed particles, masses and decay consts. in SU(4)×SU(4) broken chiral symmetry 79−40686
charmonium and asymptotic freedom in QCD 79−6327
charmonium states with small hyperfine splitting, coupling constants 79−97599
compilation of coupling constants and low-energy parameters 79−22159
conformal invariant Fermi weak interactions and weak bosons as collective modes 79−89094
conformal-invariant field theory, anomalous dimensions 80−4870
conformally invariant field theory, Wilson operators 77−41776
cosmology, role in elementary particle physics 80−27430
coupling constant singularities in QED 79−21991
coupling parameter trajectories 78−8519
deep inelastic muon hadron scatt. data, high energy, asymptotically free gauge theories predictions 77−49974
dyon-dyon interaction in predictive relativistic mechanics 79−26265
effective coupling parameters with stationary points for massless models, renormalisation group consistency 79−9292
effective Lagrangian in spontaneously broken gauge theories 79−17653
effective potential for spontaneously broken gauge theories and gauge hierarchies 80−18080
energy depend. in unified gauge field theories 77−22675
Euclidean massless spin 0, spin 1/2 electrodynamics, Fredholm determinant zeros 78−24988
f_π and g_ρ in lattice gauge theory 77−34126
Fermi superallowed decay, scalar coupling const. upper limit 77−57631
fermion pair with instantaneous interactions, relativistic bound-state equations 80−13200

elementary particle coupling constants continued
fine-struct.-const. calculated value, gravit. charge quantisation 77−26524
froissarton coupling constant, s-channel unitarity *(Russian)* 78−45799
$g\phi^4$ theory, strong coupling limit of Green functions, anharmonic oscillator appl. 78−78071
Gamow-Teller matrix elements of T=1/2 nuclei, axial-vector coupling const. renormalisation 77−74809
Glauber approach and the triple-pomeron coupling 80−68435
grand unified field theories, two-loop corrections to mixing angle and lifetime of proton 80−13249
Green's function calc. by coupling const. dispersion relations 77−45987
hadron dynamics, multiparticle prod., intermol. pot. in Feynman-Wilson gas 78−477
hadron matter, thermodynamic description, evolution, coupling const. depend., hot nucleon matter appl. *(Russian)* 79−3006
hadronic coupling constants and the nonrelativistic quark model with charmonium potential 80−37207
hadronic neutral current coupling constants, model independent determination 79−35996
hadronic neutral current struct. 78−24994
hadrons, existence of long-range forces, magnitude of coupling constants 80−13272
hard QCD processes, relations through mass singularity universality 79−22054
harmonic oscill. model, reson. total widths 77−38119
heavy quark and heavy lepton mass spectra similarity 79−67508
Higgs bosons in SU(2)×SU(2)×U(1) left-right gauge field, coupling strength 79−13017
hyperon+nucleon interactions, one boson exchange pot. approach, multichannel Schrodinger eqn. soln. 77−57556
isoscalar coupling constants, hadronic neutral current in neutrino interactions and single Z-boson hypothesis 79−54295
lattice gauge theories, effective actions 78−29239
leptonic diagonal coupling const. from neutrino data *(Russian)* 77−49950
light nuclei coupling constants from dispersion anal. of N and d scatt. amplitudes 78−29399
localised classical solution for fermions+scalar bosons in field theory, Yukawa coupling const. 78−24928
logarithmic QFT models, coupling constant nonanalyticity, UV anal. 77−49831
magntic moments and machinery of symmetry breaking 79−63477
mass dependence on QCD parameters 79−17675
massive U(1) Thirring model, S-matrix and dynamical supersymm. 77−67586
massless electrodynamics, vacuum instability, bare coupling constant Gell-Mann-Low eigenvalue condition 78−89643
matter couplings in supergravity theory 77−17895
meson-baryon interactions in u-, d-, c-quark sector 78−25011
mesons with heavy quark constituents, lifetime and branching fraction determ. 79−93404
multiquark baryons and the MIT bag model in SU(6), coupling const. and decay modes 79−97600
narrow resonances, dynamical model, mass mixing and splitting in degenerate multiplet states 78−93813
neutral current processes, factorisation and coupling constant determ. for νe, ed, and ν+hadron 80−27451
nucleon-vector meson coupling consts. 77−2837
O(3) σ-model, nonlinear, quantum fluctuations of instanton solns. *(Russian)* 78−74161
one boson exchange model, OZI rule, nucleon-nucleon-boson coupling 80−32066
OZI relations for SU(4) coupling constants with applications to tensor mesons 79−80793
parity nonconservation, coupling constants, intermediate boson mass ratio 79−9516
parity violating vector meson-pseudoscalar meson interaction, relativistic quark model 77−54102
perturbation theory at large order, choice of integration contour 79−6263
perturbative reggeon calculus, transverse correls., multiparticle prod. 77−2879
phase volumes of 3,4,5 particles, approx. formulae *(Russian)* 78−446
phenomenological analysis of single pion photoproduction in the first resonance region 78−89721
pion photoproduction, weak interaction induced parity violating assymetries 79−71758
pion-charmed baryon scatt. and coupling strengths, superconvergence sum rules 80−52532
pion-nucleus coupling constants, deduction using PCAC 79−40855
Pomeron coupling diag. to order 1/N 80−47263
pomeron-quark relative coupling strengths 77−65145
proton deep structure, renormalisation group approach, review 79−85302
pseudoscalar transition between spin-J and spin 5/2 baryon 78−50032
QCD, coupling strengths and renormalisation scale parameter, by dimens. transmutation 79−6316
QCD, infrared behaviour of effective coupling 80−42393
QCD coupling const., renormalisation prescription depend. 80−4954
QCD observables in higher order calcs. 79−9334
QCD perturbation expansions in coupling const. renormalisation by momentum space subtraction 79−63416
QCD $q\bar{q}$ running coupling constant, β-function from string model, Pade approx. 79−343
QCD running coupling const., nonperturbative determ., N struct. functions 79−75726
quark conservation at meson vertices, Zweig rule model for couplings, multiRegge phenomenology 77−82709
quark jets in e^+e^- annihilation, forward-backward asymmetries 79−97605
quark mass, electroweak contrib. 80−101990
quark-gluon, perturbation theory appl. to $e^+e^- \rightarrow$hadrons 77−38127
quark-gluon, renormalisation, unified gauge theories containing Pati-Salam model 77−6072
quarkonia from charmonium and renormalization group equations 79−22055
Racah algebra of Gln, generalised back coupling rules 80−47208
radiation gauge static pot. between fermion and antifermion, non Abelian gauge fields 78−89621
Regge pole model, NN pots., one boson exchange, coupling consts. masses 78−70346
reggeon and photon coupling relns. 79−13063

elementary particle coupling constants continued
relations between coupling consts. 80−353
renormalisability of superconductivity models, nonlinear spinor models, fermions, collective bosonic states 77−18179
renormalisation in unitary and renormalisation gauges 77−41763
semilocal duality constraints for mesons, on-shell particles, masses, couplings 78−58174
sine-Gordon model for large coupling consts., soliton scatt. matrix *(Russian)* 80−13221
SO_{11} group for interaction unification, charge and coupling constants 79−2965
soft spin 3/2 massless fermions, gravity, supersymm. 77−49869
spontaneous generation of renormalisation invariant mass in IR stable theories 78−86411
strong coupling constants in broken SU(3) 80−27423
strong gravity const. determ. from pion mass difference 77−22715
strong gravity equations, spin and torsion effects, rel. to spin of Universe 79−97116
$SU_3 \times U(1)$ gauge models and neutral current reacts. 78−89648
SU_3 couplings at scalar mesons to two pseudoscalars, S* to $\pi\pi$ and ε to $K\bar{K}$ 80−22580
$SU(2)_L \otimes SU(2)_R \otimes U(1)$ gauge models confronting neutral current data 79−22013
$SU(2) \times U(1) \times SU_F(2)$ gauge symmetry, CP violation, neutron elec. dipole moment, muon number changing process 79−89091
SU(3) theory of Yang-Mills-Higgs fermion-monopole system, topologically stable soln. 77−13888
$SU(4)_W$ symmetry, dibaryon coupling constants for γ, π and baryon interactions *(Russian)* 80−13329
SU(4), symmetry breaking effects on strong coupling const., charmed and uncharmed $\bar{B}$ BP couplings calc. 80−105802
SU(6) grand unification model, hierarchy of symmetry breakings and neutral currents 80−52446
superposed Yukawa and inverse square potentials, eigenenergy expansion 79−30281
symmetry dynamics and invariant coupling const. behaviour *(Russian)* 77−34096
Thirring model, symm., anomalous dimens. and Schwinger term 77−87900
unitarity effect of $\psi'(3684)$ on shape of $\psi''(3772)$ 79−434
vector meson-nucleon interaction, SU(3) symm., coupling consts., form factors 77−13886
vector-tensor-Pomeron couplings, nonet mass formulas 77−49883
weak axial coupling constants in nuclei, polarizability, pionic field, PCAC 77−6055
weak neutral couplings to hadrons in neutrino inclusive, semi-inclusive and elastic reactions 79−36064
weak neutral current coupling const. from νN single pion prod. data anal. 77−13911
Weinberg sum rules, derivation of meson spectrum, duality unification with chiral symm. 78−29272
Yang-Mills theory, large order calcs. 78−8511
A_1, spectral function sum rules and A_1-W coupling const. 80−27429
β decay of closed shell ± one nucleon nuclei, axial vector coupling const. quenching 78−89824
χ_c radiative decay, ψ and ψ' prod., straton coupling constants *(Chinese)* 80−42467
d(d*)N coupling constants via spectator functions 78−46011
Δ_{33} energy region, electroproduction, simple-pole model, $\gamma \mathcal{N} \Delta_{33}$ vertex 80−22625
e:μ mass ratio, EM coupling const., flux quantization model 77−79240
e^+e^-, electron type heavy neutral lepton prod., cross section and coupling const. 80−52485
e^+e^- annihilation and deep inelastic scatt., VDM approach, vector meson+photon coupling 77−46068
$e^+e^- \rightarrow b\bar{b}$, single lepton spectra, coupling strengths 79−49461
$e^+e^- \rightarrow$hadron jets, 30 GeV, strong coupling constant and QCD test 80−37283
$e^+e^- \rightarrow$hadrons, 12, 30 GeV, jets, quark fragmentation and coupling constant, QCD comparison 80−105915
$e^+e^- \rightarrow$hadrons, asymptotically free quark model predictions in complex plane 77−71522
$e^+e^- \rightarrow$hadrons, energy correls. in QCD, asymptotically free perturbation theory 79−63497
$e^+e^- \rightarrow$heavy leptons, coupling of heavy leptons to W^0 anal. 78−33051
e^+e^- high energy data from PETRA, QCD anal., QCD coupling constants 80−82985
$e^+e^- \rightarrow$multihadrons, planar three jet events, gluon bremsstrahlung, strong coupling constant 80−57617
$e^+e^- \rightarrow \pi^+\pi^-\pi^0$, 750-1100 MeV, ω and ϕ meson interference 80−105910
$e^+e^- \rightarrow t\bar{t}$, single lepton spectra, coupling strengths 79−49461
η decays of ψ's, VMD and colour model coupling const. calcs. 77−26516
η-$c\bar{c}$, η'-$c\bar{c}$ couplings from $\psi \rightarrow \eta'\gamma$, $\psi' \rightarrow \eta\gamma$ *(Russian)* 77−49962
$\eta' \rightarrow \pi\pi\eta$, $\delta\eta'\pi$ and $\delta\eta\pi$ coupling constant ratio, $\delta(980)$ quark content 80−82955
ηNN to πNN ratio, in π^-p interactions at 9 and 12 GeV/c 79−45100
f, multiparticle production in multiperipheral resonance model complemented by duality 79−36050
γp, 46-180 GeV, ω-meson photoprod. cross section, $\omega\gamma$ coupling constant 80−13319
γp, low energy scatt., one-particle exchange model 80−22617
$K^* \rightarrow K\pi\pi$ decay rate, vector meson couplings 77−30373
KN coupling const. from kaon-nucleus forward scatt. amplitudes 79−85418
KN from $^{12}C(K^\pm,K^\pm)$ scatt. amplitudes 80−32304
$\bar{K}$N reaction below 1.9 GeV, dispersion theoretic discrepancy anal., SU(3), hadron coupling 78−21457
$\bar{K}N\Lambda(1405)$, coupling const. anal. from K^-d interactions 78−8689
$\bar{K}N\Sigma(1197)$, coupling const. anal. from K^-d interactions 78−8689
$\bar{K}N\Sigma(1385)$, coupling const. anal. from K^-d interactions 78−8689
$K^-p \rightarrow \Lambda\eta$, 6 GeV/c, baryon exchange reactions, ηNN coupling constant, Λ polarisation, nucleon-Regge exchange 80−78098
$K^-p \rightarrow \Lambda\pi^0$, 6 GeV/c, baryon exchange reactions, ηNN coupling constant, Λ polarisation, nucleon-Regge exchange 80−78098
$K^\pm$p forward scatt. amplitudes, dispersion anal., effective KNY coupling constant 80−22636
$K^\pm$p scatt., $KN\Lambda$ and $KN\Sigma$ coupling constant constraints 80−32128
$\Lambda \rightarrow pe^-\bar{\nu}_e$, $|g_A/g_V|$ calc. in quark model, 56-70 octet mixing 79−389
$\mu \rightarrow e\gamma$, $\mu \rightarrow 3e$, rare decays, natural lepton models, doubly charged leptons 77−34143
μ-N, axial const. from ^2H and ^1H muon capture *(Russian)* 77−50570

elementary particle coupling constants continued
μ^+ lifetime, weak coupling const., meas. by Saclay linac beam *(French)* 79−368
$\mu^- + (A,Z) \rightarrow e^- + (A,Z)$, Z-dependence of coherent μe conversion rate in anomalous neutrinoless muon capture 80−13419
μN, deep inelastic struct. function, Nachtmann moments in QCD 80−27510
$N + \nu \rightarrow M^0$, heavy lepton prod. and decay mechanisms cross section and coupling constant *(Russian)* 79−9365
NN forward scatt., two and three pion cut contribs., nucleon exchange model 80−63103
NN interaction, coupling const. singular points for approx. Bethe-Salpeter eqns. with a nonlocal pseudopotential 78−25062
NN nonrelativistic 1-boson exchange potentials based on generalised meson field theory 78−70459
NN scattering, effective interaction in the Blankenbecler-Sugar equation in ϕ^3 theory 79−21914
NN weak coupling constant magnitude, anal. of ^{41}K data, CVC hypothesis *(Russian)* 77−6144
$\nu_\mu(\bar{\nu}_\mu)p$, 2 GeV elastic scatt., charged current/neutral current event ratio 80−57582
$\nu n \rightarrow \nu p\pi^-$, threshold pion prod., photon-neutrino weak coupling theory 77−67642
$\nu N \rightarrow X$, determ. of all neutral-current coupling constants from inclusive cross sections alone 79−13106
$\nu\nu$ effective coupling constant upper limit from high energy beam data *(Russian)* 78−89706
νP, neutral to charged current cross section ratio, coupling constant 80−27497
$pp \rightarrow \pi^+(K^+)X$, particle exchanges, coupling consts. *(Russian)* 77−50035
$p^0p\bar{p}$, const. determ. from anal. of pp elastic scatt. from 150-515 MeV 78−70396
π N forward scattering amplitudes high energy, integral axiomatic upper bounds for coupling const., logarithmic sensitivity *(Russian)* 77−13984
π nuclear coupling const., review 78−89835
π-^{3}He-^{3}H const., determ. from threshold π photoprod. and radiative π capture on ^{3}He 79−40962
π^3He^3He coupling constant determ. from $^3H(p,n)^3He$ differential cross section 78−89801
π^3He^3He coupling on basic of PCAC 80−32196
πN, pseudoscalar and pseudovector coupling to bound Dirac nucleon 78−25073
πN coupling, induced pseudoscalar nucleon form factor *(Russian)* 79−9375
πN coupling const. determ. in MIT bag model 78−78149
πN coupling constant determ. using forward dispersion relations 79−45098
πN coupling constant from simultaneous anal. of all invariant amplitudes using rational series 78−58199
πN low energy partial wave anal., cross sections, Δ^0 and Δ^{++} 80−52531
πN low energy scattering, one particle exchange model, spin 3/2 particle 78−4873
πN renormalised coupling const., NN semi-phenomenological model *(French)* 77−18311
πN scattering off-mass shell model, calc. of finite-energy sum rules 79−63517
$\pi\pi$, bounds as function of D-wave scatt. length 77−2866
$\pi\pi N\bar{N}$ partial-wave amplitudes, interior dispersion relations 77−82758
ψ and ψ' (3684) hadronic production, charmed straton content of straton sea *(Chinese)* 79−63434
ψ particles, off-mass-shell coupling consts. and radiative decays in VDM 78−70371
Q decay amplitudes, partial widths, Lorentz and SU(3) invariant coupling constants 79−26328
ρ^0, multiparticle production in multiperipheral resonance model complemented by duality 79−36050
$\rho KK/\rho\pi\pi$ ratio from $\pi^-p \rightarrow K\ \ K^+n$ and $\pi^+n \rightarrow K^-K^+p$ 6 GeV/c 77−79279
$\Sigma^- \rightarrow ne^-\bar{\nu}_e$ $|g_A/g_V|$ calc. in quark model, 56-70 octet mixing 79−389
$\Sigma p \rightarrow \Lambda X$, particle exchanges, coupling consts. *(Russian)* 77−50035
$\tau \rightarrow \nu_\tau e\nu_e$, nature of τ-ν_τ-W coupling, ν_τ mass upper limit and lifetime 79−40824
Υ states with small hyperfine splitting, coupling constants 79−97599
Y_0^* (1405) couplings, K-matrix parametrizations in $\bar{K}N$ and $\pi\Sigma$ two channel systems 78−21452
Z^0, prod. in e^+e^- collisions, important landmark 79−97567
$^{12}C(\mu^-,\nu_\mu)^{12}B$, Hartree Fock wavefunction, correlations, pseudoscalar coupling constant, capture rates, recoil nuclear polarisation 80−22774
H, parity mixing of atomic states, spin-depend. weak interaction coupling const. 78−8572
S*-δ^0 scalar meson mixing as threshold phenomenon from coupling constants 80−27477

elementary particle decay
see also electromagnetic decays; elementary particle coupling constants; hadron decay; leptonic decays; muon decay; nonleptonic decays; semileptonic decays
c(b)(t)-flavoured hadrons branching ratios and lifetimes six quark model, quark mixing angle bounds 79−71686
charmed particles, decay of short-lived particles in photoemulsion irradiated with 400 GeV/c protons *(Russian)* 79−3022
charmed particles weak decays, generalised charge symm. 78−37184
charmonium and QCD, review 78−82157
compound system, form factor behaviour on approach to asymptotically high transferred momenta *(Russian)* 77−67655
covariant polarisation density matrix analysis *(Russian)* 78−454
explosive cascade-decays of leptons. quarks, virtual photons, weak vector bosons and Higgs scalars 80−86641
exponential decay law, corrections 77−67639
flavor unification, τ decay, and b decay within the six-quark-six-lepton Weinberg-Salam model 79−35990
geometrical approach to elementary particles 80−105865
hadron production, quark fragmentation and triple Regge models, quark decay functions 80−62921
heavy lepton cascade, lifetime and branching ratios 78−33108
heavy neutral lepton radiative decay, mechanisms for supernova shell explosion *(Russian)* 79−8934
heavy quark infrared safe weak decay, dimensional regularisation techniques, gluonic corrections 80−102087

elementary particle decay continued
intermediate vector boson decay, QED and QCD radiative corrections, hadronic jets 80—73759
lepton→hadrons, coherent and inclusive, due to lepton-nucleus collisions 80—83100
lepton-quark system, quantum number laws, classification of weakly interacting particles, decays 78—82138
lifetimes, dependence of measured values on apparatus 79—22158
moment and Fokker-Planck eqns. 80—82709
n-particle decay of dual resonance, decay width, multiplicity distrib., multipion channels 78—16997
neutral weak interactions and particle decays 77—13954
nondegenerate decay system, anal. 78—447
Okubo-Zweig-Iizuka rule near new thresholds 77—2767
open systems theory, appl. to unstable particles 79—17281
particle decay in six-dimensional relativity 80—27121
phase volumes of 3,4,5 particles, approx. formulae *(Russian)* 78—446
polarisation meas. 77—22721
proton half life, Dirac approach to large number coincidences 80—27501
quantised particle lifetimes, reln. to hypothesis of quantised time 77—38106
quantum theory test using Bell-type inequality for nondicotomic observables 78—36865
quark decay function without phenomenological input 80—47247
Summer School, high energy physics, Rutherford Laboratory, England (6 to 24 September 1976) 77—41747
three particle decay, two body resonance approx., Veneziano amplitude expansion 78—82174
topological cross sections in multiplicity asymptotics, Hagedorn model *(Russian)* 80—9154
unstable particle decay, Trieste theory, rigorous inequalities 78—93869
unstable quantum states, time evolution, resolution of Zeno's paradox 78—8560
$b \to dl^+l^-$, neutral current decays, branching ratio 79—36010
$b \to sl^+l^-$, neutral current decays, branching ratios 79—36010
$B_N{}^+$-$B_N{}^0_1$ mass splitting, decay widths 79—17691
$e^+e^- \to \tau^+\tau^-$, 3.9-5 GeV, τ lifetime experimental upper limit 79—40826
$N+\nu \to M^0$, heavy lepton prod. and decay mechanisms cross section and coupling constant *(Russian)* 79—9365
ν radiative decay lifetime limits 78—448
ν with finite rest mass, radiative lifetimes 79—63568
$\nu_\mu(\bar{\nu}_\mu)N$, heavy lepton prod. and decay, differential cross sections *(Russian)* 80—105940
ν_τ, mass, lifetime, decay modes and mixing angles 80—445
$\tau \to 3\pi\nu$ decay, current algebra calcs. 79—30764
τ decay involving hadronic vector current 78—66101
$\tau \to K^*\pi\nu$, in e^+e^- annihilation, T-odd asymmetry in CP violation model *(Russian)* 80—105885
$\tau \to \mu\mu e$, flavour changing neutral current search 80—105836
$\tau \to \nu_\tau e\nu_e$, nature of τ-ν_τ-W coupling, ν_τ mass upper limit and lifetime 79—40824
$\tau \to \nu_\tau n\pi$, T-violation effects, neutrino mass *(Russian)* 80—95294
$\tau \to \nu_\tau\pi$, suppression by spin of ν_τ 78—21410
$\tau \to \nu\pi\pi$, π invariant mass distrib. predictions, hadronic decay rates 78—70352
$\tau \to \nu\rho^0\pi$, spin parity anal. 80—105941
$\tau \to \pi\nu$, decay observation, branching ratio 78—89766
$\tau \to \pi\pi\pi\pi$, π invariant mass distrib. predictions, hadronic decay rates 78—70352
τ semihadronic decay rate and branching ratio, QCD calc. 79—36119
τ^-, decays, SPEAR, Mark II detectors, recent results 80—74045
$Z \to H\gamma$, decay rate determ. in $SU(2) \times U(1)$ gauge theory 79—40717
τ decay as QCD test 80—102006

elementary particle electromagnetic interactions
see also Weinberg model
axion properties, strong T and P conservation enforcement 79—67481
bagged complex scalar field, EM interaction, fine struct. const., possible dynamic origin 80—86635
baryon resonance photocoupling, signs 79—22094
baryon resonance photocoupling anal. in relativistic quark model 78—66086
bremsstrahlung study, Rochester cross section, soft-photon region 78—62401
bubble chamber, electromagnetic shower photographs, for teachers 78—65737
Cargese lectures in physics, book 78—82130
charged particle, soft photon contrib. to Green's function, IR asymptotics, gauge transform. *(Russian)* 77—57438
charm $m(D^+)-m(D^0)$ calc., EM effects 77—2833
charmed, baryon spectrum due to chromomagnetic and electromagnetic hyperfine interaction 79—13123
charmed meson mass spectra, effect of EM interactions 80—47293
compilation of coupling constants and low-energy parameters 79—22159
cosmic ray muons and muon pairs, EM interactions, 5-1200 GeV *(Russian)* 78—73598
Coulomb-interference problem at SPS and ISR energies, operator formulation 77—54107
current algebra and electromagnetic hadron interactions, review, book contrib. 80—47240
current status in elementary particle physics 79—40651
De Rham currents, field and mag. monopoles extended singularities 78—4810
deep inelastic scatt., covariant parton model, Feynman integrals of perturbation theory 78—82221
dual electromagnetism and neutral-current interactions 79—71678
dynamical symmetry breakings in quantum chromodynamics *(Chinese)* 79—22050
eight-dimensional unified theory of weak, EM and gravit. interactions 77—37797
electro-weak interactions concept and Weinberg-Salem model verification *(Czech)* 80—22549
electron, photon and mag. monopole interactions, quantized theory 79—13004
electron- and muon-number nonconservation, new interaction 77—65128
electron-electron (muon) scatt., weak lepton interaction influence *(Russian)* 79—6333
electron-photon beams from proton accelerators, EM interaction investigation *(Russian)* 80—106214
elementary particle symmetries, axiomatic approach 79—21897

elementary particle electromagnetic interactions continued
EM cascade eqns., numerical integration, results for air, Cu, Pb and Fe 78—20602
EM pot. between nucleons 79—93524
EM shift of energy levels due to confinement, bag model 80—13287
EM-weak interference effects, LEP studies 79—97614
Feynman diagram amplitudes in cross section calcs., computer code 79—13094
fine-struct.-const. calculated value, gravit. charge quantisation 77—26524
form factor predictions and Melosh transformations 77—54105
fundamental interactions, review for teachers 78—16615
fundamental length hypothesis in a gauge theory context 80—9101
gauge formulation, $SU_\tau(2)$ internal symmetry and P- and CP-violation *(Russian)* 80—42368
gauge group theory of combined gravitational and e.m. interaction 77—80
gauge invariance, Lorentz covariance and EM props. of elementary systems 80—32037
gauge model of weak and EM interactions with SU(3)xU(1) symm. *(Russian)* 77—6074
gauge scheme of weak and electromagnetic interactions, review *(Russian)* 79—26278
hadron EM interactions, book 80—46748
hadron EM interactions, book 80—46749
hadron EM interactions, review 80—412
hadron-hadron collisions, electromagnetic pair prod., equivalent-photon method *(Russian)* 79—26353
hadronic EM current, short distance scaling, R(s) behaviour as $s \to \infty$ 79—22095
hidden gauge symmetry, appl. to elementary particle fundamental interactions 79—30658
Higgs boson couplings, charged, K_L-K_S mass differences 80—62917
Higgs bosons in gauge models with right-handed charge currents 77—49892
Higgs-Kibble mechanism and electron-muon mass ratio 78—66065
High energy behaviour of weak interactions and renormalisable theories, book contrib. 78—78164
high energy weak and EM interactions [conf. Les Houches, France (July 1976)] 79—80785
inelastic nucleon form factors, spectral representation *(Russian)* 78—37212
lepton direct production in hadron-hadron collisions, interaction models review 77—236
leptons, EM characts. and CP disturbance in $SU(3) \times U(1)$ model *(Russian)* 78—29327
leptons and quarks, EM and weak interactions, flavour $SU_3 \times U_1$ gauge model 79—97554
lowest-order EM correction in point particle scatt. 77—87978
mass splittings in quark model 77—18285
Nambu-Jona-Lasinio type unified model for gravitational and EM forces 78—65850
(non)conservation of isospin, parity, charge conjugation, and time reversal invariance in intermediate energy phys. 79—80772
nonlinear EM effects induced by vacuum polarisation and gravitational interaction, a comparison 79—97544
nonrelativistic wave eqn., second order in time, EM interaction 79—80774
nuclear interactions, isoelastic processes, one-body density matrix formalism 77—18528
nuclear weak and EM interactions, P-violation in e-nucleus scatt. 77—71479
nuclei in weak and EM processes, elementary particle method approach, book contrib. 79—97663
nucleon magnetic moments and fine struct. const., upper bounds in terms of Compton scattering cross sections 77—2836
$O(4) \otimes U(1)$ gauge model for weak and EM interactions 79—71681
P-violating neutral currents in L-R symmetric gauge model 77—82698
parity conservation, connection with absence of magnetic monpoles 77—6044
particles and fields conference, Argonne, IL, USA (Oct. 1977) 78—78130
pion magnetic polarisability using guage and relativistic invariance 78—4861
pion photoproduction, weak interaction induced parity violating assymetries 79—71758
Poincare subsymmetry, associated invariant EM field *(French)* 77—61209
polarised beams and targets in high-energy interactions, conference 77—30470
QED, fine-structure constant, coupled Maxwell and Dirac eqns., lepton and quark-like solutions 80—62894
quark decay lifetimes in Pati-Salam model 77—79243
quark models and unified field theories, review 79—80805
quarks, mass of u and d quarks from weak and EM interaction model 80—13254
radiative corrections to parity violation in atoms in $SU(3) \times U(1)$ gauge theory 78—62402
relativistic harmonic oscillator model, hadron EM interactions and props. 80—37225
relativistic particle physics, book 80—41966
relativistic wave equations for particles of unique mass, constraints, minimal coupling 80—22526
scalar one-loop integrals, soft bremsstrahlung and radiative corrections 79—75682
six-quark model, for weak and EM interactions *(Russian)* 77—67658
SL(4), common symm. group of EM and gravit. interactions 77—34112
$SO(4) \times U(1)$ model of weak and electromagnetic interactions 79—13009
soft-photon emission effects and radiative corrections for electromagnetic processes at very high energies 79—71752
spectrum-generating SU(3) and local current algebra 80—9128
spontaneous symmetry breaking with quaternionic scalar fields, $Sp(1,Q) \otimes U(1)$ group for unified gauge theory 77—61236
strangeness changing neutral currents, avoidance in gauge theories of weak and EM interactions 79—22005
strong-gravity contributions to the electromagnetic field of an elementary particle 79—36076
SU_2 gauge model, light neutral gauge boson, consequences for e^+e^- and $pp(\bar{p})$ 78—58154
SU_3 theorems, baryon octets, semileptonic decays 80—32030
$SU(2)_L \otimes SU(2)_R \otimes U(1)$ gauge models confronting neutral current data 79—22013

elementary particle electromagnetic interactions continued
SU(2)⊗U(1) gauge model of EM and weak interactions, fermion mass restriction *(Russian)* 78−89650
SU(3)×U(1)×U(1) symmetry, gauge model of weak and electromag. interactions *(Russian)* 78−45838
SU(3)×U(1) theory of weak-electromagnetic interaction with charged-boson mixing 79−35988
SU(3)⊗U(1) theory of weak and EM interactions 77−57481
supersymmetric gauge theories and their possible applications to the weak and electromagnetic interactions 79−49419
supersymmetric models of weak and electromagnetic interactions 79−26276
supersymmetric spontaneously broken theories of weak, EM and strong interactions 77−79244
supersymmetric vector-like model of lepton interaction 78−412
supersymmetry and gauge theories of weak and electromagnetic interactions 79−26208
tachyon + bradyon interactions, superluminal and subluminal EM fields 80−12902
theory of gravitation and electromagnetism from Bohm-Aharonov expt. 79−85028
$U_3(W)$-gauge unified EM-weak theory, neutral current neutrino interactions 77−26481
unified e.m.-weak Lagrangian in SU(2)×U(1) scheme *(Russian)* 77−218
unified model of weak and electromagnetic interactions based on the gauge group SU(3)×U(1) 79−22003
unified theories of weak and electromagnetic interactions 78−81908
V-A six lepton model, lepton no. conservation 77−87930
virtual phonon transmission of Coulomb forces 77−46049
virtual photon spectra, improved Weizsacker-Williams method of equivalent photons 79−40774
weak and EM phenomenology, gauge theoretical prospective, charm and flavour conservation 80−4916
weak hypercharge embedding in strong gauge groups 79−30692
weak neutral currents, status in weak and EM interactions 79−49444
Weizsacker-Williams method virtual photon spectra 79−36077
Yang-Mills theory appls., lectures given at CERN School of Physics (6-19 June 1976) 77−61173
D^+-D^0 mass difference, form factors, SU(4) coupling, vector meson dominance model 79−391
$e^+e^- \rightarrow 1^{++}$ resonance states, direct production through neutral currents 78−93891
e^+e^- annihilation, radiative corrections, review, book contrib. 80−47320
e^+e^- annihilation into boson resonance pair, multipole form factors, parametrisation of EM vertex *(Russian)* 77−74701
e^+e^- calorimetric experiments, γγ processes, tests of QCD 80−22628
$e^+e^- \rightarrow e^+e^-(\mu^+\mu^-)$ EM processes, vector resons. cross sections *(Russian)* 77−57517
$e^+e^- \rightarrow \tau^+\tau^- \rightarrow$cascade π and ρ, parity violation from weak and EM interaction interference *(Chinese)* 79−49504
eN, pion production, vector-like theories *(Russian)* 78−37221
eN deep inelastic scattering asymmetries, gauge theory predictions 79−22104
$e^-N \rightarrow e^-N\pi$, electromag. and weak process from weak neutral current interaction *(Russian)* 78−45928
ep deep inelastic scatt., many-photon exchange contrib. 80−9177
ep scatt., spin effects 80−42470
γ radiative decays, unified mechanism, form factors *(Chinese)* 77−57540
γγ collision, deep inelastic, helicity method 80−22606
γN Compton scatt., $\pi^0 \rightarrow 2\gamma$, $\eta^0 \rightarrow 2\gamma$ and N EM polarisabilities 77−18289
γp low energy scatt., one particle exchange model 78−33070
$K \rightarrow l\nu_e\gamma(l\nu_e l'^+l'^-)$ in review of weak-EM decays *(Russian)* 77−2818
Λ nucleus→Σ^0 nucleus, Σ^0 life time, Coulomb excitation method *(Russian)* 78−46114
λnγ(Z) vertex in vector-like model of weak and EM processes, appl. to K decay 77−6071
μ induced trimuon events, spin-parity selection rules 80−22603
μ-number non-conservation in gauge theories of weak interactions 77−74630
$\mu^+d \rightarrow \mu^+np$, ≤5 MeV, Coulomb break-up of deuteron and n-p off-shell effects 79−75777
μe universality breakdown of neutral weak currents in $SU_2 \times U_1$ gauge *(Russian)* 79−75712
μN scatt., deep-inelastic, EM production of trimuons 80−22619
NN electromag. interaction, one photon exchange helicity amplitudes 78−17040
NN interaction, EM phase shift calc. within relativistic model, isospin non-conservation 78−62438
np bremsstrahlung, effects of nonminimal currents and role of various couplings 78−70394
np bremsstrahlung, struct. depend. of interaction current 79−63510
ν, EM properties, weak neutral current and form factor *(Russian)* 77−61270
ν processes, weak current anomalous interaction with EM field *(Russian)* 77−6104
$\bar{\nu}$N charged-current interactions, semi-inclusive γ prod. 79−71737
p EM polarisabilities and $\gamma\gamma \rightarrow \pi\pi$ amplitude, dispersive approach 77−82743
pp, $\sqrt{s}=30.6$, 53.2 GeV, direct photon prod., γ/π^0 ratio 79−71771
$\bar{p}$p, heavy lepton prod. and decay, supersymmetrical model of weak and EM interactions *(Russian)* 80−86748
PP elastic scatt. at 20-750 MeV, EM effects 77−74707
pp→virtual gamma+hadrons soft bremsstrahlung, external emission dominance model 78−62430
$\pi \rightarrow l\nu_e\gamma(l\nu_e l'^+l'^-)$ in review of weak-EM decays *(Russian)* 77−2818
ψ mass spectra and radiative decay in light-quark model 77−18258
ρ-meson, EM form factor, elec. quadrupole and mag. dipole moments 78−12913
X(2.8)→2γ decay width, possible determ. by Coulomb photoprod. *(Chinese)* 77−57541
^{209}Bi, P violating eN pot., determ. of effects by optical rotation meas. 79−26277

elementary particle gravitational interactions
see also supergravity
affine gravity and strong interactions in SL(4,R) nonlinear representations 80−18108

elementary particle gravitational interactions continued
black holes of strong gravity, identification with elementary particles 78−16973
Borel multipliers for the Bondi-Metzner-Sachs group 80−18088
canonical quantisation of gauge fields, gravitational field *(Chinese)* 80−22266
charged particle self-interaction in black hole gravitational field 79−97275
classical pseudoparticle solutions in general relativity 78−89390
classical quark confinement from general relativity 78−58162
cosmological ν sea, EM wave propagation, torsionic background 80−77283
Dirac particle creation by gravit. fields 78−33021
Einstein relativistic particles, construction of quantal theories, appl. to two particle system 78−62347
Einstein-Cartan theory, rel. especially to elementary particle weak interactions 78−37171
equivalence principle, virtual quanta method as probe 78−36913
f-g fields, class relevant to quark confinement 80−125
f-g gravity theory, exact spherically symmetric solns. 79−319
fermion and boson fields interacting with gravitational fields 78−86208
fermion nonminimal gravit. coupling and solar neutrino problem 78−29294
fermion nonminimal gravitational coupling and the solar-neutrino problem 79−75761
fermions with gravitational interaction, press. 79−63138
Feynman diagrams, dimensionally regularised, symbolic evaluation, quantum gravity application 80−13259
Fierz-Pauli program for spin-2 fields in de Sitter space 79−21637
flat space as a gravitational instanton 79−17661
fundamental interactions, review for teachers 78−16615
gauge symmetry, max. 4-dimens., and general covariance, implications 79−63115
gauge theories and strong gravity 79−58869
general covariant group, nonlinear realisation, invariant theoretical consideration 79−35612
gravitational, electromagnetic, and nuclear theory 79−71677
gravitational charge of uniton-quark 79−63400
gravitational instantons and universal spin structs. 78−78128
gravitational interaction of spin-1/2 particles, Lorentz invariant theory 80−22257
gravitational theory of matter 79−21627
gravitationally induced CP effects, quantum gravidynamics, QCD quark sector 80−86616
gravitationally induced EM bremsstrahlung 78−24991
gravity and spin 1 gauge fields 79−21923
hadron gravitational interaction, band spinor representation of GL(n,R) 78−50000
internal rotations of spinning particles 79−22011
Kerr-like neutrino-gravitational solutions 80−95240
leptons and quarks, unification within conformal relativity 79−93343
Lorentzian gravity, appl. to hadron struct. and galaxy clusters 79−97288
massless scalar and EM field equations interacting with gravit. field, particle-like solns. 79−54290
MIT bag with de Sitter geometry 79−2988
MIT confinement scheme, geometrodynamical approach 78−89657
naked singularities, event horizons, and charged particles, test particle motion in Reissner-Nordstrom field 79−71684
Nambu-Jona-Lasinio type unified model for gravitational and EM forces 78−65850
neutron flux, gravitational interaction *(Russian)* 78−36901
Newtonian interaction between particles satisfying Dirac eqn., Einstein-Sciama force 78−32745
nonlinear EM effects induced by vacuum polarisation and gravitational interaction, a comparison 79−97544
normal flat space-time, embedding hadronic microuniverses 80−9135
particles in curved space-time, group of parallel transports 78−54602
PCAC, dimensional derivation of gravitational correction 78−21371
photino and goldstino, scatt. cross sections on matter 79−97558
Planck energy nonconserving fluctuations and strong forces 80−57551
plane gravitational wave interaction with elec. field of cloud of charged particles *(Russian)* 78−37169
Prasad-Sommerfield monopole, time depend. soln. of SU(2) Yang-Mills-Higgs system 79−273
proton mass, strong gravity explanation 78−12852
QED, fine-structure constant, coupled Maxwell and Dirac eqns., lepton and quark-like solutions 80−62894
quark confinement, event horizons around a particle surrounded by a static confinement potential 78−66075
Reissner naked singularity, spontaneous pair creation 78−24990
relativistic particles, gravitational scattering, post-linear approx. 80−27190
scalar fields, improved gravit. coupling 79−49151
self-gravitation 78−16971
separable quasipotential formulation of the relativistic dynamics for three point particles 79−12989
SO(3) field coupled to strong gravity, particle like soln. 78−4758
SO(8) extended supergravity 80−4914
soft graviton emission in scatt. processes, linearised gauge theory 78−49746
spacetime structure theory at very short distances, nonlinear sigma model 80−12979
spin, rotation and quantum effects, review 80−37203
spinor theory of general relativity, without elementary gravitons 78−8321
spontaneous origin of Newtons const., modified Einstein eqns., matter interactions in weak gravit. fields 78−12853
spontaneous symm. breaking due to gravitational interaction 78−36918
strong and gravitational interaction unified theory, hierarchy of universes, large numbers explanation 79−17654
strong gravitation and elementary particle stability 79−17660
strong gravity and Dirac numbers 78−21372
strong gravity equations, spin and torsion effects, rel. to spin of Universe 79−97116
strong gravity with torsion and the Cabibbo angle 80−4913
strong-gravity contributions to the electromagnetic field of an elementary particle 79−36076
strong-gravity model, stability under perturbation, Hamiltonian formalism 80−52453
strong-gravity solns. for Einstein's eqns. 78−24705

elementary particle gravitational interactions continued
SU(2) symmetry, classical quark confining solns. incorporating colour 79−339
SU(3) group strong interactions in gravitational field 80−91047
SU(N) conformal supergravity, gauge theories for extension 78−8577
supergravity, fundamental supergeometrodynamic theory of hadron 79−40725
supergravity, Hamiltonian formalism, quantisation and S-matrix 78−16972
supergravity, O(2) extended, exact plane wave solns. 79−25955
supergravity, unified theory of basic forces 78−50001
supergravity as gauge theory of supersymmetry 78−8576
theory of gravitation and electromagnetism from Bohm-Aharonov expt. 79−85028
twister space, complex fibration, fibration structure deformation, Einstein vacuum eqns., Maxwell's eqns. 78−12854
two-body gravidynamics 79−71683
unified gauge theory of gravitational and strong interactions 80−95016
unified theory of strong and gravitational interactions 79−17662
vector boson model from SL(2,C) gauge theory of gravitation and Yang-Mills theory 79−322
Yang-Mills instantons, space-time topology 78−8522
ν, classical, gravitational interactions 78−45833

elementary particle inclusive interactions
see also electron-positron inclusive interactions; elementary particle large momentum transfer interactions; pion-proton inclusive interactions; proton-proton inclusive interactions
ν deep inelastic scatt. in SKAT bubble chamber, 2-30 GeV 78−62390
π^-+nucleus interaction, 50 GeV, pion associative multiplicities anal. *(Russian)* 77−46191
$\pi^-\pi^-\pi^-$ semi-inclusive distrib. anal. using Kopylov-Podgoretsky-Cocconi formulation, fireball 78−89761
$(\phi^3)_6$, theory, inclusive annihilation processes, jet evolution 79−71640
additive quark model and multiparticle production off emulsion nuclei at 50 GeV 80−68491
additive quark parton model, hadronic fragmentation distribs. 78−8711
an asymptotic connection between processes of deep inelastic scattering and inclusive annihilation 79−22105
anomalous current fragmentation in high-$p_\perp$ leptoproduction 79−13134
anomalous lepton signals and inclusive particle prod. in e^+e^- annihilation 78−78198
asymptotic evaluation of high energy cross sections, functional integration method 78−54551
asymptotic relations for cross sections 77−65187
asymptotic vacuum cuts for inclusive cross-sections with weak coupling *(Russian)* 77−49928
average associative multiplicity, maximal rise in large momentum transfer processes *(Russian)* 80−42510
average multiplicity, transverse momentum and total cross section, new upper bound 79−35970
average multiplicity depend. on impact parameter and momentum transfer 80−37312
average transverse momenta of secondary particles, upper bound on modulus of vector product *(Russian)* 79−49563
axiomatic field theory, analytic structure of the 3→3 forward amplitude 80−68376
backward production on nuclei and the tube model, comments 80−52544
bag model, isobaric ensemble and multiplicity distrib. *(Russian)* 80−82952
baryon+antibaryon annihilation model, high energy, multiperipheral interpretation of dual unitarity diagrams 77−18253
baryon+baryon, single-particle distribution function structure, urbaryon model 77−18343
baryonic and electric charge distribs. in multiparticle prod., quark-parton model 77−79285
bounds for differential cross sections and distrib. function, QFT, general principles and strong interacts. at high energies 79−239
bounds on average multiplicity 77−34142
bremsstrahlung approx., quantum field model 77−50033
bremsstrahlung model of Brodsky and Gunion, comments 79−93362
broken $SU(6)_w$ analysis of electroproduction 79−93436
bubble chamber, propane, for investig. of spectra of charged and neutral particles *(Slovak)* 77−42214
C Ne+$\nu_\mu(\bar{\nu}_\mu)$, inclusive distrib. of produced hadrons 78−89854
centauro, Geminion and multipion events, quark matter hadronisation, prod. cross sections 80−47331
charge particle multiplicity and charge exchange at 40 GeV/C, effect of bubble chamber errors *(Russian)* 78−55118
charge transfer in multiparticle production processes and the quark cluster model 78−93858
charged-particle multiplicities in high-energy collisions 77−34194
charged-particle multiplicity distribs. in 100 GeV interactions 78−33101
charmed particles, inclusive semileptonic decay, struct. functions, scaling limits 78−82165
closed Regge eikonal formula, inclusive 6-point function, multiple Reggeon/Pomeron exchange contribs. 79−362
cluster concept in multiple hadron prod. 78−66177
cluster model, concepts and appls. 79−357
cluster model, multi-Regge, comparison with multiparticle transverse and longitudinal data 80−62952
Cluster problem in physics of high energy particles *(Russian)* 79−93384
clustering invariant quantities and energy inclusive measurements 79−45120
clusters in hadron multiple production processes 79−49545
collective tube model, credibility of criticism by Azimov et al., effects of target fragmentation 78−93982
colour gauge theory, quark elastic scatt. and large transverse mom. hadron prod. 78−8610
complex momenta eikonal approx., hadron-nucleus collisions at asymptotically high energies *(Russian)* 78−74294
cosmic ray events, new type of nuclear interaction in the total $E_\gamma > 10^{14}$ eV region 79−63561
cosmic ray nuclear event, ~42 TeV, high multiplicity, large transverse momenta, giant fireball 78−33105
cosmic ray-nucleus reacts., 20 TeV, balloon-borne chamber, Monte Carlo simulation 80−9309
cross section decrease at fixed angles, planarity at high energies, analyticity 80−78105

elementary particle inclusive interactions continued
cross sections, inclusive and semi-inclusive, auxiliary field theory classical solns. 79−49388
cross-section in region of large transverse momenta and singularity interaction 78−54661
cumulative hadron production off nuclei, parton recombination model 79−71773
DC K^+p, 32 GeV/c, resonance inclusive prod. cross sections, quark model comparison 78−93913
deep inelastic and semi-inclusive annihilation structure function factorisation in Bjorken limit, mass singularities 80−86713
deep inelastic hadron leptoproduction on nuclei, inclusive hadron final states 78−54741
deep inelastic inclusive neutrino interactions, 2-30 GeV, in SKAT bubble chamber 79−36060
deep inelastic lepton-hadron scatt., semiinclusive hadron prod., quark fragmentation function corrections, QCD 80−63013
deep inelastic processes book contrib. 78−82222
deep inelastic scatt., incusive observables and hard gluon emission 80−99094
deep inelstic pp, πN, eN scatt., lepton-hadron relation, multiparticle prod. phenomena, average multiplicities 78−37247
density matrix and scaling props. of cross section 77−41872
diffractive hadronic reactions, statistical description of multipion prod. 80−95260
dilepton production in hadronic collisions, review 79−49547
dimuon prod., sum rules and moments, valence quark transverse moments 78−54660
double pomeron exchange characteristics, inclusive hadron-hadron reactions, cross section 78−17003
double Reggeon representation of energy depend. of inclusive cross sections *(Russian)* 77−74737
double scattering in hadron-deuteron collisions, hadron struct. probe 77−74732
dual fermion model, inclusive single particle distribs., $\pi N \rightarrow \pi X$ appl. 78−86446
eikonal model, multiplicity distribs., KNO scaling 78−41514
electroproduction, determ. of quark fragmentation functions ratios 77−54079
electroproduction, final state hadrons, Regge-Mueller anal. 77−38176
electroproduction of hadrons, virtual photon prod., quark fragmentation region 78−54634
emulsion nuclei, 200 GeV/c inelast. interactions 78−8860
emulsion nuclei+p, 400 GeV, shower particle multiplicity 79−3145
energy inclusive meas., parton model and scaling laws 77−74733
equipartitioned jets, new tests of QCD 79−71697
exchange degeneracy evidence, Kp and πp total cross sections anal. 77−82796
factorisation of inclusive reaction in target fragmentation region 78−480
factorisation of inclusive reactions in target fragmentation region, exotic channels 78−481
factorization test relations and universality, multiperipheral model 77−79258
few-body problem connection 77−22760
Feynman scaling relations in inclusive and semi-inclusive reactions 79−35962
Feynman-gas model for semi-inclusive processes, πp appl., multiperipheral model predictions *(Russian)* 78−435
Feynman-Wilson gas, statistical model for multiparticle physics 79−22071
fine structure of inclusive and semi-inclusive spectra, fragmentation, cluster, Chew-Pignotti models *(Chinese)* 79−58984
fine structure of inclusive spectra, sum rules and Feynman-Yang scaling generalisation *(Chinese)* 79−49557
fireball mass spectrum, bootstrap condition, J-depend. 77−67626
fireball model anal. of small and large P_t pion distribs., ISR energies 77−38211
form factors, inclusive, new scale variable *(Russian)* 79−36079
formation zones, large p_T prod. on nuclei 77−50134
forward jet production meas. in high transverse momentum hadron-proton collisions 80−101989
forward scattering, single particle inclusive spectra, Cos θ plane singularities effects 80−102083
generalized Weizsacker-Williams method, single variables description 77−49937
Glauber screening eqns. in fast backward particle prod. in high energy processes, role of short range nucleus struct. 79−63670
gluon and quark jets in a recursive model motivated by quantum chromodynamics, Υ decay 80−62936
gluon and quark population evolution in QCD jets, numerical estimates 80−101987
gluon fragmentation, polarised, in e^+e^-, e^-q and hadron scattering 80−82988
gluon model, large $P_\perp$ data anal. 78−8615
gluon properties in high energy hadron reactions 78−66076
hadron+Be, 200 GeV, jets and single particle prod. at high $p\perp$ 78−45975
hadron+hadron, cluster model, field theoretic, multiperipheral production, Feynman scaling violation 80−57576
hadron+hadron, high-energy, inclusive spectra of secondary pions, Feynman scaling and statistical model 80−42502
hadron+hadron, jet production, large transverse momentum 80−42503
hadron+hadron→$\gamma\gamma$X, scaling and quark mass dependence, quark parton model 80−73749
hadron+hadron→$\mu^+\mu^-$X, QCD anal. jet recoil on large p_T muon pair 79−9416
hadron+hadron→meson+X, quark elastic scatt. as high transverse momentum meson source 77−57575
hadron+hadron high energy collisions, variables and optical concepts 80−444
hadron+hadron inclusive cross section of symmetric hadron pairs produced, hard scatt., parton model and QCD 80−63052
hadron+hadron interactions, Drell-Yan dynamics, lepton pair from $q\bar{q}$ collision, energy scaling breakdown 78−54610
hadron+nucleus, spatial temporal development, nuclear hadronic cascades 80−63040
hadron+nucleus high energy collisions modified cascade model, multiplicities energy depend. 79−59064
hadron+nucleus interactions, Fermilab energies, inclusive rapidity distribs., parton-cascade model 78−37252
hadron beam jets structure at small P_T 80−102014

elementary particle inclusive interactions continued
hadron collective interaction, particle inclusive spectrum properties, space-time model 79—40808
hadron dynamics, multiparticle prod., intermol. pot. in Feynman-Wilson gas 78—477
hadron elastic scattering and inclusive k_T^2 distrib. s-channel unitarity correl. 79—26258
hadron electroproduction, inclusive particle ratios on H and D targets 77—18291
hadron EM interactions, book 80—46749
hadron inclusive electroprod. in current fragmentation region 79—30741
hadron inclusive prod. cross sections at large P_T A-depend., quark-parton model *(Russian)* 80—86771
hadron inclusive spectrum produced at large-transverse-momentum *(Chinese)* 78—12935
hadron induced multiparticle reactions, S-1500 GeV, resonance prod. correlations, jet model *(German)* 80—91118
hadron interactions, inclusive, large momentum transfer, quark counting, EM form factors 80—68498
hadron interactions, inclusive processes, multiplicity and scaling, resonance production, additive quark model, SU(6) theory, review 80—63043
hadron interactions, multiplicity, semi-empirical formula 78—58210
hadron interactions at 24 GeV/c, sphericity by principle axis variable method 79—71767
hadron jet prod., Lorentz deformation 80—27420
hadron jets, correlating quark rearrangement model 79—2997
hadron jets, rapid parton and hadron distribution 80—86693
hadron leptoproduction, nuclear targets, quark-nucleon inclusive cross section, heavy lepton pairs 80—57607
hadron multiple generation processes, multiparticle correlations *(Russian)* 79—75807
hadron physics at high p_T 80—73743
hadron prod., large p_T transfer, multiple-scatt. theory 77—88019
hadron production, quark colour correlations *(Russian)* 79—93382
hadron production, quark fragmentation and triple Regge models, quark decay functions 80—62921
hadron production in high energy particle+nucleus collisions, sum rules, scaling law 77—57673
hadron total cross section, role of string junction 78—89676
hadron total cross sections, semiempirical formulae, three component model with SU(3) components 78—41600
hadron-hadron, direct γ production at large p_T, high energies 77—71547
hadron-hadron, in H, AL, inclusive particle distribs., QCD predictions 80—99112
hadron-hadron, p_T depend. of heavy particle prod. 77—22817
hadron-hadron, quark-gluon-parton model, constituent quarks as clusters 77—30318
hadron-hadron, waveparticle duality, hadron constituents 80—9136
hadron-hadron 3-jet collisions, charge conjugation asymmetries and trilinear gluon coupling 80—105934
hadron-hadron collisions, parton model of hard and soft processes in small p_T inclusive reactions 78—41599
hadron-hadron collisions at high energy, large transverse momentum processes *(Russian)* 79—26351
hadron-hadron hard collisions, calorimeter trigger, Ochs-Stodolsky scaling law derivation, parton model 79—17775
hadron-hadron inclusive interactions, charmed particle production, η_c, ψ and other $c\bar{c}$ bound states 80—63036
hadron-hadron interactions, multiplicity distribs., multicomponent description of energy depend. at high energy *(Russian)* 79—80859
hadron-hadron interactions, QCD appl. to meson and jet prod. 79—45076
hadron-hadron interactions at high energy, generalised hydrodynamical models 79—89131
hadron-nucleon, correl. length between created particles, multiple prod. case *(Russian)* 77—6187
hadron-nucleon interaction, multiparticle prod. 77—34192
hadron-nucleus, 50-200 GeV/c, multiparticle production, multiplicities, cross sections and ang. distribs. 80—86768
hadron-nucleus, absorptive part of scatt. amplitude, multiparticle prod., Glauber theory 78—37248
hadron-nucleus, rapidity distrib., 22.8, 50, 400 and $\gtrsim$1000 GeV in emulsion, multiperipheral models 80—91117
hadron-nucleus (nucleon), relativistic secondary multiplicities, constituent quark rescatt. 80—63034
hadron-nucleus collisions at high energy, expt. data review 77—50120
hadron-nucleus high energy reactions, multiple prod., parton-hadron cascade model *(Russian)* 78—17066
hadron-nucleus inclusive inelastic scatt. in phase space, quantum theory 80—32247
hadron-nucleus inelastic inclusive cross-sections in Reggeon field theory *(Russian)* 77—82791
hadron-nucleus interaction, multiple particle prod., absorptive part of scatt. amplitude *(Russian)* 78—17164
hadron-nucleus reactions, charged particle multiplicities, description unification 79—75986
hadronic bremsstrahlung, grand partition function determ. 78—33041
hadronic collisions, jet structure, two-jet events, glueball-Pomeron identity, dual field theory 80—63051
hadronic collisions, violation of Feynman scaling, central region, fragmentation, mixed two component model 77—26551
hadronic events, inelastic, non-diffractive, charge correlations in jets, quantum number effects 80—86764
hadronic jets, sequential decay models, nonscaling inclusive distribs. and long range correlations 79—49552
hadronic lepton pair production, QCD jets 80—62994
hadronic massive lepton pair prod., theory review, Drell-Yan model 78—89752
hadronic multiparticle reactions, models, prod. of strangeness, baryon number, charm 78—74286
hadronic multiple prod. and average charged multiplicity, strato-gluon mechanism in pp, Kp, πp *(Chinese)* 80—22586
hadronic neutral current coupling constants, model independent determination 79—35996
hadronic processes, large and small p_T behaviour 79—26268
hadronic reactions, trajectory slopes in gauge-dual-topological approach, jet multiplicity 80—18142
hadronic reactions, universal scaling law 80—18082
hadronic semi-inclusive processes, calc. of scaling props. by QCD 79—13027

elementary particle inclusive interactions continued
hadronic total cross sections, soft and hard components, model anal. 79—49546
hadroproduction of μ pairs, 39.5 GeV/c $\pi^{\pm}$, $K^{\pm}$, p, $\bar{p}$ beams on Cu target 78—62470
hard processes, large rapidity separation of baryonic number, partons, and dual topology 80—95255
hard processes, parton model and QCD, review 80—47258
hard scattering models, large transverse particle prod., cross section constraints from opposite side rapidity distribs. 78—29360
heavy meson nonleptonic and inclusive semileptonic decay, lepton spectrum calc. 79—3018
heavy quark mesons, inclusive hadronic prod. *(Russian)* 80—86770
high energy γ-ray family events, large emulsion chamber expt. on Mt. Fuji 79—63562
high energy behaviour of exclusive and inclusive cross sections 79—3047
high energy cosmic nuclei+emulsion nuclei collisions, cross sections, multiplicity distribs. 78—41744
high energy hadron-nucleus collisions, effective mass number 77—88135
high energy hadron-nucleus interactions, inclusive prod., quark-quark elastic scatt. model 78—45858
high energy hadron-nucleus interactions, mean slow particle multiplicity mass depend. 80—102081
high energy inelastic hadron reactions, π prod., scaling law, fireball model 78—74287
high energy particle-nucleus interactions, A depend. of multiplicity, cross section, rapidity, momenta distrib. 77—79291
high energy strong interactions, review, expt., theory 77—13983
high p_T hadronic jet photoprod., QCD anal., quark and gluon jets 80—42474
high p_T jet pairs, parton-parton scattering and π quark struct. functions 80—47248
high p_T processes, parton transverse momentum effects, QCD description 79—17774
high-energy hadronic collisions, classical space-time concepts 78—70420
high-energy inclusive spectra near phase-space boundary using quark fragmentation model 78—89658
high-energy two-body and inclusive reaction data 78—29370
higher order QCD jets in photoproduction 80—99087
higher-twist effects in QCD, deep inelastic scattering and the Drell-Yan process 80—102020
Homestake neutrino detector, mass composition of cosmic ray primaries, muon multiplicities meas. 79—66903
hydrodynamical description of the missing-mass clusters 79—71728
hydrodynamics and the bag model, multiparticle production, finite geometry effects 79—22044
hyperon-nucleon high energy reactions, differential cross sections, inclusive hyperon resonance prod. 77—18331
inclusive Coulomb scatt. cross section in 4th order of QED 78—78117
inclusive cross sections in scatt. angle, anal. props., ladder models with dynamical symmetry 79—93390
inclusive lepton pair prod., invariated helicity struct. funcions anal. 79—13172
inclusive lepton pair prod., P violation, quark-parton model in Weinberg-Salam theory, QCD 80—37217
inclusive negative hadron prod., comparison with π^-p, π^-n data 79—22275
inclusive production off nuclei, multiple scatt. theory extension 77—41869
inclusive strangeness changing neutral current interactions 78—8652
inclusive vector meson production in fragmentation regions of meson at small P_T 80—105931
intrinsically deformed particles, total cross sections, Chou-Yang model 77—67680
isoscalar axial-vector current between nucleon states analysis of inclusive reactions 79—93316
jet anal. in lepton-hadron deep inelastic scatt. from QCD 79—40785
jet cross sections and quark current-photon pointlike coupling, sum rules 80—32104
jet decay models, group-theoretical and four-momentum variables 80—73684
jet model, uncorrelated, implications of Bose-Einstein statistics 79—22070
jet phenomenon and Lorentz deformation 80—105806
jet production mechanism in lepton-hadron interactions, cascade and uncorrelated jet models 80—52516
jet production on nuclei, strong A depend. *(Russian)* 80—102084
jet separation by relative density method *(Russian)* 79—67616
jet struct. in hadronic lepton pair prod. ang. energy cross section, QCD 79—75806
jet studies and large transverse momentum collisions, review 79—22143
jet-mass effects and high-p_T jet production 80—52473
jets, angular distrib. of energy, QCD transverse ang. momentum distrib. 79—71726
jets in high energy collisions 79—45114
JINR experiments using Serpukhov accelerator, present and proposed *(Russian)* 79—63545
KNO scaling, possible struct. in correlations *(Russian)* 77—2887
KNO scaling and scaling in the mean for semi-inclusive processes *(Chinese)* 80—22538
large $p_{\perp}$ photoproduction, gluon fragmentation function extraction, scaling 80—105853
large p_T hadron prod., quark rearrangment model 77—50026
large p_t hadron production, lowest subprocess model, two body reactions 78—4887
large p_T hadronic collisions, QCD sensitive test, quark and gluon jets 80—57647
large p_T inclusive photoprod. and hard scatt. model 79—9417
large p_T jet prod. in hadronic collisions, QCD calc. for inclusive cross section 78—86439
large p_t processes, parton-parton cross sections constraints from angular correls. 77—71540
large p_T proton inclusive prod., quark-quark elastic scatt. 79—17773
large p_T reactions, trigger bias, two-jet picture 77—2878
large Q_T transverse momentum lepton pairs and hadron jets prod., reaction mech., perturbative QCD 79—2999
large transverse momenta hadron prod. in pionisation region, covariant parton model *(Russian)* 77—34131
large transverse momentum hadron prod. on nuclei 77—30461
large transverse momentum inclusive cross sections magnitude, hadron struct., constituent interchange model 79—431

elementary particle inclusive interactions continued
large transverse momentum trigger, multiplicities and rapidity distribs. 78—62376
leading charge flow in high energy inelastic hadron collisions 77—50020
lepton+hadron, deep inelastic scatt., QCD event states, 3-jet events 80—52515
lepton+hadron collisions, hadronic contributions to trimuon prod., quark-+antiquark annihilation 78—41551
lepton+nucleon, jet structure, cascade model and jet model 80—42471
lepton+nucleon, quark and gluon jets, Breit frame, QCD 80—62995
lepton+nucleon producing polarised baryon+anything, polarisation transfer from initial to final state 77—82746
lepton pair prod., nonfactorisability of inclusive distribs. in nonperturbative QCD 79—13085
Lepton pair production cross section using Drell Yan formula, sum rules, moments 78—54611
lepton-hadron, ξ scaling variable anal. 77—61298
lepton-hadron, local duality and precocious scaling 77—2842
lepton-hadron, quark and target mass effects, colour SU_3 theory 77—6090
lepton-hadron inclusive cross sections, kinematical scaling violation 78—8671
leptoproduction, scaling violations, colour octet model effect 79—13077
light-cone algebra anal. of inclusive charmed-particle prod. by neutrinos 77—18274
local number fluctuation in multiparticle production 80—57574
longitudinal phase space integral with leading particles 78—17058
Lorentz invariant scaling hypothesis, appl. to single particle distrib. functions 77—38214
low multiplicity diffractive dissociation, 1/N dual unitarisation scheme 79—75753
massive lepton pair hadroproduction, QCD and parton model anal. 80—42421
massive lepton pair production at large q_T, large p_T jet props. 79—54326
massive lepton pairs, transverse momentum distrib. from inclusive hadron prod. 78—89760
massless non-abelian gluon confinement and rising total cross sections 80—13264
mean charged multiplicity, energy depend., modified Heisenberg calcs. 79—40806
mean multiplicity depend. on transferred momentum, expt. and geometric approach *(Russian)* 80—95293
mean multiplicity of secondary particles in hadron-nuclear interactions, multiple scatt. theory *(Russian)* 80—68502
meson multiplicity prod. at large p_T, quark rearrangement model 77—61259
meson resonance and pion simultaneous production, correl. jet model 78—86456
meson-baryon interactions, meson spectra in forward jets, hadron cascade model anal. 80—32103
meson-nucleon, prod. of non-zero charm mesons in central region, quark model *(Russian)* 77—14008
meson-nucleon collisions, pion spectra forward-backward asymmetry, fragmentation effects, meson reson. decay 78—86457
meson-proton multiplicity data, two-component fireball model applications 79—63453
modified KNO scaling for multiple production processes 80—27526
Monte Carlo event generation with limited tranverse momentum 79—3001
multi-chain model for high energy hadron nucleus collisions 79—59042
multi-particle and inclusive reaction at high energies, review 79—17777
multi-temperature models of inclusive spectra 77—49936
multiparticle final states and shadow scatt., coherent state representation 77—18255
multiparticle hadronic reactions, phenomenological parametrisation 80—99110
multiparticle process, geometrical size, mean-square impact parameter estimate 77—14000
multiparticle prod., unitarity bounds on angular distrib. 77—38105
multiparticle prod. in hadron-hadron collisions, scaling and multiperipheral model, review *(Russian)* 77—2875
multiparticle prod. in quark-parton model, Monte Carlo method 78—41607
multiparticle production, large transverse momenta, momentum conservation, independ. emission model 78—50055
multiparticle production, sequential decay model with cluster formation, cluster mass 78—16993
multiparticle production meson ratios, statistical quark model *(Chinese)* 79—49558
multiparticle production model for high energy hadronic collisions 79—80790
multiparticle production processes, cluster formation model, math. formulation 78—478
multiparticle production processes, correls. due to energy-momentum conservation, uncorrel. jet model 78—41601
multiparticle reactions on deuterons, multiperipheral parton model anal. to rescatt. 79—22154
multiperipheral model, inclusive quantity constraints 77—30346
multiperipheral production of large and small fireballs at very high energies 80—47264
multiple hadron generating models, transition to KNO scaling *(Russian)* 79—22051
multiple hadron production and struct. from 10 GeV to 10 TeV interactions 80—57653
multiple production processes at high energy, recent results and theoretic interpretation *(Russian)* 79—63546
multiplexity distributions and total cross section at high energies 77—82789
multiplicative processes, ρ^0 meson formation cross section, pion prod., multiperipheral cluster model *(Russian)* 78—17067
multiplicities, inclusive distribs., in hadron or lepton induced reactions, quark jet universality 78—41476
multiplicities in hadronic and current induced reactions, e^+e^- annihilation, clustering 77—46070
multiplicity, average, energy depend. and scaling-in-the-mean 78—29369
multiplicity distrib. correlation moments, lower bounds, supernarrow distribs. *(Russian)* 80—37313
multiplicity distribs. and correls. at high energies, statistical treatment 78—89682
multiplicity distribs. and normalised cumulants 77—38185

elementary particle inclusive interactions continued
multiplicity distribs. for nonasymptotic energies, concept of similarity *(Russian)* 78—41522
multitemperature thermodynamical model of large P_T and large mass production 79—3004
muon scattering at Fermilab, inclusive scatt., quark models, scaling violation 80—5001
n-body decay distribution function, approx. formula 80—27488
n-particle decay of dual resonance, decay width, multiplicity distrib., multipion channels 78—16997
neutral current coupling from ν-induced inclusive and semi-inclusive pion reactions 77—74673
neutrino, inclusive charged current scatt., new quark flavours and scaling 77—82731
neutron scatt. on Pb, inelastic screening and total nuclear cross-sections 78—8824
neutron-nucleus high energy collisions, inclusive charged particle prod. 79—89308
np, nucleon charge exchange, reggeized one pion exchange model *(Russian)* 77—2888
nucleus+nucleus high energy collisions, hadron inclusive prod., scaling laws 78—33204
nucleus+nucleus high energy studies at Berkeley Bevalac, expt. data, theoretical predictions 77—50144
nucleus-nucleus and nucleon-nucleus collision model, Glauber's theory, classical transport eqn. 79—6522
Ochs-Stodolsky jet profile in iterative quark cascade models and low $p_\perp$ meson fragmentation 79—75733
p+emulsion, 200 GeV, star event containing single electron, charmed particle generation, anal. 77—61414
parent-child relationship for prompt leptons and neutrinos produced in the forward direction 79—80824
particle multiple prod. cross section in model with pomeron intercept $\alpha_P>1$ *(Russian)* 80—82959
particle production, inclusive spectra in three Reggeon limit range *(Russian)* 79—54369
parton model, large p_T region, two particle distrib. and associated multiplicity 77—82782
$pd\rightarrow Xd$, diffraction dissociation, high energy 78—25087
perturbative QCD, hard hadronic processes, e^+e^- annihilation, lepton-hadron deep inelastic scatt. 80—52477
perturbative QCD, jets, inelastic distribs., colourless clusters, scaling, multiplicity and tree evolution 80—52459
perturbative reggeon calculus, transverse correls., multiparticle prod. 77—2879
photoproduced pion inclusive distrib. in QCD, recombination model 79—85303
pion electroproduction, quark-parton model consistency 77—79254
pion multiplicity calc., target at. no. depend., statistical model anal. *(Russian)* 79—9425
polarisation in hadron cumulative prod. and large transverse momentum processes *(Russian)* 78—74293
polarised coincidence electroprod. scaling laws 77—49975
polarised hadron-hadron high-$p_\perp$ collisions, weak effects 77—30457
polarised target, beam fragmentation region, scatt. asymm. *(Russian)* 77—79292
Pomeranchuk theorem inverse, proof for logarithmically rising total cross sections, 10-2000 GeV 78—86425
pomeron building mechanism, in fragmentation region 78—89687
pomeron flavouring and rising total cross sections 77—38102
Pomeron two-gluon exchange model, quark counting, hadron-size effects for total cross sections 77—57495
production cross section for particle with large transverse momentum on nuclei *(Russian)* 77—38216
prompt lepton prod., QCD anal. 79—9346
proton beam dump expt. at CERN SPS, obs. of excess ν_e, $\bar{\nu}_e$ events 78—45978
proton interactions, beam dump expt. at CERN SPS 78—45979
proton-emulsion collisions, 67 to 400 GeV/c, energy independence, pseudorapidity distribs. for shower particles 79—75808
proton-hadron high energy collisions, hadron struct. 79—67614
proton-nucleus collisions, inclusive proton spectra A depend. at large transverse momenta, multiple collision theory *(Russian)* 77—38215
proton-nucleus inclusive single particle prod. of $\pi^\pm$, $K^\pm$ and $p^\pm$ at 28.5 GeV 77—18346
QCD, factorisation and the parton model 78—93848
QCD, hadron prod., large-transverse-momentum correl. 79—63438
QCD, hard semi-inclusive processes 78—93862
QCD, high energy behaviour of inclusive differential cross sections 78—45862
QCD, high P_T hadron prod. in pionisation region and vacuum singularity *(Russian)* 80—86772
QCD, inclusive deep-inelastic scatt., asymptotic freedom, review 80—32084
QCD, inclusive distributions in extended leading logarithms 79—13066
QCD, inclusive production at large transverse momentum, cross section 78—62369
QCD, perturbative, energy flow and energy correlations in deep inelastic scattering, infrared safety 80—27465
QCD, transverse momentum of jets in electroprod. of hadrons 78—62367
QCD, two dimens., hadron scatt., multi-Regge and inclusive reactions 78—4884
QCD, two dimens., multiparticle amplitudes 79—36029
QCD anal. of p_T^2 behaviour observed in semi-inclusive neutrino data 79—36015
QCD and short range nuclear phenomena 80—91060
QCD diagrammatic structure, deep inelastic scatt. in asymptotically free theories 79—2996
QCD extended leading logarithm approx. for inclusive distribs. and lepton pair prod. 80—379
QCD hadron jets, branching processes, multiplicity distrib., KNO scaling *(Russian)* 80—101998
QCD hadronic μ pair prod., gluon gauge depend., struct. func. calc. 79—80810
QCD higher order effects in spin-dependent deep inelastic electroproduction 80—13281
QCD jet calculus, inclusive p_T distrib. with exclusive form factors consistency 80—391
QCD jet dynamics, hadron and photon prod. at large transverse momentum 79—45077

elementary particle inclusive interactions continued
QCD multijet model, universal quark-jet fragmentation in soft hadronic reactions 80—13285
QCD predictions, high p_T processes subject to sum rules, SU(3) symmetry constraints 79—354
QCD predictions for inclusive and semi-inclusive leptoprod., hadron ang. distribs. 79—13041
QCD predictions for jet transverse momentum in leptoproduction 79—63442
QCD three jet prod. in large P_T processes, two particle inclusive distribs. 79—9342
quantum cluster decomposition of hadronic final state, stochastic theory of multiple hadron prod. 78—41507
quantum-chromodynamic predictions for inclusive spin-spin asymmetries at large transverse momentum 79—49472
quark and hadron jets, charge and energy flow in cascade models 80—102017
quark bag model, large transverse momentum processes of hadrons, EM form factors *(Russian)* 79—26308
quark fragmentation function, determ. of parameters 80—13261
quark fragmentation functions for inclusive hadron production, Regge formalism 80—68462
quark fragmentation functions in high-p_T deep inelastic processes 77—61295
quark fragmentation functions in inclusive hadron muoproduction 79—67565
quark fragmentation in P conserving jet production reactions, spin observables 79—71658
quark fragmentation jets in QCD, cascade model 80—78045
quark jet fragmentation 79—45063
quark large angle scatt., inclusive cross sections, gauge theory *(Russian)* 78—45883
quark model predictions of η and η' prod. in multiparticle reactions 78—423
quark recombination model, vector meson prod., effect on $\pi^{\pm}$ and $K^{\pm}$ fragments from proton 78—82160
quark-antiquark annihilation, small momentum transfer inclusive spectra 78—58158
quark-cascade model, particle ratios at large p_T 77—10218
quark-parton distributions model, large transverse momentum hadrons, logarithmic scale breaking 78—16989
quark-parton model, inclusive processes with large momenta *(Russian)* 77—71538
quark-parton model, leading proton-large p_T particle and proton-lepton pair correlations 79—353
rapid pionisation model, inclusive spectra height and average multiplicity growth *(Russian)* 78—89763
rapidity distrib. of large p_T particles and realistic jets 77—30334
rapidity distribution symmetry axis in hadron-hadron and hadron-nucleus collisions 77—57569
rapidity in distrib. in inclusive reacts. *(Russian)* 78—41518
Regge complex-pole model 77—41871
Reggeon model for fast hadron-nucleus inclusive cross sections *(Russian)* 78—45985
Reggeon strong coupling theory instabilities *(Russian)* 77—34139
relative semi-inclusive correl. function anal. 77—38207
ring hopping model, multichannel eikonal model, nucleon diffractive excitations, falling total cross section 78—21404
rising π inclusive cross section as series of threshold effects, multiperipheral model 78—93918
RPA scheme in multihadron production processes, high energy, strong correls. 78—41506
s-dependence of proton fragmentation by hadrons, 30-250 GeV/c 78—74291
s-dependence of proton fragmentation by hadrons 4-24 GeV/c 78—74290
S-matrix theory, inclusive coherent interference phenomena between pions 77—61206
scaling behaviour of γ/π prod. cross section ratio to distinguish large p_t inclusive interaction models 77—50032
scaling hypothesis for the rapidity distributions and information theory 80—73747
scaling in the mean, asymptotic validity 78—479
scaling in the mean, connection with Feynman scaling, semiinclusive reactions at asymptotic energies 78—29363
scaling law in strong interactions 78—41606
scaling low for inclusive production of hadrons in particle-particle collisions at high energies 78—54656
scaling of inclusive form factors with respect to a generalized scaled variable 80—417
scaling-in-the-mean functions, inclusive and semi-inclusive processes 78—4880
seagull effect in π semi-inclusive distribs. by information theory, p_L-p_T correlations 78—86458
secondary hadron multiplicity distribs., hadron prod. mech. universality test *(Russian)* 79—93477
secondary particle production in cosmic ray interaction at 10^{12} eV 80—5032
semi-inclusive deep inelastic neutrino scatt. QCD effects 79—30724
semi-inclusive distribs., renormalisation group anal. of scaling behaviour 79—30660
semi-inclusive many particle, new types, rapidity gap, scaling and exptl. results *(Chinese)* 77—74729
semi-inclusive processes, transverse momentum depend. of multiplicities 78—25028
semi-inclusive processes of multiparticle productions, scaling laws 79—30684
semi-inclusive rapidity distrib., scaling in the mean 79—93309
semi-inclusive scattering in QED 79—63388
sequential decay processes of clusters in multiparticle inclusive prod. 77—49934
single particle inclusive, distrib. in high energy collisions of heavy nuclei 78—37369
single particle inclusive distrib. at large p_T in parton models 77—79286
single particle inclusive distributions, momentum transfer components, phenomenological approach 78—89754
single particle inclusive prod. reactions, ONCPLT Fortran program for observables calcs. 77—57845
single particle semiinclusive distributions, scaling in the mean at asymptotic energies 77—57576
single-particle distrib. in cos θ, analytic props. in ladder model with asymptotically const. total cross section 79—3061

elementary particle inclusive interactions continued
single-particle distribution function structure in urbaryon model 77—18343
singular gauge fields, effect on inclusive differential cross sections 80—105782
soft gluon resummation formulae for hard parton processes in QCD 80—105842
soft hadronic processes, quark-parton model test for inclusive cross sections 79—17776
soft meson inclusive multiple prod., density matrix *(Russian)* 77—49929
space-time structure of jet hadronization 80—91024
statistical bootstrap model for hadronic matter and multiparticle reactions 77—57502
statistical model of hadron and lepton prod. for violent collisions 77—18353
statistical model of inclusive distribs., model formulation and mean field approx. 79—36041
SU(4) broken symm., duality, baryon+baryon and baryon+antibaryon exotic mesons prod. 78—89629
sum rules for single π observed inclusive reactions induced by EM or hadronic weak currents 77—34161
superinclusive cross-sections 78—41521
thermodynamic model calcs. of single particle distribs. 77—30453
three large p_T jets, hadronic prod., perturbative QCD anal., processes and formalism 80—42508
three-jet prod. in large momentum transfer reactions, perturbative QCD theory 79—93373
total and triple-Regge inclusive cross sections 78—400
total cross section ratios at high energies *(Russian)* 77—46091
total cross sections, upper bound 78—12839
totally inclusive leptoprod., scaling anal., target mass corrections in QCD parton model 80—102052
transverse momentum behaviour of hadrons, multihadron systems, and lepton pairs 79—45121
transverse momentum correlations for secondaries, rapidity cluster, stat. model 80—73754
transverse momentum distribution of particles, hydrodynamical model calcs. 78—93865
triple jet production in hadronic collisions at large transverse momentum 78—93919
triple Regge region, higher order ε terms 78—16954
triple Regge region, polarisation 77—10294
two jet model, large p_T hadronic multiplicity, colour octet exchange 78—62377
two-hadrons inclusive reactions and correl., large p_T, scale-violating quark model 78—74292
two-jet production cross section at large p_T, urbaryon rearrangement model 77—2884
uncorrelated cluster emission models 77—2801
uncorrelated jet model, Bose-Einstein and Boltzmann statistics calc. for rapidity spectrum 80—4969
uncorrelated jet model, evaluation of phase-space vols. and inclusive spectra 77—26496
uncorrelated jet model, quantum statistical correls., Bose-Einstein statistics, pion prod. 78—16992
unitary bounds on ang. distribs., role of inelastic cross section 77—30466
unitary corrections to short-range order, long range rapidity correlations 79—26315
unitary model for elast. scatt. and inclusive interactions 77—30343
universality of multiplicity distrib., hadronic bremsstrahlung 78—70419
unstable particle+nucleon, total cross section, from diffractive prod. on nuclei, multiple scatt. approach 78—41441
urbaryon rearrangement model, transverse momentum in multiple prod. processes 77—57487
vector meson inclusive prod. cross section in hadron-nucleon collisions, parton transversal motion *(Russian)* 79—67617
vector meson production in triple Regge region, absorpt. corrections 78—93867
very high energy strong interactions, review 80—440
vortex string picture and large p_T reactions 79—63415
weak (V+A) interactions of leptons, possible existence *(Russian)* 77—74678
weak charmed-baryon resonance prod., neutrino inclusive interactions, scaling behaviour 78—8645
weak neutral couplings to hadrons in neutrino inclusive, semi-inclusive and elastic reactions 79—36064
$ap \rightarrow cX$, a, $c=\pi^{\pm}$, $K^{\pm}$, p, $\bar{p}$, low P_t hadron fragmentation at 100, 175 GeV/c 79—85346
$\bar{B}B$ annihilation process, simple geometrical picture 80—95291
χ production properties from inclusive electron pair and J/ψ prod. at CERN ISR 79—36113
D(1865) charmed meson hadronic prod., cross section limits from pN 79—89211
$d+\text{nucleus} \rightarrow \pi+X$, inelastic rescatt. contrib. to cumulative meson prod. *(Russian)* 77—61334
$dA \rightarrow \pi^{-}+X$, scaling invariance of interactions of relativistic nuclei, the cumulative effect *(Russian)* 79—93611
$dd \rightarrow \pi^{0}X$, large transverse momentum, π^{0} prod. cross section, ISR energies 79—3055
$dp \rightarrow pX$, relativistic d inclusive p spectrum, cross section 77—82783
$\Delta(1236)$ inclusive prod., absorpt. corrections in triple-Regge region 77—87956
Δ inclusive production, Mueller-Regge model 79—17767
e/μ charged current $\nu(\bar{\nu})$ interaction comparison in Ne-H_2 mixture, μ-e universality 79—9363
ed, 2.3 GeV, inclusive electroprod. cross sections for final state nucleons 77—34159
$ed \rightarrow eX$, polarised deep inelastic scatt., test of Weinberg-Salam model 79—22006
$ed \rightarrow e'+X$, polarised e, parity non-conservation in inelastic scatt. 78—89719
$ed \rightarrow e'+X$, polarised electrons, asymmetric inelastic scatt., effect of odd-parity components of deuteron 79—89166
$ed \rightarrow$ hadrons, inclusive distrib. of hadrons from deep inelastic scatt. 79—89167
$e^{+}e^{-}$ annihilation and quark fragmentation functions, Monte Carlo quark-parton model 79—22119
$e^{+}e^{-}$ annihilation with polarised beams 79—36111
$e^{+}e^{-} \rightarrow X(hX)$, bound states and asymptotic limits for QCD in 2-dimens. 79—71716

elementary particle inclusive interactions continued
$e^+e^-h \to e^-X$, h=hadron, structure functions in next to leading logarithm approx., ϕ^3 field theory 80-37268
$e^-h \to e^-X$, bound states and asymptotic limits for QCD in 2-dimens. 79-71716
eN, 50, 100, 300 GeV, in emulsion, cascade showers 3-dimens. development 80-86724
eN deep elastic scatt., hadronic final states 78-78184
$eN \to eX$, generalised vector meson dominance model, sum rules 78-45810
$eN \to eX$, quark structure functions for hadrons, Drell-Yan model anal. 78-21476
$eN \to e'pX$ longitudinal-transverse separation 77-49977
$eN \to e'\pi^\pm X$, longitudinal-transverse separation 77-49977
$eN \to e\pi_s + X$, test of soft-pion theorem in inclusive pion electroprod. 79-17739
$eN \to e\pi^\pm X$, ^1H, ^2H targets, π^+/π^+ ratio, Q^2 to 4 GeV^2 77-74693
$en \to e\pi^\pm X$, π^+/π^- ratio meas. 77-18295
$eN \to e\pi^\pm X$, sum rules for polarised N 78-89718
$eN \to$ hadrons+anything, scale invariant limit on average transverse momentum 77-67659
$eN \to pX$, ^1H, ^2H targets, forward protons to $Q^2=9.5$ GeV^2 77-74690
e^-N, inclusive pion production due to $\gamma q \to \pi q'$ process, quark-parton model *(Russian)* 80-78073
$e^-N \to e^-X$, parity violating asymmetry, constraint on right-handed electron weak charge 79-17734
ep, 20.5 GeV, inclusive π^0 electroprod. in deep inelastic region 80-52520
ep, deep inelastic scatt., meson spectra in forward jets, hadron cascade model anal. 80-32103
ep, high Q^2, QCD corrections to parity-violating asymmetries 80-22618
ep, K inclusive electroproduction, K/π and K^+/K^- prod. ratios 78-37217
ep deep inelastic inclusive $K_s{}^0$ and Λ electroproduction, quark fragmentation 78-66123
ep deep inelastic scatt., density matrix appl. to scaling props. 78-8673
ep deep inelastic scatt., many-photon exchange contrib. 80-9177
$ep \to eK^+$+anything, invariant cross section, DESY studies 78-41553
$ep \to e\Lambda X$, electroprod. of forward Λ baryon near/along virtual photon direction 79-22116
$ep \to eX$, polarised deep inelastic scatt., test of model 79-22006
$ep \to eX$, SLAC data anal., parton distribution functions for polarised protons 77-82747
$ep \to e'+X$, polarised e, parity non-conservation in inelastic scatt. 78-89719
$ep \to e'nX$, π exchange, π EM struct. functions calcs. 78-70375
$ep \to e$+hadron+x, parton picture from QFT, structure function scaling behaviour 79-402
$ep \to e\gamma+X$, QCD predictions for processes involving real photons 79-6330
$ep \to epX$, photon fragmentation region, Regge pole expansion 77-54108
$ep \to epX$, pion struct. function determ. *(Russian)* 79-22097
$ep \to e\pi^\pm X$, π^+/π^- ratio meas. 77-18295
$ep \to e\pi^\pm X$, quark-parton model charged π electroprod. 79-13136
$ep \to e\pi^\pm$+anything, π^+, π^- structure function behaviour, various W and Q values 77-10262
$ep \to$ hadrons, inclusive distrib. of hadrons from deep inelastic scatt. 79-89167
ep inclusive cross-sections meas. at 50° and 60°, 6.5-19.5 GeV 77-2843
ep inclusive reactions, $e\mu$ event, associated charm quark pair creation 77-2841
ep inelastic scattering, charged hadron multiplicities, inclusive π^- distribs. 78-41552
ep scatt., longitudinal cross section and asymmetries for jets in leptoproduction 80-32106
$ep \to W^+(Z^0)+X$, inclusive cross sections, quark-parton model calcs. 79-71755
e^-p, π multiplicity and asymmetric fireballs 79-93474
$e^-p \to e^-p$+anything, virtual photon photoprod. invariant cross section 77-46058
e^-p inclusive interactions, flavour symmetry breaking in antiquark distribs. 79-36006
$e^+p \to e^+\gamma X/e^-p \to e^-\gamma X$, deep inelastic scatt., quark-parton model 77-41846
$e^\pm p \to e^\pm \gamma+X$, deep-inelastic bremsstrahlung, quark charges, colour gluon mass 78-74216
$\eta N \to$ charged particles, 200 GeV, coherent tube model 79-49554
γ+hadron$\to$lepton pair, perturbative QCD, twist-2 photon operator, parton subprocesses 80-73716
$\gamma\gamma$, jet cross sections and quark current-photon pointlike coupling, sum rules 80-32104
γN, inclusive pion production due to $\gamma q \to \pi q'$ process, quark-parton model *(Russian)* 80-78073
γN, multibody channels, review, book contrib. 80-47303
$\gamma N \to {}^\pm$+anything, 9-18 GeV, forward hemisphere 77-6134
γN collisions, charmed meson pair prod., semileptonic decay spectra 77-49952
$\gamma N \to$ jet+X, QCD cross sections 80-73715
$\gamma N \to K^\pm$+anything, 9-18 GeV, forward hemisphere 77-6134
$\gamma N \to l^+l^-X$, pol. γ, neutral current effect, Weinberg Salam model calcs., p violation 80-5000
$\gamma N \to \mu\bar{\mu}X$, QCD cross sections 80-73715
$\gamma N \to \bar{p}$+anything, 9-18 GeV, forward hemisphere 77-6134
$\gamma N \to \pi^+X$, QCD cross sections 80-73715
$\gamma N \to \psi(3.1)$+anything, cross section and N charmed quark composition 80-423
$\gamma_v N \to \pi^\pm X$, current fragmentation region, quark cascade model of deep inelastic lepton-nucleon scatt. 78-25052
γp, 40-70 GeV, inclusive $\bar{D}^0$ photoprod. cross sections, pair and associated prod. 80-91097
γp, π multiplicity and asymmetric fireballs 79-93474
$\gamma p \to (p\bar{p})p$, inclusive and exclusive $p\bar{p}$ photoprod. S(1936) prod. 80-86729
$\gamma p \to cX$, c=hadron, photon fragmentation region, Regge pole expansion 77-54108
γp cross-section observed increase, jets as source, QCD and vector-meson dominance model 80-22620
$\gamma p \to \gamma$+jet+X, perturbative QCD predictions large p_T real photon in final state 79-89165
$\gamma p \to h^\pm X$, large p_T photoprod., perturbative QCD test 80-37276
$\gamma p \to hX$, quark jet model and total cross section 79-13133

elementary particle inclusive interactions continued
$\gamma p \to hX$, SU(3)×SU(3) invariant interaction of quarks, large p_T, gluon bremsstrahlung 78-33072
$\gamma p \to \mu^+\mu^-$, cross sections, γ struct. function determ. 80-42473
$\gamma p \to pX$, 710 to 950 MeV, momentum spectrum of recoil protons 79-22108
$\gamma p \to \pi^0X$, invariant cross section at large p_T, hard scatt. model 80-22621
$\gamma p \to \pi^0$+jet+X, perturbative QCD predictions 79-89165
$\gamma p \to \pi^+\pi^-\pi^+\pi^-\pi^+\pi^-p$, diffractive production, jet-like structure 80-57606
$\gamma p \to \pi X$, large p_T, perturbative QCD 80-86723
$\gamma p \to q\bar{q}p$, quark-antiquark jet diffractive photoprod. in perturbative QCD 80-73714
$\gamma p \to W^+(Z^0)+X$, inclusive cross sections, quark-parton model calcs. 79-71755
$\gamma p \to X$, strong interaction model anal., review, book contrib. 80-47310
$hh \to \mu^+\mu^-$+jet+X, QCD anal. of recoiling jets and angular effects in large q_T pair prod. 79-45078
$h_1h_2 \to l\bar{l}X$, massive lepton pair prod., polarisation and spin effects 80-105929
$hN \to \gamma(\mu^+\mu^-)$+jet+hadrons, gluonic jets, prod. mechanism *(Russian)* 79-58986
in deep inelastic scattering, quark jet as trigger for gluon jet 80-62996
J/ψ, inclusive production cross sections, correlating quark rearrangement model 79-54320
K structure functions from inclusive prod. data, nonstrange quark distribs. 80-86715
K^0 inclusive prod. from 10 GeV/c K^+ on nuclei and hydrogen 78-4882
K^0 meson production cross section *(Russian)* 78-82394
$K^\pm \to K^\pm+X$, 140-175 GeV, differential cross-section meas. 77-18345
K^+d inclusive reactions, 4.6 GeV/c, topological cross sections, π^-, K^0, Λ prod. 77-50004
$K_S{}^0K_S{}^0$ pair rapidity correlations, quark level strangeness compensation in multiparticle production 79-36024
$K^-N \to \bar{K}^{*0}X$, inclusive cross sections and spin density matrices, 3-Reggeon model anal. *(Russian)* 79-80858
$K^-N \to \mu^+\mu^-X$, K^-/π^- structure function ratio using Drell-Yan process 80-86718
$K^+N \to \mu^+\mu$, 225 GeV/c, muon pair prod., 2 to 11 GeV/c^2, differential cross section 79-67612
$K^\pm n$, high-energy, react. differences and annihilation 78-74279
$K^\pm N \to K^\mp+X$, double hypercharge kaon exchange *(Russian)* 78-29368
$\bar{K}p$, 70 GeV/c, total and differential cross-sections for π and K production 80-63050
Kp, estimate of ω, ϕ and baryonium mixing at $t\approx0$ 79-40814
Kp, inclusive vector and tensor meson prod. in beam fragmentation region, Mueller-Regge formalism 78-17057
kp, large P_T pion^0 prod., meson structure functions, quark distrib. functions 80-86714
Kp, meson fragmentation region, meson spectra, quark cascade model 77-67689
$Kp \to \pi X$, central region, Regge Mueller approach, inclusive cross sections *(Russian)* 78-58218
$Kp \to \pi(K)(p)X$, 4-250 GeV/c, Pomeron factorisation 77-14005
K^-p, 10, 16 GeV/c, Σ^+, Σ^- inclusive prod. Λ prod. comparison 80-86766
K^-p, 110 GeV/c, charged multiplicity distrib. 80-78101
K^-p, 110 GeV/c, prod. of large $p_\perp$ single and multiparticle systems (jets) 79-85345
K^-p, 200 GeV/c, high p_T charged particle prod. and correlations 79-89199
K^-p, 32 GeV/c, inclusive cross sections and average multiplicities 77-67687
K^-p, 32 GeV/c, vector and tensor meson prod., with quark model anal. 79-80854
K^-p, 8.25 GeV/c, study of inclusive Λ, Σ^0 and $\Sigma(1385)$ prod. 79-30749
K^-p, inclusive prod. of Ξ^- and $\Xi^*(1530)$, 10 and 16 GeV/c 80-13341
K^-p, inclusive Ξ^- production at 4.2 GeV/c, triple Regge formalism 78-4875
K^-p, π multiplicity and asymmetric fireballs 79-93474
K^-p 14.3 GeV/c, inclusive and exclusive cross sections 77-82787
K^-p collisions, charged particle multiplicity, Bose distrib. 77-50022
$K^-p \to \Delta^{++}X$, 32 GeV, inclusive and total cross sections 80-105936
$K^-p \to \Delta^{=+}(1232)+X$, 16 GeV/c, cross sections 78-66169
K^-p inclusive interactions, 10, 16 GeV/c, polarisation of forward produced Λ 78-62466
K^-p interactions at 8.25 GeV/c, charge distribs. 77-82785
$K^-p \to K^-X$, 32 GeV, single and double diffractive dissociation 79-58982
$K^-p \to K^0X$, 32 GeV/c, struct. functions *(Russian)* 77-264
$K^-p \to \bar{K}^0X$, inclusive multi-Pomeron corrections in the Regge-eikonal model 79-63557
$K^-p \to \bar{K}^0X$, pseudoscalar meson prod. in triple Regge region, absorpt. corrections 78-78228
$K^-p \to \bar{K}^0(\Lambda^0)+X$, 6.5 GeV/c total inclusive cross sections, multiparticle prod. characts. 79-89188
$K^-p \to \bar{K}^{*0}X$, 7.3 GeV/c, comparison with $\pi^+n \to \rho^0X$ 77-30459
$K^-p \to \bar{K}^*(1420)X$, at 10 and 16 GeV/c 77-18338
$K^-p \to \bar{K}^*(890)X$, at 10 and 16 GeV/c 77-18338
$K^-p \to \Lambda^0$+pions, 8.25 GeV/c, resonance prod., fluctuations cluster emission model 78-93904
$K^-p \to \Lambda X$, 4.2 GeV/c, polarisation and triple Regge framework 78-45948
$K^-p \to \Lambda X$, 8.25 GeV/c, off shell $K\bar{K}$ and $p\bar{p}$ interactions, KNO scaling 80-52534
$K^-p \to \Lambda X$ or Λ(Pions) or $\Lambda p_{slow}X$, multiperipheral model with heavy clusters *(Russian)* 78-485
$K^-p \to \bar{\Lambda}+X$, 32 GeV/c, total and differential cross sections, energy dependence 80-63048
$K^-p \to \Lambda$+anything, 4.2 GeV/c, dual anal. of target fragmentation 77-57561
$K^-p \to \lambda$+pions, 4.2 GeV/c, multiplicities, hadronic temps. and ang. distribs. in $\bar{K}K$, $\bar{p}p$ annihilations 79-45101
$K^-p \to \pi^0X$, 100, 200 GeV/c high transverse momentum π^0 prod., quark scatt. 78-45976
$K^-p \to \pi X$, 32 GeV/c, struct. functions *(Russian)* 77-264
$K^-p \to \rho^0$+anything, or f+anything, 10, 16 GeV/c, central and fragmentation contribs., quark model predictions 78-62467

elementary particle inclusive interactions continued
$K^-p\to\Sigma^+$+anything, 4.2 GeV/c, dual anal. of target fragmentation 77–57561
$K^-p\to\Sigma^+(1385)+X$, 16 GeV/c, spin density matrix of $\Sigma^+(1385)$ by statistical tensor method 78–37235
$K^-p\to\sigma^\pm$ (1385)X, 32 GeV, inclusive and total cross sections 80–105936
$K^-p\to\Sigma^\pm(1385)+X$, 10, 16 GeV/c, inclusive prod. 77–26552
K^+p, 147 GeV/c, inclusive Δ^{++} prod., cross section energy depend. 80–57651
K^+p, 32 GeV/c, inclusive and semi-inclusive, Bose-Einstein interference effect 79–22152
K^+p, 32 GeV/c, vector meson inclusive spectra 79–30703
K^+p, 70 GeV/c, cross sections and charged multiplicity distribs. 80–63053
k^+p, multiple production processes regularities, Monte Carlo model 80–102082
K^+p, π multiplicity and asymmetric fireballs 79–93474
K^+p, two-particle inclusive and semi-inclusive correls. at 32 GeV/c *(Russian)* 77–88020
$K^+p\to\Delta^{++}(1232)+X^0$, 32 GeV/c 80–52540
$K^+p\to\gamma X$, 32 GeV/c, inclusive and semi-inclusive distributions for γ 80–27525
K^+p inclusive and semi-inclusive 32 GeV/c interactions, Λ and $\bar{\Lambda}$ prod. 78–21475
$K^+p\to K^0X$, 32 GeV/c, associated average charged particle multiplicities 77–2882
$K^+p\to K^0X$, 32 GeV/c, inclusive cross sections, single particle distribs. 78–41598
$K^+p\to K^0X$, 5-32 GeV/c, transverse momentum distribs. *(Russian)* 77–30467
$K^+p\to K^0X$, inclusive multi-Pomeron corrections in the Regge-eikonal model 79–63557
$K^+p\to\bar{K}^0X$, pseudoscalar meson prod. in triple Regge region, absorpt. corrections 78–78228
$K^+p\to K^0(\pi^-)$+anything, 32 GeV/c, associated multiplicities *(Russian)* 77–34197
$K^+p\to\bar{\Lambda}X$, 32 GeV/c, $\bar{\Sigma}^{*-}$ and $\bar{\Xi}^{*-}$ antibaryon resonance prod., mass enhancements 80–13340
$K^+p\to\Lambda$+anything, 4.3 GeV 78–4876
$K^+p\to pK^0X$, 32 GeV/c, total cross section and structure functions 79–40809
$K^+p\to pX$, 32 GeV/c, total cross section and structure functions 79–40809
$K^+p\to p$+anything, 16 GeV/c, study of slow inclusive protons 77–65184
$K^+p\to\pi^-X$, 32 GeV/c, associated average charged particle multiplicities 77–2882
$K^+p\to\pi^-X$, 8.2-32 GeV/c, transverse momentum distribs. *(Russian)* 77–30467
$K^+p\to\pi^-X^{+++}$ inclusive double-charge-exchange π^- prod., 100 GeV/c 78–37250
$K^+p\to\pi^-\pi^-X$, 32 GeV/c, two-pion correlations, Monte Carlo model 80–83008
$K^+p\to\pi^-\pi^-X$, inclusive distribs. in statistical model, correl. function 77–18354
$K^+p\to\pi^0X$, 32 GeV/c, inclusive and semi-inclusive distributions of π^0 80–27525
$K^+p\to X\Delta^{++}$, absorption corrections to three Reggeon formulas *(Russian)* 79–9423
$K^\pm p$, 130, 200 GeV, jet prod. cross sections, QCD anal. and scale breaking 80–99111
$K^\pm p$, 200 GeV/c, high p_T jet prod., QCD expt. test 79–89200
$K^\pm p$, 32 GeV/c, ρ, K*, ϕ inclusive prod., quark fusion model 80–32135
$K^\pm p$, fireball model, universal scaling function 80–57646
$K^\pm p$, high energy, mean charged hadron multiplicity, modified Heisenberg approach 78–45988
$K^\pm p$, high-energy, react. differences and annihilations 78–74279
$K^\pm p$, π^+/π^- inclusive ratio in quark recombination model 80–102022
$K^\pm p\to$hyperon+X, 4-16 GeV/c, unified descript. of $\Lambda,\bar{\Lambda}$, Σ^+, Ξ^- prod., urbaryon model 78–66173
$K^\pm p\to K^\pm X$, triple Pomeron coupling, Reggeon treatment 80–68488
$K^\pm p\to K^\pm$+anything, 50 to 175 GeV/c, cross sections, factorisation 77–50027
$K^\pm p\to\Lambda(\bar{\Lambda})X$, 32 GeV/c, Λ and $\bar{\Lambda}$ polarisation 79–45122
$Ld\to l'\Delta X$, deep inelastic scatt., isobar admixture possibility *(Russian)* 80–91095
$lN\to l'\pi X$, semi-inclusive deep inelastic scatt. cross sections, higher twist effects 80–32105
$lp\to lX$, scaling violation due to charm prod., conventional ideas 77–74691
$lp\to l'hX$, azimuthal depend., parton model calc. 78–93887
$MB\to l^+l^-X$, meson quark struct. functions, and Drell-Yan process 79–63551
μ pair production in hadron-hadron collisions, gluon effects, QCD predictions 78–78148
μd, 147 GeV, inclusive hadron jet behaviour, hadron spectra, quark-parton anal. 79–71757
$\mu^+\mu^+$ production in hadron-hadron collisions, small transverse momentum distrib., QCD soft gluon bremsstrahlung effects 79–75723
μN, deep inelastic scattering in emulsion, 150 GeV, intra-nuclear cascading, existence search 79–75979
μN, inclusive scatt. 96, 147, 219 GeV, nucleon struct. function determ. 80–42472
μN deep inelast. scatt., inclusive ρ^0 prod. 78–37216
μN deep inelastic scatt., hadronic final states 78–78184
$\mu N\to\mu\Upsilon X$, 209 GeV, Υ muoprod. limits from trimuon final states 80–105909
$\mu N\to\mu X$, broken colour gauge theory of integer charge quarks 80–13313
$\mu N\to\mu'h+X$, transverse parton momentum meas. 79–13076
$\mu N\to\mu\mu X$ ($\mu\mu\mu X$), 150 GeV prod. ratios 77–79268
$\mu N\to\mu\mu X/\mu N\to\mu X$ ratio, charm contrib. 77–57544
$\mu N\to\mu\psi X$, diffractive and non-diffractive ψ leptoprod. in QCD 80–424
μN scatt., deep-inelastic, EM production of trimuons 80–22619
$\mu N\to x\mu X$, x=2 or 3, charm muoprod. with small angle veto 80–47306
$\mu^-N\to$hadron shower, charm-pair production effects 80–73748
$\mu^-N\to\nu tX$, six-quarks model, upper bounds for t-quark production 80–13297
μ^+N in Fe, 280 GeV, dimuon prod. cross sections 80–91094
μ^+N in Fe, 280 GeV, trimuon event cross sections 80–99104

elementary particle inclusive interactions continued
μp, 147 GeV, inclusive hadron jet behaviour, hadron spectra, quark-parton anal. 79–71757
μp, semi-inclusive, ang. correl. tests of QCD 79–17735
μp, semi-inclusive scatt., quantum chromodynamic predictions 78–29324
μp deep inelastic scatt., inclusive cross section, lepton pair EM prod. contrib. *(Russian)* 80–105904
$\mu p\to K_s^0X$, 225 GeV, deep inelastic scatt., strange neutral particle prod. 80–105902
$\mu p\to\Lambda^0(\bar{\Lambda}^0)X$, 225 GeV, deep inelastic scatt., strange neutral particle prod. 80–105902
$\mu p\to\mu X$, deep inelastic processes, nucleon struct. function, scale breaking 78–78185
μp semi-inclusive scattering, hadronic fragmentation initiated by pointlike probes 79–49551
μ^+p inclusive hadron distribs., scaling props., quark-parton fragmentation 77–61296
N-N low multiplicity events, scaling and multiperipheral testing at cosmic ray energies 77–18342
$n+N\to(n^*\to\Lambda k\pi)X$, 45 GeV, decay prob. 77–82795
n+nucleus, high momentum study, quasi-two-body scaling, differential cross sections 77–57665
N*N, total cross sections of diffractively produced nucleon excitations 78–21481
NN, 10^{12} eV, rapidity gap distrib., Snider multiperipheral cluster model 80–73757
NN, inclusive production, low transverse momentum distrib., cluster model 77–67684
NN, prod. of non-zero charm meson in central region, quark model *(Russian)* 77–14008
NN, πN, KN, cross-sections related by sum rules, pomeron hypothesis, heavy-quark channels and threshold predictions 78–89755
$N\bar{N}$ annihilation, even-odd ratio in multipion prod. 77–22755
$N\bar{N}$ annihilation, level widths in coupled-channel problem *(Russian)* 79–93476
$NN\to\gamma X$, off-shell effects in the nucleon-nucleon system 79–80839
nN in nuclei, 200 GeV/c, inclusive backward prod., collective tube model 80–47338
NN inclusive charge exchange, parameter-free model 77–18336
$NN\to l^+l^-X$, A depend. of lepton pair prod. on atomic nuclei *(Russian)* 79–49562
NN multiplicity distributions at very high energy, universality hypothesis 77–26550
$NN\to\mu$+anything, 70 GeV, muon polarisation meas. *(Russian)* 77–6185
$N\bar{N}\to$pions, direct channel scheme based on statistical bootstrap, low-energy region 78–12924
$nN\to\bar{p}pX$, narrow struct. in $\bar{p}p$ mass spectrum, threshold to 2700 MeV/c^2 79–63511
$NN\to\pi X$, expt. review of π-prod. by (un)polarised nucleons on few-nucleon systems 79–80944
NN semi-inclusive reactions, secondary pion production, 1000 GeV, scaling phenomena 79–22157
$NN\to X$, nuclear size dependence of particle prod., hydrodynamical model 80–22593
$n\nu/p\nu$ charged current ν cross section ratio, 1-10 GeV, semi-inclusive p prod. rates 79–374
np, semi-inclusive, 19.2 GeV/c, spectra of charged secondaries *(Russian)* 77–6179
$np\to pX$, 800 MeV, proton spectra, $\pi N(1232)$ resonance 78–62437
$np\to p$+anything, inclusive charge exchange, parameter-free model 77–18336
$np\to px$, baryonium exchange, triple-Regge couplings 80–86763
np reactions, Λ production, polarisation effects, effective mass spectrometer studies 77–30412
ν, $\bar{\nu}$, inclusive neutral current interactions 78–25036
ν and $\bar{\nu}$ 'new physics' data, vectorlike quark-parton model anal. 79–9359
ν and $\bar{\nu}$ inclusive processes for neutral currents, sea quark effects, meson prod. 79–22088
ν inclusive cross section on nuclei, ν_μ representation in SU(6) 78–54626
ν inclusive prod. of charmed vector mesons 77–18273
ν interactions at high energy, leading log approx. 79–80818
$\nu(\bar{\nu})$ inclusive scattering, weak neutral currents with longitudinal cross sections, scaling 78–17007
$\nu(\bar{\nu})$-N inclusive same-sign dimuon prod., $c\bar{c}$ creation 77–49946
$\nu(\bar{\nu})N$, axial vector photon and neutral neutrino processes *(Russian)* 79–30725
$\nu(\bar{\nu})N$ inclusive scatt., scaling violation evidence, QCD test 78–89701
$\nu(\bar{\nu})N\to l^-(l^+)X$, differential cross section in scaling limit, sea quark contribution 78–37196
$\nu(\bar{\nu})N\to\mu^-(\mu^+)$+hadrons, renormalisable field theory, high energy behaviour 77–61279
$\nu(\bar{\nu})N\to\mu^-\mu^-X$, E>30 GeV, prompt like sign dimuon prod., Fe target, charm prod. 79–93395
$\nu(\bar{\nu})N\to\mu^\pm e^+e^-X$, trilepton event EM and hadronic contrib. 80–409
$\nu(\bar{\nu})N\to\mu(\mu^+)+c\bar{c}+X$, like sign dimuon prod., and b-quark prod./decay limits 79–85290
$\nu(\bar{\nu})N\to\nu(\bar{\nu})$+hadrons, neutral to charged current cross section ratio 78–8651
$\nu(\bar{\nu})N\to\nu(\bar{\nu})\pi+X$, determ. of neutral current coupling consts. 78–8649
$\nu(\bar{\nu})+N$, neutral to charged current inclusive cross-section ratio determ. 77–26511
$\nu(\bar{\nu})n\to\mu^-(\mu^+)pX$, semi-inclusive ν-scatt. and π-struct. functions 79–80819
$\nu(\bar{\nu})p$ inclusive interactions, flavour symmetry breaking in antiquark distribs. 79–36006
$\nu(\bar{\nu})p$ semi-inclusive scattering, hadronic fragmentation initiated by pointlike probes 79–49551
$\nu(\bar{\nu})p\to\mu^-(\mu^+)\Delta^{++}X$, semi-inclusive ν-scatt. and π-struct. functions 79–80819
$\bar{\nu}$ trimuon prod., EM and hadronic contrib., $\mu^+\mu^+\mu^-$ rate and distribs. 79–85291
$\bar{\nu}$ trimuon prod., $\mu^+\mu^+\mu^-$ rate, correl. with $\mu^-\mu^-\mu^+$ ν-prod. events 79–85292
$\nu_\mu(\bar{\nu}_\mu)N$ charged current total cross sections, (V-A) interactions, nucleon struct. function scaling 78–25033
$\nu_\mu(\bar{\nu}_\mu)N\to\mu^-(\mu^+)X$, struct. functions meas., quark-parton model anal. 79–58951
$\nu_\mu(\bar{\nu}_\mu)N\to\mu^\mp+X$, determ. of mass limit of weak boson 79–3012
$\nu_\mu(\bar{\nu}_\mu)N\to\mu^\mp\mu^\mp X$, $SU(2)_L\times U(1)$ gauge model with off-diagonal neutral currents 79–2923

elementary particle inclusive interactions continued

- $\nu_\mu(\bar{\nu}_\mu)N \to \mu \mp X$, colour excitation in deep inelastic scatt. 79−13099
- $\nu_\mu(\bar{\nu}_\mu)N \to \mu(\bar{\mu})$ + hadrons, phenomenology, parton model, expt. data, dimuon events *(Russian)* 77−49943
- $\nu_\mu(\bar{\nu}_\mu)N \to \nu_\mu(\bar{\nu}_\mu)$ + hadrons, gauge theories *(Russian)* 77−49943
- $\nu_\mu(\bar{\nu}_\mu)h \to \mu^\pm l^\pm + X$, charm contrib. to prod. of opposite sign dimuons 79−377
- $\nu_\tau(\bar{\nu}_\tau)N \to \tau^\pm X$, beam-dump experiment, observation of ν_τ interactions 80−22601
- ν+hadron inclusive interaction, single-lepton and dilepton prod., test of T invariance 77−34146
- $\bar{\nu}_\mu + N \to \mu^+ + X$ deep inelastic interaction at 2 to 25 GeV *(Russian)* 80−13298
- $\nu d \to \Lambda_c{}^+X$, high energy charmed baryon prod. obs. 80−105881
- νN, charged current inclusive interactions in Fe at 30-200 GeV, struct. functions, scaling phenomena 79−75764
- νN, deep-inelastic, electromagnetic radiative corrections 80−22602
- νN, inclusive charged current interactions, recent results 79−49506
- $\bar{\nu}N$, K^0 and π^- prod. rates, SU(3) symmetry violation in quark jet 80−82966
- νN, μ^+ single prod. in inclusive interaction 78−45908
- νN, semi inclusive π prod., angular asymmetries in QCD 79−9360
- νN charged current inclusive reactions below 6 GeV 77−26515
- νN charged current reacts., appl. of new scaling rule 78−89703
- $\bar{\nu}N$ charged-current interactions, semi-inclusive γ prod. 79−71737
- $\nu N \to$ hadron shower, charm-pair production effects 80−73748
- νN inclusive interactions, nondiagonal neutral currents, six quark model with slow rescaling 77−49949
- $\bar{\nu}N$ interactions, semiinclusive π production, charge ratio, Gargamelle freon data anal., weak neutral current 78−12905
- $\nu N \to \mu^- e^+ X$, quark fragmentation function 77−87968
- $\nu N \to \mu^- \mu^- \mu^+ X$, internal Drell-Yan mechanism, parton model approach 78−89656
- $\nu N \to \mu^- \mu^+ X$, quark fragmentation 77−87968
- $\bar{\nu}N \to \mu^+$ + anything, Tanikawa-Watanabe meson prod. anal. 77−61274
- $\nu N \to \mu$ + anything, or $\mu^+\mu^-$ + anything, quark-parton model, threshold effects of charm prod. 77−46041
- $\nu N \to \mu\mu X$, dimuon events, D prod., lifetime and fragmentation function 79−93397
- $\nu N \to \nu X$, broken colour gauge theory of integer charge quarks 80−13313
- $\nu N \to \nu l^+ l^-$ (+hadrons), lepton pair production suppression up to 10^5 GeV *(Russian)* 79−36065
- $\nu N \to \nu\pi X$, scale breaking effects 79−40770
- $\nu N \to \nu\psi X$, neutral current ψ prod., Z^0-gluon fusion model 80−78015
- νN single- and di-muon prod., colour excitation, weak interaction model anal. 78−45906
- $\nu N \to X$, determ. of all neutral-current coupling constants from inclusive cross sections alone 79−13106
- $\bar{\nu}_\mu N$, K^0 and Λ inclusive prod., fragmentation function and transverse momentum squared 80−32093
- $\nu_\mu N \to 3\mu X$, $SU(2)_L \times U(1)$ gauge model with off-diagonal neutral currents 79−2923
- $\nu_\mu N \to e^+ X$, $SU(2)_L \times U(1)$ gauge model with off-diagonal neutral currents 79−2923
- $\nu_\mu N \to M^0 X$, use of $\Delta\phi$ rule to disprove heavy lepton existence 79−63470
- $\nu_\mu N \to \mu^- X$, 2 to 30 GeV, characts. of deep inelastic processes *(Russian)* 79−80821
- $\nu_\mu N \to \mu^- e^+$ hadrons, Gargamelle picture anal., strange particles and charm prod. 77−54097
- $\nu_\mu N \to \mu^- e^+ X$, anal. of two-lepton events 77−6107
- $\nu_\mu N \to \mu^- e^+$ + hadrons, investigation at SCAT chamber *(Russian)* 79−58953
- $\bar{\nu}_\mu N \to \mu^+ e^- X$ in Ne 78−29329
- νp, multiple production processes regularities, Monte Carlo model 80−102082
- $\bar{\nu}p$ charged current interaction, inclusive ρ^0 prod. 80−62963
- $\bar{\nu}p$ charged current jet size, comparison with e^+e^- jets 80−22599
- νp high energy interactions, vector meson diffr. prod., charged and neutral current 78−54625
- νp inclusive interactions, ratio of neutral current to charged current cross sectins 77−79263
- $\nu p \to \mu^- D^+ X$ or $\mu^- D^{*+} p$, cross sections estimation using V+A form of charm current 77−41839
- $\nu p \to \mu^- \Lambda 3\pi^+\pi^-$, $E > 10$ GeV, inclusive 79−376
- $\nu p \to \mu^-$ + jet, greater than 10 GeV, jet props. 79−45084
- $\nu p \to \mu^- p D^{*+}$, D^0(1863) and inclusive D^{*+} (2009) prod., mass difference 79−93396
- $\bar{\nu}p \to \mu^+ X$, deep inelastic scatt., MQM description 80−47305
- $\bar{\nu}p \to \mu^+ + X$, 4.5 GeV^2, p struct. functions x depend., quark distrib. 80−32097
- p inclusive electroproduction in fireball model 78−41554
- p-nucleus collision, prompt μ prod., multiple prod. model based on lepton-hadron relation 78−29362
- $p + A \to p$ + anything, A=C, Al, Ti, Cu, Cd, Pb, inclusive backward emission of protons, 1.5 to 9.0 GeV *(Russian)* 77−10278
- p+Be(Cu)(Pb), 300 GeV, inclusive prod. of Λ^0 hyperons 78−37253
- $p + Be \to e^+ e^- X$, 30 GeV, J/ψ prod. and decay into e^+e^- 77−57570
- $p + Be \to \Lambda^0 + X$, 300 GeV/c, Λ^0 polarisation meas. 77−30458
- $p + Be \to \phi + X$, 400 GeV/c, ϕ decay modes, OZI rule 78−599
- p+d relativistic collision, super-fast π prod. 77−18362
- p+emulsion nuclei, 300, 400 GeV, search for short lived charmed particles 77−50023
- p+emulsion nuclei, 300 GeV, inclusive correl. functions 78−58279
- p+emulsion nuclei diffractive coherent prod., inclusive and exclusive channels 78−62530
- $p + Fe \to \mu^+\mu^-$ + anything, enhancement in μ pair mass spectrum at 9.5 GeV, Υ prod. 79−432
- $p + N \to \mu^-\mu^+ X$, 400 GeV, charged gluon effects, broken colour gauge model study 79−49473
- p+nucleus, 200 GeV/c, relative yields of $\pi^\pm$, $K^\pm$, p, $\bar{p}$ 78−93995
- p+nucleus, inclusive π prod., 0.78 to 5 GeV, relation to NN π prod. 78−78384
- $p + \text{nucleus} \to \mu^+ + \mu^-$ + anything, 400 GeV, high-mass dimuon continuum 78−37344
- $p + {}^{187}W$, 2 to 5 GeV/nucleon, multiplicities of secondary particles *(Russian)* 78−46066
- $p + Z \to \pi^\pm(K,p,\bar{p})X$, 28.5 Gev/c, invariant cross-sections, for P_T 0.75-2.25 GeV/c 77−30456
- $pA \to \pi^- + X$, scaling invariance of interactions of relativistic nuclei, the cumulative effect *(Russian)* 79−93611

elementary particle inclusive interactions continued

- $pC \to p(\text{pol.})X$, 100 to 400 GeV, proton polarisation in inclusive processes 79−58983
- pd, 200 GeV/c, multiplicity distribs., and rescatt. effects 78−82255
- pd, 28 GeV, multiplicity distrib., double scatt. in deuterium 79−36114
- pd, 70 GeV, $\pi^\pm$, $K^\pm$, p, $\bar{p}$ prod. with 0.5-2.2 GeV/c transverse momenta, yield ratio, QCD *(Russian)* 80−83012
- pd, neutron fragmentation and inclusive charge exchange, 195 GeV/c 77−22814
- pd coherent elastic and inelastic scatt. of 2800 GeV^2, cross sections, momentum transfer squared depend. 78−37233
- $pd \to dX$, associative multiplicity at high momentum transfer *(Russian)* 77−61333
- $\bar{p}d$ double inelastic interactions, 1.6 to 4.3 GeV/c, multiplicity distribs. 79−58969
- pd interactions, charged particle multiplicity distribs. and rescatt. effects at 19 GeV/c 79−36107
- $pd \to K^\pm$ + anything, large p_T, 200 to 400 GeV 77−22816
- $pd \to p(\bar{p})$ + anything, large p_T, 200 to 400 GeV 77−22816
- $pd \to \pi^0 X$, large transverse momentum, π^0 prod. cross section, ISR energies 79−3055
- $pd \to \pi^\pm$ + anything, large p_T, 200 to 400 GeV 77−22815
- $pd \to \pi^\pm(K^\pm)pX$, 11.75 GeV/c, meas. of left-right asymmetry far inclusive $\pi^\pm$, $K^\pm$, p prod., polarised p-beam 79−22155
- $pd \to V^0 X$, 18 GeV/c, K^0s, γ, Λ, $\bar{\Lambda}$ prod. 77−87993
- $pd \to Xd$, diffractive interaction, test of finite mass sum rule 77−22819
- $pK^- \to \Sigma^+$ + anything, beam and target fragmentation processes, triple Regge anal. 77−82786
- pn, 195 GeV/c, inclusive π^+/π^- ratio and quark distributions 79−54367
- pn, 195 GeV/c, single particle inclusive distribs. 79−75804
- pN, 22.8 GeV, cluster production, two-particle correlations 79−63550
- pN, 28 GeV in Cu, prompt neutrinos and penetrating particles 80−47336
- pN, 300 GeV, quark fragmentation functions in additive model 80−37222
- Pn, 37 GeV, diffr. dissoc. of neutrons, total cross sections 77−2873
- pN, 400 GeV, azimuthal asymmetry, cluster model anal. 79−63547
- pN, 400 GeV, in emulsion, two-particle rapidity correlation 80−63054
- pN, 400 GeV, prompt single muon prod., charm prod. cross section 79−80855
- pN, 400 GeV, rapidity gap correlations, Chew-Pignotti multiperipheral model 79−93471
- pN, 400 GeV, study in nuclear photoemulsion *(Russian)* 79−93475
- pN, 400 GeV/c in emulsion, ang. and rapidity distribs. 80−32140
- pN, 67 GeV, multiperipheral cluster production 80−73689
- pN, 67 GeV, rapidity dispersion and cluster production 80−78104
- pN, 67 GeV/c, in Be, Al, Cu, inclusive $\pi^\pm$, $K^\pm$, p, $\bar{p}$ prod. cross sections *(Russian)* 80−86769
- pN, 67 GeV/c, nuclear targets, $\pi^\pm$, $K^\pm$, p,$\bar{p}$ yields *(Russian)* 80−68501
- pN, 70 GeV, forward prompt muon yield, μ/π yield ratio *(Russian)* 79−97641
- pN, 70 GeV in emulsion, pion cluster obs. 80−86762
- pN, 70 GeV/c, multiparticle prod., principal axis variable anal. 79−36116
- pn and pp, parton-parton interaction in high transverse momentum collisions, phenomenological description 77−57574
- $pN \to$ charm particles, obs. in high resolution streamer chamber 80−73742
- $pN \to$ hadron shower, charm-pair production effects 80−73748
- pN in emulsion, 200, 400 GeV/c, multiparticle prod., azimuthal and rapidity effects 80−63035
- pN in Fe, 400 GeV/c, bottom meson prod. search in multimuon final states 80−47334
- pN in Fe, 400 GeV/c, ψ(3100) prod. 80−57650
- pN in nuclei, 2.2, 6, 8.5 GeV, p and d inclusive spectra at 162° *(Russian)* 79−97710
- $\bar{p}n$ interactions, 100 GeV/c, topological cross sections 79−54366
- $Pn \to l^+ l^- X$, scaling predictions, Drell-Yan model 80−73756
- $pN \to l\bar{l}X$, quark structure functions for hadrons, Drell-Yan model anal. 78−21476
- $pN \to \Lambda^0, \bar{\Lambda}^0$, 300 GeV, inclusive prod., triple-Regge behaviour 77−61328
- $pN \to \Lambda^0 X$, 28.5 GeV/c, Λ^0 polarisation 80−32137
- $pN \to \Lambda^0 X$, inclusive cross section, constituent-constituent multiple scatt. model for dependence on atomic number 80−83101
- $pN \to \Lambda^0 X$, Λ^0 polarisation and quark prod. mechanisms 79−63542
- $pN \to \mu^+\mu^- X$, 225 GeV/c, muon pair prod., $q\bar{q}$ annihilation model 79−63552
- $pn \to \mu^+\mu^-$ + anything, muon pair production, M quiescent mass determ. *(Hungarian)* 79−13163
- $pn \to \mu^+\mu^-$ + anything, review of data, explanation using quark models, new quarks 78−74202
- $pN \to \mu X$, 350 GeV p-Fe collisions, prompt muon prod. rate 80−37311
- $pn \to p_{slow} + x$, 195 GeV/c, triple Regge model anal., dominant π exchange 78−54657
- $pn \to pX$, 100 to 400 GeV/c, slow-proton prod., Regge trajectory 80−22646
- $pn \to pX$, 19 GeV/c pion exchange model of neutron fragmentation 79−63549
- $pn \to pX$, 195 GeV/c, hierarchy of mean multiplicities 79−36112
- $pN \to pX$, 28.3 GeV/c, Pt target, polarisation of inclusively produced protons at $p_T = 1.5$ GeV/c 78−93917
- $pN \to \pi^- X$, 3.95 to 9.7 GeV/c, inclusive π^- prod. below 62 mrad *(Russian)* 79−49538
- $pN \to \pi^- pX$, 9 GeV/c, inclusive $\pi^- p$ prod. below 188 mrad *(Russian)* 79−49538
- $pN \to \pi^0 X$, 200-400 GeV/c, inclusive π^0 prod. over large X_T and X_F ranges 80−37310
- $pn \to \pi X$, central region, Regge Mueller approach, inclusive cross sections *(Russian)* 78−58218
- pn sphericity distribution, in 70 GeV/c inelastic collisions, multiplicity depend. 79−80852
- $p^\pm n$, high-energy, react. differences and annihilation 78−74279
- $p^\pm N \to \mu^+\mu^- N$, 225 GeV/c, muon pair prod., 2 to 11 GeV/c^2, differential cross section 79−67612
- $p^\pm p \to p^\pm + X$, 140-175 GeV, differential cross-section meas. 77−18345
- ϕ inclusive and semi-inclusive prod. in thermodynamic model 77−18238
- π, structure functions from inclusive prod. data, nonstrange quark distribs. 80−86715
- π electroproduction inclusive processes, quark fragmentation function ratio determ. 77−61294

elementary particle inclusive interactions continued
  $\pi(\gamma)+A \to p+X$, effect of short range pairing correl. in cumulative nucleon prod. *(Russian)* 79−30794
  π inclusive electroproduction, quark-parton model comparison with expt. data 78−37218
  π inclusive prod., sum rules, π bremsstrahlung 78−45811
  π-Be, associative production of D^0 mesons, with muons 55 GeV/c *(Russian)* 79−3060
  π-nucleus coherent particle prod. cross-sections at 200 GeV/c 77−18360
  π-nucleus interaction, inclusive distribution of longit. velocities in range 20 to 200 GeV *(Russian)* 77−57578
  π^- ^{12}C, 40 GeV/c, Λ and $K_1{}^0$ inclusive distribs. *(Russian)* 77−34196
  π^--nucleus, one-particle inclusive distribs. of $\pi^\pm$ at 50 GeV *(Russian)* 77−50162
  π^0 high p_T prod. ang. depend., inclusive cross sections, scaling 80−91119
  π^0 inclusive photoprod. and quark-parton model 78−78189
  $\pi^\pm$ inclusive prod., central region factorization for cross section 79−6353
  $\pi^-+A \to p+$anything, A=C, Al, Ti, Cu, Cd, Pb, inclusive backward emission of protons, 1.5 to 9.0 GeV *(Russian)* 77−10278
  π^-+C, 40 GeV/c, secondary particle multiplicity off several nucleons *(Russian)* 78−484
  π^-A, 3.7 GeV, correlation parameter between π^- emitted backwards and forwards *(Russian)* 78−45984
  $\pi^-A \to \pi^0X$ with $\Delta(1240)$ slow isobar intermediate prod. in heavy nuclei, cross section *(Russian)* 78−89917
  $\pi^-Be \to D^0\bar{D}^0X$, pair production at 55 GeV/c *(Russian)* 79−3059
  π^-d, 15 MeV, charged multiplicity distribs. and rescatter probabilities 80−52545
  π^-d, charge multiplicity distribs., parity tests 79−97602
  π^-d, inclusive neutral particle prod., 205 GeV 77−67686
  $\pi^-d \to \pi^+X$, screening effect of protons in deuterons *(Russian)* 77−267
  $\pi^-d \to \pi^+X^-$, 2.6 GeV/c, d proton screening correction and Glauber parameter 80−9175
  π^+d, neutron fragmentation and inclusive charge exchange, 195 GeV/c 77−22814
  $\pi^+d \to p(N^*,\Delta^+)$, 1-5 GeV, inclusive cross-sections 77−6157
  πN, 6-200 GeV, amplitude anal. in impact parameter representation, non-zero polarisation, shell struct. *(Russian)* 80−86752
  πN exotic channels in fragmentation region, early scaling 77−18361
  πN in Al, quark jet multiple production 80−9188
  πN interaction, inclusive distribution of longit. velocities in range 20 to 200 GeV *(Russian)* 77−57578
  $\pi N \to J/\psi+X$, 27 and 40 GeV, total (J/ψ) production cross sections on Cu target *(Russian)* 78−25249
  $\pi N \to l\bar{l}X$, quark structure functions for hadrons, Drell-Yan model anal. 78−21476
  $\pi N \to \mu^+\mu^-X$, longitudinal photon polarisation from helicity ang. distrib. 80−5025
  $\pi N \to \mu^+\mu^-X$, π-struct. function determ. 79−63553
  πN scatt., spin flip dynamics and inclusive processes *(Russian)* 78−41589
  πN semi-inclusive reactions at 40 GeV/c, single particle correls., $\pi^\pm$ and γ struct. functions *(Russian)* 77−82792
  πN total cross section sum rule, reln. of sea quark distrib. and pomeron 79−63441
  π^-N, 16, 22 GeV, dimuon prod. parton intrinsic transverse momentum, QCD perturbation 80−63037
  π^-n, 40 GeV/c, charge multiplicity in forward and backward hemispheres *(Russian)* 77−265
  π^-n, 40 GeV/c, cross sections of Λ and K prod. *(Russian)* 77−6184
  π^-N, 40 GeV/c, leading and conserved mesons *(Russian)* 78−45987
  π^-n, 40 GeV/c, many pion systems in inclusive reactions, transverse momentum effects *(Russian)* 80−57654
  π^-n, 40 GeV/c, semi-inclusive $\pi^\pm$ transverse momentum distributions, statistical model anal. *(Russian)* 79−13174
  π^-N, 40 GeV/c in ^{12}C, multinuclear inclusive process correlation functions *(Russian)* 80−68500
  π^-N, 50 GeV, rapidity gap correlations, cluster emission model studies 79−93469
  π^-N, in ^{12}C, 40 GeV/c, one- and multi-nucleon interactions, secondary charged particle multiplicity *(Russian)* 80−83013
  π^-N, in ^{1}C, 5 GeV/c, π^0 and n inclusive spectra, cascade model *(Russian)* 80−68490
  π^-N collisions 27, 40 GeV/c low-mass muon pair production *(Russian)* 79−89212
  $\pi^-N \to D^{*-}+X$, 10.5 GeV/c, near threshold 78−37249
  $\pi^-N \to \gamma X$, 50 GeV, gamma prod. characteristics in emulsion reactions 80−68492
  π^-N in Be, 150, 175 GeV/c, high mass muon pair prod., Drell-Yan QCD corrections 80−13343
  π^-N in Ne, 25, 50 GeV/c, secondary particle multiplicity and multiple scatt. model anal. *(Russian)* 80−83014
  π^-N interactions, 50 GeV/c, inclusive charged π prod. in nuclear emulsion anal. 78−66168
  $\pi^-N \to \mu^+\mu^-X$, 27, 40 GeV, cross sections and differential distribs. *(Russian)* 78−89919
  $\pi^-N \to \mu^+\mu^-X$, K^-/π^- structure function ratio using Drell-Yan process 80−86718
  $\pi^-n \to pX^{--}$, 21, 205 and 360 GeV/c, reggeised one-pion-exchange 80−57649
  $\pi^-n \to$ pions$+X$, 40 GeV/c, transverse pion momenta depend. on secondary particle multiplicity *(Russian)* 78−33103
  $\pi^-N \to \psi X$, 225 GeV, bottom meson pair production limit 80−73750
  $\pi^-N \to \rho^0(\omega)X$ at 40 GeV/c, cross sections 77−18359
  π^-n semi-inclusive interaction, 40 GeV/c, charge distribution *(Russian)* 77−74739
  π^-N semi-inclusive reactions at 40 GeV/c, structure functions *(Russian)* 77−61332
  π^+n, 195 GeV/c, inclusive π^+/π^- ratio and quark distributions 79−54367
  π^+n, 195 GeV/c, single particle inclusive distribs. 79−75804
  $\pi^+n \to p_{slow}+x$, 195 GeV/c, triple Regge model anal., dominant π exchange 78−54657
  $\pi^+n \to pX$, 100 to 400 GeV/c, slow-proton prod., Regge trajectory 80−22646
  $\pi^+n \to \pi^+X$, 195 GeV/c, hierarchy of mean multiplicities 79−36112
  $\pi^+n \to \rho^0X$, 6.0 GeV/c, comparison with $K^-p \to \bar{K}^{*0}X$ 77−30459
  $\pi^\pm n$, high-energy, react. differences and annihilation 78−74279
  $\pi^\pm N \to \mu^+\mu^-X$, 225 GeV/c, muon pair prod., $q\bar{q}$ annihilation model 79−63552

elementary particle inclusive interactions continued
  $\pi^\pm N \to \rho^0X$, inclusive cross sections and spin density matrices, 3-Reggeon model anal. *(Russian)* 79−80858
  $\pi Ne \to pX$, 10.5 GeV/c, recoil nucleons, tube model anal. 77−61458
  πp, 16-GeV/c, dimuon production and obs. of low-mass continuum 78−37236
  π^-p, 150 GeV/c, leading particles and diffraction dissociation, 2-, 4- and 6-prong events 80−68486
  $\pi^-p \to \pi^+X^-$, 2.6 GeV/c, d proton screening correction and Glauber parameter 80−9175
  $\pi^\pm p \to \pi^\pm+X$, 140-175 GeV, differential cross-section meas. 77−18345
  $\pi^+\pi^-$ inclusive prod., transverse momentum correls. in cluster model 77−38134
  $\pi^\pm\pi^\pm \to$mesons, multimeson inclusive spectra and recombination model, multiquark structure functions, predictions 80−73751
  $\pi^-\pi^-\pi^-$ correlation functions, Mueller scheme with Bose-Einstein statistics 78−93915
  ψ inclusive production on 43 GeV/c π^-on Be, Cu, W, A-depend. 78−62581
  ψ prod., multimuon events in $\pi(p)+$nucleus reactions 77−30460
  $\psi\psi$ prod., correl. effects in large p_T pion events 77−26549
  $qq \to qqX$, large p_T hadronic collision jet struct., QCD calc. 79−75721
  $Be(p,h^\pm)$, 200 to 400 GeV, inclusive production of large-transverse-momentum hadrons and hadron pairs 79−89310
  $^{12}C+\pi$, 5 GeV/c, momentum spectra and mechanism of proton emission *(Russian)* 79−89334
  $^{12}C+\pi^-$, 40 GeV/c, secondary charged particle inclusive spectra, $\pi^\pm$ struct. functions *(Russian)* 78−89921
  $^{12}C+\pi^- \to p+X$, 40 GeV/c π^- momentum *(Russian)* 79−89335
  $^{12}C(\pi^-,\pi^\pm)X$, 40 GeV, multiparticle prod. mechanism, various model predictions 79−573
  Cu$+$p collisions, 400 GeV, prompt ν prod. 78−46061
  Cu$+\pi^-$, 27, 40 GeV, cross sections and differential distribs. for muon pair prod. *(Russian)* 78−89919
  Fe$+\mu \to$multimuons$+X$, 150 GeV/c, charmed particle prod. 77−38177
  Fe$+$p, 400 GeV, missing energy associated with $\mu^+\mu^-$ prod. 80−22833
  Fe$+$p inclusive react., structure function of conserved hadrons, 100-1600 GeV *(Russian)* 78−41611
  $\gamma N \to \eta X$, 9.7 GeV, inclusive η photoprod. on H- and ^{2}H-targets, ρ^0-dominance model anal. 79−63486
  $h+A \to h'+$anything, colour in production on nuclei 78−93981
  inverse problems, analytic extrapolations in high energy physics 79−49499
  $K^+p \to \pi^\pm X$, 32 GeV, topological cross sections 80−102085
  $K^\pm p$, 100 and 175 GeV/c, inclusive scatt. results from Fermilab single arm spectrometer 78−89746
  Ne$+\nu_\mu(\bar{\nu}_\mu)$, inclusive prod. of hadrons, preliminary data 78−89853
  Ne$+\pi^\pm$, 10.5 GeV/c multiplicities and inclusive moment and rapidity spectra 78−8862
  $\nu N \to 4\mu X$, radiative and hadronic production characts. 79−40771
  $\nu N \to \mu 3eX$, radiative and hadronic production characts. 79−40771
  pN, 350 GeV in Ne, $D^\pm$ prod. cross section and lifetime 80−68494
  $pN \to K_s{}^0$, 300 GeV, inclusive prod., triple-Regge behaviour 77−61328
  $\bar{p}n$, mean charged multiplicity, energy depend., modified Heisenberg calcs. 79−40806
  $\pi^-N \to \mu^+\mu^-X$, lepton ang. distrib. calc. by QCD 79−26303
  $\pi^\pm n$, mean charged multiplicity, energy depend., modified Heisenberg calcs. 79−40806
  $W(p,h^\pm)$, 200 to 400 GeV, inclusive production of large-transverse-momentum hadrons and hadron pairs 79−89310

elementary particle interaction models
  see also bootstrapping; composite models of hadrons; diffraction model; duality and dual models; peripheral models; statistical models; vector meson dominance model; Weinberg model
  $\lambda\Phi^4$ model of meson-meson interactions, dynamical symmetry restoration 77−5989
  $\pi N \to \rho X$, trajectory data, reson. and scatt. regions, compatibility *(Russian)* 78−8703
  Amado model for nd scatt., NN exchange cuts in second Born amplitude 77−2790
  angular distrib. anisotropy of particles with small relative momenta *(Russian)* 77−227
  asymptotic catastrophe, temporary freedom in lepton and quark interactions 79−85253
  axion-hadron interactions, possible strong suppression *(Russian)* 80−42387
  baryon-antibaryon harmonic oscill. pot. model, orbital matrix elements and selection rules 77−49930
  Bounds on slope of diffraction peak and zeros of absorptive differential cross sections 78−74282
  bremsstrahlung model of Brodsky and Gunion, comments 79−93362
  broken SU(3) gauge model of strong and EM interactions, scatt. lengths, baryon mag. moments 78−74133
  Cabibbo angle formula, discrete flavour symm. 78−417
  Chew-Low amplitude correction for double pion photoprod. 77−2844
  Chew-Low model, πN vertex function 78−8686
  Chew-Low model, covariant theory of off shell πN scatt. 77−6151
  Chew-Low static model, πN form factor 78−41574
  Chou-Yang model anal. of pp elastic scatt., structure of second dip 77−54120
  cluster formation in multiparticle prod. processes 77−13931
  Coherent Tube Model for very high energy inelastic interactions of deuterons 77−18347
  conference, particles and fields, Montreal, Canada (Oct. 1979) 80−73090
  confining pot., Regge poles, coupled Schrodinger eqns. 77−61219
  conformal-invariant field theory, anomalous dimensions, coupling consts. 80−4870
  contact EM terms and nuclear shadowing of high energy photons, absorpt. by nucleons and nuclei 77−49980
  conventions, naming of partial waves, Argand plot coord. systems 77−22720
  cylinder dominated model of ψ hadronic and photonic decays, pseudoscalar mixing effects 77−6120
  Deck model with absorption, nucleon diffraction dissociation, high energies 77−26548
  deep inelastic muon hadron scatt. data, high energy, asymptotically free gauge theories predictions 77−49974
  deep inelastic scattering, contrib. of twist-four operators, struct. functions 78−78187

elementary particle interaction models continued
Dirac particles, high energy scatt. by arbitrary pot. 77—57508
droplet model for high energy pp elastic scatt., ang. depend. 78—82243
dynamical model for multiplicity distribs. in πp and pp-collisions, pion prod. 78—21469
eikonal, charged secondary transverse momentum depend. on multiplicity in pp collisions 77—6177
eikonal description of nucleon-nucleon elastic polarisation data 77—13948
eikonal description of polarisation in NN elastic scatt. 77—30405
eikonal model, multiplicity distribs., KNO scaling 78—41514
eikonal model, spin depend. at high energies in pp scatt. 77—22710
eikonal model multiplicity distrib. and Koba-Nielsen-Olesen scaling *(Russian)* 79—9355
eikonal model of hadronic matter distribution of particles and nuclei 79—26317
eikonal pionisation graph summing in Lagrangian field theory 80—4973
elastic scattering amplitude, absorptive part, lower bounds on slope parameter 77—34114
extended particle model, dynamical theory of hadron interactions 77—87936
Federbush model, absence of induced counterterms e^+e^- scatt. amplitudes 78—50023
generalised optical theorem and dispersion reln. for $3 \rightarrow 3$ forward amptitude 79—22079
geometrical model of hadron hadron collisions, appl. to radii determ. for π and K 79—89137
geometrical models of hadron-hadron elastic scatt., energy depend. anal. 77—41806
hadron collective interaction, particle inclusive spectrum properties, space-time model 79—40808
hadron elastic scatt., high energy, review, optical and quasi-potential models 77—257
hadron interaction models describing multi-particle production processes, review 78—33024
hadron interactions, multiplicity, semi-empirical formula 78—58210
hadron matter, thermodynamic description, evolution, coupling const. depend., hot nucleon matter appl. *(Russian)* 79—3006
hadron multiprod., long-range correl., overlapping independent emission 78—82141
hadron-nucleus, absorptive part of scatt. amplitude, multiparticle prod., Glauber theory 78—37248
hadron-nucleus inelastic collisions, multiplicities, ang. distrib., hydrodynamic and parton models *(Russian)* 77—250
hadron-nucleus interaction, multiple particle prod., absorptive part of scatt. amplitude *(Russian)* 78—17164
hadronic bremsstrahlung models, ordinary and charge conserving, causality and unitarity breakdown 77—57486
hadronic multiparticle reactions, models, prod. of strangeness, baryon number, charm 78—74286
hard scattering models, large transverse particle prod., cross section constraints from opposite side rapidity distribs. 78—29360
high energy interactions, scaling, limited fragmentation, cosmic ray models 77—10211
high energy physics, conf., Schladming, Austria (Feb.-Mar., 1977) 78—8494
high energy strong interactions, review, expt., theory 77—13983
high-energy collisions, two-component model 79—323
hydrodynamical high-energy lepton and photon interactions *(Russian)* 77—229
hyperon-nucleon charge exchange and strangeness exchange reactions, triple Regge techniques 77—18331
inclusive processes, cross section decrease at fixed angles, planarity at high energies, analyticity 80—78105
inclusive single-particle distrib. in cos θ, analytic props. in ladder model with asymptotically const. total cross section 79—3061
inelastic final state interactions, unitarity, coupled-channel approach 77—2835
isobar model, angular crossing relations, Euclidean approx., meson+nucleon inelastic scatt. 79—13019
isobar model, unitarity, two-body discontinuities, $KN \rightarrow K\pi N$ appl. 78—418
isobar model, unitarity constraints 77—34108
isobar model and $\pi N \rightarrow \pi\pi N$ analyses 77—22776
isobar model for $ab \rightarrow jkl$, overlap integrals 77—46032
isobar models, resonance character of A_1 77—22680
iteration models, elastic reactions beyond diffraction peaks 78—93839
jet production mechanism in lepton-hadron interactions, cascade and uncorrelated jet models 80—52516
Landau's relativistic hydrodynamical model of pp to p-nucleus multiplicity ratios 77—46169
large NO(N) σ-model of meson-meson interactions, dynamical symmetry restoration 77—5989
large p_T reactions, trigger bias, two-jet picture 77—2878
large transverse momentum and large mass production in hadronic interactions review of theoretical models 79—89115
lepton direct production in hadron-hadron collisions, interaction models review 77—236
lepton-hadron relation and a new KNO-type of scaling 79—9414
leptons, topological bootstrap approach, rishon model 80—78046
massive Thirring model, four fermion interaction, conservation laws 77—41777
massive Thirring model, localised solns. in presence of external electrostatic field 77—65095
meson-baryon interactions, meson spectra in forward jets, hadron cascade model anal. 80—32103
minimal K-matrix model, three pion enhancements 77—6060
multi-temperature models of inclusive spectra 77—49936
multiparticle production model for high energy hadronic collisions 79—80790
Muskhelishvili Omnes integral equation, soln. procedure 77—13577
new particles and weak interactions, models *(Chinese)* 79—93334
nuclear decays as test of elementary particle theory, review 78—21361
nuclear primary air showers, phenomenological model 77—22028
nucleon-nucleon scattering, phase shift anals., pp at 1-500 MeV, pn at 0-425 MeV 77—54115
optical theorem violation for strong interactions 77—26504
P+f model, flavour and baryon number renormalisation 80—78050
phase modified absorption model for $\pi^- p \rightarrow \pi^0 X$ helicity non-flip amplitude 77—79288

elementary particle interaction models continued
potential model, πN local phenomenological potentials, 0-250 MeV scatt. 78—70400
potential model, Dirac eqn. with linear confining pot., symmetric model 79—364
potential model anal. of EM effects in precision anal. of low-energy np interaction data 78—93896
potential model based on Dirac eqn. with linear confining pot., asymmetric model 79—363
potential models of short distance Regge singularities 77—38147
proportionality relations in charge-exchange reactions 77—54123
pure leptonic weak interaction with induced shadow states, renormalisable theory 78—37136
quarks and leptons, topological bootstrap approach, rishon model 80—78047
quasieikonal model, hypercharge exchange reactions *(Russian)* 79—3041
quasipotential eqn., nonlocals in terms of retarded functions 78—29282
Reggeised absorption model for reaction $NN \rightarrow \Delta(1236)\Delta(1236)$ 77—6170
relativistic generalisation of linearly rising pot. 78—4768
ring hopping model, multichannel eikonal model, nucleon diffractive excitations, falling total cross section 78—21404
scalar meson dominance model, eta meson hadronic decay 78—4860
scaling property of shrinking diffraction peaks, elastic unpolarised differential cross section 77—18206
seven lepton model, quantum flavour dynamics, mixing angle, masses, spontaneous symmetry breaking 78—89652
single pion photoproduction between threshold and 16 GeV, multipole and amplitude anals. 79—3031
spectral function methods, non-relativistic two-body off-shell amplitudes 77—26643
spin dependent EM hadronic interference, pn and Λp elastic scatt. amplitudes 78—12923
spin-orbit interaction model, polarisation and spin correl., elastic NN scatt. 77—30404
spontaneous symmetry breaking in interaction of scalar field with external vector field 78—8545
strong interaction models in 6-ε dimensions 80—4919
$SU_L(24) \times SU_R(24)$ model for the unification of interactions *(Chinese)* 79—54291
$SU(2) \times U(1)$ unified gauge theory, mech. for nonconservation of muon number, $\mu \rightarrow e+\gamma$ appl. 77—30303
$SU(2) \otimes U(1) \otimes U(1)'$ gauge model of weak interactions, $\Delta I = 1/2$ enhancement 77—6073
SU(3) symmetry violation models for interactions with vector mesons, tests *(Russian)* 77—10196
SU(5), SU(6) vectorlike unified theories with unitary groups, Fermi oscillators, proton stability 77—67608
subnuclear physics, review 77—67623
supersymmetric models of weak and electromagnetic interactions 79—26276
t-channel exchange model with s-channel absorptive effects, high energy polarisation data interpretation 77—30435
total absorption model extension to include phase and spin 77—57507
twist selection rule, mass zero representation partons 80—78027
two-component model and geometric picture for high energy P-P collisions 79—58948
unconfined heavy fermion model for dimuon prod., $\nu_\mu p \rightarrow \bar{\mu}\nu_F F^+ X$, $F^+ \rightarrow \mu^+ \nu_\mu \bar{\nu}_F$ 77—18269
unitary isobar model, A_1 prod. from three π and $K^*\bar{K}$ data, partial wave anal. 79—40721
unitary model for elast. scatt. and inclusive interactions 77—30343
universality of clothed physical pomeron, geometrical pomeron, importance of asymptotically high energies 78—33047
vector meson$\rightarrow e^+e^-$, standard leptonic decay width correction, effecting pot. model predictions 78—89707
vector-like model of weak interactions, spontaneous CP violation 77—54071
weak interaction models explaining null parity violation in Bi, tests on other weak interactions 79—2974
weak interaction theory satisfying high energy unitary bounds, Weinberg model appl. *(Chinese)* 79—320
Z(N) strings and hadron structure 80—86572
d breakup, exotic final state interaction, intermediate Δ, ΔN threshold parameters 78—50043
$e^+e^- \rightarrow \mu^+\mu^-$, contribution of weak neutral currents *(Russian)* 78—62383
ep, deep inelastic scatt., meson spectra in forward jets, hadron cascade model anal. 80—32103
hh scattering, geometrical model for scatt. at ultrahigh energies, existence of dips 79—89191
$K^+ +$, 32 GeV/c, 4 and 6 body final states, principal-axis variables anal. 78—58206
$K^*\pi \rightarrow K^*\pi$, analytic quasi-unitary isobar model anal. 79—36099
$K^- d \rightarrow K^- d$ or $K^- n(p_s)$, 4.5 GeV/c, Glauber formalism, amplitudes, cross section 77—88004
$K^- {}^4He \rightarrow \pi^- \Lambda^3 He$, final state interaction model, Muskhelishvili Omnes eqn. soln., πmomentum distrib. 77—30285
$K\bar{K} \rightarrow K\bar{K}$, dispersion model, matrix N/D method *(Russian)* 78—45954
N*N, total cross sections of diffractively produced nucleon excitations 78—21481
NN inclusive charge exchange, parameter-free model 77—18336
NN interaction, EM phase shift calc. within relativistic model, isospin non-conservation 78—62438
NN polarised scatt., weak neutral current models 78—41562
NN scatt., potential models, high-energy phase shifts and off-shell react. matrices 78—45936
$N\pi \rightarrow N\pi\pi$, isobar model rescattering effects, unitarity corrections 79—71762
$N\pi\pi$ dynamics, medium energy, dispersion relations, isobar expansion for πN 80—4917
$N\pi\pi$ medium energy dynamics from πN, isobar model rescatt. corrections 80—4918
ν-induced associated production, Born term model 78—58179
$\nu_\mu e \rightarrow \nu_\mu e$, weak vector-like models, induced axial vector coupling 78—50025
νN elastic and deep-inelastic scatt., photon-neutrino weak-coupling theory, neutral lepton current 77—30358
p-nucleus collision, prompt μ prod., multiple prod. model based on lepton-hadron relation 78—29362
pd forward elastic amplitude in non-overlapping potentials model 78—45943

elementary particle interaction models continued
pd potential scattering, total cross section calcs., 200-1000 MeV, Glauber model 77−61309
$pn \to d(\pi\pi)^0$, effective two body interaction Hamiltonian, missing mass, ABC effect 78−70388
pn scattering, 50, 325 MeV, phase shift anals., single energy and energy depend. solns. 77−54116
pp, polarisation data interpretation for high energy elastic scatt., eikonal model, spin parameters 79−3048
pp, polarised 6 GeV scatt., spin depend. forces in eikonal model 80−37246
$pp \to d\pi^+$, deuteron polarisation, isobar model anal. 79−49535
pp elastic collisions, polarised, 6 GeV/c, absorpt. model 77−2858
pp elastic scattering, eikonal model, energy depend. anal. 20 to 60 GeV 79−89190
pp inelastic collisions, ρ-dominance in collision model 78−37238
pp inelastic scatt., parity violation, $\Delta(1232)$ prod. model 78−62435
$\bar{p}p$ large-angle elastic scatt., 1.5-2.06 GeV/c, optical model anal. 78−74270
pp opaqueness at high energy, factorisable eikonal model and scaling hypothesis comparison 78−74280
$pp \to pX$, leading proton spectrum, associated multiplicity distrib. in geometric bremsstrahlung model 80−37309
$p\bar{p}$ scatt. at low momenta, simple approach emphasising absorption, pot. model 79−13145
pp scattering, spin dependent eikonal amplitude, extension to pseudoscalar exchanges 79−17698
pp semiinclusive collisions, hypergeometric distrib., KNO scaling 77−2883
pp total cross section, spin dependence, relativistic model of $\Delta(1232)$ prod. 78−62436
$pp \to$ virtual gamma + hadrons soft bremsstrahlung, external emission dominance model 78−62430
$\bar{p}p \to x\pi$, model of excited hadronic matter 78−74288
$\phi\pi \to \rho\pi$, analytic quasi-unitary isobar model anal. 79−36099
π mass difference, Bars-Halpern-Yoshimura unified gauge model, perturbative calc. 77−10251
πN scatt., separable potl. model 77−6153
$\pi^- N$, 50 GeV, rapidity gap correlations, cluster emission model studies 79−93469
$\pi^- p \to p\pi^+\pi^-\pi^-$, 16 GeV/c, prism plot anal., reaction mechs. 77−6174
$\pi^- p \to \pi^0 n$, charge exchange polarisation, Gribov Reggeon calculus, derivative rule, absorpt. model alternative 77−46076
$\pi^+ p$ polarisation near backward direction, partial waves anal., comparison with model predictions 77−30421
$\pi\pi \to K\bar{K}$, dispersion model, matrix N/D method *(Russian)* 78−45954
$\pi\pi \to \pi\pi$, dispersion model, matrix N/D method *(Russian)* 78−45954
$\pi\pi$ scattering lengths, universal curve, optimal extrapolation techniques 77−46080
$\psi \to f\gamma$, form factor depend. in relativistic harmonic oscill. model 79−89156
ψ'' (3.772), ground state admixture in potential model 80−102033
$\pi d \to \pi^0 d$, 350-500 MeV, differential cross section asymm., impulse approx. with pion rescatt. terms 77−30389
$\rho K \to \rho K$, analytic quasi-unitary isobar model anal. 79−36099

elementary particle interactions
see also cosmic ray effects and interactions; elementary particle coupling constants; elementary particle electromagnetic interactions; elementary particle gravitational interactions; elementary particle inclusive interactions; elementary particle large momentum transfer interactions; elementary particle scattering; elementary particle strong interactions; elementary particle weak interactions; hadron-deuteron interactions; hadron-hadron interactions; high-energy cosmic ray interactions; lepton-deuteron interactions; lepton-hadron interactions; lepton-lepton interactions; photon-deuteron interactions; photon-hadron interactions; photon-lepton interactions; photon-photon interactions; polarisation in elementary particle interactions; quantum field theory of interactions; unified field theories; vertex functions
annihilation of particle-antiparticle pairs, possible future use as energy source 79−36054
baryon nonconservation in grand unified theories, rel. to Universe isotropy and homogeneity 80−22125
binary reactions, review of expt. investigations and comparison with theoretical models *(Russian)* 79−63530
book, annual review of nuclear science (vol.26) 77−57583
CERN experiments in 1979 80−408
cluster decomposition of many dimens. phase space, appl. to high energy collisions 80−102027
conference, particles and fields, Montreal, Canada (Oct. 1979) 80−73090
conventions, naming of partial waves, Argand plot coord. systems 77−22720
crossing relations derivation using substitution rule 79−67483
diffractive production mechanisms, high-energy, review 79−36052
dimensional considerations about elementary particles 78−33006
direct interactions, relativistic addition in point form of dynamics 79−58907
event recording and analysis by computer *(French)* 80−63496
forces between leptons and quarks, a gauge field phenomena 80−91008
fundamental constituents of matter and unification of weak and electromagnetic interactions 80−62940
graduate level textbook 80−27053
gravitation lepton-hadron, two-tensor field theories, interaction term 77−87932
gravitational baryon annihilation as type of radioactive decay *(Russian)* 77−26470
Hamiltonians, approximate relativistic, for interacting particles, canonical formalism 77−13897
heavy quarks, elementary particle physics developments, review 79−22053
heterodyning of elementary particles, radiation meas. method 80−42898
high energy physics program at BNL, equipment, experiments, future research 77−18716
high-energy physics, particles and interactions, accelerators 80−77944
nonresonant Argand loops, pseudoresonances 77−61264
off-shell effects model-independent meas. via polarisation expts. 77−18515
particle physics overview, role of CERN and FERMILAB *(Dutch)* 77−45928

elementary particle interactions continued
phase space integral, n-particle, relativistic, Monte Carlo integration program 78−33001
photon-tachyon interactions and the isotropic photon flux 80−446
polarisation in atomic and nuclear physics 80−63162
quark fragmentation parity-odd correls. 78−433
relativistic, classical interacting fields, virial theorem and stability of localised solns. 78−21342
relativistic Hamiltonian mechs., position variables 80−27123
resonance energies, complex, diverging wave functions, least squares bivariational method 78−17741
review of 30 years work by Nuclear Reactions Lab. Dubna, USSR 79−36204
Rutherford Laboratory, particle physics experiments 1979 80−105942
secondary particles from high energy reactions, detection losses correction by generator functional technique 77−6650
Summer School, high energy physics, Rutherford Laboratory, England (6 to 24 September 1976) 77−41747
superfluid as a source of all interactions 79−21620
tachyon exchange in two-body interactions 80−82960
two-body reactions, rigorous formulae for statistical errors on zeros and partial waves 78−4527
unification of fundamental forces in nature, elementary particle constituents SU(3)$_c$ gauge symmetry, review 80−27448
unified coupling scheme, world of composite nucleons 78−25000
unified theory of elementary-particle forces 80−105827

elementary particle large momentum transfer interactions
see also elementary particle inclusive interactions
anomalous current fragmentation in high-$p_\perp$ leptoproduction 79−13134
average associative multiplicity, maximal rise in large momentum transfer processes *(Russian)* 80−42510
average transverse momenta of secondary particles, upper bound on modulus of vector product *(Russian)* 79−49563
broken SU(6) parton model, spin depend struct. functions, deep inelastic lepton+nucleon appl. 78−428
canonical scaling in hadronic high-p_T processes, parton Fermi motion 78−45977
Chao-Yang statistics, particle ratios and quarks 80−27486
coherent tube model, large p_T production off nuclei, parton tubes 78−21392
colour gauge theory, quark elastic scatt. and large transverse mom. hadron prod. 78−8610
composite model of quarks, large P_T hadron prod. 78−62472
conference on high energy phys. with polarised beam and target, Argonne, USA (Oct. 1978) 79−63526
constituent interchange model, cross section normalisation 77−71486
constituent rearrangement model and hadron reactions review 79−26294
cosmic ray nuclear event, $\sim$42 TeV, high multiplicity, large transverse momenta, giant fireball 78−33105
Coulomb-nuclear interference polarisation in high energy large momentum transfer hadron reactions 77−79282
deep inelastic scatt. and lepton pair prod., covariant parton model approach to scaling 78−21431
dilepton angular correlations, test for two body QCD subprocesses 80−387
dimensional counting and Landshoff, multihadron reactions at large transverse momentum 78−33092
diquark jets in leptoprod. and large p_T reactions, fragmentation functions 78−82149
direct γ prod., large p_T, high energy hadron collisions 77−71547
Dreel-Yan processes, gluon corrections 78−8597
EAS, high transverse momentum of γ-ray bundles, $>10^{12}$ eV 79−62701
elastic quark-quark scatt. model, relations for hadron pairs 78−66092
elastic scattering, small and large momentum transfer relations *(Russian)* 80−86698
energy inclusive meas., parton model and scaling laws 77−74733
exclusive processes in QCD, baryon form factors at large momentum transfer 79−89153
extended quark model, large p_T hadron prod. 78−29342
Fermi-motion, canonical scaling of partons in hadronic high p_T processes 78−29314
fireball model anal. of small and large P_t pion distribs., ISR energies 77−38211
formation zones, large p_T prod. on nuclei 77−50134
gauge theories, large transverse momentum behaviour 77−71429
gluon model, large $P_\perp$ data anal. 78−8615
hadron+hadron, large-angle scattering, quasi-potential approach, preasymptotic effects 80−68484
hadron+hadron$\to\mu^+\mu^-$X, QCD anal. jet recoil on large ρ_T muon pair 79−9416
hadron+hadron$\to$meson+X, quark elastic scatt. as high transverse momentum meson source 77−57575
hadron+hadron collisions, particle-jet correls., quark scatt. model 78−4883
hadron+hadron inclusive cross section of symmetric hadron pairs produced, hard scatt., parton model and QCD 80−63052
hadron constituent model discrimination using large transverse momentum data 78−12881
hadron correlations at large transverse momenta, Be+p at 400 GeV/c 78−46060
hadron high-energy prod., multi-eikonal theory 77−6098
hadron inclusive prod. cross sections at large P_T A-depend., quark-parton model *(Russian)* 80−86771
hadron inclusive prod. in pionisation region, covariant parton model *(Russian)* 77−34131
hadron inclusive spectrum produced at large-transverse-momentum *(Chinese)* 78−12935
hadron interactions, inclusive, large momentum transfer, quark counting, EM form factors 80−68498
hadron jet struct. at large transverse momentum in $\gamma\gamma$ interactions 78−82225
hadron jets, correlating quark rearrangement model 79−2997
hadron physics at high p_T 80−73743
hadron production, lowest subprocess model, two body reactions, inclusive pp, πp appls. 78−4887
hadron reactions, large, small momentum transfer regions, transition point for s-depend. 77−30339
hadron-hadron collisions, dilepton ang. distribs., QCD and quark model anal. 79−80801

elementary particle large momentum transfer interactions continued
hadron-hadron collisions at high energy, large transverse momentum processes, review *(Russian)* 79−26351
hadron-hadron interactions, particle ratios and lepton prod. at large p_T, parton model 77−67620
hadron-hadron large p_T collision, weak interaction effects 78−21462
hadronic, QCD perturbation theory test, review 79−326
hadronic correlations at large transverse momenta, parton model 77−18228
hadronic events, inelastic, non-diffractive, charge correlations in jets, quantum number effects 80−86764
hadronic high momentum transfer scatt., spin meas. and polarisation review 79−63498
hadronic interactions, review of theoretical models 79−89115
hadronic large p_T phenomena, effect of parton transverse momenta, QCD Born terms 79−30716
hadronic large p_T reactions, K^+ and K^- prod. as model test, hard quark scatt. 79−40735
hadronic processes, appl. of quark parton model 79−30715
hadronic processes, large and small p_T behaviour 79−26268
hadronic processes, small and large p_T behaviour, new particle-wave duality 79−45081
hadronic prod. of large-P_T leptons and large-Q^2 lepton pairs 77−22810
hadronic reactions, hard scatt. model of urbaryons with two-jet struct. 77−41813
hard scattering models, large transverse particle prod., cross section constraints from opposite side rapidity distribs. 78−29360
hard scattering models comparison for large transverse momentum meson prod. 78−41498
heavy quark prod. in photoproduction, QCD model, possible large p_T process connection 78−78137
hierarchy in asymptotic reconstruction of spontaneously broken isotopic symmetry *(Russian)* 79−2968
high energy particle-nucleus interactions, discussion 79−30858
high p_T hadronic jet photoprod., QCD anal., quark and gluon jets 80−42474
high p_T jet pairs, parton-parton scattering and π quark struct. functions 80−47248
high p_T processes, parton transverse momentum effects, QCD description 79−17774
high P_T theory, use of polarised beams and targets, QCD tests 79−63409
high transverse momentum processes, quark-parton model anal. 78−82163
high transverse momentum scatt., two particle correlations and ϕ prod., jet trigger 78−78225
high-mass resonance enhancement by large transverse momenta selection 77−2871
high-transverse-momentum symmetric-particle-pair spectra and correlations 80−95250
inclusive cross sections magnitude, hadron struct., constituent interchange model 79−431
inclusive cross-section in region of large transverse momenta and singularity interaction 78−54661
inclusive hadron prod., large p_T transfer, multiple-scatt. theory 77−88019
inclusive hadron production in high energy particle+nucleus collisions, sum rules, scaling law 77−57673
inclusive high energy particle-nucleus interactions, A depend. of multiplicity, cross section, rapidity, momenta distrib. 77−79291
inclusive photoprod. and hard scatt. model 79−9417
inclusive processes with large momenta, quark-parton model *(Russian)* 77−71538
inclusive production cross section for particle with large transverse momentum on nuclei *(Russian)* 77−38216
inclusive production of large-transverse-momentum hadrons and hadron pairs 79−89310
inclusive single-particle distribution function structure, urbaryon model 77−18343
jet and lepton-pair prod. 79−2932
jet and lepton-pair production in high-energy lepton-hadron and hadron-hadron scattering 79−17729
jet struct., from rapidity correlations and associated multiplicities 77−49919
jet structure in high p_T events, importance of parton transverse momentum 78−432
jets and multiplicity distribs. 77−14009
kinematical scale breaking in high p_T interactions, parton fragmentation function 80−367
kinematical scale breaking in high P_T interactions 79−13064
large $p_\perp$ photoproduction, gluon fragmentation function extraction, scaling 80−105853
large p_T hadron prod. off nuclei, QCD parton model, nucleus as gluon filter 79−89110
large p_T hadronic collisions, QCD sensitive test, quark and gluon jets 80−57647
large p_T jet prod. in hadronic collisions, QCD calc. for inclusive cross section 78−86439
large p_T proton inclusive prod., quark-quark elastic scatt. 79−17773
large p_T proton production, parton models 79−40743
large Q_T transverse momentum lepton pairs and hadron jets prod., reaction mech., perturbative QCD 79−2999
large transverse momentum hadron prod. on nuclei 77−30461
large transverse momentum particle and jet prod., QCD approach 79−17761
large transverse momentum physics review, diagnosis and prognosis 78−78215
large transverse momentum trigger, multiplicities and rapidity distribs. 78−62376
large-p_T reactions, transverse quark polaris., quantum chromodynamics test 79−17741
lepton pair prod., structure function relns. at large-transverse momenta 79−17690
lepton pair production, QCD and hard-scatt. model, spin-spin asymmetries 80−63014
lepton-hadron hard reactions, scaling features, correlating quark rearrangement model 79−58939
massive μ pair prod. in hadron collisions, field theoretic parton model 77−30326
mean multiplicity depend. on transferred momentum, expt. and geometric approach *(Russian)* 80−95293

elementary particle large momentum transfer interactions continued
mean multiplicity dependence on transverse momentum *(Russian)* 77−46027
meson multiplicity prod. at large p_T, quark rearrangement model 77−61259
meson production at large p_T, interrelation between πp and pp collisions 77−50030
momentum conservation effects in large- and small-p_T prod. 77−71539
Monte Carlo event generation with limited tranverse momentum 79−3001
multiparticle production, large transverse momenta, momentum conservation, independ. emission model 78−50055
multitemperature thermodynamical model 79−3004
nonperturbative QCD effects at large momentum transfers, e^+e^- annihilation to hadrons 78−82226
nonscaling parton model, large p_T processes in hadron collisions 79−352
nucleon production in quark parton model, e^+e^-, ep and large $p_\perp$ reactions 78−21391
nucleon-nucleon potential, nuclear form factor behaviour at high transferred momenta 79−9485
opposite-side angular correlation of high-p_T particles as a probe of gluons 79−71703
parton model, large p_T region, two particle distrib. and associated multiplicity 77−82782
parton model appl. to large momentum transfer interactions, review 79−17686
parton model of large transverse momentum processes, logarithmic corrections to Bjorken scaling 77−71483
parton transverse momenta 78−21380
parton transverse momentum, large p_T processes 79−13040
parton transverse momentum effect in large $p_\perp$ reactions 78−33035
parton-parton cross sections constraints from large p_t angular correls. 77−71540
parton-parton interaction in high transverse momentum collisions, phenomenological description, pp, pn, inclusive interactions 77−57574
phenomenological two-component model for hadron constituents, large p_T spectra, pp inclusive reactions 78−25086
polarisation in hadron cumulative prod. and large transverse momentum processes *(Russian)* 78−74293
polarisation theorem for diffractive excitation at large momentum transfer, favoured helicities 77−71497
pp collisions, jet and background multiplicity distrib. associated with high P_T particle 79−26350
pp scattering, large $|t|$, q-q scatt. 79−13161
prompt lepton prod., charm as possible source 77−225
prompt lepton prod., QCD anal. 79−9346
proton-nucleus collisions, inclusive proton spectra A depend. at large transverse momenta, multiple collision theory *(Russian)* 77−38215
proton-nucleus reactions, 200-400 GeV, hadron prod. cross section 77−41967
QCD, hadron prod., large-transverse-momentum correl. 79−63438
QCD, hadron prod. at large transverse momentum 77−87949
QCD, high P_T hadron prod. in pionisation region and vacuum singularity *(Russian)* 80−86772
QCD, impulse approx. and scaling phenomena 79−22043
QCD, inclusive production at large transverse momentum, cross section 78−62369
QCD, transverse momentum distribs. of μ pairs from pN interactions, p-nucleus study 78−62375
QCD anal. of $p_T{}^2$ behaviour observed in semi-inclusive neutrino data 79−36015
QCD and hadron dynamics 79−97593
QCD and large momentum transfer processes 80−42419
QCD and polarised quarks *(Russian)* 78−74217
QCD Compton effects, quark and gluon jets 80−32101
QCD constituent-interchange to $p_T{}^{-4}$ dominance transition at high transverse momentum 79−40744
QCD effects, parton transverse momenta, large-p_T hadron prod. 78−66083
QCD gluon contribs. to large p_T reactions 78−41504
QCD in 2-D quark confinement and parton model 79−17670
QCD jet dynamics, hadron and photon prod. at large transverse momentum 79−45077
QCD opposite two hadron correl., scale violations in quark/gluon fragmentation functions 79−54299
QCD perturbation theory, nonperturbative effects on factorisation in high momentum processes 79−36016
QCD prediction for ang. distrib. of dileptons in hadron collisions 79−26300
QCD predictions, high p_T processes subject to sum rules, SU(3) symmetry constraints 79−354
QCD predictions, parton and gluon transverse momenta for large p_T particle prod. 79−40723
QCD predictions for large momentum transfer baryon prod. 79−89125
QCD predictions for large p_T hadron prod. by polarised hadrons 78−82148
QCD tests in γ-γ collisions and high p_T photon production 79−89129
QCD three jet prod. in large P_T processes, two particle inclusive distribs. 79−9342
quantum number correlations at large transverse momentum and QCD 79−9337
quantum-chromodynamic predictions for inclusive spin-spin asymmetries at large transverse momentum 79−49472
quark and parton phys., introduction, book 79−85276
quark bag model, large transverse momentum processes of hadrons, EM form factors *(Russian)* 79−26308
quark cascade model, appl. to meson spectra in e^+e^- annihilation 78−41482
quark existance studies in large p_T interactions 80−37235
quark form factor and jet cross sections, high energy asymptotics 80−32112
quark fragmentation, trigger side momentum distrib. in large P_T processes 80−42422
quark fragmentation functions in high-p_T deep inelastic processes 77−61295
quark high momentum transfer scatt., non-Abelian gauge theory *(Russian)* 78−45883
quark jet fragmentation, large momentum transfer reactions, implication of large vector meson prod. 79−345
quark rearrangement in large p_T hadron jet production 79−63454
quark rearrangement model for large p_T hadron prod. 77−50026

elementary particle large momentum transfer interactions continued
- quark-cascade model, particle ratios at large p_T 77−10218
- quark-gluon interaction in pN collisions, dimuon prod. at large transverse momenta 78−29355
- quark-parton distributions model, large transverse momentum hadrons, logarithmic scale breaking 78−16989
- quark-parton model, Large-p_T correlations in scale-breaking model 77−82704
- quark-parton model, leading proton-large p_T particle and proton-lepton pair correlations 79−353
- quark-parton model, with scaling violations, large p_T processes anal. 78−45927
- rapidity distrib. of large p_T particles and realistic jets 77−30334
- Regge cut model 77−26502
- Reggeon model for fast hadron-nucleus inclusive cross sections *(Russian)* 78−45985
- scaling behaviour of γ/π prod. cross section ratio to distinguish large p_t inclusive interaction models 77−50032
- semi-inclusive processes, transverse momentum depend. of multiplicities 78−25028
- single particle inclusive distrib. at large p_T in parton models 77−79286
- spin ang. momentum effects on clusters 77−22703
- statistical bootstrap model with spin, large transverse momenta distribs. 77−65141
- string junction model, large p_T hadron prod. 78−62380
- structure function relations, lepton pair processes at large transverse momenta 78−82214
- superconductive fireball at large p_T, mass, temp. and multiplicity 77−49922
- temperature origin in high energy strong interactions, large transverse accel. 78−37186
- three-jet prod. in large momentum transfer reactions, perturbative QCD theory 79−93373
- topological approach to high-energy large transverse momentum interactions 79−22057
- transverse momentum behaviour of hadrons, multihadron systems, and lepton pairs 79−45121
- transverse momentum distribution of particles, hydrodynamical model calcs. 78−93865
- transverse quark polarization in large P_T reactions and e^+e^- jets 79−63410
- trigger bias, two-jet picture 77−2878
- triple jet production in hadronic collisions at large transverse momentum 78−93919
- two jet model, large p_T hadronic multiplicity, colour octet exchange 78−62377
- two-hadrons inclusive reactions and correl., large p_T, scale-violating quark model 78−74292
- two-jet production cross section at large p_T, urbaryon rearrangement model 77−2884
- uncorrelated-jet model at large-p_T, momentum conservation role 77−54082
- unitarity relation, corrections to soln. for hadron elastic scatt. amplitude *(Russian)* 77−74723
- vortex string picture and large p_T reactions 79−63415
- weak effects in polarised hadron-hadron collisions 77−30457
- d EM form factors at large transferred momentum, six-quark state *(Russian)* 78−89715
- dd collisions, 4.3, 6.3, 8.9 GeV/c, d spectra high momentum struct., multiple NN scatt. model 78−89727
- $D\bar{D}$ production in large p_T hadronic collisions, $e\mu$ and eK correlation study 79−40772
- $dd \to \pi^0 X$, large transverse momentum, π^0 prod. cross section, ISR energies 79−3055
- ed, EM form factor determ., relativistic impulse approx. 77−65158
- ed, elastic and deep inelastic scatt. at large momentum transfer, quark model *(Russian)* 78−86529
- ed elastic scatt., EM form factors, relativistic harmonic oscillator model 79−54327
- ed inelastic scatt., electrodisintegration at high energy and momentum transfer, exchange currents 79−6342
- ed inelastic scatt. at high momentum transfer, scaling anal. 77−26531
- e^+e^- annihilation, DD τ decay, large timelike Q^2, conservation of vector current and current algebra 78−78155
- $eN \to$ hadrons + anything, scale invariant limit on average transverse momentum 77−67659
- $e^-N \to e^-N\pi$, electromag. and weak process from weak neutral current interaction *(Russian)* 78−45928
- $e^-\pi \to e^-$ + hadrons, spectator interaction effects in large $p_\perp$ deep inelastic processes 79−93427
- η/π^0 production ratio in inclusive large transverse momenta interactions 78−41602
- $\gamma\gamma$, jet and single particle prod. at large p_T 79−49565
- $\gamma\gamma \to$ large p_T jets, QCD predictions for processes involving real photons 79−6330
- $\gamma p \to \gamma + \text{jet} + X$, perturbative QCD predictions large p_T real photon in final state 79−89165
- $\gamma p \to h^\pm X$, large p_T photoprod., perturbative QCD test 80−37276
- $\gamma p \to hX$, SU(3)×SU(3) invariant interaction of quarks, large p_T, gluon bremsstrahlung 78−33072
- $\gamma p \to \pi^0 X$, invariant cross section at large p_T, hard scatt. model 80−22621
- $\gamma p \to \pi X$, large p_T, perturbative QCD 80−86723
- $hh \to \mu^+\mu^- + \text{jet} + X$, QCD anal. of recoiling jets and angular effects in large q_T pair prod. 79−45078
- $K^\pm d$, total cross section determ., 200 to 370 GeV/c 79−26352
- kp, large P_T pion^0 prod., meson structure functions, quark distrib. functions 80−86714
- K^-p, 110 GeV/c, prod. of large $p_\perp$ single and multiparticle systems (jets) 79−85345
- $K^-p \to \pi^0 X$, 100, 200 GeV/c high transverse momentum π^0 prod., quark scatt. 78−45976
- $K^+p \to K^0 X$, 5-32 GeV/c, transverse momentum distribs. *(Russian)* 77−30467
- $K^+p \to \pi^- X$, 8.2-32 GeV/c, transverse momentum distribs. *(Russian)* 77−30467
- $K^\pm p$, total cross section determ., 200 to 370 GeV/c 79−26352
- $lp \to l'X$, weak reaction, large transverse momenta, field theories at finite temp., symm. breaking and restoration 79−399
- μ pair transverse momentum distrib., hard interaction mechanism of constituents 77−65139

elementary particle large momentum transfer interactions continued
- μ prod. at large transverse momenta, μ polarisation meas. 77−71542
- μ prompt prod. in high p_T 400 GeV proton interactions, polarisation 77−13991
- μ^+ direct prod. in pN interactions, longit. polarisation meas. 77−2995
- μp, semi-inclusive, ang. correl. tests of QCD 79−17735
- μp, semi-inclusive scatt., quantum chromodynamic predictions 78−29324
- nd, three body systems, review of recent theoretical anal. 79−80842
- NN large angle elastic scatt., spin-spin asymmetries and flavour depend., quark interchange 80−86743
- NN large momentum transfer polarised reaction as test of strong interaction T invariance 77−30402
- $NN \to NN$, large momentum transfer, spin effects 80−22577
- NN scattering spin correl. parameters and quark-quark interactions 79−13049
- $NN \to X$, nuclear size dependence of particle prod., hydrodynamical model 80−22593
- np, elastic scatt. at large transverse momentum, spin-spin forces 78−78216
- $np \to (p\pi^-)p$ diffractive dissociation, struct. in momentum transfer 77−13992
- np elastic scattering data, comparison with theory, small and large scatt. angles 77−57566
- np large angle elastic scatt., 5-12 GeV/c, ang. distribs. 77−57565
- $p(\bar{p})p \to \gamma X$, large angle real photon prod. at large p_T, QCD anal. 80−22644
- p production, compared to π, large transverse momentum, rearrangement of hard scattered partons 80−62934
- p+Cu 400 GeV large $p_\perp$, quark search 77−79290
- p+H target, high transverse momentum π^0 and jets prod. 78−70417
- pD, phenomenological relations between large-p_T meson spectra 79−26349
- pd, total cross section determ., 200 to 370 GeV/c 79−26352
- $pd \to dX$, associative multiplicity at high momentum transfer *(Russian)* 77−61333
- $pd \to K^\pm$ + anything, large p_T, 200 to 400 GeV 77−22816
- $pd \to p(\bar{p})$ + anything, large p_T, 200 to 400 GeV 77−22816
- $pd \to \pi^0 X$, large transverse momentum, π^0 prod. cross section, ISR energies 79−3055
- $pd \to \pi^\pm$ + anything, 200 to 400 GeV 77−22815
- pp, 100, 200 GeV, elastic scatt., polarisation effects at large momentum transfer, quark model *(Russian)* 80−83005
- pp, 200 GeV/c in Be, inclusive ω prod. at large p_T, η' prod. upper limit 80−52547
- pp, 23-62 GeV, anal. of charged-particle multiplicities associated with large p_T photons 77−18358
- pp, 24, 70 GeV/c, transverse momentum distrib. anal. 77−82781
- pp, 24 GeV/c, final states with large transverse momentum particle, π and N emission 79−13159
- pp, 27 GeV/c, resonant prod. of high $p_\perp$ back-to-back gluon jets 79−93470
- pp, 31-63 GeV, direct photon prod. at large p_T, π^0/γ prod. ratio 80−63038
- pp, 52.6 GeV, large transverse momentum charged hadron at 90°, jet like structs. 80−18150
- pp, 62.4 GeV/c, direct single photon prod. at large p_T 80−91113
- pp, charged hadron prod. with large transverse momentum at 90°, 52.6 GeV interactions 79−17763
- pp, charged hadron trigger at large transverse momentum at CERN ISR 79−45117
- pp, elastic scatt., 12 to 24 GeV, leading effective trajectories, residues, anal. 79−421
- pp, elastic scattering, high P_t, spin interactions meas. 79−67608
- pp, final state struct. prod. in association with large transverse momentum π^0 79−45115
- pp, final states containing high p_T π^0 at CERN ISR 79−45119
- $p\bar{p}$, hadronic jets, possible intermediate bosons 80−18149
- pp, high p_T direct single photon prod., 30-62 GeV 80−9189
- pp, ISR energies, high p_T π^0 and single photon events, associated charged particle multiplicity 80−63039
- pp, ISR energies, inclusive high p_T ω^0 and η' prod. 80−42504
- pp, inclusive meson prod. with large transverse momentum, effective gluon model 78−8717
- pp, large P_T pion^0 prod., meson structure functions, quark distrib. functions 80−86714
- pp, large p_T two-particle correlation, hadron composite struct. 77−54085
- pp, phenomenological relations between large-p_T meson spectra 79−26349
- $\bar{p}p$, total cross section determ., 200 to 370 GeV/c 79−26352
- pp, transverse momentum fluctuations and high p_T processes in QCD 79−36014
- pp,$\bar{p}p$, Z^0 high p_T bremsstrahlung, Higgs versus quark or gluon jets 80−32063
- pp and $p\bar{p}$, Higgs-boson production at large transverse momentum in quantum chromodynamics 79−40745
- pp collisions, azimuthal correl. of high $\rho_T\pi^0$ and η with second π^0 79−85347
- pp collisions, charged and neutral multiplicities associated with large transverse momentum π^0's 79−3058
- pp collisions, constituent transverse-momentum fluctuations and hard scatt. expansion 79−17749
- pp collisions, high momentum $\pi^\pm$ and $K^\pm$ prod., 45 GeV, cross sections 78−93910
- pp collisions, large transverse momentum pions prod., correls., fireball model 78−66174
- pp collisions, meson large p_T distrib. formula, from pre-equilib. fireball state and fireball spin 79−13170
- pp collisions, multiplicities of pion, kaon or proton prod. at ISR 77−259
- pp collisions, real photon prod. at large p_T, cross section calc. 79−13149
- pp collisions at CERN ISR, charged hadron of high transverse momentum at 90°, forward particles 78−58214
- $pp \to e^+e^- X$, large p_T, reference to $\Upsilon(9.5)$, $\xi(3.5)$ and direct γ-prod. 78−89749
- pp elastic, 23 to 63 GeV, absolute differential cross section meas. 79−45103
- pp elastic amplitude, geometrical scaling real part effects 78−37232
- $\bar{p}p$ elastic scatt., constituent interchange model 77−2856
- pp elastic scatt., differential cross-section meas. at 53 GeV 77−65178
- pp elastic scatt., high energy, diffraction model with nucleon core 78−74281

elementary particle large momentum transfer interactions continued
pp elastic scatt., ISR energies, spin behaviour of ang. distribs. at large momentum transfer *(Russian)* 79—80849
pp elastic scatt., polarised cross-sections meas. at 11.75 GeV/c 78—8698
pp elastic scatt. at 201 GeV/c, large momentum transfer struct. 78—8697
pp elastic scatt. at high energy and large momentum transfer, cross-sections 78—62460
pp elastic scatt. at high energies and large momentum transfer, review *(Russian)* 80—105926
pp elastic scatt. at large transverse momentum, spin-spin forces 78—78216
$pp\to\eta X$, inclusive η prod. at high p_T at the ISR, η/π^0 cross section ratio 79—71770
pp fragmentation at high energies, quark constituents 77—34185
$pp\to\gamma X$, large p_T direct photon prod., QCD scale violation effects 79—71772
$pp\to hX$ large p_T multiplicities 77—10289
pp high p_T polarised elastic scatt., QCD explanation of asymmetries 80—13323
pp inclusive interactions, high p_T spectra and ang. multiplicity correls., phenomenological anal. 77—10292
pp inclusive interactions, π^0 prod. at large p_T at CERN ISR 79—13168
pp inclusive nonleading distrib., contributions to direct lepton spectra 77—2880
$\bar{p}p$ inelastic reactions, 22.4 GeV/c, charge asymm. at large p_t 78—476
pp interactions, hadron prod. 23.4 to 63.4 GeV, charged multiplicity density for various p_T 78—70414
pp interactions, jet fragmentation in large p_T events at ISR 79—45118
$pp\to$jets, 400 GeV, p_T plots, Monte Carlo and parton model predictions 78—89747
$pp\to K^\pm$+anything, large p_T, 200 to 400 GeV 77—22816
pp large p_T reactions, jets, dual-string approach 80—32136
pp large transverse momentum interactions, quark cascade model anal. 79—36101
$pp\to\Lambda X$, 19 GeV/c, polarisation at high transverse momenta 78—37246
$pp\to$meson+lepton pair, transverse momentum distrib. and branching ratios, proton gluon distribution 80—52537
$pp\to pX$, high p_T, spin-spin asymmetries, polarisation, hard scatt model with QCD 80—13339
$pp\to p+X$, multiplicity dependence on transverse momentum and missing mass, multiperipheral diagram anal. 79—365
$pp\to p(\bar{p})$+anything, large p_T, 200 to 400 GeV 77—22816
$pp\to$pions, 102, 400 GeV/c, transverse momentum props. 78—8713
pp polarisation asymmetry in high p_T inclusive prod., QCD and gluon models 79—40819
$pp\to pp$, high $P_T{}^2$ elastic scatt., 11.75 GeV/c, spin depend. from polarised p 79—3049
$pp\to pp$, large momentum transfer, multiple-scattering model, three-quark proton 80—63031
$pp\to pp$, Van der Waals type model 80—73740
$pp\to pp$ spin-spin interactions in high-$p_\perp{}^2$ elastic scatt. at 11.75 GeV/c 77—88009
$pp\to\pi^0$, large transverse momentum jets investig. at 52.4, 62.7 GeV 80—18151
$pp\to\pi^0X$, 100, 200 GeV/c high transverse momentum π^0 prod., quark scatt. 78—45976
$pp\to\pi^0X$, 50-400 GeV, cross sections, 0.3 to 4 GeV/c π^0 transverse momenta 77—18350
$pp\to\pi^0X$, 52.7, 62.4 GeV, inclusive prod. at very large p_T at the ISR 79—71769
$pp\to\pi^0X$, 53, 63 GeV, inclusive π^0 prod. at very large transverse momenta 78—45980
$pp\to\pi^0X$, large p_T phenomena, Bjorken scaling violation models of quarks with substructure 79—26305
$pp\to\pi^0X$, large p_T processes, pion exchange model anal. *(Russian)* 80—27527
$pp\to\pi^0X$, large transverse momentum, π^0 prod. cross section, ISR energies 79—3055
$pp\to\pi^0X$, one-gluon-exchange quark scatt. 78—8714
$pp\to\pi^0X$, parton model, polarised proton, large p_T π^0 prod. asymm. 78—12936
$pp\to\pi^0X/\pi^-p\to\pi^0X$ ratio at high-p_T, quark model explanation 77—10290
$pp\to\pi^0+X$, large p_T-π^0 spectra, quark model anal. 78—89756
$pp\to\pi^0+X$, π^0 prod. at large p_T, parton model 77—46090
$pp\to\pi^0$+anything, $\sqrt{s}=52.7$ and 62.4 GeV, prod. of high transverse momentum π^0's 78—78226
$pp\to\pi^0$+anything, large p_T, clustered parton model 77—67688
$pp\to\pi^0\pi^0$, up to 10 GeV/c, correlation of momentum of π^0 pairs 80—5011
$pp\to\pi^0\pi^0X$, large p_T, azimuthal correlations 78—89749
$pp\to\pi^++X$, inclusive reactions, ISR energies, scaling variable 77—50021
$pp\to\pi^\pm$+anything, 200 to 400 GeV 77—22815
$pp\to\pi X$, crucial spin tests of QCD approaches to large transverse momentum processes 79—63558
$pp\to\pi X$, large P_T, transversely polarised beam and target, QCD predictions 79—49553
$pp\to\pi X$, large-P_T reactions in broken color gauge theory 80—95292
$pp\to\pi+X$, high p_T jet prod., QCD perturbation theory 79—89209
pp scatt, spin dependence at large $P_T{}^2$ 80—42493
pp scatt., eikonal mechanisms at high energy 78—82256
pp scatt. cross section at high momentum transfer, geometrical scaling, energy depend. *(Russian)* 80—102064
pp single-lepton spectra at high p_T, parton p_T and gauge invariance 77—18352
π^0 high p_T prod. ang. depend., inclusive cross sections, scaling 80—91119
π^0 prod. at large p_T, pp and $\pi^\pm p$ collision 77—79287
π+H target, high transverse momentum π^0 and jets prod. 78—70417
πd interactions at large momentum transfers 77—13972
$\pi^-d\to\Delta^-p$, high energy, backward Δ^- prod. mech., Δ^{++}-Reggeon exchange *(Russian)* 79—97637
$\pi^\pm d$, total cross section determ., 200 to 370 GeV/c 79—26352
πN in Al, quark jet multiple production 80—9188
πN scattering, partial wave analysis, high energy behaviour large momentum transfer region 79—22130
πp, direct photon prod., Compton and annihilation process contrib. 80—105925
πp, large P_T pion^0 prod., meson structure functions, quark distrib. functions 80—86714
πp, real photon prod. at large p_T, QCD and CIM anals., jets 79—89185

elementary particle large momentum transfer interactions continued
$\pi p\to p$+pions, average transverse momentum, baryon exchange 77—30448
$\pi p\to\pi^0$+anything, large p_T, clustered parton model 77—67688
$\pi p\to\pi p$, large momentum transfer, multiple-scattering model, three-quark proton 80—63031
π^-p, 200, 300 GeV, relative π^+, K^+, p, $\bar{p}$ prod., charge ratios, high p_T 80—47335
π^-p, 40 GeV/c, correlation between π and accompanying large transverse momentum particle *(Russian)* 80—86758
π^-p, 40 GeV/c, particle prod. with large transversal momenta *(Russian)* 78—41609
π^-p, elastic scatt., 12 to 24 GeV, leading effective trajectories, residues, anal. 79—421
π^-p, large p_T inclusive π^0 prod., quark subprocesses 77—2885
$\pi^-p\to\eta^0n$, 3.3 GeV/c, differential cross section, helicity-flip amplitude *(Russian)* 78—45945
$\pi^-p\to\eta n$, 40 GeV/c, large momentum transfer, differential cross-section meas. *(Russian)* 78—33094
$\pi^-p\to\gamma X$, large angle real photon prod. at large p_T, QCD anal. 80—22644
$\pi^-p\to\pi^0X$, large P_T collisions, quark cascade model anal. 79—36110
$\pi^-p\to\pi^0X$, large p_T processes, pion exchange model anal. *(Russian)* 80—27527
$\pi^\pm p$, inclusive meson prod. with large transverse momentum, effective gluon model 78—8717
$\pi^\pm p$, total cross section determ., 200 to 370 GeV/c 79—26352
$\pi^\pm p\to\pi^\pm$+anything, 16 and 100 GeV/c, high transverse momentum, charge asymm. 77—18339
$\pi^\pm$single particle distribs. in pp, πp collisions, transverse momentum, rapidity depend. hard scatt. models 78—29361
$\psi\psi$ prod., correl. effects in large p_T pion events 77—26549
$qq\to qqX$, large p_T hadronic collision jet struct., QCD calc. 79—75721
Be+hadrons, 200 GeV/c, high transverse momentum jets and single particles 77—61329
Be(p,$h^\pm$), 200 to 400 GeV, inclusive production of large-transverse-momentum hadrons and hadron pairs 79—89310
ed elastic scatt. at high momentum transfer 80—82977
$\gamma N\to\eta X$, 9.7 GeV, inclusive η photoprod. on H- and ^{2}H-targets, ρ^0-dominance model anal. 79—63486
$\bar{p}p\to\mu^+\mu^-X$, scale violating effects in large q_T interactions 79—22125

elementary particle mass
see also baryon mass; lepton mass; mass differences; mass formulae; meson mass
axion mass, astrophysical limitations *(Russian)* 78—61835
axion mass from orthopositronium decay 78—78125
axion mass in SU(2)xU(1) theory 78—78080
axions and Higgs particles, astrophysical mass bounds 79—5745
bare quark masses from the transverse cut offs in e^+e^nteractions 77—18309
beautiful pseudoscalar mesons, mass scale 77—74614
bottom quark mass inequality 79—9345
charmed baryons, mass splitting, derivation using weight diagrams 80—27481
charmed current quark mass from D-meson semi-leptonic decay, current algebra treatment 79—97577
charmonium atomic physics, ψ, ψ', η_c, η_c' masses and $\psi\to\eta_c\gamma$ decay 79—40740
colour gluons, observable mass limit 77—30324
conformal relativity, bare mass theory 80—27417
cosmology, role in elementary particle physics 80—27430
fermion and Higgs boson mass constraints, Weinberg model 79—49437
fermions, charge density phase transitions in gauge theories with spontaneous symmetry breaking *(Russian)* 79—2969
fermions, light, mass hierarchy, grand unification, SU(N) theory 80—62911
fundamental constants, self-consistent values *(German)* 79—12758
gauge boson masses in flavour $SU_3\times U_1$ model, quark and lepton weak and EM interactions 79—97554
graviton rest mass, lunar ranging data anal. by Seelinger's theory 79—6040
Gross-Neveu model, mass generation, renormalisation 80—27393
hadronic structure using parton anal. of deep inelastic scattering and rel. processes 79—80803
heavy quarks, mass power law 80—62955
heavy quarks in e^+e^- annihilation 77—26494
hierarchy in asymptotic reconstruction of spontaneously broken isotopic symmetry *(Russian)* 79—2968
hierarchy of quark masses, Cabibbo angles and CP violation 79—22030
Higgs boson mass and weak interaction strength at very high energies 77—46013
high mass particle production, multitemp. thermodynamical model 79—3004
indeterminate—mass particles 79—26319
inertial mass, variation as function of age of Universe 79—80375
Kobayashi-Maskawa model, Cabibbo-like parameter and quark mass relation *(Chinese)* 80—42408
large transverse momentum and large mass production in hadronic interactions review of theoretical models 79—89115
lepton and quark spectra difference eqns., τ and toponium mass 80—22589
lepton-quark mass relation in unified theory 79—97560
light hadron mass in bag model, quark-gluon coupling constant *(Russian)* 79—67514
light Higgs boson, mass and lifetime in current algebra approach 78—45835
light quark mass spectrum in QCD 79—63427
magnetic monopole M<30GeV, CERN search 78—66176
magnetic monopoles, high mass, low vel., prod. in atmosphere 78—49262
magnetic monopoles, mass, charge, internal struct. 78—89625
magnetic monopoles, mass vanishing in supersymmetry 78—62334
magnetic quark models of elementary particle mass 79—26312
mass dependence on QCD parameters 79—17675
massless fermion representations in grand unified gauge theories 79—97553
monopoles, mass spectrum in bag model 78—24935
neutral vector bosons of very light mass 77—49898
O(10) theory of strong, weak and EM interactions, masses and mixing 80—13248
photon mass and planetary magnetic fields 77—33477

elementary particle mass continued
photon mass from fermion radiative decay 78—41456
photon rest mass, astrophysical upper limits 77—34200
photon rest mass, cosmic tests of Maxwell's eqns. 77—45708
Poincare covariant particle model with mass and spin mixing 80—32016
QCD, perturbative, colour singlet distribs. and mass damping 79—63418
QCD, perturbative contributions to quark masses 80—47249
quantisation rules and particle geometry *(French)* 80—13305
quark, chiral charge space, statistical analysis 80—42428
quark, scale depend. mass in colour gauge theory 77—30320
quark effective masses from semi-leptonic decays 78—58185
quark magnetic moment, rel. to quark mass and hadron mass in SU(3) breaking 79—13050
quark manes and flavour mixing angles based on $SU(2)_L \times SU(2)_R \times U(1)$ 79—80811
quark mass, electroweak contrib. 80—101990
quark mass dependence ambiguities in gauge theory renormalisation 79—21913
quark mass ratio, chiral perturbation in new key 80—37208
quark mass ratio from baryon mass splittings 80—42436
quark masses, isospin breaking and $\pi \rightarrow e\nu\gamma$ vector form factor 79—13111
quark masses, weak interactions and spontaneous isolation 77—34115
quark masses and Cabibbo angles 79—9332
quark masses and counting rules in chiral $SU_4 \otimes SU_4$ 79—63437
quark masses and induced strangeness-changing processes 77—57491
quark masses and mixing angles 77—82731
quark masses and numbers, bounds 78—58151
quark masses in relativistic wave eqn. models 78—74130
quarkonia from charmonium and renormalization group equations 79—22055
quarks, EM form factors in instanton fields 80—99102
quarks, mass determ. in unified weak and EM theory without scalar fields 79—75709
quarks, mass of u and d quarks from weak and EM interaction model 80—13254
quarks, third and fourth generation, mass prediction using quantised magnetic self-energy 80—18133
sixth quark mass in $SU(2)_L \times SU(2)_R \times U(1)$ gauge group 79—26291
$SU(2)_L \times SU(2)_R \times U(1)$ gauge with permutation symmetry, quark mass and Cabibbo angles 80—47232
$SU(2)_L \times U(1)$, mass hierarchies and Cabibbo angle formula 79—63420
SU(3) quark-meson σ-model, quark masses 80—47178
SU(4) mass splitting, group theory and quark model comparison 79—6290
SU(5) grand unification, heavy coloured Higgs scalars, b-quark mass 80—57543
SU(5) grand unification, strong CP violation, quark-lepton mass ratio 80—32057
SU(5) grand unified theory, t-quark mass 79—97559
t-quark mass in O(10) unified field theory 79—75708
transverse lattice QCD, hadron mass spectrum 80—57568
up quark mass 79—63461
up quark mass and chiral symmetry at infinite momentum 79—40685
up quark masslessness and $\eta \rightarrow 3\pi^0$ decay 79—40761
W-boson propagator effects in the neutrino-nucleon scattering 79—13098
weak intermediate boson masses, upper and lower bounds 77—46007
Weinberg-Salam model with two massless Higgs doublets, particle masses, perturbation constraint 80—57541
Yang-Mills theory, IR divergences and zero mass limit 80—32025
c-quark mass 0.5 or 1.5 GeV 78—45991
c-quark mass determ. in Weinberg model 77—2821
e^-/p mass ratio variation, summary of obs. evidence 79—12759
e^+e^- annihilation, heavy quark jet ang. distribs., quark mass, QCD anal. 80—42481
$K^-p \rightarrow \Lambda^0\pi^0$, strong reaction asymmetry and mass quantisation, particle struct. *(French)* 79—3043
$K^+p \rightarrow \Sigma^+\pi^+$, strong reaction asymmetry and mass quantisation, particle struct. *(French)* 79—3043
ρ-ω mixing, quark mass differences 80—37243
t-quark, mass in SU(3) horizontal symmetry 80—37230
t-quark, properties and signatures 80—37223
t-quark mass from discrete symmetries 79—63462
t-quark mass in $SU(2) \times U(1)$ 79—40710
t-quark mass predictions from Glashow determinant condition 80—86677
u- and d-quark mass generation from $SU_L(4) \times SU_R(4) \times U(1)$ gauge models 79—63419
u-quark, zero mass possibilities 78—82144
u-quark mass in SU(2)xSU(2) symmetry 78—70323
u-quark masslessness, consequences for SU(2) and SU(3) 79—22022
W, mass in SU(5) grand unified theory 80—68411
W boson, determ. of mass limit from neutrino scatt. data 79—3012
W° boson mass in e^+e^- annihilation studies 78—66100
Z, mass in SU(5) grand unified theory 80—68411
z° boson, mass constraints from e^+e^- expts. 78—37154

elementary particle scattering
see also bootstrapping; elementary particle interactions; hadron-deuteron scattering; hadron-hadron scattering; lepton-deuteron scattering; lepton-hadron scattering; lepton-lepton scattering; Mandelstam representation; photon-deuteron scattering; photon-hadron scattering; photon-lepton scattering; photon-photon scattering; polarisation in elementary particle scattering; Pomeranchuk poles and trajectories; quantum field theory of elastic scattering; Regge poles and trajectories; relativistic scattering theory; S-matrix theory
$3 \rightarrow 3$ forward amplitude, analytic struct. determ. 79—30296
ϕ^4 field theory, scatt. amplitude asymptotic behaviour, renormalisation group and slope parameter 79—49389
absorptive elastic and inelastic differential cross sections 77—87665
amplitude, analytic extrapolations, computer program, EMZERO 80—47221
analytic extrapolations towards interior points from a cut, applic. to elementary particle scatt. theory 80—12952
analyticity of forward or fixed t amplitudes, general testing method 77—57462
asymptotic bounds on derivatives of elast. scatt. amplitudes 78—12892
asymptotic theorems and polarization phenomena 79—63334
bounds on scatt. amplitudes and form factors 77—13878
CERN experiments in 1979 80—408
coherent and incoherent prod. in nuclei, multiple scatt. theory *(Russian)* 77—216

elementary particle scattering continued
conventions, naming of partial waves, Argand plot coord. systems 77—22720
Coulomb interaction in nonrelativistic quantum mech. 79—25906
diffraction peak scaling, collisions of arbitrary spin particles 77—18252
diffractive production mechanisms, high-energy, review 79—36052
diffractive states, shadow approach to elastic scatt. 77—67638
dyon-dyon nonrelativistic scatt., classical and quantum anal. 77—5985
Dyson-Jost-Lehmann representation, scaling for large-angle scatt. 77—67580
eikonal approx., backward and transverse effects 77—10205
elastic charged particle scatt., polarisation anal. Coulomb interference term, transition matrix 79—67559
elastic scattering, small and large momentum transfer relations *(Russian)* 80—86698
elastic scattering amplitude, absorptive part, lower bounds on slope parameter 77—34114
elastic scattering amplitude asymptotics in a supersymmetric theory *(Russian)* 79—75748
elastic unitarity eqn., new uniqueness condition for soln. 79—58950
electron elastic scatt., by spatially bounded mag. field 77—13834
Faddeev equations, two-potential formula, three-body scattering 80—4893
fermion-fermion scatt., very high energy weak interaction effects 79—9327
finite geometry effects in scatt. expts., numerical integration method 78—82596
forward differential cross section, t-channel singularities 77—67595
Haag-Ruelle scattering theory, charged sectors of QED, local observables framework 79—58908
hadron constituent models review, fixed angle and Regge behaviour, hard scatt., fragment X-distrib. 78—78154
half off-shell t-matrix elements for class of equivalent pots., ΛN scatt. 77—2562
high-energy, two-dimens. gauge theory anal. 77—13933
impact parameter representation *(Russian)* 80—5019
intrinsically deformed particles, high-energy collisions, Chou-Yang model 77—67680
inverse scattering at fixed energy, oscillating tail phenomenon 79—30295
local two-body interaction, off-shell phase shift 78—45516
many-body scattering, coupled channel eqns. and off shell transforms. 78—402
method of zeros for study of partial wave amplitudes 77—22752
minimal rule, Zweig Izuke rule, asymptotic hadron scatt., stiff quark line hypothesis 77—2792
Moller scatt., neutral current effects 77—2786
multiparticle amplitudes, discontinuity formulas 77—13881
multiparticle collision amplitudes, physical-region props. 77—13880
multiparticle scatt., ghost bound states and Pauli principle *(Russian)* 79—9152
Muskhelishvili-Omnes equation and final state interactions 79—67196
N-particle scatt., dynamical eqns., for transit operators 77—18428
non-relativistic scattering by stationary external metrics and Yang-Mills potentials 80—101938
off-shell, nonrelativistic two-body amplitudes, generalisation of Jost formalism 78—49687
off-shell particle scattering, total cross sections, QCD 80—68418
Pal-Bell stochastic equations for particle transport scattering theory 79—45319
particle trajectory reconstruction, elastic events fitting, fast method 77—61316
particles and fields conference, Argonne, IL, USA (Oct. 1977) 78—78130
parton model appl. to large momentum transfer interactions, review 79—17686
phase shift ambiguities, elastic spin-0—spin 1/2 scatt., partial waves 77—22669
phase space integral, n-particle, relativistic, Monte Carlo integration program 78—33001
phase-shift anal. ambiguities 77—18208
Pomeranchuk theorem inverse, proof for logarithmically rising total cross sections, 10-2000 GeV 78—86425
pomeron flip-non-flip interference term in elastic polarisation, s-channel helicity 78—50021
potential scatt. in 3-D, backscatt. and Fresnel diffraction 77—13895
proton-hadron high energy collisions, hadron struct. 79—67614
relativistic composite particle scatt., quasipotl. approach 78—404
relativistic Hamiltonian theory, high-energy representation 78—24980
representation by Penrose graphs 78—49983
S-matrix theory of relativistic elastic scatt., crossed channel struct. effects *(German)* 79—58906
scattering amplitude determ. from differential cross section, contraction mapping 77—10206
scattering amplitude determ. from differential cross-section, compactness theorems 77—10235
soft spin 3/2 massless fermions, gravity, supersymm. 77—49869
spin effects in elastic scatt. at high transmitted impulses *(Russian)* 80—5018
spinless particle scatt., plane waves on the impact parameter group *(Russian)* 79—2668
Tabakin rank-one potl. in orthogonality condition model, 3-body energy 77—18423
three-boson stimulated scatt., quantum mechanics *(Russian)* 78—78115
total cross sections, asymptotic upper bound 80—105938
transition operators, CCA class, under particle interchange, unexpected behaviour 79—75694
two-body bound state and half off-shell t-matrix parametrisation 77—18424
two-body reactions, rigorous formulae for statistical errors on zeros and partial waves 78—4527
unitarity upper bounds on amplitude phase from Holder inequality 77—57235
unitary bounds on elastic absorptive amplitudes involving total cross section, forward slope, curvature 77—49881
vector boson elast. scatt., Lorentz covariant scatt. amplitude and Compton scatt. 77—2776
Yukawa pot. scatt., separable expansion method, off-shell T matrix 78—93564
$q\bar{q}$ binary confined systems, elastic scatt. amplitudes 79—97576

elementary particle strong interactions
see also composite models of hadrons; duality and dual models; hadron classification schemes; peripheral models; quantum field theory of strong interactions
ϕ^3 theory in 6-ε dimens. SU(3)×SU(3) strong interaction model 77—82726
affine gravity and strong interactions in SL(4,R) nonlinear representations 80—18108
analytic extrapolating statistical approach, review *(Russian)* 79—3000
antiprotonic atoms, X-ray transition energies, strong interaction and $\bar{p}$ mass meas. 78—25759
asymptotic catastrophe, temporary freedom in lepton and quark interactions 79—85253
bi-scale theory of gravitational and strong interactions 79—12696
boson field in neighbourhood of classical solution, quantisation by appl. of Bogolyubov's method 78—8566
broken SU(3) gauge model of strong and EM interactions, scatt. lengths, baryon mag. moments 78—74133
Cabibbo angle and quark spectroscopy *(Russian)* 78—62351
canonical pseudoscalar-meson matrices, chiral SU(n)×SU(n) symm. of strong interactions 78—29266
canonical $SU_4 \times SU_4$ pseudoscalar meson matrix, nonlinear chiral Lagrangian 78—397
chiral gauge invariant Lagrangian, relationship to strong interactions *(Chinese)* 79—21968
chiral $SU_4 \times SU_4$ breaking and Cabibbo angle 77—74641
chiral symmetry spontaneous breaking model, multiple particle prod. *(Russian)* 77—38120
classical quark confinement from general relativity 78—58162
composite hadrons, spin depend., S-matrix theory, TeV energy range 78—58164
conference on hadron struct. and lepton-hadron interactions, Cargese, France (July 1977) 80—4473
current status in elementary particle physics 79—40651
development from the Fermi-Yang model to the quark model *(Chinese)* 79—30711
dibaryon resonance existence in ΔΔ system, potential model investigations 79—85285
Dirac's large-number hypothesis 80—18091
duality, phenomenological, strong interactions description using finite energy sum rules 77—82716
education, hadronic atom strong interaction induced level widths and shifts, WKB calc. 77—78923
effective hamiltonian for $\Delta C=1$ nonleptonic interactions in the Kobayashi-Maskawa model 80—86667
Einstein's field eqns., possible generalisation to strong interactions 78—53979
elementary length and time in the strong interaction, meson reson. width data 78—82189
exotic atoms: a new method in nuclear and elementary particle physics, review *(German)* 79—76536
extended hadrons in geometrically formulated gauge dynamics with fibre bundles 80—9141
extended particle model, dynamical theory of hadron interactions 77—87936
filling U(4) multiplets by hadrons *(Russian)* 79—22076
formalism with internal coords., partial unification of quantum theory and SU(3) classification 77—65137
fundamental interactions, review for teachers 78—16615
gauge invariance with massive gauge bosons 80—9107
general relativity, strong gravity and elementary particle theory 78—8315
geometrodynamical model of extended baryons 77—79251
gluons in e^+e^- annihilation, QCD anal. of strong interaction dynamics 79—9386
hadron+hadron high energy collisions, variables and optical concepts 80—444
hadron high-energy prod., multi-eikonal theory 77—6098
hadron interactions at 24 GeV/c, sphericity by principle axis variable method 79—71767
hadron strong interactions, theory from general relativity 79—49143
hadron-deuteron, complex ang. momenta method and increase in effective longit. distances *(Russian)* 79—49541
hadron-deuteron interaction, hadron struct. anal. 78—45955
hadronic matter, critical point exponents 79—58944
hadronic matter, statistical bootstrap model and critical behaviour 80—42430
hadronic total cross sections, soft and hard components, model anal. 79—49546
hadrons, existence of long-range forces, magnitude of coupling constants 80—13272
hadrons interacting, isospin-spin polarisations, dynamical characts. 80—32035
hard processes, parton model and QCD, review 80—47258
heavy $q\bar{q}$ systems, fine struct. and axial vector gluons 79—63431
high energy, case for discrete fireball mass spectrum, limiting temperature 77—57499
high energy behaviour of exclusive and inclusive cross sections 79—3047
high energy hadronic collisions, similarities, universality prop., reaction mechanism 78—33090
high energy strong interactions, review, expt., theory 77—13983
high-energy strong interactions, range as consequence of quantum mechanics *(Russian)* 78—4901
hot hadronic matter in early universe, relativistic eqn. of state 78—45438
inclusive processes, bremsstrahlung approx. 77—50033
introductory book using potential theory 77—223
isotopic symmetry group in strong interactions, possible geom. origin 79—17628
jet asymmetry in polarized proton collisions *(Russian)* 79—17685
kinematics in strong interaction theory 77—79246
large transverse momentum hadronic reactions, hard scatt. model of urbaryons with two-jet struct. 77—41813
LEP experiment 79—97613
lepton-hadron hard reactions, scaling features, correlating quark rearrangement model 79—58939
lepton-hadron model, determ. of N form factors 78—74256
lepton-hadron relation and the nucleon-nucleon potential 79—22207
Lie admissible formulations, math. and physical study status, strong interactions 80—37172
lightlike chiral structure of hadrons, nonleptonic hyperon decays 78—74253

elementary particle strong interactions continued
Lorentz groups, homogeneous and inhomogeneous, teaching method to illustrate difference 80—17766
many particle prod. based on hierarchy of upper bounds 78—12891
master eqn. for quantum systems with strong interactions *(Chinese)* 78—86229
meson transmission of force 77—46049
minimal rule, Zweig Izuke rule, asymptotic hadron scatt., stiff quark line hypothesis 77—2792
multipole moments for the study of mixed spin reactions 79—97611
neutron-proton mass difference, classical electrodynamic model 77—6123
non-Abelian gauge theories and mag. monopoles, strong interaction models and quark confinement 79—49367
optical theorem violation 77—26504
overlap function in high energy collisions of composite objects 77—6087
particles and fields conference, Argonne, IL, USA (Oct. 1977) 78—78130
Pauli's exclusion principle for strong interactions in hadrons, nuclei, and astrophysics 80—37206
phase-modulus correlations for forward scatt. amplitude without Froissart bound 78—401
Planck energy nonconserving fluctuations and strong forces 80—57551
polarisation expts., theoretical review 77—57564
polarisation studies at Brookhaven AGS, past, present, and future 77—30737
polarised beams and targets in high-energy interactions, conference 77—30470
polarization phenomena in hadronic reactions, review 80—52527
Pomeranchuk theorem inverse for log rising total cross sections 77—71546
pomeron-f identity 79—22077
proton mass, strong gravity explanation 78—12852
QCD, nonperturbative, fundamental scale of strong interactions 79—36002
QCD, perturbative, energy flow and energy correlations in deep inelastic scattering, infrared safety 80—27465
QCD and resonance physics, general technique for deriving sum rules 79—22058
QCD Compton effects, quark and gluon jets 80—32101
QCD development from classical Yang Mills theory, a qualitative critique 79—80804
QED, fine-structure constant, coupled Maxwell and Dirac eqns., lepton and quark-like solutions 80—62894
QFT, general principles and strong interacts. at high energies 79—239
quark cluster, model of ordinary and exotic hadrons 79—40759
quark models and unified field theories, review 79—80805
quarkonia states, heavy, strong decay into other heavy flavours, and triple-gluon vertex 80—47279
quarkonium decays into heavy quarks 79—58943
relativistic dense matter, statistical mechanics using phenomenological quantum field model 78—89814
relativistic four dimensional field theoretical model of strong interactions based on statistical bootstrap 78—29315
relativistic local renormalizable field theories, basis for quark confinement and QED 79—21893
relativistic particle physics, book 80—41966
resonance-particle system, unitary relation, phase shift anal. *(Russian)* 77—22718
scaling law in strong interactions 78—41606
separable nucleon-nucleon potentials and minimal relativity 80—27495
short range interactions, approximation by separable interactions of simple analytic form 79—85284
spin dependence in strong interactions at very high energy 78—58203
statistical bootstrap model for hadronic matter and multiparticle reactions 77—57502
stellar environment, nucl. struct. and reactions 80—72765
stochastic-field multieikonal theory, high-energy hadron dynamics 78—8634
strong and gravitational interaction unified theory, hierarchy of universes, large numbers explanation 79—17654
strong coupling constants in broken SU(3) 80—27423
strong gravity, field equations, strong interactions, de Sitter microsphere idea of hadrons 80—68111
strong interaction field theory, role of tachyons and virtual fields, book contrib. 79—58889
strong interaction models in 6-ε dimensions 80—4919
SU(2)×U(1) gauge model, chiral SU(2)×SU(2) symmetry and electron mass 80—57542
SU(3) group strong interactions in gravitational field 80—91047
SU(3) model for strong interactions quark excitation and ψ mesons 77—18198
subnuclear structure concept via dilepton prod. in hadronic collisions, historical review 79—93365
supersymmetric spontaneously broken theories of weak, EM and strong interactions 77—79244
system with interaction and stratification *(Russian)* 78—37193
T invariance, possible test in NN polarised large momentum transfer reactions 77—30402
temperature origin in high energy strong interactions, large transverse accel. 78—37186
testing strong interaction theories 79—97569
topological expansion $1/N^2$ convergence factor, stat. weight interpretation 77—54073
topological expansion asymptotic planarity 77—41821
unified gauge model with a nonlinear chiral hadron Lagrangian 80—42378
unified gauge theory of gravitational and strong interactions 80—95016
unified theory of strong and gravitational interactions 79—17662
unitarity and crossing in high energy scatt., differential cross section in diffraction region *(Russian)* 79—80764
unitary corrections to short-range order, long range rapidity correlations 79—26315
velocity of sound in hadronic matter evidence from very large transverse momenta interactions 79—71725
very high energy interactions, review 80—440
weak hypercharge embedding in strong gauge groups 79—30692
Yang-Mills theory developed around instanton, renormalisation 80—32027
$dd \rightarrow {}^3He\,n$, 1.1 to 2.5 GeV/c, energy depend., cross sections, reaction mech. 78—54643
f-mesons, spin-two interaction and general relativity, review 79—45046

elementary particle strong interactions continued
K^0-$\bar{K}^0$ mixing, strong interaction corrections in six quark model, QCD calcs. 80—82957
$K^+ \to \pi^+ e^+ e^-$, neutral-current process, strong interaction corrections 80—62968
$K^- p \to \pi^+ \Sigma^-$, box diagram calcs. unitarity corrections in strong interactions 80—91110
Λ nucleus$\to\Sigma^0$ nucleus, Σ^0 life time, Coulomb excitation method *(Russian)* 78—46114
$\mu^+ d \to \mu^+ np$, ≤ 5 MeV, Coulomb break-up of deuteron and n-p off-shell effects 79—75777
NN, Faddeev approach to strong interaction, parity non-conserving effects, predictions 79—93448
NN low energy scatt., parity violating observables, strong potentials 78—50045
$NN \to NN(NN\pi)$, isobar and peripheral model anal., and unified theory 79—80841
$\bar{N}N$ potential, imaginary part 80—32118
$\bar{N}N \to \bar{\pi}\pi\pi$, kinematic singularity free helicity amplitudes, crossing matrix anal. props. 80—95285
$N\bar{N}$ system, effects of annihilation on resonances 79—58949
$NN\pi$ amplitudes, parity violating, QCD calc. in Weinberg-Salam model and SU(4) flavour symmetry breaking 79—67520
νe elastic scattering, differential cross section, behaviour in nondiffraction region 79—58952
$\bar{p}n$ strong interaction effects on antiprotonic atoms X-rays of light nuclei 78—29867
pp, 23.4-62 GeV, scatt. amp., differential cross section from eikonal model *(Russian)* 80—57642
$\pi N \to \pi\pi N$, kinematic singularity free helicity amplitudes, crossing matrix anal. props. 80—95285
$\pi^- p$, 21 GeV, prompt e^- associated with strange particle in strong interaction, direct evidence 79—419
$\pi^+ p$, Born amplitude, unitarity sufficiency condition 79—86068
$q\bar{q}$, eikonal speculations on infrared confinement 79—36027
$q\bar{q}$ static interaction, instanton contribs. 79—12961
$^3He + \pi^-$, strong interaction shift, multiple scatt. and absorptive effects, calc. 78—62958
N*(1236) propagator, momentum depend. in N*-excitation current 80—27559

elementary particle symmetry
see also chiral symmetries; conservation laws; discrete symmetries; dynamical symmetry; helicity (elementary particles); isotopic spin (elementary particles); nonlinear symmetries; spontaneous symmetry breaking; SU_n theory; supersymmetry
0(3) dynamic symmetry of neutron in linear current mag. field, hidden symm. *(Russian)* 77—210
σ model, gauge invariant extension with EM interactions, SU(2) symm. breaking 77—30258
absorption model approx. for particles with spin, Regge cuts, crossing symmetry violation *(Russian)* 80—42435
admissible complete sets in ladders U(6,6) symmetry 78—8626
affine algebraic groups, automorphisms 79—17269
algebras, unusual, appls. in particle physics 80—27419
arbitrary-spin particles, field theory 77—34075
asymptotic symm. for charmed mesons, new duality 78—21348
atomic parity conservation, left-right symm. unified theoreies 78—70306
axiomatic approach to particle symmetries 79—21897
axion, implied by U(1) symm. 78—33037
baryon-lepton symmetry, quark mass spectrum 79—54306
bilinear symmetry-breaking in σ-model, meson mass and decay const. 77—49877
Borel multipliers for the Bondi-Metzner-Sachs group 80—18088
charge-monopole composites, Poincare invariance and parity violation 77—2762
charm scheme of subhadronic constituents, weak decay processes 78—25012
charmed baryons, weak decays, quark model framework 80—62976
charmed particles weak decays, generalised charge symm. 78—37184
classical and prequantised mechanics without Lagrangians or Hamiltonians for relativistic particles 78—74126
classical scalar and spinning particles interacting with external field 77—67557
Clebsch Gordan coefficients for meson sector in SO(8) model of elementary particles 78—58135
completely integrable equations, symm. groups *(Russian)* 77—82365
conference, group theoretical methods in physics, Austin, Texas, USA (Sep. 1978) 80—4474
conformal group as broken symm. for quarks with charm 77—10193
conformal invariance in elementary particle physics, review *(Russian)* 79—21964
conformal relativity, bare mass theory 80—27417
conformal relativity, classification of metric bosons 78—93803
conformal relativity, kinematic theory of mass 78—77706
conformal relativity, particle species classification, symms., space time origin of isospin 78—93815
conformal transformations, unitary implementability 79—21965
conservation and symmetry principles, appl. to particle systematization 79—9295
conservation law, Noether theorem 79—45034
coupling const. behaviour and invariant coupling constants *(Russian)* 77—34096
dimensional symmetry rearrangement in renormalised quantum field theory 77—5982
dual string models with non-abelian colour and flavour symm. 77—2804
dual symmetry of general type vector field, quaternion formulation *(Russian)* 78—58107
Dyal symmetry of vector and spinor fields *(Russian)* 79—30673
dynamical groups, symmetries and constants of motion for electric and mag. charges 80—101945
dynamical rearrangement of symmetry in QED 77—65122
dynamical symm. breaking, bound-state effective pot. formulation 78—8554
dyon-dyon interaction in predictive relativistic mechanics 79—26265
electroproduction structure functions studied using light cone expansion via O_4 symm. 77—41845
elementary particle properties from atomic phys. expts., parity, time-reversal 77—34578
exceptional groups, patterns of symmetry breaking 80—42356
exceptional Lie groups, basic props. 77—74611

elementary particle symmetry continued
fibre bundles almost complex manifold approach, curvature form 78—12915
finite temperature vacuum excitations for relativistic field theories with dynamical symm. breaking 77—5994
gauge hierarchy problem, proposal for elimination in unified theories 79—75707
gauge theories, symm. definition 78—32973
gauge theory, instanton solution symmetry *(Russian)* 77—38094
gauge theory phase transition with symmetry restoration 77—5984
general covariance group, unitary representations 79—21970
general light cone frame, from Galilei group to Lorentz group, appl. to Schrodinger-Pauli eqn. 77—61187
generalised Poincare group, reduction of irreducible unitary representations with respect to subgroups 77—30281
generalised statistics and quark model 77—13690
generalised symmetry algebras for para-Fermi fields 79—30676
ghost and internal symm., models on Hermitian spheres 78—70304
graded Lie algebras, Wigner Eckart theorem for tensor operators 77—45984
group theoretical foundations of classical and quantum physics, kinematical symmetry groups and state spaces 80—52008
hadron elastic scattering and inclusive k_T^2 distrib. s-channel unitarity correl. 79—26258
hadronic and electromagnetic widths of mesons in the style schemes, Sp(8) and SO(8) schemes 79—45051
hadronic cross section strength, nonlinear unitarity eqn., internal symm. restriction 78—33042
hadrons interacting, isospin-spin polarisations, dynamical characts. 80—32035
history of search for fundamental constituents of matter *(Polish)* 78—54588
hypermomentum in hadron dynamics and gravit. 78—41487
identical particle effect and symmetrization in Mueller amplitude 79—30672
induced representations, reproducing kernels, conformal group, ladder representations, SU(2,2) 77—13882
instanton, group theoretical aspects 79—97494
internal and space-time symmetry fusion, spinor charges 77—22660
internal symmetries, invariant theoretical consideration of nonlinear realizations 78—93817
invariant operators of unitary groups U(n) and SU(n) 78—8555
isospin violating effects from nonvanishing quark mass difference 79—63385
Kaluza-Klein bundle, unified theory 80—37153
Lagrangian field theory, divergence identity and dynamical symm. rearrangement 77—45963
lepton-quark and space-time symmetry 78—16967
Lie admissible algebra and nilalgebra, recent developments 78—74168
Lie admissible forces, non-self adjoint, compatible symmetry schemes 79—75696
Lie-admissible deformation of self-adjoint systems 80—101941
line reversal symmetry test in baryon exchange processes 78—78202
Lorentz invariant dual string model dimens. regularisation by hyperfunctions 78—41510
Lorentz invariant string regularised dimensionally using hyperfunctions 78—41511
manifest left-right symm., parity nonconservation via spontaneous breakdown, expt. consequences 77—57465
massive Schwinger model, consistency and Lorentz invariance 78—89613
massless field theory, conformally invariant struct. 79—30656
Melosh transform. in interacting quark theories, $U(6) \times U(6) \times O(3)$ group on null plane 79—49464
meson mass formula broken SU_N 77—6043
meson semileptonic decay, effect of symmetry breakdown *(Russian)* 79—6337
Moufang plane and octonionic quantum mechanics 78—69999
Nambu Jano-Lasinio model, symm. restoration above critical temp. 77—54054
neutral current props., Lorentz struct., internal symm., exclusive ν prod. processes 77—18267
neutron in magnetic field of linear current, system with latent symm. 0(3) *(Russian)* 77—67588
non-Abelian group spontaneous violation, gauge models and external currents *(Russian)* 77—207
nonassociative algebra, bibliography 80—36793
nonleptonic weak interactions, irregular G_u-parity term, hadronic currents 77—2770
nuclearity of C^∞ vector spaces in induced inhomogeneous Lie group representations 78—86422
null-plane $U(6)_{W,\ currents}$ identification of hadronic states, necessity for Melosh-type transforms. 77—22667
$O(4) \times U(1)$ gauge model, restrictions from νN expt. data 77—71477
O(5) form of pseudoparticle soln. in gauge theory, quantum fluctuations 77—65083
octet enhancement and Cabibbo angle in SU(3) breaking scheme 77—2785
octonion algebra, unified theories with orthogonal groups 77—46005
Okubo Zweig Iizuka rule phenomenology, rule-violating transitions 77—224
ordered hadron S-matrix, quark interpretation, selection rules 78—62322
physical fields, symmetry, causality props. 79—6270
Poincare $IO_{3,1}$, centraliser subalgebras 79—6294
Poincare $IO_{3,1}$, coordinate transforms. and centraliser subalgebra, algebra Casimirs 79—6295
Poincare subgroups, role in high energy physics models 79—97530
Poincare subsymmetry, associated invariant EM field *(French)* 77—61209
pseudoparticles, conformal symm. Lagrangian models in four dimens. space 78—374
QFT, supersymm., space time symm., internal symm. groups, relativistic invariance *(Russian)* 77—49871
quark-line rule for hadron nonets, review 79—26304
reflection groups and internal-symmetry algebras, 8-component conformal spinors 80—9112
relativistic many body theory, finite temp. and density., elementary particle symmetries 79—49403
relativistic orbital angular momentum and spin observables, Lorentz-covariance 77—6062
relativistic particle classification, representation theory, 8 nonisomorphic simply connected covering groups of O(3,1) 77—46008

elementary particle symmetry continued
relativistic wave equation, Poincare group, extended particle model 78—41414
renormalisation group transformations as symm. mappings, local Lagrangian density *(German)* 78—49953
scalar relativistic fields, symmetry groups, with self-interaction 79—30664
sequential jet decay described by an Inonu-Wigner contraction of the Lorentz group 79—17695
SL(3,R), relativistic spin selection rules 77—61215
SL(n,c) extension formulae, s_{ip} coeffs. calc. 80—4884
SO_{11} group for interaction unification, charge and coupling constants 79—2965
SO_3 monopoles, spherical symm. limits on mag. charge, gauge independent proof of Guth-Weinberg theorem 77—30231
SO_4 symmetry for classification of dibaryons and baryoniums 79—97531
SO(8)×SO(8) phenomenological symmetry, synthesis for eptons and hadrons 79—13035
spinning electron, quantum mech. rotor, dynamics, invariance requirements 78—70250
spinning particle, Lagrangian formulation of classical and quantum dynamics 77—18173
spinning particles interacting with external fields, invariance groups of relativistic eqns., SU_3 symm. 78—49962
spontaneously broken gauge theory model, ρ' vector meson, e^+e^- colliding beam data 77—2845
stepwise breaking of gauge and discrete symm. 78—29269
SU(2)×U(1) gauge models with lepton doublets and singlets, exact consequences of universality 77—54065
SU(2)×U(1) unified e.m.-weak scheme *(Russian)* 77—218
SU(3)×SU(3) model, meson spectrum, prod. and decay of new particles *(Chinese)* 77—49870
SU(3)×U(1) electroweak model, strong extension, flavour and colour gauge exchange symmetries *(Chinese)* 80—101975
SU(3) representation theory, connection with SU(3) particle classification schemes, Weyl character formula 77—34101
superconductivity and elementary particles theory, review 80—4911
supergravity, unified theory of basic forces 78—50001
symmetries and differential equations 80—105807
tensor meson dominance, internal symmetries, and meson mixing for the new particles 80—102036
three pion states, permutation group S_3 irreducible representation 79—17635
trichromatic theory and time vector in relativity theory *(French)* 78—57006
U_3(W)-gauge unified EM-weak theory, neutral current neutrino interactions 77—26481
U(1)×SU(2)×SU(2)×U(1) gauge group and weak decays 77—18214
U(1)×SU(4)$_L$×SU(4)$_R$ based weak-EM synthesis with manifest left-right symm. 78—8571
U(1) problem in generalised θ-vacua, Goldstone boson and QCD 80—52399
unified description of symmetry groups *(Russian)* 78—41436
unified field theories, E_7 group generators, 3jm factor calcs. 79—93330
unified field theory, 11-dimens. space, 7 compacted dimens., 0(8) symmetry 79—26275
unitary symmetry in baryon-antibaryon systems *(Chinese)* 80—102000
velocity operator for irreducible unitary representation of Poincare group, identification 77—49873
Weyl Lie algebra, relativistic scatt. of model particles 79—40690
Wigner rotations and associated matrices for Dirac particles 77—2761
Wigner rotations for zero mass particles *(French)* 77—41783
Yang Mills theories, high-energy gauge meson exchange reactions, factorisation, Reggeisation 77—18172
B-B, B-$\bar{B}$ scattering, models of line reversal symmetry breaking 78—62326
$\eta \to \pi^+\pi^-\pi^0$, anal. based on u_3-term of $(3,\bar{3})+(\bar{3},3)$ model 77—67657
$lp \to l'X$, weak reaction, large transverse momenta, field theories at finite temp., symm. breaking and restoration 79—399
μ-e universality and spontaneous μ-e mass splitting 77—30302
μe, mass difference, lepton number and symmetry conservation, forbidden transitions *(Chinese)* 79—13121
NN short range interaction, six quark symmetry props., nucleon colour mag. attraction *(Russian)* 80—42411
$\nu(\bar{\nu})$ scatt. on fermion targets, four symmetry relations 79—373
$\nu(\bar{\nu})$N elastic scatt., symmetry relations, current matrix elements 78—54627
ν-induced associated production, Born term model 78—58179
νN interactions, currents and symmetries, theoretical speculations following recent expt. results *(German)* 77—41837
$\bar{p}$n interactions in flight, beam target reversed symm. 78—41566
H, parity mixing, relativistic neutral current interactions and nonrelativistic pots. 79—26908

elementary particle theory
see also Bethe-Salpeter equation; complex angular momentum plane; current algebra; dispersion relations; electron theory; elementary particle interaction models; elementary particle symmetry; Feynman diagrams; form factors (elementary particles); group theoretical schemes; helicity (elementary particles); isotopic spin (elementary particles); Lee model; mass formulae; quantum field theory; S-matrix theory; scaling phenomena; structure functions; sum rules; vertex functions
advances towards a unified theory 80—91039
annihilation of particle-antiparticle pairs, possible future use as energy source 79—36054
anomalous magnetic moment, perturbative expansion divergence 80—78063
anti-commutative, self-inverse matrices and transformations in eigenvalue problems *(Chinese)* 80—101951
applied inverse problems, book 79—49017
asymmetric creation of matter and antimatter in the expanding Universe 79—75302
average multiplicity depend. on impact parameter and momentum transfer 80—37312
baryon field equation for arbitrary spin 79—63389
baryons, charmed, mag. dipole moments and mag. quarks 79—97573
basic course in modern weak-interaction theory 80—91044
Bernard Gregory 1979 lectures 80—77992
book, annual review of nuclear science (vol.26) 77—57583
boson, Green function, rainbow approach of scalar model *(Russian)* 80—68436

elementary particle theory continued
boson field in external potential, instability, Klein paradox, particle creation 77—6017
charged particle spin, theory using fluid basis for matter and energy 79—97542
charm, elementary particle theories, properties *(Spanish)* 80—73681
charm particles, implication for unified theory of elementary particles *(French)* 79—67522
charmonium state decay, nonrelativistic and relativistic theory 78—58221
classification, selection maps for quantum logics 78—29320
closed systems with nonconservative internal forces, Lie admissible quantisation, hadron struct. 80—37174
cluster decomposition of many dimens. phase space, appl. to high energy collisions 80—102027
conference on Lie admissible formulations, Cambridge, USA, (Aug. '79) 80—36765
conformal invariance in elementary particle physics, review *(Russian)* 79—21964
conformal transformations in spinor space-time 79—30674
constituents for leptons and quarks, possibilities 80—42437
cosmological approach, review, book contrib. 80—68440
cosmology, role in elementary particle physics 80—27430
crossing properties of scattering operators 80—32028
decay lifetimes, dependence of measured values on apparatus 79—22158
deuteron, relativistic space-time description and short distance effects 77—2795
dimensions, mass, elec. and mag. moments *(French)* 80—13305
discoveries during 1974-7, and associated theories *(Czech)* 78—86103
discrete spacetime, quantum numbers, uncertainty and min. entropy 77—87659
education, elementary particles, quarks and the concept of particle, Richtmyer memorial lecture 78—62286
electron model 78—29371
electron-muon symmetry of Callan-Symanzik function: two-lepton case 80—73627
elementary particle physics, information from astronomical observations 80—51935
equivalence principle, stress tensor, long-range behaviour of gravitational interactions 77—13676
equivalence theorem, path integral formulation for nonlinear case 79—12933
exclusion principle extended, particle classification anal. 78—49690
faster than light processes, causality 77—54061
Fermi quantum fields, derived from Bose quantum fields, applications 78—36928
field theory, massless equations, first-order, conformally covariant 78—29265
finite Lorentz transformation applications 77—45976
five-dimens. model of scalar bosons, O(N) symm. 78—70307
free relativistic particles, classical counterpart to Wigner's theory 77—65073
free relativistic spin-1/2 particle energy-momentum invariants and kinetic moment *(French)* 78—62287
froissaron dynamics in high-energy physics 77—61218
fundamental constants and cosmic object size, empirical relations 77—82338
fundamental interactions, review for teachers 78—16615
general relativistic particle models, and effective radius *(German)* 78—86198
general relativity conference, Trieste, Italy, 1975, July 78—8285
generalized Weizsacker-Williams method, single variables description 77—49937
graduate level textbook 80—27053
gravitational annihilation, radioactive decay 77—6075
group theory and particle theory, book 77—67589
hadron building blocks, pionic mass intervals in narrow and S-state resonances 80—105875
hadron multiplets, realisations in SU(3) from stable particles 80—9159
hadronic mass spectrum from high energy nuclear collisons 78—33049
hadronic matter, anisotropic superfluidity, analytic formulation 80—105869
hadronic structure using parton anal. of deep inelastic scattering and rel. processes 79—80803
hadrons, relation between spin, isospin, strangeness and charm 80—37183
Hamiltonian formulation for an extended particle with interacting constituents 79—63022
hard-photon theorems 77—38175
Hardy spaces, role in form factor bounds 79—30735
heavy lepton decay, selection rule, $SU_2 \times U_1$ gauge model 79—49500
heavy lepton prediction in weak interaction theories 80—73657
heavy quarks, elementary particle physics developments, review 79—22053
high energy accelerators and interactions *(German)* 79—97642
identical particle indistinguishability, field quantisation Lie algebraic approach 80—77984
individual properties of individual particles, theory, teaching approach 78—57721
indivisibility and extension concepts for elementary particles *(German)* 78—29298
infinite dimensional Lie admissible algebras, elementary particle physics 80—37177
Klein-Gordan equations with logarithmic nonlinearities, classical theory 79—5996
Lagrangian, effective, in path integral quantisation formalism 80—42325
Lagrangian, with higher derivatives, arbitrary spin fields 79—17596
Lagrangian theory of relativistic rotator, elementary particles unified model 77—41757
Lee model in EM field, mag. moment calc. using Schwinger source theory 80—42350
lepton charge, geometric interpretation *(Hungarian)* 80—73691
lepton model, heavy lepton+quark pair 77—49895
localisation concept of relativistic particles, consistency with causality 77—33883
magnetic layered theory including gravity 77—30353
magnetic monopoles, energy level calcs., Coulombian field approx. 79—26311
many-body scattering, coupled channel eqns. and off shell transforms. 78—402
mass corrections to scaling in deep inelastic processes 77—13929
massive Schwinger model in infinite momentum frame, phys. particles spectrum 77—49886

elementary particle theory continued
mathematical and elementary particle physics, conf., Austria (Feb. 1976) 77—5974
mathematical foundations of dimensional analysis and the question of fundamental units 80—42086
mathematical methods, conf. Liblice, Czechoslovakia (June 1978) 79—21891
meson model based on superposition of Klein-Gordon eqns., ϕ, f', F, K spectrum 78—58121
meson structure model with covariant oscillator potentials *(Chinese)* 78—82180
mesonic topological amplitude products, an algebraic soln. 78—81884
micrononcausal Euclidean wave functions for hadrons, virtual mesons in deuterons 78—41408
microphysics, towards an elemental grounding 78—86106
minimal time-energy uncertainty relation 79—67174
multi-eikonal theory of high-energy hadron prod. 77—6098
multilocal fields in relativisitic quantum field theory 78—37125
multiplicative baryon number conservation, $H \to \bar{H}$ oscill. upper limit, baryon to lepton transform. 79—298
multiplicity distribs. for nonasymptotic energies, concept of similarity *(Russian)* 78—41522
multipole moments for the study of mixed spin reactions 79—97611
muon model 78—29371
muon number nonconserving processes, models with doubly charged leptons 77—74613
mutually interacting charge fields, gauge theoretical formulations of elementary particle processes 78—58122
n-particle relativistic phase space integral, invariant variables, Monte Carlo calc. algorithm 79—9312
N-quantum approximation in Bronzan-Lee extended-source static model 78—8507
narrow resonance in an open channel 78—66099
neutrino as axial EM field source, symm. P-invariant broadened Maxwell eqns. *(Russian)* 78—58141
new elementary particles, theoretical predictions, recent expt. results 77—57475
nonassociativity in particle physics and Caley-Graves' octonions 80—37171
nonlinear field theory, path integrals definition, rules for transform. of variables 78—78072
nonlocal structures, shell effects 80—52391
nuclei and particles, introductory text book 78—78234
O(10) theory of strong, weak and EM interactions, masses and mixing 80—13248
open systems theory, appl. to unstable particles 79—17281
P-state particle, field current reln. and total width *(Chinese)* 78—82188
particle model based on stringlike solitons 78—62294
particle spectrum, series classification 77—74652
Pauli spin matrices, generalised, commutation rules 79—17597
Penrose theory in particle physics 78—29321
phenomenological inverse problem in elementary particle scattering 79—49498
photon double helix struct., 2 intertwined neutrinos, polarisation, helicity props. 78—37255
positivity constraints on real parts of density matrix elements 77—18207
probability concept and dynamics of extended particles in post quantum mech. theory 77—49882
proton half life, Dirac approach to large number coincidences 80—27501
quantised particle lifetimes, reln. to hypothesis of quantised time 77—38106
quantum particles in a stochastic linear potential and the temperature of hadrons 80—32087
quantum theory and structures of time and space conference, Starnberg, W.Germany (July 1978) 80—27044
radiating Weyl metric, nonstatic soln. generalisation, neutrino and EM fields 78—41210
Regge pole theory, reasons for survival, review 78—24977
relativistic centre of mass of extended particle with interacting constituents 79—17701
relativistic electron pair model of nucl. particles 79—45042
relativistic quantum mechanics formulation of space and time 78—65796
renormalisation group eqn., spontaneously broken symmetry and heavy scalar particle decoupling 80—47189
renormalised theories of particles with spin $J=1$ described by antisymmetric tensor *(Russian)* 77—13876
resonance photoproduction, Melosh transformation 77—46059
rest mass variability, theory and constraints from solar system expts. 77—45781
review of relationship between cosmology and elementary particle physics 79—101061
rotational covariance and Yang-Mills monopole 77—13870
scalar Higgs eqn., particle-like solns. *(Russian)* 78—12829
scaling of inclusive form factors with respect to a generalized scaled variable 80—417
scattering amplitude determ. from differential cross section, contraction mapping 77—10206
scattering amplitude determ. from differential cross-section, compactness theorems 77—10235
selections from 1977 Comments on Modern Physics, book 79—30181
semi-inclusive processes of multiparticle productions, scaling laws 79—30684
sequential particle order, fundamental concept for hadron physics 79—80762
sequential particle order, fundamental concept for hadron physics, S-matrix theory 79—80763
soliton dynamics in nonintegrable systems, classical solns. 78—28996
solitons with particle properties, real scalar fields anal. 77—45936
space-time approach to the description of cumulative-type processes *(German)* 80—68439
spacetime, extended conformal, interactions and dynamical groups of elementary particles 78—8290
spin, reln. to universal props. of matter 78—21329
spin 1/2 polarised particle description, spinors in 6-dimens. space *(Russian)* 77—6053
spin dependent pots. in fermion-antifermion system, annihilation width 79—9356
spinning membrane, locally supersymmetric, reparametrisation invariant action 77—79230
stable particles as building blocks of matter 80—57577

elementary particle theory continued
statistical mechanics of complex systems, linkages from fundamental particles to cosmology 79—25964
statistics, quantum characts. 78—70297
strange particle coalescence, analogy with ferromagnetism, prod. of ψ-meson 77—13951
structure and second class nucleonic currents 77—18200
structure of charged particles in Einstein's unified field theory 77—30073
$SU(2)_L \times U(1)$ primitive particle model 79—40708
$SU(4)_F \times SU(4)_C$ synthesis of strong, weak, and electromagnetic interactions 80—13255
SU(4), exact, meson-baryon four body reaction amplitudes 77—18192
Summer School, high energy physics, Rutherford Laboratory, England (6 to 24 September 1976) 77—41747
super-dense matter, phase transitions in gauge theories and cosmology, review 79—44654
superconductivity and elementary particles theory, review 80—4911
superconductivity theory development, (1950s to 1980s) *(Czech)* 80—80440
symmetry mappings, particle number conservation, baryon number conservation 77—30063
system with interaction and stratification *(Russian)* 78—37193
theoretical physics at Kharkov Inst., Ukrainian SSR *(Russian)* 79—12558
total reaction cross section calcs. without continuous spectrum wave functions *(Russian)* 79—17702
trilocal structures, expansions 80—57460
twister flat-space theory, possible bearing on quark models 77—22719
twistor struct. of hadrons, classification and masses 77—22695
twistor theory, particle models 80—13278
twistor theory appl., book 79—97485
two-particle resonances and singularities of $2 \to 3$ particle scatt. amplitude 77—49643
unified description *(German)* 77—41803
unified EM-weak interaction Adler's sum rules in source theory 77—38099
unified theory of elementary props. of matter, ideas and expts. *(German)* 77—38112
unitarity effect of $\psi'(3684)$ on shape of $\psi''(3772)$ 79—434
unitary bounds on elastic absorptive parts in terms of diffraction peak width 77—54092
unitary space of particle internal states 79—30712
units of space and time, difficulty in microscopic definition *(French)* 77—54060
unstable particles description in quantum field theory, S-matrix poles 77—6024
vectorlike theory with parity violating neutral current and natural symmetry 77—13909
Weyl's gauge field and spin 1/2 particle coupling 77—49846
Weyl Lie algebra representations as elementary particle models 79—2949
D^0 nonleptonic exclusive and semi-inclusive decays, pole model test 80—37258
e mass calc. in terms of meas. quantities 78—66180
e^+e^- annihilation Einstein Podolsky Rosen nonseparability, nonlocality in Feynman's antiparticle theory *(French)* 77—41498
μ considered as $e\bar{\nu}_e\nu_\mu$ (or $\bar{e}\nu_e\bar{\nu}_\mu$) reson. 77—6189
n-p system, EM form factors in multipole parametrisation formalism 78—17022
$N\Delta$ system, theoretical investigation of bound states and resonances 79—75749
ν mass and Pontecorvo oscills. using chronon concept in electron theory 78—36879
$\nu_\mu \to \gamma + X$, decay lifetime, mass, expt. limits 77—10234
Ω^- spin, centrifugal barriers, quantisation of $l=0$ baryon levels 77—18221

elementary particle weak interactions
see also neutral currents; quantum field theory of weak interactions; Weinberg model
$\Delta I=1/2$ enhancement, $SU(2)\otimes(1)\otimes U(1)'$ gauge model 77—6073
$\Delta I={}^1/_2$ rule, six dominance, parity violation, weak interaction theory review 78—78131
$\Delta S=0$ baryon-π amplitudes, Melosh transformation 78—12857
astrophysics and cosmology 77—25934
asymptotic catastrophe, temporary freedom in lepton and quark interactions 79—85253
asymptotic props. of elastic scatt. amplitudes, where effective number of partial waves is $L=CS^{1/2}(\ln S)^M$ 77—57470
atoms, and ions, parity nonconservation effects 79—10086
axion, Gargamelle beam dump expt. 78—50003
axion properties, strong T and P conservation enforcement 79—67481
b quark, weak interactions and multilepton final states 79—49516
b-quark, horizontal gauge symmetry, Cabibbo universality and fermion masses 80—22583
baryon, charm changing weak decays $1/2^+ \to 3/2^+ + 0^-/\gamma$ in SU(4) and $SU(8)_w$ 79—3021
baryon asymmetry of the Universe, unitarity and possible origins, comments 79—88589
basic course in modern weak-interaction theory 80—91044
bottom meson weak hadronic decays, Kobayashi-Maskawa weak current model 80—42456
bottom mesons, weak decay struct., multilepton production 79—54319
Cabibbo angle and CP violation in a gauge model with discrete symmetry 79—45028
Cabibbo angle and weak interaction invariant props. in chiral dynamics 79—71660
Cabibbo angle formula, discrete flavour symm. 78—417
Cabibbo angle in the $SU(2)_L \times U(1)$ gauge theories 79—35991
Cabibbo angle physical interpretation, weak interactions nonleptonic $\Delta I=1/2$ rule, four-quark scheme 77—22679
Cabibbo suppression and universality in SU_3 gauge model 77—67611
CERN proton synchrotron, electron ring addition, proposal for weak interaction study 78—55062
charm particle weak interaction decay, lifetime estimates, free quark model anal. 79—67544
charmed baryon nonleptonic decays, sum rules for $\Delta C=\Delta S=1$ S-wave decays 79—58957
charmed hadrons expt. data, four flavour model explanation, weak interaction scheme 78—45860
charmed particles weak decays, generalised charge symm. 78—37184

elementary particle weak interactions continued
charmed weak current group struct., chiral $SU_4 \times SU_4$ breaking 77−65118
colour-octet component of weak current, lepton-hadron correspondence 77−6077
Compton amplitude, parity violating part 77−2840
conf., weak interactions, Bloomington, USA, (May 1977) 78−414
conference on high energy phys. with polarised beam and target, Argonne, USA (Oct. 1978) 79−63526
conformal invariant Fermi weak interactions and weak bosons as collective modes 79−89094
conformally covariant spinor field equations 79−22004
cosmic ray diffusion in random magnetic field, weak particle-field interaction theory validity 79−21109
cosmological role in 'pair creation' universe, quasar model 77−5605
CP violation in weak interaction, renormalization of QCD vacuum parameter θ 79−40683
cross-sections, Lorentz contraction 77−33743
current status in elementary particle physics 79−40651
dual electromagnetism and neutral-current interactions 79−71678
dual models of weak interactions of leptons and quarks 78−66070
dynamical scaling violations, evidence from neutral current anomalies 79−17664
E_6 model, basic fermion masses and mixings 78−24972
E_7 gauge model, lepton assignments and trimuon events in neutrino scatt. 79−17709
effective hamiltonian for $\Delta C=1$ nonleptonic interactions in the Kobayashi-Maskawa model 80−86667
eight-dimensional unified theory of weak, EM and gravit. interactions 77−37797
Einstein-Cartan theory, rel. especially to elementary particle weak interactions 78−37171
electro-weak interactions concept and Weinberg-Salem model verification *(Czech)* 80−22549
electron, determ. of weak neutral current couplings 79−35994
electron nucleus weak currents, atomic X-ray spectra, parity violation *(Russian)* 79−22642
electron- and muon-number nonconservation, new interaction 77−65128
electron-electron (muon) scatt., weak lepton interaction influence *(Russian)* 79−6333
electron-nucleus polarised low energy scatt., test for weak interaction theories 77−74836
electroweak gauge models with heavy W bosons, $SU_2 \times U_1 \times U_1'$ scheme *(Russian)* 80−86652
elementary particle symmetries, axiomatic approach 79−21897
EM-weak interference effects, LEP studies 79−97614
Eotvos expts. and weak interactions, anal. 78−78129
Fermi weak interaction theory, consistent renormalisation scheme, Yang-Mills theory parallel 78−66071
fermion mass generation, regularisation 80−9090
fermion-fermion scatt., very high energy weak interaction effects 79−9327
fermions, ultra heavy, weak interactions, high energy scattering, low energy renormalisation corrections 78−93838
Feynman diagram amplitudes in cross section calcs., computer code 79−13094
four-quark scheme, $\delta I={}^1/_2$ rule, existence of K_L^0, K_S^0 77−22688
fundamental constants, self-consistent values *(German)* 79−12758
fundamental interactions, review for teachers 78−16615
fundamental nature with reference to β-decay modes *(Hungarian)* 77−26482
Gargamelle, neutrino physics history, theory and expt. 78−50027
gauge model of weak and EM interactions with SU(3)xU(1) symm. *(Russian)* 77−6074
gauge models, implications of like-sign dimuon events 77−67643
gauge models with Majorana fields and right-handed weak currents 77−22643
gauge scheme of weak and electromagnetic interactions, review *(Russian)* 79−26278
gauge theories, charm particles and observable quantities 77−34099
gauge theories applied to weak interactions, review 77−26479
gauge weak interaction model with left-handed 8 quarks and 8 leptons 77−18218
gluon exchange diagrams, effect on parity violating weak interactions 79−97565
hadron resonance decay, intermediate vector boson and high energy weak interaction detect. 79−22012
hadron-hadron weak interactions, right handed currents effects in QCD 79−13016
hadronic current, models with 4 and 6 quarks *(Russian)* 77−74616
heavy atoms, P-odd effects, weak interaction eqn., SU(2) theory, four fermion theory *(Russian)* 78−93820
heavy fermions in the standard sequential scheme 79−71748
heavy lepton decay, selection rule, $SU_2 \times U_1$ gauge model 79−49500
heavy lepton prediction in weak interaction theories 80−73657
heavy quark semileptonic decays, gluon corrections 79−17688
hidden gauge symmetry, appl. to elementary particle fundamental interactions 79−30658
Higgs boson, spontaneously broken gauge theory phenomenon, possible weak interaction model 78−74200
Higgs boson couplings, charged, K_L-K_S mass differences 80−62917
Higgs bosons, effects on experimental observables, and fermion mass scale 80−32061
Higgs bosons in gauge models with right-handed charge currents 77−49892
Higgs lattice abelian model, finite temp. behaviour 80−13260
Higgs-Kibble mechanism and electron-muon mass ratio 78−66065
High energy behaviour of weak interactions and renormalisable theories, book contrib. 78−78164
high energy unitary bounds in new theory of weak interactions *(Chinese)* 79−320
high energy weak and EM interactions [conf. Les Houches, France (July 1976)] 79−80785
historical introduction, weak interactions, book 78−78133
history, $\Delta S=\Delta Q$ selection rule violation, appl. of quantitative anal. techniques 79−53953
horizontal interaction and weak mixing angles 79−30696
inelastic final state interactions, unitarity, coupled-channel approach 77−2835
interaction models explaining null parity violation in Bi, tests on other weak interactions 79−2974

elementary particle weak interactions continued
interactions beyond Z pole 79−97568
intermediate boson mass bounds in spontaneously broken gauge theory 77−46007
intermediate boson theory with large dimensionless coupling constant, neutral currents as second order processes 77−61244
internal symmetry origin 77−45959
isotropy of Universe, entropy prod. in lepton era 78−61947
left-right symmetry, spontaneous breakdown, parity violation, leptonic right handed, currents 78−21351
LEP experiment 79−97613
lepton direct production in hadron-hadron collisions, interaction models review 77−236
lepton mixing and neutrino oscillations, cosmic neutrinos, heavy leptons, μ decay 78−82193
lepton mixing matrix, sequential Weinberg-Salem theory, CP conservation 80−47238
lepton-nucleus elastic scatt. with $0^+ \to 0^-$ nuclear transition, P nonconservation *(Russian)* 77−61402
lepton-quark symmetry, theoretical ideas about charm and flavour mixing 79−49486
lepton-quark system, quantum number laws, classification of weakly interacting particles, decays 78−82138
leptonic weak interactions, book contrib. 78−78161
leptons, EM characts. and CP disturbance in SU(3)×U(1) model *(Russian)* 78−29327
leptons and quarks, EM and weak interactions, flavour $SU_3 \times U_1$ gauge model 79−97554
manifest left-right symm., parity nonconservation via spontaneous breakdown, expt. consequences 77−57465
many-quark models, weak interactions *(Russian)* 78−33023
mass and number limits of neutral weakly interacting particles, cosmological approach 77−71000
mass scale of weak interactions 80−91045
milliweak gauge models of CP violation 80−73633
minimal anomaly-free electroweak model for several generations 80−4906
molecules, L- and R-rot., ΔE due to weak electron-nucleus interaction, P-isolation *(Russian)* 77−30793
molecules, parity-violating effects of weak interactions 80−52455
multielectron atom, parity nonconservation *(Russian)* 79−45033
multilepton events, nucleon dissociation and quark and gluon decays 77−46014
muon number nonconservation effects in gauge theory with V+A currents and heavy neutron leptons 78−8573
muonic atom, configurational mixing in shell and neutral weak muon-nucl. interaction effects obs. feasibility *(Russian)* 80−32859
muonic charge and quark-lepton analogy *(Russian)* 77−219
neutral currents, charm, dileptons and multileptons, weak interaction phys., review 79−67492
neutral transitions, vector-like weak currents, parity violation *(Russian)* 78−24995
neutral weak current interactions, review 80−73654
neutral weak interactions and particle decays 77−13954
neutral-current processes, test of single-Z-boson hypothesis 77−74639
neutral-current weak interaction without electroweak unification 80−105835
neutrino bremsstrahlung in an intense magnetic field 79−30055
neutrino experiments at high energies, total cross sections by currents, review 79−49511
neutrino historical review, detection, meas., and interactions with nuclei and nucleons 79−49002
neutrino interactions, appl. to weak interaction and nucleon struct. investigations, review 79−80823
neutrino interactions in neutron stars, pulsation damping 80−77439
neutrino reactions at high energy, weak interaction props. and hadron struct. investigation, book contrib. 79−30727
neutrinoless double β decay in ^{48}Ca, matrix element calcs. 77−30518
neutron coherent scatt., parity-violating pots., weak interaction probe 77−71599
neutron decay, weak interaction meas., coincidence type ion electron converter detector obs. 80−58100
new particles and weak interactions, models *(Chinese)* 79−93334
new physics from experiments above 100 TeV, appl. to QCD, weak interaction, and gauge theory 79−63564
non-leptonic weak interactions, book contrib. 78−78163
nonleptonic 20+15 dimens. weak interactions 79−71746
nonleptonic decays of ordinary and charmed hadrons, vector-like model 78−41545
nonleptonic weak Hamiltonian, current×current theory, SU(4) representations 79−17666
nonleptonic weak interaction, SU(4) symmetry struct., parity violating Hamiltonian 80−52456
nonleptonic weak interactions, irregular G_u-parity term, hadronic currents 77−2770
nuclear beta-decay, extended Siegert theorem 77−41924
nuclear decays as test of elementary particle theory, review 78−21361
nuclear structure, conf. 78−50059
nuclei, weak interactions and axial polarisability 77−22924
nuclei in weak and EM processes, elementary particle method approach, book contrib. 79−97663
O(4)×U(1) gauge model, restrictions from νN expt. data 77−71477
O(4)⊗U(1) gauge model for weak and EM interactions 79−71681
octet enhancement and Cabibbo angle in SU(3) breaking scheme 77−2785
optical experiments as a means of verification 79−6313
P-violating neutral currents in L-R symmetric gauge model 77−82698
P-violation in H- and He-like ions, observation impeding effects *(Russian)* 77−75078
parity nonconservation effects in atomic transitions 77−13889
parity nonconservation effects in atoms, review 77−13890
parity nonconservation in spectra of multiply charged ions 79−10087
parity nonconserving weak interaction between nuclear particles, review 77−6295
parity violating internucleon potential due to vector meson exchange, asymptotically free theories 77−10210
parity violating potentials, fermion scattering 77−79245
parity violating vector meson-pseudoscalar meson interaction, relativistic quark model 77−54102
parity violation, correl. with biomolecules optical asymm. 78−69000
parity violation and the masslessness of the neutrino 79−85258

elementary particle weak interactions continued
parity violation in neutron-proton capture 77−46165
parity-violating vector-meson-exchange internucleon potential, weak nuclear processes, modified factorisation approach 77−30418
particles and fields conference, Argonne, IL, USA (Oct. 1977) 78−78130
PCAC and weak nonleptonic strangeness changing Hamiltonian 77−71460
photino and goldstino, scatt. cross sections on matter 79−97558
photoproduction processes of charm particles with charm nonconservation *(Russian)* 78−74201
pion photoproduction, weak interaction induced parity violating assymetries 79−71758
polarised beams and targets in high-energy interactions, conference 77−30470
polarised hadron-hadron high-$p_\perp$ collisions, weak effects 77−30457
probability current and boundary conditions for wave functions of parity violating interactions 77−71459
pseudosymmetry, weak decays and gauge group U(1)×SU(2)×SU(2)×U(1) 77−18214
pure leptonic weak interaction with induced shadow states, renormalisable theory 78−37136
QCD, six-quark model, $\Delta S=1$ weak nonleptonic decays 80−22582
QED, fine-structure constant, coupled Maxwell and Dirac eqns., lepton and quark-like solutions 80−62894
quark and lepton couplings in the weak interactions 79−17665
quark decay lifetimes in Pati-Salam model 77−79243
quark flavour, crude numerical estimate in SU(2)×U(1), SU(3)×U(1), SU(2)×SU(2)×U(1) models 79−13059
quark mass spectrum, dynamical symm. breaking, weak interaction orientation to strong interaction 77−74640
quark masses, spontaneous parity violation, weak interactions of quark fields 77−34115
quark model, weak interactions, quark masses, spontaneous violation of parity 77−6054
quark models and unified field theories, review 79−80805
quark strong interactions as weak interaction symmetry breaking mechanism 80−18117
quark structure, weak interactions model 77−30313
quark-parton model, strong interactions of quarks, weak interaction *(Russian)* 77−82710
quarks, mass of u and d quarks from weak and EM interaction model 80−13254
radiative corrections in gauge theories, QCD current algebra formulation, weak interaction universality 78−93883
radiative corrections to β and μ decays in $SU(2)_L\times U(1)$ models involving 2n flavors 79−40778
radiative corrections to parity violation in atoms in SU(3)×U(1) gauge theory 78−62402
relativistic corrections to weak exchange currents and μ-p capture 79−75756
relativistic particle physics, book 80−41966
relativistic theory of P violation in many-electron atoms 80−91042
resource letter WI-1 78−16601
review of weak interaction theory 78−4822
second class axial vector currents with mesonic effects, beta-decay 77−30520
second class current in β decay of ^{20}Fe 78−50127
second threshold related to Higgs mechanism 77−57483
second-class currents and matrix elements in renormalisable field theory 77−10197
semi-leptonic weak interactions, book contrib., strangeness-conserving current, strangeness-changing decays 78−78162
semileptonic decay of charmed particles, formalism using helicity amplitudes 78−4852
semileptonic interactions with nuclei, isoelastic processes, one-body density matrix formalism 77−18528
seven lepton model, quantum flavour dynamics, mixing angle, masses, spontaneous symmetry breaking 78−89652
short distance analysis of weak interactions, asymptotically free theory 77−54068
signature, possibility of observation in future multi-TeV colliding hadron rings 77−49897
six quark model, quark mixing angle bounds 79−71686
six- and eight-quark models, weak interactions 80−99086
six-quark model, for weak and EM interactions *(Russian)* 77−67658
six-quark theory, weak interaction mixing 78−41475
SO(4)×U(1) model of weak and electromagnetic interactions 79−13009
spectrum-generating SU(3) and local current algebra 80−9128
spontaneous symmetry breaking with quaternionic scalar fields, Sp(1,Q)⊗U(1) group for unified gauge theory 77−61236
spontaneously broken chiral $U(1)_4$, weak-interaction singlet and strong CP invariance 79−80781
standard weak-EM gauge model, six-quark phenomenology and Grand Unification 80−37204
stellar interiors, sd-shell nuclei, appl. to supernovae 80−82336
strangeness changing neutral currents, avoidance in gauge theories of weak and EM interactions 79−22005
strangeness changing processes, gauge models with V+A currents, high order effects 77−22677
strength at very high energies and Higgs boson mass 77−46013
strong gravity contrib. to nucleonic axial-vector form factor in SU(3) 80−4902
strong gravity with torsion and the Cabibbo angle 80−4913
SU_2 gauge model, light neutral gauge boson, consequences for e^+e^- and $pp(\bar{p})$ 78−58154
SU_3 theorems, baryon octets, semileptonic decays 80−32030
$SU_4\times U_1$ and the origin of the Cabibbo angle, charged gauge boson mixing 80−73639
$SU(2)_L\times U(1)\times U'(1)$ left handed electro/weak model 79−54297
$SU(2)_L\times U(1)$ gauge theory, weak interactions of ultra-heavy fermions 79−75713
$SU(2)_L\times U(1)$ gauge theory of weak interactions, universal lepton mixing and mixing angles *(Russian)* 79−54298
$SU(2)_L\otimes SU(2)_R\otimes U(1)$ gauge models confronting neutral current data 79−22013
$SU(2)_L\otimes SU(2)_R\otimes U(1)$ weak model, ν mass and spontaneous P nonconservation 80−62884
SU(2)×U1 unified theory, symmetry and renormalisation 80−22551
SU(2)×U(1), gauge theory of weak interactions 78−21328

elementary particle weak interactions continued
SU(2)×U(1)×U(1) gauge model, quark-lepton correspondence in neutral and charged current interactions 79−54296
SU(2)×U(1) symmetry group, μe universality breaking in neutral current weak interactions *(Russian)* 79−58918
SU(2)×U(1) unified gauge theory, mech. for nonconservation of muon number, $\mu\rightarrow e+\gamma$ appl. 77−30303
SU(2)⊗U(1)⊗U(1) gauge model without parity violation in heavy atoms 78−82097
SU(2)⊗U(1) gauge model of EM and weak interactions, fermion mass restriction *(Russian)* 78−89650
SU(3)×U(1)×U(1) symmetry, gauge model of weak and electromag. interactions *(Russian)* 78−45838
SU(3)×U(1) gauge models, exam. of weak currents and associated features 78−16975
SU(3)×U(1) gauge theory, electro-weak interaction, helicity mixed representation 80−78013
SU(3)×U(1) modified model, quark and lepton mass hierarchy 78−89653
SU(3)×U(1) theory of weak-electromagnetic interaction with charged-boson mixing 79−35988
SU(3)⊗U(1) theory of weak and EM interactions 77−57481
SU(3) rule for weak decays of charmed and strange mesons, colour struct. of currents 78−45916
$SU(4)_L\times SU(4)_R\times U(1)$ gauge, lepton weak interaction, right currents, effective Fermi interaction const. universality *(Russian)* 79−58921
$SU(4)_LSU(4)_R\times U^Y(1)$ gauge group for lepton and quark weak interactions *(Russian)* 79−97566
SU(8) non-leptonic decay of hyperons and charmed baryons 77−49963
SU(n) group, mixing and sequential heavy lepton weak interaction *(Russian)* 79−40720
supersymmetric gauge theories and their possible applications to the weak and electromagnetic interactions 79−49419
supersymmetric models of weak and electromagnetic interactions 79−26276
supersymmetric spontaneously broken theories of weak, EM and strong interactions 77−79244
supersymmetric vector-like model of lepton interaction 78−412
supersymmetry and gauge theories of weak and electromagnetic interactions 79−26208
superweak gauge theory without charm, CP violation 77−10195
superweak interactions and the biological time direction 79−39344
superweak model of CP violation, gauge theory realisation 77−10194
symmetry breaking, and nature of weak interactions 80−27428
theory and phenomenology, graduate textbook 78−78160
three-photon vertex, weak interaction contributions 77−2787
three-triplet model, SU(2)⊗U(1) theory of weak interactions, spiral chromatic currents *(Russian)* 77−221
trimuon heavy lepton events in ν interactions, $SU(8)_L\times U(1)$ gauge model 77−79242
unconfined colour quark models, weak interactions and neutral currents *(Russian)* 80−105841
unified e.m.-weak Lagrangian in SU(2)×U(1) scheme *(Russian)* 77−218
unified model of weak and electromagnetic interactions based on the gauge group SU(3)×U(1) 79−22003
unified quartet quark model extensions, weak interactions and right-handed currents 77−22678
unified theories of weak and electromagnetic interactions 78−81908
unified theory of weak interactions of leptons and quarks, gauge model 80−22556
V+A current of charmed quarks for nonleptonic processes 77−30307
V+A theory and non-separate μ- and e-lepton number conservation 77−30367
V-A six lepton model, lepton no. conservation 77−87930
vector gauge theories, Higgs boson signature, trilepton prod. in μN reactions 77−61237
vectorlike model, spontaneous CP violation 77−54071
vectorlike model with right handed mixing 78−416
vectorlike model with six quarks, gauge theory, SU(2)×U(1), νN appl. 77−57480
vectorlike SU(3)×U(1) gauge model of weak interact. $\bar{\nu}$ reactions, neutral currents 77−41805
vectorlike theory of weak interactions 77−67613
weak and EM phenomenology, gauge theoretical prospective, charm and flavour conservation 80−4916
weak current detection in mol. physics 77−14433
weak current model with $\Delta C\neq 0$ neutral current 77−54069
weak hypercharge embedding in strong gauge groups 79−30692
weak interaction mixing angles and charmed meson nonleptonic decays 79−85294
weak interaction model with 8 quarks and 8 leptons, neutrino experiment heavy leptons *(Russian)* 79−67494
weak interaction symmetry struct. and $K\rightarrow\pi\pi$, $\pi\pi\pi$ *(Russian)* 79−22016
weak interactions, spontaneous symm. violation, strong quark interaction mechanism *(Russian)* 79−71659
weak interactions, summer school, Varenna, Italy (Jul. 1977) 80−90597
weak magnetism, review of evidence for its existence 79−49445
weak mass mixing and CP violation with heavy quarks, V-A model anal., possible meas. in e^+e^- expts. 79−30695
weak neutral currents, status in weak and EM interactions 79−49444
weak-current angles of six quark model, constraints, from K^0-$\bar{K}^0$ system 79−71685
weak-interaction mixing in the six-quark ambidextrous model of quantum flavourdynamics 79−36000
Weinberg model, exptl. test *(Russian)* 79−97564
Yang-Mills theory appls., lectures given at CERN School of Physics (6-19 June 1976) 77−61173
b-quark, weak interaction decay, lifetime estimates, free quark model anal. 79−67544
b-quark interaction with τ^--lepton, gauge model 79−40738
β decay of ^{12}B and ^{12}N, second class currents 78−50126
D charmed meson weak decays, tests via parity violation, strangeness violation and semileptonic decays 77−30368
$D^0\rightarrow K^{*-}\pi^+(K^-\pi^+)$, heavy quark weak isospin, constraints from nonleptonic transitions 79−85257
e-μ permutation symm., lepton number conservation in gauge theories 78−4777
e-μ universality possible violation and Goldberger-Treiman relation, $\pi\rightarrow e\mu$ as test 77−2739

elementary particle weak interactions continued
ee elastic scatt., possible weak interaction effects, Weinberg-Salam model estimates 79—75755
$e^-e^+ \to \mu^-\mu^+$, high energy total cross sections, Salem-Ward-Weinberg model 79—22086
e^+e^- calorimetric experiments, $\gamma\gamma$ processes, tests of QCD 80—22628
$e^+e^- \to e^+e^-$, Coulomb interf. near Z^0 pole, Bhabha luminosity monitor 79—85289
$e^+e^- \to L^+L^-$, scalar model of weak interactions 77—18264
$e^+e^- \to \mu^+\mu^-$, 30 GeV, charge asymmetry, QED and weak corrections 77—61266
$e^+e^- \to \mu^+\mu^-$, sign of weak interaction const. from odd P asymm. *(Russian)* 77—30357
$e^+e^- \to \nu\bar{\nu}\gamma$, formula for differential cross-section, including weak interaction and V-A interaction *(Russian)* 78—62385
$e^+e^- \to q\bar{q}$, high energy total cross sections, Salem-Ward-Weinberg model 79—22086
$e\bar{e}\nu_e\bar{\nu}_e$, reactive mixture, bulk viscosity 78—45565
$e\mu$ elastic scatt., possible weak interaction effects, Weinberg-Salam model estimates 79—75755
$e\ \mu^-\tau$ asymmetry, conserved currents *(Chinese)* 79—58904
eN, indications given by optical activity of heavy metal vapours *(Russian)* 77—10618
eN deep inelastic scattering asymmetries, gauge theory predictions 79—22104
eN scatt., polarised e, testing unified gauge theories prediction 79—17732
$e\ N \to e^-X$, parity violating asymmetry, constraint on right-handed electron weak charge 79—17734
eq parity violating neutral current couplings, model independent anal. 79—17737
$eZ \to Z\mu\bar{\nu}_\mu\nu_e$, muon spectra V-A theory 77—65148
η_c pseudoscalar decay const., linear potential model 77—74679
$F^+ \to \phi\pi^+(\eta\pi^+)$, heavy quark weak isospin, constraints from nonleptonic transitions 79—85257
$\gamma p \to p\nu\bar{\nu}$, energy loss from stellar bodies through ν-prod. by second class weak neutral current 79—35997
$K \to l\nu_e\gamma(l\nu_e l'^+ l'^-)$ in review of weak-EM decays *(Russian)* 77—2818
$K_s^0 \to 3\pi$, CP violation, book contrib. 78—78173
$l(\bar{l})N$, P-odd asymmetries in deep inelastic scatt. of polarised l and $\bar{l}$ *(Russian)* 79—49527
$lp \to l'X$, weak reaction, large transverse momenta, field theories at finite temp., symm. breaking and restoration 79—399
$\lambda n\gamma(Z)$ vertex in vector-like model of weak and EM processes, appl. to K decay 77—6071
μ capture by complex nuclei, universal V-A interaction, appl. to nuclear struct. studies 77—67725
μ considered as $e\bar{\nu}_e\nu_\mu$ (or $\bar{e}\nu_e\bar{\nu}_\mu$) reson. 77—6189
$\mu \to e$ transmutation, failure to observe conversion, reasons and results 79—369
μ- and e-type leptons, mixing in unified model 77—67609
μ-number non-conservation in gauge theories of weak interactions 77—74630
μ^+, muonium, phys. and chem. review *(Russian)* 77—50566
$\mu^+ \to e^+\nu\bar{\nu}$, e^+ polarisation, weak interactions and lepton number conservation 80—42444
μe universality breakdown of neutral weak currents in $SU_2 \times U_1$ gauge *(Russian)* 79—75712
$\mu\mu$, fourth order contrib. in gauge theory of weak interactions 77—38117
n electric dipole moment, CP violation in gauge theories 80—91041
N form factors, weak, asymptotic behaviour within QCD dipole and triplepole formulae 80—62987
NN, Fadeev approach to weak interaction, parity non-conserving effects, predictions 79—93448
NN low energy scatt., parity violating observables weak potentials 78—50045
NN weak coupling constant magnitude, anal. of ^{41}K data, CVC hypothesis *(Russian)* 77—6144
$NN\pi$ amplitudes, weak, sum rules and theoretical description nonleptonic hyperon decays 79—17663
$NN\pi$ partial violating amplitude, short distance effects, PCAC 77—57557
$np \to d\gamma$ process, weak interaction between nucleons *(Russian)* 79—63513
ν, $\bar{\nu}$ charged current induced one pion weak prod., $I=1/2$ resonant contrib. 80—47274
ν mass, second-order effect in Higgs coupling 79—75716
$\nu(\bar{\nu})N$ elastic scatt., symmetry relations, current matrix elements 78—54627
ν oscillations in weak interaction model 80—78014
ν processes, weak current anomalous interaction with EM field *(Russian)* 77—6104
ν-induced multilepton events, weak interaction model 78—41533
ν-N scatt., relativistic quark oscill. model, N* weak prod. *(Russian)* 77—220
ν_e-e scattering, charged- and neutral-current interference 79—89144
$\nu_\mu(\bar{\nu}_\mu)N \to \mu^-(\mu^+)X$, struct. functions meas., quark-parton model anal. 79—58951
$\nu_\mu d \to pn\nu_\mu$, neutral current induced neutrino reactions, differential and total sections 79—17708
νe elastic scattering, differential cross section, behaviour in nondiffraction region 79—58952
$\nu_\mu e$, scatt. meas., interaction gauge models *(German)* 80—37251
νN, 2 to 50 TeV, weak interaction studies with the DUMAND detector 79—63463
νN interactions, book contrib. 78—78171
$\nu n \to \mu^- p$, total cross-section and differential cross-section, estimation of nucleon mass 80—18128
$\nu N \to \nu N\pi\pi$, neutral-current cross sections for double-pion production by neutrinos 79—17712
$\nu_\mu N \to \mu^- X$, 2 to 30 GeV, characts. of deep inelastic processes *(Russian)* 79—80821
$\nu\bar{\nu}$ pair emission, stellar plasma in strong mag. field, photon-neutrino coupling theory 77—17548
$\nu p \to p2\pi^0M^0$, neutrino prod. of neutral heavy lepton in E_7 gauge model 79—17710
$\nu p^+ \to \mu^-\Delta^{++}(\nu\Delta^+)$, Δ polarisation, test of T-invariance of weak and charge currents, comment 79—67531
$\bar{\nu}p^+ \to \mu^+\Delta^0$, Δ polarisation, test of T-invariance of weak and charge currents, comment 79—67531

elementary particle weak interactions continued
$\bar{\nu}_e p \to ne^+$, interaction cross section, expt. and theoretical discrepancy, discussion *(Russian)* 79—80822
$\bar{p}p$, heavy lepton prod. and decay, supersymmetrical model of weak and EM interactions *(Russian)* 80—86748
$pp \to jet+X$, P-violating weak effects in high transverse momentum collisions, QCD anal. 79—63559
$pp \to \pi^+X$, P-violating weak effects in high transverse momentum collisions, QCD anal. 79—63559
pp scatt., <300 MeV P-odd asymmetry for pol. ρ *(Russian)* 80—102063
$\pi \to l\nu_e\gamma(l\nu_e l'^+ l'^-)$ in review of weak-EM decays *(Russian)* 77—2818
$\pi^+ \to \mu^+\nu$, muon momentum, weak interactions and lepton number conservation 80—42444
ρ^0-electroproduction, parity violating effects 80—9178
$\tau \to 3\pi\nu$ decay, current algebra calcs. 79—30764
τ heavy lepton (1782), weak interaction decay, lifetime estimates, free quark model anal. 79—67544
τ lepton, search in neutrino expts., neutrino mixing *(Russian)* 78—54604
W-boson interaction, possibility of b-quark weak interactions 79—26285
$^{35}Ar \to {}^{35}Cl\ \beta^+$ decay and anomalous Cabbibo angle 77—74807
$^{12}B \to {}^{12}Ce^-\bar{\nu}_e$, data anal., second-class currents and CVC 77—82874
^{209}Bi, P violating eN pot., determ. of effects by optical rotation meas. 79—26277
$^{12}C(\mu^-,\nu_\mu)^{12}B$, data anal., second-class currents and CVC 77—82874
H_2 ortho-para transition as means of observing weak interaction parity nonconservation *(Russian)* 80—900
$^{12}N \to {}^{12}Ce^+\nu_e$, data anal., second-class currents and CVC 77—82874
^{20}Na, β-γ directional correlation, second-class current search 77—88083
$\bar{\nu}_\mu p \to \mu^+ n$, charged current interaction, elastic cross section 79—67533

elementary particles
see also bosons; charm particles; composite particles; cosmic rays; fermions; gamma-rays; hadrons; hypothetical particles; leptons; quantum field theory; strange particles
antimatter, origin, whereabouts 80—62340
educational course, introduction for liberal arts students 79—25780
high energy physics, experimental basis *(Danish)* 79—9357
high energy physics paradigm analysis 78—20935
high-energy physics, progress and prospects 78—45989
indeterminate—mass particles 79—26319
interfaces of nuclear and chemical physics, elementary particles and biochemistry 77—6284
long lived heavy particles with fractional charge, evidence in cosmic ray events 79—2447
modern atomic and nuclear physics (book) 80—11
quarks and elementary particle physics, review 78—8493
research guiding principles 77—67174
review of particle props., leptons, mesons, bayrons 78—66179
storage rings, impact of elementary particle physics 79—72121
storage rings, impact on elementary particle physics 79—72120
survey and research *(German)* 78—486

elements (chemical)
for specific metals and non-metals see appropriate chemical names
see also element origin; element relative abundance; periodic system of elements
atomic numbers >100, nomenclature 80—3295
Auger electron emission, relax. energies, excited atom model 80—40192
compound spaces of tolerance of chemical elements, mutual relationship of compounds 79—19177
covalent elements, cohesion in condensed phases, corrections to simple Huckel approx. 78—59779
covalent elements, cohesion of σ and π bonds in condensed phases, simple Huckel approx. 78—59778
critical consts., review 78—59931
element 114, search in galena using EM isotope separator and fission track detectors 77—27203
fourth row atoms, CNDO/S method extension, parametrisation procedure *(French)* 80—9511
heavy and superheavy elements Dubna programme on synthesis and search 77—23570
mantle related thermodynamic props. and reactions at high press. and temp. 80—81874
melting, vol. change, simple model 79—55865
monotonous series based on atomic bond energy, for mech. and phys. props. calc. *(Russian)* 80—19740
noncrystalline solid element, polymorphic bonding and thermal stability 77—31597
on-line gas phase separations of ^{252}Cf fission products 77—14615
origin of the elements, review 79—97118
polymorphic phase diagrams, as function of pressure exam. 79—8289
shock adiabats, generalised 79—86839
sputtering process and sputtered ion emission, models 80—35044
supercritical nuclei, $Z>137$, relativistic Thomas-Fermi eqn. soln. *(Russian)* 78—29748
superheavy, group separation procedure using diethyldithiophosphoric acid 77—26953
superheavy elements, detection by fission activity detect. *(Russian)* 79—13358
superheavy elements, search for fission decay in Madagascar monazite 77—17105
superheavy elements, search in nature based on spontaneous fission meas. 77—29518
superheavy elements E116 and E114, theoretical chem. 77—32824
superheavy elements in monazite crystals, proton induced X-ray spectra 77—17106
transactinides, gas phase separation methods 77—26954
work functions and sublimation entropies 79—56283
XPS, position and linewidth of M-shell vacancies in Ge-Zr 78—958
$Z=100$ to 173, Dirac-Fock-Slater calcs. of energy eigenvalues and total eigenvalues 77—71739
$Z=104$, tetravalent hydride, Dirac-Fock one-centre calcs. 77—88380
$Z=106$, atomic and chemical props. by gas chromatography and aqueous chemistry, book contrib. 78—85121
$Z=114$, Dirac-Fock one-centre calcs., tetravlent hydride prediction 77—34551
$Z=114$, existence in S.American hypogene lead ores, exptl. evidence *(German)* 79—55019
$Z=118$, 172, 226, symm. and stability of $2(2l+1)$ electron configurations of elements 80—1100

elements continued
- $Z>103$ transactinides, method for rapid separation and identification 77—26952
- Bi_2S_3, superheavy element search using neutron multiplicity counter 80—4011
- Ha, (element 105), atomic and chemical props. by gas chromatography and aqueous chemistry, book contrib. 78—85121
- Li to Ne, coreless Hartree-Fock pseudopotential method 79—68188
- Rf, (element 104), atomic and chemical props. by gas chromatography and aqueous chemistry, book contrib. 78—85121

elevators *see lifts*

Eliashberg strong-coupling model *see strong-coupling superconductors*

Elinvar
- antiferromagnetic Cr-Fe-Mn Invar alloy, Elinvar charact., US wave propag. charact. 77—11640
- Elinvar, Curie point, magnetisation and susceptibility, heat treatment effects *(Russian)* 78—47973
- Cr addition effect on modulus of elasticity and thermoelastic coeff. 77—90387
- Fe base amorphous alloys, Invar and Elinvar characts. 80—29592
- Fe-B, binary alloys, giant ΔE effect and Elinvar characts. 78—76291
- Fe-B amorphous Invar alloy, elastic props., Elinvar characts. and ΔE effect 79—56595
- Fe-Cr-B, amorphous, Elinvar and Invar charact. *(Japanese)* 80—11832
- Fe-Cr-B amorphous alloys, corrosion resistance, Invar and Elinvar characts. *(Japanese)* 79—96213
- Fe-Cr-b amorphous Invar alloy, elastic props., Elinvar characts. and ΔE effect 79—56595
- Fe-Ni-Cr, struct. and mag. props., singularities during tempering *(Russian)* 80—50627
- Fe-Ni-Cr-Ti-Al Elinvar alloys, dispersion-hardened, structural transform. *(Russian)* 79—1872
- $Fe_{78}Mo_2B_{20}$, Elinvar-type behaviour 79—66091
- $Fe_{47}Ni_{43}Cr_{5.5}Te_{3.3}Al_{1.2}$, γ to γ' transformation and γ' phase form. kinetics, lattice consts. 80—35191
- Mn-Ni-Ti (Zr) systems, and mech. props. thermal expansion for different heat treatments *(Japanese)* 79—29123
- Mn-Ni-Ti(Zr), non-ferromagnetic Elinvar-type alloys 79—24566
- Mn-Ni-V(Nb)(Ta), nonferromagnetic Elivar type, mech. props. meas. 77—48473
- Mn-Pt, Elinvar props., −150 to 500°C *(Japanese)* 77—52385

ellipsometers
- *see also ellipsometry*
- automated, with pulsed tunable laser sources 77—13796
- automated device, performance characts. 78—49885
- automated Fourier-Stokes analyser ellipsometer system for in situ investigations 78—49886
- automatic ellipsometer without phase plate 77—53970
- automatic high-speed ellipsometer for industrial use 77—2682
- automatic instrument for refl. or transmitted light 77—74487
- automatic null-setting type, design and performance 77—45884
- automatic two-coordinate device 78—21205
- calculator-coupled automated ellipsometer for film thickness meas. 77—82490
- conference, Berkeley, CA, USA (Aug. 1979) 80—101665
- conference, San Diego, CA, USA (Aug. 1977) 78—54437
- digital ellipsometer using spinning analyser and photoelec. rotary encoder 79—30529
- Fourier photoellipsometers and photopolarimeters based on modulated optical rot. 78—54439
- hybrid null-photometric ellipsometer using sinusoidal optical rotation 77—61110
- in-process calibration, azimuth angle corrections 77—18070
- installation for semicondictpr surface physicochemical process study 77—18071
- instrumentation, review 80—101819
- integrating photometric rotating analyser ellipsometer, precision estimation 78—12744
- IR laser, for Si epitaxial layers meas., expt. 78—62219
- laser microellipsometers, for film thickness and optical parameters meas. *(Czech)* 77—61109
- manual to semiautomatic conversion using inexpensive mech. device 78—89526
- measurement of thin films on wafers, real time, computer assisted 80—73418
- modified O'Bryan return-path ellipsometer for film-substrate systems 79—2808
- modulated light system, for substrate and thin film meas. at 10.6 μm 78—54442
- Monin and Boutry method improvements in speed and reliability 80—47091
- normal incidence rotating sample ellipsometer 77—41667
- nulling, coupling and settling uncertainty of adjustable components 79—58771
- nulling process, convergence and speed 77—5885
- perpendicular-incidence microellipsometer 80—101824
- photometric, drift stabilization and photomultiplier linearization with feedback cct 78—54436
- photometric return path ellipsometers, for isotropic and anisotropic surfaces 78—58009
- photometric system, photomultiplier linearisation and system stabilisation 78—54441
- polarisation-modulation ellipsometer, Fortran simulation program ELLIPS 78—271
- with quarter-wave compensator, multireflection interference effects 79—12841
- return-path normal incidence null ellipsometer 77—79137
- rotating depolariser automatic ellipsometer, optical, mech., and electronic systems 78—24843
- rotating polariser ellipsometer for film-substrate system 78—8436
- rotating-compensator/analyser fixed-analyser automatic ellipsometer 77—2680
- self-nulling stepping-motor driven ellipsometer, design and performance 78—54440
- simple fixed retarder and fixed angle of incidence type, adjustment data evaluation 80—4755
- single-element rotating-polarizer ellipsometer 80—101823
- spinning analyser ellipsometer, meas. magneto-optic rotation and ellipticity *(Japanese)* 80—73419
- surface and surface layer measurements, ellipsometric method 80—52295

ellipsometers continued
- US ellipsometer design and performance 79—57196
- vacuum automatic ellipsometer for condensing film homogeneity determ 80—101825
- wavelength-scanning ellipsometer signal level regulation and dark current compensation 79—26105
- working light beam intensity, theoretical anal. 77—10092
- GaAs, Schottky barrier ellipsometric electroreflectance spectra, energy band parameters 79—99853
- Si slices surface meas., dislocation density determ. *(Hungarian)* 79—99198

ellipsometry
- *see also ellipsometers; polarimetry*
- absorbing films, optical parameters determ. by ellipsometry 80—254
- acousto-optic polarisation modulator, use in dynamic ellipsometry, polarimetry *(Russian)* 80—14472
- alloys and mixed crystals, composition determ. method 80—35615
- angle-of-incidence derivative ellipsometry and reflectometry, implementation and appl. 80—73420
- anisotropic layered media, 4×4 matrix algebra 80—106445
- anisotropic object, single zone method for ellipsometric parameter determ. 80—68240
- anisotropic reflecting media, theory of generalised ellipsometric zones 77—67491
- anodic film, automated interpretation of ellipsometer obs. 78—56902
- anodic oxide film, exam. using SIMS and ellipsometry 79—61770
- anodised films on metals, ellipsometer obs. interpretation using film form. models 80—101828
- atmosphere, boundary layer turbulence, birefringence, ellipsometric meas. 78—69453
- azimuth response function, linear nondepolarising optical system 78—65957
- biomedical application, monitoring of mol. and cellular biological processes 77—48852
- birefringent, rotating, and achromatic quarter wave plates, appl. to ellipsometry and photoelasticimetry *(French)* 80—14278
- birefringent rotating plates as modulated optical filters, polarised light meas. appl. *(French)* 77—67490
- black nickel film on Cu substrate, optical constants determ. 77—74488
- book, ellipsometry and polarised light 77—71361
- bubble film, ellipsometric meas. of thickness and refr. index 79—78463
- carbon tetrachloride, surface study, ellipticity coeff., ellipsometric method 80—84343
- Carter and Smith charts, elliptical polarization representation 80—32902
- coherent ellipsometry of Raman light scatt., four-photon spectroscopy *(Russian)* 77—58387
- compensator retardation determ. 79—26107
- compensator transmittance ratio, detector sensitivity influence 77—74484
- conducting layer, light refl. theory 80—1125
- conference, Berkeley, CA, USA (Aug. 1979) 80—101665
- conference, polarised light, San Diego, Calif., USA (Aug. 1976) 77—45881
- conference, San Diego, CA, USA (Aug. 1977) 78—54437
- corrosion inhibitor action obs., of propargyl alcohol, film growth on steel surfaces *(Rumanian)* 80—60996
- data analysis aided by derivative plots in n,κ-space 80—86378
- demonstrations with polarised light 77—45657
- depolarising optical system characterisation by automated ellipsometer 78—32855
- dielectic-semiconductor systems, immersion ellipsometric obs. *(Russian)* 79—15548
- dielectric layers on semiconducting substrate, ellipsometric monitoring 79—49272
- dielectric surfaces, small values of ellipsometric parameters meas. by photoelec. method 79—21804
- dielectric thin film, thickness measurements determ. using ellipsometer with nonmonochromatic source *(Russian)* 78—51862
- dielectric thin film refractive index and thickness, algorithm for determ. on basis of ellipsometric meas. 80—34881
- 1,2-dimyristoyl-sn-glycero-3-phosphoserine multilayers, phase transitions, temp. depend., ellipsometric study 80—108846
- 1,2-dipalmitoyl-sn-glycero-3-phosphocholine multilayers, phase transitions, temp. depend., ellipsometric study 80—108846
- discrete component Sagnac optical rate sensor, error sources 80—1342
- electrochemical surface layer obs. 78—56874
- electrochemistry, optical experimental methods 78—20022
- electrocrystallisation, recent progress in electrochem. and physical methods *(French)* 80—7510
- elliptic retarder, expt. method for optical parameters determ. 77—88941
- epitaxial growth, vapour phase, growth mode characterisation 78—87885
- epitaxy, growth modes, exp. techniques, book contrib. 80—49558
- epoxy films, in polished metal mirrors, refl.-absorpt. IR spectrosc. and ellipsometry obs. 79—78765
- factor VIII, native and modified, surface adsorption and mol. interactions, ellipsometric obs. 80—104555
- fibrinogen, native and modified, surface adsorption and mol. interactions, ellipsometric obs. 80—104555
- films, electrically conducting on transparent ceramic, ellipsometry determ. of optical consts. 79—67376
- flow-birefringence, meas. using circularly polarised laser beam 79—35813
- four-photon spectroscopy of condensed media, nonlinear spectroscopy developments 80—91860
- Gakashuin University, ellipsometry work from 1955, review 80—9019
- generalised ellipsometry with nonideal compensator 79—12840
- glass surface, ellipsometric study of zone of optical contact 80—4754
- glasses, high vol. low cost, as solar reflectors, compositions and weathering effects 80—106589
- goniometric attachment for ellipsometers 80—90883
- graphite-Br system, intercalation threshold, ellipsometric investigation 78—26760
- halfshade analyser using two polariser sheets 78—54434
- ice, surface transition layer, ellipsometric study 80—103545
- in situ, compensator inaccuracy evaluation 79—54170
- instrumentation, review 80—101819
- interface between transparent and absorbing medium, light refl. at 45° angle of incidence 79—31792
- interferometer double beam, interferometric determ. of ellipsometric phase shift 78—93757
- invariants, general theory 79—63295

ellipsometry continued
inversion problem solution using simple Monte Carlo procedure 77−41669
ion implanted layers, complex refr. index profile, ellipsometric meas. 80−93262
IR ellipsometric spectroscopy, appl. to study of adsorbed species 80−39434
IR ellipsometry of polySi-SiO_2-monoSi structure thickness 79−56287
IR material refractive index, 10.6 μm ellipsometric meas. 78−24847
Josephson junction, oxide formation process, ellipsomesric meas. *(Japanese)* 80−11561
Kerr magnetooptic effect, ellipsometric meas. 79−49271
Kramers-Kronig relations and sum rules, Lorentz oscillator model 80−102617
laser annealing, optical constants, ellipsometry observation 80−34024
linearly polarised light depolarisation effective ellipse phase and amplitude 80−86381
liquid crystal thin layer, polarised light ellipticity after passage 80−88036
material elastic anisotropy, analysis, by acoustic ellipsometry 79−47864
measuring zones theory 79−54171
metal film, on pyrex, surface roughness meas. by ellipsometry and TEM 77−20205
metal surface, perturbative calc. of elec. field 80−45108
metallic films and surfaces, nonlocal effects, theory 80−104006
metals, solid and liq., optical props. by spectroscopic ellipsometry, review 80−103929
microscopic equipment, methods, appls. and related topics, bibliography 80−73124
microscopy with an ellipsometric arrangement 80−17998
microwave wavelength diffr. ellipsometry, polarisation and refl. coeff. 79−55034
mirror substrates microroughness ellipsometric determ., effect on laser cavities 79−59791
modulation ellipsometry, freq. spectrum of output light intensity 78−41344
modulation error 80−255
Monin and Boutry method improvements in speed and reliability 80−47091
Mueller matrix ellipsometry with imperfect compensators 79−26106
Mueller-Stokes calculus, conventions and formulas 80−102618
Mueller-Stokes matrix determ. using Fourier anal. 77−42496
multiple angle incidence ellipsometry, appl. to GaAs and GaP anodic oxide systems 79−63294
multiple overlayers, effect on ellipsometric parameters 77−32457
nondestructive testing appl., in microelectronics industry 79−85161
nonmonochromatic light beam based, generalised polarisation angle method *(Russian)* 80−22419
optical adjustments to ellipsometer 79−63296
optical surfaces, ellipsometric charact. determ. using nanosecond laser pulses 80−101822
organic molecules, adsorbed, Si-SiO_2 interface as electrode for electrical and ellipsometric meas. 80−15366
organic uniaxial films, optical consts. and thickness determ. by modified ellipsometry 79−91512
overlapping Raman lines resolution by coherent ellipsometry 79−98110
oxide film, on Ti, optical consts. and thickness determ., ellipsometric method *(Russian)* 77−81164
oxides produced during Al anodisation, thickness meas. by ellipsometry 78−171
palmitic acid monolayer on water, characterisation by multiple wavelength ellipsometry 78−92136
perpendicular incidence ellipsometry, appl. to uniaxial and biaxial crysts. 77−2681
photoresist residual film on thermally oxidised Si, ellipsometric meas. 77−48266
PMMA, monolayers collapse mechanism, surface press. and ellipsometric obs. 78−43214
polarisation angles for exact ellipsometry employing real light beam *(Russian)* 78−32857
polarised light, spectral analysis, polychromatic and coherent optics *(French)* 79−50209
protein adsorption and immunological reactions at liq./solid interface 77−52948
protein adsorption expt., film thickness estimation 78−44740
pyrazine, physisorbed on Ni (111), UV spectroscopic ellipsometry obs. 79−86997
pyrocarbon coatings, refl. anisotropy and struct. determ. by perpendicular incidence microellipsometer 80−101824
quartz fused, refractive index distrib. normal to polished surface, ellipsometric meas. 79−86965
Raman, coherent, and polarised coherent active Raman spectroscopy *(Russian)* 78−55414
reflectance-aided null ellipsometry for film-substrate systems 80−101827
reflecting systems, weak anisotropy, ellipsometric obs. *(Russian)* 77−23615
reflection, transmission and scatt. of light, thin film influence *(French)* 77−34826
refractive index determination 79−26108
rhodamine dye, coherent ellipsometry determ. of third order polarisability 79−71511
rotating-analyser ellipsometers, cell window imperfection effects 80−101826
scattered light three-dimensional photoelasticimeter. Application to a blade of a compressor 79−32405
semiconductor, surface electronic props., optical spectroscopic techniques, review 80−11070
semiconductor epitaxial film optical constants meas. by far IR ellipsometry 78−93753
semiconductor film growth, multilayer systems, spectroscopic ellipsometry, review 80−103603
semiconductor process control, dielec. layers meas. 78−49887
semiconductor processing, residual film monitoring by ellipsometry 80−13124
semiconductor substrate-semicond. epitaxial layer, doping profile using ellipsometric meas. 79−99453
sensitivity threshold, sample polaris. reflectance and inhomogeneity effects 78−24846
solid-liquid interface, optical methods of study *(French)* 80−7318
spectroscopic, appl. to in situ meas. and anal. of plasma-grown GaAs oxides 80−76386

ellipsometry continued
stabilised two-frequency laser, use in ellipsometry 80−101820
steel, austenitic stainless, passive film meas., optical constants *(Japanese)* 78−85041
steel, room temp. O_2 adsorption in ultra-high vacuum system 77−20188
steel, stainless, austenitic, surface films grown in Cl^- solns., ellipsometric investig. 79−20261
steel, stainless 18-8, ellipsometric meas. of optical const. and thickness of passive film 77−21326
stress measurement in birefringent medium by fast three-dimens. ellipsometry 80−101821
substrate-thin film system with rough boundaries, ellipsometric obs. using equiv. film theory 80−2310
surface and surface layer measurements, ellipsometric method 80−52295
surface anisotropy measurement by ellipsometry 78−56452
surface films and bulk material, optical props. meas. using ellipsometry, review 79−44926
surface films and film growth examination, appl. 78−39619
surface optical spectroscopy, principles and appls. 78−16834
surface roughness meas. 80−52294
surface structure, submonolayer and monolayer films, ellipsometric study, review 80−103546
surfaces, laser-annealed, characterisation by ellipsometry 80−103544
surfaces, optical examination and monitoring, review 79−67375
techniques guide *(Japanese)* 78−24844
thickness measurement for water thin film on slightly rough quartz surface, error estimation 78−32856
thin film, optical characterisation *(French)* 79−11402
transparent film, refr. index and thickness determ. from zero refl.-induced ellipticity 78−41345
transparent film on rough metal surface, thickness meas. 79−88912
transparent films, on absorbing substrate, refr. index, thickness, ellipsometric meas. 77−52194
transparent films on Al, optical characts. meas. 77−52195
transparent films on transparent substrates, theory 80−104007
uniaxial crystals, refl. ellipsometry nonlinear eqn. inversion 80−95120
uniaxial film on nonabsorbing substrates, characterisation by multiple wavelength ellipsometry 78−92136
Van der Waals film adsorbed on graphite, two-dimensional phase transitions 80−107653
VPE of III-V ternary layers, on-time comp. determ. 78−67915
water adsorbed multilayers on quartz, surface forces, ellipsometry meas. 80−6597
wavelength-scanning polarisation-modulation ellipsometry, practical considerations 78−41343
wavelength-scanning polarisation-modulation ellipsometry, sample imperfection effect 78−24845
zone theory, single zone procedures 77−82588
Ag (110), adsorption of O_2 and CO-O_2 interaction, ellipsometry-LEED expts. 78−91542
Ag (111), ordered and damaged surfaces, O_2 adsorption, O_2+CO interaction 78−14583
Ag (111) surface, Ar ion bombardment, effect on struct. and reactivity, ellipsometry and LEED meas. 77−59192
Ag film, ellipsometric response to CO adsorption 80−103571
AgBr, adsorption of gelatin on single crystals, ellipsometric investigations 79−24779
AgI film, light-induced changes, ellipsometric meas. 78−56537
Al (111), chemisorpt. of O 78−14593
Al alloys, contamination, automated nondestructive inspection 80−16629
Al film, evaporated, corrosion in distilled water, ellipsometric obs. 77−48590
Al film, optical dielec. const. in visible region, 300 and 1.5K 77−90211
Al, porous anodisation, initial stages of oxide growth and pore initiation, ellipsometry obs. 77−1888
Al surfaces, interaction with O_2, work function changes and ellipsometric parameters 79−47831
AlN film, CVD, characterisation of film props. 78−43496
AlN-Si_3N_4 mixture film, CVD, characterisation of film props. 78−43496
Al_2O_3 anodic film peak voltage rel. to ellipsometric thickness 77−77597
Al_2O_3 anodic layer formation in H_3PO_4 solns., surface charact. 78−15603
Al_2O_3, composite film, barrier layer, ellipsometric meas. 78−67918
Al_2O_3 films, DC reactively sputtered, struct. 80−96764
Ar, liquid, surface study, ellipticity coeff., ellipsometric method 80−84343
$As_2S_3(Se_3)$, film on KCl, strain-induced refractivity anisotropy, 10.6 μ ellipsometric obs. 79−14064
Au film, ellipsometric obs. of optical props., rel. to surface roughness 79−78776
Au film, evap., temp. change and gas adsorpt. effect on opt. consts., ellipsometric obs. *(German)* 80−89081
Au film, optical dielec. const. in visible region, 300 and 1.5K 77−90211
Au, optical props., dielec. function, void model, sample effects 80−76048
Au vacuum deposition on dielectric substrates, ellipsometric and electron microscopic meas. 79−74011
Au-Ag-Cu, optical props. study using automatic nulling spectroellipsometer 80−55058
AuSn, optical props., 0.5-5 eV 78−39522
Bi film, ellipsometric obs. of optical props. 79−78776
Bi_2Te_3, anodic film form., in situ ellipsometric study 80−104318
CaF_2 crystals, mirror chips, in contact with liq. phase, ellipsometric investigation 80−11516
CdS film, ellipsometry of natural boundaries *(Russian)* 79−4866
CdTe surfaces, SIMS, Rutherford scatt. and ellipsometry 79−56046
Co-Gd(Tb)(Sm) film, magneto-optic coeff. and refr. index, ellipsometric determ. 80−71501
Co-Si interface, glassy layer, ellipsometric charact. 80−103589
Cu (110) surface, O_2 and N_2O interactions, CO reaction with adsorbed O_2, ellipsometry study 80−6635
Cu (111), interaction of O_2 and N_2O and reaction of CO with adsorbed O_2, AES, LEED and ellipsometric meas. 79−65317
Cu (111) surface, room-temp. oxidation, press. effects 79−79283
Cu adsorption of O_2, N_2O on (100) surface, reaction with CO 80−103583
Cu anode, passivating behaviour and illum. effects in alkaline soln. 80−104449
Cu film, pure and CO covered, optical consts., ellipsometry meas. 79−78645
Cu-benzotriazole (benzimidazole) thin films, ellipsometric study 80−35114

ellipsometry continued

- Cu-Xe film, metal-nonmetal transition, optical and resist. meas. 77–89818
- Fe, anodic oxidation, two phase film form., overpot. anal. 77–16737
- Fe, film growth under organic coatings, qualitative ellipsometric-electrochem. approach 80–104344
- Fe, passive film form. in phosphate soln., intensity-following ellipsometry study 80–104345
- Fe, surface films formed in inhibitive solns., optical props., protective quality 79–20260
- Fe-Cr alloys, in acid and neutral solns., thickness and optical constants of passive and transpassive films 80–66698
- Fe-Gd(Tb) film, magneto-optic coeff. and refr. index, ellipsometric determ. 80–71501
- FeO ultrathin homogeneous absorbing films, ellipsometric nucl. microanalysis data analysis, opt. consts. *(French)* 78–11011
- Fe_3O_4, film, quantitative sputter rates, AES, ellipsometry determ. 78–72661
- Ga-Xe film, metal-nonmetal transition, optical and resist. meas. 77–89818
- $Ga_{1-x}Al_xAs$, anodic oxide films, ellipsometric anal. 79–20234
- GaAlAs/GaAs heterostructures, ellipsometric assessment of epitaxial layer during growth in organometallic VPE system 79–37933
- $Ga_{1-x}Al_xAs$ LPE layers, comp. and refr. index, ellipsometry meas. 79–87011
- GaAs (111) epitaxial film, adsorption of Cs, Cs+O ellipsometric study 80–29282
- n-GaAs, anodic oxide film, exam. using SIMS and ellipsometry 79–61770
- GaAs anodic oxide film, ellipsometric and IR spectroscopic studies 80–11493
- GaAs anodic oxide system, multiple angle incidence ellipsometry, meas. at $\lambda=632.8$ nm 79–63294
- GaAs anodisation, ellipsometric study *(Japanese)* 80–97610
- GaAs, chemisorption of O_2, effect of surface index and atomic disorder AES, LEED and optical ellipsometry 79–60638
- GaAs, ion-implantation induced damage profile, ellipsometric study, annealing 80–103400
- GaAs, microscopy with an ellipsometric arrangement 80–17998
- GaAs oxide film, ellipsometry study 79–69894
- GaAs oxides, plasma-grown, in situ meas. and anal. with spectroscopic ellipsometry 80–76386
- GaAs, plasma-grown oxides, in situ anal. using spectroscopic ellipsometer 79–79138
- GaAs, Schottky barrier ellipsometric electroreflectance spectra, energy band parameters 79–99853
- GaAs, VPE by CVD, vapour-solid interface, expt. anal. *(French)* 79–33940
- GaAs VPE growth, in situ surface anal. 79–95937
- GaAs:Mg(C)(Te)(Ge), ion implanted, laser annealing, ellipsometric and Hall meas. 79–73193
- GaAs-Al interface, ellipsometric anal. methods, correl. between optical props., thickness and surface roughness meas. *(German)* 80–55215
- GaAs-GaAlAs superlattices, metalorganic VPE growth. in sites ellipsometry monitoring 80–70547
- GaAs-GaAs oxide interface layer characterisation by spectroscopic ellipsometry 80–50738
- GaAs-oxide, interface layer determ. by spectroscopic ellipsometry 79–95275
- GaAs-plasma grown oxide interface, new resonant ellipsometric technique for characterisation 79–40606
- $GaAs-SiO_2$ interface local props. *(Russian)* 78–10567
- n-$GaAs_{0.6}P_{0.4}$, anodic oxide film, exam. using SIMS and ellipsometry 79–61770
- $GaAs_{1-x}P_x$, anodic oxide films, ellipsometric anal. 79–20234
- GaP anodic oxide system, multiple angle incidence ellipsometry, meas. at $\lambda=632.8$ nm 79–63294
- GaP, ion-implanted, radiation damage, ellipsometry expts. 78–38735
- GaSe, anodic film form., in situ ellipsometric study 80–104318
- Ge, anisotropic oxidation ellipsometry meas. *(Russian)* 79–43451
- Ge, rough surface, polarisation angles, ellipsometric meas. 78–56449
- Ge, single cryst., anisotropic oxidation, ellipsometric obs. 77–70194
- Ge surface, (111), ion-bombarded and annealed, spectroscopic ellipsometry study 80–103543
- Ge surface, atomically pure, optical consts. and temp. depends. 79–65823
- Ge-Si alloy, comp. determ. using ellipsometric method 80–35615
- $Ge+Br_2$, surface reaction, rate-limiting step, ellipsometric and photochem. meas. 80–16730
- GeO amorphous semicond. films, photostructural changes by photomodulation ellipsometry 79–71510
- GeO film, optical props., rel. to possible appl. in holography 80–29816
- GeSi alloy, composition determ. by ellipsometry 79–83537
- Hg drop, optical consts. meas. from Hg-air interface, ellipsometry at spherical object 79–61326
- Hg optical props. by spectroscopic ellipsometry, review 80–103929
- In_2O_3, elec. conducting film on glass substrate, measurement of optical constants and thickness 78–60525
- InSb, ion implanted, ellipsometric study 80–60537
- InSb, refractive index and absorpt. coeff., cryst. orientation depend. 80–60536
- KCl, electron irrad., F-centre absorpt., ellipsometric obs. 78–23501
- KCl IR window material, polish layer effect, ellipsometric meas. 78–55419
- KCl surface, VUV irrad., colour centre layer, angle-of-incidence derivative ellipsometry and reflectometry 80–73420
- KCl surface, vacuum UV radiation damage, spectroscopic study 78–71758
- Li, optical props. by spectroscopic ellipsometry, review 80–103929
- LiF crystals, mirror chips, in contact with liq. phase, ellipsometric investigation 80–11516
- $MgF_2-Na_3AlF_6$ thin film deposits, quenched ageing by chopping 80–97364
- Na, optical props. by spectroscopic ellipsometry, review 80–103929
- Na_xWO_3, optical props., analysis of free- and bound-electron contribs. 77–77248
- Nb anodic oxide films, reversible optical changes 78–35580
- $Nd(NO_3)_3$, aqueous soln., single photon absorpt. band struct., electronic resons. coherent ellipsometry 80–90881
- Ni (100), adsorption of O_2 and reduction of surface oxide by H_2 80–108741

ellipsometry continued

- Ni, (110) surface, methane interaction kinetics, AES-LEED-ellipsometry 77–62756
- Ni, absorption spectrum anomalies, 2-3 eV, optical anisotropy *(French)* 78–43893
- Ni, anodic oxidation in neutral electrolyte, ellipsometric obs. 78–27673
- Ni, anodic passive film form. in NaOH soln., refl. and ellipsometric study 80–104447
- Ni, corrosion and passivation in phosphate soln., pH depend., ellipsometric study 80–104448
- Ni electrodes, electrochem.-ellipsometric studies of oxide films formed during O_2 evolution 79–16007
- Ni film, evaporated, chemisorpt. of CO, ellipsometric investig. *(German)* 80–61156
- Ni, optical consts., influence of temp. and relation to bandstruct. 80–25403
- Ni plating, surface props. of Ni after each step of activation process 78–95243
- O_2, adsorption on Ni and Ag electrodes in KOH soln. 79–61871
- Pb-In film, RF sputter anodisation, Josephson junction form., ellipsometry anal. 79–29258
- PbI_2, complex dielectric and optical consts., ellipsometric determ. 78–23425
- PbO layers on Pb films, optical props. 79–83042
- $PbO-SiO_2$ glass, leaching behaviour in dil. HNO_3, ellipsometry and AES obs. 78–23846
- PbO_x layer, ellipsometry, compensator inaccuracy evaluation 79–54170
- PbTe film, optical consts., support roughness effect 80–2882
- PdSb, optical props., 0.5-5 eV 78–39522
- Pt electrodes, polymeric surface film form. by electrooxidation of phenolic cpds., ellipsometric study 80–104450
- Ru (11$\bar{2}$0), adsorption of O_2, H_2, and CO, ellipsometry-LEED study 80–103570
- Si (111) surface, heating effects on ellipsometric parameters 77–72764
- Si, dielectric function spectra, ellipsometric determ., many-particle effects at E_1-transition 80–93363
- Si, electroreflectance, dielec. function, ellipsometric meas. 79–4790
- Si, film on Al-Cu, ellipsometric meas. technique, comparison to X-ray fluoresc. anal. 78–51840
- Si films, CVD, amorphous and polycryst., microscopic surface roughness, effective-medium models, ellipsometric expts. 80–24756
- Si, growth and thermal evaporation kinetics of oxide film on Si surface 78–3246
- Si oxides, steam grown, index of refr. ellipsometric meas. 80–75995
- Si, p-n junction, ellipsometric method of temp. meas. rel. to secondary breakdown *(Russian)* 80–11074
- n-Si, passivation, photoactivation kinetics in conc. alkali, ellipsometric investig. 77–1885
- Si, polycrystalline thin films, parameters in two absorbing layers effect on reflected light polarisation *(Polish)* 78–21095
- Si RF sputter-etched surface, cryst. damage, spectroscopic ellipsometry obs. 80–103538
- Si, rough surface, polarisation angles, ellipsometric meas. 78–56449
- Si surface, atomically pure, optical consts. and temp. depends. 79–65823
- Si surface, influence of mech. treatment, charact. by ellipsometry 78–15141
- Si surface formation during etching of thin thermally grown oxide layers, ellipsometric control *(Russian)* 80–104315
- Si, thermal oxidation, role of H_2O, ellipsometry expts. 78–27656
- Si wafer, surface characterization by ellipsometry 79–90853
- Si wafer oxidation, superthin SiO_2 film production obs. 77–76690
- Si wafers layers, multilayer ellipsometry, layer thickness and refr. index determination of layers 80–95121
- Si:$^{31}P^+$, implanted layers, characterisation by ellipsometry 79–90683
- Si:Ag, surface layer, ellipsometry 78–19121
- Si:As, CW CO_2-laser annealing, comparison with thermal annealing 80–84193
- Si:As, ion-implanted layers, ellipsometric anal. of laser annealing 79–73190
- Si:B, ion implanted, ellipsometric study for low doses, cryst. damage parameter 79–65105
- Si:P, annealing after ion implantation, ellipsometric study 80–65018
- Si:P, ion implanted, damage layer props. obs. using ellipsometric parameters *(Russian)* 77–43234
- Si-absorbing film system, ellipsometry 79–99964
- Si-Al interface, ellipsometric anal. methods, correl. between optical props., thickness and surface roughness meas. *(German)* 80–55215
- $Si-SiO_2$ interface, ESCA and ellipsometric study 79–82678
- $Si-SiO_2$ interface, thermally grown oxide, spectroscopic ellipsometric anal. 80–107659
- $Si-SiO_2$ interface layer characterisation by spectroscopic ellipsometry 80–50738
- $Si-SiO_2$ interlayer, optical evidence 79–69800
- $Si-SiO_2$ layers on Si substrate, ellipsometric meas. 77–69403
- $Si-SiO_2$-vacuum system, principal angle and azimuth determ. 78–11009
- $Si-SiO_2(Si_3N_4)$, interface layer determ. by spectroscopic ellipsometry 79–95275
- SiC, ellipsometric exam. of polytypes 78–92044
- Si_3N_4 film, thermal oxidation rate and masking effect against Si oxidation, ellipsometry meas. 78–64749
- $Si_3N_4-SiO_2$, double dielec. layer on Si substrate, parameter meas. methodology 77–63474
- SiNH films, thickness and refractive index meas., comparison of techniques 80–8957
- SiO_2 anodised layers on clean and ion bombarded Si surfaces *(Russian)* 79–24382
- SiO_2, CVD film, hydration props., ellipsometry meas. 78–22986
- SiO_2 film, Ge substrate, structure investigation 78–10297
- SiO_2 film on 6H-SiC substrate, ellipsometric meas., accuracy and sensitivity 80–77840
- SiO_2 films, desorption from Si single cryst., ellipsometric obs. 80–100410
- SiO_2 films, thickness and refractive index meas., comparison of techniques 80–8957
- SiO_2 films on Si, ellipsometric spectra, thickness determ. *(Chinese)* 80–86379
- SiO_2 HF plasma sputtered dielectric layer thickness and refractive index obs. 79–56931
- SiO_2, oxide growth in $HCl-O_2$ mixture, ellipsometric meas. 78–7073
- SiO_2, thin films on rough polycryst. Si surfaces, oxide thickness and refractive index meas. 80–93422

ellipsometry continued
SiO_2 ultrathin layers, refr. index meas. 80—103936
SiO_2-Na_2O-CaO-MgO float glass, surface SnO_2 distrib., ellipsometry and XPS study 80—84346
SiO_x thin films, deposition and characterisation study 80—80133
Sn, liq., optical props., 0.62-3.7 eV 80—75996
Sn, liq., optical props. by spectroscopic ellipsometry, review 80—103929
Sn-SnO_4-Sn junctions, oxide growth, tunnelling characts., ellipsometry meas. 79—47173
SnO_2, elec. conducting film on glass substrate, measurement of optical constants and thickness 78—60525
Ta film, optical const. var. with struct., and oxidation 77—63478
Ta film, oxidation in ambient conditions, resist. and ellipsometric meas. 79—34209
Ti anodic oxide films, reversible optical changes 78—35580
Ti, electropolished, optical props. from 1.8 to 3 eV 80—85088
Ti, substrate for thin oxide film, optical consts. determ. *(Russian)* 77—81164
VO_x, anodic film, optical anisotropy 77—20942
W, anodic oxidation, effect of electrostriction, ellipsometry meas. 78—92394
W substrate-oxide film system with rough boundaries, ellipsometric obs. using equiv. film theory 80—2310
WO_x, anodic oxide films, quadratic electro-optic and electrostrictive effects, ellipsometry 80—108184
Yb_2O_3 thin film on Cr substrate, refr. index depend. on thin film thickness 80—108290
Zn electrode, passive film form. by chrono-ellipsometry *(Japanese)* 78—68900
ZnO, ellipsometric spectroscopy of nonpolar (1$\bar{1}$00) surface 79—33651
Zr, anodic oxidation, typical valve and behaviour 77—21311

elliptical polarisation *see polarisation*

elongation
see also deformation; thermal expansion
acrylourethane coatings, radiation curable, tensile, elongation and modulus props. appl. techniques 80—66847
alloy, creep elongation, modification of Monkman-Grant relation *(Czech)* 77—63726
alloy, hyperplastic, diffusion coeffs. determ. during deform. 79—51298
alloy, precipitation hardened, containing narrow soft zones at grain boundaries, fracture toughness 77—77553
alloy, strain rate sensitivity rel. to ductility, anomalies 77—36590
aromatic polyamides, rigid and nonrigid, ultrahigh modulus fibres 79—95992
brass, M63, yield stress decrease in compression, rel. to previous elongation *(Polish)* 80—50665
α-brass, plane stress ductile fracture, prestrain effects 80—108532
αbrass, single cryst., yielding behaviour rel. to low temp. annealing treatment *(Japanese)* 80—93582
brass LMtsSKA 58-2-2-1-1, heat treatment, struct. and props. 79—83239
brittle fibre reinforced composite, static strength depend. on component separation boundaries *(Russian)* 80—76304
butadiene, stressed, microcrack generation under const. elongation, struct. depend. 77—90459
butadiene-nitrile, stressed, crack generation under const. elongation, struct. depend. 77—90459
butadiene-styrene block copolymer, oriented, isotropic, struct. changes during deformation *(Russian)* 78—88512
butyl rubber vulcanisation with resins, mech. props. *(Polish)* 79—74129
cellulose film, moisture effect on phys. and mech. props. 80—40450
cellulose hydrate, nondestructive control of mech. props. anisotropy, appl. of capacitance method 77—86277
composites, stretching, zone of disturbed stress state calc. 80—39206
Cunial MNA13-3, Mn addition effect on props. 80—21035
cylinder, plastic flow rules and Bauschinger effect parameters 78—6984
Dacron, vascular substitute, exam. of tensile fracture behaviour 78—77157
deformation strength props., simultaneous meas. of several samples, polymer films appl. 79—15896
Drucker postulate verification at high temp. 80—30025
dumbbell kinetic problem, rheology, Langevin approach 78—42633
dynamic, of material, stress/strain curve up to scabbing, meas. method 79—7348
effect of simulated fission products on mech. props. 80—73922
elastomers, effect of filler on network behaviour at high elongation 79—79049
elastomers, vulcanised, tensile failure and network fracture mechanism, particle reinforcement 80—41928
epoxy, thermomech. props., rel. to hardener type and conc. 79—1913
epoxy polymer, with low thermal expansion coeff., relative elongation at rupture 78—3094
epoxy resin systems, synthesis review, phys. and mech. props. at low temps. 80—25650
epoxy-rubber particulate composite, toughness and fracture mech. 80—71727
ethylene-base ionomers, impact tensile props. *(Japanese)* 79—96120
ethylene-Co copolymers and -SO_2 copolymers prep. by catalysis and ^{60}Co γ-radiation, mech. props. 80—66841
ethylene-propylene-diene terpolymer, sulphonated, ionically cross-linked, foam elastomer, thermo-mech. props. 78—48362
ethylene-vinyl acetate copolymers, extrusion and heavy duty films, radiation crosslinking, struct. effect 80—66844
fatigue crack growth, mechanisms 78—64703
ferritic alloy, reinforced by dispersed oxide, mech. props., modification by recovery heat treatment *(French)* 77—59837
ferrofluid droplet, interphase boundary hydrostatic characts. in uniform mag. field 80—33692
fibre reinforced laminated hybrid, tensile first cracking strain and strength 80—81175
fibres, high-strength and high tensile, equipment for testing elongation 78—56844
filled polymer mechanical properties, particle shape effect, review 80—100864
fluorocarbon foil, Ftoroplast, homogeneity study *(Polish)* 80—35278
glass, phase separated, opt. props. of elongated phases 78—27179
glass fibre reinforced Al alloy, formed by hot extrusion, mech. props. 77—24987
heat-resistant alloys, installation for mech. tests under superplasticity conditions 80—55603

elongation continued
human soft tissues, tensile stress at const. elongation, temp. effects 77—32938
Incoloy 800, creep rupture props. at 525°C 79—43437
isoprene, stressed, microcrack generation under const. elongation, struct. depend. 77—90459
jets produced by shaped explosive charges, particle size distribution in breakup 80—23957
Kapron fibres, elongation and tensile strength rel. to UV irradiation 80—25796
Kevlar 49, fibre, mech. props., environmental effects incl. sunlight, ionising rad. 77—36560
Kevlar fibres, effect of crystallinity and orientation on mech. props. *(Japanese)* 79—38952
Kevler fibre, mech. props. in aq. H_2SO_4 soln. *(Japanese)* 79—47753
Mersilene mesh, herniorrhaphic reinforcing prosthetic, mech. and struct. props., SEM study 79—74789
metal, thin-walled cylinder, elongation upon torsion 80—64386
metal wire, plastic strain during extension, temp. gradient and high density elect. current *(Russian)* 79—57049
metals, aspects of impact testing, elongation-temp. curves 79—79111
metals, thermionic emission during stretching 79—95897
metals and alloys, strength/ductility relation *(Japanese)* 79—29145
metals and alloys, yield criterion, rheological interpretation *(Russian)* 80—21014
Mylar film/adhesive/Al foil laminate, mech. interactions 80—81112
Ni alloy KhN45Yu, strength properties, dispersity of struct. effect 80—55486
Nimonic 80A, intergranular creep fracture under const. cavity density 78—60825
Nomex, fibre, mech. props., environmental effects, incl. sunlight and ionising rad. effs. 77—36560
non-linear model, constitutive equation testing with free. vol. relax. spectrum 80—6011
Nylon 6 fibre, shrinkage, influence of chain rupture during tensile deform. 79—34055
nylon fibre reinforced polypropylene, enhanced fracture strain 78—15503
nylon-6 fibre, chain rupture and tensile deform. viscosity-av. mol. wt. obs. 78—76714
organosilicon ladder polymers, struct. and phys. props., book contrib. 79—65012
Pb, hardening in intermediate state 78—47917
PBI fibre, mech. props., environmental effects, incl. sunlight and ionising rad. effs. 77—36560
pentaplast, plasticised, thermal treatment effect on props. 80—40324
PET, effect of liquid aliphatic compounds on mech. props. 80—55488
PET, stress induced crystallisation, X-ray and light scattering obs. 79—99083
PET fibre reinforced polypropylene, enhanced fracture strain 78—15503
PET film, PET, transverse constriction and stresses accompanying uniaxial orientation 78—48475
PET film, relation between deform. and rotational isomerism 77—52438
photopolymer, biaxial stress-strain test 80—40417
plastic composites 79—29162
platilon UO1, use in artificial blood pumps, fatigue resist. and mech. props. 79—84026
polethylene-polypropylene blend, extruded, thermal swelling and mech. characterisation 80—81110
polyacetylene films, tensile props. and partial alignment 80—104210
polyacrylic acid crosslinked with PVA, force rel. to elongation in swollen or contracted states 77—40434
polyalkylene tetephthalates, amorphous and cryst., durability under stretching *(Russian)* 78—88511
1,2-polybutadiene crosslinked in strain states; entanglement networks, stress-birefr. relations 80—66590
polycarbonate film, struct. and mech. props. 79—19160
polydimethylsiloxane, crosslinked, stress/strain relations from large compression to high elongation 80—66589
polydimethylsiloxane, end-linked chains, model elastomeric networks, Gaussian, nonGaussian and ultimate props. 80—103260
polydimethylsiloxane chains, with known radiative side chain amounts, model elastomeric networks prep. by sel. crosslinking 79—73106
polydimethylsiloxane end-linked chains, nonGaussian effects 80—65127
polydimethylsiloxane networks, stress-strain isotherms at high elongations to rupture point 77—40433
polyester resin, creep, uniaxial elongation under variable temperature humidity 77—52434
polyether-polyester elastomer, fine structure and mech. props. 77—59844
polyethyl acrylate atactic networks, stress-strain isotherms at high elongations to rupture point 77—40433
polyethylene: $(Dy_2 0_3)$, mech. props. and transfer to steel surfaces 80—16496
polyethylene, cross linking by energy rich radiation, mech. and elec. props. *(German)* 78—20035
polyethylene, elongated low density film, TSC 79—47106
polyethylene, elongation, conform. set change IR obs. *(Russian)* 78—37778
polyethylene, high density, lamellar struct. and plasticity micromechanism 78—23791
polyethylene, high-density, effect of fillers and moulding process parameters on strength *(Russian)* 78—60640
polyethylene, low density, γ-irrad., unixial elongation effect on elec. cond. 80—25812
polyethylene, low density melts, temp. depend. of the elongational behaviour 80—6012
polyethylene, melt, elongational flow, necking and ductile failure mechanisms 77—43267
polyethylene, of low density, determ. of avoiding of tensile cracks *(German)* 80—19874
polyethylene, photodegradation mechanism, from yield strength, elongation and mol. wt. studies *(Japanese)* 80—76311
polyethylene, photodegradation study by Fourier transform IR spectroscopy *(Japanese)* 79—24772
polyethylene, roll oriented, superstructural change during uniaxial extension *(Japanese)* 77—52422
polyethylene, solid-state extruded, exam. of props. 80—11669
polyethylene, uniaxially oriented, relation between deform. and rotational isomerism 77—52438
polyethylene, welded, exam. of neutron irrad. effects on tensile characts. *(Japanese)* 78—84918

elongation continued
polyethylene film, chain rupture and tensile deform., viscosity-av. mol. wt. obs. 78—76714
polyethylene film, elongated, elec. impulse breakdown strength temp. depend. 20 to 80°C 77—73113
polyethylene films, low density, γ-irrad., elec. cond., effect of elongation 79—4564
polyethylene films, two-layer, elongation, recovery rates meas., relaxational props. *(Russian)* 77—32663
polyethylene films modified by polyacrylonitrile grafting before, after orientating elongation, struct. *(Russian)* 77—32554
polyethylene melt, comparison of elongational behaviour at constant stress and constant strain rate 77—63753
polyethylene single crysts., force elongation meas. 79—87700
polyethylene spherulites, high density, microstruct. and mech. props. 78—42921
polyethylene stabilized with home-made antioxidants, thermal resistance *(Polish)* 79—52328
polyethylene terephthalate, chain rupture and tensile deform., viscosity-av. mol. wt. obs. 78—76714
polyethylene terephthalate, elongation, conform. set change IR obs. *(Russian)* 78—37778
polyethylene terephthalate, mech. props., influence of cryst. arrangement and noncryst. region struct. 78—76707
polyethylene terephthalate, preoriented sheet, plastic deform., anisotropic behaviour 79—8335
polyethylenes, extrusion and heavy duty films struct. parameters influence on cross-linking by radiation 80—66844
polyhydroxyethyl methacrylate swollen network filled with polyhydroxyethyl methacrylate, viscoelastic and ultimate behaviour in rubbery region 79—83247
polyimide fibre reinforced polyamide-12 80—11754
polyimides, effect of orientational stretching on thermal aging 80—11721
polyisobutylene, undiluted, mol. wt. influence on creep behaviour 80—45370
polyisobutylene fibres, stretched, crystn. kinetic study using synchrotron radiation 80—33909
polyisobutylene melt, transient shear and elongational data 77—58631
polymer, plastoelasticity theory 78—75712
polymer, rigid-chain, unity of deform. and spontaneous elongation mechanism 79—20138
polymer chain subjected to elongation, conformational microstruct. variation *(Russian)* 79—31756
polymer films and sheets 78—80590
polymer melts, elongational flow, necking and ductile failure mechanisms 77—43267
polymer melts, elongational properties, microscopic stretch history 80—23981
polymer science, conf., Pittsburgh, USA, (June, 1975) 77—38756
polymer solution, bubble elongation dynamics, modelling with viscoelastic constitutive relations 79—37388
polymeric, liq., spike-strain test relevance for network connectivity destruction by deformation 80—6001
polymers, crystalline, oriented, drawing, load elongation behaviour, fibre composite model 79—15691
polymers, hydrostatic extrusion effects on subsequent mechanical behaviour 77—90392
polymers, mech. props., temp. dependence of polymers of different struct., 4.2 to 300K 78—68746
polymers, vitreous, quasibrittle fracture 80—21094
polymers with periodic deform., longitudinal flow 80—6008
polymethacrylic acid crosslinked with PVA, force rel. to elongation in swollen or contracted states 77—40434
polyphenylene sulphide, high mol. wt. soluble resin, prep., mech. props. 80—60828
polypropylene, film and fibre, chain rupture and tensile deform., viscosity-av. mol. wt. obs. 78—76714
polypropylene, glass fibre reinforced, injection moulded discs, struct. and mech. props. 78—19706
polypropylene, melts, elongational flow, necking and ductile failure mechanisms 77—43267
polypropylene, oriented, thermooxidative degradation kinetics, durability, influence of mech. initiated processes *(Russian)* 79—24591
polypropylene nonfilaments, highly drawn, plastic deform. 78—44174
polypropylene/peanut-hull flour composite, strength 79—8365
polystyrene, high impact, under press., mech. behaviour 79—52305
polystyrene, nonisothermal rheology 77—32619
polystyrene, plastic fracture near T_g at low strain rate 77—86178
polystyrene, stress birefringence under nonisothermal conditions 78—15468
polystyrene films, amorphous, X-ray small angle scatt. near glass transition, struct. *(Russian)* 77—31606
polystyrene melts, meas. of elongation props. with universal extensional rheometer 80—6004
polystyrene monofilaments, uniaxial extension, strengthening 79—8334
polystyrene-tetrachloroxylene(tetrachlorobenzene) glassy solns., additive morphology rel. to mech. props. 79—65007
polyvinylacetate films, amorphous, X-ray small angle scatt. near glass transition, struct. *(Russian)* 77—31606
polyvinylidene fluoride, γ-ray irradiation effect on mech. props., in presence of triallyl trimellitate *(Japanese)* 77—86091
polyvinylidene fluoride film, uniaxially stretched and corona poled, piezoelec. meas. 80—25311
porcine skin, herniorrhaphic reinforcing prosthetic, mech. and struct. props., SEM study 79—74789
PVC, amorphous, orientation study by creep thermomechanical method, computer anal. 78—75561
PVC, biological media effect on. physiomech. props. 79—96168
PVC, crosslinked, mech. and thermal props. with plasticisers *(Japanese)* 79—15741
PVC, rigid, viscoelastic props. rel. to thermal, mech. history 79—5016
PVC, tensile tests, post-yield phenomena 79—91752
PVC extruded films, mech. props. *(Polish)* 79—70037
rubber, natural, crosslinked by dicumyl peroxide, modulus, swelling relations 80—59551
rubber, natural, stretching effects on glass transition, sp. ht. obs. *(German)* 78—79753
rubber, peeling initiation and propag. 78—76824
SEM, combined deformation/heating stage, acoustic emission rate meas. 80—101892
shaped strip, tension during rolling 78—84890

elongation continued
silk, natural, elongation and tensile strength rel. to UV irradiation 80—25796
silk, spider, tensile, fracture strength, elongation and ageing effects 80—41072
siloxane, temp. transitions, linear dilatometry and X-ray diffr. obs. *(Russian)* 80—59404
stainles steel, type 316, irrad. in simulated environment, tensile props. 80—34076
stainless steel, ferritic SUS 410 type, coated with organometallic complexes and Ti alkoxides 80—34078
stator windings, failure mechanisms under thermal cycling *(Japanese)* 80—104189
steel, 0Kh12G14N4Yu2, struct. after deformation under conditions of superplasticity 80—21031
steel, 12Kh18N9T-TiB_2, eutectic alloy, high temp. props. 78—84931
steel, α to γ phase transform., during rapid resistance heating, apparatus for investigation *(Slovak)* 78—19742
steel, alloy, deformation, rapid dynamic, at −196°C 80—104220
steel, alloy, tension test, computer simulation of deform. to fracture 79—11667
steel, austenitic, ASTM A533B and A542, H_2 embrittlement behavior of unirrad. steels for nuclear reactor press. vessels 79—8340
steel, austenitic, Cr-Mn, metastable, plasticity, contrib. of martensitic transform. during deform. *(Russian)* 80—30018
steel, austenitic, nitrided, creep, effect of N_2 and Ti and prior deform. 78—23789
steel, austenitic stainless, 316, surgical implant ion beam textured, stress/strain relations, fatigue characts. 78—73297
steel, austenitic stainless, biphase, ferritic, ageing and thermomech. treatment effects on struct. and props. 80—35226
steel, austenitic stainless, Cr-Ni, Mn and Mo effect on mech. props. rel. to treatment 79—96039
steel, austenitic stainless, Cr-Ni (18,8 wt.%), stress-corrosion cracking 78—85057
steel, austenitic stainless, He implanted 1.4970, high temp. fracture 77—86186
steel, austenitic stainless, metastable, transform. depend. ductility, temp. and deform. effects 78—3185
steel, austenitic stainless, stabilized, creep improvement, effect of B precipitation and hyperquenching *(French)* 78—23784
steel, austenitic stainless, stress corrosion cracking in H_2SO_4-NaCl soln., Ni and N_2 effects *(Japanese)* 79—100289
steel, austenitic stainless, type 304, cyclic creep during unbalanced tension-compression loading at elevated temp. 80—97545
steel, austenitic stainless JIS type 304, tensile test at elevated temp., high velocity 77—73302
steel, austenitic stainless Kh18N10T, strength properties, dispersity of struct. effect 80—55486
steel, C, accelerated deform. by to H_2 absorption *(Japanese)* 79—70121
steel, C, mech. props. rel. to heat treatment, ferrite-pearlite transform. *(French)* 79—20043
steel, C, plates, residual elements effect on through-thickness props. 80—66660
steel, C, tensile props. in high press. H_2 at room temp. *(Japanese)* 80—108501
steel, C, X-ray line fitting by Gram-Charlier distrib., appl. to tension test *(French)* 79—15689
steel, C-Mn, pressure vessel usage, elevated temp. mech. beahviour 78—35462
steel, Ck45, tension-compression tests, cyclic, macroscopic changes of length *(German)* 80—40424
steel, cold rolled, high strength, mech. props. 77—36527
steel, correlation links between mech. props. controlled rolling effect 80—35234
steel, Cr (13 wt.%), sintered, organometallic complex addition effects on mech. props. 80—25595
steel, Cr-Mo, cast and forged, difference in mech. props. 77—48465
steel, Cr-Mo, effect of Mo on high-temp. props. 80—85005
steel, Cr-Mo (10-14, 2-6 wt.%), heat-resist., creep-rupture strengths 80—104271
steel, Cr-Mo (2.25, 1 wt.%) annealing, high strain rate tensile props. 77—25117
steel, Cr-Mo-Ni-Nb, Nb effect on mech. props. *(German)* 80—30012
steel, Cr-Mo-V, 1% Cr, chem. comp. and struct. effect on deform. props. *(German)* 79—1888
steel, Cr-Ni-Mo-V, ductile fracture during tensile loading 80—45381
steel, creep resistant, AISI 304, residual lifetime assessment by low cycle fatigue testing *(German)* 78—15485
steel, deformation and stresses during elongation, application of Ludwig eqn. *(German)* 80—40475
steel, Fe-Mn-C austenitic, deform. twinning and mech. props. 77—59868
steel, ferrite and dual phase, mech. props., effect of Si and P 79—57063
steel, ferritic stainless, embrittlement 80—85041
steel, ferritic/austenitic high Cr, development, mech. props. and corrosion resist. 80—45422
steel, for pressure tanks, yield point influence on brittle fracture, tensile strength *(German)* 80—40539
steel, high alloy Cr-Mo-W, splat quenched, formation of metastable austenite 80—84974
steel, high C, Cr addition effect on superplasticity 79—15729
steel, high-speed, cast, mech. props. at high temps. 79—20135
steel, hot rolled, low C, low alloy, bainitic alloying addition effects on microstruct. and props. 77—36546
steel, hypereutectoid type HF-1, microstruct. effects on fracture toughness, ductility, strength 79—74255
steel, low alloy, fatigue crack nucleation under high cycle fatigue and uniaxial loading 79—79060
steel, low alloy, type 3sp, effect of temp. at end of rolling on mech. props., and coercive force 78—72799
steel, low C, brittle fracture susceptibility, low temp. deform. effects 77—56103
steel, low C, cold rolled sheet, strain rate effect on yield *(Japanese)* 79—96084
steel, low C, Mn, strain hardening parameters, electron microscope obs. 77—63690
steel, marageing, austenite formation, stability, transformation to martensite *(Russian)* 79—91646
steel, maraging, 18 wt.% Ni, tensile props., effect of aged struct. and austenite grain size 77—48511

elongation continued
- steel, maraging, (18 wt.% Ni), solution annealed, exam. of cryogenic tensile, fatigue, and fracture props. 78—92311
- steel, martensitic, high C, Co addition effect on strength *(Korean)* 78—68736
- steel, martensitic, low C wire, strain tempering by rapid heating *(Japanese)* 78—31428
- steel, Mg effect on precipitation of C and or N, and mech. props., during strain ageing *(German)* 78—35387
- steel, microalloyed, types V1599, V1600, V1286, NbCN precipitation in undeformed austenite 80—89230
- steel, mild, AC effect on fatigue and static props. 80—45372
- steel, mild, fatigue life, effect of H_2S and SO_2 gas 79—15871
- steel, mild, shear mode of ductile fracture 79—91785
- steel, Ni, welded joints on LNG carriers mech. props. and fracture toughness 80—85017
- steel, plastic flow area, determ. of relative elongation and rel. to yield point 78—23769
- steel, plasticity indices in anisothermal extension *(Russian)* 80—16378
- steel, powder forged, impact strength and fatigue strength, slag inclusion effects 77—21271
- steel, prestressed concrete wire, strain tempering by rapid heating *(Japanese)* 79—70088
- steel, quench ageing effect of Mn content on C and N precipitation and mech. props. *(German)* 78—31409
- steel, quench-hardened, exam. of anomalous plasticity when deformed *(Russian)* 79—11663
- steel, reinforcement, low, high temp. static strength testing 79—15902
- steel, sheet, rapid test for props. assessment 80—40650
- steel, spring, 60C2A, tempered under stess, influence of tempering conditions on mech. props. *(Russian)* 79—47724
- steel, stainless, 0Kh12G14N4Yu2, effect of plastic deform. on biphase struct. 78—44176
- steel, stainless, 304, creep fracture propag., elongation, tensile strength, yield stress meas. applicability of fracture mechanics parameters 78—35508
- steel, stainless, deformation, rapid dynamic, at −196°C 80—104220
- steel, stainless, even elongation and relative hardening in martensitic, transition and austenitic 78—52926
- steel, stainless, ferritic, 430 Zr, oxidation, forming and mech. props. 80—11680
- steel, stainless, ferritic, subjected to 475°C embrittlement, exam. of fracture toughness 78—84982
- steel, stainless, ferritic, tensile strain direction and roping phenomena 77—36533
- steel, stainless, fracture micromechanism when kept isothermally in sulphur pulp 80—76355
- steel, stainless, Ti stabilised, creep props. rel. to B conc. *(French)* 79—20132
- steel, stainless, two-phase ($\alpha+\gamma$), twin-related lath occurrence rel. to fracture elongation 77—90443
- steel, stainless 301, stress corrosion cracking in $MgCl_2$ soln., environment effect on initiation and propag. *(Japanese)* 80—104338
- steel, stainless 304, stress corrosion cracking in high temp. water, constant strain rate meas. 78—31565
- steel, stainless type 304 L, mech. behaviour under constant stress associated with cyclic strain 80—25767
- steel, stainless/Al laminate, sandwich sheet materials, deform. in uniaxial tension 79—57061
- steel, structural, grain size depend. of yield stress in homogeneous deformation range *(German)* 80—30013
- steel, structural, unalloyed, brittle fracture, grain size and precipitate thickness effect 78—60786
- steel, tensile testing of ultra high tensile roping wire 77—44426
- steel, TRIP, powder processing, tensile strength, ductility 78—64499
- steel, type 12KhN4MDA, deformation and fracture props. on extension and twisting *(Russian)* 80—55504
- steel, ultrahigh C, superplastic struct. development by heat treatment 80—11703
- steel, V-Nb and Cr-Mo-V-Nb, supercooled austenite isothermal decomp., struct., strength and fracture characts. 80—60966
- steel, VN precipitation after heat treatment 79—29067
- steel *(German)* 80—100869
- steel 17G1S, magnetic method of mech. prop. determ. of thick sheet 78—48600
- steel Cr-V (1.5, 0.5 wt.%), cavitation effect of temp. and C content 78—64638
- steel fibre reinforced concrete, tensile strength and ultimate strain *(Polish)* 80—21027
- steel HF-1, acoustic emission during extension, frequency content variation 77—81301
- steel mesh, herniorrhaphic reinforcing prosthetic, mech. and struct. props., SEM study 79—74789
- steel sheet, hot and cold rolled, cold formability, notched tensile test and stretch bend test *(German)* 80—61031
- steel St.3kp, ductile-brittle transition temp., variation with grain size 78—27640
- steels, austenitic stainless, stress corrosion cracking, correl. between electrochem. and mech. parameters 80—97613
- steels, types SS41, SB42, SM50A, STK55, liq. Zn embrittlement *(Japanese)* 80—81164
- stretch measurement of ribbons in industrial processes, digital instrument *(Polish)* 80—42194
- superplastic flow in unsteady and steady state regions 79—42135
- telechelic, chain extension, qualitative aspects 80—95752
- Tetron, vascular substitute, exam. of tensile fracture behaviour 78—77157
- torsional deformation testing for plastic deformation, fracture *(Hungarian)* 80—97659
- TZM-Mo alloy, mech. props., effect of exposure to high temp. He containing O_2, room temp. study 80—93639
- viscoelastic material, failure and instability in tension 80—87720
- viscoelastometer, dynamic, direct reading, automation, appls. to polymer films, fibres 79—3980
- work hardening material indentation analysis 79—8308
- wound wires, enamel insulated, elongation plus flexibility 80—20999
- Zircaloy-2, deformation instability and tensile elongation 77—32655
- Zircaloy-2, effect of simulated fission products on elongation fractography and metallography 80—649
- Zircaloy-4, H_2 effect on mech. props. *(Korean)* 79—70123
- Zircaloy-4, strain rate dependent mech. response 77—21254

elongation continued
- Ag, filament produced by glass coated melt spinning, mech. props. 77—86125
- Ag-Cu-Zn-(Cd)(Mn), solder, UTS, room temp. to 4.2K 79—57064
- Ag-Ni (10 wt.%) wire, plastically deformed, fracture struct. *(German)* 80—71744
- Al alloy 01205, mech. props. at cryogenic temps. 79—29206
- Al alloy 7075, precipitation hardening, toughness and microstruct. *(Japanese)* 78—15509
- Al alloy AL22, influence of ultrasonics application on creep during multistage ageing *(Russian)* 79—91708
- Al alloy V96Ts, superplasticity 79—52326
- Al alloy-mica particle composite, cast prep. and mech. props., bearing appl. 80—71613
- Al, alternating bending of single crysts., shear strain accumulation and microstrain distrib. *(Russian)* 78—60706
- Al and Al-Mg (5.5 wt.%), instantaneous plastic strain associated with stress increments during steady state creep 78—48478
- Al, annealing of lightly deformed samples, effect of press. *(Russian)* 78—39795
- Al, coated with anodic oxide, characterisation by tribostimulated exoemission 79—91829
- Al, elongated, deformation and recrystallisation, Rowland transform. model *(French)* 77—77498
- Al, elongated, deformed, recrystallisation, orientation relations, hard-sphere model for Rowland transform. *(French)* 77—77497
- Al, exoelectron emission under recrystallisation annealing 77—90412
- Al, impurity influence on superplasticity, elongation decrease at rupture *(Russian)* 79—91735
- Al notched bars, deform. behaviour and strength having biaxial state of stress at notch root *(Japanese)* 80—81116
- Al, plastic deform. and prominent cross slip ⟨100⟩ oriented single crystal 78—19851
- Al sheet alloy, type 2036-T4, in-plane deformation, correlation with Hill's theory 79—83260
- Al-Al_3Ni, eutectic composite, directionally solidified, thermal cycling induced distortion 78—39899
- Al-Al_4C_3, dispersion hardened physical props. meas. *(German)* 78—31415
- Al-C, dispersion hardened, effect of processing parameters on mech. props. 80—20826
- Al-Cu (33 wt.%) eutectic, superplasticity, in-situ obs. by TEM 77—28876
- Al-Cu-Mg/mica particulate composite mech. props. 80—100919
- Al-Cu-Mn-Mg-Fe-Si-Zn alloy D16, surface layers chem. composition rel. to fatigue resist., corrosion-fatigue resist. 79—29275
- Al-Cu(Ag), tensile ductility, effect of ageing and impact velocity *(Japanese)* 78—15465
- Al-Cu(Si)(Mg) binary and ternary alloys, dimensional changes in heat treatment. 80—89271
- Al-Cu(0-10 wt.%) sintered compacts, mech. props. rel. to sintering 80—76210
- Al-Mg, Mg effect on ductility, 25 to 250°C 79—100214
- Al-Mg (4 wt.%), enhanced ductility at elevated temps. 77—63740
- Al-Mg (7 wt.%), β-phase soln. behaviour and mech. props. *(Korean)* 78—11277
- Al-Mg alloy AMg6, mech. props. of welded joints, impurity effects 78—95789
- Al-Mg-Si alloys, cast, precip.-rich zones on grain boundaries, soln. heat treatment conditions effect on mech. props. 80—104176
- Al-Mn alloys, study of solidification by rapid cooling *(Japanese)* 78—88459
- Al-Ni-Co(Si), directionally solidified eutectic, morphological and mech. props. *(Russian)* 80—30057
- Al-Si casting alloys, graphite-dispersed, mech. props. and wear resist. 77—4857
- Al-Si eutectic alloys, superplasticity 80—11710
- Al-Zn (22 wt.%), superplastic strain rate sensitivity, rel. to ductility 78—31478
- Al-Zn (40 wt.%), mechanical properties after thermal cycling 78—3150
- Al-Zn alloy, flow stress, Zn content effect 79—38913
- Al-Zn eutectoid, superplastic, fracture, electron microscope obs. 78—31533
- Al-Zn-Mg, acoustic emission meas. during tensile testing, reproducibility of results 80—50782
- Al-Zn-Mg, cavitation during superplastic deform. *(Japanese)* 78—15464
- Al-Zn-Mg, plastic instability rel. to grain boundary failure at low temps. 78—56702
- Al-Zn-Ti(Mn), mech. props., Ti or Mn addition effect *(Korean)* 80—93613
- Al_2O_3, vacuum condensate, struct. and mech. props., second phase effect *(Russian)* 80—71705
- As_2S_3 glass fibre, elongation, force depend., deviations from linearity 80—45334
- Au, deformed, annealing kinetics of vacancies, elec. cond. meas. and computer simulation 78—47353
- B fibre reinforced Al composite, strength of fibre-matrix interface and tensile strength *(Russian)* 80—21005
- B fibres of various diameters, tensile strength, elasticity, elongation 78—3189
- B_2O_3 glass fibre, elongation, force depend., deviations from linearity 80—45334
- B_2O_3-SiO_2-Na_2O phase-separated glass, creep fracture morphology 80—81151
- Be, low oxide, isostatically pressed block, factors affecting tensile strength, elongation, impact resistance 77—16610
- C fibre, thermal treatment temp. effect on struct. and props. 78—23743
- C-C composite, structure model, Rosen model with fractional matrix 80—11719
- C-fibre reinforced epoxy resin, laminated structs. mech. props. 80—50672
- Co, anomalous plasticity near martensitic transform. temp. *(Russian)* 78—6971
- Co-Fe-V-Ni, mag. and mech. props., heat treatment and stress effects 80—60363
- Co-W-Cr (15,20 wt.%), surgical implant ion beam textured, stress/strain relations, fatigue characts. 78—73297
- Co-WC dispersion hardened alloy, tensile deform., volume fraction of second phase effect, simulation *(Japanese)* 79—70122
- Cu alloy, ductile fracture during tensile testing 80—45381
- Cu, bidirectional twisting, effect on elongation and ductility changes 77—44315

elongation continued
Cu, deform. instability and tensile elongation 77—32655
Cu, dislocation mean free path at 77K under elastic deform. 78—44162
Cu, ductility minimum, strain rate depend. at intermediate temps. 79—79056
Cu, extended single crystal wire, orientation of cross section ellipse 77—86115
Cu, filament produced by glass-coated melt spinning, tensile strength 77—48508
Cu, M1E, yield stress decrease in compression, rel. to previous elongation *(Polish)* 80—50665
Cu powder compacts sintering, depend. of neck form. on particle size and sintering temp. 79—28988
Cu single crysts., deformed, HVEM study of recrystn. texture 80—104179
Cu wire, electroplastic drawing X-ray diffr. anal. and mech. props. exam. *(Russian)* 79—29138
Cu-Al-Fe, mech. props. rel. to heat treatment 80—50682
Cu-Al-Fe, strength increase from intermediate annealing determ. of annealing temp. by recrystallisation 78—44136
Cu-Al-Fe (11, 2 and 1 wt.%), Fe effects on microstruct. and mech. props. *(Korean)* 77—28807
Cu-Al-Ni alloys, elongations as function of orientation calculated for the $\gamma_1' \to \beta_1''$ martensitic transformation 79—43245
Cu-Al-Si, Si effect on mech. props. and microstructure *(Korean)* 79—38903
Cu-Al-Si-C (95, 2.8, 1.8, 0.4 wt.%) fracture characts. of superplastic single phase, exam. 78—48500
Cu-BeCo (1.85, 0.29 wt.%), type CA172 (TH04), strengthened by spinodal decomp., stress relax. in bending 80—7616
Cu-Cd (1.0 wt.%), yield stress and flow stress 80—97524
Cu-Cr (0.75 wt.%), deformation characts., fully reversed cyclic strain with fatigue cracks and dislocation struct. 80—81148
Cu-Ni alloy, dislocation density during deform., comparison of electron microscopy and X-ray diffr. *(Russian)* 79—5002
Cu-Ni-Cr (28, 2.8 wt.%), spinodal alloy, microstruct. and tensile props. 78—39858
Cu-Ni-Sn (4-15, 4-8 wt.%), strip strengthened by spinodal decomp., stress relax. in bending 80—7616
Cu-Sn, graphite dispersed, wear, effect of graphite content *(Japanese)* 77—56114
Cu-Zn (0.25 wt.%), ductility minimum, strain rate depend. at intermediate temps. 79—79056
Cu-Zn-Al, reversible shape memory effect obtained by heating under constraint *(Japanese)* 79—43335
$(Fe,Ni,Co)_3V$, long-range ordered alloy for fusion reactor appl. 80—32481
Fe and Fe alloys, fast neutron irradiated at high temps., mech. props. 79—51157
Fe and Fe-Cr, flow stress, effect of cathodic, H_2 charging *(Japanese)* 79—52313
Fe, Armco, H_2 diffusion 0 to 300°C, effect on elongation tension *(Russian)* 77—66044
Fe, cast, spheroidal graphite, graphite size effect on mech. props. *(Korean)* 78—11278
Fe, cast, spheroidal graphite effects of Si and C on mechanical props. *(Korean)* 79—66114
Fe, cast, spheroidal graphite, degree of normalization effect on mech. props. *(Korean)* 79—87664
Fe, cast, thermal treatment influence on mechanical props. *(German)* 80—29980
Fe, commercial, ductile-brittle transition temp., variation with grain size 78—27640
Fe, filament produced by glass-coated melt spinning, tensile strength 77—48508
Fe, model for Luders band formation and plastic instability related with strain softening due to Johnston-Gilman-Hahn theory 79—61676
Fe polarised wire, elongation in presence of acetylene type acid corrosion inhibitors 80—55590
Fe, powder forged, impact and fatigue strengths, slag inclusion effects 77—21271
Fe, powder preforms., hot consolidated rolled strip, mech. props. 78—15338
Fe, sintered, strength and elongation, rel. to density 80—30047
Fe, sintered and pressed, props., effect of atomised Fe powder particle size distrib. 80—11601
Fe whiskers, elongation induced struct. distortion, X-ray topographic investig. 77—85121
α-Fe whiskers, pure, ductile fracture initiation, macroscopic obs. of deform. history and failure 80—85043
α-Fe whiskers, pure, ductile fracture, microscopic obs. of initiation mechanism 80—85044
Fe-C-Ni-Cr(Cu), dynamically hot pressed, mech. props., additives effect 78—60620
Fe-C(0.001 to 0.44 wt.%), C effect on low temp. brittleness *(Japanese)* 80—50711
Fe-Co-V alloy, Remendur, heat treatment effects on mech. and struct. props. 77—8846
Fe-Cr-Al (7, 5 wt.%), expt. stainless alloys, phys. and mech. props. 80—97637
Fe-Cr-Al-Y ($Y-Al_2O_3$)(Y_2O_3), preparation and exam. of mech. props. 78—52720
Fe-Cr-Mn (11.5, 3 wt.%), microduplex ferritic-martensitic steel, exam. 78—39862
Fe-Cr-Mo sintered, damping capacity and mech. props. 78—44161
Fe-Cr-Ni, two phase ($\alpha+\gamma$) alloys, transformation-induced plasticity 77—63721
Fe-Cr-Ni, two-phase ($\alpha+\gamma$), and metastable austenitic, uniform elongation peak 77—77547
Fe-Cr-Ni-C (17.2, 7.34, 0.2 wt.%) alloy, twin related laths, fracture elongation, TEM study 79—29192
Fe-Mn-Cr-C, twinning and strain induced FCC to HCP transform. 77—44248
Fe-N, neutron irrad. effects on mech. props. 79—4338
α-Fe-N solid soln., N precipitation kinetics, defects effect 77—59789
Fe-Ni (1 to 5 at.%), mech. props. below 300K *(French)* 79—8314
Fe-Ni heterogeneous alloys, ferrite, martensite and austenite phase distrib., effect on mech. props. 80—45363
Fe-Ni-C, ausformed, ductility of martensite *(Japanese)* 77—48490
Fe-Ni-C alloy, austenitic, pre-deform. effects on TRIP *(Japanese)* 77—8890

elongation continued
Fe-Ni-C alloy with single-component martensite texture, $\alpha \to \gamma$ transform., changes in shape *(Russian)* 80—104152
Fe-Ni-Cr-Ti, superalloy A286, powder, exam. of microstruct. and mech. properties 78—52979
Fe-Si (3 wt.%), electron irradiated, yield strength and elongation 80—76325
Fe-Si (3 wt.%), exam. of plastic deformation, slip band dislocation, under hydrostatic pressure 78—56695
Fe-Si (6.5 wt.%), Ni, Al and Mn additions effect on mech. and mag. props. 77—12667
$Fe-TiB_2$, eutectic alloy, high temp. props. 78—84931
Fe-Ti(Nb), internally nitrided, mech. props. 77—44307
Fe-W system, damping capacity of Gentalloy, internal friction, mech. and mag. props. 79—77679
Fe-W-Cr-Mo-Co with austenitic phase, magnetic and mech. props., cold working and ageing effects *(Japanese)* 78—60678
GdCu, electrical resistivity and length changes with temp., hysteretic behaviour 80—97600
Ge, whisker growth from vapour phase 80—15426
GeO_2 glass fibre, elongation, force depend., deviations from linearity 80—45334
Mg-Sm, phase diagram and mech. props. *(Russian)* 80—20892
Mg-Y-Nd-Zn-Zr (2,2,0.3, 0.7 wt.%), heat treatment effect on casting dimensional stability, alloy mech. props. 78—44146
MgCd wire, elongation during disorder-order transform. *(Russian)* 80—104148
Mn-Cu-Zn system, optimum heat-treatment routine for max. damping 79—87670
Mo and Mo alloy TZM, solid-state bonding, tensile strength of bond *(German)* 79—47756
Mo, electron beam melted with C additions, mech. props. *(Japanese)* 77—48449
Mo, mech. props., effect of exposure to high temp. He containing O_2, room temp. study 80—93639
Mo, mech. props., influence of temp. on singularities of deform. *(Russian)* 78—6970
Mo powder, influence of powder reduction processes on props. 80—89175
Mo-Zr-B alloy, neutron irrad. at 780-1080°C, porosity, hardening and embrittlement *(Russian)* 80—29062
Nb-low alloys, strength and ductility at high temp. and different strain rates 80—16401
Nb-W-Mo-Zr, long-term strength props., vac. level effect 80—55484
Nb-W-Zr-Ta, long-term strength props., vac. level effect 80—55484
Nb-Y, and Nb, mech. props., neutron irrad. and Y scavenging effects 77—90394
NbC, vacuum condensate, struct. and mech. props., second phase effect *(Russian)* 80—71705
Ni alloy EI867, heat resistant, mech. props., effect of prolonged elevated temp. 77—21194
Ni base alloys EhI607A and EhI929VD, fatigue strength, temp. depend. 79—15791
Ni, ductility and fracture, nonmetallic inclusions effect 80—104221
Ni, Ni-Ti (1 wt.%), serrated yielding, 77 to 723K 77—32649
Ni, oxide dispersion strengthened materials, effect of prior creep at 1365K on room temp. tensile props. 78—39857
Ni single crystal, stretched, electron microscope exam. of deformation cell structure during polygonization *(German)* 80—7651
Ni thin-walled cylinder, elongation upon torsion 80—64386
Ni-Cr machine steel, austenite grain size effects on mech. props. *(Russian)* 77—44292
Ni-Cr Nimonic alloys, mech. props., high-temp. irrad. effects 80—100885
Ni-Cr-(Al), oxide dispersion strengthened materials, effect of prior creep at 1365K on room temp. tensile props. 78—39857
Ni-Fe-Cr base superalloy, addition effect on mech. props. *(Chinese)* 80—20998
Ni-Nb-Al, eutectic, thermal cycling effect on strength and ductility *(Russian)* 79—24601
Ni-Nb-Al-(Cr), eutectic, mech. props., high press. H_2 effects 77—63779
Ni-W (45.5 wt.%), eutectic, mech. props., high press. H_2 effects 77—63779
Ni_3Al, ductility, tensile and compressive tests *(Japanese)* 77—52414
Ni_3Al, ductility in poly- and single crystals, compressive and tensile tests 78—56715
Pb, sample length effect on plasticity 78—44179
Pd, annealed, cold worked, H_2 diffusion effect on mech. props. *(Japanese)* 78—10222
$Pd_{77.5}Cu_6Si_{16.5}$, cold drawn wires, surface markings, fracture stresses 79—56997
$Pd_{80}Si_{20}$ amorphous alloy, skip deform. and crit. shear stress, using tensile testing machine 80—89321
$Pd_{80}Si_{20}$, plastic flow, fracture, slanted necking and elongation at high temps. 79—57057
Pt-Rh-W (30, 8 wt.%), intergranular embrittlement by Se vapour 80—3185
SiO_2 glass fibre, elongation, force depend., deviations from linearity 80—45334
Sn plate, rapid test for props. assessment 80—40650
Sn-Zn (9.8 wt.%), eutectic superplasticity 77—36582
Ti alloy OT4, high plasticity effect 80—35272
Ti alloys, β-annealing and controlled rate quenching effects 78—80568
α-βTi alloys, high strength, heat-treated weldments, intergranular fracture 80—21097
Ti alloys with eutectoid-forming elements, mech. props. 77—44313
Ti and Ti-Nb, plastic deform. and thermal cond., 2.5 to 10K, dislocation pinning 77—35629
Ti, mechanical props. and appls. 79—66104
Ti polycrystalline wire, electroplastic effect 79—57067
Ti, type 70A, containing 0-6000 ppm ^{3}He, sensitivity of tensile props. 80—39197
Ti-Al, age-hardened, deform., order effects in Ti_3Al and temp. effects 77—25111
Ti-Al-H, H effect on mech. props. and lattice constants 80—21036
Ti-Al-Mo-Zr, type VT-9, creep eqns. rel. to extension and compression props. 80—100875
Ti-Al-Sn (5, 2.5 wt.%) alloy, fatigue under combined alternating bending and torsional stresses 77—8923
Ti-Al-V, containing 0-6000 ppm ^{3}He, sensitivity of tensile props. 80—39197
Ti-Al-V (6,4 wt %), superplasticity, effect of temp. 80—7639

elongation continued
- Ti-Al-V (6,4 wt.%), α/β interface phase influence on tensile props. 80—30034
- Ti-Al-V (6,4 wt.%), effects of grain size on superplasticity, deformation mechanisms, microstructural characteristics 79—52323
- Ti-Al-V (6,4 wt.%), microstruct. effect of base metals on diffusion welding *(Japanese)* 80—89296
- Ti-Al-V (6,4 wt.%), surgical implant ion beam textured, stress/strain relations, fatigue characts. 78—73297
- Ti-Al-V (6,4 wt.%) superplastic alloy, maximum attainable ductility 80—60919
- Ti-Al-V (6.4 wt.%) cast alloy, with improved microstruct., mech. props. *(Japanese)* 80—71701
- β—Ti-Mo, thermal instability, hardness and tensile deform. *(Japanese)* 80—71703
- Ti-Mo-V-Al-Cr-Fe (4.8, 4.7, 5.2, 1.1, 1.0 wt.%), structural changes during heating up to 1000°C, DTA study *(Russian)* 80—93552
- Ti-TiO_2-ZrO_2-Mo, sintered struct. and mech. props. 78—60618
- α-Ti-Zr-W, effect of W impurity on mech. preps. 80—16392
- TiB_2, TiC, vacuum condensate, struct. and mech. props., second phase effect *(Russian)* 80—71705
- U-Mo (1.5 wt.%), superplastic behaviour 450 to 720°C *(French)* 79—74203
- U-Mo (2 wt.%), depleted, effect of microstruct. on mech. props. 80—108497
- U-Mo-Nb-Zr-Ti (0.75, 0.75, 0.75, 0.5 wt.%), heat treatment effect on microstruct. and mech. props. 78—23729
- V-low alloys, strength and ductility at high temp. and different strain rates 80—16401
- W alloys, deformed, vacuum technology appl., mech. props. *(German)* 79—57046
- W fibre reinforced Cu, interface porosity formation, on thermal cycling 80—30092
- W sintered rods, hot rolling with four roll passes, effect on struct. and mech. props. 79—100195
- W, with different microstructs., temp. depend. of yield strength 80—16404
- W-Ni-Fe (5(2), 5(2) wt.%) pore formation, effect on mech. props. 80—45396
- $Y_3Fe_{5-x}Al_xO_{12}$, $Y_{3-x}Gd_xFe_5O_{12}$, linear expansion 77—48024
- α-Zircaloy, strain ageing at 1000K 79—47725
- Zn, alternating bending of single crysts., shear strain accumulation and microstrain distrib. *(Russian)* 78—60706
- Zn-Al (22 wt.%), meas. of plasticity parameters under superplastic flow 78—60710
- Zn-Al (22 wt.%), superplastic, eutectoid alloy, ductility and fracture 78—60819
- Zn-Al (22 wt.%) eutectoid, superplastic, grain size effect on plastic deform. at room temp. *(Japanese)* 78—31462
- Zn-Al-Cu (18, 4 wt.%), plastic deform. at room temp., superplastic props., tensile strength *(Czech)* 80—45360
- Zn-Al(Cu), mech. and technological props. *(Polish)* 80—89286
- Zr alloys, acoustic emission during tensile testing 77—90433
- α-Zr, strain ageing at 1000K 79—47725
- Zr-Al (8.6 wt.%), fast neutron irradiated, tensile props. and fracture toughness 80—84994
- Zr-Al(8.6 wt.%), mech. props., corrosion and fast neutron irrad. influence 78—84948
- Zr-O-N system, struct. and plastic deform. *(Russian)* 78—80588
- Zr-Ru(Pd), heat treated, mech. props. and struct. 78—80571
- $ZrC_{0.97}$-$NbN_{0.93}$, $Zr_{0.5}Nb_{0.8}C_xN_{0.98-x}$, solid solns., elastic props. expansion and hardness 77—52380
- ZrO_2, ZrB_2, vacuum condensate, struct. and mech. props., second phase effect *(Russian)* 80—71705

e.m. waves *see electromagnetic waves*

embrittlement
- *see also ductile-brittle transition; hydrogen embrittlement; liquid metal embrittlement*
- Admiralty Metal, transgranular stress corrosion crack propag. 80—89402
- Al-Zn-Mg (6, 3 wt.%), water vapour embrittlement and H_2 bubble form 78—15564
- alloys, austenitic, neutron irradiation induced embrittlement, review 79—65120
- alloys, embrittling residuals categorisation by Auger electron spectroscopy 80—66739
- alloys, temper embrittlement, impurities and alloying elements role, review 80—66649
- brass, adsorpt. of Hg, effect on mech. strength, creep, fatigue, embrittlement *(Russian)* 79—29267
- chemically assisted fracture, atomic models of crack growth 80—64466
- chemically assisted fracture, general reaction rate theory and thermodynamics 80—64465
- Cl $(Co_{100-x}Fe_x)_{83}B_{17}$, $1 \leq x \leq 30$, annealing embrittlement and crystn. 80—45329
- crystal plasticity, surface effects, review 77—47505
- Duralumin, adsorpt. of Hg, effect on mech. strength, creep, fatigue, embrittlement *(Russian)* 79—29267
- engineering materials, intergranular fragility index 80—66637
- fracture, intergranular, low temp. mechanism 78—60795
- fracture mech., conf., Washington, USA (Sept. 78) 79—43422
- fusion reactor materials science 79—97899
- fusion reactor metals, He embrittlement, grain boundary cavity model 80—34075
- hardened irradiated metal, flow stress temp. depend., effect of interstitial atom clustering and embrittlement *(Russian)* 78—34538
- Inconel 600, Neutron irradiation using HFIR for evaluation as fusion reactor material 78—13324
- liquid metal, of engineering materials 79—52421
- LMFBR, effect of cracks in fast neutron embrittled hexagonal subassembly ducts 78—74446
- LMFBR materials, exam. of material requirement 78—50256
- LWR materials, pressure boundary problems, corrosion, cracking and radiation embrittlement props. 78—46142
- LWR pressure vessels, radiation embrittlement, role of ASTM 79—22435
- metal, AES study *(Chinese)* 79—38982
- metal, He-containing, high temp. embrittlement model 79—83320
- metal induced embrittlement of metals, evaluation of embrittler transport mechanisms 78—52980

embrittlement continued
- metallic glasses, annealing behaviour, thermal stability and crystn. 80—75167
- metallic glasses, mats. props. review 77—4043
- nuclear reactor pressure vessels, radiation embrittlement, allowable crack size, unstable fracture 77—10465
- polyethylene, high density, subjected to biaxial tension, effect of loading cycle asymmetry on fatigue strength 78—44215
- pseudoelastic single crystal fatigue 79—52364
- reactor materials, radiation-induced embrittlement and swelling due to void form, ASTM research 78—13231
- reversible temper embrittlement, book contrib. 78—11334
- SAP 895 (Al-Al_2O_3) alloy containing ^4He and ^3H, tensile props. 80—34129
- segregation-induced embrittlement of grain boundaries 79—83318
- solid soln., ductility, comp. effect *(Japanese)* 79—43334
- stainless steel, 18Cr-11Ni, for nuclear reactors, mech. props., neutron effects 77—34383
- steel, 0Kh16N15M3B type, He ion irradiation effect on struct. and mech. props. 78—19848
- steel, alloy, embrittlement during tempering *(Russian)* 77—90436
- steel, alloy, Fe-Ni-Cr-Sb-C effect of Ni, Sb, on temper embrittlement 78—60813
- steel, alloy, HY130, temper embrittlement due to Si intergranular segregation, effect on H_2 induced cracking 78—76735
- steel, alloy, maraging 250 grade, hot isostatically pressed powder, Ti segregation embrittlement 78—52925
- steel, alloy, Ni-Cr-Mn, type 4340 intergranular brittle fracture, exam. by impact testing and Auger spectroscopy 78—52978
- steel, alloy, Ni-Cr-Mo-V, exam. of temper embrittlement susceptibility 78—76737
- steel, alloy, temper embrittlement, comp. influence 80—66658
- steel, alloy 10G2S1 welds, fracture, subjected to low-temp. fatigue 80—89350
- steel, alloy low, Ni-Cr, tempered martensite embrittlement 80—7669
- steel, austenitic, high content of low melting additives, high temp. neutron irradiation embrittlement *(Russian)* 79—73218
- steel, austenitic stainless, embrittled by α-particle irrad. 77—69015
- steel, austenitic stainless, embrittlement by He in ^3H handling facilities 80—102285
- steel, austenitic stainless, temper embrittled, type 304, Auger spectroscopic exam. of grain boundary surface phases 78—76741
- steel, austenitic stainless, tensile stress effect on He bublbe growth 79—87684
- steel, austenitic type 304, temper embrittlement and surface segregation an AES and ionization loss spectroscopy study 79—43372
- steel, C, tempered martensite embrittlement, and retained austenite, exam. 78—56754
- steel, C-Mn elevated temp. embrittlement under impact loading 77—44366
- steel, cast automatic couplings, yield strength, crack propag. resistance and ductile-brittle transition temp. 80—104281
- steel, continuously cast, segregation at halfway cracks 80—60869
- steel, Cr, brittleness onset during high-temp. tempering *(Russian)* 77—81276
- steel, Cr, ferritic, N_2 effect on 475°C embrittlement 79—83313
- steel, Cr-Mo (2.25, 1.0 wt.%), temper embrittlement, effect of P, Sn, comp. and carbide precip. 80—85036
- steel, Cr-Mo (2.25, 1.0 wt.%), temper embrittlement, effect of Mn, Si, comp. and carbide precip. 80—85037
- steel, Cr-Mo (2.25, 1 wt.%), temper embrittlement trace elements, Mo, intercritical heat treatment effects 77—36634
- steel, Cr-Mo (3 wt.%), temper embrittlement 77—36647
- steel, Cr-Mo weld metal, trace element embrittlement suppression by creep strength effects 80—66656
- steel, Cr-Mo-(Ni-V), temper embrittlement by P and Sn, effect of rare earth additives 79—61721
- steel, Cr-Mo-V low-alloy, high-temp. ductility and crack growth, impurities effect 80—66652
- steel, Cr-Mo-V low-alloy, prior austenite grain boundary embrittlement by B 80—66657
- steel, Cr-Ni, microstruct. effect on temper brittleness *(Korean)* 79—70092
- steel, Cr-Ni (2.25, 1 wt.%), role of Mo in P-induced temper embrittlement 80—35316
- steel, Cr-Ni-C (3, 1, 0.6 wt.%), grain boundary sulphide precip. and hot ductility *(Japanese)* 80—71654
- steel, Cu, fission reactor vessels, neutron embrittled, exam. of technique for in situ thermal annealing 79—29114
- steel, effect of B on radiation embrittlement 78—691
- steel, embrittlement by impurity segregation 79—8367
- steel, failure and radiation damage *(Czech)* 80—619
- steel, ferritic, Cr-Mo (18, 2 wt.%), cold work effect on 885°F embrittlement 77—77499
- steel, ferritic, impurity defect interaction influence on radiation hardening and embrittlement 80—35199
- steel, ferritic stainless, embrittlement 80—85041
- steel, heat-treatment furnace trays, in service embrittlement, microstruct. and props. changes 77—63784
- steel, heating effect on phase composition, microstruct. and mech. props. 80—100859
- steel, high strength, 300-M, slow fatigue crack growth, threshold behaviour, temper embrittlement, impurity segregation effects 77—86152
- steel, high strength weld metal, fractography, microstructure and reheated zone toughness effects *(Japanese)* 80—108543
- steel, hot shortness, high-temp. embrittlement, residual and trace elements influence 80—66644
- steel, intergranular fracture, impurity effects 77—8842
- steel, low alloy, 15Kh2MFA and 15Kh2NMFA, neutron irrad. embrittlement, effect of P, Sb and Sn impurities 80—85055
- steel, low alloy, H_2S susceptibility, alloying effect 79—91797
- steel, low alloy, quenched, tempered martensite embrittlement, role of retained austenite and cementite 79—74251
- steel, low alloy, radiation embrittlement, heat treatment effects 78—19893
- steel, low alloy, reactor pressure vessel, effect of Mn and C content on irrad. response 79—20196
- steel, low alloy, rel. between over-heating embrittlement and behaviour of S, Auger spectroscopy anal. *(Japanese)* 79—79088
- steel, low alloy, temper embrittlement, review 79—20154

embrittlement continued
- steel, low alloy, temper embrittlement and ternary equilib. segregation 80—60958
- steel, low alloy, tempered martensite embrittlement and crack initiation *(Japanese)* 79—66149
- steel, low alloy, tempered martensite embrittlement mechanisms 79—8351
- steel, low alloy, type 10KhN1M, heat-treated, struct. and resist. to thermal embrittlement 79—15788
- steel, low alloy and C, reversible temper brittleness kinetics *(French)* 78—35498
- steel, low alloy Mn-Sb(2, 0.12 wt.%), reversibility of temper embrittlement, studied by XPS and AES 77—32667
- steel, low alloy structural, heat treated, impurities effect on embrittlement susceptibility and temper brittleness 79—38955
- steel, low C, martensitic, fracture toughness variations during tempering 78—60812
- steel, low C, stress ageing embrittlement under short term thermally stressed cycle *(Russian)* 80—60885
- steel, low C Cr-Ni, temper embrittlement by antimony, Ti addition effects 77—32683
- steel, low C Mn-V, VC effects on strength and brittleness 77—70055
- steel, low-alloy, impurities, segregation and creep embrittlement 80—66653
- steel, low-alloy structural, radiation hardening, rel. to embrittlement *(Russian)* 77—21243
- steel, machining, 12L14, effect of Pb and Te on hot-shortness mechanism 80—104190
- steel, maraging, N12K6M5TYu, fracture, influence of high-temp. thermomechanical treatment on characts. *(Russian)* 78—27591
- steel, maraging, Ni (18 wt.%), grain boundary precipitation, scanning Auger electron obs. 78—3132
- steel, maraging, thermally embrittled, TiC precipitation 77—25055
- steel, martensitic, Cr (12 wt.%), temper embrittlement 79—87722
- steel, martensitic 12% Cr, temper embrittlement 80—66650
- steel, martensitic stainless, type 05Kh13N4m, strength and embrittlement, early stages of martensite decomp. effect 80—35227
- steel, medium C, shell-shaped fracture due to B embrittlement *(Chinese)* 80—55493
- steel, mild Cr welding, 550°-850°C heating effects on structure and toughness 79—24540
- steel, mild type ASTM A36, Cl embrittling effect on fatigue crack growth rate 79—74254
- steel, Mn-Mo-Ni, embrittling effects of residual elements 80—66655
- steel, Mn-Ni-Mo, PWR pressure vessel, irrad. induced embrittlement, chemical composition effect *(French)* 79—20195
- steel, neutron irrad., additivity deviations in thermal and radiation induced embrittlement 77—73348
- steel, Ni, cryogenic fracture toughness enhancement through grain refinement 77—36651
- steel, Ni (3.5 wt.%), heavy rotor forgings, temper embrittlement, metallurgical investigations *(German)* 80—16471
- steel, Ni-Co-Mo-Ti, microfractographical features, embrittlement and grain size influence on fracture behaviour *(German)* 80—30053
- steel, Ni-Cr, (4,1, wt.%), isothermal embrittlement, AES exam. of grain boundary segregation 78—60814
- steel, Ni-Cr, cast, tempering embrittlement due to impurities, Auger spectroscopy exam. 80—11683
- steel, Ni-Cr, P doped, tempered martensite embrittlement 80—30089
- steel, Ni-Cr, P induced temper embrittlement, Mo effect 77—86148
- steel, Ni-Cr, temper embrittled, electron microscope and X-ray microstruct. obs. 79—38870
- steel, Ni-Cr, temper embrittlement, intermediate tempering treatments 80—60944
- steel, Ni-Cr, temper embrittlement by Sb, Ni, Cr effects 77—36628
- steel, Ni-Cr, temper embrittlement by Sn 77—86149
- steel, Ni-Cr low alloy, effect of Mo on tempered martensite embrittlement 80—3187
- steel, Ni-Cr temper embrittlement by P 77—40448
- steel, Ni-Cr-Mo-U, ferritic, B segregation and high temp. embrittlement 78—7040
- steel, Ni-Cr-P (0.06 wt.%), influence of intercritical heat treatment on temper embrittlement susceptibility 78—52863
- steel, Ni-Mo-Cr, embrittling effects of residual elements 80—66655
- steel, Ni-Sn, temper embrittlement, interaction detect. by Mossbauer spectroscopy 77—86176
- steel, nuclear reactor press. vessel, radiation induced embrittlement, slow neutron small angle scatt. study *(German)* 77—34390
- steel, rail, toughness, effect of Sn, SEM exam. 80—97569
- steel, rotor, Ni-Cr-Mo-V, reversible temper embrittlement 77—36656
- steel, SHE 4340, tempered martensite embrittlement 80—30084
- steel, stainless, 15Kh25T, embrittlement at 400 to 550 degrees C, grain size and cooling rate effects 78—44203
- steel, stainless, 316, neutron irradiation embrittlement, pre-irradiation treatment and composition modification 80—3171
- steel, stainless, Cr-Ni-Nb stabilised, Te vapour effect on creep and tensile props. 79—24583
- steel, stainless, due to soldering with Cu alloy solder, effect of alloying additions 79—47773
- steel, stainless, ferrite to austenite decomp. 80—93554
- steel, stainless, ferritic, Cr-Mo-Ni (29,4,2 wt.%) 77—44276
- steel, stainless, ferritic, subjected to 475°C embrittlement, exam. of fracture toughness 78—84982
- steel, stainless, ferritic and duplex, Mossbauer effect study of 475°C embrittlement 78—52933
- steel, stainless, fusion reactor He embrittlement simulation, splat cooling in development of B doping 80—30072
- steel, stainless, He cavitation, rel. to TiC precipitation 80—45399
- steel, stainless, He ion irrad., fracture behaviour, in-situ HV electron microscopy 80—29089
- steel, stainless, Kh25T, impact strength and substructure produced by deform. during cold rolling *(Russian)* 79—24535
- steel, stainless, maraging, high strength, exam. of ageing embrittlement *(Japanese)* 78—84972
- steel, stainless, maraging, type 03Kh11N10M2T2, exam. of thermal embrittlement 78—84986
- steel, stainless, maraging, type 03Kh11N10M2T, exam. of thermal brittleness 78—88526
- steel, stainless, maraging high strength, embrittlement on low temp. ageing *(Japanese)* 79—100155

embrittlement continued
- steel, stainless, martensitic, crack resistance of type VNS-2, heat treatment effects 79—100196
- steel, stainless, two phase, variation of tensile and impact strength with heat treatment 79—34085
- steel, stainless, type 316, microstruct. changes in creep ductility, SEM, TEM, optical microscopy and X-ray diffr. study 79—38927
- steel, temper control progress 78—72797
- steel, temper embrittled, grain boundary failure model for intergranular fracture modes 80—25825
- steel, temper embrittlement, effect of sp-3d impurity interactions on resistivity 79—46696
- steel, temper embrittlement, fracture mech. of grain boundary segregated phases 78—48531
- steel, temper embrittlement and embrittling intergranular segregates, Mo effects *(French)* 79—91788
- steel, tempered martensitic, type AISI 410, role of C in embrittlement phenomena 80—93652
- steel, tool, maraging, based on N12M10, exam. of hardening, crack resistance and wear *(Russian)* 79—34047
- steel, type 08Kh15N5D2T, high temp. embrittlement *(Russian)* 79—70153
- steel, type 316 stainless, Neutron irradiation using HFIR for evaluation as fusion reactor material 78—13324
- steel, ultra high strength, P induced 350°C embrittlement 79—57099
- steel, W, high C, amorphous, rapidly quenched from melt, mech. and thermal props. 79—38874
- steel 30khGSNA, low alloy, quenched, grain refinement influence on impact strength *(Russian)* 80—20974
- steel for nuclear reactor press. vessels, criteria for brittle fracture, neutron effects *(German)* 77—34389
- steel Ni-Cr, Sb doped, temper embrittlement susceptibility, intercritical heat treatment effect 78—64570
- steel pearlitic, statistical anal. of joint effect of Ni, Cu, P on irradiation embrittlement 78—71770
- steels, solute segregation and intergranular fracture 80—60957
- steels, stainless, embrittlement at temp. of 475°C 78—31503
- steels for nuclear reactor pressure vessels, neutron irrad. embrittlement, temp. effects, annealing *(German)* 77—34384
- strain ageing effect on strength and toughness, susceptibility to strain hardening 79—57028
- surface science in metallurgy, review 79—42388
- temper embrittlement kinetics, ternary and binary alloys, computer simulation 78—84953
- thermoplastics, glassy, embrittlement mech. and inelastic deform. criterion for delayed failure 78—52940
- transition metal amorphous alloys with metalloid elements, embrittlement/crystn. relationship *(Japanese)* 79—96134
- TZM-Mo alloy, mech. props., effect of exposure to high temp. He containing O_2, room temp. study 80—93639
- Zircaloy cladding, embrittlement and failure during reactor power-cooling-mismatch 78—21688
- Zircaloy fuel cladding, O embrittlement obs. 78—89947
- Zircaloy-2, Cd metal embrittlement in 300-340°C 77—16747
- Zircaloy-2, reversible embrittlement in CH_3OH/HCl 79—91833
- Ag, gas bubble embrittlement mechanism 78—60824
- $AgCl:Li^+(Na^+)(K^+)(Rb^+)$, impurities effect on plasticity, brittleness 78—14398
- Al-Cu alloy bicrystals, neutron irrad. effects on grain boundaries, intergranular fracture and precip. 77—48520
- Al-Cu-Mg-Li alloy extrusions, microstruct., embrittlement and fracture props. 80—60965
- Al-Mg_2Si (0.95 wt.%), excess Si effect on ductility 78—27580
- Al-Mg-Bi -Na, Bi additions to prevent Na embrittlement 77—86153
- Al-Mg-Ti(Zr), struct. and factors determining brittle intermediate compound form. 78—52817
- Al-Pb(Bi)(Cd), containing low melting point inclusions, impact props., temp. depend. 78—60792
- Al-Zn-Mg, crack-arrest markings on integranular stress corrosion fracture surfaces 80—89405
- Al-Zn-Mg, duplex ageing effect on tensile props. 79—91721
- Be, brittle-ductile transition, intergranular embrittlement *(Russian)* 78—3208
- α-brass, solid soln., ductility, comp. effect *(Japanese)* 79—43334
- CC TaC based hard metal, non-stoichiometric sintering, mech. props. 80—25616
- Ci-Bi (0.0115 wt.%), fracture paths, TEM study 79—27998
- Co-Ni-Mo-C, amorphous alloys, med. props. and thermal stability *(Japanese)* 80—85049
- Co-Si-B, embrittlement by crystallisation *(Japanese)* 78—48513
- Cr-Y_2O_3 dispersion hardened, oxidation and nitridation resistance, embrittlement 78—44267
- Cu polycrystals, Bi segregation embrittlement 79—83318
- Cu-Bi (0.02 wt.%) alloy, intergranular fracture, Kossel X-ray diffr. in SEM obs. 80—108579
- Cu-Bi alloys, embrittled grain boundary obs. using STEM, Cu-SiO_2 comparison 78—38730
- Cu-Bi-Fe, Fe effects on embrittlement 77—28900
- α-Cu-Ni-Zn-Pb, fire cracking, effect of pores and impurities 79—29207
- α-Cu-Zn(Al), solid soln., intermediate temp. embrittlement *(Japanese)* 79—20158
- $CuAl_2$, single cryst., embrittlement and subboundary hardening via interstitial segregation *(Russian)* 77—12679
- $Cu_{56}Zr_{44}$ metallic glass, devitrification and its effect on mech. props. 80—33893
- Fe, Armco, texture role in prestrain embrittlement 78—60796
- Fe, cast, Si, ferrite heterogenisation, phase separation and embrittlement, Si effects 79—96125
- Fe, diffusion and solid solubility of Sb, 773-873K, ion backscatt. anal., rel. to intergranular embrittlement 78—71880
- Fe, hot shortness, high-temp. embrittlement, residual and trace elements influence 80—66644
- Fe, nitrogen, impurity defect interaction influence on radiation hardening and embrittlement 80—35199
- Fe, polycrystalline, fracture surface singularities under single loading conditions *(Russian)* 80—50696
- Fe-Co-Mo-C, amorphous alloys, med. props. and thermal stability *(Japanese)* 80—85049
- Fe-Cr (25wt.%), continuously cooled, embrittlement 77—36636
- Fe-Cr (26 wt.%) effect of Ni content and austenite phase, on low temp. toughness and embrittlement 78—60754

embrittlement continued
Fe-Cr-Co, ductile magnet alloys, mech. props. 80—85001
Fe-Cr-Co-V-(Ti) hard magnets, V and V-Ti effects on mag. and mech. props. 79—91810
Fe-Cr-Mo, (30,2 wt.%) Bridgman-type, unexpected embrittlement phenomena, hydrostatic tensile test *(Japanese)* 80—55517
Fe-Cu (0.34 wt.%), neutron irradiated, field-ion microscope detection of ultra-fine defects 79—42116
Fe-Cu-Ti, improvement of irradiation-enhanced Cu embrittlement by Ti addition 79—43393
Fe-Mn 8%, type K1525 thermal cycling, effect on impact toughness 80—7608
Fe-Mn (8 wt.%), quenched, exam. of intergranular embrittlement 78—76745
Fe-Mn (8.25 wt.%), irreversible temper embrittlement, Mossbauer spectra, impact strength depend. on interstitials *(German)* 79—74235
Fe-Mn-B, B effect on intergranular embrittlement 80—108555
Fe-Ni (3 wt.%), grain boundary segregation of Sn and P embrittling additions, STEM microanal. 78—76654
Fe-Ni (3 wt.%), influence of temper embrittlement, on stress corrosion susceptibility 78—85023
Fe-Ni (3 wt.%) alloys, microanalysis of grain boundary segregation using STEM 78—35633
Fe-Ni base metallic glass, annealing embrittlement 78—64635
Fe-Ni-C, intercrystalline embrittlement in tempered martensite, elimination by reaustenitization *(Slovak)* 80—108548
Fe-Ni-Mn, martensite, aged, grain boundary embrittlement 79—96144
Fe-Ni-Mo-C, amorphous alloys, med. props. and thermal stability *(Japanese)* 80—85049
Fe-P (0.14 wt.%), cavity formation at grain boundary-subboundary interactions 77—86040
Fe-P-C, embrittlement by crystallisation *(Japanese)* 78—48513
Fe-Si-B, embrittlement by crystallisation *(Japanese)* 78—48513
Fe-Sn, grain boundary embrittlement by Sn segregation, Mossbauer study 80—7239
Fe_{40} $Ni_{40}B_{20}$, amorphous alloy, ductile-brittle transition temp., relation to composition 78—52972
$(Fe_{100-x}Ni_x)_{100-y}B_y$, metallic glass, embrittlement and crystn. 80—7685
$Fe_{40}Ni_{40}B_{20}$, metallic glass, embrittlement kinetics and crystn., quenching influence 78—68766
$Fe_{40}Ni_{40}P_{20}$, amorphous alloy, ductile-brittle transition temp., relation to composition 78—52972
$Fe_{40}Ni_{40}P_{14}B_6$, amorphous alloy, ductile-brittle transition temp., relation to composition 78—52972
$Fe_{40}Ni_{40}P_{14}B_6$, amorphous, annealed and unannealed, temp. depend. of flow stress and ductility 79—29119
$Fe_{40}Ni_{40}P_{14}B_6$ amorphous alloy, temper embrittlement 80—76295
$Fe_{40}Ni_{40}P_{14}B_6$ glass, positron lifetimes in as-received, cold-rolled, embrittled and crystallized samples 79—74177
$Fe_{40}Ni_{40}P_{20-x(B)}B_{x(B)}$, ferromagnetic metallic glass, thermal and mech. stability 77—66698
$Fe_{83}P_{17-x(B)}B_{x(B)}$, ferromagnetic, metallic glass thermal and mech. stability 77—66698
Mg-Ni-S, electroforming, mech. props. rel. to heat treatment 80—35133
Mo alloy, long-term ageing effects on ductility and microstruct. 77—44348
Mo, mech. props., effect of exposure to high temp. He containing O_2, room temp. study 80—93639
Mo, neutron irradiation effects on microcracks *(Ukrainian)* 79—77639
Mo-O system, grain boundary segregation and intergranular fracture 80—55516
Mo-O-C system, grain boundary segregation and intergranular fracture 80—55516
Mo-Ti-La-C, influence of high pressure on mech. preps. after nitriding *(Russian)* 79—57137
Mo-Zr-B alloy, neutron irrad. at 780-1080°C, porosity, hardening and embrittlement *(Russian)* 80—29062
Nb alloys, long-term ageing effects on ductility and microstructure 77—44348
Nb, neutron irrad., yield stress, fracture stress and strain *(Japanese)* 77—76472
Nb, oxidation in imperfect vac., solute O_2 level change and ductility loss 79—52452
Nb, slow strain rate embrittlement by O_2 77—28902
Ni-Be (2 wt.%), high-temp. radiation embrittlement, mechanical tests and TEM *(Russian)* 77—44331
Ni-Cr, heat-resist., high-temp. ductility and embrittlement 80—76314
Ni-Si-B, amorphous, thermal stability of ductility 80—76327
Ni-Si-B, embrittlement by crystallisation *(Japanese)* 78—48513
Ni_3Sn_2, single cryst. embrittlement and subboundary hardening via interstitial segregation *(Russian)* 77—12679
Pt crucibles, surface changes rel. to Fe anal. 80—61192
Pt-Rh-W (30, 8 wt.%), intergranular embrittlement by Se vapour 80—3185
S-metal interactions 80—55710
Sn, binding state of atoms segregated at boundary of Fe and Fe alloys, Mossbauer study 80—7232
steels, Cr-C-Mn(Ni), struct. prop. rel., design of struct. steels for high strength and toughness 80—97491
Ta, evidence for slow strain-rate embrittlement due to O_2, SEM study 79—79109
Ta-W-Hf, embrittlement, effect of composition 77—21247
Ti alloys, 685 and 6242, creep resist. and thermal stability in air and in vac., role of Si 80—30020
Ti and Ti alloys, struct. sensitivity of mech. props., alloying influence *(Russian)* 79—47748
Ti-Al-Sn-Cu-Zn, (5, 2.5, 3, 1.5 wt.%), embrittlement after high temperature long-time exposure *(Chinese)* 78—95792
Ti-Al-V-Sn (6,6,2 wt.%) solid metal embrittlement by Cd, Ag and Au 80—16551
αTi-Al-(Zr), embrittlement due to ageing 78—56673
Ti-Nb superconducting composite in Cu matrix, low temp. effects in ductility 79—57119
Ti-O, stress corrosion crack propag. in aqueous and methanolic soln. 78—19919
U-Mo (10 wt.%), gaseous O_2 and hydrogen embrittlement, exam. 78—60811
V and V-Mo, mechanical properties, O, N_2 and C addition effects 79—52356
V, oxygen impurity defect interaction influence on radiation hardening and embrittlement 80—35199

embrittlement continued
V, polycryst., O_2 effects on strength and ductility 77—36529
V-Si, strengthening by internal oxidation 80—55424
V-Zr, strengthening by internal oxidation 80—55424
W, polygonisation critical stage in single crystals deformed in compression 79—4979
W-Cu (92.8, 7.2 wt.%), liq.-phase sintered, embrittlement and interfacial impurity segregation 80—66647
W-Ni-Fe(Cu), liquid phase sintered, interfacial embrittlement 79—57101
Zr-Nb (2.5 wt.%), nuclear fuel channels, neutron effects on ultimate fracture strength, 293 to 573K 80—85054

e.m.c. *see electromagnetic compatibility*

emergency power supply
nuclear power plant, class 1E auxiliary power systems, degraded or loss of voltage protection 79—45363
nuclear power plants, safety 80—52762
nuclear power stations, IAEA nuclear safety standards program for protection, electric, instrumentation systems 79—45365
Li long life battery systems, standby power for data retention in volatile memory systems, selection criteria 80—61337
$Li-H_2O_2$ reserve power system, 600 kWh 79—48104
Ni-Cd batteries for standby power systems 80—104500
Ni-Cd system, characteristics and new developments for telephone industry applications 80—55829
Pb acid battery plants, current and future trends, telecommunications emergency power supply 80—61333
Pb-acid 'G-cell', construction and design and performance charact. for UPS systems 80—61335
Pb-acid storage batteries for uninterrupted power supply appls. 80—61334
Pb-acid system, characteristics and new developments for telephone industry applications 80—55829

e.m.f. *see electric potential*

emission nebulae *see nebulae*

emission spectra *see spectra*

emissivity
see also brightness
3 mm wavelength scattering and emission characteristics of natural media 78—3770
absorbing substances, optical consts. determ. at elevated, rel. to polarised components of emissivity *(Russian)* 77—90122
alkali metal halides, far IR emission, cryst. and melt 77—51527
alloys, oxidised, heat resistant, radiation emission props. depend. on oxidation conditions 77—43358
angular and overall emissivities for halfspace geometry, variational procedure 78—87245
apparatus for measurement 77—45844
atmospheric emissivities in tropics 79—29859
atmospheric IR properties relevant to building envelope heat losses 80—58895
atmospheric radiative flux, IR cooling rates, study of dust layer regions 78—88886
atmospheric thermal plasma, continuous emission, ionisation potential lowering and total excitation cross section 80—38705
average emissivity of various shaped volumes 77—46897
baffled blackbody diffused cavities, integrated emissivity, precise calc. 80—96180
biomedical temp. measurements, radiation balance microwave thermograph, simultaneous independent temp. and emissivity measurements 79—100692
black body monochomatic emissive power, fast calc. by nomograph 78—22257
black body radiation, photon occupation numbers 79—88869
'blackbody' IR sources 78—83059
blackbody cavities, directional emissivity calc., Monte Carlo method 80—83729
blackbody spectrum, interpretation of quantum theory, for teaching 78—54130
blackened optical surfaces, IR absorpt. rel. to stray light reduction, spectral emittance meas. 79—61449
building envelope heat radiation losses and countermeasures 80—58894
butane, total emissivity, press. depend. 78—90673
calorimetric technique for meas. total emissivity of solids and coatings at low temp. 80—17941
cellular anti-loss struct. as solar absorber, emittance distrib. at cell walls *(French)* 77—14890
chalcogenide glass, radiative emission during threshold ON-state 78—76119
characteristics expression, effective temperature *(Japanese)* 80—43602
cholesteric liquid crystal on Al evaporated surface, thermal emissivity study *(Japanese)* 77—35732
cholesteric liquid crystal semitransparent and opaque films, thermal emissivity 79—7703
cirrostratus clouds, IR emissivity meas. by remote sounding 80—82061
cirrus clouds, IR emissivity calc. from lidar and radiometer meas. 80—82060
clouds, IR emissivity in 10.5 to 12 μ band *(Russian)* 77—49167
coatings, enamel (lacquer), integrated hemispherical emissivity, bulk expt. investig. 80—19970
coatings used in industry, monochromatic emissivity in 2-25 μ range at 100 to 400°C 77—11714
colour temperature of hot bodies, exact eqns. 77—35024
conical cavity, local effective emissivity, analytic approx. soln. 80—23874
crystal, internal radiation spectral composition at high temp., energy transfer and thermionic emission 77—43359
crystalline material optical absorption meas. 80—105718
cylinder row systems, variation of heat transfer characteristics with number of rows 78—9552
cylindrical volume radiator, automatic Abel inversion, optical system 77—39040
determination from thermal rad. spectrum and optimal methods of opt. pyrometry 78—24797
diatomic gases, emissivities calc. 78—90675
dielectrics, surface heating by laser, optical temp. meas. 79—55911
diffuse wall cavity, radiation pattern, nonuniform temp. and emissivity 77—80053
dual-channel ratio thermograph counteracting skin emissivity errors 77—40892
Earth IR emission, Lambertian, of spherical surface, radiation press. on satellite *(French)* 78—81529

emissivity continued
  Earth surface, microwave emissivity remote sensing by NIMBUS-6 80—98485
  fibrous materials, IR emittance 79—95189
  fog, thermal emissivity 80—95795
  Fresnel's relations in IR, verification and determ. of emissivity and compound index *(French)* 80—84309
  galactic disc, bremsstrahlung gamma radiation emissivity and local interstellar electron spectrum 79—25417
  galactic halo, low-freq. radio emissivity rel. to electron diffusion models 78—12433
  gas, data extrapolation method 77—7506
  gas, measurement by rotation of spectral lines, optical system *(Russian)* 77—53913
  glass, IR emissivity calc., strongly absorbing media surface refl. 80—107452
  glass, thermal radiative properties from 0.32 μm to 206 μm 79—69268
  glass, thermophysical props., temp. wave methods 80—24624
  graphite, porous, heating in air atmosphere, spectral emissivity 80—19969
  graphite Knudsen cells heated by radiation, emissivity *(Japanese)* 80—13073
  gravity glass, IR emissivity, 673-1673K 80—24623
  grey cavity, apparent emission and absorpt. factors *(French)* 78—30168
  heat-radiating coatings with variable degree of blackness, efficiency 77—28027
  high temperature, measurement of small specimens of metals, alloys, structural materials appl. 79—7281
  hot solid surface, emissivity determ. by spectral method *(Russian)* 78—10200
  ionic crystallite, on substrate, IR active modes 77—1667
  IR effective emissivity meas. by natural cooling *(Japanese)* 78—29117
  IR emission spectra, during crystn., distinguishing features 80—1952
  IR emissivity meas. method and equipment 79—35812
  IR imaging systems, sensibility equation modification *(Chinese)* 80—102806
  IR radiometric meas. of object true temp., emissivity effects 77—57326
  isothermal isotropically scattering medium, influence of substrate props. on apparent emittance 77—80056
  junction device, injected carrier detect. by IR emission 79—38151
  laser modulated particulate incandescence effects in Raman scatt. diagnosis 78—20117
  liquids, opaque and diathermanous, total normal emissivity meas. at high temp. 80—102965
  measurement, emissometers refl. errors elimination by use of alternate apertures 77—10089
  measurement by thermoreceiver/gas heat exchange 77—22552
  measurement for low temp. sources, flux double modulation method 78—45634
  measurement for partially transparent materials to thermal radiation, high speed spectrometric method 79—7280
  measurement in far IR by modified Fourier spectrophotometer 77—45900
  measurement techniques for small absorpt. coeffs., using transmission, emittance and calorimetry 78—24839
  measurement using IR thermography *(French)* 80—103507
  metal, emissivity angular dependence, meas. in IR spectral region 80—34214
  metal, interference phenomena and integral emittance, during high temp. oxidation *(Russian)* 78—91458
  metal, optical props., high-temp., from emissivity ang. depend. data 78—39519
  metal, radiation characts. estimation, classical electron theory *(Russian)* 78—38859
  metal, true temp. meas. using optimal photoelectronic pyrometer 80—52223
  metal radiative characteristics, EM theory of radiation 79—7704
  metal surface, rough, hemispherical emittance 80—70434
  metal surface, thermal radiation 79—28114
  metal-insulator composite solar selective absorbers optical props. 79—52037
  metals and alloys, emissivity determ. using low-inertia opt. dilatometry 80—59684
  meteors, luminous efficiency coeff. from photographic obs. 78—96440
  methyl polymethacrylate, heat emission coeff. and cooling const., Angstrom periodic heat wave method 77—72706
  microwave radiometric methods and the problem of forest and peat fires 80—31877
  multiwavelength radiation pyrometry where reflectance is measured to estimate emissivity 80—31757
  nebulae, dusty, emissivities of non on-the-spot (OTS) models 78—85995
  nebulae, gaseous, third period elements photoionisation models and emissivity ratios 80—46640
  nonferrous metals, integral degrees of blackness 77—35725
  ocean surface, 10.5-12 μm emissivity vars. *(Russian)* 77—60384
  ocean surface, microwave thermal radiation and radiometry appls. 78—81415
  olivine, optical absorpt. spectra and radiative heat transport at high temp. 79—79818
  opaque, semitransparent materials, Kirchhoff's second law, role of reflection or diffusion *(French)* 79—36835
  oxide ceramics, thermal conductivity and emissivity at high temp. 77—28051
  p-n junctions, determ. of doping levels using nondestructive IR emission meas. 78—95338
  paint coating directional emissivity, thickness and substrate effect, light scatt. theory 80—33437
  particles, small, spherical, reformulation of radiation laws 78—87246
  photometric terminology for refl., transmission, scatt. and emission 77—74477
  polar crystals, gravitational wave induced IR emission 77—45769
  propane, total emissivity, press. depend. 78—90673
  pyrographite, IR spectral emissivity at high temperatures 80—103505
  pyrometers, two-colour, modification of emissivity response 79—93142
  radiation temperature, reflectivity, emissivity meas. of room temp. materials *(Chinese)* 80—101814
  radiative transfer between surfaces in diathermal medium, radiation anisotropy modelling 80—33435
  randomly inhomogeneous stratified media, thermal radiation calc., appl. to Earth surface *(Russian)* 78—96312

emissivity continued
  rarefied gas, convective heat transfer coeff. and surface emissivity, effect of degree of vac. 78—1693
  refractories, integral degrees of blackness 77—35725
  refractories, integral radiant capacity, calorimetric meas. method 80—65259
  refractories, spectral emittance meas. system at temp. up to 3000°C 77—22550
  rough surface, energy conservation for refl. and transmissivity 80—53188
  sapphire thermophysical props., temp. wave methods 80—24624
  schist containing clay and sand, integrated normal emissivity with low heat conductivity coeffs. 80—103504
  schist dust, integrated normal emissivity with low heat conductivity coeffs. 80—103504
  selective surface, thermal emissivity 80—7953
  semi-infinite scattering medium with refr. index greater than unity, directional emittance 79—94471
  semiconductors, temp. determ. by IR thermometry *(Spanish)* 80—47062
  semitransparent filled polymer coating, thermal radn. characts. 77—35731
  semitransparent medium, effect of radiation heat transfer in thermal cond. meas. 77—23858
  skin, effect of obliquity in clinical thermography 77—9286
  skin, influence of cosmetics and ointments on spectral emissivity 77—9285
  solar absorber, high temp., spectral selectivity, thermal emissivity calc. 80—61403
  solar absorber coatings, thermal emittance, optical technique for meas. *(Spanish)* 80—16835
  solar absorbing layers, IR spectral emittance profiles 78—25955
  solar collector DC reactively sputtered metal carbide and silicide selective surface props. 79—62029
  solar energy collection, selective surface design 79—52956
  solar energy materials, transparent, optical characts. investigation 80—20724
  solar materials radiation properties study, wide temperature range 79—94307
  solar photothermal non-selective and energy control films coatings 80—26157
  solar selective absorber coatings, reflectance, emittance, and thermal stability 80—12027
  solar selective surface absorption and IR emissivity calorimetry 79—62098
  solar-selective coatings on flat sheet, hemispherical emissivity measurement using novel calorimeter 79—80621
  solid, calorimetric method for emissivity determ. 78—62201
  solid thermophysical properties at high temp., conference, Moscow, USSR (May 1976) 77—28012
  source gas at 1273K, IR spectral radiance through atm. path 77—9493
  spectral emissivity measurement device, high-temp. materials 80—37039
  sputtered metal silicide solar selective absorbing surfaces 78—52671
  steam, total emissivity, press. depend. 78—90673
  steel, rimming, cold rolled, low alloy, radiation capacity *(Russian)* 78—14486
  steel, stainless, AISI 304, temp. variation of total hemispheric emissivity 80—15271
  steel, stainless, emittance, oxidation and surface roughness effects 80—96673
  steel, stainless, emittance meas. rel. to surface roughness parameters 80—100342
  steel, stainless, hard, and mild, optical constant dispersion and emissivity, up to 900K 78—52464
  steel, stainless, type 304, surface condition effects on IR absorptivity 79—56754
  steel, type Kh23N18, integrated normal emissivity with low heat conductivity coeffs. 80—103504
  steel stainless, solar energy collector optical props. rel. to heat treatment 78—94455
  Stefan's law, W filament elec. lamp, student expt. 78—54125
  surface emittance, determ. total hemispherical calorimetric emissometer 80—86309
  surface temperature meas. through radiance temp. and emissivity, algorithm for calc. 80—52209
  temperature fields, local equilib. in emissive medium, reconstruction 79—41874
  terrestrial surface, emissivity correction for thermal radiation interpretation 80—82092
  thermal radiation property meas. of materials 80—96181
  thermal radiation radio sources, magnetoionic modes emissivities rel. to polarisation *(Russian)* 77—91656
  thermal radio emission from exponential slab, sea ice appl. 78—28244
  thermal radio emission polarimetry, loss matrix 79—21069
  thermoelectrodes, test method 77—89556
  Tokamak, enhanced plasma-frequency radiation *(Chinese)* 80—59185
  transition metal, normal total emittance at 400 to 850K and normal spectral reflectance at room temp. 77—20813
  transition metal spectral emissivity variation with temp. *(Japanese)* 79—1517
  transition metals, temp. depend. 80—10688
  two-phase inhomogeneous media of cylindrical geometry 79—23377
  vapour pressure meas. up to 5000K, pyrometric-laser heating technique 77—1239
  water, characteristic IR emission due to latent heat of transform. 77—31754
  water droplet, IR emissivity 80—36394
  water pollution, dielectric props. and determ. of microwave emissivity 80—101142
  water vapour, data extrapolation method 77—7506
  water vapour, simple parameterisation 77—42958
  Ag, 335-1100K, polishing effect 77—39682
  Ag, expt. transient technique and theory for foils 78—43353
  Ag, total hemispherical emissivity meas. by temp. decay method 78—26708
  Al, 140-300K 77—35729
  Al, 335-1100K, polishing effect 77—39682
  Al, expt. transient technique and theory for foils 78—43353
  Al film, strips, thermal emissivity, appl. of distant-focused IR radiometer system 77—169
  Al, film integral radiation ability determ. by electron diffr. *(Russian)* 80—54413

emissivity continued
Al, total hemispherical emissivity meas. by temp. decay method 78—26708
Al, vacuum deposited, solar radiation props., grey-reflector appl. 77—20098
Al-PbS selective surfaces for solar photothermal conversion, prep., emissivity, absorptivity 80—12030
Al_2O_3, bed of coarse particles 78—47542
Al_2O_3, molten particles, complex refractive index *(Russian)* 77—55766
Au, emittance, calc. from spectral radiative and reflecting props. 77—35730
Au films, thermal phonon radiation into α-quartz substrates 79—42363
Au, normal spectral emissivity in 1-10 μm range at 100-400°C 77—11713
Au, thermal radiative props. at cryogenic temps., comparison with model predictions 77—15604
$BaSc_2O_4$, synthesis, thermal stability, emissivity, reduction processes 77—8791
$Ba_3Sc_4O_9$, synthesis, thermal stability, emissivity, reduction processes 77—8791
Be, anodised, emissivity, in 400-1000K range on function of oxide layer struct. 77—35726
Be, normal total emittance at 400 to 850K and normal spectral reflectance at room temp. 77—20813
C-H-O(-N) gas mixtures, high temp. emissivity, 4.8 μ region, shock waves 77—76027
CO, emissivity, computer calcs. 77—84386
CO_2, emissibility, correl. for high temp. and large optical thicknesses 77—15156
CaF_2-Ge(Si), cosputtered composite semiconductors, selective solar energy absorbers 79—56876
CdTe, 10.6 μm absorption meas. using thermal emission 77—1649
Ce, normal spectral emittance above 1000K 77—28028
Ce-Cu, liquid, normal spectral emissivity 80—103506
CeO_2-Mo-CeO_2 thin-film selective coatings for solar energy collectors 78—94422
Co, impure, thermal cond., resistivity, total and spectral emissivity, linear expansion coeff., 300-1700K 77—47790
Cr, emissitivty and reflectivity, oxide film thickness effect 79—82364
Cr-Cr_2O_3, black, solar selectivity at average temps. (100 to 250°C) *(French)* 80—55899
Cr-Ni-Ti alloy and steel, emissitivty and reflectivity, oxide film thickness effect 79—82364
Cu, 140-300K 77—35729
Cu, 335-1100K, polishing effect 77—39682
Cu expt. transient technique and theory for foils 78—43353
Cu films, thermal phonon radiation into α-quartz substrates 79—42363
Cu foil, total emissivity meas. by calorimetric technique 80—17941
Cu, liq., normal spectral emissivity meas., 1376 to 1687K 80—10687
Cu mirror, surface defect layer form. on mech. polishing 80—33122
Cu, molten surface layer thickness, emissivity and AES meas. 80—39261
Cu, spherically shaped crysts., surface melting, IR emission obs. 77—20050
Cu surface, total hemispherical emissivity 79—28115
Cu, total hemispherical emissivity meas. by temp. decay method 78—26708
Dy, normal spectral emittance above 1000K 77—4211
Er, normal spectral emittance above 1000K 77—4211
Fe, expt. transient technique and theory for foils 78—43353
Fe, ferromag., spectral thermal emission, partial circular polarisation 78—18806
Fe, ferromag., spectral thermal emission, partial circular polarization 79—23751
Fe, monocryst. and polycryst., thermal emission, magneto-optic circular polarisation obs. 80—70435
Fe, optical constant dispersion and emissivity, up to 900K 78—52464
Fe, polycryst., spectral thermal emission circular polarisation 79—77784
Fe-Cr-Al, blackness change in air, 1-8 micron, 1200°C, film props. depend. 77—66033
GaAs, 10.6 μm absorption meas. using thermal emission 77—1649
H_2O, warm fog and steam clouds, emission spectra variations, evidence for clusters in vapour phase 79—39849
Hf-Zr (3 wt.%), $\alpha \to \beta$ transform. temp. and entropy, emissivity 77—48424
Ir-Rh/Ir alloy, thermocouple, appl. to temp. meas. in atm. press. flame 77—86314
KBr(I), oscillatory and diffusive regime, above and below melting point, IR thermal emission spectra 78—83985
La, normal spectral emittance above 1000K 77—28028
LaB_6, emissivity at 650 nm, 1600 to 2100K 79—90806
Mo and oxide phase mixture CVD films, optical props., solar absorber appl. 77—55844
Mo, integral hemispherical degree of blackness, 1200-3000K 78—43154
Mo, liquid, spectral emissivity and brightness-temp. meas. at MP 77—43356
Mo, porous, high temp. props. 77—11894
Mo-Re, integral hemispherical degree of blackness, 1200-3000K 78—43154
Mo-W, integral hemispherical degree of blackness, 1200-3000K 78—43154
N_2-propane mixture, total emissivity, press. depend. 78—90673
NI dendrites on Al, CVD, selective solar photothermal absorber 78—52683
NaCl-KCl mixture, electrical, electromag., and acoustic props. *(Russian)* 78—30759
NaCl(Br), oscillatory and diffusive regime, above and below melting point, IR thermal emission spectra 78—83985
Nb, integral normal radiating power, high-temp. meas. technique 77—65667
Nb, liq., spectral emissivity and brightness-temp. meas. at MP 77—43356
Nb-Re(Ru)-N system, spectral emissivity, lattice parameter, initial rate of N_2 absorption *(German)* 77—4204
Nd, normal spectral emittance above 1000K 77—28028
Ni, emissitivty and reflectivity, oxide film thickness effect 79—82364
Ni, expt. transient technique and theory for foils 78—43353
Ni, polycryst., thermal emission, magneto-optic circular polarisation obs. 80—70435
Ni-Al_2O_3 composite film, selectively absorbing, optical props. 78—6798
Ni-Cr(-Fe), blackness change in air, 1-8 micron, 1200°C, film props. depend. 77—66033

emissivity continued
Ni-Cr(-W) alloys, heat-resistant, integrated hemispherical degree of blackness, specific elec. resist., oxidised surfaces 79—86912
Ni-Eu_2O_3, specific resistivity and emissivity, 1000 to 1500K 77—43675
Ni-Ge alloys, liq., integrated emissivity, electric resistivity 78—43155
Ni-NiO_x-NiS_y, black Ni, struct.-depend. thermal and optical props., rel. to solar thermal conversion 79—79404
Ni-pigmented anodic Al_2O_3, for selective absorpt. of solar energy, optical and struct. props. 80—55892
Ni_3Al-Ni_3Nb, directionally crystallised, thermal and electric cond., emissivity 77—43556
No-Ni alloy, integral emissivity in range 1200 to 1700°C 77—43357
PbS-Al coatings, absorptivity, emissivity, as function of PbS thickness 78—46731
Pd, radiance temperature at 653 nm, at melting point 79—90805
Pr, normal spectral emittance above 1000K 77—28028
Pt, emissivity, integral, meas., modulation technique 80—62672
Pt, emittance, calc. from spectral radiative and reflecting props. 77—35730
Pt, normal spectral emissivity in 1-10 μm range at 100-400°C 77—11713
Pt ribbon, melting temp. determ. from continual melting and freezing 77—51476
Re, carburised, spectral emissivity at 0.65 μm 80—75374
Re, integral hemispherical degree of blackness, 1200-3000K 78—43154
Re, specific heat, elec. cond., emissivity, 1600-2400K 78—67835
Ru, liq., spectral emissivity and brightness-temp. meas. at MP 77—43356
SO_2, emissivity, computer calcs. 77—84386
Se film, gas-evaporated, selective absorpt. characts. and emissivity 80—50998
Se layer in metal crucible, radiation emissive power theory 78—22874
Si amorphous sputtered film, solar energy selective absorber, spectral emissivity 78—83045
Si, carrier densities obs. via IR emission 77—72707
Si polycrystalline CVD film optical props. 77—77315
Si-Ti-Cr system, plasma coating on Nb, alloy substrates, radiating power 79—60529
SiC cavity radiator, spectral emissivity and radiance 77—83939
Si_2N_2O, emissivity determ. by IR thermography 77—59130
SiO_2 glass, IR spectral emissivity and absorpt. coeff. at 600 to 1700K 80—16018
SiO_2 glasses, spectral emittance at high temps. 80—96674
SiO_2, high temp. plasma, emissivity and opacity, photon group means 77—7573
SiO_2-Mo-SiO_2 thin-film selective coatings for solar energy collectors 78—94422
Sm, normal spectral emittance above 1000K 77—4211
SnO_2 films, selective, optical characterisation by thermodynamical method 80—84796
$SrZrO_3$ coatings, plasma-sprayed, spectral emittance *(French)* 78—26709
Ta, radiance temp. at melting point 77—15603
Ta surface, nonstationary heating and oxidation in low temp. plasma flow, heat and charge transfer obs. *(Russian)* 80—104341
Ta, thermal cond. and emissivity meas. using imaging furnace 80—103667
Ta-Nb(Re)(W) (50,20,0 at.%), with N_2, spectral emissivity, N_2 absorption rate, N_2 solubility, thermodynamic data *(German)* 77—25026
Te, evaporated deposition, absorptivity and emissivity 80—25473
Te film, gas-evaporated, selective absorpt. characts. and emissivity 80—50998
ThO_2 Knudsen cells heated by radiation, emissivity *(Japanese)* 80—13073
Ti, during nonstationary high temp. heating by Ar flow *(Russian)* 80—84308
Ti, liq., spectral emissivity and brightness-temp. meas. at MP 77—43356
Ti, melting point, normal spectral emittance and elec. resistivity, pulse heating method 78—91423
Ti-Al-V alloy, thermophysical meas. above 1450K, using subsecond transient technique 78—95161
UC_2, high temp. thermal diffusivity, thermal conductivity, spectral emissivity 77—28052
UO_2, liquid, reactor safety research, laser experiments *(German)* 80—42787
UO_2 spectral emissivity meas. up to 3800K 80—24625
V, integral normal emissivity in 1300-2000K range 77—35728
V, liq., spectral emissivity and brightness-temp. meas. at MP 77—43356
V, radiance temperature at melting point, surface roughness depend. 80—59683
V_2O_5, interaction with adsorbed propene, IR emission spectra obs. 79—90881
W (100), total hemispherical emissivity meas., sensitivity to O_2 adsorption 80—79964
W, CVD, optical props., solar absorber appl. 77—55844
W, emissivity angular dependence, meas. in IR spectral region 80—34214
W, emittance, calc. from spectral radiative and reflecting props. 77—35730
W, integral hemispherical degree of blackness, 1200-3000K 78—43154
W Knudsen cells heated by radiation, emissivity *(Japanese)* 80—13073
W, normal spectral emissivity in 1-10 μm range at 100-400°C 77—11713
W, normal spectral emissivity, 4.2-2800K 78—2874
W, porous, high temp. props. 77—11894
W, total hemispherical emissivity 79—10973
W-Mo-Re heat resisting alloy MVR-27-VP2, high-temp. emissivity and resistivity 77—35727
W-Re, integral hemispherical degree of blackness, 1200-3000K 78—43154
Y, normal spectral emittance above 1000K 77—28028
ZnO, black, possible use as spectrally selective coating for low temp. solar collectors 79—994
ZnSe, 10.6 μm absorption meas. using thermal emission 77—1649
ZnSe, single cryst. and film, long wave IR emission by lattice vibrs. 77—51528
Zr, integral emittance, during high temp. heating and oxidation *(Russian)* 80—39327
ZrC, stoichiometric, emissibility, integral hemispherical and monochromatic, N_2 content effect 78—91457
ZrC-Re, spectral emissivity, 1400 to 2500K, surface relief and composition 77—24420

- **emitrons** *see television camera tubes*
- **emitter-coupled logic**
  - *see also logic circuits; switching circuits*
  - processor, fast mass depend. trigger for muon pair detection 79—97954
  - programmable delay line using microstrip transmission line and temp. compensated ECL gates 79—26845
- **emitter followers**
  - high-quality voltage follower input impedance and transfer factor meas. 77—13772
- **employees** *see personnel*
- **employment**
  - *see also personnel*
  - bioengineering, career alternative for physics graduates 79—5947
  - biomedicine and the physics graduate 79—5951
  - business opportunities for the physicist's skills in applied math. anal. 79—5949
  - career changes from physics, at Ph.D. level 78—62045
  - career opportunities for physicists, changes, role of American Physics Society 78—62046
  - career opportunities for physicists, discussion 78—61966
  - career patterns of post 1970's USA physicists 78—62037
  - clinical engineering employment information sources 79—92918
  - community colleges in the USA, prospects for physicists 79—5957
  - consumer electricity supply demands fulfilment and ensuring full employment *(German)* 80—36831
  - county Government in the USA, elected positions for the physicist 79—5960
  - dynamics of funding, enrollments, curriculum and employment 78—65746
  - energy research and development, manpower needs in the USA 79—5955
  - Government career opportunities in the USA 79—5946
  - graduate PhD student subfield choice and employment prospects 78—65747
  - hiring procedure, for industrial jobs 79—5953
  - industrial applied mathematics opportunities 79—5950
  - life in a multidisciplinary government laboratory 78—62043
  - manpower studies relating to college physics teaching in the midwest 78—62039
  - non-PhD physicists, USA employment survey 78—62035
  - nonacademic physics employment, survey of employee attitudes 78—62036
  - permit-to-work certification scheme, for use in health building laboratories 80—22338
  - physicists, career development 78—62044
  - physics, education and employment, situation and prospects 78—61963
  - physics, human resources and career opportunities 78—61962
  - physics careers, employment and education, conf., Pennsylvania, USA (Aug. 1977) 78—62034
  - physics careers, employment and education, conf., Pennsylvania, USA (Aug. 1977) 79—2591
  - physics careers at Westinghouse Research 78—62041
  - physics education versus job training 78—61965
  - physics in Europe, bibliography 79—40341
  - Physics Manpower Panel of American Physical Society, employment and education trends 78—65735
  - post-doctoral appointments, tenure and multiple appointments 78—61964
  - prospects for would be PhD physicists 78—62040
  - public policy careers in the USA 79—5954
  - science career facilitation project in energy-related fields 78—61959
  - social effects of microelectronics *(Dutch)* 80—20
  - solar energy, research and application prospects for physicists 79—5958
  - supply and demand for PhD physicists, 1975 to 1986 projection 78—62038
  - technology assessment for the physicist 79—5959
  - textile and papermaking industries, opportunities for physicists 79—5952
  - unconventional jobs in unconventional companies 78—62042
  - versatility of the physicist 79—5956
  - welding engineering opportunities 79—5948
- **emulsions**
  - *see also nuclear track emulsions; photographic emulsions*
  - bituminous coal emulsification by ultrasonics 79—47997
  - n-butanol, dynamical and structural props., by chem. physics method 79—79308
  - carbon tetrachloride, emulsion dispersed, metastable phases at high press. *(French)* 77—56253
  - cavitation emulsification mechanism employing high-speed photography *(Chinese)* 78—14049
  - cluster size distribution for the Ornstein-Zernike correlation 80—97734
  - concentrated, rheological props. 80—99981
  - concentrated cylindrical systems 79—92008
  - concentrated unstable, turbulent flow in pipes 80—28537
  - creamed, vol. fraction, effect of film thickness and contract angle 80—81370
  - critical fluid, Rayleigh linewidth, simulation using emulsion 77—16324
  - n-decane, emulsion drop, efficiency of capture by bubble in noninertial flotation 80—11956
  - deposition, in pores of Al_2O_3 anodic oxide film 80—104357
  - disperser for powder, suspension and emulsion production 78—23636
  - dodecane-sodium octylbenzene sulphonate phase diagram *(French)* 79—82339
  - drop coalescence with liq. cryst., van der Waals pot. 77—12834
  - drop of water-fuel emulsion, microexplosive boiling of metastable overheated water, microblast *(Russian)* 80—74930
  - dye laser, pumped by N_2 laser 79—13962
  - electrical conductivity, H_2O-alcohol microemulsions 79—20471
  - electrical conductivity, spherical approx. *(French)* 77—45786
  - electrocapillary emulsification 78—48697
  - ethylene-vinyl acetate copolymer, powdered, prep. by emulsion polymerisation *(Japanese)* 80—104110
  - ethylene-vinyl acetate emulsion, morphology 77—48692
  - films, thinning vel., surfactant in continuous and disperse phases, Navier-Stokes eqns. 77—84305
  - films, thinning vel. and lifetime, surfactant in continuous and dispersion phases 77—84306
  - flotation of fine particles by group of bubbles, kinetics 78—53261
  - flow, relative drop-drop and drop-wall motions, slow 79—32641
  - fluorocarbon emulsions, colloidal props. 78—48703
  - gas-liquid emulsions and foams, electrical conductivity 80—11961
  - hard sphere fluid theory applic. to liq. particle dispersions 77—9129
- **emulsions** continued
  - hexadecane-H_2O-butanol-Brij 96, drop dia., comp. depend. light scatt. obs. 80—45573
  - hexadecane-H_2O-pentanol-Tween 60, drop dia., comp. depend. light scatt. obs. 80—45573
  - n-hexane droplets, coalescence in n-alcohol aqueous solns. 79—87882
  - hydrocarbon drops levitated in water, acoustically forced shape oscill. 79—47987
  - ice microcrystals, emulsion, complex dielec. permittivity meas. *(French)* 78—10821
  - inorganic emulsions, hydrophile lipophile balance temperature 78—95961
  - interfacial organic chem. processes 80—26050
  - inverse-type, coalescence of drops in uniform elec. field 78—53265
  - invert, aggregation equilibrium 79—66356
  - latex solids, agglomerating and dewatering 80—104470
  - light scattering, rel. tp percolation phenomena 80—104467
  - liquid-liquid interfaces in isolation and in interaction, review 77—47651
  - magnetic and dielectric, prep. *(German)* 78—3376
  - metal drop-oxidizing slag, oxidation kinetics 78—11153
  - methacrylic acid-methyl methacrylate statistical copolymer suspension polymerisation, stabilisation effects, viscosity 78—85157
  - micelles formation, considered as polycritical phenomena *(French)* 77—63968
  - microemulsion, border between lyophobic and lyophilic colloids, thermodynamic stability 80—40747
  - microemulsion, elec. cond., stirred percolation model 79—79314
  - microemulsion, freeze fractured, electron microscopy examination of micellar and lamellar struct. *(French)* 78—15714
  - microemulsion, struct. description of liq. particle dispersion, ultracentrifugation and small ang. neutron scatt. obs. 79—5184
  - microemulsion, structure, simple model and consequences *(French)* 80—45565
  - microemulsion, viscosity meas. *(French)* 78—61055
  - microemulsion phase equilibria, statistical thermodynamics 79—5183
  - microemulsion structural changes, light scatt. obs. 78—56920
  - microemulsion system, existence of bicontinuous zone 80—104466
  - microemulsion type systems, percolative conduction 79—100452
  - microemulsions, aerosol OT, inhomogeneous interior, fluoresc. and polarisation decay probes 80—50891
  - microemulsions, elec. cond., stirred percolation situation *(French)* 79—83512
  - microemulsions, heat transfer meas. by laser-induced thermal blooming 80—91833
  - microemulsions, lattice gas model, surfactant effects 78—23974
  - microemulsions, light-scatt., appl. of liquid state theory 80—40750
  - microemulsions, phase diagram and homogeneity gap, light scatt. and viscosity meas. 80—16736
  - microemulsions, PMR spin-lattice relax. time meas., inversion recovery method *(French)* 78—48066
  - microemulsions, quasi-elastic light scatt. 80—108755
  - microemulsions, stability, high field NMR investig. *(French)* 78—27827
  - microemulsions, stability, thermodynamic approach 78—95959
  - microemulsions, statistical mechanics 77—52677
  - microemulsions, struct., use of variable-contrast method appl. to neutron scatt. 79—16043
  - microemulsions, thermodynamic stability, theory 78—85203
  - microemulsions, thermodynamic stability 78—95962
  - microemulsions of micelles, interpretation of second virial coeff. of osmotic press. *(French)* 78—64891
  - microemulsions vs. micellar solns. 77—60131
  - multiphase, notation and terminology 78—15720
  - nonionic emulsifier blend-oil-H_2O system, ternary phase diagram 78—20074
  - nonpolar electrolyte, on anode, ion attachment and ion emission 78—65998
  - nonviscometric flow, drop suspension model, deformation and vorticity 79—60022
  - nonylphenol diethylene glycol ether-water-p-xylene system, liquid crystal stabilization of multiple emulsions 79—16046
  - oil in water microemulsion, added NaCl, light beating spectroscopy of micelles mutual diffusion coefficient 78—80793
  - oil-in-oil emulsions, particle size and stability, temp. depend. 79—20472
  - oil-in-water, electrolyte flocculation of stabilised potassium 79—43638
  - oil-water emulsification, by US, large primary oil drop breakup 79—32644
  - oil-water emulsions, pool boiling heat transfer 79—55378
  - oil-water interface, US emulsification drop form. by capillary wave instability 79—32643
  - oil-water microemulsions, osmotic press., micelle diameters, second virial coeff. *(French)* 78—20075
  - oil-water microemulsions, US attenuation and structural transitions 79—61917
  - paraffin oil, aq. emulsion, polyelectrolyte stabilised, mech. props. 79—39223
  - permittivity of nonpolar dielectrics *(French)* 78—39497
  - photographic emulsion, for spectrographic anal., calibration curve computer calcs. 78—4706
  - physical chemistry of surfaces, book 77—25310
  - poly(vinyl alcohol)-based membranes for haemodialysis *(Japanese)* 78—96115
  - polyethyl acrylate modified mortars, inner struct. and flexural props., suspension and emulsion studies *(Japanese)* 77—86092
  - polymer emulsion particles containing epoxy groups, cleavage study of epoxy groups *(Japanese)* 77—90649
  - polymerisation, homogeneous nucleation 79—29354
  - polymerisation, particle size calc., applicability of Gardon's eqns. 78—92479
  - polymerisation of polar monomer emulsions, model calc. *(Russian)* 79—34302
  - polystyrene lattice, emulsions-polymerised, particle size determ. by soap titration 80—40753
  - PVC, emulsion, melts, slip, visual observations 79—4047
  - PVC composite, MBS type multifunctional impact modifier effect on mech. and rheological props. *(Polish)* 78—52751
  - PVC plastisol, steady shear rheological behaviour 79—37274
  - SEM preparation technique for emulsion particles, freeze drying 80—62799
  - silicone oil/aqueous/organic solvent+wax, multiple phase system 78—15720
  - sodium dodecyl sulphate, dynamical and structural props., by chem. physics method 79—79308

emulsions continued
  stability, interfacial phenomena interpretation using schematic density profiles 78—60012
  stability, role of mixed emulsifiers 79—74424
  stability against coagulation 77—32843
  stability of nonaqueous emulsions in ultracentrifuge, effect of added water 78—40082
  structural aspects of microemulsions using dielectric relaxation and spin label techniques 80—26199
  surfactant solutions, aggregation, micelle and microemulsion form. 80—89547
  tetraethylene glycol dodecyl ether-H_2O, binary micellar solns. and emulsions, dielec. behaviour 80—44994
  tetraethylene glycol dodecyl ether-H_2O-heptane, binary micellar solns. and emulsions, dielec. behaviour 80—44994
  thermal radio emission from foam structures 79—29497
  thermodynamically stable emulsions 79—47993
  thin liquid film, instability and rupture 80—34279
  thin liquid films in emulsions, contact angles 80—92761
  tissue dispersions, unglycerinated, freeze-etching by appl. of oil emulsion technique 78—53594
  toluene, dynamical and structural props., by chem. physics method 79—79308
  toluene-brine microemulsion, liquid interfacial tension meas. from scatt. light intensity 80—20012
  unstable macroemulsions, rheological props. obs., non-Newtonian region obs. 77—75866
  US attenuation 79—41475
  vidicon tube, video-electronic measuring system, nuclear track emulsions 78—17493
  viscosity, dynamic, effect of inertia for dilute emulsion in pure straining motion 80—87797
  water, containing emulsion, from crack detection processes using penetrating agents, purification *(German)* 79—5517
  water, supercooled emulsified droplets, relative permitt. and cond., Maxwell-Wagner interfacial polarisation 78—52423
  water dodecane potassium oleate hexanol, micro emulsion, Rayleigh scatt., micellisation *(French)* 80—43055
  water emulsions, dielec. props. obtained after crystallisation/melting cycle 77—86381
  water in oil, supercooled, freezing, differential scanning calorimetry meas. 77—15552
  water toluene sodium dodecylsulfate butanol, micro emulsion, Rayleigh scatt., micellisation *(French)* 80—43055
  water-in-dodecane microemulsions, dielec. study of phase transition 79—28668
  water-in-dodecane microemulsions, struct. transitions in liq. cryst. phase, dielec. props. 79—28669
  water-in-hexadecane, microemulsion, dielectric behaviour, Cole-Cole type relax., temp. depend. 78—56426
  water-in-oil emulsion, boiling, bubble formation, cinemicrophotography 80—74961
  water-in-oil microemulsions, electro-optical phenomena in lyotropic liquid crystals 80—107050
  water-in-oil microemulsions, structural relaxation by thermal current anal. 80—107049
  water-in-oil-in-water, multiple phase, prep. technique 77—1953
  water-in-oil-in-water emulsions, electron micrography 78—7245
  water-oil microemulsion, thermal diffusion coeff. *(French)* 79—87880
  water-oil microemulsions, optical matching 80—61157
  water-petroleum emulsions, mean particle diameter and conc. determ. by light scatt. 80—89538
  AgBr, (100) and (111) face, influence on aggregation of sensitising dyes 79—39202
  AgBr-Ag light sensitive system, diffusion of excited states *(Russian)* 78—59101
  Al-In emulsion, solidification mechanisms at zero gravity, review 78—88458
  Al_2O_3-martensitic steel, mag. and dielec. emulsion, prep. by abrasion of steel surface 78—27826
  CS_2, emulsion theory, appl. to the permittivity of nonpolar dielectrics *(French)* 78—39497
  Fe_2O_3-martensitic steel, mag. and dielec. emulsion, prep. by abrasion of steel surface 78—27826
  H_2O-alcohol microemulsion, elec. cond. and struct. 79—20471
  H_2O-cyclohexane-sodium dodecyl sulphate-pentanol I, light scatt. study *(French)* 79—1968
  H_2O-toluol-sodium dodecyl sulphate-alcohol microemulsion, diffusion coeff., light scatt. data 78—15722
  hydrocarbon-water, emulsions, superheated, bubble nucleation 78—61056
  KCl aq. soln., lanoline emulsion, dielec. relax., 1 MHz to 70 GHz 77—77144
  KCl aqueous solution emulsions, complex permittivity meas., dielec. relax. 78—72459
  Na^+-gramicidin D, NMR study 79—43805
  Na_2SO_4 aq. soln. droplets, nucleation by $Na_2B_4O_7.10H_2O$ in emulsion *(French)* 79—1492
  $Na_2SO_4.12H_2O$ aq. soln., dodecanol additive effect near critical micelle conc. 77—73472
  Ni-Na-di-2-ethylhexyl phosphoric acid-H_2O system, droplet phenomena 77—48697

emulsions (nuclear track) *see nuclear track emulsions*

emulsoids *see emulsions*

encapsulation
  see also packaging
  composite drop formation, hydrodynamics 80—64603
  low-cost encapsulation materials for terrestrial solar cell modules 80—3522
  metal filings and wires, thermal processing encapsulated under vac. in metal tubulations 77—59810
  optical fibre waveguide cables, reinforcement, mech. props. *(German)* 78—33861
  parylene coating for $Ga_{1-x}Al_xAs$ laser diode end facet protection 79—36921
  photovoltaic cells using silicone materials, encapsulation 80—94019
  photovoltaic solar generators, ampere-hour efficiency, charging and discharge power 80—29434
  polyamide-polyurethane, enamel lacquer, far IR transmission, encapsulation of optical devices 79—55194

encapsulation continued
  polyvinyl acoustal, enamel lacquer, far IR transmission, encapsulation of optical devices 79—55194
  sheet metal, deep-drawn, for implant device encapsulation, mech. and metallographic props. *(German)* 79—8564
  single fibre optic moulded connector and encapsulated connectorised devices 78—1409
  single-mode fibre optical power divider, encapsulated etching technique 79—27420
  solar cells automated production, with wraparound contacts 80—76635
  solar cells encapsulation using ethylene-vinyl acetate double vac. technique 80—93510
  stimulator encapsulation for implantation, biomaterials 78—40416
  terrestrial photovoltaic arrays, development of glass encapsulation technique 80—94020
  terrestrial solar modules, sandwich type glass encapsulation, climatic parameters effect, economic anal. 80—45673
  thermoplastic enamel lacquer, far IR transmission, encapsulation of optical devices 79—55194
  Cu_xS-CdS solar cell improvement by Cu treatment and front contacting 79—61987
  GaAS, preliminary heated, encapsulation by sputtered deposits of Si_3N_4 and AlN *(French)* 77—32714
  GaAs, anodic oxide film, annealing effect on carrier density profile 78—88040
  GaAs by Si_3N_4, effect on laser-annealing behaviour of GaAs 79—79131
  GaAs, ion implanted, surface effects, RHEED obs. 77—1883
  GaAs, SiO_2 and Si_3N_4 encapsulants for annealing, photolum. and AES evaluation 78—27657
  GaAs:Cr, semi-insulating, Cr redistrib. during thermal annealing as function of encapsulant and implant fluence 80—84199
  GaAs:Cr,Se, ion-implanted, semi-insulating effects of Cr redistrib. on elec. characts. when encapsulated with Si_3N_4 80—59982
  GaAs:S ion implantation, SiO_2 and Si_3N_4 encapsulants effects, expt. 77—11574
  GaAs:Se, implanted, annealing with O-free CVD Si_3N_4 encapsulant 78—83834
  GaAs:Se, implanted, multilayered encapsulation using SiO_2:As and Si_3N_4 79—11715
  GaAs:Si, encapsulated by SiO_2 and Si_3N_4, ion-implanted As profiles 79—4319
  GaAs:Si encapsulated with AlN, Si_3N_4 layers, photolum., annealing effects 80—20681
  GaAs:Zn, surface conc. control 79—55758
  Si_3N_4 layers, on GaAs, encapsulation, low-energy ion beam sputtering 79—78882
  Si_3N_4 noncrystalline layers, CVD growth, encapsulant layers for annealing GaAs 79—19994
  Si_3N_4, plasma deposition, optical absorption as control test 78—35314

encoding
  see also codes; decoding
  1.5 Mb/s bipolar signal coding and decoding optical fibre link 77—27343
  analytic Fourier optics, information encoding by complex zeros 80—23628
  articulation development, possible nonlinear time varying control in feedback path 78—35870
  associative parallel-search memory, correlation search using coded key words 79—10265
  astronomical image coding in near IR, multiplex technique 77—53428
  auditory nerve fibre, insect, latency shift, neuronal time cue of sound direction 79—48274
  auditory-nerve fibre encoding of 2-tone approximations to steady-state vowels 80—61582
  binary data, holographic coding methods investig. 77—68192
  biological cell molecular computer, coding during intracellular processes of information processing 77—70400
  cochlear implantable prosthesis, information coding 80—46100
  code generator to identify time, date, and events in physiologic event recording 77—86674
  coherent coded imaging without side lobes 79—25079
  coherent codes, iterative improvement algorithm 80—87330
  coherent optical Fourier transform operator numerical accuracy improvement 79—76628
  colour coding of spatial freq. using incoherent optical processing 80—37956
  colour encoded aperture masks used for incoherent filtering of images 79—41348
  colour encoded image prod. by coherent-optical processor 77—88655
  colour film archival storage, white light processing technique 80—99637
  colour holograms, plane, information colour coding methods 78—33703
  colour images, rate distortion coding simulation for colour images 78—7361
  computer-generated double-phase holograms, Fourier transform subcells and phase coding 79—27200
  computerised classical tomography, optimum coding sequences appl. 79—8530
  digital image coding techniques, performance analysis 77—58277
  direct-reading displacement digitiser construction and coding *(Russian)* 77—9983
  discrete image tone gradation scale transform. on grid coding basis 79—10266
  drift chamber counter, missed counts and registration efficiency calc. 78—78594
  ECG numerical encoding and transmission, microprocessor appl. 77—44798
  ECG pattern classification from complete computer descriptions 80—56265
  edge detection and coding using directional masks 77—79774
  expendable bathythermograph digital recording and display system 80—46318
  Fourier holography in white light, coding of spatial and chromatic information 77—3555
  Hadamard transform image scanner, polarisation coding 77—14668
  halftone image coding rel. to visual performance characteristics 77—58280
  hearing, temporal perceptions, effects of early auditory deprivation 80—76761
  hodoscopic detector registration systems, data coding/reading block 78—78602

encoding continued
- holographic multiplexing by optical beam coding, applic. to interferometry *(French)* 77—159
- holographic pseudocolor encoding, spatial filtered imaging technique 79—18370
- image coding with far-field holograms 78—90389
- image encoding principle, optical spatial channel 77—71937
- image processing, two dimensional unitary transforms appl. 78—58928
- image restoration, 2D coded Poisson process, appl. to nuclear imaging *(French)* 79—57767
- image transmission techniques, conference, San Diego, USA (Aug. 1976) 77—79773
- information encoding and propagation in scattered fields by complex zeros 79—50238
- information encoding by complex zeros, analytic Fourier optics, comment 80—87326
- intravenous contrast angiography, improved digital real-time processing and storage 79—70624
- Ionospheric Sounding Satellite, command system, encoder *(Japanese)* 77—78609
- IR spectra, binary coded, feature selection for automated interpretation 80—3428
- line scan sensor, spatial and temporal coding of GaAs laser 78—83022
- linear predictive coded speech quality problems and expts. 80—91982
- matched filters, using optical delay line provide encoding or decoding structures 78—74983
- microminiature cooler, thermoelectric, 3-stage, for stabilisation of microelectronics elements 80—31763
- monochrome picture signal, digitally coded, level reassignment technique 78—55307
- multicolour image storage on black and white film, using crossed grating 79—31813
- multigradation image, representation in Boolean algebra 77—31071
- multiple exposure hologram generation from controlled transparencies *(Russian)* 79—94177
- multiplex holographic representations of space-variant optical processors 80—48192
- multiplex holography with chirp-modulated binary phase-coded reference-beam masks 79—27202
- multiplex image coding, astronomical IR speckle interferometry appl. *(French)* 80—67580
- multislit spatial filtered pseudocolour holographic imaging 80—53236
- myocardial ^{201}Tl scintigram anal., nonredundant coded aperture tomographic method 80—94364
- nerve cell impulse flows, determ. of quantity of useful information 78—69038
- nerve fibre membrane analogue-code conversion, ionic mechanisms 80—81575
- nerve impulse encoding, elec. processes 80—76718
- nerve impulses, phase locking of pulse encoders 79—34546
- neural communication system model, single signed integral PFM and PPM comparison 79—5268
- neural encoding model test, phase-locking meas. significance 79—2036
- noncoherent optical projection system input holograms *(Russian)* 80—14297
- nonlinear coded waveforms, optical signal processing 79—72517
- nonlinear image processing, binary pulse position encoding 78—29906
- nuclear medicine, coded aperture imaging, qualitative and quantitative 80—89843
- optical coding and decoding operations, parallel image transmission by single fibre 78—71216
- optical coding method, scene analysis 78—82924
- optical fibre digital communications, PAM-PPM signalling format 79—27190
- optical fibre network, for encoding and decoding 78—25963
- optical fibre tape for image and hologram transmission, using chromatic encoding *(French)* 79—3785
- optical image subtraction, real time grid coding and interlacing 78—33694
- optical pattern recognition, bipolar incoherent, by carrier encoding 79—50230
- optical processing, incoherent imagery system, introduction of partial coherence by holographic components 80—95853
- optical processing system for pseudo-colour encoding 77—7020
- optical pseudocolour encoding of spatial frequency information 78—87018
- optical pseudocolouring through contrast reversal filtering 79—81378
- optical pulse, fibre optic delay lines utilisation 77—83970
- optical signals, noncoherent double-scanning monochromator appl. *(Russian)* 80—5697
- optical space-variant processing of nonlinear coded waveforms, ambiguity function 79—76602
- optical spectra, direct encoding using computer interfaced vidicon TV camera 77—10114
- optical transducer, for use with windvane 79—39889
- paper tape data transmission, wavelength multiplexing, optical fibres 80—43454
- parametric coding of speech spectra, computer studies 80—96137
- patterned optical filters for solid-stage imager spectral encoding 78—66945
- PCM encoding and decoding for optical memories 80—102658
- PCM telemetry systems, air pollution detection/control appl. *(German)* 78—93003
- perceptual coding in the cosing transform domain 80—102635
- phase coding with high quality computer holograms 77—628
- photograph, pseudo-colour encoding using halftone screens and coherent filtering 77—71939
- picture coding without point by point sampling 78—33678
- picture direct transmission via single optical fibre 80—106628
- picture scrambling holographically for confidential picture taking technology 77—19208
- pictures, closed orthogonal functions, digital coding, X-ray pictures appl. 77—77965
- pitch-synchronous coding, linear prediction coding, analysis frame position influence 80—14523
- polychromatic processing technique for colour image transparencies 80—86473
- proportional counters, position-sensitive, RC-line encoded, using low-resistance, metal wire anode and active load capacitance 79—54745
- pseudo colour equidensitometry, analogue optical method 78—32903

encoding continued
- pseudocolour density encoding, white-light, using contrast reversal 80—83560
- pseudocolour density encoding of photographic materials, white light processing system 79—18360
- pseudocolour encoding, of holographic imaging, new technique 78—78963
- pseudocolour encoding of holographic images using single wavelength 78—87025
- quasistationary processes and universal codes 80—91994
- radio time signal coding and clocks for private and industrial use *(German)* 78—89445
- radiographic pictures, digital encoding, redundancy reduction 77—40850
- radiography, I isolated images using spatial frequency encoding 79—39485
- remote sensing data, cell analytical method for inland wetland photointerpretation evaluation 79—29898
- repetitive photoelec. scanning system for high resolution optical spectra accumulation 78—54456
- retinal single-photon impulse coding mechanisms *(Russian)* 78—27941
- sampling theorems in polar coordinates 80—28169
- sensory information coding, adaptation and differential sensitivity in system of detectors 77—56367
- sensory processes, information received by receptors 77—73521
- software coding for reliable data communication in reactor safety system 79—13496
- space-frequency conversions for image transmission and processing 78—71046
- space-variant holographic systems using phase-coded reference beams 78—74868
- space-variant optical processors, use of coded waveforms 79—27191
- speckle coded image subtraction configs., optimal distrib. of exposures 79—55071
- spectrometer, comparison of Fourier and Hadamard transforms 77—5922
- speech, ADPCM coded, segmental SNR measure as indicator of quality 80—33359
- speech, aspects of grammatical coding in correls. of duration for nonadjacent segments 77—56387
- speech, optimization of digital coders by exploiting human auditory masking 80—33356
- speech, parametric coding of speech spectra 80—96136
- speech, predictive and residual 80—33354
- speech, signal models for low bit-rate coding 80—106674
- speech, sub-band coding with adaptive bit allocation 80—28386
- speech, transform coding, analysis/synthesis frameworks, appls. 79—59886
- speech, using freq. domain techniques 80—33355
- speech analysis by linear predictive coding, accuracy improvement 79—46133
- speech coding using non-uniform linear prediction in transform domain 79—55277
- speech digitisation and bandwidth compression techniques, ADPCM and ADM *(Korean)* 79—59876
- speech digitization and bandwidth compression, ADPCM and ADM *(Korean)* 79—55273
- speech encoding in auditory nerve, effects of nonlinearities 80—108913
- speech parameter, encoding using vibrotactile freq. discrimination 78—11772
- speech quality and intelligibility measures and their correlations 80—91978
- speech waveform coding technique developments in Japan, review 80—33353
- steady-state vowels in auditory nerve, representation in terms of discharge rate 79—92230
- still-picture real-time Hadamard transform coding quantiser design 77—27263
- thermal viewing system, image integral scanning effectiveness 79—50402
- three-dimensional imaging by coded aperture and shadow casting techniques 79—74757
- threshold vision aspects of picture encoding 77—81509
- time code, automatic print out, EEG paper, 10 sec. intervals 77—29219
- TV, psychophysics of vision, relation to picture quality and coding limitation 77—12923
- two-dimensional image transmission by wavelength multiplexing 79—27189
- ultrasound image coding, mammograms appl. 77—81544
- US time-coordinate convertors for distance meas., design aspects *(Russian)* 78—77857
- Vibroseis system, encoding techniques 78—69474
- virtual holography, method of source and channel encoding, decoding of information 79—94185
- visual system, crayfish, coding and decoding of steady state information by patterned pulse trains 80—12105
- voice fundamental freq. into vibrotactile freq. 80—10092
- wave encoding, appl. of structural information theory of sound 77—14822
- wavelength multiplexing for information transmission 79—22906
- X-ray detector, position-sensitive, inductance-capacitance line encoding 78—12800
- X-ray image series encoding and analysis 79—83928
- X-ray imaging, coded aperture, flashing tomosynthesis 77—40848
- X-ray picture source coding for compact storage or fast transmission 78—40310
- X-ray picture transmission over voice grade telephone channels 78—44607
- X-ray tomography by grid coding 80—51206

ENDOR
- N-acetylglycine, X-irrad., stable radical electronic and mol. struct., ENDOR and ESR 80—80637
- acridine, single cryst., X-irrad., ENDOR obs. 79—87330
- actomyosin, X-irradiated ENDOR and ELDOR obs. 80—63689
- adamantane, γ-irrad., free radicals EPR and ENDOR 80—69170
- L-alanine:Cu(II), EPR and ligand-ENDOR measurements 80—44907
- β-alanine, cryst., X-irrad. producting radicals, ESR and ENDOR 79—56612
- alkaline earth fluoride:Gd^{3+}, ligand ENDOR, spin Hamiltonian and hyperfine parameters 77—43903
- alkoxy free radicals, produced by X-irrad. of hydroxy containing cpds., characterisation by ESR and ENDOR 78—95938
- α-amino acids, γ-irradiated, primary oxidation products, ESR and ENDOR 77—48754

ENDOR continued
anisotropic HFS tensors for double zeta functions with applic. to neutral radical proton interactions 77−35903
L-asparagine.H_2O, X-irrad. at room temp., ESR and ENDOR 77−40131
bacteria, photosynthesis, primary electron acceptor, EPR, ENDOR investigs. 78−77004
bacteriochlorophyll cation in soln., N atom ENDOR and proton triple resonance 78−96018
bacteriochlorophyll radicals, role in primary charge separation of Rhodopseudomonas viridis 80−63688
bacteriopheophytin b radicals, role in primary charge separation of Rhodopseudomonas viridis 80−63688
benzil, ENDOR study of geom. struct. of lowest triplet state 79−89696
benzil, ENDOR study of phase transition 79−73855
benzophenone, triplet, optically detected EPR, ENDOR and ODMR, HFS, isotope and spin-orbit effects 78−86898
benzophenone, triplet state in organic cryst., ENDOR spectra for spin density 79−64021
benzophenone-d_{10}, $^3(n,\pi^*)$ state, containing ^{13}C, in 4,4′-dibromodiphenylether, hyperfine ENDOR spectrum 78−42102
benzyl radical trapped in X-irrad. potassium hydrogen bisphenylacetate, ENDOR 77−10695
carbohydrate compounds, X-irrad., trapped electrons, ESR and ENDOR obs. 80−93161
α-chloro radical in X-irradiated 5-chlorodeoxyuridine single crysts., ESR, ENDOR 77−4916
citric acid, single cryst., X-irrad., EPR and ENDOR, 4.2K radical identification 79−65764
creatine monohydrate, single cryst., radiation damage, ENDOR obs. 78−96016
cross relaxation due to nucl. spin-spin flips *(Russian)* 77−24763
1,1-cyclobutanedicarboxylic acid, X- and γ-irrad. cryst., EI-EPR overlapping spectra resolution 77−16179
3'-cytidylic acid, X-irrad., stable radical in ribose moiety, compared with cytidine 77−25375
cytochrome c oxidase, Cu ENDOR 80−94170
deoxycytidene 5'-phosphate-H_2O, cryst., X-irrad., ESR and ENDOR obs. 79−34330
deoxycytidine 5′-phosphate, H_2O, X-irrad., 3αH radial. form., ENDOR, ESR 77−73453
dibenzenechromium-dibenzenevanadium, proton HFS data, ENDOR obs. 80−66073
p-dibromobenzene, crystal nucl. spin polarisation cross relax. study 80−29647
dicarboxylic acids, D quadrupole coupling constants, ENDOR study 78−90195
p-dichlorobenzene, triplet state symmetry, geometry, ODMR, ENDOR obs. 79−18214
diphenyl-d_{10}: diphenyl, triplet state EPR and ENDOR, 1.9K, mol. struct. implications 79−94021
diphenylmethylene, triplet state, ENDOR in $P2_1$ benzophenone, conformation and spin distrib. 77−483
dipotassium glucose-1-phosphate, X-irrad., ESR-ENDOR obs 80−60419
DTGS:VO^{2+}, ENDOR 79−99791
dulcitol, X-irrad., 4.2K, electron traps, alkoxy hyperfine coupling, ENDOR obs. 80−50863
electron spin echo envelope modulation, 2-dimens. Fourier transform 80−63680
electron-nuclear cross relaxation, spectral diffusion 78−27118
electron-nuclear-nuclear triple-reson. spectrometer 77−41662
equivalent nuclei, ENDOR fine struct., exact solns. 77−6811
F-centre ground state wave function, ENDOR and F-absorpt. data analysis 77−31978
forbidden transitions, hyperfine interactions, theory 80−50226
forbidden transitions in electron-nuclear systems 77−12254
free radicals in liq. soln., ENDOR spin-echo lineshape, density matrix 78−35064
galvinoxyl, radical in a smectic liq. cryst., ENDOR study 79−78567
glycine-$AgNO_3$, single cryst., X-irrad., oxidation product form. 77−48660
glyoxal-d_0, -d_2, triplet kinetics, microwave-saturation recovery and MIDP obs. 77−71823
haemoglobin, human, maleimide spin labeled, proton ENDOR spectra obs. 80−89719
heme-proteins, general spin Hamiltonian for determ. of ligand nucl. Zeeman and hyperfine interactions 77−85617
hippuric acid, X-irrad. single cryst., ^{14}N and ^1H ENDOR study; 80−71240
hydroxyproline HCl, X-irrad., free radical products, ENDOR meas. 78−76883
hyperfine and superhyperfine interaction parameters *(Russian)* 79−47064
inositol, X-irrad., deuteration effects, ENDROR and ESR meas. 78−73067
inositol, X-irrad., radical form. detection by ESR and ENDOR, oxidation process 78−27797
ionic crystal defects, mag. reson. studies 80−108066
ionic crystals incorporating S-state ions, expt. exam. 79−28326
isobacteriochlorins, π cation radicals, implications for NO_2^-, SO_2^- reductases 80−63684
Ka-band EPR/ENDOR spectrometer, modified, obs. of electron spin echoes at 35 GHz 80−13113
KBr(I):D, inelastic light scattering of localised vibration of interstitial H atom in alkali halides 80−88998
lanthanum ethyl sulphate=Gd^{3+}, proton position determ. by ENDOR 77−51992
lanthanum nicotinate dihydrate:Nd^{3+} cryst., H coords., EPR and ENDOR determ. 77−59005
lanthanum nicotinate dihydrate, cryst., nucl. quadrupole interactions, D atom coords., ENDOR obs. 80−97161
liquid crystal:aromatic free radical, D quadrupole splittings, ENDOR and TRIPLE reson. obs. 77−51989
lithium acetate dihydrate, γ-irrad., methyl radical, ENDOR, line-shape model appl. 79−73853
low temperature nuclear relaxation stimulated by paramagnetic impurity 79−33563
matrix ENDOR in solids, spin packet model 80−29648
methanol dehydrogenase, enzyme, electron spin echo, 35 GHz 80−13113
methanol dehydrogenase, enzyme powder, ESR and ENDOR, 9 and 35 GHz 79−70524

ENDOR continued
methanol dehydrogenase, spin echo powder ENDOR, line shape aspects 79−34485
4-methyl-2,6-di-tert-butylphenol, γ-irrad. cryst., ENDOR transitions, ELDOR detect. 78−95531
α-methyl-D-glucopyranoside, X-irrad., ESR and ENDOR study of free radicals 80−45526
α-methyl-D-glucopyranoside, X-irrad. cryst., radical form., EPR-ENDOR study 79−56613
6-methylmercaptopurine riboside, S-substituted nucleoside, ESR and ENDOR obs. 77−36766
2-methyltetrahydrofuran glass, 77K matrix ENDOR line shape model and expt. 78−6600
microwave cavity for electrons spin-echo experiments 78−82013
microwave preamplifier for ESR/ENDOR spectrometer sensitivity enhancement 78−82014
modulation-induced sidebands 77−48028
multi-level system, relax., double resonance, resistance network analogues 77−1583
multiplet struct. and energy level non-crossing, second order perturbation theory 79−72341
myosin, X-irradiated ENDOR and ELDOR obs. 80−63689
naphthalene:2-fluoronaphthalene, photoexcited triplet state X-traps, ENDOR meas. 78−39444
naphthalene:2-fluoronaphthalene(2-chloronaphthalene), triplet state X-traps, ENDOR obs. 79−33561
negative ENDOR, description by Bloch tansport eqns. 79−95678
negative enhancement and phase shift 78−39445
negative signal, theory 77−8449
nitromethyluracil, radiation-induced oxidation and reduction 77−32816
nonmetallic crystals, ENDOR of impurity centres 80−25249
organic doublet radicals in nematic and smectic liq. crysts., ENDOR obs. 80−91585
phenoxyl type radical, ^1H and ^{13}C ENDOR studies in soln. 78−94266
4-phenyl-3-thiosemicarbazide, single cryst., X-irrad., EPR, ENDOR, radical identification 79−31560
2,5-piperazinedione, X-ray damaged, ENDOR, δ proton hyperfine interaction 77−9103
point defects in crystals, book 77−47442
polycrystalline dipeptides, X-irradiated ENDOR and ELDOR obs. 80−63689
polyhydroxy compounds, X-irrad., trapped electrons, ESR and ENDOR obs. 80−93161
polynuclear system, ENDOR dynamics of F-centres, cross relax. effect 77−40151
potassium hydrogen bisphenylacetate, X-irrad., ENDOR of trapped benzyl radical 77−10695
potassium hydrogen malonate, γ-irrad. cryst., ESR and ENDOR of trapped radical 79−78524
potassium hydrogen malonate, deuterate, NQR data ($I=1$) from ENDOR expts. 80−54994
potassium hydrogen malonate, room-temperature ENDOR spectra obs. 80−106339
quartz:Ti^{3+}(Li) centres, forbidden transitions 77−90067
quick access sample system for low temp. K-band ESR and ENDOR 80−57352
quinoxaline, triplet state symmetry, geometry, ODMR, ENDOR obs. 79−18214
rare earth ions, optically excited states, EPR, ENDOR 78−43637
relaxation of nuclei due to non-Kramers paramag. ions 77−69731
resolution enhancement through multiple quantum transitions 78−19374
resonance cell for spectrometer operating in 120-350 G field 78−4671
resonant helix cell with high RF fields for steady-state experiments 79−49264
RF discrete saturation, effects of dipole reservoir 79−56626
Rochelle salt, X-irrad., radical II struct. and location, ENDOR 77−51991
ruby, consideration of dipole-dipole reservoir in nonstationary double reson. 77−4580
ruby, distant nuclei ESR and ENDOR experiments, dipole-dipole reservoir importance 80−71241
ruby, double electron-nuclear resonance at Cr^{3+} B1, B2 absorpt. lines, optical detection *(Russian)* 80−7194
ruby, ENDOR of Cr^{3+} ions, elec. field effect *(Russian)* 79−8071
ruby, equilib. between electron dipole reservoir, nuclear spins and lattice *(Russian)* 77−43904
Si:Sb(P)(As), shallow donor states with strong central cell perturbation theory 78−51933
single crystal ENDOR for NQR data ($I=1$) 80−54994
sorbitol, X-irrad., 4.2K, electron traps, alkoxy hyperfine coupling, ENDOR obs. 80−50863
spectrometer, low impedance design 80−246
spin Hamiltonian diagonalisation, theory and appls. of generalised operator transforms 77−4546
strong saturation of NMR of adjacent nuclei, influence on ESR 78−60356
succinamic acid, X-irrad., primitive radn. damage, ESR, ENDOR 78−3352
succinic acid, partially deuterated, ^1H and ^2H distant ENDOR obs. of mol. struct. parameters 80−23445
sulphides, mag. interactions of Fe group ions 79−99753
dl-tartaric acid, radiation products, ESR-ENDOR OBS. 80−55682
TCNQ salt, quinolinium $(TCNQ)_2$, mag. chain double resonance study, deuteration 80−25250
TGS:VO^{2+}, single cryst. H^2 ENDOR investig. 79−99791
TGS, ferroelec., negative ENDOR study of radiation damage 78−19373
TGS, X-irrad., glycine radicals, geom. struct. by ENDOR and INDO calc. 79−24230
TGS deuterated, X-irrad., negative ENDOR, collective motion 79−47357
l-thioproline single cryst., X-irrad., ESR and ENDOR study of radicals 80−45528
trapped electrons, ESR and ENDOR obs. 80−93161
triglycine sulphate: Cu^{2+}, cryst., struct., hyperfine coupling consts., ^1H ENDOR, isotope effects 77−71822
2,2,5-trimethyl-1,3-dioxane-4,6-dione, cryst., X-irradiated, methyl group hindered rot. tunnelling, EPR, ENDOR, and ELDOR 79−68328
tris-sarcosine calcium chloride:Mn^{2+} ferroelec. dynamics, EPR and ENDOR study 80−75972
urea-malonic acid, room-temperature ENDOR spectra obs. 80−106339

ENDOR continued
- vanadyl bisacetylacetonate, frozen soln., proton ENDOR, ligand hyperfine tensors 79−99792
- Varian HA-100D NMR spectrometer improvements for double NMR and ENDOR expts. 79−80651
- Wonderstone ENDOR cavity 78−70174
- xylitol, X-irrad., 4.2K, electron traps, alkoxy hyperfine coupling, ENDOR obs. 80−50863
- α-Al_2O_3:Co,H, Co and proton ENDOR, IR and optical spectra charge compensator nature and defect struct. 80−44956
- β-Al_2O_3-Na_2O, ENDOR meas. of defects 80−66074
- β-Al_2O_3-Na_2O, X-ray induced defects, EPR and ENDOR study 80−60456
- $AlPO_4$, synthetic berlinite, electron irrad. effects, ESR, ENDOR, optical spectral study 80−80608
- ^{27}Al, distant ENDOR and dynamic nucl. polarisation 80−2664
- BaClF, two types of F-centres, identification by ENDOR 78−60355
- BaF_2, mag. hyperfine const. and lattice distortion of V_k-centre 77−62864
- $BaF_2:Eu^{2+}$, ENDOR of ^{19}F ligands, under uniaxial stress 77−16207
- $BaMgF_4:Mn^{2+}$ ferroelec., EPR and ENDOR study, cryst. field tensor 80−71162
- BeO, ceramic and single cryst., EPR-ENDOR study of $[Li]^{\circ}$ centre 77−85569
- Be_2SiO_4:P, EPR and ENDOR 78−76295
- C-$^{+}NH_3$ radical, exchangeable H^+ hyperfine coupling, ENDOR obs. 79−36669
- $C_5H_6NNHCSNH_2$ radical, prod. in X-irrad. 1-phenyl-3-thiosemicarbazide, ESR, ENDOR 77−36770
- ^{13}C-labelled organic radicals, ^{13}C- and proton-ENDOR in soln. 78−55190
- $CaCO_3$:Mn, calcite, EPR and ENDOR absorpt. spectra of divalent Mn in single cryst. 79−47328
- CaF_2, mag. hyperfine const. and lattice distortion of V_k-centre 77−62864
- $CaF_2:Ce^{3+}$, ENDOR meas. on Ce^{3+} photochromic centre 78−19372
- $CaF_2:Ce^{3+}$, Na^+, ^{23}Na ENDOR meas. 77−69730
- $CaF_2:Eu^{2+}(Gd^{3+})$, ENDOR of ^{19}F ligands, under uniaxial stress 77−16207
- $CaF_2:Gd^{3+}$, $Li^+(K^+)$, elec. field gradient at nuclei on orthorhombic sites, vs. elec. zero-field splitting 79−87070
- $CaF_2:Gd^{3+}$, ligand ENDOR cubic centres, elec. field effect *(Russian)* 78−60357
- $CaF_2:Gd^{3+}$, S-state splitting, investigation by ESR and ENDOR at high pressure 78−52345
- $CaF_2:O_2^-$, struct. and dynamics, EPR and ENDOR obs. 79−33562
- $CaO:Gd^{3+}$, quadrupole hyperfine interaction, ENDOR 78−23370
- CdF_2:Cu, paramagnetic centre coordination, g-tensor orientation by anisotropy of ^{19}F ENDOR 80−54993
- $CdIn_2S_4:Cr^{3+}$, ESR and ENDOR 77−20692
- $CdS:Ti^{2+}$, superhyperfine interact., ENDOR study at 4.2K 80−80639
- $CeO_2:Yb^{3+}$, evidence for covalency 78−80247
- $CeO_2:Yb^{3+}$, trigonal sites of Yb^{3+}, ENDOR meas. 79−95677
- Co Schiff base complex, N,N′-ethylene-bis (salicylideniminato)-Co II pyridine doped in Znsalenpy crystal, ENDOR, EPR studies 80−34819
- Cr^{3+}, in alums, resolution enhancement through multiple quantum transitions 78−19374
- $CsCdF_3:Cr^{3+}$, ENDOR exam. of electron spin transfer 77−48089
- $CsCdF_3:Fe^{3+}$, ENDOR meas. on Fe^{3+}-F^--Cd^{2+} struct. 78−31122
- Cs_2NaYCl_6:Ce, ENDOR evidence of noncubic distortion 79−11357
- $Cs_2SO_4.Al_2(SO_4)_3.24H_2O$, $^{53}Cr^{3+}$ ENDOR Lines, RF ENDOR power and modulation freq. effects 80−75884
- $CsZnCl_4:Cu^{2+}$, electron spin echo, 35 GHz 80−13113
- Cu complex, bis-(salicyladoximato) Cu(II), ENDOR multiplet HFS, energy level non-crossing 79−72341
- Cu complex, $Cu(H_2O)_6^{2+}$, ligand hyperfine interactions, orbital angular momentum contrib. 80−96833
- Cu complex, Cu(II) bis(dithiocarbamate), ^1H ENDOR 80−87154
- Cu complex, Cu(II) impurity in α-glycine crysts., ligand ENDOR spectra 79−65765
- Cu-Cs diluted deuterated Tutton salts, electron non-Zeeman system, nuclear relaxation study 80−44951
- Fe dicyclopentadienyl-dibenzenevanadium, coalescence temps., full proton HFS tensor, ENDOR obs. 80−66073
- p-GaAs, electron-nuclear spin coupling, low field, under optical pumping conditions 77−77126
- GaAs:$^{56}Fe(^{57}Fe)$, paramag. centres, identification from ESR and ENDOR spectra 80−80600
- GaP:$^{56}Fe(^{57}Fe)(^{53}Cr)$, paramag. centres, identification from ESR and ENDOR spectra 80−80600
- GaP:Ge, ENDOR study, superhyperfine interactions 80−93210
- GaP:Mn, ENDOR of cubic $^{55}Mn^{2+}$ 79−69749
- GaP:S, ENDOR meas., symmetries, hyperfine parameters 78−72435
- GaP:Te, ENDOR meas., hyperfine interactions and elec. field gradient 79−42869
- p-GaSb, CESR, optically detected, giant Overhauser shift 79−4722
- p-GaSb, interband optical pumping, optical detection of EPR 77−28483
- KBr, ENDOR of F_A(Li) centre meas., 4.2 and 1.8K 77−63320
- KBr(Cl), F_A(Li)-centre spin-lattice relax. at 4.2K 78−91950
- $KCdF_3:Mn^{2+}$, evidence for F distortion, ligand ^{19}F ENDOR meas. 78−23369
- KCl, ENDOR line splitting by UHF field *(Russian)* 78−43678
- KCl, ENDOR of F-centres, sign of ^{41}K elec. quadrupole moment 80−34820
- KCl, F-centre hyperfine interaction parameters, press. shifts 77−8043
- KCl, self trapped exciton, off-centre configuration 79−42455
- KCl, self-trapped exciton, ENDOR 79−15377
- KCl:Ca,H, studies of localised vibrations of substitutional atomic H 78−80248
- KCl:H, dynamical superhyperfine interaction 80−2663
- KCl:H, ENDOR and ESR study of anion sites 80−108118
- KH_2AsO_4, γ-irradiated, free radicals, EPR and ENDOR study of consequences of ferroelec. transition *(French)* 80−93209
- KH_2AsO_4 irrad. ferroelec., AsO_3H^- free radical localised near impurity 77−24762
- $KH_2AsO_4:Cr^{5+}$, lateral proton config., ENDOR spectra 77−59483
- $KH_2PO_4:AsO_4^{4-}(SeO_4^{3-})$, ferroelec., low freq. fluctuations, isotope effects, EPR, ENDOR, ESCA 77−73118
- $KMgF_3$, F-centre, superhyperfine interaction, g-factor, symmetry, ENDOR obs. 80−39893
- $KMgF_3$, F-centre ENDOR study 80−108117
- $KMgF_3:Ti^{3+}$, ESR and ENDOR spectra 77−40121

ENDOR continued
- $KMgF_3:V^{2+}$, ^{51}V ENDOR meas., spin Hamiltonian parameters 79−28638
- $KMgF_3:Yb^{3+}$, perovskite type cryst., ENDOR meas. 80−80638
- $KMgF_3:Yb^{3+}$, transferred hyperfine interaction of Yb^{3+}, ENDOR meas. 78−19375
- $KZnF_3:V^{2+}$, ^{51}V ENDOR meas., spin Hamiltonian parameters 79−28638
- $KZnF_3:Yb^{3+}$, perovskite type cryst., ENDOR meas. 80−80638
- $LaCl_3:Gd^{3+}$, ^{139}La ENDOR, hyperfine and elec. quadrupole interactions 77−20749
- $La_2Mg_3(NO_3)_{12}.24H_2O:Mn^{2+}$, linear electric field effect on ground state splitting, EPR 78−80198
- $La_2Mg_3(NO_3)_{12}.24H_2O:Co^{2+}$, Ce^{3+}, relax. and ESR in magnetically cooled systems 78−88225
- $LiBaF_3:Mn^{2+}$, having inverse periodic struct., ENDOR study 80−97162
- LiF, neutron irrad., F-centres prod., hyperfine structure constants *(Japanese)* 77−69729
- LiF:H, neutron irrad., ENDOR meas. 79−11356
- α-$LiIO_3:Cr^{3+}(Fe^{3+})$, hyperfine interactions, RF discrete saturation of EPR lines 78−48032
- $Mg(NH_4)_2(SO_4)_26H_2O:VO(H_2O)_5^{2+}$, proton ENDOR meas. used to determine hyperfine coupling tensors 80−66075
- $Mg(NH_4)(SO_2)_4.6H_2O:Cu(H_2O)_6^{2+}$, ^1H ENDOR 79−73854
- MgO, ^{25}Mg superhyperfine struct. of V-type defects 77−66439
- MgO:Li, Fe(Cr), valence compensation of thermally generated $[Li]^0$ defects, EPR and ENDOR 79−77598
- MgO:Li, thermally generated $[Li]^0$ defects, valence compensation 79−77598
- $NH_4H_2AsO_4:Cr^{5+}$, ENDOR spectra 78−88224
- $NH_4H_2PO_4:AsO_4^{4-}(SeO_4^{3-})$, antiferroelec., low freq. fluctuations, isotope effects, EPR, ENDOR, ESCA 77−73118
- NO_2, radical, ENDOR and ESR obs. ^{14}N hyperfine coupling tensor 77−50455
- NO_3^{2-}, coupling consts., geometry, LCAO UHF and ENDOR data calcs. 77−14369
- NO_3^{2-}, ENDOR and ESR obs., ^{14}N hyperfine coupling and g-tensors 77−50455
- $NaF:Fe^+$, ENDOR associated with Na^+ vacancy 79−61264
- $Na_2S:Gd^{3+}$, EPR and ENDOR meas., spin-stress Hamiltonian 77−63278
- $PbF_2:Gd^{3+}$, EPR and ENDOR of Gd^{3+} at cubic sites 80−7161
- $PbF_2:Yb^{3+}$, superhyperfine interaction, ENDOR and RF discrete saturation expts. 79−73856
- l-proline monohydrate single cryst., X-irrad., ESR and ENDOR study of radicals 80−45528
- $RbAl(SO_4)_2.12H_2O$, ENDOR of $^{57}Fe^{3+}$ in trigonally distorted octahedral sites 79−38405
- $RbAl(SO_4)_2.12H_2O$, spin-Hamiltonian with trigonal S^3I terms for describing $^{57}Fe^{3+}$ ENDOR spectra 80−75885
- RbCl:Ca,H, studies of localised vibrations of substitutional atomic H 78−80248
- RbCl:H, dynamical superhyperfine interaction 80−2663
- $RbGa(SO_4)_2.12H_2O$, ENDOR of $^{57}Fe^{3+}$ in trigonally distorted octahedral sites 79−38405
- $RbGa(SO_4)_2.12H_2O$, spin-Hamiltonian with trigonal S^3I terms for describing $^{57}Fe^{3+}$ ENDOR spectra 80−75885
- Si, deformed, ENDOR of dislocation centre 78−72434
- Si, divacancy, hyperfine interactions from ENDOR meas. 79−42868
- Si, hyperfine interaction of divacancies, ENDOR meas. 77−4579
- Si:P, EPR of interacting donor centres, Overhauser effect and ENDOR 77−77085
- Si:Sb(P)(As), shallow donor electrons, hyperfine interactions, reply to Onffroy's calcs. 78−51934
- $SrCl_2:Gd^{3+}$, hyperfine interaction, X-band ENDOR 80−60457
- $SrCl_2:Gd^{3+}$, Na^+, elec. field gradient at nuclei on orthorhombic sites, vs. elec. zero-field splitting 79−87070
- SrF_2, mag. hyperfine const. and lattice distortion of V_k-centre 77−62864
- $SrF_2:Eu^{2+}$, ENDOR of ^{19}F ligands, under uniaxial stress 77−16207
- SrF_2:Yb, superhyperfine interaction of trigonal Yb^{3+} centres 78−27117
- SrO, hydrogenated, EPR and ENDOR meas. of γ-irradiated cryst. 77−8403
- SrO, neutron-irradiated single cryst., F^+ centres, ENDOR obs. 80−15824
- SrO, trapped hole defects, ENDOR and EPR spectra of V-centres 77−32255
- SrO:D, γ-irrad., V_{OD} defects, EPR and ENDOR 78−27116
- $ThO_2:Gd^{3+}$, ENDOR, nuclear mag. moment and HFS, stress-induced splitting 77−51990
- $ThO_2:Yb^{3+}$, trigonal sites of Yb^{3+}, ENDOR meas. 79−95677
- $YCl_3:^{143}Nd^{3+}(^{145}Nd^{3+})$, EPR and ENDOR spectra 79−78515
- $ZnS:Mn^{2+}$, cubic, EPR, ENDOR 77−77093
- $ZnTe:Mn^{2+}$, forbidden transitions of Mn^{2+} induced by hyperfine interactions 80−60458

energies, molecular dissociation *see molecular dissociation energies*

energy, binding *see binding energy*

energy, lattice *see lattice energy*

energy, surface *see surface energy*

energy bands *see band structure*

energy bands, electron *see band structure*

energy control *see power control*

energy conversion, direct *see direct energy conversion*

energy gap
- *see also superconducting energy gap*
- $A_{1-x}B_xC$, rapid localised non-destructive optical charact. of ternary layer *(French)* 77−62725
- adamantine family of semiconductors, props. and commercial appl. 79−42447
- adsorption rel. to dopant admixture 78−95596
- Al (001) surface, nearly-free-electron metal, origin of surface reson. states 78−95322
- alkali halide, optoelectronic props. 80−25330
- alkali metal salts with aromatic hydrocarbons, photoelectron emission and optical absorption *(Russian)* 78−80456
- amorphous, photogeneration, thermalisation model calcs., band gap *(French)* 80−75595
- amorphous, vac. evaporated, doping, transport and optical props. 80−49715

energy gap continued
- amorphous semiconductor, non-polar, mobility gap temp. variation calcs. 78—10339
- amorphous semiconductor, optical absorpt. edge shape, band edge fluctuations 77—20880
- amorphous semiconductor, tetrahedrally bonded, gap density of states 79—19545
- amorphous semiconductor film, ion bombardment effect on electronic props. 79—65125
- amorphous semiconductors, defects, band gap states 80—80215
- amorphous semiconductors, dispersive charge transport 80—39585
- amorphous semiconductors, optically induced metastable paramag. state, optical absorpt. and ESR meas. 77—40113
- amorphous solid, abnormal bonding and electronic states in forbidden energy gap 78—51942
- amorphous solids, optical absorption tail, shape 80—34946
- anthracene, solid, electronic struct., comparative ESCA study of polyacenes 78—52631
- band gap narrowing, physical mechanisms 80—15478
- band tailing due to zero-point vibrs. in perfect cryst. 79—28267
- benzene, solid, electronic struct., comparative ESCA study of polyacenes 78—52631
- binary compounds, energy gap trends, correl. with electron transfer parameters from optical spectroscopy 80—80174
- binary crystals, stability and average structure factors 78—91297
- binary solids, A^NB^{8-N}, average energy gap, quantum-dielectric-ion-depend. model 80—49571
- biological system, electron and excitation transfer, energy gap and temp. depend. 79—62187
- β-carotene, electronic struct., classical and double beam photoemission obs. 78—9285
- chalcogenide glass, charged dangling bond model reassessment 77—72813
- chalcogenide lone-pair semicond. charged impurities, effect on carrier concs., Street-Mott model 78—67984
- chalcogenides of non-transition metals, at. vol. and semicond. props. 77—20089
- chalcopyrites, refr. index dispersion 80—55057
- complex molecules, π-electron pair correl. of supercond. type, appl. to optical and mag. props. 79—54778
- compound semiconductors, electronic polarisability rel. to energy gap 80—10524
- crystal electronic spectrum, EM wave influence one-band approx. 79—33218
- degenerate nonparabolic semiconductor, rel. to acoustoelec. absorpt. 77—85269
- degenerate semiconductors, impurity band struct. for dense donors and acceptors 80—29348
- diamond, covalent semicond., depend. of energy gap on short-range order 78—84142
- diamond, nonlinear optical susceptibility, tight binding bonding orbital model 80—5784
- diamond, semiconducting, band gap temp. depend, dilation and vibr. contribs. determ. 80—10868
- diamond with local-field correction, dielec. const. calc. 80—11312
- dimers, singlet-triplet energy gap, temp. depend. 79—7809
- direct-gap crystals, one-photon absorpt., Keldysh and perturbation formulas 80—20607
- disordered semiconductor, Coulomb gap occurrence *(Russian)* 78—14658
- disordered systems, Coulomb gap computer simulation 79—51465
- dispersion reln. for energy bands and gaps, phase integral method, Mathieu pot. appl. 80—22224
- displacive ferroelectrics, connection between electron spectrum parameters and ferroelec. parameters 79—38483
- doped narrow gap semiconductor, two-channel vibronic mechanism of ferroelectric phase transitions *(Russian)* 79—56745
- doped semiconductors, impurity states, cluster model 80—20117
- education, deep one-dimens. periodic pot., zero energy gaps, Kronig-Penney model 80—62426
- education, forbidden energy gap meas. in Si and Ge p-n junctions 80—57027
- electroabsorption red shift rel. to band gap 77—1654
- electron correl. in extended systems, restricted HF calc., gap eqn. minimisation 80—54627
- electronic and spin Peierls transition, gap eqns. 80—24801
- electronic structure of solids under laser irradiation 78—91614
- exchange interactions in semiconductors and insulators, mean free path and energy gap effects 80—88522
- excitonic insulator, quasi-one-dimens. 79—90966
- excitonic insulator, tunnel breakdown theory *(Russian)* 80—29686
- excitonic phase in strong mag. field, sound absorption 77—20243
- excitons in electron-hole plasma, dynamical screening and self-energy, band gap shift to lower energy 79—15093
- ferrite, magnetoacoustic reson. in strong mag. field 80—11309
- ferroelectric crystal, absorpt. coeff. calc., Green functions method 78—10851
- field emission, effect of model hybridized energy bands 77—77349
- fluorescent planar collector-concentrators for solar energy conversion 80—45745
- GaP, reevaluation of bandgap and free exciton binding energy 78—60061
- glasses and amorphous semiconductors, band struct. and forbidden gap, review 78—75987
- graded and stepped energy band-gap MIS structures 80—2473
- graphite, diamagnetism with quasilinear dispersion law, orbital susceptibility, valence bands *(Russian)* 80—80475
- Hubbard model, narrow-band region, quasiparticles, electron relax. and transport props. 80—80151
- Hubbard model, split-band solution and energy gap, narrow-band region 80—75484
- II-IV-V_2 semiconductor, electronic struct. determ. 77—76751
- II-IV-V_2 semiconductors, electronic band struct., general model pseudopot. 78—39020
- II-VI quaternary semiconductor alloys, energy bandgap and lattice constant contours 80—103622
- II-VI semiconductor mixed crystals, two photon absorption *(Russian)* 77—20875
- II-VI semiconductors, mag. susceptibility, effect of physical parameters 80—44793
- III-V compounds, TlB^V and $A^{III}Bi$, possibility of existence with sphalerite struct. 80—33950

energy gap continued
- III-V quaternary alloy, $A_xB_yC_zD$ or $AB_xC_yD_z$, energy band gap and lattice constant 79—4296
- III-V quaternary alloys, energy bandgap and lattice consts. 78—67940
- III-V semiconductor, electronic struct. determ. 77—76751
- III-V semiconductor, energy gap and static dielectric const. 79—11062
- III-V semiconductor alloys, energy gap variation, CPA calcs. 78—43294
- III-V semiconductor solid soln., LPE, doping with groups II and IV *(Russian)* 77—80705
- III-V semiconductors, optical transitions, effect of perturbed k-selection and gap shrinkage 80—66257
- III-V semiconductors and ternary cpds., average energy gap calc. *(French)* 79—33228
- III-V ternary alloy, intrinsic bowing parameters of indirect energy gap 79—99469
- III-V ternary alloy semiconductors, bowing effect 79—95321
- insulator, many-electron systems, self-interaction corrected approach, beyond local spin density approx. 80—92844
- insulator, rel. to secondary electron escape probabilities 78—72651
- interband electronic Raman scattering, three band semiconductor, resonant EM field 78—23452
- interband Faraday effect 77—52046
- interface plasmons, longitudinal optical phonons, multilayer struct. 78—19118
- intrinsic semiconductors, indirect exchange interaction, finite temp., valence bands and energy gaps effect 80—59943
- Ising model, one dimensional, with infinite radius of interaction in transverse magnetic field 80—2587
- itinerant antiferromagnetism, antiferromag. instability and energy gap 78—31044
- leucosapphire, electronic band struct., optical props. 79—95329
- liquid semiconductor, metal-insulator transition model 77—1368
- metal, antiferromag., thermoelec. power in mag. field 80—70686
- metal-dielectric transition, two-band model, Coulomb interactions, self consistent calcs. *(Russian)* 80—80185
- metal-semiconductor interface, Schottky barrier formation, microscopic model 78—52087
- metal-semiconductor junction photoelec. phenomena, effect of dielectric gap and surface states *(Russian)* 78—84299
- metal/PbI_2/metal struct. reson. and inelastic tunnelling 80—44739
- metallic and nonmetallic solids, Fermi energies 80—2451
- metals, energy gap determ. by optical methods *(Russian)* 78—30867
- MIS negative barrier contact for induced back surface field solar cell 80—101101
- MIS structure, calc. of surface electron states using Green's function method 80—15611
- mobility edge behaviour, particle in random potential, divergence of Green's function 80—34409
- MOS structures, interface state density evaluated from charge-voltage data 79—11234
- Moss relation between refr. index and energy gap of semiconductors 80—11357
- naphthalene, solid, electronic struct., comparative ESCA study of polyacenes 78—52631
- naphthoxazole derivatives, elec. cond., thermoelec. power, energy gap, absorpt. spectra 77—32053
- narrow band gap semiconductors, physics, review 77—28112
- narrow gap semiconductor, surface states in energy gap 77—69401
- narrow-gap semiconductor, carrier quasienergy spectrum in strong EM wave field 80—92922
- narrow-gap semiconductor, recomb. instability of electron-hole plasma 80—39621
- nearly free electron model, vertex corrections 78—72054
- nonequilibrium thermodynamics of luminescent processes in solids 80—50435
- one-dimensional conductors, Peierls instability, dynamics, structural energy, pseudopot. calc. 80—54676
- one-dimensional conductors, Peierls transition temp. and 0K energy gap, mean field theory calc. 80—24782
- one-dimensional Fermi gas, energy gap, boundary conditions for renormalisation-group eqns. 78—10317
- one-dimensional homonuclear molecular systems, nature of energy gap 79—11063
- optical fibres, material dispersion 79—27377
- oxide semiconductors in photoelectrochemical conversion of solar energy, use as cell anodes 80—101120
- p-n junctions, minority carrier surface recombination velocity, lifetime, AM electron beam determ. 79—87145
- perovskite oxides, single cryst., photocond. and TSC meas. 78—43436
- phosphate glass:Yb^{3+}, excitation migration in inhomogeneous line profile, energy gap depend. 80—7407
- photodetector, threshold sensitivity for semiconductor photography 80—18017
- pnictides of non-transition metals, at. vol. and semicond. props. 77—20089
- bis cantena pol methylarsenide, energy gap depend. on As electron delocalization *(German)* 78—43296
- poly-N-vinylcarbazole—metal electrode, photoemission of electrons, photocond. meas. 79—91142
- polyacetylene, bond length alternation and energy gap, intermediate exciton formalism 80—29305
- polyacetylene, trans- and cis-isomer, electronic struct. calcs. 80—24788
- polyacetylene films, AsF_5 doped, photocond. and junction props. 80—70770
- polyacetylene films, doping investigation, insulator-metal transition, optical transmission meas. 80—103729
- polydiacetylene, extended chains with realistic model side groups, self-consistent electronic band structs. 77—39776
- polydiacetylenes, band struct., ab initio cryst. orbital method, and transport props. calc. 78—26811
- polydiacetylenes, electronic struct., cyclic vs. linear models 80—54587
- polydiacetylenes, optical props., and electronic struct., rel. to polyenes 77—23592
- polyenes, model results for π electrons 78—55128
- polyenes, optical prop., and electronic struct., rel. to polydiacetylenes 77—23592
- polyethylene, intrinsic photocond. under vacuum UV irrad. 80—70759
- polyglycine chain, electronic struct. and transport props., ab initio Hartree-Fock crystal orbital calc. 79—42448
- polyglycine chain with hydrated side group, electronic struct., transport props. 79—16146

energy gap continued
  polymer, fragment method, nonempirical, electronic struct. determ. 77—89684
  polymer UV photoconduction expts. and electronic props. 80—15572
  polymeric conjugated hydrocarbons, energy gap estimation, graph-theoretical approach 80—24789
  polymers with defects, energy bands, ab initio SCF crystal orbital calcs. 78—30884
  p-polyphenyls, band struct., mol. struct. effects calcs. *(German)* 77—47722
  porphyrin films, methine bridge substituted, surface photovolt. depend. on fabrication method 80—60119
  protein periodic models, ab initio calc. indicating insulating behaviour 77—25367
  PTFE film electret, optical spectra, band theory interpretation *(Russian)* 78—88376
  quartz, photoelectric and photoluminescent props. in fundamental absorpt. region 78—39596
  quasi-one-dimensional metallic systems, crit. behaviour, Ginzburg-Landau theory 79—56147
  quasilocal acceptor states, effects on band gap and electron mobility *(Russian)* 78—60082
  rare earth metal, effective-mass anal. carrier spectrum gap anisotropy 79—69494
  rare earth monobismuthides, LCAO calc., electronic struct. *(Russian)* 77—39777
  rare earth pnictides, prep. and props., book contrib. 80—54212
  resonant Brillouin scatt. as form of modulation spectroscopy 79—91456
  Schottky-barrier diode wavelength-modulated photoresponse spectra *(Russian)* 78—84300
  semicond. alloy, spin splitting and effective g-factor of T-holes *(Russian)* 77—51643
  semiconducting cpds., average valence-⟨4⟩ X-ray K-absorpt. edge shift and electronegativity 77—16424
  semiconducting powders, band-gap energies, photoacoustic meas. 80—70579
  semiconductor, Burstein-Moss effect, photostimulated absorption of light 80—29757
  semiconductor, covalent, molecular cluster model 78—43283
  semiconductor, disordered, Coulomb gap in energy spectrum 78—14648
  semiconductor, disordered, electroabsorption, contact excitons influence 80—10882
  semiconductor, electronic polarizability as function of Penn gap 80—49638
  semiconductor, exciton absorption, electric field effect *(Russian)* 78—43902
  semiconductor, graded-gap, internal photo-effects, excess carrier distribs. 80—107847
  semiconductor, high-power radiation propagation, rel. to interband absorption or amplification 79—76727
  semiconductor, lone-pair, localised gap states valence alteration model 77—8040
  semiconductor, meas. using piezo-reflection-retrotransmission technique *(French)* 77—28545
  semiconductor, Moss formula, refr. index rel. to energy gap 80—108173
  semiconductor, narrow-band indirect-gap, exciton instability 77—8029
  semiconductor, Penn gap, energy gap, and dielec. function 79—82520
  semiconductor, sp. ht. rel. to energy gap temp. depend. 80—54403
  semiconductor, superlattice doping, electronic states, elec. props. 79—95480
  semiconductor, temp. depend. of energy gap 80—2321
  semiconductor, two-phtoon absorption of ruby laser light, gap energy determ. 80—50373
  semiconductor, Wannier excitons, fine structure, lineshape and dispersion, review 80—44520
  semiconductor, zero-gap props. correlated to Γ_8 symmetry, review 80—6717
  semiconductor alloys, effect of lattice const. variation in band theory 80—49596
  semiconductor epitaxial layers, varizonal, parameter determ. by photoluminescence method *(Russian)* 80—108291
  semiconductor heterojunction, band-edge discontinuities and interface pot. step, two-band narrow-gap approach 80—39665
  semiconductors, disordered, light induced stationary non-equilibrium distribution of electrons, balance equation 80—39528
  semiconductors, electron states of point defects 80—39526
  semiconductors, evanescent states and complex bound structure 80—34387
  semiconductors, exciton effect in interband electronic Raman scattering 80—103946
  semiconductors, forbidden gap width, relation to refractive index, single oscillator calcs. *(Russian)* 80—71372
  semiconductors, isoelectronic series and trends in band struct. 77—89696
  semiconductors, partially disordered, density of states calcs., forbidden gap energy depth *(Russian)* 80—34347
  semiconductors, population inverted, resonant Brillouin scatt., photoelastic consts. 80—89015
  semiconductors, quasienergy spectrum, polarisation depend. in field of strong EM wave 79—69415
  semiconductors, role of excitons in dispersion effects, band gap determ. 79—65393
  semiconductors polarised light nonlinear rotation 80—93268
  semiconductors with position-dependent band gap and electron affinity, current densities 77—85210
  semimetal-exciton phase transition, microwave cond. 80—29430
  simiconducter heterojunctions, energy band profile and interface states calcs. 79—78162
  single crysts. and thin films, absorpt. edge temp. depend., gap energy changes 79—42991
  solar cell, efficiency, bandgap and temp. parameters relations 79—52935
  solid, phonon dispersion effects on nonradiative transitions 78—43926
  solid solution, density of states in forbidden band and band edge smearing 79—73418
  sputtered films, optical props. and appls. 78—72623
  superconductor, metal-insulator transition, electron pairing, effect on optical props. 80—60139
  superlattice, one-dimensional, band structure instability under strong population inversion 77—43470
  switching initiation, Anderson model 78—10524
  TCNQ salt, $(NMP)_x(Phen)_{1-x}(TCNQ)$, band filling and disorder 78—87968

energy gap continued
  TCNQ salt, K-TCNQ, energy gap, electron-phonon interaction, IR spectrum 78—15167
  tetracene, noncryst., localised valence states in forbidden gap 78—72113
  tetracene, solid, electronic struct., comparative ESCA study of polyacenes 78—52631
  tetracyanoplatinates, energy band calcs. 77—39780
  TMMC, linear antiferromag., energy gaps in spin-wave dispersion, neutron inelastic scatt. 79—91223
  transition metal pyrites, mag. and elec. props., review *(Japanese)* 78—47941
  transition metals, alloys, and cpds., XPS asymmetry of core electrons and electronic struct. parameters 80—93460
  (TTF^+) radical cation, optical props. in mixed-valence and monovalent halide salts and solns. 79—61399
  TTF-TCNQ, far IR photocond. meas. 77—32004
  tunnelling MIS structures photovoltaic energy conversion, band struct. 80—92995
  two-dimensional, Hartree-Fock soln. of CDW in mag. field 79—28302
  Urbach's rule derived from thermal fluctuations in the band-gap energy 79—33729
  UV high-power laser material, refractive props. and optical constants 80—106555
  variable band gap heterojunction laser spectral characteristics *(Russian)* 79—94236
  wide gap monocrystalline semiconductor, determ. of bulk and surface absorption coeffs., photoacoustic spectroscopy 80—4781
  a-Si:H, effect of H conc. on photovoltaic props. 79—99577
  Ag_3AsS_3, proustite, elec. cond. rel. to impurities, melt stoichiometry deviations 77—11914
  AgCl-AgBr, microcryst., halide comp. profiles, XPS 77—12850
  $AgFeSe_2(S_2)(Te_2)$, elec. props., band gap *(Russian)* 79—11116
  $AgGaS_2(Se_2)$, press. depend. of energy gap, absorption edge obs. 77—12401
  AgGaSe, direct gap semicond., exciton energy at 300K from reabsorption of luminesc. 79—78728
  $Ag_8GeS_6(Se_6)(Te_6)$, Ag_8SiSe_6, $Ag_8SnS_6(Se_6)$, absorpt. edge investigs. at phase transitions 78—35149
  Ag_8GeSe_6, polymorphic transition, absorpt. coeff. meas. 78—2257
  Ag_8GeTe_6, optical props. and polymorphism 80—45082
  β-AgI:Cu, pure and doped, photoconductivity, band struct., trap nature 79—95449
  $AgIn_5S_8$, cryst. growth and props. 78—39677
  $AgInSe_2$, press. depend. of energy gap, absorption edge obs. 77—12401
  $AgIn_5Se_8$, optical gap and low temp. depend. 79—99907
  Ag_8MSe_6, (M=Si, Ge, Sn), forbidden energy gap changes under high press., polymorphic transitions 77—51649
  Ag_8MSe_6, M=Ge,Sn,Si, absorpt. edge under hydrostatic press. 77—85740
  β-$AgSbS_2$, phase transitions, electrophysical props. 80—44316
  Ag_3SbS_3, pyrargyrite, elec. cond. rel. to impurities, melt stoichiometry deviations 77—11914
  p-Ag_2Te, electrophysical props. 77—39842
  Ag_2Te-Ag_2S system, elec. and thermal props. at 300K 78—64044
  Al (001), surface states, presence in energy gaps between muffin-tin zero and vac. level 79—60894
  Al, metallic, phonon freq., binding energy, compressibility, elastic const. and energy band gap calcs., linear pot. 80—88284
  Al-Ga-As heterostructure photocell with a transition layer 79—19655
  AlAs-GaAs (100) superlattices, band struct. 78—30868
  AlAs-GaAs monolayer crystal, two-photon absorpt. spectrum 78—52589
  AlAs-GaAs monolayered periodic cryst., optical props. 77—81079
  AlGaAs buried heterostructure lasers, gain and absorpt. spectra meas. 80—91792
  (AlGa)As, DH laser, threshold current temp. depend. 79—81431
  AlGaAs p-n diodes, I-V characts., tunnelling 80—100510
  $Al_xGa_{1-x}As$, Hall effect, press. temp. and composition depend. 80—49775
  $Al_xGa_{1-x}As$ layers, graded band gap, growth and properties 79—60645
  $Al_xGa_{1-x}As$, press. coeff. of direct band gap from optical absorpt. meas. 80—11430
  $Al_xGa_{1-x}As$:Cu, variable-gap semicond., impurity props., carrier recomb. 80—96907
  AlGaSb, growth and characts. for 1.0-1.8 μm heterojunction devices 78—6870
  $Al_xGa_{1-x}Sb$-Pd contacts, band gap depend. of barrier height 80—65685
  $Al_xGe_{1-x}Sb$, photolum. spectra 78—95602
  AlN film, chemical and plasmachem. vapour deposition, optical and other props. 77—28727
  AlN, VPE by closed space vapour process, and optical absorpt. edge 78—88371
  Al_2O_2-SiO_2, mullite 2:1 cryst., dielectric tensor components 77—48142
  Al_2O_3, noncrystalline films, opt. and elec. props. 77—51627
  Ar, liq., shock wave compression, 400 to 910 kbar 80—29101
  Ar, valence electron distrib., pseudopotential calcs. 80—2335
  As, interband, magnetorefl. for circularly polarised radiation 78—2840
  As:Ni(Ge)(S)(Se)(Te) film, amorphous, chemical modification of props. 80—49250
  As-Ge-Se system, synthesis and phys. props. of amorphous layers 77—52252
  As-Se amorphous system, photocond. props. 80—88587
  As-Se:^{197}Au, glassy, Au impurity influence, elec. cond., optical absorpt. and Mossbauer meas. 77—24558
  As-Te-Cu(Ag) system glasses, absorpt. coeff. and optical band gap 79—65829
  As_2S_3, amorphous, kinetics of photoconductivity, near fundamental absorption edge, energy gap determ. *(Russian)* 79—56263
  a-As_2S_3, energy gap meas., by Faraday rotation 80—66161
  As_2S_3 glass, determ. from elec. cond. 77—4337
  As_2S_3:Te glasses, doping influence on AC conductivity, electron transport by hopping 79—78106
  As_xS_{100-x} amorphous films, optical props. and photoinduced changes 80—60700
  As_xS_{100-x}, chalcogenide glass thin films, absorption in range of large optical densities *(Russian)* 80—11428
  As_xS_{100-x} glasses, band gap and neighbouring order *(Russian)* 79—60694
  $As_2S_3(Se_3)(Te_3)$ glass, electronic struct. calc. by extended Huckel theory 78—23012
  AsSe, molten semicond., pseudogap, elec. cond. and optical absorption meas. 77—8160

energy gap continued
$As_{1-x}Se_x$, ave. energy gap, optical freq. dielec. const. and refr. index 77–76739
As_2Se_3, cryst., electroabsorption on indirect gap 80–80812
As_2Se_3, cryst. and amorphous, optically induced absorption in band gap, picosec. dynamics 79–87439
As_2Se_3, effect of impurities on paramagnetic gap states 80–24848
As_2Se_3, molten semicond., pseudogap, elec. cond. and optical absorption meas. 77–8160
As_2Se_3, single crysts., fine struct. of direct gap from electrorefl. spectra 80–93280
$As_2Se_3Ag_x$, amorphous, optical absorpt. coeff. and DC cond. 80–54699
$As_xTe_{90-x}Ge_{10}$, $As_{35}Te_{55}Ge_{10-x}Si_x$ glasses, elec. and optical props., comp. depend. 77–24555
Au-n-$Ga_{1-x}Al_xAs$-n-GaP narrow-band variable-gap surface-barrier photoedetector 80–96944
Au-SiO_2-Si system, oxide film 16-36 Å thick, tunnel currents 80–70842
B:H amorphous films, optical band gap, thermal treatment effect 80–93415
BN, cubic, energy band and piezoelec. calcs. 78–72071
$BaAl_{12}O_{19}$, refr. index and optical absorpt. 80–66139
$Ba_{2.09}Na_{0.72}Nb_{5.02}O_{15}$, cryst. growth, monodomenisation, detwinning, optical homogeneity, composition, dielec., spectral props. 77–44151
$Ba_{2.09}Na_{0.72}O_{15}$, ferroelec., photocond. and optical absorpt. spectra. 77–8149
$Ba_{0.25}Sr_{0.75}Nb_2O_6$, ferroelec., photocond. and optical absorpt. spectra 77–8149
$Ba_{0.5}Sr_{0.5}Nb_2O_6$, electronic props. and photoresponses 80–92925
$BaTiO_3$ (001), LEED and UPS studies 80–100747
$BaTiO_3$, ferroelectric semicond. anomalous photovoltaic effect due to ionising radiation 80–29437
$BaTiO_3$, obs. by light-sensitive Rayleigh generation by surface piezoelectricity 78–43228
(Be, Al)B_{12}, wide-gap semicond., elec. cond., refl. and absorpt. spectra 80–20188
Be, electronic surface states, (001) surface, Brillouin zone 79–24047
BeS, electronic energy bands, APW and LCAO calc. 77–20236
BeSe, electronic energy bands, APW and LCAO calc. 77–20236
BeTe, electronic energy bands, APW and LCAO calc. 77–20236
Bi, band structure model parameters, deformation theory *(Russian)* 78–56067
Bi, superconducting transition temp., two-band model 80–25034
Bi-Sb, semiconducting solid solution, forbidden band width Sb-conc. depend. 77–66117
Bi-Sb, semiconductor-semimetal transition under pressure 78–34870
γ-Bi-Se phase, electronic props. 77–43493
BiI_3 film, exciton-phonon interaction, optical consts., Faraday effect., permitt. 80–59884
Bi_2O_3 film, optical energy gap, transmission spectra obs. 78–76440
$Bi_{1-x}Sb_x$, band inversion under press., Fermi surface anisotropy, galvanomag. meas. 77–51637
$Bi_{1-x}Sb_x$, far IR transmittance meas. *(Russian)* 77–44006
$Bi_{12}SiO_{20}$, film and single cryst., optical absorpt. edge and optical transitions 79–33730
BiTeI-SbTeI solid solns., form., crystn., elec., thermal props. 78–44003
C, amorphous, prepared by glow discharge method, elec. and optical props. 77–21036
C:H amorphous films, elec. cond. and optical absorpt. 80–49723
CC NiO, amorphous, charge transport in band tails 78–76026
CaB_6, electronic struct. APW and muffin-tin calcs. 80–29320
CaF_2-Ge(Si), cosputtered composite semiconductors, selective solar energy absorbers 79–56876
Cd, electronic surface states, (001) surface, Brillouin zone 79–24047
Cd-Hg, ω-phase, mag. susceptibility *(Russian)* 79–87231
$CdAs_2$ glasses, covalently bonded, energy gap correl. with average atomisation enthalpy 77–76740
Cd_3As_2, electron conc. temp. depend. heavy hole-cond. band energy gap 79–69410
Cd_3As_2 film, optical absorption edge 80–50450
Cd_3As_2, low-temp. energy band struct. and depend. of direct gap on press. and temp. 77–62822
$CdCr_2Se_4$, Mott ferromagnetic semiconductor, optical absorption edge, critical behaviour 80–97226
$CdGa_2(S_{1-x}Se_x)_4$ solid solns., band struct. behaviour w.r.t. comp. *(French)* 80–107699
$CdGa_2S_4(Se_4)$ film, optical absorpt., and energy gaps 78–11012
$CdGa_2Se_4$, thermoreflectance and visible absorpt. spectra, energy gap, cryst. field splitting 80–34945
$CdGeAs_2$, elec. and optical props., acceptor levels and energy gap determ. 77–85218
$CdGeAs_2$, optical and elec. props. 79–19590
$Cd_6Ge_3As_{11}$, press. depend. 78–72064
Cd_2GeO_4 anode for H_2O photoelectrolysis 80–108716
n-Cd_2GeO_4, electronic and cond. props. rel. to prep. conditions and defect struct. 80–107787
$CdGu_2S_{4(1-x)}Se_{4x}$, opt. absorpt., elec. cond., spectral response, thermopower 77–72862
$Cd_{1-x}Hg_xGa_2S_4$ solid solns., band struct. behaviour w.r.t. comp. *(French)* 80–107699
$Cd_xHg_{1-x}Se$, Hall coeff. and electron mobility, band parameters 79–73506
$Cd_xHg_{1-x}Te$, epitaxial graded-gap layers, elec. transport props. 77–85358
$Cd_xHg_{1-x}Te$, gap width temp. depend., absorpt. band edge meas. 78–72521
$Cd_xHg_{1-x}Te$, graded gap epitaxial layers, elec. and photoelec. props. 77–85362
$Cd_xHg_{1-x}Te$ inhomogeneous p-n junctions, elec. props. at high hydrostatic press. *(Russian)* 77–80835
$Cd_xHg_{1-x}Te$, photoconductivity under uniaxial compression, band gap 77–43657
$Cd_xHg_{1-x}Te$, temp. shift of energy gap 77–51658
$Cd_xHg_{1-x}Te$, temp. shift of energy gap, contrib. of lattice dilatation 78–51892
CdI_2, electronic struct., tight-binding calcs. 80–15446
$CdInGaS_4$:Au, single crystal, thermostimulated conductivity *(Russian)* 79–11142
$CdIn_2O_4$ anode for H_2O photoelectrolysis 80–108716
$CdIn_2S_4$, band edge study by photovoltaic effect 79–95444
$CdIn_2S_4$, photoconducting semiconductors, fundamental absorption edge 80–40130

energy gap continued
$CdIn_3Se_4$, cryst. growth, photoresponse and optical props. 78–39165
$Cd_{1-x}M_xS$ (M=Sr, Ca, Mg, Pb, Sn), solid soln., prep. and semicond. props. 80–2383
$Cd_{1-x}Mn_xSe$, fundamental optical props. 80–84751
CdO-SnO_2 DC reactively sputtered films, elec. and optical props. 80–103763
$Cd_xPb_{1-x}I_2$, photoluminescence comp. and energy depend., band gap 77–44045
CdS, charge in energy gap caused by acoustic domains 77–20822
CdS, equivalent gap alteration by light scatt. by acoustic domains 77–85687
CdS film, chemically sprayed, elec. and photocond. props. 78–34913
CdS, powder, mechanically induced localised states in energy gap 80–2354
CdS, resonance hyper-Raman light scatt. on optical photons *(Russian)* 80–14396
CdS:Bi film, spectral response characts. 78–2512
CdS:M, M=Zn, Te, doping and solid soln. prep. during VPE 77–85353
$CdSe_xTe_{1-x}$, solid solns., epitaxial layer prod. 78–23619
$CdSiP_2$, reflectance spectra at 300K 80–25407
Cd_2SnO_4 anode for H_2O photoelectrclysis 80–108716
CdTe, film, theoretical models of impurity levels 79–82557
CdTe:Cl, semi-insulating, impurity photocond. spectra, local state distrib. in band gap 80–107865
CdTe-CdS-CdSe system solid soln. single crysts., forbidden band width determ., comp. depend. 80–55083
CdTe-HgTe ideal superlattice, electronic props. calc. 80–49885
CdTe-HgTe superlattice on CdTE layers, evanescent states, tight binding calcs. 80–70611
CdTe-In_2Te_3, composition depend. of energy gap, optical absorpt. obs. 77–80728
$(CdTe)_{1-x}$-$(ZnSe)_x$ system, mutual solubility and band gap energy *(Japanese)* 77–51501
$CdTiO_3$, refl. and absorpt. coeffs. 3-3.5 eV, and refr. index dispersion *(Russian)* 78–39561
$CdTl_2Se_4$, single cryst., preparation, elec. cond. 77–24554
Cd_3X_2, X=P,As,Sb, phys. props. 78–26527
$Cd_{1-x}Zn_xS$, film, technical data, for low cost solar cell 79–48127
Ce_2ASe_5, A=Ge, Sn, diffuse refl. spectra and band gaps 79–51963
CeSb, forbidden band gap and electrotransfer parameters 80–39497
Ce_2Se_3-$SnSe_2$, solid-solution region, physical properties 78–43391
CoO, electronic struct. calc. 78–43297
CoO, self consistent energy band calc. 78–23022
Cr, antiferromag., stress depend. of Fermi surface 77–11846
Cr, antiferromag., transverse magnetoresist., electron interference oscills. 80–65534
Cr, incommensurate antiferromag., inelastic neutron scatt. meas. 80–25088
Cr, inelastic neutron scatt. expts., spin density waves 80–44818
CrAl, semicond. solid solns., depend. on antiferromag. ordering 78–67941
$Cr_{1-x}Mn_xSi_z$, semicond. props. 78–79992
$CrSi_2$, semicond. props. 78–79992
CsBr, (110) surface, electronic struct. of valence bands calc. *(Russian)* 80–75621
CsCl, (110) surface, electronic struct. of valence bands calc. *(Russian)* 80–75621
CsI, (110) surface, electronic struct. of valence bands calc. *(Russian)* 80–75621
$CsPbCl_xBr_{3-x}$, optical meas., LCAO band scheme 80–25437
Cu (111), final state band gap effects in UPS 80–89120
Cu, band structure and high-resolution normal emission UPS 80–6712
$Cu_{1-y}Ag_yInS_{2-x}Se_{2x}$, for solar photovoltaic cells 80–10982
$Cu_{1-y}Ag_yInS_{2(1-x)}Se_{2x}$, lattice consts. and band gap variations 79–78000
$Cu_{1-y}Ag_yInS_{2(1-x)}Se_{2x}$ pentenary alloy system, appl. to photovoltaic solar-energy conversion 80–35680
Cu_3Au, electrical resistivity and LRO, energy gap formation in Fermi surface 80–88533
CuBr, P exciton fine struct. 80–20091
CuCl, absorpt. coeff., 0.4-25 μm, band struct. determ. 77–73155
CuCl, defect and impurity bands, lattice consts. 80–54638
CuCl, electronic struct., self consistent all electron approach 80–2333
CuCl, self-consistent energy-band study 79–69408
CuCl, self-consistent zonal struct. calcs., electron spectrum gap *(Russian)* 80–34359
CuCl, UPS meas., electronic struct. 80–50529
CuCl, XPS and Auger spectroscopy, elec. struct. 80–29852
$CuCl_2.2H_2O$, energy gaps mag. field depend., antiferromag. reson. 79–87320
$CuGa_{0.5}In_{0.5}Se_2/Zn_{0.29}Cd_{0.71}S$ heterojunction solar cell, preparation and props. 80–101110
$CuGaS_2$, direct gap semicond., exciton energy at 300K from reabsorption of luminesc. 79–78728
$CuGaS_2$, press. depend. of energy gap, absorption edge obs. 77–12401
$CuGaS_2$-$CuGaSe_2$ system, forbidden-band width 78–35280
$CuGaS_{2-2x}Se_{2x}$, mixed crysts., band gap energy, photoluminesc. meas. 77–63454
$CuGaSe_2$, temp. depend. of fundamental absorpt. edge 78–92090
$CuGaTe_2$ and $CuInTe_2$, electroreflectance data, direct gap obs., cryst. field splitting and hybridisation degree 78–39557
$CuGaTe_2$ film, flash evaporated, growth and optical props. 79–95296
$CuGdTe_2$, synthesis and elec. props. 78–26529
$CuIn_{1-x}Ga_xSe_2$ mixed cryst., optical transmission spectrum and gap energy temp. depend. 79–65896
$CuInS_2$ film, photoconductivity effects 77–43662
$CuInSE_2$, temp. depend., 15-300K, optical absorpt. obs. 77–36266
$CuInS_2(Se_2)$ film, vacuum deposited, absorpt. coeff. 78–72621
$CuInSe_2$ film, photoconductivity effects 77–43662
$CuInSe_2$, influence of impurities and free carriers on optical props. 80–108225
$CuInSe_2$ semicond. films, optical props., 1-3 eV 78–27346
$CuInSe_2$-$CuInS_2$, solid soln., photo-EMF spectra 80–20248
$CuIn_2Se_{3.5}$, cubic ordered compound, optical gap 78–48175
$CuInTe_2$, direct energy band gap determ., electroreflectance meas. 78–2418
$CuInTe_2$ film, photoconductivity effects 77–43662
Cu_2O, energy band interactions under uniaxial compression 80–25412
Cu_2S, electromechanical props. *(Russian)* 79–11117

energy gap continued
Cu_2S, rel. to band models of Cu_2S-CdS heterojunctions *(Japanese)* 78—23154
$CuSbS_2$ crystals, growth and characterisation 80—60770
$Cu_{2-x}Te$-CdSe heterojunction, elec. and opt. props. *(Korean)* 77—51811
Cu(100), photoemission via Bloch states and evanescent band gap states, polarised synchrotron irradiation 79—61492
de Haas-van Alphen freq. and Fermi surface anisotropy press. depend. 80—59856
$Dy_{1-x}Sm_x$, magnetoresist. of polycryst. specimens in fields up to 44 kOe *(Russian)* 80—92880
$EuBi_2Te_4$, elec. cond., Hall, thermo-EMF coeffs. determ., 300-1100K 78—43386
$Eu_{1-x}{}^{2+}Eu_x{}^{3+}N_xO_{1-x}$, resist., pressure depend., semicond.-metal transition obs. 79—78104
$Eu_{1-x}{}^{2+}Nd_x{}^{3+}N_xO_{1-x}$, resist., pressure depend., semicond.-metal transition obs. 79—78104
EuO, crit. behaviour of opt. absorpt. edge 77—59418
EuO(S), effect of pressure on energy gaps 78—19239
$EuSb_2S_4(Se_4)(Te_4)$ elec. cond., Hall, thermo-EMF coeffs. determ., 300-1100K 78—43386
EuSe:Gd, mag. props. explained by band struct. 78—43324
Fe oxide films, semicond. electrode props. 79—91093
Fe_3Al, electrical resistivity and LRO, energy gap formation in Fermi surface 80—88533
$Fe_{2-x}Cr_xO_3$, elec., optical and photocond. props. 79—56262
FeF_3, thin film, optical absorpt. meas. 79—15546
FeO, electronic struct. calc. 78—43297
FeO, self consistent energy band calc. 78—23022
Fe_3O_4, hopping conduction and the Coulomb gap 80—44605
$FePS_3$, layered semiconductors, optical and electronic props. 80—70761
FeS_2, band gap temp. depend., optical absorpt. studies up to 425K 79—95758
FeS_2, pyrite, semiconducting props., energy gap press. and lattice parameter depend., Mossbauer obs. 80—44494
FeSi and $FeSi_2$, inner level ESCA spectra, many particle effects, hole lifetime *(Russian)* ·79—91560
$FeSiO_3$, UV and soft X-ray spectra, band gap determ. 79—61468
Fe_2SiO_4, UV and soft X-ray spectra, band gap determ. 79—61468
$Ga_{0.5}Al_{0.5}As$, heterostructure, cation order, effect on energy bands 79—1570
$Ga_{1-x}Al_xAs$, alternate monolayer crysts., MBE and props. exam. 78—10289
$Ga_{1-x}Al_xAs$, intervalley energy gaps, temp. junction, exptl. determ. 80—80179
$Ga_{1-x}Al_xAs$ layer, surface conc. x determ. by rapid localised non-destructive optical method *(French)* 77—62725
$Ga_{1-x}Al_xAs$, p^+-n-n^+ heterostructure, distrib. of injected carriers, forward V-I characts. *(Russian)* 80—6973
$Ga_{1-x}Al_xAs$, variation of optical transitions *(French)* 79—60708
$Ga_xAl_{1-x}As_x$ photodetector diode on GaAs substrate dark currents, tunnelling, energy gaps, effective masses 80—70805
$Ga_xAl_{1-x}P$ high-temp. solar cell with 0.3 eV band gap 80—21400
$Ga_{1-x}Al_xSb$, dispersive energy and energy gap calcs. *(French)* 79—99478
$Ga_{1-x}Al_xSb$ variable-gap p-n struct., selective photoelec. effect 77—76912
$Ga_{1-x}Al_xSb$, variation of optical transitions *(French)* 79—60708
GaAs (110) surface, electronic states near band gap 77—85290
GaAs, Auger recombination, luminesc. meas. 77—85850
GaAs, deep level photoionisation, absorpt. by derivative surface photovoltage spectroscopy 79—99575
GaAs, degenerate, impurity band struct. for dense donors and acceptors 80—29348
GaAs, direct energy gap, press. depend. up to 180 kbar 77—8020
GaAs, electron-hole plasma, ground state energy 78—84244
GaAs, heavily-doped, band gap, magnetoabsorpt. oscills. obs. 78—18960
GaAs, low-temp. absorption spectrum in presence of optical pumping 78—15188
GaAs, optical absorption spectrum dynamics using sub-ps. optical pulses 80—11431
GaAs pure and Se-doped, photoluminescence at dislocations, band gap electronic levels 79—99926
GaAs Schottky barrier diode, temp. depend. of intervalley gap, generalisation of thermionic emission theory 79—73586
GaAs, Schottky barrier ellipsometric electroreflectance spectra, energy band parameters 79—99853
GaAs, surface, distrib. of surface states 80—44692
GaAs, surface, electron struct. and Fermi level pinning by O_2 and metals 80—11066
GaAs, two-photon absorpt. spectrum, band gap luminesc. 78—10888
GaAs:Fe(Co)(Cu)(Ni), substitutional impurity elec. struct. 80—88513
GaAs-$Al_{0.4}Ga_{0.6}As$, p-n heterojunction, quantum confinement and compositional grading effects on band struct. 79—87151
GaAs-AlAs, heterostructure, effects of cation order on energy bands 80—11081
GaAs-$Ga_{1-x}Al_xAs$, variable band gap, photo-EMF 80—20296
GaAs-$Ga_{1-x}Al_xAs$ repeated monolayer heterostructure, electronic struct. 77—66197
GaAs-$Ga_{1-x}Al_xAs$ variable gap p-n junction, variable gap and photo EMFs 80—15596
GaAs-$Ge_{1-x}(GaAs)_X$ n-p heterojunctions, hydrostatic press. effect on elect. and photoelectric props. 80—20304
$(GaAs)_n$-$(AlAs)_n$, multilayer heterostructure, cation order, effect on energy bands 79—1570
$Ga_{1-x}As(Al,In)_x$, heterojunction solar cells, optimum bandgap, computer anal. 79—43767
GaAsP, VPE, lattice forbidden band composition depend. *(Hungarian)* 80—6669
$GaAs_{1-x}P_x$, piezomodulation spectra of indirect gap, zero-phonon and phonon-assisted transitions 77—48192
$GaAs_{1-x}Sb_x$, ($x \leq 0.05$), band gap, temp. depend., from edge photolum. meas. 80—71486
$GaAs_{1-x}Sb_x$ epitaxial n-n heterostructures, gap energies and interface pots., modulation electroabsorpt. meas. 79—11201
$GaAs_{1-x}Sb_x$, narrow-gap film on wide-gap GaAs, energy gap grading, optical transmission meas. 77—20943
$GaAs_{1-x}Sb_x$ ternary phase diagram, LPE, band gap and elec. props. 77—55896
$(GaAs)_{1-x}(ZnSe)_x$, LPE growth, resist., Hall effect and cathodoluminesc. meas. 77—28270

energy gap continued
GaInAsP, VPE growth and props. 80—16194
n-$Ga_xIn_{1-x}P$ photoelectrochemical cells, bandgap energy, electronic transition mode, and diffusion length 80—72070
$Ga_xIn_{1-x}P$ solid solutions, single cryst prep. and props. 80—16162
$Ga_xIn_{1-x}P$:N, Delta lattice parameter model, correl. with electronic props. 78—91560
$Ga_{1-x}In_xSb$, LPE on GaSb by stepwise grading, and characterisation 78—72745
$Ga_xIn_{1-x}Se$, fabrication, struct., elec. and optical props. 80—44180
GaN epitaxial films, cathodoluminesc. spectra 80—71496
GaN:Al, VPE grown, luminesc. and elec. props. depend. on doping conc., bound excitons 80—20688
GaP (110), electronic surface states, initial steps of O_2 chemisorption 80—49844
GaP, spectral depend. of O photoneutralisation cross-section near threshold, and band gap 79—1788
GaP:Cu, thermally and optical excited cond., deep level centres 78—72190
GaP-Ag(Au), Schottky barrier, stress effects on elec. props. 80—34512
GaP-based III-V solid solns., bonding and energy gap, mag. meas. 78—18580
GaP-liq. NH_3 soln. junctions, elec. characts. *(French)* 80—2460
GaP-ZnSe solid solutions, spectral studies *(Russian)* 79—91498
GaP_xAs_{1-x} solid solns., edge absorpt. 77—16334
GaS(Se)(Te), electronic struct., tight-binding calcs. 80—15448
$GaS_{1-x}Te_x$, solid soln., single cryst., crystallography and optical props. 79—55711
GaSb and $GaSb_xAs_{1-x}$ films, MBE growth and elec. props. 79—23863
GaSb, Auger recombination, luminesc. meas. 77—85850
GaSb, electron-hole plasma, ground state energy 78—84244
GaSb, photolum. spectra under hydrostatic press., energy shift of direct gap and L-conduction band 79—19930
GaSb, surface, electron struct. and Fermi level pinning by O_2 and metals 80—11066
n-GaSb:Te(Se), forbidden optical band gap, Moss-Burstein effect 78—88335
GaSb-InSb solid solns., heavily doped, electronic props. 77—80727
$GaSb_{1-x}As_x$-$In_{1-x}Ga_xAs$ heterojunction, prep. by MBE, transport props. 77—80827
GaSe, photocond., influence of stacking disorder 80—2422
GaSe, thin film, photoelectrical props. at high electric field *(Russian)* 79—11247
$GaSe_{1-x}S_x$, polytypes, exciton gap energies, luminesc. study 80—54611
GaTe, excitonic absorpt. edge, transmission and refl. meas. 80—40133
$Ga_{1-x}Te_x$ amorphous films, elec. cond., optical absorpt. and transparency, band gap energy 79—56335
Gd, ferromag., magneto-optical reson., optical consts. determ. 78—6657
Gd_2ASe_5, A=Ge, Sn, diffuse refl. spectra and band gaps 79—51963
Gd_2O_3, B-type monoclinic, DC(AC) elec. cond., thermoelectric power, dielectric const., temp. depends. 80—59980
β-Gd_2S_3:Nd^{3+}, spectroscopic props. from absorpt., photoluminesc. and excitation spectra 80—34968
Ge, amorphous film, annealing, effect on localised states 79—4535
Ge, energy band gap dilation and vibr. contrib. determ. 79—60703
Ge, energy gap, impurity conc. depend., calc. 80—80170
Ge, energy-gap narrowing and state filling under laser irrad. 79—42441
Ge, exciton energy gap and LA and LO momentum-conserving phonon energies 79—90965
Ge, nonlinear optical susceptibility, tight binding bonding orbital model 80—5784
Ge, photoluminesc., high excitation intensities, direct and indirect gap transitions 77—12429
Ge, picosecond optical response, effects of parametric scatt., energy-gap narrowing and state filling 80—11424
N-Ge, pressure influence on photoconductivity temp. dependence 78—76109
Ge:H, amorphous, H-states exam. 78—39059
Ge:Hg, S-type diode, elec. props. 80—20299
Ge:Pd and pure, photoelectric props., surface states *(Russian)* 80—60043
N-Ge-Bi-Se glass, elec. and optical props. 80—65550
Ge-Si cpds., effect of short-range order on direct optical gap 77—59252
Ge-Si_3N_4 system, potential barriers determ. from photoinjection carriers trapping 80—103756
Ge-Te-As-In quaternary compounds, thin sheets elec. props., thermoelec. power *(Spanish)* 77—69358
$Ge_{20}Bi_xSe_{80-x}$, semicond. glass, resist., thermoelec. power, optical absorpt. 80—88555
$Ge_{20}Bi_xSe_{70-x}Te_{10}$, semicond. glass, resist., thermoelec. power, optical absorpt. 80—88555
GeC_x, amorphous, prepared by glow discharge method, elec. and optical props. 77—21035
$GeFe_2O_4$, single crysts., elec. and mag. props, optical absorpt. spectra 80—54719
GeO_2, film, optical and electrophysical props. *(Russian)* 77—85821
GeP, thin films, vacuum-deposited, struct. characterisation 77—47691
GeS_2, energy gap and optical props. in IR region 79—51948
$GeS(Se)(Te)(O_2)$, K X-ray spectra, Ge atoms effective charge, energy-gap widths 77—28657
GeSe, single crystal, optical absorption 80—25383
$GeSe_2$, optical absorption edge 78—43901
$Ge_{0.08}Se_{0.92}$, molten semicond., pseudogap, elec. cond. and optical absorption meas. 77—8160
$Ge_{1-x}Se_x$, ave. energy gap, optical freq. dielec. const. and refr. index 77—76739
$Ge_xSn_{1-x}S(Se)$, lattice parameters, optical energy gap and IR refl. 78—23021
Ge(111)2×1, oxide layer, surface states detect optical reflectivity obs. 80—50368
H_2, highly compressed, combined representation method for use in band struct. calc. 77—89685
^3He, superfluid B-phase, collective excitations in presence of superflow 80—92744
HfO_2 film, CVD growth, struct., elec. and optical prop. characterisation 77—55891
Hg, expanded fluid, opt. gap, KKR band calcs. 77—1354
Hg, reflection spectra, electronic density of states, calc. 80—66229
$Hg_{0.75}Cd_{0.25}Te$, single crystal, reflection spectra 80—40140
$Hg_{1-x}Cd_xTe$, anodic oxide films, formation and props. 80—3212
$Hg_{1-x}Cd_xTe$ epitaxial layers, elec. props. 80—96910

energy gap continued
$Hg_{1-x}Cd_xTe$, interband magnetoreflectance 78–19448
$Hg_{1-x}Cd_xTe$, mixed crysts., band struct. and optical transitions, distorted atomic orbitals 77–69224
$Hg_{1-x}Cd_xTe$, props. and appls., book contrib. 77–39834
$Hg_{1-x}Cd_xTe$, zero-bandgap state induced by press., galvanomag. props. 77–47725
$HgCr_2Sd_{4-x}Te_x$, ferromag. semicond., zero bandgap transition 80–96783
$Hg_{1-x}Mn_xTe$, far IR studies of lattice and free carrier effects 78–39544
α-HgS, band gap shrinkage, cathodolum. under very strong excitation 77–85146
HgSe, elec. resist., high press. phase transform., band gap 80–70707
HgSe, interband absorpt. and Γ-point band structure parameters 79–47010
HgSe, interband $\Gamma_6 \rightarrow \Gamma_8$ magnetoabsorption, temp. study 80–76032
p-HgTe, inverted band struct., negative energy gap from IR absorpt. meas. 77–62820
HgTe, temp. depend. of energy gap, oscillatory magnetotransmission meas. 79–15441
HgTe-HgSe film, optical spectra in fundamental absorption edge 79–74012
IV-VI small gap semiconductor alloys, band edge parameters 80–49594
In:Sn, phonon spectrum, electron-phonon interaction *(Russian)* 78–18722
$In_{1-x}Al_xAs$, band gap, IR absorpt. spectra meas. 80–66205
InAs, band gap and effective mass, depend on impurity conc. 79–69412
n-InAs, edge luminescence band, shape depend. on degree of doping, band gap 80–7405
n-InAs, magnetophonon resonance under hydrostatic press. 77–47832
N-InAs, Moss-Burstein effect, S, Sn, Te dopants 78–64389
InAs:Zn, optical absorpt. and refl. spectra 79–91479
$(InAs)_x(CdTe)_{1-x}$, band gap and effective mass, IR spectra obs. 78–56491
$In_{1.9}As_{0.1}Se_3$, growth by chem. vap. transport, characterisation as photoelectrode 78–43994
(InGaAs)/(InGa)P, DH laser, threshold current temp. depend. 79–81431
$In_{0.53}Ga_{0.47}As$, LPE layer on InP, electron mobility and energy gap 77–24627
$In_xGa_{1-x}As$, epitaxial solid soln. film, spectral depend. of transparency, absorpt. spectra calcs. 80–45161
InGaAsP, bandgap energy by electroreflectance and photoluminesc. spectra 80–107700
InGaAsP, LPE growth techniques influence on composition 79–52130
InGaAsP, quaternary alloy, physical props. *(Japanese)* 80–15449
InGaAsP:Sn(Te)(Zn), LPE growth, influence of growth-solution dopants on distrib. coeffs. 79–47640
(InGa)(AsP)/InP, DH laser, threshold current temp. depend. 79–81431
InGaAsP-InP layers, grown by LPE techniques, lattice const., bandgap, thickness and surface morphology meas. 80–59818
$In_{0.79}Ga_{0.21}As_{0.54}P_{0.46}$, LPE layer, electroreflectance meas. 79–24290
$In_{1-x}Ga_xAs_{1-y}P_y$ layers on InP substrate, LPE growth, quaternary phase diagram, and band gaps 79–42403
$In_{1-x}Ga_xAs_yP_{1-y}$, electron effective mass from Shubnikov-de Haas meas. 80–80298
$In_{1-x}Ga_xAs_yP_{1-y}$, lattice matched to InP, band gap vs. comp., and Vegard's law demonstration 79–7782
$In_xGa_{1-x}As_yP_{1-y}$ layers on InP, LPE and opt. props. characteris. 79–28849
$In_xGa_{1-x}As_yP_{1-y}$ photodetector diode on InP substrate dark currents, tunnelling, energy gaps, effective masses 80–70805
InGaP-GaAs junction, effect of elastic strain on energy band gap and lattice parameters 79–24057
$In_{1-y}Ga_yP$-GaAs heterojunction, VPE, energy band gap and lattice parameter, lattice mismatch effects 78–95345
$In_{1-x}Ga_xSb$, energy gap, temp. depend. and photovoltaic effect 80–70746
$In_xGa_{1-x}Sb$, molecular beam epitaxy 79–47638
In_2O_3, thermally evaporated film, struct. and elec. props. 80–104066
InP, electron-hole plasma, ground state energy 78–84244
InP, free excitons in high mag. fields, band struct. 77–52129
n-InP, high field props. under high press. 78–26872
InP, reson. Raman scatt., deformation pots. 78–52495
InP, surface, electron struct. and Fermi level pinning by O_2 and metals 80–11066
InP_xAs_{1-x}, absorption edge and band gap comp. depend., bowing effect 77–4653
In_6S_7, TSC at various cooling rates *(Russian)* 80–11000
InSb (110), cleaved, gap states, field effect meas. 80–84501
InSb, absorpt. processes near bandgap, laser-induced hot electron and photocond. meas. 79–42584
n-InSb, cyclotron reson. study of conduction electrons, strong mag. field 80–2639
InSb, film, E_0, E_1 absorption edge size quantisation, optical and electroreflectance spectra 80–34998
InSb-CdTe solid solns., electroreflectance spectra, Brillouin zone transitions 80–7330
InSe, electronic struct., tight-binding calcs. 80–15448
InSe, large monocrysts. grown from nonstoichiometric melt, gap meas. 77–55882
InSe, photo-absorption of green exciton 80–80816
n-In_2Se, influence of hydrostatic press. on elec. cond. and Hall coeff. 77–55552
p-In_6Se_7, electrophysical props. 110 to 400K, thermal width of forbidden band *(Russian)* 77–35867
In_6Se_7, single cryst. prep. and electrophys. props. 79–43129
$In_{1-x}Te_x$ amorphous films, elec. cond., optical absorpt. and transparency, band gap energy 79–56335
In_2Te_3 defect semicond., photoconductivity kinetics 80–11035
$(In_2Te_3)_x$-$(Hg_3Te_3)_{1-x}$, photoelec. and luminesc. props. 77–39889
InTeBr, intermediate phase, cryst. struct. 80–100834
$(In_2Te_3)x$-$(Hg_3Te_3)_{1-x}$, $0.15 \leq x \leq 0.37$, E_g-comp. depend., spectral photo EMF meas. 77–47851
KCl, photoelectric emission in photon energy region 1.0 to 6.0 eV 80–108321
$KTaO_3$, obs. by light-sensitive Rayleigh wave generation by surface piezoelectricity 78–43228
La_2ASe_5, A=Ge, Sn, diffuse refl. spectra and band gaps 79–51963
LaOF, features of formation of band structure 79–33232
Li, cryst. and electronic props., Hartree-Fock calcs. 79–60698

energy gap continued
Li_2GeO_3, electromechanical props., band gap determ. from elec. cond. 77–8518
LiN_3, evidence for N_3^- from static and dynamic props. 78–60465
Li_3N, optical absorpt. coeffs., exciton creation, optical anisotropy 79–95796
$LiNbO_3$ doped with transition metal oxides, absorption spectra temp. depend. 77–90176
$LiNbO_3$ surfaces, ion and electron bombard., photoelectron spectroscopy and electronic props. 80–71559
$LuRhO_3$, elec., mag. and photoelectrochemical props. 80–96925
Mg, electronic surface states, (001) surface, Brillouin zone 79–24047
MgO, valence electron distrib., pseudopotential calcs. 80–2335
Mg_2SiO_4, forsterite, elec. props. 78–34833
$Mg_xZn_{1-x}Te$, high purity, luminesc. and band gap 78–68553
$Mg_xZn_{1-x}Te$, temp. depend. of energy gap, near band gap reflectivity spectra 79–28786
$MnGa_2S_4$, synthesis electrophys. props. 77–51747
MnO, electronic struct. calc. 78–43297
$MnSb_2S_4$, synthesis, electrophys. props. 77–51747
$(MnTe)_{1-x}(Bi_2Te_3)_x$ $(x \leq 0.05)$ solid solution, electrophys. props. 80–24925
MoS_2 molybdenite band structural props. rel. to supercond. and semicond. 80–96781
$MoSe_2$:Nb(Re), layered, elec. props., semicond.-metal transition 77–11922
NaCl, valence electron distrib., pseudopotential calcs. 80–2335
Na^ANO_3, (A=14,15), anomalous IR reflectivity min. in transverse-longitudinal band gap 79–56796
Na_2O-TiO_2-SiO_2 glass, elec. props. and energy gap 78–26921
Nb chalcogenides and chalcogenide halides, geometrical struct. and metal-metal bonding 80–80172
$NbSe_2$ (2H), supercond., thermodynamic props., exhibiting anisotropy and strong-coupling effect 77–12062
Nd_2ASe_5, A=Ge, Sn, diffuse refl. spectra and band gaps 79–51963
Nd_2O_3, A-type, thermoelectric power, AC cond. 78–68044
NdSb, forbidden band gap and electrotransfer parameters 80–39497
Ne, solid, rel. to optical spectra obs. of excitons 79–95340
$Ni_{1-x}Co_xS_2$, elec. cond., thermoelec. power and optical meas. 80–59986
NiO, electronic struct. calc. 78–43297
NiO, self consistent energy band calc. 78–23022
$NiPS_3$, layered semiconductors, optical and electronic props. 80–70761
P, amorphous, red, photolum. props. and band gap 80–50403
P, amorphous thin film, optical gap 79–24011
$Pb_{1-x}Cd_xS$ epitaxial layer, metastable, optical props. and electronic struct. 79–15543
$Pb_{1-x}Cd_xTe$, IR absorpt. study of Cd impurity levels, energy gaps 80–45081
$Pb_{1-x}Ge_xTe$, ferroelectric phase transition effect on forbidden band width 80–24794
$Pb_{1-x}Ge_xTe$, solubilities, elec. and optical props. 77–35940
$Pb_{1-x}Hg_xS$ film, solution-grown, struct., lattice parameters and optical band gap var. 77–69201
$Pb_{1-x}Hg_xS$, soln. growth, variable gap film for i.r. detector 77–1796
PbI_2, cryst., photocond., energy gap localised level obs. 78–43443
PbI_2, elec. props. rel. to polytypically modulated structs. 79–94971
PbI_2 polytypes, elec. cond., band gap reduction due to stacking fault levels 77–32015
PbI_2, press. depend. of band-gap excitons, 77K, optical absorpt. spectra 79–8157
PbI_2:KI alloys, fundamental abs. edge, potential as solar convertor 80–101128
$Pb_{1-x}Mn_xTe$, photovoltaic effect, p-n junction, energy gap determ. 80–92931
PbPo, electronic struct., relativistic band struct. calc. 79–4510
PbS, energy gap anomaly, relativistic band struct. calc. 79–4510
PbS, energy gap temp. depend., electron-lattice interaction, dilatation effect 79–65377
PbS epitaxial film, struct., optical and elec. props. 78–19583
$PbS_{0.1}Se_{0.9}$ 4.6 μm LED, room temp., band gap and electrolum. 80–66302
PbS(Se)(Te), energy gap and dielec. props., 77 to 373K 80–66100
PbSe, energy gap anomaly, relativistic band struct. calc. 79–4510
PbSe, energy gap temp. depend., electron-lattice interaction, dilatation effect 79–65377
PbSe, Hall effect and elec. cond. under strong anisotropic pressure 77–55549
p-$(PbSe)_{1-x}(SnTe)_x$, absorpt. edge temp. depend. *(Russian)* 78–34765
$PbSe_{1-x}Te_x$, symmetry change in cond. levels, photovoltaic effect and reflectivity obs. 78–34766
$PbSnF_4$, anionic conductor, thin films and ceramics 80–107556
$Pb_{0.65}Sn_{0.35}Se$, solid soln., elec. props. 78–39112
$Pb_{1-x}Sn_xSe$, thin film, opt. props. *(Japanese)* 77–1750
$Pb_{1-x}Sn_xSe$, transport phenomena in solid solutions with band inversion 80–107792
$Pb_{1-x}Sn_xSe$, X=0.03-0.07, monocrystal film, edge of intrinsic absorpt. *(Russian)* 80–71368
$Pb_{1-x}Sn_xSe(Te)$ epitaxial layers, growth, phase diagram, p-n junctions, optical, elec. props. 78–44029
PbSnTe/PbTe long wavelength inverted heterostructure mosaics, Fermi level temp. depend. 79–85182
$Pb_{1-x}Sn_xTe$, absorption edge shift, energy gap determ. 78–88308
$Pb_{1-x}Sn_xTe$, band struct. and phonon energies, tunnelling spectroscopy 78–72070
$Pb_{1-x}Sn_xTe$, energy band parameters from IR Faraday rotation 78–48154
$Pb_{1-x}Sn_xTe$, epitaxial layers, photolum. in mag. field 79–83033
$Pb_{1-x}Sn_xTe$ film, Burstein-Moss effect, absorpt. and photocond. spectra 78–18961
$Pb_{1-x}Sn_xTe$, hole effective mass near zero bandgap, IR refl. study 80–108205
$Pb_{1-x}Sn_xTe$, in MIS struct., tunnelling investig. of band gap and phonon energies 77–43733
$Pb_{1-x}Sn_xTe$, Mossbauer investig. of phonon softening at semicond.-semimetal transition 77–43908
$Pb_{1-x}Sn_xTe$, narrow gap, many-body interaction effects, Bloch electron scatt. lifetimes, energy renormalisation 80–49637
$Pb_{1-x}Sn_xTe$, single crysts, comparison of indirect and direct determ. methods *(German)* 78–26812
$Pb_{1-x}Sn_xTe$, single cryst. grown from vapour, photocond. meas. 79–24016

energy gap continued
- $Pb_{1-x}Sn_xTe$, $X=0.2$, monocrystal, edge of intrinsic absorpt. *(Russian)* 80—71368
- $Pb_{1-x}Sn_xTe$:In, carrier spectroscopic g-factors, magnetoresistance, temp. depend. 80—6705
- $Pb_{1-x}Sn_xTe$:In, Hall const. depend. on temp., autocompensation, band gap temp. depend. explanation 79—69527
- $Pb_{1-x}Sn_xTe$:In, Hall effect and photoconductivity *(Russian)* 80—103720
- $Pb_{1-x}Sn_xTe_{1-y}Se_y$, narrow-gap solid soln., lattice parameter, energy gap and Hall mobility of carriers 79—73154
- $Pb_{1-x}Sn_xTe_{1-y}Se_y$ solid solutions with constant lattice parameter, phase comp. 80—108417
- p-PbTe, absorpt. coeffs. meas. 77—24850
- PbTe, energy gap anomaly, relativistic band struct. calc. 79—4510
- PbTe, energy gap temp. depend., electron-lattice interaction, dilatation effect 79—65377
- PbTe, resonant scattering, photocond. 80—6910
- PbTe:Bi-PbSmTe-PbTe, epitaxial laser struct., growth, p-n junction position and lasing region 79—89908
- PdO, optical props., 0.5-5.4 eV 79—56813
- PdO, semiconductivity and stability, optical props. 78—43497
- $(Pd_xPt_{1-x})_3Fe$ atomically ordered alloy, thermoelectric power, carrier energy spin shift, mag. props. 80—29394
- Pr_2ASe_5, A=Ge, Sn, diffuse refl. spectra and band gaps 79—51963
- Pr_6O_{11}, mag. and transport props., multiphonon hopping conduction 78—19211
- PrSb, forbidden band gap and electrotransfer parameters 80—39497
- $Ru_2Ge_{3-x}Sn_x$, and $Ru_2Ge_{3-y}Si_y$, diffusionless phase transitions, elec. and mag. props. 80—96871
- S-based amorphous semicond. film, prep. by plasma decomp. of H_2S-N_2-NH_3, and characterisation 80—80422
- SMS, band struct. and semicond. metal phase transition 80—80180
- SbI_3, refl. spectra of cryst., 300-800nm, and derived optical consts. 79—87456
- Sb_2O_3 anodic layers on Sb, semicond. props. 79—56303
- Sb_2S_3, amorphous and crystalline thin films, optical consts. 79—91518
- Sb_2S_3 crystals, X-ray and DTA methods energy gap temp. dependence *(German)* 78—43119
- SbSI, band gap photoreflectance spectra near ferroelec. transition 79—38559
- SbSI-GeS_2 system glasses with and without antireflection coatings, optical props. 77—8595
- Sb_2Se_3, energy gap, light absorpt., elec. cond., photocond. meas. 78—47826
- Sb_2Se_3 single crysts., phys. prop. anomalies, 400-450K *(German)* 79—38072
- ScP, electronic struct., self-consistent Hedin-Lundqvist and Xα APW calcs. 80—29322
- Se, amorphous, defect states, SCF pseudopot. and tight-binding calc. 79—65415
- Se, amorphous layer, localised states in band gap 80—59928
- Se film, amorphous, determ. from photocond. props. *(French)* 77—72886
- Se film, noncryst., controlled vapour deposition, crystn., and optical props. 78—39696
- Se, photoelectronic behaviour, in glass transition region 80—60045
- Se, trigonal, behaviour of optical gap under press. 80—80171
- Se, trigonal, luminesc. identification of indirect transition 80—55189
- Se, X-ray sensitivity, induced photocurrents, xeroradiographic meas., pair creation energy 80—22490
- Se:Ta, electrophysical meas. rel. to control of conductivity type 77—24323
- Se-As, photoelectronic behaviour, in glass transition region 80—60045
- Se-based chalcogenide glasses, band gap variation 78—90461
- Se-Ge, amorphous, Raman spectra and average band gap 80—50327
- Si (001) surface, energy gaps in inversion layer band struct., spectroscopic determ. 79—82658
- Si (001)-SiO_2, n-inversion layer, valley splitting without effect mass approx. 80—15586
- Si, amorphous, discharge produced, optical and photocond. props. 78—39147
- Si, amorphous, effective mass theory, impurity states in band gap 79—77992
- Si, amorphous, film, hydrogenation by H diffusion, effect on elec. cond., band gap *(Korean)* 80—45326
- Si, amorphous, hydrogenated, pure and B doped, annealing effect on cond. and band gap states *(Korean)* 79—15142
- Si, amorphous, structural disorder rel. to electronic props. 78—34756
- Si, amorphous films, halogenated and hydrogenated, elec. and optical props. 80—97016
- Si, bandgap narrowing model in moderately to heavily doped material 79—99477
- Si, electron inversion layer on vicinal plane, minigaps 80—20282
- Si, energy band gap dilation and vibr. contrib. determ. 79—60703
- Si, energy gap, impurity conc. depend., calc. 80—80170
- Si film, amorphous, effects of annealing of gap states 78—72115
- Si, heavily doped, bandgap narrowing and diffusion length meas. 79—7781
- Si, heavily doped, bandgap narrowing 80—15479
- n-Si, heavily doped, meas. of minority carrier transport parameters 80—15537
- Si, heavily doped energy gap 77—43489
- Si, hydrogenated amorphous, gap states, comparison of photoemission and photocond. results 80—103724
- Si, IR photoresponse at 1.15 microns, band-gap narrowing effects 79—7864
- Si intrinsic, energy gap temp. depend. as thermodynamic problem *(German)* 77—43488
- Si, inversion layer, on vicinal plane, band structure 80—24994
- Si, Jahn-Teller distorted vacancy, electronic struct. 80—10869
- Si MOS struct., space-charge generation props. of Au 80—2475
- Si, nonlinear optical susceptibility, tight binding bonding orbital model 80—5784
- Si p-n junction, forward bias capacitance and current meas. for lifetime and band narrowing detn. 79—7892
- Si p-n junction diodes and solar cells, minority carrier diffusion length 80—107894
- Si plasma deposited amorphous hydrogenated film, optical props., annealing effect 79—56874
- Si, pn-product calc. as function of temp. and impurity conc. 77—35891
- Si, semi-empirical APW calc. of band structure 80—84424

energy gap continued
- Si, sputtered amorphous film, photocond. and electronic props., effects of annealing in plasma gas 80—44644
- Si, two-dimensional inversion layer on surface, minigap and conductivities 80—20267
- Si:F(,H), amorphous, electronic struct., orthogonalised LCAO calc. 80—44486
- Si:H, amorphous, density of states determ. using field effect 80—49937
- Si:H, amorphous, effect of gap state density on photocond. and photolum. 79—91096
- Si:H, amorphous, electronic states of hydrogenated Si, theory 79—42494
- Si:H, amorphous, glow discharge deposited, laser annealing 80—49104
- Si:H, amorphous, model for variable gap intrinsic semiconductor 80—10988
- Si:H, amorphous, RF sputtered, suitability as solar cell material 80—40864
- Si:H, amorphous thin film, ion plating, IR absorpt. meas. 80—84857
- Si:H,P, amorphous, heavily hydrogenated, high gap state densities 80—49803
- Si:H amorphous, solar cell structure, optical absorption by gap states 80—94052
- Si:H amorphous film, prep. by RF glow discharge decomp. of SiH_4, optical props. and H conc. 80—15416
- Si:H amorphous films, conductivity and temp. dependence of optical gap 80—100462
- Si:H amorphous films, ESR, optical gap and elec. cond. meas. 80—75842
- Si:H amorphous films, role of Ar in deposition process, IR absorpt. and photocond. meas. 80—50321
- Si:H amorphous sputtered films, optical gap, IR absorpt. meas. 80—50320
- Si:Mn(Fe)(Ni) amorphous films, ESR and elec. cond. 80—50171
- Si:O, O rich polycryst. film, carrier transport 78—80076
- Si:P, amorphous, CVD, defect compensation 80—54644
- Si:P, heavily doped, origin of photoluminesc. 79—56856
- Si:P, impurity cond., hopping conduction and the Coulomb gap 80—44605
- n-Si:P, piezoresist. under strong uniaxial elastic deform. 77—15858
- Si:P, strain-induced band-gap narrowing effect on P diffusion 79—55935
- Si:Pt, deep level, exam. by thermally stimulated current and capacitance techniques 79—1579
- Si-Ge, variable-gap cryst. made from solid soln. 79—66003
- Si-H, amorphous, energy gap negative-U states, Si-H-Si three centre bond model 78—91606
- Si-SiO_2 interface, (001) vicinal planes, minigaps in inversion layers, far IR absorpt. meas. 80—107919
- Si-SiO_2 MOS capacitors, relationship between trapped holes and interface states 80—70830
- Si-SiO_x-SiO_2 interface, energy gap variation 79—91148
- SiAs, monoclinic, OPW calc. 77—59255
- SiC, phys. props. and crystal growth, rel. to appl. in electrolum. devices, book contrib. 77—77299
- SiC_x, amorphous, prepared by glow discharge method, elec. and optical props. 77—21035
- $Si_xC_yH_z$ films, reactive plasma deposited, comp., IR anal., and optical props. 79—95945
- $SiH_{0.16}$ amorphous films, optical props. and photocond. near optical gap 80—50443
- SiH_x discharge produced amorphous film, gap state role in carrier transport 79—73608
- $Si_{1-x}H_x$, amorphous, gap states, DLTS 80—49656
- $Si_{1-x}H_x$:Al, amorphous, co-sputtered Al modification, electronic and optical props. 80—100461
- Si_3N_4, amorphous, charge transport in band tails 78—76026
- Si_3N_4 film, amorphous, optical props., band gap and surface roughness 77—32396
- Si_3N_4 film, plasma-activated CVD, optical prop. depend. on growth conditions 77—55892
- Si_3N_4-SiO_2:As, graded and stepped energy band-gap MIS struct. 80—2473
- Si_xN_y, amorphous, prepared by glow discharge method, elec. and optical props. 77—21035
- SiO_2, amorphous and cryst., XPS electronic band struct. interpret. 77—16454
- SiO_2, crystalline and amorphous density of states, bulk electronic struct., tight binding calcs. 80—44502
- SiO_2, film, transmission, photocond. and band gap meas. 79—73540
- SiO_2, HCl-grown oxides, characterisation of surface states using MOS transient currents 80—65696
- SiO_2, thermally grown film, optical absorption and photocond. 78—64421
- SiO_2, vitreous, photoelectric and photoluminescent props. in fundamental absorpt. region 78—39596
- SiO_2, vitreous, semi-empirical mol. orbital model, appl. to radiation compaction 79—73433
- SiO_2-TiO_2-Na_2O glass, optical absorption coeff., 2.1-3.3 eV 77—77240
- SiO_x, amorphous, ESR and hopping cond., He^+ irrad. effects 79—61213
- $Si_xO_yN_2$ film, opt. props. rel. to reactive sputter prep. conditions 77—81165
- Si(111)2×1, oxide layer, surface states detec., optical reflectivity obs. 80—50368
- Sm_2ASe_5, A=Ge, Sn, diffuse refl. spectra and band gaps 79—51963
- Sm_2O_3, B-type monoclinic, DC(AC) elec. cond., thermoelectric power, dielectric const., temp. depends. 80—59980
- SmS, semicond. thin film, absorpt. and refl. spectra, fine struct., cond. band extremum 79—69897
- SmSb, forbidden band gap and electrotransfer parameters 80—39497
- $Sn_xGe_{1-x}Te$, ferroelec. semicond. structural phase transition, X-ray study 79—37836
- SnI_2 band struct., layer model 80—44501
- $Sn_{1-x}Mn_xTe$, degenerate mag. semicond., thermoelec. power meas. 80—29392
- SnO_2, rutile, band gap assignment by two-photon spectroscopy 79—19513
- $Sn_2P_2S_6$, ferroelec., IR and Raman spectra, photocond., edge absorpt. spectra, spontaneous polarisation, forbidden gap 78—68514
- $Sn_2P_2S_6$, investigation of p-T diagram near a singular point *(Russian)* 80—88937
- $Sn_2P_2(Se_xS_{1-x})_6$, ferroelec. tricrit. phase transform., light transmission study 80—71355
- $Sn_{1-x}Pb_2Te$, elec. and struct. props. of epitaxial layers *(Russian)* 78—64147

energy gap continued
p-SnS, IR photocond., direct and indirect gaps 78−2514
SnS_2, 2H and 4H, effect of press. on optical absorpt. edge 77−77238
SnS_2, band struct., effect of polytypism 78−43293
SnS_2, cryst. growth, photoconductivity 77−85912
SnS_2, crystal growth and optical props. in visible and IR regions 77−52114
SnS_2 polytypes, electronic bandgap meas. 80−34358
$SnS_2(Se_2)$, electronic struct., tight-binding calcs. 80−15446
SnS_xSe_{2-x}, thermal changes in optical props. 78−19504
SnTe, bond gap, phase transform., optical dielec. const. meas. 80−10630
Sr, monochalcogenides, electronic energy band struct., APW calcs. 80−65439
$Sr_2Nb_2O_7$, electronic props. and photoresponses 80−92925
$SrTiO_3$, (100), LEED and UPS studies 80−100747
$SrTiO_3$ (111), O_2, H_2 and H_2O chemisorption, UPS and XPS studies, illum. effects 80−71572
$SrTiO_3$, optical absorpt. edge, absorption coeff., reflectivity, 293-853K 78−64342
Ta_2O_5 film, for MIS device, CVD and characterisation 77−4742
TaS_3, Raman spectra, CDW induced metal-semicond. transition 80−11404
Tb_2O_3, B-type monoclinic, DC(AC) elec. cond., thermoelectric power, dielectric const., temp. depends. 80−59980
Te, diffusion and cond. props., NMR investigation 79−78547
Te, energy gap, laser emission study of press. depend. 79−82521
Te, energy gap meas. under press., photocond. and transmission spectra 77−85267
Te, energy gap under press., elec. resist. and Hall effect meas. 78−30926
Te films, elec. props., 77 to 450K, thermal width of band gap 79−51698
Te, interband photocond. at up to 10 kbar, 1.6-200K 77−47850
Te, trigonal, electronic and optical props., press. depend., self consistent pseudopotential formalism 79−65838
Th_3As_4, prep. and semicond. props. 78−23087
Ti-Cr disordered alloy, gap nature of electron spectrum in region of struct. instability *(Russian)* 78−18947
TiO_2 (rutile), (001) and (110) surfaces, surface and bulk density of states calcs. 80−49858
TiO_2, cond. and valence band struct., gap anisotropy 77−47729
TiO_2, determ from elec. props. of Ti-TiO_2-Au diode 80−15617
TiO_2, indirect forbidden transitions, band struct. enhancement 80−44503
TiO_2, rutile, optoelectronic props., band struct., theory 80−80175
TiO_2 single cryst., refl. and electrorefl., energy levels 78−2871
TiO_x, UPS meas. of band struct., energy gap 78−72698
Ti_4O_7, hopping conduction and the Coulomb gap 80−44605
TiS_2, electronic struct. and props., self consistent numerical basis set LCAO calc. 77−89698
TiS_2, layer cpd., metal-insulator transitions, energy gap calcs. 79−78009
$TiSe_2$, layer cpd., metal-insulator transitions, energy gap calcs. 79−78009
$TlCl_xBr_{1-x}$, $TlBr_xI_{1-x}$, polymorphous mixed cryst. layers, opt. props. 78−23490
$TlGaS_2$-$TlGaSe_2$, phase and composition-property diagrams 80−55366
$TlGaS_2(Se_2)$ film, elec. and photoelec. props. *(Russian)* 78−52109
$TlInS_2$-$TlInSe_2$, phase and composition-property diagrams 80−55366
Tm_2O_3 film, between Al electrodes, prep. and elec. props. 80−60103
Tm_2O_3 film, electron beam deposition, elec. props., and struct. 79−87580
UO_2 and U_4O_9 single crysts., optical props. rel. to chem. bonding 77−28598
UO_2, electronic distributions by X-ray spectroscopy 80−97407
UO_2, electronic struct. and Coulomb correl. energy, XPS and bremsstrahlung spectra 80−55272
UO_2, optical props. and electronic struct. 78−68527
V, energy gap determ. by optical methods *(Russian)* 78−30867
VO_2, change in optical props. at semicond.-metal transitions 77−28597
VO_2, nonstoichiometry influence on electron struct. and metal-insulator phase transition 80−44507
V_2O_3, metallic differential refl. spectra and band struct. 77−1699
V_2O_5-B_2O_3-ZnO semiconductivity glasses, optical and modulated absorpt. spectra in band gap region 77−48189
V_2O_5-ZnO-B_2O_3 glass, sputtered, optical absorpt., band gap and Urbach tail 77−8597
VSe_2, 1T, band struct. calc. 79−95324
$W_xMo_{1-x}O_3$, absorpt. spectra and optical gap energies 79−91464
$Y_xAl_yO_z$, band gap, composition depend. 79−8161
$YFeO_3$ photoanode for photoelectrolysis of water 77−81409
YIG, elec. props. meas., 600-1500K 77−8098
YOF, band structure formation, valence band 79−33232
δ-Y_2S_3:Nd^{3+}, spectroscopic props. from absorpt., photoluminesc. and excitation spectra 80−34968
Y_3Se_4 powder, prep. and optical props. 77−28771
YbSb, forbidden band gap and electrotransfer parameters 80−39497
Zn, electronic surface states, (001) surface, Brillouin zone 79−24047
Zn-In-S thin layers, ternary phases, optical props. near long-wavelength intrinsic absorpt. edge 80−80887
Zn_3As_2, determ. of ionicity by X-ray absorption method 78−31278
Zn_3As_2, optical band-gap, absorption meas. 80−25372
Zn_3As_2, p-type semiconductor, absorption edge spectra, energy gap 79−56793
$Zn_xCd_{1-x}S$ film, prep. by soln. spray method, and struct., optical and elec. props. 78−52666
$Zn_xCd_{1-x}S$ film, prep. and use as heterojunction optical energy converters 79−95488
$Zn_xCd_{1-x}S$, film for heterojunction solar cell 77−8208
$Zn_xCd_{1-x}S$, forbidden band width, exciton refl. and luminesc. meas. 78−10947
$Zn_xCd_{1-x}S$, graded single crysts., laser or electron beam excited, luminesc. 77−85792
$Zn_xCd_{1-x}S$ monocrystal, optical and nonlinear optical characts. *(Russian)* 79−98442
$Zn_xCd_{1-x}Se$, vacuum condensates, forbidden band width determ. from transmission spectra 77−8670
$Zn_xCd_{1-x}Te$ films, absorpt. spectra in 3.0 to 5.8 eV range 79−52034
$ZnGeAs_2$, elec. cond. in solid and liq. state 77−11912
$ZnGeP_2$ bandgap absorption edge, spectra, electron transitions *(Russian)* 80−97305
$Zn_xHg_{1-x}Se$, band struct. from Shubnikov de Haas effect and hydrostatic press. meas. 80−49599
ZnO, band gap depend. on energy of zero-point vibrs., luminesc. obs. 79−73436
ZnP_2, Brillouin scattering and optical props. meas. 80−76041
α-ZnP_2, resonant Brillouin scatt. near indirect band gap 80−93350
Zn_3P_2, characteristics for photovoltaic appl. 79−7839
Zn_3P_2, determ. of ionicity by X-ray absorption method 78−31278
Zn_3P_2, direct and indirect optical transitions, metal-Zn_3P_2 contact photovoltage response 80−25402
Zn_3P_2, optical props., transition energies from transmission and refl. meas. 80−60532
Zn_3P_2, single crystal, growth, electronic and device props. 80−25551
ZnS sputtered film, interband photocond. edge *(French)* 77−8212
ZnS-ZnO, solid solns., edge emission and exciton spectra *(Russian)* 77−24899
ZnS_xSe_{1-x}, comp. depend., exciton refl. spectrum obs. 78−56071
ZnS_xSe_{1-x}, epitaxial film on CaF_2 comp. and temp. depend. of fund. band gap 80−11115
ZnSb, band struct. calc. 78−39015
ZnSe, band-edge photoluminesc., far-below band-gap excitation 80−76063
ZnSe, direct gap semicond., exciton energy at 300K from reabsorption of luminesc. 79−78728
ZnSe, single crysts., opt. band gap and Mn^{2+} EPR, effects of prep. conditions 77−47730
$ZnSiP_2$, reflectance spectra at 300K 80−25407
ZnTe, excitonic effects at E_0 and E_1 gaps, wavelength modulated reflectivity spectroscopic study 79−61400
ZnTe, pure and P(As) doped, shallow-acceptor, donor, free-exciton, and bound-exciton states 80−60667
ZnTe, two-photon absorpt. line shape near direct band gap and critical point 79−65898
ZnTe, undoped, electroreflectance of fundamental edge, exciton levels *(Japanese)* 80−20612
ZnTe:Bi, laser annealing, channelling, reflectivity spectra 80−66215
ZnTe:In(Al), pure and doped, Zn vacancy energy levels, elec. and optical props. 79−4827
ZnTe-CdSe, solid soln. formation and effects 78−27489
Zn_3X_2, X=P,As,Sb, phys. props. 78−26527
Zr-C disordered systems, Hall effect depend. on composition conc. 79−95459
ZrS_3, thermomodulated reflectivity and transmission, exciton ground state meas. 80−50357

energy gap, superconducting *see superconducting energy gap*

energy level crossing
see also Hanle effect
anharmonic oscillators, quantum theory, independent to spherically coupled, level crossing 78−77747
anticrossing effect, levels with different widths 78−55145
anticrossing spectroscopy appls. 80−23379
aromatic molecules in cryst. lattice, phosphoresc. intensity and optical nuclear polarisation, level anticrossing effects 78−91992
atom, metastable, sensitivity and level crossing role in parity nonconservation meas. 80−43005
atomic and nuclear parameters, from level crossing signals 79−3416
atomic gas, laser irrad., field avoided crossings, new transition channels 78−33477
atomic scattering theory, diffraction and angular momentum effects, level crossing of transient molecule 79−89734
atomic spectroscopy, appl. of terms level-crossing and line-crossing 78−70799
atoms, motional-Stark-effect-induced anticrossings 79−13666
atoms, oscill. strength in presence of level crossings 80−99480
avoided crossings, for exact states, model calcs., theory 79−10156
avoided surface crossing, multidimensional problem 79−89619
avoided-crossings, spurious, variationally calc., perturbation theory approach 78−5295
benzene, noncrossing and degeneracy in Hubbard models 80−14096
benzophenone $^3(n,\pi^*)$, and isotopic forms, in 4,4′-dibromodiphenylether, level anticrossings, ODMR obs. 78−2772
black holes, energy states, classical and quantum 78−12285
branch points and level crossings, multidimens. partitioning technique theory 79−6918
chloromethane, IR spectrum, evidence for $2\nu_3$ overtone 79−68226
collisional processes, nonreson. laser field effects 77−60093
cyclobutadiene, noncrossing and degeneracy in Hubbard models 80−14096
diatomic mols., spurious avoided crossing detection 80−87057
4,4′-dibromodiphenylether:benzophenone-d_{10}, optical decay constants, photoexcited triplet state near level anticrossing field 78−80250
1,8-dichlorooctane, quadrupolar relax. centres, limited spin diffusion 80−100649
Dirac Hamiltonian in presence of instanton and meron fields, fermion zero modes and level crossing 79−21927
dressed molecule, RF field, saturated absorpt. obs. 80−9648
electro-optic level-crossing effect 78−37608
fluorene: acridene, radical pair form. from excited states, optical nucl. polarisation obs. 80−14155
fluorene:acridine (phenazine)(anthracene), optical nuclear polarisation, non-crossing rule, guest-host complex 77−42339
fluoromethane, ν_3 band Lamb dips, effects of RF elec. field modulation on Stark spectra 80−52989
free radicals, spectroscopy, review, book contrib. 77−38653
gas laser, atomic constants and collision cross sections determ. by level crossing 78−50763
glyoxal, singlet-triplet coupling, double reson. and level-anticrossing spectroscopy 80−48053
halides, aryl and aryl-alkyl 193 nm photodissoc., fragment translational energy distrib. 80−48048
harmonic oscillator, $\nu=0$ level predissociation, by linear pot., line width and shift 77−75239
harmonic oscillator model in predissoc., level widths, shifts and curve crossing 78−90239
heavy particles, reson. scatt., pseudocrossing problem 79−49412
ice II, NQR of ^2D and ^{17}O 77−1617
iodomethane, RF field dressed mol. saturated absorpt. obs. 80−9648
iodomethane-d_3, ν_2 band, laser Stark saturation spectra 78−42125
iodomethane-d_3, Stark tuned level crossings and saturated absorpt., RF elec. field modulation effects 80−52989

energy level crossing continued
ions, multiply charged, highly excited states, parity nonconservation effects 80—52898
IR laser Stark spectroscopy, RF elec. field modulation effects 80—52989
Landau-Zener problem, random nature of motion role in intersecting terms problem 80—8937
laser excitation *(Rumanian)* 78—50510
laser forward scattering, two-beam polarisation method for sensitive detection of level crossing signals 80—43004
laser-induced collisional energy transfer, level crossing expansion 80—83461
lattice relaxation and time resolved polarization of emission from localized electron with level crossing 79—4840
lifetime meas. in atoms, mols., ions 77—30832
magnetic hyperfine atomic sublevels multiple anticrossings 80—27986
methane, $1B_1(1T_2)$ state, photodissoc., extended basis calcs. 78—9093
molecular collisions in laser field, multiphoton vibrational excitation enhancement, semiclassical theory 80—58350
molecular gas, laser irrad., field avoided crossings, new transition channels 78—33477
molecular pot. energy curves, non non-crossings, comment 78—78770
noncrossing rule, spurious avoided crossings, symmetry interpretation 77—57942
noncrossing rule for electronic pot. energy surfaces, role of time reversal invariance 79—54929
nuclear collective dynamics, level crossing effect 77—50042
one-electron atom, avoided crossings of reson. energy curves in external elec. field 78—17622
optical nuclear polarisation, field and orientation depend., non-crossing rule, perturbation anal. 77—42337
optical nuclear polarisation, the non-crossing rule, electronic relax. perturbation anal. 77—42338
PAA, liq. crystal, ^{14}N NQR freqs., double-reson. level crossing method 78—6602
palladiumporphin, in n-alkane, $S_1 \leftarrow S_0$ absorpt. spectrum, vibronic coupling and avoided crossing, field splitting 78—84613
palladiumporphin in n-octane cryst., lowest triplet state, ESR-optical detect. 77—58050
photon counting distribution second factorial moment meas. for level crossing detection 80—99485
resonance scattering methods in atomic spectroscopy 80—53167
resonance transfer rate of electron excitation, model of convergent terms, effect of diffusional motion of particles 80—8936
silicate glass: Cr^{3+}, optical props., 88-273K, energy levels in crossing region 78—6709
small molecules, spectroscopic techniques, review 77—54554
speckle pattern, monochromatic, amplitude and intensity spatial derivatives, statistical props. 80—53216
spectroscopy techniques, comparison with laser methods 77—30835
spurious avoided crossings, noncrossing rule calcs. 77—6661
spurious avoided crossings of pot. energy curves, eigenvectors and representation space 79—68286
three-state problem, non-noncrossings and accidental degeneracies 78—1034
transfer of oscillator strength in regions of avoided crossings, two state approx. 78—25484
xanthione, optically detected mag. reson. study of lowest excited triplet state of aromatic thioketones 78—86901
zero-field effect, selective refl. from atomic vapour 77—18856
$^4He(3^3P)$, fine struct., level crossing obs. 78—82686
Ar^+, orientation by collision with tilted surface, appl. to zero-field level crossing 77—3452
BH^{5+}, spurious avoided-crossings, variationally calc., perturbation theory approach 78—5295
Ba atomic beam, light-shift induced zero-field level crossing, optical Hanle effect 80—52947
Ba I, light shift induced zero-field level crossing 80—58220
Ba II, $6p^2P$ fine struct. g-values, laser excitation of fast ion beam 77—10645
BaO, A $^1\Sigma^+$ state, dipole moment, level crossing spectroscopy obs. 79—94040
$C^{6+}+H$, low velocity charge transfer, two-state approximation calcs. 78—42207
CN, free radical, anticrossing spectra for fine struct. consts. 79—68270
$CN(^4\Sigma^+)$, identification and characterisation by anticrossing 77—6864
CO_2, anomalous energy minima surfaces 78—86791
Cd, 5s5d states, Stark effect *(French)* 80—9543
Cd, broadening of 5^1P_1 level 80—83479
Cd II, A factors of ^{111}Cd and ^{113}Cd isotopes by hyperfine level crossing, stimulated emission 80—9564
CdH, lifetime, Λ-doubling, hyperfine struct., in $A^2\Pi$ excited states 77—58083
$^{113}CdII$, hyperfine level crossing, saturation induced in laser 79—18160
ClO_2, laser mag. reson. spectra tuned by Zeeman level crossing avoidance, perp. spectra 79—68229
Co I, odd levels, hyperfine structure by level-crossing and optical methods 77—83551
^{35}Cr, ^7P states HFS, level crossing technique, core polarisation, spin orbit interaction, config. mixing 78—78668
Cs, reson. multiphoton ionis. 79—41146
Cu complex, bis-(salicyladoximato) Cu(II), ENDOR multiplet HFS, energy level non-crossing 79—72341
Cu, crossing effect in 3249Å emission line, mag. field strength depend. 78—25491
D_2, electron impact dissoc., anticrossing signals, Doppler-profile technique 78—33619
D_2, $G(3d)^1\Sigma_g{}^+$ and $g(3d)^3\Sigma_g{}^+$ singlet-triplet anticrossing 78—42138
H, parity mixing, relativistic neutral current interactions and nonrelativistic pots. 79—26908
H, Stark-induced anticrossings, Lamb shift meas. 78—33467
H, Stark-induced anticrossings, $^2P_{3/2}$-$^2D_{3/2}$ Lamb shift meas. 78—33468
H, subnatural linewidth resolution $2^2S_{1/2}$, $2^2P_{1/2}$ level crossing, Lambshift, pulse technique 79—22669
H + highly stripped ions, energy gap and couplings at pseudocrossings 79—3526
$H+Zn^{2+}(Cd^{2+})(B^{2+})(Mg^{2+})(C^{6+})$, electron capture by slow ions, pseudo-crossing 80—43176
H_2, electron impact dissoc., anticrossing signals, Doppler-profile technique 78—33619
H_2, singlet-triplet anticrossings between ungerade states 77—14498

energy level crossing continued
H_2, singlet-triplet anticrossings, doubly excited 3^1K-$g(3d)^3\Sigma_g{}^+$ states 78—50598
$H_2{}^+$, spurious avoided-crossings, variationally calc., perturbation theory approach 78—5295
He, 1s3d config., Zeeman sublevel energies, anticrossing and degeneracy 77—23417
He, fine structure intervals, elec. field-induced anticrossing meas. 78—42031
He I, fine struct. of triplet term of 1s3d config. 79—3595
He, level crossing signals in inhomogeneous mag. field *(German)* 77—27037
He, singlet-triplet anticrossing, elec. field induced 77—14404
He^+, fine struct. obs. by beam-gas spectroscopy, level crossing resonances 80—9719
He^+, n=4 level, fine struct., level-crossing and anti-crossing reson. obs. *(French)* 78—25488
He+He, Rydberg states ang. momentum transfer, singlet-triplet anticrossing 77—88543
^3He atom forbidden singlet-triplet anticrossings, D levels 80—99491
^4He, fine structure intervals in 3^3P and n^3D states, level crossing meas. 77—14396
^4He, singlet-triplet anticrossings, ^1D and ^3D state separation, mixing 77—6738
Hg, 8^3S_1 level, Lande factor *(French)* 77—430
Hg lamp, line crossing obs. in 2537 Å line 78—9129
Hg, two photon excitation, time resolved spectroscopy 80—87075
K, fine struct. splittings of 5d and 6d states 79—76396
$KCl:PO_2{}^-$, triplet state, level anticrossing and pseudonuclear Zeeman effect, microwave ODIMR 80—39896
^{83}Kr, $4p^55p$ config., HFS meas. using level crossing technique 80—18827
Li 3^2D state, level crossing meas. 79—13832
Li, 4^2D state, fine-struct. splitting, level-crossing spectroscopy 77—83552
Li_2, MCSF accurate pot. energy curves for $^3\Sigma_u{}^+$ and $b^3\Sigma_g{}^+$ states, level crossing 77—50369
^7Li, HFS and at. lifetimes 78—66678
$Li(2p)+H_2(N_2)$, Li(2p) excitation, alignment and orientation obs. 80—63794
Mg, $3s3d^3D$ and $3s4d^3D$ states, fine-struct. meas. by level crossing spectra 79—36572
Mg II, fine struct. of ^2D and ^2F sequences by level crossing and anticrossing spectroscopy 79—6919
Mo I spectrum, lifetime meas. of excited states of $4d^55p$ and $4d^45s5p$ config. 79—13683
N, oscillator strength calc. for $^4S^0$ to ^4P sequences 78—25485
NE, disalignment collision cross sections of $2p_4$, $2s_2$ levels, mode crossing determ. 79—18162
NH_2, hyperfine level crossing spectroscopy of (0, 9, 0) and (0, 10. 0) vibr. states 78—17728
NH_2D, dipole moments effects of RF elec. field modulation on IR stark spectroscopy 80—52989
Na, laser induced zero-field effect, non-optical obs. 78—37604
Na, Rydberg states, elec. field ionisation, sensitive detection of multiple thresholds 79—7026
$Na_3Pr(C_4H_4O_5)_3.2NaClO_4.6H_2O$, single cryst., forbidden $A_1 \rightarrow A_1$ transition, mag. field induced intensification 80—50302
Ne, fine struct. obs. by beam-gas spectroscopy, level crossing resonances 80—9719
Ne, isoelectronic sequence, excitation energy and oscillator strength, level crossing anomaly, relativistic RPA calc. 80—14077
Ne, optical-optical double reson., $2p_4$ and $2s_2$ level g_J-values by mode crossing 77—50411
^{21}Ne, $2p^53p$ config., hyperfine mag. const. by laser level-crossing technique 78—50509
^{61}Ni, $3d^94p$ $^3D_2$ level, hyperfine struct., level crossing obs. *(French)* 78—41997
O_2, harmonic oscillator model in predissoc., level widths, shifts and curve crossing 78—90239
OPF_3, forbidden transitions, mol. beam elec. reson. obs. using avoided crossings 78—29775
Rb, $6^2P_{3/2}$ state, β_j Stark const. meas. 77—88424
^{87}Rb, Stark effect on $5^2P_{3/2}$ state 79—3399
SmI, Zeeman coherence, transient and stationary, polarisation spectroscopy 80—58212
Th, tensor polarisabilities of levels, level crossing method 79—10223
Tl I, $6s^26d^2D_{3/2}$ state, hyperfine struct. interaction const., mean lifetime 77—42286
^{129}Xe and ^{131}Xe, HFS of 6p, 7p, 4f and 5f levels *(French)* 79—68211
Yb, $4f^{14}6s6p$ $^3P_1$ and $^1P_1$ levels, Stark effect, tensor polarisabilities 80—87080
Yb, HFS in 6s6p $^1P_1$ state, level-crossing and anticrossing spectroscopy 77—27036
^{173}Yb, $6s6p^1P_1$ state, level crossing with additional pumping of ground state 77—34595
ZnH, lifetime, Λ-doubling and hyperfine struct. of $A^2\Pi$ excited states 77—58083

energy level transitions, atomic *see atomic spectra*

energy level transitions, molecular *see molecular spectra*

energy level transitions, nuclear *see nuclear energy level transitions*

energy levels *see energy states*

energy levels, atomic *see atomic structure*

energy levels, molecular *see molecular energy levels*

energy levels, nuclear *see nuclear energy levels*

energy levels in solids and liquids *see electron energy states (condensed matter)*

energy loss of particles
see also channelling; electron energy loss spectra; radiation effects
α-particle in air, range, energy and range straggling, stopping power meas. 78—73815
α-particle stopping power and straggling in water and tissue-equivalent liquid 80—23274
β-ray absorption, expt. using 1-ply toilet paper 77—22358
acetaldehyde, gas, stopping cross section for 0.3 to 2.0 MeV He^+ ions 78—63537
air, weakly-ionised, secondary electron distrib., produced by electron source distrib. 80—6211
alcohols, α-particle impact, 0.3-2.0 MeV, O stopping cross-sections 78—17753

energy loss of particles continued
aldehydes, molecular stopping cross section of He^+ ions and atomic stopping cross section of O 78−67746
alloys, effective atomic number from β-ray produced bremsstrahlung meas. 78−22046
alpha particle dose to respiratory airway epithelium 77−44756
alpha-particle range and stopping power, new empirical relns. 77−61671
alpha-particles, in high-density plasma, energy loss, dielec. function calcs. 77−89273
alpha-particles, stopping power and straggling in liqs., Si semicond. detect. spectrometer 78−82563
amorphous and polycryst. surfaces, anomalous yield enhancement, for 180° He^+ scatt. 79−100008
amorphous medium, neutron induced at. cascades, slowing down 77−1156
amorphous medium, radiation suppression *(Russian)* 78−30686
amorphous targets, energetic in transport, Monte Carlo program 80−102411
analytic range-energy relation for light ions in materials with atomic numbers from 1 to 92 79−93895
anisotropic medium, ionisation losses of fast charged particles *(Russian)* 78−34559
anisotropic point source in infinite medium, energy deposition 80−88228
anisotropic scatt., statistical fluctuations of collision energy losses 77−62572
anthracene, (100) and (110), scintillation response of α-particles in planar channelling and blocking expts. *(German)* 79−14869
aqueous tissue equivalent soln., alpha particle stopping power, 0.5-8 MeV 78−40334
atom-atom collision cascades localisation, impurity and thermal vibr. influence, computer simulation method 80−88227
atom-electron collisions, stopping cross section *(Russian)* 78−55901
atomic collision events, spike and shock processes 80−2105
atomic collisions in solids, book contrib. 78−75697
atomic collisions in solids, interatomic pot. 79−51173
atomic number dependence of photon and electron interactions 77−37017
atomic particle stripping analysers with solid and gaseous targets 79−1341
axial channelling, effects of dislocations on energy loss of channelled ions 77−11610
axisymmetric energy straggling, apparent higher-order Z_1 effects 78−21830
benzene, electron random motion in molecular materials, Monte Carlo anal. 77−31703
beryl, natural and synthetic, ion channelling transmission ratios 80−75277
beta flux absorption, beam unfolding calc. in segment model 77−69004
beta particle attenuation, effect of absorber postion 79−54753
beta sources, depth dose distribs. in varous materials 78−17462
Bethe stopping power formula, higher order Z_1 corrections 77−30732
Bethe stopping-power formula, higher-order Z_1 corrections 80−9479
Bethe theory, inelastic collisions of fast charged particles 78−58783
binary compound, fast ion stopping, chem. bonding effects 77−27929
binary targets, deposited energy computation 80−892
biological material photon interactions, calc. of average energy absorbed 80−45947
biological tissue, recoil nuclei specific energy losses, analytic representation 79−100680
Boltzmann transport eqn., role in radiation damage calcs. 79−77653
bound electron state in wake of swift ion in solids 77−15469
bremsstrahlung, ang. distrib. of nonrelativistic intensity calcs., program 78−87001
bremsstrahlung distrib. in water, Al, Fe and Pb, 22 MeV electron bombardment 78−59840
bremsstrahlung energy deposition as function of converter foil thickness, optimisation 77−23388
bremsstrahlung in bulk media, shielding study, Monte Carlo anal. of thick target spectra 78−59839
bremsstrahlung radiation, ang. distrib. and penetrating power 78−70657
1,3-butadienes, methyl substituted, singlet-triplet transitions, energies, relative cross-sections, $He^+(H_2^+)$ impact spectra 78−86942
butane, α-particles stopping cross-section determ. 79−49917
calorimeter, method to distinguish between electromagnetic and hadronic showers 79−748
cascade processes of particle passage through substance, fluctuations 80−92579
cellulose nitrate, detection efficiency and alpha-particle range 77−10540
cellulose nitrate, energy loss critical rate for charged particles 80−74082
cellulose nitrate plastic detector, charge resolution improvement for cosmic ray particles 79−84671
cellulose nitrate plastic detector, spallation products from energetic neutrons 78−17198
cellulose nitrate track detectors, detect. of efficiency and range meas. of alphas and protons 78−17524
channelled ions, effect of screw dislocations 78−67761
channelled protons, theory of energy loss 78−38765
channelling of 1 GeV protons, pions and deuterons in Ge crystals 77−89488
charge changing collisions of ions, relative populations 80−52835
charge deposition profiles, thin layers near irrad. material interfaces 77−27906
charged particle activation anal., are energy in ave. stopping power method 78−76963
charged particle activation anal., average stopping power method 78−48724
charged particle chemical analysis, two reactions method 78−76964
charged particle energy loss in cryst., theory 80−79847
charged particle energy loss in turbulent plasma 77−84400
charged particle hydrodynamic acoustic radiation in water *(Russian)* 77−54459
charged particle in free-electron gas, Lindhard theory of stopping power, numerical evaluation 80−893
charged particle in molecular gas, high-energy calcs. 77−6891
charged particle moving in medium, electron density fluctuations, plasmons, wakes and clusters 79−47032
charged particle stopping ratios in inhomogeneous targets, effect of multiple Coulomb scatt. 79−26854
charged particle telescope TOF system, elemental assignments of reaction products 78−86720
charged particle transport in one-dimensional finite system 77−61035

energy loss of particles continued
charged particles, completely and partially stripped, general stopping eqn. 77−62573
charged particles, review 79−95060
charged particles in matter, determ. of specific energy loss 77−67952
charged particles in matter, loss determ. by bombardment of absorbers, theory 79−26864
Cherenkov losses of relativistic neutron in conducting medium 78−5410
Cherenkov radiation from electrons in mica target, 140-250 keV *(Russian)* 78−55291
coherent bremsstrahlung from polarised electrons, asymmetry coeff. *(Russian)* 78−92139
coherent excitation of nuclei and atoms passing through crystals *(Russian)* 77−47502
collision cascades, fast charged particle bombard., of solid. defect prod. *(Russian)* 77−89492
collision cascades initiated by fast charged particles *(Russian)* 77−80561
composite interatomic potential, validity over large atomic separation 80−84225
compound nuclei as indicators in cryst. struct. anal., feasibility 77−35448
conducting medium, Cherenkov and ohmic losses of relativistic charge, unified treatment 79−12998
conference, atomic collisions in solids, Hamilton, Canada (Aug. 1979) 80−62375
conference on ion beam anal., Washington, USA (June-July 1977) 79−5194
conversion electron penetration through metallic and oxidized thin layers 80−102414
conversion electron scatt. in thin foils, depth selection, Monte Carlo calc. of energy distrib. 79−45598
convoy electrons from solids, ion vel. and Z and target material depend. 78−84692
cosmic particle dosimetry in nucl. emulsions for Apollo and Apollo-Soyuz Biostack expts. 78−20288
cosmic ray, magnetic monopole candidate, reassessment of 1975 Lexan and emulsion meas. 79−3333
cosmic ray detection, acoustic radiation by charged atomic particles in liquids, theoretical anal. 79−89526
cosmic ray heavy nuclei, LET spectra vs. absorber depth 78−20296
cosmic ray muons, radiative energy losses in ground 79−84619
cosmic ray nuclei in nuclear emulsion, appl. of energy loss params. on mass determ. 78−94175
cosmic ray particle identification from tracketch rates in minerals 79−16788
cosmic rays, Be to Mg, test of Katz's track formation theory in nuclear emulsion 79−54754
cosmic rays in supernova remnants, particles escape and adiabatic energy losses 79−16771
counter telescope for neutron induced charged particle reactions, finite geom. correction 77−57815
crystal, radiation suppression *(Russian)* 78−30686
crystal accelerator, radiative energy loss 80−23611
crystals, track form., minimal energy loss rel. to thermal cond. 78−17525
curved axial channel, motion of charged particles, effects of dislocations 77−55314
delta-electrons prod. in water by high-energy electrons and X-rays 77−29178
dense structureless media, modified treatment of low energy elastic stopping power 79−19302
depth profiling of light elements in materials with high-energy ion beams 77−59036
diamond, energy loss of protons, alpha particles and ^7Li 80−42905
diamond, half wavelength and stopping power of planar channelled protons 80−65087
diatomic molecule dissociation in thin films *(Russian)* 78−34558
diatomic positive ions, energy distrib. in drift tube 78−21257
diatomic target, slowing down of heavy ions, range and primary atom creation calcs. *(French)* 79−1473
dielectric, electron penetration, 20-50 keV, sandwich method meas. 80−6436
dielectric trapping, bremsstrahlung shielding meas. 78−78507
dielectrics, energy loss of electrons 80−24522
dielectrics, fast electron effects, space charge build up, range reduction 77−72636
Doppler shift attenuation in layered targets 80−102409
Doppler shift attenuation lifetime meas., stopping medium depend. 77−65995
Doppler-shift attenuation, γ-rays from slowing down of excited particles 77−26945
drift chamber, particle jet detection from e^+e^- reactions 79−3312
drift chamber electronics for time and pulse height meas. 79−3326
DSA meas., ion-atom interaction 79−749
DSA study of ^{28}Si lifetimes in selected materials, theoretical stopping power predictions 78−74329
dynamic screening of ions passing through solids 78−10379
effective charge theory and electronic stopping power of solids 78−67759
electron, ultrarelativistic, in periodically inhomogeneous medium *(Russian)* 77−31705
electron and positron ranges in solids, liquids and gases 79−4366
electron beam, focused, as probe of solid state, review *(Czech)* 77−24915
electron beam, sinusoidally modulated, absorption curves for various materials 77−24339
electron beam energy spectra meas. 80−895
electron beam lithography, energy loss calcs., Bethe and Spencer-Fano theories 78−87728
electron beam scatt. by plate, soln. to mixed type PDE 77−67388
electron beam scattering, in organic specimen, Monte Carlo simulation 80−100148
electron channeling pattern, large angle, generation and appl. 80−100296
electron cooling of beams in heavy particle storage rings, kinetics 77−67922
electron elastic and inelastic interactions with liq. water 80−9477
electron energy deposition in Ar, Monte Carlo calcs. 80−69242
electron energy deposition in CO_2, rel. to Venus and Mars atms. 79−45857
electron energy deposition in multilayer geometries 77−24338

energy loss of particles continued
electron energy loss by ionisation and excitation of atoms in plasma 80−33732
electron energy losses due to diffraction radiation *(Ukrainian)* 80−75278
electron flux in slab geom., high-energy radiotherapeutic field 77−81585
electron gas, energy loss of correlated charges 78−87729
electron gas, nonuniform, energy loss of charged particles 79−37748
electron gas, slow ions and atoms energy loss to electronic excitation 77−84817
electron gas, stopping power for slow neutrons, damping effects 80−65098
electron ionisation energy loss, approx. to Landau's distrib. functions 79−23664
electron mean free path, stopping and straggling 78−91367
electron probe analysis, spatial distrib. of electrons in homogeneous, isotropic target 79−43687
electron probe into solid target, diffusion model energy depend. 78−71652
electron probe penetration and energy loss characts. in solid target, diffusion model 80−96585
electron random motion in molecular materials, Monte Carlo anal. 77−31703
electron range in solids, derivation using reflected primary electron data 79−19297
electron rings, intense relativistic, deceleration by ions, stopping length 77−14282
electron slowing down in water, spatial correlation of energy deposition events 80−9473
electron transmission and backscatt. in solid layers, energy loss, 10 to 30 keV 77−59653
electron transport, continuous-slowing-down approx., adjoint Monte Carlo model 80−49269
electron transport and small angle collisions 80−165
electron transport in air and N_2, Monte Carlo calcs. 78−90042
electron transport simulation in liq. water, appl. to microdosimetry and radiobiology *(French)* 80−12202
electron-phonon inelastic scatt., passage through crystal in presence of quantised mag. field *(French)* 77−11607
electronic stopping power, Bragg's rule and Firsov's theory 80−2104
electronic stopping power, low velocity, crit. anal. of modified Firsov model 79−77660
electronic stopping power, theoretical interpretations of the energy dependence, low velocity heavy ions 79−4349
electrons, diffusion of pencil beam, ang. distrib. model 80−23273
electrons, low energy, in solids, calcs. of mean free paths and stopping powers 77−19996
electrons, monoenergetic, total stopping power, empirical relation 80−24512
electrons, random motion in dielectric media, energy loss, anal. calcs. 78−29888
electrons, ultrahigh energy, traversing cosmic blackbody photon gas, effective penetration distance 79−5742
electrons in metals, continuous slowing down approx. ranges 80−23269
electrostatic deflection type electron analysers, electron refl. ghost lines, energy loss reduction 80−18050
empirical range beta approx. 78−25401
enerfy loss and angular spread, review 78−71778
energetic ions, electronic and nucl. stopping 78−10106
energetic ions near solid surface, energy loss 80−96580
energy spectra of δ-rays produced due to high energy particles with biological systems 80−108951
energy straggling effect on cross-section to thick target yield relns. 79−26855
EPMA, stopping power and backscatt. factors, rel. to atomic number correction 78−20118
epoxides, atomic stopping cross section of O 78−67746
ESCA-ion scatt. spectroscopy-SIMS, review, chem. appls. 79−43701
ethers, α-particle impact, 0.3-2.0 MeV, O stopping cross-sections 78−17753
ethylene, stopping cross-sections using alpha particles in energy range 1.5 to 4.2 MeV 78−53510
ethylene oxide, stopping cross section for 0.3 to 2.0 MeV He^+ ions 78−63537
ethylene-tetrafluoroethylene copolymer, chem. etching of fission tracks 80−896
evaporated thin films, low energy stopping powers of ^{3}He and ^{2}H, new meas. method 79−4351
fast atom energy transfer to electrons 77−35613
fast channelled particles with low charge, energy loss calcs. 78−55899
fast charged particle beam density effect on stopping in matter 78−14180
fast charged particle traversing ferromag., dynamic mag. field, RPA 79−73230
fast electron distribution after ionisational energy loss 78−2177
fast electron retardation, ionisation cascade, degradation spectra, anal. *(Russian)* 79−27741
fast electron transfer, in external electric field, appl. of higher-order perturbation theory *(Russian)* 79−23662
fast heavy ions, elastic stopping by electrons in solids 79−51179
fast ion excited by surface grazing collision, energy loss and dissoc. 80−11523
fast molecular ion+solid (gas), excited electronic states effects 80−9687
fast moving ions traversing solid, wake-bound states, dispersive and surface effects 79−73231
fast neutron detection system, response function and efficiency calcs. 80−14056
fast proton track energy deposition and ionisation calc. and obs. 80−12196
fast test particles, slowing down, energy distrib. and spectra in infinite plasma 77−58870
fast test particles, slowing down, energy distrib. and spectra in finite plasma 77−58871
fast-moving charge near surface, self-energy 79−47138
ferromagnet, dynamic magnetic field on fast charged traversing particle 79−38423
ferromagnet, magnetic field asymmetry correction on fast moving ions 79−14862
field interface of moving particles in statistically inhomogeneous medium 79−6063
film, electron beam scatt. and energy loss during processing 77−27930

energy loss of particles continued
film, transport equation treatment of transmitted electrons *(French)* 77−80558
fission fragment excited electron generation of stress waves in metal 79−37747
fission fragment induced mol. ions desorption, electrochemical surface pot. effect *(German)* 78−6228
fission fragment recoil mass spectrometer HIAWATHA 79−9940
fission fragments, range in air, appl. of plastic and glass detectors 79−45597
fission fragments in gases, stopping powers and energy distribs. 80−78499
fluctuation in spatial distrib. of energy deposited by atomic particles 79−90709
foil, energy loss and straggling of proton and He^+ ions 78−95100
frictional quantum mechanical system, one-dimens. scatt. model for coherence in stopping power problem 80−101736
fusion pellet-target system, optimum material and design for relativistic electron beam 78−17416
fusion plasma transport, unified slowing down theory 78−18383
fusion reactor materials, range calculations using multigroup transport methods 80−34070
gamma-rays generation by fast electrons travelling through antiferroelectric or antiferromagnetic crystalline structures 78−76545
GANIL, beam stripper interaction studies 79−54721
gas, slowing down of fast atoms, using nonlinear Boltzmann eqn. 79−98196
gas, weakly-ionised, electron stopping model and secondary-electron distrib. 80−6263
gas proportional counter, relativistic electron ionisation loss, transition radiation effect 78−25389
gas proportional detectors, relativistic charged particle energy loss 77−88362
generalized transport equations in quantum theory of channelling 78−10110
graphite assembly exposed to 52 MeV protons, penetration of secondary neutrons and photons 79−76152
graphite film, relativistic excitations by inelastic electron scatt. 77−1463
hadron transmission through absorbers, Monte Carlo simulator of hadron cascade 77−30736
hadronic transmission through Fe absorbers, 0.8 to 100 GeV calcs. 78−90041
Havar foil, stopping power and multiple scatt. for low energy protons 79−31339
heavy charged particle penetration phenomena 78−71779
heavy charged particle specific energy losses meas. using densitometric method *(Russian)* 80−63482
heavy charged particle/water interaction, dose distrib. due to electrons, delta rays 80−13937
heavy charged particles, Z_1^3 contrib. to energy loss 80−10587
heavy ice, stopping power for low energy deuterons 77−35612
heavy ion beam linear energy transfer distribution calc. 79−20630
heavy ion deep inelastic processes fragments, element identification in ΔE-E telescope, computerised method 77−57839
heavy ion identification, using modified Zaidins empirical range-energy relationship, power law type algorithm anal. 77−57838
heavy ion impact on C foil, energy loss 78−55902
heavy ion irradiated target, number of point defects in displacement cascade, computational code *(French)* 79−19300
heavy ion penetration through matter, book contrib. 79−31343
heavy ion ranges, Z_1 oscillations 80−65096
heavy ion ranges in complex media, calc. 79−31337
heavy ion stopping power and low velocity projectile Z^3 effect 78−18693
heavy ions, channelled, stopping power Z_1 oscillation vel. depend. 80−65101
heavy ions, energy loss in 0.5 to 1.4 MeV/amu range 80−65103
heavy ions, experimental methods, targets and detectors, book 79−31242
heavy ions, in air, energy loss, high-energy calcs. 77−6891
heavy ions, low vel., channelling stopping power oscills. 80−103404
heavy ions, velocity stopping, theoretical analysis 78−26608
heavy ions in solids, electronic stopping cross-section, Z_2-oscills., target struct. effects 80−70285
heavy nonrelativistic ions in matter, semiclassical theory 80−84224
heavy particle track grain counting for nucl. charge determ. 78−17528
heavy particles, expt. results for W-values 80−78500
heavy particles penetrating solids, energy-angle distrib. 78−10107
heavy protons, energy-range relns., use in detection 78−58566
heavy quarks, energy-range relns., use in detection 78−58566
heavy-ion collisions, complete damping 78−21588
heavy-ion low-energy small angle multiple scatt. screening effects 79−31340
heavy-ion radiography and autoactivation techniques 79−20624
heavy-ion stopping in matter, study of nuclear and elec. mechanisms from Coulomb excitation expts. 77−10569
heavy-ion stopping-power calculations 80−78505
heavy-ion stripping, semi empirical expressions 78−13395
heayv ion lateral range calc., adaption of energy/depth distrib. program E-DEP-1 77−62571
Heidelberg Q3D mag. spectrograph, 1.4 m ΔE-E position sensitive detector 79−45566
heterogeneous media, energy deposition of slowing down particles 80−88230
heterogeneous medium, ion implantation and energy deposition, path length approx. 78−87694
high pressure proportional counters operating in pure hydrogen 79−3296
high-energy low-mass particles interaction with crystal, kinetic equation *(Russian)* 79−23660
hydrocarbon gases, additivity of stopping cross-sections for 50 to 150 keV protons 77−66853
hydrocarbon gases, proton energy loss distrib. in range 50-150 keV 77−79526
ilmenite concretes, fast neutron attenuation 79−76048
implanted ion ranges and standard deviations 78−30656
implanted ions, energy deposition profiles from range data, simple method for calc. 77−39619
implanted space charge effect on heavy charged particle range distrib. 77−24340
implanted-ion range, computing moments of energy distrib. 77−4120
improved depth resolution of channelling meas. in Rutherford backscatt. by detector tilt 79−5209
inert gas ion+oxides, energy loss spectra 78−58798

energy loss of particles continued
inhomogeneous media, ion implantation range distribs. 79—23625
insulators, secondary electron emission, free-electron scatt. theory and plasmon theory 79—8211
intense field QED in continuous medium, appl. to Thomson scatt. and Cherenkov radiation 80—27435
interaction with matter, review and bibliography *(Japanese)* 80—39149
ion, $6 \leq Z \leq 20$, stopping power systematics, Z_1-oscills., in C, Al, Ni, Ag, and Au 79—65130
ion, electronic energy loss in solids, 10-10^4 keV nucleon^{-1} 79—23666
ion backscattering and implantation, H and He ions, computer simulation, comparison of MARLOWE and TRIM codes 80—66350
ion backscattering from solid in keV range, single collision approx. 77—1772
ion backscattering under planar channelling conditions, ion-atom pot. and stopping power 80—24519
ion bombardment of solid, energy refl. coeff. depend. on target at. number 77—15470
ion energy deposition in simulated biological matter, Monte Carlo method 77—81584
ion identification with detector telescopes 79—72180
ion impact, individual orbital contrib. to electronic stopping cross section 79—23667
ion implantation, book 77—31691
ion implantation, range parameters, nucl. stopping power, ion backscatt. determ. 80—88232
ion implantation depth distrib., calc. in path-length approx. 79—23626
ion implantation depth profiles, influence of straggling using backscatt. and nucl. reacts. 78—47401
ion implantation range parameters and diffusion meas., small angle Rutherford backscatt., review 77—44108
ion range in amorphous target, Lindhard-Scharff-Schiott theory refinement 77—15473
ion scattering, lateral, in amorphous and polycryst. solids *(German)* 80—24508
ion stopping power calc. *(German)* 79—51175
ion stripping and charge state fluctuations 77—79522
ion-beam analysis, stopping power problems 80—14059
ion-lattice interactions, modelling displacement correls. in computer simulations 78—2179
ion-surface scattering, low-energy inelastic case, review 80—40212
ionic crystal, ionis. energy losses and ranges of α-particles 77—47501
ionisation spatial distrib. for 0.5 to 500 keV electron bombarded solids, empirical eqns. 79—19956
ionizing radiation and cavitation threshold 78—94774
ions, comparison of range and straggle calcs. 78—34562
ions, Firsov model at. wave functions choice 80—2103
ions, low energy surface scatt., inelastic energy loss 80—70278
ions, range, numerical method 77—71734
ions in solids, Lindhard's dielec. theory 80—65077
ions moving in condensed matter, electron density fluctuation patterns 80—24518
ions recoiling in gas, hyperfine perturbation, Scherer-Blume theory 77—46617
IR spectroscopy appl. to charged part. dose meas. in cellulose triacetate 78—94145
isotope conveyor weigher, errors caused by profile variations and shift of material 77—67933
Kapton foil, stopping power and multiple scatt. for low energy protons 79—31339
kerma partition to account for energy deposition in matter 79—66482
KERMA values, consistent set for H, C, N, and O for neutrons from 10 to 80 MeV 80—68967
ketones, molecular stopping cross section of He^+ ions and atomic stopping cross section of O 78—67746
Lenz-Jensen pot. calc. using third order approx. 78—95099
levinson's theorems in classical scattering 80—90729
LMFBR materials, electron transport method, expt. verification, energy deposition 79—22386
low energy heavy particles, total energy loss distribs. after penetration through matter 78—14385
low-energy heavy charged particle stopping power, phase effects 80—23277
low-energy heavy ions, electronic stopping power, modified Firsov formula 78—18690
magnetic monopoles, stopping-power formula 78—46242
mesonic particles, Coulomb capture in inhomogeneous matter 78—55116
metal, proton energy losses, Bohr equipartition rule 77—15467
metal and metal oxide spacecraft thermal control materials, low-energy proton effects 80—70288
metal foil, energy straggling of C and He ions 80—27905
metal foils, $Z=6$ to 79, energy loss of light 300 keV ions, using magnetic analyser 79—4350
metal surface, electron emission induced by low energy light ions 79—61482
metal surface, fast ion scatt. by plasmons, theory 80—45190
metal target preparation for stopping power meas. of channelled ions in low energy region 80—63431
metals, outer electronic shells contrib. to heavy ions stopping *(Russian)* 79—1474
metals, stopping power for 28 MeV α-particles, re-evaluation, Be, Al, Ti, V, Fe, Co, Ni, Cu, Mo, Rh, Ag, Ta, Au 78—79651
metals, stopping powers for 28.8 MeV α-particles 77—80556
metals, stopping powers for 8.78 MeV α-particles 77—80557
metaphosphate glasses, heavy ions, fission fragments energy determ. 78—17487
methane, α-particles stopping cross-section determ. 79—49917
methane, gas, total ionization created by completely stopped H^+ ions 79—46419
methane+Ne ion, nuclear stopping power and interatomic potentials 78—74549
methylpentanes, electron mobilities and penetration ranges in liq. and crit. regions 78—72220
mica, 210 keV electrons, Vavilov-Cherenkov radiation, ang. distrib. half width, spectral depend. *(Russian)* 80—71505
mica, tracklengths of I and Au ions, 0 to 1 MeV/amu 78—38767
mica, Vavilov-Cherenkov radiation ang. distribs. from 170 to 250 keV e^- *(Russian)* 79—22569
mica muscovite, iron latent tracks obs. by TEM 79—73235
microdosimetric results from ionisation chamber and proportional counter compared 80—9429

energy loss of particles continued
modified Firsov model, sensitivity to atomic electron speed 80—65100
monoenergetic electron continuous slowing down approx., range and projected range 80—78497
monopole track characteristics in plastic detectors 77—18759
MOS rectangular vol., distrib. function for ion track lengths 79—85872
multicomponent material, energetic heavy ion irrad., elastically deposited energy, numerical calc. 77—59057
multiple scatt. of particle beams, axial mag. field effect 78—70712
multiple scattering corrections to energy loss measurements for slow ions 80—95511
multiple scattering in molecular gases, target at.+energetic ion spatial correlation influence 79—27062
multiple scattering of charged particles in thin layer, Monte Carlo method, ang. deflection 78—79650
multiple scattering processes, theoretical description of elastic atom-atom scattering 79—86029
muon momentum spectrum, absolute intensity meas. 0.4 to 3.0 GeV/c 79—5720
muon transfer in gas targets 77—42445
muons, Z_1^3 correction meas. 80—78502
muons in shielded scintillator, energy loss calcs. 80—63490
MWPC, appl. as energy loss detector for the ISR 79—3331
MWPC and drift chambers, operation principles 77—83465
MWPC appl. to energy loss meas. 79—3330
NE102, proton loss by nuclear inelastic interactions 77—71729
NE213, proton loss by nuclear inelastic interactions 77—71729
NE-111 thin homogeneous scintillator foils, alpha particle energy loss and straggling 77—83472
near surface yield enhancement for He ions in noncryst. solids 80—65105
negative mesons, capture fractions conc. depend. 78—78600
negative muons, transport properties in matter, energy spectra 77—56239
negative muons, transport properties in matter 77—56238
neutron and photon, heat deposition, rate in nuclear reactor 78—29565
neutron collimated fast beam, radiation quality local distrib. 80—12247
neutron cross-sections and kerma values for C, N and O from 20 to 50 MeV 80—101217
neutron dose distributions across graphite-tissue and polythene-tissue interfaces, air/nitrogen gaps, stopping power data 80—26353
neutron energy deposition calc. using adjoint Boltzmann eqn. 79—6723
neutron energy deposition in tissue-equiv. sphere, influence of collimation 77—56482
neutron moderator energy deposition calc., role of adjoint Boltzmann eqn. 78—4974
neutron primary beam and shielding radiation quality and absorbed dose obs. 80—12281
neutron slowing down, space-depend. continuous, use for fast reactor spectrum calc. 77—54293
neutron slowing down time in hydrogenous multiplying system 77—61472
neutrons, resonance, slowing down in matter 77—50191
non-channelling ultrarelativistic particles in crystal planes, EM radiation *(Russian)* 80—45163
nonstationary distribution functions calc. 78—86758
nuclear filters, prep. from polymers using Ar ions 78—86714
nuclear stopping, ranges and straggling, in low-energy region 77—47499
nuclear stopping power, ion beam elastic collisions with target nuclei 80—34105
nuclear stopping power and interatomic potentials 78—74549
nuclear stopping powers, corrections by use of empirical multiplicative factors and screening length 79—59320
nuclear tracks, solids, formation model, etch pit parameters for light nuclei 78—13390
organic compounds, continuous slowing down approx., range difference for 0.2 to 10 MeV electrons 80—39187
particle identification systems including magnetic analysis, review 79—72181
particle transport theory, fluctuation problem, probability balance eqn. 77—37829
penetration statistics, energy loss and multiple scatt. 79—42124
Penning discharge, ion heating and collisional energy loss 77—72519
photoelectron absorption in semi-infinite targets 77—28688
photons, appl. to cosmological redshifts, critical anal. 77—9828
photons, ultrahigh energy, traversing cosmic blackbody photon gas, effective penetration distance 79—5742
pion$^-$, central axis depth-dose and stopping rate distrib. for radiobiology studies 77—52879
pion$^-$ beam stopping distrib. determ. by charge collector 78—53513
pion$^-$ capture, charged particle emission, energy spectra, LET distribs. and W-value 78—40337
pion$^-$ stopped in tissue phantom, neutron and photon dose and LET distribs. 77—52878
pions, two-dimens. visualisation of stopping pion distribs., for therapy 77—12999
PIXE, depth determ. using stopping foils 80—30310
planar channelling of α-particles, stopping power of solids 78—51602
plasma, charged particle energy losses, homogeneous superhigh freq. elec. field and ion polarisation effects *(Russian)* 79—90384
plasma, effect of turbulence on rate of energy loss by test charge 78—5872
plasma, thermalisation of energetic charged particles in fusion plasma, QED effects 77—65834
plasma cylinder, energy loss rate of charged particle with relativistic vel. 77—31485
plasma electrons, stopping power, quantum diffraction effects 78—91064
plasma sheet, excitations of wave modes and energy loss by charged particle 78—38473
PMMA, stopping power of valence electrons, Monte Carlo calcs. 79—10886
polar crystal, hot electron transport, eikonal approx. for energy loss 77—1426
polar crystal, hot electron transport, loss to single phonon modes 77—1427
polarised ferromagnetic media, decelerating ion, transient field phenomena 78—72445
polarization wake in solids, theory 77—19998
polycarbonate thin film, determ. of fission barrier in region $Z=82$, $N=126$, using electron linear accelerators 78—55104
polyethylene, electron random motion in molecular materials, Monte Carlo anal. 77—31703

energy loss of particles continued
  polyethylene, stopping cross-sections using alpha particles in energy range 1.5 to 4.2 MeV 78—53510
  polymer dielectric nuclear track detector, particle stopping power depend. on preirrad. annealing 79—72185
  polymers, continuous slowing down approx., range difference for 0.2 to 10 MeV electrons 80—39187
  polystyrene, energy losses and straggling for H^+ and He^+ beams *(Russian)* 80—84226
  polystyrene, energy straggling of H^+ and He^+ ions in 0.1 to 1.2 MeV range 77—80559
  polystyrene, gamma photon backscattering, energy dependence *(Rumanian)* 79—76316
  polystyrene, inelastic interaction of electrons, mean free path, stopping power and CSDA ranges 79—23663
  polystyrene, stopping power for 2.2 to 5.9 MeV protons 78—90040
  pore size determ. from charged particle energy loss meas. 77—71730
  positron, ultrarelativistic collimated beam, emission spectra in Si 80—7434
  positron bremsstrahlung, anomalous reduction in single cryst. 80—7433
  positron implantation profile effects, in solids of varying density 77—48273
  projectile charge dependence of stopping power 78—79655
  projectile size dependence of stopping power 80—65099
  propane, α-particles stopping cross-section determ. 79—49917
  proportional counter, energy loss of relativistc electrons and its fluctuation 78—94171
  propylene oxide, stopping cross section for 0.3 to 2.0 MeV He^+ ions 78—63537
  proton attenuation lengths in paraffin, concrete and iron around targets 80—102412
  proton beams in fluid media, acoustic signature 79—59317
  proton Bragg peak therapy, beam penetration and control in nonhomogeneous phantoms 77—70531
  proton range and stopping power, new empirade relns. 77—61671
  proton range modulator to produce uniform ^{38}K yield in bone Ca activation anal. 77—40735
  proton stopping cross-section within wide energy range, semiempirical formula *(Russian)* 78—67763
  protons, 51, 102, 153 keV, in hydrocarbon gases, energy loss distributions 77—6649
  protons, 600 MeV, luminescent detector efficiency, mass stopping power calc. 80—99346
  protons, straggling in energy loss 80—42900
  quantum theory of energy loss by test ions to plasma electrons 79—94804
  radiation damage cascades, validity of energy partitioning 78—43056
  radiational materials, spatial distrib. of H^+, He^+, D^+ ions in solids 80—6429
  radiative damping effect for ultrarelativistic channelled particles 78—67758
  radiative energy loss of electrons in thick layers of material, interpolation formulae 78—21829
  radiobiological effects and dose-LET spectra 80—26265
  rainbow scattering and orbiting of fast particles in crystals 79—99256
  range and damage distributions, Sonine expansion 79—19303
  range for transmitted, reflected, and absorbed ions and electrons, phenomenological description 79—68173
  range profile path length distrib. function 77—35615
  rare earth metals, H, and He, stopping powers meas. 80—42904
  recoil atoms of heavy ion reactions, local lattice damage, TDPAD meas. 80—84220
  recoil mixing in high-fluence ion implantation 80—65095
  recoil mixing in solids by energetic ion beams 80—59531
  recoil range distribs. of heavy mass products in deep inelastic reacts., with Au and U targets 78—66309
  relative stopping powers of light ions in solids, Rutherford backscatt. method 79—4348
  relativistic charged particle in electric field, spin rot., curved crystal. p,e^+ channelling *(Russian)* 80—63907
  relativistic electron energy loss distribs. in thin gas layers of proportional counters 80—99429
  relativistic electron ring, retarding force of image currents in resistive cylinder, stopping length 77—67918
  relativistic heavily ionising particles, energy loss, review 80—32583
  relativistic particle beam in crystal, collimation, cooling 80—42885
  relativistic particles, energy loss in solids 80—39188
  relativistic positron and electron bremsstrahlung under conditions, theory 79—19301
  resonant energy transfer from electrons to a slow electromagnetic wave 80—83545
  RNase, damage and energy deposition by low-energy ions 77—9172
  Rossi counter equivalent dose meas. in high-energy radiation fields 80—94376
  scintillation counter NE213, organic liquid, Monte Carlo calcs. of electron energy loss spectrum for incident gamma-rays 77—6613
  scintillation hodoscope for meas. of ionisation losses of relativistic particles 80—42892
  scintillator materials, data for activation assessment during spaceflight 77—23382
  secondary electron emission, energy depend. of yield, based on range-energy retardation power formula 79—47565
  semiconductor, proton energy losses, Bohr equipartition rule 77—15467
  semiconductor-metal structure, electron bombarded, energy dissipation 78—87732
  single atom detection in particle tracks 80—9475
  slow ion stopping power meas., multiple scatt. corrections 80—23278
  slowing down particles, spatial depend. of energy spectrum 79—65129
  slowing down spectra, Placzek discontinuities 77—51423
  solar flare energy spectrum simulation from monoenergetic incident proton beam 78—12786
  solid, depth profiling of ^{3}He ion implantation 78—59830
  solid, Monte Carlo simulation of energy distrib. of transmitted or backscatt. keV electrons 78—43057
  solid film, passage of electrons, linear transport theory in one-velocity approx. 79—14865
  solid-electron interaction, Monte-Carlo simulation, appl. to electron probe microanal. 77—12853
  solidified gases, energy loss of ^{4}He ions, backscattering method 79—4346
  solids, convoy electrons emerging with swift ions, vel. spectra 77—84814
  solids, stopping of energetic ions 80—42901

energy loss of particles continued
  solids, stopping values of energetic ions, predicted with energy loss model 80—88229
  solids, X-ray prod. range by 2 to 15 keV electrons, thin film and bulk targets 79—19298
  soliton solution in the wake interaction due to virtual plasmon exchange 80—65108
  spectrometer, double-focusing with ang.-resolving slit, for ion-molecule reactions 78—44426
  stable law with index $\alpha=1$ in fluctuations of ionisation loss of energy of charged particles *(Russian)* 78—62682
  STEM, effect on phase contrast 78—32960
  Stilbene, proton loss by nuclear inelastic interactions 77—71729
  stopping and straggling mean excitation energies for N, O, H_2, N_2, O_2, NO, NH_3, H_2O and N_2O 77—83473
  stopping cross-section, individual atomic orbital contrib., Hartree-Fock-Slater orbital 78—43060
  stopping cross-section meas. with thin supported films 77—30733
  stopping cross-sections, for nucl. energy level lifetimes 78—70725
  stopping power, influence of chem. effect 80—47830
  stopping power and range data compilation committee 80—9478
  stopping power dependence on physical and chemical states 80—9480
  stopping power determ. by average stopping power method 79—26852
  stopping power for low energy heavy charged particles, similarity treatment of phase effects 78—50447
  stopping power formula of Bethe, inner shell corrections 77—11608
  stopping power meas., mean excitation energy from oscillator strength distrib. 80—9481
  stopping power of liquids for alpha particles, meas. apparatus 80—88224
  stopping powers determ. from backscattered ions spectra 79—97959
  stopping powers of H in all elements, book 78—26607
  stopping powers of $Z=10$ to 18 ions, ^{22}Ne, using DSAM lifetime meas. 78—47456
  stopping-power formula, fast heavy ions 78—59846
  straggling meas. anal. by the backscatt. technique 79—4355
  stripper foils, energy straggling of heavy ion beams at tandem energies, C foil appl. 78—33353
  subsoil neutron moisture probe, lab. calibration, minimum soil sample size calcs. 77—57333
  superconducting dipole magnet, quench levels induced by proton beam spray meas. 77—26906
  superheated supercond. colloid as a total absorption detector preliminary calcs. 78—78579
  surface characts., combined ion scattering spectrocopy, SIMS, SEM, energy dispersive X-ray techniques 79—43702
  surface chemical analysis, low energy ISS compared with SIMS 78—64908
  swift ions, electron state energy shift in passing through solids 80—65107
  T-expansion solution of transport equations, Monte Carlo test 79—54752
  test particle slowing down, rarefied gas added to host, with external conservative force 79—97326
  thermonuclear target, calc. of charged particle spectra by Monte Carlo method *(Russian)* 79—37445
  thick target, energy spectrum of backscattered particles, multiple scatt. and ion effective charge deviation effect 77—81192
  thick target corrections for charged particle spectra 80—37714
  thick-target thick catcher nucl. recoil expts., anal. 78—55115
  thin dielectric track detector as particle discriminator, α dosimetry appl. 78—17511
  thin foil thickness meas. using ^{148}Gd and ^{241}Am alpha-particles 79—30417
  thin sample, structural change obs. by transmitted fission fragment energy 78—83853
  time-energy distribution of atoms in radiation damage cascade 77—1159
  tissue, heavy ion track struct., microdosimetry 77—2032
  tissue equivalent gas, total ionization created by completely stopped H^+ ions 79—46419
  tissue neutron energy deposition spectra from improved cross-section values 80—26300
  tissue substitute material formulation using basic interaction data 77—86640
  tissue-equivalent gas, energy loss of H, C, N and O ions for elastic nuclear collisions 78—86759
  tissue-equivalent gas, energy loss per ion pair for ions, 25 to 500 keV 77—35312
  tissue-equivalent gas, W-value for low energy electrons 78—15896
  tissue-equivalent gas, W-value for pion 77—56473
  TLD materials, kerma for monoenergetic neutrons, theory, expt. comparison 77—5086
  track formation and minimal energy loss in insulator crystals *(German)* 77—18757
  track formation models, depend. of mass identification scale 78—17515
  transient magnetic field effects on particles slowing in solids 80—65106
  transition metals, stopping power for 6.75 MeV protons 80—34107
  transition radiation interference effects near Cherenkov radiation threshold 80—9454
  ultracold neutrons (UCN) transmission through moving goffered foils 79—17955
  ultraheavy cosmic ray charge determ. in emulsion, Mott cross section effects 79—18084
  Vavilov energy straggling calc., validity limits 78—33405
  vinyl methyl ether, stopping cross section for 0.3 to 2.0 MeV He^+ ions 78—63537
  wake potential of swift ions in solids 77—20257
  water, absorption of high energy electrons 78—881
  water, continuous slowing down approx., range difference for 0.2 to 10 MeV electrons 80—39187
  water, electron energy deposition model, effect of 21.4 eV plasmon 77—4135
  water, heavy ion beam propag., energy loss and fragmentation of nuclei 79—54755
  water, ice and vapour, stopping cross section, 0.3 to 2.0 MeV 77—55313
  water, liq. and vap., alpha particle stopping power, 0.5-8 MeV 78—40334
  water/air mass stopping power ratios for megavolt. photon and electron beams 78—28082
  X-ray emission, due to ions moving through solids 79—83062
  X-ray emission, ions moving through solids, charge state determination 79—83061
  X-ray transition radiation, eikonal approx. 79—49422

energy loss of particles continued
α, 100 keV to 2.4 MeV, stopping power in H_2, He, N_2, O_2, CO_2, Ne, Ar, Kr, Xe 80—14057
α track registration, solid state track detectors in solutions of actinides 80—63486
α-particle, range in air, appl. of plastic and glass detectors 79—45597
α-particle range-energy relations and stopping power in tissue equivalent liquid 80—23275
β, total backscattering coefficient for thick absorbers, segment model calc. 77—72642
β emitters, identification using absorpt. coeff. in Al, accuracy 77—57837
γ 6 MeV scalar leakage flux spectra through Pb-Al and Fe-Al shields 79—85871
K^-+photonuclear emulsion nuclei, hypernuclei in hammer-like events 78—13162
p, 40 keV to 1 MeV, stopping power in H_2, He, N_2, O_2, CO_2, Ne, Ar, Kr, Xe 80—14057
p+nuclear emulsion, 400 GeV nonwhite stars 78—13097
π energy dependent mean free path length for star formation 77—23393
π^-, absorpt. length in Fe in range $15<E<140$ GeV 80—894
π^-, energy deposition spectra and radiation therapy appl. 80—26363
$\pi^- p \rightarrow \pi^0 n$ or γn, Panofsky ratio for pions, meas. using liquid H target 77—50000
Ag, electron inelastic mean free paths and energy losses, electron gas statisitcal model 79—46733
Ag, electron range, low-energies continuous-slowing-down approx. and range straggling calcs. 80—39183
Ag, electronic stopping function for He^+ and Li^+, 50-300 keV 79—69169
Ag, energy losses and straggling for H^+ and He^+ beams *(Russian)* 80—84226
Ag film, energy losses of electrons, microcalorimetric meas. 80—59543
Ag, fission fragments, Z_1 oscills. 77—76477
Ag, Li ions stopping power and straggling 80—42908
Ag, low energy stopping powers determined by time of flight techniques 79—45594
Ag, mean excitation energies from α-particle stopping power meas. 79—13615
Ag, mean excitation energy based alpha particle stopping power meas. 78—30678
Ag, multiple scatt., energy loss meas. for Ar, Kr, Xe, U 1.2 MeV ions 79—751
Ag, projectile range for $Z=8$-20, 0.0125-12.0 MeV/nucleon 78—83856
Ag, stopping power for 0.3 to 2.0 MeV ^4He ions 79—60415
Ag, stopping power for 0.3-1.5 MeV protons 79—55801
Ag, stopping power for MeV H^+, D^+, $^4He^{2+}$, $^7Li^{3+}$ ions, deviations from Bethe formula 78—26612
Ag, stopping power meas. for 4-5 MeV/N ^{16}O, ^{40}Ar, ^{65}Cu, and ^{84}Kr 78—70720
Ag, stopping ratios of 50-300 keV H^+, He^+, $^7Li^+$, and $^8Be^+$ 80—42903
Ag thin foil, proton energy straggling determ., at 0.35, 1, and 1.75 MeV, γ-emission reactions 79—4354
AgCl, defects induced by energetic ion implantation 78—17518
Al, alpha particle energy loss straggling 80—42902
Al, β-ray bremsstrahlung in thick target, 30-1300 keV 79—83049
Al, cross-section of alpha particles slowing down, stopping power *(Russian)* 77—80560
Al, determ. of width of lateral spread distribs. of MeV He ions from energy spectra 79—14860
Al, electron and proton depth-dose distribs., space-shielding appls. 80—39186
Al, electron inelastic mean free paths and energy losses, electron gas model 79—46732
Al, electron inelastic mean free paths and energy losses, electron gas statisitcal model 79—46733
Al, electron range, low-energies continuous-slowing-down approx. and range straggling calcs. 80—39183
Al, electron stopping power, 2-10.9 keV 78—43055
Al, electronic stopping function for He^+ and Li^+, 50-300 keV 79—69169
Al, energy losses and straggling for H^+ and He^+ beams *(Russian)* 80—84226
Al, energy straggling of H^+ and He^+ ions in 0.1 to 1.2 MeV range 77—80559
Al, film, electron transmission, 1-5 keV, electron MFP 77—15472
Al film, energy losses of electrons, microcalorimetric meas. 80—59543
Al foil, electron beam ionisation and energy loss processes 80—32954
Al foils, energy straggling, 5.486 MeV alpha-particles 77—80550
Al, gamma photon backscattering, energy dependence *(Rumanian)* 79—76316
Al, gamma-ray attenuation coeff. meas., 1115, 1173, 1332 keV 77—55303
Al, heavy ion ranges, 120 keV Pb ions backscatt. obs. 80—19855
Al, heavy ion ranges, He^+ backscatt. obs. 78—63796
Al, ion-induced electron emission, ion charge depend. 80—108315
Al, Li ions stopping power and straggling 80—42908
Al, low energy stopping powers determined by time of flight techniques 79—45594
Al, low mass particles, $A<16$, charge-exchange effects in energy-loss straggling 80—65104
Al, mean excitation energies from α-particle stopping power meas. 79—13615
Al, multiple scatt., energy loss meas. for Ar, Kr, Xe, U 1.2 MeV ions 79—751
Al, multiple scatt. of fast electrons and inner secondary electron generation 77—1160
Al, positron formation at surface 79—13845
Al, positron penetration depth and energy loss 80—92578
Al projected range distrib. of 5-25 keV $^4He^+$ 80—65094
Al, proton energy straggling in ion backscatt. expt. 79—37750
Al, range and range straggling of 120 keV heavy ions 79—45595
Al, range of 100 keV Pr^{2+} and Tb^{2+}, M-shell X-ray cross-sections 77—35614
Al, ranges of ^{29}Si ions meas. by (p,γ) reson. broadening, 20-100 keV 77—69023
Al, ranges of implanted 10-30 keV D^+ 78—83858
Al, single cryst., primary knocked-out atom, energy of spatial distrib., modelling of 0.2 MeV proton trajectories 79—14864
Al single crystal, $^{18}O^+$ ions implantation in channelling directions, stopping power meas. from max. range 80—65078
Al slab, fast electrons slowing down, Monte Carlo transport simulation *(French)* 78—26610
Al, stopping power and energy straggling meas., Li ion backscatt. anal. 79—3328
Al, stopping power for 0.3-1.5 MeV protons 79—55801
Al, stopping power for 6.75 MeV protons 80—34107
Al, stopping power for MeV H^+, D^+, $^4He^{2+}$, $^7Li^{3+}$, ions, deviations from Bethe formula 78—26612
Al, stopping power meas. for 4-5 MeV/N ^{16}O, ^{40}Ar, ^{65}Cu, and ^{84}Kr 78—70720
Al, stopping ratios of 50-300 keV H^+, He^+, $^7Li^+$, and $^8Be^+$ 80—42903
Al target inside magnet, hadron cascades prod. by 300 GeV protons 77—10566
Al, thin foil, Monte Carlo calcs. of electron transmission 77—80555
Al_2O_3, amorphous, range of ^{29}Si meas. by (p,γ) reson. broadening 77—69023
Al_2O_3, electron slowing-down flux spectrum, due to β-decay of neutron-activated ^{164}Dy 78—10108
Al_2O_3, stopping power and energy straggling meas., Li ion backscatt. anal. 79—3328
$^{27}Al^+$ ion ranges in Ti(Ni)(Cu)(Mo)(Ag)(Ta)(W)(Au)(Pb), meas. by (p,γ) reson. broadening 79—46729
Ar, and mixtures, photon mass attenuation and mass energy-absorpt. coeffs., 0.1 keV to 20 MeV 77—61715
Ar, electron inelastic mean free path by PES 80—4822
Ar, energy loss per ion pair for ions, 25 to 500 keV 77—35312
Ar, liquid, calorimeter, electron and proton response 80—47832
Ar, nuclear emulsion track width by photometric meas. 78—94167
Ar, restricted energy loss by ionisation of relativistic muons 77—88355
Ar^+, energy and ang. distrib. in passing through C, Cu, Ag films 80—100292
Ar+10% CH_4, Fano factor determ. from α-particle pulse height distribs. 79—76284
^{75}As, slowing down of atoms/ions with KE$\leq$5 eV by inert gases 79—31650
Au, alpha particle energy loss straggling 80—42902
Au, amorphous, bombard. by Au ions, collision cascades, computer simulation 79—46731
Au, electron beam energy losses 78—91368
Au, electron inelastic mean free paths and energy losses, electron gas statisitcal model 79—46733
Au, electron range, low-energies continuous-slowing-down approx. and range straggling calcs. 80—39183
Au, electronic stopping function for He^+ and Li^+, 50-300 keV 79—69169
Au, energy losses and straggling for H^+ and He^+ beams *(Russian)* 80—84226
Au, film, electron transmission, 1-5 keV, electron MFP 77—15472
Au film, energy losses of electrons, microcalorimetric meas. 80—59543
Au foil, integral ang. distrib. of D^+, D_2^+ and D_3^+ ions 79—93894
Au foil, relativistic electron beam deposition, field-enhanced, bremsstrahlung prod. 78—29677
Au foils, electronic energy loss of H, D, and He below 20 keV 80—42906
Au, higher order z, effects and effect of screening by bound K electron on electronic stopping of channelled ions 77—51424
Au, low energy stopping powers determined by time of flight techniques 79—45594
Au, mean excitation energies from α-particle stopping power meas. 79—13615
Au, mean excitation energy based alpha particle stopping power meas. 78—30678
Au, multiple scatt., energy loss meas. for Ar, Kr, Xe, U 1.2 MeV ions 79—751
Au, multiple scatt. of fast electrons and inner secondary electron generation 77—1160
Au, precision stopping cross section meas. for ^4He, 0.5 to 2.1 MeV 79—4353
Au, projectile range for $Z=8$-20, 0.0125-12.0 MeV/nucleon 78—83856
Au, range and range straggling of heavy radioactive ions 78—22776
Au, range distributions for 25-200 keV $^{14}N^+$ ions 80—103405
Au, stopping cross sections of protons, 350 to 650 keV, backscatt. technique 79—4352
Au, stopping power for ^{107}Ag, ^{109}Ag and ^{150}Sm 80—70284
Au, stopping power for 0.3 to 2.0 MeV ^4He ions 79—60415
Au, stopping power for 0.3-1.5 MeV protons 79—55801
Au, stopping power for MeV H^+, D^+, $^4He^{2+}$, $^7Li^{3+}$ ions, deviations from Bethe formula 78—26612
Au, stopping power meas. for 4-5 MeV/N ^{16}O, ^{40}Ar, ^{65}Cu, and ^{84}Kr 78—70720
Au, stopping power of heavy ions at 50-500 keV 77—76478
Au, stopping powers and backscatt. charge fractions for 20-150 keV H^+ and He^+ 80—42907
Au, stopping ratios of 50-300 keV H^+, He^+, $^7Li^+$, and $^8Be^+$ 80—42903
Au, thin film, anomalous stopping power effects 80—65102
Au thin foil, proton energy straggling determ., at 0.35, 1, and 1.75 MeV, γ-emission reactions 79—4354
Au-Mo-Si multiple layer structure, bombarded with P ions, calc. of P ion profile in substrate *(Russian)* 79—55771
$BaSnO_3$, powder, electron scatt. from ^{119}Sn, effective range, Mossbauer obs. 77—63345
Be film, on Pt substrate, range of primary electrons 77—4134
Be, fusion reactor material, range profiles of Li^+, appl. of (n,p) and (n,α) reactions 80—61200
Be, multiple scatt. of fast electrons and inner seconary electron generation 77—1160
Be, projected range distrib. of 5-25 keV $^4He^+$ 80—65094
Be, proton energy straggling in ion backscatt. expt. 79—37750
Be, range and range straggling of 120 keV heavy ions 79—45595
Be, stopping power for 6.75 MeV protons 80—34107
Be, stopping power for protons, 20 to 120 keV 80—91411
BeO, chemical effect, influence on stopping power 80—47830
Bi, multiple scatt., energy loss meas. for Ar, Kr, Xe, U 1.2 MeV ions 79—751
Br^{6+}, 42 MeV, stopping power and radial dose distrib. obs. in tissue-equivalent gas 80—101218
C, amorphous, ranges of implanted 10-30 keV D^+ 78—83858
C, amorphous foil, electronic energy straggling of light ions, at. number depend. 77—11612

energy loss of particles continued
C, and mixtures, photon mass attenuation and mass energy-absorpt. coeffs., 0.1 keV to 20 MeV 77—61715
C, continuous slowing down approx., range difference for 0.2 to 10 MeV electrons 80—39187
C, determ. of width of lateral spread distribs. of MeV He ions from energy spectra 79—14860
C, electronic stopping function for He$^+$ and Li$^+$, 50-300 keV 79—69169
C, electronic stopping power of heavy ions, empirical relation 80—92571
C, energy loss of fast H$_2^+$ ions 78—79653
C, energy loss straggling of protons and He ions 78—18692
C, energy-angle distrib. of Ne and Ar ions below 250 keV, test of Meyer-Klein-Wedell theory 79—49916
C, film, secondary electron emission rel. to energy loss 77—16438
C, foil, 40-100 keV He ions, electronic energy straggling 77—15471
C foil, energy loss of Ne ions (40-120 keV), and Ar ions (40-240 keV), as function of emergence ang. 79—4357
C, foil, energy loss straggling meas. for low energy protons 78—47459
C foil, heavy ion stopping powers, TOF particle identification at 2-400 keV/N 80—5435
C foil, ion irradiation, correlation of energy loss and crystallographic transform. 80—23215
C foil, OH$^+$ beam Coulomb explosion, charge state depend. 79—31649
C foil, of H$_2^+$ and HeH$^+$, moving ion pot. determ. 78—33572
C foil, passage of ^{14}N and ^{20}Ne ions, energy-angle distribs. 79—10889
C foil, transmitted H$^+$ energy loss, ang. distrib. and charge fractions 80—2102
C foil+H$^+$(C$^+$)(N$^+$)(O$^+$)(Na$^+$)(Mg$^+$)(S$^+$)(Kr$^+$), charge-state distrib. effect on photon emission, 100-400 keV 79—22814
C foils, stripping of heavy ions with energy 0.4-0.9 MeV/A, straggling, foil behaviour 78—33351
C, gamma-ray attenuation coeff. meas., 1115, 1173, 1332 keV 77—55303
C, Li ions stopping power and straggling 80—42908
C, low energy stopping powers determined by time of flight techniques 79—45594
C, multiple scatt., energy loss meas. for Ar, Kr, Xe, U 1.2 MeV ions 79—751
C, proton energy straggling in ion backscatt. expt. 79—37750
C, proton straggling determ., using 0.47 and 1.73 MeV 79—4356
C, range and range straggling of 120 keV heavy ions 79—45595
C, stopping power determ. for heavy ions, 200 to 2000 keV 79—45596
C, stopping power meas. for 4-5 MeV/N ^{16}O, ^{40}Ar, ^{65}Cu, and ^{84}Kr 78—70720
C, stopping ratios of 50-300 keV H$^+$, He$^+$, ^{7}Li$^+$, and ^{8}Be$^+$ 80—42903
C$^+$+Ne, energy loss collision spectrosc. 79—86037
CO+H$^+$, vibr. excitation, 5-90 eV, forward scatt. differential cross section 78—9228
CO$_2$, continuous slowing down approx., range difference for 0.2 to 10 MeV electrons 80—39187
CO$_2$, gas, total ionization created by completely stopped H$^+$ ions 79—46419
CO$_2$, W-value for pion$^-$ 77—56473
CaSnO$_3$, powder, electron scatt. from ^{119}Sn, effective range, Mossbauer obs. 77—63345
Cd+Te, π^- capture, radioactivity meas. 80—47831
Cd$_{0.2}$Hg$_{0.8}$Te:B, ion implanted, B range and range straggling 80—54273
CdTe, thin film, stopping power for protons and alpha particles, proton energy straggle values 77—89489
CeAl$_2$, dynamic Jahn-Teller effect, neutron energy loss obs. 79—78060
^{252}Cf fission fragment tracks in quartz glass, electron microscope obs. 78—17526
^{252}Cf, spontaneous fission, fragment ranges and kinetic energies in Al 78—94037
^{252}Cf, spontaneous fission, fragment slowing in gases 80—22875
Cl ions+Ar-methane, (isobutane), energy straggling 78—58785
CsI, proton loss by nuclear inelastic interactions 77—71729
^{130}Cs, low energy ions systematic range meas. in Ar and N$_2$ gases 79—1472
Cu, amorphous, bombard. by Ar$^+$ ions, collision cascades, computer simulation 79—46731
Cu beam dump, meas. of stopped π^+ decays with 720 MeV protons 79—45503
Cu, determ. of width of lateral spread distribs. of MeV He ions from energy spectra 79—14860
Cu, differential ranges of fission products by a coulometric method 80—65097
Cu, electron inelastic mean free paths and energy losses, electron gas statisitcal model 79—46733
Cu, electron range, low-energies continuous-slowing-down approx. and range straggling calcs. 80—39183
Cu, electron transmission and absorption, 70 keV initial energy 78—71777
Cu, electronic stopping function for He$^+$ and Li$^+$, 50-300 keV 79—69169
Cu, energy losses and straggling for H$^+$ and He$^+$ beams *(Russian)* 80—84226
Cu, energy straggling of 6.74 MeV protons 78—79641
Cu, fast electron transmission, contrib. of high-angle deflections 79—28024
Cu, film, Monte Carlo simulation of energy distrib. of low energy protons 77—15466
Cu foil, polycrystalline struct. influence on transmitted 300 keV ion energy loss 79—95057
Cu, gamma-ray attenuation coeff. meas., 1115, 1173, 1332 keV 77—55303
Cu, Li ions stopping power and straggling 80—42908
Cu, multiple scatt. of fast electrons and inner secondary electron generation 77—1160
Cu, neutron irrad., replacement sequences, calcs. using ADDES and COMENT codes 79—46714
Cu, O$^+$ implantation along channelling directions, stopping power 77—69021
Cu, projected range distrib. of 5-25 keV ^{4}He$^+$ 80—65094
Cu, projectile range for Z=8-20, 0.0125-12.0 MeV/nucleon 78—83856
Cu, range of Ni$^+$ ions, increase due to ion bombardment induced crystalline reorientation 78—26611
Cu, secondary electron yields from ion impacts, stopping power calcs. 78—11053
Cu, stopping of 3-7 MeV α-particles and 4-6 MeV protons *(Russian)* 79—51181

energy loss of particles continued
Cu, stopping power for 0.3-1.5 MeV protons 79—55801
Cu, stopping power for MeV H$^+$, D$^+$, ^{4}He^{2+}, ^{7}Li^{3+} ions, deviations from Bethe formula 78—26612
Cu, stopping powers of 100 keV protons, meas. using ion induced X-ray emission 78—48725
Cu, stopping ratios of 50-300 keV H$^+$, He$^+$, ^{7}Li$^+$, and ^{8}Be$^+$ 80—42903
Cu:O single crystal, ^{18}O$^+$ ions implantation in channelling directions, stopping power meas. from max. range 80—65078
Cu(110), Ar bombardment, fast recoil atom blocking effect 79—69172
D gas, stopping power of alpha-particles 77—18758
D, in solid absorber, large depth profile meas. by deuteron induced reactions 77—19978
DT-Pu plasma, neutron induced fission, fission fragment slowing down 79—26749
depth distrib. of self-ion damage, TEM 77—51419
dielectric track registering media, possible new sputtering mechanism 77—392
DyD$_2$, cryst. elec. field transition, neutron energy loss spectra meas. 79—78059
Eu, electron and positron multiple scatt. 80—15171
F ions, transient mag. field discontinuity in Fe(Co)(Ni) 80—24515
Fe beam stop for 500 MeV protons, secondary flux, beam intensity meas. 79—85850
Fe, continuous slowing down approx., range difference for 0.2 to 10 MeV electrons 80—39187
Fe, effect of irrad. by fast neutrons and ^{235}U fission products at 20K *(French)* 79—51159
Fe film, vacuum deposited, stopping power meas. of 0.3 to 2.6 MeV ^{4}He ions 79—3329
Fe, gamma photon backscattering, energy dependence *(Rumanian)* 79—76316
Fe, impurity atoms in hot plasma, radiation energy loss 78—18441
Fe, muon$^+$, 40 MeV, traversing magnetised plates, dynamic mag. fields 79—38422
Fe, neutron ns. slowing down time, expt. obs. 78—58319
Fe, polarised, high vel. ion recoil, transient mag. fields 77—43910
Fe, projectile range for Z=8-20, 0.0125-12.0 MeV/nucleon 78—83856
Fe, range distributions for 25-200 keV ^{14}N$^+$ ions 80—103405
Fe, stopping of 3-7 MeV α-particles *(Russian)* 79—51181
FeS$_2$, diatomic crysts. electron induced X-ray emission, channelling effects 79—56888
^{56}Fe, hadron generated cascades, energy flux absorption length, 1-20 TeV *(Russian)* 78—28468
^{56}Fe ions relativistic nuclei stopping power, Bethe theory higher order corrections 78—78599
^{212}Fr, low energy ions systematic range meas. in Ar and N$_2$ gases 79—1472
GaAs, blocking effect, backscatt. method *(Chinese)* 79—90708
GaAs, chemisorption of Cs, isobars, LEED and loss spectroscopy meas. 77—4262
GaAs, electron bombardment, absorption of energy 79—14847
GaAs, ion implantation, range distrib. calc. 79—55760
GaAs, proton range calcs. 77—76479
GaAs, proton range data and deep proton-isolated lasers 79—36923
GaAs:Sn, proton implantation and annealing behaviour *(Chinese)* 80—44224
GaAs$_{1-x}$P$_x$-SiO$_2$:N,Zn ion-implanted multiple layers, ion range distribs., secondary ion microprobe meas. 79—42129
GaSb, proton range data and deep proton-isolated lasers 79—36923
Gd, ferromag., transient mag. fields at stopping nuclei, stopping power 78—34555
Gd, stopping power and energy straggling of ^{4}He$^+$ ions in vacuum-evaporated films 80—88231
Ge, amorphous, scatt. of 2 MeV He$^+$ 77—69954
Ge, backscattered energy spectra, charged particles energy losses 79—83086
Ge, channelling effects for 15 GeV/c π^- 78—21831
Ge, channelling of 160 MeV protons, deuterons and α particles, stopping powers 79—86826
Ge, energy loss spectra of C^{2+} ions 80—65114
Ge, film, electron transmission, 1-5 keV, electron MFP 77—15472
Ge, mean excitation energy based alpha particle stopping power meas. 78—30678
Ge, positron formation at surface 79—13845
Ge, proton energy loss, 0.1-1.0 MeV 80—42909
Ge, stopping power for fast channelled α-particles 78—79654
Ge, stopping powers of 100 keV protons, meas. using ion induced X-ray emission 78—48725
H, and mixtures, photon mass attenuation and mass energy-absorpt. coeffs., 0.1 keV to 20 MeV 77—61715
H, electronic stopping power calcs. 80—2104
H gas, proton energy loss distrib. in range 50-150 KeV 77—79526
H ions, Bethe stopping power formula, higher order Z$_1$ corrections 77—30732
H ions, velocity measurement by Doppler shift of H atoms line spectra after traversing thin C foil 78—16778
H, neutron scattering, 0.1 to 14 MeV, slowing down times and distances calcs. 77—65409
H$^+$, 150 MeV scatt. in plexiglass, mean-square transverse displacement 79—6808
H$^+$, in H$_2$ gas, energy loss, high-energy calcs. 77—6891
H+H$^+$, differential energy loss cross-sections 77—46630
H$^+$+atom, Coulomb excitation, proton energy loss depend. on impact parameters *(Russian)* 80—53123
H$^+$+H$_2$, vibr. excitation, energy loss spectra, rot. sudden impact calcs. 77—88537
H$^+$+H$_2$(CO$_2$), vibr. excitation, 10-30 meV 80—58358
H$^+$+He, proton energy degradation, approx. yield spectrum 79—31643
H$_2$, α-particles stopping cross-section determ. 79—49917
H$_2$, electronic stopping power calcs. 80—2104
H$_2$ gas, ^{208}Pb stopping cross-section meas. with TOF spectroscopy 77—23569
H$_2$, neutron energy transfer 30 to 100 MeV 77—52890
H$_2^+$, collisional dissoc., excited electronic states effects 80—9687
H$_2^+$, electronic stopping power of slow mol. ions in solids 79—10888
H$_2^+$, fast ions, stopping power of carbon foils 78—79653
H$_2^+$, fast ions, thin solids 78—79652
H$_2$+Cl$^-$, 4-11 eV, inelastic scatt. 79—98202
HCl+K, ion pair form. reaction, energy loss spectra meas. 79—61849
HF+T hot atoms, energy loss 78—15691

energy loss of particles continued
$H_2^+(HeH^+)+C$ thin solid target, 50-300 keV, collisional at. physics using mol. projectiles 79−45813
H_2O, vap., fast charged particles, sum rule moment calcs. 78−5156
He beam charge fraction, emerging from solid 80−9716
He, electron and positron multiple scatt. 80−15171
He gas, energy loss and straggling of low energy alpha-particles 77−88361
He ion stopping powers and ranges in all elements 78−58565
He ions, <30 keV, stopping power in Au and nuclear collisions in Si, detector appl. 77−10546
He ions, Bethe stopping power formula, higher order Z_1 corrections 77−30732
He ions, Cu irrad., 1 to 25 keV, range profiles, reemission, blistering 78−38758
He, restricted energy loss by ionisation of relativistic muons 77−88355
He^+, energy and ang. distrib. in passing through C, Cu, Ag films 80−100292
He^+, pulse height defect in Si, meas. via field ionisation device 77−50330
$He^+ +$alkali metal, charge exchange, He metastable beam form., composition 79−89775
HeH^+, collisional dissoc., excited electronic states effects 80−9687
^3He, in solid absorber, large depth profile meas. by deuteron induced reactions 77−19978
^3He profiling, depth resolution using $^3He(d,\alpha)^1H$ reaction 78−58557
^4He, ion, backscattering anal. 79−96408
^4He stopping cross sections, 1-8.5 MeV, in H_2, He, N_2, O_2, Ne, Kr, and Xe 78−58558
^4He stopping power, 0.15 to 1 MeV, backscatt. determ. 80−88233
^4He, straggling in energy loss 80−42900
$^4He^+$ irradiation of Nb, blister skin thickness, meas.-calcs. correl. 77−35597
$^4He^{2+}$, slowing down in solids, 0.4 to 4 MeV range, calcs. 77−7776
$H(n=2)$ excitation by ion impact, precision doubly differential cross section meas. 79−45811
I^- ions of 15 MeV, stripping and charge state fluctuations in O_2 77−79522
InP, proton range data and deep proton-isolated lasers 79−36923
In_2Te_3 type semiconductors, basis of ionising radiation detectors 78−86743
$K+HCl$, ion pair form., energy loss spectra 79−34286
$K+NO_2$, ion pair form. reaction, energy loss spectra obs. 79−91921
$K+SF_6$, ion-pair form. reaction, energy loss spectra 80−55630
KBr(I), sputtering, depend. on beam energy and target temp. 79−1804
KCl, ion bombard., damage profiles, track effect anal. 77−15465
KCl(I), electron range-energy relation, thermally created lattice vacancies effect 80−92574
KI, mean free paths of 200-1500 eV electrons, XPS determ., model calc. 79−38715
^{86}Kr, stopping power meas. at 3-5 MeV/nucleon 80−102410
La, electron and positron multiple scatt. 80−15171
Li ions, 65 to 500 keV, stopping power and straggling in H_2, He, CO_2, N_2, O_2, Ne, Ar, Kr, and Xe 79−3529
Li ions, Bethe stopping power formula, higher order Z_1 corrections 77−30732
Li projectile, stopping cross section meas., chemical and target physical state influence 79−4345
Li projectiles, electronic stopping cross section meas., intermolecular interactions 80−75279
Li^+, amorphous target impact, 100 keV, electronic stopping power, models comparison 78−2180
$Li^+ + N_2$, (0.5 to 1.0 keV) energy loss spectra, ionisation, electronic and vibro-rot. transitions 77−14541
LiF, neutron ns. slowing down time, expt. obs. 78−58319
$LiNbO_3$, blocking effect, backscatt. method *(Chinese)* 79−90708
^6Li, in solid absorber, large depth profile meas. by deuteron induced reactions 77−19978
low energy He ion stopping powers calc. 79−4347
Mn, stopping power of 0.5-2.0 MeV ^4He ions, elastic backscatt. meas. 78−87730
Mo, neutron low energy interaction cross sections, gravitational spectrometer meas. 80−24521
Mo, proton energy loss, 0.1-1.0 MeV 80−42909
Mo, stopping power for 0.3-1.5 MeV protons 79−55801
Mo:H(He), depth profiles of implanted atoms, proton backscatter meas. 79−51136
N, and mixtures, photon mass attenuation and mass energy-absorpt. coeffs., 0.1 keV to 20 MeV 77−61715
N ions, 3.5 GeV, vel. spectrometry vs. depth in polyethylene 78−48896
N nuclei, track in Ilford G-5 emulsion, track with meas. 78−17488
N^+, amorphous target impact, 800 keV, electronic stopping power, models comparison 78−2180
N^+, electronic stopping power in solids, range distrib. energy depend. 80−92575
$N^{2+}+He(Ne)(Ar)$, electron capture, product ion energy loss spectra 79−36762
N_2, α-particles stopping cross-section determ. 79−49917
N_2, energy loss of H, C, N and O ions for elastic nuclear collisions 78−86759
N_2, gas, total ionization created by completely stopped H^+ ions 79−46419
N_2, liquid, absorpt. of high energy electrons 78−882
N_2, solid, interaction of 1-3 keV electron beam, range and secondary emission 79−15568
N_2, W-value for pion$^-$ 77−56473
N_2+H^+ collision, total ionis. cross section and stopping power for protons 80−69228
^{14}N ions emerging from solids, equil. charge state distribs. meas. 77−65388
^{15}N 6.5 MeV ions in solids, energy loss distrib. meas. 78−59845
$^{15}N^+$ ions in metals, ranges by $(p, \alpha\gamma)$ reson. broadening 79−37749
NaCl, F-centres near monoenergetic proton stopping region, space charge effect 78−18640.
NaCl, rock salt, average electron range in dielec., 20-50 keV, precise meas. 79−14868
NaCl+cosmic ray muons, photonuclear cross section, nuclear muon losses 77−64581
NaI, continuous slowing down approx., range difference for 0.2 to 10 MeV electrons 80−39187
NaI, proton loss by nuclear inelastic interactions 77−71729

energy loss of particles continued
Nb, projected range distrib. of 5-25 keV $^4He^+$ 80−65094
Nb_2O_5, chemical effect, influence on stopping power 80−47830
Nd, electron and positron multiple scatt. 80−15171
Ne, nuclear emulsion track width by photometric meas. 78−94167
Ne nuclei, track in Ilford G-5 emulsion, track width meas. 78−17488
Ne^+, energy and ang. distrib. in passing through C, Cu, Ag films 80−100292
^{20}Ne ions emerging from solids, equil. charge state distribs. meas. 77−65388
$^{22}Ne(4_1^+)$ from ^4He $(^{19}F,p\gamma)$, lifetime meas. by high vel. coincidence DSA method 78−33148
Ni (110), surface relax., O_2 coverage effects, medium energy ion scatt. obs. 79−28181
Ni, alpha particle energy loss straggling 80−42902
Ni, deuteron range profiles in 100 to 400 keV region, expt. and computer simulation 77−51422
Ni, electron inelastic mean free paths and energy losses, electron gas statisitcal model 79−46733
Ni, energy loss spectra of C^{2+} ions 80−65114
Ni, energy straggling of protons 79−77652
Ni film, amorphous layer covered, target prep. for channelled ion stopping power meas. 80−63431
Ni film, vacuum deposited, stopping power meas. of 0.3 to 2.6 MeV ^4He ions 79−3329
Ni, He^+ exfoliation depth and damage energy distrib., range 80−29075
Ni, Li ions stopping power and straggling 80−42908
Ni, low energy stopping powers determined by time of flight techniques 79−45594
Ni, mean excitation energies from α-particle stopping power meas. 79−13615
Ni, mean excitation energy based alpha particle stopping power meas. 78−30678
Ni, projectile range for $Z=8$-20, 0.0125-12.0 MeV/nucleon 78−83856
Ni, range and range straggling of heavy radioactive ions 78−22776
Ni, range distributions for 25-200 keV $^{14}N^+$ ions 80−103405
Ni, ranges of implanted 10-30 keV D^+ 78−83858
Ni, stopping of 3-7 MeV α-particles and 4-6 MeV protons *(Russian)* 79−51181
Ni, stopping power for ^{107}Ag, ^{109}Ag and ^{150}Sm 80−70284
Ni, stopping power for 0.3-1.5 MeV protons 79−55801
Ni, stopping power meas. for 4-5 MeV/N ^{16}O, ^{40}Ar, ^{65}Cu, and ^{84}Kr 78−70720
Ni, stopping power of 0.5-2.0 MeV ^4He ions, elastic backscatt. meas. 78−87730
Ni, stopping powers of 100 keV protons, meas. using ion induced X-ray emission 78−48725
$Ni:K^+(Ba^+)$, ion implantation, effect on inelastic refl. and energy losses of fast primary electrons 78−55900
Ni:O single crystal, $^{18}O^+$ ions implantation in channelling directions, stopping power meas. from max. range 80−65078
O, and mixtures, photon mass attenuation and mass energy-absorpt. coeffs., 0.1 keV to 20 MeV 77−61715
O ion, range calc., number of primary atoms created in diatomic target *(French)* 79−1473
O ions, non-equilibrium charge state distrib. charge exchange cross-sections in solid targets 80−65109
O ions, transient mag. field discontinuity in Fe(Co)(Ni) 80−24515
$O^- + Ne(Ar)(Kr)$, 0.2-1 keV, elastic and inelastic reduced differential cross-sections 80−32829
$^{16}O^{x+}+Al$, energy-loss straggling, charge exchange effects 78−58799
Pb, gamma photon backscattering, energy dependence *(Rumanian)* 79−76316
Pb, gamma-ray attenuation coeff. meas., 1115, 1173, 1332 keV 77−55303
Pb, photon showers produced by 150 MeV electrons 77−10563
^{208}Pb, stopping power meas. at 3-5 MeV/nucleon 80−102410
Pd-C solid solution, dechannelling of α-particles by C atoms *(French)* 79−7643
Pt (111), relax. effects, and thermal vibrs., medium energy ion scatt. 79−28182
^{79}Rb, low energy ions systematic range meas. in Ar and N_2 gases 79−1472
^{187}Re, slowing down of recoil atoms in W, WSe_2, Nb 77−4136
S ion charge distrib., 70-140 MeV, through C and Be foils 78−13364
S^{4+}, travelling in solids, $K\alpha$ X-ray spectra 80−100706
Sc, electron and positron multiple scatt. 80−15171
Sc, stopping powers of 100 keV protons, meas. using ion induced X-ray emission 78−48725
Se, Li ions stopping power and straggling 80−42908
Se, mean excitation energies from α-particle stopping power meas. 79−13615
Si, amorphous, asymmetrical profile of ion implanted P 79−46693
Si, amorphous, heavy ion ranges, He^+ backscatt. obs. 78−63796
Si, amorphous, implanted ion trajectory and spatial distrib., Monte Carlo simulation 77−11611
Si, amorphous foil, electronic energy straggling of light ions, at. number depend. 77−11612
Si, and SiO_2 on Si, ranges of implanted B^+ and B^{2+} 77−31687
Si, ang. distribs. of 6.6 MeV protons, 12.5 MeV deuterons, and 24 MeV α-particles 78−29720
Si, anomalous passage of positrons, expt. 79−95052
Si, blistering due to 400 to 1800 keV $^4He^+$ ions, modal range determ. 80−100289
Si, blocking effect, backscatt. method *(Chinese)* 79−90708
Si, channelled and random proton stopping power, 30-1000 keV 78−67760
Si, channelled protons to valence electrons, dielec. calc. 77−55312
Si, channelling of 1 MeV He ions with greater-than-random energy loss rates 77−80564
Si, channelling of 160 MeV protons, deuterons and α particles, stopping powers 79−86826
Si, channelling of π^- and π^+ 79−60414
Si detector, anal. of $\Delta E,E$ particle identification 77−88348
Si, electron bombardment, absorption of energy 79−14847
Si, electron channelling patterns, contrast mechanisms, lattice-defect images, in SEM 79−27884
Si, electron inelastic mean free paths and energy losses, electron gas statisitcal model 79−46733
Si, electronic stopping powers of hydrogen in Si (100) wafers below 140 keV 79−4334

energy loss of particles continued
- Si, energy deposition in heavy-ion path using Monte Carlo transport anal. of delta rays in track 80—39185
- Si, energy loss and multiple scattering of non-channelled α-particles *(German)* 80—59544
- Si, energy loss of non-channelled α-particles, interpretation using averaged continuum pot. 78—30683
- Si, feeding-in and blocking of 2 MeV protons, simple diffusion model 78—22782
- Si, half wavelength and stopping power of planar channelled protons 80—65087
- Si, heavy ion ranges, 120 keV Pb ions backscatt. obs. 80—19855
- Si, impurity atoms in hot plasma, radiation energy loss 78—18441
- Si, inelastic stopping of medium energy light ions, channelling meas. 77—59058
- Si, ion penetration, computer program 80—88185
- Si, mean excitation energy based alpha particle stopping power meas. 78—30678
- Si, positron formation at surface 79—13845
- Si, proton energy loss, 0.1-1.0 MeV 80—42909
- Si, proton energy straggling in ion backscatt. expt. 79—37750
- Si, proton random and aligned stopping powers, 80 to 300 keV, backscatt. meas. 77—27931
- Si, random and channelled energy loss for positive and negative, 2-15 GeV/c pions, kaons and protons 79—3332
- Si, range and range straggling of 120 keV heavy ions 79—45595
- Si, range distribs. of energetic protons, Monte Carlo computer simulation 78—22777
- Si, range of 100 keV Pr^{2+} and Tb^{2+}, M-shell X-ray cross-sections 77—35614
- Si, range parameters of protons implanted at 0.5 to 300 keV 80—44242
- Si semiconductor counters, response to relativistic pions, electrons and protons 79—13597
- Si solid state detector telescopes, neutral particle background effects 78—28472
- Si, stopping power for channelled 160 MeV α particles, expt. 78—26613
- Si surface barrier detectors, energy distrib. functions of low energy H and ^{3}He ions 77—6652
- Si thin detector, ionisation energy loss of relativistic electrons 78—55117
- Si:^{11}B, amorphous, calc. of implanted-ion range and energy-deposition distrib. 77—7748
- Si:B, ion implanted, comparison of range and range straggling 77—55293
- Si:B impurity range distrib. determ. by $^{10}B(n,\alpha)^7Li$ reaction 78—11585
- Si:N, ion implantation, refractive index, IR spectra, ion range and straggling meas. 80—34020
- Si:O, ion-implanted between 2 and 20 MeV, range and range straggling 80—44241
- Si-SiO_2, two layer system, P^+-ion penetration tails, expt. and computer anal. 80—75249
- Si+C ion, nuclear stopping power and interatomic potentials 78—74549
- SiC distribution profiles of 30 keV Al ions using Lindhard-Scharff-Schiott model *(German)* 80—15172
- Si_3N_4-SiO_2:N,Zn ion-implanted multiple layers, ion range distribs., secondary ion microprobe meas. 79—42129
- SiO_2, glass, ion implanted, radiation effect on chem. stability 77—1158
- SiO_2 massive dielectric target, 5-25 keV electrons penetration characts. 80—70260
- Sn, charged particle stopping power meas. by 100 keV proton induced X-ray emission 79—45593
- Sn, continuous slowing down approx., range difference for 0.2 to 10 MeV electrons 80—39187
- Sn, gamma-ray attenuation coeff. meas., 1115, 1173, 1332 keV 77—55303
- Sn, stopping power for 6.75 MeV protons 80—34107
- SnO_2, powder, electron scatt. from ^{119}Sn, effective range, Mossbauer obs. 77—63345
- ^{119}Sn, thin foil, 19.6 keV conversion e^- energy, ang. contrib., Monte Carlo calc. 79—11360
- Ta, range and range straggling of heavy radioactive ions 78—22776
- Ta, ranges of light ions meas. by (p,γ) reson. broadening, 20-100 keV 77—69023
- Ta, stopping power for 0.3-1.5 MeV protons 79—55801
- Ta, transmission channelling of MeV ions to study edge dislocations, expt. setup 80—29098
- TaO, energetic heavy ion irrad., elastically deposited energy, numerical calc. 77—59057
- Ta_2O_5, amorphous, range of ^{27}Al meas. by (p,γ) reson. broadening 77—69023
- Ta_2O_5, chemical effect, influence on stopping power 80—47830
- Te, Li ions stopping power and straggling 80—42908
- Ti, energy loss spectra of C^{2+} ions 80—65114
- Ti film, on Be(Ag) substrate, range of primary electrons 77—4134
- Ti, neutron low energy interaction cross sections, gravitational spectrometer meas. 80—24521
- Ti, projectile range for Z=8-20, 0.0125-12.0 MeV/nucleon 78—83856
- Ti, stopping of 3-7 MeV α-particles *(Russian)* 79—51181
- Ti, stopping power for 0.3-1.5 MeV protons 79—55801
- Ti, stopping power of 0.5-2.0 MeV ^{4}He ions, elastic backscatt. meas. 78—87730
- TiO_2, chemical effect, influence on stopping power 80—47830
- U, continuous slowing down approx., range difference for 0.2 to 10 MeV electrons 80—39187
- U ion, range calc., number of primary atoms created in diatomic target *(French)* 79—1473
- UO_2 film, vacuum evaporated, He^+ ion energy loss parameter 78—50253
- UO_2 fission fragment, range calc., number of primary atoms created in diatomic target *(French)* 79—1473
- UO_2 neutron transmission temp. depend. 79—82265
- ^{235}U, fission recoils, chem. effects, energy deposition efficiencies, surface conditions depend. 78—80776
- ^{238}U, stopping power meas. at 3-5 MeV/nucleon 80—102410
- $^{238}U(p,nf)$, multiple scatt. effect due to filling in of blocking patterns 78—21617
- $^{238}U(p,xnf)$, lifetime of second chance fission at threshold, in UO_2 single cryst. 78—17259
- V, neutron low energy interaction cross sections, gravitational spectrometer meas. 80—24521
- W (110), D^+ depth distrib., effect of surface impurities, channelling model 79—1451
- W, atomic density, effect on proton energy loss and dechannelling 80—65088

energy loss of particles continued
- W, backscattered energy spectra, charged particles energy losses 79—83086
- W, channelled proton energy losses 77—1161
- W crystal, backscatt. energy spectra, channelling particles energy loss determ. 78—2181
- W, enhanced penetration of low energy He along ⟨100⟩ channel 80—65093
- W, ion implantation, $^4He^+$ range profile and ^{4}He diffusivity meas. 79—33022
- W, neutron low energy interaction cross sections, gravitational spectrometer meas. 80—24521
- W, secondary electron yields from ion impacts, stopping power calcs. 78—11053
- W, single cryst., proton integral dechannelling functions *(Russian)* 78—10111
- W, stopping power for 0.3-1.5 MeV protons 79—55801
- W-EuS emitter junction, energy loss of field emitted electrons 77—81201
- $Xe+Xe^+$, 0.3-1.2 MeV, multiple N- and M-shell excitation, inelastic energy loss meas. 79—852
- ^{132}Xe, stopping power meas. at 3-5 MeV/nucleon 80—102410
- Y, charged particle stopping power meas. by 100 keV proton induced X-ray emission 79—45593
- Y, electron and positron multiple scatt. 80—15171
- Y, mean excitation energy based alpha particle stopping power meas. 78—30678
- Yb, electron and positron multiple scatt. 80—15171
- $YbCu_2Si_2$, mag. 4f Zeeman-level power spectrum using diffuse mag. neutron scatt. 79—60775
- Zn, stopping power for 0.3-1.5 MeV protons 79—55801
- Zn, stopping power for 6.75 MeV protons 80—34107
- Zn, stopping power of 0.5-2.0 MeV ^{4}He ions, elastic backscatt. meas. 78—87730
- Zn+Se, π^- capture, radioactivity meas. 80—47831
- ZnO, chemical effect, influence on stopping power 80—47830
- ZnO, spacecraft thermal control material, low-energy proton effects 80—70288
- ZnS, diatomic crysts. electron induced X-ray emission, channelling effects 79—56888
- ZnSe, diatomic crysts. electron induced X-ray emission, channelling effects 79—56888
- ZnTe, thin film, stopping power for protons and alpha particles, proton energy straggle values 77—89489
- Zr, gamma-ray attenuation coeff. meas., 1115, 1173, 1332 keV 77—55303
- Zr, range distributions for 25-200 keV $^{14}N^+$ ions 80—103405
- Zr, ranges of implanted 10-30 keV D^+ 78—83858

energy measurement *see power measurement*

energy-range relations *see energy loss of particles*

energy resources
- *see also fuel; solar energy concentrators; solar power; wind power*
- 1978 state and long-term assessment, in US conditions 79—52863
- advanced energy conversion for electrical power generation *(Japanese)* 80—93865
- advanced energy systems for industrial appls., assessment of nuclear- and coal-based systems 80—16771
- alternate, economic considerations 79—87940
- alternative energy resources, review *(Italian)* 80—66917
- alternative energy sources, conf. Miami, FL USA (Dec. 1979) 80—55772
- alternative energy sources, energy accounting study 80—76589
- alternative energy sources and environmental problems, Ispra Research Centre activities, w.r.t. EEC policy 79—97770
- alternative energy strategies, development of solar-based renewable resources, review 80—30417
- alternative energy technologies and strategies, assessment using the Reference Energy System 80—30421
- alternative technologies, cost analysis 79—48041
- alternative versus conventional energy sources, economic comparison *(German)* 80—72002
- ambient energy systems for energy conservation 80—61316
- assessments of nuclear systems and use of nuclear power, review 79—45334
- Austria, development possibilities of energy resources, review *(German)* 80—21355
- automobile propulsion using H_2 and electric power, comparative evaluation 80—16769
- bioenergy conversion systems, efficiency improvements 80—30511
- biofuel, large-scale prod. of ethanol and methanol from biomass, review 79—52864
- biomass, an alternative to fossil hydrocarbons 79—87985
- biomass, combustion of agricultural waste as supplementary boiler fuel, environmental and economic consequences 80—40809
- biomass, ethanol production through wood hydrolysis 79—48039
- biomass, review of possible energy conversion processes *(French)* 80—93843
- biomass conversion technology 80—89601
- biomass energy, development, availability, and storage possibilities *(French)* 80—89587
- biomass energy conversion, energy sources for rural development 80—30509
- biomass energy production and the photosynthetic pathway 80—61393
- biomass for energy production, economic eval. *(Swedish)* 80—93844
- biomass gasification process, Garrett Energy Research 79—48040
- biomass production utilising geothermal low temp. heat 80—66932
- Brazil's energy consumption, oil resources and economic and technical difficulties *(French)* 80—55777
- break-even rating of nuclear and conventional power. technico-economic parameters 79—79362
- brown coal basins of Hungary, Eocene, geophys. exploration *(Hungarian)* 80—104938
- Bullaren lineament, SW.Sweden, heat extraction potential 80—76602
- Canadian renewable energy industry, solar and biomass conversion technology *(French)* 79—87971
- coal and hydrocarbons, exploration via refl. seismology, book 78—96162
- coal conversion processes, appl. of non-fossil-derives H_2 for synthetic fuel manufacture 79—74483
- coal energy utilisation technology in Japan overview 79—96413
- coal fired power stations, review of conventional and advanced systems 80—35625

energy resources continued
coal gas production using HTR 80—11996
coal gasification and liquefaction 78—53012
cold water pipe designs for ocean thermal energy conversion plants 80—45725
comparability study of fission and fusion reactors w.r.t. safety, costs and development time 79—59114
comparative evaluation of fossil fuel and advanced generating systems 80—40808
comparative risk assessment of energy systems 80—30423
comparative social impact of alternative electrical energy generating technologies 78—9003
concept of energy, review 79—96412
conf., 14th Intersociety energy conversion eng. conf. [Boston, MA, USA (Aug. 1979)] 80—31424
conf. on non-fossil fuel and non-nuclear fuel energy strategies, Hawaii (Jan. 1979) 80—27030
conf. San Diego, CA, USA (Feb. 1980) 80—62395
conference on nuclear power and its fuel cycle, Salzburg, Austria (May 1977) 79—26504
conservation, energy-efficient houses and industrial processes 80—30422
conservation, hard and soft paths compared 80—89584
conservation in the OECD 1980 to 2000, book 80—35654
conservation system using waste heat, Kitakyushu regional system *(Japanese)* 80—21386
crisis in energy supply, review 79—66396
demand and conservation in US residential and commercial buildings 80—26121
denatured Th cycle in symbiotic systems, potential role 79—26484
development and technology, surface science rel. problem areas 78—88553
development role of Sandia Laboratories' photometrics division 78—58077
developments up to year 2000, demand and technology forecasting *(French)* 79—92048
digester gas cogeneration facilities Los Angeles 80—30514
domestic water and space heating by new technologies, energy and direct economic effects, evaluation 79—92049
driven magnetic fusion reactors, conf., Erice-Trapani, Italy (Sept. 1978) 80—41948
economic aspects, ECE (Economic Commission for Europe) policy 80—26119
economic assessment of alternative energy strategies 80—30424
economic assessment of future energy schemes, domestic solar heating appl. 79—48044
economic choice for rural India, methodology 80—104499
economic demand in RGW countries, long term plan *(German)* 80—55770
education, alternative energy sources, solar and atmospheric 78—69951
education, applied science CNAA degree course at Kingston Polytechnic 79—35454
education, conservation effects on resource usage, integral expressions 78—69941
education, energy option for undergraduates 80—31447
effect of Harrisburg failure on nuclear power development *(Swedish)* 79—92056
electrical generation, alternatives, evaluation rel. to environmental impact, capacity factor, public acceptance 79—87938
electricity supply industry, effects of world energy resources on economy *(German)* 80—89583
elementary particle-antiparticle annihilation, possible future use as energy source 79—36054
energy conservation in Britain, main options 80—76620
energy conversion engineering, alternative energy sources *(Japanese)* 80—26105
energy modelling and forecasting at US ERDA 78—49629
energy R&D in the United Kingdom, energy resources 79—43710
energy science and technology in Belorussian SSR, historical review *(Russian)* 79—35516
energy transfer by electric power generation and utilisation, economic case 80—16777
energy-political questions nationally and internationally for West Germany *(German)* 80—101072
ethanol, as petrol substitute, increased use in USA *(Dutch)* 80—72004
Finnish energy policy up to year 2000 *(Finnish)* 80—50928
fission reactor fuel preparation and reprocessing, aspects 77—88267
Florida Regional Energy Action Committee system for citizens' technical input 79—79363
forecasting models and their validity 80—89582
forecasting of future energy requirements 79—57348
forecasts of energy supply, (late 1970's till 2000) *(German)* 79—96411
fossil fuelled advanced energy conversion systems, review 80—16772
French nuclear power generation programme *(French)* 79—26732
French plan VII, energy forecasting 78—49628
fusion and energy sufficiency 79—81090
fusion as a future power source, plasma confinement and technological problems 79—26752
fusion energy, utility requirements and economics 79—76145
fusion energy commercialisation, research review 79—76146
fusion energy trends 79—6763
fusion power, energy policy, prospective role 80—13843
fusion power, plasma and the controlled thermonuclear reaction, review of practical problems of energy prod. 79—93826
fusion reactor, research program strategy 79—59251
fusion reactors, synthetic fuel production appl. 80—13864
fusion reactors, use as process heat source for secondary energies 80—13863
fusion technology progress 78—62607
fusion within a European energy strategy 80—45652
future energy concepts, review 79—61936
future energy sources *(Korean)* 80—55771
future energy strategies effects on atm. CO_2 conc., rel. to global climate 79—83640
future reserves projections to 2050 *(Dutch)* 80—61221
gas, unconventional resources, public sector R&D investment allocation 79—79365
gas deposits, distribution related to Earth's rotation and local geological conditions *(Russian)* 79—83545
gas turbine power stations, off shore, electricity generation, off shore gas utilisation 80—21360

energy resources continued
geopressured geothermal energy production plant, environmental effects 80—97764
geothermal, 5 MW pilot plant, anal. of binary thermodynamic cycle with dual boiling 80—97763
geothermal, advanced geopressured and hot dry rock reservoirs, technical feasibility 80—40823
geothermal, coaxial well for space heating and cooling 80—66933
geothermal, economics of electric power generation 80—35635
geothermal, feasibility and demonstration of low-grade heat energy from deep aquifers, Canada 80—61278
geothermal, future prospects in world energy strategy 80—72012
geothermal, heat extraction from hot dry crustal rock via hydraulic fracture 79—74491
geothermal, hot dry rock geothermal energy development program 80—55801
geothermal, hot dry rock project, Los Alamos Scientific Lab. *(German)* 77—91086
geothermal, overall view *(French)* 80—40804
geothermal, Portugese 1951-78 development, Azores area *(Portuguese)* 79—79373
geothermal, renewable energy sources, Rumania *(Rumanian)* 80—35639
geothermal, space heating appls., system design and economic anal. 80—30379
geothermal, strategy and prospects for future development 80—30376
geothermal, technological aspects of exploitation 80—55799
geothermal, temp. gradient distrib. and geological struct. in Izmir-Seferihisar, Turkey 80—56441
geothermal, utilisation factor in power plants 80—16779
geothermal aquifers, reservoir lifetime and heat recovery factor, for urban heating 79—74492
geothermal district heating system, planning assessment, financing and design optimisation 80—61279
geothermal drilling research in the United States 80—55800
geothermal electric power generation, types of plants 80—61276
geothermal electric power generation 80—66937
geothermal electricity generation costing methods, quantitative comparison 80—3487
geothermal energy, development, availability, and storage possibilities *(French)* 80—89587
geothermal energy, environmental problems, air and water pollution, subsidence, induced seismicity, blowouts, noise, review 80—55797
geothermal energy, exploitation in France for spaceheating 79—79372
geothermal energy, heat extraction from hot dry rock masses 78—61378
geothermal energy, high-temp. electronics development 80—11997
geothermal energy, low grade, future uses in France *(French)* 77—53022
geothermal energy, review 79—29447
geothermal energy, utilisation factor *(Japanese)* 80—21371
geothermal energy, utilisation for thermal and electric energy, geochem. engineering and materials 80—61275
geothermal energy 79—35507
geothermal energy and biofuel production in agriculture 80—66932
geothermal energy at Grass Valley, Nevada, USA, microseism survey 80—21647
geothermal energy extraction, liq. flow pattern in system with three-dimens. filtration zone 77—49037
geothermal energy extraction from penny-shaped reservoir made in hot dry rock 80—108784
geothermal energy in California, economic and technological aspects 80—30377
geothermal energy in Holland, prospects *(Dutch)* 80—35634
geothermal energy in Hungary, non-electric usage 80—76601
geothermal energy in Italy, survey *(Italian)* 79—24889
geothermal energy in Sweden, investigations in Bohus granite area 80—85631
geothermal energy investigations in Sweden 79—74488
geothermal energy potential 79—70427
geothermal energy prospecting by geophys. methods, review 78—7803
geothermal energy prospects in Brazil 79—74487
geothermal energy recovery from hot dry rock, use of weighted brine 80—101076
geothermal energy resource exploitation, conf. Sept., Landerello, Italy 80—81418
geothermal energy resources, in Great Britain 79—17166
geothermal energy resources, low enthalpy, in Denmark 79—74489
geothermal energy resources for electricity generation, discounted cash flow anal. 80—85263
geothermal energy resources in Oregon, USA, elec. and EM sounding obs. 80—97761
geothermal energy resources utilisation possibilities *(German)* 80—108785
geothermal energy utilisation thermodynamic aspects *(German)* 79—96416
geothermal exploration in Iceland, volcanological methods 79—74877
geothermal generation of power, review 79—87965
geothermal heat extraction from hot dry rock, siting criteria and appl. to Switzerland 79—39275
geothermal hot water for controlled horticulture 80—108783
geothermal potential and heat flow meas. in Egypt 79—74490
geothermal potential of Caledonian granites in Britain, geochemical and geophysical evidence 79—74486
geothermal potential of Kirishma region (Japan) evaluation using resistivity sounding 80—11998
geothermal power, availability accounting *(Japanese)* 80—16780
geothermal power, demonstration projects for technical and economic feasibility 80—66936
geothermal power, near-term supply curve for elec. appls. based on prod. costs 80—61277
geothermal power 79—70426
geothermal power at Geysers, Calif., USA, net energy anal. of elec. energy generated 80—45629
geothermal power developments and environmental pollution 80—61470
geothermal power for heating purposes *(Slovak)* 79—87963
geothermal power stations, economics and risk assessment 80—30378
geothermal research by IR scanning, image processing 77—64458
geothermal research in Netherlands *(Dutch)* 78—61415
geothermal reservoir, transient steam flow, Kawah Kamojang, Java 80—77018
geothermal reservoir at Raft River, Idaho, USA, borehole geophys. study 80—21672

energy resources continued
- geothermal reservoir exploitation, finite difference modelling 80—55798
- geothermal reservoirs, mathematical modelling of heat and mass transfer 80—55802
- geothermal resource assessment of United States 79—70428
- geothermal resource development, power station planning and siting 80—66935
- geothermal resource field development for electric power generation 80—66934
- geothermal resources, exploration via seismic noise sources mapping 77—81828
- geothermal resources, in Coast Plutonic Complex of S.British Columbia, Canada 79—70429
- geothermal resources, low-temp., in E.United States 80—85264
- geothermal resources for elect. generation or direct heat utilisation, review 80—35636
- geothermal resources in Japan, thirty promising sites 79—96417
- geothermal resources in USA, National Exploration Program 80—72011
- geothermal resources utilisation, systems aspects, computerised decision anal., social-economic anal. 80—30380
- geothermal saturated strata maintained by linear, ring batteries of wells, heat exchange 80—45630
- geothermal technology, development into an exact science 80—61781
- global energy demand growth, contrib. of alternative supply systems 80—30420
- global nuclear power is alternate source of energy, prospects and issues 80—7897
- global options for short-range alternative energy strategies, development of hydro power and biomass conversion 80—30418
- global perspectives and options for long-range energy strategies 80—30419
- global problems and energy, nuclear power 78—45454
- global problems soln., scientific and social approaches 77—74185
- Green River oil shales, anal. of depend. of thermal transport parameters on organic content 79—79817
- H, thermochemical production by H_2O decomp., optimum temp. conditions utilizing HTGR nuclear heat 80—35781
- H-fuelled passenger bus, design 80—40924
- Hawaii, wind and insolation as alternative energy resources 80—45623
- Hawaii Geothermal Project, groundwater geochem. study 80—72567
- health physicist role in development of safe sources 78—36088
- heat and energy savings and coordination and planning of resources expansion *(Russian)* 80—89585
- heat recovery system at Green Bay sewerage wastewater facility 79—83610
- heat supply from nuclear reactors and coal combustion, appl. study 78—37455
- heavy quark physics, practical appls. in energy sources and storage 79—9426
- high power restrictions imposed by physical laws 77—5616
- high-temperature power-technological industrial processes use of nuclear power, reviews 79—26729
- hot dry rock geothermal reservoir fracture mapping techniques 80—81419
- HTR nuclear long distance energy system, heat transport by chemical circuit 80—7905
- HTR plant with methane reformers for long distance energy system 80—7906
- human factors of energy research 80—30425
- human health risk, comparison of conventional and nonconventional technologies 79—87956
- hybrid solar/H fuel system producing high energy 80—45809
- hydrocarbon deposits in Rumania, geothermal gradients meas. *(Rumanian)* 77—29266
- hydrocarbons production by photosynthesis 80—89661
- hydroelectric potential in Scottish Highlands 80—7911
- hydroelectric power, application potential 80—30372
- hydropower potential in Burundi 80—81417
- India's wind energy potential and utilisation, as supplement to solar power 79—61942
- industrial utilisation of energy, book 80—61222
- instrumentation 80—72001
- integrated reactor systems fuel strategy, review of future nuclear energy options 79—49696
- interacting energy resource processing systems, energy effectiveness and environmental impact 80—40847
- Iran, feasibility of energy self-sufficiency through decentralised use of renewable resources 80—35658
- irrigation plants using solar or wind power, comparison w.r.t. cost, maintenance and reliability 79—70425
- Israel's coastal plain (1967 to 1976) temp. and global radiation meas., for appl. to design of solar heating systems 79—80003
- Italy's electric power requirements, nuclear programme, pumped storage hydroelectric integration 79—26733
- LMFBR prospects, reln. to world energy resources 79—97888
- LNG, transport and storage hazards 80—45620
- logistic substitution model, appl. to energy systems 80—89600
- management program for industrial energy conservation incl. computer controlled plant 80—40849
- marine structures for energy conversion 79—43712
- materials problems and basic research needs 78—86703
- materials research for advanced energy technology, appl. of crystallography, review 79—96429
- Maui offshore gas field, in New Zealand 80—26103
- methane, combustible gas production from organic wastes using bacteria 80—7898
- methane reforming by nuclear steam for coal hydrogasification 80—30325
- MIDCON conference, Dallas, USA, Dec. 1978 79—87939
- modelling for policy anal. 79—83578
- multicriterial optimization of the development of nuclear power in the framework of the perspectives of COMECON 80—7900
- municipal refuse, utilisation of heat energy 80—66919
- national energy and nuclear power system plans of the Federal Republic of Germany 79—26506
- national energy planning optimisation model 79—57350
- national energy policy anal. and planning models 80—101071
- national energy programme of USA, nuclear power, fuel enrichment and waste disposal 79—26686
- natural gas/solar energy transition strategy 80—30414

energy resources continued
- natural resource conservation, energy analysis approach criticised *(French)* 79—57349
- neutronics rel. to energy problem 77—26827
- new energy source contributions to heating, transport and power generation *(French, English)* 80—21356
- Newfoundland, offshore oil and gas production, associated problems 79—87946
- non-electric fusion energy applications 80—42866
- non-nuclear, non-fossil sources, utilisation, W.Germany *(German)* 77—9426
- non-nuclear energy systems, accidents and unscheduled events 79—52861
- nuclear, FBR development, US 1977 policy and future prospects 79—49828
- nuclear, fission and fusion processes *(Portuguese)* 77—3189
- nuclear, world resources up to year 2020, review 78—685
- nuclear energy, future role, fuel cycles, reactor types *(German)* 78—29579
- nuclear energy strategy, Japan, possibility of FFHR 80—42868
- nuclear fuel cycle, benefit-cost analysis 78—8957
- nuclear fusion, research, review 79—49839
- nuclear heat utilisation for centralised heating systems 80—7899
- nuclear power, nonelectrical energy production, review 79—26728
- nuclear power, significance as energy source in USSR *(Russian)* 79—26592
- nuclear power, US energy policy 80—81426
- nuclear power and US energy policymaking, suggested revision of production/consumption patterns 80—66954
- nuclear power appl. to centralised heat supply and central heating 79—26730
- nuclear power appl. to district heating systems 78—37454
- nuclear power engineering development, mathematical modelling 80—7901
- nuclear reactor strategies in a global context 79—87937
- ocean energy potential 80—66956
- ocean energy sources, new technological developments 79—43723
- ocean energy sources and their exploitation 80—89588
- ocean surface wave power resource estimate 77—41062
- ocean thermal energy, development, availability, and storage possibilities *(French)* 80—89587
- ocean thermal energy, HNO_3 cycle process for extraction 78—53660
- ocean thermal energy, renewable power source, review 79—5503
- ocean thermal energy conversion, prospects 79—87960
- ocean thermal energy conversion, review of engng. problems for technical and economic development 80—3486
- ocean thermal energy conversion concept 79—83577
- Ocean Thermal Energy Conversion platform environmental impact assessment 80—45726
- ocean thermal energy conversion programme, review 79—92066
- ocean thermal energy conversion to electricity *(French)* 80—21389
- ocean thermal gradients, power plant design 78—16059
- ocean wind waves, energy utilization, power generation 77—9446
- oil and gas bearing provinces of Ukrainian SSR, digital seismic prospecting 79—96836
- oil shale in situ extraction processes, US DOE 1979 R and D program 80—40812
- oil shales of Green River, USA, thermal decomposition rel. to elec. cond. obs. 80—104495
- oil supply and demand model structure 79—79369
- oil-shale, Colorado's Green River Formation, vertical modified in-situ processes 79—48049
- oil-shale, prerefining, in situ, hydrotreatment at 1500 and 2200 psig 79—48047
- oil-shale refining, jet fuels production, by surface and in situ technology 79—48048
- oils, shale, from five different sources, comparison w.r.t. boiling-point composition, elemental content and physical properties 79—48050
- Pakistan, hydroelect. pot. for future electricity demand, review 79—34423
- peat resource management policy formulation, systems approach 80—30324
- pegmatite ores in Tanco mine area, SE.Manitoba, in Canada, exploration methods 79—48577
- petroleum generation in SW block of Los Angeles Basin, rel. to thermal subsidence 80—3967
- photosynthesis energy factory as an integrated bioconversion system, technoeconomic analysis of an photosynthesis energy factory as an integrated bioconversion system 80—30510
- photovoltaic cells, current production and future prospects *(French)* 79—100531
- photovoltaic cells, Galileo works activities *(Italian)* 80—60029
- photovoltaic conversion comparative evaluation *(Italian)* 80—60023
- planning in Arab world, with aid of computer 80—26122
- policy, energy requirements in United States in year 2000 for stable social progress 79—79385
- policy process models, oil price decontrol and synthetic fuels commercialisation 79—83546
- possible options *(Spanish)* 79—66397
- potential resources for USA, prospects 79—79368
- power from the rain 80—7910
- power generation, hydroelectric, economic assessment of fuel savings *(Russian)* 80—97760
- power generation by thermonuclear reactions 77—65330
- power station waste heat utilisation for fish farming and agriculture *(German)* 80—101080
- power stations, steam-gas combined, based on natural gas resources from North Sea, economics and possibilities *(Norwegian)* 80—101073
- R and D at the Canada Centre for Mineral and Energy Technology 80—35656
- Raft River geothermal area, Idaho, seismic refr. study 80—3963
- rate of consumption, exponential growth 78—86049
- recycling materials for energy convservation, review 80—21388
- reduced form approach to combining energy models, methodological issues 79—79386
- reference Energy Systems as applied to regional energy policy 80—35657
- remote communities novel energy concepts, technical and economic aspects 79—48078
- renewable, economic assessment for UK power supply system 79—48043
- renewable, energy technologies economic assessment 79—48045
- renewable, future energy concepts, Conf. London, England (Jan.-Feb. 1979) 79—43709

energy resources continued
renewable energy options for developing countries 80—30426
renewable energy source utilisation in developing countries 79—57351
renewable energy sources and the environment 79—79411
renewable energy sources in West Germany, review *(German)* 79—87958
research and development in Britain, general survey *(German)* 80—72000
review, worldwide variation of energy production, future Hungarian energy requirements *(Hungarian)* 78—70580
review of energy resources, reactor accidents, radioactive waste disposal 78—50413
review of long-term energy systems and the role of nuclear and solar energy 80—66918
review of new sources including solar and wave energy *(Spanish)* 80—81420
risk assessment of energy production *(Japanese)* 79—83543
risk assessment of energy technologies, conventional vs. non-conventional 79—52862
rural electrification, energy economies and national policies, in developing countries 79—48042
salinity gradient power utilising vapour pressure differences in water 80—76652
seawater, electrical energy tapping 79—5504
seismic prospecting techniques for oil resources *(French, English)* 80—21362
social cost and benefit of energy strategy *(German)* 80—51017
solar, availability concept based on climatology, Canada 77—25762
solar, geothermal, hydrogen energy, and coal gasification and liquefaction, Japan's energy programme 80—3478
solar and wind energy, complementary nature 79—92062
solar energy, research, applications, water heating, space heating, air conditioning and hothouse heating *(French)* 79—100487
solar energy availability estimation 78—81344
solar energy utilisation methods and overall energy resources survey *(Czech)* 79—83565
solar energy utilization, direct and indirect *(German)* 80—3489
solar fuels prod. by photochemical conversion and chemical storage 79—66413
solar intensity obs., global insolation on horizontal and tilted surfaces 78—81275
solar photochemical energy conversion, nonbiological 77—86331
solar power, alternative fuel source, predictions for future and technical-economic possibilities 80—89591
solar power, global energy option *(French)* 79—100496
solar power, technological economics, current criteria based *(French)* 79—100495
solar power satellite, construction in space, fabrication methods, materials, tools 80—21377
solar power water-heating systems, design method 79—83629
solar radiation data for Hong Kong, statistical study 80—26112
solar water heaters, aluminium alloy rolled-welded heating panels production and use 79—96421
solar-energy installations, high-temperature, paraboloid concentrator, radiant flux control 79—96420
solar-radiation meter, automatic 80—89592
Southern African solar energy resources and requirements 79—57383
space as radiation sink, nonconventional energy sources 79—43750
St. Lucia, Sulphur Springs geothermal field model 80—94494
status and development trends, in late 1970s 79—57347
submarine geothermal resources 77—37171
supply, transition from fossil fuel to nuclear and regenerative sources, technical, economic and ecological aspects 80—66955
supply and demand, United States government analyses, review 80—30320
Swedish energy policy up to the year 1990 *(Swedish)* 79—87982
synergetic aspects of solar energy and the fast breeder reactor 80—7907
synthesis of energy system, soft solar energy option 80—76614
system modelling, New Zealand appl. 80—76590
technological forecasting, uK energy modelling system 80—72003
terrestrial heat, extraction by hydraulic fracturing of rock, growth rate of penny-shaped crack 77—29289
N.Thailand, hot springs and geothermal gradients 80—94495
thermochemical production of H_2, process assessment and economics *(French, English)* 77—86309
thermoclines, solar thermal energy resource for enhanced hydroelectric power production 79—92060
Third World energy stragegy 80—21387
tidal energy, flexible water barriers and compressed air energy 80—61273
tidal power, Korea, prefeasibility study 80—61271
tides as alternative energy sources, appraisal 78—86091
Travale-Radicondoli geothermal area (Tuscany), dipole elec. sounding method appl. 80—97762
trithermal absorption cycle process for upgrading waste heat 80—35731
Turkey, nuclear power prod., utilisation and safety 80—3481
UK primary energy consumption, changing structure of final demand 80—26101
UN Economic Commission for Europe report, book 79—100544
unconventional energy systems, exam. of material requirements 78—50255
undergraduate physics projects 77—13530
United States, available energy resources, 1985-2000 period 79—43711
urban district heating, review 80—26118
US energy strategy, role of hybrid nuclear reactors 80—42743
USA, utilisation of indigenous fuels to replace petroleum and natural gas, future strategy 80—30321
USA developments, by means of technological innovations, federal regulations influence 80—16763
USA National Energy Plan, role of solar technology 79—57392
USA-Japanese cooperation in science and technology 79—58518
utilisation and economics, effects of US National Energy Act 80—3499
utilisation in USA, city lights obs. by satellite 80—104494
waste heat, industrial applications of warm water at 58°C 80—40848
waste heat recovery using the indirect Brayton energy recovery system 80—35726
water power, potential, regional analysis method 79—83557
water power, review of possible developments in Sweden *(Swedish)* 80—93847
water power development, feasibility, economics 80—61274
wave energy convertor array power available 78—81216

energy resources continued
wave power, development, availability, and storage possibilities *(French)* 80—89587
wave power utilisation *(German)* 77—66927
wave-energy by submerged reson. ducts, 2-dimens. anal. 79—50743
wavepower review 77—81919
waves, forces on floating or submerged bodies, sand bars, wave power machines appls. 77—13090
wind, availability data in high plain regions of S.W. USA 77—37343
wind, electric power generation, application for high rise flats *(German)* 77—70739
wind, energy pattern factor meas., analogue technique appl. 77—81964
wind, turbines spacing in large arrays 77—73797
wind characteristics for energy conversion systems, variance anal. 78—49100
wind energy survey anemometer and recording instrumentation 77—33222
wind energy utilization, surface wind speeds run duration anal. appl. 79—100916
wind power plants, experimental projects in progress, design problems and results achieved *(Italian)* 80—72007
wind power potential estimation using power laws 78—92912
wind power potential in the Pacific Northwest 79—83549
wind power resources evaluation for use in rural areas, w.r.t. economic and social aspects 79—70416
wind power statistics 77—70765
wood energy in W.Virginia 80—72006
world distribution of commercial energy consumption (1950 to 1975) 80—26120
world energy economy, role of cryogenics *(Rumanian)* 80—7933
world energy situation, future requirements and challenges 80—50927
world oil resource estimates (1949-79) *(French, English)* 80—21365
worldwide energy prospects, synthesis of studies published in 1976 and 1977 *(French)* 79—29443
Yugoslavia, energy conversions in the S.R. Croatia *(Croatian)* 80—3475
Yugoslavia, energy delivered to consumers in the S.R. Croatia *(Croatian)* 80—3473
Yugoslavia, primary energy balance in S.R. Croatia *(Croatian)* 80—3472
Yugoslavia, regional energy consumption in S.R. Croatia *(Croatian)* 80—3474
H_2 production, comparison of thermochem. and electrochem. methods 80—16826
H as the solar energy translator 80—30608
H biological photoprod. using sunlight, review 80—45777
H biological prod. by solar energy conversion, coupling of hydrogenase and chloroplast photosystems 80—45778
H, biophotolytic production from H_2O 80—61457
H cryogenic storage, liquefaction processes, storage and distrib. equipt. 80—45784
H, demand and supply of hydrogen as chemical feedstock in the USA 80—45817
H, electro-/thermochemical prod. from H_2O by Westinghouse sulphur cycle 80—55940
H electrochemical prod., solid polymer electrolyte water electrolysis status for large scale hydrogen production 80—30605
H electrochemical/thermochem. prod. using S cycle, laboratory prod. model and electrolyser development 80—30602
H electrolytic prod. by H_2O decomposition in acid molten electrolytes at 220 to 320°C 80—45769
H, electrolytic prod. by inorganic-membrane-electrolyte H_2O electrolysis 80—45804
H, electrolytic prod. using mobile generator 80—45805
H electrolytic production *(Spanish)* 80—35766
H energy, industrial appls. of liquid and gaseous H 80—45801
H energy, production, storage, transmission, [Conf. Zurich, Switzerland. (Aug. 1978)] 80—22144
H energy, R and D programs, review 80—45802
H energy prospects 80—45799
H, energy storage in FeTi, surface segregation, catalytic effect on hydrogenation 80—45814
H energy utilisation in the nuclear, solar and fossil fuel energy strategies 80—45798
H generation, photoelectrolysis of water in sunlight 78—19143
H, industrial scale, production from natural gas, naphtha, coal review 80—35791
H laser-fusion prod. by radiolytic-thermochem. cycles 80—45811
H, metal hydride storage, diffusion-rate-limited hydriding and dehydriding kinetics 80—35764
H, optimal development strategies for a whole energy system based on hydrogen 80—45795
H, photoassisted production, reactions of H_2O with C and ethylene over Pt/TiO_2 80—55703
H photochemical prod., H_2O photolysis using fission pumped gas lasers 80—45810
H photochemical prod. by H_2O photolysis using sunlight 80—45776
H photoelectrochemical prod., solar beam-assisted electrolyser applied to Yokohama marks 5 and 6 [system for hydrogen production] systems 80—45768
H photoelectrochemical prod. using TiO_2-Si solar cell hybrid electrodes 80—45775
H, photoelectrolytic prod. from H_2O, storage efficiency estimate 80—51016
H photoelectrolytic production by H_2O decomposition using sunlight, review 80—45774
H, photolytic prod. using biological and artificial catalysts 80—61444
H plasmochemical prod. by H_2O decomposition in non-equilib. plasma 80—45773
H prod. by H_2O pyrolysis using solar thermal energy 80—45770
H prod. by H_2O solar photolysis by engineering methods using biological materials *(Japanese)* 80—45765
H prod. by high temp. electrolysis using fusion heat 80—51012
H production, EPRI R and D program for electric utility industry, review 80—30610
H production, exergetic/energetic/economic anal. of electrolytic, thermochem. and hybrid processes 80—55938
H production, storage, and utilisation for domestic appls., Hydrogen Homestead project 80—40921
H, production, techno-economic evaluation using OPTIMO code 80—45797

energy resources continued
H production, thermochemical or hybrid cycles of hydrogen production techno-economical comparison with water electrolysis 80—45796
H production, thermochemical water-splitting cycles based on Ce and alkaline earth phosphates 80—55945
H production and distrib., US safety regulations and standards, bibliography 80—41976
H production and utilisation, EEC R and D program review 80—45821
H production by photobiological energy conversion 79—70456
H production by pressurised coal gasification 80—30609
H production by Westinghouse electrochem./thermochem. S-cycle process 80—45808
H production for solar energy utilisation 80—51014
H production from coal using steam-Fe process, development status 80—55942
H production from fusion reactors coupled with high temp. electrolysis 80—45771
H production from H_2O by two-stage plasmochemical cycle 80—45772
H production on illuminated transition metal surfaces, tight binding model 80—45812
H production using fusion reactor heat and gas dynamic compression heating 80—35793
H, production using HBr electrolysis 80—35777
H production using HTGR nuclear heat source 80—45803
H production using hybrid electrochem./thermochem. cycles, search for electrochem. reactions 80—45807
H production utilising nuclear energy, global energetic system, mathematical model *(Rumanian)* 80—35623
H, radiolytic/thermal cycles 80—51011
H, solar-thermochemical prod. of H_2O appl. of fixed mirror solar concentrators 80—45767
H, storable conc. of atomic H in T-impregnated crystalline solid H_2 80—30594
H storage, development of low cost Ni-rare earth hydrides 80—45791
H storage, effect of the interstitial hole size and electron concentration on complex metal hydride formation [for H storage] 80—45789
H storage, electrolysis-based technology R and D at BNL, review 80—40920
H storage, high temp. hydrides for vehicular appls. 80—45793
H storage, kinetics of hydrogen absorption and desorption by ternary $LaNi_5$ type intermetallic compounds 80—45813
H storage, $LaNi_{5-y}Al_y$ alloys and their hydrides, metallurgical, structural and thermodynamic props. 80—45816
H storage, $SmCo_5$ hydriding kinetics, inverse over pressure effect 80—55944
H storage, sorption props. of Al-containing Laves phase intermetallics 80—45794
H storage, technological aspects and characteristics of industrial hydride reservoirs 80—45792
H storage, use of Ti binary alloys for solid metal hydride storage 80—45786
H storage and distrib., potential for pipeline transmission in Switzerland 80—45780
H storage and distribution, problem rel. to use of natural gas distrib. eqpt. 80—45779
H storage and utilisation using metal hydrides 80—45785
H storage by metal hydrides for automotive propulsion 80—40922
H storage by use of cryoadsorbents 80—45783
H storage materials, design criteria; thermodynamics, absorpt. kinetics, economics and materials science 80—55943
H storage using $CeMg_{11}V(Cr)(Mn)(Fe)(Co)$ alloy hydrides 80—51009
H storage using cubic metal binary alloys 80—45787
H storage using FeTi hydrides, struct., heat of soln., diffusion and hydriding kinetics 80—40930
H storage using intermetallic Ni_5La *(Russian)* 80—55937
H storage using $LaNi_5$, effect of Ni, Ce, Co alloying additions on H_2 absorption 80—45790
H storage using $LaNi_5$, self restoring of active surface 80—45815
H storage using metal hydrides, numerical physical property data 80—40929
H storage using small scale NH_3 prod. 80—45782
H storage using Ti-Zr-Cr-Mn/$LaNi_5$ hydriding alloy mixtures 80—45788
H synfuel prod. by high temp. electrolysis using fusion energy 80—35792
H synfuel prod. from fusion power using hybrid thermochem. $Bi_2O_3.SO_3$ cycle 80—40931
H synthetic chloroplasts 80—30508
H, thermochem. prod. by H_2O decomposition using Mg-I cycle 80—35786
H, thermochem. prod. using the Mark-13 process, status report 80—30606
H thermochemical prod., engineering impact on the validity of the Mark-16 thermochem. cycle 80—45806
H, thermochemical prod. by H_2O decomposition, equilibrium effects in high press. prod. 80—35775
H, thermochemical prod. by H_2O decomposition, impact of thermal burdens and kinetics 80—35787
H thermochemical prod. by H_2O decomposition using solar energy 80—40919
H, thermochemical prod. by H_2O pyrolysis, computer thermodynamic anal. and optimisation 80—45766
H thermochemical prod. by H_2O decomposition, review 80—45800
H, thermochemical prod. by high temp. H_2O decomposition using solar energy 80—45822
H, thermochemical prod. from H_2O, noncorrosive two-reaction low temp. cycles based on mordenite-hosted redox reactions 80—55939
H thermochemical prod. using $Bi_2(SO_4)_3$ cycle, process engng. design 80—30599
H, thermochemical prod. using SO_2-I_2 water splitting cycle 80—30600
H, thermochemical prod. using S-Br cycle, development of lab.-scale plant 80—35774
H, thermochemical prod. using Br-Ca-Fe H_2O-decomposition cycles 80—35784
H, thermochemical prod. using General Atomic S-I cycle for H_2O decomposition 80—55941
H, thermochemical production, irreversibility anal. of separation schemes from binary gas mixtures 80—35767
H, thermochemical production, H_2O decomposition using S compounds, feasibility anal. 80—35768
H, thermochemical production, H_2O decomposition using S-I cycle 80—35769

energy resources continued
H, thermochemical production, H_2O decomposition using S-I cycle, process eng. and bench-scale studies 80—35770
H, thermochemical production, HI decomposition and H separation 80—35771
H, thermochemical production, by HBr pyrolysis 80—35772
H, thermochemical production, $SO_2/H_2O/X_2$ reactions ($X_2=Br_2$, I_2) 80—35773
H, thermochemical production, HBr decomposition using $FeBr_2$ and Fe_3O_4 80—35778
H, thermochemical production, H_2O decomposition using S cycles, thermochem. anal. of energy balance 80—35779
H, thermochemical production from H_2O, development of two new thermochem. cycles at ORNL 80—35780
H, thermochemical production using ZnSe cycle, chemical and process design studies 80—35782
H, thermochemical production using Ce-Cl cycle 80—35783
H, thermochemical production using Hg-I ANL-4 cycle 80—35785
H, thermochemical production by steam reforming of methane, kinetic anal. 80—35788
H thermochemical production by coal gasification using steam 80—35789
H thermochemical production using air blown coal gasification, economics 80—35790
H, thermochemical production using fusion energy source 80—51010
H, thermoelectrochemical prod. using H_2SO_4-SO_2 cycle, electrochem. aspects 80—35776
H thermoelectrochemical prod. utilising electrolyzer and fuel cell 80—45718
H, thermoelectrochemical prod. using NaCl 80—55946
H, use of H_2/O_2 combustor for supplementary steam generation during peak periods 80—30330
H-fuelled railway motive power systems 80—40923
H_2 as energy vector, production, use, storage and transportation, (conf. Brussels, Belgium. Oct 1978) 79—74511
H_2, chemical feedstock, supply and demand in USA (conf. Houston, Texas (Dec. 1977)) 80—16765
H_2, electrochemical prod., development of high efficiency alkaline electrolysis technology 80—30601
H_2 energy bibliography 80—12863
H_2 energy bibliography (1974-79) 80—26173
H_2 energy economy, R&D programmes 80—26171
H_2 from falling water, 1978 overview and prospects in USA 79—52958
H_2 gas, photosynthesis prod. by green algae, turnover times and pool sizes 80—16821
H_2 microbial production from replenishable resources 80—16768
H_2, prod. from coal, water and electrons 79—61962
H_2 production and utilisation, EEC R&D program progress and results 80—16767
H_2 production by electrolysis, development of electrolysers *(French)* 80—7803
H_2 production by H_2O decomposition using solar energy conversion 80—97813
H_2 production by KOH electrolysis, materials, geometry and characts. of electrolyser cell 79—74397
H_2 production by medium temp. high press. water electrolysis 79—74398
H_2 production by polynaphthoquinone-SO_2-I_2 system for H_2O decomposition 80—16825
H_2 production by solar photochemical decomposition of H_2O 80—16822
H_2 production by steam reforming of natural gas, chemical kinetics 80—97815
H_2 production using high temp. reactors 80—97814
H_2 production using hybrid cycles with HBr electrolysis 80—97816
H_2 production using thermoelectrochem. cycles 80—16820
H_2 production using thiazine dye-Fe photoelectrochem. cells, instabilities 80—16814
H_2 storage, thermodynamic and structural properties of $LaNi_{5-y}Al_y$ compounds and their related hydrides 80—16847
H_2 storage as MgH_2 hydriding and dehydriding kinetics obs. by press. sweep method 80—35765
H_2, thermochem. prod., H_2O pyrolysis using Fe-Cl cycle, chem. engineering anal. 80—97811
H_2, thermochemical prep. by H_2O dissoc. using S-I cycle 80—16823
H_2 thermochemical prod. by H_2O dissoc. using Sb-I-Ca process 80—16824
H_2, thermochemical production using H_2SO_4-SO_2 cycle, electrochem. aspects 80—97812
H_2-methane mixture properties for hydrogen supplementation of natural gas 80—45781
H_2O, thermochemical cycles of high temp. decomposition, thermodynamic method of research *(French)* 79—96295
Li concentrations in McDermitt Caldera, in Nevada and Oregon, geological survey 79—48478
Li deposits and potential, Quebec and Atlantic Provinces, in Canada, report 79—48481
Li, occurrence in flint clay and related rock types in United States, preliminary survey 79—48475
Li ores in Horse Spring Formation Miocene rocks, Clark County, Nevada, report 79—48474
Li, ores in United Kingdom, brief assessment 79—48476
Li pegmatite ores in Western Superior Province, in Canadian Shield, distribution and petrogenesis 79—48480
Li requirements for fusion power plants, survey 79—45401
Li resources, energy reserves of D-T fusion, recovery costs 78—46162
Li resources, Yellowknife area, in NW.Canada, report 79—48482
Li resources and potentials, NW.Ontario, Manitoba, Saskatchewan, in Canada, estimation 79—48483
Li rich brines in SW.Bolivia, chemical composition and distribution 79—48479
Pu as energy resource, availability, health hazards, nuclear weapon proliferation 77—46286
Pu fuelled LMFBR need, nuclear proliferation, W.German perspective 79—71895
Pu, source and availability of fuel for breeder reactor programme 77—61625
U complex, $[UO_2(CO_3)_3]^{4-}$, vibr. and low-temp. optical spectra, rel. to U recovery from oceans 79—73939
U exploration, LANDSAT data merged with geol. and geophysics data 80—56651
U exploration and prospecting methods 80—85768
U exploration in developing countries, facts and trends 80—16764

energy resources continued
U, extraction from seawater by polymer-bound macrocyclic hexaketone 79—92052
U, international resources assessment 80—99215
U ore bodies ground level radiometric surveys, overburden effects correction techniques 79—88485
U, reactor fuel supply, exploration and production capacities, review 79—22388
U resource conservation using pebble bed prebreeder reactor 79—49697
U resource information economic value estimation 79—83547
U resources, consumption and 30 year fuel commitments for Canada and the world, 1975-2025 78—82456
U resources and accessibility, reliability of nuclear fuel supply 80—99216
U, review of Australian resources 79—87941
U supply, Canada's role 78—86627
U_3O_8 demand projections using a diaggregated market penetration model 80—99214
U_3O_8 recovery from seawater, R and D program 80—99217
^{235}U, recovery from enrichment plant tailings by laser isotope separation 80—83212

energy states
see also atomic structure; electron energy states (condensed matter); energy level crossing; molecular energy levels; nuclear energy levels; population inversion
't Hooft magnetic monopole, energy levels in the Prasad-Sommerfield limit 79—54268
B.I.P. An interactive graphic system for indexing energy bands of model polymers 79—59608
bound state problems, scattering theory calc. 79—92979
Coulomb potential, modified, S-wave energy levels 78—41918
dispersion reln. for energy bands and gaps, phase integral method, Mathieu pot. appl. 80—22224
education, composite potential well, energy level determ. using Green's function factorisation theorem 79—97148
education, quantum mechanics, spherically symmetric pots., ladder operators, energy levels and degeneracy 78—62013
education, recursive method for partition function calc., average energy calc., APL program 79—9050
eigenvalues, Temple's lower bound, generalisation 79—88823
Fermi gas, slightly non-ideal one-dimens., spectral ground state, energy determ. method *(Russian)* 78—62149
flat rotator in field of circularly polarised wave, quasienergy states 78—54596
gamma ray incoherent scattering, spectrometer for electronic momentum distribs. investigation *(German)* 77—41741
infinite-well potential, soln. using SO(2), for teachers 77—33791
loss energy states of nonstationary quantum systems 78—49719
many fermion systems, energy lower bound 80—17860
matrix elements of $\delta(r_1)$, approx. wavefunction 80—47860
metal at low temperature investigation *(German)* 77—13753
orbital angular momentum eigenvalues, integralness calcs. 80—67977
oscillator in coherent state, quantum nondemolition meas. 78—54228
permutation matrices using graphical methods of spin algebras, Serber coupling 79—6833
perturbed energies, 2nd order, coupled HF iterative procedure, geometric approx. 79—9991
quantum chemistry, optimum scaling in a Monte Carlo method 79—6832
quantum dissipative systems, time evolution of state vector 80—12935
Schrodinger equation nonseparable potentials, vibr. energy level semiclassical calc. 80—8832
screened Coulomb potentials, energy levels, nonperturbative approach 78—41917
spin-1 system, periodic perturbation, analogue of Shirley's eqn. 77—3248
tensor virial theorem, quantum mechanical generalisation for Born-Oppenheimer approx., atoms, mols. 78—86182
three resonantly interacting particles, level spectrum 77—17860
weak external gauge fields, energy levels, modified functional measure 78—49973
Ar, momentum density of electrons, two-gamma positron annihilation determ. 77—69211
H, recombining plasma, population inversion using collisional-radiative model 79—46423

energy states in solids and liquids *see electron energy states (condensed matter)*

energy storage
see also capacitor storage; direct energy conversion; energy storage devices
100 MWh, peak-shaving battery plants, Zn-Cl_2 79—48119
290 MW compressed air storage power station, construction and commissioning 80—16842
advanced compressed air energy storage concepts utilising thermal energy storage, cost anal. 80—30581
advanced energy conversion and storage, electric utility appls. 80—16793
air based solar heating systems, phase charge energy storage, optimum physical properties 79—43742
alternative concepts, Conf., Chicago, IL, USA, Nov. (1978) 80—23123
alternative energy sources, conf. Miami, FL USA (Dec. 1979) 80—55772
alumina sphere packed bed thermal storage analysis 79—57486
atomic device for trapping energy 77—88604
autonomous and hybrid solar thermal electric plant energy storage requirements 79—57494
batteries, electric vehicle and power storage appl. 80—72031
batteries for transport and stationary appl., advanced systems development 79—43756
battery appls. and developments, conf., Brussels, Belgium (Jan. 1979) 80—72032
Battery Energy Storage Test facility, test programs and data processing 80—30449
book 80—51974
Canadian R and D program for energy storage and conversion, review 79—29457
chemical, 'Solchem' solar power project 80—50994
chemical, H_2SO_4-H_2O chemical heat pump energy storage system 80—30515
chemical bond thermal energy storage feasibility 79—57495
chemical conversion and storage of solar energy, book 80—86045
chemical fuel production by solar energy conversion 80—61318
chemical systems for solar radiation storage, long-term efficiency of iterative cyclic reactions 80—45764

energy storage continued
coal underground conversion, integrated fuel-generation and power-generation concept, using electrochemical engines 79—48053
compound parabolic concentrator heat transport to storage 79—62102
compressed air, fluids engineering aspects, Conf., San Francisco, CA, USA (Dec. 1978) 79—83550
compressed air, hydraulic compressor performance analysis 79—83639
compressed air, optimum design w.r.t. economics 80—26167
compressed air energy storage, anal. of moist air cycling in porous rock reservoirs 80—30575
compressed air energy storage electric power systems, conceptual design 79—88006
compressed air energy storage in Galesville sandstone, phys. and chem. stability at elevated temp. and press. 80—30576
compressed air energy storage in hard rock caverns, stability and design criteria 80—30574
compressed air energy storage plants, turbomachinery options 80—30578
compressed air energy storage power plant using coal-fired fluid bed combustor, technical assessment 80—30573
compressed air rock reservoirs, geologic conditions 80—30577
compressed air storage, basic and advanced concepts feasibility 79—43793
compressed air storage plant, ejector augmentation of air supply 79—48189
compressed-air, champagne effect modelling, improved cavern design 79—83638
conf., 14th Intersociety energy conversion eng. conf. [Boston, MA, USA (Aug. 1979)] 80—31424
conversion, Conf., San Diego, CA, USA (Aug 1978) 79—48038
cool storage as a means for residential air conditioning electrical load management 80—30590
cylindrical annulus phase-change energy storage simulation 79—57478
diesel-driven chiller system simulation, with multi-tank thermal storage system, for large commercial buildings 79—48187
distribution systems for centralised heat source 79—48184
domestic wind power system including storage, simulation analysis 79—92058
electrets appl., membrane, polyelectrolyte 80—26177
EM accelerators/launchers with pulsed energy storage 80—35756
environmental impact of energy storage technology development 80—61471
farmhouse heating solar energy collection and thermal storage system 79—57482
fast ion transport in solids, conf., Lake Geneva, USA (May 1979) 80—57006
fast ion transport in solids, conf., Lake Geneva, USA (May 1979) 80—105427
finned heat pipe latent thermal energy storage system performance 79—57487
fluidized bed heat storage, baffled heat transfer anal. 80—30592
flywheel, composite, for regenerative braking of electric vehicles 79—48185
flywheel and hot water storage systems for 10 kWe solar power pack 79—57469
flywheel energy storage and conversion system for photovoltaic appl., economic anal. 80—94116
French energy research projects *(French)* 79—74497
fusion reactor, ohmic heating energy storage for power reactor, costing 78—58495
fusion reactor, T-10M Tokamak, normal and supercond. inductive energy storage and switching 78—55018
fusion reactor, TEXT, pulsed homopolar generator power supply, engineering and design 78—55016
fusion reactor, TFTR, energy conversion and storage systems, fault detection and protection 80—95431
fusion reactor, Tokamak, commercial, plasma driving system requirements 78—54954
fusion reactor inductive storage technology, new applications, review 78—55019
future energy concepts, Conf. London, England (Jan.-Feb. 1979) 79—43709
H_2 absorption in thin film hydriding alloys, $LaNi_5$ and $SmCo_5$ 80—65238
H, thermochemical production by H_2O decomp., optimum temp. conditions utilizing HTGR nuclear heat 80—35781
H-fuelled passenger bus, design 80—40924
heat energy storage units, thermodynamic optima 79—57471
heat storage, periodic, heat-carrying fluid and storage material transport kinetics 79—3901
heat storage in a solar heating system using Na salt hydrates 80—67005
heat storage in passive solar heated building using concrete block under concrete slab 80—55922
heat storage in solar heating system using Na salt hydrates, based on extra water principle 80—67006
heat storage tank, energy saving control system for air conditioning *(Japanese)* 80—72087
heating of residential house, solar and wind energy combination, Danish design 79—57411
heavy quark physics, practical appls. in energy sources and storage 79—9426
high temperature storage for a wind energy system 80—55920
homopolar generator design for fusion reactor energy storage 80—68953
hot water storage tank, heat loss rel. to thermal insulation *(Japanese)* 80—5918
houses thermal environmental control in Northern India, using roof for heat and coolness storage 79—62151
hybrid solar/H fuel system producing high energy 80—45809
hybrid thermal energy storage system, transient simulation 80—30588
hybrid thermal energy storage with water systems, eval. using analytical models 80—30589
hydrides appl., metallic 79—43792
hydro-photovoltaic plants, peak power generation economics and reliability 80—45706
hydrocarbon oils as thermal storage media for solar central power appls., specific heat variations and their economic implications 79—100540
hydrogen storage in metals, use of metal-metal contacts to prevent escape 80—24595
hydrogen storage materials *(French)* 79—66419
inductive storage bank, appl. to N_2 high-current discharge 80—10450
inductive storage systems for cylindrical imploding plasma drives 80—70019

energy storage continued
inorganic salt hydrate melts, nucleation, thermal storage appl. 79—66417
insolation stability characterisation by stochastic time series 79—57396
International Solar Energy Congress, New Delhi (1978) 79—57357
large-scale elec. energy storage, review 80—89676
latent heat solar energy storage system, heat transfer eqns., numerical soln. 80—55926
latent heat storage, physical and chemical processes at low temps. 80—72091
latent heat storage materials, high temp. corrosion resistance and thermodynamic stability 80—30582
latent heat thermal energy storage materials, eval. of molten alkali carbonates 80—30586
latent-heat thermal energy storage materials, energy density and materials cost *(Japanese)* 80—26168
liquid metal rotor energy storage device, secondary flow due to Alfven waves 77—39353
load levelling in electrical utilities, Li-FeS$_2$ batteries appl., industrial participation in ANL development program 79—48113
long-term solar energy storage in native rock 79—57474
lossless energy-storing system, thermodynamic limits to nonlinearity 79—54090
marine photosynthesis; available, usable and stored radiant energy 79—39313
materials needs, in energy conservation and storage 80—66958
materials problems and basic research needs 78—86703
mechanical, commercialisation risks of underground pumped hydro and compressed air storage 80—16841
mechanical, compressed air and underground pumped hydro storage, comparison 80—40910
mechanical energy storage systems for electric vehicles, effect on performance 80—30579
metal hydride chemical heat pumps, materials and performance characts. 80—40927
metal hydrides use as energy conversion media, review *(Japanese)* 80—55934
micellar system, photoinduced redox processes kinetics, intramicellar electron transfer 78—92603
NaOH fusion for heat storage, heat utilisation for turbo-alternator unit *(French)* 80—40915
northern solar house long-term storage systems 79—57473
nuclear district heating schemes, heat transport and storage 79—39321
oceans, heat storage rel. to Earth global heat balance annual var. 78—73300
off-peak, underground pressurized hot water storage 79—43789
OTEC (ocean thermal energy conversion) plants 79—61958
paraffin latent heat storage system theory and expt. 79—57484
paraffin plate heat storage element, fusion, periodic solidification, heat transfer kinetics *(French)* 80—40913
paraffin wax, solar energy storage heat transfer characts. 80—55921
passive rock bed storage system for domestic solar air heating 79—57490
PCM wall thermal storage, design criteria 80—35759
PCM wall thermal storage, modelling 80—35758
pebble layer heat exchange investigation, solar energy storage 80—21374
phase change energy storage for air-based solar heating systems 80—35762
phase change material physical and chemical props. for space heating and cooling 79—57479
phase change materials, thermal energy storage, cycle life tester 80—72090
photogalvanic, EDTA-methylene blue cell appl. 80—21406
photovoltaic energy systems, assessment of suitable energy storage media and concepts 80—30562
power systems, review 79—24913
pulse current generator, capacitive energy stores, ultrapowerful, improved service life development problems 79—81089
pulsed energy storage in fusion device 77—74984
pulsed power conversion with inductive storage 78—55029
rare earth intermetallics for H storage 80—21416
reservoirs, pumped water, compressed air, batteries 80—35755
residential annual cycle energy storage, ice storage and three-coil heat pump 80—55917
salt-gradient solar ponds, performance characts. 80—30551
salty solar ponds, stability criteria for saturated ponds 80—30552
seasonal storage of solar energy 79—57472
social implications of solar and H$_2$ energy storage and electric vehicles 80—67001
solar, by thermo-electrochemical H$_2$ prod. *(French)* 79—24918
solar, desalination process appl. multistage flash evaporation, demonstration project 80—61283
solar, large-scale thermal power generation potential 79—43749
solar, review of methods 80—55916
solar, thermal chemical conversion cycles appl. 79—100537
solar air conditioner with flywheel-storage system 79—52909
solar chemical reactor theory and designs *(French)* 80—7916
solar chemical reactors, industrial appls. to chemical and thermal storage *(French)* 80—55815
solar chemical storage, chemical bond energy of SiO$_2$ and ammoniates undergoing thermal decomposition 80—76656
solar chemistry research and developments *(French)* 80—11999
solar collector, water-trickle type, with massive concrete slab for heat storage 80—108814
solar collector design and suntracking control for PORSHE concept 80—61425
solar collector-cum-storage water heater transient behaviour model 79—62088
solar dwelling independent of servicing networks, digital simulation 79—62149
solar energy, chem. energetics role *(French)* 80—7917
solar energy, chemical storage, effect of micellar phase on photo-induced reactions 80—89678
solar energy, storage and power supply for building heating, optimal conditions *(French)* 80—61297
solar energy accumulation by soil in shed hothouse 80—21373
solar energy chemical conversion and storage using norbornadiene-quadricyclene photoisomeric interconversion 80—89664
solar energy chemical storage, photo-induced electron transfer reactions in solution, organised assemblies and at interfaces 80—89677
solar energy chemical storage, photosensitization mechanisms for energy storing isomerizations 80—89679
solar energy chemical storage 79—66413
solar energy chemical storage using novel photocyclization reactions of 1-alkenyl-2-pyridones 80—89680
solar energy collection and storage, latent heat diode walls, space heating *(French)* 80—61298
solar energy collection and storage, space heating *(French)* 80—61299
solar energy conversion, liquid thermal storage tanks, thermal stratification enhancement 80—40918
solar energy conversion and storage using artificial photosynthetic systems 80—89662
solar energy direct photoelectrochem. conversion and storage 79—62015
solar energy earth storage and utilisation, technical and economic aspects 79—57475
solar energy electricity storage, battery appls. potential 80—72067
solar energy short-term storage monolithic structures 79—57489
solar energy storage, molten salts, heat transfer salt *(French)* 80—61434
solar energy storage apparatus, dimension determ. from statistical model of solar radiation *(French)* 79—29812
solar energy storage as hydrogen from bromine from hydrogen bromide 79—57470
solar energy storage by metal hydride, review 80—61455
solar energy storage in compressed air 79—57468
solar energy storage methods for large-scale appls., eval. 80—89675
solar energy storage system, ammoniated salt heat pump using MgCl$_2$, CaCl$_2$, NH$_4$Cl 80—81484
solar energy storage tank, Markovian model of behaviour *(French)* 79—24912
solar energy storage using chemical potential changes associated with drying of zeolites 80—51006
solar energy system with dual-source heat pump and long-term storage 79—57453
solar energy systems for buildings, passive, use of thermal modelling and 'predicted percentage dissatisfied' 79—62145
solar energy thermal storage, numerical simulation of energy transfer by conduction and radiation *(French)* 79—24916
solar energy thermal storage by latent heat of fusion of mineral salts *(French)* 79—24915
solar energy thermal storage eutectic molten salt mixtures, enthalpy of fusion estimation *(French)* 79—24914
solar heat collection and storage system evolution 79—62085
solar heat pump and thermal storage system based on CaCl$_2$ and methanol vapour reaction for space heating 80—85307
solar heat short- and long-term storage, stratification effects 79—57488
solar heat storage in buildings using inexpensive systems 80—51004
solar heating system, annual cycle thermal energy storage, sensitivity anal. 80—67007
solar hot water systems analysis and optimisation 79—57461
solar hothouse with closed moisture cycle, temp. regime 80—21375
solar HVAC system, thermal storage, materials, labour and insulation costs 80—72088
solar integrated collector-heat storage systems for heating and ventilation 80—51002
solar pond interaction with ground thermal storage 79—62093
solar pond viscosity stabilisation by organic thickeners 79—62094
solar ponds, daily performance characts. of shallow solar ponds 80—30554
solar ponds, economics and performance characts. of salty and saltless ponds 80—30553
solar ponds, non-convecting, review 80—61407
solar ponds for thermal conversion/storage 80—30550
solar power, direct conversion and storage, review of developments, review 79—43741
solar power plant thermal storage unit analysis 79—57493
solar power systems, combined generation/storage, using Ca(OH)$_2$ 79—43790
solar power sytems 77—73798
solar space heating, two-tank storage system using seasonal and diurnal tanks 80—72016
solar space heating using rock storage, thermal performance 80—45732
solar system, 32 kWe, total energy project 79—52912
solar thermal energy accumulator using stones, operating principles *(German)* 80—72085
solar thermal energy storage by chemically driven heat pumps 79—57476
solar water heater with built-in storage 79—57454
solar-H$_2$ energy systems, review 80—61447
solar-H$_2$ systems using metal hydrides 80—61464
solar-powered opencycle chemical heat pump/energy storage system 80—30512
southern Iranian solar pond performance simulation 79—62096
space heating, all-year solar energy collection and storage system 79—62074
spaced metallic plate utilisation for solar thermal storage 79—57492
subsistence-economy chicken-breeding solar energy storage regulation expt. 79—57485
superconducting magnetic energy storage applic. for particle accelerators and power networks 78—25360
superconducting magnetic energy storage system with superconducting rotary machines as I/O system *(Japanese)* 80—85306
superconductive, 1970-9 development at Wisconsin University, Madison (USA) 80—26176
supercritical liquid air storage plant for elec. energy 78—74006
technology and solar energy use, worldwide trends *(German)* 80—72086
thermal, American Society of Heating, Refrigerating, and Air-Conditioning Engineers, activities overview 80—16844
thermal, based on reversible dissociation of SO$_3$, solar power plant appl. 79—48186
thermal, by sensitive, latent heat, dynamic model *(French)* 80—40917
thermal, commercialisation risks of customer side-of-the-meter thermal storage 80—16841
thermal, for solar power systems, 1978 development status 79—48095
thermal, heat transfer processes in the solidification of inorganic hydrates *(Japanese)* 80—6372
thermal, high efficiency, for utility appl. 79—48188
thermal, high temp. storage using the latent heat method *(French)* 80—40912
thermal, integrated solar collector-heat storage systems for heating and ventilation of buildings 80—45758
thermal, materials props. and selection, 1978 status and developments *(Japanese)* 80—7960
thermal, molten salt thermal conductivity *(Japanese)* 80—6573

energy storage continued
- thermal, optimally distrib. insulation for in-ground heat storage tanks 80—94119
- thermal, phase change material, melt time and heat flux relations 79—74546
- thermal, porous medium with circulating heat transfer fluid *(French)* 80—40916
- thermal, rock bed storage for solar energy systems, comparison of meas. and predicted performance 80—67004
- thermal, short term storage for low temp. solar heating appls. 80—55918
- thermal, SO_4/H_2O vapour mixture in heat pump mode 80—26169
- thermal, solar central receiver program, heliostat, receiver and storage subsystems 80—30404
- thermal, solar energy storage for space heating appl. *(German)* 80—26152
- thermal, solar thermal conversion, collectors, storage systems, energy transport and economics, review 80—51003
- thermal, Toshiba Solar House No. 1 performance 79—57458
- thermal, underground constant flow solar collector/storage system 80—21412
- thermal, underground storage systems, review 80—26170
- thermal, underwater storage containers transmission lines and control systems 80—55924
- thermal, using hot liquids, CEGB research review 79—43788
- thermal, using phase change material, time variation of storage and release 80—67008
- thermal, waste heat utilization with annual aquifer storage for space heating appls. 80—97809
- thermal and electrochem., using molten salts, physical props. data compilation 79—92090
- thermal energy storage, appl. to waste heat recovery in food processing industry 80—30585
- thermal energy storage, US DOE research program for aquifer waste heat utilisation 80—97808
- thermal energy storage and transmission, electric utility appls. 80—30583
- thermal energy storage for electric utility applications 80—16843
- thermal energy storage for solar appls. 80—72089
- thermal energy storage in aquifers, expt. anal. 80—30591
- thermal energy storage in aquifers for a solar power plant 80—55925
- thermal energy storage in industry and power stations 80—67002
- thermal energy storage in salt hydrates for solar heating systems, storage material props. 80—101134
- thermal energy storage using plastic crystal phase transitions 79—57480
- thermal energy transport using benzene/cyclohexane reversible chemical reaction systems 80—67009
- thermal fluid selection for long-distance heat transmission, theoretical model 80—35761
- thermal phase change storage medium, new type, thermal properties 79—43787
- thermal regenerator, periodic flow type, transient performance 78—59389
- thermal regenerator performance, gas heat storage effect 78—5647
- thermal storage, convolution model of packed bed units 80—94118
- thermal storage assisted heat pumps using phase change materials 80—35733
- thermal storage by molten salts *(French)* 79—70466
- thermal storage for solar energy utilisation 80—45759
- thermal storage for solar heating and cooling of buildings, Shenandoah Solar Recreational Center 80—45757
- thermal storage in density stratified fluids and phase change materials 80—67003
- thermal storage in solar heating appls. in northern latitudes, insolation modelling 80—66941
- thermal storage of solar energy 80—51005
- thermal storage of solar energy using chabazitic tuff, a zeolitic rock 80—94117
- Thermocrete heat storage material development 79—57483
- Tokamak power plants, impact of technology and maintainability on economic aspects 80—27807
- Tokamak reactor cycles 78—62661
- transfer from low voltage capacitor bank to high inductance with air pulse transformer 78—49860
- Trombe-Michel wall using phase change materials, solar energy collection and thermal storage 80—55909
- two-phase thermosyphon feasibility for solar energy transport and storage 79—57491
- unconventional energy systems, exam. of material requirements 78—50255
- underground aquifer storage of hot water from solar energy collectors 79—57477
- underground hydroelectric pumped storage, geologic conditions 80—30577
- underground pressurised saturated hot water storage for peak lopping appls. 80—76653
- underground thermal storage in the operation of solar ponds 80—40911
- undersea hot water storage system 80—45763
- unit helium requirements for superconductive energy applications in the USA 78—89999
- utility, Li-Si alloy/FeS cells appl., research and development at Atomics International 79—48115
- wind energy storage systems simulation model, SIMWEST program package 79—52872
- wind generation of electricity, in dwelling independent of servicing network 79—61943
- $Ag-H_2$ battery cells, long-life, light-weight, spacecraft appl. 79—48108
- $Ag-H_2$ electrochemical cell design using rolled stack configuration 80—101084
- BaO reversible oxidation energy storage system feasibility 79—83637
- CO_2, electrochem. reduction for use in energy storage 78—92490
- $CaCl_2.2CH_3OH$, solar heat pump and thermal storage system for space heating 80—85307
- $CaCl_2.6H_2O$ heat of fusion system for solar energy storage 80—16846
- $CaCl_2.6H_2O$, heat transfer props. for heat of fusion energy storage 80—76654
- $CaO-Ca(OH)_2$ reversible hydration-dehydration for solar energy storage 80—97810
- Ce_xMg_y, hydrogen storage materials *(French)* 79—66419
- FeTi, hydrogen storage, annealing effects *(Japanese)* 79—100542
- H absorption-desorption characts. on $TiCo_{1-x}Mn_x$ 80—96735
- H as energy transport system, prospects 79—66418
- H as the solar energy translator 80—30608
- H biological photoprod. using sunlight, review 80—45777

energy storage continued
- H biological prod. by solar energy conversion, coupling of hydrogenase and chloroplast photosystems 80—45778
- H, biophotolytic production from H_2O 80—61457
- H cryogenic storage, liquefaction processes, storage and distrib. equipt. 80—45784
- H, cryogenic storage and refuelling for automobiles 80—30604
- H, demand and supply of hydrogen as chemical feedstock in the USA 80—45817
- H, effect of steel embrittlement on design requisites for H energy systems 80—30109
- H, electro-/thermochemical prod. from H_2O by Westinghouse sulphur cycle 80—55940
- H electrochemical prod., solid polymer electrolyte water electrolysis status for large scale hydrogen production 80—30605
- H electrochemical/thermochem. prod. using S cycle, laboratory prod. model and electrolyser development 80—30602
- H electrolytic prod. by H_2O decomposition in acid molten electrolytes at 220 to 320°C 80—45769
- H, electrolytic prod. by inorganic-membrane-electrolyte H_2O electrolysis 80—45804
- H, electrolytic prod. using mobile generator 80—45805
- H electrolytic production *(Spanish)* 80—35766
- H energy, industrial appls. of liquid and gaseous H 80—45801
- H energy, R and D programs, review 80—45802
- H energy prospects 80—45799
- H, energy storage in FeTi, surface segregation, catalytic effect on hydrogenation 80—45814
- H energy utilisation in the nuclear, solar and fossil fuel energy strategies 80—45798
- H fuel storage and distrib. for automotive vehicles, techno-economic feasibility study 80—45820
- H, industrial scale, production from natural gas, naphtha, coal review 80—35791
- H, kinetics of hydrogen absorption and desorption by ternary $LaNi_5$ type intermetallic compounds 80—45813
- H laser-fusion prod. by radiolytic-thermochem. cycles 80—45811
- H, liquid fuel for commercial aircraft, production and liquefaction facilities 80—45818
- H, metal hydride heat pump as topping cycle for power generation 80—40928
- H, metal hydride storage, diffusion-rate-limited hydriding and dehydriding kinetics 80—35764
- H, optimal development strategies for a whole energy system based on hydrogen 80—45795
- H, photoassisted production, reactions of H_2O with C and ethylene over Pt/TiO_2 80—55703
- H photochemical prod., H_2O photolysis using fission pumped gas lasers 80—45810
- H photochemical prod. by H_2O photolysis using sunlight 80—45776
- H photoelectrochemical prod., solar beam-assisted electrolyser applied to Yokohama marks 5 and 6 [system for hydrogen production] systems 80—45768
- H photoelectrochemical prod. using TiO_2-Si solar cell hybrid electrodes 80—45775
- H, photoelectrolytic prod. from H_2O, storage efficiency estimate 80—51016
- H photoelectrolytic production by H_2O decomposition using sunlight, review 80—45774
- H plasmochemical prod. by H_2O decomposition in non-equilib. plasma 80—45773
- H prod. by H_2O pyrolysis using solar thermal energy 80—45770
- H prod. by H_2O solar photolysis by engineering methods using biological materials *(Japanese)* 80—45765
- H prod. by high temp. electrolysis using fusion heat 80—51012
- H production, EPRI R and D program for electric utility industry, review 80—30610
- H production, exergetic/energetic/economic anal. of electrolytic, thermochem. and hybrid processes 80—55938
- H production, storage, and utilisation for domestic appls., Hydrogen Homestead project 80—40921
- H, production, techno-economic evaluation using OPTIMO code 80—45797
- H production, thermochemical or hybrid cycles of hydrogen production techno-economical comparison with water electrolysis 80—45796
- H production, thermochemical water-splitting cycles based on Ce and alkaline earth phosphates 80—55945
- H production and distrib., US safety regulations and standards, bibliography 80—41976
- H production and utilisation, EEC R and D program review 80—45821
- H production by pressurised coal gasification 80—30609
- H production by Westinghouse electrochem./thermochem. S-cycle process 80—45808
- H production for solar energy utilisation 80—51014
- H production from coal using steam-Fe process, development status 80—55942
- H production from fusion reactors coupled with high temp. electrolysis 80—45771
- H production from H_2O by two-stage plasmochemical cycle 80—45772
- H production on illuminated transition metal surfaces, tight binding model 80—45812
- H production using fusion reactor heat and gas dynamic compression heating 80—35793
- H, production using HBr electrolysis 80—35777
- H production using HTGR nuclear heat source 80—45803
- H production using hybrid electrochem./thermochem. cycles, search for electrochem. reactions 80—45807
- H, radiolytic/thermal cycles 80—51011
- H, solar-thermochemical prod. of H_2O appl. of fixed mirror solar concentrators 80—45767
- H sorption at press. up to 1500 atm. on rare earth alloys, RM_x ($M=Co$, Ni) 80—97819
- H, storable conc. of atomic H in T-impregnated crystalline solid H_2 80—30594
- H storage, development of low cost Ni-rare earth hydrides 80—45791
- H storage, effect of the interstitial hole size and electron concentration on complex metal hydride formation [for H storage] 80—45789
- H storage, electrolysis-based technology R and D at BNL, review 80—40920
- H storage, high temp. hydrides for vehicular appls. 80—45793

energy storage continued
- H storage, $LaNi_{5-y}Al_y$ alloys and their hydrides, metallurgical, structural and thermodynamic props. 80–45816
- H storage, $SmCo_5$ hydriding kinetics, inverse over pressure effect 80–55944
- H storage, sorption props. of Al-containing Laves phase intermetallics 80–45794
- H storage, technological aspects and characteristics of industrial hydride reservoirs 80–45792
- H storage, transmission and distribution, review 80–30596
- H storage, use of Ti binary alloys for solid metal hydride storage 80–45786
- H storage and distrib., potential for pipeline transmission in Switzerland 80–45780
- H storage and distribution, problem rel. to use of natural gas distrib. eqpt. 80–45779
- H storage and utilisation using metal hydrides 80–45785
- H storage by $LaNi_5$, effect of O_2, H_2, H_2O, SO_2 on surface segregation *(German)* 80–51008
- H storage by metal hydrides for automotive propulsion 80–40922
- H storage by use of cryoadsorbents 80–45783
- H storage in metal hydrides 80–61445
- H storage in metals, book contrib. 80–26175
- H storage materials, design criteria; thermodynamics, absorpt. kinetics, economics and materials science 80–55943
- H storage materials, H diffusion in $Ti_2NiH_2(FeTiH)(LaNi_5H_6)$, neutron diffr. obs. 80–51013
- H storage using $CeMg_{11}V(Cr)(Mn)(Fe)(Co)$ alloy hydrides 80–51009
- H storage using cubic metal binary alloys 80–45787
- H storage using electrochem. reduction of CO_2 80–7934
- H storage using FeTi hydrides, struct., heat of soln., diffusion and hydriding kinetics 80–40930
- H storage using $LaNi_5$, effect of Ni, Ce, Co alloying additions on H_2 absorption 80–45790
- H storage using $LaNi_5$, self restoring of active surface 80–45815
- H storage using metal hydrides, numerical physical property data 80–40929
- H storage using rare earth alloy hydrides, props., book contrib. 80–45291
- H storage using small scale NH_3 prod. 80–45782
- H storage using Ti-Zr-Cr-Mn/$LaNi_5$ hydriding alloy mixtures 80–45788
- H storage using VH and VD, expt. exam. of isotope effects 80–45281
- H, survey of liquid hydrogen container technology for highway vehicle fuel system applications 80–30607
- H synfuel prod. by high temp. electrolysis using fusion energy 80–35792
- H synfuel prod. from fusion power using hybrid thermochem. $Bi_2O_3.SO_3$ cycle 80–40931
- H synthetic chloroplasts 80–30508
- H, thermochem. prod. by H_2O decomposition using Mg-I cycle 80–35786
- H, thermochem. prod. using the Mark-13 process, status report 80–30606
- H thermochemical prod., engineering impact on the validity of the Mark-16 thermochem. cycle 80–45806
- H, thermochemical prod. by H_2O decomposition, equilibrium effects in high press. prod. 80–35775
- H, thermochemical prod. by H_2O decomposition, impact of thermal burdens and kinetics 80–35787
- H thermochemical prod. by H_2O decomposition using solar energy 80–40919
- H, thermochemical prod. by H_2O pyrolysis, computer thermodynamic anal. and optimisation 80–45766
- H thermochemical prod. by H_2O decomposition, review 80–45800
- H, thermochemical prod. by high temp. H_2O decomposition using solar energy 80–45822
- H, thermochemical prod. from H_2O, noncorrosive two-reaction low temp. cycles based on mordenite-hosted redox reactions 80–55939
- H thermochemical prod. using $Bi_2(SO_4)_3$ cycle, process engng. design 80–30599
- H, thermochemical prod. using SO_2-I_2 water splitting cycle 80–30600
- H, thermochemical prod. using S-Br cycle, development of lab.-scale plant 80–35774
- H, thermochemical prod. using Br-Ca-Fe H_2O-decomposition cycles 80–35784
- H, thermochemical prod. using General Atomic S-I cycle for H_2O decomposition 80–55941
- H, thermochemical production, irreversibility anal. of separation schemes from binary gas mixtures 80–35767
- H, thermochemical production, H_2O decomposition using S compounds, feasibility anal. 80–35768
- H, thermochemical production, H_2O decomposition using S-I cycle 80–35769
- H, thermochemical production, H_2O decomposition using S-I cycle, process eng. and bench-scale studies 80–35770
- H, thermochemical production, HI decomposition and H separation 80–35771
- H, thermochemical production, by HBr pyrolysis 80–35772
- H, thermochemical production, $SO_2/H_2O/X_2$ reactions ($X_2=Br_2, I_2$) 80–35773
- H, thermochemical production, HBr decomposition using $FeBr_2$ and Fe_3O_4 80–35778
- H, thermochemical production, H_2O decomposition using S cycles, thermochem. anal. of energy balance 80–35779
- H, thermochemical production from H_2O, development of two new thermochem. cycles at ORNL 80–35780
- H, thermochemical production using ZnSe cycle, chemical and process design studies 80–35782
- H, thermochemical production using Ce-Cl cycle 80–35783
- H, thermochemical production using Hg-I ANL-4 cycle 80–35785
- H, thermochemical production by steam reforming of methane, kinetic anal. 80–35788
- H thermochemical production by coal gasification using steam 80–35789
- H thermochemical production using air blown coal gasification, economics 80–35790
- H, thermochemical production using fusion energy source 80–51010
- H, thermoelectrochemical prod. using H_2SO_4-SO_2 cycle, electrochem. aspects 80–35776
- H thermoelectrochemical prod. utilising electrolyzer and fuel cell 80–45718
- H, thermoelectrochemical prod. using NaCl 80–55946

energy storage continued
- H transportation, suitability of contemporary gas distrib. equipment 80–30603
- H-fuelled railway motive power systems 80–40923
- H-rich synthetic fuel prod. and transportation for solar energy utilisation 80–51015
- H_2 and O_2 production from H_2O using solar energy, eval. of a hybrid process 80–104519
- H_2 as an energy source 80–108816
- H_2, atomic at 1K, energy storage appls. *(German)* 80–89681
- H_2, biologically-assisted production, use of polymeric viologen mediators in a bioreactor based on hydrogenase-catalysed $Na_2S_2O_4$ decomposition 80–61460
- H_2 bulk storage using TiFe-based hydrides 80–61463
- H_2, by alloys hydrogenation, alloy bonding theory approach 78–18786
- H_2, by $NdNi_5$ and $LaNi_4Cu$ intermetallics, cell volumes and desorption pressures correlation 78–22860
- H_2, comparison of technologies and economics for fixed site storage 80–67011
- H_2 distribution in natural gas equipment, operating, safety and material problems 80–61468
- H_2, electrochemical prod., development of high efficiency alkaline electrolysis technology 80–30601
- H_2 electrolytic production by high temp. steam electrolysis 80–61440
- H_2 electrolytic production, development and operation of advanced electrolysis cell 80–61441
- H_2 electrolytic production, design and operation of advanced H_2O electrolysers, review 80–61449
- H_2 energy bibliography (1974-79) 80–26173
- H_2 energy research programs in Japan 80–61435
- H_2 fuelled vehicles, design and engine modifications with Fe-Ti hydride storage 80–40925
- H_2, HYCSOS chemical heat pump, low grade heat enhancement using $LaNi_{5-x}Al_x$ 80–61467
- H_2 in rare-earth and Th-transition metal intermetallics, desorption isotherms depend. on d-bandfilling 78–18912
- H_2, liquid automobile fuel, cryogenic storage, and semiautomatic refueling station 80–40926
- H_2, photobiological prod., key enzymes and biochem. systems, tech. problems of H_2 prod., review 80–61446
- H_2 photochemical production by H_2O dissociation utilising solar energy, review 80–61452
- H_2, photochemical production using visible light on aqueous solns. of a Ru complex 80–85192
- H_2 photoelectrochemical production using solar energy and Zn(Mg)(Cr)(Ni) phthalocyanine dyes *(French)* 80–55936
- H_2 photolytic production using chlorophyll-catalysed H_2O photolysis and solar energy storage 80–61458
- H_2 production, H_2O electrolysis module design, geometry, capacity, operating temps., pressures, electrode types 80–72098
- H_2 production, wind energy conversion schemes, South African feasibility study 79–43714
- H_2 production and storage utilising solar energy conversion, book 80–57017
- H_2 production by alkaline electrolysis using inorganic-membrane-electrolyte 80–72092
- H_2 production by biological and biochemical solar energy conversion, review 80–61454
- H_2 production by direct solar energy conversion at sea, review 80–61456
- H_2 production by direct thermal decomposition of H_2O utilising solar energy, thermodynamics, review 80–61450
- H_2 production by H_2O electrolysis, nucleate boiling, vapour bubble behaviour, heat and mass diffusion 80–67013
- H_2 production by H_2O electrolysis, compression and storage 80–72097
- H_2 production by H_2O electrolysis in fused NaOH 80–76660
- H_2 production by H_2O photolysis using solar radiation, feasibility of large scale generation 80–72095
- H_2 production by H_2O radiolysis, thermoradiation dehydrogenation using nuclear power, kinetic anal. 80–67010
- H_2 production by H_2O solar photolysis using Pt/(chlorophyll a.$2H_2O$) reaction 80–89663
- H_2 production by solid polymer electrolyte H_2O electrolysis 80–61442
- H_2 production by solid polymer electrolyte H_2O electrolysis 80–67012
- H_2, production from natural gas, naphtha and coal on industrial scale 80–61438
- H_2 production from water using biomass feedstock and bromination process 80–61459
- H_2 production in fusion-synfuel blanket, thermal hydraulics 80–106176
- H_2 production using Mg(Al)(Fe)(Co)(Ni)(Cu)(Zn) sulphates for solar energy storage *(French)* 80–55935
- H_2, review 80–61453
- H_2 solution in $TiCr_{1.8}$, enthalpy, solubility and mol. vibr. determ., comparison with soln. in metals and binary alloys 80–79951
- H_2 storage, high pressure gas storage using microcavity structures 80–61462
- H_2 storage, thermodynamic and structural properties of $LaNi_{5-y}Al_y$ compounds and their related hydrides 80–16847
- H_2 storage, transmission and distrib., review 80–61439
- H_2, storage as metal hydrides, props. and appls. 80–76661
- H_2 storage as MgH_2 hydriding and dehydriding kinetics obs. by press. sweep method 80–35765
- H_2 storage at fixed sites for distribution 80–61461
- H_2 storage in amorphous plasma-sprayed Sm-Co, effect of H_2 atm. on crystn. and mag. props. 80–64898
- H_2 storage in Fe-Ti hydrides, specific heat meas. at room temp. 80–65248
- H_2, storage in form of metal hydrides 80–72096
- H_2 storage in $LaNi_5$-type ternary alloys, absorption and desorption kinetics 80–55932
- H_2, storage properties of $Zr(V_{1-x}Co_x)_2$, rel. to electronic struct. 80–76662
- H_2 storage using hydride beds, thermal transport enhancement using high conductivity materials 80–61466
- H_2 storage using Mg-La(Ce)(mischmetal) alloys 80–72093
- H_2, thermal efficiency of H_2 compression using hydrides 80–61465
- H_2 thermo-electro-chemical production by Westinghouse H_2SO_4 process, heat penalty and economic anal. 80–61437
- H_2 thermochemical compression for hydride thermosorption, theory *(Ukrainian)* 80–76657
- H_2 thermochemical prod. by H_2O decomposition utilising solar heat 80–61451

energy storage continued
- H_2, thermochemical production by H_2O pyrolysis 80—55928
- H_2 thermochemical production, based on reactions of $CeTiO_2$ for water-splitting 80—55929
- H_2 thermochemical production using open-loop cycles 80—55930
- H_2, thermochemical production, engineering impact on the validity of the mark-16 thermochemical cycle 80—55931
- H_2 thermochemical production, plasmochemical H_2O decomposition using nuclear energy source 80—61436
- H_2 thermochemical production using fusion energy using metal oxide thermochem. cycles 80—76658
- H_2 thermochemical production by Mark-13 cycle, development of laboratory-scale plant 80—76659
- H_2 underground storage in aquifers, physical, chemical, energy aspects 80—55933
- H_2, using $LaNi_5$, fundamentals and appl. 78—18785
- H_2, using Ti-Mn alloy systems *(Japanese)* 80—61443
- H_2/hydrocarbon fuel prod. via biomass conversion wastes by solar H_2O photoelectrolysis 80—89653
- H_2-Br_2 cell for energy storage appls. 80—72029
- H_2-Cl_2 cell, electrochemically regenerative, mass and heat balances 80—3503
- H_2-methane mixture properties for hydrogen supplementation of natural gas 80—45781
- KCl-CuCl eutectic fused salt, potential as intermediate temp. solar heat transfer and storage medium 80—101135
- La_xMg_y, hydrogen storage materials *(French)* 79—66419
- Li-FeS battery eng. problems for elec. load levelling plant design 80—30457
- $Li_{1-y}Ti_{1+y}S_2$, intercalation chemistry and electrochemical energy storage 79—100541
- NaOH, liq., thermal storage, steel corrosion, appl. in accumulation type steam generator *(French)* 80—40914
- NaOH-8% $NaNO_3$ phase change thermal storage for solar total energy system 79—57481
- Pb-Ca batteries, float current 80—12004
- $TiFe_{0.8}Be_{0.2}$ alloys for H_2 storage 80—97817
- Zr-Ni alloy, H_2 storage in form of capsules *(French)* 79—92091

energy storage devices
- 500 V homopolar generator for Tokamak device power supply 78—5957
- advanced electrochemical energy systems, future needs and developments 78—8197
- Argonne National Laboratory energy storage and transfer program 78—55031
- batteries for solar electricity storage, Systems optimisation of solar cell/battery 80—51007
- book 80—51974
- cryogenic inductive energy storage device for LASL fusion reactor 77—23284
- duplex chemical system for storage and transport of heat from LWR, district heating 78—37460
- economic assessment 79—48183
- economic assessment and optimization of energy storage systems 80—40909
- fast discharging homopolar demonstration model as fusion reactor pulsed power supply 77—23283
- flywheel, regenerative energy storage system for electric vehicle propulsion 80—30564
- flywheel energy accumulatsrs, stationary, for industrial undertakings, economic assessment *(German)* 80—35757
- flywheel energy storage interface unit for photovoltaic applications 80—30571
- flywheel energy storage system, rotating flywheel in an evacuated casing 80—30570
- flywheel energy storage system 80—30569
- flywheel energy storage system for electric utilities, study 79—96486
- flywheel energy storage system for JT-60 toroidal field coil 78—62662
- flywheel energy storage unit for a high power energy source for vehicular appls. 80—30580
- flywheel rotor design utilising natural cellulosic materials for energy storage appls. 80—30568
- flywheel rotor with high energy density 80—30565
- flywheel system for storage and conversion of energy from wind turbine 80—30572
- flywheels, development of low loss magnetic bearings 80—30566
- flywheels, performance of retainerless bearings 80—30567
- fuel cell appls. in space power systems 80—30465
- fusion reactor, inductive and rotating machinery energy storage and transfer 79—85782
- fusion reactor, Shiva Faraday rot. coils, circuit and mag. anal. 78—54951
- fusion reactor, use of homopolar generator for inductive energy storage 78—54948
- heat storage device, off-peak, ambient temp. observer/predictor control system 80—66950
- high energy gas laser facility, energy storage system design 78—55030
- homopolar generator, radially stacked drum type, for Tokamak Ohmic heating coils 78—13337
- homopolar generator for Tokamak device power supply 78—5958
- homopolar machine, fast discharging, 10 MJ model, for fusion device 78—13335
- homopolar machine with superconducting field coils, design and appl. 78—54927
- hybrid drives with flywheel energy storage, automobile appls. *(German)* 80—30563
- inductive, two-stage opening switch technique, for high inductive voltage generation 78—55034
- inductive storage element, pulsed discharge into fluid gap, electrohydraulic effect *(Russian)* 80—100117
- inductive storage systems motor-generator sets, voltage protection scheme 78—55037
- inductive storage unit for laser pumping, design and construction 79—89916
- inductive storage unit used to pump SF_6-H_2 laser 79—98409
- inductor for high power impulse production, features *(German)* 78—50293
- large-scale elec. energy storage, review 80—89676
- membrane-lined thermal storage systems 80—55919
- metal hydride system for H_2-fuelled vehicles 80—45819

energy storage devices continued
- methanol based heat pumps for storage of solar thermal energy 80—30587
- motor-generator system for fusion power reactor energy storage 78—5044
- phase-change, energy storage unit sizing for air-based solar heating systems 80—7922
- pulsed, DC vacuum interrupter, tests 78—74489
- pulsed superconducting coil, 1.5 MJ, and cryostat, performance tests 79—49259
- Redox flow cells, electrochem. energy storage for utility appls. 80—30456
- secondary batteries, 1979 status and prospects *(Japanese)* 80—76655
- secondary batteries, powered by forced ionisation 79—43755
- secondary cells, Ni-Cd, plastic-bonded electrodes positive active layer study 80—101088
- secondary cells with C-air electrodes in alkaline electrolytes, ageing mechanism study 80—101087
- solar chemical heat pump/storage system for air conditioning 80—55886
- solar energy terrestrial uses, photovoltaic units combined with storage batteries *(German)* 80—55840
- solar heating system components, optimal insulation, numerical sensitivity anal. 80—35745
- solar photoelectrolysis with semiconductor electrodes for solar energy conversion and storage, review 79—74533
- solar seasonal storage devices, economic optimisation of storage capacity and collector area 80—101133
- solar storage tank, buried, hemispherical, heat cond. to environment, series soln. 79—3891
- solar thermal energy storage bed, heat transfer and heat storage characts. 80—55927
- solar thermal power plant storage systems, survey *(Japanese)* 79—79379
- solar-powered absorption cycle with energy storage, theoretical anal. 80—55885
- superconducting coil energy storage power supply 79—34442
- superconducting magnetic device, He requirements for superconducting power network 79—50897
- superconducting magnetic energy storage for electric power system stabilizaion 80—30611
- superconducting magnetic energy storage system, switching technology in theta-pinch fusion reactor 77—23285
- superconductive energy storage magnet, single layer, design and cost-related parameters 80—108815
- thermal energy storage by latent heat of fusion *(French)* 79—3893
- thermal energy storage in a packed bed of iron spheres with liquid sodium coolant, thermocline broadening 80—45762
- thermal energy storage material cylinders, heat transfer during melting 79—3894
- thermal energy storage system for a Stirling engine powered highway vehicle 80—30584
- thermal energy storage tank, thermal stratification during charging 79—3890
- thermal storage cell for high temperature solar systems 80—55923
- thermal storage in fluid/solid packed beds, design and rating *(French)* 80—61433
- thermal storage systems, electric utility load management appls. 80—16845
- thermal storage unit, sensible-heat, solid, transient response 79—3892
- Tokamak, Texas exptl., homopolar generator, eddy currents, EM forces (torques), due to misalignment 78—54953
- Tokamak EF coil energy transfer supercond. solenoids and phase-shifting bridge 79—31213
- Tokamak energy storage superconducting solenoids 78—66369
- vacuum mag. energy systems, fast switching into external load, for pellet fusion 78—13339
- H-Cl electrochemically regenerative fuel cell, electrode kinetics and cell perform. 80—89610
- Na-S batteries, energy storage for peak power generation 80—30455
- Na-S battery for load levelling appls. 80—30453
- Nb-Ti filamentary superconductor critical current density rel. to thermal treatment 79—33440
- Zn-Br_2 battery for utility energy storage appls. 80—30450
- Zn-Br_2 non-circulating storage batteries 80—30451
- ZnCl hydrate battery system, design fabrication and testing of 5 MWh system at BEST Facility 80—35763

energy transfer collisions, molecular *see molecular inelastic collisions*

engineering
- *see also biomedical engineering; civil engineering; design engineering; electrical engineering; environmental engineering; maintenance engineering; mechanical engineering; naval engineering; project engineering; systems engineering; value engineering*
- biological analogues 78—8214
- design, creativity testing 80—27062
- earthquake engineering, implications of seismic body waves propag. in S. Kanto Region *(Japanese)* 80—94481
- education, physics, engineering and teacher training at Loughborough University of Technology 79—35455
- education, physics joint honours degree course at Manchester University 79—35456
- education modern methods and instructional media roles 80—27064
- educational courses, for professional engineers, economic costs and course contents considerations 79—80414
- electronics design course curriculum study, overview 80—27063
- engineering-science summer programme 79—2588
- imaginative engineering through education and experience, conference, Williamsburg (1977) 77—71164
- liberal arts-engineering courses, interaction with a physics dept. 77—64898
- materials science and engineering as a multidiscipline 79—38726
- scientific ideas originating in engineering 78—8213
- sociotechnical systems: the new engineering frontier—a sketch for an engineering school plan 80—31445
- undergraduate engineering education, physics requirements 79—44656
- university engineering course, first semester subjects and projects *(French)* 80—27066
- C fibres, engineering applications, production requirements and mech. props. 80—89168

engineering applications of computing *see engineering computing*

engineering computing
- *see also aerospace computing; chemical engineering computing; civil engineering computing; communications computing; control engineering*

engineering computing continued
- *computing; electrical engineering computing; electronic engineering computing; mechanical engineering computing; nuclear engineering computing*
- applications of finite-element and finite-difference methods 78−57765
- automatic dimensional analysis using symbolic maths. 77−57173
- axially symmetric hollow collectors for high temp. solar installations, radiative heat transfer computation 78−79093
- CAD of windows as passive solar collectors, using interactive program 79−62146
- climatic test chambers, automation using microprocessor programmers 80−21430
- designer work station link for ES computers 79−30442
- diesel-driven chiller system simulation, with multi-tank thermal storage system, for large commercial buildings appl. 79−48187
- environmental noise, urban, systematic evaluation and control *(Japanese)* 79−88033
- ESCA spectrometer retarding lens system, computer optimisation 77−13827
- flat plate solar concentrator performance calc. using programmable desk calculators 77−75691
- flow and mass transport through porous media, linear equations systems solution, unsymmetric, sparse 77−80210
- forced-circulation solar water heater analysis and expt. 79−62043
- full unsymmetric matrices, out of core eqn. solver 78−45477
- geometrical optics, programmable pocket calculator appls. 79−58468
- geothermal binary cycle, hydrocarbon working fluid selection 79−48091
- gyrocompass levelling and setting for gyrostabilised platforms *(Russian)* 80−52190
- heat pump simulation, solar boosted 79−57414
- heating of single family dwellings, heat pump appl. 79−43784
- house energy conservation measures obs. and evaluation, Philips expt. house (West German project) 79−61951
- induction motor, polyphase, at no-load, nonlinear magnetostatic field determ. 78−33647
- lens design optimisation, Version 14 program 78−90488
- lens system design with extended depth of focus, Version 14 optimisation program 78−90489
- MHD conversion channel plasma flow computation by finite difference method 78−22470
- microcomputer appl. in photometric technique *(German)* 77−74480
- noise, forecasting program for sound press. level in closed building *(French)* 78−13856
- nuclear reactor optimal control using Walsh function variational synthesis technique 77−38347
- oil recovery from Utah tar sand deposit, by in situ combustion 79−48046
- OTF calculation using gaussian quadrature, rel. to lens system design 78−90383
- pipeline compressible flow and heat transfer simulation program 77−19638
- potential flow about bodies of revolution, general analytic method 78−1629
- radioisotope thermoelectric generator, selenide, power degradation predictions 79−48148
- solar air conditioner performance prediction, based on LiBr absorption devices 79−62134
- solar air conditioning system simulation, using evacuated tubular collectors 79−61949
- solar building analysis and design, using Cal-ERDA programs 79−57456
- solar flat plate collector thermal performance testing 79−62061
- solar furnace temp. meas. using digital pyrometry system 77−37896
- solar heating, of dwelling independent of servicing networks 79−62149
- solar heating of buildings, thermal performance evaluation 79−57467
- solar input and solar data computation for engineering of solar systems, transients simulation 80−94060
- solar space heating system analysis, based on Markov chain models 79−61950
- solar total energy system, for US Army base buildings, conceptual design and large-scale expt. 79−52899
- solution generation by programmable pocket calculator, engineering training course appl. 80−6
- sound amplifying systems in halls, model *(French)* 79−37090
- speech intelligibility in auditorium, computer evaluation *(French)* 79−37095
- steam pressure and temp. in relation to enthalpy and entropy *(German)* 78−59532
- Stirling cycle machines optimisation, free piston design 79−48172
- Stirling engine simulation, research, JPL laboratory 79−48171
- structural analysis, dynamic, soln. of quadratic eigenproblems 77−89017
- vibration-acoustic diagnostics, random signal patterns recognition *(Slovak)* 79−18612
- water resource management, gaming-simulation appl. in Hunter River Valley, New South Wales 79−57517
- wave propagation problems, numerical anal. based on finite element method *(Japanese)* 78−28928
- wind energy storage systems, SIMWEST program package 79−52872
- zoom lens design by pocket calculator 78−55423

engineering facilities
- *see also test facilities*
- general performance parameter for meas. facilities, engineering formula 77−67404
- high speed cine photography, in industrial engineering environment 78−37099
- hot cell manipulator remote decontamination facility and repair station 79−9911

engineering societies *see societies*

engines
- *see also aerospace engines; heat engines; internal combustion engines; ion engines; propulsion*
- diesel engine, freq. response and multiple coherence function of noise generation system 77−7254
- engine intake noise, high freq., ray-theory approach 80−69595
- nuclear piston engine concept involving pulsed quasisteady-state gaseous-core reactor 77−34423
- H_2 fuelled vehicles, design and engine modifications with Fe-Ti hydride storage 80−40925

entertainment *see sports and entertainment*

enthalpy
- *see also heat of ......*
- acetonitrile binary liq. mixtures, excess thermodynamic functions, complex formation 79−52736
- acetonitrile-water mixture, electrolyte transfer, thermodynamic props. 80−3395
- acrolein, s-trans and s-cis, trapping from thermal mol. beams and UV-induced isomerisation in Ar matrices, enthalpy determ. 80−97688
- adsorbed macromolecules, conform. and thermodynamics at liq./solid interface 77−11782
- air enthalpy meas. by LiCl humidity sensors 80−90858
- air flows in triple point shock configurations, anal. thermodynamics *(Russian)* 79−32569
- β-Al_2O_3-Na_2O, mechanism of diffusion 80−2202
- alcohol-inert soln., assoc. soln. thermodynamics, enthalpy, Gibbs free energy 78−31670
- alcohol-unassociated active component liquid mixtures, associated soln. theory, thermodynamic parameters 80−7836
- alkali halide, migration enthalpy and entropy for cation vacancy motion 77−35750
- alkali halides, free energy of formation of vacancy determ. 77−76597
- alkali isoalkanoates, thermal behaviour, differential scanning calorimetry 78−34600
- alkali metal fluoroaluminates, dissoc. enthalpies, mass spectrometric determ., heat of form. 80−97720
- alkali metal halides, molten binary mixtures, excess enthalpies calc. 80−3397
- alkali metal nitrates, lattice energies and related thermodynamic props. 77−51344
- alkali metals, liq., density, enthalpy, up to 1500 bars 77−84821
- alloy, thermodynamic and structural changes in deform. twinning 78−2139
- alloys, enthalpy of mixing, ‘const. vol. alloy’ formulation 79−28111
- bacteriorhodopsin, enthalpy changes during photochemical cycle 79−34602
- BCC metal hydrides, geometric and electronic contribs. to thermodynamic props. 79−46815
- benzaldehyde, in polymer matrix, dielec. absorption, Eyring parameters 79−4761
- benzene+cyclohexane, excess enthalpy, calorimetric cell 79−58689
- benzene-cyclohexane (methane) vapour mixture, excess enthalpy meas. appl. of differential-flow mixing calorimeter 78−12700
- 3,4-benzo-1,6-methano(10)-annulene, mol. geom. and gas phase thermodynamic props., minimisation scheme 78−78829
- benzyl cyanides, α-substituted, in dil. soln., dielec. absorpt. obs., enthalpy of activation 80−55019
- binary alloys, activity of most oxidizable element *(French)* 79−61868
- binary liquid mixtures, mol., intermol. props. from excess enthalpies 77−44503
- binary metallic solid solns., thermodynamic quantities rel. to vacancy and diffusion characts. 79−95204
- binary mixtures, models, distance parameter geometric averaging, excess free enthalpies *(German)* 77−32825
- biomolecules+chloranil, charge transfer interaction, equilib. const., enthalpy and entropy determ., mol. polarisability 80−89708
- biopolymers, reversible unfolding, mol. field theory 79−34479
- boranes, nido and arachno, bond length-bases bond enthalpies 80−30265
- brass, martensite stability 79−91650
- brass, vacancy form. enthalpy, determ. from threshold temp. for positron trapping in vacancies 78−80433
- brass, vacancy formation enthalpy, composition depend., position annihilation obs. in Cu rich phase 79−95872
- α,βbromonaphthalenes, thermodynamic functions calcs. 298-1500K 77−31418
- butane, liq., enthalpy difference between rot. isomers, IR spectrosc. obs. 80−106404
- t-butyl acetate, rot. isomerism, dielect. and Raman spectra 80−106328
- t-butyl formate, rot. isomerism, dielect. and Raman spectra 80−106328
- calculation using pocket calculator, data-base library formation 77−67391
- caloric function derivation for liquids and gases 80−13017
- calorimeter, corrosive gases and liquids, particularly N_2O_4 77−79097
- calorimeter, for meas. of enthalpies of solids and liquids in 1200-3000K range *(French)* 77−13754
- calorimetric probes for gas stream enthalpy meas., calibration 78−70126
- cation-exchange sorption microcalorimetry, automatic micro-injection system 78−24777
- ceramic, calc. for solids and liqs. 77−43348
- chalcogenide spinels, thermal stability, thermochemical, thermodynamic and crystallochemical props. 77−51519
- chemical reaction, linear free enthalpy relation validity, thermodynamic foundation *(German)* 79−34351
- chloromethyl formate(-d_1,d_2,d_3), gas, solid. and liq., IR spectra assignments and struct. 80−32715
- β-chloronaphthalene, thermodynamic functions calcs. 298-1500K 77−31418
- o-chlorotoluene(-benzene), liq. and dilute soln., microwave absorption and relax. processes 79−82920
- cholesteryl myristate, polymorphism of blue phase, DTA and microscopy meas. 79−37819
- cholesteryl nonanoate, polymorphism of blue phase, DTA and microscopy meas. 79−37819
- computer generated phase diagrams 78−83928
- α-corundum, 800-2300K 77−47592
- α-corundum, enthalpy, 800-2300K, empirical eqn. 78−14478
- cresols, ideal gas thermodynamic props. 78−75250
- crystal hydrates, thermodynamic functions, Karapetyants-Rozenfeld equation *(Russian)* 79−66332
- cubic margules solution model, miscibility gap and crit. point behaviour 78−59925
- cyclohexanal, liq., viscoelastic and structural relax., US rel. and absorption meas. 78−26634
- cyclohexane-benzene (methane) vapour mixture, excess enthalpy meas., appl. of differential-flow mixing calorimeter 78−12700
- diamantane, sp. ht., thermodynamics of transition and fusion 79−55899
- o-dichlorobenzene(-benzene), liq. and dilute soln., microwave absorption and relax. processes 79−82920
- diffusion, activation enthalpy and entropy and defect form., basic thermodynamic relation, validity limit 78−47557

enthalpy continued
digital automatic thermodynamic enthalpy and specific heat determ. equipment 78−57951
dil. soln., dielectric relax., solid rotator phase 79−42890
dimers, dissociating, in nonisothermal ideal gas phase, stationary state anal. 78−76848
diphenyl mixture, superheated cap. and liq., enthalpy, press. depend. 78−42702
dispersed two-phase single-component system, modification of charact. functions by interphase boundary and surface tension 77−90647
DNA in water-ethanol solns., enthalpy of B-A transition 77−70412
dodecylamine ($-NH_2$)/H_2O_2 and deuterated cpd., liquid crystal, phase relationships, isotope effects 79−19358
electrolyte, strong, conc. solns., thermodynamic props. of mixed electrolytes and Harned rule basis 79−90506
electrolyte, strong, lattice-like network of ions thermodynamic quantities 78−35699
enthalpy-entropy compensation effect, separation of chemical from statistical effects 77−21412
enthalpy-entropy compensation effect, statistical analysis, van't Hoff and Arrhenius data 77−21411
equations of state calculation methods *(German)* 78−34588
ethylene, diatomics-in-mols., semiempirical valence bond π-electron theory 80−99461
ethylene + N_2, gaseous, excess enthalpy, determ. by flow calorimetry 78−91057
ethylmethylether(-d_3), low freq. vibr. spectra, methyl torsional pot. functions, internal rot. 79−26978
excess enthalpy and excess entropy functions derivation by direct method from TX phase diagram, heats of mixing calc. 80−75366
ferromagnetic binary alloys, strictly regular, quasi chemical model 78−39316
flame, laminar mixed-mode forced-free diffusion type, on vert. burning fuel slab 78−91033
flow, transient, two-phase, flow reversal prediction LOCA conditions 78−94811
flow calorimeter for condensable gases, low temp. and high press., design and eval. 80−37033
flow calorimeter for condensable gases, low temp. and high press., computer program prediction and exptl. data comparison 80−37034
fluid, multiphase system, vapour bubble collapse, charact. functions 78−18156
fluorobenzene(-benzene), liq. and dilute soln., microwave absorption and relax. processes 79−82920
fluoroform(-d_1)-trimethylamine-Ar(Kr), cryospectroscopic IR study of association 77−468
furfuraldehyde, liquid isomers rot. barrier and enthaply difference, US meas. 77−20016
gas mixtures containing common polar and nonpolar components 77−31417
glass making system, continuous, energy balance 80−89189
glass structure, isobaric variation, phenomenological theory *(French)* 80−59393
glasses, order parameter model, vol. and enthalpy relax. 80−88008
glasses, thermal behaviour during heating or cooling, retardation kinetics 77−4049
glutarate complexes in aqueous soln., enthalpy and entropy meas. *(Italian)* 79−19378
graph-like state of matter, LCGI schemes, expt. data statistical anal. 78−15696
graphite, pyrolytic commercial, high-temp. thermal and mech. props. 80−75372
graphite-halogen intercalation compound, calorimetric study of order disorder transform. 79−52206
graphite-HNO_3 intercalation compounds, differential scanning calorimetry investigation 79−42234
n-hexane+cyclohexone, excess enthalpy, calorimetric cell 79−58689
p,n-hexyloxybenzylideneamino-p′-chlorobenzene, liq. cryst., sp. ht. meas. 78−22831
high-pressure asymmetric mixture vapour-liquid equilibrium calc. 79−4408
HOAB, liq. cryst. phase transitions, specific ht. meas. 79−33075
hydrocarbons, heavy liq., vapour press. and enthalpies of vaporisation by group-contrib. method 80−40726
hydrocarbons, thermodynamic props., optimum incremental diagram calc. method *(German)* 78−51702
intercalation compound electrodes, thermodynamic and transport props. 80−66963
interface segregation through cooling 79−43294
intermetallic phase with B2 structure, relationship between enthalpy of form. and disorder parameter 77−7878
intermetallic phases, B2 struct., substitutional and triple defects, enthalpies of formation 80−96520
ion solvation, correlation of total and partial enthalpies, vel. to nucleation energy barrier 80−89514
ionic crystals, migration volumes calc. 80−103324
isotactic polypropylene/butene-1 copolymers, soln. grown crystals, props. 77−55247
isothermal displacement calorimeter, for positive excess enthalpies 78−89483
kaolinite, decomposition 77−52627
liquid, saturated, low press. enthalpy function, corresponding states and pseudocriticals 78−31672
liquid alloys of actinides and lanthanides, thermodynamic props. 77−55366
liquid crystals, thermal parameters, transition temps. and latent heats 78−22832
liquid mixture, adsorption on solid, equilib., thermodynamics correlations 78−84045
liquid mixture, modified Heil-Prausnitz eqn. for excess Gibbs energy 77−62652
liquid mixtures, excess enthalpy 79−23733
liquid-vapour critical region, empirical description from coexistence data 77−27973
liquids, order parameter model, vol. and enthalpy relax. 80−88008
lithium n-alkanoates, long-chain, thermal and phase props. 77−62619
lysozyme, cryst., dynamic sp. ht. capacity meas. 80−21447
metal, critical temp. determ. by exploding wires method, liquid metal enthalpy 78−6149
metal, degree of deform. effect on thermophys. props. at high temps. 78−26694

enthalpy continued
metal, first transition systems, survey of regular solution parameters 77−44220
metal, self- and impurity diffusion, connection between preexponential factor and activation enthalpy 77−69111
metal, standard free enthalpy of oxidation meas. *(French)* 79−61867
metal, thermodynamic props. of grain and phase boundaries, review *(German)* 79−34012
metal, vacancies, energy charact. *(Russian)* 77−24314
metal, vacancy formation parameters and Gruneisen constant 78−22709
metal calc. for solids and liqs. 77−43348
metal film resistor, resistance fluctuations from spontaneous enthalpy fluctuations 78−72217
metal halides, calc. for solid and liq. phases 77−43349
metal hydrides use as energy conversion media, review *(Japanese)* 80−55934
metal ions complex formation with carboxylic acids in aqueous soln. *(Italian)* 77−48669
metal-H systems, solvus line interpretation, enthalpy change 79−15655
metallic melts, three-component, enthalpies of form. *(Russian)* 79−51277
metals, heat content correlation under fast heating *(Russian)* 80−70426
metals, purification and thermodynamics, possibilities in space environment 79−46816
metals and intermetallic cmpd., monovacancy form. enthalpy 79−90649
methane-benzene (cyclohexane) vapour mixture, excess enthalpy meas. appl. of differential-flow mixing calorimeter 78−12700
1,5-methano(10)-annulene, mol. geom. and gas phase thermodynamic props., minimisation scheme 78−78829
methyl alcohol, intermol. interaction, thermodynamic parameters determ. from chem. shifts of functional groups 79−64068
micellar systems, aqueous, thermochemistry 80−61133
microemulsions, stability, high field NMR investig. *(French)* 78−27827
mixtures, perturbed hard chain theory, thermodynamic props., appls. in chem. technology 79−34343
molten salt mixtures, binary, excess thermodynamic props. and US vel. *(French)* 77−27943
multicomponent systems, phase diagrams and thermodynamic data, electrochem. determ. 80−71922
multidimensional conduction phase change problems, effect of density change, enthalpy model 77−42699
naphthalene-tetracyanobenzene, order-disorder transition, heat capacity and thermodynamic props., 5 to 300K 79−33100
natural gas mixtures, simulated, enthalpy and phase equil., correl. with modified Starling eqn. 80−61127
nematic liquid crystals, sp. ht., thermodynamic props. 77−39678
neodymium ethyl sulphate, cryst. c-axis demag. from 25000G, magnetohydrodynamic props. to 0.01K 77−20599
neodymium ethyl sulphate hydrate, spherical single crystal, magnetothermodynamic props. 77−55365
network thermodynamics with entropy stripping 78−7223
nonelectrolyte aqueous solutions, lattice model approach 79−32876
1-octanol, dielec. consts., solvent struct., effect of H bonding solutes, chain length 77−48674
cis-9-octodecenoic acid+cyclohexane excess enthalpy, calorimetric cell 79−58689
organic compounds, enthalpies and related thermodynamic functions 79−42276
organo tin dichlorides, tetrahedral, dilute soln., dielec. and thermodynamic behaviour, microwave region 77−36170
oxidation-reduction reactions in undifferentiated Earth, thermal effects 79−25218
partition coefficients, theoretical calc. of isovalent impurities with due regard for excess entropy of mixing in solid soln. and melt 79−65015
pentane, liq., enthalpy difference between rot. isomers, IR spectrosc. obs. 80−106404
PET, thermodynamic equilib. melting parameters, effect of annealing 78−71837
phenol, ideal gas thermodynamic props. 78−75250
phenylcyclohexanes, nematic, low melting liq. crysts. with positive dielec. anisotropy, phys. props. 77−43148
piezoelectric plate HF vibrations, two-dimensional eqns. 77−39143
pipeline compressible flow and heat transfer simulation program 77−19638
planetary probe shock layer thermodynamics, reduction-of-ionisation-pot. model 77−9651
plasmatron gas average enthalpy, forced heat exchange calcs. *(Russian)* 80−38724
polar compounds, liq. props. representation, by modified Redlich-Kwong eqn. of state 78−34590
polar liquids, solns., mol. rot., kinetics 77−51984
poly (trioxane), melting behaviour, simultaneous thermogravimetric and differential scanning calorimetric meas. 77−76529
polyamide-12 plasticized with sulphonamides, relaxation props. *(Russian)* 80−55031
polybutylene terephthalate, semicryst., mech. props., effect of annealing below glass temp. 77−25066
polycarbonate, glassy, temp. drop during deform. 78−15456
polycarbonate, glassy state, enthalpy relax., thermal density fluctuations 80−59678
polycarbonate, highly hot-drawn, mechanical prop. and phys. struct. changes 78−14293
polyethylene, low-density, environmental stress cracking, surfactant soln. effect 80−89376
polyethylene terephthalate, effect of excess thermodynamic props. versus struct. form. on dynamic moduli 77−86053
polymer, amorphous, enthalpy relax. rel. to T_g 77−52278
polymer glass, isobaric vol. and enthalpy recovery, transparent multiparameter theory 80−24375
polymer glasses, aged, enthalpic state determ. by scanning calorimetry 80−6528
polymer glasses, enthalpy relax., scanning calorimetry technique 80−90851
polystyrene, annealed, enthalpic retardation times 80−19959
polystyrene, atactic, effect of excess thermodynamic props. versus struct. form. on dynamic moduli 77−86053
polystyrene glasses, transition temp. and thermodynamic state 78−75819
polyvinyl acetate, struct. relax., enthalpy and elec. polarisation obs. 79−41978
porous insulation filled cavity wall, forced and free convective heat loss 77−75909

enthalpy continued
propylene, computer generated phase diagrams 78—83928
protein supramolecular structures, calorimetric and van't Hoff enthalpies of assembly comparison 77—90717
PTFE, $H_2(D_2)$ solubility and diffusion, activation enthalpy 78—79775
pure gas, enthalpy, Carlson-Thodos van der Waals eqn. calcs. 80—83878
PVC, thermodynamic props. *(German)* 77—28024
PWR fuel assembly, lumped subchannel model anal. of enthalpy transfer 79—76063
pyrolysis of solid particle, cyclic dynamics 79—47897
real gas, nonpolar, ideal eqn. of state curve features 78—1776
refractory compounds heat of formation determ. using self-propagating high-temp. synthesis 80—3392
refractory oxide, high temp. props. conf., Odeillo, France (June/July 1977) 79—100125
resistor, fluctuations in resistance and enthalpy, response to current changes 78—34871
Schiff's base compounds, double axis, Siamese Twin type liq. crysts., thermal and X-ray obs. 80—39312
Schottky defect, possibility of enthalpy decreasing with increasing temp. 80—2012
semiconductors, asymmetry in displacement energy for Frenkel-pair prod. 78—2116
shock waves in material with linear shock wave-particle vel. relation 77—69042
silicate glasses from igneous rocks, high temp. thermal props. 77—33055
sodium n-alkanoates, long-chain, thermal and phase props. 77—62619
solid, formation volume of vacancies calc. 79—19244
solid electrolytes, fabrication and props. 80—70463
solute hydrophobic interaction, mol. aggregation, free energy, entropy and enthalpy, scaled particle theory 77—84609
solute interaction energy, const. press. and const. vol. condition effects 78—38856
sonic boom, nonlinear propag., including asymm. effects, numerical soln. program 77—72326
steel, Ni-Co-C (9, 4, 0.2 wt.%) enthalpy, sp. ht. to 2000K 79—10960
stored energy, and increment in heat capacity due to plastic deform. 80—54302
superplastic flow, activation enthalpy determ. from strain rate changes in tensile tests 80—81127
TBBA, liq. cryst., metastable phase, thermodynamic props., differential scanning calorimetry meas. 78—94985
thermochemical analyser, continuous flow, high sensitivity 79—92022
thiophene- or benzene-light alcohol binary system isobaric liquid-vapour equilibrium *(Spanish)* 79—77738
thiorhodites, $M_xRh_{3-x}S_4$ (M=Cu,Co,Fe), thermal stability and thermochem. props. 79—86904
thiospinels, thermodynamic stability, enthalpy of form. 79—52737
tolualdehyde, dil. soln., dielectric relax., solid rotator phase 79—42890
transition metal alloys, binary, energy of formation 77—15341
transition metal disilicides, chem. linkage, enthalpy, above 1200K 77—90324
transition metals, liquid, thermal volume expansion, MP to BP 79—90802
s-triazine, sp.ht. 130-380K, melting enthalpy and solid-state transition 79—46812
trifluoromethane, PVT study by Burnett method 77—42949
unstable compounds, free energy of formation calcs., FORTRAN program for ternary phase equilibria. 80—10683
vacancies in crystal in temp. gradient, conc. rel. to enthalpy 80—49217
vacancy formation enthalpy measurements, via positron experiments 78—47337
vaporising coolant enthalpy for cryodevice initial cooling *(Russian)* 78—70130
water, heat of ionisation, calorimetric meas. on enthalpies of reaction of I_2O_5 79—70359
water, random network model, liq. and ice polymorphs enthalpy and heat content 80—64869
water, vap., dimerization, from thermal cond. meas., 373K 78—44359
water vapour, dissociated, thermodynamic props. *(Japanese)* 77—80263
Ag thin evaporated films, rel. between microstruct. and excess free energy, TEM 80—70427
Ag-Ge eutectic alloy, heat capacity meas. over temp. range 800-1200K *(French)* 80—88331
Ag-Pb-Te, phase equilibrium *(German)* 79—34018
AgBr, determ. of ionic transport processes 77—89578
AgBr(Cl), formation vol. of Frenkel defect 78—79606
AgCl, determ. of ionic transport processes 77—89578
AgCl-NaCl molten solns., activities and surface tension 80—10748
$AgGaTe_2$, Debye temp., standard entropies and enthalpies, sp. ht. meas. 78—30769
$AgInTe_2$, Debye temp., standard entropies and enthalpies, sp. ht. meas. 78—30769
$AgPO_3$-AgBr(Cl)(I) system glasses, soln. calorimetry obs., thermodynamic activity correl. with ionic cond. *(French)* 79—33102
$AgPO_3$-AgI glass system, solution calorimetry, enthalpy of formation *(French)* 78—64527
Ag_2Se, X-ray determ. of inclusion function 77—76559
$Ag_2Tl_6I_{10}$, one-dimensional ionic conduction 79—7707
Al alloy, calorimetric studies on 700 series, matrix precipitate charact. of 7075 77—86036
Al, self-interstitial interaction with solutes, resistivity meas. 78—47331
Al, vacancy form. enthalpy, simultaneous positron lifetime and momentum meas. 78—47335
Al, vacancy formation enthalpy, positron annihilation spectroscopy 78—67707
Al-Cu (4 wt.%), relationship between enthalpy, yield strength, and size of Guinier-Preston zone *(French)* 78—19767
Al-Ga, enthalpy of mixing, 'const. vol. alloy' formulation 79—28111
Al-Ga(Sn), ab initio calcs. of partial enthalpy and result for enthalpy of mixing 79—43197
Al-In, enthalpy of mixing, 'const. vol. alloy' formulation 79—28111
Al-Mn(Fe)(Co)(Ni), liquid alloys, thermodynamic charact. calc. *(Russian)* 78—27475
Al-Tl, enthalpy of mixing, 'const. vol. alloy' formulation 79—28111
Al-Zn (10 wt.%), ageing behaviour, calorimetric study 80—45328
Al_2O_3, alumina, adsorpt. of saturated hydrocarbons, gas-solid chromatography based on compensation effect 80—26053
α-Al_2O_3, synthetic sapphire, enthalpy determ., 900-1900K, use as calorimetry reference standard 79—42275

enthalpy continued
Ar, vapour press., entropy and enthalpy, thermodynamic consistency, two-parameter eqn. 77—80613
$Ar+Xe^+$, $XeAr^+$ form., dissoc. energy, reaction equilib. and rate consts. 80—61071
As_2Se_3 glass, heat capacity and struct. relaxation of enthalpy 77—55360
As_2Se_3-As_2Te_3, liquid, mixture enthalpies *(German)* 79—77770
$(AsSe)_{1-x}Te_x$ glasses, thermal props. and viscosity, temp. and conc. depend. 77—76324
Au, heat content between 300.05 and T (T from 400 to 1000K) drop calorimetry *(French)* 80—10682
Au-Al, liq. alloy, thermodynamic activities and enthalpies 80—19960
Au-Ni, liquid alloy system, determ. of thermodynamic props. using Knudson effusion method, phase diagram calc. *(German)* 78—51707
Au-Sn, zeta and AuSn phases, heats of form. and heat contents 80—60837
Au-Sn liquid alloys, Sn activity *(Japanese)* 78—6901
Au-Zn, liq., thermodynamic props. *(German)* 80—49386
BF_2 radical, thermomechanical studies by mass spectrometry, enthalpy of form. and ionisation pot. determ., chem. bonds 80—81382
$B_nH_n^{2-}$ anions, bond enthalpies 80—30266
BaO-B_2O_3-V_2O_5 glass, oxidation-reduction of V, thermodynamics 80—85169
$BaZrO_3$, high-temp. enthalpy and specific heat, method of mixtures 77—35712
Bas and B_6As, standard values of thermodynamic functions 77—24414
Bi_2O_3, energies of formation, solid-state electrochemical techniques 80—6527
Bi_2Se_3-Bi_2Te_3, liquid, mixture enthalpies *(German)* 79—77770
C, synthetic mats., 50-3000K 77—84942
$CaCu_5$, γ-phase in Ca-Cu system, calorimetric determ. of enthalpy of form. *(French)* 80—84915
CaF_2, association parameters of $[Me^{3+}$-$Fi^-]$ dipoles (Me=Metal), ionic cond. meas. 78—30788
CaO-MgO-SiO_2, melts, mixing enthalpy, 1700-1873K 78—79785
$CaWO_4$, cryst. growth from solns. in melts, kinetics parameters and thermodynamic props. 80—59424
Cd-In-Sb, liq. alloy, Cd thermodynamic activities, Gibbs free mixing enthalpy *(German)* 80—45279
Cd-Pb-Bi melts, enthalpies of form. *(Russian)* 79—51277
Cd-Zn-Hg alloys, liq., comp. and temp. depend. of Hg VP, activity, free energy and enthalpy *(Russian)* 77—20087
$CdAs_2$ glasses, covalently bonded, energy gap correl. with average atomisation enthalpy 77—76740
CdP_4, thermodynamic functions, 55-300K 80—34203
CdSb, thermodynamic props. 79—77767
$CdTl_2Te_4$, single and polycryst. samples, linear expansion, heat capacity and thermodynamic props. 80—103489
$CeCo_5$, adsorption and desorption charact. of H_2 *(Japanese)* 77—47667
Cl^- hydration complexes, gas phase, electrostatic calcs. 80—100055
$ClNO_2$, kinetics of thermal decomposition *(German)* 78—95924
Co-Ni interface, intrinsic interdiffusion coeffs. and activation enthalpies 77—84998
CoB, thermophysical props., 296-2000K 78—14477
$Co_{1-x}O$ single crystal of controlled stoichiometry, ^{60}Co self-diffusion 77—43369
γ-CoSe, d-electron deficit model, electrochem. meas. of free enthalpy *(French)* 78—30605
Cr, enthalpy and specific heat, empirical eqn. *(Russian)* 80—92683
$CrAl_2S_4$, thermodynamic stability, enthalpy of form. 79—52737
ϵ-Cr_2N phase, analysis of expt. results of Mills and Schwerdtfeger to yield partial enthalpy and entropy 78—52783
Cr_2S_3, enthalpy and specific heat, temp. depend. 80—54406
Cu dilute binary solid solutions, enthalpies of mixing and excess free enthalpies *(French)* 80—107427
Cu, heat content between 300.05 and T (T from 400 to 1000K) drop calorimetry *(French)* 80—10682
Cu, liq., surface tension rel. to temp., surface enthalpy, entropy 78—38912
Cu, monovacancy formation enthalpy 79—65217
Cu, self-interstitial interaction with solutes, resistivity meas. 78—47331
Cu-Al (In), eutectic systems, specific phase boundary enthalpy, calorimetric study *(German)* 79—29016
Cu-Al-Ni alloys, entropy and enthalpy of martensitic transformation, calcs. 79—43245
Cu-Ge-O, phase diagram and thermodynamics, electrochem. study 80—50617
Cu-Ni-Sn, liq. alloy, mixing enthalpies determ. using a SETARAM high temp. calorimeter *(German)* 80—44324
Cu-Sb, thermodynamic investigation 78—39750
β- Cu-Zn(47.4 wt.%), heat content between 300.05 and T (T from 400 to 1000K) drop calorimetry *(French)* 80—10682
$CuInSe_2(S_2)(Te_2)$, Debye temp., standard entropies and enthalpies, sp. ht. meas. 78—30769
CuO-Cu_2O-TiO_2, phase equilibria, thermodynamics of Cu_3TiO_4 phase 80—55374
$CuSe_2$, CuSe, Cu_3Se_2 and Cu_2Se, thermodynamic props., 298 to 420K *(Russian)* 77—69098
$Cu_xZn_{1-x}SiF_6.6H_2O$, heat capacities and thermodynamic props., 14 to 300K, cooperative Jahn-Teller transition 80—21314
D_2O, eqn. of state, up to 380°C and 1000 bar, derived functions 78—26655
D_2O, liq., ionisation const., thermodynamic props. determ., 298-523K 77—32821
D_2O, vapour, mol. association entropy and enthalpy, thermal cond. meas. 80—7777
$DyFeO_3$, thermodynamic props. 79—77771
$Dy_3Fe_5O_{12}$, thermodynamic props. 79—77771
$EuPO_4$, enthalpy and heat capacity, 298.15-1600K 77—12559
$Eu_5Sn_3S_{12}$, mag. and thermodynamic props., metamagnetism 80—60273
Fe alloys, component interaction parameters, enthalpy and mixing energy *(Russian)* 80—54382
Fe, α-, γ-, liq., thermodynamic data *(German)* 80—40328
Fe base melt, thermodynamic props. *(Russian)* 77—55363
Fe complex, bis(N,N-diethyldithiocarbamato)-iron chloride, ferromag., sp. ht. meas., 0.4-20K 78—19258
Fe, low temperature deform., strain-rate cycling and stress relaxation tests *(Japanese)* 78—52876
Fe-Al (0.069 and 0.158 wt.%), internally oxidised, low temp. deform. *(Japanese)* 78—52876

enthalpy continued
- Fe-C solid solution, volume effects on enthalpy and internal energy 78—75839
- Fe-Co, free enthalpy data, thermodynamic activity determ. at 1500K 77—59751
- Fe-Co ordered alloys, enthalpy of form. 78—48376
- Fe-Cu(-C), alloyed with graphitising elements, geometrical thermodynamics *(Russian)* 79—52261
- Fe-Mo, ferritic, thermodynamics and solubility of C and ferrite 77—36456
- Fe-Mo austenite, thermodynamics of C 77—36457
- Fe-Ni alloys, enthalpy change between $\alpha' \rightarrow \gamma$ and $\alpha \rightarrow \gamma$ transformations 80—93550
- Fe-Ni(Cu)(Al)(Si) liquid alloys, thermodynamic characts. calc. *(Russian)* 80—15264
- Fe-O, exam. of thermodynamic data, using a computer aided strategy 79—11592
- α-Fe-V, dilute alloy, Mossbauer diffusion line broadening, exponential fitting evaluation 78—52379
- FeB, thermophysical props., 296-2000K 78—14477
- $Fe_{32}Ni_{36}Cr_{14}P_{12}B_6$ metallic glass, effect of pre-ageing on glass transition temp. 80—100326
- FeS-Ni_3S_2-Cu_2 S melt, enthalpy *(Russian)* 78—95730
- Ga-alloys, thermodynamic properties 78—14480
- Ga-Te, solid and liq. alloys, thermodynamic props. 80—35567
- GaAs(Sb), high-temp. thermodynamic data and quantitative fits to liquidus line 77—63637
- Ge, entropy and enthalpy of vacancy form., comparison of theory with quenching expts. 77—11872
- Ge-Te binary glass, eutectic, DSC obs., thermodynamic and thermokinetic characts. 80—39309
- GeP, thermodynamic characts. 10-300K, interatomic bond elasticity 80—59677
- GeTe, enthalpy and specific heat, 0 to 860°C, polymorphic transitions obs. 77—43350
- H, bond energy, chem. substitution influence 80—37718
- H_2CO_3, enthalpies of ionis. 79—57284
- HCl aqueous soln., H^+ mobility, 15, 25, 40°C, up to 5000 atm 78—10207
- H_2O, vapour, mol. association entropy and enthalpy, thermal cond. meas. 80—7777
- H_2O-acetic acid, liq. mixture, thermodynamic excess functions, calorimetric meas. 77—52666
- $HO_2.H_2O(NH_3)$ complex form., ab initio calcs., min. energy configs. 77—14340
- He, supercritical, laminar free convection heat transfer, analytical study 79—23311
- He, thermodynamic props., in range 20 to 1500°C and 1 to 100 bar *(German)* 79—69266
- ^{4}He, superfluid, transient heat transport 80—10715
- HfS_2, enthalpy and specific heat, temp. depend. 80—54406
- HgTe-CdTe(ZnTe) solid solns. form., equil. vacancy conc. changes 77—43208
- $HuO_2P(As)O_4.4H_2O$, water deficiency, enthalpy of dehydration, thermogravimetric anal. 80—65251
- I, activation enthalpy of diffusion in mixed solvents 78—14492
- I^- hydration complexes, gas phase, electrostatic calcs. 80—100055
- In, measurement of enthalpy of fusion by adiabatic calorimetry 80—37037
- In-Tl liquid alloy, thermodynamic props. and struct. *(German)* 77—48400
- InAs(Sb), high temp. thermodynamic data, quantitative fits to liquidus line 77—63637
- InSb-Pb(Bi), thermodynamic prop. *(German)* 78—75847
- Ir, thermophysical props. at temps. up to 7000K 80—103497
- KCl:Sr, Ca, simultaneous diffusion, coefficients meas. 78—79813
- $KHSO_4:Fe^{3+}$, DC cond. meas., mechanism 80—65285
- K_2O-Al_2O_3 system, high temp. thermodynamics and phase equilibria 78—80521
- K_xO_y, thermodynamic props. 80—29184
- $K_2O.nB_2O_3$ (n=6, 4, 3), heat of soln. *(Japanese)* 77—77802
- Kr, vapour press., entropy and enthalpy, thermodynamic consistency, two-parameter eqn. 77—80613
- $LaBO_3$ (B=V, Cr, Mn, Fe, Co, Ni), chem. stability X-ray and thermal anal. 79—79242
- $LaCrO_3$, sp. ht., enthalpy, entropy, 298-900K, polymorphic transition 77—69094
- $LaNi_5$, adsorption and desorption charact. of H_2 *(Japanese)* 77—47667
- $LaNi_5$/H system, thermodynamics of H trapping 80—107444
- $LaNi_{5-x}Fe_x(Cr_x)$, Fe and Cr electron hydride formation, X-ray and SEM obs. *(Japanese)* 79—43202
- $La_{10}W_2O_{21}$, enthalpy and heat capacity at high temp. 80—70424
- α-La_2WO_6, enthalpy and heat capacity at high temp. 80—70424
- $La_6W_2O_{15}$, enthalpy and heat capacity at high temp. 80—70424
- Li-Pb, liq. alloy, enthalpies of mixing, calorimetric study *(German)* 80—2170
- Li-Tl(In)(Bi), liquid alloys, calorimetry study *(German)* 80—25664
- LiAl, β phase thermodynamic props., chem. diffusion coeff., electrochem. meas. 80—39308
- $LiBF_4$, thermal decomposition, equilib. decomposition press. and enthalpy of form. 79—91983
- $LiCrO_2$, evaporation, as a corrosion product in compatability experiment of Li_2O pellets with Fe-Ni-Cr alloys, mass spectrometric study 79—73301
- Li_6NBr_3, $Li_{13}N_4Br$, ionic transport 79—73336
- $Li_2O.nB_2O_3$ (n=6, 4, 3), heat of soln. *(Japanese)* 77—77802
- Mg partial molar thermodynamic data from EMF and calorimetric meas. of Mg-In liquid solns. 80—55359
- Mg-Ga system, thermodynamic props. of metastable and glassy phases *(German)* 79—52743
- $MgAl_2O_4$ spinel refractory, enthalpy and specific heat determs. 80—88334
- $MgCr_2O_4$, spinel refractory, enthalpy and specific heat determs. 80—88334
- MgO, single crysts., activation enthalpy and activation free enthalpy for creep 79—43262
- $Mg_yU_{1-y}O_{2+x}$, thermodynamics from EMF meas., high Mg conc. 78—43143
- Mn^{2+} ions, solvation enthalpies in various solvents *(French)* 79—69264
- MnP, and Mn_2P, enthalpy and heat capacity at high temp. 77—11704

enthalpy continued
- Mn_2P, heat capacity, mag. entropy and thermodynamic functions 77—80630
- Mo, standard ref. material, enthalpy and heat capacity 78—18792
- Mo, temperature standard reference material, USA National Bureau of Standards 80—47009
- MoS_2, entropy, enthalpy and specific heat, temp. depend. 500 to 1700K 80—15260
- Mos_2, enthalpy and specific heat, temp. depend. 80—54406
- N-Fe solid soln. in equilibrium with N_2 gas, partial molar enthalpy and excess entropy 80—60838
- N_2, arc jet enthalpy meas. by fast miniature total calorimetric probe 78—67486
- NH_4NO_3 aqueous solution, enthalpies of dilution and relative apparent molar enthalpies, dissociated soln. case 80—50876
- NH_4NO_3, standard enthalpy of soln. in water, standard thermodynamic state search 80—50877
- $NO^+ + 2N_2 \rightleftharpoons NO^+.N_2 + N_2$, rate const., enthalpy and bond strength 77—16809
- N_2O_4, dissociated, enthalpy, 310-782K 78—73073
- N_2O_4 dissociating coolant, O_2 generation time constant, enthalpy change *(Russian)* 78—58345
- Na thermodynamic props. for reactor safety analysis 79—13478
- Na-Ga liquid alloy, thermodynamic props. 79—37854
- Na-Sn liq. alloys, thermodynamic props. by EMF meas. with β-Al_20_3-Ba_2 electrolytes 79—19379
- Na-Te system, liq., electrochem. determ. of thermodynamic props. rel. to temp. 77—1245
- $NaAlCl_4$, relative enthalpy to 573K and standard enthalpy of form., molar enthalpy of fusion 80—50878
- NaAu(Ag), mol. dissoc. energy, third law enthalpy and heat of formation, mass spectra 78—40033
- NaCl, Schottky defect, formation enthalpy, entropy, temp. effects, correction 78—10039
- $NaCl:Pb^{2+}$, activation energy for clustering of Pb^{2+} vacancy pairs 77—72610
- NaCl-graphite interface, elec. cond. 78—52060
- NaF:Ca, migration enthalpy and entropy, TSC obs. 80—54716
- $NaNO_2$, enthalpy of soln. and dilution, obs. 78—80781
- Na_2O-SiO_2, melt, EMF meas., partial molar enthalpy and entropy 80—6525
- Na_2O-SiO_2 glass, interpretation of data 79—95183
- $Na_2O.nB_2O_3$ (n=6, 4 or 3), heats of soln. *(Japanese)* 77—77802
- $NaPO_3$, heat content between 300.05 and T (T from 400 to 1000K) drop calorimetry *(French)* 80—10682
- $NaUO_3$, ht. capacity and thermodyn. props., 5-350K 77—43343
- Nb, enthalpy and heat capacity determ. 78—71866
- Nb, liq. and solid, enthalpy meas. by levitation calorimetry 80—103499
- Nb, solute trapping of H, symmetry of O-H pair 80—108488
- Nb-Mo alloy, solubility of H_2 77—89542
- Nb-Re(Ru)-N, α-solid soln., thermodynamics *(German)* 77—12600
- NbS_2, enthalpy and specific heat, temp. depend. 80—54406
- Ne, molar volumes and thermodynamic props., 25 to 150C, up to 7 kbar 77—42957
- Ni base melt, thermodynamic props. *(Russian)* 77—55363
- Ni Ga, defect struct. 78—30608
- Ni, oxidation, diffusion enthalpy and entropy 78—7084
- Ni^{2+} ions, solvation enthalpies in various solvents *(French)* 79—69264
- Ni-Fe alloy, oxidation, diffusion enthalpy and entropy 78—7084
- Ni-In, thermodynamic props., phase diagram 77—55949
- Ni-Si liquid alloys, thermodynamic props., enthalpy of mixing *(Russian)* 80—34207
- β-NiSe, d-electron deficit model, electrochem. meas. of free enthalpy *(French)* 78—30605
- $Ni_{0.685}Zn_{0.177}Fe_{2.138}O_{4+\gamma}$, phase diagram, therm. anal. 79—78945
- Pb, positron annihilation, Doppler broadening, 4.2 to 600K 79—47540
- Pb-Ag, liquid alloy, exam. of thermodynamic props. using solid oxide galvanic cell 78—75851
- β'PbIn, thermodynamic analysis 77—36455
- PbO-GeO_2 melt, thermodynamic study 77—59760
- PbO-$PbSO_4$ system, discussion of thermodynamics of oxide-sulphate melts 79—82358
- PbO-$PbSO_4$ system, thermodynamics 79—82359
- PbO-TiO_2, solid phase reactions, thermodynamic anal. 77—12603
- PbTe, enthalpy of formation *(Russian)* 80—15267
- PbTe-SnTe, solid soln., enthalpy of formation *(Russian)* 80—15267
- Pd-Ni(Si), melt, struct. and physical-chemical props., thermodynamic props. *(Russian)* 78—18536
- Pd-Ti liquid alloy, mass spectrometric study of high temp. thermodynamic stability 78—15369
- PrF_3, heat capacity from 5 to 350K, entropy enthalpy, Planck function 79—46811
- Pt-H solid solutions, thermodynamics 79—77756
- Pu, liq., meas. using neutron heating 77—20078
- Pu-Ga (1-8.56 at.%) alloys, enthalpy sp. ht. determ. at elevated temp. 78—78458
- $PuC_{0.82(1.49)}$, high temp. enthalpies 80—49384
- $R_{1-x}Co_x$, rare earth amorphous alloys, thermal stability, elec. cond. enthalpy 80—100172
- Rb, molten, meas. in 320 to 1220K range 77—35711
- $RuTe_2$, decomposition press. and thermodynamic props. 78—3366
- Sb_2O_3, energies of formation, solid-state electrochemical techniques 80—6527
- Sb_2Se_3-Sb_2Te_3, liquid, mixture enthalpies *(German)* 79—77770
- Sc_2O_3, solid, enthalpy investig. at high temp. 80—103498
- $ScPO_4$, enthalpy and heat capacity, 298.15-1600K 77—12559
- Se, monoclinic to trigonal conversion, thermodynamic stability and associated investigs. 80—24592
- Se-Bi bilayers chemical reactions, differential scanning calorimetry technique and obs. results 78—2398
- Si, entropy and enthalpy of vacancy form., comparison of theory with quenching expts. 77—11872
- Si:P, doping element incorporation, temp. depend. in CVD epitaxy 80—45234
- Si-Mn(Fe)(Co)(Ni), liquid alloys, thermodynamic charact. calc. *(Russian)* 78—27475
- β-SiC, thermodynamic props., temp. depend., 5 to 300K 80—96666
- SiO_2 glass, densified, enthalpy variation, heat of dissolution obs. *(French)* 79—34015
- SiP, thermodynamic characts. 10-300K, interatomic bond elasticity 80—59677

enthalpy continued
- $SmCo_5$, adsorption and desorption charact. of H_2 *(Japanese)* 77–47667
- SmO, dissoc. energy, mass spectrometric determ., rel. to EuO 77–58199
- Sm_2WO_6 and $Sm_{14}W_4O_{33}$, high-temp. enthalpy and specific heat 80–34205
- Sn, thermally induced vacancies, positron trapping 80–89083
- Sn-Pb alloys, stress relaxation and activation enthalpy 79–74190
- Sn-Te liquid alloy, thermodynamic meas. 77–73271
- SnTe, enthalpy of formation *(Russian)* 80–15267
- $SrCl_2$, anion diffusion mechanism 80–2201
- $SrWO_4$ cryst. growth, from Na_2WO_4 melts, thermodynamic props. 80–107084
- $SrZrO_3$, high-temp. enthalpy and specific heat, method of mixtures 77–35712
- Ta, 2400 to 3270K, mass calorimetry meas. *(Russian)* 77–66031
- TaS_2, enthalpy and specific heat, temp. depend. 80–54406
- Te, and heat capacity, 0 to 750°C 77–11705
- Th-Mo(Re), high temp. phase diagram, thermodynamic props. of refractory metal solutes in liquid Th 77–25022
- ThC_n(n=1 to 6), Knudsen effusion mass spectrometric investigations, enthalpies and heat of formation calcs. 80–66858
- Ti-Cu system, appl. of metal-hydrogen equilibration determ. thermodynamic props. 79–77772
- Ti-Ir system, high temp. thermodynamic investig. of Ir-rich portion by Knudsen cell mass spectrometry 77–12595
- Ti-O system, O/Ti<1, high-temp. thermodynamics using Tian-Calvet microcalorimetry 78–85190
- $TiCr_{1.8}$, H and D soln., enthalpy, solubility and mol. vibr. determ., comparison with soln. in metals and binary alloys 80–79951
- TiCu intermetallic compounds, decomposition reaction by H_2 absorption *(Japanese)* 78–23668
- TiO_2 polymorphs, transform. enthalpy 79–100131
- TiO_2, slightly reduced rutile, diffusion of Ti 78–79799
- Ti_3O_5-V; semicond.-metal transition, resist., enthalpy and mag. susceptibility changes obs. 77–62965
- TiS, vaporisation chemistry and thermodynamics, computer-automated simultaneous Knudsen-torsion effusion 80–48837
- TlCl(Cl_2), vap. press. and thermodynamics 80–6503
- TlH_2PO_4, thermodynamics props. of solid phase transitions, heat capacity 79–10966
- $(U,Pu)O_{2\pm x}$, cluster model approach to thermodynamic props. 77–20093
- U, liq., meas. using neutron heating 77–20078
- U-Mo(Re), high temp. phase diagram, thermodynamic props. of refractory metal solutes in liquid U 77–25022
- U(C,N), N vapour pressures and thermodyanmic props. 80–84918
- UC_x, partial molar thermodynamic quantities, semi-invariant cumulants method 80–65250
- UH_3, UD_3, dissoc., isotope effect 80–26174
- UN, N vapour pressures and thermodynamic props. 80–84918
- UO_2, electronic struct. contribs. to excess enthalpy at 3000K and in liq. phase 80–15265
- U_3O_8, λ-type heat capacity anomalies 77–20080
- U_4O_{9-y}, doped, phase transitions, heat capacity meas. 77–18664
- $UO_2F_2(Cl_2)(Br_2)$, high temp. enthalpy increments and thermodynamic functions 80–29189
- $(U_{0.8}Pu_{0.2})C$, enthalpy, 1039 to 2421K 77–74920
- U_3Si, heat capacity and thermodynamic props., 1 to 1203K 77–72697
- V, enthalpy and heat capacity determ. 78–71866
- V, thermophysical props. at temps. up to 7000K 80–103497
- V-Cr alloys, absorption of H_2, thermodynamic parameters 78–87862
- V_2S_3, enthalpy and specific heat, temp. depend. 80–54406
- V_3S_4-V_5S_8 system, exam. of thermodynamic props. at temp. from 650 to 800°C 78–52784
- $V_xW_{1-x}O_2$, phase relations, vacuum seal study and DTA obs. 79–100122
- W, meas. in 1500-2800K range using calorimeter *(French)* 77–13754
- W, relative enthalpy, 273 to 1173K, electronic heat capacity coeff. 80–103496
- W, vacancies, quenching and recovery invest., resist. and TEM study 80–39074
- W_aBr_b, enthalpy determ. by mass spectroscopy 78–11584
- WO_aBr_b, enthalpy determ. by mass spectroscopy 78–11584
- Xe, vapour press., entropy and enthalpy, thermodynamic consistency, two-parameter eqn. 77–80613
- Y-Ni, liquid alloys, enthalpy struct. *(Russian)* 78–27474
- Y_2O_3, calorimetric meas. of enthalpy, heat of fusion, heat of high temp. phase transition 77–28020
- ZnAl (18.75 wt.%), supercooling phase β break up kinetics *(Polish)* 80–25654
- $ZnAl_2S_4$ and $ZnCr_2S_4$, thermodynamic stability, enthalpy of form. 79–52737
- $Zn_3(OH)_4(NO_3)_2$, sp. ht., 5-300K, thermodynamic props. 79–55900
- $Zn(OH)(NO)_3.H_2O$, sp. ht., 5-300K, thermodynamic props. 79–55900
- $Zn_5(OH)_8(NO_3)_2.2H_2O$, sp. ht., 5-300K, thermodynamic props. 79–55900
- Zr-Nb (1 wt.%), tensile props., 295 to 773K 79–8318
- $Zr(HPO_4)_2$, amorphous, crystalline, enthalpy of formation 80–6518
- ZrI_4, high-temp. enthalpy, X-ray powder diffr. data 80–107446
- ZrI_4, thermodynamics of vaporisation and high temp. enthalpy 78–91432
- ZrN, in homogeneity range, high-temp. thermodynamic characts. 77–77464
- ZrO_2, enthalpy and heat capacity at 1100-2500K 80–103472

entropy
- *see also entropy of substances*
- a-Entropy for generalized observables 79–71389
- a-entropy for spectrally absolutely continuous observables 79–54087
- adsorbed monolayer, vibr. contrib. to thermodynamic props. *(French)* 77–4261
- adsorbed multicentre particles, configuraional and entropy and blocking coeff. 77–60118
- adsorption thermodynamics, symmetrical, case of noninert adsorbent 80–80059
- alloys, concentrated, excess vibr. entropy and local environment effects 77–76498
- anisotropic solids with magnetic symm., unified dynamic theory 78–77713
- antiferromagnet, 3-dimens. Ising model, with finite entropy at zero temp. 77–40021

entropy continued
- antiferromagnetic Ising lattice, degeneracy at crit. mag. field and zero temp. 79–8007
- Baierlein's entropy theorem, limitation on quantum-mechanical extension 77–83
- Belousov-Zhabotinskii reaction, chaotic oscills. 79–5151
- Bianchi type-I universe, entropy per particle in early stage 77–17732
- Bianchi type-I universes, entropy prod. and viscous dissipation 78–8179
- binary system, isobaric and isothermal phase transform., exchange processes, entropy meas. *(German)* 80–90798
- bioenergetics, entropy changes 80–3609
- biological intracellular energy transform., phys. aspects 77–86462
- biological systems, entropy of fluctuations, time evolution, NMR obs. 79–53017
- biomolecules+chloranil, charge transfer interaction, equilib. const., enthalpy and entropy determ., mol. polarisability 80–89708
- black hole entropy, sense or not 80–52092
- black hole thermodynamics and entropy 80–4613
- black holes, primordial, entropy generation in evaporation *(Russian)* 77–22266
- body oscillating in supersonic stream, entropy and total energy 79–86456
- Boltzmann's theorem 79–40459
- Boltzmann distribution in the distribution limit, maximisation of entropy of degree β *(Italian)* 79–93083
- Boltzmann-Gibbs-Shannon generalised entropy, unique characterisation 77–5747
- Bose lattice gas, statistical systems with well defined entropy 79–30395
- Brownian motion, new term in stochastic calculation, in terms of excess entropy 79–67227
- Brownian motion and NMR spin relax., book 78–15054
- bures distance and relative entropy 80–84
- calculation with computer simulation 77–22504
- caloric function derivation for liquids and gases 80–13017
- Carleman model, increase of entropy 79–80558
- Carnot cycle, systematics at positive and negative Kelvin temps. 80–42178
- cavity, single-mode photon emission/radiation, Gibbs vs. information theoretic entropies 78–16765
- characterisation by generalised probability distribution 78–6163
- charged droplets metastable state *(Czech)* 78–86231
- chemical equilibrium, entropy gradient, heuristic approach 79–48991
- chemical impurities, entropy and enthalpy of solution 78–51691
- chemical local equilibrium, chemical affinity, theory 77–12823
- chemical reaction kinetics, mixing entropy for activation barrier 78–19993
- chemisorption kinetics, power adsorption isotherm, entropy correction 80–40734
- classical entropy, relationship with quantum-mechanical entropy 80–73298
- classical spins, linear chain, with random Dzyaloshinski-Moriya interactions, exactly soluble model 79–61118
- classical statistical mechanics, entropy definition for arbitrary phase space densities 79–63185
- clusters of atoms, phase transitions, thermodynamics calcs. 77–59096
- coherent radiation beams, thermodynamic processes 78–32752
- collision processes, information theoretic maximal entropy theory, rel. to scatt. theory 78–81888
- collisional entropy production, classical theory 79–10162
- commuting macro-observables, entropy conserving eqns. 79–44855
- complex molecular systems, collision phenomena by stochastic model, observables distribs. and information entropy 78–25640
- complixity and time in physics *(Chinese)* 80–81285
- composite system approach to thermodynamic stability 79–12752
- concavity of quantum mechanical or classical entropy 80–27158
- conductors, rigid, thermodynamic anal., hyperbolic heat conduction eqn. 80–64334
- continuous boson system, entropy density of quasifree states 79–142
- continuous distribution based on non-standard anal., new definition 80–82736
- continuous quantum systems, variational principle for pressure, entropy, free energy, convexity consequences 79–40453
- continuum physics axioms and entropy concept *(French, English)* 80–8941
- continuum thermodynamics, entropy and hidden variables 77–33963
- continuum thermodynamics, objection to entropy as primitive concept 78–12659
- correlated disorder in 1-D system at 0K 77–16022
- cosmological baryon excess, finite temp. gauge theory effects, entropy 80–51933
- cosmological fluctuations, spontaneous prod. 80–94902
- cosmological fluid, viscous phenomena and entropy in early universe 77–82337
- cosmology, entropy prod. in very early universe 78–32624
- cosmology, shock damping and entropy prod. in relativistic simple waves 77–17725
- critical binary mixture, entropy fluctuations, light beating spectroscopy 77–10119
- crystal growth from solution, mechanism role of solvent-solute interactions, surface entropy factor 77–24281
- crystal model teaching aid *(Hungarian)* 77–64906
- crystallisation, percolation theory, Lindemann melting criterion and thermodynamic props. 79–28081
- cybernetic-thermodynamic and mathematical approaches *(French)* 77–5787
- Davies model of heat cond., entropy prod. in open quantum systems 79–88899
- defects, or inhomogenities, entropy of formation equation validity 80–79960
- definitions of entropy by Boltzmann and Clausius, reversible processes 77–10
- dense fluids, kinetic theory, entropy abalance eqn. and irreversible thermodynamics 79–94758
- dense hard core system, transport coeffs., entropy 77–62656
- density matrices convergence and entropy 77–30046
- density matrices with continuous entropy for quantum mechanical system 80–13024
- density matrix calc. of entropy 78–62148
- density matrix entropy, definition with respect to observable 78–45586
- deterministic dynamics to probabilistic descriptions 80–68029

entropy continued
- diffusion potential, concept. rel. to Maxwell's eqns. and irreversible thermodynamics 79−63171
- diffusion with wave fronts, definition *(French)* 77−67386
- dimensionless entropies, simplification of thermodynamic calcs. 80−13019
- dipole relaxation in electric field, teaching 80−90625
- discontinuous systems, time depend. of entropy prod., stationary states 78−61043
- discrete Markov system 79−17340
- discrete systems, fundamentals of dissipation inequalities 80−27251
- disequilibrium theory applied to two-spin Glauber model 80−31669
- dislocation motion, activation entropy, computation 80−39083
- dislocations and melting in two and three dimensions 80−103454
- disorder parameter, phase transition theory, rel. to entropy 80−52146
- disordered and amorphous mag. materials, position entropy solids, exchange and anisotropy noise 79−11295
- dissipation inequality fundamentals, field formulation, continuous systems case 80−36960
- dynamical theory of irreversible processes and the microscopic interpretation of nonequilibrium entropy 79−30402
- early Universe, inhomogeneity and origin of entropy 80−62350
- education, Brownian motion, melting, surface tension and rubber networks, thermodynamic anal. 80−73132
- education, geometrical analogy for the formal definition of entropy 80−51990
- efficiency and existence of entropy in classical thermodynamics 78−54324
- elastic materials, non-hyperelastic, thermodynamic behaviour, mathematical model 80−73290
- elastic media, dissipative, relativistic electrodynamics 80−73219
- electrical circuit, slowly modulated dissipative steady state, dQ=TdS far from equilib. 78−81934
- electrode systems, nonequilib. polaris. states props. overvoltage theory, in book, for teachers 78−8205
- EM classical single-mode fields with given degrees of coherence, max. entropy 78−50697
- ensemble density matrix form., with off-diagonal (coherent) constraints 77−74314
- ensemble of max. entropy, formula derivation 77−33930
- enthalpy-entropy compensation effect, separation of chemical from statistical effects 77−21412
- enthalpy-entropy compensation effect, statistical analysis, van't Hoff and Arrhenius data 77−21411
- entropic uncertainty relation from quantum mechs. state function 78−21009
- Euler flow in two dimensions, periodic, construction of stationary measures 79−93085
- excess enthalpy and excess entropy functions derivation by direct method from TX phase diagram, heats of mixing calc. 80−75366
- existence for elastic systems, efficiency of cyclic processes 77−57290
- ferrite, two-sublattice, thermodynamic functions in mag. field *(Russian)* 77−32197
- ferroelectric ice model, triangular lattice 77−82463
- fission reactor neutron gas, nonequilibrium thermodynamics *(Japanese)* 78−62595
- fluid, multiphase system, vapour bubble collapse, charact. functions 78−18156
- fluid, simple, thermodynamic props. in hard-sphere reference system 77−76575
- fluid, with anisotropic spatially inhomogeneous viscosity, frictional force and torque 79−37367
- fluid mixture, unified theory of dynamics and thermodynamics *(Japanese)* 78−8244
- fluids, classical, linear irreversible thermodynamics, derivation 79−2740
- fluids, polarisable and magnetisable, thermodynamic theory in electromag. EM fields 77−57291
- fluids interacting with Kihara potential, thermodynamic props. using cell theory with holes *(Spanish)* 77−72400
- fluvial geomorphology, entropy concepts reevaluation 80−12453
- flux, theorem for justification of generally postulated form *(French)* 77−13720
- flux, theory *(French)* 77−57293
- flux equations, heat of transport and heat of soln. 79−99323
- fracture, rupture time, entropy criterion estimate 80−55535
- fracture initiation, numerical anal. 77−75861
- freezing, first principles order-parameter theory 79−77718
- Freidrichs model, Lyapunov function evaluation 78−73876
- function space entropy density, diffusion induced, Onsager-Machlup function 79−17375
- fundamental convective heat transfer, entropy generation 80−38411
- fusion of liquids with spherical- and linear-like mols. 79−82318
- Ganymede image restoration by maximum entropy method 77−60624
- gas, monatomic, time average problem, statistical entropy change over constant energy path 80−68123
- gas, quantum square-well pot. gas, low-temp. 79−55443
- gas flows, entropy prod. determ. using Boltzmann's H-theorem, Knudsen effusion 80−106867
- gas mixtures containing common polar and nonpolar components 77−31417
- gas system entropy waves dissipation, power plant appl. 80−19395
- gaseous diffusion in stressed thermoelastic solid, thermodynamic struct. 78−51065
- gaseous univalent ions, solvation entropy, one-layer continuum model 79−47959
- gases, ideal, entropy of mixing, Gibbs paradox, indistinguishability 80−57226
- general props. review of implications in statistical mechanics 78−73955
- generalised, basic props. 77−5746
- generalized Liouville equation, entropy, and dynamic systems containing limit cycles 79−21648
- generation, heat transfer augmentation techniques 80−79118
- Gibbs adsorption equation, phenomenological interface theory 79−23834
- Gibbs eqn., generalised, second-order fluids 80−24331
- Gibbs equation, generalised, heat fluctuations 79−76940
- Gibbs mixing entropy paradox, quantum gases 78−49588
- Gibbsian Distribution on the Lorenz attractor, 1-dimens. Ising model representation 79−97331
- glutarate complexes in aqueous soln., enthalpy and entropy meas. *(Italian)* 79−19378
- grand canonical ensemble, entropy function representation 77−74306

entropy continued
- granular materials, shear deformation, entropy model 80−84233
- granular materials, thermoelasticity theory 80−42066
- granular materials flow, micropolar continuum theory 79−35565
- gravitation and entropy prod. 78−12638
- gravothermal catastrophe and negative specific heat of self-gravitating systems 78−93593
- ground-state entropy and algebraic order at low temperatures 80−86234
- H-theorem for the (modified) nonlinear Enskog equation 79−60242
- hard hexagon model, site entropy 80−42152
- hard-sphere fluid, modified nonlinear Enskog eqn., entropy function 78−63526
- heat engine, quantum open system model 79−44894
- heat engines, minimum entropy prod. and optimisation 80−85297
- Heisenberg ferromagnets, entropy 79−65635
- high spin/low spin transition, model including lattice dynamics 77−63202
- homogeneous cosmological models, entropy prod., viscous damping of anisotropy, Bianchi type-I spaces 78−49572
- hot Universe perturbations, primordial struct. evol. 80−105411
- Hubbard model, cluster-variation method in two-site approx. at high temp. 80−7071
- Hubbard model, single band with infinite repulsion on 2×2×2 lattice, thermodynamic props. 79−87225
- Hubbard model, two-point doubly degenerate in half-filled case, thermodynamics 77−4492
- hypersonic two-dimens. flow behind compression shock, entropy layer 78−1691
- image restoration with max. entropy, entropy expression 78−42283
- imaging system fundamental limits and degrees of freedom 77−50630
- increase principle, collection of thermally interacting systems, for teachers 77−33785
- information, irreversibility and statistical equilib. 77−2603
- information entropy, and law of large numbers, opacity of statistics *(French)* 80−73288
- information measures and thermodynamic criteria of motion 80−8947
- information of comparison under generalized additivity and non-additivity 79−85105
- information process mathematical and thermodynamic aspects *(French)* 77−5789
- information theoretic approach, exptl. and inherent uncertainties 80−82733
- information theory of measurement systems, construction using concept of entropy 79−93088
- information uncertainty 79−40506
- inhomogeneous medium, effective cond., iteration series and variational estimates, Herring method 80−70663
- interacting quantum gas, nonequilibrium entropy, low-density approx. 79−21684
- interfaces of two bulk phases, non-equilibrium thermodynamics including EM effects 80−13021
- interfacial entropy, elec. and mag. interfacial polarisation *(French)* 79−7050
- interfacial systems, entropy prod. at surface, nonequilib. thermodynamics 77−33966
- intergalactic hot gas in clusters of galaxy, temp. and entropy 80−17660
- internal stress fields caused by lattice defects, entropy 80−39067
- invariant transforms. of entropy prod., extended irreversible thermodynamics 80−73293
- inversion problems, information theoretical approach 80−27210
- ion+molecule, entropy change, enthalpy of form., equilib. consts., thermochemistry 80−30233
- ion beam as drifting gas, cf. optical approach 79−31788
- ionic solvation, electrostatic free energy, multilayered continuum model 79−57282
- irreversible entropy change, detailed imbalance of stochastic process 77−49700
- irreversible thermodynamics, coupling and uncoupling of forces 79−58664
- isentropic explosion compression of matter, profiling of explosion shock waves 77−56228
- isentropic explosion compression of matter nonhomogeneous transition layer for shock wave profiling 77−56229
- Ising 2D regular model, frustration effects 80−39784
- Ising model, bond random, ferromagnetic-antiferromag. mixture, triangular cactus tree, statistical theory 80−75702
- Ising model, disordered, thermodynamic pot., ferro-and antiferromagnetic bonds, mag. moment and entropy *(Russian)* 79−19714
- Ising model, Toulouse frustration effect 79−24167
- Ising spin glass, Sherrington Kirkpatrick model, entropy calc. 80−20411
- Ising spin systems with random bonds, thermodynamic props. at low temp. 79−28532
- Ising spins randomly located, with oscillatory exchange interactions 79−42778
- Ising system with S=1, thermodynamics, uniaxial anisotropy 79−49173
- Ising systems, frustrated, interface entropy, phase transitions 79−19711
- isothermal bulk relaxation, entropy production monotonicity 77−68097
- isotropic elastic-plastic materials, thermodynamic theory, global entropy inequality 80−1436
- isotropic materials, differential type, entropy flux *(French)* 77−14887
- K-entropy, non-equilib. quantum statistical mechanics, stochastic transport processes 77−5749
- kinetic theory of dense fluids, derivation, transport coeffs., soln. of kinetic eqn. by moment method 79−54032
- Kolmogorov entropy, dynamical system phase space trajectory divergence, numerical anal. 77−26149
- Kolmogorov entropy, quantum generalisation 78−86232
- Kolmogorov entropy as a disorder parameter, heuristic approach 79−35654
- LA fluctuations in solids, polarisation of scattered light 77−81113
- laser model, stochastic, entropy and stability 79−50279
- laser theory, statistical mechanics of open systems *(Japanese)* 79−76658
- laser theory, statistical mechanics of open systems *(Japanese)* 79−76659
- lattice, gas, entropy and phase transitions in partially ordered sets 78−77808
- lattice gas, phase transition on partial orders, entropy 79−63158
- light scattering by dielectric particles, statistical theory 80−32913
- liquid, simple, transport coeffs. and internal energy relation, hard sphere model 77−76284

entropy continued
liquid, viscosity temp. var., ratio of viscous flow energy to vaporisation energy 77—31793
liquid, viscous flow mechanism, Ree Eyring theory extension 77—31794
liquid alloys, binary, ab initio calcs. 77—47599
liquid crystal, orienting action of US related to theorem of min. entropy prod. 79—77498
liquid crystals, mean field theory of model anisotropic pot. of rank >2 79—60268
liquid mixture, modified Heil-Prausnitz eqn. for excess Gibbs energy 77—62652
liquid mixtures, combinatorial entropy, lattice model expressions 80—31693
liquid-vapour critical region, empirical description from coexistence data 77—27973
living systems, thermodynamic, informational and structural entropies *(Russian)* 79—20511
local equilibrium hypothesis extension 80—27249
Lorentzian shape, deduction from maximum entropy principle 78—21056
Lyapunov characteristic numbers and Kolmogorov entropy of a four-dimensional mapping 80—46978
Lyapunov variable, entropy and meas. in quantum mechs. 80—77739
macromolecular configurational entropic force, Brownian motion entropy calc. 77—34791
macrostructural nonequilibrium entropy *(Russian)* 78—77826
magnetic Stirling cycles, new appl. for mag. materials 77—85450
magnetofluid, self-gravitating, local behaviour of congruences 78—89384
many worlds cosmology, entropy per baryon 77—53714
many-particle systems, distrib. functions and thermodynamic functions 77—57273
master operators, with extremal entropy prod. 79—2714
material with internal variables, condition equivalent to existence of non-equilibrium entropy and temp. 79—44890
maximal entropy distrib. determ., using variational technique with Lagrange multipliers 78—24754
maximal entropy distribution subject to constraints, algorithm 79—49183
maximisation, chemically organising effects 77—26107
maximisation controversy, for teaching 79—58477
maximum entropy histograms 77—78961
maximum entropy principle anal., relative freq. reln. and appls. 78—73948
maximum entropy spectral estimation of frequency and arrival angle 80—96129
Maxwell demon and correspondence between information and entropy 80—86241
Maxwell-Boltzmann statistical distrib. function of ideal gaseous assembly 80—17858
measure definition from oriented graph complexity 77—71176
measure of degree of material organisation using information quantity based on entropy *(Polish)* 80—57232
melting curve maximum phenomenon, computer simulation using two species soft core model 78—6146
metabolism, energy conservation 77—81459
metallic glasses, flow behaviour, entropy model 77—24345
metals under stress, thermally and radiation induced creep, constitutive relns. 77—90413
meteors, nonequilibrium thermodynamic model 80—4308
microemulsions, stability, high field NMR investig. *(French)* 78—27827
micropolar fluids, thermodynamical aspects, non-linear approach 80—105598
micropolar thermoelastic solids, entropy inequality and accel. waves 78—47538
Migdal-like approximation, quantum spin systems 80—34649
minimum entropy production, principle formulation 80—13018
mixing and entropy 79—71348
mixtures, simple, non-equilib. thermodynamics 80—76543
mixtures of interacting continua, thermodynamics and nature of 2nd law 79—26016
molecular liquids and solids, dissipation functions, conservation laws 77—45817
molecular model *(Hungarian)* 77—64903
molecular relaxation in entropy and macroscopic disequilibrium, isothermal vibr. relax. 77—6896
molecular relaxation in entropy macroscopic disequilibrium, Markovian relax. 77—14539
molecular scattering angular distrib. information content, angular entropy 77—54583
molecules, without internal rot., ground state heat capacity and entropy MINDO/3 calc. 78—33450
multicomponent systems, phase diagrams and thermodynamic data, electrochem. determ. 80—71922
multiple choice examination, entropy state and evaluation of understanding 79—58457
multispectral images, region extraction and classification by entropy index 79—58130
muscle thermodynamic cycles, temp.-entropic relations 79—53049
N-body generalised entropy, time derivatives calcs. 77—5781
N-boson system, generalised entropy, time derivatives calcs. 77—5781
N-fermion system, generalised entropy, time derivatives calcs. 77—5781
network thermodynamics with entropy stripping 78—7223
neural signal space entropy, neurodynamic basis of Weber's and Steven's laws 77—73516
neutron gas, highly rarefied, non-equilibrium thermodynamics under creative and destructive reactions 79—12747
neutron gas system in stationary power reactor with decoupling thermodynamics and distrib. function 80—86950
non-equilibrium thermodynamics, De Donder-Meixner transformations 80—8944
non-equilibrium thermodynamics of continuous media 80—8943
non-Hamiltonian perturbations, reduced distrib. functions and entropy prod. 77—9950
non-increasing entropy on quantum logic 77—17850
non-Markovian quantum stochastic processes and their entropy 79—49163
non-Newtonian fluid, creeping flow, variational principles, entropy prod. 77—75946
non-stationary thermodynamics of polarisable and magnetisable dissipative fluid media 80—47002
nonelectrolyte aqueous solutions, lattice model approach 79—32876
nonequilibrium, Lyapunov variables, ergodic props. of classical systems 79—2739
entropy continued
nonequilibrium entropy and symmetry principle of transport coefficients 79—21683
nonequilibrium expressions for entropy, thermodynamic quantities, using density series expansion 78—8371
nonequilibrium steady states 79—6068
nonequilibrium thermodynamics, stochastic measures 80—86240
nonisothermal system, equilib. distribs. and detailed balance relations 79—36737
nonlinear mechanics eqns. and entropy growth across a shock, symmetric form 80—69705
nonlinear response of a system in connection with entropy maximum 80—95047
nonprobabilistic measures of information with biological applications *(French)* 77—9160
nuclear spin thermodynamics 80—54964
observable in Hilbert space, continuity props. of entropy 77—60970
one particle distributions, entropy bounds 80—62607
one-dimensional classical spin chain with random interactions, exact calcs. 79—4687
one-dimensional disordered system withshort-range order, struct. and model and config. entropy 77—80422
open system, stochastic model, entropy prod. 78—4574
operational statistics and quantum logic 80—17903
optical instabilities from the entropy production point of view 79—80560
optical systems, entropy and neguentropy *(French)* 80—102608
Ott relativistic temperature variation, comment on derivation 80—86084
parametric linear systems, time delays, optimality, control coordination and entropy *(French)* 77—9161
partition coefficients, theoretical calc. of isovalent impurities with due regard for excess entropy of mixing in solid soln. and melt 79—65015
perfect gas, with finite particle number, metric entropy as function of energy 79—17326
perfect gas model *(Hungarian)* 77—64904
phase transitions, first-order, finite-size rounding rel. to entropy, system size 80—59623
photoluminescent crystal, minimum entropy prod. rel. to the dynamical behaviour of trapped electrons *(French)* 77—77263
photoluminescent crystal trap depths, appl. of thermodynamics of single particle *(French)* 77—77264
photosynthesis, balance of entropy 79—92181
plasma, ordered motion in ring, mag. field effect, decreasing entropy 78—59553
plasma, prod. by anomalous drift wave transport 78—75263
plasma, relativistic Boltzmann theory, entropy production, reference frame 78—22547
plasma-beam system, entropy theorem and plasma waves spontaneous emission 78—69677
plastic deformation, steady-state, irreversible thermodynamic description 78—72831
plastic material, Muller's entropy principle restrictions on constitutive eqns. *(Japanese)* 78—9578
point mass in plane convex region, stochastic transition and entropy 78—54288
polymer attached to surface, dynamics, bead and spring model 78—75931
polymer globule elasticity 77—70404
polymer solutions, conc., Adam-Gibbs theory, for viscoelasticity and glass transition 78—83353
polytype relative stabilities, entropy contribs. 80—100197
press. by Monte Carlo computer simulation 78—4564
probability distrib. of discrete scheme, maximisation of entropy of degree β *(Italian)* 79—93082
production, effect of electrochem. processes 79—70330
production deceleration, hydrodynamical eqns. 78—93094
quantum amount of information and maximum work 79—63142
quantum coherence effects and the second law of thermodynamics 79—6025
quantum crystal, ground-state lattice vacancies and Bose-Einstein condensation 77—7943
quantum dynamical semigroups, entropy prod. 78—57883
quantum information theory, comments on recent studies 77—17851
quantum irreversible kinetic eqn. for strongly interacting system, increasing entropy 78—54300
quantum lattice, conditional entropy in microcanonical ensemble 79—80555
quantum nonlinear reversible dynamical evolution, entropy and superposition 77—60961
quantum numbers, uncertainty, min. entropy and discrete spacetime 77—87659
quantum state entropy using covariant and contravariant symbols 80—52068
quantum statistical thermodynamics, rigorous information theoretic derivation 77—74338
quantum systems undergoing time evolution 77—30051
radiation entropy and its role during photosynthesis 80—108858
radiation entropy estimation by weight functions 78—408
radiative equilibrium, entropy variation 79—98599
radioactive contamination in aquatic organisms, evaluation by statistical and information theory 78—53535
radiographic granularity, of screen-film systems, assessment by entropy method 80—98070
radiographic images, evaluation by entropy, appl. to development process 79—12914
random EM wave field, anal. by maximum entropy method *(French)* 79—68926
random exchange Heisenberg antiferromagnetic chain, exchange-coupled pair model 80—20423
random spin systems, non-analyticity of entropy and Nernst's law 78—2692
random-bond Ising chain, entropy, depend. on temp. and mag. field 79—1679
random-bond Ising chain, ground-state energy, magnetostriction and zero-point entropy calcs. 79—7957
Rayleigh gas, irreversible processes, generalisation to non-equilib. systems *(Russian)* 78—54329
reacting reversible small bimolecular systems, numerical anal. of statistical functions 78—64831
relative entropy, information-theoretic discussion 79—71360
relative entropy and Wigner-Yanase-Dyson-Lieb concavity in interpolation theory 77—49580

entropy continued
- relativistic EM fluid flows, geometry 79–58601
- relativistic kinetic theory, scalar proper time and vectorial relativistic entropy 77–22461
- relativistic scalar entropy in Robertson-Walker universes 79–62939
- relativistic self inductive fluids, stress energy tensor and entropy generation 79–18975
- relativistic thermodynamics, entropy law 78–8373
- relativistic thermodynamics of chemically reacting fluids 79–64801
- resonance fluorescence, detailed balance, Lyapunov stability and entropy 79–13941
- reticulocyte blood count data analysis by maximum entropy spectral estimate 77–78017
- role in information theory *(French)* 80–27247
- rubber model *(Hungarian)* 77–64905
- Schottky defect, possibility of enthalpy decreasing with increasing temp. 80–2012
- second law, according to principle of max. entropy prod. *(German)* 77–65016
- second principle, Clausius-Planck inequality as local formulation 78–45585
- second-order constitutive equations of hydrodynamics, dynamical interpret. 80–36860
- Segal entropy, characterization in W algorithm 79–17378
- Segal entropy and principle of least interference 77–79043
- self-gravitating system of N parallel plane sheets, Kolmogorov entropy 79–80562
- sensory processes, information received by receptors 77–73521
- shock wave, plane, magnetogasdynamic, variable strength 79–98813
- simple metal, liquid, entropies and struct. factors 77–7656
- smectic C phase and smectic C-smectic A transition, induced dipole model 79–90527
- soft discs, two-dimens. melting, phase transition boundary 80–96629
- solid, entropy of solubility of substitutional impurities 77–4202
- solidification, stability analysis, interfacial surface entropy effect in heat balance 78–26464
- solids, polarisable and magnetisable, theory of in electromag. fields 77–57291
- solute hydrophobic interaction, mol. aggregation, free energy, entropy and enthalpy, scaled particle theory 77–84609
- sonic boom, nonlinear propag., including asymm. effects, numerical soln. program 77–72326
- special relativistic implications 80–47003
- spectra search systems, computer-aided, efficiency eval. using information theory *(German)* 80–37003
- spectral entropy method for distinguishing regular and irregular motion of Hamiltonian systems 80–4629
- spin glass, exchange energy, residual entropy and number of minima *(French)* 77–66322
- spin glass, Sherrington-Kirkpatrick model, thermodynamic props. 79–51797
- spin relaxation and linear irreversible processes, role of entropy prod. 77–20678
- spin wave parametric excitation, stochastic auto-oscills., Kolmogorov entropy *(Russian)* 80–75749
- stars, rotating Newtonian, specific entropy distrib. rel. to secular instability 78–53922
- stars, struct. eqns. for given entropy distrib. 79–66993
- statistical entropy, and law of large numbers, opacity of statistics *(French)* 80–73288
- statistical interference as maximal entropy state 77–61040
- statistical mechanics, entropy, information theory *(French)* 79–63178
- stellar clusters equilibrium statistical mechanics, steepest-descent technique 77–45496
- stellar degenerate C core, entropy rel. to collapse triggering by thermonuclear burning 78–65608
- sticking condition for fluid at solid boundary, entropy change 78–83359
- still-picture real-time Hadamard transform coding quantiser design 77–27263
- stochastic self-oscillations and turbulence, review 80–4537
- straight line processes *(French)* 77–61037
- student laboratory experiment, Pb block lowered into liq. nitrogen 79–71194
- submerged turbulent isothermal jet development and min. entropy prod. principle 79–77199
- subsonic nozzle flow, response to acoustic and entropy disturbances 77–75958
- super resolution and cost of entropy 79–89862
- superadditivity and concavity, black hole systems 80–98867
- superposition principle and entropy 77–60969
- supersaturated vapour, critical clusters, theory and Monte Carlo simulation, review 80–82734
- surface thermodynamics, equilib. and nonequilib. processes, review 77–44505
- teacher resource paper on entropy an rubbery elasticity 80–17777
- terrestrial planet, cratered surface entropy 80–101541
- tetranuclear cluster, eigenvalues spectrum of spin Hamiltonian calc., thermodynamics props. *(French)* 77–35902
- thermal conduction, sign of d^2S/dt^2 80–36959
- thermal diffusion, entropy production minimum theorem, generalisation thermal cond. coeff. depend. *(French)* 78–73943
- thermodynamic, information theory relationship *(French)* 77–5788
- thermodynamic properties, of interacting particle ensemble, by simulation of stochastic disordering 77–87697
- thermodynamics of solids, corrections from electron-phonon interactions 80–49387
- thermoelastic effect, lattice dynamics and energy channelling 78–22786
- thermoluminescence, minimum entropy prod. 79–28845
- thermoluminescent process, entropy production 78–23539
- thermomechanics, derivation of jump condition 78–87250
- thermorheological behaviour and coupling problem of struct. materials 77–3718
- thermorigid dielectrics, nonlinear thermodynamic theory 80–10149
- thermotropic systems of rodlike molecules with orientation-depend. interactions 80–33883
- time asymmetry, rel. to black hole thermodynamics 77–2451
- time evolving system, markovian density operator, generalised H-theorem 79–49184
- TLD elements, transmitted information 80–89860
- transport processes, nonlinear, hydrodynamics 80–22310

entropy continued
- turbojet engine noise interaction of entropy fluctuations with turbine blade rows 77–80149
- two-dimensional lattice, cluster expansion method 78–34942
- two-level quantum dynamics, representations of Kossakowski conditions 78–20989
- Universe, consequences of using concept of entropy 78–4418
- universe, entropy chaotic cosmology 77–57112
- Universe, entropy per baryon rel. to isotropy and homogeneity 80–22125
- universe, stiff, specific entropy rel. to primordial black holes minimum mass *(Russian)* 80–51802
- Universe, weak interactions and isotropy 78–61947
- Universe initial regularity, effects of matter-antimatter symmetry breaking 80–22124
- unstable particles, entropy balance eqn. on Markovian approx. 79–80554
- unsteady compressible flow, dissipative thermodynamic effects 78–26136
- vacancy entropy of formation due to anharmonic effects 77–62521
- valence transition, entropy and phase diagram 80–59877
- van der Waals complex, formation, role of entropy 80–7840
- Van der Waals gases, adiabatic and isothermal spinodal curves 80–92034
- vaporisation entropy/surface tension relation near melting point *(Japanese)* 79–99397
- variation conceptual treatments *(German)* 77–41561
- variational principle for Z_+^N action on compact space 77–53825
- variational thermodynamics of viscous compressible heat conducting fluids 77–50868
- viscoelastic flow, continuum thermodynamic theory, configurational entropy effects 78–1621
- viscoelastic fluid theory, entropy effects 77–14971
- Vlasov eqn. and entropy, collective, nonHamiltonian model 77–5745
- von Laue's theorem of partially coherent radiation entropy, quantum statistical proof 79–17373
- von Neumann entropy and entropies of meas. 78–54229
- wear, entropy production model 80–74815
- Wehrls entropy conjecture proof, Bloch coherent spin states analogous problem 78–89418
- X-Y model, spin 1/2, thermodynamic props. in three dimens., high temp. series expsn. 78–47930
- Al-Ga(In)(Sn), interpretation of metallic phase diagrams, entropy of mixing 79–42274
- Au-Zn, liq., thermodynamic props. *(German)* 80–49386
- Bi_2O_3, energies of formation, solid-state electrochemical techniques 80–6527
- $CaWO_4$, cryst. growth from solns. in melts, kinetics parameters and thermodynamic props. 80–59424
- $CdCr_2X_4$ (X=S,Se), excess entropy terms 79–86905
- Cl^- hydration complexes, gas phase, electrostatic calcs. 80–100055
- $CoCr_2S_4$, excess entropy terms 79–86905
- $Co(NH_3)_5\ Br^{2+}$, aquation, polyelectrolyte catalysis, high pressure effect 80–55656
- $Co(NH_3)_5Br^{2+}\ +OH^-$, polyelectrolyte catalysis, high pressure effect 80–55657
- $CsHF_2$, heat capacities, transitions and melting 79–10967
- Cu based dilute alloys, enthalpy of formation and excess entropy 80–55347
- Cu, NMR study on nuclear ordering below 1 μK 80–93187
- Cu-Al-Ni alloys, entropy and enthalpy of martensitic transformation, calcs. 79–43245
- $CuCr_2X_4$ (X=S,Se,Te), excess entropy terms 79–86905
- $CuSO_4$ soln., electrochemical analogue of Benard instability, isothermal and potentiostatic conditions 80–76530
- D_2O, eqn. of state, up to 380°C and 1000 bar, derived functions 78–26655
- $DyFeO_3$, thermodynamic props. 79–77771
- $Dy_3Fe_5O_{12}$, thermodynamic props. 79–77771
- Fe, α-, γ-, liq., thermodynamic data *(German)* 80–40328
- $FeCr_2S_4$, excess entropy terms 79–86905
- G_2-B_2O_3 melt, thermodynamic props. from mass spectroscopy 80–39318
- Ga, liquid, effective pair potential and entropy *(French)* 78–14267
- Ga-alloys, thermodynamic properties 78–14480
- Ga_2Se_2, sublimation growth, closed tube, enthalpy from mass flow and press. meas. 77–63550
- Ga_2Se_3, evaporation, thermodynamic props. 80–54365
- $H+H_2$, reaction probability, max. entropy derivation, statistical theories 80–66781
- H_2O-acetic acid, liq. mixture, thermodynamic excess functions, calorimetric meas. 77–52666
- $(H_2O)_n$, n=8, 64, cluster thermodynamics calcs. using Monte Carlo method 77–58219
- He, thermodynamic props., in range 20 to 1500°C and 1 to 100 bar *(German)* 79–69266
- ^4He, liquid, Bose-Einstein condensate near lambda point 77–15645
- ^4He, superfluid, surface tension and surface entropy 78–10235
- I^- hydration complexes, gas phase, electrostatic calcs. 80–100055
- K_2O-Al_2O_3 system, high temp. thermodynamics and phase equilibria 78–80521
- $LaBO_3$ (B=V, Cr, Mn, Fe, Co, Ni), chem. stability X-ray and thermal anal. 79–79242
- $La_{1-x}Ca_xNi_5$, role of entropy change during H_2 sorption 78–91533
- $La(Ni_{1-x}Cu_x)_5$, role of entropy change during H_2 sorption 78–91533
- Li_3N, heat capacity 5 to 350K, thermochem. props. to 1086K 78–92500
- MoS_2, entropy, enthalpy and specific heat, temp. depend. 500 to 1700K 80–15260
- Nb-H, interstitial position of H from entropy of soln. 77–65989
- Ni-Cu, liq., activity meas. of O_2 by EMF method *(Japanese)* 80–54408
- Pd-H, interstitial position of H from entropy of soln. 77–65989
- Pd-H, solid soln., excess entropies, variation of H solubility with pressure 79–46846
- Sb_2O_3, energies of formation, solid-state electrochemical techniques 80–6527
- SmF, vaporisation, sublimation, Knudsen effusion method 80–6508
- $SrWO_4$ cryst. growth, from Na_2WO_4 melts, thermodynamic props. 80–107084
- Ta-H, interstitial position of H from entropy of soln. 77–65989
- $TaB_{2.11}$, heat capacity thermodynamic properties from 5 to 350K 78–91446
- Ti-Cu system, appl. of metal-hydrogen equilibration determ. thermodynamic props. 79–77772
- $TiB_{1.964}$, heat capacity thermodynamic properties from 5 to 350K 78–91446

entropy of substances
acetone vapour, mol. assoc., monomer-dimer equilib., thermal cond. meas., MO calcs. 79—52647
acetonitrile-water mixture, electrolyte transfer, thermodynamic props. 80—3395
aeroacoustic fluid dynamic equations, acoustic energy conservation, vibrational relaxation effects 78—90566
aerodynamically generated noise, especially jet noise *(French)* 78—14002
aliphatic acids, thermodynamics of adsorption at air/aqueous soln. interface 80—10752
aliphatic alcohol, thermodynamics of adsorption at air/aqueous soln. interface 80—10752
alkali halide, migration enthalpy and entropy for cation vacancy motion 77—35750
alkali halides, free energy of formation of vacancy determ. 77—76597
alkali halides, heat and entropy of evaporation, Trouton's rule generalisation 79—77735
alkali halides, NaCl and CsCl type structs., comparison of migration entropy for cation and anion vacancy motion 77—62519
alkali metal,thermodynamics of melting *(Russian)* 78—71840
alkali metal chlorides, thermal diffusion in H_2O, D_2O, potentiometric calcs. 78—18807
alkali metals, anharmonic effects in thermodynamics *(Russian)* 78—43145
alkaline earth fluoride, doped with trivalent rare earths, migration entropy for bound fluorine motion 80—71303
1-alkanols, liq., H-bond order temp. depend. from Hildebrand rule 80—7838
N,N′-bis(p-alkoxybenzylidene)-α,α'-bi-p-toluidines, nematic phase, synthesis, thermodynamic props., gas-liq. chromatographic anal. 79—90763
alkylammonium zinc tetrachloride cpds., high temp. phase transitions 80—54372
alkylene-di-ammonium cadmium chloride, influence of C atoms and metal ions on structural phase transitions 78—2256
alloys, $L1_2$ and $L1_0$ superstructure atomic ordering phase diagrams, order-disorder transition 80—38989
amalgams, liq., mixing, excess entropy, vibr. contrib. *(Russian)* 79—51263
anilines, substituted, in benzene, dielectric relax. and mutual viscosity, obs., entropy calc. 79—38449
anthracene, chemical thermodynamic props. 80—21312
anthracene, thermodynamic function calc. using cell model 77—7879
atomic and plastic crystals, melting transitions, thermodynamic props. 80—96452
benzene-hexa-n-hexanoate, phase transitions and mesophase form., sp. ht. and IR spectra, 13 to 393K 80—79955
2,3-benzo-1,6-methano(10)-annulene, mol. geom. and gas phase thermodynamic props., minimisation scheme 78—78829
benzylideneanilines, thermal parameters for cryst.-mesophase and cryst.-cryst. transitions 77—11679
binary, segregating alloy, theory of surface effects 79—19435
binary alloy melt, influence of associate formation on thermodynamic quantities 79—66329
binary ordering alloy, theory of surface effects 79—19434
bis-tetraethylammonium tetrachloronickelate, heat capacity, structural transitions 79—65209
bis-tetraethylammonium tetrachlorozincate, heat capacity, structural transitions 79—65209
block copolymers, microphase separation, thermodynamic treatment *(Chinese)* 80—79947
brass, calorimetric investigation of thermodynamic props. 79—52172
brass, liquid, thermodynamic props. *(German)* 80—66482
brass, martensite stability 79—91650
α,βbromonaphthalenes, thermodynamic functions calcs. 298-1500K 77—31418
Carnot cycles, transform. temp. and latent heat under applied stress, rel. to shape memory effect 77—28874
cast iron-steel mixture, interaction of Zr, formation reaction thermodynamics *(Russian)* 80—55645
chalcogenide glass, partial values and structure features 79—41969
chalcogenide spinels, thermal stability, thermochemical, thermodynamic and crystallochemical props. 77—51519
chemical spinodal, estimation 79—8271
chloroform-tetrahydrofuran system, excess free energies and vols. 79—82357
β-chloronaphthalene, thermodynamic functions calcs. 298-1500K 77—31418
o-chlorotoluene(-benzene), liq. and dilute soln., microwave absorption and relax. processes 79—82920
COC, liq. cryst., test of tricriticality 80—10648
communal entropy and glass transition, theory 80—70131
composite, glass transition model 77—84901
computer generated phase diagrams 78—83928
copolymer globule model, orientationally-ordered liq. cryst. state *(Russian)* 80—59389
cresols, ideal gas thermodynamic props. 78—75250
crystal hydrates, thermodynamic functions, Karapetyants-Rozenfeld equation *(Russian)* 79—66332
crystal orientational disordering, thermodynamic props., stat. mech. model 80—96453
crystal thermodynamics in statistical theory, density Fourier coeffs., stress tenser, internal energy 80—13025
cyclic ethers-HF H-bonded complexes, calorimetry, IR spectra and MO calcs. 79—52738
cyclo-hexyl-ammonium-copper-trichloride, specific heat, ferromagnetic chain system 80—103491
cyclohexanol plastic cryst. phase, glass transition temp., press. depend. 80—49135
degenerate semiconductor, entropy production and choice of heat flux 77—15778
di(alkylammonium)$CdCl_2Br_2$, solid-solid phase transitions 80—84290
dialkyl ammonium cadmium chloride, influence of C ions and metal ions on structural phase transition 78—2256
dialkyl ammonium manganese chloride, influence of C ions and metal ions on structural phase transition 78—2256
dialkyl phthalates, plasticizers, surface tension, contact angle, surface energy, entropy determ. *(Japanese)* 77—31843
diamantane, sp. ht., thermodynamics of transition and fusion 79—55899
o-dichlorobenzene(-benzene), liq. and dilute soln., microwave absorption and relax. processes 79—82920

entropy of substances continued
dielectric fluid, Debye absorption at crit. liq.-vapour transition 80—100322
diffusion, activation enthalpy and entropy and defect form., basic thermodynamic relation, validity limit 78—47557
difluorodiazine, cis-trans isomerisation, mechanism and kinetics, CNDO/2 study 77—90589
dimensionless, simplification of thermodynamic calc. 79—91984
4,7-dioxaoctanal, equilib. anionic polymerisation, −90 to −68°C, polar substituent effects 78—88631
disordered solids, excess entropy 80—38914
DNA, entropy nature of B-A transition 79—92130
elasto-plastic metal-dislocation system, stress-activated dislocation motion, thermodynamic theory *(Chinese)* 78—83868
elastomers, block copolymers, generalised elasticity theory, domain cross-linkage vol. 77—39229
elements, anomalous entropies of fusion, deviations from Richard's rule 77—47601
elements, work functions and sublimation entropies 79—56283
entropy change on melting of simple substances, thermal expansion, configurational entropy 80—59630
ethane-C mol. sieve system, adsorptive pot. distrib., entropy, enthalpy 77—72778
ethanol, plural glass-transitions, thermodynamic functions 78—38820
ethylene oxide-d_0, -d_4, centrifugal distortion const., thermodynamic functions 79—41149
ethylene sulphide, centrifugal distortion const., thermodynamic functions 79—41149
ethylene-CO copolymer, highly alternating, melting and internal motion 77—51474
FCC metals and alloys, grain boundary energy and self-diffusion, effect of solute segregation 78—15412
ferroelectric, eight-site order-disorder model, influence of tunnelling 80—2709
ferroelectrics and ferromagnetics, theoretical development 78—43815
ferromagnetic metals, thermodynamic props. 79—91245
flexible chain polymer, topomorphism and phase dualism 78—14265
fluid with nearly spherically symmetric molecules, thermodynamic perturbation theory 80—14985
fluorobenzene(-benzene), liq. and dilute soln., microwave absorption and relax. processes 79—82920
gas adsorption, on solid adsorbents, thermodynamics *(Rumanian)* 80—10786
gas solubility, entropy of soln. in binary nonpolar solvent mixtures 79—52745
glass transition, soft-sphere model, mol. dynamics study 80—49343
glass-forming liquids, viscous flow and valence config. theory 80—14756
glass-forming melts, exam. of isobaric-isothermal pots. in glass transition interval 79—7681
glass-forming systems, structure and thermodynamics *(German)* 80—38924
glasses, liq.-phase separated, phase comp., temp. depend. 80—16289
glasses, polymerised, statistical thermodynamics, short and long range props. 77—27834
glyceryl tristearate, soln. growth, surface entropy factor calc. 78—42934
grain boundary entropy computation in computer simulation 78—30647
graphite, adsorption of O_2, graphical determ. of entropy of adsorpt. *(French)* 77—11790
graphite-halogen intercalation compound, calorimetric study of order disorder transform. 79—52206
graphite-HNO_3 intercalation compounds, differential scanning calorimetry investigation 79—42234
Heisenberg linear chain, with nearest and next-nearest neighbour interactions 77—63059
p-n-heptyloxybenzylidene-p-aminobenzoic acid, smectic C to nematic transition 79—33076
2,4-hexadiynyl-1,6-bis(p-toluenesulphonate), programmed temp. and DSC obs., cryst. forms and polymerisation kinetics 79—43583
hexamethylene tetramine, cryst. growth kinetics from soln., role of solvent-solute interactions 77—24282
p,n-hexyloxybenzylideneamino-p′-chlorobenzene, liq. cryst., sp. ht. meas. 78—22831
HOAB, liq. cryst. phase transitions, specific ht. meas. 79—33075
homovalent disordered solid alloy, entropy-vol. correlation 78—63868
Hubbard model, computer renormalisation-group technique 79—19716
hydrocarbon liquid, residual energy and entropy, rel. to liq. and mol. structs. 78—71869
hydrocarbons, saturated open-chain, transport behaviour of excess electrons and props. 80—39643
hydrocarbons, thermodynamic props., optimum incremental diagram calc. method *(German)* 78—51702
ice, polarisation processes, in lattice, Kirkwood's theory rel. to thermodynamics of irreversible processes 79—38447
ice, polarisation processes, in lattice, thermodynamics of irreversible processes, universal relation 79—38446
ice, VII to VIII transition, lattice model 78—10187
ice, vitreous, sp. ht., entropy and 'glass transition' 77—51520
II-VI compounds, heat and entropy of evaporation, Trouton's rule generalisation 79—77735
immiscible liquid binary cycle temp.-entropy diagrams 78—157
impurity distribution on growing crysts. from melt 78—52656
interstitial-FCC soln., thermodynamics based on kinetic considerations 77—62651
ionic crystals, migration volumes calc. 80—103324
ionic crystals, vibrational surface modes, vibrational contributions to surface thermodynamic functions 77—47659
ionic molecules, vapours, thermodynamic properties, classical partition function, dimens. anal. 80—43829
isobutyric acid-water, mixture, heat of transport, crit. exponent 80—15277
isotropic media, linear dynamical eqns. of state, general formalism 78—93639
KCl-$BaCl_2$ system, solid solns., phase diagram, enthalpy of soln., vibr. entropy. 78—39751
layered crystal, electron gas statistical and thermodynamic props. *(Russian)* 79—87051
Lennard-Jones (100) crystal-liquid interface, structure 78—91284
liquid, configurational properties near glass transition 78—26662
liquid alloy, thermodynamic ab initio calcs. 77—47602
liquid crystal, binary mixtures, phase transition, entropy, relation to smectic plane tilt angle 80—65203

entropy of substances continued
- liquid crystal surface, statistical thermodynamics, local order parameter 80−88023
- liquid crystals, phase transitions up to 3 kbar, transition enthalpy, entropy 77−20051
- liquid crystals, thermodynamic props. calc. 80−103464
- liquid metal, electronic theory of thermodynamics and struct., summer school lecture series 80−6353
- liquid metal, interatomic forces and thermodynamic props., hard-sphere model 77−47321
- liquid metal, surface entropy using hard-sphere model 79−37906
- liquid metal enthalpy meas. up to 2100K 80−4715
- liquid metals, electron component of entropy *(Russian)* 79−23747
- liquid metals, mixing volumes, pseudopotential method 79−37846
- liquid transition metal, electronic states densities from struct. and entropy data 77−1347
- liquid-glass transition, free volume approach, thermodynamic behaviour 80−1940
- liquids, polar, thermodynamics, electrostatic approximations using Onsager model 80−55693
- lysozyme, cryst., dynamic sp. ht. capacity meas. 80−21447
- macromolecules, crystallisation thermodynamics, various degrees of coiling 78−51445
- martensite energy due to order inherited from austenite 77−28813
- material interfaces, entropy inequality 77−15678
- MBBA, nematic-isotropic transition, isothermal compressibility and thermal expansion coeff. meas. 79−99301
- MBBA, volume meas. and phase transitions at high press. 79−90764
- mesomorphic mixtures, binary phase diagrams, thermodynamic props., diamag. anisotropy 78−95139
- metal, allotropic transform., anharmonicity, effects due to thermal expansion and Gruneisen parameters 79−52207
- metal, complete thermodynamic eqns. of state 80−24561
- metal, diffusion, correlation with entropy of fusion 78−43109
- metal, entropy and lattice parameter relation 77−36464
- metal, entropy production and choice of heat flux 77−15778
- metal, entropy/free energy relation 78−15368
- metal, equation of state, isentropic expansion method 78−91414
- metal, first transition systems, survey of regular solution parameters 77−44220
- metal, formation entropy per vacancy, anal. of exptl. data 78−75657
- metal, HCP, regular soln. model for interstitial soln. 77−15591
- metal, self- and impurity diffusion, connection between preexponential factor and activation enthalpy 77−69111
- metal, thermal expansion coeff. of defect-entropy volume 78−26707
- metal, thermodynamic props. of grain and phase boundaries, review *(German)* 79−34012
- metal, vacancies, energy charact. *(Russian)* 77−24314
- metal, vacancy formation parameters and Gruneisen constant 78−22709
- metal ions complex formation with carboxylic acids in aqueous soln. *(Italian)* 77−48669
- metallic glass, thermal stability, validity of energy and entropy interfacial tension models 78−91255
- metals, dislocations and shock compression, thermodynamics 80−100235
- metals, entropies and heats of fusion 80−103458
- metals, entropy of fusion and allotropic behaviour, exam. of correlation and modification of Richard's rule 78−71838
- methane, entropy and sp. ht., 0.4 to 28K, spin-species conversion 77−28015
- methane, liq., thermodynamic perturbation theory, equilib. props. 79−64976
- methane, melting transitions, thermodynamic props., positional disordering energies 80−96452
- methane-d_1, tunnelling states and nuclear spin conversion 79−10944
- methane-d_1(-d_2,-d_3), solid, struct. of phase III from thermodynamic meas. 79−82193
- methane-d_2, orientational ordering and tunnelling states meas. 79−10963
- methane-d_4, solid, thermodynamic props. calc. using significant structures method, 6 to 87K 80−24616
- 1,5-methano(10)-annulene, mol. geom. and gas phase thermodynamic props., minimisation scheme 78−78829
- methyl alcohol, intermol. interaction, thermodynamic parameters determ. from chem. shifts of functional groups 79−64068
- micellar systems, aqueous, thermochemistry 80−61133
- minerals, dislocations and shock compression, thermodynamics 80−100235
- mischmetal-$Ni_{5-x}Al_x$ ternary alloys, Al addition effects on structural and H_2 absorpt. props. 79−52761
- molecular liquids, glass transition temp., press. depend. 80−49135
- monolayer, anomalous thermal effects, statistical mechanics 80−15367
- monolayer, interfacial, thermodynamic treatment, excess quantities, adsorbed and spread layers 80−40732
- multicomponent polymer system, liq.-liq. phase separation, thermodynamic aspects of polymer compatability 78−14469
- naphthalene, thermodynamic function calc. using cell model 77−7879
- naphthalene-tetracyanobenzene, order-disorder transition, heat capacity and thermodynamic props., 5 to 300K 79−33100
- narrow-band solids, entropy, depend. on mag. ordering 79−56112
- nematic liquid crystals, sp. ht., thermodynamic props. 77−39678
- neodymium ethyl sulphate, cryst. c-axis demag. from 25000G, magnetohydrodynamic props. to 0.01K 77−20599
- neodymium ethyl sulphate hydrate, spherical single crystal, magnetothermodynamic props. 77−55365
- nylon 6 and 66, necking stress *(Japanese)* 77−56037
- n-octanal, equilib. anionic polymerisation, −90 to −68°C, polar substituent effects 78−88631
- 1-octanol, dielec. consts., solvent struct., effect of H bonding solutes, chain length 77−48674
- octaphenylcyclotetrasiloxane, phase behaviour and nucleation kinetics 80−29168
- one component plasma fluid, derivation of eqn. of state in strong coupling 80−33741
- organic compounds, enthalpies and related thermodynamic functions 79−42276
- organic compounds, high-press. expansivity determ. by piezo-thermal anal. 77−72705
- organic eutectic, heat of fusion and excess thermodynamic functions 78−3104
- organic liquids, glasses and glassy crystals, entropy of struct. disorder, rel. to mol. struct. 79−65219
- organic liquids, polar and nonpolar, entropies of vaporisation 78−26676

entropy of substances continued
- organic molecules, information content, thermodynamic props., electropy (bondtropy) theory 77−54500
- organo tin dichlorides, tetrahedral, dilute soln., dielec. and thermodynamic behaviour, microwave region 77−36170
- PET, thermodynamic equilib. melting parameters, effect of annealing 78−71837
- phenanthrene, chemical thermodynamic props. 80−21312
- phenol, ideal gas thermodynamic props. 78−75250
- phenylthiobenzoate derivatives, thermodynamic and mesomorphic props. 77−11678
- phytanic acid, in phospholipid bilayers, struct., order parameters, liq. cryst. transition, entropy 79−83713
- phytol in phospholipid bilayers, struct., order parameters, liq. cryst. transition, entropy 79−83713
- plasma, electrostatically turbulent, definition and Boltzmann H theorem 77−76081
- plastic crystal, glass transition temp., press. depend. 80−49135
- polar liquids, solns., mol. rot., kinetics 77−51984
- polarisable hard sphere fluid, thermodynamic props. 79−42277
- polyalkyl methacrylates, oriented stretched membrane, gas diffusion, entropy correl. theory 79−69291
- polyamide-12 plasticized with sulphonamides, relaxation props. *(Russian)* 80−55031
- 1,4-cis-polybutadiene, stereoregular, recrystn. in partial melting temp. region *(Russian)* 80−6495
- polychlorotrifluoroethylene, necking stress *(Japanese)* 77−56037
- polydiethylsiloxane chains, dipole moments 78−78844
- polydiphenylsiloxane, thermodynamics of fusion 80−84280
- polyethylene, necking stress *(Japanese)* 77−56037
- polyethylene (orthorhombic), intermol. pot. functions, force consts., vibr. assignments, thermodynamic props. 77−39639
- polyethylene oxide, aq. salt soln., meas.-based thermodynamic quantities 78−75525
- polyethymethylene, necking stress *(Japanese)* 77−56037
- polymer, multicomponent, homopolymer blends, macroscopic phase separation 80−45289
- polymer, polydisperse, glass transition temp., mol. mass depend. 80−92656
- polymer chains in cubic lattice solvent, thermodynamic props., Monte Carlo method, computer simulation *(Russian)* 77−31787
- polymer crystal and melt, stat. thermodynamics using Midha-Nanda cryst. state theory 79−41979
- polymer crystallisation, thermodynamic analysis of nucleation *(Russian)* 77−19881
- polymer mixtures, compatible, glass-transition temps. 79−46789
- polymer mixtures, thermodynamics, review 79−1506
- polymer protonated and deuterated mixtures, partial miscibility 80−107037
- polymeric fluids, entropy effects in viscoelasticity 78−9618
- polymers, cryst., hard-elastic fibres, morphology mech. props., mechanisms, review 77−32612
- polymers, equation of state *(German)* 79−82309
- polymers, solidification, as dissipative process 80−65205
- polyoxide chains, config. partition functions, entropy, (CH_2)y-o- repeat unit 78−17829
- polyphenyl ether, glass transition temp., press. depend. 80−49135
- polypropylene, necking stress *(Japanese)* 77−56037
- polystyrene, glassy, thermally activated deform. 79−20126
- polyterephthalate, necking stress *(Japanese)* 77−56037
- polythene melts of high density, viscosity meas., entropy and compressibility *(German)* 78−67162
- propylene, computer generated phase diagrams 78−83928
- proximity sandwiches, thermodynamics of second order phase transitions 79−56408
- PTFE, necking stress *(Japanese)* 77−56037
- PTFE copolymer, melting point, cryst. struct., modification *(Russian)* 77−31607
- PVC, thermodynamic props. *(German)* 77−28024
- pyrazine, cryst. phases, entropy changes and struct. implications 80−54397
- pyridine, deuterium substituted, Raman and IR vibr. spectra 80−84739
- quenched magnetic system, statistical thermodynamics 77−66363
- rare earth (III) complexes, cysteinates, thermodynamics of form. 80−89515
- rare earth alloys, config. entropy and stability of intermetallic hydrides 77−84949
- rare earth metals, liq., entropies 77−69100
- rare earth rhodium borides, RRh_4B_4, NMR and sp. ht. in supercond. and mag. ordered phases 80−7037
- Schiff's base compounds, double axis, Siamese Twin type liq. crysts., thermal and X-ray obs. 80−39312
- Schiff's bases, nematic phys. props. 79−99057
- semicarbazide hydrochloride, phase transition, IR spectra and thermal study 79−37833
- semiconductor, entropy of fusion allowing for dissociation at melting point 77−55348
- semiconductor defects, entropy of ionisation and temp. variation of ionisation levels 77−11871
- semiconductor electronic component of entropy of fusion 78−47503
- silicate minerals, thermodynamics and lattice vibr. props. 79−100830
- silicates, entropy estimates at 298K from molar vols. 77−1243
- simple compounds and elements, entropy of melting 77−59101
- single metals, monovacancy formation parameters, temp. depend., pseudopot. theory 78−75658
- sodium tetraborate glass, melt, temp. depend. of high viscosity property *(Russian)* 80−39336
- solid, formation volume of vacancies calc. 79−19244
- solid solution, heterovalent, use of expt. data to estimate energy of soln. 80−54380
- solid-gas surface reaction, nonequilibrium thermodynamic anal. 79−79285
- solid-liquid interface free energy anisotropy clustering influence 80−80054
- solution, different-sized mols., orientation effects, surface region, lattice model 79−1540
- solution growth, surface entropy factor calc. 78−42934
- spin glass, mean field approx. 78−52280
- spin glass, Sherrington-Kirkpatrick model, finite system, low temp., susceptibility, entropy 78−34993
- spin glass, statistical thermodynamics 77−66363

entropy of substances continued
spin glass, thermodynamics, virial expansion vs. T^{-1} expansion 77—66362
spin glasses, towards a mean field theory 79—99704
spin system, random thermodynamic props. using Bethe-Peierls-Weiss approx. 79—78387
spinels, entropy of cation transitions 79—11812
steel, aluminising, thermodynamic anal. of phase transforms. 80—76413
steel, medium and high C, deformation ageing, entropy, free energy, dislocations *(Russian)* 80—66581
strong-coupling superconductors, meas. of small changes in entropy 77—33988
strontium calcium tartrate tetrahydrate, gel grown mixed single crystals, defect characterisation 80—2027
substitutional impurities in solids, entropy and volume of solution 80—15253
succinonitrile, low entropy of fusion plastic crystal, dendritic growth, expt. test of theory 77—35842
superconductor with paramag. impurities, transport entropy of vortices 77—20506
superlattice, electron gas statistical and thermodynamic props. *(Russian)* 79—87051
TBBA, liq. cryst., metastable phase, thermodynamic props., differential scanning calorimetry meas. 78—94985
TCNB-pyrene 1:1 charge transfer complex, heat capacity, 10-300K, and entropy of transition 77—11702
TCNQ anion radical salts, phase transitions, solid solns., thermodynamic props. 77—47571
TCNQ salt, Qn $(TCNQ)_2$, configurational entropy, thermoelec. power meas. 80—34432
TCNQ salt QCTCNO, strong Coulomb correlations 79—56203
tetra-n-pentylammonium salts, molten, thermodynamic props., cation struct. 79—55639
1,1,1,3-tetrachloropropane, Raman and IR obs. of rot. isomerism, entropy difference between vapour and liq. phase isomer *(Russian)* 79—31529
thermodynamic equation for liquidus line of narrow homogeneity range compound 77—35716
α-tocopherol in phospholipid bilayers, struct., order parameters, liq. cryst. transition, entropy 79—83713
transition and noble metal dilute alloys, Einstein's temp. and vibrational entropy, rel. to electronic struct. 78—83900
transition metal, Einstein temp. and vibr. entropy, semiquantitative calc. 78—2221
transition metal, fusion entropy, electronic contrib. 79—42217
transition metals, 3d, liquid, electronic contrib., Percus-Yevick eqn. soln. *(Japanese)* 77—76579
1,1,1-trifluoro-3-chloropropane, Raman and IR obs. of rot. isomerism, entropy difference between vapour and liq. phase isomer *(Russian)* 79—31529
trifluoromethane, PVT study by Burnett method 77—42949
vacancies in metals 77—27879
vacancy formation parameters from specific heat data 80—75221
vacancy in crystal, excess entropy 77—11542
vibration entropy and mean square atomic displacements due to defects in crysts. *(French)* 79—28064
viscous liquid, glass transition, mol. mechanism for thermodynamic second order transition 78—2237
viscous liquids, glass transition, nonconfig. contribs. to excess entropy 80—92654
water, autoadsorption and surface entropy in 20-50° temp. range 77—28065
water, isentropic decompression from crustal and mantle press., thermodynamics 79—79769
water, random network model, entropy calc. 80—64870
water, vap., dimerization, from thermal cond. meas., 373K 78—44359
water vapour, dissociated, thermodynamic props. *(Japanese)* 77—80263
wet resin, glass transition model 77—84901
Wolff model, thermodynamic props., local moments in dil. alloys, var. method 80—65781
xylideneaniline-p′-benzonitri 80—44328
Ag, specific entropy and surface heat determ. as function of temp. *(German)* 80—6619
AgBr, determ. of ionic transport processes 77—89578
AgBr, migration entropy of Na^+ diffusion 79—14965
AgBr, photographic emulsion, adsorpt. of Br^-, cyanine, thermodynamics 78—32908
AgCl, determ. of ionic transport processes 77—89578
AgCl, solubility in methanol+water mixtures 77—47579
AgCl-NaCl molten solns., activities and surface tension 80—10748
$AgCl_xBr_{1-x}$, binary melt, Ag solubility, temp. and conc. depend. 80—10677
$AgClO_4$ benzene, complex, heat capacity 78—75843
$AgFeSe_2$, thermographic investigation of phase transitions *(Russian)* 80—10661
$AgFeTe_2$, thermographic investigation of phase transitions *(Russian)* 80—10661
$AgGaTe_2$, Debye temp., standard entropies and enthalpies, sp. ht. meas. 78—30769
Ag_8GeSe_6, polymorphic transition, absorpt. coeff. meas. 78—2257
α-AgI, superionic cond., statistical thermodynamic description *(French)* 80—65281
$AgInTe_2$, Debye temp., standard entropies and enthalpies, sp. ht. meas. 78—30769
$AgNa(NO_2)_2$, single cryst., specific heat anomaly, −90-55°C, ferroelec. transition entropy 77—77157
Ag_3SI, superionic conductor, ordered phase struct. 78—83792
Ag_3SI, superionic cond., phase transition and cryst. structs., sp. ht., neutron and X-ray diffr. obs. 80—10662
$Ag_2Se(Te)$, thermodynamics of phase changes *(Russian)* 77—73459
Al alloy, calorimetric studies on 700 series, matrix precipitate charact. of 7075 77—86036
Al, elastic grain boundary responses, thermodynamic props., computer calc. 77—39593
Al, liq., thermodynamic props., pseudopot. calc. *(Russian)* 79—46549
Al, monovacancy thermodynamic parameter calcs., temp. dependence 78—2114
Al, specific entropy and surface heat determ. as function of temp. *(German)* 80—6619
Al-Li-Mg, estimation of isothermal sections of phase diagram 79—11567
Al-Mn(Fe)(Co)(Ni), liquid alloys, thermodynamic charact. calc. *(Russian)* 78—27475

entropy of substances continued
Al-Ti(-Si), nucleation entropy and grain refinement 79—91627
Al_cMg_{1-c} liquid alloys, vols. and entropies of mixing, calc. 80—75363
Al_2O_3, alumina, adsorpt. of saturated hydrocarbons, gas-solid chromatography based on compensation effect 80—26053
alkali metals, liquid, internal energy, heat of mixing, entropy, dielectric function 80—88340
^{241}Am metal, 15 to 300K 77—28019
Ar, liq., variational eqn. of state and entropy 79—28070
Ar, melting transitions, thermodynamic props., positional disordering energies 80—96452
Ar, vapour press., entropy and enthalpy, thermodynamic consistency, two-parameter eqn. 77—80613
Ar-Kr, liq. mixture, excess thermodynamic props. 78—75836
AsI_3, enthalpy, entropy of melting 78—34598
Au-Fe, liq., thermodynamic mixing effects, mass spectrometric meas. eval. *(German)* 77—59123
Au-Sn liquid alloys, Sn activity *(Japanese)* 78—6901
$BaCl_2(F_2)$, sp. ht meas., Schottky-type diffuse phase transitions, defect form. energies and entropies 80—107441
$BaNiO_3$, form. entropy and tolerance factor 80—34204
$BaTiO_3$, form. entropy and tolerance factor 80—34204
$BaTiO_3$, thermodynamic props. 77—39680
Ba_3WO_6, Ba_2WO_5, and $BaWO_4$, chem. thermodynamics, galvanic cell study 80—21315
$BaZrO_3$, form. entropy and tolerance factor 80—34204
Bas and B_6As, standard values of thermodynamic functions 77—24414
Bi, equilib. vacancy conc., thermal expansion meas. 77—59007
BiI_3, enthalpy, entropy of melting 78—34598
δ-Bi_2O_3, thermoelectric power rel. to fast ionic conduction 80—107549
δ-$(Bi_2O_3)_{1-x}(Y_2O_3)_x$, thermoelectric power rel. to fast ionic conduction 80—107549
Br_2, liq., entropy, computer simulation, Widom method 79—77486
CO, liq., thermodynamic perturbation theory, equilib. props. 79—64976
CO_2, isentropic decompression from crustal and mantle press., thermodynamics 79—79769
CO_2, liq., thermodynamic perturbation theory, equilib. props. 79—64976
$CO_2(g)$, standard enthalpies of solution and formation, standard Gibbs energies of formation and standard entropy 79—57285
$Ca_3Al_2Si_3O_{12}$, garnet, thermophysical props., 5 to 600K 79—60517
CaF_2, association parameters of $[Me^{3+}$-$Fi^-]$ dipoles (Me=Metal), ionic cond. meas. 78—30788
CaF_2, Frenkel defect, entropy of form., Green function calc. 80—19898
$CaGa_2O_4$ and $CaGa_4O_7$, cryst., thermodynamic parameters of reactions of form., thermodynamic stability 80—108726
$Ca(NO_3)_2$-H_2O solns., ice I homogeneous nucleation temp., slow vitrification mechanism 78—26666
CaO-ZrO_2 solid soln., thermodynamic investig., by EMF method 77—36485
$Ca(O_2)_2$, standard heat, entropy and free energy of form. 79—87869
$CaSnO_3$, form. entropy and tolerance factor 80—34204
$CaTiO_3$, form. entropy and tolerance factor 80—34204
$CaZrO_3$, form. entropy and tolerance factor 80—34204
Cd-As, liq. alloys, thermodynamic props. and cpd. formation 77—1238
$Cd_{0.010}Fe_{2.990}O_4$, heat capacity investigation of dopant effects on mag. disordering temp. 80—25143
$CdGeP_2$, CdP_2, Cd_3P_2 of formation 77—90634
CdP_4, thermodynamic functions, 55-300K 80—34203
CdS, polytype relative stabilities, entropy contribs. 80—100197
CdS(Se), reaction with Sn chalcogenides, thermodynamic anal. 80—40728
CdSb, free energy and heat of formation 79—77768
CdSb, thermodynamic props. 79—77767
$CdTiO_3$, form. entropy and tolerance factor 80—34204
$CdTl_2Te_4$, single and polycryst. samples, linear expansion, heat capacity and thermodynamic props. 80—103489
CeB_6, anomalous sp. ht. intrinsic mag. phase transitions obs. 80—108027
^{249}Cf, vapour pressure, thermodynamic functions 80—6509
Cl_2, liq., entropy, computer simulation, Widom method 79—77486
$ClNO_2$, kinetics of thermal decomposition *(German)* 78—95924
ClO_3F, heat capacity, permittivity, thermodynamic props., 2.7 to 160K 77—35713
CoB, thermophysical props., 296-2000K 78—14477
$CoSO_4$, aq. soln., viscosity meas., viscous flow activation energy, entropy *(Japanese)* 77—43363
Cr, specific heat of strained and annealed samples 79—38331
Cr-Ge, thermophysical props., at elevated temp. 80—103493
CrAs, heat capacity, enthalpy increments, thermodynamic props., 5 to 1280K 78—91450
CrF_2, heat capacity, entropy, 10-300K, mag. ordering effects 79—87264
CrF_2, thermodynamic props. meas., electrochem. method 77—7874
$Cr_{11}Ge_8$, Cr_3Ge, thermodynamic functions 77—84948
$Cr_{12}Ge_{19}$, CrGe, thermodynamic props. 77—36779
ε-Cr_2N phase, analysis of expt. results of Mills and Schwerdtfeger to yield partial enthalpy and entropy 78—52783
Cr_2O_3-Al_2O_3 solid solution, electrochemical determ. of activity 78—44391
$CrSb_2$, heat capacity and thermodynamic props., mag. transition, enthalpy of decomposition 78—43591
Cs, liq., vapour press., thermodynamic functions determ., Knudsen-effusion radiotracer method 78—26678
Cs-CsCl, liq. mixture, enthalpy of fusion, Gibbs energy of mixing and excess entropy 80—19947
CsN_3, heat capacity from 5 to 350K 79—55901
(Cu,Ag)X, (X=Cl, Br, I), molten, thermoelec. power determ. 78—26711
Cu, elastic grain boundary responses, thermodynamic props., computer calc. 77—39593
Cu, entropy factors for vacancy formation and migration 78—75866
Cu, liq., surface tension rel. to temp., surface enthalpy, entropy 78—38912
Cu, vacancies, formation entropy, diffusion const. by determinant and Green's function methods 79—77595
Cu-Al, heat capacity of phases, 233 to 800K, heat of transform. and entropy 77—47589
Cu-Ge-O, phase diagram and thermodynamics, electrochem. study 80—50617
Cu-In alloy, thermodynamics, calorimetric exam. *(French)* 77—21105
Cu-In liquid alloy, thermodynamic props., potentiometric exam. *(French)* 77—59126
Cu-Mn, dil., mag. heat capacity, conc. and temp. depend. 79—61164

entropy of substances continued
CuAu, order-disorder transform., band theory for internal energy, configurational entropy 79−19539
Cu_3Au type antiferromagnet Ising lattice, finite entropy at T=0, phase transition 77−89958
$CuCl_xBr_{1-x}$, binary melt, Cu solubility, temp. and conc. depend. 80−10677
$CuCr_2O_4$, heat capacity, entropy, polymorphic transition, 298-1000K 78−10196
CuF_2, heat capacity, entropy, 10-300K, mag. ordering effects 79−87264
CuI, γ and β phases, phonon contribs. to Gibbs free energy and entropy 77−80633
$CuInSe_2(S_2)(Te_2)$, Debye temp., standard entropies and enthalpies, sp. ht. meas. 78−30769
CuMn spin glass, specific heat and entropy 80−60354
$Cu(NO_3)_2.2^1/_2H_2O$, singlet ground-state system, mag. props., short-range ordered state 78−23289
$CuO-Cu_2O-TiO_2$, phase equilibria, thermodynamics of Cu_3TiO_4 phase 80−55374
Cu_2S, $Cu_{1.8}S$, $\alpha \rightarrow \beta$ transition, thermographic investigation of heats, entropies and activation energies 80−88314
$CuSO_4$, aq. soln., viscosity meas., viscous flow activation energy, entropy *(Japanese)* 77−43363
$CuSe_2$, CuSe, Cu_3Se_2 and Cu_2Se, thermodynamic props., 298 to 420K *(Russian)* 77−69098
$Cu_xZn_{1-x}SiF_6.6H_2O$, heat capacities and thermodynamic props., 14 to 300K, cooperative Jahn-Teller transition 80−21314
$CuZr_2+H_2$, 550 to 850°C, absorption isotherms, thermodynamics 79−87841
D_2, solid, melting curve, meas. of P, V, T and longitudinal sound velocity 79−37814
D_2O, liq., ionisation const., thermodynamic props. determ., 298-523K 77−32821
D_2O, vapour, mol. association entropy and enthalpy, thermal cond. meas. 80−7777
Dy, mag. characts. in strong mag. field 77−89936
$DyAl_2$, sp. ht. and thermal props., 5 to 300K 77−43342
$DyCo_2$, field induced vol. magnetostriction 78−91920
DyF_3, thermodynamic props., galvanic cell meas. 80−21316
$DyFe_2H_x$, thermodynamic props., H_2 desorption isotherm meas. 80−89516
Er, specific heat and compression curves 79−51272
$ErAl_2$, sp. ht. and thermal props., 5 to 300K 77−43342
$ErCo_2$, field induced vol. magnetostriction 78−91920
ErF_3, thermodynamic props., galvanic cell meas. 80−21316
$ErFe_2H_x$, thermodynamic props., H_2 desorption isotherm meas. 80−89516
EuB_6, ferromag. and antiferromag. sp. ht meas., 1.8-77K 80−65948
$EuCl_3$, heat capacity and Schottky anomaly, 5 to 350K, entropy 77−47588
$Eu_5Sn_3S_{12}$, mag. and thermodynamic props., metamagnetism 80−60273
$Eu_xSr_{1-x}S$, ferromagnet-spin glass transition, mag. ordering, mag. susceptibility and neutron scatt. meas. 80−50135
Fe, BCC, computer simulation of entropy of $^1/_2\langle 111\rangle\{110\}$ edge dislocation 78−67716
Fe, BCC, vib. entropy of $^1/_2$ $\langle 111\rangle$ $\{110\}$ edge dislocations 78−63768
Fe complex, bis(N,N-diethyldithiocarbamato)-iron chloride, ferromag., sp. ht. meas., 0.4-20K 78−19258
Fe, paramagnetic mag. entropy 77−63081
Fe, phase transition thermodynamics 78−18769
α-Fe vacancies, formation entropy, diffusion const., determinant and Green's function methods 79−77595
Fe-C system, mixing variables, activities and entropies calc., short range order model *(German)* 80−25655
α-Fe-Cr solid soln., thermodynamic activity of components 79−38797
Fe-Cu liquid alloy, heats of mixing, mixing entropies *(Russian)* 80−65224
Fe-Cu(-C), alloyed with graphitising elements, geometrical thermodynamics *(Russian)* 79−52261
Fe-Mo, ferritic, thermodynamics and solubility of C and ferrite 77−36456
Fe-Mo austenite, thermodynamics of C 77−36457
Fe-Ni(Cu)(Al)(Si) liquid alloys, thermodynamic characts. calc. *(Russian)* 80−15264
Fe-O, exam. of thermodynamic data, using a computer aided strategy 79−11592
FeB, thermophysical props., 296-2000K 78−14477
$Fe(CO)_5$, chem. thermodynamics 78−18799
$Fe_{(1-x)}Co_xCl_2.2H_2O$, antiferromag. random mixture, sp. ht. meas. 79−65678
Fe_2Mo, standard Gibbs energies, enthalpies, entropies of formation 78−61042
Fe_3Mo_2, standard Gibbs energies, enthalpies, entropies of formation 78−61042
$FeMoO_3$, standard Gibbs energies, enthalpies, entropies of formation 78−61042
Fe_3O_4, anomalous sp. ht. obs. at 10K 77−85454
Fe_3O_4, low temp. phase, sp. ht. and elec. cond. 77−59308
FeS_2, marcasite and pyrite phases sp. ht., thermodynamics of transform. 77−28016
$Fe_{0.9}S$, ferrimag. transition, mag., thermodynamic props., kinetics 79−47280
GaAs (110), adsorption of Cs 77−72794
GaAs(Sb), high-temp. thermodynamic data and quantitative fits to liquidus line 77−63637
Ga_2O_3, entropy of beta→alpha transformation 77−36489
β''-Ga_2O_3-Na_2O-K_2O mixed crystals, cond. anomaly 79−46838
Ga_2Se_2, sublimation growth, closed tube, entropy from mass flow and press. meas. 77−63550
$Ga_xV_{1-x}O_2$, resistivity, EPR, enthalpy and entropy meas., rel. to semicond.-metal transition 78−88004
$GdCl_3$, heat capacity, 5 to 350K entropy 77−47588
$Gd_{0.1}Mo_6Se_8$, mag. supercond., entropy depend. on temp. 79−56380
Ge, amorphous, first order transition to metallic liquid, calc. of transition temp., enthalpy and entropy 79−69227
Ge, entropy and enthalpy of vacancy form., comparison of theory with quenching expts. 77−11872
Ge, thermodynamic functions and normalised moments 79−51279
Ge-Mn, liq., calorimetric investigation of heats of mixing, and entropies of mixing 79−95165
Ge-Sn, liq. alloys, thermodyn. props. 77−51518

entropy of substances continued
Ge-Te binary glass, eutectic, DSC obs., thermodynamic and thermokinetic characts. 80−39309
GeH_4, heat capacity, dielectric const., thermodynamic props. 78−83967
GeP, thermodynamic characts. 10-300K, interatomic bond elasticity 80−59677
H_2, solid, melting curve, meas. of P, V, T and longitudinal sound velocity 79−37814
HCO_3^-(aq), standard enthalpies of solution and formation, standard Gibbs energies of formation and standard entropy 79−57285
HF chemical laser, pulsed, evolution, irreversible thermodynamic anal. 79−31887
HF, vibr. relax. entropy deficiency and vibr. entropy 79−36743
H_2O, vapour, mol. association entropy and enthalpy, thermal cond. meas. 80−7777
HOCO and HOCO*, thermochem. props., 100-300K 78−27805
$HO_2.H_2O(NH_3)$ complex form., ab initio calcs., min. energy configs. 77−14340
HSO, thermochem. props. 79−5173
^{3}He, adsorbed on Vycor glass under press., nature of phases, entropy and magnetisation expts. 80−49458
^{3}He, BCC, four-spin interaction effects on ordering processes 77−39721
^{3}He, liq. B-phase at equilib., formalism 80−88384
^{3}He, significant structure theory, thermodynamic props. 78−51774
^{3}He, solid, nuclear spin ordering in applied mag. fields 77−51568
^{3}He, solid, ordering obs. at melting press. in high mag. fields 80−84341
^{3}He, solid, spin ordered, melting press. and entropy 80−84340
^{3}He, solid, struct. of vacancy induced spin polarons 79−95244
^{3}He, solid magnet, spin-lattice models 80−88394
^{3}He, superfluid, A-phase, orbital solitary wave solution 77−31824
^{3}He, superfluid, fountain press., sp. ht. and thermal cond. meas. 77−35782
^{3}He, superfluid A-phase, entropy production and non-linear hydrodynamic eqns. 77−80668
^{3}He-^{4}He 6.4% soln., entropy of transfer 79−56013
^{3}He-Z near A. phase transition, collective oscill. hybridisaiton *(Russian)* 80−80020
^{4}He films adsorbed on graphite, transition temp., entropies, internal energies and heats of desorption, vapour press. meas. 80−2238
^{4}He, HCP→FCC transition, temp. hysteresis 78−56021
^{4}He, liq., dynamic scaling near λ point 79−14977
^{4}He, liq., entropy meas. under press. between 0.7 and 1.35K 78−56004
^{4}He, liq., phonon dispersion curve from entropy meas. down to 0.75K 77−7922
^{4}He, quantum cryst., ground-state lattice vacancies and Bose-Einstein condensation 77−7943
^{4}He, solid, 0.1 to 0.82K, and density at freezing 77−7925
^{4}He, solid-fluid, eqn. of state, melting props. under press. 80−96721
^{4}He superfluid, acoustic vibration field density of states in piecewise const. parameter media 80−6483
^{4}He, superfluid, elementary excitations below 1K, exptl. evidence for interactions, entropy meas. 77−85006
^{4}He, superfluid, roton lifetime effects on thermodynamic props. 79−55957
^{4}He, superfluid, roton-roton interactions and thermodynamic props. 79−60571
^{4}He, superfluid, second sound damping, crit. dynamics below T_λ 80−10727
^{4}He, superfluid, thermodynamic props. determ. from sound velocity data 77−15649
^{4}He, superfluid, thermodynamic versus neutron meas. at low temp. 79−51327
^{4}He, superfluid, under press. *(French)* 77−72726
$HfB_{2.036}$, $HfC_{0.968}$, ht. capacity, thermodyn. props., 5-350K 77−47590
$Hg(NH_3)_2Br_2$, $Hg(NH_3)_2Cl_2$, thermodynamic study of disorder 79−28109
HgS(Se), reaction with Sn chalcogenides, thermodynamic anal. 80−40728
HgTe-CdTe(ZnTe) solid solns. form., equil. vacancy conc. changes 77−43208
Ho, sp. ht., using lattice dynamical model for HCP metals 79−51273
$HoCo_2$, field induced vol. magnetostriction 78−91920
HoF_3, thermodynamic props., galvanic cell meas. 80−21316
I_2 solid charge-transfer complexes, determ. of thermodynamic form. values 80−45540
In-Cd, soft mode, latent heats and entropies of fusion 79−46786
In-Tl, BCC alloys, stability and elastic consts., US vel. 79−42133
In-Tl, soft mode, latent heats and entropies of fusion 79−46786
In-Tl liquid alloy, thermodynamic props. and struct. *(German)* 77−48400
InAs, heat and entropy of melting, assessment by quantitative thermography 77−15550
InAs(Sb), high temp. thermodynamic data, quantitative fits to liquidus line 77−63637
InI_x, x=1,2,3, thermodynamic props. 77−40572
IrO_2 anodic amorphous film, electrochromism isotherms, internal entropy 80−50300
K, liquid, equation of state, press. and entropy along melting curve 77−47540
K, thermodynamics of melting at high pressures 78−91426
K-Rb, internal energy, heat of mixing, entropy, dielectric function 80−88340
KCl, aqueous film on Hg, secondary electrocapillary effects, interfacial tension and entropy 77−55420
KCl, entropy change associated with substitutional anion defects calc. 78−79782
KCl, entropy changes associated with formation of defects, Schottky defects 77−62552
KCl:$Na^+(Rb^+)(Ag^+)$, entropy changes associated with point defects form. calcs. 77−7741
KCl:Sr, Ca, simultaneous diffusion, coefficients meas. 78−79813
$K_3Fe(Cn)_6$, mag. and thermodynamic props. below 0.4K in mag. fields 79−56542
$K_2Mn_2(SO_4)_3$, phase transition press. effect, dielectric const. meas. 79−37834
KN_3, heat capacity from 5 to 350K 79−55901
KNO_2, polymorphism, calorimetric investigation 78−75827
K_2OsCl_6, low temp. sp. ht. and thermodynamic props. near phase transition 77−39655
K_2ReCl_6, low temp. sp. ht. and thermodynamic props. near phase transition 77−39655

entropy of substances continued
K_2SO_4, effusion studies of vaporisation/decomposition 79−95153
Kr, vapour press., entropy and enthalpy, thermodynamic consistency, two-parameter eqn. 77−80613
$LaCrO_3$, sp. ht., enthalpy, entropy, 298-900K, polymorphic transition 77−69094
LaF_3, heat capacity of 350K, enthalpy to 1477K, calorimetric determ. 78−79781
$LaMnO_3$, stoichiometric manganite form. reaction, thermodynamic characts. 80−108727
$LaNi_5$/H system, thermodynamics of H trapping 80−107444
$LaNi_{5-x}Al_x$ ternary alloys, Al addition effects on structural and H_2 absorpt. props. 79−52761
Li, entropy and enthalpy of solution of H 78−51692
Li, thermodynamics of melting at high pressures 78−91426
Li-Pb liquid compound forming alloy, entropy of mixing 80−88328
Li-Sb(Bi), thermodynamic props., 355-600°C 78−34634
LiAl, β phase thermodynamic props., chem. diffusion coeff., electrochem. meas. 80−39308
$LiAlCl_4$, solid and molten electrolyte, thermodynamic stability 80−107447
$LiAlH_4$, molar heat capacity, thermodynamic props., 10 to 300K 80−44329
Li_3AlH_6, molar heat capacity, thermodynamic props., 10 to 300K 80−44329
$LiBF_4$, thermal decomposition, equilib. decomposition press. and enthalpy of form. 79−91983
Li_2MoO_4, Li_2MoO_7, $Li_2Mo_3O_{10}$ and $Li_2Mo_4O_{13}$, thermodynamic props. 77−12822
Li_3N, vaporisation, studied by Knudsen effusion method 80−92662
$Li_{x+2}P_xO_{3x+1}$, polyphosphate, melting and crystallisation 80−70376
$LuAl_2$, sp. ht. and thermal props., 5 to 300K 77−43342
Mg partial molar thermodynamic data from EMF and calorimetric meas. of Mg-In liquid solns. 80−55359
Mg, phonon spectrum and thermodynamic functions, inelastic coherent cold neutron scatt. *(Russian)* 78−55917
Mg-Ga alloys, form. enthalpies and excess entropies, differential scanning calorimetry *(German)* 79−51278
Mg-Ga system, thermodynamic props. of metastable and glassy phases *(German)* 79−52743
$MgIn_2O_4$ free energy, entropy of form. 78−91433
$Mg(NH_3)_6(ClO_4)_2$, phase exam. by adiabatic calorimetry and X-ray diffr. methods 78−63854
$Mg_yU_{1-y}O_{2+x}$, thermodynamics from EMF meas., high Mg conc. 78−43143
Mn, solubility of N_2, 650-1030°C, 13-25 at.% N range 79−90783
Mn-Ge, thermophysical props., at elevated temp. 80−103493
MnAs, soft mode, energy and entropy, competition with energy and entropy of spin system 79−10908
$Mn_{0.27}Co_{0.73}Cl_2.6H_2O$, antiferromag., sp. ht. meas., phase transition obs. 79−78415
MnF_2, heat capacity and entropy, 10 to 300K, mag. ordering contrib. 77−16080
Mn_3GaN, sp. ht., 6 to 350K, mag. and crystallographic phase transitions 80−71060
Mn_2P, heat capacity, mag. entropy and thermodynamic functions 77−80630
$MnSO_4$, aq. solns., viscosity meas., viscous flow activation energy, entropy *(Japanese)* 77−43363
MnSe, and $MnSe_2$, thermodynamic props. 80−19958
Mn_3ZnN, sp. ht., 6 to 350K, mag. and crystallographic phase transitions 80−71060
MoF_5, vapour, thermodynamic props. calc. 78−38826
MoO_2, Gibbs energies of form., form. enthalpies and standard entropies 79−52742
Mo_4O_{11}, Gibbs energies of form., form. enthalpies and standard entropies 79−52742
N-Fe solid soln. in equilibrium with N_2 gas, partial molar enthalpy and excess entropy 80−60838
N_2, liq., thermodynamic perturbation theory, equilib. props. 79−64976
Na entropy and enthalpy of solution of O(N)(C)(H) 78−51692
Na, liquid, entropy calc. using phonon theory of liquids 80−39310
Na, liquid, eqn. of state and thermodynamic props. at high temp. and density 79−55902
Na, liquid, equation of state, press. and entropy along melting curve 77−47540
Na, monovacancy thermodynamic parameter calcs., temp. dependence 78−2114
Na-Cs, internal energy, heat of mixing, entropy, dielectric function 80−88340
Na-Cs, liq., struct. factor, free energy of mixing, and electrochem. pot., thermodynamic calc. 80−96436
Na-Ga liquid alloy, thermodynamic props. 79−37854
Na-K, internal energy, heat of mixing, entropy, dielectric function 80−88340
Na-Sn liq. alloys, thermodynamic props. by EMF meas. with β-Al_2O_3-Ba_2 electrolytes 79−19379
Na-Te system, liq., electrochem. determ. of thermodynamic props. rel. to temp. 77−1245
$NaAlH_4$ and Na_3AlH_6, molar heat capacity and thermodynamic functions, 10 to 300K 80−65243
$NaAsO_2$ aq. solns., O exchange between $AsO_2(OH_2)^-$, and water 78−92459
Na_2CO_3(s), $NaHCO_3$(s), standard enthalpies of solution and formation, standard Gibbs energies of formation and standard entropy 79−57285
NaCl, Schottky defect, formation enthalpy, entropy, temp. effects, correction 78−10039
NaF:Ca, migration enthalpy and entropy, TSC obs. 80−54716
NaI:Ca^{2+}, pure and doped, lattice defects, entropy and enthalpy of formation and migration 80−96687
$NaNH_4SO_4.2H_2O$, ferroelec. and thermal props. 78−83968
NaO_2, physical mechanisms of phase transitions 80−6381
Na_2O-SiO_2, melt, EMF meas., partial molar enthalpy and entropy 80−6525
Na_2UBr_6, phase transformations, elec. cond. and entropy meas., synthesis *(French)* 78−79763
$NaUO_3$, ht. capacity and thermodyn. props., 5-350K 77−43343
Nb-H system, enthalpy and entropy changes for non-stoichiometric hydride formation 79−52741
Nb-H(D) system, solubility, entropy and enthalpy, isotope effects 77−20069

entropy of substances continued
Nb-Re(Ru)-N, α-solid soln., thermodynamics *(German)* 77−12600
NdF_3, enthalpy, entropy, heat capacity and Planck function from 5 to 350K 80−15257
Ne, molar volumes and thermodynamic props., 25 to 150C, up to 7 kbar 77−42957
Ni alloys, aluminising, thermodynamic anal. of phase transforms. 80−76413
Ni, H adsorption, on (100)(110)(111) surfaces, inert model 80−50889
Ni, oxidation, diffusion enthalpy and entropy 78−7084
Ni-Au alloys, surface segreg., surface energy and solute strain energy effects 77−72760
Ni-Fe alloy, oxidation, diffusion enthalpy and entropy 78−7084
Ni-In, thermodynamic props., phase diagram 77−55949
Ni-Si liquid alloys, thermodynamic props., enthalpy of mixing *(Russian)* 80−34207
$NiAl_2O_4$, entropy of form. determ. using solid electrolyte twin thermocell 78−27812
$NiCl_2$-tetra-n-butylammonium iodide melts, densities and kinematic viscosities 79−77793
$Ni(H_2O)_6(ClO_4)_2$, specific heat meas., 90 to 376K, phase transitions 78−83970
$Ni(NH_3)_6(NO_3)_2$, jumpwise vol. change in structural phase transition 79−42233
NiO, entropy of form. determ. using solid electrolyte twin thermocell 78−27812
NiS_2, high press. effect on mag. transition temps. 78−91866
$Ni_{1-x}S$, metal-semimetal transition, lattice dynamics and thermodynamic props. 80−29324
O_2, liq., thermodynamic perturbation theory, equilib. props. 79−64976
$Os(CO)_5$, chem. thermodynamics 78−18799
P, crystalline to amorphous transition, thermodynamic functions 80−54354
PLZT ceramics, diffuse phase transitions and thermodynamics 80−29694
Pb, evaporation in shock compression release waves *(Russian)* 78−18761
Pb, thermodynamic characterisation, by isobaric expansion meas. 80−103494
Pb-Ag, liquid alloy, exam. of thermodynamic props. using solid oxide galvanic cell 78−75851
Pb-In (40-60 at.%), type II superconducting Ettingshausen effect, transport entropy of vortices 78−56272
Pb-Pd, liq. alloy activity by effusion method *(German)* 79−29023
Pb-Sn, lamellar eutectic alloy, proximity effect, entropies, free energies and transition temps. 77−51849
$PbCl_2$-MCl, (M=Li, Na, K, RB, Cs), molten systems, thermoelec. power 77−62658
PbF_2, sp. ht. meas., Schottky-type diffuse phase transitions, defect form. energies and entropies 80−107441
$Pb_5Ge_3O_{11}$, dynamic central peaks and phonon interactions near structural phase transitions 78−83903
$Pb_{40}In_{60}$, mixed state supercond., Hall and Ettingshausen effects, vortex entropy transport 80−44780
PbO-GeO_2 melt, thermodynamic study 77−59760
PbSe, enthalpy, heat capacity, 300 to 1480K 79−60523
$Pb(Zr,Ti,Ge)O_3$, antiferro-ferroelectric transition 78−95565
Pd, H adsorption, on (111)(110) surfaces, inert model 80−50889
Pd-Ag-H, alloys, 25-50% Ag, thermodynamic props., 555-700K 79−65216
Pd-Au:$H_2(D_2)$, thermodynamic props. at 555 and 700K, vibr. freqs. and excess entropies 80−29186
Pd-Cu, H solubility enthalpy and entropy, effect on elec. cond. 77−35699
Pd-Cu-H(D) dilute alloy soln., thermodynamic props. at high-temp. 79−99334
Pd-D, crystallite size effects, simultaneous sorption and X-ray study 80−65237
Pd-H system, enthalpy and entropy changes for non-stoichiometric hydride formation 79−52741
Pd-Mn dilute alloys, mag. ordering, sp. ht. calc. by Monte Carlo method 77−77030
Pd-Ni(Si), melt, struct. and physical-chemical props., thermodynamic props. *(Russian)* 78−18536
Pd-Pt alloys, soln. of H_3, partial thermodynamic parameters determ. 77−66027
Pd-Rh alloys, soln. of H_2, partial thermodynamic parameters determ. 77−66027
Pr-Al liquid alloys, atomic interactions, thermodynamic props. *(Russian)* 80−39307
PrF_3, heat capacity from 5 to 350K, entropy enthalpy, Planck function 79−46811
$Pr(OH)_3$, electronic heat capacity, 0.45 to 4.2K, phase transition at 1.21K 80−59673
Pt.(111), H adsorption, inert surface model 80−50889
Pt, chemisorption of H, entropy, temp. and press. effects 78−84059
Pt-H solid solutions, thermodynamics 79−77756
PuN, heat capacity, at low temps. 79−24168
$PuRu_2$, intermetallic cpd., sublimation thermodynamics 80−96639
Rb, liquid, equation of state, press. and entropy along melting curve 77−47540
Rb, thermodynamics of melting at high pressures 78−91426
Rb-Hg liquid amalgams, thermodynamic props. determ. from conc. cell EMFs 77−1246
RbI, vaporisation thermodynamics, mass-loss Knudsen effusion, mass spectrometry 79−28093
RbN_3, heat capacity from 5 to 350K 79−55901
$Ru(CO)_{5(g)}$, chem. thermodynamics 78−18799
$RuTe_2$, decomposition press. and thermodynamic props. 78−3366
S-Se(Te)(Tl), liq. semicond., bonding energies and entropies, mag. susceptibility meas. 80−49082
S_7, Raman and IR spectra, vibr. anal., force consts., thermodynamic functions 78−50545
$SbCl_5$, phase diagram to 43 kbar 80−2144
SbI_3, enthalpy, entropy of melting 78−34598
Sb_xSe_y (x=0 to 4; y=1 to 4) molecular species formed in vaporisation of solid $SbSe_3$, thermodynamic props. 80−11943
ScP, thermodynamics and high temp. vaporisation 80−88310
$Sc_{0.8}S$, order-disorder transition, ionic model appl. 80−107096
Sc_xS, high temp. vaporisation, enthalpy, atomisation, dissoc. energies 77−1223

entropy of substances continued
- α-Se, monoclinic, heat capacities and thermodynamic properties, 3-300K 78−95162
- Se, monoclinic to trigonal conversion, thermodynamic stability and associated investigs. 80−24592
- SeTe liquid alloy, effect of branched chain polymers on bond equilib. 80−24348
- Si, entropy and enthalpy of vacancy form., comparison of theory with quenching expts. 77−11872
- Si, self diffusion entropy 80−29211
- Si-Mn(Fe)(Co)(Ni), liquid alloys, thermodynamic charact. calc. *(Russian)* 78−27475
- SiC, polytype relative stabilities, entropy contribs. 80−100197
- β-SiC, thermodynamic props., temp. depend., 5 to 300K 80−96666
- SiO_2-K_2O, thermodynamic approach to ionic conds., statistical model of chem. potential 79−46833
- SiO_2-Na_2O, thermodynamic approach to ionic conds., statistical model of chem. potential 79−46833
- SiP, thermodynamic characts. 10-300K, interatomic bond elasticity 80−59677
- $SmCl_3$, heat capacity and Schottky anomaly, 5 to 350K, entropy 77−47588
- SmS, high-pressure mixed-valence phase, diagram and electronic entropy, neutron diffr. obs. 79−33267
- Sn, single cryst., equilib. vacancy conc., length and lattice parameter change meas. 79−60352
- Sn-Te liquid alloy, thermodynamic meas. 77−73271
- $SnCl_2.2H_2O$, high temp. entropy of ionic model for phase transition 78−55949
- $SnSe_2$, rel. to p-T projection of phase diag. of SnSe-Se 78−27485
- $SnSe_2$, sublimation, temp. depend. of equilib. constants 80−88312
- Sr, specific heat and thermodynamic props. 5-350K 78−47534
- Sr^+, hydration, gas phase clustering mass spectra, thermodynamics, bonding 77−16814
- $SrCl_2$, anion diffusion mechanism 80−2201
- $SrCl_2$, sp. ht. meas., Schottky-type diffuse phase transitions, defect form. energies and entropies 80−107441
- $SrSi_2$, phase diagram, 10 to 40 kbar, 600 to 1200°C, polymorphic transform. 80−29165
- $SrTiO_3$, dynamic central peaks and phonon interactions near structural phase transitions 78−83903
- $SrTiO_3$, form. entropy and tolerance factor 80−34204
- $SrTiO_3$, thermodynamic props. 77−39680
- $SrZrO_3$, form. entropy and tolerance factor 80−34204
- Ta-D, dil. soln., high temp. thermodynamics 78−43128
- Ta-H, dil. soln., high temp. thermodynamics 78−43128
- Ta-O, dil. soln., high temp. thermodynamics 78−43128
- $TaH_{0.75}$, calorimetric study of phase transform. 77−48426
- $TaSe_2$ (2H), microscopic model of CDWs lattice dynamics in commensurate phase 77−89719
- Tb, mag. characts. in strong mag. field 77−89936
- Tb, sp. ht., using lattice dynamical model for HCP metals 79−51273
- $TbPO_4$, sp. ht., 0.5-10K 78−52298
- TcF_6, heat capacity, entropy Gibbs energy, 2.23-350K 78−38852
- Te alloy, intermetallic, melting entropy and molar specific heat 79−29024
- Th-Gd spin glass, low temp. sp. ht. 79−51795
- Th_3As_4, heat capacity meas., 3-500K 80−88769
- ThH_2, $ThH_{3.75}$, heat capacity and thermodynamic props. to 1000K 78−91451
- Ti-Co alloys, absorpt. of H_2, press.-composition-temp. relationships, enthalpy, entropy 80−2267
- Ti-Co alloys, absorpt. of H_2, thermodynamic parameters calc. 80−2268
- Ti-Ni alloys, absorpt. of H_2, press.-composition-temp. relationships, enthalpy, entropy 80−2267
- Ti-Ni alloys, absorpt. of H_2, thermodynamic parameters calc. 80−2268
- α-Ti-O solid soln., hexagonal, thermodynamics 78−3098
- $TiBe_2$, cubic Laves compound, sp. ht. rel. to intinerant antiferromag. 79−82356
- $(Ti_{0.99}V_{0.01})_2O_3$ spin glass, sp. ht. anomaly and entropy change 79−56546
- Tl-Te alloy, liq., bond equilib. theory for electronic props., thermochemistry 77−89365
- $TlCl(Cl_2)$, vap. press. and thermodynamics 80−6503
- TlN_3, heat capacity from 5 to 350K 79−55901
- TlS_x, struct. from radial electron density distrib. curves, entropies of melting and crystallisation 79−23527
- Tl_2SO_4, elec. cond. rel. to thermodynamic props. in phase transitions 77−39690
- Tl_xSe_{1-x}, liquid semiconductor, diamagnetism and paramagnetism, dangling bond paramag. centres, mag. susceptibility obs. 80−44797
- TmF_3, thermodynamic props., galvanic cell meas. 80−21316
- $(U,Pu)O_{2\pm x}$, cluster model approach to thermodynamic props. 77−20093
- U, liquid, electronic density of states, shock vaporization technique 80−29300
- UAs, sp. ht. meas., 5-300K, mag. transition obs. 80−50101
- U_3As_4, heat capacity, 5-300K, ferromag. transition obs. 80−88769
- $UAs_2(Sb_2)$, heat capacities, antiferromag.-paramag. transitions 78−76253
- UC_x, partial molar thermodynamic quantities, semi-invariant cumulants method 80−65250
- UF_4, vaporisation behaviour 80−84283
- UH_3, UD_3, dissoc., isotope effect 80−26174
- UO_{2+x}, configurational entropy of defect complexes, Mayer cluster theory calcs. 79−77591
- U_3O_8, λ-type heat capacity anomalies 77−20080
- U_4O_{9-y}, doped, phase transitions, heat capacity meas. 77−18664
- UPt, weak ferromag., magnon heat capacity, magnetisation and mag. entropy 77−24685
- U_3Si, heat capacity and thermodynamic props., 1 to 1203K 77−72697
- V-Cr alloys, absorption of H_2, thermodynamic parameters 78−87862
- V-Ge, thermophysical props., at elevated temp. 80−103493
- $V_2Hf_{1-x}Zr_x$, normal and supercond. state, transition temps., mag. susceptibility and specific heat determ. *(Russian)* 80−60132
- VN_{1-x}, vacancy ordered structure in cubic mononitride phase, transition entropy determ. 78−43011
- VO_2+I_2 transport react., thermochem., appl. to MoO_2:V cryst. growth 79−43116
- V_3O_5, spin order, one-dimensional, Neel transition 80−39799
- V_5O_9, metal-insulator phase transition temp. depend. on press. 80−29327

entropy of substances continued
- V_6O_{11}, metal-insulator phase transition temp. depend. on press. 80−29327
- V_6O_{11} single crystals, heat capacity anomaly at 172K 78−10197
- V_nO_{2n-1}, Magneli phases, sp. hts. 0.4 to 50K 79−42774
- V_3S_4-V_5S_8 system, exam. of thermodynamic props. at temp. from 650 to 800°C 78−52784
- VSb_2, free-energy, heat and entropy of formation, 430-600°C *(Ukrainian)* 80−7837
- VSi_2, thermodynamic props. determ. using ternary phase equilibria 78−91449
- V_3Si, thermodynamic props. determ. using ternary phase equilibria 78−91449
- V_5Si_3, thermodynamic props. determ. using ternary phase equilibria 78−91449
- WO_3, force field, normal coord. anal., kinetic consts. method, thermodynamic props. 78−25504
- Xe, vapour press., entropy and enthalpy, thermodynamic consistency, two-parameter eqn. 77−80613
- YIG, dissociation press. and Gibbs energy of form. 79−11816
- $YNi_{5-x}Al_x$ ternary alloys, Al addition effects on structural and H_2 absorpt. props. 79−52761
- YbGaG, mag. props. between 44-600 mK 80−80517
- Zn-bearing binary substitutional solutions, thermodynamics 80−44337
- Zn-S system, Zn-rich liquidus, 1000-1300°C 78−18747
- $ZnFe_2O_4$, heat capacity investigation of dopant effects on mag. disordering temp. 80−25143
- $Zn_xFe_yO_4$, heat capacity investigation of dopant effects on mag. disordering temp. 80−25143
- $ZnGeP_2$ dissoc. press., vapour comp. and press., thermodynamic characts. 77−24934
- $Zn_3(OH)_4(NO_3)_2$, sp. ht., 5-300K, thermodynamic props. 79−55900
- $Zn(OH)(NO)_3.H_2O$, sp. ht., 5-300K, thermodynamic props. 79−55900
- $Zn_5(OH)_8(NO_3)_2.2H_2O$, sp. ht., 5-300K, thermodynamic props. 79−55900
- ZnS, polytype relative stabilities, entropy contribs. 80−100197
- $ZnSO_4$, aq. solns., viscosity meas., viscous flow activation energy, entropy *(Japanese)* 77−43363
- ZnS(Se), reaction with Sn chalcogenides, thermodynamic anal. 80−40728
- ZnX_2, ZnXY, X and Y=halogen, matrix isolation IR and Raman spectra 78−55171
- ZrI_4, high-temp. enthalpy, X-ray powder diffr. data 80−107446
- ZrI_4, thermodynamics of vaporisation and high temp. enthalpy 78−91432

environmental engineering
- *see also air conditioning; cooling; ergonomics; lighting; safety; space heating; temperature control; ventilation*
- acoustic planning of plants, technical and economic advantages 80−3561
- advances in environmental science and engineering, book 80−105448
- aircraft noise identification system by correlation technique 79−23131
- applied mechanics computing, conference, New York (1976) 77−67285
- buildings, noise control of mechanical services equipment at design stage 79−18598
- BWR plants, I-131 airborne emission data for environmental impact evaluation 77−38391
- coal conversion technologies, health and environmental effects 80−81493
- community noise, exp. study outdoor sound propagation over hard ground for distances under 200 ft 79−18600
- control equipment noise reduction, steam power, chemical, petrochemical industries appl. 78−51002
- curricula for undergraduate courses 78−77644
- curriculum, interdisciplinary, faculty requirements 79−12553
- developing countries' architectural design for solar energy environmental control 79−57449
- dust control, measurement methods *(Hungarian)* 80−35810
- ELMO-G quiet running vacuum pumps and compressors for plant noise reduction 80−5872
- energy overview course for general audiences 77−37681
- fusion reactors, JT-60, seismic anal., design changes 80−95425
- gas chromatography-mass spectroscopy technique in environmental study *(Japanese)* 79−29496
- heat pumps, energy and environmental considerations in extending appls. 77−17976
- high electric field biological effects on human nervous systems 80−89739
- hydropower reservoir lakes and dams construction, environment protection aspects *(German)* 80−30373
- industrial machinery, sound power determ., environmental corrections 77−39153
- instrumentation for pollution control 78−24363
- Iranian solar town conceptual development 80−35645
- laser fusion generating stations, safety, environmental effects 78−50337
- laser fusion reactor, environment and safety features 78−50333
- metrological servicing in USSR ministry of land reclamation and water management 79−96496
- noise, urban, computer aided evaluation and control *(Japanese)* 79−88033
- noise control program for General Motors Corporation, computerised noise modelling 80−43542
- noise control standards, criteria 79−18597
- noise levels in hospitals, measurement 80−51025
- nuclear fuel cycle impact assessment, oceanic and geological disposal, use of box model method *(Japanese)* 80−9346
- nuclear power generation, safety aspects *(Japanese)* 77−83112
- nuclear power plants, environment protection problems during construction *(French)* 80−76663
- nuclear power plants, environmental research data implementation *(French)* 80−74037
- nuclear power plants, environmental studies organisation *(French)* 80−76664
- nuclear power plants, hydrobiological studies, conception and data obtained *(French)* 80−76665
- power plant effects on environment, protection measures *(German)* 80−26574
- radioactivity meas., fly-ash radioactivity meas., environmental protection *(Polish)* 77−14318
- RWE environment protection organisation outline and functions *(German)* 80−101552
- safety and environmental pollution *(German)* 80−63370

environmental engineering continued
timekeeping clock synchronisation and comparison problems and equipment 77—71302
trace analysis *(Japanese)* 77—87116
transformer substation, audible noise, effect on urban environment 77—3701
transportation effects, public, future outlook 80—35621
USSR metrological provisions for water conservation 79—96495
working position illumination, factors affecting good vision and efficiency *(Spanish)* 80—3638
CO monitoring using automatic functional check *(German)* 77—53883
Si photovoltaic industry, environmental control, economic and ecological requirements 80—94026

environmental requirements *see environmental engineering*

environmental testing
see also corrosion testing
acoustic, aircraft and missiles, effect of intense noise on equipment 79—3853
air pollution monitoring networks, automatic systems 78—93009
Aryabhata, Indian scientific satellite, magnetic testing 78—40793
automated GMN-K gravity meters, marine testing *(Russian)* 79—39953
birefringent filter mechanical tuning techniques 80—102834
cabled fibre, temp. effect on transmission loss and pulse delay distortion 78—1407
chamber, Oblako universal gas-water vapour generator, humidity test facility 80—62653
climatic, features of McKinley laboratory for aerospace testing 79—16798
climatic test chambers, automation using microprocessor programmers 80—21430
coatings in space environment 78—85827
component reliability tests in thermal neutron environment 78—21787
composite insulating materials, fatigue behaviour, influence of superposition of elec., mech. and environmental stresses 80—97590
curriculum, interdisciplinary, faculty requirements 79—12553
Darrieus rotar windmill arrays, wake interaction, wind tunnel simulation 80—61245
electric soil moisture gauges, testing procedure 77—78481
electrical contact materials, corrosion test *(German)* 80—55561
electronic components, space radiation environment effects, laboratory simulation 80—94689
electronic systems role in environmental monitoring in India 77—41146
epoxy polymers, high temp./press. materials test for undersea environment 78—3213
equivalent continuous noise levels, instrument design, electronic 77—65654
European nonreflective solar cell qualification 79—96477
fibre optical cable, buried, transmission characts. meas. *(German)* 78—33865
filters for airborne radioactive particles, Winfrith, double automatic Pollak counter 78—33301
graphite fibre filled polyimide composite laminates, space environment, phys. and mech. response 80—81140
high efficiency particulate air filters, efficiency testing at large pressure transients rel. to nuclear facility safety 79—81020
hybrid fibre optic/electrical connector, environmentally sealed, multispin, cylindrical 79—41457
Inconel 718, environment effect on high temp. fatigue crack growth 80—30090
industrial aerodynamics, conference, Aachen 80—17712
industrial machinery, acoustic environment improvement for in situ meas. 77—39155
Isaacs wave-energy pump, field tests around Hawaii 79—57354
materials testing, environmental simulation *(German)* 79—20314
medium-range data transmission optical cables 77—39096
modified Andersen impactor and All Weather Sampler Inlet, wind tunnel tests 78—3926
multilayer dielectric enhanced mirrors for 2 to 6 μm 79—14086
multiple shaker testers, production and military applications 80—64276
nuclear facilities *(German)* 80—35356
ocean current meters, for continental shelf deployment, development and testing 79—5674
optical coating requirements in United States military specifications 80—48365
optics in adverse environments, conf., San Diego, USA (Aug. 1977) 78—82976
paradigm for environmental considerations in material system design and testing 80—26192
photographic film, Skylab environmental effects 77—60620
photovoltaic modules testing, reliability and performance 80—94063
PIXE analysis of trace elements in environmental samples *(Chinese)* 79—61925
pneumopress, for extracting interstitial water from marine sediments 80—26643
polyethelene tubes and sheets, light resistance investigation under natural climatic conditions 80—21127
polyurethane, high temp./press. materials test for undersea environment 78—3213
PWR containment vessel wall electrical penetration tests *(Japanese)* 79—6747
random loading 79—87803
SAW device production and test programme progress report 78—59206
snowgauge measurements, Canada, accuracy 79—70818
soil warming, waste heat from nuclear power station 78—37463
solar array sample accelerated thermal cycling facility 79—96458
solar photovoltaic flat panel procurement, qualification test results 80—94064
space qualification of optical instruments, using long duration exposure facility 78—85826
Space Shuttle, environmental effects during launch and reentry 78—85681
Space Shuttle payload verification requirements 78—85812
steel, stainless, 18Cr-2Mo-Ti, atmospheric corrosion 80—85078
submerged self-contained buoy station, expt. launchings 80—26642
tactical rugged lightweight fibre-optic cable performance 79—37025
terrestrial solar cell reliability, accelerated stress testing 79—74528
terrestrial solar cells, accelerated stress testing 79—92083
thermal meas. using digital systems 78—81966
thin dust layers, particle size effects automatic correction, computer appls. in spectrometry 79—83539

environmental testing continued
thin solar cells, advanced module technique 80—94041
Ultra Lightweight Panel solar array development and testing 79—96473
Viking Lander environmental test programme 77—56810
Ag, corrosion in atmosphere, environmental test 79—66205
Al-brass tubes, passivation treatment for atmospheric corrosion protection during storage and transport 80—85079
Al-Cu-Mg-Fe-Ni, Hiduminium RR58, crack propag. rates in air and salt soln. 80—21063
Al-Si-Cu, LM30, crack propag. rates in air and salt soln. 80—21063
CO_2 conc. regulation in climatic cabinets for corrosion testing *(German)* 78—53069
Cu, corrosion in atmosphere, environmental test 79—66205
Cu-Ni-Zn alloy, surface comp., outdoor exposure influence 80—59770
Cu-Sn alloy, surface comp., outdoor exposure influence 80—59770
Cu-Zn alloys, surface comp., outdoor exposure influence 80—59770
$Cu_{2-x}S$-CdS ceramic solar cells, solar batteries operating characts. 80—93874
GaAlAs-GaAs DH laser diodes, long-life diodes for optical fibre communication 80—48246
$Li/SOCl_2$ cells, abuse tests 80—97776
$LiAl-NaAlCl_4-MoCl_5$ thermal battery test results 79—29459
Ni, corrosion in atmosphere, environmental test 79—66205
$Ni-H_2$ battery for satellite energy storage 80—81430
Si solar cells, base resist. influence on temp. characts., temp. cycling 80—89618
Ti-Al-Mo-V (8, 1, 1 wt.%), environmental fatigue crack propag., texture influence 79—91802
Ti-Al-V (6, 4 wt.%), environmental fatigue crack propag., texture influence 79—91802
W protective coatings, CVD, for components in contact with HTR-He 79—626

epitaxial growth
see also liquid phase epitaxial growth; vapour phase epitaxial growth
alkali halide, lattice fitting role in epitaxy 78—34728
basic methods, thermodynamic and kinetic growth *(German)* 79—43142
binary systems containing one chemical cmpd., reaction kinetics and diffusion *(Russian)* 79—87014
book, current topics in material science 80—46747
chalcogenides, epitaxial growth, role of lattice fitting 78—34728
chemical problems, book 77—12524
covalently bonded materials, surface reconstruction effects, review 77—89669
crystalline polymer, epitaxial crystallisation on surface of drawn polytetrafluoroethylene 78—14626
diamond, olivine inclusion epitaxy 77—78173
diamond-like semiconductor film epitaxial growth, computer simulation 80—70560
directory of crystal growth and solid state materials production and research 79—65988
disorientation degree, of layers on monocrystn. supports, determ. by interferometry *(Russian)* 80—24748
electronics appl., 1979 technology status *(French)* 79—95928
ferrite garnet film growth, automatic machine 78—27418
III-V semiconductors, radiative recomb. and related phenomena, conference, Prague, Czechoslovakia (Sept. 1979) 80—51940
implanted amorphous layer reordering 77—76435
incommensurate epitaxies at finite temps., substrate pot. effect 80—88451
large misfit systems, epitaxy and misfit dislocations 80—24767
lattice misfit in epitaxy 79—46970
localized, morphology analysis 79—99089
materials science, current topics, book 79—69966
metal condensation on alkali halide, nucleus saturation density and epitaxy 78—18928
metal films, on alkali halide substrates, nucleation and growth, surface study techniques, review 80—10809
metals, epitaxial growth, role of lattice fitting 78—34728
metastable compound synthesis with high supercond. transition temp. 80—93024
method of depositing quasi-single cryst. film on any other film 77—32536
mode of growth, numerical confirmation of Palmberg's criterion 77—11812
monolayers on crystal substrate, orientational ordering of incommensurate structure, static distortion waves 77—59235
nucleation theory 78—75961
orientation mechanism, determ. for model system of AgCl on TGS 79—11022
polyoxymethylene, epitaxial growth on KBr single crystal *(Japanese)* 78—56054
rare-earth dihydride epitaxial films, growth and struct. 79—37936
review, growth modes, book contrib. 80—49558
review, struct. and topological aspects, state of art *(French)* 79—4483
semiconductor epitaxial structures, atomic diffusion 77—85110
semiconductor film-substrate boundary, epitaxial interface form. and transition regions 80—10821
semiconductor materials preparation, late 1970s innovations 80—6666
semiconductors, laser annealing after ion implantation, temp. distrib. 80—54265
solar cells, materials aspect, review 80—50971
solid films and surfaces, conference, Tokyo, Japan (Jul. 78) 80—10739
solid phase epitaxy, book contrib. 79—1825
solid phase epitaxy *(Japanese)* 79—38738
stepped substrate-adsorbed layer interaction, selective effect on epitaxy 78—14616
surface structure, distribution of defects, LEED 80—44402
ternary semiconductors, chalcopyrite struct., RHEED exam. of epitaxial overgrowth *(German)* 79—11042
TGS, crystallisation by epitaxial germination *(French)* 77—21040
TGS, epitaxial growth method from soln., on Ag layer 77—32536
thin film Congress Loughborough, England, (Sept. 1978) 79—77949
Udimet 700, superalloy, convective processes during epitaxial regrowth 79—69919
Ag-Cu (6.6% at.wt.), convective processes during epitaxial regrowth, expt. results 79—69919
AgCl, on Ag, form. by Cl adsorption, RHEED 78—14642
Al film, epitaxial growth on MgO, effect of weak interfacial interactions 77—1325

epitaxial growth continued
Al film, influence of predeposited island film on crystallisation of continuous film 78−18930
Ar adsorption on graphite, orientational epitaxy in self-consistent phonon approx. 79−95261
Au film, influence of predeposited island film on crystallisation of continuous film 78−18930
Au-Ge contacts on GaAs, SEM and TEM obs. of struct. 80−100522
CdS, epitaxial layers on Cd single crystal, direct synthesis and struct. 78−68628
CdS-CdTe solar cells fabrication, thin film *(Japanese)* 79−87992
Cu, adsorbed on W, FIM and FEM obs. of nucleation, epitaxial growth on interface form. 78−26800
Fe growth on Cu(111), supersaturation and mode of growth, LEED and AES exam. 78−18929
GaAs, ion-implanted, laser pulse annealing of amorphous surface layer, TEM 80−55436
GaAs-metal ohmic contacts, solid phase epitaxy formation, AES and channelling meas. 79−60658
GaP films on Si, epitaxial crystallisation by nanosecond laser pulses 80−107674
Ge, amorphous, growth rate of crystallisation, Raman spectroscopy study 80−44227
Ge, amorphous layer, comparison of laser and electron beam pulsed annealing 79−69374
Ge, amorphous layer, on single cryst. Si, heteroepitaxy by laser annealing 79−77952
Ge films on semicondcuting substrates with diamond structure, computer model of autoepitaxial growth 79−95927
Ge, ion-implanted amorphous, epitaxial regrowth on Ge 77−35835
Ge, solid-phase epitaxial growth through PdGe layers, channelling and backscatt. obs. 77−85936
$K_xLi_{1-x}NbO$ films, epitaxial growth by melting on $K_{1.5}Bi_{1.0}Nb_{5.1}O_{15}$ substrate 79−33204
$MgAl_2O_4$, spinel, epitaxial growth by solid-state reaction of MgO with molten Al 77−8751
$MgO:Li^+(Na^+)$, precipitation rel. to dislocations *(French)* 79−51163
Nb_3Si, ion implantation synthesis, supercond. transition temp. optimization 79−38218
Ni, ion-implanted and virgin, laser irrad. effect, epitaxial lattice regrowth 80−108306
Pd-Si structure, epitaxial silicide growth, LEED and AES study 80−103590
Pd_2Si film on Si, substrate temp. effect on microstruct., TEM obs. 78−14621
Pt_2Si film formation, AES exam. to characterise impurity effects 79−15054
Si, amorphous, epitaxial regrowth by pulsed laser beam 78−91554
Si, amorphous, epitaxial regrowth, structure and impurities effect 80−84401
Si, amorphous, laser-induced epitaxial regrowth, substrate and doping effects 79−56082
Si, amorphous, Si implanted, substrate-orientation depend. of epitaxial regrowth rate 78−79900
Si, amorphous deposited, laser induced epitaxy 79−69372
Si amorphous film, vacuum deposited, microscopic voids, gas absorpt., crystn. study 80−49534
Si, amorphous layer, comparison of laser and electron beam pulsed annealing 79−69374
Si, amorphous layer, epitaxial growth by laser annealing 78−79899
Si amorphous layer, ion-beam induced epitaxial regrowth 79−69378
Si amorphous layer, solar furnace annealing to induce solid-phase epitaxy 80−2277
Si, amorphous layer crystn., effect of ^{16}O, ^{12}C, ^{14}N and inert gases 78−14623
Si amorphous layers, on Si substrates, deposited and ion-implanted, laser-annealing behaviour 79−69373
Si, amorphous layers, recrystallisation, pulsed laser annealing 80−65404
Si bridging epitaxy from Si windows onto SiO_2, ruby laser pulse annealing 80−44441
Si, crystal defects in integrated circuits, review 78−88547
Si, defects, solid-phase epitaxy process, rel. to Si dissolution into Al 78−95188
Si electron beam deposited film, epitaxy by pulsed laser annealing 78−56055
Si epitaxial growth on porous Si layer, struct. 79−1557
Si epitaxial layer, large-area uniform growth through Al film by solid epitaxy 78−3033
Si epitaxial layer regrowth due to laser annealing mechanism, liquid and solid phase regimes 80−100712
Si, epitaxial regrowth of thin amorphised layers by laser annealing, absorpt. coeff. influence 79−46968
Si, epitaxy by solid phase crystn. of amorphous film 78−19663
Si film, crystallographic orientation using surface relief grating and laser crystn. 79−95277
Si, graphoepitaxy on fused SiO_2 using surface micropatterns and laser crystn. 80−70554
Si implanted with ^{31}P, ^{75}As, ^{11}B, amorphous layer reordering 78−14622
Si, ion implantation, high dose, solid phase epitaxial regrowth 80−103380
Si, ion implanted, annealing by ion beam heating 80−103382
Si, ion implanted, difference between ruby and Nd:YAG laser annealing 79−37723
Si, ion implanted, laser annealed, elec. props. and annealing kinetics 79−69508
Si, ion-implanted layers, crystn. by ns laser pulses, TEM and RHEED 80−100421
Si, ion-implanted layers, epitaxial regrowth by laser beam and flash annealing 80−100420
Si, laser annealing after ion implantation, temp. distrib. 80−54265
Si, laser irrad., anisotropic melting and epitaxial regrowth, surface struct. 79−33163
Si layers, solid phase epitaxial growth temp. depend. 78−10305
Si layers, solid phase epitaxial growth, crystalline qualities, ^4He backscatt. and TEM exam. 78−10306
Si, local mechanical defects, annealing and effect on autoepitaxial growth *(Russian)* 80−7701
Si, planarized solid state epitaxy for Schottky barrier diodes 78−35302
Si, silicide forming systems, solid phase epitaxy 78−23613
Si, solid phase epitaxial growth through Al film 79−24432

epitaxial growth continued
Si, solid phase epitaxy, Si⟨100⟩/Pd_2Si system, dissoc. mechanism 77−7980
Si solid phase grown, structural obs. 78−2397
Si, solid-phase epitaxial growth, rapid 77−21022
Si, solid-phase epitaxial growth stages in Si(crystal)-Pd_2Si-Si(amorphous) system 77−85114
Si, solid-phase epitaxy in Si (100)/Pd_2Si/Si (amorphous) system, radioactive tracer obs. 77−89663
Si, solid-state epitaxial growth of amorphous layer 80−10803
Si substrate solar cells, upgraded metallurgical grade, epitaxial growth 80−93905
Si surface, reduction growth, autoepitaxy *(Russian)* 80−107672
Si, surface structures after pulsed laser annealing, LEED obs. 80−54494
Si:Ar, ion implanted, amorphous, epitaxial regrowth 79−10868
Si:Ar, ion-implanted, epitaxial regrowth by laser annealing, microstruct. 80−84404
Si:As, CW laser annealing mechanism, annealed spot size, solid phase epitaxial regrowth 79−78798
Si:As, ion implanted, laser annealed, lattice defects, epitaxial regrowth 80−103334
Si:As, ion implanted, pulsed laser annealing, partial solid-state regrowth 80−103591
Si:As, ion implanted, two-step annealing, TEM study 79−82249
Si:As, ion-implanted, CW IR laser annealing 80−34022
Si:As,Sb, amorphous, damage depend. of epitaxial regrowth during annealing 78−47679
Si:Bi, ion-implanted, solid phase epitaxial growth during annealing, supersaturated solid soln. form. 80−103384
Si:In(Sb), incorporation of implanted impurities during amorphous layer regrowth 79−55761
Si:Ne(Ar)(Kr), amorphous, implanted and sputtered, epitaxial regrowth, influence of noble gas atoms 80−2289
Si:Ne(Kr), ion implanted, amorphous, epitaxial regrowth 79−10869
Si:Sb, epitaxial regrowth of amorphous layers created by high-dose Sb implantation 78−30654
Si:Sb,P, double implants, residual defect reduction after damage anneal 80−88170
Si/Pd system, solid phase epitaxial growth control by C ion implantation 80−75466
Si-Al interface, solid phase epitaxial growth of Si 80−34324
Si-Al solid-phase epitaxial growth, substrate effects, SIMS and backscatt. spectra 79−42421
Si-$CoSi_2$Si, double heteroepitaxy, solid phase and MBE 80−104063
Si-Pd_2Si heterostructure growth by solid-phase epitaxy from Si (111)-Pd-Si (amorphous) 77−51617
Si-Pd_2Si Schottky barrier diode grown by solid phase epitaxy 77−80837
Si-Pd-Si structure, epitaxial growth, backscattering and transmission electron microscopy studies of layered structures 80−80123
SiC epitaxial layers, crystallographic orientation effects on polytype stabilization and transform. 79−42413
Si(111) reconstructed 7×7 surface superlattices, microdomain model 80−107625
Si⟨111⟩/Al/Si, growth kinetics of ⟨111⟩ Si through Al layer by solid phase epitaxy 79−28236
Te-Se-CdO struct., fabrication and characts. 78−76106
Tl-Se-$TlInSe_2$, struct. and growth peculiarities, epitaxial heterojunctions *(Russian)* 79−11038

epitaxial layers
see also magnetic epitaxial layers; metallic epitaxial layers; semiconductor epitaxial layers
anthraquinone, UV light effect on nucleation during crystallisation on anthracene surface 80−75478
anthrone, UV light effect on nucleation during crystallisation on anthracene surface 80−75478
benzene, on metal (111) substrates, surface struct., LEED obs. 79−86969
benzoic acid, ENSH method of oriented thin film growth 79−99443
commensurability in one dimension at nonzero T 79−35655
conductivity, rectangular waveguide, control rect. E_{112} mode resonator, sensitivity analysis *(Russian)* 77−18052
diamond-graphite epitaxial film deposition on diamond substrate 77−4271
dislocation energy near epitaxial interface 77−43457
dislocation structure at stress measurement, theory 80−2017
durene, ENSH method of oriented thin film growth 79−99443
ferroelectric, appl. of electron microprobe methods 80−44443
film/substrate interface, misfit dislocation obs. using electron microscopy 80−103605
heteroepitaxial, misfit, strain and dislocations, book contrib. 79−82499
heteroepitaxial layers, dislocation structures, problems of formation 80−15100
heterojunction, compositionally graded, misfit dislocation energy calc. 77−59237
ice, on metal (111) substrates, surface struct., LEED obs. 79−86969
island mobility, one-dimens. model sinusoidal pot. 80−44457
islands, equilibrium struct., one-dimens. model 79−15035
LPE film property control, regression eqns. 79−33200
magnetoresistance, unified weak-field, for cubic and noncubic (001)- and (111)-oriented epitaxial films and surface layers 79−47110
monolayer, 2-D, and 1-D electron gas and 2-D Coulomb gas, family of mappings 80−34346
multilayer heteroepitaxial structure, stress calc. 77−72798
multilayers, solid, liquid, dielec. consts. meas. at microwave freqs. 79−2791
naphthalene, ENSH method of oriented thin film growth 79−99443
naphthalene, on metal (111) substrates, surface struct., LEED obs. 79−86969
n-nitroaniline, UV light effect on nucleation during crystallisation on anthracene surface 80−75478
NMP-TCNQ, oriented, prep. by vacuum evaporation and properties obs. 79−15040
orientation mechanism, determ. for model system of AgCl on TGS 79−11022
periodic misfit-dislocation networks, electron diffr. 78−59815
phthalocyanine, metal-free, molecular imaging and phase transformations using electric microscopy 79−33198
polyethylene, epitaxial crystallisation, IR investig., macromol. struct. changes 77−35493

epitaxial layers continued
polyethylene crystal, preferred orientation relationship, epitaxy 78—67923
polyoxyethylene, epitaxial crystallisation, IR investig., macromol. struct. changes 77—35493
polyurethanes, epitaxial crystallisation, IR investig., macromol. struct. changes 77—35493
resistance meas., using meter based on spreading resistance probes *(Polish)* 79—88981
snow, epitaxial relationship during three dimensional dendrite form. 79—23875
solid-solid interface, chemistry and physics, book contrib. 79—1551
steel, magnetite film formation at metal scale interface, during cooling 78—88575
structure and properties, basic relationship 78—6236
superlattices, one- and two-dimens., possibility of X-ray and electron diffr. struct. determ. 80—54560
surface relief obs. of single crystals using epitaxial replicas 77—51577
TGS epitaxial thin film, IR absorption spectra *(French)* 78—35129
TGS-d, TGSe-d, IR transmission spectra *(French)* 78—72742
TGSe, IR trichroism, epitaxial prop. process 77—63475
three-dimensional epitaxial crystallite nucleation at substrate grain boundaries 77—76707
thulium phthalocyanine, mol. image in high resolution electron microscopy, radiation damage effect 80—107203
transition regions, formation and reduction methods, size effects, review 78—14630
X-ray double-crystal method using nonparallel setting for lattice mismatch meas. between epitaxial layers and substrates 79—28235
X-ray fluorescence and diffr. anal. 80—3451
AgBr, conductance, reversible variations meas. 78—10588
AgBr, thin epitaxial layer, surface ionic cond., lattice disorder, space charge region 77—11730
AgBr(Cl) vapour-deposited epitaxial film, surface structure 80—59814
AgCl, Cl_2 adsorption on Ag, energetics and structures 79—87000
AgCl, on Ag, form. by Cl adsorption, RHEED 78—14642
Al_xCy, on diamond 77—72758
AlN, epitaxial film growth by MBE, physical and optical props. 80—2293
BP wafers, epitaxial growth by thermal decomp. of $B_2H_6+PH_3$, struct. imperfections 77—62774
BaO, cathode poisoning due to O_2, CO_2, and S, surface anal. 79—42600
BaO, single cryst. on Ir, electron affinity, conduction band edge position, low energy electron reflection spectra 78—14790
BaO, surface pot. meas., cond. band edge, electron affinity, LEER 77—24606
$BaTiO_3$, exoelectron emission obs. of phase transition 79—74069
$BaTiO_3$, ferroelectric, appl. of electron microprobe methods 80—44443
$BaTiO_3$, vacuum condensates, epitaxial growth on $SrTiO_3$ crysts., electron diffr. and TEM anal. 79—15051
Bi epitaxial film, twinning, electron diffr. 77—35838
Bi, epitaxial films, grain boundary struct., electron microscopy obs. *(Russian)* 79—46671
Bi epitaxial films, size effect in elec. props. 80—54813
Bi film, elec. cond., obs. of epitaxial growth mechanism *(French)* 78—84329
Bi, magnetoresist., EM meas. in mag. fields up to 85 kG 77—32095
Bi, orientation on mica, effect of deposition parameters 77—28085
Bi-Sb, bicrystal rearrangement of grid of nonconformity dislocations on (111) interface during heating 79—28215
$Bi_{0.9}Sb_{0.1}$, epitaxial film, defect struct. and galvanomagnetic props. 77—89889
$Bi_{1-x}Sb_x$ epitaxial layers, effect of film thickness on elec. props. *(Russian)* 79—11244
$Bi_{12}SiO_{20}$:Nd, light absorpt. and transmission spectra, photoluminescence spectrum, optical absorpt. coeff. 79—74001
$Bi_{12}TiO_{20}$, RF sputtered epitaxial film on $Bi_{12}GeO_{20}$, for optical waveguiding 78—9462
$(BiTm)_3(FeGa)_5O_{12}$ ion implanted epitaxial garnet film, bubble domains, cryst. struct. disorder 80—93150
CaO, on Mo, secondary electron emission, struct. effects, LEED and AES expts. 78—2959
$Co_xMg_{1-x}O$, EPR of Co^{2+} *(Russian)* 80—11251
CoO, XPS obs. of formation on Co (0001) 80—66396
Cr_2O_3-Cr black, solar collector coating, microstruct., FIM and SEM obs. 80—26166
Cu, epitaxy in aqu. oxidation of (001) single crystal 80—11844
Cu_2O, on Cu (111), misfit dislocations, TEM obs. 78—14629
Cu_2O, on Cu(111), misfit dislocation annealing, TEM obs. 79—82228
Cu_2S, epitaxial overgrowths on Cu films, characts., TEM and RHEED obs. 78—84101
Cu_2S, epitaxial overgrowths on Cu(111), struct. and morphology 79—82494
$Cu_{2-x}S$, digenite, electron diffr. 77—85117
Fe-Cr, oxidation, in H_2/H_2O vapour mixtures, epitaxial oxide phase formation, effect on oxidation 78—88568
$Ga_xAl_{1-x}N$, epitaxial film, cathodoluminesc. 80—25469
GaAs, VPE by single flat temp. zone method, elec. props. 79—95526
GaAs:Si(Cr), LPE, spiral growth patterns, dopants role 77—72800
Ge, epitaxial layer deposition by vacuum pyrolysis 78—52676
$KNdP_4O_{12}$ epitaxially grown waveguide, laser operation at 1.051 μm 79—18423
Kr, epitaxial monolayer on graphite, second order phase transform. obs. by LEED 77—76687
Kr monolayer, on graphite, misfit dislocations and lattice parameters, model 78—34708
LaB_6:C, AES, LEED and energy-loss spectra study of C layer on (100) surface 77—62715
$Li_{1-x}Na_xNbO_3$, LPE, growth and temp. coeff. of SAW velocity 78—43227
$LiNbO_3$ film on Al_2O_3, optical guided wave mode conversion by Love waves 79—46055
MgO:Be epitaxial layers, vacuum UV luminescence 80—11480
MnO, EPR spectra of ceramic and epitaxial monocrystalline thin film samples *(Russian)* 80—11252
NH_3, on metal (111) substrates, surface struct., LEED obs. 79—86969
Na (111) surface, epitaxial film, electron induced dissociation 80—6646
Nb_3Ge, high T_c film with impurity expanded lattice, form. and stabilisation 79—56099
$Nd(Ga,Cr)_3(BO_3)_4$, cryst. growth by LPE, Nd^{3+} fluorescence, lattice constants 80—29883

epitaxial layers continued
NdP_5O_{14} single crystals grown from polyphosphoric acids, morphology control 80—15395
$Nd_{0.14}Y_{0.86}P_5O_{14}$ epitaxial layer an $Gd_{0.33}Y_{0.67}P_5O_{14}$, growth lasing 77—46722
$Ni_3B_7O_{13}Cl$, boracite, on Cr-Cl boracite, gas phase synthesis of epitaxial layers 79—60650
$NiSi_2$ epitaxial film on (111) Si substrate, interfacial order, backscatter, channelling study 80—65390
PbS, surface relief of NaCl single crystals using epitaxial replicas 77—51577
Pd_2Si epitaxial islands on Si (001) substrate 80—96748
$(SN)_x$, acoustic and optical phonons, Raman, i.r. and transmission spectra 77—4642
$(SN)_x$, elec. resist., 0.03-8.9K, possible supercond. 77—15970
$(SN)_x$, optical props. and plasmon dispersion from electron energy loss spectra 77—35882
Sb, epitaxial growth of electrodeposits on oriented single crystal Au and Ag 78—43267
Si:Al epitaxial layers, nuclear microanalysis of Al impurities $^{27}Al(d,\alpha)^{25}Mg$ 80—61193
Si:Bi, ion-implanted, solid phase epitaxial growth during annealing, supersaturated solid soln. form. 80—103384
SiC, epitaxial film, effect of impurities on polymorphism during growth 80—15414
SiC, polytypic forms determ. from Kikuchi electron diffr. patterns 77—31566
SiC, reaction-bonded , 'REFEL', microstruct. characterization 80—97490
SrO, on Mo (110), secondary electron emission and struct., LEED and AES expts. 78—2958
$TlBiTe_2$, struct. anomalies, TEM 77—11824
TlBr, polymorphism, XPS obs. 80—97398
TlCl, polymorphism, XPS obs. 80—97398
TlI, on KCl, epitaxial growth habit rel. to optical scatt. 77—50738
UO_2 epitaxial films, epitaxial, channelling studies 79—49683
W epitaxy on W(110) substrate, work function meas., LEED investigation 80—80103
W layers on Mo, exam. of epitaxial orientation, and deposition *(Russian)* 79—11039
Xe monolayer, on graphite, misfit dislocations and lattice parameters, model 78—34708
ZnO monocrystal and RF sputtered heteroepitaxial film, SAW attenuation comparison 79—56063

epitaxy *see epitaxial growth*

EPR line breadth
alaninium copper tetrahalides, exchange, mag. anisotropy, and spin diffusion contribs. to EPR linewidth 80—80597
alkali halide:Ag film, EPR and optical exam. of Ag impurity centres 77—85562
alkali halides, ^{14}N impurities, molecular point defects, EPR isotropic hyperfine triplets 80—2636
ammonium acetate, irrad. crysts., freq. swept ELDOR obs. at 77K, resolution of spin packets 79—95686
anisotropic media, line broadening of ESR spectra of spin probes 77—12203
anthracene, EPR linewidth of triplet excitons 78—15011
anthracene, EPR of triplet excitons, source of residual linewidth 79—15338
anthracene-tetracyanobenzene charge-transfer complex, EPR of triplet excitons, phase transitions 77—28425
antisymmetric exchange effects on mag. reson. and relax. 77—59448
α-B, rhombohedral, magnetic props. and ESR spectra 80—20452
benzil, free radical adducts, organometallic group dynamic migration, EPR 77—58049
benzophenone, migration of triplet excitons, EPR profiles and phosphoresc. decay data 80—84641
BEPC, nematic liquid crystals, EPR of slowly tumbling VO^{2+} spin probes 79—50985
biomolecular EPR and saturation transfer EPR spectra at high microwave field intensities 79—34488
biradical metal chelates, rot. motion in polar solvents, rel. to ESR lineshape 80—27994
bottlenecked EPR, singly, doubly, multiply bottlenecked systems 78—27078
broadening effects associated with cryst. imperfections, theory 78—35021
d-camphor, NO diffusion, ELDOR, self-diffusion 77—1618
carbonisation, ESR study of kinetics, mesophase formation 79—96045
CBOOA:nitroxide, liq. cryst. phase transition study by electron spin relax. *(French)* 79—55874
CESR line profile, indirect spin spin interaction 79—28616
CESR line-width and g-shift anisotropy, singularities, appl. to Ag 77—20705
CESR transmission, surface relax. effects 79—61218
charge transfer crystals, mixed, exciton transport, low-dimensional, statistical model and experiments 80—65461
computation, fast, EPR (ST-EPR) spectra, master supermatrix eqn. soln. 78—62213
conducting media, EPR line shape, magnetoresist. effect 80—84638
copper di-isopropyldiselenophosphate, soln. anisotropic g and hyperfine tensors, ESR linewidth meas. 79—85978
copper formate urea hydrate, two dimens. antiferromagnet, EPR, temp. depend. 80—54937
copper phthalocyanine, polycrystalline, forbidden ESR transition 79—95638
crystal orientation dependence of ESR line profile 80—15786
cyclodextrin, trapped electrons in cryst. matrices, ESR, optical absorption spectra 78—80768
cyclohexane, NO diffusion, ELDOR, self-diffusion 77—1618
$DEM(TCNQ)_2$, ESR study 80—97127
di(ethyleneammonium) manganese tetrachloride, 2-dimens., EPR linewidth and spin-dimens. crossover 77—69670
diamond, ultradisperse, ESR, particle size and lattice microdistortions 80—97140
3,3′-diethyl-2,2′-selenacyanine-$[TCNQ]_2$, elec. cond., and quasi-two-dimensional mag. props. 78—6564
diethylammonium copper chloride, non-Lorentzian EPR lineshape and magnetostatic modes 77—43862
diethylammonium manganese chloride, 20 spin diffusion, EPR linewidth meas. 79—47289

EPR line breadth continued
diethylammonium manganese chloride, Heisenberg magnet, spin diffusion, EPR study 80—66019
diethylammonium manganese chloride, planar Heisenberg magnet, spin diffusion, EPR study 80—15793
5,6-dihydro-6-methyluracil, X-ray irrad., free radical form; ESR spectra obs. 80—50189
dilute paramagnet, mag. reson. linewidth due to two-particle interaction 77—90012
dimethyl ammonium copper manganese tetrachloride, EPR study *(German)* 80—54941
dipolar interaction, reduction by off-resonance phonon avalanche 77—63260
directional field dependence of ESR and relaxation 78—91931
DPPH, polycryst., forbidden EPR transition 78—48044
dynamic Jahn-Teller effect in ESR spectra, Green's functions calcs. 80—84643
echo decay beats, coherent averaging of electron spins by rotary echoes 79—42823
enhancement of longit. paramag. susceptibility under inhomogeneous broadening conditions 78—19308
ESR spectrometry, anal., cavity loading effects 78—7253
ESR spectroscopy, spectra collection and anal. using KRS-4200 minicomputer *(German)* 78—57998
exchange narrowing including spin correlations and local field contribs. 77—40060
F- and F$_A$-centres, EPR and spatial extn. of relaxed excited state 79—73812
fast relaxing centres, in paramag. cryst., spin-lattice relax. *(Russian)* 79—15340
ferric haemoglobin chains, crystalline state disorder and hyperfine component line widths 79—34482
ferric haemoglobin single crystals, contribs. to EPR line width 79—34484
ferroelectrics, EPR spectra above crit. temp., cluster theory for dynamic crit. phenomena 78—6566
ferromagnet, quasi-two-dimensional, EPR at high temp. *(Russian)* 80—11243
ferromagnet, with anisotropic exchange, homogeneous relax., time const. calc. 77—16149
ferromagnetic semiconductor, CESR in strong alternating electric field 78—35038
ferromagnetic semiconductor, CESR line width, two-magnon exchange splitting 80—29621
free radical EPR saturation corrections 77—48963
free radicals in nonviscous soln., electron spin-echo theory 77—3386
free radicals in soln., spin exchange and EPR broadening 78—52357
gas phase, EPR linewidths and intermol. pots., quantum calcs. 77—34665
Gaussian second derivative lines, modulation broadening calcs. 77—16147
graphite, EPR, effect of motional averaging, anisotropy, skin effect rel. to heat treatment and neutron irradiation *(French)* 80—34752
graphite, polycryst., EPR meas. rel. to temp., crystallite orientation, paramag. suscept. 78—35023
graphite intercalaction compounds with acceptor molecules, CESR 78—48042
graphite lamellar cpds. with Li, K, Rb, HNO$_3$ and SO$_3$, EPR studies 80—44902
guanidinium aluminium sulphate hexahydrate:Mn^{2+}, NMR 78—91939
Heisenberg one dimensional magnet, single ion anisotropy, magic angle line width in high temp. limit 77—51870
hyperfine ESR spectra, exchange effect *(French)* 79—4717
inhomogeneous systems, line broadening, spin-spin and spin-lattice relax. rate meas. 80—58292
instrument cavities, TE$_{011}$ and TE$_{102}$, inhomogeneous static fields, spurious line feature obs. 80—31833
lanthanum ethyl sulphate:Gd^{3+}, EPR lineshape distortion in weak fields with zero-field splitting 77—48034
layer structures, ML$_4$ dimer (M=metal, L=ligand), exchange interaction temp. depend., appl. to EPR linewidth 78—19306
lipid bilayers, spin-labelled, pure, EPR lineshape evidence of phase transitions 78—69004
lipids, from rat liver and hepatoma mitochondria, stochastic EPR anal. 78—76984
liquid, electron spin echo phase memory decay, generalised cumulant expansions appl. 79—11334
liver tissue, mouse, appearance of free radical centres on low temp. oxidation 78—69013
logarithmic divergency removal, quantising mag. fields *(Russian)* 80—34755
longitudinal detection, electron-spin double reson., signal depend. on relax. times 77—81030
Lorentzian second derivative lines, modulation broadening calcs. 77—16147
low-dimensional correlated spin systems, exchange narrowing theory 79—11335
magnetically dilute crystal, with strong spin-spin interaction, EPR conc. depend. 79—42826
magneto-microwave effects, rel. to ESR, review 77—69667
magnets, EPR line shape 78—91926
manganese acetate tetrahydrate, single cryst., ESR spectra, temp. depend. 77—43877
manganese copper formate dihydrate, conc. depend. of EPR linewidth 79—38376
manganese stearate: cadmium stearate, dil. quasi two-dimensional, ESR line width 80—71155
manganese stearate monolayer, two-dimensional mag., prep. and characterisation 78—31097
mesophase pitch, magnetically-oriented, phys. props., mol. struct. 80—64885
metal, CESR and inhomogeneous broadening due to local moments 79—99769
metal, CESR line shape, strong surface relax. case *(Russian)* 78—56378
metal, paramagnetic, CESR spin-orbit perturbation, spin-phonon scatt. 77—63285
metal film, CESR line width and shape, surface relax. contrib. *(Russian)* 77—32260
metallic monopnictides:Gd, coupling between 4f electrons and conduction electrons, EPR linewidth 78—52347
metals, cond. electron and spin scatt. due to dislocations 80—75856
metals, conduction-electron spin flip by phonons, expt. data anal. 79—61219

EPR line breadth continued
metals, electron bottleneck effect, impurity spin relax. and EPR linewidth 79—28589
metals, non-S-state impurities, coupled ESR 79—47326
methanol dehydrogenase, enzyme powder, ESR and ENDOR, 9 and 35 GHz 79—70524
methylammonium aluminiumselenate:Cr^{3+}, EPR and linewidth anomaly 77—12191
methylammoniumgallium sulphate:Cr^{3+}, EPR and linewidth anomaly 77—12191
methylene-d$_0$, -d$_2$, in Xe matrix, EPR, temp. depend. 78—5255
MgO:Cr^{3+}, single cryst., ESR linewidth 80—29605
molecular aggregates, triplet, ESR line shape in solid matrix, fine and HFS 78—58878
molecular crystal, triplet exciton excess EPR linewidth, orientational order effect 78—72389
molecular one-dimensional systems, electronic collective excitons, EPR response 77—31960
molecular polycrystals, effect of high hydrostatic press., EPR meas. 78—19307
naphthalene, triplet exciton annihilation and triplet spin relax. 80—29792
naphthalene, triplet pairs in naphthalene-d$_8$, ESR, nonreson. 78—64257
naphthalene-d$_8$:naphthalene-h$_8$ cryst., triplet excitons in A-B pairs, origin of inhomogen. broadened ESR lines 78—91623
naphthalene-TCNB, charge-transfer cryst., donor mol. orient. and dynamics 79—32926
nearly-one-dimensional paramagnet, self-consistent diffusion coeff. for analysis of EPR linewidth 77—80997
nematic liquid crystal, ESR of symmetrical three-spin systems, slow motional spectra 77—36135
nitroxide spin probes, unresolved hyperfine broadening convection in EPR, linewidth and Heisenberg spin exchange freq. determ. 80—71180
oxide glasses, charact. by magnetic resonance and optical absorption of metallic probe ions *(Japanese)* 79—95640
paramagnets, conc., ESR line shift, phonon relax. influence 78—88171
partial summations for slow tumbling radicals 77—36134
partially ordered ensemble, calc. of orientational distrib. function from line shape 79—87305
peroxylamine disulphonate, EPR lineshape, dispersion vs. absorpt. plots, modulation broadening and instrumental distortion 80—58290
Phase V, nematic, transient response to redirected mag. field, EPR study 80—33879
phenanthrene-d$_{10}$, oriented in biphenyl, triplet zero-field splittings, conc. depend. 78—2773
phospholipid membrane, polar head motion, NMR and EPR linewidth study using TCNQ$^-$ ion-radical *(French)* 80—45865
piperdinyloxy 2,2,6,6-tetramethyl radical, recrystallised samples, EPR study 80—100615
polar liquids, electron solvation, spectral changes 77—73501
poly-4-vinyl-pyridine soln., local density of monomer units, spin label obs. 80—44099
poly-4-vinylpyridine, intramol. mobility and local density in soln. spin mark method obs. *(Russian)* 80—70107
poly-4-vinylpyridine, mol. dynamics and local density in conc. soln., spin mark method obs. *(Russian)* 80—70108
trans-polyacetylene, and AsF$_5$ doped, EPR 79—42835
polyacetylene, mag. soliton defect ESR study 80—80590
polyacetylene, undoped, thermally activated mobile defect, temp. EPR line broadening 80—43218
polycarbonate:tri-p-tolylamine amorphous film, elec. and mag. props 80—49959
polystyrene, spin-labelled, EPR, end group mobility, temp. and solvent depend. 78—56368
praseodymium ethylsulphate:Sm, one-dimens. X-Y system, spin dynamics, electron spin echo meas. 80—66031
1,3-propanediammonium MnCl$_4$, 2-dimens. antiferromagnet, with dipolar broadening, spin diffusion, EPR obs. 79—38371
1-3-propanediammonium-CuCl$_4$, ferromag., antisymmetric and anisotropic exchange, EPR linewidth 78—10761
pulse shape of second harmonic generated by two level system 78—60327
pyrene-d$_{10}$, EPR line shape of photo-excited triplet state, in cryst. and glass 79—24210
pyrocarbons, EPR, effect of motional averaging, anisotropy, skin effect rel. to heat treatment and neutron irradiation *(French)* 80—34752
pyromellitic dianhydride-phenanthrene, single cryst., charge-transfer triplet excitons, spin polaris. 79—11069
quartz:Fe^{3+}, EPR for phase transform., reduced signal above 670K 77—90016
quasi-one dimensional organic systems, ESR 78—52358
quasi-one-dimensional organic metals, electron spin relax., temp. depend., Peierls fluctuations, EPR meas. 79—73802
quasirandomly oriented centres, appl. to radiation damage centres in bone 77—21667
quinolinium (TCNQ)$_2$, random exchange Neisenberg antiferromag. chain, intermediate field magnetisation meas. 80—103857
radical pair with axial symmetry, EPR parameters and linewidth components 78—6573
rare earth alloy, dil., anisotropic exchange Hamiltonian, rel. to ESR spectrum 77—20696
rare earth alloys, dil., ESR linewidth of rare-earth ions 78—68373
rare earth impurity, ESR, exchange induced broadening in low lying crystalline field system 80—108062
rare earth pseudobinary intermetallic compounds, ESR studies 80—108064
rare earth trichloride hexahydrate:Gd^{3+}, EPR meas. 78—15017
rare earth trichloride hexahydrates, Tb to Yb, EPR of Gd^{3+}, spin Hamiltonian parameters 77—36128
rare-earth magnets, low-frequency modes 78—88087
RE-1306 radiospectrometer improvement for crystals obs., use of LF modulation of magnetic field 80—57350
ruby, distant nuclei ESR and ENDOR experiments, dipole-dipole reservoir importance 80—71241
ruby, ESR and NMR correl. line broadening effect assoc. with external mag. field inhomogeneities 80—50227
saturation of inhomogeneously broadened line under bottleneck phonon, conditions *(Russian)* 79—8040
semiconductor and semimetal powders, EPR, effect of mag. field depend. of elec. parameters 79—99749
semiconductor with transition metal impurity states, EPR linewidth calc. 80—80599
semiquinones in protic solvents, saturation behaviour, ESR 77—6808

EPR line breadth continued
- silica gel, Mn^{2+} adsorption rel. to H_2O adsorpt., EPR study 79—5180
- simulated spectra, compensation for integerisation errors 79—33537
- sodium decanoate-n-decanol-H_2O system, lamellar G-phase, orientational-order, EPR investigation 80—24355
- solid, partially ordered, orientational distrib. from NMR and EPR line shapes 78—35048
- spectrum analysis, polynomial regression and nonderivative search technique 77—14461
- spin diffusion and spin-lattice relaxation in paramagnetic crystals 79—33525
- spin glass, EPR freq. rel. to Larmor freq., spin correlations, dipolar energy *(French)* 79—61198
- spin glasses, freezing of EPR relaxation rates 79—99713
- spin labels, water soluble, factors restricting diffusion, rel. to biological use 77—86436
- spin system with weak exchange couplings, EPR spectrum 78—64258
- spin systems, longit. paramag. suscept. inhomog. broadening conditions 78—88169
- sugar carbons, EPR in transition range 80—34751
- superconductors, slightly dirty, EPR relaxation time, thermal behaviour 79—47195
- systems with anisotropic g-tensor, EPR spectra, extra absorpt. peaks 79—51839
- TANOL, linear chain-like organic free radical, EPR line widths 78—39404
- TCNE$^-$, anionic spin probe for ESR of amphiphilic liq. cryst. 78—75548
- TCNE, electron donor-acceptor complexes, EPR *(German)* 78—55187
- TCNQ, electron donor-acceptor complexes, EPR *(German)* 78—55187
- TCNQ salt, 1,1′-diethyl-2,2′-cyanine-$[TCNQ]_2$, electric and mag. props. 79—42523
- TCNQ salt, 1-ethyl-3′-methyl-2,2′-quinoselenacyanine-$(TCNQ)_2$, EPR linewidth, angular and temp. depend. 78—76313
- TCNQ salt, 1-methyl-3′-ethyl-2,2′-quinoselenacyanine-$[TCNQ]_2$, two-dimens. ferromag., EPR 77—16148
- TCNQ salt, 3,3′-diethyl-6,6′-dimethyl-2,2′-thiacyanine-$(TCNQ)_2$ EPR linewidth, angular and temp. depend. 78—76313
- TCNQ salt, $(TSeF)_x(TTF)_{1-x}$-TCNQ, struct., elec. and mag. props., review 80—20158
- TCNQ salt, K-TCNQ, EPR linewidth, ang. and freq. depend. 80—80591
- TCNQ salt, $Mn(TCNQ)_2$, mag. props. 77—85558
- TCNQ salt, $NMP_{0.63}phenazine_{0.37}TCNQ$, mag. susceptibility, 0.03-4.2K 80—25191
- TCNQ salt, $Qn(TCNQ)_2$, Heisenberg antiferromag. chain for low temp. thermometry and cooling, EPR expts. 79—63217
- TCNQ salts, $Mn(TCNQ)_2$ and hydrates, mag. and elec. props. 79—82767
- TCNQ salts, n-methylacridium $(TCNQ)_2$, 2,2′bipyridinium $(TCNQ)_2$ and $Qn(TCNQ)_2$, with asymmetric donors, mag. susceptibility, 0.035-4.2K 80—25190
- TCNQ-TMTTF phases comparison with TTF-TCNQ, ESR 77—40116
- 1,2,4,5-tetrachlorobenzene, triplet exciton, ESR and optical absorption lines 80—96791
- 1,2,4,5-tetrachlorobenzene, triplet excitons, ESR and ODMR 78—43681
- tetramethylaminelithium(0), $Li(CH_3NH_2)_4$, existence, conduction- and localised-electron spin reson. 80—66035
- tetramethylammonium manganese trichloride, ESR meas., evidence for two paramag. species 79—61208
- tetramethylphenylenediamine chlorate, EPR investig. of exchange interaction 77—40114
- TGS:Cr^{3+}, EPR obs. of fluctuations near phase transition 78—43820
- three-spin systems in nematic liq. cryst., EPR 77—14463
- TMMC:Cu, EPR linewidth freq. depend., spin dynamics 80—15794
- TMMC, exchange-narrowed EPR linewidth, temp. depend. 78—52292
- TMMC, half-field EPR transitions in 1-D Heisenberg paramagnet 79—51843
- TMMC, linear Heisenberg antiferromagnet, EPR half-field transitions 80—15792
- TMMC, one dimensional antiferromagnet, EPR expts. 80—20454
- TMMC, one-dimens. Heisenberg magnet, EPR sidebands 78—88163
- TMMC, one-dimensional paramag., anomalous freq. depend. of EPR linewidth 80—15784
- $(TMTSF)_2PF_6$, ESR g-factor, linewidth, spin susceptibility, metal-insulator transition 80—103887
- $(TMTSF)_2PF_6$ (AsF_6), linear-chain conductor, semicond.-metal transition in small elec. field 80—103730
- TMTTF salts, $(TMTTF)_2$-X, ($X=BF_4{}^-$, $ClO_4{}^-$, SCN^-, $PF_6{}^-$, Br^-), physical props. 79—47085
- transient ESR line profiles, $S=I={}^1/_2$ system, calcs. 78—88170
- transition metal, paramagnetic-NO· radical interactions, EPR spectra rel. to dipolar interactions 79—95647
- transmission electron spin resonance, experimental methods *(Japanese)* 79—75563
- tri-p-tolylamine and its paramag. radical cation, disordered mol. solid, direct obs. of superexchange 80—39848
- trigonal exchange clusters of three nuclei, randomly oriented in polycrystalline system, ESR line profiles 77—28430
- trimer heteronuclear exchange clusters, ESR line profile 79—42828
- triple-ion species of alkali metals, ESR spectral hyperfine multiplets, linewidth effects 77—83624
- triplet exciton motion, influence on EPR line shape of pairs of differently oriented molecules 79—69427
- triplet excitons, quasi-coherent, in pairs of differently oriented mols., EPR line shape 78—43631
- trishydrazyl radical in s-butylbenzene, slowly slowly tumbling triradicals EPR 80—32748
- TTF-TCNQ type salt, trimethylene-TTF-TCNQ, unsymmetric cation, phys. props. 78—76059
- TTT_2-$(I_3)_{1+x}$, physical props., elec., mag. and optical meas. 80—24908
- two-dimensional antiferromagnets, diffusion-controlled mode coupling, EPR linewidth 79—51844
- two-dimensional heisenberg ferromagnet, open diffusion effects *(Russian)* 77—32201
- vanadyl octaethylporphyrin, radical cation EPR linewidth inversion, relax. theory 77—10693
- vibronic system, motional narrowing of lines 77—4547
- violanthrone, free radical, EPR meas. 78—27094
- vitamin B_{12b}:B_{12r}, cryst. growth, orientation, ESR obs. 79—34486
- in weak magnetic fields with zero-field splitting, line shape distortion 77—48034

EPR line breadth continued
- xanthine oxidase (dehydrogenase), EPR, mag. spin-spin dipolar interaction 80—53026
- Ag, CESR, influence of freq. and surface effects 79—51856
- Ag film, CESR linewidth exam., sample size effect 79—33536
- Ag foil, or film, conduction electron spin disorientation at surface 80—75855
- Ag-Dy, dil., EPR linewidth anisotropy and mag. field depend., internal stress effects 79—33532
- Ag-Er, dil., reflection EPR residual linewidth 77—81004
- $AgBr_{1-x}Cl_x$, self-trapped holes, Jahn-Teller and reorientation effects in ESR 78—64273
- AgCl, excited states, optically detected EPR 79—8073
- Al, CESR lineshape and A/B and g-values 77—63284
- Al, CESR linewidth, freq. effects 78—10775
- Al, with plastic surface coating, g-factor and spin relax. time of cond. electrons 77—32258
- Al, with plastic surface coating, CESR obs. at 60 GHz in refl. spectrometer 77—32259
- Al:Fe(Cu), CESR, effect of ion implantation 77—20701
- Al_2O_3:Cr^{3+}, inhomogeneous spin system, time evolution towards saturated state 80—88869
- Al_2O_3:Cr^{3+}, new method for spin-lattice relax. time, inhomogeneously broadened ESR lines 79—15343
- Al_2O_3:Fe^{3+}, dynamic nuclear polarisation, correl. ESR and NMR strain-broadening effects 77—48090
- Al_2O_3:Ni(Cr), thermally detected EPR of Ni^{3+}, Cr^{2+}, Cr^{3+} and Cr^{4+} ions 77—63273
- β-Al_2O_3-Na_2O, EPR and optical absorpt. studies of X-ray produced defects 78—95517
- β-Al_2O_3-Na_2O_3:Ag^{2+}, EPR measurements 78—95515
- β-Al_2O_3.Na_2O:Cu, EPR, localisation of Cu^{2+} and linewidth effect 78—39395
- $AlPO_4$:Fe^{3+}, EPR, α-β phase transition 77—90016
- As_2Se_3, and As_4Se_5Ge glasses, struct. changes, Mn^{2+} EPR expts. 78—79534
- As_xSe_{100-x}:Mn^{2+}, $0 \leq x \leq 70$, EPR, composition depend. and struct. 77—24736
- As_xTe_{100-x}:Mn^{2+}, $40 \leq x \leq 70$, EPR, composition depend. and struct. 77—24736
- $As_4Te_5Ge(Si)$ glass, struct. changes, Mn^{2+} EPR expts. 78—79534
- Au-Er, dil., cold-worked, EPR expts. 80—39864
- Au-Er, dil., EPR at 100 mK to 1K 80—66028
- Au-Er film, stress-induced g-shift, ESR meas. on Er 77—51951
- Au-Fe solid soln. alloys, reson. and relax. effects 79—82865
- Au-Gd, dil., crystal-field splitting of localised Gd^{3+} moments, ESR obs. 79—82869
- Au-Yb, dil., EPR at 100 mK to 1K 80—66028
- β-B, rhombohedral, EPR, book contrib. 78—48041
- β-B, rhombohedral, EPR anisotropy 80—25183
- BC, EPR, book contrib. intensity correl. with elec. cond., Hall coeff., book contrib. 78—48041
- $BaBr_2.2H_2O$:VO^{2+}, EPR meas. 77—16145
- $BaCl_2.2H_2O$:VO^{2+}, EPR meas. 77—16145
- $BaMnF_4$, ESR linewidth and reson. field for Mn^{2+}, 25 to 300K, spin diffusion 77—69681
- $BaTiO_3$, antireson. in EPR spectra of Fe^{3+} ions *(Russian)* 80—11257
- BrF_6, EPR spectra, ‘NMR’ transitions, mol. symmetry 77—46580
- C films with high conductivity, prep. and props. 80—80983
- C-C composites, existence diagram and properties *(French)* 78—64517
- CO_2-$O_2{}^-$ radical, on MgO surface, ESR spectrum, mobility effects 80—43076
- C_3O_2 polymer, preparation, spectra rel. to polymerisation temp. electron spin resonance 77—32239
- CaF_2:Gd^{3+}-M$^+$, (M=Li, Na, K, Rb, Cs, Ag), electric field effect expts., EPR line breadths, lattice distortions 78—80210
- CaF_2:Tm^{2+}, ultra-low nuclear spin temp., low field behaviour, EPR study 80—100614
- $CaMoO_4$:Er^{3+}, phase relax. time rel. to g-factor anisotropy, electron spin echo obs. 80—29615
- $CaMoO_4$:Fe^{3+}, single crystals, structure and kinetics, EPR meas. 79—99760
- $CaMoO_4$:Mo^{5+}, g-factor, ground state, line broadening, EPR obs. 80—39863
- CaO, line broadening of EPR and zero phonon lines of F centres 78—43686
- CaO:Ag^{2+}, EPR spectrum, static, quasistatic and quasidynamic Jahn-Teller effect 77—85561
- $CaWO_4$:Yb^{3+}(Nd^{3+}), phase relax. time rel. to g-factor anisotropy, electron spin echo obs. 80—29615
- $CdCr_2S_4$, EPR line profiles in paramag. and ferromag. phases 79—28602
- $CdCr_2S_4$, Heisenberg ferromag., obs. of dynamic dipolar crossover, ESR linewidths meas. 79—24209
- $CdCr_2S_4$, single crysts., EPR linewidth near Curie point, temp. and susceptibility depend. 77—63272
- $CdCr_2S_4(Se_4)$, 100-300K, spin-lattice relax. 77—51942
- $CdCr_2Se_4$, Crit. relax. processes, mag. reson. expts. 80—60425
- $CdCr_2Se_4$, crit. speeding-up of spin-relax. 78—48028
- $CdCr_2Se_4$:Cu(Ag), ferromag. reson. and ESR line widths 80—60413
- CdF_2:Gd^{3+}, investigation of superhyperfine struct. in EPR spectra 79—51851
- $Cd_{1-x}Mn_xTe$, EPR, mag. crit. point 80—39851
- CdS:Mn$^+$, cryst., X-band ESR 78—2730
- Ce^{3+}, in Van Vleck paramagnets, EPR meas. 77—12199
- $CePd_3$-Gd, EPR of Gd^{3+} impurities in host with interconfig. fluctuations 78—56377
- ClF_6, EPR spectra, mol. symmetry, INDO calcs. 77—46580
- $CoSO_4.7H_2O$:Mn^{2+}, host spin-lattice relax. narrowing in single cryst. 78—27079
- Cr complex, influence of anisotropy of spin-Hamiltonian parameters on EPR spectra *(Russian)* 77—28432
- CrB_3, crit. spin-relax. in hard mag. direction 78—72390
- $CrBr_3$, modulation of exchange integral, contrib. to temp. depend. of exchange interaction 77—69484
- $Cr_2(CrO_4)_3$, ferromagnet, ESR spectra near Curie temp. 79—8042
- CrN, antiferromagnetic EPR spectra, binding energy, isotropic exchange and ordering *(German)* 80—80604
- Cr_2O_3, near Neel temp. 78—23327
- Cr_2O_3-Al_2O_3, antiferromag. cluster stability, 300-5200K 77—20683
- CsBr, second relaxed excited state of F-centre, optically detected EPR 79—87335

EPR line breadth continued
$Cs_2HfCl_6:Mn^{2+}$, ESR of mol. jumps, zero-field splitting tensor 77—51944
$CsMnBr_3$, EPR linewidth anisotropies 80—103878
$CsMnCl_3$, electron resonance linewidth anisotropy 79—28588
$CsMn_{1-x}Co_xCl_3.2H_2O$, impure Heisenberg linear chain, EPR meas. 78—43634
$CsMnF_3$, solid and molten paramag. high-temp. e.p.r. linewidth meas. 77—4548
$CsNiF_3$, one-dimens. anisotropic paramagnet, EPR meas. 79—73799
CsO_2, low temp. phases, mag. order, EPR and antiferromag. reson. 79—95630
$Cs_2ZrCl_6:Mn^{2+}$, ESR of mol. jumps, zero-field splitting tensor 77—51944
Cu, CESR, influence of freq. and surface effects 79—51856
Cu, CESR linewidth and *g*-value, freq. and temp. influence, 4.2-50K 79—87318
Cu, CESR meas., 4.2K, selective transmission method 78—39401
Cu complex, catena-μ-isothiocyanato-(N′-pyridylmethylene-N″-salicyloylhydrazinato-NN′O) copper (II), EPR and visible spectra 80—5566
Cu complex, Cu-glycine in water, EPR spectral parameters, temp. depend. 80—2623
Cu complex, Cu(II) impurity in α-glycine crysts., ligand ENDOR spectra 79—65765
Cu complex, Cu(II)-L-asparagin complexes, ESR spectra, mag. and bonding parameters 78—23326
Cu complex, diaquobis(2,3-dihydroxy-2-methyl propanato) copper(II), cryst., EPR, room-temp. 79—82861
Cu complex, N,N′-ethylenebis (salicylaldiminato) copper (II)-thiourea, in solns., bond strength and hyperfine linewidth, EPR 80—74186
Cu complex, N,N′-o-phenylenebis (salicylaldiminato) copper (II)-thiourea, in solns., bond strength and hyperfine linewidth, EPR 80—74186
Cu complexes, with L-glutamic acid and DL-aspartic acid, EPR, bonding and hyperfine linewidth 78—25572
Cu complexes with glycine, in aqueous soln., EPR meas. 77—36115
Cu foil, conduction electron spin disorientation at surface 80—75855
Cu II complexes, 5-coord., ESR and optical absorpt. spectra 79—64020
Cu oxalate complex with aliphatic amines, X-band ESR line width 77—20687
Cu, surface spin-flip probability from TESR 78—91953
Cu-Mn, exchange-coupled localised moments, Korringa relaxation rate 80—75851
$CuCl_2.2H_2O$, EPR linewidth and relax., effect of antisymmetric exchange 77—59448
$CuCl_2.2H_2O$, nearly one dimensional mag. system, EPR line shape 79—99759
$CuCl_2.2H_2O$, X-band ESR magneto-microwave effects 77—28434
$CuCr_2Se_4$, Crit. relax. processes, mag. reson. expts. 80—60425
$CuF_2.2H_2O$, X-band ESR powder spectrum and related magneto-microwave effects 79—24214
$Cu_{75}Mn_{25}$, spin glass, EPR line breadth, exchange-narrowed 79—15345
$Cu(NH_3)_n(ClO_4)_2$, ($n=4$ or 5), EPR parameters and dilatometry 80—39850
$Cu(NH_3)_4SO_4.H_2O$, EPR around Neel temp. 78—39390
$Cu(NH_4SO_4)_2.6H_2O$, X-band ESR magneto-microwave effects 77—28434
$Cu(ethylenediamine)_2{}^{2+}$, electron tunnelling probability as function of distance for chem. reactions 78—80759
Dy^{3+}, in Van Vleck paramagnets, EPR meas. 77—12199
EuB_6, pure single crystals, magnetic and electric props. 80—11260
EuB_6, single and bulk polycryst., EPR, temp. and freq. depend. 79—28606
$Eu_xLa_{1-x}Al_2$, cryst. fields and exchange parameters, ESR meas. 80—71175
EuO, critical EPR spin dynamics, sample shape and temp. depend. 77—32244
$EuO_{1-x}N_x$, ferromag., temp. variation of EPR linewidth *(French)* 77—85547
Fe^{3+} transferrin, EPR spectrum analysis, polynomial regression and non-derivative search technique 77—14461
$FeCl_4{}^-$ in organic solvents, dilute, ESR linewidths *(German)* 80—11258
$Fe_{32}Ni_{36}Cr_{14}P_{12}B_6$, Metglas 2826A, EPR at 20 GHz 80—75848
Fe_2O_3 ultrafine particles in PTFE matrix, EPR and Mossbauer study 80—100625
Fe_2O_3-NiO-Na_2O-Li_2O-B_2O_3-SiO_2 glass, EPR meas. of exchange interactions 77—32243
$GaAs:Co^{2+}$, EPR expts., y-factor determ. 78—76301
$GaAs:Cr^{2+}$, effect of uniaxial stress and temp. variation on Cr^{2+} centre, EPR expts. 79—95636
p-GaAs:Fe, temp. depend., 4.2-330K 77—12195
p-GaSb, interband optical pumping, optical detection of EPR 77—28483
Gd, EPR linewidth and spin-spin relax. near T_c 78—68369
Gd^{3+} impurity ions, EPR spectra, linewidth narrowing due to spin-lattice relax. of lanthanide Kramers host ions 80—108061
Gd^{3+}, in Van Vleck paramagnets, EPR meas. 77—12199
$GdAl_2$-$GdCo_2$ system, EPR and mag. props. 79—33478
GdAs(Sb)(Bi), antiferomag., EPR meas., Neel temp. determ. 77—32242
$Gd(Co_xIr_{1-x})_2$, C15 Laves phase struct., g shift, linewidth EPR meas., Fermi level movement interpretation 79—61210
$GdCrO_3$, Neel point to 700K 80—39849
$Gd_{1-x}Dy_xAl_2$, EPR bottleneck, Dy substitution effect 77—63281
$Gd_{0.5}Dy_yY_{0.5-y}Ir_2$, effect of dil. Dy substitution on Gd ESR 79—82868
$Gd(Fe_xAl_{1-x})_2$, magnetic behavior 80—108079
$Gd_xLa_{1-x}Al_2$, cryst. fields and exchange parameters, ESR meas. 80—71175
$Gd_xLa_{1-x}Pd_3$, EPR of Gd, g-factor and thermal broadening, temp. and comp. depend. 77—48048
$Gd_2Ni_{17-x}Al_x$, EPR of Gd^{3+} ions 80—97139
GdS(Se), antiferromag., EPR meas., Neel temp. determ. 77—32242
Ge, amorphous, EPR 78—88167
Ge, amorphous, ESR and DC cond. 77—48032
Ge-Al film, amorphous, EPR meas. 78—80212
Ge-Cu film, amorphous, EPR meas. 78—80212
GeTe, degenerate semiconductor, EPR experiments on Mn^{2+} 79—11339
H_2O^-, trapped in γ-irrad., Y-type zeolites, ESR obs. 77—9099
$HgCr_{2-x}Al_xSe_4$ and $HgCr_{2-x}Ga_xSe_4$, temp. depend. of ESR linewidth, 105-300K 80—71161
$HgCr_2Se_{4-x}S_x$, 100-300K, spin-lattice relax. 77—51942
$HgCr_2Se_{4-x}S_x$, temp. depend. of EPR line intensity 78—27074
$Hg_{1-x}Mn_xTe$, EPR investigation of ordering effects 79—47330

EPR line breadth continued
$HoVO_4:Gd$, indirect superhyperfine interaction, EPR line width meas. 80—2633
I, atomic ESR spectra, broadening by He, O_2 and HI 79—68205
K-ethylamine-ethylenediamine, soln., ion-pairing and EPR 79—78502
KBr:Li(Na), F_A centres, optical detection of ESR 79—99793
KCl:Na, F_B centres, optical detection of ESR 79—99793
KCl(Br), second relaxed excited state of F-centre, optically detected EPR 79—87335
$K_2Cr_5F_{17}$, monocrystal, cryst. field and mag. props., EPR and optical absorpt. spectra 79—19773
K_2CuF_4, two-dimens. ferromagnet, half-field EPR line 79—19765
KD_2AsO_4, Cr^{5+} EPR, line shape and elec. field effect 79—11336
$KHSO_4:SO_3{}^-$, X-irradiated, ESR saturation 78—80220
$KMgF_3:Ni^{2+}$, EPR meas., g-factor, spin-orbit coupling const. and mag. moment determ. 77—80999
$KMnF_3$, EPR antiferromag. reson. linewidths near Neel point, exchange interactions *(Russian)* 77—8386
$KMnF_3$, solid and molten paramag., high-temp. e.p.r. linewidth meas. 77—4548
K_2MnF_4, 2-dimens. antiferromagnet, with dipolar broadening, spin diffusion, EPR obs. 79—38371
K_2MnF_4, two-dimens. antiferromag., diffusion-controlled mode coupling, EPR linewidth 79—51844
$K_3Mn_2F_7$, crit. EPR line broadening near Neel temp. 80—71165
$K_2Mn_cMg_{1-c}F_4$, impurities effect on EPR spectra 79—91283
$K_2Mn_xMg_{1-x}F_4$, impure two-dimensional system, ESR line reson. shift due to low symmetric spin distrib. 80—93162
$K_2Mn_xMg_{1-x}F_4$, two-dimensional antiferromag., ESR meas. 77—36121
KN_3, X-irradiated, N defect, EPR obs. 79—82870
KO_2, low temp. phases, mag. order, EPR and antiferromag. reson. 79—95630
$K_2Pt(CN)_4Br_{0.3}.3H_2O$, quasi one-dimens. conductor, EPR linewidth 80—54938
La-Gd, exchange-coupled localised moments, Korringa relaxation rate 80—75851
$LaBe_{13}:Er$, ESR, appl. of exchange induced broadening in low lying crystalline field system 80—108062
$La_xEu_{1-x}B_6$, EPR linewidth conc. depend., $Sr_xEu_{1-x}B_6$ comparison, exchange interaction in EuB_6 80—20457
LaH_x, $x=2.3$ to 2.98, EPR investigation 79—78513
$LaNi_5$-Gd, dil., ESR spectra, fine struct. and random stresses 80—25203
$(La_2O_3)_{0.95}(CeO_2)_{0.05}:Mn^{2+}$, X-band EPR study 80—60409
$La_{3-x}V_xS_4:Gd^{3+}$ localised moment-conduction electron interact., ESR obs. 78—88183
$La_{3-x}\square_xS_4:Gd^{3+}$, localised moment-cond. electron interactions, EPR data interpretation 77—63280
Li, Pauli susceptibility meas. by CESR transmission 79—61217
$Li_3AsO_4:CrO_4{}^{3-}$, EPR, 4.2K, cryst. field parameters 79—28586
$LiCl:Ni^{2+}$, EPR meas. of Ni^{2+} vacancy dipoles 79—28594
$LiCrO_2$, EPR of Cr^{3+} ion, g-factor and effective mag. moment 77—73073
$LiCrX_2$, $X=S$, Se, EPR meas., g-factors, effective mag. moments, and dipolar shifts 79—8043
$LiCuCl_3.2H_2O$, EPR linewidth and relax., effect of antisymmetric exchange 77—59448
LiF, neutron irradiated, ESR of Li metals *(Japanese)* 79—82858
LiH, EPR line shape of Li colloids created by γ-irrad. 77—77097
LiH, F-center, dynamic and NEDOR polarisation meas. *(French)* 77—28481
$Li_3PO_4:CrO_4{}^{3-}$, EPR, 4.2K, cryst. field parameters 79—28586
$Li_3VO_4:CrO_4{}^{3-}$, EPR, 4.2K, cryst. field parameters 79—28586
$Lu_2V_2O_7$, pyrochlore struct., mag. props. 78—72335
Mg-Mn, dil., mag. props., EPR meas. 79—73804
Mg_6MnO_8, EPR in magnesium-manganese spinel *(Russian)* 78—91936
$MgO:Ag^{2+}$, EPR spectrum, static, quasistatic and quasidynamic Jahn-Teller effect 77—85561
$MgO:Co^{2+}$, ESR linewidths of Co^{2+} 80—80596
MgO:Cr, Co, optical and ESR studies 80—50175
$MgO:Fe^{2+}$, phonon-induced transition interf. in EPR and IR spectra, ion-lattice coupling 77—51945
$MgO:Mn^{2+}$, clustering of mag. ions, study method 80—11155
$MgO:Ni^{2+}$, elastic interaction of mag. centres, EPR line width meas. 78—19315
Mn complexes in solution, hyperfine linewidth in EPR spectra 78—91937
Mn II-lecithin lipid-water system, NMR and EPR obs. 80—61168
Mn^+, in soln., EPR relax. probe 78—31104
Mn^{2+} compounds, strongly exchange coupled, solid and liq. states, 300-1450K 77—73077
$Mn_3Al_2Si_3O_{12}$, amorphous, spin-glass, insulating, Mn^{2+} mag. reson. 80—65918
$MnCl_2$-KCl system, molten, EPR spectra, linewidth study 78—88173
MnF_2, molten, superexchange, EPR linewidth 79—19774
MnF_2, solid and molten paramag., high-temp. EPR linewidth meas. 77—4548
MnO, EPR spectra of ceramic and epitaxial monocrystalline thin film samples *(Russian)* 80—11252
γ-MnOOH, antiferromag., prep. and mag. props., EPR meas. 79—87310
$xMnO.(100-x)[19TeO_2.PbO]$ glasses, EPR studies of Mn^{2+} ion distribution 80—71167
MnTe, magnetic resonance at high hydrostatic pressure 78—76247
Mo complex, influence of anisotropy of spin-Hamiltonian parameters on EPR spectra *(Russian)* 77—28432
$(NH_3$-$(CH_2)_2$-$NH_3)Cd_{1-x}Mn_xCl_4$, Mn^{2+} single ions, clusters and layers, ESR study 79—78507
$(NH_4)_2Cd_5Fe_3Al(SO_4)_{12}.18H_2O$, EPR above ferrimag. transition 78—10762
$NH_4H_2ASO_4$-$NH_4H_2PO_4$, EPR spectra of central peak fluctuations 78—91932
NO, EPR line shape in solvating mixtures 78—33532
NO· radicals, saturation transfer EPR effects anal. using hole-burning concept 79—94022
Na, CESR, influence of freq. and surface effects 79—51856
Na, Pauli susceptibility meas. by CESR transmission 79—61217
Na-ice condensate, EPR lineshape second moment, electron solvation struct. 78—3440
NaCl, second relaxed excited state of F-centre, optically detected EPR 79—87335
$Ni(BF_4)_2.6H_2O$, EPR, cryst. field symmetry 79—28593
$Ni_xMg_{1-x}O$, EPR in magnetoconcentrated solid solution *(Russian)* 80—39856

EPR line breadth continued
$Ni(NH_3)_6(ClO_4)_2$, EPR determ. of phase transition temp., line shape anal. 77−20063
$Ni(NH_3)_6(PF_6)_2$, EPR investig. of struct. transition 77−20679
$NiSiF_6.6H_2O$, EPR line shape, Tanaka-Kondo method 80−29602
$NiSiF_6.6H_2O$, ESR spectra at low temperatures and high pressures 78−52339
$NiSiF_6.6H_2O$, single cryst., EPR, 77-300K, Debye temp. 77−85551
O_2, diffusion coeff. in liqs. determ. by ESR line widths 78−91929
O_2 liquid, EPR temp. depend. *(Russian)* 78−31103
O_2, liquid, exchange interaction, EPR absorpt. line shape anal. 80−71158
α-$PVW_{17}O_{40}{}^{5-}$, α_2-$P_2VW_{17}O_{12}{}^{8-}$, aq. soln., hydrodynamic radii from ESR line width 79−78504
$Pb_5Ge_3O_{11}$:Gd^{3+}, discrete saturation of ESR, due to superhyperfine interaction 77−28440
Pb_2MnF_6, antiferromag. and superionic conductor, EPR and NMR meas. 79−99366
$PbMoO_4$:Fe^{3+}, single crystals, structure and kinetics, EPR meas. 79−99760
$Pb_3(PO_4)_2$:Gd^{3+}, EPR near ferroelastic transition point 79−15350
PbS film, appearance of EPR centres in initial form. stage *(Russian)* 77−63283
PrAs(Bi)(P)(Sb):Gd, EPR relax. of impurity in Van Vleck paramag., host ion fluctuation spectra 77−48049
$PrIn_3$:Gd, EPR relax. of impurity in Van Vleck paramag., host ion fluctuation spectra 77−48049
$PrIn_3$:Gd, indirect nuclear exchange interactions, ESR-linewidth meas., sp. ht. determ. 80−103825
$PrNi_5$-Gd, dil., single crystal, ESR study 80−75850
$PrNi_{5-x}Gd_x$, nucl. cooling agent, relax. and exchange, EPR and NMR study 80−25237
PrSb:Gd, ESR study, relaxation narrowing 79−99765
$Pt(NH_3)_4CuCl_4$, ferromag., antisymmetric and anisotropic exchange, EPR linewidth 78−10761
RbCl:Cu, X-irrad., ESR of noncentral Cu^0 atoms, 20-180K 77−24739
RbCl:Eu^{2+}, EPR of $^{153}Eu^{2+}$ and $^{151}Eu^{2+}$ 80−11259
$RbIn(MoO_4)_2$:Fe^{3+} monocrystals, EPR spectrum in the phase transition neighbourhood 80−2624
$RbMnBr_3$, EPR linewidth anisotropies 80−103878
$RbMnF_3$, solid and molten paramag., high-temp. EPR linewidth meas. 77−4548
$RbMnF_3$:$Fe^{2+}(Co^{2+})$, high-temperature EPR linewidth, impurity fast relax. effects 77−85556
$Rb_2Mn_xMg_{1-x}F_4$, spin dynamics near percolation threshold, EPR study 80−39859
RbO_2, low temp. phases, mag. order, EPR and antiferromag. reson. 79−95630
$Sc_{0.995}Gd_{0.005}H_{1.9}$, low temp. anomaly, Gd^{3+} EPR linewidth and X-ray meas. 77−69687
$ScH_{1.9}$:Pt, Gd, effect of Pt on Gd^{3+} ESR lineshape 78−68371
Si, amorphous, EPR 78−88167
Si, amorphous, ESR and DC cond. 77−48032
Si, amorphous, ESR linewidth, exchange interaction effect 79−61216
Si, amorphous, undoped and B doped, ESR-linewidth temp. depend. meas. 80−20459
Si amorphous film, saturation meas. on ESR signals 79−33535
n-Si, EPR linewidth, Orbach relax. process, conc. depend. 80−44901
Si, EPR of radiation defects, temp. depend. 78−15023
n-Si, heavily-doped, EPR near metal-nonmetal transition 77−28446
Si, ion implanted, EPR line shape exam. of amorphous centres 79−28587
Si:B, ESR at zero and small external stress, interpreted in spin Hamiltonians 78−43641
Si:B, elastic strength of O and C, determ. from ESR linewidth 79−19764
Si:Fe, anisotropic broadening of linewidth in EPR spectra of Fe^0 77−66417
Si:Fe^0, spin relax. rate ang. depend. for pulsed saturation of inhomogeneously broadened ESR line 79−65721
Si:Fe^0 interstitial localisation, EPR spectrum 79−1582
Si:Fe(Cr), EPR line intensity and widths, temp. depend. 79−28604
Si:In amorphous films, EPR, elec. cond., and magnetoresist. 80−50160
n-Si:P, heavily depend., spin-lattice relax. at high temp. 78−39403
Si:P, heavily doped, 100 GHz ESR of impurity band 79−95631
Si:P, ion implanted, resist. changes induced by ESR 78−68377
Si:P, ion-implanted layers, CESR meas., impurity distrib. inhomogeneity 78−2738
Si:P, polycryst., CVD, elec. activation of impurities, EPR obs. 80−34774
Si:P amorphous films, doping and annealing effects on localized states, ESR meas. 79−38380
Si-Au, amorphous, ESR linewidth var. with temp. and comp. 77−48033
Si-B amorphous film, plasma deposited, characterization 79−69828
Si-Ge alloys, temp. depend. of ESR line intensity of surface centres 77−32246
Si-Ge amorphous films, effects of annealing and crystn., ESR microstruct. and elec. meas. 78−26790
Si-SiO_2 interface, electrically active paramag. centres detect., photocond. reson. obs. 80−50185
SiF_3Cl^-, radical anion struct. and ESR spectrum 78−25571
$Si_{1-x}Ge_x$ amorphous, ESR centres, effect of annealing 77−55701
SiO_2 gel, adsorption curves of O_2, EPR *(Russian)* 79−52776
SiO_2 surface defects, influence of adsorbed O_2 EPR spectra 80−7163
SmB_6:$Gd^{3+}(Eu^{2+})$, mixed valence compound, ESR g-shifts and linewidths 78−48035
$Sm_2Mg_3(NO_3)_{12}.24H_2O$:$Mn^{2+}$, EPR spectra, 77-298K 79−15342
SnTe:Mn, EPR as probe of phase transitions 80−15790
$(SnTe)_{1-x}(MnTe)_x$, ESR, effect of Mn ion conc. on line width and area 78−35026
$Sr_xEu_{1-x}B_6$, EPR linewidth conc. depend., $La_xEu_{1-x}B_6$ comparison, exchange interaction in EuB_6 80−20457
SrO:Ag^{2+}, EPR spectrum, static, quasistatic and quasidynamic Jahn-Teller effect 77−85561
SrO:Cu^{2+}, phonon-induced tunnel hopping, ESR obs. 79−69714
$SrTbO_3$, EPR study of perovskite struct. 77−69685
$SrTiO_3$, EPR of Fe^{3+}-V_O centre, above T_c 80−39870
$SrTiO_3$:Fe, photochromic Fe^{5+} in non-cubic local fields, EPR spectra near structural phase transition 77−40127
$SrTiO_3$:Fe^{3+}, order-disorder and central peak behaviour, EPR study 80−75970

EPR line breadth continued
ThH_2:Er^{3+}, EPR of Er localised electron mag. states, Kondo effect 80−25202
Th_4H_{15}:Er^{3+}, EPR of Er localised electron mag. states, Kondo effect 80−25202
TiO_2:Fe, rutile, ESR meas. 80−54945
$TmAsO_4$:Gd, cooperative Jahn-Teller system, dipolar and random strain effects 77−40124
$Tm_3Ga_5O_{12}$:$Cf^{3+}(Yb^{3+})(Gd^{3+})$, Van Vleck paramagnet, EPR g-shifts and linewidths, temp. depend. 77−66419
$TmVO_4$:Gd^{3+}, EPR linewidth temp. var., random strains due to Jahn-Teller effect 77−12200
$Tm_2V_2O_7$, pyrochlore struct., mag. props. 78−72335
V_2O_5-CuO-BaO glass, unpaired electron localisation, ESR study 80−66026
$VW_5O_{19}{}^{4-}$, aq. soln., hydrodynamic radii from ESR line width 79−78504
YAG:M^{3+}, ESR absorption spectra, line broadening of Fe^{3+}, Cr^{3+}, Gd^{3+} 78−91940
$YCrO_3$, Neel point to 700K 80−39849
$YbCl_3.6H_2O$:Gd^{3+}, EPR, temp. depend., spin-lattice relax. time 80−93173
$Yb_2V_2O_7$, pyrochlore struct., mag. props. 78−72335
zinc formatedihydrate: Co, spin lattice relax. of Co^{2+} ions 80−75847
$Zn(BF_4)_26H_2O$:Ni, phase transition study, EPR of diluted Ni^{2+}, 98-298K 80−75846
$ZnCr_2Se_4$, 100-300K, spin-lattice relax. 77−51942
ZnO:Li, optically detected ESR, donor-acceptor pairs, line broadening 78−80256
ZnS, microregions disorientation degree anal. by birefringence, ESK and decoration methods 79−60389
$(ZrO_2)_{0.9}(Y_2O_3)_{0.1}$:Cr, Mn, stabilised single crystal, EPR of Mn^{2+} and Cr^{3+} obs. 80−66024
$(ZrO_2)_{0.9}(Y_2O_3)_{0.1}$:Ti, γ-irrad., ESR of trigonal centres, attributed to Ti^{3+} at cation sites 77−24740
$ZrSiO_4$, natural, radiation defect centre, EPR obs. 80−75853

epsilon meson resonances *see eta meson resonances*

equalisers
see also attenuation equalisers
32 Mb/s step-index optical fibre repeater equaliser *(German)* 78−33881
equalisers as universal sound quality control instruments *(German)* 79−64399
fibre optic communication repeater design, high impedance input, equalisation cct. *(Italian)* 77−50758
multimode fibre optical equaliser conversion function 77−23747
optical communication conference, Munich (1977) *(German)* 78−33854
optical fibre, nonlinear, post decision type, communications appl. 78−30052
optical fibre nonlinear equalisation by shaping filter *(German)* 78−33882
outdoor classical music sound reinforcement systems compared 80−92011
periodic dielectric rod array optical delay equalisation characteristics 78−5578
room acoustics correction, using Shure analyser *(German)* 80−58873
satellite digital data, radiometric correction and equalisation 79−74587
SAW transversal using SAW tapped delay line and PIN diode control ccts., characts. 79−68532
speech processing by autocorrelation function, spectral domain equalizer 80−1383
step-index fibre transmission system variable equaliser 79−55243
transformless broadband equaliser of US transducers, design algorithm 79−94436
US transducer lumped wideband equaliser design optimisation 79−46159

equations
see also Bethe-Salpeter equation; differential equations; equations of state; functional equations; integral equations; nonlinear equations
algebra, appl. to symm. of non-differential eqns. of phys. *(Russian)* 77−78952
asymptotic results for model eqn. for low Reynolds no. flow 79−14371
black holes, spherically symmetric, perturbations, linearised Einstein-Maxwell eqns. 80−72992
Bouguer formula of 1749, appl. to gravity corrections derivation 79−29692
continuity eqn. review of numerical solns. 77−26153
convolution equation solution, problems arising, auditory appl. 80−94147
electromagnetism, Maxwell's equations, form of distributions *(French)* 79−97221
Fokker-Planck equation, numerical integration and star clusters evolution 80−36675
geodesy, telluroid definition and three-dimensional mapping eqns. 78−65171
geodesy, three-dimensional mapping eqns. for non-rigid Earth models *(German)* 78−73304
Green and Ampt infiltration eqn., effective capillary press. estimation 78−3844
Hartmann interpolation equation for refractive index, TI-59 calculator program 79−98451
Hill's equation in celestial mechanics, new exact method *(Chinese)* 80−105152
interstellar rocket, three-dimensional eqn. of motion for relativistic navigation problem 79−21136
Jacobi's virial equation soln. for nonconservative systems, anal. of depend. on parameters 80−4243
linear equations systems solution, unsymmetric, sparse, computer program 77−80210
multiquadratic equations, appl. to interpolation method in geodesy *(German)* 78−15951
Navier equation of dynamic elasticity, appl. of tensor spherical harmonics 80−98296
Pfaff's equations of motion in dynamics, appls. to satellite theory 79−12386
pure harmonic tide in canal, eqns. of motion quadratic resistance term linearisation 78−69369
secular equation of the 4th order, L-matrix approx. vs. HLFS methods, mol. force consts. appl. 79−36556
stellar hydrodynamics equations, for thin disc galaxies 79−25706

equations of state
see also equations of state of gases; equations of state of liquids; equations of state of solids; phase transformations; thermodynamics
$1/n$ expansion up to $1/n^2$, eqn. of state and correlation function 78—89412
adsorbed gases, on heterogeneous surface energy distrib. function, virial anal. 77—28080
adsorbed phase, virial expansion, eqn. of state and isotherms *(German)* 78—95235
adsorption, virial theory, critical discussion 80—54506
alkali metal, law of corresponding states, pseudopotential theory 77—59095
anisotropic spheres, adiabatic contraction in general relativity 80—36489
asymptotic freedom and dense baryonic matter 79—62738
atoms, bound system, generalised virial theorem and dipole sum rules 78—21088
binary mixture of hard spheres and square-well molecules, quantum corrections to eqn. of state 80—6338
binary mixtures, vapour-liquid critical volume estimation 77—39662
black holes, primordial, self-similar growth for general sound speed case 79—5856
Bose gas, ideal, virial series 80—42139
Bose system condensed, crit. behaviour, renormalisation group approach 78—41231
catastrophe theory, appl. to eqn. of state for gas-liq. transition 77—59092
charged fluid, gas-liq. transition theory 79—82327
chemically reacting nonequilibrium turbulent shear flow, prediction model *(German)* 79—18973
classical fluid, elementary molecular theory 77—19859
cold matter in Einstein-Cartan gravitation theory, static spherical configurations 78—49308
commensurability in one dimension at nonzero T 79—35655
computer generated phase diagrams 78—83928
condensed matter, SCF theory, orbital and pot. functions calc., eq. of state 80—44463
condensed phase, lattice gas model 78—73931
corresponding states theory, thermodynamic props. 80—54338
coulombic potentials, two virial theorems 77—3429
critical point region eqns. of state, thermodynamical scaling hypothesis 77—74341
crystals with three particle interactions, state eqns. with account of collective oscillations *(Russian)* 78—70086
dense hadronic matter, in asymptotically free gauge theory, neutron stars eqn. of state 78—36627
dense matter, U(1) symm. gauge model, eqn. of state 78—62500
differential renormalisation-group generators, exact and approx. 78—77825
distribution of zeros, eqn. of state, fundamental relations, Cauchy type integral 78—4577
Earth, eqn. of state fits to lower mantle and outer core 78—85522
Earth inner core eqns. of state 77—73695
Earth interior, thermal model and eqn. of state 78—15982
Earth lower mantle, thermodynamically based eqn. of state 80—26473
Earth mantle, eqn. of state and stresses due to phase changes in subduction zones 77—73718
electron beams, stationary state diagrams 80—18985
electron gas, classical diamagnetism, Gibbs method *(Russian)* 78—73918
empirical, optimisation of number of coeffs. 80—17904
ferrofluids, phase diagrams and eqn. of state 80—60280
ferromagnetic fluid, molecule system eqn. of state, exchange interactions, spin independent forces 77—59412
flow, stratified, environmental, finite element analysis, book contrib. 79—34875
fluid, equation of state and Euler's turbine eqn. *(Rumanian)* 78—79400
fluid, one dimens., Kirkwood modified Tait eqn. of state 78—8372
fluid of rigid spherocylinders, virial eqn. of state 78—63836
fluid with triangular-well potential, eqn. of state, quantum corrections 79—69222
fluids, of hard spherocylinders, dumbbells and spheres, equations of state, theory 79—50970
fluids with assoc. mols., van der Waals type eqn. of state 77—967
free boson gas in weak external pot. 80—86203
free electron gas, n-dimens., eqn. of state *(Spanish)* 80—82718
freezing, molecular theory, eqn. of state, free energy, from 1st BBGKY eqn. 78—67804
fused hard spheres eqn. of state near close packed limit 77—84881
gas, Mayer theorem appl. to case of arbitrary interaction between gas particles 77—82478
gas-liquid interface, irreversible thermodynamics, eqn. of state 78—51800
general equation of state of matter 78—43095
glass transition, soft-sphere model, mol. dynamics study 80—49343
graphite/inert gas adsorption, modified Buckingham pot., virial coeff. anal. 79—65312
grinding, physical theory, eqn. of state *(Russian)* 79—74267
hadron gas, non-ideal, eqn. of state appl. to universe Friedmann model *(Russian)* 79—44649
hadron system, gravit. collapse, rel. to contraction of closed oscillating Universe *(Russian)* 80—4466
hadronic matter, eqn. of state for relativistic quantum gas model 79—9349
hard core fluid with Yukawa tail, eqn. of state 80—24330
hard core trigonal mols. on triangular lattice, phase transition, eqns. of state 77—59089
hard disc fluid, sixth and seventh virial coeffs. 78—91047
hard disc mixture, eqn. of state, compressibility and phase behaviour, mol. dynamics simulation 77—51291
hard discs system, fifth virial coeff. calc. method 77—26263
hard disk system, solid-fluid transition 79—88900
hard dumb-bells, interaction site mol. statistical thermodynamics 77—55222
hard dumbbells 77—30119
hard heteronuclear dumb-bell fluid, thermodynamic props., eqn. of state 78—38599
hard sphere, semiclassical fluid, equilib. props., quantum corrections 78—18522
hard sphere fluid, series expansion calcs. 80—44092
hard spherocylinders, Monte Carlo simulation 78—91046
hard-core particle system, zero separation theorem, virial coeff. 77—26261
hard-particle fluids, series representation of eqn. of state 80—6337

equations of state continued
hard-sphere equation of state, vap.-liq. equilib. 77—4181
hard-sphere fluid, eqns. of state, transport data, glass transaction 77—4182
hard-sphere fluid, interacting with wall, virial coeffs., in surface tension 79—23808
heavy ion collisions, high energy, depend. of total pion prod. cross sections on eqn. of state 78—41772
Heisenberg ferromagnet, eqn. of state, using modified Gell-Mann Low renormalisation group 77—63225
Heisenberg system, parametric representation in crit. region 78—79741
heteronuclear hard dumbbells 77—30085
high pressure vapour-liquid equilibrium, quantitative description 79—1486
high temperature matter, comp. and adiabatic index 79—44354
hot hadronic matter in early universe, relativistic eqn. of state 78—45438
hot nuclear matter, eqn. of state determ. 79—93538
hydrocarbon-$CO_2(H_2S)(N_2)(CO)$ mixtures, phase equilib. calcs., modified Soave eqn. of state 79—19353
hydrocarbons, phase equilib. calcs., modified Soave eqn. of state 79—19352
ideal Fermi gas, thermodynamics and eqn. of state 77—30147
incompressible matter, in bimetric gravit. theory 77—33329
inert gas, thermodynamic props. in critical region 78—6139
infinite dilution activity coeffs. determ. from total press. VLE data, eqn. of state influence 80—40727
infinite finite temperature baryon matter, Green's function formalism, quantum correction 78—13000
insoluble monolayer, ionised, of surfactant, thermodynamic eqn. of state 79—8450
insoluble monolayers, thermodynamic eqn. of state for uncharged films 78—85195
interacting bosons, second and third virial coeffs. calc. 77—26264
interacting neutron fluid at high temp., eqn. of state, supernovae hydrodynamics 79—2718
interfacial order parameter profile near critical point, renormalisation group approach 78—6200
interstellar medium, eqns. of state rel. to role of OB stars in interstellar clouds form. 80—109506
inverse-6 potential, exact fourth and fifth virial coeffs. 80—42174
ionisation potential, Koopman's virial scaling corrections, appl. to He, Ne and Ar series 79—45655
Ising model, one-dimensional transverse-field, in complex longitudinal field, real-space renormalization group method, T=0 80—103806
Ising model, pair and triplet interactions, mean-field eqn. of state 77—16021
Ising model, three dimensional, crit. exponents, scaled eqn. of state 77—8262
isostere equation of absorbed state, comparison with that based on John's isotherm eqn. 79—42368
isothermal neutron star core 79—62864
isotropic media, linear dynamical eqns. of state, general formalism 78—93639
isotropic media, linear dynamical equations of state 80—22314
Kantowski-Sachs cosmological model, global struct. 78—24584
Lane-Emden problem, series soln. 78—36559
lattice gas model, three phase eqns. of state 78—22818
Lennard Jones 6-12 fluid, Pade approximant for eqn. of state 77—3905
Lennard Jones polymer, eqn. of state, collapse transition 77—19117
Lennard-Jones fluid, eqn. of state, Monte Carlo and perturbation theory 77—76519
Lennard-Jones fluid, equation of state 79—73083
Lennard-Jones fluid, hypernetted-chain eqn. of state 78—67800
Lennard-Jones two-dimens. fluid, Percus Yevick eqn., radial distrib. function, critical point 77—76272
lipid monolayer, statistical mech. theory 78—73141
liquid fuel-fission gas bubble mixtures, equation of state 80—47568
liquid-vapour equilibrium, Van der Waals' eqn. of state, heat of evaporation 78—51640
liquid-vapour phase equilib., modified Redlich-Kwong eqn. of state 78—83908
liquid-vapour transition, non-Ising-like effects, eqn. of state, renormalisation group calc. 80—84286
many body theory, eqn. of state 80—42183
many-body systems, resons., extended virial theorem, complex acaling, Schrodinger operators 79—21575
matter at supernuclear densities, neutron star test of models 77—78812
mechanics analogy with thermodynamics symplectic struct. 79—71174
membrane system, closed, vesicular, mechano-chemistry 77—60189
metal surface, high-intensity laser beam interaction 80—19600
metals, eqns. of state based on free energy expressions, isothermal compression moduli *(Russian)* 79—90753
methane, molecules interacting via Kihara pot. with spherical core *(Spanish)* 77—31749
microemulsions of micelles, interpretation of second virial coeff. of osmotic press. *(French)* 78—64891
micropolar current and heat conducting magnetically-saturated solid, field eqns. 78—36845
Mie-Gruneisen eqn. of state, generalisation 78—96194
minimum energy reaction paths, virial theory implications 80—97686
mixtures, vapour-liquid equilibria, mixing rules in equations of state 80—19902
modified cell theory, eqn. of state for hard spheres 80—103445
modified Soave equation of state for phase equilib. calcs. systems containing hydrogen 79—95118
molecular force constants, virial theorem, appls. 78—41904
molecular force fields, virial theorem appls., zero virial reaction coords. and diatomic pots. 79—31433
molecular system, with N associating particles, free energy, virial expansion 77—55336
molecules in applied elec. field, virial relations 80—53087
multicomponent mixtures, vapour-liquid equilibria predictions, statistical thermodynamic approach 77—55335
multicomponent systems, and multiphase systems, mean-field state eqns. 77—20040
multicomponent systems, critical props. prediction from eqn. of state 77—57289
multicritical (order O) magnetisation eqn. of state, renormalisation group calc. 78—31085
multistage multicomponent separation, calc. using thermodynamic props. from SRK/PR eqn. of state 79—34346

equations of state continued
Murnaghan equation compared with exponential equation of state 77−11661
neutron gas, finite temperature 77−67715
neutron gas interactions at high density and temp., supernova models appl. 77−33330
neutron star matter, eqn. of state rel. to max. mass 77−33545
neutron stars, eqn. of state with pion condensate rel. to cooling 80−77443
neutron stars, mass-radius relation, obs. constraints, dense matter eqn. of state 80−46597
neutron stars, maximum mass, Brans-Dicke theory 77−33543
neutron stars, microscopic eqns. of state rel. to struct. 77−64790
neutron stars, nonrotating, eqn. of state and bounds on mass 77−45477
neutron stars, rotating, eqns. of state rel. to props. in bi-metric theory of gravitation 80−90466
neutron stars, stability against pulsations with anisotropic eqn. of state 77−13378
neutron stars with equation of state given by nuclear Thomas-Fermi model 79−48840
neutron-proton electron mixture with zero charge density, eqn. of state, rel. to supernova explosions 77−53416
neutrons, relativistic, ultra-degenerate, non-interacting gas, Fermi energy and eqn. of state in intense mag. field 78−89401
neutrons, warm degenerate matter 79−84810
non-Newtonian shear flow, eqns. of state 79−23344
nonanalytic, modification for low density limit, appl. to ethylene 79−46779
nonpolar binary mixture, partial molar vol. prediction from Lee-Kesler eqn. of state 80−10632
nonspherical molecular system, second dielec. virial coeff. 77−45814
nuclear matter, π condensed, eqn. of state of finite temp. 79−3110
nuclear matter, hot 79−63619
nuclear matter with neutrinos retention, eqn. of state and chemical comp. 78−96390
nuclear reactor mats., crit. consts., review 78−59931
nucleon gas, weakly degnerate, virial coeffs., eqn. of state, species concentrations 77−15658
nucleon matter, eqn. of state at subnuclear densities 80−77278
one component plasma fluid, derivation of eqn. of state in strong coupling 80−33741
one parameter family 77−13722
ordered colloidal dispersion, electrostatically stabilised, polydispersity and osmotic press. 79−74428
p-α-τ equation of state in Lagrangian codes 79−68771
N Pacific Ocean waters, densities rel. to comp. and eqn. of state 78−73391
Peng-Robinson and Benedict-Webb-Rubin equations, calculations using TI-59 80−77738
percolation, universal critical amplitude ratios 80−101765
Percus-Yevick eqn. of state for sticky hard rod gas 78−9933
perturbed-hard-sphere eqn. of state applicable to sub- and supercritical temps. 79−19350
phase equilibria, enthalpies, equations of state calculation methods *(German)* 78−34588
plasma, classical one-component, improved equation of state 80−83887
plasma, equation of state, activity expansion *(Chinese)* 80−43863
plasma, high-Z, Saha's ionisation eqn. soln., input for opacity calcs. 77−39412
plasma, nonideal 78−75261
plasma, one-component, virial pressure 80−38536
plasma, one-component asymptotic fluid eqn. of state, Monte Carlo calcs. 77−24527
plasma, pulsed solid breakdown, blow off, shock waves 77−27688
plasma, quantum statistical theory 78−91627
plasma, superdense, compression, role of eqn. of state and boundary press. profile, simulation 78−83589
polar fluids, improved corresponding states method, second virial coeffs. 78−14120
polyatomic fluids, convex nonspherical particles with nonpolar and multipolar forces 80−15213
polydisperse hard-disc systems, equations of state, particle size effects 78−73947
polydisperse hard-sphere systems, equations of state, particle size effects 78−73947
polymer, single ring, Lennard-Jones model, eqn. of state calcs. 78−5379
polymer chain, virial expansion, two parameter expansion 79−72450
polymer flocculation and stabilisation, concentration effects 80−45569
polymers, adsorbed, excluded vol. effects, Monte Carlo investigation 79−95259
propylene, computer generated phase diagrams 78−83928
propylene, equation of state for gas-liq. transition, catastrophe theory 77−59092
quantum virial theorem, derivation for teachers 79−71193
quark matter, Gibbs energy rel. to baryon to quark matter transition 77−5424
quark matter, phenomenological equation of state, neutron star appl. 79−63424
quark stars, eqn. of state and possibility of existence 77−45471
quark stars, possible existence, 2nd order perturbation theory 80−26889
quark stars with 'realistic' equations of state 78−73725
random spin system, $1/n$ expansion 78−62173
Redlich-Kwong, modified parameters, appl. to vapour-liquid equilib. 77−39659
relativistic gas of interacting particles, phase vol. approx. 78−41225
relativistic plasma, virial theorem 77−89299
relativistic quantum ideal gas of massive particles, eqns. of state 79−2721
renormalisation group eqns. and thermodynamic anomalies near tricritical point *(Russian)* 80−13027
saturated vapour volume, eqn. 79−95119
scaling equation of state derived from the pseudospinodal, liq.-gas system 80−44286
scaling equation of state for boson system, renormalisation group transformation 78−12643
scaling function for eqn. of state in $1/n$ and ε expansions 77−87718
search procedure, based on step-wise least-squares technique 80−19900
seawater, P-V-T props. calculated from US derived eqn. of state 79−25264
second virial coeff. for Mie m-n potential 77−7835

equations of state continued
second virial coeff. inversion for complete pot. energy functions 80−91628
second virial coefficient, functional equations 80−103442
second virial coefficient, low temp., S-matrix pole representation 77−37834
second virial coefficient, trace formulas for time delay 77−82476
second virial coefficient data, complete iterative inversion method calcs. 80−83448
simple fluid, hard and soft core eqns. of state, termination temps. 79−82305
simple fluid, hard and soft core eqns. of state, termination temps. for Lennard-Jones m,n pot. 79−82306
simple fluid, hard and soft core eqns. of state, termination temps. and 2nd virial coeff. 79−82307
simple systems, equilib. and the thermodynamic state surface *(Hungarian)* 79−26014
sine-Gordon chain, $T\neq 0$, commensurability, phase-torque eqn. of state 80−39251
single phase liquids, thermodynamic stability limit and eqns. of state 80−92037
spherically symmetric fluid, general relativity, equation of state, no slow uniform contraction 80−62544
spin systems, tricritical phase transition, eqn. of state, critical exponents, logarithmic corrections 78−27048
square well fluid, eqn. of state well width depend., Monte Carlo calc. 80−64853
square well fluid, mean spherical approx. and optimized cluster theory 78−26407
stability limit of liquid and crystal phase, three-parameter law of corresponding matter 80−49340
standards for single substances and mixtures 78−14481
stars under gravitational collapse 79−97014
stellar collapsing core, Thomas-Fermi model of warm nuclei 80−51648
stellar partial ionisation zones, eqns. of state 78−28653
Stockmayer-type polarisable mols., N-particle dynamics 77−68089
superdense celestial bodies, theory 80−67773
superdense matter, hydrodynamic model, nonlinear pion+pion chiral Lagrangian, $e^+ + e^-$ and $p+p$ collisions 78−32966
superdense matter, nuclear size correction to relativistic Thomas-Fermi model 78−29413
superdense matter and stellar collapse, eqn. of state 79−16996
superdense neutron matter, relativistic theory and eqn. of state 78−45349
supernovae, effects of core eqn. of state on outcome of stellar collapse 80−85928
systems of soft diatomic mols., eqn. of state, Monte Carlo simulation 77−26262
Tait equation, constants 78−18736
Teit's equation modification in critical region *(Russian)* 77−27976
tensor virial theorem, quantum mechanical generalisation for Born-Oppenheimer approx., atoms, mols. 78−86182
testing fundamental equations of state for practical applicability 80−4684
tetrafluoromethane-trifluoromethane-chlorotrifluoromethane, vapour-liq. equilib. compositions, calc. 80−19925
theories rel. to high-compression data *(German)* 78−81148
thermally dissociated matter, comp. and eqn. of state 77−33476
thermodynamic speed of sound, virial form 77−27406
Thomas-Fermi equation of state, radiation press., high temp., coupling to high-density electron plasma 77−3925
Thomas-Fermi model quasiclassical corrections, electron density, eqns. of state 78−25404
Thomas-Fermi shell model, at high press. and temp. 78−79738
Thomas-Fermi thermodynamic functions, quantum and exchange corrections *(Russian)* 77−9953
three-parameter eqn. of state, critical compressibility factor correlation 78−2226
transition metal-hydrogen systems, eqn. for multiplateau isotherm, lattice expansion role 80−39252
tricritical coexistence in three dimensions, multicomponent limit 80−19907
tricritical points and thermodynamic quantity singularities, renormalisation group method *(Russian)* 77−69071
two-component flow, with phase transitions, thermodynamic processes 77−27584
two-component ionic mixture, eqn. of state and phase separation in uniform background 78−21058
two-dimensional fluid, adsorption isotherm, summation of virial expansion for eqn. of state 79−15007
two-dimensional fluid, with 12-6 pot., fourth virial coeff. 78−59723
universe, stiff, eqn. of state renormalisation by primordial black holes form. *(Russian)* 80−51802
van der Waals theory generalised 78−38602
vapour-liquid equilibria, algorithm for calcs. 80−19903
vapour-liquid equilibria, generalised method for calc. and prediction at high press. 78−87780
vapour-liquid equilibrium, generalised one-parameter Redlich-Kwong eqn., mixtures 78−34589
virial coeff. theory anal. of Kr adsorption on graphitized carbon black 78−34697
virial equation, truncation errors 78−87764
virial equations, second-order tensor, for stellar mag. configurations linear oscills. 79−44461
virial expansion and Kirkwood-Salsburg eqn. for many-body pots. 77−5744
virial inequalities, quantum and relativistic 80−62609
virial theorem and Born-Oppenheimer approx. at different order of perturbation *(French)* 77−49617
virial theorem and scale transformations, for teaching 80−17763
virial theorem in general relativity, consequences for spherical symmetry stability 79−21593
virial theorems for coulombic potentials 77−3429
viscoelastic medium, eqn. of state for shock-wave struct. 78−9594
water, between 350 and 1000°C (0 to 10 GPa) and between 100 to 350°C (200 MPa to melting curve) 80−15214
water-entrained gas flow, force on moving body 78−63480
weakly random system, limit $n\to\infty$, scaling function for eqn. of state 78−73953
Wilson-Kogut renormalisation group calcs. 79−97249

equations of state continued
zeros distribution, eqns. of state, phase transitions with circular distrib. of singularities 79—58666
$N\bar{N}$, relativistic interacting system, eqn. of state using Regge-type interaction amplitude *(Russian)* 77—79032
Ar, gas-liquid-solid equilibrium, eqn. of state 80—24563
Ar, molecules interacting via Kihara pot. with spherical core *(Spanish)* 77—31749
Ar, thermodynamic behaviour, improved analytical representation 80—54339
CO, second virial coeffs. 80—83440
CO+Ar(He)(Ne)(Kr)(Xe), intermol. pot. energy surfaces from electron gas model, ang., distance, and vibr. depend. 79—3520
CO_2, molecules interacting via Kihara pot. with spherical core *(Spanish)* 77—31749
Cs, plasma, eqn. of state, 30-140 atm, 3000-4000K, by adiabatic compression 78—14132
Cs plasma, eqn. of state 78—42711
Cs, plasma, highly ionised, conductivity and eqn. of state 78—26323
H atom gas with unsaturated electron shells, third virial coeff. calcs. 79—90752
H, spin-polarised, mag. eqn. of state 80—100374
H_2, solubility in high press. He 80—10674
HCl-H_2O, p-V-T relations up to 773K and 1500 bars 78—43096
H_2O, polarisability tensor components, virial theorem calcs. 80—53087
He II, excitation spectrum and second virial coefficient calc. 80—102549
^{3}He, equations of state, 3.3 to 14K *(Russian)* 78—83912
^{4}He, equations of state, 3.3 to 14K *(Russian)* 78—83912
Kr, molecular dynamics simulations, three effective interactions 79—69224
Li plasma, elec. cond. at 12.5-50 MPa, $(7\text{-}50)\times10^3$K 80—64685
Li-D equation of state under extreme conditions, solid state to plasma region 80—69976
Li_2, second virial coeffs., Konowalow MCSCF potential calcs. 80—23312
N_2, second virial coeffs. 80—83440
N_2-Ar-O_2, liq. vap. equilib. prediction using cubic eqn. of state 78—18737
N_π ground state, second virial coeffs. calcs., 6000 to 20000K 77—14524
Na isoelectronic sequence, hypervirial theorem, screening parameters and oscill. strengths 79—6882
NaCl, adsorption of Ar, gas-solid virial anal. 77—55444
Ne, adsorption on Xe-plated graphite, virial coeffs. 78—18904
Ne solid, solubility in high press. He 80—10674
SF_6, pair polarisability anisotropy, point atom polarisability approx. calcs. 80—87244
SiO, nearly degenerate $G^1\Pi$-$I^1\Pi$ energy spectra, predissoc., extended virial theorem 79—22771
UO_2, vapour press. meas. up to 500K, critical point data prediction, present state of art 79—45347
Xe+CO(N_2), ^{129}Xe chem. shielding, second virial coeff. 78—66563
Y_2O_3 plasma, eqn. of state investig. 80—75027

equations of state of gases
$\gamma>5/3$ gas accreted by Schwarzschild black hole, eqn. of state softening 79—17011
adsorption on homogeneous solid, surface second virial coeff. 80—45558
n-alkane+Ar mixtures, intermol. pot. using Kihara model with spherical cores 77—54591
n-alkanes, Bender eqns. of state 78—26656
benzene, P-V-T relations, 5-300 MPa and 323-683K range 77—69069
benzene, vapour-flow calorimetry 78—91058
binary gas mixtures, nonspherical mols., second virial coeffs. calc. 78—75247
binary mixtures at high press., phase equilibria, critical phenomena calcs. 77—35664
binary solutions of dense liquids and gases, isothermal eqn. of state calcs. *(Russian)* 80—88292
binary vapours, enthalpies of mixing 80—93791
buoyant flow, thermally driven, equations of motion 79—23334
Burnett data reduction, fast least-squares method 78—47082
Charles' law, student expt. 78—36783
chemical potential, near crit. density, Thom's catastrophe theory 78—91063
chlorotrifluoromethane, compressibility, 298 to 348K, Burnett expansion obs. 79—27733
clusters in imperfect vapour, eqn. of state 77—31413
clusters in imperfect vapour, nucleation theory 77—35289
collision processes, kinetic theory, density effects expts. 78—12468
compressed gas, radial distrib. function hard sphere model 80—69961
condensable gases, modified Redlich-Kwong eqn. predictions, comparison with flow calorimeter data 80—37034
convection, natural, in confined region between two horizontal ducts for variable fluid properties 79—23321
dense gas, eqn. including nonadditive and quantum effects 78—5838
dense monatomic gas, quasiclassical approx. 77—55125
diatomic mol. gases, quantum partition functs., virial coeffs., by path integration 77—15146
dielectric second virial coeffs., van der Waals dimers struct. 77—46611
dissociation equilibrium, phase space allocation 79—27746
entropy, quantum square-well pot. gas, low-temp. 79—55443
ethane, gas, second virial coeffs., intermol. pot. at low temp. 79—46416
ethanol vapour, isothermal Joule-Thomson coefficient, equation of state 80—24119
ethyl chloride, second dielec. virial coeffs. *(German)* 79—32729
ethylene, μ, ρ and T-surfaces, global behaviour, rel. to catastrophe theory 78—26226
ethylene, gas, second virial coeffs., intermol. pot. at low temp. 79—46416
Fisher's droplet model, pure filled vap.-liq. nucleation theory 77—62626
fluorocarbon-hydrocarbon mixtures press. second virial coeff., graph theory prediction 80—43823
fluorocarbons, press. second virial coeff., graph theory prediction 80—43823
fluorocarbons, press. second virial coeffs., walks on graphs method 80—7841
fluoromethane, fluid, second dielec. virial coeff. calc. 78—22449
fluoromethanes, and perfluoroethane, NMR gas-to-liquid shifts, 2nd-virial coeff. of chem. shielding validity 79—85976
fourth virial coefficient and structural consistency, for inverse power pots. 79—99047
Freon 12, P-V-T relation determ., student lab. apparatus 79—62970

equations of state of gases continued
gas, virial expansions for dielec. and refr. indices, rel. to collision-induced absorption bands 79—86547
gas mixtures, third virial coeffs., nonadditive dispersion interactions effects 78—67299
gaseous mixtures at high pressure, phase equilib. calc. 77—35291
halomethanes, second dielectric virial coeff. of polar gas, temp. depend. *(German)* 78—26234
hard sphere gas, 2nd virial coeff., high temp. quantum corrections 77—76012
hard-core fluid, with Yukawa tail, eqn. of state, Monte Carlo results 78—26410
hard-sphere fluid, eqn. of state, quantum corrections 78—34592
hard-sphere fluid, Yukawa tail pot., eqn. of state study 79—42211
hard-sphere gas, rel. density of state, second virial coeff. 77—27641
heterogeneous nonideal chemically reacting system, comp., thermodynamic props. calcs. 80—76492
hexafluorides, universal eqns. of state and thermodynamic similarity 77—35290
high temperature vapours, appl. of laser pulse heating 80—52230
high-pressure gas equation-of-state meas. interferometry 80—77810
hydrocarbon-simple fluid gas streams, second virial coeffs. calcs. 78—1777
hydrocarbons, press. second virial coeff., graph theory prediction 80—43823
hydrocarbons, press. second virial coeffs., walks on graphs method 80—7841
hydrocarbons, second virial coeff., empirical eqn. 77—58831
hydrocarbons and mixtures, second virial coeffs. calcs. incl. angular coordinates 77—19659
ideal gas, derivation with nonspecular enclosure wall reflection 77—13545
ideal gas law, virial theorem for open systems 77—37804
ideal gases, solns., basic props. kinetic derivation from elastic collision processes 78—91048
imperfect gas, van der Waals eqn. of state derivation 77—89221
inert gases, second virial coeffs., intermol. pot. at low temp. 79—46416
ionisation, partial, in gas dynamics, computational method 78—38447
Kirkwood superposition approximation, $\chi'(r)$ nondiagrammatic cluster props. 77—47129
Lennard-Jones gas, second virial coeff., closed form 80—28084
Lennard-Jones gas, second virial coeff. calc. using equilib. Wigner distrib. function variational principle 80—4685
Lennard-Jones gas, third virial coeffs., empirical eqns. 78—94876
Lennard-Jones low temp. gas, eqn. of state, integral eqn. and perturbation method 78—26228
Mayer function, delta-function expansion, virial coeffs. appls. 79—4221
metal, equation of state, isentropic expansion method 78—91414
methane, μ, ρ and T-surfaces, global behaviour, rel. to catastrophe theory 78—26226
methane, dense gaseous and liq., thermal cond.-viscosity correlation, up to 500 atm., 95-500 K 77—80657
methane, gas, second virial coeffs., intermol. pot. at low temp. 79—46416
methane, intermol. pair pot. energy function 77—10721
methane, second refractivity virial coeff. direct determ. 77—15158
methanol vapour, isothermal Joule-Thomson coefficient, equation of state 80—24119
methyl halides, second dielec. virial coeffs. *(German)* 79—32729
methylpropylketone, P-v-T data, 270-670K, 1-800 bar *(Russian)* 77—39661
mixture of two gases, Krichevskii-Kazarnovskii equation, virial coeff. consideration 77—11294
mixtures, liquid-vapour equilibrium, thermodynamic props. using modified Redlich-Kwong eqn. of state 77—36775
mixtures, perturbed hard chain theory, thermodynamic props., appl. in chem. technology 79—34343
mixtures, vapour-liq., equilibria, fugacity coeff. calc., pseudocritical method 77—27972
monatomic gas, collision-induced light scatt. at intermediate density, integrated intensity, appl. to Ar 80—24124
multipole gases, second virial coeff. meas. 80—69959
neopentane, virial coefficient, meas. at various temps. using differential Burnett apparatus 80—22373
nonequilibrium fission bubble behaviour during fast transients in oxide fuel 78—8916
nonideal gas, self association theory 79—29347
nonideal gas in gravitational field, partition function, eqn. of state 80—6198
nonpolar gases, eqn. for prediction of third virial coefficients 80—33717
nonpolar molecular system, arbitrary symmetry, virial coeffs. 78—9743
one-component systems, isothermal eqn. of state using thermodynamic perturb. theory *(Russian)* 80—49335
phenol, vapour, viscosity coeff. and second virial coeff., conformity with Lennard-Jones pot. *(German)* 79—32732
point particle system, grand partition function, zero distrib., logarithmic interaction 77—11296
polar fluid, second dielec. virial coeff. calc. 78—22449
polar gas, 2nd and 3rd virial coeffs. calc., including nonadditive interactions 77—76013
polar gas, second virial coefficients for four-parameter model 78—14121
polar molecules interaction, Wooley pot., 2nd virial coeff. 77—65831
polar-quadrupolar gas mixtures, interaction second virial coeff. 79—32728
polyatomic gas viscosity related to Cp and molal vol. 78—34248
polyatomic molecules, quadrupolar and dipolar, numerical evaluation of second virial coeff. 78—91050
polyatomic substances, thermal eqns. of states *(French)* 78—91413
potential, predictive ability for dilute gas, bulk and microscopic data 79—81250
potential energy functions extracted from second virial coefficient data 79—72381
pressure, 'stress' calculation and virial theorem 79—37433
propane, compressibility, virial coeffs., Burnett method 78—47083
propane-propene mixtures, compressibility, virial coeffs., Burnett method 78—47083
propene, compressibility, virial coeffs., Burnett method 78—47083
propylene, μ, ρ and T-surfaces, global behaviour, rel. to catastrophe theory 78—26226
pure components, liq.-vapour equilib. and thermodynamic props. using modified Redlich-Kwong eqn. of state 77—36775
pure fluids, augmented van der Waals theory 78—18518

equations of state of gases continued
reactor fuel vapour expansion work energy calcs., effect of eqn. of state uncertainties 78—8940
real gas, nonpolar, ideal eqn. of state curve features 78—1776
real gas, P ρ T surfaces, butterfly catastrophe, from N_2, CO_2, Xe, propene and ethylene data 79—86546
real gas, theory and expt. comparison 79—86548
real gas, use of correl. relations of thermal vel. components 79—72981
real gas thermodynamics, Van der Waals model approach 80—38515
real gas version of de Saint Venant and Wantzel gasdynamic formulae *(German)* 79—18974
real gases, μ, ρ and T-surfaces, global behaviour, rel. to catastrophe theory 78—26226
real gases, eqns. of state, limits of validity *(Italian)* 79—41781
real gases, new eqn. of state *(Ukrainian)* 78—67297
Redlich-Kwong equation of state, modification to polar gases 78—9742
saturated steam parameters in reactor containments with escape of coolant, simplified calc. 80—68764
second virial coeff., in weak coupling limit, temp. depend. upper bound on partial wave contrib. 79—30356
second virial coefficient, triangular-well pot. gas, quantum correction 79—64818
second virial coefficient from the scattering operator 78—24730
second virial viscosity coefficient, temp. depend. 80—19543
square well potential gas, eqn. of state, parametric eqn. calcs. 77—89220
steam, saturated and superheated, up to 800°C 79—14908
sticky hard sphere fluid, eqn. of state, Percus-Yevick approx, 79—60240
supersaturated vapour, equilib. press. depend. on nucleating drop radius 80—69960
Tait eqn., new form, const. determ. for gases, liquids at press. of 3 to 10 kbar 79—86867
thermodynamic functions of gases, liquids by computer simulation 79—86866
thermodynamic properties of mixtures containing common polar and nonpolar components 77—31417
thermophysical props. inversion, anisotropic pot. energy function generation 80—99531
thermophysical props. tabulated for mixture composition certification 78—80818
third virial coefficient, nonadditive interactions effects calcs. 77—30122
transport coeff. for real gases *(Russian)* 79—10624
trifluoromethane, PVT study by Burnett method 77—42949
two-dimens. neutral Coulomb gas, bounds for classical canonical partition function 77—26227
unlike molecules, force constants, transport and virial coefficients, law of corresponding states calcs. 79—98848
vapour pressure, prediction using equation of state 80—103443
virial coeffs., quantum mech. second, square-well plus hard core pot. 78—1778
water, uniform and two-phase states, thermodynamic model interpolation 80—24565
water, vap., averaged potential for complex polar fluids 80—48833
water vapour, perturbed-hard-sphere eqn. of state 80—96331
weakly ionised gas non-ideal behaviour, virial eqn. of state and fugacity coeffs. 80—79424
weakly relativistic gas, equilib. distrib. and eqn. of state 79—21649
Wigner-Kirkwood expansion of second virial coeff., convergence accel. 78—91052
Ar, adiabatic compression to 25 kbar 79—86549
Ar, adsorbed on Xe-plated graphite, virial coeffs. and interatomic pots. 77—9125
Ar, Clausius-Mossotti second virial coefficient 80—79426
Ar, force constant props., 12-6 pot. model 78—13563
Ar, gas const. meas. by acoustical interferometry 77—7492
Ar gas constant determ. from speed of sound meas. 78—9746
Ar, phase transition, anharmonic cryst.-gas transition 80—6510
Ar, positive column, contracted, balance equations anal. 80—6312
Ar, second virial coeffs. from compressibility meas., mol. pot. parameters calc. *(Spanish)* 77—47133
Ar, sublimation temp. determination at very low pressures *(Croatian)* 79—28094
Ar, virial coefficient, meas. at various temps. using differential Burnett apparatus 80—22373
Ar-He, heat of mixing, low press., theories comparison 78—26230
Ar-Kr, pair pot. energy functions, gas phase bulk property reproduction 77—27642
Ar-SF_6, thermophysical props., second virial and diffusion coeffs., thermal diffusion factors 78—42699
Ar_2, interatomic potential single parameter 80—48059
CO, heat capacity, calc. by modified Redlich-Kwong eqn. of state 80—69963
CO-He, heat of mixing, low press., theories comparison 78—26230
CO_2, gas, second virial coeffs., intermol. pot. at low temp. 79—46416
CO_2, non-symmetric parametric eqn. of state for extended crit. region 77—35296
n-D_2, fluid, eqn. of state from P-V-T and US vel. meas. up to 20 kbar 78—63837
D_2O, saturated and superheated steam, eqn. of state up to 500°C 78—79401
F_2, gas, second virial coeffs., intermol. pot. at low temp. 79—46416
F_6S-Ar, compressibility 0 to 50°C, second virial coeffs. calcs. 77—15147
F_6S-Kr, compressibility 0 to 50°C, second virial coeffs. calcs. 77—15147
H, thermodynamic props. and eqns. of state in stellar conditions 79—35241
H_2 and isotopes, 4 to 30K 77—72674
n-H_2, equation of state from PVT and sound vel. meas., 75-307K, 2-20 kbar 77—62609
HCl, acid vapour, eqn. of state 78—79402
HCl, dilute gas, sp. ht. simulated with Lennard-Jones 12-6 pot. 80—1917
H_2O, metastable state, fundamental equation 80—103447
He, accurate empirical intermol. pot. 79—68291
He, Clausius-Mossotti second virial coefficient 80—79426
He, dense, semi-empirical eqn. of state and compressibility factors 77—7499
He, dielec. const. gas thermometry, 4-27K, and eqn. of state 79—63222
He, in confined region between two horizontal ducts for variable fluid properties 79—23321
He, second virial coeff., 0-500°C, two-temp. gas-expansion method 78—55711
He, thermodynamic props. and eqns. of state in stellar conditions 79—35241
He, third virial coeffs. calcs. using realistic Beck pair potential 78—94880
He-Xe, eqn. of state, Monte Carlo calcs. 80—59158
He+Ar, interatomic pot. well depth, SPFD pot., diffusion, viscosity and second virial coeff. 80—5599
He+H_2(HD)(HT), interaction second virial coeff. nonspherical pot. terms effects 77—3432
^{4}He, gas, second virial coeff., acoustic determ., 1.28-2.13K 80—69965
^{4}He, polarisability, second and third virial coeffs. meas. 4.2 to 27.1K 80—43825
^{4}He, Wigner-Kirkwood expansion of second virial coeff., convergence accel. 78—91052
IF_5, second virial coeff. meas., Lennard-Jones pot. determ. *(German)* 77—19658
Kr gas structure, three-body-contrib., neutron diffr. obs 80—43820
Kr, gas structure by neutron diffr., three-body pot. contrib. 79—90358
Kr, second virial coeffs. from compressibility meas., mol. pot. parameters calc. *(Spanish)* 77—47133
MoF_6, second virial coeff. meas., Lennard-Jones pot. determ. *(German)* 77—19658
N_2, cryogenic, shock wave-boundary layer interaction *(German)* 78—71370
N_2, dilute gas transport props. calcs. 77—72399
N_2, gas, second virial coeffs., intermol. pot. at low temp. 79—46416
N_2, μ, ρ and T-surfaces, global behaviour, rel. to catastrophe theory 78—26226
N_2, pair pot. 2nd virial coeff., nonproduct integration algorithm calc. 77—47128
N_2, press.-density depend. at high density, functional depend. using osculating curves 79—93109
N_2 structural second virial coeff., intermol. pot. and mag. scatt. 80—78678
N_2, thermodynamic and transport props., consistent correlation using Lennard-Jones (12-6) and Buckingham (exp-6) pots. 78—91045
NH_3, assoc. mols., struct. and dynamics, atom-atom pots., gas, solid and liq., props. 80—23487
NH_3, fluid, second dielec. virial coeff. calc. 78—22449
NO_2-N_2O_4 system, self-association theory 79—29347
Ne, Clausius-Mossotti second virial coefficient 80—79426
Ne, transport properties, exponential 6-pot. model parameters 77—47130
O_2, gas, second virial coeffs., intermol. pot. at low temp. 79—46416
O_2, μ, ρ and T-surfaces, global behaviour, rel. to catastrophe theory 78—26226
O_2, structural second virial coeff., intermol. pot. and mag. scatt. 80—78678
PF_5, second virial coeff. meas., Lennard-Jones pot. determ. *(German)* 77—19658
SF_6, gas, thermodynamical and spectral props., effect of angle-dependent part of dispersion forces 80—43138
SF_6, second virial coeffs. from compressibility meas., mol. pot. parameters calc. *(Spanish)* 77—47133
T_2, fluid, equations of state deduced from P-V-T and US meas. up to 20 kbar 79—23696
(U,Pu)N, self-consistent normal fluid eqn. of state, press., density, and enthalpy of vaporisation calc. 78—8909
(U,Pu)O_2, vapour press. eqn. of state, VENUS-II code studies 78—8908
UO_2 effective eqn.-of-state meas. to determ. vapour pressure, rel. to LMFBR safety 79—31036
UO_2 vapour, saturated, thermodynamic state and gas kinetic relaxation to 5000K 80—13593
WF_6, second virial coeff. meas., Lennard-Jones pot. determ. *(German)* 77—19658
Xe, high temp. and presssure, rel. to fission gas behaviour in fast reactor 79—67860
Xe, thermodynamic properties formulation, 161.36 to 800K and 0 to 350 MPa 77—51468

equations of state of liquids
Alfven wave system, eqn. of state, thermodynamic props., Bose-Einstein statistics 78—87397
alkali metal, law of corresponding states, microscopic basis 77—47539
alkali metals, crystalline and alkaline, eqns. of state, zero compression isotherms *(Russian)* 80—103446
alkali metals, equations of state and density meas. installation 77—43307
alkali nitrates, molten, pVT data, internal energies, eqn. of state 78—43098
alkali nitrates, molten, pVT data, thermal press. coeffs., compressibilities 78—43097
n-alkanes, Bender eqns. of state 78—26656
athermal polymer in strong soln., size and eqn. of state, screened convolution approx. 79—60257
p-azoxyanisole, nematic eqn. of state, incorporating short-range orient. order. 77—55237
benzene, equation of state studied using statistical theory results 80—84276
benzene, P-V-T relations, 5-300 MPa and 323-683K range 77—69069
binary hydrocarbon mixtures, critical points calc. using Soave eqn. of state 77—1209
binary liquid mixtures, viscous flow props., mol. thermodynamic theory 78—2280
binary mixtures at high press., phase equilibria, critical phenomena calcs. 77—35664
binary nonelectrolyte liquid mixture, hard sphere eqns. of state 78—47495
binary solutions of dense liquids and gases, isothermal eqn. of state calcs. *(Russian)* 80—88292
branched polymer molecules, second virial coeff., chain length effects calcs. 78—37775
1,3-butyleneglycol, density rel. to temp. and pressure *(Russian)* 79—10890
carbon tetrachloride, equation of state studied using statistical theory results 80—84276
CBOOA, liq. cryst.-isotropic transition at high press., P-V-T eqn. of state 79—95135
cellulose trinitrate, in soln., gel-like aggregate form. rel. to configuration 77—31036
charged hard sphere dense classical fluid, equation of state and crit. point 80—64849
classical fluids, thermodynamic behaviour near crit. point, book contrib. 79—60479

equations of state of liquids continued
- classical one-dimens. Lennard-Jones type system, eqn. of state 80−24562
- Clausius eqn. of state, thermodynamic props. calc. 78−83909
- Clausius modified eqn. *(French)* 78−91412
- coexistence curve of liquid system with global eqn. of state 79−1487
- corresponding states correlation for thermal cond. 77−59155
- Coulombic system, statistical mechs., eqn. of state in restricted primitive model 77−7644
- critical point, scaling and extended scaling eqns. of state implementation, program 79−46780
- dense fluid, with square-well+hard core pot., equilib. props., quantum corrections 79−27891
- dense fluid monolayer, eqn. of state, appl. to alcohol monolayer on water 78−6195
- diblock copolymer solution, second virial coeff., perturbation theory 80−29148
- o-dichlorobenzene, liq. mixtures, excess vols. and eqns. of state 77−29036
- dielectric liquids, critical point and eqn. of state investig. by optothermodynamic method *(Russian)* 79−33068
- dumbbells, nearly-Hookean, dilute soln., rheological equation of state 80−100321
- dynamic viscosity and heat cond. coeffs., linear relationship 77−7884
- EBBA, pVT data and viscosity-press. behaviour 78−94989
- ethane, fluid, saturated, compressed, sound velocity meas., compressibility, sp. ht. determ. 77−76488
- ethane, thermophysical props. from 90 to 600K at press. up to 700 bar 77−84940
- ethanol, Benedict-Webb-Rubin parameters 77−39660
- fatty-acid monolayer, on water, eqn. of state, liq.-gas crit. region 77−76520
- ferromagnetic fluid, 1D Ising and 3D Heisenberg solns. 77−85478
- fluid-solid surface interaction, two-particle correlation function 78−79880
- fluoromethanes, and perfluoroethane, NMR gas-to-liquid shifts, 2nd-virial coeff. of chem. shielding validity 79−85976
- fourth virial coefficient and structural consistency, for inverse power pots. 79−99047
- fused hard sphere fluids, equations of state, virial coeffs., Monte Carlo simulation 80−54095
- Gibbs-Duhem equation, appl. to water/magma systems 78−57205
- glass forming liquids, vol. relax. 80−96429
- Green's function Monte Carlo method for quantum hard spheres radial distrib. function 79−54005
- group contribution mol. model of liqs. and solns. 77−58932
- Gruneisen coeff., semi-empirical eqn., temp. and lattice distortion parameter depend. 77−31785
- hard core fluid with two-Yukawa tail, appl. to Ar 80−59618
- hard core fluids, asymptotic behaviour of virial expansions 80−88010
- hard core fluids, distrib. functions and equation of state, zero-separation theorem 80−44089
- hard disc fluid, infinite dilution solute chemical pot. by Monte Carlo simulation 80−88009
- hard oblate spherocylinders, Monte Carlo virial coeffs. 78−26400
- hard polyatomic molecular fluid, virial press., Monte Carlo method 77−89357
- hard rod fluid, phase transitions, rotational and liquid-crystalline, 1-D model 80−54090
- hard sphere, surface tension, compressibility, bulk modulus press. coeffs. and Rao's acoustical parameter 80−80027
- hard sphere fluid, fifth to tenth virial coeffs. calcs. 77−72671
- hard sphere mixture, nonadditive dias., perturbation theory, double reference system 78−38597
- hard spheres, partition functions, Miller's method 78−71828
- hard spheres, quantum mechanical virial coeff., two point Pade approx. 80−79657
- hard spheres mixtures, equations of state for calc. thermodynamic props. 80−84301
- hard- and soft-core equations of state 79−55635
- hard-core fluid with Yukawa tail, eqn. of state, Monte Carlo results 78−26410
- hard-sphere fluid, eqn. of state, quantum corrections 78−34592
- hard-sphere fluid, Yukawa tail pot., eqn. of state study 79−42211
- hard-sphere liquids, equations of state and evaluation of isothermal compressibility 79−73285
- heavy water dynamic viscosity coefficient in supercritical region of parameters of state, experimental investigation 78−67845
- n-heptadecane, short-chain mol. liq., statistical thermodynamics 79−73084
- heteronuclear hard dumbbells 77−30085
- hexafluorides, universal eqns. of state and thermodynamic similarity 77−35290
- n-hexane, superheated liq., US wave vel., adiabatic compressibility, heat capacity 78−2198
- high pressure, refr. index vs. press. and strain 79−33668
- hydrocarbon+CO_2(H_2S) mixtures, vapour-liq. equilibrium, crit. locus curve, Soave eqn. 78−83913
- hydrocarbon liquid, residual energy and entropy, rel. to liq. and mol. structs. 78−71869
- hydrocarbons, shock compression, dynamic high press. eqns. of state 80−6450
- ionic solution, charged square well model, virial osmotic coeffs. 79−4217
- Isopar-M, pressure-volume isotherms determ., use in deep-sea instrument float 77−25786
- isothermal bulk modulus and compressibility, intermol. interaction *(Russian)* 77−35658
- lattice gas virial coefficients, hard rectangular parallelepipeds and cubes on simple cubic lattice 79−97308
- Lennard-Jones fluid, 2-dimens. eqns. of state, comparison with expt. 79−69223
- light scattering, ratio of Brillouin to total scatt. intensity 78−52515
- linear polymer molecules, second virial coeff., chain length effects calcs. 78−37775
- liquid, under high press., refr. index vs. density 79−28712
- liquids, simple, thermodynamically self-consistent theories, radial distrib. function, functional derivative 80−92435
- 2,6-lutidine-water, fluid film, crit. phenomena, scaling, law of corresponding states 79−90787
- MBBA, liq. cryst.-isotropic transition at high press., P-V-T eqn. of state 79−95135
- MBBA, pVT data and viscosity-press. behaviour 78−94989

equations of state of liquids continued
- metal, and triplet and higher correlations in long wavelength limit 77−11453
- metals, eqn. of state parameters rel. to Earth core energetics 77−15536
- metals, isothermal compressibility and eqn. of state at m.p. 80−79673
- metals, lattice model, metal-nonmetal transition, eqn. of state, phase diagrams 77−69220
- metals and alloys, geometrical model, soft sphere static approx. eqn. of state 78−42892
- methane, dense gaseous and liq., thermal cond.-viscosity correlation, up to 500 atm., 95-500 K 77−80657
- methane-propane(pentane)(n-heptane)(n-decane)(H_2S) mixtures, densities calc., van der Waals model 78−79740
- methylpropylketone, P-v-T data, 270-670K, 1-800 bar *(Russian)* 77−39661
- mixture, of hard convex body fluids, pair correlation function 80−6484
- mixtures, asymmetric, Henry's constants and second virial coefficients from perturbed-hard-chain theory 80−96621
- mixtures, liquid-vapour equilibrium, thermodynamic props. using modified Redlich-Kwong eqn. of state 77−36775
- mixtures, perturbed hard chain theory, thermodynamic props., appl. in chem. technology 79−34343
- mixtures, vapour-liq., equilibria, fugacity coeff. calc., pseudocritical method 77−27972
- molecular liquid, thermodynamic functions, interaction site model calc. 78−71661
- molten salt mixtures, binary, excess thermodynamic props. and US vel. *(French)* 77−27943
- molten salts, compressibility hard sphere calcs. 77−51295
- monodisperse latex, simulation study of eqn. of state of simple liquid 77−63964
- monodisperse polymer solution, 2nd virial coeff., renormalisation group calc. 79−10777
- nematic liquid crystal, derivation 77−47560
- nematic liquid crystal, eqn. of state, incorporating short-range orient. order 77−55237
- nematic liquid crystal, eqn. of state for Maier-Saupe model 77−35474
- nematic liquid crystals, equation of state, anistropic props., perturbation theory 78−67645
- nematic-isotropic transition, Onsager's orientational order theory 78−79750
- n-nonane, short chain mol. liquid, statistical thermodynamics 79−64974
- nonlinear piezo-optical and linear elasto-optical behaviour 79−78650
- nonpolar liquids, soft nonspherical repulsions, effect on props. 77−68903
- oil-water microemulsions, osmotic press., micelle diameters, second virial coeff. *(French)* 78−20075
- one-component systems, isothermal eqn. of state using thermodynamic perturb. theory *(Russian)* 80−49335
- PAA, nematic, equation of state, anistropic props., perturbation theory 78−67645
- PAA, nematic liq. cryst. 77−47560
- n-paraffins, generalised eqn. of state from acoustical meas. 78−51642
- perfluorocyclobutane, dense fluid, self-diffusion, shear viscosity, density, and temp. depend., NMR 77−36152
- PET, P-V-T relationships 80−107400
- polar compounds, liq. props. representation, by modified Redlich-Kwong eqn. of state 78−34590
- poly-4-methylpentene-1, P-V-T relationships 80−107400
- polyacrylamide, aq. soln., thermodynamic props., light scatt. obs. *(Russian)* 80−71439
- polybutadiene and butadiene-styrene in tetrahydrofuran, second virial coeffs. 80−65188
- polybutene-1, P-V-T relationships 80−107400
- polyethylene, branched, P-V-T relationships 80−107400
- polymer, dil. soln., light scattering charact. of thermodynamic props., solvent and mol. wt. effect 80−16717
- polymer, isotropically swollen networks, vol. depend. of elastic eqn. of state 78−67832
- polymer branched chains, chain length, mol. architecture rel. to second virial coeff. 78−94964
- polymer Gruneisen formulation of p-V equation of state 78−30733
- polymer liquid, Ising fluid equation of state 77−51469
- polymer melt, eqn. of state analysis w.r.t. Ising fluid model 80−79907
- polymer mixtures, thermodynamics, review 79−1506
- polymer solution, complex coacervation, virial expsn. method 79−77750
- polymer solution, second virial coeff., segment cloud model, chain length and branching study 80−24559
- polymer solution, virial coefficients and osmotic press. 79−90751
- polymeric liquid, entropic elasticity and time temp. superposition principle, thermodynamic eqn. of state 78−63406
- polyolefin melts, eqns. of state analysis w.r.t. Simha-Somcynsky hole theory 79−37807
- polypropylene, P-V-T relationships 80−107400
- polystyrene mixture solutions, second virial coeff. light scatt. meas. 78−14438
- polystyrene solutions, light scatt., mol. parameters, computer anal. assessment 79−1766
- polysulphone, glass and melt, PVT props., glass transition 79−14911
- polysulphone, P-V-T relationships 80−107400
- power-law liquid, dil. suspensions of dipole dumbbells, rheological eqns. of state and shear flow in elec. field 79−86473
- Prandtl number, eqn. of state analogy and linear relations with transport props. 77−59156
- propylene, search procedure, based on step-wise least-squares technique 80−19900
- PTFE, P-V-T relationships 80−107400
- pure components, liq.-vapour equilib. and thermodynamic props. using modified Redlich-Kwong eqn. of state 77−36775
- pure fluids, augmented van der Waals theory 78−18518
- Rao's acoustical constant, temp. depend., from C_l-parameter 80−6462
- Redlich-Kwong-Soave eqn. of state, modification 78−38808
- Redlich-Kwong-Soave eqn. of state, modified, generalisation 77−27968
- rigid sphere model and evaluation of surface tension of liquids 79−56040
- seawater, eqn. for open ocean salinity, temp. and press. ranges 77−66922
- seawater, eqn. of state at high press. 80−101369
- seawater, equation of state for bounded depths *(Russian)* 77−60424
- seawater, Knudsen-Ekman equation of state, possible replacement 77−33083
- seawater, use for PVT props. of lake waters 77−49095

equations of state of liquids continued
second virial coeff. meas. apparatus, for pure organic cpds. and mixtures 80—44289
shock augmentation by bubble flow 77—3853
significant liquid structure theory, liquid-vapour transition, reduced eqn. of state for real fluids 79—32869
significant structure theory, critical pt. exponents calc. 77—7837
simple fluids, hard and soft-core eqns. of state, termination temps., Kihara pot. 80—70360
simple fluids, hard- and soft-core eqns. of state, characteristic curves 79—55861
simple fluids, hard-core equations of state, C_p extrema loci 79—60474
simple fluids, hard-core equations of state, characteristic curves 79—55862
simple liqs. with repulsive forces, thermodynamically selfconsistent theory 80—75139
simple liquid intermolecular interaction, extremal values 78—87602
solubility parameters, calc. from eqn. of state 77—11660
square well+hard core fluid, quantum corrections 79—7535
square-well+Sutherland (∞,6) fluid, perturbation theory 77—11455
square-well fluid, eqn. of state and thermodynamic props. 77—7834
square-well fluid, nonclassical crit. behaviour 80—44291
square-well liquids, equation of state, acoustic properties 79—99270
square-well-potential fluid, Yvon-Born-Green crit. exponent determ. 79—65169
sticky hard sphere fluid, eqn. of state, Percus-Yevick approx, 79—60240
structural relaxation times, smoothed cell potential model 77—27796
superheated liquid, spinodal, hole thoery 80—19232
surface tension, statistical mechanical theory 79—82414
Tait eqn., new form, const. determ. for gases, liquids at press. of 3 to 10 kbar 79—86867
ternary liquid-liquid equilibria, associated soln. theory capabilities 78—83910
thermodynamic functions of gases, liquids by computer simulation 79—86866
thin liquid film, instability and rupture 80—34279
unassociated liquids, estimate of props. 79—51232
vapour pressure, prediction using equation of state 80—103443
vinyl polymers, precip. from solns., temp. determ. *(German)* 80—85208
virial coefficents, review of liquid theory 77—7653
virial series divergence for hard discs and spheres at closest packing 79—94859
viscoelastic fluid flow, eqns. of state and motion, direct numerical soln. 79—60021
water, eqn. of state determ. from sound speed eqn., spl. vol. and compressibility 77—47538
water, liq., internal press. isobars, anomaly short-range order influence 77—65944
water, liq., solubility in compressed air 78—34631
water, PVT props., density meas., 150-350°C, saturation to 1 kbar 78—34594
water, saline and pure max. density points meas. 78—57900
water, uniform and two-phase states, thermodynamic model interpolation 80—24565
water pollutants, volatile, second virial coefficients, empirical correl. 79—52965
Ar, liq., equation of state, square-well model calcs. 77—84883
Ar, liq., equation of state studied using statistical theory results 80—84276
Ar, liq., variational eqn. of state and entropy 79—28070
Ar modified droplet model, mean droplet interaction below T_c 80—70363
Ar, μ, ρ and T-surfaces, global behaviour, rel. to catastrophe theory 78—26226
Ar, T_c, P_c, V_c, from eqn. of state 78—2228
CO, vaporisation temp. and press., state eqn. *(French)* 77—43323
Cs, determ. from PVT data 80—24564
Cs, expt. PVT data 80—19905
Cs, T_c, P_c, V_c, from eqn. of state 78—2228
Cs, volume and compressibility up to 22 kbar, eqn. of state 77—47541
Cu, equation of state, isentropic expansion method 78—91414
n-D_2, fluid, eqn. of state from P-V-T and US vel. meas. up to 20 kbar 78—63837
D_2O, eqn. of state, up to 380°C and 1000 bar 78—26655
D_2O, liquid, volumetric and derived thermal characteristics at low temp. and high pressure 80—107352
F, hard sphere model with attractive interactions 80—96434
Fe, eqn. of state in Earth's core conditions 77—73694
H_2 and isotopes, 4 to 30K 77—72674
H_2, eqn. of state of solid and liq. phases, metallic phase *(Russian)* 79—19354
n-H_2, equation of state from PVT and sound vel. meas., 75-307K, 2-20 kbar 77—62609
p-H_2, equil. bulk props., perturbation theory approach and quantum effects *(Russian)* 77—89551
H_2, perturbation theory and quantum effects, thermodynamic props. and quantum stat. corrections *(Russian)* 78—22867
H_2O, metastable state, fundamental equation 80—103447
H_2O, modified droplet model, mean droplet interaction below T_c 80—70363
He, accurate empirical intermol. pot. 79—68291
He films, physisorbed low-density submonolayer thermodynamics, potential scatt. theory calcs. 79—95243
He, T_c, P_c, V_c, from eqn. of state 78—2228
^{3}He, equation of state and crit. exponents near liq.-vapour crit. point 80—24707
^{3}He-^{4}He mixture, equation of state and crit. exponents near liq.-vapour crit. point 80—24707
^{4}He, Lennard-Jones model at 0K, props. using Monte Carlo method 79—82401
^{4}He, second and third virial coeffs., meas. from 2.6 to 27.1K 79—37808
^{4}He superfluid, isochores between 25 bar and melting curve 78—14523
^{4}He superfluid film, modified eqn. of state, mech. reson. meas. 80—24692
Hg, electrical and thermodynamic props. in metal-semicond. transition range 80—20144
Hg expanded liquid, simultaneous investigation of eqn. of state and elec. cond. 77—55337
Hg, P-V-T relations for temperatures of 40 to 240°C and press. up to 1400 kg cm^{-2} 78—6140
Hg, soft-sphere equation of state 79—55863
Hg, T_c, P_c, V_c, from eqn. of state 78—2228

equations of state of liquids continued
K, equation of state, press. and entropy along melting curve 77—47540
K, T_c, P_c, V_c, from eqn. of state 78—2228
K, volume and compressibility up to 14 kbar, eqn. of state 77—47541
Kr, T_c, P_c, V_c, from eqn. of state 78—2228
$LiNO_3$-$NaNO_3$-$AgNO_3$, molten salt mixture, excess thermodynamic props. and US vel. *(French)* 77—31720
N_2, liq., second virial coeffs., 77.3 to 90.1K 79—90754
N_2+methane, liquid mixture, press. effect on excess thermodynamic functions 78—47494
Na, determ. from PVT data 80—24564
Na equation of state, melting curve 80—103448
Na, equation of state, press. and entropy along melting curve 77—47540
Na, expt. PVT data 80—19905
Na, liquid, eqn. of state and thermodynamic props. at high temp. and density 79—55902
Na, T_c, P_c, V_c, from eqn. of state 78—2228
Na, volume and compressibility up to 22 kbar, eqn. of state 77—47541
NaCl, interpolational eqn. of state with allowance for melting, vaporis., dissoc. and ionis. processes 80—24566
Ne, T_c, P_c, V_c, from eqn. of state 78—2228
Ne-H_2 mixture, liquid vapour phase equilib., sound vel., compressibility, thermodynamic perturbation theory obs. *(Russian)* 80—39306
Ne-Kr, partially miscible mixture, high press. mol. dynamics using Lennard-Jones pot. 79—41929
O_2, modified droplet model, mean droplet interaction below T_c 80—70363
O_2, vaporisation temp. and press., state eqn. *(French)* 77—43323
Pb, equation of state, isentropic expansion method 78—91414
Pb, evaporation in shock compression release waves *(Russian)* 78—18761
Rb, determ. from PVT data 80—24564
Rb, equation of state, press. and entropy along melting curve 77—47540
Rb, expt. PVT data 80—19905
Rb, liquid, expanded, eqn. of state, transport up to 1700°C, 400 bar 80—2136
Rb, T_c, P_c, V_c, from eqn. of state 78—2228
S, eqn. of state determ., crit. props. and mol. comp. 80—49336
SF_6, liq., near crit. point, optical props. meas. 77—72673
Se, electronic transport props., equation of state, to 1900K and 1800 bars 80—65574
Se, eqn. of state determ., crit. props. and mol. comp. 80—49336
T_2, fluid, equations of state deduced from P-V-T and US meas. up to 20 kbar 79—23696
(U,Pu)N, self-consistent normal fluid eqn. of state, press., density, and enthalpy of vaporisation calc. 78—8909
(U,Pu)O_2 fuels, eqn. of state up to 5000K, high-temp. laser technique 77—27971
UO_2, liquid, eqn. of state 79—14910
Xe, liquid-vapour coexisting densities, nonlinear crossover, scaling corrections 77—84913
Xe, μ, ρ and T-surfaces, global behaviour, rel. to catastrophe theory 78—26226
Xe, T_c, P_c, V_c, from eqn. of state 78—2228
Xe, thermodynamic properties formulation, 161.36 to 800K and 0 to 350 MPa 77—51468

equations of state of solids
adiabatic shear explanation 77—14924
alkali halides, polymorphic phase transition 77—80618
alkali metals, atomic properties, pseudopot. calcs. 77—89512
alkali metals, bulk modulus and eqns. of state under press. 80—88293
alkali metals, crystalline and alkaline, eqns. of state, zero compression isotherms *(Russian)* 80—103446
alkali metals, equation of state and vol. depend. of thermodynamic props., pseudopot. theory 78—18738
alkali metals, law of corresponding states 77—15535
alkali metals, partial pressure contributions to equation of state 80—107401
alloy, rel. to variation in interatomic interaction and lattice parameters during ordering *(Russian)* 77—81255
amorphous soft-core systems, low temp., mol. dynamic studies 80—6359
anorthite, thermal eqn. of state up to 120 GPa, appl. to Earth mantle 80—109136
approximate equation of state of condensed substances, shock adiabats calcs. 77—35657
atomic solid, Gruneisen formulation of p-V equation of state 78—30733
benzene, crystalline, press.-vol.-temp. relations 78—22819
benzene, mol. reorientationally disordered phases, thermodynamics 79—46782
bond percolation model, site-cluster distribs. and eqn. of state 77—74329
bulk moduli, Wachtman's eqn., and temp. depend. 78—75799
chain networks, static and dynamic entanglements, contrib. to equilib. shear modulus 80—28126
classical n-vector model, eqn. of state in 1/n expansion 77—65005
classical solid solutions, beyond-mean-field approx. 77—20039
critical region, nonasymptotic terms *(Russian)* 77—28402
crystals, anharmonic, with complex lattice, equations of state 80—107399
cubic metals, press.-vol. relations calc., pseudopotential method 77—11662
densely packed crystals with strong sixth-order anharmonicity, eqns. of state 80—92637
diamond, compressibility, appl. of Murnaghan eqn. of state, Morse pot. 80—79861
discrete structure solids, mathematical models for stress relaxation and deformation 77—14923
dynamic, shock wave expts. *(German)* 78—59858
Earth interior, Gruneisen function evaluated in harmonic approx. 80—72474
Einstein's work in solid-state theory, geophysical importance *(German)* 79—86848
elastic deformation, thermodynamics of, eqn. of state for solids 80—96589
elements, generalised shock adiabats 79—86839
finite strain equations of state, evaluation using lattice model 80—96620
fourth order quasi-harmonic, solids of cubic and tetragonal symm. 77—69068
furan, mol. reorientationally disordered phases, thermodynamics 79—46782
glassy linear polymer, mol. model *(Russian)* 77—62610
granular materials flow, micropolar continuum theory 79—35565

equations of state of solids continued
  graphitised C black, adsorption of inert gases, gas-solid virial coeffs. 78—75928
  Gruneisen coefficient at Earth interior conditions 80—72474
  Gruneisen parameter and adiabatic compressibility, simple model 77—11706
  guanidine aluminium sulphate hexahydrate:Cr^{3+}, ESR spectra fine struct. 80—93169
  high pressure, appl. to alkali halides 78—55935
  homogeneous isotropic material, high press. eqn. of state and sound vels. to fourth order elastic consts. 79—37806
  Hugoniot curves of third and fourth order for cubic crystals *(French)* 77—11634
  inert gas solids, isotherms 77—20041
  ionic crystals, binding forces and eqns. of state, inner electron contrib., calc. 80—64950
  ionic crystals, temp. expansion of Bogolyubov chains *(Russian)* 77—27949
  ionic solids, many-body effects on fourth-order elastic consts. 77—76483
  isentrope extrapolation in high pressure region, isotropic compression case 80—24532
  Ising-like system parametric eqn. of state 77—30102
  isothermal equations of state, P-V relation, elements and selected compounds *(Chinese)* 78—79739
  isothermal Murnaghan eqn., appl. to CsCl, CsBr, CsI *(Chinese)* 77—7836
  isotropic magnet, Goldstone mode singularities eqn. of state, magnetisation curve, perturbation theory calcs. 78—43607
  lattice constant fluctuations, influence on thermal props. of cryst. 79—77715
  lattice constant fluctuations, rel. to theory of eqn. of state for crystals 78—30732
  lattice-lattice scaling, reln. to scaled eqn. of state, appl. to Ising model 78—70067
  material stability under high press., eqns. of state *(Chinese)* 80—6461
  materials under pressure *(French)* 79—95117
  matter behind wave front, eqn. of state *(Chinese)* 79—82308
  metal, complete thermodynamic eqns. of state 80—24561
  metal, Gruneisen coeff. rel. to press. depend. of Poisson ratio 77—47504
  metal, monovalent, low temp. eqn. of state 78—22820
  metal, plasticity, dynamic, governing relations, elastic energy 79—43328
  metal, simple, non muffin-tin corrections to eqn. of state *(French)* 80—59906
  metal, thermal expansivity determ. 77—27970
  metal plastic deformation, influence of mech. vibrations 78—60722
  metallic hydrides, props. suggesting H_3^+ type clusters 77—35660
  metals, shock wave compression, reduced Hugoniot curve and eqn. of state *(Chinese)* 80—44259
  metals between 300-200000K for all press., numerical calcs. for Cu, Al *(French)* 77—72672
  methane, crystalline, struct. and compression at high press., room temp. 80—107199
  Mie-Gruneisen equation of state, appl. to planetary interiors 78—29072
  minerals, eqns. of state for metastable phases 77—70639
  minerals pressure-density path, effect of viscosity on release adiabat meas. 80—51388
  minerals relevant to Earth interior geophysics, Hildebrand equation of state 80—56464
  molecular solids, intermol. forces and eqn. of state, pseudoharmonic approx. calcs. 78—30731
  molecular solids, melting curves, Lennard-Jones Devonshire theory 80—65201
  noncubic crystals, eqn. of state model, shock wave studies appl. 79—14883
  nonuniformly stressed crystal, statics and kinetics of vacancies *(Russian)* 78—55863
  nuclear reactor core mats., constitutive eqn. 78—80598
  ordered alloy, applicability of semiempirical function of binding energy *(Russian)* 77—15533
  orthorhombic crystal, Hugoniot curves, elastic anisotropy effect *(French)* 78—18735
  piezoelectric crystal, acoustic activity and other effects due to spatial dispersion 78—2808
  planetary physics, comparison of eqn. of state theories using high-compression exptl. data 79—20779
  plastic material, Muller's entropy principle restrictions on constitutive eqns. *(Japanese)* 78—9578
  poly(alkyl methacrylate), vitreous state, thermal cond., hole theory of liqs., press. 78—84013
  poly [nitrilo-bis(phenylamino)phosphoranetriyl]s, synthesis and characterisation *(Italian)* 77—66755
  polyethylene, equation of state for semicrystalline, crystalline polymers 80—65187
  polyethylene, orthorhombic and triclinic lattices, eqns. of state 79—28069
  polymer, flexible chain collapse 78—87628
  polymer, Gruneisen formulation of p-V equation of state 78—30733
  polymers, equation of state *(German)* 79—82309
  polypropylene, isotactic, equation of state for semicrystalline, crystalline polymers 80—65187
  polysulphone, glass and melt, PVT props., glass transition 79—14911
  polyvinylidene fluoride, equation of state, compression ratios, theory 80—10634
  porous solid, generalised p-α model, eqn. of state, sound vel. 80—65154
  quartz, fused, second press. derivatives of elastic moduli, US vel. meas. 79—23670
  quartz, porous, Hugoniot synthesis at high pressures 79—95080
  reinforced plastics, equations of state, taking account of mech. damage 80—97553
  second Hugoniot relationship 77—35659
  semi-infinite systems, critical behaviour 78—4563
  shock wave propagation, in smoothly-varying density condensed medium 77—75844
  shock waves and the dimensionless Hugoniot eqn. of state 79—69191
  shock waves in material with linear shock wave-particle vel. relation 77—69042
  silicate minerals, seismic eqn. of state rel. to seismic parameter Φ and phonon cond. 79—39707
  silicate rocks, quartz-stishovite transitions, shock wave processes 79—88347
  simple crystalline lattice with central force bonds, thermal eqn. of state and elastic consts. *(Russian)* 78—14437

equations of state of solids continued
  spin glass, quenched random impurities, dynamics, replicas and frustration approaches 80—34673
  spin glasses, Ising type random bond, scaling, eqn. of state and instability 79—73753
  statistical mech. treatment of phase transitions impurity states 78—64004
  steel, high-strength, dynamic yield strengths, phase transition press. and Hugoniot parameters 80—75331
  stishovite, compression to 100 kbar, eqn. of state from bulk modulus 77—17085
  stishovite, polycrystalline, US vels. and Murnaghan P-V trajectories 77—5189
  superionic crystals, phase transitions 78—75826
  surface tension of solids, eqn. of state anal. 80—6618
  Tait equation of state, high press. and isothermal bulk modulus 77—84882
  tetrachloroisophthalonitrile, vapour press. by effusion method, solid phase eqn. of state 80—49350
  TGS, eqn. of state near ferroelec. Curie temp., including tunnel effect 77—12342
  thermal pressure in solid and eqn. of state, computer simulation 78—34593
  transition metal, eqn. of state, s- and d-contribs. 78—91633
  transition metal alloy, ground state properties, self-consistent calc. 78—91587
  transition metals, 4d, theory of energy bands, s and d contrib. to eqn. of state 78—30865
  uniaxial stress component, effect on eqns. of state determ. with opposed-anvil X-ray apparatus 80—49301
  van der Waal's crystal P-V-T diagram, Holmholtz free energy, mean-field model, for teaching 77—33784
  van der Waals crystal, Bogolyubov chain temp. expansion *(Russian)* 77—13705
  viscoelastic materials, eqn. of state for class of viscoelastic deforms. 78—26060
  Ag, low temp. eqn. of state appl. to thermal expansivity 79—60476
  Al and its alloys, dynamic determ. of Gruneisen coeff. 77—24418
  Al, constitutive equation for porous materials with strength, press. effects 80—79875
  Al, electronic Gruneisen parameter in shock Hugoniot eqn. of state 80—10635
  Al, eqn. of state from statistical electronic free energy 79—99495
  Al, Gruneisen coeff. depend. on specific volume, phonon spectra calcs. 79—65165
  Al Hugoniot curves of third and fourth order for cubic crystals *(French)* 77—11634
  Al, load relaxation, plastic deform. theory and plastic eqn. of state 78—27554
  Al, porous, Hugoniot synthesis at high pressures 79—95080
  Al, shock wave data, 'solid Hugoniot' rel. to 'fluid Hugoniot' 80—65155
  Al, sp. ht. meas., 0-100 kbar, eqn. of state comparison 77—51512
  Al, under very high dynamic load *(German)* 78—59858
  Al, zero-temperature equation of state, statistical model with density gradient correction 80—15215
  Ar, solid, density at melting and isochoric equations of state 78—83915
  Ar, solid, self consistent field calcs. of isotherms and thermodynamic props. *(Russian)* 80—10633
  Ar, thermal eqn. of state and elastic consts., calc. *(Russian)* 78—14437
  As_2Se_3 glass, mech. props. var. due to high press. phase change 77—76481
  Au, low temp. eqn. of state appl. to thermal expansivity 79—60476
  Be, eqn. of state from statistical electronic free energy 79—99495
  Be, solid-state models, comparison 80—75332
  Be, zero-temperature equation of state, statistical model with density gradient correction 80—15215
  Ca, zero-temperature equation of state, statistical model with density gradient correction 80—15215
  CaO, eqn. of state at high press., appl. to Earth core and mantle 80—109122
  Cd, Hugoniot curves, elastic anisotropy effect *(French)* 78—18735
  Cd, phonon spectra and eqn. of state, pseudopot. method *(Russian)* 77—24367
  CdTe, equation of state 79—82310
  CdTe, relations pressure-volume under high pressure 80—39219
  Ce, high pressure phase transition, anomalous Gruneisen parameter behaviour 80—79934
  $CrBr_3$, parametric representation of the equation of state of a Heisenberg system in the critical region 78—79741
  CsCl, phonon dispersion, temp. induced phase transition, deformable shell model calcs. 79—77698
  Cu crystal, cohesion and vacancy form., electron statistical model 80—54169
  Cu, eqn. of state from statistical electronic free energy 79—99495
  Cu, shock compressed, release isentropes, eqn. of state at high energy density *(Russian)* 80—54340
  Cu, shock wave compression, reduced Hugoniot curve and eqn. of state *(Chinese)* 80—44259
  Cu, shock wave data, 'solid Hugoniot' rel. to 'fluid Hugoniot' 80—65155
  Cu, sp. ht. meas., 0-100 kbar, eqn. of state comparison 77—51512
  Cu_3Au, applicability of semiempirical function of binding energy *(Russian)* 77—15533
  D_2, at high pressure 79—46781
  D_2, mol. solid, 4.2K isotherm, ortho-para depend. 79—7670
  Fe, BCC, shock wave simulation using Morse pot. 78—2196
  Fe close-packed phases, eqns. of state and implications for Earth core 79—20780
  Fe, P-V-T data for Lennard-Jones potential, computer expt. 78—75800
  Fe, shock wave compression, reduced Hugoniot curve and eqn. of state *(Chinese)* 80—44259
  ϵ-Fe, vol. eqn. of state under static press. conditions, rel. to Earth core-mantle models 80—19904
  FeO, eqn. of state at high press., appl. to Earth core and mantle 80—109122
  FeS_2, pyrite, eqn. of state, rel. to constraints on Earth S content 79—70789
  $Fe_{0.9}S$, pyrrhotite, eqn. of state, rel. to constraints on Earth S content 79—70789
  GaAs, equation of state 79—82310
  GaSb, relations pressure-volume under high pressure 80—39219
  Ge, eqn. of state, under press. 78—75801
  Ge, metallic, high press. 79—60475

equations of state of solids continued
H_2 and isotopes, 4 to 30K 77—72674
H_2, at high pressure 79—46781
H_2, energy in vol. range 10 to 60 a.u./atom, allowance for three-particle interactions *(Russian)* 78—38654
H_2, eqn. of state of megabar press. using z-pinch method *(Russian)* 79—33071
H_2, equation of state for α-N_2 and HCP type lattices, at 0K 77—47537
n-H_2, equation of state from PVT and sound vel. meas., 75-307K, 2-20 kbar 77—62609
p-H_2, FCC, equation of state and lattice dynamics, temp. depend. 77—76521
H_2, metal phase, eqn. of state, thermodynamic pot. *(Hungarian)* 79—14909
H_2, metallic, eqn. of state and thermodynamic potential *(Russian)* 77—89519
H_2, metallic and molecular, transition press. and eqns. of state calc. 78—26685
H_2, metallic phase, eqn. of state of solid and liq. phases *(Russian)* 79—19354
H_2, quadrupolar glass, press. meas. 80—34271
p-H_2, solid, anisotropic contribs. to ground state props. 78—83914
H_2, solid, equation of state, intramol. zero pt. energy contrib., total sublimation energy 78—71829
^{4}He, HCP, ground-state props. 80—44389
^{4}He, Lennard-Jones model at 0K, props. using Monte Carlo method 79—82401
^{4}He, solid-fluid, eqn. of state, melting props. under press. 80—96721
InSb, equation of state 79—82310
InSb, relations pressure-volume under high pressure 80—39219
KBr crystals, binding forces and eqns. of state, inner electron contrib., calc. 80—64950
KBr, shock adiabatic, nonparametric equation of state 78—10121
KCl, thermal expansion, compressibility and melting calcs. 79—33069
Kr, solid, density at melting and isochoric equations of state 78—83915
Li, zero-temperature equation of state, statistical model with density gradient correction 80—15215
LiBr, shock adiabatic, nonparametric equation of state 78—10121
LiH, electronic struct., equation of state, insulator-metal phase transition 79—33234
LiH, electronic struct. and equation of state up to 100 Mbar 77—1361
$(Mg,Fe)_2SiO_4$, shock deform. expts., Hugoniot data implications 80—94497
Mg, phonon spectra and eqn. of state, pseudopot. method *(Russian)* 77—24367
Mg, shock wave compression, reduced Hugoniot curve and eqn. of state *(Chinese)* 80—44259
Mg_2SiO_4, forsterite, single-cryst., shock wave compression 79—84242
Mg0, vol. eqn. of state under static press. conditions, rel. to Earth core-mantle models 80—19904
Mo, shock compression to 2.0 TPa, by nuclear explosion, Hugoniot determ. 77—84841
Na equation of state, melting curve 80—103448
NaBr, shock adiabatic, nonparametric equation of state 78—10121
NaCl, eqn. of state, effect of Gruneisen parameter 79—51233
NaCl, eqn. of state to 32 kbar and 500°C, length change meas. 80—70361
NaCl, high press. eqn. of state and sound vels. to fourth order elastic consts., 270 kbar 79—37806
NaCl, interpolational eqn. of state with allowance for melting, vaporis., dissoc. and ionis. processes 80—24566
NaCl, isothermal eqn. of state, length change meas. technique 77—1210
NaCl primary press. gauge, failure of central force model 77—15492
NaCl, thermal expansion, compressibility and melting calcs. 79—33069
Ne, P-V-T data for Morse pot., computer expt. 78—75800
Ni, sp. ht. meas., 0-100 kbar, eqn. of state comparison 77—51512
Pb, shock compressed, release isentropes, eqn. of state at high energy density *(Russian)* 80—54340
PbS, first-principles calc. of eqn. of states 80—49649
PbS, thermomech. props., SCF Xα scatt. wave theory 78—71704
$Pb(Zr_xTi_{1-x})O_3$, meas. of Hugoniot curve with commercial manganin stress gauges 80—70362
Pd:H, elastic props. of dilute solid solutions 78—75706
Pd-Zn, $L1_0$ type intermetallic phase, X-ray diffr. study of lattic compression 80—49182
PuO_2 nuclear fuel, thermodynamic props. 80—13592
RbF(Cl)(Br), shock adiabatic, nonparametric equation of state 78—10121
$RbHSO_4$, acoustic and dielectric props. near phase transition 80—55053
Si, eqn. of state, under press. 78—75801
Si, metallic, high press. 79—60475
β-Sn, equation of state under press. 79—33070
p-H, solid, constant volume heat capacity and eqn. of state, temp. depend. 80—65334
Th, electronic states under press. 80—54600
TiO_2, rutile phase, shock induced phase transition anisotropic behaviour 80—103475
U, Hugoniot data, ultrahigh press. (TPa) shockwave from underground nuclear explosion 80—59580
UO_2, elastic props. at high press., US meas. 77—4141
UO_2 nuclear fuel, thermodynamic props. 80—13592
W, Hugoniot, rel. to shock compression data, 1223K 77—55320
W, porous, room temp. shock compression expts., Hugoniot states, 0.6-7.6 GPa 77—84842
WC-Co, elastic moduli and their press. derivatives 79—83248
Xe, solid, high press. equation of state 79—37809
Xe, solid, zero temp. isotherm, APW calc. 79—73128
ZnS, equation of state 79—82310

equilibrium, chemical *see chemical equilibrium*

equilibrium, phase *see phase equilibrium*

equilibrium constants *see chemical equilibrium*

equilibrium diagrams *see phase diagrams*

equivalence classes
see also automata theory
visual stimuli equivalence classes, model neural network 78—69064

equivalent circuits
see also network analysis; network parameters; network synthesis
Acetabularia cell electrical parameters and equiv. cct. 77—56350
acoustic field, equiv. circuit using finite element method *(Japanese)* 77—50790

equivalent circuits continued
acoustic field, finite-element approach 79—7238
acoustic surface wave resonators, characts. from Fabry-Perot cavity anal. 77—39131
acoustic wave propagation in anisotropic rods of rectangular cross-section 78—1463
acoustic wave propagation in composite thin-plates, equivalent microwave network analysis 79—3820
active vibration-suppression systems, block diagram 78—18098
acupuncture, transient impedance between stimulation points 79—43977
angular spectrum of EM field, elec. network equivalent 78—78867
bar-shaped resonators excited electromechanically in flexural vibration 77—42677
cardiac conduction and propag., equiv. cct. 78—31791
cardiovascular system, analogue circuit and compartmental model, normal and defective states 79—57700
cascaded gratings, transmission response 77—23835
cell electric circuit model, alternating signal interaction 78—77011
cell electric circuit model, alternating signal interaction 78—77012
charge sensitive preamplifiers, signal and noise response 78—33404
Cole-Cole dielectric relaxation distrib. function, circuit model 80—7291
complex US vibratory systems, equiv. circuit anal. 78—50997
compliance, variable, arterial compliance appl. 80—41097
composite piezoelectric transducers, dynamic lumped parameters 78—18142
conduction MHD pump with current leakage, equivalent circuit *(Russian)* 78—26346
conduction MHD systems, feedback and self-excitation threshold calcs. *(Russian)* 77—47108
contactless electrostatic-acoustic transducer equivalent cct. analysis 77—19507
dental electrosurgery, evaluation of patient elec. load by analogue cct. 77—40912
dielectric material ageing anal. *(Bulgarian)* 77—66467
dielectrics, liquid, electrical model of conductivity *(Russian)* 77—8101
discharges, transversely inhomogeneous, equivalent circuit treatment 77—62419
discontinuous metal film, AC equivalent circuit anal. 79—51690
education, elec. electric energy density in dissipative medium by cct. analogue 78—36759
electric field strength, dissipative media, for teachers 79—40319
electroacoustic transducers, four-pole network model rel. to dynamic behaviour anal. 78—9518
electrochemical convertors, conc. type, for elec. signals, diffusion theory of conc. networks 78—61026
electrochemical electrodes, current distribution, network-type equivalent cct. investig. 78—35705
electromechanical filter torsional mode transducer analysis 77—27436
electrometric circuit switching by magnetically controlled contact 77—79108
electrometric voltmeter input capacitance absorption meas. 77—79107
electroretinographic response rel. to vars. of visual performance during day 78—77051
electrosurgical passive grounded electrode/patient equivalent circuit analysis 77—78025
epithelium, tight, impedance anal. using distributed resistance model 79—62201
equatorial electrojet, equivalent circuit anal. of neutral wind effects 78—57392
explosive mag. generator, magnetic accumulation in plane liner, flux loss and equiv. cct. 79—14571
filter design, band-pass, with SAW *(Czech)* 80—19201
flexural-mode mechanical filter resonances 77—27435
glottal sound source, self-oscillating model *(Japanese)* 78—92654
glow discharge, transversely inhomogeneous, stability, equiv. cct. theory 78—51373
gravimeter, LaCoste and Romberg, equivalent ccts. rel. to vibr. characts. *(Japanese)* 78—65400
gravitational wave antennas, with and without piezoelectric ceramics, elec. equivalent circuits 78—73915
Gunn domain transient behaviour and associated equivalent circuits 78—19043
heart, source impedance and internal reactive power in infarcted left ventricle 77—37007
heart polyphase harmonic generator model and application to ECG 77—60278
heat capacity evaluation, electrical analogy 79—10453
HF electrodeless discharges, second stage with external magnetic field applied to plasma, investigation by equivalent circuit approach 80—24296
HF second-step discharge meas. and equivalent cct. 79—7505
high-power US transducer performance rel. to ceramic location 79—50561
human body *(Russian)* 79—53295
human skin impedance change 77—81773
interacting SAW transducer equivalent circuits 77—27456
interdigital transducers, equiv. cct. parameters from surface waves dispersion relations 77—39187
ionosphere low latitude dynamo current system, equivalent mesh cct. rel. to seasonal vars. 80—8479
IR detectors, microwave-biased extrinsic photoconductors, performance anal. 78—49898
Josephson junction, solns. of nonlinear eqn. of resistively shunted model 78—2628
Josephson junctions, coupled, I-V charact., model calc. 80—84559
Josephson weak-link, simplification of resistively shunted junction model 77—72946
Jupiter ionosphere, current cct. rel. to decametric radiation modulation by Io 78—89110
large-area solar cell electrical characterisation accuracy 79—96454
laser discharge, stimulated reactive oscills., laser-elec. circuit Q 77—58315
leg electrical impedance freq. characts. *(Japanese)* 80—56252
local tract area function, estimation by adaptive deconvolution and adaptive speech anal. system *(Japanese)* 78—92658
lumped parameter equiv. ccts. for HF transducers, quarter-wave matching characts. 80—1397
magnetostrictive, transducer in presence of eddy currents, mobility analogy equivalent cct. 80—48540
magnetostrictive transducer terminated in arbitrary elec. impedance, elec. cct. anal. 78—5627

equivalent circuits continued
MHD convertors, with non-uniform gas *(Italian)* 80—3525
MHD generator, channel electrical characts., equivalent ccts. 80—75106
MHD generator, diagonal channel equivalent energy circuit 79—55571
MHD generator, diagonal type, end effects anal. by means of equivalent cct. *(Japanese)* 78—87505
microwave transducer, thermoelectric using hot carrier semicond. 77—10109
MIS structure, elec. parameter meas. of second order equivalent ccts. 80—57332
MISIM structure impedance and equivalent cct. 77—62998
modular chirp Z transform equivalent to two-lens optical Fourier transform 78—78943
MOS capacitor formed over p-on-n semiconductor structure, G-V characts. 80—100532
MOS capacitor photovoltage characterisation 78—10573
multielectrode composite piezoceramic bar, equivalent elec. cct. 77—46877
multilevel generation-recomb. noise spectra, appl. of equivalent network methods 77—43674
nerve axon, leading edge approx. 77—12903
network thermodynamic two-port element, representation of salt, current coupled flow 79—34505
neural membrane two-factor two-mode model 78—7330
neuron model of burst generation, FET analogue 77—44630
noncontact EM transducer design improvement 79—46151
nonlinear magnetic field simulator for electromagnetic fields anal. *(Japanese)* 80—95756
ohmic resist. of glass meas. from equivalent circuit 79—33110
one-port SAW resonators, config. and cct. anal. 78—63258
opto-acoustic transducer, for biomed. diagnostic imaging, equiv. cct. and simulation 77—60283
overlay ridge waveguide SAW mode analysis 79—46100
p^+-n diode under forward bias, effects of radiation-induced deep levels on admittance 78—23157
p-n heterojunction differential admittance theory in the presence of surface electron states 80—96981
p-n junction, small signal equivalent circuit, finite carrier multiplication 80—65664
photoconductor image charge transfer to electrographic film 80—101864
piezo-transducer, broadband matching for acousto-optical devices *(Russian)* 80—64329
piezoactive complex vibratory systems, matrices of parameters for six-pole equivalent circuits 77—68304
piezoceramic cylinders, short axially polarized annular, calculation of equivalent circuit parameters 80—5901
piezoceramic microwelding transducer component oscillation amplitudes 79—26046
piezoceramic sphere, radially polarised, equivalent cct. parameters calc. 80—14538
piezoelectric modulation transducers for alternating pressures 78—77891
piezoelectric polymer transducers, effect of acoustic radiation on equivalent circuit 79—94380
piezoelectric thickness vibrator, equivalent ccts. rel. to digital computer simulation 77—88998
piezoelectric transducer with inhomogeneous acoustic load 79—32174
piezoelectric transducers, acoustically loaded, expt. method for equivalent circuit parameter determination 78—51036
plasma resonator, electron-beam excited, explosive instability 80—28693
polyacrylonitrile, pyrolyzed, surface layer, anal. of elec. cond. mechanism by impedance diagram *(Japanese)* 78—23148
porous layers, equivalent cct. for acoustic impedance, appl. to reson. absorbers damping *(German)* 77—14825
positive column *(German)* 77—58909
rare earth iron magnetostrictive underwater sound transducer, equivalent cct. 78—13881
resistance and capacitance determ., lecture demonstration 78—69938
respiratory ventilator model and design optimisation 79—20713
rod outer segment adaptation anal. based on a simple equiv. cct. 78—73157
SAW bandpass filters, two-port model 77—62117
SAW delay line complex transfer coeff. calc., Shockley-Ramo induced current theorem 79—7264
SAW EM transducer harmonic operation 79—46152
SAW metallic gratings, equivalent circuit of step discontinuity, rel. to SAW devices 80—33389
SAW resonator reflector and transducer characteristic effects 77—39168
SAW storage correlator equivalent circuit models 78—9506
SAW transducers, equivalent circuit model 77—46870
Schottky-barrier metal-semiconductor junction carrier migration and equivalent cct. analysis *(Russian)* 78—84294
semiconductor modelling, bulk, negative-cond., transverse spreading of high-field domain 79—1602
shock excited oscillator for US flaw detectors, piezoelectric transducer matching 77—73422
skeletal muscle fibre with helicoidal T system, linear elec. props. 78—80852
skin impedance parameter dispersion and correlation 79—29518
skin impedance simulation w.r.t. Cole-Cole circular arc law 77—5101
skin resistance during square-wave elec. pulses of 1 to 10 mA, rel. to nerve stimulation 78—31929
slot impedance of rectangular conductor, transient field anal. using Bubnof-Galerkin method *(Polish)* 77—54643
solar cells, faulty, scanning light spot anal. 80—89625
solar energy systems, electrical analogue simulator development 80—30382
soliton line constructed from an equivalent cct. of undamped spiking lasers 79—3673
sonar transducer, Langevin type, made from $Pb(Zr,Ti)O_3$ type 1 ceramic, performance characts. 80—79095
spectrum analyser for radar signal processing 78—78942
ST-quartz SAW resonators and coupled resonator filters 77—39174
strip-coupled varactor SAW convolvers, parametric cct. anal. 78—71245
superconducting junction with linear periodic current phase relation, AC Josephson like effect 77—32124
superconductors, composite, and normal conductors, transient loss analysis and measurements using equivalent circuit technique 79—60978
symmetrical Lamb wave scatt. at pair of thin slots 79—47868
systemic vasculature, importance of non-linear contribs. 78—44549
tapered piezoelectric bar transducer with transversely polarised piezoceramic, equivalent cct., capacitance and admittance 78—1537

equivalent circuits continued
thermoelectric coolers, electrical analogue simulation of transient behaviour 78—21140
Tokamak simulation, equivalent cct. model and mag. field diffusion eqns. 77—84409
US transducer thickness mode design, computer simulation using Thevenin equivalent ccts. 78—30143
vibrating bars, transverse-mode, equivalent electrical networks and appls. 79—68469
water content meas. capacitance transducer systematic error reduction 77—79082
Ag/(α-AgI) interface, impedance meas., equivalent circuit parameters. calc., electrolyte defect struct. 78—59975
CO_2 waveguide laser, pulsed operation 78—42353
CdS, piezoelectric thin-film transducers, electromechanical coupling meas. and equivalent cct. 77—23840
CdSe, MIS thin film capacitance, theory 79—87156
Cr, discontinuous thin film, AC equivalent circuit anal. 79—51690
Cu film, complex impedance, IR transmission and refl. meas. 79—78216
GaAs oxidation saturation and MOS diode equivalent cct. 78—47875
GeSe amorphouse sputtered film, DC and AC behaviour, effect of contact material 79—95513
InSb, MIS thin film capacitance, theory 79—87156
Na_2CO_3 electrolyte, silent discharges elec. characts., expt. *(Korean)* 78—40057
Pb-acid battery charge determ. from internal impedance 79—96436
Si reverse-biased p-n junction DC characteristics interpretation *(Polish)* 78—91761
Si SAW delay line design, inclusion of cond., equivalent cct. 77—88989
Si:Zn p-n junctions, I-V characts. using exact DC circuit model 79—95476
Ta-Ta_2O_5-Au capacitive system, freq. depend. of dissipation factor, dielectric const., conductance *(Spanish)* 77—69426
n—TiO_2-electrolyte interface, equivalent circuit elements from impedance meas. 80—39669
ZnO-based nonohmic ceramic, dielec. dispersion and equiv. circuit 77—73110

erbium
see also nuclei with......
adsorption and absorption of $H_2(D_2)$ 77—4257
adsorption on W, field emission electron study 80—100393
Anderson-Gruneisen parameter, temp. depend., third-order elastic consts. calc. 79—46776
atom, absolute oscill. strengths of spectral lines 79—85928
atom, keV electron impact, L X-ray prod. cross section 79—18293
atom, L-shell internal excitation accompanying L-capture 80—95726
atom, L-X-ray emission, new satellite 77—10620
atom, photoabsorpt. spectra 77—88417
atom, spectral lines, relative oscill. strengths determ. 77—83657
atom X-ray emission spectrum, electronic quadrupole transition $L_2M_3(\beta_{17})$ 79—98018
axon, squid giant, compensation of potential changes produced by Er ion with applied potentials 79—16181
borate glass:Er^{3+}, $^4I_{13/2}$ level relax. 79—87476
Debye-Waller factor and Lindemann parameter, temp. depend., lattice dynamical model calcs. 80—59610
diffusion of ^{198}Au, anisotropy, interstitial solute diffusion mechanism 80—29223
elastic constants, magnetoelastic contrib. 80—15777
electron irradiated, defect annealing, recovery spectra 79—23648
film, elec. resist., thickness depend., effect of presence of dihydride 77—51829
film, elec. resist. results 78—84326
film, evap., CO effect on work function 78—39188
film, magnetoelastic excitations, phonon spectroscopy and forbidden transitions 79—82853
film, O_2 and H_2 contamination effect on elec. resist. 77—80856
film, reaction with H_2O vapour, spectroscopic and X-ray diffr. obs. 77—40575
film, vacuum-evaporated, elec. resist., thickness depend. 77—76956
film, work function, effects of O_2 sorption 78—19125
fluoride, MF_2:Er^{3+}, (M=Ba,Ca,Cd), far IR Stark and Zeeman splitting 77—48190
glass:Er^{3+}, nonradiative decay and multiphonon relax. 77—85802
glass:Er^{3+}, polarised luminesc. 78—48224
glass:Yb^{3+},Er^{3+}, stimulated emission 77—50675
Hall constant and elec. resist., 80-700K *(Russian)* 78—60110
hyperfine structure of odd isotopes, two step photoionisation, mass filtration *(Russian)* 77—46550
impurity in nonmag. host, anisotropic exchange Hamiltonian, rel. to ESR spectrum 77—20696
ion implantation, nonradiative transitions on crystals, laser active media 79—31911
isotope separation, laser two-step photoionisation 78—46461
kaonic atom, radiationless mixing, even-even X-ray yield *(Russian)* 77—61880
$KZnF_3$:Er excitation of 650 GHz phonons in spin-lattice relax. 78—27089
L-line emission spectrum diagram line 80—84808
laser evaporation and condensation in H_2 and Ar atmospheres 79—10941
lattice dynamics, thermal expansion, bulk modulus calcs. 77—20022
liquid, struct. factors, high temp. X-ray diffr. obs. 79—7544
magnetic aftereffect obs. 77—8364
magnetisation, quantum jump 80—60369
magnetisation in strong pulsed mag. field, differential susceptibility meas. *(Russian)* 79—19729
optical absorption in paramagnetic and antiferromagnetic states *(Russian)* 78—56497
perovskite:Er^{3+}, ESR spectrum, higher order Zeeman effects 79—99766
plastic deformation, substructured changes, stress-strain diagrams and microhardness meas. *(Russian)* 79—52296
point defect production during electron irrad. at low temp. 80—49273
powder, hydride form. under water vap. 79—91997
rare earth compound:Er^{3+}, phosphors active layer effective thickness calc. *(Russian)* 79—43039
scheelite:Er^{3+}, ESR spectrum, higher order Zeeman effects 79—99766
silicate glass: Er^{3+}, $^4I_{13/2}$ level relax. 79—87476
silicide thin film formation on (100) and (111)Si substrate, backscattering study 80—70542
specific heat, and compression curves 79—51272

erbium continued
specific heat, mag. contrib. 79−28538
spectral emittance above 1000K 77−4211
spin wave exam. 78−56306
spin wave theory in strongly anisotropic magnets 77−63151
thin layer chromatography 78−20105
TmBi:Er, ESR of non S-state ions 77−43881
US attenuation, longitudinal, in mag. ordered region and out phase transitions 77−28422
US attenuation in mag. field, temp. and field depend. 79−91279
US attenuation near magnetic transitions at 53.9 and 83.8K 79−55837
vaporisation, heat of sublimation, meas. 80−103471
X-ray L_{III} absorption discontinuity, bidirectional orbital interpretation 77−16423
Ag:Er, orbit-lattice coupling, nonuniform strain effects 78−88182
Al:Er, orbit-lattice coupling, nonuniform strain effects 78−88182
$BaF_2:Er^{3+}$, fluoresc., importance of defect clustering 79−33827
$BaF_2:Er^{3+}$, fluoresc. spectra of charge compensated cryst., multiphonon and energy transfer relax. 79−87496
$BaF_2:Er^{3+}$, single-site multiphonon and energy transfer relax. 78−52547
$BaO\text{-}B_2O_3:UO_2^{2+} \rightarrow Er^{3+}$ glass, energy transfer 78−2895
$BaWO_4:Er^{3+}$, spin-lattice and spin-spin relax. times, electron spin echo obs. 79−28609
$BaY_2F_8:Er^{3+}$, ESR spectra and spin-lattice relax. 80−11263
$BeF_2\text{-}KF\text{-}CaF_2\text{-}AlF_3:Er^{3+}$ glass, multiphonon relax., fluoresc. obs. 78−15219
$Bi_{12}GeO_{20}:Er$, luminesc., emission and excitation spectra 80−103975
$Bi_4Ge_3O_{12}:Er^{3+}$, host-sensitised energy transfer, laser time resolved spectroscopy 79−83013
$Bi_4Ge_3O_{12}:Er^{3+}$ crystal growth, spectral and laser props. 80−45115
$CaF_2:Er$, defect structure, quenching effect, dielec. relax. and optical absorption 80−65031
$CaF_2:Er$, γ-irrad., photostimulated luminesc. meas. 77−66538
$CaF_2:Er$, hydrogenated and deuterated, optical and EPR specra 79−61209
$CaF_2:Er$, near-Debye dielectric responses 80−71291
$CaF_2:Er^{3+}$, fluoresc. spectra of charge compensated cryst., multiphonon and energy transfer relax. 79−87496
$CaF_2:Er^{3+}$, fluorite, defect equilibria cluster control 79−99231
$CaF_2:Er^{3+}$ laser fluoresc. of Er^{3+} sites, defect equilibria 78−6748
$CaF_2:Yb^{3+}$, Er^{3+}, and $CdF_2\text{-}CaF_2:Yb^{3+}$, Er^{3+}, IR to visible upconverting system 77−44035
$CaF_2\text{-}YF_3:Er^{3+}$, stimulated emission 77−52135
$CaMoO_4:Er^{3+}$, phase relax., EPR spin echo expts. 79−99767
$CaMoO_4:Er^{3+}$, phase relax. time rel. to g-factor anisotropy, electron spin echo obs. 80−29615
$CaSO_4:Eu$, gamma-irradiated valency conversions in rare-earth ions 80−55198
$Ca_{1-x}Sr_xF_2:Er^{3+}$ mixed crystal, luminesc. transition, inhomogeneous line broadening calc. 80−97332
$CaWO_4:Er$, spectroscopic parameters calcs. 80−50379
$CaWO_4:Er^{3+}$, magnetocaloric behaviour, cryst. field theory 77−4520
$CaWO_4:Er^{3+}$, phase relaxation, spin echo meas. 78−68375
$CaYAlO_4:Er^{3+}$, absorpt. and luminesc. spectra 77−69901
$CdF_2:Er^{3+}$, selective monochromatic excitation of $^4S_{1/2}$-$^4I_{15/2}$ transition *(French)* 77−85765
$CdF_2:Er^{3+}$, Tm^{3+}, evidence for $Er^{3+} \rightleftharpoons Tm^{3+}$ energy transfers, fluoresc. expts. 80−60655
$CdInGaS_4:Er^{3+}$, cryst. field parameters, thermal and mag. props. calc. 77−20540
$CdIn_2S_4:Er^{3+}$, cryst. field parameters, thermal and mag. props. calc. 77−20540
$CdS:Er^{3+}$, spectra of different emission centres *(Russian)* 77−16356
$CePt_2$, ESR of Er^{3+} 79−87315
$Cs_2NaRCl_6:Er^{3+}$, R=lanthanide, EPR parameters and interpret. 77−59456
^{A}ER, A=167,168, absolute atomic masses 79−89228
Er III $4f^{12}$ configuration, spectra calcs. by configuration superposition *(Russian)* 80−14080
Er, magnetisation and susceptibility in basal plane in strong mag. field *(Russian)* 80−50145
Er^{3+} amino acid complexes, supersensitive transition intensities, spectra *(Russian)* 77−88461
Er^{3+}, dual action on transmitter release at frog neuromuscular synapse 78−35834
Er^{3+}, intermediate coupling props., relativistic average of config. wavefunctions applicability 78−17574
Er^{3+}, local symmetry in frozen aq. solns., EPR and local electric field effect 77−16169
Er^{3+}, luminesc. sensitisation by Yb^{3+}, in liq., efficiency *(Russian)* 78−90116
Er^{3+}, non-radiative energy transfer from Eu^{3+} in dimethylsulphoxide 79−47510
Er^{3+}, Yb^{3+}:glass, Nd laser radiation energy conversion *(Russian)* 77−62013
$Er^{3+}:CaF_2$ crystal laser, hologram form. at 2.76 μm, laser emission linewidth meas. 79−10270
$Er^{3+}:KGd(WO_4)_2$, stimulated emission by subsidiary transitions 79−3696
$Er^{3+}:KLu(WO_4)_2$, room temp. stimulated emission obs. 80−106527
$Er^{3+}:Lu_3Al_5O_{12}$, 3-μm crystal laser functional scheme, stimulated emission 80−43339
Er^{3+}:trifluoride, VUV fluorescence and tunable coherent sources from 1650 to 2600 Å 77−688
Er^{3+}:YAG pulse periodic laser with high activator conc. 79−10320
Er^{3+}:YErAG, $^4I_{11/2}$ to $^4I_{13/2}$ laser transition cross section, luminesc. energy 77−79833
$Er^{3+}:Yb^{3+}$ in liq. media, luminesc. cooperative sensitisation 80−2827
$Er\text{-}H_2$ system, work function changes correlated with phase changes, elec. resist. meas. 77−11828
Er^{3+}-doped trifluorides, vacuum-UV excitation spectra 78−80381
$ErAG:Er^{3+}$, 3 μm stimulated emission at room temp. 77−42541
GaP:ER, magnetic susceptibility, impurity states 79−61044
$GdAlO_3:Er^{3+}$, $^4S_{3/2}$ to $^4I_{9/2}$ transition laser action, optical and luminescence spectra 80−16082
$Gd_3Ga_5O_{12}:Er^{3+}$, stimulated emission 79−91466
H, and He, stopping powers meas. 80−42904
$KMgF_3:Er^{3+}$, Orbach-Aminor paramag. relax. processes, phonon bottleneck 79−28610
KYF_4, KY_2F_7, KY_3F_{10}, Er^{3+} and Yb^{3+} doped, IR excitation curves for visible luminesc. 79−33795

erbium continued
$KY(WO_4)_2:Er^{3+}$, stimulated emission at 300K 80−34951
$LaBe_{13}:Er$, ESR, appl. of exchange induced broadening in low lying crystalline field system 80−108062
$LaBe_{13}:Er$, ESR, crystalline field single ion effects 78−84481
$LaBe_{13}:Er$, ESR spectra, Er spin-spin exchange broadening 78−23338
LaBi:Er, ESR of non S-state ions 77−43881
$LaF_3:Er$, cryst. field anal. of triply ionised ion spectra 80−2796
$LaF_3:Er^{3+}$, impurity centre interaction with external. elec. field 77−89727
$LaF_3:Er^{3+}$, optically excited, direct-process spin-lattice relaxation 80−93378
$LaF_3:Er^{3+}$, spin-lattice relax. meas. in excited $^4S_{3/2}$ state by purely optical method 79−19923
$La_2O_2S:Yb^{3+}$,Er^{3+}, IR excited visible luminesc. of Er^{3+} 78−2910
$La_2S_3.3Ga_2S_3:Er^{3+}$ glass, fluoresc., and possibility of lasing 78−23514
$LiYF_4:Er^{3+}$, ESR, nonlinear effect of elec. field 80−2635
$LiYF_4:Er^{3+}$, electron-irrad. induced defects, optical and EPR study 80−66238
$LiYF_4:Er^{3+}$, magnetocaloric behaviour, cryst. field theory 77−4520
$LiYFd_4:Er^{3+}$, optical spectra and multifreq. stimulated emission 79−56818
$(Lu,Er)_3Al_5O_{12}:Er^{3+}$, stimulated emission 77−52135
$LuAlO_3:Er^{3+}$, $^4S_{3/2}$ to $^4I_{9/2}$ transition laser action, optical and luminescence spectra 80−16082
$Lu_3Al_5O_{12}:Er^{3+}$, 3 μm stimulated emission at room temp. 77−42541
$Lu_3Al_5O_{12}:Er^{3+}$, absorpt., luminesc., stimulated emission 77−32402
$Lu_3Al_5O_{12}:Er^{3+}$, sensitized stimulated emission at 3 microns 80−53302
$Lu_3Al_5O_{12}:Er^{3+}(Ho^{3+})$, stimulated radn., electron-phonon interaction *(Russian)* 77−8605
$LuBe_{13}:Er$, ESR, crystalline field single ion effects 78−84481
$LuCrO_3:Er^{3+}$, doping effect on ^{53}Cr NMR in domain walls 80−71219
$LuYScO_3:Er^{3+}$, thermolum. meas. 80−97354
$MgO:Er^{3+}$, Γ_8 quartets, orbit-lattice interaction, e.p.r. under stress 77−1591
$MgO:Er^{3+}$, spin-lattice interaction in Γ_8 quartets, models tested for EPR data 78−23336
$MnF_2:Er^{3+}$, fluorescence props. 79−73994
$Na_2O\text{-}TeO_2:Er^{3+}$ glass, luminesc. quenching by OH and OD *(Russian)* 79−28839
$POCl_3:ZrCl_4:Nd^{3+}(Er^{3+})$, radiative transition probabilities within 4f configs. 77−8617
$POCl_3\text{-}ZrCl_4:Yb^{3+}$, Er^{3+}, energy transfer from Yb^{3+} to Er^{3+}, agglomeration formation 78−64405
PrBi:Er, ESR of non S-state ions 77−43881
$RbMnF_3:Er$, unirradiated and electron irrad., energy transfer 80−108254
$RbMnF_3:Er^{3+}$, absorption, emission, excitation and lifetime meas. 80−71460
$SRF_2:Er^{3+}$, laser excitation of single ion and clustered ion sites 77−69879
$ScH_x:Er$, ESP determ, of proton locations 80−34768
$ScH_x:Er$, ESR evidence of octahedral site occupation 79−78512
$ScH_x:Er$, proton distrib. and site energies, ESR meas. 80−59509
$Sc_2(WO_4)_3:Er^{3+}$, growth, solubility, absorption spectrum and thermal expansion meas. 77−36391
$SeOCl_2:Er^{3+}$, $SbCl_5$ acidified, Racah and Judd-Ofelt parameters in laser liqs. 80−106516
$SrF_2:Er$, activation vol. for interstitial motion, dielec. const. meas. 80−49412
$SrF_2:Er$, dipolar complex exam. 79−38435
$SrF_2:Er$, far IR spectra 79−33736
$SrF_2:Er^{3+}$, fluoresc. spectra of charge compensated cryst., multiphonon and energy transfer relax. 79−87496
$SrWO_4:Er^{3+}$, spin-lattice and spin-spin relax. times, electron spin echo obs. 79−28609
$Tb(OH)_3:Er^{3+}$, ferromag., anisotropic exchange effects in optical spectra 78−80141
$Tb(OH)_3:Er^{3+}$, g-values and hyperfine interaction parameters, calc. for Er^{3+} 79−15123
$ThBe_{13}:Er$, ESR, crystalline field single ion effects 78−84481
$ThH_2:Er^{3+}$, EPR of Er localised electron mag. states, Kondo effect 80−25202
$Th_4H_{15}:Er^{3+}$, EPR of Er localised electron mag. states, Kondo effect 80−25202
$YA\text{-}O_3:Er^{3+}$, pulsed laser action, $^4S_{3/2}$ to $^4I_{9/2}$ transition laser action, optical and luminescence spectra 80−16082
YAG:Er, elastic wave damping, 300 to 1500 MHz, impurity effects 80−92602
YAG:Er, US attenuation 77−89500
$YAG:Er^{3+}$, 3 μm stimulated emission at room temp. 77−42541
$YAG:Er^{3+}$, crystal field theory, Er^{3+} behaviour in tetragonal field 77−8259
$YAG:Er^{3+}$, oscillator strengths of impurities, 5000 to 30000 cm^{-1} 79−4830
$YAG:Er^{3+}(Er^{3+}, Ga^{3+})$, LPE and luminesc. 78−64408
$YAG:Er^{3+}(Ho^{3+})$, stimulated radn., electron-phonon interaction *(Russian)* 77−8605
$YAlO_3:Er^{3+}$, free-ion-model cryst.-field calc. 77−43545
$Y_3Al_5O_{12}:Er^{3+}$, stimulated emission 77−52135
$YE+AG:Er^{3+}$, laser material, radiative and nonradiative transitions, conc. quenching 77−16391
$YF_3:Er^{3+}$, Yb^{3+}, IR excitation curves for visible luminesc. 79−33795
$YF_3:Yb,Er$, IR to visible light conversion, effect of temperature on efficiency *(Russian)* 77−28628
$YF_3:Yb,Er$, IR to visible radiation transform., limit yield *(Russian)* 79−28838
$YF_3:Yb,Er$, limit efficiency of transformation of IR to visible radiation 80−29784
$(Y_{0.8}Gd_{0.2})AlO_3:Er^{3+}$, spectroscopic props. 77−85791
$YH_3:Er$, Mossbauer spectra of Er^{3+}, gyromagnetic ratios and cryst. field parameters determ. 78−19388
$YH_x:Er$, proton distrib. and site energies, ESR meas. 80−59509
YOCl:Yb,Er, anti-Stokes luminesc., temp. depend. *(Russian)* 78−6764
$YOCl:Yb^{3+}$, Er^{3+}, anti-Stokes luminesc., 4.2 to 293K 77−59609
$Y(OH)_3:Er^{3+}$, g-values and hyperfine interaction parameters, calc. for Er^{3+} 79−15123
$Y_2SiO_5:Er^{3+}$, EPR and spin-lattice relax. 80−108063
$YVO_4:Er^{3+}$, energy transfer laser time-resolved spectroscopy 78−27306
$YVO_4:Er^{3+}$, Yb^{3+}, IR excitation curves for visible luminesc. 79−33795
$(Y_{0.80}Yb_{0.19}Er_{0.01})F_3$ phosphors, IR to visible conversion 78−48210
Zn tellurite: Er^{3+} glass, visible green emission 79−15523

erbium continued
ZnIn$_2$S$_4$:Er^{3+}, cryst. field parameters, thermal and mag. props. calc. 77–20540
ZnO:Er, electrolum. brightness, field strength and freq. depend. 80–100696
ZnO:Er, phosphor, photoluminesc. and electroluminesc. spectra 79–11457
ZnO:Er, phosphors, photo- and electroluminesc. 77–12428
ZnO:Er(Ag), photoluminescence and electroluminescence 78–27327
ZnS:Cu,Er,Cl film, ageing and forming, DC electroluminesc., impact excitation 79–47522
ZnS:Er diodes, electrolum. 79–33840
ZnS:Er phosphors, optical scintillation mechanism 79–56867
ZnS:Er^{3+}, ion-implanted, annealing, cathodolum. obs. 80–2868
ZnS:Er^{3+}, luminesc. centres with cubic symmetry 79–38636
ZrH$_x$:Er, (x=1.5 and 1.85), Mossbauer spectra 80–20527
ZrSiO$_4$:Er, anisotropic mag. susceptibility meas. 77–43806

erbium alloys
dilute, ESR linewidth of rare-earth ions 78–68373
rare earth intermetallics, RAl$_2$-Er, dil., (R=La, Yb, Lu), EPR and mag. susceptibility 80–15797
Ag-Er, dil., cryst. field and spin exchange parameters, susceptibility and ESR expts. 77–40129
Ag-Er, dil., reflection EPR residual linewidth 77–81004
Ag-Er film, stress-induced g-anisotropy, EPR of Er 77–85566
Al-Er, dil., lattice location of ^{169}Er ions after implantation, Mossbauer effect of ^{169}Tm 78–39460
Al-Er, dil., supercond., order parameter dynamics and collective modes, pair tunnelling meas. 79–56409
Al-Er, dil., transmission ESR and expts. 77–20704
Al-Er film, spin-flip scatt. and supercond. order parameter dynamics 79–78267
Au-Er, dil., cold-worked, EPR expts. 80–39864
Au-Er, dil., EPR at 100 mK to 1K 80–66028
Au-Er, ESR studies 80–108064
Au-Er film, stress-induced g-shift, ESR meas. on Er 77–51951
α-Ce-Er, dil., ESR study of mag. prop 78–39398
CePd$_3$-Er, dil., EPR 80–25201
CePd$_3$-Er, dil., low field mag. susceptibility, electro-nuclear effects 80–60189
Co-Zr-Er alloys, mag. annealing effect, effect of Er on induced uniaxial mag. anisotropy 80–39771
Co$_{67}$Er$_{33}$ amorphous alloy, sputtered, local order and amorphous struct. 80–88061
Er-Au, dil., Mossbauer exam. of mag. hyperfine field at ^{197}Au impurity 78–88244
Er-Cd, dil., elec. field gradient, at ^{111}Cd impurities, temp. depend. 79–28642
Er-Co-Ni, cryst. struct. and H$_2$ capacity 77–89543
Er-Fe amorphous alloys, mag. props. 79–90557
Er-Fe-Al(Mn)(Co), cryst. struct. and H$_2$ capacity 77–89543
Er-Fe-O system, O-stabilised intermetallic Er$_{12}$Fe$_{32}$O$_2$, prep. and characterisation 77–8956
Er-H$_2$ system, work function changes correlated with phase changes, elec. resist. meas. 77–11828
Er-La, HCP, mag. phase diagram, neutron diffr. meas. 80–70950
Er-Ta, dil., elec. field gradient at ^{181}Ta, temp. depend., TDPAC meas. 79–95689
Er-Ta, dil., mag. hyperfine field determ., TOPAC meas. 79–91330
Er-Tb, elasticity modulus, ΔE-effect, internal friction, magnetic transformations *(Russian)* 79–91723
ErAg, amorphous, bulk mag. props., field, time and temp. depends. 77–89932
ErAl$_2$, anisotropic magnetostriction, temp. depend. 80–39841
ErAl$_2$, conduction electron spin and orbital polarisation effects 78–80228
ErAl$_2$, cryst. field volume magnetostriction calc. 79–8029
ErAl$_2$, sp. ht. and thermal props., 5 to 300K 77–43342
ErAl$_3$, 15 layer rhombohedral struct., mag. struct. 77–63104
ErAu$_3$, mag. props. *(German)* 79–51761
Er$_2$Au, mag. props., 4.2-300K 79–7972
ErAuNi$_4$, mag. props. 77–20595
Er$_3$Au$_3$Sb$_4$, mag. suscept. meas., 4 to 300K 79–51742
ErBi, electronic struct., LCAO calc. *(Russian)* 77–39777
Er$_c$Ce$_{1-c}$Pd$_3$, cryst. field spectra, neutron scatt. study 80–50047
ErCo$_2$, amorphous, mag. correlations, neutron exam. 79–73682
ErCo$_2$, amorphous, mag. correlations, neutron exam. 79–73683
ErCo$_2$, elec. resistivity, thermopower, X-ray struct. meas. 80–24874
ErCo$_2$, field induced vol. magnetostriction 78–91920
ErCo$_2$, mag. excitation spectrum, neutron inelastic scatt. obs. 79–78351
ErCo$_2$, mag. excitations, RPA theory 80–65830
ErCo$_2$, magnetocryst. anisotropy props. by ^{57}Fe Mossbauer spectroscopy 77–63328
ErCo$_2$, spontaneous vol. magnetostriction and thermal expansion meas. 77–12183
ErCo$_3$, absorption of H$_2$, 77-300K 79–23737
ErCo$_3$, ErCo$_6$ and Er$_2$Co$_{17}$, Kerr effect determ. of domain structure, Bloch wall energy 80–39805
ErCo$_3$-H$_2$, phase equilibria, from dissociation isotherms 80–50591
ErCo$_{5.6}$, easy magnetisation direction 78–84415
ErCo$_6$, domain wall grooving due to mech. polishing 79–70232
ErCo$_x$, sorption at press. up to 1500 atm. 80–97819
Er$_{1-x}$Co$_x$, amorphous alloys, thermal stability, elec. cond. enthalpy 80–100172
Er$_2$Co$_{17}$, domain wall grooving due to mech. polishing 79–70232
Er$_2$Co$_{17}$, magnetisation, magnetocryst. anisotropy and magnetostriction 77–8303
Er$_2$Co$_{17}$, single cryst., magnetostriction const. temp. depend., 78 to 300K 79–51836
Er$_4$Co$_3$, cryst. field effect on mag. moment direction, neutron diffr. meas. 78–80132
Er$_{65}$Co$_{35}$, amorphous, amg. ordering, susceptibility, magnetisation and hysteresis meas. 78–68190
ErCoAl, mag. props. 78–2659
ErCo$_3$B$_2$, ferromag. ordering and saturation moments 77–24711
(ErCo$_2$)$_x$(ErAl$_2$)$_{1-x}$, mag. and struct. investigations of intermetallic systems 78–95440
Er$_2$(Co$_{1-x}$Fe$_x$)$_{17}$, mag. anisotropy and intersublattice exchange interactions 78–31066

erbium alloys continued
Er$_2$Co$_{17-x}$Fe$_x$(Mn$_x$)(Ni$_x$), saturation magnetisation, Curie temp., easy direction, and anisotropy field 77–8304
Er$_2$Co$_{17-x}$M, M=Fe, Mn, Ni, magnetisation, Curie temp., anisotropy 77–89947
Er$_2$Co$_{17-x}$M$_x$, M=Cr, Ni, effect of substitution on mag. props. 79–78363
ErCo$_{5-x}$Ni$_x$ ferrimagnetic series, magnetisation, coercive field meas. 78–91896
Er$_2$(Co$_{1-x}$Ni$_x$)$_{17}$, mag. anisotropy and intersublattice exchange interactions 78–31066
ErCu, cubic antiferromag., mag. excitations inelastic neutron scatt. meas. 78–72341
ErCu, magnetic excitations 80–25115
ErFe$_2$, crystal field interaction contribution to specific heat 80–39788
ErFe$_2$, Czochralski growth, and cryst. quality determ. 77–8742
ErFe$_2$, effect of H on sublattice magnetization, elastic neutron scatt. obs. 79–78327
ErFe$_2$, electronic heat capacity coeffs. 80–39787
ErFe$_2$, excited state spin waves inelastic scatt. meas. 78–76234
ErFe$_2$, highly magnetostrictive props. 77–12180
ErFe$_2$, lattice dynamics, Mossbauer spectra 80–19888
ErFe$_2$, Laves phase, cryst. field effects on spin wave dispersion relations 78–84408
ErFe$_2$, mag. excitations, RPA theory 80–65830
ErFe$_2$, magnetostriction in polycryst. samples 77–73065
ErFe$_2$ powders, mag. and hysteresis props. *(Russian)* 79–42800
ErFe$_2$, spin excitations, neutron scatt. obs. 77–63153
ErFe$_2$, spin waves, exchange interaction, neutron scatt. study 79–47267
ErFe$_2$, spontaneous magnetoelastic distortion, X-ray diffr. expts. 77–63253
ErFe$_2$ surface, effect of H and O adsorption, spin polarised photoemission study 80–29854
ErFe$_2$-LuFe$_2$ (10, 90 wt.%), mag. props., 80-1300K *(Russian)* 80–75750
ErFe$_2$-YFe$_2$ (30, 70 wt.%), mag. props., 80-1300K *(Russian)* 80–75750
ErFe$_3$, 47K magnetic anomaly, point charge crystal field model 77–20517
ErFe$_3$ and Er$_6$Fe$_{23}$, magnetostriction, room temp. to 80K 80–65993
ErFe$_3$, H$_2$ sorption, mag. and struct. props. of hydrides 80–34831
ErFe$_3$, mag. anomalies at 47 and 131K 77–63134
ErFe$_3$, mag. struct., powder neutron diffr. meas. 78–2651
ErFe$_3$, Mossbauer and magnetisation investig. of 47K mag. anomaly, atomic rearrangement 77–20766
Er$_{1-x}$Fe$_x$, amorphous film, cosputtered, struct. and mag. props. 78–60323
Er$_6$Fe$_{23}$, lower critical field 80–20414
Er$_6$Fe$_{23}$, magnetostriction, temp. depend., 20 to 350K 80–65994
ErFeAl, scatter order cpd., mag. props. 77–51891
ErFe$_4$Al$_8$, mag. props. 78–52250
ErFe$_4$Al$_8$, neutron diffr. exam., mag. struct. 78–10656
(Er$_{65}$Fe$_{35}$)$_{100-x}$B$_x$ glasses, mag. props. 79–73693
Er(Fe$_{1-x}$Co$_x$)$_3$, spin reorientation, easy axis of magnetisation 80–25144
Er$_2$Fe$_3$Co$_{14}$, Kerr effect determ. of domain structure, Bloch wall energy 80–39805
ErFe$_2$Ge$_2$, magnetisation, 4.2-273K 77–8310
ErFe$_2$H$_{3.9}$, mag. props. and lattice consts., effect of hydrogen absorpt. 77–20561
ErFe$_2$H$_x$, multiplateau absorpt. isotherms, theory 80–103564
ErFe$_2$H$_x$, thermodynamic props., H$_2$ desorption isotherm meas. 80–89516
Er(Fe$_{1-x}$Mn$_x$)$_2$, phase struct., mag. and Mossbauer meas. 77–20563
Er(Fe$_{1-x}$Mn$_x$)$_2$, struct. determ. by X-ray diffr. *(Russian)* 77–76358
Er$_6$(Fe$_{1-x}$Mn$_x$)$_{23}$, mag. props. and mol. field coeffs. 78–39319
ErFe$_2$Si$_2$, mag. props. 4.2 to 950K 77–20544
Er$_2$Fe$_4$Si$_9$ and ErFeSi$_3$, cryst. struct. and mag. suscept., temp. depend. *(Russian)* 78–34957
ErGa, antiferromag., mag. props., 4.2 to 350K 77–63230
ErGa$_2$, mag susceptibility, 1.5-300K and Neel temp. 78–68184
Er$_6$Ga$_{1.5}$Ni$_{2.5}$, struct. determ. by X-ray powder method *(Ukrainian)* 80–39001
Er$_{1-x}$Gd$_x$Al$_2$, effective mol. field at ^{167}Er, NMR meas. 80–71197
Er$_{1-x}$Gd$_x$Al$_2$, nuclear hyperfine field, quadrupolar splitting, NMR study 80–39888
Er$_{1-x}$Ho$_x$Rh$_4$B$_4$, mag. and supercond. transitions, cryst. field effects 80–107950
Er$_2$In, mag. props. 80–108009
Er$_3$In, mag. props., 4.2 to 270K 79–56512
Er$_5$Ir$_2$, cryst. struct. 80–96473
Er$_x$La$_{1-x}$Be$_{13}$, ESR studies 80–108064
Er$_x$La$_{1-x}$Be$_{13}$, mag. sp. ht. and ESR, cryst. field interactions 80–60290
Er$_x$La$_{1-x}$Cu, antiferromagnetic, mag. and resist. behaviour 80–34412
ErMg, mag. props., neutron diffraction and magnetisation meas. 77–16045
ErMg, Mossbauer spectroscopy and mag. props. 77–85624
ErMn$_{12}$, mag. interactions, mag. meas. and neutron diffr. 77–63103
Er$_6$Mn$_{23}$, magnetic moments, magnetisation 80–25094
Er$_6$Mn$_{23}$, noncollinear mag. struct., magnetization meas. 79–78322
ErNi$_2$, Mossbauer effect of ^{57}Fe 77–69743
ErNi$_5$, cryst. field parameters in ferromag., paramag. states, susceptibility meas. 77–63139
ErNi$_x$, sorption at press. up to 1500 atm. 80–97819
Er$_2$Ni$_{17}$, magnetic structure by neutron diffr. 77–73000
ErNi$_{0.6}$Cu$_{0.4}$, sp. ht. and modulated mag. struct. 77–32167
ErNiSi$_3$, mag. susceptibility, 80-1200K *(Russian)* 77–66281
Er$_3$Os, cryst. struct. 80–96474
ErPd$_3$, specific heat at low temp. 80–20413
Er$_5$Pd$_2$, mag. props. 77–20547
ErPt$_5$, low temp. mag. susceptibility 80–93075
Er$_2$Pt, mag. susceptibility meas., mag. transitions obs. 80–60222
Er$_3$Pt$_4$, mag. props., 4.2 to 160K 79–78343
Er$_5$Pt$_4$, isotypic with Pu$_5$Rh$_4$, X-ray cryst. struct. refinement anal. 79–4271
ErRh$_4$B$_4$, reentrant supercond., mag ordering, neutron diffr. obs. 78–14879
ErRh$_4$B$_4$, supercond., electronic props. of Er^{3+} using Mossbauer effect in ^{166}Sr 79–56651
ErRh$_4$B$_4$, supercond. and mag. props. 79–4631
ErRh$_4$B$_4$, supercond. and mag. props., influence of mag. fields 79–56374
ErRh$_{1.1}$Sn$_{3.6}$, new supercond./mag. cpds., X-ray powder diffr. data 80–100215

erbium alloys continued
$ErRh_{1.1}Sn_{3.6}$, synthesis, supercond. and mag. props. 80—100547
$Er_{1-x}Sm_xCo_2Ni_3$, giant intrinsic magnetic hardness 78—56347
$Er_{1-x}Tm_xRh_4B_4$, mag. and supercond. transitions, cryst. field effects 80—107950
$(Er_xY_{1-x})Al_2$, cryst. field splitting, inelastic neutron scatt. data 80—44551
$Er_xY_{1-x}Al_2$, mag. props. meas. and neutron diffr. data 80—7126
$Er_xY_{1-x}Cu$, antiferromagnetic, mag. and resist. behaviour 80—34412
ErZn, magnetoelastic and quadrupolar couplings 78—52328
ErZn, magnetoelastic consts. 78—15005
ErZn, preferred mag. domain orientation, and microstructural defects, magnetostriction meas. 79—73769
Gd-Er, mag. anisotropy, magnetisation meas. 77—12115
Gd-Er, magnetic and electric hyperfine fields at Gd, NMR spin echo 77—77123
$Gd_xEr_{1-x}Rh_4B_4$, effects of Gd ion on supercond. transition temp., mag. transition temp. and upper crit. field 79—56392
$Gd_xEr_{1-x}Rh_4B_4$, ferromag. and structural transitions, low temp. calorimetric meas. 79—55888
$(La,Er)Al_2$, cryst. field parameters, inelastic neutron scatt. study 79—23937
La-Er, superconducting, EPR for localised Er mag. moments *(Russian)* 77—47931
Mg-Er (<25%), struct. and props. 79—96001
$Mg_{1-x}Er_x$, dil., cryst. field interactions, neutron scatt. spectra 80—50048
Ni-Er ion implanted surface alloys, solid solubility and radiation-induced disorder, backscatt. obs. 79—46692
Pd-Er, dilute alloy, EPR spectrum, effect of fine and hyperfine interactions 78—19323
Pd-Er, dynamic Jahn-Teller effect of Er^{3+} 79—73478
Pd-Er, fine struct. of Er^{3+}, dynamic Jahn-Teller effect of electronic Γ_8 quartet 77—35895
Sc-Er, dil., high field magnetisation 78—56292
$Sm_xEr_{1-x}Co_5$, temp. compensated magnetic material, mag. and struct. characterisation 78—68177
Tb-Er, Kaufman approach to calc. of intra-rare earth phase diagrams 80—25657
Tb-Er, magnetisation process of helical spin struct., neutron diffr. and magnetisation meas. 77—43850
Th-Er (1 at.%), Heisenberg exchange, residual resist. meas. 80—75558
Ti-Er, dispersoid effect on deform. 79—24530
Ti-Er(Y), effects of Er and Y additives on deformation behaviour 80—81121
$(Y,Er)Al_2$, cryst. field parameters, inelastic neutron scatt. study 79—23937
Y-Er, mag. susceptibility, 4.2 to 300K, Neel temps. 79—19735
Y-Er, surface, high-freq. elec. cond. dispersion function, effects of polishing and annealing 78—19506
YAl_2-Er, dil., EPR, $Er^{3+}\Gamma_8$ ground state 80—15798
$Y_{1-x}Er_x$, dil., cryst. field interactions, neutron scatt. spectra 80—50048
$Y_xEr_{1-x}Al_2$, paramag. anisotropy 80—39737
$(Zr_{1-x}Er_x)_3Rh$, amorphous, influence of mag. ordering on supercond. props. 80—29511

erbium compounds
see also erbium alloys
erbium ethylsulphate, cryst. laser-excited fluoresc. intensity 79—33751
$ErCO_3Y^{3-}$, (Y=ethylenediaminetetracetate ion), formation constants *(French)* 80—104458
ferrite aluminates, prep. 77—85970
formate, IR spectra and phase transitions, under pressure 78—31179
phthalocyanine solutions, bleaching by ruby laser beam 78—30030
triethyl sulphate, single cryst., H^+ coords., NMR 80—97152
Al_2O_3-Er_2O_3 system, high temp. phase diagrams 80—40340
CEr_2S_4, spinel, crystal struct. *(French)* 78—91326
CaF_2:ErF_3, clustering, defect struct., NMR study 78—80229
CdF_2:FrF_3 films, electroluminesc. meas. *(French)* 79—11471
$CsEr(MoO_4)$, permittivity temp. depend., polymorphic transition 80—92670
$Cs_2NaErCl_6$, Raman spectra 77—77205
$Dy_xEr_{1-x}FeO_3$, transition to antiferromag. state, Dy^{3+} conc. effects 77—66319
ERN, vaporization enthalpy, Knudsen cell vaporization of rare earth nitrides 79—10936
$(Er,Nd)_3PO_7$, IR and Raman spectra, vibr. assignments, cryst. struct. characts. 80—97258
$(Er,Tb,Gd_3)Fe_5O_{12}$ plate, pseudouniaxial, domain struct., magneto-optical obs. 80—11221
Er complex, diphthalocyanine complex, electrochromism *(Japanese)* 80—20611
Er complex, $ErL_6(ClO_4)_3$, L=tetramethyl, urea, struct. 77—62512
ErAG, facet formation 78—63687
ErAG:Er^{3+}, 3 μm stimulated emission at room temp. 77—42541
$ErAgSe_2$, cryst. struct. determ. *(French)* 77—47413
$ErAl_2$, crystal field study rel. to $La_{0.9}Er_{0.1}Al_2$ 78—76036
$ErAl_3(BO_3)_4$, and $(Y,Er)Al_3,(BO_3)_4$, crystallisation and growth characts., density and composition 80—35080
ErAlG:Ho, Tm, Et⇄Ho and Er⇄Tm energy transfer, fluorescence meas. 78—27305
$Er_3Al_{5-x}Ga_xO_{12}$, LPE, spectroscopic props. 80—93419
$ErAl_3[BO_3]_4$, thermal stability, X-ray struct. anal., refractive indices 79—4297
$ErAsO_4$, ferroelectricity, dielec. meas. 80—60515
ErB_{12}, nature of magnetism *(Russian)* 78—31049
ErB_4, antiferromag. props. *(French)* 77—20566
ErB_4, cryst. and mag. struct., neutron diffr. meas. 80—15692
ErB_4, Czochralski crystal growth 79—95920
ErB_4, mag. and elec. props., metallic character 80—20386
ErB_4, mag. phase diagram, neutron diffr. study 80—50091
ErB_4, theory of metamagnetic transitions *(Russian)* 78—95436
ErBi, thermal expansion, thermal cond., 300-900K 78—91453
$(ErBi)_3Fe_{5-x}Ga_xO_{12}$ film, ferrimag., splitting of domains into layers 77—28420
$Er(C_2O_4)(C_2O_4H).3H_2O$, single cryst., mag. susceptibility, 1.5-20K, g-factors 77—77094
$ErCl_3$, aquo complex form., in aq. chloride soln., coord., X-ray diffr. obs. 79—64975
$ErCl_3(AlCl_3)_x$, vap. complexes, absorpt. spectra, 6000-44000 cm^{-1}, relax. props. 78—62799
$Er(ClO_4)_3$, osmotic coeffs. 80—45556

erbium compounds continued
$ErCl_3.6H_2O$, single cryst., H^+ coords., NMR 80—97152
$ErCl_3.6H_2O$:Gd^{3+}, spin Hamiltonian parameters EPR meas. 77—36128
$ErCl_3.6H_2O$-$TbCl_3.6H_2O$, in DMWO soln., $Tb^{3+}\rightarrow Er^{3+}$ energy transfer mechanism 80—5498
$ErCoO_3$, ^{59}Co NMR, quadrupolar and hyperfine interactions 79—15366
$ErCo_2Si_2$, mag. props. 80—107988
$ErCrO_3$, dynamic spin reorientation process, magneto-optical meas. 77—69590
$ErCrO_3$, field-induced spin reorientation relax. 79—78402
$ErCrO_3$, mag. field induced spin reorientation, optical Zeeman absorpt. spectra 79—61398
$ErCrO_3$, magnetisation, NMR freq. temps. depend. weak ferromagnetic-antiferromagnetic spin reorientation transition 80—29631
$ErCrO_3$, phonon Raman spectra rel. to mag. ordering 77—52100
$ErCrO_3$, spin-reorientation, optical obs. 77—63201
$ErCrO_3$:^{53}Cr, NMR frequencies, anomalous behaviour at low temps., 2-8K *(Russian)* 78—43650
ErD_2 thin film, degradation during film processing, investigation 80—101047
ErD_2, thin film, reaction with H_2O vapour, spectroscopic and X-ray diffr. obs. 77—40575
ErD_2:He, tailored low Z impurity distribs. in solids, distrib. evaluation by proton backscatt. technique 79—5199
$ErD_{2-x}T_x$ films, on Cr underlays on Cu substrates, vacuum deposition conditions for optimum hydriding 79—78891
$Er_{0.8}Dy_{0.2}FeO_3$, mixed orthoferrite crystals, ^{57}Fe NMR in spin reorientation range 78—15039
$(ErEu)_3(FeGa)_5O_{12}$ film, for mag. writing and magneto-optical displays 78—6349
$Er_2EuFe_{5-x}Ga_xO_{12}$, rag-domain garnet film, controlled variation of props. under O_2 annealing 79—15328
ErF_3, bomb calorimetric determ. of enthalpy of formation 80—50879
ErF_3, crystal growth by Bridgman-Stockbarger method 78—52660
ErF_3, single cryst. ^{19}F NMR, ligand hyperfine field interactions 77—48067
ErF_3, standard enthalpy of formation 79—91990
ErF_3, thermodynamic props., galvanic cell meas. 80—21316
$ErFe_2B_2$, compounds with $CeAl_2Ga_2$ structure type *(Ukrainian)* 79—32970
$ErFe_3(BO_3)_4$, solubility in Bi_2O_3-B_2O_3 melt and crystallisation 80—19736
$ErFe(CN)_6.5H_2O$, powder, elec. transport props. obs. 80—70701
$ErFe_2H_{3.65}$, $ErFe_2H_{4.12}$, Mossbauer spectra, electronic and structural studies 80—15860
$ErFe_2H_n$, pressure-composition-temperature phase diagram 80—3010
$ErFe_2H_x$, mag. props. 80—25095
$Er_3Fe_{5-x}In_xO_{12}$, lattice consts., T_c, mag. saturation, K-absorpt. and Mossbauer spectra, 80K *(Russian)* 77—20954
$ErFeO_3$, far IR spectra 78—88303
$ErFeO_3$, field induced spin reorientation, Mossbauer spectroscopy 80—65878
$ErFeO_3$, low-temperature spin reorientation 79—65683
$ErFeO_3$, parameters of interaction between rare earth and Fe ions, theory and expt. 79—73705
$ErFeO_3$, Raman scatt. from magnons, anisotropy consts. determ. 80—66178
$ErFeO_3$, SAW meas. of magnetoelastic effects 80—75839
$ErFeO_3$, second-order reorientation transition, NMR signal relax. 77—90066
$ErFeO_3$, sound velocity meas. at high press., spin-reorientation transition 78—76254
$ErFeO_3$, spin flip, Faraday effect and absorption spectrum meas. 77—43842
$ErFeO_3$, temp. depend. of neutron depolarisation factor meas. near spin reorientation transition 77—16053
$ErFeO_3$, weak ferromag., high freq. props. in ordering region of spin system, antiferromag. reson. study *(Russian)* 80—2644
$ErFeO_3$, weak ferromagnet, μSR study 80—93226
$ErFeO_3$:Co, Ti, effects of Co and Ti ions on cryst. growth 77—28711
$Er_3Fe_5O_{12}$, low temp. CVD epitaxial film growth and mag. props. 79—42406
ErGa garnet, crystal field theory of Er^{3+} ion behaviour 77—8259
$Er_{1-x}Gd_xRh_4B_4$, supercond. and mag. transitions at press. up to 19 kbar 79—38236
$Er_{1-x}Gd_xRh_4B_4$, supercond., phase diagrams and upper crit. fields 80—2531
$Er_{1-x}Gd_xRh_4B_4$, ternary superconductor, mag. interactions 79—73613
$Er_2Ge_2O_7$, opt. absorpt. spectra, cryst. field parameters 77—48196
ErH_2, electronic struct. 79—28268
ErH_2, form. from Er by laser evaporation and condensation in H_2 79—10941
ErH_2, lattice thermal expansion and point defect form. energy 77—51524
ErH_2, synchrotron XPS obs., rel. to theory for metal dihydrides 80—55275
ErH_3, cryst. fields and mag. props. 78—68181
ErH_3, Mossbauer spectra of Er^{3+}, gyromagnetic ratios and cryst. field parameters determ. 78—19388
$ErH_2(D_2)$, mag. props., 1.5 to 10K, Mossbauer meas. 79—78578
$Er_{0.3}Ho_{0.7}FeO_3$, mixed orthoferrite crystals, ^{57}Fe NMR in spin reorientation range 78—15039
$(Er_{0.6}Ho_{0.4})Rh_4B_4$, reentrant supercond., magnetisation meas. near lower crit. temp. 80—25043
$Er_{1-x}Ho_xRh_4B_4$, ferromagnet, sp. ht anomaly at lower superconducting transition temp. 79—47194
$Er_{1-x}Ho_xRh_4B_4$, re-entrant supercond. and mag. ordering 78—60240
$Er_{1-x}Ho_xRh_4B_4$, supercond., phase diagrams and upper crit. fields 80—2531
$(Er_{1-x}Ho_x)Rh_4B_4$, superconducting ferromag., Josephson effect, point contact junction meas. 80—7043
$(Er_{1-x}Ho_x)Rh_4B_4$, superconductive and mag. interactions, hydrostatic press. effect 80—49973
$Er_{1-x}Ho_xRh_4B_4$, ternary superconductor, mag. interactions 79—73613
$Er_{1-x}Ho_xRh_4B_4$ type cpds., supercond., phase stratification *(Russian)* 79—42685
ErIG, high-field magnetisation, low temp. mag. anisotropy 80—75802
ErIG, magnetic props. of single cryst., 4.2-600K 79—78341
ErIG, spontaneous Faraday rot. rel. to sublattice magnetisation 80—66159
ErIG, superexchange operator and cryst. field interactions 80—59931
$Er_2M_3(BO_3)_4$, M=Ba,Cu, thin-film capacitor mats., synthesis and props. 77—48128

erbium compounds continued
$Er_2(MoO_4)_3$, DC electrical cond., 650 to 1150K 79–60831
$Er_2(MoO_4)_3$, mag. susceptibility, ferromagnetism, mol. field theory 78–34966
$ErMo_6S_8$, long range mag. order in supercond. state 79–65653
$Er_{1.2}Mo_6S_8$, mag. ordering in supercond. state, resist. and AC susceptibility meas. 78–19194
$ErMo_6S_8(Se_8)$, ternary superconductor, paramagnetic relax. effects 78–68112
$ErMo_6Se_8$, crystal field excitations, inelastic neutron scatt. obs. 79–78321
$ErMo_6Se_8$, mag. ordering and supercond., neutron diffr. 78–68125
$ErMo_6Se_8$, mag. supercond., neutron scatt. obs. 80–70952
$Er_xMo_6Se_8$, long-range antiferromag. order and supercond. coexistence 78–10715
ErN, miscibility with UC *(German)* 80–96654
$ErNbO_4$, ^{93}Nb NQR spectra, 77 to 450K 79–38401
$ErNbO_4$-$CaWO_4$, phase transitions of fergusonite-scheelite *(French)* 80–19942
$ErNi_2Si_2$, mag. props., 4.2-200K 80–84602
ErO, vac. deposited films, struct. changes due to annealing 79–77741
ErO_x film, in MIM struct., nonstoichiometry effects on elec. cond. 79–1635
ErO_x films, phase transforms. 77–62784
ErO_x, nonstoichiometric film, short-range order characts. and its effect on elec. behaviour 79–99435
Er_2O_3, 300 to 900K, mag. susceptibility and Curie temp. meas. 78–56288
Er_2O_3 densely sintered and granular ceramics prep. physicomechanical props. 77–32548
Er_2O_3, Hf diffusion, vol. and grain boundary diffusion coeffs., tracer sectioning technique 79–7712
Er_2O_3, mag. susceptibility, elec. cond. and dielectric const., hopping cond. 77–12083
Er_2O_3, powdered cryst., high resolution optoacoustic spectroscopy 80–31898
Er_2O_3, pure and HfO_2-doped polycryst., Er self-diffusion 80–29207
Er_2O_3 sesquioxide, Raman spectra 78–19478
Er_2O_3, solid, photoacoustic spectra 78–58044
Er_2O_3, XPS, charging effects on core-level binding energies 79–24409
Er_2O_3:CaO, elec. cond. and nonstoichiometry 79–11112
Er_2O_3-GeO_2 system cpds., physicochem. characteris. 80–97469
Er_2O_3-Ta, oxide grain growth at interface 77–81245
$3Er_2O_3$-Ta_2O_5 refractories, prep. and anal. 77–48384
Er_2O_3-TiO_2-WO_3-PbO, glass form., refr. indices and density meas. 77–90312
Er_2O_3-ZrO_2, subsolidus phase relations, X-ray diffr. and thermal expansion exam. 78–31382
$Er_2O_3+VO_2$, high-pressure reaction, cryst. struct. and mag. props. of $ErVO_3$ 80–19773
Er_xO_y film, struct., electron microscope and diffr. obs. 79–11028
ErOCl, tetragonal, lattice coupling with cubic and hexagonal ZnS and ZnSe, heterojunctions 79–60919
$Er(OH)_3$, g-values and hyperfine interaction parameters, calc. for Er^{3+} 79–15123
$Er(OH)_3$, Mossbauer spectra, cryst. field and mag. props. 80–15873
$ErOHCO_3$, synthesis of rare earth carbonates under hydrothermal conditions 78–72714
$Er_4O_2(OH)_8.HNO_3$, gel-grown, cryst. struct. 77–35528
$Er_2O_2SO_4$, antiferromag., mag. props. 1.6 to 40K 79–33464
$Er_2O_2SO_4$, antiferromag., specific heat, 0.6 to 30K 79–33487
ErP, energy spectrum calcs. in one-electron approx. 78–15250
$Er(PO_3)_3$ glass, Faraday resonance effect in pulsed mag. field, optical freq. EPR *(Russian)* 80–2734
$ErPO_4$, cryst., IR spectra, complex anions internal vibrs. resonance splitting 80–34907
$ErPO_4$, IR and Raman spectra 80–34904
$ErPO_4$-$Pb_2P_2O_7$, solubility curves for high temp.-melts for growth of single crysts. 78–95687
ErP_5O_{14}, single cryst., radiative and non-radiative transitions 79–19920
ErP_5O_{14}, X-ray cryst. struct. determ. 80–96486
$ErRh_4B_4$,, NMR and sp. ht. in supercond. and mag. ordered phases 80–7037
$ErRh_4B_4$, cryst. struct., X-ray diffr. 77–89423
$ErRh_4B_4$, ferromag. superconductor, vortex phase 80–80441
$ErRh_4B_4$, film, sputter deposition and low temp. props. 80–2948
$ErRh_4B_4$, high supercond. transition temp. 77–89893
$ErRh_4B_4$, long ferromag. supercond., metastable supercond. state 80–103771
$ErRh_4B_4$, mag. supercond., NMR study of ^{11}B 80–107957
$ErRh_4B_4$, Mossbauer spectra 80–15926
$ErRh_4B_4$, supercond., electronic struct. and reentrant magnetism 78–10340
$ErRh_4B_4$, supercond., re-entrant magnetism, energy band calcs. 78–52140
$ErRh_4B_4$, supercond., thermal cond. between 0.05 and 4K 79–60967
$ErRh_4B_4$, supercond. transition temp., upper critical field, local spin fluctuations 79–38250
$ErRh_4B_4$, superconductivity destruction at onset of long-range mag. order 77–76994
$ErRh_4B_4$, superconducting and mag. transitions, alpha particle irradiation damage effects 79–60954
$ErRh_4B_4$, superconducting and normal state props. 79–73632
$ErRh_4B_4$, superconducting, magnetic dilemma 80–75680
$ErRh_4B_4$, superconducting thin films, critical mag. field 80–75693
$ErRh_4B_4$, superconductor, neutron scatt. exam. of mag. phase 79–73680
$ErRh_4B_4$, ternary superconductor, paramagnetic relax. effects 78–68112
$ErRh_4B_4$, ternary superconductor, mag. interactions 79–73613
ErS, heat carrier scatt., thermal and elec. cond. from 5-400K 79–14974
Er_2S_3, polymorphic transforms. on impact compression 77–47575
Er_2S_3-Ga_2S_3 system, phase diag. *(French)* 78–3108
ErSb, cryst. field effects on transport props. 78–72133
ErSb, crystal field effect in thermal expansion 78–19305
$ErScO_3$, synthesis and lattice const. 78–30593
Er_2Se_3, elec. resist., thermoelectromotive force, temp. depend., 300 to 1400K *(Russian)* 78–84243
Er_2Se_3, mag. susceptibility 77–40032
$Er_2(SeO_4)_3.8H_2O$, thermal decomp. and IR spectra 80–3319
Er_2SiO_5:Ho^{3+}, single cryst., luminesc. and stimulated emission 77–69895
C-,D-$Er_2Si_2O_7$, single cryst. flux growth 79–52097
(ErSm)FeO_3, spin reorientation, Faraday rot. meas. 77–8547
$Er_2Sr_3(BO_3)_4$, cryst. struct. from X-ray diffr. meas. 77–89419
$ErT_{1.8}$, ^3He thermal desorption, comparison of aged and ^4He implanted samples 77–60102
ErT_2, film, surface oxide form. and interfacial metal loss, AAS, XES 78–31733
ErT_x, ^3He outgassing after ^3H decay, ^3H conc. effects 77–60100
$ErTaO_4$, heat of form. 79–83494
Er_2Te_3, films, prep., elec. props. 78–43494
Er_2Te_3, magnetic susceptibility meas., cryst. field interpretation 80–11156
$ErTiO_3$, bulk mag. and struct. props., ferrimag. order 80–107993
$ErTiO_3$, magnetic structure determination, neutron scatt. study 80–65809
$Er_{0.5}Tm_{0.5}FeO_3$, mixed orthoferrite crystals, ^{57}Fe NMR in spin reorientation range 78–15039
$ErVO_3$, produced by $Er_2O_3+VO_2$ high-press. reaction, cryst. struct. and mag. props. meas. 80–19773
$ErVO_4$, phonon resistivity mag. field depend. in paramag. phase 80–2226
$ErVO_4$:Ho^{3+}, CW and pulsed laser emission at 2.0416 μm 77–19254
$Er_2(WO_4)_3$, mag. props., 300 to 900K 79–28510
Er_2WO_6, growth from soln. in melt 77–1806
$Er_xY_{3-x}Fe_5O_{12}$, garnet, mag. anisotropy and magnetostriction 80–11189
$Er_xY_{3-x}Fe_5O_{12}$, spin reorientation transitions 78–2686
$Er_xY_{1-x}Rh_4B_4$, mag. and supercond. transitions 80–70874
$Er_xY_{1-x}Rh_4B_4$, supercond. phase transitions, recentering temp. to normal ferromag. state 80–7024
Er_2ZrS_5, mag. and sp. ht. meas. on polycrystalline samples 78–23253
$Er_2[Pt(CN)_4]_3.21H_2O$, phase transitions, X-ray study and spectroscopic study 79–60506
$(Eu,Er)_3(Ga,Fe)_5O_{22}/(Y,Sm)_3(Ga,Fe)_5O_{12}$ double-layer self-biasing garnet films, dynamic behaviour of domain walls 80–34722
$EuEr_2Ga_{0.7}Fe_{4.3}O_{12}$, garnet thin films, magnetisation orientation, temp. depend. 80–71125
$Gd_xEr_{1-x}Rh_4B_4$, mag. and supercond. transitions 78–68127
$Gd_xEr_{1-x}Rh_4B_4$, mag. ordering near supercond. region 79–73696
GdF_3-ErF_3, stabilisation of rhombic β-YF_3 type struct. 78–67700
HfO_2:Er_2O_3, elastic props., sonic reson. meas. 80–7612
$Ho_{0.7}Er_{0.3}FeO_3$, crystn. on seeds, layer morphology 78–72041
β-KEr_3F_{10}, cryst. struct. *(French)* 78–51500
$K_2Er(NO_3)_5$, cryst. struct. by X-ray diffr., cryst. binding 78–42988
KF-ErF_3, phase diagram 80–92645
$LaNbO_4$, ^{93}Nb and ^{139}La NQR spectra 79–38401
$LiY_{0.416}Er_{0.5}Tm_{0.067}Ho_{0.017}F_4$, Stockbarger single cryst., charact. of solidification behaviour 77–24948
$(Lu,Er)_3Al_5O_{12}$:Er^{3+}, stimulated emission 77–52135
$NaEr(SO_4)_2$, cryst. struct. by X-ray diffr. *(French)* 78–42990
$Na_{5-x}Li_xErSi_4O_{12}$, solid electrolytes for Na/TiS_2 cells, synthesis, characts. and utilisation 80–107518
$Rb_5Er(MoO_4)_4$, cryst. struct. 77–62510
$(Sm,Er)(Ga,Fe)_5O_{12}$, LPE, non-grooved film, thermomag. writing 78–76278
$Sm_{0.7}Er_{0.3}FeO_3$ spin reorientation photomagnetic motor 78–2695
$Tb_{0.7}Er_{1.3}Gd_{1.0}Al_{0.2}Fe_{4.8}O_{12}$, garnet plate, domain struct. 80–2602
TiO_2-Er_2O_3 system, dislocation mechanism of diffusion processes 79–77837
$TlEr(MoO_4)_2$, fluoresc. spectra at 77, 300K 79–56848
$TlEr(WO_4)_2$, fluoresc. spectra at 77, 300K 79–56848
$TlR(MO_4)_2$, R=Eu, Dy, Er; M=Mo, W, luminesc. *(Russian)* 78–48229
YE+AG:Er^{3+}, laser material, radiative and nonradiative transitions, conc. quenching 77–16391
$(YErCa)_3(Fe\ Ge)_5O_{12}$, mag. loss and domain wall mobility 80–65980
$(YErCa)_3(Fe_{5-x}Ge_x)O_{12}$ film, high g, for mag. bubble applics. 77–85529
YErIG, magnetisation anomalies in strong mag. fields *(Russian)* 77–43854
$Y_{1-x-y}R_xEr_yAlO_3$, $Y_{1-x-y}R_xEr_yScO_3$, stimulated emission of Er^{3+} ions 78–6705
$Y_{1-x-y}Yb_xEr_yOCl$, Er ion excited state decay and population *(Russian)* 80–100694
ZnS:Cu, Er, Na, phosphor, mechanism of sensitisation effect of Cu and Na ions 77–16369

erection
290 MW compressed air storage power station, construction and commissioning 80–16842
breeder reactor, Super Phoenix, construction report *(French)* 79–63803
LWR power station construction in France, standardisation advantages *(French)* 78–58397
nuclear power stations, public hearings in Japan 80–47599
nuclear reactor containment structures, design and construction, ACI-ASME code of practice impact 80–798
PWRs, 900 MW, in France, construction report *(French)* 79–63801
shrouded wind turbine, pilot plant construction 80–66931
vertical axis wind turbines 80–66929
waste management centre, features 77–88229
wind turbine, variable pitch vertical axis, 2.4 m dia. prototype 80–61265

ergodic theorem *see statistical mechanics*

ergonomics
see also human factors; man machine systems
acoustic noise effect on performance of a psychomotor task, sorting during 90 dB(A) of pink noise 80–64283
brain potentials, synchronous and asynchronous, space-time organisation formal anal. *(Russian)* 77–52767
car drivers, work spectacles and functional visual fields *(Italian)* 80–108875
design of materials satisfying acoustical and mechanical criteria 80–64234
effect of vibration on reading numeric displays 80–104582
energy expenditure in man, simple apparatus for meas. 79–92415
ergometer for small-animal research 80–101295
human factor studies, conf., San Francisco, USA (Oct. 1977) 78–48742
open-plan offices, role of acoustic screening 80–87650
psychophysical laboratory unit organisation and meas. system for persons with impaired locomotor system *(Croatian)* 78–44667
radiological diagnostic equipment, ergonomic design problems *(German)* 79–74729
recording studios, leisure facilities for performers 80–69601

ergonomics continued
- repetitive muscular contraction, localised fatigue evaluation from EMG power spectrum 78—57103
- respirator, narcosis, ergonometric design *(German)* 79—2163

erosion
- Alpine permafrost environment, mass-wasting by rock glaciers 77—81934
- Antarctic meteorites, trace element contents, weathering effect 80—56784
- Antarctica, glacial weathering rel. to silica budget of Antarctic waters 78—20436
- arroyo cutting near Santa Fe, New Mexico 77—70698
- SW Atlantic, abyssal circulation increase during Late Pliocene rel. to global climatic cooling 78—40645
- Atlantic coastline, behaviour in Landes and Basque regions *(French)* 80—76987
- NE Atlantic continental margin, sediments differential deposition and distrib. by bottom currents 80—12372
- N Atlantic continental slope, submarine canyons and valleys origin and development 77—21713
- Badlands slope development, importance of mass movement and piping 80—41468
- Baltic beach scouring and detritus accumulation in short-term disturbance *(Russian)* 80—36288
- E Baltic coast littoral drift regime and dynamics *(Russian)* 78—36147
- Baltic coastal beach scouring and accumulation by moderate sea disturbances *(Russian)* 80—81867
- SE.Baltic mainland shore moderately accumulative section morphodynamics *(Russian)* 80—67359
- SE.Baltic shore zone dynamic classification *(Russian)* 78—36146
- SE Baltic shore zone subdivision into lithomorphodynamic sections *(Russian)* 78—36148
- basal hills in Darling Downs, SE.Queensland, slope profiles of cycloidal form 78—44820
- beach deposits sedimentary material differentiation and bedding form. dynamico 80—26496
- beach erosion prediction rel. to rising water level 77—91150
- beach rock erosional features morphological zonation 79—48447
- beach sedimentology of Mustang and Padre Islands, time series approach 78—77211
- bed forms and unsteady flow, classification 77—45036
- bedrock freeze-thaw weathering in Colorado front range alpine zone 80—31039
- Blake Plateau, Late Cenozoic erosion rel. to Gulf Stream vel. fluctuations 80—12432
- boat wake effects on shoreline of Lake Manapouri 79—25278
- building stones, characterizing weathering processes *(German)* 77—86270
- Cape Basin, S. Atlantic, scour and deposition at Walvis Ridge base 77—91103
- channel bottom, kinematic characts. of nonuniform flow, limiting stability, erosion 80—94547
- channel network evolution in mature drainage basins, relief factor 77—66932
- channel turbulence characts. and deform. in inshore zone 77—78258
- chemical weathering of rock, meas. technique using U isotope ratio 80—77142
- cirques in Bear River Range, north-central Utah, numerical anal. 80—72510
- cliff erosion, wave induced rel. to erosive force of waves 78—20388
- climatic change and erosion cycle reversal 77—64338
- coastal erosion in Florida 79—57911
- cohesionless bottom sediments, limiting stability in turbulent channel flow, erosion 80—94546
- cohesionless soils on channel bottom and sloping sides, onset of motion 80—94548
- cohesive sediments, modelling of transport, erosion and deposition 78—15994
- Colorado River in Grand Canyon, control of rapids and pools 79—62537
- continental ice sheets, erosion 79—25276
- cratering record, crater prod. rate 79—66699
- cratering record, current obs. status 79—66698
- craters, on Earth, Moon and Mars, morphological evolutionary tracks 77—91134
- cultivated loamy soils, Belgium, splash and wash 78—73410
- Cumberland Peninsula, Baffin Is., tors, felsenmeer and glaciation 78—61442
- Cumberland Peninsula, Baffin Island, hornblende grain etching, age and palaeoclimate indicator 80—8307
- Deimos, loose material downslope movement obs. 80—94737
- differential erosion, transient heat flux with exponential heat source distrib. 79—57887
- drainage density and channel network geometry, post-Hortonian studies 79—20874
- drainage headwater development, modelling 79—20875
- dune ridge morphodynamic characteristics on spit of Kurshyu Nyariya, abrasional section *(Russian)* 78—36149
- dust storms, Great Plains, USA, lessons 79—29486
- electric arc duration-erosion correl. in relay contacts, atmosphere effect *(French)* 77—72518
- eolian sediment transport during dust storms, Slims River Valley, Yukon territory 79—5552
- evolution of surface features of Earth, endogenic and exogenic forces 80—3972
- fixed dunes, Sahel, central Niger, erosion 78—81225
- flowing water erosion, bed scallops and ripples sizes 79—27628
- forested watershed Oesling, Luxembourg, chemical erosion 77—81930
- gabbro weathering, Quebec, geomorphological conditions 78—28230
- Galilean satellites, ice sputtering and water products contrib. to Jupiter magnetosphere 78—45268
- geomorphological processes, conf., Louvain, Belgium (Apr. 1976) 77—81923
- Georges River, Sydney, changes in urban water resource 77—70697
- glacial erosion, effect on terrestrial heat flow palaeoclimatic and topographic corrections 79—34767
- glacial erosion of bedrock rel. to gravel clasts in Newfoundland fjords 77—17148
- Gondwana, Late Palaeozoic glacial erosion, evidence from garnets 79—100874
- Grand River, Ontario, geomorphic effects of catastrophic flood 78—28248

erosion continued
- granitic clasts selective weathering 79—92532
- granodiorite weathering, REE mobility and fractionation 79—62512
- granular bed material, erosional capacity of smoothly varying streams, particle size 80—94545
- Great Lakes shoreline erosion, meas. of W. Lake Michigan 79—5542
- W Greenland, Canadian Shield erosion rel. to continental margin Mesozoic and Cenozoic sediments 79—62479
- Grote Nete basin, Belgium, geomorphology *(Flemish)* 78—61452
- Gulf of Gdansk, lithodynamical processes, theoretical anal. and scale model tests *(Polish)* 78—40540
- gully erosion, gravel pad appls. *(French)* 79—62533
- gully erosion on vegetated screes in Black Mountain, Carmarthenshire 77—44992
- Hong Kong badlands, slopewash patterns and rates 78—20441
- Hurricane Agnes storm and flood, geomorphic effects, SE.Pennsylvania 78—77280
- icy permafrost in NE.British Columbia, distrib. and sensitivity to erosion 78—77277
- impact erosion and meteorite bombardment 78—57476
- Indian rivers, chemical and sediment load input into world oceans 79—34870
- inshore submarine slope cross-profile changes and littoral drift balance *(Russian)* 78—15989
- interfluvial area of Minija and Sventoji, marginal formations structures *(Russian)* 77—25708
- interplanetary and interstellar ice grains, low energy cosmic ray erosion 78—45177
- interstellar grains, destruction by sputtering 78—45382
- Iowa, wind-aligned drainage in loess 80—41467
- island groups in Scotia Sea, Antarctica, glacial erosion rel. to max. ice extent 78—20450
- karst depressions, areal growth rates, ages 79—48484
- kimberlite pipes, erosion depth rel. to exploration geophysics techniques 80—51393
- Labrador, Canadian Shield erosion rel. to continental margin Mesozoic and Cenozoic sediments 79—62479
- Lake Eyre North, S.Australia, bottom profile rel. to inshore scouring 78—69376
- Lake Superior, shoreline inheritance in coastal histories 77—33112
- Lake Vanern, Sweden, wind, fetch and water depth rel. to sediment distrib. 77—66934
- land surfaces, erosional potentials generation from topographic information, LEAP programs 77—33075
- landform development, simulation of baselevel lowering, weathering and denudation 77—81932
- landform erosion simulation program 80—85650
- landscape evolution and around Sagar, Madhya Pradesh, India 77—21813
- landscape periodicity, slope deposits, soil pattern and erosion in small catchment area 78—11924
- landscapes, soils and erosion, Wither Hills, New Zealand 78—88864
- landslides, hydrogeological conditions rel. to stability, rheology *(Russian)* 77—25683
- landslides, relationship to rainfall, Kitakyushu City, Japan *(Japanese)* 78—88848
- landslip/debris flow, Bilsdale, North York Moors, 1976 September 79—48524
- laser techniques for rain impact and erosion recording 79—62610
- limestone, erosion under soil due to acid waters 77—45023
- limestone, estimation of short-term vars. in erosion processes 77—81935
- limestone cave systems, development in dimensions of length and depth 79—62531
- littoral alterations, Messina coastline, Sicily *(Italian)* 79—5469
- loamy sand, Flanders hilly region, quantitative rill and gully erosion study 77—81936
- loess erosion and redeposition by water, expt., micromorphology 77—81925
- lunar rocks, erosion mechanisms rel. to microcrater and accretionary grain populations development 80—94732
- Macdonald Valley River, NSW, catastrophic channel changes in 1949-1955 period 78—16065
- Mahone Bay, Nova Scotia, Late Quaternary glacial erosion history 78—77232
- Mantaro landslide, Peru, seismological and geological aspects 78—96248
- marble in Pikikiruna Range karst, solution processes 79—74906
- Mars, chaotic terrain erosion rel. to fossil H_2O liquid-ice interfaces 78—65539
- Mars, CO_2 permafrost as erosive agent rel. to topography 78—65535
- Mars, dust redistrib. and erosion during one Mars year from Viking landers imaging obs. 79—80265
- Mars, erosion rel. to aeolian sedimentation, comparison with Earth 80—31042
- Mars, erosion rel. to crater streaks form. in Chryse Planitia, early Viking results 78—65534
- Mars fretted terrain, erosional debris flow 78—65537
- Mars outflow channels erosion, implications of sediment transport modes in channelised water flows 80—98363
- Mars polar regions, stepped topography origin 78—65536
- meteorite, Holbrook chondrite, chem. alterations due to terrestrial weathering 79—71007
- meteorite impact crater discovered in central Alaska with LANDSAT imagery 77—91136
- mineral, dissolution under Earth surface conditions, rate control 79—20817
- minerals, impact abrasion by windblown dust or snow 77—70647
- minerals, weathering profile evolution simulation by aq. soln. *(French)* 77—60438
- minerals surface weathering reactions, stability, thermochem. calcs. 77—44969
- Mississippi basin, magnitude and freq. of transport of solids by streams 77—78235
- montane arroyos and gully development 79—74905
- montmorillonite neoformation by post-depositional subsurface weathering in slope deposit 78—73367
- mountain aerial photography, colour film types compared 77—29500
- mudslide potential situations, meteorological parameters critical values, Caucasus mountains 79—39782
- Nahal Yael, Israel, arid watershed, climatic variations, hillslope study 80—8342
- natural slopes, failure surfaces propag. 79—39719

erosion continued
central New England, denudation rate determined from estuarine sedimentation 79—92550
New England submarine canyons, bedrock geology 78—73356
Norwegian-Greenland basin continental slope, submarine canyons and valleys origin and development 77—21713
ocean waves on erodable base, bottom vel. and scouring 78—49029
oceanic rifted ridges, submarine erosion rel. to ophiolitic breccias in E. Ligurian Apennines 77—86881
Pacific basin, chemical erosion of continents, sedimentation rates and sea levels 79—88365
pebbles, wear in river headwaters 79—92557
pipe, particulate suspension flow, sticking probability and erosion, data correlations 79—41744
plant condition monitoring in nuclear power generating industry, review 80—47612
Point Pelee, SW.Ontario, erosion rel. to geomorphology and landscape elements origin 78—92857
Pomme de Terre River, Missouri, USA, Holocene erosion and climate 80—51446
potential landslide sites mapping, digital simulation 77—37204
quartz grains in Einbeck, W.Germany, loess profile, weathering rel. to stratigraphy *(German)* 79—20823
quartz silt, resistance to isotopic exchange when buried and weathered 79—39709
rainfall simulation for lab. water erosion expts. 77—81931
rainfall simulator, portable, for soil erosion studies in difficult terrain 78—20537
rainsplash erosion of sandy soils, field study 79—20879
regolith reprocessing by cratering, erosion of material layer which loses charact. props. 80—62053
remotely sensed data acquisition and processing, developing countries appl. 79—34963
riffle formation model 78—63482
river bank erosion rate, obs. in Devon, England 80—105002
river channel enlargement, effect on bankfull discharge 80—8369
river flow and sediments to bed evolution *(Russian)* 77—29330
riverbeds, channel deformations, hydraulic modelling 80—77024
rivers, stable numerical model of local scour 77—21809
rivers denudation, fallacy of stream equilib. assumption 77—78236
rock weathering, elements water-rock partition coeffs. rel. to sea and river water comps. 79—44200
Rockall Trough, hydrographic and geological inferences from near-bottom traverse 79—62483
rockfall from cliff face, seasonal variation obs. in N.Ireland 80—105001
Rotoehu Ash weathering in Bay of Plenty district, New Zealand 78—85558
Rubble Creek landslide, British Columbia, during 19th century, potential slide area 79—5477
Runswick Bay, N.Yorkshire, coastal ground movement 80—36285
salts, dissolving and outwashing from soil and rock, hydromechanical treatment *(Russian)* 78—77279
sand barrier beach shoreline accumulative section, protective dune ridge morphodynamics *(Russian)* 80—36287
sand barrier beach shoreline transit section, protective dune ridge morphodynamics *(Russian)* 80—36286
sandy channel, rate and time of deform. due to artificially compressed flow 77—78259
scalar partial differential eqns., variational principles 79—30255
scree slope rockfall model 77—44990
sea-floor basalt, rare earth elements behavior during weathering 79—57910
sediment movement behaviour, current, wave and wind effects *(French)* 77—78151
sediment transport for desert watersheds in erodible materials 78—20442
sedimentary geochemistry, environments and processes involving an aqueous phase 77—86888
sedimentary material in Atlantic Ocean, shore abrasion 79—2217
sedimentary organic matter, subaerial weathering effects 78—57206
sedimentation and erosion, problems rel. to water supply, research needs 78—61444
sediments and pollution, society's needs and professional opportunities 77—64342
sediments of old coast formations of E.Lithuanian upland *(Russian)* 78—16012
severe local storm, Pennsylvania, predictibility of location and damage 77—66965
sheet flow on smooth surface, hydraulics, simulated rainfall effects 77—81926
sheetwash and rainsplash, soil entrainment, slope angle effects 79—74908
shore platform formation on SE. coast of Izu peninsula, Japan 78—81147
shoreline erosion, Croatan and Pamlico Sounds, N.Carolina, LANDSAT imagery appl. 79—39701
Sierra Nevada, California, glacial deposits, relative dating techniques from weathering 80—8451
silicate rocks, chem. denudation rates in tropical catchments 78—73414
slope recession in Onefour Badlands, Alberta, Canada, rel. to moisture regimes 79—92552
slope stability and valley form. in glacial outwash deposits, Norfolk, England 79—20880
slopewash and wind action, Quaternary morphogenesis in Belgium 77—81924
small watersheds, effect of urbanisation on kinetic energy distribs. and erosion 79—25275
snad grain surface texture rel. to wind vel. conditions 80—41443
soil, weathering age from U and Ac series nuclides radioactive disequilibrium 80—4014
soil, wind tunnel simulation, effects on fine dust production 79—20834
soil development models and slope models 77—81933
soil erodibility factor rel. to aggregate stability and micromorphological props. 79—48522
soil erosion by Hortonian overland flow, magnitude and freq. 77—70701
soil erosion prior to overland flow, time and aggregate size rel. to crusting process 79—20876
soil erosion processes meas. in German area of Moselle river valley 77—81937
soil loss factors rel. to flow, runoff creep and rainwash 77—45028
soil or sand, frequency tracker for laser Doppler anemometry, lab. expt. 79—72968
soil weathering, geochemical study and elemental redistrib. 78—7634
solute loading and chem. denudation rate mapping in Devon, England 78—69375
splash erosion, animal activity and sediment supply in forested catchment 77—81928
splash erosion and colluvium form. beneath deciduous woodland, Luxembourg Ardennes 77—81929
Squamish River, British Columbia, mean flow struct. in meanders rel. to channel migration 79—62532
stationary sphere on boundary of similar spheres, drag coeff. function extension *(French)* 78—36211
stone movement through snow creep, 1963-75 period, Mt. Twynam, Australia 78—69374
streambank erosion, stereometric meas. 80—17421
streams, straight, alluvial, unsteady flow and individual dunes modification 79—62535
submarine canyon heads, relief development processes, Black Sea 78—44803
submarine canyons south of Iceland, obs. 80—90068
submarine pillow basalts, seafloor weathering effects on geomag. palaeointensities determ. 80—3927
surface water chemistry and weathering processes, Absaroka Mts., Wyoming 78—32125
tabular iceberg, off Newfoundland Grand Banks, deterioration 77—56646
talus slopes angles, repose angles and shearing resistance angles 78—20405
talus slopes angles, repose angles and shearing resistance angles, comment 78—20406
thick water film in turbulent flow over impermeable slope, erosion and sedimentation *(French)* 80—43692
tholeiitic basalts, rare earth elements behaviour during submarine weathering 78—73369
Tolaga Bay Flats basin, recent alluvial infilling estimation using tephra marker beds 78—11925
topsoil mineralogy, Ngunguru Basin, New Zealand 78—85557
tracer theory, nonsteady state systems 79—5646
tropical weathering, effect on electrical and EM meas. 79—88246
underwater margins of W.Spitsbergen, glacial morphogenesis and sea floor morphology 80—26494
unit sediment graph 79—79902
urban erosion and sedimentation prediction and control 77—37282
urban hydrology and sediment control, symposium, Lexington (1976) 77—37266
urban stormwater and sediment discharge, deterministic model 77—37273
US National Shoreline Erosion Control Demonstration Program, review 78—16163
Vajont rock slide (Italy, 1963) analysis, new approach 79—8633
valley incisions widening by soil fall in forested Keuper area, Luxembourg 77—81927
Vema Channel, increased transport of Antarctic Bottom Water during last ice age 77—21798
Victoria Falls, erosion rate and Batoka Gorge archaeological dates 77—2184
volcanosedimentary levels, S.Pacific, neoformation and weathering *(French)* 78—73353
water erosion characteristics in Siberia, Russian plains and central Asia 78—61449
watershed geochemistry, aqueous solns. control by soil materials 78—20445
watershed geomorphology, relative scales of time and effectiveness of climate 78—81229
watersheds sediment prod. long-term patterns following road construction and logging 79—84322
weathering, correction method in seismic sounding 79—44255
weathering model in palaeomag. field intensity meas. on ancient fired clays 78—61328
Westend basin, S.Pennines, England, slope form and basal stream relationships 77—45025
wind action on sub-Antarctic Marion Island 80—31093
wind erosion and suspended dust deposition, wind speeds and particle concs. 78—40623
wind erosion threshold velocities, tests with portable wind tunnel 79—70826
wind erosiveness in New Zealand, index 79—5579
Yangtze River middle reaches, channel development after completion of aritficial cutoffs 79—44210
Yellowstone Lake, seismic refl. and refr. surveys and palaeomag. study 78—49049
$CaCO_3$ accumulations, erosion effects in Ontong-Java Plateau box cores 80—61793
Cr_3C_2-(WC)-Ni, sintered, cavitation erosion resistance *(Japanese)* 77—52500
Mg mass balance in continental runoff 79—34859
U bearing natural samples, water erosion rel. to U series disequilibrium 79—16466

error analysis
see also error correction; error detection
absorbing-emitting media, integro-differential energy eqn. soln., validity range of differential approx. 78—5644
accuracy and efficiency test for bicubic spline interpolation 80—17405
acetylene-d_0, ($-d_2$), IR intensities, relative error anal. 78—58686
acoustic logging, errors of statistical signal processing *(Russian)* 79—39939
acoustic logging, phase-freq. charact. effect on transmission accuracy of analogue signals *(Russian)* 79—39940
acoustic travelling-wave equipment in active-impedance termination method, error estimation 79—94429
aerosol meas. by lidar, error analysis and simulation 80—26617
angiography, comparison of convolution and ray tracing computations of small blood vessel images 77—48863
angular meas., method *(Russian)* 79—97345
approximation errors for boundary layer equations *(German)* 79—86416
approximation method for solution of nonlinear integral equation with error estimation for problems in heat or mass transfer *(Russian)* 78—57879
artificial Earth satellites radial and cross track errors analysis 77—45297
artificial satellite motion, error evaluation, averaging method for canonical eqns. *(French)* 77—67028

error analysis continued
- artificial satellite motion, error evaluation, averaging method for canonical eqns. *(French)* 77−67029
- artificial satellites, effective isotropic radiated power, error anal. using calibrated radio star 78−93070
- astrometric observations, systematic errors, spectral anal. of obs. series *(Russian)* 78−73614
- astronomical observations errors, optimum linear estimation of mathematical expectation and standard deviation *(Russian)* 80−12673
- astronomical photoelectric photometry, zero point drift 79−53735
- atmospheric precipitable water, computation from upper air data 79−34886
- atmospheric precipitation acidity measurement, error anal. applied to indirect methods 80−72108
- atomic frequency standard prediction error analysis 78−57906
- average-value voltage transducer *(Russian)* 78−45649
- background noise levels in United Kingdom, prediction model 77−14843
- ballistic galvanometer, error due to non-transient impulses, integral expression 80−86349
- beam formation, eccentric, error anal. 79−3920
- bell type volume dynamic systems for gas flow meas. 78−75239
- bias error, system noise, parameters computed from C, T, P and V profiles 80−8445
- blood flow calc. by indicator dilution, pulsatile error analysis 77−60225
- brain isotope distribution reconstruction, error anal. for instrument design 80−3772
- broadband filter radiometry, solar spectral distribution monitoring 77−53163
- bromomethane(-d_1,d_2,d_3), F and G sum rules as vibr. intensity data error indicators 79−3494
- Brorfelde transit circle, diameter corrections 80−105164
- Burgers eqn. calcs., mesh Reynolds number, computational accuracy 79−3997
- Cauchy problem for Laplace's eqn., solution approximation 77−78966
- chemical analysis, multicomponent analysis computations based on Kalman filtering 80−40772
- chemical reaction kinetics, temp. integral approximating eqns. accuracy 78−92445
- cineroentgenography, quantitative biplane method, error propag. 78−73224
- clinical thermography, eval. of distortion 80−3750
- code AROSA for quantal Coulomb excitation calcs. 77−2550
- coherence functions and input/output quantities, statistical errors in meas. 79−3965
- coherent Doppler anemometer for turbulent vel. meas., potential accuracy anal. *(Russian)* 78−71406
- compensator retardation determ. 79−26107
- complex moduli of viscoelastic materials, coated beam technique 79−27565
- composition of several error distribution functions, determ. method 77−13731
- Compton effect, multiple scatt. corrections, error bounds 78−16959
- concentration meas. kinetic reaction equation parameter determ. *(German)* 77−66782
- concentricity, round parts, profile determ. *(German)* 80−57249
- contacting surface depth and shape determ., random and sytematic errors *(Russian)* 79−39935
- control rod reactivity meas. error analysis 79−9783
- convective heat transfer coefficient measurement using heat-flux sensor, error anal. 79−94463
- correlation methods, signal parameter meas. 80−57241
- corrosion rates, error anal. in using 2 and 3 electrode polarisation resist. meas. 80−100930
- cosmic ray data selection and preprocessing in realistic error evaluation 77−53337
- covariance estimation, of stationary, ergodic processes, with non zero mean value *(French)* 79−80513
- crystallography, electron densities, thermal smearing, limited resolution effects 78−71635
- D-region, electron density profiles from gyrowave interaction expt., error anal. 79−5705
- DC currents, low, new system of meas. 80−82791
- differential equations systems, linear, nonlinear, asymptotic method using projection iteration *(Russian)* 77−57169
- diffusion-convection const. coeff. eqn., centred differencing, box scheme, mesh size, errors 77−7386
- digital fibre optical communication system, average error probability calc. 80−53228
- digital tachometers 80−90832
- digital time pulse thermometer, technical description and error anal. *(Russian)* 79−49228
- digitising error from period and freq. counting techniques 78−61570
- directional-hemispheric reflectance factor scale establishment, Van den Akker method 78−77967
- displacements, strain and stress error nodal lines in finite elements 79−2606
- dose variation in X-ray epilation for tinea capitis 77−9267
- dual-wavelength spectrophotometry, precision, theoretical assessment 78−29163
- dynamic system, two representations of sensitivity and error analysis 77−60900
- Earth tide observations processing, errors combination rel. to monthly data sets weighting *(Russian)* 78−88789
- eclipsing variable stars, Fourier analysis of light curves, error anal. in freq. domain 80−31214
- education, least squares fit, uncertainty calc. 78−86068
- EEG slope descriptor computation, time and frequency domain comparison 78−57115
- eigenvalue systems of second order differential eqns., numerical soln., matching method 78−8232
- elasto plastic problems 78−1578
- elastostatics, error estimates of finite element approx. 80−8793
- electron diffraction patterns, of textures, reflection sphere curvature influence on reflection location geometry 80−87996
- electron micrograph computer image processing, error sensitivity as resolution limit 79−71570
- electron microscope autoradiographs, iterative anal., sample sizes and confidence limits 79−35896
- electronic meas. systems, statistical methods appl. *(Polish)* 79−88902
- electrooptical distance meas. instruments, Zeiss ELDI 2 type, error anal. *(German)* 79−21081

error analysis continued
- evapotranspiration meas., Bowen ratio precision 77−33122
- evolutionary problems, error anal. of finite difference, finite element and spectral methods 80−46815
- experimental data interpretation, chemical analysis appl. 78−77827
- experimental design, unbiased regression, practical appls. 79−97184
- experimental measurement, review of error statements 79−85110
- fast reactor, few group constants for reactivity calcs., errors *(Czech)* 77−71639
- fast reactors, error anal. of computational models 79−97750
- ferrites, disaccommodation meas. *(Bulgarian)* 78−21181
- film refractive index and thickness meas., error anal. of SYNCANG and SYNCWANG methods 78−8439
- fission afterheat, sensitivity to errors in fission product data 77−26841
- fission reactor, uncertainty analysis and stored-energy calcs. 79−93698
- fission track dating method, standard error estimation 80−36419
- flotation integrating gyroscope, dynamic errors 79−93135
- flow, incompressible and viscous, finite elements for numerical simulation, error estimates 79−1151
- flow, turbulent, complex geometry, finite difference techniques accuracy 80−19357
- flow rate transducer dynamic error determ. 77−72386
- fluorescence de-excitation function recording, one-quantum method, error anal. *(Russian)* 77−65925
- forward looking IR system, radiometric accuracy 77−82604
- Fourier transform spectrometry, finite zero filling error estimates 80−37061
- fracture toughness value determination by compact testing 80−45451
- frequencies synthesis by extension of Southwell-Dunkerley methods, errors 77−39217
- galaxies, luminosity classifications, systematic and accidental errors 79−12510
- galaxy photometry, reduction to B_T system of Ames, Reiz and Zwicky catalogues of Virgo cluster area 79−58411
- gas absorption analyser, mean risk criterion *(Russian)* 78−70088
- gas-liquid chromatography, quantitative anal., systematic errors 78−31722
- general relativity, Lense-Thirring effect, relativity test, counter-orbiting satellites 78−45554
- geodesy, props. of Gauss-Helmert least-squares adjustment model *(German)* 78−61309
- geodetic measuring instruments, periodic errors determ. via spectral anal. *(German)* 77−87131
- geodetic networks connection problems, stiffening problem, error anal. 80−81799
- geodetic observations goodness, factor anal. determ. rel. to recent crustal movements estimation 79−57840
- geopotential, harmonic coeffs., determ. error *(Russian)* 79−5439
- geostrophic ocean currents, relative press. topography and relative vel., calc. accuracy 79−39758
- glass, failure prediction technique derived from fracture mech. 77−7343
- graded index fibre, error estimates fo first order WKB calc. method 80−87488
- gravity base points, repeated meas. accuracy estimation *(Chinese)* 80−76892
- gyrohorizon with harmonic and random swinging *(Russian)* 78−62194
- heat conduction, boundary value problems, error analysis of determined thermophysical characteristics 79−81687
- heat conduction parameters, from transient temp. data, correl. ARIMA errors 79−76938
- high precision voltage meas. automatic error correction using iterative method *(Russian)* 78−70089
- holographic interferometry, nonlinear recording, fringe location errors 79−76633
- hot-wire anemometer temp. compensation errors estimation *(Russian)* 78−57345
- hysteresis-free magnetic *(Russian)* 78−86305
- image correlation with geometric distortion effect on local accuracy 78−71040
- indicating measuring instruments, error estimation *(Croatian)* 78−57886
- industrial chromatograph dynamic error estimation 77−77853
- industrial chromatograph static error determ. and correction 77−81446
- inertial navigation system, for error analysis of inertial navigation system 80−36411
- Information Measuring System error computation considering communication channel characts. 78−73957
- information-meas. system accuracy, influence of residual voltages 78−77828
- initial boundary value problem for three dimensional heat equation, Rothe's line method *(German)* 78−30147
- integration of ODEs 77−9874
- IR complex refr. index spectra, FT interferometry, errors in liquid-cell expts. 77−87814
- IR radiation brightness unit reproduction, USSR standard 78−45699
- IR radiation thermometer, −10 to +600°C range, solid-state, features *(German)* 77−82513
- land-use map accuracy testing, sampling designs 80−17226
- laser flash method, error evaluation in heating disc 77−6552
- laser freq. and vel. of light meas., interference methods, accuracy 78−17997
- laser power calculations, laser models, sources of error 80−48207
- least squares method, generalisation 80−62028
- least-squares parameters, rounding errors 78−158
- LEED calculations, reliability factors 80−49058
- lens centring error tolerance study *(German)* 78−33806
- light spot location photocathode of quantum detect. accuracy estimation 78−77832
- linear algebraic systems, penalty function techniques for constraint definition 77−41467
- linear elasticity, finite error approx., error estimates for continuous time approx. 80−52024
- linear Navier-Stokes equations. numerical solution using finite difference method 78−38268
- liquid, simple equilib. theories, review 80−38887
- Lohmann hologram, detour phase error 79−41351
- low-loss dielectric microwave measurement in the E_{010} resonator, numerical error analysis *(Polish)* 78−70153
- marine air temp. sensor error analysis 77−78437
- marine geophysical surveys, trackline crossover differences as accuracy indication 79−39893

error analysis continued
- maximum likelihood test in estimation of exptl. inaccuracies, applic. to equilib. data 77—9867
- measurement data processing system error analysis 78—41288
- measurement error determination techniques, meas. of mass 80—57237
- measurement errors, random, simulation (Monte Carlo) method, teaching appl. 78—86062
- measurement errors reduction, using microprocessors *(Czech)* 78—8398
- measurement instruments, rack and pinion types, indication error reduction *(Polish)* 78—49818
- measurement systematic multiplicative algorithm *(Russian)* 80—86245
- measurement theory contribution to measuring process intensification *(German)* 80—36966
- measuring instrument total error estimate, approx. methods 78—16769
- meteorological pilot balloon position meas., error anal. of double-theodolite data 79—21051
- microwave reflection coeff. meas., calibration error evaluation 79—21768
- mixed finite element method for elasto-plastic plates 78—28929
- Monte Carlo biased transport calcs. optimisation, prediction of statistical error 79—58654
- Monte Carlo transport calcs., error anal. 79—80548
- multiple input/output data, system identification 77—37750
- multiple measuring systems 79—26049
- myoelectric processor and human operator dynamic error performance 79—96714
- N-body problem, numerical solution accuracy 80—21896
- Navier-Stokes equations, finite difference soln. errors 80—17807
- neutron group cross sections fitting integral meas., adjustment 79—93679
- neutron transport theory code, automated approach to quantitative error anal. 77—67788
- NMR absorption peak voltmeter cct. error analysis *(Russian)* 79—26079
- nonlinear partial differential eqns., Galerkin method error analysis 77—78986
- nonlinear variation eqns., convergence of finite element solns. 78—86127
- nonstationary Poisson train intensity meas. error analysis 79—67246
- nosetip recession meas. using implanted radioactive sources 78—16272
- nuclear power stations, gross operator error rates, evaluation of operator reliability 79—45371
- numerical analysis of Stirling cycle, with aid of computer 79—48170
- numerical integration, error estimation by means of Fourier series *(Japanese)* 79—2612
- numerical quadrature formulae, error term evaluation 79—30207
- oblique entry US inspection of welds, defect coord. meas., error anal. 78—40008
- oceanic geoid computations, accuracy 80—21608
- oceanographic data buoys, environmental data quality estimates 77—5364
- optical communication channel, error probability calc. charact. function method, intersymbol interference 80—53227
- optical receivers, photo diode, amplifier and resistance *(Italian)* 77—54775
- optimum interpolation analysis, role of obs. errors in meteorology 80—8383
- ordinary differential eqn. extended difference soln. *(German)* 79—21538
- orthophoto mapping, accuracy prediction 77—40970
- overdetermined windfinding systems, error anal. 80—17399
- parameter estimation appl. to physiological systems, accuracy anal. 78—31762
- particle track inverse momentum, error estimation using Wind's quintic spline method 79—22563
- pendulum accelerometers vibration errors *(Russian)* 78—77874
- perturbation method error bounds, comparison theorem 77—13574
- phase cyclic meas. ambiguity elimination *(Russian)* 79—6072
- photographic zenith tube obs. for time and latit. determ., meas. errors estimation 77—56816
- photometer and photocolorimeter reading errors 78—12742
- photometry radiation energy unit reproduction 78—45670
- planar angle meas. using rotating ring laser *(Russian)* 77—38942
- planet surface gravit. potentia, satellite model error estimation 79—96935
- plasma, diagnostics, axial symmetry, error estimate of optical methods 77—84500
- plasma, inverse-bremsstrahlung absorption rate in an intense laser field 80—24201
- plasma, low-temperatures meas., dynamic thermocouple technique 77—76203
- plasma density diagnostics using short-circuit effect 79—23460
- plasma diagnostics of radial profiles axisymmetric plasma Abel eqn. soln. accuracy 77—84506
- plasma distribution functions, meas. error using finite size electrostatic analyser 79—55562
- plasticity with hardening, mixed finite element method appl. 78—9577
- polarimeter, precision, systematic errors, instrumental errors *(German)* 78—272
- polarisation torque-measuring system *(Russian)* 80—52191
- pollutant advection eqn. integration 77—13118
- polymer lightguide attenuation coeffs. meas., data anal., accuracy 79—1005
- potential field data, constrained inversion, use of pseudohyperellipsoids 80—85752
- propagation of systematic and random errors, math. analysis for practising engineers *(German)* 80—31703
- pulsed light rangefinder, amplitude error in presence of signal fluctuations 80—28332
- radiation conversion method for IR laser wavelength meas. 79—7175
- radiation measurement using integrating detectors, environmental monitoring appl. 77—38428
- radiative transfer through turbid atmosphere, single-scatt. solution 79—16663
- radiochemical determination of ^{89}Sr and ^{90}Sr, comparison of methods 77—16873
- rain-rate estimates from attenuating radar, error analysis 78—73540
- rainfall rate meas. from weighing raingauge records 77—49126
- random vortex methods for two dimens. large Reynolds number flow, errors 78—42614
- relative humidity of air, control, error comparison for various sensors, accuracy 77—10034
- relaxation time meas., simulation, systematic and random error effects 80—37062
- relaxation time measurements, bounded error anal. of expt. distribs. 79—88924

error analysis continued
- remote reference magnetotellurics, random error derivations relating to impedance 80—12335
- remote sensing, error probability estimation without ground truth and known a priori probabilities 77—56746
- reservoir storage size sampling error 78—61466
- residual gravity anomalies interpretation *(Russian)* 79—88232
- residual stress meas., Alignment Error of the hole-drilling method 79—81823
- RMS digital voltmeter calibrator for VLF 78—86293
- road traffic noise monitoring, errors between sampled data and continuous data 79—81618
- satellite-to-satellite statistical orbit determ. error analysis 78—65486
- scattering phase shifts, first order error estimates in approx. calcs. 79—58573
- Schrodinger eqn. alternating direction method 78—21011
- Schrodinger partial wave equation, Numerov algorithm solutions, roundoff error study 79—2643
- Seasat scanning multichannel microwave radiometer, antenna pattern corrections error analysis algorithm 80—94683
- seismic refraction method, vel. determ. and error anal. 80—90229
- shells of revolution, max. principles and pointwise error estimates for torsion 78—18180
- sky photographs, star position meas. error reduction by Gaussian freq. distribution curves *(German)* 77—17384
- snow storage determ. for small high Arctic basins, error anal. 79—70817
- sonar, deterministic and random error model of multibeam hydrographic system 79—3873
- sound power measurement techniques, error propag. anal. 80—48529
- spaced receiver drift experiments, triangle size effect 79—53635
- specific activity determination, procedure optimisation and error anal. 77—6645
- spectra search systems, computer-aided, efficiency eval. using information theory *(German)* 80—37003
- spectral analyser principal error classification and assessment 78—41326
- spectral coefficient error numerical calc. 79—75571
- spectral radiation detectors, calibration and error anal. 78—46177
- spectroscopic measurement, convergence of iterative deconvolution technique, effect of errors 77—53849
- speech analysis, error evaluation for linear predictive using small anal. segment *(Japanese)* 78—31824
- spin-lattice relaxation measurements by optimised inversion recovery 77—48072
- standards comparison, capacitance-inductance, transformer ratio bridge *(Polish)* 79—80645
- star catalogue FK4, systematic errors *(French)* 77—87282
- star tracker error evaluation in optoelectronic direction finders 79—75075
- statistical mechanics, continued fraction error bounds, for complex transport coeffs. and spectral functions 79—12744
- steel, electrical sheet, wattmeter unit for measuring specific losses, system errors 79—91893
- stellar absolute luminosity calibrations, error discussion rel. to consistency 80—62111
- Stokes problem with conforming Lagrangian finite elements, soln. error estimates *(French)* 78—62085
- strain gauge with screw tenso-resistor, linearity anal. *(Russian)* 78—89475
- Sturm-Liouville, error estimation 78—81818
- summation using piecewise-polynomial distribution functions 77—67246
- surface current mapping by Coastal Ocean Dynamics Radar 80—46316
- tenso-resistive strain gauge output error *(Russian)* 78—89474
- thermal conductivity measurement method, normal to thin film, error anal. 78—90682
- thermal convertor AC-DC transfer errors determ., absolute method 78—93643
- thermal diffusivity measurement method, by pulse expt., error anal. 79—32208
- thermocouples, sheathed, electrical shunting and leakage errors, model 78—4618
- three-layer dielectric reflectivity standard error analysis 77—79727
- time signal multifreq. transmission ambiguity detection 77—87741
- time-domain measurement, mm-wave circular waveguide 77—18020
- Tokyo meridian circle obs., true external errors, from SAO 158687 occultation by Uranus 78—28487
- tolerated errors in determining transfer-function parameters of temperature transducers 78—73959
- tomographic system error propagation, hybrid anal. 78—40327
- triangulation ranging using beta density angular errors 79—72758
- triaxial electrostatic gyroscope *(Russian)* 79—88947
- trigonometric parallaxes, external error estimation 77—67087
- turbulence, two-dimens., ergodic behaviour 80—28494
- two body problem, time transformations and local truncation errors 77—22053
- two body problem, time transformations effect on local truncation errors 77—22052
- two-rotor gyrocompass intercardinal error anal. *(Russian)* 79—30460
- underground water mineralisation, reliability anal. of geophys. estimation *(Polish)* 77—73862
- undersampled images, bounds on errors in reconstruction 79—89858
- underwater sound, CW propag. loss meas. rel. to background ambient noise levels estimation 77—84046
- unnotched samples, fatigue limit, estimation of scale relationship, error anal. 79—15793
- US shadow immersion exam. of defects, dimension determ., error anal. 78—44305
- US testing, oblique entry inspection, random error of defect coord. meas., anal. 78—40006
- US testing, pulsed thickness gauge, inspection of tapered profiles, error anal. 78—40007
- UV backscatter expt., airborne, for O_3 distrib. determ., error anal. 78—92985
- variable-potential coulometer analyser integration error analysis 80—93831
- vehicle noise meas. using correlation techniques, expt. 77—68349
- visco-plastic steady-state flow finite element solns. 77—5670
- Weibull wind speed distrib. parameters, vertical extrapolation formulae, errors 78—92916
- wire strain gauge in heat cycling condition, method *(Russian)* 78—65916
- X-ray crystallography, struct. factors, accuracy assessment 78—71636

error analysis continued
X-ray small-angle scattering, information content and error anal., Shannon sampling 80—59340
X-ray sources, point-like, positions determ., lunar occultations optimisation 79—92652
CO_2-laser long-path absorption system for air pollution monitoring, computerised 79—25340
^{14}C absolute dating using low altitude European tree-ring calibration 78—16195
Cs freq. standard, error due to second order Doppler shift 77—87745
H frequency standard undisturbed transition evaluation 77—79066
Kr gas structure, three-body-contrib., neutron diffr. obs 80—43820
NH_3-$N_2(H_2)(Ne)(Ar)(Kr)(Xe)$, as R(1,1) vibr-rot. line parameters, ν_2 band, using CO_2 laser light 79—3444
Pt resistance thermometer calibration characts. linearisation methods *(Russian)* 78—70123
Pt resistance thermometers, temp. range influence on error to nonlinearity *(Russian)* 80—90841
^{222}Rn alpha-scintillation counting, statistical counting error calc. 77—3211
SiC, failure prediction technique derived from fracture mech. 77—7343
W ribbon-filament temperature lamps, radiation error estimation 80—64128

error compensation
see also error correction
aspherical surface diamond turning machine development 80—1372
digital temp. meas. instrument with automatic error compensation of thermoelectric thermometer 79—75526
direct-reading photometry system with automatic instability correction 79—26099
displacement A/D convertor with multichannel phase shifter 77—5823
dual-channel ratio thermograph counteracting skin emissivity errors 77—40892
electro-mechanical sensors, mechanical compensation methods influence on error characts. *(German)* 78—16786
ellipsometer with quarter-wave compensator, multireflection interference effects 79—12841
EPR of free radicals, simulated spectra, compensation for integerisation errors 79—33537
Epstein permeameter, 25 cm, parallel stray mangetic flux compensation *(Polish)* 79—2798
ferrite pot core pressure transducer development and compensation 79—75519
fluxmeter measurement range extension 78—57993
force meas. rod bending moment compensation by parallel resistors *(German)* 77—79078
Fourier transform spectrometer, SNR enhancement by elec. filter compensation of slide velocity errors 80—95151
geodetic levelling, new development in compensator levels, systematic errors reduction *(German)* 77—2289
gradient index spherical lens design for selfcoupled optical pickup system 80—14427
gyrotachometer, error autocompensation at angle vibr. of base *(Russian)* 78—16782
interferometer comparator error, length meas. appl. 78—4587
interferometric measurement of sphericity standards *(German)* 80—87569
laser adaptive optical control with closed-loop estimation and predictive filtering 77—19298
laser beam propagation in atmosphere, thermal blooming, mirror deform. for phase compensation 80—8423
multiactuator mirrors, wavefront error compensation capabilities 79—59797
multijunction thermal convertor AC/DC transfer, Thomson effect error reduction 80—103679
optical multilayer coating production with continuous thickness reoptimisation 79—76890
optical multilayer filters, non normal incidence, optical monitoring, allowable tolerances *(French)* 80—87526
optical rotating table eccentricity error compensation 79—71415
optical systems, error compensators, calc. procedure 80—28296
optical wavefront distortion compensation in real time 77—17219
path difference measurement on anisotropic materials 80—4758
photoelectric transducer for linear displacement meas. 79—50404
photon counting spectroscopic system, error optimisation of dead time determ. *(Spanish)* 79—80693
pulse counting, high precision, limitations, optimal conditions 77—54463
strain gauge, Hg-in-rubber, for plethysmography, temp. drift error and compensation 77—52900
strain gauge load cells, stabilisation and compensation of temp. dependent errors *(German)* 79—35717
strain gauge transducer compensation linearisation by shunt resistors 78—12688
strain gauges, error compensation 77—84198
telescope triple-prism beam deflection compensation 79—75105
thermal sighter-radiometer for temp. meas., signal drift compensation unit 79—35830
thermoresistive convertor error compensation methods *(Russian)* 80—73363

error correction
absolute radiometer instrumental correction theory improvement 77—82585
adaptive laser resonator techniques for CO_2 laser, phase error correction 79—59729
aircraft noise measurement, microphone height depend. errors correction 77—23813
arc, DC, AC, for spectrochem. anal., correlation between anal. signals, plasma parameter changes 79—52828
astrolabe catalogue of San Fernando, coordinates corrections *(French)* 77—78653
astrometric observations with transit instrument, elimination of systematic errors *(Russian)* 78—73615
astrometry, lateral refr. elimination from absolute declinations observed by micrometric method *(Russian)* 79—96890
atmosphere measurements by double theodolite technique, control of inherent uncertainties 80—77160
atmospheric mean temperatures, divisional and state, in Indiana, correction for non-climatic trends 80—51524
atmospheric precipitation, optical array probe small-particle response and particle concs. correction 80—51577

error correction continued
atomic absorpt. spectroscopy, spectral interference correction 77—77825
Auguer electron spectroscopy, mag. field effects correction via blanking heating cct. 77—29078
Bethe stopping-power formula, higher-order Z_1 corrections 80—9479
buoy wave data analyses noise correction functions and error sources 80—46302
cerebral blood flow meas., lateral counting corrections 79—8536
chemical kinetics meas. computational processing iterative optimisation techniques 77—32765
chopping pyrometer for remote meas. below 200°C *(German)* 80—86313
chromel-alumel thermocouple readings, stability prediction 77—87760
clock synchronisation cct., error monitoring correction appl. 78—73970
cone absorption calorimeter for pulsed laser meas. 80—98980
data logger mean square error minimisation by analogue computer *(Russian)* 77—9994
diffraction grating residual ruling errors, magnetostrictive correction method 79—50454
Earth EM sounding, VLF-EM profiles topographic correction based on model studies 80—101452
Earth gravitational field, corrections for atmospheric masses influence 79—57841
Earth tide meas., correction for M_2 freq. oceanic tides 77—9316
eccentricity of rotating cylinder, error calc. in viscosity meas. *(German)* 78—67291
electron diffraction patterns, of textures, reflection sphere curvature influence on reflection location geometry 80—87996
electron microprobe analysis X-ray interferences correction, graphical method 79—43707
electron probe anal., corrections, quantitative, effect of electron incidence angle 79—39270
electron probe anal., quantitative, correction procedure 79—43686
electron probe analysis, ZAF-correction procedures for biological bulk specimens 79—44073
ellipsometer, polarisation-modulation, Fortran simulation program ELLIPS 78—271
emissometers, refl. errors elimination by use of alternate instruments 77—10089
ephemeris time, correction determ. from photographic obs. of Sun annular eclipse (1976, April 29) *(German)* 79—44335
exponential clipped photon autocorrel. spectra, data anal. 79—2837
eye, computer assisted examination, Refractor III system 79—29650
FK4 catalogue, right ascension and declination corrections from meridian obs. *(Russian)* 77—71016
flow curve correction by FORTRAN program *(German)* 78—79394
flow meas. in chemical industry, VDI and DIN specifications *(German)* 77—42946
flowmeters, correction factor appls. for blunting of diaphragm input rim 78—75240
fluorescence anal., computerised correction for excitation beam absorpt. 77—77818
fluorescence polarisation measurements, correction for finite apertures 78—21224
galaxy photometry, reduction to B_T system of Ames, Reiz and Zwicky catalogues of Virgo cluster area 79—58411
geodesy, parameter accuracy improvement by choice and quality of obs. 79—44078
geodesy, refinement of short arc satellite altimetry adjustment model 77—60336
geomagnetic palaeointensity determination, ARM correction method 79—34968
geophysical data analysis, random values separation *(Russian)* 79—74983
Geos 3 altimeter data, error model for geoid undulations and gravity anomalies recovery 80—3896
Geos-3 altimeter data, error correction rel. to geoid undulation and anomaly estimation 77—64178
gravimetric networks, adjustment *(German)* 79—44084
hydrometeorological fields, probabilistic models for error correction *(Russian)* 77—56697
hygrometer, Meteorological Office Mk3, frostpoint meas. systematic error 78—73538
imaging system shading effects and countermeasures 78—78922
industrial chromatograph static error determ. and correction 77—81446
instrument operation speed increase, additive-iterative correction method *(Russian)* 78—89423
instrumental distortion correction 79—54116
interpolation error operator, digital time series error detect. and correction 78—3963
ion potentiometric continuous analysis, calibration method for minimizing errors 78—35748
iris diaphragm photometry, nonuniform background correction 80—12680
Large Space Telescope mirror figure control, adaptive optical techniques 77—22076
laser Doppler velocimeters, signal processing using counters, biasing elimination method 78—1773
laser range measurements, atmospheric correction determ. *(Russian)* 80—12674
light scattering by solns., correction for effects of contaminating dust particles 77—37959
linear dichroism measurement, fictitious signal elimination via polarisation scrambling 78—4683
lunar ephemeris, Earth oblateness effects, corrections 77—22043
Mars, photographic positional obs. with 400 mm astrograph, atmospheric dispersion and phase corrections *(Russian)* 79—44395
Maryland-Argonne gravit. radiation detector, bias and errors elimination 77—22476
measurement systems, automatic error correction methods 79—80566
measurement theory contribution to measuring process intensification *(German)* 80—36966
measuring instrument inspection, optimal error correction signal 78—77829
meteorology, surface synoptic obs., automatic real-time quality control 78—92920
microtron, scheme for correcting orbit 77—65366
monochromator scanning control system using microprocessor, spectral line shift correction *(Japanese)* 80—57384
MPP-1 stationary precision proton magnetometer, error elimination and calibration 79—53535

error correction continued
- nephelometer, integrating, ang. truncation error in fog droplet size range 77—70861
- neutron activation anal., computerised, correction procedure, detection limit, standardisation 77—44544
- neutron spectrometer, angular-displacement precision control with fast error-signal transducer 78—186
- ocean microwave radiometry, correction for external sources and intervening atmosphere 78—81416
- optical and photoelectric pyrometry, measurement correction, reference wavelength 77—45847
- passive value parameter transducer *(Russian)* 78—49819
- photogrammetry, SEM appls., simplfied numerical transform. for distortion correction *(German)* 79—17572
- plasma chromatography, baseline corrector for boxcar integrator instruments 77—52717
- powder reflections, computer program for determining multiplicities, correction for $\bar{3}1m$ Laue symmetry 79—10759
- precision levelling with two-fluid tiltmeter 77—21919
- primary meas. transducer error twin-circuit correction *(Russian)* 79—71404
- pyrgeometer performance improvement 77—70860
- radiation quality factor, lineal energy correction for saturation effects 80—26376
- radiotherapy megavoltage depth-dose value corrections due to reduced backscatt. thickness 77—48871
- rocks tensile strength indirect measurements, two-dimensional theoretical soln. correction 79—29883
- satellite digital data, radiometric correction and equalisation 79—74587
- satellite imagery, filtering to remove cloud cover 77—56744
- satellite laser tracking data, ray tracing evaluation of refraction errors 79—8588
- secondary electron emission spectroscopy, cascade background correction, Auger peaks, Cu(110) surface appl. 79—43079
- seismic prospecting, minimisation of distortion caused by geophone-ground coupling 79—44256
- seismic sounding, weathering correction method 79—44255
- seismic surveys, residual static and crossdip corrections simultaneous estimation 79—92500
- seismic surveys, zero time identification rel. to mis-ties correction 77—21916
- seismometer, long-period, drift corrections using borehole seismometer with stable period *(Japanese)* 80—67417
- SIMS, computerised system for energy spectra determ. 80—3423
- soil-structure interaction effect on seismometer readings, seismogram correction 79—16685
- space research, spacecraft mag. field correction via dual magnetometer method 78—77459
- stars photoelectric positions, chromatic refr. correction tables *(Russian)* 79—96889
- stellar Balmer discontinuities, correction for line blocking 77—45419
- stellar trigonometric parallaxes statistical anal. corrections 77—64743
- strain indicator for semiconductor strain gauges, correction for gauge resist. and gauge factor 77—71313
- systematic uncertainties, randomisation and quantitative assessment 80—98869
- temperature measurement error due to cond. along sensor leads 77—13752
- temperature measurement in polymer melts, thermocouple heat loss correction 77—65034
- terrestrial heat flow measurment, vertical groundwater movement correction 80—3969
- theodolite, reduction of influence of vertical axis error on horizontal angle meas. *(German)* 79—44278
- thermocouple dynamic error correction cct. 78—77909
- thermocouple psychrometry, effect of and correction for different wet and dry bulb response 80—98472
- thin-wire resistance thermometer, dynamic error correction 79—12801
- tomographic image, with aid of computer simulation 80—85470
- transverse section picture reconstruction, correction functions and statistical noise 77—12989
- ultrasound B-mode scans, speckle reduction 78—22233
- US wave velocity measurement, elimination of transducer bond corrections via capacitative transducer 77—46873
- UV fluorescence lifetime determ., correction of instrumental time response var. with wavelength 78—5374
- vibration meas. via laser interferometry, thermal and mechanical drifts elimination 77—118
- voltmeter frequency error reduction using eccentric and elastic transducer *(Bulgarian)* 77—61082
- Wilson's sound speed meas. reevaluation for pure water 77—23794
- X-ray fluoresc. anal., correction procedures, accurate coeff. method 77—56311
- X-ray fluoresc. anal., energy dispersive, erroneous peaks, removal 77—56314
- X-ray fluoresc. anal., of powdered samples, additivity of effective coeffs. for X-ray absorpt. 79—24856
- X-ray fluoresc. anal. absorpt. correction, effective wavelength calc. 79—24855
- X-ray fluoresc. anal. using matrix correctional procedure, appls. to alloys, Al_2O_3-supported catalysts 78—80817
- X-ray fluorescence anal., interelement correction, models, computer program, appls. to alloys 77—56315
- X-ray fluorescence anal., matrix correction, computer program *(German)* 80—3427
- X-ray spectral anal., theoretical correction parameters rel. to chem. composition of steels 78—61108
- X-ray spectroscopic anal., mathematical correction procedures, review 77—56308
- zodiacal light UV observation from D2B-Aura satellite, extraneous light evaluation 79—58299
- O_2 partial pressure on blood sample, polarographic method, error reduction 78—7470

error correction codes
- high data rate acoustic telemetry system design 80—43573
- speech transmission, forward and backward prediction in adaptive differential PCM over nonideal channels 80—99902

error detection
- *see also error analysis*
- Aanderaa Ni-coated current meter, pressure-induced direction error 80—4121
- Earth crust stress meas. by overcoring, error detect. by diagnostic stress-relief curves 79—29886
- ECG, computer processing, measurement error determ. 80—94401
- ECG computer-assisted interpretation, routine automated quality control 78—40394
- eye, computer assisted examination, Refractor III system 79—29650
- geodesy, systematic errors detect. by hypothesis tests using adjustment in sections *(German)* 79—44083
- IC, pattern overlay errors, automatic meas., using EL-1 lithographic system 79—21868
- interpolation error operator, digital time series error detect. and correction 78—3963
- noise level meter, method *(Russian)* 79—67244
- optical storage focus error detection, skew beam and Foucault knife-edge techniques 80—102649
- workpiece quality control by optical correlation 77—50644

error recovery (computers) *see system failure and recovery*

error statistics
- 800 Mbit/s optical transmission experiments with dispersion-free fibres at 1.5 μm 80—58680
- automobile exhaust emission meas. and testing procedures, survey *(German)* 77—73839
- binary optical communication system, atm. scintillation effects 77—71943
- chemical anal. by counting meas. calibration determs., statistical uncertainties of anals. 78—92533
- chromel-alumel thermocouples, investigation 78—24794
- covariance estimation, of stationary, ergodic processes, with non zero mean value *(French)* 79—80513
- digital EMG processor and three-state myoelectric control design 79—53283
- digital fibre optic communication systems error probability anal. 78—46775
- digital fibre-optic transmission system average error probability 77—27380
- dynamic emission computed tomography, quantitative pots. 78—77105
- elastic vibrations parameters evaluation, statistical and dynamic errors determ. *(Russian)* 80—38181
- EPR anal., precision investig., Cu (II) complex appl. 77—56261
- error prediction in meas. of probability densities *(French)* 78—57885
- fibre optic systems, digital, error probability with inter-symbol interference and additive noise 79—89855
- fibre-optic system repeater error rate calc. approaches compared 77—54672
- fission track dating method, standard error estimation 80—36419
- Fourier spectroscopy, delay compensation, sampling error reduction 79—30566
- geodesy, systematic errors detect. by hypothesis tests using adjustment in sections *(German)* 79—44083
- hierarchical systems, calibration errors influence on end item performance 80—98788
- holographic interferometry, errors in small vector displacements meas., statistical anal. 78—78953
- holographic memory, data readout reliability by optoelectronic channel 79—27216
- holographic storage data error probability in $LiNbO_3$:Fe electro-optic crystal 80—43304
- image detection in the presence of speckle 79—45909
- image registration using material information 80—99664
- instrument mechanism analysis, linear *(Hungarian)* 78—49823
- integrated probability distribution for sum of two or more constituents 77—17940
- inverse filter which is optimum in error-distrib. sense, stability characts. 78—81424
- laser wavelength determ., random/systematic errors statistical estimation 78—17996
- lens, errors in thickness and reference vertex distances, statistics 78—1314
- measurement data equal accuracy verification, correlation anal. 78—8378
- measurement errors, random, simulation (Monte Carlo) method, teaching appl. 78—86062
- measurement rounding error uncertainty anal. *(German)* 77—87721
- measuring instrument total error estimate, approx. methods 78—16769
- multidimensional Gaussian max. likelihood classifiers error probability estimation 77—78540
- NMR analysis system, LAOCOON3-type, reliability efficiency and error estimates 78—258
- non-Gaussian distribution laws for statistical error theory generalisation *(German)* 80—22315
- nonGaussian error limits, distribution and probability curves *(German)* 80—36967
- optical channel conditioning against intersymbol interference and timing errors *(Italian)* 77—23622
- optical communication using two-photon laser, optimum control of quantum noise 78—71049
- optical discrete PPM signal reception accuracy *(Russian)* 79—94171
- optical fibre communication systems, computer design aids 80—28350
- optical fibre digital transmission error probability, quantum noise effects *(Italian)* 77—23623
- optical fibre nonlinear equalisation by shaping filter *(German)* 78—33882
- optical fibre system, timing error tolerant waveforms 80—14293
- optical signal receivers, optimal and nonoptimal, logical structs. efficiency comparison, simulation *(Russian)* 78—71041
- optimum design of expts. on exponential absorpt., statistical errors anal. 78—885
- photoelectric transducers with astatic characteristics, statistical error determ. 78—93760
- probabilities of error in research statistical interpretation 80—90658
- quantum radiation from a point source, angular coords. determ. 77—65050
- radiation monitoring, continuous collecting and counting 79—54603
- remote sensing, error anal. of ill-conditioned data, inversion technique 77—66992
- rubber testing, statistical anal., method variance *(Polish)* 77—28962
- scanning optoelectronic device with multielement photodetector, error probabilities 77—58455

error statistics continued
- single-mode obs. distributions, invalid data rejection algorithm *(Russian)* 79—21690
- steady-state process, probability characts. error calcs. 80—42145
- stochastic processes, correl. functions, finite-time averaging, statistical error 78—20946
- surveying, interpolation via linear prediction errors *(German)* 77—9321
- traffice noise, sampling errors with gamma headway distributions 77—84072
- transducer, pulsed frequency, continuous random signals errors evaluation, by means of computer simulation 77—74386
- transducer precision model, angle-digital quantities conversion error evaluation 77—82498
- transverse section reconstruction, statistical errors, effects of projection angle number and projection sampling 77—52869
- turbulent atmosphere, optical DPSK system performance 78—42293
- two-scale meter, max. likelihood method, probability density function 77—61047
- wandering in turbulent atm., error probability in binary signal reception 79—10337
- AlGaAs DH laser preamplifier to improve optical receiver sensitivity 80—53316

errors

see also coding errors; measurement errors; roundoff errors
- acid, weak, ionisation in aq. soln., rate const. meas., elec. field jump method errors 79—43611
- active noise-suppression, influence of random errors on acoustic fields compensation 77—14852
- active sound absorption, errors rel. to attainable noise reduction, appl. of Huygens principle *(French)* 77—14840
- active vibration suppression systems, errors in compensating sources placement criteria 78—18099
- aerosols, Mie optical cross-sections calcs., sensitivity to size distribs. sampling errors 77—2243
- airport wind reports, error freq. rel. to wind components averaging time 77—17177
- N. Atlantic Ocean mesoscale currents, errors from use of geostrophic approximation *(Russian)* 77—49071
- atmosphere electron content from ATS-6 satellite radio beacon, meas. and anal. errors 79—48611
- atmosphere transmittance, algorithm accuracies 80—101429
- atmospheric transmittance, profile depend., line parameter vars. 78—77322
- beta emitters, identification using absorpt. coeff. in Al, accuracy 77—57837
- bromomethane (-d_1, d_2, d_3), exptl. vibr. intensity data error indication by F and G sum rules 79—72364
- calorimeter, double compensated, for absolute beam intensity meas., design, accuracy 77—6631
- chemical analysis, instrumental, minicomputer appls., errors 78—92543
- chemical data base, error detect. by text searching 77—37678
- computed tomography, offset detector, interleaving vs. separate processing 80—30877
- computerised hologram generation, quantisation error minimisation method 77—83836
- crystal face orientation error rel. to axis, shear wave meas. 77—35006
- diamond machined optical surface specification 80—48472
- distance measurement, electro-optical, nonperiodic errors rel. to use of plane mirrors *(German)* 77—9324
- double radio sources, observational selection in ang. size-redshift test 77—57100
- drift tube array, meas. of alignment error by hot wire method *(Japanese)* 77—61638
- Earth gravity field, errors due to atmospheric masses influence latit./seasonal depend. 79—57841
- Earth surface temperature in mountainous terrain, diurnal var. prediction and errors 80—82011
- Earth underparameterised models, random data errors treatment in linear inference theory 78—49000
- ECG, His-bundle activity detect., theoretical anal. of error during signal averaging 80—94392
- ECG telephone transmission, analogue and digital, errors and noise 80—94398
- elastodynamics, linear, discrete time approx. of initial boundary value problems, error estimates 80—73175
- electrocardiographic data processing, filtering and sampling 78—24162
- ellipsoidal concentrators, shaping errors, effects on radiant energy characteristics 79—96418
- examination marks, reliability, in electronic engineering educational courses 79—75305
- f_0F_2 monthly median values, mean square deviations of long-range forecast 77—60513
- fission products in reactor, decay power, sensitivity to uncertainty in yields 77—6494
- flow, of liq., thermal markers for vel. field meas., error reduction 78—91036
- flow rate convertor, EM, optimal mag. system design 79—77313
- Fourier spectrometer, effect of random errors in sampling interval on spread function 80—18020
- Fourier transform spectroscopy, minicomputer appls., errors 78—92543
- geomagnetic declination field near Earth surface, error in analytic representation 78—73307
- geophysical anomalies anal., effect of meas. and theoretical errors on regional background separation *(Russian)* 78—40703
- geopotential models, accuracy 79—25183
- heat of adsorption, isosteric, determ. using contact pot. difference meas. 79—66347
- holographic interferometer instrument errors for narrow reference beam 77—640
- image alignment errors due to aliasing 80—106480
- interstellar molecular spectra, predicted radioastronomical freqs. accuracy, determ. from OH spectrum 79—48666
- kilogram mass standard, air buoyancy correction for different materials *(German)* 77—82483
- laser tracker, target induced pointing noise 78—5519
- linear thermal conduction eqn., errors of differential-difference approx. *(Russian)* 78—38173
- liquid radial distribution functions, method of reducing termination errors 80—24332

errors continued
- magnetic field computation, by Schwarz-Christoffel mapping function numerical integration *(German)* 79—89826
- mass spectroscopic ion sampling, across small diameter hole, mass discrimination errors 77—56273
- molecular spectra, r-centroid approximation accuracy 79—89661
- molecular spectral line broadening semiclassical straight line vs. curved trajectories 79—45765
- musical sounds, digital meter for tonal error meas. *(German)* 77—830
- myoelectrically controlled systems, five-state, error rate obs. 80—72376
- neutrino physics, errors on ratios of small numbers of events 80—105879
- neutron capture cross sections for fission products, statistical adjustment method, error evaluation 77—6498
- nuclear power stations, HTGR risk assessment, operator actions, event and fault tree anal. 80—63330
- nuclear reactor in-core 78—82476
- nuclear standard cross sections, uncertainties and correls. in evaluated data sets 77—23196
- nutation, errors rel. to tidal effects in time-service obs. 79—96733
- object reconstruction from projections, influence of detector arrays fixed errors 78—4743
- ocean chemistry, confusion of mathematical notation for element residence times 77—86937
- open channel acoustic flowmeters, design, calibration and errors 78—55701
- optical element fabrication and assembly, centration errors 80—9980
- oscillator strengths, absolute, for Fe group elements second spectra, error and correction 77—3310
- perturbed energies, 2nd order, coupled HF iterative procedure, geometric approx. 79—9991
- photodetector, integral error, matching to weighting function *(German)* 80—31876
- plasma rarefied flow around bodies, ion density computation accuracy 79—50849
- pyrometry, methodological error elimination 77—126
- radiotherapy, pelvic radiation portal reproduction 78—35928
- rectilinear scanning, error due to radionuclide decay 78—3590
- refractive error stability of contact lens wearers 80—108879
- road traffic noise with interrupted flow, errors of prediction methods 77—62106
- seismic surface waves, inversion of dispersion data with random errors 77—73681
- seismology, interval vel. estimation error and geological model 77—86790
- solar energy concentrators, generalised optical design technique, consideration of various errors 80—95979
- solar X-ray images quantitative interpretation, filter ratio method errors 79—40085
- spatial lattice distance, accurate and precise meas. *(German)* 80—19666
- spectrochemical quantitative analysis, absorption spectra 79—100461
- spectrophotometer recording errors caused by discrete removal of information 79—49301
- star catalogue coord. system orientation errors, effect on planetary ephemerides *(Russian)* 80—51640
- stellar spectral classification prediction from uvbyβ photometry, errors 80—67700
- stereo-pair images, correlation error prediction 80—102636
- surfactant inhibition of electrochem. reaction rate, random error effect on characteristic parameters 80—40705
- system reliability in face of human (operator) errors, bibliography 80—94940
- temperature integral, approximative eqns., accuracy analysis 80—36834
- tensile test, regulated, strength and deform. characteristic values, consistency *(German)* 80—93712
- three-body problem, limited circular, Delaunay-Hill method averaging error estimation *(Russian)* 80—8530
- torquemeter, capacitive, with digital display *(German)* 77—34006
- Varshni V and Lennard-Jones pots., 3rd order WKBJ eigenvalues 79—6982
- virial equation, truncation errors 78—87764
- VMOS dynamic memory, 65536-bit, investigation of alpha-particle induced soft errors 80—88223
- X-ray diffraction errors due to TDS, effects on atomic parameters and electron density distrib. 77—19819
- X-ray powder diffr. anal., reference intensity ratios determ. methods, errors 77—70385
- e^+e^- physics, errors on ratios of small numbers of events 80—105879
- H II regions radio emission analysis, consequences of improper analytic methods 78—54000
- He, 0-16.5 eV electron scatt., R-matrix calc. 79—36768
- O_3, sextic centrifugal distortion consts. calc. 79—59430
- OH radical calculated densities in troposphere and stratosphere, uncertainties 79—53426

Esaki diodes *see tunnel diodes*

Esaki effect *see tunnelling*

ESCA *see electron spectroscopy; spectrochemical analysis; X-ray photoelectron spectra*

estimation theory

see also information theory
- absorbed dose, bounded estimate using linear programming 78—37452
- acoustic emitter delay and Doppler parameters, max. likelihood estimation 78—9503
- acoustic image improvement using statistical estimation theory 79—46115
- acoustic reflection in discrete layered media, structure estimation accuracy 79—23108
- algebraic structure and finite dimensional nonlinear estimation 79—5975
- astronomical observations errors, optimum linear estimation of mathematical expectation and standard deviation *(Russian)* 80—12673
- asymptotic theory of statistical estimation, regularity versus nonregularity comparison 80—52003
- bilinear system Volterra-kernel estimation 79—26512
- blind deconvolution, zero phase blurring function estimation 80—106482
- bounded flux-at-a-point estimators 79—587
- conference on pattern recognition and signal processing, Paris, France (June/July 1978) 79—59864
- convergence speed of a posteriori variance estimation *(German)* 79—100984
- daily precipitation stochastic models, estimation of Fourier coeffs. to describe parameters seasonal vars. 79—53481
- film-grain noise degraded image estimation 78—54479

estimation theory continued
film-grain noise degraded images, nonlinear detection and estimation 77—50627
flood frequency analysis, appl. of incomplete means estimation procedure 79—88378
hail-prevention operations, cost effectiveness estimation methods anal. 78—93013
identifiable sound source location from time differences of arrival 80—91951
instrumental variables, regression model *(German)* 78—29080
laser adaptive optical control with closed-loop estimation and predictive filtering 77—19298
linear state estimator design, updating budget, meas. theory 80—95058
LMFBR-subassembly outlet computerised temp. monitoring techniques 78—8948
log Pearson type 3 distrib., T-year event and asymptotic standard error by max. likelihood theory, comment 80—12461
maximum entropy spectral analysis, power estimation method 79—16691
meteorology, maximum likelihood estimates for parameters of mth extreme value distrib. 77—78332
meteorology inverse problems, estimation theory appls. 79—35018
nonlinear recursive estimation procedure, convergence and hybrid simulation 77—53850
nuclear reaction rate Monte Carlo estimators, unified definition 78—58334
optical phase tracking, Fourier series and estimation appl. 78—25812
partitioned sub-optimal linear estimator, separate channel implementation 80—94949
passive sonar, errors in range and bearing estimation 80—79030
phase-coherence detector and estimator, formed via overlapped FFT 79—59870
radionuclide angiocardiography determ. of ventricular ejection fraction, correction of noisy data 77—48868
regional air quality, estimation using GMDH 79—57544
rock specimens impulse response estimation, numerical method and appl. to laboratory data 79—80049
seismic data filtering and smoothing, least-squared error, stationary and nonstationary 80—4158
seismic surveys, residual static and crossdip corrections simultaneous estimation 79—92500
seismic wave field parameters optimal estimation *(Russian)* 78—28177
signal-dependent film-grain noise, optimal image estimation 80—102659
singular compensation problems, hypothesis tests *(German)* 78—44758
stationary point processes, estimation procedures 77—2517
statistical thermodynamics from statistical theory of estimation 78—54328
stereology, estimation of linear functionals by max. likelihood 77—61056
thermal diffusivity of solid, iterative estimation method 80—43603
thermal properties, simultaneous evaluation, nonlinear estimation procedure 79—94478
time series, conference, Nottingham, England (Mar. 1977) 80—82580
time-averaged areal mean of precipitation, estimation and network design 79—79901
tomography reconstructions with limited data using estimation theory 80—30883
truncated exponential density sequence, estimator asymptotic variance comparison 78—12539
undersea acoustic transponders, locations optimal estimation 79—5684
underwater sound, Confidence bounds for magnitude-squared coherence estimates 78—66979
variance-covariance-component estimation of Helmert type, introduction 80—101318

eta meson resonances
$\eta\to\pi^+\pi^-\gamma$, one-loop approx. in quantum chiral theory 78—25041
η' meson as pseudoscalar gluon, current sum rule saturation in QCD *(Russian)* 79—71718
charmonium atomic physics, ψ, ψ', η_c, η_c' masses and $\psi\to\eta_c\gamma$ decay 79—40740
chiral SU(4)×SU(4) model, scalar meson decays 78—4801
integral and fractional charged quark model test using η and η' props. 80—32074
$m_{\eta c}{}^2 = m_\psi{}^2 - (m_\rho{}^2 - m_\pi{}^2) = (3000 \pm 20\ \mathrm{MeV})^2$ after all 79—85288
mixing of gluon bound states and quark-antiquark states, η and η' appl. 80—47255
multiparticle reactions, quark model predictions of η and η' prod. 78—423
nonperturbative QCD, large N_c, QCD bag model, instantons and η' mass 80—57559
pseudoscalar and vector meson decays, triangular quark diagram anomalies, ψ, η and η' appl. *(Russian)* 80—42455
$SU(4)\otimes SU(4)$ broken chiral model, η mixing 78—12836
three gluon coupling hadronic signature, η' in gluon jets, QCD vertex 79—75727
E(1420) assignment of η' in broken SU(3) plus SU(2) 77—38144
$e^+e^-\to e^+e^-X$, $X=e^+e^-$, $\mu^+\mu^-$, $\pi^+\pi^-$, η', photon-photon interactions, QED test 79—93425
$e^+e \to e^+e^-\eta'$ (958), radiative width in two photon interaction 79—89174
$e^+e^-\to\eta'(X^0)\gamma$, generalised VMD theory 77—10268
$e^+e^-\to\psi X$, estimate of inclusive ψ and $\psi\eta_c$ prod., QCD anal. of cross section 79—85308
η, η' and η_c, mixing and decays in nonrelativistic quark model for QCD idea 78—82166
η-$c\bar{c}$, η'-$c\bar{c}$ couplings from $\psi\to\eta'\gamma$, $\psi'\to\eta\gamma$ *(Russian)* 77—49962
η-η', pseudoscalar meson mixing, phenomenological model with radial excitations in mass matrix 79—54316
η-η' mixing angle and relative radiative decay rates $\Gamma(\psi\to\eta\gamma)/\Gamma(\psi\to\eta'\gamma)$ 80—9173
η_C, coherent prod. and baryon-antibaryon pair decay 78—21421
η_c, mass and other props, review from theoretical models 80—102025
η_c and η_c', mass prediction using QCD 80—22590
η_c meson hadronic decay 78—8664
η_c prod. and hadronic decay, charmonium model 78—41502
η', QCD sum rules for mass, possible pseudoscalar gluonium, instanton effects 80—388
$\eta'\to2\gamma$, nonet mixing and gluon effects in current quark framework 79—80799
$\eta'\to3\pi$, isospin violating effects from nonvanishing quark mass difference 79—63385
$\eta'(957)$ meson, quark model description for prod. and decay 80—62970

eta meson resonances continued
$\eta'(958)$, spin-parity test from collinear prod. and decay 78—41543
$\eta'(958)$ spin parity assignment, $K^-p\to\eta'\Lambda$, 4.2 GeV/c 77—82769
$\eta'(958)\to4\pi$, decay mode in broken $SU_6\times O(3)$ quark model 79—36071
$\eta'(958)\to\gamma\gamma$, total width meas. using known $\gamma\gamma$ branching ratio 79—54343
η' assignment in SU(4) spectral function sum rules 77—38143
η' $c\bar{c}$ component, Okubo mass formula and $\psi\to\eta'\gamma$ 77—6116
$\eta'\to\eta\pi\pi$, amplitude satisfying Adler conditions, relativistic quark pair creation model 80—95262
$\eta'\to\eta\pi\pi$, current algebra calcs. with symmetry breaking, inconsistency with expt. 79—13114
$\eta'\to\eta\pi\pi$, finite dispersion relation calc. of decay rate 78—41542
$\eta'\to\gamma\gamma(\pi^+\pi^-\gamma)$, chiral quark model anal. *(Russian)* 80—105900
η' mass and quark mass ratio 78—8584
$\eta'\to\mu^+\mu^-\gamma$, in π^-p interactions at 25 and 33 GeV/c, form factors *(Russian)* 80—4984
$\eta'\to\pi^+\pi^-\gamma\gamma(\pi^+\pi^-\pi^+\pi^-\gamma\gamma)$, rare decay modes near production threshold from $\pi^-p\to\eta'n$ reaction 80—9171
$\eta'\to\pi\pi\eta$, $\delta\eta'\pi$ and $\delta\eta\pi$ coupling constant ratio, $\delta(980)$ quark content 80—82955
$\eta'\to\pi\pi\gamma$, nonet mixing and gluon effects in current quark framework 79—80799
$\eta'\to\rho\gamma$, radiative widths, δ and S* background, SU(3) and VDM anal. 80—419
$\eta'_c\to\psi\gamma$, charmonium, hyperfine interaction, nonperturbative treatment 80—62944
$\eta''(2.8)$ radiative decay, charmed quark content of ω and ϕ mesons 77—71511
from π^-p mass spectrum 80—27498
$\gamma p\to\eta^0p$, phtotproduction cross-section asymm. for 1.39 to 1.78 GeV polarised photons *(Russian)* 77—79273
$\gamma p\to\pi^0p$, 0.6 to 1.8 GeV, backward angles, η-cusp 80—57609
$J/\psi\to\eta(\eta')\gamma$ decay rate, QCD sum rules 80—52497
K^-p, η and ω prod. at 10 and 16 GeV/c 77—34191
$K^-p\to\eta'\Lambda$, 4.2 GeV/c, total and differential cross sections, forward production peaks 79—40801
$P\to\gamma l^+l^-$, EM characts. for pseudoscalar meson decay in nonlocal quark model *(Russian)* 80—102050
pp, 200 GeV/c in Be, inclusive ω prod. at large p_T, η' prod. upper limit 80—52547
pp, ISR energies, inclusive high p_T ω^0 and η' prod. 80—42504
$\bar{p}p$ resonant annihilation, η_c charmonium state prod. cross section 80—82991
$\pi^-p\to\eta'n$, 15-40 GeV/c, differential cross section and singlet-octet mixing angle 79—54361
$\pi^-p\to\eta(\eta')n$, 8.45 GeV/c, differential cross section ratio, η' decay branching 80—78094
$\pi^-p\to\pi^-\pi^+n$, narrow epsilon resonance under rho 80—5021
$\pi^+p\to\pi^+\pi^-\Delta^{++}$, narrow epsilon resonance under rho 80—5021
$\pi^\pm p$, η and ω prod. at 10 and 16 GeV/c 77—34191
$\psi\to3\gamma$, heavy narrow state search, η' and η_c branching ratios 80—57600
$\psi\to\eta(\eta')\gamma$, SU_3 violation, symmetry breaking and decay amplitudes 80—52499
$\psi\to\eta(\eta')\gamma$, Ward identity anal., η,η' quark-glue struct. 80—42449
$X^0\to\gamma\gamma$, prod. in $\pi^-p\to X^0n$, four-momentum transfer region 0.38-0.79 $(\mathrm{GeV}/c)^2$ 77—67656
$X^0\to\pi^+\pi^-$ decay, 1 GeV/c^2, prod. in $\pi^-p\to X^0n$ 77—67670
$\eta_c(2830)$, OZI rule breaking in decays 79—97597

eta mesons
0^--mesons in broken SU(4), improved mass formula 77—30352
η_q prod. cross section ratio in quark parton model *(Korean)* 80—27466
baryon decay, η modes, hadronic interaction symm. 77—30379
charmonium atomic physics, ψ, ψ', η_c, η_c' masses and $\psi\to\eta_c\gamma$ decay 79—40740
charmonium photoprod., gluon-exchange model 78—74214
cosmic ray-nucleus reacts., 20 TeV, balloon-borne chamber, Monte Carlo simulation 80—9309
current algebra theorems for U(1) Goldstone boson rel. to η' 79—89081
decay constants, smoothness and spin-zero charm mesons in broken chiral SU(4)×SU(4) symmetry 79—58900
decay constants from Weinberg type sum rules 79—54336
EM decay, η-η' mixing and gluons 80—62981
extended PCAC+Veneziano type model, Goldberger Treiman relations, $\eta\to\gamma\gamma$or $\pi^+\pi^-\gamma$ 78—21354
free η^+ meson gas, creation in nuclear matter with neutrinos retention 78—96390
gauge theory, non-Abelian, tunnelling effects, phase coherence and mass in η, η' mesons 79—93287
hadron-hadron inclusive interactions, charmed particle production, η_c, ψ and other $c\bar{c}$ bound states 80—63036
integral and fractional charged quark model test using η and η' props. 80—32074
light quark mass and low energy η meson interactions *(Russian)* 79—67513
$M_\psi - M_{\eta(c)}$ and $M_\Upsilon - M_{\eta(b)}$ lower bounds, concave and convex pots. 80—91057
mass, quark-gluon model, virtual annihilation mech. 79—351
mass formulae and mixing in SU(8) and $SU_W(8)$ symmetries *(Russian)* 78—66097
meson strong decay, 2 quark-antiquark pair model 80—52496
mesonic octet decays, chiral QFT description using one loop approx. *(Russian)* 79—63471
MIT bag model, PCAC effects, pion field exchange energy, η mass 79—93378
mixing of η, η', η_c, charm-quark-to-strange-quark mass ratio 79—93312
mixing of gluon bound states and quark-antiquark states, η and η' appl. 80—47255
multimesonic decays of charmonium states in a constant matrix element quark model 79—26298
multiparticle reactions, quark model predictions of η and η' prod. 78—423
N-flavour quark model, axial-vector current anomaly, decay constants and η-η'-η_c problem 79—13045
nonleptonic decays of charmed mesons and chiral Lagrangians *(Russian)* 79—30732
production in ${}^6\mathrm{Li}(\gamma,\eta){}^6\mathrm{Li}$, partial cross section meas. 77—65220
pseudoscalar and vector meson decays, triangular quark diagram anomalies, ψ, η and η' appl. *(Russian)* 80—42455
pseudoscalar decay const., linear potential model 77—74679

eta mesons continued
quark model with 4 quarks pseudoscalar meson masses 77-46021
trajectory mixing scheme, dual planar theory 77-13942
vacuum symmetry, decay consts., mixing consts. in SU(3)×SU(1) QCD 80-27483
b quark$\to\psi(\eta_c)+$X, B branching ratios assuring colour suppression 80-37259
$c\bar{c}$ component, Okubo mass formula and $\psi\to\eta'\gamma$ 77-6116
e^+e annihilation, 3.1-5.2 GeV, DASP results 80-42483
e^+e^- annihilation, 6 GeV, η_c existence, possible $c\bar{c}c\bar{c}$ state 77-82755
$e^+e^-\to e^+e^-\eta_c$, two photon process, numerical distrib. studies 79-13142
$e^+e^-\to\eta$, 4-5.2 GeV, F, F* masses determ. 77-87988
$e^+e^-\to\eta X$, $F\to\eta\pi$ F meson prod. characts. 79-26338
$ep\to ep\eta$, meas. in S_{11} (1535) reson. region 78-50038
$ep\to ep\eta$ at S_{11}(1535) resonance, longit. to transverse cross sections ratio 78-78194
η, η' and η_c, mixing and decays in nonrelativistic quark model for QCD idea 78-82166
$\eta\to2\gamma$, η-problem of meson masses, quark charges, colour model 77-57542
$\eta\to2\gamma$, nonet mixing and gluon effects in current quark framework 79-80799
$\eta\to2\gamma$, study of γ-ray spectrum in $\pi^-p\to\eta n$. 15 to 40 GeV/c 79-58978
$\eta\to3\pi$, nonet mixing and gluon effects in current quark framework 79-80799
$\eta\to3\pi$ chiral symmetry breaking, Dashen mass formula, baryon mass differences 79-289
$\eta\to3\pi$ width, quark pair creation model 77-41841
$\eta\to3\pi^0$, decay rate, up quark masslessness 79-40761
$\eta\to3\pi^\circ$, chiral SU(4)×SU(4) breaking and tadpole term 80-22532
η(549), η'(958) with inert component, gluon bound state 78-74226
$\eta(\eta')\to\gamma\gamma$, quark model tests 80-78067
$\eta\to\gamma e^+e^-$, form factor slope calc., VDM 78-58181
$\eta\to\gamma\gamma$, radiative widths, δ and S* background, SU(3) and VDM anal. 80-419
$\eta\to\gamma\gamma(\pi^+\pi^-\gamma)$, chiral quark model anal. *(Russian)* 80-105900
$\eta\to\gamma\mu^+\mu^-$, vector dominance model *(Russian)* 79-58954
$\eta\to\mu^+\mu^-\gamma$, branching ratio and η EM form factor 80-105899
$\eta\to\mu^+\mu^-\gamma$, mass spectrum 79-9367
$\eta\to\mu^+\mu^-\gamma$, obs. in π^-p collisions at 25 GeV/c *(Russian)* 79-22090
$\eta\to\pi^0\gamma\gamma$, $\pi^+\pi^-\pi^0\gamma$, $\pi^+\pi^-\gamma\gamma$, scalar meson dominance model 78-4860
$\eta\to\pi^0\nu\bar{\nu}$, presence of second class neutral currents 79-26284
$\eta\to\pi^+\pi^-\gamma$, quantum chiral theory, decay width determ. *(Russian)* 78-41544
$\eta\to\pi^+\pi^-\pi^0$, anal. based on u_3-term of $(3,\bar{3})+(\bar{3},3)$ model 77-67657
$\eta\to\pi^+\pi^-\pi^0$, decay width 78-70362
$\eta\to\pi^+\pi^-\pi^0$, on-mass-shell current algebra, SU(3)×SU(3) σ model 77-34151
$\eta\to\pi^\circ\gamma\gamma$ decay rate 77-10270
$\eta\to\pi\pi\gamma$, nonet mixing and gluon effects in current quark framework 79-80799
$\eta\to\pi\pi\gamma$, quark loop model, SU(3) splitting of quark masses 80-62990
$\eta\to\rho\gamma(\gamma\gamma)$, C-even meson radiative decay, SU(3), and VDM anals. *(Russian)* 80-68460
η/π^0 prod. ratio at high transverse momenta 78-41602
η-$c\bar{c}$, η'-$c\bar{c}$ couplings from $\psi\to\eta'\gamma$, $\psi'\to\eta\gamma$ *(Russian)* 77-49962
η-η' complex, quark-line rule in $\pi^+p\to\eta\Delta^{++}$, $\pi^-p\to\eta n$, $p\bar{p}\to\pi^+\pi^-\eta$ 77-30330
η-η' mixing angle and relative radiative decay rates $\Gamma(\psi\to\eta\gamma)/\Gamma(\psi\to\eta'\gamma)$ 80-9173
η^0, backward ω^0 and η^0 prod. in π^-p interactions at 9 and 12 GeV/c 79-45100
$\eta^0\to\gamma+(e^+e^-)$, EM bound states, approx. Bethe-Salpeter wave function *(Chinese)* 80-42448
$\eta^0\to\gamma+(\mu^+\mu^-)$, EM bound states, approx. Bethe-Salpeter wave function *(Chinese)* 80-42448
$\eta^0\to\gamma\gamma(\pi^0\gamma\gamma)(\pi^0\pi^0\pi^0)$, neutral decay channels, possible $3\pi^0$ system *(Russian)* 80-42454
η^0-π^0 mixing effects and $\Delta S=1$ nonleptonic weak decays 80-4991
η_c, candidate evidence from SPEAR, crystal ball detector, recent results 80-74046
η_c, interpretation of X(2.88) obs. in $\pi^-p\to\gamma\gamma n$ 79-22150
η_c, predictions of existence by extrapolation methods 78-93863
η_c, production cross sections in e^+e^- colliding beams, two-photon processes 79-36089
η_c(2.83), instantons and spin forces between massive quarks 78-37173
η_c associated with gluon, hadronic prod. 80-105846
$\eta_c\to\gamma+$anything, OZI rule violating decay in QCD 78-89709
η_c mass determ. from QCD sum rules 78-74223
η_c mass from dispersion sum rules in QCD, identification with X(2.83) *(Russian)* 78-89681
η'(958)$\to\gamma\gamma$, decay rate, axial-vector current divergences 80-9172
$\eta'\to\eta\pi\pi$, current algebra calcs. with symmetry breaking, inconsistency with expt. 79-13114
$\eta'\to\eta\pi\pi$, current algebra techniques, pole plus remainder model, chiral symmetry breaking and QCD 80-62972
$\eta'\to\omega\gamma$, decay rate obs. in $\pi^-p\to\pi^+\pi^-3\gamma n$ 77-74683
$\eta\rightleftharpoons\pi^0$, effects of EM mixing on pn mass difference *(Russian)* 78-74255
$\gamma\to\eta d$, differential cross-section calc. using resonance model 79-93432
$\gamma d\to\eta d$, coherent photoproduction impulse approximation 77-82749
$J/\psi\to\eta_c\gamma$, radiational decays in charmonium *(Russian)* 80-13308
$J/\psi\to\eta(\eta')\gamma$ decay rate, QCD sum rules 80-52497
$K^-p\to\eta\Lambda$, 4.2 GeV/c, total and differential cross sections, forward production peaks 79-40801
$K^-p\to\Lambda\eta$, 6 GeV/c, baryon exchange reactions, ηNN coupling constant, Λ polarisation, nucleon-Regge exchange 80-78098
$\nu\to3\Pi$, broken nonlinear chiral SU(3)×SU(3) dynamics *(Russian)* 77-65117
$P\to\gamma l^+l^-$, EM characts. for pseudoscalar meson decay in nonlocal quark model *(Russian)* 80-102050
pp, 400 GeV/c, inclusive and semiinclusive prod. of π^0, $K_s{}^0$, Λ^0, $\bar{\Lambda}^0$, Σ^0, $\bar{\Sigma}^0$, η^0, ω^0 79-93472
$\bar{p}p$ annihilation, low energy, prompt e^+e^-, ω^0 and η^0 prod., inclusive prod. rates 80-42506
$pp\to\eta X$, inclusive η prod. at high p_T at the ISR, η/π^0 cross section ratio 79-71770
pp inclusive interaction, 30 to 50 GeV η meson prod. 80-5023
$\bar{p}p$ inclusive prod. of π^-,η,ρ^0,ω,f, mesons at 0.7 GeV/c 77-65170
$\bar{p}p\to\pi^0\eta^0$, 1.1-2.0 GeV/c, differential cross sections in T and U meson region 79-9393

eta mesons continued
πN scatt., isospin violation from π^0-η mixing, partial wave anal., N*(1540) struct. 80-27426
π^-p, 100 GeV/c, π^0 and η inclusive prod. in all neutral mode 79-13165
π^-p elastic scatt. near η threshold, cusp discontinuity, nonspin-flip elastic amplitude 80-22635
$\pi^-p\to\eta^0n$, 3.3 GeV/c, differential cross section, helicity-flip amplitude *(Russian)* 78-45945
$\pi^-p\to\eta^0\pi^+\pi^-n$, D, E, and δ mesons obs. at 12 and 15 GeV/c 79-3052
$\pi^-p\to\eta^\circ\pi^+\pi^-n$, D, E, and δ mesons, obs. at 12 and 15 GeV/c 79-9410
$\pi^-p\to\eta X$, pseudoscalar meson prod. in triple Regge region, absorpt. corrections 78-78228
$\pi^-p\to\eta'n$, cross-section over momentum range 15 to 40 GeV/c *(Russian)* 79-89194
$\pi^-p\to\eta'n$, Regge pole model with phenomenological residue functions 80-102077
$\pi^-p\to\eta(\eta')n$, 8.45 GeV/c, differential cross section ratio, η' decay branching 80-78094
$\pi^-p\to\eta\eta n$, 40 GeV/c, production cross sections and $\eta\eta$ angular distribs. *(Russian)* 78-78223
$\pi^-p\to\eta n$, 1171 to 2267 MeV/c polarised cross section meas., partial wave anal. in resonance region 79-89182
$\pi^-p\to\eta n$, 15-40 GeV/c, cross sections and spin-flip amplitudes *(Russian)* 79-67609
$\pi^-p\to\eta\pi^+\pi^-n$, axial vector and pseudoscalar resonances near 1.275 GeV, D mesons 79-30747
$\pi^-p\to n\epsilon^0$, 1.3 to 3.8 GeV/c, differential and total cross-sections 80-83000
$\pi^-p\to\pi^0(\eta)+$anything, absorptive corrections using Regge pole amplitude 77-38204
π^+p, 32 GeV/c, π and ρ^0 inclusive prod., f and η cross section estimates *(Russian)* 80-68499
$\pi^\pm p$, 100 GeV/c, π^0 and η inclusive prod. in triple Regge region 79-13164
$\pi^\pm p$ 100 GeV/c, π^0 and η inclusive prod., triple Regge theory test 79-6349
$\psi\to3\gamma$, heavy narrow state search, η' and η_c branching ratios 80-57600
$\psi\to\eta(\eta')\gamma$, SU_3 violation, symmetry breaking and decay amplitudes 80-52499
$\psi\to\eta(\eta')\gamma$, Ward identity anal., η,η' quark-glue struct. 80-42449
$\psi\to\eta\gamma$, conflict with single parameter scheme for radiative decays of vector mesons 80-86720
$\psi\to\eta\gamma$, radiative decays, vector dominance model 79-26330
$\psi'\to\psi+\eta$, two gluon mechanism, Υ dynamics test 78-89665
$\psi'\to\psi\eta$, Ward identity anal., η,η' quark-glue struct. 80-42449
$\psi'\to\psi\pi^0(\eta)$, SU_2 violation, symmetry breaking and decay amplitudes 80-52499
$\psi'\to\psi\eta$, OZI rule violating transition, unitary corrections using dual model 79-26330
$\Upsilon\to\eta\gamma$ or $\eta'\gamma$, other hadronic and two body charmed and strange modes 78-78175
$\Upsilon'\to\Upsilon+\eta$, two gluon mechanism, Υ dynamics test 78-89665
$X^0(958)\to\eta\pi\pi$, ηX^0 mixing angle, broken SU(6)×O(3) quark model 79-17721
$\eta\to\pi^0e^+e^-$, presence of second class neutral currents 79-26284
$\gamma N\to\eta X$, 9.7 GeV, inclusive η photoprod. on H- and ^{2}H-targets, ρ^0-dominance model anal. 79-63486
^{6}Li$(\gamma,\eta)^6$Li, $E_\gamma=3.56$ MeV, partial photoproduction cross-section calc. *(Russian)* 79-9547
$\pi^-p\to\eta n$, 724-2723 MeV/c, differential cross sections, baryon resonance non-zero couplings 79-71761
$\pi^-p\to\eta n$, Fermilab energy, Regge pole model 79-17762
Xe$+\pi^-$, 3.2 GeV/c, π^0, η, ω, f meson prod. determ. of meson-N total cross sections *(Russian)* 79-22122
Xe$+\pi^-$ 3.2 GeV/c, intermediate Δ^- prod. in π^0 and η prod. *(Russian)* 79-36280

etalons *see interferometers*

etchants *see etching*

etching
see also crystal defects; dislocation etching; sputter etching
ABS-2 plastic, etching rate rel. to electroless Cu adhesion *(Russian)* 78-35542
active abrasive conc. determ. by static method based on etch figure stars count 80-74544
alpha particle revelation characteristics, and heating of cellulose nitrate plastics 79-49910
anisotropic track etching in olivine crystals using WN solution 79-26836
apatite, mean etchable fission track length, high fission track densities determ. 77-82041
bimetallic welded joints, heterogeneous, metallographic anal., etcharts and etching regimes 80-40635
biological specimens, new freeze-etch unit 79-5423
blazed ion-etched holographic grating prod., high spectroscopic qualities 79-76847
boride coatings, method of revealing structural components 80-21228
borosilicate glass, phase separation effect on HF etch rate 78-11208
borosilicate glass, surface struct. rel. to HF etching and stressed state 79-100276
brass, sphere, dissolution in H_2SO_4 in elec. field *(Russian)* 77-4867
brass, surface microstruct. changes on immersion in $CuSO_4+H_2SO_4+HI$ soln. 78-19945
bronzes, ancient, chem. polishing and etching for metallographic exam. 78-356
capacitance meas. for etching power determ. 77-44377
cellulose acetate, bulk and track etch rate studies 79-31338
cellulose nitrate, effect of high γ-doses on etching characts., dosimetry appl. 79-31224
cellulose nitrate, etching behaviour, nuclear track detector 78-17485
cellulose nitrate, nuclear track detectors, etch induction time, particle identification parameter 78-17486
cellulose nitrate, proton, $H_2{}^+$ mol. ion, and heavy ion irrad., track prod., etching obs. 78-86757
cellulose nitrate (CN) detectors, effect of pre-irrad. thermal treatment on track revealing props. 78-94168
cellulose nitrate CA8015, calibration for fast neutron dosimetry 79-49907
cellulose nitrate LR115, neutron personnel dosimetry at high energy accelerators 78-20284
cellulose nitrate track detectors, bulk etch rate studies 79-36482

etching continued
- cellulose nitrate track detectors, CA80-15 and LR-115, etch pits due to Rn and Tn alpha particles 78—855
- cellulose nitrate track detectors, direct dosimetry in π^- beams 78—20281
- ceramics, archaeological, dating by alpha-recoil tracks in mica 78—70237
- charged particle tracks in isotropic detectors, kinetics 77—79512
- CMOS ICs electrically active stacking faults, anomalous leakage currents 79—78191
- Cr plates, for photomasks, prep. by vacuum deposition, etching ability *(Russian)* 79—33203
- CR-39 plastic, electrochem. etching, optimum conditions 80—95505
- CR-39 polymeric nuclear track detector, props. and appls. 78—94170
- CR-39 thermoset plastic nuclear track recorder, etching in hot NaOH 78—74535
- DH, stripe geometry injection lasers, monolithic passivated, fabrication by selective chemical etching 77—10925
- diacel plastic track detector, track diameter meas. of alpha particles, etching 79—49911
- diamond:Sb, implanted, radiation damage and annealing study 80—100263
- diamond, natural octahedron, etching at high temp. and pressure 80—39097
- diamond, synthetic, oxidized in fused salts, etch features 80—97604
- diamond, synthetic, topographic structures and origin *(German)* 77—85036
- diamond crystals, synthetic, etch-pit formation on cube faces, electron microscopy obs. 80—75232
- dielectric film, optical monitoring of etching 79—52412
- diffraction gratings, photoresist and GaAs, exposure and etching time optimalisation 80—23816
- diffused Si pressure transducer, stress conc. at transverse gauges 78—12711
- N,N-dimethyl-p-nitrosoaniline, coherent anti-Stokes Raman spectra, negative peak intensities 77—72805
- dry etched inorganic resist. for lithographic appl. 79—24633
- dry etched line edge profiles, computer simulation 80—71780
- edge etch process for minimum geometry windows on poly Si surface 78—31550
- electrochemical, comparison of fast neutron induced tracks in plastics 80—23154
- electrochemical, effect of AC component on capacitance of Al foil, electrolytic capacitors appl. *(Polish)* 80—35420
- electrochemical, with rotating cathode, residual stress meas. in ring-shaped specimens 77—25212
- electrochemical etching, of neutron-induced tracks in plastic detectors using HV 50 Hz supply 78—86738
- electrochemical etching of fast neutron induced recoil tracks in cellulose triacetate 80—91406
- electrochemical etching of particle tracks in plastic foils, HV AC power supply 77—10541
- electrochemical etching studies of the CR-39 plastic solid state nuclear track detectors 80—91391
- electrochemical track etching in plastic foils, for charged particle detect. 78—17521
- electrode, interpretation of selective etching, electrochem. props 80—7703
- electrolytic capacitors effect of electrical parameters of Al foil capacitors *(Polish)* 80—30245
- electrolytic deep etching 78—31604
- electron microscopy on etched thin foils, comparative SEM, STEM and TEM analysis 80—100144
- ethylene-tetrafluoroethylene copolymer, chem. etching of fission tracks 80—896
- fatty acid film, $(CH_3(CH_2)_nCOOH)$, etching in glow discharge 77—16506
- feldspar, crystalline track detector, etching characts. anisotropy 77—46465
- ferrites, Mn-Zn, machining effect obs., on magnetisation curves *(Japanese)* 77—21295
- ferrogarnet crystal, surface layer damage thickness meas. 79—5106
- ferrographite, sintered, porous, electrolytic prep. 79—52530
- fibre tip lens fabrication and smoothing 78—33923
- fibre-optic power divider, single-mode, fabrication using encapsulated etching technique 79—50433
- field ion (emission) microscope tip prep. from sheet and block metal 78—7155
- films, preparation using low pressure plasmas 77—40361
- fission fragment track registration in crysts., development efficiencies, etchant (etching conditions) depend. 78—66454
- fluorene, γ-irrad., void form. 80—2068
- fluorocarbon glow discharges, plasma polymerising and etching, mass spectrometric obs. 77—32790
- freeze-etch device, for electron microscope laboratories 78—8474
- freeze-etching improvement using evaporated film 80—85558
- freeze-etching results interpretation 78—28141
- geodesic optical lens prod. by anisotropic etching 80—10047
- glass, chemically strengthened, stress profile determ. using scatt. light 80—30186
- glass, diffusion profiles analysis, grinding and etching techniques comparison 78—26732
- glass, etching rate temp. and conc. depend. 77—10533
- glass, surface treatment, improvement in mech. and optical props. recent progress *(Japanese)* 79—79141
- glass fibre, elastic moduli, thermal history depend. *(Japanese)* 80—45333
- glass hardening, etching in hydrofluoric acid effect by low temp. ion exchange 77—44373
- glass shell, built-up, local strengthening influence on supporting capacity 80—71714
- glass track detectors, effects of pre-irradiation and conditions on etching 80—37702
- glasses, effect of temp. on etching appl. to particle track visualisation 79—76290
- glassy passivation films on Si substrates, appl. of silicates to flaw detection 77—39745
- graphite composites containing refractory carbides, electrochem. etching for microscope section preparation 77—28949
- Hastelloy-X, Ni-Cr-Fe-Mo, cyclic oxidation resist. improvement by high temp. etching treatment 80—97627
- hexafluoroethane, RF discharge chem., added acetylene effect, mechanistic model for fluorocarbon plasmas 80—84017

etching continued
- hologram recording on semiconductor, photochem. etching control 80—28179
- holographic grating, fine, made of positive photoresist AZ2400, anal. of two-dimensional etching effect on profile 78—82928
- holographic pattern etching into Si wafer 77—34840
- horizontally dipped LPE film, inhomogeneities, spin wave reson. meas. 79—91298
- hydrothermal etching method 80—50790
- III-V semiconductor, surface microhardness depend. on surface treatment method 78—15560
- Inco 718, fatigued specimens, plastic zone size 77—25150
- Inconel 625, organic contamination removal by plasma cleaning and etching 80—97645
- Inconel X-750 foil, surface pretreatment for improved coating adherence 79—15877
- n-InSb, surface recomb. vel., repeated cyclic surface treatment effects 77—32065
- insulating film for semicond. devices, props., rel. to deposition conditions 78—23612
- intaglio imaging with nuclear particles 78—65993
- ion, effect on surface features, theoretical, experiments study *(Japanese)* 77—32483
- ion beam utilisation for etching and film deposition, review 77—32522
- ion etching, technological appls. of ion-induced sputtering, review 77—44107
- ion milling, string segment motion algorithm 80—71779
- ion milling (ion beam etching), bibliography for 1975-1978 period 80—4
- ion optic precision magnet homogenising surface coils 79—41329
- ion-beam, by oblique incidence pattern fabrication *(Japanese)* 79—74271
- ion-beam, reactive, appl. for microstructure fabrication, review 79—15844
- ionic cleaning, plasma accelerator with closed drift of electrons for ion beam formation *(Russian)* 79—38993
- Josephson junction fabrication by ion implantation, electron beam lithography and dry etching 80—88693
- junction laser diffusion and rooftop etching technique 80—1227
- kink nucleation and propagation along steps of finite length, modelling 77—31669
- laser induced gas etching technique 77—63815
- lavsan film, Ar ion-bombarded, KOH etching for micropore filters preparation 78—3305
- leucosapphire, Cr influence as impurity on thermochem. etching 80—88190
- Lexan, bulk and track etch rate studies 79—31338
- Lexan polycarbonate, thermolum. radiation-induced EPR of free radicals and track etchability 79—76295
- Lexan polycarbonate track detectors, direct dosimetry in π^- beams 78—20281
- lithography, heavy ion, tool for object investigation and replication 80—90931
- low-pressure plasma applications to surface treatment 79—94824
- LR-115 plastic track detector, etching behaviour 80—99423
- lunar crystals, etchable ranges of heavy-ion tracks 77—30734
- lunar fines, etching by adsorbed water effect of annealing temp. 77—60632
- macroscopic examination procedures for failure analysis 79—66254
- macroscopic metal catalysts, morphology and etching processes, review 80—7856
- magnetic bubble memory device prod., ion beam etching 79—78487
- Makrofol, neutron personnel dosimetry at high energy accelerators 78—20284
- Makrofol KG in KOH solution, bulk etching rate, light ion tracks 77—67942
- Makrofol polycarbonate, electrochemical etching of neutron induced tracks, appl. to dosimetry 78—20282
- metal, high melting point, electrolytic polishing and etching to reveal struct. *(German, English)* 80—89417
- metal, ion beam texturing 77—44402
- metal, laser-photoinduced etching, photodissociation of dissolved complexed halogens in soln. 80—100929
- metal, surface layer dissolution, effect of rate on softening during plastic strain 78—39957
- metal film, galvanic effects in wet-chemical etching of metal films 80—25915
- metal film, optical etching, diffr. grating effects 77—19263
- metal foil photoetching profile, quantitative obs. 78—39943
- metal sheet for manufacture of scales and grids, one-sided etching 79—32102
- metal spheres, electromechanical polishing and etching 80—68188
- metal surface, plasma cleaning and etching, removal of C 80—97645
- metal surface free energy for BCC, FCC and HCP structs. etch pit depend. 80—29258
- metal-containing plasma polymerised fluorocarbon films, deposition, struct., and polymerisation mechanism 79—78928
- metallographic sections, in situ, cathodic device 79—39067
- metallography, quantitative methodology *(French)* 80—30205
- meteoritic crystals, etchable ranges of heavy-ion tracks 77—30734
- methylamine, aq., effect on polyethylene terephthalate, chem. stress cracking 79—57131
- mica, bulk and track etch rate studies 79—31338
- microcapillary system, staged, tortuous, for haemodialysis and ultrafiltration 77—37107
- microfabrication by ion-beam etching 79—78807
- MIS solar cells, etched slotted mask for direct deposition of metal contact pattern 80—97786
- MNOS device, high temperature annealing, effect on Si_3N_4 stress, interface charge density and memory props. 79—87158
- multi-detector electrochemical etching and automatic scanning system 79—26837
- muscovite, fission track etching and annealing anal., dating appl. 78—32036
- muscovite mica, crystalline track detector, etching characts. anisotropy 77—46465
- narrow double-current-confinement channelled-substrate-planar laser fabrication by double etching 80—64073
- natural quartz SSNTD, etching characts. 80—91401
- neutron fluence meas. using fission foils of ^{235}U, ^{238}U, ^{237}Np used for neutron fluence meas. 78—13177
- nuclear filters, prep. from polymers using Ar ions 78—86714

etching continued
nuclear tracks, etched, statistical distrib. of quadratic holes on planar surface, computer simulation 80—37705
nuclear tracks, solids, formation model, etch pit parameters for light nuclei 78—13390
Oberhoffer etch, suitability for identifying surface defects 79—43525
olivine from Marjalahti meteorite, cosmic ray tracks 78—36414
optical components, polishing defects obs. by etching 77—75724
optical fibre refractive index dip removal by etching method 79—14120
optical fibre-photodiode alignment by etched Si structure 80—53430
optical glass ceramic, (sital) surface operation parameters, selection using bending strength tests 79—32101
optical reticle and scale fabrication, cyclohexadiene-1,3 pleinomer photoresist 79—27452
orthodontic adhesive joints, adherend topography effects 77—52916
oxide films, anodically and thermally grown, XPS study 80—16141
p-n junction, method for determining dopant and defect distribs. in diffusion layer 79—37727
particle track detectors, electron microscopy of etch pits 80—99424
Permalloy, conductor crossing effect on bubble propagation margins 80—29588
Permalloy narrow stripes, permeability 77—89987
Permalloy sputtered film, bevelling by chemical etching, for this film mag. header 78—92375
phlogopite, fission track etching and annealing, chronological application 79—84230
phosphosilicate films, deposited, P conc. meas. 79—69014
phosphosilicate glass, CVD, P conc. meas. 77—80533
photofabricated profile quantitative exam., etch factor meas. 79—61779
photographic emulsion grains, latent image distrib., etching and recrystn. effects of solns. 80—77890
phthalic anhydride spherulites, cryst. growth from melt 79—32930
planar optical waveguide interconnection method 80—58671
plasma chemistry, appl. to IC fabrication 79—79252
plasma etched SAW resonator ageing effects 77—39148
plasma etching, electron or ion bombardment, Ar^{+} enhancement 79—82073
plasma etching, mech., review 79—83348
plasma etching, problems with creating vacuum *(French)* 80—101803
plasma etching and plasma deposition, glow discharge phenomena 79—69993
plasma etching characts., effect of dark space in RF glow discharge 79—15830
plasma etching control using optical reflection methods 79—57127
plasma etching during NMOS VLSI circuits manufacture process and problems *(Norwegian)* 80—60090
plasma etching techniques in semiconductor manufacture 79—20238
plasma industrial utilisation, synthesis, powder, metallurgical and surface treatments, review *(French)* 80—96398
plasma reactor for materials research good processing 77—40362
plasmachemical reactors for surface layer removal, regime parameters *(Russian)* 80—54050
plastic, etching rate temp. and conc. depend. 77—10533
plastic detectors, isotope resolution 77—79511
plastic foils for neutron dosimeters, electrochem. etching prep. techniques 79—76298
plastic track detectors, processing 77—38560
poly(4-methylpentene-1), isotactic, permanganic etchant for TEM obs. 80—21132
polycarbonate film, fission track etching characts., UV and ageing effects 79—76296
polycarbonate foil electrochemical etching for dosimetry, bulk etching rate evaluation 78—78506
polycarbonate foils, detection of low energy ^{4}He, ^{12}C, ^{14}N, ^{16}O ions, etching props. 78—13391
polycarbonate track detector, electrochemically etched, meas. of low neutron fluences 80—32577
polyethylene, linear, bulk-crystallised, morphology study 79—32918
polyethylene, permanganic etchant for TEM obs. 80—21132
polyethylene terephthalate, irradiated with radiations with linear energy losses, peculiarities in chemical etching 78—39934
polyethylene terephthalate, selective chem. etching using primary amines 79—57130
polyethylene terephthalate fibres, chem. stress cracking after exposure to aq. methylamine 79—57131
polyethylene-terephthalate track detector, electrochemically etched, meas. of low neutron fluences 80—32577
polymer film, plasma etching and cleaning 80—1855
polymer multicomponent systems, selective electron beam etching 78—45603
polymeric detector particle track diameter rel. to etching time *(French)* 80—9463
polymers, for electron microscopy, plasma etching combined replica technique *(Russian)* 79—32923
polypropylene, fracture exam. using microscopic obs. *(German, English)* 79—20186
polypropylene, permanganic etchant for TEM obs. 80—21132
polysiloxane homopolymers and random-block copolymers, surface degradation, with HF soln. 78—15554
polysiloxane plasma polymerised film growth on GaAs substrate, dry etching process 80—25575
polystyrene, high impact, etching in CrO_3-H_2SO_4 soln. *(Russian)* 80—81223
polyurethane:rhodamine 6G film, laser, etched cavity 77—7140
polyvinylidene fluoride, chem. etching of fission tracks, growth of fine holes, TEM, SEM study 79—76297
positive resist, plasma etching durability, additive effects 80—66683
PVC-chlorinated polyethylene blend, optical characterisation methods 79—8408
quartz, dissolution of grown synthetic quartz inside the autoclaves 78—63911
quartz, etch features for determ. of quartz grain source 77—70650
quartz, natural crystals, fission fragment track development anisotropy 77—1149
quartz, synthetic, as-grown and etched cobbled Z-surfaces, SEM obs. *(French)* 80—24719
quartz, synthetic, line defects, etch tunnels and X-ray topography 77—76406
quartz, theory of etchihg in HF 78—27666
quartz, track retaining props. for high temp. in-core neutron fluence meas. 77—75032

etching continued
quartz inclusion morphology for thermolum. dating, effect of HF etching 78—70240
quartz SAW resonator deep etching 78—59248
α-quartz seed plate fracture strength, etching and annealing effects 77—36661
quartz surface, chemical polishing by etching 78—60858
rare earth garnets, preparation, substrate and epitaxial layer surface quality control, X-ray topography *(German)* 77—55432
reactive ion etching, reactant supply 79—83349
redeposition, problem in RF sputter etching of structures of micron dimensions 77—44388
residual stress measurement using holographic interferometry and etching 77—52577
ruby, Cr influence as impurity on thermochem. etching 80—88190
sapphire, etching of arrays of orifices using Pt-Cr composite layer mask 80—3216
sapphire substrates, prep. for GaN epitaxy 78—39929
SAW deeply-etched resonators, long-term aging improvement 79—55290
semiconductor, anodic etching, physicochemical parameters for maximum resolution 79—74276
semiconductor, laser-photoinduced etching, photodissociation of dissolved complexed halogens in soln. 80—100929
semiconductor, photochemical etching mechanism 77—16709
semiconductor, photosensitive etching in nonoxidising etchants 80—78813
semiconductor, RF etch sputtering under controlled atmosphere 77—44397
semiconductor etching method using Au pellets, Si solid-state detector manufacture 77—28917
semiconductor films, production of oblique cuts 80—104309
semiconductor IC production, plasma CVD equipment for insulating films 80—25572
semiconductor photosensitive etching for hologram recording, attainable spatial freqs. 80—69343
semiconductor structures and devices, plasma etching methods *(Slovak)* 80—40564
semiconductor thin sample etching for electron microscope exam. 80—86272
shadow mask etching for ion implantation 78—6086
p-Si, anodic etching for discriminating between elec. active and inactive defects 80—108605
single surface electrochemical etching of charged particle tracks, simple set-up 79—76283
single-mode fibre optical power divider, encapsulated etching technique 79—27420
sintered materials, porous, electrolytic preparation 79—52530
Sitalls, soln. rate in alkali soln. 80—16531
soda lime glass track registration, HF etching conditions effect 80—52815
soda-lime and reactor waste glasses, reaction with water, determ. of diffusion controlled hydration and surface etching 79—54519
soda-lime glass track detector etching in NH_4HF_2, NaOH and KOH aq. solns. 79—26816
solar cell, fabrication process, Si single cryst. cells 79—61977
solid state nuclear track detectors, development of etched nuclear tracks 80—91384
solid state nuclear track detectors, effect of etching conditions on energy resolution of phosphate glass and polycarbonate detectors 80—91390
solid state nuclear track detectors, past and future uses 78—17484
solid state nuclear track detectors, review 80—37696
solid state nuclear track detectors, track registration and development efficiency 80—91385
solid state nuclear track detectors, track registration and development efficiency 80—91386
solid state nuclear track detectors, visualization of latent damage trails etching, decoration and observation techniques, review 80—91382
spherical end faced coupling fibre fabrication by selective etching/melting 80—53492
spray-freezing unit for prep. of specimens for freeze-etching 77—41581
stainless steel, photoetching, props. of liq. photoresists 78—39942
steel, alloy, V-W-Mo-Cr, exam. of carbide transformation 80—16299
steel, austenitic stainless, cast struct., determination of origin using etching techniques 78—39985
steel, austenitic stainless, phosphide analysis using nonaqueous electrolyte potentiostatic etching method *(Japanese)* 80—89221
steel, austenitic stainless, precipitates and grain orientation by non aqueous electrolyte potentiostatic etching method *(Japanese)* 80—15102
steel, C, explosively fractured, struct. of white etching band 79—61722
steel, C, hot plastic deform., vac. colour etching investigation 80—61036
steel, C, phosphide analysis using nonaqueous electrolyte potentiostatic etching method *(Japanese)* 80—89221
steel, carbonitrided, case struct. investigation by warm electrolytic etching 80—35414
steel, Cr, cold roll, frictional heating surface damage 80—76289
steel, Cr, ferritic, oxide scale etching 79—70204
steel, Cr-Mo-V type X 41 CrMoV 5 1, austenized, carbide detection by etching *(German, English)* 79—91884
steel, Cr-Ni-Al, intergranular crack investigation by etching *(Chinese)* 79—43457
steel, CrNi, etchability of austenite *(German, English)* 80—11860
steel, dual phase, improved etching technique for percent martensite determ. 80—16624
steel, etchant for revealing austenite grain boundaries 80—85098
steel, ferritic stainless, phosphide analysis using nonaqueous electrolyte potentiostatic etching method *(Japanese)* 80—89221
steel, fracture obs., shell-shaped fracture 77—25153
steel, high alloy, potentiostatic development of structures 78—95887
steel, high speed, tempered, etching reagents for austenite grain boundaries 78—80704
steel, high strength dual phase, martensite/bainite differentation using improved etching technique 80—100951
steel, high-speed, eutectic carbide structure, determ. by SEM 78—85075
steel, low alloy, exam. of microstructure, in type PZhK-1000 soldered joint by metallography 79—52257
steel, low C, cold rolled sheet, Cu effect on recrystallization texture *(Chinese)* 79—74173
steel, low-C-Si, LS1.2, LS1.5, phase transformation 80—45302
steel, martensitic, dendritic structure assessment with Elypovist electropolisher 77—52565

etching continued
- steel, martensitic-ageing, etching technique, for revealing struct. inhomogeneities 80—61035
- steel, medium C, internal cracks in continuous casting billet and rolling products *(Chinese)* 79—43375
- steel, mild, etching method for revealing plastic deformation 78—72825
- steel, mild, photoetched profiles 80—25907
- steel, Nb microalloyed dual phase, etching technique 80—71809
- steel, sphere, dissolution in H_2SO_4 in elec. field *(Russian)* 77—4867
- steel, stainless, Cr-Ni-Ti, metallographic detection of $(Ti,Ni)_6C$ 80—66721
- steel, stainless, determ. of fracture surface orientation, due to stress corrosion cracking *(Japanese)* 78—53025
- steel, stainless, ferritic Ti stabilised, changes in structure and mech. props., after alkali bath etching *(Russian)* 79—29271
- steel, stainless, gas liberation in vac., effect of different methods of surface treatment *(Russian)* 80—45429
- steel, stainless, intercrystallite corrosion, testing using potentiostatic etching method 78—7113
- steel, stainless, martensitic new etchant to reveal prior austenite grain boundaries 78—3290
- steel, stainless, martensitically ageing, techniques for revealing microstruct. characts. 79—70241
- steel, stainless, metallographic technique for detection of ferromagnetic δ-ferrite to paramagnetic σ-phase 79—61816
- steel, stainless, O_2 desorpt. during laser irrad., etching, AES study 80—66338
- steel, stainless, photoetched profiles, quantitative examination 79—20268
- steel, stainless, surface cleaning by H^+ bombard., AES study 78—53022
- steel, stainless, type photomachining 410, diffused H_2 during etching, lack of evidence for H_2 effect 79—74246
- steel, surface state influence on etching effect 80—81235
- steel, thermal etching displaying hardening structure 77—40487
- steel, tool, low alloy, methods of revealing austenitic grain 80—25949
- steel, tool, martensitic hardened, reagent for revealing austenitic grain size 80—21207
- steel, W-Mo, types R6M5 and R6M5K5, decarburising layer evaluation 80—21164
- steel, X5CrNiTi26.6, ferrite-austenitic struct., optical and electron microscopy 78—84848
- steel cladding, B distrib., particle track etch technique 77—57719
- steel medium C, type 45, electroerosion, white-layer structures detection method 79—52485
- steel mild, etching of plastic zones 77—60013
- steel sheet, surface anal. by ion etching and atomic absorpt. spectroscopy *(German)* 80—81377
- steels, C and stainless, fatigue crack propag. and crystallographic orientation *(Japanese)* 78—7027
- steels, high-purity and commercially based, containing 10 wt.%W or 5 wt.%Mo, tempering behaviour 80—7600
- steels, obs. and anal. of sulphides, using non-aqueous electrolyte-potentiostatic etching method *(Japanese)* 80—89433
- steels, stainless, surface characterisation rel. to adhesive bonding chem. etching, SEM, AES, XPS and electron probe microanal. 80—88416
- surface relief gratings, 3200 Å period fabrication, effect on film growth 78—84089
- technique for revealing plastic zone in Al 78—72955
- TEM specimen preparation by chemical etching 77—52589
- TEM specimen preparation using photochem. etching *(German, English)* 77—56202
- thin film deposition process, line-edge profile simulation appl. 80—104068
- thin foils from multilayer heterostructures, prep. and ion etching 79—12779
- tourmaline, fission track etching and annealing, thermal retention 77—82042
- track etch detectors, neutron energy depend. and threshold energy 80—61703
- track etch imaging, model of directional effects 77—18739
- transition metal silicides, refractory for ICs, review 80—100820
- triglycine sulphate, deuterated, reticulated target for pyroelectric vidicon, IR imaging 80—77858
- triode plasma etching 79—47789
- Udimet 700, microstruct. of resolidified zones formed by laser melting single crysts. 79—78953
- uniform depth profiling, in XPS, using saddle field ion source 78—48708
- Vacuum Society conf., San Francisco, USA (Nov. 1978) 79—77862
- vacuum technique problems, with modern semiconductor processes *(German)* 80—86330
- wear study, analytical surface tool, review 78—64718
- weld, specimen prep. for TEM obs. 77—60029
- wire, device for uniform electrolytic removal of surface layers for residual stress determ. 78—60918
- wire, rolled, vibr. etching, parameters, vibr. freq. meter 79—14356
- Zircaloy-2, hot-pressed, influence of diffused C on structure and oxidation 80—61016
- zircon, improved etching techniques for fission track dating 77—29457
- Ag epitaxial growth, on W-ribbon substrate, in UHV, cryst. orientation determ. by etching *(German)* 79—65994
- Ag, etching by graphite suspension method in 0.5 H_2SO_4 soln. *(Japanese)* 80—35406
- Ag, injection of vacancies by electrochem. etching at high temp. *(German)* 80—49219
- Ag-Cu (6.2 at.%), with discontinuous precipitates, quantitative struct. anal. using SEM 79—43527
- AgBr microcrystals, Herschel effect, $Na_2S_2O_3$ etching soln. effects *(Russian)* 79—5167
- AgCl, ionic space charge and dissolution 80—107431
- Ag_3Sn, containing Au, etching technique for alloys and amalgams 78—3291
- (Al,Ga)As DH wafer, Al distrib. meas. 77—7994
- Al alloy, 2024-T3, adherend surface, chem. comp., effects of chem. and thermal treatments 78—39939
- Al and Al alloy anodised oxide films, for adhesive bonding appls., AES and SEM study 80—66689
- Al and its alloys, reactive ion etching, preferential lateral chemical etching 79—83371
- Al, etched, electronic props. of surface *(Russian)* 78—15569
- Al etching surfactant evaluation 77—77646
- Al film, and native oxide film, etching in carbon tetrachloride plasmas 80—76407

etching continued
- Al foils, etching wastes appl. to corundum ceramics prod. 80—108376
- Al lithographic sheet, AC etching 80—35547
- Al, negative corona 80—40593
- Al plasma etching, undercutting phenomena 80—97635
- Al, reactive ion etching by discharge impedance monitoring, end-point determ. 79—83372
- Al solid electrolytic capacitors, pit etching method for improving freq. and temp. characts. 80—100944
- Al surface, plasma cleaning and etching, removal of C 80—97645
- Al, surface energy and adhesion props. 80—10774
- Al, transfer etch control in chemical polishing 80—16599
- Al-Al_3Ni two-phase matrix, Al electrolytic etching in $AlCl_3$ molten salts 78—3280
- Al-Cu (0.5 to 4.6 wt.%), cathode foil for electrolytic capacitors, relationship between comp., struct., and etchability 79—74314
- Al-Mg alloys, overheating effects on microstruct. and props. 77—63698
- Al-Pd eutectic, microstruct. morphology 80—3018
- Al-poly-Si Schottky-barrier solar cells, grain boundary effects on electrical behaviour 80—85279
- Al-Ti, solid soln., unidirectionally solidified, segregation patterns revealed by etching 79—47693
- Al-Zn-Mg/Al-Mg filler welds, weld fusion boundary structure 80—39459
- AlCu, electron microscope spot prep. of deform. bands 79—15922
- (AlGa)As DH lasers, comparison of 'normal' lasers and lasers exhibiting light jumps 80—106519
- $Al_xGa_{1-x}As$, solid soln., controlled electrochemical and selective etching, integrated optics appl. 77—14814
- $Al_xGa_{1-x}As$-GaAs, DH integrated optics development 80—33240
- AlN-Si_3N_4 CVD film preparation and props. 77—77408
- Al_2O_3, cutting tools, effect of acid etching on cutting performance 79—96169
- Al_2O_3 single crystals, soln. in M_2O-V_2O_5 (M=Li, Na, K) and $NaVO_3$-KVO_3 melts 80—20910
- α-Al_2O_3, thermal etching *(German, English)* 78—60934
- β-Al_2O_3-Na_2O, thermal etching *(German, English)* 78—60934
- Al_2O_3-TiC sinter products, grain size meas. by combination etching process 79—74334
- $Al_2(SO_4)_3$-$K_2SO_4.2PH_2O$, rel. between etch pits or growth hillocks and dislocations on (111) faces 79—77602
- As_2S_3 chalcogenide film surface relief hologram selective etching *(Russian)* 79—94181
- As_2S_3 chalcogenide glass films, photographic Ag photodoping to produce negative relief image 80—59490
- As_2S_3 film, diffr. efficiency of continuously etched gratings 78—38019
- As_2S_3 film, effect of light exposure and heat cycling 78—94417
- As_2S_3 film, vacuum deposited, selective etching characts. obs. *(Russian)* 80—3207
- As_2S_3, inorganic resist, optical monitoring of etching 79—52412
- As_2Se_3 chalcogenide film surface relief hologram selective etching *(Russian)* 79—94181
- As_3Se_2 chalcogenide film surface relief hologram selective etching *(Russian)* 79—94181
- $AsSe_{1.5}Bi_{0.05}$ glasses, soln. rate in alkali solns. 80—16531
- Au, ^{18}F recoil ranges by irradiation of O_2 with ^3He and ^4He particles 80—71931
- Au, electroplate, delineation of hard from soft by etching 78—3292
- Au film on Cr adhesion layer, etching, SEM anal. of abnormal undercutting 79—5075
- Au thin films, with nm-sized pores, prep. from Au-Ge eutectic films by etching 80—16227
- Au-CdS junction diodes, chemically etched CdS cryst. surfaces effect on barrier layer 80—44722
- Au-GaAs, film-substrate interface alloying behaviour, electron microscopic study 79—60652
- Au-GaAs Schottky barrier solar cells, effect of interfacial oxide layer on cell characts. 80—61365
- Au-Si Schottky contact elec. props. rel. to AES 77—85322
- BP, by HCl gas, temp. and HCl conc. effects 77—86205
- $BaAl_{12}O_{19}$, Czochralski cryst. growth, quality examination by polarisation microscopy, etching and X-ray topography 79—24428
- BaF_2 crystal, selective etching and dissolution kinetics 80—71775
- BaF_2, formation and growth of oxidation centres result of O^{2-} diffusion 80—7706
- $BaSO_4$, single cryst., neutron bombard. effect on struct. 78—63793
- Be-Cu strip surface quality and preparation 80—50779
- BiO-SiO_2 films, on Si, dopant distrib. pattern study using chem. etching 79—86812
- $6Bi_2O_3.GeO_2$, single crysts., selective etching in HNO_3, Bi_2 and H_2O_2 solns. 79—99201
- BiSb, dendritic growth, transverse striations photomicrograph 77—4277
- $Bi_xSi_yO_z$ films on Si, form. kinetics and props. 80—35358
- Bi_2Te_3, surface prep. by etching for electroplating elec. contacts 80—108647
- C and low-alloy steel inherent austenitic grain size determ., exam. of methods used 78—85071
- C fibres, electrolytic oxidation treatment for struct. studies 78—22649
- C fibres, oxidation, surface props. *(French)* 78—44238
- $CaCO_3$ calcite, neutron irrad. effects 77—39617
- $CaCO_3$ single crystals, effect of defect struct. charact. on X-ray diffr. 79—65089
- $CaHPO_4.2H_2O$, brushite, obs. of etch pits on as grown faces 79—73169
- $Ca_5(PO_4)_3F$, dislocation struct. exam. *(Russian)* 78—63770
- Ca_3SiO_3, hydrated, composition and morphology 78—26755
- $CaTiSiO_5$, sphere, effects of thermal annealing on track etching rate 78—65435
- Cd-Sn alloy, superconductivity and microstructure 80—107949
- $Cd_xHg_{1-x}Te$, comp. in successive layers determ. by chem. polishing etching of surface 77—7868
- $Cd_xHg_{1-x}Te$, surface microhardness depend. on surface treatment method 78—15560
- CdS, CdSe, growth rate, sublimation rate and etching behaviour along polar axis 80—24387
- CdS, polycrystn. layers on CdS substrate, electron microscope study of surface struct. 78—22940
- CdS, semicond. film, contoured anodic photodissolution 79—74277
- CdS, single cryst., surface treatment effects on photoluminesc., struct. and optical props. *(Russian)* 78—15224
- CdS thin film solar cell fabrication, HCl etching 80—81474
- CdS-Cu_2S heterojunction, elec. and photoelec. characts., effect of etching of CdS 78—80048

etching continued

- CdS-InP(GaAs) heterojunction prep. by CdS CVD and etching 78—52062
- CdSe photoanode improved efficiency by photoelectrochem. etching 80—104512
- CdTe, surface layers formed by etchants, XPS meas. 78—44240
- Co-Gd film, amorphous, prep. conditions influence on supernetwork struct. 77—76709
- Co_5Sm sintered magnet, effect of surface conditions on mag. props. 79—28556
- Cr, film, defects and mechanical stability, different deposition methods *(Bulgarian)* 80—44438
- Cr film, reversal etching in gas plasma, reaction mechanism, AES and XPS obs. 80—16564
- CsI, selective etching 78—19911
- Cu, dislocation path length after pulse loading 78—30630
- Cu, fatigued specimens, 'etch pit slip', SEM obs. 79—100258
- Cu, grain boundary character, revealed by etching and slip line continuity 79—33001
- Cu, H_2O_3/H_2SO_4 etching system 79—96227
- Cu selective surfaces on Al-Cu alloy, chemical brightening and etching 79—62037
- Cu single crystal spheres, dissolution, formation of etch pits, surface structure study using SEM 79—23735
- Cu single crystals, neutron irradiated, secondary slip 80—88161
- Cu surface, plasma cleaning and etching, removal of C 80—97645
- Cu surface, surface cleaning by H^+ bombard., AES study 78—53022
- Cu-Si(Sb), dil., chemical etching and X-ray topography obs. of cellular struct. *(French)* 79—96249
- CuO selective surfaces on Al-Cu alloy, chemical brightening and etching 79—62037
- CuO surface, contaminated, cleaning treatments, ion scatt. anal. 78—53307
- Cu_2O, creep substruct. under compression, X-ray diffr. study 78—95785
- Cu_2S-CdS thin film solar cells, Cu_2S layer separation, struct. 79—95282
- Cu_xS-CdS solar cell, p-n junction shape and struct. 77—55599
- EuB_6, growth by soln. method, struct., mech. and elec. props. 80—16168
- Fe, cast, austenitic grain size determ. 80—81255
- Fe, pure, initial grain boundaries effect on cold-rolling and annealing textures *(Japanese)* 80—35205
- Fe, sintered, influence of metallographic treatment on pore analysis 80—76417
- Fe-Cr, microstructural study of oxidation, selective etching 78—44245
- Fe-Ni-Cr, high Ni content, intergranular corrosion, effect of Cr *(French)* 80—7708
- Fe-Ni-Cr alloy, cast, etching methods for determ. of primary struct. 78—23888
- Fe-Si, etch figure method appl. *(Chinese)* 80—21194
- Fe-Si (2-8 wt.%), single crysts., growth striations, X-ray studies 80—79774
- Fe-Si (3 wt.%), single crystal, colour etching of striations 77—70253
- Fe-Si (3 wt.%), square etch pit characts., subgrain misorientation and mag. domain patterns 77—25199
- Fe-Si (3wt.%), quantitative determ. of grain orientation and textile by etch figure method *(Chinese)* 78—11233
- α-Fe_2O_3, haematite, etch figure shapes on most stable faces *(French)* 77—16707
- α-Fe_2O_3, interpretation of microcrysts. observed on faces (01.2) *(French)* 79—51038
- α- Fe_2O_3, mutual orientations and morphology obs. *(French)* 79—37647
- (Ga,Al)As narrow double-current-confinement channelled-substrate planar laser fabrication, double etching technique 80—74371
- GaAS, (110) oriented, preferential chemical etching of blazed gratings 79—37067
- $Ga_{0.7}Al_{0.3}As$-GaAs chemically etched mirror lasers, optical coupling effect 77—72000
- $Ga_{1-x}Al_xAs$ LPE crystals for DH laser, LEDs, TEM obs. of Ge, Si-doped epitaxial layers 79—1556
- GaAs, anodised, interfacial reactions, Raman scatt. obs. 80—49544
- GaAs, back etching and growth by liq. phase epitaxy, surface morphology obs. 80—29287
- GaAs based MOS capacitors, scanning photovoltage investigation 80—80396
- GaAs, chem. etched surface, Auger characterisation 77—25169
- GaAs, chem. etching and ion-bombardment effects, during ESCA 78—92171
- GaAs, chem. prep. of surfaces, and AES and XPS characterisation 77—90477
- GaAs, chemical etching processes, review 78—95832
- GaAs conducting MIS structures and metal-semicond. structures, effects of ultrathin oxides 79—1626
- GaAs, defect revealing etchant, electrochem. process in $NH_4OH:H_2O$ 78—6060
- GaAs, diffraction gratings prod. by interference photoetching 77—46805
- GaAs, epitaxial growth and etching rate meas. method 77—35829
- GaAs, epitaxial layer, controlled electrochemical and selective etching, integrated optics appl. 77—14814
- GaAs epitaxial layers, non-doped, from Ga-$AsCl_3$-H_2 system, TEM and RHEED study of micromorphology and defects 79—65340
- GaAs, epitaxy on semiinsulating GaAs, elec. props. of transitional layers rel. to growth conditions 77—15977
- GaAs, epitaxy using TMG and AsH_3, chloride etching effect 78—76606
- GaAs, etch pit pattern made by light irradiated electrolytic etching 79—95012
- GaAs etch solns. containing H_2O_2, correl. between etch and surface film characts. 80—71770
- GaAs, etchant, universal, multipurpose 78—53008
- GaAs, etching by water vapour rate 80—16519
- GaAs, etching soln. system H_3PO_4-H_2O_2-H_2O for MESFET fabrication 78—11379
- GaAs, facet formation by preferential etching in $1NH_4OH$-$2H_2O_2$ *(Japanese)* 78—44242
- GaAs homoepitaxial interface, thermal degradation 77—11988
- GaAs, impurity distribs. by chemical methods 77—43237
- GaAs integrated optical circuits by wet chemical etching 79—32092
- GaAs LPE in situ etchback calibration 79—83114
- GaAs LPE layers, dopant tracing of terrace growth 78—75948
- GaAs, laser annealed, etched, Rutherford scattering spectra, TEM study 79—79127
- GaAs, laser-induced microscopic etching 80—76379

etching continued

- GaAs, peculiarities of plasma region reflection, effect of surface treatment methods *(Russian)* 79—69827
- n-GaAs, preferential photoelectrochemical dissolution in Fe(III) based etches 78—7066
- GaAs, selective etching in nonaqueous bromine and iodine solns. 77—40453
- GaAs, selective in situ vapour etch of substrate and growth 80—2958
- GaAs, semi-insulating, magnetophotoconductivity as function of etching time 79—56265
- GaAs surface morphology during etching with H_2O vapour 80—39094
- GaAs, VPE, hole diffusion lengths, surface prep. and heat treatment effects, etchant evaluation 80—15627
- GaAs, vapor-phase etching, mechanisms and kinetics 80—100934
- GaAs, vapour phase etching and polishing with $AsCl_3$ 78—3243
- GaAs wafer, double-etching technique for submicron channel fabrication, laser fabrication appl. 80—74387
- GaAs wafer, H_3PO_4-H_2O_2-H_2O etching solution system and its kinetics 79—20229
- GaAs:Cd, effect of As vapour press. on etch pit density and junction depth 78—26937
- GaAs:Zn(Si)(Sn), etching rel. to dopant and carrier conc. 77—16704
- GaAs-$Al_xGa_{1-x}As$ integrated optics structs., dry processing 77—27383
- n-GaAs-electrolyte interface, surface pretreatment rel. to photocurrent, spectral response 80—3204
- GaAs-$Ga_{1-x}Al_xAs$ multilayer struct., growth over preferentially etched channels, MBE 77—40388
- GaAs-GaAlAs embedded stripe DH laser with polycryst. GaAsP, etched mirrors 77—75549
- GaAs-GaAlAs heterostructure, GaAs preferential etching, using O_2 and CCl_2F_2 mixture 79—8373
- GaAs-GaAlAs laser, degraded, characterisation by selective etching and photoetching 80—48252
- GaAs-SiO_2 interface local props. *(Russian)* 78—10567
- $GaAs_{0.6}P_{0.4}$, VPE, hole diffusion lengths, surface prep. and heat treatment effects, etchant evaluation 80—15627
- GaAs(Sb), electrochemical sectioning and surface finishing 80—108611
- GaInAsP/InP system, chemical etching, fabricating laser diodes and integrated optical circuits 80—38030
- GaInAsP-InP DH laser, LPE and wet chem. etching techniques for integration 79—98388
- GaInAsP-InP DH lasers made by melt-back method, operating characteristics 80—48287
- GaInAsP-InP stripe laser, etched mirrors fabricated by wet chem. etch 80—99744
- $Ga_xIn_{1-x}P$ electrode, in aqueous electrolytes, impedance meas. *(French)* 79—87153
- $Ga_xIn_{1-x}P$, real struct. exam. by electron microscopy and channelling 78—2143
- GaP (001), dislocation etch pits 78—14351
- GaP (100) thermal and vap. phase etching in H_2-HCl-PH_3, obs. 77—77612
- GaP, chemical etching processes, review 78—95832
- GaP, epitaxial layer, carrier recomb. at dislocations 77—20932
- GaP, etching in aqua regia and bromine-methanol-water solns. 78—68833
- GaP, LEC crystal, etch pit obs. 77—76387
- GaP LED, surface treatment effect on surface recomb. vel. and leakage current 77—20410
- GaP, polished, technique for uniform etching 78—39928
- GaP, surface layers produced by chemical treatment, comp. and struct. 79—96173
- GaP, vapor-phase etching, mechanisms and kinetics 80—100934
- GaP:Mg, ion implanted, elec. profiles 79—77628
- GaP:Te, struct. imperfections, prep. and doping effects 77—89451
- GaP-GaAlP-GaP LPE layers, etch pit patterns 79—51445
- $GaPO_4$ film growth on GaP, XPS exam. 78—31552
- GaSb, p-type, effects of accumulation layer on photocond. *(French)* 77—24582
- GaSe, basal plane orientation determ. in vertical Bridgman grown single crysts. 78—19658
- $(Gd,Bi)_3$,$(Fe,Al,Ga)_5O_{12}$ LPE film, 180° Bloch wall pinning at etched nucl. tracks 78—39376
- $Gd_3Ga_5O_{12}$, garnet substrate, surface polishing, damage, abrasion, brittle fracture model *(German)* 77—73357
- $Gd_3Ga_5O_{12}$ single crystal polishing characteristics, comparison chemical, mechanical methods, magnetic bubble device appl. *(Japanese)* 79—5067
- $Gd_2(MoO_4)_3$, ferroelectric domain decoration 78—10862
- Ge, black, solar selective absorber characterisation 80—80112
- Ge, chemical etching processes, review 78—95832
- Ge, cross-slip of single dissociated screw dislocations, double etching and X-ray topography studies 80—15104
- Ge film, amorphous, prep. conditions influence on supernetwork struct. 77—76709
- Ge film black, solar selective absorber surface 79—29484
- Ge, laser initiated etching 77—25308
- Ge, microflaw vol. conc. determ., etching method 79—24688
- Ge, polycrystalline epitaxial film, exam. of growth kinetics and props. 80—55304
- Ge, rough surface, polarisation angles, ellipsometric meas. 78—56449
- Ge surface, line tension induced dislocation motion, obs. by etching and X-ray topography 79—82212
- Ge:Ga, heavily doped, structure defect evolution during heating *(Russian)* 78—43026
- Ge-metal contacts, surface electron state spectrum surface treatment effects *(Russian)* 80—34497
- Ge-metal Schottky barrier junction, surface electron states spectrum *(Russian)* 78—84297
- GeTe, machining effects on electrophys. props. 77—86199
- 40% HF acid, neutron fluence meas. using mica and plastic as fission fragment track detectors 78—13346
- H_2SO_4 etchant, for revealing struct. inhomogeneities in martensite-ageing steel 80—61035
- HfC, etchant for revealing microstructure 80—85097
- InAs anodic oxide films prep. and props. 80—55553
- $InAs_{1-x}Sb_x$-InAs stepwise-graded struct., steady-state LPE, etching, investig. 77—21042
- $In_{1-x}Ga_xAs$, LPE growth on InP, electron probe anal. of etched surface 79—23862

etching continued
- InGaAsP LPE layers on InP substrate, material selective chemical etching 79—70188
- InP (100) surfaces, chem. treatment effects on comp. and nature 79—47794
- InP, effects of baking time on purity and morphology 78—6862
- n-InP, epitaxial layer, (100) surface chemistry, ESCA study 80—103552
- InP, LPE growth on GaAs, etching and electron probe anal. 79—11526
- InP, laser-induced microscopic etching 80—76379
- InP, MIS diode prep. by anodic oxidation 79—74270
- InP p-n junction, grain boundary etching 80—96541
- InP, photolum. depend on surface treatment 79—78727
- InP substrates, chem. etching by H_2O_2-H_2SO_4-H_2O soln. 80—35360
- InP substrates, HCl etching speed and polarity obs., with aid of laser beams *(Slovak)* 78—56575
- InP substrates preparation, etching and polishing in Br-methyl alcohol solution *(Slovak)* 78—56576
- InP, VPE, etch pit density, dislocation density 79—87569
- n-InSb, elec. props. changes during ht. treatment 77—85213
- InSb, low defect crystal growth by InN doping, IR detector appl. 80—20780
- InSb, magnetically frozen-out, evidence of surface cond. from etching expts. 79—47152
- n-InSb, magnetotransport experiments, surface treatment induced effects 80—34468
- InSb, optical constants and oxidation with various surface treatment *(Russian)* 80—88955
- n-InSb, phonon-assisted cyclotron reson. strongly depend. on surface condition 80—70755
- InSb, refractive index and absorpt. coeff., cryst. orientation depend. 80—60536
- InSb, single crystal, chem. and ion etching, surface changes *(French)* 80—108614
- InSb, single crystal, etching of {111} plane, rates and activation energies 77—12723
- InSb, surface analysis, X-ray photoelectron spectra, surface oxidation-etchant correlation 78—56029
- $KBr:PbI_2$, single crysts. grown from aq. soln., growth striations obs. 77—1089
- KCl, cryst., etch hillocks on (100) cleavage planes 77—4109
- KCl:Ba, γ-irradiation, defect struct., X-ray and chemical etching exam. 77—84793
- $KClO_4$, cryst. growth from gelatin gels, exam. of growth and morphology 80—7488
- $KClO_4$ single crystals, gel growth, temp. effects etching 79—78862
- KH_2PO_4 crystals, rel. between selective and total soln. 80—39103
- $KNbO_3$, dopant effect on domain struct., etching study 79—56749
- $KNbO_3:Al^{3+}$, dopant effect on domain struct., etching study 79—56749
- $KNbO_3:Ba^{2+}$, dopant effect on domain struct., etching study 79—56749
- La-N-C system, metallographic investigation *(German, English)* 77—52600
- LaB_6, growth by soln. method, struct. mech. and elec. props. 80—16168
- LiF, electron irradiated, defects, selective etching and electron microscopy *(Russian)* 77—47488
- $LiNbO_3$ crystals, low temp. polarisation reversal, study of domains 79—61322
- $LiNbO_3$, microfabrication by ion-bombardment enhanced etching 78—76779
- $LiNbO_3$, reversed polarity layer at positive domain surface, heat-induced, etching investig. 77—63383
- $LiNbO_3$, ridge struct. fabrication by CF_4 plasma etching 80—28357
- $LiNbO_3$, Ti diffused optical waveguide, ferrolectric domain inversion 79—94338
- $LiNbO_3$:Ti narrow ridge optical waveguides and electro-optical, ion-bombardment-enhanced etching 80—38133
- $LiNdP_4O_{12}$, grown by top seeded pulling technique, possible laser material 80—25542
- LiO_2 pellets, sintered, exam. of microstructure 78—72749
- MgO, anisotropy of grinding damage, chem. polishing and etching 79—47793
- MgO crystals, etching and polishing, inorganic or organic acids effect 80—40573
- MgO crystals, etching behaviour rel. to chem. reactions 80—3229
- MgO crystals, kinetics and mechanism of dissoln., etch rates in H_2SO_4 solns. 79—79136
- MgO, etching in acids, kinetics and mechanism of dissolution 78—85014
- MgO, etching on {100} faces by H_3PO_4 acid 78—67714
- MgO, polycrystalline, grain growth and grain boundary migration, pore effects *(Japanese)* 78—19701
- Mg_2Si0_4, etch pits in cleaved faces, revealing low angle boundaries 79—14818
- Mn-Zn ferrite single crystals, mech. polishing effect on mag. props. *(Japanese)* 80—16569
- $Mn_xFe_{3-x}O_4$ film, spin wave reson., effect of etching 77—16183
- MnZn ferrites, abrasive wear measurement appl. *(Japanese)* 78—39917
- MnZn ferrites, doped; determ. of grain boundary composition, using Auger spectroscopy *(German)* 79—23618
- Mo film on Si surface, $MoSi_2$ form. conditions *(French)* 78—43270
- Mo, sintered, thermal and elec. conds., 50-800°C, microstructure 78—43352
- MoF_6 reduction by H, chemical kinetics eqn., adsorbed component interactions *(Russian)* 80—35569
- $(NH_4)_2SO_4$, mechanically twinned, orthorhombic, search for antiphase boundaries 79—37715
- NaCl, electron irradiated, defects, selective etching and electron microscopy *(Russian)* 77—47488
- NaCl, etch pits on cleaved surfaces, oriented overgrowths 77—73359
- NaCl, etched cleavages, moisture effect on spiral and terraces steps 77—4251
- NaCl, plastically deformed, glide on {111} planes 79—82234
- NaCl, single cryst., crack healing at low temp. 77—36622
- NaCl-KCl mixed crystal, growth, X-ray exam. and microstruct. 78—44001
- Na_2O-CaO-SiO_2, plates, exam. of Hertz crack branching 78—72887
- Na_2O-ZrO_2-SiO_2 glass, treated with 2 N solns. of $NaCO_3$ and NaOH, surface layer comp. 80—35366
- Nb, mono- and polycrystn., crystallographic orientation, etching technique determ. 80—71814
- Nb-N(O)(C) system, specimen prep. for metallography *(German, English)* 80—89439
- NbC, etchant for revealing microstructure 80—85097

etching continued
- Ni (100) and (110) surface at open circuit in H_3PO_4, changes in surface struct. after anodic etching 79—61777
- Ni alloy EhI698, new etchant for revealing microstructure 80—25934
- Ni-Cr alloy, cast, etching methods for determ. of primary struct. 78—23888
- Ni-Fe films, coercivity control for single-level masking bubble devices using surface modification and intermediate layers 79—51816
- NiO, interface for xerographic Se photoreceptor on flexible Ni foils 78—29184
- NiO_2 single crystals, welding, optical and SEM study 79—65097
- Ni_xP_{1-x} surface, laser produced ripple patterns 77—79878
- PLZT, ferroelectric domain struct. obs. by SEM and optical microscopy *(Japanese)* 78—15136
- Pb, high purity microstructural investigation by etching with aqueous $HClO_4$ 77—56205
- Pb, Pb alloys, metallographic preparation using pH controlled silica gel and superior microetchant 80—16623
- Pb, sphere, dissolution in H_2SO_4 in elec. field *(Russian)* 77—4867
- $PbMoO_4$, hollock growht origin in gel growth 80—49139
- $PbNb_2O_6$, ferroelectric thick crystals, domain formation and dislocation loops 78—60410
- PbO glass, strength, effect of HNO_3 etching 77—56124
- PbO-SiO_2 binary glasses, Pb depth profiles after acid etching, α-particle backscatt. 79—79343
- PbO-SiO_2 films, on Si, dopant distrib. pattern study using chem. etching 79—86812
- PbS, plastic deform. on compression along ⟨100⟩ direction 79—28036
- $Pb_xSi_yO_z$ films on Si, form. kinetics and props. 80—35358
- $Pb_xSn_{1-x}Te$ surfaces, fractured and etched, Raman scatt. spectra of monolayer oxide and Te films 77—48211
- PbTe-PbSnTe heterjunction, misfit dislocations, etch pit and electron probe study 79—77926
- $PbTiO_3$, spontaneous polaris. shielding destruction by polishing and scribing 79—15427
- Pd-Si-Cu metallic glass tips, appl. as electron field emission source 79—8229
- Pu, $\beta \rightarrow \alpha$ and $\gamma \rightarrow \alpha$ transforms., microstructures and kinetics 77—25048
- $Sb_xSi_yO_z$ films on Si, form. kinetics and props. 80—35358
- Se-Ge amorphous films, obliquely deposited, photoinduced chem. changes 80—76385
- Se_{90}-Te_{10} alloy crystals, growth and cleavage 78—88421
- Se_xTe_{1-x}, growth of single crystals by Czochralski method 80—66423
- Si (001) wafer, pyramidal hillocks, TEM obs. during chemical etching 80—70508
- Si, (100) and (110), anisotropic etching for fabrication of 3-D microstructures 79—15826
- Si, (100) and (110), anisotropic etching 79—15827
- Si (111), growth and etching vectors, adsorption and step reconstruction 79—23548
- Si amorphous film, anisotropic etching phenomenon, appl. as solar selective absorber surfaces 80—72054
- Si amorphous films, laser beam annealing, optical information storage possibilities 79—87515
- Si and its cpds., chemical aspects of fluorocarbon plasma etching 79—83350
- Si, anisotropic etching by $CCl_4(+O_2)$ gas plasma 77—32701
- Si, anomalous etch structures using ethylenediamine-pyrocatechol-water based etchants and their elimination 80—81217
- Si based MOS capacitors, scanning photovoltage investigation 80—80396
- Si blazed holographic grating fabrication by selective etching 80—74320
- Si, CVD layers, change of etch rate associated with amorphous to crystalline transition 78—7064
- Si, CVD mechanism, book contrib. 79—69991
- Si, chem. etching, comp. selection, geometry effects 77—21299
- Si, chemical etching processes, review 78—95832
- Si, chemical staining due to suboxide form. 78—35540
- Si chip manufacture for fibre alignment in lightguide cable connectors 80—64188
- Si compounds, plasma etching, gas flow-rate depend. 80—97603
- Si, controlled etching in catalysed ethylenediamine-pyrocatechol-water solns. 80—3223
- Si, cross-slip of single dissociated screw disclocations, double etching and X-ray topography studies 80—15104
- Si, Czochralski grown crystal, O precip., nucleation behaviour and dislocation loop form. *(Japanese)* 80—59664
- Si, Czochralski wafers, oxidation induced stacking fault sources 77—7737
- Si Czochralski wave, oxid. induced stacking fault, oxygen content influence 78—10062
- Si, Czochralski-grown, oxide precip. form. process 80—49364
- Si, defects, electrically active, correl. of electrolytic etch and surface photovoltage methods 79—77929
- Si, diffraction grating, rectangular profile, fabricated from single cryst. 80—38093
- Si dislocation free, quantitative determ. of microdefect density by preferential chem. etching 80—65001
- Si, dislocation-free Czochralski-grown, detection of microamounts of O *(German)* 78—26592
- Si, epitaxial (111) surface, etching observation of stacking faults, dislocations, S-pits, etch pits *(Chinese)* 80—70197
- Si epitaxial detector fabrication, crystal growth and preferential etching 78—37505
- Si epitaxial detectors, chemical preferential etching 77—79509
- Si epitaxial film concentrated inhomogeneity detection by selective etching *(Russian)* 78—10298
- Si epitaxial growth, in $SiCl_4$-HCl-H_2 system, model based on flow graph, depend. of gas phase etching and growth rate on process parameters 79—42405
- Si epitaxial layers on metallurgical-grade polycryst. substrates, characteris. 79—28967
- Si, epitaxial wafer, saucer pit microdefects reduction by intrinsic gettering 80—75450
- Si epitaxial wafers, role of metallic contamination in formation of 'saucer' pit defects 77—39588
- Si, etch rate loading effect and temp. depend. in CF_4 plasma 79—34167
- Si, etching by CF_4, plasma deposition reactor gas phase characts., mass spectra 80—70566
- Si, etching by tetrafluoromethane plasma, mechanism 79—15832
- Si, etching in He-F_2 plasma, etch rates, mass spectra, direct ion sampling study 80—79510
- Si, etching using XeF_2 vapour, adsorption/desorption process 79—43449

etching continued
- Si, etching with CF_4 in diode system 79–61759
- Si, film, amorphous, prep. conditions influence on supernetwork struct. 77–76709
- Si film, MBE, cryst. defect props., substrate treatment effects 80–70551
- Si film, on sapphire, new etchant 78–7070
- Si, gas phase etching, with HCl-H_2 mixture 79–96165
- Si, HCl etching, effect of O_2 traces 79–91818
- Si, HCl oxidation conditions for stacking fault nuclei gettering and undesirable etching 78–68830
- n-Si high-temp. vacuum etching, p-n junction photodetectivity 78–95355
- Si, monocryst. etching by Br, high-power Ar laser beam initiation *(Russian)* 77–73358
- Si, new preferential etch for defects in (100) and (111) oriented n- and p-type cryst. 77–59954
- Si, optical waveguides along both sides of groove 80–96006
- Si oxidation in HCl-O_2 atms., Si etching and SiO_2 bubble form. 77–63823
- Si, oxidation-induced Frank sessile dislocation loops, struct. change 80–75228
- Si, oxidation-induced stacking faults, distinction between clean and decorated faults by etching 80–79818
- Si photovoltaic low series resistance concentrator for high intensity appl. 80–93940
- Si, plasma etching, control of relative etch rates 77–44390
- Si, plasma etching in Freon plasma, for microelectronics appls. 80–3080
- Si polycrystalline films, anomalous etching effects 77–77613
- Si preferentially to produce high density multichannel optical waveguides 77–794
- Si, reactive ion beam etching expts., selectivity, anisotropy 80–104308
- Si, reactive ion etching in CF_4 plasma, competitive mech. 79–91816
- Si, reactivity with organic nitrogen compound, rel. to polishing *(Russian)* 79–70192
- Si, rough surface, polarisation angles, ellipsometric meas. 78–56449
- Si, Schottky diode ageing, influence of metal electrode O diffusion coeffs. 79–99620
- Si semiconductor plates, control of quality of surface treatment, using Al spraying technique 80–60989
- Si, single cryst., electrolytic buffing using non-abrasive electrolyte *(Japanese)* 77–4862
- Si, single-tip and multitip cathodes, fabrication, and photofield emission characts. 78–2976
- Si solar cells, junction formation techniques using spray-on polymer dopants, cost effective, high throughput 80–94014
- Si spectroscopic applications of structures produced by orientation-dependent etching 80–93668
- Si substrates, reactive ion etching 79–83351
- Si surface, decontamination of Au impurities by etching 80–55559
- Si, surface, etched and heat-treated, optically stimulated ESR investigation 80–11245
- Si surface, line tension induced dislocation motion, obs. by etching and X-ray topography 79–82212
- Si surface, plasma etching as diagnostic technique 77–44385
- Si surfaces, influencing microstruct. deform. process by impurity type, etching study *(German)* 79–65107
- Si surfaces etched in CF_4 or CF_4-O_2 plasma, morphology 80–93671
- Si, thermally induced microdefect form., C and O role 80–11439
- Si, V-grooves formed by etching, phosphosilicate glass bridge struct. 80–104312
- Si, vertical etching, at very high aspect ratios, review 80–50744
- Si wafer, automatic meas. system for resist. profiles 80–39574
- Si wafer, chemically etched, surface roughness by gas adsorption techniques 80–15398
- Si wafer, Czochralski grown, precipitation during high temp. oxidation 78–11381
- Si wafer, HCl etching, smooth or pitted surface struct., gas phase comp. effect 78–11360
- Si wafer, oxidation induced stacking faults, surface vs. bulk nucleation 77–62545
- Si wafer, shrinkage and annihilation of stacking faults 77–39598
- Si, wafer, suppression of oxidation stacking fault generation by preannealing in N_2 atm. 78–30648
- Si wafers, Au contamination during plasma etching 80–19831
- Si wafers, Czochralski grown, crystal defects, photoluminesc. topographic obs. 79–1432
- Si wafers, etched in HCl, exam. of bunch formation 78–68831
- Si wafers, floating-zone, etch struct. on microdefects as affected by dopants and surface treatment 80–79773
- Si, wafers, HCl etched, surface morphology, etch pit origin 79–96166
- Si wafers, preparation of preselected areas for TEM 78–24887
- Si:B, selective etching by NaOH soln. 79–70189
- Si:P, As, chem. etching, thick epitaxial layers prod. for dopant conc. investigations by neutron activation anal. 79–37728
- Si/SiO_2 interface, precise wet-chemical etching, using rapidly rotating sample 80–93669
- Si-based technology for hemispherical laser fusion target fabrication 79–89495
- Si-containing films, formed by reaction of Si with organic compounds of N, struct. investigation 79–87009
- Si-Ni(Pt)(Al) Schottky diode, type II localised interface states, Si surface prep. effects 78–39210
- Si-SiO_2, etch rate of removal of ion implanted SiO_2 determ. lay optical method 79–23629
- Si-SiO_2 film, crater-edge profiling in interface anal., ion beam etching and AES 77–1323
- Si-SiO_2 interface, effect of oxidation time and temp. using AES 80–35359
- Si-SiO_2 wafer thinning for TEM 77–89352
- Si-undoped poly Si interface, in oxidation process, defects generation 80–40571
- $Si+XeF_2(F_2)(Cl_2)$ plasma etching, electron or ion bombardment, Ar^+ enhancement 79–82073
- α-SiC, epitaxial layer, impurity macroincorporation, distrib. of Al, B, N and P 77–69192
- β-SiC, fluidised bed deposited coatings for nucl. fuel granules, microstructural obs. by SEM 77–14233
- α-SiC, lattice absorpt. bands in IR spectra, surface treatment effects 77–52071
- SiC-H_2 system, thermodynamic analysis 77–86347
- Si_3N_4 antireflection coating for solar cells, reactive plasma process for forming metal grid patterns 80–93990

etching continued
- Si_3N_4 CVD film etching in acidic fluoride media 78–7071
- Si_3N_4, enhanced etching by ion beam, localised substrate heating effects 78–51573
- Si_3N_4, etch rate loading effect and temp. depend. in CF_4 plasma 79–34167
- Si_3N_4, etching with CF_4 in diode system 79–61759
- Si_3N_4 film, CVD, etching in acidic fluoride media 78–39927
- Si_3N_4 film, plasma etching, role of chemisorpt. of CF_4, CF_3H, CF_3Cl, CF_2Cl_2 and CCl_4 79–11714
- Si_3N_4 films, plasma deposited over substrate steps, fast etching phenomenon 79–34168
- Si_3N_4 layers produced by ion implantation, oxidation inhibition and etching 80–103374
- Si_3N_4, low temp. deposition using microwave-excited active N_2 78–84718
- Si_3N_4 on Si, optical monitoring of etching using grating 78–76775
- Si_3N_4, surface etching by laser-generated free radicals 80–71772
- $Si_3N_4+XeF_2(Cl_2)(F_2)$, plasma etching, electron or ion bombardment, Ar^+ enhancement 79–82073
- Si_4N_4, ion-implanted, enhanced etching in buffered HF solns. 78–72903
- $Si_3N_4(SiO_2)$ plasma etching, plasma processes involved in dry processing using CF_4 active etchant species 80–79581
- SiO_2 film, preferential etching on Si substrate, plasma reactive sputter etching 77–20448
- SiO_2 DryOx process using anhydrous HF, microelectronic appls. 77–77606
- SiO_2, etch rate loading effect and temp. depend. in CF_4 plasma 79–34167
- SiO_2, etching characts. in trifluoromethane gas plasma 80–76392
- SiO_2, etching in He-F_2 plasma, etch rates, mass spectra, direct ion sampling study 80–79510
- SiO_2, etching with CF_4 in diode system 79–61759
- SiO_2, fabrication of surface relief struct. with linewidth below 2000 Å 78–42478
- SiO_2, film, formation from tetraalkoxysilanes in O_2 current, props. 77–44170
- SiO_2 film, prep. using high press. O_2, residual stress, chemical etch rate, refr. index and density meas. 80–71768
- SiO_2 film, spin-on oxide, phys. and cond. meas. 77–43762
- SiO_2 film deposition from SiH_2Cl_2 on Si 77–77407
- SiO_2 films sputtered in H-Ar mixed gas, enhanced step coverage 80–75470
- SiO_2, fused, slide glass surface, Ca^{2+} ion deposition as inhibitor to alkaline attack 80–50737
- SiO_2, glass, ion implanted, radiation effect on chem. stability 77–1158
- SiO_2, HF vapour phase etching, prod. viability for semicond. manufacturing and reaction model 80–81219
- SiO_2 layers, passivating, deposition by plasma decomp. in planar reactor, etching rate 78–88430
- SiO_2 magnetron sputtered film, oblique deposition effect on growth rate, etching rate, and struct. *(Japanese)* 80–54555
- SiO_2, masking film in alkaline etching 80–71771
- SiO_2 on Si, optical monitoring of etching using grating 78–76775
- SiO_2, plasma etching, control of relative etch rates 77–44390
- SiO_2, plasma etching with hexafluoroethane in radial flow reactor 80–76391
- SiO_2, plasma-chemical etching, spectroscopy 80–85243
- SiO_2, RF sputtered films, anomalous etching phenomenon 80–3226
- SiO_2, reactive ion beam etching expts., selectivity, anisotropy 80–104308
- SiO_2 relief, plasma etching, tapered wall prod. 80–97606
- SiO_2, sputtered, reactive ion etching in CF_4 plasma, competitive mech. 79–91816
- SiO_2, surface etching by laser-generated free radicals 80–71772
- SiO_2, surfaces etched in CF_4 or CF_4-O_2 plasma 80–93671
- SiO_2 thermal film, freon ion beam etching, IR study *(Russian)* 80–76095
- SiO_2 thin thermally grown oxide layers etching in HCl, ellipsometric control of Si surface form. *(Russian)* 80–104315
- SiO_2, uniform film prep. by pyrolysis of tetraethoxysilane 77–40379
- SiO_2 wafers, Au contamination during plasma etching 80–19831
- SiO_2-Al_2O_3-B_2O_3 glass mech. strength increased by etching 80–97609
- SiO_2-Na_2O-CaO, electrochemically coloured, chemical composition and structure of surface layers 78–84758
- SiO_2-P_2O_5 glass film, CVD, P conc. profile by etch rate technique 80–96450
- SiO_2-Si (n-type) interface, electrochem. etching 77–11799
- $Si_lO_mN_p$, CVD from SiH_4-CO_2-NH_3-H_2 system, physicochem. props. 78–38978
- $SmB_4(B_6)$, growth by soln. method, struct. and mech. props. 80–16168
- $SmCO_5$, etched microparticles, Barkhausen discontinuity, nucleation, and domain wall pinning 79–87288
- Sn, CVD onto GaAs surface, anal. of conditions 79–87584
- Sn, white crystals, dislocation reactions 79–86796
- Sn-Ni electroplated alloy, etch rates using quartz cryst. microbalance, contact resist. 77–59981
- Sn-Ni metastable alloy, surface film comp., time depend., XPS 78–60870
- SnO_2:P, CVD growth and etching characts., doping effects 80–107667
- Ta-N(O)(C) system, specimen prep. for metallography *(German, English)* 80–89439
- TaC, etchant for revealing microstructure 80–85097
- Te, galvanomagnetic props., surface layer effects reduced by etching 77–51769
- Te, growth of single crystals by Czochralski method 80–66423
- Te, single crysts., Czochralski growth, etch pit orientation study 79–43133
- Ti alloys VT23 and VT15, etching as a function of struct. *(Russian)* 78–15568
- Ti-Al-Mo-(Cr), etching as a function of struct. *(Russian)* 78–15568
- α-β Ti-Mn alloys, etching and electropolishing to reveal α and β-grain size 78–3254
- Ti-V (15.5 wt.%), {332} deformation twins, optical microscopy study 79–79047
- TiO_2 electrodes, effect of processing variables on photoelectrochem. props 80–6975
- U conc. in blood meas. by thermal neutron induced fission, chem. etching, conc. rel. to leukaemia 80–21532
- U prospecting using microdistrib. anal. of Siwalik vertebrate fossils by nuclear Track Etch tech. 80–98489
- UO_2-zircaloy-4, reaction kinetics at high temps., O_2 diffusion 80–16667

etching continued
V-N(O)(C) system, specimen prep. for metallography *(German, English)* 80−89439
W [310] tip, prep. from rolled sheet 80−97447
W, stacking fault stability determ. 80−96548
W surface wetting by liquid Cu depend. on preliminary surface treatment *(Russian)* 80−35388
W, whisker fabrication, AC and DC electrochem. etching 78−43278
W-Ni sintered alloy, etching 79−29323
WS_2, single cryst., growth by direct vapour transport, pit density determ. by etching 79−28904
$(YEuTmCa)_3(FeGe)_5$ bubble garnet films, ion-implanted, mag. susceptibility meas. 79−47311
$(YEuYbCa)_3(FeGe)_5O_{12}$ bubble films, Ne^+-implanted, cryst. and mag. props., X-ray diffr. obs. 79−38362
YIG, single crysts. grown by floating zone method, quality eval. of etching and optical microscopy, ferromag. resonance linewidth meas. 79−19990
YbB_6, growth by soln. method, struct. and mech. props. 80−16168
Zn, isothermal annealing effect at 400-410°C, on dislocation struct. in monocrystals *(Russian)* 79−20082
Zn_3As_2-ZnSe(ZnTe) solid solutions, single cryst., phase equilib. and props. 80−16283
$ZnGeP_2$, Br_2-methanol etching soln. for crystallographic axes determ. 78−35541
ZnO film, for SAW transducers, Al electrode micro-fabrication technique 77−80042
ZnO, ZnS, growth rate, sublimation rate and etching behaviour along polar axis 80−24387
ZnO_2, polycrystn., determ. of crystallographic orientation of grains 79−69049
ZnS, (110) cleavage stratigraphic etch patterns, displacements 77−7680
ZnS ion beam etching, topographic changes, amorphisation, luminescence study 80−76078
ZnSe, crystallographic polarity and etching behaviour 77−85030
ZrB_2, etching method using H_3PO_4 and H_2SO_4, effect of Pt 78−44339

ether drift *see special relativity*

Ettingshausen effect *see thermomagnetic effects*

europium
see also nuclei with ......
abundance in HD 18474 giant star *(Spanish)* 79−25605
adsorption by Al_2O_3, radioactive waste storage 80−99240
alkali halide:Eu^{2+}, spin-Hamiltonian parameters, superposition model calcs. 80−96830
alkali halide:Eu^{2+} , spin Hamiltonian, cryst. field consts. calcs. 79−51537
alkali halide:Eu^{2+} phosphor, explosive loading method form., spectra, luminesc. characts. *(Russian)* 78−35212
alkali metal halides:Eu^{2+}, single cryst. optical absorpt. spectra 80−45117
alkaline earth fluoride:Eu^{2+}, model of ligand hyperfine interaction 80−6792
alkaline earth halides:Eu^{2+}, fluorescence lifetime and quantum efficiency for 5d→4f transitions 80−100681
aluminate:Eu^{2+}, Mn^{2+}, luminescence, efficiency of $Eu^{2+}\rightarrow Mn^{2+}$ energy transfer, struct. effects 77−8629
aluminates:Mn, Eu, red Mn^{2+}-luminesc. 79−61420
atom, absorpt. spectrum, 1300-2200 Å 80−932
atom, absorpt. spectrum in Schumann region, 1750-2200 Å 77−34581
atom, absorption spectra of 4d→f transitions in 40-300 Å range 77−3298
atom, absorption spectrum, 2100-7200 Å, wavelengths, intensities, J- and g_J-values determ. 77−14383
atom, autoionising states excitation in electron collisions *(Russian)* 79−86073
atom, coexistence of 'collapse' and 'blow' states 80−32587
atom, electron impact excitation cross section, Born and Ochkur approx. 80−87230
atom, electron impact excitation of spectral lines 79−3579
atom, excitation transfer cross section, luminesc. meas. *(Russian)* 77−61706
atom, excited state lifetime meas. using cw dye-laser 79−89636
atom, HFS, many-body and relativistic effects 78−37565
atom, hyperfine interaction calc., relativistic many-body approach 77−46504
atom, in inert gas matrix, pseudolocalised vibr. modes, UV/vis. spectra 78−46289
atom, Kα line widths, precise meas. 78−62761
atom, K-shell X-ray energy, excitation mode depend. 79−26926
atom, L_I X-ray fluoresc. and Coster-Kronig yields 77−30814
atom, L-emission spectrum, $L_{II}N_{II}$ forbidden transition obs. 77−23451
atom, laser isotope separation by two step photoionisation 77−61720
atom, photoabsorpt. spectra 77−88417
atom, spin relaxation of $^8S_{7/2}$ ground state in noble gases 77−58131
atom, superfluorescence, visible, cooperative reson. Stokes radiation 80−5500
atom, UV photoelectron spectra, config. interaction effects 77−50413
atom, visible Dicke superradiant transitions *(French)* 79−45690
atom, visible Dicke-superradiant transitions 79−45692
atom, VUV emission spectra, 5p electron excitation by electron impact 77−68007
band structure and Fermi surface 77−62814
BCC, self-diffusion coeff. meas. *(French)* 77−15616
calibo glass:Eu^{3+}, Ho^{3+}, energy transfer 78−76510
calibo glass:Eu, Br, quantum efficiency of non-radiative energy transfer 79−33832
determination, by at. fluoresc. anal. with pulsed dye laser excitation *(Russian)* 78−35774
electrical resistance, effect of mag. field near Neel point 77−8073
electrical resistance anomaly below Neel temperature 77−11889
electrical resistivity of solid and liquid phases, thermopower, melting temp. 80−59955
electroluminescence activator in La_2O_3, Y_2O_3, Y_2O_2S, comparison 77−20927
electron and positron multiple scatt. 80−15171
electronic struct. investigation by electron spectroscopy method 80−92812
EPR, g-shift determ. 77−48045
exchange integral, spiral spin configuration, ab initio calc. 79−47275
Fermi surface and helical spin ordering 77−4291
film, optical cond. meas. 78−76112

europium continued
germanate glass:Bi^{3+},Eu^{3+}, time resolved spectra for Bi-Eu energy transfer 79−33748
glass:Eu^{3+}, fluorescence linewidth, anomalous, theory 80−50404
glass:Eu^{3+}, polarised luminesc. 78−48224
glass:Eu^{3+}, spectral line inhomogeneous broadening, electron excitation migration *(Russian)* 77−48200
glass:Eu^{3+}, spectroscopic props. of excited states of ions, laser induced fluorescence line narrowing meas. 79−38641
glass:Eu^{3+}, vibronic spectra, impurity complex model 78−19516
hyperfine interactions, high press. Mossbauer expts. 78−43714
inert gas:Eu, absorpt. and emission spectra, phonon sidebands 79−43021
isotope separation, laser two-step photoionisation 78−46461
laser self-terminating transitions in Eu atoms and ions 77−75493
liquid, divalent, electrical resist. 79−38039
liquid, resist. and thermoelec. power, t-matrix calc. 78−26840
luminescence of ions in soln., solvent effects on band intensities *(Russian)* 77−55828
magnetic and structural transitions, X-ray K-line shift, 77-1000K *(Russian)* 77−4518
magnetic anisotropy of helicoidal struct., magnetisation, 4.2-300K *(Russian)* 79−56499
magnetoresistance, irreversible component rel. to antiferromag. struct. *(Russian)* 77−35920
magnetoresistance, longit., at low temps. and up to 80 kG 77−55515
Mossbauer isomer shift and magnetic hyperfine field, press. effect 78−52386
nitrate glass: Eu^{3+} struct. reorganisation in glass transition interval, polarised luminesc. obs. 80−45141
Oklo natural fission reactors, migration in core sample, appl. to dating of reactions *(French)* 80−21760
orthovanadate:Eu^{3+}, spectroscopic props. 77−16363
phosphor:Eu^{3+}, rel. band intensities in luminesc. spectra *(Russian)* 77−48238
photochemical separation from lanthanide mixtures in aq. soln. 78−31660
polarisation paramagnetism, saturation *(Russian)* 79−47232
Precambrian Fe formations, rare earth elements evidence for changing oxidation states 77−64284
protein: Eu^{3+}, luminesc. spectra and binding centres 78−15754
purification, laser induced photochem. separation methods, review 79−61883
rare earth oxysulphide, R_2O_2S:Eu^{3+}, branching ratios for fluoresc. 79−33807
rare earth oxysulphides:Eu^{3+}, luminescence decay 78−15214
rare earth phosphates:Eu^{3+}, vac. UV luminesc.-excitation spectra 77−85774
rare earth phosphates:Eu, electronic-vibr. spectra rel. to struct. 79−56850
rare earth phosphors, Ln_2O_2S:Eu, Raman spectra, lattice vibrs. 79−78669
relativistic band struct. calcs., unoccupied 4f level calc., Fermi level, atomic configuration 80−49584
silicate galss:Eu^{3+}, fluoresc. linewidth variation, electron-phonon coupling 78−19531
specimen preparation for TEM by ion beam thinning *(German, English)* 80−11861
structural and electronic changes under 200 kbar press. and above 80−24588
thermal conductivity at low temps. *(Russian)* 79−11100
thermal conductivity elec. and thermal magnetoresist., at low temps. 77−69301
transport properties at high temp., scatt. mechanisms 77−15825
tungstates:Eu, electronic-vibr. spectra rel. to struct. 79−56850
X-ray photoabsorption near 3d edges 77−38645
AlN:Eu, luminescence at high excitation levels 77−1721
α-Al_2O_3:Er, crystal defects from X-ray irradiation, F-centres, X-ray luminesc. obs. 80−55176
Al_2O_3:Eu, surface luminesc. centres excitation characts. 78−52560
Al_2O_3-La_2O_3:Eu^{3+} system, optical and struct. exam. 77−4674
$Al_2(WO_4)_3$:Eu, and undoped crystals, luminesc. obs. 80−89047
Ar:Eu, matrix isolated, obs. of Stokes and anti-Stokes vibrational sidebands in emission spectra 77−73164
Ba aluminate:Eu, effect of non-stoichiometry on luminesc. 78−68550
$BaCaLu_2F_{10}$, site occupancy from excitation and emission spectra *(French)* 77−81145
$BaCl_2$:Eu^{2+}, EPR, electrostatic versus superposition model 78−23337
BaF_2:Eu^{2+}, ENDOR of ^{19}F ligands, under uniaxial stress 77−16207
BaF_2:Eu^{2+}, spin-lattice coeffs., meas. using uniaxial stress method 77−36129
BaFCl:Eu X-ray intensifying screen 78−11735
$BaMg_2Al_{16}O_{27}$:Eu^{2+} phosphor, for low press. fluoresc. lamp, luminesc. characts. 78−10960
BaO-B_2O_3: UO_2^{2+}, Eu^{3+} glass, nonradiative energy transfer 77−59602
$Ba_3(PO_4)_2$:Eu, X-ray phosphor, study of emission and trapping centres 79−8197
BaR_2O_4:Eu^{3+}, luminesc. 77−52156
$Ba_5SiO_4Br_6$:Eu, blue emitting X-ray luminescent material for intensifying screens *(French)* 80−66260
$Ba_5SiO_4Cl_6$:Eu, blue-emitting phosphor high quenching temp. 80−16076
$(Ba_xSr_{1-x})SO_4$:Eu mixed crystal series, X-ray diffr. study of miscibility 80−2168
$BaTiO_3$:Eu(Sm), absorption spectra, Ti^{3+} ion and Z-centre formation 77−24871
BaY_2F_8:Eu^{2+}, R^{3+}, energy transfer from Eu^{2+} to trivalent rare earth ion 79−91490
BeF_2:Eu^{3+} glass, luminesc. of Eu^{3+}, transition probabilities 80−80845
BeF_2:Eu^{3+} glass, struct. and optical props. 80−84067
BeF_2:Eu^{3+} glass, struct., Monte Carlo simulations 80−96448
$Bi_2Al_4O_9$:Eu^{3+}, luminesc. expts. 80−60656
$Bi_2W_2O_9$:Eu, energy transfer and luminesc. props. 80−55177
$CaEO_4$:Eu^{3+}, energy transfer after red edge excitation 78−52552
CaF:Eu, dimer reorientation activation volume 80−107285
CaF_2:Eu, CaF_2:Eu,Mn(Gd), single crystal predisintegration phenomena, SEM cathodolum. obs. 80−59502
CaF_2:Eu, capture of thermalised positrons by activator impurities 77−40299
CaF_2:Eu, oxidation and reduction of Eu, EPR and optical studies 80−25199
CaF_2:Eu, thermolum. in presence of lanthanide impurities 80−2870
CaF_2:Eu, X-ray luminesc. 79−99933

europium continued
$CaF_2:Eu^{2+}$, circular polarisation in luminesc. and optical orientation 78-6740
$CaF_2:Eu^{2+}$, ENDOR of ^{19}F ligands, under uniaxial stress 77-16207
$CaF_2:Eu^{2+}$, energy transfer to luminesc. centres, pulsed excitation obs. 77-85781
$CaF_2:Eu^{2+}$, nuclear spin diffusion barrier, ^{19}F NMR Obs. 78-64282
$CaF_2:Eu^{2+}$, photoluminesc. mag. circ. polaris. 80-89056
$CaF_2:Eu^{2+}$, second order perturbation in vibronic system 78-30893
$CaF_2:Eu^{2+}$, short high-energy pulse induced X-ray luminesc., anomalous kinetics 77-59608
$CaF_2:Eu^{2+}$, Sm^{2+}, relaxed resonance acoustic phonons in vibronic anti-Stokes luminescence *(Russian)* 80-93404
$CaF_2:Eu^{2+}$, tunable optical detection and generation of THz phonons 79-65149
$CaF_2:Eu^{2+}$, two-photon absorpt. spectra exam. of excited state of Eu^{2+} 77-77261
$CaF_2:Eu^{2+}$, X-ray excited luminesc., $^5D_0$-$^7F_1$ transition 80-2842
$CaF_2:Eu^{2+}$, X-ray induced luminesc. kinetics, energy transfer processes 79-8181
$CaF_2:Eu^{2+}$ single cryst., temp. depend. of second-order spin-lattice coeffs. 77-90029
$CaF_2:Eu^{3+}$, ^{19}F NMR studies 80-60429
$CaF_2:Eu^{3+}$, dielec. spectrum 77-36171
$CaF_2:Eu^{3+}$, one- and two-photon luminesc. excitation spectra 79-83023
$CaF_2:Eu^{3+}$, VUV absorpt. spectra, dopant clustering 80-108230
$CaF_2:Gd^{3+}$, Eu^{2+}, natural, EPR study of impurity centres 78-19318
$CaF_2:Sm^{2+}(Eu^{2+})$, cubic crysts., vibronic spectra, induced dichroism method 77-81131
$CaLaGaO_4:Eu^{3+}$, luminesc. of α- and β-phases 77-90186
$CaLaGaO_4:Eu^{3+},Bi^{3+}$, luminesc. influenced by struct. transition 78-6773
CaO:Eu, phosphor, isothermal decay 80-55156
CaO:Eu,Tb phosphor emission under X-ray excitation 79-52011
CaO(S),Eu^{2+} to Eu^{3+}, charge transfer *(Russian)* 78-72403
$Ca(PO_3)_2:Eu^{3+}$, amorphous, phonon-assisted site-to-site electronic energy transfer, fluoresc. line narrowing obs. 77-81140
$Ca(PO_3)_2:Eu^{3+}$, anomalous spectral props. 79-38614
CaS:Tb,Eu phosphors, fluoresc. spectra under X-ray excitation 80-16083
$CaSO_4$:Eu, origin of thermoluminescence 77-85813
$CaSO_4$:Eu phosphors, fluorescence spectra, thermolum. glow curve 80-2879
$CaS(Se):Eu^{2+}$, emission and excitation spectra obs. 80-55162
$Ca_3Y_2Ge_3O_{12}:Eu^{3+}$, garnets, prep., struct., luminesc., absorpt. spectra, Eu^{3+} localisation 77-69884
$CdBr_2:Eu^{2+}$, layered, temp. depend. of consts. in ESR Hamiltonian, 16-300K *(Russian)* 77-32254
CdF_2:Eu, role of solution and precipitation phenomena on ITC spectra 80-7265
CdF_2:Eu, semicond., symmetry of optical centres, optical and elec. props. 77-59592
$CdF_2:Eu^{2+}$, EPR spectra, hydrostatic press. and temp. effects 80-84648
$CdF_2:Eu^{3+}$, electroluminescence spectra from 400 to 700 nm *(Russian)* 77-69916
$CdF_2:Eu^{3+}$, luminesc., charge transfer states 79-33799
$CdF_2:Eu^{3+}$, luminesc. spectra conc. and annealing depend. 79-65917
$CsDy(MoO_4)_2:Eu^{3+}$, anomalous effect of impurity on struct. phase transition temp. *(Russian)* 77-69083
$CsI:Eu^{3+}$, cryst., influence of impurities on yield stress 79-15748
Er^{3+} doped phosphors, IR excitation and absorpt. and emission spectra *(Russian)* 79-52021
$^{152,154}Eu$ fixation in solid/liquid systems 79-13530
Eu I, 5p spectra collective excitation, rel. to double photoionis. 77-50387
Eu I, high resolution study of $4f^76s^2 \rightarrow 4f^76s6p$ 79-54790
Eu I, isotope shift meas., level classification in $4f^65d6s^2$ and $4f^75d6p$ configs. 77-30831
Eu II, lifetimes of $^7P_{2\text{-}4}$, $^9P_{3\text{-}5}$ excited levels 79-3407
Eu III, two-electron single-photon transition in electron-atom collisions *(Russian)* 79-68319
Eu^+, electron impact, resonant line excitation 78-82847
Eu^+, IR transition probability meas. 79-6897
Eu^+ metastable states in discharge plasma, anomalously high speed deexcitation, modulation of induced radiation obs. 80-44014
^{151}Eu (^{153}Eu) excitation transfer, effect on selective photoionisation 80-99538
Eu^{2+} activated phosphors, luminesc. efficiency, temp. and high pressure 78-23508
Eu^{2+}, broadband luminesc. in fluorite struct. crysts. 79-65923
Eu^{2+} doped microcrystals, unusual optical emission 79-73992
Eu^{2+}, ground state, fourth-order spin-Hamiltonian parameters 77-69278
Eu^{2+} impurities in cubic crystals, 5d→4f radiative transition probability calc. 80-71474
Eu^{2+} in aqueous solution, multiphoton excitation and emission 78-94222
Eu^{2+}, in metallic hosts, Kondo effect 80-39739
Eu^{2+}, isomer shift in fluorites, Mossbauer studies 79-56649
Eu^{3+} activated rare earth oxysulphides and oxyhalides 79-56849
Eu^{3+} fluoresc. lineshape in glass, temp., time and conc. depend., two-phonon Raman scatt. 78-64406
Eu^{3+} fluorescence spectra in rare earth oxyhalides *(French)* 80-89042
Eu^{3+} in aq. soln. MCD spectrum, sign inversion 77-34669
Eu^{3+} in molten $LiNO_3$-KNO_3, transition probabilities in absorpt. and fluoresc. spectra 79-50085
Eu^{3+}, in soln., non-radiative transitions as Forster's energy transfer to solvent vibrations 80-1014
Eu^{3+}, intracavity enhancement of absorpt. in nanosecond regime 78-78839
$Eu^{3+} \rightarrow Nd^{3+}$ diffusion-limited energy transfer in Na borate glass 78-31238
Eu^{3+}, non-radiative energy transfer to Pr^{3+} and Er^{3+} in dimethylsulphoxide 79-47510
Eu^{3+}, nonradiative $^5D_1$-$^5D_0$ transition in various solvents 79-3479
Eu^{3+}, rare-earth ions, charge transfer and crystal field theory 80-70654
Eu^{3+} soln., luminesc. quantum yield spectral depend. 80-2838
Eu-W-O, reaction system, thermodynamics, mass spectrometric obs. 77-77748
$Eu+H^+$, atomic K-shell ionis., X-ray emission 79-18280
$Eu+H^+$, two-step laser isotope enrichment using charge transfer ionisation 79-867

europium continued
$Eu+O_2$, reaction cross-section, energy depend. 77-9054
Eu+Sr, absorptive collisional energy transfer, laser induced excitation spectra 80-63584
Eu+Sr, laser induced collisional energy transfer profile, high resolution study 80-83471
$Eu^{3+}+UO_2^{3+}$ solution, nuclear pumped liq. lasers, LASL program 80-64011
^{151}Eu, ^{153}Eu, two-step laser photoionisation *(Russian)* 77-6952
^{152}Eu, X-ray emission probabilities per decay 80-14027
Eu*+Sr, light-induced collisional energy transfer 78-50614
$Eu^*+Sr+h\omega \rightarrow Eu+Sr^{**}$, photon assisted collisional energy transfer 78-90285
$GdBO_3:Eu^{3+}$ and $GdBO_3:Bi^{3+},Eu^{3+}$, vacuum UV excitation spectra and quantum efficiencies 79-28811
$GdNbTiO_6:Eu^{3+}$ emission under UV excitation 78-6770
$Gd_2O_3:Eu^{3+}$, luminesc., rel. to crystallographic data 79-33793
$Gd_2O_2S:Eu^{3+}$, luminesc., excitation spectra, cooperative phonon sidebands 79-33771
$GdVO_4:Eu^{3+}$, absorption and fluoresc. spectra, SU(2) chain *(French)* 78-28912
$GdVO_4:Eu^{3+}$, ligand field parameters, computed from fluoresc. and absorption data 78-2453
$Gd_xZr_{1-x}O_{2-x/2}:Tb^{3+}(Eu^{3+})$, energy transfer, luminesc. 79-51999
He-Eu ionic gas discharge laser, increasing energy parameters *(Russian)* 77-58320
He-Eu pulsed laser, pumping rate and electron density meas. 80-9868
$HfO_2:Eu^{n+}$, impurity valence transitions 77-51694
$KBr:Eu^{2+}$, spin Hamiltonian cryst. field consts. calcs. 79-38035
KBr:Eu(Yb), electron-irrad., photostimulated luminesc., ionic processes 78-52561
KBr(Cl):Eu, Z_2-centre investig. by EPR and optical absorpt. 77-16177
KCl:Eu, additively coloured, ESR obs. of $^{2+}$ complex 77-16170
KCl:Eu, Eu^{2+} concentration effect on lattice parameter and density of crystals 80-88169
KCl:Eu, flow stress 77-36577
KCl:Eu, impurity conc. determ. by optical absorpt. meas. 77-32409
KCl:Eu, injection electrolum., fields up to 10^4 V cm^{-1} 77-12445
KCl:Eu, OH^-, EPR meas. on Eu^{2+} complex 78-10773
KCl:Eu crystallophosphores, aggregation of $Eu^{2+}v_c^-$ centres *(Russian)* 78-43909
KCl:Eu IR laser window lattice equilibrium obs. 79-14055
$KCl:Eu^{2+}$, cation impurity-vacancy pairs, effect of X-rays 79-55778
$KCl:Eu^{2+}$, γ-irrad., photostimulated low temp. recomb. luminesc. 80-11435
$KCl:Eu^{2+}$, lattice defect equilib. optical absorpt. and cond. studies 80-29767
$KCl:Eu^{2+}$, optical absorpt. meas. for Eu^{2+} conc. determ. 79-51137
$KCl:Eu^{2+}$, radiationless transitions, photoacoustic spectra 77-32405
$KCl:Eu^{2+}$, radiationless processes 78-80391
$KCl:Eu^{2+}$, spin Hamiltonian cryst. field consts. calcs. 79-38035
$KCl:Eu^{2+}$, zero phonon lines, time-resolved fluoresc. spectra 77-77269
$KCl:Eu^{2+}$ crystals, photostimulated afterglow investigation at room temp. 80-108259
KCl(Br):Eu, Eu^{2+} ESR meas. 78-80209
$KF+Eu^{2+}$, cryst., hyperfine splitting, EPR 78-2733
$KI:Er^{2+}$, elec. field effect on mech. of recomb. 78-80397
KI:Eu, electron-irrad., photostimulated luminesc., ionic processes 78-52561
$KMgF_3:Eu^{2+}$, f-f transition, cryst. field parameters calc. 77-15805
$KMgF_3:Eu^{2+}$, Zeeman absorpt. and luminesc. spectra *(Russian)* 77-69872
$KY_3F_{10}:Eu^{2+}$, luminescence 79-78746
$KY_3F_{10}:Eu^{3+}$, cryst. field parameters and intensity parameters, J-mixing effects 80-59932
$KY_3F_{10}:Eu^{3+}$, fluoresc. intensity, 77 to 4K, cryst. field parameters of Eu^{3+} 78-72580
$KY_3F_{10}:Eu^{3+}$, fluoresc. decay, radiative and nonradiative transition probabilities 78-72581
$KZnF_3:Eu^{2+}$ f-f transition, cryst. field parameters calc. 77-15805
$Khu_3F_{10}:Eu^{3+}$, site occupancy from excitation and emission spectra *(French)* 77-81145
$La:Eu^{2+}$, liquid, γ-ray spectra observation of exchange interaction 80-84672
$LaAl_2:Gd^{3+}(Eu^{2+})$, cryst. field parameters, relax. rates 78-84482
LaF_3:Eu, cryst. field anal. of triply ionised ion spectra 80-2796
$LaF_3:Eu^{3+}$, absorpt and laser fluoresc. spectra 77-52159
$LaNbO_4:Eu^{3+}$, single cryst., photoluminesc. obs., vibronic transition dichroism 77-69890
La_2O_2S:Eu, high press. effect on luminesc. efficiency and lifetime, charge transfer absorpt. 80-66266
La_2O_2S:Eu, slow phosphoresc., high press. study 80-80839
$La_2O_2S:Eu^{3+}$, luminesc., excitation spectra, cooperative phonon sidebands 79-33771
$LiBaAlF_6:Eu^{2+}$, luminesc., band emission and line emission 79-28810
LiCl-KCl:Ln^{n+}, fused eutectic, electrolytic behaviour *(Japanese)* 79-16009
LiF:Eu, impurity effect on elec. cond. 79-7709
$LiNbO_3:Eu^{3+}$, Cr^{3+}, exciton migration, laser time-resolved spectra obs. 79-69861
$LiNbO_3:Eu^{3+}$, luminesc. props., Li/Nb ratio effect 80-97323
Li_2O-$B_2O_3:Eu^{3+}$ glass, laser induced fluoresc. line narrowing, struct. 79-38613
$Li_{14}ZnTa_4O_{18}$:Eu, fluorescence and cryst. symm. 77-24886
$Lu_2O_2S:Eu_3^+$, luminesc., excitation spectra, cooperative phonon sidebands 79-33771
$LuVO_4:Eu^{3+}$, absorption and fluoresc. spectra, SU(2) chain *(French)* 78-28912
$LuVO_4:Eu^{3+}$, ligand field parameters, computed from fluoresc. and absorption data 78-2453
$Lu_2(WO_4)_3$:Eu, and undoped crystals, luminesc. obs. 80-89047
$MgS:Eu^{2+}$, emission and excitation spectra obs. 80-55162
$MgS:Eu^{2+}$ phosphors, anal. of absorption spectra $4f^{N+1} \rightarrow 4f^N5d$-6s 80-7383
$MnF_2:Eu^{3+}$, fluorescence props. 79-73994
$Na_{56}(AlO_2)_{56}.(SiO_2)_{136}:Eu^{3+}$, Y-type zeolite, luminesc. props. 79-83017
$NaBr:Eu^{2+},Ho^{3+}$, single cryst., cluster luminesc. centres *(Russian)* 77-20922
$NaBr:Ho^{3+},Eu^{2+}$, single cryst. synthesis, rel. to purification methods 77-8744

europium continued
- NaCl:Eu, secondary Eu phase dissolution, EPR and optical absorpt. study 80−96655
- NaCl:Eu^{2+}, ESR and elec. field effects 77−28441
- NaCl:Eu^{2+}, optical absorpt. meas. for Eu^{2+} conc. determ. 79−51137
- NaCl:Eu^{2+}, oriented growth and cryst. struct. of precipitated phases 80−24303
- NaCl:Eu^{2+}, reorient. of Eu^{2+}-vacancy complexes, ESR method using elec. field effect 79−99768
- NaCl:Eu^{2+}, spin Hamiltonian cryst. field consts. calcs. 79−38035
- NaCl-NaF:Eu^{2+}, point defects, ionic thermal current and optical meas. 80−6403
- NaCl(Br):Eu, Eu^{2+} ESR meas. 78−80209
- NaF+Eu^{2+}, cryst., hyperfine splitting, EPR 78−2733
- NaMgF$_3$:Eu$^+$, Zeeman absorpt. and luminesc. spectra *(Russian)* 77−69872
- Na$_2$O-Al$_2$O$_3$-P$_2$O$_5$:Eu glasses, fluorescence line narrowing meas. *(French)* 80−34975
- NaPO$_3$:Eu^{3+}, luminesc. of Eu^{3+}, transition probabilities 80−80845
- PbFCl:Eu^{2+} crystal field splitting, parametrisation of temperature dependence 78−91652
- Pb$_3$(PO$_4$)$_2$:Gd^{3+}(Eu^{2+}), EPR spectra of α- and β-phases 80−11261
- RbCl:Eu, electron-irrad., photostimulated luminesc., ionic processes 78−52561
- RbCl:Eu, γ-irrad., thermoluminesc., EPR meas. 78−84670
- RbCl:Eu^{2+}, EPR of ^{153}Eu^{2+} and ^{151}Eu^{2+} 80−11259
- RbCl:Eu^{2+}, optical absorpt. meas. for Eu^{2+} conc. determ. 79−51137
- RbCl:Eu^{2+}, tetragonal sites, spin Hamiltonian parameters, EPR and UV absorpt. spectra obs. 80−50177
- RbCl(Br):Eu, Eu^{2+} ESR meas. 78−80209
- RbF+Eu^{2+}, cryst., hyperfine splitting, EPR 78−2733
- Rb$_2$InOH(SeO$_4$)$_2$.H$_2$O:Eu^{3+}, synthesis and luminesc. 79−91488
- Sc$_2$(WO$_4$)$_3$:Eu, and undoped crystals, luminesc. obs. 80−89047
- Sc$_x$Y$_{0.95-x}$Sm$_{0.05}$, ^{153}Eu isomer shift, at. vol. depend. 77−43915
- SmB$_6$:Eu^{2+}, mixed balence compound, ESR g-shifts and linewidths 78−48035
- SmFe$_2$(Co$_2$)(Ni$_2$):Eu^{3+}, hyperfine interactions and exchange fields acting on Eu^{3+}, Mossbauer obs. 77−63338
- SmS:Eu, excited-state exchange interactions, EPR meas. 78−68374
- Sm$_3$S$_4$:Eu, excited-state exchange interactions, EPR meas. 78−68374
- SmSe:Eu, excited-state exchange interactions, EPR meas. 78−68374
- SnO$_2$:Eu film, RF cosputtering, cryst. site of Eu, cathodolum. obs. 77−7987
- SnO$_2$:Eu powder phosphor, prep., low energy electron excitation 78−39608
- SnO$_2$:Eu^{3+}, luminesc. and charge compensation 77−28618
- SnO$_2$:Eu^{3+}, luminesc. and charge compensation 78−76532
- SrB$_2$O$_4$:Eu^{2+}, luminesc. of high-press. phases 80−100680
- SrF$_2$:Eu, dipolar complex exam. 79−38435
- SrF$_2$:Eu^{2+}, circular polarisation in luminesc. and optical orientation 78−6740
- SrF$_2$:Eu^{2+}, ENDOR of ^{19}F ligands, under uniaxial stress 77−16207
- SrF$_2$:Eu^{2+}, phonon spectroscopy, phonon pulse spatial, spectral and temporal evolution 78−34580
- SrF$_2$:Eu^{2+}, spectral, spatial and temporal phonon spectroscopy, new spectrometer 78−83892
- SrF$_2$:Eu^{2+}, superfine struct. in EPR obs. 77−1593
- SrF$_2$:Eu^{2+}, tunable optical detection and generation of THz phonons 79−65149
- SrF$_2$:Eu^{2+}, two-photon absorpt. spectra exam. of excited state of Eu^{2+} 77−77261
- SrR$_2$O$_4$:Eu^{3+}, luminesc. 77−52156
- SrTiO$_3$:Eu(Sm), absorption spectra, Ti^{3+} ion and Z-centre formation 77−24871
- TaS$_2$-Eu intercalation compound, CDW's and superlattice patterns 77−47746
- (Y,Gd)BO$_3$:Eu^{3+}, phosphor, vac. UV excitation spectra, appl. to gas discharge display 80−2816
- YAG:En^{3+}, cathodolum. efficiency rel. to activator conc. 80−11479
- YAG:Eu^{3+}, cathodolum. intensity, temp. depend., comparative study with other YAG:R^{3+} crysts. 79−99953
- YAG:Eu^{3+}, reson. fluoresc. spectra, showing multiple Eu^{3+} sites 80−2812
- YBO$_3$:Bi^{3+},Eu^{3+}, vacuum UV excitation spectra and quantum efficiencies 79−28811
- YIG:Eu,Pb, bubble domain film, magnetocrystalline anisotropy coeff. reduction, by Pb addition 79−11329
- YNbTiO$_6$:Eu^{3+} emission under UV excitation 78−6770
- Y$_2$O$_3$:Eu, cathodoluminesc. investig., appl. to cathode ray tube screening 80−108282
- Y$_2$O$_3$:Eu, fluoresc., cathodoluminesc. and thermal quenching 79−47488
- Y$_2$O$_3$:Eu, surface luminesc. centres excitation characts. 78−52560
- Y$_2$O$_3$:Eu sintered slice, DC electroluminesc., impact excitation 79−47522
- Y$_2$O$_3$:Eu^{3+}, absorpt. spectra, fluoresc., electron beam excitation 78−92093
- Y$_2$O$_3$:Eu^{3+}, cubic, laser-induced polarised fluoresc., Stark levels and cryst. field parameters 79−95838
- Y$_2$O$_3$:Eu^{3+}, quantum yield in candoluminescence process by low energy H$^+$ ion bombard. 79−65930
- Y$_2$O$_2$S:Eu, high press. effect on luminesc. efficiency and lifetime, charge transfer absorpt. 80−66266
- Y$_2$O$_2$S:Eu, phosphor, temp. meas. by line shift method 77−13750
- Y$_2$O$_2$S:Eu phosphor, luminescence saturation effects due to N$_2$ laser and cathode-ray excitation 80−40151
- Y$_2$O$_2$S:Eu phosphor, particles of different sizes, prep. by flux method 77−44140
- Y$_2$O$_2$S:Eu^{3+}, luminesc., excitation spectra, cooperative phonon sidebands 79−33771
- Y$_2$O$_2$S:Eu^{3+}, temp. and viscosity depend. of colour coords. 80−40149
- Y$_2$O$_2$S:Tb^{3+},Eu^{3+}, energy transfer mechanism 78−6793
- YVO$_4$:Eu, cathodoluminesc. investig., appl. to cathode ray tube screening 80−108282
- YVO$_4$:Eu, cluster electron struct., X-alpha calc., emission spectra 78−2898
- YVO$_4$:Eu, fluoresc., cathodoluminesc. and thermal quenching 79−47488
- YVO$_4$:Eu^{3+}, absorption and fluoresc. spectra, SU(2) chain *(French)* 78−28912
- YVO$_4$:Eu^{3+}, absorpt. spectra, fluoresc., electron beam excitation 78−92093
- YVO$_4$:Eu^{3+}, energy transfer, laser time-resolved spectroscopy 78−27306
- YVO$_4$:Eu^{3+}, laser site-selection spectroscopy investigation 78−68556
- YVO$_4$:Eu^{3+}, ligand field parameters, computed from fluoresc. and absorption data 78−2453
- YVO$_4$:Eu^{3+} phosphor, cathodoluminesc. and photon statistics 77−59621
- Y$_2$WO$_6$:Eu, noncontinuum model for energy transfer 79−33800
- Y$_2$WO$_6$:Eu^{3+}, luminesc., rel. to crystallographic data 79−33793
- Y$_6$WO$_{12}$:Eu^{3+}, crystal struct., fluorescence spectra, exam. 78−52558
- ZnS:Eu^{3+}, origin of red fluoresc., occurrence of rare earth oxysulphide inclusions *(French)* 77−69875
- ZrF$_4$:Eu^{3+} glass, luminesc. of Eu^{3+}, transition probabilities 80−80845

europium alloys
- indirect magnetic interactions, NMR anal. 80−71193
- mixed valence, role of phonons and Coulomb interactions 79−38032
- Mossbauer effect isomer shift, charge density at nucleus, trends 77−48112
- noble metal-Eu, dil., hyperfine fields of rare earth impurity, calc. 80−15486
- valence fluctuations, role of charge screening 78−51944
- valence fluctuations, thermal occupation effects 78−72118
- Ba-Eu, phase diag. *(Russian)* 78−80514
- Bi$_3$Sr$_{1-x}$Eu$_x$, supercond. and mag. ordering 78−56252
- Dy-Eu, mag. props. at low temp. in high mag. fields 79−56570
- (Eu,Sn)Mo$_6$S$_8$, ternary superconductor, mag. interactions 79−73613
- Eu-Ag, amorphous, formation and mag. props. 79−91216
- Eu-As system, cryst. struct. of phases formed 78−26493
- Eu-Cd compounds, Mossbauer effect, mag. props. and lattice consts. 77−36164
- Eu-Ga alloys, phase diagrams, struct. and comp. *(Russian)* 79−52163
- Eu-transition metal intermetallics, valence fluctuations 78−91649
- Eu+t$_2$, high press. Mossbauer spectra, interconfig. charge fluctuations 77−63341
- EuAg$_5$, cond. electron spin polarisation 77−63136
- EuAl$_2$, and EuAl$_4$, hyperfine interactions, high press. Mossbauer expts. 78−43714
- EuAl$_2$Ga$_2$, synthesis, NMR and X-ray absorpt. studies 80−108083
- Eu$_{11}$As$_{10}$, Eu$_5$As$_{10}$, Eu$_{3+x}$As, Eu$_5$As$_3$, Eu$_4$As$_2$O, cryst. struct. 78−18585
- Eu$_5$As$_3$, cryst. struct. of high and low temp. phases 78−75626
- EuAu$_5$, cond. electron spin polarisation 77−63136
- Eu$_{0.95}$Ba$_{0.05}$Pt$_2$, ^{151}Eu Mossbauer studies at high press. 80−39923
- EuBe$_{13}$:Gd, Van Vleck paramagnet, exchange parameters, ESR determ. 77−4557
- Eu$_x$Ca$_{1-x}$, mag. ordering temp. conc. depend., Eu mag. hyperfine field temp. depend. 78−14971
- EuCu$_2$, and EuCu$_5$, hyperfine interactions, high press. Mossbauer expts. 78−43714
- EuCu$_5$, cond. electron spin polarisation 77−63136
- EuCu$_5$(Pt$_2$)(Pd$_2$), indirect exchange, spin echo NMR meas. 80−15822
- EuCu$_2$Si$_2$, fluctuating valence system, quadrupole interaction temp. depend. 80−54972
- EuCu$_2$Si$_2$, interconfiguration fluctuation, NMR expts. 80−66069
- EuCu$_2$Si$_2$, valence fluctuation and temp. depend. of Cu nuclear quadrupole interaction 80−15818
- EuCu$_2$Si$_2$, XPS studies, valence band, 4-f region 78−6831
- EuFe$_4$Al$_8$, mag. ordered, mixed valency of Eu, X-ray, susceptibility and Mossbauer spectra studies 79−19728
- EuIr$_2$, superconductivity 79−78248
- Eu$_x$La$_{1-x}$Al$_2$, binding energy and workfunction charges using XPES 80−33928
- Eu$_x$La$_{1-x}$Al$_2$, cryst. fields and exchange parameters, ESR meas. 80−71175
- Eu$_x$La$_{1-x}$Al$_2$, dil. EPR, cryst. fields and effective exchange interaction 80−66029
- Eu$_{0.25}$La$_{0.75}$Rh$_2$, high press. Mossbauer spectra, interconfig. charge fluctuations 77−63341
- Eu$_{1-x}$La$_x$S, electron struct., lattice consts., X-ray spectral study *(Russian)* 80−100432
- EuMg$_5$, Mossbauer effect, effective moments, mag. ordering temp. and isomer shifts 80−34833
- Eu$_2$Mg$_{17}$, Mossbauer effect, effective moments, mag. ordering temp. and isomer shifts 80−34833
- EuMg$_2$H$_x$, Mossbauer effect exam. 78−48094
- Eu(Ni$_{1-x}$Cu$_x$)$_5$, mixed valency, isomer shift temp. depend. 78−84511
- EuNi$_x$Cu$_{5-x}$, mixed valency of Eu, Mossbauer expts. 78−52407
- EuNi$_5$H$_x$, Mossbauer effect exam. 78−48094
- EuNi$_x$Zn$_{5-x}$, mixed valency of Eu, Mossbauer expts. 78−52407
- EuPd, mech. of H absorption, Mossbauer, mag. and X-ray diffr. meas. 78−38846
- EuPd$_2$, elec. field gradient, spin echo NMR meas. 80−20509
- EuPt$_2$, ^{151}Eu Mossbauer studies at high press. 80−39923
- EuPt$_2$, elec. field gradient, spin echo NMR meas. 80−20509
- EuPt$_x$ compounds, partial valence change, ^{151}Eu Mossbauer and magnetisation obs. 80−70167
- EuRh$_2$, H$_2$ absorbing, degradation by cycling 78−34628
- EuRh$_2$, mech. of H absorption, Mossbauer, mag. and X-ray diffr. meas. 78−38846
- EuRh$_{2-x}$Pt$_x$, intermediate-valance state, XPS obs. 77−28687
- EuSn$_3$, hyperfine interactions, high press. Mossbauer expts. 78−43714
- EuZn$_5$, cond. electron spin polarisation 77−63136
- Fe-Eu, dil., hyperfine interaction of ^{153}Eu, Mossbauer effect meas. 78−43703
- Gd-Eu, mag. props. at low temp. in high mag. fields 79−56570
- Gd-Eu, magnetocrystalline anisotropy, magnetisation and torque curve meas. 80−65859
- Ho-Eu, mag. props. at low temp. in high mag. fields 79−56570
- La-Eu, dil., DHCP, impurity effects on supercond. T$_c$, electron pair breaking 77−36013
- La-Eu, EPR investig. of local moment, correl. with supercond. props. 77−63282
- LaEu, mag. supercond., phase diagram, bulk susceptibility meas. 77−59353
- La$_{1-x}$Eu$_x$Al$_2$, cryst. field splitting and spin-spin interaction of Eu^{2+}, ESR meas. 78−68370
- La$_{0.9}$Eu$_{0.1}$Ni$_{4.6}$Mn$_{0.4}$, absorption-desorption props. of H$_2$, degradation mechanism, Mossbauer study 80−88431
- Mg-Eu, dil. alloy, mag. suscept. meas. 77−89925
- MgEu, dil. alloy, cold worked, valence transform. of Eu due to defect association, mag. suscept. and Mossbauer meas. 77−51404
- Pr-Eu, dil., magnetisation, Mossbauer spectra 80−15928
- PrEu, magnetic interactions, Mossbauer spectra quadrupole splitting, crystal field parameters 80−39907

europium alloys continued
ScAl$_2$-Eu, intermediate valence on Eu ions, Mossbauer isomer shift 80−84587
Sm-Eu, dil., mag. and elec. hyperfine interac., TDPAD obs., paramag. behaviour, exchange integral 80−103908
Yb-Eu alloys, mag. ordering, magnetisation meas. 80−7081

europium compounds
see also europium alloys
chalcogenides, anomalous Hall effect, analysis 77−20344
chalcogenides, anomalous Hall effect, impurity scatt. 78−39131
chalcogenides, cond. band spin struct. 80−71577
chalcogenides, heavily doped mag. semiconductors, effect of carriers' statistics on indirect exchange 77−69280
chalcogenides, mag. polaron stability 80−96803
chalcogenides, magnetic exciton states optical props. 77−31948
chalcogenides, magnetic semiconductor, light scatt. exam. 79−61372
chalcogenides, multiphonon inelastic light scatt., hot recomb. 77−8559
chalcogenides, paramag., spin-disorder-induced Raman scatt. 78−19474
chalcogenides, paramagnetic, optical orientation of 4f electrons, transverse and longit. pumping 77−69799
chalcogenides, Raman scatt. near mag. phase transitions 79−47458
chalcogenides, resonant Raman scatt. 77−55787
chalcogenides, resonant Raman scattering model via magnetic exciton in ferromagnetic phase 80−93326
chalcogenides, spin-dependent Raman scatt. from phonons 80−97274
chalcogenides, spin-disorder Raman scatt., mag. phase depend., theory 78−10887
chalcopnictides, Eu$_4$Y$_2$X, (Y=pnictogen, X=chalcogen), anti-Th$_3$P$_4$ type struct. 79−65048
chelate, fluoresc. lifetime, depend. on optical environment 80−9630
complexes, luminesc. spectra, electronic-vibr. transitions 77−52171
crystal field and Slater parameters and coordination 78−6771
domain boundary mobility, effect of easy magnetization axis inclination 78−19293
double metaphosphates with alkali metals or H, luminesc. props. 80−100675
ethylsulphate nonahydrate, MCD due to mag. dipole transitions 77−24825
europium B-diketone chelate solns., fluoresc. quenching by appl. voltage, display devices appl. 79−87497
EuSb$_4$S$_7$, single cryst. growth, and X-ray anal. 79−100033
EuSe, photocond. and photodiffusive voltage spectra 80−96940
formate, IR spectra and phase transitions, under pressure 78−31179
growth from PbO-B$_2$O$_3$ based flux, prop. depend. on Pb content 80−39824
ionic, magnetic interaction potential 78−10682
monochalcogenides, anti-stokes luminesc. 78−60515
monochalcogenides, multiphonon inelastic light scatt. 77−90144
monochalcogenides, Raman light scatt., phonons and valence fluctuations, review 77−63415
niobates, mixed metal, Eu oxidation state, mag. props., Mossbauer study 80−66080
phosphors, liq., using aprotonic solvents 80−20686
phthalocyanine solutions, bleaching by ruby laser beam 78−30030
piperidinium salts, emission spectra, ligand field symmetries 79−61413
pyrochlores, Eu$_2$Z$_2$O$_7$, (Z=Ti, Ru, Ir, Mo, Sn, Zr, Pb, Pt and Hf), elec. field gradient, Mossbauer expt. 79−8077
selenides X-ray phase anal. 77−11514
sulphides, EuRS$_4$, R=La, Ce, Pr, Nd, Sm, Gd, elec. cond. meas. 80−65555
tantalates, mixed metal, Eu oxidation state, mag. props., Mossbauer study 80−66080
ternary metal oxides, DC electrolum. 77−77300
tetrabutylammonium europium yttrium isothiocyanate, conc.-depend. electron-phonon coupling, and self-quenching 80−60657
tetrahedral complexes, ligand struct., rel. to luminesc. spectra satellite intensity *(Russian)* 78−72603
X-ray L-absorption spectra, 'white line' absorpt. maximum, chem. shifts 77−58042
(YSmEuCa)$_3$(FeGe)$_5$O$_{12}$, garnet film, ion implanted, bubble domain props. 78−88152
o, Heisenberg ferromagnet, spin dynamics, neutron scatt. expts. 77−20619
Al$_2$O$_3$-Eu$_2$O$_3$, phase diagrams at high temps., exam. 78−44114
Al$_2$O$_3$-Eu$_2$O$_3$ system, phase diagram at high temp. *(Japanese)* 80−40339
β-Al$_2$O$_3$-EuO, X-ray diffuse scatt. 78−71725
Ba$_2$EuFaO$_6$, luminescence Raman spectra, means for localisation of binding energy levels *(German)* 78−88304
Ba$_2$EuNbO$_6$, luminescence Raman spectra, means for localisation of binding energy levels *(German)* 78−88304
BeF$_2$-KF-CaF$_2$-AlF$_3$-EuF$_3$ fluoroberyllate glass, Eu^{3+} fluoresc. linewidth 80−66285
C$_6$Eu intercalation compounds, three dimensional continuous melting 80−59631
Ca$_{1-x}$Eu$_x$Si$_2$, solid solns., α-ThSi$_2$ struct. type, comp. and press depend. 78−91322
CdF$_2$:EuF$_3$ films, electroluminesc. meas. *(French)* 79−11471
Ce$_x$Eu$_{1-x}$B$_6$, mag. susceptibility, 80-1000K 79−73674
CsCa$_{0.95-x}$Mg$_x$Eu$_{0.05}$F$_3$, blue luminesc. obs. 77−32428
Cs$_3$EuF$_6$, CsEu$_2$F$_7$, cryst. struct. by X-ray diffr., equilib. in CsF-EuF$_3$ *(French)* 78−44107
CsF-EuF$_3$ system, thermal anal. and X-ray diffr., phase equilibria *(French)* 78−44107
Cs$_2$NaEuCl$_6$, luminescence Raman spectra, means for localisation of binding energy levels *(German)* 78−88304
Cs$_2$NaEuCl$_6$, mag. dipole transitions ^{5}D$_3$→^{7}F$_4$, interpretation 79−42505
Cs$_2$NaEuCl$_6$, Raman spectra 77−77205
Cs$_2$NaY$_{0.99}$Eu$_{0.01}$Cl$_6$, cryst. field parameters of Eu^{3+} ion 77−31983
EUIG:Pb, valence of Pb in Fe-garnets 77−47480
(ErEu)$_3$(FeGa)$_5$O$_{12}$ film, for mag. writing and magneto-optical displays 78−6549
Er$_2$EuFe$_{5-x}$Ga$_x$O$_{12}$, rag-domain garnet film, controlled variation of props. under O$_2$ annealing 79−15328
(Eu,Er)$_3$(Ga,Fe)$_5$O$_{22}$/(Y,Sm)$_3$(Ga,Fe)$_5$O$_{12}$ double-layer self-biasing garnet films, dynamic behaviour of domain walls 80−34722
(Eu,La,Ca)$_3$(Fe,Ga,Al)$_5$O$_{12}$ film, LPE growth and induced orthorhombic anisotropy 77−20652
(Eu,Lu)$_3$(Fe,Al)$_5$O$_{12}$ film, epitaxial, increased domain wall velocities, due to orthorhombic anisotropy 77−20653

europium compounds continued
(Eu,Lu)$_3$Fe$_5$O$_{12}$ epitaxial film, induced orthorhombic anisotropy 77−69640
(Eu,Lu)$_3$Fe$_5$O$_{12}$, epitaxial film, orthorhombic mag. anisotropy 78−19290
(Eu,Lu)$_3$Fe$_5$O$_{12}$, submicron bubble films on rare earth-Ga garnet substrates, prep. and mag. props. 78−91909
(Eu,Lu)$_3$Fe$_5$O$_{12}$:Ga(Al)(Ca,Ge), bubble material, dynamic characterisation, comparison between transport and FMR methods 80−39833
(Eu, Pb)MnO$_3$, flux growth 79−83113
(Eu,Y)$_3$Fe$_5$O$_{12}$, low temp. CVD epitaxial film growth and mag. props. 79−42406
(Eu,Yb)$_3$Fe$_5$O$_{12}$, low temp. CVD epitaxial film growth and mag. props. 79−42406
Eu chalcogenide mag. semiconductors, modulation spectroscopy *(Japanese)* 77−24862
Eu complex, (Et$_4$N)$_3$ [Eu(NCS)$_6$], Eu^{3+} ion site symm. 78−84656
Eu complex, benzoylacetonate, energy transfer at high pressures 78−52541
Eu complex, benzoyltrifluoro-acetone-chelate, refr. index determ. of fluoresc. films 80−40175
Eu complex, Eu(III) β-diketonates, Mossbauer studies 79−61286
Eu complex, europium benzoyltrifluoroacetane chelate layers, fluorescence lifetime changes induced by variable optical environments 80−93386
Eu complex, fast reactions, pulsed selective photoexcitation, rate determ., spectral method 77−86336
Eu complex, with benzoylacetone, isotropic solns., Eu^{3+} luminesc. excitation spectra and polaris. spectra 79−87487
Eu complex Eu dibenzoylmethane chelate with piperidine, vibronic and IR spectra 79−82981
Eu complex of L-histidine, influence of metal-to-ligand ratio on energy transfer to Tb complex of L-histidine 80−32763
Eu complex-benzophenone, triplet-triplet energy transfer, viscosity and temp. depend. 79−87847
Eu complexes, intermol. energy transfer to Tb complexes in aq. soln. 80−25426
Eu complexes, intermol. energy transfer to Tb complexes in aq. soln. 80−25427
Eu complexes at surface of vesicular phospholipid membranes dispersion, luminescence spectra 79−79478
Eu solid solutions with lanthanides, monosulfides, and oxides, vacant d states, X-ray absorpt. 80−103623
Eu^{2+} solutions, cyclic photoredox quantum yields, solar energy conversion 77−90627
Eu^{3+} compounds, chloride, sulphate, nitrate, carbonate, oxalate and acetate, Mossbauer study 79−99801
Eu-As-S, glass forming region, Raman and IR obs. *(French)* 79−99080
Eu-B-C ternary and binary boundary systems, preparation techniques, X-ray analysis 80−60840
Eu-Bi system, X-ray powder diffr. data for phases Eu$_5$Bi$_3$, Eu$_4$Bi$_3$, Eu$_{11}$Bi$_{10}$ 79−51075
Eu-Ce(Pr)-Fe-O system, solid solns. of ferrogarnet and ferroperovskite type 78−27488
Eu-Fe garnet, light mag. linear birefringence and dichroism near absorption band *(Russian)* 80−55063
Eu-S system, L-X-ray absorpt. spectroscopy, conc. of ions with various numbers of f electrons 77−28646
Eu-salt solutions, frozen, Mossbauer parameters depend. on pH and halide conc., Eu(III) complexes form. 78−3330
Eu-Sb system, X-ray powder diffr. data for phases Eu$_5$Sb$_3$, Eu$_{11}$Sb$_{10}$, Eu$_2$Sb$_3$ 79−51075
Eu-Sr-S, spin glass materials, mag. field dependence of susceptibility peak 80−103840
Eu-Te, chalcogenides, exam. of crystal-chemical characts. 79−1407
EuAlO$_3$:Co, Ti, effects of Co and Ti ions on cryst. growth 77−28711
EuAl$_2$S$_4$, mag. susceptibility and EPR meas. 80−71173
Eu(Al$_{0.5}$Ta$_{0.5}$)O$_3$, mag. props. 77−4587
EuAl$_3$[BO$_3$]$_4$, thermal stability, X-ray struct. anal., refractive indices 79−4297
Eu$_2$As$_2$, single cryst. struct. refinement, X-ray diffr. 77−19817
Eu$_3$As$_4$, X-ray cryst. struct. determ. 79−99135
Eu$_4$As$_3$, new synthesis, trigonal anti-Th$_3$P$_4$-type compound, X-ray characterisation 79−37687
Eu$_4$As$_3$, X-ray cryst. struct. anal. 80−39013
Eu$_5$As$_4$, cryst. struct. determ., symmetrical version of Sm$_5$Ge$_4$-type struct. 78−63710
EuAsO$_4$, ferroelectricity, dielec. meas. 80−60515
EuAsO$_4$:Gd, dynamical interactions, EPR meas. 80−7162
Eu$_4$As$_2$O, X-ray cryst. struct. determ., least squares refinement 78−9999
Eu$_3$As$_3$.TaO, X-ray cryst. struct. determ. 80−33940
EuB$_6$, ^{11}B nucl. quadrupole interaction, NMR meas. 80−2660
EuB$_6$, (La,Eu)B$_6$, (Eu,Y)B$_6$, (Eu,Ba)B$_6$, single crystal growth for thermionic emission 78−92183
EuB$_6$, absorber material for fast reactor control appl. 78−8919
EuB$_6$, correlation between mag. struct. and elec. props. 77−63192
EuB$_6$, elec. cond. under hydrostatic press. 79−7832
EuB$_6$, electrical transport under press. 79−87101
EuB$_6$, electronic struct., transport and mag. props. 80−96782
EuB$_6$, exchange interaction, EPR obs. in Sr$_x$Eu$_{1-x}$B$_6$ and La$_x$Eu$_{1-x}$B$_6$ 80−20457
EuB$_6$, ferromag., mag. props. 80−2561
EuB$_6$, ferromag., spin-polarised energy band struct., APW calc. 80−96779
EuB$_6$, ferromag. and antiferromag. sp. ht meas., 1.8-77K 80−65948
EuB$_6$, growth by soln. method, struct., mech. and elec. props. 80−16168
EuB$_6$, Hall effect and resistivity data, ferromagnetic ordering temp., pressure depend. 80−60010
EuB$_6$, low temp. nucl. spin-lattice and spin-spin relax. times meas. 77−90063
EuB$_6$, mag., transport and thermal props. 79−73738
EuB$_6$, pure single crystals, magnetic and electric props. 80−11260
EuB$_6$, resist., Hall effect, and magnetoresist. under hydrostatic press., 4.2 to 300K 80−96879
EuB$_6$, resistivity press. variation, lattice consts. 80−100456
EuB$_6$, simple crystal, prep., floating zone technique 77−85934
EuB$_6$, single and bulk polycryst., EPR, temp. and freq. depend. 79−28606
EuB$_6$, synthesis and hot pressing fabrication for appl. to neutron absorbing core control material 78−8904
EuB$_6$, thermal expansion, X-ray method, room temp. to 1300 C 80−96670

europium compounds continued

- EuB_6, valence mixed state, Kondo lattice, Anderson localisation models *(Japanese)* 78−51945
- EuB_6, valence state of Eu, X-ray line displacement meas. 80−70633
- EuB_6-CrB_2 quasibinary cross section 77−86001
- $EuB_{6-x}C_x$, magnetic and elec. props. 78−91842
- $EuB_{6-x}C_x$, magnetisation, effects of C 80−25163
- $EuB_{6-x}C_x$, Mossbauer spectra, cond. electrons effect 80−20545
- $EuB_{6-x}C_x$, pure and doped, mag. and transport props. 80−54689
- EuB_2O_4, X-ray single cryst. struct. determ., Patterson synthesis 79−19204
- EuB_4O_7, X-ray cryst. struct. determ. 80−107135
- $Eu_3B_2O_6$, synthesis, struct. and mag. props. 77−89934
- $Eu_2B_5O_9Cl(Br)$, synthesis and characterisation 80−39039
- $Eu_{0.5}Ba_{0.5}TiO_3$, ferromag., ferroelec., ceramic, Curie temps. determ. 78−68230
- $EuBi_2Te_4$, elec. cond., Hall, thermo-EMF coeffs. determ., 300-1100K 78−43386
- $EuBr_2$, vaporisation thermodynamics, enthalpy sublimation 78−22837
- $EuBr_{1.5}Cl_{0.5}$, preparation and characterisation 79−77571
- EuC_6, intercalation cpd. with graphite, synthesis and struct. 80−44184
- $Eu_{3-x}Ca_xSi_xFe_{5-x}O_{12}$, bubble film, LPE growth induced anisotropy 77−20659
- $EuCl_2$, $EuCl_2$-$EuCl_3$, $EuCl_2.HCl$, mag. props., 77-292K 78−52197
- $EuCl_2$, matrix isolated, Mossbauer effect, isomer shift and quadrupole splittings obs. 78−46377
- $EuCl_3$, heat capacity and Schottky anomaly, 5 to 350K, entropy 77−47588
- $EuCl_3$, solns., $^7F_0 \rightarrow {}^5D_1$ and $^7F_1 \rightarrow {}^5D_0$ transitions, MCD 79−31566
- $EuCl_3$-$NaPO_3$-H_2O system, Eu polyphosphates form. at 0°C 80−35515
- $Eu(ClO_4)_3$, aq. soln., Eu^{3+} $^5D_{0,1,2} \leftarrow {}^7F_{0,1,2}$ transitions, MCD and absorpt. spectra 78−19446
- $EuCl_3.6H_2O:Gd^{3+}$, EPR spectrum, g-tensor and zero-field splitting 77−55706
- $EuCl_3.6H_2O$-$NdCl_3.6H_2O(HoCl_3.6H_2O)$, in DMSO soln., $Eu^{3+} \rightarrow Nd^{3+}(Ho^{3+})$ radiationless energy transfer 80−5499
- $EuCo_2Ge_2$, magnetism and hyperfine interactions 78−76228
- $EuCoO_3$, anomalous $^{57}Fe^m$ charge states, Mossbauer study 80−40017
- $EuCo_2Si_2$, cryst. struct. and valence state 77−76375
- $EuCrO_3$, long term mag. ordering, antiferromagnetic resonance study *(Russian)* 80−54953
- $Eu_{1-p}Cr_2S_{4-p}(Se_{4-p})$, modulation of intergrowth struct. 79−94967
- $EuCu_2Ge_2$, cryst. struct. and valence state 77−76375
- $EuCu_2Ge_2$, magnetism and hyperfine interactions 78−76228
- Eu_2CuO_4, catalytic props., mag. and elec. props. 79−66350
- $EuCuSi_3$, cryst. struct. and valence state 77−76375
- $EuCu_2Si_2$, mixed valence system, X-ray absorption spectroscopic study 80−80906
- $EuEr_2Ga_{0.7}Fe_{4.3}O_{12}$, garnet thin films, magnetisation orientation, temp. depend. 80−71125
- $Eu_{1-x}{}^{2+}Eu_x{}^{3+}N_xO_{1-x}$, resist., pressure depend., semicond.-metal transition obs. 79−78104
- EuF_2, thermal props. *(German)* 80−81355
- EuF_2, thermodynamic data compared with SrF_2 *(German)* 80−81355
- EuF_3, mol. force, compliance and Coriolis consts. 79−31726
- EuF_3, thermal stability in vacuum 78−7183
- EuFX mised halides, synthesis and lattice parameters 78−30594
- $EuFe_2Ge_2$, magnetism and hyperfine interactions 78−76228
- $EuFeO_3$, cryst. domain wall energy density determ. 77−1567
- $EuFeO_3$, minute single crystal domain struct. 77−20646
- $EuFeO_3$, thermodynamic study of form. 78−48685
- $Eu_3Fe_5O_{12}$, thermodyn. props. 77−84947
- $Eu_3Fe_5O_{12}$, thermodynamic stability 77−52662
- $EuFe_2Si_2$, cryst. struct. and valence state 77−76375
- $EuGa_3(BO_3)_4$, luminesc. spectra, local symmetry of rare earth ion determ. 80−16095
- $EuGa(In)_2X_4$, X=S,Se,Te, prep. and props. 77−85214
- $Eu_3Ga_5O_{12}$, sp. ht. meas., 0.4-90K 77−55680
- $EuGa_2S_4$, cryst. struct. determ. by direct methods with MULTAN 76 *(French)* 79−37669
- $EuGa_2S_4(Se_4)$, mag. susceptibility and EPR meas. 80−71173
- EuGaYIG film, bubble dynamics, anisotropy depend., ferromag. reson. expts. 77−63240
- EuGaYIG:Cr, epitaxial garnet film, interaction pot. of domain walls with localised stress fields 80−44889
- $Eu_{1-x}Gd_xO$, mag. props., transport meas. 80−97117
- $Eu_{1-x}Gd_xO$, mag. semicond., specific heat and magnetocaloric effect 79−69688
- $Eu_{1-x}Gd_xO_{1-x}N_x$, ferromag. semicond., prep., ferromag. props. *(French)* 77−69550
- $EuGd_2S_4$, nonstoichiometric, elec. transport props., semicond. and metallic cond. 80−107786
- $Eu_{1-x}Gd_xS$, concentrated system with ferromag. and antiferromag. interactions, spin-glass props. 80−34639
- $Eu_{1-x}Gd_xS$ films, mag. and elec. props. 80−15766
- $Eu_{1-x}Gd_xS$, spin glass, transition temp., freq. depend. 80−97113
- $Eu_2(GeO_4)O$, X-ray cryst. struct. determ. 79−99140
- Eu_2GeS_4, X-ray cryst. struct., thiogermanate ion *(French)* 80−15066
- $Eu_3Ge_3S_9$, X-ray cryst. struct. determ. *(French)* 79−7587
- EuIG bubble domain film, magnetocrystalline anisotropy coeff. reduction, by Pb addition 79−11329
- EuIG, non-cryst., Mossbauer and magnetisation studies 80−44979
- EuIG, noncrystalline, Mossbauer and magnetisation data 80−34828
- EuIG:Ga(Al), pure and doped, mag. anisotropy, magnetisation meas. 80−60240
- EuIG:Pb film saturation magnetisation improved by Sb^{5+} substitution 80−54926
- EuIG:Sb(Ca)(Ti), growth from PbO-B_2O_3 based flux, prop. depend. on Pb content 80−39824
- EuIG:Si, magnetoresistance meas. 79−78120
- EuIG+Pb, (100) LPE film, magnetocryst. anisotropy and lattice mismatch 77−20647
- Eu(III) complexes, f-f transition probabilities, ligand polarisation model, anisotropic contribs. 80−53049
- Eu(III) complexes with gluconate ions, reduction, polarographic behaviour 78−92568
- Eu_2IrH_5, prep., cryst. struct., mag. and elec. props. 80−88117
- $Eu_2Ir_2O_7$, pyrochlore, sp. ht. below 20K, Debye temp. 80−65241
- $Eu_xLa_{1-x}Ta_7O_{10}$, polycryst., luminesc. and excitation spectra 80−60659
- $EuLiH_3$, transferred hyperfine fields at Eu nuclei, NMR meas. 80−71195

europium compounds continued

- $(EuLu)_3(FeAl)_5O_{12}$, film epitaxial growth on Gd_3GaO_{12} substrate, mag. props. 80−65402
- $(EuLu)_3Fe_5O_{12}$, Ga, Al or (Ca,Ge) substituted, mag. props. and growth of 2 μm bubbles 78−91910
- $Eu_{2.9}Lu_{0.1}Fe_5O_{12}$:Si magnetoresistance meas. 79−78120
- $Eu(Lu_{0.5}Ta_{0.5})O_3$, mag props. 77−4587
- $Eu(Lu_{0.5}Ta_{0.5})O_3$, mag. props. 77−4587
- $Eu_2Mg_3(NO_3)_{12}.24H_2O$, Zeeman effect in ahsorpt. spectrum 77−63402
- $Eu(Mg_{0.5}W_{0.5})O_3$, mag. props. 77−4587
- $EuMn_2Ge_2$, magnetism and hyperfine interactions 78−76228
- $EuMn_2P_2(As_2,Sb_2)$, pnictides with Ce_2O_2S-type struct. 79−65055
- $EuMo_6S_8$, Chevrel phase, RE mag. isolation and supercond. 80−44470
- $EuMo_6S_8$, Chevrel phase, mag. interactions, LMTO energy band studies 80−70606
- $Eu_xMo_6Se_8$, mag. props., 0.7 to 295K 77−32113
- EuN-EuO solid soln., ^{151}Eu Mossbauer spectroscopy 78−6610
- $Eu(NCS)_3$ solns., luminesc. quenching of Eu^{3+}, charge transfer states 77−90190
- $Eu(NO_3)_3.6H_2O$, isotropic solns., Eu^{3+} luminesc. excitation spectra and polaris. spectra 79−87487
- $EuNa_2Mg_2(VO_4)_3$, disordered, thermal quenching of luminesc. 80−71472
- $EuNbO_4$-$CaWO_4$, phase transitions of fergusonite-scheelite *(French)* 80−19942
- $Eu_2Nb_2O_7$-$Sr_2Nb_2O_7$, new system preparation 78−42994
- $Eu_{1-x}{}^{2+}Nd_x{}^{3+}N_xO_{1-x}$, resist., pressure depend., semicond.-metal transition obs. 79−78104
- $EuNi_2Ge_2$, cryst. struct. and valence state 77−76375
- $EuNi_2Ge_2$, magnetism and hyperfine interactions 78−76228
- $EuNiSi_3$, cryst. struct. and valence state 77−76375
- $EuNi_2Si_2$, cryst. struct. and valence state 77−76375
- EuO, ^{153}Eu spin-spin relax. time and Suhl-Nakamura interaction 77−69722
- EuO (100), disordered, LEED and electron spectroscopy 79−28178
- EuO (100), EELS, Eu valence in surface region and high energy giant reson. 80−84816
- EuO (100), surface struct., LEED study 80−39396
- EuO, anomalies in transport props. under hydrostatic press. due to bound mag. polaron 77−20372
- EuO, anti-Stokes luminesc., magnon assisted 78−31252
- EuO, band struct., linear combination of muffin-tin orbitals calcs. 78−2407
- EuO, Brillouin-Mandelstam scattering from thermal and excited magnons 80−70980
- EuO, crit. behaviour of opt. absorpt. edge 77−59418
- EuO, critical EPR spin dynamics, sample shape and temp. depend. 77−32244
- EuO, cryst. and electronic struct., mag., elec., and optical props., book contrib. 80−39760
- EuO, cryst. field parameters due to $4f^{N-1}5D$ configs. 80−80230
- EuO, Curie temp. raising by impurity addition *(Russian)* 77−47994
- EuO, degenerate ferromag. semiconductor, mechanism of transition to insulating state *(Russian)* 77−8024
- EuO, dissoc. energy, mass spectrometric determ., rel. to EuO 77−58199
- EuO, dynamic dipolar cross over 78−76339
- EuO, electron correls., defects, metal-insulator transition 78−63960
- EuO, electronic struct. and props., mol. cluster approx. 77−11852
- EuO, electronic struct. investigation by electron spectroscopy method 80−92812
- EuO, electronic structure, octahedral clusters, determ. by X_α method 78−10350
- EuO, Eu doped, temp. depend. of carrier conc. and mag. susceptibility 77−69483
- EuO, Eu rich, insulator-metal transition, model Hamiltonian 78−2422
- EuO, Eu-rich, IR absorpt. spectra, 4.2 to 300K, transitions assoc. with O vacancies 77−52142
- EuO, excitation of spin waves by current carriers, magnetisation and elec. cond. reduction *(Russian)* 79−7981
- EuO, ferromag., light scatt. from bulk and surface spin waves 79−28778
- EuO, ferromag., magnetostatic theory of response functions, appl. to Brillouin scatt. 79−61083
- EuO, ferromag. reson. and nonlinear phenomena 79−28627
- EuO, ferromag. semicond., absorpt. edge and cond. band width 77−36267
- EuO, ferromag. semicond., electronic spectrum, influence of finite carrier conc. 78−76220
- EuO, ferromagnetic, mag. field effect on optical absorpt. edge, piezotransmission spectra 78−95578
- EuO, ferromagnetic electronic structure, absorption, thermoreflection and thermotransmission spectra *(French)* 80−97300
- EuO, ferromagnetic piezotransmission behaviour in magnetic field 80−97272
- EuO, ferromagnetic resonance and dielectric losses 78−2748
- EuO film, thermomag. effects for reversible holographic storage 77−34851
- EuO film for thermomagnetic recording, anisotropy of resolving power 80−20404
- EuO film threshold characteristics in holographic and bit recording *(Russian)* 80−63944
- EuO, HF conductivity meas. 79−33304
- EuO, Heisenberg ferromagnet, exchange interactions, neutron scatt. expts. 77−20579
- EuO, Heisenberg ferromagnet, static crit. props., neutron scatt. expts. 77−20618
- EuO, Heisenberg ferromag. semicond., hyperfine and exchange interactions 77−69530
- EuO, hydrostatic press. effects on elec. resist. in temp. range 3 to 300K 79−23968
- EuO, light absorpt. during ferromag. reson. *(Russian)* 79−28618
- EuO, light scatt. by spin waves 80−45086
- EuO, light scatt. from bulk and surface spin waves 78−19497
- EuO, light scatt. from spin waves and magneto-optic hysteresis meas. 80−97244
- EuO, light-induced metal-insulator transition, mol. mag. polarons 77−4396
- EuO, mag. form factor of Eu^{2+}, solid state effects 78−2653
- EuO, mag. semicond., dielec. and optical props. 78−10824
- EuO, mag. semicond., s-f model, intermediate coupling theory 79−95326
- EuO, mag. struct. and transition temp., indirect exchange 78−91860
- EuO, magnetic semiconductor, piezoresistance effect, 4.2 to 300K 80−34450

europium compounds continued
EuO magnetic semiconductor, quasiparticle lifetimes, CPA study 80—65443
EuO, magnetic susceptibility, quasiphase transition 79—65684
EuO, magnetic susceptibility critical exponent, corrections to scaling 80—103846
EuO, magnetocaloric effect in high magnetic fields 80—25140
EuO, magnetostriction, spin-spin correl. function, above T_c 77—4541
EuO, microwave and DC cond., dielec. const., 1.7 to 300K 77—20347
EuO, microwave cond., influence of mag. ordering 79—69544
EuO, Mossbauer line, exchange narrowing 77—85627
EuO, nonstoichiometric film with excess EU, optical magneto-optical and elec. props. 79—8204
EuO nonstoichiometric film, ESR spectra and exchange interaction 80—93176
EuO, optical orientation of f-electrons, Curie temp. variation due to exchange interactions *(Russian)* 79—15431
EuO, origin of exchange interaction 78—10675
EuO, photoelectron anomalous transport phenomena 78—23114
EuO, quadrupole coupling due to lattice imperfections 78—76347
EuO, Raman scatt. and phonon dispersion 77—55786
EuO, reflectivity spectra near absorpt. edge 79—47471
EuO, resolution as hologram recording material 77—83834
EuO, rotation of polarisation plane in very high mag. field 78—92054
EuO, single crystal enriched in ^{17}O, growth from melt in sealed Mo crucible 77—4734
EuO, spin assisted Raman scatt. theory 78—43866
EuO, spin order and fluctuations, Raman scatt. study 80—97273
EuO, spin system heating by drifting current carriers, magnon-phonon system energy transfer *(Russian)* 80—29541
EuO, spin wave damping, theory compared with expt. 78—52237
EuO, spin wave lifetime, theory compared with expt. 80—60228
EuO, spin-dependent Raman scattering 79—95782
EuO, spin-disorder induced phonon Raman scatt. 78—60457
EuO, stoichiometric, crit. behaviour of piezotransmission at Curie temp. 77—85688
EuO, surface magnons and surface mag. struct. 77—36066
EuO, transmission and resistivity, stress modulation effect near Curie temperature 80—96874
EuO, transport properties at ferromag. reson. 78—68387
EuO type mag. semicond., with impurities, semicond.-metal transition and instability phenomena 77—59257
EuO, zero-field critical relax. rate, mode-coupling theory 77—69593
EuO, zero-wave vector kinetic coefficient near T_c 79—73714
EuO:Eu, doped ferromag. semicond., carrier density and mag. susceptibility rel. to M-S transition 77—72820
EuO:Gd, 4f-photoelectron spin polarization, temp. depend. 79—78842
EuO:Gd, critical specific heat depend. on doping, microwave cond. 79—95602
EuO:Gd, elec. cond. under hydrostatic press., Curie temp. 80—96881
EuO:Gd, electron mobility below Curie temp. 78—91696
EuO:Gd, ferromag. semicond., electron spin polarisation and conduction band struct. 80—65449
EuO:Gd, mag. props. and instability phenomena 79—1666
EuO:Gd, pure and doped, elec., mag., and optical props. rel. to electronic conc. 80—96880
EuO:Gd, surface depolarisation of photoelectrons 78—15286
EuO:Gd, surface mag. props. 80—71566
EuO:La, metallic, photothreshold, correl. and exchange energy of electron gas 77—62852
EuO:La, photothreshold reduction by mag. induced space charge layer 78—72692
EuO:La(Gd), photoelectron spin polarisation, temp. depend. 77—69966
EuO:La(Gd), photothreshold changes below mag. ordering temp. 80—97406
EuO:Sm^{3+}, hyperfine field at Sm, TDPAC meas. 80—93215
EuO:Yb(Sm), electron transition and valence state of impurities, X-ray spectroscopy and structural anal. 78—39064
EuO-EuN solid soln., ^{151}Eu Mossbauer spectroscopy 78—6610
EuO-GdN solid soln., ^{151}Eu Mossbauer spectroscopy 78—6610
EuO-NdN solid soln., ^{151}Eu Mossbauer spectroscopy 78—6610
$EuO_{1-\delta}$ films, Faraday effect dispersion rel. to electronic struct., visible and IR spectra 80—45162
$EuO_{1-\delta}$ single crystals, Faraday effect, near IR, effect of carriers 80—71395
$EuO_{1-\Delta}$, thin film, Faraday effect dispersion and transmission, 0.5-1.1 μ, 20.4 and 77K, anion vacancies 79—19945
$EuO_{1.05}$, specific heat, mag. phase transition 77—36077
$Eu_{1-x}O$, optical absorpt. spectra at metal insulator transition 78—10928
Eu_2O, Eu_2O_2, atomisation energies and stand. ht. of formation 77—54622
Eu_2O, Eu_2O_2, Eu_2OS, dissoc. energies and ht. of formation 77—47569
Eu_2O_3, absorber material for fast reactor control appl. 78—8919
Eu_2O_3, activator in Na_2O-B_2O_3-SiO_2 glass, exam. of distribution by absorption study 79—4832
Eu_2O_3, appl. to LMFBR control 78—50261
Eu_2O_3, C→B transformation 77—11688
Eu_2O_3 ceramic powder, in situ deposition of metal coating, cermet form. 77—32713
B-Eu_2O_3, cryst. struct. refinement from X-ray scattering data 79—37672
Eu_2O_3, cubic to monoclinic transform. 77—8815
Eu_2O_3, elec. cond., thermoelec. power, dielectric const. 79—69763
Eu_2O_3, for controlling fast reactor, irrad. behaviour 78—37409
Eu_2O_3, from reactive evaporation, struct. and polymorphic transform. 79—51441
Eu_2O_3 LMFBR control material, integral capture cross section meas. in CFRMF 77—26760
Eu_2O_3, large single crystals, production and props. rel. to structural anisotropy *(French)* 77—36396
Eu_2O_3, mech. and physical props. rel. to reactor control rod appl. 78—21641
Eu_2O_3, microhardness anisotropy of single cryst. *(French)* 77—52489
Eu_2O_3, monoclinic, growth from molten NaF solvent 78—19653
Eu_2O_3, photoacoustic spectra, spectrometer sample cell design investig. 77—74520
Eu_2O_3, sintering kinetics 78—52731
Eu_2O_3, thermophysical props. and neutron absorpt. 80—103488
Eu_2O_3:Gd, neutron activation anal. of Gd impurity 77—16874
Eu_2O_3-Gd_2O_3-Ta_2O_5 system at 25, 50 and 75 mole.% Ta_2O_5, cross section investig. 77—12607
Eu_2O_3-MoO_3, phase diag. 77—48408
Eu_2O_3-R_2O_3-Ta_2O_5, R=La, Gd, Y, quasibinary cross sections 77—90333
Eu_2O_3-Sc_2O_3-Ta_2O_5 system, orthotantalate section, X-ray diffr. and luminesc. obs., conc. depend. 80—54205
Eu_2O_3-Ta_2O_5, microcracking, elastic props., internal friction 78—92326
Eu_2O_3-Y_2O_3 solid soln. phases, synthesis 80—104132
Eu_2O_3-Y_2O_3-Ta_2O_5, struct., phase form., luminesc. and X-ray diffr., obs. *(Russian)* 78—6765
Eu_2O_3-ZrO_2, phase decay 77—86002
$Eu_2O_3+EuPO_4$ in Mo crucible, $EuMoO_4$ and $EuMoO_3$ atomisation energy 78—40073
Eu_3O_4, inelastic light scatt. 77—55788
Eu_3O_4, mixed valence system, inelastic light scatt., photoluminesc. 77—90145
Eu_xO_y film, dielec. props. rel. to annealing 79—99636
Eu_xO_y film, struct., electron microscope and diffr. obs. 79—11028
$EuO_iF^{-}_{8-2i}$ defect structure, stabilisation of Eu^{2+} in fluorites 79—56649
$Eu(OH)_3$, cryst. struct. 80—24424
$Eu(OH)_3$, heat capacity from near 5 to 350K, lattice and Schottky contribs. 80—49374
$Eu(OH)_3$, mol., XPES, satellite phenomena 79—27035
$EuO_{1-x}N_x$, blocking of valence fluctuations, ^{151}Eu Mossbauer spectra 80—2678
$EuO_{1-x}N_x$, ferromag., temp. variation of EPR linewidth *(French)* 77—85547
$EuO_{1-x}N_x$, ferromag. semicond., elec. and mag. props. *(French)* 78—79993
EuO(S), effect of pressure on energy gaps 78—19239
EuO(S), spin polarisation of field-emitted electrons 77—40337
EuO(S):Gd, indirect exchange 78—23264
Eu_2O_2S, cooperative optical absorption obs. in luminesc. excitation spectra 78—27308
EuO(S)(Se) electronic props., effect of electron-ion spin coupling 77—28359
EuO(S)(Se)(Te), exchange interaction mechanisms, theory compared with expt. *(Russian)* 78—39312
EuO(S)(Se)(Te), phase transition spectroscopy 77—63426
EuO(S)(Se)(Te), spin order and fluctuations, Raman scatt. study 80—97273
EuO(Se), complex elec. cond. anomalies 80—107812
EuO(g), thermochem. props. 77—14604
$EuOs_4Sb_{12}$, prep. and cryst. struct. 80—100211
$EuPO_2$, $EuPO_3$, gases, thermochem. props. 79—66334
$Eu(PO_3)_3$ and $Eu(PO_3)_3.6H_2O$, form. in $EuCl_3$-$NaPO_3$-H_2O system at 0°C 80—35515
$EuPO_4$, enthalpy and heat capacity, 298.15-1600K 77—12559
$EuPO_4$ in Mo crucible, $EuMoO_4$ and $EuMoO_3$ atomisation energy 78—40073
EuP_5O_{14}, 4f-level press. depend., fluorescence exam. 77—72841
EuP_5O_{14}, luminesc. of Eu^{3+}, transition probabilities 80—80845
EuP_5O_{14}, luminesc. spectra 77—52155
Eu_3PO_7 and $(Eu,Nd)PO_7$, IR and Raman spectra, vibr. assignments, cryst. struct. characts. 80—97258
$Eu_5(PO_4)_3OH$, prep. from sulphate, X-ray diffr. and IR spectrosc. 80—29893
$Eu_{1-x}{}^{2}R_x{}^{+}O_{1-x}$ (R=Nd, Eu, Gd), lattice parameters, mag. and elec. props. 80—100578
$Eu(ReO_4)_3.4H_2O$, $(ReO_4)^-$ ion vibrs. rel. to static field, Raman investig. *(Russian)* 78—76470
$Eu(ReO_4)_3.4H_2O$, Raman spectra, $(ReO_4)^-$ ion normal vibrs. rel. to static field 79—65858
$EuRu_4Sb_{12}$, prep. and cryst. struct. 80—100211
EuS, amorphous, on W, memory effect in field emission 80—89126
EuS, conduction band density of states, redistrib. near ferromag. saturation 78—67939
EuS covered W tip, field emission of monoenergetic spin-polarised electrons 77—85899
EuS, cryst. and electronic struct., mag., elec., and optical props., book contrib. 80—39760
EuS, defect struct., etch pitting and electron microscopic obs. 79—27989
EuS, electronic struct. and props., mol. cluster approx. 77—11852
EuS, Eu_2S, EuS_2, Eu_2S_2, Eu_2OS, dissoc. energies and ht. of formation 77—47569
EuS, evaporation, thermodynamic data 78—2248
EuS, exchange magnetostriction in paramagnetic phase 79—78492
EuS, ferromag., on W, electron field emission 79—8230
EuS, ferromag. semicond., optical spin orientation, Curie temp. increase 77—20627
EuS, ferromag. semicond., absorpt. edge and cond. band width 77—36267
EuS, ferromag. semicond. film, Hanle effect, optical orientation time consts. meas. 77—40214
EuS, ferromag. semicond., high field susceptibility, spin waves 80—75735
EuS, ferromagnetic electronic structure, absorption, thermoreflection and thermotransmission spectra *(French)* 80—97300
EuS, ferromagnetic film, optically induced magnetisation amplification, Curie temp. increase *(Russian)* 77—24719
EuS, film, anisotropic growth on amorphous substrate 77—12547
EuS film, influence of prep. on mag. props. 79—24201
EuS, film, intrinsic demagnetising fields 78—10735
EuS, film, mag. surface reconstruction, ferromag. reson. 78—10781
EuS film, magnetic props. using transverse Kerr and Voigt effects 77—52054
EuS film, struct., elec. and opt. prop. changes during annealing in air 77—7983
EuS films, ferromag., optical spectra and light scatt. from spin waves 80—16116
EuS films, mag. and elec. props. rel. to stoichiometry and defects 80—97122
EuS films, thermoreflectance spectra below Curie temp. 77—66550
EuS, heat capacity near ferromag. transition 78—47986
EuS, Heisenberg ferromagnet, exchange interactions, neutron scatt. expts. 77—20579
EuS, Heisenberg ferromagnet, static crit. props., neutron scatt. expts. 77—20618
EuS, Heisenberg ferromag. semicond., hyperfine and exchange interactions 77—69530
EuS, hyperfine field and magnetisation temp. depend., NMR meas. 77—8422
EuS, light scatt. from spin waves and magneto-optic hysteresis meas. 80—97244

europium compounds continued
EuS, mag. phase depend. Raman scatt. 78−10886
EuS, mag. semicond., s-f model, intermediate coupling theory 79−95326
EuS, mag. semiconductors, excitation spectrum, temp. and band occupation depend. 80−49588
EuS, mag. struct. and transition temp., indirect exchange 78−91860
EuS, origin of exchange interaction 78−10675
EuS, phonon anomalies and electron-lattice coupling 80−39490
EuS, pure and Gd doped, electronic struct., mag. exchange and elec. transport props. 78−87974
EuS, Raman scatt. and phonon dispersion 77−55786
EuS, red shift of absorpt. edge for mag. saturation 79−61342
EuS, single cryst., high-field susceptibility meas., temp. range 2.5 to 16.5K 80−84589
EuS, spin assisted Raman scatt. theory 78−43866
EuS, spin filter effect on W 80−45221
EuS, spin order and fluctuations, Raman scatt. study 80−97273
EuS, spin polarised tunnelling and mixed spin states in conduction band 79−52085
EuS, spin relax. in crit. region 78−52270
EuS, spin relaxation crit. behaviour 78−76251
EuS, spin-assisted phonon Raman scatt., mag. phase depend. 80−71413
EuS, spin-disorder induced phonon Raman scatt. 78−60457
EuS, surface magnons and surface mag. struct. 77−36066
EuS, thermal stability in air, 20-900°C 77−52519
EuS, thermo- and magnetorefl. spectra, dynamical spin fluctuation effect on exciton state 77−52126
EuS, thin film, Brillouin scattering from spin waves 80−65843
EuS, three dimens. Heisenberg ferromagnet, crit. relax. spectra mag. susceptibility 79−8000
EuS, transferred hyperfine interacs. 77−69741
EuS, vaporisation thermodynamics, Knudsen cell mass spectra 77−47569
EuS:Sn^{2+}, Mossbauer spectra, Sn^{2+} transferred hyperfine fields 80−15887
EuS:Yb(Sm), electron transition and valence state of impurities, X-ray spectroscopy and structural anal. 78−39064
EuS-Ga_2S_3-GeS_2, chalcogenide glasses, conditions of form. of glassy prod. *(French)* 80−100325
EuS-metal contact, electrical switching exam. 78−68085
EuS-W emitter junction, energy loss of field emitted electrons 77−81201
EuS-W interface, electron spin polarisation in field emission 78−35265
EuS_x film, vacuum deposited, composition depend. on substrate temp. and deposition rate 78−84107
Eu_3S_4, inelastic light scatt., photoluminesc., anomalous vibr. 77−48229
Eu_3S_4, inelastic light scatt. 77−55788
Eu_3S_4, metal-insulator transition, cond. processes 80−96787
Eu_3S_4, mixed valence system, inelastic light scatt., photoluminesc. 77−90145
Eu_3S_4, single cryst., X-ray cryst. struct. refinement *(French)* 79−23579
$EuSO_4$, sp. ht. and susceptibility meas. 78−14977
$Eu_2(SO_4)_3.8H_2O$, mag. props., thermal var., cryst. field reduced matrix elements 77−51875
$EuS_{1-x}Se_x$, mag. phase diagram, from temp. depend. of magnetisation 80−7105
$EuSb_2$, cryst. struct. and antiferromag. props. 79−32973
Eu_2Sb_3, cryst. struct., elec. and mag. props. 80−33958
$EuSb_2S_4(Se_4)(Te_4)$ elec. cond., Hall, thermo-EMF coeffs. determ., 300-1100K 78−43386
$EuSb_2Se_4$, single cryst. growth, and X-ray anal. 79−100033
EuSe, annealed, AC conductivity and dielectric anomaly 80−34445
EuSe, atomic interaction effects in X-ray emission spectra *(Russian)* 79−69905
EuSe, bound mag. polaron, temp. and field depend. of resist. 79−90976
EuSe, cryst. and electronic struct., mag., elec., and optical props., book contrib. 80−39760
EuSe, dynamical conductivity in high mag. fields 79−78118
EuSe, first- and second-order Raman scatt. near T_N 79−61374
EuSe, giant negative magnetoresistance, anomalous carrier density mag. field depend. 80−49774
EuSe, HF conductivity meas. 79−33304
EuSe, Hall effect, elec. cond. and magnetoresistance temp. depend. 79−33296
EuSe, Heisenberg ferromag. semicond., hyperfine and exchange interactions 77−69530
EuSe, high field Faraday rot., 1.7-3 eV 77−52131
EuSe, mag. ordered phase, first order Raman scatt. theory 77−85723
EuSe, mag. phase depend. Raman scatt. 78−10886
EuSe, mag. phase stability, theory 77−63183
EuSe, mag. semicond., dielec. and optical props. 78−10824
EuSe, mag. struct. and transition temp., indirect exchange 78−91860
EuSe, magnetic phase transitions, thermal modulation spectroscopy study *(French)* 80−97301
EuSe, metamagnetic, magnetostriction ferrons 78−88160
EuSe, microwave and DC cond., dielec. const., 1.7 to 300K 77−20347
EuSe, MnO-type antiferromag. spin order, Faraday rotation obs. 77−47974
EuSe, optical absorption exam., electron phonon interactions 78−10923
EuSe, photomagnetisation, photoinduced heterojunctions 77−63259
EuSe, polarisability of shallow donors, permittivity meas. 80−24833
EuSe, Raman scatt. and phonon dispersion 77−55786
EuSe, Raman scatt. near mag. phase transitions 79−61373
EuSe, spin assisted Raman scatt. theory 78−43866
EuSe, spin config. stabilisation by lattice distortion 78−52251
EuSe, spin order and fluctuations, Raman scatt. study 80−97273
EuSe, spin structs., mol. field theory 78−31054
EuSe, spin-assisted phonon Raman scatt., mag. phase depend. 80−71413
EuSe, spin-disorder induced phonon Raman scatt. 78−60457
EuSe, superexchange interaction parameters, many-electron model calc. 79−7988
EuSe, surface magnons and surface mag. struct. 77−36066
EuSe, VPE by hot-wall technique 80−80958
EuSe:Gd, mag. props. explained by band struct. 78−43324
$EuSe_{1-x}Te_x$, transferred hyperfine fields at Eu nuclei, NMR meas. 80−71195
$EuSi_2$, high-pressure phase transform., cryst. struct. 77−35693
$EuSi_2$, valence band struct. *(Russian)* 79−15076
$Eu_{0.14}Si_{0.31}O_{0.55}$ glass, optical, magnetic, and magneto-optical props., chemical clustering 79−42951
$Eu_{0.14}Si_{0.31}O_{0.55}$, insulating amorphous mag., optical, mag., and magneto-optical props. 79−61344
β-Eu_2SiO_4, cryst. struct. *(French)* 78−47293

europium compounds continued
$Eu_{0.98}Sm_{0.02}O$, ferromag. semicond., elec. cond. meas. 80 to 370K, press. effect to 20 kbar 77−51751
$Eu_{1-x}Sm_xO$, ferromag. semiconductor with elevated Curie temp. 77−51903
$Eu_{1-x}Sm_xO$, mag. semicond., thermodynamics of mag. quasimols. 78−19266
$EuSm_2S_4$, mag. props. 78−68237
$Eu_{1-x}Sm_xS$, ESR, exchange interaction, susceptibility, elec. cond., thermoelectric power 80−93174
$Eu_{1-x}Sm_xS$, electron config. of Sm ions, X-ray L-absorpt. spectroscopy 80−60715
$Eu_{1-x}Sm_xS$, electronic transition in Sm impurity ions, rel. to exchange interactions, L absorpt. spectra 77−59644
$Eu_xSn_{1-x}Mo_6S_8$, Chevrel phase supercond. cond. electron polarisation by Eu^{2+}, effect on supercond. props. 79−56650
$Eu_ySn_xMo_6S_8$, supercond. props. 80−97023
$Eu_zSn_{1-z}Mo_6S_y$, supercond., mag. props. 77−69447
$Eu_xSn_{1-x}Mo_6Sn_8$ (Se_8), ternary superconductor, paramagnetic relax. effects 78−68112
$(Eu_{1-x}Sn_x)S$, high press. Mossbauer exam. of Curie temp. and transferred hyperfine field 79−56643
Eu_2SnS_4, cryst. struct. *(French)* 79−86757
$Eu_3Sn_2S_7$, cryst. struct. *(French)* 78−18597
$Eu_3Sn_2S_7$, cryst. struct. *(French)* 79−86757
$Eu_4Sn_2S_9$, cryst. struct. *(French)* 79−86757
$Eu_5Sn_3S_{12}$, cryst. struct. determ. *(French)* 77−47388
$Eu_5Sn_3S_{12}$, cryst. struct. *(French)* 79−86757
$Eu_5Sn_3S_{12}$, mag. and thermodynamic props., metamagnetism 80−60273
$(Eu_{1-x}Sn_x)Se$, high press. Mossbauer exam. of Curie temp. and transferred hyperfine field 79−56643
(Eu_xSr_{1-x}) S dilute, spin-cluster freezing observation by low-freq. mag. absorpt. 79−78404
$Eu_{1-x}Sr_xCoO_3$, electronic and mag. props., itinerant ferromagnetism obs. 78−10660
$Eu_xSr_{1-x}M_4O_{11}$, M=Nb, Ta, electrophys. and mag. props. 77−89760
$Eu_xSr_{1-x}O$, ferromag. ordering and photoluminesc. 77−66313
$Eu_{0.4}Sr_{0.6}S$, spin glass, spin dynamics, neutron scatt. study 80−65907
$Eu_{1-x}Sr_xS$, exciton refl. spectra 80−2782
$Eu_{1-x}Sr_xS$, non-metallic system, spin glass behaviour 79−24175
$Eu_xSr_{1-x}S$, blocking of pairs and spin glass freezing 79−61174
$Eu_xSr_{1-x}S$, chalcogenide-like system, crit. conc. for ferromagnet-spin glass transition 80−34662
$Eu_xSr_{1-x}S$, dil. insulator spin-glass versus blocking 80−34641
$(Eu_xSr_{1-x})S$, dilute, magnetic 'blocking' 79−78348
$Eu_xSr_{1-x}S$, dilute Heisenberg magnet, complex susceptibility of blocked spins 80−15740
$Eu_xSr_{1-x}S$, ferromag. ordering and photoluminesc. 77−66313
$Eu_xSr_{1-x}S$, ferromagnet-spin glass transition, mag. ordering, mag. susceptibility and neutron scatt. meas. 80−50135
$Eu_xSr_{1-x}S$, Heisenberg spin glass system, excitations 80−84610
$Eu_xSr_{1-x}S$, insulating spin glass, mag. props. 80−2589
$Eu_xSr_{1-x}S$, insulating spin-glass, sp. ht. near ferromag. onset 80−34667
$Eu_xSr_{1-x}S$, insulating spin glass, sp. ht. near ferromag. onset 80−97106
$Eu_xSr_{1-x}S$, mag. clusters, spinodal decomp. trend 80−65923
$Eu_xSr_{1-x}S$, mag. ordering temp. conc. depend., Eu mag. hyperfine field temp. depend. 78−14971
$Eu_xSr_{1-x}S$, mag. ordering in dil. Ising and Heisenberg systems with competing interactions 80−65914
$Eu_xSr_{1-x}S$, magneto-optical redshift in absorpt. and photoluminesc., mag. short-range order 80−71388
$Eu_xSr_{1-x}S$, non-metallic spin glass system 79−61175
$Eu_xSr_{1-x}S$, onset of ferromagnetism for x near 0.5 neutron diffr. obs. 79−24181
$Eu_xSr_{1-x}S$, paramag. susceptibility, expt. and comparison with high temp. series expansion 80−60176
$Eu_xSr_{1-x}S$, spin glass, spin wave modes and low temp. sp. ht. 80−80538
$Eu_xSr_{1-x}S$, spin glass, transition temp., freq. depend. 80−97113
$Eu_xSr_{1-x}S$, spin glass to ferromag. transition, neutron scatt. and susceptibility meas. 80−60254
$Eu_xSr_{1-x}S$, spin-glass props. and mag. transition 80−97105
$(Eu_xSr_{1-x})S$, transferred hyperfine fields, NMR 80−71196
$(Eu_xSr_{1-x})S$, very dil., magnetisation dynamics 80−65915
$Eu_xSr_{1-x}SO_4$, mag. ordering temp. conc. depend., Eu mag. hyperfine field temp. depend. 78−14971
$Eu_{1-x}Sr_xSi_2$, solid solns., α-$ThSi_2$ struct. type, comp. and press depend. 78−91322
$Eu_{1-x}Sr_xSi_2$, solid solution with type $SrSi_2$ struct., lattice parameters at high press. 80−54203
$Eu_{1-x}Sr_xVO_{3-0.1x}$, elec. cond. and mag. susceptibility, temp. depend., 77-300K 77−47816
$EuTaO_4$, heat of form: 79−83494
$Eu_2Ta_2O_7$-$Sr_2Ta_2O_7$, new system preparation 78−42994
EuTe 79−61373
EuTe, antiferromag. FCC lattice of second kind, surface magnons and mag. structs. 78−23261
EuTe, antiferromag. semicond., Raman scatt., spin-phonon interactions 80−66185
EuTe, antiferromagnet, phonon Raman scatt. from spin superstructures 80−16030
EuTe, cryst. and electronic struct., mag., elec., and optical props., book contrib. 80−39760
EuTe, exchange and superlattice band splittings, magneto-optical meas. in high mag. fields 79−61342
EuTe, field depend. correl. function theory of Raman scatt. near antiferromag.-paramag. transition 78−68490
EuTe, Heisenberg ferromag. semicond., hyperfine and exchange interactions 77−69530
EuTe, high field Faraday rot., 1.7-3 eV 77−52131
EuTe, high-temperature evaporation and reactivity 80−103469
EuTe, light scatt. by magnons 77−69805
EuTe, mag. 'Bragg' scatt. obs. through Raman scatt. 80−66179
EuTe, mag. ordered phase, first order Raman scatt. theory 77−85723
EuTe, mag. semicond., antiferromag. reson. meas. 80−44926
EuTe, mag. struct. and transition temp., indirect exchange 78−91860
EuTe, magnetic impurity states, mag. and transport props. 80−96913
EuTe, magnetic phase transitions, thermal modulation spectroscopy study *(French)* 80−97301
EuTe, Neel temp. and hyperfine interactions, press. depend. up to 60 kbar, ^{151}Eu Mossbauer obs. 77−63181
EuTe, optical absorpt. in high mag. field 79−28726

europium compounds continued
EuTe, Raman scatt. and phonon dispersion 77−55786
EuTe, Raman scatt. exam. 79−61375
EuTe, spin alignment, high field Faraday rotation expt. 77−63401
EuTe, spin order and fluctuations, Raman scatt. study 80−97273
EuTe, spin-assisted phonon Raman scatt., mag. phase depend. 80−71413
EuTe, spin-dependent Raman scattering 79−95782
EuTe, spin-disorder induced phonon Raman scatt. 78−60457
EuTe:Sn^{2+}, Mossbauer spectra, Sn^{2+} transferred hyperfine fields 80−15887
$EuTi_{1.5}W_{0.5}O_6$, Stark sublevels in mag. suscept. and luminesc. 77−51876
EuTm-CaGe, magnetic FE garnet film, LPE growth and composition 78−23634
$EuTm_2Fe_5O_{12}$ film , CaGe substituted, LPE growth kinetics 78−31349
$EuVO_4$, electron energy loss spectra, primary excitation processes in cathodolum. 79−11490
$EuVO_4$:Gd, dynamical interactions, EPR meas. 80−7162
Eu_2VO_4, prep. and props. 77−15379
$Eu_3V_2O_7$, prep. and props. 77−15379
$Eu_3VTa_2O_9$, prep., characterisation and mag. props. 78−26535
$Eu_2(WO_4)_3$, mag. susceptibility, elec. cond. and dielec. const. meas. 77−11916
$Eu_2(WO_4)_3$, mag. susceptibility, paramag. Curie temp., 300-900K 79−82753
$Eu_2(WO_4)_3$, molar mag. susceptibility meas., 4.2-900K 77−4507
$Eu_2(WO_4)_3$, molar mag. susceptibility, DC elec. cond., thermopower meas. 79−15172
Eu_2WO_6, growth from soln. in melt 77−1806
Eu_xWO_3-Sn_yWO_3, prep. and struct. of mixed W bronzes 77−4085
EuX type magnetic semiconductors, physical props. and possible applications 78−2474
EuX, X=chalcogen, antiStokes luminesc. 77−63455
$(EuX_6)^{3-}$, (X=Br, Cl), spectral hypersensitive intensity, ligand polarisability contrib. 78−51946
$Eu_{1-y}X_yS$ (X=Sr,Gd), spin-disorder-induced Raman scatt. from phonons, expt. investigation 80−20635
$Eu_{1-y}X_yS$ (X=Sr,Gd), spin-disorder-induced Raman scatt. from phonons, theory 80−20636
EuX(X=0,S,Se) 80−20635
EuX(X=0,S,Se), spin-disorder-induced Raman scatt. from phonons, theory 80−20636
$(EuY)_3(FeGa)_5O_{11}$, ferrite garnet film, mag. bubble motion delay 79−91269
$Eu_{0.6}Y_{2.4}Ga_{1.26}Fe_{3.74}O_{12}$ garnet film, Walker oscills., detection by mag. bubble collapse 78−68318
$Eu_{0.6}Y_{2.4}Ga_{1.26}Fe_{3.74}O_{12}$ garnet film, dynamic bubble-collapse determ. of domain wall motion oscillation 79−78454
$Eu_zY_{3-z}Ga_tFe_{5-t}O_{12}$, epitaxial garnet films, props. at compensation points 80−39823
$Eu_{0.8}Y_{0.2}S$, Debye-Waller factor, X-ray diffr. meas. 77−11659
$Eu_{1-x}Yb_xO$, solid soln., ferromag. semicond., increase of exchange interaction 78−88109
$Eu_{1-x}Yb_xS$, solid soln., ferromag. semicond., increase of exchange interaction 78−88109
$Eu_{1-x}Yb_xTe$, $(0<x<1)$, mag. semicond., elec., mag. and optical props. 80−97070
$Eu_2[Pt(CN)_4]_3.18H_2O$, nonradiative energy transfer from tunable donor states to Eu^{3+} 79−43018
$Gd_xEu_{1-x}B_6$, solid solns., mag. susceptibility, 80 to 1000K *(Russian)* 80−88713
HfO_2:Eu_2O_3, elastic props., sonic reson. meas. 80−7612
HfO_2-Eu_2O_3, phase composition in HfO_2-rich region, X-ray anal. 77−12609
HfO_2-Eu_2O_3, phase equilibrium, 960 to 1900°C, X-ray anal. 78−23688
HfO_2-EuO_2 system, liquidus determ. from thermal anal. *(Ukrainian)* 79−96007
$K_5Eu(MoO_4)_4$, electric dipole transition cross section and effective site symmetry of Eu^{3+} 78−52556
$K_{0.5}Eu_{0.5}Nb_2O_6$, ^{93}Nb NQR spectra, 77 to 450K 79−38401
$KEu(PO_3)_4$, cryst. struct. 77−43188
$K_3Eu(PO_4)_2$, synthesis and IR spectra 80−16019
KF-EuF_3 system, composition of phases determ. by DTA and X-ray crystallography *(French)* 77−68945
La_{1-x} Eu_x B_6 solid solutions, cryst. lattice defectiveness, mag. susceptibility and elec. conductivity 80−15083
$La_xEu_{1-x}B_6$, EPR linewidth conc. depend., $Sr_xEu_{1-x}B_6$ comparison, exchange interaction in EuB_6 80−20457
$La_xEu_{1-x}B_6$ solid solns., thermal cond., 300 to 2000K 80−59741
$LiY_{1-x}Eu_xP_4O_{12}$ phosphor, prep. and fluoresc. 77−48219
$Na_2Eu_3(NH_2)_8$, cryst. struct. and cryst. chemistry *(German)* 79−51080
$Na_3Eu(PO_4)_2$, synthesis and IR spectra 80−16019
$Na_3La_{0.98}Eu_{0.02}(VO_4)_2$, luminesc. spectrum 77−4673
$Nd_xEu_{1-x}B_6$ solid solution, mag. susceptibility, lattice parameters, Weiss temp. 80−29535
Ni-Eu_2O_3, specific resistivity and emissivity, 1000 to 1500K 77−43675
$RbCa_{0.95-x}Mg_xEu_{0.05}F_3$, green luminesc. obs. 77−32428
$RbEu_3F_{10}$, crystal struct., X-ray studies *(French)* 80−33955
Rb_3EuF_6, Rb_2EuF_5, $RbEu_2F_7$, $RbEu_3F_{10}$, cryst. struct., X-ray diffr., equilib. in RbF-EuF_3 *(French)* 78−44107
$Rb_3Eu(PO_4)_2$, synthesis and IR spectra 80−16019
RbF-EuF_3 system, thermal anal. and X-ray diffr., phase equilibria *(French)* 78−44107
Si_3N_4-SiC-Eu_2O_3, reactively sintered, microstruct. and strength 80−25631
$Sm_{1-x}Eu_xS$, valence transition under high press. 79−73551
$Sn_{0.5}Eu_{0.5}Mo_6S_8$, supercond., spin polarisation, NMR, Mossbauer effect and bulk magnetisation meas. 77−43782
$Sn_{0.75}Eu_{0.25}Mo_6S_8$, Chevrel phase supercond., spin-depairing interaction, Mossbauer obs. 80−25258
$Sn_{1-x}Eu_xMo_6S_8$, supercond., Mossbauer effect, struct. phase transition 77−12290
$Sn_{1.2(1-x)}Eu_xMo_{6.35}S_8$, supercond. transition temp., upper critical field, local spin fluctuations 79−38250
$Sr_xEu_{1-x}B_6$, EPR linewidth conc. depend., $La_xEu_{1-x}B_6$ comparison, exchange interaction in EuB_6 80−20457
$Sr_{1-x}Eu_xB_2O_4$, luminesc. props. 80−34972
$Sr_{1-x}Eu_xB_4O_7$, luminesc. props. 80−34972
$Sr_{1-x}Eu_xB_6O_{10}$, luminesc. props. 80−34972
$SrEuFeO_4$, Neel temp. and spin reorientation, Mossbauer study 80−39934

europium compounds continued
$SrEu_2Fe_2O_7$, ferrite, Mossbauer effect study of hyperfine interactions, spin reorientation 78−19383
$Sr_{2x}Eu_{2-2x}NbO_4$, synthesis and props. 77−52265
$Sr_{1-x}Eu_xS$, dilute spin glass, mag. props. 79−78386
$SrO.Eu_{1-x}Sr_xVO_{3-0.1x}$, solid solns., elec. and mag. props. 77−89819
Sr_2TiO_4-Eu_2O_3, synthesis, luminesc. of materials 79−11534
$TlEu(MoO_4)_2$, fluoresc. spectra at 77, 300K 79−56848
$TlEu(WO_4)_2$, fluoresc. spectra at 77, 300K 79−56848
$TlR(MO_4)_2$, R=Eu, Dy, Er; M=Mo, W, luminesc. *(Russian)* 78−48229
$Tm_{1-x}Eu_xSe$, semicond. with valence instabilities, cryst. chem. considerations 80−100213
$Tm_{1-x}Eu_xSe$, valence changes, semicond.-metal transition 80−20086
$Tm_{1-x}Eu_xSe$, valence instabilities, phase diagram 80−70651
TmSe-EuSe, semiconductor-metal transitions 80−96953
W/EuS field emitters, electron emission current depend. on annealing temp., mag. props. 80−16160
$(Y,Eu,Lu,Ca)_3(Fe,Ge)_5O_{12}$, bubble memory chip, dynamic conversion comparison with $(Y,Sm,Lu,Ca)_3(Fe,Ge)_5O_{12}$ 78−68319
$(Y,Eu,Tm,Ca)_3(Fe,Ge)_5O_{12}$, Ca, Ge substituted garnet LPE films, elec. props., charge imbalance, Seebeck effect 78−68101
$(Y,Eu,Tm,Ca)_3(Fe,Ge)_5O_{12}$ garnet film coercivity, new annealing method 78−84459
$(Y, Eu, Yb, Ca)_3(Ge, Fe)_5O_{12}$, bubble film, LPE on $Gd_3Ga_5O_{12}$, mismatch and faceting 77−20657
$(Y,Eu)_3(Fe,Ga)_5O_{12}$, epitaxial, cylindrical mag. domain struct., radial wall motion effect *(Russian)* 77−8373
$(Y,Eu)_3(Fe,Ga)_5O_{12}$, LPE growth from molybdate fluxes, bubble props. 78−68322
$(Y,Eu)_3(Ga,Fe)_5O_{12}$ film, bubble wall state stability obs. 77−20651
$(YCaEuYb)_3(FeGe)_5O_{12}$, LPE, stripe end motion, effect of in-plane field 78−68330
$(YEuCa)_3(FeGeSi)_5O_{12}$, mag. loss and domain wall mobility 80−65980
$(YEu)_3(FeGa)_5O_{12}$ rigid magnetic bubble transition to normal behaviour 78−95501
$(YEu)_3(FeGa)_5O_{13}$, LPE growth, uniaxial magnetocryst. anisotropy 77−8766
$Y_{2.35}Eu_{0.65}Ga_{1.2}Fe_{3.8}O_{12}$, bubble translation vel., ion-implantation effects 78−68327
$(YEuLuCa)_3(FeGe)_5O_{12}$ film, stable state of bubbles containing Bloch lines 78−76281
YEuLuCaGe garnets, 7 μm-period bubble devices 80−44887
$Y_{1-x}Eu_xP_3O_9$ phosphor, prep. and fluoresc. 77−48219
YEuTmCa garnet bubble films, domain wall transition 79−56584
$(YEuTmCa)_3(FeGe)_5$ bubble garnet films, ion-implanted, mag. susceptibility meas. 79−47311
YEuTmCaGe garnets, 7 μm-period bubble devices 80−44887
$(YEuTmCa)_3(GeFe)_5O_{12}$ film, Bloch loop punch-through in mag. bubbles 77−59437
$Y_{1.52}Eu_{0.3}Tm_{0.3}Ca_{0.88}Ge_{0.88}Fe_{4.12}O_{12}$, bubble translation vel., ion-implantation effects 78−68327
$(YEuTm)_3(FeGa)_5O_{12}$ film, dynamic props. of bubble domains by high speed photography 80−15771
$(YEuTm)_3(FeGa)_5O_{12}$ garnet film, bubble domain steady state motion on a circle 80−29589
YEuTmGa garnet bubble film, dynamic diffuse wall deform. 80−54927
$(YEuTm)_3(GaFe_5)O_{12}$ ferrite garnet films, mag. bubbles, translational motion, mechanism for inertial effects 80−100606
$Y_{1.57}Eu_{0.78}Tm_{0.65}Ga_{1.05}Fe_{3.95}O_{12}$ film, gradient propagation, overshoot and creep 78−19291
$(YEuYbCa)_3(FeGe)_5O_{12}$, ion-implanted, in-plane mag. field effects on bubble props. 77−85521
$(YEuYbCa)_3(FeGe)_5O_{12}$ film, mag. σ-bubbles, automation props. 78−88150
$(YEuYbCa)_3(FeGe)_5O_{12}$ bubble films, Ne^+-implanted, cryst. and mag. props., X-ray diffr. obs. 79−38362
$(YEuYbCa)_3(FeGe)_5O_{12}$ film, isolated straight stripe domain dynamic props. 79−33514
$(YEuYbCa)_3(FeGe)_5O_{12}$, garnet film, isolated straight stripe domain, dynamic behaviour 80−39809
$(YEuYbCa)_3(GeFe)_5O_{12}$ bubble film with ion-implanted layer, FMR study 80−2643
$(YEuYb)_3(FeGa)_5O_{12}$, LPE, stripe end motion, effect of in-plane field 78−68330
Y_2O_3-Lu_2O_3-Eu_2O_3-CaO-GeO_2-Fe_2O_3-PbO-B_2O_3 system, garnet crystn. fields 78−43995
(ZrF_4-BaF_2-ThF_4)-EuF_2 system, glass forming region, prep. and props. 79−91633

eutectic alloys
anomalous eutectic, acicular, nonequilib. crystn. anal. *(Russian)* 80−25678
binary, distribution coeffs., estimation from Van Laar and Hayes-Chipman relations 80−84293
binary eutectic alloys, solidification anal. considering temp. and solute distrib., numerical soln. *(Japanese)* 78−39757
binary eutectic system, steady state lamellar solidification, self consistent theory 77−70041
binary melts, appl. of quasichem. method of cluster components *(Russian)* 77−80623
binary system, eutectic conc. calc., graphic representation of equations *(Russian)* 77−66622
binary systems of eutectic type, phase diagrams, approximations, appls. 78−43094
β′ brass, eutectoid, microstruct. obs. 77−36553
cast iron, hypereutectic, transform. of cementite to austenite 77−52318
composite growth by eutectoid or solid-state decomposition 78−44056
crystallisation course in condensed eutectic systems, computer calc. 77−86018
dendrite growth−the coupled zone 80−97489
directional solidification, effect of thermal parameters, two-dimens. heat transfer model 78−88456
directionally solidified, contact melting kinetics, mass transfer during solidification *(Russian)* 77−52310
eutectics, HgTe-PbTe and Au-PbTe, prep. and thermoelectric behaviour characts. 80−107774
fibre reinforced composite prep. by crystallizing metallic and metal-ceramic eutectics *(Polish)* 79−20008
glassy alloy prod. using low temp. melt spinning device 80−100825
growth from stirred melt, off-eutectic comp. 77−8808

eutectic alloys continued
high temp., borides and silicides as reinforcing phases *(German)* 77—48368
lamellar eutectoids(ic), stability principles 80—89195
metallic glass, composition, mech. props., simulation 80—49117
Moire fringe study 77—60020
monotectic composite growth 79—56970
multiphase, metallography 79—61823
multiphase solidification theory 78—95740
nontransition element/alkali metal systems, direct calorimetric exam. 78—84775
phase volume fraction determ. using manual point count practice 78—53052
quasi binary eutectic systems, with inclusive phases, hardness, transform., decomposition *(Russian)* 80—97572
refractory oxide-metal eutectic system 77—36483
regular eutectic composite, plane faced growth criterion *(Russian)* 79—56968
rim zone formation *(Russian)* 77—85988
single grained, directionally solidified, anisotropic yielding behaviour 80—103412
skin technology, industrial appl. of space processing 79—28991
solidification mechanisms, contribution of microgravity expts. 78—88457
steel, 12Kh18N9T-TiB_2, high temp. props. 78—84931
steel, alloy, type 11Kh18M, eutectic carbide composition change due to heating 80—16353
steel, C, autectic, sintered, isothermal transformation behaviour, porosity effects 80—3031
steel, C, hypo-eutectoid naturally fibrous composites, strength analysis 78—3190
steel, Co-Si-Cr-Mo, alloying additions effect on pearlite interlamellar spacing *(German)* 80—40327
steel, Cr-Mn eutectoid, pearlite growth kinetics and partitioning 80—29963
steel, deformed eutectoid C_2 back stress decrease on annealing and H embrittlement 80—20981
steel, eutectic 1080, fatigue life improvement by thermomech. processing 80—25732
steel, eutectoid, activation energy of oxidation in wear 77—52507
steel, eutectoid, high strength, unnotched specimens, fatigue crack init. and propag. 77—56098
steel, eutectoid, mech. behaviour, thermomech. treatment effects 80—84970
steel, eutectoid and hypoeutectoid viscoelasticity under transformational superplasticity *(Japanese)* 77—52416
steel, high purity plain C, eutectoid, alloying additions effect on pearlite interlamellar spacing *(German)* 80—40327
steel, high-speed, eutectic carbide structure, determ. by SEM 78—85075
steel, hypereutectoid, type FS-01, HF-1, brittle fracture, fragmentation due to blast loading 80—50699
steel, hypereutectoid type HF-1, microstruct. effects on fracture toughness, ductility, strength 79—74255
steel, notch toughness, tempering at moderate temps., effect of quenching temp. 77—21193
steel, pearlitic eutectoid, crack initiation and effective grain size for cleavage fracture 80—30085
steel, plain C eutectoid, schematic isothermal transform. diagram 78—48393
steel, V, carbide eutectic presence, solidification and struct. 80—50624
steel M16C, low C, natural discrete microlamellar composite *(Russian)* 78—39810
steel pearlite, annealed, hot fatigued, eutectoid, spheroidization 77—52374
steel-Cu M3 bimetal, eutectic alloy, crack development, failure energy capacity *(Russian)* 80—40480
superalloy, aluminite coating, improvement by sputtering *(French)* 79—29278
surface energy considerations 78—44152
transition, eutectic, use in temp. calibration of X-ray diffractometer furnace *(Japanese)* 79—6128
transversely-isotropic metallic materials, constitutive eqn. for modelling secondary creep 78—6974
unidirectional crystallisation, containing enhanced amounts of reinforcing phase *(Rumanian)* 79—29035
unidirectionally solidified, solidification and morphology relationship 80—25684
welded joint, microstructural and chemical heterogeneity 79—29096
yield point analysis 77—8875
Ag-Bi, discrete eutectic form. mechanism *(Russian)* 77—66634
Ag-Cu, directionally solidified, obs. of cutting deform. zone *(Japanese)* 78—15422
Ag-Cu, highly deformed eutectic composite wire, anomalous props., fibre diameter and foreign atom effects *(German)* 77—36566
Ag-Cu, mechanism of lamellar spacing adjustment 78—31395
Ag-Cu (39.9 at.%), eutectic composites, solidification and deform. *(Czech)* 77—59773
Ag-Cu alloy filaments, prod. by glass coated melt spinning, microstruct. and tensile strength 79—91667
Ag-Cu eutectic and off-eutectic alloys, thermal stability 77—25077
Ag-Cu eutectic composite wire, HF conductivity and skin effect 79—33305
Ag-Ge, liq. eutectic, struct. by neutron diffr. 78—18537
Ag-Ge, X-ray spectral exam. *(Russian)* 77—63489
Ag-Ge eutectic alloy, heat capacity meas. over temp. range 800-1200K *(French)* 80—88331
Ag-Si, X-ray spectral exam. *(Russian)* 77—63489
Ag-Sm system, phase diagram, eutectic temps., microstruct. *(German)* 80—104119
Ag-Tl, eutectic liquid alloy, structural features, interatomic interaction *(Russian)* 79—77494
Al alloys, effect of alloying elements on cond. 80—3205
Al alloys, superplastic, tensile deform. behaviour *(Japanese)* 78—27558
Al-Ag_2Al, eutectic alloy, exam. of terminal solid solubility limits 78—76633
Al-Al_2 eutectic, abrasive fragmentation *(Czech)* 78—64715
Al-Al_2Cu, aligned eutectic, precipitation, TEM and microhardness meas. 78—27529
Al-Al_2Cu eutectic, radial growth, in-situ obs. of solidification interfaces with 1 MeV electron microscope 79—87574
Al-Al_3Ni, aligned, eutectic alloy, mech. behaviour at high strain rates 78—39855

eutectic alloys continued
Al-Al_3Ni, effect of some thermal parameters on the directional solidification process 78—88456
Al-Al_3Ni, electrolytic prep. of Al_3Ni fibres, SEM and anodic polarisation studies 80—100817
Al-Al_3Ni, eutectic, creep model 77—36588
Al-Al_3Ni, eutectic composite, directionally solidified, thermal cycling induced distortion 78—39899
Al-Al_3Ni directionally solidified eutectic, microstructural degradation in temp. gradient 78—3145
Al-Al_3Ni directionally solidified eutectic alloy, struct. and mech. props. *(Korean)* 80—29944
Al-Al_3Ni eutectic, cryst. struct., orientation, electron microscopy, computer calcs. *(German)* 77—72582
Al-Al_3Ni eutectic, temp. gradients, microstructural changes 80—84971
Al-Al_3Ni eutectic, thermal stability in temp. gradient 79—61611
Al-Al_3Ni eutectic composite, substructural matrix hardening *(Russian)* 77—21162
Al-Al_3Ni eutectic composite, structural response to shape variations 79—83190
Al-Al_3Ti, peritectic transform. 77—16564
Al-Al_4Ca, eutectic alloy, unidirectionally solidified, exam. of growth and crystallography 78—72771
Al-Al_4Cin eutectic alloy, extruded and unidirectionally solidified, corrosion a neutral NaCl soln. 80—21154
Al-Al_6Fe, fibre reinforced eutectic, deformation behaviour by rolling, TEM and SEM study 79—29129
Al-Al_6Fe eutectic, thermal stability rel. to soaking times 77—21131
Al-based, unidirectionally solidified, solidification and morphology relationship 80—25684
Al-Ca-Zn (5,5 wt.%) superplastic sheet alloy, mechanical properties, superplastic forming behaviour 80—60920
Al-Cu (33 wt.%) eutectic, superplasticity, in-situ obs. by TEM 77—28876
Al-Cu (33 wt.%) eutectic, solidification under reduced gravity, behaviour of suspended Al_2O_3 particles *(German)* 80—60853
Al-Cu alloys, hypo- and hyper-eutectic, dendrite coarsening during solidification 77—63651
Al-Cu eutectic alloy, cooling rate in rapid solidification, estimation from cell spacing 80—50623
Al-Cu eutectic melts, struct. determ. *(Russian)* 77—80408
Al-Cu hypoeutectic, solidification cycle, thermal anal. 80—29945
Al-$CuAl_2$, directionally solidified eutectic alloy, effect of heat treatment 77—55977
Al-$CuAl_2$, directionally solidified eutectic, structural changes during strength tests *(Russian)* 80—7543
Al-$CuAl_2$, eutectic system, interlamellar spacing meas. 77—36492
Al-$CuAl_2$ aligned, fracture, effect of growth speed, orientation, environment 77—28907
Al-$CuAl_2$ eutectic, deformed, thermal stability 77—52348
Al-$CuAl_2$ eutectic, heat treatment and interlamellar spacing effect on tensile deformation 80—29979
Al-$CuAl_2$ eutectic, superplastic behaviour during compressive deform. 77—52429
Al-$CuAl_2$ eutectic, thermal instability in temp. gradient 78—52851
Al-$CuAl_2$ eutectics, microstruct. after solidification, heat pipe influence 80—76243
Al-$CuAl_2$ lamellar composite, stress and temp. depend. of creep 79—52330
Al-$CuAl_2$ lamellar eutectic, computer simulation of two dimensional Zn diffusion 78—30799
Al-Fe, plastically deformed, influence of microstruct. on energy stored 78—84894
Al-Fe-Si, eutectic alloy growth, by twinning plane propagation *(French)* 78—60667
Al-$FeAl_3$, unidirectionally solidified eutectic, α-liq. interface stability 77—63650
Al-Ge, directionally solidified lamellar eutectics, specimen prep. for TEM *(German, English)* 78—95885
Al-Ge, X-ray spectral exam. *(Russian)* 77—63489
Al-Mn alloys, study of solidification by rapid cooling *(Japanese)* 78—88459
Al-Ni eutectic alloy, directional solidification using electroslag remelting 79—61578
Al-Ni-Co, directionally solidified ternary eutectic morphology *(Czech)* 77—59772
Al-Ni-Co(Si), directionally solidified eutectic, morphological and mech. props. *(Russian)* 80—30057
Al-Ni-Si, eutectic, unidirectional solidification 77—16565
Al-Pd eutectic, microstruct. morphology 80—3018
Al-Si, and Al-Si-Na eutectic melts, struct. determ. *(Russian)* 77—80408
Al-Si, eutectic colonies morphology by stereometric microanal. *(Russian)* 77—81247
Al-Si, hypereutectic silumins, P and Na modification 78—84792
Al-Si, inoculated with NaCl+KCl+NaF, effect on morphology of eutectic columns *(Russian)* 79—15684
Al-Si, off-eutectic alloy growth from stirred melt 77—8809
Al-Si, quasiisotropic, rheological deformation theory 80—79165
Al-Si, unidirectionally solidified eutectic alloy grow at different rates, Vickers hardness 77—36654
Al-Si (16 wt.%) melt, fivefold twinned Si cryst. growth, crytallographic study 80—2942
Al-Si eutectic, depend. between min. creep rate and time of beginning of secondary creep *(Czech)* 80—35267
Al-Si eutectic, directionally solidified, tensile props. 78—64531
Al-Si eutectic, high temp. creep, two regimes of flow, modified Dorn eqn. anal. 79—74215
Al-Si eutectic, Na, Sb and Sr alloying addition effects on microstructure *(French)* 78—64548
Al-Si eutectic, pressure effect on metal-die heat transfer coeffs. during solidification 80—7544
Al-Si eutectic alloy, banded struct., SEM and optical microscopy 80—104144
Al-Si eutectic alloy, hardness rel. to tensile and compressive strength 79—52354
Al-Si eutectic alloys, superplasticity 80—11710
Al-Si eutectics and hypoeutectics, mech. props. and thermal cond., P impurity effect 79—83271
Al-Si hypereutectic alloy, dissolution and primary crystallization of Si *(French)* 77—59832
Al-Si hypereutectic alloy, wear resistance 77—77593

eutectic alloys continued

Al-Si(Ge) eutectic alloys in screened ohmic contacts for solar cells 80—94090

Al-Sn, discrete eutectic formation mechanism *(Russian)* 77—66634

Al-Zn, tension deformed superplastic specimens, instantaneous strain rate variation *(Russian)* 79—79033

Al-Zn alloy, solid state eutectoid transformation 79—74146

Al-Zn eutectoid, superplastic, fracture, electron microscope obs. 78—31533

Al-Zn eutectoid, superplasticity, test machine rigidity effect 79—70250

Al-Zn eutectoid alloy, sensitivity analysis of torsion method in evaluating superplasticity indicators 77—56179

Al-Zn(Cu)(Ni), mechanism of lamellar spacing adjustment 78—31395

Al-ζ(AlAg) eutectic and off-eutectic alloys, thermal stability 77—25077

(Al-Zn):Cd eutectic system, cellular growth, unidirectional solidification investig. *(Korean)* 77—28805

As-Pb, eutectic, temp. determ. up to 35 kbar 77—85989

Au-Co, liquidus line determ. by mag. meas. 80—60250

Au-Ge, liquid quenched, exam. of phase decomposition 78—48371

Au-Ge eutectic films, prep. of Au films with nm-sized pores by etching 80—16227

Au-Ge/GaInAsP, ohmic contact, elec. characts. 80—80376

Au-Si thin film double layer, silicide form., electron diffr. study 80—80005

AuSn$_4$-Sn, eutectic struct., faceting and morphological regularity 79—61573

AuSn$_4$-Sn, unidirectionally solidified, X-ray diffr. anal. of crystal struct. 78—91308

Bi-Cd eutectic alloy, directionally solidified, contact melting kinetics, mass transfer during solidification *(Russian)* 77—52310

Bi-Cd(Sn), eutectic, contact melting kinetics *(Russian)* 80—70377

Bi-MnBi, directionally solidified composite, processing parameter role on mag. props. 80—35352

Bi-MnBi, mag. props. singularities, electron microscope exam. *(Russian)* 78—39363

Bi-MnBi directionally solidified eutectic alloys, struct. and mag. props. 79—51815

Bi-MnBi eutectic, directional crystallisation and microstruct. *(Russian)* 77—55915

Bi-MnBi eutectic composites, microstructure and mag. props., annealing effect 79—82827

Bi-MnBi eutectic region, of Bi-Mn phase diagram 80—81034

Bi-Pb-Sn, eutectic alloys, struct. instability and absence of superplasticity *(Russian)* 77—8882

Bi-Pb(Sn)(Tl), complex-regular eutectics, structural modification 78—23695

BiTe-In(Gn,Sn)Te system, physicochemical anal., eutectic type phase diagram with solid soln. region 77—16556

(Cd-Bi)-Sn, eutectic alloy, directionally solidified, contact melting kinetics, mass transfer during solidification *(Russian)* 77—52310

Cd-Cd$_3$Ag, peritectic transform. 77—16564

Cd-CuCd$_3$, off-eutectic alloys, controlled grain growth *(Japanese)* 77—55958

Cd-Ge broken lamellar eutectic composite, tensile and compressive props. 80—71694

Cd-Pb, high pressure effects, eutectic temp. 80—55361

Cd-Sn, eutectic alloys, struct. instability and absence of superplasticity *(Russian)* 77—8882

Cd-Sn binary system, high press. study 80—93539

Cd-Tl binary alloy system at high press. 80—97461

Cd-Zn, directionally solidified lamellar eutectics, specimen prep. for TEM *(German, English)* 78—95885

Cd-Zn alloys, splat-quenched, X-ray diffr., SEM and TEM study of struct. 79—66077

Cd-Zn binary systems, melts, elec. resist., 0-700°C 80—65517

Cd-Zn eutectic, microstruct. degradation, role of temp. fluctuations 77—4766

Cd-Zn eutectic and off-eutectic alloys, stability 77—25077

Cd-Zn eutectics, microstruct. after solidification, heat pipe influence 80—76243

(Co,Cr,Ni)-TaC, eutectic alloy, directionally solidified, struct. defects, autoradiographic investig. *(Russian)* 77—25038

(Co,Cr)-(Co,Cr)$_7$C$_3$, eutectic creep model 77—36588

(Co,Cr)-(Cr,Co)$_7$C$_3$, eutectic alloy, directionally solidified, struct. defects, autoradiographic investig. *(Russian)* 77—25038

(Co,Cr)(Co,Cr)$_7$C$_3$ eutectic composite, creep anisotropy 78—19840

(Co,Ni)-Cr$_{23}$C$_6$ eutectic, microstruct. effect on fracture energy 80—7662

Co base alloy, creep-fatigue interaction in aligned eutectic and solid soln. 80—108554

Co-(Cr,Co)$_7$C$_3$ eutectic, oxidation effect on toughness and strength 80—89404

Co-Al-Cr(Nb)(Ta), eutectic alloys, charact. by melting, oxidation resistance and composition 78—52768

Co-Al-Nb, monovariant directionally solidified eutectics, struct. and mech. props. *(Russian)* 78—92254

Co-B (6.6 at.%), columnar alloys, metallographic obs. of eutectic struct. *(Russian)* 78—27469

Co-C-TaC directional eutectic, high-strength, interphase boundaries *(Russian)* 79—38812

Co-Co$_2$Sn *(Russian)* 79—74182

Co-CoAl eutectic, invariant composition redeterm. 78—3099

Co-Cr, fibrous eutectic, thermal stability 77—36547

Co-Cr-Al-C eutectic alloy, thermal cyclic loading, exam. 78—48496

Co-Cr-C eutectic, creep and fatigue crack propag. 78—39859

Co-Cr-C eutectic alloy, thermal conductivity and electric resist. at high temp. 80—103668

Co-Cr-C-Al (39, 2.2, 2 wt.%), directionally solidified eutectic alloy, Larson Miller C const. 79—70162

Co-Cr-Mo (Zr)(Nb)(Ta), eutectic alloys, charact. by melting, oxidation resistance and composition 78—52768

Co-Cr-Ni-TaC, directionally solidified eutectic, mech. props. and sruct., thermal cycling effects *(Russian)* 78—92282

Co-Cr-NiTaC eutectic, directionally solidified, ~~micro~~structural stability 79—38815

Co-Cr-Nr-TaC eutectic alloys, fatigue, microstructure effects 78—23803

Co-Cr-Zr, thermodynamically calculated phase diagram 79—91617

Co-Cr(VC)((Ti,V)C)-(Al), eutectic alloy, unidirectional solidification, oxidation and tensile tests 78—52790

Co-Ge eutectic alloys, X-ray spectral investig. of electron struct. 77—44087

Co-Nb(W)(Mo)(Ti)-Si, directionally solidified eutectics 79—61575

eutectic alloys continued

Co-Ni-Cr-Ta-C (10, 10, 14, 1 wt.%), aligned eutectic, directionally solidified, fatigue crack propag. 78—27624

Co-Si, directionally solidified eutectic composite alloy, form. and strength 77—90294

Co-Si-Nb(Zr), eutectic alloys, charact. by melting, oxidation resistance and composition 78—52768

Co-Sm-Sn-Co$_{17}$Sm$_2$ eutectic fibre composite, coercive force 77—40084

Co-Ti (22 at.%), amorphous eutectic phase 80—55360

Co-VC (12 wt.%), directionally solidified eutectic, oxidation 80—11821

Co-WC, levitation quenching 77—59711

(Co-Ni)-Cr$_{23}$C$_6$ eutectic alloy, directionally soldified, microstruct. and crystallography 78—48390

Co(Cr,Ni)-TaC fibrous eutectic, deformed, thermal stability of microstruct. *(Russian)* 79—1895

Cr steel, austenite, abnormal decomposition kinetics and mechanism *(Russian)* 80—55344

Cr-(Cr,Co)$_7$C$_3$ eutectic, oxidation effect on toughness and strength 80—89404

Cr$_7$C$_3$ fibre reinforced Cr alloy 73C, directionally solidified eutectic, fatigue crack propag. 77—36635

Cu-Al, directionally solidified eutectic composite alloy, form. and strength 77—90294

Cu-Al, eutectic composition, exam. of high temp. mechanical behaviour *(French)* 78—72818

Cu-Al (In), eutectic systems, specific phase boundary enthalpy, calorimetric study *(German)* 79—29016

Cu-Al eutectic alloy, unidirection transform. controlled by heat flow *(Japanese)* 78—15386

Cu-Al hypoeutectic alloy, water-quenched, tensile fatigue strength at high temp. in vacuo *(Japanese)* 78—72837

Cu-Al(In), lamellar eutectoids, calorimetric determ. of interfacial enthalpy 78—60668

Cu-Cr, eutectic, effect of comp. and solidification conditions on microstruct. *(Russian)* 79—29037

Cu-Cr (1.45 wt.%), unidirectionally solidified eutectic, cooperative growth 77—90341

Cu-Cr eutectic, thermal stability in temp. gradient 79—61611

Cu-Cu Zr eutectic composite, struct. and props., heat treatment and crystn. rate influence *(Russian)* 79—38813

Cu-Cu$_6$Y eutectic alloy, cast and directionally solidified, struct. and props. *(Russian)* 80—104138

Cu-Ge-La, Cu+Misch metal, eutectic alloy, internally oxidised, mech props. *(Japanese)* 77—52411

β-Cu-In, directionally transformed eutectoid, morphology exam. by metallography *(German)* 78—92257

β-Cu-In, unidirectionally transformed eutectoid, lamellar microstructure, influence of grain boundaries on thermal stability 78—72795

β-Cu-In eutectic, unidirectionally decomposed discontinuous coarsening reaction 78—27472

Cu-In eutectoid, coarsening at 829K 79—1885

Cu-In eutectoid, directional eutectoid decomposition growth, crystallography 80—29874

Cu-Nb$_2$Sr, multifilamentary supercond. composites, in situ formed, critical currents 79—65625

Cu-Sb alloy, splat-quenched, energy dispersive X-ray diffr. 78—23728

Cu-Sb melt, eutectic struct. by neutron diffr., isotopic substitution 78—47233

Cu-Si, melt, enthalpy of formation at 1370K 80—26042

Cu$_{60}$Zr$_{40}$, metallic glass, composition, mech. props., simulation 80—49117

Fe, cast, eutectic solidification, expt. study by quantitative metallography 79—24516

Fe, cast, grey eutectic transform. mechanism *(Russian)* 80—20924

Fe, cast, vermicellular, eutectic cell struct. *(Rumanian)* 79—74167

Fe, gray, Mg bearing, high strength, eutectic grain determ. by Si reverse liquation 79—15886

Fe group transition metal metalloid binary alloys, metallic glass form., eutectic composition 79—74133

Fe-Al eutectic alloy, duplex crystals, unit cell parameters, appl. of Weissenberg technique 78—67684

Fe-B, columnar alloys, metallographic obs. of eutectic struct. *(Russian)* 78—27469

Fe-B, eutectic, crystallisation *(Russian)* 79—70087

Fe-B glass, crystallisation kinetics, elec. resist. meas. 79—4254

Fe-B(-Si), glassy, field-induced mag. anisotropy near eutectic comp. 80—93110

Fe-C, lamellar eutectoid, calorimetric determ. of interfacial enthalpy 78—60668

Fe-C, pearlite, eutectoid alloy, efficiency of directional transformation on orientated growth 78—76642

Fe-C, pre-eutectic melt, struct. anomalies *(Russian)* 77—28794

Fe-C eutectic, solidification cycle, thermal anal. 80—29945

Fe-C-H phase diagram, effect of H on eutectoid equilib. *(Russian)* 79—15648

Fe-C-Si, high purity, vacuum melted, nodular graphite form. 80—108452

Fe-Cr-Al-TaC (13.5, 3.7, 9 wt.%) eutectic alloy, directionally solidified, thermal cycling effects on microstruct. 77—32686

Fe-Cr-Ta, eutectic alloy, exam. of eutectic temp., composition, and oxidation resistance 78—52767

Fe-Fe$_x$Sb, *(Russian)* 79—74182

Fe-Mo-C, eutectoid transform. of δ-ferrite 77—16570

Fe-MoS$_2$, exam. of props., using differential thermal analysis, and metallography *(Russian)* 79—15653

Fe-MuS eutectics, unidirectional solidification *(German)* 80—100827

Fe-Si-Ti(Zr)(V)(Nb), eutectic alloy, exam. of eutectic temp., composition, and oxidation resistance 78—52767

Fe-V-S-(C), sulphide nature exam. by X-ray spectral anal., solidification effects *(Russian)* 79—52191

Fe-VC alloys, struct. and mech. props. 79—52171

FeCoC, unidirectionally transformed eutectoid, crystallography of herringbone pearlite, TEM obs. 78—31399

FeSi-Fe$_2$Si$_5$ eutectic, FeSi$_2$ formation, annealing temp. and time effects 79—24512

α-Fe$_2$Si$_5$-ϵ-FeSi, orientation relationships 78—31397

Fe$_2$Ti-Fe eutectic alloy, directional solidification singularities *(Russian)* 78—68678

Ga/rare earth systems, direct calorimetric exam. 78—84775

Ga-In-WSe$_2$ eutectic alloy, self-lubricating, struct. and props. 79—100267

eutectic alloys continued
GaSb based eutectics, thermal cond. and diffusivity, 300-700K, phonon mechanism 80—103526
Ge-Au eutectic alloys, field ion sources 80—97414
Ge-GaP system, phase analysis 78—23674
Ge-InP system, phase analysis 78—23674
Ge-Sb, eutectic alloy, exam. of morphology during solidification *(Russian)* 79—34022
Ge-Sb eutectic alloy, crystallisation in electric field *(Russian)* 77—52311
HfC-HfB$_2$, wear in vacuum, role of boride phase 80—21113
HfC-HfBr$_2$, preparation and high temp. antifriction props. 79—1918
Hg-Tl, phase limits, determ. by enthalpy functions along liquidus *(French)* 80—84911
Hg-Tl amalgam, viscosity meas. 80—88349
In-Bi (22 at.%), directionally grown eutectic two phase superconductors, magnetisation behaviour 77—28293
In-Bi alloy system at high press. and temp. 78—92238
In-Ga alloy, electrode metal-solvent interaction rel. to elec. double layer struct., adsorpt. 78—61023
In-Sn-Sb, liquid state, structure of eutectic alloy 78—42890
In-Zn binary system, melts, elec. resist., 0-700°C 80—65517
InAs-FeAs, growth from melt, electrical props. 77—11911
In$_2$Bi-In, thin lamellar eutectic strips, unidirectionally solidified, morphologic and crystallographic study *(French)* 77—55264
InSb based eutectics, thermal cond. and diffusivity, 300-700K, phonon mechanism 80—103526
InSb-MnSb eutectic alloy, temp. depend. of conductivity and Hall effect, field depend. of Hall coeff. 77—24566
InSb-NiSb, eutectic alloy, Te-doped, electrophys. props. 77—35955
Ir-Y eutectic alloy, supercond. transition enhancement due to lattice softening 80—103775
K-Na(22 wt.%), dense plasma in arc, elec. and heat conds., two-probe diagnostics 80—38560
Li-Pb eutectic alloys for fusion reactor solid breeder blankets, reactions with water 80—102297
Li-Pb-cooled blanket for tandem mirror fusion reactor, neutronic anal. 80—99273
Mg/Mg$_2$Cu eutectic, hydriding and dehydriding kinetics obs. by press. sweep method 80—35765
Mg-Al, unidirectional solidification, method for determ. of diffusion and thermal diffusion coeffs. in molten Mg 78—30772
Mg-Fe, unidirectional solidification, method for determ. of diffusion and thermal diffusion coeffs. in molten Mg 78—30772
Mg-Ho alloys, phase diagrams and transformations, Ho solubility *(Russian)* 79—52162
Mg-Mg$_2$Ni eutectic alloy and Mg$_2$Ni, catalytic effect in hydrogenation, surface analysis 80—30283
Mg-Si, unidirectional solidification, method for determ. of diffusion and thermal diffusion coeffs. in molten Mg 78—30772
Mn-Bi eutectic alloy, mag. anisotropy 78—68220
Mn-Pt (<29 at.%), eutectoid transform., antiferromag. struct. transform. *(French)* 78—92259
Mn$_{0.6}$Ga$_{0.4}$Sb, eutectics, galvanomag. props., thermo EMF 77—15869
Mo-Mo$_2$C(HfC)(TiC)(ZrC), eutectic formation of regular struct., crystn. *(Russian)* 80—66496
Mo-TiN (3.5 vol.%), failure characts. exam. 78—68788
Mo-Ti(Zr)(Hf)-N, exam. of phase equilibria *(Russian)* 79—29018
Nb-Mo-Al-(Cr) eutectic directionally crystallised alloy, heat resistance, alloy struct. *(Russian)* 80—40481
Nb-Nb$_2$C, directional crystn. using plasma heating 78—60569
Nb-Nb$_2$C eutectic composites, directionally solidified, growth crystallography and lamellar to rod transition 77—32569
Nb-Nb-Al-(Cr), γ/γ'-δ type eutectic, fatigue, effect of composition and microstruct. 78—48520
Nb-Th, eutectic composition 80—100828
Nd-Tl phase diagram, intermediate phases 78—60653
Ni/Ni$_3$Al-Ni$_3$Nb, directionally solidified lamellar eutectic alloy, deform. anisotropy and fracture 77—36604
Ni/Ni$_3$Al-Ni$_3$Nb eutectic, directionally solidified, plastic deformation *(Russian)* 78—39843
Ni/Ni$_3$Al+Ni$_3$Nb, directionally solidified eutectic alloy, crack growth rate under creep fatigue conditions 79—52361
Ni-Al-Cr$_3$C$_2$, directionally solidified, oxidation resistance, influence of Y 80—89409
Ni-Al-Cr$_3$C$_2$, eutectic, directionally solidified, high-temp. oxidation 80—50775
Ni-Al-Cr$_3$C$_2$, eutectic, Al$_2$O$_3$ coatings for oxidation resist. 80—50776
γ/γ-Ni-Al-Nb, aligned eutectic alloy, H$_2$ embrittlement 77—8951
Ni-Al-Ti, eutectic alloy charact. by melting temp., composition and oxidation resistance 78—52771
Ni-B (3 at.%), columnar alloys, metallographic obs. of eutectic struct. *(Russian)* 78—27469
Ni-based, in gas turbines, Ni-Cr-Al coatings, use of diffusion barrier 79—24673
Ni-based, unidirectionally solidified, solidification and morphology relationship 80—25684
Ni-based eutectic alloys, struct. and props. *(Russian)* 77—21129
Ni-based TaC eutectic, directionally solidified, elastic moduli 80—84984
Ni-C. exam. of metastable phase diagrams, at high temp. and pressure *(Russian)* 79—56955
Ni-Co-Cr-Ta-Al-W-Mo-Ti, cast, phase volume fraction determ. using manual point count practice 78—53052
Ni-Cr-Al-Cr-Hf-Zr-C, directionally solidified eutectic with (Hf,Zr)C reinforcement, precipitation, and thermal cycling 78—44057
Ni-Cr-Al-TaC, eutectic composite, microstructure, fatigue props. 80—85038
Ni-Cr-Nb-Al eutectic alloys, sulphidation/oxidation at high temps., corrosion mechanism 78—72934
Ni-Cr-NbC (18, 10 wt.%) eutectic composite, unidirectional solidification, thermal cycling, temp. range effect on microstructural degradation 80—89272
Ni-Cr-TaC directional eutectic, high-strength, interphase boundaries *(Russian)* 79—38812
Ni-Cr-TaC eutectic-like composite, obs. of interfacial diffusion by high resolution TEM 79—4432
Ni-Cr-Ti(Nb)(Zr), eutectic alloy charact. by melting temp., composition and oxidation resistance 78—52771
γ-Ni-γ'-Ni$_3$Al-TaC fibre reinforced eutectic, oxidation protection 77—40475
Ni-Mo-Al eutectics, unidirectional solidification 77—4769

eutectic alloys continued
Ni-Nb-Al, eutectic, thermal cycling effect on strength and ductility *(Russian)* 79—24601
Ni-Nb-Al, unidirectionally solidified γ/γ'-δ eutectic, fatigue crack propag. 79—29184
Ni-Nb-Al (21,2.5 wt.%), eutectic aligned alloy, mech. behaviour at high strain rates 78—39855
Ni-Nb-Al (25, 2.5 wt.%), directionally solidified γ/γ'-δ eutectic, growth conditions on struct. 80—11639
Ni-Nb-Al-(Cr), eutectic, mech. props., high press. H$_2$ effects 77—63779
Ni-Nb-Cr-Al, directionally solidified eutectic superalloy, high temp. oxidation resistant coatings 78—39937
γ/γ'-δ-Ni-Nb-Cr-Al (20, 6, 2.5 wt.%), growth kinetics of γ' precipitates 77—40424
Ni-NbC (10 wt.%), directional solidification and struct. *(Russian)* 80—84922
Ni-NbC eutectic, microstructure and strength depend. on composition and crystallisation conditions *(Russian)* 79—100128
Ni-Ni$_2$B eutectic, high temp. X-ray anal. 80—71639
Ni-Ni$_3$Al-Cr$_3$C$_2$ eutectic composite, creep 77—40431
Ni-Ni$_3$Ti eutectic alloys, solidification 77—70042
Ni-Ta-C, composites of γ+TaC 77—85965
Ni-TaC, eutectic alloy, fibre reinforced, directionally solidified, anisotropic yielding behaviour 79—11675
Ni-W (45.5 wt.%), eutectic, mech. props., high press. H$_2$ effects 77—63779
Ni-W directionally solidified eutectic composite, foil prep. for TEM 78—53072
NiAl-Cr, eutectic, directionally solidified, temp. behaviour of misfit dislocations *(German)* 78—3119
NiAl-V join, phase relations and eutectic directional solidification 78—31396
Ni$_3$Al-Ni$_3$Nb, ^{63}Ni diffusion rate rel. to struct. defects *(Russian)* 78—2288
Ni$_3$Al-Ni$_3$Nb, directionally crystallised, thermal and electric cond., emissivity 77—43556
Ni$_3$Al-Ni$_3$Nb, directionally crystallised eutectic, influence of prolonged annealing on microstructs. and props. *(Russian)* 79—74182
Ni$_3$Al-Ni$_3$Nb, eutectic, temp. and thermal cycling influence on oxidation 80—45417
Ni$_3$Al-Ni$_3$Nb, eutectic alloy, crack development, failure energy capacity *(Russian)* 80—40480
Ni$_3$Al-Ni$_3$Nb directional eutectic, oxidation and interaction with protective coatings *(Russian)* 77—52526
Ni$_3$Al-Ni$_3$Nb eutectic, directionally solidified, high-temp. oxidation mechanism 80—16544
Ni$_3$Al-Ni$_3$Nb eutectic alloy, aluminide coating microstruct. exam. 78—15593
Ni$_3$Al(γ')-Ni$_3$Nb(δ), directionally solidified, deformation substruct. and slip systems 79—8326
Ni(Cr)/Ni$_3$Al-Ni$_3$Nb directional eutectic, oxidation and interaction with protective coatings *(Russian)* 77—52526
Ni$_3$Nb platelet reinforced Ni base alloy 77—36635
NiTaC, eutectic alloys, chem. incompatibility of ceramic nitrides for directionally solidifying 80—81046
NiTaC eutectic superalloy, casting, furnace atm. effects 80—84880
NiTaC eutectics, high cycle fatigue at room temp. 80—16459
NiTaC-13, directionally solidified eutectic alloy, chem. compatibility with ceramic materials 79—87623
Ni$_3$Ti-Ni eutectic alloy, directional solidification singularities *(Russian)* 78—68678
Pb-Ag eutectic alloy, microstruct. coarsening under isothermal and temp. gradient conditions 79—20079
Pb-Bi eutectic alloy flow rate meas. apparatus 77—79412
Pb-Bi eutectic melt, in contact with Cu, mutual indentation *(Russian)* 77—59853
Pb-Cd lamellar eutectic composite, pair potential meas. 79—33396
Pb-Cu, hypoeutectic, grain refinement, and structural stability by S, Se and Te additions *(German)* 80—55387
Pb-Sb, thermal analysis in non-faceted/faceted eutectic systems 80—71637
Pb-Sb eutectic alloys, solidification in space environment 79—47671
Pb-Sn, directionally solidified lamellar eutectic, deform. induced microstruct. instability 77—32623
Pb-Sn, directionally solidified, perfection and stability of lamellar struct. *(French)* 77—77468
Pb-Sn, directionally solidified, periodic array of supercond.-normal contacts, supercurrent and dynamic resist. 78—34928
Pb-Sn, eutectic, electron emission avalanche obs., during isothermal superplastic deform., *(Russian)* 77—48324
Pb-Sn, eutectic, superplastic behaviour, grain size effect 80—7635
Pb-Sn, eutectic alloy, plastic deform., work hardening *(German)* 78—92279
Pb-Sn, eutectic alloys, struct. instability and absence of superplasticity *(Russian)* 77—8882
Pb-Sn, lamellar eutectic alloy, proximity effect, entropies, free energies and transition temps. 77—51849
Pb-Sn, off-eutectic alloy growth from stirred melt 77—8809
Pb-Sn, proximity and pinning effect up to 7K *(French)* 77—51858
Pb-Sn, spiral growth phenomenon 77—48419
Pb-Sn, superplastic deform. of circular sheets *(French)* 77—28871
Pb-Sn, superplastic deform., appl. of SEM specimen holder for cold tensile deform. expts. *(French)* 77—36704
Pb-Sn, superplastic eutectic, roll load and torque necessary for rolling *(French)* 78—95761
Pb-Sn, undercooled eutectic, compositional variations at various gravity levels 77—52314
Pb-Sn (62 wt.%), intercrystalline and interface boundary sliding, tensile tests, SEM obs. 79—38886
Pb-Sn (62 wt.%), superplastic eutectic, exceptional ductility 78—27579
Pb-Sn directionally solidified eutectic alloy, morphology and crystallography 77—90340
Pb-Sn eutectic, cavitation during superplastic flow, affecting factors 78—60728
Pb-Sn eutectic, strain rate sensitivity index, expt. comparison of different methods 80—3144
Pb-Sn eutectic, superplastic, anelasticity effect on stress relaxation 78—31443
Pb-Sn eutectic alloy, high temp. deform. 77—16637
Pb-Sn eutectic alloy, superplastic deform. at relatively high strain rates 79—57042

eutectic alloys continued
- Pb-Sn microduplex eutectic, cavitation during superplastic flow due to hard particles 77−36575
- Pb-Sn-Cd, eutectic and monovariant eutectic, ingot struct. 78−15388
- Pb-Sn-Cd, monovariant eutectic and eutectic alloys, ingot struct. 77−63656
- Pb-Zn, off-eutectic alloys, controlled grain growth *(Japanese)* 77−55958
- Pb_4Li, ISSEC selection for fusion reactor 80−57950
- PbSe-$PbCl_2$, eutectic crystallisation, visual monitoring 77−44237
- Pd-Cd, unidirectionally solidified, tensile and compressive props. 78−27567
- PdAl-Fe(Ni), phase diagrams, eutectic points and solubility *(Russian)* 80−40333
- $Pd_{80}Si_{20}$, metallic glass, composition, mech. props., simulation 80−49117
- Sb-Ge, unidirectionally solidified, exam. of compressive props. and struct. 78−68730
- Si-Al, silumin, crystn. of eutectic phases *(Russian)* 80−29942
- Si-Au eutectic alloys, field ion sources 80−97414
- SiC-B eutectic alloys, struct. of crystallising graphite 79−38829
- Sn-Bi, eutectic, superplastic anisotropy *(German)* 80−25808
- Sn-Bi, thermal analysis in non-faceted/faceted eutectic systems 80−71637
- Sn-Bi alloy, splat-quenched, energy dispersive X-ray diffr. 78−23728
- Sn-Cd, interface undercooling-growth vel. relationship, horizontal and vertical solidification 79−8294
- Sn-Pb, eutectic system, interlamellar spacing meas. 77−36492
- Sn-Pb (26%), liq. eutectic alloy Seebeck coeff. 80−84463
- Sn-Pb composition anal. of PCBs using beta-backscatter gauge 80−16631
- Sn-Pb eutectic, strain rate sensitivity of flow stresses, grain boundary sliding during superplastic, non-superplastic deform. 80−7645
- Sn-Pb eutectic, struct. and plasticity, thermomech. treatment effects *(Russian)* 78−60686
- Sn-Pb eutectic alloy, inelastic behaviour 77−48471
- Sn-Pb-(Bi)(Ag)(Sb) (Cu), microduplex eutectic, cavitation during superplastic flow 78−48457
- Sn-Zn (9.8 wt.%), eutectic superplasticity 77−36582
- Sn-Zn eutectic, liq., appl. to drilling of steel, cutting conditions rel. to tool parameters *(Russian)* 79−34187
- SnPb eutectic alloy, Mossbauer spectra, isomer shifts 79−82903
- Te-$(Bi_xSb_{1-x})_2Te_3$, electrophys. props., directed crystn. conditions influence and comp. depend. 80−107827
- Te-Ge eutectic alloy, glassy, crystn. mechanism 78−22836
- Te-Tl, eutectic liquid alloy, structural features, interatomic interaction *(Russian)* 79−77494
- Ti-Ag (10 to 17.5 wt.%), eutectoid system, $\beta \rightarrow \alpha_m$ transform., nucleation kinetics 80−97474
- Ti-Ag(Au)(Si), existence of β to α_m phase transformation 78−44123
- Ti-Au, (9.9 wt.%), eutectoid system, $\beta \rightarrow \alpha_m$ transform., nucleation kinetics 80−97474
- Ti-Bi(Co)(Cr)(Cu)(Fe)(Mn)(Ni)(Pb)(Pd)(Pt), eutectoid decomposition 79−24491
- Ti-Th, eutectic composition 80−100828
- TiC-TiB_2, friction characts., comp. depend., 20-1000°C 80−3203
- TiC-TiB_2, preparation and high temp. antifriction props. 79−1918
- TiC-TiB_2, wear in vacuum, role of boride phase 80−21113
- TiC-TiB_2 alloys, composition effect on surface layer rupture at various temps. 80−25879
- Tl-Bi-Hg alloys, phase diagrams and equilib. *(Russian)* 79−52166
- W-W_2C, directional crystn. using plasma heating 78−60569
- W-ZrC (25 wt.%), eutectic alloy, thermionic emission and adsorption props. 79−69951
- W-ZrC(-Re) eutectic alloy, Re effect on breaking stress, lattice parameters, electron struct. *(Russian)* 79−1845
- WC-TiC-Co, powder for plasma arc sprayed coating 78−15591
- Zn-22 wt.% Al superplastic eutectoid alloy tensile deformation obs. *(Japanese)* 79−90714
- Zn-Al, unidirectional eutectic, FCC phase, preferred orientation 80−29973
- Zn-Al, unidirectionally solidified eutectic, morphology and crystallography 77−48421
- Zn-Al (22 at.%), superplastic, microscopic examination of internal void formation 80−16383
- Zn-Al (22 wt.%), eutectoid, low stress and superplastic creep behaviour 80−81120
- Zn-Al (22 wt.%), superplastic eutectoid cavitation evidence 77−63741
- Zn-Al (22 wt.%), superplastic, eutectoid alloy, ductility and fracture 78−60819
- Zn-Al (22 wt.%), superplastic eutectoid, concurrent grain growth and deformation mechanism 79−74222
- Zn-Al (22 wt.%) eutectoid, superplastic, factors affecting ductility 77−86097
- Zn-Al (22 wt.%) eutectoid, superplastic, grain size effect on plastic deform. at room temp. *(Japanese)* 78−31462
- Zn-Al (22 wt.%) superplastic alloy, cavitation and neck form. 80−30022
- Zn-Al eutectic alloy, uni-directionally solidified, damping capacity *(Japanese)* 80−16364
- Zn-Al eutectoid, superplasticity, study by electron microscopy 77−48479
- Zn-Al eutectoid alloy, straining at elev. temp., whisker crystal 79−29087
- Zn-Al eutectoid alloy sheets, creep bulging 80−1439
- Zn-Al eutectoid superplastic alloy, fatigue, microstruct. obs. and frequency effect 77−36659
- Zn-Ge, eutectic, stereomorphology using SEM, TEM and optical microscopy *(Russian)* 79−52187
- Zn-Pb melt, immiscible component distrib. in crossed EM fields *(Russian)* 77−48396
- Zn-Sn, specific elec. resist., temp. and conc. depend., 20-800°C 79−82571
- Zn-Sn(Bi), discrete eutectic formation mechanism *(Russian)* 77−66634
- Zr-C, exam. of metastable phase diagrams, at high temp. and pressure *(Russian)* 79−56955
- Zr-Fe, amorphous alloy quenched by levitation method, crystallisation 79−55669
- Zr-ZrC, eutectic formation of regular struct., crystn. *(Russian)* 80−66496
- ZrC-W (75 wt.%) eutectic refractory alloys, smelting in suspended states, components distrib. *(Russian)* 80−19913
- ZrC-ZrB_2, friction characts., comp. depend., 20-1400°C 80−3203
- ZrC-ZrB_2, preparation and high temp. antifriction props. 79−1918
- ZrC-ZrB_2, wear in vacuum, role of boride phase 80−21113

eutectic structure
- borophosphate glasses, effect of F on props. 78−67657
- cast iron, hypereutectic, transform. of cementite to austenite 77−52318
- chlorobenzene-cis-decalin mixtures, phase transitions and dielec. behaviour study in 77-330K 80−29680
- coarsening during and after unidirectional growth 78−35379
- crystallisation, stability in presence of external perturbations *(Russian)* 80−16291
- diffusional crystal growth mechanisms 80−3059
- eutectic crystal-melt system, interphase boundary struct., Monte Carlo method study 80−1950
- eutectics, HgTe-PbTe and Au-PbTe, prep. and thermoelectric behaviour characts. 80−107774
- ferrous eutectic liquids, exam. of structures 78−71668
- irregular eutectic, branching limited growth 80−81042
- lamellar eutectoids(ic), stability principles 80−89195
- modification of eutectic morphology, state-of-the-art 78−31394
- multi-component crystal growth, kinetic equation theory, binary system crystallisation 80−88071
- naphthalene-catechol eutectic struct., crystallisation behaviour 79−55868
- naphthalene-p-chloronitrobenzene eutectic system, phase diagrams and crystn. 77−47551
- oxide eutectics, directionally solidified, crystallography and microstruct. 79−78950
- pattern selection in non-equilib. processes, marginal stability theory, eutectic solidification model 80−60852
- polyoxyethylene-glutaric acid eutectic, melting and crystn. 80−28924
- steel, low alloy, low C grain boundary proeutectoid ferrite formation, direct obs. method 80−3074
- ternary systems containing more than three phases, eutectic like and peritectic like reactions 80−29928
- unidirectionally solidified eutectic alloys, solidification and morphology relationship 80−25684
- Zircaloy-4/stainless steel, diffusion bonding in presence of Fe intermediate layer 79−10987
- Ag-Cu (50 at.%), splat-cooled, struct. of γ' extended solid solution 78−3147
- Al-$Al_{21}Pt_5$ eutectic alloys, unidirectionally solidified, struct. study 80−108394
- Al-Al_3Ni eutectic, cryst. struct., orientation, electron microscopy, computer calcs. *(German)* 77−72582
- Al-based eutectic alloys, unidirectionally solidified, solidification and morphology relationship 80−25684
- Al-Cu, splat-quenched, microstruct. thickness and comp. depend., TEM 77−8863
- Al-$CuAl_2$, directionally solidified eutectic alloy, effect of heat treatment 77−55977
- Al-$CuAl_2$, directionally solidified eutectic, structural changes during strength tests *(Russian)* 80−7543
- Al-Pd eutectic, microstruct. morphology 80−3018
- Al-Si, eutectic colonies morphology by stereometric microanal. *(Russian)* 77−81247
- Al-Si alloy, quasiisotropic, rheological deformation theory 80−79165
- Al-Zn(Cu)(Ni), ingots, solidified, formation of equiaxed eutectic grains *(Japanese)* 78−39756
- (Al-Zn):Cd eutectic system, cellular growth, unidirectional solidification investig. *(Korean)* 77−28805
- Au-Ge contacts on GaAs, SEM and TEM obs. of struct. 80−100522
- BPO_4-SiO_2 system, new data to prevent B_2O_3 or P_2O_5 loss at elevated temp. 80−20914
- Bi-MnBi directionally solidified eutectic alloys, struct. and mag. props. 79−51815
- Bi-MnBi eutectic, directional crystallisation and microstruct. *(Russian)* 77−55915
- Bi-Pb(Sn)(Tl), complex-regular eutectics, structural modification 78−23695
- $Bi_{0.52}Sb_{1.48}Te_3$ thermoelec. solid soln., homogeneity, effects of prep. method 78−52698
- BiTeI, formation of lamellar and fibrous microstruct. due to beam heating in electron microscope 79−20024
- CaF_2-AlF_3-Na_3AlF_6(-Al_2O_3), phase equilibria, X-ray diffr. and DTA meas. 80−108409
- Cd-Zn alloys, splat-quenched, X-ray diffr., SEM and TEM study of struct. 79−66077
- Cd-Zn eutectic, microstruct. degradation, role of temp. fluctuations 77−4766
- $Cd(PO_3)_2$-$Sr(PO_3)_2$, physicochemical investigation 78−44102
- Co-Al-Nb, monovariant directionally solidified eutectics, struct. and mech. props. *(Russian)* 78−92254
- $CoCl_2$-KCl-NaCl system, melting diagram investigation by thermographic anal. *(Russian)* 78−3111
- $CoCl_2$-NaCl purification by H_2 reduction, of Co, exam. of conductivity *(Russian)* 79−28981
- Cr-C facing alloys, effect of B on phase composition and facings props. during abrasive wear 80−21117
- Cu-Si-Te, phase equilib., DTA and metallographic anal. *(French)* 79−52182
- Fe, cast, eutectic cells microstruct., crystallisation kinetics *(Polish)* 79−52186
- Fe, eutectic grain in grey Fe, method of size determ. 77−72529
- Fe-C-Mg, cast iron, graphite phase obs. *(Russian)* 77−59744
- Fe-Cr(W)-M, (M=Si,Mo,Ni,Mn,P,Cr), cellular growth of S-pearlite formed by carburisation 80−108486
- Fe-M, (M=Cr,W,Mo,V,Ti), morphology and growth kinetics of δ-pearlite formed by carburisation 80−108485
- Fe-Mn-C, cast iron and steel, Mn effects on struct. 78−23696
- Fe-Ni martensitic alloys, age hardening, eutectoidal transformation 79−47736
- Fe-Ni-Cr (35, 15 wt.%) superalloy, stress rupture and tensile props., C and B additions effect *(Chinese)* 80−104244
- FeO-FeS, mag. susceptibility, eutectic phase diagram *(Russian)* 80−15682
- α-Fe_2Si_5-ϵ-FeSi, orientation relationships 78−31397
- GaAs-Si eutectic alloy, effect of crystallisation rate on microhardness 79−96110
- Ga_2S_3-PbS system, phase diagram and crystallographic study *(French)* 80−29937
- GaSb-GaAs-Ge system, props. and struct. 80−20232
- GaSb-Ge eutectic alloy, effect of crystallisation rate on microhardness 79−96110
- InAs-FeAs, growth from melt, electrical props. 77−11911

eutectic structure continued
  InSb-Ge eutectic alloy, effect of crystallisation rate on microhardness 79—96110
  InSb-NiSb, eutectic, intraband magneto-optical studies, far IR transmission spectra 79—61371
  InSb-NiSb eutectic, struct. and optical props., IR polariser appl. 80—45078
  InSb-Sb eutectic solidification, interface demarcation expts. 79—43228
  $KAsO_3$-K_3AsO_4, phase diag. 78—23681
  KCl-CuCl eutectic fused salt, potential as intermediate temp. solar heat transfer and storage medium 80—101135
  $LaCrO_3$-W(Mo)(Cr) eutectics, prep. and microstruct. 80—108380
  La_2O_2S-Ga_2S_3 system, phase diagram determ. by DTA and X-ray diffr. *(French)* 77—43309
  LiCl-KCl molten eutectic mixture, PbS solubility product and Li_2S solubility 80—54387
  LiCl-LiF molten eutectic mixture, PbS solubility product and Li_2S solubility 80—54387
  $MgBr_2$-ABr (A=Cs, Rb, K, Na, Tl), thermochemical and struct. investigation *(German)* 79—1423
  Mn_2SiO_4-MnO eutectic composite, EFG die-top geom. effect on solidification interface shape 77—48420
  Mo-TiC lamellar eutectic composite, deformation and strength, room temp. to 2073K *(Japanese)* 80—71702
  $NaVO_3$-BaV_2O_6-SrV_2O_6, phase diagrams, simple eutectic system 78—48379
  Na_2WO_4-Pb_2WO_4-WO_3 system investigation, crystn. from melt, coordination compounds form. 79—52189
  Nb-Mo-Al-(Cr) eutectic directionally crystallised alloy, heat resistance, alloy struct. *(Russian)* 80—40481
  NbC-NbB_2, phase relns. 78—23677
  Ni, B-containing diffusion layer formation *(Russian)* 77—48570
  Ni, B-containing multicomponent diffusion layer formation *(Russian)* 77—44400
  Ni/Ni_3Al+Ni_3Nb, directionally solidified eutectic alloy, crack growth rate under creep fatigue conditions 79—52361
  Ni-based eutectic alloys, struct. and props. *(Russian)* 77—21129
  Ni-based eutectic alloys, unidirectionally solidified, solidification and morphology relationship 80—25684
  Ni-Nb-Al (25, 2.5 wt.%), directionally solidified γ/γ'-δ eutectic, growth conditions on struct. 80—11639
  Ni-NbC eutectic, microstructure and strength depend. on composition and crystallisation conditions *(Russian)* 79—100128
  NiAl-V join, phase relations and eutectic directional solidification 78—31396
  Ni_3Al-Ni_3Nb eutectic alloy, aluminide coating microstruct. exam. 78—15593
  NiO-CuO, equilibrium relations 80—55375
  Pb-Sn, controlled solidification, monograin growth, selection and struct. *(French)* 77—16568
  Pb-Sn, ingots, solidified, formation of equiaxed eutectic grains *(Japanese)* 78—39756
  Pb-Sn, lamellar eutectic stability and growth struct., fault formation 79—96019
  Pb-Sn, unidirectionally solidified eutectic, lamellar microstructure, influence of grain boundaries on thermal stability 78—72795
  PbS(Se)(Te)-NiSb eutectic system, crystn. 79—52190
  PbS(Te)-Sb eutectic system, crystn. 79—52190
  Sc-Fe system phase diag. *(Ukrainian)* 78—84773
  Si-Al, silumin, crystn. of eutectic phases *(Russian)* 80—29942
  SiC-B_4C eutectic, directional solidification, growth and mech. props. 79—91638
  Sn-Zn, ingots, solidified, formation of equiaxed eutectic grains *(Japanese)* 78—39756
  SnSe-Tl_2Se, phase diagram, DTA and X-ray diffr. peritectic decomposition *(French)* 77—51471
  SnSe-TlSe, phase diagram 100-900°C *(French)* 79—83180
  TaC-TaB_2, exam. of high temp. friction and wear, and deformation behaviour 79—34152
  TaC-TaB_2, phase diag., solubilities, reactions 77—63643
  Te-based eutectics, crystn. rate effect on electrophys. props. mutual solubility effect 80—60774
  Te-Bi_2Te_3 oriented eutectic, microhardness, influence of size of phases *(Russian)* 78—92322
  Te-Sb_2Te_3 oriented eutectic, microhardness, influence of size of phases *(Russian)* 78—92322
  Ti-ZrO_2(HfO_2), eutectic system metallographic investigation *(Russian)* 77—66629
  TiC-Ni, reaction kinetics under simulated liq.-phase sintering 78—52746
  TiO-ZrO_2, pseudo binary system, effect of Ti addition on struct. and props. of zirconia 79—11583
  Tl-Pb-S system, phase diagram quasibinary Tl_2S-PbS section obs. 80—55372
  V-ZrO_2(HfO_2), eutectic system, metallographic investigation *(Russian)* 77—66629
  $YCrO_3$-W(Mo)(Cr) eutectics, prep. and microstruct. 80—108380
  Zn-Al, unidirectionally solidified eutectic, morphology and crystallography 77—48421
  Zn-Sn(Bi) alloys, morphology and mechanism of formation of eutectic *(Russian)* 78—6916
  $ZnAl_2S_4$-$ZnIn_2S_4$, phase relationships, 800 to 1050°C 79—1852
  ZnS-Al_2S_3, phase relationships, 720 to 1110°C 79—1852
  ZrO_2-Nd_2O_3(Sm_2O_3)(Dy_2O_3) eutectic, unidirectional solidification, microstruct. and crystallographic characterization 80—35176

eutectoid steel *see carbon steel*

evaluation
  see also computer selection and evaluation; function evaluation; information retrieval system evaluation
  abdominal and pelvic diagnosis, US and computed tomography evaluation 78—61228
  aortic concave-convex pivoting disc valve prosthesis, hydrodynamic evaluation 79—84027
  astronomical data files, critical examination 77—78832
  building heat loss diagnostics, IR image evaluation requirements 80—86424
  clinical ECG real-time telephone transmission usefulness and reliability 78—57108
  data evaluation, on Intel 8080A, materials testing, X-ray emission analyser *(Hungarian)* 79—43522

evaluation continued
  dereverberation process evaluation by normal and impaired listeners 80—91974
  developing countries' solar energy evaluation by energy balances 79—57388
  edge operator evaluation test procedure 79—75646
  electrophotographic film evaluation apparatus 79—93244
  eye movement in target tracking using EOG 80—109057
  flat solar collector, energy and economic analyses 78—83236
  fluid volume evaluation in spherical vat with deformable metal diaphragm 77—57310
  glottal area waveform synthetic and natural speech comparison 77—77919
  holographic interferogram quantitative evaluation procedures *(German)* 80—87344
  international collaboration among calibration services 80—101773
  International Nuclear Fuel Cycle Evaluation, midterm assessment *(German)* 79—89370
  IR aspherical lens and surface evaluation 77—39019
  IR material and lens evaluation interferometer 77—39121
  ischaemic cardiac disease determ., heartbeat interval analysis and questionnaire evaluation 79—39580
  lubricant evaluation, of oils used in cold rolling of steel 80—85068
  lubricants, ester-type, thin-film test for meas. of oxidation and evaporation 80—40626
  magnetic particle inspection oxides, evaluation 80—40657
  magnetically hard material demagnetisation curve evaluation 80—90869
  monochromator stray light transmission meas. and evaluation 77—38030
  nondestructive evaluation transducer figure of merit 77—27457
  nuclear power plant siting evaluation, environmental impact probabilistic assessment model 79—79412
  optical comparator, for fine sieves evaluation 80—37068
  optical instrument evaluation definition and test criteria 77—39119
  optical sensor system simulation and evaluation 80—96030
  physical optics farfield inverse scatt., mathematical inversion technique for nondestructive eval. 80—69580
  porcelain, elec., comparative assessment of methods of determ. strength 80—40429
  POSITRON, evaluating system for positron annihilation R-40 computer meas. 79—78787
  reactor emergency cooling model validation by Loss of Fluid Test Facility 79—80981
  solar energy Implementation Centre proposals 79—57394
  solar flat plate collector performance evaluation 79—62091
  solar heating system economic evaluation and optimisation 80—35644
  Solar Thermal Electric Power System technical and economic evaluation for Japan 79—57441
  solid propellant stress transducer evaluation 80—81245
  standard sample homogeneity evaluation, optimal obs. planning 80—93721
  stellar data in machine-readable catalogues, critical evaluation 77—78830
  stellar photometric data, critical evaluation 77—78831
  strain evaluation by specimen-grating photograph electro-optical processing 77—39266
  superfluous, meas. elimination, precision evaluation 80—90805
  US computerised tomography scanner evaluation 79—48301
  US transducer evaluation in exptl. and theoretical domains 79—46153
  ventricular arrhythmia detector, arrhythmia data base of American Heart Association 79—62391
  Visible and Infrared Radiometer evaluation from SeaSat-A surface temp. obs. 80—46325
  X-ray image quality evaluation, visual and objective methods 77—25543
  Cs Hanle effect magnetometer characteristics and evaluation results 77—79586

evaporated layer production *see vapour deposition*

evaporation
  see also drying; field evaporation
  accommodation coefficients, effects on evaporation and condensation *(Japanese)* 78—81933
  acoustic reflection from liquid surface, influence of condensation and evaporation 79—46097
  adsorbed monolayers, permeation and evaporation resistance, attractive forces effects 78—67892
  aerosol, charged spray, evaporation in elec. field *(French)* 77—29054
  aerosol, from medical nebulizer, droplet size distrib., evaporation effect 78—24084
  aerosol, single droplet, size and mass meas. using electrodynamic balance 80—89535
  aerosol, ultradisperse condensational, formation by plasma-jet powder evaporation *(Russian)* 80—55721
  aerosol drop, submicron size evap. in continuum and non-continuum regimes 79—43639
  aerosol solid particles, diffusive evaporation, laser spectrochemical analysis 79—92040
  air humidity diurnal variation over continents, absorpt. in hygroscopic soil layer 79—29825
  air-sea interaction, stratification effect *(French)* 80—31085
  alkali halide, molecular processes of condensation and evaporation 79—69237
  alkali halide, morphology of growth and evaporation surface 78—79544
  alkali metal-ammonia solutions containing cryptands, metal anion and trapped electrons form. by evap. 79—100340
  alloy, binary, surface dehomogenisation during evaporation and ion sputtering 77—73207
  Amazon Basin, water recycling, ^{18}O conc. study 80—81955
  S.America, water balance rel. to water vapour transport in atmosphere 79—29820
  α-amino acids, mass spectrometers study of evaporation 77—86402
  approx. soln. for damage by pulsed discharge 77—39500
  aqueous aerosol, optical thickness change due to CO_2 laser pulses 77—75591
  atmosphere, continental maps of evapotranspiration *(German)* 80—98368
  atmosphere, evaporation calc. using measured wind, temp. and humidity profiles 77—17194
  atmosphere, surface evaporation rate parameterization for numerical modelling 77—91222
  atmosphere, surface evaporation rate rel. to steam fog form. in Fenland 80—98431

evaporation continued
atmosphere at Kew, monthly potential evaporation totals for 1698-1976 period 78—7724
atmosphere boundary layer, evaporation studies using portable differential psychrometer system 80—105072
atmosphere micrometeorology during hot spells of 1976, role of evaporation latent heat 79—79961
atomised liquid dropwise evaporation, mist cooling 80—6506
Baltic Sea region, evaporation-precipitation during IHP 78—44865
benzene adsorbent mesopores, capillary evaporation and struct. 80—107614
binary liquid drops, nucleate boiling evaporation on heated surface 77—27531
binary solution spray evaporation in gas flow 77—39331
$Bo_2 \rightarrow BO_2$ 80—65252
boiling point drying by volumetric abs. of RF and MW EM energy, heat and mass transfer characts. 80—79130
bubble, of vap., with microlayer, universal growth relations 78—71266
bubble motion and bubble-droplets in immiscible liq., photographic obs. method *(German)* 79—72931
bubbles, evaporating, surface condensation of vapours of high boiling substance 80—59021
calorimeter for liquid evaporation rate meas. 77—87764
canopy interception, measure of loss from hydrologic budget 78—11928
canopy resistances for partially wet canopies 78—44904
canopy temp. thermal scanner meas. to estimate evapotranspiration 77—5324
capillary and porous surfaces, liquid boiling and evap. heat transfer 78—94526
capillary device construction for liquid introduction into analytic mass spectrometer 80—4805
capillary pore, evaporation from digital surface, mass transfer kinetics 78—51233
carbowax in benzene, evaporation, vapour press. determ. from gaseous diffusion coeff. 80—10654
Caspian Sea, evaporation processes, evaluation of temporal spectral density *(Russian)* 77—5337
cathode spots on Ag, Ni, Cu, and W vac. arc discharge electrodes, model 78—91179
charged droplets evaporation and motion in electric field 78—42669
charged particle, effect of electrostatic field on rate of evaporation 77—27585
classical liquids, phase transitions, book contrib. 79—60481
climate, evaporation rel. to water balance of Britain, 50000 yr BP to present day 80—72566
climate, soil and vegetation, annual evapotranspiration value 79—79895
climate, soil and vegetation, annual water balance dynamics 79—79896
climate, soil and vegetation, water balance dynamics 79—79893
cloud, warm cumulus, three-dimens. numerical model with microphysical processes *(Russian)* 78—88884
cloud droplet spectra evolution, effects of mixing, lab. expt. 77—70778
cloud medium evaporation by CO_2 laser radiation, self-focusing possibility 79—27306
cloud particles, effects of nearest neighbour interactions on evaporation rate 77—2209
coastal muds, interstitial water isotopic behaviour during evaporation *(French)* 79—79811
condenser efficiency and performance enhancement, evaporative cooling *(German)* 79—72781
contact angle and solid surface prop. effects 79—77867
cooling, on vapour cooled transmitter tubes, physical fundamentals *(German)* 77—11114
cooling, radiation effect on heat transfer and Lewis no. *(German)* 79—41562
cooling of porous heat-producing element 79—32213
cooling pond, heat transfer processes evaluation 78—61458
cooling system based on porous heat emitting element, hydrodynamic and thermal characts. *(Russian)* 77—67430
cooling system based on porous heat emitting element, stability anal. *(Russian)* 77—71322
croplets, in mist flow 77—55350
cryogenic liquid surface, floating insulation beads effect on evaporation rate 77—30164
cryogens, porous solids, gradientless heat transfer, cryogenic liq. crystn. 79—59903
crystal, Langmuir torsion effusion meas., recoil force correction factors 78—75929
crystal growth, stochastic models, diffusion and relax. kinetics 79—37642
crystal rough surface smoothing, during evaporation or condensation 80—103470
cultured cells preparation for SEM by air drying from org. solvents 77—48965
cutting fluid, hydrolysed polyacrylonitrile based, operational characteristics 80—89359
cylindrical capillary, mass transfer kinetics during evaporation, BGK eqn. basis 77—47044
desalination evaporator, falling-film, with vertically finned surfaces, hydrodynamics and heat transfer 80—58891
desalination units, evaporator-condenser film-type, horizontal tube, configuration effect on heat transfer 80—53604
desert formation mechanisms 77—70707
desorption, damped oscillatory evaporation of single crysts., empirical discussion 79—65327
desorption, nonstationary evaporation of single crysts., phenomenological model 79—65328
detonation of unmixed liq.-gas mixture with surface evap., fluid dynamical characts. *(Russian)* 78—55630
di-butyl-sebacate, HV evaporation, mass transfer in evaporating space *(Japanese)* 80—50558
dielectric surface, nonlinearly-absorbing, laser-induced evap. 78—80438
Douglas fir, evapotranspiration determ. using weighing lysimeter 77—64353
drop, asymptotic evaporation, convection and Jakob number 77—59108
drop, diffusional evap. in EM radiation field 78—43112
drop, evaporation in vap., slow viscous flow, heat flow asymmetry effect 77—75966
drop, laser irradiated, explosive evap. criteria 77—953
drop electrification by evaporation or vapour condensation *(French)* 78—61511
drop evaporation, in EM field, theory 79—72787
drop evaporation in turbulent gas jet 77—55077

evaporation continued
drop evaporation rate in forced convective flow with transverse sound fields 78—51224
drop fragmentation by laser 79—7169
drop in air stream, temp. during transient evaporation *(Russian)* 78—38827
drop of soln. moving in hot gas, solvent evaporation 77—65783
drop of soln. moving in hot gas, solvent evaporation 77—68673
drop of solution, slow evaporation 79—90847
droplet, evaporation rel. to aerosol particles precip. 80—7869
droplet, nonequilibrium evaporation and condensation, quasisteady theory 79—99394
droplet evaporation, diff. coeffs., vap. press. and Lennard-Jones pot. function determ. 77—80262
droplet evaporation, modelled by wet porous sphere, heat-transfer meas. 78—59268
droplet evaporation in const. cross flow, with and without gas. chem. reaction 77—35214
droplet evaporation on heated surfaces, theory 78—87785
droplet evaporation on shell, temp. fields 78—9546
droplet in turbulent gas flow, evaporation rel. to aerosol particles precip. 80—7870
droplets of soln. dispersed in gas flow, heat and mass transfer during evaporation 78—90998
droplets on surface, theory 79—59909
drops, evaporating in vert. hot air tunnel, heat radiation effect 79—46400
drops in still air 77—85027
drops of atomised liquid *(Russian)* 78—38828
drops of binary liq. mixtures, evaporation under free convection conditions 77—84121
drought in semi-arid regions, effects of albedo change 78—32128
dryness line localisation on all continents *(German)* 77—17179
eccentric spherical fluid shell, heat and mass transfer at large Peclet number 77—27520
electrode, deterioration by conc. heat fluxes in pulse discharge 77—51251
electrode, evaporation rate from cathode spot in vac. arcs. 80—49024
energy budgets, Priestley-Taylor large scale evaporation, comments and reply 77—45039
ethanol, evaporating meniscus profile, evaporative heat flux 79—77868
ethanol, rate var. with vap. press. 78—18758
ethanol evaporating meniscus, capillary flow heat transfer model anal. 79—82416
evaporating droplets in immiscible liq., theoretical anal. 79—23193
evaporating interline region, const. heat flux model 78—38178
evaporation with natural convection, simultaneous heat and mass transfer in laminar boundary layer, numerical anal. *(French)* 80—53778
evaporation-effusion problem, rarefied regime, nonlinear numerical soln. 80—6167
evaporator design, for gas phase electron diffraction 80—57424
evaporimeters, thermal insulation calc. 79—29803
evapotranspiration, actual/potential relationship 80—41465
evapotranspiration, remote sensing using Nimbus 5 satellite IR radiometer, evaluation *(French)* 77—17156
evapotranspiration climatonomy model of Lake Ontario drainage basin 77—5266
evapotranspiration estimation, advection-aridity approach 80—8366
evapotranspiration from soil, Canterbury, New Zealand, comparison of methods for estimating 77—53092
evapotranspiration meas. in Douglas fir forest, canopy resistance calc. 77—60432
expanding vapour bubble, anal. of reactive forces exerted by evaporating molecules 78—1548
explosive evaporation of cylindrical shell inner layer on collapse *(Russian)* 77—58714
extended liquid masses, film boiling heat transfer, partial evaporation method 78—90668
falling evaporating thin film, interfacial phenomena effect on interline region on hot spot rewetting 79—86321
falling film evaporator, after-polycondensation of polycaprolactam *(Japanese)* 79—70325
Fe-N system, fine particles growth, prep. by reactive gas evaporation technique, lattice consts. and habit study 79—56919
ferrous metallurgy, surface purification using laser and N_2 jet 78—92392
film, unsteady evaporation 78—42519
fission reactor, evaporative removal of Na from components 79—93735
flow-through reservoir, vel. and temp. fields, num. simulation 77—17152
fluidised beds of inert particles, moisture evaporation 77—15113
fogs formation theory and prediction 78—61522
forest canopy, evaporation of intercepted rain, comments 77—25727
forest evapotranspiration determined using Bow ratio and eddy correl. meas. 80—31103
forested land evaporation, Priestley-Taylor eqn. 80—31102
fuel droplet evaporation at elevated press. and temp., math. model investig. 77—52675
fuel droplet on hot surface, evap. and ignition 79—96310
fuel droplet on hot surface, evap. and ignition 79—96311
gas, in contact with condensed phase, hydrodynamic eqn. and slip boundary condition 80—14791
gas mixture, multicomponent, transport equations near catalytic surfaces 80—43821
gas-porous electrode, mass exchange in transport zones 77—32801
gas-side mass transfer coeff., diffusivity effect 79—18684
glass, optical K8, advanced evaporation mechanism under laser irrad. 77—79887
glazed solar cooler soln. regenerator, thermotechnical characts. 79—83620
grain boundary groove evolution in presence of evaporation 78—14364
grain boundary grooving under action of surface diffusion and evaporation or corrosion 80—39397
grain boundary grooving under influence of evaporation or corrosion 79—28179
grooved horizontal conduit, film mass transfer enhancement 79—72947
groundwater dynamics in plane regions during time varying seepage and evaporation *(Russian)* 79—79878
heat conduction, unsteady, in quarter plane, appl. to bubble growth 78—75045
heat pipe, evaporator section, evap. and vap. flow between parallel planes 80—10115
heat pipe wick, liq. evaporation, drop carry-over phenomena in capillary struct., obs. 79—18948

evaporation continued
heat pipes zone, heat exchange mechanism and vapour formation laws 80—24023
heated tubes, alternate dry and rewet, flow boiling, obstruction effects 79—1181
heterogeneous medium, laser irrad., prebreakdown stage evaporation *(Russian)* 79—24393
horizontal elliptical conduits, turbulent film evaporation and condensation 79—1182
S.Humberside, 1949-76 summer months, evaporation and rainfall 77—73819
hydrodynamic instability of evaporating interface 77—908
hydrology, force-restore method for ground surface temp. prediction 80—98469
hydrology, parameterisation of evaporation from nonsaturated surfaces 79—53372
hydrometeor precipitation from anvil clouds, melting and evaporation 80—17323
hypersonic gas flow, radiant heat and evaporative cooling 78—91028
ice, evaporation in planetary atmospheres rel. to ice-covered rivers on Mars 80—17526
ice crystals, epitaxial, influence of environmental saturation and elec. field on growth and evaporation 79—42408
ice precipitation layers, evaporation effects at base, theory and radar obs. 77—78312
impacted droplets, spray evaporator for spacecraft thermal control systems 80—29160
India, climatic water balance 77—64408
industrial, using geothermal power, feasibility assessment 79—48086
infinite plate, thin liquid film evaporation, surface temp. and heat transfer 80—64346
intense evaporation and condensation, molecular kinetics anal. 79—86330
intensive evaporation processes, lifetime of drop rapidly evaporating in a heated gas medium *(Russian)* 80—74725
intensive evaporation processes, mechanism 78—30746
internally finned tubes, refrigerant 22, evaporative heat transfer and pressure drop 80—5919
ion wind enhancement of evaporation into a laminar air stream 80—53773
jets acting on surface, hydrocarbon evaporation 79—72919
kinetic analysis, BGK eqn. 77—11683
kinetic theory, disequilibrium conditions 78—79755
kinetic theory, evaporation, condensation, linear, nonlinear problems 78—75802
kinetic theory, hydrodynamic eqn. and slip boundary condition 78—63903
kinetic theory of one-dimensional evaporation and condensation problem *(Japanese)* 78—81932
kinetic theory treatment of nonlinear half-space 79—27500
Lake Biwa basin, hydrological cycle, system theoretic study *(Japanese)* 77—81951
Lake Erie, heat storage and advection 77—41078
lake evaporation, climatological estimates 80—12449
lake Flevo, Netherlands, Priestley-Taylor evaporation model of shallow lake 80—51443
Lake Magadi basin (Kenya), evaporation rel. to hydrochemistry 77—49098
Lake Ontario, evaporation during IFYGL 79—2318
lakes, summertime evaporation, simple determ. method 77—5352
lakes and rivers, evaporation from surface, scaling theory 80—109179
land surfaces, diurnal vars. of evaporation 79—57987
laser beam surface evaporation, spectral-line absorption 79—19951
laser radiation action on condensed medium, hydrodynamic effects 80—93439
laser-evaporated material, quasisteady crater evolution, heat cond. anal. 77—48283
leaf water in cedar-hemlock catchment, silicone antitranspirant effects on streamflow 77—78272
Leidenfrost effect, demonstrations 78—81744
liquefied natural gas spilled on water, spreading and evap. investig. 78—26748
liquid, absorbing intense IR radiation, behaviour of pressure 80—102749
liquid, boiling at wall, nucleation, influence of dissolved gases 77—76537
liquid, spontaneously evaporating, critical discharge from channel 78—59456
liquid coolant, porous evaporative cooling for subcritical, critical, supercritical coolant parameters 79—55372
liquid drop in immiscible liquid, evaporation, surface tension effects 77—47648
liquid droplet, idealised models for preheat stage 78—94586
liquid evaporation in circulating gas, porous channel temp. determ., obs. 79—72943
liquid film, evaporating, interline heat sink capability, optical and thermophsyical props. depend. 78—71276
liquid film, evaporating heat transfer model 78—30154
liquid film, falling, laminar, evaporation model 79—46305
liquid film, falling, laminar, transport augmentation by surface waves 78—71343
liquid films on horizontal tubes, combined boiling and evaporation 79—81882
liquid He dewar, heat anal., reduction of evaporation rate 79—75533
liquid in capillary, evaporation above boiling point 77—66019
liquid metals, incipient boiling press. signal and evaporation coeff. meas. 79—77734
liquid mixture, shallow, laser separation, thermal mechanism 80—5925
liquid thin film, evaporation and breakdown driven by shear stresses 80—38410
liquid-gas interface, Stefan flow of binary mixture, with evap. or condensation 79—37381
liquids, low-press. evaporation, interface thermodynamic model 80—2252
liquids rapidly evaporating at reduced press., stability rel. to lateral press. variations 79—95146
Lithuania, karst lake replenishment *(Russian)* 79—8643
lubricant vapour pressure and evap. rate in vacuum, determ. using ambient press. meas. 78—29123
lubricants, ester-type, thin-film test for meas. of oxidation and evaporation 80—40626
mass spectrometer effusion for thermodynamic props. determ., surface evaporation effects and elimination 77—184
mass transfer in cylindrical channel with evaporation and condensation at walls 80—6101

evaporation continued
meniscus of air-liquid interface 79—14224
metal, evaporation under laser irradiation *(German)* 78—52599
metal evaporation losses, reduction, by inert gas atmospheres 79—42230
metal layers, thin, atomic absorption analysis with laser atomisation 80—30308
metal pulse evaporation under laser irrad., metal-insulator transition 77—81181
metal surface, electron beam impact, time-varying evaporation 79—10942
metal surface, electron beam impact, time-varying evaporation, metastable state lifetime 79—10943
metal surface, flash mechanism caused by monochromatic laser radiation 79—95878
metal surface, high-intensity laser beam interaction 80—19600
metal target, recoil impulse on microsecond CO_2 laser irrad. 77—36322
metal tip profile change meas. for evaporation rate determ. 77—24403
metallic target, post-crit. stationary plasma form. by TEA-CO_2 laser irrad. 77—1004
metallurgical melts, vacuum thermogravimetric device for evaporation kinetics determination 77—37865
metals and alloys, thermodynamic props., evaporation, optical spectral method appls., review *(Russian)* 78—75822
meteoric matter, evaporated, mass spectrum of particles formed in condensation 79—71005
methanol-H_2O mixture, evaporating droplets in air, temp. modelling *(German)* 80—2243
microlayer, formation and evaporation, theory 78—9536
monolayer permeation and evaporation resistance, hard disc fluid model 78—34678
monolayers, on water surface, depend. of evaporation resist. on chain length 79—28196
monsoon, digital simulation of evaporation phase, development of moisture eqn. 77—56712
Monte Carlo simulation diffusion and evaporation on (100) surface of FCC crystal 78—30836
Moon, devolatilisation in fission origin model 79—30000
multistage flash evaporation phenomena 78—2246
NaCl crystals, air cleaved, anisotropy of round evaporation spirals, electron microscopy study 79—73300
natural surfaces, Penman's eqn. modification 77—70781
natural water surfaces in Armenian SSR, evaporation calc. 78—7673
natural waters, evap. var. with salinity and temp. 77—53083
nitrate solutions, highly active, precipitation of Mo compounds during evaporation 78—37426
nucleate pool boiling heat transfer including microlayer evap., model development 77—42833
nucleation, microscopic theory *(Russian)* 78—67801
ocean warm wavy surface, lab. study of evaporation 77—86924
open solar regenerator, heat and mass transfer coefficients, moisture evaporation 80—38238
organic solvent evaporation, internal heating by IR irrad. 78—87237
paramagnetic vapours and condensing materials, apparatus for susceptibility meas., 300-1600K *(Russian)* 79—93178
Parana river basin, atmospheric moisture inflow and outflow rel. to water balance *(Russian)* 77—53090
particle, EM wave irradiated, evaporation, diffusion approx. 80—44308
particle, spherical, transient heat-mass exchange 79—7276
perspiration mass transfer coefficients and clothing models 79—92158
pine forest wet canopy evap. meas. 78—61460
plane evaporation boundary instability in laser radiation-matter interactions *(Russian)* 80—76111
polar and nonpolar liqs., absolute evaporation rate meas. 78—2244
polymers, high-temp. pyrolysis, heat transfer processes at gas/solid surface *(Russian)* 80—61152
polyorganosiloxane, thermogravimetric assessment of stability at high temps. 77—52704
polyphenyl ether in benzene, evaporation, vapour press. determ. from gaseous diffusion coeff. 80—10654
polystyrene, spherical pellets, ablation rates in Q-pinch plasma 77—89265
pool water, flash evaporation phenomena 78—2245
porous body, sublimation, heat, mass transfer from parallel capillaries 79—37395
porous cermet, heat transfer and stability for moving evaporating coolant 80—64563
porous medium, drying, evaporation characteristics determ. *(Russian)* 79—37134
porous surfaces, wind tunnel for evap. rate from soil samples *(French)* 77—80684
porous wall evaporation cooling system, liquid component temperature state *(Russian)* 79—32664
potential evaporation from soil, water and crop surfaces, eqn. adaptable to remote sensing use 77—64334
Priestley and Taylor α parameter for high latitudes 78—3833
Priestley-Taylor model, soil moisture influence on evaporation 78—24314
psychometric constant γ, pressure depend. 77—53149
PWR/BWR power stations, waste-water treatment plants, engineering experience 77—6543
quasisteady half-space problem, gas kinetics theory and expt. 80—6106
quasisteady one-dimens. problem, entropy-balance relation 80—6168
rainfall from nimbostratus, effect on mesoscale unsaturated downdraughts, numerical anal. 80—8400
rainfall interception by forests, analytical model, evaporation 79—79966
rare earth hexaborides, powders, evaporation 77—89535
rarefied flow, boundary conditions for gasdynamic eqns. in presence of evap., condensation and chem. reactions 77—47042
rate monitor with quartz sensor 79—28921
refractory carbides, thermodynamic evap. characts., cluster-component calcs. 78—51704
refractory metal, evaporation in inert gas atmosphere *(German)* 79—55879
regional evapotranspiration, determ. from upper air meteorological data 77—91171
regional evapotranspiration calc. using planetary boundary layer theory 77—25716
reservoir, well-mixed shallow water, evaporation estimation model 78—20453
restoration, evaporation and melting of materials in high temp. gas flow *(Russian)* 80—39271
river watershed evaporative losses, Tigris and Euphrates 80—81957

evaporation continued
river/atmosphere time dependent, single dimensional heat exchange, analysis *(Bulgarian)* 78—57221
sea-atmosphere heat-transfer expts. *(Russian)* 78—81206
seawater boundary layer during evaporation, optical interferometry *(Russian)* 80—61919
semi-microscopic description of evaporation and condensation 80—39254
semiconductor, bulk evaporation, injection of nonequilibrium vacancies 80—39273
semiinfinite porous media, heat cond., phase transitions effects 78—94523
sensitivity and variance analysis of evaporation and evapotranspiration models 77—25717
shallow lake evaporation, simple model 79—39767
shells, creation of finite perturbations by use of laser beam 79—18849
simultaneous melting and evaporation due to area heat source *(German)* 78—59282
snow cover of Yakutia (USSR), evap. and evolution 77—73768
snowpack evaporation during chinooks along eastern slopes of Rocky Mountains, Alberta 79—79883
soil drying, evaporation, solar radiation and atm. temp. effect 80—8373
soil moisture, role in flood forecasting model 80—81951
soil moisture deficit estimation from meteorological factors 79—20890
soil water, evaporation rel. to ground surface temp. and moisture content, vegetation layer effects 78—73373
solar desaliniation unit with evaporation chamber, test results 80—96178
solar evaporation and refrigeration units, assurance of specified energy parameter values, statistical analysis 80—93848
solar flare plasma, evaporative cooling 78—40890
solar nebula, primitive dust material evaporation metamorphism 79—58279
solar regenerator of hygroscopic solutions, for air dehumidification 79—57464
solid H_2 pellet ablation, in Tokamak plasma 77—89264
solution, aq.-organic, 25°C, solute/water rel. evap. rates 78—34614
spherical condensed phase, rel. to motion in uniform vapour gas flow, kinetic theory 78—1725
spherical droplet, evaporation and condensational growth, mass transport calcs. 80—97736
spherical liquid droplets, nonlinear condensation and evaporation 78—63902
statistical mechanical theory of the kinetics of phase transitions, review, book contrib. 80—73270
steam-generating pipe, containing porous deposits, mass transfer (impurities) 78—38398
stearic acid, evaporating cryst. surfaces in vacuum 79—77740
subarctic and tundra surfaces, evap. equilib. model 78—61459
superheated liquid, under intense EM irrad., effect of spinodal singularities *(Russian)* 77—89533
surface self-diffusion consts. from growth or evaporation spiral evolution kinetics, appl. to NaCl and KCl 79—65301
surface water in India, evaporation rel. to overall assessment of resources 77—56662
surfaces subject to cooling effects, nonlinear eqns. numerical soln. *(German)* 80—58893
TEM meas. of evap. coeff. 78—18909
thermal plumes development, effect of condensation *(French)* 79—23192
thermosiphons, two-phase heat exchange in supply zone, anal. 80—19387
thermosyphon, two-phase, heat and mass transfer in evaporation zone 79—1048
thin absorbing films, laser-induced removal, two-phase mechanism 80—97384
thin film evaporator grooves, fluid evaporation and boiling heat transfer 80—38227
thin films fabrication techniques 80—76176
thin liquid films with extensive evaporation, heat transfer *(German)* 80—99920
Tokamak, Diva, metal impurities origin, arcing ion sputtering, evap. 78—59691
transparent solid dielectric, laser evaporation, analytic eqns. 80—35014
turbulent air-water mass transfer under varied stratification conditions 79—84389
turbulent exchange coefficients for sensible heat and H_2O vapour under advection conditions 78—92907
two-dimensional Lennard-Jones system, phase transitions, calc. 80—59621
two-phase evaporating and condensing flows, system mean void fraction model 78—42520
two-phase flow, dryout region of forced convection evaporation, heat transfer coeff. 78—90988
two-surface problem of evaporation and condensation, in presence of noncondensable gas 80—6169
vacuum evaporation from finite surfaces 77—59099
vaporising liquid layer at nonadiabatic evaporation, binary laminar boundary layer flow *(German)* 80—1588
vapour, kinetic theory of evaporation and condensation between concentric cylinders and spheres 77—62629
vapour bubbles, oscillating, evaporation-condensation resonance frequency 80—19488
vapour dispersion, near surface of evaporation 77—51487
vapour distribution between parallel plates, condensation, evaporation 77—3847
vapour permeability mechanism of porous bodies 77—58782
vapour pressure, ultra low, determ. by submicron droplet evaporation 79—88993
vapour-gas phase, heat and mass transfer during evaporation of fluid 77—55354
vegetation-atmosphere interaction, simplified one-dimens. theory 78—61479
vertical evaporating circuit, heat exchange calc. and optimisation *(Russian)* 77—71321
volatile binary solution, theory of evaporation, of large drops 79—10931
volatile liquids, dispersion of gases into atmosphere *(Dutch)* 79—79425
volatile solvent, evaporation from multi-component droplets, in stream of air 77—56255
vortex filament form. from ascending flows over evap. liquid 78—63440
water, bulk evaporation coeffs. depend. on air-water interfacial conditions, isotopic method determ. 78—85576
water, deep evaporation characterisation, from homogeneous porous medium *(French)* 78—59468
water, evaporation coefficient, reply to comments 78—75912

evaporation continued
water, evaporation coefficient, variation with observation conditions 78—75909
water, evaporation coefficients, comments 78—75911
water, evaporation through monolayer free and monolayer covered surfaces, temp. gradients meas. 80—88402
water, rate var. with vap. press. 78—18758
water, saturated (subcooled), crit. discharge through differently shaped channels 78—55681
water, surface cooling, apparent evaporation coeff. 80—2148
water adsorbed on IR optical material, evaporation rel. to surface breakdown 80—35020
water aerosol, evaporation during transport through atmosphere *(Russian)* 79—88408
water condensation number, from micron size drop evaporation and growth rate determ. 79—90774
water drop evaporation by 10.6 μm laser radiation 77—75589
water drop thermal explosion by high-power laser radiation 77—75590
water droplet, laser induced evaporation, diffusion coeff. temp. depend. 77—20062
water droplet clouds, rate of evaporation, stability 79—52782
water droplet evaporation, heat transfer characts., on heated surfaces 78—59269
water droplet evaporation and microclimatic modification 77—17248
water droplet forced convection and heat transfer rel. to vapour conc. *(Chinese)* 79—23185
water droplets suspended in turbulent flow, evaporation rate rel. to $Ca(CO_3H)_2$ soln. drops 79—90771
water drops, evaporation and condensation in air, quasi-steady approximation 77—21854
water drops, large, falling at terminal velocity in air, wind tunnel investigation of evaporation rate 80—56541
water evaporation coefficients, comments 78—75910
water evaporative cooling, convection and mass transfer, fog formation in boundary layers 80—79293
water evaporative cooling, heat and mass transfer coeffs., fog formation effects 80—79294
water loss meas. from small animals by dew-point hygrometry 78—20326
water surface, radiation balance meas. 79—20889
weighing apparatus for hydraulic lysimeter in the Western Australian cereal belt 79—12276
wetting fluids, evaporating menisci 80—29248
wind influence on evaporation from Earth surface *(Spanish)* 78—44965
Ag electrode, evaporation rate from cathode spot in vac. arcs. 80—49024
Ag, fine particles prep. by vacuum evap. onto running oil substrate 79—28925
Ag, ultrafine powder, role of evap. during sintering 78—64505
Ag-Hg amalgam, lattice const., temp. depend., explained in terms of Hg evaporation 78—26704
$AgAsS_2$, dissociation pressures and their temp. depend. 79—52640
Ag_3AsS_2, dissociation pressures and their temp. depend. 79—52640
AgBr, thin layers, evaporation conditions, photoresponse *(Bulgarian)* 78—78017
Al, vacuum evaporation appl. of TiB_2-TiC and TiB_2-BN for crucibles 79—74094
Al, vapour deposition on substrates, splash-free, using modified W helix 78—52689
Al-Cu, successive dilution method for reproducible control 77—69994
Al-Mg-Zn alloys, evaporation effect of alloying elements Mg and Zn in in-situ EM studies 80—103388
Al_2O_3, fine powder, prep. by evaporative decomposition of solns. 78—39725
Au electrode, evaporation rate from cathode spot in vac. arcs. 80—49024
B_2O_3-GeO_2 system melts evaporation coeffs. 79—65180
$BaZrO_3$(s), evaporation and standard ht. of formation 77—25302
BeO, heated on W, thermal anal. using mass spectrometric, technique, vaporisation behaviour 80—79932
Bi_2Te_3-Bi_2Se_3 thermoelectric alloys, diffusion and evaporation of volatile component during prep. 80—35118
$CaAl_2O_4$, fine powder, prep. by evaporative decomposition of solns. 78—39725
CaO, heated on W, thermal anal. using mass spectrometric, technique, vaporisation behaviour 80—79932
Cd electrode, evaporation rate from cathode spot in vacuum arcs 79—37566
Cd, inert gas effect on rate of evaporation 80—84285
Cd, influence of source material and shape on sublimation props. 78—80474
$CdCr_2Se_4$, evap., mass spectra 78—53238
CdS, crystal growth from vapour, evaporation theory and surface kinetics 77—76335
CdSe, comp. and evap. kinetics on vacuum heating, effects on deposited film characts. 77—85940
CdSe, influence of source material and shape on sublimation props. 78—80474
CdTe:Cu, doping effects on evaporation kinetics and electronic props. during high-temp. annealing in vacuum 78—22743
Co, particle formation by evap., electron microscopy obs. of interaction processes 80—104053
Co, ultrafine particles prepared by vacuum evap. on running oil substrate, mag. behaviour 79—28565
CoO, evaporation curve struct. from AC arc electrodes *(Russian)* 78—3051
Cr-Zr source improvement, diffusion barrier layer deposition for IC metallurgy 80—76163
Cs, flash evaporation in pulsed high-density atomic source 78—17825
Cs ion evaporation isotherms, from W single cryst. faces 79—24829
Cs_2CrO_4, mol. beam obs. of evap., saturated vapour press., 656.8 to 1151K 80—107411
Cu, by absorption of Nd laser pulse, numerical anal. *(Russian)* 77—40312
Cu exploding, wire accelerated evaporation of fast drops colliding with target *(Russian)* 77—15570
Cu-Ag, liquid, diffusion-limited evaporation for const. comp. film prep. 77—21038
Cu-Ag (Pb)(Bi), evaporation of Ag, Pb, Bi in vacuum induction melting 77—28742
Cu-Ag(Bi)-O, evaporation of Ag, Bi in vacuum induction melting 77—28742
Cu-Ag(Pb)(Bi)(Ag-O)(Bi-O)(Si-S), stirred at different speeds under press., evaporation of Ag, Pb, Bi, S 77—47555

evaporation continued
  Cu-Ni, evaporation limited segregation 80−70513
  $CuCl_2$-water solution, Nd-glass laser radiation induced vaporisation, press. history 80−2153
  Cu_2S, $Cu_{1.8}S$, $\alpha \rightarrow \beta$ transition, thermographic investigation of heats, entropies and activation energies 80−88314
  DyI_3/CsI/Hg arc, time varying arc constrictions due to periodic metal iodide condensation-evaporation discussion 79−60205
  Dy_2O_3-based ceramic, preparation, mech. props. 77−24998
  Er, laser evaporation and condensation in H_2 and Ar atmospheres 79−10941
  EuS, thermodynamic data 78−2248
  EuTe, high-temperature evaporation and reactivity 80−103469
  Fe electrode, evaporation rate from cathode spot in vacuum arcs 79−37566
  Fe, particle formation by evap., electron microscopy obs. of interaction processes 80−104053
  Fe, ultrafine particles prepared by vacuum evap. on running oil substrate, mag. behaviour 79−28565
  Fe-C(Si)(Mn)-S melt, S evaporation *(Russian)* 78−19716
  Fe-Ni-Co base alloys, composition changes during electron radiation melting *(Russian)* 78−19718
  FeO-Fe_2O_3, evaporation curve struct. from AC arc electrodes *(Russian)* 78−3051
  α-Fe_2O_3, prep. by evaporative decomposition of $Fe(NO_3)_3.6H_2O$ soln. 79−20011
  GaAs:Te, ion implanted, surface crystallinity and stoichiometry of laser annealed samples 79−73198
  GaP (100) thermal and vap. phase etching in H_2-HCl-PH_3, obs. 77−77612
  Ga_2Se_3, evaporation, thermodynamic props. 80−54365
  Gd, populations of metastable levels during electron beam evap. 77−57926
  GeS, film on Ge, evaporation, thermogravimetric, electron microscopy investigs. 77−15715
  H_3BO_3 evaporation from seawater, major source of atm. B 79−2293
  HTO, atmospheric condensation-evaporation model 77−29326
  He, liq., withdrawal from liquefier 79−67306
  He, liquid, evaporation loss minimisation during expansion and transfer 77−30166
  ^3He-^4He mixture systems, evaporation and condensation 79−65283
  ^3He-^4He mixtures, evaporation and condensation meas., weak coupling model anal. 79−51366
  ^3He-^4He system, evaporation and condensation mechanism 79−77858
  ^4He, superfluid, evaporation by rotons and phonons, heat-pulse technique 79−33135
  ^4He, superfluid, evaporation through narrow channels 79−60578
  ^4He, superfluid, interface conditions between liq. and vapour 80−10723
  ^4He, superfluid, sound pulse amplitude meas. method sound transform. at free surface 80−54451
  ^4He superfluid films, geometry induced third sound splitting 80−96712
  Hg, deposition, on W, evaporation energies 80−107666
  Hg, droplets, film boiling 78−14453
  $In_{1-x}Ga_xP$, solid soln., evaporation of P during LPE 79−95948
  InSb, evaporation kinetics, rel. to film growth 78−3050
  Ir electrode, evaporation rate from cathode spot in vac. arcs. 80−49024
  Ir, evaporation/oxidation kinetics 77−36691
  K, boiling, in tubes, superheat and instability 77−35136
  KBr, rot. of vacuum thermal etch pits 78−87674
  K_2CO_3 melt in combustion prods. medium, vaporisation of drops 79−57290
  Li-LiH, evaporation diagram at high liq. phase hydride concs. 77−35681
  $LiCrO_2$, evaporation, as a corrosion product in compatability experiment of Li_2O pellets with Fe-Ni-Cr alloys, mass spectrometric study 79−73301
  LiF, condensation and evaporation in monomers, dimers and trimers, mol. beam method *(German)* 77−85052
  $Mg+O_2 \rightleftharpoons MgO+O$, shock-tube study of evap. and oxidation kinetics 80−16651
  MgO, heated on W, thermal anal. using mass spectrometric, technique, vaporisation behaviour 80−79932
  $MoSe_2$, evaporation, mass spectroscopic investigation 77−76530
  N_2 adsorbent mesopores, capillary evaporation and struct. 80−107614
  N_2, capillary condensation and evap., apparatus and calc. method 80−2150
  N_2, capillary condensation and evap., scanning curves within B-type hysteresis loops 80−2151
  N_2, evaporating in horizontal tube, local heat transfer coeff. 77−23959
  N_2O_4, evaporation in enclosed containers, N_2 medium, 1.12-4.96 gauge atm. 77−47564
  Na evaporation from slot type capillary structs., crit. heat fluxes 80−74854
  Na evaporation in Ar atm., fog formation, expt. theory comparison 77−55352
  Na heat pipes, evap. process, sonic limits to power transfer 79−18672
  Na, liquid, evaporation from capillary-porous struct., capillary restriction in initial stages 80−107609
  NaCl, (100), (110) and (111) surfaces annealed in vac. 400-800°C, evap. struct. 77−15572
  NaCl, cleavage faces, evaporation pattern determ. by decoration method in electron microscopy *(German)* 80−107626
  NaCl crystal rough surface smoothing, during evaporation or condensation 80−103470
  NaCl, evaporating cryst. surfaces, successive monatomic step trains with different density 80−29254
  NaCl, evaporating surface, step motion obs. and simulation 78−26766
  NaCl, evaporation coeff. meas. by TEM 78−18909
  NaCl, rocksalt (h10) faces, terrace like step trains, evaporation, TEM obs. 77−35801
  NaCl, single cryst. in vac., influence of dislocations on evaporation 79−10935
  NaCl soln., no particle fragmentation during evaporation 77−91189
  NaCl, solution, droplet evaporation in laminar gaseous stream *(French)* 77−51102
  NaCl-$CaCl_2$, electrolyte mixture, evaporation from multi-component droplets, in stream of air 77−56255
  Na_2O-B_2O_3-GeO_2 system glass-forming melts, mass spectrometry obs. of thermodynamic props. 80−97468
  Na_2O-B_2O_3-GeO_2 vitreous melts, thermodynamic props. from mass spectra 80−65253

evaporation continued
  Nb coated Mo, Ti, evaporation, carburisation and diffusion behaviour 77−44410
  $NbSe_2$, thermal dissociation 78−44370
  Nb_3Si, supercond., A15 film, electron beam evaporation 80−29284
  Ni, particle formation by evap., electron microscopy obs. of interaction processes 80−104053
  Ni, ultrafine particles prepared by vacuum evap. on running oil substrate, mag. behaviour 79−28565
  Ni-Al, melt, short-range order and microinhomogeneity, rel. to NiAl form. 77−35466
  Ni-W (2%), Mg diffusion meas., 970-1330K, appl. of vapour collect and AES method 78−75876
  NiO, evaporation curve struct. from AC arc electrodes *(Russian)* 78−3051
  Pb, evaporation in shock compression release waves *(Russian)* 78−18761
  Pb, evaporation under action of laser beam, recoil press. behaviour 80−25501
  Pb multicomponent glasses, alkali evaporation, mass spectrometry study, thermal anal. 79−74464
  Pb particles, evaporation in arc plasma, integral eqn. method calcs. 78−1942
  Pd electrode, evaporation rate from cathode spot in vac. arcs. 80−49024
  Re, metal losses during annealing in O_2, air, water vapour, high temp., low press. *(German)* 77−8856
  Rh electrode, evaporation rate from cathode spot in vac. arcs. 80−49024
  Sb, cleavage faces, evaporation pattern determ. by decoration method in electron microscopy *(German)* 80−107626
  Sb_2Te_3, cleavage faces, evaporation pattern determ. by decoration method in electron microscopy *(German)* 80−107626
  Se, evaporation kinetics from temp. programmed large area source 77−69996
  $Se_{5,6}$, influence of source material and shape on sublimation props. 78−80474
  Si, growth and thermal evaporation kinetics of oxide film on Si surface 78−3246
  Si, reactions with metal oxides, general features, glass form. 79−11819
  Si:As, segregation and desorption kinetics for evaporation of As 79−99410
  Si:P, Czochralski growth, dopant evaporation coeffs., resistivity distrib. 77−16487
  Si:Sb, laser doping, evaporation loss and diffusion of Sb, under pulsed laser irrad. 80−59508
  SiC, ceramic, mass loss in inert gas stream *(Russian)* 79−7686
  SiO_2, particle, EM wave irradiated, evaporation, diffusion approx. 80−44308
  SiO_2-water system, inorg. polymer struct. form., globular crystn. 80−101042
  Sn-S system, use of boiling points to investigate vapour pressure 80−54361
  $SnSe_2$, rel. to p-T projection of phase diag. of SnSe-Se 78−27485
  soil, surface moisture content parametrization, use in atm. prediction models 78−49052
  Ta, thermoelectron emission, S impurity atom effects, electron spectra *(Russian)* 77−8712
  $TaSe_2$, evaporation, mass spectroscopic anal. 77−76530
  $ThCl_4$, thermodynamics of vaporisation and melting 79−60492
  TiN, synthesis using enhanced reactive evaporation 80−2953
  $(U,Pu)C_{1\pm x}$, evap. behaviour, 1500-2458°C 77−27994
  W, surface, self-diffusion coeff. at very high temp. using theory on tip evolution by capillarity forces and evaporation 79−11011
  Yb_2O_3-based ceramic, preparation, mech. props. 77−24998
  YbTe, high-temperature evaporation and reactivity 80−103469
  Zn electrode, evaporation rate from cathode spot in vacuum arcs 79−37566
  Zn, inert gas effect on rate of evaporation 80−84285
  $(Zn_{0.2}Co_{0.8}(Ni_{0.8}))O.Al_2O_3$, ZnO evaporation in vac. 80−59640
  ZnS, laser evaporated film, microstruct. TEM obs. 79−82479
  ZrO_2-Nd_2O_3 system, solid solns., evaporation, mass spectroscopy investig., thermodynamics 79−10938

Evershed effect *see sunspots*

evolution (biological)
  abiogenetic synthesis rel. to vulcanism and Hg-sensitised photoreactions 77−37173
  acetonitrile, possible source of amino acids on primitive Earth 80−4112
  acid-labile amino acid precursors in Murchison meteorite, chromatographic fractionation 77−64707
  acid-labile amino acid precursors in Murchison meteorite, peptides and amino acylamides 77−64708
  ageing, energy-saving strategy of reduced error regulation 78−11789
  amino acid formation by ^{60}Co to γ-ray irradiation of HCN solns. 77−37410
  amino acid formation in ultrasound in water masses of primordial Earth 77−37409
  amino acid photoresolution, rel. to origin of optical activity in life 77−40634
  amino acids, high energy radiation effects and chemical evolution 77−63937
  anthropic principle of cosmology, rel. to physical world struct. 79−48973
  arogenesis correlation with geomagnetic field reversals *(Russian)* 78−36089
  asteroidal terrestrial cratering, plate tectonics and evolution of life 78−96421
  binocularity and stereopsis in the evolution of vertebrate vision 80−12144
  biological transformations theory, dynamical similarity 79−34469
  biosatellite Cosmos-782, biological expts. 80−61710
  bird frontal vision, rel. to visual Wulst retinotopic organisation 80−12098
  calcareous plankton, origin rel. to dynamic models of deep-sea sedimentation 78−15988
  chance and origin of life 78−69269
  chemical evolution, energetics of reactions in aqueous solns. on primitive Earth 77−33189
  chemical evolution, rel. to evolution of Earth crust 78−40666
  comets as origin of terrestrial life 80−51672
  Cretaceous-Tertiary environment, effect of nearby supernova explosion 78−32499

evolution continued
Cretaceous-Tertiary extinctions, effects of solar flares and stratospheric aeronomy 78—32215
Cretaceous-Tertiary extinctions, effects of solar luminosity vars. and super solar flares 78—32435
Cretaceous-Tertiary extinctions, geomag. field effects 78—32013
Cretaceous-Tertiary extinctions, possible terrestrial and extra-terrestrial causes 78—31999
Darwinian revolution, applicability of Planck's principle 79—62991
dinosaurs extinction, date from Cretaceous-Tertiary boundary sediments magnetostratigraphy, biostratigraphy and geochronology 79—57888
dynamic processes on Earth, extraterrestrial causes, rel. to extinction of life 78—92820
early Earth regolith formation and origin of life 78—85698
ecological disasters and ice ages, prod. by Earth-comet close approach 78—53714
elliptical galaxies, lack of spiral arms and lifebearing planets 77—64845
environment evolution, available elements during Earth history rel. to life evolution 79—80030
extinctions at end of Cretaceous, astronomical evidence rel. to supernova hypothesis 78—32500
extraterrestrial life, criteria for technology evolution on planets supporting biosphere 77—71018
ferredoxins, evolution of chloroplast-type from S. platensis [2Fe-2S] type and struct. of latter 80—94165
geomagnetic field influence, possible mechanism 77—90977
hominid evolution, palaeomag. results and ages at Makapansgat and Swarthkrans sites 77—25637
instability of evolving systems, elastic stability theory and catastrophe theory approaches 78—44442
interstellar cold grains as seeds of life 77—91606
interstellar dust grains as possible cold sources of life 79—21203
interstellar molecules in prebiological evolution 80—94726
interstellar prebiotic molecules, assoc. with grain clumps 77—26042
Isua sediments, W.Greenland, isotope averages and Archaean C and O cycles 79—84262
land life emergence, implications of atmospheric O_3 content evolution 80—98400
life on primitive Earth, P availability 78—20518
living and lifeless matter, complementarity 79—66436
magnetic field of Earth, role in evolution 80—104883
mammalian extinctions rel. to groundwater variations 78—36215
Mars information from Viking mission, appl. to Earth 77—78709
mathematical model 79—12060
molecular chirality rel. to biological mols. origin and evolution *(Russian)* 77—52739
Neogene evolution, palaeontology and geology of Pakistan 78—24269
ocean chemistry, effects of changes on biological evolution 77—56653
optical asymmetry correl. with parity violating weak interaction 78—69000
optical purity of living beings, origin through β-decay 78—40459
optically active molecules and polarised bremsstrahlung 77—63938
organic compound synthesis on primitive Earth, volcanic processes 77—64434
origin of life, astrochemistry and organic mols. form. 78—73660
origin of life, chem. evolution (bibliography) 80—90620
origin of life, from origin of universe to earliest geological times 78—69923
origin of life, implications of thiocyanate in Red Sea brine 79—57975
origin of life, mol. biophys. basis 80—94158
origin of life, molecular evolution and exobiology, interdisciplinary course 79—21485
origin of life, monomers to polymers 78—69461
origin of life, pre-biotic era 78—69460
origin of life, rel. to evolution of lunar orbit 77—29671
origin of life, role of complex interstellar organic compounds 78—24543
origin of life, role of mineral surfaces 77—91273
palaeoatmosphere O_3 content rel. to biological evolution 77—78425
palynofloral change at Cretaceous-Tertiary, boundary, Rb/Sr age from Hell Creek, Montana (Z coal) 80—94487
panspermia hypothesis, trace elements 77—32968
peptide formation in prebiotic era with clay catalysts 77—64435
Phanerozoic diversification of life, effect of O abundance in palaeoaquatic environment 78—44879
photochemical formation of self-sustaining coacervates, rel. to origin of life, review 78—11611
photosynthetising organisms, chlorophyll pigment redox pots. rel. to evolutionary development 77—56337
polymer formation, interstellar molecules and prebiological evolution 79—92842
prebiological compounds, form. in volcanic processes 78—40667
prebiological molecular evolution, as physico-chemical processes 77—60331
prebiotic chemical evolution, far UV irradiation effects on primitive model atmospheres 78—40668
prebiotic molecules in Martian dust clouds 77—64688
prebiotic oceans, soluble organic matter scavenging 77—64436
primitive Earth, volcanic processes role in organic compounds evolution 78—32230
protein evolution, molecular clock test using Panamanian sea urchins 79—92134
quartz fibres, possible role as templates for biopolymers 79—39345
reducing to neutral biosphere, length of transition period 78—20519
review of ecology and systematics (book) 80—67945
self-organisation, origin of information 77—32868
space colonisation consequences 78—4187
superweak interactions and the biological time direction 79—39344
symbiosis and origin of life 77—90979
C_3O_2 polymers in primitive atmosphere rel. to living systems genetic code 79—83690

EXAPT *see problem oriented languages*

exchange forces in nucleus *see nuclear forces*

exchange interactions (electron)
see also antiferromagnetism; ferromagnetism; RKKY interaction; superexchange interactions
^{3}He, solid, two parameter model of mag. and thermal props., spin exchange 80—49461
actinide monopnictides, anomalous mag. props., planar coupling theory 80—60245

exchange interactions continued
actinide systems, nearly ferromag., coupled d- and f-band model 77—63211
adsorbed layers, autoionisation bands due to one-centre resonances, theory 80—59790
alaninium copper tetrahalides, exchange, mag. anisotropy, and spin diffusion contribs. to EPR linewidth 80—80597
alkali dithioferrates (III), electronic struct. and hyperfine interactions, Xα calcs. 80—100448
alkali halide, exchange charge polarisation, dielectric const., Dick and Overhauser model 78—55832
alkali halides, vacuum UV absorption spectra, exciton splitting rel. to exchange interaction 78—23494
alkali metal, electron-electron scatt. in terms of dielec. and vertex functions 79—95351
alkali metal+inert gas, role of different interactions in intramultiplet relax. at nonresonant interactions 77—6902
alkali metal-ammonia solns., spin site exchange mechanism for electron relax. times 78—27077
alkali metals, lattice dynamics, a priori pseudopot. calc., cond.-core exchange approxs. 77—72662
alkali metals, magnetic property volume depend., Knight shifts, electron spin response 80—88729
alkylammonium compounds, $(C_nH_{2n+1}NH_3)_2CuCl_4$ and $(C_6H_5C_mH_{2m}NH_3)_2CuCl_4$, interlayer exchange field 77—20714
alloy, binary, with mixed ferro- and antiferromag. exchange, magnetisation, phenomenological theory *(German)* 78—56297
alloys, dil., Kondo coupling, hyperfine and exchange interactions 79—65647
alloys, magnetic anisotropy, influence of local symmetry *(Russian)* 80—93109
aluminoborate glass, Fe and Cr ion interaction, mag. and spectral props. 80—103883
amorphous alloy resistivity, contrib. of mag. ordering *(French)* 77—89746
amorphous alloys, indirect exchange interaction and paramag. Curie temp. 80—75752
amorphous alloys 77—16054
amorphous ferromagnet, random model spin wave spectrum 77—89918
amorphous ferromagnets, dispersion rels. and spin-wave spectroscopy *(Russian)* 79—7983
amorphous ferromagnets, ferromag. saturation, spatially random magnetostatic, magnetocrystalline, magnetostrictive and exchange fluctuations 78—60277
amorphous ferromagnets, possibility of low temp. phase below ferromag. phase 79—4674
amorphous Heisenberg and Ising chains, thermodynamics 80—108022
amorphous Heisenberg ferromagnet, spin wave excitations and magnetization curve 79—15292
amorphous Heisenberg ferromagnet, variational cluster method 80—39728
amorphous magnet, finite temperature calculations, random anisotropy model 78—80112
amorphous magnet, indirect exchange interaction 79—65669
amorphous magnetic metals and alloys, high temp. thermodynamic props. 77—16078
amorphous magnetic system, microwave absorption spectra, calc. 80—50469
amorphous substance, ferromag. or spin glass transitions 78—2690
Anderson model, orbitally degenerate, exchange coupling in atomic limit, rel. to two-site Hubbard model 80—108000
Anderson-localised states, intrastate and interstate interactions 80—20113
anisotropic antiferromagnet, phase transition, with external mag. field 79—11316
anisotropic exchange interactions, effect on singlet ground state system 80—65852
anisotropic ferromagnet with biquadratic exchange, crit. temp. 77—12124
anisotropic ferromagnet with biquadratic exchange, critical temp. 77—40075
anisotropic linear spin chain, two-magnon problem with arbitrary interaction radius 78—72320
anisotropic magnet, low-temperature properties 79—65633
anisotropic magnet mixture, Heisenberg spin system by Monte Carlo simulation 79—78408
Anisotropic magnetic ordering via combined spin and orbital exchange scattering of conduction electrons 80—65863
anisotropic magnets, spin wave theory 77—20576
anisotropic spin-phonon coupling model, exact solutions *(Russian)* 80—100590
antiferrimagnet, two-sublattice, spin waves, magnetocaloric effect 78—31073
antiferrodielectrics with antiferromag. intrasublattice exchange interaction 79—38352
antiferromagnet, amorphous, spin waves, exchange fluctuations, calc. 80—65847
antiferromagnet, dil. paired, bond dilution problem, CPA theory 79—78389
antiferromagnet, easy plane, specific props. 79—1665
antiferromagnet, FCC, Ising model, mag. phase diagram, ordering, Monte Carlo calc. 80—103833
antiferromagnet, linear chain, biquadratic exchange interaction effects 77—63062
antiferromagnet, mag. excitations within local exchange approx. 77—69517
antiferromagnet, magnetoelastic coupling in nonlinear acoustic phenomena, exchange interaction effects *(Russian)* 77—90010
antiferromagnet, magnetoelasticity, exchange enhancement 79—87299
antiferromagnet, mechanism for hard excitation of spin waves *(Russian)* 78—19235
antiferromagnet, second-order phase transition, weakening of effect of fluctuation in order parameter near crit. point 79—15316
antiferromagnet, spin-1, with biquadratic exchange, sublattice magnetisation and Neel temp., RPA 77—47953
antiferromagnet, transversely anisotropic, spin-wave theory of paramag. phase boundary 77—69552
antiferromagnet, two-magnon Raman scatt., temp. effects 77—48178
antiferromagnet, uniaxial, influence of field direction and single-ion anisotropy on phase diagram 77—16072
antiferromagnet, weakly anisotropic, effective anharmonicity of elastic subsystem 77—69658

exchange interactions continued
- antiferromagnet chain, renormalisation group nearest neighbour interactions 80—60357
- antiferromagnet cubic, with exactly-known ground state 78—43540
- antiferromagnetic, triang., spin wave theory 79—7978
- antiferromagnetic exchange-coupled one-dimens. anisotropic chain with S=1/2, comparison with expts. 77—20530
- antiferromagnetic garnet, absorpt. and luminesc. spectra, cryst. field and exchange interactions 77—73154
- antiferromagnetic garnets, review 77—80952
- antiferromagnetic metal, with paramag. impurities, Neel temp., impurity conc. depend calc. 78—68232
- antiferromagnetic semiconductor, magnon-spin flip excitations in Raman scatt., g-factors 77—66494
- antiferromagnetic semiconductor, theory of Raman scatt. due to magnon-spin flip excitation 77—36209
- asperomagnetism, short-range order, in Heisenberg magnet 80—65941
- 9-aza-bicyclo (3,3,1)nonan-3-one-9-oxyl, dimerisation, ESR, NO radical pair exchange 78—19330
- BCC Ising model with competing interactions, fluction-induced first-order transition 80—20424
- Berthollides, chaotic mag. states 78—56330
- binary alloy, annealed Ising ferromagnet 78—47927
- binary alloys, mag. interactions effects on phase separation 78—27047
- bipolarons, localised, in ionic crystals 78—67957
- biquadratic exchange systems, low temp. spectrum and elementary excitation damping 77—72969
- bis(diethylammonium) copper tetrachloride, mag. susceptibility, EPR spectra 78—68193
- bisgalvinoxyl biradical, cryst., spin-spin dipolar and exchange interactions 78—52356
- Bloch electron system, exchange correction to dielec. function, local exchange approx. 77—1384
- Bloembergen-Rowland approximation, indirect exchange interaction, mean free path effects 80—60238
- borides, transition metal, rare earth, and actinide, mag. props., book contrib. 78—47978
- borosilicate glass, Fe and Cr ion interaction, mag. and spectral props. 80—103883
- bound excitons in local density approximation 79—47022
- bubble device materials, single-layer, ion-implantable small, design and development 79—82844
- CeAg$_x$In$_{1-x}$, cubic to tetragonal phase transform., conc. dependence by resist. meas. 78—2252
- channel model in exchange theory 78—14950
- channel model in exchange theory 78—39311
- channel model in isotropic exchange theory 77—47783
- charge ordered crystals, mag. props., energy spectrum, triplet excitations 78—18979
- charge ordered state and collective excitations 77—28136
- charge transfer allowance in effective Hamiltonian method, technique 78—68001
- chemically induced dynamic spin polarisation, orientation depend. 80—63656
- Chichibabin's hydrocarbon, ESR spectra, electron exchange integral 78—50562
- CIDN(E)P, in two-dimensional fluid, and Heisenberg spin exchange 80—14157
- close packed lattices of ferro- and antiferromag. exchange integrals, glass-like phase 78—10697
- cobalt formate dihydrate, ordered state, paramag. cross relax. *(Japanese)* 77—43873
- collectivised electrons and localised spins, thermodynamic props. 77—8257
- complex, Mn(C$_5$H$_5$NO)$_6$(BF$_4$)$_2$, mag sp. hit below 1K 77—89968
- complex compounds, calc. of probability of electronic excitation energy transfer 79—69478
- composite permanent magnet, magnetostatic and exchange interactions 77—69536
- compressible magnet with exchange anisotropy, crit. behaviour 78—39354
- conducting ferromagnets, surface impedance resonance depend. *(Russian)* 79—91089
- conduction-electron polarisation at nucl. sites due to indirect exchange interaction 80—34619
- conductivity electrons-localized d(f) electrons, exchange interaction, energy within Hartree-Fock theory *(Russian)* 78—43580
- contact hyperfine interaction, influence of exchange hybridisation of impaired s electron with ligand electrons 77—15806
- copper, benzoate, one-dimens. antiferromag., heat capacity, field-induced crossover of spin-dimensionality 80—97099
- copper acetate, deuterated, dimeric, single crysts., inelastic neutron scatt. 80—92867
- copper acetate monohydrate, pure quadrupole reson., covalency 77—16205
- copper benzoate, antiferromag. reson. below 1K, Neel temp. determ. 78—39407
- copper diethyldithiocarbamate single crystal, EPR exchange coupled pairs, low temp. hyperfine anomaly 77—90021
- copper dipyridine dichloride, antiferromag. reson. below 1K 79—28619
- copper tetrammine sulphate monohydrate, evidence for exchange coupled quadratic nets 77—24705
- Covalency and hyperfine interaction on the impurity ion in crystals 78—23063
- covalent elements, cohesion in condensed phases, corrections to simple Huckel approx. 78—59779
- covalent semiconductors, vacancy screening, dielec. const., exchange correl. pot., Thomas-Fermi description 80—44528
- crossover, field-induced, in mag. chain, scaling theory 80—54904
- crystal field model of Invar effects in weak and strong ferromagnets 79—56484
- crystal with strong s-d exchange, mag. susceptibility and Curie-Weiss law *(Russian)* 80—25068
- crystals, mag. struct., exchange multiplets 80—60202
- cubic semiconductor, exchange splitting of excitons 79—42467
- cubic semiconductor, long-range exchange splitting of excitons 77—51671
- cubic spinels, appl. of determinant method *(French)* 80—54854
- cyclohexyl ammonium copper chloride, one dimensional spin $^1/_2$ ferromag., mag. props. 80—71000
- degenerate electron system, low-freq. polarisability, RPA calc. with temp. correction 79—95354

exchange interactions continued
- degenerate narrow bands, intraatomic Coulomb and exchange energies 80—84452
- density function formalism, exchange and correl., in at., mol. and solid 77—14367
- density functionals in unrestricted Hartree-Fock theory 79—89583
- density matrix formalism for coupled dynamical systems 78—95522
- diagrammatic Green function technique appl. to cryst. field systems with exchange 78—68130
- dialkylammonium copper chlorides nearly two dimens. Heisenberg ferromagnet, NMR study of magnetisation 77—85586
- dialkylammonium copper tetrachllride, ferromag., static and dynamic mag. props. 80—50074
- diamond, ESR studies, review 78—95521
- diamond, exchange interaction of N paramag. centres, spin density delocalisation 80—39847
- dielectric response of solids, approxs. for treatment of local field effects 79—47033
- dielectric thin slab. magneto-exchange modes with arbitrary pinning 77—63261
- diethylammonium copper tetrabromide, mag. struct., NMR meas. 80—71192
- diisopropylammonium copper chloride, mag. interactions, susceptibility, 2-230K 80—60237
- dilute alloy, exchange field, conc. depend. 77—47970
- dilute alloys, long-range interaction of mag. impurities 78—19216
- dilute alloys, mag. ordering of impurities, random phase approx. and conc. limits 79—24187
- dilute alloys, Wolff-Clogston model, effective exchange interactions calcs. 78—34812
- dilute ferromagnets, with site and bond disorders, Curie temp. 77—59407
- dilute rare earth in metal, effective exchange interaction model 80—25127
- dilute RKKY spin glass, Bethe-Peierls theory 78—39351
- diluted ferromagnets, mag. excitations, appl. of recursion method 78—23223
- diluted Ising and Heisenberg magnets with competing interactions, phase diagrams and mag. props. 80—34672
- diluted Ising and Heisenberg systems with competing interactions, mag. ordering, appl. to Eu$_x$Sr$_{1-x}$S 80—65914
- dimers, singlet-triplet energy gap, temp. depend. 79—7809
- dimethyl ammonium copper chloride, nearly two-dimensional ferromag., nucl. transverse relax. rates meas. 77—81024
- dimethylammonium copper chloride, magneto-optical props., 0.03-13.5 eV 77—52132
- dimethylammonium copper tetra(chlorobromide), mag. susceptibility, 1 to 30K, mag. phase transition 79—4675
- dimethylammonium copper tetrachloride, ferromag., quasi two-dimensional, ordering temp., press. depend. 80—84601
- dipole-exchange spin waves in cylindrical ferromag. *(Chinese)* 78—6521
- dipropylammonium copper chloride, nearly 2D ferromag., spin wave theory 77—85436
- dipropylammonium manganese tetrachloride, and tetrabromide, two-dimens. antiferromagnet, spin canting and exchange 80—34620
- Dirac exchange and relativistic corrections, effective EM potential in Thomas-Fermi atomic model 79—89614
- direct-gap semiconductors, charged excitons 77—62840
- disordered and amorphous mag. materials, position entropy solids, exchange and anisotropy noise 79—11295
- disordered anisotropic antiferromagnet. random field effects 80—2580
- disordered binary alloy, mag., with mixed exchange interaction, crit. behaviour *(Russian)* 79—1675
- disordered condensed media, with impurities, energy transfer 80—80217
- disordered Heisenberg binary magnetic alloy with mixed exchange interaction, compensation point *(Russian)* 77—51898
- disordered linear chain, exchange probability distrib., Hubbard model 78—10641
- domain wall micromagnetic dynamics, numerical model 78—72381
- doped electrode junction, tunnelling, Kondo scatt., coherence distance 78—31001
- double exchange, infinitely strong s-d coupling *(Russian)* 77—8264
- double exchange mechanism theory 77—24689
- DPPH, exchange integral determ. by ESR in weak Zeeman fields 78—2740
- DPPH, polycryst., forbidden EPR transition 78—48044
- DPPH-benzene complex, ht. capacity, 0.55-20K, mag. susceptibility, 0.4-300K 78—56317
- dynamical local field corrections in dielectric function 80—88500
- effective exchange interactions and magnetic ground state of strongly correlated electrons 79—61036
- effective field models in magnetism, unifying theory 77—32136
- elastic compliance, cooperative mag. contrib., exchange striction mechanism 77—40108
- electron gas, degenerate, response functions, memory function kinetic eqn. approach 79—49159
- electron gas, dielec. function, freq. dependent exchange correction 77—35880
- electron gas, dielectric function, dynamical exchange decoupling, plasmon dispersion, SDW and CDW 80—59900
- electron gas, dielectric function, dynamical exchange effects 80—54629
- electron gas, exchange and correlation effects, self consistent theory 77—85161
- electron gas, inhomogeneous, exchange effects and nonzero temps. 80—84444
- electron gas, inhomogeneous nonlocal approx. to exchange energy 78—138
- electron gas, interacting, elec. cond. 78—95276
- electron gas, optical props. in generalised HF approx. 80—24825
- electron gas, quasi-one-dimensional, inhomogeneity effects, eval. of exchange hole and exchange pot. 79—65397
- electron gas, relativistic, spin-polarised, Bloch theory 80—15465
- electron gas, spin polarised, exchange and correl. energy 77—85163
- electron gas, two-dimens. longit. and transverse dielec. function including exchange correls 77—66133
- electron gas, two-dimensional, internal energy, specific heat effective mass, temp. depend. 80—75513
- electron gas with surface, Green function theory, exchange and correlation effects 77—8164
- electron liquid, local field factor, freq. depend., dynamical exchange effects 80—29342
- electron liquid, local field factor freq. depend. 79—38009

exchange interactions continued
  electron liquid with any spin polarisation, correlation energy, local exchange-correlation pot. 79—65399
  electron scattering, exchange perturbation theory 80—78709
  electron-electron interactions, role in kinetic exchange 78—34974
  electron-hole liquid, quasi two dimensional in strong mag. fields *(Russian)* 78—34781
  electron-ion system, multiplicity and pseudomultiplicity 77—1389
  electron-nuclear quadrupole coupling induced by exchange interaction 79—73850
  EPR concentration dependence in magnetically diluted crystals with strong spin-spin interaction 79—42826
  EPR line profile in systems with randomly oriented 77—28430
  EPR linewidth and relax., effect of antisymmetric exchange 77—59448
  EPR of heteropairs with strong exchange coupling, hyperfine struct. 78—72395
  ESR spectra, hyperfine, exchange effects and lineshape *(French)* 79—4717
  exchange and dipoles coupled ferromags., light scatt. from mag. surfaces, response theory 79—42820
  exchange narrowing including spin correlations and local field contribs. 77—40060
  Falicov-Kimball model at atomic limit 80—65505
  α-Fe, mag. ordering affecting homodiffusion coeff., 511-1200°C 79—73711
  Fermi fluid with paramagnetic impurities, spin wave spectrum *(Russian)* 79—23915
  Fermi one dimensional gas with long range potential, renormalisation group, exchange, Umklapp interactions 80—2351
  fermion system, exchange contrib. to surface energy infinite barrier model 79—85067
  ferredoxin, Fe atoms at active centre, exchange integral of antiferromag. interaction 80—76697
  ferredoxin synthetic analogues, $[Fe_4S_4(SR)_4]^{3-}$ clusters, Mossbauer effect, EPR, and mag. props. 80—41057
  ferrimagnetic Neel mode with helical mode, coupling energy study *(French)* 80—70999
  ferrites, ferroelec., coupled ferroelec. and spin waves, exchange interactions 80—70995
  ferrites, hexagonal, model, two-sublattice uniaxial systems with strong antisymmetric exchange 78—47971
  ferrites, inhomogeneous exchange interaction influence on ferromagnetic resonance line moments 80—75864
  ferroelectric antiferromagnet, coupled ferroelec.-magnetoelastic waves 77—51935
  ferroelectric antiferromagnets, exchange enhancement of the magnetoelectric coupling 78—88159
  ferroelectric with H bonds, exchange integral press. depend. *(Russian)* 78—35097
  ferromagnet, amorphous, Ising model, Curie temp., exchange integral fluctuation effects 80—50121
  ferromagnet, anisotropic, spin one, Callen's decoupling approx. 77—8258
  ferromagnet, anisotropic exchange interaction, random phase and Callen approximations *(Japanese)* 79—95560
  ferromagnet, chain type, with uniaxial exchange, localised one-magnon states in presence of impurity *(Russian)* 77—63143
  ferromagnet, diluted, two-dimens., with anisotropic exchange interaction, excitation spectra 77—43826
  ferromagnet, dislocation effects on phys. props. at $T \neq 0K$ *(Russian)* 77—8378
  ferromagnet, effects of biquadratic exchange and uniaxial anisotropy on T_c 80—60329
  ferromagnet, Heisenberg model, two-magnon reson. in absence of bound states, calc. 80—60423
  ferromagnet, high freq. crit. dynamics above T_c *(Russian)* 78—10718
  ferromagnet, insulator-metal transition, s-d exchange interaction effects 78—2421
  ferromagnet, inter-atomic interaction effect on dynamic susceptibility, RPA calcs. 79—65662
  ferromagnet, light scatt. by spin waves 80—45086
  ferromagnet, linear mag. birefr. *(Russian)* 80—93284
  ferromagnet, magnetisation at low temp., disorder induced behaviour 78—52234
  ferromagnet, magnon-phonon interactions, Heisenberg exchange red. 80—80494
  ferromagnet, one dimensional, effect of biquadratic exchange on solitary waves 80—65836
  ferromagnet, one-dimensional, with biquadratic exchange, solitary excitations 78—76232
  ferromagnet, one-dimensional localised nuclear magnon modes 80—93098
  ferromagnet, photoelectric effect rel. to saturation magnetisation 80—65618
  ferromagnet, planar, US attenuation, spin-phonon coupling, magnons and magnetostriction contrib., calc. 80—34611
  ferromagnet, random anisotropy amorphous, initial magnetisation, remanence and coercivity 77—80964
  ferromagnet, rel. to domain interaction with mag. monopole 77—40078
  ferromagnet, surface magnetoelastic waves in the presence of exchange interactions and pinning of surface spins 78—80186
  ferromagnet, three dimens., N-magnon coupled states *(Russian)* 77—12111
  ferromagnet, two dimensional diluted, spin wave spectrum 77—66287
  ferromagnet, uniaxial, coercive force associated with domain boundary pinning on plane defects *(Russian)* 78—6543
  ferromagnet, uniaxial, with random exchange bonds of different signs, spin waves 78—76233
  ferromagnet, uniaxial with single-ion and exchange anisotropies, magnetisation in transverse mag. field 78—56277
  ferromagnet, with anisotropic exchange, homogeneous relax., time const. calc. 77—16149
  ferromagnet, with exchange-anisotropy and dipolar interaction, crit. dynamics 77—36086
  ferromagnet film, spin wave propagation near surface 78—68308
  ferromagnetic, mag. excitations within local exchange approx. 77—69517
  ferromagnetic array of pseudospin $S=1/2$, nearest neighbours anisotropic exchange mag. stability at 0K 77—1547
  ferromagnetic binary alloys, strictly regular, quasi chemical model 78—39316
  ferromagnetic degenerate semiconductor, magnon spectrum near instability of homogeneous state 79—28516

exchange interactions continued
  ferromagnetic elements, conduction electrons and s-d exchange interaction 78—19021
  ferromagnetic exchange interaction, role in X-ray threshold 77—90219
  ferromagnetic film, tangentially magnetized, spin wave instability 78—2712
  ferromagnetic film, two-layer exchange coupled, mag. reversal, exchange energy const. *(Russian)* 77—59435
  ferromagnetic fluid, 1D Ising and 3D Heisenberg solns. 77—85478
  ferromagnetic fluid, molecule system eqn. of state, exchange interactions, spin independent forces 77—59412
  ferromagnetic interaction obeying Kanamori-Goodenough rules 78—39307
  ferromagnetic Ising model, band-mixed square-lattice: approx. crit. surface 80—70921
  ferromagnetic linear chains of spin 1/2 particles, one-magnon states 78—14946
  ferromagnetic metal, anomalous magnetooptic effects near Curie temp., s-f exchange model 80—2736
  ferromagnetic metal, magnon and cond. electron relax. processes *(Russian)* 80—7102
  ferromagnetic metallic glass, hyperfine field and spin wave excitations, $T^{3/2}$ depend. 78—10672
  ferromagnetic metals, dislocation drag by conduction electrons 80—24451
  ferromagnetic metals, s-d exchange interactions, effect on attenuation of spin waves *(Russian)* 79—19730
  ferromagnetic metals, simple theory of spin-wave relax. 78—19231
  ferromagnetic metals, zero temp. magnon exchange effects 77—51897
  ferromagnetic nonmetallic film, stand exchange mode determ. 80—2565
  ferromagnetic porous material, coercive field 78—14984
  ferromagnetic semiconductor, anomalous Hall effect, s-f model 78—10478
  ferromagnetic semiconductor, autolocalised electron states 78—51924
  ferromagnetic semiconductor, nonlinear magnetoelec. effect, depend. on s-d exchange 77—20676
  ferromagnetic semiconductor, Raman scatt. due to magnon-spin flip of cond. electrons 77—20839
  ferromagnetic semiconductor, spectrum of quantum spin waves in field of strong EM wave 78—91857
  ferromagnetic semiconductor, wide-gap, nonlinear galvanomag. effects 77—39862
  ferromagnetic semiconductor with defects, exchange Hamiltonian 79—82777
  ferromagnetic semiconductors, giant blue shift of absorption edge *(Russian)* 77—32401
  ferromagnetic semiconductors, mag. excitations, light scatt. 77—63161
  ferromagnetic single crystal with cubic symmetry, mag. and magnetoelastic props. 79—15332
  ferromagnetic spin-one system, quadrupolar to paramagnetic phase transition 77—80934
  ferromagnetic system, random spherical model in nonzero mag. field 77—55677
  ferromagnetic systems, singlet-triplet, excitation spectrum, double-time Green's functions 80—84603
  ferromagnetic thin film, with nearest neighbour and next nearest neighbour exchange interactions spin-wave excitations 79—73783
  ferromagnetism, itinerant, effective Hamiltonian 80—11150
  ferromagnetism, manyelectron exchange Hamiltonian in theory 78—19199
  ferromagnetism of disordered systems, review 80—29513
  ferromagnets, amorphous, Curie temp. depend. on nearest neighbour fluctuations 80—50120
  ferromagnets, Heisenberg and planar, exact results for spin-wave renormalisation 79—69660
  ferromagnets, metallic, spin wave damping, magnetisation relax. 78—88106
  ferromagnets, random, large exchange interaction, Green function theory 78—6537
  ferromagnets, spin polarised LEED, exchange correlation effects, calc. 79—99686
  ferromagnets, uniaxial, US attenuation and kinetic coeffs. near crit. point, renormalisation group theory 79—4715
  ferromagnets and antiferromagnets, transverse dynamical susceptibility within the local exchange approx. 78—76229
  ferromagnets crystal, $S \geq 1$, ground state of mag. polaron *(Russian)* 77—63142
  ferromagnets with double exchange, quantum theory 78—19204
  ferromangetic conductor, electric field response and electrofluctuation instability *(Russian)* 78—56083
  ferrous formate dihydrate, paramagnetic specific heat, decoration iteration transformation anal. 80—70938
  film, rel. to micromagnetic dynamics in domain walls, numerical model 78—72382
  films, ferromagnetic, perpendicularly magnetised, surface and vol. magnetoelastic waves *(Russian)* 80—93151
  free energy, random magnetic system 78—2634
  free radicals in soln., spin exchange and EPR broadening 78—52357
  Frenkel excitons, optical resonance 78—91621
  p-GaAs, spin relaxation of photoelectrons 77—85207
  gapless semiconductor, effect of nonlocal pot. on hole energy spectrum in mag. field 78—39017
  gapless semiconductor valence band in mag. field 80—49600
  garnets magnetic excitations 79—99695
  garnets with Fe^{3+} ions in tetrahedral sublattice, mag. ordering and bond geometry 77—32163
  giant intrinsic magnetic hardness, review 78—48004
  gradient approx. to exchange correlation energy functional 79—90983
  graphite, electronic struct. exact exchange HF calcs. 80—65438
  guanidine aluminium sulphate hexahydrate:Cr^{3+}, ESR spectra fine struct. 80—93169
  guanidine aluminium sulphate hexahydrate type ferroelectrics, ESR of Fe^{3+} exchange pairs 77—90022
  guanidinium vanadium sulphate hexahydrate, singlet ground state system, low temp. mag. props. 80—44843
  harmonic rotor model, interactions, spirals and phase transitions with and without long range order 80—60350
  heat magnetization in the singlet-triplet model 78—64211
  heavily doped semiconductor, n-type, disordered mag. system, hierarchy of exchange interactions 80—80235
  heavy rare-earth alloys, mag. ordering temps., Heisenberg exchange 79—61103

exchange interactions continued
Heisenberg and biquadratic exchange, eigenstates of short chains of spin-1 atoms 77—55652
Heisenberg antiferromagnet, ABX$_3$-type, exchange interaction and zero-point spin reduction 77—12080
Heisenberg antiferromagnet, dil., CPA calc. 78—68263
Heisenberg antiferromagnet, dil. with random first- and second-neighbour exchange bonds, CPA theory 78—52187
Heisenberg antiferromagnet, one-dimens., impure, mag. susceptibility 80—60168
Heisenberg chain, ferromag., with biquadratic exchange, spin correl. length, susceptibility and spin diffusion *(Russian)* 77—69568
Heisenberg classical compressible model, phase transition exam., anisotropic exchange 77—59414
Heisenberg exchange integral, in nonorthogonal basis, for anti- and ferromag. systems 78—2641
Heisenberg exchange interaction Hamiltonian, eigenvalues and eigenvectors 79—78289
Heisenberg FCC ferromagnet, surface spin instabilities 77—69475
Heisenberg ferromag. localised magnons around surface impurity *(Russian)* 78—84376
Heisenberg ferromagnet, amorphisation, anisotropically distrib. exchange forces *(Russian)* 77—85408
Heisenberg ferromagnet, anisotropic, with biquadratic exchange interaction and uniaxial anisotropy, Curie temp. 80—7118
Heisenberg ferromagnet, biquadratic exchange, Green's function method, Hamiltonian and Curie temp. 80—15675
Heisenberg ferromagnet, dil., CPA theory, spin-wave stiffness and Curie temp. 78—31080
Heisenberg ferromagnet, dil., localisation of excitations near percolation threshold 79—15271
Heisenberg ferromagnet, equivalence of large biquadratic exchange to small uniaxial single ion anisotropy 79—78292
Heisenberg ferromagnet, isotropic with biquadratic exchange 78—39344
Heisenberg ferromagnet, low-dimens., crit. temp. *(Russian)* 78—23274
Heisenberg ferromagnet, spin-one, with biquadratic and uniaxial anisotropy, Curie temp. 79—61123
Heisenberg ferromagnet, structural disorder effects on Curie temp. 79—78417
Heisenberg ferromagnet, structurally and chemically disordered, critical behaviour 77—43838
Heisenberg ferromagnet, with biquadratic exchange, first-order quadrupolar transition 77—69571
Heisenberg ferromagnet, with biquadratic exchange 77—63060
Heisenberg ferromagnet, with biquadratic exchange interaction 78—34999
Heisenberg ferromagnet with biquadratic exchange 79—38338
Heisenberg ferromagnet with higher-order exchange interactions, thermodynamic props. 79—42770
Heisenberg ferromagnet with s-d exchange interactions, Curie temp. 78—19255
Heisenberg ferromagnetic system with biquadratic exchange interactions, spin wave theory *(Chinese)* 80—88755
Heisenberg film, spin-one isotropic, quadratic interactions, quadrupolar-paramag. T_c 78—64210
Heisenberg film, spin-one isotropic, with biquadratic interactions, phase transition 77—20611
Heisenberg Hamiltonian generalisation for case of atomic system with variable atomic spin value 78—14669
Heisenberg linear spin systems, dynamical spin correlation functions 78—31035
Heisenberg magnet, classical one-dimensional, with biquadratic exchange interaction, correlation functions and susceptibility calc. 77—36048
Heisenberg magnets, with two kinds of exchange interactions, surface magnons and surface spin arrangements 77—36043
Heisenberg model, disordered ferromag. states, random exchange integrals 80—80550
Heisenberg model, disordered spin system, commutator and anticommutator Green's functions 79—51792
Heisenberg model, generalised, with biquadratic exchange, partially aligned mean-field ground states 78—23227
Heisenberg model, with anisotropic biquadratic exchange interaction, two-magnon bound states 77—28356
Heisenberg model with biquadratic exchange, Hamiltonian and two-spin eigenstates 77—72968
Heisenberg multi-quadratic isotropic model, LRO, phase transf., exchange interactions *(Chinese)* 80—88756
Heisenberg open finite chains, zero field, susceptibility calc. as function of reduced temp. 77—51868
Heisenberg paramagnet, dil., dynamics at high temp. 77—28355
Heisenberg paramagnet, dil., uniaxial anisotropy, frequency moments of spin correlation function 78—84377
Heisenberg paramagnet, exchange bond dilution, freq. moments of spin correl. function 80—50030
Heisenberg paramagnet, sixth frequency function of relaxation shape function 78—39348
Heisenberg spin glass, spin diffusion 78—6538
Heisenberg-Ising chain, correlation functions at $T=0$ 79—24123
helical order and its onset at Lifshitz point 78—34996
Heusler alloy, Mn-containing hyperfine field and magnetic behaviour 79—78360
Heusler alloy, Mn-containing theory of spin waves 79—78354
Heusler alloys, ferromag. alignment rel. to conduction electron polarisation 80—60235
Hubbard antiferromag. semiconductor, electron correlations, weak coupling 78—67969
Hubbard Hamiltonian, kinetic exchange interaction in narrow S-band 77—55655
Hubbard model, doubly degenerate, functional integral approach 79—99711
Hubbard model, spin-wave excitations in narrow s-band, including intersite exchange interactions 77—16033
Hubbard model, two band, magnetic behaviour 78—80119
ilvaite, Fe temp. depend. oxidation states, electron hopping, Mossbauer spectra, X-ray diffr. obs. 78—2779
impurity centres, exchange interaction due to phonons *(Russian)* 78—79678
impurity centres exchange interaction caused by elementary excitations in solids, temp. depends. 80—25193
indirect exchange between local moments, cyclotron reson. effect 77—40051

exchange interactions continued
indirect exchange in Bloembergen-Rowland approx., ellipsoidal Fermi surface and relax. process effects 80—107754
indirect exchange interaction through narrow conduction zones *(Russian)* 79—4538
induced moment systems, effect of spin fluctuations 80—2585
induced-moment singlet-triplet model, high-temp. series expansion 79—73653
induced-moment singlet-triplet model, rel. between ground-state moment and crit. temp. 79—78282
inhomogeneous electron gas, exchange energy *(Russian)* 77—72830
inhomogeneous electron gas at jellium surface, exchange energy 80—10901
inhomogeneous electron system, exchange and correlation 78—18985
inhomogeneous electron systems, exchange and correlation effects calc. 80—20104
inhomogeneous relativistic electron gas 79—28304
inhomogeneous system, electron gas model, exchange pot. charge density depend. 80—54626
insulating solids, long exchange paths between mag. ions pairs, singlet-triplet separation determ. 77—69283
insulator, localised surface impurity modes 77—1545
insulators, mag., interference effects in NMR line shape 77—8435
interatomic electron interactions, effect of electron correl. 79—38010
interatomic interactions between electrons 78—64017
intermediate-valence systems, magnetic-nonmagnetic transitions, heuristic model 79—73718
intermetallic compounds, containing d-transition metal, hydrogenated, magnetism 80—34609
intrinsic semiconductor, indirect exchange 77—80924
intrinsic semiconductors, indirect exchange interaction, finite temp., valence bands and energy gaps effect 80—59943
Invar, local moment model 79—56505
Invar, rel. to elec. transport props. and Invar features *(Russian)* 78—14710
Invar films, exchange interaction depend. on lattice parameter, spin-wave reson. and magnetisation meas. *(Russian)* 79—42751
(iron, chromium) carboxylates, heteronuclear trimer exchange clusters, ESR spectra 80—80603
iron porphyrin chlorides, X-ray, EPR and mag. susceptibility obs., intermol. exchange interaction 78—10765
Ising and Heisenberg ferromagnets with biquadratic exchange, uniaxial anisotropy, susceptibility calc. 79—99670
Ising and Heisenberg inhomogeneous mixture, quenched system, critical temp. 80—88770
Ising chain, with next-nearest neighbour interactions, mag. responses to spin-Peierls transition 80—71054
Ising double chain, compressible, mag. susceptibility and thermodynamic props. 79—15320
Ising ferro and antiferromagnet random bond mixture, on s.c. lattice, phase transition 77—12131
Ising ferromagnet, annealed, of binary alloys 77—59368
Ising ferromagnet, disordering, short-range mag. order 80—50119
Ising ferromagnet and antiferromagnet, two-dimens. square, ground state, apparent 3-spin interactions 80—88709
Ising magnet, random, with frustration, zero-temp. props. from series expansions 79—61129
Ising model, logarithmic exchange interaction, Monte Carlo simulation 79—19712
Ising model, mixed, renormalisation group calc. 79—56547
Ising model, random-bond, upper bond to sp. ht. on Nishimori's line 80—71068
Ising model, spin glass state, mixed nearest-neighbour exchange interaction 78—39341
Ising model, surface magnetic order, Cayley tree approx. 77—72964
Ising paramagnet, transverse, spectral density approach 77—80897
Ising paramagnet in transverse field 77—8260
Ising quadratic two-dimensional ferromagnet with three spin interactions 80—2542
Ising quenched bond model, statistical theory of random ordered phase 77—12075
Ising $S=1$, $^1/_2$ mixture, one-dimens., random, mag. props., spin distrib. 78—95407
Ising site model, random mixtures, Monte Carlo simulation 78—73935
Ising system, finite, statistically layered, crit. phenomena 78—95446
Ising two-dimens. lattice, next-nearest neighbour interaction, impurity effect on sp. ht. 77—89957
isotropic exchange theory, channel model 77—73019
itinerant electron antiferromagnet, effects of paramagnetic impurities on Neel temperature 79—4678
itinerant electron antiferromagnetic matrix, local moments, spin Hamiltonian 80—34626
itinerant electron ferromagnetism, local exchange model 77—72994
itinerant electron ferromagnets, elastic props. and electronic struct. 80—66001
itinerant electron model, susceptibility, local exchange approx. calc. 80—60169
itinerant magnets, anomalous sound attenuation near mag. transition temp. 78—15004
itinerant to local moment magnetism transition with comp. 77—72984
Jansen-Byers Brown exchange perturbation theory, transformation operator 77—28380
kinetic exchange interaction, doubly degenerate narrow bands 78—23263
Kondo Hamiltonians, s-d exchange, ground states, renormalisation group calcs. 80—50046
Kondo Hamiltonians with non-zero ground-state spin 79—51746
Kondo lattice, phase diagram 80—7077
lanthanide ions, finite ligand size and Sternheimer antiscreening 79—19561
lattice dynamics, cubic metal, Sharma-Joshi model, correl. exchange effects 80—10613
layer structures, ML$_4$ dimer (M=metal, L=ligand), exchange interaction temp. depend., appl. to EPR linewidth 78—19306
layered compounds, effect of exchange on CDWs 78—60078
lightly doped, 1/f noise for hopping conduction, theory 80—44683
Lindhard dielectric function for degenerate electron gas, exchange contrib. 77—51685
localised model for systems with double-exchange coupling 79—38318
long-range correlation of localised spins in s-d exchange model 77—16043
long-range exchange interactions 77—69531

exchange interactions continued
Lorentz-Lorenz formula, microscopical derivation 78—92014
low-dimensional correlated spin systems, exchange narrowing theory 79—11335
luminescence quenching parameters, donor-acceptor exchange mechanism 80—2840
magnet, ordering temps. determ. by Bethe-Peierls-Weiss (BPW) method 80—54912
magnetic 3d impurity in non-magnetic metal, effective ion Hamiltonian 78—64016
magnetic alloys, conc., density of states, Kondo effect, theory 80—65780
magnetic chains, spin 1/2 Ising and classical Heisenberg models with alternating exhange, static props. 79—82737
magnetic crystal, sound velocity temp. depend. anomaly 77—72891
magnetic electron gas induced by van Vleck ion, spin polarisation 79—56176
magnetic excitations, applic. of submillimetric spectroscopy 77—40135
magnetic film two-layer, exchange-coupled, switching, differential permeability *(Russian)* 78—27061
magnetic impurity ion in mag. ordered cryst., optical absorpt., exchange interaction effects 77—16355
magnetic insulators, indirect exchange interactions, polar model study 78—88110
magnetic insulators, perovskite-like struct., supertransferred hyperfine interaction 78—14913
magnetic insulators with Jahn-Teller ions, temp. depend. of exchange integrals 80—103827
magnetic ions interaction in insulator, degenerate orbitals 79—91010
magnetic materials, symmetry and macroscopic dynamics 80—107973
magnetic ordering due to exchange-crystal splitting 79—8010
magnetic resonance line, exchange narrowing at low temp. *(Russian)* 78—56366
magnetic semiconductor, doped, electron struct. and indirect exchange mechanisms 80—25123
magnetic semiconductor, doping effects on echange interaction mechanism 78—31064
magnetic semiconductor, double exchange and small-polaron hopping 79—19591
magnetic semiconductor, exchange interaction mechanisms, theory compared with expt. *(Russian)* 78—39312
magnetic semiconductor, indirect exchange interaction, mean free path effects 80—97088
magnetic semiconductor, multispin indirect exchange *(Russian)* 78—56311
magnetic semiconductor, with impurities, semicond.-metal transition and instability phenomena 77—59257
magnetic semiconductors, electron propag., s-d model, red shift theory 77—51736
magnetic structure, neutron diffraction patterns, group theoretical, exchange Hamiltonian symm. anal. *(Russian)* 79—65648
magnetic structures, neutron diffr., symmetry anal., group theoretical group anal. of exchange Hamiltonian 80—29527
magnetic susceptibility of cryst. with strong s-d exchange *(Russian)* 78—56283
magnetic susceptibility of $s=1/2$ crystallographic two sublattice system 78—14914
magnetic systems with random interactions, upper bounds to be quenched free energy 80—103845
magnetic transitions, first-order, intrinsic volume magnetostriction concept 80—29562
magnetic-atom cluster, spin Hamiltonian for direct exchange interaction 77—20519
magnetically ordered crystals, exchange symm., mag. struct. *(Russian)* 80—65785
magnetically ordered singlet ground state system, nucl. spin Hamiltonian 79—28496
magnetically soft cylinders, micromagnetics of curling configurations 79—82826
magnets, mixed, competing spin glass and mag. order, phase diagrams, crit. points 80—39802
magnon elementary excitations damping *(Russian)* 79—28515
magnon problem, anisotropic spin chain with exchange interaction 78—6502
manganese acetate tetrahydrate, Heisenberg ferrimag. magnetisation 79—47304
manganese aluminosilicate glass, insulating spin glass, exchange dipole optical transition 80—40136
manganese copper formate dihydrate, conc. depend. of EPR linewidth 79—38376
manganese stearate: cadmium stearate, dil. quasi two-dimensional, ESR line width 80—71155
many-electron systems, self-interaction corrected approach, beyond local spin density approx. 80—92844
Mattis model, modified, mag. relax. 80—65947
metal, 3d, X-ray emission and XPS broadening, many-body effects and intra-atomic exchange 77—44090
metal, conduction electron coupling with moments of 3d and 4f ions 78—60090
metal, d-band, generalized pseudopotential theory, density functional formulation 78—10389
metal, electron gas, correlation effects on polarisation 80—54628
metal, electron-phonon interaction, magnetism influence 77—73040
metal, electron-phonon interaction effects on spin susceptibility 80—93108
metal, exchange enhancement of electron-phonon coupling 78—47968
metal, ferromagnetic, longitudinal spin susceptibility 79—61078
metal, ferromagnetic, many-electron direct exchange interaction 79—69667
metal, indirect coupling between localised mag. moments by narrow band electrons 80—70942
metal, inhomogeneous electron system, nonlocal exchange and correlation 78—56097
metal, magnetic impurity, model of resonance level in Kondo problem *(Russian)* 78—80129
metal, pressure equation derived, Hartree-Fock approx. 78—72103
metal, supercond. as probe of mag. state of local moments 77—20491
metal, superconductivity and ferromagnetism 79—73616
metal, surface energy calc., exchange contrib., convergence of gradient expansion 77—43684
metal, wake potential for fast ion pairs, self consistent calc. 78—34792

exchange interactions continued
metal conduction electron photoemission spectrum, effect of recoil on shake-up spectra, infinite summation method 80—50526
metal hydrides, rare earth and intermetallic, electronic and mag. props., Mossbauer study 80—34830
metal ions, exchange coupled, pair hamiltonian, coupled representation matrix 78—48026
metal surface, dynamic image pot. for tunnelling electrons 80—49874
metal surface, exchange-correlation hole 78—80037
metal surface, gradient correction to electron exchange-correl. energy 77—43691
metal surface, step potential model, static semiclassical response of bounded electron gas 78—72221
metal surfaces, exchange and correlation energy, wave vector anal. 80—20273
metal with incomplete shell, core photoelectron spectra, spin-depend. final-state interactions 77—69965
metal with incomplete shell, spin-depend. final-state interactions in core photoelectron spectra 77—20981
metal with incomplete shell, spin-depend. final-state interactions in core photoelectron spectra 77—20982
metallic monopnictides:Gd, coupling between 4f electrons and conduction electrons, EPR linewidth 78—52347
metallic rare earths, conference, St. Pierre-de-Chartreuse, France (Sept. 1978) 80—12844
metallic substances, retention and exchange of 4f electrons *(Dutch)* 79—1587
metallic surface energy, exchange and correl. contrib., wave-vector decomp. 80—75615
metals, core overlap interactions 77—47759
metals, cubic, cohesion and Cauchy discrepancy 80—54170
metals, electric properties calc., book 79—28274
metals, hybrid exchange interaction of localised moments 77—28381
metals, inelastic neutron scatt. cross-section, effect of cryst. field 79—65642
metals, simple, electron-electron interaction, self-consistent perturbation theory based on Hartree-Fock theory 79—95357
metals, spin- and charge-density oscillations 77—11886
metals, spin-orbit coupling enhancement of 3d ions 79—47069
metals, with mag. impurities, kinetic exchange interaction, Curie-Weiss high temp. susceptibility 79—33457
metals, X-ray photoelectron and absorpt. spectra, edge singularities in spin-depend. final-state interactions 78—6810
metamagnet, compressible, renormalisation group theory of pseudocritical point 80—60337
metamagnetic insulators theory, microscopic model *(Russian)* 77—43798
metamagnetic transitions, theory 77—16076
metastable polarised crystals, decay kinetics, exchange magnon-phonon interactions *(Russian)* 80—7060
methylcyclohexane, trapped electron charge distribs., optical transitions 77—28139
3-methylpentane, trapped electron charge distribs., optical transitions 77—28139
microscopic model for the exchange-inversion transition 79—56548
mixed valence cpds., exchange coupled ions, electron transfer, optical intervalence transition 80—44556
mixed valence state, electronic structure 79—11092
molecular crystal, dipole-dipole interaction rel. to internal vibr. 78—47476
molecular crystals, charge-transfer electron-exciton bound states 77—43543
Mossbauer line, exchange narrowing 77—85627
Mossbauer spectrum, magnetic ion exchange interaction effects 79—95696
multielectron system, weakly delocalised, direct exchange 77—40050
multiple scattering method, eliminating α exchange parameter 80—103652
multivalley semicond., biexciton props. 77—66120
N,N′-dioxy-2, 6-diazoadamantane, exchange interaction, spin density delocalisation 78—9056
naphthalene $^1B_{2u}$ resonance pairs, energy denominator depend. of excitons absorpt. 77—39783
narrow conduction bands, allowance for correl. effects 78—47933
Neel mode, ferrimagnetic-helical [hh0] mode coupling vector model *(French)* 80—75770
NMR bandshape, complex exchange-broadened, iterative computer anal. 79—35805
NMR hybrid relaxation and multiple pulse methods for studying chemical, physical and spin exchange 80—80629
NMR lineshape exchange narrowing, for Heisenberg paramag. 77—69717
noncollinear magnetic order and spin wave spectrum in presence of competing exchange interactions 80—65834
nonequilibrium superconductors, ferromag. ordering of quasi-particles and rise of domains 80—107958
nonmagnetic metal, s-d exchange model exact solution, mag. susceptibility, mag. impurity interactions *(Russian)* 80—70943
nucleation centre formation in mag. phase transitions of first kind 78—2683
one dimensional spin-1/2 XY model, finite temp. transverse autocorrelation function 80—50024
one dimensional system, Kondo lattice and weak antiferromagnetism 77—73038
one-dimensional antiferromagnet, with antisymmetric exchange, Green's function theory 79—15290
one-dimensional classical planar model in applied magnetic field 80—15729
one-dimensional classical spin chain with random interactions, exact calcs. 79—4687
one-dimensional ferromagnet with biquadratic exchange, solitary bound states of magnons and lattice deform. 79—19732
one-dimensional magnetic compounds, orbital interaction 78—6494
one-dimensional magnetic system, spin anisotropy and exchange alternation 80—34644
one-dimensional random Glauber model, magnetisation relax. 80—80523
one-dimensional semi-infinite chain, enhanced surface exchange interaction, mag. relax. 80—29558
one-dimensional systems, exchange effects in plasmon dispersion 78—91628
one-dimensional systems, exchange effects in plasmon dispersion 79—60741

exchange interactions continued
one-spin ferromagnet, high temp. series expansion for mag. susceptibility and sp. ht. 80—25148
orbital functional theory for exchange and correl., local spin density approx., self interaction correction 79—76347
orbital interaction and chemical bonds. Exchange repulsion and rehybridization in chemical reactions 78—85142
ordered magnetic cpds., selective sublattice dilution, percolation problem 80—103850
paramagnet, anisotropic, spin dynamics, exchange-bond dilution effects 80—88763
paramagnetic centres, quadrupole relaxation transitions due to carrier exchange scattering 79—73803
paramagnetic to helicoidal or sinuosidal state transition *(Russian)* 77—63193
paramagnets, high-temp., quadrupolar exchange effects on spin dynamics 79—61038
periodic structure, electron-exciton complex auto ionisation *(Russian)* 80—49611
periodic systems electronic struct., LCAO SCF ab initio HF calcs. method 80—65419
Permalloy film, with-small surface anisotropy, ferromag. reson. 77—69701
Permalloy-Co film, domain walls, magnetisation ripple *(Russian)* 79—47314
phase diagram of magnets with two-sublattices *(Russian)* 78—23268
phenyl alkyl ammonium copper chloride, quasi-two-dimens. Heisenberg ferromag., mag. props. 77—66273
polaritons, multi-component, reflectance spectrum 78—87921
polyarylenealkyls, colour, EPR, electron density delocalisation degree determ. *(Russian)* 80—7152
polyene, linear, band gap calcs. 77—31969
polyvinyl alcohol film containing Cu^{2+} complexes, photoconductivity 80—107849
porous anisotropic magnets, approach to mag. saturation 80—93146
1-3-propanediammonium-$CuCl_4$, ferromag., antisymmetric and anisotropic exchange, EPR linewidth 78—10761
pseudopotential form factor determ., exchange interaction and correlation effects 80—49639
pseudospins, $S=1/2$, simple cubic array, with anisotropic exchange between nearest neighbours, ground state configs. 78—72340
quantal spin system, classical representation and scaling props. of spin Hamiltonians 78—14919
quantum crystal, magnetically ordered, phenomenological theory 77—7944
quasi-one-dimensional metals, narrow-band, exchange-correlation effects on plasmons and on CDW instability 80—44525
quenched random alloy with competing anisotropies, decoupled tetracrit. point 77—12138
quenched random spin systems, spin glass and related orderings 78—10706
quinolinium $(TCNQ)_2$, random exchange Neisenberg antiferromag. chain, intermediate field magnetisation meas. 80—103857
quinolinium manganese (II) chloride monohydrate, crystal struct. and mag. susceptibility 79—19239
radical pairs, electron spin motion, diamag.-paramag. exchange, mag. field effect 79—98123
random, and 'frustration effect' 78—68212
random binary magnetic systems, quenched, Neel temp. calc. 77—89963
random binary system, mag. transition temp. and sp. ht. 77—77065
random chain of classical spins, statistical mechanics 78—10630
random collinear states, Gaussian internal mol. field distrib. 77—16016
random exchange Heisenberg antiferromagnetic chain, exchange-coupled pair model 80—20423
random ferromagnet, with long-range interactions, dynamics 77—89942
random isotropic dipolar magnet, absence of ferromag. long range order 79—28546
random mixture of ferro- and antiferromag. exchange interactions, high temp. expansion 78—23280
random quenched mixtures, ferro- and antiferromagnetic exchanges 77—51864
random quenched site model, competing exchange energies and competing anisotropy energies 80—29552
randomly diluted Heisenberg spin system with anisotropic exchange coupling, crit. temp. 79—99702
randomly located Ising spins with oscillatory exchange interactions 79—42778
rare earth alloy, dil., anisotropic exchange Hamiltonian, rel. to ESR spectrum 77—20696
rare earth alloys, amorphous, magnetoresistivity, exchange scatt. model 78—95287
rare earth alloys, amorphous, random anisotropy antiferromag. model 78—95428
rare earth alloys, dil., ESR linewidth of rare-earth ions 78—68373
rare earth alloys, mag. phase diagram 78—10684
rare earth alloys, magnetic properties, impurity effects, CPA calc. 80—44784
rare earth alloys, RCo_2 and R_2Fe_{17}, Invar props. 79—56593
rare earth alloys, RZn_{12} and RCu_4Al_8, mag. struct. and interactions 80—25092
rare earth amorphous alloys, antiferromagnetism, mol. field approx. 78—80142
rare earth amorphous alloys, random mag. anisotropy, antiferromag., Monte Carlo calcs. 79—33471
rare earth and rare earth intermetallic hydrides, magnetic properties, effect of hydrogenation 78—68210
rare earth antiferromagnet, magnetic excitation, appl. to DySb 79—78358
rare earth binary insulating compounds, exchange interactions, paramag. susceptibility expts. 80—60177
rare earth chalcogenides, cryst. field splitting, press. depend. 80—24852
rare earth compounds, connection between exchange field and Fe and Co moments 77—1551
rare earth compounds, effect of cryst. field on inelastic neutron scatt. cross-section 77—55659
rare earth compounds, Kramers, temp. renormalised spectrum of mag. excitations, cryst. field level ordering 77—20516
rare earth ethyl sulphate:Gd^{3+}, host lattice effects on EPR spectra 77—69684
rare earth garnets, anisotropy due to cryst. elec. field and exchange 77—69543

exchange interactions continued
rare earth impurities in s-band metals, Kondo anomaly 78—52208
rare earth impurity, ESR, exchange induced broadening in low lying crystalline field system 80—108062
rare earth intermetallic compounds, quadrupolar interactions, parastriction 80—60400
rare earth intermetallic cpds., mag. props., book contrib. 80—39759
rare earth intermetallics, AB_2, ($A=Y$, La, Ce, Lu; $B=Ir$, Rh) 77—85564
rare earth intermetallics, cubic, exchange coulombic contrib. of cond. electrons to cryst. elec. field 79—95376
rare earth intermetallics, cubic, magnetic order effects on cryst. field parameters 77—40019
rare earth intermetallics, RAl_2, exchange modification of cond. bands 79—82568
rare earth intermetallics, RAl_2-Gd(Er)(Dy)(Nd), dil., ($R=La$, Yb, Lu), EPR and mag. susceptibility 80—15797
rare earth intermetallics, RPt, ($R=Gd$, Tb, Dy, Ho, Er, Tm), structs. and mag. props. 80—50069
rare earth ions, energy transfer rates, unified method using standard tensor calc. *(French)* 78—79965
rare earth ions in solids, indirect exchange between localised moments *(Russian)* 79—87237
rare earth iron intermetallics, RFe_2, ($R=Sc$, Lu, Y), mag. props., 80-1300K *(Russian)* 80—75750
rare earth metal, 4f levels, obs. by bremsstrahlung isochromat and XPS spectroscopy 79—24411
rare earth metal, anomalous sound attenuation near mag. transition temp. 78—15004
rare earth metal, conduction electron interactions, anisotropic 80—15492
rare earth metal, electron interactions rel. to lattice props. *(Russian)* 77—35901
rare earth metal, magnetic properties, nonlinear s-f exchange interaction effect 80—15711
rare earth metal, s-core levels multiplet splitting, exchange correl. 78—10407
rare earth metal impurity in metallic host, exchange interaction, electrical resistivity 80—84453
rare earth metal S-states in metals, anomalous cryst. field splittings 79—19563
rare earth metals, ferromagnetic theory of low-temp. and freq. depend. of extraordinary kinetic effects *(Russian)* 79—91408
rare earth metals, mag. excitations, neutron inelastic scatt., review 79—47265
rare earth metals, magnon dispersions in ferromag. and screw structs., nonlinear s-f exchange interaction effect 80—75746
rare earth mixed ferrite-chromites, mechanism of polarisation of rare earth ions 79—42740
rare earth molybdenum selenides, supercond., mag. props., 0.7 to 295K 77—32113
rare earth nuclei in cubic cpds., self polarisation field calc. 80—15487
rare earth orthoferrites, parameters of interaction between rare earth and Fe ions, theory and expt. 79—73705
rare earth orthovanadites, indirect exchange 78—34977
rare earth palladinides, R_3Pd_4, mag. props. 77—47980
rare earth pnictides, cryst. field splitting, press. depend. 80—24852
rare earth pseudobinary intermetallic compounds, ESR studies 80—108064
rare earth sesquioxides, cubic, indirect exchange interactions Anderson model 79—95585
rare earth sesquioxides, exchange interactions, paramag. susceptibility expts. 80—60177
rare earth superconductors, upper crit. fields in the dirty limit, depend. on intra- and interaction exchange interactions 79—56461
rare earth ternary compounds, coexistence of superconductivity and long-range magnetic order 79—11264
rare earth-Al_2 (Zn), mag. coupling mechanism 79—4655
rare earth-Al Laves phase intermetallics, RAl_2, $R=Gd$, Ho, Dy, Tb, cubic Laves phase compounds, exchange striction determ. 80—44895
rare earth-Co alloy, mag. anisotropy origin 79—38319
rare earth-cobalt intermetallics, R_4Co_3, cryst. field effect on mag. moment direction, neutron diffr. meas. 78—80132
rare earth-Cu intermetallic compds. single crysts., mag. props. 80—54892
rare earth-Fe alloy, amorphous, random anisotropy model, generalised mol. field calcs. 77—28345
rare earth-gold amorphous alloys, R_4Au, anisotropy versus exchange 80—34624
rare earth-iron, RFe_2, Laves phase intermetallics, ordered and paramagnetic phases, mean field exchange consts. 80—50084
rare earth-nonmagnetic metal intermetallic cpds., struct. and props., review 79—95377
rare earth-transition metal (4f-3d) intermetallic cpds., mag. moment and mag. anisotropy 80—25107
rare earth-transition metal alloys, amorphous, Hubbard hamiltonian, mag. props. 77—72985
rare earth-transition metal alloys, cryst. and amorphous, mag. props. 77—73008
rare earths, spin waves and excitations 78—84407
rare earths in metallic environment, mag. moments 78—6515
rare-earth alloys, amorphous study of hysteresis effects using Monte Carlo technique 79—1686
rare-earth impurities in s-p hosts, self-polarization hyperfine fields 79—33456
rare-earth metals, US attenuation, exchange striction, and spin-phonon interaction 79—33518
reciprocal lattice expansion, Hartree-Fock exchange term, LCAO calcs. 78—47691
ruby:Cr^{3+}, exchange integral, pressure depend., test of theory 78—87741
ruby, energy transfer time const. between single Cr^{3+} and Cr^{3+} pairs 79—38627
ruby, luminesc., ground state of Cr(III) pair 79—33782
ruby, piezo-spectroscopy of exchange coupled Cr^{3+} pairs 79—33783
$S=1$, singlet ground state systems, mag. props. 80—11157
SCF calcs., electron exchange and correlation phenomena, effect of local electron speed 79—95356
screw spin ordered state through dipole-dipole interaction 78—39337
semiconducting surface inversion layers, exchange and correl. 80—75618
semiconductor, antiferromagnetic, spin-magnetomagnon resonance 80—2566
semiconductor, doped with mag. impurity, ordering mechanism 80—2572

exchange interactions continued
  semiconductor, exchange and correlation energies, local field effects 78—39044
  semiconductor, exciton and impurity states, unified theory, for arbitrary mag. field 80—39511
  semiconductor, intrinsic, indirect exchange interaction, finite temp. effects 80—71003
  semiconductor, intrinsic, indirect interactions between localised mag. moments 78—43578
  semiconductor, metamagnetic, magnetostriction ferrons 78—88160
  semiconductor, spin relax., in quantising mag. field, effect of carriers 78—72388
  semiconductor, spin relax. of deep impurity centres, exchange scatt. 77—43870
  semiconductor, Wannier-Mott polaritons in mag. fields, review 78—2437
  semiconductor, zincblende-type, exchange splitting of donor-acceptor pairs 77—20263
  semiconductor based spin glasses, conduction electron produced exchange interaction between localised spins *(Russian)* 79—82799
  semiconductor-based spin glass, indirect exchange interaction of localised spins 80—88768
  semiconductors, antiferromagnetic resonance rel. to surface impedance, magnetoelastic contrib. 80—50200
  semiconductors, indirect exchange interaction between localised moments 80—93079
  semiconductors, magnetic, electron spectrum, light absorpt. spectrum, calcs. 80—2793
  semiconductors, mixed, containing paramag. atoms, Landau levels and interband Faraday rot., appl. to $Cd_{1-x}Mn_xTe$ 79—61348
  semiconductors, zero gap, indirect exchange interaction 79—61094
  semiconductors, zero-gap, indirect-exchange interactions 80—29370
  semiconductors and insulators, mean free path and energy gap effects 80—88522
  semiinfinite, effect of next nearest neighbour coupling 77—73014
  simple metals, ground state energy, structural expansion 80—88497
  singlet ground state system in mag. field, anisotropic exchange interaction effect on props. 79—91224
  soft magnetic metals, ideal, AC response 78—64223
  soft X-ray thresholds, exchange effects, renormalisation group theory 78—31280
  specific heat of two-dimens. electron gas, exchange interaction contrib., calc. 80—44331
  spin chain with nearest and next nearest neighbour interactions 77—47955
  spin deviation states in spin-1 system with Heisenberg and biquadratic exchange 78—84378
  spin function recoupling method, wave function calcs. 77—47782
  spin glass, crit. props., simple soluble model 77—12141
  spin glass, exchange energy, residual entropy and number of minima *(French)* 77—66322
  spin glass, frustration concept 79—38328
  spin glass, local exchange invariance concept 78—60288
  spin glass, low temp. Lorentz number assuming exchange interactions between electrons 79—19567
  spin glass, phase diagrams and order parameters, Oguchi-Kaneyoshi method 80—15727
  spin glass, random-bond Ising model with continuous distrib. of exchange interactions 77—43837
  spin glass freezing temp., conc., Fermi-momentum depend. 78—14970
  spin glass transition in system with competing ferromag. and antiferromag. interaction 77—20616
  spin glasses, anisotropic, crossover effects 79—65692
  spin glasses, freezing of EPR relaxation rates, exchange narrowing 79—99713
  spin glasses, one-dimens., with antiferromag. exchange 80—25231
  spin glasses, recent progress in numerical simulation 79—69689
  spin reduction in systems with orbital degeneracy 77—51873
  spin system, exchange energy near singular points or lines 80—93106
  spin system, thermodynamics, contrib. of spin-phonon interaction 78—2635
  spin system with double electron exchange order-order transitions 77—4522
  spin systems with three-atom exchange, elementary excitations 78—84404
  spin wave theory in strongly anisotropic magnets 77—63151
  spin waves, space disordered media phenomenological Lagrangian, exchange, relativistic interactions *(Russian)* 80—29537
  spin waves in medium with nonequilib.-oriented spins *(Russian)* 77—80923
  spin waves in strongly anisotropic magnets, canonical transform theory 78—68197
  spin waves in weak antiferromagnetic exchange field system 78—43577
  spin waves in weak exchange field systems 78—43576
  spin-1/2 cubic lattice, with anisotropic exchange, configs. 80—65926
  spin-fluctuation resistivity, low-temp., effect of pot. scatt. 77—15840
  spin-glass, one-dimens., sp. ht. and mag. susceptibility calcs. 80—7120
  spin-Hamiltonian formalism for exchange-coupled pairs of paramag. ions, second-order corrections 78—68133
  spinel ferrites, thermoelectric power, effect of exchange interactions 78—43422
  spinel structures, electroconductivity and electron exchange 78—84207
  spinel systems, prop.-comp. relationship, electron exchange effect *(Russian)* 78—47524
  spinels, electron exchange between Fe^{2+} and Fe^{3+} on octahedral sites 77—69752
  standing spinwave resonance in film with nearest and next-nearest neighbour exchange 78—68390
  Sternheimer valence shielding-antishielding factor including exchange, ions of interest in Mossbauer spectra 77—85182
  strip films, bulk and surface spin oscills., mag. reson. 80—97149
  superconducting film, depend. of crit. conc. of paramag. impurities on mag. field 78—14863
  superconductivity, exchange enhancement of electron-phonon coupling 79—7930
  superconductor, slightly dirty, CESR due to exchange and spin-orbit scatt. 77—28300
  superconductor with magnetic impurities, coexistence of superconductivity and ferromag., BCS and Zener models 80—88676
  superconductors, slightly dirty, EPR relaxation time, thermal behaviour 79—47195

exchange interactions continued
  superconductors, spin susceptibility of conductivity electrons, spatial dispersion *(Russian)* 79—51719
  superconductors with paramag. impurities, NMR theory in singlet state 79—28445
  superradiance, dynamical behaviour in model mag. insulator 80—87358
  surface, density-density correlation function, exchange corrections 78—14786
  symmetrical clusters, higher order isotropic exchange 77—51712
  symmetry breaking effects on excitons in cubic and wurtzite structs., unified theory 77—20246
  TCNQ alkali salt, spin-Peierls transition, 1-D antiferromag. Heisenberg model 80—29395
  TCNQ complexes, disordered, thermodynamics of random exchange models 80—103826
  TCNQ salt, MEM$(TCNQ)_2$, phase transitions, elec. cond., ESR, mag. susceptibility study 80—24981
  TCNQ salt, Mn$(TCNQ)_2$, mag. props. 77—85558
  TCNQ salt, N-n-butyl-quinolinium $(TCNQ)_2$, ESR spectrum fine struct. splitting 80—44904
  TCNQ salt, $NMP_{0.63}phenazine_{0.37}TCNQ$, mag. susceptibility, 0.03-4.2K 80—25191
  TCNQ salt, Qn$(TCNQ)_2$, one-dimens. spin glass with antiferromag. exchange, Knight shift meas. 80—25231
  TCNQ salts, n-methylacridium $(TCNQ)_2$, 2,2′bipyridinium $(TCNQ)_2$ and Qn$(TCNQ)_2$, with asymmetric donors, mag. susceptibility, 0.035-4.2K 80—25190
  TCNQ salts 78—6356
  1,2,4,5-tetrachlorobenzene, excited triplet state dimer, intermol. exchange integral, isotope effect 80—15826
  1,2,4,5-tetrachlorobenzene, triplet excitons, zero field ODMR 80—88891
  tetramer clusters, ESR spectra, spin Hamiltonian analysis 77—28429
  tetramethylphenylenediamine chlorate, EPR investig. of exchange interaction 77—40114
  tetranuclear cluster, eigenvalues spectrum of spin Hamiltonian calc., thermodynamics props. *(French)* 77—35902
  tetrathiotetracene, charge transfer state parameters, evaluation by mag. field effect *(Russian)* 80—10924
  three-spin systems in nematic liq. cryst., EPR 77—14463
  TMMC:M, impurity (M) effects on Neel temp. and low temp. mag. susceptibility 78—88113
  TMMC, antiferromag. coupling in linear chains, molecular orbital approach 78—52239
  TMMC, exchange-narrowed EPR linewidth, temp. depend. 78—52292
  TMNB, ferromag. chains with easy-plane anisotropy, exchange const., anisotropy const. and g-value 77—80927
  TMNC, ferromag. chains with easy-plane anisotropy, exchange const., anisotropy const. and g-value 77—80927
  $[TMPD^+]_2[Cu_xNi_{1-x}(mnt)_2]$, ESR obs. of triplet excitons and Cu(II) ions, mag. interactions 79—95633
  transition metal, chemisorption of H, effect of surface spin fluctuations 80—75613
  transition metal, 3d, s-core levels multiplet splitting, exchange correl. 78—10407
  transition metal, band model, mag. susceptibility of exchange-enhanced paramagnet 78—2644
  transition metal clusters, symmetric, higher-order isotropic exchange, Schrodinger model 79—7955
  transition metal complexes, mag. exchange in $s=1/2$ systems 78—43553
  transition metal compounds, 3d-cation solids, mag. ordering at low temps., exchange perturbation theory 77—69529
  transition metal compounds, $M(O)(F_2)(Cl_2)(Br_2)(I_2)$, 90° exchange interactions 79—69666
  transition metal compounds, pd^N $(N=7,8,9)$ electron system in cubic crystal field, energy matrices *(Japanese)* 79—42504
  transition metal compounds and dil. alloys, mag. ordering phenomena in high mag. fields 80—50075
  transition metal cpds., carboxylates, sulphates and chlorides, exchange interaction mechanism 78—10411
  transition metal intercalates of Ni and Ta dichalcogenides, magnetic susceptibility, function of temp. 80—39756
  transition metal ion pairs, anisotropic exchange parameters 79—11093
  transition metal ion pairs, simply reducible symmetry group crystal fields, kinetic exchange theory 80—39541
  3d-transition metal ions, s-doublet struct., appl. of exchange correlation mass operator approx. 80—106266
  transition metal ions in crysts., two-centre exchange interactions between orbitally degenerate ions 79—15126
  transition metal magnetic clusters, neutron inelastic scatt., review 80—50083
  transition metal monosulphides of first-row, XPES and UV PES 80—20760
  transition metal surface, spin fluctuations 78—95451
  transition metal vanadates 78—51991
  transition metal-rare earth alloys, amorphous, mag. props., mean field anal. 79—4701
  transition metal-rare earth dil. alloy, hyperfine field of rare earth impurity 79—1588
  transition metals, direct exchange between $3d^n$ ions 79—69668
  transition metals, energy of cohesion calc., Hubbard Hamiltonian with exchange interaction 77—69261
  triangular Ising lattice with anisotropic interactions 78—47926
  trimer heteronuclear exchange clusters, ESR line profile 79—42828
  trimethylammonium cobalt trichloride, metamagnet, AC susceptibility and exchange consts. 80—70961
  trimethylammonium copper chloride dihydrate, mag. props., evidence for lattice dimensionality 77—89967
  trimethylammonium copper heptachloride, one-dimens. ferromag., mag. susceptibility, 2 to 300K 79—61077
  trimethylammonium manganese bromide, mag., anisotropy, biquadratic exchange 78—14952
  trinuclear clusters with half-integral spins, ESR theory, inc. anisotropy effect in antisymmetric exchange 77—8391
  TTF(MBDT) spin-Peierls transition, mag. exchange interactions, mag. props. 80—25138
  TTF-CuBDT, inter- and intra-chain exchange couplings, proton spin-lattice relax. time meas. 80—71220
  TTF-TCNQ, microscopic model for three low temp. phases 79—73303
  $TTF.PtS_4C_4(CF_3)_4$, quasi-one-dimensional cpd., exchange, thermal and mag. study 78—68209

exchange interactions continued
- two or three electrons, interacting with localised mag. moment, wave function determ. *(French)* 79—12636
- two-dimensional electron fluid, second order exchange energy, correlation energy 80—107729
- two-dimensional Ising spin glass, crit. temp. 80—11206
- two-dimensional quantum plasma in mag. field, exchange energy 77—72904
- two-sublattice ferromagnet, biquadratic exchange effects 77—4502
- two-sublattice magnetic substances, mag. transitions due to exchange-striction mechanism *(Russian)* 77—47995
- two-sublattice magnetic system with fourth-order uniaxial anisotropy and strong antisymmetric exchange in transverse mag. field 79—56530
- two-sublattice system, with strong antisymm. exchange and fourth order anisotropy, mag. configs. 78—68167
- uniaxial ferromagnet, in transverse mag. field, quantum theory *(Russian)* 79—15297
- uniaxial Heisenberg antiferromagnet, phase diagrams 80—15730
- uniaxial magnet, free energy of system with weak exchange interactions and high mag. anisotropy *(Russian)* 78—68213
- vanadyl carboxylates, EPR and mag. susceptibility, near one-dimens. antiferromagn. 77—63265
- violanthrone, free radical, EPR meas. 78—27094
- wavevector-dependent spin susceptibility, variational principle 78—91586
- weak exchange interaction between atoms or ions orbitally degenerate ground states, atomic second quantisation method 80—32604
- weakly disordered uniaxial ferromagnet, phase transition *(Russian)* 78—23291
- Wigner condensation, localisation of electrons in a magnetic field 79—60752
- Wigner crystallisation, -density-functional theory 79—42477
- Wolff model, effective mag. interactions between impurity and conduction electrons 78—68143
- wurtzite-type crystals, deform. effects on biexcitons, electron-hole exchange interaction 77—52038
- X-ray plasmon scatt. by solids, electron exchange energy influence 79—56884
- X-ray plasmon scattering, plasmon cut off wave vector electron exchange energy effect 80—50458
- X-Y model, biquadratic, spin one, variation of Curie temp. 80—97102
- X-Y model for linear chain, struct. transition under external mag. field and stress 77—12126
- X-Y quasi-one-dimens. system anisotropic, spin-Peierls phase transition, tricritical point 80—25142
- zinc bisdiethyldithiocarbamate:Cu^{2+}, exchange interaction of Cu^{2+}-Cu^{2+} pairs, spin-lattice relax. 78—48034
- zincblende structure semiconductor in intermediate mag. field, exciton spectra 78—18969
- Ag, valence-core electron exchange interactions, local approx. 80—91416
- Ag-Mn alloys, dilute, low temp. elec. resist. *(Russian)* 78—68024
- Ag-Mn film, supercond. proximity effect and pair breaking, normal state mag. interactions 77—63035
- Al, plasmon dispersion, dynamical exchange effects 79—51509
- Al-Li, Fermi surface impurity scatt. 79—56114
- Ar, solid, energy bands, depend. on choice of exchange-correlation pot. 80—70607
- As-Se-Tl system, chalcogenide glasses, NMR spin-lattice relax. time meas. 79—95671
- Au alloys, dil., conduction electron-local moment interactions using dHvA waveshape anal. 79—77981
- Au-Cr Kondo alloy, effect of press. on resistivity 78—79978
- Au-Fe alloy, dil., Mossbauer exam. in spin glass regime 79—61289
- Au-Gd(Y), dil., conduction electron-local moment exchange interaction meas. 80—60191
- Au-V, dil., ^{51}V CW NMR line width anal., RKKY broadening 78—15033
- Au-Yb, dil. alloy, high field nuclear relax. of ^{173}Yb, anisotropic cond.-electron exchange 77—8434
- Au-Yb dilute, NMR investig. of anisotropic cond. electron exchange 77—63309
- BN, electronic struct., exact exchange HF calcs. 80—65438
- $BaCa_{1/2}Ru_{2/3}O_3$, biquadratic exchange interaction between Ru^{5+} ions in (Ru_2O_9) clusters 77—20580
- $Ba_3Fe_{2-x}Ho_xUO_9$, $O \leq x \leq 1.2$, perovskites, struct. and mag. props. *(French)* 78—18612
- $Ba_2Fe_{18}O_{27}$, hexagonal ferrite, W-struct., Mossbauer spectra of Fe^{3+} and Fe^{2+} 78—88242
- $BaMnF_4$, struct. and mag. transitions, magnon dispersion curves, nearest neighbour exchange consts. 79—42760
- $Ba_4NbRu_3O_{12}$ and $Ba_4TaRu_3O_{12}$, $(Ru_3O_{12})^{13-}$ cluster obs. in presence of orbital degeneracy and spin-orbit coupling *(French)* 80—70655
- BaO-V_2O_5-CuO, P_2O_5-V_2O_5-CaO-CuO glasses, EPR, Cu impurity effect on elec. props. 79—51849
- BaO-V_2O_5-CuO semiconducting glasses, impurity effects, elec. resist. and EPR study 80—103692
- $BaX_{1/3}Ru_{2/3}O_3$ (X=Ca, Cd, Mg, Sr), crystal struct., mag. susceptibility and exchange integrals *(French)* 77—16037
- Be, noncubic crystal, temp. depend. of elec. field gradient 79—99515
- Be, spin susceptibility, electronic effective mass, spin density functional calcs. 78—43291
- Be, X-ray plasmon scatt., electron exchange energy influence 79—56884
- $Be_3Al_2Si_6O_{18}$:Cr^{3+}, EPR spectra, exchange-coupled pairs 79—28596
- Bi, band struct., empirical pseudopot., correl. effects 78—18955
- $BiFeO_3$, pyroelectric-antiferromag., magnetoelectric effect *(Russian)* 78—43625
- $Bi_7Ti_{2.5}Sn_{0.5}Fe_3O_{21}$, layered ferroelec. antiferromag., superparamagnetism, Mossbauer spectra obs. 77—51999
- $CD_{1-x}In_xCr_2S_4$, ferromagnetic spinel, Cr^{3+} exchange interaction mechanism, Cr^{2+} relaxation, EPR line width depend. 79—69715
- CO catalytic oxidation on spinel type ferrites, role of mag. exchange interactions 78—56916
- CaF_2:Dy^{3+}, EPR of colour centres, spin-spin interaction of pair of Dy^{3+} ions *(Russian)* 79—69751
- $CaLaFeO_4$, two-dimens. mag. ordered, structural and mag. props. *(French)* 80—70173
- $Ca_2LaFe_3O_8$, physico-chemical characterisation, Mossbauer exam. and mag. props. *(French)* 77—28494
- $(Ca_{1-x}Mg_x)RuO_3$, mag. props. 78—27027
- $(Ca_{1-x}Sr_x)RuO_3$, mag. props. 78—27027
- Cd, noncubic crystal, temp. depend. of elec. field gradient 79—99515

exchange interactions continued
- Cd-Cr, dil., estimates of s-d interaction from supercond. transition temp. and mag. susceptibility 78—43561
- Cd-Cr(Mn)(Ni), dil., mag. and supercond. props. 79—38237
- $Cd_{1-x}Mn_xTe$, exchange interaction, magneto-optical spectra 80—25348
- $Cd_{1-x}Ag_xCr_2Se_4$, Ag acceptor states effect on exchange interaction 80—20397
- $CdBr_2$:Co^{2+}, exchange-coupled Co^{2+} pairs, optical absorpt. and Zeeman studies 80—66242
- $CdCl_2$:Fe^{2+}, magneto optical study, ferromagnetically coupled Fe(II) pairs 78—6711
- $CdCr_2O_4(S_4)(Se_4)$, magnetic exchange interactions 77—24690
- $CdCr_2S_4$, EPR line profiles in paramag. and ferromag. phases 79—28602
- $CdCr_2S_4$:Cu, magnetic microregions caused by s-d exchange 77—77050
- $CdCr_2S_4$:In(Ga), resist. and magnetoresist. meas., effect of donor impurities 79—19608
- $CdCr_2S_4(Se_4)$, spontaneous magnetisation temp. depend., nuclear resonance freq. depend. *(French)* 80—80483
- $CdCrSe_4$, ferromag. semiconductor, mag. props. near Curie pt., doping effects 79—1670
- $CdCr_2Se_4$, ferromag. semicond., conc. anomalies rel. to red shift of absorpt. edge 80—70732
- $CdCr_2Se_4$:Ag(Gd), doping effects on exchange interaction 78—43579
- $CdCr_2Se_4$:In(Ga)(Cu), magnetic microregions caused by s-d exchange 77—77050
- $CdCr_2Se_4$-$ZnCr_2Se_4$, single cryst., mag. props. 79—28526
- $Cd_{1-x}In_xCr_2S_{4-x}P_x$, ferromagnetic spinel, Cr^{3+} exchange interaction mechanism, Cr^{2+} relaxation, EPR line width depend. 79—69715
- $Cd_{1-x}In_xCr_2Se_4$, electric, photoelectric and mag. props., metal-semicond. transition *(Russian)* 80—54738
- $Cd_xMn_{1-x}Fe_2O_4$, substitution effect on mag. struct. and exchange interaction *(Russian)* 78—47949
- CdMnTe, exciton ground state, magnetic field influence 80—54616
- $Cd_{1-x}Mn_xTe$, effect of Mn $3d^5$ states on band struct., exciton refl. struct. in mag. field 79—11094
- $Cd_{1-x}Mn_xTe$, indirect exchange interaction 80—97087
- $Cd_{1-x}Mn_xTe$, semimagnetic, exchange interactions between localised and delocalised electrons 80—97245
- CdS, doped, amorphous antiferromagnet model, susceptibility and spin-flip Raman scatt. meas. 80—97057
- CdS, electron-exciton elastic scatt. cross sections, central field and exchange approxs. 77—62919
- CdS, model $S={}^1/_2$ amorphous antiferromagnet, spin polarisation 78—52288
- CdS, photocond. cryst. characterisation of electron-trap responsible for acoustic holographic echoes *(French)* 79—19544
- CdSe, electron-exciton elastic scatt. cross sections, central field and exchange approxs. 77—62919
- Ce compounds, Anderson model, exchange parameter, Kondo temp., mag. susceptibility 79—1656
- Ce compounds, Kondo coupling, hyperfine and exchange interactions 79—65647
- Ce compounds with group V elements, antiferromag., temp.-renormalised longit. mag. excitations 77—51862
- α-Ce, exchange-enhanced, elec. resist. T^2 depend., press. effect 80—96845
- Ce monochalcogenides, cryst. field effects, phase transitions 80—24853
- Ce monopnictides, anomalous mag. props., planar coupling theory 80—60245
- Ce monopnictides, cryst. field effects, phase transitions 80—24853
- Ce^{3+}, in Van Vleck paramagnets, EPR meas. 77—12199
- $CeAl_2$, mag. ordering, neutron diffr. meas. 78—6518
- Ce_3Al_{11}, competition between ferro- and antiferromag. interactions 80—60258
- CeB_6, anomalous sp. ht. intrinsic mag. phase transitions obs. 80—108027
- CeB_6, mag. and electronic props. 80—71048
- CeBi(Sb), anisotropic mag. ordering and mag. structural transitions 79—78324
- CeC_2, mag. props. 80—108008
- $CeCl_3(Br_3)$, interaction parameters, high freq. meas. of adiabatic differential susceptibility 78—68211
- $CeCu_4$ Knight shifts and mag. susceptibility 79—95656
- $CeCu_5$, Knight shift and mag. susceptibilities 79—95656
- $Ce_xDy_{1-x}C_2$, mag. props. 80—108008
- CeF_3, ^{19}F spin-lattice relax. and mag. couplings 79—65753
- $CeFe_2$, ferromagnetic cpds., mean field exchange consts., Stoner itinerant model calcs. 80—50084
- $Ce_x(La_{0.76}Y_{0.24})_{1-x}Bi$, mag. phase diagrams 79—56535
- $Ce_x(La_{0.76}Y_{0.24})_{1-x}Sb$, mag. phase diagrams, exchange interaction variation-thermodynamic model 79—65673
- CeM_2:Nd^{3+}, M=Ru, Rh, Ir, ESR investigation 79—78514
- $Ce_2Mg_3(NO_3)_{12}.24H_2O$, ground state with dipole-dipole and exchange interactions in external mag. field 80—84582
- CeSb, ferromag., mag. excitation spectrum, inelastic neutron scatt. obs. 79—78352
- CeSb, mag. excitations dispersion 80—25121
- CeSb, mag. phase transitions, zero applied mag. field 78—31070
- CeSb, mag. transition, effect of applied mag. field 78—43590
- CeSb, press. effect. on mag. props. 78—23315
- $CeSn_3(Pb_3)(In_3)$, crystalline elec. field parameters, exchange and Coulomb contrib. 77—20278
- CeX (X=P, As, Sb, Bi), neutron inelastic scatt. expts. 80—19674
- $Ce_{0.08}Y_{0.92}Sb$, dilute f-electron system in cluster regime, crystal field and exchange splittings 80—97062
- CeZn, cryst. field and exchange effects, inelastic neutron scatt. study 80—24855
- Co (0001), photoemission, exchange-split energy-band dispersions 80—35059
- Co complex, Co II high spin binuclear species, magnetic exchange and anisotropic susceptibilities 78—39308
- Co complex, $CoCl_2(indazole)_2$, linear chain ferromagnetism 79—56519
- Co complex, $CoCl_2(pyrazole)_2$, linear chain ferromagnetism 79—56519
- Co complex, $Co(C_5H_5NO)_6(ClO_4)_2$ and $Co(C_5H_5NO)_6(BF_4)_2$, $S={}^1/_2$ XY magnet, sp. ht. below 1K 77—55682
- Co complex, $Co(C_5H_5NO)_6(NO_3)_2$, simple cubic X-Y mag., specific heat, mag. exchange anisotropy meas. 78—39346
- Co complex, $Co(II)(1,2,4\text{-triazole})_2(NCS)_2$ quasi two-dimens. canted S=1/2 antiferromag. 80—70976
- Co complex, tetra-μ-benzoato-bis(4-methylquinoline)dicobalt II, triclinic cryst., antiferromag. exchange 78—39309

exchange interactions continued
Co, energy band dispersion and mag. exchange splitting, angle-resolved photoemission meas. 80—71567
Co, energy band dispersions and mag. exchange splitting 80—76146
Co, FCC single-crystals, NMR freq. depend. on interatomic distances 79—69748
Co, ferromagnetic, calc. hyperfine fields and their press. derivations 80—6796
Co, liquid, Hall effect, band struct. and exchange scatt. 80—80250
Co, UPS, single cryst. and polycryst. film, electronic struct. 78—11081
Co-B alloys, amorphous, mag. moment and exchange stiffness constant 79—1662
Co-CoO films, evaporated, exchange anisotropy 80—88841
Co-Fe alloys, FCC structure, average mag. moment, conc. depend. 78—88099
Co-Ni fine particles, anhysteretic growth of exchange fixed remanent states 77—16116
$CoAl_xGa_{2-x}O_4$, mag. interactions, susceptibility obs., 4.2 to 300K 79—15294
$CoBr_2$, magnetic excitations, neutron scatt. investigation 80—39761
$CoBr_2.2H_2O$, metamagnetic, relax. phenomena at phase transitions 79—24164
$CoBr_2.2H_2O$, phase transitions in ferrimag. state 77—63191
$CoCl_2$, antiferromag., elementary excitations 77—69519
$CoCl_2$, antiferromag., mag. excitations, mag. neutron inelastic-scatt. meas. 77—85437
$CoCl_2$, antiferromag. elementary-excitations, electronic Raman scatt. meas. 77—80922
$CoCl_2$, antiferromagnetic resonance, effect of hydrostatic pressure *(Russian)* 78—35042
$CoCl_26H_2O$, g-tensor and exchange parameters, mag. reson. studies 79—87324
$CoCl_2.2NC_5H_5$, quasione dimens. Ising system, thermodynamic props. 78—27042
$(Co_{1-x}Mn_x)_2B$, $0 \leq x \leq 1$, magnetisation, lattice consts., press. depend. of Curie temp. rel. to pair interaction model 80—7137
$CoNb_2O_6$, Co^{2+}-Co^{2+} interaction, susceptibility and magnetisation, 3.3-300K 77—8282
CoO, antiferromag. mag. excitations, spin wave model, neutron scatt. study 79—51766
CoP-NiCoP, composite ferromag. film, exchange coupling between soft and hard layers, FMR obs. 79—78448
$CoRh_xGa_{2-x}O_4$, mag. interactions, susceptibility obs., 4.2-1000K 79—15293
Co_2SnO_4, $CoMg(Zn)SnO_4$ and $Co_{2-x}Mg_2TiO_4$, magnetic props., short-range ordering 77—32155
$Co_{1-x}Te$, fluctuating localised mag. moments, d band motion, Mossbauer study 80—65768
CoU_2S_5, mag. struct., exchange energy, magnetisation and neutron diffr. expts. 78—68170
$Co_{2-y}Zn_yTiO_4$, spinel series, exchange integrals, mag. struct. and coercive force, magnetisation meas. 77—69507
Cr alloy, localised magnetic moments in band antiferromagnets, impurity interactions *(Russian)* 80—54888
Cr complex, dinuclear, exchange interactions, neutron inelastic scatt. obs. 77—55502
Cr complex, trimeric clusters, low temp. mag. props. 78—76261
Cr complex, trivalent dimer, mol. electronic excitations, neutron inelastic scatt. 77—47985
Cr oxides, XPS study, electron binding energies, spin orbit splittings, exchange splittings 79—78839
Cr^{3+} clusters in mol. complexes, interference effects in neutron scatt. 77—85544
Cr-Al, elementary excitations, exchange stiffness const., inelastic neutron scatt. study 79—47294
Cr-Fe, dilute, localised moment cluster model, ferromagnetic exchange coupling 80—39774
Cr-Fe(Co) alloys, dil., exchange interactions 77—47986
CrAs, anisotropy of compressibility 79—7648
$CrBr_3$, modulation of exchange integral, contrib. to temp. depend. of exchange interaction 77—69484
$CrBr_3(Cl_3)$, two-dimensional mag. insulators, cryst. field spectra, mag. circular dichroism 79—47058
$CrBr_3(Cl_3)$, two-dimensional mag. insulator, cryst. field splitting, spectroscopic g-factors 79—47059
$Cr_xMn_{1-x}As$, antiferromagnetic-ferromagnetic transition, mag. moment and elec. resist. meas. 80—15718
$Cr_xMn_{1-x}As$, antiferromag. to ferromag. transitions, superexchange-double exchange mag. coupling, susceptibility and resist. obs. 80—50070
CrN, antiferromagnetic EPR spectra, binding energy, isotropic exchange and ordering *(German)* 80—80604
Cr_2O_3, elastic consts., distance depend. of mag. interactions, US vel. meas. 77—4539
Cr_2O_3, exchange parameters including temp. effects 79—24153
Cr_2O_3:$^{119}Sn^{4+}$, Mossbauer spectra *(French)* 79—24248
$(Cr_4(OH)_6(NH_3)_{12})Cl_6.4H_2O$, exchange interactions in Cr^{3+} clusters, inelastic neutron scatt. obs. and Heisenberg Hamiltonian calc. 79—78359
$Cr_4(OH)_6(NH_3)_{12}Cl_6.4H_2O$, exchange coupled mol. Cr^{3+} tetramers, inelastic neutron scatt. 80—65792
$CrSb_{1-x}As_x$, exchange striction and press. effect on Neel temp. 77—63189
Cr_5Te_6, high press. effects on magnetisation and mag. transitions, 77 to 360K 77—77057
$CrTe_{1-x}Se_x$ (Sb_x), Curie temp., high press. and doping effects *(Russian)* 77—12125
$CsCdBr_3$:Gd^{3+}, EPR spectra of mag. coupled Gd^{3+} ions 78—35032
$CsCoCl_3$, Co^{2+} ions, theoretical Raman spectra 78—10878
Cs_2CoCl_4, heat capacity below 1K, rel. to $S=1/2$ linear chain XY model 77—59415
Cs_2CoCl_4, paramag. mag. exchange rel. to low temp. mag. characts. 77—55669
$CsCoCl_3.2D_2O$, crit. behaviour along metamag. phase transition 77—59409
$CsCoCl_3.2H_2O$ interchain exchange low temp. susceptibility 78—19240
$Cs_3Cr_2Br_9$, Cr (III) trigonal pair, exchange interactions, absorpt., MCD and Zeeman spectra 78—19009
$Cs_2Cr_2Cl_9$, Cr (III) trigonal pair, exchange interactions, theory 78—19008
$Cs_3Cr_2Cl_9$, optical absorpt., MCD, exchange interactions 78—10917
$CsFeCl_3$, linear chain ferromag., optical absorpt. and dichroism in mag. field 77—77237

exchange interactions continued
$CsFeCl_3$, single cryst. mag. susceptibility meas. 77—20560
Cs_2FeF_5, mag. struct. and one-dimens. antiferromagnetism 80—60209
CsMgCl:Cr^{3+},Mo^{3+}, Cr^{3+}-Mo^{3+} exchange coupled pair, EPR study 79—42830
$CsMgCl_3(Br_3)$:Gd^{3+}, EPR spectra of mag. coupled Gd^{3+} ions 78—35032
$CsMnCl_3.2H_2O$, antiferromag. reson. and two-magnon absorpt. 79—61234
$CsMnCl_3.2H_2O$, Heisenberg antiferromag., linear mag. birefringence meas. 77—16277
$CsMnCl_3.2H_2O$, linear antiferromagnet, specific heat, exchange interactions and anisotropy effects 77—1556
$CsMnCl_3.2H_2O$, subthreshold two-magnon absorpt., depend. on freq., temp. and mag. field, exchange coupling const. *(Russian)* 80—71184
$CsMn_{1-x}Co_xCl_3.2H_2O$, impure Heisenberg linear chain, EPR meas. 78—43634
$CsMnF_3$, magnon absorption and luminesc. 80—7400
$CsMnF_3$, solid and molten paramag. high-temp. e.p.r. linewidth meas. 77—4548
$CsMnF_3$, spin-wave dispersion relations, neutron inelastic scatt. obs. 77—51895
$CsNiCl_3$, antiferromag. coupling in linear chains, molecular orbital approach 78—52239
$CsNiF_3$, demagnetising effects on antiferromag. reson. 80—15803
$CsNiF_3$, double-excitonic optical transition intensity, exchange and dimensionality effects 77—69591
$CsNiF_3$, in mag. field, spin wave dispersion, inelastic neutron scatt. 77—77046
$CsNiF_3$, quasi-one-dimensional ferromagnet, subthreshold parallel pumping of magnons 80—75745
$CsNiF_3$, single cryst. mag. susceptibility meas. 77—20560
CsO_2, low temp. phases, mag. order, EPR and antiferromag. reson. 79—95630
$CsVCl_3$, antiferromag. coupling in linear chains, molecular orbital approach 78—52239
$CsVX_3$, X=Br, Cl, I, mag. props. *(French)* 77—16059
Cu complex, 1,2-ethanediammonium tetrachlorocuprate, layered struct. mag. susceptibility 80—7094
Cu complex, $[C_6H_5(CH_2)_nNH_3]_2CuCl_4$, n=1,2,3, two-dimens. ferromagnet, NMR and mag. susceptibility 77—16058
Cu complex, chloride monodimethylsulfoxide, spin $^1/_2$ ferromag. Heisenberg linear chain, cryst. struct. and mag. susceptibility 80—15706
Cu complex, chloride tetramethylsulfoxide, spin $^1/_2$ ferromag. Heisenberg linear chain, cryst. struct. and mag. susceptibility 80—15706
Cu complex, $Cu_3Cl_6(H_2O)_2.2$ tetramethylsulphone, mag. interactions, susceptibility, 2-230K 80—60237
Cu complex, diaquobis(2,3-dihydroxy-2-methyl propanato) copper(II), cryst., EPR, room-temp. 79—82861
Cu complex, hexa(pyridine-N-oxide)$(ClO_4)_2$, Heisenberg antiferromag., mag. props. and sp. ht. 78—23287
Cu complex, strong antisymmetric exchange 78—34976
Cu complex, substituted Cu(II) acetates, exchange interactions, EPR, struct. 79—42829
Cu complex, tetrameric Cu(II) complex, higher-order spin coupling 79—99690
Cu complexes, involving metal-metal exchange interaction, shifts in X-ray K-absorption edge 77—16422
Cu complexes, with tridentate Schiff bases, exchange interactions, EPR, mag. susceptibility 78—23324
Cu, magnetic susceptibility, thermal density of states, non-local exchange-correlation effects 78—14924
Cu, NMR study on nuclear ordering below 1 μK 80—93187
Cu, spin density wave fluctuations in nuclear spins, susceptibility, internal energy 80—50115
Cu-Al-Fe, dil. liq. alloy, localised mag. state interactions *(German)* 77—1539
Cu-Co heterobinuclear complex, cryst., mag. susceptibility of Cu-Co$(fsa)_2$ en, $3H_2O$ 80—2556
Cu-Mn, exchange-coupled localised moments, Korringa relaxation rate 80—75851
Cu-Mn, molecular field distribution function in disordered Ising model *(Russian)* 80—54859
Cu-Mn alloys, Mn K X-ray emission and XPS lines, width and asymm. 78—19605
Cu-Mn dilute alloys, local moment fluctuations, NMR meas. 77—63091
Cu-Mn spin glasses, spin dynamics, neutron scatt. meas. 79—8002
$CuBeF_4.5H_2O$, NMR, interactions between paramag. ion system and antiferromag. linear chains 77—63295
CuBr, direct gap semiconductors, charged excitons 77—62840
CuBr, piezo-optical effects on excitons, importance of k-linear terms 79—95802
CuCl, direct-gap semiconductors, charged excitons 77—62840
$CuCl_2$, anhydrous, single cryst., mag. behaviour in low temp. ordered phase 79—7974
$CuCl_2$, anhydrous paramagnetic phase, mag. susceptibility depend. on temp. 79—7965
$CuCl_2.2H_2O$, antiferromag. to paramag. transition, high field magnetisation meas. 78—64204
$CuCl_2.2H_2O$, EPR linewidth and relax., effect of antisymmetric exchange 77—59448
$CuCl_2.2H_2O$, influence of high hydrostatic press. on intermediate state associated with spin flopping 78—35020
$CuCl_2.2H_2O$, submillimetre ESR meas. using pulsed high mag. field 80—44905
$CuCr_2Se_{4-x}Y_x$, (Y=Cl, Br), magnetisation, Curie const. 79—91225
n-$CuInS_2$, mag. props., obs. 80—70939
$CuK_2Cl_4.2H_2O$, Heisenberg ferromag., mag. props. at high press. 77—69512
$CuK_2Cl_4.2H_2O$, proton spin-lattice relax. and exchange interactions, temp. depend. 79—95663
$Cu_{75}Mn_{25}$, spin glass, EPR line breadth, exchange-narrowed 79—15345
Cu_2MnAl, dynamical mag. susceptibility, spin waves, calc. from band struct. 80—54871
$Cu(NH_4)_2Br_4.2H_2O$, Heisenberg ferromag., mag. props. at high press. 77—69512
$Cu(NH_4)_2Br_4.2H_2O$ Heisenberg ferromagnet, mag. props. in mag. field 80—34637
$Cu(NH_3)_4SO_4.H_2O$, submillimetre ESR meas. using pulsed high mag. field 80—44905
$Cu(NO_3)_2.2^1/_2H_2O$, singlet ground-state system, mag. props., short-range ordered state 78—23289

exchange interactions continued
Cu_2O, electron-exciton scatt. cross sections, central field and exchange approxs. 77−62919
Cu_2O, energy band interactions under uniaxial compression 80−25412
Cu_2O, even-parity excitons assignment, from two-photon spectrum 80−6731
Cu_2O, optical absorpt. due to paraexciton, exchange energy and g-factors 77−28596
$CuSe_2O_5$, strongly antiferromag. coupled Cu linear chain, orbital props. 80−100580
$Cu_xZn_{1-x}ZrF_6.6H_2O$, distortions of nearest Jahn-Teller $[Cu(H_2O)_6]^{2+}$ centres 78−68000
dimethylammonium manganese tetrachloride, 2D Heisenberg antiferromag., spin wave anal. 80−54879
Dy film, helimag. order, surface deform., exchange and single-ion magnetocrystalline anisotropy energy 77−66390
Dy, spin wave exam. 78−56306
Dy^{3+}, in Van Vleck paramagnets, EPR meas. 77−12199
Dy-Co amorphous film, prep. by dual-source evaporation, mag. props. 77−89988
Dy-Sn alloy, hyperfine fields acting on diamag. impurities and anisotropic exchange, Mossbauer spectra 77−1625
Dy-Th, single cryst., mag. susceptibility, transitions, anisotropy 80−54873
Dy-Y alloy, rel. to scatt. of cond. electrons by spin disorder 78−47778
DyAG, antiferromag., induced staggered mag. fields 80−65810
$DyCo_{3.4}$, amorphous, mag. props. 77−32177
Dy_2Co_{17}, hyperfine interactions and cryst. field effects, Mossbauer spectra 80−2369
Dy_2Fe_{17}, hyperfine interactions and cryst. field effects, Mossbauer spectra 80−2369
$DyFeO_3$, non Heisenberg R-Fe exchange interaction, behaviour in mag. field *(Russian)* 80−2568
DyH_2, mag. and crystal field props. from ^{161}Dy Mossbauer studies 79−95692
DyH_3, mag. and crystal field props. from ^{161}Dy Mossbauer studies 79−95692
$Dy_{0.5}Ho_{0.5}FeO_3$, mag. transitions, influence of Dy^{3+}, Ho^{3+} ground states 77−89955
DyIG, magneto-optical absorption, near IR 80−40094
DySb, biquadratic exchange interactions, magnetisation above Neel point 77−69533
DySb, magnetic excitations 79−78358
DySb, quadrupole interactions above T_N 79−78304
$Dy_{1-x}Sm_x$, magnetoresist. of polycryst. specimens in fields up to 44 kOe *(Russian)* 80−92880
Dy_2ZrS_5, mag. and sp. ht. meas. on polycrystalline samples 78−23253
Er, paramagnetic and antiferromagnetic states, optical absorption *(Russian)* 78−56497
Er, spin wave exam. 78−56306
ErB_4, theory of metamagnetic transitions *(Russian)* 78−95436
$ErCo_2$, mag. excitation spectrum, neutron inelastic scatt. obs. 79−78351
$Er_2(Co_{1-x}Fe_x)_{17}$, mag. anisotropy and intersublattice exchange interactions 78−31066
$Er_2(Co_{1-x}Ni_x)_{17}$, mag. anisotropy and intersublattice exchange interactions 78−31066
$ErCrO_3$, mag. field induced spin reorientation, optical Zeeman absorpt. spectra 79−61398
ErCu, cubic antiferromag., mag. excitations inelastic neutron scatt. meas. 78−72341
$ErFe_2$, effect of H on sublattice magnetization, elastic neutron scatt. obs. 79−78327
$ErFe_2$, spin excitations, neutron scatt. obs. 77−63153
$ErFe_2$, spin waves, exchange interaction, neutron scatt. study 79−47267
$ErFe_2$-YFe_2, and $ErFe_2$-$LuFe_2$, mag. props., 80-1300K *(Russian)* 80−75750
$ErFeO_3$, parameters of interaction between rare earth and Fe ions, theory and expt. 79−73705
ErIG, magnetic props. of single cryst., 4.2-600K 79−78341
$Er_xY_{1-x}Rh_4B_4$, supercond. phase transitions, recentering temp. to normal ferromag. state 80−7024
ErZn, magnetoelastic and quadrupolar couplings 78−52328
Er_2ZrS_5, mag. and sp. ht. meas. on polycrystalline samples 78−23253
Eu chalcogenides, anomalous Hall effect, analysis 77−20344
Eu chalcogenides, exchange and superlattice band splittings, magneto-optical study in high mag. fields 79−61342
Eu, exchange integral, spiral spin configuration, ab initio calcs. 79−47275
Eu solid solutions with lanthanides, monosulfides, and oxides, vacant d states, X-ray absorpt. 80−103623
Eu^{2+}, in metallic hosts, Kondo effect 80−39739
Eu^{2+}-ionic compounds, magnetic interaction potential 78−10682
$Eu(Al_{0.5}Ta_{0.5})O_3$, mag. props. 77−4587
$EuAsO_4$:Gd, dynamical interactions, EPR meas. 80−7162
$EuB_{6-x}C_x$, Mossbauer spectra, cond. electrons effect 80−20545
$EuBe_{13}$:Gd, Van Vleck paramagnet, ESR determ. 77−4557
$EuCu_5(Pt_2)(Pd_2)$, indirect exchange, spin echo NMR meas. 80−15822
$Eu_{1-x}Gd_xS$ films, mag. and elec. props. 80−15766
$Eu_xLa_{1-x}Al_2$, cryst. fields and exchange parameters, ESR meas. 80−71175
$Eu_xLa_{1-x}Al_2$, dil. EPR, cryst. fields and effective exchange interaction 80−66029
$Eu(Lu_{0.5}Ta_{0.5})O_3$, mag props. 77−4587
$Eu(Lu_{0.5}Ta_{0.5})O_3$, mag. props. 77−4587
$Eu(Mg_{0.5}W_{0.5})O_3$, mag. props. 77−4587
EuO, Curie temp. raising by impurity addition *(Russian)* 77−47994
EuO, Eu doped, temp. depend. of carrier conc. and mag. susceptibility 77−69483
EuO, Heisenberg ferromagnet, exchange interactions, neutron scatt. expts. 77−20579
EuO, light scatt. by spin waves 80−45086
EuO, mag. struct. and transition temp., indirect exchange 78−91860
EuO nonstoichiometric film, ESR spectra and exchange interaction 80−93176
EuO, optical orientation of f-electrons, Curie temp. variation due to exchange interactions *(Russian)* 79−15431
EuO, origin of exchange interaction 78−10675
EuO:Gd, surface mag. props. 80−71566
EuO:La, metallic, photothreshold, correl. and exchange energy of electron gas 77−62852
EuO:Sm^{3+}, hyperfine field at Sm, TDPAC meas. 80−93215

exchange interactions continued
EuO:Yb(Sm), electron transition and valence state of impurities, X-ray spectroscopy and structural anal. 78−39064
$EuO_{1-\delta}$ films, Faraday effect dispersion rel. to electronic struct., visible and IR spectra 80−45162
$EuO_{1-x}N_x$, ferromag., temp. variation of EPR linewidth, exchange field calc. *(French)* 77−85547
EuO(S), effect of pressure on energy gaps 78−19239
EuO(S):Gd, indirect exchange 78−23264
EuO(S)(Se), surface magnons and surface mag. struct. 77−36066
EuO(S)(Se)(Te), cryst. and electronic struct., mag., elec., and optical props., book contrib. 80−39760
EuO(S)(Se)(Te), exchange interaction mechanisms, theory compared with expt. *(Russian)* 78−39312
EuO(S)(Se)(Te), Heisenberg ferromag. semicond., hyperfine and exchange interactions 77−69530
EuO(s), mag. semicond., s-f model, intermediate coupling theory 79−95326
EuS, conduction band density of states, redistrib. near ferromag. saturation 78−67939
EuS, exchange magnetostriction in paramagnetic phase 79−78492
EuS, film, intrinsic demagnetising fields 78−10735
EuS, Heisenberg ferromagnet, exchange interactions, neutron scatt. expts. 77−20579
EuS, mag. struct. and transition temp., indirect exchange 78−91860
EuS, origin of exchange interaction 78−10675
EuS, pure and Gd doped, electronic struct., mag. exchange and elec. transport props. 78−87974
EuS, single cryst., high-field susceptibility meas., temp. range 2.5 to 16.5K 80−84589
EuS, transferred hyperfine interacs. 77−69741
EuS:Yb(Sm), electron transition and valence state of impurities, X-ray spectroscopy and structural anal. 78−39064
EuSe, mag. struct. and transition temp., indirect exchange 78−91860
EuSe, spin structs., mol. field theory 78−31054
$Eu_{0.14}Si_{0.31}O_{0.55}$ glass, optical, magnetic, and magneto-optical props., chemical clustering 79−42951
$Eu_{1-x}Sm_xO$, ferromag. semiconductor with elevated Curie temp. 77−51903
$Eu_{1-x}Sm_xS$, ESR, exchange interaction, susceptibility, elec. cond., thermoelectric power 80−93174
$Eu_{1-x}Sm_xS$, electronic transition in Sm impurity ions, rel. to exchange interactions, L absorpt. spectra 77−59644
$Eu_xSr_{1-x}S$, chalcogenide-like system, crit. conc. for ferromagnet-spin glass transition 80−34662
$Eu_xSr_{1-x}S$, ferromagnet-spin glass transition, mag. ordering, mag. susceptibility and neutron scatt. meas. 80−50135
$Eu_xSr_{1-x}S$, insulating spin glass, mag. props. 80−2589
EuTe, mag. semicond., antiferromag. reson. meas. 80−44926
EuTe, mag. struct. and transition temp., indirect exchange 78−91860
EuTe, rel. to press. effects on Neel temp. and hyperfine interactions 77−63181
$EuVO_4$:Gd, dynamical interactions, EPR meas. 80−7162
$Eu_{1-x}Yb_xO$, solid soln., ferromag. semicond., increase of exchange interaction 78−88109
$Eu_{1-x}Yb_xS$, solid soln., ferromag. semicond., increase of exchange interaction 78−88109
Fe (111), photoemission, exchange-split energy-band dispersions 80−35059
Fe alloys, FCC, Invar effect, model 80−25105
Fe based ternary alloys, Coulomb and exchange scatt. amplitudes, spin dependent residual resistivities 78−64033
Fe complex, bis(N,N-diethyldithiocarbamato)-iron chloride, ferromag., sp. ht. meas., 0.4-20K 78−19258
Fe complex, $Fe(Br)[S_2CN(C_2H_5)_2]_2$, 3-D Ising ferromag., cryst. susceptibility, 1.5-20K 80−20390
Fe complex, $Fe(Cl)[S_2CN(C_2H_5)_2]_2$, susceptibility near critical pt. 79−24147
Fe complex, $Fe(Cl)[S_2Cn(C_2H_5)_2]_2$, 3-D Ising ferromag., cryst. susceptibility, 1.5-20K 80−20390
Fe complex, $Fe(1,2,4\text{-triazole})_2(NCS)_2$, quasi-2-dimens. $S={}^1/_2$ antiferromag., mag. props., hidden canting 80−107986
Fe complex, hexa(pyridine-N-oxide)$(ClO_4)_2$, sp. ht., comparison with simple cubic $S=1/2$ Ising magnet 78−23290
Fe complex, iodobis(morpholyldithiocarbamate), allotropes, intermol. exchange interactions 77−8455
Fe complexes, S-bridged binuclear, orbitally dependent exchange 77−24688
Fe, de Haas-van Alphen effect and exchange splitting, effect of pressure *(Russian)* 78−95252
Fe dilute alloys, itinerant 3d electron spin density oscills. around solute atoms 77−72978
Fe, energy band dispersion and mag. exchange splitting, angle-resolved photoemission meas. 80−71567
Fe, ferromag. nonrelativistic LCAO energy band calc. 78−10343
Fe, ferromagnetic, calc. hyperfine fields and their press. derivations 80−6796
Fe, ferromagnetic, cluster method, environmental effects 78−95405
Fe garnets, sublattice magnetisation curves, Mossbaeur study 80−75808
Fe group, mol. Jahn-Teller reson. states as possible antecedents to magnetism 80−75701
Fe, intercell exchange energy, Hartree-Fock approx. 80−60239
Fe, light scatt. by spin waves 80−45086
Fe, liquid, Hall effect, band struct. and exchange scatt. 80−80250
Fe, photoemission and electronic spectra, exchange splitting 77−4717
Fe, spin susceptibility, high-field, spin-density functional formalism 80−70959
Fe^{3+} clusters in mol. complexes, interference effects in neutron scatt. 77−85544
Fe-Al-Fe, phase diagram, microscopic model 80−34630
Fe-Co-Ni-Al, Si alloying of mag. hard alloys *(Russian)* 79−73765
Fe-Cr, Invar alloy, explanation of phys. anomalies *(Russian)* 78−88112
Fe-Cr (70-92 at.%), coexistence of ferro- and antiferromagnetism *(Russian)* 78−47955
Fe-Cr-Ni, mag. state at low temps. *(Russian)* 78−56298
Fe-Gd film, amorphous, mag. props., mean field analysis 78−64236
Fe-La(Zr) amorphous films, mag. props., Mossbauer effect and magnetisation meas. 79−69701
Fe-Mn-P-B-Al metallic glass, exchange anisotropy 77−16068
Fe-Ni, Invar alloy, explanation of phys. anomalies *(Russian)* 78−88112

exchange interactions continued

γ-Fe-Ni, local magnetisation of Fe atoms, Mossbauer effect meas. 80−75891
γ-Fe-Ni, Mossbauer exam. 79−56640
Fe-Ni alloys, Invar effect explanation in localised moment model *(Russian)* 77−76580
Fe-Ni FCC alloys, invar effect by local moment model 77−90006
Fe-Ni film, $\alpha\rightarrow\gamma$ transition, Mossbauer effect *(Russian)* 77−40154
Fe-Ni/Fe, bimetal film, exchange const. determ. from hysteresis loops *(Russian)* 77−48015
Fe-Ni/pure Fe exchange coupled films, mag. reversals, hard layer thickness effects *(Russian)* 78−56359
Fe-Ni-Mn alloy, rel. to temp. coeff. of linear expansion *(Russian)* 77−80634
Fe-Ni(Cr), Invar, exchange interactions between ferromag. and antiferromag. components 80−29545
Fe-Rh alloys, spin wave spectrum in antiferromag. and ferromag. phases, inelastic neutron spectrometry 77−63158
Fe-Si, spin- and charge-density oscillations 77−11886
Fe-V alloys, BCC, ferromag., polarised neutron diffr., appl. of multiband CPA theory 77−77033
Fe-Y(Lu) amorphous films, mag. props., Mossbauer effect and magnetisation meas. 79−69701
Fe_2 magnetism, randomised exchange field theory 80−39733
Fe_3B, mag. props., ^{57}Fe Mossbauer spectra meas. 79−95693
$Fe_{80}B_{20}$, amorphous ferromag., hyperfine field distrib., Mossbauer effect 78−60371
Fe_xB_{100-x}, amorphous, mag. props., ^{57}Fe Mossbauer spectra and magnetisation meas. 79−95693
$Fe_{80}B_{20-x}M_x$, M=C, Si, P, Ge, amorphous, effect of metalloids on mag. props. 79−11304
$FeBO_3$, magnon dispersion by light scatt. and ferromag. reson. 77−55668
$FeBO_3$, spin wave dispersion at small wavevectors, Brillouin scatt. and ferromag. reson. 78−47962
$Fe_{78}B_{12}Si_{10}$, amorphous ferromagnet, long and short range exchange interactions, Mossbauer spectra and interpretation 79−56526
$FeCO_3$, antiferromag., siderite, Raman spectra obs. 77−85708
$FeCO_3$, siderite, Fe^{2+} Mossbauer spectrum, ligand field theory 77−16212
$FeCl_2$, magnetic excitation in presence of transverse field, ferromag. reson. 78−19335
FeCo disordered alloys, Mossbauer spectra, hyperfine mag. field distrib., Curie temp. 80−7198
$(Fe_{1-x}Co_x)_{77}Si_{10}B_{13}$, amorphous, mag. moments at 0K, Curie temp., mag. interactions 79−4670
$(Fe_{1-x}Cr_x)_2O_3$, Mossbauer exam. of mag. struct. 77−24694
$Fe_{1-x}Cu_xCr_2S_4$, mag. semicond., mag. props. and elec. cond. *(Japanese)* 79−47111
$Fe_xCu_{1-x}Rh_2S_4$, mag. tetrahedral intrasublattice interaction, X-ray, magnetisation and Mossbauer expts. 78−52241
FeF_2:Mn, antiferromag. reson. and local magnon mode, FIR laser study 80−66042
FeF_2:Mn, Heisenberg antiferromagnet, impurity thermodynamics, NMR meas. 79−61098
FeF_3, amorphous, noncryst. magnet with antiferromag. interactions 79−91228
FeF_3, amorphous, struct. and mag. props., computer model 80−96446
$FeGe_2$, antiferromag., biquadratic exchange 80−2371
FeI, magnon energies, phase transitions of eight sublattice model 77−59463
FeI_2, antiferromag. struct., four spin exchange interaction 78−14948
FeI_2, eight sublattices model, exchange coupling parameters 77−69498
$Fe_{1-x}M_xCl_2$, disordered, Mn spin excitations by microwave absorption at high freqs. 80−34759
$Fe_{2-x}M_xP_{1-y}As_y$, (M=Mn,Fe, Co,Ni), band model of mag. props. 77−40029
$Fe_{3-x}Mg_xO_4$, Verwey transition, Mossbauer study 80−39942
$(Fe_{1-x}Mn_x)Si$, US vel. rel. to mag. struct. and phase transforms *(Russian)* 77−47976
Fe_2MoO_4, electron exchange between $Fe^{2+}-Fe^{3+}$ ions on tetrahedral and octahedral sites, Mossbauer spectra 79−78585
$(Fe_xMo_{1-x})_{75}P_{16}B_6Al_3$, amorphous, effects of Mo on mag. props., Mossbauer meas. 79−73859
$(Fe_xNi_{1-x})_{80}B_{20}$, amorphous, Mossbauer spectra, mag. props. 80−15843
$Fe_{32}Ni_{36}Cr_{14}P_{12}B_6$, amorphous ferromagnet, long and short range exchange interactions, Mossbauer spectra and interpretation 79−56526
$Fe_{3-x}Ni_xO_4$, low temp. Mossbauer spectra, electron transfer and spin density distribution 78−52404
$(Fe_{1-x}Ni_x)_2P$, Curie temp., press. depend. meas. 80−97091
$(Fe_{1-x}Ni_x)_2P$, mag. props. 78−23248
α-Fe_2O_3, exchange parameters including temp. effects 79−24153
Fe_2O_3-NiO-Na_2O-Li_2O-B_2O_3-SiO_2 glass, EPR meas. of exchange interactions 77−32243
Fe_3O_4, Mossbauer linewidth of octahedral Fe 77−66446
Fe_xO, antiferromag., surface magnetism probe by photoelec. currents 77−73214
Fe_zO, non-stoichiometric, mag. struct., neutron diffr. exam. 79−42737
$Fe_3O_{4-x}F_x$, low temp. Mossbauer spectra, electron transfer and spin density distribution 78−52404
Fe_2P, magnetisation, susceptibility, thermal expsn. 79−11302
$Fe_{2-x}P$, first order ferro- to paramag. transition, 216K, susceptibility obs. 78−39322
$Fe_{80}P_{20}$, binary amorphous ferromagnet, Mossbauer study 80−34829
$Fe_{80}P_{20-x}C_x(Si_x)(Ge_x)$, amorphous, size effect of metalloids on mag. props. 80−84594
Fe_3Pt Invar alloy, anomalous Curie const., susceptibility meas. 80−75731
Fe_3Pt Invar alloy, thermal expansion and spontaneous magnetisation, Invar anomalies, low spin model 80−71001
FeS, structural chem., influence of itinerant 3d electrons and valence-band holes 79−23563
FeS, zinc blende type, crystallographic and Mossbauer obs. 78−87650
FeS, zinc blende type, mag. struct. *(French)* 78−91846
$Fe_{0.996}S$, antiferromag., energy dispersion of spin waves, inelastic neutron scatt. meas. 77−69522
$FeSO_4$, α- and β-forms, magnetic interactions, neutron inelastic scatt. study 80−107980
$Fe_{1-x}Te$, fluctuating localised mag. moments, d band motion, Mossbauer study 80−65768

exchange interactions continued

$FeTiO_3$, ilmenite, lunar and terrestrial, cell dimensions and antiferromagnetism 77−21764
FeU_2S_5, mag. struct., exchange energy, magnetisation and neutron diffr. expts. 78−68170
$Fe_{1-x}Zn_xF_2$, dil. antiferromag., electronic and mag. props., Raman scatt. and optical absorpt. study 80−108207
$Fe_xZn_{1-x}F_2$, Neel temp. mag. cone depend., CPA calcs. 78−88122
$Fe_{3-x}Zn_xO_4$ low temp. Mossbauer spectra, electron transfer and spin density distribution 78−52404
$Fe_{80}b_{20-x}C_x(Si_x)(Ge_x)$, amorphous, size effect of metalloids on mag. props. 80−84594
GaAs, effective dielectric function calc., exchange interaction effects 79−99494
GaAs, exchange interaction, analytical and nonanalytical parts, from polariton spectra in mag. fields 80−50367
GaAs, surface states, band struct. by discontinuous potential method 80−20276
GaAs:Fe, exchange-coupled pairs, ESR 79−11343
GaP:Fe, electron exchange via val. band between Fe acceptor centres, Mossbauer spectra 77−55741
GaP:Te(S), nucl. relax. rel. to donor density 80−11284
Gd alloys, amorphous, mag. props. and ferromag. reson. 80−54952
Gd compounds, NaCl type, exchange striction 78−84409
Gd, ferromag., magneto-optical reson., optical consts. determ. 78−6657
Gd in CsCl type alloys, exchange between localised 4f and cond. electrons 77−63279
Gd, spin wave exam. 78−56306
Gd, spin wave temp. depend., exchange coupling role 78−68199
Gd^{3+} Gd-ionic compounds, magnetic interaction potential 78−10682
Gd^{3+}, in Van Vleck paramagnets, EPR meas. 77−12199
Gd-Au(Ni), amorphous ferromag., mag. and transport meas. 77−89930
Gd-Co, and Gd-Co-Mo films, amorphous, mag. props., annealing effects 78−64235
Gd-Co amorphous film, sputtered perpendicular mag. anisotropy 79−56576
Gd-Co-Fe film, amorphous, bias-sputtered, uniaxial perpendicular anisotropy 78−64234
Gd-Dy, magnetostriction contrib. to thermal expansion *(Russian)* 77−12184
Gd-Dy alloy, mag. anisotropy, magnetisation meas. 77−12115
Gd-Er alloy, mag. anisotropy, magnetisation meas. 77−12115
Gd-Fe, DC bias RF sputtered film, mag. props. 77−16124
Gd-Fe, mag. moment of Fe, multiplet splitting in photoemission 79−78846
Gd-Fe amorphous film, prep. by dual-source evaporation, mag. props. 77−89988
Gd-Fe film, amorphous, mag. props., annealing effects 78−64235
Gd-Fe(Co), mag. interactions, exchange fields, mol. field model 77−4498
Gd-Ho alloy, mag. anisotropy, magnetisation meas. 77−12115
Gd-La, magneto-optic reson. *(Russian)* 79−47426
Gd-Ni, ferromag., elec. resist. temp. depend. 80−96843
$GdAg_{1-x}In_x$, magnetic transition temp., effect of hydrostatic press. 78−76244
$GdAl_4$, mag. props., mag. exchange strength 77−85440
$Gd(Al_{1-x}Cu_x)_2$, C15 struct., elec. resist., comp. depend. 78−14705
$Gd(Al_{1-x}Cu_x)_2$, thermoelec. power, exchange interactions 80−24881
$GdAlO_3$, canted antiferromagnetic, Mossbauer meas. 80−97171
$GdAlO_3:Cr^{3+}$, mag. field effects on fluoresc. 80−2850
GdAuSn, mag. props. 77−85439
$Gd(CO_xNi_{1-x})_2$, mag. interactions, effects on moments *(Rumanian)* 79−15296
$GdCl_3$, interaction parameters, high freq. meas. of adiabatic differential susceptibility 78−68211
$GdCo_x$, mag. interactions, effects on moments *(Rumanian)* 79−15296
$Gd_2Co_6Al_{11}$, NMR and mag. susceptibility 79−15367
$Gd(Co_xFe_{1-x})_2$, mag. props., composition and temp. depend. 79−15289
$Gd_{6.9}Co_{74.0}Mo_{12.8}Ar_{6.3}$, amorphous film, spin wave reson. 79−73823
$GdCo_{5c}Ni_{5-5c}$, intrinsic coercivity, anisotropy, exchange and cryst. field interactions 80−75806
$GdCrO_3$, magnetisation, appl. of molecular field theory 79−4637
$Gd_2Cu_6Al_{11}$, NMR and mag. susceptibility 79−15367
GdCuSn, mag. props. 77−85439
$Gd(Fe_xAl_{1-x})_2$, magnetic behavior 80−108079
$GdFeO_3$ orthoferrite, rare earth-Fe interactions 79−56525
$Gd_3Ga_5O_{12}$, magnetic interactions and short range order 79−78401
$Gd_{0.99}Ho_{0.01}(Rh_{1-x}Fe_x)_2$, spin echo meas. on ^{165}Ho, quenching effect of Fe substitution 78−48079
GdIG, spin wave intrinsic relaxation, magnon damping at low temps. 80−29543
$Gd_xLa_{1-x}Al_2$, cryst. fields and exchange parameters, ESR meas. 80−71175
$Gd_xLa_{1-x}Be_{13}$, $0.001 \lesssim x \lesssim 1$, EPR, indirect exchange, bottleneck effect 77−16171
$Gd_xLa_{1-x}Pd_3$, EPR of Gd, g-factor and thermal broadening, temp. and comp. depend. 77−48048
$Gd_xLa_{1-x}Pd_3$, ESR linewidths, g-shifts, effective electron interaction, spin-lattice relax., spin-flip scatt. 78−68372
GdMg, canted mag. struct. in S-ion compound, neutron diffr. obs. 78−34962
$GdNi_x$, (x=3, 3.5, 8.5), ferrimag., mag. reson. above and below Curie temp. 80−97148
$Gd_2Ni_{17-x}Al_x$, EPR of Gd^{3+} ions 80−97139
GdP, electronic struct., mag. exchange and elec. transport props. 78−87974
GdS, electronic struct., mag. exchange and elec. transport props. 78−87974
GdS, low temp. phase transitions, mag. moment orientation, spin flip 79−99700
GdSe, low temp. phase transitions, mag. moment orientation, spin flip 79−99700
GdTe, low temp. phase transitions, mag. moment orientation, spin flip 79−99700
$GdVO_4$, hyperfine field and exchange interactions, Mossbauer meas. 79−47370
$(Gd_xY_{1-x})Co_2$, mag. interactions, effects on moments *(Rumanian)* 79−15296
$(Gd_xY_{1-x})Fe_2$, Fe mag. behaviour, FMR measurements, mag. props., Vangsness relation anal. 79−78336
$(Gd_xY_{1-x})Fe_2$, high temp. mag. behaviour 77−1538

exchange interactions continued
$Gd_xY_{1-x}Fe_2$, s-d exchange interaction integral, change due to hydrostatic compression 78—88199
$Gd_xY_{1-x}Fe_3$, saturation magnetisation, magnetostriction, Curie temp., ferrimag. ordering, exchange field *(Russian)* 78—68343
Gd_2ZrS_5, mag. and sp. ht. meas. on polycrystalline samples 78—23253
Ge, effective dielectric function calc., exchange interaction effects 79—99494
Ge, recombination at dislocations 79—38023
Ge, spectral diffusion in acceptor-hole system at low temp., ultrasonic hole-burning expt. 80—92610
H solid, spin-aligned, rapid decay mechanisms at 0K in large magnetic fields 77—72741
H^- ground state, evaluation, failure of local exchange approx. 77—47758
H_2, liq. metal, electron kinetic eqn. with exchange, elec. resist. 79—15131
H_3, relative magnitudes of direct and indirect exchange, Heitler-London calcs. 80—69069
^3He adsorbed layers, antiferromag. indirect exchange 79—99389
^3He, BCC, first-neighbour mag. interaction sign 78—14538
^3He, BCC, four-spin interaction effects on ordering processes 77—39721
^3He, BCC, meas. from 3 to 300 mK 79—33153
^3He, BCC lattice, quadruple exchange in Heisenberg antiferromagnet 77—89616
^3He, BCC solid, exptl. mag. props., four spin exchange explanation 79—69319
^3He film, theory of motional inhibition of interlayer quantum tunnelling 80—54466
^3He, HCP, and adsorbed ^3He with triangular lattice, exchange and mag. order 80—107606
^3He, liq., exchange model 80—88387
^3He liquid, exchange model, antiferromagnetic exchange field, susceptibility-specific heat ratio *(French)* 80—80019
^3He, solid, four spin exchange model and magnetism 80—92752
^3He, solid, phenomenological treatment of exchange effects in high-temp. limit 77—35795
^3He, solid, spin diffusion in BCC and HCP phases *(Russian)* 77—35794
^3He, solid BCC, four spin exchange, susceptibility behaviour below 10 mK 78—10253
^3He, solid BCC, nucl. spin mag. ordering with spin exchange 77—89615
^3He, solid BCC, physical origin of large four spin exchange 79—56031
^3He, solid locked in magnetism 79—56033
^3He, submonolayer on Grafoil, vacancy induced ferromag. 78—14536
^3He with C particles, pulsed NMR, mag. susceptibility surface induced ferromagnetism, antiferromagnetic exchange interaction 78—79844
HgCdTe, interband magnetoabsorption and band struct. 79—82959
$HgCr_2O_4(S_4)(Se_4)$, magnetic exchange interactions 77—24690
$HgCr_2Se_4$, spontaneous magnetisation temp. depend., nuclear resonance freq. depend. *(French)* 80—80483
$Hg_{1-x}Fe_xTe$ mixed crystals, zero gap, magneto-optical evidence of exchange interactions 80—45045
HgMnTe, interband magnetoabsorption and band struct. 79—82959
HgMnTe, semimagnetic semiconductor, band structure, transport phenomena 79—95331
$Hg_{1-x}Mn_xTe$, energy levels at Γ-point in intense mag. fields, Shubnikov-de Haas effect meas. 80—24951
$Hg_{1-x}Mn_xTe$, exchange interaction effect on $\Gamma_8 \rightarrow \Gamma_8$ magnetoabsorption 79—61351
$Hg_{1-x}Mn_xTe$, indirect exchange interaction 79—61094
$Hg_{1-x}Mn_xTe$, indirect exchange interaction 80—97087
$Hg_{1-x}Mn_xTe$, mag. props., 4.2-300K 77—4508
$Hg_{1-x}Mn_xTe$ mixed crystals, zero gap, effect of exchange on interband magneto-absorption 78—23443
$Hg_{1-x}Mn_xTe$, non-parabolic zero-gap semicond., indirect exchange interaction 80—80498
n-$Hg_{1-x}Mn_xTe$, quantum transport phenomena, exchange interaction influence 78—76093
$Hg_{1-x}Mn_xTe$, semimagnetic, exchange interactions between localised and delocalised electrons 80—97245
$Hg_{1-x}Mn_xTe$, semimetallic, giant spin splitting induced by exchange interactions 77—28150
$Hg_{1-x}Mn_xTe$, transverse magnetoresistance in quantised mag. fields 80—96922
$Hg_{1-x}Mn_xTe$, zero-gap semicond., indirect-exchange interactions 80—29370
HgTe, zero-gap semicond., absorpt. spectrum in mag. field 80—11370
Ho-Co amorphous film, prep. by dual-source evaporation, mag. props. 77—89988
$HoAl_2$, biquadratic pair coupling from mag. anisotropy 77—28383
$HoAl_2$, magnetisation and neutron diffr. meas., cryst. field and exchange 77—63163
$HoCo_2$, ground state spin excitations, inelastic nneutron scatt. study 80—50077
$HoCrO_3$, magneto-optical investig. of Ho-Cr and Ho-Ho interactions 77—52055
$HoFe_2$, effect of H on sublattice magnetization, elastic neutron scatt. obs. 79—78327
$HoFeO_3$ orthoferrite, rare earth-Fe interactions 79—56525
$Ho_xTb_{1-x}Fe_2$, single cryst., spin orientations 78—84425
$Ho_xY_{1-x}F_3$, calc. of $Ho^{3+} \rightarrow Ho^{3+}$ energy transfer rates *(French)* 78—79966
HoZn, magnetoelastic and quadrupolar couplings 78—52328
$In_xGa_{1-x}As$, epitaxial solid soln. film, spectral depend. of transparency, absorpt. spectra calcs. 80—45161
InP, exchange interaction, analytical and nonanalytical parts, from polariton spectra in mag. fields 80—50367
KCl, perturbed M-centre triplet state, M-F centre exchange mechanisms 79—69884
$KClO_4$, X-irrad., ESR spectra of O_3^- and ClO_3 exchange-coupled to O_2 78—64856
K_2CrCl_4, ionic ferromag., temp. depend. intensity in optical absorption 77—12399
$KCrO_2$, two-dimensional antiferromag., mag. props. *(French)* 78—23251
$K_2CuCl_4.2H_2O$, paramag. single cryst., PMR temp. depend., hyperfine const. and exchange interaction *(Korean)* 80—29630
$K_2CuCl_4.2H_2O$ structure compounds, 3-dimens. ferromag., exchange anisotropy by NMR 77—55714
$K_2CuCl_4.2H_2O$, thermal effects in mag. exchange interaction 77—16067
$KCuF_3$, chain-like antiferromag., parallel susceptibility 78—80137

exchange interactions continued
$KCuF_3$, nearly 1-D spin-$^1/_2$ antiferromagnet, spin wave energy dispersion 80—2551
$KCuF_3$, one-dimens. antiferromag., spin waves, neutron scatt. study 80—65848
K_2CuF_4, 2-D ferromagnet, optical and magneto-optical props. 77—52062
K_2CuF_4, Curie temp. XY-like anisotropy effect, inter-layer exchange 77—59406
K_2CuF_4, nearly two-dimensional ferromag. nucl. transverse relax. rates meas. 77—81024
$K_2Cu_{1-x}Mn_xF_4$, Cu-Mn exchange interaction, optical determ. 78—72551
$K_2Cu_{1-x}Zn_xF_4$, two-dimens., ferromag., spin wave excitations 78—80140
$(KF)_n$-FeF_3, antiferromagnetic systems, dimensionality and spin reduction effects, Mossbauer study 80—39947
$KFeCl_3$, linear chain ferromag., optical absorpt. and dichroism in mag. field 77—77237
K_2FeF_4, Raman scatt. in two dimens. antiferromagnet 78—19488
K_2FeF_5, mag. struct. and one-dimens. antiferromagnetism 80—60209
K_2FeF_5, one-dimens. antiferromag., single cryst. Mossbauer spectra 78—23376
K_2FeF_5, one-dimensional antiferromag., neutron diffr. and mag. meas. *(French)* 79—47241
$K_{10}(Fe_3O(SO_4)_6(H_2O)_3)_2.12H_2O$, mag. exchange interaction of trinucl. Fe^{3+} complex *(German)* 78—14947
$KI{:}Tl^+$, pre-resonant enhancement of Raman scatt. 80—7354
K_2IrCl_6, thermal expansion meas. near antiferromag. transition 77—20610
$KM_{nx}Mg_{1-x}F_3$, randomly diluted Heisenberg paramag. nucl. relax. 80—60444
$KMgF_3{:}Mn^{2+}$, exchange and spin-orbit interactions, optical spectra study 79—95817
$KMgF_3$:Ni, Co, emission from Ni-Ni and Ni-Co pairs, exchange coupling const. 79—33788
$KMgF_3{:}Ni^{2+}$, absorpt., MCD and emission spectra 79—51953
$KMnF_3$, EPR antiferromag. reson. linewidths near Neel point, exchange interactions *(Russian)* 77—8386
$KMnF_3$, solid and molten paramag., high-temp. e.p.r. linewidth meas. 77—4548
K_2MnF_4-Ni^{2+}, and undoped, magnon spectra, Raman, far IR and fluorescence meas. 77—20573
$K_3Mn_2F_7$, double-layer antiferromag., mag. prop. meas. and calc. 77—55666
$K_3Mn_2F_7$, two magnon Raman scatt., magnon dispersion, susceptibility, Green's function methods 80—50340
$KMn_{0.1}Zn_{0.9}F_3$, exchange interaction determ. by neutron scatt. 79—47274
$KMn_{0.18}Zn_{0.82}F_3$, excitation of Mn^+ clusters, neutron scatt. 78—68200
$KNiF_3$ and K_2NiF_4, MCD and stress linear dichroism on double excitonic transitions 77—52051
$KNiF_3$, and K_2NiF_4, double-excitonic optical transition intensity, exchange and dimensionality effects 77—69591
$KNiF_3$, refr. index, isotropic exchange contrib. 77—69808
KO_2, low temp. phases, mag. order, EPR and antiferromag. reson. 79—95630
K_2ReCl_6, thermal expansion meas. near antiferromag. transition 77—20610
$KZnF_3$, Cu^{2+} and Mn^{2+} exchange interactions, luminesc. line temp. depend. 79—69480
$KZnF_3$, exchange interactions of transition metal ions in orbitally degenerated excited states 80—65512
$KZnF_3{:}Mn^{2+}$, exchange and spin-orbit interactions, optical spectra study 79—95817
$KZnF_3{:}Ni^{2+}$, absorpt., MCD and emission spectra 79—51953
$KZnF_3{:}Ni^{2+}$, Mn^{2+}, interference transition electric dipole mechanism 80—34896
$K_2Zn(ZrF_6)_2.6H_2O{:}CO^{2+}$, anisotropic exchange interactions between Co^{2+} ions, ESR spectra 79—95637
$(La,Ce)B_6$, low temp. mag. props. 79—61043
$(La,Gd)Al_2$, dil. alloy, magnetoresistivity determ. 79—73495
$La{:}Eu^{2+}$, liquid, γ-ray spectra observation of exchange interaction 80—84672
La-Fe alloy, amorphous, sputtered at high rate, mag. props. 80—75753
La-Fe bulk amorphous alloys, mag. props. *(Japanese)* 79—95588
La-Gd, exchange-coupled localised moments, Korringa relaxation rate 80—75851
La-P-Ce, dilute, NMR investig. of anisotropic cond. electron exchange 77—63309
LaAg, band calcs., rel. to mag. and electronic props. and martensitic transform. 77—8014
$LaAlO_3$, exchange interactions of transition metal ions in orbitally degenerated excited states 80—65512
$LaBe_{13}$:Er, ESR, appl. of exchange induced broadening in low lying crystalline field system 80—108062
$LaBe_{13}$:Er, ESR spectra, Er spin-spin exchange broadening 78—23338
$LaBe_{13}$-Er(Dy), dil., ESR, crystalline elec. field splitting, exchange parameters 78—52348
$(La_{1-x}Gd_x)Al_2$, dil., reverse resistance anomaly 78—76054
$(La_{.993}Lu_{.007})_{1-x}Gd_xRu_2$, exchange enhanced supercond., compensation effect on H_{c2} 77—4474
$LaM_2{:}Nd^{3+}$, M=Ru, Rh, Ir, Pt, ESR investigation 79—78514
$La_2(MnO_3)_3$, hydrostatic press. effect on mag. struct., neutron diffr. 77—51886
$(La_{0.5}Na_{0.5})RuO_3$, mag. props. 78—27027
$(LaNd)Sn_3$, containing Nd impurities, supercond. and normal state props. 80—49967
$LaNi_5$:Gd, ESR, exchange induced g-shift, H_2 uptake effect 77—4556
$LaNi_{1-x}Co_xO_3$, mag. props. 77—85411
$La_{1-x}Tb_xAl_2$, competing paramag. anisotropy from cryst. field and indirect quadrupolar coupling 80—60180
$La_2Zn_3(NO_3)_{12}.24H_2O{:}Mn^{2+}$, pair spectra and mag. props. of Mn^{2+} 77—8396
$La_2Zn_3(NO_3)_{12}.24H_2O{:}CO^{2+}$, Mn^{2+}, Ni^{2+}, mag. exchange interactions, EPR 77—36118
Li K edge, exchange effects 77—4702
Li, local orbital energy bands using Kohn-Sham and near Hartree-Fock exchange 78—30866
Li-Mg alloy, BCC, paramag. enhancement *(Russian)* 77—51878
$LiCrO_2$, two-dimensional antiferromag., mag. props. *(French)* 78—23251
$LiCuCl_3.2H_2O$, EPR linewidth and relax., effect of antisymmetric exchange 77—59448
LiF, F-centre, excited state, optical absorption 77—20267

exchange interactions continued
LiF, ground and excited state props., local density formalism 78—10349
$Li_{0.13}Fe_{2.87}O_4$, acoustic spin wave dispersion branch, exchange const., neutron scatt. study 79—47266
$LiGa_5O_8:Cr^{3+}$, antisymmetric exchange interaction, EPR study 79—47331
$Li_2Mn_xTi_{1-x}O_3$, EPR exam. of antiferromag. props. 78—15015
LiMnZn ferrites, elementary coupling energy to lattice of Mn^{3+} ions, depend. on T_c 77—69534
Lu-Gd, dil., positive exchange Kondo system, magnetisation and resist. 78—68158
$LuCo_2$, mag. interactions, effects on moments *(Rumanian)* 79—15296
$LuFe_2$, ferromagnetic cpds., mean field exchange consts., Stoner itinerant model calcs. 80—50084
$LuRh_4B_4$, superconducting and normal state props. 79—73632
$Lu_2V_2O_7$, pyrochlore struct., mag. props. 78—72335
Mg, spin susceptibility, electronic effective mass, spin density functional calcs. 78—43291
Mg-Mn, dil., mag. props., EPR meas. 79—73804
Mg-Mn, dil. alloy, de Haas-van Alphen effect, exchange interaction, Kondo effect 78—88093
$MgAlO_4:Cr^{3+}$, exchange parameters of Cr^{3+} pairs, optical and EPR meas. 77—69282
$MgAl_2O_4:Cr^{3+}$, exchange parameters determ. from emission and luminesc. excitation spectra 77—52160
$MgEr_2S_4$, magnetisation and susceptibility, exchange interactions obs. 78—52242
$MgF_2:Co^{2+}(Mn^{2+})$, Coulomb and exchange interaction consts. optical spectra line assignment, new technique 80—45124
$MgFe_2O_4$, Mossbauer study 79—47375
Mg_6MnO_8, EPR in magnesium-manganese spinel *(Russian)* 78—91936
$Mg_{1-x}Mn_xTe_2$, random dil. antiferromagnet, mag. props. 80—54870
MgO:Cr, Co, optical and ESR studies 80—50175
$MgO:Fe^{3+}$ single cryst., exchange energy 80—96834
$MgO:Ni^{2+}$, near IR luminesc. from isolated and exchange-coupled Ni^{2+} ion pairs, temp. depend. 80—93382
Mn complex, manganese (II)(1,2,4-triazole)$_2$(NCS)$_2$, 2-dimens. Heisenberg antiferromag., mag. props. 78—72336
Mn compounds, crysts. with spin-forbidden transitions, two-photon light absorption *(Russian)* 77—48185
Mn oxides, XPS study, electron binding energies, spin orbit splittings, exchange splittings 79—78839
Mn^{2+} compounds, strongly exchange coupled, solid and liq. states, EPR and NMR, 300-1450K 77—73077
Mn^{2+}, Fermi contact interaction, spin density distrib., X_α calc. 77—54514
Mn-Bi mictomagnetic alloy, mag., elec. and elastic props. *(Russian)* 80—108028
Mn^{2+}-Cu^{2+} coupled pair, ESR spectrum, strong isotropic exchange model 80—29606
$Mn(CN)_3.(H_2O)_{0.57}$, mag. interactions, theory 80—97085
$MnCl_2$-KCl system, molten, EPR spectra, linewidth study 78—88173
MnCoSi, effect of press on mag. transition temp. *(Russian)* 80—25137
$Mn_3Cr_2Ge_3O_{12}$ garnet, antiferromag. ordering *(Russian)* 78—80146
$Mn_{2-x}Cr_xSb$, exchange-inversion interaction and acoustical magnon soft mode 77—40049
$Mn_{1-x}Cu_xSb$ film, ferromag. reson. 78—31114
$MnEr_2S_4$, magnetisation and susceptibility, exchange interactions obs. 78—52242
MnF_2, antiferromagnetic phase stability limit near spin-flop boundary 78—10683
MnF_2, local mag. ordering above Neel point, EPR *(German)* 77—36125
MnF_2, mag. anisotropy at OK 79—33473
MnF_2, solid and molten paramag., high-temp. EPR linewidth meas. 77—4548
$MnF_2:Ni^{2+}$, IR fluoresc., field depend., exchange energy 78—68543
$Mn_{1-x}Fe_xAs$, mag. props. in ground state *(Russian)* 78—56294
$MnFe_2O_4$, exchange splitting of ionic S-state, neutron spectra 78—52240
$Mn_xFe_{3-x}O_4$ ferrite film, exchange interaction depend. on conduction electrons *(Russian)* 80—34621
$Mn_xFe_{3-x}O_4$ film, spin wave reson., exchange const. 77—16183
Mn_3Ge, triangular spin ordering, weak ferromagnetism 79—47237
$Mn_xMg_{1-x}S$, mag. props. 77—66244
$Mn_xMg_{1-x}S$ solid solution, mag. props. 78—60269
$Mn_xMg_{1-x}Y_2S_4$, magnetisation and susceptibility, exchange interactions obs. 78—52242
Mn_4N, mag. struct. non-collinearity, neutron diffr. obs. 80—65796
$Mn(Nb_{0.5}Ta_{0.5})_2O_6$, random and spin-flop magnet, neutron crit. scatt. 79—24169
$Mn(Nb_{0.5}Ta_{0.5})_2O_6$, spin flop magnet, four dimens. phase diagram and multicrit. phenomena 79—15304
MnP, ferro-spiral transition, neutron scatt. studies 80—65876
$Mn_xPd_{82-x}Ged_{18}$, amorphous alloys, mag. props. 78—91906
$MnS_2(Se_2)(Te_2)$, antiferromagnetic ordering, effective electron model 77—47975
$MnS_2(Se_2)(Te_2)$, mag. ordering, 2 cation, 2-anion indirect exchange interactions *(French)* 78—43566
Mn_2Sb, spin-wave dispersion relations, exchange interactions, neutron inelastic scatt. 80—65832
$MnSe_2$, pyrite struct., mag. suscept. and thermal expansion 77—32176
β-$MnSeO_4$, mag. interactions 79—78361
α-$MnSeO_4$, magnetic interactions, neutron inelastic scatt. study 80—107980
MnSi, itinerant electron helical mag., ESR 77—59446
Mn_3Sn, triangular spin ordering, weak ferromagnetism 79—47237
α-$MnSo_4$, mag. interactions 79—78361
$MnTe_2$, pyrite struct., susceptibility, 4.2-450K, exchange consts. 77—77040
$Mn_{1-x}Ti_xAs$, ferro- to paramag. transition, press. effect up to 7 kbar 77—89954
MnY_2S_4, magnetisation and susceptibility, exchange interactions obs. 78—52242
$Mn_{1-c}Zn_cF_2$, Heisenberg antiferromag., linear mag. birefringence meas. 77—16277
Mo, exchange and correlation screening, self-consistent density-functional representation 79—60748
Mo, nuclear indirect interaction, NMR line shape anal. 78—52360
Mo-Fe, dil., Kondo effect of RKKY interaction and sd exchange parameter 78—31052
$(NH_4)_2Co(SO_4)_2.6H_2O$, submillimetre ESR meas. using pulsed high mag. field 80—44905

exchange interactions continued
$(NH_4)_2CuBr_4.2H_2O$, ferromag., static and dynamic mag. props. 80—50074
$(NH_4)_2CuCl_4.2H_2O$, submillimetre ESR meas. using pulsed high mag. field 80—44905
$(NH_3)_2FeF_5$, quasi two-dimens. antiferromagnet, Mossbauer study 80—39947
NH_4FeF_4, mag. and Mossbauer obs. *(French)* 78—19389
$N_2H_6FeF_5$, one-dimens. magnetism, mag. suscept. and Mossbauer reson. exam. 77—51893
$NaCeS_2$, mag. susceptibility, 3.7 to 297K, extended mol. field model 79—87227
$NaCrO_2$, two-dimensional antiferromag., mag. props. *(French)* 78—23251
NaF, ab-initio calc. of cohesion energy, compressibility and density 78—71782
NaO_2, physical mechanisms of phase transitions 80—6381
Na_2O-$B_2O_3:Cu^{2+}$, Mn^{2+} glasses, Cu^{2+}-Mn^{2+} interaction studied by ESR 80—93166
Nb, electronic structure, APW calcs., self-consistency and exchange effects 77—66109
Nb oxides, XPS study, electron binding energies, spin orbit splittings, exchange splittings 79—78839
NbC, self consistent APW-Xα calc., electronic struct. 77—20237
NbN, self consistent APW-Xα calc., electronic struct. 77—20237
$NdAl_2$, mag. excitation spectrum, neutron inelastic scatt. 78—10673
$NdAl_2$, mag. excitations, cubic cryst. field and isotropic Heisenberg exchange models 77—63154
Nd_xCo_{1-x} film, amorphous, mag. props. meas. 78—68312
$Nd(Co_{1-x}Cu_x)_5$, coercive force temp. depend., short-range exchange fluctuations 79—82823
NdF_3, ^{19}F spin-lattice relax. and mag. couplings 79—65753
Nd_xFe_{1-x} film, amorphous, mag. props. meas. 78—68312
NdSb, mag. excitation spectrum, neutron inelastic scatt. 77—63152
$NdSn_3(In_3)(Pb_3)(Pd_3)$, crystalline elec. field parameters, exchange and Coulomb contrib. 77—20278
$NdVO_3$-$CaVO_3$ solid solns., mag. props. rel. to cryst. struct. 78—43571
Ne, solid, energy bands, depend. on choice of exchange-correlation pot. 80—70607
Ne, solid, rel. to optical spectra obs. of excitons 79—95340
Ni (111), band struct. and temp.-depend. mag. exchange splitting, angle resolved photoemission obs. 78—60546
Ni (111), photoemission, exchange-split energy-band dispersions 80—35059
Ni alloys, mag. moment distrib. 77—32178
Ni, band struct. and multielectron excitations, angle-resolved photoemission determ. 80—76147
Ni based ternary alloys, Coulomb and exchange scatt. amplitudes, spin dependent residual resistivities 78—64033
Ni complex, $(Ni(C_2H_5NO)_6)(NO_3)_2$, field induced level crossing and cryst. struct. 79—47070
Ni complex, hexa(pyridine-N-oxide)$(ClO_4)_2$, field-induced mag. ordering in S=1 singlet ground-state 78—23288
Ni, effective exchange parameter, q-depend, intra-atomic interaction 79—4542
Ni, electronic and magnetic props., spin split energy band dispersions 79—78829
Ni, energy band dispersion and mag. exchange splitting, angle-resolved photoemission meas. 80—71567
Ni, exchange splitting of 3d bands, angle-resolved photoemission meas. 80—71568
Ni, ferro- to paramag. transition, angular resolved photoemission 78—68603
Ni, ferromag., energy bands, self-consistent calcs., exchange splitting 79—19509
Ni, ferromag., exchange integral maximisation, neutron scatt. obs. and ten-fold degenerate Hubbard model comparison 80—71004
Ni, ferromag., exchange splitting, angle-resolved photoemission meas. 78—43985
Ni, ferromag. props., teaching expt. 80—82608
Ni, ferromagnetic, calc. hyperfine fields and their press. derivations 80—6796
Ni fibres, magnetisation reversal 77—69625
Ni film, granular, tunnelling of spin-polarised electrons and magnetoresist., exchange effects 77—12024
Ni film, spin wave resonance 79—33542
Ni, liquid, Hall effect, band struct. and exchange scatt. 80—80250
Ni, magnetisation in pulsed field up to 320 kOe, 283 to 693K, band theory *(Russian)* 77—80920
Ni, Si ion projectile bound s electron polaris. rel. to transient mag. fields 79—33023
Ni, spin-wave exchange stiffness const. 77—4510
Ni, surface electronic structure, rigid exchange splitting model 77—11977
Ni, valence-band photoemission spectra, self-energy corrections effect 80—11534
Ni wire in Ag matrix, coercivity meas. 77—20642
Ni-Co, elementary excitations, exchange stiffness const., inelastic neutron scatt. study 79—47294
Ni-Co, ferromagnetic resonance, surface anisotropy 78—95526
Ni-Co film, spin wave resonance 79—33542
Ni-Co thin films, spin-wave reson. obs., exchange stiffness const. 80—44924
Ni-Cr, elementary excitations, exchange stiffness const., inelastic neutron scatt. study 79—47294
Ni-Cu alloy, nearly ferromag., spin-glass-like distrib. of interaction fields 79—91243
Ni-Fe, elementary excitations, exchange stiffness const., inelastic neutron scatt. study 79—47294
Ni-Fe film, unidirectional anisotropy by exchange coupling, appl. to biasing of magnetoresist. read head 78—91907
Ni-Fe Invar, thermal expansion and spontaneous magnetisation, Invar anomalies, low spin model 80—71001
Ni-Fe Invar alloy, thermoelectric power temp. and mag. field depend. 78—26849
Ni-Fe oxidised film, extraordinary viscous wall motion at extreme vel. 78—14997
Ni-Fe/Mn interface, mag. surface effects, dead layers and exchange anisotropy 77—24718
Ni-Mn alloy, disordered, exchange-anisotropy field, magnetisation curves 78—72365

exchange interactions continued
Ni-Mn alloy, disordered, mag. struct., high field twist deform. 78—68166
Ni-Mn alloy, disordered FCC, stiffness const., single cryst. neutron inelastic scatt. meas. 77—20558
Ni-Pd, high mag. field effects, mag. isotherms near Curie point, exchange splitting energies 80—60272
Ni-Pd, mag. moment distrib., one-mag.-species model calc. 80—65788
Ni-Rh, mag. moment distrib., one-mag.-species model calc. 80—65788
Ni-V, elementary excitations, exchange stiffness const., inelastic neutron scatt. study 79—47294
$(NiAl)_{1-x}M_x$, M=3d transition metal, elec. resist. and magnetoresist. 77—43580
NiAs crystal lattice alloys and cpds., mag. transitions, mag. field and high press. effects 79—82780
$NiBr_2$, ^1Eg spin-forbidden transition, temp. depend. and magnetoabsorpt. 78—48151
$Ni(BrO_3)_2.6H_2O$, low temp. EPR meas. 77—81001
$NiBr_2.6H_2O$, antiferromag. ordering and paramag. behaviour 78—14941
$NiCl_2.2H_2O$, mag. phase diagram and exchange parameters 77—77054
$NiCl_2.6H_2O$, antiferromag., phase diagram, low temp. canted paramag. boundary, bicritical point 79—47282
$Ni_xCo_{3-x}O$, composition depend antiferromagnetic-ferrimagnetic ordering, mag. susceptibility meas. 80—70973
NiFe alloys, spin-wave exchange stiffness const. calcs., weak ferromagnetism 77—4510
NiFe disordered alloys, Mossbauer spectra, hyperfine mag. field distrib., Curie temp. 80—7198
Ni_3Fe disordered alloys, Mossbauer spectra, hyperfine mag. field distrib., Curie temp. 80—7198
$NiFe_2O_4$, exchange integrals from magnetisation meas. 79—47273
Ni_3Mn, thermoremanent magnetisation and blocking temp. 80—34601
Ni_xMn_{1-x} disordered alloy, mag. interactions exam. 77—24687
$(Ni_{0.75}Mn_{0.25})_{82}Si_{10}B_8$, amorphous, exchange anisotropy, mag. susceptibility meas., 4.2K to room temp. 80—11186
NiO (001), surface layers, sublattice magnetisation temp. depend., LEED exam. 78—27018
NiO (100), antiferromag., LEED calcs. of exchange refls. 78—14949
NiO, exchange striction 78—56309
NiO, surface sublattice magnetis., temp. depend., determ. using low energy electron exchange scatt. *(Japanese)* 77—55700
NiO:Cr, effect of Cr additives on structure parameters *(Bulgarian)* 80—44319
NiO:Fe, exchange anisotropy of Ni-ferrite precipitates 79—28520
$NiPtCl_6.6H_2O$, singlet-ground-state magnets, ESR at low temps. 80—97132
$NiSnCl_6,6H_2O$, singlet-ground-state magnets, ESR at low temps. 80—97132
$NiSnCl_6.6H_2O$, ESR line shift at very low temps. 78—56375
$Ni_{1-x}Te$, fluctuating localised mag. moments, d band motion, Mossbauer study 80—65768
NiZn ferrite, exchange integrals, magnetisation data and mol. field theory 78—19241
$Ni_{1-x}Zn_xFe_2O_4$, statistical model and phase transform. *(German)* 77—85473
Ni(001) surface states, surface magnetisation, electron spin polarisation 80—88612
Ni(110), mag. exchange splitting of electronic surface states 80—88610
O_2, liquid, exchange interaction, EPR absorpt. line shape anal. 80—71158
$Pb_{1-x}Mn_xTe$, single cryst., mag. susceptibility 79—73672
$PbMo_6S_8$, influence of Fe on superconduction transition temp., and mag. props. *(Russian)* 79—42686
$Pb_{0.9}Sn_{0.1}F_2$, NMR study of F atom motion *(French)* 80—100622
$Pb_{1-x}Sn_xTe$, diamag. reson. *(Russian)* 78—23347
PbTe:Fe, single crystals, state and behaviour of Fe, mag. props. 80—93080
Pd, band model, mag. susceptibility of exchange-enhanced paramagnet 78—2644
Pd, CESR expts. using transmission technique 78—91954
Pd, electronic struct., effects of press. and alloying with Ru, Rh, Ag, and Rh+Ag 78—91581
Pd-Co-P amorphous alloy, mag. an elec. props. 77—40043
Pd-Cr, dil., appearance of mag. order for Cr impurities in exchange enhanced hosts 79—4690
Pd-Fe, molecular field distribution function in disordered Ising model *(Russian)* 80—54859
Pd-Fe alloys, dil., spin polarisation effect on hyperfine interactions, anal. of Mossbauer meas. *(Russian)* 79—47055
Pd-Fe alloys, disordered FCC, exchange stiffness consts., temp. depend. of magnetisation 77—69528
Pd-Fe type dil. ferromag. alloys, spin wave propag. *(Russian)* 77—12110
Pd-Mn alloy, spin glass, low temp. spin dynamics, numerical studies 79—78385
Pd-Rh-Ag, magnetic susceptibility press. depend., d-band deform. and exchange var. 77—47967
$Pd_{0.98}Fe_{0.01}$ $Gd_{0.01}$, Pd-Gd exchange const., neutron diffuse scatt. meas. 80—71002
$Pd_{0.98}Fe_{0.01}Gd_{0.01}$, ferromag., Pd-Gd exchange const. and Pd polarisation, neutron scatt. meas. 80—25122
$(Pd_{1-y}M_y)_{100-x}Fe_x$, M=Ag, Rh, exchange-enhanced alloys, mag. ordering 79—61050
PdMn, giant moment-spin glass high field magnetisation, exchange parameter, saturation moment estimation 79—61143
$Pd_2MnIn_{1-y}Sb_y$, Heusler alloy, mag. order obs. 80—29528
$Pd_2MnIn_{1-x}Sn$, and $Pd_2MnIn_{1-y}Sb$, Heusler alloys, mag. order, disorder effects 80—88723
$Pd_2MnIn_{1-x}Sn_1-_x$, mag. order exam. 77—40036
$Pd_2MnSn_{1-x}Sb_x$, mag. order exam. 77—40036
$Pd_{95}Rh_5$, low-temp. spin-fluctuation resist., effect of pot. scatt., effect of Ni addition 77—15840
$(Pd_{95}Rh_5)Co$, exchange enhanced system, AC susceptibility meas. 77—16096
Pr, magnetic excitations, exchange, crystal field and magnetoelastic interactions 80—2563
$PrAl_{2-x}Ag_x$, cryst. field and exchange interactions 77—63076
PrAs(Bi)(P)(Sb):Gd, EPR relax. of impurity in Van Vleck paramag., host ion fluctuation spectra 77—48049
$PrBe_{13}$:Gd, Van Vleck paramagnet, ESR determ. 77—4557
$Pr_{1-x}Ca_xMnO_3$, struct. and magnetisation study 80—65804

exchange interactions continued
$PrCo_2$, strongly exchange-enhanced paramagnetism, susceptibility 80—60179
$Pr(Co_{1-x}Cu_x)_5$, coercive force temp. depend., short-range exchange fluctuations 79—82823
$Pr(Co_{1-x}Cu_x)_5$, magnetocrystalline anisotropy exam. 78—39315
$PrCu_4$ and $PrCu_5$, Knight shift, mag. susceptibilities 79—95570
PrEu(Gd), magnetic interactions, Mossbauer spectra quadrupole splitting, crystal field parameters 80—39907
PrF_3, ^{19}F spin-lattice relax. and mag. couplings 79—65753
PrF_3, crystal field split levels, inelastic neutron scatt. study 79—47065
$PrFe_2$, Laves phase, mag. props., Mossbauer spectra, crystalline field mag. anisotropy 80—65851
$PrIn_3$, nucl. orientation of ^{144}Pm in singlet ground state, exchange interaction and cryst. field splitting obs. 80—71275
$PrIn_3$:Gd, EPR relax. of impurity in Van Vleck paramag., host ion fluctuation spectra 77—48049
$PrIn_3$:Gd, indirect nuclear exchange interactions, ESR-linewidth meas., sp. ht. determ. 80—103825
$PrNi_5$, nucl. cooling agent, relax. and exchange, EPR and NMR study 80—25237
$PrNi_5$-Gd, dil., single crystal, ESR study 80—75850
PrP, nonstoichiometric, with singlet ground state, induced van Vleck ferromag. spin glass 77—66378
PrSb, mag. excitations, press. depend., inelastic neutron scatt. meas. 78—10699
PrSb(Bi), Gd ESR, Gd-Pr exchange, conduction electron effects 79—69719
$PrSn_3(Pb_3)(In_3)(Pd_3)$, crystalline elec. field parameters, exchange and Coulomb contrib. 77—20278
Pr_3Tl, exchange-coupled singlet-groundstate system, central model 77—77060
Pr_3Tl, induced ferromag., mag. props. under hydrostatic press. 78—56315
Pt, band model, mag. susceptibility of exchange-enhanced paramagnet 78—2644
Pt cluster, conduction electron density oscills., NMR spin-echo meas., indirect exchange interaction 80—44954
Pt-Co, magnetostatic and exchange interactions in composite magnets 77—69536
Pt-Cr, dil., appearance of mag. order for Cr impurities in exchange enhanced hosts 79—4690
$Pt(NH_3)_4CuCl_4$, ferromag., antisymmetric and anisotropic exchange, EPR linewidth 78—10761
Rb, lattice dynamical props., conduction-core exchange, Lindgren approx. 79—1481
Rb, valence-core electron exchange interactions, local approx. 80—91416
$RbCoF_3$, antiferromag., anisotropic exchange, dispersion relations of mag. excitations 77—69532
$Rb_2CuBr_4.2H_2O$, ferromag., static and dynamic mag. props. 80—50074
$Rb_2CuX_4.2H_2O$, (X=Cl, Br), fine struct. due to indirect coupling of nuclear spins 79—78541
$(RbF)_n$-FeF_3, antiferromagnetic systems, dimensionality and spin reduction effects, Mossbauer study 80—39947
$RbFeCl_3$, linear chain ferromag., optical absorpt. and dichroism in mag. field 77—77237
$RbFeCl_3.2H_2O$, 2D Ising system, crit. fluctuations, Mossbauer spectra study 80—44842
$RbFeCl_3.2H_2O$, pseudo-one-dimens. canted Ising antiferromag., spin cluster reson. 79—61235
Rb_2FeF_5, 1D antiferromagnetic system, Mossbauer investigation 78—95533
Rb_2FeF_5, mag. struct. and one-dimens. antiferromagnetism 80—60209
$RbMnCl_3$, high-pressure cubic phase, mag. props. 79—47260
Rb_2MnCl_4, 2D Heisenberg antiferromag. spin wave analysis 80—54879
$RbMnF_3$, solid and molten paramag., high-temp. EPR linewidth meas. 77—4548
$RbMnF_3:Fe^{2+}(Co^{2+})$, high-temperature EPR linewidth, impurity fast relax. effects 77—85556
$RbMnF_3$:Ni, antiferromag., exchange splitting of $^3T_{2g}E$ state, fluorescence meas. 77—12419
$Rb_3Mn_2F_7$, double-layer antiferromag., mag. prop. meas. and calc. 77—55666
$Rb_2Mn_xMg_{1-x}F_4$, random magnetic-nonmagnetic 2-dimens. antiferromag., spin fluctuation dynamics 77—63147
$RbNiF_3$ and Rb_2NiF_4, MCD and stress linear dichroism on double excitonic transitions 77—52051
RbO_2, low temp. phases, mag. order, EPR and antiferromag. reson. 79—95630
$RbVCl_3$, mag. props. *(French)* 77—16059
Rh-Fe, dil., anti-Kondo effect, de Haas-van Alphen obs. 79—73427
Rh_2MnX, (X=Al, Ga, In, Tl, Sn, Pb, Sb), Heusler and Heusler-related cpds., mag. and cryst. props. 77—20568
RuF_5, mag. props. 80—15707
Sc, spin susceptibility, exchange correlation enhancement 77—85167
Sc-Gd, dil., reverse resist. anomaly and negative magnetoresist. 80—84459
$ScAl_2$-Er(Dy)(Nd), dil., EPR and mag. susceptibility 80—15797
ScP, electronic struct., self-consistent Hedin-Lundqvist and $X\alpha$ APW calcs. 80—29322
ScP, energy band struct., exchange-correl. pot. effects, APW calcs. 80—29321
Si (100)-SiO_2 inversion layers, exchange and correl. contribs. to subband energies 79—42654
Si, amorphous, ESR linewidth, exchange interaction effect 79—61216
Si, amorphous, undoped and B doped, ESR-linewidth temp. depend. meas. 80—20459
Si, effective dielectric function calc., exchange interaction effects 79—99494
Si, electron-exciton elastic scatt. cross sections, central field and exchange approxs. 77—62919
Si MOS inversion layer, subband struct., many body effects 78—64131
Si n-channel (100) inversion layer, valley splittings, enhancement by many-body effects 77—85331
Si, phonon-mediated intervalley electron-electron interaction 78—95125
Si, recombination at dislocations 79—38023
Si, spin dependent effects, theory 78—23342
Si, spin-depend. recomb. at exchange-coupled dislocation centres 77—89725
Si, vacancy screening, dielec. const., exchange correl. pot., Thomas-Fermi description 80—44528
Si, valence band model, nonlocal exchange and correl. pot. 77—43492

exchange interactions continued
SiC, laser Raman spin-flip scatt. from excitons, luminesc. 80−80786
Si(100), inversion layer, interaction induced transition at low density 80−15581
$Sm,(Co,M)_{17}$, (M=Fe, Mn, Cr), exchange and crystal field parameters, anisotropy meas. 77−69535
Sm compounds, mixed valence, metals or small gap insulators, two-band Hubbard Hamiltonian 80−34399
Sm intermetallics temp. depend. of Sm^{3+} magnetisation, exchange and cryst. field effects 77−8302
Sm^{3+} in magnetically ordered Sm compounds, crystal-field effects on crossover temp. of magnetisation 79−69656
Sm^{3+} in ordered compounds magnetisation temp. depend., exchange and cryst. field effects 77−51890
Sm-Eu alloy, dil., mag. and elec. hyperfine interac., TDPAD obs., paramag. behaviour, exchange integral 80−103908
$SmAl_2$, exchange and cryst. field effects 80−24857
SmB_6:Gd^{3+}(Eu^{2+}), mixed valence compound, ESR g-shifts and linewidths 78−48035
$SmCo_5$, and $SmCo_{3.5}Cu_{1.5}$, anisotropy and coercivity, Kerr effect, magnetisation and aftereffect expts. 77−8300
$SmCo_5$, exchange and cryst. field effects 80−24857
$SmCo_5$, sintered, mag. props. *(German)* 77−43852
$SmCo_5$, temp. depend. of Sm^{3+} magnetisation, exchange and cryst. field effects 77−8302
$SmCo_5$, temp. depend. of Sm mag. form factor, polarized neutron expts. 79−78329
$SmCo_x$-Fe composite permanent magnet material, mag. props. 77−40089
$Sm_2(Co_{1-x}Al_x)_{17}$ *(Russian)* 78−64202
$Sm_2(Co_{1-x}Fe_x)_{17}$, anisotropy consts., conc. and temp. depend. *(Russian)* 78−64202
$SmCo_{5c}Ni_{5-5C}$, exchange fluctuations and giant intrinsic mag. hardness 78−56310
$Sm_2Co_{17-x}Ni_x$, effect of Ni on mag. props. 78−68296
SmF_3, ^{19}F spin-lattice relax. and mag. couplings 79−65753
$SmFe_2$, ferromagnetic-ferrimag. cpds., mean field exchange consts., Stoner itinerant model calcs. 80−50084
$SmFe_2(Co_2)(Ni_2)$, hyperfine interactions and exchange fields acting on Eu^{3+}, Mossbauer obs. 77−63338
$Sm_{1-x}La_xS$, mag. suscept., moment, impurity effects, indirect exchange interaction 78−68147
SmN, magnetic props., neutron diffr. and mag. susceptibility meas. 80−50036
$SmNi_{5-x}Cu_x$, giant intrinsic mag. hardness due to randomised cryst. field interactions 78−68208
SmS:Eu, excited-state exchange interactions, EPR meas. 78−68374
Sm_3S_4:Eu, excited-state exchange interactions, EPR meas. 78−68374
SmSe:Eu, excited-state exchange interactions, EPR meas. 78−68374
Sm_3Se_4, valence fluctuation, mag. susceptibility meas. 80−97056
$Sm_xY_{3-x}Fe_5O_{12}$, magnetostriction comp. depend., 78 to 300K 77−77082
Sm_2ZrS_5, mag. and sp. ht. meas. on polycrystalline samples 78−23253
$Sn_{0.75}Eu_{0.25}Mo_6S_8$, Chevrel phase supercond., spin-depairing interaction, Mossbauer obs. 80−25258
SnTe:Mn, NMR shift meas. 80−97154
$(SrCaR)_2(Cr_xGa_{1-x})O_4$, R=La or Sm, mag. 2-D oxide, phys. props. 78−47974
$SrCl_2$, O_2^- pair centre EPR spectrum 77−24742
$Sr_2Fe_xRu_{1-x}O_4$ solid soln., Mossbauer spectrosc. study 80−50235
$SrLaFeO_4$, mag. and cryst. struct. determ. *(French)* 80−54866
$SrR_2Fe_2O_7$ series, mag. struct. and spin reorientation, neutron diffr. and Mossbauer meas. 77−69503
Ta, electronic structure, APW calcs., self-consistency and exchange effects 77−66109
^{181}Ta nuclear acoustic reson. line shapes, quadrupole exchange contrib. 79−61242
Tb-Ho film, helimag. order, surface deform., exchange and single-ion magnetocrystalline anisotropy energy 77−66390
Tb-Sc(Y)(La)(Lu)(Yb)(Mg)(Th), mag. ordering temps., susceptibility meas. 80−25136
Tb-Y, magnon component of elec. resist., s-f exchange parameter 77−15827
Tb-Y-Zn, magnetic props. conc. and temp. depend. *(Russian)* 77−47989
Tb-Y(Gd), mag. ordering temp. and indirect exchange integrals *(Russian)* 79−95590
$TbAg_{1-x}Zn_x$ solid solns., mag. props. *(Russian)* 77−77049
$TbCo_2$, magnetocrystalline anisotropy and spontaneous magnetostriction 80−75831
$TbCo_2$, spontaneous distortion, mag. props. due to cryst. field, exchange field, magnetoelastic energy 79−61096
$TbCo_{5.1}$, sublattice magnetisation, temp. depend., neutron diffr. anal. *(Russian)* 80−103815
$TbFe_2$, amorphous, Mossbauer spectra *(French)* 80−25261
$TbFeO_3$, mag. phase transitions, Van Vleck interaction and R-Fe exchange *(Russian)* 79−61105
$TbFeO_3$, magnetisation exam. 77−24681
$Tb(OH)_3$:Er^{3+}, ferromag., anisotropic exchange effects in optical spectra 78−80141
TbP (As)(Sb)(Bi), mag. transitions, quadrupolar interaction effects 80−80512
$Tb_{1-x}Y_x$ alloy, helicoidal antiferromag. to ferromag. transition 78−10687
$(Tb_{1-x}Y_x)_3Co$, mag. props. and transitions, conc. depend. *(Russian)* 78−10671
$Tb_xY_{1-x}Co_{5+0.1x}$, exchange interactions and magnetocrystalline anisotropy 80−34618
$Tb_cY_{1-c}Sb$, elec. resist., cryst. field and exchange interaction contribs. 80−39556
TbZn, mag. excitations meas. 80−70979
Tb_2ZrS_5, mag. and sp. ht. meas. on polycrystalline samples 78−23253
$TeCr_2O_6$, exchange interactions within binuclear entity $(Cr_2O_{10})^{14-}$ 80−60236
Th-Gd(Tb)(Dy)(Ho)(Er)(Tm)(Lu) (1 at.%), Heisenberg exchange, residual resist. meas. 80−75558
$ThRu_2$:Nd^{3+}, supercond. state, ESR investigation 79−78514
Ti oxides, XPS study, electron binding energies, spin orbit splittings, exchange splittings 79−78839
TiO_2:Ta, Ti^{3+}-Ti^{3+} exchange interaction *(French)* 77−89945
TiO_2-P_2O_5 glasses, reduced, mag. susceptibility, 1 to 400K, mag. exchange between Ti^{3+} ions 79−73691
$(Ti_{1-x}V_x)_2O_3$, spin-glass props., 0.05-300K 80−25149

exchange interactions continued
Tm, from anisotropy meas. on Gd-Tm alloys 78−68216
Tm pnictides, van Vleck paramag., relax., host exchange parameters 78−2735
Tm-Zn, paramagnetism, mag. excitations, exchanges interactions 80−88718
$TmAsO_4$, optical side bands, absorpt. spectra in mag. fields 77−52123
$TmBe_{13}$:Gd, Van Vleck paramagnet, ESR determ. 77−4557
$TmFeO_3$, parameters of interaction between rare earth and Fe ions, theory and expt. 79−73705
TmSb, metallic, elec. resistivity, 4f-quadrupole charge distrib. 80−24873
TmSb:Gd, Gd ESR, Gd-Pr exchange, conduction electron effects 79−69719
TmSe, intermediate valence cpd., susceptibility, single-ion approach 80−70935
TmSe, mag. props. 80−97086
TmSe, valence mixing, mag. props. obs. 80−70648
$Tm_xSe_yTe_{1-y}$, magnetic ordering studies *(German)* 80−54882
$Tm_2V_2O_7$, pyrochlore struct., mag. props. 78−72335
TmZn, cooperative Jahn-Teller effect 78−67998
U complex, UCl_4.3DMBA(.3MAA), mag. exchange interaction 79−78303
U_3As_4, magnetisation in strong fields, 4.2 to 200K anisotropy and exchange forces 80−54886
UAs(Sb), anisotropic mag. ordering and mag. structural transitions 79−78324
UBe_{13}:Gd, Van Vleck paramagnet, ESR determ. 77−4557
UCu_5, mag. props. and NMR 77−20734
UN, single crystal, mag. props. 77−77042
UN, sound velocity temp. depend. anomaly 77−72891
UN, sound velocity temp. depend. anomaly in elastic consts. determ. 77−72892
$U_2N_2As(P)(S)(Se)$, susceptibility, 4.2-1000K, cryst. field and exchange interactions 77−20569
US, electronic struct. calc. 78−91615
US(Se)(Te), electronic struct. and exchange band splitting, optical refl. meas. 80−66226
V, electronic structure, APW calcs., self-consistency and exchange effects 77−66109
V oxides, XPS study, electron binding energies, spin orbit splittings, exchange splittings 79−78839
VF_2, nearly one-dimensional, paramag. susceptibility 79−15278
VI_2, antiferromag., zone-boundary phonon Raman scattering, modulation of exchange interaction 80−11386
V_2O_3-Al_2O_3 solid soln., interactions between V atoms, comp. and temp. depend. of mag. susceptibility 77−8056
V_2O_3-M_2O_3, M=Ti, Cr, struct. and mag. props. 78−27041
V_2O_5-CuO-BaO glass, unpaired electron localisation, ESR study 80−66026
V_3O_5, spin order, one-dimensional, Neel transition 80−39799
$VS_2(SE_2)$ (1T), electronic struct. using nonspherical cryst. pot. 80−44498
W, exchange and correlation screening, self-consistent density-functional representation 79−60748
WCr_2O_6, exchange interactions within binuclear entity $(Cr_2O_{10})^{14-}$ 80−60236
WV_2O_6, exchange interactions within binuclear entity $(V_2O_{10})^{14-}$ 80−60236
WV_2O_6, magnetic susceptibility, behaviour in terms of quasi-isolated binuclear units 80−97073
$(Y,Ca)_3(Fe,Ge)_5O_{12}$ LPE layer, exchange stiffness coeffs., 30-300K 79−78464
$(Y,Ca)_3(Fe)_2(FeGe)_3O_{12}$ film, exchange const., ferromag. reson. meas. 79−8023
$(Y,Eu)_3(Ga,Fe)_5O_{12}$ film, bubble wall state stability obs. 77−20651
$(Y,Lu)_3(Fe,Sc)_5O_{12}$ LPE layer, exchange stiffness coeffs., 30-300K 79−78464
$(Y,Sm,Ca)_3(Ge,Fe)_5O_{12}$ film, bubble wall state stability obs. 77−20651
Y-Co, amorphous alloy film, spin reson. meas., exchange stiffness 78−68389
Y-Fe alloys, mag. interactions, effects on moments *(Rumanian)* 79−15296
Y-Fe(Co), mag. interactions, exchange fields, mol. field model 77−4498
Y-Gd, dil., reverse resist. anomaly and negative magnetoresist. 80−84459
YAl_2-Er(Dy)(Nd), dil., EPR and mag. susceptibility 80−15797
YCo_3, amorphous ferromagnet, exchange dominated surface modes 78−52359
YCo_x, mag. interactions, effects on moments *(Rumanian)* 79−15296
$Y_2Co_{17-x}Ni_x$, effect of Ni or mag. props. 78−68296
YF_3, crystal field parameters acting on rare earth ions 79−69475
YFe_2, amorphous concentrated spin glass, susceptibility, Mossbauer and neutron scatt. meas. 80−39783
YFe_2, ferromagnetic cpds., mean field exchange consts., Stoner itinerant model calcs. 80−50084
$YFe_{1-x}Cr_xO_3$, weak ferrimagnet, anomalous mag. props. explained by exchange interactions *(Russian)* 77−69538
$Y_3Fe_{5-x}Sc_xO_{12}$, local spin struct., Mossbauer obs. 77−32305
$Y_3Ga_5O_{12}$-$Y_3Fe_5O_{12}$ garnets, EPR spectra of ferric ions 77−66414
$Y_{1-x}GdCo_5$, exchange interactions and magnetocrystalline anisotropy 80−34618
$Y_{3-x}Gd_xFe_5O_{12}$, mag. phase diagrams, mag. transitions, exchange interaction *(Russian)* 80−54896
$Y_{1-x}Gd_xRh_4B_4$, mag. supercond., anomalous temp. depend. of upper crit. fields 80−29510
YIG bubble films, light scatt. from spin waves, hysteresis meas. by Voigt effect 80−15770
YIG, refr. index, isotropic exchange and higher-order anisotropic mag. contribs. 77−69808
YIG, thick epilayer, unpinned magnetostatic modes 77−63290
YIG, thin ferromagnetic film, exchange interaction constant, from paramag. resonance spectra of spin waves 79−42811
YM_2:Nd^{3+}, M=Rh, Ir, Pt, ESR investigation 79−78514
$Y_6(Mn_{0.75}Fe_{0.25})_{23}$, mag. scatter state, hysteresis loops 78−56350
$Y_6(Mn_{1-x}Fe_x)_{23}$, hydriding characts. and mag. props. 77−69527
$Y_{1-x}Nd_xCo_5$, exchange interactions and magnetocrystalline anisotropy 80−34618
$Y_{1-x}R_xCo_5$, R=Gd,Tb,Nd, ferrimag., magnetisation, exchange interactions, mag. anisotropy 80−80565
$Y_{1.62}Sm_{0.21}Lu_{0.27}Cu_{0.9}Ge_{0.9}Fe_{4.1}O_{12}$, implanted bubble garnet, anisotropy profile, FMR study 80−7103

exchange interactions continued
- $YbFe_2$, cryst. elec. field and exchange interac., ^{170}Yb Mossbauer obs., magnetostriction contrib. 80–108124
- $YbFe_2$, Mossbauer spectra, cryst. elec. field and exchange interaction 79–47368
- $Yb_2V_2O_7$, pyrochlore struct., mag. props. 78–72335
- Zn, noncubic crystal, temp. depend. of elec. field gradient 79–99515
- Zn-Cr, dil., mag. anisotropy, 0.001 to 2K 78–68157
- $ZnCr_2O_4(S_4)(Se_4)$, magnetic exchange interactions 77–24690
- $ZnCr_2Se_4$, screw spin struct., neutron diffr. exam. 78–27019
- $ZnGa_2O_4{:}Cr^{3+}$, weak exchange interaction determ., ESR study 80–93107
- $Zn_{1-x}Ge_xFe_{2-x}{}^{3+}Fe_{2x}{}^{2+}O_4$, double exchange magnetism, Mossbauer study 80–66087
- $Zn_{1-x}Ge_xFe_2O_4$, spinel series, obs. by Mossbauer spectroscopy of electron hoppings 78–43754
- $Zn_xMn_{1-x}Fe_2O_4$, substitution effect on mag. struct. and exchange interaction *(Russian)* 78–47949
- $Zn_{1-x}Ni_xCr_2S_4$, spin struct., mag. props. meas. 77–85428
- $Zn_xNi_{1-x}Fe_2O_4$, magnetic props. rel. to localised canting model 77–32161
- ZnO accumulation layers, electrolytic contact quantisation, self consistent quantum calcs. effective mass approx. 79–60920
- ZnO, electron-exciton elastic scatt. cross sections, central field and exchange approxs. 77–62919
- ZnS, natural and stress induced birefringence dispersion 78–6651
- ZnSe, cubic, magnetoreflectance of Γ_6-Γ_8 exciton ground state 78–23495
- ZnSe, magnetoreflectance of exciton-polaritons, semiclassical treatment 79–99857
- $ZnSiF_6{:}Cu^{2+}$, spin-spin interactions of impurity pairs *(Russian)* 78–72397
- ZnTe:Mn, mag. field splitting α n=2 exciton state *(Russian)* 78–79940
- ZnTi ferrites, electron exchange between Fe^{2+} and Fe^{3+}, paramag., Mossbauer spectra and susceptibility meas. 77–63327
- $ZrZn_2$, phonon contrib. to Stoner enhancement factor, ferromag. and possible superconductivity 80–25070

exchange models *see peripheral models*

exchanges (chemical) *see chemical exchanges*

exchanges (telephone) *see telephone exchanges*

excimer lasers
- activation and deactivation rates in high-power lasers 79–941
- applications of excimer systems, book contrib. 79–81441
- atom+vibrationally excited molecule reactions, rel. to high power lasers 79–5155
- atomic and molecular lasers appl. to collision physics 80–63596
- backward Raman amplifier for excimer laser pulse compression, parasitic superfluoresc. suppression 80–69453
- blue-green laser technology for ocean optics 77–78458
- Blumline type discharge laser, single switch operation 78–13727
- book, gaseous electronics and gas lasers 80–73120
- book 79–81415
- book contrib. 77–50665
- bound-free excimer lasers, radiative and kinetic mechanisms 77–88697
- chemical lasers, thermally initiated, utilizing excited atoms, feasibility in visible 79–89898
- closed-cycle high-energy pulsed lasers, investigation and management of acoustic waves 80–38153
- computer modelling, at. and mol. processes 80–23661
- conference, Charleston, USA (Sept. 1979) 80–27039
- corrosive gas laser systems, capacitance manometer design and perform. 79–36909
- CW lasers, homogeneously broadened, with uniform distribution loss, exam. of output power 78–55332
- diluent in XeCl laser, performance 79–94212
- discharge pumped, design and performance 78–46639
- discharge pumped multiwavelength lasers *(Chinese)* 80–102703
- discharge pumping, self-sustained UV preionised 80–28219
- double discharge, improved beam quality using unstable cavity 77–72007
- electric discharge pumped excimer laser model 80–58516
- electron beam coaxial excitation system for high power excimer lasers 80–53310
- electron beam pumped laser, interferometric technique for transient phase shift meas. 80–1195
- electron beam sustained, long pulse high current gun 77–88733
- electron beam system for laser excitation, coaxial diode 80–86509
- electron gun, long-pulse, high-current, for e-beam sustained excimer lasers 78–29967
- electronic structure, pot. energy curves, radiative transition probabilities, quantum mech. calcs. 79–10284
- electronic structure and radiative transitions of excimer systems, book contrib. 79–81416
- electronic transition laser development 79–946
- electronic transition lasers, conf., Snowmass Village, USA (Sept. 1976) 78–63076
- energy storage and nonstoring advanced lasers for fusion appls. 78–79027
- engineering aspects, colloquium, London, England (Nov. 1978) 79–31940
- excimer laser Raman pulse compression for appl. to laser fusion 79–59756
- excimer laser Raman pulse compressor systems for laser fusion 79–59757
- excitation mechanisms, review 80–9865
- excitation technique, performance characteristics, review *(Japanese)* 78–33723
- Group VIA photolytic laser systems, for fusion research 78–59002
- halogen molecule UV excimer lasers, review 77–34877
- halogens, diatomic, kinetics and energy flow, expt. characts., book contrib. 79–81417
- high-efficiency, high-power lasers for fusion appl. *(Japanese)* 78–5486
- high-power lasers and appls., conf., Munich, Germany (June 1977) 79–964
- inert gas, at. and mol. collision processes 80–53263
- inert gas, electroionisation discharge, negative cathode pot. drop 80–79615
- inert gas, excited mols. form., rate const. determ. 80–9859
- inert gas, stimulated emission kinetics in nonself-sustained elec. discharge 78–50753

excimer lasers continued
- inert gas dimer ions, $A^2\Sigma_{1/2u}{}^+ \rightarrow D^2\Sigma_{1/2g}{}^+$ system, theoretical absorption spectrum 80–32734
- inert gas excimer and exciplex oscillators, VUV and XUV pulse generation 79–3688
- inert gas excimers, kinetics and energy flow, expt. characts., book contrib. 79–81417
- inert gas fluoride, discharge and electron beam pumped, review 78–71083
- inert gas fluoride, XF*, $X^+ + F^- + X \rightarrow XF^* + X$ ionic recomb. 78–46574
- inert gas fluoride exciplex laser pumping efficiency 78–74892
- inert gas fluoride laser, using NF_3-inert gas mixture, long pulse UV emission *(French)* 78–58982
- inert gas fluoride laser system, $X_2{}^+ + F^- \rightarrow (X_2F)^*$, recomb. rates 78–46576
- inert gas fluorides, covalent and ionic states, ab initio CI calcs. 78–78634
- inert gas halide, appl. to nonlinear optical processes in atoms and mols. 79–59745
- inert gas halide, at. and mol. collision processes 80–53263
- inert gas halide, development of miniature high-power high-press. UV and IR lasers 78–46642
- inert gas halide, discharge excited, optical loss mechanisms and tuning performance 80–32970
- inert gas halide, discharge excited, preionisation technique 80–23714
- inert gas halide, frequency conversion in atomic or mol. media 79–36965
- inert gas halide, gas recirculating system, purification by Ti gettering 78–46617
- inert gas halide, power and efficiency, review 79–937
- inert gas halide, stable-unstable resonator for beam control 80–23722
- inert gas halide, TEA, operating and beam characts. 79–59715
- inert gas halide avalanche discharge lasers, characts. and parametric behaviour 80–37998
- inert gas halide electronic transition laser, quantum chem. 80–32971
- inert gas halide excimer laser, electron beam excited, efficiency 80–53278
- inert gas halide excimers, book contrib. 79–81418
- inert gas halide high power lasers, const. E/N pumping 77–88711
- inert gas halide high-power lasers, efficiency and energy scaling, review 79–36887
- inert gas halide laser, discharge excited, gas composition and lifetime studies 80–53268
- inert gas halide laser compatible materials, gas purification techniques 80–38037
- inert gas halide lasers, 60-ns electron beam excitation 80–74340
- inert gas halide lasers, e-beam sustained, glow discharge stability 79–55117
- inert gas halide lasers, operation and use in photochem. 80–9860
- inert gas halide lasers, pumped by transverse elec. discharge devices 79–41373
- inert gas halide lasers, use in mol. photolytic dissoc. obs. of Se_2 80–11935
- inert gas halide VUV lasers, pumped by travelling-wave discharges, 170 to 250 nm range 79–41372
- inert gas halides, exciplex mol. form., rel. to laser operation 80–81318
- inert gas halides, high power and efficiency, review 78–33728
- inert gas halides, III(1/2)-II(1/2) transition 79–94211
- inert gas halides, kinetic processes 78–63098
- inert gas halides, laser mechanism, excitation methods and appls. 80–95871
- inert gas halides, pumping technology 77–88767
- inert gas halides, triatomic, as laser candidates 80–28220
- inert gas halides, UV emission spectra, pressure and temp. depend. 80–28209
- inert gas halogen excimer laser principles, performance and applications 78–55342
- inert gas halogen exciplex, spontaneous and superfluoresc. emission, pumping of I laser 77–34883
- inert gas metastable atoms, photoionisation rel. to laser development 78–13476
- inert gas mixture, electrophotoionization discharge, laser pumping 80–91781
- inert gas molecule, population inversion in high press. short discharge 77–71974
- inert gas monohalides, UV excimer lasers, review 77–34877
- inert gas nuclear pumped lasers, prod. efficiency of excited states 80–63998
- inert gas oxide amplifiers, appl. and performance 78–63085
- inert gas oxides, kinetics and energy flow, expt. characts., book contrib. 79–81417
- inert gas-halide lasers, halide mol. negative ion prod. rates 80–18938
- inert gas-halogen bearing molecule three-component mixture, self-sustained electric photoionization discharge 80–54073
- inert gas-halogen excimer lasers, electron beam controlled discharge pumping 77–10893
- inert gas-halogen mixtures, UV laser output from elec. discharge after X-ray preionisation 79–64205
- inert gases, electron beam excited, absorpt. characts. 78–82948
- inert gases, self-sustained discharge possibility with bulk photoionisation impurities 80–75113
- inert halide lasers, emission spectra, efficiencies, pulse energy, appls. 78–58993
- intense lasing with HCl halogen donor 78–90411
- ion-molecule processes in lasers, excitation methods 80–28221
- ionisation instability buildup of nonself-sustained discharge laser 80–9858
- isotope separation pulse power requirements 79–13972
- kinetics simulation of high-power gas lasers 79–59676
- laser-radar observations of stratospheric O_3, excimer laser appls. 80–17410
- mercuric halide dissociation lasers, discharge pumping 78–79009
- metal atom oxidation reactions, kinetics of chemilum. emitter form. and quenching 78–63107
- metal halide vapours, quantum efficiency of fluoresc. excited by photodissociation 79–81421
- metal oxide, temp. depend. of chemilum. reactions, activation energies for excited state form. 78–66818
- metal vapour excimers, book contrib. 79–81419
- metal vapour laser discharges, stability criteria 78–66802

excimer lasers continued
nuclear generated plasmas, ^{3}He and $^{235}UF_6$ excitation, spectra obs. 80—83997
nuclear pumping, inert gas media 78—17916
optically pumped CW dimer lasers, Li_2, Na_2, K_2, Bi_2, S_2, Te_2, and I_2 80—14322
optically pumped mol. lasers, review 80—58519
organic material forming quasi-one-dimensional crystals 80—23673
oscillation and amplification, high output and efficiency 78—66807
oscillatory excimer emission, analytic quantum mech. model 79—59675
photochemical applications 79—98379
photoionisation excimer laser characts. 80—102712
photopreionization-stabilized discharge scheme for inert gas halogen excimer lasers 80—33009
physical processes and performances 80—32962
preionisation techniques, spark and corona preionisers 80—33016
progress and development 80—14326
pulsed and CW optically pumped lasers for novel applications in spectroscopy and kinetics 78—90413
pumping, quasi-reson. energy and charge exchange processes, new transitions 80—58526
pumping by barrier tunnelling for exciplex lasers 78—17908
radioactive source preionisation of visible and UV discharge lasers 78—63096
rare gas halide lasers, high repetition rate, multiple cct. pulse generator 78—94399
recombination processes, book contrib. 77—50663
review 77—34877
review of lasers with wide-band optical pumping 79—31885
stability enhancement of electron beam sustained laser discharge 79—98381
surface metallization studies for excimer laser electrodes 80—19048
technology advances, conf., Washington, USA (Mar. 1978) 79—36911
tesla discharge as spectroscopic source for excimer laser transitions study 80—274
theory and application, reviews 79—59684
tunable UV and visible lasers 78—59029
UV, using pulsed discharge pumping, design and operation 79—31946
UV absorption spectra for inert gas dimers 78—17680
UV laser *(Japanese)* 79—3686
UV molecular lasers with transverse electronic pumping, review *(French)* 79—31880
UV nonlinear optical processes using excimer lasers 80—38060
UV range, new perspectives *(German)* 80—53309
UV/visible gas lasers, appls. in commercial photochemical processes, review 79—55123
vacuum UV coherent sources, and freq. up-conversion 77—7067
visible wavelength lasers, gasdynamic and acoustic management 79—36937
volume high-pressure discharge with photoionization for laser pumping 80—54058
XeF laser wavelenghts, transient absorpt. in electron-beam excited inert gases 80—83592
$Ar\text{-}F_2$, proton excited mixtures, energy transfer processes 78—66647
$Ar\text{-}F_2$ excimer laser, kinetics of excimer formation 80—14328
$Ar\text{-}Hg\text{-}Cl_2$, elec. discharge, electron inelastic collision props. 80—79617
$Ar\text{-}I_2$, low electron beam excitation rates 79—86163
$Ar\text{-}Kr\text{-}F_2$, nucl. pumped laser, high energy beam deposition 80—63999
$Ar\text{-}Kr\text{-}F_2$, proton excited mixtures, energy transfer processes 78—66647
$Ar\text{-}Kr\text{-}F_2$ excimer laser, kinetics of excimer formation 80—14328
$Ar\text{-}Kr\text{-}F_2$ mixture, electron beam pumped, spectroscopy and kinetics of 248, 414 nm bands 78—63081
$Ar\text{-}N_2$, electron-beam-excited laser lines at 337.1, 357.7, and 380.5 nm, gain conditions 79—86166
$Ar\text{-}N_2$, intense proton beam pumping 78—78998
$Ar\text{-}N_2$, proton beam pumped, laser actqn at 3577 Å 80—9861
$Ar\text{-}N_2$ electron beam pumped laser characts. at 25-350°C 78—58984
$Ar\text{-}N_2$ laser, electron beam excited, gain measurements using amplified spontaneous emission 80—37986
$Ar\text{-}N_2$ mixture, electron beam pumped, lasing obs. at 337, 358, 380 and 406 nm 80—102700
$Ar\text{-}N_2$ mixture, lasing at four lines 80—99713
$Ar\text{-}Xe\text{-}F_2$, proton excited mixtures, energy transfer processes 78—66647
$Ar\text{-}Xe\text{-}NF_3$ mixture, fluorescence from e-beam excitation at low temp. and high press. *(French)* 78—58727
Ar-Xe-tetrachloromethane excimer discharge laser 79—13957
$Ar^{+}+Cl^{-}(F^{-})$ in Ar, high press. ion-ion recomb. rate calcs. 78—31621
Ar_2, electron beam excited, absorpt. characts. 78—82948
Ar_2, electron-beam pumped, visible absorpt. rel. to laser development 79—59671
Ar_2, excimer laser action in coaxial field emission diode, comparison with Kr_2, Xe_2 80—28201
Ar_2, tunable vac. UV action 80—48215
$Ar_2{}^{+}$, electronic states, pot. curves, with/without spin-orbit interaction 78—33443
ArCl superfluorescent laser, discharge-pumped, laser action at 175 nm 77—38859
ArF, 50 mJ double discharge excimer laser, spectroscopy and characts. 78—63082
ArF, Ar_2F, time depend. emission meas., $Ar\text{-}Kr\text{-}F_2$ laser mixture kinetics 80—32768
ArF, closed cycle characts. 80—33030
ArF, closed cycle flow type, operating characts. 80—43349
ArF, discharge laser, operating characts. 79—22937
ArF discharge laser, steady state amplification 80—5726
ArF, double discharge laser, operating parameters, discharge characts. 77—88704
ArF, double discharge laser, prism tuning 78—37892
ArF, electron quenching rate consts. meas. by fluoresc. anal., laser implications 80—32969
ArF excimer laser, electron-beam pumped, efficiency and gain 80—78844
ArF excimer laser multiphoton ionisation mass spectra 80—81381
ArF, excimers, power superluminescence, in elec. discharge *(Russian)* 77—7621
ArF, high efficiency laser, photolysis of OCSe producing Se 80—33032
ArF laser, excimer gas-discharge tunable, intense laser oscill. obs. 77—38862
ArF, laser emission, ab initio config. interaction calcs. on electronic states 78—63083
ArF, laser expts. on $^{2}\Sigma\text{-}^{2}\Sigma$ transitions 78—63080

excimer lasers continued
ArF laser pump source, tunable efficient VUV generation using stimulated Raman scatt. in H_2 80—38072
ArF, providing high-power stimulated radiation in Ar and F lines 77—83858
ArF, pump radiation for HgBr dissociation laser 78—13695
ArF, Raman shifting of laser wavelengths 77—75539
ArF, stimulated Raman scatt. of excimer laser wavelengths for new lines in UV 79—59755
ArF superradiance laser excited by electric discharge 77—19236
ArF, UV preionised transverse discharge laser, theoretical model 79—22938
ArF, UV preionized discharge pumped laser 77—10889
ArF*, Ar_2F^*, kinetics of proton-excited $Ar\text{-}F_2$ mixtures, time-resolved and time-integrated spectra 79—36883
ArF*, electron beam pumped, dominant formation and quenching processes 79—938
Ar_2F^*, radiative lifetimes, quenching rate consts., emission spectra 78—46577
ArO, lasing, low-lying electronic states, ab initio config. interaction calcs. 78—63084
$Ar_2(^{3}\Sigma_u{}^{+})+N_2$, quenching, fast absorption spectrophotometry 79—54940
ArXeF*, gain meas. at 4416 Å 78—50758
$Ar_2{}^{*}$, electron impact ionisation cross sections in binary encounter approx. 79—68320
$Ar_2{}^{*}$, excimers and excimer lasers 80—48217
Bi_2, optically pumped continuous laser oscill. 79—933
Bi_2, vap., optically pumped, laser action 78—71081
Br_2, optically pumped at 532 nm, lasing obs. in visible and near IR 78—63094
Br_2, optically pumped laser, operation 78—25858
Br_2, UV laser transitions, electronic designation 79—944
BrCl, time-resolved fluoresc. of $a^{3}\Pi_0{}^{+}$ state 78—63093
$Br_2{}^{*}$, excitation mechanism in $Ar\text{-}Br_2$ system 77—31096
$Br_2{}^{*}$ laser, excitation mechanism in $Ar\text{-}Br_2$ system 77—31096
CN ($A^{2}\Pi$), chem. prod., CN number densities for gain, emission and absorpt. meas. 78—63112
CN radicals, electronic transition laser, using C_3F_7CN and $(CN)_2C_4F_8$ photodissociation 78—50769
CO* prod. from $Ar^{*}+CO_2$, use in laser systems 80—63824
$C^{3}\Pi_u$ effective lifetime in N and air 80—102704
CdHg excimer system, absorpt. meas. 80—48007
CdHg, positive gain measurements or 470 nm continuum band 78—66805
CdHg* excimer, kinetic model of sustained discharge excitation 78—66804
CdHg*, metal vapour exciplex laser, stability criteria 78—66802
$Cd^{*}{}_2$, 470 nm absorber, multiconfiguration SCF calcs. 80—27963
Cl_2, laser oscillation on 2580 Å band system, axial electron beam excitation of $He\text{-}Cl_2$ 79—31879
ClF, interhalogen UV laser on 285 nm band, fluoresc. and laser oscill. obs. 79—76674
ClF UV laser system 80—83597
Cs-Xe solar-pumped MHD excimer laser, modelling 80—95873
Cs_2, fluoresc. spectra, kinetics, laser candidate 79—64027
CsXe, form. and dissociation rates, fluoresc. meas. 78—1216
$F^{-}+Ar^{+}(Ar_2{}^{+})(Kr^{+})(Kr_2{}^{+})$, in Ar, high press. ion-ion recomb. rate calcs. 78—31621
F_2 discharge pumped laser, 1578 Å emission 79—31877
F_2 molecular laser, high power, electron beam excited 79—932
F_2 UV laser system 80—83597
F_2, VUV high-power laser, laser-induced fusion 78—58996
F_2, valence electronic states, $^{1}\Pi_u \leftarrow X^{1}\Sigma_g{}^{+}$ absorption spectrum 79—63920
F_2-Ne(He) mixtures VUV emissions, mol. F_2 laser at 1575 Å 77—75487
GeO, produced in $Ge+N_2O$ reaction, kinetics of chemilum. emitter form. and quenching 78—63107
H_2, high-power, vac. UV emission at high pulse repetition freq. 78—29977
H_2 laser, VUV, with sealed gas-discharge tube 80—74399
H_2, Lyman system nonsaturated laser line intensity obs. 78—71089
H_2, transversely excited, oscill. characts. in vacuum UV region *(Japanese)* 78—22148
H_2 VUV laser, compact high repetition rate for scientific appl. 78—37899
H_2, vac. UV, appl. to mol. photoionisation in mass spectrometer 77—88606
H_2, vac. UV discharge, elementary processes 78—9370
H_2, vacuum UV, high power, excited by longit. elec. discharges *(German)* 78—37896
H_2, vacuum UV lasing 77—7067
$H_2(a^{3}\Sigma_g{}^{+}\rightarrow b^{3}\Sigma_u{}^{+})$ continuum emission excited by low-energy Ar^{+} collisions, UV laser appl. 79—41200
$HbBr(B^{2}\Sigma^{+}{}_{1/2})$, rate coeffs. for collisional quenching, time resolved emission obs. 79—89705
He and He^{+}, $3^{3}P$ and $4^{2}F$ levels excitation with electron beams, radiation decay obs. 80—43188
$He\text{-}F_2$, dissociative electron attachment, rate coeffs., appl. to lasers 78—46575
$He\text{-}Xe\text{-}F_2$ mixture, pulsed avalanche discharge at high gas press., homogeneous form. conditions 80—49027
He_2 dimer, electron-beam pumped, anal. of feasibility of stimulated vacuum UV radiation 80—9857
Hg halide electrically excited dissociation laser, kinetic processes 80—38013
Hg halide electronic transition laser, quantum chem. 80—32971
Hg halide lasers, efficiency of different pumping methods, review 79—36886
Hg-Cs, vac. UV laser, charge exchange pumping 77—31095
Hg-Xe(Kr)(Ar), fluoresc. emission, high press., electron beam excitation, laser appl. 77—34676
Hg_2, 335 nm optically pumped, signal gain 78—999
Hg_2 as energy storage medium, energy extraction from metastable excimers 79—59677
Hg_2, dissociative recomb. and optical transmissions meas. in high press. discharge 80—37816
Hg_2 excimer states, energy transfer kinetics 78—63090
Hg_2 excimers in constricted positive column, radial intensity distrib. meas. 78—63091
Hg_2, high press. transverse discharge for high efficiency, elec. and optical props. 78—63092
Hg_2, photoassoc. processes and laser applics. 80—9649

excimer lasers continued
- HgBr, 502 nm stimulated emission, prolonged optical pumping of $HgBr_2$ 79—18414
- HgBr, ab initio CI calcs., spectroscopic parameters 79—72245
- HgBr, $B^2\Sigma_{1/2}^+ \rightarrow X^2\sigma_{1/2}^+$ band at 5018 Å 77—83856
- HgBr $B^2\Sigma_{1/2}^+ \rightarrow X^2\Sigma_{1/2}^+$ laser, sustained discharge excitation 78—42342
- HgBr, B→X transition radiative lifetime, charge transfer model 78—17719
- HgBr dissociation laser is elec. discharge 78—50768
- HgBr, dissociation of $HgBr_2$, oscillator and oscillator-amplifier expts. 80—48232
- HgBr electrically excited dissociation laser, kinetic processes 80—38013
- HgBr, electrically excited dissoc. of $HgBr_2$, kinetic processes 80—48231
- HgBr, laser action on B→X bands, 5018 Å 77—88709
- HgBr, laser photolysis prep., laser induced fluoresc., collisional quenching processes 80—38014
- HgBr laser using dissociative excitation of $HgBr_2$, extraction efficiency increased by N_2 addition 80—38012
- HgBr, visible laser action due to $HgBr_2$ photodissociation 77—88710
- HgBr, visible laser transitions at 5018 Å and 4984 Å 79—939
- $HgBr_2$+ inert gas metastable atom ($N_2(A^3\Sigma_u^+)$), dissoc. excitation 80—63774
- HgCl, ab initio CI calcs., spectroscopic parameters 79—72245
- HgCl $B^2\Sigma_{1/2}^+ \rightarrow X^2\Sigma_{1/2}^+$ laser, sustained discharge excitation 78—42342
- HgCl, $B^2\Sigma^+ \rightarrow X^2\Sigma^+$ band, electron beam excited Ar/Xe/Hg/CCl_4(CCl_3Br) mixtures 78—13683
- HgCl, B→X transition radiative lifetime, charge transfer model 78—17719
- HgCl discharge laser, electron beam sustained, operation, appls. 78—59043
- HgCl, laser action obs. at 5576 Å 77—83855
- HgCl, laser action on B→X bands, 5576 Å 77—88709
- HgCl, photodissociation cross section, laser extraction efficiency 80—32972
- HgCl, photodissociation calcs., laser efficiency 80—48047
- HgCl, visible laser transition at 5576 Å 79—939
- HgCl(B→X) laser, photolytic pumping, HgCl(B) state radiative lifetime meas. 78—94390
- $HgCl_2(Br_2)$, low lying excited state electronic struct. and photodissoc., appl. to lasers 80—63560
- HgCl*, laser action using electron-beam-controlled discharge pumping 78—42325
- HgCl*, metal vapour excimer laser, stability criteria 78—66802
- HgCl*(B1/2), fluoresc., collisional quenching kinetics 78—94269
- HgH, two-level laser system, discharge simulations 80—74351
- HgI, B→X transition radiative lifetime, charge transfer model 78—17719
- HgTl excimer laser, kinetics, optical excitation obs. 80—58527
- HgTl optically excited excimers, upper state kinetics 80—37831
- HgX (X=F, Cl, Br, I), three-body ion-ion recombination rates 78—63068
- I_2, B-X system superfluoresc. emission obs., 1.1 to 1.3 μm 79—81412
- I_2, CW, optically pumped, performance 78—17912
- I_2, CW optically pumped, laser oscill. 0.57 to 1.35 μm 79—943
- I_2, efficient laser action on 342 nm band, ArF laser pumping 80—99703
- I_2 laser, three-level, pumped by CW dye laser 80—63993
- I_2 laser, with programmed mag. field 78—33750
- I_2 molecule B-X electron transition during Cu vapour laser optical pumping *(Russian)* 80—78845
- I_2 molecule pumped by Cu vapour laser, pulsed stimulated emission due to electronic transitions 80—14330
- I_2, optical pumping, quasi-tunable IR emission, appl. to absorption meas. 77—42551
- I_2, optically pumped, lasing obs. on 342 nm band 78—79008
- I_2, optically pumped continuous laser, 583-1338 nm 78—17962
- I_2, optically pumped laser, I_2 transition moment from gain 79—54917
- I_2, optically pumped UV, 1 μs pulse emission at 342 nm 77—79811
- I_2, oscillatory excimer emission, analytic quantum mech. model 79—59675
- I_2 UV laser, quartz flashlamp pumped, pulse-periodic operation 80—53279
- I_2, UV laser transitions, electronic designation 79—944
- I_2+Ar(Ne)(tetrafluoromethane), D-state lifetime and UV laser action 77—14471
- IF emission spectrum and form. kinetics in electron-beam-produced plasma 80—102533
- KXe, dye laser induced emission, excimer bands and uses 80—9650
- Kr-Xe-F_2 excimer laser, kinetics of excimer formation 80—14328
- Kr_2, electron-beam pumped, visible absorpt. rel. to laser development 79—59671
- Kr_2, excimer laser action in coaxial field emission diode, comparison with Ar_2, Xe_2 80—28201
- Kr_2, kinetics of optically excited electronic states 78—63059
- Kr_2^+, electronic states, pot. curves, with/without spin-orbit interaction 78—33443
- KrCl, B and C states, energy ordering from temp. depend. of emission spectra 80—78837
- KrCl laser, lifetime extension by H addition 80—91773
- KrCl, laser expts. on $^2\Sigma$-$^2\Sigma$ transitions 78—63080
- KrCl, stimulated emission obs. from electron beam excited Ar-Kr-Cl_2 mixture 77—672
- KrCl, stimulated Raman scatt. of excimer laser wavelengths for new lines in UV 79—59755
- KrF, 0.8 J multi-atm. laser, glow discharge characts. 78—58992
- KrF, 1/4J discharge pumped laser 78—74927
- KrF 1J avalanche discharge laser unstable resonator expts., beam divergence 80—74404
- KrF, 25 J unstable resonator oscillator, injection locking 80—28218
- KrF, absorpt. spectra of $ArKr^+$, ab initio calc. of potential energy curves 78—74568
- KrF, closed cycle characts. 80—33030
- KrF, closed cycle flow type, operating characts. 80—43349
- KrF, development of dielectric mirror *(Japanese)* 79—72588
- KrF, diffraction-limited laser, with negative branch unstable resonator 77—38937
- KrF, discharge and electron beam pumped, review 78—71083
- KrF, discharge excited laser operation at elevated temps., transitions, output power 80—43359
- KrF, discharge laser, operating characts. 79—22937
- KrF discharge laser, steady state amplification 80—5726
- KrF, discharge pumped laser, efficient amplification 78—78997

excimer lasers continued
- KrF discharge pumped laser, circuit and UV preioniser parameters effect 79—55143
- KrF discharge pumped laser, stable-unstable resonator for beam control 80—23722
- KrF discharge pumped laser, energy extraction, collisional coupling between B, C and D-states 80—28213
- KrF, double discharge laser amplifier, small signal gain meas. 77—79807
- KrF, double discharge laser, operating parameters, discharge characts. 77—88704
- KrF, double discharge laser, prism tuning 78—37892
- KrF, e-beam pumped Kr-F_2 mixtures, form. and quenching processes 78—42322
- KrF, efficiency optimisation, photoionisation cross sections for excited states of Kr and Ar 77—75110
- KrF, efficient 1/4 J laser with corona preionisation 79—59713
- KrF efficient discharge-pumped laser, amplification characts. 79—59679
- KrF, efficient short pulse lasing 80—28217
- KrF, elec. discharge laser, pulsed, high-power UV emission *(Russian)* 77—79808
- KrF, electric discharge pumped laser, model for UV preionisation 77—23658
- KrF, electrically excited laser, theoretical model 78—42321
- KrF electroionisation laser, energetic, threshold and spectral characts. 80—99705
- KrF, electron beam controlled discharge laser, plasma elec. characts. 79—59680
- KrF, electron beam pumped, high press. UV emission 78—25866
- KrF, electron beam pumped laser system at 2 to 7 MW/cm^3 excitation rates 80—32968
- KrF, electron beam pumped laser medium, time depend. fluoresc. spectrum in high current density range 80—78842
- KrF, electron beam stabilised, electron kinetics 77—83888
- KrF, electron beam sustained discharge excitation, threshold power density meas. 78—63078
- KrF, electron impact deexcitation, low energy cross-sections and rate consts. 80—1071
- KrF, electron quenching rate consts. meas. by fluoresc. anal., laser implications 80—32969
- KrF electron-beam pumped laser, performance model 80—53273
- KrF electron-beam-excited amplifier, master-oscillator power-amplifier expt. for gain coeff. and saturation intensity determ. 80—48222
- KrF excimer laser, passive mode-locking using saturable absorber dyes 80—1244
- KrF, excimer laser pumped dye laser *(Chinese)* 80—1234
- KrF excimer lasers, lasing action *(Chinese)* 79—59682
- KrF, excimer lasers, state of art 80—95879
- KrF, excimers, power superluminesc. in elec. discharge *(Russian)* 77—7621
- KrF, excimers and excimer lasers 80—48217
- KrF, fast discharge laser in NF_3, N_2F_4 or SF_6 mixtures 77—31097
- KrF, fluoresc. spectrum, theoretical modelling using electronic potential curves 78—63086
- KrF, for pumping of UV dye lasers 79—10301
- KrF, formation and quenching of electronic excited states 77—673
- KrF, high brightness performance using high magnification unstable resonator 79—59716
- KrF, high efficiency laser with short pulse electron excitation 80—33032
- KrF, high pulse rate, 10 W excimer laser 78—42348
- KrF, high-power, dye laser pumping characterisation at 248 nm 80—1199
- KrF high-power electron-beam pumped lasers, optical performance 78—46640
- KrF high-power laser, efficiency and energy scaling 79—36887
- KrF high-power laser, X-ray preionisation 80—33031
- KrF injection locked unstable resonator discharge laser, narrow linewidth and high spatial quality 80—53323
- KrF, injection-locked narrow-band discharge laser, using unstable resonator cavity 78—25893
- KrF, kinetics simulation of high-power gas lasers 79—59676
- KrF, Kr_2F, in electron beam pumped Ar-Kr-F_2 mixture, spectroscopy and kinetics of 248, 414 nm bands 78—63081
- KrF, Kr_2F, time depend. emission meas., Ar-Kr-F_2 laser mixture kinetics 80—32768
- KrF laser, collisional coupling between B, C, D states from fluoresc. meas., influence on energy extraction 80—1189
- KrF laser, e-beam sustained, glow discharge stability 79—55117
- KrF laser, electron beam pumped, with Ne-Ar diluent 79—22936
- KrF laser, electron-beam sustained discharge excitation, threshold power density meas. 77—88699
- KrF laser, kinetic model, limiting behaviour and scaling 80—78838
- KrF laser action in return-current discharge-excited F_2/Kr/He mixtures 78—94920
- KrF laser beam, Raman pulse compression, for fusion expts. 78—59086
- KrF laser compatible materials, gas purification techniques 80—38037
- KrF laser driven methane backward Raman amplifier, high-efficiency energy extraction 80—106533
- KrF, laser emission, ab initio config. interaction calcs. on electronic states 78—63083
- KrF laser excitation of tunable UV Ce:LiYF_4 laser 80—38022
- KrF laser induced preionization of XeCl discharge 80—84020
- KrF, laser performance, collisional quenching rates 78—63066
- KrF, laser spectrum, discharge-pumped, absorption bands and lines, assignment 78—79004
- KrF linac-excited gas mixture, UV fluoresc. meas. 80—28216
- KrF, meas. of basic reaction parameters 78—13578
- KrF mini-laser operation at high repetition rate 80—74396
- KrF, operating and beam characts. 79—59715
- KrF oscillator at excitation rates of 2-7 MW/cm^3 80—5727
- KrF, photoionisation excimer laser characts. 80—102712
- KrF, power and efficiency, review 79—937
- KrF pump laser, scaled Raman pulse compression experiments at 248 nm 80—38071
- KrF, radiative lifetime and quenching 78—63063
- KrF, Raman pulse compression for appl. to laser fusion 79—59756
- KrF, Raman shifting of laser wavelengths 77—75539
- KrF, review of basic properties *(Japanese)* 78—33723
- KrF, simple high-power TEA laser operating in UV 79—94251
- KrF, small signal gain meas. and kinetic modelling 78—63077
- KrF, spark-preionised large-vol. discharge laser 78—1218

excimer lasers continued
KrF, stability enhancement of electron beam sustained laser discharge 79−98381
KrF, stimulated Raman scatt. of excimer laser wavelengths for new lines in UV 79−59755
KrF superradiance laser excited by electric discharge 77−19236
KrF, UV bound-free emission after electron excitation 77−27279
KrF, UV discharge laser, emission spectra 77−79809
KrF, UV excimer laser, fast helical pin discharge, 50 μJ 77−23660
KrF, UV preionised transverse discharge laser, theoretical model 79−22938
KrF, UV preionized discharge pumped laser 77−10889
KrF, using corona preioniser 80−33016
KrF, water dielec. Blumlein-driven fast elec. discharge pulser 79−10318
KrF X-ray-preionized high-pressure laser 79−18403
Kr_2F, absorpt. in near UV wing of 410 nm band, fluoresc. efficiency 80−14323
KrF* constant E/N pumped high-power laser, parametric study 78−42346
KrF* discharge laser, 248 nm pumping of dye laser 79−954
KrF* discharge laser, pump for tunable narrow bandwidth 2 MW dye lasers 79−41378
KrF*, discharge pumped, influence of electron-F_2 collisions 78−42326
KrF*, elec. discharge excimer lasers, stimulated emission 79−31884
KrF*, electron beam controlled laser, plasma processes 79−930
KrF*, electron beam pumped, dominant formation and quenching processes 79−938
KrF*, electron beam pumped laser, pulse shape and laser-energy extraction, model and expt. comparison 79−98345
KrF*, excimer laser, electron beam controlled discharge pumping 77−10893
KrF*, Kr_2F*, kinetics of proton-excited KrF_2 mixtures, time-resolved and time-integrated spectra 79−36883
KrF* laser, gain and absorption meas. 77−79802
KrF* laser, generation of high-spectral-brightness tunable XUV radiation at 83 nm 80−91846
KrF* laser, influence of F_2 dissociation and degree of ionisation 78−50756
KrF* laser discharges, electron beam sustained, instability onset 78−63065
KrF* laser system, trimer form. rates 80−50831
KrF* nuclear pumped lasers, excited state prod. rate and fission power pulse shape matching 80−63998
KrF*, three-body quenching by Ar and broad-band emission at 415 nm 77−75486
KrF* tunable ultrahigh spectral brightness excimer laser source 80−64046
KrF*, waveguide laser excited by capacitively coupled discharge 78−94391
KrF*+Ar(Kr)+Ar(Kr), recomb. rate consts., 300 to 800K, appl. to KrF* laser efficiency 79−45930
KrF*+Ar(Kr)+Ar(Kr)→Ar(Kr)KrF*+Ar(Kr) recombination rate consts. calc. 77−75488
Kr_2F*, gain meas. at 4416 Å 78−50758
Kr_2F*, radiative lifetime and quenching rate consts. 78−63056
KrO, high press., optical gain profile near 5577 Å 77−68204
KrO, lasing, low-lying electronic states, ab initio config. interaction calcs. 78−63084
Kr_2*, excimers and excimer lasers 80−48217
Kr_2*, radiative lifetime and quenching rate consts. 78−63056
Kr_2*, stimulated emission kinetics in nonself-sustained elec. discharge 78−50753
La-F_2(ClF)(Cl_2)(SF_6), visible chem. laser development from reactions yielding visible chemilum. 78−63111
Li_2, $^3\Sigma_g{}^+$-$^3\Sigma_u{}^+$ excimer emission, ab initio calcs. 80−91608
Li_2, gerade excited electronic states, pulsed optical-optical double reson. spectroscopy, laser medium 79−81220
Li_2, laser, continuous, optically pumped 78−87046
Li_2 laser, proposed, implications of crossing of a $^3\pi_u$ state pot. with $^3\Sigma_u{}^+$ pot. 77−50369
Mg_2 $A^1\Sigma_u{}^+$-$X^1\Sigma_g{}^+$ system, discrete and continuous Franck Condon factors, J-depend. 78−66811
MgXe excimer bands, emission intensities and excited-state densities meas. 80−92413
N_2, 3371 Å, fringe visibility curve 78−46695
N_2, 3371 to 1124 Å conversion by nonresonant freq. tripling in compressed Kr gas 79−64279
N_2, 337.1 nm emission, high specific power, high pulse repetition freq. 79−45932
N_2, capacitor modification 77−14735
N_2, ceramic capacitor failure elimination 78−33740
N_2, coherent radiation from unstable resonator 77−71994
N_2 compact LEA laser, for sub-nanosecond pulse generation 79−76708
N_2, development of miniature high-power high-press. UV and IR lasers 78−46642
N_2 discharge laser, photopreionisation stabilised, high-power, ultraminiature 79−22977
N_2, effect of SF_6 on lasing characts. 77−65591
N_2 electron impact excitation, rate coeffs., momentum transfer cross-section 78−78819
N_2 electron-beam-sustained discharge stability model 78−71608
N_2, employing electron seeding technique, performance 77−71997
N_2, energy transfer from Ar, 3371 and 3577 Å laser emission, kinetic model 78−5465
N_2, first positive system, for optical fibre meas. 78−59020
N_2 helical TE laser, tube geometry simplification 80−69406
N_2 helical TE laser with circular beam cross section 80−33023
N_2 high power discharge laser excited through high dielectric constant ceramic materials 80−58572
N_2 high power inexpensive laser for student laboratory 77−23687
N_2, high power UV lasers, travelling wave excitation via low-impedance high-voltage pulsers 77−3608
N_2 high-power pulsed laser manufacture and reliability 77−19331
N_2, high-press., UV *(Japanese)* 78−55346
N_2, home-built, design improvements 78−46612
N_2, IR laser transition, excitation process 80−87383
N_2, interference-free coaxial system, construction and operational anal 77−38918
N_2, LG-21 serial, org. dye accessory invertor 77−68224
N_2 laser, 406 nm emission on C→B band 80−64047

excimer lasers continued
N_2 laser, appl. of pulsed transversally excited discharge *(French)* 80−107009
N_2 laser, construction and properties, axial or cross-field discharge 80−69418
N_2 laser, electrode configuration for high peak powers and high repetition rates 78−55379
N_2 laser, high-power, TE, UV, using Blumlein transmission line, construction characts. *(Korean)* 79−22971
N_2 laser, high-press., effect of SF_6 addition 78−25859
N_2 laser, segmented equiv. circuits and rate eqns. *(Chinese)* 79−50282
N_2 laser, stimulated emission kinetics under pulse-periodic conditions 79−64212
N_2 laser, superrad., inexpensive construction *(Korean)* 78−22147
N_2 laser, time shape of laser pulse 79−7120
N_2 laser, UV, discharge-excited, improvement in efficiency *(Japanese)* 78−33724
N_2 laser 337.1 nm transition, rotational struct. variation 80−78836
N_2, laser channel dynamic behaviour, spontaneous emissions obs. *(German)* 78−25867
N_2 laser discharge dynamic characts., power supply circuit 79−18446
N_2 laser discharge emission model and meas. 78−71093
N_2 laser for pumping dye lasers with spectral narrowing 78−25903
N_2 laser pump for tunable dye laser oscillator-amplifier system *(Japanese)* 79−68406
N_2 laser pumped DFB dye laser, tunable single ps pulse generation 79−55147
N_2 laser pumped dye laser, construction and performance of laser and pumping source *(Japanese)* 77−58341
N_2 laser pumped unstable ring resonator dye laser 80−53326
N_2 laser transitions, Ar($^3P_2$)+N_2($C^3\Pi_u$) excitation transfer cross section, radiative lifetime 79−27246
N_2 laser-pumped dye laser, generation of tunable ultrashort light pulses *(German)* 79−27275
N_2 lasers, pulsed operation, characteristic data comparison 79−10287
N_2, metal-ceramic discharge chamber, with transverse excitation 80−48285
N_2, miniaturised atmospheric press. laser 77−54733
N_2 mixing with dye laser in $NH_4H_2PO_4$ for 0.68-1.1 μm output 77−27314
N_2 molecule $\omega \rightarrow a$, $a \rightarrow a'$ electron transitions, strong near IR generation *(Russian)* 79−76676
N_2 multi-stage TEA laser 80−95912
N_2 multichannel Blumlein type laser, elec. and optical characts. 79−59719
N_2, new laser struct. *(French)* 77−61971
N_2, oscillator-amplifier laser system in 337 nm band 77−14748
N_2, oscillator-amplifier system using press.-depend formative time lag of discharge 80−14354
N_2, oscillatory circuit with current breaker for discharge excitation 77−14759
N_2, photostabilised UV laser, gain, fluoresc., and energy extraction characts. 79−7118
N_2, practical design of high-power laser 77−42545
N_2, pulsed, interfacing with higher freq. electro-optic instrumentation 77−50698
N_2 pulsed laser, construction and theoretical explanation *(Slovak)* 80−95874
N_2, pulsed laser with damping capacitors, dynamics *(German)* 77−10957
N_2, pump for dye laser, conversion to UV radiation in nonlinear crysts. 77−743
N_2, pumped by relativistic electron beam, numerical model 77−75492
N_2, pumping 0.915 to 1.04 μm of IR dye laser 77−61969
N_2, pumping dye laser, short tunable pulses 77−7126
N_2, reliable, high-power, design 77−706
N_2 Schenck-Metcalf laser, capacitor modification 79−18439
N_2, sealed off miniature high-power laser 78−22143
N_2, sealed system with 10 kHz pulse repetition freq. 77−58344
N_2, simple and reliable atm. press. laser 79−55150
N_2, simple high-power TEA laser operating in UV 79−94251
N_2, single freq. emission, superradiance line splitting 77−75495
N_2 small-size discrete-capacitor laser 77−660
N_2, stimulated emission kinetics under pulse-periodic conditions, theory 79−59689
N_2 superfluorescent UV laser, demonstration 80−105475
N_2, superradiant, fast helical pin discharge, 4.5 mJ 77−23660
N_2 superradiant UV laser, method for brightness increase 79−36917
N_2, TE, anal. of time variation of discharge channel voltage by Pockels effect 78−90412
N_2, TEA, for sub ns spectroscopy, modified elec. field 78−17964
N_2, TEA, pump for dye laser amplifier system 78−82984
N_2 TEA high-power laser using modified Marx generator 80−1229
N_2 TEA laser, compact high power, modification 78−90427
N_2 TEA pulsed UV laser 77−68228
N_2, TEA system, coherent UV generation, synchronisation technique 78−17949
N_2, transient discharge stage calcs. 77−666
N_2, transverse excited $C^3\Pi_u \rightarrow B^3\Pi_g$(0-0) UV laser band, spectroscopic rot. anal. 79−7115
N_2, transverse excited $C^3\Pi_u$-$B^3\Pi_g$ (0-0) UV laser band, spectroscopic analysis 79−76671
N_2, travelling wave, pump for short resonator tunable dye laser 80−48291
N_2, travelling wave pulsed 79−59685
N_2 UV emitting simple and reliable laser, with H_2 thyratron switch 79−27290
N_2 UV laser, long pulse from N_2-CF_4 mixture 78−63067
N_2 UV laser, travelling-wave corona excitation 77−7121
N_2, UV laser *(Russian)* 77−83859
N_2 UV lasers, performance and operation *(Polish)* 79−55124
N_2 UV multichannel laser, short duration pulse generation 79−969
N_2 UV pulsed laser with Blumlein pulse generator, fabrication *(Japanese)* 80−69417
N_2 UV TEA lasers 79−41388
N_2, with discrete ceramic capacitors in Blumlein-type circuit 77−19330
$N_2{}^+$, gain and saturation 78−79001
N_2-Ar, stimulated emission obs. at 337.1, 357.7 and 380.5 nm 78−17925
N_2-F_2 mixture, fast Blumlein discharge excited, intense 3371 Å laser emission 79−41365

excimer lasers continued
N_2-He plasma, laser produced, high press. amplified stimulated emission 80—78843
N_2-SF_6 laser, UV, discharge-excited, improvement in efficiency *(Japanese)* 78—33724
N_2-SF_6 pulsed discharge laser with CW X-ray preionisation 80—95910
NF, $b^1\Sigma^+$ state, enhancement by I laser pumping, lasing potential 78—79012
NF, chem. pumped electronic transition laser system, chem. and scale-up 78—63103
NF, excited, lasing potential, prod. by $N+O_2F$ reaction 78—63106
NF, lasing due to electronic transitions, H_2+NF_2 chain reaction kinetics 79—89899
NF_3, disappearance and appearance in excimer lasers, reaction kinetics 77—38860
NF_3, reaction kinetics 77—38860
NF_3-N_2(Ar)(He), electron attachment coeffs. using swarm techniques 80—53915
$NF(a^1\Delta)+I(^2P_{1/2})$ system, electronic angular momentum transfer, chem. kinetic model 78—63104
$NF(b^1\Sigma^+)$ enhancement by I laser pumping 78—63105
Na, diatomic mol., CW laser oscill. 77—38861
Na-Xe, high-power discharges, models 80—69373
Na-Xe vapour, high power discharge, potential excimer laser 78—82957
Na_2, $^3\Sigma_g{}^+$-$^3\Sigma_u{}^+$ excimer emission, ab initio calcs. 80—91608
Na_2, continuous laser oscill., optical pumping 77—88706
Na_2, gain optimisation on $A\rightarrow X$ transitions, Na-Xe discharge kinetic model 78—63088
Na_2, laser, continuous, optically pumped 78—87046
Na_2 laser action obs. in Na high press. discharge lamp 77—31091
Na_2, laser excited broadband violet emission, 420 to 457 nm 78—79006
Na_2 optically-pumped three-level dimer lasers, amplification profiles and dynamic Stark effect 79—41367
NaXe, gain optimisation on $A\rightarrow X$ transitions, Na-Xe discharge kinetic model 78—63088
Ne-NF_3, long pulse UV laser emission in electron beam excited supersonic flow 78—66801
NeF, ionic excited states of Ne_2F 78—25452
Ne^*+Xe, chemiionis. in metastable state collisions 79—68306
$Ne_2{}^*$, electron impact ionisation cross sections in binary encounter approx. 79—68320
O_2, high energy pulsed laser feasibility at 1.27 μm, O_3 photolysis 78—63117
O_2, possible high energy laser at 1.27 μm 79—13950
Rb_2, mol. spectra, population inversion, high-power laser appls. 77—3406
S_2, chem. pumped laser emitting visible radiation, construction possibility 79—13960
S_2 laser, optically pumped, lasing obs. 470 to 480 nm 78—63095
S_2, optically pumped superfluorescence molecular laser 80—63990
S_2, tunable visible and UV laser, $B^3\Sigma_u{}^-$-$X^3\Sigma_g{}^-$ transition 77—42522
Sc-F_2(ClF)(Cl_2)(SF_6)(Br_2), visible chem. laser development from reactions yielding visible chemilum. 78—63111
ScF supersonic mixing flame, spontaneous emission, electronic transition chem. laser pot. 78—66817
SiF, chemilum. obs. of $A^2\Sigma^+$ and $a^4\Sigma^-$ states 78—66816
SnO, produced in $Sn+N_2O(O_2)(O)$ reactions, kinetics of chemilum. emitter form. and quenching 78—63107
SrF, temp. depend. of chemilum. reactions, activation energies for excited state form. 78—66818
Te_2, optically pumped continuous laser oscill., 550 to 660 nm 79—933
Tl-Hg, excimer band emission from electron beam initiated discharge in TlI-Hg 80—78841
Tl-Hg, possibility of creation from UV preionised discharge 79—55119
Tl-Hg excimer, emission pressure and temp. depend., blue band gain, RF excited discharge 79—22941
Tl-Xe, electric discharge excitation of Tl in high-press. Xe 80—49025
Tl-Xe, excimer band emission from electron beam initiated discharge in TlI-Xe 80—78840
Xe, atm. press. and low e-beam excitation rates, expt. studies 80—78863
Xe VUV high-power repetitive, tunable laser 80—5758
Xe-F two module discharge laser, gain and temporal characts. 80—87385
Xe_2 coaxial-diode tunable vacuum UV excimer laser systems 77—54738
Xe_2, e-beam excited, 193 nm absorpt. studies 80—43323
Xe_2, efficient vac. UV laser, 172 nm at 6 atm 78—50793
Xe_2, electron beam excited, 193 nm absorpt. meas. rel. to 172 nm laser pulse termination 80—28200
Xe_2, electron-beam pumped, visible absorpt. rel. to laser development 79—59671
Xe_2 excimer laser, electron beam excitation, VUV fluoresc., lasing 80—87379
Xe_2, excimer laser action in coaxial field emission diode, comparison with Ar_2, Kr_2 80—28201
Xe_2, excimer radiation excited by radial electron beam 79—94239
Xe_2, fluoresc. decay of $O_u{}^+$ and 1_u states, rad. decay consts. 79—86009
Xe_2, large-scale laser, gas purity 78—87063
Xe_2, laser performance for atm. press. and microsecond electron beam excitation 80—28199
Xe_2 laser pulse temporal evolution, cavity mirror depend. 79—76732
Xe_2, near atm. press. operation 78—17905
Xe_2, performance as photolytic driver at low electron beam excitation rates 80—32963
Xe_2, review of basic properties *(Japanese)* 78—33723
Xe_2, simple VUV high press. laser, with coaxial electron beam pumping 79—974
$Xe_2{}^+$, electronic states, pot. curves, with/without spin-orbit interaction 78—33443
XeBr, B and C states, energy ordering from temp. depend. of emission spectra 80—78837
XeBr electric discharge pumped laser *(Chinese)* 80—102701
XeBr, energy decrease mechanism 80—28243
XeBr, high-energy lasing in elec. discharge 78—55340
XeBr laser, electron beam excited, experimental study 79—98347
XeBr, UV bound-free emission after electron excitation 77—27279
XeCl 80—53323
XeCl avalanche discharge laser, D and B state coupling, population depletion 80—28214
XeCl, B and C states, energy ordering from temp. depend. of emission spectra 80—78837
XeCl, closed cycle characts. 80—33030
XeCl, closed cycle flow type, operating characts. 80—43349
XeCl, discharge excited, preionisation technique 80—23714

excimer lasers continued
XeCl discharge laser, energy characts. 80—48228
XeCl effective laser performance with combined pumping, discharge stability by short electron beam 79—94250
XeCl, efficient discharge pumping, 3080 Å emission 77—42524
XeCl, efficient laser output at 308 nm, electron-beam excitation 79—59678
XeCl, efficient Raman conversion of radiation in Ba vapour 78—79069
XeCl, electric discharge excimer laser with intense preionisation 80—63991
XeCl electroionisation laser, energetic, threshold and spectral characts. 80—99705
XeCl, electron-beam pumped, emission spectrum, saturation intensity, optical absorpt. 79—927
XeCl, electron-beam pumped excimer laser *(Japanese)* 79—64208
XeCl, energy curves and transition moments 80—28210
XeCl excimer laser, electron beam controlled discharge, construction and operation 78—63125
XeCl excimer laser, high power, discharge pumped 78—55375
XeCl excimer laser, long-life operation 79—41366
XeCl excimer laser radar, stratospheric O_3 layer meas. 79—16681
XeCl, excimers and excimer lasers 80—48217
XeCl, excited by discharge stabilised by electron beam 80—63992
XeCl frequency-tuned laser, coherent tunable vacuum UV near H Ly-β transition 80—99798
XeCl high specific power long-pulse supersonic flow laser at 308 nm 80—48221
XeCl, high-energy subnanosecond pulse amplification 80—99770
XeCl, intense lasing with HCl halogen donor 78—90411
XeCl laser, $B\rightarrow X$, form. and quenching kinetics 80—74341
XeCl laser, discharge stabilisation with 50 nsec electron beam 80—23716
XeCl laser, electron beam excitation *(Russian)* 78—22115
XeCl laser, electron beam, beam-stabilized discharge and fast discharge excitations 80—28204
XeCl laser, lifetime extension by H addition 80—91773
XeCl laser, pumping for dye lasers 79—59691
XeCl laser, transient optical absorpt. meas. 79—55115
XeCl laser pulse backward Raman compression in Pb vapour 80—19068
XeCl laser radiation, efficient Raman conversion in metal vapours 79—23025
XeCl laser radiation, third harmonic conversion in Ar 79—89962
XeCl mini-laser operation at high repetition rate 80—74396
XeCl molecule excited by electron beam, stimulated emission obs. 80—32966
XeCl, relax. and quenching rate consts., emission spectra modelling 80—28211
XeCl, stimulated Raman scatt. of excimer laser wavelengths for new lines in UV 79—59755
XeCl, UV discharge laser, emission spectra 77—79809
XeCl, UV picosecond pulse amplification 80—74372
XeCl, UV preionised discharge pumped laser, improved performance 78—37906
XeCl UV preionised simple compact laser, elec. and gain characts. 80—28206
XeCl, using chlorinated hydrocarbons as Cl donors 78—79007
XeCl+HCl(inert gas atom), ground state destruction, quenching rate consts. meas. 80—63758
Xe_2Cl, triatomic excimer, transient gain meas. at 488.0, 497.6, 514.5 nm 80—58511
Xe_2Cl triatomic excimer laser in visible 80—64048
XeCl(B) formation in electron beam assisted Xe/HCl laser discharge 80—63988
XeCl*, elec. discharge excimer lasers, stimulated emission 79—31884
XeCl* excimer laser, electron-beam-excited discharge in Ar-Xe-CCl_4 79—18408
XeF, 1 μs pulse production, electron beam excitation 77—14692
XeF, 1 μsec pulse lasing, cold cathode electron beam initiation 78—63079
XeF 2 kHz repetition rate laser action at 351, 353 nm 79—59714
XeF, (B,C) state prod. and kinetics, XeF_2 photolysis with VUV radiation 80—32975
XeF, B and C-state kinetics with self-sustained discharge pumping 80—28212
XeF, B- and C-state fluoresc. rel. to laser efficiency 79—41368
XeF, broadband emission origin 80—38007
XeF, C-A blue-green, multipass amplification and tuning 80—43346
XeF, C-A blue-green band, gain meas. at 488 and 475.9 nm 79—45929
XeF, closed cycle characts. 80—33030
XeF, closed cycle flow type, operating characts. 80—43349
XeF, diffraction-limited laser, with negative branch unstable resonator 77—38937
XeF, direct pumping by electron beam pulses, gain and laser oscill. obs. in blue-green 80—102699
XeF, discharge and electron beam pumped, review 78—71083
XeF, discharge excited laser operation at elevated temps., transitions, output power 80—43359
XeF discharge laser, gain and fluorescence meas. at high energy loading 77—79844
XeF discharge laser for transient phase shift meas. in electron beam pumped lasers 80—1195
XeF discharge pumped laser at 490 nm 79—89893
XeF discharge-excited laser, high repetition rate operation with gas recycling 79—973
XeF, double discharge laser amplifier, small signal gain meas. 77—79807
XeF, double discharge laser, operating parameters, discharge characts. 77—88704
XeF, double pulse fast discharge driven laser, optimal timing and power enhancement 78—63132
XeF, efficient operating conditions with electron beam stabilisation 80—38006
XeF, efficient Raman conversion of laser output, 351 to 585 nm 77—58377
XeF, electric discharge pumped laser, model for UV preionisation 77—23658
XeF electric discharge laser, energy and spectral characts. changes on press. increase 79—64214
XeF electric discharge laser at 490 nm 79—89890
XeF, electric discharge excimer laser with intense preionisation 80—63991
XeF electroionisation laser, energetic, threshold and spectral characts. 80—99705

excimer lasers continued

- XeF, electron beam controlled discharge pumping 77—23657
- XeF, electron beam controlled, output power, efficiency 78—82951
- XeF, electron beam controlled Ne stabilised laser 79—972
- XeF, electron beam excited, long pulse operation 78—50794
- XeF, electron beam excitation, kinetics scheme 78—78999
- XeF, electron beam pumped multiatmosphere laser, Ne diluent 77—88705
- XeF, electron beam pumped laser, gain, fluoresc. and laser output at 351, 488 nm 80—28215
- XeF electron beam pumped laser, energy, time and spectral characts. 80—38005
- XeF, electron beam sustained discharge excitation, threshold power density meas. 78—63078
- XeF, electron impact deexcitation, low energy cross-sections and rate consts. 80—1071
- XeF, electron quenching rate consts. meas. by fluoresc. anal., laser implications 80—32969
- XeF electron-beam pumped laser at 486 nm 79—89892
- XeF electron-beam-pumped laser, characts., 300-600K 80—78839
- XeF, energy curves and transition moments 80—28210
- XeF, energy ordering of excited states, rel. to fluoresc. and laser action 78—74887
- XeF excimer, Blumlein driven, high-repetition rate operation, gas recycling 77—58337
- XeF, excimer laser pumped dye laser *(Chinese)* 80—1234
- XeF, excimers, power superluminesc. in elec. discharge *(Russian)* 77—7621
- XeF, excited by discharge stabilised by electron beam 80—63992
- XeF, formation and quenching of electronic excited states 77—673
- XeF, from photodissoc. of XeF_2, $B(1/2)$-$X^2\Sigma^+$ transition, stimulated emission 78—71097
- XeF, ground state kinetics, multilevel model of energy transfer 80—99707
- XeF ground-state dynamics in laser discharge 79—18404
- XeF, high press. discharge, UV ps. pulse amplification 77—88768
- XeF, high press. UV laser, electron beam excited *(Russian)* 77—14696
- XeF, high pulse repetition freq. laser action, appl. of multiple-circuit pulse generator 78—94399
- XeF, high repetition rate transverse flow laser 78—46620
- XeF, high-intensity short pulse generation, oscillator-optical gate-amplifier system 80—38038
- XeF high-power electron-beam pumped lasers, optical performance 78—46640
- XeF high-pressure supersonic flow electronic transition laser, with pulsed blowdown and electron gun facility 79—59723
- XeF, influence of diluent gas 78—9365
- XeF, injection locking, cross relax. rates 78—17909
- XeF, kinetics simulation of high-power gas lasers 79—59676
- XeF laser, discharge-pumped, spectroscopic study at high resolution 78—37873
- XeF laser, electron beam stabilised discharge *(Russian)* 78—25894
- XeF laser, electron beam, beam-stabilized discharge and fast discharge excitations 80—28204
- XeF laser, electron beam excited, gain measurements using amplified spontaneous emission 80—37986
- XeF laser, electron-beam sustained discharge excitation, threshold power density meas. 77—88699
- XeF laser, excitation by microsecond electron beam 79—59686
- XeF laser, excited states quenching of electron beam excited media 79—18406
- XeF laser, high-repetition rate operation, gas recycling 77—58337
- XeF laser, output control by injection locking 80—74405
- XeF laser, transverse discharge in $Xe+He+NF_3$, time and energy characts. *(Russian)* 78—25861
- XeF, laser action on C→A transition, pumping mechanisms, kinetics and efficiencies 80—32967
- XeF laser efficiency improvement at elevated temps. 79—45957
- XeF, laser emission, ab initio config. interaction calcs. on electronic states 78—63083
- XeF laser excited by proton beam, stimulated emission at 351, 353 nm 79—98344
- XeF laser line, 353 nm, picosecond gain and saturation meas. 78—17910
- XeF laser performance, ground state population effect 80—63987
- XeF laser using Ar-Xe-NF_3 mixture, discharge stabilised by short-pulse electron beam 80—14358
- XeF laser using XeF_2 photodissociation, fluoresc. and laser performance 80—32976
- XeF laser wavelength transient absorpt. in electron beam excited inert gases 80—32644
- XeF linac-excited gas mixture, UV fluoresc. meas. 80—28216
- XeF, long pulse electron beam excited laser 79—940
- XeF, long pulse UV laser emission in electron beam excited supersonic flow 78—66801
- XeF molecule formed by XeF_2 photodissociation, laser action due to bound-free C(3/2)-A(3/2) transition 80—14334
- XeF, nuclear pumping possibility 78—17916
- XeF, optically excited by incoherent Xe_2* radiation, B→X band emission 78—87044
- XeF, photodissociation by Xe_2*, excimers inducing blue-green excimer lasing, laser spectra 79—68382
- XeF, photoionization-stabilised self-sustained, energy extraction efficiencies 79—41369
- XeF, ps laser pulse amplifier 77—14736
- XeF pumped Tm:$LiYF_4$, excimer excited storage laser 80—33003
- XeF, relax. and quenching rate consts., emission spectra modelling 80—28211
- XeF, review of basic properties *(Japanese)* 78—33723
- XeF, scalable multiatmosphere high power laser 77—71995
- XeF, self-sustained discharge laser, kinetic processes 78—74888
- XeF, self-sustained discharge pumping 80—28219
- XeF, simple high-power TEA laser operating in UV 79—94251
- XeF, spark-preionised large-vol. discharge laser 78—1218
- XeF, spontaneous emission lifetime meas. of C→A band 79—31874
- XeF superradiance laser excited by electric discharge 77—19236
- XeF, superradiant laser, gain saturation effects 78—66808
- XeF, temperature depend. absorpt. processes in Ne-Xe-NF_3 mixtures 80—1188
- XeF, transverse discharge-excited laser, active mode locking 77—23656
- XeF, transverse-discharge laser, increased efficiency 79—72595
- XeF, UV discharge laser, emission spectra 77—79809

excimer lasers continued

- XeF, UV laser, longit. elec. discharge *(Russian)* 78—1220
- XeF, UV preionised discharge pumped, 10 kHz repetition rate 80—33029
- XeF, UV preionized discharge pumped laser 77—10889
- XeF waveguide laser operation on 351, 353 nm transitions 79—22942
- XeF(B) nuclear pumping, candidate laser fusion driver 79—86171
- XeF(Cl)(Br), covalent and ionic states, spectroscopic props., ab initio CI calc., laser emission 78—90092
- XeF(Cl)(Br) excimer lasers, lasing action *(Chinese)* 79—59682
- XeF* ($C_{1/2}$), radiative lifetime meas. 78—63087
- XeF*, broadband emission origin 80—28202
- XeF*, elec. discharge excimer lasers, stimulated emission 79—31884
- XeF*, fluoresc. intensity, two- and three-body quenching by Ar, Xe 77—58053
- XeF*, formation and quenching in Ne-Xe-F_2 laser mixtures 78—42324
- XeF* gas-discharge excimer laser, kinetics 80—48226
- XeF* laser mixture, Ne- and Ar-rich, absorption 78—63062
- XeF* laser system, trimer form. rates 80—50831
- XeF*, lifetime and collisional quenching meas., XeF_2 photolysis 78—33545
- XeF* nuclear pumped laser obs. 80—63996
- XeF*, waveguide laser excited by capacitively coupled discharge 78—94391
- XeF*-UF_6, nuclear pumped excimer fusion lasers, kinetic model 79—18410
- XeI, UV bound-free emission after electron excitation 77—27279
- XeO, lasing, low-lying electronic states, ab initio config. interaction calcs. 78—63084
- XeO, luminesc. meas. of $O(^1S)$ absolute quantum yield in photolysis of CO_2, N_2O 80—35561
- XeO, optical pumping, ^1S-^1D transition, 0.54 μm emission 77—667
- XeO, photochem. laser performance, 0.54 μm stimulated emission 79—45938
- XeO photochemical laser, energy characts., kinetic model of physicochem. processes 80—28228
- XeO*, green emission on electron beam pumping, population inversion kinetics 77—23661
- XeO*, mol. laser emitting at green wavelengths, population inversion kinetics 77—23661
- Xe_2*, excimers and excimer lasers 80—48217
- Xe_2*, vacuum UV lasing 77—7067
- xeCl excimer laser, lasing action *(Chinese)* 79—55126
- Y-F_2(ClF)(Cl_2)(SF_6)(Br_2)(IBr), visible chem. laser development from reactions yielding visible chemilum. 78—63111
- YCl supersonic mixing flame, spontaneous emission, electronic transition chem. laser pot. 78—66817
- YO, temp. depend. of chemilum. reactions, activation energies for excited state form. 78—66818
- ZnHg, optical pumping of Zn reson. line, optical and kinetic props. 78—58991

excimers

- *see also excimer lasers*
- alkali metal salt solution, Ar saturated, sonoluminesc. as acoustic cavitation probe 79—60437
- m-aminoacetophenone+t-amyl alcohol, in soln., fluoresc. and absorpt. spectra, excimer form. 78—78737
- 1-(N-p-anisyl-N-methyl)-amino-3-anthryl-(9)-propane, intramol. exciplex formation 77—58059
- anthracene, γ-irradiated, temp. depend. of photolum. *(Russian)* 78—56511
- anthracene, excimer fluoresc. lifetime and quantum yield in soln. 77—6834
- anthracene, excimer form. in soln. and cryst., fluoresc. study 79—45759
- anthracene, noncryst. solid, excimers, time resolved fluoresc. obs. 79—52006
- anthracene intramolecular excimer in 1,3-dianthrylpropane, direct obs. 80—48029
- anthracene-aliphatic amine, photochemically induced H isotope exchange 79—11771
- anthracene-N,N-diethylaniline exciplex, intersystem crossing 77—30905
- anthracene-tetracene amorphous films, host-guest energy transfer 78—60505
- anthracene/trans, trans-2,4-hexadiene-exciplex, fluoresc. rel. to photodimerization 77—3401
- anthracenes, exciplex form. with amines, form. kinetics and luminesc. props. 80—66792
- 9-anthroic acid, excimer-type transition polaris. 79—50062
- bis(9-anthryloxy)polyoxaalkanes,, intramolecular excimer form. and photodimerisation, kinetic anal., rate constants determ. 80—66800
- aromatic hydrocarbon soln., delayed fluoresc., mag. field effect, excimer form. 77—14479
- aromatic hydrocarbons, excimer decay dynamics, rate const. rel. to solvent 78—58729
- aromatic hydrocarbons-amine, π-axciplexes, intermolecular interactions 80—43134
- 1,2-benzanthracene, monomer and excimer fluoresc. in soln., triplet-triplet annihilation and mag. field depend. 78—78738
- benzene, nanosecond laser photolysis 80—66825
- benzene-benzene (anthracene) dimers, ground and excited states, EHT calc. 79—36553
- benzil triplet-anisole, reversible exciplex form., phosphorescence, photostationary and transient obs., simulation 78—9182
- benzophenone-N,N-dimethylaniline, intramolecular exciplex systems, laser photolysis obs. 80—35550
- 1,12-benzperylene exciplexes, radiative and radiationless decay 77—6817
- 3,4-benzpyrene, monomer and excimer fluoresc. in soln., triplet-triplet annihilation and mag. field depend. 78—78738
- bimetallic cluster, photoselective bimetallic aggregation, review 80—53182
- C-A blue-green band, gain meas. at 488 and 475.9 nm 79—45929
- N-carbazolyl-$(CH_2)_n$-tetrachlorophthalimide, (n=2,3,4,7) intramol. electron donor-acceptor system, photophys. 78—82763
- chromophores, $^1O_2$, annihilation luminesc., in polymer matrices 77—88488
- conformational mobility, fluorescence obs. 80—63877
- 9-cyano anthracene-dimethyl aniline, exciplex, fluoresc. of vap., 185-231°C 78—74693
- 9-cyano anthracene-tributyl amine, exciplex, fluoresc. of vap., 185-231°C 78—74693

excimers continued
9-cyano anthracene-triethyl amine, exciplex, fluoresc. of vap., 185-231°C 78—74693
9-cyanoanthracene:perylene, exciplex emission 78—60513
9-cyanoanthracene, cryst., excimer emission, spectra, photochem. and multiphonon processes 78—10914
9-cyanoanthracene, luminesc., excimeric species 78—84637
9-cyanoanthracene, metastable crystal, structure 78—6757
9-cyanoanthracene, quenching of solid state photodimerisation reaction by cryst. doping 78—68547
9-cyanoanthracene excimer emission, in glassy and cryst. matrices 79—11445
9-cyanoanthracenes-N,N-dimethylaniline, fluoresc. exciplex emission in gas phase 79—68250
Davydov splitting theory, excitonic parameters, split absorption bands, organic molecular aggregates *(Spanish)* 79—59437
di(1-pyrenylmethyleneoxycarbonyl) alkanes, intramol. excimer emission 78—70862
dianthracene, photodissoc., electronically excited products 78—27790
dianthronylidene ethane, luminescent excimer geometries, intermol. shift 78—27294
diarylalkane, in isooctane soln. triplet excimer form., phosphoresc., delayed fluoresc., triplet-triplet absorption 78—25597
1,3-dibiphenylpropane, intramol. excimer form., kinetic and thermodynamic obs. 79—13750
9,10-dicyanoanthracene, exciplexes, electronic struct. by electro-optical expts. 78—25581
dicyanoanthryl-naphthyl, intramol. exciplex, fluoresc. quenching by pyridine (γ-picoline), triple exciplex form. 79—50061
N,N-diethyl-4-phenyl-butylamine, fluoresc. spectra intramol. exciplex formation, fluoresc. spectra 79—59499
dimethoxyphenyl-1,1-dicyanomethylene, donor-acceptor systems, fluoresc., through-band interaction 79—13751
dimethylaminophenyl-(methylene)$_n$-(1-pyrenyl), intramolecular charge transfer, heteroexcimer formation processes 78—27783
9,10-dimethylanthracene, conc. solns., fluoresc. quenching by anthracene and derivatives 78—17711
2:3dimethylnaphthalene, in polystyrene matrix, singlet O_2 induced excimer fluoresc. 77—6832
α,α-dinaphthylalkanes, absorpt. spectra and phosphoresc. in soln., triplet excimers 78—62816
dinaphthylalkanes, triplet-triplet annihilation of excimers in soln. 78—86904
dinaphthylamine, fluoresc. in soln., intramol. excimer and exciplex form. 78—62836
dinucleoside phosphates, polaris. spectra, excimer phosphoresc. and fluoresc. 79—34497
2,6-diphenyl-1,4-benzoquinone+aromatic amine, triplet exciplex quenching, H-transfer mechanism 79—79228
donor excimers, effect on resonant energy transfer *(Russian)* 78—76530
electrochemiluminescence, excimer-monomer emission ratio 78—31640
electronic structure and radiative transitions of excimer systems, book contrib. 79—81416
10,10′-ethanediylidenedianthrone, fluoresc. efficiency, mol. geom. effects in two cryst. structs. 77—18953
ethylene, CW CO_2-laser irrad., low-press., chem. relax. 79—74404
exciplex quenching, FMO calcs. 77—48655
exciplexes, electronic struct. by electro-optical expts. 78—25581
flexible chain molecules, mutual interpenetration, fluorescence obs. 80—63877
fluoradene, absorpt. and fluoresc. in solvents, excimer form., aggregation 77—79625
fluorene:phenazine, excimer form. transient EPR phenomena, wide-band detect. 77—13793
fluorene, in polystyrene matrix, singlet O_2 induced excimer fluoresc. 77—6832
fluoresc. decay, elec. field depend., quantum theoretical model 79—98133
fluorescence, relative yield following triplet-triplet annihilation, reencounter effects 78—33538
gas mixture, self sustained volume photoionisation discharge existence conditions 80—79610
heteroexcimers, intramolecular, picosecond time-resolved fluorescence studies 80—83401
impurity centres, electron-phonon coupling from structured optical spectra, review 80—89038
inerg gas excited molecules formation, rate const. determ. 80—9859
inert gas afterglow, excimer form., VUV emission obs. at low press. 80—38755
inert gas fluorides, excimer emission bands *(Russian)* 77—71885
inert gas halides, emission spectra, open-shell closed-shell interaction, electron gas model 77—30879
inert gas halides, excimer emission from electron beam produced plasma 80—43887
inert gas halides, exciplex mol. form., rel. to laser operation 80—81318
inert gas-alkali metal excimer molecule, possibility of existence 79—76354
inert gas-halogen bearing molecule three-component mixture, self-sustained electric photoionization discharge 80—54073
inert gas-SF_6 mixture, formation of inert gas fluorides in AC discharge 80—64817
intramolecular donor-acceptor systems, fluoresc., through-band interaction 79—13751
lepidopterene exciplex, luminesc. intramolecular anthracene-ethylene exciplex, mol. geometry-fluoresc. relationship 78—58728
metal vapour excimers, book contrib. 79—81419
methacrylate polymer, carbazolyl substituted, excimer and charge transfer complex trapping of excitons 80—34367
methine dyes, spectral props., solvent effects 80—69181
micelle-confined molecules reaction, diffusion-controlled, luminesc. quenching, excimer form. 80—50890
molecule formation in plasma by halide ion recomb. or alkali metal charge exchange 80—75026
Na_2, laser-excited, emission bands obs. in visible and IR 80—48036
naphthalene, adsorbed on silica gel surface, biphasic photochemistry, time-resolved spectra 80—30252
naphthalene, fluoresc. and phosphoresc., singlet/triplet excimers conform. difference 77—14469
naphthalene, microcryst. and evaporated film, excimer emission 80—2823
naphthalene, singlet and triplet excimer interactions, exciton resons. 80—95535

excimers continued
naphthalene, triplet excimer conformation, σ-π interaction transitions 77—6701
1-naphthyl methacrylate-9-vinylanthracene copolymer, time-resolved fluoresc. spectra 78—80401
1-β-naphthyl-2-N-piperidinoethane, intramol. exciplex form., ground state conform. control 80—102547
nuclei acid base stacked dimer, origin of excimer states in extended Huckel method 80—35832
nucleic acid bases, excited states formation, EHT calc. 79—13651
organic solid state chemistry, conf., Waltham, USA (June 1978) 79—46990
palladium-octaethylporphyrin, gas phase delayed fluoresc. and phosphoresc., triplet excimer formation 80—18884
α-perylene, excitation spectra of exciton fission in organic crystals 78—92116
perylene, exciton fission in excimer forming cryst., fluoresc. 79—15511
perylene, fluoresc., exciton fission in excimer forming cryst. dynamics 79—61423
α-perylene crystal, emission spectra, temp. variation and pair states 78—27300
phenanthrene, triplet state conc. quenching in propan-1,2-diol *77—75196
phosphatidylcholine bilayers, fluidity changes and phase transitions, intramol. excimer fluoresc. obs. 80—85342
phthalamide derivative with aromatic amine, exciplex formation and fluoresc. quenching 79—87848
phthalimide derivative-tetramethyldiaminodiphenylmethane exciplexes, luminesc. props. 77—68070
phthalocyanine, metal-free, solid, fluoresc., lifetimes temp. depend., polymorphic modification 78—80388
PMMA film, doped, time resolved absorpt. spectra, decay kinetics of exciplex state 80—84098
poly (ar-methylstyrene)s, steric effects on excimer formation, fluorescence spectra exam. 80—25430
poly-1-naphthyl methacrylate, time-resolved fluoresc. spectra 78—80401
poly-1-vinyl napthalene, excimer dissoc., time resolved fluoresc. spectra 78—33643
poly-1-vinylnaphthalene solution, time-resolved fluoresc. spectroscopy, excimer form. and dissoc. 79—38637
poly-9-vinyl carbazole, fluoresc. props. 78—84647
poly-N-vinyl carbazole, pulsed laser excitation, time resolved fluoresc., 80—89041
poly-N-vinylcarbazole, in polymer film, excimer fluoresc., high press. effects 80—34966
poly-N-vinylcarbazole, soln., picosecond time-resolved fluoresc. by pulse radiolysis 80—28122
polyacenaphthalene, glassy soln., fluoresc. yield, polarisation and decay., temp. depend. 80—89043
polyacenaphthalene-methylmethacrylate copolymer 80—89043
polymer matrix, decreased stabilisation energy of excimers and exciplexes 80—25431
polymers, intra- and intermolecular nonradiative energy transfer 77—34792
polymers containing carbazole units, optically active, fluoresc. props. 78—84647
polynucleotides, polaris. spectra, excimer phosphoresc. and fluoresc. 79—34497
polystyrene, steric effects on excimer formation, fluorescence spectra exam. 80—25430
polystyrene photophysical behaviour, solvent effect obs. *(Spanish)* 79—57267
polystyrene solution, time-resolved fluoresc. spectroscopy, excimer form. and dissoc. 79—38637
porphyrins in liquid crystal, oriented photoexcited triplets, EPR study 80—84636
pyrene:rubicen(coronen), exciton migration and energy transfer, temp. depend., model 78—79932
pyrene, adsorbed on silica gel surface, biphasic photochemistry, time-resolved spectra 80—30252
pyrene, emission from triplet state in electrochemical at low temps. 77—77307
pyrene, excimer fluoresc., struct. depend. in cryst. 77—75200
pyrene, excimer form. process, ps laser fluoresc. obs. 79—11448
pyrene, in polystyrene, excimer fluorescence 79—68249
pyrene, in polystyrene matrix, singlet O_2 induced excimer fluoresc. 77—6832
pyrene, monomer and excimer fluoresc. in soln., triplet-triplet annihilation and mag. field depend. 78—78738
pyrene+N,N-dimethylaniline (deuterate)(3,5 dimethoxy-N,N-dimethylaniline), geminate recomb., solvent, isotope, mag. field effects 78—56888
pyrene crystals, anomalous emission excited near absorption edge 80—100682
pyrene dodecanoic acid, lateral diffusion at air-water interface, monomer excimer dynamics 80—92693
pyrene excimer fluorescence, erythrocyte membrane fluidity changes after X-irrad. obs. 80—72262
pyrene excimer formation in micellar surfactant solns., distributional effects 78—64855
pyrene excimer formation in micelle, time-resolved spectra 79—79298
pyrene solutions, emission spectra 77—30910
pyrene-3-sodium sulphonate solubilised in didodecyldimethylammonium bromide-benzene inverted micelles 80—3417
pyrene-diethyl aniline in acetonitrile-toluene, triplet exciplex state in pulsed laser photolysis 77—16836
pyrene-N,N-diethylaniline exciplex, visible spectra obs., picosec. laser photolysis, solvent polarity depend. 77—38677
pyrene-N,N-dimethylaniline heteroexcimer systems, micellar solns., fluoresc., photoinduced electron transfer 78—25590
pyrene-sodium 5-[1-pyrenyl]pentanoate intramicellar excimer formation in CTAC and SDS micelles, fluoresc. probe 80—16733
1-pyrene-sodium sulphonate, excimer form. in inverse micelles, fluoresc. probe 77—88491
pyrenophanes, excimer fluoresc., struct. depend. in cryst. 77—75200
resonance energy transfer, donor excimers effect 79—95825
sodium dodecyl sulphate micelles, diarylalkane intramolecular excimer formation, microfluidity and fluoresc. meas. 78—80791
solid-state reaction, excimer form. 79—47917
styrene-method methacrylate copolymer glassy soln., excimer form., energy migration, fluoresc. depolarisation meas. 78—70986

excimers continued
tetracyanobenzene+methylated benzene, fluorescent exciplex form., electronic relax. 80-5573
thionine triplet+haloanilines, electron transfer reaction, radical yield meas. 80-3330
thionine-monohaloaniline triplet exciplex, quenching position dependent heavy atom effect, intersystem crossing 78-53197
triplet exciplexes, rapid rot., spin-selective depopulation of sublevels, heavy atom-induced mag. field effect 80-95552
vibrational transitions, Franck-Condon matrix elements 80-9645
2-vinylnaphthalene-methyl methacrylate copolymer glassy soln., excimer form., energy migration, fluoresc. depolarisation meas. 78-70986
xanthione, solns., triplet state quenching by ground state xanthione 78-42180
zinc pyrochlorophyllide in nematic liquid crystals, oriented photoexcited triplets, EPR study 80-84636
Ag, matrix isolated, fluoresc. spectra. excimeric bond effects 78-50498
Ar:$O_2(N_2)$, long-wave UV luminesc. *(Russian)* 78-88347
Ar-F_2 mixtures, low-press. excimer form. and quenching by e-beam excitation 79-50071
Ar-Kr-F_2 mixture, nucl. induced excimer fluoresc. for I laser excitation 80-78846
Ar+HCN(H_2O), electron excitation of Ar* and Ar_2*, fluoresc. and dissoc. energy transfer collisions 77-14580
Ar+N_2, bimol. and three body quenching, reson. state $^1P_1$, $^3P_1$ and excimer Ar atoms 79-3540
Ar_2 $^1\Sigma_u^+$ excimer state, photoionis. cross section 78-70882
Ar_2, excited state pot. curves, ab initio CI calc. 78-78643
ArCl*, excimer formation rate consts., B state radiative lifetimes, quenching, VUV excitation 80-55631
ArF, Ar_2F, electronic struct., pot. energy curves, radiative transition probability calcs. 77-57879
ArF, excimers, power superluminescence, in elec. discharge *(Russian)* 77-7621
ArF, proton excited mixtures, energy transfer processes 78-66647
ArF*, formation and quenching kinetics 77-88482
ArH exciplex emission obs. in rarefied Ar-H_2 plasma jet *(French)* 80-48054
$Ar_2(^3\Sigma_u^+)$+N_2, quenching, fast absorption spectrophotometry 79-54940
Ar_2*, electron impact ionisation cross sections in binary encounter approx. 79-68320
Ar_2*, electron-beam excited, time-resolved fluoresc. spectra 79-813
Ar_2*, excimers and excimer lasers 80-48217
Cd_2 as 470 nm absorber, multiconfig. SCF calcs. 80-32731
Cd_2, quenching and predissociation, possible excimer laser 80-32770
$CdGa_2$, excimer visible emission spectra in RF discharge, vibr. struct. 79-18201
CdHg, excimer kinetics and transmission meas. 80-37832
CdHg excimer system, absorpt. meas. 80-48007
Cd^*_2, 470 nm absorber, multiconfiguration SCF calcs. 80-27963
Cd_2* excimer, fluoresc. band shape, decay rates 78-70866
Cs, multiphoton ionisation spectroscopy, molecular satellites of 6^2S-7^2P doublet 78-17632
Cs-inert gas molecule, excimer transitions, absorpt. spectra 77-475
CsAr, 6dσ states, multiphoton laser spectrosc. obs. 79-85974
CsHe absorption bands associated with forbidden Cs transitions 79-27005
CsHe(Ne)(Ar)(Kr)(Xe), excited state IR emission bands 80-14140
CsKr, 6dσ states, multiphoton laser spectrosc. obs. 79-85974
CsXe excimer, laser-excited fluoresc. in Cs-Xe mixture, pumping, level scheme 78-86909
CsXe excimer laser, form. and dissociation rates, fluoresc. meas. 78-1216
1,6-di-(N-carbazolyl)-2,4 hexadiin, cryst. struct., luminesc., γ-ray polymerisation 78-18629
GaKr, low-lying electronic states, PE curves, transition moments, emission coeffs. 79-6894
H_4 excimer, electronic and geom. struct., ab initio CI calc. 79-76348
H_4, excited potential energy hypersurfaces, trapezoidal geometry, rel. to photochem. 2s+2s processes 77-30797
H_4, ground and excited states, SCF MO CI calcs. 77-6693
He_2 excimer potentials, long range, from He+He differential cross-sections 79-81167
$He_2(A,C^1\Sigma_{u,g}^+)$, long-range excimer pot. determ., high resolution at. beam expt. 77-42371
Hg positive column, high press., excimer densities and destruction mechanisms 78-5967
Hg-Ar(Kr)(Xe) mixtures, prebreakdown discharges, Hg excimer formation 79-77433
Hg-Xe(Kr)(Ar), fluoresc. emission, high press., electron beam excitation, laser appl. 77-34676
Hg_2, dissociative recomb. and optical transmissions meas. in high press. discharge 80-37816
Hg_2, emission and form. kinetics, sequential two-photon absorpt. expt. 80-32767
Hg_2, excimer fluorescence, electron beam and optically produced systems 77-27107
Hg_2, optical pumping, continuous emission obs. 78-5296
Hg_2, photoassoc., spectroscopy and kinetic processes of high-lying vibronic states, laser applics. 80-9649
Hg_2, photoassociated, collision-induced predissoc. with Hg 79-31626
Hg_2, quenching and predissociation, possible excimer laser 80-32770
HgBr emission intensity, $HgBr_2$ dissociative excitation by inert gas and N_2 metastables 80-40687
HgBr, polarised photofluoresc. spectroscopy, $HgBr_2$ photodissociation by ArF laser 80-37841
HgBr(B→X) radiative lifetime, laser induced fluorescence 77-30900
HgTl optically excited excimers, upper state kinetics 80-37831
HgXe, excited molecule formation 77-23519
HgXe, fluoresc. spectra, pot. curves and binding energy 78-66581
KXe, dye laser induced emission, excimer bands and uses 80-9650
KXe_n exciplexes (n=1-4), visible emission bands 78-78746
K(5S)Xe, K(5S)Kr, excimer, visible emission band, exptl. results relative to theory 78-82779
Kr:N_2O, photoluminesc. from KrO (^1S) excimers 78-68544
Kr_2, in non-self-maintained high-press. discharge, ionis. instability *(Russian)* 77-84557
KrCl*, excimer formation rate consts., B state radiative lifetimes, quenching, VUV excitation 80-55631
KrCl*+Xe, substitution efficiency during excitation in transverse AC electric discharge 80-50850

excimers continued
KrF, electron impact deexcitation, low energy cross-sections and rate consts. 80-1071
KrF, electron impact deexcitation cross sections and rate consts. calcs. 80-32848
KrF, electronic states, ab initio CI calcs., spin-orbit coupling, pot. curves, dissoc. energy, dipole moments 77-38619
KrF, excimers, power superluminesc. in elec. discharge *(Russian)* 77-7621
KrF, excimers and excimer lasers 80-48217
KrF, laser spectrum, discharge-pumped, absorption bands and lines, assignment 78-79004
KrF(B), excimer, collisional quenching rates, photolysis meas. 78-63066
KrF*, bound-free emission spectra, simulation 78-29806
KrF*, excimer electronic struct., config. interaction, electrostatic model 78-927
KrF*+Ar(Kr)+Ar(Kr), recomb. rate consts., 300 to 800K, appl. to KrF* laser efficiency 79-45930
Kr_2*, excimers and excimer lasers 80-48217
Li_2, $^3\Sigma_g^+$-$^3\Sigma_u^+$ excimer emission, ab initio calcs. 80-91608
Li_2, $A^1\Sigma_u^+$ state, radiative lifetime 77-27104
Li_2, spectroscopy and structure, triplet excimer continuum emission 80-32769
Mg_2 excimer system, laser induced fluoresc. 78-33548
Mg_2, Mg_2^+, electronic struct., pot. energy curves, multiconfig. SCF calcs. 78-5124
Mg(^3P)+K(Ca), energy transfer and excimer form. in flowing afterglow 77-60049
NF_3, disappearance and appearance in excimer lasers, reaction kinetics 77-38860
Na+Kr(Xe), excimer bands, multiperturber interactions 78-66497
Na_2, $^3\Sigma_g^+$-$^3\Sigma_u^+$ excimer emission, ab initio calcs. 80-91608
Na_2, form., collision-produced diffuse violet emission band obs. 79-27026
Na_2, spectroscopy and structure, triplet excimer continuum emission 80-32769
Na_2, triplet satellite band obs. in self-broadened D-line very far blue wing 80-95688
NaAr, ground and excited state pot. curves, dispersed fluoresc. spectrum 79-98140
Na(4S)Xe, Na(4S)Kr, excimer, visible emission band, exptl. results relative to theory 78-82779
Ne:O_2 (N_2), long-wave UV luminesc. *(Russian)* 78-88347
Ne_2*, electron impact ionisation cross sections in binary encounter approx. 79-68320
Ne_2* potential energy curves of several excited states transient absorption spectra assignment 79-41115
OCS photodissociation by Kr_2* excimer in OCS-N_2-SF_6 laser, electric dipole forbidden transition 79-68389
P_2-PO, exciplex, chemiluminesc., reduced press. system 77-32795
$(PO_2)_2$*, excimer, chemiluminesc., reduced press. system 77-32795
Rb-inert gas molecule, excimer transitions, absorpt. spectra 77-475
RbXe*, far-wing line spectra undulations, semiclassical methods 77-61808
SF_6-R-He(Ar) ternary mixtures, formation of inert gas fluorides in AC discharge 80-64817
Tl, green line superradiance, selective optical excitation and inversions via excimer channel using Tl-Hg and Tl-Cd-Ar systems 79-50281
Tl-Hg, prod. in UV preionised discharge 79-55119
TlHg excimer, fluoresc. at 4590 and 6560 Å, possible laser action 77-6837
$U_2O_4H^{4+}$ exciplex, in UO_2 aq. soln., time resolved luminesc. spectra 79-61417
Xe:N_2O, photoluminesc. from XeO (^1D) excimers 78-68544
Xe-$Br_2(Cl_2)$(HCl) mixtures, low-press. excimer form. and quenching by e-beam excitation 79-50071
Xe+Ne, quenching of excited Xe*($^3P_2$, $^3P_1$, $^1P_1$) states 80-63578
Xe_2, time-resolved excitation using synchrotron radiation *(French)* 77-88483
Xe_2, VUV radn. emission, radiative lifetimes 79-27089
Xe_2^+ excimer form. in pulsed discharge, visible emission obs. 80-38754
XeBr, emission and form. kinetics, sequential two-photon absorpt. expt. 80-32767
XeBr, UV transient absorption following flash photolysis of Xe-Br_2 79-61879
XeCl, excimer emission band at 235.5 nm 77-18935
XeCl, excimers and excimer lasers 80-48217
XeCl, UV transient absorption following flash photolysis for Xe-Cl_2 79-61879
XeCl* emission spectrum obs., in Xe(6s,$^3P_2$)+RCl reactive quenching 79-100344
XeCl* spectra, for Xe(6s,$^3P_2$)+RCl vibr. energy disposal assignment 79-100345
XeCl*+Kr, substitution efficiency during excitation in transverse AC electric discharge 80-50850
XeF, electron impact deexcitation, low energy cross-sections and rate consts. 80-1071
XeF, electron impact deexcitation cross sections and rate consts. calcs. 80-32848
XeF, excimers, power superluminesc. in elec. discharge *(Russian)* 77-7621
XeF, transfer and quenching rate constants for (III, 1/2) and (II, 3/2) states 79-16003
XeF*, fluoresc. intensity, two- and three-body quenching by Ar, Xe 77-58053
XeF*, formation by XeF_2+Ar(Kr)(Xe) metastable states reaction, mechanisms 77-30897
XeF*, in enhanced quenching of Xe+F by intense laser light, computer modelling 78-55232
XeF*(C1/2), excited state radiative lifetime meas. 77-34671
XeI*, emission spectrum, from Xe-I_2 77-6843
XeI*, production via laser absorpt. processes at 193 nm, quenching kinetics 80-91466
XeO, luminesc. meas. of O(^1S) absolute quantum yield in photolysis of CO_2, N_2O 80-35561
XeOH exciplex, UV emission 78-37653
XeO*, mol. laser emitting at green wavelengths, population inversion kinetics 77-23661
Xe_2*, excimers and excimer lasers 80-48217
Xe_2*, synchrotron radiation excited, time resolved spectroscopy 80-69092

excimers continued
- Xe_2*, Xe_2^+, Xe_2, pot. energy curves, relativistic ab initio effective core pots. 78−86800
- Zn_2, quenching and predissociation, possible excimer laser 80−32770
- $ZnGa_2$, excimer visible emission spectra in RF discharge, vibr. struct. 79−18201

exciplexes *see excimers*

excitonic molecules
- anthracene, cryst., exciton aggregate possible form. under intense optical pumping, fluoresc. spectra 80−84772
- antiferromagnetic biexcitons in critical temp. range 79−95601
- biexciton binding energy, influence of lattice polarisation 77−8028
- biexciton bounded state pot., many-exciton effects 79−60717
- biexciton luminescence, influence of free excitons on profile 77−4684
- biexciton virtual formation in renormalisation of polaritons 79−99490
- biexcitons, nonlinear laser spectrosc., multiphoton transitions 80−84433
- biexcitons recombination, polariton effects 78−23033
- binding energy, variational calc. 80−10891
- binding energy in mag. field *(Russian)* 79−78011
- Bose condensed, long range order, superfluidity 77−43514
- Bose-condensed excitonic molecules, emission spectrum 77−11856
- change of binding type and dissoc. in strong mag. field 78−62744
- condensation effects of excitons, review 78−2427
- diatomic bound molecules with zero bond order, excited biexcitons 78−9049
- direct semiconductor, exciton luminescence in longitudinal optical photon sideband, formation time 79−61438
- elementary excitations in one-dimensional systems with resonance interaction 79−99489
- excitonic molecule, Bose condensation, optical response 77−43512
- Frenkel biexcitons, eigenstates and transition spectra 80−88480
- indirect band gap semiconductors, excitonic absorption band shape calc. 79−78015
- macromolecule, circular dichroism, exciton dimer and helix-free particle absorption 79−94116
- many-valley semiconductor, bound multi-exciton complexes, density-matrix functional approach 80−96794
- methyl iodide, biexciton states, IR absorpt. exam. 77−89714
- molecular crystal, charge transfer biexciton spectra, theory 77−51664
- molecular crystal, singlet and triplet biexciton spectra 78−10366
- multiexciton complexes in semiconductor, binding energy *(Russian)* 78−10372
- multivalley semicond. 77−66120
- organic solids, charged excitonic complexes, coupled states, exciton interaction with charge carriers study 80−20090
- perylene crystal, molecular exciton system, resonance Raman and fluorescence studies, dynamical effects 80−66169
- polar crystal, biexciton, lowest triplet state 79−56137
- polar crystals, biexciton stability 78−76002
- polar semiconductor, exciton-neutral donor and biexciton complexes 79−90968
- polyethylene, pristine and radiation-damaged film, electron energy loss spectra 79−81312
- population dynamics, collision effects 77−85149
- resonant Raman scattering and luminescence 79−95763
- secondary radiation, optical orientation effects 79−83010
- semiconductor, anisotropic, binding energy of exciton complexes 79−15088
- semiconductor, biexcitons, one-photon radiative recomb. 80−70621
- semiconductor, diamagnetic susceptibility of excitonic molecules *(Russian)* 80−7074
- semiconductor, luminescence, coherent conversion of excitons and photons to biexcitons *(Russian)* 79−47508
- semiconductor, polariton dispersion change by virtual biexciton form. under laser irrad. 79−38607
- semiconductor, single-quantum radiative recomb. of biexcitons due to biexciton-exciton interactions 80−96793
- semiconductor, two-polariton decay of excitonic mols. at 2K 79−95339
- semiconductor, wurtzite-type, emission lineshape of excitonic mols., polariton states 77−20918
- semiconductor film, Bose-Einstein condensation of excitons 77−28127
- semiconductor film, exciton complexes, form. and dissoc. 79−95343
- semiconductors, coherent biexcitons, two-photon nutation effect *(Russian)* 80−59892
- semiconductors, high density excitons and biexcitons, recomb. radiation bands profiles, time depend. 80−45140
- semiconductors, highly excited, condensation and pairing, interacting boson theory without anomalous propagators 77−33942
- semiconductors, multiple bound excitons, density functional calc. 80−10889
- semiconductors, particle complexes, $N=1$ to ∞, book contrib. 80−80194
- semiconductors, two-photon nutation of coherent biexcitons 80−80191
- structure two-photon processes 77−51675
- surface biexciton in polar semicond., binding energy calc. 80−96796
- theory, luminescence spectra of crysts., biexcitonic states classification 77−69238
- TTF-TCNQ, two-chain Fermi gas, response behaviour 80−2381
- two photon transitions to exciton and biexciton states, selection rules 77−69240
- two-photon excitation of first vibr. state 79−7789
- uniaxially compressed crystal, exciton molecule radiation *(Russian)* 80−108264
- wurtzite-type crystals, deform. effects on biexcitons 77−52038
- AgBr, electron-hole liq. and biexciton pocket, luminesc. obs. 78−15216
- AgBr excitonic mols., time-resolved luminesc. line obs. 77−69888
- CO_2, $\nu_2+\nu_2$ biexciton transition in Raman spectra 77−48158
- CdS, biexciton, low intensity nonlinear coherent mixing study 80−49619
- CdS, biexciton fluoresc. line shape 77−44059
- CdS, biexciton levels, luminescence-assisted two-photon spectra 80−29795
- CdS, biexcitonic luminesc. for allowed and forbidden polarisation 77−44040
- CdS, biexcitonic state existence, 2.5 MeV binding energy *(Russian)* 77−39788
- CdS electronic two- and one-photon Raman scatt. via biexcitons, stimulated config. obs. mag. field shift 80−103963
- CdS, emission and transmission spectra, excitonic mols. effect 77−44062
- CdS, emission lineshape of excitonic mols., polariton states 77−20918
- CdS, excitation spectroscopy, relation between I_2 bound exciton line and CdS excitonic molecule line 80−40153

excitonic molecules continued
- CdS, exciton condensation effects on refr. index 77−20818
- CdS, excitonic mol. emission, strain induced splitting 77−44060
- CdS, excitonic mol. transitions, optical gain and induced absorpt. spectra 80−11438
- CdS, highly excited cryst., biexciton, impurity transition and electron-hole plasma 79−15092
- CdS, luminesc. of I_2 bound exciton and excitonic mol. 79−91492
- CdS, photocond., spectral depend. at high excitation intensity, exciton effects 80−65619
- CdS, ps decay kinetics of luminesc., streak camera obs. 79−78752
- CdS, reson. Raman Scatt. under two-photon excitation of excitonic mols. 78−52486
- CdS, two-photon Raman scatt. via biexcitons, angle- and polarisation depend. 79−87446
- CdS, virtually excited biexcitons polaritons dispersion, two photon Raman scatt. 80−45067
- CdS(Se), magnetooptic study of P line at high excitations, biexciton binding energy values 78−48220
- CdSe, biexcitonic state existence, 1.2 MeV binding energy *(Russian)* 77−39788
- CdSe, excitonic mol. transitions, optical gain and induced absorpt. spectra 80−11438
- $Cd_{1-x}Zn_xS$ heteroepitaxial single-cryst. layers, photoluminesc. props. 80−100692
- CuBr, biexciton dispersion, two-photon absorpt. 80−76045
- CuBr, biexciton luminesc. 77−44056
- CuBr, biexciton two-photon absorption 79−47480
- CuBr, biexciton two-photon absorpt. 80−11432
- CuBr, excitonic mols., two photon generation 77−43511
- CuCl, biexciton first excited state, LO phonon assisted two-photon absorption 77−40260
- CuCl, biexciton luminesc. 77−44056
- CuCl, biexciton luminesc., subnanosecond time resolved spectroscopy 77−73167
- CuCl, biexciton resonant two-photon absorption 78−23491
- CuCl, biexciton two-photon absorpt. 80−11432
- CuCl, biexcitons, two-photon absorption and luminesc. 77−43513
- CuCl, biexcitons existence, review 77−69239
- CuCl, dielectric function for semiconductors with high exciton conc. 80−84443
- CuCl, direct creation of high biexciton density at $K=0$, two-photon absorpt. and emission spectra 79−33727
- CuCl, exciton mol. creation by pure and phonon-assisted two-photon transitions 78−63987
- CuCl, exciton spatial dispersion determ., two-photon Raman scatt. via excitonic mol. state 80−60595
- CuCl, excitonic mol., two-photon excitation via polariton state 80−54612
- CuCl, excitonic mol. luminesc. spectra, picosecond time anal. 78−52548
- CuCl, excitonic molecules, secondary emission under two-photon reson. excitation 80−11468
- CuCl, excitonic mols., ps time resolved luminesc. spectra 77−16383
- CuCl, excitonic mols., two photon generation 77−43511
- CuCl, excitonic polariton-polariton resonance scattering 79−24306
- CuCl, fission of relaxed excitonic mols. into upper and lower branch polaritons induced by M_L emission 80−11380
- CuCl, induced absorption due to exciton-biexciton transitions 78−15187
- CuCl, light mixing induced by giant two-photon absorpt. of excitonic mols. 78−42383
- CuCl, luminesc. and reson. Raman scatt. of excitonic mols. 79−33814
- CuCl, luminesc. of excitonic mols. 80−2817
- CuCl, luminesc. spectra, excitonic mol. reson. two phonon excitation 78−19514
- CuCl, nonlinear light absorpt., picosec. pulse, exciton-biexciton transitions 79−47483
- CuCl, phonon interaction of excitonic molecule 80−50316
- CuCl, phonon-assisted two-photon absorpt. of excitonic mol., bare-exciton approach 79−78702
- CuCl, ps. luminesc. spectra, resonantly excited excitonic mols. 78−19555
- CuCl, psec time resolved spectroscopy, excitonic mols. 79−47500
- CuCl, relaxation of excitonic molecules generated by two-photon excitation, forward Raman scatt. 78−2838
- CuCl, reson. coherent nonlinear scatt., biexciton autoionising states 79−51978
- CuCl, reson. Raman scatt. and luminesc. of biexcitons 79−38618
- CuCl, reson. Raman scatt. and luminesc. due to excitonic mols. 79−91425
- CuCl, reson. Raman scatt. and luminesc. under two-photon excitation 79−95765
- CuCl, reson. two-photon excitation of excitonic mol. using circ. polarised light 78−84566
- CuCl, resonantly excited excitonic molecules, time resolved spectroscopy 78−92109
- CuCl, time resolved exciton-biexciton transitions, UV excitation, luminescence spectra 79−69883
- CuCl, time-resolved study of induced absorption due to exciton-biexciton transitions 79−38658
- CuCl, two-photon absorpt. and luminesc., biexcitons 80−11434
- CuCl, two-photon reson. scatt. in excitonic mol., population instability 79−28826
- CuCl, two-photon reson. Raman scatt. and luminesc. of excitonic mols. 79−28819
- GaAs, biexciton stability, appl. of theory for polar crysts. 78−76002
- GaP:Zn, luminesc., acceptor-bound multiple excitons 80−11476
- GaSe, deep free and constrained excitons and biexcitons, collective interactions *(Russian)* 80−66282
- Ge, biexciton and trion existence, photolum. *(Russian)* 80−16088
- Ge, bound exciton complexes, density functional calc. 80−10890
- Ge, exciton mol. by phonon-assisted two-photon absorpt., theory 78−48197
- Ge, exciton mol. creation by pure and phonon-assisted two-photon transitions 78−63987
- HgI_2, red, liminesc. and Raman scatt., biexcitons and exciton-phonon interactions 79−61424
- HgI_2, red, luminesc., excitation spectra on M-band 79−28822
- InP:Bi, isoelectronic impurity states, emission and absorpt. obs. 79−42491
- MnF_2, biexciton decay, time resolved laser spectra 78−75999
- N_2, active solid, surface excitation prod. by at. beam deposition, stimulated emission 79−99911
- N_2 crystals, luminesc. and biexcitons 79−69893

excitonic molecules continued
  NaCl, bi-exciton luminescence possibility 80—40167
  α-O$_2$, cryst., exciton, exciton-magnon, and biexciton absorpt. at 1.5K 80—84750
  α-O$_2$, cryst., exciton effects, spectra *(Russian)* 79—47481
  O$_2$, cryst., polyexciton light absorpt. *(Russian)* 78—27251
  α-O$_2$ crystals, absorpt. line polarisation biexciton existence *(Russian)* 80—108242
  α-O$_2$ crystals, absorption line biexciton polarisation *(Russian)* 80—89028
  Si, biexcitons, photoluminesc. spectrum exam. 78—47705
  n-Si, bound excitons and bound multiexciton complexes, excitation spectra 80—96792
  Si, bound multiexciton complexes, luminesc. 80—10888
  Si, diamagnetism of excitons and biexcitons, recomb. spectra *(Russian)* 80—7412
  Si, electron-hole liquid, free excitons, biexciton gas, luminesc. 80—6750
  Si, exciton-plasma transitions, dense electron-hole system portrait composition *(Russian)* 80—49622
  Si, excitonic molecules, thermodynamics, luminesc. 80—25442
  Si, uniaxially deformed, photoluminesc., biexcitons *(Russian)* 77—59611
  Si, uniaxially stressed, excitonic molecule emission spectra, electron valley degeneracy effects 80—60669
  Si:B(Li)(P), piezospectroscopic studies of bound multiexciton complexes 80—16006
  Si:Ga, luminescence fine struct. from bound exciton and multiexciton complexes 77—32430
  Si:P, bound multiexciton complexes, shell model 77—31953
  ZnO, biexciton levels, luminescence-assisted two-photon spectra 80—29795
  ZnO, excitonic mol. emission, strain induced splitting 77—44060
  ZnO, excitonic mol. transitions, optical gain and induced absorpt. spectra 80—11438
  ZnO, excitonic molecule transitions, M-band emission 79—78742
  ZnO, existence of biexcitons, reson. two-photon Raman scatt. 79—19889
  ZnO, highly excited, biexciton states, M-band luminescence 79—78744
  ZnO, multiparticle exciton complexes, luminesc. spectra *(Russian)* 80—16090
  ZnO, optical gain and induced absorption from excitonic mols. 78—84609
  ZnO, stimulated two-photon emission from excitonic molecules 79—28815
  ZnSe, blende type struct., luminesc. under high excitation 79—19928
  ZnSe, luminesc., reson. Raman scatt. due to excitonic mols. 79—33816
  ZnTe, blende type struct., luminesc. under high excitation 79—19928

excitons
  see also excitonic molecules; phonon-exciton interactions
  absorption band, integrated intensity 78—72084
  absorption spectra, dislocations effect on band profile 80—16070
  absorption spectra, exciton peak, temp. depend., calc. 80—59885
  acceptor-donor-acceptor complex, Frenkel excitons and ionic excited states 80—92824
  acenaphthylene, orientational disorder, spectroscopic exam. 78—14670
  additional light waves near region of exciton absorpt. and luminesc. in crystal 80—2340
  adenine film, polycryst., energy conversion processes, quantum yields, 4 to 10 eV 80—88589
  alkali bromides and iodides, self-trapped exciton and F-centre form. by picosecond laser pulses 80—10546
  alkali cyanides, mol. excitons, X-ray excited emission spectra obs. 80—66287
  alkali halide, defect formation, model of excitonic mech. 78—91337
  alkali halide, excitonic mechanism of defect form. 77—47737
  alkali halide, polarization dichroism in the optical spectra of Jahn-Teller excitons 79—69435
  alkali halide crystal, defect formation in thermal equilibrium state of self-localised exciton 80—44205
  alkali halide crystals, exciton mechanism of complex active centre formation at fracture 79—33033
  alkali halide crysts., photoemission on mech. stimulation, mechanism *(German)* 77—85819
  alkali halide film, low energy electron scatt. 78—26928
  alkali halides, defect form., model of excitonic mechanism 78—38696
  alkali halides, electron sputtering mechanisms involving excitons 77—55857
  alkali halides, F-centres, formation time 80—15477
  alkali halides, photoelectric yield spectra, 10 to 40 eV photon energy 79—28887
  alkali halides, self trapped exciton, optical detection of spin relax. processes 78—60358
  alkali halides, thermoreflect. spectrum, 5 to 9 eV, electronic struct. 77—81123
  alkali halides, vacuum UV absorption spectra, exciton splitting rel. to exchange interaction 78—23494
  alkali iodides, free exciton reson. luminesc. lines 77—77272
  alkali metal film, inert gas impurities, metal-insulator transition, optical absorption and cond. 77—24598
  alkali metal film, inert gas impurities, optical spectra, rel. to inert gas solids 77—24878
  alkali metal halides, defect production in cation sublattice, mechanisms 80—96510
  alkali metal halides, irradiated, annealing 78—92494
  alkaline earth fluoride, EPR of triplet state of self-trapped excitons 78—43684
  alkaline earth oxides photoluminescent spectra of surface states 79—47505
  alkane:toluene, radiolysis at 77K, luminesc., excited singlet toluene form., energy transfer mechanism 77—16846
  n-alkanes, single cryst., γ-irrad., ESR, energy deposition rel. to alkyl radical form. 77—16844
  amorphous semiconductor with Gaussian random pot , exciton effects on absorpt. spectra 77—16273
  Anderson localisation of mol. excitons, substitutionally disordered systems 77—89733
  anisotropic crystal, additional light waves and boundary conditions 77—73121
  anisotropic crystal, exciton-impurity complexes *(Russian)* 77—80741
  anisotropic crystals, exciton diffusion and relax. time *(Russian)* 77—80742
  anisotropic excitons, longitudinal-transverse splitting 78—2431

excitons continued
  anisotropic magnetic crystals, theory of excitons *(Russian)* 79—7786
  annihilation phenomena in low dimensionality finite lattice, master eqn. 80—92821
  anomatic hydrocarbon high density excitation effects on fluoresc. 79—1782
  anthracene: tetracene, singlet exciton trapping mechanism, fluoresc. mag. field modulation obs. 77—77267
  anthracene:acridine(carbazole), fluoresc., structural traps for singlet excitons 78—19542
  anthracene:rhodamine, triplet exciton density, isotope substitution effect, in weak mag. field 77—90184
  anthracene:tetracene, crysts., triplet kinetics model *(German)* 79—4518
  anthracene:tetracene, fluorescence decay with X-irrad., energy transfer by excitons 77—20915
  anthracene:tetracene, nonlinear quenching of fluoresc. 79—65924
  anthracene:tetracene, singlet exciton fission, fluoresc. in mag. field 79—69877
  anthracene:tetracene crysts., mag. field modulation of scintillation under α-irrad. 77—48256
  anthracene, α-induced radical production beyond Bragg peak 79—24773
  anthracene, α-particle tracks, excited states, creation and evolution 78—43934
  anthracene, coherent exciton scatt. and recomb. 80—39510
  anthracene, cryst., exciton aggregate possible form. under intense optical pumping, fluoresc. spectra 80—84772
  anthracene, cryst., heat pulse propag., exciton condensation, time-resolved fluoresc. spectra 80—84771
  anthracene, cryst., triplet exciton pair kinematics, diffusion model 78—79931
  anthracene, cryst., with electrolytic contacts, photocurrent anomalous behaviour, current-volt. characts. 77—39933
  anthracene, Davydov splitting of lowest singlet exciton under high press. 77—72823
  anthracene, electron irrad., creation and evolution of excited states, scintillation obs. 78—92128
  anthracene, EPR linewidth of triplet excitons 78—15011
  anthracene, EPR of triplet excitons, source of residual linewidth 79—15338
  anthracene, excitation spectra of exciton fission in organic crystals 78—92116
  anthracene, exciton bands, dipolar lattice sums *(Japanese)* 77—43167
  anthracene, exciton sounding of α-particle induced radiation defects 77—12423
  anthracene, fluoresc. from (001) surface and sub-surface excitons 79—33763
  anthracene, high exciton conc., low temp. fluoresc. *(Russian)* 77—28623
  anthracene, IR spectra, strong anharmonicity effects *(Russian)* 77—66511
  anthracene, isotopically mixed cryst., exciton dynamics 80—29329
  anthracene, laser-induced photocond., excited charge carriers 77—28211
  anthracene, lifetimes of exciton-polariton luminesc. 79—33761
  anthracene, liq. chromatography, sublimation, zone refining, exciton fluoresc., mobility meas., melt grown crystal 79—38736
  anthracene, nonlinear fluorescence quenching 78—52562
  anthracene, O-O exciton absorption bands, thermomodulation study 78—39563
  anthracene, orientationally disordered cryst., lattice relax. effect 80—107278
  anthracene, photocond. spectrum induced by excitons *(Japanese)* 80—29440
  anthracene, photon-emitting singlet excitons spatial distrib. 79—83009
  anthracene, polarised refl., surface excitons, Davydov splitting 77—16327
  anthracene, polarised reflection spectra, surface and vol. exciton coupling, vibronic states 78—72543
  anthracene, polariton effects in transmission and absorpt. spectra in thin crysts. 77—20886
  anthracene, protection against radiation damage, exciton effects 80—29055
  anthracene, pulsed electron excitation, triplet excitons, spectral and electrical investigations 80—92828
  anthracene, pure and doped, singlet exciton diffusion lengths, fluoresc. quenching by dye 78—43923
  anthracene, reflectivity and fluoresc. of (001) surfaces, sub-surface exciton states 79—15508
  anthracene, reson. Raman emission and hot luminesc. *(Russian)* 79—61377
  anthracene, single cryst., piezomodulated reflection spectra 79—61392
  anthracene, single cryst., X-radiation damage recovery, using triplet state exciton probe 78—75694
  anthracene, single cryst., X-ray radiation damage, delayed fluoresc. meas. *(Japanese)* 79—37736
  anthracene, single cryst. triplet excitation form. 79—69437
  anthracene, single cryst. with photoinduced local centres, luminesc. 79—61433
  anthracene, singlet and triplet excitons as probes for photochem. reactivity 79—74406
  anthracene, singlet exciton annihilation kinetics 79—19926
  anthracene, singlet exciton fission, fluoresc. in mag. field 79—69877
  anthracene, singlet exciton fission, prompt and delayed fluoresc. mag. field depend., temp. effects 78—52540
  anthracene, singlet exciton transitions, energies and oscillator strengths, boson theory with PPP wavefunctions 80—92820
  anthracene, singlet-triplet absorpt. spectra, 2-300K, photoexcitation spectra 78—43890
  anthracene, temperature independent intersystem crossing 78—39030
  anthracene, theory of fission of singlet Frenkel exciton into two localised triplet excitons 79—23901
  anthracene, thick crystals, excitation spectrum of fluorescence 80—76068
  anthracene, thin film vacuum deposited, exciton reflection spectra *(Russian)* 78—15194
  anthracene, total reflection spectra, site shift surface exciton dispersion 77—77233
  anthracene, triplet exciton absorpt. lines 79—47475
  anthracene, triplet exciton trapping, structural imperfections and delayed fluorescence 78—68551
  anthracene, triplet exciton trapping by dislocations 78—30871
  anthracene, triplet excitons, phosphoresc. and delayed fluoresc. excitation spectra 78—63986
  anthracene, triplet-exciton fine struct., high resolution optical meas. 80—45099

excitons continued

- anthracene crystal, resonance secondary emission, Raman scatt. in exciton absorpt. region *(Russian)* 80—40120
- anthracene crystal, singlet-triplet exciton annihilation 78—31240
- anthracene crystal, triplet exciton absorpt., high resolution photoconductivity spectroscopy 78—10504
- anthracene crystals, α-particle induced scintillation, mag. field effects 80—40161
- anthracene crystals, local biexciton formation, luminesc. spectra *(Russian)* 78—2428
- anthracene crystals, orientationally disordered, exciton trap depths 80—88481
- anthracene crystals, resonance Raman spectra sensitivity to exciting light intensity *(Russian)* 78—52504
- anthracene crysts., dissoc. near charged defect 77—51669
- anthracene crysts., nonlinear fluorescence quenching, recomb. of free excitons 80—7397
- anthracene films, optical props., comparison between free and optical contact mounting 80—89079
- anthracene iostopic mixed crystals, exciton spectra 79—38602
- anthracene like crysts., charge-transfer electron-exciton bound states, theory 78—10365
- anthracene mol. cryst., exciton-lattice interaction and exciton absorption line shape 78—18968
- anthracene single cryst., Frenkel exciton spectra at dielectric and conducting layer interfaces 80—44510
- anthracene-Au interface, energy transfer 77—85775
- anthracene-Au interface exciton luminescence Frenkel exciton metallic quenching *(Russian)* 80—50421
- anthracene-d_{10}-s-tetracyanobenzene, rotational mode coupling in phase transition 78—71827
- anthracene-dimethylpyromellitimide, cryst., triplet exciton pairs, EPR spectra 77—43906
- anthracene-dimethylpyromellitimide CCT crystals, mutual annihilation of triplet excitons 78—19543
- anthracene-dimethylpyromellitimide charge-transfer complex, photoconductivity mechanism 77—47860
- anthracene-phenanthreen-TCNB, exciton transport obs. 80—65461
- anthracene-phenanthrene-tetracyanobenzene, CT-cryst., mini-excitons and lattice dynamics, ESR, optical and Raman spectra 80—60406
- anthracene-pyromellitic dianhydride, cryst., charge transfer exciton transitions, refl. spectra obs. 78—72540
- anthracene-pyromellitic dianhydride complex, optical and photoelectric props. *(Russian)* 80—15570
- anthracene-quartz interface exciton luminescence, Frenkel exciton metallic quenching *(Russian)* 80—50421
- anthracene-TCNB charge transfer crystal, EPR spectra of triplet excitons, and Raman spectra 78—26817
- anthracene-tetracene amorphous films, host-guest energy transfer 78—60505
- anthracene-tetracenebenzene, triplet excitons annihilation, mag. reson. sign reversal 79—65769
- anthracene-tetracyanobenzene, triplet exciton annihilation, mag. double reson. *(Russian)* 78—19380
- anthracene-tetracyanobenzene charge-transfer complex, EPR of triplet excitons, phase transitions 77—28425
- anthracene-tetracyanobenzene charge-transfer complex, RYDMR of triplet excitons annihilation 78—39448
- anthracene-tetracyanobenzene cryst., triplet exciton annihilation, time correlated delay fluoresc., ODMR 80—39895
- anthracene-tetracyanobenzene cryst., triplet excitons, zero-field EPR splitting temp. depend. 78—10748
- anthracene-tetracyanobenzene crysts., deuteration effect on phase transition, triplet state EPR study 80—50163
- anthracene/TCNB, charge-transfer cryst., fluoresc., 1.2-300K, mobile triplet excitons 78—43913
- antiferromagnetic, light absorption in freq. region of exciton and exciton-magnon transitions 77—48149
- antiferromagnetic, noncollinear, exciton-magnon light absorpt. at $T \neq O$ *(Russian)* 78—23482
- antiferromagnetic extended Hubbard chain, excitonic effects on optical absorption 79—61323
- antiferromagnetic Hubbard chain, interband absorpt., Peierls dimerisation, excitonic effects 80—25072
- antiferromagnetics, with displaced 3d-ions, mech. of electric dipole absorption of light *(Russian)* 77—32406
- antiferromagnets, exciton motion 80—70617
- antiferromagnets, magnon parametric generation with impulses at Brillouin zone boundary *(Russian)* 80—29540
- aromatic hydrocarbons, doped mol. crysts., singlet host exciton nonradiative heterofission 77—28122
- aromatic organic macromolecules, energy-gain satellite in C(1s) XPS 79—1813
- aromatic-hydrocarbon crystals, model for fission of singlet excitons into triplet-exciton pairs 78—14672
- astaxanthin, aq. soln., aggregate, reson. Raman spectra, and IR spectra, exciton interactions 78—31770
- bacterial photosynthesis, light collection and harvesting processes investig. on psec. time scale 77—90743
- benzene, cryst., molecular exciton cluster states and spectra 77—66123
- benzene, IR spectra, vibr. exciton cluster states, percolation and pairwise interactions 78—43844
- benzene, isotropically mixed crysts., singlet and triplet exciton percolation theory 78—26818
- benzene, liq., vibr. excitons, reson. energy transfer and local struct., IR spectra 77—75145
- benzophenone, charge carrier generation and mobility 78—84231
- benzophenone, cryst., charge carrier generation by exciton-exciton collisions 80—88568
- benzophenone, cryst., phosphoresc. spectra and decay time, temp. depend. 79—87479
- benzophenone, migration of triplet excitons, EPR profiles and phosphoresc. decay data 80—84641
- benzophenone, triplet exciton absorpt. lines 79—38563
- betamethylnaphthalene in $C_{10}D_8$, exciton percolation and coherence 77—59258
- biexcitons, many exciton effects, appl. to CuBr(Cl) 78—51901
- bimolecular exciton recombination kinetics, limited by anisotropic diffusion 77—4295
- binding energy and lifetime in free carrier gas 79—33238
- binding energy of exciton-neutral donor complexes 79—60715

excitons continued

- binding energy of small radius excitons, freq. depend. optical phonon contrib. 77—69236
- binding energy to neutral acceptor, calcs. using atomic-like variable wave function 78—79937
- binding to neutral donor 77—31949
- bioenergetics, solitons, muscle contraction mechanism 79—96508
- biological membranes as excitonic superconductors *(Russian)* 78—23190
- biomembrane active transport and energy transformation, quantum mechanism 78—53364
- biphenyl, cryst., electronic absorpt. and refl. spectra 78—64377
- bipolariton dispersion laws 77—51677
- bistability and anomalies in absorption and resonance scattering of intense light 79—95803
- book 80—41951
- Bose condensation and superdiamag. current prod. possibility 80—65456
- Bose condensation of Frenkel excitons, optical props. of condensate 77—55485
- Bose condensed, long range order, superfluidity 77—43514
- Bose gas, with anisotropic dispersion laws, phase transitions, sp. ht. and excitons *(Russian)* 77—4229
- Bose-condensated electron-hole fluid, phase fixation, excitonic and spin superfluidity 78—30872
- Bose-Einstein condensation and excitons in living systems 80—30640
- Bose-Einstein condensation of Frenkel excitons in mol. cryst. 77—62838
- bound, in semiconductors, review, book contrib. 80—44519
- bound, in spherical model, low lying excited states 80—10883
- bound excitons, ground state energies for all mass ratios 79—60729
- bound excitons in local density approximation 79—47022
- bounded crystals, auxiliary boundary conditions in theory of additional light waves and excitons *(Russian)* 78—56080
- Brillouin scattering, resonant, analogy to modulation spectroscopy *(Japanese)* 78—68526
- Brillouin scattering of exciton polaritons and additional boundary conditions 79—95795
- canted magnetic structured materials, exciton spectra, optical props. 80—70622
- carbazolyl substituted diacetylene monomer cryst., ODMR and triplet state kinetics 78—76355
- chalcogenide glass, mech. for electron-hole recomb. 78—72196
- chalcogenide glasses, non-radiative recombination of electron-hole pairs 78—6759
- chalcogenide semiconductors, optical and elec. props., comparison with SiO_2 78—6721
- charge ordered crystals, mag. props., energy spectrum, triplet excitations 78—18979
- charge transfer complex high density excitation effects on fluoresc. 79—1782
- charge transfer crystals, mixed, exciton transport, low-dimensional, statistical model and experiments 80—65461
- chlorophyll, a and b, lowest singlet-singlet transition, solvent effects 79—24952
- chlorophyll, fluorescence quenching, exciton annihilation excited state absorption and stimulated emission 79—98137
- chlorophyll-a arrays, exciton transition calculations 78—35802
- chloroplast photosystems, exciton annihilation at 100K 77—25371
- cholesteryl caprinate, liq. cryst. mesophase electron emission 79—55664
- chromophone aggregates in Frenkel exciton model, dynamic perturbation effects on circular dichroism intensity 80—93273
- chromophore excitonic interaction in Halobacterium halobium purple membrane 77—21497
- coherent and incoherent motion in continuous time random walk framework 80—59882
- coherent pairing, microscopic theory 77—8026
- coherent phonons and excitons in biological systems, Bose condensation 80—67042
- complex particle emission, pre-equilibrium exciton model anal. 78—66280
- condensation and liquefaction in strong mag. field, RPA and variational calcs. 78—63984
- condensation effects of excitons, review 78—2427
- condensation kinetics 78—10370
- conference, luminescence, Paris (July 1978) 79—33755
- conference, Tomakomai, Japan (Sept. 1975) 77—43510
- contact exciton, screening and quenching 80—29334
- convalent crystals, fundamental absorption band struct. in quasimolecular model 77—24868
- copper phthalocyanine film, photocelectrochem. behaviour on SnO_2 electrodes 80—15626
- coronene, protection against radiation damage, exciton effects 80—29055
- coupled coherent-incoherent motion, rel. to mean square displacement 79—19519
- covalent crystal, dynamical correlation effects on quasiparticle Bloch states 80—88499
- cryst. with defects 78—60478
- crystal luminescence, polariton mechanism, reabsorption, spatial dispersion effects, boundaries *(Russian)* 80—55186
- crystal optical characteristics, relax. processes exciton dispersion 80—107709
- crystal-vacuum interface, light reflection and transmission coeffs., additional boundary conditions 80—34870
- CTIP, exciton surface polaritons at room temp. 79—47476
- cubic crystal, theory of large-radius exctions 78—47710
- cubic crystals, calc. of binding energy of X-ray excitons 78—2435
- cubic crystals, III-V and II-VI, luminesc. polarisation and hot-exciton orientation and decoupling 78—6733
- cubic semiconductor, exchange splitting of excitons 79—42467
- cubic semiconductor, long-range exchange splitting 77—51671
- cubic symmetry cryst., quadrupole exciton theory 80—103632
- current states and domains in systems with electron-hole pairing 80—54614
- cyanine dye, crysts., extraordinary exciton polaritons in refl. spectra, macroscopic dielec. theory 77—89715
- 9-cyanoanthracene, cryst., polarised refl. spectra at 2K, 360-460 nm, dielec. function 79—91461
- cyclododecatrienetriyne, model for exciton theory of excited states in poly-1,4-hexadiyn-1,6-diol bis(p-toluene sulphonate) 77—80733
- γ-cyclopropyl-bis (1,3,3-trimethylindolenine-2-yl)pentamethinium fluoroborate, exciton surface polaritons, reflecting faces obs. 80—65645
- Davydov splitting, mol. cryst. with complex lattice 79—56132
- Davydov splitting theory, excitonic parameters, split absorption bands, organic molecular aggregates *(Spanish)* 79—59437

excitons continued
defect theory and processes, review 80—2009
degenerate semiconductor, exciton dispersion 77—69248
degenerate semiconductors, electric field influence on exciton states, Stark effect 80—54617
degenerate valence band semiconductors, polariton effect 79—15102
diamagnetic, odd states, oscillator strengths, and optical absorption line positions 79—11072
diamond, natural, free exciton luminesc. line shape 80—40165
diamond, role of electron-hole interaction in optical spectra, review 80—45113
p-diamond, synthetic, semicond., photocond. bands due to ionisation of indirect excitons 79—69550
diamond and sphalerite type crystals, energy levels of indirect excitons 80—15457
diamond and sphalerite type crystals, with spin-orbit interaction, indirect exciton energy levels 80—24804
diamond structure, energy levels of direct exciton formed by split-off valence band 78—91624
diamond-type crystals, energy levels of Mott excitons 78—6282
p-dibromobenzene, cryst. electronic and vibr. energy transfer and relax. 78—31229
1,4-dibromonaphthalene, k-k scatt., exciton dephasing time-resolved phosphoresc. obs. 80—11458
1,4-dibromonaphthalene, optical props., struct. disorder effects 78—52525
1,4-dibromonaphthalene, proton spin relaxation by optically excited triplet states 79—19810
dibromonaphthalene, quasilinear chain excitons, Stark effects 80—97239
1,4-dibromonaphthalene, S_0 to T_1 exciton transition, optical dephasing time and lineshape function 78—15183
(1,4)-dibromonaphthalene, triplet exciton scatt., absorpt. spectra 78—6696
1,4-dibromonaphthalene, triplet-triplet exciton annihilation in quasi-1-dimens. cryst. 78—27297
9,10-dichloroanthracene, cryst., singlet-triplet absorpt. spectra, delayed fluoresc. 77—8619
9,10-dichloroanthracene, mag. field effect on exciton processes and photodetrapping 77—4668
9,10-dichloroanthracene, quasi 1D α-cryst., exciton transitions, optical refl. spectra obs. 77—81116
p-dichlorobenzene($-d_4$), mixed cryst. phases, mol. reorientations and intermol. interactions, Raman obs. 79—28751
p-dichlorobenzene-p-dibromobenzene, mol. cryst., intermol. mixing of electronic states 77—85768
p-dichlorobenzene-p-dibromobenzene, solid soln., local struct. and triplet energy migration 78—60489
p-dichlorobenzene-p-dibromobenzene mixed crysts., triplet exciton migration, time resolved emission spectroscopy 80—89052
4,4′-dichlorobenzophenone, cryst., X-traps, rel. populations, elec. field effect 77—12414
4-4′ dichlorobenzophenone, triplet exciton absorpt. lines 79—38563
4,4′-dichlorobenzophenone single crysts., mutual annihilation of triplet excitons, 1.5 and 4.2K, phosphoresc. obs. 80—80850
dielectric, exciton, possibility of current state *(Russian)* 79—60726
dielectric, inhomogeneous current state phase transition, free energy *(Russian)* 80—84703
dielectric, spatially dispersive, boundary conditions for polarisation waves 79—61296
dielectric, spin-orbit interaction, effect on electron-hole pairing *(Russian)* 79—7790
dielectric function of electron-hole plasma, influence of two-particle states 79—56154
dielectric layer, natural EM oscillations excitation by stream of electrons or EM field 80—34378
dielectric medium, steady propag. of coherent light pulse, effect of spatial dispersion 79—72480
dielectric surfaces, phenomenological model for optical props. 80—20605
dielectric susceptibility, mol. cryst. with extended defects, exciton contrib. 77—55486
dielectric theory of interacting exciton reson. 78—14673
1,1′-diethyl-2,2′-cyanine iodide, neat and mixed crysts., visible absorption and emission spectra assignments 77—1692
diethylammonium manganese chloride, antiferromag., magnon sideband exam. by absorpt. spectra 77—12108
diethylammonium manganese tetrachloride, quasi two-dimensional antiferromag., magnon sideband in absorption spectra 78—43895
diffusion and annihilation, inhomogeneous surface layer effect *(Russian)* 79—60730
Diffusion of excitons and energy transfer to impurity molecules *(Russian)* 78—27282
1,4-dihalonaphthalenes, binary solid solns. lattice stability, mol. motions 78—31182
dimer triplet state line shape, small excitons, appl. to phenazine, naphthalene, tetrachlorobenzene 80—48041
dimers, adiabatic theory of exciton interactions 77—30852
dimers, bandshape prediction, incoherent exciton scatt. model 78—42132
diphenyl:(benzophenone, naphthalene), triplet exciton diffusion, phosphoresc. obs. 78—10964
diphenyl:naphthalene, benzophenone, phosphoresc., triplet diffusion excitons 78—63985
direct gap semiconductors, exciton energy determ., electron beam excited luminesc. 79—38680
direct-gap semiconductors, charged excitons 77—62840
disordered molecular system, exciton percolation, book contrib. 77—36297
disordered system, exact solution for diffusion const. 78—22885
disordered systems, electronic energy transfer, generalized master eqn. 80—57221
dispersive media, localised states of Wannier exciton type, bound state energy 77—43506
dissociation energy of exciton-neutral donor complexes 80—34364
DNA-acridine orange complexes, energy transfer after dye laser excitation 79—2005
droplets, energy condensation, comparison with ball lightning *(Russian)* 80—107712
durene-naphthalene melt, exciton diffusion, percolation approach 80—2390
dye crystal, CTIP, exciton surface polaritons detect. by ATR spectra at 295K 79—4818
dye monomolecular layers, energy transfer between sensitizers and acceptors 80—80861

excitons continued
dynamical screening and self-energy, in electron-hole plasma 79—15093
dynamical screening of excitons by free carriers 78—39031
echo, under single-pulse excitation conditions 79—73450
eigenstates of excitons near a surface 79—37994
electrical conductivity of excitonic and optical insulators with nonequilibrium distrib. of quasiparticles 77—15888
electrically induced light absorption and deep excitons 77—43973
electron correlation and bound excitons 77—85150
electron hole plasma, excitons, influence of dynamical effects 78—76004
electron-hole binding accompanied by Wannier-Mott exciton form. 80—59887
electron-hole binding and exciton formation *(Russian)* 80—65468
electron-hole drop, instability and motion, recombination flow, exciton gas *(Russian)* 80—15458
electron-hole liquids, relation between bulk compressibility and surface energy 80—65465
electron-hole pair states, singlet charge density formulation of exchange effects 80—20094
electron-hole paired systems, ferromagnetic ordering phase diagram 80—97097
electron-hole plasma nucleation, time evolution 80—49616
electron-hole system, phase transition during formation of exciton condensate *(Russian)* 78—60060
electronic elementary excitations in far UV, core level exciton and core hole polarisation 78—39032
electronic elementary excitations in far UV and X-ray region, appl. to GaAs(P)(Sb) 79—95346
electronic state of excitations and their phonon coupling 79—60719
electronic transitions, optical dephasing times and line shape functions 78—35162
elementary excitations in crystals, dielectric theory 78—60076
energy density and flux in exciton reson. region 78—48201
energy levels, influence of exciton gas and electron-hole plasma 80—96795
energy levels near hard walls, Green's theorem calc. 79—78014
energy transfer rates for coherent and incoherent motion 79—90973
EPR, optical detection in excited state *(Japanese)* 77—81029
EPR line shape of pairs of differently oriented molecules, effect of coupled coherent and incoherent motion of triplet excitons 79—69427
EPR of triplet excitons, model Hamiltonian, Kubo-Tomita approximation 77—24734
ethyl substituted ammonium halides, exciton absorpt. spectra 79—28782
ethylammoniumtetrachlorochromate, optical absorption intensity, short-range spin correlation 80—108185
ethylbenzocarbazole, soln., luminesc., effect of electronic excitation energy vibr. 80—55174
exact derivation of a generalized master equation for the motion of excitons 78—87911
exciton, insulator, differential thermo EMF, temp. depend. *(Russian)* 78—72182
exciton condensation in electron-hole drops *(Russian)* 79—19522
exciton echo intensity, closely spaced energy levels effect 77—20244
exciton insulator, coexistence of ferromag. and ferroelec. ordering 78—18973
exciton-coherent light nonlinear interaction theory 77—54754
exciton-impurity interaction rel. to absorption band shape *(Russian)* 77—52146
exciton-ionised donor complex, binding energy, effective electron-hole interaction pot. 78—67949
exciton-ionized donor complex, Eulerian angle separation within effective mass approx. 79—51495
exciton-photon interaction, exciton absorpt. lineshape, polariton and wave models 79—38564
excitonic insulators, study of coherence factors 78—76338
excitonic phase, collective excitation modes under strong mag. field *(Japanese)* 77—43502
excitonic phase transition in mag. field, quantum renormalization group 79—87045
excitonic polaritons, classical and quantum mechanical aspects *(French)* 80—103634
excitonic wave-phonon coupling, struct. transitions 77—15775
extremely anisotropic crystals, free excitons and exciton-impurity complexes, generation, theory 80—39509
extrinsic crystals, exciton migration theory 79—87043
Fermi resonance and two particle excitation 79—69436
Fermi system, excitons in electron-hole plasma 79—90969
ferromagnet, and Peierls antiferromagnet, two-parameter Landau expansion 79—23907
ferromagnet, excitonic, zero-sound excitations, Fermi liq. model 80—93101
ferromagnet, incommensurate mag. structs., inhomogeneous magnetisation *(Russian)* 80—29566
ferromagnet, refractive index, magnetic contribution 79—28727
ferromagnet, spin-lattice relax., light and US absorption *(Russian)* 79—7960
ferromagnetic dielectric, crit. behaviour of exciton relaxation consts. 78—84442
ferromagnetic metal, exciton condensation effects on props., Hubbard model 80—60171
ferromagnetic-paramagnetic transition, exciton migration in crit. region 79—73440
film, Wannier excitons 79—69426
fluorene:pyrene-d_{10}, exciton-guest, triplet-triplet annihilation, impurity traps effects 80—25433
fluorene:pyrene-d_{10}, single cryst., host-guest triplet pairs, mag. field effect 80—60649
fluorene, exciton band struct., two-photon fluoresc. excitation 78—64402
fluorene, lowest singlet state, exciton band struct. calc. 78—63983
fluorene, near 6K, two-photon excitation spectrum, g-exciton states location 78—64393
fracture, ionisation wave generation, microbreakdown mechanism 79—33032
free and autolocalised, coexisting in cryst. 78—6274
Frenkel, weakly excited, energy bands calculation in number representation *(Japanese)* 80—107714
Frenkel exciton formation in LEED theory of mol. crystals 78—38592
Frenkel exciton spectrum under the condition of Bose condensation 79—56133
Frenkel exciton system, phase transition and exciton-photon coupling 78—23024

excitons continued
- Frenkel exciton-charge transfer state mixing near charged defect model of photocond. 77—51663
- Frenkel excitons, high density system, collective excitations 77—43501
- Frenkel excitons, kinematical interaction at light absorption and luminesc. 78—10359
- Frenkel excitons, memory function for migration process *(Russian)* 77—47740
- Frenkel excitons, optical resonance 78—91621
- Frenkel excitons, superfluidity for DLRO or ODLRO 77—43516
- Frenkel excitons interaction resulting in polariton kinematical levels optical absorption line broadening 80—10892
- Frenkel type exciton solitary waves, damping and modification 77—62833
- fusion of Frenkel excitons in exciton-phonon field 77—55484
- GaP, reevaluation of bandgap and free exciton binding energy 78—60061
- GaSe$_{1-x}$Sx, exciton spectrum nature and anisotropy of electron bands near absorption edge *(Russian)* 79—51483
- GG GaS, indirect exciton exam. 78—39029
- granular metal-semiconductor system, exciton enhancement of supercond. transition temp. 79—7921
- graphite, photoemission, C 1s core-electron line shape, excitonic effects, Fermi energy and hole density of states 80—29848
- ground state of two- and three-dimens. excitonic molecule 78—72076
- Haken-Strobl model, three-dimensional, mean-square displacement of particle *(Russian)* 80—39506
- halides, vacancy-interstitial pair prod. by electron-hole recomb. 79—4530
- heavily doped semicond., photoemission lineshapes of impurity levels, p-wave resonance 80—76154
- Heisenberg Hamiltonian generalisation for case of atomic system with variable atomic spin value 78—14669
- hexamethylbenzene, exciton band struct. for first singlet state 77—55483
- HF characteristics at low temps., multiphoton absorpt., tunnelling under dimensional quantisation effect *(Russian)* 78—68073
- Hubbard antiferromagnetic semiconductor, collective excitations, weak coupling limit 78—19210
- hydroxygallium phthalocyanine, exciton electroabsorpt., optical density spectra 77—85746
- ice, cubic, LCMO calc. of energy bands 77—51656
- II-VI and III-V cryst., excitons detect., precision method 79—19906
- II-VI compounds, magnetoreflectance of exciton-polaritons 79—91410
- II-VI semiconductor mixed crystal, comp. disorder-induced broadening for free excitons 79—15479
- II-VI semiconductors, highly excited blend type involving free particle scatt. 79—38648
- II-VI semiconductors, photoreflection exciton spectra *(Russian)* 77—20874
- III-V semiconductors, magneto-optical spectra of free excitons, manifestation of electron-hole exchange effects 77—59561
- impurity doped solid, electronic excitation spatial diffusion meas. by degenerate four-wave mixing 79—64274
- impurity interaction, absorpt. line shape, linear impurity conc. approx., validity criterion *(Russian)* 80—49620
- induced moment paramagnet, singlet ground state, mag. fluctuations 77—4482
- inelastic biexciton-biexciton collision, effect on radiative recombination of biexcitons 79—15529
- inert gas, atom and solid, excitons 78—39034
- inert gas, solid, dead layer effects in UV reflectance of excitons 78—72553
- inert gas, solid, electron impact excited, exciton recomb. spectrum, temp. variation 78—48239
- inert gas crystal, benzene-doped, luminescence excitation investig. 77—77276
- inert gas crystals, excitons exam. 78—51898
- inert gas crystals, intermediate-radius excitons *(Russian)* 79—11068
- inert gas solid, electronic struct. of self-trapped excitons 79—19525
- inert gas solid, VUV luminesc. from excitons 79—43020
- inert gas solids, band struct. and excitons, book contrib. 77—47731
- inert gas solids, benzene doped, energy transfer processes, excitons, photoemission, luminescence spectra 77—69886
- inert gas solids, collective excitations and EELS, calc. 80—92842
- inert gas solids, core excitons, nonstructural theory 78—84148
- inert gas solids, exciton states, nonstructural theory using effective mass approx. 78—84147
- inert gas solids, luminesc., self-trapped exciton 79—38605
- inert gases, solid, absorption spectra of self-trapped excitons 78—43879
- inert gases, solid, electronic excitations, nonstructural theory 78—79942
- inert gases, solid, exciton states, intermediate coupling interaction 78—67952
- inhomogeneous state of exciton ferromagnet *(Russian)* 78—88132
- insulator, coherence factors and transport props. 79—28291
- insulator, Coulomb interaction effects on tunnelling 77—8051
- insulator, excitonic, condensate flows in mag. field, charge and mass transport *(Russian)* 79—11108
- insulator, quasi-one-dimens. 79—90966
- insulator, semiinfinite, spatial dispersion influence on EM props. 77—24814
- insulator in mag. field, two-band model 80—80192
- insulators, theory of plasmon exciton coupling 78—23032
- insulators, tightly bound, collective excitations 79—51492
- insulators with spontaneous currents, impurity scatt. effect on phase transitions 80—80242
- interaction with screw dislocation 78—10361
- interband transitions and currents in systems with electron-hole pairing 78—72302
- internal structure, review, book contrib. 80—44518
- iodomethane, thin single cryst., IR spectra anal., Fermi-Davydov intensity distrib. 77—59577
- ionic crystal, exciton mechanism model for defect form. 80—80187
- ionic crystal, free and self-trapped Wannier-Mott excitons, thermal mutual transitions *(Russian)* 79—38003
- ionic crystal, fundamental luminescence at high ionisation levels *(Russian)* 80—103985
- ionic crystal, intrinsic electronic excitations and defects, review *(Russian)* 80—10881
- ionic crystal containing self-localising excitons, cathodolum. 78—6785
- ionic crystals, anomalous props. of positronium atom, exciton state 78—2433
- ionic crystals, electronic excitation decay into radiation defects, review 78—47420

excitons continued
- ionic crystals, imperfect, positron stabilisation 80—40182
- ionic crystals, luminesc. of free and self-trapped excitons 79—33757
- Ising model, nonlinear excitations and coherent states in transverse field 80—68143
- ketones, mol. cryst., interband transitions, triplet-triplet absorptions 79—11452
- kinematical levels arising from Frenkel excitons interaction 79—56134
- kinematical multi-level exciton schemes 78—39028
- Knight shift, triplet exciton contrib. 77—59472
- laser action in dense exciton systems 77—75531
- laser pulse propagation in solid under conditions of excitonic state resonance 80—87430
- lattice, deformable, local and global stabilities of electron 80—54620
- lattice migration, diffusive and percolative excitons 80—59879
- lattice vibration effect on exciton motion, inner potential energy, ground state, effective mass *(Chinese)* 80—54610
- layer materials with stacking faults, fine structure splitting of ground state excitons 77—51665
- layered compounds, modulation spectroscopy, book contrib. 77—40267
- layered compounds, optical props., book contrib. 77—44023
- layered crystal, light absorption by excitons, interlayer hoppings *(Russian)* 78—68532
- layered crystal, wave functions, exciton spectrum, light absorpt. *(Russian)* 80—100436
- layered semiconductor, exciton spectrum calc. *(Russian)* 77—1378
- layered semiconductor plate, exciton light absorption *(Russian)* 77—85750
- layered semiconductors, exciton spectra in case of strong anisotropy 77—51666
- leucosapphire, electronic band struct., optical props. 79—95329
- lifetime of carriers and excitons before self trapping 77—85236
- light reflectivity in exciton region for arbitrary surface pot. 79—38568
- light scattering by excitons localised at dislocations 78—60479
- LiH, cubic, vibronic struct. and anisotropy of excitons, refl. and edge luminesc. spectra 78—23523
- linear chain doublet exciton, with exponential memory, exact dynamical soln. 78—39027
- linear chain system, exciton model of supercond. 78—6476
- linear conductor, interchain coupling role 78—6294
- linear crystal, donor-acceptor complex, Frenkel excitons and ionic excited state mixing 79—99485
- linear molecular crystal, effect of mixing between Frenkel excitons and charge transfer states on charge carrier transfer 79—33242
- linear molecular crystal, mixing of Frenkel excitons and ionic excited states 77—15771
- linear molecular crystal, mixing of Frenkel excitons and ionic excited states 77—15772
- localisation of motion 77—31962
- low frequency excitations in exciton dielectric type system with doping *(Russian)* 80—15459
- low-dimensional crystals, excitonic superfluidity 78—6359
- luminescence, exciton, RF coherence and polarisation 78—10937
- luminescence spectra, surface polaritons and Brewster waves *(Russian)* 79—43033
- lutein, aq. soln., aggregate, reson. Raman spectra, and IR spectra, exciton interactions 78—31770
- macrometals as possible excitonic superconductors 79—42688
- magnetic ions interaction in insulator, degenerate orbitals 79—91010
- magnetically ordered dielectric, review *(Russian)* 77—80943
- magneto-optical crystals, spectra of hybrid excitations from transverse photons, excitons, magnons interactions 78—80320
- many-valley semiconductors, donor impurity levels and excitons, shallow-deep instabilities 80—75520
- mechanical surface excitons, interaction with radiation, refl. and transmission spectra 79—15098
- memory fading in generalized master eqn. of excitation transfer 80—49610
- merocyanine organic solar cells, photovoltaic props. in terms of exciton transport 79—43763
- metal, damping of excited molecules located above surface 78—92160
- metal-dielectric contact, exciton quenching and excited state props. 77—4416
- metallic crystals, low-dimensional, excitonic 'superfluidity' 77—20248
- metals, exciton effects on X-ray absorption edges 80—108298
- methacrylate polymer, carbazolyl substituted, excimer and charge transfer complex trapping of excitons 80—34367
- methyl iodide, liquefied gas solns. bound exciton model for Rydberg bands 78—31214
- methyl substituted ammonium halides, UV exciton absorpt. bands 78—72547
- methylammoniumtetrachlorochromate, optical absorption intensity, short-range spin correlation 80—108185
- mixed crystal, exciton self-trapping 79—37991
- mixed crystal theory, qual. tests, energy denominator depend. of naphthalene reson. pairs 77—39783
- mixed crystals, exciton percolation migration dynamics 77—1372
- mixed crystals, reson. Raman scatt. of light by longitudinal optical phonons 77—28577
- mixed crystals with indirect band struct., no-phonon struct. from Wannier exciton model 78—43898
- mixed organic solids, triplet exciton transport at crit. conc., Anderson localization or delocalization 79—15087
- molecular aggregates, density operator description of excitons, excitonic motion in 1-D finite chain 79—37997
- molecular aggregates, optical spectra, near strong coupling limit, Green's function model 77—83774
- molecular aggregates in non-resonant matrix, excitonic motion, density operator theory *(French)* 78—10357
- molecular biophysics, systems with dipole-dipole interactions 79—11882
- molecular chains in non-resonant matrix, excitonic state optical response, density operator theory *(French)* 78—10358
- molecular cryst., dipolar exciton band struct., optical model 77—15770
- molecular cryst., triplet exciton annihilation and triplet exciton quenching by free radicals, analytical form of mag. field depend. of rate consts. 79—15094
- molecular crystal, band structure, excitonic processes, trap distrib. 80—6720
- molecular crystal, charge-transfer electron-exciton bound states, theory 78—10365

excitons continued
molecular crystal, coherent 1-dimens. exciton transport and impurity scatt. 78—14666
molecular crystal, coherent pairing of excitons in reson. EM field, biexciton spectra 77—47736
molecular crystal, collective props. of mol. excitons 77—15774
molecular crystal, dipole plasma 77—85168
molecular crystal, dipole plasma oscillations, Bose-Einstein condensation of excitons *(Russian)* 78—84155
molecular crystal, dislocation excitons 79—65388
molecular crystal, disordered, transport of energy of electron excitations 77—40283
molecular crystal, exciton band spin-orbit coupling 78—39025
molecular crystal, exciton bandwidth effects on electron-phonon coupling 77—4172
molecular crystal, exciton density of states, effect of struct. disorder 79—28288
molecular crystal, exciton scatt. by lattice defects, absorpt. line shape 79—38576
molecular crystal, exciton transport, variational method 78—30870
molecular crystal, exciton trapping and self-trapping 77—31947
molecular crystal, Frenkel exciton, coupled coherent and incoherent motion 77—35870
molecular crystal, Frenkel excitons, effect on charge carrier transfer 78—79936
molecular crystal, generalised master eqns. under delocalised initial conditions 79—26003
molecular crystal, ground state energy of exciton gas and liq. 79—95341
molecular crystal, high power light pulse coherent interaction with exciton-impurity centres 80—55146
molecular crystal, impurity effect on exciton band absorption 78—27268
molecular crystal, impurity reson. interaction effects 77—1396
molecular crystal, kinematical interaction of excitons and Davydov splitting 79—82528
molecular crystal, LEED, Frenkel exciton influence, diagram formalism 78—47217
molecular crystal, LEED differential cross-section, Frenkel excitons effects 78—51398
molecular crystal, LEED specular beam intensity, bulk Frenkel exciton effects 78—51399
molecular crystal, light absorpt. with excitation of singlet and double triplet excitons *(Russian)* 77—15773
molecular crystal, mixing between Frenkel excitons, and charge transfer states, effect on charge carrier transfer 77—89707
molecular crystal, quasi-one-dimensional, exciton wave scatt. by impurity 79—78012
molecular crystal, second-quantisation representation of exciton states 78—23030
molecular crystal, sensitised fluoresc., energy transfer rate 79—38586
molecular crystal, sensitised luminesc. calc. for trapping models using momentum-space theory of exciton transport 80—11447
molecular crystal, stimulated Mandelshtam-Brillouin scatt., dipole-plasma oscills. 80—1278
molecular crystal, surface exciton energy calc. 77—20400
molecular crystal, surface exciton levels, radiation corrections 80—34962
molecular crystal, surface excitons theory 77—15927
molecular crystal, trapping, detrapping and heterofusion using kinetic eqns. 79—87044
molecular crystal, triplet exciton excess EPR linewidth, orientational order effect 78—72389
molecular crystal impure, exciton transport, local defect scatt. 77—8025
molecular crystal with spatially disperse media, self induced transparency 77—7162
molecular crystal-metal interface, exciton decay, random-walk model 78—10356
molecular crystal/electrolyte interface, illuminated, space charge behaviour 78—84290
molecular crystals, biexcitonic level splitting 78—10362
molecular crystals, charge-transfer electron-exciton bound states 77—43543
molecular crystals, coherent exciton scatt. and recomb. 80—39510
molecular crystals, diffusion mediated exciton processes, mag. field depend. of fission and fusion 79—37998
molecular crystals, disordered, incoherent, electronic energy transfer in impurity band 80—75525
molecular crystals, effects of impurity scatt. and transport topology on trapping 78—95263
molecular crystals, electronic energy transfer, review, book contrib. 77—39789
molecular crystals, electronic excitation energy transfer, external elec. field effect 80—84431
molecular crystals, energy transport dynamics, picosec. transient-grating method 78—72079
molecular crystals, exciton annihilation at high exciton densities, Suna equation calcs. 79—78016
molecular crystals, exciton interband transitions absorpt. band shapes 77—20876
molecular crystals, exciton propagation and memory effect at low temp. 78—67947
molecular crystals, exciton transport in strong intersite coupling limit, long-range transfer states 79—37995
molecular crystals, exciton-lattice interaction and exciton absorption line shape 78—18968
molecular crystals, exciton-phonon coupling and exciton transport 80—84430
molecular crystals, neutron scattering and exciton spectrum due to impurities 78—91622
molecular crystals, optical absorpt. line shape of excitons, two-time correl. function calcs. 79—44795
molecular crystals, optical props., struct. disorder effects 78—52525
molecular crystals, phononless exciton band lineshape, excitation transfer, stochastic models 80—107711
molecular crystals, semi-infinite, with surface point defect, exciton states 80—20271
molecular crystals, shallow traps, spin triplet population temp. depend. 77—1371
molecular crystals, spectroscopy, bibliography (1977) 80—7317
molecular crystals, spectroscopy, bibliography for 1976 78—72585
molecular crystals, struct. disorder effect on optical props. 77—90165
molecular crystals, two particle exciton-phonon interactions, optical absorpt. line shapes theory 80—55120

excitons continued
molecular crystals, weakly disordered theory of time evolution of exciton coherence 80—65455
molecular crystals long-range energy transfer combined with isotropic or anisotropic diffusion 79—11461
molecular crysts., electron-hole interaction, two-exciton dissoc. terms 78—39024
molecular crysts., extraordinary exciton polaritons in refl. spectra, macroscopic dielec. theory 77—89715
molecular cystals, triplet exciton pairs, mag. reson., fluoresc. modulation detect. 77—43906
molecular organic crystals, triexcitons, theory 79—33787
molecular pair, fluoresc. depolarisation, using stochastic Liouville eqn. with radiative terms 80—16074
molecular solid, disordered, exciton migration, dynamical approach 79—65916
molecular solid, electronic polaris. energy, quantum dynamic rel. to classical microelectrostatic approach 78—52427
molecular solid, fading memory as insufficient condition for exciton diffusion 79—19520
molecular solid, localisation of mol. ion or exciton states 79—47048
molecular solid, triplet exciton system, motional correlation effects, model 78—75997
molecular solids, electronic energy transport, picosec. transient grating technique obs. 79—47028
molecular solids, interaction with 0-15 eV electrons, formation of charged excitonic complexes 80—107708
molecular solids, Raman, fluoresc. and nonlinear props. 79—33702
molecular systems, biophys. effects of solitons and excitons 80—51044
MOS, many-body effects in n-Si inversion layers, excitation to higher subbands 77—62997
motion, coupled coherent and incoherent, kernel of generalized master eqn. determ. 79—51497
Mott excitons in crossed fields 77—4299
Mott insulators, excitonic spin polarons, appl. of Nagaoka's theorem for electron-Hole pair 80—107978
Mott-Wannier exciton in polar crystal, binding energy 77—39786
MTPA(TCNQ)$_2$ radical salt, triplet exciton system, motional correlation effects, model 78—75997
multi-component, LT mixed mode, dispersion relation 80—65470
multicomponent exciton gas, composition calc. 80—49618
Nakajima Zwanzig's generalised master equation, integro-differential eqn. kernel evaluation, exciton motion appl. 78—86123
Nakajima-Zwanzig generalised master eqn. for coupled coherent and incoherent exciton motion, Born approx. 79—60723
Nakajima-Zwanzig generalised master eqn. for exciton motion in mol. crysts. 80—65462
naphthalene:β-chloronaphthalene, reaction rate constants of triplet excitons 78—80407
naphthalene:anthmacene, singlet exciton energy transfer dynamics, time resolved spectra 79—83032
naphthalene:anthracene, cryst. energy transport and luminesc. at room temp. and 4.2K 79—56828
naphthalene:anthracene, pure and doped, delayed fluoresc. *(French)* 80—80846
naphthalene:anthracene, two-photon picosec. excitation, sensitised fluoresc. kinetics 79—47516
naphthalene:benzofuran, luminescence spectra and intensity, 1.6-77K 79—87477
naphthalene:indole, luminescence spectra and intensity, 1.6-77K 79—87477
naphthalene:thionaphthalene, luminescence spectra and intensity, 1.6-77K 79—87477
naphthalene, 2-methylnaphthalene and anthracene doped, single cryst., sensitised fluoresc. 78—68548
naphthalene, $^1B_{2u}$ supertransfer, exciton percolation, fluoresc. spectra obs. 77—55482
naphthalene, a-exciton lineshape, exciton-photon coupling 79—33243
naphthalene, a-exciton temp. depend. scatt., optical absorpt. profile 78—72088
naphthalene, cryst., singlet exciton interactions, prompt fluoresc. decay 78—60500
naphthalene, cryst., singlet exciton interactions fluoresc. decay 79—47027
naphthalene, crystalline, singlet exciton diffusion coeff. meas., fluorescence quenching anal. 78—67945
naphthalene, doped, fluoresc., impurity centre struct. depend. *(Russian)* 77—48231
naphthalene, electron excitation energy transfer efficiency, temp. depend. *(Russian)* 77—52182
naphthalene, exciton migration, variable range cluster model 79—33762
naphthalene, fluorescence decay induced by electron pulse, exciton interactions 77—16403
naphthalene, in durene and perdeutero-naphthalene mixed crystals, photon-echo decay 78—42388
naphthalene, isotopic mixed cryst., phospheresc., photoselection of pure initial triplet states 78—35189
naphthalene, long range exciton percolation, superexchange, energy denominator 77—28609
naphthalene, mag. effects on delayed fluoresc. at high and low triplet exciton density 77—8634
naphthalene, nonlinear fluorescence quenching 78—52562
naphthalene, singlet and triplet excimer interactions, exciton resons. 80—95535
naphthalene, singlet and triplet exciton percolation, tunnelling and thermalisation 80—84432
naphthalene, singlet exciton transitions, energies and oscillator strengths, boson theory with PPP wavefunctions 80—92820
naphthalene, theory of fission of singlet Frenkel exciton into two localised triplet excitons 79—23901
naphthalene, triplet exciton annihilation and triplet spin relax. 80—29792
naphthalene, triplet exciton annihilation at high triplet densities 79—37996
naphthalene, triplet exciton tunnelling, crit. concs. 79—15086
naphthalene, triplet excitons, phosphoresc. and delayed fluoresc. excitation spectra 78—63986
naphthalene, vibr. relax. studied by four wave mixing (CARS), spectral lineshapes obs. 80—80762
naphthalene $^1B_{2u}$ resonance pairs, energy denominator depend. of excitons absorpt. 77—39783
naphthalene β-chloronaphthalene, optically induced detrapping of triplet excitons 79—28828

excitons continued
naphthalene anthracene doped, decay times and diffusion coeffs. of singlet excitons, under press. 77—20911
naphthalene charge transfer complexes, cryst., vibr., factor group splittings 79—7658
naphthalene cryst., anthracene doped, fluoresc., two-photon excited 78—68560
naphthalene crysts., nonlinear fluorescence quenching, recomb. of free excitons 80—7397
naphthalene in $C_{10}D_8$, exciton percolation and coherence 77—59258
naphthalene mixed crystal, time resolved excitation migration, triplet and singlet critical concs. 79—78010
naphthalene pair ($C_{10}H_8$) in $C_{10}D_8$ host, mini-exciton obs., electron spin echo and ODMR 77—4559
naphthalene-β-naphthol, concentration effects in exciton absorption region 80—108241
naphthalene-β-naphthol mixed mol. cryst., multiplet struct. of electron absorption spectra 77—1706
naphthalene-β-naphthol mixture, exciton absorpt. depolarisation 80—103972
naphthalene-d_0, in naphthalene-d_8 cryst., mol. pair mini-exciton form., electron spin echo and ODMR 77—72822
naphthalene-d_4(d_8) crystal, with isotopic impurities, Rashba effect, luminescence spectra, impurity states 80—29768
naphthalene-d_8:naphthalene, betamethylnaphthalene, $^1B_{2u}$ naphthalene exciton percolation kinetics, exciton coherency 79—33750
naphthalene-d_8:naphthalene, symmetry reduction obs. of deformed crysts. by absorbt. spectrum method 79—15504
naphthalene-d_8:naphthalene-h_8 cryst., triplet excitons in A-B pairs, origin of inhomogen. broadened ESR lines 78—91623
naphthalene-h_8 and -d_8 mixed crystal, two-dimens. lattice, cluster-cluster interactions, model inhomogeneous distribs. 79—23922
naphthalene-h_8 and d_8, isotopic mixed crystals, exciton spectra in IR region 80—71400
naphthalene-h_8-naphthalene-d_8 mixed crystal, monomer cluster states 79—15089
naphthalene-h_8-naphthalene-d_8-β-methylnaphthalene, mixed cryst., dynamic exciton percolation, photosynthesis simulation 77—28124
naphthalene-TCNB, charge-transfer cryst., donor mol. orient. and dynamics 79—32926
naphthalene-tetrachlorophthalic anhydride charge-transfer cryst., electronic states 77—32415
naphthalenes, phonon satellite narrowing in local exciton luminesc. *(Russian)* 79—47507
narrow band gap semiconductor, antiferromag. in strong mag. field *(Russian)* 77—28387
narrow gap semiconductor, diamagnetic excitons in two-band Dirac model 80—59888
neutral bound excitons, accurate binding energies, variational method calc. 80—107715
neutron scattering by excitons, theory 80—29330
neutron scattering from equilibrium and non-equilibrium phonons, excitons and polaritons 80—84032
p-nitroaniline, exciton level directional dispersion, absorpt. band profiles 78—48192
p-nitrotoluene crystal film, exciton spectrum, IR absorpt. and Raman scatt. 80—80771
NMR under optical pumping conditions 80—25253
nondegenerate semicondcutor, three exciton radiative recomb. producing biexcitons 78—39603
nonequilibrium excitonic insulator, possible diffusion instability 80—59891
nonequilibrium populations and nonlinear response 79—28285
nonequilibrium semiconductor with electron-hole pairing, mag. moment quantum oscills. *(Russian)* 77—28131
nonlinear luminescence quenching at high pumping levels, microscopic theory 80—89040
nonstationary processes 80—107710
nuclear matter, particle-particle collision probability, vol. integral using preequilibrium exciton model 78—70477
nuclear preequilibrium decay, exciton model formulation, reply to comments 78—78354
nuclear spin relaxation via contact hyperfine interaction with excitons 77—51983
one-dimensional molecular chain, collective excitations, solitons *(Russian)* 77—4305
one-dimensional molecular chain, collective model for conformons 80—15456
one-dimensional molecular crystal, soliton-like solns. of eqns. for excitations 78—84149
one-dimensional molecular lattice, soliton motion, thermal vibrations *(Russian)* 80—54321
one-dimensional substitutionally disordered system, energy transfer, coherence, tunnelling, thermal promotion 78—56078
one-dimensional system, energy and charge transport theory *(German)* 80—15506
one-dimensional two-band model, free electron-hole pairs and exciton-polariton 80—29331
optical absorption by excitons 77—80734
optical absorption of diamagnetic excitons in crossed mag. and elec. field 78—10874
optical data storage, requirements and attainable bandwidths *(Russian)* 77—10841
optical reflectivity, microscopic calc., excitons in semi-infinite crystals 79—69430
organic charge transfer complexes, refl. spectra, excitons 79—47477
organic charge transfer crystals, transport props., phase transitions, mol. dynamic *(German)* 80—39507
organic crystals, exciton surface polaritons 79—4519
organic crystals, kinetic model of triplet exciton dynamics 78—67948
organic mixed crystals, energy transfer 78—76515
organic molecular cryst., singlet-triplet-triplet triexciton bound states 78—2426
organic molecular crystal, doped, two-particle electronic excitation, optical cooperative excitation 80—93368
organic molecular crystals, optical spin alignment, phosphoresc. *(Russian)* 78—84652
organic molecular crysts., charge carrier generation by exciton-exciton collisions 80—88568
organic molecular solid, space group C_{2h}^5, triplet excitons energy band struct. 78—6276

excitons continued
organic monolayer/metallic substrate, exciton-surface plasmon interaction 79—69569
organic solid, exciton motion effect on proton relax. 78—14671
organic solid state chemistry, conf., Waltham, USA (June 1978) 79—46990
organic solids, charged excitonic complexes, coupled states, exciton interaction with charge carriers study 80—20090
organic solids, cryst. and amorphous, optical spectra, Urbach rule, struct. disorder effect 78—23479
oxide semiconductor crystals, with forbidden energy gap, review of spectroscopic props. 78—2876
pentacene, in p-terphenyl, electronic excitation transport, acousto-optical effects 78—72079
pentacene, singlet exciton transitions, energies and oscillator strengths, boson theory with PPP wavefunctions 80—92820
pentamethinium cyanine dye, single cryst. excitation of singlet excitons 79—51626
percolation and coherence 77—59258
percolation model, one-dimens., spectral diffusion 78—80411
perfect crystals, low-temp. exciton luminesc. 79—56826
periodic structure, electron-exciton complex auto ionisation *(Russian)* 80—49611
perylene, α- and β-crysts. and soln., polarised reflection and absorption spectra 77—8598
perylene, cryst., fluoresc. spectra, time-resolved, excimer and excitons 79—78724
perylene, excitation spectra of exciton fission in organic crystals 78—92116
perylene, exciton fission in excimer forming cryst., fluoresc. 79—15511
perylene, fluoresc., exciton fission in excimer forming cryst. dynamics 79—61423
phase diagram of exciton in phonon field 78—6277
phase transition to incommensurate excitonic phase 80—75510
phenanthrene:anthracene, cryst., triplet-triplet annihilation, shallow traps effect, 77-293K 79—11446
phenanthrene:anthracene, delayed fluores. of cryst. in mag. field 79—52023
phenanthrene, mol. cryst., thermolum. build-up 78—27334
phenanthrene-PMDA, spin polarization of charge-transfer excitons, EPR meas. 79—19766
phenanthrene-pyromellitic acid dianhydride, single cryst., EPR, delocalised and localised charge transfer excitons 77—85545
phenanthrene-pyromellitic dianhydride, single cryst., charge-transfer triplet excitons, spin polaris. 79—11069
phenol, cryst., mol. vibrs., factor group splittings 80—16021
phonon-exciton interaction 77—28125
phosphors, thermoluminescence, UV dosimetry 80—853
photoexciton dispersion in mag. field *(Russian)* 78—48152
photoexcitons, possibility of exptl. determ. of nature of additional boundary conditions 77—69250
photon-exciton-phonon system, coupled, density matrix eqn. solved 77—85156
photosynthetic membrane, in vivo, light collection and exciton dynamics 79—48215
photosynthetic membranes, anal. of laser-induced fluorescence with Pauli master eqn. 79—39350
photosynthetic membranes, exciton dynamics, picosecond pulse train study 79—8483
photosynthetic unit, bimol. quenching of excitons and fluoresc. 77—16908
phthalic anhydride, vibr. excitons reson. interaction in IR and Raman spectra *(Russian)* 79—61386
picosecond spectroscopy, book contrib. 77—65057
polar, layered material, quenching of excitonic diamag. shifts 79—19526
polar crystal, effective electron-hole interaction for intermediate and strong electron-phonon coupling 77—80735
polar crystal, Frenkel exciton effective mass temp. depend., lattice displacement interactions *(Chinese)* 80—84429
polar crystal model, instabilities in electron energy spectrum, metallic state stability criterion 79—82524
polar crystal model, instabilities in electron energy spectrum, max. polarity state 79—82534
polar crystals, exciton interaction pot., polaron effects 77—24523
polar semiconductor, effective exciton-exciton interaction 79—42465
polar semiconductor, effective Hamiltonian for few-particle systems 77—15776
polar semiconductor, exciton, energies, oscillator strengths, and phonon side bands 80—44512
polar semiconductor, exciton dispersion, influence of optical phonons, variational method for effective exciton mass 79—15091
polar semiconductor, exciton-dispersion 80—6741
polar semiconductor, exciton-neutral donor and biexciton complexes 79—90968
polar semiconductor, excitons bound to ionised donors, binding energy calc. 77—28128
polar semiconductor, impurity levels, influence of electron-phonon coupling 78—64007
polar semiconductor, theory of excitons bound to neutral impurities 79—73441
polar semiconductors, biexcitons, variational wave functions 78—23031
polar semiconductors, hot exciton scatt. accompanied by transitions to excited states, phonon interactions 80—44516
polariton-exciton dispersion curve 79—33244
polaritonic Bose condensation, effects of superfluidity 78—18976
polaron effects 80—24811
polaron mass of exciton 79—95344
poly(2-vinyl pyridine), electronic struct., molecular-ion states and dielectric props. 79—37969
poly(5,7-dodecadiyne-1, 12-diol-bis phenylurethane), visible refl. spectra, photocond., excitons 77—81117
poly(N-vinylcarbazole) film, fluoresc. and phosphoresc., energy transfer mechanism 80—16112
poly (ar-methylstyrene)s, steric effects on excimer formation, fluorescence spectra exam. 80—25430
poly-1,6-di-N-carbazolyl-2,4-hexadiyne, synthesis, thermal expansion, photocond., optical transition 78—76858
poly-2,4-hexadiyn-1,6-diol bis(p-toluene sulphonate), exciton theory of excited states 77—80733
poly-2,4-hexadiyne-1,6-diol bis (p-toluene sulfonate), exciton surface polaritons, reflecting faces obs. 80—65645

excitons continued
poly-2,4-hexadiyne-1,6-diol bis (p-toluene sulphonate), cryst., exciton surface polaritons, reflectivity of (100) face, 295K 78—80372
poly-2-vinylpyridine, electron energy loss spectra, for optical and dielec. props. 79—15569
poly-N-vinylbenzocarbazole, soln., luminesc., effect of electronic excitation energy vibr. 80—55174
poly-N-vinylcarbazole film, triplet-triplet energy transfer, chemiluminesc. 78—43944
poly-N-vinylcarbazole-biacetyl, triplet exciton quenching, exciton trapping model 80—66267
polyacetylene:AsF_5, X-ray absorpt. meas. of mol. struct., orientation and charge transfer 80—25486
polyacetylene, bond length alternation and energy gap, intermediate exciton formalism 80—29305
polyacetylene, intrinsic conformational defect states 80—65500
polycarbonate, photoconductivity, UV-IR light, absorpt. and photoluminescence. spectra *(Japanese)* 78—34857
polydiacetylene, extended chains with realistic model side groups, self-consistent electronic band structs. 77—39776
polydiacetylene, intrinsic conformational defect states 80—65500
polydiacetylene, single crystal, electroreflectance and electroabsorption spectra, π-electron system and excitonic transitions 79—78653
polydiacetylenes, excited singlet state electronic struct., band and excitonic models 78—91620
polyene, linear, band gap calcs. 77—31969
polyene band struct. calc., excitons in polyene chain 78—26816
polyene chain, collective excitations and optical absorpt. 79—47019
polyene chain, excitonic state, wave function calcs. 80—20098
polyethylene, pristine and radiation-damaged film, electron energy loss spectra 79—81312
polyethylene naphthalate, photoconductivity, UV-IR light, absorpt. and photoluminescence. spectra *(Japanese)* 78—34857
polyethylene terephthalate, photoconductivity, UV-IR light, absorpt. and photoluminescence. spectra *(Japanese)* 78—34857
polymer:trimethylamine, field-depend. UV photogeneration of holes, polymer composition depend. 78—76104
polymer, conjugated and saturated chain, electronic struct., review 80—59860
polymer, magneto-optical props., MCD, Frenkel exciton model 78—10873
polymer solution, rigid, exciton transport 79—69431
polymers and molecular crysts., vibronic spectra exam. 78—67778
polymethinium dye, excitonic fluoresc., absorpt. trapping spectra 78—27302
polyparaxylyrene, photoconductivity, UV-IR light, absorpt. and photoluminescence. spectra *(Japanese)* 78—34857
polypeptides, β-form, vibronic exciton approach to NV_1 absorption band 77—79626
polystyrene, electron energy loss spectra, for optical and dielec. props. 79—15569
polystyrene, photoconductivity, UV-IR light, absorpt. and photoluminescence. spectra *(Japanese)* 78—34857
polystyrene, steric effects on excimer formation, fluorescence spectra exam. 80—25430
polyvinylbenzocarbazole, weak solution, intramolecular energy transfer by singlet and triplet excitons 80—34971
polyvinylcarbazole, exciton migration, luminesc. and quenching *(Russian)* 77—36275
polyvinylcarbazole, fluoresc., photooxide quenching, exciton migration effects 79—56830
polyvinylcarbazole, weak solutions, intramolecular energy transfer by singlet and triplet excitons 80—34971
pre-equilibrium exciton model, mean lifetimes 79—93601
prequilibrium decay, differences of alternate formulations, possible exciton formulation errors 78—70507
proximity effect at low temp. for exciton insulator 79—73643
proximity effects in transitions to exciton phases 79—28296
PTS, exciton surface polaritons at room temp. 79—47476
PTS polydiacetylene single cryst. reflection spectra, exciton site splitting 78—31211
PTZ:PMDA, purification, growth, struct., optical and elec. props. 80—54216
pyrene:rubicen(coronen), exciton migration and energy transfer, temp. depend., model 78—79932
pyrene, band structure, excitonic processes, trap distrib. 80—6720
pyrene, crystalline, EPR spectrum of triplet excitons 78—27076
pyrene, excimer form. process, ps laser fluoresc. obs. 79—11448
pyrene, luminescence of free and self-trapped excitons 80—108250
pyrene, perylene doped, decay times and diffusion coeffs. of singlet excitons, under press. 77—20911
pyrene, triplet exciton absorpt. lines 79—47475
pyrene, triplet state, excitonic energy transfer, phosphoresc. and delayed fluoresc., 2 to 300K 80—84776
quantum defect theory, analogy to Rydberg states 78—51902
quantum field theory of solids, book 77—31922
quartz, photoelectric and photoluminescent props. in fundamental absorpt. region 78—39596
quasi-coherent-triplet excitons in pairs of differently oriented mols., EPR line shape 78—43631
quasi-one-dimensional metals, narrow-band, exchange-correlation effects on plasmons and on CDW instability 80—44525
quasi-one-dimensional systems, Peierls transition, possible pairing of spatially separated electrons and holes 79—15085
quasifree, impurity trapping, finite coherence effects 80—59880
Raman excitation profiles and mol. spectra synthesis, vibronic and exciton-in-mol. theory 78—42076
Raman scattering, reson., second-order, theory for case of strong excitonic effects 78—76460
Raman scattering, two-photon reson., by excitons via intermediate excitonic mol., polarisation and polariton effects 78—10880
Raman scattering on excitons, polaritons in crysts. *(Rumanian)* 77—48172
rare earth metals, neutron inelastic mag. scatt., book contrib. 77—89944
rare gas crystal, pure and benzene-doped, photoelectron emission, exciton states 77—44116
rate processes in condensed media, anharmonicity effects 79—19349
reaction yield detected mag. reson. spectra, evolution, degenerate energy levels, triplet excitons 79—19378
reflectance spectrum, calc., multi-component polaritons 78—87921
relaxation constant of final state in excitonic molecule 79—95763

excitons continued
relaxation times in solid-state theory and one-dimensional molecular systems *(Russian)* 80—100640
resonance excitation in crystals, light scatt., polarisation, specular refl., theory 80—50356
resonance light scattering and hot luminesc. of self-trapping excitons 80—93336
resonance Raman scattering and luminescence of excitons in self-trapping process 80—20689
resonance region, energy transfer by normal modes 77—89705
resonant Brillouin scattering via exciton-polaritons, theory 80—50353
resonant Raman scattering via virtual exciton 80—71412
resonant secondary radiation, hot luminesc. *(Russian)* 79—52018
review of work at Ukrainian SSR Acad. of Science *(Russian)* 79—47026
rhodamine dyes, methanol-water solns., triplet state EPR spectra, aggregation, mol. orientation 77—48031
Rydberg states in condensed matter, appl. to doped solid rare gases and H_2 79—69425
sapphire, pure and doped, luminesc. centres 79—33791
Schiff's base, thin layer samples, mechanism of change carrier photogeneration *(Russian)* 77—32045
Schottky barrier, excitonic refl. of light 80—10885
Schottky barrier field, exciton reflection band burning *(Russian)* 79—47479
self induced transparency, steady-state exciton-photon pulse dispersion law 78—30028
self induced transparency 77—42575
self-diffraction of light by excitons 80—53389
self-induced transparency, dispersion law of steady-state exciton-photon pulses 79—27336
self-induced transparency, two-photon interaction of laser radiation with Frenkel excitons 78—25931
self-induced transparency in exciton part of spectrum 78—33786
semi-infinite crystals, linear wave vector effects on optical props. 77—85721
semiconducting film, exciton oscillator strength, EM wave-polaritan propagation, reflective power *(Russian)* 79—99491
semiconducting films, exciton polariton attenuation, spatial dispersion effect 80—20097
semiconductor, anomalous props. of positronium atom, exciton state 78—2433
semiconductor, bound exciton recombination, phonon replicas 79—38649
semiconductor, characts. of two-photon absorption under reson. conditions 77—90170
semiconductor, coexisting phases in electron-hole plasma 77—1374
semiconductor, collective magnetoexciton transition under action of light *(Russian)* 78—79939
semiconductor, core excitons, binding energy in effective mass approx. 80—24808
semiconductor, crit. points for electron-hole system 80—44511
semiconductor, cubic, in mag. field, exciton states 80—24807
semiconductor, diamagnetic excitons in strong elec. field 79—38002
semiconductor, dielectric liq. of Wannier-Mott excitons 80—65458
semiconductor, direct band gap type, polariton theory of reson. electronic Raman scatt. on neutral donor levels 80—108194
semiconductor, direct band-gap, polariton emission spectrum, exciton kinetics influence 78—14676
semiconductor, direct-gap, polariton luminesc., under strong excitation conditions, exciton gas model 77—8650
semiconductor, disordered, electroabsorption, contact excitons influence 80—10882
semiconductor, donor van der Waals interactions, spectral lineshapes 80—11450
semiconductor, effect of free carriers on exciton luminescence 78—48226
semiconductor, effect of surface space charge region 78—43939
semiconductor, electron-hole droplet nucleation, Fokker Planck treatment 80—6732
semiconductor, EM properties, general lecture 78—27173
semiconductor, exciton absorption, electric field effect *(Russian)* 78—43902
semiconductor, exciton and impurity states, unified theory, for arbitrary mag. field 80—39511
semiconductor, exciton and impurity states theory 79—82526
semiconductor, exciton condensation, microwave cond., book contrib. 80—11043
semiconductor, exciton ferromagnetism 79—28293
semiconductor, exciton-plasma transition 79—28295
semiconductor, excitonic molecule creation by two-photon absorpt. 77—20247
semiconductor, excitonic surface potential 78—76000
semiconductor, excitons and nonlocal optical props. 79—95345
semiconductor, far IR spectroscopy, appl. of far IR lasers 80—31914
semiconductor, fundamental light absorption, in field of strong EM wave 77—52032
semiconductor, high-conc. exciton and biexciton emission 78—6725
semiconductor, highly excited excitation induced optical absorption 77—44025
semiconductor, highly excited states, ps spectroscopy 77—48245
semiconductor, impure, exciton absorpt. line shape calc. *(Russian)* 78—10934
semiconductor, indirect excitons 77—69247
semiconductor, layered, electron-hole liquid exam. 78—18975
semiconductor, light absorption, temp. depend., exciton-exciton and -phonon interactions *(Russian)* 77—40265
semiconductor, luminesc. due to exciton-electron scatt., calc. 77—16379
semiconductor, luminescence, coherent conversion of excitons and photons to biexcitons *(Russian)* 79—47508
semiconductor, mag. ordering in systems with low carrier densities 78—2684
semiconductor, multilayer, exciton Stark effect 79—19528
semiconductor, narrow-band indirect-gap, exciton instability 77—8029
semiconductor, natural EM oscillations excitation by stream of electrons or EM field 80—34378
semiconductor, noncrystalline, mag. freeze out effect 78—43281
semiconductor, nonlinear coherence phenomena in exciton region 80—99806
semiconductor, ODMR appl. to recombination processes 79—42871
semiconductor, optical absorpt., Coulomb screening influence, exciton ionisation energy 78—72568
semiconductor, optical excitations, many particle effects 79—87046

excitons continued
- semiconductor, optical non-locality phenomena near exciton reson. 79—95794
- semiconductor, optical transform. of biexcitons 77—62844
- semiconductor, plasma model of exciton gas *(Russian)* 77—11860
- semiconductor, quasi-one- and quasi-two-dimens., exciton self-localisation *(Russian)* 77—31956
- semiconductor, quasi-one-dimens., many-exciton instability condition 77—43507
- semiconductor, quasi-one-dimensional, light absorpt. and Raman scatt., large exciton form. 77—16272
- semiconductor, reson. in fundamental absorpt. region, quasi-mol. model interpretation 78—76490
- semiconductor, resonant Brillouin scattering of exciton polaritons 80—93357
- semiconductor, resonant Raman and Brillouin spectroscopy, review, book contrib. 80—49624
- semiconductor, single-quantum radiative recomb. of biexcitons due to biexciton-exciton interactions 80—96793
- semiconductor, size quantised, superlattice state 78—39142
- semiconductor, surface state excitons 77—51799
- semiconductor, tetravalent, fundamental absorpt. spectra, direct interband transitions 78—63972
- semiconductor, theory of charge transport partly dissociated excitons and impurity atoms 80—44581
- semiconductor, thermodynamics of electron-hole system 78—43304
- semiconductor, three-band, absorpt. of weak EM wave in presence of intensive one 79—61325
- semiconductor, two-dimensional electron-hole systems in high mag. fields, phase transitions 80—49608
- semiconductor, variable-gap, exciton drift length 77—28129
- semiconductor, Wannier excitons, fine structure, lineshape and dispersion, review 80—44520
- semiconductor, with neutral impurities, exciton spectrum, conc. depend. *(Russian)* 78—2894
- semiconductor epitaxial layer, polariton wave packet propag. in exciton reson. 80—2345
- semiconductor film, Bose-Einstein condensation of excitons 77—28127
- semiconductor film, exciton complexes, form. and dissoc. 79—95343
- semiconductor film, Mott exciton spectrum in mag. field 78—34780
- semiconductor film, neutral exciton-donor complex dissoc. energy 77—55488
- semiconductor film, size-quantised, EM wave absorpt. coeff. in coherent hypersonic wave field 80—29819
- semiconductor film, Wannier-Mott exciton states *(Russian)* 78—79943
- semiconductor films, exciton light absorption coefficient *(Russian)* 80—71504
- semiconductor films, free exciton polaritons, energy dissipation 79—95870
- semiconductor films, two-photon absorption, exciton effects *(Russian)* 80—40174
- semiconductor in highly excited state, thermodynamic theory, photocond. 77—47742
- semiconductor layer structure, laser-induced photolum. and collective effects *(Russian)* 79—95830
- semiconductor luminescence, PH band profile, exciton-electron interactions 80—20702
- semiconductor multiple bound excitons, binding energy calc. 78—51900
- semiconductor or semimetal, screened and localised impurity states in 'optical' and exciton insulators *(Russian)* 77—62870
- semiconductor physics in high mag. fields, review *(Japanese)* 80—50192
- semiconductor submillimetric-wave spectroscopy 79—33221
- semiconductor surface spectroscopy, exciton effects, theory 80—49856
- semiconductor thin film, Coulomb interaction depend. on film thickness, exciton binding energies *(Russian)* 79—78027
- semiconductor thin films, ion implanted, optical and luminesc. props. 80—60699
- semiconductor with dipole impurities, light absorption 79—28796
- semiconductor with nonparabolic bands, diamag. excitons, optical absorpt. in mag. field 77—55487
- semiconductor with nonspherical bands, diamag. excitons and Franz-Keldysh effect 78—72554
- semiconductor with polytype layers, interface exciton states 78—26819
- semiconductor with wurtzite structure, natural optical activity *(Russian)* 79—78647
- semiconductor-metal, surface exciton modes for plane and spherical interfaces 78—64113
- semiconductors, Auger and radiative recombination of acceptor bound excitons 79—47023
- semiconductors, binding energies of core excitons, effective mass approx. 79—73439
- semiconductors, binding energy in exciton-impurity systems, Haynes rule 79—15112
- semiconductors, core exciton binding energies 80—80188
- semiconductors, disordered, phonon-assisted interband optical absorption 80—34947
- semiconductors, doped, shallow impurity states, Hubbard bands and donor excitonic states, HF calc. 80—100443
- semiconductors, exciton and domain luminesc., book 80—82588
- semiconductors, exciton condensation and electron hole liquids, state-of-the-art 80—49625
- semiconductors, exciton effect in interband electronic Raman scattering 80—103946
- semiconductors, exciton-impurity state with low binding energy 80—103646
- semiconductors, excitons in mag. field, exciton-phonon interaction 80—24806
- semiconductors, high density excitons and biexcitons, recomb. radiation bands profiles, time depend. 80—45140
- semiconductors, highly excited, condensation and pairing, interacting boson theory without anomalous propagators 77—33942
- semiconductors, interimpurity radiative recombination, intermediate exciton state *(Russian)* 80—49621
- semiconductors, low carrier density, lasing action, exciton Bose condensate charact. function 79—64233
- semiconductors, magneto-optical expts., MG field production and appls. 79—71491
- semiconductors, optical transitions between deep impurity centre levels 79—61410
- semiconductors, particle complexes, $N=1$ to ∞, book contrib. 80—80194

excitons continued
- semiconductors, photoexciton waves, restrictions imposed on nature of additional boundary conditions 79—28789
- semiconductors, recombination, conference, Southampton, England (Aug.-Sept. 1978) 79—38087
- semiconductors, recombination processes, review 79—38088
- semiconductors, review, book contrib. 80—44517
- semiconductors, role of excitons in dispersion effects, band gap determ. 79—65393
- semiconductors, spin orientation by optical pumping, review 79—38410
- semiconductors, two-dimensional, Mott exciton formation in high mag. fields *(Russian)* 80—65467
- semiconductors, two-photon light absorption by excitons in static elec. field 80—11364
- semiconductors, uniaxial, exciton light absorpt. spectra depend. on crystal anisotropy *(Russian)* 80—50386
- semiconductors, with nonspherical bands, exciton absorpt. in crossed fields 79—69432
- semiconductors and dielectrics, broadband, spectral contour for strong exciton bands 78—27194
- semiconductors with degenerate valence band, diamg. excitons, and oscillatory magnetoabsorpt. of GaSb 77—76754
- semiconductors with direct band gaps, exciton-polariton interactions, Green's function approach 80—92831
- semiconductors with optically anisotropic energy bands, antiresonance states of diamagnetic excitons 79—51500
- semimetal, excitonic and gas-liquid type transition of electron-hole system in strong mag. field 79—60718
- semimetal, excitonic phase and gas-liquid transition in strong mag. field 79—4514
- semimetal, excitonic transition in strong mag. field, HF approx. 78—23028
- semimetal, mixed superconducting-excitonic insulator phase, diamagnetism, virtual intraband transitions 80—2520
- semimetal, pressure induced transition to state with strongly anisotropic electron-hole pairing 77—47735
- semimetal film, quantised, in high mag. field, thermodynamics of electrons *(Russian)* 79—56341
- semimetal-exciton phase transition, microwave cond. 80—29430
- semimetallic system, critical temp. depend. on band gap for dielectric-supercond. transition *(Russian)* 79—65578
- semimetallic thin film, Coulomb interaction depend. on film thickness, exciton binding energies *(Russian)* 79—78027
- semimetals, exciton phase, transport effect in strong mag. fields 78—87977
- semimetals, two-dimensional, electron-hole rearrangements in high mag. fields 79—87028
- short-range ordered mag. cluster pinning by localised optical excitation 78—68279
- Si, multiple bound exciton states, valley-orbit splitting 79—60725
- singlet ground state system, line shape of mag. excitations, diagrammatic expansion calc. 77—69482
- small-polaronic glass, dynamics of optically induced props. 80—49630
- solid solution, nondiagonal disordered system, excitation spectrum 80—15429
- solid state physics, conf. Munster, Germany (March 1979) 80—41941
- solid state resonances, interactions *(German)* 79—42456
- solid-state theory, introduction, book 79—33215
- soliton wave packet propag., superfluidity of Bose condensed excitons and photons 78—22178
- spatial dispersion exponential model, boundary conditions *(Russian)* 80—75994
- spatially dispersive media, optical boundary value problem 80—45024
- spatially dispersive medium, exciton polaritons, absorption theory 80—54618
- spatially extended systems, stochastic Liouville eqn. rel. to generalized master eqn. 78—45581
- spatially nonlocal transfer rates in exciton transport, local intersite matrix elements 78—14667
- spectra of diffuse reflection and photoluminesc. *(Russian)* 79—11447
- spectral absorption range, spatial dispersion theory *(Russian)* 79—61405
- spectroscopy, polariton dispersion 80—54613
- spectroscopy using synchrotron radiation 77—20882
- square lattice, percolation and cluster distrib. variable range interactions, exciton cluster model, layers 79—30379
- statistical props. at high concentrations, parastatistics description 77—51674
- stilbene:rhodamine-6Zh, luminesc. of adsorbed mols., excitonic energy transfer to surface 78—31255
- stilbene, adsorbed rhodamine 6Zh, mol. cryst., role of excitonic and radiative mechs. of energy transport 80—108276
- trans-stilbene, cryst., triplet excitons, $S_0 \rightarrow T_1$ transition 78—76518
- stilbene, pulsed electron excitation, triplet excitons, spectral and electrical investigations 80—92828
- stilbene, single cryst., free charges and excitons generated by electron pulses 78—63988
- stilbene, single cryst. under pulsed electron excitation, triplet exciton, optical absorpt. spectrum 79—7838
- stilbene, thin single cryst., IR spectra anal. Fermi-Davydov intensity distrib. 77—59577
- stochastic exciton lattice coupling, exciton line shapes and migration 79—11070
- superconductivity, exciton and polariton mechanisms 79—60959
- superconductivity, excitonic, possibility 79—38243
- superconductivity, high temp., possible mechanism based on metallic excitonium formation 79—38244
- superconductor layered crystals, excitonic pair formation *(Russian)* 77—36016
- superfluidity, Bose condensation, DLRO and ODLRO 77—43515
- superradiance and free induction decay, theory 79—37992
- superradiance in solid state physics, review 79—51988
- surface, surface self-trapped states *(Japanese)* 80—2445
- surface channel, quasitwo dimens. excitons and plasmons at different carrier conc. 78—60063
- surface exciton energies and radii 80—92829
- surface exciton polaritons, attenuated total reflection spectra 77—24867
- surface exciton polaritons, book contrib., review 80—49623
- surface exciton-polariton *(Japanese)* 77—39910
- surface excitons in mixed molecular crystals, theory 79—47135
- surface polariton effects in spontaneous emission, effects of spatial dispersion 78—34879

excitons continued
surface potential effects on phase of exciton wave *(Russian)* 77—89708
surface state, binding energies and wave functions 77—66192
surface-exciton polaritons, dispersion theory 78—72089
symmetry breaking effects on excitons in cubic and wurtzite structs., unified theory 77—20246
system with electron-hole pairing, collective excitations *(Russian)* 79—51501
$TCNQ^0$, crysts., extraordinary exciton polaritons in refl. spectra, macroscopic dielec. theory 77—89715
TCNQ, exciton surface polaritons at room temp. 79—47476
TCNQ, single crystal, exciton surface polaritons, attenuated total reflection spectra 79—91460
TCNQ complex salts, mag. props., ESR meas. 79—56603
TCNQ compounds, dimensionality of triplet excitons 78—91974
TCNQ salt, decamethylferrocenium, monomeric and dimeric, optical and EELS study 80—100660
TCNQ salts, Rb^+TCNQ^-, and TMB^+TCNQ^-, triplet exciton dipolar splitting tensors rel. to mag. susceptibility 77—62839
TCNQ salts, simple, triplet exciton obs. by ESR 78—10373
TCNQ-M_2P charge transfer complex, triplet spin excitons, EPR spectra 78—80192
TCNQ-pyrene complex, evaporated layers and single crysts., photocond. *(Russian)* 78—6416
teracene, photoionisation of triplet excitons 77—62837
p-terphenyl, cryst., exciton phosphoresc. at 300K 80—108277
p-terphenyl, cryst., highly excited states decay, mag. field effects 78—10962
p-terphenyl, triplet exciton annihilation and triplet spin relax. 80—29792
tetracene:pentacene, exciton migration, picosec. meas. 78—15207
tetracene:pentacene, pressure-induced phase transition, mag. field effect on guest fluoresc. 79—33083
tetracene:pentacene, thermally activated heterofission, fluoresc. 77—85787
tetracene, cryst., fluoresc. decay time, synchrotron radiation excitation 77—4675
tetracene, cryst., prompt fluoresc., mag. field depend. 77—85788
tetracene, cryst., singlet exciton fission rate const. RYDMR spectra meas. 78—91619
tetracene, cryst., triplet exciton pair kinematics, diffusion model, prompt fluoresc. decay 78—79931
tetracene, cryst., triplet exciton pairs, EPR spectra 77—43906
tetracene, excimer luminesc. spectra, 4.2-300K 79—87478
tetracene, fluoresc. time decay, exciton interaction depend. 77—8618
tetracene, photoluminescence spectra, 4.2-300K, phase transition and excitons 79—4847
tetracene, single cryst., exciton interactions, ps laser pulse intensity depend. 77—63448
tetracene, singlet exciton fission, kinematic theory 78—87913
tetracene, singlet exciton fission and fluorescence, mag. field depend. 78—39026
tetracene, singlet exciton transitions, energies and oscillator strengths, boson theory with PPP wavefunctions 80—92820
tetracene, spatial distrib. of electrolum. and recomb. process 79—19938
tetracene, theory of fission of singlet Frenkel exciton into two localised triplet excitons 79—23901
tetracene, triplet exciton diffusion and double photon absorpt., delayed fluoresc. obs. 77—36287
tetracene single crystals, exciton refl. spectra, 4.2 to 300K 79—47478
tetracene surface states, electric field effects, exciton-charge carrier interactions *(Russian)* 80—24989
1,2,4,5-tetrachlorobenzene, excited triplet state dimer, intermol. exchange integral, isotope effect 80—15826
1,2,4,5-tetrachlorobenzene, exciton migration and trapping, X-trap phosphoresc. 79—1780
1,2,4,5-tetrachlorobenzene, exciton states in crystals and dimers 80—70620
1,2,4,5-tetrachlorobenzene, impurity induced states, spin dephasing, spin coherence expts. 78—84498
1,2,4,5-tetrachlorobenzene, linear chain triplet excitons, electron spin-echo and ODMR 78—76357
1,2,4,5-tetrachlorobenzene, localised excitations thermal promotion to exciton band, impurity states effect 78—52539
1,2,4,5-tetrachlorobenzene, mol. cryst., coherent 1-dimens. exciton transport and impurity scatt. 78—14666
tetrachlorobenzene, mol. crystal, exciton band spin-orbit coupling 78—39025
1,2,4,5-tetrachlorobenzene, mol. solid, heat pulses, phonon-induced delocalisation of trapped excited triplet states 80—89053
1,2,4,5-tetrachlorobenzene, proton spin relaxation by optically excited triplet states 79—19810
tetrachlorobenzene, pure and doped crysts., triplet exciton trapping, phosphoresc. spectra 77—85766
1,2,4,5-tetrachlorobenzene, triplet energy transfer in substitutionally disordered system 79—52000
1,2,4,5-tetrachlorobenzene, triplet exciton, ESR and optical absorption lines 80—96791
tetrachlorobenzene, triplet exciton spectral line shape, 2-45K 78—19498
1,2,4,5-tetrachlorobenzene, triplet excitons, ESR and ODMR 78—43681
1,2,4,5 tetrachlorobenzene, triplet excitons, high. mag field, spin-lattice relax. study 80—20517
1,2,4,5-tetrachlorobenzene, triplet excitons, zero field ODMR 80—88891
1,2,4,5-tetrachlorobenzene, triplet state spin-lattice relax. in cryst. and matrix isolated mol. 79—11449
tetrahedral semiconductors, exciton binding energy, Haben methods for single isotropic parabolic energy bands 79—56140
tetramethylammonium manganese chloride, energy migration rel. to impurity trap behaviour 77—55811
thin crystal, interference spectra, size quantisation of excitons 78—47708
third harmonic generation under reson. conditions *(Russian)* 79—31997
thymine film, polycryst., energy conversion processes, quantum yields, 4 to 10 eV 80—88589
$TiSe_2$, anomalous behaviour and excitonic insulator mechanism 77—39782
$[TMPD^+]_2[Cu_xNi_{1-x}(mnt)_2]$, ESR obs. of triplet excitons and Cu(II) ions, mag. interactions 79—95633
transfer rates, effect of nucl. degrees of freedom 78—60057
transition into excitonic phase, boundary effects 78—76003
transition metal dichalcogenides, modulation spectroscopy obs. 78—80377
transition metal hexafluorides, density of exciton states, two-particle and mixed cryst. spectra 78—2829

excitons continued
trialkylammonium, iodides, absorpt. and luminesc. spectra of self-localized excitons 80—97340
trifluoroiodomethane, liquefied gas solns. bound exciton model for Rydberg bands 78—31214
triphenylmethylphosphonium-TCNQ, paramag. echo from triplet excitons obs. 77—28130
triplet exciton annihilation rate, magnetic field depend. effect of spin-lattice relaxation 80—65459
triplet excitons, condensation in mag. field 80—2341
(TTF^+) radical cation, optical props. in mixed-valence and monovalent halide salts and solns. 79—61399
TTF-TCNQ, core exciton exam. by inelastic electron scatt. 77—4296
TTF-TCNQ, mol. core excitons, high energy electron inelastic-scatt. spectra 77—69235
TTT, dark cond. and photocond. effect of strong mag. field, at charge carrier injection *(Russian)* 79—69607
tunnel self-trapping of electrons or Frenkel excitons, theory *(Russian)* 78—60192
two photon transitions to exciton and biexciton states, selection rules 77—69240
two-dimensional crystals, exciton-exciton and exciton-electron interactions in luminesc. spectra 77—52179
two-dimensional excitonic phase in strong mag. field 78—43308
two-photon reson. Raman scatt. by excitons via intermediate excitonic mol. 77—52086
ultrashort laser pulses, interaction with condensed matter *(German)* 79—27335
uniaxial crystal, macroscopic exciton luminesc. characts., high reabsorption conditions 78—19545
unified treatment, tightly- and weakly-bound excitons Wannier representation 78—43301
uranyl acetates, cubic crysts., optical spectra fine struct. 77—1693
uranyl propionates, cubic crysts., optical spectra fine struct. 77—1693
Urbach's rule derived from thermal fluctuations in the band-gap energy 79—33729
US attenuation in excitonic phase in strong mag. field 77—20243
vanadyl phthalocyanine, exciton electroabsorpt., optical density spectra 77—85746
vibrational IR excitons, spectra *(Russian)* 78—15173
vinyl acetate, model for exciton theory of excited states in poly-2,4-hexadiyn-1,6-diol bis(p-toluene sulphonate) 77—80733
Wannier, single site theory in disordered semiconductors, general consideration 79—99486
Wannier and Frenkel excitons, simple model for unified treatment 79—69422
Wannier exciton binding energy in strong anisotropic crystals 77—28126
Wannier exciton-polaritons, real space wave eqn. 80—39508
Wannier excitons, electronic spectrum, in quasi-two-dimensional structures 80—65460
Wannier excitons, laplace transform method in two-photon spectroscopy theory 79—10084
Wannier excitons, radiative decay in thin crystal fields 80—92823
Wannier-Mott, interactions with screw dislocations *(Russian)* 79—4513
Wannier-Mott excitons in layer structures and near interface of two media 77—66124
Wannier-Mott polaritons in mag. fields, review 78—2437
waves, excitonic, dispersion relation in correlated electron system 77—11861
wire, exciton energy spectrum and light absorption *(Russian)* 77—62832
wurtzite-type crystals, magnetopolaritons 79—78019
wurtzite-type semiconductor, with electron-hole exchange interaction, energy levels of A and B excitons 79—51494
X-ray exciton in strong mag. field, energy spectrum and wave functions, hole mobility effect *(Russian)* 79—95338
zeaxanthin, aq. soln., aggregate, reson. Raman spectra, and IR spectra, exciton interactions 78—31770
zincblend structure, energy levels of direct exciton formed by split-off valence band 78—91624
zincblende structure semiconductor in intermediate mag. field, exciton spectra 78—18969
Ag halide, EPR of triplet state of self-trapped excitons 78—43684
Ag halides, physical props. rel. to photographic processes 79—19555
Ag halides, tetrahedrally coordinated, semiempirical band struct. model 77—51655
AgBr, Bose-Einstein condensation of triplet excitons 77—44057
AgBr, cyclotron reson. of polarons at high density excitation 80—75859
AgBr, decay of proposed Bose-Einstein condensed excitons 78—15221
AgBr, dispersive phonon modes, reson. Raman scatt. obs. 78—10896
AgBr, EPR of excitons, detected in X-ray excited luminesc. spectra at 4K 77—55732
AgBr, electron simulation, luminescence and hidden image formation *(Russian)* 79—47515
AgBr, electron-hole liq. and biexciton pocket, luminesc. obs. 78—15216
AgBr, exciton absorpt. at high excitation rates 80—2343
AgBr, exciton relax. by intervalley scatt., reson. Raman meas. 79—33713
AgBr, exciton relaxation by intervalley scattering 80—20644
AgBr, excitonic mol. recomb., photoluminesc. 77—8633
AgBr, highly excited, time resolved luminesc., recomb. of excitonic mols. 77—69889
AgBr, indirect near edge emission, 1.5-50K 77—16380
AgBr, luminesc. band shape of free excitons, at high exciton density, calc. 77—81148
AgBr, new shoulder in luminesc. spectra, triplet excitons 80—20706
AgBr, optical absorpt. of indirect exciton in high mag. field 78—60486
AgBr, photoluminesc. study of excitons in high mag. fields 80—80843
AgBr, radiative recomb. of indirect excitons at high concs. 78—6732
AgBr, shoulder in luminesc. spectra due to triplet excitons 79—15525
AgBr, Stark effect on I-bound exciton 79—28719
AgBr, time resolved luminesc. spectra at high excitation density 79—78751
AgCl, AgCl:AgBr, X-ray and ultraviolet effects, ODMR 78—79933
AgCl, and Br doped, EPR of excitons, detected in X-ray excited luminesc. spectra at 4K 77—55732
AgCl, cryst. luminesc. and photovoltaic effect kinetics 78—64391
AgCl, electron simulation, luminescence and hidden image formation *(Russian)* 79—47515
AgCl, optical absorpt. of indirect exciton in high mag. field 78—60486
AgCl, optically detected EPR of excited states rel. to luminesc. 77—12256

excitons continued
- AgCl, photoconductivity and photoluminesc., 6.8 to 80K, exciton and valence band states 77–43644
- AgGaS$_2$, elec. field influence on absorpt. spectrum, exciton parameters and energy of impurity levels *(Russian)* 77–69860
- AgGaSe, direct gap semicond., exciton energy at 300K from reabsorption of luminesc. 79–78728
- AgGaSe$_2$, reabsorpt. of excitonic luminesc. in direct band gap semiconds. 77–63469
- β-AgI, 2H and 4H polytypes, exciton refl. spectra at 4.2K 79–69860
- β-AgI (4H), visible spectra, reflected light phase and amplitude, exciton resonance 80–45110
- β-AgI, exciton luminesc. of 2H and 4H polytypes 77–85783
- β-AgI, exciton refl. spectra, optical activity *(Russian)* 78–64380
- AgI film, crystallisation, exciton absorption spectra meas. 77–35483
- β-AgI thin film, exciton spectrum 80–55216
- AgN$_3$, optical absorpt. spectra, and photoemission, electron band scheme 79–100015
- Ag$_2$O, exciton luminesc. spectra, mag. field influence 80–80860
- Ag$_2$O, photoconductivity of crystals grown under hydrothermal conditions 78–14765
- Ag$_2$O, quadrupole exciton transition and struct. of optical absorpt. edge 79–38569
- Al-Formvar-Sn coupled films, Ginzburg's excitonic supercond. model 80–97039
- Al-SiO$_2$-Si structure, positive interface charge, exciton and H diffusion models 80–2471
- AlAs-GaAs monolayer crystal, two-photon absorpt. spectrum 78–52589
- AlAs(Sb), fine structure of lowest exciton state *(Russian)* 80–96801
- Al$_x$Ga$_{1-x}$As:N, photoluminesc. and optical absorpt. spectra of N impurity bound-excitons 79–47496
- Al$_x$Ga$_{1-x}$As-GaAs quantum-well heterostruct., exciton in recomb. 80–103990
- Al$_x$Ga$_{1-x}$P, photoluminescence excitation spectra, bound excitons, Al conc. depend. 80–20687
- AlN, absorpt. edge shape interpretation, Wannier excitons absorpt. in charge impurity elec. field 80–66233
- AlN, excitation, luminescence, reflection spectra in fund. absorpt. region 78–10956
- AlN, luminesc. excitation spectrum and band struct. 80–84783
- AlNH$_4$(SO$_4$)$_2$:Cr^{3+}, optical spectral, crystal field, spin orbit and exciton interactions 80–34958
- Al$_2$O$_3$ monolayer, core excitons and inner well resonances in surface soft X-ray absorpt. spectra 80–40187
- AlSb, indirect exciton dispersion, 'camel's back' 79–73447
- Ar atoms in Ne matrix, radiative and nonradiative lifetimes in excited states 80–69106
- Ar, condensed electron beam excited, exciton radiative lifetimes 80–6727
- Ar, cryst., luminesc., absorpt. spectra, free, self-localised excitons coexistence *(Russian)* 78–31231
- Ar, liquid, triplet state of self-trapped exciton states, evidence of existence, luminescence meas. 78–72608
- Ar, liquid and solid, absorpt. and luminesc. spectra of self-trapped excitons 79–65893
- Ar, optical absorpt. and luminesc. spectra, obs. of relaxed exciton states 77–52082
- Ar, solid, n=1 surface excitons and LO-TO splittings of bulk excitons 79–73445
- Ar, solid, self-trapped exciton, pseudopotential method 79–82529
- Ar, solid, surface excitons 77–76892
- Ar, solid gaseous, valence and inner shell excitonic band struct. 80–6735
- Ar:OCS, O(^{1}S) and S(^{1}S) photodissociative prod., photoluminesc. excitation spectra, exciton energy transfer 80–89508
- Ar:Xe, liq. 0-1.4 g cm^{-3}, vac. UV absorpt. spectra, Wannier impurity states 77–77232
- Ar:Xe film, solid, competition between electronic energy transfer and relax., photoelectron spectra 77–24929
- As$_2$S$_3$, amorphous, luminesc. and optically detected ESR, photoinduced struct. change 80–50399
- a-As$_2$S$_3$, rel. to luminesc. with short decay time 78–2906
- As$_2$S$_3$:Fe glass, photolum. and ESR, Fe impurities as non-radiative recomb. centres 80–29788
- As$_2$S$_{3-x}$Se$_x$, amorphous, picosecond relax. of optically induced absorption 80–97302
- a-As$_2$Se$_3$, rel. to luminesc. with short decay time 78–2906
- Au-GaS, Schottky-barrier electroreflectance spectra under uniaxial stress 79–56767
- Au-Ge Schottky diode, phonon energies, barrier heights, photovoltage spectra 78–64112
- AuCl, luminesc., excitons 80–2839
- BaMnF$_4$, low temp. phonon, and exciton effects on polarisation 79–42905
- BaO, logarithmic derivative reflectance spectra 80–11429
- BaO, surface states, reflectance spectra, impurity effects 77–20873
- Ba[Pt(CN)$_4$].4H$_2$O, polarised time-resolved emission spectra 79–33811
- Bi hole pocket, far-IR magnetospectroscopy, electron-electron interaction effects 77–77211
- Bi$_4$Ge$_3$O$_{12}$:Er^{3+}, host-sensitised energy transfer, laser time resolved spectroscopy 79–83013
- BiI$_3$, excitonic shifts of quasiatomic optical core to cond. band transitions, UPS obs. 78–11079
- BiI$_3$ film, exciton peaks, temp. depend. 90-270K, and press. depend. up to 3500 atm. 77–36265
- BiI$_3$, layered compound, exciton spectra, surface and stacking fault effects 80–40134
- BiI$_3$, layered single crystal, band-edge excitons, optical constant meas. *(Russian)* 77–90171
- BiI$_3$ single crystals, refl., absorpt. and photoluminesc. spectra, exciton transitions 77–52164
- BiI$_3$, structure, exciton states and physicochem. characteristics *(Russian)* 80–100435
- (CH$_4$)NMnCl$_3$, nearly-one-dimensional cpd., energy migration rel. to impurity trap behaviour 77–55811
- CO, cryst. at 5K, absorpt. and emission spectra, exciton interpretation 79–87481
- CO-Ar, cryst. at 5K, absorpt. and emission spectra, exciton interpretation 79–87481
- CO-Ne, cryst. at 5K, absorpt. and emission spectra, exciton interpretation 79–87481

excitons continued
- CO$_2$, isotopically mixed crysts., IR spectra ν_2 vibr. exciton band 77–73136
- C$_3$PbCl$_3$, single crysts., X-ray and photoluminesc., and reflection spectra 77–69896
- CS$_2$, liquefied gas solns. bound exciton model for Rydberg bands 78–31214
- CaF$_2$:Eu^{2+}, energy transfer to luminesc. centres, pulsed excitation obs. 77–85781
- CaF$_2$:Eu^{2+}, short high-energy pulse induced X-ray luminesc., anomalous kinetics 77–59608
- CaF$_2$:Eu^{2+}, X-ray induced luminesc. kinetics, energy transfer processes 79–8181
- CaF$_2$:Y, absorpt. spectra, radiation defect formation energy, F to M centre conversion kinetics 79–65079
- CaO, electronic band struct., combined tight-binding and pseudopot. approach 77–47728
- CaO, single cryst., tribolum. obs. 79–52031
- Cd$_{1-x}$ Mn$_x$Te, exchange interaction, magneto-optical spectra 80–25348
- CdBr$_2$, optical refl. spectra, exciton bands obs. around optical gap 78–15192
- CdBr$_2$(I$_2$), exciton spectra, temp. and press. effects 77–20881
- CdCl$_2$, optical refl. spectra, exciton bands obs. around optical gap 78–15192
- CdCl$_2$-CdBr$_2$, solid soln., luminesc., optical absorpt. 78–19538
- CdGa$_2$S$_4$, direct excitons, refl. spectra 79–90972
- CdI$_2$ (Br$_2$), cathodoluminescence, 300 and 80K *(Russian)* 79–78760
- CdI$_2$ crystals, photolysis obs. *(Russian)* 80–7833
- CdI$_2$, luminesc., relaxed excitonic states 79–33758
- (CdI$_2$)$_x$(PbI$_2$)$_{1-x}$, reflection and luminesc. spectra obs. 77–8648
- CdMnTe crystals, exciton binding energy, magnetoabsorption and magnetoreflectivity 79–38523
- CdMnTe, exciton ground state, magnetic field influence 80–54616
- Cd$_{1-x}$Mn$_x$Te, effect of Mn 3d^5 states on band struct., exciton refl. struct. in mag. field 79–11094
- Cd$_{1-x}$Mn$_x$Te, exchange induced ionization of bound excitons, luminesc. meas. 80–97328
- Cd$_{1-x}$Mn$_x$Te, magneto-optical props. of free excitons rel. Mn^{2+} ions spin alignment 79–47419
- Cd$_{1-x}$Mn$_x$Te mixed cryst., giant exciton Faraday rotation 78–27260
- Cd$_{1-x}$Mn$_x$Te mixed crystals, excitonic magnetoabsorption 80–40095
- Cd$_{1-x}$Mn$_x$Te, semimagnetic, exchange interactions between localised and delocalised electrons 80–97245
- Cd$_x$Pb$_{1-x}$I$_2$, photoluminescence comp. and energy depend., band gap 77–44045
- CdS, A$_{n=1}$-exciton, reflectance and thermoreflectance spectra, spatial dispersion and angle of incidence effects 80–25409
- CdS, A-exciton-polariton, time depend. optical spectrosc. obs. 78–80376
- CdS active surface, exciton stimulated emission and superradiance refl. spectra, props. 80–25411
- CdS, additional waves and polariton dispersion, reflectivity, transmittivity spectra 80–71443
- CdS, attenuation of transmitted light in exciton region, polarisation, coherence, scatt. 77–69852
- CdS, Auger effects in donor acceptor pair spectra 80–20707
- CdS, B exciton-polariton, reson. Brillouin scatt. 79–33717
- CdS, biexciton, low intensity nonlinear coherent mixing study 80–49619
- CdS, Brillouin scatt. of forbidden polaritons 79–33722
- CdS, cathodolum. in red and exciton regions, surface treatment influence 77–77303
- CdS, creation of 2P excitons by two photon magneto-absorption 78–2432
- CdS crystals, one-photon pumping, active layer structure, light amplification 80–78858
- CdS crystals, radiative recombination, high excitation rates 80–108269
- CdS, deform. effects on exciton excitation spectra 78–35191
- CdS, electron-exciton elastic scatt. cross sections, central field and exchange approxs. 77–62919
- CdS, electron-exciton inelastic collision cross sections 79–90967
- CdS, electron-hole liquid, non-equilib. transmission spectroscopy meas. 77–20883
- CdS, electron-hole pairs behaviour in energetic ion tracks 80–65457
- CdS, electron-hole plasma, gain and refl. spectra study 80–66227
- CdS, energy transfer by normal modes in exciton reson. region 77–89705
- CdS epitaxial layers on sapphire, exciton struct. of absorpt., photoluminesc. and photocond. spectra 80–89027
- CdS, excitation spectroscopy, relation between I$_2$ bound exciton line and CdS excitonic molecule line 80–40153
- CdS, exciton absorpt. at low temps. *(Russian)* 78–48195
- CdS, exciton cathodoluminesc. of semicond. with surface pot. barriers 78–88366
- CdS, exciton condensation, photoluminesc. spectra 80–25448
- CdS, exciton luminescence, surface recombination, space-charge-layer effects 78–80410
- CdS, exciton obs. in thin surface layers, refl. spectrum *(Russian)* 78–2877
- CdS, exciton optical and luminescence spectra characts. near dislocation slip bands 80–45111
- CdS, exciton polaritons, optical response 77–69792
- CdS, exciton polaritons, Brillouin scatt. efficiency, additional boundary conditions 79–73960
- CdS, exciton resonant secondary emission spectrum temporal evolution 79–51499
- CdS, exciton spectra anomalies, surface state effects 78–18974
- CdS, exciton spectrum of high-density gas of nonequilib. carriers 79–38567
- CdS, exciton-contrib. to reflection spectrum at high excitation intensities 78–43900
- CdS, excitonic polariton reflectance, quantitative anal. in spectral range of A-exciton 79–15480
- CdS, excitonic polariton reflectance, B-exciton and k-linear term 80–7369
- CdS, excitonic region, nonlinear optical meas., 4.2K 78–68531
- CdS film, exciton exhibiting spatial dispersion, reflectivity, polariton standing-wave struct. 79–4865
- CdS, fine struct. of two-photon absorption, luminesc. meas. 77–24893
- CdS, group velocity of light near exciton resonance 77–24863
- CdS, high intensity excited, exciton reflection spectra, reflection struct. 80–20692

excitons continued
CdS, highly excited, stimulated emission processes, exciton-exciton (electron) scatt. 80—97307
CdS, impact ionisation of excitons, photocond. and photolum. meas. 79—56266
CdS, induced absorption and gain from high density excitons 78—68533
CdS, induced absorption in energy ranges of exciton and exciton-biexciton transitions 78—72548
CdS, influence of Lamb US waves on exciton spectra *(Russian)* 80—7374
CdS, influence of surface annihilation of excitons on cathodolum. meas. 77—20937
CdS, interaction of excitons with charged impurities 78—43906
CdS, intrinsic exciton fine struct., two-photon absorption 77—12397
CdS, irrad. with high doses of fast reactor neutrons, exciton reflection spectra 79—73221
CdS, laser action in dense exciton systems 77—75531
CdS laser irrad. native defect formation, influence on photoelectric props., IR luminescence *(Russian)* 80—11039
CdS, laser thresholds and stimulated emission, intrinsic recomb. processes 79—15489
CdS, luminesc. and gain spectra of two-photon excited excitons 79—33815
CdS, luminesc. of $\mathrm{I_2}$ bound exciton and excitonic mol. 79—91492
CdS, $\mathrm{M_1}$-$\mathrm{M_2}$ luminesc. band, assignment to exciton-impurity complexes 77—8649
CdS, magnetoreflectance and magnetoluminesc. of A exciton 78—39597
CdS, mol. model for exciton-impurity complexes 77—80740
CdS, nonlinear optical suscept., resonant excitonic contrib. 77—3633
CdS, ODMR, bound excitons 78—80253
CdS, obs. of forbidden Brillouin scatt. near exciton reson. 78—15180
CdS, optical activity in exciton spectra region, reflectance spectra 79—28707
CdS, photocond., spectral depend. at high excitation intensity, exciton effects 80—65619
CdS, photocond. peaks due to exciton transition and S vacancies 77—8131
CdS, photoexciton waves, restrictions imposed on nature of additional boundary conditions 79—28789
CdS, photorefl. in exciton region, surface layer influence 78—76489
CdS plane parallel slab, optical const. determ. methods 80—60531
CdS, ps decay kinetics of luminesc., streak camera obs. 79—78752
CdS, Raman shift dispersion near exciton reson., two-phonon cascade processes 80—11405
CdS, reflectance, transmittance and luminesc. spectra, light group vel. near exciton reson. *(Russian)* 77—69857
CdS, reson. Brillouin scatt. of exciton polaritons 80—11418
CdS, reson. dispersion of Brillouin shift 78—35160
CdS, reson. Raman scatt., temp. depend. polarisation, A-exciton 77—12386
CdS, reson. Raman scatt., second-order, theory for case of strong excitonic effects 78—76460
CdS, reson. scatt. of exciton-polaritons second emission under monochromatic excitation 77—1717
CdS, resonance hyper-Raman light scatt. on optical photons *(Russian)* 80—14396
CdS, single cryst., bound excitons in surface layers, luminesc. obs. 79—28294
CdS, single cryst., laser emission following single-photon excitation *(Russian)* 78—37889
CdS single crystal, laser emission at one-photon excitation *(Russian)* 77—79835
CdS single crystals, Roentgenoluminescence, exciton interactions *(Russian)* 80—2853
CdS, spatial diffusion of excitons under intense excitation 77—44061
CdS, spatial dispersion and surface layer effects on the phase of reflected light *(Russian)* 78—35182
CdS, spatial dispersion effects, exciton decay const. depend. *(Russian)* 78—72086
CdS, spectral anal. of luminesc. of high density excitons 79—11451
CdS, spontaneous and stimulated emission from electron-hole plasmas 77—69241
CdS, spontaneous optical activity in exciton spectrum *(Russian)* 78—35167
CdS, stimulated emission under $\mathrm{N_2}$ laser excitation 77—14723
CdS, stimulated emission and optical gain in dense exciton system 79—33731
CdS, subMM radiation excitation by $\mathrm{N_2}$ laser pulse 80—60678
CdS, submillimetre laser emission due to transitions between free exciton level 79—27261
CdS, surface photovoltage in exciton absorpt. range 78—19119
CdS, thermoreflectance spectra, additional boundary conditions in terms of optical constants 79—15478
CdS, three-branch exciton-polariton dispersion, direct meas. by reson. Brillouin scatt. 80—60620
CdS, transmission spectra, region of exciton reson., spatial dispersion effects 79—78704
CdS, two-phonon resonant Brillouin scatt. 78—84597
CdS, two-photon absorpt., excitons *(Russian)* 78—39571
CdS, Wannier exciton and Wannier-exciton-ionised-donor complex, binding energies of lowest excited states 80—34363
CdS, Wannier exciton-ionised donor complex, binding energy 80—44509
CdS, wavelength dependence of pressure coefficients of birefringence 77—20820
CdS, wurtzite structure, natural optical activity *(Russian)* 79—78647
CdS:Cl, extrinsic, exciton absorption 78—72569
CdS:Cl, resonant Raman scatt. exam. 78—39546
CdS:F(Cl), shallow donors electronic Raman scatt., reson. enhancement 80—45068
CdS:In, two-photon absorpt. spectra exam. of effects of screening of exciton continuum 79—8166
CdS:$\mathrm{Li^+(N^+)(Ne^+)(P^+)}$, ion-implanted, edge emissions 77—77274
CdS:Li(Cu), pure and doped, electrodiffusion of shallow donors, photocurrent, TSC, and exciton luminesc. meas. 80—79992
CdS:Mn(Co), intensity and spectral distrib. of luminescence *(Russian)* 77—16392
CdS:Ni, exciton reflection spectra 78—72557
CdS/$\mathrm{LiNbO_3}$ system SAW convolution signal photoenhancement obs. 77—27431
CdS(Se), magnetopolaritons in wurtzite-type crystals 79—78019

excitons continued
CdS(Se), magnetoreflectance spectra of anisotropic II-VI semiconds. by mag. field modulation 77—66519
CdS(Se), ps. spectra, high density exciton system 78—19553
CdS(Se), ps. spectra, high density exciton system 78—19554
CdS(Se), single cryst., band parameters from optical exciton spectra 79—47021
$\mathrm{CdS(Se)_3}$ excitons and Landau levels meas. by magneto-optical spectroscopy apparatus 77—34032
$\mathrm{CdS_{0.4}Se_{0.6}}$, reson. excitation of excitons by ultrashort freq.-tunable light pulser 78—46728
$\mathrm{CdS_{1-x}Se_x}$, comp. disorder-induced broadening for free excitons 79—15479
$\mathrm{CdS_{1-x}Se_x}$ mixed crystals, free excitons, disorder effects 80—34365
$\mathrm{CdS_{1-x}Se_x}$, mixed crystals, deformation effects on free excitons 80—76073
$\mathrm{CdS_{1-x}Se_x}$ single crysts., photocond. and excitonic luminesc. under high laser excitation 78—23127
$\mathrm{CdS_xSe_{1-x}}$ mixed crystals, exciton spectra 78—92131
$\mathrm{CdS_xTe_{1-x}}$, emission spectra at high excitation levels *(Russian)* 79—74004
$\mathrm{CdS_xTe_{1-x}}$, low temp. photoluminesc. *(Russian)* 78—43931
CdSe, collisions between hot excitons and hot electrons 80—7415
CdSe, dynamic holographic gratings based on excitons 77—3556
CdSe, electron-exciton elastic scatt. cross sections, central field and exchange approxs. 77—62919
CdSe, electron-exciton inelastic collision cross sections 79—90967
CdSe, electrorefl. and photocurrent of ground state excitons 79—99905
CdSe film, as-deposited and recrystallised, struct. and fund. optical absorpt. 77—1753
CdSe, hexagonal, Coulomb interaction at $\mathrm{E_1}$ interband transition 78—19507
CdSe, high intensity excited, exciton reflection spectra, reflection struct. 80—20692
n-CdSe, laser excited stimulated emission, optical gain spectrum 80—76050
CdSe, magnetoreflectance and magnetoluminesc. of A exciton 78—39597
CdSe, mol. model for exciton-impurity complexes 77—80740
n-CdSe, negative photocond., optical excitation of exciton-impurity complexes 77—15905
CdSe, optical gain spectra, exciton collision processes and electron-hole plasma 79—28814
CdSe, oriented single-crystal films, edge luminescence at high excitation levels 77—1720
CdSe, polarisation correl. of resonant Raman scatt. or hot luminesc. 80—25384
CdSe, radiative recomb. process, P-band, 2-psec time resolution 79—24346
CdSe, resonant Brillouin scatt. via free and bound excitons 79—24330
CdSe single crysts., exciton luminesc. and polarisation spectra under one- and two-photon excitation 79—65391
CdSe, single crysts., luminesc. of electron-hole plasma 80—60675
CdSe, thin films, exciton piezotransmission 79—24380
CdSe, wavelength dependence of pressure coefficients of birefringence 77—20820
CdSe:Fe, exciton electroreflectance spectra, impurity effects 77—16335
CdSe:Li, pure and doped, reson. Raman and Brillouin scatt., elastic exciton-defect scatt. 80—80788
$\mathrm{CdSiP_2}$, pseudodirect bandgap semiconductor, natural birefringence 79—65834
CdTe crystals, exciton luminescence spectra rel. to shallow impurity conc. 80—97335
CdTe, electron-hole liquid formation in pure and doped crystals, luminesc. study *(Russian)* 80—55184
CdTe, excitation spectra, resonant Raman scatt. versus hot electron effects 79—38645
CdTe, exciton magnetoreflectance spectra, multicomponent polaritons, Zeeman splitting 80—88974
CdTe film, exciton spectra, press. and temp. depend. 80—80886
CdTe, low temp. luminesc. *(Russian)* 79—91497
CdTe, luminescence and reflect. investig. of excitons, stress and Zeeman splitting 77—40281
p-CdTe, photocond., photoluminesc., spectral studies 80—88593
CdTe, recombination radiation due to high-density excitons 80—93392
CdTe, reson. Raman scatt. by excitonic polaritons 80—11396
n-CdTe, single crystal, photoreflectance, temp. depend. of exciton spectra *(Russian)* 78—23488
CdTe, spatial dispersion rel. to exciton reflection spectra *(Russian)* 80—40126
CdTe:$\mathrm{Mn^{2+}}$, exciton refl. spectra and mag. susceptibility 80—66253
CdTe:$\mathrm{Mn^{2+}}$, luminesc. and magnetooptic reson., mag. field effect 80—93390
CdTe:$\mathrm{Mn^{2+}}$, magneto-optical and microwave-optical double reson. meas. of exciton band *(Russian)* 77—81087
CdTe:Mn(Fe)(Ni), exciton refl., photoluminesc., and mag. suscept. meas., influence of impurities 77—39787
CdTe:V,Cr, optical props. meas. 79—73969
CdTe:Yb, exciton emission, cathodoluminescence 78—39033
$\mathrm{CoCO_3}$, exciton and magnon excitation spectra *(Russian)* 78—23467
$\mathrm{CoCO_3}$, LF exciton and Raman spectra, one-magnon and two-magnon scatt. 80—93333
$\mathrm{CoCO_3}$, two-sublattice noncollinear antiferromag., exciton-magnon light absorpt. mechanisms *(Russian)* 80—89017
$\mathrm{CoCO_3}$, weak ferromagnet, optic study of spin wave spectrum *(Russian)* 79—47263
$\mathrm{CoCO_3}$, weak ferromagnet, light absorpt. dichroism and mag. config. *(Russian)* 79—87457
$\mathrm{CoCl_2}$, antiferromag., elementary excitations 77—69519
$\mathrm{CoCl_2}$, antiferromag. elementary-excitations, electronic Raman scatt. meas. 77—80922
Cr, antiferromagnetic, phase fixation, excitonic and spin superfluidity of electron-hole pairs 78—30872
Cs halides, electronic struct. of self-trapped excitons magneto-optic props. 79—33805
CsBr, luminesc., mag. circ. polaris., self-trapped excitons, EPR 79—33805
CsBr, luminesc. polarisation for free and bound excitons 78—10942
CsBr, self-trapped excitons, magneto-optical props., 1.3-50K 80—49606
$\mathrm{CsCoBr_3}$, quasi ID Ising antiferromag., polarised Raman scatt. from mag. excitations 80—66182

excitons continued
$CsCoCl_3$, 10 Ising antiferromag., mag. excitations, electronic Raman and IR absorption spectra 78—2668
CsF, EPR of self trapped exciton and MCd meas. 77—48091
CsI, correl. between UV emission band at 300 nm and self-trapped excitons, 4.2K 78—75998
CsI, luminesc., mag. circ. polaris., self-trapped excitons 79—33805
CsI, pure and Na(Tl)-doped, luminesc. from bound excitons, UV absorpt. and EPR 77—77282
CsI, self-trapped exciton electronic struct., semi-empirical mol. orbital method 80—49605
CsI, self-trapped excitons, magneto-optical props., 1.3-50K 80—49606
CsI:Na, electronic struct. and luminesc. 80—16080
CsI:Na, localised excitons, absorption and emission 77—32425
CsI:Na, photoluminescence spectra and lineshapes anal., exciton energies 77—77281
CsI:Na, self-trapped exciton emission polarisation 80—49607
CsI:Na, tunnelling recomb. of electron-hole pair, optical detection of ESR and circ. dichroism 79—47360
$CsI:Na^+(K^+)$, luminesc. processes 80—103989
$CsMnCl_3.2H_2O$, antiferromag. insulator, self-trapping of excitons 80—70619
$CsMnCl_3.2H_2O$, nonequilibrium magnon population obtained by optical pumping *(Russian)* 80—11457
$CsMnCl_3.2H_2O$, quasi-one-dimensional antiferromag., luminesc. enhancement in mag. field *(Russian)* 79—91487
$CsMnF_3$, exciton migration, excitation and luminesc. study *(Russian)* 80—66264
$CsMnF_3$, exciton-magnon interactions in optical transition, absorpt. and emission spectra meas. 80—70981
$CsMnF_3$, mag. field- and temp.-depend. of light absorption spectra 78—52528
$CsMnF_3$, magnon absorption and luminesc. 80—7400
$CsNiF_3$, double-excitonic optical transition intensity, exchange and dimensionality effects 77—69591
$CsPbCl_3$, electronic struct. and optical props. in fundamental absorpt. region 80—93367
$CsPbCl_3$, exciton states, magneto-optical investigation 80—29328
$^{133}Cs(n,\gamma)^{134}Cs$, $E_n = 14.1$ MeV, γ emission exciton model *(Russian)* 79—13302
Cu halides, tetrahedrally coordinated, semiempirical band struct. model 77—51655
$CuAlS_{2x}Se_{2(1-x)}$, excitonic structure, phase-shift-difference spectra 78—2872
CuBr, 1S exciton triplet state, magneto-optical props. 80—25345
CuBr, direct gap semiconductors, charged excitons 77—62840
CuBr, dispersion of multicomponent exciton polaritons, hyper-Raman emission spectra 80—20096
CuBr, emission spectra after two-photon excitation, Raman scatt. 79—47518
CuBr, evaporated film, magneto-optical effects on exciton bands 78—72624
CuBr, exciton absorpt. band shape, dielectric const. real part derivatives *(Russian)* 80—25413
CuBr, exciton bands, oscillator forces, temp. depend. *(Russian)* 79—28284
CuBr, multiplet struct. of P-excitons due to valence band degeneracy 78—39035
CuBr, P exciton fine struct. 80—20091
CuBr, piezo-optical effects on excitons, importance of k-linear terms 79—95802
CuBr, single oriented crystals., electroreflectance, exciton transitions 77—66517
CuBr, surface exciton polariton, ATR meas. 77—77236
CuBr-Ag system, spectral distrib. of photosensitivity *(Russian)* 78—56535
CuBr(Cl), biexcitons, many exciton effects 78—51901
CuCl, biexciton luminescence and two photon Raman emission, polarisation props. 78—80406
CuCl, Bose-Einstein condensation of biexcitons 79—56138
CuCl, decay time mas. of biexcitonic photoluminesc. 78—10935
CuCl, direct-gap semiconductors, charged excitons 77—62840
CuCl, electron-hole pairs behaviour in energetic ion tracks 80—65457
CuCl, electronic struct., ab initio HF SCF MO calcs. of $CuCl_4^{3-}$ cluster 78—95262
CuCl, emission spectra after two-photon excitation, Raman scatt. 79—47518
CuCl, evaporated film, magneto-optical effects on exciton bands 78—72624
CuCl, exciton bands, oscillator forces, temp. depend. *(Russian)* 79—28284
CuCl, exciton luminesc., reabsorpt. and polariton effects 80—50430
CuCl, exciton spectra, extended effective mass theory 79—69424
CuCl, excitonic polariton, picosecond time of flight meas. 80—29337
CuCl, excitons bound to neutral donor impurities, magneto absorption spectra 79—56816
CuCl, existence of charged excitons 78—76496
CuCl film, exciton absorption bands *(Russian)* 79—51985
CuCl, giant two-photon absorption into excitonic mol., anomalous dispersion of excitonic polariton 78—27211
CuCl, H^+ irrad., luminesc., high density excitons in particle tracks 79—47020
CuCl, induced absorption due to exciton-biexciton transitions 78—15187
CuCl, interface supercond., piezoelec. hypothesis 80—60128
CuCl, luminesc. and Raman processes under reson. two-photon excitation 79—33796
CuCl, luminesc. from Bose-condensed state of biexcitons 79—23905
CuCl, nonlinear light absorpt., picosec. pulse, exciton-biexciton transitions 79—47483
CuCl, optical consts. in exciton absorption region, spectral depend. *(Russian)* 77—81125
CuCl, picosecond spectroscopy of secondary radiation from resonantly excited excitonic molecules 79—15461
CuCl, polariton, prop. times at energies near transverse exciton 79—28297
CuCl, polariton effects in resonant Raman scatt. 78—10881
CuCl, possibility of excitonic dielectric-supercond. phase transition 77—43797
CuCl, possibility of high temp. superconductivity 79—51711
CuCl, Raman and luminesc. processes under reson. two-photon excitation of excitonic mol. 79—8143

excitons continued
CuCl, reson. two-photon Raman scatt., excitonic polariton dispersion 78—72509
CuCl, resonant emission, lifetime of excitons 77—69887
CuCl, resonantly excited excitonic molecules, time resolved spectroscopy 78—92109
CuCl, surface exciton polariton, ATR meas. 77—77236
CuCl, third-order nonlinear optical spectroscopy 77—23713
CuCl, time resolved exciton-biexciton transitions, UV excitation, luminescence spectra 79—69883
CuCl, time-resolved study of induced absorption due to exciton-biexciton transitions 79—38658
CuCl, two-photon reson. Raman scatt. with recoiling excitonic polariton 77—36223
CuCl, two-photon reson. Raman scatt., recoil of upper-branch excitonic polariton 78—27212
CuCl, two-photon resonant Raman scatt. via biexcitons 78—43302
CuCl, UV spectra, Γ_1 biexciton level, appl. of nonlinear spectroscopic technique 79—8156
CuCl, Urbach rule at excitonic absorpt. edge, theoretical model tests 80—50299
CuCl, Z_3-exciton, temp. dependent TPA linewidth 78—67946
CuCl:Ag system, light sensitivity spectrum, exciton struct. *(Russian)* 79—51985
CuCl-Ag system, photosensitivity spectrum in region of CuCl exciton absorpt. *(Russian)* 79—78707
CuCl(Br), charged excitons, band struct., electron-hole exchange interaction 77—69233
CuCl(Br)(I), electron-exciton inelastic collision cross sections 79—90967
$CuGaS_2$, direct gap semicond., exciton energy at 300K from reabsorption of luminesc. 79—78728
$CuGaS_2$, exciton absorption energies, appl. of modulated phase-shift-difference method 78—39565
$CuGaS_2$, reabsorpt. of excitonic luminesc. in direct band gap semiconds. 77—63469
$CuGaS_2$, reson. Raman scatt. by extraordinary phonons obs. 77—85704
$CuGaS_{2-2x}Se_{2x}$, mixed crysts., free exciton decay in luminescence spectra 77—63454
$CuGaS_{2x}Se_{2(1-x)}$, excitonic structure, phase-shift-difference spectra 78—2872
$CuGaSe_2$, photoluminesc. spectra at 76K 79—38655
γ-CuI crystalline film, excitonic spectra *(French)* 79—78771
$CuInS_2$, optical and elec. phenomena 78—39605
CuO_2, width of reson. Raman scatt. enhancement profiles, phenon-lifetime contrib. 79—19883
Cu_2O, 1s yellow exciton, lineshape studies by reson. Raman scatt. 78—76465
Cu_2O, electro-optic effects due to the Stark splitting of energy bands 79—82950
Cu_2O, electron-exciton inelastic collision cross sections 79—90967
Cu_2O, electron-exciton scatt. cross sections, central field and exchange approxs. 77—62919
Cu_2O, energy band interactions under uniaxial compression 80—25412
Cu_2O, even-parity excitons assignment, from two-photon spectrum 80—6731
Cu_2O, exciton luminesc. spectra, mag. field influence 80—80860
Cu_2O, exciton spectra, extended effective mass theory 79—69423
Cu_2O, exciton spectrum, effect of isotopic substitution 78—67955
Cu_2O, excitons and structural defects at low temp. 78—84255
Cu_2O, fine struct. of exciton spectrum 78—18972
Cu_2O, optical absorpt. due to paraexciton in strong mag. field 77—28596
Cu_2O, ortho and para exciton lifetime meas. 80—6730
Cu_2O, photoconductivity in 1S excitonic line 80—34366
Cu_2O, photoconductivity of crystals grown under hydrothermal conditions 78—14765
Cu_2O, polar semicond., effective exciton-exciton interaction 79—42465
Cu_2O, relationship between interband transitions and spectrum of diagmagnetic excitons in moderate mag. fields 79—91412
Cu_2O, reson. Raman scatt., yellow and green excitonic series 78—72511
Cu_2O, reson. Raman scatt. from stress-split forbidden excitons 80—93332
Cu_2O, sample thickness depend. of exciton polariton absorption coeff. 80—34941
Cu_2O, self-induced transmission and radiation echo for intraseries and interseries exciton transitions 78—5528
Cu_2O, self-induced transparency, two-photon interaction of laser radiation with Frenkel excitons 78—25931
Cu_2O, theory of large-radius excitons 78—47710
Cu_2O, uniaxial stress effects on excitons 80—60589
Cu_2O, yellow exciton series, silver impurity influence on spectrum 78—64388
Cu_2O, yellow exciton states investig. by forbidden resonant Raman scatt. 77—48165
$Cu_2O:Ag^+$, exciton-neutral and exciton-charged impurity scatt. cross sections 80—70618
$Cu_2O:Ag^+$, yellow series line width, exciton-impurity scatt. 78—64386
Cu_2O:Cd, dipolar and quadrupolar bound excitons, absorption spectrum *(Russian)* 78—92099
Cu_2O:He(Na)(Cd), ion-implanted, resonance Raman studies of annealing 79—55765
D_2, solid, fundamental absorption spectra, 10 to 40 eV at 2K, using synchrotron radiation 79—73967
$DyCrO_3$, Cr^{3+} exciton-Dy^{3+} spinflip absorpt. 77—73153
Eu chalcogenides, resonant Raman scatt. 77—55787
Eu chalcogenides, resonant Raman scattering model via magnetic exciton in ferromagnetic phase 80—93326
Eu-chalcogenides, magnetic exciton states optical props. 77—31948
EuS, thermo- and magnetorefl. spectra, dynamical spin fluctuation effect on exciton state 77—52126
$Eu_{1-x}Sr_xS$, exciton refl. spectra 80—2782
$FeBO_3$, mag. linear dichroism and absorpt. spectra, exciton-magnon absorpt. mechanism 80—66160
Fe_3BO_6, polarised absorpt. spectra in range of $^6A_1 \rightarrow {}^4T_1$, $^4T_2$ transitions 77—52092
$FeBr_2$, metamagnetic, optical study of mag. phase diagram 78—56312
$FeBr_2$, optical props. around Neel temp. 79—78658
$FeCl_2$, optical props. around Neel temp. 79—78658
$FeCl_3$-graphite, intercalation compound, Fermi level lowering and core exciton spectrum, EELS study 79—74036
$FeCl_2.2D_2O$, metamagnetic, excitonic Davydov splitting in Raman spectrum 79—33704

excitons continued
- FeF_3, thin film, optical absorpt. meas., excitonic peaks 79−15546
- $Fe_{1-x}Mn_xCl_2$, disordered, Raman scatt. from Fe^{2+} and Neel temp. 80−60579
- $Fe_{1-x}Mn_xCl_2$, low-lying electronic excitations in antiferromag. and paramag. phases Raman scatt. study 80−71414
- FeS_2, optical absorpt. 79−43002
- GE, microwave cyclotron resonance lineshape, magnetoplasma interference effect, reinterpretation of excitonic polaron 78−43287
- Ga, reson. photoemission shake-up and Auger processes at 3p photothreshold 80−100748
- Ga-group V semiconductors, electroreflectance spectroscopy using synchrotron rad. 78−10912
- GaAs, (110) surface, electronic struct. of clean and O_2 covered surface 77−43685
- GaAs, acceptor bound exciton Auger and radiative transition rates, radiative recomb. 80−6733
- GaAs core exciton binding energies 80−80188
- GaAs, deep trap study by free exciton refl. spectra 79−60761
- GaAs, donor-acceptor-type complex 80−80837
- GaAs, electron-exciton collision influence on luminescence line profile due to bound excitons 80−29800
- GaAs, electronic surface props., interaction with Au and O adsorbate layers 77−20385
- GaAs epilayers, high-quality, sharp-line transitions due to donor-acceptor recomb. 78−6768
- GaAs epitaxial layer, photoluminesc. defect complex 80−29804
- GaAs, epitaxial layers, multiexciton complex bound to neutral acceptors, photoluminesc. obs. 79−87503
- GaAs, exchange interaction, analytical and nonanalytical parts, from polariton spectra in mag. fields 80−50367
- GaAs, excited luminescence, influence of IR illumination 80−76072
- GaAs, exciton effects in photocond., photoluminesc. 80−96797
- GaAs, exciton ground state and oscillatory absorption spectra in mag. fields, variational calc. 79−11071
- n-GaAs, exciton luminescence, excitation intensity depend. 78−52554
- GaAs, exciton motion under external electric field 79−56135
- GaAs, exciton parameters near absorption edge 79−73448
- GaAs, exciton quenching, obs. at room temp. using electrolyte electroreflectance 80−60546
- GaAs, exciton-polariton reflectance spectra, exciton impact ionization and illum. intensity effects 79−42943
- GaAs, excitonic polariton reson. interaction with LA phonons 78−60481
- GaAs, excitons, diamond like semiconductor, variational calculation of binding energies 78−79938
- GaAs, excitons in arbitrary mag. fields 80−96798
- GaAs FET structure, sharp line photolum. spectra 78−72248
- GaAs, fine structure of lowest exciton state *(Russian)* 80−96801
- GaAs, hot electrons and exciton-electron collision under external elec. field 78−43928
- GaAs, impact ionisation of excitons 79−38079
- GaAs, impurity states and core excitons, binding energies, perturb. theory 80−49659
- GaAs, interaction of excitons with charged impurities 78−43906
- GaAs, low-temp. absorption spectrum in presence of optical pumping 78−15188
- GaAs, luminescence by laser excitation, photocarrier thermalisation and polariton kinetics 77−66533
- p-GaAs, MBE grown, photolum. lines due to defect-induced bound exciton radiative recomb. 80−103974
- GaAs MOS and Schottky systems, electromodulated reabsorption of luminesc. 79−15524
- GaAs, nonlinear refractive index dispersion at helium temp. 78−2820
- GaAs, optical absorption spectrum dynamics using sub-ps. optical pulses 80−11431
- GaAs, photoabsorption and magnetoabsorption effects 77−16332
- GaAs, photocarrier thermalisation by laser excitation spectroscopy 78−31250
- GaAs, photoexcited, band edge absorpt. dynamics 79−19879
- GaAs, photoluminescence at low temp., free exciton recomb. mechanisms *(Russian)* 77−32438
- GaAs, polar semiconductor, collisions between hot excitons and hot electrons 80−7415
- GaAs, reson. Brillouin scatt. of exciton polaritons 80−11418
- GaAs, reson. polariton fluoresc. obs. 77−85785
- p-GaAs, spin relaxation of photoelectrons 77−85207
- GaAs surface, O_2 sorption and excitonic effects, photoemission expts. 77−85055
- GaAs, surface exciton energy 80−92829
- GaAs, two-photon absorpt. spectrum, band gap luminesc. 78−10888
- GaAs, two-photon electroabsorption by excitons 79−42944
- GaAs, weakly excited, luminesc. from exciton polaritons, based on exciton-electron collisions 79−83020
- GaAs:Co VPE layers, bound-exciton luminesc., Zeeman anal. 79−95818
- n-GaAs-Al surface barrier diodes, influence of exciton effects on photo-EMF spectrum 78−10557
- GaAs-Au, quenching of exciton luminesc. by surface elec. field 80−29801
- GaAs-GaAlAs heterostructures, saturation of free exciton absorption 79−61454
- GaAs-metal diode, surface-barrier, excitons effect on photocurrent 79−82670
- $GaAs_{1-x}P_x$, bound exciton, luminesc. reson. excitation 79−95840
- $GaAs_{1-x}P_x$, indirect-gap, evidence for exciton localization by alloy fluctuations, photolum. 80−66276
- $GaAs_{1-x}P_x$:N, $0.6<x<1$, photoluminesc., comp. depend. 78−52546
- $GaAs_{1-x}P_x$:N, photoluminesc. and optical absorpt. spectra of N impurity bound-excitons 79−47496
- $GaAs_{1-x}P_x$(Te), bound exciton stress depend., piezoluminescence, photoluminescence 80−80206
- $Ga_xIn_{1-x}P$, with indirect band struct., radiative recomb. of free excitons, cathodolum. meas. 77−90202
- $Ga_xIn_{1-x}P$:N layers, LPE growth, luminesc. and direct exptl. obs. of band struct. effects 77−52157
- $Ga_{1-x}In_xSe$, energy bands near absorpt. edge, transmission and photoluminesc. spectra 79−83022
- $Ga_{1-x}In_xSe$, exciton spectrum nature and anisotropy of electron bands near absorption edge *(Russian)* 79−51483
- GaN epitaxial layers, exciton cathodolum. *(Russian)* 78−76543
- GaN epitaxial layers, exciton cathode luminesc. 79−65933

excitons continued
- GaN, stimulated emission under high one and two quantum excitation 78−35171
- GaN:Al, VPE grown, luminesc. and elec. props. depend. on doping conc., bound excitons 80−20688
- GaP (110), surface excitonic binding energy for relaxed cleavage surface 78−91744
- GaP, anomalous photoeffect on connected excitons *(Russian)* 80−92929
- GaP, bound excitons in spherical model, low lying excited states 80−10883
- GaP, camel's back excitons, rel. to band structure 78−47707
- GaP, complex form of donor energy levels, optical spectra anal. 78−23045
- GaP, core exciton binding energies 80−80188
- GaP, core levels, temp. depend. of conduction band and core exciton energies 80−24828
- GaP, deformation potentials of direct and indirect absorpt. edges 79−69854
- GaP, donor states theory, camel's back struct. influence 80−59921
- GaP, electron-hole plasma luminesc. 79−38651
- GaP, excited 1s-level of S-bound excitons 79−82996
- GaP, fine struct. of indirect exciton 78−19509
- GaP, first order Mott transition of exciton gas 78−76535
- GaP, green luminesc. efficiency, review 77−28636
- GaP, ground state of indirect free exciton 77−51670
- GaP, hyperbolic singularity of dispersion law of excitons 79−42466
- GaP, indirect exciton dispersion, 'camel's back' 79−73447
- GaP, indirect exciton fine struct. in absorpt. spectrum, stress effects 79−42986
- GaP, indirect exciton fine struct. and effect of uniaxial stress 79−95805
- n-GaP, LPE, minority carrier bulk lifetime and diffusion coeff. meas. 77−11932
- n-GaP, LPE, non-radiative recombination 78−19565
- GaP, MCD of phonon-assisted exciton transitions 78−92053
- GaP, Mott transition of exciton gas, cathodoluminesc. 79−33845
- GaP, optical absorption and struct. of acceptor centres 78−48205
- GaP, piezo-modulated spectroscopic investigation of N and N-N pairs, bound exciton 77−66474
- GaP, reson. photoemission shake-up and Auger processes at 3p photothreshold 80−100748
- GaP, S-bound exciton stress depend. 80−29333
- GaP, shallow impurity states, free exciton binding energy 78−79960
- GaP, spectral depend. of O photoneutralisation cross-section near threshold, and band gap 79−1788
- p-GaP, spin-flip Raman scattering, review 80−108209
- GaP:Bi,N, photoluminesc., electroluminesc., 4.2 to 300K, excitons and hole traps 80−108275
- GaP:Bi(N), luminesc. decay kinetics 79−38646
- GaP:N, bound exciton absorpt. line asymmetry, electroabsorption spectra 80−71459
- GaP:N, bound excitons, low temp. photoluminesc. thermal quenching 77−48228
- GaP:N, excited states of excitons bound to NN_i pairs, fluoresc. obs. 77−44039
- GaP:N, photoluminesc., temp. depend., exciton recombination mechanism 78−88355
- GaP:N, radiative recomb. of electron-hole liq. 79−73442
- GaP:N, spin dependent exciton recombination at N_2 isoelectronic traps 77−69734
- GaP:N, temp. modulated photoluminesc. 77−55818
- GaP:N, temp.-modulated photoluminesc., phonon assisted tunnelling process 78−23511
- GaP:S, effects of uniaxial stress on luminesc. 79−78739
- GaP:S, ground and excited states of bound exciton complex, stress effects 80−65463
- GaP:S(Se), donor bound exciton excited states 80−66284
- GaP:S(Se)(Te), pot.-depend. g-values and quenched diamag., props. of donor states 77−62861
- GaP:S(Se)(Te), pot.-depend. g-values and quenched diamag., pseudoacceptors D^0, X 77−62862
- GaP:Zn,O, Auger coeff. from luminesc. decay and Hall effect 77−48226
- GaP:Zn,O, Auger coeff. from luminesc. efficiency and Hall effect 77−48227
- GaP:Zn,O LED, 76K electrolum, spectrum, γ-irrad, and forward bias effects 79−78756
- GaP:Zn(Mg)(Cd), multiple bound excitons, photoluminesc. obs. 79−95837
- GaP_xAs_{1-x}, N doped, alloying induced shift between excitation and luminesc. of N bound exciton 79−52013
- GaP_xAs_{1-x}:N, luminesc. of N bound state excitons, local-environment effects 80−100691
- GaS, electrolum. and electroabsorpt., 77K 77−48247
- GaS, indirect excitons *(Russian)* 77−89709
- GaS layer crystal, differential indirect exciton spectra 79−8159
- GaS, optical absorption edge under hydrostatic press. 78−23487
- GaS, optical detection of triplet excitons 80−29650
- GaS, reflectivity from 4 to 32 eV, Kramers-Kronig anal. 80−34943
- α-Ga_2S_3, defect semicond., optical absorption meas. 78−15186
- GaS(Se), absorpt. edge, exciton levels and Raman scatt., press. effects above 40 kbar 77−48187
- GaS(Se), reson. Brillouin scatt. 80−89010
- GaS_xSe_{1-x}, indirect exciton spectrum and phase transition, luminesc. and absorption spectra 79−8160
- GaS_xSe_{1-x}, recomb. radiation intensity, temp. depend. *(Russian)* 79−33830
- GaSb, bound excitons at doubly ionisable acceptors 79−42459
- GaSb, core exciton binding energies 80−80188
- GaSb, degenerate valence band, diamag. excitons and oscillatory magnetoabsorpt. 77−76754
- GaSb, electrorefl. spectra from 0.6 to 26 eV 77−20825
- GaSb, interaction of exciton recombination with LO phonons 79−38647
- GaSb, oscillatory magnetoabsorption and excitons 77−55777
- GaSe, absorpt. and electroabsorpt. near indirect edge 77−20827
- GaSe, absorpt. spectra, electron-hole system at high densities 77−69854
- GaSe and GaS_xSe_{1-x}, multiphonon reson. Raman scatt., excitonic transition 77−59574
- GaSe, anisotropy effects on electroreflectance spectra at oblique incidence 77−52042
- GaSe based layer crystals, three dimensional electron state nature near absorpt. edge 79−90960
- GaSe, cathodolum., 115 and 285K 79−87512

excitons continued
GaSe, deep free and constrained excitons and biexcitons, collective interactions *(Russian)* 80—66282
GaSe, direct exciton excited state hot luminescence, band struct. props. 80—55183
GaSe, electron beam excited free exciton luminesc. 79—19940
GaSe, electron-phonon interaction and optical props. 80—34942
GaSe, excitation spectra and structural props., X-ray Laue diagrams and optical transmission *(French)* 80—50358
GaSe, exciton, excitation-induced absorption and luminesc. 78—60516
GaSe exciton absorpt., change under a pulsed dye laser 78—92088
GaSe, exciton absorpt. spectra, additional light wave 77—63445
GaSe, exciton absorption under intense excitation 77—77235
GaSe, exciton absorption spectrum, polariton effects 77—85747
GaSe, exciton luminesc. kinetics, intermediate electron-hole states 80—93389
GaSe, exciton magneto-optical spectra 80—25347
GaSe, exciton spectra at 4.2K rel. to layer struct. 77—16336
GaSe excitonic spectra fine struct., reflection and transmission spectra *(Russian)* 80—55126
GaSe, fine struct. of exciton spectrum 78—39567
GaSe, highly excited, polarisation of luminesc. spectra and electron-hole plasma radiation 77—52169
GaSe, highly excited photoluminesc. exciton-exciton and exciton-carrier scatt. 77—48244
GaSe, interlayer interaction and exciton spectra study 77—52165
GaSe, lamellar crystal, exciton translational mass from magneto-Stark effect *(Russian)* 78—48153
GaSe, luminesc. emitted by electron-hole plasma 77—85795
GaSe, luminesc. from exciton-electron and exciton-exciton collisions 77—52168
GaSe, luminescence and absorpt. spectrum in region of high-energy resonance 77—44044
GaSe, magnetoluminesc. at 4.2K 79—61345
GaSe, optical detection of triplet exciton reson. 79—33567
GaSe, optical excitation, excitonic spectra, stimulated luminesc. 80—40132
GaSe, optical orientation and free exciton alignment on reson. excitation *(Russian)* 77—69812
GaSe, optical orientation and alignment of free excitons, on resonant excitation *(Russian)* 77—90196
GaSe, photolum. under strong optical excitation 79—24364
GaSe, photoluminescence between 4.2 and 40K 78—10974
GaSe, photovoltaic spectra 80—20240
GaSe, polarized exciton luminesc. 78—6734
GaSe, population dynamics and spin relax. of excitons 77—66122
GaSe, pressure-induced polytypic transforms. and edge absorpt., exciton lines 77—28595
GaSe, radiative decay of direct and indirect excitons 78—10975
GaSe, radiative transitions, cathodoluminescence 78—10997
GaSe, reflectivity from 4 to 32 eV, Kramers-Kronig anal. 80—34943
GaSe, reson. light scatt., luminesc. and Raman spectra 79—38615
GaSe, single cryst., dispersion of refr. indices and exciton absorption 79—73947
GaSe, spontaneous and stimulated emissions due to exciton-electron and exciton-exciton collisions 77—32421
GaSe, stacking disorder effect on Wannier excitons 77—62834
GaSe thin films, electroabsorpt. spectra, exciton line splitting 80—107716
GaSe, triplet excitons ODMR 80—25252
GaSe, triplet indirect bound exciton, level anticrossing effect on magnetolum. 79—47513
GaSe, type II crysts., triplet exciton resonances 79—47359
GaSe:Cu(Cd, Sb), photovoltaic spectra 80—20240
GaSe-SnO_2 heterojunction, elec. props. and electrolum. spectra 77—59328
$GaSe_{1-x}S_x$, polytypes, exciton gap energies, luminesc. study 80—54611
$GaSe_{1-x}S_x$, stimulated photoluminesc. excitons role 77—48201
$GaSe_xS_{1-x}$, layered semicond., electroabsorpt. in fundamental absorpt. edge region 77—52043
$GaSe_{0.9}Te_{0.1}$, undulation spectra associated with acceptor complexes 78—80392
$GaSe_{1-x}Te_x$, energy bands near absorpt. edge, transmission and photoluminesc. spectra 79—83022
$GaSe_{1-x}Te_x$, room temp. electroreflectance meas. 77—12361
$GaSe_xTe_{1-x}$ mixed crystals, excitonic structures, absorption spectra 79—61401
$GaSe_xTe_{1-x}$, solid solns., exciton luminesc. 78—10992
GaTe, exciton polariton effect on absorpt. edge, thickness depend. of absorpt. 80—20665
GaTe, excitonic absorpt. edge, transmission and refl. meas. 80—40133
GaTe, laser modulated reflectance meas. 77—63424
GaTe, single cryst. prep. and electroabsorpt. spectra investig. 80—103968
GaTe:Sn, electroabsorption spectra 79—19901
$GaTe_{1-x}Se_x$, exciton spectrum nature and anisotropy of electron bands near absorption edge *(Russian)* 79—51483
Ge, absorption edge, hydrostatic press. effects 77—43994
Ge, amorphous, possible ABB-type excitonic superconductor *(Chinese)* 80—7029
Ge, amorphous/cryst. interface, supercond. mechanism 80—44783
Ge, carrier relaxation rate temp. depend. and pair density in large electron-hole drop 80—75509
Ge, condensation of electron-hole drops in supersaturated gas of free excitons 77—69242
Ge, cyclotron reson., exciton and electron-hole drop diffusion coeffs. 77—48055
Ge, cyclotron resonance peaks under high excitation 77—48056
Ge, diamagnetic excitons, fundamental absorption edge, Faraday config. 79—8144
Ge, dispersion law of indirect excitons 80—24805
Ge, E_1-optical struct. from electroreflectance spectra 78—43897
Ge, elec. cond., optically injected carrier density and temp. depend. 78—68046
Ge, electron interaction with many excitons 78—26823
Ge, electron-hole drop and exciton atmosphere 80—6748
Ge, electron-hole drop formation, nucleation phenomena, free excitons 79—33240
Ge, electron-hole drop motion at low exciton densities 77—47865
Ge, electron-hole droplets, transient photoluminesc. intensities 78—88353
Ge, electron-hole drops, laser Doppler velocimetry 77—43504
Ge exciton and electron-hole drop decay, far IR magnetoabsorption obs. 77—40252

excitons continued
Ge, exciton condensate and electron-hole droplet, metastable state, effect of illumination and high-frequency heating 79—15097
Ge, exciton condensation, electron-hole drop investigation in UHF field, nucleation *(Russian)* 80—80193
Ge, exciton condensation, light scatt. by electron-hole drops 80—84435
Ge, exciton condensation, microwave cond. below 1K, book contrib. 80—8997
Ge, exciton condensation, microwave studies, book 80—10886
Ge, exciton condensation, microwave cond., book contrib. 80—11040
Ge, exciton condensation, microwave breakdown, luminesc., book contrib. 80—11471
Ge, exciton contrib. to oscillatory magnetophotocond. 79—15180
Ge, exciton effects on intervalence band transitions 77—4297
Ge, exciton energy gap and LA and LO momentum-conserving phonon energies 79—90965
Ge, exciton gas, entropy ionisation, luminesc. meas. 78—35196
Ge, exciton luminesc. polarisation in mag. field *(Russian)* 77—12436
Ge, exciton microwave breakdown, electron-hole drops, book contrib. 80—11041
Ge, exciton recombination with emission of single phonon, luminesc. replicas, detect. and anal. 79—60728
Ge, excitons, influence of temp. on high freq. breakdown in presence of electron-hole drops 78—26820
Ge, excitons bound to acceptors, Auger transition rates 78—34778
Ge, far IR magneto-absorption of donor-bound excitons, pseudo-acceptor model 77—63418
Ge, far IR magnetoabsorption, excitons, electron-hole drops and impurities 78—6664
Ge, far IR magnetoabsorption of free and bound excitons 78—52474
Ge, far-IR absorpt. spectra interpret. 77—40233
Ge, HF breakdown of excitons effect on kinetic of electron hole droplets *(Russian)* 77—59260
Ge, highly degenerate multicomponent plasma thermodynamic props., electron-hole drop transition 80—33739
Ge, highly excited, theory of electron-hole plasma 78—10363
Ge, indirect exciton excited states 78—30873
Ge, indirect excitons, photoexcitation spectra, 2.0-2.6 meV 77—44051
Ge, influence of dislocations on free-exciton lifetime 78—60064
Ge, interband Faraday ellipticity 78—92052
Ge, luminescence line shape of free exciton, electron-hole droplet binding energy 77—44041
Ge, luminescence meas., presence of trions, molecules and excitons above Mott density 77—80737
Ge, microwave absorption by nonequilib. current carriers, book contrib. 80—11042
Ge, microwave exciton breakdown and luminesc., under one- and two-photon excitation 77—31955
Ge, microwave exciton discharge, collision frequency, hot carrier temp. determ. *(Russian)* 79—65507
Ge, Mott transition of exciton gas in equilib. with electron-hole droplets 77—4298
Ge, nonequilibrium charge carrier-mag. field interaction electron-hole drops, recombination *(Russian)* 80—75511
Ge, optical absorption from indirect transitions at high mag. fields 79—47441
Ge, oscillatory exciton breakdown, microwave cond. 80—103716
Ge, partly dissociated excitons and impurity atoms system, collisional processes, charge transport theory 80—44581
Ge, phase diagram of electron-hole fluid in low temp. photoexcited semicond. 77—69237
Ge, phonon-assisted exciton emission, temp. depend. of relative integrated intensities 77—1375
Ge, pure, magnetic phase transition between electron-hole drops and free-excitons 78—6278
Ge, rest friction of electron-hole drops *(Russian)* 79—42463
Ge strain-confined large electron-hole drop characteristics 80—65469
Ge, strain-narrowing of luminesc. line from excitons 79—24356
Ge, stressed, α_1 and α_3 electron-hole droplet luminesc. 79—28820
Ge, stressed, recombination luminescence from hot carriers in electron-hole droplets 78—6754
Ge, stressed cryst., props. of strain-confined electron-hole liquid 79—7787
Ge, thermal relaxation time, laser heating effect at 1.3K , book contrib. 80—11519
Ge:As, recomb. of donor bound excitons, luminesc. intensity decay 80—25441
Ge:As(Bi), donor bound exciton luminesc. and absorpt. 80—29777
Ge:In (Sb) and pure cryst., kinetics of strain-confined large electron-hole drop and its clinging exciton system 80—75508
Ge:P, bound-exciton luminesc. and absorpt. 79—87469
n-Ge:Sb, exciton absorption 78—6688
GeO_2, tetragonal, exciton struct. in UV absorption edge 78—48199
GeS, electron-hole interaction in d-electron excitations, photoelectron and optical spectra 78—34776
GeS, exciton luminescence 78—52555
GeS, physical basis for Urbach's rule 80—93366
GeSe, optical absorption edge meas. 77—63430
$GeSe_2$ amorphous film, laser induced light absorpt. oscillation, exciton model 80—50446
$GeSe_2$ amorphous film, laser induced oscillatory phenomena 80—84711
$GeSe_2$, exciton absorpt., transmission spectra of cryst., glasses and amorphous samples 79—15485
H_2, cryst. ortho-para mixtures, vibr. coherence decay 80—78903
H_2 crystal, exciton states, intermediately bound-exciton theory 77—69234
H_2, solid, fundamental absorption spectra, 10 to 40 eV at 2K, using synchrotron radiation 79—73967
H_4, excited potential energy hypersurfaces, trapezoidal geometry, rel. to photochem. 2s+2s processes 77—30797
He:Xe, 0.04-0.1 g cm^{-3}, vac. UV absorpt. spectra, Wannier impurity states 77—77232
Hg fluid, expanded, optical absorpt., excitonic and continuum states 79—95801
$Hg_{0.75}Cd_{0.25}Te$, thermorefl. spectra, effect of excitons on E_1 and $E_1+\Delta_1$ structs. 80—16057
$Hg_{1-x}Cd_xTe$, acceptor bound exciton Auger and radiative transition rates, radiative recomb. 80—6733
$Hg_{1-x}Cd_xTe$, near band-gap photoluminesc., bound exciton luminesc. obs. 80—103973
HgI_2, cooperative fluoresc. by excitonic reson. pumping 79—33732
HgI_2, electrons and holes cyclotron reson. 78—72061
HgI_2, emission spectra in highly excited state 77—52167

excitons continued
HgI$_2$, exciton study by wave length modulated reflectivity, band parameters 77–51667
HgI$_2$, excitons, spectral obs. 78–23492
HgI$_2$, phonon-assisted recomb. of free electron-hole pair 78–23521
HgI$_2$, red, reson. Raman scatt. and luminesc. 78–84579
HgI$_2$, red, resonant Raman scatt. in B-exciton and band to band transition regions 79–61381
HgI$_2$, red anisotropic polariton dispersion, reson. Brillouin scatt. 80–7366
HgI$_2$, rel. to stimulated emission and optical gain, 80K 78–33738
HgI$_2$, stimulated emission at high exciton density, temp. depend. 78–84608
HgI$_2$, stimulated photoluminesc. excitons role 77–48201
α-HgS, green cathodoluminesc., impurity effects 78–2924
In$_{1-x}$Al$_x$P:Bi(N)(Zn,O) radiative recombination at isoelectronic centres 79–52027
InAs, fine struct. of diamag. excitons, oscillatory magnetoabsorpt. obs. 78–18971
InBr, metastable exciton emission, electron excitation mechanism 77–66546
In$_{0.53}$Ga$_{0.47}$As, interband magnetoabsorption study, quasi-Ge model application 80–50304
In$_{1-x}$Ga$_x$As$_y$P$_{1-y}$, oscillatory magneto-transmission, band parameters 79–60707
In$_{0.3}$Ga$_{0.7}$P, N free and implanted, photoluminescence study 80–97322
In$_{1-x}$Ga$_x$P:Bi(N)(Zn,O) radiative recombination at isoelectronic centres 79–52027
In$_x$Ga$_{1-x}$Se single crystals, exciton absorption spectra 80–20663
InI, orthorhombic, reflection spectra, exciton transition 79–24333
InP, deep trap study by free exciton refl. spectra 79–60761
InP, exchange interaction, analytical and nonanalytical parts, from polariton spectra in mag. fields 80–50367
InP, exciton localisation at impurity pairs 79–37999
InP, excitons bound to neutral donors in VPE layers, luminesc. and absorpt. obs. 79–42460
InP, free excitons in high mag. fields, band struct. 77–52129
InP, luminescence, hot electron effects 80–66277
InP, polar semiconductor, collisions between hot excitons and hot electrons 80–7415
InP, reflection spectra, optical functions, exciton peaks *(Russian)* 80–50372
InP:Bi, uniaxial stress effect on free and Bi-bound excitons 79–56854
InP-Au, Schottky barriers, electroreflectance spectra 77–43698
InSb, absorpt. edge, exciton struct. 80–93321
InSb, interaction of exciton recombination with LO phonons 79–38647
p-InSb, photoexcited exciton spin-flip scatt. 80–74434
p-InSb, spin-flip Raman scattering, review 80–108209
InSb-Au Schottky barrier, photovoltaic spectra and magneto-optical transitions, Landau levels and excitons 77–47858
InSe, direct gap exciton exam. by magneto-optics and photoconductivity 79–19527
InSe, exciton absorpt. spectra, additional light wave 77–63445
InSe, excitonic absorpt. edge 78–88352
γ-InSe, fundamental absorpt. edge 80–2781
InSe, high field magnetoabsorpt. of hydrogenic excitons at second direct gap 80–6729
InSe, layer cpd., reson. Raman scatt. at higher Mo exciton edge 79–28764
InSe, opt. props. new fundamental absorpt. edge 77–16330
InSe, optical props. near fundamental absorption edge 77–12434
InSe, photo-absorption of green exciton 80–80816
InSe, photoelec. props. 79–73543
InSe, reflectivity from 4 to 32 eV, Kramers-Kronig anal. 80–34943
InSe, spin orbit split off valence bands, exciton transitions, Hopfield's quasicubic model, visible absorpt. spectrum 80–50370
InSe, wavelength modulated optical absorption above fundamental edge 78–27255
IrF$_6$ neat and mixed cryst., exciton splitting, quenching by Jahn-Teller interaction 79–38540
KAg$_4$I$_5$, superionic film, elec. ionic cond. and electron spectra 80–6543
KBr, cation defects creation mechanism 80–75224
KBr, colour centre form. under polarised UV irrad., dichroism in absorption spectra 80–107232
KBr, decay and time resolved emission spectra from σ-excitons produced by heavy-ion irradiation 80–89071
KBr, heavy ion irrad., σ and π exciton emission spectra, 4.2K 78–76534
KBr, optical conversion, luminesc. and colour centre formation 79–24354
KBr, self-trapped exciton and F-centre form. 79–73443
KBr, self-trapped exciton form. via thermally induced defect reactions 80–60687
KBr, two photon absorpt., 2p excitons relax., F-centre 79–91462
KBr:I, energy transfer due to excitons and holes under host sensitization 79–15526
KBr:I, luminesc., exciton and hole migration to I$^-$ sites 79–38626
KBr:Li, radiative recomb. of localised excitons 78–72605
KBr:Li$^+$(Na$^+$), electronic struct. of (V$_K$e)$_A$ 78–95269
KBr:NO$_2$, Na effect of Na$^+$ impurity on self-trapped hole *(Japanese)* 78–67982
KBr:Na, exciton-like state disturbance in radioluminesc. *(Russian)* 77–85805
KBr:Na, X-irrad., luminesc. from self-trapped excitons 77–28614
KBr(Cl), X-ray irrad., tunnelling recomb. luminesc. 80–2873
KCN, ionic mol. cryst., exciton struct. 78–79935
KCN$_x$-KCl$_{1-x}$, finite-freq. local field catastrophe with appl. to spectra 79–51491
KCN$_x$Cl$_{1-x}$, finite field local field catastrophe phenomena in spectra 80–92830
K$^+$CN$_x^-$Cl$^-_{1-x}$, influence of structural disorder on exciton spectra 80–108224
KCl, axial shift of self-trapped exciton, semiempirical calc. 80–2339
KCl crystal, F-H centre formation by opt. conversion of self-trapped excitons 78–91335
KCl, F- and H-centre production by nonradiative decay of self-trapped exciton 78–23042
KCl, F-centre formation, short-pulse optical exam. of exciton relax. 79–42061
KCl, F-centre formation at highly excited triplet states of self-trapped excitons 80–76066
KCl, positronium states near defects in cationic sublattice 80–16121

excitons continued
KCl, self trapped exciton, off-centre configuration 79–42455
KCl, self-trapped exciton luminesc. 77–48225
KCl, self-trapped exciton, ENDOR 79–15377
KCl, X-ray irrad., thermoluminescence, TSC and thermal stability 79–95859
KCl:Cu$^+$, exciton bands, optical absorpt. and MCD spectra 80–80821
KCl:I, luminesc. at low temp. 80–2818
KCl:Na$^+$, self trapped excitons, optical absorption and emission 77–43503
KCl-KBr mixed crystal, containing defects, mag. quenching of positronium states 77–8680
KCl(Br), cation defects creation mechanism 80–75224
KCl(Br)(I), electronic struct. of self-trapped excitons calc. 77–39784
K$_2$CoF$_4$, 2-dimens. Ising antiferromag., mag. excitons, Raman scatt. obs. 80–66181
K$_2$CoF$_4$, two dimensional Ising antiferromag., mag. exciton energies determ. 77–12389
K$_2$CrCl$_4$, ionic ferromag., temp. depend. intensity in optical absorption 77–12399
KF, self-trapped exciton, ODMR spectra 79–28286
KF(Br)(Cl)(I), K$^+$3p core excitons, refl. spectra study, low temp. 80–29759
KI, edge emission of excitons 77–59606
KI, exciton diffusion, luminesc. quenching, meas. 4 to 77K 77–32433
KI, free exciton-F$^-$ centres interaction, electron excited emission 79–83036
KI, intrinsic luminesc. quenching, by X-ray induced coloration 78–19539
KI, luminesc. due to free excitons, line shapes 79–33803
KI, luminesc. lines due to n=2 free exciton state of Wannier series 80–29776
KI, luminesc. polarisation for free and bound excitons 78–10942
KI, piezo-optical study of excitons 80–16055
KI, self trapped exciton form. time at $^1\Sigma_u{}^+$ state under pulsed electron beam in ps range 80–97347
KI, self-trapped excitons and F-centres, picosec. range form., absorpt. bands 78–19515
KI, self-trapped exciton form. via thermally induced defect reactions 80–60687
KI, zero phonon and LO phonon assisted luminesc. of free excitons 79–28799
KI:Cu$^+$, exciton bands, optical absorpt. and MCD spectra 80–80821
KMF$_3$, M=Mg, Ni, Co, Mn, reflectivity, 8-60 eV, excitonic struct. 77–20871
KMgF$_3$, extreme UV spectra, 9-30 eV 78–23486
KMnF$_3$, antiferromag., multi-magnon luminesc. sidebands 78–76525
KMnF$_3$, antiferromag. cryst., luminesc. enhancement in mag. field, exciton model *(Russian)* 77–48214
KMnF$_3$, exciton and exciton-magnon emission 79–33779
KMnF$_3$, exciton dynamics by time resolved emission spectroscopy 80–54615
KMnF$_3$, exciton line and magnon satellite in UV spectrum at high press. *(Russian)* 79–4517
KMnF$_3$, stress-induced phase transition, optical props. meas. 77–20067
K$_2$MnF$_4$, quadratic layer antiferromag., intrinsic emission obs. 77–20906
KNiF$_3$ and K$_2$NiF$_4$, MCD and stress linear dichroism on double excitonic transitions 77–52051
KNiF$_3$, and K$_2$NiF$_4$, double-excitonic optical transition intensity, exchange and dimensionality effects 77–69591
KNiF$_3$, electronic UV laser excited Raman, scatt. by mag. excitons 78–68492
KNiF$_3$, K$_2$NiF$_4$, antiferromag., two-exciton transition 77–32398
K$_2$NiF$_4$, electronic UV laser excited Raman, scatt. by mag. excitons 78–68492
Kr atoms in Ne matrix, radiative and nonradiative lifetimes in excited states 80–69106
Kr, film, absorpt. in exciton region 78–52529
Kr, liquid, triplet state of self-trapped exciton states, evidence of existence, luminescence meas. 78–72608
Kr, liquid and solid, absorpt. and luminesc. spectra of self-trapped excitons 79–65893
Kr, solid, core excitons, integral eqn. formalism, isolated atoms and cryst. 78–47704
Kr, solid, n=1 surface excitons and LO-TO splittings of bulk excitons 79–73445
Kr, solid, self-trapped exciton, pseudopotential method 79–82529
Kr, solid, surface excitons 77–76892
Kr:N$_2$O, cryodeposited film, exciton-enhanced KrO excimer luminescence 77–36288
Kr:N$_2$O, photoluminesc. from KrO (^{1}S) excimers 78–68544
Kr:OCS, O(^{1}S) and S(^{1}S) photodissociative prod., photoluminesc. excitation spectra, exciton energy transfer 80–89508
LiD, luminesc. of free and localised excitons, UV, X-ray and electron irrad. luminesc. 79–87483
LiD(H), excitons and exciton-phonon interaction, refl. spectra meas. 4.9 to 5.3 eV 77–44019
LiF, crystal, electron emission under uniaxial compresssion 80–7483
LiF film, electronic excitations, inelastic electron scatt. spectra 77–32479
LiF, ground and excited state props., local density formalism 78–10349
LiF, R core exciton thermotransmission and absorpt. spectra, line shapes, forbidden and allowed excitons 79–73968
LiF, self-trapped exciton, ODMR spectra 79–28286
LiH (D), single crystals, electronic excitations, review *(Russian)* 78–72574
LiH, excitons, reflection, cathodolum. and photocond.-excitation spectra 78–10989
LiH, ionic cond., thermocurrent and photocond., defect and electronic props. 77–15621
LiH, luminesc. of free and localised excitons, UV, X-ray and electron irrad. luminesc. 79–87483
LiH, motion and relax. of free excitons, luminesc. spectra 79–43037
LiH, single crysts., refl. photolum., cathodolum., and photocond. meas. 77–52186
LiH, UV induced luminescence 77–85784
LiH:LiF, luminesc. of free and localised excitons, UV, X-ray and electron irrad. luminesc. 79–87483
LiH(D), isotope effect on Wannier-Mott exciton levels 80–103633
LiH(D), resonant Raman scattering in crystals with self-trapping excitons 80–7344

excitons continued
LiI crystal, emission spectra under UV-light excitation at 77K 78−92110
$Li_{1-x}K_xI$, intrinsic optical absorpt. spectra 78−23500
Li_3N, optical absorpt. coeffs., exciton creation, optical anisotropy 79−95796
$Li_{1-x}Na_xBr(I)$, intrinsic optical absorpt. spectra 78−23500
$LiNbO_3$, exciton migration, laser time-resolved spectra obs. 79−69861
$Li_{1-x}Rb_xI$, intrinsic optical absorpt. spectra 78−23500
MgF_2, cryst., Roentgenoluminesc., exciton emission *(Russian)* 78−95609
MgF_2, optical absortion following pulsed electron irrad., 100-500K 79−8164
MgF_2, transient absorption and luminesc. following electron beam excitation 77−69920
MgO, crystal, electron emission under uniaxial compresssion 80−7483
MgO, electronic band struct., combined tight-binding and pseudopot. approach 77−47728
MgO, electronic excitations and luminescence, review *(Russian)* 78−72575
MgO, exciton luminesc. spectrum, fine struct. 80−20715
MgO, single cryst., tribolum. obs. 79−52031
$MgO:Al^{3+}$, positron annihilation meas. 77−8681
MgO:Be epitaxial layers, vacuum UV luminescence 80−11480
MgO:Sn(Al), energy transfer in luminescent crystals 78−10998
$Mg_xZn_{1-x}Te$, temp. depend. of energy gap, near band gap reflectivity spectra 79−28786
$MnAs_{0.88}P_{0.12}$, excitonic absorpt., derivative refl. spectra 80−25406
$Mn_xCd_{1-x}Se$ single crysts., photoluminesc., composition depend. 80−80854
MnF_2, antiferromag., multi-magnon luminesc. sidebands 78−76525
MnF_2, fluorescence props. 79−73994
MnF_2, local mag. ordering above Neel point, EPR *(German)* 77−36125
MnF_2, MCD spectrum, Zeeman splitting of purely excitonic lines 77−40262
MnF_2, one-magnon luminesc. sidebands of excitonic transition 78−60517
MnF_2, two-exciton light absorption, with four-photon excitation *(Russian)* 78−35186
MnF_2, two-exciton many photon absorption, effect of statistical props. of light on intensity *(Russian)* 78−95589
$MnF_2:Eu^{3+}(Er^{3+})$, fluorescence props. 79−73994
MoF_6, cryst., overall vibr. band struct., excitons 77−90136
MoF_6 crysts., density of exciton states, two-particle and mixed cryst. spectra 78−2829
MoF_6, orthorhombic crysts., Raman spectra, int./external mode separation and factor group anal. 77−90135
MoS_2, 2H phase, far IR magnetoabsorption and refr. index meas. 77−24847
MoS_2, mag. circular dichroism 79−23900
$MoS_2(Se_2)$, effect of uniaxial stress on excitonic optical spectra 78−84606
$MoS_2(2H)$, electro-absorpt. edge spectra, cryst. thermal modulation, exciton state field ionisation 79−61395
$MoSe_2$, exciton spectra 80−97296
$MoSe_2$, mag. circular dichroism 79−23900
α-N_2, mol. cryst., theory of time evolution of exciton coherence 80−65455
α-N_2, solid, coherent loss of vibr. and librational excitations 79−86852
N_2, solid, exciton-phonon coupling in strong coupling limit, temp. depend. 80−92616
N_2, solid, UV spectra, phonon induced exciton fine struct. 79−15477
N_2, solid, vacuum UV luminesc., 8K 78−10958
NH_3, cryst., radiolysis yield, temp. effects, Arrhenius depend. 77−48662
NH_4Br, thermorefl. spectra, band energy anal. 77−12402
NH_4Br:Tl, and pure crystals, luminesc., VUV irradiated at 80K *(Russian)* 80−84763
NH_4Cl, thermorefl. spectra, band energy anal. 77−12402
NH_4I, thermorefl. spectra, band energy anal. 77−12402
NO, $3s\sigma(A^2\Sigma^+)$, in Ar Kr Xe matrices, Rydberg state ‘bubbles’, reson. fluoresc. obs. 77−83636
N_2O crystal, vibrational exciton bands, impurity modes 77−28560
NaBr(:I), exciton ionisation and decay, photoluminesc. in elec. field 77−44046
NaBr(Cl), F-centre formation, short-pulse optical exam. of exciton relax. 79−42061
NaCl, crystal, electron emission under uniaxial compresssion 80−7483
NaCl, electron and ion beam excited luminesc. spectra 79−52026
NaCl, exciton luminesc. obs. 77−12449
NaCl, excitons at $L_{II,III}$ absorption edge of Cl^-, decay characts. thermolum. meas. 77−28121
NaCl, luminesc. singlet from triplet self-trapped excitons 79−99936
NaCl, luminescence excited by vacuum UV lasers 78−10941
NaCl, mechanoluminesc. peaks, microbreakdown mechanism, generation of ionisation waves 79−33032
NaCl, optical conversion, luminesc. and colour centre formation 79−24354
NaCl, photoemission exam. of Na^+-2p core excitons 78−43982
NaCl, pure and doped, 20K X-ray irradiation, thermolum. and recovery processes 80−93412
NaCl, search for IR absorption by triplet self-trapped excitons 78−56473
NaCl, self-trapped exciton form. via thermally induced defect reactions 80−60687
NaCl:Ag, irrad. with synchrotron radiation, thermolum. light-sum spectrum of L absorpt. edge of Cl^- 79−15540
NaCl:Ag, thermolum. light sum storage by ultrasoft X-rays 77−20939
NaCl:Br, host-sensitized luminesc., energy transfer due to excitons and holes 79−38590
$NaCl:Ca^{2+}$, X-ray induced luminescence 78−23516
NaCl(Br), X-ray or UV irradiated, cation defects creation mechanism 80−75224
NaF, self-trapped exciton, ODMR spectra 79−28286
NaI and $NaI:Tl^+$, intrinsic and impurity induced luminesc., exciton diffusion 77−16367
NaI, exciton luminesc., characteristics near absorption edge 78−88363
NaI, luminesc. polarisation for free and bound excitons 78−10942
NaI, motion of free excitons and their self-localisation 80−2342
NaI, resonant Raman scattering in crystals with self-trapping excitons 80−7344
NaI, thermal dissoc. of photoproduced excitons at UV band edge, recomb. luminesc. obs. 80−50412

excitons continued
$NaMgF_3$, extreme UV spectra, 9-30 eV 78−23486
$NaMnCl_3$, antiferromagnet, exciton self-localisation luminesc. and excitation spectra *(Russian)* 80−11456
$NaMnCl_3$, antiferromag. insulator, self-trapping of excitons 80−70619
$NaNO_2$, cryst., delayed fluoresc., triplet excitons, dopant effects 78−10963
$NaNO_2$, cryst., triplet excitons, localised states, zero-field ODMR, dopant effects 78−15062
$NaNiF_3$, electronic UV laser excited Raman, scatt. by mag. excitons 78−68492
Na_xWO_3, cubic, final-state effects in XPS 77−90251
$NbS_2Cl_2(Br_2)(I_2)$, absorpt. edge spectrum, fine struct. 80−66219
$^{93}Nb(n,\gamma)^{94}Nb$, $E_n=14.1$ MeV, γ emission exciton model *(Russian)* 79−13302
Ne, crystalline, Frenkel exciton calc. 79−23906
Ne, crystalline, self-localized exciton, cavity radius, wave function and energy 80−6737
Ne, liquid and solid, absorpt. and luminesc. spectra of self-trapped excitons 79−65893
Ne, solid, bulk and surface excitons, transmission and refl. spectra obs. 79−95340
Ne, solid, bulk excitons, expt. 80−92827
Ne, solid, bulk excitons, theory 80−92826
Ne, solid, doped with Xe and benzene, energy transfer 77−32416
Ne, solid, large-gap insulator, valence excitons, integral eqn. method calc. 77−11858
Ne, solid, lattice relax. model of n=1 exciton emission 79−47492
Ne, solid, n=1 surface excitons and LO-TO splittings of bulk excitons 79−73445
Ne, solid, pure and Xe, Kr, Ar doped, photoemission yields and reflectance spectra, exciton dynamics 77−28123
Ne, solid, quasi-line emission in transitions between excited states *(Russian)* 79−91494
Ne, solid and gaseous, excitons 78−23026
Ne:Ar(Kr)(Xe), luminesc. in vacuum-UV excitation of guest atoms by free and relaxed excitons 79−15519
Ne:H, exciton states and L_α,L_β emission 80−93372
$Ne:O_2$ (N_2), long-wave UV luminesc. *(Russian)* 78−88347
Ne:Xe, liq., 0.1-0.65 g cm^{-3}, vac. UV absorpt. spectra, Wannier impurity states 77−77232
Ne:Xe film, solid, competition between electronic energy transfer and relax., photoelectron spectra 77−24929
Ne:Xe(Ar), electronic relax. cascades in Wannier and Frenkel type exciton states 79−33759
Ne_2, solid, a priori calc. of n=1 valence exciton 78−10364
NiF_2, electronic UV laser excited Raman, scatt. by mag. excitons 78−68492
α-O_2, antiferromagnetic polycrystal, splitting of exciton absorpt. lines in mag. field *(Russian)* 80−103943
α-O_2, cryst., exciton, exciton-magnon, and biexciton absorpt. at 1.5K 80−84750
α-O_2, cryst., exciton effects, spectra *(Russian)* 79−47481
α-O_2 crystals, spin ordering effect on light absorpt. *(Russian)* 80−89029
α-O_2 crysts., absorption band at 1.3K, $^1\Sigma_u^- \leftarrow {}^3\Sigma_g^-$ transition *(Russian)* 77−48186
α-O_2, elementary excitations, effect of mag. anisotropy *(Russian)* 78−76317
O_2 isotopically mixed crystals, IR absorption spectra (7000-15000 cm^{-1}) at 1.5K *(Russian)* 77−32362
OCS, lattice dynamics and phonon sidebands of vibr. excitons calc. 77−20028
Pb halides, above-edge cathodolum. from metastable excitons 78−6786
$PbBr_2$, metastable exciton emission, electron excitation mechanism 77−66546
$PbBr_2$, reflectance spectra, exciton peaks 77−24870
$PbBr_2$, single cryst., photolum. meas. 77−69882
$PbBr_2(Cl_2)$, exciton spectra, temp. and press. effects 77−20881
$PbBr_2(Cl_2)$, light sensitive material, regularities in exciton states 77−20885
$PbCl_2$, metastable exciton emission, electron excitation mechanism 77−66546
$PbCl_2$, single cryst., photolum. meas. 77−69882
$PbCl_2$:NaCl, trapped exciton states, absorption spectra 80−50383
$PbCl_{2-2x}Br_{2x}$, luminesc. and reflection spectra *(Russian)* 80−84762
$PbCl_{2-2x}I_{2x}$, orthorhombic, absorpt. spectra 77−59633
PbF_2 optical props. 77−32394
β-PbF_2, single cryst., photolum. meas. 77−69882
PbFBr(Cl), reflectance spectra, exciton peaks 77−24870
PbFCl, single cryst., photoluminesc. 77−16375
$PbF_2(Cl_2)(Br_2)$, lowest exciton states 78−72082
$Pb_{1-x}Ge_xTe$, ferroelectric phase transition effect on forbidden band width 80−24794
PbI_2 (2H), angular depend. magnetoluminesc. 79−43029
PbI_2 (2H), layer cpd., band parameter determ. 79−95332
PbI_2 (2H), photolum. spectrum, in strong photoexciton mixing region 78−48223
PbI_2, cooperative fluoresc. by excitonic reson. pumping 79−33732
PbI_2, cryst., photochem. phenomena investig. *(Russian)* 78−35204
PbI_2 crystals, exciton condensation, excitation and luminesc. study 80−55182
PbI_2 direct gap polar semicond., electron hole liquid phase diagram *(Russian)* 80−93314
PbI_2 direct gap semiconductor, exciton lifetime and condensation threshold, luminescence spectra 80−34981
PbI_2, electronic struct. and exciton problem, photoelectron spectra meas. 77−63540
PbI_2, emission spectra, 80K, high excitation intensity effects at different pump wave lengths 77−52170
PbI_2, exciton absorpt. band shape, dielectric const. real part derivatives *(Russian)* 80−25413
PbI_2, exciton magneto-optical spectra 80−25347
PbI_2, exciton spectra depend. on strong excitation, crystal transmission 79−69433
PbI_2, exciton states, high field magnetoabsorption 77−52130
PbI_2, excitonic shifts of quasiatomic optical core to cond. band transitions, UPS obs. 78−11079
PbI_2, excitons in spatially dispersive medium, absorption theory 80−54618

excitons continued
PbI_2, film, fundamental absorption edge, complex dielec. const. *(Russian)* 77—40266
PbI_2, film, highly excited, oscillator strength of excitons, absorpt. and emission spectra 78—76001
PbI_2, film, spectral depend. of optical consts. on fundamental absorption edge *(Russian)* 77—16415
PbI_2, film exciton spectrum, Faraday rot. 77—20944
PbI_2, film intercalated with pyridine, UV absorpt. spectrum, Frenkel excitons 77—24864
PbI_2, first-order 2H-4H polytype transition, exciton spectroscopic study 80—59647
PbI_2 laminar semicond., phase transition of first kind by exciton spectroscopy *(Russian)* 79—82334
PbI_2, layered compound, exciton spectra, surface and stacking fault effects 80—40134
PbI_2, layered cryst., photoluminesc., and reflection spectra obs. 78—6726
PbI_2, longitudinal-transverse splitting of anisotropic excitons 78—2431
PbI_2, metastable exciton emission, electron excitation mechanism 77—66546
PbI_2, optical props. 77—32394
PbI_2, photocond. induced by polaritons at band-edge 79—95450
PbI_2, photoexciton interaction, luminescence spectra, polariton dispersion diagram 80—93397
PbI_2, photoluminesc. spectra, generation of stimulated radiation 77—8647
PbI_2, press. depend. of band-gap excitons, 77K, optical absorpt. spectra 79—8157
PbI_2 single crysts., resonant and nonresonant Raman spectra 77—69823
PbI_2, stimulated photoluminesc. excitons role 77—48201
PbI_2, two-photon absorpt. spectrum 77—52118
PbI_2:KI, trapped exciton states, absorption spectra 80—50383
PbI_2-Ag system, effect of bound and free exciton states on light sensitivity *(Russian)* 78—71169
PbI_2-$PbBr_2$, optical spectra, solid soln. struct. 78—48247
PbO, single crysts., exciton and impurity luminesc. 80—60674
PbO, visible absorpt. spectra rel. to indirect exciton transitions 80—60628
Pr, magnetic ordering due uniaxial stress, mag. excitons by neutron scatt. 78—84467
PrSb, mag. excitations, press. depend., inelastic neutron scatt. meas. 78—10699
PrSb, pressure-induced antiferromag., neutron scatt. study 80—39750
Pr_3Tl, exchange-coupled singlet-groundstate system, central model 77—77060
$Pt(NH_3)_4SO_4$, cryst., absorption spectrum *(French)* 79—28784
Rb halides, high-resolution spectroscopy in far UV 77—66484
$RbAg_4I_5$ superionic films, elec. cond. and optical absorpt. studies 79—99355
RbBr (I), optical absorpt. centre formation time meas. 80—40081
RbBr, self trapped exciton form. time at $^1\Sigma_u^+$ state under pulsed electron beam in ps range 80—97347
RbBr, two photon absorpt., 2p excitons relax., F-centre 79—91462
RbCl(Br), cation defects creation mechanism 80—75224
$RbCoF_4$, 2-dimens. Ising antiferromag., mag. excitons, Raman scatt. obs. 80—66181
Rb_2CrCl_4, optical absorption intensity, short-range spin correlation 80—108185
Rb_2CrCl_4, zone centre magnon gap determ., exciton-magnon combination band meas. 79—61082
RbF-CsF, solid solution, fundamental absorption 79—11433
RbI, edge emission of excitons 77—59606
RbI, intrinsic luminesc. quenching, by X-ray induced coloration 78—19539
RbI, two photon absorpt., 2p excitons relax., F-centre 79—91462
RbI, zero phonon and LO phonon assisted luminesc. of free excitons 79—28799
$RbMnCl_4$, quadratic layer antiferromag., intrinsic emission obs. 77—20906
Rb_2MnCl, layer antiferromag., optical absorpt., temp. and mag. field depend. 80—20661
$RbMnF_3$, antiferromag., multi-magnon luminesc. sidebands 78—76525
$RbMnF_3$, exciton and exciton-magnon emission 79—33779
$RbMnF_3$, reflectivity, 8-60 eV, excitonic struct. 77—20871
$RbNiF_3$ and Rb_2NiF_4, MCD and stress linear dichroism on double excitonic transitions 77—52051
Ru complex, Ru(2,2′-bipyridine)$_3Cl_2$-$6H_2O$, photocond., optical absorpt. and fluoresc. 77—80807
S, orthorhombic, photogeneration of charge carriers 80—107844
SbI_3 film, exciton peaks, temp. depend., 90-270K, and press. depend., up to 3500 atm. 77—36265
SbI_3, layered compound, exciton spectra, surface and stacking fault effects 80—40134
SbI_3, refl. spectra of cryst., 300-800nm, and derived optical consts. 79—87456
Se, exciton luminesc. in trigonal form 79—33802
Se, trigonal, cathodolum. at 10K *(German)* 78—2923
Se, trigonal, indirect exciton ground states, photoluminescence 79—24361
Si (111) 7×7 surface, giant core-exciton effects, electron energy loss spectra and XPS 77—24600
Si (2p) optical transitions, final state effects, soft X-ray electroreflectance study 77—66553
Si, amorphous, electron-hole recombination, mech. 78—72196
Si, amorphous, phonon interaction in luminescence 78—43927
Si, amorphous, photo-induced changes in elec. props., defect states 79—82553
Si, amorphous, possible ABB-type excitonic superconductor *(Chinese)* 80—7029
Si, amorphous/cryst. interface, supercond. mechanism 80—44783
Si, Auger recombination, localized and free carrier comparison 79—38090
Si, bound exciton lifetimes for acceptors 77—80738
Si, bound exciton-dopant Auger lifetimes 78—18970
n-Si, bound excitons and bound multiexciton complexes, excitation spectra 80—96792
Si, bound-exciton spectral lines, conc. broadening at high impurity concs. 80—80826
Si, continuum-exciton effect in optical spectrum 80—25416
Si, core exciton binding energies 80—80188
Si, core levels, temp. depend. of conduction band and core exciton energies 80—24828

excitons continued
Si, deformed, recomb. radiation from electron-hole drops and free excitons 77—8641
Si, diamagnetism of excitons and biexcitons, recomb. spectra *(Russian)* 80—7412
Si, dispersion law of indirect excitons 80—24805
Si, donor bound excitons and bound multiexciton complexes 77—40282
Si, electron-exciton elastic scatt. cross sections, central field and exchange approxs. 77—62919
Si, electron-exciton inelastic collision cross sections 79—90967
Si, electron-hole liquid, free excitons, biexciton gas, luminesc. 80—6750
Si, electron-hole liquid, spatial condensation of strain-confined excitons and excitonic mols. 78—39592
Si, electron-hole liquid and exciton and biexciton gas in elastically deformed cryst. *(Russian)* 78—34782
Si, emission spectra, excitons bound to isoelectronic trap 79—33772
Si, exciton and deformation pot. fine struct. 78—88301
Si, exciton ground state splitting 80—6736
Si exciton luminescence in mag. field or under uniaxial stress 78—27322
Si, exciton-impurity complexes, emission spectra, Zeeman splitting *(Russian)* 78—64413
Si, exciton-plasma Mott transition, luminescence spectra 77—62836
Si, excitonic molecules, thermodynamics, luminesc. 80—25442
Si, excitons, far IR absorption 78—31201
Si, excitons and electron-hole drops, phonon assisted luminescence lineshape 79—99942
Si, excitons and electron-hole liquid, luminesc. 80—6746
Si, excitons bound to acceptors, Auger transition rates 78—34778
Si, fine structure of lowest exciton state *(Russian)* 80—96801
Si, free excitons, drift and diffusion, luminesc. obs. 80—84434
Si, ground state of indirect free exciton 77—51670
Si, H_2^+ irrad., annihilation of free excitons, inelastic scatt. by SiH_4 mols., photolum. obs. 78—19561
Si, high purity, exciton lifetime, temp. depend., photoluminesc. meas. 80—44508
Si, highly excited, theory of electron-hole plasma 78—10363
Si, hole localisation, solid solubility, excitonic Auger lifetime of acceptors 80—20216
Si, impurity content characterisation, exciton luminesc. 80—60653
Si, impurity doping influence on free-exciton absorpt. 77—69861
Si, impurity states and core excitons, binding energies, perturb. theory 80—49659
Si, intrinsic, radiative recombination probability *(German)* 79—61441
Si, intrinsic, two-phonon assisted free exciton recomb. radiation 78—2922
Si, LO and TO phonon assisted free exciton luminesc. 79—33833
Si, luminesc., simultaneous kinetics of drops and excitons during drop formation 77—48222
Si, luminescence of multiparticle exciton-impurity groups 79—83003
Si, mass-anisotropy exciton splitting determ. 78—6685
Si, multiple band excitons, binding-energy calc. 78—34775
Si, non-equilib. orientation of electrons in electron-hole droplets in mag. field *(Russian)* 77—36294
Si, nonradiative recombination and luminesc. 79—33770
Si, obs. of cyclotron reson. absorptions due to excitonic ion and excitonic mol. ion 77—73082
Si, optical excitations, many particle effects 79—87046
Si, optical spectrum, many particle effects, band struct. 80—89024
Si, phonon induced intervalley transitions, violation of selection rules 78—30875
Si, phonon-assisted exciton emission, temp. depend. of relative integrated intensities 77—1375
Si, photoexcited, highly stressed, electronic Raman scatt. and antireson. 80—29737
Si, plastically deformed, hot-exciton luminesc. as function of strain 78—88361
Si, polarisation of recombination radiation from multiparticle exciton-impurity complexes, induced by uniaxial deform. *(Russian)* 79—78754
Si, pure and heavily doped, 2p core levels and core exciton binding energy, photoemission obs. 78—76583
Si, recombination luminescence, electron-hole drop, excitons orientation in mag. field 78—88362
Si, role of electron-hole interaction in optical spectra, review 80—45113
Si, shallow impurities, photolum. anal. 78—23512
Si, splitting of 1s excitons, derivative spectra of optical absorption 77—69249
Si, surface space charge layer, anisotropic and tilted valley systems, absorption 77—85726
n- Si, surface space-charge layer, intersubband-cyclotron combined reson. 78—68063
Si, uniaxial stress effects and excited states for multiple bound excitons 78—6281
Si: Li, absorpt. and luminesc. transitions involving exciton excited hole states 79—78038
Si:Al, bound exciton and bound multiexciton complexes, electronic structure, luminesc. obs. 79—56139
Si:Al, bound exciton and multiple bound electron luminesc., fine struct. 77—48221
Si:Al, bound-exciton absorption 78—56507
Si:Al, localised exciton bound to isoelectronic trap 80—66283
Si:Al, valley-orbit splitting of bound exciton states 79—28290
Si:Al(B)(P), bound multiexciton complexes, work function thermodynamic determ. 78—72078
Si:As(Li)(P), luminesc., stress effects on donor exciton satellites 77—85786
Si:As(Sb)(Bi)(P), luminescence associated with transitions from bound exciton excited states 78—23534
Si:B, antiferromagnetic ordering of holes, recombination radiation polarisation *(Russian)* 80—45121
Si:B, bound many-exciton complexes, luminescence spectra, mag. props. 80—103994
Si:B, bound multiexciton luminesc., recomb. kinetics 79—38591
Si:B, many-body exciton-impurity complexes, stress depend. of photolum. meas. 79—28833
Si:B,In, sharp line series in near-band-edge photolum. 80—16092
Si:B recombination emission polarisation of bonded multiple-exciton complexes in mag. field *(Russian)* 78—2905
Si:B(Al)(Ga)(In)(Tl) luminescence spectra, bound exciton lines, fine structure 78—15233
Si:B(Ga), even-parity acceptor excited states, bound exciton two hole transitions 77—85793

excitons continued
Si:B(P), recombination spectra of bound multiexciton complexes, Zeeman splitting *(Russian)* 79−38526
Si:B(P), uniaxially stressed, impurity-assisted intervalley scatt., photoluminesc. obs. 80−34979
Si:Ga, bound-exciton absorption 78−56507
Si:Ga(Al), edge luminesc. spectra of acceptors, multiexciton complexes 78−56517
Si:In, bound exciton photolum. obs. 78−95607
Si:In, bound-exciton absorption 78−56507
Si:In, capture cross section of excitons on neutral In impurities, photoluminesc. decay 78−6760
Si:K, bound exciton luminescence in mag. field *(Russian)* 80−108278
Si:I, obs. of donor exciton in far IR transmission meas. 79−91477
Si:Li, bound exciton complexes associated with Li, photolum. meas. 79−28823
Si:Li, luminesc. of bound exciton and bound multiexciton complexes 79−28821
Si:Li, photolum. of bound exciton and bound multiexciton complex, Zeeman effect 80−108265
Si:P, absorpt. due to creation of bound excitons 78−23025
Si:P, acceptor bound multiexciton complex recomb., shell model, luminesc. line splitting 78−6275
Si:P, bound exciton and multiexciton complex struct., luminesc. obs. 77−81138
Si:P, excitation density depend. of cathodoluminesc. from bound multiexciton complexes 78−72609
Si:P, exciton complexes bound to impurities, resolved fine structure 77−62843
Si:P, exciton two-electron luminesc., temp. and impurity-conc. depend. 78−39585
Si:P, expt. evidence against shell model of bound multiexciton complexes 78−10368
Si:P, heavily doped, IR bound-exciton luminesc. spectra 78−15211
Si:P, luminesc. lines, multiexciton complexes and unaixial stress 78−92114
Si:P, luminescence circular polarisation, emission by many exciton complexes 80−93398
Si:P, model for exciton bound to donor pair, photolum. data anal. 79−51498
Si:P, photolum. obs. of donor pairs 79−52014
Si:P, satellite of bound excitons, transient decay 80−11466
Si:P, temp. depend. of anomalous struct. in wavelength-derivative absorption spectra 77−52143
Si:P bound multiexciton complexes, expt. evidence for shell model 78−39036
Si:P(B), multiple-particle exciton-impurity complex form. *(Russian)* 78−43925
Si:Sb(As)(P), bound excitons and bound multiexciton complexes for shallow donors, luminesc. meas. 79−24363
Si:Tl, optical absorption and photolum. of bound exciton 78−88359
α-SiC, 6H, excited states, photoluminesc. efficiency 78−39604
SiC, (6H), radiation damaged, luminesc. 80−25462
β-SiC, cubic, conduction band minima location and shape determ. 77−85141
SiC, donor exciton satellites, multiple bound excitons 77−11857
SiC, laser Raman spin-flip scatt. from excitons, luminesc. 80−80786
SiC polytypes, free exciton luminesc. meas., phonon energies 80−80852
p-SiC, spin-flip Raman scattering, review 80−108209
SiC, spin-flip scatt. of laser light from photoexcited excitons 80−93330
SiC, struct. of spectrum of excitons bound to neutral B atoms 78−19523
p-SiC:B (4H), absorption spectra of bound excitons 78−88338
Si_3N_4-GaAs structure, photoluminesc. and collective effects 78−6727
SiO_2, amorphous, optical and elec. props., comparison with chalcogenide semiconds. 78−6721
SiO_2, core levels, temp. depend. of conduction band and core exciton energies 80−24828
SiO_2, exciton study, luminescent centres as exciton detectors 80−66278
SiO_2, film, diode expt. for detecting photoluminescence and excitons 79−73540
SiO_2, fused, broken bond defect generation mechanisms 80−88044
SiO_2 glass, electronic struct. and optical props. 80−2790
SiO_2 in MOS struct., exciton transport rel. to surface states 78−34901
SiO_2, intrinsic luminescence 80−16098
SiO_2 monolayer, core excitons and inner well resonances in surface soft X-ray absorpt. spectra 80−40187
SiO_2, vitreous, exam. of electron excitations and intrinsic defects 78−87905
SiO_2, vitreous, photoelectric and photoluminescent props. in fundamental absorpt. region 78−39596
$Sm_{1-x}Ca_xS$, XPS, electronic struct. excitonic effects, insulator to metal transition 78−43988
$Sm_{1-x}Gd_xS$, XPS, electronic struct. excitonic effects, insulator to metal transition 78−43988
$Sm_{1-x}Th_xS$, XPS, electronic struct. excitonic effects, insulator to metal transition 78−43988
$Sm_{1-x}Y_xS$, XPS, electronic struct. excitonic effects, insulator to metal transition 78−43988
SnI_2 band struct., layer model 80−44501
SnI_2 film, absorpt. spectrum *(Russian)* 79−43056
SnI_2, single crysts. and film, optical props. 77−32437
SnO_2 defective crystals, exciton-impurity complex luminescence spectra *(Russian)* 79−65926
SnO_2, exciton luminescence spectra, absorpt. spectra 80−89064
SnO_2, rutile, band gap assignment by two-photon spectroscopy 79−19513
SnS, electron-hole interaction in d-electron excitations, photoelectron and optical spectra 78−34776
$SrCl_2:Cu^+$, exciton bands, optical absorpt. and MCD spectra 80−80821
SrO, logarithmic derivative reflectance spectra 80−11429
SrO, luminesc. band edge, 4-6.5 eV, optical absorpt., photoluminesc., cathodoluminescence, photocond. obs. 80−50411
SrO, single cryst., tribolum. obs. 79−52031
SrO, surface states, refl. spectra, impurity effects 77−20873
$SrTiO_3$, energy band struct., two-photon absorption spectra study 80−15453
TCNQ salts, mag. props. 77−43869
$TTF.CuS_4C_4(CF_3)_4$, spin-Peierls system, nucl. spin-lattice relax. process 78−19361
$Tb(OH)_3$, exciton dynamics within an inhomogeneously broadened line, luminesc. spectra 80−50407

excitons continued
$Tb(OH)_3$, sign of energy dispersion of one dimens. excitons, time resolved spectroscopy 77−1377
TbP, mag. excitations above antiferromag. ordering temp., inelastic neutron scatt. obs. 80−50112
TbP, magnetic Γ_1-Γ_4 exciton, inelastic neutron scatt. study 80−11159
$Tb_xY_{1-x}PO_4$, H_2 VUV laser excitation, fluoresc. decay characts. 78−60510
$^{159}Tb(n,\gamma)^{160}Tb$, $E_n = 14.1$ MeV, γ emission exciton model *(Russian)* 79−13302
Te, simultaneous absorpt. of three photons, selection rule, exciton peak on absorpt. edge 78−43303
ThF_4, 5d X-ray spectra 78−88382
ThO_2, 5d X-ray spectra 78−88382
TiO_2, exciton luminescence spectra, absorpt. spectra 80−89064
TiO_2, fine struct. in intrinsic absorpt. edge 79−42987
TiO_2, resolved quadrupolar transition, absorpt. spectra obs., 1.6K 78−27259
$TiSe_2$, UPS, excitonic instability indicated from study of band struct. 78−56069
Tl halides, polar semicond., binding energy of Wannier excitons 77−69232
TlBr, electromodulation spectroscopy of excitons 79−73444
TlBr, hot-exciton effects, luminesc. excitation spectra 77−32434
TlBr, phonon struct. of forbidden-indirect transitions 79−61393
TlBr, piezoreflectance of first exciton band obs. 78−64347
TlBr, reson. Raman scatt., forbidden one phonon and intervalley scatt. at direct exciton 80−45073
TlBr, resonant polaron coupling and excitons under mag. field 80−71383
TlBr, two indirect excitons decay to direct and indirect excitons 77−44058
TlBr(Cl), light sensitive material, regularities in exciton states 77−20885
TlCl, electromodulation spectroscopy of excitons 79−73444
TlCl, hot-exciton effects, luminesc. excitation spectra 77−32434
TlCl, magnetoreflectance of $X_6^+ \times X_6^-$ exciton meas. 79−38525
TlCl, phonon struct. of forbidden-indirect transitions 79−61393
TlCl, piezoreflectance of first exciton band obs. 78−64347
TlCl, piezoreflectance spectra of first exciton band 77−12357
TlCl, role of electron-hole interaction in optical spectra, review 80−45113
TlCl, two indirect excitons decay to direct and indirect excitons 77−44058
TlCl, Urbach rule at excitonic absorpt. edge, theoretical model tests 80−50299
TlCl-TlBr mixed crystal, reflectivity spectra meas. 77−85743
TlCl(Br), Wannier exciton-ionised donor complexes, binding energy calc. 80−49609
$TlGaS_{2x}Se_{2(1-x)}$, solid soln., fundamental optical absorpt. edge 80−25408
$TlGaS_xSe_{2-x}$, optical and photoelectric props., composition depend. 79−15183
TlI with CsCl struct., exciton magnetoabsorption 77−28593
$TlInS_xSe_{2-x}$ solid solution, optical and photoelectric props. 79−11179
UF_6, cryst., overall vibr. band struct., excitons 77−90136
UF_6 crysts., density of exciton states, two-particle and mixed cryst. spectra 78−2829
UF_6, orthorhombic crysts., Raman spectra, int./external mode separation and factor group anal. 77−90135
UO_2 complexes, cubic crysts., low temp. optical spectra *(Russian)* 78−92083
USb, neutron inelastic scatt. meas., phonon spectra, mag. response, anisotropy 80−50065
WF_6, cryst., overall vibr. band struct., excitons 77−90136
WF_6 crysts., density of exciton states, two-particle and mixed cryst. spectra 78−2829
WF_6, orthorhombic crysts., Raman spectra, int./external mode separation and factor group anal. 77−90135
WS_2 films, exciton peaks in absorpt. spectra, press. and temp. depend. 79−51496
WS_2, mag. circular dichroism 79−23900
$WS_2(Se_2)$, effect of uniaxial stress on excitonic optical spectra 78−84606
WSe_2, mag. circular dichroism 79−23900
WSe_2, refl. spectra and photovoltaic effect, 1.5-3.2 eV, 4.1-300K 79−47470
Xe atoms in Ne matrix, radiative and nonradiative lifetimes in excited states 80−69106
Xe, condensed electron beam excited, exciton radiative lifetimes 80−6727
Xe, crystal, edge hot emission, free exciton luminesc. *(Russian)* 79−15520
Xe, crystalline, polariton effects, reflectivity, absorpt., and resonant luminesc. spectra calcs. 80−20095
Xe, liq., UV reflection spectra, density depend., excitonic band evolution 77−77246
Xe, liquid, ionisation and scintillation, application to radiation detectors, review *(Japanese)* 78−35206
Xe, liquid, triplet state of self-trapped exciton states, evidence of existence, luminescence meas. 78−72608
Xe, solid, core excitons, integral eqn. formalism, isolated atoms and cryst. 78−47704
Xe, solid, luminesc. from self trapped excitons (excimers) 79−1785
Xe, solid, n=1 surface excitons and LO-TO splittings of bulk excitons 79−73445
Xe, solid, self-trapped exciton, pseudopotential method 79−82529
Xe, solid, self-trapped exciton emission bands 80−20697
Xe, solid, surface excitons 77−76892
Xe, solid, synchrotron irradiation pulse excitation photoluminesc. decay, exciton generation 78−6746
$Xe:N_2O$, photoluminesc. from XeO (^1D) excimers 78−68544
$YAG:Ce^{3+}(Eu^{3+})(Gd^{3+})(Tb^{3+})$, cathodoluminesc. efficiency rel. to activator conc. 80−11479
$YCrO_3$, antiferromag., exciton absorption lines obs. during field induced spin-reorientation 77−63397
Y_2O_3, autolocalised excitons *(Russian)* 79−19523
Y_2O_3, reflection spectra, Kramers-Kronig anal. of optical characts. 79−8161
YVO_4, pure and Bi^{3+} doped, absorpt. and emission props., excitons 79−38592
$YVO_4:Eu^{3+}(Er^{3+})$, energy transfer, laser time-resolved spectroscopy 78−27306

excitons continued
$YVO_4:Nd^{3+}$, energy transfer processes, laser-excited time-resolved spectroscopy 80—84765
$ZnAs_2$ Schottky diodes, elec. and photoelec. props., excitons 80—65653
$Zn_xCd_{1-x}S$, bound-exciton lines, compositional fluctuation-induced broadening 80—2846
$Zn_xCd_{1-x}S$ epitaxial layers, elec. resist. and luminescence obs. 78—19540
$Zn_xCd_{1-x}S$, forbidden band width, exciton refl. and luminesc. meas. 78—10947
$Zn_xCd_{1-x}S$ monocrystal, optical and nonlinear optical characts. *(Russian)* 79—98442
$Zn_xCd_{1-x}S$, reflectivity spectrum, excitons and energy band struct. 77—55804
$Zn_xCd_{1-x}S$, resonance Raman scatt. involving exciton complexes 80—16039
$Zn_xCd_{1-x}S(Te)$, solid soln., broadening of exciton states, depend. on conc. 79—73449
$Zn_xCd_{1-x}Se$, exciton reflection spectra anomalies *(Russian)* 80—97304
$Zn_xCd_{1-x}Te$, relaxation processes, emission spectra *(Russian)* 78—72598
$Zn_xCd_{1-x}Te$, reson. Raman scatt. of light by longitudinal optical phonons 77—28577
$Zn_xCd_{1-x}Te$, resonant Brillouin scattering *(Japanese)* 79—15474
$ZnCr_2O_4$, antiferromag. spinel, absorpt. and luminesc. spectra 80—66225
$ZnGeP_2$, pseudodirect bandgap semiconductor, natural birefringence 79—65834
ZnO, ang. depend. of reflection spectra and directional dispersion of anisotropic exciton polaritons 78—31216
ZnO, attenuation of transmitted light in exciton region, polarisation, coherence, scatt. 77—69852
ZnO, band gap depend. on energy of zero-point vibrs., luminesc. obs. 79—73436
ZnO, electron-exciton elastic scatt. cross sections, central field and exchange approxs. 77—62919
ZnO, electron-exciton inelastic collision cross sections 79—90967
ZnO, electron-hole plasma, gain and refl. spectra study 80—66227
ZnO epitaxial film, UV luminesc. due to radiative annihilation of excitons 79—11468
ZnO, excited states of bound excitons, photoluminesc. obs. 80—44513
ZnO, exciton luminesc., 16 to 77K 80—97329
ZnO, laser thresholds and stimulated emission, intrinsic recomb. processes 79—15489
ZnO, negative photocond. by excitation of exciton-impurity complexes, recomb. mechanism *(Russian)* 79—28379
ZnO, optical gain spectra, direct recording using laser modulation 78—66834
ZnO phosphors, origin of UV emission 78—64400
ZnO powders, UV luminesc. spectral distrib., comparison with single crysts., excitons role 80—55167
ZnO, reflection spectra, exciton reflection at high excitation levels 77—69853
ZnO, surface exciton dispersion relations, additional boundary conditions 77—43687
ZnO, surface exciton polariton, nonlinear optical excitation 77—59259
ZnO, surface exciton polaritons, ATR obs., book contrib. 79—42620
ZnO, surface exciton polaritons, nonlinear optical excitation and dispersion relation 79—82657
ZnO, Zeeman splitting of A1-exciton emission lines, k-linear term effects 78—52563
ZnO:Li(Na), band-edge emission obs. 77—20933
ZnP_2, cathodoluminesc. 4.2 to 200K 79—52028
ZnP_2, monoclinic, cathodoluminesc. spectra exam. 79—15534
ZnP_2 Schottky diodes, elec. and photoelec. props., excitons 80—65653
ZnS, cathodolum. emission spectra, exciton lines 80—76084
ZnS, natural and stress induced birefringence dispersion 78—6651
ZnS phosphor, exciton struct. in luminesc. excitation spectra 77—52176
ZnS, temp. coeffs. of charact. reflectivity struct. 77—85745
ZnS:Al,Cu(Ag)(Au) phosphors, luminesc. excitation spectra and exciton struct. 80—55164
ZnS:Al(Te) phosphors, luminesc. excitation spectra and exciton struct. 80—55165
ZnS:Cu,Cl, exciton refl. spectra, hexagonal struct. 77—44021
$ZnS:Mn^{2+}$ phosphors, luminesc. excitation spectra and exciton struct. 80—55164
ZnS:Mn(Al)(Te), luminesc., exciton struct. 79—33801
$ZnS:TbF_3$, photoelectroluminescence, effect of electron-hole pairs 78—27328
ZnS-O, single cryst., fast neutron irrad., optical props. 78—27331
ZnS-ZnO, solid solns., edge emission and exciton spectra *(Russian)* 77—24899
ZnS_xSe_{1-x}, band gap, comp. depend., exciton refl. spectrum obs. 78—56071
ZnS(Se)(Te), thermoreflectance spectra, at energies from absorption edges to 9 eV *(Japanese)* 79—11436
ZnSe, attenuated total refl. spectra of surface exciton polariton 77—36262
ZnSe, blende type struct., luminesc. under high excitation 79—19928
ZnSe, blue photoluminesc. excited with strong laser radiation 80—93391
ZnSe crystal, exciton reflection spectra, control of exciton-free surface layer thickness 80—7373
ZnSe, cubic, magnetoreflectance of Γ_6-Γ_8 exciton ground state 78—23495
ZnSe, cubic, magnetoreflection of s-excitons 78—60426
ZnSe, cubic, valence band parameters, magnetoreflectance of Γ_6-Γ_8 exciton 78—60056
ZnSe, direct gap semicond., exciton energy at 300K from reabsorption of luminesc. 79—78728
ZnSe, exciton emission, halfwidths, thermal and optical activation energies obs. *(French)* 80—66268
ZnSe, exciton refl. spectra, temp. depend. 80—59886
ZnSe, exciton-impurity complex, electroabsorption meas. 79—15484
ZnSe LED, blue electrolum. due to bound excitons 77—32441
ZnSe, magnetoreflectance of exciton-polaritons, semiclassical treatment 79—99857
ZnSe, near band edge photoluminescence, electron-hole recombination 80—80835
ZnSe, polaritons, reson. Brillouin scatt., heavy and light excitons 79—99898
ZnSe, reabsorpt. of excitonic luminesc. in direct band gap semiconds. 77—63469

excitons continued
ZnSe, relaxation processes in Raman scattering and exciton luminescence under resonant excitation 80—25386
ZnSe, reson. Brillouin scatt. near ground state exciton energy region 79—61390
ZnSe, resonance Raman scatt., exciton-polariton luminescence *(Russian)* 80—97287
ZnSe, resonant Brillouin scatt. by injected acoustic waves 77—12394
ZnSe single crystal, exciton photolum. and refl. spectra, 4-90K *(Russian)* 77—66540
ZnSe, single crysts., opt. band gap and Mn^{2+} EPR, effects of prep. conditions 77—47730
ZnSe, temp. coeffs. of charact. reflectivity struct. 77—85745
ZnSe, thermally treated crystals, photoluminesc. 80—60661
ZnSe, two photon absorpt. by envelope-hole coupled exciton states, polarisation depend. 77—66522
ZnSe, two-photon absorpt., envelope-hole coupled exciton states 77—52124
ZnSe, undoped and doped, pair spectra, edge emission and shallow acceptors 77—28611
ZnSe, valence-band parameters and g-factors from free-exciton magnets reflectance 79—73905
ZnSe:Ag, low-temp. photolum. meas. 77—20912
ZnSe:Al(Ga)(In), single cryst., doping, blue luminesc. 78—39584
ZnSe:Cu, discovery of bound exciton, electroabsorption 80—45038
ZnSe:In, Li, binding energy of excitons bound to donor-acceptor pairs, electron-phonon coupling 77—4689
ZnSe:Ni, evidence for exciton binding at Ni impurity sites, photolum. excitation spectrum 80—45135
$(ZnSe)_x(CdTe)_{1-x}$, low temp. photoluminesc. *(Russian)* 78—43931
ZnSe(Te), fine structure of lowest exciton state *(Russian)* 80—96801
$ZnSiAs_2$, pseudodirect bandgap semiconductor, natural birefringence 79—65834
$ZnSiP_2$, pseudodirect bandgap semiconductor, natural birefringence 79—65834
ZnTE, relaxation processes in Raman scattering and exciton luminescence under resonant excitation 80—25386
p-ZnTe 79—43028
ZnTe, band parameters from bound exciton, donor-acceptor pair excitation luminescence 78—92111
ZnTe, blende type struct., luminesc. under high excitation 79—19928
ZnTe crystals, polariton effects in luminesc. 80—103988
ZnTe crystals, secondary radiation polarization and relaxation of optical excitation 80—11399
ZnTe, edge luminesc. excited by electron bombard. 80—66308
ZnTe, exciton localisation at impurity pairs 79—37999
ZnTe, excitonic complexes, stress splitting of luminesc. lines 77—4672
ZnTe, excitonic effects at E_0 and E_1 gaps, wavelength modulated reflectivity spectroscopic study 79—61400
ZnTe film, exciton spectra, press. and temp. depend. 80—80886
ZnTe, free exciton refl., surface layer effects 78—76493
ZnTe, free-exciton emission band under high-intensity photoexcitation 79—73993
ZnTe, high purity acceptor bound and free exciton states 79—99941
ZnTe, high quality p-type cryst., predominant acceptors 78—60504
ZnTe, I_4 bound exciton, magneto-optical meas. 77—20836
ZnTe, laser thresholds and stimulated emission, intrinsic recomb. processes 79—15489
ZnTe, luminesc., donor-acceptor-pair excitation spectroscopy 80—25456
ZnTe, luminescence spectra struct. surface and volume polaritons *(Russian)* 80—16089
ZnTe, magneto-optical effect, I_2 bound exciton 77—12432
ZnTe, magnetoreflectance meas. on Γ_6-Γ_8 exciton 78—6656
ZnTe, photoluminesc., donor and acceptor excited states 79—38622
ZnTe, pure and P(As) doped, shallow-acceptor, donor, free-exciton, and bound-exciton states 80—60667
ZnTe, radiative recombination involving free particle scatt. 79—38648
ZnTe, Raman scatt. and exciton luminesc. under reson. excitation 79—38617
ZnTe, real structure effect on luminescence and absorption spectra, dislocations 80—16085
ZnTe, refined, undoped, Cu acceptor, optical absorption and photoluminesc. meas. 80—34970
ZnTe, relax. processes at high excitation levels, Bose-Einstein condensation of excitons 78—48219
ZnTe, relax. times of secondary radiations, circular polarisation correlation 79—28816
ZnTe, relaxation processes, emission spectra *(Russian)* 78—72598
ZnTe, reson. Brillouin scatt., injected acoustic domains obs. 78—19493
ZnTe, resonance Raman scatt. of excitonic polaritons by LO and acoustic phonons 79—65879
ZnTe, secondary emission, transient behaviour under band-to-band excitation 80—108266
ZnTe, shape of reflectance and thermoreflectance spectra 79—11430
ZnTe, single cryst., anomalous struct. of exciton refl. spectra 77—44020
p-ZnTe, single crystal *(Russian)* 78—23488
p-ZnTe, spin-flip Raman scattering, review 80—108209
ZnTe, temp. depend. of Raman scatt. and exciton luminesc. spectra 78—39586
ZnTe, two-photon absorption line shape exciton effect and valence band degeneracy depend. 79—65898
ZnTe, undoped, electroreflectance of fundamental edge, exciton levels *(Japanese)* 80—20612
ZnTe, valence band parameters and free exciton reduced mass, free exciton magnetoreflectance 80—45046
ZnTe:Ag, containing dislocation loops, optical absorption-edge fine struct. 78—43905
ZnTe:Ag, real structure effect on luminescence and absorption spectra, dislocations 80—16085
ZnTe:Cr(Mn)(Fe), exciton refl. spectra 80—2806
ZnTe:Li(Cl)(Al)(In), ion implanted and annealed, photoluminesc. meas. 78—15208
ZnTe:Mn, exciton refl. band, giant mag. splitting *(Russian)* 78—56079
ZnTe:Mn, mag. field splitting α n=2 exciton state *(Russian)* 78—79940
ZnTe:O, deep centres, photocapacitance detection 79—95362
ZnTe:P, pure and doped, electron and exciton excited states of neutral donor 80—34393
Zr, liquid, ionisation and scintillation, application to radiation detectors, review *(Japanese)* 78—35206
ZrS_3, excitonic transition, reson. Raman spectra, Franck-Condon factors 80—97252

excitons continued
  ZrS_3, photolum. from excitons 80−66274
  ZrS_3, thermomodulated reflectivity and transmission 80−50357

executive programs *see supervisory and executive programs*

exhibitions
  chemical analysis, Munich (1978), microprocessors and millivoltmeters appl. *(German)* 79−20482
  Michigan Space Center and model solar system 78−69653
  pollution control equipment for metals industry 79−66432

exobiology *see extraterrestrial life*

exoelectron emission
  apparatus for exoelectron emission by electron impact *(Japanese)* 79−100029
  attenuation length, escape depth and probability for excited electrons in solids 78−76593
  creep monitoring 77−44312
  crystal defects role, unified nature *(Russian)* 77−55872
  deformed solids under tensile loads, automated installation of metallographic and exoemission obs. 80−50792
  dosimeter, exoemissive, automation of testing 79−6770
  energy and angular distribs. 77−85904
  exoelectron emission defectoscopy, metal fatigue strength prediction 78−76807
  exoemission defectoscopy in initial stages of fatigue fracture 78−53126
  exoemission phenomena, TSC, thermionic emission, book contribution 80−80954
  fatigue damage, development rate by exoelectron meas. 80−25835
  fatigue damage early prediction by acoustic and exoelectron emission 78−53170
  fatigue damage measurement by laser scanning, exoelectron display 77−73391
  insulators, trap struct. anal. by fractional glow techique 79−11078
  ionic crystal, ion-electron mechanoemission mechanism 78−3002
  ionic crystals, photostimulated electron emission after photoexcitation, diffusion approach 78−52641
  measurement apparatus for chemically stimulated, photostimulated and tribostimulated exoelectrons 77−90260
  metal, exoelectron emission from surface during fatigue damage 78−44217
  metal, vacancy diffusion during plastic deform., possibility of stimulated electron emission obs. *(Russian)* 79−5007
  oxidised surface, oxidising conditions effect on thermally stimulated exoelectron emission *(Japanese)* 80−89127
  patch field, Maxwellian exoelectron energy distrib., simulation 77−85905
  ruby laser rod, exoemission parameter rel. to optical strength 77−732
  semiconductors, exoelectronic emission, mechs., sensitivity meas., surface study appls. 77−52228
  solid, thermally stimulated processes 78−10828
  solids, high energy electron emission, influence of structure and props. *(German)* 79−52317
  stainless steel, exoelectron emission by electron impact *(Japanese)* 79−100029
  steel, hardened, exoelectron emission from torsion fatigue damage 77−86142
  steel, stainless, effect of gas press. and sample temp. during slow electron excitation 79−61505
  steel, stainless, exoelectron emission centre form. by slow electron impact 79−52088
  steel bearing balls, exoelectron emission for surface fatigue wear testing 78−39960
  technological strength and nondestructive methods of testing during heat treatment 78−85090
  tensile deformation of flat samples, meas. equipment using exoelectron emission 77−77679
  thermally stimulated, electronic detect. instrumentation for dosimetry *(Spanish)* 77−32958
  thermally stimulated, meas. by windowless Geiger-Muller gas flow counter 77−79505
  thermostimulated processes appl. to radiation dosimetry and dating 78−11004
  triboemission from oxide covered metals, meas. apparatus 77−90260
  for tribomechanical surface treatment *(German)* 77−4870
  TSEE, role of surface pot. 77−8732
  TSEE from insulating layers, Monte Carlo method simulation *(German)* 80−2932
  wear and metal fatigue cracking observation technique 77−81202
  Ag, deformed, exoelectron emission and electron energy distrib. 80−7481
  Al alloys, oxide-covered, characteristic emission of negatively charged particles during tensile deform. 78−92179
  Al anodic films, acoustic and electron-emission during deform. 80−80143
  Al, anodised, photostimulated exoelectron emission, effect of oxide thickness 78−80461
  Al, chemisorption of O_2, photon and electron emission as indicators of intermediate states 80−39439
  Al, deformation enhanced photoemission meas. 77−32511
  Al, etched, electronic props. of surface *(Russian)* 78−15569
  Al, exoelectron emission under recrystallisation annealing 77−90412
  Al, exoelectron photoemission enhanced by slip steps, plasmon reson. theory 78−15300
  Al, fatigue enhanced optically stimulated electron emission 77−4719
  Al, oxide covered, tensile deform. in high vac., particle and photon emission 78−39672
  Al, polycrystalline, abrasion, deform., fatigue, study by exoelectron microscope *(Japanese)* 78−74108
  Al polycrystalline, exoelectron emission under tensile deform. and fracture *(Japanese)* 77−55870
  Al, polycrystalline, fatigue damage detection by exoelectron emission meas. *(Japanese)* 77−55871
  Al, surface fatigue damage meas. by photostimulated exoelectron emission 78−19876
  Al, surface subjected to friction, wear, exoelectron emission, rel. to O_2, H_2O, gaseous adsorpt. 79−1816
  Al, tribomechanically activated, optically stimulated exoelectron emission *(German)* 78−48290
  Al, tribomechanically activated, photostimulated electron emission 79−33905
  $Al\text{-}Al_2O_3\text{-}Ag$ structure, electron bombard, charge accumulation kinetics, exoelectron emission obs. 77−51825

exoelectron emission continued
  $\alpha\text{-}Al_2O_3$, complex glow spectra, improvement of fractional glow technique, thermally stimulated exoelectron emission 79−65984
  Al_2O_3, exoelectron emission, energy and ang. distrib. anal. *(German)* 78−92180
  Al_2O_3:Li, TSEE, Li doping effects 80−80953
  Au condensed films on NaCl, ion bombarded, film growth, thermally stimulated exoelectron emission 80−50537
  Au, deformed, exoelectron emission and electron energy distrib. 80−7481
  $BaSO_4$, TSEE and surface charging, simultaneous meas. 80−29864
  $BaTiO_3$, anisotropic emission of exoelectrons ferroelec. phase transitions *(Russian)* 78−48291
  $BaTiO_3$, electron exoemission unipolarity associated with phase transitions 80−97415
  $BaTiO_3$, epitaxial films and single domain crysts., exoelectron emission obs. of phase transition 79−74069
  $BaTiO_3$, exoelectron emission during phase transition, orientational depend. 79−69786
  Be (0001) oxidised surfaces, internal electron source contrib. to TSEE trap population 80−16161
  BeO, anomalous exoemission, laser irrad., electron trap ionisation *(Russian)* 77−1792
  BeO ceramic, unlapped and lapped with diamond powder, thermally stimulated exoelectron emission 78−11086
  BeO, ceramic and single cryst., EPR-ENDOR study of $[Li]^\circ$ centre 77−85569
  BeO ceramics, thermally stimulated exoelectron max., effect of H_2 adsorption 79−43109
  BeO, ceramics, thermally stimulated exoelectron emission *(German)* 79−100028
  BeO ceramics, thermostimulated exoemission and adsorption centres 78−27386
  BeO discs, thermally stimulated exoelectron emission and thermolum. sensitisation 78−35277
  BeO, exoelectron emission from hydrated and dehydrated surfaces 80−11545
  BeO, field-assisted thermally stimulated exoelectron emission 80−100761
  BeO, film, TSEE, low energy electron impact excitation 77−12505
  BeO, photostimulated exoelectronic emission under discontinuous stimulation 80−108329
  BeO, radiation dosimetry *(Japanese)* 79−83110
  BeO reactively evaporated film, elec. and optical props. 77−32512
  BeO, TSEE, effect of surface SiO_2 80−76159
  BeO, thermally stimulated exoelectron emission, influence of desorption processes 77−85906
  BeO:Li, ceramics, thermally stimulated exoelectron emission *(German)* 79−100028
  Bi_2S_3, photostimulated electron emission, cryst. growth conditions depend. 77−44135
  $CaSO_4$, radiation dosimetry *(Japanese)* 79−83110
  Cu film, struct., oxidation, and exoelectron emission rel. to bulk samples *(Russian)* 79−37927
  Cu surface subjected to friction, wear, exoelectron emission, rel. to O_2, H_2O, gaseous adsorpt. 79−1816
  Cu, thermally stimulated exo-electron emission 80−11547
  Cu-Zn, thermally stimulated exo-electron emission 80−11547
  Fe, surface subjected to friction, wear, exoelectron emission, rel. to O_2, H_2O, gaseous adsorpt. 79−1816
  KCl, single cryst., electron beam irrad. optically simulated exoelectron study 79−95908
  LiF (TLD-100), thermoluminescent response to 0.1-5 keV electrons 79−95852
  LiF, evaporated film, thermally stimulated exoelectron emission rel. to thermolum. 79−47602
  LiF, mech. excitation, luminesc. electron emission, friction, static electrification, meas. method *(German)* 77−24904
  LiF, powder energy distrib. of TSEE 77−12504
  LiF, radiation dosimetry *(Japanese)* 79−83110
  LiF, thermally stimulated exoemission, radiation defects and adsorpt. centres 78−11087
  LiF, thermostimulated exoemission, adsorbed layer effects 78−11085
  LiF:Mg, effects of grain size on thermolum. and thermally stimulated exoelectron emission 79−15536
  $LiNbO_3$:Fe, exoelectron emission in pyroeffect regime 80−76158
  $LiNbO_3$:Fe, influence of anomalous photovoltaic effect on exoelectron emission 79−28374
  Mg, clean annealed surface, exoelectron emission during O_2 and Cl_2 adsorption 78−39671
  MgO, exoelectron emission, mean energy, temp. depend. 80−76160
  MgO, single crystal, thermal and optical stimulation processes of V-centres *(Japanese)* 80−11485
  MgO, thermally stimulated exoelectron emission *(German)* 80−66404
  Mo, quenched sample, UV photoelectron spectra, exoelectron-like emission 79−15587
  NaCl, deform. process, exoemission and desorption meas. *(Russian)* 78−75708
  NaCl, emission of Cl atoms during V_k centre decomposition 80−10578
  NaF, single crystal, TSEE by electron bombardment 78−6836
  Ni film, struct., oxidation, and exoelectron emission rel. to bulk samples *(Russian)* 79−37927
  Ni, oxide covered, tensile deform. in high vac., particle and photon emission 78−39672
  Ni, surface subjected to friction, wear, exoelectron emission, rel. to O_2, H_2O, gaseous adsorpt. 79−1816
  NiO, powder compact surface, oxidising conditions effect on thermally stimulated exoelectron emission *(Japanese)* 80−89127
  NiO, single cryst. cleavage plane, oxidising conditions effect on thermally stimulated exoelectron emission *(Japanese)* 80−89127
  Pt, tension-strained, thermostimulated exoelectron emission, excitation mechanism *(Russian)* 80−71581
  n-Si, effect of surface polishing rel. to defect distrib. in surface layer 80−40239
  SiO_2-Si structure P^+ bombardment damage, exoelectron emission obs. 78−95383
  SnO_2 layers, study using Mossbauer effect 78−31124
  Ta_2O_5, anodic film, thermally stimulated exo-electron emission 80−11546
  Ta_2O_5 anodic films, reanodisation effect on exoelectron emission 79−43110
  Ta_2O_5/Ta, heat-treated anodic film, exoelectron emission and radiation dosimetry *(Japanese)* 79−83110

exoelectron emission continued
- ^{182}Ta-containing Ta sheet, radioactive electron emission spectrum (exoelectrons), surface elec. field and Auger effects 78−72705
- TiO$_2$, thermally stimulated exoelectron emission *(German)* 80−66404
- V$_2$O$_5$, thermally stimulated exoelectron emission *(German)* 80−66404
- Zn, thermally stimulated exo-electron emission 80−11547
- ZnO, thermally stimulated exoelectron emission *(German)* 80−66404
- ZrO$_2$ films on Zr alloys, exoelectronic emission props. and energy-band parameters 79−91571

exosphere
- collision dominated, vel. distrib. function 77−82136
- cosmic antiproton-proton flux ratio at top of atmosphere 78−40783
- dayside sub-solar H bulge 77−21957
- density and temperature, AEROS and TAIYO satellite results 80−46340
- electron density and temp. meas., night time, 2500 km altitude 79−16730
- escape of ions to space, ion chem. and low altitude accel. effects 80−85798
- exobase, H density and temp. from Lyman alpha absorpt. and polarisation meas. 77−29526
- extinction meas. by OSO-8 French expt. 77−21963
- geocoronal H conc. models, Hα emission rates and solar Lyman β flux 77−25808
- geocoronal Lyman α Doppler line profiles 80−12579
- geomagnetic density and temp. effect propag. 79−48593
- global composition and temp. during quiet times 77−33227
- global temperatures and densities under active solar conditions 77−33234
- H global density distrib. vars., escape fluxes 78−93023
- H latitude vars., rel. to polar wind, heating and charge exchange processes 78−93024
- ion-exosphere, rot. effects on plasma distrib. 77−2301
- ionosphere-protonosphere interaction, dynamic model 77−45220
- Lyman α emission in antisolar direction on Earth's night side 77−87138
- Lyman α scattering in geocoronal models, effect on rocket meas. of proton fluxes 77−53273
- neutral temperature and winds, geomag. disturbances effects 80−26658
- neutral temperature observations 80−56661
- outgoing longwave radiation estimation from meteorological variables in numerical models 78−49192
- primitive exosphere, neutral and electron temps. 78−40754
- protonosphere depletion assoc. with mag. storm, and recovery 80−85784
- satellite atoms in collisionless exosphere, depletion by radiation press. 79−96933
- satellite particle exospheres of planets, appl. to Earth 79−101097
- Space Shuttle, orbital environment 78−36430
- Space Shuttle orbiting molecular beam laboratory 78−35242
- temperature, determ. from ionospheric obs. using numerical simulation 77−53268
- temperature, from incoherent scatt. radar and satellite meas. 77−33224
- temperature, global model based on meas. from Fabry-Perot interferometer on OGO-6 satellite 77−53265
- temperature, global model using optical and incoherent scatter meas. 78−36343
- temperature, models seasonal vars. at solar max. and low geomag. activity 78−57376
- temperature, rel. to Hα airglow semi-annual vars. 78−28360
- temperature, rel. to heating by solar wind energy 77−37471
- temperature, representation by sum of series in Legendre polynomials 78−45063
- temperature determ. by ground meas. of ionosphere and O I 6300 Å line 77−67003
- temperature diurnal variation, effect on densities derived from near-circular satellite orbits 80−21867
- temperature variations, appl. to neutral atmosphere semi-empirical models 79−21085
- temperatures of high latit. exosphere, geomag. activity effects 80−109286
- thermal escape of H and He, assoc. non-Maxwellian effects 79−80264
- thermal escape of molecules, non-Maxwellian effects 80−46419
- thermosphere-exosphere transition layer, structure, temps., H escape 79−66845
- thermosphere-exosphere transition region, reduced H temp. 77−33225
- trapping region, quasiperiodic electron density pulsations, satellite detection 80−4198
- whistler-mode wave rel. to sweepers in HF and VHF bands 78−16231
- wind enhanced thermal escape, collisional modifications 77−49204
- H atoms vel. distrib. from OGO-5 meas. of Lyman α emission 78−61642
- H density distrib. at exobase near solar minimum 78−45067
- H density near exobase, local perturbations inferred from Lyman α airglow meas. 78−24400
- H distribution and escape, charge exchange effects 77−29674
- H escape at low O$_2$ levels, photochem. model 77−56784
- H escape flux, charge exchange induced, diurnal and solar cycle vars. 78−93022
- H, escape rate due to charge exchange with hot plasmaspheric ions 77−37469
- H thermal escape, influence of thermosphere 63 μm radiation field 79−80066
- H$^+$ loss during solar cycle, charge exchange processes 78−93021
- He seasonal-latitudinal var. from He I 584 Å dayglow emission 79−75007
- He$^+$, outflow from terrestrial ionosphere 78−49221
- Li$^+$ diffusion and ion-neutral interactions, laser sounding obs. *(French)* 80−82115
- O atom corona, of fast atoms during solar max., airglow obs. 80−101469
- O atoms, polar corona atom distrib. 80−82120

exotic atoms
- *see also hadronic atoms; muonic atoms*
- atomic spectral line shifts for heavy quark atoms 78−62965
- charmonium, spectra, interaction with external quantised EM field, H-like atom 79−68332
- chemical structure studies with positrons and mesons, review 79−79277
- coherent multistep transitions, interference effects 77−71896
- Conference on meson-nuclear physics, Houston, USA (Mar. 1979) 79−85489

exotic atoms continued
- double exotic atoms, lifetimes, main decay modes, production mechanism of $(\pi^\pm\mu^\pm)$ $(K^\pm\mu^\pm)$, $(\mu^+\mu^-)$, $(\pi^+\pi^-)_p$, $(\Sigma^\pm\mu^\pm)$ $(\Xi^-\mu^+)$, $(\Omega^-\mu^+)$, $(\Omega^-\pi^+)$ 80−14258
- excited state lifetime calc. using Bethe-Salpeter eqn. 77−27208
- high energy physics, conf., Schladming, Austria (Feb.-Mar., 1977) 78−8494
- hyperfine splitting, recoil corrections calcs. 78−50667
- light exotic atoms, L-shell refilling rate, theory 77−12469
- light nuclei, with unequal numbers of protons and neutrons, radioactive decay 78−89831
- monopole H atom, spectra, energy levels, transition probabilities *(Chinese)* 78−90322
- nuclear bound states of k−, $\bar{p}$ and Σ 80−13399
- nuclear electric moment determ. from exotic atom X-ray meas., review 78−50061
- nuclear moments, E2 and E4, from HFS, review 78−37265
- nuclear size, strong interaction effects, expt. tests of QED, review *(German)* 79−76536
- pionic and muonic atoms prod. by 'pion factories' 78−21791
- positron atomic shells, quantum mech. anal. 79−10235
- production and characts., review *(Hungarian)* 78−13630
- review, props., EM and strong interaction effects within the atoms 78−9281
- spectral line intensities and selection rules, exotic atoms with monopoles *(Chinese)* 79−36800
- supernuclei containing bound states of charmed baryons, existence, decay, phys. significance 77−79320
- Ω hyperon atoms, Coulomb level fine splitting *(Russian)* 79−22871
- $\bar{p}$p and $\bar{p}$d formed in liquid hydrogen and deuterium, mechanisms, quasi-nuclear mesons *(Russian)* 77−50569
- $\bar{p}$p atom and N$\bar{N}$ nucl. interaction, radiative transitions 78−25065
- $\pi\mu$ atom, energy levels, fine struct. and Lamb shift calc. *(Russian)* 79−31744
- Σ^-n dibaryon decay in exotic atoms 80−9762
- F .e$^+$, positron energy levels, rel. to Rydberg levels of Na, NO 79−86089
- H anomalous isotopes, including quarks of unit charge, search using cyclotron 77−61879
- H, exotic superheavy, search in terrestrial substances *(Chinese)* 79−59605
- H$^-$, bound states in mag. field, binding anal., variational calcs. 80−42940
- H-like atoms, quadrupole moments 78−90072
- H-positron bound state, effective one-body pot. to prove absence 78−82871
- ^{A}H, A=1,2,3, $\bar{p}$ radiative atomic recombination, antiprotonic atoms 80−83527
- He mesoatoms, π^-, μ^-, K$^-$, p$^-$ atoms, energy spectra, wave functions *(Russian)* 78−55264
- ^{4}He, muonic, formation and hyperfine struct. 80−91707
- Li, mesoatoms, π^-, μ^-, K$^-$, p$^-$ atoms, energy spectra, wave functions *(Russian)* 78−55264
- p$\bar{p}$ atom, nucl. level shift and radiative transitions *(Russian)* 80−28121

expanding universe *see cosmology*

expansion, thermal *see thermal expansion*

expansion chambers *see cloud chambers*

exploding foils *see exploding wires and foils*

exploding wires and foils
- *see also discharges (electric); plasma production*
- accelerators, direct-action, using inductive storage device with commutation by exploding conductors 80−68974
- atomic emission spectroscopy, exploding foil excitation, parametric investig., Cd, Ni anal. appl. 77−12840
- burst phase, simulation by one-dimens. MHD code 80−75080
- coaxial high current discharge, exploding cylindrical foils in air, compression and expansion 80−38841
- composite wires, exploding, hypervel. and temp. amplification 79−41853
- conductor, MHD kink instability 80−6307
- conductors, in water obs., for varying cross section/length ratio *(Russian)* 77−7612
- continuum radiation, spectral radiant intensity meas. 78−91134
- critical temp. determ. by exploding wires method, liquid metal enthalpy 78−6149
- current wave, EM field nonlinear diffusion 77−51254
- cylindrical blast wave high-speed photography for material impact testing 79−79189
- cylindrical foil explosion in air, elec. characts. 79−55597
- cylindrical foil in air, elec. explosion, high current shunt pinch props. 79−64950
- destructive explosion mechanism, short heating time scale 77−62424
- discharge in RCL circuit with greatly nonlinear resistance *(Russian)* 79−41854
- electric detonation in vac., Xe, He, N$_2$ atoms, discharge characts. *(Russian)* 77−11435
- electric strength recovery rate, following explosion of wire *(Russian)* 78−22592
- electrical generator with resistive load, design and performance 77−55195
- electrically exploded foil opening switches, basic performance 80−70019
- electrically exploded foils, heating and burst phenomena 77−39488
- electrohydraulic forming of circular metal sheet 80−84866
- electron beam self-acceleration, due to exploding conductor *(Russian)* 77−13824
- electron emission, explosive, effect of press. on cathode 80−49034
- electron emission, minimal current *(Russian)* 77−15256
- electron emission spectra produced by exploding wire photon sources, yield and energy meas. 78−31299
- EM implosion of foil, SHIVA pulsed radn. source expt. 78−14190
- exploding wire, nonthermal IR and X-ray emission 79−4187
- explosive electron emission 79−50914
- explosive emission diode, plasma pot. oscills., probe diagnostics 80−6284
- explosive emission multiple-tip cathodes, improved stability 79−64887
- explosive-magnetic generators, energy take-off to inductive load using circuit breaking 80−59323
- fused metal foil operating switch for inductively driven plasma implosions generation 80−70018
- fusion reactor high-voltage production using underwater exploding foil fuse 78−54948
- fusion reactor ignition by controlled supercritical fission 77−15221

exploding wires and foils continued
- fusion reactor inductive storage technology, new applications, review 78—55019
- high current relativistic electron beam retardation distance in dense plasma *(Russian)* 80—14911
- high-speed photographic recording, of exploding wires 78—41365
- laser-heated exploding wires, X-ray emission 79—10685
- liquid cavity collapse, accompanied by RF emission 80—87790
- liquid thread explosions, fusion plasma prod. 77—15220
- metal atom oxidation laser, pure rotational HF laser oscills. 77—14701
- metal atom oxidation lasers, book contrib. 77—10913
- metal damage by intense EM radiation, kinetic mechanism 77—20167
- metal foil plasmas, short term radiative processes obs. 79—82083
- metal surface, electrical pulsed discharge action under air environment *(Russian)* 77—43091
- metal vapour, thermal instability elec. cond. 78—1868
- MHD calc., pulse generator characts. 77—55196
- MHD generator, model with central exploding wire or outer cylinder *(Russian)* 77—51245
- MHD instability effects in imploding plasma liners 80—75081
- microsecond stratified pulsed discharge 80—87975
- miniature exploding foil, pulsed laser stereophotography 78—41364
- multiple-wire implosion in transmission line generators, hot plasma efficient prod. 80—48929
- nonlinear evolution of exploded wire plasma, numerical simulation 78—83605
- oscillograms processing, with aid of microcomputer and main-frame computer *(Russian)* 80—28854
- particles resulting, investigation by microscopy and size *(Russian)* 79—37558
- photoemission spectra for Ag and C, total primary yields for exploding wire radiator source 80—32773
- plasma, convective instability in inhomogeneous mag. field 78—67340
- plasma nonlinear evolution, numerical simulation 78—14197
- plasma prod., nonlinear diffusion in exploding wires 78—14191
- plasma production, inner shell X-ray spectra 77—27720
- plasma production, MHD sausage instability, wavelength determ. 77—47238
- plasma production, X-ray diagnostics 78—5909
- plastic plate velocity measurement, as continuum, by streak camera technique 78—37095
- potential drop across exploded foil, theory of expt. determ. 78—71515
- Rayleigh-Taylor instability in imploding foil plasma, two dimens. simulation 78—47156
- relativistic electron beam, propag. in air, preformed plasma column 77—87875
- skin effect, current distribution in LC circuit *(Russian)* 80—19628
- solving transient process in electrical explosion of conductor in restricted volume of liquid *(Russian)* 80—100088
- spiral wire underwater explosion characteristics *(Russian)* 79—94809
- stratified pulsed discharge with limited surface area 80—87974
- structural inhomogeneity and MHD sausage instability, arc chains, grain size and annealing 79—41904
- switch, 100 kA, explosively actuated, 70 μs opening time 78—8984
- thin film excitation, anal. spectrosc. appls. 79—40618
- underwater, form. and propag. of compression wave *(Japanese)* 77—72329
- underwater wire explosion, shock wave propag. *(German)* 77—76244
- underwater wire explosive metal forming, Al membrane plastic deform. 79—100208
- unduloids, X-ray diffr. obs., preferred grain orientations, lattice distortions, zonal texture 77—36568
- voltage pulse rel. to conductor inhomogeneities 77—19798
- wire, resistance increase phase, elec. characts., applications 77—55192
- wire explosion plasma production, diagnostics by Bartels method 79—10686
- wire in LC-loop, initial stages of elec. explosion, heating rate depend. 80—24287
- X-ray emission spectra, of exploded wire plasma 77—68872
- X-ray line emission from single and multiple exploding wires 77—84519
- X-ray line spectra from exploded-wire array, plasma temp. and density 79—55457
- X-ray spectra from exploded-wire plasmas, spatial resolution techniques 78—14188
- Al, cylindrical foil, elec. explosion, current distrib. in high current shunting discharge 79—41855
- Al foil, elec. explosion, dielec. breakdown 78—67388
- Al, foil, elec. explosion, immersion medium effects 78—67389
- Al foil fuse, electrically exploded, surrounding medium effect 80—103207
- Al foil in quartz dust, electrical explosion for accelerator application 80—6314
- Al, photoemission spectrum for exploding wire radiator source, Boltzmann eqn. soln. 79—26949
- Au, photoemission spectrum for exploding wire radiator source, Boltzmann eqn. soln. 79—26949
- Co, exploding wire, elec. resist. at high temp., submicrosec. pulse heating meas. 77—89747
- Cs, exploding wire, striations produced at supercrit. press. 79—64952
- Cs, plasma, highly ionised, conductivity and eqn. of state 78—26323
- Cs, plasma diagnostics by wire explosion 78—71516
- Cu bridge wires mesh, appl. to large area detonators 77—10001
- Cu double wire explosion, optical flashes, photographic appl. 80—1865
- Cu exploding foils, rapid mag. energy transfer, conductivity law *(French)* 78—91135
- Cu foil, elec. explosion, dielec. breakdown 78—67388
- Cu, laser using exploding wire *(Russian)* 77—38863
- Cu, quasistatic model for exploding wire with inductive energy bank, resistivity meas. 78—47199
- Cu wire, exploding underwater, in closed chamber, vap. bubbles, air effect *(Japanese)* 78—22596
- Cu wire, transient current pulsed heating, explosive inhomogeneous boiling explosive 78—38562
- Cu, wire evaporation of fast drops colliding with target *(Russian)* 77—15570
- Fe exploded wire, X-ray line emission and plasma conditions 78—59670
- Fe, exploding wire, elec. resist. at high temp., submicrosec. pulse heating meas. 77—89747
- K plasma in arc and capillary devices, optical props. 80—24244
- Li, ionisation and radiation dynamics simulation 78—83606

exploding wires and foils continued
- Li wire high energy density exploding plasma, holographic interferometry, self pinching, charge density 79—77436
- Mo XXXI-XXXIV spectra from exploded Mo wire plasmas 79—1295
- N_2 discharge, high-current, with inductive storage bank, exploding wire-initiated 80—10450
- Ni, exploding wire, elec. resistivity in fast RCL circuit 77—31995
- Ni, exploding wire, elec. resist. at high temp., submicrosec. pulse heating meas. 77—89747
- Ni, wire, pulsed heating in ultrahigh vacuum, anomalous electron emission 79—55598
- W exploding wire, peripheral arc initiation 78—87559
- W, wire, pulsed heating in ultrahigh vacuum, anomalous electron emission 79—55598

explosion bubbles *see bubbles*

explosions
- *see also accidents; detonation; nuclear explosions; safety; shock waves*
- acoustic pressure wave from linear explosion source *(Ukrainian)* 79—76901
- acoustic signal propagation from explosive source, time constant derivation 80—48485
- air, variable energy blast wave, shock trajectories, flow field densities 77—68620
- air suspension homobaric flow in presence of physicochemical transform. 80—87820
- Alpine Longitudinal Profile 1975, first results from explosion seismology 77—49172
- S.Central America, shallow crustal struct. from seismic data 77—56609
- anaesthetics, rel. to electrostatic volt., capacitance and energy storage characts. of human body 77—40954
- anisotropic explosion of rotating, self-gravitating uniform spheroids, astrophysical appls. 79—8822
- Asama Volcano, spectral studies of explosion earthquakes assoc. with 1973 eruptions *(Japanese)* 80—67340
- asymmetrical explosions, blast wave propag. 77—75939
- atmosphere, 2D calcs. 79—46345
- atmospheric explosions, attenuation of blast waves 77—31155
- axially symmetric explosion in magnetogasdynamics 80—62007
- axially symmetric medium, thermal radiation effects, astron. radiosources appl. 77—87249
- axisymmetric media, flow variables behind shock surface due to point explosion 79—68736
- black hole explosions, theory of optical and radio detect. 77—53622
- black hole explosions, upper limit of radio pulse emission rate 77—87469
- black hole universal origin and exploding black holes 78—8178
- black holes, primordial, explosion rate upper limit from gamma-ray bursts search 80—67911
- blast propagation, statistics of amplitude and spectrum 78—63224
- blast wave, with transport props., self-similar soln. 77—68621
- blast wave problem in conducting gas 79—37414
- blast waves, spherical, time-depend. energy deposition 78—9655
- bore hole explosion, elastic wave emitter model 77—33005
- borehole explosions, mechanical impulse of plates *(Russian)* 79—62455
- buried source, ground vibrations from seismic detonation 77—73667
- cathode spots of the first kind, erosion rate resistivity and thermal cond. depend., explosive model 79—14630
- cavity, cylindrical in compressible liq., dynamics, underwater explosion appl. 79—7385
- centrifuge cratering 80—72522
- chemical explosion induced, nuclear power plant protection 77—38351
- chemically reacting ideal gases mixture, explosion and implosion analysis 77—60066
- chloroform, variable energy blast wave, shock trajectories, flow field densities 77—68620
- circular cylinder pressure rise caused by surface explosions *(Japanese)* 79—76994
- cloud development, effect of explosions *(Chinese)* 80—82042
- coating by explosive cladding, technique for metals and alloys 78—3260
- collapsing gas, self-similar problem of strong explosion 79—90284
- compressed multicomponent mixture, pt. explosion 80—24044
- concrete slab, explosive shock resist., tensile fracture 80—85065
- conducting, magnetisable, incompressible media, explosion interactions *(Russian)* 77—55037
- containment vessel, cylindrical, submerged, dynamic plastic response, design formulae 80—83759
- containment vessel research 77—58594
- cool flame explosion, during piston compression, time predicted by Livengood-Wu integral method 78—15675
- crater formation modelling, meteorite impact effects 80—90088
- cratering explosion, pulsed hydrodynamic model 78—51180
- cratering phenomena, small scale, in geologic materials, photographic study 78—37093
- craters, coherently overturned flaps produced by hydrodynamic type wave motion 78—57209
- critical parameters of thermal explosion analysis 80—11891
- cyclotrimethylene trinitramine, high explosive, fracture surface energy determ. 77—44337
- cylindrical implosion, flow development, numerical anal. 79—4040
- damage for buildings caused by shaking, new data *(German)* 79—62444
- dense plasma generation by ionised gaseous filament explosion 78—71507
- detectors of explosive materials evaluation, for use in nuclear facilities 79—89451
- detonation, similarity and differences between conditions for initiation and failure 80—103038
- detonation velocity transient of Composition B-3 and PBX-9404 79—86450
- detonation wave magnification by pulsation energy 80—59075
- Diablo Range, California, P-velocity models from earthquake and explosion arrival times inversion 79—12094
- dielectric, thermal explosion theory in strong elec. field 79—91954
- dielectric constants and losses of explosive mixtures below 100 kHz 78—56422
- disc galaxies nuclei, superdense gaseous cores form. rel. to periodic explosions 80—90526
- disturbance wave-head amplification in homogeneous explosion in chem. reacting atm. 79—27658
- disturbances in viscoelastic spherical shell immersed in liquid 79—81734
- dust explosion, flame propag. vel., uniform dispersion of single sized particles 80—66803
- dynamic parameters of seismic sources 79—84141

explosions continued
elastic wave generation and mutual conversion of longitudinal and surface waves 77—70610
elastic wave parameters time vars. rel. to earthquake prediction problems 79—57870
elastic waves from weak explosion in deformed elastic material 77—56598
electric breakdown of detonation products 79—10736
electrical conductivity of high temp. imperfect gas *(Russian)* 80—100072
electron explosive emission regime, quasiplane cathode processes 78—75460
evaporation of cylindrical shell inner layer on collapse *(Russian)* 77—58714
explosion-induced accel. of cylindrical metal liners, form stability anal. 78—83425
explosive device detection using NMR techniques 79—6158
explosive heating due to projectile impact, numerical anal. 77—72142
explosive instability upon interaction of localized and nonlocalized waves 80—31530
ferrite powders, mag. props., explosive shock treatment effects 79—52395
field emitter vacuum breakdown, external mag. field effects, transition period 80—38824
flame sensor-trigger device for explosion barrier in underground mines 80—52313
foam, explosive charge detonation, shock wave parameters 77—15062
fragmentation of asteroids and artificial satellites in orbit 78—53858
galactic nuclei, explosions, rel. to very large H II regions form. 80—56951
galaxies, multiple explosion model of extended radio objects 80—41894
in galaxies, source and nature of explosions in nuclei 78—96546
Galaxy nucleus explosion, rel. to origin of North Polar Spur *(Russian)* 78—41072
gas cloud explosions, nuclear power plant blast effects 77—38350
gasdynamic disturbances, small amplitude, in exploding atmosphere 79—32574
Geysers geothermal field, California, explosions and microearthquakes study 80—3964
graphite, shock wave, prod. by explosion, vel. meas. 80—59074
Gurney equations for multilayer metal fragments 79—86367
hazardous atmospheres, max. explosion press. affected by low ambient temp. 78—44380
homogeneous explosives, electrical polarisation with initiation of shock wave detonation 79—100378
hydrodynamic cumulation regimes during lining collapse, cumulative jet 80—69891
hyperdetonation eccentric shock wave, approx. soln. 78—67070
hyperdetonation shock wave passage through jump like nonhomogeneity 78—67069
ignimbrite/sea water explosions, volcanic ash generation 80—26480
impulsive discharge noise, balloon burst and engine exhaust systems, acoustic pulse parameters determ. 78—90588
industrial explosions, causes, detection, and suppression 80—31725
initial shock parameters for explosion in rarefied gas 80—53815
instability collision mode stabilisation by drifting effects, Thirring instability *(Russian)* 80—43920
interfacial waves launched by an explosive line-source in a submerged elastic half-space 78—75088
ionospheric disturbances accompanying earthquakes and explosions 80—36451
IR emission meas. using versatile sensitive radiometer 77—70887
isentropic explosion compression of matter, profiling of explosion shock waves 77—56228
isentropic explosion compression of matter nonhomogeneous transition layer for shock wave profiling 77—56229
isothermal blast waves, one-dimens. in mag. field, mathematical theory 80—28532
N.E.Japan, upper mantle regionality from explosion seismic obs. 77—37167
jets produced by shaped explosive charges, particle size distribution in breakup 80—23957
large scale thermal explosions, propagation analysis 79—86449
laser focused on air, emission processes affecting development of explosion 79—7417
late stage equivalence of near-surface explosions 78—61353
Leidenfrost effect, demonstrations 78—81744
Liaoning Province, China, crustal thickness from gravity and seismic obs. *(Chinese)* 80—12349
liquid with ring shaped explosive, toroidal gaseous cavity one-dimens. pulsation 78—83423
in liquids, slow detonation, vapour explosions and bubble reson. explosions *(German)* 78—34150
LMFBR shock-induced fragmentation and detonating thermal explosions 79—13475
LMFBR thermal explosion hazards, review of present understanding and simulation expts. 78—82464
LWR, post-LOCA γ-ray energy redistrib. and effects 78—13280
LWR hypothetical core meltdown, vapour explosion potentials at high interface temp. 79—13476
LWR steam explosion pressure buildup estimation 79—13473
LWR steam explosion triggering expts. with oxidised Corium-E simulants 79—13472
M82, exploding, galaxy hypothesis questioned 79—75279
magnetized spheroids, anisotropic explosions 80—67532
metal powder explosive compaction 78—64501
metallic shell, explosive expansion, deform. and rupture modes and mechanisms 80—85064
metallic shell, explosive expansion, rupture behaviour 80—85063
meteorite explosion, Tunguska, Siberia, shock wave effects, model, computation 77—5507
meteorite impact and impact-explosive craters, destruction asymm. *(Russian)* 77—9726
meteorite in inhomogeneous atm., shock wave propag. 77—66973
meteoroids, in atm., shock waves producing geomag. disturbances 77—13139
methyl isocyanide, laser initiated thermal isomerisation, thermal explosion 78—80725
methyl isocyanide, thermal explosion, scaling laws 78—15676
microscopic metal points, explosive emission characts. 77—7624
mines and quarries, recording system for blast noise meas. 77—88984

explosions continued
mining explosions near Centralia, Washington, search for time-depend. P-wave travel times 78—44788
molten glass/water thermal interaction, nucl. reactor appl. 78—46149
molten LWR core material, thermal interaction with water 78—17383
molten metal-reactor coolant interaction, vapour film collapse expts. 79—13474
multishock problem in cylindrical symm., particle trajectory method, explosion near ground 78—1692
nanosecond gas discharge, explosive emission 78—9889
neutron generation by implosion of D_2 gas target 78—54869
NGC 1275, explosive phenomena in nuclei of radiogalaxy 80—26970
nuclear power stations, industrial activities nearby causing hazards 80—78408
nuclear reactor, impulse-initiated gas release triggering vapour explosion 78—17384
nuclear reactor, LOCA causing core meltdown, vapour explosion caused by water entrapment with melt 78—17382
nuclear reactor accident conditions, molten fuel+coolant interactions 77—23225
ocean, acoustic bottom loss measurement using multipath resolution 79—5652
ocean blast wave propagation, theory for stratified ocean *(Russian)* 80—81904
oceanic long range explosion expt., preliminary report 77—73679
off-centre point explosion in spheroid 78—63450
pentaerythritol tetranitrate, high explosive, fracture surface energy determ. 77—44337
phase plane method for seismic signals anal. 79—66843
photographic emulsions, preparation, explosion hazard of ammoniated silver salt solns. 78—4727
piezoresistive C gauge for low shock pressure meas. 79—1278
planar explosion mag. generator with resistive load, work performance optimisation 79—6156
planar laser explosion near a target in air 80—19601
plane hyperdetonation wave generation, optimum conditions 78—67068
plasma, explosion compression profiled via nonhomogeneous external layer 78—22534
plate, elastic, explosive shock wave 77—89060
PMMA, radical form. in explosive loading, electron spin reson. obs. 80—63678
point explosion in arbitrary atmosphere with radiative heat transfer 78—53708
primordial black hole explosions, search for optical pulses 77—57006
primordial black holes explosions, limits on microsecond cosmic radio bursts 79—17119
props. gas cavity expansion, soil dilatation after explosion in brittle rock 79—8608
propulsion of bodies in plane and cylindrical symm. 77—58544
quarry blasting, sound propag. expts. 79—24928
quarrying, use of electronic transient recorders for meas. explosion noise and vibration 80—67023
radiating stars, similarity solns. for central explosions 78—32443
ray method for solving gas dynamics equations *(Russian)* 79—27659
ray parameter-epicentral distance curves for point source on boundary 78—61336
Rayleigh-Taylor instability, boundary between products and surrounding atm. *(Russian)* 78—26135
reactive material ignition by heated surface, asymptotic anal. 78—7206
reflection of explosion waves from plane surface *(Russian)* 78—87361
residual stress formation in explosive welding 79—83285
rock rupture by elastic shock wave superposition in multiple detonations *(Russian)* 77—35082
rocks, explosions, spalling, tensile stresses 79—7324
S-wave propag. from explosion in transversely isotropic medium 78—81110
sea explosion waves, comparison of empirical and theoretical laws of parameter variation 80—36325
seismic events identification, appl. of non-linear stochastic models 79—16396
seismic explosions at Tateyama, Japan, appl. to seismic waves vel. change in S.Kanto area *(Japanese)* 80—67338
seismic fan shooting and least-squares analysis of non-layered anomalous vel. zones. 79—57857
seismic line-up axis time shift correction algorithm *(Russian)* 79—62613
seismic magnitude bias in network meas. rel. to identification criteria 77—40989
seismic radiation from a finite cylindrical explosive source 78—61340
seismic velocity time variance from multiple explosive sources, Hollister, California 78—44779
seismic wave generation, explosive versus nonexplosive sources *(Russian)* 77—9377
seismic wave reflection at wide angles, travel times 78—65202
seismic wave spectra forecasting from preliminary detonations 77—44930
shallow water horizontal spatial coherence meas. 78—5605
shaped charge jet formation, Pugh-Eichelberger-Rostoker solution representation 79—94692
shock adiabatic, given surface charge, appl. charged grid explosion *(Russian)* 77—65812
shock initiation, vol. of activation determ. 80—16683
shock tube, high-speed shock generation, using explosives 78—26156
shock wave, reflection from a plane, peculiarities 79—90281
shock wave front formation process, explosion due to inertial plate drive by pressure pulse 80—53811
shock wave propagation in hollow circular cylinder *(Japanese)* 80—10175
shock wave propagation in inhomogeneous atmosphere 79—55426
shock wave propagation investigations on suitability of piezoelectric and magnetoelastic detectors *(Polish)* 80—79351
shock waves, explosive charges of finite radius, energy hypothesis 78—55658
shock waves instability in a relaxing medium 80—100013
shock waves interaction with free ocean surface 79—2287
shock waves on Earth and in space 78—3897
sliding discharge, guided, explosive emission phenomena 80—19649
soil, wave interaction, stresses and strains 77—86801
solar chromosphere flares, initial phase parameters determ. from gas-dynamic explosion model 80—62104
solid-liquid model for explosion in ground 78—96158
source depth in marine seismology from explosive sink rates 79—34753

explosions continued
spark generator for dust explosion hazard assessment and gas ignition 78—57983
spherical shocks reflected from real and ideal surfaces, photogrammetry 77—72328
spiral galaxies, normal, post-explosion gas depletion in central regions 80—62272
stars, relativistic dynamics of radiating shell 79—21271
steady-state detonation velocity effect of physical homogeneity 79—94641
steam explosions, energy conversion, efficiency of LWR core materials 79—85648
steam explosions, hydrodynamic fragmentation, acoustic cavitation mechanism 79—85650
steam explosions with molten Fe oxides 79—85649
steel, low C, quenched, hardening during explosive forming 79—87650
steel, spalling prod. by sheet charge explosion and collision of plate 78—44198
steel butt weld structure and mech. props., explosive treatment effects 79—24541
stellar collapse and explosion, massive star core hydrodynamics 79—16995
stellar magnetospheric explosions, role of gravitational instabilities 78—28655
sterilisers, ethylene oxide, evaluation of effectiveness and hazards 77—60269
strong curvilinear shock wave, with arbitrary profile, evolution in inhomogeneous medium 79—14428
supernova core, Rayleigh-Taylor convective overturn rel. to explosion 80—77429
surface waves generated by shallow underwater explosions 79—2288
suspension explosives immersed in hydrostatic pressure field, detonation *(Polish)* 79—64700
thermal explosion, critical condits., step function reaction rate approx. 78—92480
thermal explosion theory for slab with time periodic surface temp. variation 80—43604
thermal explosion with heat loss, spatially homogeneous model 77—70303
thermal explosions, fragmentation requirements for detonation 78—71368
thermal explosions, heat balance and reactant consumption 77—90601
thermal explosions and the disappearance of criticality at small activation energies: exact results for the slab 80—7793
thermal explosions with reactant consumption, criticality phase-plane anal. 79—86530
thermal homogeneous, influence of reactant consumption on critical conditions 78—92483
thermal instability of vibr.-excited mol. gas, appl. to surface ignition *(Russian)* 78—56895
thermal reactor, steam explosion propagation phenomena, multidimensional aspects 79—89420
thermal wave propag., effect of mass released 79—41713
thermally conducting gas, point explosion 79—41714
Tokyo, base rock depth, seismic wave obs. from explosions *(Japanese)* 77—64232
Tunguska event, comet impact theories confirmed 78—7642
Tunguska event, thermal explosion of porous meteoroid, model 78—61813
Tunguska meteorite, energy, atm. inhomogeneity, comment 78—20424
ultrahigh vacuum discharge cathode erosion minimum conditions 78—75461
underground, model studies in halite and aleurolite 77—52999
underground explosion, seismic radiation pattern 80—61780
underwater, acoustic sources, distrib. of measured bubble pulse periods 79—5495
underwater, generation of sonomagnetic pulses 80—43510
underwater, ray and wave models evaluation and data interpretation 77—11068
underwater, scaling law for shock waves 77—14838
underwater, shallow, determination of acoustic source levels 80—19131
underwater, source depth determ. from spectra obs. at long ranges 77—7243
underwater explosion generation of sound pulse, nonlinear region 80—56493
underwater explosion of detonating gas with high initial bulk energy density 80—5867
underwater explosion shock waves, comment on weak shock soln. 79—90068
underwater explosions, book contrib. 77—47035
underwater explosions, shock wave interactions 80—14746
underwater explosions, surface effects, review 80—14745
underwater explosive shock waves, formulation of weak shock soln. 80—10070
unsteady MHD eqn. solns., for explosion in non-homogeneous media, num. anal. 79—64778
vacuum technique problems, with modern semiconductor processes *(German)* 80—86330
viscous fluid under cyclic deform., self-heating, hydrodynamic thermal explosion 80—58993
volcano, magma mixing as acid explosive eruption triggering mechanism 77—53027
vortex ring generation in dusty buoyant thermal following near-ground explosion 79—48561
water, explosive shock wave propagation, energy hypothesis 80—92179
in water, isothermal flows behind shock wave 77—89159
Yumenoshima explosions and seismic investigation of Tokyo base rock *(Japanese)* 80—41403
Al_2O_3, powder, phase composition, sintering, effect of explosive treatment 77—21079
Cl_2-H_2 mixture, detonation initiation, nonequilib. physicochem. process simulation 80—38431
Cu/Cu single crystal, explosion clad bonding, TEM obs. 77—62763
H_2-F_2-O_2, chem. laser mixture, multiatm., spontaneous explosions 78—73044
H_2-O_2 mixture, explosion limits as stochastic phenomenon 77—21387
Hg+water systems, drop fragmentation rel. to thermal explosion detonation requirements 78—71368
in Li/SO_2 cells, differential scanning calorimetry studies 79—52919
Pb(Zr, Ti)O_3, piezoceramic, explosive synthesis 77—16525

explosions continued
PuO_2 and (Pu,U)O_2 assemblies, fission and explosive energy releases 77—65295
SF_6 mixtures, laser initiated explosions, chemilum. in near UV, visible and IR 78—48674

exposure meters *see photometers*

extended Huckel theory calculations *see EHT calculations*

extensive air showers *see cosmic ray showers and bursts*

extensometers
absolute interferometric dilatometer 77—45832
bricks, extensometer for meas. of linear expansion due to freezing 78—53062
capacitance type AC dilatometer for piezoelectric and electrostriction const. meas. 80—77747
capacitance-torsion balance for measuring small stresses and strains 78—73988
chain-loading fibre tensometer for meas. glass fibre tensile strength *(Japanese)* 80—55610
cholesteryl laurate, crystallisation kinetics and phase transitions, differential scanning dilatometric obs. 79—69230
computerised for plastic and rubber industry 77—26284
conductive paper transducer output signal fluidity reduction 77—57318
counterbalanced pushrod vacuum dilatometer for low-strength materials 79—12762
description, and appl. to buildings and public works *(French)* 77—5828
design principles and props., thermal and thermomechanical cycle generation *(French)* 78—31598
dielectric layer, heat transfer coeff. meas., dilatometer method 78—45616
differential, precision, opticomechanical, for 20 to 1200°C range 77—74390
differential capacitance displacement transducer with low power lock-in amplifier 77—49710
differential dilatometer for detecting volume changes in specimen under H_2 attack 79—17395
differential dilatometer for reduced average coeff. of linear expansion meas. for solids at high temp. 78—193
differential scanning dilatometer, low temp., exam. of design, appl. to stainless steel, V_3Si *(Russian)* 79—34224
diffracting gauge principle, strain meas. appl. 79—85119
dilatometer, high-temp., for meas. shrinkage kinetics of liquid-containing ceramic materials 79—17396
dilatometer, ultrahigh vacuum, construction *(French)* 78—12670
dilatometer for Poisson ratio determ. of nearly incompressible elastomers 79—11733
dilatometer for PVT meas. of liquids and plastic crystals at low temperature 80—68208
dilatometer for small linear expansion temp. coeffs. 78—77957
dilatometer of parallel-plate capacitor design, thermal expansion meas. 77—51523
dilatometers, tube type, calibration, standards 78—12669
dilatometric anal. of thermophysical props. 77—71316
dilatometric measurements, high temp. method accuracy 80—73308
dilatometric method for study of dimensional anomalies in metallic materials rel. to crystal struct. *(French)* 79—52563
dilatometric titration, pressure transducing instrum. appls. 77—36810
dilatometry and its versatility in metallurgical studies. I *(French)* 78—65919
dilatometry with pressure transducing instrumentation, apparent molar vol. of NaOH in water 78—75702
dilution dilatometer for excess vol. meas. 77—48678
dynamic signals treatment from strain gauges *(French)* 80—22352
emissivity determination, metals and alloys, using low-inertia opt. dilatometry 80—59684
fatigue tests with axial and diametral extensometers 78—85062
fluid, heat capacity, thermal expansion, simultaneous meas., dilatometric meas. 77—84131
glasses, automatic recording dilatometer *(Japanese)* 79—70291
Hall effect extensometer for simple shear meas. in polymers 79—23286
high pressure, high temp. dilatometer, construction and appl. 77—37844
for high-pressure phase transformation obs. in polymers *(Russian)* 77—17950
high-temperature dilatometer for thin wires 79—97380
induction, temp. compensated, displacement meas. appl. 79—17394
laser extensometer, comparative anal. with rod extensometers 77—64452
laser extensometer with scanning beam modulation, improved gauging precision 78—57896
linear thermal expansion coeff. unit, 4.2 to 90K, USSR state standard 78—37001
liquid crystals, phase transitions, differential scanning dilatometric obs. 79—69230
liquid specific heat and thermal expansivity, simultaneous determ. by dilatometric method 77—87758
low cycle fatigue testing extensometer for anisotropic materials 79—24695
low-temperature differential dilatometer for measuring linear expansion coeffs. in 4 to 80K range 80—17922
metallic bellows dilatometer, calibration 77—82487
metals and alloys, use of dilatometric methods *(French)* 79—5100
mould material deformation meas. at high temp., apparatus 78—3266
nuclear fuel cladding strain meas., microprocessor-controlled microwave extensometer 78—33240
optical dilatometer, for thermal expansion coeff. determ. of fibres, films and polymers 80—45454
photoresistor dilatometer, for polymer materials testing 80—81251
pneumatic extensometer for large deformations *(Russian)* 78—77901
polymers, hygroscopic, lateral extensometer, appl. to creep testing of nylon-6,6 78—95883
porcelain-metal cermet, stress determ., meas. method *(German)* 80—76425
quartz dilatometer based on mechanotron for meas. linear expansion coeff. 80—105639
quartz dilatometer with capacitance transducer 77—13736
rolling mill performance monitoring appl. 77—41590
second-order transitions in metals, high-speed dilatometry 77—89951
skin extensometer for in vivo meas. of human skin biomech. props. 77—44704
small-size, for wide range of strains in tension and in torsion 77—40439
specific heat determination, rapid dilatometric method 79—86327
standard samples for dilatometry 78—26699

extensometers continued
- steel, C, decomposition of supercooled austenite, exam. of carbide formation *(Russian)* 78—35388
- strain gauge meas. system, semiconductor, rolling mill force meas. appl. 78—41296
- testing installations, high-temp., high precision absolute interference dilatometer 79—35677
- thermal diffusivity, improved dilatometric method 77—41597
- thermal expansion of solids meas., 25°C to 1600°C, using alumina tube 78—36965
- thermomechanical and linear dilatometric testing, automatic recording device 80—11858
- tower extensometer for tension testing rigid plastics 79—83410
- vitreous SiO_2 tube dilatometer for thermal expansion meas. of solids, −195 to 1000°C 79—26026
- volume dilatometer for polymers 78—5706
- volumetric dilatometer, design, exam. of petroleum asphalts 78—57939
- Al-Al_2O_3 alloys, dilatometric method for studying relaxation of conc. of defects 77—55288
- Si cell for precise measurement of thermal expansion at low temps., results for Cu, NaF 80—37027

external flows
- buoyancy cross-flow effects on longitudinal boundary layer flow 77—58687
- circular cylinders, surface-roughness effects on mean flow, turbulent boundary layers 80—92128
- circular cylinders of high aspect ratio at $Re \ll 1$, drag coeff. 80—48832
- convection, mixed forced/free, from horizontal plate, in porous medium 77—75908
- cylinder, transverse curvature and turbulence effects on axisymmetric liquid flow *(Russian)* 80—59015
- cylinder wake, external turbulence effects 78—94665
- ellipsoid in inviscid flow, surface pressure distrib. 80—48831
- fluid-elastically coupled coaxial cylindrical shells, response to external flow 77—89063
- formation from self-gravitating gas cloud, rotation and Kelvin-Helmholtz instability 79—46287
- free surface gravity flow, finite element anal. with variable domain 78—79294
- gas cloud, self-gravitating rotation and Kelvin-Helmholtz instability 79—46287
- heat transfer bibliography 78—63425
- ideal gas supersonic flow around blunt wedge, sonic line shape 80—64577
- inviscid conical flowfield structure about external axial corners 79—94646
- jet flow, viscous, with surface tension, finite element soln. 78—79349
- jet noise, external boundary-layer flow effect in flight 77—75901
- longitudinal blunt circular cylinder, axisymmetric separated and reattached flow, turbulence 80—79285
- non-Newtonian flow along thin needle, vel. profile, skin friction 78—67229
- nozzle in different jet regimes, internal and external flows, separation and wakes 80—100023
- oscillating, struct. and development of turbulent boundary layer 80—19353
- Oseen's linearised flow eqns. for low Reynolds flow past cylindrical bodies 80—53739
- rectangular body, laminar flow, separation bubble and stagnation line 80—64514
- separated supersonic boundary layer, moderate injection with reattachment, shear layer 79—32562
- sphere immersed in a fluidised bed, mass transfer *(French)* 80—92214
- stagnation flow turbulence about circular cylinder, visual study 80—96248
- steady flow about blunt bodies, finite difference methods 80—96280
- steady viscous flow past circular cylinder, numerical study, vortices and separation 80—92108
- steam condensation on external entrance length of cooled rot. tube 77—75906
- Stokes flow, slender body theory for viscous incompressible fluid 80—92160
- streaming in vicinity of plate possessing propagating longitudinal strain wave 80—87758
- streamline flow round an array of profiles in a magnetic field perpendicular to the plane of the flow 80—83856
- supersonic viscous flows, interactive numerical calc. procedure 77—31326
- transonic flow problems soln. using method of decomp. 77—58725
- turbomachines, boundary layer charact., influence of external flow turbulence 80—87811
- turbulence, book 78—90839
- turbulence, book contrib. 77—58653
- turbulent boundary layer struct. with low external flow turbulence *(Russian)* 79—68689
- turbulent heat transfer measurements in axisymmetric external separated and reattached flows 80—10234
- unsteady transitional and turbulent boundary layers, expt. and calc. methods *(French)* 78—75125
- viscous flow past circular cylinder, two coord. systems description 77—58643
- wing, supersonic gas flow, numerical method and routine 80—38440

extraordinary ray *see birefringence*

extrapolation
- adsorption isotherm, John's method, linearity range implication 80—34293
- analytic extrapolations towards interior points from a cut, applic. to elementary particle scatt. theory 80—12952
- animal carcinogenicity expts. low-dose-rate data extrapolation 77—56327
- atmospheric hail volume model extrapolation from surface meas. 77—21871
- creep rupture data analysis, development of correlation and extrapolation methods 80—58975
- emissivity of gases, data extrapolation method 77—7506
- external mag. field, analytical extrapolation into two-dimens. magnetised body *(German)* 79—48393
- fusion reactor materials science 79—97899
- gravitational and magnetic anomalies extrapolation, equivalence principle *(Russian)* 79—39926
- Josephson junctions, voltage response, functional relation, extrapolation technique for accelerating computation 80—107963

extrapolation continued
- Langmuir probe characteristics at low plasma densities, numerical analysis 78—63592
- magnetic and gravitational anomalies extrapolation, equivalence principle *(Russian)* 79—39926
- magnetic multicritical behaviour, two-variable approximants using series extrapolation method 77—66336
- molecular orbitals, effective convergence to complete orbital bases and at HF limit through systematic Gaussian primitive sequences 80—14065
- monatomic gas, collision-induced light scatt. at intermediate density, integrated intensity, appl. to Ar 80—24124
- multidimensional interpolation by polynomial roots 80—18778
- multiparameter discounted least squares, extrapolation 77—17792
- neutron point kinetics, smoothing and extrapolation method 77—65252
- orbital amplitudes of nuclei, extrapolation procedure, gaussian basis set and nucl. cusp eqn. 78—74560
- partial differential equations., methods 78—36810
- periodic solns., numerical extrapolation 78—69663
- pion pion scattering lengths, universal curve, optimal extrapolation techniques 77—46080
- potential fields extrapolation, numerical techniques and geophysical appls. *(Russian)* 79—74988
- proton form factor extrapolation using Pade type approximants 79—6341
- PWR core, large, appl. of coarse-mesh finite difference eqns. for k_{eff} and peak power factors 78—17305
- rate equations for elevated temperature creep 80—65141
- SCF calculations, simplified extrapolation procedure 78—82604
- Stokes eqns. approx., stationary 77—14976
- structure factor extrapolation into low-angle scatt. region 77—51289
- subsonic and slightly supercritical aerodynamic flow, rapid finite-difference computation 77—23979
- temperature prediction method for inverse heat cond. problem for solid cylinder 79—94449
- thermal conductivity and viscosity of pure liquids and gases, interpolation formulae *(Dutch)* 78—12661
- thermal expansion of solids at high temp., calc. using extrapolated estimate 79—86909
- time scale realisation models and predictions 78—57907
- whistler extrapolation, comparison of systematic errors in different methods 77—53334
- whistler extrapolation via linear-Q anal. and extrapolation factor, systematic errors 77—53333
- Co (VII), semiempirical investigation of spectra 78—33434
- Ni (VIII), semiempirical investigation of spectra 78—33434

extraterrestrial atmospheres
- *see also comets; planetary atmospheres; stellar atmospheres*
- comet comae, effect of solar photodissociative ionisation 80—90370
- Comet Kohoutek (1973 XII), ion tail dynamical response to solar wind interaction 80—85897
- Comet West (1976 VI), coma mols. and dust distrib., visible emission profiles 80—101562
- cometary atmospheres, opposition effect detect. from BV photometry 80—31258
- cometary coma, C production model 79—16885
- comets, electric current and mag. field struct. 79—40141
- comets, interplanetary shock waves interaction 77—22032
- comets, photoelectron fluxes in atmospheres 79—2520
- comets neutral atmospheres, average random walk model for mol. phot. dissociation 80—77351
- Galilean satellites, max. permissible exospheric temps. calc. 79—70989
- Galilean satellites magnetospheres, plasma and mag. field perturbations 80—46465
- Ganymede, atmosphere erosion by radiation belt energetic atomic particles 80—72736
- Ganymede, O atmosphere stability 77—29708
- Ganymede, stellar occultation obs. by Voyager 1 rel. to exospheric atmosphere 80—26792
- Io, atmospheric models with NH_3, N_2 and Na 77—37559
- Io, global SO_2 abundance upper limit 80—77332
- Io Na cloud, solar radiation press. as cause of east-west asymmetries 80—36560
- Io plasma torus, effects on Jupiter kilometric radiation ray tracing 80—72866
- Io plasma torus, effects on Jupiter kilometric radiation spatial and temporal distrib. 80—77328
- Io plasma torus, Voyager 1 EUV spectrum obs. 80—26792
- Io plasma torus, Voyager 1 plasma waves obs. 80—26795
- Io plasma torus, Voyager 1 radio astronomy obs. 80—26796
- Io SO_2 frost controlled gaseous atmosphere, evidence from UV obs. 80—36561
- lunar volatile emissions, detect. techniques 79—44385
- Moon, atmosphere and meteoritic flux transformation 78—61768
- Moon, dust transport on lunar surface 80—8558
- Moon, plasma near surface, radiosource occultation obs. 80—8559
- Moon, surface interaction with exospheric atmosphere 78—49351
- Moon exosphere simulation, Monte Carlo methods 80—67588
- Moon exosphere simulation, Monte Carlo methods 80—67589
- Periodic Comet Stephan-Oterma (1980g), total visual magnitudes and coma diameters, (1980 September 7 to 11) 80—109397
- satellites of outer planets, atm. dynamics 79—75125
- Titan, Axel dust props., Mie theory 77—37565
- Titan, Kuiper bands detect. in spectrum 78—85898
- Titan, NH_3 atmospheric abundance 78—12142
- Titan, photochemistry of hydrocarbons in atm. 79—53766
- Titan, props. from IR spectrum from 0.8 to 2.5 microns 80—21946
- Titan, upper ionosphere photoionisation 77—60720
- Titan atmosphere, non-Maxwellian effects assoc. with H_2 thermal escape 79—80264
- Titan atmosphere, photochemical aerosols identification 80—31249
- Titan atmosphere, photochemical models 80—36567
- Titan atmospheric aerosol distribution, constraint 79—96964
- Triton, image tube spectra, 6800-9000 Å, search for possible atm., methane upper limit 79—16880
- Triton, satellite with atmosphere, IR spectrum obs. 80—21945
- Io, Na and H clouds 77—64695
- Io, Na I, Ca I, Fe I, and Mg I emission lines in spectrum 79—21223

extraterrestrial life
- alien probe flux density calc. 78—81563
- apparent absence on Earth, significance, rel. to search for extraterrestrial intelligence 80—4277

- **extraterrestrial life** continued
  - artificial objects located at Earth-Moon libration points, unsuccessful search 80–98647
  - bacteriophage ϕX174 DNA, possible message from extraterrestrial intelligence 79–53738
  - bibliography, chem. evolution and the origin of life 80–90620
  - broadcast strategies and source position for advanced civilizations 77–91449
  - CETI, 1.5 mm as optimum wavelength region 79–40094
  - CETI failure possibilities 77–49316
  - CETI from Earth satellite orbit 78–61758
  - CETI from Earth satellite orbit 80–4275
  - civilisations possible self-annihilation through thermonuclear war 78–81562
  - colonisation of interstellar space, extent and Drake eqn. 80–56724
  - colonisation of solar system 77–49263
  - comets, primordial, elementary life forms origin in radiogenically melted interiors 80–67659
  - comets as origin of terrestrial life 80–51672
  - communication, call signals struct. 77–13257
  - communication by mutual search strategy 80–56723
  - communication problems *(Czech)* 77–9678
  - communication with civilisation around other stars 78–16314
  - communication with extraterrestrial intelligence, international conference discussion and conclusions *(German)* 77–56845
  - communications, possibilities using neutral H line 79–35152
  - contaminant terrestrial microorganisms, limitations to growth on outer planets 77–41355
  - detection from nucelar waste spectrum in stellar spectra 80–82230
  - Dyson spheres, mass and energy requirements rel. to IR emission 78–69710
  - Earthlike planet prevalence in Universe and possibility of higher biological organisms 80–41735
  - elliptical galaxies, lack of spiral arms and lifebearing planets 77–64845
  - ETI signals search, obs. program using existing facilities 80–4266
  - exotic life and exobiology, characts. 78–69708
  - extinction at UV wavelengths, role of biochemical chromophores 80–26945
  - fundamental dimensionless numbers and possibility of life, historical data in cosmic cycle 79–80245
  - fundamental dimensionless numbers and possibility of life, Machian variational cosmology 79–80246
  - galactic communicative civilizations, formalism and numerical calc. 77–91448
  - inGalaxy, probabilities 79–48692
  - in globular clusters, search of OH and H_2O lines 80–56725
  - habitable planets in Galaxy, number 79–40221
  - habitable zones about main sequence stars 79–40188
  - habitable zones around main-sequence stars rel. to climatic models 80–82049
  - habital planets around multiple stars, computer simulations 79–2559
  - human colonisation consequences 78–4187
  - interstellar and prebiotic organic chemistry 77–37641
  - interstellar arks, cosmic-ray shielding 77–49264
  - interstellar bacterial grains, prod. of 3μ spectral feature in galactic IR sources 80–62227
  - interstellar cold grains as seeds of life 77–91606
  - interstellar colonisation 78–61756
  - interstellar communication, binary stars use as time markers 79–101092
  - interstellar communication, review of theory 80–4271
  - interstellar communication, signalling strategy 78–61757
  - interstellar communication, timing strategy 78–16313
  - interstellar communications, preferred freq., 4.8 GHz formaldehyde line 79–16845
  - interstellar dust grains as possible cold sources of life 79–21203
  - interstellar formation of living matter rel. to interstellar molecules 79–84836
  - interstellar grains, possible identification with bacteria, algae and virus particles 80–31341
  - interstellar human civilisation likelihood 78–81561
  - interstellar molecules, galactochemistry and origin of life 78–12338
  - interstellar molecules in prebiological evolution 80–94726
  - interstellar search systems, antenna concepts 78–28545
  - interstellar travel and communication, bibliography 78–81564
  - interstellar travel and communication, bibliography 80–101677
  - laser signals detect. likelihood, instrumentation 80–4276
  - manned interstellar flight and colonisation of other systems 77–71017
  - Mars, biological implications of Viking mission 79–8872
  - Mars, organic compound search by Viking, final conclusions 80–67627
  - Mars, photosynthetic microorganism response, model 79–40114
  - Mars, Viking and search for life, gas exchange expt. indicators 77–37549
  - Mars, Viking biological expts. 78–20711
  - Mars, Viking biological expts. findings 78–65542
  - Mars, Viking biological investigation, preliminary results 77–17415
  - Mars, Viking biological investigations review and status 79–80263
  - Mars, Viking C assimilation expts. 78–20708
  - Mars, Viking gas exchange expt. 78–20710
  - Mars, Viking labelled release biology expt. 77–56863
  - Mars, Viking labelled release expt., radiorespirometry 77–37548
  - Mars, Viking labelled release expt., results 78–20709
  - Mars, Viking Lander 1 life detection expt., chemical interpretation 78–32382
  - Mars, Viking lander camera search for life 78–20697
  - Mars, Viking Landers and unsuccessfull search for life 78–49367
  - Mars, Viking mission and search for life 77–25969
  - Mars, Viking mission results 80–82255
  - Mars, Viking project and search for organic life *(Swedish)* 77–22128
  - Mars, Viking pyrolytic release expt., C assimilation meas. 77–41346
  - Mars, Viking results–life or active soil chemistry 77–37546
  - Mars lander sterilisation and biological expt. containment 77–17327
  - microwave observational approach 78–61759
  - multiple stars and the number of habitable planets in the Galaxy 77–37511
  - narrowband radio signals near H I 21 cm line, all-sky search 77–29661
  - narrowband signals of extraterrestrial origin, search at 21 cm wavelength 79–25521
  - non-chemical life-form, crystalline physiology model 77–90978
  - nonsolar planets, search methods, IR interferometry from Earth orbit 79–53737
- **extraterrestrial life** continued
  - Nova Cygni 1975, synchrosignal for extraterrestrial civilizations 78–28546
  - origin of life, molecular evolution and exobiology, interdisciplinary course 79–21485
  - panspermia hypothesis, trace elements 77–32968
  - prebiotic molecules in Martian dust clouds 77–64688
  - radio contact problems 78–69707
  - radio emission leakage in interstellar communication, Earth model 78–57474
  - radio search for extraterrestrial intelligent signals 77–17386
  - radiocommunication, efficiency of signals associated with natural phenomena *(Russian)* 78–40842
  - radiocommunication possibilities, use of Moon *(Czech)* 77–9677
  - radiocommunication using Sun as gravitational lens 80–62040
  - search for civilisations, SETI scenario approach 77–67048
  - search for extraterrestrial intelligence, implications for telecommunication 77–33361
  - search for extraterrestrial intelligence (SETI), consensus 79–40093
  - search for intelligent life in Galaxy, geophysical importance 79–53736
  - search for signals from extraterrestrial civilisations, simulation approach 80–62039
  - SETI, radio emissions 80–4273
  - SETI, systems analysis 80–4274
  - SETI at 18 cm, high sensitivity search 80–82229
  - SETI strategies 80–4270
  - SETI strategy in microwaves 80–4265
  - signal processing equipment in SETI programme 78–69709
  - signals from extraterrestrial civilisations using X-rays from neutron star accretion 77–53432
  - signals from extraterrestrial civilizations, search by synchronous dispersion reception 80–4264
  - soils, planetary chemical-biological search possibilities 79–40176
  - space colonisation, teaching 79–44663
  - technology evolution on planets supporting biosphere, criteria 77–71018
  - telecommunications requirements for search for extraterrestrial intelligence 78–32319
  - Viking lander biology expts., review 77–91407
  - Viking lander biology instrument 78–49347
  - Viking programme, biological expts. *(Hungarian)* 79–44329
- **extraterrestrial radiofrequency radiation** *see radiofrequency cosmic radiation*
- **extremum control** *see optimal control*
- **extrusion**
  - carboxymethylcellulose soln., flow in profile channel of extrusion head 79–98780
  - composite superconductors, fabrication 77–24989
  - continuous extrusion of metal powders for electrical industry appl. 79–95968
  - die entry flow, kinematics and stability 79–60026
  - ethylene-methyl acrylate, random copolymer, review 80–108330
  - ethylene-vinyl acetate copolymers, extrusion and heavy duty films, radiation crosslinking, struct. effect 80–66844
  - extended plane fluid sheet, swelling finite element anal. 79–37277
  - glass fibre, forming process, characts., anal. techniques 80–58827
  - glass-ceramic, hot extrusion prep., and microstruct. 77–32552
  - glass-fibre reinforced Al-alloys, hot extrusion, heat-treatment 77–24988
  - glass-fibre reinforced Al-alloys, hot extrusion prep. and props. 77–24987
  - glass-fibre reinforced PET, order-disorder transitions during extrusion 80–50633
  - green bodies, extruded, slip-cast and isostatically pressed, binder distrib. 78–27448
  - helical shape extrusion from round billets 79–29102
  - high strain rate processes, review 80–84864
  - hydroextrusion under hydrodynamic lubrication conditions *(Russian)* 79–38852
  - hydrostatic extrusion, hot and cold, adaptation of conventional press *(French)* 77–57344
  - hydrostatic forming, novel appls. 77–44191
  - invariant system with switched element, design and evaluation for heat processes control during extrusion of plastic materials *(Russian)* 80–100854
  - metal, hydroextrusion, effect of longitudinal US vibrs. 79–96046
  - metal extrusion process, stress and deform. anal. 77–48364
  - metal hydroextrusion process, boundary-value problem *(Russian)* 79–10505
  - metals, hydroextrusion, effect of longitudinal US oscills. *(Russian)* 79–34071
  - multiple hole extrusion 80–35236
  - nonferrous metal, semi-brittle, high-speed backward extrusion using superimposed hydrostatic press. 80–84865
  - nonisothermal flow of anomalously viscous liquids in channels of screw extruders 80–19305
  - Nylon 6, plasticized with NH_3, deformation by solid-state extrusion 80–25736
  - Nylon-12, hydrostatic extrusion, struct. change *(Japanese)* 79–15693
  - plastic flow of cylindrical body, axisymmetrically deformed *(Russian)* 79–7300
  - plastic resins, secondary coating of optical fibres, effect on transmission props. 80–58704
  - plastics sheet blowing and extruding, process identification for automatic process control *(German)* 80–81023
  - PMMA, hydrostatic extrusion 80–108479
  - PMMA femoral cement compactor for total hip replacement 79–79688
  - polethylene-polypropylene blend, extruded, thermal swelling and mech. characterisation 80–81110
  - poly(vinylidene fluoride) orientation, solid state deformation by coextrusion 80–40394
  - polybutene-1 film, tubular-extended, anal. of orientational and form birefringence 80–29712
  - polyethylene, amorphous-cryst., highly oriented, plastic deform. rel. to supermol. struct. *(Russian)* 79–51010
  - polyethylene, direct ram extrusion, correlation between chain-folding and tensile modulus 77–44209
  - polyethylene, high density, elongational flow induced extrusion *(Japanese)* 79–91614
  - polyethylene, high density, hydrostatic extrusion behaviour 80–50649
  - polyethylene, high density, self-reinforced thermoplastic, extrusion 79–15699
  - polyethylene, high density, solid state coextrusion, geometric factors effect 80–71704

extrusion continued
- polyethylene, high density, solid state coextrusion, technique for ultradrawing thermoplastics 80—84979
- polyethylene, high density extruded fibres, morphology effect on physical and mech. props. 79—83235
- polyethylene, high modulus filaments, form. from melt, cryst. nucleation effects 79—70034
- polyethylene, high-density, solid-state coextrusion, mol. wt. distrib. effect 80—104212
- polyethylene, high-density fibres, extrusion conditions influence on thermal props. and morphology 79—61617
- polyethylene, high-density fibres, solid-state extruded, form. props. 79—70035
- polyethylene, high-density ultradrawn, extrusion ratio influence on tensile props. 79—61618
- polyethylene, hydrostatic extrusion, deform. of crystalline and amorphous, and thermosetting resins 79—38875
- polyethylene, solid-state extruded, exam. of props. 80—11669
- polyethylene, ultra-oriented high density, shrinkage as meas. of deformation efficiency 80—40398
- polyethylene, ultrahigh mol. wt., processing methods for artificial joint appl. 79—84001
- polyethylene fibre, high-strength high-modulus, morphology and tensile prop. relations 80—103264
- polyethylene fibres, high density, ultra oriented, physical, mech. props. 80—25649
- polyethylene film, minimum running thickness, biaxial extensional flow study 80—100993
- polyethylene melt, flow in profile channel of extrusion head 79—98780
- polyethylene melt, high density, oscillating flow during extrusion, model anal. 80—100016
- polyethylene melt, oscillatory flow through capillary 80—103046
- polyethylenes, extrusion and heavy duty films struct. parameters influence on cross-linking by radiation 80—66844
- polymer melt, shear stress over wide shear rate range, in falling coaxial cylinder, rheometer 79—7363
- polymer melts, extrusion at constant deform. rate 78—68744
- polymer science and technology, book 78—48363
- polymer soln. through capillary, flow instability and electrostatic effects 79—60035
- polymers, anal. of mechanics of solid phase extrusion 80—39204
- polymers, hydrostatic extrusion, deform. of crystalline and amorphous, and thermosetting resins 79—38875
- polyolefins, ultra-high modulus, production by tensile drawing and hydrostatic extrusion 80—81022
- polypropylene melt, flow in profile channel of extrusion head 79—98780
- polystyrene melt, molecular weight effects in die swell and in shear rheology 79—94575
- polystyrene-polypropylene(polyethylene) mixtures, elastic moduli, phase struct. effect *(Polish)* 79—70107
- polythene, ultraoriented, microhardness, extrusion conditions effect 80—50704
- porous body, densification during hot extrusion 77—44189
- porous preforms, die filling and densification in hot extrusion forging 78—23645
- prealloyed powder blending, composite materials fatigue and tensile props. *(French)* 80—20850
- PVA soln., flow in profile channel of extrusion head 79—98780
- PVC, amorphous-cryst., highly oriented, plastic deform. rel. to supermol. struct. *(Russian)* 79—51010
- PVC, asbestos reinforced, CIR/Palram process preparation, mechanical and thermal properties measurements 79—66106
- PVC extruded films, effect of chlorinated polyethylene as impact modifier *(Polish)* 79—70037
- PVC rigid, flow and therm. stability 79—64618
- reverse cold impact extrusion, appl. of ultrasonic radial oscillations *(Russian)* 80—97441
- rigid-ideal plastic, process using orthotropy concept of Hill, kinematically determined problems *(German)* 80—1445
- rubber toughened plastics, ABS- and AAS-resin, flow props., effect of heating and shearing hysteresis *(Japanese)* 79—94685
- shear band formation models, in rolling and extrusion 80—3152
- shear band formation models, in rolling and extrusion 80—11666
- spherical shell, three layer, stress/strain relations *(Russian)* 80—3122
- steel, alloy, high speed, cutting tools, carbide heterogeneity change during hot extrusion 80—16390
- steel, high C, type UB, hydrostatic extrusion influence on struct. and props. *(Russian)* 77—56022
- steel, sintered, mech. props., effect of small cold reduction 79—39048
- steel, structural martensitic, corrosion resist. under stress effect of strain ageing with hydroextrusion *(Russian)* 79—38853
- steel, TRIP, warm extrusion, process control and tensile props. 80—16338
- steel, W-Mo, tool, hydrostatic extrusion and tempering, wear resistance effect 80—50728
- steels, tool, cold hydrostatic extrusion rel. to struct., props. 79—20068
- steels, tool, type U10A and R6M5, phase comp. and phys. props. after hydrostatic extrusion 79—96053
- thermally induced extrudate swell, Galerkin method 80—79312
- thermoelectric materials, extruded from ceramic blanks, recrystn. and elec. props. 79—43267
- thermoelectric materials, extruded materials with tetradymite struct., primary and in situ recrystn., elec. props. 79—43266
- thermoplastic sheet, extruded, thickness adjustment and cooling between calender rolls 79—68597
- viscous drag continuous extrusion 77—55912
- Ag halide optical fibres, extrusion, visible and IR transmission 80—58829
- Al alloy compacts, specific press. for extrusion 79—20070
- Al alloys, extrusion, purity effect on fracture props. 79—100248
- Al billet, hot extrusion, nonsteady state temp. distrib., numerical method 80—60886
- Al, numerical smoothing of flow patterns 80—7625
- Al plastic flow in plain strain extrusion, photographic appl. 80—7626
- Al-alloys, extruded, mech. props. 78—11151
- Al-C, dispersion hardened, effect of processing parameters on mech. props. 80—20826
- Al-C alloys, dispersion hardened exam. of production method using pressed powders 80—16244
- Al-Cu-Mn-Mg, type D16, substruct. anisotropy and decomp. as subboundaries in extruded rods *(Russian)* 77—25095

extrusion continued
- Al-extrusions, pick-up formation 78—39882
- Al-Mg-Si, deformed, orientation of recrystallisation nuclei 79—91681
- Al-Zn-Mg, polygonized struct. in extrusions, thermal stability and mech. props. 80—50659
- Al-Zn-Mg alloys, role of dispersed transition metal intermetallic compounds 79—96088
- Be, ultra fine-grained, recrystn. after deform. 79—52239
- n-$Bi_2(Te,Se)_3$ semiconducting solid solns., plastic deform. during hot extrusion 79—20143
- Bi_2Te_3-Sb_2Te_3 composite billet, diffusion during plastic deformation *(Russian)* 79—23767
- p-Bi_2Te_3-Sb_2Te_3 semiconducting solid solns., plastic deform. during hot extrusion 79—20143
- Bi_2Te_3-Sb_2Te_3 solid solns., plastically deformed by hot extrusion, diffusion meas. using micro-X-ray spectrum anal. 79—14954
- n-$Bi_2Te_{2.88}Se_{0.12}$, extrusion deformed, powder dispersion degree influence on thermal and elec. props. *(Russian)* 80—39366
- Cu, extruded at 77K, defect struct. and elastic limit *(Russian)* 80—30016
- Cu, stress removal during annealing after hydrostatic extrusion 79—83215
- Cu-Ge(Sn)(Sb) alloys, stress removal during annealing after hydrostatic extrusion 79—83215
- Cu-Nb_2Sn composite wires, prep. and superconducting props. 78—31026
- Fe, Armco, hydrostatic extrusion in fluence on struct. and props. *(Russian)* 77—56022
- Fe-Cr-Al, ODS alloys, prep. and props. 78—52720
- Fe-oxide dispersed alloys, fabrication by hot extrusion 77—25063
- Fe-P-S composite sintered bearing materials manufacture, wear intensities 80—20881
- Mn-Al-C alloy, anisotropic, permanent magnet appl., properties and production *(German)* 79—8309
- Mn-Al-C anisotropic permanent mag., cryst. orientation and form., X-ray diffr. anal. 79—82778
- Mo, single crysts., pressure masgnitude influence in hydroextrusion on plastic strain mechanism *(Russian)* 80—21009
- Mo-Zr-C (0.063, 0.06 wt.%) alloys, ageing, effect of cold deform. by hydrostatic extrusion 79—57001
- Mo-Zr-C (0.63, 0.06 wt.%), quenched and deformed, structural changes during heating to ageing temp. *(Russian)* 79—1879
- Nb-Ti, wire drawn and hydrostatically extruded supercond., crit. current density 79—38275
- Nb_3Sn A15 composite superconductors, hydrostatic extrusion *(French)* 80—104090
- Nb_3Sn multifilament supercond. wire, hydrostatic extrusion processing 79—33976
- Nb_3Sn-Cu superconducting composites, produced by cold extrusion of fine powders 79—38767
- NbTi multifilament supercond. wire, hydrostatic extrusion processing 79—33976
- Ni, dislocation structure evolution after hydroextrusion *(Russian)* 80—96530
- Ni powder, sintered, use of extruded porous materials as fuel cell electrodes 80—40853
- Ni-Ti (48 at.%), annealed and rolled electron microscope and probe analysis of structure 79—100189
- p-$Sb_{1.48}Bi_{0.52}Te_3$, extrusion deformed, powder dispersion degree influence on thermal and elec. props. *(Russian)* 80—39366
- $Sb_{1.48}Bi_{0.52}Te_3$, obtained by zone crystallisation, effect of extrusion and annealing on elec. props. 79—96038
- Sn bronze, extruded atomized powders, struct. and props. 79—38763
- Sn bronze powders, air atomised, densification and pressure requirements during extrusion 77—59713
- Ti-6Al-4V, stress distrib. for steady axisymmetric extrusion 80—3103
- Ti-Al-V (6, 4 wt.%), temp. distrib. for steady axisymmetric extrusion 80—11670
- Ti-Al-V (6, 4 wt.%), temp. distrib. for steady axisymmetric extrusion numerical results 80—11671
- Ti-Mo (Zr) (Nb), sintered, manufacture and exam. of props. 79—95975
- TiAl, manufacture by extrusion of blended elemental powders 77—28750
- V_3Ga, hydrostatic extrusion feasibility *(Russian)* 77—21215
- Y_2O_3 stabilised ZrO_2, ultrafine-grained, fabrication and flexural strength 77—1829
- Zr_3Al-base alloys, tube forming 77—8784
- ZrO_2, partially stabilized, props. and appl. to extrusion dies 80—97507

eye
- *see also contact lenses; vision*
- aberrations, high-order, subjective meas. 77—1994
- aberrations, monochromatic, subjective meas. 78—35837
- aberrations and aphakia 77—29146
- abnormal movements control method using audio feedback 80—41156
- acceleration forces at eye level experienced with rotation on the horizontal bar 80—45937
- accommodation, reaction and response times obs. 80—67073
- accommodation, temporal stability of the dark focus 79—43867
- accommodation absence during perceptual reversal of Necker cubes 80—41037
- accommodation and vergence static behaviour, computer simulation of interactive dual-feedback system 80—94205
- accommodation as a function of object form 79—11930
- accommodation dynamics, range nonlinearity 79—83770
- accommodation in infants, photorefractive study 80—56028
- accommodation microfluctuation dynamics studied with highly sensitive IR optometer 80—81580
- accommodation microfluctuations in humans 80—12124
- accommodation orthoptics, objective assessment of dynamic insufficiency 80—45884
- accommodation response, depend. on spatial freq. spectrum of observed object 77—25422
- accommodation response, effects of colour 78—69042
- accommodation response dynamics rel. to spatial freq., ocular MTF 79—53134
- accommodation time and rest position, computer-controlled tachystoscope meas. *(German)* 79—2143
- accommodative, bias towards intermediate viewing distances, Mandelbaum effect 79—79518
- accommodative changes in humans induced by positional ghanges rel. to gravity 77—48789

eye continued
accommodative responsiveness rel. to contrast sensitivity for sinusoidal gratings 80—61552
adaptation, technique for estimating the contrib. of photomech. responses 80—85547
adaptation 78—15834
adaptive model using accommodation index, human eye 80—51073
aerial image modulation lowering, contribs. of retina and eye optical system 80—81584
afferent visual systems of cat and rhesus monkey, responses to wavelength contrast 80—56030
alignment development in cats 78—27955
amacrine cells in Necturus retina, independ. γ-aminobutyric acid- and glycine-releasing neurons 78—35848
amblyopia, acuity and contour interactions across the visual field, expt. obs. 80—56038
amblyopia, human, differences in neural basis, effect of mean luminance 80—72156
amblyopia, lack of normalcy of dominant eye 80—97898
amblyopia, monocular, prevalence among anisometropes 80—67071
amblyopia, visual acuity and contrast sensitivity rel. to stimulated region of the retina 80—45893
ametropia, expt. obs. of speckle motion in laser refraction 80—45879
analogue analyser for on-line eye movement detection 79—79699
animal eye technology use in better lens and mirror design 80—28295
anisometropia, artificially induced, effect on separable binocular processes 80—45906
aquatic eyes, retinoscopy, refractive error considerations 80—61750
aqueous humor flow rate determination by fluorescein tracer model 79—43943
aqueous temperature stabilisation, laser induced temp. changes and model 77—40713
arthropod visual cell membrane cond. control 78—15831
astigmatic amblyopia, study 79—11922
astigmatism, refractive, evaluation and control of DuraSoft contract lenses 79—34706
astigmatism in infants 79—57642
astigmatism in infants meas. by photorefraction 79—62242
astigmatism induced by pterygium 78—40139
astigmatism of central and peripheral cornea, asymm. meas. by photokeratoscopy 78—64981
atka fish, dynamics of cornea colour 77—36926
ATPase cytochemical localisation in developing retina of teleost 77—70454
axial length, meas. by ultrasonography, obs. on Hirschberg test 79—34551
axial length meas. using controlled weight direct contact US ophthalmological transducer 78—20239
axon-bearing horizontal cells, teleost retina, functionality obs. 80—51084
barnacle photoreceptor visual response rel. to metarhodopsin transitions 78—69050
bathoproducts of rhodopsin, isorhodopsin I, and isorhodopsin II 80—51088
bifoveate retina of lizard, light microscopic study 80—101165
binocular eye movements during accommodation vergence 78—61186
binocular retinal image motion during active head rotation 80—72158
binocular summation, eye accommodative-vergence state rel. to binocular instrument collimation 78—53417
binocular synchronism monitoring, prolonged monolateral occlusion, electro-oculographic response 79—20543
binocular vergence dynamic components step stimulation 79—79550
binocular vision, artificial aniseikonia, geometrical explanation of induced size effect 80—72173
binocular vision, fusional vergence eye movements rel. to fixation disparity 80—56031
binocular vision, visual sensitivity of one eye 79—20544
binocular vision deprived humans, binocular interactions tuned to size and orientation 80—81606
bioelectric recording from human retina and cortex 80—12111
biomedical stimulus device for characterizing temporal MTFs in man 80—51204
bipolar cell, catfish, receptive field and input signals 77—12921
bipolar cell, on-centre, effect on polarisation of horizontal cells in carp 79—16207
bird migration and homing, physicochem. mechanism for mag. field detect. 77—52811
blink elicitation and measurement, human infant appl. 80—56293
blink rate, human, long-term trends 80—35879
blink reflex, 1st component in rabbit and man 79—74649
blink reflex, afferent pathways, human 79—43864
blink reflex, effects of elec. stimulus freq. during rest and a task 80—61547
blink reflex studies in stroke patients, role of dynamic sensory perception 80—3641
blink response to startle evoking stimuli in humans, excitatory and inhibitory components 78—77050
blinking and suppression of visual stimulation 80—97909
blue cone signals in red-green opponent-colour ganglion cells, macaque retina 79—79549
blue receptor distrib. in primates revealed by spectral photic damage and histochem. response expts. 80—12130
blue-sensitive cones, non-contribution to luminance 80—51098
Boll, Franz, (1849 to 1879), investigator of retinal pigments, biography 78—20927
Boll's phenomenon concerning retinal pigments, effect of illum., colour photography obs. 78—24072
brain stem auditory evoked potentials and blink reflex in quiescent multiple sclerosis 80—67091
caloric nystagmus, air and water, mathematical model 79—24983
cancer incidence and prevalence 78—3472
catadioptric systems, matrix optics 79—94167
cataract, cold, form. in young rat lens, phase separation of protein-water mixture 78—11640
cataract development in micr irrad. at different ages 78—20232
cataract formation in rabbits and monkeys under acute microwave irrad. 79—5326
cataract formation in vitro, rel. to protein synthesis control and intracellular Na^+/K^+ ratio 78—11646
cataract microstructure meas., picosecond range-gated light scatt. technique 79—8584
cataractous lens, NMR study of state of water *(Hungarian)* 78—64986

eye continued
cataractous lens, optical transmission at 430 nm and blue field entoptoscopy 80—45883
cataractous lenses, PIXE elemental anal. 80—21468
cataracts, visual acuity obs. *(Italian)* 79—79539
center-surround retinal ganglion cells: receptive field organization with special reference to light-dark adaptation 80—12104
centrifugal fibres to eye in nonavian vertebrate, source revealed by horseradish peroxidase transport 77—36921
cephalopod visual cells, effect of illum. on squid rhodopsin membrane at oil-water interface 77—44646
cerebellar stimulation and eye movement in cats 80—30719
cerebral palsied children, film projection system for eye movement monitoring 79—16329
chemical and physical aspects *(Dutch)* 77—9188
choroidal blood flow, non-invasive meas. 77—40704
choroidal blood flow meas., theoretical basis using radioactive inert gas 79—92349
chromatic aberration, effect of yellow ocular filter, fish eye 80—8046
chromatic aberration meas. with chromoretinoscopy 80—81581
chromatic aberration rel. to accommodation, meas. using dynamic laser speckle pattern 80—81582
chromatic border perception, by R and G cones in trichromatic eye 79—57658
chromatic mechanisms exposed by colour substitution pupil response 79—92221
chromatic stereopsis, opposition of photometric and dioptric factors *(Italian)* 78—56986
chromoretinoscopy, longit. chromatic aberration meas. 78—56967
chromoretinoscopy and its instrumentation 80—94201
cinema photography 80—67186
circadian rhythm in Limulus lateral eye, mediation by efferent optic nerve fibres 77—90783
clinical perimetry, glossary of basic information *(Italian)* 79—39413
coagulation of eye tissue, using OK-2 laser ophthalmocoagulator 79—11991
colour CRT-observer interaction 77—77901
colour discrimination ability in the white region, evaluation 80—16941
compensatory movements to miniature rotations, rabbit, retinal image stability implications 80—45890
compound eye, Dipteran, small signal phototransduction 80—35882
compound eye of Cicindela tranquebarica herbst, fine struct. 80—85382
compound eye of green lacewing, light reflectance 79—96554
compound eye of worker honey bee, cell junctions, electron microscopy 80—85383
computer assisted examination, Refractor III system 79—29650
computer-assisted examination, evaluation of Refractor III system for subjective exam. 78—3622
concomitancy testing, new method 80—94305
conditioning auditory stimuli and the cutaneous eyeblink reflex, human obs. 80—67090
cone, computer-driven hardware model, response obs. 80—72402
cone activity, correl. with horizontal cell morphology, goldfish retina 80—45900
cone afterimages, interchangeable background obs. 80—45902
cone and rod involvement in grating detection and resolution 78—92626
cone cell of tiger salamander, hardware model 78—44505
cone dark adaption, foveal and parafoveal, effect of background 79—43914
cone interactions at high flicker frequencies 78—35857
cone ionic channel closure, turtle 78—15830
cone light adaption, frog, receptor rel. to ganglion sensitivity changes 79—48253
cone outer segments, light-induced changes in membrane current, tiger salamander and turtle 80—108899
cone pigment ecology in teleost fish 78—69041
cone pigments, intraretinal distrib. in certain teleost fish 79—74667
cone receptor, inhomogeneous waveguide model and Stiles-Crawford effect 77—90797
cone saturation, human, function of ambient intensity 79—2049
cone sensitivity to flicker, primate, during light and dark adaptation, ERG obs. 79—43900
cone specific c-wave in turtle retina 78—69060
cone spectral mechanisms, ERG and psychophysical obs. 80—61565
cone system, attenuation during rapid dark-adaption, frog 79—62253
cone voltage-current relationships, turtle, origin of non-linearity 79—74659
cones, evidence for equivalent-background hypothesis 80—16931
cones, post-receptoral adaption obs. 79—79548
cones, single and double, intraspecific evidence for function in teleost retina 79—62248
constant esotropia with anomalous correspondence, home visual therapy 80—8207
contact lens, circular, tear film dynamics and O_2 tension 78—48929
contact lens, hard gas-permeable type, O_2 tension underneath 78—3473
contact lens, hydrogel, change in lens power due to flexure 79—11917
contact lens rotation on toric corneas, nonprism and prism-ballast hydrogel lenses 78—3474
contact lenses, hydrogel, light transmission 79—11918
contact lenses, ultra-thin, corneal-edema response 79—34552
continuous movement monitoring, proportional-integral adaptive system *(German)* 79—16320
contrast effects on smooth-pursuit eye movement velocity 79—43891
contrast sensitivity as a function of position on the retina 80—61561
contrast sensitivity function 77—25442
contrast sensitivity rel. to stimulus onset and image motion 80—16938
contrast sensitivity to narrow-band CRT phosphors 79—11933
contrast threshold response of human eye based on Tiffany data anal. 80—51093
contrast thresholds versus border enhancement, scatt. light effect 80—94213
convergence and divergence, large and sustained improvement after short isometric exercise 80—8049
convergence insufficiency rel. to school achievement 80—8048
cornea, beagle, capillary endotherlial cells, repair of sublethal radiation damage 79—100672
cornea, low-angle light scattering meas. apparatus 77—5123
cornea formation, human, models 78—35840
cornea O_2 flux, meas. when covered by soft contact lens 79—34705
cornea sensitivity in normal human eyes 80—12093
cornea thickness, human, topographic pachometry meas. 79—11921

eye continued
corneal apex position determ. in normal eye by photoelectronic keratoscopic analysis 80—41003
corneal curvature alteration by elec. heating, rabbit expt. 77—40665
corneal curvature meas., simple photokeratoscope 78—3624
corneal damage induced by near-UV laser, cumulative effects 80—85448
corneal edema with contact lenses under closed-eye conditions 79—96553
corneal environment, osmotic responses to contact lenses 80—12078
corneal epithelium, predictive equation for IR laser damage 79—25031
corneal flash surface calc. rel. to system for recording eye movement 80—30713
corneal hydration endothelial control theory 78—35841
corneal image, photokeratoscopic technique 77—1993
corneal mechanised trepan control 79—29659
corneal O_2 flux when covered by a soft contact lens, humans 79—34549
corneal oedema, effect of peripherally fenestrated contact lenses 78—3470
corneal polarisation cross obs. at human cornea 79—8503
corneal pressures due to soft contact lenses and corneal asymmetry 80—104621
corneal scattering, contact lens wear, border-enhancement spread, subjective monitoring method 79—29641
corneal sensitivity and thickness after wearing PMMA and gas-permeable contact lenses 80—61544
corneal stroma, small angle X-ray and neutron diffr. study 79—11923
corneal temperature range, implications in prediction of laser thermal damage 80—108848
corneal temperatures, normal and laser injured rabbits 79—11919
corneal topography using moire contour fringes 80—26316
corneas, canine, γ and negative pion irradiation of microvasculature 79—43964
corrective saccades, effects of altering visual feedback 78—40150
cortical cells as bar and edge detectors or spatial freq. filters 80—12109
cortical plasticity in monocularly deprived immobilized kittens, eye movement dependence 80—81588
critical duration changes during dark adaptation 80—51094
critical flicker freq. for sensitivity difference meas. of retina *(Japanese)* 79—8512
critical flicker fusion freq., river lamprey 79—74663
crustacea with scotopic eyes, screening pigment effects on spectral sensitivity 78—65009
crustacean eyes and polarisation sensitivity 78—7350
cryoprobe, for medical surgery 80—56274
α-crystallin, of calf eye lens, small angle X-ray scattering study 79—11891
crystalline lens, normal and cataractous, H_2O proton relax. 77—60203
crystalline lens accommodative efficiency rel. to anterior chamber depths 79—83765
cyclofusional response, human, effect of stimulus size 78—61187
cyclorotatory trained voluntary eye movements, influence on egocentric orientation 78—92633
cyprinid retina, model of function at outer plexiform layer 80—12103
dark-adaption, comments on the testing of 2 prominent hypotheses 80—108896
deep convexiclivate fovea as directional focus indicator 78—48789
defocus, psychophys. and electrophysiological effects 77—90768
deformation due to intraocular press. changes, holographic interferometry meas. 79—20720
depth of field, wavelength dependence obs. and calc. 79—62240
depth of focus rel. to minimal blur disc, human eye 79—8505
detached retinal tears computer localisation for scleral buckling procedure 78—7529
detection, effect of photon noise 80—61559
detective quantum efficiency of human eye 78—56976
development of eye and retina of kittens 80—12113
diabetic blindness prevention with ophthalmic photography 80—16920
diabetic retinopathy therapy, laser photocoagulation efficiency factors 79—79622
diagnosis, ophthalmological instrument design and construction 78—15918
dichromat, large-field colour naming with rods bleached 80—12126
dioptric corrections of age dependent isopters 79—20539
dioptric effects of optical parameter changes, math. model, rel. to contact lenses 78—3477
Dipteran fly neural superposition eye, rhabdomere visual axis misalignments 77—64032
direction of gaze, determ. method using Listing's law 79—34677
disc vascularity in Down's Syndrome 80—67069
diseases of optic nerve, tracts and visual cortex, annual review of ophthalmic literature 78—3475
displacement thresholds, foveal and peripheral, rel. to stimulus luminance, line length, movement duration 80—101183
distance measurement between eye surface point and needle tip within eye, geometric method 79—53273
divergence excess, prevalence and management 80—35877
divergence excess strabismus, optometric therapy 80—97902
divergence paralysis, association with papillar oedema *(Italian)* 79—79520
dose during brain computerised tomography 79—92389
Drosophila mutant with phototransduction defect 77—90777
eccentric fixation with secondary visual feedback 79—79522
education, cornea, radius of curvature, quantitative geometric optics expt. 78—62004
education, human eye, artificial model, physics laboratory for medical students 78—62003
EEG alpha rhythm, result of corneal-retinal potential modulation obs. 79—34535
efferent commands, perceptually monitored and unmonitored, smooth pursuit eye movements 79—53104
elasticity of sclera and choroid in humans, rel. to scleral rigidity and accommodation 78—80907
electrical phosphene threshold, rel. to Rashbass' model 77—25428
electro oculography, computerised diagnostic system 80—21566
electro-oculogram light induced amplification effect, time const. 78—15827
electro-oculogram light-induced amplification, quantification in clinical practice 77—90771
electro-oculographic activity, computerised meas. during sleep 79—74781
electro-oculographic amplification induced by macular light adaptation in various retinal diseases 77—90773
electro-oculographic ratio, rod and cone contribution 79—11925

eye continued
electro-oculographic response, comparison between binocular and monocular recordings 77—48791
electro-oculographic response, interocular comparison while reading printed material 79—20536
electro-oculographic response, recording and interpretation review *(Italian)* 78—73156
electro-oculographic response interocular comparison, unpredictability of residual long-term effects 78—53392
electro-oculography, on-line system for quantitative study of ocular kinetics 79—34699
electronystagmography signal processing *(French)* 77—37078
electronystagmography system for vestibular testing, microprocessor-based 4-channel 80—41293
electroretinogram, adaptation-overlap model, response to laser stimuli 79—74650
electroretinogram, automatic meas. of b-wave amplitude and peak latency *(German)* 78—80993
electroretinogram, DC registered, off-responses in humans 77—44647
electroretinogram, E- and b-wave analogue model, retinal expression of inductive reactance 77—48797
electroretinogram, effects of light adaptation, frog 77—44650
electroretinogram, elicited with sinusoidal flicker, component anal. 79—74660
electroretinogram, frog, rod and cone generation of wavelets 78—48799
electroretinogram, human, DC registered, influence of ethyl alcohol 79—2052
electroretinogram, human, real-time computer for first- and second-order Wiener kernels 79—12046
electroretinogram, human, white noise analysis 79—1995
electroretinogram, increment spectral sensitivities of primate late receptor pot. and b-wave 77—70461
electroretinogram, photopic, freq. response characts. meas. with synchronous detect. 77—48796
electroretinogram e-wave, frog, rel. to ganglion cell activity and rod responses 79—48254
electroretinogram of albinos 79—53099
electroretinogram P III component model, luminance variations 77—81495
electroretinogram signals computer anal. 79—8559
electroretinograms of epigeous and cave-dwelling harvest spiders *(French)* 79—53093
electroretinographic observations of insect compound eye 79—53100
electroretinographic response rel. to vars. of visual performance during day 78—77051
electroretinographic species difference within the leopard frog complex 79—62254
electroretinography, clinical, use of Mingograph ink-jet recorder 78—92731
electroretinography improved electrode, design and standardisation 79—92401
ellipsosomes in fish cones, ultrastruct. and staining props. 79—11924
empty-field myopia correction on dark-focus of accommodation basis 79—53131
endoparietal eye of Limulus polyphemus, spectral sensitivity 80—41029
energy uptake in the first step of visual excitation 80—30724
entoptic phenomena 79—53106
EOG, three-electrode array, in communication interface for non-vocal physically handicapped 77—25603
epiphysis, frog, characts. of slow pots. 80—56029
ERG, effects of conducting media inhomogeneities 80—51078
ERG, human, nonlinear kernels 80—61545
ERG, human corneal, frequency domain anal. 80—45888
ERG, oscillatory pots., analogue circuit model and frog obs. 80—89750
ERG, rabbit, dynamic light-dark adaptation 80—35887
ERG, suprafusion, theoretical retinal anal. 80—56020
ERG, Wiener kernels and freq. response functions, human retina, obs. 80—45887
ERG B-wave of ground squirrel, spectral components 80—51082
ERG photostimulus calibration by standard photometer and photodiode 80—8222
ERG recording, computer assisted standardised quantitative method 80—109048
evoked potentials, speed methods for vision assessment, normal and amblyopic eyes 80—61661
exotrope, intermittent, of divergence excess type, panoramic viewing, visual acuity and anomalous retinal correspondence 80—51076
extrafoveal retina, Bezold-Brucke phenomena 80—45898
extrafoveal spectral sensitivity during dark adaptation 80—45896
extraocular eye muscle force duction tests after administration of succinylcholine or pancuronium 80—26255
extraocular motor unit activity, electromyographic recording in man during fixation and saccades 79—16203
extraocular muscle system mechs. model for clinical ophthalmology 78—40155
extraocular muscles, relative tensions 79—34554
extrinsic muscle nerve terminals 78—56970
eye, direction-selective cells formation modelling in developing retina 80—30721
eye movement meas. using elliptical projection 78—15931
eyeblink, human, dynamics model 78—61167
falconiform eye, depression in deep fovea acting as telephoto lens system 78—88705
far peripheral retina, spectral sensitivity 80—104586
figure perception, role of eye movements 80—101186
fine movement recording through closed eyelid, piezoelec. transducer 78—35988
fish, chromatic aberration and effect on refr. state 78—64985
fixation changes in transverse plane at eye level, Hering's law of equal innervation 78—61184
fixation disparity rel. to rapid prism adaption 80—16929
fixation distance changes, ecular translation and cyclotorsion obs. 80—89752
fixation stability observations, proprioceptive information and autokinesis considerations 80—51086
fixation-sensitive areas in the eyes of the walking fly, Calliphora erythrocephala 79—43904
fluorescein angiography of the ocular fundus 80—67185
fluorescence angiography, colour and black and white, use of interference filters 78—48856

eye continued

- focus on retina, best value for various fixation distances, phakic and aphakic eyes 80—108882
- foreign body detect. using computerised tomography 78—3577
- fovea, human, diameter meas. expt. 79—30
- foveal fixation, functional test based on differential cone directional sensitivity 80—85399
- foveal increment threshold, lateral effect of oscill. of peripheral luminance gratings 80—108904
- foveal tritan vision, colour naming evidence 79—83780
- foveal vision, mental scanning mechanism 79—5280
- foveal vision, mental scanning mechanism 79—2066
- frog, Rana esculenta, under-corrected lens rel. to comparable aerial and underwater vision 78—7344
- Fuchs's endothelial dystrophy, optometric management 79—83994
- fundus oculi tissue, thermal effects on exposure to laser radiation 80—26261
- fundus photographs, automatic assembly using blood vessel structure 79—83991
- fundus photography in optometric practice 80—67183
- fusional amplitude deterioration in diabetic people 80—26224
- ganglion cell on and off processes, spatial distrib., anal. of receptor inputs 79—100606
- ganglion cell response to far violet light, macaque 78—11656
- gaze-evoked nystagmus, analogue model 78—27938
- glare, adverse consequences in aviation 79—11932
- glass lenses, effectiveness in reducing eye exposure 79—92394
- glasses, conventional, value for X-ray protection 79—88202
- glasses, prescription meas. 80—67981
- glaucoma, early diagnosis by meas. of internal eye pressure 79—25140
- glaucoma diagnosis and therapy, importance of tonometry 78—40383
- glaucoma diagnosis by digital processing of optic nerve head images 78—81043
- glaucoma surgery, Nd:glass laser with freq. doubling capability 78—40403
- goldfish, adult, eye growth, optics 77—44645
- goniophotography in optometry 80—67182
- gonioscopic method for grading of the anterior chamber angle 80—108993
- gonioscopy, foot-operated camera trip for Nikon photo slit lamp 78—80986
- grating free scanning, production of patterned retinal exposure obs. 80—56034
- green-rod pigment of frog, Rana temporaria, long-lived photoproducts 77—25433
- habituation, dishabituation and generalisation induced by colour flashes 77—12918
- Haidinger's brushes, recent explanation and their clinical use 80—45880
- heterophoria, prism-induced, oculomotor adaption 80—108880
- hierarchical detection structures in vision 79—79523
- historical paper by Jean Mery written in 1704 80—57050
- holocamera, clinically useful, for 3-D microscopy of unanaesthetised eye 78—48863
- holocamera for 3-D micrography of the alert human eye 80—98057
- holographic diagnosis of human eye 80—12209
- holography application *(Japanese)* 79—79515
- holography applications in ophthalmology 80—67200
- horizontal cells, nonlinear characts. of spatial summation in receptive field, model 80—26232
- horseshoe crab, anal. of adapting bump model 78—73160
- hue change with eccentricity, rod and cone contribs. 80—45904
- hue change with rod intrusion during dark-adaptation 80—51104
- human eye defects rel. to visual nondestructive testing *(German)* 77—86488
- human eye movements recording using opto-television method *(Russian)* 77—12909
- human retina model for props. of vision 78—77655
- human retinal blood flow meas. by laser Doppler velocimeter 79—79623
- hummingbird colour vision to near UV light 80—97914
- hydrodynamic model of aqueous flow in posterior chamber 78—69122
- hypermetropia rel. to chromatic aberration in small animals 78—40140
- hyperopic eye functional visual acuity at intermediate range 78—48791
- illumination and reflection edges, recognition by human visual system 80—94209
- image contrast and its dependence on luminosity, physical model *(Italian)* 79—62261
- image degradation by irregular retinal mosaic 78—20177
- image formation, ocular optics and evolution 77—1991
- image matching with the eye, effects of pictorial noise 80—51113
- information capacity 78—11661
- information processing within retina and lateral geniculate nucleus 79—74648
- injury potential of propelled objects, assessment system 80—21591
- insect colour vision, effected by one visual pigment and filters 80—94212
- insect compound eye, anatomy and operation 78—7343
- insect compound eye, internal desynchronisation of bilaterally organised circadian oscillators 78—80875
- insect eye slow cell resonses, colour adaptation 78—64988
- insect visual neurones, sexual differences 80—41010
- insects which turn and look 77—90769
- instability in dark, proprioception 77—86495
- instrument focusing to take account of eye accommodation 80—101811
- intensity discrimination capacity of tree shrew retinal ganglion cells 80—61556
- intra-ocular pressure measurement, non-contact tonometer, status report 77—2063
- intra-ocular pressure measurement using sonics and coherent optics 77—81548
- intraocular fluid dynamics meas. by minicomputer-based system 78—24130
- intraocular lens implant evaluation 78—81061
- intraocular pressure measurement, applanation tonometer correls. 78—77047
- intraocular pressure measurement, evaluation of Pneuma-Tonometer 79—34678
- intraocular pressure measurement, for glaucoma, comparison of Schiotz standard tonometer and applanation tonometer 78—48915
- intraocular pressure survey, pediatric patient emphasis 80—30712
- intraocular pressure telemetry monitoring 78—3632
- IR. effects on eyes, safety *(Japanese)* 78—35881
- IR nonlinear perception in 800-1355 nm range 80—12123

eye continued

- IR radiation effects evaluation, from GaAs laser diodes *(German)* 78—20241
- IR recording retinoscope for accommodation monitoring 80—36055
- iris coloboma, selective atrophy in lateral geniculate nucl., cat 78—3471
- isobaric gas counterdiffusion in rabbit eye 80—30718
- isorhodopsin chromophore conform. and orientation in frog disc membrane 78—64980
- jerk nystagmus, some new findings 80—67074
- keratoconus, position of corneal apex 80—94200
- kitten, optical quality development 78—64982
- kitten, optical surface development 78—64983
- kitten cornea optical development 78—64984
- Kuhne, Friedrich Wilhelm, (1837 to 1900), chem. processes in retina, biography 78—20928
- L-type horizontal cells, dynamic interaction in receptive field 80—26233
- laser applications in ophthalmology 77—90869
- laser damage, fast pulses 78—48827
- laser endoscopy, associated ophthalmic hazards 79—79598
- laser IR pulse irrad. of human eye, max. permissible exposure for safety 77—37009
- laser iridectomy, energy required, hazards and techniques 78—11713
- laser maximum permissible exposure, 1.54 μm wavelength, human eye 79—11966
- laser picosecond pulse maximum permissible exposure 79—25033
- laser pupillometer, especially suitable for anesthetised cats 79—48317
- laser radiation dosimetry 80—12268
- laser safety eyewear, filter glasses 79—39525
- laser trabeculotomy in glaucoma treatment 78—53470
- laser-induced retinal morphological and functional changes and safe energy levels 80—3712
- lateral inhibition in composite eye of limulus, expt. *(French)* 80—89705
- length measurement, accurate, by US echo-oculometer 77—37030
- lens, bovine, rheological analysis 77—90767
- lens, calf, γ-crystallin, single cryst., X-ray diffr. low resolution struct. anal. 79—16130
- lens, cryst., elec. props. of struct. components in frog 79—24982
- lens, human, aspheric curvatures 78—11642
- lens, human and calf, light scatt. and reversible cataracts 80—56019
- lens, induced optical anisotropy fluctuation 78—35838
- lens, light scatt., appl. of random density and orientation fluctuation theory 79—62241
- lens, normal and senile cataractous, PMR study of state of water 78—64987
- lens, radiation protection for patients and users 79—92393
- lens, verterbrate, as system for study of mol. processes 77—90770
- lens accommodation, interpositus neuron control obs. 80—21469
- lens aperture, rel. to depth of focus, appl. to reading with relaxed eye 78—12489
- lens dose estimation in cranial irradiation of acute lymphocytic leukemia 79—88198
- lens fibre damage after laser irradiation, rat 79—39374
- lens formation models, human 77—25423
- lens hazards from high-energy beta-rays 78—65131
- lens low molecular weight protein obs. and prep. 80—16921
- lens opacification in mice exposed to 14 MeV neutrons 78—65097
- lens pigmentation, human, in vivo, independ. of UV light exposure 77—60202
- lens pigmentation in humans rel. to UV light exposure 78—65100
- lens protein, organisation in fibre cell 77—90766
- lens protein composition obs. during senile nuclear cataract development 79—62236
- lenses, crystalline, of humans, fish and birds, state of water, NMR meas. 79—48212
- lid closure and refractive error in macaque monkeys 78—35839
- light adaptation, multiple intracellular contribs., Limulus ommatidia 79—43896
- light adsorption, recovery of retina sensitivity of silver carp *(Chinese)* 79—2056
- light sequence bar, electronically controlled, for EOG study of eye pursuit movements *(German)* 80—36058
- light-adapted photoreceptors, sensitivity changing mechanisms evaluation 79—79543
- light-damaged eye of albino rat, photoreceptor survival, ERG 77—36927
- lightness normalisation with rods and cones 79—100609
- Limulus lateral eye, phase-locked responses 77—86491
- Limulus ommatidia, resonant response of neural model to double freq. stimulation 80—76734
- Limulus ventral nerve photoreceptor response height vs. stimulus intensity curve 78—69058
- lipid function in excitable membranes 80—12095
- long-term growth and shortsightedness model 79—83768
- luminance difference thresholds of foveal vision, uniform surrounding luminance effects *(Japanese)* 79—24988
- luminance flicker enhancement by colour-opponent mechanisms, monkey obs. 80—61549
- luminosity-type cells in the turtle retina, short-wavelength input 80—41012
- lumirhodopsin, photoconversion at 77K, quantum efficiency estimation 80—67081
- Macular pigment, role in polarised light detect., meas. technique 80—61560
- magnetophosphenes, quantitative anal. of thresholds 80—72184
- malignant melanoma treatment near optic disc using small ^{60}Co beams 78—35929
- masking-induced sensitivity changes in Limulus photoreceptors 80—41024
- mathematical model for eye tracking movements of acoustic targets 78—80870
- mental activity evoking pupil dilation, link with intelligence 80—61532
- metarhodopsin transition, triggering of light-induced change in Ca binding, rod disk membranes 80—94211
- 8-methoxypsoralen detection in ocular lens, rel. to psoriasis treatment with photosensitising agent 78—15937
- microcomputer-controlled visual stimulator for eye movement and visual evoked pots. study 80—41350
- microsaccades, role in high acuity observational tasks 80—108893
- microsaccades during finely guided visuomotor tasks 77—9198
- microscope, scanning mirror, with optical sectioning characts., ophthalmology appls. 80—85461

eye continued
  microtremor clinical recording, using piezoelec. strain gauge transducer 78—96109
  microvilli membrane fragment protonic and ionic processes, of cephalopod visual cell 78—73159
  microwave cataractogenesis, expt. investigations 80—35965
  microwave induced hazardous thermal stresses in ocular lens of human eye 78—80914
  microwave repeated exposure, 9.3 GHz, ocular pathology absence in unanaesthetized monkeys 79—53191
  microwave-induced non linear thermoelastic vibrations of human eye lens 79—83853
  minicomputer system, automatic visual stimuli, hand and eye movement monitoring *(French)* 79—34682
  molecular mechanism for initial process 80—51089
  monocular deprivation, unequal, alternating, cause of asymmetric visual fields in cats 80—104584
  monocular fixation and acuity in amblyopic and normal eyes 78—48801
  monocular light exclusion, reduction of retinal directional sensitivity obs. 80—81592
  monocular vergence movements produced by external visual feedback 80—108883
  motility, glossary of terms *(Italian)* 80—16919
  motility, rel. to visual motor development 80—12121
  motility test in strabismus and amblyopia evaluation, computer administration and analysis via PAL8 program 78—48784
  motion and vision, stabilised spatio-temporal threshold surface 80—16926
  motion kinetics in moving target pursuit, oculomotor abnormalities in neurological disorders detect. 80—108888
  motor control in cephalopods, cerebellar-type system 77—12914
  motor systems, eye and hand, optimal response in pointing at visual target 80—56079
  motor systems of eye and hand, optimal response in pointing at a visual target 80—61567
  mouse, effect of high-LET ^{20}Ne on brain, eye and other head structs. 79—66489
  movement, minicomputer processing of dual Purkinje image eye-tracker data 79—29645
  movement, role in hand movement control 80—26237
  movement, three-dimens. visual stimulus deflector 78—48945
  movement activity in paradoxical sleep, occipital spikes in visually defective children 79—16185
  movement amplitudes, information used by the perceptual and oculomotor systems 80—35885
  movement control, vestibular mechanisms, book contrib. 79—96588
  movement control during single unit recording in pigmented rat 77—81767
  movement detection, one-way, in fruitfly visual system 79—39415
  movement during radiograph scanning, microprocessor equipment for analysis 79—25130
  movement hierarchical control 79—83763
  movement hierarchical control model 77—25429
  movement in luminance edge threshold effect, stabilised viewing conditions 80—81589
  movement meas. using ocular mag. search coil 79—74798
  movement measurement, IR technique *(French)* 77—36916
  movement measurement, laser Doppler technique 79—92322
  movement measurements, for cognitive processes based on visual fixation points 78—31816
  movement mechanism, transient charact., human 77—77894
  movement monitoring, signal detect. via phase-locked sampling in mag. search coil 79—25124
  movement monitors, compensation for distortion 80—56244
  movement of eye, on-line computers for research 80—41329
  movement phase plane meas., antiaircraft tracking operator performance anal. 78—15825
  movement potentials of superior colliculus of awake cats 77—60208
  movement recording, vertical and lateral, single channel method 79—16205
  movement recording system, for clinical appl. 78—3623
  movement recording using non-contacting US transducer system 78—7414
  movement tracking and regulation test station *(German)* 79—16321
  movements, additivity of fusional vergence and pursuit eye movements 80—35884
  movements, corrective saccadic, for refixation amplitudes of 10° or less 79—43886
  movements, nonadditivity of vergence and saccadic components 78—69095
  movements, role in detection of stationary structs., theoretical model 80—81594
  movements, vel. precision in smooth pursuit 79—57656
  movements, vergence and version, reciprocal innervation model 77—48798
  movements and contrast resolution, sensitivity variations in visual system 79—53088
  movements control, effects of frontal eye field and superior colliculus ablations 80—72154
  movements during learning-set form., monkey 78—77057
  movements in paralysed cats induced by drugs and sympathetic stimulation 80—51083
  movements of African chameleons, spontaneous saccade timing 78—69053
  movements while reading, annotated bibliography 78—53394
  movements while reading, interocular comparison for normal and amblyopic subjects 78—53393
  MTF of defocused optical system for incoherent monochromatic light, human eye 80—67072
  multilayer mirror optics of animal eyes 79—57643
  myopia, corrected and uncorrected, effect of pupil size on visual acuity 80—45882
  myopia, extreme, produced by modest change in early visual experience 79—53085
  myopia, Prentice Memorial Lecture [optometry] 80—27089
  myopia, spherical error of refraction, statistical anal. of biological theory 80—45881
  myopia and eye enlargement after neonatal lid fusion in monkeys 77—29145
  myopia associated with incipient cataract *(Italian)* 79—62238
  myopia in developing chicks following monocular and binocular lid closure 80—61543

eye continued
  myoscope MG 23, two channel, ocular muscle measurement, myasthenia gravis diagnosis appl. 77—37085
  Nephrops norvegicus (L.), circadian rhythmicity, neurohumoral basis 80—108889
  neural discharge phase-locking to periodic stimuli 79—83775
  neural diseases, quantitative EOG and CT obs. 80—36070
  neural interactions, difference differential eqns., periodic solns. 77—86489
  neural network dynamical response, effect of boundaries, Limulus retina 80—30717
  neural response evaluation and statistical judgement to sinusoidal stimulation with superimposed drift and noise 79—88068
  neural superposition compound eye of male Bibionidae expt. obs. 79—43874
  neurons, cat eye, stereotaxic method for recording from single cells 80—89913
  night convergence and presbyopia *(Spanish)* 80—89746
  non-ionising radiation absorption , hot spots study, stochastic model 78—35884
  nonlinear visual processing in cat's retina, model 80—85385
  nonlinearity, analytical derivation 80—67082
  nuclear stars, rel. to light flashes obs. on Skylab 4 77—5089
  nystagmic movements, caloric, mathematical model 77—73525
  nystagmus, automatic on-line anal. *(German)* 80—76846
  nystagmus, congenital, orientational detect. modification obs. 80—56039
  nystagmus analysis, microprocessor based instrum. 77—44799
  nystagmus analysis system using microprocessor 77—48917
  ocellus of phalangium opilio, electrical response 79—53095
  ocular axial dimensions, development following eyelid suture in cat 79—43870
  ocular contusion injury from propelled objects, evaluation model 79—43955
  ocular following reflex elicited from retinal periphery, cat 77—60206
  ocular fundus reflectometry 78—48861
  ocular hazard of short pulse Ar laser irradiation, primates 79—25030
  ocular pulse measurement, electronic/US system for carotid occlusion diagnosis 77—37081
  ocular tonometry through sonic excitation and laser Doppler velocimetry 80—56152
  oculomotor control system, expt. set-up for clinical investigation, visual, acoustic, vestibular stimulations 78—80990
  oculomotor control system signal flow diagram 77—25415
  oculomotor control system synthesis photoelectric matrix method appl. *(Korean)* 77—90779
  oculomotor deficiencies, association of symptoms with meas. 79—96556
  oculomotor performance in smooth pursuit of targets, effect of luminance 79—48268
  oculomotor slow control, effect of expectations, periodic target steps 79—100604
  oculomotor slow control, effect of expectations, single target displacements 79—100605
  oculomotor system parameter identification, strabismus appl. 78—3478
  on line eye movement recorders, problems use 80—41331
  operations, photographic documentation using model 310 surgical microscope 80—56161
  ophthalmic fluorophotometry, improved slit-lamp fluorophotometer 79—92326
  ophthalmic photography, external 80—67180
  ophthalmic photography instrumentation, survey of clinical impressions 80—67188
  ophthalmic tissue signature characterisation by US frequency-domain analysis 77—40857
  ophthalmological diagnosis, US contact stabilisation method 77—25523
  ophthalmological instruments and eye models in teaching, training and education 80—51993
  ophthalmological tissue differentiation, digitisation of HF US signals 78—80935
  ophthalmological treatment with photocoagulation systems *(Croatian)* 78—44581
  ophthalmology, appl. of picosecond optical range gating 77—81549
  ophthalmology, holography appl. 78—7342
  ophthalmology, research and training, TV appl. *(German)* 78—24157
  ophthalmology and physics, review 79—53084
  ophthalmology diagnosis, computer assisted 78—92739
  ophthalmoscope, for interior and refraction error exams. 77—81606
  ophthalmoscope, hand-type, supplementary unit for photoelectric measurements 78—48907
  optic disc changes meas. using retinal stereophotogrammetry, glaucoma detect. appl. 80—3757
  optic disc topography, meas. by laser contour angiography error model 77—60236
  optic lobe neurosecretory cells of Poekilocerus pictus, effects of visual stimulation 79—5279
  optic nerve, tracts and visual cortex diseases, ophthalmic literature review 79—83762
  optic nerve fibre arrangement in cat, non-retinotopic 80—30720
  optic nerve fibre layer, river lamprey, light- and electron-microscopic obs. 79—43879
  optic nerve fibre topography in tectum retinal projection, cichlid fishes 79—48250
  optic tectum, pigeon, single cell spatial- and temporal-freq. selectivity 80—41016
  optic tectum, pigeon, single-neuron responses to moving sine-wave gratings 80—41015
  optic tract fibres, receptive field props., tree shrew 79—48252
  optic-nerve head, congenital malformations 79—92213
  optical characteristics of human eye, instrument reading appl. *(Hungarian)* 78—11641
  optical line spread width judgement, merits of Gaussian moment 80—16924
  optical mechanism of image formation in Limulus eye 79—83767
  optical system, retina contrib. to modulation lowering, aerial images *(French)* 79—34553
  optics, first order, of typical and myopic eyes 78—44499
  optokinetic movement inversion in anterior visual field, albino rabbit 78—77052
  optokinetic nystagmus, evaluation of a simple study device 80—56299
  optokinetic nystagmus study of spatial vision, normal and reeler mutant mouse obs. 80—41032
  optokinetic reactions, rabbit, rel. to visual streak 79—43884

eye continued
optokinetic reactions in man elicited by localised retinal motion stimuli 80—45889
optokinetic reflex, mathematical model 80—41008
optokinetic responses in brain lesions, EEG and electro-oculographic correlative study 80—8055
optokinetic stimulation device, expt. and clinical appls. 80—3844
optokinetic stimulus pattern by computer graphics for study of optokinetic nystagmus 79—44008
optokinetic torsional tracking, influences of skeletal musculature reflexes 79—53087
optometric education in Nigeria, three year programme 79—25781
orbit, direct coronal computerised tomography by using a dedicated head scanner 80—56177
orbital disease, appl. obs. computerised tomography scanning 80—56174
orbital mass lesion patients, advantages of a fourth generation computerised tomography scanner 80—56176
orbital tissue visualisation by A-scan echography 77—77953
orbital trauma evaluation by computed tomography 80—56175
orientation sensitivity of visual movement detection system activating landing response of blowflies 80—101176
orthokeratology, refr. error rel. to corneal power 78—48786
oscillatory responses of the Limulus retina 80—101166
otpical line spread width judgement, merits of Gaussian moment 80—16923
outer isopter perimetric response variability obs. in old subjects 80—108894
particle induced visual phenomena in space 78—20297
pattern induced flicker colours, sensory process sensitivity to short time delays 78—96048
perceived motion, role in smooth pursuit eye movements 79—100618
perception, adaptive filters and eye movements 79—53153
perceptive field sizes fovea and periphery, light- and dark-adapted obs. 80—61574
perimetric examination in visual physiology *(Italian)* 79—62244
peripheral contrast sensitivity for sine-wave gratings and single periods 80—61562
peripheral retina colour vision, hue and saturation of spectral lights 77—52788
peripheral retina colour vision, spectral sensitivity functions 77—52787
peripheral retinal optical image quality variation obs. 79—83766
peripheral saccades, latency obs. 80—12089
perspective distortion in photography, eye as simple lens 80—17734
phasic pupillary light reflex and visual evokes potentials, simultaneous anal. 80—26226
photochemical reactions in retina, excitation by pulsed luminescence diode *(German)* 79—16250
photocoagulation application of lasers 77—77961
photocoagulation using ruby laser, colour discrimination time variability 78—53401
photoconvertible pigment states and excitation, prolonged depolarising afterpot., blowfly 80—8060
photodocumentation, conf., Birmingham, USA (Dec. 1977) 80—62362
photography, accessory fill-in flash for the Nikon photo-slit lamp 80—36056
photography, new instrumentation and techniques 80—67187
photokeratography using moire techniques 77—21590
photopigment and receptor props. in Drosophila compound eye and ocellar receptors 80—8063
photopigment rapid conversions in blowfly visual sense cells, effect on receptor pot., pupillary response 80—8062
photopigments and pseudo-pigments, spectral sensitivity and neural interaction 77—25425
photoreceptor, barnacle, conditioning light effect modification by metarhodopsin absorpt. of light 80—8064
photoreceptor, barnacle, effects on prolonged depolarising afterpot. of Mn^{2+}, Ca^{2+} 80—8051
photoreceptor, barnacle, props. of on-transient of intracellular response 80—8052
photoreceptor, barnacle, upper limit on translational diffusion of visual pigment 80—8053
photoreceptor bleaching and adaption reversal by microsecond flashes 79—79542
photoreceptor cell disk membrane, photoinduction of pot. 79—70548
photoreceptor cells, daily rhythms and vision research 78—61176
photoreceptor directional sensitivity, coherence and polarisation obs. 79—100610
photoreceptor electric response, in invertebrates and vertebrates, quantitative model 77—44656
photoreceptor fluorescence rel. to UV sensitivity, fly 79—92219
photoreceptor form dichroism in vertebrates 78—56969
photoreceptor function, rel. to prolonged depolarising afterpot. 78—15832
photoreceptor light adaptation, Ca^{2+} ion as putative intracellular messenger 78—15833
photoreceptor membrane, lipid free radical oxidation kinetics rel. to lipid composition 78—80872
photoreceptor membrane, protein-lipid interactions on peroxide oxidation of lipids 77—21522
photoreceptor membrane interfacial pots., light-induced 80—72161
photoreceptor membrane lipid-rhodopsin interactions 80—12094
photoreceptor membrane photostable pigments and possible role 78—15837
photoreceptor membrane potential reconstruction from simultaneous intra- and extracellular recordings, S. atlantica 77—86494
photoreceptor membrane rhodopsin orientation model 77—90775
photoreceptor membrane viscosity and component dynamics, recombination kinetics method 79—39366
photoreceptor membranes, dynamic aspects of molecular texture 79—79519
photoreceptor membranes, incorporation into a multilamellar film 80—89907
photoreceptor models, vertebrate, response waveforms 79—43894
photoreceptor mutant of Drosophila, protein role in intermediate steps of phototransduction 77—48799
photoreceptor of Calliphora erythrocephala, appl. of quasi-white random signals 77—73528
photoreceptor optics, formalism and excitation 80—61540
photoreceptor rod cells, vertebrate, visual transduction, book contrib. 79—96561
photoreceptor sensitising pigment, fly 77—90796

eye continued
photoreceptor sensitivity increase following light illumination, frog expts. 80—51095
photoreceptor shedding in the frog retina 80—12096
photoreceptor signals at visual threshold, turtle obs. 80—56042
photoreceptor synaptic activity in isolated frog retina, Co ion effects 78—48797
photoreceptor transduction, determ. of pigment transition or state coupled to excitation 80—8054
photoreceptor transduction process, reversible events 80—51102
photoreceptors, arthropod, prolonged light-induced cond. change on recovery from anoxia 77—12915
photoreceptors, bullfrog, effect of temp. on rapid dark adaptation 79—43883
photoreceptors, light propag. in twisted anisotropic media 78—63004
photoreceptors, Limulus ventral eye, effects of removing extracellular Ca^{2+} on excitation and adaptation 77—9190
photoreceptors, ventral, light-induced conductance changes in Limulus 79—8506
photoreceptors, vertebrate, light-activated GTPase 78—3481
photoreceptors of Limulus ventral eye, sensitivity rel. to Ca^{2+} injection and light adaptation 78—44500
photoreceptors of nocturnal gecko, patency in outer segments 78—48796
photoresponse suppression during anoxia, role of Ca^{2+}, Limulus 79—62252
photosensory membrane of Limulus ventral nerve photoreceptor, effect of extracellular Ca/Na ratio 78—69067
photostable pigments, function in fly photoreceptors 80—8058
physiology review 80—56023
picture processing, psychology, computer appls. 80—41330
pigeon visual pigments, oil droplets and spectral sensitivity 78—11655
pigment absorption spectral band shapes, lognormal distribution curve description 79—53110
pigment changes in rainbow trout, in response to temp. 77—48788
pigment reactions, coupling of charge stabilisation, torsion and bond alternation 78—64999
pigment responses to prolactin in trout, effect of thiourea 78—69065
pigment solutions, flash photolysis, time resolved difference spectra, temp. var. 77—25434
pigment system kinetics, bistable system meas. appl. 78—92624
pigment system kinetics, mathematical anal. 78—92623
pigmentary retinal epithelium of trout, chromatographic detect. of indolic cpds. *(French)* 79—53115
pigments, visual and purple membrane, charge stabilisation mechanism 79—34500
pigments in isolated retina of chicken and pigeon 77—44667
pineal eye rel. to swimming behaviour in Xenopus tadpoles 78—64978
polarised light retinal photography of monkey eye 78—40163
polyenals, related to visual chromophores, absorpt. spectra rel. to chain length 79—34494
polyenals related to visual chromophores, emission spectra 79—34495
polyenones related to visual chromophores, absorpt. spectra rel. to chain length 79—34494
polyenones related to visual chromophores, emission spectra 79—34495
position determination for communications system, IR system 80—76821
position information accuracy for motor control 77—81491
position measurement, method for implantation of mag. search coils 80—85548
position measurement from surface-recorded ERG 80—26400
position sense, Listing's law and perception of vertical 77—44686
postero-anterior radiography, method for eye dose reduction 79—92388
prawn's eye, optical model of cornea image form. by thin film metal mesh *(Japanese)* 77—25421
presbyopia, visual response experiments after awakening from sleep 77—90790
primary glaucoma etiopathogenesis 80—12086
projector having a thermoplastic target and operator's eye, characts. 80—96023
proprioception, input to horizontal oculomotor system of crayfish, expt. obs. 80—72181
proptosis diagnosis, contrib. of echography 78—28023
protection against beta radiation, effectiveness of ophthalmic lenses 77—66862
protection from scatt. radiation during mantle-field therapy 79—92396
protection shield for the fluoroscopist 79—92398
psychophysiological function of the human eye *(Czech)* 80—21472
pupil, closed-circuit TV infrared electropupillometer design *(Japanese)* 77—66870
pupil, human, normal and diseased, model for computer simulation 77—77895
pupil diameter and depth-of-field of human eye as meas. by laser speckle 78—15826
pupil diameter of observer's eye, effect of electron-optical convertor screen luminance 80—35890
pupil noise amplitude control, interaction of sensory and motor mechanisms 78—64998
pupil response as indicator of visual function, pupilometry equipment 78—40154
pupil responses, human, instrumentation for automated study 80—36164
pupillary escape, positive off-diagonal kernels as correlates of dynamic process 80—26229
pupillary light reflex system, modelling and identification 80—61554
pupillary near reflex static and dynamic characteristics *(Japanese)* 79—29524
pupillary reflex of noncollaborating subjects, contact lens pupillography electronics 78—40381
pupillary response to light, gekkonid lizards 79—57653
pupillary sphincter, light-induced Ca release in photosensitive vertebrate smooth muscle 78—64994
pupillary system, human, same-signed 1st and 2nd degree kernels 80—26228
pupillometer, Fick-Broca, modification to overcome problems 79—5276
pupillometer, objective device using counter-rot. perspex blocks 78—81000
pupillomotor latent period 77—60200
pupilometry, instrumentation for stimulating and monitoring human pupil 78—48911
pursuit after-nystagmus obs. 80—41018
pursuit movements in absence of target, perceptual effect 78—73162
pursuit movements of disappearing moving target 78—61174

eye continued
Raman spectroscopy with intensified Vidicon detectors, appl. to intact bovine lens protein 79—29525
rapid action and movements during the jump, theoretical anal. 79—79521
rapid eye movement analysis during sleep 80—76870
rapid eye movement automatic detect. system and normative data 79—74771
rapid eye movements, computer analysis 78—48900
rapid eye movements, computerised anal. method, REM sleep period appl. *(Japanese)* 80—41273
rat eye refractive state 77—81493
ray-tracing for physiological optics 77—25420
readaptation after dazzle, multidimensional functional model *(German)* 79—16208
reading through pinholes, for teaching 80—17765
reading without a fovea 80—76748
receptor adaptation, spectral sensitivities and photopigments, fly 77—29149
receptor cell outer segment, bovine, Ca^{2+}-depend. ATPase activity 77—29147
receptor optics and orientation, vertebrate 80—81585
red-absorbing visual pigment of butterflies, rhodopsin 80—3646
red-green dichromats, wavelength variation in directional sensitivity obs. 80—45903
red-green opponent channel, short-wave cone input obs. 80—41028
reduced eye, expts. in life science labs. 80—82617
refraction deduced from speckle movement in laser refr. 80—41001
refraction estimate dependence on visual task 79—62237
refraction measurement, automated subjective optometer 78—35971
refraction scotomata rel. to eye chromatic aberration 79—62239
refractive error, AO SR III Subjective Refraction System compared with phoropter 79—83953
refractive error, meas. using modified Foucault knife-edge test 77—4999
refractive error meas. using dynamic laser speckle pattern 80—81583
refractive error measurement using Humphrey Vision Analyser, reliability and validity 78—61265
refractive keratoplasty, theory and computations of optical modification to cornea 80—35875
refractive power, rat, estimation by pattern evoked cortical potentials 77—70455
refractive state, optical system for autorefractor 79—25127
refractive state, rabbit, variation with eccentricity, correct. for oblique astigmatism 79—43869
refractive state of ground squirrel 80—67070
refractor, automatic, optical system 78—61274
Refractor III system, computer-assisted eye examination 79—34698
REM detecting machine, portable 79—92410
removal at birth, producing excessive bilateral branching in rat, Co filling method 77—21520
response properties of fly visual systems 80—41021
retina, albino rabbit, X-ray effects, SEM obs. 80—104674
retina, blood flow, photon correlation velocimetry 77—90828
retina, bovine, R2 component of early receptor pot. rel. to metarhodopsin II form. 80—97904
retina, carp, neuronal architecture of on and off pathways to ganglion cells 78—44502
retina, cat, contrast gain control 79—79536
retina, cat, transfer function for spatial freqs. *(Spanish)* 79—62247
retina, cephalopod, dark adaption dynamics 79—79541
retina, cephalopod, extracellularly-recorded photoreceptor pots. 79—62245
retina, chicken, visual pigments and oil droplets 77—73530
retina, current research and study, selected review 80—30710
retina, dark-adapted, time integrative props. 78—53399
retina, developing, transient intraplexiform neuron, histogenesis of inverted amacrine cell, chick 77—90765
retina, excitation and interaction, review, book contrib. 79—5282
retina, frog, GABA and lateral spread and tonic activity 79—74661
retina, frog, morphometric anal. of internal horizontal cells 80—108892
retina, frog, near IR transmission of rods rapid light-induced changes 79—74658
retina, goldfish, X-like and not X-like cells obs. 79—43837
retina, grey squirrel, bipolar and horizontal cells, Golgi morphology and receptor connections 78—48795
retina, inner, of teleosts and reptiles, proximal negative response 77—21521
retina, lateral spread of light adaptation, rat 77—44659
retina, light-adapted, of carp, intercellular junctions between pigmentary epithelium and cones *(French)* 77—12911
retina, light-damaged, rhodopsin content and electroretinographic sensitivity, rat 77—64033
retina, light-induced transient thermal response 78—7340
retina, Limulus, temp. dependence of dynamic response 79—43866
retina, mammalian, localisation of cholinergic synapses 79—57654
retina, of river lamprey, electroretinogram recordings 77—60205
retina, pigeon, antidromic invasion of ganglion cells 79—43881
retina, pigeon, extensive lateral transmission in inner plexiform layer 77—48794
retina, pigeon, graded pots. accompanying antidromic invasion 79—43882
retina, pigeon, non-directional and directional ganglion cells 79—57655
retina, primate, temp. rise and tissue damage due to Ar laser irrad. 78—44559
retina, rat, rod and cone-type photoreceptors in post-equatorial region, electron microscopy 80—85384
retina, rat, rod elec. model, early receptor pot. generation 79—57647
retina, roach, post-receptoral neurons, adaption effects in elec. responses 79—79534
retina, serial reconstruct. of adjacent ganglion cells 80—89749
retina, significance of antidromic potentiation and induced activity 80—12092
retina, snapping turtle, mixed rod-cone responses in horizontal cells 79—79533
retina, teleost, enhancement of hyperpolarising S-potentials of surround illumination 79—2051
retina, toad, evidence for passive electrotonic interactions in red rods 78—92627
retina, turtle, modes of chromatic interactions 78—7347
retina chromaticity horizontal cells of turtle, synapse mechanisms 80—51079
retina detachment, math. model 78—44536

eye continued
retina early receptor potential, quantum mechanical model 79—57644
retina electrical activity and lipid peroxidation 79—43885
retina injuries, magnetoretinographic meas. using SQUID magnetometer 80—104702
retina neural networks between cone and photopic L-type horizontal cells 79—83782
retina of carp, colour coded S-potentials, latency measurement 79—53097
retina of cat, neural path real time simulation *(Spanish)* 78—96046
retina of developing frog eye, free radical reactions rel. to mitosis, daily vars. 77—56376
retina of Limulus, spatially synchronised oscillatory response theory 78—73158
retina of turtle, horizontal cells influence on bipolar cells' membrane pot. 78—88708
retina of vertebrate, optical tiering 77—32886
retina origin from both sides of embryonic brain, optic chiasma crossing problem 79—62250
retina outer plexiform layer lateral interactions after atropine block of horizontal cells, turtle 77—70457
retina photoreceptor membrane, light and GTP-regulated GTPase interaction 80—45897
retina physiology, single cell studies on lower vertebrates, book contrib. 79—96558
retina receptor layer current spatial distribution, frog, electrical model 77—40666
retina rod outer segments and disc membranes, bovine, trace elements, PIXE determ. 79—48012
retina structure in whistling ducks rel. to feeding habits 78—53391
retina thermal injury following laser irrad., asymptotic rate process calcs. 78—80916
retina-lamina connectivity, polarisation sensitivity, crustaceae 79—2054
retinal$_1$, all-trans, valence bands, XPS obs. 78—24030
retinal anatomy and physiology, reprint of 1877 paper 78—20932
retinal autofluorescence in land snails 79—53103
retinal b-wave currents, frog 79—57652
retinal bipolar cell dark noise and stability of rod rhodopsin 78—11644
retinal bipolar cells, dogfish, visual signal transmission near absolute threshold 79—79535
retinal bipolar cells, frog, Golgi study 78—56968
retinal bipolar cells, struct. basis for on- and off-centre responses 78—44503
retinal blood flow, laser Doppler meas. 78—69174
retinal camera with infrared TV obs. *(German)* 79—2145
retinal cell sensitivity to movement of stimuli and flickers, histochem., frog 77—86490
retinal cells of cat, spatio-temporal model 78—92621
retinal chemical processes, reprint of 1879 paper 78—20933
retinal chromophore, reson. Raman spectra obs. of struct. 80—94168
retinal chromophore transition dipole moment, orientational changes obs. 80—41023
retinal cone chromatic organisation, baboon, using light-stimulated NBT reduction 77—64031
retinal cone mechanism saturation, blue-sensitive receptors 77—29151
retinal cone pigments, human spectrophotometry, annotated bibliography *(Italian)* 79—62256
retinal damage by 325 nm He-Cd laser radiation 78—69136
retinal damage by visible light, role of singlet O 78—15858
retinal damage from a white-light laser, thresholds and mechanisms, rhesus monkey obs. 80—108955
retinal damage from suprathreshold Q-switch laser exposure 79—5274
retinal degeneration, hereditary, cone inputs to ganglion cells 80—8056
retinal degeneration in dystrophic rats, light-induced, action spectrum 80—41118
retinal degeneration in RCS rats raised under ambient light levels 79—43887
retinal diffusion, two-stage, rel. to flicker sensitivity 79—74657
retinal diffusion and eye optics quality, OTF and light scatt. characterisation 80—41004
retinal diseases, literature review (1975-76) 78—35836
retinal distribution of illuminance, universal mathematical expression *(German)* 79—92214
retinal excitation, molecular mechanism for initial process 79—100598
retinal feature mapping in freely moving eye with precise control of retinal stimulus position 80—12097
retinal ganglion cell activity in ground squirrel under halothane anaesthesia 78—40147
retinal ganglion cell activity induced by ELF mag. fields, method for study 80—56321
retinal ganglion cell firing patterns, implications for separate ON and OFF processes goldfish 77—70458
retinal ganglion cell functional pathways, book contrib. 79—96559
retinal ganglion cell layer, cat, newly identified presumptive microneurones population 80—67077
retinal ganglion cell of cat, refractoriness in maintained discharge 78—64991
retinal ganglion cell of frog, excitatory and inhibitory processes giving rise to delayed response 79—2055
retinal ganglion cell response to sinusoidal flicker, mudpuppy 78—48798
retinal ganglion cell responses in dark-reared rats 79—53102
retinal ganglion cell responses to flashing and moving stimuli, mudpuppy 77—12917
retinal ganglion cell types, of cat, visual resolution and receptive field size 80—56037
retinal ganglion cells, abnormal response in Siamese cats 77—90785
retinal ganglion cells, bovine, size and distrib. 79—100596
retinal ganglion cells, cat, nonlinear analysis in freq. domain 78—48793
retinal ganglion cells, class I, in the toad, Bufo spinulosus 80—85393
retinal ganglion cells, displaced, projection on accessory optic system, pigeon 77—90781
retinal ganglion cells, frog, species differences in optimal stimulus sizes 77—21519
retinal ganglion cells, goldfish, effects of photic stimulation upon var. of interspike intervals 77—70460
retinal ganglion cells, macaque, macular pigmentation and spectral sensitivity 79—43877
retinal ganglion cells, mudpuppy, hyperpolarising ON/OFF responses 77—25427
retinal ganglion cells, Necturus, responses to stationary and moving stimuli 77—70459

eye continued
- retinal ganglion cells, orientation bias, cat expts. 80—94206
- retinal ganglion cells, rat, adaptation pools and excitation receptive fields 78—7356
- retinal ganglion cells, responses to stationary and moving stimuli 80—51080
- retinal ganglion cells, scotopic increment thresholds 79—79558
- retinal ganglion cells, struct. basis for on- and off-centre responses 77—1997
- retinal ganglion cells, suppression of maintained activity 79—79537
- retinal ganglion cells, surround- to centre-type response transition by receptive field centre darkening 77—44649
- retinal ganglion cells action pots., goldfish, function of lighting conditions 79—43888
- retinal ganglion cells in the galago, size and tropographic arrangement 80—67078
- retinal ganglion cells of 3 week old kittens, physiological props. 77—36922
- retinal ganglion cells of a tree shrew, definition of neural response and incremental sensitivity 80—41011
- retinal ganglion cells of cat, response patterns for moving contours 78—69059
- retinal ganglion cells of pigeon, concentric receptive fields 77—44653
- retinal ganglioside synthesis, chick, light stimulation 77—9189
- retinal horizontal cell, oscillatory responses 78—31813
- retinal horizontal cell reaction to non-uniform illum., model 77—56375
- retinal horizontal cell receptive field centre/surround interaction model 77—86497
- retinal horizontal cells, amplification of graded pots. 77—32889
- retinal horizontal cells, response to monochromatic light 77—81500
- retinal image cinematographic recording, accommodation microfluctuation appl. 80—81579
- retinal image displacements and saccadic eye movements, adaption to altered relationship 79—43911
- retinal image light distrib., cat 78—48790
- retinal image motion, effect on vision in coloured light 80—51105
- retinal image stabilisation 80—12088
- retinal image stabilisation quality during small body rotations in man 79—100595
- retinal image study, computer controlled laser interferometer using acoustooptic modulators 80—56294
- retinal images, defocused and spatially filtered, stereoscopic acuity 80—101177
- retinal information processing, computer model 77—66814
- retinal injury, permanent, due to over-exposure 79—62295
- retinal injury, thermally-induced, due to high optical-radiation doses 80—3710
- retinal injury mechanics, laser exposure limits 79—66485
- retinal internal circulation visualisation using Purkinje's methods 78—69043
- retinal L-type horizontal cells, nonlinearity in dynamic characts. 79—100603
- retinal lesions, incidence prior to retinal detachment *(Italian)* 79—79514
- retinal light intensity 2-dimens. profiles from laser-irrad. monkey eye 78—40141
- retinal light responses, simultaneous recording by extra- and intracellular electrodes in crayfish 78—69055
- retinal mechanisms of visual latency in Bufo marinus, electroretinogram obs. 79—48255
- retinal models, experimentation, program framework 79—53108
- retinal nerve fibre atrophy development computer evaluation 77—40856
- retinal neuron, variability of interspike intervals during sustained firing, model 77—86492
- retinal neuron firing rates, lack of predictability from interspike interval statistics 80—67075
- retinal neuron interspike intervals variability, model dynamics 79—24984
- retinal neuronal network, interactions between photoreceptors and horizontal cells 78—11648
- retinal neuronal network of photoreceptors and horizontal cells 78—3482
- retinal neurones, differential labelling by ^{3}H-2-deoxyglucose 79—92447
- retinal neurons, catfish, spatiotemporal testing and modelling 80—41005
- retinal neurons, spatio-temporal receptive field meas. 79—57649
- retinal neurons studies, appl. of white noise anal. *(Japanese)* 79—66471
- retinal on-centre bipolar cell, ionic mechanisms of rod and cone signals 78—61177
- retinal photocoagulation by laser beam, temp. and bleaching dynamic meas. *(German)* 79—2098
- retinal photoreceptor and horizontal cell synaptic connections 77—90787
- retinal photoreceptor model, FET cct. realisation 80—56027
- retinal photoreceptors, response increase and noise decrease by circadian clock in Limulus brain 80—94210
- retinal pigment epithelium, defective phagocytosis of isolated rod outer segments RCS rat cells 78—11647
- retinal pigment epithelium, identification of membrane protein binding retinol 77—21515
- retinal pigment epithelium, variations in phagosome content rel. to cyclic lighting 77—90772
- retinal pigment epithelium phagocytosis, RCS rat 79—34561
- retinal processing, nonlinear, generalised model 79—53107
- retinal R/G horizontal cells, light intensity and response amplitude relation 79—5281
- retinal receptor directional sensitivity, flicker effects 80—8057
- retinal receptor model, input intensity adaptive 77—90786
- retinal receptors, human, modal pattern stability, with wavelength, inhomogeneous waveguide model 79—8504
- retinal research and study, selected review 80—108874
- retinal resolving power meas. by laser interferometry 80—36066
- retinal response, expected waiting time 80—51091
- retinal responsivity compression, V-log I functions and increment thresholds 78—61181
- retinal rod, localisation of Na^{+}, K^{+}-ATPase and Ca^{2+}-activated Mg^{2+}-depend. ATPase 77—44652
- retinal rod discs, intradiscal surface, photoreceptor membrane carbohydrate 77—4998
- retinal rod external segment mag. anisotropy decrease after total photolysis 77—52838
- retinal rod outer segment membranes and liposomes of extracted phospholipids, proton spin-lattice relax. rates 77—90782
- retinal rod outer segments, birefr. analysis 78—56954
- retinal rod outer segments, presence of Lubrol activated latent Na^{+}, K^{+}-ATPase 77—12920

eye continued
- retinal rod photoreceptor membrane orientation in intact eye, X-ray diffr. 77—48790
- retinal rods, thermal activation of visual transduction mechanism 79—74651
- retinal Schiff bases, Raman spectra modelling of rhodopsin and bacteriorhodopsin chromophores 79—62190
- retinal sensitivity, monochromatic stimuli, large eccentricities 79—5285
- retinal single-photon impulse coding mechanisms *(Russian)* 78—27941
- retinal site of transient tritanopia 79—88078
- retinal spectral sensitivity to light it has scattered, human 77—9193
- retinal spectral-response characteristics model, light propag. through human eye 79—92215
- retinal stimulation by Ra 79—71213
- retinal streak, turtle, orientation of horizontal cell axon terminals 79—74653
- retinal synaptic transmission effectiveness, neurone regulator model 79—57645
- retinal tissue damage, by single ultrashort laser light pulses 78—96065
- retinal-image movement rel. to eye rotation, contact lens/spectacle system for correction 79—53281
- retinals, catalysed cis-trans isomerisation by crude tissue extracts 78—64925
- retinas, goldfish, dorsal rel. to ventral areas obs. 79—43880
- retinoblastoma treated with ^{60}Co applicator 77—81550
- retinol-binding proteins in retinal pigment epithelium 79—20525
- retinomotor activity, local control in fish 79—2047
- retinoscopic and subjective measurements, discrepancy, effect of age 79—34550
- retinoscopic and subjective refraction discrepancy, polarisation effect 79—83764
- retinoscopic artifact obs. in rabbits 79—48247
- retinoscopy, near and cycloplegic, in early primary schoolchildren 80—8047
- retinoscopy, theory including aperture stops 78—85308
- retinoscopy artefact in rat and rabbit eyes, origin at retina/vitreous interface obs. 80—51075
- retinoscopy of infants at distance, limits of normal and anomalous reflexes 78—61170
- retinoscopy using He-Ne laser retinoscope 80—41159
- retinotectal projection development, Gierer-Meinhardt eqns. appl. 80—56022
- retinotectal projection development, mathematical model *(Japanese)* 80—21467
- retinotectal projection in goldfish to an inappropriate region with a reversal in polarity 80—72153
- retinula cell response properties, fly 77—44658
- retinula peripheral cells within Drosophila visual mutants, response to monochromatic white-noise 78—69078
- retinular cell spectral sensitivities in bumblebees, optical method meas. 79—2057
- retinular cells, arthropod, light-induced membrane cond. change rel. to membrane pot. 77—5001
- retrolental fibroplasia, A-mode ultrasonography and oculometry 80—89816
- rhabdom spectral absorption, crayfish visual pigment, photoproduct and pH sensitivity 78—65008
- rhabdomere transmittance decrease due to blue light, rel. to desensitisation of peripheral photoreceptors 78—64993
- rhodopsin, bovine, kinetics of NaBH$_3$CN reduction 78—64926
- rhodopsin, vertebrate, chromophore orientation obs. 80—40959
- rhodopsin and its photoproducts, directional absorpt. props. obs. 80—51090
- rhodopsin flash photolysis, rabbit retina 78—76996
- rhodopsin formation, opsin recognition of longit. length of retinal isomer 78—61137
- rhodopsin P499$_1$ and porphyropsin P522$_2$, paired visual pigments in goldfish 79—53111
- rhodopsin phosphorylation as possible mechanism of visual adaptation 78—15836
- rhodopsin photoproduct kinetics in frog retinas, rapid scanning microspectrophotometer meas. 78—92763
- rhodopsin regeneration in frog, effect of MS-222 anaesthetic 77—36925
- rhodopsin thermal stability in photoreceptor membrane, role of lipids, PMR spectroscopy 80—35874
- rhodopsins of oceanic decapods, absorpt. spectra 78—61182
- rod, amphibian, dark adaptation processes 78—15835
- rod, Ca-depend. regenerative responses 78—3480
- rod and cone activities, large field early light adaptation 79—53117
- rod disc membrane ion transport props. 78—15829
- rod disc membrane phosphodiesterase control 79—79527
- rod early receptor potential isolation from frog retina 78—69066
- rod ERG, human, dark-adapted a-wave response function obs. 80—56036
- rod ERG, human, rel. to psychophysical responses in light and dark adaptation 78—69063
- rod ERG of mudpuppy, effect of dim red backgrounds 78—69062
- rod external segment fragment suspension, Ca^{2+} activity rel. to illum. 77—36918
- rod external segment membrane, phospholipid auto-oxidation during conform. changes 77—21523
- rod external segment surface membrane, lateral diffusion of rhodopsin 78—15828
- rod network in turtle retina, elec. spread 78—80874
- rod outer segment, Rana pipiens, birefringence meas. of struct. inhomogeneities 78—77048
- rod outer segment adaptation anal. based on a simple equiv. cct. 78—73157
- rod outer segment and interstitial matrix of rat, refr. index difference determ. using waveguide parameter 79—5277
- rod outer segment birefringence changes following intense light flashes, frog 77—90789
- rod outer segment birefringence gradient, struct. interpretation, 3-dielectric layer model 79—83771
- rod outer segment disc shedding in rat retina, rel. to cyclic lighting 77—32887
- rod outer segment membrane current, light-induced fluctuations recorded in single toad rod 77—86493
- rod outer segment phagocytosis obs., rat 79—62249
- rod outer segment shedding, intraocular initiation 78—85309
- rod outer segment tip shedding in frog retina, rel. to light stimulation 77—29148

eye continued
rod outer segments, accel. membrane renewal after light exposure 77−64035
rod outer segments, intact, GTP hydrolysis rel. to transmitter cycle in visual excitation 79−83773
rod outer segments, shedding behaviour under constant light, darkness 79−2050
rod outer segments, spread of activation and desensitisation 80−35881
rod outer segments, vertebrate, role of Ca and H ions as transmitters 77−90776
rod outer segments membrane current fluctuations 79−79530
rod outer segments membrane current obs. 79−79529
rod outer segments pots., frog, local stimulation and adaption obs. 79−79528
rod outer sements, isolated, photoresponses, frog 79−43890
rod photoreceptor disc membrane, cooperative conform. change induced by bleaching 77−81499
rod photoreceptor membrane, pot. regulation by cyclic GMP 79−74654
rod photoreceptor model sensitivity, depend. on level of background light intensity 78−20179
rod photoreceptors, vertebrate, opposing effects of Ca^{2+} and Ba^{2+} 79−24990
rod photoresponse, contrib. of Cs^{+}-sensitive cond. increase 78−44501
rod receptor orientation local variations 78−40175
rod threshold, human, influence of cones stimulated by contrast flashes 78−69074
rod threshold, neighbouring cone influence 79−53116
rod-cone interaction, spatial patterns 80−16930
rod-cone interaction obs. 79−100607
rod/cone system interactions in goldfish retina 78−35853
rods, frog, bleaching and background adaption 79−79532
rods, role in iconic storage 79−24987
rods, threshold rel. to pigment in Xenopus 79−79526
rods, toad, effects of Ba^{2+} on dark-adapted intensity-response curve 79−79531
rods, toad, effects of Ca^{2+} on intensity-response curve 79−53091
rods, toad, spontaneous quantal events induced by pigment bleaching 80−108895
saccade, oblique, obs. of curvature using scleral coil technique 77−48793
saccades, counting accuracy obs. 79−43889
saccades, differential responses of 'simple' and 'complex' cells of cat's striate cortex 80−85394
saccades, large, error-correcting mechanisms 78−61175
saccades, primary and secondary for goals defined by instructions 79−43878
saccades, small, lack of useful purpose considerations 80−61553
saccades, small, role in counting 77−25456
saccades, two-dimens., accuracy in absence of continuing retinal stimulation 78−7341
saccadic and vergence eye movements, reciprocal innervation model 78−31811
saccadic eye movement control system, digital analogue simulation 77−44654
saccadic eye movement controller, adaptive considerations 78−27949
saccadic eye movement simulation, grey-out elimination 79−43910
saccadic eye movements, small, perceptual function 80−61577
saccadic eye movements and visual stability 79−2068
saccadic eye-movement system, processing of direction and magnitude obs. 80−56035
saccadic latency predictability in a novel voluntary oculomotor task 80−72157
saccadic movements, binocular, synchrony 77−36934
saccadic movements anal., voluntary nystagmus nature investigation 78−3476
saccadic movements during changes in fixation to stimuli at different distances 77−32895
saccadic ocular dysmetria simulation using sampled-data model 77−56373
saccadic omission, grey-out obs. 79−43909
saccadic suppression, exogenous and endogenous contribs. 77−40671
saccadic suppression by corollary discharge in the locust 79−92217
saccadic system, anal. by double step stimuli 80−41014
scanning eye movement target point selection 78−24066
schematic eye for the opossum 79−62243
schematic eyes, reduced, for vertebrates, table including computed longitudinal chromatic aberrations 80−51074
schematic for the rat 79−74647
scotopic hues of simultaneous contrast 79−53122
screening-pigment migration in retinula cells of crayfish, spectral sensitivity 80−72165
senile macular degeneration, colour discrimination rel. to visual acuity 80−108897
sensitisation effect, rectilinear stimuli 79−2062
serous retinopathy, monolateral central, colour discrimination in 23 patients 79−5286
shark visual system 78−15824
shields, individualised, for electron beam therapy and low-energy photon irrad. 80−109040
short-wavelength cone pathways, response saturation, colour opponent mechanisms control 80−41017
silicone rubber, vulcanizing, possible substitute for damaged/diseased parts of eye 79−74788
simulator of human visual system *(Russian)* 80−76877
single-epoch somatosensory evoked vertex potential, time window for electro-ocular monitoring 79−96535
slit lamp, hand-held, with lid opener for ocular exam. 80−67179
slit lamp photodocumentation of ocular structure 80−67181
smallest channel in early human vision 80−101178
smooth eye tracking, motion perception in absence of real movement 79−2075
smooth movements, oculomotor and perceptual localisation 79−74680
smooth pursuit eye movements, perceived motion obs. 80−3649
smooth pursuit movements, target position and vel. as stimuli 80−85392
spatial localisation during pursuit eye movements 80−51081
spectacle, role in visual optics of snake eye 77−36917
spectral eye fatigue, school lighting effects 80−76732
spectral reflectance photography of the ocular fundus 80−67184
spectral sensitivity of human eye, colour coordinates number triple *(Russian)* 80−76741
spectral sensitivity of human eye, deductive derivation of mathematical model *(Russian)* 80−76740

eye continued
spectral sensitivity of the goldfish, cone mechanisms identification 80−56043
spectrally-opponent responses in ground squirrel optic nerve 80−35883
specular reflections by polaroid films, pot. eye hazard 80−85447
spherical aberration, contrib. of cornea and lens 79−100597
spheroidal degeneration of cornea and conjunctiva, pathology 80−12085
stereo-ophthalmoscope 110, for viewing of fundus oculi 78−48905
stereo-ophthalmoscope 110, stereophotography of fundus 78−48906
stereophotography, using camera slit lamp, ophthalmic applications 78−48904
stereoscope vergence, convergence and divergence independence obs. 80−30714
Stiles-Crawford function, specification of directionality 80−45907
Stiles-Crawford function peak shift with wavelength 78−92631
stimulus onsets and offsets, response of visual mechanisms 80−16937
strabismic amblyopia, optical aberrations rel. to visual loss 78−48788
strabismic amblyopia in infants 80−30715
strabismic cats, eye movement obs. 80−89748
strabismus, fusional convergence ranges using random dot stereograms, operant conditioning 80−108900
strabismus and amblyopia, eye movement analysis by computerised ocular motility test system 80−41299
striate cortex functional architecture quantitative model 80−89747
striated muscle, bovine, physico-chemical anal. of contractile proteins 77−90819
superior colliculus in rat, plasticity of developing visual system, sensory deprivation effects 78−88706
superposition images formed by refl. in eyes of some oceanic decapod crustacea 77−4997
synaptic projections formation mechanism in arthropod visual system 78−88707
tapered parabolic-index fibre waveguide model 79−76803
tapetum lucidum, cat, morphology obs. 80−108878
target tracking, eye movement evaluation using EOG 80−109057
tear measurement, slit lamp fluorophotometer 77−2064
tecta termination bands, eye-specific, three-eyed frogs 79−62251
tectal units, goldfish, centre-surround organisation and receptive field interactions 79−79538
television ophthalmoscope image processor/graphics system 77−81633
thermal-flash protective devices for eye. PLZT electrooptic shutters 77−46808
threshold, transient increase due to combined changes in propagation direction and polarisation plane 80−51096
tissue examination by multiple internal reflection IR spectroscopy 77−9304
tonometer, applanation, for intraocular pressure meas. 80−30833
torsion and visual tilt, mediation by different binocular processes 80−41035
torsion in response to tilted visual stimulus 80−45891
torsional movements, binocular coordination in cyclofusional reponse 79−2048
torsional movements, rapid phase, in humans 78−69045
tracking as sequential input adaptive process 79−88074
tracking communication system feasibility for nonverbal cerebral palsy children 79−83981
tracking movements rel. to illusion of movement 77−86500
tracking system, accurate three-dimens. 78−48944
transduction in photoreceptors with bistable pigments, prolonged depolarising afterpot., obs. 80−8050
transient sensitisation by a contrast flash 80−72162
transient tritanopia at the level of the ERG b-wave 79−100614
trichromatic colour matching, high-level, rel. to pigment-bleaching hypothesis 80−35891
TV pupillometer, anal. of dynamic performance *(Japanese)* 79−39545
two eyes constituting separate visual channels, expts. 80−97923
two-dimensional movement meas. with ferromag. contact ring 79−5387
US impediography, quantitative characterisation of lesions in vivo 80−17039
US in ophthalmic diagnosis 80−81673
US ophthalmological diagnostics and therapy *(Croatian)* 78−44570
US ophthalmological signal acquisition and image enhancement 78−57045
US ophthalmoscope, eye axial distances meas. 80−36032
US pulse scatt. 77−37008
UV effects, review 78−80917
UV effects 300 to 400 nm, literature review 78−57042
vascularised cornea, fluorescence angiography, using camera slit lamp 78−48855
ventral photoreceptors, Limulus, excitation by photons and fluoride ions 80−8065
vergence and accommodation static behaviour, computer simulation of interactive dual-feedback system 80−94205
vergence control, role of spatial freq. tuned channels 80−101170
vergence eye movement role in stereoscopic perception of space 78−85315
vergence movement of rabbits in visuomotor behaviour 79−43892
vergence movements, heuristic feedback system model 77−21517
vertebrate cornea, transparent layered structure thickness monitor 78−92737
vertebrate retina modelling and simulation, extended networks 80−108884
vertebrate retina neuronal activities modelling and simulation 80−85386
vertebrate retinal horizontal cells, spatial integration, computer analysis 77−36920
vertebrate retinas, outer segment layer, light-induced Ca fluxes 80−94207
vertical fixation disparity, correction by horizontal prism 80−67281
vertical movement elementary detectors of fruitfly 79−34558
vestibular control of oculomotor and postural mechanisms 80−72151
vestibular nuclei neurons in goldfish, model with ocular proprioception 78−40142
vestibular nystagmus, Alexander's law model 80−35878
vestibular nystagmus, computer anal. of irregularities indicating central vestibular disorders 78−81036
vestibulo-ocular reflex, horizontal, linear system anal. appl. to alert rhesus monkey 79−100600
vestibuloocular reflex of cat, quick phase generation model 78−56971
vision model using optical engineering theory concepts 79−96555
vision sharpness improvement, optical devices and apparatus *(Hungarian)* 78−15823

eye continued
visual activity lateral impedance theory, Markov processes appl. 79—2046
visual acuity threshold variation, study of research literature *(French)* 79—5283
visual field modifications in ocular and neuro-ophthalmological pathology, perimetry glossary *(Italian)* 79—79540
visual field plotting using eye movement response 80—8045
visual performance after blue light exposure, rhesus monkey 79—53114
visual pigment, steady-state composition in rainbow trout 80—51097
visual pigment chromophores, models, spectroscopic and photochemical studies 80—30723
visual pigment composition of rainbow trout 79—43899
visual pigment processes and prolonged pupillary responses in insect photoreceptor cells 80—8061
Visual pigment systems, implications of bistability 80—8059
visual pigments, conf., Florence, Italy (Sep. 1978) 80—4468
visual pigments, resonance Raman studies of the primary photochemical event 80—41020
visual sensitivity and adaption, conf., Guildford, England (Sept. 1978) 79—79516
visual stimulator for flicker fusion expt. 78—96053
visual-motor development in the cat, eye movement obs. 79—83774
vitamin A receptors in normal and dystrophic human retina 77—21514
vitreous humour, human, viscoelasticity, in vivo obs. 80—56077
vitreous sample, human, viscoelasticity determ. by Weissenberg rheogoniometer 79—92266
vitreous surgery via pars plana, instrument design 78—81056
wavelength discrimination near absolute visual threshold, goldfish 79—48264
X-ray computerised tomography for diagnosis of eye-socket *(German)* 79—100727
^{60}Co therapy for Hodgkin's disease, gonadal and eye doses 79—96665
O_2 transmural transport to retina, mathematical model 79—34583

F-centres
see also A-centres; M-centres; R-centres; Z-centres
alkali bromides and iodides, self-trapped exciton and F-centre form. by picosecond laser pulses 80—10546
alkali chlorides, positron-trapping colour centre dynamics, positron annihilation study 80—108294
alkali halide:H^-(D^-), local modes and colour centre absorpt. bands, analogy 80—60632
alkali halide, activated crystal, absolute quantum yield of stored light sums *(Russian)* 79—56851
alkali halide, binding energies of positron to F and F′ colour centres 78—87667
alkali halide, defect formation, model of excitonic mech. 78—91337
alkali halide, F-centre, stabilisation process in first colouring stage 79—19246
alkali halide, F-centres, vibronic problem in higher excited states 78—10931
alkali halide, gamma irradiated, positron annihilation 79—23643
alkali halide, impurity pseudopotential screening 79—15121
alkali halide, irrad., colloidal centre growth, model 77—19946
alkali halide, molecular model for F_A(II)-centre emission process 77—28616
alkali halide, positron localisation at negatively charged centres 77—8055
alkali halide, with oppositely charged defect centres, autoionisation-tunnel relax. of electron excitation 78—72112
alkali halide, X-irrad., elec. breakdown, temp. and F-centre conc. depend. *(Russian)* 77—8504
alkali halide crystal, deformation, electrical voltage generation 79—56256
alkali halide crystal, irrad., chemiluminesc. process during dissolution *(Russian)* 78—92133
alkali halide crystals, binding energy of F_{e+}', M_{e+}' and R_{e+}' centres, positron trapping 79—69460
alkali halide crystals, deformation spectroscopy, dislocation interactions with electron and hole centres 78—10983
alkali halide crystals, exciton mechanism of complex active centre formation at fracture 79—33033
alkali halide crystals, optical breakdown, role of colloidal particles 80—50270
alkali halide crystals, radiation damage products, impurities and colour centres *(German)* 78—10086
alkali halide crystals, tunable CW IR lasers using F_A(II), F_B(II), M and F_2^+ centres 77—88725
alkali halide crystals, X-ray irradiated, luminescence during release of pressure 79—65939
alkali halide CW single mode colour centre lasers, freq. behaviour and linewidth 77—88728
alkali halide F-centres, cation vacancy model, rot. mechanism 77—76393
alkali halide hologram, high-efficiency recording by selective colloidal centre destruction 80—63955
alkali halide host cryst. F-centre lasers, tunable IR emission 78—59030
alkali halides, bound polarons, vibronic theory, appl. to F-centre excited states 78—84150
alkali halides, cryst., F-centre decay, temp. effects, Arrhenius depend., rel. to NH_3 radiolysis 77—48662
alkali halides, defect form., model of excitonic mechanism 78—38696
alkali halides, divalent cation doped, irradiated, first-stage F-centre prod. 80—107231
alkali halides, doped, F-centre accumulation efficiency temp. depend. 77—76394
alkali halides, emission band of F-centre 80—76071
alkali halides, EPR in relaxed excited state of F-centres, detection via saturated optical pumping 78—6606
alkali halides, extended-ion approximation and pressure shifts in F-band energies 80—49223
alkali halides, F_A-centre optical absorpt., estimate using symmetry-adapted wave functions 80—11448
alkali halides, F_A-centre optical absorption, lattice statics theory 79—43004
alkali halides, F^--centres, thermal and photolytic decay processes 78—95053
alkali halides, F-centre, cluster-Bethe lattice treatment 78—63762
alkali halides, F-centre absorption energy calc. 79—78715
alkali halides, F-centre accumulation, radiation induced, temp. depend. 80—59460
alkali halides, F-centre photoionisation, semicontinuum model 79—99509

F-centres continued
alkali halides, F-centre trapping of conduction electrons, photocond. study 78—56179
alkali halides, F-centres, ESR in different states of relaxed configuration 80—108067
alkali halides, F-centres, first order Raman scatt. *(French)* 78—2828
alkali halides, F-centres, formation time 80—15477
alkali halides, F-centres, optical pumping, spin-orbit and hyperfine coupling 77—16360
alkali halides, gamma and additively coloured, dissolving in pure water, lyoluminesc. mechanism 80—100693
alkali halides, influence of purity of crystals on stability of F-centres and interstitials 78—91336
alkali halides, interstitial motion during radiation damage and sputtering processes 80—54230
alkali halides, light amplification at activator centres 80—2795
alkali halides, luminesc., colour centres and radiation-tunnel transition 79—4846
alkali halides, luminescence quenching of F-centres 80—50417
alkali halides, photodichroic, as optical processing elements 78—83056
alkali halides, positively charged long-lived excited states and spontaneous tunnel transitions 79—82552
alkali halides, relaxed excited state of F-centre, vibronic theory of Stark effects 77—85691
alkali halides, resonance Raman scattering, electron-phonon interaction for F centres 78—68519
alkali halides, saddle-point configuration, molecular model parameter 80—107234
alkali halides, spin lattice relax. and g-shift 80—15799
alkali halides, XPS, trapped electrons at F-centres and anion defects, photoionis. cross sections 77—90249
alkali halides, Z_1-centres, peculiarities of thermolum. 80—103999
alkali halides with NaCl struct., F-centre absorpt. and ground state 77—62524
alkali halides with NaCl structure, F-centre emission and relaxed excited state 79—42060
alkali metal chloride crystal, F centre energy level shift and splitting in O^- field 80—70640
alkali metal halides, F-centre coupling to lattice modes 79—77596
alkali metal halides, F-centre luminesc. rel. to cryst. chemical parameters 80—29780
alkali metal halides, F-colouring role of impurities 80—64995
alkali metal halides, irradiated, annealing 78—92494
alkaline earth fluoride crystals, colour centre thermal stability 78—83811
alkaline earth fluorides, F-centre annealing and intrinsic luminesc. 79—65937
alkaline earth fluorides, radiation damage and photochromism in doped and undoped crysts. 79—51148
alkaline earth oxides and fluorides, F-centre luminesc. rel. to cryst. chemical parameters 80—29780
borate glass, containing Ag_2O, ESR obs. of electron trap centres 77—20697
diffusion-controlled defect recombination, quasi-steady radius, tunnelling and elastic interaction *(Russian)* 80—10908
dilute metal solutions in molten salts, optical absorption, F-centre model for bound state 80—89023
dislocation field effect, dislocation photoconduction spectrum *(Hungarian)* 80—51977
dislocation influence on optical props. 80—108234
electron levels, temp. depend. shift calcs. 77—28599
EPR and spatial extn. of relaxed excited state 79—73812
EPR in relaxed excited state, via mag. circular polarisation of emission 79—24232
ground state wave function, ENDOR and F-absorpt. data analysis 77—31978
halides, form. photochem., review 78—63763
halides, vacancy-interstitial pair prod. by electron-hole recomb. 79—4530
ionic crystals, efficiency of radiation-induced F-centre accumulation *(Russian)* 79—69102
ionic crystals, radiation defect accumulation temp. depend. 80—19803
ionic crystals, surface F centres, electronic struct., numerical soln. of one electron Schrodinger eqn. 78—64091
ionic crystals with intermediate polaron coupling, magneto-optical effects in shallow F-centres 80—20615
KBr, γ-irradiated and additively coloured, chemiluminescence origin *(Russian)* 77—32453
KCl, pure and Ba-doped, γ-irrad., point defect form. and interaction, X-ray and optical studies 79—65078
KCl crystal surface, electron bombard., absorpt. investigated by use of lateral light waves 78—4707
KCN, relax. times of F-centres meas. at 83K phase transition 77—59458
laser, continuously tunable near IR *(German)* 80—1207
laser, F II centre, cavity design incorporating polarisation beam splitters 79—45960
laser, pulsed broadly tunable IR 79—76706
laser design, tunable CW for spectroscopy and photochemistry 78—94397
laser spectroscopy, struct. and quantum optics 77—52147
laser used for IR optogalvanic spectrosc. of He positive column discharge 80—78563
lasers, colour centre, thermal strains in active elements, theory 80—91804
lasers, spectral sources appl. 79—36900
luminescence, temp. depend. of stress-induced polarisation 79—56857
3-methylpentane glass, electron-ion pair polarisation, γ-irrad. induced current and IR photocurrent 77—69768
molten salt, metal dilute solns., optical absorption 79—19899
NaCl, dislocation charge photostimulated variation kinetics *(Russian)* 80—79806
nonradiative quenching of hot luminesc. in F centres 80—11467
optical absorption bandshape calc. for transition to state with Jahn-Teller and spin orbit couplings 80—55135
oxides, excited states of F-centres 78—64006
polynuclear system, ENDOR dynamics of F-centres, cross relax. effect 77—40151
potassium halides, F-centres, optical pumping, spin-orbit and hyperfine coupling 77—16359
primary F-H pair, annihilation probability of components in thermoactivated motion *(Russian)* 78—14340
pseudo-Jahn-Teller effect, cubic, linear, rotational invariance 80—15482

F-centres continued
relaxed excited state, spin polarisation, saturated optical pumping 79—15522
relaxed excited states, vibronic model of stress effects 78—95118
sapphire, F-centre, fluorescence decay below 75K 80—60664
sapphire, F-type centre induction, 6.1 eV optical absorpt. band 78—88332
sapphire, luminesc. of F centre 79—73990
sapphire, neutron bombard., F-centre fluorescence, photoluminescence 80—100676
shell-model crystal, electron-phonon interactions effect of F-centre on shell screening 77—72825
space distribution, pair correl. function 79—60361
transition metal oxides, XPS, trapped electrons at F-centres and anion defects, photoionis. cross sections 77—90249
tunable IR lasers with F_A(II) and F_B(II) colour centres 78—90420
vibronic scheme of relaxed excited state 79—90989
Zeeman interaction, relativistic corrections and very small g-shifts, contrib. to EPR 78—72393
α-Al_2O_3, additively coloured single crystal, luminescence *(Russian)* 80—55169
α-Al_2O_3, crystal defects from X-ray irradiation, F-centres, X-ray luminesc. obs. 80—55176
Al_2O_3, neutron irrad., EPR spectra, F^+-centres 77—4558
Al_2O_3, neutron irradiated, electron centres, optical spectra exam. 77—63440
Al_2O_3, optical props. of F-centre 79—43003
α-Al_2O_3:Er(Cr), crystal defects from X-ray irradiation, F-centres, X-ray luminesc. obs. 80—55176
Al_2O_3:Si, Ti, pure and doped, luminescence, optical absorpt. and colour centres 79—87501
Al_2O_3:Si thermoluminescent phosphor, annealing characts. and nature of traps 77—85817
β-Al_2O_3-$K_2O(Na_2O)(H_3O^+)$, ESR of paramag. defects in cond. planes 80—29617
β-Al_2O_3-Na_2O, EPR and optical absorpt. studies of X-ray produced defects 78—95517
β-Al_2O_3-Na_2O, X-ray induced defects, EPR and ENDOR study 80—60456
$BaBr_2$:K^+, X-irradiated, perturbed F-centre, EPR and optical absorption 77—68966
$BaCl_2(Br_2)$, absorpt. spectra calc. and EPR spectra analysis 77—48203
BaClF, two types of F-centres, identification by ENDOR 78—60355
BaF_2, F-centres, muffin-tin approx. inadequacy 78—63761
BaF_2, thermoluminesc. and F-centre annealing, after neutron irrad. 80—7422
BaF_2:RF_3, cryst., absorpt. spectra, γ-ray effects 77—12409
BaFBr, X- and γ-irrad., thermolum. and optical absorpt. spectra 79—95857
BaFCl crystals, F-centres, X- and γ-irradiation, thermoluminescence and optical absorption spectra 80—45155
$BaSO_4$, X-ray irrad., electron and holes traps, g-factors, ESR obs. 80—50183
$BaTiO_3$, H_2-reduced, elec. cond. mechanism, EPR, resist. and Seebeck coeff. meas. 80—10976
BeO, F-centre exam., pseudopotential calc. 78—43328
CSI:Na cryst., V_K-Na^0 centre pairs, tunnelling recomb. 78—91952
Ca fluorapatites, carbonated, B-type, EPR of F^+-centre after X-irrad. *(French)* 80—108065
CaF_2, additively coloured, photothermal bleaching of Ca colloids 79—15500
CaF_2, F-centre growth by neutron irrad. 79—55788
CaF_2, F-centres, muffin-tin approx. inadequacy 78—63761
CaF_2, natural fluorite colouring, effect of impurities on absorpt. spectra 79—56822
CaF_2, thermolum., F-centre annealing after neutron irrad. at 20K 79—55787
CaF_2, thermoluminesc. and F-centre annealing, after neutron irrad. 80—7422
CaF_2:Co, X-irrad., F-centre form., optical absorpt. spectra and dichroism obs. 79—42998
CaF_2:M, M=Mn, Fe, Co, Ni, X-irrad., impurity effects on defect prod. 80—92525
CaF_2:O, absorption, ionic cond. and thermal depolarisation 78—14502
CaF_2:Y, absorpt. spectra, radiation defect formation energy, F to M centre conversion kinetics 79—65079
CaO, $^3T_{1u}$ of F-centre, EPR, unaxial stress effects 78—48040
CaO, $^3T_{1u}$ state of F-centre, ODMR spectra 78—43685
CaO, $^3T_{1u}$ state of F-centre, paramag. relax. optical detect. 78—43687
CaO, chemisorption of O_2, adsorboluminescence from surface F-centres 80—20723
CaO, EPR of colour centres, 295K *(Russian)* 80—84649
CaO, electron irradiated, photocond. and luminesc. meas., F-centre electronic struct. determ. 78—6409
CaO, electronic struct. calc. of F-centre, absorpt. and luminesc. bands 77—62859
CaO, F^+ centre, dynamic Jahn-Teller effect 79—28327
CaO, F^+ centre in octahedral Jahn-Teller system 79—42499
CaO F^+-centre, Lie group theory aspects of Jahn-Teller effect 77—20279
CaO, F-centre, selective excitation, detection of EPR 78—43688
CaO F-centre luminesc. and PMDR 79—95832
CaO, F-centres, $^3T_{1u}$ relaxed excited state, uniaxial stress effect and spin-lattice coupling 78—72405
CaO, F-centres, laser selective excitation and double reson. in Jahn-Teller systems 78—19379
CaO, line broadening of EPR and zero phonon lines of F centres 78—43686
CaO, luminesc. single cryst., sharp IR absorpt. lines 77—1704
CaO, obs. of dipolar induced spin dephasing, coherent optical-microwave spectroscopy 80—103900
CaO, phosphoresc. F-centre, phonon assisted conversion of Jahn-Teller states, ODMR under uniaxial stress 78—48084
CaO, photoionisation of F-centre, luminesc. and photocond. meas. 80—66270
CaO, random intrinsic strain effect on ODMR, PMDR, of F-centre in Jahn Teller states 78—84499
CaO, relax. in $^3T_{1u}$ state of F centres 80—24443
CaO, tunable optical gain at 3600 Å using F^+ centres 79—45947
$Ca_3(PO_4)_2$-$CaCl_2$:F^-, EPR of electron excess centres 78—10772
CaS, EPR of colour centres, 295K *(Russian)* 80—84649

F-centres continued
CaS phosphor, deep capture centres obs. 78—10951
CdS, electron and hole trapped centres, EPR, photoluminescence, photoconductivity study 80—108071
Cs halides, elec. field gradient at F_{Z1} electron site 78—22713
Cs halides, F_x-centres, variational calc. of energy levels 79—82204
Cs halides, F-centre energy levels, ion-size effects, calc. 80—96519
Cs halides, F-centres, first excited degenerate states, props. of electron-phonon interaction 78—63824
Cs-halide, optical response function from Jahn-Teller systems, F-band absorpt. band shape 79—43005
CsBr, electron-phonon interactions of F-centres, first-order Raman scatt. 78—64370
CsBr, F-centre absorpt., uniaxial stress effects 80—60634
CsBr, F-centres, EPR in relaxed excited state, detection via saturated optical pumping 78—6606
CsBr, F-centres, relaxed excited state, ESR, detected via optical pumping 78—43693
CsBr, first-order Raman off- and on-reson. scatt. induced by F-centres 78—92073
CsBr, second relaxed excited state of F-centre, optically detected EPR 79—87335
CsBr:Cl(F), luminescence investig. of F_H-centre lifetime 77—20917
CsBr:Cu^+, X-ray irrad., thermoluminesc. 80—16107
CsBr(Cl), spin-lattice relax. of F-centres, magneto-optical meas. 77—43884
CsCl, electron-phonon interactions of F-centres, first-order Raman scatt. 78—64370
CsCl, F- and F_H-centres, luminesc. meas. 78—10397
CsCl, F-centres, EPR in relaxed excited state, detection via saturated optical pumping 78—6606
CsCl, F-centres, relaxed excited state, ESR, detected via optical pumping 78—43693
CsCl, first-order Raman off- and on-reson. scatt. induced by F-centres 78—92073
CsCl, impurity and defect sites, elec. field gradient calc. 79—78034
CsCl:Cu^+, X-ray irrad., thermoluminesc. 80—16107
CsCl(Br)(I), ESR in relaxed excited state, isotropic superhyperfine interaction consts. 79—65733
CsF, doped with F-centres, first order Raman scatt. 78—52492
CsF, electron-phonon interactions of F-centres, first-order Raman scatt. 78—64370
CsF, F-centre ground state distortion fields and optical absorption 80—55140
CsF, optical absorption bandshape calc. for transition to state with Jahn-Teller and spin orbit couplings 80—55135
CsI, correl. between UV emission band at 300 nm and self-trapped excitons, 4.2K 78—75998
CsI, F- and F_H-centres, luminesc. meas. 78—10397
CuCl, defect and impurity bands, lattice consts. 80—54638
Cu_2O, positive and negative photomemory, IR luminesc. spectra, illum. effect 79—69557
D_2O ice, crystalline, irrad., temp. depend. of trapped electrons, 77 to 6K 79—83474
EuO, reflectivity spectra near absorpt. edge 79—47471
GeO_2, radiation damaged, paramag. point defects, F-centres, ESR, absorpt. spectra 78—80213
HfO_2, stabilised, low temp. induced centres, ESR meas. 78—72409
KBr, additively coloured crystal, depend. of bleaching kinetics on F-light intensities, holographic storage *(Russian)* 79—27351
KBr bicrystal, rel. to Ag^+ injection transport and grain boundary mobility, electrodecoration obs. 80—2214
KBr, change of state of F-centres due to electrostatic field *(Russian)* 79—58827
KBr, colour centre form. under polarised UV irrad., dichroism in absorption spectra 80—107232
KBr, defect accumulation under electron irrad. at 4K 80—107233
KBr, diffusion-controlled defect recombination, quasi-steady radius, tunnelling and elastic interaction *(Russian)* 80—10908
KBr, doped with F-centres, Raman spectra meas. excitation in F and K bands 80—16027
KBr, dynamic equilib. between F and F_2 centres at room temp. 79—51103
KBr, efficiency of creation of X_3^- centres in X-rayed alkali halides *(Russian)* 78—71731
KBr, electrolytically coloured single cryst., ionic SCL current, F-centre diffusion 77—62937
KBr, electron irrad., F-centre formation kinetics, interstitial stabilisation mechanism 79—69103
KBr, electron irrad. at 4K, role of V_K centres in equilib. among centres 78—67712
KBr, electron irradiated, defect accumulation kinetics of low temps. 80—10577
KBr, F-centre lifetime, perturbation effects, luminesc. meas. 80—108252
KBr, F-centre luminesc., MCD effects 78—39598
KBr, F-centre radiative lifetime meas. near 65K 80—25439
KBr, F-centre spin-lattice relax., theory and MCD meas., phonon-modulated HFS 77—43883
KBr, gamma-irrad., hologram recording by F-centre bleaching 80—78814
KBr, interaction between F- and α-centres, luminesc. meas. 79—73988
KBr, irrad., colour centres and thermolum. 77—85815
KBr, kinetic eqns. of formation of F-centres and V_4-centres 78—67713
KBr photochromic materials, F→M transform., electrostatic field control of optical information recording *(Russian)* 80—48370
KBr, radiation-induced F-centre accumulation efficiency *(Russian)* 79—69102
KBr, recomb. in ionic crysts., defect interaction 80—84206
KBr, recomb. in ionic crysts., defect interactions 80—84207
KBr, self-trapped exciton and F-centre form. 79—73443
KBr, self-trapped exciton form. via thermally induced defect reactions 80—60687
KBr, spectral distrib. of triplet to singlet luminesc. of F_2 centre 77—59601
KBr, spin-lattice relaxation time of relaxed excited state of F-centre, MCD meas. 79—61350
KBr, Stark effect in F-centre emission 77—63434
KBr, transient infrared absorption of bound polarons 78—92071
KBr, two photon absorpt., 2p excitons relax., F-centre 79—91462
KBr, V- and X-centres accumulation *(Russian)* 80—54228
KBr whisker, X-irrad., defect form., thermolum. and ionic cond. obs. *(Russian)* 78—84666

F-centres continued
- KBr, whiskers, F-centre accummulation and track effects due to X-ray irrad. 80—39484
- KBr, with F-centres, vol. holograms diffr. efficiency 77—19205
- KBr, X-irrad., F-centre role in thermoluminescence 80—20720
- KBr, X-irrad., thermally stimulated and tunnelling luminescence 78—72606
- KBr:Ca, $F \rightarrow Z_1$ colour centre conversion, hologram recording appls. 78—17877
- KBr:Eu(Yb), electron-irrad., photostimulated luminesc., ionic processes 78—52561
- KBr:Na(Rb)(Cs), microcrystalline powders, isothermal decay of colour centres 80—2804
- KBr:Rb^+, F- and H-centre form. and annealing, impurity interactions 77—76396
- KBr:Sr, X-irradiated, first-stage F-centre production 77—76395
- KBr(Cl), X-ray irrad., tunnelling recomb. luminesc. 80—2873
- KBr(Cl)(F), spin-orbit interaction of relaxed excited state of F-centres 77—15808
- KBr(Cl)(I), electron-spin memory and magnetic-circular-dichroic effects in F-centre luminesc. 80—29794
- KBr(Cl)(I):Tl^+, recomb. luminesc. kinetics 77—16366
- KBr(F), orbital g-factor and spin-orbit splitting of F-centre excited state, magnetoabsorpt. and MCD 78—2886
- KBr(I), photostimulated recomb., electron spin polarisation 80—60673
- KBr(I): $O^{2-}(S^{2-})(Se^{2-})(Te^{2-})$, low temperature photochemistry on chalcogen vacancy centres 78—18641
- KCN, F-centre emission spectrum 77—12420
- KCN, F-centres, optical props. 78—2892
- KCN, optical F centres and phase transitions 78—56504
- KCN-KCl mixed crystals, F-centre optical absorpt. half width 77—81134
- KCl (Br) crystals, thermally stimulated luminescence accompanying recombination of V_F and F centres 80—55201
- KCl, absence of energy transfer between F- and M-centres 79—99935
- KCl and KCl:S, change of state of F-centres due to electrostatic field *(Russian)* 79—58827
- KCl, and KCl-AgCl, surface positron and positronium states, positron annihilation expts. *(Russian)* 78—39623
- KCl, coloured, trap-controlled photoelectron mobility, transit-time expts. 77—72880
- KCl, cryst. γ-irrad., holographic information recording appls. *(Russian)* 79—27218
- KCl crystal, F-H centre formation by opt. conversion of self-trapped excitons 78—91335
- KCl, distant F-centre pairs, ODNMR 78—68414
- KCl, ENDOR line splitting by UHF field *(Russian)* 78—43678
- KCl, ENDOR of F-centres, sign of ^{41}K elec. quadrupole moment 80—34820
- KCl, efficiency of creation of X_3^- centres in X-rayed alkali halides *(Russian)* 78—71731
- KCl, electrolytically coloured single cryst., ionic SCL current, F-centre diffusion 77—62937
- KCl, electron injection, F-centre formation efficiency 78—63790
- KCl, electron irrad., F-centre absorpt., ellipsometric obs. 78—23501
- KCl, electron-irrad., positron-capture centres, thermal annealing kinetics 79—95875
- KCl, F centre, EPR in relaxed excited state, via mag. circular polarisation of emission 79—24232
- KCl, F centre pairs, ODMR, close and distant pairs 78—43691
- KCl, F- and H-centre production by nonradiative decay of self-trapped exciton 78—23042
- KCl, F-F′ conversion at room temp. 78—51539
- KCl, F-center pairs, light excitation, mag. field and resonance effects on absorption bands 78—92094
- KCl, F-centre, wave functions and spin densities, pseudopot. calc. 79—4533
- KCl, F-centre first excited state radiationless decay, cluster model 77—52158
- KCl, F-centre form. and dissociation under pulsed electron irrad. 78—18643
- KCl, F-centre form. by electron irrad., efficiency penetration depth 77—51370
- KCl, F-centre formation, short-pulse optical exam. of exciton relax. 79—42061
- KCl, F-centre formation efficiency, dependence on lattice vacancy concentration 79—82203
- KCl, F-centre formation at highly excited triplet states of self-trapped excitons 80—76066
- KCl, F-centre hyperfine interaction parameters, press. shifts 77—8043
- KCl, F-centre luminesc., MCD effects 78—39598
- KCl, F-centre phonon many-mode interaction, absorption band shape 78—2883
- KCl, F-centre relaxation kinetics, temp. depend. following electron irrad. 80—92527
- KCl, first order reson. Raman spectra, line shape freq. depend. 77—32370
- KCl, gamma irrad. relationship between thermolum. and deform. luminesc. 79—19942
- KCl, γ-irrad., F-centre absorpt., flash-stimulated changes 80—92524
- KCl, γ-irradiated, photo- and thermoluminesc., F-centre interstitial recomb. 77—44036
- KCl, γ-radiation effect on 10.6 μ absorpt. coeff. assoc. with F-aggregate centres 77—4661
- KCl, hologram recording by photodichroic F_A centres at room temp. 77—34846
- KCl, ion bombard., damage profiles, track effect anal. 77—15465
- KCl, irradiated, determ. of molar extinction coeff. and oscillator strength of V_2-centre *(Russian)* 78—80384
- KCl, laser stimulated luminesc. 78—6749
- KCl, luminesc. excitation spectra of F-aggregate centres, 400-900 nm. *(Russian)* 78—10980
- KCl, M-centres, F-centre sensitised luminesc. 77—4681
- KCl, optical breakdown, γ-irrad. effects, rel. to appl. in high power lasers 77—8507
- KCl, perturbed M-centre triplet state, M-F centre exchange mechanisms 79—69884
- KCl, photo-induced F-centres, hologram recording 80—28174
- KCl, photoelec. effect produced by far UV light, memory effect 79—24008
- KCl, positively charged long-lived excited states and spontaneous tunnel transitions 79—82552

F-centres continued
- KCl, positron annihilation in colour centres 77—73185
- KCl, press. shifts of F-centre hyperfine interaction parameters 78—79957
- KCl, pure and Pb^{2+}-doped, X-irrad., quenching effects on thermal glow curves 78—27333
- KCl, radiation damaged, proton and $^4He^+$ channelling, F-centre production, optical absorpt. meas. 78—79656
- KCl, radiative tunnel transitions in negatively charged colour centre systems 80—49655
- KCl, room temp. X-irrad., first stage F-centre form. 78—67709
- KCl single crystals, F-band absorpt. and thermolum. under DC field and X-ray irrad. 79—65910
- KCl, spectral distrib. of triplet to singlet luminesc. of F_2 centre 77—59601
- KCl surface, VUV irrad., colour centre layer, angle-of-incidence derivative ellipsometry and reflectometry 80—73420
- KCl surface, vacuum UV radiation damage, spectroscopic study 78—71758
- KCl, temp. depend. of F-colouring efficiency 80—44204
- KCl, thermal annealing of F, V_2-, V_3-centres *(Russian)* 80—54229
- KCl, thermoluminesc., halogen and alkali impurity effects 80—97352
- KCl, undoped and Pb- or NO_3^--doped, colloid centre formation, absorpt. spectra, 300-1000 nm 79—78710
- KCl, V- and X-centres accumulation *(Russian)* 80—54228
- KCl, whiskers, F-centre accummulation and track effects due to X-ray irrad. 80—39484
- KCl, with F-centres, vol. holograms diffr. efficiency 77—19205
- KCl, X-centres thermal decay process, activation energy *(Russian)* 79—90651
- KCl, X-irrad., thermally stimulated and tunnelling luminescence 78—72606
- KCl, X-ray irrad., thermoluminescence, TSC and thermal stability 79—95859
- KCl, X-ray irradiated, first-stage F-centre prod. 80—107231
- KCl:Ag, X-irrad., thermoluminesc. study of Ag centres 80—80874
- KCl:Ca, $F \rightarrow Z_1$ colour centre conversion, hologram recording appls. 78—17877
- KCl:Ca, vol. holographic grating, modulation characts. using F to Z_1 colour centre conversion 79—94197
- KCl:Ca, Z_4 centres, thermal and optical bleaching 80—19802
- KCl:Cd, EPR of anisotropic Cd_F^+ centres, similarity to Z-centres 77—77101
- KCl:Eu, luminescence and absorption of color centres in RbCl:Cu and KCl:Eu crystals 78—92118
- KCl:Eu^{2+}, F centres and 220-nm optical-absorption band, creation by X-rays 79—55778
- KCl:Ga(In), ESR of impurity centres, impurity optical absorpt. bands 80—29618
- KCl:I(Br), colouration under two-photon excitation, absorption spectra 78—84618
- KCl:K, F-centre coloured, for highly efficient holographic storage 78—37833
- KCl:Li, additively coloured, luminesc. material for IR region *(Russian)* 78—15209
- KCl:Li, self-induced resonant optical rotation 79—65831
- KCl:Li^+,Na^+, F_A(II) to F_B(II) centre crystals, CW laser oscill. with extended tuning range 80—32997
- KCl:Na, absorption from relaxed excited state by F_A and F_B centres 77—44031
- KCl:Na, F_B centre energy levels 80—107738
- KCl:Na, F_B centres, optical detection of ESR 79—99793
- KCl:Na and pure, hologram recording through $F \rightarrow X$ conversion 80—48190
- KCl:Na^+, F_B(II) colour centres, tunable CW laser action obs. 77—83877
- KCl:Na^+, R-centre exam., uniaxial stress effects on zero-phonon lines 78—47371
- KCl:OH^-, image effect in previously electrolytically coloured crystals 78—22714
- KCl:Pb, additive coloration 77—68967
- KCl:Pb, colouring, room temp., influence of conc. and aggregation state of Pb 78—14339
- KCl:Pb^{2+}, γ-irrad., rel. to props. 78—31262
- KCl:Pb^{2+}, pure and doped, electrolytically coloured, elec. cond. and optical absorpt. meas. 80—100668
- KCl:Pb^{2+}, X-ray irrad., electron-trapped centres, Pb^+ and Pb^0, optical absorpt. spectra 80—71461
- KCl:Sr, thermally pre-treated, glow curves 80—25470
- KCl:Sr^{2+}, X-irrad., thermolum., impurity aggregation, trapping centre form. 78—88367
- KCl:Sr^{2+}, X-irradiated, thermolum. decay, effect of impurity aggregation 77—85814
- KCl:Sr(Ca), thermoluminescence and colour centre thermal stability in irradiated sample 78—43941
- KCl:Tl, ESR of trapped electron and hole centres 79—78516
- KCl:Tl, thermal glow of trapped electron and hole centres 79—78762
- KCl:Tl and KCl, F-centre production by positive ions and X-rays 78—38760
- KCl:Tl F-centre form. by electron irrad., efficiency penetration depth 77—51370
- KCl:Tl^+, optical absorpt. spectra following X-irrad., F- and V-centres 79—99912
- KCl:Tl^{2+}, hole mechanisms of H- can F-centre production, thermolum. obs. 77—16407
- KCl-Ba, X-ray irrad. cryst., thermoluminescence spectra 80—20719
- KCl-$BaTiO_3$, composite cryst., F-centres, thermoluminesc., DC field and X-irrad. effects 78—2926
- KCl-KH, F- and U-centre redistrib. at end of proton tracks, microspectrophotometric anal. 80—10583
- KCl-KH cryst. stimulated by X-radiation, spatial redistribution of F and U centers 79—14804
- KCl-Mg, X-irrad. and F-bleached, optical and ESR spectra 77—48052
- KCl-Na, F_A, F_B and F_C-centres, wave functions and energy level of bound states 77—8049
- KCl(Br), coloured, irrad. damage during positron bombardment 78—63791
- KCl(Br), F-centre emission, mag. circular polarisation 80—108251
- KCl(Br), second relaxed excited state of F-centre, optically detected EPR 79—87335
- KCl_xBr_{1-x}, mixed crystals, thermolum. and optical absorption studies 80—104000

F-centres continued
KCl(I), electron range-energy relation, thermally created lattice vacancies effect 80−92574
KClIn, absolute quantum output of low-inertial energy transmission *(Russian)* 77−32429
KF, deformation coloration 77−76397
KF, IR absorpt. spectra from relaxed excited states of F-centres 77−69868
KF:Hg^{2+}, electrolytic colouration 78−75665
KF(Cl)(Br), mag. props. of relaxed excited state of F-centre, vibronic theory 78−60502
KI, containing F-centres, Raman scatt. calc. 77−16306
KI doped with F-centres, mag. vibr. Raman scatt. 77−4636
KI, efficiency of creation of X_3^- centres in X-rayed alkali halides *(Russian)* 78−71731
KI, electrolytically coloured single cryst., ionic SCL current, F-centre diffusion 77−62937
KI, F-centre effect on particularities in vac. evaporated Cr film growth 79−82496
KI, F-centre luminesc., MCD effects 78−39598
KI, free exciton-F$^-$ centres interaction, electron excited emission 79−83036
KI, mag. circular dichroism in luminesc. of F-centres 77−20919
KI, recomb. luminesc. of H-centre and F-centre electrons *(Russian)* 78−80402
KI, self trapped exciton form. time at $^1\Sigma_u{}^+$ state under pulsed electron beam in ps range 80−97347
KI, self-trapped excitons and F-centres, picosec. range form., absorpt. bands 78−19515
KI, self-trapped exciton form. via thermally induced defect reactions 80−60687
KI, spectral distrib. of triplet to singlet luminesc. of F_2 centre 77−59601
KI, spin-lattice relaxation time of relaxed excited state of F-centre, MCD meas. 79−61350
KI, Stark effect in F-centre emission 77−63434
KI:Eu, electron-irrad., photostimulated luminesc., ionic processes 78−52561
KI:S^{2-}, impurity-vacancy dipole UV absorpt. and ionic thermocurrent, F-centre form. 77−36271
KI:S^{2-}, photochemical reaction, F-centre production 78−64861
KI:Tl, cryst., induced recomb. emission 79−4845
KI(Br), irradiated at room temp., thermolum. and F-centre thermal stability 78−84669
KMgF$_3$, F-centre, superhyperfine interaction, g-factor, symmetry, ENDOR obs. 80−39893
KMgF$_3$, F-centre ENDOR study 80−108117
KX:Tl^{2+}, (X=Br, Cl, I), F-centres energy levels change 79−65075
LaF$_3$, gamma-irrad. induced coloration and role of impurities 77−35586
Li halides, F-band energies press. effect 78−60086
LiCl, electron irrad., F-centre emission 78−60501
LiCl, press. shifts of F-centre hyperfine interaction parameters 78−79957
LiCl, radiation effects on decay time of F-centre emission 80−93381
LiCl:Cd, EPR of anisotropic Cd$_F{}^+$ centres, similarity to Z-centres 77−77101
LiF, 3 MeV electron induced, F, F$_2$, F$_2{}^+$, R$_1$, R$_2$ and F$_2$ colour centre obs., IR spectra obs. *(Russian)* 77−48210
LiF, coherent freq. tunable radiation generation in F-centres, 0.6 to 1.26 μm range 79−36902
LiF, coherent radiation generation in F$_2$-centres 78−50782
LiF crystal, tunable laser via F$_2{}^+$/F$_2{}^-$-centres, 0.88 to 1.25 microns 77−75529
LiF, electron irrad., transport of valence band holes, optical absorpt. obs. 79−99188
LiF, excited state, optical absorption 77−20267
LiF, F centre study by mol. SCF calcs. 80−44530
LiF, F-centre electronic struct. determ. using LCAO method, appl. of cubic harmonic expansion 77−20268
LiF, F-centres, defect electron struct., extended-ion model calcs. 80−59907
LiF, high-energy particle bombard., F-centre creation, optical meas. and model 77−47497
LiF, influence of neutron irrad. temp. on F-aggregate centre form. 78−72561
LiF, irrad. at pile temp., higher F aggregate centres produced during thermal annealing 77−43212
LiF, irradiated and plastically deformed, thermoluminesc. defect centres 77−1740
LiF, neutron irrad., F-centres prod., hyperfine structure constants *(Japanese)* 77−69729
LiF, radiation damaged, proton and ^{4}He$^+$ channelling, F-centre production, optical absorpt. meas. 78−79656
LiF, thermoluminescence mechanisms following gamma irradiation 77−59625
LiF, thermostimulated exoemission, adsorbed layer effects 78−11085
LiF, V$_k$ and F centres, efficiency of formation, temp. depend. 79−7600
LiF:Hg^{2+}, electrolytic colouration 78−75665
LiF:Mg,Ti, (TLD-100), optical bleaching of defect centres 79−19911
LiF:Mg,Ti, defect states, ESR and ionic cond. study 80−108058
LiF:Mg^{2+}(CO^{2+}), X-ray induced UV absorpt., band shapes, F- and Z-centers 77−20889
LiH, defect form. at low temp., EPR, thermolum. and TSC study 80−107222
LiH, F-center, dynamic and NEDOR polarisation meas. *(French)* 77−28481
LiH, F-centres, dynamic nucl. polarisation, solid effect meas. *(French)* 77−81028
LiH, formation and annihilation of Li colloids and H bubbles 80−107228
LiI crystal, irradiated at low temps., optical absorption spectra 80−45123
Li$_2$O, neutron irradiated, ESR of F$^+$, O$^-$, H^0 and colloidal Li centres 78−2737
Li$_2$O pellets, sintered, neutron irradiated, ESR study 80−92566
LiYF$_4$, electron-irrad. induced defects, optical and EPR study, impurity effects 80−66238
MgAl$_2$O$_4$, radiation damage, optical absorpt., F-centres 80−64994
MgAl$_2$O$_4$, thermochemical coloration and annealing 79−91468
MgF$_2$, optical absorption following pulsed electron irrad., 100-500K 79−8164

F-centres continued
MgF$_2$, primary pair of radiation defects, energy of form., colour centre conversion rates *(Russian)* 78−6055
MgF$_2$, transient absorption and luminesc. following electron beam excitation 77−69920
MgF$_2$:Fe^{2+}, γ-irrad., F-centres, Fe^{2+} ion hole traps, absorpt. and EPR meas. 79−7598
MgO, chemisorption of O$_2$, adsorboluminescence from surface F-centres 80−20723
MgO, defect centres, thermolum. examination 78−15235
MgO, F centre luminesc., effects of uniaxial stress and ODMR 80−20690
MgO, γ-irrad. polycryst., isothermal luminesc., recomb. of electron from F$_s{}^+$ centres 80−34985
MgO, ion irrad. induced vol. changes, optical absorpt. expts. 77−59053
MgO, radiation induced O interstitials, EPR meas. 78−55866
MgO, thermochemical coloration and annealing 79−91468
Na$_6$Al$_6$(Si$_{0.99}$Ge$_{0.01}$)$_6$O$_{24}$.2NaBr, Ge-doped sodalite powders, UV absorpt. band 80−71452
Na$_6$Al$_6$Si$_6$O$_{24}$, zeolite, luminescence and coloration *(Russian)* 78−72578
Na$_4$Al$_3$Si$_3$O$_{12}$Cl:Br,Ge, sodalite, reflectance and luminescence obs. 79−4839
Na$_8$(Al$_6$Si$_6$O$_{24}$)Cl$_2$, sodalite, photochromism, ESR and optical spectra obs. 77−32407
Na$_8$(Al$_6$Si$_6$O$_{24}$)Cl$_2$, sodalite, electronic struct. of F-centre 80−2356
Na$_8$Al$_6$Si$_6$O$_{24}$F$_2$(Cl)(Br)(I), sodalite, luminescence and coloration *(Russian)* 78−72578
Na$_6$Al$_6$Si$_6$O$_{24}$(NaX)$_{2n}$, X=Cl, Br or I, sodalites, thermal destruction of colour centres *(Russian)* 80−84169
Na$_3$Al$_6$Si$_6$O$_{24}$X$_2$, optically erasable colouring and luminesc. *(Russian)* 77−85801
Na$_8$Al$_6$Si$_6$O$_{24}$.Cl(Br)(I), cathodochromic sodalites, coloured crysts., tunnel and recomb. luminesc., temp. depend. *(Russian)* 80−66261
Na$_6$Al$_6$Si$_6$O$_{24}$.NaX$_{(2-n)}$, (X=Cl, Br, I), X-ray irrad., thermal-erase cathodochromism and dihalide mol. centres *(Russian)* 80−66236
NaBr, F-centre decay 79−11442
NaBr, lifetime of colour centres 78−92115
NaBr powder coloured in electrodeless discharge, reflectance spectra, thermoluminescence props. 78−6796
NaBr, Stark effect of F-centre obs. 77−1707
NaBr(Cl), F-centre formation, short-pulse optical exam. of exciton relax. 79−42061
NaBr(Cl), spin-lattice relax. of F-centres, magneto-optical meas. 77−43884
NaBr(I), optically activated F→F′ centre conversion in mag. field 80−108253
NaCN, optical F centres and phase transitions 78−56504
NaCl, absorpt. spectra, influence of elec. field 80−2794
NaCl, amplitude phase hologram recording on colloid type centres *(Russian)* 80−69347
NaCl, containing Na colloids, first-order Raman spectra 79−73943
NaCl crystal with aggregate colour centres, photocond. kinetics 78−19100
NaCl crystals, electronic and hole centres and surface, quantum-chemical calcs. 80−65489
NaCl crystals with dipole O colour centres, radiation colouring and holographic recording 80−48187
NaCl, efficiency of creation of X$_3{}^-$ centres in X-rayed alkali halides *(Russian)* 78−71731
NaCl, electronic structure calculation, CNDO semi-empirical methods *(Russian)* 80−10909
NaCl, F-centers, laser irrad. optical bleaching kinetics 80−66244
NaCl, F-centre, wave functions and spin densities, pseudopot. calc. 79−4533
NaCl, F-centre aggregation, initial stage study by Raman scatt. 79−56791
NaCl, F-centre interactions and local distortions *(French)* 78−43016
NaCl, F-centre space distrib., pair correl. function 79−60361
NaCl, F-centres near monoenergetic proton stopping region, space charge effect 78−18640
NaCl, filamentary crystal, vacancy-enriched surface layers 78−51536
NaCl, gamma irradiated, optical bleaching of colour centres, F-aggregate centre form. 79−95813
NaCl, γ-irrad., F-centres form., energy storage 79−82264
NaCl, γ-irrad., F-stimulated inversion of sign of dislocation charge 80−59475
NaCl, γ-irradiated, F→M phototransformation, effect on aquoluminescence 80−7418
NaCl, γ-radiation effect on 10.6 μ absorpt. coeff. assoc. with F-aggregate centres 77−4661
NaCl, hologram recording, F-centre bleaching by 633 nm light 79−22922
NaCl, irradiated, at 80K, thermolum. processes 80−34990
NaCl, irradiated, determ. of molar extinction coeff. and oscillator strength of V$_2$-centre *(Russian)* 78−80384
NaCl, optically bleached and X-irrad., relation between F- and C-centres 77−72613
NaCl, photoplastic effect *(Japanese)* 79−82279
NaCl plates, hologram recording, F-centre conversion to R, M centres 78−17878
NaCl, positron annihilation in colour centres 77−73185
NaCl, press. shifts of F-centre hyperfine interaction parameters 78−79957
NaCl, pure and doped, 20K X-ray irradiation, thermolum. and recovery processes 80−93412
NaCl, quantum-chem. calcs. of electronic and hole centres and surface 80−20118
NaCl, radiation damaged, proton and ^{4}He$^+$ channelling, F-centre production, optical absorpt. meas. 78−79656
NaCl, second relaxed excited state of F-centre, optically detected EPR 79−87335
NaCl, self-trapped exciton form. via thermally induced defect reactions 80−60687
NaCl, thermal expansion meas. after X-ray irrad., F-centre bleaching 80−44338
NaCl, thermoluminesc. and optical absorpt., simultaneous DC field and X-irrad. 79−99956
NaCl, transient infrared absorption of bound polarons 78−91642
NaCl, V- and X-centres accumulation *(Russian)* 80−54228
NaCl, X-centres thermal decay process, activation energy *(Russian)* 79−90651

F-centres continued
NaCl, X-irrad., F-thermal bleaching 77—89433
NaCl, X-ray irrad., F-centre accumulation and rad. hardening *(Russian)* 78—51538
NaCl:Ag, absorpt. spectra, influence of elec. field 80—2794
NaCl:Ca, microhardness and thermoluminescence, hardness-quenching temp. variation 80—29813
NaCl:Cd, EPR of anisotropic Cd_F^+ centres, similarity to Z-centres 77—77101
NaCl:Cu, X-irrad., thermoluminesc., F-centres 79—33849
NaCl:Cu^+, electrolytically coloured, electron trapping, optical absorpt. 80—100672
NaCl:Cu^+, X-irrad., anisotropic Cu centre anal. 79—78714
NaCl:Cu^+, X-ray irrad., role of Cu^+ in thermoluminesc. 78—56526
NaCl:Ga(In), ESR of impurity centres, impurity optical absorpt. bands 80—29618
NaCl:Mn^{2+}, radiation-induced colouring, room temp. kinetics 79—55736
NaCl:Mn^{2+}, thermolum. spectra, mechanisms 80—80873
NaCl:Mn^{2+}, X-ray irradiated, thermolum. and EPR 77—81161
NaCl:Mn^{2+}(Zn^{2+})(Sn^{2+}), electrolytically coloured, CESR 77—16174
NaCl:OH^-, UV and IR absorpt. spectra, colour centres transformation 79—28791
NaCl:Pb, colouring, room temp., influence of conc. and aggregation state of Pb 78—14339
NaCl:Zn^+, X-irrad., EPR and optical absorpt. 78—43642
NaCl(Br), orbital g-factor and spin-orbit splitting of F-centre excited state, magnetoabsorpt. and MCD 78—2886
NaCl(F), irradiated at room temp., thermolum. and F-centre thermal stability 78—84669
NaF, excess electron colour centre obs. 77—16343
NaF, F-centre, wave functions and spin densities, pseudopot. calc. 79—4533
NaF, laser stimulated luminesc. 78—6749
NaF, radiation damaged, proton and $^4He^+$ channelling, F-centre production, optical absorpt. meas. 78—79656
NaF, two-photon absorpt. cross sections of N_1 and $F_3{}^+$ centres 79—73991
NaF:Hg^{2+}, electrolytic colouration 78—75665
NaF:Mn, role of Mn^{2+} in thermolum. 80—97353
NaF:U, luminesc. spectra, Vibr. struct. 80—80840
NaI, X- or γ-irrad., colour centre formation and accumulation *(Russian)* 77—65978
NaI:F, electron-lattice coupling of F-centres, optical props. 80—60641
$NaMgF_3$, defects induced by X- and vacuum UV irrad., optical and elec. study 80—107319
$NaMgF_3$, optical absorpt. of radiation produced defects 77—28604
NaN_3, UV irradiated, F-centre ESR 77—28444
NaN_3, UV irradiated, polarised optical absorpt. of $F_2{}^+$-, F-centres 77—28605
NaX:Tl^{2+}, (X=Br, Cl, I), F-centres energy levels change 79—65075
NdF_3, gamma-irrad. induced coloration 77—35586
β-PbF_2, γ-irrad., F-band region spectrum, impurity effects 77—44026
PrF_3, gamma-ray induced coloration 77—35586
RbBr, self trapped exciton form. time at $^1\Sigma_u{}^+$ state under pulsed electron beam in ps range 80—97347
RbBr, Stark effect in F-centre emission 77—63434
RbBr, suprapure, thermolum. glow and emission studies at room temp. 80—7423
RbBr, two photon absorpt., 2p excitons relax., F-centre 79—91462
RbBr(Cl) F centre, EPR in relaxed excited state, via mag. circular polarisation of emission 79—24232
RbBr(I), parallel and perpendicular Stark effect of F-centre 77—1703
RbCN, ferroelasticity and F- and M-centres absorpt. 79—87475
$RbCaF_3$, optical absorpt. of radiation produced defects 77—28604
RbCl ESR in relaxed excited state, isotropic superhyperfine interaction consts. 79—65733
RbCl, electron bombard., colour centre photoemission, surface contamination and escape depth 80—66392
RbCl, undoped and Sn doped, γ-irrad. crysts., thermolum. and emission, 300 to 560K 79—15539
RbCl:Ca^{2+}, thermolum. and optical absorption studies 80—104002
RbCl:Eu, electron-irrad., photostimulated luminesc., ionic processes 78—52561
RbCl:Eu, luminescence and absorption of color centres in RbCl:Cu and KCl:Eu crystals 78—92118
RbCl:H^-, defect pairs of F-centres and U-centres, Raman meas. 79—7599
RbCl:Li^+, new off-centre defect system, studied with dielec. techniques under hydrostatic press., behaviour of F_A(Li) centres 79—19834
RbCl:Li^+,Na^+, F_A(II) to F_B(II) centre crystals, CW laser oscill. with extended tuning range 80—32997
RbCl:Mg, γ-irrad., thermoluminesc. 79—47528
RbCl:Na^+, F_B(II) colour centres, tunable CW laser operation obs. 77—83877
RbCl(Br), F-centre emission, mag. circular polarisation 80—108251
RbI, photostimulated recomb., electron spin polarisation 80—60673
RbI, Stark effect in F-centre emission 77—63434
RbI, two photon absorpt., 2p excitons relax., F-centre 79—91462
$RbMgF_3$, irradiated, thermal conductivity 78—22909
$RbMgF_3$:Mn, low-temp. radiation damage, optical absorption meas. 78—22761
$RbMnF_3$:Fr, pure and doped, unirradiated and electron irrad., energy transfer 80—108254
$RbNgF_3$, radiation defect F,M,R-centre absorpt., emission, excitation spectra 79—43000
^{85,87}RbCl isotope enriched cryst., optical registration of EPR F-centres *(Russian)* 80—103886
$SrCl_2$, F-centre production mechanism, radiolysis exam. 79—23602
$SrCl_2$:K^+(Na^+)(Rb^+) X-irradiated, recomb. luminesc. between trapped electron and self trapped holes 77—73162
SrF_2, F-centres, muffin-tin approx. inadequacy 78—63761
SrF_2, F-centres, single-phonon Raman scatt. meas. 77—20844
SrF_2, neutron irrad., role of F-centres in thermoluminesc. 79—19941
SrF_2, Q-switching of ruby laser by saturated absorption 78—71157
SrF_2, thermoluminesc. and F-centre annealing, after neutron irrad. 80—7422
SrF_2:CeF_3(GdF_3)(TbF_3), absorpt. spectra of γ-irrad. cryst., 77K, 200-700 nm 78—84615
SrO, electronic struct. of F-centre 78—30887
SrO, irradiated, low temp. photocond. 77—39891

F-centres continued
SrO, neutron- or proton-irrad., F^+ centre fluoresc. yield and lifetime, 5 to 140K 80—55181
SrO, neutron-irradiated single cryst., F^+ centres, ENDOR obs. 80—15824
SrO, proton, neutron irradiated, fluorescence from anion vacancies, F^+ centre model 78—48221
Y_2O_3, formation and changes in point defects, EPR, optical transitions and thermolum. spectra 78—2118
Y_2O_3:Zr^{3+}, F-centre charge state, ESR and thermally stimulated luminesc. obs. 80—60418
ZnO, defect struct. calc., doping effects 80—107218
ZnO, F^+-centre exam., ground and first excited energy level 77—39800
ZnO, F-centre exam., pseudopotential calc. 78—43328
ZnO:Li, electron irrad., F^+ centre, photosensitivity of e.p.r. spectrum 77—1594
ZnS, additively coloured or neutron irradiated, near IR emission 77—90199
ZnS, electron irrad., ESR 79—91293
ZnS, F-centre exam., pseudopotential calc. 78—43328
ZnS phosphor, deep capture centres obs. 78—10951
ZnS, tight binding calc., F-centres, and isoelectronic defects 77—20266
ZnS, tight-binding model of F-centre 77—89729
ZrO_2 1.6H_2O, anion defect formation and annealing during thermal decomp. in vacuum 77—51366
ZrO_2, stabilised, low temp. induced centres, ESR meas. 78—72409
ZrS:O_4, X-irradiated, trapping and emission centres, thermolum. meas. 80—89076

F_2-centres *see M-centres*

F_3-centres *see R-centres*

F_A-centres *see A-centres*

F-layer *see F-region*

F-region
absorption events at high latits. 77—21987
acoustic gravity waves role in generation of spread-F and ionospheric scintillation 79—66868
airglow, anal. of consistency of ground-based obs. with satellite results 80—98496
airglow of at. O rel. to short wave radio absorpt. 80—77184
artificial spread-F generation by parametric instability 77—45247
artificially-injected gases dispersal in night-time atm. 78—65460
aurora associated with magnetospheric cusp 80—90273
auroral convection over 60°≤Λ≤75°: Millstone Hill incoherent scatter obs. 80—67454
auroral electric field, description based on plasma interaction with geomag. field 80—46342
auroral F-region, plasma drifts comparison with E-region irregularity drifts 77—33262
auroral F-region ionosphere form. role. of neutral winds and particle precip. 79—44296
auroral patches and deteched arcs, equatorward of auroral oval, Isis 2 obs. of particle precip. 79—70911
bottomside equatorial spread-F rel. to Ba cloud striations 79—75022
bottomside spread-F, equatorial, assoc. with night-time ionospheric scintillations 79—44292
bubbles in equatorial spread F, nonlinear evolution 80—85801
bubbles seen in topside soundings of spread F, characts. 80—85800
collision frequency of electrons with O and N_2 79—53641
collisional Rayleigh-Taylor instability in equatorial spread F 80—82138
collisionless electrostatic drift waves, linear theory, space plasma appls. 79—1305
convecting F_2-layer at high latitudes, numerical model 78—28391
convective electric field determ. from rocket meas. of thermal ion spectra 78—57386
cosmic radio noise absorpt. rel. to mag. storms at Delhi 78—69589
critical frequency, rel. to ionosphere global scale electrodynamic coupling of high and low latit. regions 80—77194
critical frequency small scale fluctuations at Kodaikanal 79—16745
current convective instability in auroral F-region 80—72680
current convective instability in diffuse aurora 79—70907
daily variability of midlatitude winter F-region 78—16240
daytime drift obs., tests of electrodynamic consistency 77—70934
diffusion eqns. with large temp. differences between interacting species 79—66857
diffusion equations, coupled time-dependent, numerical method using self-diffusion coeff. 80—109285
diffusion inhomogeneities, small-scale, dissipative parametric generation 78—69580
diffusion-recombination parameters 77—53300
disappearance, due to Earth encounter with interstellar cloud 78—57292
disturbances, large scale periodic, Faraday fading of satellite 40 MHz signals 80—101475
drift instability, generation by action of strong radio wave 77—91344
drift meas. at Tiruchirapalli, India, 1973-75 period 79—53639
drift variability above Tiruchirapalli, rel. to electrojet strength 80—82129
drifts over Tiruchirapalli, India, daily variations 79—84580
dynamics, Sturm-Liouville problem 77—13149
dynamics in equatorial region 78—36376
electric field induced drifts, incoherent scatt. radar obs. 77—29576
electric field irregularities at low latits., rel. to spread-F and plasma irregularities 77—53290
electric field oscills. meas. near auroral arc, assoc. with MHD wave 78—65457
electric field wavelike fluctuations obs. at Ft. Churchill, Canada 77—21982
electric fields, poleward-directed, at subauroral latits. 78—88970
electric fields rel. to ionospheric currents and mag. vars. 77—87166
electrodynamics, polarisation elec. field rel. to E-region solar tidal dynamo field 78—36391
electron conc. profiles during sunrise and sunset 79—88526
electron concentration var. with height, improved model 78—49214
electron content and atmospheric gravity waves at high magnetic dip station 77—53277
electron density, AEROS and TAIYO satellite results 80—46340
electron density, latitude var. 78—36375
electron density and ion vel. during isolated substorm incoherent scatter radar meas. 78—65452
electron density distrib. and total electron content near mag. equator 79—75028
electron density disturbances during local heating 77—29543

F-region continued
- electron density disturbances nonlinear saturation, strong radiowave effects 78—28378
- electron density enhancements beneath magnetospheric cusp 78—28389
- electron density fluctuations, power spectra rel. to travelling ionospheric disturbances and assoc. gravity waves 78—28394
- electron density inhomogeneity, thermodiffusion mechanism *(Russian)* 80—85791
- electron density irregularities from plasma reson. phenomena obs. by rocket-borne relax. sounding expt. 79—8767
- electron density max., harmonic analysis and periodicities 78—57383
- electron density model distribs. 79—88536
- electron density profile from energetic particle and spread-F obs. 78—36383
- electron energy distrib. above aurora, secondary peaks driving instability 80—82135
- electron heat conduction importance in energy balance 78—61649
- electron loss coefficients, diffusion-recomb. parameters 77—13156
- electron precipitation, transient response to F-region and topside ionosphere 77—78566
- electron temp. model, Aeros-A data compared to radar obs. 80—67465
- electron temp. models using electron density height profiles 77—60540
- electron temperatures, theory and obs. 79—48618
- electron-neutral collision frequency upper limit 79—84573
- electrons collision frequency at sunrise and sunset 77—13174
- ELF ion plasma oscills. in Nike-Apache rocket apogee region 79—40012
- ELF waves assoc. with equatorial spread-F, satellite obs. 79—35051
- energetic electrons spectra, meas. by Hadamard energy spectrometer *(Japanese)* 80—94637
- enhanced ionisation during winter, charged particles transfer mechanism 78—45108
- equatorial, drift measurement of Ba cloud, spaced receiver technique 80—72678
- equatorial, modelling of H_2 gas release effects 79—16741
- equatorial, neutral winds determ. from O I 6300 Å nightglow Doppler shifts 78—81473
- equatorial, solar cycle effects on elec. fields 78—28405
- equatorial anomaly, counter electrojet assoc. changes, upward drifts reversal 80—109292
- equatorial anomaly, counter electrojet assoc. changes, upward drift reversal obs. 80—109297
- equatorial anomaly, solar cycle and seasonal variation of electron content 80—41622
- equatorial anomaly in electron distrib. 80—41602
- equatorial elec. fields during mag. disturbances, auroral and equatorial meas. 80—31160
- equatorial elec. fields during mag. disturbances, interplanetary mag. field effect 80—26676
- equatorial F-region, plasma bubbles and irregularities 77—87156
- equatorial F-region, topside and bottomside, review of struct. 78—36373
- equatorial F-region irregularity patches, localised origin 78—77404
- equatorial ionisation motions from Sq current distrib. 77—21981
- equatorial ionosphere spread-F echoes in HF and VHF bands, theoretical model 78—85764
- equatorial irregularities, radar obs. 77—29566
- equatorial irregularity experiment (Equion) for spread-F obs. 77—33266
- equatorial Mg^+ ion distrib. from Mg II 2800 Å airglow obs. 80—26673
- equatorial north-south aligned airglow depletions and F-layer irregularities 78—45074
- equatorial scintillations model from in situ meas. 77—13180
- equatorial spread F, nonlinear theory of collisional Rayleigh-Taylor instability 78—32270
- equatorial spread-F, 3-metre irregularities due to plasma instability 80—41624
- equatorial spread-F, artificial control technique 78—69602
- equatorial spread-F, artificially created, initial report on ionosphere modification 78—88972
- equatorial spread-F, causing VHF scintillations 77—17289
- equatorial spread-F, coincident radar and rocket obs. 80—105111
- equatorial spread-F, geomag. disturbance effects 79—35044
- equatorial spread-F, high freq. drift waves with wavelengths below ion gyroradius 78—88973
- equatorial spread-F, in situ irregularity spectra rel. to ionospheric scintillation calcs. 78—28415
- equatorial spread-F, nonlinear Rayleigh-Taylor instability 79—16748
- equatorial spread-F, onset during post-midnight period 80—4166
- equatorial spread-F, plasma instabilities obs. by Spacelab-borne Langmuir probe 77—21947
- equatorial spread-F, range-type, occurrence 79—35045
- equatorial spread-F, Rayleigh-Taylor and wind-driven instabilities of nighttime ionosphere 79—96855
- equatorial spread-F, role of steepened structs. and drift waves 79—2431
- equatorial spread-F, seasonal and solar cycle vars. in American zone 80—109298
- equatorial spread-F, solar cycle effects at Huancayo 78—61647
- equatorial spread-F, two-dimens. turbulence 79—2432
- equatorial spread-F, VHF scattering 78—61661
- equatorial spread-F and F-layer height 79—88535
- equatorial spread-F and ionospheric holes, ion chemistry and transport 78—88982
- equatorial spread-F and threshold height 77—29561
- equatorial spread-F configs. correl. with geomag. activity 79—101007
- equatorial spread-F in American and Indian zones, seasonal var. 80—72689
- equatorial spread-F irregularities, spatial relationship with plasma bubbles 80—67457
- equatorial spread-F irregularities and electron depletion, radar obs. 80—41611
- equatorial spread-F irregularities drifting patches, support for ionospheric spatial reson. mechanism 79—21095
- equatorial spread-F irregularities from spaced fading records, Thumba, India 79—88543
- equatorial spread-F meas. by Altair incoherent scatter radar 80—61927
- equatorial spread-F onset, height control 79—16734
- equatorial spread-F onset characts. 78—69562
- equatorial spread-F rel. to F-peak and bottomside electron density 79—53643
- equatorial spread-F rel. to interplanetary mag. field reversal 79—16747
- equatorial stratified irregularities movement, time and magnetic dependence 80—8470
- equatorial vertical drifts depend. on season and solar cycle 80—31159

F-region continued
- f_0F2, relationship to O I 6300 Å airglow 78—36354
- f_0F_2, correl. with riometer meas. of ionospheric radio wave absorpt. 78—85763
- f_0F_2, geomag. activity effects 80—8480
- f_0F_2, median values obs. over S.Atlantic Ocean 78—81505
- f_0F_2, spectral components temporal and spatial distrib. 78—49211
- f_0F_2, vars. rel. to thermospheric storms 77—9583
- f_0F_2 and electron content latit. var. in subauroral zone 77—13164
- f_0F_2 determ. from satellite obs. of HF noise 77—53292
- f_0F_2 diurnal var. at equatorial latitudes and counter electrojet 79—48600
- f_0F_2 monthly median values, verification of long-range forecast 77—60513
- f_0F_2 variations correl. with stratospheric O_3 content vars. 78—45098
- f_0F_2 variations during stratospheric winter warmings 77—29550
- F_1-F_2 transition region, neutral gas temperature during low solar activity 79—88519
- F_1-layer, auroral ion vel. distrib. for polarisation collision model 77—45241
- F_1-layer, dynamical effect obs. 79—12340
- F_1-layer, ion comp. and temp. profiles from incoherent scatter radar studies 80—72654
- F_1-layer, mid-latitude, mean diurnal var. of O^+, NO^+, $O_2{}^+$ and $N_2{}^+$ ions 79—96856
- F_1-layer at nighttime, ion composition near mag. equator 80—72683
- F_2 layer of quiet night ionosphere, calculated and measured decay rates comparison 78—81493
- F_2 layer seasonal anomaly rel. to composition changes 77—33252
- F_2-layer, analytic description of geometric parameters maps by spherical functions 79—53616
- F_2-layer, bottomside, electron depletion obs. assoc. with mid-latit. ionosphere trough 80—109300
- F_2-layer, chem. depletion of O^+ by H_2O and CO_2 injection 80—12610
- F_2-layer, electron density long-period variation f_0 evidence 80—56667
- F_2-layer, electron density vars. rel. to magnetosphere-ionosphere electrodynamic interaction 78—28372
- F_2-layer, equatorial, vertical ionospheric soundings 77—17276
- F_2-layer, geometrical parameters and critical frequencies, solar activity dependence study 80—4182
- F_2-layer, global distrib. of electron density rel. to elec. fields in closed magnetosphere 77—64514
- F_2-layer, ionization balance disturbance by radiowave heating 77—17274
- F_2-layer, low-latit., vertical motions during prolonged and isolated mag. storms 77—37479
- F_2-layer, lunar tide over Japan 79—2436
- F_2-layer, MHD wave propag. characts. 77—2298
- F_2-layer, MHD waves ducted propag. 77—2299
- F_2-layer, midlatitude storms in daytime and nighttime 79—8757
- F_2-layer, N(h) variations at midnight 77—17275
- F_2-layer, night-time, over Arecibo, seasonal mean struct. 80—31163
- F_2-layer, nighttime height rel. to aeronomic parameters 79—8745
- F_2-layer, nighttime electron density at Ootacamund, India, from ATS-6 satellite radio beacon meas. 79—48611
- F_2-layer, parameters at high latitude during quiet conditions 80—105106
- F_2-layer, parameters rel. to parameters of neutral atmosphere at fixed height 77—91346
- F_2-layer, peak electron densities in main trough region, empirical model 78—28417
- F_2-layer, plasma continuity eqn., comparative anal. of numerical soln. methods 78—69578
- F_2-layer, post-sunset decay rel. to protonosphere induced proton flow 78—49222
- F_2-layer, response to August 1972 mag. storms 77—25858
- F_2-layer, response to solar mag. sector crossing 79—35030
- F_2-layer, scintillation of signals from extraterrestrial radio noise sources in mid-latit. trough 78—73574
- F_2-layer, seasonal difference in ionisation and height due to neutrals 80—61951
- F_2-layer, temp. and thickness from vertical sounding and incoherent scatt. 77—45221
- F_2-layer, temporary vars. in critical freq., rel. to solar activity 77—67008
- F_2-layer, vars. of multiple rays on short radio waves 77—21972
- F_2-layer, vertical drift assoc. with polar substorm 79—53618
- F_2-layer, zonal and meridional elec. fields effects in evening sector 78—69571
- F_2-layer at middle latitudes, electron density oscills. rel. to lunar tide 78—61655
- F_2-layer at middle latitudes, ion and neutral gas vel. oscills. rel. to lunar tide 78—61656
- F_2-layer critical freq. determ. using topside HF noise meas. 79—8756
- F_2-layer critical freq. during sunspot minimum 79—25397
- F_2-layer critical frequency, forenoon bite-out characts. 78—65453
- F_2-layer daytime, simulation, selection of aeronomic parameters system 78—45087
- F_2-layer during daytime, servo model 80—101486
- F_2-layer electron density, mag. storm effects 80—61970
- F_2-layer equatorial anomaly development, role of ambipolar diffusion 77—13168
- F_2-layer field-aligned and field-perpendicular vels. theory 78—85760
- F_2-layer height, model effects on thermospheric calcs. 78—36345
- F_2-layer ionisation through a solar cycle, (1958-69), SW radiocommunication appl. 80—41626
- F_2-layer nighttime ionisation latit. depend., var. in solar activity cycle 79—53617
- F_2-layer noon ionization seasonal var. at dip-conjugate places 77—33259
- F_2-layer noontime critical frequency variation through a solar cycle, SW radio communication appl. 79—21102
- F_2-layer $O_2{}^+$ source rel. to charge exchange of $O^+(^2D)$ metastable ions 79—58141
- F_2-layer of mid-latit. ionosphere, internal gravity waves day and night effects 79—58150
- F_2-layer over Gauhati, penetration freq. study, India 77—5394
- F_2-layer peak from Atmosphere Explorer C 78—28354
- F_2-layer thermal plasma interhemispheric flow in closed mag. flux tube, sunspot min. conditions 78—93035
- F_2-layer variations, hemispherical differences rel. to neutral atmosphere 78—69603
- F_2-layer vertical sounding, radio signal Doppler spectrum and arrival angle meas. *(Russian)* 78—61651
- F_2-layer waves, comparison with waves in OH emission layer 78—45065

F-region continued
F_2-peak altitude determination using global model based on M3000 values 79—101020
F_2-region, meteorological perturbations due to gravity waves at sunspot minimum *(Italian)* 79—29922
F_2-region, nighttime thermal balance at mid-latitudes 79—84583
F_2-region neutral winds, Navier-Stokes eqns. *(French)* 79—35031
$f_{min}F$ in mid-latit. nighttime ionosphere, effect of interplanetary mag. field 79—58151
F-lacuna events rel. to state of ionosphere 78—93036
F-lacunae, geographical distrib. and simultaneity of occurrence 80—4193
F-layer artificially created hole, convergent lens for radiotelescope 77—78571
F-layer irregularity zone and O I 6300 Å emission meas. in midnight sector 78—12038
fading records over Tiruchirapalli (1973-5), cross spectral anal. 80—101478
field-aligned irregularity excitation and thermal parametric instability 78—77419
general circulation at altitudes $>$100 km, empirical model 78—61664
global electron temp. distrib. model, 300-700 km altitude 80—67464
gradient drift instability, high-altitude limit 78—88984
gradient-drift instability, nonlinear effects 80—36455
gravity effect on instability formation conditions 79—96858
gravity waves, obs. during tornado outbreak (1974 April 3) 78—85753
gravity waves in high-latit. F-region, obs. using fixed freq. sounding 79—25390
h_mF_2, geomag. activity effects 80—8480
heat flow eqns. with large temp. differences between interacting species 79—66857
heating by powerful radio emission with random modulation of carrier freq. 80—109310
heating effects by powerful radiowaves, calc. *(Russian)* 78—32278
height and electron content changes at midlatit. during mag. storms 77—21984
HF and MF signals refl. from spread-F, fading anal. 79—101005
HF backscatter curtains rel. to plasmapause location 79—58165
HF communication at low latitudes, problems and solns. 77—70921
HF Doppler observations associated with spread-F 79—70918
HF max. usable freq. prediction algorithm, MINIMUF-3 79—25372
HF phase path records, anomalous var. over daytime Waltair 77—70924
HF radiowave forecasting scattering by induced ionospheric irregularities, expt. *(Russian)* 77—29553
HF signal, group path variations from modulation envelope measurements 80—51597
high-latitude overhead horizontal current, influence on mag. D-component vars. 79—75037
hmF_2, high-latit. behaviour along noon-midnight meridian under quiet conditions 79—40004
holes created artificially by H_2 or H_2O releases 78—40752
incoherent scatter from nighttime F-region, rel. to neutral atmosphere parameters var. *(Portuguese)* 80—41584
internal gravity waves, generation of small-scale inhomogeneities 78—45100
ion cloud releases, E-region induced disturbances 78—61657
ion concentration depletion experiment, thermal ion obs. 80—41620
ion convection and midlatit. ionisation trough form. 79—2429
ion convection at high-latitude, nighttime 80—85797
ion velocity distribs. in high-latit. regions 79—101018
ion-drag effects 80—17432
ionisation, by solar flares X-ray and EUV emission, models 77—5515
ionisation, geomag. control and possible coupling mechanism 77—9598
ionisation enhancements, rel. to localised nighttime auroral zone scintillation enhancements 80—98506
ionisation equinoxial asymmetry due to ionizing agency outside solar system 77—29559
ionisation measurements, rel. to mesosphere, NO conc. geomag. control 79—8651
ionization irregularities drift meas. from first and second order refl. 79—53642
ionosphere quasiperiodic scintillations, rel. t E_s and spread-F activity 77—91361
irregularities, drift vels. from ATS-6 140 MHz Faraday rot. records 78—69599
irregularities, equatorial, evolution and scatt. effects on trans-ionospheric radiowaves 79—29933
irregularities and background density of equator region, VHF and UHF radar obs. 80—77222
irregularities and scintillations in equatorial region, VHF radar maps 78—36382
irregularities in situ meas. by OGO-6 correl. with scintillation meas. 77—21977
irregularities rel. to backscatter obs. at 3 m wavelength 79—12338
irregularities rel. to O I 6300 Å mid-latitude nightglow fluctuations 78—49194
irregularity model, reconciliation with sunspot cycle vars. in spread-F occurrence 77—41262
Joule dissipation of elec. currents during equatorial spread-F events 78—45127
large-scale artificial inhomogeneity spectrum 80—98515
large-scale horizontal winds in presence of vertical vel., relaxation time 77—78561
LF field strength meas. on single-hop path 77—29547
LF sound waves relax. absorpt. *(Russian)* 78—65356
low density regions at high altitudes, rel. to equatorial spread-F 79—62671
lunar tidal effect on spread F 79—80070
magnetic storm of June 1972 causing disturbance, thermosphere-ionosphere coupling 80—41617
magnetic storms affecting electron composition, 140 MHz obs. 80—101471
mesoscale waves in D-region and F-region, temporal vars. 80—8483
MHD waves, as cause of simultaneous ionospheric and geomag. oscills. 77—9615
mid-latitude spread-F, coupling between conjugate stations 77—53304
midlatitude, parameters diurnal behaviour in summer 79—84570
midlatitude, reaction to neutral atm. disturbances 77—25805
midlatitude convection electric fields, occurrence rel. to ring current development 78—57395
midlatitude F-region, electron density depressions under relatively quiet geomag. conditions 78—36385

F-region continued
midlatitude magnetically quiet nighttime F_2-region, math. model 79—62650
midlatitude neutral winds and temps. during 1976 March 26 magnetic storm 79—53594
midlatitude spread-F, depend. on geomag. vars. and solar cycle 78—36389
midlatitude wind source, energetic neutral atom precipitation 79—70913
modification by release of highly reactive molecules, diffusion aspects 77—21988
morphological studies of rising equatorial spread F bubbles 78—77410
motions in equatorial F-region, deduction from Sq currents 78—96344
n_2F_2 annual vars. with latit. and solar activity level 78—69577
neutral and ion winds in polar region 77—45209
neutral temperature at nighttime, during equatorial spread-F activity, OI spectra 80—41587
neutral winds, determ. from ionosonde meas. of hmF2 at low latit. mag. conjugate regions 78—81477
neutral winds and ion drifts in polar region 77—87173
neutral zonal winds, contrib. to interhemispheric ion transport 80—98509
nightside F-region, distortion prod. by plasmasphere substorm elec. fields 79—40009
nighttime dynamics from airglow features mapping 78—88980
nighttime electron density maintenance rel. to neutral winds 77—29555
nighttime equatorial, coexistence of km and m scale irregularities, radar and scintillation obs. 79—2427
nighttime F-region, geostationary satellite signals latit. scintillation at 137 MHz 79—25388
nighttime Hall and Pedersen cond. comparison 77—41260
nighttime height vertical movement correl. with solar wind mag. field 77—13147
nighttime ionization by energetic particles, 120-200 km altitude 79—62666
nighttime seasonal electron density anomaly 78—69566
NmF2, low latit. features of annual and semiannual periodicities in America and India 77—53306
noctural F-region heights over Arecibo, band struct. 79—66863
nonstationary nighttime disturbances produced by internal gravity waves 78—73565
Pc 1 geomagnetic pulsation sources, location using ULF goniometer techniques *(French)* 79—70890
peak electron densities of F_2-layer, comparison of CCIR predictions with in situ meas. 78—57394
peak electron density, diurnal and solar cycle variation 80—61949
Perkins spread-F instability, effects of E-region coupling 78—40755
perturbation by electron precipitation in cleft region during substorm 80—101483
photoelectrons, energy loss and spectral features deduced by plasma line technique 77—45227
plasma ambipolar diffusion in gravit. field, analytical solns. of eqn. 77—78562
plasma cloud, intermediate wavelength E×B gradient drift instability 80—105114
plasma cloud striations, study of outer scale size 80—90279
plasma clouds, deform. and striation, multilevel model with recomb. chemistry 77—25834
plasma clouds, nonlinear stabilization of E×B gradient drift 79—58162
plasma density variations in negative ionospheric storms, simulation using neutral comp. data 79—25393
plasma drifts above Saint-Santin on quiet days, seasonal vars. 79—101011
plasma dynamics, vertical displacement during substorms 80—4184
plasma flow, var. in topside and F-layer, ionospheric-protonospheric interaction model calcs. 80—4180
plasma instabilities and fine struct. 80—21869
plasma instability, electron-ion collisions effects 78—45097
plasma interactions with EM radiation *(Russian)* 78—32277
polar cap and auroral zone, math. model 78—65458
polar F-region, winds and drifts 77—33274
polar substorms, equatorial-auroral ionosphere coupling 78—32291
polarisation field, nighttime maintenance of equatorial ionisation 80—4192
predawn, conjugate photoelectrons, rocket obs. 79—29931
probing at dm wavelengths, aspect depend. characts. 79—88547
protonosphere-F-region nighttime proton fluxes 78—93034
protonosphere-ionosphere coupling, postsunset obs. with Arecibo radar 79—70915
quasitrapped electrons, 100 MeV, in geomag. field 200-250 km above equator *(Russian)* 78—49223
radar measurement, incoherent scatter, systematic error due to noise contamination 78—49225
radar observation method, meas. of auroral zone elec. field 80—51573
radio waves, phase path changes due to gravity waves 79—35043
radiosource scintillation obs., ionospheric irregularities determ. 79—84579
radiowave absorption separation from cosmic radio noise absorpt. 78—85769
radiowave heating using HF signal, plasma line enhancement 80—82140
radiowave influence on nonhomogeneity appearance connected with current instability *(Russian)* 78—49200
radiowave propag., generalized magnetoionic formulae 80—61963
radiowave propagation in F2 layer, crit. freq., solar influence 79—2423
radiowave scintillation, nighttime equatorial F-region 80—26681
radiowave scintillation, signal-statistical and morphological model 79—58185
radiowave scintillation rel. to aurora 77—87158
radiowave scintillation studies using ATS-6 radio beacons at Delhi 78—69600
radiowaves modulation instability 77—25814
random and anisotropic irregularities at low latits. 79—88532
range and freq. spread F rel. to solar cycle 78—32292
Rayleigh-Taylor gravitation-induced instability, rel. to equatorial spread-F 78—69595
response to geomagnetic storms at field line L=4, electron data anal. 80—8472
satellite radio signals amplitude scintillations rel. to spread-F and sporadic-E over Brisbane 78—49209
scintillations at GHz freqs. power spectra model comp. 77—45233
scintillations obs., at Lunping Observatory, geomagnetic activity influence 79—88545
seasonal anomaly in S.America and S.Atlantic 77—17277

F-region continued
semidiurnal tide in the meridional wind at F region heights at low latitudes 79—53596
short period oscills. during cyclonic weather conditions 78—16234
small amplitude short period waves from radio reflection virtual height meas. 77—73906
small-scale inhomogeneities, ionogram and OGO 6 satellite obs. 77—33265
solar activity affecting temp. and electron density 80—46337
spatial resonance effect in nighttime equatorial F-region 78—96341
spectral analysis of wave perturbation 80—21873
spread F bubble drift velocity, radar obs. 80—51598
spread-F, midlatitude, occurrence during mag. storms 79—29924
spread-F, props. of plasma bubbles near dawn terminator in topside ionosphere 79—101016
spread-F, range and frequency spread occurrence at Kodaikanal 80—72676
spread-F activity at southern mid-latitudes, rel. to scintillation regions horizontal struct. 79—12339
spread-F and magnetic activity at Kodaikanal, India 79—88542
spread-F bubbles, nonlinear Rayleigh-Taylor mode theory in two dimensions 78—88986
spread-F formation 80—72712
spread-F in equatorial ionograms assoc. with horizontal elec. field reversal 78—69560
spread-F in equatorial ionosphere, assoc. with radio scintillations 80—77191
spread-F intensity, at Halley Bay high latitude station, India 79—75034
spread-F occurrence following geomag. activity, time delay latit. depend. 80—8481
spread-F parameters, related to geomag. disturbance index 80—8471
spread-F plasma bubbles in equatorial topside region 80—72694
spread-F recurrence, relationship to ionospheric height rises and polar mag. substorms 78—81494
spread-F simultaneous occurrence at magnetically conjugate points 77—21994
stationary nighttime F-layer, analytical model 78—73564
strong mag. storms affecting equatorial f_0 80—77197
structure, calc. and obs., AE-C satellite and incoherent scatter radar obs. 78—49203
structure variations rel. to thermospheric diurnal tide seasonal-latitudinal struct. 78—77377
sudden frequency deviations and phase anomalies due to solar flares *(Italian)* 78—96345
sunlit F-region, neutral wind southward midnight surge, Chatanika radar obs. 77—33233
SW radio propag., weak large-scale inhomogeneities effect of auroral ionosphere 79—101017
temperature, satellite meas. rel. to incoherent scatter radar results 79—2435
temperature and ion chemistry at nighttime, 400-450 km altitude, Ogo 6 data 80—90267
temperature and wind measurement Fabry-Perot-interferometer imaging system appl. 80—101441
temperature domains, nonlinear stationary 79—35052
temperature meas. by satellite and incoherent scatter radar 78—36394
temperatures, meas. at Malvern and S. Santin 77—91360
thermal parametric instability, effect of recomb. processes and plasma nonisothermability 80—61967
TID phenomena at nighttime, distrib. and occurrence 80—77206
TID phenomena in F-region, influences of thermosphere winds 80—109305
topside profile determ. by single meas. 77—56739
total electron content, geomag. activity effects 80—8480
transequatorial propag. in 144 MHz amateur radio band, forward scattering at rising plasma bubbles 79—35057
travelling disturbances, directional filtering 79—62661
travelling disturbances, frequency of occurrence over Waltair, India 79—40011
travelling disturbances, possible correl. with jet stream activity 78—69601
travelling disturbances characts. over Thumba 78—69590
travelling disturbances rel. to reson. coupling of ionisation waves and acoustic gravity waves 77—25832
travelling disturbances study using multistation rapid-run ionosondes 78—93041
travelling ionospheric disturbance obs. by HF Doppler sounder array 79—48619
travelling ionospheric disturbances, in F1 region, phase path technique obs. 80—36436
travelling ionospheric disturbances (TIDs), prod. by gravity waves, Hooke perturbation formula testing 79—40005
troposphere-ionosphere coupling during 1973 November 20 isolated tornadoes 79—70851
trough region auroral patches and detached arcs characts., Isis 2 obs. 79—70910
unresolved spread-F, a result of pulse spreading 77—78557
VHF absorpt. winter anomaly over Delhi 77—64522
VHF multi-satellite scintillations correl. with spread-F and sporadic-E increase over Brisbane 77—53297
VHF radar aurora and strong HF backscatt. comparison 80—61960
VHF scintillation late evening enhancements at low latits. 79—75031
VLF cross meridian refraction at 500-600 km altitude 80—46339
VLF electrostatic emissions form. mechanism at high latits. 78—93037
wavelike vars. in path of totality of 1976 October 23 solar eclipse 79—66865
wind negatively correlat. to elec. field, nocturnal radar reflection data 80—41603
winds affecting O^+ and H^+ equal ionisation level 80—90280
winter anomaly causes 80—85793
winter high-latitude, 300 km altitude, AE-C thermal plasma obs. 79—16740
winter nighttime ionosphere distortions at L=4 77—87165
zonal wind during Joule heating, computed bounds 79—21084
zonal winds, estimation during Joule heating using incoherent scatter techniques 78—36344
Ba cloud release, computer simulation of gradient drift instability 80—85802
Ba striated clouds, electron density struct. meas. 78—88974
F_2-layer, plasma ambipolar diffusion and vertical drift at low latitude 80—101472

F-region continued
F_2-layer electron density var. with latitude during geomag. storm. 80—101474
Fe^+ ions, distrib., on high latitude F-region 79—16736
He^+ escape fluxes from polar ionospheres, calcs. 79—35037
Mg II equatorial airglow altitude distrib. 79—2418
N atom and O ions in dynamic model, daytime high-latitude 80—72693
N_2 airglow solar activity effect on (0,0) second positive band 77—70902
N_2^+, electron impact dissociative recomb. coeffs. inferred from Atmosphere Explorer meas., objections 78—86957
N_2^+ photochem. rel. to solar cycle phase 80—85783
$N(^2D)$ chemistry from airglow and atm. comp. meas. 78—16241
NmF_2, high-latit. behaviour along noon-midnight meridian under quiet conditions 79—40004
O I, red line luminesc. amplification by radiowave anomalous absorpt. *(Russian)* 79—29925
O I 6300 Å line correl. with electron content in nighttime F-region 77—67007
O^+ and H^+ daily vars. at mid-latitudes at sunspot max. 79—58167
O^+-O, resonant charge transfer cross-section, collision freq. and energy transfer rate 77—45231
$O^+ + N_2$ reaction, effects of soft electron precip. on N_2 vibr. energy distrib. 77—33261
$O^+ + N_2(O_2)$, excited ion reactions, charge transfer coeffs. at thermal energy 80—95721
$O^+ + N_2(O_2)$, reaction rates, 300-900K 79—8434
$O^{+*} + N_2(O_2)$, metastable ion reactions, rate consts. and ion mobility at 300K 80—95722

f-values *see oscillator strengths*

faces (crystal) *see crystal faces*

facsimile
see also video signals
educational display appl. *(Japanese)* 78—20924
Gaussian spot synthesized image facsimile fine structure 79—76604
ground receiving system, Earth survey data 77—82012
laser facsimile printing comprising real-time diffr.-limited reading, transmission and printing of large images 77—42559
METEOSAT 1 weather satellite pictures, amateur reception *(German)* 80—81982
picture direct transmission via single optical fibre 80—106628
random halftone contact screens, transmittance control of tone reproduction 78—66775
weather chart transmission for military appls. 80—90206
weather facsimile (WEFAX), expanded digital system 79—66817
weather satellite picture processor for TIROS-N series, visible and IR pictures 80—67439

facsimile communication *see facsimile*

facsimile document reproduction *see photocopying*

facsimile equipment
fibre optic sheet prod., appl. for image convertors in facsimile input system 78—42477
laser galvanometer scanning system, CAD 77—58475
marine radiofacsimile weather chart receiver and recorder 80—46297
radio weather chart, facsimile machine 77—70878
TIROS-N weather satellite, detection circuits and sync pulses 79—53577
Viking Ground Reconstruction Equipment for facsimile picture recording 77—38051
Viking Lander camera design 77—41285
Viking Lander camera performance and data reduction 77—41286
weather-satellite picture facsimile machine, constructional details 77—21870
weather-satellite picture facsimile machine, sample-and-hold detector and line dividers 77—17260
weather-satellite picture facsimile machine 77—9558
weather-satellite picture facsimile machine 77—29629
X-ray picture laser scanning system for digital image transmission over telephone channel 78—80953
GaAs laser facsimile printer 80—30207

facsimile signals *see video signals*

facsimile transmission *see facsimile*

faculae *see Sun*

fading
see also radiowave propagation
15 GHz propagation losses on long-range air-to-ground transmission 77—17218
30 GHz signals, thunderstorms 78—3854
atmosphere, turbulent, conditional fading statistics of scintillation 78—66757
auroral radio echo, ion-acoustic, short term characts. 78—45080
E-region, fading records over Tiruchirapalli (1973-5), full correl. anal. 80—101473
Earth-satellite paths, 11.5 GHz, annual and annual-worst-month statistics of fading 78—57238
HF and MF signals refl. from spread-F, fading anal. 79—101005
HF fading ionospheric reflection channel, delay and Doppler power spectra 79—8765
HF signal fluctuations energy spectra in auroral zone 77—17284
HF signals, allowance for fadings in computation of single-hop paths 77—91352
HF sky-wave received signal level determination for communication link 78—85758
ionosphere, closely-spaced receiver technique for horizontal drift meas. 78—40743
ionosphere, E- and F-regions over Tiruchirapalli (1973-5), cross spectral anal. 80—101478
ionosphere, electron prod. and loss rates, satellite meas. 79—35047
ionosphere, scintillations induced by cloud of sporadic-E layer 77—37477
ionosphere, spaced fading obs. of ionisation irregularity drift motion 80—82133
ionosphere electron density of Delhi and latitudinal depend., INTASAT Faraday fading obs. 80—109293
ionosphere Faraday fading records, mean field height determ. using Q-T position 80—8482
ionosphere night-time scintillations at mag. equator fading rates 79—44292
ionosphere sounding, filtering effect on drift parameters determined by full correl. anal. 78—65450
ionospheric absorption, Gauhati, India 77—41261

fading continued

- Jupiter probe-to-relay communication MFSK frequency acquisition and tracking 77—64613
- LF field strength meas. on single-hop path 77—29547
- LF radiowave absorpt. events rel. to meteoric ionization 79—48608
- LF signals attenuation due to meteor trains 78—40726
- low angle tropospheric fading meas. of satellite signals *(French)* 78—49069
- medium wave broadcasting, interference fading *(Russian)* 79—40018
- MF band, polarisation coupling loss and sea gain effects 79—5709
- MF radiowave field strength digital measurement equipment *(Japanese)* 77—82051
- microwave link, scintillation fading meas. at 100 and 36 GHz, wavelength depend. 77—41110
- microwave link at 19 GHz over 35 km, attenuation meas., effects of rain and multipath propag. 79—88453
- microwave links, 11 GHz, fading due to rain, snow and multipath propag. 77—91206
- microwave propagation under multipath conditions, expt. investigation *(Russian)* 77—5392
- microwave rain attenuation, 11.6 GHz, diversity meas. at Etam and Lenox, West Virginia 79—79922
- Mitra-type fading near travelling ionospheric disturbances, cross spectral anal. 80—82128
- multipath fading and radio refractivity meas. at 11, 19 and 36 GHz on 7.5 km path 77—41111
- multipath fading and rain attenuation on terrestrial radio links, 7 to 15 GHz 79—16630
- quasiperiodic scintillations, morphological and ionospheric aspects 77—91361
- radio lens in ionosphere, UHF and VHF fading patterns 77—53299
- radio signals ionospheric propag., meteor trail ionization effects 79—101001
- radio waves, diffr. from discrete and homogeneously structured ionospheric irregularities 79—48612
- radiowave polarisation fading records, spectra interpretation 77—60527
- radiowave scintillation studies using ATS-6 radio beacons at Delhi 78—69600
- radiowaves, Faraday fading of 40 MHz signals, ionospheric irregularities characts. 77—13166
- rain attenuation of radiowaves meas., microwave radio link projected design appls. *(Slovenian)* 80—46217
- rain attenuation on satellite-Earth path at 11.4 and 14 GHz by radiometric meas. *(French)* 78—49066
- rain slant path attenuation statistics prediction at various locations 78—24344
- refractive index microstructure and scintillation fading meas. in tropical region 79—16629
- satellite links, ionospheric wave disturbances effect on polarisation fading freq., simulation 78—69572
- satellite radio links, due to ionospheric radio lenses 78—7833
- scintillation levels of synchronous satellite beacons at equatorial and high latitudes, empirical models 79—58182
- spaced fading records, correlation analysis, occurrence of negative V_c^2 79—88540
- spaced fading records, equatorial spread-F irregularities 79—88543
- spaced receiver drift experiments, triangle size effect 79—53635
- spaced receiver drift expt., triangle size effect, ground diffr. pattern estimation errors 79—88525
- spaced receiver fading obs. at Thumba 80—109296
- spaced receiver fading records, nature of ionospheric irregularities determ. 79—88532
- sporadic-E affecting ELF wave propag. at nighttime 80—77202
- sporadic-E layer, VHF fading evidence for F-region disturbances 80—101475
- synthetic aperture radar image coherent-optical simulation 77—50632
- troposphere, radiosonde meas. and spectral anal. of LOS fading 80—56568
- turbulence and wavelength effect on scintillation fading at mm. wavelengths 78—85623
- underwater sound in deep ocean, source-motion rel. to amplitude fades 77—62088
- VHF satellite signals, 40 MHz, ionospheric characts. determ. 79—88529
- VHF satellite signals, 40 MHz, scintillations obs. at Kurukshetra 79—88527
- VHF signals from satellite radio beacons, ionospheric scintillations 79—53634
- VLF atmospherics anomalies rel. to rainy days over Calcutta 80—82127

failure, electrical *see electrical faults*

failure (mechanical)

- *see also fracture; mechanical strength; plastic deformation*
- adhesion, locus of failure, implications for adhesion meas. 80—50818
- adhesive failure, and thin film adhesion 80—50820
- adhesive joint failure, adhesive/electronically conducting substrate, exam. of electrochemical aspects 78—60979
- alloys, statistical model, in conditions of monotonous cyclic loading *(Bulgarian)* 80—70296
- asymptotic time to failure of a mechanical system of parallel members 78—83240
- bimetal, failure during fatigue testing, electron microscope obs. *(Russian)* 78—23808
- brittle fibre reinforced composite, failure, mathematical simulation 78—3221
- BWR, pellet-cladding interaction related failures during manoeuvring operations 78—21743
- cantilevers, randomly excited, first passage failure 79—46241
- composite, physics of strength, kinetics of failure 78—3206
- composite materials, tension stability, deformation up to failure *(Russian)* 80—75289
- composites under complex loading, failure criteria 80—81206
- conference, reliability and stress anal., San Francisco, CA, USA, 1975 80—8740
- crack growth, discussion of different stages 77—68536
- E-glass fibre reinforced epoxy, eval. of tensor polynomial and Hoffman strength theories 78—19830
- fibre reinforced composite, role of binding agent 79—1912
- fibre reinforced laminate, nonlinear response 77—70107
- fibre reinforced metals, fatigue limit *(German)* 78—72859
- flood levees, failure rel. to reliability anal. 77—91182

failure continued

- FTR, mechanical failure of subassembly ducts and its effects on transition-phase analysis 79—85667
- FTR subassembly failure pattern under transient overpower accident 79—31006
- geological materials failure, role of acoustic fluidisation 80—85653
- glass fabric reinforced polyester, biaxial stress failure surface under static and fatigue loading 78—72836
- glass reinforced plastics, static and fatigue failure, fracture mechanics 78—19898
- granite cylinders, failure under impact loading, brittle fracture process 77—86864
- granular material, particle crushing under high triaxial stresses *(Japanese)* 78—15466
- graphite fibre reinforced epoxy, laminated plate under tension, stacking sequence and lay up angle effect on free edge stresses round hole 78—88524
- HTGR fuel element failure mechanisms and fission product release 80—13586
- ice shelves, floating, tidal flexure cracks, fracture mechanics 78—69368
- laminated plate under tension, stacking sequence and lay up angle effect on free edge stresses round hole 78—88524
- LMFBR-type steam generator, consequences of intentional steam tube failure 79—54544
- LWR, condenser tube failures 78—21715
- machine fault diagnosis, vibr. anal., bispectrum method 79—8404
- machine parts, safety factor determ. during cyclic loading taking account of initial stresses 80—43675
- metals, statistical model in conditions of monotonous cyclic loading *(Bulgarian)* 80—70296
- piezoceramic benders, circular, bond stresses anal. and failure probability 78—21124
- polyhedral sandwich domes, elastic behaviour, failure, practical investigation and numerical simulation 78—59309
- polymer, deformation, failure, kinetic model *(Russian)* 78—72832
- polymer, failure build-up on micro- and macro-level 77—70172
- prestressed media with moving phase boundaries, dynamics, continuum theory of failure 78—18238
- PTFE/graphite bond in H_3PO_4 environment, electrochemical exam. of joint failure 78—60979
- ring shaped bodies, collapse *(German)* 78—87258
- rock, scale invariant properties 78—3758
- rock failure precursors during anelastic deformation 78—61405
- solar cell life prediction using physical chemical failure progression modelling 80—61370
- stator windings, failure mechanisms under thermal cycling *(Japanese)* 80—104189
- steel, low-alloy sheet, welded hydraulic turbine volute chamber, strength and toughness 78—68820
- steel, structural, subject to low temp. low cycle fatigue, failure charact. 77—70174
- steel vessels, internal pulsed loads, effect of scale. geometry and filler on strength 78—21659
- surface profilometry, role in diagnosis 80—66676
- surface wave scatt. from ellipitical cracks for failure prediction 80—55608
- viscoelastic material, failure and instability in tension 80—87720
- Al, surface wave scatt. from elliptical cracks for failure prediction 80—55608
- B fibre reinforced epoxy, tensile anal. of edge notch 77—70159
- B fibre reinforced epoxy, eval. of tensor polynomial and Hoffman strength theories 78—19830
- KH_2PO_3, mechanically treated single crystal, depth and struct. of disturbed layer *(Russian)* 78—23839
- Mo-Zr-Ti-C(0.1, 0.15, 0.004 wt.%), alloy TsM2A, cavitation failure mechanism 77—70169
- SiC, hot pressed, brittle fracture and subcritical crack growth 78—72885
- Si_3N_4, hot pressed, flawed plate under combined stresses, failure prediction 78—72884
- Si_3N_4, hot pressed, surface wave scatt. from elliptical cracks for failure prediction 80—55608
- SiO_2 fibres, fused, failure predictions based on fatigue strength 78—71293

failure analysis

- *see also electrical faults; wear*
- 14th Annual Reliability Physics Symposium, Las Vegas (1976) 77—40514
- aerospace guidance computer AgSu intermetallic particle contamination detection using X-ray 78—21313
- aircraft metal fatigue crack detection using nondestructive evaluation (NDE) methods 80—71826
- cardiac pacemaker RF susceptibility tests 78—48935
- CMOS microcircuit, scanning electron microscope and mass spectrometry appl. 78—21264
- component reliability tests in thermal neutron environment 78—21787
- component unavailability and failure intensity 77—83063
- coronary care unit equipment failure finding and prediction 78—44648
- corrosion failure, metallographic anal. 79—61836
- cylinder elastic orthotropic brittle, under axisymmetric thermal and press. loading failure probability anal. 78—34078
- ductile crack growth 79—90724
- electrical components, mathematical simulation of life *(Spanish)* 79—21532
- electrode longevity analysis 77—81750
- electron linear accelerator, computer prediction and diagnosis of failures of systems 79—693
- electronic piece parts reliability evaluation by neutron radiography 78—31610
- endocardial electrode lead and pacemaker failure, actuarial analysis 80—30945
- fatigue failure, rupture, continuous damage mechs., uniaxial homogeneous state of stress 80—74806
- fault conditions diagnosis based on tree logic and probabilistic importance, appl. to nuclear power plant 77—6549
- fault tree technique and electron fractography 78—53071
- ferrofluid susceptibility meas. device and method *(Czech)* 77—26345
- fibre bundle time-dependent failure, probabilistic model 77—3798
- fibre reinforced composite failure analysis by acoustic emission 78—80691

failure analysis continued

- filament wound material, lamination theory for failure envelope prediction under biaxial loading 79—38931
- fission reactor system reliability prediction, appl. of Bayes eqn. 77—67797
- fission reactors, CRBR shutdown system, Markovian reliability anal. 80—27761
- fission reactors, failure probability distrib. from observed failure data, beta distrib. 80—63335
- fission reactors, shutdown heat removal system failure, fault tree, common-cause anal. 80—63334
- fission reactors, shutdown heat removal systems, reliability fault tree anal. and β-factor method 80—63331
- fractography, fractures preservation and cleaning 80—71866
- glass fibre reinforced composite, failure anal. by fault tree technique 79—29193
- glassy materials, compression cracking theory and failure 80—7677
- graphite fibre reinforced epoxy, stress transfer to brittle coating, failure 79—96106
- graphite reinforced epoxy steel scarf joint, adhesively bonded, exam. of failure 78—92350
- IC relaibility assessment by scanning electron microscope 78—24902
- implanted prosthesis failure analysis techniques and results 80—89906
- instrument CAD considerations *(Hungarian)* 79—93134
- kinetic equations of failure in complex programs of cyclic loading 79—64592
- kinetics and stability 77—883
- light duty electrical contact reliability assessment methods 78—29219
- LMFBR, SNR-300, HCDA anal. by failure incoherence modelling, HOPE computer code 77—88237
- load-bearing structures, behaviour prediction of materials degradation 79—34133
- LSI circuits, wafer defect classification using modified scanning electron microscope 79—21876
- LWR fuel element reliability, materials science aspects 79—67855
- mechanics of failure rel. to strength 79—64591
- metallisation corrosion, IR microscopy technique 80—98976
- metallography, failure analysis appl., conf., Houston, USA (July 1977) 79—61832
- metals structural failures, for industrial appl. 80—76429
- microelectronic device bonds, glass-metal seals and weld metal, Auger spectroscopy appl. 78—24900
- micromechanical models in risk anal. 80—108572
- nuclear electric power plants, failure anal. and failure prevention 77—79450
- nuclear power plant safety systems, common mode failures, appl. *(German)* 78—694
- nuclear reactor, assessment by reliability technique 77—30653
- nuclear reactor components, design by analysis 77—3095
- nuclear reactor emergency core cooling system motor operated valves, failure criteria 78—70592
- nuclear reactor pressure components, common cause failures 79—18012
- nuclear reactor redundancy systems, common mode failures 80—13641
- nuclear reactor structural reliability, time-depend. nature modelling 79—18013
- nuclear reactor structure, probabilistic failure mechanics anal. 77—81317
- nuclear steam supply, emergency core cooling system motor operated valves, failure mode anal. 78—54866
- op amp, type 108, radiation hardening by modified processing, failure anal. 77—18751
- plastic polycrystalline body, energy criterion for failure 77—4823
- plates, symmetrically laminated cross-ply rectangular, initial flexural failure anal. 80—64461
- PWR pressure vessel failure probability from pressure transients, OCTAVIA computer code 79—18011
- PWR pressure vessel reliability, failure anal. 77—74962
- PWRs, auxiliary feedwater system, fault tree anal. 78—54867
- reactor safeguard system common-mode failure analysis 78—29618
- reactor steam generator tube perform. anal., corrosion failure 79—59178
- reliability physics, conference, Las Vegas (1977) 77—79086
- replication, NDT anal. and inspection technique 78—11467
- safety determ. from defect evaluation rel. to fracture mech. *(German)* 80—100908
- scanning electron microscope obs. 78—27710
- semiconductors, SEM electron beam irradiation damage and contamination 78—29217
- solar array sample accelerated thermal cycling facility 79—96458
- solar cell fault analysis using scanning light spot and distrib. network model 80—81473
- spacecraft materials failure, metallurgical exam. 80—71868
- spacecraft systems, evaluation of acceptance testing 79—16797
- stress corrosion cracking failure, predictive approaches 80—97611
- surgical implants, in human body, failure anal. 79—62407
- tagged assembly failure location analysis program 79—13486
- thermistor bolometers, anal. methods 78—24795
- tools comparison and selection 80—71865
- VVER-440 reactors, emergency operating conditions following main circulation pipe failure, computer-aided analysis 79—9823
- Ag-Zn cells, test methods evaluation 79—48105
- Au, thin film, electrotransport-induced failure site, minor constituents effects 79—23763
- Cu electrodeposition on Su, reliability 78—24901
- GaAs FET, SEM electron beam technique 78—29216
- H maser failure mode identification 77—37862
- Si:As, neutron damage mechs. in IR detectors 78—30668
- W, filament, incandescent lamps, creep, failure, life prediction 78—84927

fallout

- *see also air pollution*
- 1976 fallout in air and rain over United Kingdom 77—73847
- atmosphere dust, radioactive fallout results to end of (1978) 79—79997
- atmospheric radiation environment, mass integral scaling 77—46406
- S.Australia, T fallout in rainfall and wine samples 78—11960
- beta activity meas., 1973 to 1975, for rain and dust fallout *(German)* 77—64420
- Bikini lagoon, coral alpha emitters, solid-state track detection 78—53661
- Bulgaria, radionuclide composition and activity over Bulgaria in 1976 79—88018
- Chiltern, Oxon. (1951-1977), dose rate, air ionisation, radioactive fallout 79—6775

fallout continued

- Chinese 19th nucl. test explosion, fallout γ-ray spectra anal. using Ge(li) detector *(Japanese)* 79—31219
- Chinese explosion 1977 Sept. 18, time distrib. and anal. fallout particles 79—25796
- Chinese nuclear explosion, Jan. 1976, anal. of fission products 77—26884
- Chinese nuclear explosions, props. of highly radioactive particles *(Japanese)* 79—63813
- Chinese nuclear test explosion, September 1976, hot particle anal. from γ-spectra *(Japanese)* 78—82519
- Chinese nuclear weapon tests, fresh fallout anal. using beta counting technique 79—92106
- community shelters for protection from radioactive fallout 80—5338
- W.Cumbria, Pu and ^{137}Cs concs. in environmental samples and possible maritime effect 80—108817
- damping coefficients 78—92961
- Danube River, distrib. of artificial radionuclides at mile 34, 1976 79—39323
- Devon Island ice cap, NWT, artificial radioactivity layers 77—5250
- dust captured by wind from Earth's surface, radioactive fallout *(Russian)* 80—16869
- education, nuclear fallout radioactivity γ-ray detection and anal., Chinese fission bomb anal. 78—49596
- environmental radioactivity meas. in the EEC, 1977, for air, deposition, water and milk 79—62162
- environmental radioactivity prior to the Kori nuclear power plant operation 79—6773
- N.Europe air radionuclide conc., due to Chinese nucl. explosion 80—108826
- fallout nuclide determination for 19th Chinese nuclear test 79—54601
- fission products, washout by rain *(Spanish)* 79—92399
- Flin Flon, Manitoba, fallout in vicinity of base metal smelter 80—55959
- gamma radiation, effectiveness of soil as shielding 78—5059
- Hudson River estuary, man-made radionuclides and sedimentation 77—2183
- India, ^{32}Si, ^{210}Pb, 2^{22}Na, ^{35}S and ^{7}Be in rain, 1965-71 obs. 80—41526
- Japan, ^{137}Cs and K contents in low-teens in areas of different fallout level 77—90922
- Japan atomic bombs, radiation doses received by survivors residing in USA 77—9260
- Lake Huron, shore contamination from radioactive fallout 77—86897
- Lake sediment radioactivity, mixing by benthic organisms 78—16060
- LMFBR, accidental Na release as peroxide aerosol, effect on tomato and lettuce *(French)* 78—8997
- magnetic particle fallout recorded in recent ombrotrophic peat sections 78—61519
- Nagasaki atomic bomb fallout effects 78—85393
- neutral particle transport in 2-D, appl. of space angle synthesis 77—83107
- Nevada test site, nuclear testing fallout possible association with childhood leukaemia 80—12186
- nuclear fission aerosol products, bioindication using needles of common pine tree 79—100550
- nuclear installations, environmental surveillance programme, Spanish experience 77—65336
- nuclear tests, Chinese 80—27820
- nuclear weapons testing, radionuclide distributions in oceans and marine sediments 78—13344
- nuclides determ., 19th Chinese test 78—82520
- radioactive fallout in air and rain, results to end of 1977 78—82535
- radioactive fallout on Milan 1976-7, influence of Chinese nuclear expts. *(Italian)* 78—58501
- radioactive fallout water deactivation using sorption props. of clinoptilolite, vermiculite, bentonite 79—43995
- radioisotopes distrib. in ocean, turbulent exchange intensity determ. *(Russian)* 79—39744
- radionuclide inhalation reduction using indoor shelter after nuclear accident 77—34478
- radionuclide ratios in wet and dry deposition samples, USA, 1976 Jun.-1977 Dec. 79—29807
- radionuclides decomposition in glaciers 80—40934
- rain, radioactive fallout results to end of (1978) 79—79997
- reactor accidents, struct. shielding against gamma-ray sources, dose reduction factors 78—13251
- reactor airborne plume deposition estimation model evaluation 78—94148
- Ross Ice Shelf, Antarctica, artificial radionuclides depositional history 79—88027
- satellite Cosmos 954, estimating fallout on Great Slave Lake 79—85830
- scavenging, in-cloud, rel. to aerosol particle size, mechanisms 78—16108
- sediment mixing and accumulation, fallout tracer obs. 80—81864
- soil and vegetation, surface β-activity caused by nuclear explosion products, depend. on isotope vertical migration 78—86700
- soil samples, meas. trace radionuclide L X-ray detection 78—49020
- Taiwan, 1971 to 1975 period 77—90918
- time-variant atmosphere dispersion model 77—49207
- transuranic nuclides depositional history in S.Greenland firn layers 77—86953
- tropopause, ^{7}Be, ^{137}Cs and shortlived fission product concs. *(German)* 77—29408
- tropospheric fallout fluxes of Pb, Cd, Cu, Zn, Ag in Antarctica and Greenland 79—58007
- Ural disaster questioned, possible fallout from atmospheric test 80—76666
- water, sensitive sampling method for radioactivity meas. 79—39768
- ^{137}Cs, conc. variations in Baltic Sea 1973 to 1975 79—92100
- ^{241}Am, conc. in thermonuclear test debris, collected near Bikini Atoll 78—96103
- ^{241}Am concentrations concs. in drinking water and organic fertiliser 77—56488
- ^{241}Am, concs. in sediments from coastal basins off California and Mexico 80—98303
- ^{241}Am soil concs., in situ gamma anal. and sampling data comparison, Nevada 77—64143
- ^{14}C, bomb-produced, distrib. in equatorial Atlantic, upwelling rate estimation 79—39726
- ^{14}C fallout from nucl. weapons testing, human radiation burden 77—64091
- ^{14}C fallout from nucl. weapons testing, use as biological tracer 77—64162
- ^{14}C pollution of Atlantic from nucl. weapons tests 80—89683

fallout continued
  ^{113}Cd^{m}, in marine organisms and sediment around Marshall Island nucl. test site 80—109174
  Cl^{-} ion concentrations in river, spring waters in Okinawa Honto, origin *(Japanese)* 79—39324
  ^{242}Cm and ^{244}Cm in global fallout, lichen sample results 78—57263
  ^{137}Cs body burden in Japanese from 1967 to 1975 77—9283
  ^{137}Cs, dating of salt marsh sedimentation rates 78—96247
  ^{137}Cs excretion in urine vs. total excreta following continuous intake of ^{137}Cs in fall-out 78—20294
  ^{137}Cs fallout in arid watersheds, phys. and chem. parameters affecting transport 78—61461
  ^{137}Cs in alpine tundra habitats, effects of phys. habitat factors and plant morphology 77—37058
  ^{137}Cs levels in soils and vegetation of W.Malaysia 78—73263
  ^{137}Cs movement and loss in small lake 78—24317
  ^{137}Cs radioactive fallout and lacustrine sedimentation rates 80—4048
  ^{137}Cs, runoff coeff. from surfaces of river basin soils 79—44212
  ^{55}Fe and stable Fe forms and availability in oceanic aerosols 79—12241
  ^{3}H, conc. in atmospheric precip., rivers, and seas, USSR 79—74560
  ^{3}H from weapons testing, rel. to reactor release detect. by atm. water vapour ^{3}H meas. 78—11988
  ^{131}I population thyroid dose in USA after Chinese atm. nucl. weapons tests 78—77116
  Na$_2$O aerosol gravitational fallout rate, validation of computer code for fast reactor accident anal. 80—18535
  ^{210}Pb from nucl. explosions in environment 78—21774
  ^{210}Pb tropospheric residence time 78—85396
  ^{239,240}Pu, conc. in thermonuclear test debris, collected near Bikini Atoll 78—96103
  Pu, A=239, 240, concs. in drinking water and organic fertiliser 77—56488
  Pu distribution in Ohio soils, local and stratospheric sources 78—16015
  Pu fallout detection using fission tracks prod. with neutron irrad. spectra 80—95479
  Pu in alkaline, saline lakes 80—97826
  Pu isotopes in Antarctic snow layers, deposition and accumulation 79—70820
  Pu, remote contamination and total inventory from Rocky Flats, mass spectroscopic anal. 77—73739
  Pu, U, and Th, metal separation by column extraction chromatography 78—44421
  ^{239}Pu soil concs., in situ gamma anal. and sampling data comparison, Nevada 77—64143
  ^{241}Pu concentrations in Swedish reindeer lichens, radiochem. anal. 78—15912
  ^{241}Pu, concs. in sediments from coastal basins off California and Mexico 80—98303
  ^{90}Sr and T conc. and distrib. in N.Atlantic surface water 78—65345
  ^{90}Sr and T in N.Pacific surface water during 1974, conc. meas. 80—26181
  ^{90}Sr, conc. variations in Baltic Sea 1973 to 1975 79—92100
  ^{90}Sr in human bone, Yugoslavia 77—56490
  ^{90}Sr, runoff coeff. from surfaces of river basin soils 79—44212
  ^{90}Sr tropospheric residence time 78—85396
  T, concentrations in Caspian Sea 79—34858
  T fallout at South Pole in 1954-1978 snow samples 80—16867
  ^{99}Tc accumulation by plants 77—56489
  ^{132}Te in lower troposphere, airborne levels and lifetime 79—12242
  ^{95}Zr from Chinese atmospheric thermonuclear explosions, appl. to stratospheric transport parametrisation 79—2342

Faraday effect
  acetylene, Verdet consts., ab initio calcs. 77—3390
  anthracene, Faraday spectrum, sign rel. to mag. field strength *(German)* 77—36204
  antiferromagnetic heavily doped semiconductors, Faraday light depolarisation in mixed mag. states 80—29726
  atomic Faraday effect, analytical appl. 80—9538
  atomic forward reson. scatt. spectrometry using magneto-optical effect *(Japanese)* 78—76956
  atomic resonant media, nonlinear Faraday effect 79—32001
  atomic system, magnetoelec. susceptibility in static mag. field 78—55143
  atomic system, nonlinear variations in strong mag. field 80—79429
  atomic systems, nonlinear magnetoelec. susceptibility, Faraday effect, laser intensity depend. 78—59076
  ATS-6 radio beacon signals, Faraday rot. modulation rel. to travelling ionospheric disturbances 79—21101
  ATS-6 satellite radio beacon, Faraday rot. meas. at Ootacamund, India 79—48611
  auroral radioscattering anisotropy, from 42 MHz polarisation investig. 77—21968
  benzene, Faraday spectrum, sign rel. to mag. field strength *(German)* 77—36204
  biphenylic bridged systems, appl. of Faraday rot. data to conform anal. 77—65495
  bond magnetic rotations, Faraday effect determ. of additive props. 77—30746
  bubble collapse field, anisotropy field, and domain wall mobility, magneto-optic meas. 77—85534
  4C+36.11, extragalactic source, Faraday rot. in S232 rel. to mag. field strength 80—51840
  chalcogenide spinels, Faraday effect optical isolators for CO$_2$ laser system 78—50816
  chloroform molecule, liq. phase, Faraday rot. dispersion near vibr. reson. 79—91413
  circularly polarised light, right- and left-handedness, sign conventions for magneto-optical effects *(Japanese)* 78—23433
  compact extragalactic radio sources, electron-positron pair prod. rel. to Faraday rot. 78—73770
  compact optical circulator for near-infrared region 79—23063
  Crab Nebula, Faraday rot. obs. during solar control occultations 77—45593
  cubic crystals, paramagnetic nonlinear Faraday effect, EM wave propagation *(Russian)* 80—80761
  D-region, improved Faraday rotation expt. for electron conc. rocket meas. 77—9543
  D-region, lower, Faraday rot. and absorpt. calcs. rel. to electron density meas. 80—31162
  dialkylammonium copper chlorides, mag. and struct. transitions, IR absorption 77—52097

Faraday effect continued
  dipropylammonium coppertetrabromide, Faraday effect obs. of mag. struct., and domains 77—63399
  Dirac-spinor form of Maxwell's eqns., polarised light beams in gravitational fields 78—50696
  disordered system of two level atoms, Hall and Faraday effect theory 79—51601
  disordered systems, phononless Faraday effect 79—38524
  dispersion and Faraday rotation associated with point-imperfections 78—19449
  dispersion of opt. characts. in amplification range, freq. spectrum of stimulated emission, calcs. *(Russian)* 77—54757
  dye ring laser, CW, optical diode to enforce one-direction travelling wave operation 80—69427
  electric current measurement, AC, using magneto-optical methods, principles and advantages *(Polish)* 80—105676
  electro-optic voltage dividers, capacitor type, current meas. appl. *(Italian)* 77—26339
  ellipsometry without phase plate, using Faraday effect modulation 77—53970
  EM wave propagation in isotropic medium with nonstationary mag. gyrotropy *(Russian)* 77—28555
  ESR saturation, influence on Faraday effect 79—15442
  ESR saturation, influence on magneto-optical effects, allowance for dipole-dipole reservoir of electron spins 79—15442
  extragalactic radio sources, Faraday rot. rel. to Galaxy turbulent struct. 78—20885
  extragalactic radiosources, origin of rot. measures 77—5584
  extragalactic radiosources, rot. measures interpretation 77—60836
  Faraday rotation in galaxies and quasar absorption lines *(Russian)* 79—40273
  ferrites, EM wave effects on mag. and optical props., lecture 78—27031
  ferrofluid, mag. birefringence pulsed field meas. 79—82943
  ferromagnet, microwave modulation of light using magnetodynamic resonance 80—71393
  ferromagnetic metal, anomalous magnetooptic effects near Curie temp., s-f exchange model 80—2736
  fibre Faraday rotators in fibre Raman lasers 80—58775
  film, mag. domain width meas. in in-plane field 77—4534
  filter, freq. locking of CW dye laser to Ne absorpt. lines 79—22989
  formaldehyde, mag. rot. spectrum, A^{1}A$_2$ state, singlet-triplet perturbations 79—98126
  free electron gas, inverse Faraday effect and cyclotron freq. radiation shift *(Russian)* 77—8033
  fusion reactor, Shiva Faraday rot. coils, circuit and mag. anal. 78—54951
  G120.1+1.4, Tycho's SNR, rot. measure and turbulent struct. 79—88718
  galactic magnetic field from Faraday rotation of extragalactic radiosources 79—58430
  galactic magnetic fields config. from Faraday rot. data, M51 appl. 79—48934
  galactic radiation, distributed, linear polarization obs. results processing optimal algorithm selection *(Russian)* 77—91441
  garnet epitaxial film, Faraday effect and magnetometrical meas. 78—52317
  garnet film waveguide, magnetooptical effects 77—3650
  garnet films, for magneto-optic appls., substituted rare earth garnet substrate crystals 78—31351
  garnet films, meas. using magnetooptical apparatus 80—105680
  garnet optical waveguide, with high Faraday rotation, mode degeneracy 78—94454
  garnet thin film waveguide, magneto-optical effects 77—54802
  garnets, ferro- and paramag., gyromag. ratio determ. by magneto-optical method *(Russian)* 77—32356
  garnets, IR refl., ATR, Voigt and Faraday expts. 80—66180
  gas lasers, freq. selection, using Faraday effect in active medium 78—1257
  geostationary satellite VHF Faraday rotation mea. for ionospheric electron content 78—61599
  glass, photochromic, types FkhS-3, S-4, S-4a and FkhPP, exam. of magnetooptical rotation 78—88284
  glass, transducer material, comparison with quartz 78—48149
  gyrotropic layer, 4×4 interference matrix 79—55054
  high speed magneto-optic camera system, for obs. of mag. bubble domain devices 77—79186
  Hubbard model, Green function method, conc. depend. of Hall and Verdet coeffs. 80—80240
  imaging by magneto-optics, domain struct. obs. 77—48151
  implosion heating experiment, Faraday rot. meas. 77—39456
  inhomogeneously magnetised media, Faraday effect, polarisation plane rotation *(Russian)* 80—66154
  inhomogeneously magnetised solid, calc. 80—16015
  integrated isolator using Faraday and Cotton-Mouton effects 77—79966
  intensity dependent, nonlinear refr. index effect 77—77181
  intergalactic magnetic fields and Faraday rotation of extragalactic radio sources 80—22086
  intergalactic medium Faraday rotation 77—26066
  intergalactic rotation measures and cosmology 78—28800
  invariant molecular tensors, definition in origin change, refraction and Faraday, effect 80—53363
  inverse, polarisation ellipse rot. calcs. *(Russian)* 77—66483
  inverse effect in circumterrestrial plasma *(Russian)* 80—4190
  ionic crystals with intermediate polaron coupling, magneto-optical effects in shallow F-centres 80—20615
  ionosphere, Faraday effect meas at 140 MHz using two-channel polarimeter first results 80—61912
  ionosphere, Faraday rot. meas. rel. to dissimilar forms of equatorial anomaly in E.Asia and India 80—109301
  ionosphere, irregularities drift vels. from ATS-6 140 MHz Faraday rot. records 78—69599
  ionosphere, total electron content meas. at Gauhati, using ATS-6 140 MHz transmissions 78—69598
  ionosphere, total electron content obs. at Kurukshetra, suing ATS-6 140 MHz transmissions 78—69597
  ionosphere, VHF scintillation rel. to peculiar Faraday rotation fluctuations 78—61663
  ionosphere Faraday fading records, mean field height determ. using Q-T position 80—8482
  ionospheric radiowave propag., Faraday rotation measurements at Ootacamund 79—88533

Faraday effect continued
- IR glass, Verdet const. 77—73132
- isolator for integrated optics using Faraday and Cotton-Mouton effects 77—88964
- Kramers-Kronig transforms, Fourier method numerical soln. by computer 78—2825
- laser beam radial intensity distrib. formation by use of Faraday effect 77—54746
- laser output power external stabilisation using Faraday effect, control unit design *(German)* 79—18455
- laser radiation frequency spectrum control, phase polarisation method 77—75583
- lightguide, magneto-optical props., weak microwave field meas. 80—73463
- linear and nonlinear effects in system with dispersion and mag. ordering 77—52058
- liquid, new optical effects, elec. analogue of Faraday effect 77—81085
- liquid, pure, organic and inorganic, Verdet consts., pulsed mag. field meas. 80—16012
- low Verdet constant material in Faraday rotator 80—69520
- M87 radio emission, Faraday rot. in radio/X-ray halo 80—67844
- magnetic domain boundaries study, structure and movement *(Dutch)* 77—63242
- magnetic field prod. and meas. 78—8425
- magnetic film, domain wall struct. by Faraday effect 79—65702
- magnetic films, magnetooptical interference 79—28724
- magnetic materials, transparent, optical studies of phase transitions 77—66481
- magnetic pulsed 70-T system with long operational life, Faraday effect meas. 80—42243
- magnetic thin film, spectral conversion of optical radiation 79—64344
- magnetic white dwarfs, Faraday effect and depolarization of optical emission 79—97002
- magneto-microwave effects, rel. to EPR 77—55853
- magneto-optic current sensing with birefringent fibres 79—75544
- magnetometer, elimination of mag. contrib. of sample holder 79—21788
- magnetooptical parameter sums, sum rule analogue 79—89697
- meas. device with accuracy up to 0.001°, using receiving microscope, reading microscope and recording unit 80—47087
- measurement in pulsed mag. field 80—80758
- measurement of magneto-optic rotation and ellipticity, spinning analyser ellipsometer *(Japanese)* 80—73419
- megagauss magnetic field production and appl. to solid-state magneto-optical spectroscopy 79—71491
- MHD devices, plasma ionization instability, dynamic suppression, switching modelling 80—59308
- microwave, rel. to ESR, review 77—69667
- $Mn_{1-x}Cu_xSb$ films, $0 \leq X \leq 0.3$, magneto-optical props. 79—51981
- modulation of polarisation, small ang., beam in diamag. glass *(Korean)* 78—50918
- moment summation method 77—27102
- MOS structure, 2D electron gas, far IR Faraday rotation 80—80389
- Mossbauer radiation at oblique incidence to magnetically ordered absorber 80—50236
- multilayer structure, multiple internal reflections effect on Faraday rot. 78—48148
- multiphonon effects on dispersion, Faraday rot., associated with point imperfections 78—43839
- naphthalene, Faraday spectrum, sign rel. to mag. field strength *(German)* 77—36204
- Neel ferrimagnets, phase transitions, field-induced spin-orientational 80—75767
- neodymium oxydiacetate, magneto-optical rotatory dispersion and oxid absorption spectra 79—91409
- optical fibre, highly birefringent, Faraday rotation 80—58672
- optical instrum., for high elec. current meas. 77—2669
- optical instrumentation, atomic and mol. structure determ. 78—54466
- optical quanta counting procedure, magneto-optical transition radiation, Cherenkov radiation *(Russian)* 80—80760
- optically active material, nonreciprocal Faraday effect *(Russian)* 78—55298
- oscillator strength measurement using reson. Faraday effect in monochromatic light 80—23363
- paramagnetic centre crystals, nonlinear optical Faraday effect 80—99811
- paramagnetic glass, Faraday effect in pulsed megagauss field 77—69804
- paramagnetic system with quadrupole splitting, magneto-optical effects, magnetic resonance saturation 80—60404
- Permalloy, films, Faraday rotation effect dispersion 80—40092
- plasma, hot, mag. field determ. using Faraday rot. *(Rumanian)* 80—87950
- plasma, inhomogeneous, magnetised, polarisation transfer eqn. and Faraday rot. tensor 79—84662
- plasma, inhomogeneous magnetised, Faraday rot. in polarisation transfer eqn. 77—84436
- plasma, laser gas discharge, Faraday rot. diagnostics 80—43981
- plasma electron density and mag. field meas. in high-β fusion expts. 80—49008
- plastic:Eu^{3+}, Faraday rotation sign oscill. in very strong mag. fields *(Russian)* 80—88973
- polarimeter, precision, systematic errors, instrumental errors *(German)* 78—272
- polarimeter magnetic potential difference calc. 77—82587
- polarisation ellipse, rel. to MCD and Faraday rot. meas. 77—43975
- polarisation propagator calculations of frequency-dependent polarisabilities, Verdet constants, and energy weighted sum rules 78—58647
- polarisation-sensitive nonlinear spectroscopy, improved geometry 80—1285
- polyethylene glycol, mol. polarisability from Faraday effect 78—58726
- PT asymmetry and four-fold EM degeneracy lifting, appl. to ring laser mode splitting, optical prop. effects 80—23606
- QSO radio emission, Faraday rotation and cosmological magnetic fields 80—22087
- quartz, molten, stimulated Mandel'shtam-Brillouin scattering in a magnetic field 79—76762
- quartz, transducer material, comparison with glass 78—48149
- quasi-homogeneous magneto-optically active media, Muller and Jones matrices 79—8126
- radio signals Faraday rot. obs. for ionospheric total electron content determ. 77—33249
- radio sources, extragalactic, intracluster Faraday rot. obs. 79—75285
- radio sources Faraday rotation measures, computation method 80—4263

Faraday effect continued
- radiosources, Faraday rotation in variable sources, upper limits 77—91660
- radiosources, red shifts and rot. measures, Universe isotropy test 77—2502
- radiowaves, Faraday fading of 40 MHz signals, ionospheric irregularities characts. 77—13166
- rare earth compounds, paramagnetic, Faraday and Cotton-Mouton effects for acoustic phonons 78—52476
- rare earth garnet thin films, macroscopic magn. props., magneto-optical expts. 80—46764
- rare earth garnets, RIG, (R=Tb, Dy, Ho, Er), spontaneous Faraday rot. rel. to sublattice magnetisation 80—66159
- rare earth iron garnet, Faraday rotation from empirical scaling model 77—81083
- rare earth iron garnet single crystal films, synthesis and props., review 78—48013
- rare earth iron silicides, $R_2Fe_4Si_9$ and $RFeSi_3$, cryst. struct. and mag. suscept., temp. depend. *(Russian)* 78—34957
- rare earth orthoferrite, linear dichroism influence on Faraday effect 80—2737
- rare earth orthoferrite, $RFeO_3$, spin reorientation and magneto-optical effects *(Japanese)* 79—47414
- rare earth systems, crystal field effects 78—67987
- rarefied magnetoactive plasma, polarised radiation transfer 79—92669
- reflectivity, normal, superconvergent sum rules 77—85678
- resonance medium, high power radiation polarisation ellipse, mag. rot. *(Russian)* 78—70794
- reverse field pinch, Faraday rot. diagnostics for internal mag. field 80—43976
- ring laser, unidirectional system efficiency comparison *(French)* 79—76717
- rotator, low loss, and appl. for isolator design 77—58447
- satellite links, ionospheric wave disturbances effect on polarisation fading freq., simulation 78—69572
- semiconductor, Faraday rotation in presence of attractive traps 78—76081
- semiconductor, Faraday rotation in the presence of deep repulsive traps 80—29724
- semiconductor, meas. using IR magneto-optic polarimeter 77—34014
- semiconductor, nonradiative multiphonon carrier capture by deep neutral traps 80—6871
- semiconductor, p-type, Faraday effect due to free holes 80—97247
- semiconductors, mixed, containing paramag. atoms, Landau levels and interband Faraday rot., appl. to $Cd_{1-x}Mn_xTe$ 79—61348
- semiconductors, role of excitons in dispersion effects, band gap determ. 79—65393
- semiconductors, spin orientation by optical pumping, review 79—38410
- semiconductors and dielectrics, broadband, spectral contour for strong exciton bands 78—27194
- semiconductors free-carrier concentration, contactless meas., IR polarimeters, Faraday effect 77—73135
- single-mode optical fibre using injection DH laser light source 80—48245
- solar corona, Helios 1 occultation expt. results 78—20790
- spin-dependent magneto-optical rotation for free radicals and for singlet-triplet transitions 79—10129
- stimulated backward light scatt., Faraday effect, theory 77—34910
- stimulated Brillouin backscattering in laser heated solenoid 78—71511
- stimulated Brillouin scattering in media with induced anisotropy 78—1304
- superconductor Faraday effect obs. in polarising microscope 80—70892
- tarotion, effects of pulsewidth 78—71540
- Tokamak, poloidal field meas. by far IR polarimetry 79—32794
- toroidal controlled fusion poloidal mag. field meas. by far IR Faraday rotation 80—59303
- toroidal plasma, modulated submillimetre-laser polarimeter for meas. of Faraday rotation 79—46474
- transparent magnetic materials *(Japanese)* 80—11369
- transparent synchrotron astronomical sources, internal Faraday rot. effect 80—72760
- TTF-TCNQ, Hall mobility using Faraday rot. method at 9.3 GHz 77—47801
- type II superconductor, flux-line gradients and pinning forces, Faraday obs. 77—24651
- uniaxial crystals, Faraday effect at ε-isotropic point 77—12367
- Vela supernova remnant, rot. measure and turbulent struct. 80—51836
- Vela X supernova remnant, rot. measure and depolarisation ratio 80—56909
- VHF signals from satellite radio beacons, ionospheric scintillations 79—53634
- water-methanol(ethanol)(acetic acid), liq., Verdet const., pulsed mag. field meas. 80—16012
- Z-pinch, azimuthal mag. field meas. using Faraday rot. 78—9832
- AgBr, optical absorpt. of indirect exciton in high mag. field 78—60486
- AgCl, optical absorpt. of indirect exciton in high mag. field 78—60486
- Ar ion laser radiation, Faraday effect, polarisation plane negative rot. 79—98424
- a-As_2S_3, energy gap meas., by Faraday rotation 80—66161
- As_2S_3, non-cryst., 0.7-2 μm 77—16307
- Be, freq.-depend. polarisabilities and Verdet consts., calcs. 78—62781
- Bi, Faraday effect and magnetic circular dichroism 80—83399
- Bi, vapour, optical activity, Faraday effect, parity nonconservation, mag. transitions *(Russian)* 80—55070
- Bi_2, vap. phase Faraday effect, P-invariance in M1 transitions, calc. 78—82805
- BiI_3 film, exciton-phonon interaction, optical consts., Faraday effect., permitt. 80—59884
- $Bi_{1-x}Sb_x$, far IR magnetoabsorption, band struct. study 80—50351
- CO, freq.-depend. polarisabilities and Verdet consts., calcs. 78—62781
- $CaF_2:Ce^{3+}$, Kapitza limited spin-bath relax., paramag. Faraday effect meas. at liq. He temp. 79—95642
- $CaF_2:U^{3+}$, anomalous magnetooptic props., optical detection of ESR and cross-relax. resonances 80—93287
- $CdCr_2S_4$ ferromag. semicond. film, props. 78—76175
- $CdCr_2S_4$, ferromagnetic semiconductor films, prep. and props. *(Japanese)* 79—47308
- $CdCr_2S_4$, hot pressed, Faraday effect isolation 10.6 μm, damage tests 77—46750
- $CdCr_2S_4$, magnetic semicond., resonance Raman scatt., mag. circular polarisation props. 80—50341

Faraday effect continued
$CdCr_2S_4(Se_4)$, spin depend. phonon Raman scatt., band struct. 78–68491
$CdCr_2Se_4$ film, absorpt. and Faraday effect 78–2936
$CdCr_2Se_4$ film, mag. linear and circular dichroism and Faraday rot. 79–99966
$CdCr_2Se_4$ films, mag. hysteresis, domain struct., mag. viscosity 80–25169
$CdCr_2Se_4$, mag. semicond., domain struct. by IR Faraday effect 79–95604
$Cd_{1-x}Fe_xCr_2S_4$ series of magnetic semiconductors, magneto-optical effects, expt. *(Japanese)* 77–40212
$Cd_{1-x}Mn_xTe$, Faraday rot. meas. up to 150 T 80–29722
$Cd_{1-x}Mn_xTe$, interband Faraday rot., appl. of mixed semicond. calcs. 79–61348
$Cd_{1-x}Mn_xTe$ mixed cryst., giant exciton Faraday rotation 78–27260
p-CdP_2, Faraday rot., inherent optical activity dispersion *(Russian)* 78–35119
CdS, amorphous antiferromag., mag. props. of dilute neutral donors 79–78367
CdS crystal, magnetic field intensity meas. by obs. of Faraday effect 78–93739
CdS, donors, EPR and spin-lattice relax., Faraday rot. meas. 80–54939
CdS, magneto-optical effects in field up to 200 T 77–52059
CdS, model $S={}^1/_2$ amorphous antiferromagnet, spin polarisation 78–52288
CdS:In, spin flip Raman scatt., electron dynamics 78–80342
CdSe, resonant Faraday effect, optical orientation of excitonic polaritons 77–69821
CdTe AC Faraday rotation devices for far IR laser intracavity polarisation modulation 80–58613
$CdTe:Mn^{2+}$, magneto-optical and microwave-optical double reson. meas. of exciton band *(Russian)* 77–81087
$CeCl_3$, Raman spectra circ. polaris., Faraday effect phonon state splitting 78–43855
CeF_3, Faraday rot., paramag. temp. *(French)* 79–65841
$Ce_cLa_{1-c}F_3$, Raman spectra circ. polaris., Faraday effect phonon state splitting 78–43855
$(Co,Cr,Fe)_3O_4$, $(Co,Rh,Fe)_3O_4$ film magnetooptical switches, for laser beam synchronisation 80–58615
Co, Faraday rotation in X-ray region 79–82958
Co-Pt films, mag. and magneto-optic props., appl. to holographic and bit-by-bit storage 79–33512
$CoCr_2S_4$, Faraday effect, appl. to CO_2 laser systems, radiation damage resist. 78–95579
$Co_xFe_{3-x-y}Cr_yO_4$, epitaxial, magneto-optical props., effect of Cr^{3+} 78–52590
$CoFe_2O_4$ film, Faraday rot., birefr. 77–1663
$Co_xFe_{3-x}O_4$, single cryst. mag. films, holograms recording and thermomagnetic writing 78–55324
Cs, $7P_{3/2}$-$6S_{1/2}$ transition, photon-echo quantum beats obs. 80–23373
CuBr, evaporated film, magneto-optical effects on exciton bands 78–72624
CuCl, evaporated film, magneto-optical effects on exciton bands 78–72624
$CuCl_2.2H_2O$, X-band ESR magneto-microwave effects 77–28434
$CuF_2.2H_2O$, X-band ESR powder spectrum and related magneto-microwave effects 79–24214
n-$CuInSe_2$, effective electron mass, IR free-carrier Faraday rot. meas. 77–55783
$Cu(NH_4SO_4)_2.6H_2O$, X-band ESR magneto-microwave effects 77–28434
DyAG, crit., tricrit., and crossover phenomena, light scatt. 78–68251
$DyFeO_3$, influence of mag. field on Faraday effect 78–27196
$DyFeO_3$, phase domains, polarisation microscope obs. 77–28407
$DyFeO_3$, spin reorientation, Faraday rot. meas. 77–8547
$DyFeO_3$, spin reorientation near Morin temp., magnetooptical exam. 78–68284
$DyFeO_3$; linear dichroism influence on Faraday effect 80–2737
DyIG, mag. and magnetooptical props., temp. and field depends. 77–89927
$DyPO_4$, metamagnet, phase diagrams, investigation by Faraday rot. and light-scattering technique 79–28544
$(Er,Tb,Gd_3)Fe_5O_{12}$ plate, pseudouniaxial, domain struct., magneto-optical obs. 80–11221
$ErFeO_3$, spin flip, Faraday effect and absorption spectrum meas. 77–43842
$Er(PO_3)_3$ glass, Faraday resonance effect in pulsed mag. field, optical freq. EPR *(Russian)* 80–2734
$(ErSm)FeO_3$, spin reorientation, Faraday rot. meas. 77–8547
EuO film threshold characteristics in holographic and bit recording *(Russian)* 80–63944
EuO, nonstoichiometric film with excess EU, Faraday rot. angle 79–8204
EuO, rotation of polarisation plane in very high mag. field 78–92054
$EuO_{1-\delta}$ films, Faraday effect dispersion rel. to electronic struct., visible and IR spectra 80–45162
$EuO_{1-\delta}$ single crystals, Faraday effect, near IR, effect of carriers 80–71395
$EuO_{1-\Delta}$, thin film, Faraday effect dispersion and transmission, 0.5-1.1 μ, 20.4 and 77K, anion vacancies 79–19945
EuSe, high field Faraday rot., 1.7-3 eV 77–52131
EuSe, MnO-type antiferromag. spin order, Faraday rotation obs. 77–47974
$Eu_{0.14}Si_{0.31}O_{0.55}$ glass, optical, magnetic, and magneto-optical props., chemical clustering 79–42951
$Eu_{0.14}Si_{0.31}O_{0.55}$, insulating amorphous mag., optical, mag., and magneto-optical props. 79–61344
EuTe, exchange and superlattice band splittings, magneto-optical meas. in high mag. fields 79–61342
EuTe, high field Faraday rot., 1.7-3 eV 77–52131
EuTe, spin alignment, high field Faraday rotation expt. 77–63401
FH, freq.-depend. polarisabilities and Verdet consts., calcs. 78–62781
Fe-Mn(0 to 80 wt.%), paramagnetic susceptibility by Faraday method, band model interpretation *(Russian)* 77–20545
Fe-Pt films, mag. and magneto-optic props., appl. to holographic and bit-by-bit storage 79–33512
$FeBO_3$, Faraday effect, polaris. ellipse rot. 77–20834
Fe_3BO_6, Faraday rotation and birefringence 80–100650
$FeBr_2$, Faraday rotation in pulsed mag. field, linear absorpt. const. 80–45041

Faraday effect continued
$FeBr_2$, multicritical behaviour 77–4627
$FeCO_3$, mag. field drawn destruction of antiferromag. destruction, light depolarisation at mag. transform. *(Russian)* 78–23432
$(Fe_yNi_{1-y})_{1-x}(SiO)_x$, dielec. effect on magnetisation and Faraday rot. *(Russian)* 78–39298
Fe_3O_4, IR refl., ATR, Voigt and Faraday expts. 80–66180
FePd epitaxial film, vacuum-deposited, for thermomag. recording, mag. and magneto-optical props. *(Russian)* 78–60319
FePt epitaxial film, vacuum-deposited, for thermomag. recording, mag. and magneto-optical props. *(Russian)* 78–60319
GaAs, exciton ground state and oscillatory absorption spectra in mag. fields, variational calc. 79–11071
GaAs, interband Faraday rotation, Roth theory calcs. 77–52046
n-GaAs, Verdet const., free carrier density depend. 78–56462
GaP:Fe, optical absorption spectrum and Faraday effect 80–108245
GaSb, E_1 and $E_1+\Delta_1$ edges using electroreflectance, Franz-Keldysh oscills., high mag. fields 77–66518
GaSb, interband Faraday rot., Roth theory calcs. 77–52046
GaSe, Faraday rot. near absorpt. edge, optical dispersion meas. 80–80757
GaSe, optical orientation and free exciton alignment on reson. excitation *(Russian)* 77–69812
$(Gd, Bi)_2$ $(Fe, Ga)_5O_{12}$ magneto-optic LPE garnet films, high-energy heavy ion irrad., props. 80–71390
Gd-Co amorphous films, struct. and mag. anisotropy 80–20438
Gd-Co amorphous thin film, mag. and optical props., conc. depend 79–19748
$GdCrO_3$, Faraday rot. and linear birefr. meas., 0.8 to 2 μm 77–77180
GdFeBi, amorphous ferrimag. films, magneto-optical props., optical spectra 80–76008
$(Gd_{1-x}Fe_x)_{1-y}Bi_y$ amorphous films, saturation magnetisation, Kerr and Faraday rotation 80–40093
$Gd_3Ga_5O_{12}$, IR refl., ATR, Voigt and Faraday expts. 80–66180
GdIG, IR refl., ATR, Voigt and Faraday expts. 80–66180
GdIG, spin struct. obs. by Faraday rotation expts. in fields up to 200 T 77–69809
GdIG, spin-orientation phase transitions, magneto-optic and visual exam. 77–24675
$(GdPrBi)_3(FeGaIn)_5O_{12}$, pure and In^{3+} doped, near IR absorpt. and Faraday rot. 78–95580
Ge, electron-hole drops, IR magnetoplasma absorptions 80–6728
Ge, Faraday rotation and ellipticity, interband transitions, comparison with Si 77–52048
Ge, interband Faraday ellipticity 78–92052
Ge, interband Faraday rotation, Roth theory calcs. 77–52046
n-Ge, microwave Faraday effect in strong mag. field 77–1662
Ge, piezoreflectance, at E_1 and $E_1+\Delta_1$ edges, high mag. field 77–77245
Ge, standard measures of magnetooptical rotation of plane of polarisation in IR region 80–60551
Ge, transmission Faraday rot., due to intervalence band transitions 79–38521
H_2, Verdet consts., ab initio calcs. 77–3390
H_2O, Faraday rot., sum rule moment calc. 78–5156
He, freq.-depend. polarisabilities and Verdet consts., calcs. 78–62781
He-Ne laser simultaneous oscillation at 0.63 μ and 3.39 μ in mag. field, and with Brewster windows 79–68381
Hg cell, enhanced Faraday effect for reversible depolarisation, communication scrambling appl. 77–42596
Hg, nuclear magnetic moment ratio of odd isotopes *(French)* 77–75081
$Hg_{1-x}Cd_xTe$, Faraday effect at CO_2 laser freq. 78–64348
$Hg_{1-x}Cd_xTe$ mixed crysts., magneto-opt. obs., semicond. config., semimetal-semicond. transition 77–73131
HgTe, long-wavelength magneto-absorptions 80–11397
HoIG, anomalous Faraday behaviour, mag. props. 79–82955
HoIG, Faraday rotation, mag. field depend., 4.2 to 300K, magneto-optical coeffs. 78–95577
HoIG, mag. permeability, Faraday rotation expts. 77–16287
HoIG, spin reorientation from Faraday effect meas. 79–51780
I photodissociation laser oscillator or amplifier, Faraday rot. in active medium 79–10296
I_2, use as test mol. in modern spectroscopy, review 78–90317
InAs, interband Faraday rot., Roth theory calcs. 77–52046
$In_{0.53}Ga_{0.47}As$, interband magnetoabsorption study, quasi-Ge model application 80–50304
InP, Faraday interband effect subjected to quantising mag. fields 80–97246
InP, oscillatory interband magnetoabsorption meas. 79–73909
InSb, 100 W average power 10.6 μm isolator based on interband Faraday effect 79–59706
InSb, doping depend. of high-field donor spectra 77–90175
p-InSb, elec. instability and oscills. of transparency in transverse mag. field 78–6407
n-InSb, Faraday effect in strong EM fields 80–93286
n-InSb, freq. depend. cond. tensor in quantising mag. fields *(German)* 80–29419
InSb, intensity depend. interband Faraday rot. obs., saturation and reson. enhancement effects 80–108186
InSb, interband Faraday rot., Roth theory calcs. 77–52046
n-InSb, propagation of magnetoplasma waves, Faraday geometry, effect of strong electric field 79–65510
InSb, standards for magnetooptical rotation, charge carrier density determ. in semiconductors 80–60551
n-InSb submillimetric-wave free-carrier Faraday effect in strong longitudinal elec. field 80–66164
p-In_6Se_7, Faraday meas. of mag. susceptibility, 110 to 400K *(Russian)* 77–35867
$KMgF_3:Ni^{2+}$, acoustic Faraday and Cotton-Mouton effects, theory 80–65987
$KMnF_3$, Faraday effect mechanism in paramag. phase 80–60552
KTb_3F_{10}, mag., optical, magneto-optical behaviour 78–68484
KTb_3F_{10}, temp., field and wavelength depend. 78–72542
Kr, rotation of plane of polarisation close to reson. 79–41129
Li, microwave Faraday effect, relation to CESR 79–99855
$Li_{0.5}Fe_{2.5}O_4$, domain struct. in (110) and (111) plates, Faraday effect meas. 79–61180
$LiTbF_4$, $LiTb_{0.5}Y_{0.5}F_4$, and $LiTb_{0.25}Gd_{0.75}F_4$, temp., field and wavelength depend. 78–72542
$LiTbF_4$, mag., optical, magneto-optical behaviour 78–68484
$(Lu,Bi)Fe_5O_{12}$, magneto-optic colour effects 78–23308
$MgFe_2O_4$, Faraday rotation in X-ray region 79–82958

Faraday effect continued
- Mn-Cu-Ni-Bi, magneto-optic film for storage appl. 77—12165
- MnBi film, ferromag., diffr. efficiency of mag. holograms, Faraday effect 77—32355
- MnBi film anisotropy field intensity meas. by Faraday rotation *(Russian)* 77—12162
- MnCuBi film, for mag. storage appl., prep. by RF sputtering, and props. 77—8369
- $MnCu_{1-x}Dy_xBi_{0.86}$ film, mag. and magneto-optic props., appl. as storage medium 77—8550
- $MnSb_{1-x}Sn_x$ films, Faraday rotation, optical absorpt. coeffs. 80—97242
- NO vibr. overtone band, mag. rot. spectrosc. obs. 80—86446
- Na, oscillator strength measurement using reson. Faraday effect in monochromatic light 80—23363
- Na, rotation of plane of polarisation close to reson. 79—41129
- $NaBrO_3$, dispersion of Faraday effect 80—2731
- $NaClO_3$, dispersion of Faraday effect 80—2731
- Na_2O-B_2O_3-CoO glass, Co^{2+} ion activated, magneto-opt. study 79—65844
- Na_2O-GeO_2-CoO glass, Co^{2+} ion activated, magneto-opt. study 79—65844
- Na_2O-SiO_2 glass, magnetooptical props. 78—80318
- Na_2O-SiO_2-CoO glass, Co^{2+} ion activated, magneto-opt. study 79—65844
- Na_2O-SiO_2-$Pr_2O_3(Ho_2O_3)$ glass, magneto-optical props. 79—65894
- $Na_2O.SiO_2$-Tb_2O_3 glass magnetooptical study 80—88976
- Nb, cylindrical specimen, flux-line gradients and pinning forces, Faraday obs. 77—24651
- Nb, plastic deform., Shubnikov phase penetration, Faraday effect obs. 79—82731
- Nb, plastically deformed, flux density gradients and pinning forces, Faraday effect obs. 79—61010
- Nb, type II superconductor, Faraday effect, flux density gradient determ. 79—24113
- Nb_3Sn, flux density gradient determ. by Faraday effect 80—107969
- NdF_3, Faraday rot., paramag. temp. *(French)* 79—65841
- Ne discharge Faraday filter, dye laser freq. locking to absorpt. lines 77—79870
- Ne, magnetorotation of 6328 Å line, absorpt. coeff. for $3s_2$-$2p_4$ transition 77—71768
- Ni, Faraday rotation in X-ray region 79—82958
- Ni film, temp. depend. of magneto-optical effects 77—81167
- Ni films, Faraday rotation effect dispersion 80—40092
- Ni, paramag. region, Fe and Co impurity effects on susceptibility, Faraday obs. *(Russian)* 80—88731
- O_2, liq., Faraday effect anomalous dispersion 79—99856
- OH, fundamental vibr. band, mag. rot. spectrosc. obs. 80—86446
- P_2O_5 glasses for laser amplifiers and optical isolators 78—25885
- $Pb_5Ge_3O_{11}$, uniaxial ferroelectric, optical activity dispersion 78—48141
- $Pb_{1-x}Ge_xTe$ magnetoplasma reflectivity and transmission spectra 80—71428
- PbI_2, film exciton spectrum, Faraday rot. 77—20944
- $PbMoO_4$, Faraday rotation, interband optical transitions *(Russian)* 80—55071
- PbSe, electron gas magnetisation, energy band parameters determ., use of Faraday effect 80—45047
- PbSe, Faraday effect and electron gas magnetisation, Kane two band model calcs. *(Russian)* 80—34899
- $Pb_{1-x}Sn_xTe$, electroreflectance, Faraday rot., elec. band struct. parameters 77—66113
- $Pb_{1-x}Sn_xTe$, energy band parameters from IR Faraday rotation 78—48154
- $Pb_{1-x}Sn_xTe$, Faraday effect and electron gas magnetisation, Kane two band model calcs. *(Russian)* 80—34899
- p-PbTe, IR reflection and Faraday rotation angle meas. 77—1680
- PbTe-SnTe compound semiconductors, lattice instability by mm-wave magnetoplasma refl. 80—54336
- $(PrGdYb)_{3-x}Bi_x(FeAl)_5O_{12}$ system, LPE growth and magnetooptical props. 79—65842
- $Pr_xY_{3-x}Fe_{5-y}O_{12}$ film, IR absorpt. and Faraday rot. spectra 77—52093
- Rb cell, enhanced Faraday effect for reversible depolarisation, communication scrambling appl. 77—42596
- $RbMnCl_3$, high-pressure cubic phase, mag. props. 79—47260
- $RbMnF_3$, Faraday effect mechanism in paramag. phase 80—60552
- n-Si, effective mass from intraband Faraday rot. and Hall effect 77—52049
- n-Si, Faraday rot. temp. depend., effective mass determ. 80—71392
- Si, Faraday rotation and ellipticity, interband transitions, comparison with Ge 77—52048
- SiO_2-Na_2O-Nd_2O_3 glass, magneto-optical props., absorpt. spectrum 80—88969
- $SmFeO_3$, orthoferrite, anisotropy of Faraday rotation 79—61341
- $Tb_3Fe_5O_{12}$, Faraday rotation in high transient mag. fields 77—69810
- $Tb_3Fe_5O_{12}$, quasiantiferromag. state magnetised along two-fold symmetry axis, mag. phase diagram 77—69564
- TbGa garnet, Verdet const. meas. with pulsed mag. field 78—68486
- TbIG, anisotropic garnet, mag. struct., magnetisation and Faraday rotation obs. 78—68169
- TbIG, Faraday rot., temp. and high mag. field depend. 79—95736
- TbIG, Faraday rotation and transition of spin config. at high mag. fields 80—39776
- TbY ferrite garnet, Tb^{3+} energy level inversion, Faraday effect *(Russian)* 79—47418
- Te conduction band parameters, interband magnetoabsorption meas. in Faraday configuration 77—89695
- Te, optical activity, de Haas-van Alphen oscillations and cond. band parameters 80—54605
- $Tl_2(Te_xSe_{1-x})$ mixtures, liq., electrical conductivity, magnetic susceptibility 80—88715
- $Tm_{2.2}Bi_{0.8}Fe_{3.5}Ga_{1.5}O_{12}$ epitaxial film, Faraday effect and domain struct. near compensation point 77—20838
- $Tm_{2.7}Bi_{0.3}Ga_{0.3}Co_xFe_{4.7-x}O_{12}$, Co ion concentration effect on mag. props. close to mag. compensation point *(Russian)* 79—73788
- $TmFeO_3$, domain struct. in spin reorientation region, Faraday effect obs. 77—20835
- UO_2, electronic transitions, crystal field effects and phonons, phase transition 80—97303
- $(Y,Gd,Yb)_{3-x}Bi_x(Fe,Al)_5O_{12}$, garnet single cryst. film, possible bubble appl. 78—6552
- $(Y,Gd,Yb)_{3-x}Bi_x(Fe,Al)_5O_{12}$, LPE, for magneto-optical appls. 78—48341

Faraday effect continued
- $(Y,Gd,Yb)_3(Fe,Ga)_5O_{12}$ film, magnetisation processes and domain struct. near compensation temp. 78—14996
- $(Y,Sm,Ca)_3(Fe,Ge)_4O_{12}$, garnet thin film, mag. anisotropy, Faraday effect meas. 79—42812
- $Y_2BiFe_{3.8}Ga_{1.2}O_{12}$ film, colour contrast between different domains 77—12166
- $Y_2BiFe_{3.8}Ga_{1.2}O_{12}$ film, magnetooptic interference of light 77—32458
- $Y_{2.7}Bi_{0.3}Fe_{3.8}Ga_{1.2}O_{12}$ epitaxial film, mag. domains in microwave mag. field, Faraday obs. 78—19295
- $Y_{3-2x}Ca_{2x}Fe_{5-x}V_xO_{12}$, single cryst., Faraday effect and opt. props. 77—1660[illegible]
- $YCrO_3$, mag. circular dichroism and Faraday rotation in R-lines region 79—28725
- $YFe_{1-x}Co_{x/2}Ti_{x/2}O_3$, orthoferrite, anisotropy of Faraday rotation 79—61341
- $YFe_{1-x}Ga_xO_3$, zone refined, exam. of Curie point and magnetisation 79—4673
- $YFe_{4.5}Ga_{0.5}O_{12}$ domains, neutron dpolarisation and Faraday rotation study 80—93137
- $Y_3Fe_{4.5}Ga_{0.5}O_{12}$, domain struct., neutron depolarisation and Faraday rot. 80—71084
- $YFeO_3$, Faraday rotation anisotropy 77—20837
- $YFeO_3$, influence of mag. field on Faraday effect 78—27196
- $YFeO_3$ monocrystalline, mag. field depend. of magnetic domain *(Korean)* 78—68337
- $YFeO_3$ orthoferrite, weak ferromagnet domain struct. near Neel temp. 79—99739
- $YFeO_3$:Co^{2+}, Ti^{4+}, spin reorientation, Faraday rot. meas. 77—8547
- $Y_3Fe_{5-x}Sc_xO_{12}$, garnets, magnetooptical spectra, 15000-21000 cm^{-1} 77—90131
- $Y_3Ga_xFe_{5-x}O_{12}$, Faraday rot., 1.06 μm, 100-300K 77—52059
- $Y_3Ga_xFe_{5-x}O_{12}$, HF Faraday light modulator, optical characts. crystal struct. depend. 77—39052
- $Y_3Ga_xFe_{5-x}O_{12}$, spin struct. obs. by Faraday rotation expts. in fields up to 200 T 77—69809
- $Y_{2.6}Gd_{0.4}Fe_{3.9}Ga_{1.1}O_{12}$, epitaxial uniaxial film, mag. phase diagram, optical expts. *(Russian)* 77—48022
- YIG, computer optical isolator for near IR region 78—83104
- YIG, Faraday effect, influence of mag. field on sublattice contributions 80—88975
- YIG, Faraday rot. rel. to sublattice magnetisation 79—33675
- YIG Faraday rotation optical isolator, intensity fluctuation suppression in $LiNdP_4O_{12}$ laser 79—81437
- YIG, high field magneto-optical study 77—85749
- YIG LPE film, optical waveguide in mag. strip domains *(French)* 77—83979
- YIG, light diffr. by banded domain struct. *(Russian)* 78—15150
- YIG, MCD meas. by retardation modulation technique 80—16014
- YIG, mag. and magneto-optic props., temp. and exchange field depend. 77—24824
- YIG magnetic bubble domain grating, light diffr. *(German)* 79—95737
- YIG, one-magnon Raman scatt., Faraday rot. 80—66156
- YIG, single cryst., Neel lines, Faraday effect obs. 78—64216
- YIG, spin struct. obs. by Faraday rotation expts. in fields up to 200 T 77—69809
- YIG, superexchange and applied field depend. of Faraday rot. induced by elec. dipole transitions 77—36206
- YIG thin film gyromag. waveguide, on GGG substrate, optical propag. props. Faraday effect 80—74513
- YIG, YGaIG, Faraday effect and IR radiation modulation 79—10403
- YIG:Tb garnet, Faraday effect in strong mag. field *(Russian)* 80—100651
- $(YLaBi)_3(FeGa)_5O_{12}$, pure and In^{3+} doped, near IR absorpt. and Faraday rot. 78—95580
- YRBiFe garnets, epitaxial films, R=Gd+Yb, Faraday effect and phys. props. 77—69928
- $(YRBi)_3(FeAl)_5O_{12}$ films, R=Gd, Yb, Faraday effect in transverse mag. field, orientation depend. 80—88971
- YbIG, IR Faraday rotation meas. 77—43978
- YbIG, mag. permeability, Faraday rotation expts. 77—16287
- ZnO(S)(Se), high field Faraday rotation, 6.5K 79—38522
- ZnP_2, tetragonal, interband Faraday effect *(Russian)* 78—72490
- ZnSe, magnetoreflectance of exciton-polaritons, semiclassical treatment 79—99857
- ZnSe, visible optical isolator 77—75657

farming
- 150 kW solar powered irrigation facility, design 79—96427
- bean and corn seed growth effects of constant mag. field *(Russian)* 79—83811
- East African swidden farming, computer processed LANDSAT data interpretation 77—78494
- farmhouse heating solar energy collection and thermal storage system 79—57482
- field burning practice, downwind particulate pollution 80—97836
- fish stock count by acoustic target strength meas. of individual fish, comparative anal. 80—19129
- grazing, hydrologic impact on infiltration 79—2325
- heat from nuclear plant, agricultural uses *(French)* 78—5060
- Large Area Crop Inventory Experiment, LANDSAT image registration accuracy meas. 77—26421
- photometric interpretation process for crop monitoring 80—42251
- photovoltaic powered 20-hp DC/AC irrigation system and 3-kW N generator 80—89645
- physics in agriculture, various applications 80—31481
- sheep grazing rel. to gully erosion on vegetated screes in Black Mountain, Carmarthenshire 77—44992
- solar energy utilisation in India, reflector-concentrator modified Stirling engine unit and aqua-ammonia absorber gas turbine unit developments for farm power needs in India 79—62024
- solar heating and cooling, passive, of poultry sheds 79—70437
- subsistence-economy chicken-breeding solar energy storage regulation expt. 79—57485
- thermal energy balance in leaves, crops, hot and cold blooded animals 77—32875
- wild oat weed control using microwave techniques 77—81531

fast amplifiers *see pulse amplifiers*

fast Fourier transforms
- acoustic narrow band signals, bearing estimation in oceanic environment, comparison with Prony algorithms 77—46855

fast Fourier transforms continued
AES/APS self-convolution inversion, FFT and digital signal processing 79—71430
air coils, FFT calc. of mag. fields 80—74280
air coils, magnetostatic field FFT calcs., linear system theory 80—32868
analysers, high real time, applications 79—1041
atom+molecule, collision dynamics, classical trajectory problem Fourier transform method 79—98189
auto and cross-correlation analysis techniques on-board spacecraft *(French)* 79—70925
baffled piston wideband acoustic near- and far-field transients 79—46154
beams and rods, dispersive waves, experimental study using FFT 79—46275
beatquency domain, frequency content of heart rate Fourier analysis 77—81595
cochlear macromechanics, time domain solutions 79—88087
computational physics, review *(Russian)* 77—5650
computerised tomography image reconstruction, interpolation effect 78—77110
convection, natural, in closed container, numerical simulation 78—46969
convolution of large arrays, using number theoretic transforms 78—22092
cosmic gamma-ray burst sources, location via periodic slot collimator using FFT analysis 77—64647
data buoy wideband wave directional spectra, real-time telemetry 80—46305
demagnetising field, calc. by FFT 79—38355
digital signal anal. of Dutch vowels 79—3858
Dirichlet problem, response function method for fast soln. of Laplace eqn. 78—86119
double beam interferometer for background suppression and spectral detection 80—95129
dynamic heat transfer meas. at Mach 8, digital Fourier anal., boundary layer transition 80—14682
ECG data compression, quantisation studies 80—26396
EEG alternations, power spectral analysis 80—30924
EEG analysis, using short epoch Fourier transforms, automated system 77—44824
EEG frequency analyser, real-time, microprocessor monitored 78—57092
electrochemical data interpolation, fast Fourier transform method 79—16061
electron microscopy, image processing, optical diffraction and filtering, fast Fourier transforms 80—30956
EM scattering from buried wires, fast Fourier transform 79—16369
faradaic admittance, rapid drop time on-line FFT meas. 78—92544
faradaic admittance, SYDAGES system for on-line FFT meas. 78—20090
fast-scanning Fourier spectrometer automatic adjustment method 79—80705
fibre optics transmission characts. meas. by computerised signal processing system 79—76876
fluctuation anal. of signals from nuclear reactor ex-core ion-chamber 77—54312
fluctuations generation with arbitrary power spectrum, algorithm 78—73927
fluid dynamics, pseudo-spectral FFT technique, non-periodic problems 78—59359
fluid simulation of plasmas, MHD particle code 79—68948
fluorescence, and laser Raman decay times, evaluation water pollution detect. appl. 78—81444
forced vibr. problems, dynamic influence coeff. 77—72233
FOURGEN, fast Fourier transform program generator 77—41466
Fourier hologram machine synthesis *(Czech)* 78—66784
gamma ray spectra anal., fast Fourier transform *(Chinese)* 80—77762
gamma-ray spectral anal. *(Japanese)* 78—90047
generalised Gram-Charlier series with application to the sum of log-normal variates 77—37736
geomagnetic field microstructure separation, digital filtering methods 78—69480
geophysics, time series filtering with time variant operators, convolution and Fourier transform 77—87082
gravimetric estimation technique using FFT, inertial navigation systems appls. 79—25376
gravity and magnetic anomalies of arbitrary bodies, FFT method for rapid computation 77—41186
heart fourth sound studied by FFT 80—94397
heterogeneous charge transfer kinetic effects, deconvolution by FFT faradaic admittance meas. 78—20091
holographic, image digital reconstruction with limited-length arithmetic register *(Russian)* 79—22910
image recognition by generalised harmonic analysis *(Russian)* 80—63930
image reconstruction by modified back projection methods, reconstruction error determ. 78—33682
image restoration for invariant pointspread functions 80—69332
interferogram analysis, point spread function and OTF determ. for optical system testing 79—76616
interferometer signals processing, far IR, use of microcomputer 77—2689
jet engine noise meas., flowing duct sound separation probe 78—13878
laser anemometry, flow statistics retrieval via photon correl., fast Fourier transform appl. 77—3896
laser gyro performance analysis 80—9933
linear time dependent partial differential eqns., solns. by Laplace transform and FFT 78—57763
linear wave motions study using FFT, NDT appl. 80—92038
long-wavelength hologram image reconstruction microcomputer system 78—1196
macromolecular structure factor calc. 77—51268
magnetic field reduction to pole, fast Fourier series algorithm 77—5333
microwave holography using quadratically spaced linear antenna array, microcomputer processing 80—32938
modal anal., formulations for numerical calcs. 78—57767
myocardial perfusion images using ^{201}Tl, quantitative evaluation methods 79—39479
neural network simulation method 77—1986
neutron and X-ray diffraction data from amorphous materials 77—58928
night vision system testing image scanner 77—39102
nuclear reactor component vibration investigation using fast Fourier transform analysers 80—63315
numerical integration of macroscopic semiconductor equations, applications *(German)* 77—69319

fast Fourier transforms continued
optical fibre diameter measurement using fast Fourier transform 80—91894
optical systems analysis using two-dimensional FFT algorithm 80—78986
passive sonar system adaptive processor 78—5622
plano-plano interferometer modes, FFT computation, Fresnel numbers 80—86392
plasma diagnostics, of subnsec. laser fusion implosion, streak photo. FFT technique 79—71945
positron camera, 3-dimens. imaging using Fourier techniques 77—32951
power spectrum for equally spaced time series of finite length, computing methods 77—45190
proton recoil data, frequency filtering 78—46240
pulmonary vascularity automated diagnosis from chest roentgenograms 77—60248
pulsed laser Doppler velocimeter signal processing, FFT and pulse-pair estimation 79—77322
radio astronomy, interference-excising correlator using FFT cross-power spectrum anal. 79—75110
radiography, fast Fourier digital quantum mottle anal. appl. to rare earth intensifiers 77—52868
radiometry of flat finite wave tank, three-dimensional vector modelling and restoration of meas. 77—22599
radiosources, two-dimensional max. entropy reconstruction of radio brightness 78—28534
remotely sensed Earth imagery, atmospheric blurring removal 79—88517
room reverberation decay curve meas., FFT methods and errors *(Japanese)* 79—27468
rotationally invariant two-variable functions, computer implementation of Hankel transform 77—74209
SAW chirp filter FFT processor 78—87209
SAW-based discrete Fourier transformers 79—18613
sediment classification by ocean subbottom acoustic Q meas. 80—46168
seismic common-depth-point stacking, appl. of multirate digital filtering approach to interpolation 79—29876
seismic data processing, using frequency filter method *(Chinese)* 79—96838
seismic waveforms extrapolation appl. 79—34978
seismology, rapid convolution and correl. *(Russian)* 79—39959
SEM diffractogram online computation 80—70095
simple introduction 79—75328
solar type IV radio events, FFT anal. rel. to pulsating structs. 78—96455
spatial filters, square root type phase image differential linear intensity output digital simulation 78—33839
speckle imaging phase estimation, FFT-based algorithm 79—76605
spectral analysis for teachers 78—81750
spectral entropy method for distinguishing regular and irregular motion of Hamiltonian systems 80—4629
spectrum analyser appl. *(Spanish)* 80—90825
speech adaptive noise cancellation by short-time Fourier transform 80—91976
staircase voltammograms, synthesis, anal., convolution, devolution 77—25336
symmetrised neutron transport eqn., fast Fourier transform method solns. 78—78435
Three Array Processor beamforming system 80—43550
time-domain measurement, mm-wave circular waveguide 77—18020
tissue US signal analysis methods 79—57737
tomograph noise filtering, lung boundaries determ. using neuristic search 78—73240
US attenuation in breast malignant tumour, freq. depend. 80—45996
voltammetry, cyclic, AC, on-line digital FFT faradaic admittance data acquisition 78—61118
X-ray scattering data, calc. from variety of models, computer program using fast Fourier transform algorithm 77—76256
zero crossing and FFT speech recognition systems compared 79—76917
^{57}Fe Mossbauer spectroscopy, added precision 77—88327

fast-response computer systems
X-ray cylindrical scanning multiaxial computerised tomography unit 78—80956

fastening *see joining processes*

fatigue
for corrosion fatigue see stress corrosion cracking; for thermal fatigue see thermal stress cracking
see also fatigue cracks; fatigue testing
accumulation of damages, theory 77—14968
acetal copolymer, notches effect on fatigue strength 80—25857
acoustic emission 80—97673
acoustic emission signals distrib. anal., fatigue life prediction 80—25852
acoustic loading, fatigue stength installation 79—83426
adhesive, reinforced, fatigue resistance 77—4834
after-effects in thermo-elasticity 80—106724
aircraft engine inlet guide vanes, acoustic fatigue due to intake flow distortions 80—53542
aircraft parts, microfractographic fracture analysis exam., SEM exam. *(Japanese)* 78—52950
aircraft struct., in service problems 77—86158
AK4-1 alloy, sheet mat., fatigue and corrosion fatigue strengths, coatings effects *(Russian)* 78—11397
Al alloy, type AK4-1T1, effect of high temp. ageing, on endurance of thin walled joints 78—80570
Al alloy, type D20, fatigue damage inspection, on basis of change in natural oscillations freq. 79—57116
alloy, thermal cycling fracture 78—60839
alloy structural steel, electron fractographic pattern of fatigue fracture under cyclic loading 77—56094
alloy V93, fatigue strength, effect of residual stresses and cold working 77—56101
alloys, high temperature, creep failure criteria 80—65150
alloys, ion implantation in tribology and corrosion science, overview 79—14830
amorphous polymers, intrinsic time to fracture criterion 78—92320
amplitude transformation procedure, for fatigue life prediction 78—68796
analysis of complex components 77—72246
aortic valve tissue, porcine, glutaraldehyde-treated, mech. fatigue study 80—67112
austenitic alloys in hot water, low cycle fatigue, appl. to nuclear reactors 77—4871
automotive materials, microfractography appl. to ductile failure, brittle fracture, crack studies 77—56199

fatigue continued
axially symmetric body, subject to cyclic heat loading elastoplastic strain 78—5672
bar, dynamic stability, subjected to impulse loading 78—46901
bimetal, failure during fatigue testing, electron microscope obs. *(Russian)* 78—23808
bimetal, obtained by facing, static and fatigue strength, obtained by facing 77—90457
bluntly notched members, fatigue life estimates 80—100999
body force method, to calculate stress intensity factors, for crack, in arbitrarily shaped plate 78—90775
bone, compact, fatigue damage, residual strength and stiffness 77—90834
bone, deformation under unloading and repeated loading 78—3546
brass, adsorpt. of Hg, effect on mech. strength, creep, fatigue, embrittlement *(Russian)* 79—29267
brass, burst acoustic emission during Bauschinger effect 77—48475
brass, cyclic creep and fracture under stress-controlled cyclic conditions 79—74232
α- brass, effect of mean stress on high temp. fatigue 79—20153
brass, fatigue hardening and high cycle fatigue under reversed bending 79—20180
brass, fretting fatigue 77—86164
brass, martensite form. in cyclic transform., reproducibilities 77—16582
brass, spring alloys, microplastic deform. and endurance limit 80—81197
α-β brass, two phase bicrystal, fatigue 80—108520
brittle material, strain rate dependent effect of specimen vol. on strength 77—56085
butadienepstyrene, surface phenomena in struct. rearrangement after deform. *(German)* 78—19913
C Fe Armco, cumulative fatigue damage at US freqs., thermal activation 77—70181
cables design and testing, optical fibre, w.r.t. stress-strain behaviour 80—69551
cast materials for nuclear appls., low-angle fatigue and fatigue crack growth rates 80—5240
central receiver solar power stations, solar receiver tube thermal stresses, fatigue aspects 80—40908
ceramic endoprostheses (total hips), mech. and tribological props. *(German)* 79—84005
ceramic hip endoprostheses, fatigue strength *(German)* 77—56514
ceramics, subcrit. crack extension charact. *(German)* 80—100888
complex shaped large scale part, statistical eval. of service life 79—91798
complex stress state, equivalent stress in theory of fatigue fracture 80—79230
composite insulating materials, fatigue behaviour, influence of superposition of elec., mech. and environmental stresses 80—97590
composite laminates, proof test and fatigue study 80—93643
composite material, fracture and fatigue, review 78—68781
composite materials, fatigue strength determ. under plane stress state condition 80—16475
composite materials, lecture *(Japanese)* 77—8928
composite materials, reliability, exam. of mech. strengths and fatigue characts., review 80—11762
composites, fibre reinforced, fatigue damage under pulsating tensile stress 79—100237
concrete, compressive fatigue life, estimate of distrib., statistical method *(Japanese)* 78—11328
concrete, fatigue, applicability of Palmgren Miner partial damage hypothesis 78—11316
concrete, fatigue, load-deform. behaviour *(German)* 79—11693
concrete, fatigue strength rel. to static strength *(Japanese)* 78—11329
concrete, prestressed beam, fatigue strength of cold-worked non prestressed reinforcement 79—96123
concrete, unreinforced, fatigue strength under cyclic loads obs. *(Dutch)* 78—52945
concrete column, strength estimation by US pulse velocity method, aggregate variation effects 77—63867
conference, Cambridge, England, Mar. (1977) 77—86102
conference on fusion reactor materials [Miami Beach, Florida, Jan. 1979] 80—31407
consistent creep and rupture properties for creep-fatigue evaluation of nuclear components 80—35329
Constantan, fatigue, grain size effect 77—21260
contact stress anal. involving fretting fatigue loadings, computer soln. 78—34096
corrosion, review 77—8991
coupled dynamic problems of thermoviscoelasticity quasilinearisation method 77—72188
crack development kinetics, with varied rigidity under low cycle loading 77—90464
cracks, circular, forced torsional oscillations at low frequencies 80—53703
cumulative damage, continuum theory 77—31255
cumulative damage, under random loads algorithm of hysteresis loop counting 80—21064
cumulative damage model 79—44736
cumulative damage rule, exam. of new model 78—92358
cumulative damage stochastic model, fatigue and wear life test data anal. 79—18823
cumulative damage stochastic model 79—18822
cumulative damage theory for fatigue failure 78—75101
cup and cone fatigue fracture, electron fractographic obs. *(Japanese)* 78—72838
curve, spread of parameters, influence on fatigue life *(Russian)* 79—98667
cyclic creep, enhnaced, high temp. theory for polycrystalline materials 78—7018
cyclic programmed loading, accumulation of damaging energy *(Russian)* 79—91777
cyclic strain hysteresis loop, width and area determ. 78—26056
cylinder, circular, fatigue propag. of internal crack 80—48645
cylinder, short, visioelastic, expt. and theoretical investigation of heat evolution in cyclic compression 78—13929
cylinder, thin-walled, fatigue under biaxial stress *(Japanese)* 77—48537
cylinder under pulsating internal press., limit and life prediction 78—55595
D16 alloy, sheet mat., fatigue and corrosion fatigue strengths, coatings effects *(Russian)* 78—11397
damage accumulation, in various structs., under steady and programmed loads 79—57114
damage accumulation in nonstationary low cycle rigid loading 77—16686

fatigue continued
damage accumulation investigation during unsteady low cycle loading under stress control 78—7041
damage analysis under nonproportional cycling 80—97556
damage model of creep-fatigue interaction 79—77008
damage parameter in continual fracture mechanics review *(Polish)* 79—32382
damage rupture, phenomenological approach to plasticity, creep and fatigue *(French)* 79—37245
damage summation, determinate and statistical models 79—90188
damage summation 77—3781
design elements, reliability rating during fatigue failure 78—79275
design fatigue analysis, use of fracture mechanics, exam. 78—90794
diamond, sintered compact, fracture and fatigue 79—52352
diamond grain configuration in high temp. creep and fatigue 77—21221
discriminating specimens, for fatigue research 80—39213
dislocation behaviour, in fatigue, friction and back stress from hysteresis loops 80—3176
dislocation behaviour, loop patch props. in fatigue cycling 79—90725
dislocation behaviour 77—24352
dislocation behaviour during fatigue, friction stress and back stress from hysteresis loop anal. 79—42076
dislocation creep under cylcic stressing, physical model and theoretical eqns. 78—39833
dislocation structures, and fracture surfaces in fatigue *(Japanese)* 80—65144
dislocation substructure effects 77—86140
dough moulding compound, exam. of tensile and fatigue props. 79—20152
Duralumin, adsorpt. of Hg, effect on mech. strength, creep, fatigue, embrittlement *(Russian)* 79—29267
elastic creep fatigue rules fo ASME B&PV code case 1592 78—44211
elastic fatigue limit determ. 78—3269
electronic devices, failure analysis of metal parts using fractography 79—61811
engineering materials, elev. temp. fatigue interactions 77—86173
engineering materials, elev. temp. fatigue props. 79—5061
engineering materials at elev. temp. 78—80646
epoxide resin, amine-cured, crack propag. 78—27596
epoxide resin cured with aliphatic dicarboxylic acids, fatigue behaviour *(Japanese)* 79—79092
epoxy, glass microsphere filled, low-cycle fatigue 80—40517
epoxy, mech. props., 20 to 300°C *(French)* 77—56018
epoxy laminate, fatigue residual strength degradation model and theory of periodic proof tests 77—70158
epoxy resin, heat generated by fatigue *(Spanish)* 80—11736
epoxy resin, low temp. fatigue, tensile strength, Young's modulus *(German)* 78—76748
equations relating contact fatigue life to material, lubricant and operating variables 79—96107
exoelectron emission defectoscopy, metal fatigue strength prediction 78—76807
exoemission defectoscopy in initial stages of fatigue fracture 78—53126
failure, rupture, continuous damage mechs., uniaxial homogeneous state of stress 80—74806
failure characts. of steel 15G2AFDps, effect of loading freq. and temp., SEM exam. of failure surface 78—84995
failure of angle ply laminates 77—4833
failure origin areas, metallographic charact. 79—61835
failure prediction by dynamic correlation intensity 78—11483
failure similarity, statistical theory 80—38330
fatigue, random process effect on life 79—66160
fatigue damage, development rate by exoelectron meas. 80—25835
fatigue limit, in bi-freq. loading 80—104289
fatigue strength, low cycle steels and welds, relationship to static tensile props. 78—64684
ferromagnetic solids, magnetomechanical effects, magnetostriction, hysteresis, stress, yielding, fatigue damage, crack growth *(Polish)* 80—71150
fiberglass materials, fatigue damage effects on light scatt. 79—11706
fibre, single-mode, numerical aperture effects 80—69548
fibre bundles, stochastic strength and fatigue 78—79262
fibre reinforced composite, fatigue damage, early detection by NDT 77—28951
fibre reinforced composite aircraft materials, design allowables 80—81204
fibre reinforced composites, conf., London, England June (1977) 78—15489
fibre reinforced composites, materials properties, unsolved problems, review 77—4843
fibre reinforced composites 78—68767
fibre reinforced ionomer composites, fatigue strength, dynamic viscoelastic props. and fracture surface exam. *(Japanese)* 78—92339
fibre reinforced laminated composite, reliability anal. approach to fatigue life dispersion *(Japanese)* 79—61704
fibre reinforced metals, fatigue limit *(German)* 78—72859
fibre reinforced plastics, temp. increase under uniform plane bending fatigue test *(Japanese)* 78—44200
fibre reinforced plastics, under random loadings, mathematical model and digital simulation *(Japanese)* 80—85032
fibreglass plastics, fatigue lifetime prediction based on cumulative damage 80—11776
fibres, optical, high-strength, use of surface compression cladding 80—69549
flexural fatigue and surface abrasion 78—15504
flexural properties, unidirectional GRP, transverse direction 79—66138
float glass, exam. of dynamic fatigue 78—80631
foil, push-pull straining device for h.v. electron microscope in-situ deform. 77—4875
Fort St. Vrain HTGR, He circulators, development and testing 79—67821
fracture analysis of rotating disks under torque 80—43668
fracture mechanisms review 80—35296
fracture toughness determ., use of fatigue fracture toughness 79—46747
fracture toughness determ. from fatigue test results in circular bending 78—15526
fracture toughness test by impact-fatigue method *(Chinese)* 80—3258
fretting effect 80—16482
fretting effects 77—16688
fretting fatigue, stress intensity factors 79—90184
fretting fatigue 77—4152
friction stress method for cyclic inelastic behaviour of metals 77—4855

fatigue continued
fusion reactor blanket, thermal stresses and cyclic creep-fatigue 78—62655
fusion reactor first wall/blanket system, thermal-hydraulics and fatigue life modelling 78—58453
fusion reactor first-wall structures, fatigue life criteria 80—86980
fusion reactor limiters; thermal and stress environment effects 80—32461
fusion reactor materials, material requirements exam., review 78—50257
gas turbine engine discs and blades design eval. of strength under thermocycling 77—70179
geometry effects 78—67132
glass, C and glass/C hybrid reinforced plastics, fatigue props. and flexural rigidity *(Japanese)* 80—55510
glass, fracture and fatigue, crack tip radii influence 80—89335
glass, minimum life prediction, uncertainty 77—16665
glass, static fatigue, reexamination of limit 77—90458
glass, static fatigue, review 77—40441
glass, surface treatment, improvement in mech. and optical props. recent progress *(Japanese)* 79—79141
glass and ceramics, strength and failure predictions 77—21256
glass fabric reinforced plastic laminate, fatigue strength rel. to test frequency 79—8362
glass fabric reinforced polyester, biaxial stress failure surface under static and fatigue loading 78—72836
glass fibre reinforced composite, fatigue failure, role of shear deform. 78—15494
glass fibre reinforced composite, shear fatigue 78—15493
glass fibre reinforced epoxy, as electrical insulation for Tokamak toroidal field coils, mech. props. 78—64610
glass fibre reinforced epoxy, fatigue damage in cyclic bending 79—100256
glass fibre reinforced epoxy, struts for superconductive storage magnets, mech. props. 80—25824
glass fibre reinforced epoxy-phenolic binder, exam. of short cycle fatigue strength under compression 80—11759
glass fibre reinforced Kinel, mech. props., 20 to 300°C *(French)* 77—56018
glass fibre reinforced plastic, fatigue fracture kinetics studied by diffusion scatt. of luminous fluxes 80—76446
glass fibre reinforced plastic, fatigue processes, review 80—81176
glass fibre reinforced plastic, fatigue strength in shear in plane of reinforcement 77—32690
glass fibre reinforced plastic, flexural fatigue props. *(Japanese)* 79—20171
glass fibre reinforced plastic, laminate, fatigue strength under normal and interlaminar shear stresses 80—11758
glass fibre reinforced plastic, strain disintegration under repeated static load 80—11756
glass fibre reinforced plastic laminates, strength and deformability, artificial ageing effect 80—60893
glass fibre reinforced plastic tube under cyclic pressurisation 78—68761
glass fibre reinforced plastics, cyclic strength in complex stressed state 80—3181
glass fibre reinforced plastics, stress conc. effect on spread of strength and fatigue life *(Japanese)* 79—96117
glass fibre reinforced poly- and vinylester, fatigue and flexural strength 79—8364
glass fibre reinforced polyester, compressive fatigue tests at cryogenic temps. 80—25870
glass fibre reinforced polyester, struts for superconductive storage magnets, mech. props. 80—25824
glass fibre reinforced polyester 80—25856
glass fibre reinforced polyester resin laminate cantilever, bending fatigue strength, cyclic freq. effect *(Japanese)* 80—55507
glass fibre reinforced polymer, fatigue life, determ. from reheat temp. 79—61724
glass fibre reinforced resins, fatigue damage in notched samples 78—15496
glass fibre reinforced vinyl ester matrix, axial fatigue failure sequence and mechanism 78—68773
glass fibre-reinforced vinyl esters, fatigue life-limiting parameters 80—11746
glass fibres, epoxy-acrylate coated, static and dynamic fatigue, tensile strength 79—1906
glass fibres, fatigue failure probability 79—32045
glass fibres, tensile strength and fatigue 77—3662
glass optical fibre, epoxy-acrylate coated, strength and static fatigue 78—1386
glass optical fibres, UV-cured, epoxy-acrylate coated, environmental effect on long-term strength 78—5582
glass opticalfibres 79—46062
glass plastic, fatigue strength, loading frequency effect 77—52484
glass reinforced plastic, acoustic emission investigation of deformation and fracture 77—16756
glass reinforced plastic, low cycle tensile fatigue strength anisotropy 77—66697
glass reinforced plastics, static and fatigue failure, fracture mechanics 78—19898
glass reinforced polyamide 6, fatigue strength after heat treatment, ageing and coating of Al-containing lacquer *(Polish)* 80—89347
glass reinforced polyester, internal reinforcement joints under static and fatigue loading 79—91776
glasses, mech. strength fracture dynamics, behaviour forecasting *(French)* 77—73344
glassfibre reinforced composites, accumulating of fatigue damage using diffuse light transmission *(Russian)* 78—19896
graphite, cyclic fatigue, influence of stress cycle and neutron irrad. 79—52335
graphite, Goodman diagram determ. 77—56078
graphite fibre-reinforced epoxy, impact damaged, acoustic emission 79—91875
graphite fibre reinforced epoxy, notched, biaxial fatigue loading 78—19879
graphite fibre reinforced epoxy, notched, fatigue initiation 77—52471
graphite fibre reinforced epoxy, US attenuation as an indicator of fatigue life 80—85118
graphite fibre reinforced epoxy laminate tension-compression fatigue loading, fatigue residual strength degradation model, comparison with expt. results for 78—35491
graphite fibre reinforced polyester, pultruded fibres, interlaminar shear fatigue 78—56742

fatigue continued
graphite reinforced epoxy, scale effect in fatigue 79—91780
graphite reinforced epoxy angle ply laminates, statistical fatigue in shear 79—11690
graphite/epoxy laminate, T300/5208, proof testing under cyclic tension-tension fatigue 80—81249
graphite/epoxy laminates, statistical fatigue, high load effect 80—93642
graphite/epoxy laminates fatigue characts. under compression loading 78—84971
gum and C black filled vulcanisates, rubber, natural and styrene/butadiene, unixial and equibiaxial fatigue 79—8363
Haigh diagram determ. using fatigue tester *(Polish)* 79—74327
Hastelloy X, high temp. low cycle fatigue strength *(Japanese)* 77—59910
heat resisting, types EhI598, ZhS6KP, and 1, fatigue under mech. and thermal stress 79—66164
heat-resistant alloys, fatigue under conds. of mech. and thermal stress loading 79—87726
high cycle fatigue diagram based on dynamic severity criterion 78—60759
high strength materials, strengthening *(Japanese)* 78—15513
high strength structural mats., microstruct. influences on fatigue and fracture resist. 78—56728
high temp., hold time effects, cavitation nucleation, creep interaction 78—60734
high temp. fatigue, review 78—56773
high temperature fracture under cyclic loading, book contrib. 79—66171
high-alloy bearing, LTMT effects on ht. resist. and contact fatigue resist. 77—44354
high-temperature alloys, thermal fatigue props. 80—21071
hip total replacements, welds in stems of cast Co-Cr femoral components 78—44697
holographic interferometry appl. to NDT 79—8420
HTGR, structural materials, effect of coolant impurities on mech. props. *(German)* 78—25297
hydrostatic stress-sensitive relationship for biaxial stress conditions 80—74805
hydroxylapatite, dense, fatique and fracture strength from diametral tests, after various treatments 80—60953
impression fatigue 80—25861
In 519 high temp. low-cycle fatigue behaviour for nuclear process heat appl. 80—628
Inco 718, fatigued specimens, plastic zone size 77—25150
Incoloy 800, 600 and 718, press. vessel, fatigue design criteria 78—60758
Incoloy 800, and 800 H, low cycle fatigue behaviour comparison 79—43438
Incoloy 800, austenitic, creep fatigue interaction at 600°C 78—64672
Incoloy 800, austenitic, fatigue at elevated temps., second phase form. effect 77—36637
Incoloy 800, creep and fatigue props. in high temp. gas cooled reactor He environment 79—47776
Incoloy 800, design codes and lifetime prediction aspects for nuclear and non nuclear appls. 79—47778
Incoloy 800, mechanical props., heat treatment and appl., conf., Petten, Netherlands (March 1978) 79—43296
Incoloy 800, solution annealed, low and high cycle fatigue correlation 79—43439
Incoloy 800 H, 617, high temp. low-cycle fatigue behaviour for nuclear process heat appl. 80—628
Incoloy 800H, high temp. low cycle fatigue, ageing and cold working effect 79—43277
Incoloy 800H, high temp.-low cycle fatigue, ageing and cold working effect on initial stress/strain curve 79—47720
Incoloy-800, annealed, mech. behaviour anal. for elevated-temp. LMFBR appl. 80—18428
Incoloy-800, creep-fatigue interaction 77—70113
Inconel 718, high temp. fretting fatigue, fatigue and fretting wear 80—3197
Inconel 718, low cycle fatigue at 298 and 823K 77—86151
Inconel 718, surface flawed tensile bars, utility in cyclic life studies 77—21342
Inconel X-750 foil, surface pretreatment for improved coating adherence 79—15877
inelastic deform. mechanism, fatigue testing in air and corrosive environments *(Russian)* 79—52432
influence function method, fracture mechs. and residual fatigue life anal. of power station cracked components 77—80109
Kevlar 49 fibre reinforced composite, shear fatigue 78—15493
Kevlar-29, flexural fatigue and surface abrasion 78—15504
Kinel 5504, mech. props. 20 to 300°C *(French)* 77—56018
laminate, anal. 80—104253
laminate, multidirectional, general fatigue failure criterion and test program 80—7658
life, prediction of Miner damage distribution by Bayesian method *(Japanese)* 79—59942
life calc. prediction *(German)* 77—7336
life calc. under combined torsion and bending 77—11148
life determination for structural elements, based on fatigue crack propag. theory 80—81182
life dispersion in rolling contact, new model 78—59349
life distrib., estimation of three parameters of Weibull distrib. *(Japanese)* 79—59943
life distribution estimation, from S-N curve *(Japanese)* 80—71737
life estimation of structures from programmed elastoplastic loading results 77—56102
life prediction, cumulative damage rule, base on knee point of S-N curve 77—25156
life prediction computer based 80—21251
life prediction of cooling hole configs., fracture mechanics applic. 77—54924
life prediction using computer modelling, cyclic stress/strain curves 80—19290
lightguide fibre, ensuring mechanical reliability 80—79001
limit, statistical interpretation on basis of extreme theory 80—30056
limit under combined stress 77—73314
limits and curves, sloping branches, correlation relationships *(Russian)* 79—77018
linear fracture mechanics parameters, in fatigue life estimation, sensitivity study *(Japanese)* 80—64468
load transport problems 77—86159

fatigue continued
- load-bearing structures, behaviour prediction of materials degradation 79—34133
- Long-life notch strength reduction due to local biaxial state of stress 78—9612
- longevity, probabilistic description 77—63770
- low cycle, charact. determ. using digital computers 79—100263
- low cycle expt. at elevated temps., frequency effect 77—48553
- low cycle fatigue, design of structural elements, review 77—3788
- low-alloy cast steel, high-strength, fracture toughness 77—56109
- low-cycle fatigue, method of approximating curves in rigid loading 80—21078
- low-cycle fatigue, rel. between fatigue crack growth rate props. 80—5987
- material under random complex state of stress, hybrid simulation 77—42786
- material with heterogeneous struct., fracture mechanism 78—67127
- mechanical surface structure damage, action of plastic deformations *(French)* 80—30011
- mechanisms, thermally activated, activation energy calcs. *(Russian)* 80—16436
- metal, crack initiation and propagation studies *(German)* 77—77587
- metal, exoelectron emission from surface during fatigue damage 78—44217
- metal, fatigue damage accumulated by combination of alternately applied over- and under-stresses *(Japanese)* 80—35306
- metal, fatigue damage examination using two-crystal X-ray spectrometer method 79—52481
- metal, fatigue failure, similarity eqns. in components with stress concentration factors, coeff. anal. 78—39907
- metal, fatigue failure, similarity eqns. in components with stress conc. factors, error estimation 78—39908
- metal, fatigue fracture-stacking fault energy correlation *(Russian)* 78—15499
- metal, fatigued, relationship between stress and point defect cluster density 80—10592
- metal, FCC, polycrystn., fatigued, behaviour model during plastic deformation *(German)* 80—21023
- metal, lives up to crack initiation 78—7050
- metal, notched, cyclic stress/strain behaviour, random fatigue life *(German)* 80—100907
- metal, notched, fatigue under alternately over- and under-stresses *(Japanese)* 80—35307
- metal, plastic flow, role of osmotic forces in low cycle fatigue, vacancy generation *(Russian)* 79—60430
- metal, recovered dislocation substructure, prod. and utility, review 77—84749
- metal, stochastic model for fatigue under repeated stress or strain 77—56107
- metal, strain criteria for fatigue at high cycle loading 79—61712
- metal, surface layer transform. and failure, kinetic charact., under dry friction 77—52506
- metal fatigue, eddy current sensors, tuning method 80—21231
- metal fatigue analysis, inversion of strain-life, and strain-stress relationships 80—16428
- metal fatigue analysis, inversion of strain-life and strain-stress anal. 80—19289
- metal fatigue crack detection using nondestructive evaluation (NDE) methods 80—71826
- metal fatigue tests for plastic deformation *(Hungarian)* 80—97665
- metal structures, inelastic anal. 78—70586
- metal-metal metal-polymer sliding, wear mechanisms, review 79—70174
- metallic glasses, mats. props. review 77—4043
- metallic materials, fatigue life distrib. theoretical obs. near fatigue limit 80—59569
- metals, fatigue failure, book 78—76747
- metals, fatigue resistance, processes leading to failure 80—94907
- metals, inelastic cyclic strain under nonuniform stress state conditions, residual stresses effect 80—81132
- metals, single phase FCC, cyclic deform. long range stress changes 80—54308
- metals *(Japanese)* 77—8929
- metals and alloys, cyclic strength in nonisothermal loading, exam. of method and equipment 78—85096
- metals and alloys, fatigue behaviour, vacuum effect, review 80—35309
- Mg alloy MA12, fatigue failure in air and vacuum 79—91800
- micro plastic strain energy criterion applied to reversed biaxial fatigue 78—63391
- micromechanisms of crack extension, conf., Cambridge, England (March 1980) 80—105421
- mild steel, fluctuating overstresses, effects 77—90524
- model for elastic materials with freq. independent Q 79—86384
- mortar specimens, repeated impact bending load study *(Japanese)* 80—93622
- multi-stage nature, review 77—21269
- multiaxial creep-fatigue damage, determ. of strain range 79—7650
- nonsteady temp. field computation, rel. to thermal part of mech. hysteresis 79—3905
- North Sea structures 77—86160
- notch and size effect, new method for calc. 78—63389
- notch fatigue behaviour, multiaxial stress-strain approx. 77—40446
- notch fatigue life predictions, using smooth bar fatigue data 78—63387
- notched and bend specimens with equivalent geometries *(German)* 77—86271
- notched bodies, exam. of fatigue limit 78—71291
- notched bodies *(Czech)* 79—70166
- notched components, generalised design procedure for estimating fatigue life 78—63388
- notched member fatigue life predictions combining crack initiation and propagation 80—38328
- notched plates, fatigue life estimation based on elastopolastic anal. *(Japanese)* 79—18814
- notched plates, monotonic and cyclic loaded, exam. of elastic-plastic stress-strain behaviour 78—63390
- notched specimen, gust loading test results, appl. of relative Miner rule 79—83308
- nuclear power plant system, optimisation with regard to design, materials and testing *(German)* 80—42739
- nuclear reactor structural alloys, time-depend. fatigue behaviour 79—1909
- nuclear reactor structural materials assessment, AISI 316 and 9Cr-1Mo steels, for UK LMFBR 78—86581

fatigue continued
- nuclear reactors, high temp. 79—6745
- numerical expressions of fatigue results *(Japanese)* 80—62455
- numerical modelling of fatigue, crack, creep and corrosion test results, review 78—30243
- Nylon 6, pressurized heat treatment effect on fatigue props. 79—87669
- nylon 6 fibres, highly oriented, fatigue process, struct. changes 77—90447
- optical CVD fibres having surface compression, fatigue characts. 79—46064
- optical fibre, UV cured epoxy acrylate coated, zero stress ageing effect on strength 80—58753
- optical fibre fatigue strength, environmental and temp. effects 78—46835
- optical fibre high-temperature fatigue strength and OH^- stress-induced corrosion 78—1387
- optical fibre tensile and fatigue strength 77—7211
- optical fibre transmission, dispersion, and strength characteristics 79—37021
- optical fibres, GeO_2-$B_2O_3SiO_2$, ageing effects of moisture on fatigue and tensile strength 80—66539
- optical fibres, high-strength metal-coated advances in reduction in microbending loss 79—46066
- optical fibres, mech. reliability 80—91909
- optical fibres, plastic-coated fused silica, ageing and static fatigue 79—46067
- optical fibres, static fatigue effect on breaking strain 78—30060
- optical fibres, surface compressive strength, increase after ageing under load 79—46065
- optical fibres, tensile strength and static fatigue, analysis using Weibull distribution for optimum design 80—85011
- optical fibres, UV curable epoxy acrylate coated, long-term mech. behaviour 78—95802
- optical fibres coated with Si_3N_4 for improved fatigue 79—50470
- optical glass fibres, fatigue failure prediction, appl. of fracture mech. theory 79—998
- optical waveguide fibre, screen tested, fatigue strength meas. 80—19098
- optical waveguide fibre cladding composition effect on stress corrosion and fatigue 77—3664
- PA6, loss factor rel. to fatigue strength *(Polish)* 77—28904
- palliative treatments for fretting fatigue, review 80—21126
- parameter inaccuracy effect on calc. of material service life under high cycle random loading *(Slovak)* 78—18251
- particle dispersed composite, fatigue life anal., reliability concept *(Japanese)* 79—29200
- parts with stress raisers, endurance limit in asymmetric cycling 79—94558
- Permendur 49, ordered and disordered, clean mild wear 80—16508
- photomachining type 410, evidence for lack of H_2 embrittlement in failure 79—74246
- piezoelectric ceramic, bend and compressive strength, stressing rate effect 77—52409
- piezoelectric material, fractographic features of fatigue 79—52374
- plastic, flexural fatigue props. *(Japanese)* 79—20171
- plastic bodies break-up *(Russian)* 77—80121
- plastic extension control during fatigue tests 77—25220
- plastic solid, loosening and fracture 77—89071
- plastic zones, monotonic and cyclic, eval. 77—72239
- plastically prestrained materials and components, high cycle fatigue *(Czechoslovakian)* 77—32680
- platilon UO1, use in artificial blood pumps, fatigue resist. and mech. props. 79—84026
- PMMA, electric phenomena in process of deform. and failure, role in fracture mechanism 77—44344
- PMMA, fatigue life enhancement, prior crazing 80—89331
- PMMA, fracture toughness under biaxial stress 78—76760
- PMMA, lifetime reduction under cyclic loading 77—66695
- PMMA and PPMA, glassy state, cyclic loading effects on internal damping, shear modulus, heat capacity and density 77—43275
- PMMAF fatigue life in stepped and stationary nonisothermal cyclic loading 77—28905
- polyamide 6, reinforced and unreinforced, fatigue fracture types under circular flexural loading *(German)* 79—70170
- polycaproamide, deformability props. in cyclic extension-compression 79—20183
- polyester cloth reinforced epoxy resin, fatigue strength and reliability under repeated impact tensile load *(Japanese)* 79—61703
- polyester moulding compounds, cyclic loading and strength 77—81310
- polyethylene, ageing in extreme cold climate *(Russian)* 77—59897
- polyethylene, high density, fracture fatigue kinetics, IR absorption spectra 78—11323
- polyethylene, high density, subjected to biaxial tension, effect of loading cycle asymmetry on fatigue strength 78—44215
- polyethylene, low-density, fatigue fracture surfaces produced by monatonic and cyclic loading 80—40510
- polyethylene, ultra-high molecular weight, linear, impact fatigue response 79—100242
- polyethylene terephthalate, fatigue failure under cyclic loading, overstress in chem. bonds 79—57106
- polyethylene wear against dry stainless steel in unidirectional motion 79—20212
- polymer, crack tip failure mechanism modelling 80—108565
- polymer, gas environment effects 77—4845
- polymer endoprosthetic joint, fatigue life 80—40521
- polymer lifetime reduction under cyclic loading 77—66695
- polymer materials, fatigue life, determ. from reheat temp. 79—61724
- polymer-polymer and metal-polymer sliding wear mechanisms, review 79—70174
- polymers, cryst., hard-elastic fibres, morphology mech. props., mechanisms, review 77—32612
- polymers, fatigue, fracture 79—43425
- polymers, fracture and fatigue, review 78—68781
- polymide 6, glass fibre reinforced and unreinforced, fatigue under rotary bending *(German)* 79—15782
- polypropylene, creep and failure under low frequency cyclic loading 77—1858
- polypropylene, microstruct. changes during large strain cyclic deform. 80—66627
- polystyrene, fatigue behaviour, cyclically loaded, mean stress effect 78—52968
- polystyrene, temp. and environmental effects on fatigue fracture 79—79079

fatigue continued

- polystyrene amorphous film, cyclically fatigued, molecular behaviour 80−35310
- polystyrene fracture surfaces prod. by monotonic and cyclic loading 79−47768
- polystyrenes, monodisperse, static and dynamic props., mol. wt. effect 78−84938
- powder metallurgy, fatigue strength significance *(German)* 80−60946
- power engineering problems 77−86157
- power transmission cables, pipe-type, low-cycle fatigue tests 80−7731
- prealloyed powder blending, composite materials fatigue and tensile props. *(French)* 80−20850
- prediction over wide range of frequencies 77−11631
- pressure vessel alloys, fatigue design curves using modified Langer eqn. 80−30107
- probability model rel. to linear fracture mechanics 78−27637
- prosthetic aortic valve, Reul-Ghista optimal tri-leaflet Avcothane design performance 78−44736
- prosthetic hip joints, fatigue strength of Co base alloys 79−48375
- pseudoelastic single crystal fatigue 79−52364
- PVC, fatigue life, influence of cyclic loading conditions 80−76350
- PVC, thermal history and treatment effect on mech. props. 79−4986
- PVC with mineral fillers, mech. props. 80−21042
- radial impeller blades, unsteady aerodynamic forces and moments, singularity method obs. 80−58952
- rain-flow calcs. for wide band random stress process 78−11332
- random, time series determ. of transfer functions 80−33526
- rectangular parallelepiped, fatigue fracture in complex stress state 80−79229
- refractory, high-temp. stress relaxation during alternating torsional loading 77−16636
- reinforced polymers, fatigue and damage accumulation 78−15490
- reliability under multiple-amplitude loads 79−79072
- Rene 95, as hot isostatically pressed (HIP) and HIP+forged, low cycle fatigue 80−25854
- residual strength based on strength life equal rank assumption 78−67094
- residual stress data sheets, changes due to fatigue *(Japanese)* 77−4841
- review 77−4150
- rod and plate, fatigue strength in bending, small number load cycles 77−86183
- rolling contact, fracture mech. approach 80−23961
- rolling contact fatigue life, traction and microgeometry effects 79−20205
- rolls in hot strip mills, contact fatigue failure 80−60950
- rotating circular disc 77−73327
- rotating cylinder 78−30238
- roving glass cloth fibre reinforced polyester resin cumulative damage fatigue *(Japanese)* 77−8941
- rubberized cloth, service life determ. under cyclic load 78−31535
- S-N curves determination from accelerated fatigue data, analytical method 78−35475
- safety, interrelation between stress and magnitude of safety and fatigue crack *(German)* 79−32385
- satin woven glass cloth fibre reinforced plastic, fatigue life under random loading *(Japanese)* 80−55509
- scale effect in the resistance to fatigue in the complex stressed state 80−74807
- shakedown of deformable plastic structure, approx. methods, fatigue 77−54900
- silica optical fibres, ageing polymer-coated fused specimens in pH solns., tensile strength and dynamic fatigue 79−46063
- single crysts., fatigued age-hardenable, dislocation structure *(German)* 80−54247
- slab, semi-infinte, stress amplitudes and fatigue damage resulting from cyclic Hertzian compression 77−19567
- solar collectors with multilayer cylinder heat exchangers, heat balance eqn. and thermal stress anal. 80−58977
- spectral method of rating life under action of random loads 77−19570
- stainless cast high-strength steel, fracture toughness 77−56109
- stainless steel, 18Cr-11Ni, for nuclear reactors, mech. props., neutron effects 77−34383
- stainless steel, 304, tensile stress effects on high-cycle fatigue 78−86603
- stainless steel, type 304 tubular specimens, biaxial fatigue damage at elevated temps. 77−28939
- stainless steel wire reinforced Al sheet, prod. by explosive compaction, and mech. props. 77−32542
- statistical methods for creep, fatigue and fracture data analysis 80−58936
- statistical size effect for fracture probability functions 77−50995
- statistical treatment, maintenance procedures 79−43538
- steel, 0.22% C type, impact fatigue tests under −50°C low temp. atm. 77−52450
- steel, 0.22% C type impact fatigue strength under −100°C low temp. atm. 77−52451
- steel, 0.45% C, annealed, roller, macroscopic and microscopic changes in surface layer due to rolling contact 77−77518
- steel, 0.45% C, annealed, roller, rolling contact fatigue life, effect of changing rolling direction 77−77519
- steel, 0.7% C, welded zone, fatigue strength and microstruct. *(Japanese)* 80−89339
- steel, 0Kh16N15M3B, irradiation effects on resistance to cyclic elastoplastic deformation 79−91767
- steel, 10Kh11N20T3R, brittle fracture susceptibility rel. to grain size *(Russian)* 77−59901
- steel, 12Cr1MoV, thermal fatigue and creep effect in fracture 80−104297
- steel, 14G2AFD and 15G2AFDps, fatigue resistance when strengthened by nitrides and welded joints 78−95790
- steel, 15G2AFDps and boiler steel, fracture toughness determ. from fatigue test results in circular bending 78−15526
- steel, 22K and 09G2S, residual stress change in conc. zone in cyclic loading 78−3224
- steel, 316L, low-cycle *(French)* 77−28903
- steel, 4140 compact, fatigue crack growth delay, yield strength, neg. stress ratio depend. 78−3210
- steel, 45, EHI961, EHI437B, fatigue strength, effect of residual stresses and cold working 77−56101
- steel, (0.36 wt.% C) Ni-Cr-Mo, electroslag refined, fracture toughness and fatigue behaviour 80−81171
- steel, age-hardenable, relation between fatigue S-N and P-N charact., definite fatigue limit *(Japanese)* 77−8938
- steel, AISI 1010, low-cycle fatigue at temps. up to 1200°F 78−35516

tigue continued

- steel, AISI 1045, laser transform. hardening, fatigue and wear rates 79−70198
- steel, AISI 4340, positron lifetime and X-ray particle size meas. during high cycle fatigue 79−5053
- steel, Al-Cr-Mo, nitride hardened roller, surface fatigue failure under pure rolling and sliding rolling contacts 79−79183
- steel, Al-Cr-Mo, nitride hardened rollers, surface fatigue resistance under pure rolling and sliding-rolling contacts 79−79184
- steel, Al-killed, fatigue life for program loading of multiple repeated two step stresses *(Japanese)* 80−66632
- steel, alloy, 15KhM1 and 20KhM1, plastic deform. with thermal cycling 80−89310
- steel, alloy, 16GNMA, stress conc. effect on endurance under repeated static loading conds. 79−43412
- steel, alloy, carburized case parameters, effect on props. of 20Kh3MVFA and 12Kh2N4A 78−52989
- steel, alloy, Cr-Mo-V, fatigue, failure probability based on residual strength 78−68797
- steel, alloy, fatigue strength and fracture, diamond grinding effect 80−55532
- steel, alloy, fracture and fracture energy, subject to static, impact and repeated impact bending 77−63799
- steel, alloy, JIS SNCM8, crack propagation vel. in delayed failure under cyclic load, temp. and freq. depend. 79−43381
- steel, alloy, mechanical properties, morphology, transform. kinetics and composition interrelations 77−86146
- steel, alloy, Ni-Cr-Mo, SNCM8, mech. stre-ngth under combined alternating strength 78−64690
- steel, alloy, quenched carbonitrided, multicycle fatigue failure 80−104283
- steel, alloy, static and fatigue strength, tension and compression test results 78−95810
- steel, alloy, type 25Gs, increasing fatigue resistance by surface plastic deformation 78−88530
- steel, alloy, type 25KhNZMFA, fatigue strength characts. rel. to absolute dimensions and stress conc. 79−43410
- steel, alloy 10G2S1 welds, fracture, subjected to low-temp. fatigue 80−89350
- steel, alloy cyclic strength after strain hardening and tempering, precip. hardened 40FT, and 40 78−52988
- steel, alloy St. 3sp, weld, deformation criteria of low cycle failure 78−39875
- steel, and alloy, fatigue strength improvement, by subcritical quenching 78−44153
- steel, anisotropic rolled plate, torsional fatigue in middle and high cycle fatigue ranges *(Japanese)* 77−12691
- steel, annealed, limit stress, effect of specimen length 77−44357
- steel, API 5LX-X60, pipe fatigue strength under cyclic internal pressure, inner surface defects 79−38980
- steel, ASTM A588, fatigue test of fillet weld, practical aspects of anal. 78−64682
- steel, ATSI 9310, fretting, selected fretting resistant surface treatments 79−29223
- steel, austenitic, fatigue after plastic deform. sequences *(French)* 79−20131
- steel, austenitic, low-alloy, and C, fatigue limit during bending, inelastic strain effects 77−44355
- steel, austenitic, martensitic transform., alternating elastic stressing effects 77−86029
- steel, austenitic, mechanical strength, effect of mech. and heat treatment 77−12659
- steel, austenitic, precipitation of $Cr_{23}C_6$ at grain boundaries 78−84846
- steel, austenitic, stainless, life prediction of high temp. low cycle fatigue, strain rate effect 79−8360
- steel, austenitic, under creep and cyclic loading at 823K *(German)* 77−90435
- steel, austenitic and ferritic stainless, fatigue, effect of struct. and work hardening rate *(French)* 77−63783
- steel, austenitic metastable, fatigue, effect of deformation-induced martensitic transformation *(Japanese)* 78−15514
- steel, austenitic stainless, 304 and 316, creep-fatigue interaction 77−70113
- steel, austenitic stainless, 316, surgical implant ion beam textured, stress/strain relations, fatigue characts. 78−73297
- steel, austenitic stainless, equivalent alternating stress from two-level multiple-step wave *(Japanese)* 78−92333
- steel, austenitic stainless, fast neutron irrad., effect on mech. props. 78−92309
- steel, austenitic stainless, fatigue and cyclic stress-strain characts. austenite-martensite transform. effect 80−21109
- steel, austenitic stainless, fatigue crack propag., stable and unstable, role of precipitation 80−40534
- steel, austenitic stainless, fatigue damage, under sawtooth wave strain cycling at elevated temp. *(Japanese)* 78−84977
- steel, austenitic stainless, fatigue under static and cyclic heating fractographic peculiarities, electron microscope obs. *(Russian)* 77−52465
- steel, austenitic stainless, fretting corrosion of orthopaedic implant materials by bone cement 80−104813
- steel, austenitic stainless, fusion reactor blanket struct. material, low cycle fatigue behaviour 80−30073
- steel, austenitic stainless, high temp. low cycle fatigue resist. under superimposed stresses at two freqs. 80−25832
- steel, austenitic stainless, martensitic transform. effect during static and fatigue loading 77−52325
- steel, austenitic stainless, neutron irradiated OKh16N15M3B, reactor structural material, low-cycle fatigue study 79−91793
- steel, austenitic stainless, nonsensitized, fatigue strength, intergranular corrosion effect *(Japanese)* 80−85027
- steel, austenitic stainless, shot-peening effect 79−87733
- steel, austenitic stainless, stressing conditions, influence on fatigue behaviour *(French)* 78−68776
- steel, austenitic stainless, supercond. magnets, mech. and phys. props. at 4K 80−86976
- steel, austenitic stainless, thermal fatigue, fractographic features of failure 80−76349
- steel, austenitic stainless, type 316, effect of hold times on fatigue life, explanation in terms of grain boundary sliding damage 78−72851
- steel, austenitic stainless, type 321S12, fatigue cycling in $R=-1$ loadings 80−35317

fatigue continued
steel, austenitic stainless, type SUS 304, low cycle fatigue strength reduction factor *(Japanese)* 80—104259
steel, austenitic stainless, types 304 and 316, environment effect on crack growth, under creep and fatigue conditions 80—85035
steel, austenitic stainless in liq. Na, mechanical props., review 79—20150
steel, austenitic stainless low-cycle fatigue, effect of mean plastic strain and stress factor 77—63766
steel, austenitic stainless type 304, time-depend. fatigue, mechanistic model 80—100925
steel, austenitic stainless type SUS 316, low cycle fatigue tests, freq. effect on notch sensitivity at elevated temps. *(Japanese)* 80—104260
steel, ball bearing, fatigue damage, influence of dispersed phases in martensitic matrix 80—108549
steel, ball bearing, martensitic decay during rolling contact fatigue 77—32682
steel, ball bearing with modified chem. comp., improved rolling contact fatigue 78—64732
steel, bearing, corrosion resistant, rolling element fatigue life 79—20090
steel, C, bar, round, subject to combined static and repeated bending and torsion, fatigue strength criterion 80—40496
steel, C, contact fatigue strength, effect of austenite grain size 79—100254
steel, C, cumulative damage rule, based on reduction in fatigue limit, experimental confirmation 78—92358
steel, C, cyclic loading and fracture toughness 80—35298
steel, C, EN8, Mo coated, fretting wear and fatigue strength assessment 78—88583
steel, C, failure mechanisms in impact fatigue 80—40493
steel, C, fatigue damage accompanying nonstationary modes of cyclical loading, coeff. of heredity *(Russian)* 79—52349
steel, C, fatigue damage accumulation and nonuniform microscopic strains, development features 79—91770
steel, C, fatigue failure in type 45, strength charact. 79—52373
steel, C, fatigue life, reliability analysis, reliability-based design safe lives *(Japanese)* 77—8939
steel, C, fatigue life prediction under programmed loading *(Japanese)* 79—20167
steel, C, fatigue limit, in plane specimen, microfatigue cracks and understressing effects *(Japanese)* 77—52480
steel, C, fatigue strength and damping capacity, short term cyclic overload effect 79—66157
steel, C, fretting fatigue damage, SEM exam. 78—88541
steel, C, inclusions, influence on toughness and fatigue props. 80—40533
steel, C, notched, fatigue damage detection, using optical correlation technique 78—35511
steel, C, rolling contact fatigue, tufftriding effect on 0.2% C cylindrical specimen 80—100954
steel, C, rotating bending fatigue strength, high tensile load effect during stress cycling *(Japanese)* 77—52477
steel, C, rotating bending fatigue strength, periodic high tensile load effects *(Japanese)* 78—11313
steel, C, S15C, crack propag. under combined creep and fatigue, J-integral approach *(Japanese)* 79—83303
steel, C, S15C, S35C, S55C, rotating bending fatigue strength, annealing in vacuum effects *(Japanese)* 78—11314
steel, C, spring, compressed, patented wire, reverse elastic aftereffect and fatigue strength 79—38881
steel, C, strain ageing and fatigue limit 80—40378
steel, C, strain ageing contribution to fatigue hardening 78—23817
steel, C, structural strength, increase by high temp. mech. treatment with austenite isothermal decomp. 79—24555
steel, C, torsional prework effect on fatigue strength, crack propagation *(Japanese)* 80—55514
steel, C, type 45 and 1Kh2M, fatigue strength, of notched specimens with regard for cyclic plastic strains 79—43414
steel, C, type S15CK, tufftrided, fatigue strength at elevated temp., under reversed axial strength *(Japanese)* 78—84980
steel, C, type SFVV1, low cycle fatigue strength reduction factor *(Japanese)* 80—104259
steel, C, unnotched, fatigue life estimation, under combined torsion and bending *(Japanese)* 80—93647
steel, C, X-ray diffraction correlation between cyclic loading and residual stress *(German)* 78—48583
steel, C (0.18 wt.%), fatigue strength, atmospheric press. effect *(Japanese)* 77—77573
steel, C (0.1 to 1.15 wt.%), fatigue, mean stress effects *(German)* 78—56721
steel, C (0.1-1.15 wt.%), fatigue under reversed tension-compression stresses, photoelasticity investig. *(German)* 78—31493
steel, C (0.21 wt.%), loading wave shape effect on deform., failure, impact tensile strength of smooth specimen *(Japanese)* 79—29146
steel, C (0.54 wt.%), torsional fatigue process, obs. by electron microscope *(Japanese)* 77—12690
steel, C and alloy, restricted durability, subject to pure bending with rotation 77—90431
steel, C and low alloy, size effect in bending fatigue strength and its prediction 79—43411
steel, C and Ni-Cr surface hardened, rolling contact fatigue failure 80—16608
steel, C-Mn, threshold stress intensity range in fatigue 80—30058
steel, C-Mn-(Cr), structural changes during stress cycling after heat treatment and cold rolling *(Russian)* 78—19787
steel, C-Mn-V and Cr-Mo-V, power station component, fracture toughness and fatigue characts. 79—20192
steel, carburised, fracture resistance 79—24612
steel, carburised, with non martensitic microstruct. at surface, fatigue *(Japanese)* 77—48535
steel, carburized, fractography of fatigue fractures 77—86137
steel, carburized fatigue, non-martensitic struct. effect, rel. to mean stress and residual stress *(Japanese)* 78—7024
steel, case hardened, MnCr, shot peening effect on bending fatigue strength *(German)* 78—56777
steel, case-carburized, low alloy, rolling contact fatigue 78—35518
steel, casecarburized and hardened, relationship between fatigue strength and case hardness distrib. *(Japanese)* 79—61782
steel, cast, fatigue strength probability characts. determ. 77—70173
steel, cast, mech. props., fatigue behaviour, influence of microdiscontinuities, review 78—35512
steel, cast 20KhML, deform. resistance and low cycle fatigue in pure shear creep effect 78—3192

fatigue continued
steel, CC Ti-C, threshold fatigue behaviour, effect of grain size and yield strength 79—91790
steel, CK10, structural, fatigue softening tests, temp. and freq. depend. of stress-strain behaviour, cyclic loading *(German)* 79—38888
steel, Ck35N and 37MnSi5, fatigue strength estimation, separation method suitability *(German)* 78—27644
steel, Ck45, tension-compression tests, cyclic, macroscopic changes of length *(German)* 80—40424
steel, Co-Cr casting, fatigue at welds, hip replacement appl. 78—44697
steel, constructional, fracture toughness in cyclic loading 78—72860
steel, Cr, exam. of surface layer after electrochemical treatment, effect on mech. props. *(Russian)* 80—7727
steel, Cr (12 wt.%), thermomechanical treatment, high temperature, effect on props. and struct. *(Czechoslovakian)* 77—32603
steel, Cr (13 wt.%), fatigue, effect of toughness *(Japanese)* 78—7025
steel, Cr plated, high strength, with and without surface strengthening prior to plating 79—39051
steel, Cr-Mn, low-cycle fatigue at 20 and −196°C 80—81196
steel, Cr-Mo, hardened, fatigue life, effect of programmed load history *(Japanese)* 79—20160
steel, Cr-Mo, high tension, delayed fracture, fundamental study *(Japanese)* 77—48531
steel, Cr-Mo, high-temp. props. and constitutive equations 79—34146
steel, Cr-Mo, martensite to ferrite transform. by fatigue deform. *(French)* 79—66056
steel, Cr-Mo, notched specimens, fatigue strength distrib. *(Japanese)* 80—66633
steel, Cr-Mo (2.25, 1 wt.%), creep and high temp. low-cycle fatigue tests 80—85061
steel, Cr-Mo (2.25, 1 wt.%), creep-fatigue testing from thermal transient effects in CRBRP reactor 78—21660
steel, Cr-Mo (2.25, 1 wt.%), oxidation effect on hold time fatigue behaviour 80—30161
steel, Cr-Mo (2.25, 1 wt.%) pipe, high temp. fatigue and creep strength 80—85060
steel, Cr-Mo-V, creep fatigue interaction 78—60841
steel, Cr-Mo-V, creep fatigue interactions obs., strain controlled and load controlled tests 78—44214
steel, Cr-Mo-V, creep/fatigue interaction 78—64632
steel, Cr-Mo-V, high-temp. cumulative damage for stage I crack growth 78—19883
steel, Cr-Mo-V, low alloy, creep fatigue interaction 78—64673
steel, Cr-Mo-V, Low-cycle fatigue under out-of-phase loading conditions 78—7051
steel, Cr-Mo-V (0.5, 0.5, 0.25 wt.%), heat treated, microstructure effect on threshold region fatigue 78—56757
steel, Cr-Mo-V and stainless, biaxial cyclic deformation behaviour 80—16431
steel, Cr-Mo-V-W, crack-growth and thermal-mech. fatigue 80—21072
steel, Cr-Ni, case hardened rollers, surface fatigue failure under pure rolling and sliding rolling contacts 79—52472
steel, Cr-Ni, rolled and sintered, to produce capillary structured filter material, exam. of mech. props., and production 80—16235
steel, Cr-Ni (32,8), two phase austenite-ferrite alloy, fatigue behaviour *(Japanese)* 79—79091
steel, Cr-V, hardened sping, surface finish effect on fatigue strength *(Japanese)* 79—61708
steel, creep and fatigue fracture prevention 78—60837
steel, creep resistant, AISI 304, residual lifetime assessment by low cycle fatigue testing *(German)* 78—15485
steel, creep-resistant, creep rupture under variable stress and temp. *(German)* 79—24597
steel, CrMo, cast, fatigue tests under varying stress amplitude and varying temp., amplitude damage *(Japanese)* 78—27605
steel, CrMoV, creep and creep strength under alternate tension/compression *(Czech)* 77—63728
steel, cyclic creep and mean stress influence on fatigue life *(Czech)* 79—43403
steel, deformation and fracture resistance due to low-cycle fatigue in plane bending 79—66166
steel, dual-phase, notched, fatigue 79—100253
steel, electroless Ni plated, fatigue strength, effect of P content of Ni film *(Japanese)* 77—52478
steel, eutectoid, mech. behaviour, thermomech. treatment effects 80—84970
steel, fatigue, impact loading, friction, wear in surface active media *(Russian)* 79—29268
steel, fatigue, low cycle, test results, least square deviation method 77—63796
steel, fatigue, variable and constant amplitude 79—61711
steel, fatigue and cyclic plasticity rel. to struct. inhomogeneity 80—81184
steel, fatigue and tensile props., of heat resisting bars, type SUH 660-B and SUH 310-B at elevated temps. 79—38979
steel, fatigue damage and crack propagation, classification zone approach 77—56106
steel, fatigue damaged, fracture toughness 80—89353
steel, fatigue fracture after Fe and Ce diffusion coating, microstruct. investigation *(Russian)* 79—52446
steel, fatigue life, influence of cyclic loading conditions 80—76350
steel, fatigue life, load sequence effects *(Polish)* 79—34135
steel, fatigue life, structural parameters and chem. comp. effects, rel. to test parameters 77—59928
steel, fatigue life enhancement by ion implantation 79—1910
steel, fatigue life prediction for fillet welded attachments, under service loadings 78—64683
steel, fatigue limit assessment, progressive load methods *(German)* 80—61058
steel, fatigue limit estimation when subject to bending loads 77—21281
steel, fatigue reliability under random loads 79—79066
steel, fatigue resistance of heat-resistant 12Kh1MF, 15Kh1M1F and 1Kh18N12T at normal and elevated temps. 77—90466
steel, fatigue strength, low cycle overload effect 80—60967
steel, fatigue strength, statistical prop. *(Japanese)* 79—20169
steel, fatigue strength during two-freq. loading, stress conc. effect 79—52347
steel, fatigue strength of 30 KhGSNA, 12 KhN3A, effect of friction in abrasive medium after hardening 78—35507
steel, fatigue strength with stress concentrator, mean compressive stress effect 77—21264

fatigue continued
steel, fatigue testing, low cycle, effect of testing method on fatigue 79−52515
steel, fatigue with programmed loading, damage accumulation, nomogram 79−38964
steel, ferrite-pearlite, cyclic behaviour, fatigue, chem. comp. and microstruct. effects 78−60833
steel, ferritic, Cr-Mo (2.25, 1 wt.%), annealed, time depend. strain controlled fatigue, nuclear steam generator appl. 77−8915
steel, ferritic, MA 956, oxide dispersion strengthened, mech. props. and damping behaviour 79−47702
steel, ferritic, static yield props., changes during fatigue cycling 78−23790
steel, ferritic-pearlitic, low C, low alloy, low temp. effects on fatigue strength 79−5057
steel, fibre reinforced Al, fracture mechanics under fatigue *(Czech)* 78−64629
steel, finite life characteristics, notch effects *(German)* 77−90434
steel, fracture in low-cycle fatigue tests in H_2 *(Russian)* 80−76332
steel, fracture toughness, influence of low-cycle damage 78−72873
steel, fracture toughness and dynamic strength, surface active agent effects *(Russian)* 78−56812
steel, grinding effect with Elbor wheel 78−48540
steel, hardened, exoelectron emission from torsion fatigue damage 77−86142
steel, heat treated SCM3, SNCM8 and SUS403, statistical fatigue props. *(Japanese)* 77−48532
steel, heat treatment with induction heating, 78−92285
steel, high C, piano wire, mean stress effect on low cycle torsional fatigue life *(Japanese)* 79−96114
steel, high C, weld heat affected zone, impact and fatigue props. *(Japanese)* 80−11668
steel, high Mn mandrels, wear resist., surface layer chem. comp. influence *(Russian)* 79−52444
steel, high Nb, HSLA, low temp. fatigue props. 80−40490
steel, high Ni, medium C, impact fatigue strength 79−79104
steel, high speed type M-50 and 18-4-1, fracture and fatigue 80−16457
steel, high strength, 33Kh35NMVFA, low cycle fatigue fractures, electron microscope exam. *(Russian)* 78−31512
steel, high strength, low alloy, low cycle fatigue, composition, thickness effects 79−57100
steel, high strength, low alloy, response to cyclic plastic deform. 78−7035
steel, high strength, shell, stress distrib. around notch, beyond fatigue limit 78−13928
steel, high strength, types EP810VD and EP842, effect of stress conc. on fatigue strength at elevated temps. 79−57115
steel, high strength low alloy, high strain fatigue behaviour 77−86180
steel, high-strength, 30KhGSA and Kh12M, low cycle fatigue 79−87724
steel, high-strength, criteria for determining struct. strength and reliability 77−60021
steel, high-strength, endurance in air and NaCl soln., loading freq. effects *(Russian)* 78−56810
steel, high-strength, fatigue, interaction effects between trace impurities and environment 80−66651
steel, high-strength, low cycle fatigue, hysteresis loops, cyclic strain curves, fatigue diagrams *(Polish)* 80−66638
steel, high-strength, type 4340, new inhibitors for crack arrestment in corrosion fatigue 80−100941
steel, high-strength and mild, fatigue of V-bent specimens 77−16681
steel, hot forging die type, fractography *(Japanese)* 80−108547
steel, induction hardened, static bending strength and correlation between static strength and endurance limit *(Japanese)* 77−70108
steel, induction hardened sheet, inhomogeneity and distrib. of residual stresses effect on fatigue *(Japanese)* 78−31518
steel, inelastic cyclic deform. and fatigue 77−63795
steel, inelastic deform. mechanism, fatigue testing in air and corrosive environments *(Russian)* 79−52432
steel, influence on positron annihilation 78−76551
steel, Kh16N6, fatigue in gaseous H_2 *(Russian)* 78−31509
steel, low, C, rimmed and killed, exam. of impact fatigue behaviour *(Japanese)* 78−88528
steel, low alloy, fatigue fractographs *(Japanese)* 78−92335
steel, low alloy, high strength, fatigue crack growth, in presence of welding residual stresses *(Russian)* 80−71739
steel, low alloy, high strength, residual stresses during low cycle fatigue 79−29201
steel, low alloy, St 52-3, structural, fracture toughness, fatigue precracking and grain size effect 78−60782
steel, low alloy, type 4340, quenched and tempered, effect of plastic strain followed by ageing, on torsion fatigue resistance 78−92360
steel, low alloy structural, type 30KhGSA, effect of thermomech. treatment on strength, fracture toughness and fatigue props. 80−11676
steel, low and medium C, fatigue failure, inelastic response, energy criterion 77−73333
steel, low and medium C, fatigue strength, small defect effect 80−104255
steel, low C, cyclic loading, change in mech. props. rel. to heat treatment 80−104282
steel, low C, cyclic plasticity and low cycle fatigue life 80−21058
steel, low C, cyclic plasticity and low cycle fatigue life in variable amplitude loading 80−16433
steel, low C, cyclic strain ageing effect on crit. stress for crack propag. 79−34124
steel, low C, cyclic stress-strain response under spectrum loading *(Slovak)* 78−19886
steel, low C, dynamics of cyclic plastic deform. and fatigue life at low temps. 77−16670
steel, low C, dynamics of cyclic plastic deform. at low temps. *(Czechoslovakian)* 77−32679
steel, low C, fatigue, limit, statistical interpretation on basis of extreme theory 80−30056
steel, low C, fatigue, low cycle, cyclic stress-strain curve eval. 77−44347
steel, low C, fatigue damage, under sawtooth wave strain cycling at elevated temp. *(Japanese)* 78−84977
steel, low C, fatigue endurance limit, metallurgical technology and mech. treatment effect 80−55536
steel, low C, fatigue fractographs *(Japanese)* 78−92335
steel, low C, fatigue life, variable strain ranges *(Czech)* 80−60956
steel, low C, fatigue life under programmed loading including stress lower than fatigue limit *(Japanese)* 77−8934

tigue continued
steel, low C, fatigue limit, strain ageing effect *(Japanese)* 77−8933
steel, low C, fatigue strength, effect of loading type, cross section shape, and specimen edge finish *(Japanese)* 79−8343
steel, low C, fatigue strength under rotating bending and torsion, understressing effects *(Japanese)* 78−44201
steel, low C, ferritic, static yield prop. changes during fatigue cycling 77−52427
steel, low C, fractographic study of stage 1 cracking, endurance limit *(Japanese)* 77−8936
steel, low C, gas nitrocarburized, cyclic stressing 79−57098
steel, low C, grain size effect on fatigue strength, high temps. 78−68759
steel, low C, hysteresis loop behaviour under fatigue load, dislocations model 79−74197
steel, low C, improvement of props. by ion implantation 80−16601
steel, low C, long life corrosion fatigue strength under continuous and alternate immersion in 1% NaCl *(Japanese)* 77−12736
steel, low C, low cycle fatigue, cumulative damage, absorbed plastic energy anal. 79−38932
steel, low C, low cycle fatigue props. with variable strain ranges *(Czech)* 80−45390
steel, low C, low endurance fatigue at low temps. 77−21274
steel, low C, push-pull fatigue strength, effect of tensile preload on plastic strain range *(Japanese)* 78−64625
steel, low C, slip band expt. studies during fatigue process 80−45374
steel, low C, stress-controlled and strain-controlled tests, S/N curves comparison *(German)* 80−40476
steel, low C, temp. effect on hysteresis loop under cyclic load *(Japanese)* 79−20096
steel, low C, thermomechanically processed, martensitic fibre development, fatigue fracture 78−64572
steel, low C, thin walled tubes, low endurance, under bending and torsion 77−86129
steel, low C, tufftrided, fatigue strength ahd microstructure change by reversed stressing *(Japanese)* 78−15511
steel, low C, type 38NCD4, fatigue life improvement by N ion implantation, dose depend. 80−76328
steel, low C, type AISI 1010, effect of Se, Te additions on fatigue props. 78−92359
steel, low C, under rotating bending and torsion, overstressing effects *(Japanese)* 77−8935
steel, low C, weldable, precipitation hardening rel. to low cycle fatigue *(Czech)* 79−15686
steel, low C, with various strain ageing potentials, tension compression fatigue *(Japanese)* 79−20162
steel, low C and Cr-V, fatigue strength and fatigue failure at complicated states of stress 77−56057
steel, low C and mild, fatigue deformation, phenomenological exam. 78−64691
steel, low C fatigue, stability of energy dissipative charact. 77−21209
steel, low C fatigued, appl. of microbeam X-ray technique to plastic zone size evaluation 80−3199
steel, low C S10C, fatigue strength under repeated stresses of superposed wave pattern *(Japanese)* 79−61705
steel, low C-Cu composite plates, vol. fraction and residual stress, effect on fatigue strength *(Japanese)* 79−8349
steel, low-alloy, case carburised, retained austenite effect on contact fatigue strength 80−30096
steel, low-alloy 12GN2MFAYu, heat treated, testing temp. influence on fatigue strength *(Russian)* 80−40501
steel, low-C, fatigue strength, low-cycle, effect of shock wave press. 79−29205
steel, low-C, fatigue strength and crack propag. behaviour under impact program loading conditions *(Japanese)* 80−66635
steel, low-C, gas nitrocarburised, aged, fatigue behaviour 80−40514
steel, maraging, (18 wt.% Ni), solution annealed, exam. of cryogenic tensile, fatigue, and fracture props. 78−92311
steel, maraging, DI52, low cycle fatigue in gaseous H_2 *(Russian)* 78−35478
steel, maraging, Ni-Co-Mo (18, 8, 5 wt.%), fatigue strength charact. *(German)* 77−21241
steel, maraging N18K9M5T, crack propag. resistance under stress corrosion 77−70224
steel, martensitic, fatigue crack propag., effect of intercrystalline fracture associated with temper brittleness *(French)* 80−16463
steel, martensitic, fatigue life, low-cycle, temp. and strain rate effects 80−85056
steel, martensitic, low C without Ni, for deep-well sucker rods, corrosion fatigue 80−55588
steel, martensitic, size effect during rotating beam fatigue tests 80−7674
steel, martensitic and austenitic, fatigue, scale effect, structural parameter effect in rotary bending *(French)* 78−23822
steel, martensitic ferritic struct., fracture toughness *(Russian)* 77−77560
steel, martensitic stainless types 403 and 616, temp. depend. of low cycle fatigue behaviour 80−7667
steel, medium C, behaviour under combined fatigue and wear 78−3236
steel, medium C, difference between strain energy changes during repeated bending and rotatory bending fatigue tests *(Japanese)* 78−39894
steel, medium C, electrolytic Fe coated, distrib. of bounded fatigue limits 80−81198
steel, medium C, fatigue behaviour of NiAl precipitation hardening 78−84983
steel, medium C, fatigue failure, alloying influence *(Russian)* 80−21081
steel, medium C, fretting fatigue, microstructural and environment effects 78−64734
steel, medium C, low-cycle fatigue effect of mean plastic strain and stress factor 77−63766
steel, medium C, S 45 C, influence of mean strain on low-cycle torsional fatigue life *(Japanese)* 79−8348
steel, medium C, tempered, normalised or quenched, statistical property of fatigue limit, press-fitted axles *(Japanese)* 77−12693
steel, medium C, type 45, sheet, working life, effect of dynamic loading type 77−21278
steel, medium C type JIS S45C, multiple notched specimens, fatigue props. 79−61729
steel, mild, AC effect on fatigue and static props. 80−45372
steel, mild, biaxial fatigue, data compilation and anal. 77−4856
steel, mild, cantilever beams, structural response under random loading conditions, memory model 77−3784

fatigue continued
  steel, mild, cyclic strain enhanced dissolution in NH_4NO_3, corrosion fatigue props. 80—85083
  steel, mild, fatigue crack initiation 77—86163
  steel, mild, fatigue limit, effect of grain size, cold work, temp., loading frequency 77—32685
  steel, mild, fatigue strength, effect of grinding surface *(Japanese)* 77—48533
  steel, mild, friction welded joint, strain distrib. and fatigue damage under rotary bending *(Japanese)* 80—30076
  steel, mild, high temp. fatigue, effect of temp. variation 78—64685
  steel, mild, interface between corrosion fatigue and stress corrosion cracking 77—86172
  steel, mild, notch effect on impact fatigue strength *(Japanese)* 79—43400
  steel, mild, origin of spherical particles on fatigue fracture surfaces and ferrograms 79—79112
  steel, mild, plastic deform. during fatigue, detection by Barkhausen noise meas. 79—43524
  steel, mild, shot-peening effect 79—87733
  steel, mild, tensile and cyclic loading effect in Barkhausen noise 80—40560
  steel, mild, time dependent plastic relaxation at crack tip, fracture implications 77—63765
  steel, mild, with different grain sizes, surface strengthening by high frequency loading *(Czechoslovakian)* 77—28934
  steel, mild, with different sensitivities to strain ageing, cyclic plastic strain amplitude *(Japanese)* 77—8932
  steel, mild, with small flaws elastic-plastic anal. of fatigue limit 80—21069
  steel, mild, work hardening and strain ageing during fatigue *(Japanese)* 77—8931
  steel, mild and stainless, fretting wear, role of adhesion and delamination 78—35533
  steel, Mn, solutioning of castings in salt baths 78—23871
  steel, Mn-Cr, blank hardened, shot peening effect on bending fatigue strength *(German)* 78—35402
  steel, Mn-Cr, normalised, shot peening effect on bending fatigue strength *(German)* 78—35401
  steel, Mn-Cr, tempered, case hardened, shot peening effect on bending fatigue strength *(German)* 79—24645
  steel, Mn-Si, fatigue, level of prior cyclic stresses effect 80—89348
  steel, Mn-Si, for springs, metallographic study, present phases rel. to mech. props. *(French)* 80—21090
  steel, MnCr (16, 5 wt.%), bending fatigue behaviour improvement by surface treatment *(German)* 78—84957
  steel, Ni, cross girder connections, fatigue strength, design stress 78—64700
  steel, Ni, high-strength, impact fatigue strength, heat treatment conditions effect 80—76285
  steel, Ni (23 wt.%), crack propag. in the presence of H_2 *(French)* 78—15517
  steel, Ni (9 and 5 wt.%), for liquefied natural gas appls., material and weld props. 79—61736
  steel, Ni-Cr, case hardened rollers, macroscopic and microscopic changes in surface layer due to rolling contact 77—77518
  steel, Ni-Cr, case-hardened, surface durability in rolling contact fatigue testing 77—63684
  steel, Ni-Cr, case-hardened roller, rolling contact fatigue life, effect of changing rolling direction 77—77519
  steel, Ni-Cr-Mo, bar, subject to combined static and repeated bending and torsion fatigue strength criterion 80—40496
  steel, Ni-Cr-Mo (2.5 wt.%), elevated temp. fatigue, effect of zero load rest period 77—8943
  steel, Ni-G rollers, case hardened, surface durability in pure rolling and sliding-rolling contacts 79—61739
  steel, Ni-P plated, electroless, fatigue strength and plated layer microstruct. *(Japanese)* 80—93645
  steel, Ni-Ti, high-alloy, precipitation hardening, fatigue strength 79—79103
  steel, nitriding, mag. field effect 79—57153
  steel, notch sensitivity in fatigue 78—60757
  steel, notched 1018, air fatigue in endurance limit range 77—36631
  steel, notched specimens in sea water, endurance limit enhancement, specimen size, freq. effects 80—93678
  steel, oxide inclusions 78—23648
  steel, pearlitic, fatigue, metallographic aspects 78—60828
  steel, plain C, type 304 and type 316 stainless, fatigue damage indicators, non-desructive 80—25932
  steel, plain C, X-ray diffr. study of low cycle fatigue damage 77—66700
  steel, plain C having ferrite-martensite mixed structs., microstructural parameters effect on fatigue strength *(Japanese)* 80—71735
  steel, plasticity depend. on hydrostatic press. in low-angle fatigue, Manson-Coffin coeff. *(Russian)* 79—61651
  steel, plate, type SM50A for weld struct., statistical fatigue props. 79—96146
  steel, powder forged, fatigue, surface treatment effect 80—85048
  steel, powder forged, impact strength and fatigue strength, slag inclusion effects 77—21271
  steel, powder forged for carburizing appl., core props., mech. props. 78—15339
  steel, pressure vessel, fatigue design criteria 78—60758
  steel, pressure vessel type, H_2 effect on corrosion, fatigue strength and embrittlent *(French)* 79—47770
  steel, quenched, notch sensitivity, effect of tempering temp. 77—1846
  steel, quenched surface layer hardness rel. to adsorption contact fatigue *(Ukrainian)* 80—40478
  steel, railway bridge, expt. determ. of coeff. of excess dynamic fatigue stress *(French)* 79—34151
  steel, reinforced Al and Cu based composites, fatigue strength, surface layer effects 77—12697
  steel, reinforcing wires, high strength, microstruct. obs. *(Czech)* 79—43342
  steel, relaxation of residual stress with fatigue loading 77—56051
  steel, reliability under multiple-amplitude loads 79—79072
  steel, rolled, anisotropic, fatigue fracture surface obs. *(Japanese)* 80—108546
  steel, rolled plates, anisotropic, fatigue behaviour under cyclic torsion 77—44326
  steel, rolls for cold-rolling mills, surface hardening, contact fatigue strength 79—24664

fatigue continued
  steel, S20, 45, 0.1%C types, fatigue-freq. relationship 79—11707
  steel, S45C, low-cycle torsional fatigue under multiple repeated loads *(Japanese)* 77—8925
  steel, semi-high speed, martensite degradation due to fatigue *(French)* 79—91615
  steel, shafts, type 45, fatigue strength improvement after glow discharge treatment 80—108573
  steel, sheets bonded with low density polyethylene, static fatigue *(French)* 80—108522
  steel, short-cycle, fatigue, stress concentration effect 78—95859
  steel, sintered constructional, resistance to cyclic impact loads 77—77583
  steel, spring alloys, microplastic deform. and endurance limit 80—81197
  steel, spring wire and springs, type 60S2A and 50KhFA, stress tempering effect on mech. props. 79—66085
  steel, St.3, fatigue fracture near slot shaped stress concentrators 77—1870
  steel, St 37-3 and St 52-3, fracture mech. specimen, effect of fatigue precracking condition *(German)* 77—21240
  steel, stainless, 304, annealed and 9% prestrained, cyclic hardening and softening, room temp. 77—52483
  steel, stainless, 304, creep/fatigue interaction at elevated temps. 77—86174
  steel, stainless, 304, thermal fatigue and strength estimation, creep fatigue interaction 79—11708
  steel, stainless, 304 and 316, creep-fatigue life, strainrange partitioning applic. 77—77586
  steel, stainless, 316, 304, LMFBR primary piping materials, mech. props., review 77—25151
  steel, stainless, 316, creep fatigue interaction failure 78—80652
  steel, stainless, annealed, low-cycle fatigue push-pull specimens, theory and expt. 78—27641
  steel, stainless, austenitic, deform. substruct. and annealing, stacking fault tetrahedra form 80—107282
  steel, stainless, fatigue, high temp. under isothermal and thermal cycling conditions 78—60836
  steel, stainless, fatigue failure kinetics, effect of water 80—55585
  steel, stainless, FBR fuel pin cladding strain under transient testing 80—18425
  steel, stainless, FBR fuel rod cladding damage correl. for rod perform. predictions 80—18424
  steel, stainless, Harrington rod implant failure analysis 79—79686
  steel, stainless, Kh18N10T, low-cycle fatigue characts., gaseous, pure H_2 effects *(Russian)* 79—15764
  steel, stainless, martensitic, SUS 403-B, temp. and strain rate effect on low cycle fatigue *(Japanese)* 79—87717
  steel, stainless, martensitic SUS 403-B, high temp. rotating bending fatigue *(Japanese)* 77—59906
  steel, stainless, martensitic SUS 403-B, high temp. rotating bending fatigue 78—60756
  steel, stainless, Mn-N, low cycle fatigue 77—36646
  steel, stainless, neutron irradiation effect on low cycle fatigue and tensile props. at 298K 80—30059
  steel, stainless, nickelless, low cycle fatigue 80—35326
  steel, stainless, orthopaedic, type En58J, Mo ion-plating, corrosion fatigue 80—66694
  steel, stainless, plastic zones around creep and fatigue cracks at 650°C 78—48523
  steel, stainless, prestrained, heat treatment effect on fatigue strength *(Czech)* 78—60747
  steel, stainless, reversibility of plastic strain during fatigue with martensitic transform. 78—31526
  steel, stainless, strain induced martensitic transform. effect on low cycle fatigue 77—55965
  steel, stainless, SUS 304, creep-fatigue interaction, creep effect *(Japanese)* 79—83264
  steel, stainless, SUS 304B, tufftrided, fatigue strength *(Japanese)* 77—77572
  steel, stainless, SUS 316, creep-fatigue interaction at 600°C 79—34123
  steel, stainless, SUS 321, thermal ageing effect on high temp. low cycle fatigue life *(Japanese)* 80—29988
  steel, stainless, type 07Kh16N6, heat treatment 79—66158
  steel, stainless, type 304, corrosion fatigue and stress corrosion cracking, in boiling NaOH 80—7719
  steel, stainless, type 304, grain boundary sliding in isothermal and thermal fatigue *(Japanese)* 78—84979
  steel, stainless, type 304, solution-annealed and thermally aged, correl. of high- and low-cycle fatigue data 78—15532
  steel, stainless, type 304, uniaxial damage accumulation law for time depend. loading with creep-fatigue interaction 79—83324
  steel, stainless, type 316, cyclic creep behaviour, as func. of max. applied stress 78—48460
  steel, stainless, type 316, low cycle fatigue props. in vac., fracture mode 80—85021
  steel, stainless 12kh18N9T, wire, mechanical and heat treatment effect on static and cyclical strength *(Russian)* 78—35410
  steel, stainless 304, crack initiation obs. in low-cycle fatigue specimens 77—52490
  steel, stainless 304, crack propagation under fatigue-creep conditions and fractography *(Japanese)* 80—104267
  steel, stainless 304, cyclic deformation behaviour at elevated temps. 79—52322
  steel, stainless 304, cyclic plasticity, exponential stress-strain law 77—25157
  steel, stainless 304, elevated temp. low cycle fatigue, heat treatment effect 78—27626
  steel, stainless 304, stress crack initiation in chloride soln., role of corrosion pits *(Japanese)* 78—92397
  steel, stainless 304 sol. of annealed and thermally-aged, high-cycle fatigue behaviour 80—100923
  steel, stainless 316, fusion reactor first wall, thermal stress and creep fatigue limitations 79—76132
  steel, stainless AISI 304, low cycle fatigue at 649°C, substructural development 77—32664
  steel, stainless and Cr-Mo-V, high temp. low cycle biaxial fatigue 80—30063
  steel, stainless and ferritic, damping, logarithmic decrement meas. by torsion pendulum *(German)* 79—74195
  steel, stainless and low alloy, PWR primary circuit constituent materials, design features verification *(French)* 79—17976
  steel, stainless fatigue props. at elevated temps. 78—27643

fatigue continued
- steel, stainless type 316, monotonic and cyclic biaxial loading at room temp. 78—52928
- steel, stainless type XM-19, influence of recrystn. behaviour on mech. props. 79—83213
- steel, statistical fatigue props. of SM50A for welded structures *(Japanese)* 79—20168
- steel, strain-hardened subsurface layer, residual stress change in fatigue 80—81185
- steel, strengthened by surface plastic deform., tempering effect on physicomech. props. *(Russian)* 78—35409
- steel, structural, brittleness susceptibility rel. to heat treatment 79—24620
- steel, structural, fatigue softening, temp. and load freq. influence *(German)* 79—61614
- steel, structural, low temp. fatigue strength 77—21273
- steel, structural, resistance to low endurance fatigue fracture, in biaxial stress 78—15531
- steel, structural, subject to low temp. low cycle fatigue, failure charact. 77—70174
- steel, structured, fatigue life distrib., statistical anal., mixed Weibull distrib. *(Japanese)* 78—72841
- steel, tempering effect on fatigue strength 80—60891
- steel, tensile prestrained strength of anisotropic rolled steel, rot.-bending fatigue tests, slip bands 78—27590
- steel, thermal cycling fracture 78—60839
- steel, total life estimation of notched and cracked members 79—77015
- steel, TRIP, fatigue strength 80—108552
- steel, tufftrided, fatigue strength estimated from heat generation in specimen *(Japanese)* 77—52476
- steel, tufftrided, fatigue strength under reversed torsion *(Japanese)* 79—61707
- steel, tufftrided, hardened, fatigue life, effect of programmed load history *(Japanese)* 79—20160
- steel, tufftrided, S15CK smooth specimens, fatigue strength, strengthening mechanisms *(Japanese)* 78—27609
- steel, tufftrided, type S15CK, fatigue strength, estimation of size effect *(Japanese)* 80—81166
- steel, type 20, fatigue, low cycle, exam. of damage accumulation rule, for loading in air and H impregnating medium 78—64649
- steel, type 304, faceted fracture surfaces, selected area channelling patterns 77—77565
- steel, type 33Kh3SNMVFA, high-strength, failure accompanying cyclical elastoplastic straining *(Russian)* 79—70152
- steel, type 4Kh5MFS, 5KhNM, 5KhNMFS, stress conc. effect on low-cycle fracture results 79—87697
- steel, type Ck22 and St52-3, under cyclic stress, damping behaviour and fatigue strength correlation *(German)* 80—39211
- steel, type IN-787, for use in Arctic, low temp. effects on mech. props. 80—76310
- steel, type Man-Ten, and KQC-100, fatigue life estimates of bluntly notched members 80—100999
- steel, type SAE 1008, finite fatigue life distribs., various load-time histories 80—97589
- steel, types 15Kh2NMFA and 45, fatigue tests, low cycle, material variance distrib. law 79—91799
- steel, unalloyed, high temp. short term fatigue tests 79—66233
- steel, unnotched C-35, cumulative damage rule based on knee point of S-N curve 77—25156
- steel, unnotched samples, fatigue limit, estimation of scale relationship, error anal. 79—15793
- steel, US strengthening treatment effect on fatigue resistance 80—81193
- steel, V strengthened dual phase, deform. and fracture props. 78—48467
- steel, water accelerated fatigue, lubricant additive effects 78—64710
- steel, WC reinforced surface layer, serviceability improvement by Ni, Cu-Ni, V alloying additions 77—21290
- steel, welded joints, durability in repeated impact loading, low temp. effects 77—63800
- steel, work-hardenable, N26T low magnetic phase, fatigue strength effect of surface treatment 77—48546
- steel *(French)* 80—66670
- steel 03Kh13Ag19, fatigue damage inspection, on basis of change in natural oscillations freq. 79—57116
- steel 12Kh18N10T, fatigue damage inspection, on basis of change in natural oscillations freq. 79—57116
- steel 1Kh17N2Sh, fatigue failure, surface finishing influence 80—60972
- steel 1Kh18N9T, physico-mech. props. after boring in metallic melts *(Russian)* 78—56736
- steel 35KhN2VL, deoxidation effect on fatigue and endurance limit in wear tests varying P and S content *(Russian)* 78—35523
- steel 40Kh, notch sensitivity under cyclic impact loads 78—3220
- steel 45, fracture surface obs. during fatigue failure 77—86185
- steel 60S2 and 55S2GF, elastic and fatigue charact. 77—21267
- steel AISI 304 tubes, fatigue crack growth under mixed loading conditions 77—3114
- steel austenitic stainless, fatigue, low cycle, temp. and strain rate effects *(Japanese)* 79—29198
- steel ball bearing, fatigued, phase changes, nomenclature 80—89198
- steel beams with bracket plates welded to tension flange 78—7008
- steel bearing, surface-ground, residual stress fatigue property comparison 80—60975
- steel brittle transition temp. meas. by hardness testing *(Japanese)* 79—87797
- steel C, fatigue life and cumulative fatigue damage under const. stress cycling, plastic strain range effect *(Japanese)* 77—8940
- steel C, fatigued, strengthening by surface plastic deformation 78—88505
- steel C, high tensile load, during stress cycling on push-pull fatigue strength *(Japanese)* 78—92332
- steel C, types AISI 1008, 1020, 1035, renitrogenized 1010 and 1522, dynamic strain ageing, tensile notch impact and fatigue props. 79—43288
- steel core/steel tube duplex reinforcing member, behaviour under cyclic loading, core element geometry effects 77—28894
- steel Cr-Mn (13, 19 wt.%), for liquefied natural gas appls., material and weld props. 79—61736
- steel drill tubing, exam. of cyclic cracking resistance *(Russian)* 79—15767
- steel fatigue in surface active media, adsorption facilitation mech. 80—55586
- steel fibre reinforced Al, fatigue strength *(Czech)* 78—60748
- steel fibre reinforced Cu, fatigue 79—29221

tigue continued
- steel finite life characteristics, temperature change effects, torsion cycle tests *(German)* 78—7004
- steel JIS-SNCM8, fatigue under in-plane combined axial loading and torsion 79—96147
- steel Kh18N10T, substructure after low-endurance fatigue in pure bending *(Russian)* 77—81311
- steel Kh18N9T, fractographic features of rupture, rel. to struct. changes 77—63801
- steel low C, fatigue strength of notched specimen, low-temp. quenching and quench ageing effects 79—100173
- steel N22, crack movement rate during cyclic deform., internal microstress effects 78—3225
- steel OKh18N10T, subjected to low temp. thermal cycling, temp. depend. of yield point *(Russian)* 78—48489
- steel plate, high tensile strength, fatigue props. of butt welded joint 78—80649
- steel plates, fatigue substructures after high cycle vibrs. 77—8945
- steel reinforced concrete slabs, connected via shear connectors, exam. of fatigue in shear connectors, exam. of method 79—43539
- steel rod reinforced concrete, laterized columns, random axial loading, compressive strength to failure 78—27614
- steel rolled, low-cycle torsional and push-pull fatigue anisotropy 78—27589
- steel shafts testing 80—3184
- steel ShKh15, fatigue strength and residual stress distrib., machining method effects 78—31528
- steel structural bars, subjected to plastic bending, random fatigue analysis *(Japanese)* 78—27619
- steel structures, appl. of risk analysis to brittle fracture and fatigue 78—56768
- steel SW7M, low-cycle fatigue at high hardness levels *(Polish)* 80—89323
- steel wire, high C, fatigue and fracture 80—55531
- steel wires, drawn and annealed, tensile fatigue and tensile strength under cyclic stress *(Japanese)* 78—15507
- steel-Al-steel plate, fatigue damage analysis and life predictor 77—25120
- steel-steel bimetal rolled plate, low-cycle fatigue in bending 79—91794
- steels, C, H_2 embrittlement after patenting and cold deform. *(Russian)* 79—29175
- steels, Cr and Cr-Ni-Mo refining effect on low cycle fatigue strength, resistance to hydrogen embrittlement 78—44208
- steels, effect of tensile and rolling prestrains 77—52455
- steels, heat-treated, nature of high sensitivity to stress raisers 80—21051
- steels, low C S25C, medium C S45C, Cr-Mo SMC3, statistical fatigue props. eval., heat-to-heat variations 78—7048
- steels, low-C, aged after quenching, rel. between micro-cracks and coaxing effect *(Japanese)* 80—81159
- steels, S 45 C, SK 5 SCM 3, SNCM 8 and SUS 403, heat treated JIS, statistical fatigue props. 78—44222
- steels and alloys, fatigue limit, static and cyclic loading 80—71755
- strain gauges, small high-elongation foil, as fatigue damage indicators 79—32417
- strength estimation under multicomponent loads 77—54933
- strength prediction, U_0* procedure using Woehler tests *(German)* 80—71850
- stress analysis, experimental, conf., Bradford, England (Sept. 1978) 80—17718
- stress intensity factor crack opening displacement relationship for compact tension specimen 78—90778
- stress intensity factors for circumferential crack from notch in round tensile bar 79—41618
- stress-cycle asymmetry degree, determ. problem 79—90187
- stress/strain relations in nonsteady cyclic load 77—89073
- striation form., three dimensional strain compatibility model 79—1908
- structural components, cumulative damage technique 77—50986
- structural fatigue life rel. to element uncertainty 79—27593
- structural steels and alloys, conf., Kiev, USSR (Sep. 1976) 77—59921
- structure components, damage sum 78—55589
- submarine cables, wire fracture modes and mech. props. correl. with fatigue life 78—35520
- superalloy, microstructure resulting from alloying and heat treatment, effect on creep, fatigue, fracture strength 78—11246
- surface, mech. and corrosion props. improvement using US energy *(Rumanian)* 79—15821
- surface coatings, materials conservation and optimum tribological performance 80—34130
- surface damage, plastic deformation cause in fatigue, wear, fretting and rolling fatigue 80—40537
- test data, statistical anal. *(Japanese)* 80—62452
- test result spread of cast gas turbine blades, rel. to design and technological factors 77—63797
- tests, improving accuracy with axial loading, specimen fixing 79—83428
- thermal energy losses and steady state temp. field calc. 77—19571
- thermoplastic, deform. at low cycle loading 77—70122
- thermosetting polymers, fibre-reinforced, 4.2-300K 77—25160
- threshold stress intensity range 80—30058
- timber butt-joint, with metal plate connectors, rotating bending fatigue *(Japanese)* 80—3175
- time to fracture under static and cyclic loads 77—70176
- tip of propagating fatigue crack, strain distrib. meas. by Moire fringe multiplication method 77—80124
- Tokamaks, lifetime of reactor components 80—32445
- TORUS II Tokamak, toroidal field coil, fatigue test results 80—13928
- total life estimation of notched and cracked members 79—77015
- two step program loading involving impact load, fatigue strength and damage accumulation *(Japanese)* 79—66148
- U-shaped bellows design, low cycle fatigue life, elastoplastic anal. 79—37247
- UHV fatigue drive, design and performance 80—86328
- uniaxial damage accumulation law for time depend. loading with creep-fatigue interaction 79—83324
- unnotched samples, fatigue limit, estimation of scale relationship, error anal. 79—15793
- US atomizer, construction, fatigue strength, elec. characts. 78—81959
- valve tissue, glutaraldehyde preserved, stress/strain and fatigue behaviour 78—40217
- vibrating mechanical structures, realistic fatigue modelling 78—31517
- wear, steady, mechanism anal. by fatigue theory as stochastic process 80—11789

fatigue continued
- Weibull distribution, adding static and dynamic fatigue effects 80—70298
- Weibull distribution, three parameter estimation rel. to parameter estimation of fatigue life distrib. *(Japanese)* 80—65130
- weld fatigue assessment 80—3179
- welded construction, beam loaded, stress conc. effect *(German)* 79—34150
- welded joints, flash, fatigue strength obs., under heating and cooling cycles, microstructures influence 79—15760
- welded joints, low cycle fatigue anal. 77—3789
- wire-rope pendants, overload effects on fatigue damage 78—7052
- Zircaloy-2 fuel tubes, cumulative damage fatigue tests at room temp. and 300°C 80—93638
- Zircaloy-2 fuel tubes, low cycle fatigue studies at room temp., 300 and 350°C 80—93637
- Zircaloy-4, tensional stress cycling 80—3168
- Ag, fatigued, relationship between stress and point defect cluster density 80—10592
- Ag, fatigued single crystal, annealing of deform. struct. 78—3204
- Ag-Pd-Cu, contact-spring props., fatigue and spring limit *(Japanese)* 79—29117
- Al, adhesively bonded and weld bonded aircraft struct. subjected to acoustic excitation, determ. of sonic fatigue life 78—92351
- Al aircraft alloy, fatigue resistance improvement by laser shock 80—93654
- Al alloy, 2024-T3, notched sample fatigue damage detection via optical correlation technique 78—35511
- Al alloy, 51S, modified by misch metal, for space appl. 80—55466
- Al alloy, accumulation of damages in stress concentration zones in alternating creep and fatigue 79—100261
- Al alloy, deformation and fracture resistance due to low-cycle fatigue in plane bending 79—66166
- Al alloy, fatigue damage, sum distribs. during programmed tests at 120°C 78—23809
- Al alloy, fatigue endurance scatter in transitional region of fatigue curve *(Russian)* 78—56738
- Al alloy, fatigue life distrib., statistical anal., mixed Weibull distrib. *(Japanese)* 78—72841
- Al alloy, fatigue life estimation from creep rupture data *(Japanese)* 79—79089
- Al alloy, inelastic cyclic deform. and fatigue 77—63795
- Al alloy, low-cycle fatigue strength, isothermal hardening effect 79—38863
- Al alloy, residual stress relax. rel. to temp., load cycling, aircraft struct. appl. 78—7053
- Al alloy, total life estimation of notched and cracked members 79—77015
- Al alloy, type 2024-T3, fatigue deformation and crack growth, holographic study 80—25836
- Al alloy, yield surface of material subjected to combined cyclic loadings 78—84905
- Al alloy 01420, welded joint fatigue life improvement, vacuum annealing appl. 80—7597
- Al alloy 2017-T3, part-through crack propagation, by alternating bending stress *(Japanese)* 78—27607
- Al alloy 2017A, low-cycle fatigue, effect of direction of first half-cycle *(French)* 77—25236
- Al alloy 2024, creep crack growth rate, temp. and cyclic load effect *(Japanese)* 79—83302
- Al alloy 2024, loading sequence, normal and reversed sequence effect 78—68791
- Al alloy 2024-T3, work hardening in surface layers and bulk during fatigue 78—48428
- Al alloy 2219-T87, sheet, fatigue tested, fracture surface rotation mechanism 80—11764
- Al alloy 7050, fatigue, effect of intermediate thermomech. treatments 79—8352
- Al alloy 7075, modified, fatigue and failure mechanisms 79—100252
- Al alloy 7075-Tb, coldworked fastener holes, elastic-plastic boundary layer determ. 79—34066
- Al alloy AK4-1T1, endurance at elev. temp. of strip with loaded hole 77—86181
- Al alloy AMg6, residual stress change in conc. zone in cyclic loading 78—3224
- Al alloy adhesively bonded laminates, axial fatigue 80—40491
- Al alloy Al 7075-T651, microcrack closure load development for stage I and II cracking 77—86150
- Al alloy D16, fatigue props. eval. 79—15750
- Al alloy D16, fatigue testing, low cycle, effect of testing method on fatigue 79—52515
- Al alloy D16AT, fatigue life, struct. and microhardness, working conditions effect 80—55525
- Al alloy JIS A5083-O, notch sensitivity in fatigue 78—60757
- Al alloy JIS A5083-0, multiple notched specimens, fatigue props. 79—61729
- Al alloy RR58, low cycle fatigue at 423K, prior treatment effect 80—104254
- Al alloy V93, high strength, notch sensitivity in static and repeated loading 78—27639
- Al alloys, (5083, 6061, 2219), supercond. magnets, mech. and phys. props. at 4K 80—86976
- Al alloys, anodic oxides influence 77—44408
- Al alloys, critical stress intensity factor determ., fatigue tests on notched specimens *(French)* 78—35502
- Al alloys, extrusion, purity effect on fracture props. 79—100248
- Al alloys, fatigue of fillet welds, peening effect 79—91853
- Al alloys, laser generated stress waves, effect on microstruct., hardness and strength 79—69192
- Al alloys, preliminary forging effects on struct. and mech. props. of extruded sections *(Russian)* 78—80564
- Al alloys, types 2017A, 2014, 2618A, 7049A, 7050, 7075, low-cycle fatigue *(French)* 79—74250
- Al alloys 7075-T6 and 2024-T3, crack propag./wear rate relationship 78—3232
- Al alloys A5083 and A7075, statistical fatigue props. 79—5060
- Al alloys D16T and AK4-1T1, fatigue life, effect of stress cycle asymmetry, shape of fatigue curves 77—1873
- Al, and Al alloys 6061 and 2024, burst acoustic emission during Bauschinger effect 77—48475
- Al bronze, superplastic low cycle fatigue 78—27632

fatigue continued
- Al, cold rolled, X-ray diffr. and optical microscope exam. of fatigue damage *(Japanese)* 78—84976
- Al, cyclic loading, change in mech. props. rel. to heat treatment 80—104282
- Al, deformation enhanced photoemission meas. 77—32511
- Al, dislocation struct. change during cyclic straining at high temps. 78—44218
- Al, fatigue, effect of pre-existing subgrains 79—5041
- Al, fatigue characteristics, low-cycle, theoretical predictions and expt. 78—27641
- Al, fatigue damage, test temp. effects *(Japanese)* 77—52475
- Al, fatigue enhanced optically stimulated electron emission 77—4719
- Al, fatigue hardening at various test freqs. 79—24539
- Al, fatigue induced dislocation struct. and hardening, exam. *(Japanese)* 78—64624
- Al, fatigue life, influence of cyclic loading conditions 80—76350
- Al foil, modification of texture by fatigue, X-ray diffr. exam. 78—88477
- Al, high purity, cyclic torsional deform., factors influencing ductility 77—56031
- Al, high temp., cyclic grain boundary migration phenomena 80—85053
- Al, high temp. fracture, SEM obs. 77—59918
- Al, mech. props., 20 to 300°C *(French)* 77—56018
- Al, mechanical deformation with superimposed insonation, volume effects 78—60723
- Al, plastic flow, role of osmotic forces in low angle fatigue, vacancy generation *(Russian)* 79—60430
- Al, polycrystalline, abrasion, deform., fatigue, study by exoelectron microscope *(Japanese)* 78—74108
- Al, polycrystalline, fatigue damage detection by exoelectron emission meas. *(Japanese)* 77—55871
- Al, pure, grain size effect *(Japanese)* 77—59911
- Al, struct. changes during cyclic deform. *(Russian)* 77—25127
- Al, surface fatigue damage meas. by photostimulated exoelectron emission 78—19876
- Al, surface fatigued single crystal, inhomogeneous positron trapping 77—90216
- Al, torsional fatigue and bending tests 79—43521
- Al wire, torsion fatigue strength and fibre texture 77—48549
- Al/polyethylene/Al sandwich construction, flexural fatigue props. *(Japanese)* 78—56751
- Al-Ag (15 wt.%), precipitation hardenend cyclic stress-strain response 78—35412
- Al-Ag (7.27 wt.%), peculiarities exhibited during fatigue loading *(Chinese)* 80—71723
- Al-alloy, type 2024, fatigue life prediction, X-ray diffr. method 80—25837
- Al-alloy, type AK4-1-T1, internally heated low-cycle fatigue resist. 80—21077
- Al-alloy type 7075-T6, effect of shot peening on fatigue behaviour 79—79102
- Al-bronze, input energy, hysteresis, and fracture in low cycle buckling fatigue, superelastic range 78—31527
- Al-Cu, high strength, type 2024-T3, crack growth, fatigue induced surface deform., holographic detect. 80—85120
- Al-Cu (4 wt.%) partially coherent precipitation hardened alloy, high temp. cyclic deform. 80—25710
- Al-Cu (4.2 wt.%), precipitation strengthened, solute depletion at fatigue facets, AES study 79—38973
- Al-Cu (5 wt.%), fatigue strength, coarse precipitation effect *(German)* 79—91660
- Al-Cu alloy D16, riveted, low-cycle fatigue strength 80—30097
- Al-Cu alloy RR58, high strain fatigue life, prior treatment effect 78—60835
- Al-Cu-Mg, rolled plate fatigue charact. *(Russian)* 80—16437
- Al-Cu-Mg alloy, influence of plastic deformation on fatigue limits, for prestrained components 78—68799
- Al-Cu-Mg-Mn-Si-Fe, endurance with cyclic bending, effect of loading conditions 80—50724
- Al-Cu-Mg-Si-Mn alloy AK8, fatigue strength, effect of residual stresses and cold working 77—56101
- Al-Cu-Mg-(Ag), effect of addition on fatigue microstructure relationships 80—40483
- Al-Cu-Mn (6.3,0.3 wt.%), alloy Al 2219-T851, crack closure load development for surface microcracks 77—86226
- Al-Cu(Zn-Mg), age hardening, conditions leading to localised plastic deform. and fracture in slip bands during fatigue 78—64670
- Al-Fe-Si commercial alloy, elevated temp. low cycle fatigue behaviour under rotating bending 79—47766
- Al-Mg (2.4 wt.%) alloy, solution-treated, grain size effects on fatigue strength 77—4839
- Al-Mg (4.4 and 6 wt.%), for liquefied natural gas appls., material and weld props. 79—61736
- Al-Mg (5 wt.%), hardness-flow stress rel. during strain-controlled bending fatigue 79—74245
- Al-Mg alloy AMg6, fatigue, random process effect on life 79—66160
- Al-Mg single crystal, fatigue deform. 79—91747
- Al-Mg-Li alloy 01420, riveted, low-cycle fatigue strength 80—30097
- Al-Mg-Mn alloy AMG-6M, endurance determ. by dimensionless damageability curves 79—96141
- Al-Mg-Si, type 6061-T6, 6063-T6, effective stress range factor in fatigue 80—100924
- Al-Mg-Zn-Cu, type 7050, calorimetric study of fatigue induced microstructural changes 80—85034
- Al-Mg-(Ag), effect of addition on fatigue microstructure relationships 80—40483
- Al-Si (1 wt.%), hardness-flow stress rel. during strain-controlled bending fatigue 79—74245
- Al-Zn, type 7075-T6, coldworked hole specimens, residual stresses, fracture mech. anal. 80—97587
- Al-Zn (3.9 wt.%), single crysts., fatigued age-hardenable, dislocation structure *(German)* 80—54247
- Al-Zn (6.5 at.%), fatigue props., effect of ageing and thermomech. treatment 78—27620
- Al-Zn-Mg and Al alloy 7050, age hardenable, microstruct., effect of monotonic and cyclic straining 77—36633
- Al-Zn-Mg-Cu, alloy 7075, fatigue, loading sequence, normal and reversed sequence effect 78—68791
- Al-Zn-Mg-(Zr), low cycle fatigue, grain refinement effect 77—44345
- Al_2O_3, cyclic fatigue in direct push-pull, exam. 78—56746
- Al_2O_3, impact fatigue 77—56048

fatigue continued
Al_2O_3, polycrystalline, slip band form. under fatigue stress, Schmid factor effect *(Korean)* 78−44199
Al_2O_3, polycrystn., high-temp. fatigue and strength 80−60954
Al_2O_3, porous, sintered, delayed failure, static fatigue in distilled water 78−64750
Al_2O_3, vitreous-bonded, eval. of proof testing to assure against delayed failure 78−84954
Al_2O_3-Mo (20 wt.%) cermet, ZrO_2 crystal addition effect on thermal fatigue resistance 80−40528
As_2Se_3, film, amorphous, fatigue and recovery of electrophotographic props. 78−21253
As_2Se_3 layers for electrophotographic use *(German)* 80−42283
Au, wear, atmos. press. effect, rel. to fatigue 77−70189
B epoxy laminate, notched, fatigue damage 78−3215
B fibre reinforced Al, impact behaviour under fatigue 80−7661
B fibre reinforced Al alloy 6061, cross plied laminate, tension-compression fatigue 79−38940
B fibre reinforced epoxy resin laminate, fatigue damage, stiffness/strength comparison 77−90451
B fibre reinforced Mg, exam. of fatigue props. and corrosion 80−11751
B thin wires, fatigue limit and tensile strength 80−25834
Be, hot-extruded, fracture in impact, static tensile and fatigue tests *(Russian)* 77−52458
C fibre, flexural fatigue and surface abrasion 78−15504
C fibre and glass fibre hybrid reinforced plastics, review of physical properties 80−55496
C fibre composite/metal joint, fatigue research 78−15497
C fibre reinforced Al, mech. props. 80−11708
C fibre reinforced composites, mech. props., rel. to aircraft appl. 77−81289
C fibre reinforced composite, shear fatigue 78−15493
C fibre reinforced composites for spacecraft use, prep., props. and struct. 80−71625
C fibre reinforced Cu composite, fatigue strength under constant strain *(Russian)* 78−95796
C fibre reinforced epoxy, fatigue strength 78−15495
C fibre reinforced Kinel, mech. props., 20 to 300°C *(French)* 77−56018
C fibre reinforced plastic, multi-directional reinforcement, fatigue 78−15491
C fibre reinforced plastic laminates, axial and short beam shear fatigue 78−15492
C fibre reinforced plastic, ±45° orientation, creep, fatigue, repeated loading and crack growth 78−68729
C fibre reinforced plastic, fatigue failure mechanism identification, AE detection using piezoelectric strain gauge 79−96239
C fibre reinforced plastic, SEM obs. of fatigue 80−11737
C fibre reinforced plastics, fatigue behaviour visualised by moire fringe method 80−21110
C fibre-reinforced plastic joints, fatigue life, stress distrib. analysis 80−55497
C glass fibre hybrid plastics, review of mech. props 79−20107
C, isotropic pyrolytic, for biomedical devices, mech. props. 78−65150
C-fibre reinforced epoxy resin, laminated structs. mech. props. 80−50672
Co alloy, X-40, creep-fatigue interaction at high-temp. 78−84958
Co base alloy, creep-fatigue interaction in aligned eutectic and solid soln. 80−108554
Co base superalloy, rupture life, prior temperature cycling effect 78−60840
Co-B-Si amorphous alloy, liq. quenched, elec. resist. and cyclic deform. 80−59949
Co-base superalloy, machine thixocast, mech. prop. deficiencies 79−74244
Co-Cr-Mo alloy shoulder prosthesis, wear and fatigue tests 80−26415
Co-Cr-Nr-TaC eutectic alloys, fatigue, microstructure effects 78−23803
Co-Ni alloy, slip charact., and fatigue, FCC twinning and FCC to HCP martensite transform. effect 80−35182
Co-Ni-Cr-Mo, hip joint anchorage stem, superior fatigue strength, high corrosion resist. 79−29671
Co-superalloy, cast, high temperature fatigue behaviour 80−40485
Co-W-Cr (15,20 wt.%), surgical implant ion beam textured, stress/strain relations, fatigue characts. 78−73297
Cr-Mo, structural carbonitrided at low temps., rotating bending fatigue strength *(Japanese)* 77−48534
Cr-Mo steel types JIS SCMV 2, SCMV 3 and SCMV 4, high-temp. high-cycle fatigue props., press. vessel appls. *(Japanese)* 80−93650
Cr-Ni, fatigue, low cycle, test results, least square deviation method 77−63796
Cr-Ni-Mo steel, low-cycle fatigue in sea water, mechanism *(Russian)* 77−59970
Cr-V-B-Y system, fatigue strength and fatigue fracture at 20 and 1100°C, SEM study 80−3194
Cr_3C_2-(WC)-Ni, sintered, cavitation erosion resistance *(Japanese)* 77−52500
Cu alloy, fatigue cavitation, high temp. 77−36658
Cu alloys, low-cycle fatigue and cyclic creep, −196-20°C 80−100913
Cu and alloys, inelastic cyclic deform. and fatigue 77−63795
Cu, annealed, positron lifetime changes during cyclic fatigue 79−43060
Cu, cold-drawn, low-cycle fatigue, effect of mean plastic strain and stress factor 77−63766
Cu, creep-fatigue failures, damage concept appl. 80−40535
Cu, creep-fatigue interaction of polycryst. specimens at elevated temp., hydrostatic press. effect on crack behaviour 77−59890
Cu, crystallographic fatigue fracture of single crystal 77−44352
Cu, cyclic loading, change in mech. props. rel. to heat treatment 80−104282
Cu, cyclic strain hardening under deform. at various temps. 79−43273
Cu, cyclic work hardening during frequency change fatigue tests *(German)* 79−34068
Cu, cyclic work hardening frequency effects *(German)* 79−29090
Cu, fatigue behaviour effect of Zn, Au diffused coatings 78−72850
Cu, fatigue hardening and failure at intermediate life 77−48548
Cu, fatigue hardening and high cycle fatigue under reversed bending 79−20180
Cu, fatigue of single crystals and low const. plastic strain amplitude 79−20174
Cu, fatigued, relationship between stress and point defect cluster density 80−10592
Cu, fatigued, structural changes, damping and modulus 77−28906
Cu, fatigued high-purity polycrystals, temp. depend. of flow stress 77−44316

tigue continued
Cu, fatigued polycrystals, impure, temp. depend. of flow stress 77−44317
Cu fatigued polycrystals, point defect cluster rel. with yield stress temp. depend. 78−6989
Cu, fatigued specimens, 'etch pit slip', SEM obs. 79−100258
Cu, grain boundary morphology effect on void form. 78−48533
Cu, grain-boundary sliding component in high temp. fatigue 80−50706
Cu, high purity, low cycle fatigue, cumulative damage, absorbed plastic energy anal. 79−38932
Cu, high purity, small-angle neutron scatt. from pores in high temp. fatigue 79−14795
Cu, intrinsic stacking fault energy, effect on cyclic hardening 79−11638
Cu, low-temp. fatigue, effect of ambient environment *(Russian)* 77−59896
Cu, modulus meas. during high frequency fatigue *(German)* 77−59938
Cu, pure, fatigue crack propagation, effect of stacking fault energy as deduced from dislocation patterns, TEM study 79−61719
Cu, single crystal, fatigue and fretting initiated fatigue, crystallographic orientation effect 77−70182
Cu, single crysts., fatigued, random strain amplitude cycling 80−3146
Cu, single crysts., hysteresis behaviour implications rel. to fatigue, plastic strain cycling 80−3191
Cu, wear, atmos. press. effect., rel. to fatigue 77−70189
α-Cu-Al, single crystal, low cycle fatigue 79−43405
Cu-Al, single crysts., hysteresis behaviour implications rel. to fatigue, plastic strain cycling 80−3191
Cu-Al (10 wt.%), annealed, tensile fatigue strength at high temp. in vacuum *(Japanese)* 78−35493
Cu-Al (10 wt.%) alloy, water-quenched, tensile fatigue strength at high temp. in vacuo *(Japanese)* 78−72837
Cu-Al (5 wt.%), subjected to tension-compression fatigue, deform. and fracture strength *(Japanese)* 80−93644
Cu-Al (5.5, 7.3, 6.3 and 2.5 wt.%), Hg embrittlement under cyclic loading 77−86225
Cu-Al (7.9 wt.%), burst acoustic emission during Bauschinger effect 77−48475
α-Cu-Al single crystal, strain burst during low cycle fatigue 80−25866
Cu-Al-Ni (14.5, 3 wt.%), polycrystalline, pseudoelastic, cyclic stress strain response 77−86144
Cu-Al-Ni (14.5, 3 wt.%), fatigued, polycrystn., pseudoelastic, dislocation and martensite substructs. 79−82223
Cu-Co (2 wt.%), single crysts., fatigued age-hardenable, dislocation structure *(German)* 80−54247
Cu-Cr (1 wt.%), exam. of low cycle fatigue props. at elevated temp. 78−64674
Cu-Cr-Zr-Mg (0.5, 0.1, 0.03 wt.%), exam. of low cycle fatigue props. at elevated temp. 78−64674
Cu-Ni, Ni atom cluster break up, slip band formation, point defect motion 79−57096
α-Cu-Sn, cyclic work hardening frequency effects *(German)* 79−29090
A-Cu-Sn, cyclic work hardening during frequency change fatigue tests *(German)* 79−34068
Cu-Zn (36 wt.%), hardness-flow stress rel. during strain-controlled bending fatigue 79−74245
Cu-Zn-Al, martensitic phase transformation effect on low cycle fatigue behaviour 80−7666
Cu-Zn-Al, polycrystn., β-phase, fatigue life, intergranular cracking 79−38974
Cu-Zn-Al, pseudoelastic alloy, exam. of fatigue props. 78−76744
CuNiCr, IN838, heat treatment effect on fatigue and corrosion fatigue behaviour 80−20982
Fe, [110] and [410] single crysts., push-pull fatigue 79−74257
Fe alloy, cast, Young's modulus and microstructure *(German)* 77−25090
Fe alloys, universal diags. of cohesive strength *(Russian)* 78−56733
Fe and Fe alloys, fatigue rel. to US attenuation at large strain amplitudes 77−1182
Fe, Armco, cyclic loading and fracture toughness 80−35298
Fe, Armco, deform. strengthening during low-cycle fatigue in H gas *(Russian)* 77−52460
Fe, Armco, fatigue micromechanism *(Russian)* 78−23818
Fe, Armco low-cycle fatigue, electric field effects 77−1868
Fe, cast, fatigue strength, effect of notches and effective sectional area, for cast Fe with various graphite sizes *(Japanese)* 78−64626
Fe cast, low-cycle fatigue 80−16474
Fe, cast, low-cycle fatigue, theory 80−89349
Fe, cast, nodular, transition from quasistatic to fatigue fracture under low cycle loading 79−66167
Fe, cast, pearlitic, residual compressivel stress distrib. effect on resultant stress conc. in notched samples 78−92336
Fe, cast, rare-earth-Mg nodular, fracture toughness and fatigue *(Chinese)* 78−95791
Fe, cast nodular, high strength, low cycle fatigue 79−57112
Fe, cast spheroidal graphite, pipe, fatigue strength 80−16419
Fe, casting, fatigue strength, section size and surface struct. effect *(Japanese)* 79−20170
Fe chromised layers, fatigue fracture kinetics study by reverse bend tests *(Russian)* 78−31511
Fe electrolytic coated medium C steel, distrib. of bounded fatigue limits 80−81198
Fe, electroplated with soft Fe coating, fatigue fracture, struct. characts. 80−55524
Fe, fatigue fracture kinetics at various deform. amplitudes, vacuum effects 77−4851
Fe, fatigue fracture strength and failure, at 77K after cyclic loading at room temp. 78−84996
α-Fe, influence of C and ZrH_2 on static and cyclic creep behaviour 78−39856
Fe polycrystalline, two ferromag. methods for eval. of fatigue limit 80−89438
Fe, powder forged, impact and fatigue strengths, slag inclusion effects 77−21271
Fe, pure, strain ageing and fatigue *(Japanese)* 79−20161
Fe, sintered, fatigue, metallographic obs. 78−64646
Fe, slip-initiation phenomenon by fatigue, appl. to stress meas. 80−45342
Fe, static loading over wide deform. and temp. range, acoustic emission, fracture, plastic flow 77−90425
Fe, tensile strength and cyclic tensile fatigue strength at high temp. in vacuum, BCC and FCC phases *(Japanese)* 79−100251

fatigue continued
Fe waisted cylinders, fatigue, exam. of Miner's rule 78—64689
Fe-Al-(Nb), fatigue deform. 77—44350
Fe-B-Si amorphous alloy, liq. quenched, elec. resist. and cyclic deform. 80—59949
Fe-C (0.16 wt.%) hardness-flow stress rel. during strain-controlled bending fatigue 79—74245
Fe-Cr-Ni (20,15 wt.%), low cycle fatigue life under hold time conditions, grain size effect 77—77577
Fe-Ni, brittle transgranular and intergranular fatigue crack growth rate, yield strength effect 78—68786
Fe-Ni (25 wt.%), and single phase, solidified from undercooled melt, mech. props. 77—48540
Fe-Si (3 wt.%) BCC single crystals, low cycle fatigue *(French)* 79—20177
Fe-Si (3.72 wt.%) fatigue failure in vacuum and air 78—68789
$Fe_{29}Ni_{49}P_{14}B_6Si_{12}$, Metglas fibre reinforced mortar, fracture props. 79—70159
α-Ge_ySe_{1-y}, photoluminescence and fatigue effects 78—84648
Mg alloy MA12, fatigue, low temp. effect 80—55529
Mg alloy MA15, fatigue, random process effect on life 79—66160
Mg, burst acoustic emission during Bauschinger effect 77—48475
Mg, cyclic hardening of single crystal 78—64552
Mg-Al (0.8 wt.%), grain-boundary sliding component in high temp. fatigue 80—50706
Mg-Zn-Zr rare earth alloy, mech. props., effect of microshrinkage during solidifaction 79—43234
MgO single cryst., impact wear characts. 80—76374
Mn-Cu, fatigue, stability of energy dissipative charact. 77—21209
Mo alloy, TsM-10, fatigue fracture mechanism, dislocation struct. *(Russian)* 77—32674
Mo alloys, fusion reactor first wall and blanket material, props. for struct. appl. 80—30071
Mo, fatigue charact., effect of Ni and Re surface doping on mech. props. *(Russian)* 80—7660
Mo, fatigue of single crystals, dislocation struct. and strain localisation *(Russian)* 80—71741
Mo polycrystn., cyclically deformed, dislocation arrangements 80—108506
Mo reinforced Al and Cu based composites, fatigue strength, surface layer effects 77—12697
Mo single crystals, simulating initial stage of deformation in fatigue loading 80—35328
Mo single crysts., substruct. variation during fatigue, kinetics *(Russian)* 78—60742
Mo, single crysts., work hardening and softening in cyclic strain 80—20957
Mo, sintered, fusion reactor blanket struct. material, low cycle fatigue behaviour 80—30073
Mo, strain localisation and fatigue, glide plane shearing stress 80—7683
Mo-B-Al-C, alloy TsM-10 rolled, recrystallised, deformed system, behaviour under cyclic loading 79—91795
Mo-B-Al-C system, fractography of static and fatigue fracture 79—87729
Mo-Re alloy, type MR47VP, fractographic of static and fatigue fracture 79—87729
Mo-Re alloy MR47-VP, dislocation struct. and fatigue damage during room temp. deform. *(Russian)* 79—20111
Mo-Ti-Zr alloy TZM, fatigue and plastic flow, irradiation effects 77—52466
Mo-Ti(B)-Zr(Al)-C, stress cycling at room temp. *(Russian)* 77—25148
Na ML-3 circuit for testing mech. props. of structural materials of LMFBRs *(Spanish)* 80—55595
Na_2O-CaO glass, strength and failure predictions 77—21256
Na_2O-CaO-SiO_2 glass, Hertzian fracture characts., comp. influence 78—31522
Nb alloys, fusion reactor first wall and blanket material, props. for struct. appl. 80—30071
Nb and Nb-Zr (1 wt.%), fusion reactor blanket struct. material, low cycle fatigue behaviour 80—30073
Nb fatigue strength, surface layer effects 77—12697
Nb, fusion reactor first wall material, cyclic deform. tests 80—30074
Nb, oxidation kinetics, abnormal, at high temp. 79—29289
Nb-H, fatigue 79—11695
Nb-Mo steel, HSLA, low temp. fatigue props. 80—40490
Nb-Nb-Al-(Cr), γ/γ'-δ type eutectic, fatigue, effect of composition and microstruct. 78—48520
Nb-Ti superconducting composites, crit. current changes and fatigue damage after 4.2K strain cycling 77—28323
Nb_3Sn fatigue effects in unidirectional composites, computer simulated model 80—35289
Ni alloy, fatigue and cyclic plasticity rel. to struct. inhomogeneity 80—81184
Ni alloy, heat resistant, fatigue limit comparison in torsion and tension-compression 80—81181
Ni alloy, high temp., fatigue strength, temp. depend. 77—56100
Ni alloy EHI437BVD, inelastic cyclic deform. and fatigue 77—63795
Ni alloy EhI867, effect of structural state on fatigue and heat resistance *(Russian)* 79—34140
Ni alloys, damping, logarithmic decrement meas. by torsion pendulum *(German)* 79—74195
Ni base alloys EhI607A and EhI929VD, fatigue strength, temp. depend. 79—15791
Ni base heat resistant casting alloy, fatigue resistance, microstruct. obs. 79—66159
Ni base superalloy, rupture life, prior temperature cycling effect 78—60840
Ni base superalloy IN 100, corrosion resistant intermetallic coating, microstruct. effect on mech. props. 78—85058
Ni, electrical resistivity and stress amplitude change during push-pull fatigue 79—91792
Ni, high temperature cyclic deformation 80—16429
Ni, pure and alloyed, and fibre reinforced, at elevated temps. 77—52353
Ni, push-pull fatigued polycrystals, point defects, elec. excess resist. meas. 80—100910
Ni spring alloys, microplastic deform. and endurance limit 80—81197
Ni, wear, atmos. press. effect, rel. to fatigue 77—70189
Ni-Al, CC Ni-Al (42 at.%), Al_2O_3 growth, morphology and spalling model 78—53030
Ni-Al-Cr-Mo-Ti-W-(Co) alloys EhI 826 and EhI 929, reverse elastic after effect under loading 78—39829

fatigue continued
Ni-base alloy creep, corrosion and fatigue testing for appl. in nucl. process heat system 78—13237
Ni-Co (10 wt.%), cast single phase, solidified from undercooled melt, mech. props. 77—48540
Ni-Co-Cr, type E1929VD, effect of stress conc. on fatigue strength at elevated temps. 79—57115
Ni-Co-Cr-Al-Ti-Mo superalloy IN738, casking porosity removal using hydrostatic press. sintering 80—55322
Ni-Cr, creep-fatigue failures, damage concept appl. 80—40535
Ni-Cr, wrought, fatigue at high temp., microstruct. assessment 79—29208
Ni-Cr superalloy, interactions between creep and low cycle fatigue *(Chinese)* 80—66572
Ni-Cr-Al-TaC, eutectic composite, microstructure, fatigue props. 80—85038
Ni-Cr-Co base superalloy APK1, hot isostatically pressed, heat treatment, fracture props. 77—73251
Ni-Cr-Co superalloy IN-792, crack growth resistance, metallurgical effects 77—36655
Ni-Cr-Co-Al alloy IN-738, uniaxial damage accumulation law for time depend. loading with creep-fatigue interaction 79—83324
Ni-Cr-Co-Ti-Mo-W-Al (14, 9.8, 5, 4, 3.9, 3 wt.%), low cycle fatigue, prior heat treatment effect 80—60962
Ni-Cr-Ta-Ti-Si, EP557 precipitation hardening alloy, mech. props., heat treatment effect 80—60877
Ni-Cr-Ti-Co-W-Al-Mo alloys AF-115 and AF2 1DA, superalloy powder compacts, fatigue origins 78—48521
Ni-Cr-W-Co-Ti heat resistant alloy ZhS6K, fatigue resistance, heat treatment and protective coating effects 77—81320
Ni-Cu (30 wt.%), cast single phase, solidified from undercooled melt, mech. props. 77—48540
Ni-Fe-Cr (18, 18 wt.%) superalloy, mech. props., 4-295K 77—44327
Ni-Fe(Co) alloys, fatigued, struct. and cyclic stress strain, influence of stacking fault energy and atomic size-module-interactions *(German)* 79—42082
Ni-Mo-Cr, type E1867, effect of stress conc. on fatigue strength at elevated temps. 79—57115
Ni-ThO_2, dispersion strengthened, high temperature cyclic deformation 80—16430
Ni-Ti, martensitic phase transformation effect on low cycle fatigue behaviour 80—7666
NiTaC eutectics, high cycle fatigue at room temp. 80—16459
Pb, cyclic grain boundary migration during high temp. fatigue 80—39111
Pb-Sb-Te-Cu-Sn, influence of specimen and grain size on mech. props. *(Russian)* 77—81297
Si, failure in strong melt grown single crysts. 78—3205
SiC, abrasive paper, variables affecting degradation 79—43444
SiC, self bonded, exam. of fracture 79—20149
Si_3N_4, high temp. thermal fatigue, role of activation energy of slow crack growth 77—44340
Si_3N_4, high-speed rolling bearings, fatigue strength 80—93655
Si_3N_4, hot pressed, strength and life prediction 80—3173
Si_3N_4, static fatigue, fitting of data to iterative trivariant analysis 78—76732
Si_3N_4, stress corrosion 77—8917
SiO_2 fibre lightguides, fused, zero stress strength reduction and transitions in static fatigue 80—87523
SiO_2 fibres, fused, failure predictions based on fatigue strength 78—71293
SiO_2, fused, fibres, lifetime predictions, applicability of crack velocity date 77—52467
SiO_2, fused silica fibres, high-strength epoxy-acrylate coated, dynamic and static fatigue 78—1385
SiO_2, fused silica fibre lightguide, static fatigue transitions 80—58744
steel, C, annealed S45C, multiple repeated low cycle torsion fatigue under controlled strain *(Japanese)* 78—27610
Ti alloy, creep and long-term strength under cyclic loading 78—3191
Ti alloy, cyclic creep 77—81323
Ti alloy, deformation field investigation in danger zone of sheet 77—16654
Ti alloy, fretting wear, role of adhesion and delamination 78—35533
Ti alloy, mechanical props. at high temp., effect of Pt ion plating 79—29156
Ti alloy, microstruct. and mech. props., room and elevated temps. 77—36554
Ti alloy, microstructure resulting from heat treatment, alloying, effect on creep, fatigue, fracture strength 78—11246
Ti alloy 685, β-processed, fatigue behaviour 77—90453
Ti alloy fatigue, stability of energy dissipative charact. 77—21209
Ti alloy TA6V, fatigue, low cycle, and microfractography *(French)* 77—70168
Ti alloy TA6ZrSD, low cycle fatigue at 450°C *(French)* 79—70169
Ti alloy VT20, endurance in cyclic bending 77—63798
Ti alloy VT20, phase composition and structure effect on mech. props. 79—38958
Ti alloy VT3-1, fatigue failure, surface finishing influence 80—60972
Ti alloy VT6, cyclic strength under programmed loading 78—7043
Ti alloy VT9, fatigue strength estimation after US hardening 77—12746
β-Ti alloys, annealed, faceted fracture 79—57102
Ti alloys, β-annealing and controlled rate quenching effects 78—80568
Ti alloys, data handbook of low temp. mech. and phys. props. 80—22153
Ti alloys, universal diags. of cohesive strength *(Russian)* 78—56733
Ti alloys VT5-1 and VT14, fatigue testing, low cycle, effect of testing method on fatigue 79—52515
Ti, beta III powder compact, fatigue origins 77—44351
Ti, commercial purity, cyclic behaviour and delayed softening 77—36641
α-Ti, fatigue crack growth, influence of grain orientation, SEM study 80—108550
Ti, fatigue damage, SEM, X-ray diffr. and surface trace anal. 80—85040
Ti, fatigue fracture surface microstruct., electron microscope obs. 78—60834
Ti, high purity, data handbook of low temp. mech. and phys. props. 80—22153
Ti, laser generated stress waves, effect on microstruct. hardness and strength 79—69192
Ti, mech. props., 20 to 300°C *(French)* 77—56018
Ti, mechanical deformation with superimposed insonation, volume effects 78—60723

fatigue continued

- Ti, notched sample, fatigue damage detection via optical correlation technique 78—35511
- Ti, sintered, fatigue strength, oxidation effect 79—96137
- Ti-Al (4 wt.%), sintered, long-time strength 80—40529
- Ti-Al-Cr-Mo system, VTZ-1 alloy, microstruct. influence on fatigue characts. 80—3195
- Ti-Al-Cr-Mo-Fe(V)(Zr), effect of structure and heat treatment on tensile strength, ductility, fatigue limit and notch sensitivity 78—56711
- Ti-Al-Cr-Mo-U, alloy VT22, phase composition and fatigue strength 78—3219
- Ti-Al-Cr-Mo-V(Fe), low cycle fatigue in repeated tension 80—76348
- Ti-Al-Mn, endurance with cyclic bending, effect of loading conditions 80—50724
- Ti-Al-Mo-Sn alloy, elastically and plastically deformed, positron annihilation meas. of deformation 80—21038
- Ti-Al-Sn (5, 2.5 wt.%) alloy, fatigue under combined alternating bending and torsional stresses 77—8923
- Ti-Al-Sn-Zr-Mo-Si-O-H, Si, O, H effects on fatigue, fracture and creep charact. 79—11697
- Ti-Al-U (6,4 wt.%), low and high cycle fatigue rupture at same load 78—3217
- Ti-Al-V, alloy 685, fatigue life, creep and dynamic strain ageing effect, 25 to 400°C *(French)* 80—45384
- Ti-Al-V (Mo-Sn)(Zr), environmental effects in alloy fretting, effect on fatigue props. 78—56787
- Ti-Al-V (6, 4 wt.%), cavitation induced erosion, under mill annealed, soln. treated and aged, and beta annealed conditions 79—8371
- Ti-Al-V (6, 4 wt.%), fretting corrosion of orthopaedic implant materials by bone cement 80—104813
- Ti-Al-V (6, 4 wt.%), friction characts. improvement by O_2 dissolution and controlled surface hardening *(French)* 80—45401
- Ti-Al-V (6, 4 wt.%), improvement of props. by ion implantation 80—16601
- Ti-Al-V (6,4 wt.%), fretting fatigue behaviour of temps. up to 600°C 80—21104
- Ti-Al-V (6,4 wt.%), H related fatigue fracture 80—76344
- Ti-Al-V (6,4 wt.%), high temp. fretting fatigue, fatigue and fretting wear 80—3197
- Ti-Al-V (6,4 wt.%), surface residual stresses, surface topography, fatigue behaviour 79—52366
- Ti-Al-V (6,4 wt.%), surgical implant ion beam textured, stress/strain relations, fatigue characts. 78—73297
- Ti-Al-V (6,4 wt.%), sustained loading charact. and H_2 effects 78—48515
- Ti-Al-V(6,4 wt.%), environmental fatigue crack propag. 77—36632
- αTi-Al-(Zr), embrittlement due to ageing 78—56673
- β-Ti-Mn, exam. of reloading yield points 78—72822
- Ti-Mo-V-Fe-Al (8,8,2,3, wt.%), exam. of stress controlled fatigue response 79—61734
- β-Ti-V (40 at.%), BCC, flow stress asymmetry and cyclic stress-strain response 77—36583
- Ti-V (40 at.%), BCC, single crystal, fatigue and slip 78—19854
- Ti-V-Fe-Al (10, 2, 3 wt.%), fracture toughness and stress corrosion resistance 80—100904
- Ti_3Al, cyclic deform., dislocation struct. 78—7003
- TiC layers, on steel and cemented carbides, load-bearing capacities 80—40606
- U-Mo (10 wt.%), commercial alloys, influence of metallurgical factors on fracture processes *(French)* 78—60751
- V alloy, fusion reactor first wall, thermal stress and creep fatigue limitations 79—76132
- V alloys, fusion reactor first wall and blanket material, props. for struct. appl. 80—30071
- V, and V-H, fusion reactor first wall material, cyclic deform. tests 80—30074
- W alloy, nonlinear compliance curves, caused by crack closure and fracture tests 77—56064
- W, cyclically deformed, electrical resistivity 77—52491
- W fibre reinforced Cu composite, hardening in two-phase material 77—52448
- W-Re, thin wires, fatigue limit and tensile strength 80—25834
- WC-Co (10%) alloy, high cycle fatigue, optical microscopy and SEM obs. 77—52494
- WC-Co hard-alloy cermets, strength, fatigue, static tests 79—29314
- Zn single crystals, fatigue failure at low temp., under low-freq. cyclic loads *(Russian)* 79—61697
- Zn, tension cycle close to soft loading, accumulation of damages, theory 77—14968
- Zn-Al eutectoid superplastic alloy, fatigue, microstruct. obs. and frequency effect 77—36659
- α-Zr and Zircaloy 2, fatigue, 20 to 700°C 77—70154
- α-Zr, grain-boundary sliding component in high temp. fatigue 80—50706
- Zr-Sn, grain-boundary migration during fatigue at 600 to 775°C 80—16443

fatigue cracks

- 2056 MW nuclear reactor pressure tubes cracking 78—82463
- acoustic emission monitoring 78—27706
- acoustic emission signals distrib. anal., fatigue life prediction 80—25852
- adhesively bonded metallic panels, 2-ply, finite element and integral eqns. anal. of fatigue crack growth 78—92347
- AE detection in aircraft wing test 78—60925
- aircraft wing, tests using acoustic emission source technique 77—16769
- Al alloy 2024-T3, fatigue crack closure with negative stress ratio, following single tensile overloads 78—64687
- Al alloy 7075-T6, fatigue crack propag. rate rel. to accumulated plastic strain rate, cold work effect *(Japanese)* 79—96115
- alloy steels, delayed retardation phenomena of fatigue crack growth, exam. 78—56745
- alloy structural steel, electron fractographic pattern of fatigue fracture under cyclic loading 77—56094
- alloys, dislocation pile-up model, fatigue crack nucleation at intermetallic particles 79—69189
- alloys, high-strength, subcritical crack growth 79—43494
- annular fatigue crack prod. in cylindrical specimens *(Russian)* 77—52559
- asymptotic stress intensity factors for fatigue crack-growth calculations 80—108529
- bending crack test, for fatigue crack propag. laws determ. *(French)* 77—51007
- biaxial stress field, stress ratio effect on fatigue crack growth 77—58617

tigue cracks continued

- bleeding system, used for flaw detection in aircraft industry 79—66226
- blunting and growth, prediction of threshold stress intensity using dislocation model 78—79662
- boiler steel fatigue crack propagation test results *(Hungarian)* 79—83293
- brass, crack propagation properties in rotating bending fatigue tests 77—32669
- α-brass, dislocation structure around crack tips in early stage of fatigue 78—60830
- α-brass, fatigue crack growth micromechanisms at low stress intensities 80—108570
- α-brass, fatigue crack propag., role of dislocation substruct. 80—60963
- α-brass, fractographic obs. of cracks in early stages of fatigue *(Japanese)* 78—7023
- brittle fracture, stability problem, three-dimensional linearised theory *(Russian)* 78—55606
- C-shaped fracture-toughness test specimens, stress, strain and deflection meas. 78—19963
- calculated model for initiation period *(Russian)* 77—25143
- cantilever beam method to investigate J_{Ic} and J_{Iscc} *(Chinese)* 78—15488
- cast materials for nuclear appls., low-angle fatigue and fatigue crack growth rates 80—5240
- cement, Portland, static and fatigue cracking morphology, SEM obs. 77—52493
- cement based materials, fatigue hardening 79—29086
- ceramics, lifetimes and slow crack growth prediction *(German)* 80—104250
- ceramics, subcrit. crack extension meas. with double-torsion specimens *(German)* 80—104359
- close-growth relationship *(German)* 77—7789
- closure, computer model, based on surface roughness and residual strain 77—73347
- closure, influence of mech. factors 78—67100
- closure analysis in fatigue crack growth 79—18825
- closure and delay effect under variable amplitude loading, finite element anal. 77—73331
- closure determ. using elec. pot. method, cf compliance method 78—5701
- closure in single overload cycles in single-edge-notched specimens 77—56066
- coke, breakage behaviour rel. to struct. 80—85026
- cold worked hole, expt. study of fatigue crack initiation and growth 79—79063
- complex stress 77—86175
- complex structure fatigue life prediction using critical location concept 78—59348
- compliance calibration, expt., of WOL specimen 78—19798
- composite material crack tip fatigue behaviour and stress state study *(Japanese)* 80—28470
- compressive load effect 80—30065
- compressive max. shear crack initiation and propag. 77—56065
- computer analysis of crack propagation 77—35094
- computer simulation of crack propagation, based on crack closure concept 78—68793
- computer simulation of propag., model based on Elber's eqn. *(Japanese)* 78—7030
- computer simulation of propag. based on BCS model *(Japanese)* 78—7029
- conference, Sheffield, England, 27-29 Aug. 1979 80—22132
- corrosion fatigue 77—4151
- corrosion-fatigue crack initiation in metals 77—40468
- corrosion-fatigue resistance, specimen with V-shaped stress concentrator and annular cracks *(Russian)* 77—16702
- crack closure, and delay effects under mode I spectrum loading, elastic-plastic anal. 80—19282
- crack closure related to crack propag., prediction method for crack growth 78—67099
- crack growth, anal., crack tip deform. modelling 79—41626
- crack growth measurement using acoustic emission, instrum., expt. 77—73421
- crack growth prediction methods, review 77—50983
- crack length indirect measurement during a fatigue test *(French)* 79—20312
- crack path prediction by finite element method *(Japanese)* 78—42568
- crack propag. estimation method in pre-strained and mean stressed samples 80—21067
- crack propagation, brittle amorphous solids 78—75721
- crack propagation, quantifying the parameters 80—100891
- crack propagation, under variable stresses *(Japanese)* 80—86028
- crack tip, plastic deform., metallographic anal. by recrystn. 80—85029
- crack-tip slip band blocked by grain boundaries, simple model 79—50665
- cracked sample stress meas. by US phase shift detection 77—28971
- cracking resistance investigation apparatus, for constructional materials in vacuum and gaseous media *(Russian)* 77—28940
- cracking-resistance evaluation, apparatus for rapid determ. of K_{Iscc} 77—77671
- cumulative damage approach using local stress/strain concepts for fatigue-life prediction 77—50984
- cumulative damage laws for initiation and stage I propag. 78—18248
- cumulative damage model, fatigue crack growth appl. 80—79232
- cup and cone fatigue fracture, electron fractographic obs. *(Japanese)* 78—72838
- current aspects 77—86156
- cyclic compression, behaviour study *(Japanese)* 79—50667
- cyclically loaded structures, effects of periodic proof and nondestructive testing 79—15946
- cylinder, hollow with internal circular crack, axially symmetric torsion determ. 80—64456
- cylindrical specimens, fatigue and crack generating and meas. device 79—52508
- damage parameter, energy based, for fatigue and creep-fatigue appl. 78—59347
- delay due to single cycle overload, analyt. prediction 78—5687
- depth meas. in threaded part of drill pipe by US inspection 79—1930
- design based on crack initiation and propag. *(Japanese)* 78—27611
- detection and rating by acoustic emission, review 80—104380
- development, fracture mech. 79—27588
- development in real structures, appl. to aircraft design 78—56769
- development under high-temp. single-stage, low cyclic loads, appl. to steel Kh18N10T 79—43389
- device for producing fatigue cracks in specimens 80—61051

fatigue cracks continued
diamond, cracking and fatigue under repeated indentations 77—59905
dimensions, recording method and sensor 77—63856
dislocation diffusion mech. of form. 78—60829
dislocation model, threshold stress intensity 78—18244
dislocation substruct. 77—86161
ductile materials, acoustic emission and fracture 77—56059
Dugdale crack closure analysis, under const. amplitude loading 79—50650
Dugdale crack model, continuous damage approach, to fatigue process 78—90780
Duralumin, fatigue cracks development, intermetallic inclusion influence 79—38962
dynamic fatigue tests, statistical reproducibility of crack propag. parameter 80—25842
dynamic treatment of growth *(Japanese)* 78—34084
early stage problems 78—56758
effective stress range factors in fatigue crack propag. 80—100924
elastic transpositions, numerical calc. 80—74809
elastic-plastic, growth under load cycling 77—59913
elastoplastic body, depend. of crack opening and plastic zone size on type of stress state 79—14348
electrical detection method 77—73382
electrically cond. materials, pulsed elec. meas. method *(French)* 79—29324
energy criteria in rupture and fatigue *(French)* 78—90771
energy-balance approach to fatigue crack growth 78—90773
epoxy resin, low temp. fatigue, tensile strength, Young's modulus *(German)* 78—76748
eutectoid thermomechanically treated, textural studies 80—29978
fatigue crack growth, model prediction, two coupled differential equations 78—67103
fatigue crack propag., plastic work role 79—79070
fission reactor cladding, strain ratcheting during power cycling 80—16442
fission reactor fatigue loading, growth of underclad flaws 79—22429
fission reactor materials, failure analysis by remote fatigue crack growth meas. system 80—68790
flaw detector for revealing fatigue cracks 79—66244
fracture mech., conf., Washington, USA (Sept. 78) 79—43422
fracture mechanic anal. of growth *(Japanese)* 77—77575
fracture mechanics anal. *(Japanese)* 78—7026
fracture mechanics parameters, applicability to creep, fatigue crack propag., at evalated temp., exam. using various materials *(Japanese)* 78—52962
fracture surface struct., effect of fracture surface closure mechanisms *(German)* 77—25159
fretting fatigue crack, initiation and propag. 77—73353
friction welded joints, strain distrib. and fatigue cracks of joint's subjected to repeated torsion *(Japanese)* 79—8350
fusion reactor first wall materials development evaluations, fatigue crack growth testing optimisation 80—35444
gas turbine airfoils, protective coatings, degradation characts. and methods of application 79—24670
glass fabric reinforced organic-matrix, interlaminar fracture studies 80—55495
glass fibre reinforced epoxy, interlaminar crack growth during fatigue 80—11763
glass fibre reinforced polycarbonate, fatigue crack propag., mean stress effect *(Japanese)* 79—66151
graphite fabric reinforced organic-matrix, interlaminar fracture studies 80—55495
graphite reinforced epoxy steel scarf joint, adhesively bonded, exam. of failure 78—92350
growth, assessment of threshold 78—63392
growth, closure, prediction and fracture mechanics 79—50653
growth, in diffusion model 79—72860
growth, investigation method for constant amplitude of stress-intensity coeff. 77—40491
growth, mechanisms, crack geometry 78—64703
growth, model prediction, two coupled differential equations 78—67103
growth, parameter representation 79—68650
growth at high-temp., fracture mech. appl., review 79—41628
growth data, three component model anal. 80—3161
growth dependence on loading parameters, phenomenological model 80—38340
growth eqn., stress intensity factor rationalisation 79—41620
growth model, notch anal. of fracture approach 78—52984
growth near free surface, BCS model 77—3774
growth prediction, aircraft structures, under flight-by-flight loading 79—50651
growth prediction methods, model development 78—34074
growth propagation, delayed retardation phenomenon, from single overload 78—92317
growth rate, K_{1c} range depend. *(Russian)* 77—59899
growth rate correlation 77—48544
growth rate data, effect of meas. precision and data processing procedures on variability 79—61817
growth rate determ., phenomenological eqn. based on fracture mechanics *(German)* 77—21262
growth rate prediction, using phenomenological approach 78—67101
growth rate rel. to loading cycle parameters, review *(Russian)* 79—28038
growth rate testing, COD technique for crack length meas. 77—56170
growth rates and kinetic diags. of fatigue fracture *(Russian)* 78—11456
growth rates cumulative damage, under random loads algorithm of hysteresis loop counting 80—21064
growth retardation model, based on critical damage approach 80—99960
growth testing, using computer-controlled stress intensity gradient technique 80—76432
growth threshold, practical implications 77—86169
growth under variable amplitude loads *(Japanese)* 78—7033
Hastelloy X, high temp. low cycle fatigue tests, ductility, fracture 77—90523
Hastelloy-X, fatigue crack propag. at elevated temps. in solid solution strengthened superalloys 78—39895
Hastelloy-X, low cycle fatigue crack propagation at 25°C and 760°C 80—104270
Haynes alloy 188, fatigue crack propag. at elevated temps. in solid solution strengthened superalloys 78—39895
hybrid bodies, propagation of multiple ended fatigue crack 78—68801

fatigue cracks continued
hydraulic component fatigue crack acoustic emission inspection 77—40513
impact bending, specimen parameter effect on crack propag. 77—86242
impact test, finite element analysis 78—68806
in plane strain displacement near crack tip at high temp., optical meas. 79—32412
IN-100, fatigue crack growth retardation at elevated temp. 80—3158
inclined-strip-yield crack tip plasticity model, appl. to fatigue crack growth 80—38333
Incoloy 800, fatigue crack behaviour in bending and pull-push modes 77—81315
Inconel, fatigue crack growth rate in high temp., high purity oxygenated water 80—40622
Inconel, pressure vessel bottom, subcritical crack growth in ligament between instrumentation rods 79—22428
Inconel 600 and 718 in liquid Na environment, fatigue crack propag. 80—40624
Inconel 718, environment effect on high temp. fatigue crack growth 80—30090
initiation, microscopic aspects *(Japanese)* 77—28898
initiation, rel. to grain boundaries, stress gradients and cross slip 77—27890
initiation in low cycle range *(German)* 79—15781
internal, finite element calc. of fatigue growth 80—1472
internal elliptic cracks in thick plate, fatigue growth calcs. 77—80112
internal fatigue crack growth in vacuum 78—56729
iron, Armco, effect of low temps. and heat treatment on growth rate of fatigue cracks 79—57027
j integral applications for short fatigue cracks at notches 80—38332
life prediction in initiation and propag. stages, review 79—68596
linear viscoelastic body, opening and closing of growing crack under alternating tensile and compressive loads 79—23282
low cycle, test machine rigidity effect on kinetics 78—15632
low-cycle fatigue, rel. between fatigue crack growth rate props. 80—5987
LWR, risk-sensitive Markovian policies for detection and maintenance of fatigue cracks in pressure vessels 79—54534
macroscopic residual stress at tip, X-ray obs. and finite element anal. *(Slovak)* 78—19885
martensitic steel, fatigue crack nucleation, rotating beam determ. of true min. stress *(French)* 77—25122
metal, cyclic and damage constitutive laws, calculation methods *(French)* 79—43408
metal, fatigue crack growth micromechanisms at high stress 80—108569
metal, growth rate characts., fracture mechanics fatigue design methods 78—7034
metal, overload effect on fatigue crack growth, fracture toughness prediction *(Polish)* 79—34134
metal fatigue crack detection using nondestructive evaluation (NDE) methods 80—71826
metal propagation and initiation, high frequency, US meas. 78—60978
metal structural part, fatigue crack propag., new approach 78—56752
metallic alloys, fracture toughness and fatigue crack growth data, compendium of sources 78—84963
metallic material, fatigue cracking, cyclic fracture toughness determ., critical state *(Russian)* 79—29173
metallic materials, distrib. characts. of fatigue crack propag. life *(Japanese)* 80—25847
metallic materials, fatigue life distrib. theoretical obs. near fatigue limit 80—59569
metallic materials, tenacity parameters 80—60973
metallic structures initial fatigue quality characterisation using equivalent-initial-flaw-size distribution 80—58978
metals, fatigue crack growth rate, expt. programme for determ. in thickness direction 79—57168
metals, fatigue failure, book 78—76747
metals, fatigue lives, eval. using crack initiation model *(Japanese)* 80—104258
metals, fatigue resistance, processes leading to failure 80—94907
metals, fracture toughness charact. in fatigue 79—15790
metals, growth calc. 78—27638
metals, growth rate in thickness direction, expt. programme 79—57168
metals, US device for determining growth rate 78—60917
metals and alloys, growth at low stress intensities 77—86167
micro and macro fracture mechanics, exam. of brittle fracture and fatigue crack growth 78—60774
microcrystalline alloys, metastable, rapidly quenched particulates, props. appl. and production 80—84887
microscopic aspects of initiation *(Japanese)* 77—32678
microwave detection of third-order nonlinearities 80—55594
mixed spatial elasticity problems, variational soln. *(Russian)* 79—9110
moire system, using fringe multiplication method for strain field anal. around a fatigue crack 79—36832
Multimet, fatigue crack propag. at elevated temps. in solid solution strengthened superalloys 78—39895
new measurement and observation techniques 80—45463
Nimanic 80A, inhomogeneity effect of cyclin strain on crack initiation 78—48532
Nimonic 105, overaged, creep and fatigue crack growth 77—86138
Nimonic PE16, fatigue crack growth rate, temp. effect 77—77568
nonpropagating, analytical explanation, strain intensity factor criterion 79—68655
nonpropagation in specimen with crack *(Japanese)* 77—77571
notch analysis for fracture toughness and fatigue crack propagation threshold 77—35086
notch contribution to crack length 77—65715
notch effects and surface hardening effects on growth 77—86165
notch fatigue cracks, propag. and initiation, elastic-plastic fracture mechanics 80—38329
notched beam, fatigue crack emanates from notch root, fracture strength 78—72866
notched components, fatigue crack growth 78—83329
notched member fatigue life predictions combining crack initiation and propagation 80—38328
notched plates, fatigue crack growth prediction, under variable amplitude loading history 78—18233
notched plates, fatigue strength 78—9601
nuclear components, struct. integrity assessment mat. prop. variations 78—89953
nuclear reactor materials, PWR, H_2-assisted fatigue-crack growth model 80—71745

fatigue cracks continued
nucleation from particles, statistical aspects, expt. test 80—89345
nucleation mechanism, effect of dislocation substructure 77—86140
numerical method of processing propag. data 77—73320
nylon 66, fatigue crack propagation, effect of moisture 80—3166
optical fibres, plastic coated fused silica, dynamic fatigue data reliability 78—87166
Paris differential eqn., numerical calculation of parameters 78—63384
Paris eqn. for crack growth, C and m parameters 78—18243
phase defect inspection for determ. of moment of origin of fatigue cracks 79—52578
pinion, cracking of accidentally nitrided keyway, leading to fatigue 77—32694
plastic blunting process during propag., additional evidence 77—63781
plastic wake zone effect on fatigue crack propag. investigated with optical interference technique 80—55502
plastic work during fatigue crack propag. 77—56068
plastic zone at tip of fatigue cracks, X-ray diffr. study 77—56058
plastics, fatigue fracture props. correl. with viscoelastic damping 78—52993
plates and pipes, fatigue crack growth model for part-through flaws 80—10197
PMMA, effect of temp. on freq. sensitivity of fatigue crack propag. 78—76762
PMMA, fatigue crack growth rate freq. depend. 79—74256
PMMA, fatigue crack growth under biaxial stress 79—70144
PMMA, fracture under biaxial stresses, simple testing technique 77—73383
polyacetal, exam. of fatigue crack propag. 78—48497
polycarbonate, craze roles in fatigue 79—29183
polycarbonate, cyclic deformation and craze growth 78—76759
polycarbonate, effect of temp. on freq. sensitivity of fatigue crack propag. 78—76762
polycarbonate, fatigue crack propag., mol. wt. depend. 80—50700
polycarbonate, glassy, fatigue crack initiation in high strain fatigue tests 80—97564
polyethylene, fatigue, fractographic study 80—30101
polyethylene, fatigue crack growth charact. 80—30100
polymer, fatigue crack growth, model 78—15506
polymer, glassy, generality of discontinuous fatigue crack growth 77—32677
polymer, viscoelastic, fatigue, fractographic study 80—30101
polymer, viscoelastic, fatigue crack growth charact. 80—30100
polymer-metal sliding, wear eqn. in terms of fatigue and topography of sliding surfaces 80—108597
polymeric fibres, cyclic tension endurance, Prevorsek-Lyons theory 78—52967
polymers, fatigue crack growth model 79—70160
polymers, fatigue crack growth model 79—70161
polypropylene, crystalline, morphological aspects of crack growth 78—76761
polypropylene, microstruct. changes during large strain cyclic deform. 80—66627
polysulphone, effect of temp. on freq. sensitivity of fatigue crack propag. 78—76762
potential methods, for crack length determ. of fatigued specimens *(German)* 80—81167
prediction in structural element 79—66165
prediction of growth rate, theory, mechanism, expt. results 77—86166
pressure vessels, AE during fatigue crack expansion 80—108675
pressure vessels, elastoplastic fracture modelling, acoustic emission 80—35303
propagation, behaviour, initial, 1st. stage *(Japanese)* 77—48539
propagation, continuum mechanics model 78—5692
propagation, data anal., new method 77—73321
propagation, effect of 2- or 3-dimensional macrodefect *(Japanese)* 80—104261
propagation, fracture of practical materials, anal., recent developments, review 79—43428
propagation, in deformable media with nonlinear characteristics, model 78—63393
propagation, model, low cycle, cyclic stress-strain response determinations 79—68653
propagation, theoretical expl. of delaying effects of overloads 78—67093
propagation and strain softening under hydrostatic press. 77—16691
propagation and strain softening under hydrostatic press. 77—16692
propagation at stress amplitude below fatigue limit *(Japanese)* 79—19315
propagation behaviour, under stress amplitude, below fatigue limit on fatigue life *(Japanese)* 78—92331
propagation in biaxial stress field 77—50994
propagation in ductile-brittle transition temp. range 77—59929
propagation investigations, US testing equipment 80—81247
propagation kinetics in circular cylinder with annular crack *(Russian)* 77—70145
propagation model for strain hardening materials 78—18236
propagation rate, mechanical property effects of materials 78—90776
propagation theory, threshold derivation, Paris regime crack growth rate 78—83338
propagation theory, threshold derivation 78—83337
propagation under variable amplitude loading, math. model 80—16414
pseudoelastic single crystal fatigue 79—52364
PVC, effects of mol. wt. and plasticiser on fatigue crack propagation rates 79—5044
PVC, fatigue crack growth rate, tensile cyclic tests 79—5043
PVC, glassy, fatigue crack initiation in high strain fatigue tests 80—97564
PVC, plasticised, fatigue, fractographic study 80—30101
PVC, plasticised, fatigue crack growth charact. 80—30100
PVC, rigid, fatigue crack growth, under biaxial stress 79—70144
PWR pressure components reliability and residual life evaluation and precipitation 79—20191
PWR pressure vessel reliability, failure anal. 77—74962
quasibrittle body with internal determ. of crack growth kinetics and life expectancy 78—63383
quasistatic growth under cyclic loading and displacement 79—10531
radial-bolt-hole cracks in mechanically fastened aircraft structs., measurement of size using Doppler shift 80—55597
radiography, effect of stress on crack detection 80—40653
radiography inspection, improved 77—86262

tigue cracks continued
refractories, fatigue, effect of texture/crack relationship *(German)* 80—25829
refractories, fatigue behavior, effect of texture and crack kinetics, AE anal. *(German)* 80—21061
relation between da/dN and K_I *(Chinese)* 79—41611
Rene 95, Ni based superalloy, effect of grain size and gamma prime size, on fatigue crack propag. 78—64686
retardation at elev. temp., hold time effect of single overload 79—79068
rock, dilatancy anisotropy and response to large cyclic loads 80—21715
SAW, harmonic generation at unbonded interfaces and fatigue cracks 78—90562
SEM of bulk specimens using imaging of subgrains 80—66609
semi-elliptical fault fatigue propagation, three-dimensional anal. *(French)* 79—23283
servo-hydraulic test system, for fatigue crack propagation studies under biaxial loading 80—76431
shaft or axle type components, crack propagation and residual strength, problems specification 78—51120
short cracks, exam. of propagation 80—10196
silicide coatings, on steel, exam. of fracture processes 78—44206
β-Sn, cryst., fatigue crack propag. mechanism 80—25861
spectrum growth under cyclic compressive-compressive loads 78—79267
speed of subcritical development and plastic disintegration 77—3782
stable growth props. 79—68648
stainless steel, double cantilever sample, stress meas., US technique 77—25219
stainless steel, types 304 and 308, fatigue crack growth at elevated temps. 77—46288
static fatigue limit in the thermal activation approach to subcritical crack growth 80—30075
statistical approach to fracture, fatigue crack growth of defects 80—1487
statistical size effect for fracture probability functions 77—50995
statistics of crack growth data 77—24351
steady state growth rate, empirical formulations for anal. and prediction trends 77—90450
steel, 00Kh12N3D, 15Kh2NMFA, loading freq. effect on fatigue crack development 79—87727
steel, 0.40/0.50 C, crack growth, Weibull analysis 78—92319
steel, 0.54% C, fatigue crack accel. and closure in rotating bending tests, in annealed or quenched/tempered state 79—43383
steel, 1045, fatigue crack growth testing, decreasing stress intensity technique, computer-controlled 78—72949
steel, 17KhG2SAFR, 45 and fatigue cracking under cyclic bending, 40 kH *(Russian)* 78—31506
steel, 18% Ni maraging, fatigue strength, effect of soln. treatment and inclusions 78—23805
steel, 20, fatigue endurance tests in moist H_2S *(Russian)* 78—31510
steel, 35, fracture characteristics, notch sharpness effect in impact tests 79—52536
steel, 4140, fatigue crack initiation and microcrack growth 79—24617
steel, 4140 compact, fatigue crack growth delay, yield strength, neg. stress ratio depend. 78—3210
steel, 45, depth length relationship of fatigue crack developing in circular specimens during bending 79—11705
steel, (0.36 wt.% C) Ni-Cr-Mo, electroslag refined, fracture toughness and fatigue behaviour 80—81171
steel, A516-60, press. vessels, fatigue crack growth rate 77—77585
steel, A533 B, fatigue crack propagation, grain size and temp. effects 78—56727
steel, A533 grade B, class 1, in PWR coolant, fatigue crack growth 77—77584
steel, A533B alloy, fatigue crack growth of irradiated pressure vessel steels in simulated, reactor-grade water environment 80—97582
steel, A553, fatigue crack growth, delayed retardation phenomena, stress ratio at baseline loading effect 79—79065
steel, acoustic emission anal., during fatigue crack growth 77—56090
steel, AISI 4140, cyclic crack opening displacement behaviour during high-amplitude block loading 80—45375
steel, Al-killed, fatigue life for program loading of multiple repeated two step stresses *(Japanese)* 80—66632
steel, alloy, HP9-4-20, retained austenite influence on fatigue crack propagation 80—16432
steel, alloy, HY140, fatigue crack initiation and propag. at notch tip 78—80647
steel, alloy, HY180, fatigue crack initiation and propag. at notch tip 78—80647
steel, alloy, Ni (5.5 wt.%), fatigue fracture toughness, crack propag., at low temp. 78—68823
steel, alloy, Ni-Co-Mo, fatigue crack growth, during impact tests exam. of kinetics 78—88525
steel, alloy, Ni-Cr-Mo, alloys SNCM8, SAE 4161, heat treated, residual stress at fatigue fracture surface *(Japanese)* 78—64622
steel, alloy, quenched and tempered, fatigue crack propag., effect of mean stress 77—59914
steel, alloy, Si-Mn(Mn-Cr), heat treated, exam. of microfractographic aspects of fatigue cracks *(Japanese)* 78—52959
steel, alloy, ultrahigh-strength, near threshold fatigue crack propag., microstructure effects 77—86168
steel, alloy 18G2AV, residual stress distrib. effect on fatigue crack growth 79—57111
steel, anisotropic rolled plate, fatigue crack growth, rel. to laminated struct. and inclusions 78—92313
steel, API 5LX-X60, pipe fatigue strength under cyclic internal pressure, inner surface defects 79—38980
steel, austenitic, creep fatigue cycling, electric crack growth 79—29209
steel, austenitic, martensitic transform. at propagating fatigue crack 78—19745
steel, austenitic, overheated, ESR, low alloy, fatigue crack growth rate 79—34141
steel, austenitic, precipitation hardening, effect on fatigue strength 78—84829
steel, austenitic 03KhAG19, fatigue crack development at normal and low temps., struct. effects *(Russian)* 78—35480
steel, austenitic stainless, effect of irrad. and other factors on fatigue crack propagation 79—20194
steel, austenitic stainless, fatigue crack growth rates in type 316, effects of overloads on growth rate 78—64688
steel, austenitic stainless, fatigue crack propagation, effect of neutron irradiation 80—97583

fatigue cracks continued
  steel, austenitic stainless, fatigue crack propagation, influence of neutron irradiation 80—97584
  steel, austenitic stainless, fusion reactor first-wall and blanket material, mech. props. 80—34074
  steel, austenitic stainless, low-cycle fatigued at high temps., crack obs. 77—1874
  steel, austenitic stainless, neutron irrad. effects on fatigue crack propag. 80—29069
  steel, austenitic stainless, type 07Kh25N12G2T, US monitoring of fatigue crack growth 78—60917
  steel, austenitic stainless, type 304, 316, crack growth behaviour at elevated temp., freq. effects 79—83326
  steel, austenitic stainless, types 304 and 316, environment effect on crack growth, under creep and fatigue conditions 80—85035
  steel, austenitic stainless in liq. Na, mechanical props., review 79—20150
  steel, austenitic stainless type 304, time-depend. fatigue, mechanistic model 80—100925
  steel, austenitic stainless type SUS 316, low cycle fatigue tests, freq. effect on notch sensitivity at elevated temps. *(Japanese)* 80—104260
  steel, ball bearing, fatigue damage, influence of dispersed phases in martensitic matrix 80—108549
  steel, ball bearing, heat treated, fatigue crack propag. 79—20188
  steel, brass clad plate/roll bonded Ni clad, fatigue crack growth behaviour 80—40484
  steel, C, and high strength, fatigue crack propag. under periodic overstressing, design criterion *(Japanese)* 79—20166
  steel, C, crack initiation and propagation life under repeated impact tensile loads *(Japanese)* 80—104264
  steel, C, failure mechanisms in impact fatigue 80—40493
  steel, C, fatigue, residual stress and crack growth expts., notch and surface treatment effects 79—8356
  steel, C, fatigue crack exam. using slip initiation phenomena *(Japanese)* 77—8930
  steel, C, fatigue crack features, in S 35 C and SK 5, anal. by precision matching method *(Japanese)* 78—52955
  steel, C, fatigue crack growth in air and seawater, under constant amplitude and random loading 78—64679
  steel, C, fatigue crack growth rate in high temp., high purity oxygenated water 80—40622
  steel, C, fatigue crack propag., crack closure, dislocation struct., electron microscopy obs. *(Japanese)* 80—25845
  steel, C, fatigue crack propag., transient effects 77—56053
  steel, C, fatigue crack propag., transient effects *(Czech)* 77—63775
  steel, C, fatigue crack propag. and crack closure, of part through cracks *(Japanese)* 78—72842
  steel, C, fatigue crack propag. and fractography under periodic overstressing, exam. *(Japanese)* 78—52958
  steel, C, fatigue crack propag. in biaxial stress fields 80—40494
  steel, C, fatigue crack propagation in sheet, influence of struct. of ferrite-pearlite bands *(French)* 80—76338
  steel, C, fatigue subsurface crack initiation, result of residual stresses 80—25833
  steel, C, fracture dynamics at high frequency loading *(Czech)* 80—45391
  steel, C, heat treated, exam. of microfractographic aspects of fatigue cracks *(Japanese)* 78—52959
  steel, C, non-propagating microcrack, opening and closing behaviour in rotating bending and torsional fatigue *(Japanese)* 80—25846
  steel, C, transition from initiation to propagation of fatigue cracks 78—68802
  steel, C, type 45, crack form. mechanism during fatigue 79—38957
  steel, C, wear charact. of worn surface layer under lubrication *(Japanese)* 78—35526
  steel, C and alloy, notched beam, fatigue crack emanates from notch root, fracture strength 78—72866
  steel, C-Mn, fatigue crack growth retardation following load reduction 79—70141
  steel, case hardening and carbonitriding treatment, mech. props. testing *(French)* 77—59991
  steel, cast, fatigue from cast-to-shape notches 77—16679
  steel, cast, plain C, C-Mn and low-alloy fatigue from notches 77—16678
  steel, Co-Cr-Mo, type HY 180 correl. between advanced NDT evaluation methods and fracture mech. parameters 80—97675
  steel, Cr, cast, fracture toughness and fatigue crack propagation, structural components of hydro-turbines, in water and air 78—68822
  steel, Cr-Cu-Mn, fatigue crack propag. rate eval. by J integral method *(Japanese)* 79—8346
  steel, Cr-Mo, impact fatigue crack growth at low temps. *(Japanese)* 80—104266
  steel, Cr-Mo, Mn-V, V, fracture toughness, pressure vessel appl. *(Czech)* 79—79094
  steel, Cr-Mo, notched specimens, fatigue strength distrib. *(Japanese)* 80—66633
  steel, Cr-Mo, notched specimens, statistical eval. of fatigue life and fatigue limit and life distrib. *(Japanese)* 79—61702
  steel, Cr-Mo (2.25,1 wt.%), exposed to H_2-H_2O-H_2S environment, fatigue crack growth 80—40623
  steel, Cr-Mo-V, brittle failure, heat treatment and influence of cold plastic deform. 78—72858
  steel, Cr-Mo-V, cast, strain intensity approach of high temperature fatigue crack growth and failure 79—20175
  steel, Cr-Mo-V, fatigue crack growth rate and threshold under oxidising conditions 79—20272
  steel, Cr-Mo-V, low cycle fatigue crack propag. at a notch under pulsating load 80—40492
  steel, Cr-Mo-V (1 wt.%) oxidation assisted crack growth during high cycle fatigue at 550°C 77—16742
  steel, Cr-Mo-V alloy, crack growth during strain fatigue at 825K 78—39890
  steel, Cr-Ni-Mn, AISI 4340, correl. between advanced NDT evaluation methods and fracture mech. parameters 80—97675
  steel, crack propagation, struct. effects 79—52370
  steel, crack propagation properties in rotating bending fatigue tests 77—32669
  steel, cracking resistance of high-strength 40Kh and 35KhGSA, tempering temp. influence *(Russian)* 79—52252
  steel, Cu-Zn, brass clad, fatigue crack growth behaviour 80—40484
  steel, cyclic fatigue loading, effect of plastic zone size, −196°C to room temp. *(German)* 79—1915

fatigue cracks continued
  steel, ductile structural, fatigue crack propag. rate and striation spacing 80—93635
  steel, duplex ferrite-martensite, microstructure resistance optimisation 80—40482
  steel, eutectoid, fatigue crack tip props. in rotary bending and cyclic torsion 77—32668
  steel, eutectoid, high strength, unnotched specimens, fatigue crack init. and propag. 77—56098
  steel, fatigue crack, decrease in growth rate after thermal treatment and reduced load *(Russian)* 77—25142
  steel, fatigue crack depth meas. by US technique 77—9006
  steel, fatigue crack growth, exam. of some aspects 78—56772
  steel, fatigue crack growth eqn., correlation of threshold stress intensity factor, review 79—34127
  steel, fatigue crack propag., data anal., new method 77—73321
  steel, fatigue crack propag., quantifying the parameters 80—100891
  steel, fatigue crack propag., single overload effect 77—86170
  steel, fatigue crack propag. data, Weibull anal. 80—16416
  steel, fatigue crack propag. in weld 77—81324
  steel, fatigue crack propag. kinetics *(Russian)* 77—70146
  steel, fatigue crack propag. near to threshold stress intensity 80—100898
  steel, fatigue crack propag. rate and stress intensity factor at varying stress ratio 78—7049
  steel, fatigue crack propag. under random loading 78—76726
  steel, fatigue crack propagation rate in types 15KP, ST3, 15G and 10G251 with different yield strengths 78—52987
  steel, fatigue crack tip plastic deform., X-ray diffr. investigation *(Russian)* 80—104251
  steel, fatigue cracking, statistical theories of scale effect, expt. verification *(Russian)* 77—28884
  steel, fatigue cracking diagrams *(Russian)* 79—29301
  steel, fatigue damage and crack propagation, classification zone approach 77—56106
  steel, ferritic, clad with austenitic steel 309, US detection of undercladding microcracks *(Italian)* 80—108683
  steel, ferritic-martensitic, fatigue crack tip plastic zone *(Japanese)* 80—71738
  steel, ferritic-pearlitic, fatigue crack development, load-cycle assymmetry coeff. effect 79—87710
  steel, fracture mechanics appl. to H_2 embrittlement under press. *(French)* 78—23821
  steel, fracture micromechanisms, fracture toughness, exam. 78—56766
  steel, fracture toughness charact. in fatigue 79—15790
  steel, hardened and casecarburized, fatigue crack initiation, propag. and termination, notch depth effects *(Japanese)* 78—7022
  steel, heat treated high strength, X-ray diffr. anal. of residual stress 80—3200
  steel, high C, pearlitic, non-metallic inclusion effect on threshold behaviour of fatigue 79—91786
  steel, high Nb, HSLA, low temp. fatigue props. 80—40490
  steel, high strength, 300-M, slow fatigue crack growth, threshold behaviour, temper embrittlement, impurity segregation effects 77—86152
  steel, high strength, crack growth anal., variable amplitude block loading effects 77—8953
  steel, high strength, fatigue crack growth 78—64697
  steel, high strength, fatigue crack initiation and early growth 78—7009
  steel, high strength, fatigue crack propag., stress intensity threshold levels 77—73324
  steel, high strength, fatigue crack propag. and fractography under periodic overstressing, exam. *(Japanese)* 78—52958
  steel, high strength, increasing resistance to cracking, use of overheating before quenching *(Russian)* 77—25135
  steel, high strength, low alloy, fatigue crack growth from a surface flaw 78—68803
  steel, high strength, strain concentration and occurrence of fatigue cracks in welded joint *(Japanese)* 77—90452
  steel, high strength, WT 80C, fatigue crack propag. and crack closure behaviour, under various loading conditions 78—68795
  steel, high strength 4340, fatigue crack growth resistance, fracture mechanism effect *(Japanese)* 80—104265
  steel, high strength alloy, near threshold fatigue crack growth, prior austenite grain size effect 78—39903
  steel, high strength HP 9-4-20, retained austenite influence on fatigue crack propag. 80—21106
  steel, high strength low alloy, plastic work during fatigue crack propag. 77—56068
  steel, high tensile strength, base plate and welded joints, exam. of fatigue crack growth rate *(Japanese)* 78—52956
  steel, high-strength, fatigue crack growth rate and crack tip shapes, cyclic bending *(Russian)* 80—71740
  steel, HT60, fatigue crack propag. work coeff. 80—16422
  steel, HT80, fatigue crack closure over stress ratio range, stress intensity threshold 78—80619
  steel, HY140 and HY180, fatigue crack init. at notch tip, early stage propag. *(Japanese)* 78—7021
  steel, hybrid bodies, propagation of multiple ended fatigue crack 78—68801
  steel, kinetics of fatigue crack propagation 78—68804
  steel, low alloy, 10KhSND, 16G2AF, welded joint low-cycle fatigue during crack form. and propag. during biaxial bending 79—11704
  steel, low alloy, A533B, fatigue crack prop. 78—35517
  steel, low alloy, BS 4360-50C, stress ratio and freq. effect on fatigue crack growth 80—21068
  steel, low alloy, constructional, fatigue cracking in corrosive media 78—85081
  steel, low alloy, crack propag. anal. in delayed fracture under repeated load, internal friction model 79—79064
  steel, low alloy, creep crack growth, microstruct., fatigue effects 80—7672
  steel, low alloy, exam. of fatigue crack growth, and Paris Law parameter relationship 78—92343
  steel, low alloy, fatigue crack growth rate in high temp., high purity oxygenated water 80—40622
  steel, low alloy, fatigue crack nucleation under high cycle fatigue and uniaxial loading 79—79060
  steel, low alloy, fatigue crack propag. in deaerated distilled water 77—25177
  steel, low alloy, high strength, fatigue crack growth, in presence of welding residual stresses *(Russian)* 80—71739

fatigue cracks continued
- steel, low alloy, microstruct. effects on fatigue at intermediate and high crack growth rates 79−74247
- steel, low alloy, precracked, crack growth and propag., repeating load effect in delayed failure 78−19861
- steel, low alloy, Q1N, fatigue crack growth under random load, mean stress and amplitude distrib. 77−73319
- steel, low alloy, tempered martensite embrittlement and crack initiation *(Japanese)* 79−66149
- steel, low alloy, thermally fatigued, fracture toughness 78−72872
- steel, low and medium C, fatigue crack growth rate, kinetic eqn. of temp. depend. *(Russian)* 77−25136
- steel, low C, and hardened and tempered, impact specimen fractures, stress concentrator sharpness effect on size of tough component 78−7015
- steel, low C, annealed, fatigue crack propag. law under elastic-plastic and general yield conditions *(Japanese)* 77−48538
- steel, low C, crack propagation energy rel. to temp., time factors 79−29179
- steel, low C, effect of heat treatment on resistance to fatigue crack propag. 80−11675
- steel, low C, fatigue crack plasticity, effect of water vapour 78−64678
- steel, low C, fatigue crack propag. and crack closure behaviour, under various loading conditions 78−68795
- steel, low C, fatigue crack propag. and cumulative damage under periodic overstressing *(Japanese)* 77−12692
- steel, low C, fatigue crack propag. prestrain effect *(Japanese)* 79−96116
- steel, low C, fatigue crack propagation in smooth specimen, strain ageing effect *(Japanese)* 79−20163
- steel, low C, fatigue crack tip, observation of crack closure phenomena, by electron microscopy 78−68794
- steel, low C, high cycle fatigue, crack initiation model *(Japanese)* 80−104258
- steel, low C, low temp. effect on rate and fractographic features of fatigue cracks 78−39909
- steel, low C, prior austenite grain size, effect on near threshold fatigue crack growth 78−92341
- steel, low C, prior austenite grain size, effect on near threshold fatigue crack growth 78−92342
- steel, low C, S 35 C, annealed, crack initiation life, anal. of smooth and notched specimens *(Japanese)* 79−8347
- steel, low C, specimens with notch and fatigue crack, fracture surface features 79−43417
- steel, low C, type AISI 1018, microstruct. effects on fatigue crack growth 79−61718
- steel, low C 08Kp sheet, development at temps. of +20 and −160 degrees C 78−35505
- steel, low C alloy, SNCM2, waveform effect on corrosion fatigue crack growth in NaCl soln. 80−21163
- steel, low C ferritic, fatigue crack growth micromechanisms at low stress intensities 80−108570
- steel, low-alloy samples with fatigue crack, work of crack propag. and fracture toughness 79−38959
- steel, low-C, fatigue strength and crack propag. behaviour under impact program loading conditions *(Japanese)* 80−66635
- steel, low-C, types 535C, SB 42-B, fatigue crack propag. and crack closure behaviour under plain strain conditions *(Japanese)* 80−81160
- steel, maraging, fatigue crack growth, during impact tests, exam. of kinetics 78−88525
- steel, maraging, Ni (18 wt.%), fatigue crack initiation and propag. in earlier stage *(Japanese)* 77−8937
- steel, maraging, Ni (18 wt.%), with aged struct. at low temp., delayed failure crack and fracture toughness 78−7047
- steel, maraging, precipitation hardening, struct. and fracture *(German)* 79−61696
- steel, maraging, type 200, effect of freq. on cyclic crack growth in salt water environment 78−64680
- steel, maraging and low-alloy, electron fractographic analysis of fatigue fractures 79−38965
- steel, maraging type with 18% Ni, ageing treatment effect on fatigue crack propag. 80−16411
- steel, martensite and ferrite-pearlite, fatigue crack growth rates, stress ratio dependence 79−70148
- steel, martensitic, fatigue crack form. associated with cyclic slip deform. along prior austenite grain boundaries 78−60831
- steel, martensitic, low tempered, high strength, fatigue crack, propag. rate *(Czech)* 78−64770
- steel, martensitic, Ni-Cr-Mo, fatigue crack initiation and propag. in water 77−9000
- steel, martensitic-ferritic, sub-surface strengthening model for non-propag. fatigue crack 80−21070
- steel, medium C, fatigue crack propagation under repeated two-step loadings above and below threshold condition *(Japanese)* 79−38945
- steel, metastable austenitic stainless, fatigue damage, static and dynamic simultaneous obs. *(French)* 78−88516
- steel, mild, acoustic emission monitoring during crack propagation 79−86313
- steel, mild, annealed, fatigue crack init., microstructure and strain ageing effect 77−86162
- steel, mild, creep in low endurance fatigue 78−19865
- steel, mild, exam. of fatigue damage, using thermography 78−92356
- steel, mild, fatigue crack arrest and retardation, load stepdown effect 80−108527
- steel, mild, fatigue crack growth from a surface flaw 78−68803
- steel, mild, fatigue crack growth in compression, notch effect 80−30065
- steel, mild, fatigue crack initiation, fractographic exam. *(Japanese)* 78−52957
- steel, mild, fatigue crack initiation 77−86163
- steel, mild, fatigue crack propag., stress ratio effect *(Japanese)* 79−38946
- steel, mild, fatigue crack propagation, stress ratio effect 80−71733
- steel, mild, fractography study of shear mode fatigue crack growth by etch pits *(Japanese)* 80−108545
- steel, mild, fracture toughness meas. with reinforced-double-cantilever-beam specimen 77−4842
- steel, mild, low cycle fatigue crack propag. at a notch under pulsating load 80−40492
- steel, mild, mode II fatigue crack growth threshold 78−92362
- steel, mild, plastic deform. around fatigue cracks, X-ray microbeam and recrystn. studies 80−35258

tigue cracks continued
- steel, mild, precracked Charpy bars, plasticity spread 80−16415
- steel, mild, programmed fatigue crack propag., crack tip residual stresses 77−36644
- steel, mild, stress history effect on fatigue crack retardation 78−64627
- steel, mild, with small flaws elastic-plastic anal. of fatigue limit 80−21069
- steel, mild plates, fatigue crack propag. estimation method in pre-strained and mean stressed samples 80−21067
- steel, mild type ASTM A36, Cl embrittling effect on fatigue crack growth rate 79−74254
- steel, Ni, microstruct., plastic zone size and crack propag. 78−60790
- steel, Ni-Cr, case-hardened, surface durability in rolling contact fatigue testing 77−63684
- steel, Ni-Cr-Mo, Ni effect on fracture toughness, heat treatment effect *(Korean)* 79−91781
- steel, Ni-Cr-Mo increase of crack initiation time in delayed fracture by fatigue accumulation *(Japanese)* 78−11312
- steel, Ni-Cr-Mo-V, fatigue crack growth rate, specimen thickness and stress relief effect 77−40445
- steel, Ni-Mo-V, fatigue crack growth, H_2 gas environment effect *(Japanese)* 80−104340
- steel, Ni-Si-Nb (1.5,0.02,0.03 wt.%), fatigue crack growth under bending *(French)* 80−21089
- steel, NiCr, random load fatigue crack propag. 78−64692
- steel, non-irradiated and irradiated specimens, autoclaves for fatigue crack growth tests *(German)* 80−45467
- steel, notched specimens in sea water, endurance limit enhancement, specimen size, freq. effects 80−93678
- steel, perlite, with Ni-Cr steel anticorrosion coatings, viscous-failure characts. from dynamic failure energy 79−43391
- steel, plain C having ferrite-martensite mixed structs., microstructural parameters effect on fatigue strength *(Japanese)* 80−71735
- steel, potential-drop crack detection system 79−34225
- steel, powder-forged, fracture toughness 79−66155
- steel, precipitation hardening, strength and struct. *(German)* 79−47701
- steel, pressure vessel, ASME SA-387 grade D, fatigue crack growth, liquid Na environment effects 77−8997
- steel, PWR pressure components, mechanical factors affecting reliability *(French)* 79−20198
- steel, quenched, tempered, intergranular failure during fatigue crack growth 79−8357
- steel, rail and structural, fatigue crack growth 78−64695
- steel, rolled, effect of inclusions on torsional fatigue 78−92314
- steel, rolled plates, anisotropic, fatigue behaviour under cyclic torsion 77−44326
- steel, RSt 37-2, fatigue crack length determ. in fracture mechanics by electric potential technique of RSt 37-2 *(German)* 78−15486
- steel, Si-Mn, ferrite-pearlite structs., fatigue crack propagation *(Russian)* 79−34126
- steel, sintered, fracture of residual pores 80−76352
- steel, SNCM8, HT80, A553, fatigue crack growth, delayed retardation phenomenon, from single overload 78−92317
- steel, St.3ps, 18 Gps, 09 G2S, fatigue crack resistance, temp. effect 79−52375
- steel, stainless, 304, fatigue crack growth at room temp., crack closure and cycle ratio effect 79−70139
- steel, stainless, 304, thermal fatigue strength *(Japanese)* 79−83306
- steel, stainless, 304 and 316, fatigue crack growth in PWR environment 79−66170
- steel, stainless, 316, crack propag. in low cycle fatigue below 600°C, SEM obs. 78−64631
- steel, stainless, 316, surface finish effect on low-cycle fatigue at 400°C 79−29277
- steel, stainless, A612 grade B, effect of temp. and R-ratio on fatigue crack growth 80−3159
- steel, stainless, AISI 304, dislocation substruct. around fatigue cracks, SEM obs. 78−15516
- steel, stainless, austenitic and ferritic, fatigue crack propagation in single crysts., orientation depend. 79−29167
- steel, stainless, corrosive environment effect on fatigue crack growth rate 80−55584
- steel, stainless, crack propag. at high temp. under low cycle loading 78−60838
- steel, stainless, dislocation struct. adjacent to fatigue crack tips 77−36643
- steel, stainless, fatigue crack growth behaviour in air and high-C liquid Na, carburization studies 80−40625
- steel, stainless, fatigue crack growth rate in high temp., high purity oxygenated water 80−40622
- steel, stainless, fatigue crack morphology of type 304 cycled at const. stress amplitude at elev. temps. 78−64671
- steel, stainless, fatigue crack propag. rate and stress intensity factor at varying stress ratio 78−7049
- steel, stainless, fatigue props. of low-fluence neutron irrad. samples 80−97585
- steel, stainless, ferritic, BCC cryst., fagigue cracking rel. to cryst. orient. *(French)* 79−20178
- steel, stainless, fracture toughness improvement by applying Pb-Sn-Cd coating to crack tip 79−43416
- steel, stainless, growth, plastic zone form. 78−64702
- steel, stainless, highly deformed zone and cyclic strain history near fatigue crack tip *(Japanese)* 79−34145
- steel, stainless, Kh18N10T, crack development under high-temp. single-stage, low cyclic loads 79−43389
- steel, stainless, low fatigue crack growth rate 78−64701
- steel, stainless, low-cycle fatigue characteristics of neutron irrad. samples 80−97586
- steel, stainless, orthopaedic fixation devices, failure, SEM exam. of fatigue crack surfaces and microstructure 78−77156
- steel, stainless, ring notched samples, charge in fatigue crack growth rate 80−50716
- steel, stainless, SUS304, fatigue crack closure over stress ratio range, stress intensity threshold 78−80619
- steel, stainless, SUS 316, creep-fatigue interaction at 600°C 79−34123
- steel, stainless, type 309, low-cycle fatigue, effects of notches on crack initiation 79−74249
- steel, stainless, type 316, fatigue crack propagation, J-integral application 80−35332
- steel, stainless, type 316, microstruct. changes in creep ductility, SEM, TEM, optical microscopy and X-ray diffr. study 79−38927

fatigue cracks continued
steel, stainless 304, creep and fatigue crack propag. at elevated temps., fract. mech. and fractography 77−21279
steel, stainless 304 and 308 and weld material, fatigue crack propag. in neutron irradiation 78−23815
steel, stainless 316, dislocation substruct. prod. by elev. temp. fatigue crack propag., TEM obs. 78−19863
steel, stainless 316, fatigue behaviour of materials containing significant amounts of irrad.-induced He 80−100917
steel, stainless 316, fatigue testing fixture, elev. temp. appl. 79−57185
steel, stainless 316, low cycle fatigue life, relation with striation spacing, and macroscopic crack growth at 625°C 78−11317
steel, stainless AISI 316, fatigue crack growth, effect of grain size on threshold stress intensity 78−44216
steel, stainless and Cr-Mo-V, initiation and growth of cracks in biaxial fatigue 80−30064
steel, stainless austenitic welds, time domain approach to crack location and sizing 80−50781
steel, stainless cold-worked austenitic, fatigue and creep crack growth at elevated temp. 78−48524
steel, stainless martensitic, high alloy, fatigue cracks, effect of chem. comp. and heat treatment *(Russian)* 77−25144
steel, stainless SUS 304, fatigue crack propag. work coeff. 80−16422
steel, stainless type 304, effects of waveshape on crack initiation in low-cycle fatigue 79−79108
steel, stainless type 316, thermally aged, accelerated creep-fatigue crack propag. 80−89326
steel, steam turbogenerator rotors, fatigue crack initiation and growth, from macroscopic slag inclusions 78−64681
steel, structural, crack growth under cyclic load, stress intensity factor 79−87709
steel, structural sheet, high-cycle fatigue crack growth under in-plane biaxial loads 80−40495
steel, temp. effect on fatigue failure *(Russian)* 78−88517
steel, Ti microalloyed structural, precipitation hardening, struct. and fracture *(German)* 79−61696
steel, tool, acoustic emission monitoring during crack propagation 79−86313
steel, tool, hardened, crack propag. under cyclic load *(German)* 79−24596
steel, TRIP, fatigue crack propagation 78−64696
steel, tufftrided, observation of fatigue fracture surface *(Japanese)* 78−52951
steel, tufftrided, residual stress and fatigue crack propag. *(Japanese)* 77−48536
steel, type 26NCDV14, fatigue cracking under polymodal stress *(French)* 79−91787
steel, type A533B, fatigue crack propag., metallographic and fractographic anal. 79−83325
steel, type CSN 12060, random fluctuation intensity of fatigue crack growth *(Czech)* 80−30079
steel, type Man-Ten, and KQC-100, fatigue life estimates of bluntly notched members 80−100999
steel, type N18K9M5T, maraging, rate of movement change of fatigue cracks as result of ageing *(Russian)* 79−70149
steel, ultrahigh strength, effects of strength and grain size on near-threshold fatigue crack growth 78−64704
steel, ultrahigh strength, near-threshold fatigue crack propagation, load cycle and cyclic strength effects 78−11331
steel 10GN2MFA, effect of low temps. and heat treatment on growth rate of fatigue cracks 79−57027
steel 10GN2MFA, fatigue crack development at low temps. 79−57110
steel 45, cracking resistance under impact loading *(Russian)* 77−25138
steel 45, effect of low temps. and heat treatment on growth rate of fatigue cracks 79−57027
steel 45, fractional fatigue, microcrack formation in surface layers 77−86193
steel brass, explosively bonded and roll bonded, clad plate, fatigue crack growth *(Japanese)* 79−61706
steel component strengthened by surface plastic deformation anal. 78−88529
steel core/steel tube duplex reinforced metal sheet, fatigue crack growth 77−28894
steel fibre reinforced Al alloy D16T, sheet reinforced by Ti alloy butt straps, fatigue 79−100262
steel low C, notched, fatigue strength, crack propagation, plastic torsional prework depend. *(Japanese)* 79−15744
steel plate, austenitic stainless, creep and fatigue fracture, expts. and finite element analysis *(Japanese)* 80−50694
steel plates, explosively clad, fatigue crack propagation behaviour *(Japanese)* 80−104262
steel reinforcement in concrete, fatigue crack growth 80−30060
steel rollers, case-hardened, nitrided, surface failure, durability 78−84959
steel U8, hydrogenation effects on fatigue crack propag. *(Russian)* 78−56800
steel welded joint impact strength, preheating and tempering effects 79−24542
steel/Ni, explosively bonded and roll bonded clad plate, fatigue crack growth *(Japanese)* 79−61706
steels, 08kp and 03Kh13AG19, cyclic and static fracture toughness, low temp. effect *(Russian)* 79−52344
steels, austenitic stainless, crack propag. rates under high-temp. low cycle fatigue conditions 80−21088
steels, C and stainless, fatigue crack propag. and crystallographic orientation *(Japanese)* 78−7027
steels, mild and type 304, fatigue crack growth and threshold measured at very high frequencies 80−71742
steels, stainless 00Kh12N3D and constructional 15 Kh2NMFA, fatigue crack development *(Russian)* 79−29174
stereo viewing technique for crack tip displacements 79−24700
stochastic model for fatigue crack propag. 80−53701
stress intensity threshold level determ. method 78−5700
stress/strain distrib. meas. inside plastic zone of notched sheet, fatigue crack propag. *(Japanese)* 78−6981
stresses due to acoustically induced vibration aircraft skin panels, prediction of edge crack growth 80−69737
stretch zone width and striation spacing. The comparison of theories and experiments 80−85051
strip under residual stress, crack-contact and free-end problem 77−65720

fatigue cracks continued
structural bonded joints, fatigue crack growth of adhesive bond line cracks 78−92346
structural fatigue crack acoustic emission monitoring 77−32755
subcritical development, effect of stress state on rate of development 78−79276
surface contact fatigue onset, mag. detection system 79−20330
surface crack propagation in bending 77−72238
surface crack shape change in bending fatigue, resonant fatiguing apparatus 78−72950
surface damage, plastic deformation cause in fatigue, wear, fretting and rolling fatigue 80−40537
surface reaction, and transport controlled crack growth, model 80−75299
tensile to shear fracture mode transition, in fatigue crack propogation 79−79101
test machine for fatigue cracking kinetics in pure bending *(Russian)* 79−52477
theoretical model 78−39906
thermal detection 78−92423
threshold for cracking after overloadings, rel. to efficient stress intensity factor *(French)* 77−72247
threshold stress intensity for crack growth, prediction using dislocation model 78−83870
tip of blunt notch, plastic yielding during static and fatigue loading 79−77010
tip of propagating fatigue crack, strain distrib. meas. by Moire fringe multiplication method 77−80124
turbine blades, fatigue crack detect., strobed hologram method 78−35624
type HT80, delayed retardation phenomena of fatigue crack growth, exam. 78−56745
Udimet 700, high temp. fatigue crack growth, fracture mech. approach 79−52340
Udimet 700, Ni-Co-Cr-Ti, hold time effects on high temp. fatigue crack growth 79−5036
ultrasonic evaluation, development of reference fatigue cracks, book contrib. 79−100327
US test procedure for early detect. and remaining life prediction 80−71848
US visualization, advantages over pulse-echo methods 80−66738
weakest link model, for prediction of crack growth rate 78−90797
wedge-crack development, fatigue-life model in creep region, under stationary and non-stationary loading 78−38248
weld defects, toughness, crack growth anal. 79−43429
weld joint, fatigue crack progress, acoustic emission frequency determ. *(German)* 78−19971
welded component fatigue life and crack propag. analysis with internal stresses 77−77576
welded joints, strain concentration zone detection by holographic interferometry 77−40512
X-ray microbeam meas. of local stress, appl. to fatigue crack growth *(Japanese)* 78−64793
Al alloy, 2024-T3, crack closure 78−72833
Al alloy, 2024-T3, fatigue crack propag., statistical nature 80−35330
Al alloy, 2618 A, crack closure effect *(French)* 79−20172
Al alloy, 5083-0, fatigue crack growth and fracture resistance meas., at 295, 111, 76 and 4K 78−35509
Al alloy, 5083-0, pressure vessel material, delay effects 78−35515
Al alloy, 7050, plastic work during fatigue crack propag. 77−56068
Al alloy, 7075-T6, crack-closure in single overload cycle in single-edge-notched specimens 77−56066
Al alloy, 7175 T 651, crack tip opening under cyclic loading, effect of environmental and R-ratio 80−45377
Al alloy, AU2GN fatigue crack propagation under alternating shear band *(French)* 78−44191
Al alloy, A2017, A5083, fatigue crack growth, delayed retardation phenomenon, from single overload 78−92317
Al alloy, adhesive-bonded-laminated, fatigue props. 80−50695
Al alloy, commercial, slow fatigue crack growth and threshold behaviour in air and vacuum 80−30062
Al alloy, crack opening displacement, expt. and FEM study 78−68811
Al alloy, effect of frequency changes on fatigue crack growth 78−64693
Al alloy, fatigue crack growth, Paris's law 78−39902
Al alloy, fatigue crack growth, crack closure 78−80650
Al alloy, fatigue crack growth in type BS2L71, effect of mean stress and thickness 79−61710
Al alloy, fatigue crack propag. in air and vacuum *(French)* 78−15518
Al alloy, fatigue crack propag. and fractography under periodic overstressing, exam. *(Japanese)* 78−52958
Al alloy, fatigue crack propagation under repeated two-step loadings above and below threshold condition *(Japanese)* 79−38945
Al alloy, fatigue crack propag. near threshold conditions, environment and load ratio effects 80−55522
Al alloy, fracture toughness testing with eddy current sensor 80−45459
Al alloy, high strength, fatigue crack propag. and fatigue life, shallow notch effect *(Japanese)* 79−29199
Al alloy, loading freq. effect on fatigue growth rate 78−83873
Al alloy, low and medium C, fatigue crack growth rate, kinetic eqn. of temp. depend. *(Russian)* 77−25136
Al alloy, low fatigue crack growth rate 78−64701
Al alloy, plastic zone form. and fatigue crack growth 78−64702
Al alloy, type 2024-T3, fatigue deformation and crack growth, holographic study 80−25836
Al alloy, type 2024-T4 and 2124-T4, fatigue crack initiation and microcrack growth 79−79100
Al alloy, types L73 and L88, fatigue crack propagation, stress ratio effect 80−71733
Al alloy 2024-T3, effect of stress level on fatigue crack delay behaviour 78−68790
Al alloy 2024-T3, fatigue crack propag., load interaction effects 77−56055
Al alloy 2024-T3, threshold stress intensity range, physical interpretation during fatigue loading *(German)* 78−19888
Al alloy 2024-T3 77−56049
Al alloy 2024-T3 and 7075-T6, fatigue crack propag. at low ΔK 79−83291
Al alloy 2024-T351, fatigue crack propagation, model, low cycle, cyclic stress-strain response determination 79−68653
Al alloy 2024-T351, retardation in vacuum 79−79069
Al alloy 2024-T351 fatigue crack propag., residual stress distrib. 79−70146

fatigue cracks continued
- Al alloy 2024-T4, compact shear specimen, finite element anal. rel. to fracture 80—16423
- Al alloy 2219-T851, fatigue crack initiation, effect of intermetallic comp. and microstruct. 79—5054
- Al alloy 2219-T851, microcrack closure phenomena 79—57097
- Al alloy 2219-T851, noncontinuum crack tip deform. of surface cracks 80—104273
- Al alloy 5056, fatigue crack growth in ultrahigh vacuum *(Japanese)* 77—56088
- Al alloy 7050, crack propagation and closure, tensile overloads effects 79—43384
- Al alloy 7050-T76, crack propagation rate and crack closure, mean stress effects 79—52336
- Al alloy 7075, comparative US response of machined slots and fatigue cracks 77—40506
- Al alloy 7075, influence of overageing at 175°C on fatigue crack growth rate *(French)* 77—56010
- Al alloy 7075, precipitation hardening, toughness and microstruct. *(Japanese)* 78—15509
- Al alloy 7075-T6 fatigue crack propag., stress ratio effect *(Japanese)* 79—38946
- Al alloy 7075-T7351, early growth of fretting fatigue cracks 80—35345
- Al alloy 7075-T7351, fretting fatigue crack form. 80—35344
- Al alloy AU2GN, variation of crack opening-load diagram with fatigue crack growth rate 77—66691
- Al alloy A5083-0, fatigue crack propag. and closure, repeated loading under low stress intensity *(Japanese)* 80—30077
- Al alloy A5085, fatigue crack growth, delayed retardation phenomena, stress ratio at baseline loading effect 79—79065
- Al alloy adhesively bonded laminates, axial fatigue 80—40491
- Al alloy BS 2L71, crack closure during fatigue crack growth, for two thicknesses 78—68792
- Al alloy bimaterial laminates, crack growth 80—16424
- Al alloy D16, cyclic and static fracture toughness, low temp. effect *(Russian)* 79—52344
- Al alloy extrusion type 7050, tests 77—36703
- Al alloy fatigue crack growth, stage I, effect of liquid environment 77—86164
- Al alloy fatigue cracked alloy 7075 T6, repair machining and inspection of components 78—80689
- Al alloy JIS A5058, fatigue crack propag. rate and stress intensity factor at varying stress ratio 78—7049
- Al alloy lug, fatigue crack growth 80—30061
- Al alloy RR58, fatigue crack propag., 293 to 463K 77—16672
- Al alloy sheets, type 7075-T6 used in aircraft, early detection of fatigue cracks 80—66730
- Al alloy type 7010-T7651, high toughness, cyclic and monotonic crack propag. 80—108528
- Al alloys, A356 T6 and 2219-T851, fatigue crack growth testing, decreasing stress intensity technique, computer-controlled 78—72949
- Al alloys, crack opening stress level in fatigue, determ. by eddy current technique 80—16617
- Al alloys, D16AT, V95AT-1 fatigue crack, microfractographic charact., low temp. effects *(Russian)* 77—70147
- Al alloys, D16At and V95A, fatigue crack growth *(Russian)* 77—52463
- Al alloys, delayed retardation phenomena of fatigue crack growth, exam. 78—56745
- Al alloys, epoxy bonded sheet, fatigue crack initiation, propagation 79—15776
- Al alloys, fatigue, microcrack development, acoustic SHG study 80—35440
- Al alloys, fatigue crack arrest, corrosive environment, at low stress intensities 78—92415
- Al alloys, fatigue crack closure 80—16420
- Al alloys, fatigue crack growth rate change on decreasing temp. in D16AT and V95A sheets *(Russian)* 77—59894
- Al alloys, fatigue crack growth, exam. of some aspects 78—56772
- Al alloys, fatigue crack initiation, computer simulation 80—100893
- Al alloys, fatigue crack propagation rates, stress intensity factors *(French)* 77—25154
- Al alloys, fatigue crack propag., effect of overloads *(French)* 78—19892
- Al alloys, fatigue crack propag., mechanism of overload effect 78—56730
- Al alloys, fatigue crack propag. under periodic overstressing, design criterion *(Japanese)* 79—20166
- Al alloys, fatigue cracking diagrams *(Russian)* 79—29301
- Al alloys, fracture micromechanisms, fracture toughness, exam. 78—56766
- Al alloys, fracture relief formed in fatigue crack growth, rel. to failure mechanism 80—76347
- Al alloys, high strength, cyclic plastic strain damage eval. and summation 79—57060
- Al alloys, microstruct. effects on strength, fracture toughness, fatigue cracks 79—43434
- Al alloys, steady-state fatigue crack growth rate behaviour 79—43432
- Al alloys 2024-T3 and 2219, fatigue crack growth, R-curve concept appl. 79—61733
- Al alloys 2024-T4, 2219-T861, overaged 2219, fatigue crack propag., plastic work role 79—79070
- Al alloys selection using fracture mechanics 78—56725
- Al, bicrystal, fatigue crack initiation, crystal boundary effects *(Japanese)* 78—92328
- Al, bicrystal, fatigue crack initiation along crystal boundaries *(Japanese)* 79—70163
- Al bicrystals, fatigue crack initiation, cryst. boundary effect 80—55537
- Al bicrystals, isoaxial, fatigue crack initiation in grain boundary affected regions *(Japanese)* 80—89338
- Al, cold rolled, annealed, fatigue crack propag. rate, temp. effect 78—39904
- Al, cold rolled and annealed, substruct. near fatigue crack tip, X-ray microbeam technique exam. *(Japanese)* 78—64621
- Al, fatigue crack initiation, model using probabilistic technique 78—68800
- Al, fatigue crack initiation, pre-existing subgrain effect 80—97565
- Al, fatigue crack propag., grain size effect *(Japanese)* 78—39889
- Al, fatigue crack propag., quantifying the parameters 80—100891
- Al, fatigue crack propagation rates, stress intensity factors *(French)* 77—25154
- Al, US fatigue crack propagation obs. 77—40451
- Al-304 stainless steel laminate composite, fatigue crack nucleation and propagation 79—100244

fatigue cracks continued
- Al-alloy, 7175, fatigue crack closure in vacuum and air 80—21065
- Al-alloy, NP8, fatigue crack propag. 80—40538
- Al-alloy type 2124 T351, crack tip closure assessment by electron fractography 80—19875
- Al-alloys, type 2024-T3 and 7475-T761, gust spectrum fatigue crack propag. 80—21105
- Al-Cu, crack advance during fatigue, effect of cyclic hardening and COD 77—16675
- Al-Cu, high strength, type 2024-T3, crack growth, fatigue induced surface deform., holographic detect. 80—85120
- Al-Cu, O transport during fatigue crack growth 78—52981
- Al-Cu, type 1100, synchrotron radiation microradiography 80—85121
- Al-Cu, type 2024, fractography of fatigue 80—40488
- Al-Cu, type 2219-T851, fracture mechanics and surface chemistry of fatigue crack growth 80—81168
- Al-Cu (4 wt.%), aged to contain Guinier Preston zones, crystallographic fatigue crack growth 78—60832
- Al-Cu (4 wt.%), fatigue crack propag. role of adsorption in H_2S, Hg and moist air *(French)* 78—15580
- Al-Cu (4 wt.%), interparticle spacing influence on cyclic deformation and fatigue crack propag. 79—61717
- Al-Cu (4 wt.%), precipitation hardened and fatigued alloys, solute loss at fracture surface, EPMA exam. 78—39893
- Al-Cu alloy 1201, thermomech. treatment effect on strength characts. and fracture toughness *(Russian)* 80—40391
- Al-Cu-Mg, alloy 2124-T351, crack tip closure assessment by electronfractography 80—16427
- Al-Cu-Mg, alloy Al2048, early stages of fatigue crack propag. 77—63780
- Al-Cu-Mg, alloys A-U4, A-U4G1, A-U2GN, effect of environment on fatigue crack growth 78—64677
- Al-Cu-Mg alloy D16T, fatigue cracking under cyclic bending *(Russian)* 78—31506
- Al-Cu-Mg-Fe-Ni, Hiduminium RR58, crack propag. rates in air and salt soln. 80—21063
- Al-Cu-Mg-Li alloy extrusions, microstruct., embrittlement and fracture props. 80—60965
- Al-Cu-Mg-Mn (4.5, 1.5, 0.6, wt.%), alloy 2024-T81, plates, adhesively bonded, exam. of fatigue crack growth 78—92349
- Al-Cu-Mg-Mn-Si-Fe, subcritical crack growth under static plane stress 80—55528
- Al-Cu-Mn, type 2219, edge effects of fatigue crack closure 80—3189
- Al-Cu-Mn, type 2219, synchrotron radiation microradiography 80—85121
- Al-Cu-Mn (6.3, 0.3 wt.%), Al 2219-T851, fatigue crack initiation and early propag. 77—32684
- Al-Cu-Mn (6.3, 0.3 wt.%), alloy Al 2219-T851, crack closure load meas. during fatigue 77—63870
- Al-Cu-Mn-Mg-Fe-Si, corrosive environment effect on fatigue crack growth rate 80—55584
- Al-Mg, alloy A5083-O, fatigue crack propag. and crack closure behaviour under plain strain conditions *(Japanese)* 80—81160
- Al-Mg, subcritical crack growth under static plane stress 80—55528
- Al-Mg-Si, dispersoid effect on fatigue crack propag. 79—43420
- Al-Mn-Mg laminated composite, fatigue fracture, fatigue strength enhancement 79—87725
- Al-Si-Cu, LM30, crack propag. rates in air and salt soln. 80—21063
- Al-Zn, type 7075-T6, coldworked hole specimens, residual stresses, fracture mech. anal. 80—97587
- Al-Zn-Cu-Mg (V95T1), subcritical crack growth under static plane stress 80—55528
- Al-Zn-Mg, atmosphere effect on fatigue crack propag. *(Japanese)* 80—81161
- Al-Zn-Mg, fatigue crack propag., stage I 77—36653
- Al-Zn-Mg, fractographic stage I fatigue facets 77—16680
- Al-Zn-Mg, O transport during fatigue crack growth 78—52981
- Al-Zn-Mg, type 7075, fractography of fatigue 80—40488
- Al-Zn-Mg (3,1.5 wt.%), precipitation hardened and fatigued alloys, solute loss at fracture surface, EPMA exam. 78—39893
- Al-Zn-Mg (4.5, 2.5 wt.%), fatigue crack propag. 77—86171
- Al-Zn-Mg (6.0, 2.5 wt.%), aged, grain, size depend. of fracture toughness 78—48495
- Al-Zn-Mg-Cu, alloy 7075-T6, fatigue crack closure with negative stress ratio, following single tensile overloads 78—64687
- Al-Zn-Mg-Cu (6,2, xwt.%) type alloy, fatigue crack propag., Cu content and recryst. effect 80—60960
- Al-Zn-Mg-Cu alloy, laminated, adhesively bonded alloy 7075-T6, exam. of fracture resistance 78—76754
- Al-Zn-Mg-Cu-Co (6.5, 2.5, 1.5, 0.4 wt.%), fatigue crack propag. 80—55521
- Al-Zn-Mg-Cu-Co-Fe-Si, powder alloy, fatigue crack tip plasticity, from load interactions 80—21066
- Al-Zn-Mg-Cu-Cr, (5.6, 2.5, 1.6, 0.3 wt.%), laminates, 8 and 22 layers, adhesively bonded exam. of fatigue crack propag. 78—92345
- Al-Zn-Mg-Cu-Cr, (5.6, 2.5, 1.6, 0.3 wt.%), alloy 7075, plates, adhesively bonded, exam. of fatigue crack growths 78—92348
- Al-Zn-Mg-(Zr) alloy, microstruct. effect on fatigue crack growth 80—3164
- Al-Zn-(Mg), age hardenable single crystal, fatigue and fatigue cracks *(German)* 77—16689
- Al_2O_3, vitreous-bonded, eval. of proof testing to assure against delayed failure 78—84954
- AlZnMgCuO.5, crack propag. under monotone and cyclic load 78—7006
- B fibre reinforced Al alloy D16T, sheet reinforced by Ti alloy butt straps, fatigue 79—100262
- $Ba_xSr_{1-x}Nb_2O_6$, growth defects 78—38640
- Be, high-strength, fracture toughness determ. 77—73336
- C fibre reinforced plastic, ±45° orientation, creep, fatigue, repeated loading and crack growth 78—68729
- C steel, crack initiation lives at stresses near endurance limit, probability distribs. 77—86127
- C steel, fatigue, residual stresses, surface cracks *(Japanese)* 77—25121
- C steel, fatigue crack propagation, effect of mean stress on crack closure 77—73315
- C steel, impact-fatigue strength , notch strength, rel. to comp. and ductility of core 77—56093
- CU, US fatigue crack propagation obs. 77—40451
- Co-Cr-C eutectic, creep and fatigue crack propag. 78—39859
- Co-Ni-Cr-Ta-C (10, 10, 14, 1 wt.%), aligned eutectic, directionally solidified, fatigue crack propag. 78—27624

fatigue cracks continued
Co-superalloy, cast, high temperature fatigue behaviour 80–40485
Cr_7C_3 fibre reinforced Cr alloy 73C, directionally solidified eutectic, fatigue crack propag. 77–36635
Cu, crack nucleation and stage I propag. in high strain fatigue, microscopic and interferometric obs. 78–52936
Cu, crack nucleation and stage I propag. in high strain fatigue, mechanism 78–52937
Cu, cracks in earlier stages of fatigue, fractography *(Japanese)* 77–8924
Cu, cracks in fatigue early stages, direct obs. of substruct. by electron microscope *(Japanese)* 78–7028
Cu, creep-rupture interaction, crack behaviour 79–52334
Cu, cyclic hardening role in crack nucleation at high strain amplitude 78–64633
Cu, deformation band, role in fatigue crack nucleation and propag. 79–24585
Cu, dislocation structure, around tips of propagating fatigue cracks 79–29211
Cu, ductile fatigue crack growth mechanism in single crystals, in situ SEM obs. 79–61695
Cu, fatigue crack growth and threshold measured at very high frequencies 80–71742
Cu, fatigue crack initiation, model using probabilistic technique 78–68800
Cu, fatigue crack propag., role of dislocation substruct. 80–60963
Cu, fatigue crack propag., influence of specimen thickness *(German)* 80–66669
Cu, fatigue crack propagation, model, low cycle, cyclic stress-strain response determination 79–68653
Cu, fatigued, early stage crack tip dislocation morphology, electron microscope obs. 78–27628
Cu single crystal film, electrodeposited, fatigue cracks *(Japanese)* 78–84975
Cu-Al, fatigue cracks, propagation, model, low cycle, cyclic stress-strain response determinations 79–68653
Cu-Al (9 wt.%), deformed, fatigue crack propag. 78–27621
Cu-Al (9 wt.%), sudden mean stress variations during fatigue crack propag. 80–7668
Cu-Al (9 wt.%) deformed, dispersed, ordered, microcalorimetry of plastic zones during fatigue crack propag. 79–47769
Cu-Co, age hardenable single crystal., fatigue and fatigue cracks *(German)* 77–16689
Cu-Co (2 at.%), age hardened, stage I fatigue crack propag. 78–3203
Cu-Cr (0.75 wt.%), deformation characts., fully reversed cyclic strain with fatigue cracks and dislocation struct. 80–81148
Fe, [110] and [410] single crysts., push-pull fatigue 79–74257
Fe, Armco, crack and slip band form. during US fatigue 78–56723
Fe, Armco, fatigue crack propag., influence of specimen thickness *(German)* 80–66669
Fe, Armco, fatigue cracking under 23 kHz loading at 23°, 60° and 100°C 78–60763
Fe, Armco, plastic zone around fatigue crack, vac. effect 80–100914
α-Fe, crack initiation study at low-cycle fatigue using slip bands *(Slovak)* 79–38949
Fe, dislocation struct. around fatigue cracks, exam. *(Japanese)* 78–64623
Fe, dislocation struct. at tip of fatigue crack 77–4107
Fe, dislocation struct. round fatigue cracks 78–48519
Fe, ductile, influence of crack tip sharpness and morphology of graphite on K_{1c} *(Chinese)* 80–81144
Fe, fatigue crack propag., crack closure, dislocation struct., electron microscopy obs. *(Japanese)* 80–25845
Fe, fatigue crack propag., low temp. 80–35311
Fe, foil, fatigue crack, low growth rate, microstruct. round top 77–16674
Fe, low-temperature fatigue crack propagation 78–72876
Fe, pure, fatigue crack direct obs. by SEM, propag. mechanism *(Japanese)* 79–20164
α-Fe, TEM on struct. round fatigue cracks 77–12699
Fe/Cu composite, prop. of fatigue crack crossing interface under residual thermal stress effect 80–45371
Fe-C (0.64 wt.%), fatigue crack bifurcation 80–71748
Fe-C (0.64 wt.%), quasicleavage during fatigue crack propag., pearlitic microstruct. effect 79–11702
Fe-C system, effect of microstruct. on fatigue crack propagation 79–79097
Fe-Cr-Mo (26, 1 wt.%), single crysts. and polycrysts. strain rate influence on low cycle fatigue props. 80–3126
Fe-Cu-C, fatigue behaviour for tempering at 500°C, precip. hardening 77–40442
Fe-Ni(Mo), solid soln., cyclic stress-strain props., depend. of fatigue crack growth rate 77–4853
Fe-Si, fatigue fracture fractography in broad strain-amplitude range, in air and vacuum 80–81186
Fe-Si, grain oriented, fatigue crack direct obs. by SEM, propag. mechanism *(Japanese)* 79–20164
Fe-Si, low-temperature fatigue crack propagation 78–72876
Fe-Si (2.4 wt.%), ductile fatigue crack growth mechanism in single crystals, in situ SEM obs. 79–61695
Fe-Si (3 wt.%), BCC, crystallographic depend. of fatigue crack propag. *(Japanese)* 77–48528
Fe-Si (3 wt.%), BCC, transcrystal fatigue crack propag. mechanism *(Japanese)* 77–48529
Fe-Si (3 wt.%), fatigue crack propag. work coeff. 80–16422
Fe-Si (3 wt.%), single crysts. and polycrysts. strain rate influence on low cycle fatigue props. 80–3126
Fe-Si(Ni), fatigue crack propag., low temp. 80–35311
Fe(-Ni)(-Si), BCC, cyclic cleavage crack growth model for fatigue 80–55519
Mg alloy, MA12, structural state effect on life and in fatigue crack generation in air and in vacuo 79–87728
Mg alloy MA12, thermally strengthened, fatigue cracking in air and vacuum *(Russian)* 78–35481
Mg alloys MA12, fatigue crack growth in air and vacuum 79–15792
Mn alloy MA12, fatigue fracture, structural state effect in air 79–91796
Mo alloys, fusion reactor first-wall and blanket material, mech. props. 80–34074
Mo, powder specimens, fatigue and threshold behaviour under high cycle fatigue 80–40487

fatigue cracks continued
Mo-W alloy, fatigue and threshold behaviour under high cycle fatigue 80–40487
Nb alloys, fusion reactor first-wall and blanket material, mech. props. 80–34074
Nb, fusion reactor first wall material, cyclic deform. tests 80–30074
Nb-Mo steel, HSLA, low temp. fatigue props. 80–40490
Ni alloy, kinetics of fatigue crack propagation 78–68804
Ni alloy 718, fatigue crack growth at 298 and 823K, frequency and wave form effects 78–64636
Ni base alloy, directionally solidified, fatigue crack propag. 77–36639
Ni base alloy IN 738 LC, overaged, creep and fatigue crack growth 77–86138
Ni base superalloy, fatigue crack opening load variation with meas. location 80–16425
Ni, cyclic flow stress and microstructural changes during multiple step testing at elevated temperatures 79–91746
Ni, fatigue crack propag. qualitative stereoscopic fractography obs. 79–96143
Ni, fatigue cracks, use of SEM in quantitative stereofractographic anal. 78–80645
Ni, pure, fatigue crack propagation, quantitative stereoscopic fractography study 79–74238
Ni superalloy Mar-M200, slow fatigue crack propagation rate meas. using high freq. resonant technique 78–52983
Ni/Ni_3Al+Ni_3Nb, directionally solidified eutectic alloy, crack growth rate under creep fatigue conditions 79–52361
Ni-Al (7.2 wt.%), fatigue crack propag., plastic work role 79–79070
Ni-Al-Cr superalloy IN-100, crack retardation at elev. temp., hold time effect of single overload 79–79068
Ni-base alloys, Nimonic PE-16, type 718 and type 625, neutron irrad. effects on fatigue crack propag. 80–29069
Ni-base superalloy, microscopic inhomogeneity of plastic strain influence on fatigue cracks *(German)* 80–40470
Ni-Co-Cr-Al-Y coating, electron beam deposited, for Ni-base superalloy, fatigue crack initiation and propag. 78–11438
Ni-Co-Cr-Mo-Ti-Al Nimonic 105, loading frequency and environmental effects on high temp. fatigue crack growth 78–64675
Ni-Cr, microstruct. effects in low-cycle fatigue tests 77–56108
Ni-Cr, O transport, during fatigue crack growth, exam. 78–52981
Ni-Cr-Co-Al-Ti-W-Ta-Mo, IN 738 LC, loading frequency and environmental effects on high temp. fatigue crack growth 78–64675
Ni-Cr-Mo-V steel disc, rolling contact fatigue and residual stress on contact surface 77–32671
Ni-Fe-Cr-Nb-Ta-Mo alloy, fatigue crack growth, stress ratio and hold-time effects 80–40531
Ni-Nb-Al, unidirectionally solidified γ/γ'-δ eutectic, fatigue crack propag. 79–29184
Ni_3Nb platelet reinforced Ni base alloy 77–36635
NiTi, thermoelastic martensites, fatigue crack growth rates 79–29166
TZM powder alloys, fatigue and threshold behaviour under high cycle fatigue 80–40487
α-β Ti alloy, fatigue crack initiation from notches 77–21259
Ti alloy, fatigue crack propag. kinetics *(Russian)* 77–70146
Ti alloy, fracture toughness testing with eddy current sensor 80–45459
Ti alloy, kinetics of fatigue crack propagation 78–68804
Ti alloy TA6V, toughness and rate of fatigue, cracking, structural morphology effects *(French)* 77–77579
Ti alloy VT3-1, fracture toughness improvement by applying Pb-Sn-Cd coating to crack tip 79–43416
$\alpha+\beta$Ti alloys, colony size effect on fatigue crack growth on Widmanstatten struct. 80–30094
Ti alloys, fatigue crack growth, exam. of some aspects 78–56772
Ti alloys, fatigue crack propagation resistance, grain size effect, exam. 80–11765
Ti alloys, fusion reactor first-wall and blanket material, mech. props. 80–34074
Ti alloys, toughness and behaviour under dynamic loads *(French)* 80–45383
Ti, crack closure mechanism by examining crack profile and monitoring crack mouth opening displacement 80–16434
Ti, fatigue crack closure mechanism 80–21107
Ti fatigue crack growth, exam. of O transport 78–52981
α-Ti, fatigue crack growth, influence of grain orientation, SEM study 80–108550
α-Ti, fatigue crack growth micromechanisms at low stress intensities 80–108570
Ti, fatigue cracking, initial stage under bending and torsion *(Japanese)* 79–20165
Ti, fatigue damage, SEM, X-ray diffr. and surface trace anal. 80–85040
Ti-11, fatigue crack propag. under dwell time conditions 78–80639
Ti-11, unstable shear modes in fatigued β-annealed specimens 78–84984
Ti-A-V (6, 4 wt.%), castings, fatigue crack initiation 79–29186
Ti-Al-Mo-V (8, 1, 1 wt.%), environmental fatigue crack propag., texture influence 79–91802
Ti-Al-Sn-Zr (6.19, 1.92, 1.43 wt.%), fatigue cracking characteristics of β annealed microstruct. 79–5051
Ti-Al-Sn-Zr (6.19, 1.92, 1.43 wt.%), fatigue fracture facet investigation by selected area electron channelling 80–89344
$\alpha+\beta$-Ti-Al-Sn-Zr-Mo-Cr, low cycle fatigue crack nucleation and early growth 79–8354
Ti-Al-Sn-Zr-Mo-Si (6, 2, 4, 2, 0.1 wt.%), effect of elevated temperature and environment 80–40486
Ti-Al-V, (6.7, 4.3 wt.%), fatigue crack growth and fracture resistance enhancement, due to annealing 78–35510
β-Ti-Al-V, annealed, differing interstitial O content, fatigue crack propag. resist. 79–11696
Ti-Al-V (6, 4, wt.%), delayed retardation phenomena of fatigue crack growth, exam. 78–56745
Ti-Al-V (6, 4 wt.%), environmental fatigue crack propag., texture influence 79–91802
Ti-Al-V (6, 4 wt.%), fatigue crack growth data 77–73332
Ti-Al-V (6, 4 wt.%), fatigue crack propag. under dwell time conditions 78–80639
Ti-Al-V (6, 4 wt.%), gust spectrum fatigue crack propag. 80–21105
Ti-Al-V (6, 4 wt.%), hot isostatically pressed casting, fatigue crack initiation 79–79078
Ti-Al-V (6, 4 wt.%), texture effect on fatigue crack path 78–27633
Ti-Al-V (6, 4 wt.%), Widmanstatten, microstructurally sensitive fatigue crack growth obs. 78–27627

fatigue cracks continued
  Ti-Al-V (6,4 wt.%), alloy plate, fatigue crack propag. under in-plane loading, expts. 79—52337
  Ti-Al-V (6,4 wt.%), alloy plate, fatigue crack propag. under in-plane loading, anal. 79—52338
  Ti-Al-V (6,4 wt.%), β-annealed, subsurface fatigue crack initiation 80—108553
  Ti-Al-V (6,4 wt.%), cyclic stress-strain response 77—21170
  Ti-Al-V (6,4 wt.%), surface residual stresses, surface topography, fatigue behaviour 79—52366
  Ti-Al-V (6,4 wt.%) alloy, fatigue crack growth, influence of dwell-time 79—43380
  Ti-Al-V (6,4 wt.%) alloy, fatigue crack closure eval. with electric potential method 79—50678
  Ti-Al-V-Sn (5.5, 5.3, 2.3 wt.%) fatigue crack growth and fracture resistance enhancement, due to annealing 78—35510
  Ti-Al-V-Sn (6, 6, 2 wt.%), fatigue crack growth, cyclic freq. and microstruct. influence 80—55515
  Ti-Al-V-(Mo), Widmanstatten, quantitative anal. of microstruct. effect on fatigue crack growth 79—79071
  Ti-Al-Zr (6,5 wt.%), alloy IMI 685, SEM exam. of crack growth 78—72849
  Ti-Al-Zr-Mo-Si (5.97, 4.73, 0.49, 0.34 wt.%), fatigue fracture facet investigation by selected area electron channelling 80—89344
  Ti-Al-Zr-Mo-Si (6, 5, 0.5, 0.25 wt.%), β-processed, fatigue props., hold time effect 80—60961
  Ti-alloy, IMI-685, unstable shear modes in fatigued β-annealed specimens 78—84984
  Ti-Cu, struct. damage and internal fatigue cracks *(French)* 77—73341
  β-Ti-Mo-V-Fe-Al (8,8,2,3 wt.%), metastable, high cycle fatigue crack initation, grain size effect 77—86145
  Ti-V (27 and 30 wt.%), fatigue crack propag., in single and poly. crystals 79—5048
  Ti-V (40 at.%), microcracks intersecting fatigue crack, exam of origin 78—80638
  β-Ti-V metastable alloys, fatigue crack propag. 80—60964
  V alloys, fusion reactor first-wall and blanket material, mech. props. 80—34074
  V, and V-H, fusion reactor first wall material, cyclic deform. tests 80—30074
  V-H, H effect on fatigue crack propag. 78—48516
  W arc welds, fatigue crack growth behaviour in air and high-C liquid Na, carburization studies 80—40625
  Zr,Nb (2.5 wt.%), interaction of hydride, stress, and crack growth at 600K, metallographic obs. 77—12695
  Zr base alloy, fatigue crack propag., role of adsorption in H_2S, Hg and moist air *(French)* 78—15580
  Zr-Nb, pressure tube alloy, initiation COD as fracture criterion 78—72862

fatigue failure *see fatigue*

fatigue fracture *see fatigue*

fatigue life *see fatigue*

fatigue testing
  for corrosion fatigue testing, see corrosion testing
  accelerated fatigue-resistance evaluation by programmed stress-amplitude increase, Al alloys appl. 77—73386
  acetal homopolymer, exam. of bending strength, using new method 78—53056
  acoustic emission method, use of standard equipment and background noise effects elimination, expt. 77—73423
  acoustic emission monitoring, new technique 77—28938
  acoustic emission signals interpretation 77—9030
  acoustic emission system for monitoring components and struct. in severe fatigue noise environment 77—63869
  acoustically active material, fatigue strength testing installation, electric and magnetic field effects 78—39995
  alloy, high-temperature low-cycle fatigue strength at const. and variable temps., cycle period effect 78—7127
  alloy, light, durability during random loading, approx. determ. method 77—48610
  alloy steel samples, spherical, subjected to forced bending *(Croatian)* 77—36712
  alloys, heat-resistant, thermal stress cracking resist. evaluation method 80—3260
  annular fatigue crack prod. in cylindrical specimens *(Russian)* 77—52559
  anodised Al rods, humidity and coating thickness effects on fatigue in reversed torsion 77—25205
  austenitic steel, Cr-Ni alloyed, Ti stabilised, nuclear reactor pipeline appl. *(Hungarian)* 77—18658
  automatic detection of crack initiation life of welded joint *(Japanese)* 80—30189
  automatic unit 77—56209
  automation, of installation control for low-cycle fatigue tests 79—15926
  automotive materials, microfractography appl. to ductile failure, brittle fracture, crack studies 77—56199
  B fibre reinforced Al, real-time NDT during fatigue loading 77—86264
  bearings, Weibull distrib. statistical interference 79—52473
  under biaxial strain at elevated temps., cumulative damage tests, exposure times 77—28939
  bituminous mixes, fatigue strength, effect of mix and test variables 77—63881
  boiler steel fatigue crack propagation test results *(Hungarian)* 79—83293
  boundary technique, cost saving method for fatigue data, theory, practice, experience eval. *(German)* 77—86266
  brittle materials, static, fatigue testing, method 79—29314
  C-shaped fatigue specimen 78—68867
  ceramics, lifetimes and slow crack growth prediction *(German)* 80—104250
  ceramics, subcrit. crack extension meas. with double-torsion specimens *(German)* 80—104359
  composite, fatigue life and static strength testing, sample size estimation 79—91867
  composite materials, critical factors for frequency dependent processes 77—8903
  composite T-beams, repeated loading effects 77—86253
  composites, appl. of exptl. methods to fracture 80—11869
  computer controlled system, conf., Haifa, Israel, (July 1977) 79—15683

fatigue testing continued
  computer-controlled system for fatigue testing under simulated service loading 79—15885
  concrete, running fatigue test, determ. of loading-deform. charact. and internal damping *(German)* 77—25229
  constructional material fatigue resistance test under asymmetric loading 78—85083
  contact fatigue limit testing machine, for metals, alloys under vibrating load 80—55617
  corrosion bending fatigue machine, multi-specimen 79—39060
  crack, low cycle, test machine rigidity effect on kinetics 78—15632
  crack dimensions, recording method and sensor 77—63856
  crack growth kinetics for constant ΔK 77—40491
  crack growth measurement using acoustic emission, instrum., expt. 77—73421
  crack growth rate testing, COD technique for crack length meas. 77—56170
  crack growth rates, meas. method based on crack opening 80—61032
  crack growth rates and kinetic diags. of fatigue fracture *(Russian)* 78—11456
  crack growth testing, decreasing stress intensity technique, computer-controlled 78—72949
  crack length indirect measurement during a fatigue test *(French)* 79—20312
  crack propag. meas. and crack closure at low stress intensity level by unloading elastic compliance method *(Japanese)* 77—9016
  crack propagation in shaft or axle type components, problems specification 78—51120
  crack propagation testing machine using Shimadzu Servopulser Dynatec *(Japanese)* 80—25973
  cracking in corrosive medium and low cycle loading, meas. equipment 77—77676
  cracking resist. testing *(Russian)* 79—29301
  cracking resistance investigation apparatus, for constructional materials in vacuum and gaseous media *(Russian)* 77—28940
  creep and fatigue testing installation for wide range of strain rates 80—76447
  cryostat, He for prolonged low-cycle fatigue testing 79—52491
  cycle ductility determ. in low cycle tests 78—56835
  cyclic elastoplastic bending, recording deform. curves and working life 79—52499
  cyclic life, utility of surface-flawed tensile bars 77—21342
  cyclic simple shear testing apparatus for granular materials 77—90578
  cyclic strength tests, long term, exam. of severe-load testing equipment design 79—52521
  cyclic stress-strain curve determination *(Czech)* 80—89434
  cyclic thermal effects in discs, device to study disc strength 77—63880
  cyclic toughness determ. in low-cycle fatigue testing of plane specimens in simple bending *(Russian)* 77—52560
  damage measurement by laser scanning, exoelectron display 77—73391
  damage process recording and analysis method 79—52487
  data analysis for lifetime predictions for ceramics 78—95870
  data computer processing, methodological problems of automating on short-term fatigue tests 79—15931
  deflection measurement device, specimen under cyclic cantilever bending 80—21227
  denture base materials, multi-station machine for fatigue testing 80—108648
  denture base polymers, test machine 80—66712
  device for high temp. short term tests 79—66233
  die components, apparatus for determining fatigue resistance 80—16627
  digital computer control of mech. tests, review 79—43508
  digital simulation of environmental processes rel. to fatigue 77—40499
  eddy current transducer, for monitoring fatigue crack growth 80—45460
  electrohydraulic fatigue apparatus for testing at cryogenic temperature 80—35463
  endurance determ. method over wide range of load asymmetry 78—56836
  equivalent alternating stress from two-level multiple-step wave *(Japanese)* 78—92333
  equivalent alternating stress from two-level multiple-step wave or mutiple-level multiple-step wave *(Japanese)* 78—92334
  fastening materials, specimen for testing 80—61050
  fatigue stages in repeated loading by ref. to microfractographic characts. 77—40490
  fibre reinforced shell-type structures, strength estimation using limit state method 79—18820
  fibres, biaxial rotation fatigue testing, torque development 80—71840
  fibres, fatigue tester based on rot. over wire for use in different environments 77—44421
  fibres, using biaxial rotation test 79—97381
  filament yarn under cyclic tension, study *(Japanese)* 77—36701
  fixture, elev. temp. appl. 79—57185
  force meas. rod bending moment compensation by parallel resistors *(German)* 77—79078
  fracture resistance, delayed, test-piece dimensions influence *(Russian)* 79—52478
  fretting fatigue, device for investigation in contact zones between shaft and embracing part 79—57171
  fretting fatigue development, sonic monitoring 77—12770
  fretting fatigue in vacuum apparatus for investigation 78—15640
  fretting fatigue testing apparatus in vacuo 79—39084
  fusion reactor, PDX toroidal field coil joint fatigue testing 80—91252
  fusion reactor, TFTR, vacuum vessel bellows, strength and fatigue anal. 80—95455
  fusion reactor first wall materials development evaluations, fatigue crack growth testing optimisation 80—35444
  graphite fibre reinforced epoxy laminate tension-compression fatigue loading, fatigue residual strength degradation model, comparison with expt. results for 78—35491
  graphite reinforced epoxy, combined torsional-bending fatigue tests 77—28951
  Hastelloy X, high temp. low cycle fatigue tests, ductility, fracture 77—90523
  heat resistant materials, high temp. fatigue testing machine 80—25954
  HS-188 alloy, elevated temp. fatigue anal. 77—40509
  hydraulic machine adapted for low-cycle fatigue testing 79—57175
  hysteresis energy-temp. rise relation *(Japanese)* 77—77682
  impact bending, specimen parameter effect on crack propag. 77—86242
  impact fatigue testing machine 78—56838
  impact test equipment for use at high-temp. 79—52492

fatigue testing continued
inclusion effects, statistical analysis, deriv. of specific fatigue criterion *(French)* 77−73379
installation, GRM-2, modernisation for programmed low cycle tests 80−25940
irradiated material in elastoplastic region, systems of remote meas. of forces and deform. in cyclic tests 77−90546
laboratory complex for fatigue testing with variation of low-temp. conditions 78−27723
laboratory tests automation, using 500 kN and 2.5 MN ATE *(Czech)* 80−66710
laminate, multidirectional, general fatigue failure criterion and test program 80−7658
large cross-section materials *(Russian)* 77−52557
life determ. in stepped loading 77−86280
life prediction and design, review 77−16475
life prediction method for conditions of multistep cyclic loading 80−76346
life prediction techniques, appl. of computer for materials substitution 79−61820
life testing, effect of program load including peak load *(Japanese)* 77−9015
life testing of springs universal machine 78−11479
loading mode stabilisation 77−86247
loads and load histories, test methods devel. 80−100970
low cycle bending and torsional fatigue testing machine 79−43521
low cycle fatigue, of metals. method of testing, effect on fatigue 79−52515
low cycle fatigue and plasticity testing, specimen verification 80−30202
low cycle fatigue testing extensometer for anisotropic materials 79−24695
low cycle tests of shear connectors, instrumentation and data acquisition procedure 79−43539
low temperature thermal cycling unit 77−77666
low-cycle fatigue, effect of direction of first half-cycle *(French)* 77−25236
low-cycle fatigue tests with axial and diametral extensometers 78−85062
low-cycle nonisothermal loading, strain relations and failure criteria investig. method 79−52486
low-cycle pure bending tester for several specimens simultaneously 80−55607
low-cycle testing unit for use in vacuum and at high temp. 79−52503
machine, low-cycle, far sheet material bending to −196°C 80−55616
machine, materials in pure bending 77−1906
machine, stress amplitude stabilising system 79−52501
machine for long fatigue tests under varying load conditions 78−60909
machines, crank driven, electromech. system for stabilisation and programming static load 78−64801
macro X-ray fractography, fatigue failure anal. *(Japanese)* 78−11464
magnetic field of test machine, effect on results 79−91890
martensitic steel, fatigue crack nucleation, rotating beam determ. of true min. stress *(French)* 77−25122
materials testing under alternate force and thermal loading, installation 78−11481
metal, data processing of test results *(Japanese)* 77−9013
metal, fatigue and inelasticity testing apparatus in symmetrical bending mode, 36 to 330 Hz 78−27722
metal, fatigue testing at US frequency, hardness change 77−44440
metal, magnetic, and SEM exam. of fatigue, dynamic strength problems *(German)* 77−86272
metal, resistance to plastic deform. under HF vibrs. rel. to surface treatment *(Russian)* 77−52400
metal, stress concentration sensitivity, scale factor effect on fatigue strength 79−39064
metal fatigue monitoring by US velocity and attenuation meas. 78−60970
metal in atomised NaCl solutions, fatigue strength testing unit 77−77677
metallic materials, tenacity parameters 80−60973
metals, adiabatic heating as cause of low cycle fatigue failure 77−21339
metals, fatigue crack growth rate, expt. programme for determ. in thickness direction 79−57168
metals, low-cycle failure investigation, elec. resist. meas. appl. 80−85109
metals, method using EM pulsator 80−89440
metals, rationalisation of test methods 80−25936
metals and alloys, thermal stress cracking, installation for −180 to 1100°C 80−3266
metastable austenitic steels, test machine and fatigue strength temp. dependence *(Japanese)* 80−71842
microbellows, cyclic strength exam. procedure at low temp. 77−90547
micromachine for low-frequency fatigue testing of materials by pure bending 79−29317
mild steel, fluctuating overstresses, effects 77−90524
mill stand in-situ fatigue testing, devices for automatic emergency protecting *(Russian)* 80−93717
NDT for early prediction by acoustic and exoelectron emission 78−53170
nonisothermal and low cycle isothermal tests, with complex loading apparatus design 80−25939
notched plates, fatigue strength 78−9601
nuclear power engineering materials certification testing for safety and reliability 80−78360
nuclear steam generator tubes testing and evaluation, using CIS/DASIO system *(Czech)* 80−63301
optical fibre, dynamic fatigue and strength degradation 80−58719
optical fibre mechanical testing, optical degradation under tensile stress, fatigue, defects *(French)* 77−72074
optical high-strength fibre production and prooftesting 80−64204
optical strong fibres, fatigue strength and flaw size distribution 77−11056
optimal periodic proof test based on cost-effective and reliability criteria 77−63838
piping, high frequency fatigue testing under symmetrical and asymmetrical loading 77−86246
plastic, machine under axial load 77−66734
plastic extension control device 77−25220
plastics, apparatus for comparison of fatigue limits under shock and harmonic loading 77−63855
plastics, bending fatigue, exam. of new method of testing 78−53056
plastics, endurance testing machine 77−52580

fatigue testing continued
plastics, viscoelastic, fatigue testing, using hollow cylindrical specimens *(German)* 78−44292
plate testing under alternating flexure, pneumatic test equipment 78−7119
PMMA, fracture under biaxial stresses, simple testing technique 77−73383
polyethylene pipes, lifetime determ., crack growth in thermoplastics under various conditions 78−39981
polymer, fatigue testing apparatus in plane stressed state 78−3300
polymer cyclic deformation amplitude, automatic meas., apparatus design 78−85082
programmed, two-frequency, using EM resonance machine 79−96232
prosthetic trileaflet aortic valve, optimum design and in vitro testing 77−56541
radial-bolt-hole cracks in mechanically fastened aircraft structs., measurement of size using Doppler shift 80−55597
random signal analysis applic. 77−44453
real-time fatigue damage assessment method 79−43546
reinforced plastic, fatigue mech., charact. and defect detection 79−24687
reinforced polymer, fatigue testing machine, materials in pure bending 77−1906
resistance, influence of test specimen form *(Russian)* 79−15884
resistance threaded connections 77−81373
resonant bending fatigue apparatus for approx. determ. of dislocation density 77−86279
resonant electromagnetic fatigue tester, features *(French)* 78−56870
rupture strength testing under cycic loading, AIMA-5 machine modification 79−52506
S-N curves determination from accelerated fatigue data, analytical method 78−35475
servo-hydraulic testing machines 80−108649
sheet material, Bauschinger effect determ. using tension-tension loading cycle 77−52570
sheet materials, attachment for testing during sign alternating loading 77−52579
skew hole-containing specimens 77−44420
smooth test pieces, method of estimating scale relationship of endurance limit 78−60914
solar cell interconnector fatigue resistance tests 79−96457
stainless steel rod adaptor, failure anal. in Fast Burst Reactor 77−54307
standards, terms and symbols definitions, statistical methods *(French)* 79−91862
statistical analysis of crack growth data 77−24351
statistical analysis of nonstationary loading, methods comparison 79−52488
steam turbine rotor steel type EI-415 77−25238
steel, austenitic stainless, plastic deform. build-up during low cycle fatigue *(Russian)* 77−25207
steel, austenitic stainless, US fatigue meas. 80−40489
steel, austenitic stainless type SUS 316, low cycle fatigue tests, freq. effect on notch sensitivity at elevated temps. *(Japanese)* 80−104260
steel, ball, fatigue life prediction, fully automatic X-ray diffr. apparatus *(Japanese)* 79−39076
steel, C, crack initiation and propagation life under repeated impact tensile loads *(Japanese)* 80−104264
steel, C-Cr (1.0, 1.5 wt.%), 52100 bearing steel, control of surface residual stress by heat treatment 80−97501
steel, case hardening and carbonitriding treatment, mech. props. testing *(French)* 77−59991
steel, cyclic stress-strain and failure testing, effect of meas. stress and mean strain *(German)* 77−21338
steel, fatigue crack propag. under random loading 78−76726
steel, fatigue testing, exam. of scale relationship of endurance limit 78−60914
steel, G-Mo type, welded joints, thermal fatigue testing 78−3278
steel, heat treated rimmed, statistical study on fatigue life distrib. in long life region *(Japanese)* 77−12755
steel, heat-treated, toughness factor statistics *(Russian)* 77−44418
steel, life scatter and loading conditions reproduction methods 77−70262
steel, low C, low-cycle failure investigation, elec. resist. meas. appl. 80−85109
steel, medium C, type 45, sheet, working life, effect of dynamic loading type 77−21278
steel, mild, fatigue softening and hardening detected from Barkhausen noise 80−76428
steel, non-irradiated and irradiated specimens, autoclaves for fatigue crack growth tests *(German)* 80−45467
steel, pressure vessel, acoustic emission during loading by pulsating internal press. *(German)* 78−19973
steel, rotating bending fatigue tests in hydrostatic environment 77−21343
steel, spring, fatigue life testing, universal machine 78−11479
steel, structural, nondestructive method of struct. damage investig. using cyclic loading effects and mag. characts. 78−3275
steel, structural, rate of damage detection by fatigue testing of instrumentation *(German)* 78−19972
steel, type SAE 1008, finite fatigue life distribs., various load-time histories 80−97589
steel, weldable, fatigue data, low and high cycle compatibility *(Czech)* 80−89343
steel 15G2AFDps, fatigue to brittle fracture transition at low temp., stress raiser effect 77−12696
steel 45, fatigue strength determ. apparatus, in corrosive environment under complex stress *(Russian)* 77−77657
steel bearing balls, exoelectron emission for surface fatigue wear testing 78−39960
steel discs, austenitic and ferritic biaxial fatigue testing under changing temps. *(German)* 80−71759
steel weld fatigue life estimation, multichannel NDT monitor 78−56846
steels 30KhGSNA and VNS-2 fatigue life diagrams plotting 79−70246
stepwise changes, fatigue strength rapid eval. method 79−52489
stiffened plates, tests on interactive buckling 78−71286
strain and damage electrical measurement method *(French)* 80−71854
strain range partitioning method for anal. of material creep fatigue behaviour 80−104361
stranded rope with independent wire rope core *(Japanese)* 77−9014
strength determ. for independently applied biaxial stresses *(German)* 80−21238
strength testing, long-term of specimens with fatigue crack 78−7131
stress concentrator effects *(Russian)* 78−56831

fatigue testing continued
- superconducting material, in normal and superconducting states 78—19959
- surface contact fatigue onset, mag. detection system 79—20330
- techniques review, and fatigue life prediction techniques 80—21251
- tension-compression fatigue testing machines, characterisation of materials under cyclic loading at high temperature *(French)* 78—15628
- test machine, automatic control 77—56181
- test machine for fatigue cracking kinetics in pure bending *(Russian)* 79—52477
- texile fibres, multistation apparatus using biaxial rotation over a pin 80—66726
- thermal cycling of loaded materials, testing equipment, IMASh-9-66 machine attachment 77—77678
- thermal detection of cracks 78—92423
- thermal fatigue of high-melting material sheets, testing device 80—25955
- thermal fatigue testing system for structural materials, metals 77—90525
- thermal-cycling effects at temps. from 200 to 430K 77—86248
- thin sheet materials, plane bending, at high loading freq. 78—31607
- two-axis tensile test machine, for static and dynamic tests *(French)* 78—15627
- ultrasonic and acoustic emission detection of fatigue damage, book contrib. 79—100326
- US determination of magnification and resonance length of samples 79—15948
- US fatigue cycling, radius optimisation of specimen with circ. gauge profile 79—79190
- US fatigue systems, deform. amplitude determ. 80—97676
- US testing of different materials with equivalent vibration charact. 80—11847
- varying temperature unit for fatigue testing, automatic control 77—77667
- vibrating bench, automated design, exam. of gas turbine blades 78—64800
- weld joint, fatigue crack progress, acoustic emission frequency determ. *(German)* 78—19971
- wire, fatigue probability diagram plotting 79—52490
- wire, testing method, error reduction 79—52493
- wire fatigue properties, fast testing method using 23 kHz US frequency 80—89460
- Woehler tests, U_0* procedure for reliable prediction of random fatigue strength *(German)* 80—71850
- Zircaloy-2 fuel tubes, cumulative damage fatigue tests at room temp. and 300°C 80—93638
- Zircaloy-2 fuel tubes, low cycle fatigue studies at room temp., 300 and 350°C 80—93637
- Al alloy, 5083-0, pressure vessel material, delay effects 78—35515
- Al alloy, corrosion fatigue testing, galvanostatic vs. potentiostatic control 77—40467
- Al alloy, fatigue testing, exam. of scale relationship of endurance limit 78—60914
- Al alloy 2024, fatigue damage detection by optical correlation 78—27717
- Al alloy 2024-T3, Alclad, dimpled loaded-hole fatigue strength, effect of interf. 78—72948
- Al alloy V95T1, endurance determ. method over wide range of load asymmetry 78—56836
- Al alloys, struct., accelerated fatigue test method 80—100981
- Al, deform. enhanced photoemission meas. 77—32511
- Al, plastic deform. build-up during low cycle fatigue *(Russian)* 77—25207
- Al-Mg alloy AMg5, welded structures, machine for fatigue life investigation 79—52566
- B fibre reinforced epoxy resin, real-time NDT during fatigue loading 77—86264
- Cu, dislocation density in fatigue, approx. determ. by resonant bending fatigue apparatus 77—86279
- Cu, electrical grade, fatigue damage eval. from freq. change of natural vibrs. 79—52498
- Cu, plastic deform. build-up during low cycle fatigue *(Russian)* 77—25207
- Cu-Cr (0.75 wt.%), deformation characts., fully reversed cyclic strain with fatigue cracks and dislocation struct. 80—81148
- Fe/Cu composite, prop. of fatigue crack crossing interface under residual thermal stress effect 80—45371
- Mo, fusion reactor appl., quick heating thermal fatigue test, ultra-high vac. environment *(Japanese)* 80—93716
- Nb-Ta fibre reinforced Cu, fatigue testing in normal and superconducting states 78—19959
- Nb_3Sn, filamentary, fatigue tests on small coils 78—64652
- Ni, plastic deform. build-up during low cycle fatigue *(Russian)* 77—25207
- Ni-Cr, microstruct. effects in low-cycle fatigue tests 77—56108
- Ni-Cr-Mo-V steel disc, rolling contact fatigue and residual stress on contact surface 77—32671
- Ti alloy VT-20, fatigue life diagrams plotting 79—70246
- Ti-V-Cr-Al (13, 11, 3 wt.%) alloy spring wire, torsional fatigue props. 77—77649

fault currents
- *see also flashover; leakage currents; short-circuit currents*
- biological effects and protection 80—56330
- flameproof coating for PVC insulated cables, composition, tests *(Russian)* 78—68828
- fusion reactor, JT-60, fault current anal. in grounding system 80—99307
- vacuum arc plasma, fault current limiter mode, temp. distrib. diagnostics 78—9851

fault location
- 600 MW pulsed energy convertors for toroidal field coil, design philosophy 78—58496
- digital multimeter, Avo DA117, overview of field servicing appls. 80—68210
- ECG cable continuity tester 77—77997
- electrical thermometers, functional fault detect. using electronic devices, report *(German)* 78—81972
- fault detection by scanning acoustic microscopy 77—80040
- IC testing, photoacoustic microscopy appl. 80—14525
- industrial NDT computed transverse axial tomography system 80—89430
- long-haul communications optical fibre fault location method 80—64193
- moving material fault test rig *(German)* 80—11855
- nuclear power plant loose parts monitoring techniques and experience 79—3211

fault location continued
- optical cable, meas. methods *(German)* 79—14097
- optical fibre, on-site defect location and transmission loss eval. 79—3801
- optical fibre cables for field trials, meas. methods *(German)* 78—50922
- optical fibre time-domain reflectometer with gated photomultiplier receiver 77—65620
- optical fibres, backscatter meas. 80—64183
- optical fibres, using time-domain reflectometer 79—64355
- optical time domain reflectometry by photon counting 80—95122
- regenerative fibre-optic transmission system supervisory line codes *(German)* 78—33884
- remote diagnostic techniques used in Viking lander operations 78—57426
- semiconductor circuits, employing new voltmeter impedance multiplier 77—41649
- shift register reliability assessment by scanning electron microscope 78—29215
- traction motor, circuit fault detection by NDT method 79—39097
- US testing, foreshortened projected distance concept *(German)* 80—16625
- SiO_2 film, local defects detection by electrolytic decoration *(Bulgarian)* 78—60896

fault-tolerant computing
- computerised reactor safety systems, design, specification and implementation 79—63783
- ECG analysis systems 77—44811

faults, electrical *see electrical faults*

f.d.m. *see frequency division multiplexing*

feature extraction *see pattern recognition*

feedback
- *see also control systems; control theory*
- 3.39 μm He-Ne laser frequency stabilisation without FM 79—55152
- afferent elec. nerve stimulation with ref. to prosthesis sensory feedback 77—90962
- afferent nerve stimulation in below-elbow amputees 78—57125
- alpha rhythm, human, feedback control from central area 80—40988
- ambulatory neuromuscular activation control model 79—57638
- amplifying system, distributed feedback due to meeting of oppositely propag. noise waves, beats *(Russian)* 77—71965
- analogue and digital optical image processing, feedback systems 80—102650
- arm movements controlled by peripheral feedback, in humans, simulation 78—80891
- articulation development, possible nonlinear time varying control in feedback path 78—35870
- artificial arm, supplemental sensory feedback for below elbow amputee 77—40931
- artificial cold resistors, electronic feedback cct. 78—32750
- artificial hand with sensory feedback, production 80—36191
- artificial heart, electronic pressure control with fast variable aperture valve *(French)* 77—40928
- artificial limb control appl. 78—15923
- artificial sensory feedback system, stimulation freq. discriminability 78—44714
- assisted reverberation in outdoor environment, use of delayed feedback 78—13825
- at-power reactor noise, second-order coherent functions 78—94070
- auditory feedback, effect on guitar playing intensity and speech prod. 78—85322
- auditory perception nonlinear model with autocorrel. feedback 80—81615
- auroral arcs global formation, numerical simulation in feedback theory 80—67446
- automatic digital magnetic recording system in Tihany Observatory 79—39989
- bio- and neurocybernetic models of the living being 79—53018
- biochemical multiple-loop negative feedback control networks, oscills., periodic metabolic systems 78—85285
- biofeedback, physiological responses control appl. *(Japanese)* 77—44830
- biofeedback, student demonstration 79—44677
- biofeedback control of alpha wave amplitude and frequency *(Japanese)* 77—44626
- biofeedback devices for control of unconscious physiological processes 78—35992
- biofeedback therapy technique and application *(German)* 79—16341
- biomedical IC differential amplifiers 77—48891
- biosphere-albedo feedback and climate modeling 79—53508
- bistable element array generation by liquid crystal light valve and optical feedback 80—48442
- bistable TV-optical feedback system using optical flip-flops 80—53354
- blood pressure control, mechanical-chemical balloon implant 79—20712
- boiling water reactor optimal control, regulator problem, feedback control laws 77—54315
- bone functional adaptation model and thermodynamic consideration *(Japanese)* 78—7316
- BWR void reactivity feedback, statistical weight factor 79—9702
- cell growth regulation, effects of cell density and metabolite flux on dynamics 78—85296
- cell growth regulation, effects of cell density and metabolite flux on dynamics 78—88701
- cell population auto-activation, math. model 78—77017
- cellular control of gene expression by positive feedback, differential eqns. 79—66460
- chest wall compliance meas. with biofeedback using 2-electrode oesophageal-balloon catheter 77—52905
- climatology, ice-cap albedo feedback rel. to energy-balance models stability theorem 80—56594
- cognitron, feedback-type, self-organising neural network with associative memory 78—56962
- conduction MHD systems, feedback and self-excitation threshold calcs. *(Russian)* 77—47108
- controlled particle suspension system for laser initiated target expt. mag. mirror fusion facility 78—1864
- coronary perfusion pressure programmable control circuit 79—92278
- digital simulation of neuron *(Polish)* 79—16189
- diode detectors, wide-gap, of IR radiation, positive feedback 78—24863
- disturbed cell renewal control system modelling and simulation 79—29510
- driven-sweep generator scan velocity transducer 78—57925
- EEG feedback training, techniques and clinical appls. 78—36043
- electro-optical device with feedback, multi-functional 79—32055

feedback continued
electron microscope, UHV, const.-load tensile device and appls. to materials science 78—11462
electron-optical convertor, multielectron scintillation statistics 79—72695
electronic cooling of resonant gravity gradiometers 79—49222
electrostatic generator terminal voltage on-line feedback stabilisation using digital computer 78—82004
electrostatic wattmeter with automatic voltage feedback for torque balance 77—82569
EMG biofeedback device 79—96706
EMG control enhancement using predictor feedback technology 77—48952
EMG feedback in therapeutic aid for disabled children 78—36048
endocrine tumours, silent, feedback system cell number change effects, steady-state anal. 79—20526
eye, vergence movements, heuristic feedback system model 77—21517
feedback stabilization of an l=0,1,2 high-beta stellarator 78—75404
Fermilab booster, low level RF system 79—76205
Fermilab booster, transverse instabilities suppression, fast feedback system 77—83298
fine muscular control rehabilitation using ramp threshold feedback 79—83996
fission reactor suboptimal control system, response improvement by param. imbedding method 77—34421
fixed-frequency laser beam scanning device 78—59135
flexible band-pass filtering using coherent optical feedback 79—94166
force and strain meas., spring-mass-damping system, dynamic errors *(German)* 79—12794
four-arm bridge measuring circuits with linearised characteristics *(Russian)* 79—12820
Fourier transform spectrometer, high resolution ruggedized 80—95152
fusion reactor, flute mode axial feedback stabilisation 77—80344
gas stripping column, periodically cycled, feedback control, simulations 79—1231
geophones, electromechanical feedback for low freq. equipment *(Russian)* 79—62618
heat exchangers, parallel and counter-flow, weighted residuals method and modal control 79—3898
high-speed optical systems at 0.85 μm, modal noise and optical feedback 80—87323
hind-limb reflex movements, chelonian, simulation 79—74642
hot-film anemometers, testing strategy for freq. optimisation 78—26218
hybrid image processing system, space and time picture oscillation, by active incoherent feedback 78—58924
image feedback computer contrast control expts. *(Japanese)* 79—22903
image processing, hybrid optical and TV system with feedback 77—61922
image processing on-axis coherent optical feedback system 77—50631
image sharpening telescope, atm. distortion compensation 77—49294
incoherent feedback optical system 78—66924
injection laser automatic level control by optoelectronic feedback *(German)* 78—33883
instrument science appls. 79—21687
integrated astable optical multivibrator using Mach-Zehnder interferometric optical switches 80—87560
interferometer for precision linear displacement meas. 80—27285
intracranial pressure regulation, nonlinear parametric feedback model 79—96599
IR laser interferometer, length measuring, alignment using laser feedback 80—37075
ISR RF cavities, beam load compensation, feedback system 77—83294
laser frequency stabiliser using electronic servocontrol system 78—1240
laser primary regulated dual power supply 79—98396
laser-fibre transverse coupling and front-mirror monitoring for feedback control of laser transmitters 80—33151
light feedback suppression, from optical fibre into diode laser 79—1004
light source, stabilisation by negative feedback *(Russian)* 77—49762
lipid bilayer hydrophobic ion interactions, inner volt. clamping method 78—28129
LPE film property control, regression eqns. 79—33200
machine tool position feedback by laser interferometer 80—73438
mass spectrometer, ion-cyclotron reson. type, optically-coupled feedback emission current regulator 77—61150
master-slave manipulator power-assisted grip system 79—9212
membrane potentials tracing system, using amplifier for voltage clamping *(German)* 78—61285
Michelson interferometer, active stabilization by electrooptically tuned laser 80—86386
microdensitometer precision focus control 79—58769
microphotometer for intensity registration of spectra, feedback system *(Russian)* 77—13244
mirrorless electrooptic device with feedback, optical multistable operations 79—32051
monochromatic light source with electronically variable wavelength 80—102791
MOST, short channel, output impedance, thermal feedback effects *(French)* 80—15609
motoneurones excited by phasic muscle stretches, discharge pattern shaping, recurrent inhibitory feedback effects 78—85303
multidither adaptive optics, estimation and control 77—50757
muscle control system Ia feedback pathway correlations, origin and nature 79—24977
muscle length reflex control, servosystem simulation 79—57639
MW impulse generator system, for ion cyclotron heating, fusion reactor 78—70635
myofeedback prosthesis with sense of touch, operating experience 80—36190
myopotential controlled elec. operated hand with sensory feedback 79—57815
nerve stimulation, noradrenaline release regulated by α-adrenoceptor mediated negative feedback 77—29139
neural adaptation and transient responses due to inhibitory feedback 79—92206
neural pacemaker phase control 78—11631
neuron population, local, model performance 79—20531
neutral beam power supply, series switch/regulator system, 40 kV, 80 A, 10 ms, for fusion reactor 78—66366
noise analysis of power reactor, simulation using nucleate boiling noise generator 78—54840
nonlinear image processing with optical feedback *(Russian)* 77—58258

feedback continued
nonstationary nonlinear vibratory system feedback oeration effects 79—14316
NQR scanning spectrometer, improved super-regenerative oscillator and quench generator 78—8429
nuclear fuel cycle, GASP IV simulation model 78—41847
nuclear reactor constrained feedback control system design 77—88257
nuclear reactor core 78—54860
nuclear spectroscopy systems, active zero-pole cancellation feedback loop 79—9972
ocean-atmosphere system, interannual variability 79—2330
oculomotor control system synthesis photoelectric matrix method appl. *(Korean)* 77—90779
optical coherent feedback, flexible filter operations 80—87337
optical feedback effects on saturated absorpt. signals, suppression by phase modulation of refl. light 78—21225
optical feedback in incoherently illuminated systems 80—87336
optical feedback in lasers *(Chinese)* 79—81405
optical feedback processing by TV-optical method 80—87335
optical fibre nonlinear equalisation by shaping filter *(German)* 78—33882
optical image processing, analogue and digital, feedback, review 80—102639
optical incoherent feedback using TV 80—87334
optical information processing, feedback techniques 79—55062
optical modulators, temp.-compensated, control method 77—42611
optical processor, confocal feedback system for partial differential eqn. analogue soln. 80—102630
optical systems, noisy image restoration 78—63020
optically levitated particles, feedback stabilisation 77—27290
optimal feedback control of plasma parameters in Tokamak 79—64891
oscillating control system theory 77—25360
parallel-connected transducer systems, integral parameters determ. 77—17939
photoelectric inclinometer, sensitivity stabilization by negative feedback *(Russian)* 78—4012
photomultiplier gain stabilisation with high counting rate, feedback resistor series effect appl. 80—106232
photomultipliers, logarithmic scale using AGC *(Czech)* 77—5884
physiological pressure transducer design with negative feedback 77—48910
planar biped finite state control, appl. to walking and sitting 80—16986
plasma, control of stellarator-Tokamak hybrid system 77—72468
plasma, drift-cyclotron instability, pot. feedback control 77—19689
plasma, feedback stabilisation of flute oscills. in direct traps *(Russian)* 77—47184
plasma, flute oscills. suppression by regulator with cross feedback *(Russian)* 78—26262
plasma, grooved instability, self-adjusting feedback system for stabilisation *(Russian)* 77—68767
plasma, in multiple mag. mirror, axial feedback stabilisation of flute mode instability 78—75408
plasma, multimode instability control by state feedback 79—77357
plasma, Scyllac feedback-sector expt. 77—72473
plasma, Scyllac ordering, instabilities, sharp-boundary dynamical model 77—51216
plasma, tearing mode suppression by feedback system *(Russian)* 78—22535
plasma, toroidal filament, stabilisation of current instabilities *(Russian)* 77—76185
plasma disruptive instability in TO-1 Tokamak, feedback stabilisation *(Russian)* 79—55546
plasma drift-cyclotron instability, feedback stabilisation, appl. to polar cusp plasma 78—7838
plasma equilibrium feedback control in ORMAK 77—3976
plasma instabilities, feedback controller development 79—50853
plasma instability, suppression by feedback method automatic control, stabilisation methods 78—63564
plasma mirror trap, feedback suppression of spatial channelling instability modes *(Russian)* 77—47243
plasma mirror trap, transfer function meas. 77—51215
plasma oscillations control by linear feedback system *(Russian)* 78—38469
pneumatic micrometer with positive feedback system *(Japanese)* 79—93101
portable easy-operation long-period seismometer, peripheral stabilising device 78—65399
preamplifier circuit in Fourier spectrometer, using InSb photodiode, improved noise compensation 80—73474
pressure transducer temperature coefficient sensitivity, compensated using positive feedback 80—17928
prosthesis, sensory feedback system for above knee prosthesis *(Japanese)* 80—72372
prosthetics sensory feedback, human tracking performance with afferent elec. nerve stimulation 80—17195
proton (antiproton) beam in storage ring, stochastic cooling anal. 80—5420
PS booster at CERN, longit. active damping system electronics, tracking band pass filters 77—83297
PWR core Doppler spatial weight factor 79—9713
PWR differential rod worth and feedback coeff. online estimation system 79—9798
radiochemical purity quality control by rapid feedback system 77—90900
real time optical signal processors with feedback control 77—23620
RF charged-particle separator power recovery, for synchrotron 78—66440
RF feedback, in integrated cct. Robinson oscillator for NMR detect. 77—74475
river aeration system subject to random disturbances, optimal control 78—16078
rotor vibration control appl. *(Russian)* 78—70116
satellites attitude control, inertially fixed pitch stabilisation by solar radiation press. 80—101523
Scyllac feedback stabilisation 77—24129
Scyllac fusion reactor, feedback stabilisation system 78—54887
segmented bidirectional amplifier SAW oscillator 78—1528
seismographs, feedback-controlled wide-band, design, rel. to undesired side effects 79—39909
seismometer, miniature, wideband, with force feedback, design 79—16698
seismometer, miniature wideband horizontal-component 78—24382

feedback continued
seismometers, EM and hybrid instruments, developments 79—39906
seismometers, wide-band feedback instrument 79—39907
SEM, voltage meas. via new electron energy analyser using feedback loop 77—54019
semiconductor injection laser, external optical feedback effect on props. 80—58535
semiconductor laser, output power and coherence length in incoherent feedback 79—98412
semiconductor laser direct PCM improvement by optical feedback 78—1287
semiconductor laser nonlinear distortions on modulation linearity improvement by negative feedback *(German)* 80—69395
sensory feedback code comparison using electrocutaneous tracking, for prosthetics 78—69255
simultaneous feedback control of bias and modulation currents for injection lasers 80—43332
skeletal muscle rhythmic oscillation simulation and analysis 78—31806
SLAC beam, feedback system for steering and energy correction in beam switchyard 79—93852
solar heating and cooling systems, optimisation, using continuous flow control 79—62127
solid laser Q-switching by optomechanical shutter 79—72609
solid state delayed auditory feedback system for speech therapy 77—13028
speech, nasalisation in normal and hypernasal speakers, effects of feedback filtering 80—35921
stabilised rectifier unit 78—4643
stability criterion for feedback control of unstable waves 77—5671
stammerer fluency aid using delayed auditory feedback, body-worn aid 80—56283
static induction transistors, one-dimens. potential profile anal. 79—56290
steam generator channel, once-through, flow dynamic stability, influence of press. loss components *(Czech)* 77—3148
stick insect leg position control mechanism open loop analysis 77—36907
storage ring, feedback-stabilised, resonator wall instability caused by ponderomotive forces 80—5418
storage rings, single feedback systems for simultaneous damping of horizontal and longitudinal coherent oscillations 79—72075
stratosphere, model, temp. feedback effect on O_3 conc. 78—28277
stream pollution controller design via pole assignment 77—60434
structural vibration testing, using electromag. forcing device, use of feedback to reduce harmonics 79—20298
stuttering, fundamental freq., effects of delayed auditory feedback and masking 80—35922
submillimetric-wave negative-feedback-loop thermistor bolometer 79—44931
superconducting heavy-ion resonator, microprocessor based feedback system 77—88292
TEXTOR vessel, plasma position, feedback control calcs., response time behaviour 79—98959
thermal feedback, in dialable ampere current source with ppm/h stability 77—50320
thermionic emission triode, with auxiliary discharge, rectifying parameters 79—64925
tilt meters, photoelectric, with negative feedback, block diagrams anal. *(Russian)* 78—88948
time variant filter performance in 1/f noise, Si(Li) detector-opto feedback FET system 77—57830
time varying systems, stability anal. 78—37
TO-1 Tokamak, kink instability, feedback stabilisation 80—28634
Tokamak, ISX, dynamics and feedback control 78—71528
Tokamak, major disruption suppression by tearing modes stabilisation 80—10422
Tokamak plasma equilibrium, feedback control 78—55738
Tokamak power reactor, position control and sensor requirements 78—5035
Tokamaks, feedback stabilisation of magnetic islands 80—28638
tracking Michelson interferometer stability improvement *(Russian)* 78—29149
trapped electron instability, feedback diagnostic 78—51350
TV optical operational amplifier 79—94327
two-channel amplifier section with common negative feedback loop 78—9042
two-resonator CRM oscillator with external feedback 80—87362
two-wavelength optical phase control system 80—33140
upper-limb prosthesis neuroelec. control 78—44704
US beam power meas. calorimeter bridge for 1 to 15 MHz 77—27446
ventilation feedback control in small infants after open-heart surgery 79—70710
vestibular research, rotating room acceleration and damping 79—84048
video biofeedback for alpha monitoring of brain activity 78—20299
visceral function voluntary control, electrophysiological concept 78—35827
visual feedback effects on corrective saccades 78—40150
voice amplification, adaptive method for feedback suppression *(German)* 80—106676
voltage-sensitive preamplifier, output stabilisation by pole-zero cancellation 77—61088
walking, connections between different legs, quantitative model 80—101161
walking, individual leg control, model 80—101160
wastewater treatment, distributed digital processing and closed loop computer control 80—45824
water quality controller, observer-based, polluted river stream appl. 77—81938
waveguide, hollow-core rectangular, propagation losses at 10.6 μm for distributed feedback appl. 80—38101
weight control through behavioural engineering using videotape biofeedback and subliminal communication 77—78040
whole-body hyperthermia with oesophageal temp. feedback control 79—92423
X-ray fluoresc. spectrometry using pulsed X-ray excitation, for environmental anal. 77—56319
X-ray preamplifier with pulsed drain feedback 79—6249
X-ray spectrometer, Si(Li) detector, preamplifier with drain feedback 78—66448
ZGS, low level beam diagnostics for polarised proton operation 77—83311
He-Ne $^{127}I_2$ stabilised laser source for Michelson interferometer, optical feedback obs. 80—106545

feedback continued
$Pb_{1-x}Sn_xSe$ laser, optical feedback effects on performance, external cavity modes 80—32981
SO_2 gas pollution of Osaka city, optimal discharge control 79—52993

feeds, antenna *see antenna feeders*

Fermi-Dirac statistics *see quantum statistical mechanics*

Fermi gas *see fermion systems*

Fermi level
A15 compounds, new aspect of superconductivity, Fermi level rel. to electron-phonon interaction 79—7927
A15 compounds, quasi-one-dimens., theoretical group anal. of electron spectrum 79—82511
A15 superconductors, supercond. and phonon softening in unstable systems 79—65587
alkaline earth fluorides, orbital binding energy and ionicity relations, XPS meas. 80—97399
alloys, binary ordered, residual resist., s-d hybridisation effect 80—39559
amorphous semiconductor, conductivity, thermopower and statistical shift 79—95434
amorphous semiconductors, gap states, electronic behaviour 78—2452
amorphous semiconductors, thermopower, conductivity, statistical shift, doping effects 79—69537
Anderson localisation problem, cond. numerical studies 80—49673
Anderson model, electrical resistivity, for wide range of Coulomb coupling parameters 80—2373
asymmetric Anderson model, ground state fundamental nature 79—90932
chalcogenide, charge transfer, influence of cryst. field 79—99516
chalcogenide glass, localised gap states, Mott-street model 79—37968
chalcogenide glasses, defect states 78—39066
chalcogenide glasses, field effect, localised states and electronic transport 77—66187
chalcogenide lone-pair semicond. charged impurities, effect on carrier concs., Street-Mott model 78—67984
complex tight binding systems, surface density of states determ. 80—20272
defect semiconductor, or insulator, carrier densities, elec. cond. and Fermi level 77—43532
degenerate semiconductor, with nonparabolic energy bands, magnetic quantisation 78—30864
density of states, normal systems 78—23004
diamond cubic structure, kink formation and migration, rel. to Fermi level 79—82218
diode model for spectral sensitivity 77—41716
disordered metallic structure, calc. of Fermi level 79—33217
disordered semiconductors, recomb. radiation spectrum *(Russian)* 79—4855
disordered systems, Coulomb gap computer simulation 79—51465
electron gas, perturbed, p-wave electronic recoil spectra 80—107724
electron-hole plasma, strongly degenerate, helical density waves 80—15550
excitonic insulator in mag. field, two-band model 80—80192
extended systems, HF density of states, appl. to thin films and polymers 80—6689
extrinsic semiconductor, Fermi level eqns. 79—99472
extrinsic semiconductors, carrier concs. and Fermi levels 77—66112
FCC clusters, size and shape depend., tight binding approximation 78—79920
Fermi gas, one dimensional with backward scatt., gap renormalisation 80—24818
Fermi-Dirac integral $\mathcal{F}_{1/2}(\eta)$ approx. 78—22997
ferromagnetic metal surface, Fermi level shift by charging, mag. moment and hyperfine splitting 77—20677
GaSb surface, Au overlayer, adatom interactions, photoemission obs. 79—33898
glass, conduction and valence bands props., review 77—66106
glasses, defect reactions, ionicity dependence, negative-U states 80—88510
graphite, diamagnetism with quasilinear dispersion law, orbital susceptibility, valence bands *(Russian)* 80—80475
graphite, electronic props., self-consistent LCAO calc. 78—51887
graphite, intercalated with Br_2, far IR magnetorefl. expts. 77—40228
graphite, photoemission, C 1s core-electron line shape, excitonic effects, Fermi energy and hole density of states 80—29848
graphite intercalation compound, interaction between one or two s orbitals *(French)* 80—65440
graphite intercalation compounds, electronic props. in dil. limit 77—47714
graphite intercalation compounds, interband Landau level transitions, magnetorefl. 77—52095
graphite intercalation cpds., K-point effective masses and Fermi level shifts, magnetorefl. study 80—50305
graphite intercalation cpds., mag. susceptibility, tight-binding model 80—44796
graphite intercalation cpds. with alkali metal, interlayer screening and mag. susceptibility 80—44794
graphite-$FeCl_3$ intercalation cpd., electronic excitation spectrum, high resolution EELS meas. 80—45182
Heine-Abarenkov optimised potential for 27 elements, radial Schrodinger eqn. soln. 77—11833
III-V semiconductor Schottky barrier formation, Fermi-level pinning, defect mech. 78—95358
III-V semiconductor-oxide interface states, photoemission obs. of energy levels induced by adsorpt. 80—93000
inflowing structure, Anderson localisation, elec. cond. temp. depend. *(Russian)* 80—103639
insulator-semicond. interface, impurity-band hopping conduction in surface layers 80—75649
insulators, noncryst., electron density captured at traps, liberated to conduction band 78—87946
intermediate valence system, local polaron model 80—107717
lamellar graphite acceptor intercalation cpds., charge distrib. in c direction 78—87935
lightly doped semiconductors, impurity band struct. 79—69461
liquid metal, integrated density of states, expression in Roth's effective-medium approx., generalisation of Friedel formula 79—99467
liquid metals of groups IIB, IIIB, and IV, thermoelectric power, pseudopotential calc. 80—59959
local mixed valence model, exact limit 77—51705
metal, effect of impurities on electronic struct. 78—47692

Fermi level continued
metal, plasma oscillations, Fermi level position effect on excitation energies for band transitions 79—99493
metal film, size quantised, energies and Fermi level of electrons 77—15749
metal lattice heating by radiation, plasma effects, degenerate electron gas calcs. 80—70742
metal surface, inert gas bombard., 1.05 keV, electron yields, Fermi energy estimate 78—52611
metal-semiconductor interface, disordered, supercond. 80—20347
metal-semiconductor interface, Schottky barrier formation, microscopic model 78—52087
metal-semiconductor-metal junction, tunnelling phenomena in terms of exact method and WKBJ approx. 80—20329
metallic and nonmetallic solids, Fermi energies 80—2451
metals, Doppler broadening of positron annihilation line 79—43057
metals and alloys, electrons at Fermi surface, book 80—105445
MIS, HF capacitance, minimum value and position 77—85338
MIS structure, high- and low-freq. steady state capacitance 80—54796
mixed valence metals, elementary excitation damping, electron specific heat 79—95180
mixed valence state, electronic structure 79—11092
MOST channels, quasi-Fermi level gradient distrib., Hall voltage 80—29481
nondegenerate strongly doped compensated semicond., electron props. *(Russian)* 77—11839
one dimensional Fermi gas model in relation to spin and field theoretical models 80—24816
one-dimensional disordered system, numerical expt., Coulomb gap *(Russian)* 77—31932
one-dimensional metal, disordered, with half-filled band, rel. to elec. cond. *(Russian)* 77—80769
p-n junction theory, Fletcher's boundary conditions 79—73571
periodic systems electronic struct., LCAO SCF ab initio HF calcs. method 80—65419
photoconductivity-controlled imaging systems, limitations on sensitivity 80—6907
phthalocyanine thin layers, metal-free, mobility and thermally stimulated polarisation meas. 79—73527
phthalocyanines, UV photoemission, valence band struct. 77—85884
pnictides, charge transfer, influence of cryst. field 79—99516
polyacetylene, trans- and cis-isomer, electronic struct. calcs. 80—24788
polystyrene films on metal substrates, electrode effect on carrier injection, TSC, I-V characts. 80—34463
polysulphur nitride, pure and brominated, electronic model for high cond. 80—24923
α-quartz, energy level schemes, Fermi level-electrochemical potential level coincidence, quantum yield spectrum 79—69400
rare earth, liquid, divalent electrical resist. 79—38039
rare earth, liquid, trivalent, electrical resist. 79—42514
rare earth aluminate, scandate and zironate film coatings, electrophys. props. w.r.t. prep. technology 80—60781
rare earth element submonolayer films, electronic phase transitions, heat of absorption 80—24736
rare earth metal, 4f levels, obs. by bremsstrahlung isochromat and XPS spectroscopy 79—24411
rare earth metals, 4f level energy position relative to Fermi energy 80—6764
rare earth metals, density of 4f states below and above Fermi level, XPS and bremsstrahlung isochromat spectroscopy 80—76140
rare earth metals, position of unoccupied 4f levels, APS meas. 80—16125
semiconductor, amorphous, non-polaronic, cond. and thermopower near band edge 80—49719
semiconductor, bonding and transport properties 79—90950
semiconductor, doped and strongly compensated, fluctuation pot. and density of states *(Russian)* 79—95366
semiconductor, effect of random var. in impurity conc., n-Si appl. 79—51470
semiconductor, Fermi level, monotonous shift with increasing temp. 80—92809
semiconductor, polaronic hopping conduction at low temp. 78—51906
semiconductor junction device quasi-equilib. assumption, quasi-Fermi level approach 79—91128
semiconductor junction device quasi-equilib. assumption, quasi-Fermi level calcs. 79—91129
semiconductor with parabolic bands, empirical approx. for Fermi energy 79—7770
semiconductor-electrolyte contact, electrolytic decomposition and photodecomposition 78—95357
semiconductor-metal interfaces, intrinsic surface states and Fermi-level pinning 78—95319
semiconductors, isothermal and non-isothermal C-V deep level meas. using Schottky contacts 80—88515
semiconductors, temp. depend. electronic cond. 80—59975
semiconductors, thermally stimulated relaxation processes, book contribution 80—80295
simiconducter heterojunctions, energy band profile and interface states calcs. 79—78162
simple metals, Fermi energy, density of states 77—76730
solar cells n-type Schottky barrier, theoretical anal. of band edges, Fermi levels 80—50975
space charge limited current with diffusion theory, for exponential trap distribution 80—10992
substitutional alloys of intermediate valence systems, static mag. susceptibility con. and temp. depend. 80—84586
superconducting alloy, theory of upper crit. field 77—63038
superconductor critical temp. depend. on radiation defects, electron density of states calcs. 80—44758
transition metal alloys, binary, state density curves, relation between short-range order and Fermi level position, CPA calculations 80—107687
transition metal alloys, heats of formation, tight binding theory, moments approach 79—61891
transition metal carbides, complex phases with NaCl struct., microhardness rel. to electronic structure 77—90438
transition metal carbides, d-metal, band struct. calc., Fermi level *(Russian)* 78—39019
d-transition metal hydride, mag. suscept. and quasirigid model *(Russian)* 78—26805
transition metal monoantimonides, electronic struct. determ. 77—4290
transition metals, ferromag., dil. H electronic struct. 80—70638

Fermi level continued
transition metals, supercond., effect of s-, d-electron hybridisation *(Russian)* 78—39243
TTF(I)$_{0.71}$, physical props., Fermi energy scaling of metal-insulator transition temp. 77—8081
TTF(SeCN)$_{0.54}$ and TTF(SCN)$_{0.54}$, Fermi energy scaling of metal-insulator transition temp. 77—8081
TTF-TCNQ, electronic struct. near Fermi level, tunnelling spectra 77—85126
TTF-TCNQ, physical props., Fermi energy scaling of metal-insulator transition temp. 77—8081
X-ray K- and L-emission bandwidths from characteristic electron energy loss values 79—83057
zincblende-symmetry narrow-gap semicond., Fermi energy and Fermi-Dirac integrals 80—70604
Ag, thin film deposited on Si, work function *(French)* 80—80353
Ag_3SbS_3, pyrargyrite, thermoelec. and photoelec. work functions, Fermi level and electron affinity *(Russian)* 77—15939
Al (001), enhanced photoexcitation 80—80937
Al, direct nonvertical interband transitions at large wave vectors, electron energy loss meas. 78—34759
Al film, supercond., meas. of effective quasiparticle recombination times, density of electronic states at Fermi level 79—38264
Al, singular struct. in density of levels 79—77997
Al surface, (100), 9-23 eV photoionis., spatially-varying photon field effects 80—2921
Al, thin film deposited on Si, work function *(French)* 80—80353
Al-Al_2O_3-SnTe, junction, tunnelling, Fermi level depend. on carrier conc., influence of surface states 80—25016
Al-Al_2O_3-SnTe structure, tunnelling characts., model anal. 80—29480
Al-anodised Ta_2O_3/native oxide-n-GaAs MOS structure evaluation 80—84514
AlB_2, band struct. and density of states, metallic behaviour 77—59249
$Al_xGa_{1-x}As$, analytic approx. for Fermi energy 78—63973
Al_2O_3, amorphous, energy level schemes, Fermi level-electrochemical potential level coincidence, quantum yield spectrum 79—69400
Al_2O_3-Ca_3SiO_5, solid solution, exam. of lattice defects 79—95167
As, interband, magnetorefl. for circularly polarised radiation 78—2840
a-As, opt. and elec. props. 77—39894
As:Ni(Ge)(S)(Se)(Te) film, amorphous, chemical modification of props. 80—49250
AsF_5-intercalated graphite, mag. spin susceptibility, density of states at Fermi energy 79—7966
As_2S_3 vitreous, Ag, Cu, Sn and Ge impurities infleunce on electrophys. props. 77—76826
As_2Se_3:X (X=Cu, Ag, Tl, I, Ge), effect of doping, NMR meas. 80—11282
Au-3d transition metal alloys, UPS study, localised states 80—93449
Au-n-Si Schottky barrier solar cells, recombination in space charge region 80—61351
Au-Si interface, valence band and core levels, Si diffusion, alloy form., photoelectron spectra obs. 80—45205
Be, electronic struct., NMR study 80—108085
BeB_2, band struct. and density of states, metallic behaviour 77—59249
BeNi, dil., electronic struct., NMR study 80—108085
Bi, chemical shift of X-ray L-absorption edge 79—52044
Bi, dielectric anomalies, electronic relax. times at far IR frequencies 77—24513
Bi electron properties, carrier spectrum 78—84137
Bi, empirical pseudopot., temp. and press. depend. 78—18955
Bi, freq. mixing of de Haas-van Alphen oscills., quantum variations of Fermi energy 77—80721
Bi, giant quantum attenuation anomalies of sound waves at high mag. field, temp. and freq. depend. 80—70587
Bi, intravalley electron-phonon scatt. non parabolicity, thermoelectric power 79—99539
Bi, Shubnikov-de Haas effect in high mag. fields 80—2404
Bi:Sn(Pb), carrier dispersion law, cyclotron masses rel. to Fermi level 77—20345
Bi-Sb, semiconducting, lattice dielec. const., comp. depend. 80—39516
C:H films, amorphous, elec. props., chem. modifications 80—84523
CaSb, resist., susceptibility and thermopower rel. to electronic struct. 78—67935
Cd-Hg, ω-phase, mag. susceptibility *(Russian)* 79—87231
Cd_3As_2, highly doped, Shubnikov-de Haas type oscills. in optical transmission 79—61352
Cd_3As_2 platelet, single vap.-grown cryst., passive annealing, Fermi energy variation 80—45223
$Cd_xHg_{1-x}Te$, graded gap epitaxial layers, elec. and photoelec. props. 77—85362
$Cd_xHg_{1-x}Te$, intrinsic carriers, Fermi level calc. rel. to conc. 77—55481
CdS, photoanode, difference between Fermi level and bottom of cond. band 79—62013
CdS:Cu, Fermi level position, luminesc., and photosensitivity, electron irrad. effects *(Russian)* 78—14652
CdS:Li film, chemical bath deposited, photocond. and optical props. quasi-Fermi levels 80—2426
CdS-metal interface, chemical reactions and local charge redistrib., Fermi level-pinning 79—19661
CdSe platelets, determ. of localised level energies by Fermi level statistics 77—31980
CdSe-metal interface, chemical reactions and local charge redistrib., Fermi level pinning 79—19661
p-$CdSiAs_2$, electron irrad. elec. props. annealing, lattice defects 80—100465
CdTe:Cl, heavily doped, elec. and photoluminesc. investig. of defect interactions 77—39603
β-Ce, electronic energy band calcs. by KKR method 79—95317
Ce, electronic structure vol. depend., rigorous cellular method, γ- and α-forms 77—20233
$Ce_{3-x}S_4$, $Ce_{3-x}Sm_xS_4$, elec. cond. mechanism, thermoelec. power, Hall and absorpt. coeffs. 77—24559
$CeSn_3$, polarised neutron study of induced magnetisation 80—34594
Co, liq., density of states of d-band, heat of vaporisation 78—95253
Co, UPS, single cryst. and polycryst. film, electronic struct. 78—11081
Co-Mn alloys, Nernst-Ettinghausen effect and electrical resistivity *(Russian)* 78—14714
Cr alloys, localised magnetic moments in band antiferromagnets, impurity interactions *(Russian)* 80—54888
Cr, single Q-state, antiferromag. phase, rel. to band struct. 77—15759
Cr_2O_3, electronic struct. study by XPS 80—25518

Fermi level continued

- Cr_3Si, mag. susceptibility, 2 to 300K, rel. to electron energy spectrum 80−60185
- Cr_3Si, specific heat at low temps., electron density of states, Debye temp. *(Russian)* 80−54398
- Cu (100) monolayer, self consistent electronic struct. 80−6926
- Cu, hot cathodoluminescence study, electron-hole recombination 80−93410
- Cu-alloys, dil., optical props. and electronic struct. 78−35164
- Cu_2MnAl, alloy, Fermi energy calc. by nonrelativistic SAPW method 79−4507
- $Cu_{2-x}S$-CdS heterojunction V-I characteristic and max. photovoltage, long-term changes *(Russian)* 78−43468
- ErH_2, electronic struct. 79−28268
- Eu, electronic struct. investigation by electron spectroscopy method 80−92812
- Eu, relativistic band struct. calcs., unoccupied 4f level calc., Fermi level, atomic configuration 80−49584
- Eu-transition metal intermetallics, valence fluctuations 78−91649
- EuO, electronic struct. investigation by electron spectroscopy method 80−92812
- Fe, energy bands, tight binding calc. *(Korean)* 79−51479
- Fe, UPS, density of states determ. 78−52623
- Fe-Co(Cr), electron state density and elec. resist. 80−39558
- Fe-Mn(Ni), electron state density and elec. resist. 80−39558
- $FeCl_3$-graphite, intercalation compound, Fermi level lowering and core exciton spectrum, EELS study 79−74036
- $Fe_{0.65}Ni_{0.35}$, UPS, density of states determ. 78−52623
- $Fe_{1-x}O$, wustite phase, surface elec. props. 78−76133
- Fe_3O_4, electron energy band theory, thermodynamic functions *(Korean)* 79−7785
- Fe_7S_8, pyrrhotite, thermocond. and thermoelec. power 80−96926
- GaAlAs, surface vacancies, bound state energy levels calc. 80−80340
- GaAs, chemisorpt. of O_2 and thin oxide layer form., review of synchrotron radiation meas. 79−60637
- GaAs epitaxial layers, contact pot. difference, rel. to Fermi level stabilisation 77−20403
- GaAs, MBE (001) layers, work function meas. 80−49870
- GaAs, surface, electron struct. and Fermi level pinning by O_2 and metals 80−11066
- n-GaAs, surface states, photoemission yield obs. 77−16459
- GaAs surfaces (110) and (111)As, UPS and LEED 78−91514
- GaAs, UPS, 5-450 eV, surface states, oxidation behaviour 77−66579
- n-GaAs, valence band studies of clean and O_2 exposed surfaces 78−43298
- GaAs:Ar^+-metal, semi-insulating layer capacitor, Fermi level pinning 79−56316
- p-GaAs:Cd, (110) cleaved surface, defect-induced surface states 80−6925
- GaAs:Cr, current voltage characterisation, deep levels and Fermi level determ. 79−7823
- n-GaAs:Cr, semi-insulating, contact effects, trapping levels 78−10465
- GaAs:Cr, semi-insulating, I-V characts. and photocond. spectra dependencies on Fermi level 79−99576
- GaAs:Cr, semiinsulating, I-V characts., photocond., Fermi level, and deep levels 78−39118
- GaAs-metal interface, metal-induced chem. reactions and surface states 80−20311
- GaAs(Sb), Schottky barrier and semicond./insulator interface states formation 80−49906
- GaP (110), electronic surface states, initial steps of O_2 chemisorption 80−49844
- GaP, cleaved (110) surface, electron surface props. 80−11067
- GaP, minority carrier quasi-Fermi level meas. in illuminated photoelectrolysis cell 77−85308
- GaP, stabilisation of electron-hole liquid by camel's back 80−6740
- GaP, temp. depend. of Fermi Level, calc. 80−39491
- GaP:Cr_2O_3, growth, dopant distribution, elec. resist. 78−34531
- GaP(As)(Sb), electronic surface props., contact potential difference and photoemission expts. 77−47884
- GaSb films, amorphous and cryst., vac. evaporated, Elec. cond. thermoelec. power and optical absorpt. 80−2504
- GaSb, photoemission investig. of surface states, effects of O_2 and alkali metals 77−48312
- GaSb, surface, electron struct. and Fermi level pinning by O_2 and metals 80−11066
- GaSb, UPS, 5-450 eV, surface states, oxidation behaviour 77−66579
- n-GaSb:Te(Se), forbidden optical band gap, Moss-Burstein effect 78−88335
- Gd in CsCl type alloys, exchange between localised 4f and cond. electrons 77−63279
- Gd, magnetic crystalline anisotropy, Fermi level, electronic density of states 80−84596
- $Gd(Co_xIr_{1-x})_2$, C15 Laves phase struct., g shift, linewidth EPR meas., Fermi level movement interpretation 79−61210
- $Gd(Co_xIr_{1-x})_2$, rel. to comp. depend. of struct. and mag. moments 79−86743
- Ge, amorphous film, annealing, effect on localised states 79−4535
- Ge, Fermi level, minority carrier conc., effective intrinsic conc., Einstein relation 77−85209
- N-Ge, pressure influence on photoconductivity temp. dependence 78−76109
- Ge, X-ray emission spectra formation, role of nonequilibrium electron density *(Russian)* 77−63490
- n-Ge:Sb, fast electron irrad. at 77K, radiation defect changes by annealing at 220K 79−37737
- Ge:Sb(As)(Ga), fast-neutron irradiated, shallow radiation defect levels, electronic props. 78−23049
- Ge:Sb(Ga), amorphous, doping effects on Fermi level, electrical meas. 79−42546
- Ge-SiO_2-p^+Si tunnel junctions, for determ. of AC cond. of amorphous Ge 77−24608
- Ge-Te-As-In quaternary compounds, elec. props., Hall effect *(Spanish)* 77−69344
- $GeBi_2Te_4$, Hall const., thermoelec. power, and elec. cond. 80−29407
- $Ge_{0.8}Si_{0.2}$, elec. cond., density of states, impurity and temp. depend 80−65568
- p-GeTe, reflectance, and thermorefl. spectra 80−80814
- HfC_xN_{1-x}, X-ray valence photoelectron spectrum, 4f signal calc. 80−66391

Fermi level continued

- $Hg_{1-x}Cd_xTe$, optical absorpt., quasilocal acceptor level effects, theory 80−92853
- $Hg_{1-x}Cd_xTe$, zero-bandgap state induced by press., galvanomag. props. 77−47725
- HgSe, Dingle temp. exam. 79−65358
- HgSe, Shubnikov-de Haas oscills. in pulsed mag. field, Fermi energy var. 77−15873
- p-HgTe, experimental and theoretical study of the dynamic dielectric function 78−92069
- HgTe, Γ_8 symm. acceptor centre hole mag. props. *(Russian)* 80−88733
- In-Mn, dil., film, ion implanted, supercond, and mag. props. 77−15987
- n-InAs, edge luminescence band, shape depend. on degree of doping, band gap 80−7405
- InAs, electron surface props., contact potential difference and photoemission expts. 77−47884
- n-InAs, transport props., influence of higher energy bands, calcs. 79−19598
- InAs-GaSb superlattice, cyclotron resonance, energy level quantisation 79−73430
- InP, and $In_xGa_{1-x}As_yP_{1-y}$ binary and quaternary cpds., surface and dielec.-semicond. interface props. 80−93001
- InP, Fermi level pinning on exposure to O_2 79−60637
- InP, Schottky barrier and semicond./insulator interface states formation 80−49906
- InP, surface, electron struct. and Fermi level pinning by O_2 and metals 80−11066
- InP, surface vacancies, bound state energy levels calc. 80−80340
- InP, temp. depend. of Fermi Level, calc. 80−39491
- n-InP-metal surface barrier struct., props. 79−11223
- n-InSb, magnetophonon effect in non parabolic band 79−37962
- In_2Te_3-type semiconductor, mechanism of electrically inactive impurities 80−24834
- KC_8, intercalated graphite, electronic and cryst. struct. 80−44472
- KCl, photoelectric emission in photon energy region 1.0 to 6.0 eV 80−108321
- La, electronic structure vol. depend., rigorous cellular method 77−20233
- $La_{1-x}M_xCrO_3$, M=Mg, Sr, electronic struct. study by XPS 80−25518
- La_2O_3, electronic struct. study by XPS 80−25518
- $Li_2Ag_{2-x}In_x$, optical props., struct., energy bands, interband transitions 78−72539
- Li_5B_4, molecular and electronic struct. 80−20107
- LiC_6, and LiC_{12}, intercalation cpds., electronic struct. calcs. 80−70613
- LiC_6, spatial distribution of valence electrons 79−37983
- $Li_2Cd_{2-x}In_x$, optical props., struct., energy bands, interband transitions 78−72539
- Lu, Compton profiles, electronic configurations 80−11501
- $LuH_{2.05}$, Compton profiles, electronic configurations 80−11501
- $LuRhO_3$, elec., mag. and photoelectrochemical props. 80−96925
- Mg-Bi alloy, liq., far IR reflectivity rel. to possible transport processes 78−2827
- MgB_2, band struct. and density of states, metallic behaviour 77−59249
- MnP, spin polarised energy band struct., electronic specific heat, APW calcs. 80−65431
- MnSb, resist., susceptibility and thermopower rel. to electronic struct. 78−67935
- MnSi, electronic energy band struct., self-consistent APW calc. 80−65433
- Mo (001) surface, electronic susceptibility and surface phase transition 79−33169
- Mo (100), sharp peak in UPS near Fermi level 77−52220
- Mo (100), surface resonances, photoemission and field emission meas. 79−4593
- Na, equilibrium struct. and phys. props., pseudopot. method 80−96778
- Nb-Ni glass, photoemission spectra meas. 77−55867
- Nb_3Al, band struct. and density of states from self-consistent pseudopotentials 79−69401
- Nb_3Au, BCC, density of states, comparison with A-15 78−80095
- Nb_3Ge, A15 superconductor, rel. between transition temp. and density of states 79−15247
- Nb_3Ge, band struct. and density of states from self-consistent pseudopotentials 79−69401
- Nb_3Ge, superconducting hybridisation and bonding, XPS exam. 78−2988
- $NbSe_2$ pure and intercalated with ethylenediamine, positron annihilation study 80−84801
- $NbSe_3$, chemical bonding and dimensionality 78−75992
- Nb_3Sn, fast neutron irradiation, effect on critical current density 78−19197
- Ni, near-Fermi part of energy band struct. from PES 80−2328
- Ni, UPS, density of states determ. 78−52623
- β-Ni-Al, X-ray absorpt. spectra meas., Fermi level location 80−35005
- Ni-Cu, Ni-rich, temp. depend. resist. 80−10943
- Ni-Ti, Ni-rich, temp. depend. resist. 80−10943
- $Ni_3(Fe,M)$, M=Cr,Mo,W, elec. resist., temp. depend. anomalies, Hall and Nernst-Ettinghausen effects *(Russian)* 80−10942
- Ni_3Fe alloys, low-temperature specific heat, long and short range order effects 80−100339
- NiSb, bandstructure and density of states calc. 80−70580
- NiSb, resist., susceptibility and thermopower rel. to electronic struct. 78−67935
- PBSnTe/PbTe long wavelength inverted heterostructure mosaics, energy gap temp. depend. 79−85182
- Pb, chemical shift of X-ray L-absorption edge 79−52044
- Pb film, supercond., meas. of effective quasiparticle recombination times, density of electronic states at Fermi level 79−38264
- $Pb_{1-x}Ge_xTe$:Ga, Fermi level stabilization, transport props. meas., 77-400K 78−56065
- $Pb_{1-x}Ge_xTe$:Ga, influence of hydrostatic compression on elec. props. 79−73516
- PbO-SiO_2 glass, reduced channel-plate, variable range hopping conductivity 80−107466
- PbS, (100), angular resolved UV photoemission 78−2989
- PbS (100) surface, electronic struct., O_2 adsorption effects, UPS study 80−54756
- n-$Pb_{0.94}Sn_{0.06}Se$ solid solns., Burstein-Moss effect and energy band struct. 80−40118
- $Pb_{1-x}Sn_xSe$, (x=0.125), pressure induced band inversion, effect on energy spectrum *(Russian)* 78−39007
- n-$Pb_{0.82}Sn_{0.18}Te$, conduction band struct., determ. by Shubnikov-de Haas meas. 78−2504

Fermi level continued
$Pb_{0.82}Sn_{0.18}Te$, thermomagnetic, thermoelectric props., valence band struct. *(Russian)* 80-54724
$Pb_{1-x}Sn_xTe$:Ge, anomalous behaviour of impurity centres under press. *(Russian)* 80-65491
$Pb_{1-x}Sn_xTe$:In, high temp. Fermi level position 79-90948
$Pb_{1-x}Sn_xTe$:In, semiconductor-metal-semiconductor transitions under press. 80-34491
$PbTe_{1-y}Se_y$:In, high temp. Fermi level position 79-90948
Pd, hydride and alloys, electronic band struct., comparative study of electric and mag. props. 78-95259
Pd-Al alloys, Fermi level position rel. to mixing behaviour, Al activity, thermodynamic props. *(German)* 78-75835
Pd-Ni, dil., Zeeman splitting of cond. electrons 77-11884
Pd-Si, metallic glasses, XPS and UPS studies 79-74062
Pd-Si(-Cu), amorphous, Hall effect meas. and electronic struct. 80-75551
Pd-Zr alloy, activity coeff. rel. to electronic props. *(German)* 77-20084
$Pd_{1-y}Ag_yH_x$, superconducting transition temp., APW band struct. calcs. 78-95393
$Pd_{80}Si_{20}$, amorphous, electronic struct. calc. 79-87032
Pt chain compounds, one dimens. conductors, Fermi wavevector determ., X-ray scatt. obs. 80-44187
Pt-Al(In)(Sn) alloys, Fermi energy influence on thermodynamic props. *(German)* 80-24619
Pt-transition metal, dil., impurity resist. 80-92875
Pt-Zr alloy, activity coeffs. rel. to electronic props. *(German)* 77-20084
Pt_3Sn, electronic struct., calc. using linear-muffin-tin-orbitals method 77-24516
ReB_2, electron struct., Fermi energy and surface, bonding 80-20076
$(SN)_x$, brominated, struct. and elec. props. 80-24914
$(SN)_x$, electronic struct., X-ray and UV photoemission obs., OPW and pseudopot. calcs. 78-6832
$(SN)_x$, quantum chem. calcs. of electronic struct. 78-6257
$(SN)_x$, quasi-one-dimens., theoretical group anal. of electron spectrum 79-82511
$(SN)_x$ single crystals, tunnelling spectroscopy investigation *(Japanese)* 80-49954
$(SN)_x$, temp.-depend. of elec. resist. and mag. susceptibility, density of states determ. 77-51877
Sb, de Haas-van Alphen effect, effective mass, Fermi levels 78-75982
Sb, partial Fermi levels of electrons and holes, press. depend. 77-43490
Sb:Te, de Haas-van Alphen effect, effective mass, Fermi levels 78-75982
Sb-Sn, dil., de Haas-van Alphen effect, effective mass, Fermi levels 78-75982
SbSe, amorphous thin film high field charge transport and quasi-Fermi level location 80-70863
ScH_2, electronic struct., band theory 79-78006
Si (100) surface, pairing model, electronic pot., charge density, Fermi energy and surface density of states 77-47875
Si (111) surface, Al overlayers, theoretical study 78-95366
Si, amorphous, doped, density of states determ. from transport meas. 80-49720
Si, amorphous, doped, non-polaronic cond. and thermopower near band edge 80-49719
Si, amorphous, doped, photoconductivity and recomb. meas. 77-89800
Si, amorphous, in contact with electrolyte, Schottky barriers at interface 79-78169
Si, amorphous, photo-induced changes in elec. props., defect states 79-82553
Si, amorphous, position of Fermi level, spectroscopic and transport determ. 80-6706
Si, amorphous film, Fermi energy shift with substitutional doping 79-46998
Si, amorphous presence of acceptor states around Fermi level 78-2445
Si, determ. of Fermi level from reson. tunnelling through Si-SiO_2 double barriers 77-80846
Si, doped amorphous, transport props., conductivity, thermopower, temp. depend. 79-73512
n-Si, effect of random var. in impurity conc. on Fermi level 79-51470
n-Si, efficiency of radiation defect generation by electron bombardment, influence of Fermi energy 77-11596
Si, electron irrad., limiting position of Fermi level, elec. cond. and optical absorpt. meas. 79-65484
Si, Fermi level, minority carrier conc., effective intrinsic conc., Einstein relation 77-85209
Si film, amorphous, effects of annealing of gap states 78-72115
Si, interstitials in radiation defect formation 77-15461
p-Si, inversion layer, screening effect and quantum transport in strong mag. fields 78-19155
p-Si, neutron irradiated, elec. props. 78-51939
Si, vacancy, possible Anderson negative-U system 80-2358
Si, X-ray emission spectra formation, role of nonequilibrium electron density *(Russian)* 77-63490
Si:As, amorphous, field effect and thermoelectric power 79-33289
Si:B(P), amorphous, photo- and dark conductivity 77-28216
Si:Fe^0 interstitial localisation, EPR spectrum 79-1582
Si:H, amorphous, doped, Fermi level position, photoelectron spectra 79-47592
Si:H, amorphous, Schottky diodes, elec. props., light-induced effects 80-103741
a-Si:H/Pt, Schottky diode, influence of prep. conditions on forward bias currents 79-78171
Si:H(F), amorphous, Schottky barrier profiles, depletion region width 80-49871
Si:Li, amorphous, elec. cond. and thermopower 79-73537
Si:Li, amorphous, electron transport, depend. on non-linear statistical shift of Fermi level 79-69142
Si:Na^+, variation of cond. in two-dimensional impurity band with Fermi level position 79-95510
Si:Ni(Co)(Mn), influence of neutron irradiation as elec. props. 78-55895
Si:O, O rich polycryst. film, carrier transport 78-80076
Si:P, amorphous, substitutionally doped CVD, electrical props. 79-99566
Si:P, CVD amorphous film, electronic density of states 79-46993
n-Si:P, edge dislocation energy level, differential capacitance meas. 79-23927
$Si_{1-x}B_x$:H, amorphous films, thermopower and cond. for mixed band and broad tail state cond. 80-49786
p-SiC:Be, Fermi level, Fermi distrib. and activity coeff. calc. 77-1365

Fermi level continued
$Si_{1-x}H_x$:Al, amorphous, co-sputtered Al modification, electronic and optical props. 80-100461
SiO_2, amorphous, energy level schemes, Fermi level-electrochemical potential level coincidence, quantum yield spectrum 79-69400
SiO_2, amorphous and cryst., XPS electronic band struct. interpret. 77-16454
SiO_x, core level shifts, nature of bonding 77-84698
Sm compounds, mixed valence, metals or small gap insulators, two-band Hubbard Hamiltonian 80-34399
SmB_6, mixed valent semicond., transport props. and electonic struct., review 80-96877
$SrTiO_{3-x}$-In contacts, differential capacitance, elec. field depend. permittivity effect 80-54779
TaH_x, H diffusion and electronic struct., pulsed NMR obs. 80-54967
$TaSe_3$, effect of press. on supercond. transition temp. 79-91182
TbZn, ferromag., thermoelec. power, temp. depend. and crit. behaviour 80-96852
TcB_2, electron struct., Fermi energy and surface, bonding 80-20076
Te-transition metal, liq. semicond., elec. props. 80-96870
$ThC_{0.75}$, specific heat, Fermi level density of states 80-10680
$ThC_{0.6}N_{0.4}$, specific heat, Fermi level density of states 80-10680
ThC_xN_y, NMR, Knight shift and spin-lattice relax. 80-100621
$Th_4H_{15}(D_{15})$ normal and supercond., low-temp. spt. ht., density of states at Fermi level 77-4466
ThP, specific heat, Fermi level density of states 80-10680
Ti (0001), with adsorbed N (1×1) layer, underlayer geometry, electronic struct. calcs. and UPS meas. 80-54751
Ti (0001) film, electronic struct., Fermi level, surface states, GO calcs. 80-6927
Ti, electronic structure of omega and alpha phases, nonrelativistic APW method 79-90952
Ti, liq., density of states of d-band, heat of vaporisation 78-95253
Ti-Cr disordered alloy, gap nature of electron spectrum in region of struct. instability *(Russian)* 78-18947
Ti-Ni, martensite transform. B2-B19′, optical props. and electron struct. *(Russian)* 80-34878
TiC, soft X-ray emission, excitation pot. spectra, excited level binding energy 80-35009
TiC_{1-x}, substoichiometric, electronic density of states 80-2319
TiH_x, temp. depend. of thermo-EMF coeff., 100 to 350K 77-11944
TiI_4, temp. depend. of thermo-EMF coeff., 100 to 350K 77-11944
TiN, soft X-ray emission, excitation pot. spectra, excited level binding energy 80-35009
TiN_{1-x}, substoichiometric, electronic density of states, CPA method calcs. 80-88464
TiO_2:Nb, Seebeck coeff., Fermi level temp. depend. 79-11161
Tl_xTe_{1-x}, liq., rigid band behaviour, elec. cond. and thermopower 77-35845
V, electronic density of states, effective mass, electron-phonon interaction, Coulomb pseudopot. *(Russian)* 78-26804
VC, soft X-ray emission, excitation pot. spectra, excited level binding energy 80-35009
$V_{0.75-x}Ga_{0.25+x}$ ^{51}V, nucl. spin-lattice relax. time, annealing and neutron effects 79-82710
VN, soft X-ray emission, excitation pot. spectra, excited level binding energy 80-35009
$VN_{0.74}$ and $VN_{0.89}$, low-temp. specific heat and superconducting critical temp. meas., density of states 80-54835
$V_{2-x}Nb_3Hf$, NMR of ^{51}V and mag. susceptibility, 20-300K *(Russian)* 80-93192
V_3Si, electron spectrum characts., mag. susceptibility depend. on resistivity ratio 79-95320
V_3Si, magnetic susceptibility, density of states model for lattice transformation in A-15 compounds 80-65219
V_3Si, NMR of ^{51}V above and below 21K struct. transition *(Russian)* 80-34796
V_3Si, neutron irrad., sound velocity, magnetic susceptibility and upper critical field 78-88074
V_3Si, neutron-irrad., ht. capacity and resistivity 78-88075
W (100), surface resonances, photoemission and field emission meas. 79-4593
YH_2, electronic struct., band theory 79-78006
ZnS-metal interface, metal-induced chem. reactions and surface states 80-20311
a-ZnSe, elec. and optical meas., Mott-type model for amorphous semicond. 78-2414
p-ZnSe:Li(Na)(N)(P), LPE layers, photocapacitance and photocond. meas. 79-99572
p-$ZnSiAs_2$, electron irrad. elec. props. annealing, lattice defects 80-100465
Zr, electronic structure of omega and alpha phases, nonrelativistic APW method 79-90952
Zr-Nb-Mo, phonon spectra anomalies, lattice dynamics calculations, superconductivity parameters 79-7655
Zr-Pd, metallic glasses, electronic props. and supercond. 79-73486

Fermi liquid *see fermion systems*

Fermi resonance
acetic acid-d_0(-d_1), Fermi reson., IR spectra band profiles 80-60569
acetone, liq., C-C stretching mode relax., Fermi reson. influence 80-25352
1-azacarbazole, IR spectra, Fermi reson., H-bonding *(German)* 77-12392
7-azaindole, IR spectra, Fermi reson., H-bonding *(German)* 77-12392
benzene, SVL fluoresc. band intensities, Franck-Condon factors, Fermi reson. 77-10700
benzene-Br_2 complex, cryst., IR spectrum assignments, site symmetry, rel. to benzene 77-36217
benzene-d_0, -d_6, vapour absorpt. spectrum, band intensities meas. 79-81212
biphenyl, luminescence spectrum intensity distribution 79-3476
bromoacetylene, microwave spectrum, r_5-struct., dipole moment, quadrupole coupling consts., vibr. excited states 77-79606
t-butyl alcohol, and deuterates, gaseous and matrix IR spectra, liq. Raman spectra, vibr. assignment 79-10113
carboxylic acid dimer, Fermi reson. 79-31501
p-chlorobenzaldehyde and deuterated derivs., vibrational spectra 79-3441
crystal, theory 77-1666
dichlorodifluoromethane, IR spectrum and mol. force field 79-72309

Fermi resonance continued
ethylene, IR multiphoton excitation, optoacoustic meas. 80−1038
ethylene(-d_1,d_2), high-resolution UPS, mol. ion vibr. assignments, symmetry 79−27032
ethylene carbonate, Fermi reson., isotopic substitution meas. 78−86870
ethylene-d_1, ν_9 B-type band analysis, ground state rot. parameters 77−42316
ethylene-d_1, IR absorpt., ν_{12} and $\nu_2+\nu_9$ bands, rot. consts., Fermi and Coriolis coupling consts. 77−27070
exciton spectra, Fermi resonance and two particle excitation 79−69436
finite nucleus model for the Fermi contact interaction 79−36601
fluorobenzene, IR vibr. spectra 79−13713
formate esters-d_1, Fermi reson. parameters 80−48103
formic acid monomer, vib. spectra and normal coordinate analysis 77−58003
formic acid-d_0, -d_2, OH(OD) stretching, vibr. band struct. 77−6751
ice, D_2O-H_2O, intramolecular stretching spectrum, role of Fermi resonance 79−93973
ice, II and IX, deuterated forms, 10K, OD stretching bands interpretation 78−2836
iodomethane, thin single cryst., IR spectra anal., Fermi-Davydov intensity distrib. 77−59577
lattice local vibrations, two phonon spectrum 78−18723
lithium formate, and deuterated, parametric light scatt., Fermi reson. of polaritons 77−90150
lithium formate, Fermi reson. of optical phonons with two particle state zone, interference effects *(Russian)* 77−90149
methanethiol, ab initio force consts., anharmonic vibr. 78−21898
methanol, ab initio force consts., anharmonic vibr. 78−21898
methanol, aqueous, damped coupled oscillator model used to study Fermi resonance 80−69152
methanol-d_1, H-bonded in soln., ν_s(OD) band 79−18183
methyl alcohol-d_3, Fermi resonance due to large amplitude vibrs. 80−83519
methyl cyanide, isotopically substituted species, IR spectra, vibr. freq. displacements, harmonic pot. function 78−42057
methyl iodide, mag. hyperfine struct. of quadrupole spectra *(Russian)* 77−34622
N-methylacetamide, solid, Fermi resons. 80−97266
methylamine, ab initio force consts., anharmonic vibr. 78−21898
molecular crystal with isotopic impurity molecule, phonon spectrum under Fermi resonance 78−34583
molecule, theory 77−1666
multidimensional systems, semiclassical calc. of bound states 80−963
neutron scattering, inelastic, optical phonon strong anharmonicity effects 77−31739
PAN fibre, pre-oxidised, IR absorpt. 77−28561
phase transitions soft modes and dipole relaxations 78−91409
polariton, EM wave dispersion 80−2344
polariton Fermi reson. as detection of weakly polar vibrs. 79−7791
polariton Fermi resonance, Raman spectra in band of many-particle states 80−25374
trans-polyacetylene obtained by polymerisation on TiO_2, Raman spectrum *(Spanish)* 80−88988
polyatomic molecules, radiationless transitions, Fermi resons. and quasidiscrete spectrum 80−95665
polymethylene, extended chain, C-H stretching band struct., Fermi reson., Raman spectrum 80−5552
polymethylene chain, vibr. spectra, CH stretching region, struct. and assignments 78−70991
pyridines and water complex, Raman spectra, Fermi reson. in ν_8 region 79−89679
Raman light scatt. efficiency, comparison of various crystals *(Russian)* 77−52104
stilbene, thin single cryst., IR spectra anal. Fermi-Davydov intensity distrib. 77−59577
tetrafluoromethane, IR spectrum, Fermi reson. sequences, cubic pot. energy, anharmonicity consts. 77−10674
s-tetrazine, visible absorpt. band assignment, vibr. anal. 78−994
toluene sulphonate diacetylene polymer, vibr. modes, strain depend. using Raman spectra 80−20626
toluene-d_5, liq., vibr.-vibr. near resonant energy transfer, Raman spectra 77−61836
s-triazine(-d_3), gas phase IR band contours obs., computer simulation 77−6774
tricyclo(3.3.0.$0^{2.6}$)octane, liq., Raman spectrum, vibr. assignments 77−61753
vibrational-rotational line intensities, accidental resonances effect 77−18987
XH_2 molecules 1:2 complexes, H-bonding fluctuation hypothesis, IR and Raman vibr. spectra 77−34632
$_2$, photoluminesc. spectrum, ^{31}P Fermi interaction, hyperfine struct. 78−33536
BO_2, fluoresc. excitation spectra, vibronic level fluoresc., Fermi reson., force field 77−79643
CO_2, dipole moment functions 80−87094
CO_2, Fermi reson, effect on vibr. bands relative intensities 80−965
CO_2, in various solvents, IR absorpt. spectrum, Fermi-reson. doublet and intermolecular interactions 80−18856
CO_2, isotropic Raman scatt., Fermi reson. vibr.-rot. spectra 77−38741
CO_2, near critical point Rayleigh and Raman scatt., Fermi diad 80−80765
CO_2, rot.-vibr. bands, absorpt. coeff. calc. method, Fermi reson. effect on spectral lines 80−32696
CO_2, solid, Fermi reson. press. tuning, Raman spectra 80−93293
CO_2, spectra, Fermi reson. and classical motion 80−28000
CO_2, Σ-diads, Raman spectra, O isotope effects 77−83610
$^{12}C^{16}O_2$, vibr.-rot. Raman spectrum, in Fermi reson. region 78−42073
$^{13}C^{16}O_2$, emission spectrum near 4.5 μm, nu_3 region spectroscopic consts. 77−38664
$C^{18}O_2$, Raman spectra in Fermi reson. region 78−74664
COS^+, photoionis. reson. study of ($^2\Pi$) and ($^2\Sigma^+$) states, vibr. freqs., ionis. pot. 78−29821
CS_2^+, photoionis. reson. study of ($^2\Pi$) and ($^2\Sigma^+$) states, vibr. freqs., ionis. pot. 78−29821
$CaSO_4$, in KBr(KI) crysts., SO_4^{2-} vibr. spectra, press.-scanned Fermi reson. spectroscopy appl. 79−73937
CdTe:S, reson. interaction of local S vibr. with lattice phonons 77−11654
ClCN, and isotopic derivatives, rot. depend. 78−94227

Fermi resonance continued
ClCN, and isotopic species, force field calc., freqs., rot. consts. 79−22692
$GaCl_3(I_3)$, gaseous, Raman spectra, struct., Fermi reson. and thermodynamic functions 77−18929
H bonded systems, IR spectra, theoretical interpretation 79−31519
H bonds, IR spectra, theoretical interpretation 79−31519
H-bonded systems, frequency shift rel. to IR bandwidth 80−99502
H-bonds, IR spectra, ν_s band interpretation 78−58653
HCN, and isotopic derivatives, rot. depend. 78−94227
HCO, ν_2 fundamental band, laser mag. reson. spectra 78−5256
HIO_3 crystals, anharmonicity effects in Raman spectra 80−25379
HIO_3, polariton Fermi-resonance and dissociated phonon states *(Russian)* 80−20634
H_2O, electronic ground state, SCF HF and CI calcs, pot. energy hypersurface, spectroscopic consts. 78−50473
H_2O, in D_2O ice I_c, decoupled vibr. spectra 80−52984
$KB_5O_8.4H_2O$, polariton Fermi reson., spontaneous parametric light scatt. 78−87923
KCN_xKCl_{1-x}, phase transition and OCN^- vibr. spectrum 78−43093
α-$LiIO_3$, Fermi resonance in surface polariton spectra *(Russian)* 80−71423
MoF_6, cryst., overall vibr. band struct., excitons 77−90136
MoF_6, orthorhombic crysts., Raman spectra, int./external mode separation and factor group anal. 77−90135
NCO, $A^2\Sigma$ state, Fermi resonance and vibr. relax. in solid Ar 78−5212
ND_4Cl, ordered phase, Raman spectrum, dipole and polarisability derivatives 77−52072
NH_3 in benzene(CCl_4)(pentane) Fermi resonance, solvent and phase depend. 80−47960
NH_3, pure, Raman scatt., high press., high temp. 77−27077
NH_4Cl crystal, polariton light scattering spectra in zone of dissociated states 79−47029
NH_4Cl, ordered phase Raman spectrum, dipole and polarisability derivatives 77−52072
N_2O, dipole moment functions 80−87094
$NaNO_2$, Raman and IR spectra, destructive Fermi reson. 77−16309
SO_2, IR spectra, $\nu_1+\nu_2$ combination band, rot.-vibr. anal. 78−5225
UF_6, cryst., overall vibr. band struct., excitons 77−90136
UF_6, orthorhombic crysts., Raman spectra, int./external mode separation and factor group anal. 77−90135
WF_6, cryst., overall vibr. band struct., excitons 77−90136
WF_6, orthorhombic crysts., Raman spectra, int./external mode separation and factor group anal. 77−90135

Fermi surface
actinide intermetallic compounds, Fermi surface meas. 80−6698
actinide metals, Fermi surface meas. 80−6698
actinide metals and compounds, nearly magnetic, thermoelec. power 78−84197
actinides, band structure Fermi surface, magnetisation density 78−84140
Ag, anisotropy of electron-phonon collision frequency on Fermi surface, RF size effect 77−15750
alkali metals, Fermi surface topological changes due to uniaxial stresses 80−92810
alloy, dil., mag. ordering of localised spins and effective mass on Fermi surface 77−1541
alloy, Fermi surface and phase stability 77−77459
alloy, high resolution high intensity apparatus for positron annihilation meas. 78−23008
alloy, rel. to stabilisation of long-period superlattices 79−95348
alloys, dil., of polyvalent and noble metals, deviations from Matthiessen rule 80−65525
alloys, positron annihilation CPA calc. for spatial and momentum distrib. 77−80720
alloys, positron annihilation technique in Fermiology 79−69902
anisotropic metal, with impurities, long-range interactions of spins 79−47092
anisotropic superconductors, upper critical field theory 80−75692
α-brass, electronic momentum densities by two-dimensional angular correlation of annihilation radiation 78−91605
Chevrel phase materials, indirect meas. of Fermi surface parameters 79−60686
conductors with Fermi surface in form of corrugated cylinder, EM excitations 79−33224
crystalline films, dispersion law and struct. transition, Fermi line geometry, acoustic spectrum, resist. min. *(Russian)* 79−7764
α-Cu-Ge, Fermi surface, high resolution positron annihilation study 78−6261
cubic harmonics product representation 77−13588
curve calculation method *(French)* 80−2318
de Haas-van Alphen effect, FFT anal. 79−42434
de Haas-van Alphen effect in metals, intermetallic compounds and dilute alloys 79−99473
dilute alloy, mag. ordering rel. to effective mass on Fermi surface 77−20550
dilute alloys, electron self-energy, Fermi surface changes and generalized golden rule 80−10858
dimension determ. using de Haas-van Alphen effect 77−24511
dipole-nuclear acoustic resonance, electron band struct. influence, in cubic metal 79−19787
disordered alloy, positron annihilation, Fermi surface study, review 80−44480
disordered alloys, short range order diffuse electron scatt. 78−87595
Doppler-shifted cyclotron resonance, anomalous propag. of US waves 79−73429
doppleron propagation in inclined mag. field spectrum, decay, polarisation study, Fermi surface model 80−44922
double magic nuclei, self consistent description *(Russian)* 78−33120
double magic nuclei, self consistent description of low lying collective states *(Russian)* 78−89783
edge dislocation screening in metals and superconductors, metal softening *(Russian)* 80−64997
electron field emission, from high-index crystallographic faces, scatt. approach 77−48323
electron liquid, cyclotron reson. at skipping orbits *(Russian)* 78−72240
electron sound absorpt. coeff. Fermi surface local geometry changes *(Russian)* 80−15437
electron-electron scatt. and elec. resistivity of metals 79−95396
electron-phonon interaction, expt. test of rigid muffin tin approximation 79−65364

Fermi surface continued
electronic Fermi fluid, instabilities in mag. field *(Russian)* 79—11073
electronically driven phonon anomalies and phase transforms. 78—63834
Eliashberg eqns., numerical solns., Fermi surface calcs. 77—1514
exciton dielectric, inhomogeneous current state phase transition, free energy *(Russian)* 80—84703
exciton ferromagnet, spin-lattice relax., light and US absorption *(Russian)* 79—7960
FCC binary alloys, short-range order diffuse scattering, Fermi surface imaging *(Japanese)* 79—7776
Fermi gas, one dimensional with backward scatt., gap renormalisation 80—24818
Fermi momenta determ. from Fourier anal. of Compton profiles 77—4285
Fermi surface volume depend. 79—65365
ferromagnet, electron transport with arbitrarily oriented ellipsoidal Fermi surfaces, cyclotron wave excitation 78—23006
ferromagnetic metal, electron-magnon mass enhancement 77—15748
Fourier method, symmetrized for interpolating band-structure results 79—73419
graphite, band theory, Fermi surface constructed, ab initio energy band calc. 77—11841
graphite, band theory, press. effects on Fermi surface 77—85131
graphite, galvanomagnetic effects, trigonal warping of constant energy surfaces 78—87987
graphite acceptor intercalation cpds., C_nBr and C_nNO_3H, electronic struct., quantum-magnetothermal oscills. 80—44478
graphite acceptor intercalation cpds., modulated electronic struct. 79—95310
graphite intercalation compounds, props. and appls. 78—71711
graphite intercalation cpds., C_nK, de Haas-van Alphen effect, cyclotron reson., and transport props. 80—44479
graphite intercalation cpds., Fermi surface and transport props., LCAO model 80—80159
graphite-AsF_5 intercalation compounds, de Haas-van Alphen effect, charge transfer rate 80—54595
graphite-AsF_5 intercalation compounds, resist. data indicative of cylindrical Fermi surface 79—99590
graphite-Br_2, intercalation process 78—63965
graphite-K intercalation compounds, electronic props., de Haas-van Alphen effects and Fermi surfaces 80—75498
graphite-K intercalation compounds, electronic props., resistivity, Hall effect and magnetoresistance 80—75585
graphite-K intercalation compounds, Fermi surface, transport and supercond. props. 79—65367
hexagonal compensated metal, chemical pot. shift due to coupled orbit conduction 79—28273
HMTSF-TCNQ, obs. of the de Haas-Shubnikov oscills. 78—84201
Hume-Rothery alloys, magnetism 78—95417
Hume-Rothery Phases, electronic struct., main features 79—23883
indirect exchange in Bloembergen-Rowland approx., ellipsoidal Fermi surface and relax. process effects 80—107754
intermediate state, thermal cond., Fermi surface shape and topology effects *(Russian)* 78—72314
intermediate state superconductor, kinetic props. of corrugated and thread struct., sound attenuation *(Russian)* 80—54843
intermediate valence metals, renormalisation of collective excitations, acoustic wave vel. near electronic transition 79—82539
ionicity and struct., interrelation, appl. to zincblende, rocksalt and wurtzite structs. and amorphous semiconductors 77—1093
isotropic metals, CDW, Fermi-surface instability 78—79947
IV-VI semiconductors, crystal structure and symmetry of electron spectra, doping effects *(Russian)* 79—7696
KKR calc. of energy bands 80—34355
Knight shift theory near Fermi surface points with changing topology *(Russian)* 80—34794
layered crystals, thermodynamic pot. in quantizing mag. field, conc. depend. *(Russian)* 79—15071
local flattening effect of acoustic wave absorpt. and dispersion *(Russian)* 79—51471
magnetic field sweeper and recorder drive for de Haas-van Alphen type phenomena 77—67474
magnetic oscillations, Fermi surfaces and high magnetic fields 79—73423
mapping from one-dimens. Fourier transform of Compton effect 77—39764
metal, acoustic breakdown, electron energy spectrum *(Russian)* 78—18948
metal, antiferromag., thermoelec. power in mag. field 80—70686
metal, charge screening and Friedel oscillations of electron density *(Russian)* 78—79951
metal, closed Fermi surface, galvanomagnetic phenomena, in intermediate magnetic fields *(Russian)* 78—34822
metal, compensated, with closed Fermi surface, Hall coeff. temp. depend. 77—8074
metal, dispersion relation for ordinary cyclotron waves, spherical Fermi surface 77—55474
metal, effect of impurities on electronic struct. 78—47692
metal, effect of nonlocal potential, phase shift parametrisation scheme 78—43289
metal, electron-electron scatt. 79—38045
metal, electron-lattice interaction effect on equilib. struct. form. *(Russian)* 80—34380
metal, electron-phonon and electron-impurity collision frequencies, RF size effect method 77—20227
metal, Fermi surface local geometry ultrasonic absorpt. ang. depend., Pippard oscill. spectrum *(Russian)* 79—19507
metal, Fermi surface topological transition, electron-phonon interaction contrib. calc. 80—6697
metal, ferromagnetic, spin wave propagation, deformation oscillation of Fermi surface 79—7982
metal, Lifshitz transitions and tunnelling effect 78—91591
metal, local geometry effects on phonon spectrum, acoustic props. *(Russian)* 77—55333
metal, longwave sound, absorpt. coeff., in phase transition of $2^1/_2$ kind *(Russian)* 78—39008
metal, magnetic surface states induced linear magnetoresistance 79—60798
metal, normal, thin films, tunnel electron injection, Fermi surface terrace, from tunnel current *(Russian)* 79—19696
metal, phonon spectra, singularities caused by local geometry of Fermi surface 78—91401

Fermi surface continued
metal, Pippard sound-attenuation oscillating angular depend. *(Russian)* 80—103613
metal, RF size effect, line shape, exactly solvable models 78—43429
metal, RF size effect, small-angle scatt., exactly solvable models 78—47821
metal, soft X-ray emission spectra and Fermi surface, contrib. of John Bardeen 80—57057
metal, sound absorpt. coefficient at phase transition of order $2^1/_2$, effect of geometry of const. energy surfaces 77—39769
metal, strained, interpolation functions for Fermi surface 80—65425
metal, surface impedance in mag. field, cyclotron waves 77—89787
metal, surface impedance in magnetic field, Azbel-Kaner cyclotron resonance 78—87901
metal, thermal resist. calc., role of electron diffusion over Fermi surface 77—62894
metal, with multiply-connected Fermi surface, SAW absorpt., mag. field effect *(Russian)* 77—31936
metal and semiconductor surfaces, electrostatic interaction of charges influence of Fermi surface shape 80—24996
metal crystal with and without surfaces, asymptotic displaced charge round impurities 79—95364
metal spherical Fermi surface, cyclotron reson. line shape and cyclotron waves 78—95251
metal surface region, electrostatic energy and screened charge interaction for different Fermi surface shape 80—70631
metal with open Fermi surface, intrinsic magnetoresist. 77—11899
metal with several carrier groups, acoustic attenuation in strong mag. field *(Russian)* 77—47868
metal-dielectric transition, two-band model, Coulomb interactions, self consistent calcs. *(Russian)* 80—80185
metallic filaments, Tomonaga-Luttinger model, quasi-1D generalisation *(Russian)* 79—51560
metallic films, ultrasound attenuation, size magnetoacoustic effect *(Russian)* 80—107869
metallic slab, theory of Larmor waves, Fermi-liquid interactions, Fermi-surface and g-tensor anisotropy 79—69397
metallic ultrathin filaments, dielectric and superconducting fluctuations, Peierls transition *(Russian)* 80—65742
metals, anomalous sound propag. by cond. electrons 80—11048
metals, charge perturbations around impurities 77—85582
metals, effect of alloying on Fermi surface and Dingle temp. 77—47719
metals, electron theory, internal press. 80—92802
metals, Fermi surface geometry, effect on sound absorpt. and vel. 79—7775
metals, ground state energy, structural expansion, HF approx. 80—65420
metals, hybrid, exchange interaction of localised moments rel. to Fermi surface 77—28381
metals, inelastic scatt. of fast electron, plasma oscillations effect 80—100439
metals, mag. field effects on positron annihilation 77—62803
metals, microwave transmission, time-of-flight effects in Fermi vel. determ., calc. 80—20238
metals, nearly-free-electron, holelike Fermi surface, Hall coeff. and magnetocond. tensor 79—4547
metals, noble, dilute alloys, solute vacancy binding energy, Dingle temp. 80—49177
metals, positron annihilation expts., electronic struct. and Fermi surface studies 80—54594
metals, positron annihilation technique in Fermiology 79—69902
metals, quantum magneto-dimensional effects, open Fermi surfaces, conduction electrons *(Russian)* 80—80487
metals, sound absorpt. and dispersion, Fermi surface flattening 78—91596
metals, sound absorption and dispersion temp. depend. associated with Fermi surface plateaus *(Russian)* 80—65166
metals, uniaxial ferrogmagnetic, influence of anisotropic fluctuations on elec. resist. near T_c 79—91038
metals, with open Fermi surfaces, galvanomag. effects, static skin effect *(Russian)* 80—29389
metals, X-ray photoemission line shape, Fermi surface excitations, book contrib. 79—61499
metals and alloys, electrons at Fermi surface, book 80—105445
modulated structures, electron energies and Fermi surface 79—94929
neutron stars, neutrino cooling in pion-condensed phase 78—45351
noble metals, monovalent, magnetic susceptibility, impurities effect, Fermi surface effects 79—91207
noble metals, positron annihilation data anal. by Mijnarends' method 77—20223
noble metals, TEP calc. 77—24549
noble metals and their dil. alloys, electronic struct., de Haas-van Alphen studies, book contrib. 79—37967
nohle metal, g-factor on the Fermi surface 78—18949
normal metals, low temp. resistivity, correl. with electron-phonon scatt. anisotropy 79—56190
paramagnetic limit, Fermi surface dielectric gap *(Russian)* 80—2533
Pb, Fermi surface model from silicone-rubber mould *(Japanese)* 77—26277
phase transition with valency change, sound vel. renormalisation *(Russian)* 78—79963
phonon anomaly near Fermi surface topological transition 78—95120
polyacetylene:AsF_5, mag. susceptibility, Fermi surface density of states, semicond.-metal transition 79—95566
positron annihilation radiation apparatus, multicounter two-dimensional ang. correlation, momentum density meas. 78—10331
pure crystalline materials, review of Fermi surface studies 78—10334
pyrolytic graphite, magnetoresistance positive-negative transition *(Russian)* 80—96923
quasi-one-dimensional electron-phonon system, electron jump effect on phase tansition *(Russian)* 80—92673
radial distribution function, derivation from exptl. Compton profiles 78—15244
rare earth alloys, magnetic and electronic phase transitions 79—87254
rare earth metal compounds, high temp. paramagnetic-supercond. phase transitions, mag. cell symm. *(Russian)* 79—78255
rare earth metals, electronic sound attenuation anomalies at transition to helical phase, Fermi surface topology *(Russian)* 80—92807
rare earth metals, mag. structs., nonspherical Fermi surface in RKKY theory 77—63227
rare earths, band structure Fermi surface, magnetisation density 78—84140

Fermi surface continued
self energy, density functional approximation 77—15751
semiconductor, electron spectra in mag. and US fields *(Russian)* 77—62801
semiconductor with elliptical isoenergetic surface, photon drag theory 77—1443
semimetal, phonon spectrum, influence of mag. field induced quasi-local levels 78—18946
simple metals, model pseudopot. appl. to various props. 80—59845
sound attenuation in magnetic field at the $2^{1}/_{2}$-order phase transition *(Russian)* 80—100487
spin-splitting factor for Landau levels from de Haas-van Alphen effect first 3 harmonics 77—20226
squared electron-phonon coupling constant, tight-binding calc. in transition metals and alloys 79—1571
superconducting band gap anisotropy, Eliashberg eqns., review *(Spanish)* 80—84544
superconducting film, Pauli paramagnetism and Fermi surface topology changes under press. 78—2612
superconductor, magnetic, Fermi surface nesting effect on mag. instability 80—54831
superconductor, US attenuation and Fermi surface topology *(Russian)* 78—23203
superconductor order parameter singularities, tunnelling currents, Fermi surface calcs. *(Russian)* 80—80458
superconductors, polyvalent metals, Brillouin zone boundary influence on Coloumb interactions 80—24827
superconductors, strongly anisotropic, nonmag. impurities effect on supercond. transition temp. 80—93035
superconductors, thermal conductivity at Lifshitz electronic transition point *(Russian)* 80—11135
superconductors with dielectric gap in Fermi surface, exceeding of paramag. limit *(Russian)* 78—95402
surface impedance in mag. field 77—89786
topology by two-dimens. angular correlation annihilation radiation, appl. to Cu 79—65359
transition metal, 3d, paramag., energy band calcs. 78—91608
transition metal, 4d BCC, electron-phonon interactions 79—95107
transition metal, Fermi surface, stress depend., from quantum oscill. effects 78—91597
transition metal alloys, elastic properties, vol. depend. 78—95103
transition metal compounds, reduced ionisation potentials as parameters in superconducting transition temp. calcs. 80—75671
transition metal dichalcogenides, 2H polytype, rel. to Hall coeff. sign reversals 77—80795
transition metal dichalcogenides, phys. props. and CDWs, review *(Japanese)* 80—49635
transition metal dichalcogenides, US characts. rel. to Fermi surface geometry *(Russian)* 78—34749
transition metal dihydrides, band struct. and electronic props., electron-phonon coupling 79—47011
transition metal layer compounds, Fermi surface anisotropy effect on struct. transitions 77—51661
transition metals, 3d, systematics of electron momentum distribs. 78—18950
transition metals, electron-phonon coupling, electronic aspects 77—69255
TTF-TCNQ, band struct., Fermi surface and density of states, LCAO calc. 78—60048
type II superconductor, clean cubic, anisotropy of generalised Ginzburg-Landau parameters 79—4630
weak-coupling superconductor, effect of electron-phonon renormalisation on thermodynamics 79—99655
AS_xSb_{1-x} thermomagnetic EMF, temp. and mag. flux density *(Russian)* 80—11022
Ag, curvature factor, interpretation of de Haas-van Alphen oscillation amplitudes 79—47000
Ag, cyclotron mass and Fermi velocity meas. by de Haas-van Alphen effect 77—76734
Ag, electronic contribution to thermal cond. at low temps. 79—95384
Ag, Fermi surface and thermoelec. power, de Haas-van Alphen calc. 79—4503
Ag, Fermi velocity from proximity effect tunnelling 78—51875
Ag film, size effect in thermoelec. power, MFP and Fermi surface 77—69433
Ag, microwave size effect, open orbit, and obs. of solid state reson. 79—51621
Ag, size effect, ballistic-type field penetration at 45 GHz, 3 MHz 80—44634
Ag, surface anisotropy meas. by positron annihilation 77—20222
Ag, surface impedance in mag. field, doppleron propag. 77—51642
Ag, surface Landau level resonances, effect of k_H-broadening 79—65533
Ag-Al, short-range order, X-ray and electron diffr. study 80—54173
Ag-In(Sn), HCP ζ-phase, magnetic susceptibility 78—47946
α-Ag-Mg, disordered, rel. to interpretation of electron diffr. obs. of short range order diffuse scatt. 77—84596
β′-AgMg, de Haas-van Alphen effect, LMTO band struct. and Fermi surface 78—75984
$AgTe_2I$, Fermi surface meas. by Shubnikov-de Haas effect 77—39767
Al alloy, dil., Hall coeff., calc. by 4-OPW approx. 78—76052
Al alloys, dil., screening charge anisotropy around impurities, nucl. quadrupole couplings meas. 77—32286
Al, anisotropic electron scattering, Hall coefficient, path integral calc. 79—91027
Al, anisotropic Fermi vel., surface Landau level reson. 78—10333
Al, anomalous behaviour of low temp. magnetoresistivity *(Russian)* 77—31998
Al, band struct. effects on electrical and thermal cond. 78—34820
Al, cryst. and polycryst., inhomogeneity effects on galvanomagnetic props. 78—60109
Al, de Haas van Alphen technique 78—2412
Al, determ. by γ-ray angular correl. meas. 79—4869
Al, EM excitation in metals with anisotropic Fermi surface 77—39768
Al, EM generation of ultrasound, obs. of anomalies 78—84131
Al, elec. resist. and magnetoresist., anisotropic temp. depend. *(Russian)* 79—11103
Al, electron-phonon collision frequencies, RF size effect, Fermi surface study 79—90945
Al, electron-phonon scattering rates, anisotropic, meas. on Fermi surface 78—87753
Al, electronic momentum densities by two-dimensional angular correlation of annihilation radiation 78—91605

Fermi surface continued
Al, Fermi surface, scattering anisotropy of conduction electrons on dislocations *(Russian)* 78—60051
Al, Fermi surface under homogeneous strain, local pseudopot. model 80—29308
Al, impurity low-field galvanomag. coeffs., 4 OPW calcs. 77—69304
Al, low-field galvanomag. props., Fermi surface and defect struct. effects 77—4323
Al, magnetic breakdown, quantum phenomena *(Russian)* 78—43290
Al, magnetomorphic oscillations, magnetoresist. and Hall coeff. meas. 77—28159
Al, magnetoresist., mag. breakdown, open trajectories, temp. depend. *(Russian)* 77—35921
Al, magnetoresistance, path integral method calc. 80—65537
Al, positron annihilation, ang. correl. meas., electronic momentum density calcs. 77—4284
Al, positron annihilation studies using high-density proportional chambers 80—25478
Al, quantum oscills. of thermal EMF under mag. breakdown conditions *(Russian)* 77—69305
Al, quasi-particle properties, anisotropic, electron-phonon interaction study 77—43480
Al, quenched, irradiated, anisotropic electron scatt. on defects 79—95397
Al rel. to Sondheimer size effect, phonon-limited mean path, 1.8-12K 80—49698
Al, Sondheimer oscillation 79—87085
Al, struct. stability 77—8015
Al, superconducting band gap anisotropy and Fermi surface anisotropy *(Spanish)* 80—84544
Al, US quantum oscillation exam of third-zone Fermi surface 78—47695
Al-Cr(Mn), anisotropic electron scattering, Hall coefficient, path integral calc. 79—91027
Al-Ga(Ag), dil, Hall coeff. by OPW Fermi surface model 80—6816
Al-Ge(Mg)(Zn)(Ga), dil., electronic transport coeffs. for point defect scatt., 4-OPW calc. 79—42531
Al-Li, Fermi surface impurity scatt. 79—56114
AlB_2 electronic struct. calcs. 78—2417
Au alloys, dil., conduction electron-local moment interactions using dHvA waveshape anal. 79—77981
Au, conduction electron g-factor meas. 77—35859
Au, conduction electron scatt. from vacancies 77—76735
Au, curvature factor, interpretation of de Haas-van Alphen oscillation amplitudes 79—47000
Au, cyclotron mass and Fermi velocity meas. by de Hass-van Alphen effect 77—76734
Au, Fermi surface and thermoelec. power, de Haas-van Alphen calc. 79—4503
Au, Fermi surface orbit integrals, tetrahedron method, cyclotron mass orientation depend. 80—44476
Au, g-factor determ. from de Haas van Alphen meas. 77—11847
Au, quenched and annealed, cond. electron scatt., de Haas-van Alphen Dingle temp. meas. 77—89688
Au, self-consistent relativistic band struct. 80—75501
Au, surface anisotropy meas. by positron annihilation 77—20222
Au-Ag film, thermoelectric power and resist. meas., MFP and Fermi surface meas. 77—51826
Au-In(Sn), HCP ζ-phase, magnetic susceptibility 78—47946
β′-Au-Mg, de Haas-van Alphen effect, relativistic LMTO bandstructure, Fermi surface 79—37959
Au-Pd(Zn), disordered, rel. to interpretation of electron diffr. obs. of short range order diffuse scatt. 77—84596
$AuCu_3$, ordered, band struct. and optical props. at 30K 79—60696
$AuTe_2I$, Fermi surface determ. by Shubnikov de Haas effect 77—51639
Be, Fermi surface, stress-induced changes 80—96770
Be, Fermi surface stress induced changes calcs., principal cross sectional areas 79—60684
Be, orbital magnetism, effect of energy spectrum features *(Russian)* 77—85414
Be, quantum oscillations of thermal EMF under mag. breakdown conditions *(Russian)* 77—69305
Bi, $2^{1}/_{2}$ order electron phase transition under extension *(Russian)* 78—75981
Bi, acoustic waves, giant quantum attenuation at high mag. fields, angular depend. *(Japanese)* 79—4585
Bi, band structure model parameters, deformation theory *(Russian)* 78—56067
Bi, deformation calculations, band struct. variation, electron phase transitions due to deform. *(Russian)* 80—65137
Bi, diffusion size effects 79—60824
Bi, diffusion thermoelectric power in mag. field, calcs. 78—56167
Bi, electrical resistivity due to electron-phonon scatt. on small cylindrical Fermi surface 79—4562
Bi, electron band models, simultaneous meas. of giant quantum oscills. and diamag. reson. 78—14653
Bi, electron isoenergetic surface, variation of connectivity under press. *(Russian)* 78—60050
Bi, electron isoenergic surface coherence var. under press. *(Russian)* 77—55476
Bi electron properties, carrier spectrum 78—84137
Bi, energy dispersion of electron Fermi surface, deform. model and k.p. calcs. 79—51469
Bi, energy spectrum changes under strong uniaxial compression, Shubnikov-de Haas effect 77—28098
Bi, energy spectrum variation under strong uniaxial tension 79—73432
Bi, Fermi surface, change in connectivity under press. 79—73431
Bi, Fermi surface changes due to strong elastic tensile strains *(Russian)* 77—85133
Bi film, non-extremal cross sections of isoenergy surfaces, tunnel spectroscopy determ. *(Russian)* 77—8011
Bi, giant quantum attenuation of sound, anomalous temp. depend. 77—76728
Bi, giant quantum attenuation anomalies of sound waves at high mag. field, extra attenuation peaks 80—70588
Bi, Landau level spin splitting factor, US exam. 77—20281
Bi, magnetoresistance, high temp. oscills., props. *(Russian)* 80—65606
Bi, microwave magneto-absorption, NENP Cohen model 77—39766
Bi, quantum-EM excitations 80—88471
Bi, review of electronic props. 77—15742
Bi, Shubnikov-de Haas effect and Fermi surface under strong uniaxial deform. 77—43474
Bi, Shubnikov-de Haas effect *(Russian)* 79—7840

Fermi surface continued

- Bi, single crystal, drift velocity of charge carriers *(Russian)* 78—84208
- Bi, skipping electrons cyclotron resonance, electron-electron interaction parameter determ. 80—34351
- Bi, thin cylindrical monocryst., dimens. oscills. of longitudinal magnetoresist. *(Russian)* 77—8124
- Bi, transverse magnetoresist. high-temp. oscills., rel. to Fermi surface *(Russian)* 77—24570
- Bi type, semimetals, electron heating due to acoustic phonon scatt. *(Russian)* 80—10991
- Bi whiskers, elec. resist. under strain *(Russian)* 79—91164
- Bi whiskers, electron transition on simple extension, elec. resist. and magnetoresist. meas. *(Russian)* 80—29422
- Bi, whiskers, hardness, elec. props. *(Russian)* 78—51874
- Bi:Sn(Pb), carrier dispersion law, hole cyclotron masses rel. to Fermi surface vol. 77—20345
- Bi-Sb, semiconduct., e.m. wave propag. perpendicular to mag. field 79—82517
- Bi-Sb narrow gap semiconductor, EM wave propagation in direction parallel to mag. field 78—80014
- Bi-Te, electron isoenergetic surface, variation of connectivity under press. *(Russian)* 78—60050
- $BiIn_2$, dHvA effect, Fermi surface determ., free-electron model 77—15744
- BiSb, alloys, semimetallic, camera, dispersion relations 80—59854
- BiSb, hybrid resonance in a quantising magnetic field, spin splitting parameter 78—67933
- p-$Bi_{0.9}Sb_{0.1}$, Fermi surface anisotropy var. on press. induced transition to gapless state *(Russian)* 77—43483
- n-$Bi_{0.924}Sb_{0.076}$, energy spectrum variation under strong uniaxial tension 79—73432
- n-$Bi_{0.924}Sb_{0.076}$, one-ellipsoid to two-ellipsoid fermi surface transition in extended cryst. *(Russian)* 78—14657
- $Bi_{1-x}Sb_x$, band inversion under press., Fermi surface anisotropy, galvanomag. meas. 77—51637
- $Bi_{1-x}Sb_x$, deformation calculations, band struct. variation, electron phase transitions due to deform. *(Russian)* 80—65137
- n-$Bi_{1-x}Sb_x$, determ. carrier dispersion relation parameters 79—38107
- $Bi_{1-x}Sb_x$, EM wave propag. for rot. of mag. field from Faraday to Voigt config. 80—84419
- $Bi_{1-x}Sb_x$, galvanomag. props., energy spectrum *(Russian)* 79—56248
- $Bi_{1-x}Sb_x$, non-ellipsoidal Fermi surface, cyclotron reson. meas. at 35 and 70 GHz 77—62804
- $Bi_{1-x}Sb_x$, semicond. alloy, EM wave propag. in direction perpendicular to mag. field 79—60687
- $Bi_{1-x}Sb_x$ semiconducting alloy, band struct. study, Shubnikov-de Haas effect *(Russian)* 80—80181
- $Bi_{1-x}Sb_x$, Shubnikov-de Haas effect, Abrikosov-Falkovskii treatment of Fermi surface anisotropy *(Russian)* 78—43285
- $Bi_{86}Sb_{14}$:Te, single crystal, dispersion of magnetoplasma waves *(Russian)* 80—70739
- $(Bi_{1-x}Sb_x)_2Te_3$, highest valence band struct., Shubnikov-de Haas effect 78—14661
- Br-graphite, intercalation cpd., magnetothermal oscill. and charge-density waves 80—11199
- CBr_x, graphite intercalated, de Haas-van Alphen effect and cyclotron reson. 80—44479
- C_8K, K-graphite intercalation compound, electronic struct. using semi-empirical tight-binding scheme 78—6255
- $C_{24}Rb$, graphite intercalated, de Haas-van Alphen effect, cyclotron reson., and transport props. 80—44479
- $C_{12n}(SbCl_5)$, magnetothermal oscill. and electronic struct. 78—84129
- Cd, 3rd band sheet, effective electron mass and relaxation time, Azbel'-Kaner high freq. cyclotron reson. meas. 79—11056
- Cd and Cd-Mg, Fermi surface press. derivatives, de Haas-van Alphen effect meas. 77—43477
- Cd, anisotropy of free-electrons momenta distribution, positron annihilation meas. 77—36309
- Cd, band structure, density of states and Fermi surface, APW calc. 77—20232
- Cd, carrier mean free path, temp. depend. doppleron obs. 79—7822
- Cd, de Haas-van Alphen effect under press., Fermi surface and pseudopot. form factors 77—43475
- Cd, de Haas-van Alphen effect and mag. breakdown *(Russian)* 77—80722
- Cd, Fermi surface, stress-induced changes 80—96770
- Cd, Fermi surface changes under uniaxial compression 78—51876
- Cd, Fermi surface stress induced changes calcs., principal cross sectional areas 79—60684
- Cd film, elec. cond., classical size effect 77—89881
- Cd, inversion of cyclotron resonance data 78—91593
- Cd, phonon anomalies, calc. based on model electron-ion potential and spherical Fermi surface 79—99285
- Cd, positron annihilation data anal. by Mijnarends' method 77—20223
- Cd, size oscillations in magnetocond. 77—4324
- Cd, strain depend., from US vel. oscills. 78—84133
- Cd US attenuation due to conduction electrons 79—46754
- Cd, US attenuation of conduction electrons calc. 78—91588
- Cd, US attenuation of conduction electrons, shear waves calc. 78—91589
- Cd whisker, rel. to anomalous stress depend. of supercond T_c 77—39989
- Cd-Mg alloys, positron annihilation meas. of Fermi surface 79—56113
- Ce, renormalisation of collective excitations, acoustic wave vel. near electronic transition 79—82539
- Co, de Haas van Alphen oscill., effective mass 78—87900
- Co, Fermi surface under press., de Haas-van Alphen effect meas. 80—75499
- Co, ferromag., HCP, electronic struct. calcs., band props. 78—39012
- Co, ferromag., spin subband level position determ. by de Haas-van Alphen meas. under press. *(Russian)* 79—90947
- Co, HCP, positron annihilation meas. of electronic struct. 77—20224
- Co, itinerant ferromag., Fermi surface and single particle excitations 80—34350
- $Co_{92}Fe_8$, FCC, electronic struct., ang. correlation of positron annihilation γ-quanta, meas. 80—10864
- Cr, antiferromag., electron interference oscills. and spin-density-wave energy gaps at Fermi surface 80—49574
- Cr, antiferromag., stress depend. of Fermi surface 77—11846
- Cr, antiferromag., stress depend. of spin density wave state 77—63257
- Cr, antiferromagnetic, pressure effect on Fermi surface by de Haas-van Alphen effect *(Russian)* 80—6701

Fermi surface continued

- Cr, band struct. and Fermi surface, angular correl. of positron annihilation radiation 78—6260
- Cr, band structure and Fermi suface of paramag. solid *(Russian)* 79—65375
- Cr, diffuse electron scatt. *(Russian)* 80—103438
- Cr, Fermi surface under press., de Haas-van Alphen effect meas. 80—75499
- Cr, Neel temperature and Fermi energy, nonmag. impurity effects 80—65888
- Cr, paramagnetic, Hartree band struct., Fermi surface, nesting wave vector 80—49583
- Cr, phase transition at T_N 79—4676
- Cr-Si, dilute alloy, mag. susceptibility and Neel temp. meas. 80—71017
- CrN, electron struct. calc. 80—49587
- Cs, Fermi surface, de Haas-van Alphen meas. 78—2411
- Cs, Fermi surface and quasiparticle props., density functional approx. 80—96771
- Cs, Fermi-surface press. dependence 80—96772
- Cs, metal impurity effect on residual elec. resistance *(Russian)* 80—84457
- Cs, model pseudopot. for Fermi surface distortion and phonon dispersion calc. 77—15737
- Cu, conduction electron g-factor, Fermi surface 78—23011
- Cu, curvature factor, interpretation of de Haas-van Alphen oscillation amplitudes 79—47000
- Cu, cyclotron mass and Fermi velocity meas. by de Haas-van Alphen effect 77—76734
- Cu, determ. by γ-ray angular correl. meas. 79—4869
- Cu, elec. resist., electron-electron scatt., Fermi surface calc. 78—64023
- Cu, electron-phonon enhancement factor on Fermi surface 77—1357
- Cu, electronic contribution to thermal cond. at low temps. 79—95384
- Cu, electronic transport properties, OPW calcs. 77—43553
- Cu, Fermi surface, electron mass enhancement, orthornormal function enhancement 80—96777
- Cu, Fermi surface and thermoelec. power, de Haas-van Alphen calc. 79—4503
- Cu, Fermi surface orbit integrals, tetrahedron method, cyclotron mass orientation depend. 80—44476
- Cu, Fermi surface orbit integrals, tetrahedron method, Dingle temps. for 3d transition metal impurities 80—44477
- Cu, Fermi surface studies by the positron annihilation technique 79—82515
- Cu, Fermi surface topology by two dimens. angular correlation of annihilation radiation 79—65359
- Cu film, electron transport props., struct. defects role 77—40117
- Cu, impurity and electron-phonon scattering rates for orbit on Fermi surface 79—69541
- Cu, monocryst., Hall resist., anisotropic temp. depend. rel. to Fermi surface 77—62897
- Cu monocrystals, positron annihilation quanta ang. correl., point defect effects 77—76729
- Cu, polycryst., transverse magnetoresistance, effective medium approx. 79—87083
- Cu, positron annihilation studies using high-density proportional chambers 80—25478
- Cu, quenched, Hall coefficient, relaxation times, Fermi surface 80—84460
- Cu, self-energy nonlocality effect 77—62805
- Cu, strained, interpolation functions for Fermi surface 80—65425
- Cu, umklapp annihilation of positrons, rot.-specimen method 78—2410
- Cu:Ni, Dingle temps. calcs., tetrahedron method 80—6699
- Cu-Al, optical composition modulation spectra, dielec. const. var., Fermi surface and electronic level shifts 80—6707
- Cu-Pd, Fermi surface comp. depend. by positron annihilation ang. correl. 77—76727
- Cu-Pd(Pt), disordered, rel. to reinterpretation of electron diffr. obs. of short range order diffuse scatt. 77—84596
- Cu-Zn, optical composition modulation spectra, dielec. const. var., Fermi surface and electronic level shifts 80—6707
- Cu_3Au, electrical resistivity and LRO, energy gap formation in Fermi surface 80—88533
- CuH dilute alloy, Hall coefficient, relaxation times, Fermi surface 80—84460
- Cu_2Mg, electronic struct. volume depend. 79—65366
- $Cu_2Mo_6S_8$, normal state and superconducting property measurements 78—91660
- $Cu_xMo_6S_8$, normal-state electronic props., Fermi surface and supercond. parameter derivations 79—60850
- Cu_cNi_{1-c}, Fermi surface of concentrated paramag. alloys 78—95257
- Cu_2Sb, linear muffin-tin calc. for Fermi surface 77—62802
- de Haas-van Alphen freq. and Fermi surface anisotropy press. depend. 80—59856
- ErH_2, electronic struct. 79—28268
- Eu, band struct. and Fermi surface 77—62814
- Eu, Fermi surface and helical spin ordering 77—4291
- Fe, electronic structure, positron annihilation meas. 79—91524
- Fe, Fermi surface under press., de Haas-van Alphen effect meas. 80—75499
- Fe, ferromag., effect of pressure on electron struct. *(Russian)* 79—77987
- Fe, ferromag. nonrelativistic LCAO energy band calc. 78—10343
- Fe, itinerant ferromag., Fermi surface and single particle excitations 80—34350
- Fe, mag. breakdown and Hall resist., theory and model calcs. 80—75552
- Fe whiskers, galvanomag. size effects, spherical Fermi surface model anal. 78—14709
- Fe_3Al, electrical resistivity and LRO, energy gap formation in Fermi surface 80—88533
- $FeGe_2$, antiferromag., Fermi surface, stress effects, oscillatory magnetostriction and torque meas. 80—103616
- $FeGe_2$, antiferromagnet, de Haas-van Alphen effect 79—4505
- $FeGe_2$, Fermi surface press. depend., de Haas-van Alphen method 77—43478
- Ga, de Haas-van Alphen effect, expt. and interpretation 78—84132
- Ga, electronic struct. under pressure, Fermi surface meas. using magnetoacoustic technique *(Russian)* 77—47716
- Ga film, monoclinic, elec. cond., classical size effect 77—89881
- Ga, oscillatory magnetoresist. meas., Fermi surface model 77—62898
- Ga, spiral cyclstron waves excited by US in open Fermi surface metals *(Russian)* 79—99771

Fermi surface continued
Ga, thermopower quantum oscillations 80–15505
GaAs (100) surface, self-consistent electronic calc., rel. to Fermi surface instability 77–20382
GaAs-$Ga_{1-x}Al_xAs$ superlattice, sub-band dimensionality 78–63981
Gd, band structure and Fermi surface using KKR formalism 79–77993
Gd, de Haas-van Alphen effect 78–84138
Gd, de Haas-van Alphen effect, Fermi surface 80–15435
Gd, Fermi surface and de Haas-van Alphen effect frequencies meas. 77–69217
Gd, ferromag. Fermi surface and band struct., press. effects, dHvA expts. 78–14656
Gd, HCP, ferromag. band struct. and Fermi surface, KKR band calcs. 77–62815
Gd, magnetoresistance anisotropy, Fermi surface model 79–91025
Gd pnictides, band struct., semicond.-metal trend 77–28111
Gd, thermoelectric power anisotropy at high temp. 79–23952
Gd-Dy, magnetostriction contrib. to thermal expansion *(Russian)* 77–12184
H_2, solid, electronic struct., HF calc. using plane wave basis 79–7772
$Hg_{3-\delta}AsF_6$, Fermi-surface of incommensurate Hg-chain compounds 79–56115
$Hg_{3-\delta}AsF_6$, quasi one-dimensional, anomalous magnetoresistance 80–24884
$Hg_{3-x}AsF_6$, linear chain metallic cpd., square Fermi surface model for conduction 80–6822
$Hg_{3-x}AsF_6$, linear chain cpd., open orbits, induced torque meas. 80–29309
HgSe,, Fermi surface anisotropy parameters, magneto-optical effect 80–25350
In, electron scattering rates, RF size effect meas. under multiple-turn conditions 78–14654
In, Fermi surface dimensions, ab initio KKRZ calc. 77–89686
In, Fermi surface dimensions, RF size effect meas., KKRZ calc. 77–89687
In, Lifshits transition, electron-phonon interaction 80–29502
In, magnetothermopower giant oscills., mag. breakdown 77–8075
In, RF size effect signals, anomalous behaviour 79–4502
In, relativistic energy bands, density of states, and optical spectra, KKRZ calc. 79–51478
In, stress depend. of supercond. parameters 77–12045
In, superconducting energy gap and phonon frequencies under press., tunnelling meas. 77–32112
In, US absorption and dispersion, lineshape studies of quantum oscills., anomalous behaviour 78–63966
In whisker, rel. to alloying addition effects on stress depend. of supercond. T_c 77–39988
In:Sn, phonon spectrum, electron-phonon interaction *(Russian)* 78–18722
α-In-Sn, stress depend. of supercond. parameters 77–12045
In-Sn alloy, Lifshits transition, electron-phonon interaction 80–29502
InBi, Fermi surface and band struct., press. effects 77–39779
In_2Bi, de Haas-van Alphen effect 78–91594
n-InSb, helicon wave propag., quantum mechanical features 79–42571
β-In_3Sn, band struct. and Fermi surface calc. using model pseudopot. 77–28103
K, Fermi surface distortion 80–2325
K, intermediate-wavelength cyclotron waves and Fermi-liq. effects 79–77986
K, Larmor wave spectrum 79–69397
K, MAPW calcs. using nonlocal screened exchange pot. 77–1359
K, metal impurity effect on residual elec. resistance *(Russian)* 80–84457
K, model pseudopot. for Fermi surface distortion and phonon dispersion calc. 77–15737
K, pressure dependence of Fermi surface, de Haas-van Alphen meas. 78–26807
K, ultrasonic attenuation at low temp., spherical Fermi surface model 80–84255
K-Na, dil., dynamical props. of quasiparticle excitations, de Haas-van Alphen effect meas. 78–84128
K-Rb(Na), dil., anisotropy of electron-impurity scatt. in K, de Haas-van Alphen effect meas. 78–18943
K-Rb(Na), dil., anisotropic scatt. of conduction electrons by impurities 78–18944
KC_8, intercalated graphite, electronic and cryst. struct. 80–44472
n-$KTaO_3$, ang. var. of extremal areas of Fermi surface 79–73426
$LaAl_2$, calc. of energy band-structure and Fermi surface by APW method 80–70590
$LaAl_2$, de Haas-van Alphen effect, Fermi surface 80–15436
$LaAl_2$, electronic struct., APW method and local-spin-density approx. 80–65434
$LaAl_2$, magnetoresist. and de Haas-van Alphen effect, Fermi surface model 79–15069
LaB_6, de Haas-van Alphen effect and Fermi surface 77–15743
LaB_6, de Haas-van Alphen effect, low-field 80–75497
LaB_6, electronic struct., APW method and local-spin-density approx. 80–65434
LaB_6, metallic, energy bands and bonding 77–43486
LaB_6, metallic, energy band structure and Fermi surface, self-consistent APW method 77–69221
LaB_6, synthesis and props. *(Japanese)* 80–40255
Li, cryst. and electronic props., Hartree-Fock calcs. 79–60698
Li, Fermi surface and quasiparticle props., density functional approx. 80–96771
Li, impurity and conduction electron scatt. at 4.2K *(Russian)* 77–35931
Li MIM struct., electron-phonon interaction function investigation by microcontact spectroscopy 79–95108
Li, struct. stability 77–8015
Li-Mg alloy, X-ray Compton scatt. 77–16421
LiC_6, band struct., density of states and Fermi surface props. 79–37982
$LiCd_{1-x}Tl_x$, intermetallic, X-ray and Knight shift meas. of ^{205}Tl and ^{113}Cd 79–42851
metals, model pseudopotential calcs., elastic consts., spin susceptibility, Fermi surface distortions 78–79922
Mg, anisotropy of free-electrons momenta distribution, positron annihilation meas. 77–36309
Mg, cross section, KKR calc. using potentials with exchange and correlation 79–11060

Fermi surface continued
Mg, Fermi surface, stress induced changes, kinetic, pot. energy contrib. 79–60683
Mg, Fermi surface changes under uniaxial compression 78–51876
Mg, Fermi surface stress induced changes calcs., principal cross sectional areas 79–60684
Mg film, Fuchs Sondheimer theory, size effect, elec. cond., Fermi surfaces 79–99637
Mg, Hall resistivity, 1.7-300K, up to 2 T, cyclotron motion breakdown 77–89751
Mg, positron annihilation data anal. by Mijnarends' method 77–20223
Mg, quantum interference effect in transverse magnetoresistance 77–35854
Mg, quantum interference effect in transverse magnetoresistance 77–35855
Mg, quantum interference effect in transverse magnetoresistance 77–35856
Mg, quantum oscills. of thermal EMF under mag. breakdown conditions *(Russian)* 77–69305
Mg US attenuation due to conduction electrons 79–46754
Mg, US attenuation of conduction electrons calc. 78–91588
Mg, US attenuation of conduction electrons, shear waves calc. 78–91589
Mg-In dil. alloys, effect of alloying on Fermi surface, de Haas-van Alphen effect meas. 77–76732
Mg-In dil. alloys, effect of alloying on Fermi surface, pseudopot. model 77–76733
Mg-Li dil. alloys, effect of alloying on Fermi surface, de Haas-van Alphen effect meas. 77–76732
Mg-Li dil. alloys, effect of alloying on Fermi surface, pseudopot. model 77–76733
MgB_2, LCAO calc. 79–90957
$MgCu_2$, Fermi surface investig. by de Haas-van Alphen effect 77–35857
β'-MgHg, energy bands and Fermi surface calc. 77–43481
β'-MgTl, energy bands and Fermi surface calc. 77–43481
MgTl, fermi surface exam. by de Haas-van Alphen effect 78–34752
MnP, elec. resist. of different mag. phases, temp. depend. 80–54691
Mo, band struct. and Fermi surface angular correl. of positron annihilation radiation 78–6260
Mo, cyclotron effective mass and identification of carriers on Fermi surface 79–65372
Mo, cyclotron resonance by microwave transmission and carrier identification on Fermi surface 79–60685
Mo, dielec. function and energy loss function, APW band struct. calc. 77–62850
Mo, differential characteristics in (100) and (110) planes *(Russian)* 79–87038
Mo, diffuse electron scatt. *(Russian)* 80–103438
Mo, effective mass meas. and electron velocities 80–96773
Mo, electron scatt. mech., RF size effect study *(Russian)* 79–37965
Mo, electron-electron scatt., doppleron damping meas. 79–37963
Mo, electronic props., first-principles nonlocal pseudopot. approach 79–95319
Mo, Fermi surface, homogeneous strain response 78–34753
Mo, Fermi surface ang. shear deform. 79–77985
Mo, Fermi surface press. depend., surface impedance and US attenuation oscills. in mag. field 77–43476
Mo hole ellipsoid scatt. rate temp. dependence, magnetoacoustic obs. 79–51472
Mo, longwave dopplerons, nonlocal Hall effect, surface impedance, size effect *(Russian)* 80–80253
Mo, magnetoacoustic studies, to 500 MHz 78–91604
Mo, precision investigation using RF size effect 79–77984
Mo, RF size effect meas. *(Russian)* 79–95311
Mo, RF surface impedance, new type of oscills. 79–15070
Mo, stress depend., hybridised nearly-free-electron tight-binding model 77–15757
Mo, vol. depend. of extremal cross sectional areas of Fermi surface from de Haas-van Alphen meas. 80–70589
MoO_2, effect of press. *(Russian)* 79–77988
MoO_2, Fermi surface calcs. 78–67934
MoO_2:Re(V), current carrier sign, Fermi surface cross section variations *(Russian)* 80–84420
MoS_2 intercalation compounds, reaction with alkali and alkali earth metals, band struct., superconductivity 78–26541
Na, Fermi surface distortion 80–2325
Na, Fermi surface distortions, model pot. 80–80157
Na MIM struct., electron-phonon interaction function investigation by microcontact spectroscopy 79–95108
Na, metal impurity effect on residual elec. resistance *(Russian)* 80–84457
Na, size oscillations in magnetocond. 77–4324
Nb, de Haas-van Alphen study of Fermi surface, cyclotron effective masses, mag. breakdown effects, KKR calcs. 78–43288
Nb, dielec. function and energy loss function, APW band struct. calc. 77–62850
Nb, diffuse electron scatt. *(Russian)* 80–103438
Nb, electron-phonon spectral function and mass enhancement 78–26988
Nb, electronic and optical properties 78–91612
Nb, electronic structure, APW calcs., self-consistency and exchange effects 77–66109
Nb, Eliashberg eqns., numerical solns. Fermi surface calcs. 77–1514
Nb, Fermi surface, electron mass enhancement, orthornormal function enhancement 80–96777
Nb, Fermi surface, Fermi velocity, electron-phonon interaction parameter 79–7778
Nb films, supercond. props. and electronic density of states *(Russian)* 79–28439
Nb, high field de Haas van Alphen spectroscopy 79–73425
Nb hole ellipsoid scatt. rate temp. dependence, magnetoacoustic obs. 79–51472
Nb, optical properties and electronic props. 79–42439
Nb, quasiparticle velocity, anisotropic many-body effects 79–33223
Nb, supercond., rel. to magnetoresist. and mag. breakdown in field up to 175 kOe *(Russian)* 77–20492
Nb-Al, diffuse electron scatt. *(Russian)* 80–103438
Nb-Mo, BCC, press. derivatives of elastic moduli, Fermi surface topological changes, band struct. 79–61639
Nb-Zr alloy, BCC-ω phase transition, electronically driven nature, rel. to Fermi surface features 80–103433
NbC, phonon anomaly rel. to Fermi surface 77–11853

Fermi surface continued
NbO_2, electronic band struct., optical props., generalised susceptibility, struct. transition 79—95328
NbS_2, 2H layer cpd., electronic susceptibility and CDWs 78—39040
Nb_3Sb, de Haas-van Alphen effect and Fermi surface 78—6262
$NbSe_2$, 2H layer cpd., electronic susceptibility and CDWs 78—39040
$NbSe_2$, 2H polytype, Fermi surface and CDWs 77—51641
$NbSe_2$, 2H polytype, layered cpd., thermal props. at CDW transitions 77—47750
$NbSe_2$ (2H), electronic response function including electron-phonon matrix elements 79—28300
$NbSe_2$ (2H), metallic layer cpd., reconstructed band struct. and Fermi surface 79—95312
$NbSe_3$ and $Nb_{1-x}Ta_xSe_3$, thermoelec. power meas., 10-300K 80—20177
$NbSe_3$, CDW form., supercond. and Fermi surface determ., press. study 80—70891
$NbSe_3$, Fermi surface, press. effects, Shubnikov-de Haas effect meas. at 1.5K 80—20068
$NbSe_3$, linear chain metal, anomalous transport props. 78—14718
$NbSe_3$, mag. susceptibility, CDW effect 80—88716
$NbSe_3$, non-ohmic transport props. near phase tranistions 78—72213
$NbSe_3$, oscillatory magnetotransport, Fermi surface anisotropy, Hall effect, g-factor, Dingle temp. 78—51975
$NbSe_3$, quantum oscillation, Fermi surface exam: 78—60049
$NbSe_3$, satellite electron diffr. below 59K, Fermi surface features 78—84136
$NbSe_2$(2H), layered metallic magnetoresist. and Fermi surface above and below CDW onset temp. 79—19578
Nb_3Sn, A-15 cubic phase, band calc. using APW method 79—56120
Nb_3Sn, A-15 superconductor, dHvA effect 78—75985
Nb_3Sn, normal state, Fermi surface, APW band calc. and de Haas-van Alphen oscills. 79—65369
Ni and Ni alloys, tunnel currents, spin polarisation, simple band theory interpretation 79—78451
Ni band structure, rel. to lattice const., spin polarised APW calc. 80—20073
Ni, dHvA effect, absolute amplitude, Fermi surface neck 77—85134
Ni, electronic and magnetic props., spin split energy band dispersions 79—78829
Ni, Fermi surface under press., de Haas-van Alphen effect meas. 80—75499
Ni, ferromag., de Haas-van Alphen effect, press. effects *(Russian)* 78—2413
Ni, ferromag., effect of pressure on electron struct. *(Russian)* 79—77987
Ni, ferromag., Fermi surface determ. 77—11843
Ni, ferromag., self-consistent calc. of energy bands 77—39774
Ni, ferromagnetic, Fermi surface and band struct. 78—6267
Ni, itinerant ferromag., Fermi surface and single particle excitations 80—34350
Ni, mag. anisotropy, $X_{2\text{spin down}}$ hole pocket in Fermi surface 78—39314
Ni, mag. excitations variation of de Haas-van Alphen frequency 79—8019
Ni-Cu-Mn alloys, mag. and galvanomag. meas. 77—89928
β'-NiAl, electronic struct. and optical props. 80—97228
Ni_3Al, itinerant ferromag., Fermi surface and single particle excitations 80—34350
Ni_3(Fe,M), M=Cu, Cr, Mo, W, kinetic phenomena rel. to ordering and electron struct. *(Russian)* 78—76043
Os, correlation effect of crystal pot., RAPW calcs. 78—6265
Os, thermal EMF quantum oscills. *(Russian)* 80—88543
Pb, ab initio band struct. calcs. 80—75502
Pb and Pb-Mg, dil., resistivity, multiple plane wave calc., Fermi surface, vel. and band struct. 77—51723
Pb, cyclotron reson., anisotropy, line shape, relax. time and identification of orbits 77—35853
Pb, cyclotron reson., tipping effect of mag. field 77—35852
Pb, cyclotron reson. obs. *(Japanese)* 78—23009
Pb, de Haas-van Alphen effect, mag. induction oscillation 77—62806
Pb, de Haas-van Alphen effect obs. *(Japanese)* 78—23010
Pb, de Haas-van Alphen γ oscill. for [011] symmetry direction 79—90944
Pb, effective cyclotron masses of central and noncentral ζ orbits, de Haas-van Alphen effect 78—63968
Pb, Fermi surface, uniaxial stress depend. 79—65362
Pb, Fermi surface and non-muffin-tin energy bands, calc. 80—20072
Pb, neutron irrad. effect on cyclotron reson. *(Russian)* 77—69216
$PbMo_6S_8$, normal state and superconducting property measurements 78—91660
$PbMo_6S_8$, normal-state electronic props., Fermi surface and supercond. parameter derivations 79—60850
$Pb_{1-x}Sn_xGe$:In, press.-induced transition to gapless state, galvanomag. effects 78—19108
$Pb_{1-x}Sn_xSe$, (x=0.125), pressure induced band inversion, effect on energy spectrum *(Russian)* 78—39007
$Pb_{1-x}Sn_xSe$, determ. of anisotropy coeff. of Fermi surface, magnetoresist. meas. 78—51878
$Pb_{1-x}Sn_xSe$, energy band parameter determ. from Shubnikov-de Haas effect 77—69227
$Pb_{0.82}Sn_{0.18}Te$ solid solution, energy band spectrum characts., Hall effect meas. 77—76737
$Pb_{1-x}Sn_xTe$, diamag. reson. *(Russian)* 78—23347
$Pb_{1-x}Sn_xTe$ narrow gap solid alloys, hole Fermi surface, galvanomag. and oscill. effect obs. *(Russian)* 77—69345
$Pb_{1-x}Sn_xTe$:In, nonequilib. metallic state *(Russian)* 79—33300
p-PbTe, Fermi surface parameters depend. on carrier density, Shubnikov-de Haas oscills. 79—42435
Pd, electron-phonon interaction, expt. test of rigid muffin tin approximation 79—65364
Pd, electron-phonon parameters and supercond. p-state pairing 80—25041
Pd, extremal cross section, press. derivative, determ. by de Haas-van Alphen meas. 79—11055
Pd, Fermi radii, Fermi velocities and many body enhancement 79—65363
Pd, g tensor of d holes near X point in Brillouin zone 79—23890
Pd, generalised susceptibilities and phonon anomalies, band struct. calcs. 79—90953
Pd, high field de Haas van Alphen spectroscopy 79—73425
Pd, Knight shift calcs. 79—56620

Fermi surface continued
Pd, stress depend., oscillatory magnetostriction and de Haas-van Alphen torque obs. 78—91602
Pd-Cu compound, KKR electronic struct. 80—59864
Pd-H, dil., electronic states, de Haas Haas-van Alphen effect meas. 77—47718
Pd-H, electronic states from de Haas-van Alphen measurements 79—7777
Pd-H dilute alloy, de Haas-van Alphen oscill. freq., absolute amplitude, Dingle temp. 80—49575
Pd-Rh-Ag, mag. susceptibility, pressure effect up to 4000 atms. 77—16142
PdH, electronic struct. and proton spin-lattice relax. calc. 78—67937
PdH_x, electronic states calc. 79—7769
α-PdH_x, electronic states and Fermi surface props. 80—29310
PdSb, de Haas-van Alphen effect, Fermi surface 79—7773
PdSb, electronic struct., optical transitions, Fermi surface 78—51885
$PdTe_2$, bandstructure, Fermi surface, LMTO method 78—6264
Pr, de Haas-van Alphen effect, Fermi surface 80—15435
Pr, de Haas-van Alphen freq. determ. 79—11054
Pt, de Haas van Alphen obs. 78—91601
Pt, Fermi surface 78—47693
Pt, generalised susceptibilities and phonon anomalies, band struct. calcs. 79—90953
Pt, high field de Haas van Alphen spectroscopy 79—73425
Pt, mag. field induced conduction electron , polarisation, magnetisation density, and neut neutron mag. form factor 78—18945
Pt_3Mn, mag. excitation dispersion relation 80—25090
Pt_3Sn, Fermi surface, de Haas-van Alphen effect meas. 77—24514
Rb, Fermi surface, de Haas-van Alphen meas. 78—2411
Rb, Fermi surface and quasiparticle props., density functional approx. 80—96771
Rb, Fermi-surface press. dependence 80—96772
Rb, metal impurity effect on residual elec. resistance *(Russian)* 80—84457
Rb, model pseudopot. for Fermi surface distortion and phonon dispersion calc. 77—15737
Rb, quasiparticle dynamics, density-functional approx. 79—60682
Rb-K, dil., dynamical props. of quasiparticle excitations, de Haas-van Alphen effect meas. 78—84128
Re, Fermi surface, determ. from RF size effect 79—23889
Re, Fermi surface, Landau quantum oscill. meas. in magnetostriction, stress and strain derivatives 80—107691
Re, Fermi surface, RF size effect, temp. depend. 80—65424
Re, Fermi surface hydrostatic press. depend., de Haas-van Alphen phase shift meas. 80—54593
Re, RF size effect, Fermi surface dimensions determ. 78—91598
Re, single crystal, size effect in elec. resistivity *(Russian)* 78—87961
Re, strain depend., from US vel. oscills. 78—84133
Re, stress depend., quantum oscills. obs. 78—91599
ReB_2, electron struct., Fermi energy and surface, bonding 80—20076
ReO_3, de Haas-van Alphen frequencies as function of press. 79—19505
ReO_3, mag. breakdown above compressibility collapse transition 80—103617
ReO_3, open orbits in cryst., EM induction meas. 79—73421
ReO_3, phase transition at high press., Fermi surface and X-ray studies 79—65188
ReO_3, positron annihilation, Fermi surface shape 79—46997
Rh, de Haas-van Alphen effect 77—35851
Rh-Fe, dil., anti-Kondo effect, de Haas-van Alphen obs. 79—73427
Ru, electronic structure and mag. breakdown, galvanomag. props. obs., 1.3-20.4K 78—91600
Ru, Fermi surface, influence of press. *(Russian)* 79—4501
Ru, Fermi surface energy spectrum, de Haas-van Alphen effect *(Russian)* 79—37964
Ru, single crystal, size effect in elec. resistivity *(Russian)* 78—87961
Ru, thermopower and magnetoresistance meas., mag. breakdown 78—47766
$(SN)_x$, electronic struct. and opt. props. 78—6256
$(SN)_x$, polycryst. films, single crysts., UPS, valence band struct. 77—69967
$(SN)_x$, polymeric, electronic structure, semi-empirical pseudopotential calc. 77—72812
Sb, carrier energy spectrum, effect of hydrostatic pressure 78—87903
Sb, carrier transport, magnetoresistivity, field-dependent tensor study 80—39609
Sb, de Haas-van Alphen effect, effective mass, Fermi levels 78—75982
Sb, electronic band struct. changes due to plane straining effects *(Russian)* 80—54602
Sb, electronic struct., depend. on hydrostatic pressure 80—80158
Sb, energy spectrum variation under strong uniaxial tension 79—73432
Sb, quantum oscillations of vel. of sound meas. in mag. field 78—39004
Sb, tension effect *(Russian)* 78—75980
Sb:Te, de Haas-van Alphen effect, effective mass, Fermi levels 78—75982
Sb-Ge (1.2 to 2.2 at.%), carrier transport, magnetoresistivity, field-dependent tensor study 80—39609
Sb-Sn, dil., de Haas-van Alphen effect, effective mass, Fermi levels 78—75982
Sb-Sn (0.5 to 1.0 at.%), carrier transport, magnetoresistivity, field-dependent tensor study 80—39609
$Sb_{1-x}Bi_x$ alloys, Shubnikov-de Haas *(Russian)* 78—23007
Sc_3In, itinerant electron ferromag., NMR and relax. 78—6586
Si, inversion layer, interacting electron system, cyclotron reson. 78—87902
Si inversion layers, resolution of Shubnikov-de Haas paradoxes 80—39648
Si, surface space charge layer, anisotropic and tilted valley systems, absorption 77—85726
Si:B, heavily doped, paramagnetic props., anomalous hole spin susceptibility *(Russian)* 80—54861
SiP_2 with pyrite struct., Fermi surface calc. 80—65427
Sn, Fermi surface, dilational strain depend., elastic moduli and torque obs. 80—70586
β-Sn, Fermi surface, electronic momentum densities, positron annihilation obs. 80—6696
Sn, Fermi surface press. depend., surface impedance quantum oscills. in mag. field 77—47717
β-Sn, Fermi surface press. depend., de Haas-van Alphen meas. 79—73422
Sn, magnetic breakdown orbits 80—103615

Fermi surface continued
Sn, sound absorption giant resonance, produced by coherent mag. breakthrough *(Russian)* 80−6700
Sn, stress depend. of supercond. parameters 77−12045
Sn, supercond., quasiparticle recomb. time and normal electronic density of states at Fermi surface from tunnel junction expts. 79−24108
Sn, white, band masses and deformation pots., OPW pseudopotential model 80−100430
Sn, white, cyclotron effective masses, US attenuation meas. 77−15753
Sn, white, Fermi surface, dilational strain depend., OPW calcs. 80−84418
Sn, white, US quantum oscillations exam. at 0.1K 78−47694
SnO_2:Sb transparent conductive coatings for Cu_2S-CdS solar cells 79−61992
$SrTiO_3$:Nb, Fermi surface meas., oscillatory magnetothermal effect study 79−65357
Ta, electronic props. and reflectivity, iterative empirical pseudopot. calc. 77−76745
Ta, electronic structure, APW calcs., self-consistency and exchange effects 77−66109
Ta, optical properties and electronic props. 79−42439
Ta-W BCC, press. derivatives of elastic moduli, Fermi surface topological changes, band struct. 79−61639
TaC, phonon anomaly rel. to Fermi surface 77−11853
TaN, energy band struct. calc., symmetrised APW method 80−96784
TaS_2, 1T, quasi-octahedral layer compound, band struct. and Fermi surfaces 77−76747
TaS_2, 1T polytype, intercalated with Li(Na)(K)(Eu), CDW's and superlattice patterns 77−47746
TaS_2, $1T_2$ polytype, incommensurate periodic lattice distortions, real space TEM rel. to Fermi surface 77−47432
TaS_2 (1T) and (2H), bonding and charge density wave phase transitions 80−44282
TaS_2 (2H), quantum oscillations and Fermi surface 79−37960
TaS_2 ($4H_b$), Fermi surface calcs. 77−51640
TaS_2 (4Hb) layer cpd., oscillatory magnetotransport obs. 77−85241
4Hb-TaS_2, charge transfer and charge density waves 78−79926
$TaS_2(Se_2)$, 2H and 4Hb polytypes, layered cpd., thermal props. at CDW transitions 77−47750
$TaSe_2$, 1T, quasi-octahedral layer compound, band struct. and Fermi surface 77−76747
$TaSe_2$, 2H, CDW 77−76736
$TaSe_2$ (2H), Fermi surface, de Haas van Alphen meas. 77−20229
$TaSe_2$ (2H), magnetoresistance in commensurate CDW state, Fermi surface topology 77−43576
$TaSe_2$/(2H) layer cpd., oscillatory magnetotransport obs. 77−85241
Tb, thermoelectric power anisotropy at high temp. ·79−23952
Tb-Y, Fermi surface topology var., mag. and elec. props. *(Russian)* 77−80723
Tb-Y, magnetostriction, mag. and elec. props. 78−27068
Tb-Y, magnon component of elec. resist., rel. to Fermi surface struct. 77−15827
Tc, Fermi surface, constant-energy-search KKR band theory calc. 77−89689
Tc, superconductivity and Fermi surface calcs. 80−70873
TcB_2, electron struct., Fermi energy and surface, bonding 80−20076
Th, correlation effect of crystal pot., RAPW calcs. 78−6265
Th, electronic states under press. 80−54600
Th, Fermi surface press. depend., de Haas van Alphen meas. 78−39006
Ti alloys, Fermi sphere limiting electronic capacitance, Brillouin zones *(Russian)* 80−92808
Ti-Cr, diffuse electron scatt. *(Russian)* 80−103438
Ti-Mo, diffuse electron scatt. *(Russian)* 80−103438
Ti-Nb, diffuse electron scatt. *(Russian)* 80−103438
Ti-Ni, electron phase transition XPS, optical spectra and mag. susceptibility meas. 80−19943
Ti-V-Cr, BCC, press. derivatives of elastic moduli, Fermi surface topological changes, band struct. 79−61639
$TiBe_2$, de Haas-van Alphen effect, Fermi surface, theory 80−103614
TiH_2, electronic density of states and tetragonal distortion, APW calc. 79−37986
TiO, electron struct. calc. 80−49587
TiO, Fermi surface and de Haas-van Alphen effect *(Russian)* 80−49573
$Ti_{1+x}S_2$, short-range order, conc. modulations, rel. to Fermi surface effects 77−19936
$Ti_{1+x}Se_2$, superlattic form., phase transform., Fermi surface instability 77−15383
Tl, band struct. by LMTO method 77−39773
Tl, band structure and fermi surface using relativistic APW calc., optical spectra interpretation 77−20231
Tl film, Fuchs Sondheimer theory, size effect, elec. cond., Fermi surfaces 79−99637
Tl, mag. breakdown, electron energy spectrum 78−10335
Tl, nonlinear helicon resonance due to open-orbit conduction 80−2324
Tl, relativistic Green's function theory 79−82512
α-U, electronic band struct. and props. 80−10861
α-U, Fermi surface and effective masses, de Haas-van Alphen meas. 80−65426
UAsS(Se)(Te), positron annihilation ang. distrib., valence electrons and Fermi surface 77−28093
UGe_3, compensated metal, topological props. of Fermi surface, magnetoresist. meas. 78−6350
UGe_3, de Haas-van Alphen effect, band struct. calc. 78−72068
UGe_3, spin fluctuation phenomena, band struct. calcs. and de Haas-van Alphen meas. 77−20225
UIr_3, uncompensated metal, topological props. of Fermi surface, magnetoresist. meas. 78−6350
$UIr_3(Rh_3)$, de Haas-van Alphen effect 77−28099
$UP_2(Sb_2)(As_2)$, positron annihilation ang. distrib., valence electrons and Fermi surface 77−28093
V, amorphous film, supercond. props., gaseous impurities effect *(Russian)* 78−72301
V, electron-phonon coupling constant calc. *(Russian)* 80−70624
V, electronic structure, APW calcs., self-consistency and exchange effects 77−66109
V, electronic structure, model potential calcs. *(Russian)* 80−100431
V, energy bands, calcs. using LCGO method 78−91608
V, energy bands, Compton profile, optical cond., SCF LCAO calcs. Gaussian orbitals 78−47698

Fermi surface continued
V, Fermi surface area, effective heat, optical masses, surface anisotropy critical temp. depend. *(Russian)* 79−90943
V, Fermi surface topology, associated plane wave calcs. 78−14660
V, magnetoresistance and thermopower behaviour 79−33222
V, optical properties and electronic props. 79−42439
VN-CrN system solid solns., electrophys. and galvanomag. props. 77−24567
VO, investigation of Fermi surface from electron energy spectrum *(Russian)* 80−75496
VSe_2, 1T, quasi-octahedral layer compound, band struct. and Fermi surface 77−76747
VSe_2, 1T polytype, layer cpd., thermal props. at CDW transition 77−47750
VSe_2 (1T), Fermi surface calcs. 77−51640
VSe_2, angle-resolved UPS, Fermi surface determ. 80−55257
VSe_2, k-dependent photohole scatt. in photoemission 79−56912
V_3Si, A-15 superconductor, dHvA effect 78−75985
V_3Si, determ. by γ-ray angular correl. meas. 79−4869
V_3Si, Fermi surface, positron annihilation meas. 79−87039
V_3Si, Fermi surface determ. by positron annihilation 80−2326
V_3Si, Fermi surface studies by the positron annihilation technique 79−82515
V_3Si, Fermi surface topology, positron annihilation meas. 79−56117
V_3Si, mixed state A15 struct., Gibbs free energy and lower crit. field temp. depend. 77−55643
V_3Si, normal state, Fermi surface, de Haas-van Alphen oscills. 79−65369
V_3Si, quasi-one-dimens. band struct. 78−19596
W, (110) surface, conduction electron interaction with diffracting electrons *(Russian)* 80−79643
W, electron-electron scatt. 79−38045
W, Fermi surface, uniaxial strain depend., quantum oscills. in magnetostriction, US vel., with torque 77−28094
W, Fermi surface press. depend., surface impedance and US attenuation oscills. in mag. field 77−43476
W, Fermi velocity calc., linear muffin-tin orbital method 79−28272
W, Fermi velocity calc. 79−4504
W hole ellipsoid scatt. rate temp. dependence, magnetoacoustic obs. 79−51472
W, longwave dopplerons, nonlocal Hall effect, surface impedance, size effect *(Russian)* 80−80253
W, magnetoacoustic studies, to 500 MHz 78−91604
W plate, impedance oscillations in mag. field 78−39140
W, RF surface impedance, new type of oscills. 79−15070
W thin plate, oscillations of surface impedance in circularly polarised RF fields *(Russian)* 78−39144
WO_2, effect of press. *(Russian)* 79−77988
WO_2, Fermi surface calcs. 78−67934
Y, de Haas-van Alphen effect, Fermi surface 80−15435
Y, Fermi surface and de Haas-van Alphen effect 78−75983
Y, thermoelectric power anisotropy at high temp. 79−23952
Y-Gd, de Haas-van Alphen effect, Fermi surface 80−15435
YAl_2, de Haas-van Alphen effect 78−91590
YB_6, metallic, energy bands and bonding 77−43486
YS, electronic instability and phonon softening, APW calc. 80−29323
YS, superconductor, resonances in generalised susceptibility and phonon anomalies 79−60443
YZn, self-consistent energy bands and Fermi surface 77−72814
Yb, FCC, Fermi surface parameters, de Haas-van Alphen effect, press. depend. 77−28092
Zn, anisotropy and temp. depend. of electron-phonon mass enhancement 77−15745
Zn, anisotropy of free-electrons momenta distribution, positron annihilation meas. 77−36309
Zn, band structure, density of states and Fermi surface, APW calc. 77−20232
Zn, cyclotron mass and superconducting energy gap calc. as a function of Fermi surface position 79−69625
Zn, de Haas-van Alphen effect under press., Fermi surface and pseudopot. form factors 77−43475
Zn, de Haas-van Alphen effect, oscill. freq., 1-140 bar *(Russian)* 79−19506
Zn, electrical and thermal resist. calc. 79−69489
Zn, Fermi surface, stress-induced changes 79−82516
Zn, Fermi surface changes under uniaxial compression 78−51876
Zn, Fermi surface stress induced changes calcs., principal cross sectional areas 79−60684
Zn, Fermi surface-Brillouin zone interaction, XPS obs. 79−52078
Zn, Hall effect, analysis at high temp. 78−2465
Zn, magnetoresist. anisotropy change under stress, rel. to Fermi surface topology *(Russian)* 77−62907
Zn, monocryst., electron motion, Hall effect and Fermi surface 77−47793
Zn, quantum oscills. of thermal EMF under mag. breakdown conditions *(Russian)* 77−69305
Zn, superconducting, ultrasonic attenuation 78−88071
Zn US attenuation due to conduction electrons 79−46754
Zn, US attenuation of conduction electrons calc. 78−91588
Zn, US attenuation of conduction electrons, shear waves calc. 78−91589
Zn:Al, residual resistivity, numerical calc., Fermi surface and multiple plane wave band struct. 77−51722
Zn-Al, dil., impurity quasi-particle lifetimes and pseudopotential form factor 78−47734
ZnTe clean and adsorbed O_2 (110) surfaces, UV photoemission spectra *(Japanese)* 80−93456
Zr, de Haas-van Alphen studies in high mag. fields, Fermi surface model 80−6702
Zr-Hf, mag. susceptibility, elec. cond., Hall conc. thermoEMF conc. depend. *(Russian)* 80−39551
Zr-Ti, alloy, mag. susceptibility, elec. cond., Hall conc. thermoEMF conc. depend. *(Russian)* 80−39551
ZrB_2, Fermi surface, de Haas-van Alphen effect meas. 78−84134
$Zr_xHf_{1-x}V_2$, polycrystalline superconductor, resist. and mag. susceptibility, transition temp., temp. depend. 80−25113
$ZrZn_2$, de Haas-van Alphen effect, Fermi surface, theory 80−103614

Fermi-Thomas model *see Thomas-Fermi model*

fermion systems
see also electron gas; liquid helium-3
$4k_F$ response function in Tomonaga model 79−93039

fermion systems continued
- algebraic approach, equilib. states and hierarchy of stability 77—22491
- algebraic models with non-Abelian gauge group U(1) and superselection rates 77—30266
- alkali halide crystals, defect fermion properties, ionic cond. calcs. 80—59457
- Anderson impurities, interacting, pair, Fermi-liq. theory 80—44803
- anisotropic Fermi liquid, mag. order and transitions, phenomenological theory *(Russian)* 77—36038
- antiferromagnetic Fermi liquid, critical phenomena, neutron scatt., Neel point *(Russian)* 80—71077
- antisymmetrisation effects in Jastrow cluster expansion for nucl. matter 77—10352
- asymmetric nuclear matter, isospin and density waves, Landau theory 78—66235
- baryon asymmetry of the Universe, unitarity and possible origins, comments 79—88589
- baryon interactions through scalar meson field viar Yukawa-like interaction 79—67225
- binary disordered system, effective-medium and augmented space method, pseudofermion approach 79—60668
- binary mixed crystals, phonon frequency spectra, travelling pseudofermion approx. 79—77704
- Birman-Schwinger bounds for the Laplacian with point interactions 80—137
- Born-Green-Yvon eqns. for strongly interacting Fermi systems 79—71363
- Born-Green-Yvon equations, for strongly interacting Fermi systems 79—49161
- Bose description of fermions, model 77—53833
- Bose modes, spin-1/2 approx. in quantum theory 79—6047
- boson scattering, variational method 79—255
- boson-fermion interacting system, coherent states on Lie groups and evolution operator 78—36932
- boson-fermion system, semiclassical anal. approach 80—27401
- boson-like excitations, effect on props. just above 2nd order transition 77—61015
- broken SU_2 symmetry field, two-dimensional isotopic model *(Russian)* 80—73616
- C*-algebras of two body interactions, existence of scatt. theory of time automorphism groups 80—31972
- canonical formalism, tensor product composition of algebras 77—71177
- charge density phase transitions in gauge theories with spontaneous symmetry breaking *(Russian)* 79—2969
- charged fermion system, in random external field, dielec. instability 77—85170
- charged particles, method of collective variables 79—88873
- charged relativistic, semi-classical, two-body problem, new approach 78—29284
- classification of states, spin 1/2, using chain of subgroups of unitary scheme 79—63597
- cluster approximation for an infinite-dimensional determinant 79—80503
- coherent states of Fermi operators and the path integral 79—2717
- cold relativistic neutron gas, study of massive neutron cores 79—35292
- configuration interaction and coupled cluster solns., analytic continuation 78—62147
- confinement and bosonisation, quantum sine-Gordon field theory, quark confinement 78—86442
- contractions of expansions of fermion operators 80—17834
- correlation function Euler eqn. when closed-form energy is used 77—49674
- correlation functions, dielectric function 79—85071
- crystal, mag. props. of vacancies *(Russian)* 79—46881
- cyclotron wave measurements, Fermi-liquid parameter determ. 78—60069
- deformable-jellium model, self-consistent long-range order in terms of non-plane-wave HF states 79—19533
- degenerate Anderson model, fermi liq. theory 79—90935
- degenerate electron liquid, compression modulus, perturbative calc. 80—36942
- degenerate Fermi gas, distrib. functions with allowance for pairing correlations 79—40458
- degenerate Fermi liquid, metallic density spin correlations *(Russian)* 78—43321
- degenerate many fermion system in exp. S form, linked valence expansions 78—41654
- degenerate many fermion theory, cf. with perturbation theory 77—6254
- degenerate many fermion theory on expS form 77—6253
- degenerate system, heavy impurity mobility 80—70493
- delta function fermion gas, solitons and HF solns. 78—49755
- dense Fermi systems, energy expectation values, numerical study of Fermi hypernetted chain method 79—40874
- dense matter, transport props., neutron stars appl. 79—67236
- density gradient expansion for kinetic energy 78—34794
- density matrix and spin-depend. correlations, appl. to normal liq. ^{3}He 79—73369
- density-potential relation, exact, one-dimens. local density approx. 79—25972
- diagonalisation of the quadratic fermion Hamiltonian with a linear part 79—40445
- diffusion equation for semiclassical bosons and fermions 79—40446
- disorder variables and para-fermions in two-dimensional statistical mechanics 80—98853
- disordered Fermi systems, in two dimensions, interaction effects 80—75655
- disordered solid, Fermi glass, theory for localised electrons 77—39807
- disordered system, elementary excitation exam. 78—56086
- dispersion energies and excitation parameters 77—74319
- double well anharmonic oscillator, 1-d system, effect of fermions upon tunnelling 78—16689
- dressed fermion bubble, real-space equivalent calcs. 80—101751
- dressed fermions in Abelian gauge theories 78—82093
- eigenvalue spectra widths, symmetry, Wigner coeffs. 80—18213
- eigenvalue spectrum of interacting massive fermions in one-dimens. 77—8035
- electron charge ordering, Peierls distortion, quasi one-dimensional spinless fermion model 79—87050
- electron Fermi liquid in metallic thin films with mag. impurities, collective excitation spectrum *(Russian)* 77—62846
- electron fluid with paramagnetic impurities, spin wave spectrum *(Russian)* 79—23915
- electron liquid, 2-dimens., cluster expansion 79—55461
- electron liquid, density response function 78—67961

fermion systems continued
- electron liquid, dynamic structure factor 79—78023
- electron liquid, excitation spectrum, memory-function approach 77—39791
- electron liquid, excitations 79—4522
- electron liquid, local field factor, freq. depend., absence of logarithmic singularity 80—29343
- electron liquid, local field factor, freq. depend., dynamical exchange effects 80—29342
- electron liquid, local field factor freq. depend. 79—38009
- electron liquid, spin-dependent, correlation energies for local spin density calcs. 80—107725
- electron liquid, two dimensional, lattice model 78—67964
- electron liquid on liq. He surface, high freq. cond. electron correlation effects 80—107589
- electron liquids, two-dimens., short-range order onset, thermodynamic props. 78—43454
- electron liquids, two-dimensional, self-diffusion constant, molecular dynamics 80—34372
- electron system, two-dimensional, melting curve, phase diagram 80—57179
- electron-hole liquid, microscopic theory *(Russian)* 78—51905
- electron-positron pair production in field of longitudinal electric wave *(Russian)* 79—6300
- electronic Fermi fluid, instabilities in mag. field *(Russian)* 79—11073
- electrons in magnetic and electromagnetic fields, Bloch functions, Jacobi ϑ-function determ. 80—36941
- Euclidean fermion-boson systems on lattice, appl. to field theory 78—45559
- exciton dielectric type system with doping, low freq. excitations *(Russian)* 80—15459
- extended Fermi system, optimum Jastrow function 78—8761
- extended Fermi systems, hypernetted-chain calcs., convergence props. 78—24733
- extended Fermi-hypernetted chain scheme, Landau parameters calc., transport coeffs., Jastrow theory 77—41529
- extended system, energy expectation value per particle, lack of $O(A^{-1})$ contribution in Iwamoto-Yamada expansion 78—60081
- Fermi and Bose quasi-particles in lattice system *(Russian)* 79—75462
- Fermi fluids, nonlinear response of equilibrium strongly coupled fluids 77—7930
- Fermi fluids, nonlinear response of strongly coupled fluids, appl. to polarisation diags. 77—7931
- Fermi fluids, propagation techniques for equilibrium strongly coupled fluids 77—7932
- Fermi gas, one-dimensional theory, correlation functions 80—22278
- Fermi gas, slightly non-ideal one-dimens., spectral ground state, energy determ. method *(Russian)* 78—62149
- Fermi gas, vacuum ground state, nuclear matter theory calc. 79—40876
- Fermi gas model in 1-D, review 79—58636
- Fermi gas model in 1-D 79—58635
- Fermi golden rule and Markov master eqns. 78—36935
- Fermi liquid model of magnetism, susceptibility maximum in 4d and 5d transition metals 77—4480
- Fermi liquids, computation of second order energies using reference spectrum Euler eqn. 79—71359
- Fermi one dimensional gas with long range potential, renormalisation group, exchange, Umklapp interactions 80—2351
- Fermi-Bose similarity, parafermi and parabose algebras 77—30091
- fermion clusters, many particle correlations, method of transition density operators 78—49763
- fermion matter with spin depend. correlations, variational theory 79—63614
- fermion system, two-body propagations with dynamic effective interactions 77—41896
- fermions on the hypertorus 78—74149
- ferromagnetic Fermi liquid, multicomponent, g-factor 77—80724
- ferromagnetic Fermi liquid, stability conditions 79—47224
- ferromagnetic Fermi-liquid model, electron-impurity system hydrodynamics, elec. cond. 80—103835
- ferromagnetic metals, zero temp., magnon exchange effects 77—51897
- ferromagnetism, itinerant, local band theory, Fermi-liq. theory 78—31040
- ferromagnetism, metallic, criterion for Fermi liq. picture 77—66231
- Feshbach-Villars transformation, bosons, fermions 77—87647
- FHNC equations, derivation 79—54048
- FHNC expression for the three-body term of the kinetic energy in the Jackson-Feenberg form 79—67682
- finite Fermi systems, symmetrized correl. functions, renormalisation procedure 78—4555
- fluid-dynamical approximation for finite Fermi systems 79—89259
- four-fermion Lagrangian interaction, fermion number conservation spontaneous breakdown 77—67584
- free energy independence for 1-D systems 79—40448
- free-fermion condition for generalised vertices 78—93622
- functional integral formalism for quantum spin systems 80—82714
- gapless superconductors, antilinear operators, pairing for broken time reversal symmetry systems 79—51716
- generalised Federbush model, current definition, perturbation calcs., gauge transformations 79—6297
- generalised ferrion chromodynamics, eqns. of motion and lagrangian density 79—93358
- generalized Grassmann algebras with applications to Fermi systems 80—57174
- generator coordinate method and the theory of metals 79—28299
- giant MIT bag, hot quark matter, from relativistic ideal Fermi gas 80—99083
- Goldstone system with off-diagonal disorder, freq., spectrum of lattice vibrations, pseudofermion approx. 79—60466
- gravitating fermions, thermodynamic functions 79—80552
- gravitating fermions, thermodynamic potentials 79—80551
- ground state, Fermi-hypernetted chain methods, convergence props. 78—16727
- ground state energy of fermion liquid 77—85010
- Hamiltonian approx., with Bose-Fermi and Fermi-Fermi cross interactions 79—85062
- hard sphere Fermi gas Jastrow correlations 79—40451
- hard-sphere Fermi system, energy and momentum distrib., Jastrow variational wave functions 80—73261
- Hartree Fock solns. 80—98852
- Hartree-Fock states in thermodynamic limit, low-density clustering 78—54296

fermion systems continued
heavy ion+nucleus reactions, friction force, gas kinetic model 77−30621
Heisenberg eqns. on C* algebra of quasilocal observables, boson and fermion systems 78−57854
heuristic Hamiltonian for fermions interacting via meson fields 77−6022
HF approximations, thermodynamic Fermi systems 80−4642
with higher symmetries, energy spectrum 77−5698
homeopolar excitations in a one-dimensional system of spinless fermions with nonlocal interaction 79−97318
hydrodynamic equations in external fields 80−36944
hydrodynamics of Fermi superfluids, time-depend. BCS formalism, compared with He II, finite nuclear systems 78−22920
hypernetted chain calcs. for model nuclear matter 78−8759
ideal Fermi gas, thermodynamics and eqn. of state 77−30117
ideal Fermi gas, ultradegenerate, ground state press. 79−58471
inequalities for fermion density matrices 79−6044
infinite, irreversible dynamics 77−82451
infinite Fermi system, asymptotic behaviour of mass operator near Fermi energy 77−71271
infinite nuclear matter, response function, quantum field theory of fermion systems 78−70480
infinite system, Fermi hypernetted chain method for state depend. Jastrow correl. functions 78−32757
inhomogeneous, dynamic linear density response 79−97299
inhomogeneous electron liquids, variational approach, appl. to metallic H_2 79−38013
instanton solns. for coupled nonlinear scalar and fermion fields 77−79220
integral evaluation 79−40449
interacting fermi system, partition function, trace calcs. 78−29043
interacting neutron fluid at high temp., eqn. of state, supernovae hydrodynamics 79−2718
interacting particles, Tomonaga model, 3-D analogue *(Russian)* 78−71900
interaction theory of nuclear and atomic struct. models, singlet paired fermions 79−9180
irreversible behaviour in quantum statistical mechs., singular coupling and weak coupling limits 77−45790
itinerant electron system, weakly ferromagnetic ground state, Fermi liquid theoretical study 79−4646
itinerant strongly interaction fermion system, uniform paramagnon theory 77−69577
Jackson-Feenberg form of the kinetic energy in the chain and FHNC approximations 79−67681
Jastow and exact many fermion theories, comparison 77−17908
Jastrow theory, momentum distrib. of boson and fermion systems 78−45561
Jastrow theory, variational problem 77−33944
Jastrow wavefunction, hypernetted chain method applied to Fermi and Bose systems 80−17866
kinetic energy, Jackson-Feenberg form in chain, hyperchain and Percus-Yevick approx. 79−93035
kinetic theory of normal Fermi liquids 78−87841
kinetic theory of nucl. fluids 78−8763
Kirkwood-Salzburg integral eqn. solns. for boson and fermion systems *(Ukrainian)* 79−93036
Landau Fermi liquid parameters, extended Jastrow theory 77−41534
lattice fermions, Dirac fields and Thirring fields, spontaneous breaking of chiral symm. 78−24962
lattice gauge theories with fermions, phase transitions and renormalised struct. 78−82105
level densities, appl. of cluster expansion theory *(Spanish)* 79−88868
linear fermion systems, molecular field models, and the KMS condition *(German)* 79−9178
liquid-gas transition, zero temp. 77−39710
local symmetry groups and fermion families 79−13030
low density Fermi liquids in mag. field, theory *(Russian)* 78−59999
low-dimensional systems, infrared problems and phase transitions of continuous order 78−6286
Luttinger model, preservation of sum rules for 1p-Green function 77−9956
magnetic Fermi liquid, temp. mag. transitions 77−69563
magnetic Fermi liquid in external mag. field *(Russian)* 77−47952
magnetic ordering temperature in Fermi liq. close to phase transition *(Russian)* 79−78427
magnetic susceptibility, Fermi liquid description for temp. variation 77−63049
magnetic susceptibility of Fermi liq., temp. depend. 79−65628
magnetic susceptibility quantum oscillations, low temp., mag. instabilities in electron liq. *(Russian)* 78−87928
many body systems, Tamm-Dancoff method based on SO(2N+1) regular representation 79−35629
many fermion energy calculations 78−66238
many fermion systems, asymptotic nature of perturbation theory 80−46967
many fermion systems, energy lower bound 80−17860
many-body fermion energy lower bound models 77−37809
many-body theory based on SO(2N+1) Lie algebra of fermion operators 77−67374
many-fermion quantum mechanics, coherent-state representation 80−94988
many-fermion system, Monte Carlo simulation 78−12644
many-fermion system, wave-number-depend. susceptibility, low temp. and long wavelength, anal. struct. 77−40016
many-fermion two- and three dimens. density oscills., Tomonaga boson operators 78−41232
massive neutron star, fermionic matter, coupled Dirac-Einstein eqns., self consistent soln. 78−73731
massless, isospin 3/2, coupled to N-pseudoparticle field 79−6298
matrix equations for two-fermion systems with magnetic interactions 79−21904
meson exchanges and finite Fermi system theory 77−74774
metal film, electron liquid oscills. *(Russian)* 78−43315
metal theory, two-component Fermi liq. model of nonferromagnetic d-metals *(Russian)* 77−51683
metallic film, electron Fermi liquid, microscopic theory *(Russian)* 77−35999
metallic state, Fermi liquid theory of effect of spin fluctuations 77−62853
metallic ultrathin filaments, dielectric and superconducting fluctuations, Peierls transition *(Russian)* 80−65742

fermion systems continued
metals, localised dynamic perturbations 80−73262
metals and superconductors, Fermi liquid correl. function 79−61225
micro- and macrocoherence relation *(German)* 80−31660
mixed valence impurity model, Fermi liq. theory, Ward identities 80−34401
model fluid eqn. of state via lowest order constrained method, nuclear matter 77−18443
momentum and positional uncertainty, for states of N identical fermions with spin 79−35583
momentum distrib., Fermi-hypernetted-chain theory 80−82716
N-body generalised entropy, time derivatives calcs. 77−5781
N-fermion problem, few-body reduction, model systems 79−6043
N-fermion problem, improved lower bounds 78−54292
N-fermion problem, incorrect lower bounds 78−65865
n-fermion problem, new approximation method 77−2610
N-fermion translation invariant systems, derivation of energy lower bound models 78−65866
N-level systems in contact with singular Fermi reservoir 77−22487
N-particle Schrodinger eqn., macroscopic behaviour, superconductor and fermion systems 78−60242
N-representability density operators, necessary conditions 77−5759
nearly ferromagnetic Fermi systems, spin-conserving approx. spin susceptibility 78−47982
nearly ferromagnetic Fermi systems, temp. depend. of spin susceptibility 79−8008
neutral gravitating fermion system, equilibrium states 80−31692
neutrino+antineutrino system, relativistic kinetic theory, Wigner functions 77−26239
neutrino component of $e\bar{e}\nu_e\bar{\nu}_e$ mixture, transport eqn. 77−33941
neutrino system, kinetic equation 77−33940
neutrino-antineutrino gas, transport coeff. values *(French)* 79−30388
neutrino-antineutrino mixture, transport props. 78−93625
neutrino-electron mixture, influence of spin and Weinberg-angle on bulk viscosity 77−61223
neutrinos+antineutrinos gas, transport coeff., thermal diffusion *(French)* 78−86217
neutron gas, highly rarefied, non-equilibrium thermodynamics under creative and destructive reactions 79−12747
neutron matter, Landau parameters, extended Jastrow theory 77−41534
neutron star matter, abnormal phase 78−20849
neutron star model, appl. of Schrodinger eqn. 77−49418
neutrons, relativistic, ultra-degenerate, non-interacting gas, Fermi energy and eqn. of state in intense mag. field 78−89401
non-relativistic fermions, Ward identity 80−86633
nonlinear fermion system of self-interacting particles, field patterns 78−16909
nonlocal properties of fermionic matter in strong gravitational fields 79−26210
nonrelativistic, self-energy and inter-fermion Coulomb-Yukawa forces, quantum theory 78−29047
nonrelativistic para-Fermi gas, thermodynamic and mag. props. 79−25974
normal Fermi liq., mag. ordering at absolute zero 79−38344
normal Fermi liquid, transition from first sound to zero sound 77−89609
normal liquid, finite temp. contribs. to mag. susceptibility 78−10246
normal liquid viscosity in finite geometry 80−24702
normal quantum fluid, kinetic theory, transport props. 78−77799
nuclear and neutron matter N-N potentials, variational calcs. 78−37292
nuclear dynamics, adiabatic TDHF limit versus TDHF, in soluble model 78−50113
nuclear field theory, path integral techniques, Fermi systems with two body force interactions 78−50096
nuclear field theory of Fermi systems in an external field, path integrals 78−93954
nuclear many body problem, boson-fermion descript. *(Chinese)* 78−82297
nuclear matter, elongated soliton type wave solutions, finite amplitude wave propagation *(Russian)* 80−13397
nuclear matter, thermodynamic model, shear viscosity temp. dependence 78−62499
nuclear matter model, momentum distrib., Fermi-hypernetted-chain theory 80−82716
nuclear matter model calc. with fermion lowest order constrained variational method 77−14053
nuclear matter theory, one pion exchange processes, condensate effects 77−6276
nuclear partition functions at high temperature rel. to pre-supernova stellar collapse 79−101059
nuclear shell-model basis of interacting boson model, correspondence between fermion and boson states and operators 80−52593
nuclear spin-dependent parameters in Landau-Migdal theory 77−82844
nuclei, classification of states, unitary scheme 80−42550
nucleon fluid, excitation to N*(1234) state, lowest order constrained variational calcs. 79−40864
nucleon gas, weakly degenerate, virial coeffs., eqn. of state, species concentrations 77−15658
nucleon systems, spin density wave and π^0 condensation 77−61368
nucleons, energy density formalism calcs. 77−46121
one dimensional, thermodynamics by cluster expansions 77−41535
one dimensional continuous quantum systems, limit Gibbs state 78−93599
one dimensional Fermi gas, planar theory 78−45519
one dimensional Fermi gas model in relation to spin and field theoretical models 80−24816
one particle distributions, entropy bounds 80−62607
one-body dissipation of nuclear deformation collective energy, semiclassical approx. *(Russian)* 78−86502
one-dimens. Fermi gas, classical calc. of correl. function 79−40461
one-dimensional, and plane xy model, behaviour of correlation functions 78−56091
one-dimensional, cluster expansion methods and thermodynamics 78−6289
one-dimensional, dynamic mag. susceptibility calc., bound magnon states 78−6290
one-dimensional, electron-phonon interaction in adiabatic approx. for supercond. state *(Russian)* 77−47753
one-dimensional backward-scattering model with generalised coupling const., variational soln. 78−66036
one-dimensional Fermi gas, correl. functions, classical calc. 78−34790

fermion systems continued
one-dimensional Fermi gas model with two charact. energies, scaling theory 78—6287
one-dimensional Fermi gas with backscattering, coupling between charge and spin degrees of freedom 80—17861
one-dimensional many-body system, SCF approx. 77—62699
one-dimensional system, strongly interacting, Efetov-Larkin model 78—6288
one-dimensional system, three-loop scaling eqns. using renormalisation group method 79—80508
one-dimensional systems, variational soln. of sine-Gordon theory and Luther-Emery backward scatt. model for one-dimens. systems 79—40447
open quantum systems with time-dependent Hamiltonians and their linear response 79—44852
operator manifolds, expansion and completeness theorems 79—59331
operator ordering, functional integrals 80—62574
optimal correl. function in hypernetted chain approx. 77—64996
orthonormalisation method, appl. to j-j coupling of fermions in single j-shell 78—81922
pairing Hamiltonian, general, approximate solns., by variational method 78—36931
pairing-force interaction many-fermion system, energy calc. 78—8339
para-Bose operator, explicit representations 79—85064
para-Fermi algebra representation 78—65867
para-Fermi quantization in the representation of SO(n) 80—86554
para-Grassmann algebras and para-Fermi systems 79—44783
para-Grassmann algebras with applications to para-Fermi systems 80—57175
parafermi operators, fixed order matrix elements 79—54044
parafermi statistics, Lie algebraic aspects of quantum statistics 79—54045
paramagnetic, with Coulomb interactions, susceptibility temp. var. 77—40017
paramagnetic metals, temp. depend. of susceptibility, microscopic Fermi liq. theory 77—28364
paramagnon theories below three dimensions for itinerant strongly interacting fermion system 79—38298
partial level density for widely varying values of the range of interaction 80—58120
Pauli principle in Euclidean geometry, for teaching 80—17768
Peierls phase transition, in one-dimens. conductor 79—60806
perturbation theory, system exhibiting dynamic symmetry breaking 79—143
photons as para-fermion composites, limitations 79—40704
plasma long-wave oscillation damping calc. *(Russian)* 78—75302
Poincare supersymmetry, parafermion generalisation 79—17626
QCD of highly condensed matter 78—70267
QED, nonlinear approach, charged fermion fields 79—97545
QED on lattice, vacuum polarisation in one-loop approx., SLAC fermion lattice action 79—85249
quadratic Hamiltonian diagonalisation 80—82719
quantization of time dependent self-consistent fields and finite boson representations for many-fermion system 79—6048
quantum crystal, soln. of Fermi-Bose quasiparticle 79—28173
quantum crystals, melting curves low temp. anomalies rel. to neutron stars 78—24757
quantum crystals of spinless fermions, collective modes, vacancy motion-lattice vibr. coupling 79—86960
quantum mechanics of ground state 80—82713
quantum spin systems, Fermi systems and group extensions in Weyl quantisation procedure 80—8905
quantum thermodynamic system, high-order perturbation expansion 80—4635
quark currents, fermion collective motions, Green's functions 79—93348
quark gas, nonAbelian gauge field theory 78—21341
quark gas magnetisation in intense mag. field 79—85061
quasi one-dimensional spin lattice coupled system, collective modes 80—24896
quasi-one-dimensional, electronic density of states *(Russian)* 80—6755
quasi-one-dimensional systems, three-dimens. ordering in system of weakly coupled chains 78—6295
quasiparticle pairing at arbitrary densities, soluble model 77—6252
quasiparticle renormalisation of memory function approach for response functions 78—8345
radial distribution function for hard-sphere fermions, zero and finite temps. 78—14530
radiation gauge static pot. between fermion and antifermion, non Abelian gauge fields 78—89621
reduced density matrices 78—16731
relativistic Fermi-Bose system quantisation, by compensated functional method *(Russian)* 80—42142
relativistic fermion fields, bosonisation, Luttinger model, thermodynamic correlation functions 80—68356
relativistic kinetic eqns. 77—67376
relativistic kinetic theory of $e\nu_e$ and $e\nu_\mu$ systems, transport coeffs. 79—21680
relativistic quantum ideal gas of massive particles, eqns. of state 79—2721
representability conditions for rotationally invariant density matrices, group theory appl. to generation 79—88870
review of methods in quantum field theory 78—8338
rotating fermion systems, quantum mech. treatment 79—17337
Schrodinger fluid velocity field, fermion system moments of inertia 78—65868
self consistent RPA for three body forces in Fermi systems 78—89810
semi-free gas and collective coordinates model, for ground state 79—54040
semiclassical approach to lattice theories of nonrelativistic fermion model and Gross Neveu model 78—16724
semiclassical density matrix, fermion system in one body pot. 78—65872
semiconductor, electron-hole liquid, prod. and props. at low temp. 79—82527
shell model level densities in evaporation calculations 79—45241
short-range forces and surface tension 77—57596
SHRIMP energy lower bound model, derivation for translation-invariant many-fermion systems 78—29046
single particle occupation probability and one body density matrix, cluster analysis 77—4233
single particle response function in finite and infinite Fermi systems 77—82457

fermion systems continued
six-fermion interaction, possible evidence from super trimuons 79—71743
SO(2N+1) algebra, time-dependent Hartree-Bogoliubov theory, quantisation 80—62575
SO(2N+1) operator representation and wave functions of fermion many-body systems 78—41227
solution of the Dirac equation with anomalous magnetic moment 78—82133
specific heat, depend. on spectrum fluctuation 77—61010
spectral function calculation, time depend. approach 79—43096
spherical nuclei, self consistent theory of finite Fermi systems and low lying collective states 79—45130
spin dependent pots. in fermion-antifermion system, annihilation width 79—9356
spin ordering in Fermi liquids 77—15779
spin polarised hard core Fermi gas, ground state energy 78—43197
spin susceptibility, absence of T^2lnT term 78—10692
spin systems and Fermi systems quantisation 79—58627
spin/isospin saturated system, two-body distribution function, direct and exchange sum rules 80—27212
spinless fermion systems, Coulomb repulsion, bond alternation, Peierls distortion, HF approx. 80—44524
stability conditions for normal Fermi liqs., microscopic proof 78—135
star with neutron core, gravitational equilib. relativistic treatment 78—57570
strong coupling asymptotic behaviour for solvable field theory 77—54048
strongly interacting, d=2 paramagnon problem, rel. to fluctuation problems with long-range forces 77—13701
superconducting Fermi-liquid, electromagnetic response, formal solutions 80—100548
superfluid, eqns. of motion for field operators and energy spectrum for isotropic systems 78—36926
superfluid, hydrodynamical action functional *(Russian)* 77—47639
superfluid, microscopic derivation of hydrodynamic equations, appl. to ^{3}He-B 79—46865
superfluid as a source of all interactions 79—21620
superfluid degenerate fermi gas, hydrodynamic eqns. allowing for finite coherence length *(Russian)* 80—12989
superfluid Fermi gas, hydrodynamic action and Bose spectrum 78—139
superfluid Fermi liquid, small-gap excitations at zero temp. and in acoustic limit 79—7725
superfluid Fermi liquids, stability conditions, small-gap spin excitations 78—87839
superfluid Fermi systems, appl. to low density hard sphere systems 79—51339
superfluid Fermi systems, binary expansion in microscopic theory 79—51338
superfluid neutron fluid, stationary flow in $^3P_2$ paired state *(Russian)* 80—103527
superfluids, microscopic theory 79—65281
superspace with Fermi and Bose coords., appl. to graded Lie bundles and supergravity 77—26143
surface energy, exchange contrib. infinite barrier model 79—85067
surface props., thickness and energy 80—52600
surfaces, quasiclassical boundary conditions for Fermi liquids 80—4641
symmetries and statistical behavior in fermion systems in nuclei 80—9248
T-approximation, viscosity coeff. of ^{3}He *(Russian)* 79—21655
T-approximation in theory of normal Fermi liq. *(Russian)* 77—79030
T-approximation in theory of normal Fermi liq. *(Russian)* 77—82453
TCNQ, generalised Wigner lattices and band motion effects 80—24815
temperatures, inverse, equilibrium states, C*-algebra and continuous one-parameter automorphism group 80—82712
thermodynamics, appl. of class of dissipative evolutions 80—46960
thermodynamics of pair production in a nondegenerate Fermi gas 79—44356
tight-binding spinless many fermion system 80—42143
time dependent Hartree Fock approx., fermion system appl. 78—49780
Tomonaga fermions and three-dimens. Dirac eqn. 79—58633
transition metal, d-metals, electron Fermi liquid oscillations *(Russian)* 79—90979
transition metals, 4d and 5d, susceptibility max. and grand Fermi-liq. effect 77—63082
transition metals, 4d and 5d, susceptibility maximum, Fermi liquid model of magnetism 77—4480
transverse sound, soln. to dispersion eqn., with nonzero Landau F_2 77—20150
trilocal structures, secular eqn. 80—90776
trimer ground states, quantum exchange effects 78—1117
TTF-TCNQ, two-chain Fermi gas, response behaviour 80—2381
two-body operators with dynamic effective interactions, t-channel 77—41898
two-body propagators with dynamic effective interactions, s-channel 77—41897
two-body propagators with dynamic effective interactions s-channel 77—41897
two-chain Fermi gas, linear conductors 79—40462
two-component Coulomb Fermi liq., unusual phase diagrams 79—63137
two-component degenerate charged Fermi liquid, EM wave scatt. *(Russian)* 77—7928
two-dimensional quantum systems at zero temp., liquid to gas phase transitions 78—77798
uniqueness theorem for anticommutation relations and commutation relations of quantum spin systems 79—12713
unstable fermion system, semigroup law, canonical description 80—8907
variational wave function, three-body correlations 78—87834
Ward identities for charged and neutral Fermi liquids 77—41530
weakly imperfect 1D gas, correlation functions *(Russian)* 79—49160
Weyl quantization of classical spin systems quantum spins and Fermi systems 80—31585
Yang-Mills pseudoparticles, fermion Green's functions 78—54548
Yukawa interaction among fermions, asymptotic estimates in perturbation theory 77—30092
zero-fermion modes in models with spontaneous symmetry-breaking 80—18105
zincblende-symmetry narrow-gap semicond., Fermi energy and Fermi-Dirac integrals 80—70604
(e,e′), deep inelastic, meson exchange currents from Fermi gas model 78—66268
$e\bar{e}\nu_e\bar{\nu}_e$, reactive mixture, bulk viscosity 78—45565

fermion systems continued
$e\bar{e}\nu_e\bar{\nu}_e$ mixture, covariant transport eqns., collision terms from Weinberg Salam theory 77−74315
$F_1 \rightarrow F_2\gamma$, nondiagonal transition amplitude for arbitrary fermion charges *(Russian)* 80−86722
$L^0 \rightarrow \nu_L\mu^+\mu^-$, heavy lepton spin, massless spin 3/2 ν four fermion interaction 79−13175
$N\bar{N}$, relativistic interacting system, eqn. of state using Regge-type interaction amplitude *(Russian)* 77−79032
Bi hole pocket, far-IR magnetospectroscopy, electron-electron interaction effects 77−77211
Bi, skipping electrons cyclotron resonance, electron-electron interaction parameter determ. 80−34351
D, atomic, Fermi fluid, stabilisation 80−100374
Ge, electron-hole drop phase separation, due to uniaxial stressing 78−84145
^{3}He, ground state of polarised and unpolarised fluid, Monte Carlo calcs. 80−92748
^{3}He, specific heat second layer adsorbed on Grafoil 78−87843
^{4}He-^{3}He, dilute soln., low temp., ^{4}He effective interaction 80−10734
^{208}Pb region, finite Fermi systems, review 78−537
Sc, mag. susceptibility, temp. depend., theoretical explanation 78−47944
YCo_2, high-field magnetisation, Fermi liquid model 79−11303

fermions
see also baryons; fermion systems; leptons
boson field operator constructed from even number of fermion field operators 80−27416
bound states from instantons 78−78087
confinement, strongly coupled lattice gauge field theory 79−2905
coupled to pseudoparticle gauge field, Dirac operator eigenvalues 77−67569
dual fermion model, inclusive single particle distribs., $\pi N \rightarrow \pi X$ appl. 78−86446
E_6 model, basic fermion masses and mixings 78−24972
equivalence principle test for spin-$^1/_2$ particles 79−12707
expectation values using program SCHOONSCHIP 78−74555
fermion-antifermion eqn., appl. to positronium, Breit eqn. 78−62963
Fisk-Tait equation for spin-3/2 particles 79−17623
Friedmann cosmological models, fermion pair creation by gravit. field and singularity *(Russian)* 78−93493
generations in grand unified theories, SU(8) model 80−78012
gravitational creation of odd numbers of fermions 80−32048
gravitational interaction, press. 79−63138
Gross-Neveu model and self-consistent β-function method, fermion mass generation 79−49466
independent, 1-dimens. density-pot. rel., local density approx. 78−29045
instanton-fermion coupling in two dimens., using perturbation theory for fermion sector 79−67475
long wavelength spin susceptibility from particle-particle scattering, logarithmic temp. control 80−7124
many-fermion theory, expS or coupled cluster form 78−29048
mass, gauge theories with short range chiral invariance *(Russian)* 77−10187
mass generation, regularisation, gauge dependence 80−9090
mass hierarchy, light fermions, grand unification, SU(N) theory 80−62911
massless, in background metric, conformal anomaly in dimens. regularised theory 77−26210
massless, quantum electrodynamics of Schwinger model, perturbation anal. 77−65109
massless fermion coupled to single axial vector field in U(1) model, AAA triangle diagram 79−35965
micro- and macrocoherence relation *(German)* 80−31660
non-perturbative quantum field theory, lattice renormalisation construction 80−9098
nonlinear super-Poincare fermion, quantisation in bag like formulation 80−4923
nonstationary gravitational field, creation of fermion pairs *(Russian)* 77−74635
pair creation near Friedmann singularity, energy density and press. *(Russian)* 77−57114
phase locked cavity, inertial mass and anomalous ang. momentum, fermion model 80−86159
quantum electrodynamics review *(Hungarian)* 78−37159
quantum field theory, fermion-boson correspondence, spinor field quantisation 78−8496
quantum field theory, large order perturb. theory, more than one coupling constant 80−77940
quark and lepton mass determ., unified weak and EM theory without scalar fields 79−75709
Reggeization of elementary fermions in arbitrary renormalizable gauge theories 80−68367
relativistic bound state of fermion and antifermion, fermion fields, quark model 78−82151
relativistic bound-state equations for fermion pair with instantaneous interactions 80−13200
relativistic quantum theory with correct conservation laws 80−82677
scattering by force centre anal. *(Russian)* 79−5998
Schwinger model, Ward identity, fermion axial vector current divergence, chiral invariant regulator field 80−57524
self-energy calculation, covariant formulation of relativistic Hamiltonian theory *(Russian)* 80−9087
soft spin 3/2 massless fermions, gravity, supersymm. 77−49869
soliton-fermion connection in extended particle field theory 77−26454
spin rotation by precession during neutron interferometry 80−32584
spinor Bethe Salpeter and Goldstein eqns., fermion-boson coupling, numerical soln. 78−86400
strong external fields, fermion and boson interactions 78−49987
SU(2)×U(1) model, fermion and Higgs multiplet structure, universality 80−62909
SU(2)⊗U(1) gauge model of EM and weak interactions, fermion mass restriction *(Russian)* 78−89650
SU(3)-symmetric gauge theory, static gluon pots., appl. to fermions 79−12967
SU(5) grand unification, superheavy fermions and proton lifetime *(Russian)* 80−91036
thermodynamics of gravitating fermions rel. to atmospheric temp. inversion 79−57994
ultra heavy, weak interactions, high energy scattering, low energy renormalisation corrections 78−93838

fermions continued
unification of fermions and bosons, interacting model 79−21629
unification of fermions and bosons, math. structures and phys. questions 79−21630
unification of fermions and bosons, physical foundations of local (algebraic) approach 79−21628
unified gauge theories, electroweak mixing angle, sequential triplets scheme of fermions 80−86650
unified scalar-free theory, order-R vacuum functional, with spontaneous scale breaking 80−78003
Universe, isotropic models, regularisation of fermion stress-energy tensor 78−81725
vortex solutions and fermions in Abelian and non-Abelian gauge theories 79−12959
Young's double beam interference experiment with spinor and vector waves 78−89363
$F^+ \rightarrow \mu^+\nu_\mu\bar{\nu}_F$, unconfined heavy fermion model for dimuon events in $\nu_\mu p \rightarrow \bar{\mu}\nu_F F^+ X$ 77−18269
$\nu(\bar{\nu})$ scatt. on fermion targets, four symmetry relations 79−373
$^3He_3$, ground state binding energy, Faddeev-UPE method 79−72377

fermium
see also nuclei with ......
No entries

fermium compounds
aqueous solution, electrochem. props., thermodynamic props., radiopolarography 77−29040

ferrimagnetic properties of substances
see also ferrimagnetism; ferrites; garnets; magnetic semiconductors
amorphous films of rare earth transition metal system, preparation by co-sputtering 79−56928
anisotropy energy density 80−88742
$(CaO.6Fe_2O_3)_{97}(La_2O_3)_3$ compounds, effects of Nd_2O_3 substitution on magnetic props. *(Japanese)* 80−108010
$CoCr_2S_4$ films, galvanomagnetic and thermoelec. props. 80−54717
ferrites, universal hysteresis loop for soft ferrimag. polycryst. 77−69620
ferrites of divalent metals, prep. by double decomp. reaction, mag. characts. *(French)* 79−33463
ferrous-formate dihydrate, mag. system model, mag. sp. ht. *(Japanese)* 78−31091
garnet, doped magnetic, ang. variation of induced anisotropy, symm. of centres 78−2676
garnet, epitaxial film, mag. bubble props., permanent local modification by laser annealing 80−2612
garnet film, domain obs. by SEM 77−69646
garnet film, minimum bubble drive field, ion implantation effect 77−24721
garnet film, uniaxial, cubic anisotropy effect 77−89998
garnet films, (111)-oriented, cubic anisotropy meas. 80−54924
garnets, bubble domain memory appls., growth requirements 77−20660
garnets, dynamics of mag. domain walls and bubbles 77−69599
light scattering, one-magnon, effect of quadratic magneto-opt. coupling 79−11407
manganese acetate tetrahydrate, Heisenberg ferrimag. magnetisation 79−47304
$MgAl_{2-x}Fe_xO_4$ solid solution system, solid state properties study 80−93094
$Mn_{1.98-x}Cr_xFe_{0.02}Sb$, Mossbauer effect exam. 78−68432
oxides, $RCu_3Mn_4O_{12}$, R=La to Lu, Y, synthesis and mag. props. 80−75717
oxides with perovskite struct., neutron diffr., ferri- and ferromag. props. 78−52214
perovskite-like oxides, $ACu_3B_4O_{12}$ subseries, synthesis, struct. and mag. props. 77−68960
perovskites, $(AA')(BB')O_6$, ion valency pairs determ. from lattice consts. 77−43195
rare earth alloys, amorphous, mag. props. rel. to struct., review 79−15298
rare earth alloys, R_2Pt (R=Gd, Tb, Dy, Ho, Er), magnetic susceptibility meas., mag. transition obs. 80−60222
rare earth alloys, R_3Pt_4, R=Nd, Gd, Tb, Dy, Ho, Er, Tm, mag. props., 4.2 to 160K 79−78343
rare earth alloys, $R(Fe_xRh_{1-x})_2$, mag. props., Mossbauer spectra 80−25108
rare earth intermetallics, RFe_2 and $R(Co_{0.98}\,Fe_{0.02})_2$, magnetostrictive material, changes in vibr. modes near mag. phase transition 79−90736
rare earth iron alloy, amorphous film, cosputtered, struct. and mag. props. 78−60323
rare earth orthoferrite, $RFeO_3$, spin reorientation and magneto-optical effects *(Japanese)* 79−47414
rare earth titanium oxides, $RTiO_3$ type, bulk mag. and struct. props., ferrimag. order 80−107993
rare earth-Ag alloy, amorphous, model calcs., of mag. props. 80−84616
rare earth-Co amorphous film, sputtered, in-plane anisotropy induced by rare gas annealing 78−84458
rare earth-Co systems, anomalous Hall effect and Kerr rotation obs. 77−11897
rare earth-cobalt intermetallics, RCo_2, sublattice magnetisation, powder neutron diffr. meas. 79−19725
rare earth-Fe alloy, RFe_2 (R=Tb, Dy, Ho and Y) crit. phenomena, Mossbauer exam. 78−52403
rare earth-Fe alloys, amorphous and crystalline, small angle neutron scatt. study of mag. order and mag. microstruct. 79−15283
rare earth-Fe alloys, RFe_2, temp. depend of coercivity 79−61185
rare earth-transition metal alloy amorphous film, magnetostriction, dipolar mechanism 78−95502
rare earth-transition metal alloys, amorphous, ferrimag., spin arrangements in large fields 80−75718
rare earth-transition metal alloys, disordered, magnetisation behaviour 80−71099
rare earth-transition metal alloys amorphous thin films, anisotropic mag. and microstruct. props. 78−95487
rare earth-transition metal amorphous thin films for thermomag. recording 80−20403
rare earth-transition metal film, amorphous, microstruct., TEM obs. 78−72018
rare earth-transition metal film, amorphous, microstruct. and magnetism 78−64230
RF materials, dispersion props. 79−73772
semiconductors, magnetic, static magnetic properties, mean field approach 80−7090

ferrimagnetic properties of substances continued
spinel, magnetostriction effects from Mn^{3+}, Co^{2+} and Fe^{2+} ions 79—91277
spinel structure ferrite, magnetisation using Neel's mol. field theory 79—87223
Supertransferred hyperfine interaction in magnetic insulators. I. Theoretical considerations 77—85403
suspension, rel. to magnetochem. separation 77—20628
titanomagnetite, monodomain behaviour in multiphase oxidised material 77—60366
titanomagnetite in basalts, mag. coupling in partial self-reversal assoc. with increased mag. viscosity 77—73717
titanomagnetites, domain struct. var. with temp. 78—65272
transition metal-rare earth alloys, amorphous, mag. props., mean field anal. 79—4701
TTF-bis-dithiolene metal complex compounds, donor-acceptor type, one-dimens. mag. variety and props. 77—66271
$Au_2(Mn,Z)_2$, Heusler alloy, ($Z=Al$, Cu, Ga, In or Zn), magnetic order and coupling 79—38303
$BaCo_2(AsO_4)_2$, magnetic field effect on mag. ordering neutron diffr. obs. 80—50053
$BaCo_2(AsO_4)_2$, planar X-Y model, mag. ordering 77—66256
$Ba_3Co_{2+x}Ti_xFe_{24-2x}O_{41}$, z-type ferroxplan, effect of Co^{2+} ions 77—36094
$Ba_3Fe_{2-x}Lu_xUO_9$, crystallographic and mag. props. *(French)* 77—15380
$BaFe_{12}O_{19}$, nucl. spin-lattice and spin-spin relax. in domain walls 77—69610
Ba_2FeReO_6, seignettomagnets with perovskite struct. 79—38459
Ba_2MnReO_6, seignettomagnets with perovskite struct. 79—38459
$BaNi_2M_xFe_{16-x}O_{27}$, effect of $M=Sc^{3+}$ or In^{3+} on props. 77—47978
BaO-Fe_2O_3-B_2O_3 glass, splat cooled, low temp. micromagnetism 80—34660
BaO-Fe_2O_3-(Na_2O) glass, rapidly quenched, mag. and ferrimag. props. 80—75744
$Ba_3WFe_2O_9$ and $Ba_3WFe_2O_{8.42}$, crystallographic and mag. props., comparative study 80—103303
Ca, Ge-substituted garnet, LPE growth atm. effects on bubble props. 77—20655
CaO-Fe_2O_3-B_2O_3 glasses, phys. props. rel. to struct. and comp. 78—23331
$Cd_{1-x}Fe_xCr_2S_4$, Fe II electronic struct., Mossbauer spectra 80—15876
$(Co,Cr,Fe)_3O_4$, $(Co,Rh,Fe)_3O_4$ film magnetooptical switches, for laser beam synchronisation 80—58615
Co-Gd amorphous film, struct., mag. anisotropy consts., saturation magnetisation *(Russian)* 79—99735
Co-Gd-Mo, amorphous film, mag. props., temp. depend. 78—10734
Co-Gd-Mo-Ar film, amorphous, mag. props. 78—80182
Co-Gd-Mo(Au) alloy film, amorphous, Hall effect 77—85347
$CoBr_2.2H_2O$, phase transitions in ferrimag. state 77—63191
$CoCr_2S_4$, CVD grown, surface microstruct. 79—4905
$CoCr_2S_4$, Faraday effect, appl. to CO_2 laser systems, radiation damage resist. 78—95579
$CoCr_2S_4$, ferrimag. semicond., magnetocrystalline anisotropy 80—71012
$Co_{0.7}Cu_{0.3}Cr_2S_{4-x}Se_x$, ferrimag. chalcospinel, paramag. susceptibility 80—15681
$Co_{1-x}Fe_xCr_2S_4$, ferrimag. spinel semicond., Curie temp. variation with composition and elec. props. 77—15849
$CoFe_2Se_4$, low-temp. thermal expansion anomalies and isothermal compressibility, mag. ordering and magnetorestriction 79—38363
$Co_{3-x}Ni_xO_4$, $0 \leq x \leq 1.1$, struct., semicond.-semimetal transition, Seebeck coeff. 78—87972
Co_2SnO_4, paramagnetic props. and short-range ordering 77—32155
$Co_{2-y}Zn_yTiO_4$, cation distrib. and mag. props. 78—14939
CrO_2, single particle material for tape and disc manufacture, prep., props., and appls. 78—52308
$CrPr_2S_4$, synthesis, single crystal growth, mag. and elec. props. 79—78857
$CsCoBr_3$, ID Ising antiferromagnet, spin dependent Raman scattering from phonons and electronic excitations 80—103948
$CsCoBr_3$, quasi one dimensional antiferromag., magnon Raman scatt. 80—11395
$CsMn_{1-x}Co_xF_3$, ferrimag., mag. props. and cryst. struct. 77—77056
$CsMnF_3$, mag. props. above T_n, NMR obs. of induced ferrimagnetism 79—99780
$CsMn_{1-x}Ni_xF_3$, ferrimag., mag. props. and cryst. struct. 77—77056
$Cs_{1-x}Rb_xMF_3$ ($M=Mg$, Co, Ni, Zn), hexagonal fluoride perovskite structural evolution by cationic substitution *(French)* 80—24430
Cu-Mn ferrites, heat treatment effect on props. 77—28838
$CuCr_2O_4$-$CuFe_2O_4$ (2 mol.%), Mossbauer expts., existence of Fe^{2+} 78—43721
Cu_2SeO_4, ferrimag., spontaneous magnetisation meas. 77—63128
D-$_{12}Fe_{32}O_2$, anomalous magnetisation, compensated to uncompensated mag. arrangement transition 78—52254
Dy-Fe, amorphous ferrimag. film, mag. props. and Curie point writing 77—12164
Dy-Fe, amorphous film, Kerr readout characts. 79—15439
$DyCo_{3.4}$, amorphous, mag. props. 77—32177
$DyCo_5$, rotational type spin reorientation, collinear to canted spin struct. change 77—63214
$Dy_{0.25}Co_{0.75}$ film, amorphous, displacement of mag. compensation temp. by elastic stress *(Russian)* 78—19284
DyFe amorphous film, Mossbauer and mag. meas. 80—15844
$DyFe_2$, amorphous, mag. struct., US meas. 79—99683
$Dy(Fe_xNi_{1-x})$, mag. interactions, mol. field model 77—73010
$Dy(Fe_xNi_{1-x})_2$, mag. behaviour, susceptibility and Mossbauer expts., 4.2-1300K 78—52235
$DyFeO_3$, bubble domain struct. temp. depend. 77—69647
$DyFeO_3$, orthoferrite, domain struct. and hysteresis props. 77—77071
$DyFeO_3$, phase domains, polarisation microscope obs. 77—28407
$Dy_3Fe_5O_{12}$, formation mechanism from metallic oxides 77—48376
Dy_6Mn_{23}, magnetic moments, magnetisation 80—25094
Dy_6Mn_{23}, noncollinear mag. struct., magnetization meas. 79—78322
Dy_2Ni_{17}, magnetic struct. by neutron diffr. and Mossbauer spectra *(French)* 77—32165
$Dy_2O_2SO_4$, mag. ordering, magnetisation, AC susceptibility and Zeeman effect meas. 80—60205
$Dy_2O_2SO_4$, magnetic struct. in antiferromag. and ferrimag. states 80—15695
$DyPt_5$, low temp. mag. susceptibility 80—93075
$Dy_{0.7}Tb_{0.3}Fe_2$, magnetostrictive material, liq. phase sintering 78—64493
ErB_4, mag. phase diagram, neutron diffr. study 80—50091

ferrimagnetic properties of substances continued
$(ErBi)_3Fe_{5-x}Ga_xO_{12}$ film, ferrimag., splitting of domains into layers 77—28420
$ErCo_2$, mag. excitation spectrum, neutron inelastic scatt. obs. 79—78351
$ErCo_3$, $ErCo_6$, and Er_2Co_{17}, Kerr effect determ. of domain structure, Bloch wall energy 80—39805
$ErCo_{5.6}$, easy magnetisation direction 78—84415
Er_4Co_3, cryst. field effect on mag. moment direction, neutron diffr. meas. 78—80132
$ErCo_2(Fe_2)$, mag. excitations, RPA theory 80—65830
$ErCo_{5-x}Ni_x$ series, magnetisation, coercive field meas. 78—91896
$ErFe_2$, effect of H on sublattice magnetization, elastic neutron scatt. obs. 79—78327
$ErFe_2$, excited state spin waves inelastic scatt. meas. 78—76234
$ErFe_2$, spin waves, exchange interaction, neutron scatt. study 79—47267
$ErFe_3$, H_2 sorption, mag. and struct. props. of hydrides 80—34831
Er_6Fe_{23}, lower critical field 80—20414
$Er(Fe_{1-x}Co_x)_3$, spin reorientation, easy axis of magnetisation 80—25144
$Er_2Fe_3Co_{14}$, Kerr effect determ. of domain structure, Bloch wall energy 80—39805
$ErFe_2H_x$, mag. props. 80—25095
$Er_6(Fe_{1-x}Mn_x)_{23}$, mag. props. and mol. field coeffs. 78—39319
Er_6Mn_{23}, magnetic moments, magnetisation 80—25094
Er_6Mn_{23}, noncollinear mag. struct., magnetization meas. 79—78322
Er_2Ni_{17}, magnetic structure by neutron diffr. 77—73000
$Er_xY_{3-x}Fe_5O_{12}$, spin reorientation transitions 78—2686
$Eu_{3-x}Ca_xSi_xFe_{5-x}O_{12}$, bubble film, LPE growth induced anisotropy 77—20659
EuIG+Pb, (100) LPE film, magnetocryst. anisotropy and lattice mismatch 77—20647
$Eu_{1-x}{}^{2+}Nd_x{}^{3+}O_{1-x}N_x$, lattice parameters, mag. and elec. props. 80—100578
EuSe, cryst. and electronic struct., mag., elec., and optical props., book contrib. 80—39760
EuSe, mag. ordered phase, first order Raman scatt. theory 77—85723
EuSe, mag. phase depend. Raman scatt. 78—10886
EuSe, spin structs., mol. field theory 78—31054
EuTe, mag. ordered phase, first order Raman scatt. theory 77—85723
Fe-Gd amorphous films with comp. gradient, volume and surface hysteresis *(Russian)* 78—88148
Fe-Gd film, amorphous, mag. props., mean field analysis 78—64236
Fe-Gd film, amorphous, O_2 contamination effects on mag. props. 78—64231
Fe-Mn-P-B-Al metallic glass, exchange anisotropy 77—16068
Fe-Pd alloy, mag. struct. determ., neutron scatt., Mossbauer and mag. meas. *(Russian)* 78—2648
Fe-R alloys, mag. elastic properties 78—52331
$FeAl_{2-x}Cr_xO_4$, spinel, elec. cond. behaviour during oxidation 79—19593
γ-$(Fe_{1/3}Al_{2/3-y}Cr_y)_2O_3$, lacunar spinels, elec. cond. behaviour during oxidation 79—19593
$FeCl_2.2H_2O$, and $FeCl_2.2D_2O$, Raman scatt. at metamagnetic phase transitions, mag. hysteresis 78—14958
$FeCl_2.2H_2O$, metamagnetic, resonant magnon-optical phonon coupling 79—28773
$FeCoF_5.2H_2O$, ferrimag. props., suscept. and transitions, 3-296K 79—87240
$Fe_{3-x}Co_xO_4$, Mossbauer spectra, effect of Fe^{2+} conc. 77—69754
$Fe_{1-x}Cr_xBO_3$, magnetisation, 4.2-600K 78—68187
$FeCr_{2-x}In_xSe_4$, struct. and mag. props., comp. depend. 77—66262
$FeCr_2S_4$, ferrimag. semicond., elementary step growth on surface of vapour grown cryst. 77—76649
$FeCr_2S_4$, Mossbauer spectra, second order phase transition 80—20539
$FeCr_2S_4$, normal ferrimag. spinel, NMR studies 2-77K *(Russian)* 79—19785
$FeCr_2S_4$, pure and doped, CVD grown, surface struct., elec. props. and band struct. 79—4905
$FeCr_2S_4$, vapour grown, struct. and stoichiometry, X-ray fluoresc. anal. 79—4263
$Fe_{0.5}Cu_{0.5}Cr_2S_4$, ESR spectra, elec. and mag. props., Curie temp. 80—97137
$Fe_{1-x}Cu_xCr_2S_4$, Hall effect and magnetoresist. 79—78119
$Fe_2F_5.2H_2O$, ferrimagnetism, susceptibility obs. 5-300K, phase transition 79—4658
Fe_5LiO_8, magnetoelectric-effect and magnetisation process 79—1688
$Fe_{2(1-y)}Mg_{1+y}Ti_yO_4$ spinel, incomplete mag. ordering, static magnetisation and Mossbauer meas. 77—16056
$Fe_{2(1-y)}Mg_{(1+y)}Ti_yO_4$, Mossbauer spectra anal., model 80—20560
$Fe_{1.4}Mg_{1.3-x}Zn_xTi_{0.3}O_4$ spinel system, X-ray diffraction, Fe Mossbauer effect 80—88900
$Fe_{2.1-x}Mn_xAs$, $0 \leq x \leq 2.1$, mag. phase transitions 78—2679
$Fe_{3-x}Ni_xO_4$, Mossbauer spectra, effect of Fe^{2+} conc. 77—69754
γ-Fe_2O_3 acicular particles, coercivity increase by Co ferrite surface crystn. 80—44866
γ-Fe_2O_3, clean and SiO_2 coated, reduction temp. influence on coercivities, coercivity factors and rheological props. 79—69698
γ-Fe_2O_3, hyperfine mag. field at ^{119}Sn, Mossbauer expt. 80—50232
γ-Fe_2O_3, magnetisation distribution in isolated transitions 80—29580
γ-Fe_2O_3 particles, growing Fe-Co ferrite, coercivity increase 79—56571
γ-Fe_2O_3 powders, influence of densification on mag. props. 78—95481
γ-Fe_2O_3 recording tapes, orientation, Mossbauer, X-ray and electron microscope meas. 77—16219
γ-Fe_2O_3, sat. moment *(French)* 77—85431
γ-Fe_2O_3, single mag. particle, remanent coercive force and remanent loop meas. 78—95480
α-Fe_2O_3, single particle material for tape and disc manufacture, prep., props., and appls. 78—52308
γ-Fe_2O_3 small particles, noncollinearity as crystallite-size effect, Mossbauer study 80—39939
γ-Fe_2O_3:Co, impact-induced demagnetisation, magnetostriction and coercive force, appl. in mag. recording 77—16111
γ- Fe_2O_3:Co powder, increased coercivity by epitaxial doping 79—82833
γ- Fe_2O_3-Fe_3O_4, lodestone, microstructure and mag. props., source of mag. hardening 79—82828
$Fe_{3-x}O_4$, vacancy diffusion from relax. of deviations from stoichiometry 79—23769
Fe_3O_4, 3d-photoelectron spectrum, final state effects, compared with Fe_xO 77—69964
Fe_3O_4 (magnetite), mag. susceptibility under hydrostatic press. and implications for tectonomagnetism 80—26504
Fe_3O_4 (magnetite), multidomain particles magnetisation 79—66686

ferrimagnetic properties of substances continued
Fe_3O_4 (magnetite), piezomag. response depth depend. rel. to tectonomagnetism as earthquake precursor 80—26465
Fe_3O_4 and $Fe_{3-x}Ti_xO_4$, IR transmission spectra changes at Verwey temp. 77—85714
Fe_3O_4, anomalous sp. ht. obs. at 10K 77—85454
Fe_3O_4, Co modified, synthesis with autoclave in H_2 atm. 80—35117
Fe_3O_4, crit. exponents meas. by polarized neutron scatt. 80—44828
Fe_3O_4 film, prep. by reactive condensation and mag. props. 78—64241
Fe_3O_4, hydrothermal growth in Au capsule in presence of H_2 77—1793
Fe_3O_4, hyperfine field temp. depend., Mossbauer meas. near Verwey transition 77—69749
Fe_3O_4, hyperfine fields and spin densities below 20K 78—52405
Fe_3O_4, low temp. phase, sp. ht. and elec. cond. 77—59308
Fe_3O_4, low temp. phase 77—69751
Fe_3O_4, mag. crit. scatt., neutron spectroscopy 77—20614
Fe_3O_4, mag. relax., permeability and loss tangent determ. at 4.2 to 300K 77—32263
Fe_3O_4, magnetic after-effect by valency fluctuations assoc. with cond. transition 77—8365
Fe_3O_4, magnetically biased, linear and bilinear magnetoelec. susceptibility, 4.2K 77—40106
Fe_3O_4, magnetite, change in state due to applied mag. fields obs. in magnetoresistance meas. 77—43623
Fe_3O_4, magnetite, charge order-disorder and metal-insulator transition 77—20241
Fe_3O_4, magnetite, coercive force spectrum at high temps. rel. to thermal activation below blocking temp. 77—91111
Fe_3O_4, magnetite, comparison of anhysteretic remanence and thermoremanence 77—5191
Fe_3O_4, magnetite, electronic cond. mechanisms, review 77—20314
Fe_3O_4, magnetite, electronic struct. at low temps., NMR anal. 78—67686
Fe_3O_4, magnetite, ferrimag. reson. at 9.3 GHz near Verwey temp., g-factors *(French)* 78—91959
Fe_3O_4, magnetite, grain size limits for pseudosingle domain behaviour, rel. to palaeomagnetism 80—11215
Fe_3O_4, magnetite, low temp. phase, magnetocryst. anisotropy 77—20584
Fe_3O_4, magnetite, low temp. phase transition, magneto-optical exam. 78—27193
Fe_3O_4, magnetite, magnetoelec. effect at 77K and cryst. symm. 80—29593
Fe_3O_4, magnetite, magnetoelec. effect at 77K, elec. field depend. of mag. anisotropy 80—29594
Fe_3O_4, magnetite, magnetoresist., applied mag. field effects 80—80301
Fe_3O_4, magnetite, Mossbauer spectra of low temp. phase 80—20541
Fe_3O_4, magnetite, oxidation rate anomaly at Curie temp. 79—96298
Fe_3O_4, magnetite, phase transition, X-ray diffr. meas. 80—15238
Fe_3O_4, magnetite, polarisation screening effect on charge ordering, pure ionic model 78—6272
Fe_3O_4, magnetite, reduced A-site moments, polarised neutron study 79—47253
Fe_3O_4, magnetite, TRM props. of single-domain, pseudo-single-domain and multidomain particles 78—40544
Fe_3O_4, magnetite, X-ray diffr. investig. of low temp. phase symm. 77—15364
Fe_3O_4, magnetite film, coercive force and lattice const. 78—2707
Fe_3O_4, magnetite Mossbauer spectra, mag. dipolar and elec. quadrupole effects 80—20544
Fe_3O_4, magnetite particles, interaction fields effect on hysteretic props. 80—54921
Fe_3O_4, magneto-electric effect temp. depend. at 10K 79—78498
Fe_3O_4, magneto-optical refl. spectra by equatorial Kerr effect *(Russian)* 77—32400
Fe_3O_4, magnetoelastic coupling effect on anisotropy below transition temp. 77—69657
Fe_3O_4, metallic phase, photocond. and mag. permeab., photoinduced changes 80—15566
Fe_3O_4, monoclinic phase, saturation magnetisation near Verwey temp. 77—77038
Fe_3O_4, Mossbauer linewidth of octahedral Fe 77—66446
Fe_3O_4, NMR exam. of low temp. phase 78—56401
Fe_3O_4, NMR of low temp. phase, electron ordering anal. 78—56402
Fe_3O_4, nuclear gamma reson. investig. of high temp. electronic struct. 77—20751
Fe_3O_4 particles, nonstoichiometric, morphology and enhanced coercivity, Mossbauer meas. 80—7132
Fe_3O_4 powder, oxidation to γ-Fe_2O_3, coercivity changes 80—44864
Fe_3O_4, selective excitation double Mossbauer exam. of electron hopping 77—69750
Fe_3O_4 single cryst., Mossbauer γ-ray diffr. 77—84600
Fe_3O_4, spin polarised photoemission, surface magnetism 79—52083
Fe_3O_4, typical spontaneous symmetry breakdown in solid state 80—34737
Fe_3O_4:Co, impact-induced demagnetisation, magnetostriction and coercive force, appl. in mag. recording 77—16111
Fe_3O_4:Sn, hyperfine field temp. depend., Mossbauer meas. near Verwey transition 77—69749
Fe_3O_4:Zn, and pure, influence of mag. order on charge delocalisation, Mossbauer spectra 78—68423
$Fe_3O_4/\gamma Fe_2O_3$ surface layers formed on small Fe particles, Mossbauer expts. 79—8081
δ-FeO(OH) and its solid solns. synthesis, X-ray diffr. and TEM studies 80—29891
δ-FeO(OH) crystallites, TEM imaging investigation 80—39096
FeOOH gels, Mossbauer spectra, mag. props. 80—11303
$Fe_{0.9}S$, ferrimag. transition, mag., thermodynamic props., kinetics 79—47280
Fe_7S_8, pyrrhotite, thermocond. and thermoelec. power 80—96926
Fe_9S_{10}, antiferro- to ferrimag. transition, Mossbauer and mag. exam., diffusion of Fe during transition 79—73716
Fe_9S_{10}, polytypism, Fe diffusion near antiferromag. to ferrimag. transition 80—44830
Fe_3Se_4, mag. props., 4.2-600K 78—43570
Fe_3Se_4, thermal expansion, compressibility, magnetisation, susceptibility and magnetostriction 77—66318
Fe_7Se_8, 3c struct., spin axis transition 78—14967
Fe_7Se_8, test of Okazaki's 3c and 4c superstruct. model, Mossbauer expt. 77—66445
$Fe_{3-x}Sn_xO_4$, mag. hyperfine fields, ^{57}Fe and ^{119}Sn Mossbauer spectra 80—39944
$Fe_{1-y}Zn_{3y/2}O_3$, solid soln. prep., struct. and mag. moment 78—52228

ferrimagnetic properties of substances continued
$FrCr_2S_4$, second-order phase transition, Mossbauer spectra 80—20569
$GDCo_2$, forced vol. magnetostriction and induced moment 77—36106
$(Gd,Bi)_3(Fe,Ga)_5O_{12}$, LPE film, coercivity, influence of nuclear tracks 79—51829
$(Gd,Tm,Y)_3(Ga,Fe)_5O_{12}$, bubble domain gradient propag., elliptical distortion and bias compensation 78—19292
Gd alloys, pseudobinary Laves phases, mag. reson. 79—87323
Gd-Co, amorphous, RF sputtered, prep. and props. 79—1693
Gd-Co, amorphous film, anisotropy due to resputtering effect 77—89989
Gd-Co, and Gd-Co-Mo films, amorphous, mag. props., annealing effects 78—64235
Gd-Co, evaporated amorphous film, perpendicular anisotropy by controlled O_2 contamination 77—89990
Gd-Co, film, evaporated and sputtered, struct. and mag. anistoropy, electron microscopy 79—56578
Gd-Co amorphous film, magnetisation processes near compensation point 77—69644
Gd-Co amorphous films, annealed, short-range order and perpendicular mag. anisotropy 80—15765
Gd-Co amorphous films, correlation between struct. and mag. props. *(Chinese)* 80—54532
Gd-Co amorphous films, mag. anisotropy, static and ferromag. reson. expts. 79—33477
Gd-Co amorphous films, RF sputtered, magnetisation ripple effects 80—11232
Gd-Co amorphous sputtered films, magnetoelastic contrib. to perpendicular anisotropy, internal stress meas. 78—95490
Gd-Co amorphous sputtered film, magnetostriction and anisotropy 80—39821
Gd-Co amorphous thin film, mag. and optical props., conc. depend 79—19748
Gd-Co amorphous thin films, crystn. process and domain struct. *(Chinese)* 80—54533
Gd-Co based amorphous sputtered films, microstruct. variability and mag. anisotropy, implanted ion effects 80—88459
Gd-Co film, amorphous, Ar sputtered, struct. 78—63946
Gd-Co film, amorphous, for bubble device appl., prep. and perpendicular anisotropy 77—69641
Gd-Co film, amorphous, inverted and biased loops 77—89996
Gd-Co film, amorphous, magnetisation processes near compensation point 77—40101
Gd-Co film, amorphous, phase separation as source of perpendicular anisotropy 78—64244
Gd-Co film, amorphous, preferential resputtering effect induced anisotropic distrib. of atomic pairs 78—63950
Gd-Co film, amorphous, selective resputtering-induced anisotropy 78—72376
Gd-Co film, amorphous ferrimagnet, mag. anisotropy, effect of ion bombard. during prep. 79—1692
Gd-Co film, amorphous ferrimagnet, anisotropic short range order effects on mag. props. 79—1691
Gd-Co film, bias-sputtered, dipolar mechanisms for mag. anisotropy 78—64233
Gd-Co film, sputtered, inert gas incorporation effect on uniaxial anisotropy 78—64232
Gd-Co films, anomalous magneto-optical hysteresis loops obs. 77—12174
Gd-Co sputtered amorphous films, resistivity anomalies, 42 to 300K *(Chinese)* 80—7001
Gd-Co sputtered films, preparation process, props. 77—59688
Gd-Co-Fe film, amorphous, bias-sputtered, uniaxial perpendicular anisotropy 78—64234
Gd-Co-Mo alloy film, amorphous ion implantation damage effects 77—89991
Gd-Co-Mo film, amorphous, Ar sputtered, struct. 78—63946
Gd-Co-Mo film, amorphous, in-plane susceptibility near compensation point 78—64238
Gd-Co-Mo film, bubble dynamics 77—89997
Gd-Co(-Au) amorphous film, domain wall dynamics near compensation point 79—1696
Gd-Co(-Au) film, ferrimag. amorphous, coated with Permalloy films, mag. props. 79—1695
Gd-Co(-Mo) films, amorphous, inhomogeneities of mangetization and anisotropy 79—65698
Gd-Co(Fe) amorphous films, microstruct. and mag. anisotropy 79—82838
Gd-Fe, amorphous film, Kerr readout characts. 79—15439
Gd-Fe, amorphous film, stress induced anisotropy 77—89989
Gd-Fe, co-evap. amorphous film, anomalous hysteresis loop, domains obs. 77—89995
Gd-Fe amorphous films with CeO_2 coatings, Kerr magneto-optical effect enhancement 79—19866
Gd-Fe amorphous sputtered films, magnetoelastic contrib. to perpendicular anisotropy, internal stress meas. 78—95490
Gd-Fe film, amorphous, in-situ ion beam sputtered, microstruct. and Lorentz mag. struct. 78—63947
Gd-Fe film, amorphous, mag. props., annealing effects 78—64235
Gd-Fe film, amorphous, preferential resputtering effect induced anisotropic distrib. of atomic pairs 78—63950
Gd-Fe(Co) amorphous films, O_2 adsorption, effect on perpendicular anisotropy 80—34713
Gd-Mn(-Co) alloys, amorphous, ferrimag. props. and Hall effect 79—73692
GdCo, amorphous film, MCD *(Japanese)* 78—39530
GdCo sputtered amorphous film, third elements effect on mag. anisotropy 79—91260
$GdCo_2$, ^{59}Co hyperfine field, temp. depend. splitting 77—8447
$Gd_{1-x}Co_x$ amorphous thin film, magnetostriction 79—91281
$Gd_{1-x}Co_x$ film, amorphous, Curie and compensation temps., effect of O or Ar impurity 77—40093
$Gd_{1-x}Co_x$, film, resistivity, Hall effect, domain wall density 78—76169
$Gd_{65}Co_{35}$, amorphous, amg. ordering, susceptibility, magnetisation and hysteresis meas. 78—68190
$(Gd_xCo_{1-x})_{1-y}Ar_y$ amorphous films, effective anisotropy field, ferromag. reson. obs. 80—71123
GdCoAu amorphous film, bias field depend. of domain drag propagated bubble domains 79—78471
GdCoMo film, amorphous, sputtered, ferrimag., in-plane susceptibility near compensation point 78—64240
$Gd_{6.9}Co_{74.0}Mo_{12.8}Ar_{6.3}$, amorphous film, spin wave reson. 79—73823
GdFe amorphous film, Mossbauer and mag. meas. 80—15844

ferrimagnetic properties of substances continued
GdFe homogeneous amorphous films, compensation point switching, magneto-optical Kerr signal anal. 80−15726
$GdFe_2$ films, electron beam deposited, amorphous and cryst., mag. and struct. props. 79−4710
Gd_xFe_{1-x} film, mm-wave ferrimag. reson. using optically pumped waveguide laser source 77−55710
$Gd(Fe_xAl_{1-x})_2$, magnetic behavior 80−108079
GdFeBi, amorphous ferrimag. films, magneto-optical props., optical spectra 80−76008
$(Gd_{1-x}Fe_x)_{1-y}Bi_y$ amorphous films, saturation magnetisation, Kerr and Faraday rotation 80−40093
GdFe(Co), amorphous film, XPS meas. 79−87295
$Gd(Fe_xCo_{1-x})_2$, ferromag. reson. of pseudobinary cubic compounds 78−91961
$Gd_3Fe_5O_{12}$, formation mechanism from metallic oxides 77−48376
$Gd_3Fe_5O_{12}$, nucl. gamma reson., anomalous behaviour of intensity 77−12289
GdIG, one-magnon light scatt. with and without compensation temps. 78−31062
GdIG, spin-orientation phase transitions, magneto-optic and visual exam. 77−24675
$Gd_{1-x}M_x$, M=Co, Ni, Fe, temp. depend. of magnetisation 77−77043
Gd_6Mn_{23}, magnetic moments, magnetisation 80−25094
Gd_6Mn_{23}, noncollinear mag. struct., magnetization meas. 79−78322
$GdNi_x$, (x=3, 3.5, 8.5), ferrimag., mag. reson. above and below Curie temp. 80−97148
Gd_xNi_{1-x} sputtered amorphous films, mag. props. and Hall meas. 78−95488
$Gd_2Ni_{17-x}Al_x$, mag. behaviour in paramagnetic region 79−73675
$(GdPrBi)_3(FeGaIn)_5O_{12}$, pure and In^{3+} doped, near IR absorpt. and Faraday rot. 78−95580
$Gd_xY_{1-x}Co_2$, transferred hyperfine interactions, ^{155}Gd Mossbauer effect and ^{165}Ho NMR expts. 77−63339
$Gd_xY_{1-x}Fe_2$, effective g-values, ferromag. reson. meas. 77−20720
$(Gd_xY_{1-x})Fe_2$, Fe mag. behaviour, FMR measurements, mag. props., Vangsness relation anal. 79−78336
$(Gd_xY_{1-x})Fe_2$, high temp. mag. behaviour 77−1538
$Gd_xY_{1-x}Fe_3$, saturation magnetisation, magnetostriction, Curie temp., ferrimag. ordering, exchange field *(Russian)* 78−68343
$Gd_{1.8}Y_{1.2}Fe_5O_{12}$, nucl. gamma reson., anomalous behaviour of intensity 77−12289
$Ge_xZn_{1-x}Fe_2O_4$, ferrimagnetism and ion distrib. 77−12103
Ho-Co film, evaporated, struct. and mag. anistoropy, electron microscopy 79−56578
$HoCo_2$, ground state spin excitations, inelastic nneutron scatt. study 80−50077
$HoCo_2$, mag.excitations, neutron inelastic scatt. meas. 80−60231
$HoCo_3$, Ho_2Co_7, $HoCo_{5.5}$ and Ho_2Co_{17}, Kerr effect determ. of domain structure, Bloch wall energy 80−39806
Ho_2Co_{17}, spin wave excitations, 4.8 and 78K 80−60230
Ho_4Co_3, cryst. field effect on mag. moment direction, neutron diffr. meas. 78−80132
Ho_xCo_{1-x} amorphous films, microstruct. and mag. anisotropy 79−82838
$HoCo_{5.5-x}Mn_x(Fe_x)(Ni_x)(Cu_x)$, cryst. struct. and mag. props. 80−75800
$HoFe_2$, effect of H on sublattice magnetization, elastic neutron scatt. obs. 79−78327
$HoFe_2$, spin wave and cryst. field excitations, neutron scatt. 78−68196
$Ho_2Fe_3Co_{14}$, Kerr effect determ. of domain structure, Bloch wall energy 80−39806
$HoFe_2H_x$, mag. props. 80−25095
$Ho(Fe_xNi_{1-x})$, mag. interactions, mol. field model 77−73010
$Ho(Fe_xNi_{1-x})_2$, mag. behaviour, susceptibility and Mossbauer expts., 4.2-1300K 78−52235
$Ho_{12}Fe_{32}O_2$, struct. and ferrimag. props., neutron diffr. obs. 79−78319
HoIG, Faraday rotation, mag. field depend., 4.2 to 300K, magneto-optical coeffs. 78−95577
Ho_2Ni_{17}, ferrimag. struct., neutron diffr. expt., cryst. field calcs. 77−73001
$Ho_2O_2SO_4$, mag. ordering, magnetisation, AC susceptibility and Zeeman effect meas. 80−60205
$Ho_2O_2SO_4$, magnetic phase diagram, magnetisation and mag. susceptibility meas. 80−15720
$Ho_2O_2SO_4$, magnetic struct. in antiferromag. and ferrimag. states 80−15695
HoSb, mag. phase diagram, quadrupolar interactions 80−65820
$IrMn_{1+x}Sb$ alloys, crystal struct., and mag. props. 78−34466
$K_5V_3F_{14}$, ferrimagnetic props., ordering temp. and anisotropy *(French)* 77−47990
Li ferrite, $Fe(Li_{0.55}Fe_{0.45})O_4$, one-magnon light scatt. with and without compensation temps. 78−31062
Li-Cr ferrite, $Fe(Li_{0.5}Fe_{0.25}Cr_{1.25})O_4$, one-magnon light scatt. with and without compensation temps. 78−31062
Li-Zn ferrite, magnetic props., effect of V_2O_5 addition *(Japanese)* 77−28415
Li-Zn ferrites, characts. and appl. *(German)* 77−80953
$Li_{0.5}Al_xFe_{2.5-x}O_4$, polycrystalline, ferromag. reson. absorpt. curves, stress effects *(Russian)* 77−20713
$Li_2B_2O_4$-$LiFe_5O_8$ glass, rapidly quenched, mag. and ferrimag. props. 80−75744
$LiFe_5O_8$, hysteresis and other mag. props. rel. to microstruct., TEM investig. 77−20636
$(Li_{0.5}Fe_{2.5}O_4)_{0.8}(CuFe_2O_4)_{0.2}$, struct., magnetic props., rectangular hysteresis loop 77−20645
$LiMnCrF_6$, ferrimagnetic, magnetic props. *(French)* 79−1668
Li_2O-NiO-O_2, phase diagram and mag. props. of $Li_xNi_{1-x}O_{1\pm y}$ 78−48380
LiZn ferrospinel, sequence of mag. transforms. *(Russian)* 78−19252
$Li_{0.5-z/2}Zn_xFe_{2.5-z/2}O_4$, field magnetisation and susceptibility 79−82762
$(Lu, La, Y, Ca)_3(Ge, Fe)_5O_{12}$, temperature compensated high mobility bubble garnet, LPE and props. 77−20656
$MgAl_ySc_xFe_{2-x-y}O_4$, X-ray spectra, Mossbauer spectra, electronic struct. of Fe and Sc 77−28647
$MgFe_{2-y}Al_yO_4$, with added Co, effect of Na_2O admixture on props. 77−36423
$MgFe_2O_4$, Mossbauer study 79−47375
$Mg_xFe_{3-x}O_4$, cation redistribution, effect of composition and thermal treatment 79−27966
$MgGa_xFe_{2-x}0_4$, spinel struct., neutron diffr. exam. 77−12096
Mn metallic perovskite, structural instability *(French)* 79−100123

ferrimagnetic properties of substances continued
Mn-Zn ferrite, domain struct. and initial permeability, effect of O nonstoichiometry 78−35001
Mn-Zn ferrites, mag. parameters, determ. from RF susceptibility 79−82769
$Mn_2As_xSb_{1-x}$, $0<x<0.25$, specific magnetisation, temp. dependence, 300 to 600K 78−76248
Mn_3C, Mn_5C_2, $Mn_{15}C_4$, Mn_7C_3 and $Mn_{23}C_6$, mag. susceptibility temp. depend. 79−51754
$Mn(CN)_3.(H_2O)_{0.57}$, mag. interactions, theory 80−97085
$Mn_{1+x}Cr_{2-x}O_4$, noncollinear ferrimagnets, induced anisotropy 77−73022
$Mn_{1.88}Cr_{0.12}Sb$, antiferromag.-ferrimag. transition, neutron crit. scatt. and crossover effect 80−71023
$Mn_{1.88}Cr_{0.12}Sb$, magnon renormalisation 77−69520
$Mn_{1.88}Cr_{0.12}Sb$, thermomagnetic props., antiferromag. to ferrimag. transition 77−63194
$MnCr_{2-x}V_xS_4$, mag. struct., Yafet-Kittel to Neel ferrimagnet transition temp. 77−66264
$Mn_{1-x}Cu_xCr_2S_4$. phase relationships and mag. phase diagram 79−78374
Mn_4F, non-collinear component in mag. struct. 80−25089
MnFe ferrite, mechanically induced anisotropy, effect on mag. permeability 78−47970
$Mn_{1-x}Fe_xCr_2S_4$, Fe II electronic struct., Mossbauer spectra 80−15876
$Mn_xFe_{3-x}O_4$ film, spin wave reson., exchange const. 77−16183
$Mn_xFe_{3-x}O_{4+\gamma}$, average directional order, cation valency and repartition on A- and B-sites *(French)* 78−39369
$Mn_xFe_{3-x}O_{4+y}$, prep., resist., hysteresis loop and mag. disaccommodation *(Spanish)* 77−73045
$Mn_{2-x}Fe_xSb$, mag. struct. and spin flop transition, ^{57}Fe Mossbauer expts. 77−66261
$Mn_{2-x}Fe_xSb$, Mossbauer effect exam. 78−68432
Mn_2Sb, Bi-modified, mag. first order phase transition 79−51777
Mn_2Sb, domain and domain wall resons. in ^{55}Mn NMR spectrum 80−25219
Mn_2Sb, hyperfine fields of ^{121}Sb in several mag. phases 79−28650
Mn_2Sb, large anisotropy in mag. hyperfine field at ^{121}Sb, Mossbauer spectra meas. 77−73101
Mn_2Sb, spin-wave dispersion relations, exchange interactions, neutron inelastic scatt. 80−65832
$Mn_2Sb_{1-x}Bi_x$, temp. depend. of magnetisation *(Japanese)* 79−78375
$Mn_{1+x}Sb_{1-x}Sn_x$, nuclear Zeeman effect, Mossbauer meas. 79−28654
$Mn_{1.77}Sn$, 170K transitions temp. in ferrimag. state, pressure and γ-irrad. effects 77−51902
$Mn_{2-x}V_xSb$, $0.08\leq x\leq 0.25$, mag. props. modification by V 77−36071
MnZn ferrite, anomalous thermal change of permeability near Curie point 77−20638
MnZn ferrite, mag. relax., permeability and loss tangent determ. at 4.2 to 300K 77−32263
MnZn ferrite, mag.-mechanical-microstruct. interaction 77−1578
MnZn ferrite, mechanically induced anisotropy, effect on mag. permeability 78−47970
$(NH_4)_2Cd_5Fe_3Al(SO_4)_{12}.18H_2O$, EPR above ferrimag. transition 78−10762
$NaMnCrF_6$, ferrimagnetic, magnetic props. *(French)* 79−1668
$NaMnCrF_6$, mag. struct., neutron Laue diffr. method 80−70951
$NaMnCrF_6$, magnetic struct., neutron Laue diffr. study *(French)* 79−99682
$Na_2O.2Al_2O_3.5SiO_2{:}Fe^{3+}$, Mossbauer effect and magnetometric exam. 78−6613
$Nd_{50}Ag_{50}$, amorphous, mag. props. 80−60182
Nd_2O_3, magnetisation and mag. susceptibility Curie-Weiss behaviour 77−4505
$NdPt_5$, low temp. mag. susceptibility 80−93075
Ni, spontaneous magnetostriction determ. method, molecular field theory study *(Russian)* 80−50157
Ni-Fe oxidised film, extraordinary viscous wall motion at extreme vel. 78−14997
Ni-Zn ferrite, electrical cond., Seebeck coeff. and saturation magnetisation 77−20315
Ni-Zn ferrite:Co^{2+}, synthesis of optimal quality recording head mat. 77−52272
Ni-Zn ferrites, mag. recording head props. rel. to manuf. from schoenite-type solid solns. 77−85496
$NiCo_2O_4$, ferrimagnetic spinel, neutron diffr. study 79−99681
$Ni_xCo_{3-x}O$, composition depend antiferromagnetic-ferrimagnetic ordering, mag. susceptibility meas. 80−70973
$NiCr_2O_4$, ^{61}Ni Mossbauer effect studies of hyperfine interactions, mag. dipole and elec. quadrupole 78−43746
$NiCr_2O_4$, sign of net mag. hyperfine field, ^{61}Ni Mossbauer study 80−39946
$NiFe_{2-t}Al_tO_4$, cryst. and mag. props. 78−14940
$NiFeO_4$, induced ferrimagnetism, temp. depend. of sublattice magnetisation, Mossbauer study 77−66280
$NiFe_2O_4$, hysteresis and other mag. props. rel. to microstruct., TEM investig. 77−20636
$NiFe_2O_4$ precipitation from silicate glass, Mossbauer study 80−54998
$NiFe_2O_4$-Fe_2O_3, effects of excess Fe_2O_3 on mag. props. 77−85495
NiO, thin films with spinel-type defect structure, FMR study 80−39877
NiZn ferrite, mag.-mechanical-microstruct. interactions 77−1578
NiZn ferrite, magnetic props., porosity and grain size effects 77−36095
NiZn ferrite, magnetic field effect on Rayleigh wave attenuation 78−6557
NiZnCo ferrite, excess Fe type, saturation magnetostriction meas., oxidation effects 79−82852
$Ni_xZn_{1-x}Mn_2O_4$, mag. props. 78−43573
$NpAs_2$, magnetic props., 4.2 to 77K, Mossbauer study 80−39937
Pb_2FeReO_6, seignettomagnets with perovskite struct. 79−38459
Pd-Fe (25-55 at.%) ^{57}Fe effective field and mag. struct., Mossbauer and magnetisation expts. *(Russian)* 77−90085
Pt_3Cr, ferrimag., magnetisation density, polarised neutron diffr. meas. 80−60204
$RbNiF_3$, MCD and stress linear dichroism on double excitonic transitions 77−52051
$RbNiF_3$ spin lattice, susceptibility, Heisenberg model *(Russian)* 80−65893
$SmCo_5$ powder alloy, densification by cold working 77−4753
$SmFe_2$, ferromagnetic-ferrimag. cpds., mean field exchange consts., Stoner itinerant model calcs. 80−50084
$Sm_6Mn_{23-x}Fe_x$, magnetic behaviour, temp. and comp. depend. 80−93090
SmTmIG, epitaxial layer with submicron bubbles, mag. props. 77−12172

ferrimagnetic properties of substances continued

- $Sm_xY_{3-x}Fe_5O_{12}$, mag. anisotropy, meas. temp., depend. 78−19247
- $Sm_xY_{3-x}Fe_5O_{12}$, spin reorientation transitons 78−2686
- $SnCo_2O_4$ spinel, mag. props. 77−1543
- $SrFe_8Al_4O_{19}$, thin film LPE growth and mag. props. 80−80992
- Sr_2FeReO_6, seignettomagnets with perovskite struct. 79−38459
- Sr_2MnReO_6, seignettomagnets with perovskite struct. 79−38459
- $SrO.nFe_2O_3$ isotropic ferrite magnets, manuf. process and mag. props. *(Japanese)* 80−29915
- $Sr_xZn_2Y(Y=Ba_{2-x}Fe_{12}O_{22})$, x=0, 1, 1.6, mag. moments reorientation 80−44851
- Tb-Fe, amorphous ferrimag. film, thermomag. writing using He-Ne laser 77−12163
- Tb-Fe, amorphous ferrimag. film, mag. props. and Curie point writing 77−12164
- Tb-Fe, amorphous film, Kerr readout characts. 79−15439
- Tb-Fe amorphous film, thermomag. contact printing 77−89986
- Tb-Fe amorphous thin films, magnetic after-effect, Kerr magneto-optic effect obs. 80−97123
- Tb-Fe film, undoped and O-doped, amorphous, microstruct. and mag. props. 79−91273
- Tb-Fe sputtered films, amorphous, mag. aftereffect due to domain well motion 79−73780
- $TbCo_2$, magnetocrystalline anisotropy and spontaneous magnetostriction 80−75831
- $TbCo_2$, origin of magnetostriction 79−78499
- $Tb_{0.27}Dy_{0.73}Fe_2$, domain configurations, obs. by Kerr effect and synchrotron radiation topographs 78−64215
- $Tb_{0.27}Dy_{0.73}Fe_2$, LF magnetoelastic effects 78−68348
- $TbFe_2$, amorphous, mag. struct., US meas. 79−99683
- $TbFe_2$, domain configurations, obs. by Kerr effect and synchrotron radiation topographs 78−64215
- $TbFe_3$, mag. struct., powder neutron diffr. determ. 79−78328
- Tb_xFe_{1-x} film, amorphous, magnetostriction and magnetisation 78−68305
- $Tb_3Fe_5O_{12}$, mag. phase transition exam. 79−19736
- $Tb_3Fe_5O_{12}$, weak field mag. transition, magneto-optical and magnetisation meas. 77−69551
- TbIG, X-ray topographic obs. of domain evolution in mag. field 77−69600
- Tb_2Ni_{17}, magnetic structure by neutron diffr. 77−73000
- $ThCu_3Mn_4O_{12}$, mag. structure, neutron diffr. powder data, 430K ferrimag. T_c 77−69502
- $ThCu_3Mn_4O_{12}$, mag. struct. of new perovskite-type ferrimag. 78−52222
- $ThFe_5$, mag. props., ferrimag. moment arrangement 79−33475
- Tm, magnetisation, uniaxial anisotropy, mean field model 78−2660
- $Tm_{2.2}Bi_{0.8}Fe_{3.5}Ga_{1.5}O_{12}$ epitaxial film, Faraday effect and domain struct. near compensation point 77−20838
- $TmCo_5$, easy magnetisation direction 78−84415
- $TmFe_2$, low temp. magnetisation and magnetostriction 78−64249
- $TmFe_2H_x$, mag. props. 80−25095
- Tm_2Ni_{17}, magnetic structure by neutron diffr. 77−73000
- $TmPt_5$, low temp. mag. susceptibility 80−93075
- UAs, magnetisation, ferrimag. spin struct. 80−7088
- UFe_2, magnetisation, neutron diffr. and Mossbauer expts. 77−63137
- U_2S_3, sp. ht. at low temps., mag. behaviour 80−60353
- $V_xTi_{1-x}S_2$, elec. and mag. props. 79−65504
- $(Y,Eu,Sm)_3(Ga,Fe)_5O_{12}$ film, mag. loss and bubble dynamics 77−8371
- $(Y, Eu, Yb, Ca)_3(Ge, Fe)_5O_{12}$, bubble film, LPE on $Gd_3Ga_5O_{12}$, mismatch and faceting 77−20657
- $(Y,Gd,Yb,Bi)_3(Ga,Al,Fe)_5O_{12}$, bubble conversion to anomalous behaviour 78−23309
- $(Y,Gd,Yb)_3(Fe,Ga)_5O_{12}$ film, magnetisation processes and domain struct. near compensation temp. 78−14996
- $(Y, Sm, Lu, Ca)_3(Fe, Ge)_5O_{12}$:$Ne^+$, film, S=1 bubbles dynamic props., temp. depend. 77−20658
- $(Y,Sm,Lu,Ca)_3(Fe,Ge)_5O_{12}$ bubble magnetic garnet film, LPE grown, props., $CaCO_3/GeO_2$ molar ratio influence 80−50152
- $(Y,Sm)_3(Ga,Fe)_5O_{12}$ films, growth from melt, growth property control 78−27395
- Y alloys, pseudobinary Laves phases, mag. reson. 79−87323
- $(YBi)_3Fe_{5-x}Ga_xO_{12}$ film, ferrimag., splitting of domains into layers 77−28420
- YCaSmTmGeIG, epitaxial layer with submicron bubbles, mag. props. 77−12172
- $Y_{1-x}Co_x$, temp. depend. of magnetisation 77−77043
- $(YEuYbCa)_3(FeGe)_5O_{12}$, ion-implanted, in-plane mag. field effects on bubble props. 77−85521
- YFe_x film, ($x\simeq2$), magnetoelastic excitations obs. 78−68307
- Y_xFe_{1-x} amorphous films, microstruct. and mag. anisotropy 79−82838
- $YFe_{0.62}Cr_{0.38}O_3$, compensation of weakly ferrimag. moment 79−8035
- $YFe_{1-x}Cr_{\alpha}O_3$, reorientational transitions, mag. and neutron diffr. exam. 77−12097
- $YFe_{1-x}Cr_xO_3$, weak ferrimagnet, anomalous mag. props. explained by exchange interactions *(Russian)* 77−69538
- $YFeO_3$, bubble domain struct. temp. depend. 77−69647
- $YFeO_3$:Co, NMR of ^{57}Fe, spin echo 78−91987
- $Y_3Fe_5O_{12}$, formation mechanism from metallic oxides 77−48376
- $Y_3Fe_{5-x}Si_xO_{12}$, photoinduced jumps of permeability 79−28564
- $Y_3Ga_xFe_{5-x}O_{12}$ film, growth kinetics of film with cylindrical mag. domains 77−1577
- $Y_{3-3x-2z}Gd_{3x}Ca_{2z}Fe_{5-z-u}V_zSi_uCo_uO_{12}$, mag. props., effect of V substitution 77−20582
- $(YGdYbBi)_3$ $(FeAl)_5O_{12}$ epitaxial film, diffuse domain wall, bubble domain expansion 80−25170
- $Y_{1.3}GdYb_{0.7}GaO_{12}$, epitaxial film, ferromagnetic reson. exam. 77−85579
- YIG, Barkhausen effect *(German)* 78−14986
- YIG, Bloch wall mobility, effect of dynamic change in wall struct. *(Russian)* 78−2698
- YIG dielectric layered struct. magnetostatic bulk wave steering 80−25166
- YIG, dynamic characts. of domain walls, low temp. behaviour 77−69598
- YIG epitaxial film and cryst., bound magnetostatic waves controlled by field gradients 78−95425
- YIG film, ferrimag., determ. of freq. of magnetostatic modes 77−36104
- YIG film, surface effects in spin wave reson. 77−16182
- YIG, homogeneous crit. relax. in dipole region *(Russian)* 78−10782
- YIG, interaction force between 180° domain wall and edge dislocation 77−28408
- YIG, intrinsic microwave emission, coupling to waveguide system, magnon system cooling 77−24912

ferrimagnetic properties of substances continued

- YIG, mag. and magneto-optic props., temp. and exchange field depend. 77−24824
- YIG multilayered film, magnetostatic spectrum 78−23350
- YIG, one-magnon light scatt. with and without compensation temps. 78−31062
- YIG, optical spectroscopic exam. of ferromag. reson. *(Russian)* 77−48057
- YIG, relax. after spin wave excitation in ferrite *(Russian)* 79−19783
- YIG, spinwave dispersion curves 78−19230
- YIG substrates, magnetoelastic surface waves, magnetostatic reson. anal. 80−20441
- YIG, universal hysteresis loop for soft ferrimag. polycryst. 77−69620
- YIG:Ca film, strong mag. reson. of Fe^{4+} 78−48047
- YIG:Ca films, rapid O diffusion at 25 to 250°C 77−85120
- YIG:Fe^{2+}, magnetostriction const. temp. depend., ferromag. reson. meas. 77−40103
- YIG:Si, relative Fe^{2+} ion conc. depend. 77−48150
- YIG:Si, thermomagnetic processing and illum. effects on mag. props. *(Russian)* 77−8410
- YIG:$Si^{4+}(Ti^{4+})(Zr^{4+})$, X-ray induced change in initial permeability 78−19280
- YIG:Sn, IR absorpt. and MCD 78−19447
- YIG-rare earth garnet solid solutions, magnetisation temp. depend. calcs. 80−20388
- $(YLaBi)_3(FeGa)_5O_{12}$, pure and In^{3+} doped, near IR absorpt. and Faraday rot. 78−95580
- Y_6Mn_{23}, ferrimag., mag. interactions, polarized neutron diffr. meas. 79−78322
- Y_6Mn_{23}, magnetic moments, magnetisation 80−25094
- $Y_{2.5}Pr_{0.5-x}Ca_xFe_5O_{12}$, magnetic aftereffect exam. 78−23304
- $Y_{1-x}R_xCo_5$, R=Gd,Tb,Nd, ferrimag., magnetisation, exchange interactions, mag. anisotropy 80−80565
- $Y_{3-y}Sm_yFe_{5-x}Ga_xO_{12}$ film, LPE growth induced mag. anisotropy 78−2709
- $Y_{2.6}Sm_{0.4}Ga_{1.2}Fe_{3.8}O_{12}$ film, ion-implanted, bubble domain behaviour 77−12177
- $YbFe_2$, Laves phase compounds, synthesis, mag. props., ^{57}Fe Mossbauer effect 78−10807
- $YbFe_2$, Mossbauer spectra, cryst. elec. field and exchange interaction 79−47368
- $YbFe_2$, preparation and mag. props. 80−25259
- YbIG, mean field phase diagrams 78−23269
- $ZnFe_2O_4$, neutron damage effects, superparamag. state replacement cascades 77−16051
- $Zn_{0.005}Fe_{2.995}O_4$, phase transitions, neutron elastic scatt. and resist. meas. 77−28000
- $Zn_xMn_{1-x}Fe_2O_4$, Mossbauer spectra exam. 77−40155
- $Zn_{1-x}Ni_xCr_2S_4$, spin struct., mag. props. meas. 77−85428
- $Zn_xNi_{1-x}Fe_2O_4$, magnetic props. rel. to localised canting model 77−32161

ferrimagnetic resonance

- advances in basic magnetism during past twenty-five years 80−36791
- ferrimagnetic spheroids 77−73013
- ferrite cylinder, ferrimag. reson. modes in semi-infinite boundary system 77−63288
- ferrite sphere plane EM wave scatt. at arbitrary angle to mag. field *(Russian)* 79−15358
- ferrites, LPE growth and characterisation 78−68640
- ferrites, soft and microwave, grain-size effects on mag. props., review 78−64222
- garnet, LPE film, domain dynamics in microwave field 77−20663
- garnet, substituted polycryst., low FMR linewidth, relax. processes 77−20718
- magnetic bubble films, spin wave and magnetoelastic resonance meas. 78−91913
- nonpiezoelectric dielectric, polarisation echo and polarisation avalanche signal form. *(Russian)* 79−61297
- review of magnetic resonance, book contrib. 80−11242
- spinel ferrite, LPE growth, film quality, mag. meas. 78−11136
- uniaxial two-sublattice ferrimagnet, ferrimag. reson. near mag. compensation temp. 77−51963
- α-Al_2O_3:Fe, ferrimagnetic resonance exam. precipitate nature and size determ. 78−48405
- Fe_3O_4, magnetite, ferrimag. reson. at 9.3 GHz near Verwey temp., g-factors *(French)* 78−91959
- $(Gd,Tm,Y)_3(Fe,Ga)_5O_{12}$ LPE garnet thin films, magnetocrystalline anisotropy 80−93147
- $GdFe_2$ films, electron beam deposited, amorphous and cryst., mag. and struct. props. 79−4710
- Gd_xFe_{1-x} film, mm-wave ferrimag. reson. using optically pumped waveguide laser source 77−55710
- $Gd(Fe_xAl_{1-x})_2$, magnetic behavior 80−108079
- $GdNi_x$, (x=3, 3.5, 8.5), ferrimag., mag. reson. above and below Curie temp. 80−97148
- $(Ho_{0.58}Tb_{0.2}Dy_{0.22})Fe_2$, microwave mag. props. 80−65860
- $Li_{0.5}Fe_{2.5-x}Cr_xO_4$ press. depend. of anisotropy consts. 80−65865
- $Li_{0.5}Fe_{2.5}O_4$, LPE growth on spinel substrate crystals, ferrimagnetic resonance exam. 78−76613
- $Mg_xFe_{3-x}O_{4-y}$ precipitates, g-factor, ferrimag. reson. meas. 78−60337
- MgO, mag. anisotropy, ionic distrib. and composition of magnesioferrite precipitates, ferrimag. reson. study 77−69699
- $Sm_{0.4}Y_{2.6}Fe_{3.8}Ga_{1.2}O_{12}$ epitaxial films, uniaxial mag. anisotropy, ferrimag. reson. study 80−80577
- SnCaV garnet polycrystal, ferrimag. resonance loss rel. to grain size 77−85581
- $Y_{3-x}Ca_{2x}Fe_{2-y}In_yFe_{3-x}V_xO_{12}$, first magnetocryst. anisotropy const., ferrimag. reson obs. 78−68218
- $Y_{3-y}Ca_yFe_{2-y}Zr_yFe_3O_{12}$, first magnetocryst. anisotropy const., ferrimag. reson obs. 78−68218
- $Y_{3-3x-2z}Gd_{3x}Ca_{2z}Fe_{5-z-u}V_zSi_uCo_uO_{12}$, mag. props., effect of V substitution 77−20582
- YIG, epitaxial, temp. stabilisation of ferrimag. reson. field by Ga, La substitution 77−77104
- YIG, FMR line broadening, two-magnon scatt. contribs. 77−20711
- $Y_{3-x}La_xFe_{5-y}Ga_yO_{12}$, mag. bubble film, low freq. ferrimag. reson. 78−31110

ferrimagnetism

- *see also ferrimagnetic properties of substances*
- amorphous alloy, dipolar mechanisms for mag. anisotropy 78−64233

ferrimagnetism continued
- amorphous ferrimagnet, molecular field theory, struct. fluctuations 77—40018
- amorphous ferrimagnetic alloy, mag. anisotropy from dipolar interactions 79—87252
- amorphous magnetism, Curie temperature and mag. excitation spectrum 78—10693
- amorphous thin films, struct. and mag. props., review 80—93148
- biquadratic systems, spin 3/2, elementary excitations in antiquadrupolar, ferrimag. and ferromag. phases 79—51763
- Bloch wall oscills., viscosity coeffs. freq. depend., permeability and mag. losses 80—71094
- cubic ferrimagnet, mag. phase diagram, domain struct. analysis *(Russian)* 78—19249
- dilute, sequence of mag. transforms. *(Russian)* 78—19252
- effective field models in magnetism, unifying theory 77—32136
- elastic properties of magnetic materials, review 80—7142
- EM wave propagation on lossy ferrimagnetic slab, modal spectrum 79—86111
- ferrimagnetic Neel mode with helical mode, coupling energy study *(French)* 80—70999
- film, uniaxial epitaxial, induced canted mag. struct., problem of domain wall broadening 78—35016
- indirect hyperfine and superexchange interactions 77—69537
- isotropic three-sublattice ferrimagnet, magnetisation 80—2605
- light diffraction by mag. bubbles in ferrimag. single cryst. layer *(German)* 79—56769
- magnetic polaritons in two sub-lattice ferrimagnets 80—65845
- magnetic torque near compensation point, of ferrimag. materials 79—33472
- magnetisation curves, spin reorientational phase transitions 79—82785
- magnetisation theoretical models, for uniparametric materials 80—65960
- magnetocaloric effect, mag. field direction effect 79—78379
- magnetostatic waves bound by DC mag. field gradients 77—89941
- materials with high uniaxial anisotropy 78—43581
- metamagnetic transitions in crystals with low exchange fields, ferrimagnetic phase *(Russian)* 77—32188
- Neel ferrimagnet, field-induced spin-orientational phase transitions 80—2576
- Neel ferrimagnets, phase transitions, field-induced spin-orientational 80—75767
- Neel mode, ferrimagnetic-helical [hh0] mode coupling vector model *(French)* 80—75770
- neutron diffr., integrated intensity heats, crystal and mag. struct. determ. 80—44079
- one-magnon light scatt., temp dependence, two-sublattice systems 78—31061
- orthorhombic ferrimagnets, domain wall motion at near sonic velocity, magnetoelastic interactions 80—34683
- parametric excitation of sound near phase transition point 79—69710
- polaritons in ferrimagnets, mag. susceptibility 80—7095
- powders, ferromag. and ferrimag., conc. characts. of magnetic props. 77—73052
- semiconductor, cyclotron-magnon reson. 79—69725
- semiconductor, magnetomagnon reson. 79—69663
- semiinfinite, effect of next nearest neighbour coupling 77—73014
- spheroids, magnetostatic modes 77—73013
- spin polarised electron emission from mag. materials, review 77—73215
- spin-wave rays, effect of ellipticity on propagation vector 79—1659
- two-sublattice biquadratic systems, phase transitions 79—99710
- uniaxial two-sublattice ferrimagnet, energy spectrum, magnetisation, and crit. field, Green function method 80—25060
- uniaxial two-sublattice ferrimagnet, ferrimag. reson. near mag. compensation temp. 77—51963
- uniaxial two-sublattice ferrimagnet, magnetisation intensity, crit. fields in applied fields *(Russian)* 78—68285
- X-ray K absorption edge meas. for ferrimag.-material anal. 78—35226
- zero point effect in ferrimag. and antiquadrupolar biquadratic systems 79—91201
- Ho-YIG, magnetic props. in strong fields at low temp., Ising approx. calcs. *(Russian)* 80—54920

ferrite applications
- *see also ferrite devices*
- accelerating resonator for ion synchrotron, with tunable freq. from 2.5 to 30.8 MHz 79—97914
- ferrite-garnet film, waveguide light propag. charact., integrated optics appl. *(Russian)* 78—1346
- ferrite/steel composite bar magnet, large size, for mobile appls. 78—93740
- nuclear reactor, mild steel structures, oxide thickness monitor 77—67806
- proton synchrotrons, magnetisation of ferrites in tunable accelerating resonators 80—68983
- quadrupole mass analyser-field ionis. source interfacing, ferrite insert, repeller electrode 77—18125
- relativistic electron ring azimuthal oscillations in resonator with stabilising medium *(Russian)* 78—29889
- $Sm_{0.7}Er_{0.3}FeO_3$ spin reorientation photomagnetic motor 78—2695
- $YFeO_3$, thermomag. recording in surface layer of orthoferrite 79—24165

ferrite devices
- *see also ferrite applications; magnetostatic wave devices*
- accelerating structure, self accel. of strong electron beam 77—23609
- core, strength improvement method, SiO_2 and Bi_2O_3 additions, mag. characts. 79—24484
- direct-reading displacement digitiser construction and coding *(Russian)* 77—9983
- disc, isotropic, topographs of resonant vibrations 79—64394
- ELF antenna for Magion satellite for 0.1 to 16 kHz freq. range *(Czech)* 80—85775
- even harmonic ferrite probes with axial rectangular pulse excitation, anal. 77—77704
- ferritometer testing, using DC magnetic field 77—16766
- Hall probes, temp. matching, small mag. field detection 79—40592
- hydrostatic pressure effect on ferrite props. of pressure sensors *(Polish)* 80—31707
- magnetoelastic transducer, with increased mechanical strength *(Polish)* 79—40549
- microstructural depend. of operating characts. 78—88548
- phase shifters, azimuthally magnetised, soln. of differential eqns. in terms of Bessel and Neumann functions 79—55025
- pot core pressure transducer development and compensation 79—75519

ferrite devices continued
- pyromagnetic detector for wideband laser radiation *(Russian)* 79—93220
- quarter wave absorbers, C-band, NiZn ferrite appl. 79—38386
- Rogowskii loop with ferrite core, precision meas. of high-power current pulse 78—4639
- sensors, shrinking and thermal tension estimations in epoxy resins appl. *(Polish)* 80—35456
- synchrotron miniature pulse deflector construction 78—82545
- transducer of small displacement, reluctance, 'Polfer' ferrite cores appl. *(Polish)* 78—29100
- UHF microtron system with ferrite gate, frequency responses 77—46430
- Li, fine particle, for arc plasma spraying mm-wave phase shifter 78—64469
- MnZn ferrite disc, excitation of radial mode vibration due to AC 79—69708
- $(Y,Gd)_3(Fe,Ga)_5O_{12}$, thin film lightguide, noninteracting mode conversion *(Russian)* 78—1347
- $(YBiEr)_3(FeGa)_5O_{12}$ ferrite-garnet film, micron cylindrical mag. domains, high recording density 80—65978

ferrites
- *see also ferrimagnetic properties of substances; ferrimagnetism; ferrite applications; ferrite devices*
- 350 NNI ferrite for use in superhigh vacuum systems, prep. 80—108478
- 2000 NN type ring, self-accel. caused by high-current electron beam interruption 80—4809
- adsorption of CO, catalytic oxidation, IR spectrosc. investig. 80—89524
- alkali metal solvent-ferrite quasibinary systems, dissociation 77—40573
- anomalous permeability in Polder-Smit region 78—19278
- antiferroelectric, coupled magnetoelec. oscills. and high freq. susceptibility tensor *(Russian)* 80—93152
- austenitic steel neutron-irradiated weld toughness rel. to ferrite content 79—83327
- bubble film struct., EM and RHEED, Mn and Mn-Cu ferrites 77—11801
- $(CaO.6Fe_2O_3)_{97}(La_2O_3)_3$ compounds, effects of Nd_2O_3 substitution on magnetic props. *(Japanese)* 80—108010
- ceramic, microstructure and physical props. 78—72756
- CO_2 ferrite, crystal structure, X-ray absorpt. spectra, chemical shifts 80—88118
- coercive force dependence microscopic packing density, of hard ferrite particles, model *(German)* 77—20639
- composite garnet ferrite epitaxial film ferromag. resonance obs. 77—85578
- composite semiconductor-ferrite struct., surface magnetostatic spin wave interactions *(Russian)* 80—88739
- composition determination, interelement effects by X-ray fluorescence analysis 78—85259
- critical dynamics, influence of static impurities *(Russian)* 78—10713
- crystal growth for mag. appl., book 79—69967
- cubic ferrite garnet, diffracted light polarisation characts., spin and magnetoelastic waves 80—20614
- Curie temperature meas., by magnetic method *(Czech)* 79—93176
- cylinder, ferrimag. reson. modes in semi-infinite boundary system 77—63288
- cylindrical magnetic bubble domain memory materials 79—61194
- densification of compacts during hydrostatic pressing 80—25629
- dielectric constant measurement for rods in mode E_{010} resonators 79—71483
- dielectric constants and permeability of microwave ferrites *(Chinese)* 80—66096
- dielectric-ferrite interface, physics of microwave reflection, Renard analysis of lateral shift 79—76557
- dilute ferrimagnet, sequence of magnetic transforms. *(Russian)* 78—19252
- disaccommodation meas., errors analysis *(Bulgarian)* 78—21181
- dispersive props., effect of sample size 80—39878
- domain boundary movement, thickness depend. *(Russian)* 78—43611
- electron-stimulated absorption of bulk spin waves 80—70992
- electronic conduction mechanisms, review 77—20314
- EM wave effects on mag. and optical props., lecture 78—27031
- EM wave propagation in transversly magnetised ferrite, anal. *(Russian)* 78—37791
- EM wave scattering, at arbitrary angle to mag. field, ferrite-sphere scatt. *(Russian)* 79—15358
- epilayers for bubble application 80—39829
- epitaxial ferrite garnet film growth, automatic machine 78—27418
- epitaxial ferrite-garnet films with inversion layers, behaviour of cylindrical mag. domains, visual tracking method 80—71139
- fast firing in kilns with jet burners 78—64496
- ferrite F-600, suspension in caster oil, residual magnetisation *(Russian)* 79—1689
- ferrite materials and components, laboratory meas. automation *(Polish)* 80—101789
- ferrite-semiconductor film struct., cyclotron resonance in static elec. mag. fields 80—29624
- ferrite-semiconductor hybrid struct., magnetoelastic wave interaction with drifting carriers 80—54934
- ferrite-semiconductor structure, EM wave excitation and amplification 80—6891
- ferrite-semiconductor structure, transverse galvanomag. effect *(Russian)* 77—24569
- ferrite-semiconductor structure with volume magnetostatic waves, effect of convolution 80—54761
- ferroelectric ferrites, coupled ferroelec. and spin waves, exchange interactions 80—70995
- ferromagnetic resonance absorpt. line intensity and shape 77—90041
- film, magnetostriction const., mag. saturation and internal stress, ferromag. reson. determ. *(Russian)* 77—16126
- film, prep. by plasma jet spraying microstruct. and magnetic props. 78—6546
- film, reactive RF sputtering prep., high mag. recording density 77—12528
- films, plasma sputtering, influence of heating support on struct. and props. *(Russian)* 79—78445
- flux quantisation 78—80136
- FMR absorptiuon, in low resistivity cylinder 79—1718
- frequency tripling of spin waves due to longitudinal pumping excitation *(Russian)* 80—88740

ferrites continued
garnet, optic axes determ. using two sublattice model mag. birefr. 77—8555
garnet epitaxial layer, flaw detection method 78—2719
garnet film, ion-implanted, hard mag. bubble suppression mechanism 80—44890
garnet film, local conc. of effective mass of domain boundaries *(Russian)* 77—12179
garnet-ferrite film thickness meas. with UM-2 monochromator interference attachment 78—3035
Geothite synthesis by ammoniacal method, prep. of Fe_2O_3 77—28741
grade 2000NM1, effect of CaO, MgO and SiO_2 impurities on props. 77—40412
hexaferrites, $M(BaFe_{12}O_{19})$, mag. characts. correlation with substituting ions at. nos. *(Russian)* 79—91218
hexagonal, local lattice distortions, use of Mossbauer effect 78—43745
hexagonal, LPE growth on nonmag. spinel substrate by isothermal dipping method 77—12552
hexagonal, mag. anisotropy 77—20581
hexagonal, model, two-sublattice uniaxial systems with strong antisymmetric exchange 78—47971
hexagonal, with M, W and Y structures containing Fe^{2+} and Fe^{3+} mag. ions, saturation moment and anisotropy 80—71009
hexagonal ferrite films, growth by LPE 78—3062
hexagonal planar ferrite slab, magnetostatic modes 77—24731
hot pressed coprecipitated, for appl. to mag. heads 77—85968
hot pressing, charge:oxidizer ratio 77—48379
hot pressing ferrite and ceramic, bulk interaction *(Russian)* 80—40277
hydrothermal crystallisation, for mag. appl., review, book contrib. 79—69974
hysteresis loop rectangularity, inverse domain vol. depend. *(Russian)* 78—76270
hysteresis loop rectangularity rel. to anisotropy in polycryst. mat. 78—27056
hysteresis loops, formation processes 80—39813
indirect hyperfine and superexchange interactions 77—69537
industrial ferrites type 1500 NMZ and 2000 NMI, mag. susceptibility depend. on heating *(Russian)* 80—108603
inhomogeneous exchange interaction influence on ferromagnetic resonance line moments 80—75864
internal friction, rel. to dislocation movement *(Polish)* 79—95026
inverse spinel ferrite, mol. field theory 79—61021
ionic diffusion and dislocation movement during creep deform. *(Japanese)* 77—28039
laser induced explosion 77—40308
light diffr. by magnetisation inhomogeneities, multiple refl. 80—2733
lightguide, ferrite film, for nonreciprocal optical systems 80—99880
limiting hysteresis loop and number of easy magnetisation axes connection *(Russian)* 78—72364
LPE growth 77—89673
LPE growth and characterisation 78—68640
M type anisotropic, powder prep. and, sintered, effect of powder and pressing technology on alignment *(German)* 79—24472
magnetic aftereffect, measurement system 79—82834
magnetic anisotropy constant, contrib. of Fe^{2+} ion 79—33476
magnetic bubble field distribution meas. by InSb ultramicro Hall element 79—56585
magnetic bubble materials, props. and preparation models, review *(Rumanian)* 80—93149
magnetic permeability, initial, determination for toroidal samples as function of temp. 80—57346
magnetic permeability, meas. method, UHF waves total internal reflect. 78—57994
magnetic permeability meas. at 9.5 GHz, precision test unit 77—74465
magnetically hard materials, technology, development *(Polish)* 77—89973
magnetically-soft materials, mag. characts. determ. methods, review 79—40593
magnetisation effect on RF dispersion of permeability *(Russian)* 79—4700
magnetisation precession, nonlinear homogeneous, stability *(Russian)* 78—48001
magnetised, nonreciprocal refl. of EM waves 78—71006
magnetised rod, propap., interference and relax. of magnetostatic waves, magneto-optical obs. 79—73704
magnetite, classical reaction force density meas. in material media at LF 79—64141
magnetization, regulation in expts. on self-acceleration of electron beam 80—63425
magneto-microwave Kerr effect, K-band interferometer 80—52263
magneto-microwave Kerr effect *(German)* 78—2742
magnetoacoustic resonance in strong mag. field 80—11309
magnetoelastic waves, shear, horizontal, integral representation 77—90009
magnetostatic oscills., in single crystal ferrite with domain struct. *(Russian)* 77—32236
magnetostatic wave instability in ferrite-semicond. composite struct., theory 77—12186
magnetostriction constants, effects of compression 77—40109
magnetostriction due to Co^{2+} ions, effect of excited states 80—65990
magnetostrictive, relationship between static parameters and piezoactivity 78—95507
magnetostrictive ferrites, magnetising field influence on amplitude depend. of mechanical props. 78—2723
manufacture, modified technology development *(German)* 77—21073
mechanical strength, effect of temp. for 2000NM and 2BA ferrites 80—7753
microstructure role in characteristics, review 78—88548
microwave absorbing ferrite-dielectric composite 77—7880
microwave and soft, grain-size effects on mag. props. 78—64222
microwave ferrite mag. props., grain size effect 78—10722
microwave ferrite structures, interference effects 77—160
microwave ferrites, saturation magnetisation determ. *(German)* 79—67357
microwave flaw detection 78—53122
Mossbauer spectroscopy, effect of neighbours on hyperfine field 80—39931
natural gyromagnetic resonance and effective anisotropy *(French)* 77—1629
Ni-Zn ferrites, mag. param. 78—35005
nickel calcine, reactivity, contact I-V meas. 77—85975

ferrites continued
orthoferrite cryst. films, local coercivity of domains boundaries *(Russian)* 80—80578
orthoferrite garnet, mag. bubble lattice nucleation obs. 78—76283
orthoferrites, regular domain structs., magneto-optical characts., optoelectronics appls. 80—40098
orthoferrites, skew cylindrical mag. domains, light modulator appl. anal. 79—38360
orthoferrites, struct. of domain walls 80—34684
orthoferrites, weak ferromagnetism, single ion anisotropy contrib. 80—25126
orthoferrites near spin-flip temp., magnetoelastic waves 78—19301
parametric spin wave excitation *(Russian)* 80—93099
partially magnetised, diagonal components of permeability tensor and resonance 79—47306
partially magnetised, magneto-microwave Kerr effect 78—48003
partially magnetised, modified expression for permeability tensor 77—73048
partially magnetised, tensor permeability 77—89981
pearlite ferrite, plastic anisotropy 79—91772
permanent magnet ferrites, forming 78—64495
permeability, frequency dispersion determination using Kramers-Kronig relation 78—39355
permeability tensor element in Polder-Smit region 77—36090
phase composition, in magnetic field, use of DTA-TG-DTG *(Polish)* 78—31393
phase transforms. near compensation pt., theory *(Russian)* 77—8312
plasma sputtering, struct. props. and phys.-chem. transform. *(Russian)* 79—38739
plate, domain boundary crit. velocity *(Russian)* 78—35015
polycrystalline, dynamic mag. susceptibility rel. to ferromag. reson. *(Russian)* 77—66267
polycrystalline, ferromagnetic reson. curves, theory and meas. method *(Russian)* 77—20713
polycrystalline, X-ray diffr. struct. anal., chem. anal. *(German)* 77—72598
polycrystalline ferrites, anisotropy const. meas. 80—97090
polycrystalline ferromagnetic reson. theory applicability limits *(Russian)* 77—55709
powder, formation during calcining of sulphate mixture 77—63608
powder, grain size meas. by electron microscopy, sample prep. *(German)* 78—56833
powder, single-phase, conditions for formation from solid solutions schoenite-type salts 77—16524
powders, influence of CoO and CuO alloying on physicomechanical characts. *(Russian)* 77—66600
powders, mag. props., explosive shock treatment effects 79—52395
powders with high specific surface, manufacture using freeze-dry method *(German)* 77—63603
'Pulsed ferrite core tests for 50-ns linear induction accelerator' 79—690
pyromagnetic detector for IR Nd laser pulses 77—82606
rare earth ferrite aluminates, prep. 77—85970
rare earth ferrite garnets, phase transitions, field-induced spin-orientational 80—75767
rare earth ferrite-garnets, compensation temp., rare earth ion influence 79—51775
rare earth garnets-$R_xR'_{3-x}Fe_{5-t}M_tO_{12}$, R,R′-rare earths, on Y ions, $Mp=Al^{3+}$, $Ga^{3+}Sc^{3+}$, In^{3+}, effect of ion replacements on lattice constant 79—1408
rare earth orthoferrite, linear dichroism influence on Faraday effect 80—2737
rare earth orthoferrite, phonon slowing down of domain wall *(Russian)* 79—33503
rare earth orthoferrite, $RFeO_3$, spin reorientation and magneto-optical effects *(Japanese)* 79—47414
rare earth orthoferrite, second-order reorientation transition, NMR signal relax. 77—90066
rare earth orthoferrite, Sn^{4+}-doped, indirect Sn^{4+}-O^{2-}-Fe^{3+} interactions 77—11887
rare earth orthoferrite, stripe domain struct. near spin-reorientation points 77—24707
rare earth orthoferrites, domain wall dynamics 80—65957
rare earth orthoferrites, mag. anisotropy in cryst. field approx. 80—60241
rare earth orthoferrites, mag. dipole anisotropy and magnetostriction 79—73710
rare earth orthoferrites, muon states, local mag. fields 80—75911
rare earth orthoferrites, Neel point, cation depend. *(Japanese)* 77—43834
rare earth orthoferrites, parameters of interaction between rare earth and Fe ions, theory and expt. 79—73705
rare earth orthoferrites, Raman scatt. from magnons, anisotropy consts. determ. 80—66178
rare earth orthoferrites and orthochromites, exchange interactions 78—60279
rare-earth orthoferrite, cubic anisotropy consts. 80—11190
rare-earth orthoferrite, domain wall crit. vel. 79—38354
reduction using plasma methods *(Russian)* 80—7700
rod with domain structure, magnetostatic waves and internal field *(Russian)* 78—76236
rods, magnetised longitudinally, surface mode propag. 80—54878
semiconductor-ferrite layer structure, EMF created by spin-wave, effect of current 80—11072
semiconductor-ferrite layer structure, influence of Hall effect on spin wave spectron and amplification by current 79—11308
semiconductor-ferrite layered struct., interaction of spin waves with hot carriers 79—15291
semiconductor-ferrite layered structs., SHF spin wave interaction with electrons, review 79—95507
semiconductor-ferrite structure, nonlinearity and conditions of existence of convective instability 78—72241
semiconductor-ferrite structure, reson. galvanomagnetic phenomena in semicond. 78—87989
semiconductor-ferrite structure, surface magnetostatic wave instability 78—76235
semiconductor-ferrite structure, surface spin waves, current-induced amplification, effect of static state inhomogeneity 79—28519
semiconductor-ferrite-semiconductor structure, absolute instability of magnetostatic surface waves interacting with drifting carriers 78—95486
sheet, magnetised, excitation of surface EM waves 78—10747
sintering, strength and mag. props., vacuum effects 79—70028

ferrites continued
slab, transversely magnetised, adjacent to semicond., mag. surface wave amplification 78−72339
soft, production and props. 80−88801
soft, spray firing for presintered powder prep. 80−89181
sound propagation, nonlinear effects of magnetoelastic interactions 77−27413
sphere, small anisotropic, excitation by pot. field 77−43890
sphere with magnetic anisotropy, EM plane wave, anal. *(Russian)* 77−75373
spheres, magnetisation, resonance oscillation freq. determ. 80−71106
spheroids, magnetostatic modes 77−73013
spin wave amplification in layer in semicond.-ferrite struct. 79−65668
spin wave instability in ferrite-semicond. layer struct. with negative differential conductance 80−25118
spin wave instability on approaching FMR *(Russian)* 78−76318
spin wave relaxation processes 79−82771
spin waves, parametrically excited, amplitude restriction mechanisms *(Russian)* 77−32182
spin waves, parametrically excited, spectral density *(Russian)* 79−4667
spin waves line width, suitability for microwave appl. characterisation 77−20571
spin-reorientation transitions in rare-earth magnets, review 77−36073
spinel, DC resistivity depend. on substitutions 80−44565
spinel, LPE growth on nonmag. spinel substrate by isothermal dipping method 77−12552
spinel ferrites, electrical resistivity and hardness 77−43596
spinel ferrites, thermoelectric power, effect of exchange interactions 78−43422
spinel films, LPE growth and props., SIMS, X-ray diffr., and spin wave reson. obs. 80−34323
spinel type, catalytic oxidation of CO, role of mag. exchange interactions 78−56916
spinel-type, thermodynamic stability, dissociation and phase relations *(Japanese)* 80−55378
spinels, dielec. permeability tensor and transmittance, transition to single lattice struct. *(Russian)* 79−87465
spinels, mag. crit. point behaviour 80−60342
spinels, magneto-optical refl. spectra by equatorial Kerr effect *(Russian)* 77−32400
spinels, normal and inverse, solid state chem. expts. for students 80−36815
spinels, single crystals, growth by Bridgman technique, book contrib. 79−69977
square hysteresis loop magnetisation mechanism and conditions 80−29577
stable magnetic bubbles near compensation point 77−40099
steel, alloy, Cr-C (12, 0.2 wt.%) growth of grain boundary ferrite allotriomorphs, photoemission electron microscope exam. 78−88468
steel, austenitic stainless, ferritic, single phase ferritic solidification in welds, exam. 80−7546
steel, duplex ferrite-martensite, microstructure resistance optimisation 80−40482
substrates, adhesive Cu layers prep. *(Polish)* 78−35537
Supertransferred hyperfine interaction in magnetic insulators. I. Theoretical considerations 77−85403
surface magnetostatic wave, travelling-wave amplification anal. using Maxwell equations *(Japanese)* 78−6560
surface spin wave amplification in ferrite-n-GaAs layer struct. *(Russian)* 77−73016
synthetic, inhomogeneity, nonstoichiometry and lattice defects 77−35547
thermodynamic functions of two-sublattice ferrite in mag. field *(Russian)* 77−32197
thin films, Brillouin scattering from spin waves 80−65843
universal hysteresis loop for soft ferrimag. polycryst. 77−69620
unmagnetised polycrystalline, gyrotropic susceptibility and effective anisotropy 78−64224
US testing 78−53084
void, conc. and dimensions determ. by acoustic charact. 80−35472
wave heam propagation in longitudinally magnetised gyrotropic media *(Russian)* 80−23607
window cores, magnetoelastic props., compressive stresses influence measurements using photo stress method *(Polish)* 80−93134
X-ray K absorption edge meas. for ferrimag.-material anal. 78−35226
β-Al_2O_3-K_2O/K ferrite, interfaces and solid soln., thermal expansion and lattice parameter variations 78−55959
$B_2O_3.Fe_2O_3.2CoO$, mag. props. up to 1200K transitions and magnetisation curves 77−36069
$B_2O_3.Fe_2O_3.2MgO$, mag. props. up to 1200K transitions and magnetisation curves 77−36069
$B_2O_3.Fe_2O_3.nMO$ (M=Fe, Co, Ni, Cu, Mg), synthesis and mag. props. 80−20384
$B_2O_3.Fe_2O_3.nMO$, (n=2 or 4, M=Mg, Co, Ni, Cu), mag. props., transitions 80−75763
$(Ba,Sr)Fe_{12}O_{19}$, Ferroxdure, developments and research 78−84455
Ba ferrite, FMR in uniaxial crystal plate with bubble domain lattice 80−93182
Ba ferrite compounds, microsyntactic intergrowth and cryst. defects, TEM obs. 79−10858
Ba ferrite crystals, etch pitting, of hard magnetic ferrite crystals *(German)* 78−26568
Ba ferrite platelets in multidomain state and at saturation, FMR absorpt. 79−42841
Ba ferrite powder, effect of lattice defects on coercivity *(German)* 79−24194
Ba ferrites, lattice imaging 78−30522
Ba, Hall effect 79−38109
Ba, Hall effect and electrical conductivity 79−42564
Ba hexaferrite, Fe_2O_3-Fe_3O_4 equilibrium in BaO-B_2O_3 melt rel. to prep. 77−36428
Ba hexaferrite, irradiated by fast neutrons, mag. props. 80−97116
Ba hexaferrites, mech. and mag. props. 79−70151
Ba, plastic magnet appl. anisotropic, based on moulding ferromagnetic powder material with plastics *(Japanese)* 80−60829
$Ba_2Co_{1.65}Fe_{0.35}{}^{2+}Fe_{28}{}^{3+}O_{46}$, temp.-mag. field phase diagram, torque method 80−60276
$BaCo_{1\ 5}Fe_{16.5}O_{27}$, type W ferrite, spin reorientation 78−60301
$BaCo_{1.65}Fe_{16.35}O_{27}$, spin reorientation obs. using magneticaloric effect *(Russian)* 77−32195
$Ba_3Co_{2+x}Ti_xFe_{24-2x}O_{41}$, z-type ferroxplan, effect of Co^{2+} ions 77−36094

ferrites continued
$Ba_2Co_{1.75}Zn_{0.25}Fe_{12}O_{22}$, trigonal ferrite, mag. anisotropy 79−73709
$Ba_2Co_{2x}Zn_{2-2x}Fe_{12}O_{22}$, mechanically oriented, topotactic prod. technique, mag. props. 80−35140
$BaFe^{2+}{}_2Fe^{3+}{}_{16}O_{27}$, metal deficient, hexagonal with W struct., chemical instability 78−27662
$BaFe_{12-x}M_xO_{19}$ (M=Al, Ga, Sc, In) ferrites, mag. props. and struct. 80−15690
$BaFe_{12-2x}M_xTi_xO_{19}$ (M=Co, Ni, Zn), mag. props. determ. 80−75759
$BaFe_{12}O_{19}$, bubble and stripe lattice domain wall oscills. 80−97115
$BaFe_{12}O_{19}$, Ca^{2+} substitution effect on hexaferrite lattice and mag. props. 80−60243
$BaFe_{12}O_{19}$, discontinuous growth, effect of equilib. segreg. at boundaries 77−51336
$BaFe_{12}O_{19}$, effect of impurity concentrations, and sintering conditions on grain size *(German)* 79−23630
$BaFe_{12}O_{19}$, ferrite, DC cond., dielec. props., lattice consts. 80−80272
$BaFe_{12}O_{19}$, Hall effect, magnetisation and elec. resist., 30 to 80°C 77−51766
$BaFe_{12}O_{19}$, hexagonal ferrite, local lattice distortions, use of Mossbauer effect 78−43745
$BaFe_{12}O_{19}$, high field Mossbauer effect on ^{57}Fe at room temp. and 4.2K 79−24238
$BaFe_{12}O_{19}$, M type hexaferrite, Fe ion dynamic characts. in bipyramidal position, nucl. γ reson. 79−95697
$BaFe_{12}O_{19}$ microparticles, magnetisation reversal, hysteresis loop obs. 80−75813
$BaFe_{12}O_{19}$, nucl. spin-lattice and spin-spin relax. in domain walls 77−69610
$BaFe_{12}O_{19}$ particles, magnetic domain study by colloid-SEM method 80−97120
$BaFe_{12}O_{19}$ plate, with cylindrical domain struct., ferromag. reson. at arbitrary magnetisation 77−81017
$BaFe_{12}O_{19}$ powder, chemical plating with Co, Co-P, Ni-P and Cu 80−25593
$BaFe_{12}O_{19}$ powder, hysteresis of microwave absorpt. and magnetisation reversal 80−75814
$BaFe_{12}O_{19}$, powder, milled and annealed, phase composition, lattice conts. and crystallite size 80−71677
$BaFe_{12}O_{19}$ powders, fast reaction presintering 80−97445
$BaFe_2O_4$, $BaFe_{12}O_{19}$, formation, dilatometric investigs. 78−27459
$BaFe_2O_4$, free energy of form. 77−4924
δ-$BaFe_2O_4$ room-temp. formation and polymorphism *(German)* 80−44192
$BaFe_2O_4$-Fe_2O_3-$ZnFe_2O_2$ system, phase relations at 1200°C 78−72767
$Ba_2Fe_{18}O_{27}$, hexagonal ferrite, W-struct., Mossbauer spectra of Fe^{3+} and Fe^{2+} 78−88242
$Ba_2Fe_6O_{11}$, cryst. struct. *(French)* 79−86755
$BaFe_4Ti_2O_{11}$, R-type hexaferrite, spin struct. and mag. props. 78−52216
$BaLa_2Fe_2O_7$, Mossbauer exam. of mag. struct. 77−40157
$Ba_2Mg_2Fe_{12}O_{22}$, hexagonal ferrite, with anisotropic g-factor, ferromag. reson. 77−69700
$BaNi_2M_xFe_{16-x}O_{27}$, effect of $M=Sc^{3+}$ or In^{3+} on props. 77−47978
BaO-Fe_2O_3, chemically coprecipitated, mag. props., orientation 80−15763
BaO-Fe_2O_3 system, splat cooled phases struct., magnetisation and susceptibility 300-1100K *(French)* 77−48017
BaO-SiO_2-Fe_2O_3 permanent mag. ceramics, exam. of phase diagram, using X-ray analysis, optical microscopy, electron probe anal., and thermal analysis *(German)* 79−29012
$BaO.6Fe_2O_3$, ferrite polycryst., depend. of domain width on sample thickness 80−108031
$BaO.n\ Fe_2O_3$, magnet, effect of SiO_2 on texture and densification behaviour *(German)* 79−24631
$BaSr_xCa_{1-x}Fe_4O_8$, substituted hexagonal ferrites, mag. split Mossbauer spectra obs. and X-ray struct. data 80−71250
$BaZn_{1.38}Co_{0.62}Fe_{16}O_{27}$, W-type hexaferrite cryst., first order magnetisation processes 78−95472
$Ba_2Zn_{2-2x}Cu_{2x}Fe_{12}O_{22}$, hexagonal ferrites, prep. and mag. characterisation 79−1727
$BaZn_2Fe_{16\ x}Al_xO_{27}$, saturation magnetisation, anisotropy field and Mossbauer meas. 77−69508
$BaZn_2Fe_{16\ x}M_xO_{27}$ (M=Al, Ga, In, Sc), mag. props. and Mossbauer effect 80−75766
$Ba_2Zn_2Fe_{12}O_{22}$, anisotropic magnetisation and susceptibility 78−84411
$Ba_2Zn_2Fe_{12}O_{22}$, model for low mag. moment, magnetisation meas., 5-1375K 78−2655
$Ba_3Zn_2Fe_{24}O_{41}$, ferromag. reson., low power nonlinear effects 80−75861
BamSrmPb hexaferrites, prep. by cernet procedure, mag. props. 77−32174
$BiBi_4Ti_3FeO_{15}$, perovskite-like layer-type ferroelec. magnetic cpd., Mossbauer expts., 80-1200K 78−64329
$BiFeO_3$, pyroelectric-antiferromag., magnetoelectric effect *(Russian)* 78−43625
BiTm ferrite garnet coating on $LiNbO_3$:Ti optical waveguide *(Russian)* 77−42623
$(BiTm)_3(FeGaTm)_3O_{12}$, layer separation of domain struct. 80−44857
$Bi_xYb_{3-x}Fe_5O_{12}$ LPE film, phase grating integrated optic coupler-modulator 77−11048
Ca ferrite, composition and mag. props., anisotropy field, magnetisation 80−71109
Ca ferrite magnets, anisotropic, BaO substitution effect on mag. props. *(Japanese)* 79−99697
$Ca_2(Al,Fe,Cr)O_5$ solid soln., planar interfaces, TEM obs. 80−65008
$Ca_xFe_{3\ x}O_4$, Ca^{2+}, Mossbauer study 78−10814
$CaLaFeO_4$, two-dimens. mag. ordered, structural and mag. props. *(French)* 80−70173
$Ca_2LaFe_3O_8$, Fe replacement by diamag. cation, Neel temp. *(French)* 79−73712
$Ca_2LaFe_3O_8$, physico-chemical characterisation, Mossbauer exam. and mag. props. *(French)* 77−28494
$Ca_xNi_{1-x}Fe_2O_4$, initial permeability and Curie temp. 80−25130
$Ca_xNi_{1-x}Fe_2O_4$, X-ray struct. anal., determ. of lattice constant and interplanar distances *(French)* 80−96487
CaO-Al_2O_3-Fe_2O_3, and resonance spectroscopy study *(Russian)* 77−55733
CaO-Fe_2O_3-B_2O_3 glasses, phys. props. rel. to struct. and comp. 78−23331
CaO-SrO-Fe_2O_3 system, phase relations, Sr hexaferrite field occurrence 80−93545

ferrites continued

$(CaO.nFe_2O_3)_{100-x}(La_2O_3)_x$ ferrite, permanent mag. material, mag. props. and preparation 79—83148
CaV ferrite garnet, large grained, mag. props. 78—64222
$CdFe_2O_4$, synthesis 77—16523
$Cd_{0.010}Fe_{2.990}O_4$, heat capacity investigation of dopant effects on mag. disordering temp. 80—25143
$Cd_xFe_{3-x}O_4$, collective electron states, ^{57}Fe Mossbauer meas. 77—69748
CdNi ferrite, quadrupole interaction, cation distrib. influence 78—2776
$Cd_{0.8}Ni_{0.2}Fe_2O_4$ ferrite, Fe spin relaxation Mossbauer study, mag. hyperfine struct. *(Russian)* 80—15932
$Cd_xNi_{1-x}Fe_2O_4$, mag. behaviour, Mossbauser meas. 78—52390
$CeFeO_3$, enthalpy of formation determ. from heat of oxidation, calorimetric investig. 77—25300
$CeFe_2O_4$, prep. by double decomp. reaction, mag. characts. *(French)* 79—33463
$(Co,Cr,Fe)_3O_4$, $(Co,Rh,Fe)_3O_4$ film magnetooptical switches, for laser beam synchronisation 80—58615
Co, crystalline anisotropy, FMR meas. 77—8408
Co ferrite, growth on fine acicular γ-Fe_2O_3 particles 80—29871
Co ferrite film prep. by vac. evaporation and annealing 77—85939
$CoAl_{2-x}Fe_xO_4$, cation distrib., lattice parameter determ., X-ray diffr. exam. 79—69088
$CoAl_tFe_{2-t}O_4$, Kerr effect, magneto-optical refl. spectra 79—82954
$Co_{1.8}BaFe_{0.2}Fe_{16}O_{27}$, influence of spin-reorientation on magnetoelastic props. *(Russian)* 79—8028
$Co_{1.8}BaFe_{0.2}{}^{2+}Fe_{16}{}^{3+}O_{27}(Co_{1.8}W)$, magnetoelastic props. under spin-reorientation conditions 79—69709
$CoCr_xFe_{2-x}O_4$, magneto-optical refl. spectra by equatorial Kerr effect *(Russian)* 77—32400
$Co_xFe_{3-x-y}Cr_yO_4$, epitaxial, magneto-optical props., effect of Cr^{3+} 78—52590
$Co_x{}^{2+}Fe_{1-x}{}^{2+}Fe_2{}^{3+}O_4$ ferrites, effect of Fe^{2+} on Mossbauer parameters 78—76360
$Co_x{}^{2+}Fe_{1-x}{}^{2+}Fe_2{}^{3+}O_4$, Mossbauer parameters, effect of Fe^{2+}, Zeeman patterns 79—28647
$CoFe_2O_4$, cation self-diffusion, 1231 to 1390°C, vacancy migration mechanism 77—1260
$CoFe_2O_4$, epitaxial layer prod. by chem. transport 77—81224
$CoFe_2O_4$ film, Faraday rot., birefr. 77—1663
$CoFe_2O_4$, fine particles, surface effects on saturation magnetisation 77—69630
$CoFe_2O_4$ formation rate consts. meas. by Mossbauer effect 78—68875
$CoFe_2O_4$ mag. fluid particles, comp., struct., and mag. props. 80—60374
$CoFe_2O_4$, mag. hyperfine fields, Mossbauer spectra 80—108139
$CoFe_2O_4$, superexchange interactions, three-sublattice anal. 79—61095
$CoFe_2O_4$ synthesis, chem., thermal histories rel. to fine cryst. struct. 79—43186
$CoFe_2O_4$, thermally induced surface chemistry and struct., XPS 78—22939
$CoFe_2O_4$ ultrafine particles, prep. and mag. props. 80—71116
$Co_{1-x}Fe_{2+x}O_4$, prep. by wet and ceramic methods, struct., mag. and surface props. 78—52307
$Co_{1-y}Fe_{2+y}O_4$ ferrite, $-0.1\leq y\leq 0.1$, surface composition, AES 78—14557
$Co_xFe_{3-x}O_4$ film, magnetooptic recording material, mag. and magnetooptic props. 77—20832
$Co_xFe_{3-x}O_4$, single cryst. mag. films, holograms recording and thermomagnetic writing 78—55324
$Co_{0.25}Mn_{0.75}Fe_2O_4$, ferromag. reson. in frozen lattice model, anisotropy consts. 79—51859
$Co_{0.08}(Ni,Cu)_{0.92}Fe_2O_4$ sphere, rotational hysteresis, mag. field strength and orientation depend. *(Russian)* 77—16110
$Co_x(Ni_{0.5}Cu_{0.5})_{1-x}Fe_2O_4$ ferrite, relation between elec. cond. and mag. anisotropy 80—75548
$Co_xNi_{1-x}Fe_2O_4$, induced mag. anisotropy consts., conc. and temp. depend. 80—108001
CoNiZn ferrites, Fe excess, complex permeab. var. with annealing temp. 77—89979
CoZn, chemical shift in X-ray absorpt. spectra, effective changes 78—6811
$Co_xZn_{1-x}Fe_2O_4$, elastic behaviour, mag. field and temp. depend. 79—87301
$Co_xZn_{1-x}Fe_2O_4$, ferrite, DC cond., dielec. props., lattice consts. 80—80272
$Co_{0.0031}Zn_{0.5676}Ni_{0.4293}Fe_2O_4$, single phase powder, from solid solution of schoenite-type salt 77—16524
Cu ferrite films, Mn-, Ni- and Al-substituted, LPE growth 80—96752
Cu ferrites, crystallisation of monocrystals from high temp. soln. 78—60561
Cu-Mg-FeO system spinel solid solns., synthesis, struct., and mag. props. 79—52142
Cu-Mn ferrites, heat treatment effect on props. 77—28838
CuCoNi ferrite magnetoacoustic oscills. rel. to microstruct. 77—85536
CuFeCrMn spinel oxides, struct. determ., mag. states of Mn^{3+} ions *(Russian)* 78—19227
$CuFe_2O_4$, Jahn-Teller type crystal distortions 80—103904
$CuFe_2O_4$, LPE grown, domain struct. rel. to tetragonal distortion 78—92205
$CuFe_2O_4$, superexchange interactions, three-sublattice anal. 79—61095
$CuFe_2O_4$, thermally induced surface chem. and struct. 78—22939
$Cu_{0.5}Fe_{2.5}O_4$, ferrite, determination of specific heat at 298-800K 80—2579
$Cu_{0.5}Fe_{2.5}O_4$-$ZnFe_2O_4$, cation distrib., mag. moment, Mossbauer spectra, chem. anal. 80—75210
$Cu_{1-x}Fe_{2+x}O_4$, cation distrib. and valence state 78—63732
$Cu_{1-x}Fe_{2+x}O_4$, elec. resist., Seebeck coeffs., 20 to 900°C, cation distrib. 79—4575
CuO-CdO-Fe_2O_3, sintered ferrite, preparation, mag. susceptibility, DC resistivity 80—34598
CuO-ZnO-Fe_2O_3, sintered ferrite, preparation, mag. susceptibility, DC resistivity 80—34598
$Dy_xEr_{1-x}FeO_3$, transition to antiferromag. state, Dy^{3+} conc. effects 77—66319
$DyFe_{0.998}Co_{0.002}O_3$, mag. transition, NMR meas. 78—27036
$DyFe_{0.998}Co_{0.002}O_3$, orthoferrite, freq. and relax. of ^{57}Fe NMR signal near Morin spin-reorientation phase transition 79—69744
$DyFe_{1-x}Co_xO_3$, magnetostriction, thermal expansion and elastic moduli near Morin point 77—8383
$DyFeO_3$, bubble domain struct. temp. depend. 77—69647

ferrites continued

$DyFeO_3$, field induced spin reorientation, Mossbauer spectroscopy 80—65878
$DyFeO_3$, influence of mag. field on Faraday effect 78—27196
$DyFeO_3$, mag. field induced intermediate state, magneto-optical effect meas. 77—55672
$DyFeO_3$, non Heisenberg R-Fe exchange interaction, behaviour in mag. field *(Russian)* 80—2568
$DyFeO_3$, phase domains, polarisation microscope obs. 77—28407
$DyFeO_3$ single crystal, mag. domain width, temp. depend. 4.2 to 293K 77—40100
$DyFeO_3$, spin reorientation, Faraday rot. meas. 77—8547
$DyFeO_3$, spin reorientation near Morin temp., magnetooptical exam. 78—68284
$DyFeO_3$, spin reorientation transitions induced by magnetic fields, Mossbauer study 80—71246
$DyFeO_3$, spontaneous magnetostriction 79—56599
$DyFeO_3$, weak ferromagnet, μSR study 80—93226
$DyFeO_3$:Al^{3+}, Morin transition, mag. vacancies effect *(Russian)* 78—27039
$Dy_3Fe_5O_{12}$, formation mechanism from metallic oxides 77—48376
$DyFeO_3$; linear dichroism influence on Faraday effect 80—2737
$Dy_{0.5}Ho_{0.5}FeO_3$, mag. transitions, influence of Dy^{3+}, Ho^{3+} ground states 77—89955
$Dy_{0.5}Ho_{0.5}FeO_3$ orthoferrite, domain struct., temp. depend. 80—71086
$Dy_{0.7}La_{0.3}FeO_3$, reorientational phase transitions, influence of La^{3+} ions 80—7108
$Dy_xTb_{1-x}FeO_3$ orthoferrites, Dy^{3+} and Tb^{3+} contribs. to anisotropy const. *(Russian)* 77—89946
$Dy_xTm_{1-x}FeO_3$, transition to antiferromag. state, Dy^{3+} conc. effects 77—66319
$Er_{0.8}Dy_{0.2}FeO_3$, mixed orthoferrite crystals, ^{57}Fe NMR in spin reorientation range 78—15039
$ErFeO_3$, field induced spin reorientation, Mossbauer spectroscopy 80—65878
$ErFeO_3$, low-temperature spin reorientation 79—65683
$ErFeO_3$, parameters of interaction between rare earth and Fe ions, theory and expt. 79—73705
$ErFeO_3$, SAW meas. of magnetoelastic effects 80—75839
$ErFeO_3$, second-order reorientation transition, NMR signal relax. 77—90066
$ErFeO_3$, sound velocity meas. at high press., spin-reorientation transition 78—76254
$ErFeO_3$, temp. depend. of neutron depolarisation factor meas. near spin reorientation transition 77—16053
$ErFeO_3$, weak ferromagnet, μSR study 80—93226
$ErFeO_3$:Co, Ti, effects of Co and Ti ions on cryst. growth 77—28711
$Er_{0.3}Ho_{0.7}FeO_3$, mixed orthoferrite crystals, ^{57}Fe NMR in spin reorientation range 78—15039
$(ErSm)FeO_3$, spin reorientation, Faraday rot. meas. 77—8547
$Er_{0.5}Tm_{0.5}FeO_3$, mixed orthoferrite crystals, ^{57}Fe NMR in spin reorientation range 78—15039
Eu-Ce(Pr)-Fe-O system, solid solns. of ferrogarnet and ferroperovskite type 78—27488
$EuFeO_3$, cryst. domain wall energy density determ. 77—1567
$EuFeO_3$, minute single crystal domain struct. 77—20646
$EuFeO_3$, thermodynamic study of form. 78—48685
$(EuY)_3(FeGa)_5O_{11}$, ferrite garnet film, mag. bubble motion delay 79—91269
$Fe_{3-x}Al_xO_4$, cation distrib., mag. and other phys. props. 77—43818
$FeBMO_4$, M=Mg, Cu, Co, Ni, mag. props. meas. 80—34607
$FeCoCrO_4$ spinel, elec. resistivity, temp. var. 79—38065
$Fe_{3-x}Co_xO_4$, charge transfer, ion distribs., Mossbauer effect 77—20767
$Fe_{3-x}Co_xO_4$, Mossbauer spectra, effect of Fe^{2+} conc. 77—69754
$Fe_{3-x}Cr_xO_4$, electron transfer and spin density distribs., Mossbauer spectra 79—24243
$Fe_{3-x}In_xO_4$, ferrospinels, cation distrib., Curie point and magnetisation meas. 79—42095
$Fe_{10.92}K_{1.55}O_{17}$, ferrite, cryst. struct., nonstoichiometry, ion-ion correlations 80—88130
$Fe(Li_{0.5}Fe_{1.5-x/8}Mn_{x/8})O_4$ $0\leq x\leq 2$ spinel system, X-ray diffr. anal. of loss of order on Cr substitution 79—73178
Fe_5LiO_8, magnetoelec. effect interpretation by magneto-cryst. anisotropy *(French)* 79—33515
$(Fe_{0.19}{}^{2+}Mg_{0.56}{}^{2+}Mn_{0.25})$ $[Fe_{1.87}{}^{3+}Al_{0.13}{}^{3+}]O_4{}^{2-}$, influence of Fe^{2+} ion substitution on electron hopping, Mossbauer study 80—71247
$(Fe_{0.55}{}^{2+}Mg_{0.32}{}^{2+}Mn_{0.03}{}^{2+}Cu_{0.10}{}^{2+})$ $[Fe_{1.74}{}^{3+}Al_{0.26}{}^{3+}]O_4{}^{2-}$, influence of Fe^{2+} ion substitution on electron hopping, Mossbauer study 80—71247
$Fe_{3-x}Mg_xO_4$, Verwey transition, Mossbauer study 80—39942
$FeNiBO_4$, $FeNi_2BO_5$, Mossbauer spectra, mag. relax. 80—15889
$Fe_{3-x}Ni_xO_4$, low temp. Mossbauer spectra, electron transfer and spin density distribution 78—52404
$Fe_{3-x}Ni_xO_4$, Mossbauer spectra, effect of Fe^{2+} conc. 77—69754
$Fe_{1.985}Ni_{0.975-x}Zn_xCo_{0.04}O_{4+\gamma}$, elementary coupling energy of Co^{2+} to lattice 77—1549
γ-Fe_2O_3, fine particles, surface effects on saturation magnetisation 77—69630
Fe_2O_3-BaO-CoO system, phase comp. and mag. props., Bi_2O_3 additions effect 79—29032
α-Fe_2O_3-Li_2O, structural and thermal phase behaviour from mag., spectral and thermal studies 80—2673
Fe_2O_3-NiO-ZnO-CoO (15.1, 17.6, 0.6 wt.%) ferrite, effect of electron beam machining on surface layer 79—34178
$Fe_{3-\Delta}O_4$, mag. aftereffects near Verwey temp. 79—87294
Fe_3O_4, dielec. function and polar Kerr rotation, 0.5-3.6 eV 80—66221
Fe_3O_4, doped, electron correls. above and below Verwey transition, Green function theory 77—51687
Fe_3O_4, effect of Al ion on formation and structure *(Japanese)* 77—59727
Fe_3O_4, electronic struct. and charge density oscills. near Verwey transition, Mossbauer expt. 78—27150
Fe_3O_4, hyperfine fields and spin densities below 20K 78—52405
Fe_3O_4, hyperfine mag. field at ^{119}Sn, Mossbauer expt. 80—50232
Fe_3O_4, IR refl., ATR, Voigt and Faraday expts. 80—66180
Fe_3O_4, inverse spinel ferrite, spontaneous magnetisation, mag. field theory 80—25104
Fe_3O_4, low temp. phase ionic ordering, NMR *(Russian)* 78—23354
Fe_3O_4, magnetisation using Neel's mol. field theory 79—87223
Fe_3O_4, magnetite, charge carriers, optical props. 80—34874
Fe_3O_4, magnetite, defect content, gas-phase comp. effects 77—43336

ferrites continued
Fe_3O_4, magnetite, low temp. phase transition, magneto-optical exam. 78−27193
Fe_3O_4, magnetite, precip. with urea, prep. and props. 80−20854
Fe_3O_4, magnetite cylinder, EM ang. momentum observation 79−55027
Fe_3O_4, magnetocrystalline anisotropy, anomolies in magnetostriction and elastic constants 80−60244
Fe_3O_4 particles, entrapped in drug carrying microsphere, intravascular mag. guidance method 78−73188
Fe_3O_4, phase transition, pseudospin analysis 78−10157
Fe_3O_4, photocond. 70-130K, temp. range including metal-semicond. transition *(Russian)* 78−56178
Fe_3O_4, relax effects, Mossbauer expt. using selective excitation method 78−25375
Fe_3O_4, single cryst., surface magnetism, spin polarized photoemission 78−52622
Fe_3O_4, spherulitic film growth, elec. and mag. props. 78−68627
Fe_3O_4, superexchange interactions, three-sublattice anal. 79−61095
Fe_3O_4, tetrahedral-site Fe^{3+} ion, spin-transfer due to covalency 79−15285
Fe_3O_4, ultrafine particles in ferrofluid, superparamag. and ferromag. reson. 78−15026
Fe_3O_4-$FeTiO_4$ solid soln. spinels, domain wall formation inhibition, effect on bulk mag. props. 80−11220
$Fe_3O_{4-x}F_x$ ($0\leq x\leq 0.25$), Mossbauer spectra 78−15075
$Fe_3O_{4-x}F_x$, low temp. Mossbauer spectra, electron transfer and spin density distribution 78−52404
$Fe_3O_{4-x}F_x$ substituted magnetite, low temp. resistivity, Seebeck coeff., thermopower 80−20234
FeTi ferrite, H trapping study by high resolution autoradiography and degassing *(French)* 77−81368
$Fe_{3-x}Zn_xO_4$ low temp. Mossbauer spectra, electron transfer and spin density distribution 78−52404
β-Ga_2O_3-K_2O/K ferrite, interfaces and solid soln., thermal expansion and lattice parameter variations 78−55959
$GdFeO_3$ orthoferrite, rare earth-Fe interactions 79−56525
$Gd_3Fe_5O_{12}$, formation mechanism from metallic oxides 77−48376
$Gd_3Fe_5O_{12}$, nucl. gamma reson., anomalous behaviour of intensity 77−12289
GdIG single crystal plates for magnetooptical information storage 79−7997
$Gd_{1.8}Y_{1.2}Fe_5O_{12}$, nucl. gamma reson., anomalous behaviour of intensity 77−12289
$GeFeO_3$, field induced spin reorientation temp. depend. 77−63200
$Ho_{0.5}Dy_{0.5}FeO_3$ orthoferrite, domain wall struct., stability conditions, Morin transition, anisotropy const. 80−34684
$Ho_{0.7}Er_{0.3}FeO_3$, crystn. on seeds, layer morphology 78−72041
$HoFeO_3$, field induced spin reorientation, Mossbauer spectroscopy 80−65878
$HoFeO_3$ orthoferrite, rare earth-Fe interactions 79−56525
$K_{1+x}Fe_yGa_{11-y}O_{17}$, electron hopping and excitation at room temp., ^{51}Fe Mossbauer spectra 80−25257
KFe_2O_3, β'' phase, mag. props., hyperfine interactions, Mossbauer study 80−20524
$K_{1+x}Fe_{11}O_{17}$, ionic cond. and chemical diffusion 77−47618
$K_2O.6Fe_2O_3$: divalent metal oxide, electronic and ionic cond. 79−87135
$LIFe_5O_8$, absolute struct. and space group determ. by electron microscopy 77−62454
La ferrite, composition and mag. props., anisotropy field, magnetisation 80−71109
$LaFe_{1-x}D_xO_3$:Sn, D=Al, Ga or Sc, Mossbauer effect, hyperfine mag. fields at Sn 77−24772
$LaFeO_3$, doped, effect of doping on hyperfine fields, supertransfer model 79−47057
$LaFeO_3$, electronic struct., super transfer effects, Mossbauer expt. 78−27150
$LaFeO_3$, thermodynamic study of form. 78−48685
$LaFe_{12}O_{19}$, high field Mossbauer effect on ^{57}Fe at room temp. and 4.2K 79−24238
$La_{1-x}Na_xFeO_{3-x}$, defect perovskite system, Mossbauer effect 77−36159
(Li,Na,Cu,Zn) ferrites, nonceramic synthesis, electrochem. investig. 78−35339
Li ferrite, cladding on plastic foil, thermal deform. *(Polish)* 80−30002
Li ferrite, electrical cond., thermoelectricity, magnetoresistance meas. 78−19039
Li ferrite, $Fe(Li_{0.55}Fe_{0.45})O_4$, one-magnon light scatt. with and without compensation temps. 78−31062
Li ferrite, ferromag. reson., linear elec. field shift 79−1716
Li ferrite, linear electric field effects in mag. anisotropy and ferromag. reson. 80−65854
Li ferrite, reduction, phase transitions 80−55642
Li ferrite film, magnetic circular and linear dichroism, temp. depend. 79−69815
Li ferrites, MW dielectric losses, causes and reduction *(Chinese)* 80−75930
Li ferrites, porous, porosity effect on saturation of magnetisation 80−108036
Li matrix ferrites, coercivity, synthesis, thermostability control 80−80569
Li-Co ferrite, mag. anisotropy induced by thermomag. treatment, ionic order effect, magnetostriction meas. 80−103830
Li-containing, conditions for obtaining high-density one-phase mag. ceramic 79−52141
Li-containing ferrite-BiO_2, phase diagrams and sintering conditions 79−52141
Li-Cr ferrite, $Fe(Li_{0.5}Fe_{0.25}Cr_{1.25})O_4$, one-magnon light scatt. with and without compensation temps. 78−31062
Li-ferrite, ultrafine powders, prod. by cryochemical, freeze drying, spray drying or soln. techniques 80−55336
Li-Na ferrite powders, props. rel. to Fe_2O_3 chem., thermal, mech. historical 79−11539
Li-Ti, microwave props. 77−40082
Li-Zn, (Li, Zn, Ti, Cr substituted), Mossbauer spectrometry, effect of supertransferred hyperfine fields and relaxation *(French)* 80−80654
Li-Zn, characts. and apol. *(German)* 77−80953
Li-Zn ferrite, magnetic props., effect of V_2O_5 addition *(Japanese)* 77−28415
$Li_{0.5}$ $Fe_{2.5}O_4$, microwave material, mag. props., review 79−33504
LiAl ferrite, substituted ferrospinel, spin configuration determ. *(Russian)* 77−32162
$LiAl_xFe_{5-x}O_8$, IR spectra, ionic ordering in absence of fine struct. 77−8583
$Li_{0.5}Al_xFe_{2.5-x}O_4$ and $Li_{0.5}Ga_xFe_{2.5-x}O_4$, polycrystalline, ferromag. reson. theory *(Russian)* 77−55709
$Li_{0.5}Al_xFe_{2.5-x}O_4$, polycrystalline, ferromag. reson. absorpt. curves, stress effects *(Russian)* 77−20713
LiCd ferrite, dielec. const. and loss meas., 50-10^6 Hz 77−77135
LiCr ferrite, elec. resist., thermoelec. power and Nernst-Ettingshausen meas. near compensation point 78−10487
$LiCr_xFe_{5-x}O_8$, IR spectra, ionic ordering in absence of fine struct. 77−8583
$Li_{0.5}Fe_{2.17}Al_{0.33}O_4$:Co, single cryst., domain struct., mag. annealing effect depend. on induced anisotropy 78−68290
$Li_{0.5}Fe_{2.5-x}Al_xO_4$ ($0\leq x\leq 0.68$) films, LPE 80−29884
$Li_{0.5}Fe_{2.5\ x}Cr_xO_4$, mag. anisotropy, ferromag. reson. meas. 77−69542
$Li_{0.5}Fe_{2.5-x}Cr_xO_4$ press. depend. of anisotropy consts. 80−65865
$Li_{0.5}Fe_{1.25}Ga_{1.25}O_4$, ferrimag. with local canted struct. thermal expansion anomalies 79−73762
$LiFe_5O_8$, elec. props. 77−80641
$LiFe_5O_8$, hysteresis and other mag. props. rel. to microstruct., TEM investig. 77−20636
$LiFe_5O_8$, material loss and high-temp. phase transition 78−64534
$LiFe_5O_8$, microstruct. and magnetic props., electron microscope obs. 79−87290
$LiFe_5O_8$, second order magnetoelectric effect 77−66409
$LiFe_5O_8$, spinel, mixed cond. using four-point DC techniques 79−60877
$LiFe_5O_8$, vacuum annealed, tetragonal γ-phase obs. with TEM 80−11661
$Li_{0.13}Fe_{2.87}O_4$, acoustic spin wave dispersion branch, exchange const., neutron scatt. study 79−47266
$Li_{0.5}Fe_{2.5}O_4$, antiphase domains, broadened X-ray diffr. line anal. 78−26578
$Li_{0.5}Fe_{2.5}O_4$, domain struct. in (110) and (111) plates, Faraday effect meas. 79−61180
$Li_{0.5}Fe_{2.5}O_4$, effects of low-melting additive on struct. and dielec. props. 77−85494
$Li_{0.5}Fe_{2.5}O_4$, ferritisation of Li_2CO_3 77−52269
$Li_{0.5}Fe_{2.5}O_4$, ht. treatment conditions effect on superlattice formation 77−84922
$Li_{0.5}Fe_{2.5}O_4$, LPE growth on spinel substrate crystals, ferrimagnetic resonance exam. 78−76613
$Li_{0.5}Fe_{2.5}O_4$, linear elec. field shift of ferromag. reson. field 79−78530
$Li_{0.5}Fe_{2.5}O_4$, magnetic domain walls, mobility 80−2600
$Li_{0.5}Fe_{2.5}O_4$, magneto-optical Kerr effect, reflectivity spectra 80−66157
$Li_{0.5}Fe_{2.5}O_4$, magnetooptical spectra, polar Kerr rotation, dielectric tensor elements spectra 80−40091
$Li_{0.5}Fe_{2.5}O_4$ milled ferrite powder, substruct. and sinterability 80−84894
$Li_{0.5}Fe_{2.5}O_4$, neutron-irrad., mag. spectra *(Russian)* 77−44092
$Li_{0.5}Fe_{2.5}O_4$, polar Kerr rotation spectra, 2-5.7 eV, comparative study with YIG 79−47413
$Li_{0.5}Fe_{2.5}O_4$ Ru substitution effect on struct. and mag. props., and max. solubility determ. 80−75364
$Li_{0.5}Fe_{2.5}O_4$, slow neutron polariser, by single cryst. (222) refl. 80−49052
$Li_{0.5}Fe_{2.5}O_4$, spinel ferrite, prep. by thermal treatment of spray-dried formates, scanning electron microscope examination 79−24482
$Li_{0.5}Fe_{2.5}O_4$, superexchange interactions, three-sublattice anal. 79−61095
$Li_{0.5}Fe_{2.5}O_4$, uniaxial anisotropy energy, elec. field depend. 78−68346
$Li_{0.5}Fe_{2.5}O_4$-$Bi_2O_3(V_2O_5)$ systems, phase diagrams, sintering conditions 78−35366
$Li_{0.5}Fe_{2.5}O_4$-$CuFe_2O_4$-$MnFe_2O_4$, structural characteristics and mag. props. of solid solutions 77−35696
$Li_{0.5}Fe_{2.5}O_4$-$CuFe_2O_4$-$ZnFe_2O_4$, order-disorder transition, quadratic transformation *(French)* 78−76447
$Li_{0.5}Fe_{2.5}O_4$-$LiNb(Ta)O_3$, in situ composite growth, phase diag., melting relns. 77−21132
$Li_{1-x}Fe_{5-x}O_8$:Co, single cryst., domain struct., mag. annealing effect depend. on induced anisotropy 78−68290
Li_5FeO_4, compatibility of Fe-Ni-Cr alloy with Li_2O pellets, mass spectrometric study of Li_5FeO_4 evaporation 79−8385
$(Li_{0.5}Fe_{2.5}O_4)_{0.8}(CuFe_2O_4)_{0.2}$, struct., magnetic props., rectangular hysteresis loop 77−20645
$Li_{0.17}Fe_{2.17}Zn_{0.66}O_4$, ferrimag. with local canted struct. thermal expansion anomalies 79−73762
LiGa ferrite, substituted ferrospinel, spin configuration determ. *(Russian)* 77−32162
$Li_{0.5}Ga_{0.095}Fe_{1.55}O_4$ ferrites, linear magnetostriction in weak field, 150 to 300K *(Russian)* 77−80983
$Li_{0.5}Ga_xFe_{2.5-x}O_4$, superexchange interaction parameters, Mossbauer spectra obs. 77−51899
$Li_{0.5(1-x)}Mn_x$ $Fe_{2.5-0.5}O_4$, rectangular hysteresis loop, microstruct. form. 77−12718
$Li_{0.5}Mn_{0.15}Fe_{2.35}O_4$ ferrite cores with rectangular hysteresis loops, pulse parameters, effect of Fe_2O_3 heat treatment 80−60370
LiMnSc ferrites, role of intergranular microstresses in control of coercive force 77−20640
LiMnZn, elementary coupling energy to lattice of Mn^3 ions, depend. on T_c 77−69534
LiNa effect of sintering temp. on oxidation kinetics, conductivity meas. 77−21298
$Li_{0.4}Na_{0.1}Fe_{2.5}O_4$, and $Li_{0.3}Na_{0.2}Fe_{2.5}O_4$, form. X-ray, chem. and mag. anal. 77−36424
$Li_{0.5-x}Na_xFe_{2.5}O_4$, Na_2CO_3 effects on ferrite formation 78−27458
$Li_{0.45}Ni_{0.1}$, $Fe_{2.45}O_4$, sintering, mag. props., rare earth oxide additive effects *(Japanese)* 77−66602
Li_2O-Fe_2O_3-$Pr_6O_{11}(Er_2O_3)(CeO_2)(Eu_2O_3)$, Hall effect and magnetoresist. 78−34849
LiTi, Mossbauer study, relax. and supertransferred hyperfine fields 80−39941
LiTi, substituted ferrite, cation distribution, Mossbauer, X-ray, neutron diffr. study 80−28975
LiTiZn ferrites, elec. resist., mag. props., effect of Bi addition 78−95474
LiTiZn microwave ferrites, effects of Mn and Bi additives, expt. *(German)* 77−28411
LiZn ferrite, dielec. const. and loss meas., 50-10^6 Hz 77−77135
LiZn ferrospinels, mol. field. coeff. conc. depend. 80−97114
LiZn, Mossbauer study, relax. and supertransferred hyperfine fields 80−39941
LiZn, substituted ferrite, cation distribution, Mossbauer, X-ray, neutron diffr. study 80−28975
$Li_{0.2}Zn_{0.6}Fe_{2.2}O_4$, ferrite, mag. ordering at low temp. *(Russian)* 77−32171

ferrites continued
  $Li_{0.44}Zn_{0.09}Fe_{2.47}O_4$, ordering, elect. of V_2O_5 additions 77–35532
  $Li_{0.5-z/2}Zn_xFe_{2.5-z/2}O_4$, field magnetisation and susceptibility 79–82762
  $Li_{0.5(1-x)}Zn_xFe_{2.5-0.5x}O_4$, cryst. struct., neutron and X-ray diffr. obs. *(Russian)* 77–31645
  $Li_{0.5(1-x)}Zn_xFe_{2.5-0.5x}O_4$, canted spin struct., neutron diffr. study 78–68175
  Mg $(Fe,In)_2O_4$:Pb,Pt film, LPE 77–77436
  Mg ferrite, crystal lattice defectiveness and degree of inversion, effect of synthesis temp. 77–11501
  Mg ferrite, sintered, cation redistribution, microstructural effects 77–55356
  Mg-Cu-Mn-Ni-Fe-O, UHF ferrites, synthesis, physicochem. state, mag. and dielec. parameters 79–11536
  Mg-Mn ferrite, finely divided, synthesis 77–28773
  $Mg_{0.7}Cu_{0.3}Fe_2O_{4+\delta}$, disaccommodation and accommodation 77–20641
  $MgFe_{2-y}Al_yO_4$, with added Co, effect of Na_2O admixture on props. 77–36423
  $MgFe_2O_4$, epilayer, perpendicular anisotropy 80–39769
  $MgFe_2O_4$, form. mechanism in mixture of metallic oxide powders 77–63609
  $MgFe_2O_4$, LPE growth, film quality, mag. meas. 78–11136
  $MgFe_2O_4$, Mossbauer effect determ. of cation distrib. temp. depend. 77–8481
  $MgFe_2O_4$, prep. by double decomp. reaction, mag. characts. *(French)* 79–33463
  $MgFe_2O_4$, sintered, cation ordering, grain size effects 78–39763
  $MgFe_2O_4$-Co_3O_4 solid soln. spinels, domain wall formation inhibition, effect on bulk mag. props. 80–11220
  $MgFe_2O_4+ZnO$, powders, cation mutual diffusion coeffs. calc. 77–15635
  $Mg_{0.5}Fe_{2.5}O_4$, ferrimag. epilayer, superparamag. interface, mag. props., FMR 78–95492
  $Mg_xFe_{3-x}O_4$, cation redistribution, effect of composition and thermal treatment 79–27966
  $Mg_xFe_{3-x}O_4$, cation redistrib., lattice const. 79–60338
  $Mg_xFe_{3-x}O_4$ crystals, first mag. anisotropy const., 7-295K 80–65855
  $Mg_xFe_{3-x}O_4$, magnetostriction consts., 80 to 320K 78–95503
  $Mg_xFe_{3-x}O_4$, polycryst., Verwey type transition, resist., magnetisation, Mossbauer effect and permeability obs. 80–75764
  $(MgFe_2O_4)_{1-\gamma}(Mn_3O_4)_\gamma$, polycrystalline, coercive forces 78–39366
  $(MgFe_2O_4)_{x-1}(Mn_3O_4)_x$, soft ferrite, squareness ratio and max. induction 79–99730
  $MgGa_xFe_{2-x}0_4$, spinel struct., neutron diffr. exam. 77–12096
  $MgIn_xFe_{2-x}O_4$ and $MgSc_xFe_{2-x}O_4$, Mossbauer spectra, elec. and mag. props. *(Russian)* 77–69737
  $MgM^{3+}{}_xFe_{2-x}O_4$, M=In,Al,Cr,Sc, comp. effects on ferrite characts. 78–52305
  MgMn ferrite, electrical cond., thermoelectricity, magnetoresistance meas. 78–19039
  MgMn ferrite, reaction during ferrite form. X-ray phase and mag. anal., contact volt. amperometry 77–21068
  MgMn ferrite CVD epitaxial layers, bubble domains in remanence and demagnetised states 77–85516
  MgMn, film, magnetostriction const., mag. saturation, and internal stresses *(Russian)* 77–16126
  MgMn, mag. noise features at low temps. *(Russian)* 78–27060
  $Mg_{0.8}Mn_{0.2}Fe_{1.8}Al_{0.2}O_4$, grade 6SChl ferrite, milling conditions effect on fine cryst. struct. and activity 79–24483
  MgMnZn ferrite, ultrafine powder, prod. by cryochemical, freeze drying, spray drying or soln. techniques 80–55336
  MgO-ZnO-Fe_2O_3, sintered ferrite, preparation, mag. susceptibility, DC resistivity 80–34598
  MgO-ZnO-Fe_2O_3-Cr_2O_3 system spinels, IR absorpt. spectra, short-range order 79–42957
  (MgO-Fe_2O_3-Cr_2O_3-TiO_2):Na_2O, powder, prep., heat treatment, Na_2O impurity effect on props. 77–16528
  MgZn solid solns., thermodynamic props. 77–21116
  $Mg_{0.25}Zn_{0.75}Fe_2O_4$, ferrite, DC cond., dielec. props., lattice consts. 80–80272
  (Mn,Ni,Zn) ferrite single cryst., flame fusion cryst. growth, conc. change 77–77369
  $(Mn,Zn)Fe_2O_4$:Si, Ca, Ti, second phase effect on elec. and mag. props. 80–60986
  Mn ferrite, magnetic permeability, photoinduced reduction *(Rumanian)* 80–75794
  Mn ferrites, Fe^{2+} ion contrib. to induced anisotropy and mag. aftereffect 77–36101
  Mn ferrites, Fe-excess, charge carriers, optical props. 80–34874
  Mn, monocrystalline epitaxial layers, surface spin-wave modes in ferromag. reson. 78–2743
  Mn, photogalvanomagnetic effects 80–34483
  Mn-Zn, permittivity anal. and meas. *(Russian)* 79–15391
  Mn-Zn, single-crystal, machining effect obs., on magnetisation curves *(Japanese)* 77–21295
  Mn-Zn ferrite, domain struct. and initial permeability, effect of O nonstoichiometry 78–35001
  Mn-Zn ferrite, extraordinary Hall effect 79–51615
  Mn-Zn ferrite, oxidation-reduction equilib. and struct. defects 77–20189
  Mn-Zn ferrite, single crystal, electrolytic buffing studies *(Japanese)* 77–86259
  Mn-Zn ferrite, single crystal, surface damaged layer study *(Japanese)* 77–86260
  Mn-Zn ferrite powder, spray dried calcination 77–12558
  Mn-Zn ferrites, grain boundary exam. using TEM and AES 80–107268
  Mn-Zn ferrites, mag. parameters, determ. from RF susceptibility 79–82769
  Mn-Zn ferrospinels, carrier transfer phenomena 80–54727
  MnFe ferrite, mechanically induced anisotropy, effect on mag. permeability 78–47970
  MnFe ferrites, reson., effect of EM propagation 78–64277
  $MnFe_{2-x}In_xO_4$, magnetic props., In substitution effects *(Russian)* 78–91849
  $MnFeO_2$:^{55}Mn, NMR freq. dynamical shift for nuclei in domain walls *(Russian)* 77–40148
  $MnFe_2O_3$, superexchange interactions, three-sublattice anal. 79–61095
  $MnFe_2O_4$, additional spin echo of ^{55}Mn nuclei 80–60455
  $MnFe_2O_4$, discontinuous growth, effect of equilib. segreg. at boundaries 77–51336
  $MnFe_2O_4$, exchange splitting of ionic S-state, neutron spectra 78–52240

ferrites continued
  $MnFe_2O_4$, ferrite, dynamic shift of NMR freq. of nuclei located in domain walls 80–15823
  $MnFe_2O_4$ film, bulk and surface spin waves, spin wave reson. expts. 79–73826
  $MnFe_2O_4$ magnetic moments and high field susceptibilities, spin model 77–28376
  $MnFe_2O_4$, nuclear reson. and relax. from domains and domain walls 77–8448
  $MnFe_2O_4$, prep. by double decomp. reaction, mag. characts. *(French)* 79–33463
  $MnFe_2O_4$, valence states, NMR investig. *(Czech)* 78–72420
  $MnFe_2O_4$, valency states, NMR 77–51987
  $MnFe_2O_4$:Sn, hyperfine mag. fields at ^{119}Sn and ^{57}Fe nuclei, influence of press. 79–99811
  $Mn_{0.82}Fe_{2.18}O_4$, anelasticity, 280 to 730K, 125 kHz vibr. study 78–87740
  $Mn_{1-x}Fe_{2+x}O_{4+\delta}$, ferrites, homogeneity region, cluster component model 78–35367
  $Mn_{1+x}Fe_{2-x}O_4$, magnetostriction meas., inversion degree influence 77–73070
  $Mn_xFe_{3-x}O_4$, dielec. function and polar Kerr rotation, 0.5-3.6 e▼ 80–66221
  $Mn_xFe_{3-x}O_4$ epitaxial films, mag. and reson. props. 80–50149
  $Mn_xFe_{3-x}O_4$ ferrite film, exchange interaction depend. on conduction electrons *(Russian)* 80–34621
  $Mn_xFe_{3-x}O_4$ film, spin wave reson., exchange const. 77–16183
  $Mn_xFe_{3-x}O_4$ NMR of Mn^{3+} in B-sites 78–35061
  $Mn_xFe_{3-x}O_4$, optical props. 80–20606
  $y(Mn_xFe_{3-x}O_4)$-$(1-y)B_2O_3$ glasses, elec. and struct. props., 400-1000K 79–51575
  $Mn_xFe_{3-x}O_{4+\gamma}$, average directional order, cation valency and repartition on A- and B-sites *(French)* 78–39369
  $Mn_xFe_{3-x}O_{4+y}$, prep., resist., hysteresis loop and mag. disaccommodation *(Spanish)* 77–73045
  MnMg ferrite, products if reaction of ferrogel with $MnCl_2$ solution 77–12582
  MnMgZn, accurate chemical comp. determ. by instrument-aided neutron activation anal. 79–29438
  MnO-MgO-ZnO-Fe_2O_3, grade 1.3 VT ferrite formation from hydroxides 77–90302
  MnO-ZnO-MgO-Fe_2O_3 ferrites, effect of Fe^{2+} ion on initial permeability 77–8357
  $(Mn_xSn_{1-x})Fe_2O_4$ thin film LPE on Bridgman grown Zn_2TiO_4 substrate 79–100065
  MnZn, combined Sn-Ti substitutions, improved props. *(German)* 77–20644
  MnZn, commercial grade, microstruct. rel. to mag. props. 80–34009
  MnZn ferrite, anomalous thermal change of permeability near Curie point 77–20638
  MnZn ferrite, appreciable SiO_2 content, origin of core losses, microstructure and mag. props. 78–64225
  MnZn ferrite, combined Bridgeman-zone levelling cryst. growth technique 80–35076
  MnZn ferrite, high cond., magneto-microwave Kerr effect 77–43888
  MnZn ferrite, initial mag. permeability rel. to mag. anisotropy 80–80557
  MnZn ferrite, mag. anisotropy, effect on recording head characts. 80–39765
  MnZn ferrite, mag. loss accommodation depend. on freq. and amplitude of mag. field *(Russian)* 80–34686
  MnZn ferrite, mag. permeability accommodation depend. on mag. field *(Russian)* 80–34685
  MnZn ferrite, mag. relax., permeability and loss tangent determ. at 4.2 to 300K 77–32263
  MnZn ferrite, mag. susceptibility freq. spectrum, effect of pressure 78–95420
  MnZn ferrite, mag.-mechanical-microstruct. interaction 77–1578
  MnZn ferrite, mechanically induced anisotropy, effect on mag. permeability 78–47970
  MnZn ferrite, microstructure and initial permeability, presintering process effect 80–89367
  MnZn ferrite, MoO_3 addition effect on grain growth kinetics and densification 79–61550
  MnZn ferrite, nonstoichiometric, neutronographic determ. of cation distrib. *(Bulgarian)* 78–83656
  MnZn ferrite, O_2 stoichiometry effect on fracture 80–25826
  MnZn ferrite, optical refl. and electroreflection spectra obs. 78–27262
  MnZn ferrite, polycrystalline, doped, DC resist. 78–47788
  MnZn ferrite, post sintering cooling rate effects on props. 77–63604
  MnZn ferrite, prep. and magnetic props. 78–19254
  MnZn ferrite, quantitative anal., using X-ray fluorescence 78–40090
  MnZn ferrite, spray dried agglomerates, compaction response, fracture, deform. 79–43172
  MnZn ferrite, surface damaged layer, mag. domain obs. by taper section SEM 77–59423
  MnZn ferrite, temperature dependence of Hall mobility 78–30944
  MnZn ferrite, thermal cond. of single crystals 77–36079
  MnZn ferrite, Ti substituted, vacancy contents and phase equilibria 80–29012
  MnZn ferrite, wall topography change induced by external press. 80–34734
  MnZn ferrite disc, excitation of radial mode vibration due to AC 79–69708
  MnZn ferrite fabricated by hot isostatic pressing, recording head appl. 80–35139
  MnZn ferrite fillers for elastic mag. materials, prep. and props. 79–52143
  MnZn ferrite particles, mag. filtration from air streams 77–4945
  MnZn ferrite powder prep., wet method 80–89180
  MnZn ferrite powders, reactive, mag. materials obtained by compaction 80–89182
  MnZn ferrite single cryst., Bridgman growth and appl. *(Chinese)* 79–33928
  MnZn ferrite single cryst., high temp. phase transform. characts., growth techniques *(Chinese)* 79–33927
  MnZn ferrite single crystals, growth by Bridgman technique, book contrib. 79–69977
  MnZn ferrites, abrasive wear investigation *(Japanese)* 78–39917
  MnZn ferrites, cationic distrib. and Curie temp. *(Russian)* 79–91232

ferrites continued
MnZn ferrites, doped; determ. of grain boundary composition, using Auger spectroscopy *(German)* 79—23618
MnZn ferrites, effect of In additives on electron-ionic struct. *(Ukrainian)* 79—52046
MnZn ferrites, elec. cond. mechanism in paramag. and ferrimag. phases 80—15524
MnZn ferrites, field depend. of mag. permeability accommodation *(Russian)* 79—69694
MnZn ferrites, hot pressed, mechanism of protective action of Zn0 coating *(Russian)* 79—15822
MnZn ferrites, impurity induced exaggerated grain growth 78—92222
MnZn ferrites, internal friction and ΔE effect depend. on demagnetisation method 80—80584
MnZn ferrites, mag. domains on worked surfaces 79—99722
MnZn ferrites, neutron diffr. exam. of influence of technology on mag. and cryst. parameters 79—42741
MnZn ferrites, phase equilibria, use in manufacture of spinel ferrites 79—11596
MnZn ferrites, post sinter-cooling rates effects 80—89369
MnZn ferrites, thin struct. of $K\beta_5$ and $L\alpha_{1,2}$ emission bands of Fe *(Ukrainian)* 79—78790
MnZn ferrites, Ti substituted, mag. permeab. meas., grain boundary comp. AES obs. 78—95473
MnZn ferrous ferrite, initial mag. permeability second-order magnetocrystalline anisotropy influence 80—88820
MnZn ferrous ferrites, mag. permeability stress depend. 80—88822
MnZn, form. of comp. heterogeneity during high-temp. sintering 80—60818
MnZn, gas phase fluorination for improved props. 78—52306
MnZn, initial mag. permeabilities under low temp. reactor irrad. 77—36093
MnZn, laser drilling and cutting, anal. of results using computer model 79—70180
MnZn low loss, highly stable, study *(Slovene)* 78—27055
MnZn, mag. permeability spectra, 0.001-100 MHz range *(Russian)* 77—8355
MnZn, natural, intrasite cation ordering and clustering 77—12259
MnZn, polished, worked layer magnetic characts. determ. by electron diffraction method *(Japanese)* 78—10742
MnZn, polydispersive spin relax. near Curie temp., mag. susceptibility meas. 77—69513
MnZn, pressing powder, spray dried, pressing behaviour and props. 80—11617
MnZn, props. rel. to raw materials *(German)* 77—21074
MnZn, weak mag. losses, microcalorimetric meas. 77—51926
MnZn-ferroferrites, sintered, microstruct., TEM study *(Dutch)* 80—2036
$Mn_{1.18}Zn_{0.06}Co_{0.01}Fe_{1.75}O_4$, transport props. near Curie points 78—88100
$Mn_{0.4}Zn_{0.42}Fe_{2.16}O_{4+x}$, permeability, rel. to intrinsic mag. props. 79—4702
$Mn_{0.510}Zn_{0.417}Fe_{2.073}O_{4+\delta}$ relationship between magnetic permeability and stoichiometry 79—42799
$Mn_{0.53}Zn_{0.35}Fe_{2.12}O_4$, and Ti substituted, acoustic losses 79—24207
$Mn_{0.7}Zn_{0.1}Fe_{2.2}O_4$, temp. depend. of microwave resistivity 79—69540
$(Mn_{0.7}Zn_{0.3})_xFe_yO_4$, electromag. props. rel. to Fe content 78—43613
$Mn_{1-x}Zn_xFe_2O_4$, noncollinear mag. structure, Mossbauer spectrum 77—69501
$Mn_{1-x}Zn_xFe_2O_4$, prepared by wet method, neutron diffr. and high field Mossbauer expts. 80—75719
$Na_{0.9}Ti_{1.1}Fe_{0.9}O_4$, short period β-alumina type cpds., cryst. struct. and superionic cond. 80—107499
$NdFeO_3$, mag. transition, NMR meas. 78—27036
$NdFeO_3$, magnetic struct., time of flight neutron diffr. method 77—8280
Ni ferrite, quenched, Neel temp. and initial susceptibility 80—75762
Ni ferrite with domain struct., FMR absorpt. line intensity and shape 77—90041
Ni ferrite-$BaTiO_3$, piezomagnetic-piezoelectric sintered two-phase composite, magnetoelec. conversion 77—12181
Ni, gas phase fluorination for improved props. 78—52306
Ni, internal friction and modulus defect at US freqs. 79—19762
Ni-Co-Zn ferrite, exam. of electromag. characteristics 79—1409
Ni-ferrite, ultrafine powder, prod. by cryochemical, freeze drying, spray drying or soln. techniques 80—55336
Ni-ferrite powders, form. in presence of Li_2SO_4-Na_2SO_4 molten salts, prep. and characts. 80—84869
Ni-Zn ferrite, elastic moduli temp. and composition depend. 78—26617
Ni-Zn ferrite, electrical cond., Seebeck coeff. and saturation magnetisation 77—20315
Ni-Zn ferrite, grain size depend. of grain boundary sliding *(Japanese)* 80—15120
Ni-Zn ferrite, high temp. behaviour of grain boundaries under bending stress *(Japanese)* 77—1875
Ni-Zn ferrite, neutron irrad., mag. spectra, domain wall behaviour 77—48006
Ni-Zn ferrite:Co^{2+}, synthesis of optimal quality recording head mat. 77—52272
Ni-Zn ferrites, comp., lattice imperfections, sintering 78—3080
Ni-Zn ferrites, hot-pressed, key props. 78—15348
Ni-Zn ferrites, mag. recording head props. rel. to manuf. from schoenite-type solid solns. 77—85496
Ni-Zn ferrites, polycrystalline, grain boundary slip *(Japanese)* 77—63764
Ni-Zn ferrites 600 NN and M450 NNI, Curie point radiative shift due to neutron irrad. *(Russian)* 80—39775
Ni-Zn-Co, synthesis from solid solns. of schoenite-type salts 80—93511
$NiAl_tFe_{2-t}O_4$, Kerr effect, magneto-optical refl. spectra 79—82954
$Ni_{1-x}Cd_xFe_2O_4$, mag. props. rel. to ionic struct. 80—75756
$Ni_{1-x}Cd_xFe_2O_4$, mag. thermal expansion anomaly 77—69595
NiCo ferrite, induced mag. anisotropy, hysteresis loops, Barkhausen effect *(Russian)* 78—64203
$Ni_{2-x}Co_xBaFe_{16}O_{27}$, ferromagnetic reson., anisotropy and g-factor, spin-orbit interactions 77—24749
$Ni_{0.5-x}Co_xZn_{0.5}Fe_2O_4$ ferrospinal solid solutions, cryst. lattice defects and props. 80—19796
$NiCr_xFe_{2-x}O_4$, magneto-otpical refl. spectra by equatorial Kerr effect *(Russian)* 77—32400
NiFe, prep. of single crystal by chem. transport with $TeCl_4$ 80—104051
$NiFe_{2-x}Al_xO_4$, ^{57}Fe and ^{61}Ni Mossbauer spectra 80—39940
$NiFe_{2-x}Al_xO_4$, cation distrib. calc. from equilib. conditions 78—22701

ferrites continued
$NiFe_{2-x}Al_xO_4$, stress-induced anisotropy in LPE grown single cryst. films, domain struct. 79—28238
$Ni_{0.51}{}^{2+}Fe_{0.46}{}^{2+}Fe_{1.95}{}^{3+}O_4{}^{2-}$, elec. resistivity above 300K 79—78099
$Ni_{0.89}{}^{2+}Fe_{0.13}{}^{2+}Fe_{2.11}{}^{3+}O_4{}^{2-}$, elec. resistivity above 300K 79—78099
$NiFe_{2-x}Mn_xO_4$, cell dimens. determ. 78—26526
$NiFeO_4$, induced ferrimagnetism, temp. depend. of sublattice magnetisation, Mossbauer study 77—66280
$NiFe_2O_4$, domain wall size and mag. losses in freq. spectra 77—85481
$NiFe_2O_4$, effect of sintering in air in range 1373-1773K on lattice parameter 79—19208
$NiFe_2O_4$, exchange integrals from magnetisation meas. 79—47273
$NiFe_2O_4$ ferrite, mag. props., neutron irrad. 80—103858
$NiFe_2O_4$ form. mechanism in mixture of metallic oxide powders 77—63609
$NiFe_2O_4$, hysteresis and other mag. props. rel. to microstruct., TEM investig. 77—20636
$NiFe_2O_4$, LPE growth, film quality, mag. meas. 78—11136
$NiFe_2O_4$, mag. anisotropy compensation under neutron irrad. 80—75807
$NiFe_2O_4$ mag. fluid particles, comp., struct., and mag. props. 80—60374
$NiFe_2O_4$, microstruct. and magnetic props., electron microscope obs. 79—87290
$NiFe_2O_4$ milled ferrite powder, substruct. and sinterability 80—84894
$NiFe_2O_4$, parametric excitation of spin waves in samples with regular domain struct. *(Russian)* 77—32183
$NiFe_2O_4$ precipitation process from silicate glass, ESR study, effective g value, transition temp. 80—25194
$NiFe_2O_4$, prep. by double decomp. reaction, mag. characts. *(French)* 79—33463
$NiFe_2O_4$, single cryst. prep. by chem. transport 78—23589
$NiFe_2O_4$, soft ferrite, squareness ratio and max. induction 79—99730
$NiFe_2O_4$, superexchange interactions, three-sublattice anal. 79—61095
$NiFe_2O_4$, thermally induced surface chemistry and struct., XPS 78—22939
$NiFe_2O_4$:Ir^{4+}, mag. anisotropy, single ion contrib., octahedral sites 77—4511
$NiFe_2O_4$-$BuTiO_3$, in situ composite growth, phase diag., melting relns. 77—21132
$NiFe_2O_4$-Fe_2O_3, effects of excess Fe_2O_3 on mag. props. 77—85495
$NiFe_2O_4+ZnO$, powders, cation mutual diffusion coeffs. calc. 77—15635
$Ni_{0.33}Fe_{2.33}O_4$, {001} ⟨110⟩ glide system, room temp. TEM obs. 79—90660
$Ni_{1-x}Fe_{2+x}O_4$, mag. anisotropy constant, contrib. of Fe^{2+} ion 79—33476
$Ni_xFe_{3-x-\Delta}O_4$, mag. aftereffects 79—56572
$Ni_xFe_{3-x}O_4$, DC and low freq. cond. and influence of microstruct. 80—70699
$Ni_xFe_{3-x}O_4$, magnetostriction, 80 to 300K, depend. on comp. and electron ordering on octahedral sites 80—65995
$Ni_xFe_{3-x}O_4$, solubility in high-temp. aqueous soln., appl. to PWR 78—4987
$Ni_xFe_{3-x}O_4$, spinels, fine particles, magnetic properties obs. 80—71031
$Ni_xFe_{3-x}O_4$, $x<1$, anomalous microwave loss 79—69540
NiO reaction with Fe_2O_3, ferrite formation, microstruct. obs. 79—87834
NiO:Fe, exchange anisotropy of Ni-ferrite precipitates 79—28520
NiO-CdO-Fe_2O_3 system, phase equilibria 79—11582
Ni_2Sc_2W, mag. order 77—63120
NiZn, exchange integrals, magnetisation data and mol. field theory 78—19241
NiZn ferrite, dielec. props., Jahn-Teller ion effects 80—97181
NiZn ferrite, effect of reactor radiation on mag. props. 77—32215
NiZn ferrite, mag. susceptibility freq. spectrum, effect of pressure 78—95420
NiZn ferrite, mag.-mechanical-microstruct. interactions 77—1578
NiZn ferrite, magnetic props., porosity and grain size effects 77—36095
NiZn ferrite, magnetic field effect on Rayleigh wave attenuation 78—6557
NiZn ferrite, wall topography change induced by external press. 80—34734
NiZn ferrite quarter wave type absorber 79—38386
NiZn ferrites, comp., X-ray diffr. and saturation magnetisation obs. 78—18617
NiZn ferrites, density and mag. props., isostatic pressure effect 80—60816
NiZn ferrites, internal friction and ΔE effect depend. on demagnetisation method 80—80584
NiZn ferrites, Mossbauer effect and IR spectra 78—64300
NiZn ferrites, nonstoichiometric, initial susceptibility and microstruct. 80—84591
NiZn ferrites, substituted ferrospinel, spin configuration determ. *(Russian)* 77—32162
NiZn ferrites, V_2O_5induced mag. aftereffects 80—60379
NiZn ferrites under high press., grain growth *(Chinese)* 78—52825
NiZn, formation by reaction of NiO-ZnO solid soln. with Fe_2O_3, mechanism and kinetics 80—3309
NiZn, laser drilling and cutting, anal. of results using computer model 79—70180
NiZn, magnetoelastic Villari effect 80—88847
NiZn, prep. of single crystal by chem. transport with $TeCl_4$ 80—104051
NiZn, ZrO_2 additions influence on sintering and physicochem. props. 80—108369
NiZnCo ferrite, excess Fe type, saturation magnetostriction meas., oxidation effects 79—82852
NiZnCo ferrite, model of photomagnetic effect 77—43853
NiZnCo ferrite, quantitative anal., using X-ray fluorescence 78—40090
NiZnCo ferrites, switching time and coeff., hydrostatic press. effect 80—88802
NiZnCo ferrites, temp. stability, effect of Fe content and processing conditions 79—28993
NiZnCo ferrites, voltage response under sinusoidal and pulse magnetisation effected by hydrostatic press. 80—88846
$Ni_{0.25}Zn_{0.75}Fe_2O_4$, Mossbauer study, spin fluctuations 80—60471
$Ni_{0.25}Zn_{0.75}Fe_2O_4$, Mossbauer study, noncollinear spin struct. 80—60472
$Ni_{0.25}Zn_{0.75}Fe_2O_4$, structural phase transition, X-ray and neutron diffr. study 80—79735
$Ni_{0.32}Zn_{0.68}Fe_2O_4$, mag. props. and neutron damage 77—47973
$Ni_{0.32}Zn_{0.68}Fe_2O_4$, microstructure and magnetic props., effects of silica content, sintering temp. and sintering time 79—87746
$Ni_{0.36}Zn_{0.64}Fe_2O_4$, normal grain growth 78—72796
$Ni_{0.38}Zn_{0.62}Fe_2O_4$, preparation, Mossbauer study 80—50231
$Ni_{0.4}Zn_{0.6}Fe_2O_4$, conditions for max. resistivity 77—21065
$(Ni_{0.47}Zn_{0.53})_{1-x}Fe_{2+x}O_4$, recording head medium 77—86187

ferrites continued

- $Ni_{0.5}Zn_{0.5}Fe_2O_4$ coarse grain polycryst. ferrite, diffusional creep *(Japanese)* 80−104238
- $Ni_{0.5}Zn_{0.5}Fe_2O_4$, Hall mobility, elec. cond. and carrier conc., 30 to 180°C 77−51765
- $Ni_{0.685}Zn_{0.177}Fe_{2.138}O_{4+\gamma}$, phase diagram, therm. anal. 79−78945
- $Ni_{0.71}Zn_{0.29}Fe_2O_4$ and $Ni_{0.57}Zn_{0.43}Fe_2O_4$, form. kinetics 79−83159
- $Ni_{0.8}Zn_{0.2}Fe_2O_4$, twisted tubular polycryst. sample in axial mag. field, circular magnetisation 77−32230
- $Ni_{0.85}Zn_{0.15}Fe_2O_4$, ferrite, mag. anisotropy compensation under neutron irrad. 80−75807
- $Ni_{1-x}Zn_xFe_2O_4$, LPE growth, film quality, mag. meas. 78−11136
- $Ni_{1-x}Zn_xFe_2O_4$, polycryst., domain wall energy rel. to anisotropy 80−71090
- $Ni_{1-x}Zn_xFe_2O_4$ spinel, low-temp. transitions and spin configurations, Mossbauer study 78−27144
- $Ni_{1-x}Zn_xFe_2O_4$, statistical model and phase transform. *(German)* 77−85473
- $(Ni_xZn_{1-x})_{0.5}Fe_2O_4$, spontaneous vibr. modes excited by reversible magnetostriction 79−56587
- $Ni_xZn_{1-x}Fe_2O_4$, catalytic oxidation of CO, mag. props., kinetic parameters and composition depend. 80−16723
- $Ni_xZn_{1-x}Fe_2O_4$, crystal growth from BaO-B_2O_3-ZnO-NiO-Fe_2O_3 melt, exam. of crystal props. 80−40249
- $Ni_{1-x}Zn_xO$ reaction with Fe_2O_3, ferrite formation, microstruct. obs. 79−87834
- $PbFe_{12-x}Ga_xO_{19}$ ferrite, single cryst., ferromag. reson. 80−50193
- $PbFe_{12}O_{19}$, bubble and stripe lattice domain wall oscills. 80−97115
- $PbFe_{12}O_{19}$ hexagonal ferrite amorphous films for mag. bubble memories, materials review *(Polish)* 80−34715
- $PbFe_{12}O_{19}$, single crystal, Mossbauer spectra 80−84670
- $PrFeO_3$, magnetic struct., time of flight neutron diffr. method 77−8280
- $PrFeO_3$, thermodynamic study of form. 78−48685
- $RFeO_3$ amorphous films for mag. bubble memories, materials review *(Polish)* 80−34715
- $SmFeO_3$, HF susceptibility, crit. divergence in spin reorientation temp. region *(Japanese)* 77−43836
- $SmFeO_3$, magnetisation direction angle meas. in spin reorientation region 77−26366
- $SmFeO_3$, magnetostriction meas. in spin reorientation region 78−2721
- $SmFeO_3$, orthoferrite, anisotropy of Faraday rotation 79−61341
- $Sm_{0.05}Tb_{0.45}FeO_3$, singularities of domain struct. in spin-flip region 78−19272
- $Sm_{0.55}Tb_{0.45}FeO_3$, orthoferrite cryst., domain memory effect *(Russian)* 77−55693
- $Sm_{0.55}Tb_{0.45}FeO_3$ orthoferrite, optical and magneto-optical props. 79−61396
- $Sm_xTb_{1-x}FeO_3$, gyrotropic props. and birefringence, in spin reorientation range 80−7324
- $Sm_xTb_{1-x}FeO_3$, mag. reorientation, temp. *(Russian)* 79−87263
- $Sm_xTb_{1-x}FeO_3$ orthoferrites, crystallo-optical props. 79−42027
- $Sm_xTb_{1-x}FeO_3$, rotation of polarisation plane, ang. depend. 77−43961
- Sr ferrite crystals, etch pitting, of hard magnetic ferrite crystals *(German)* 78−26568
- Sr, plastic magnet appl., anisotropic, based on moulding ferromagnetic powder material with plastics *(Japanese)* 80−60829
- $(Sr/Ba)(Fe/Al/Ga)_{12}O_{19}$ solid soln. crystal for hexaferrite layer substrate *(German)* 78−23672
- $SrEu_2Fe_2O_7$, ferrite, Mossbauer effect study of hyperfine interactions, spin reorientation 78−19383
- $Sr(Fe_{7.2}Al_{4.8})O_{19}$, minute single crystal domain struct. 77−20646
- $Sr(Fe_xAl_{12-x})O_{19}$, cryst. domain wall energy density determ. 77−1567
- $SrFe_{12-x}Cr_xO_{19}$, effects of substitution of Fe by Cr, Mossbauer spectra 80−2674
- $SrFe_{12-x}Cr_xO_{19}$, hexagonal ferrite series, Mossbauer study 80−71258
- $SrFe_6Ga_6O_{19}$ ferrite, mag. struct., Mossbauer study 80−93087
- $SrFe_{12}O_{19}$ and $Sr_4Fe_6O_{13}$, Mossbauer spectra 80−15882
- $SrFe_{12}O_{19}$, Ca^{2+} additives effect on hexaferrite lattice and mag. props. 80−60243
- $SrFe_{12}O_{19}$ ceramic compact, sublattice magnetisation and textures 78−68426
- $SrFe_{12}O_{19}$, exam. of factors affecting reaction kinetics, thermal analysis *(German)* 79−24471
- $SrFe_{12}O_{19}$, ferrite, powder effect of SiO_2 during sintering, exam. of grain growth and phase diagram *(German)* 79−24473
- $SrFe_{12}O_{19}$, formation from α-Fe_2O_3 and $SrCO_3$ 77−8786
- $SrFe_{12}O_{19}$, hysteresis loops, formation processes 80−39813
- $SrFe_{12}O_{19}$, M type hexaferrite, Fe ion dynamic characts. in bipyramidal position, nucl. γ reson. 79−95697
- $SrFe_{12}O_{19}$, mag. props., effect of Sr dissolution by milling in water 77−25000
- $SrFe_{12}O_{19}$ micropowder, high coercivity, obtained by extended wet milling, prep. and mag. props. 77−8776
- $SrFe_{12}O_{19}$, microstruct. and magnetic props., electron microscope obs. 79−87290
- $SrFe_{12}O_{19}$, powder, chemical plating with Co, Co-P, Ni-P and Cu 80−25593
- $SrFe_{12}O_{19}$, prep. by fluidized bed technique, ceramic and magnetic props. 79−43445
- $SrFe_{12}O_{19}$:Si, Sr, second phase effect on elec. and mag. props. 80−60986
- $Sr_6Fe_{10}O_{22}$-Fe_2O_3-$ZnFe_2O_4$ system, phase relations at 1100°C 78−68676
- $Sr_7Fe_{10}O_{22}$, mag. props. and spin order 78−52232
- SrO-Fe_2O_3 system, non-existence of single phase $SrFe_2O_4$, Mossbauer expts. 80−29178
- SrO-SiO_2-Fe_2O_3, permanent mag. ceramics, exam. of phase diagram, using X-ray analysis, optical microscopy, electron probe anal., and thermal analysis *(German)* 79−29012
- $SrO.6Fe_2O_3$, ultrafine, microstruct. development during sintering, mag. props. 79−70022
- $SrO.nFe_2O_3$ isotropic ferrite magnets, manuf. process and mag. props. *(Japanese)* 80−29915
- $SrR_2Fe_2O_7$, (R=Pr,Nd,Sm,Eu,Gd or Tb), Mossbauer exam. of mag. struct. 77−40157
- $SrR_2Fe_2O_7$ series, mag. struct. and spin reorientation, neutron diffr. and Mossbauer meas. 77−69503
- $SrTb_2Fe_2O_7$, ferrite, Mossbauer effect study of hyperfine interactions, spin reorientation 78−19383
- $Sr_xZn_2Y(Y=Ba_{2-x}Fe_{12}O_{22})$, x=0, 1, 1.6, mag. moments reorientation 80−44851
- $TbFeO_3$, mag. phase transitions, Van Vleck interaction and R-Fe exchange *(Russian)* 79−61105

ferrites continued

- $TbFeO_3$, mag. susceptibility, temp. depend., effective field at Tb ion sites 80−75742
- $TbFeO_3$, metamag. phase transitions, mag. struct. instability *(Russian)* 79−61107
- $TbFeO_3$, ortho-ferrite, electron spin relax. time temp. depend. 77−90026
- $TbFeO_3$ static effective mag. field acting on ^{160}Dy nucleus 77−90074
- $TbFeO_3$, thermodynamic props. 77−36078
- TbIG, mag. linear double refr., two-sublattice model *(Russian)* 79−28728
- TbY ferrite garnet, Tb^{3+} energy level inversion, Faraday effect *(Russian)* 79−47418
- $Tb_xY_{3-x}Fe_5O_{12}$, spin-reorientation phase transitions, neutron depolarisation factor 78−27037
- Ti, magnetisation effect on channelling and blocking of proton beam 77−69022
- TiO_2-Fe_2O_3-CaO-V_2O_5 system ferrites, TiO_2 content and thermomag. effects on dielec. props. 77−43927
- $Tm_{2.7}Bi_{0.3}Ga_{0.3}Co_xFe_{4.7-x}O_{12}$, Co ion concentration effect on mag. props. close to mag. compensation point *(Russian)* 79−73788
- $TmFeO_3$, acoustic vel. and attenuation shifts at spin reorientation phase transition 80−65986
- $TmFeO_3$, domain struct. in spin reorientation region, Faraday effect obs. 77−20835
- $TmFeO_3$, magnetoelastic props. at spin reorientation region 77−8382
- $TmFeO_3$, orthoferrite, vel. of planar domain wall 78−72363
- $TmFeO_3$, parameters of interaction between rare earth and Fe ions, theory and expt. 79−73705
- $TmFeO_3$, temp. depend. of neutron depolarisation factor meas. near spin reorientation transition 77−16053
- $(Y,Gd,Yb)_{3-x}Bi_x(Fe,Al)_5O_{12}$, LPE, for magneto-optical appls. 78−48341
- $(Y,Sm,Ca)_3(Fe,Ge,Si)_5O_{12}$ single-crystal films, props. 78−64247
- Y ferrite-garnet, porous polycrystal, law of approach to saturation *(Russian)* 78−47956
- Y orthoferrite, magneto-optical controlled transparencies, page composers 78−50932
- $Y_{3-x}Bi_xFe_5O_{12}$, ferrite-garnet formation 78−52737
- $(Y_{3-x}Ca_x)[Fe_{2-x}Sn_x](Fe_3)O_{12}$, Mossbauer spectra of Fe^{27} and Sn^{119} nuclei 79−95578
- $(YEuTm)_3(GaFe_5)O_{12}$ ferrite garnet films, mag. bubbles, translational motion, mechanism for inertial effects 80−100606
- $YFe_{1-x}Co_xO_3$, reorientation transitions, neutron diffr., mag. behaviour *(Russian)* 77−24678
- $YFe_{1-x}Co_{x/2}Ti_{x/2}O_3$, anomalous decrease of spontaneous magnetisation in spin reorientation region 77−36059
- $YFe_{1-x}Co_{x/2}Ti_{x/2}O_3$, magnetostriction meas. in spin reorientation region 78−2721
- $YFe_{1-x}Co_{x/2}Ti_{x/2}O_3$, orthoferrite, anisotropy of Faraday rotation 79−61341
- $YFe_{0.62}Cr_{0.38}O_3$, compensation of weakly ferrimag. moment 79−8035
- $YFe_{1-x}Cr_\alpha O_3$, reorientational transitions, mag. and neutron diffr. exam. 77−12097
- $YFe_{1-x}Cr_xO_3$, weak ferrimagnet, anomalous mag. props. explained by exchange interactions *(Russian)* 77−69538
- $YFe_{1-x}Ga_xO_3$, zone refined, exam. of Curie point and magnetisation 79−4673
- $Y_3Fe_{5-x}Ga_xO_{12}$, inhomogeneous stress effect on ferromagnetic resonance 79−24219
- $YFe_{1-x}Mn_xO_3$ orthoferrite, spin reorientation, mag. torque meas. 78−47979
- $YFeO_3$, Bloch, Neel and head to head domain wall mobilities 77−1562
- $YFeO_3$, Bloch, Neel and head to head wall vels. 78−68287
- $YFeO_3$, bubble domain struct. temp. depend. 77−69647
- $YFeO_3$, Co^{2+} substituted, reorientational transitions 77−59419
- $YFeO_3$, domain boundary inertia during mag. reversals *(Russian)* 80−88776
- $YFeO_3$, domain wall motion, magnetoelastic coupling 79−78435
- $YFeO_3$, domain walls vel. *(Russian)* 79−28553
- $YFeO_3$, Faraday rotation anisotropy 77−20837
- $YFeO_3$, hydrothermal synthesis, mag. struct. 77−47972
- $YFeO_3$, induced spin reorientation near Neel point 78−19267
- $YFeO_3$, influence of mag. field on Faraday effect 78−27196
- $YFeO_3$, mag. anisotropy in cryst. field approx. 80−60241
- $YFeO_3$, mag. bubble stray field distrib. meas. using micro Hall element 77−40097
- $YFeO_3$, mag. domain walls, photomagnetic effects, ^{57}Fe NMR obs. 78−95464
- $YFeO_3$ monocrystalline, mag. field depend. of magnetic domain *(Korean)* 78−68337
- $YFeO_3$, orthoferrite, vel. of planar domain wall 78−72363
- $YFeO_3$, orthoferrite, domain boundary vel. exceeding limiting vel. *(Russian)* 79−24192
- $YFeO_3$ orthoferrite, weak ferromagnet domain struct. near Neel temp. 79−99739
- $YFeO_3$, orthoferrite, crit. domain wall vel. 80−71135
- $YFeO_3$ photoanode for photoelectrolysis of water 77−81409
- $YFeO_3$ plate, anisotropy of domain wall velocity, magneto-optical obs. 79−99725
- $YFeO_3$ platelets, domain wall mobility, dynamic coercivity 78−91884
- $YFeO_3$, skew bubble domains, stripe domains 77−89999
- $YFeO_3$, solubility in aq. KOH under hydrothermal conditions 77−39677
- $YFeO_3$, spin-wave damping of domain walls 79−42795
- $YFeO_3$, thermodynamic study of form. 78−48685
- $YFeO_3$, thermomag. recording in surface layer of orthoferrite 79−24165
- $YFeO_3$, transit time meas. of domain-wall mobilities, magnetostatic and magnetoacoustic effects 79−42794
- $YFeO_3$, weak ferromagnet, domain wall motion and velocity *(Russian)* 80−54917
- $YFeO_3$, weak-ferromagnet, domain boundary dynamics *(Russian)* 79−73768
- $YFeO_3$:Co, NMR of ^{57}Fe, spin echo 78−91987
- $YFeO_3$:Co^{2+}, Ti^{4+}, spin reorientation, Faraday rot. meas. 77−8547
- $YFeO_3$:Co^{2+}, weak ferromagnetism, single ion anisotropy contrib. 80−25126
- $Y_3Fe_5O_{12}$, formation mechanism from metallic oxides 77−48376
- $Y_3Fe_5O_{12}$, growth rel. to physicochem. investig. of $Y(OH)_3$-α-$FeOOH$ system 77−40418
- $Y_3Fe_{5-x}Sc_xO_{12}$, local spin struct., Mossbauer obs. 77−32305
- $Y_3GaFe_4O_{12}$, mag. props. meas. in high mag. fields, review *(Japanese)* 78−52303

ferrites continued
$(YGdTm)_3(FeGa)_5O_{12}$ epitaxial film, formation of lattice of cylindrical mag. domains from stripe domains *(Russian)* 80—80579
$Y_{0.9}Gd_{1.1}Yb_{0.7}Bi_{0.3}Al_{0.9}Ga_{0.2}Fe_{3.9}O_{12}$ films, cylindrical mag. domain form. *(Russian)* 77—40098
$(YGdYbBi)_3(FeAl)_5O_{12}$ ferrite-garnet films, effect of in-plane field on dynamics of domain walls 80—65979
YIG, light diffr. by banded domain struct. *(Russian)* 78—15150
YIG, mag. linear double refr., two-sublattice model *(Russian)* 79—28728
YIG, relax. after spin wave excitation in ferrite *(Russian)* 79—19783
YIG, single cryst., high temp. dislocation mobility 79—19255
YIG, spin wave instability, parametrically excited spin waves distribs. *(Russian)* 79—38317
YIG, substituted, effect of electron bombardment on mag. and elec. props. 79—42103
YIG, thermodynamic props. 77—36078
YIG-Ge layered struct., anisotropy of EMF under nonlinear ferromag. reson. conditions 77—8417
Y_2O_3-Fe_2O_3 systems, solid-phase reacts., $Y_3Fe_5O_{12}$ form. 78—44062
$YbFeO_3$:Co, mag. struct. factors, neutron diffr. study 79—47248
Zn ferrite, production by mechanochemical reactions by grinding in ball mill 79—20014
$Zn_2BaFe_{12}O_{22}$, mag. phase transitions, magnetostriction temp. depend. *(Russian)* 78—34983
$Zn_2Ba_2Fe_{12}O_{22}$, phase transition, mag. props. *(Russian)* 79—51837
$Zn_xCn_{0.1}Fe_{2.9}O_4$, Cu, Zn substituted magnetite, domain wall resonance, mag. props. 80—15756
$ZnCrFeO_4$, ferrite spinel, unsupported and SiO_2 supported, structural and catalytic studies 80—44191
$ZnCr_xFe_{2-x}O_4$, Mossbauer spectra, quadrupole splitting, Debye temp. 80—93218
$Zn_xCu_{0.1}Fe_{2.9-x}O_4$, ferromag. relax. 80—60422
$Zn_xCu_{0.1}Fe_{2.9-x}O_4$, ferromag. reson., g-factors, Jahn-Teller ion effects 80—66043
$Zn_xCu_{1-x}Fe_2O_4$, mag. props., Mossbauer spectra 79—87344
$Zn_xFe_yMn_zFe_2O_4$, ferrite, production from Fe_2O_3, effect of impurities on props. *(German)* 79—4925
$ZnFeO_4$, ferrite spinel, structural and catalytic studies 80—44191
$ZnFe_2O_4$, cation distrib., preference energy determ. by neutron irrad. method 77—15384
$ZnFe_2O_4$, duplex struct. formation during sintering, grain growth study 79—11541
$ZnFe_2O_4$, heat capacity investigation of dopant effects on mag. disordering temp. 80—25143
$ZnFe_2O_4$, LPE growth, film quality, mag. meas. 78—11136
$ZnFe_2O_4$, neutron damage effects, superparamag. state replacement cascades 77—16051
$ZnFe_2O_4$, single cryst. prep. by chemical transport 77—16482
$ZnFe_2O_4+NiO_2(MgO)$ powders, cation mutual diffusion coeffs. calc. 77—15635
$Zn_xFe_{3-x}O_4$, collective electron states, ^{57}Fe Mossbauer meas. 77—69748
$Zn_xFe_{3-x}O_4$ ferrite, mag. struct., Mossbauer spectra and magnetisation study, 4.2K 80—103818
$Zn_xFe_{3-x}O_4$, ferromag. reson., g-factors, Jahn-Teller ion effects 80—66043
$Zn_xFe_{3-x}O_4$, mag. ordering and domain wall relax. 77—8336
$Zn_xFe_{3-x}O_4$, Mossbauer exam. of relax. phenomena 77—8479
$Zn_xFe_yO_4$, heat capacity investigation of dopant effects on mag. disordering temp. 80—25143
$Zn_cM_{1-c}Fe_2O_4$, $M=Ni^{2+}$, Co^{2+}, Fe^{2+}, $Zn_cMFe_{2-c}O_{4-c}F_c$, $M=Ni^{2+}$, Co^{2+}, calc. of saturation magnetisation by cluster components 77—43817
ZnMn ferrites, prepared by wet chemical and ceramic methods, comparison of struct. and mag. props. *(German)* 79—24470
$Zn_{0.8}Mn_{0.2}Fe_2O_4$, spin interaction, neutron diffr. and Mossbauer effect meas. 77—4501
$Zn_xMn_{1-x}Fe_2O_4$, Mossbauer spectra exam. 77—40155
$Zn_xMn_{1-x}Fe_2O_4$, substitution effect on mag. struct. and exchange interaction *(Russian)* 78—47949
$Zn_{0.3}{}^{2+}Mn_{0.7}{}^{2+}Mn_y{}^{3+}Fe_{2-y}{}^{3+}O_4$, Mossbauer hyperfine field meas. 77—81033
$Zn_{0.7}Ni_{0.3}Fe_2O_4$ film, epitaxial deposition, comp. and mag. prop. obs. using Mossbauer effect 79—38748
$Zn_{0.75}Ni_{0.25}Fe_2O_4$, mixed ferrite-spinel, helicoidal struct. 79—47242
$Zn_{1-x}Ni_xFe_2O_4$, heat treatment and sintering effect on porosity 80—25610
$Zn_xNi_{1-x}Fe_2O_4$, magnetic props. rel. to localised canting model 77—32161
$Zn_xNi_{1-x}Fe_2O_4$, Mossbauer spectra, mag. hyperfine struct. 80—15877
ZnO reaction with Fe_2O_3, ferrite formation, microstruct. obs. 79—87834
ZnTi ferrites, electron exchange between Fe^{2+} and Fe^{3+}, paramag., Mossbauer spectra and susceptibility meas. 77—63327
Zn_2Y, magnetostatic volume waves, magnetocrystalline anisotropy effects, group delay 79—78355

ferroacoustic resonance
conducting ferromagnets, magnon spectra and magnetoacoustic reson. singularities *(Russian)* 80—50154
Ni, electromagnetically excited acoustic waves at low temp. 77—77081

ferroelasticity
see also shape memory effects
alkali metal double molybdates, $M^IM^{III}(MoO_4)_2$, $M^{III}=Al,Sc,Fe,In$, struct. transitions phenomenological approach 78—51674
alkali metal double tungstates, $M^IM^{III}(WO_4)_2$, $M^{III}=Sc,In$, struct. transitions, phenomenological approach 78—51674
aniline hydrobromide, ferroelastic, acoustic softening near transition temp. 80—96617
aniline hydrobromide, ferroelastic phase transition, Raman scatt. study 80—108195
aniline-HBr, ferroelasticity, orthorhombic to monoclinic phase transition, X-ray scatt. 80—39276
benzil, phase transition study be simultaneous Raman-scatt. and domain-struct. investigations 79—60504
boracites, spontaneous birefr., meas. and appl., ferroelectric/ferroelastic phases 79—15434
Brillouin scattering spectroscopy, dynamical aspects 80—55115
commensurate ferroic, elucidation with model of 'situations' and 'oriates' 78—26651
conference, Leningrad, USSR (1977) 79—15406
crystalline phase transitions, symmetry determined phenomena 79—46800

ferroelasticity continued
defect structure near phase transition pt., effect on solid props. *(Russian)* 79—37838
dicalcium strontium propionate, ferroelasticity and opt. activity rel. to transition 78—76420
dicalcium strontium propionate, ferroelasticity and optical activity rel. to transition 77—76547
dislocation-phonon interactions, phase transition effects in proper ferroelastic 80—59600
domain well, roughening transition suppression by long range elastic forces 80—75991
electronic micropositioning with ferroelastic-ferroelectrics 79—17392
ferrodistortive spin-phonon systems, crit. props. 80—88315
ferroelectric-elastic phase transition, modelling, appl. to KH_2PO_4 and $LiNH_4C_4H_4O_6.2H_2O$ *(Russian)* 80—75961
ferroic crystals, prototypic point group, physical props., model 80—80715
ferroic phase, second-order transition between prototypic and commensurate, thermal behaviour of soft modes 77—85662
ferroic phase transitions, non-mag., unified classification 80—70387
ferroics, nonmagnetic secondary and higher-order, order-parameter symmetries for the phase transitions 77—85668
ferroics, secondary, polycryst., poling effects 77—16102
gyrotropic phase transitions 78—71852
gyrotropy, an implicity form of ferroicity 79—73286
incommensurate twin plane *(Japanese)* 80—29034
isopropyl ammonium chloroplatinate and chlorostannate, ferroelastic transition, thermal, optical, and elastic meas. 79—28096
lithium ammonium tartrate, ferroelectric and ferroelastic transitions, Brillouin scatt. meas. 79—33716
lithium ammonium tartrate, piezoelec., proper ferroelastic transition 78—2812
lithium ammonium tartrate monohydrate, in paraelec. phase, Brillouin scatt. 78—64373
lithium ammonium tartrate monohydrate, spontaneous shear strain, X-ray obs. 78—56433
lithium ammonium tartrate monohydrate, struct. phase transitions, light scatt. meas. 79—95774
macroscopic quadrupole effects as method of obs. of struct. transforms in crysts. 80—71321
memory alloy, pseudoelastic, model for first-order phase transition 80—92642
nonideal ferroelastic crystals, domain struct. 78—2191
phase transitions, ferroelectric and structural refractive indices and electro-optics 79—19850
piezoelectric semiconductor, dissipative, amplification of spin waves 79—24000
polymorphic transition region, mech. hysteresis 80—79942
prototype and prototypic phase explained 78—38833
prototype temperature setting rel. to soft modes 78—63833
α- quartz, ferrobielastic hysteresis 80—19869
quartz, ferroelastoelectricity, expt. 80—40078
quartz ferrobielastic twinning coercive stress obs. 78—59854
rare earth molybdates, cryst. growth, cryst. chem., and phys. props., book contrib. 80—44194
Rochelle salt, phase transition mechanisms by optical spectroscopy, elastic moduli 79—15411
Rochelle salt, phase transitions, free energy in symm. group representation of parent phase 79—69790
Sapriel's W′-wall, struct. determ. 80—34866
second-order transitions, cryst. unit cell modification, group theoretical anal. 79—37830
squaric acid, ferroelasticity, elastic hysteresis loop and domain struct. 79—55814
structural phase transition induced refractive index changes in crysts. 80—16000
tanane, crit. behaviour near ferroelec.-ferroelastic transition 78—52459
Tanane, ferroelec. ferroelastic transition, X-ray and optical expts. 78—15110
tetramethylammonium tetrachlorocuprate crystal, incommensurate-ferroelastic (commensurate) phase transition obs. 80—75352
tetramethylammonium zinc tetrachloride, ^{13}C NMR and PMR study of incommensurate phase transition 80—34863
transitions, order parameter symm., free energy expansions 80—49164
tris-sarcosine calcium chloride:Mn^{2+} ferroelec. dynamics, EPR and ENDOR study 80—75972
tris-sarcosine calcium chloride, ferroelec., ferroelasticity and hypothetical hexagonal to orthorhombic phase transition 77—63377
trisarcosine calcium chloride crystals, ferroelec., electrooptic and ferroelastic props. 80—34865
TSCC ferroelastic monodomain crysts., dielec. behaviour 79—42888
TTF-TCNQ powder, phase transition at 49K 77—89539
$Ba_2AgNb_5O_{15}$, $Ba_2AgTa_5O_{15}$, ferroelec. and ferroelastic props. *(French)* 79—24266
$BaCl_2.2H_2O$, cryst. struct. determ. by neutron diffr. 78—75639
$BaCl_2.2H_2O$, ferroelastic effect obs. 79—28033
$Ba_2NaNb_5O_{15}$, ferroelastic transition sequence, cooperative pseudo-Jahn-Teller model 77—35689
$Ba_2NaNb_5O_{15}$, high-pressure phase transitions, ferroelastic phase 79—7687
$Ba_2NaNb_5O_{15}$, incommensurate refls. near ferroelastic transition, neutron and X-ray precession obs. 80—70395
$Ba_2NaNb_5O_{15}$, low temp. ferroelectric transitions, birefr. and dielec. meas. 79—38499
$Ba_2NaNb_5O_{15}$, phase transition at high press., Raman scatt. obs. 79—55884
$Ba_2NaNb_5O_{15}$, transition with increasing symm. on cooling 77—16265
$BaTiO_3$, effect of phase transformation on fracture behaviour 78—48507
$BaTiO_3$ family, unified phenomenological theory, spherical system of transition parameters 77—31751
$BaTiO_3$, ferroic materials, fracture processes 80—79869
Bi_3GeVO_9, dielec. props. and twin struct. 77—12350
$BiVO_4$, cryst. growth and struct. 80—35078
$BiVO_4$, ferroelastic, observation of soft optical phonon 78—2856
$BiVO_4$, ferroelastic domains, electron microscopy and electron diffr. obs. 80—100254
$BiVO_4$, ferroelastic phase transition, thermodynamic theory 79—37832
$BiVO_4$, ferroelastic phase transition, birefringence meas. using rotating-analyser method 80—80742
$BiVO_4$, ferroelastic phase transition, birefringence meas. at simultaneous high pressure and temp. 80—80743
$BiVO_4$, ferroelastic transition, soft optical phonon mechanism 79—51230

ferroelasticity continued
$BiVO_4$, linear coupling between soft optical and ferroelastic acoustic modes 78—79716
$BiVO_4$, struct. and ferroelastic phase transition 80—29004
Cs_2CrO_4, effects on domain struct., new ferroelastic revealed 78—18702
CsH_2PO_4, domain obs. in paraelectric phase 79—24277
$Cs_2NaM^{3+}Cl_6$ (M^{3+}=Bi,Nd,Pr), ferroelastic phase transitions, thermal expansion, elasticity, and X-ray anal. 80—70393
$Cs_2NaM^{3+}Cl_6$, (M=Bi,Nd,Pr), struct. transitions, polarisation optical expts. 79—99318
$Cu_3B_7O_{13}Cl(Br)$, piezoelectric, elastic and electromechanical coefficients *(French)* 78—39504
$DyVO_4$ Jahn-Teller crystal, deform. induced transitions, elastic and dielectric characts. *(Russian)* 80—80726
$ErNbO_4$, ^{93}Nb NQR spectra, 77 to 450K 79—38401
$Fe_2(MoO_4)_3$, cryst. struct. and twinning behaviour 80—33967
β-$Gd_2(MoO_4)_3$, antiferromag., polarised ferroelec., ferroelastic, magnetothermodynamics 79—7996
$Gd_2(MoO_4)_3$, antiphase boundaries and phase transforms., electron microscope obs. 78—15134
$Gd_2(MoO_4)_3$, electron microscope exam. of ferroelec. and ferroelastic props., domain walls and cryst. defects 77—69786
$Gd_2(MoO_4)_3$, ferroelastic, laser-induced twinning 77—76422
$Gd_2(MoO_4)_3$, ferroelec. and ferroelastic, electron microscopic study 77—85675
$Gd_2(MoO_4)_3$, ferroelec. ferroelastic, domain wall motion, crit. field var. 77—81075
$Gd_2(MoO_4)_3$, ferroelec.-ferroelastic, photolum. and photocond. meas. 80—84768
$Gd_2(MoO_4)_3$, piezoelectric and electrostriction coeffs. near ferroelastic transition *(French)* 77—40182
$Gd_2(MoO_4)_3$, variable frequency SAW resonator on ferroelectric-ferroelastics 78—33977
H_3BO_3, ferroelastic state shift and domain wall angle 78—43063
Hg_2Br_2, ferroelastic, Brillouin and Raman scatt. spectra 79—95770
Hg_2Br_2, ferroelastic phase, softening of acoustic and optical modes 79—33064
Hg_2Br_2, improper ferroelastic, soft mode props. in Raman spectra 77—36246
Hg_2Br_2, nonintrinsic ferroelastic, thermal expansion and thermodynamic potential 80—88344
Hg_2Cl_2, ferroelastic transition, refr. index, 80 to 300K 79—82941
Hg_2Cl_2, improper ferroelastic, soft mode props. in Raman spectra 77—36246
Hg_2Cl_2, neutron and Raman scatt. studies, ferroelastic transitions 80—76015
Hg_2Cl_2 prototype phase, soft mode, inelastic neutron scattering, Raman effect 78—91411
Hg_2Cl_2 single crysts., IR refl. spectra and ferroelasticity 79—99889
Hg_2Cl_2, sp. ht., 100-273K 77—59064
Hg_2Cl_2, thermal expansion and ferroelastic $D^{17}{}_{4h}\rightarrow D^{17}{}_{2h}$ transition 79—99337
$K_2Ba(NO_2)_2$, elastic props. 80—96588
$K_2Ba(NO_2)_4$, ferroelastic, Raman spectra and phase transition 79—56800
$K_2Ba(NO_2)_4$, new ferroelastic, phase transitions, optical and electrical props. 79—55887
KCN, dipolar impurity tunnelling model, elastic interaction and const. 78—71826
KCN, optical F centres and phase transitions 78—56504
$KCN:HCN^-$, structural props. using ESR 80—25205
KCN-KCl mixed system, order-disorder transition, dielec. props. meas. 78—15112
KCN-KCl mixed system, order-disorder transition, Raman spectra obs. 78—15113
KCN_x-KCl_{1-x}, finite-freq. local field catastrophe with appl. to spectra 79—51491
$K_2Cd_2(SO_4)_3$, ferroelastic phase transition, X-ray diffr. and dielec. temp. depend. meas. 79—55882
$K_2Cd_2(SO_4)_3$, melt growth and ferroelastic transition, and K_2SO_4-$CdSO_4$ phase diagram 78—31335
$K_2Cd_2(SO_4)_3$, piezoelec. langbeinite-type, cryst. struct. and ferroelastic transform. 78—6036
$K_2Cd_2(SO_4)_3$, piezoelectric, cryst. struct., near ferroelastic transition 78—42984
$KCl_{1-x}CN_x$, dipolar impurity tunnelling model, elastic interaction and const. 78—71826
K_2CrO_4, effects on domain struct., new ferroelastic revealed 78—18702
$K(D_xH_{1-x})(SeO_3)_2$, anelastic and elastic infra-low freq. props. 80—70304
$KD_3(SeO_3)_2$, ferroelastic transition, EPR 80—7148
$KD_3(SeO_3)_2$, optical and dielec. props. near ferroelastic phase transition 79—38518
$KD_3(SeO_3)_2$, phase transition, neutron scatt. study 80—75351
$K_{0.5}Eu_{0.5}Nb_2O_6$, ^{93}Nb NQR spectra, 77 to 450K 79—38401
$KFe(MoO_4)_2$, ferroelastic domain struct. *(Russian)* 79—90719
$KFe(MoO_4)_2$, phase transitions at 312 and 139K 80—70396
KH_2PO_4, appl. of γ-ray diffractometry to twinned crystals study 79—68987
KH_2PO_4, differential γ-ray diffractometry, exam. of ferroelectric-ferroelastic cryst. in cyclic fields 79—38511
KH_2PO_4, dislocation strain decoration and static central peak 79—99263
KH_2PO_4, ferroelastic cryst., appl. of γ-ray diffractometry 77—8533
KH_2PO_4, ferroelectric-ferroelastic phase transition, γ-ray diffr. 78—43819
$KH_3(SeO_3)_2$, acoustic phonon softening, US vel. meas. 78—14429
$KH_3(SeO_3)_2$ and $KD_3(SeO_3)_2$, ferroelastic phase transition, mech. stress effect 80—70394
$KH_3(SeO_3)_2$, dislocation strain decoration and static central peak 79—99263
$KH_3(SeO_3)_2$, ferroelastic transition under uniaxial press., EPR study 80—59562
$KH_3(SeO_3)_2$, $KD_3(SeO_3)_2$, second-order ferroelastic phase transitions, piezo-opt. props. obs. 78—95558
$KH_3(SeO_3)_2$, lattice consts. and thermal expansion tensors, X-ray diffr. meas. 79—37856
$KH_3(SeO_3)_2$, low-frequency elastic props., −190 to 50°C 79—37759
$KH_3(SeO_3)_2$, optical and dielec. props. near ferroelastic phase transition 79—38518
$KH_3(SeO_3)_2$, phase transition, acoustic phonon softening 77—27997
$KH_3(SeO_3)_2$, proton NMR study about paraelastic-ferroelastic transition 78—23363

ferroelasticity continued
$KH_3(SeO_3)_2$, slightly deuterated, central peak obs. in Brillouin spectra 78—64374
$KH_3(SeO_3)_2:Cr^{3+}$, EPR, ferroelectric phase transition 79—65716
$KH_3(SeO_3)_2:Cr^{3+}$, ferroelastic material, EPR, 77-300K 78—60331
$KIn(WO_4)_2$, ferroelastic domain struct. *(Russian)* 79—90719
$K_2Pt(CN)_4Br_{0.3}.3H_2O$, specific heat and ferroelastic behaviour 78—91447
K_2SO_4, ferroelastic props. 78—2251
$KSc(MoO_4)_2$, quadrupole interaction const., influence of phase transition, NMR meas. 77—16206
$KSc(MoO_4)_2$, soft modes and Raman spectrum at ferroelastic phase transitions 79—47450
K_2SeO_4, ferroelastic props. 78—2251
K_2SeO_4, thermal expansion, phase transitions, 77-190K 77—16263
$K_{0.5}Tm_{0.5}Nb_2O_6$, ^{93}Nb NQR spectra, 77 to 450K 79—38401
$K_4Zn(MoO_4)_3$, domain struct. and phase transition, ferroelastic behaviour 77—62581
$(La,Nd)P_5O_{14}$, optical props., ferroelastic phase transition induced 79—95731
$LaBnO_4$, single cryst., grown by Czochralski method, exhibiting ferroelasticity 77—52247
$LaNbO_4$, ^{93}Nb and ^{139}La NQR spectra 79—38401
$LaNbO_4$ crystals, ferroelastic, w′ walls, temp. depend. 80—10560
$LaNbO_4$, ferroelastic, cryst. struct. and twinning struct. 79—27965
$LaNbO_4$, ferroelastic phase transition exam. 77—27934
$LaNbO_4$, Raman scatt. and fluoresc. spectra 80—20625
LaP_5O_{14}, continuous ferroelastic transition elastic and mechanical props. 80—92668
LaP_5O_{14}, coupling effects between soft optic and acoustic modes at ferroelastic transition 80—70358
LaP_5O_{14}, ferroelastic transition, soft acoustic mode 77—11656
LaP_5O_{14}, ferroelastic phase transition, thermal expansion and elastic consts. tensors 79—42236
LaP_5O_{14}, ferroelastic transition, polarised Raman study 80—16035
β-$LiNH_4SO_4$, lattice modes and phase transition, polarised Raman meas. 77—20859
$LiNH_4SO_4$, press.-temp. phase diagram, NMR and SHG meas. 78—23690
lithium ammonium tartrate monohydrate ferroelastic phase transition *(Japanese)* 79—77747
MoO_3-M_2O_2 system, M=trivalent metal, solid-state chem., review 77—24288
$(NH_4)_2BeF_4$, elastic compliance, US attenuation and piezo-coeffis., 170 and 190K 79—51918
$NH_4HSO_4:VO^{2+}$, ferroelastic, inernal strains, ferroelec. transitions, EPR 79—47400
NH_4NBeF_4, successive phase transitions, dielec. and optical props. obs. 80—50275
$(NH_4)_2SO_4$, phase transition mechanisms by optical spectroscopy, elastic moduli 79—15411
$(NH_4)_2SO_4$-type crystals, ferroelastic, ferrielectric, and incommensurate phase transitions *(Japanese)* 79—65811
$NaAl(MoO_4)_2$, domain struct., phase transition, and dielec. props. 79—56748
$NaAl(MoO_4)_2$, ferroelastic, domain struct. obs. 77—15483
NaCN, optical F centres and phase transitions 78—56504
Na_2CO_3, phys. props. related to phase transitions 80—96643
Na_2CO_3, structural modulation, theory 77—35535
$NaFe(MoO_4)_2$, domain struct., phase transition, and dielec. props. 79—56748
$NaH_3(SeO_3)_2$, domain struct. realignment and Barkhausen effect 80—71361
$(Na_{5-x}Nd_x)(W_{3-2x}Nb_{2x})O_9F_5$, ferroelastic-ferroelectric material *(French)* 79—99834
$Na_5W_3O_9F_5$, single cryst., prep., optical and dielec. studies *(French)* 80—15994
$NdNbO_4$, ferroelastic, cryst. struct. and twinning struct. 79—27965
$NdNbO_4$, ferroelastic domain wall motion, stress-strain hysteresis curve 77—43271
$NdNbO_4$, single cryst. grown by Czochralski method, exhibiting ferroelasticity 77—52247
NdP_5O_{14}, ferroelastic, spectroscopy, ferroelastic/ferroelectric coupling, soft optic mode frequencies 79—19845
NdP_5O_{14}, ferroelastic, Raman scatt. from soft phonons, 4.2-600K, monoclinic-orthorhombic transition temp. 79—51962
NdP_5O_{14}, ferroelastic, hydrostatic press. effect on phase transition temp. 80—70293
NdP_5O_{14}, sp. hts. near ferroelastic phase transitions 78—63863
$Pb_2AgNb_5O_{15}$, $Pb_2AgTa_5O_{15}$, ferroelec. and ferroelastic props. *(French)* 79—24266
$Pb_{0.27}K_{0.56}Nb_{0.91}Ta_{4.15}O_{15}$, coupled ferroelastic-ferroelectric props. 77—59543
$Pb_2KNb_{5-x}Ta_xO_{15}$, ferroelastic-ferroelectric coupling, dielec. props. 79—38433
$Pb_{2.07}K_{0.56}Nb_{0.91}Ta_{4.15}O_{15}$, tetragonal tungsten bronze type, ferroelastic-ferroelectric coupling *(French)* 77—28522
$Pb_3(NO_4)_2$, press. induced ferroelastic phase transition, neutron diffr. study 79—73308
Pb_3O_4, IR and Raman study of structural phase transitions *(French)* 78—84582
$Pb_2(PO_4)_2$, ferroelastic, switching processes 78—2192
$Pb_3(PO_4)_2$, crit. behaviour of polar modes near ferroelastic phase transition 79—95750
$Pb_3(PO_4)_2$, deform. hysteresis loop 77—51432
$Pb_3(PO_4)_2$, domain struct., EM study *(French)* 80—44216
$Pb_3(PO_4)_2$, ferroelastic, bending stress effect on domain struct. *(Russian)* 77—39623
$Pb_3(PO_4)_2$ ferroelastic, dielec. consts. and birefringence meas. 78—2793
$Pb_3(PO_4)_2$, ferroelastic, switching processes in pulse mech. field 78—59853
$Pb_3(PO_4)_2$, ferroelastic, Raman scatt. by soft vibr. involved in ferroelastic phase transition 80—16040
$Pb_3(PO_4)_2$, ferroelastic, dielectric anomalies, phase transitions, permittivity, relaxation *(Russian)* 80—71293
$Pb_3(PO_4)_2$, ferroelastic transition, X-ray diffr. and scatt. *(French)* 77—31769
$Pb_3(PO_4)_2$, ferroelastic transition, soft modes, inelastic neutron scatt. obs. 77—31772
$Pb_3(PO_4)_2$, ferroelastic domain struct., twinning analysis by pseudosymmetry 77—76421

ferroelasticity continued
- $Pb_3(PO_4)_2$, ferroelastic transformations and struct. as function of temp., neutron diffr. study 79—19188
- $Pb_3(PO_4)_2$, ferroelastic phase transition, thermodynamic theory 79—37832
- $Pb_3(PO_4)_2$, ferroelastic phase, structure domains, electron microscope obs. 79—42078
- $Pb_3(PO_4)_2$, ferroelastic phase transition, inelastic neutron scatt. *(French)* 80—24584
- $Pb_3(PO_4)_2$, nonintrinsic ferroelastic properties 78—91374
- $Pb_3(PO_4)_2$, phase transition at 180°C, dielectric meas. 79—37831
- $Pb_3(PO_4)_2$, temp. depend. of lattice parameters and spontaneous strain 80—29170
- $Pb_3(PO_4)_2{:}Gd^{3+}$, EPR near ferroelastic transition point 79—15350
- $Pb_3(PO_4)_2{:}Gd^{3+}(Eu^{2+})$, EPR spectra of α- and β-phases 80—11261
- $Pb_3(PO_4)_2{:}Mn^{2+}$, EPR study around ferroelastic transition point of $Pb_3(PO_4)_2$ 78—76303
- $Pb_3(PO_4)_2$-$Pb_3(VO_4)_2$, direct obs. 77—21203
- $Pb_3(PO_4)_2$-$Pb_3(VO_4)_2$ mixed crystal, crit. stress and phase diagram temp. depend. 78—26623
- $Pb_3(P_{0.95}V_{0.05}O_4)_2$, ferroelastic transition, soft mode, inelastic neutron scatt. study 80—70357
- $Pb_3(P_{1-x}V_xO_4)_2$, ferroelastic, acoustooptic props. of single crysts. and solid solns. 79—69809
- $Pb_3(P_{1-x}V_xO_4)_2$, $x=0.1, 0.2$, Raman scatt. by low freq. vibrs. 80—55111
- $Pb_3(P_xV_{1-x}O_4)_2$, ferroelastic phase transitions, lattice dynamics, dielec. and optical props. meas. 77—55334
- $Pb_3(P_xV_{1-x}O_4)_2$, ferroelastic phase transition, DTA, dilatometric and Brillouin scatt. study 80—70398
- $Pb_3(VO_4)_2$, ferroelastic, phase transitions, boundary walls 80—107419
- $Pb_3(VO_4)_2$, ferroelastic phase transition, thermodynamic theory 79—37832
- $Pb_3(VO_4)_2$-$Pb_3(PO_4)_3$ solid solutions, ferroelastic, dielec. consts. and birefringence meas. 78—2793
- $Pb_3(VO_4)_3$, ferroelastic, dielec. consts. and birefringence meas. 78—2793
- $Pb(Zr,Ti)O_3$, ferroic materials, fracture processes 80—79869
- PrP_5O_{14}, sp. hts. near ferroelastic phase transitions 78—63863
- PtGeSe, ferroelastic, cryst. struct. models 77—19927
- RbCN, ferroelasticity and F- and M-centres absorpt. 79—87475
- $RbCaF_3$, first order improper ferroelastic phase transition at 194K, phenomenological description 80—70397
- $RbCaF_3$, thermal props. near phase transition 78—75850
- Rb_2CrO_4, effects on domain struct., new ferroelastic revealed 78—18702
- RbH_2PO_4, ferroelectric-ferroelastic phase transition, γ-ray diffr. 78—43819
- $RbH_3(SeO_3)_2$, crystal lattice monoclinic distortion determ. by phase transition from elec. meas. results 79—73887
- $Rb_2Hg(CN)_4$, spinel, ferroelasticity and phase transformation 79—7646
- Sb_5O_7I, ferroelastic, Raman scatt. and symm. aspects of phase transition 77—8578
- Sb_5O_7I, polytype 2MA, ferroelectric, ferroelastic, Raman scattering and symmetry anal. 79—38550
- Sb_5O_7I polytypes, cryst. growth, struct., ferroelastic and ferroelec. props. 78—31309
- Sb_5O_7I, polytypes 2MC and 2MA, photoferroelastic phenomena 79—95447
- SnF_2, phase transitions, X-ray diffr., elec. cond. and thermal analysis 80—100329
- SnF_2, second order $\beta \rightleftarrows \gamma$ transition, neutron diffr. and NMR obs. 80—107095
- $Sr_2AgNb_5O_{15}$, $Sr_2AgTa_5O_{15}$, ferroelec. and ferroelastic props. *(French)* 79—24266
- $Tb(MoO_4)_3$ cryst. struct. in ferroelec., ferroelastic, antiferroelec. and paraelastic phases 80—75205
- $Tb_2(MoO_4)_2$, ferroelectric-ferroelastic crystal, room temp. crystal struct., X-ray scatt. 80—28978
- $Tb_2(MoO_4)_3$, thermal expansivity and spontaneous strain temp. depend. 79—14943
- TeO_2, press.-induced ferroelastic transition and internal displacement, soft effective elastic const. meas. 79—73240
- $TlCdF_3$, thermal props. near phase transition 78—75850
- $TlCdF_3$, third and fourth order elastic consts., press. depend. near phase transition *(French)* 80—34116
- VO_2, ferroelastic metal-insulator transition, electronically triggered crystallographic phase transition 80—70614
- WO_3, acoustic instability near monoclinic orthorhombic phase transition, X-ray scatt. 80—65215
- $YbNbO_4$, ^{93}Nb NQR spectra, 77 to 450K 79—38401
- $YbNbO_4$, ferroelastic phase transition exam. 77—27934

ferroelectric Curie temperature
- copper formate tetrahydrate, dielec. props. under hydrostatic press. 77—20789
- crystals with noncentral ions, ferroelec. transitions rel. to spontaneous polarisation 80—15991
- diglycine nitrate, cryst. growth, dielec. and electromech. props. 80—2701
- displacive ferroelectrics, connection between electron spectrum parameters and ferroelec. parameters 79—38483
- displacive type ferroelectrics with impurities, lattice dynamics 79—28061
- domain struct. near first-order phase transition resembling second-order transition 80—93139
- doped narrow gap semiconductor, two-channel vibronic mechanism of ferroelectric phase transitions *(Russian)* 79—56745
- electrometer ferroelectric modulator temperature stabilisation 77—82550
- electrometer ferroelectric second-harmonic modulator design 77—82549
- extended defect system, phase transform., critical props. 80—103455
- extrinsic ferroelectrics, transition, polarisation, dielectric divergence 80—80718
- ferroelectric films, surface effects on phase transitions, local spontaneous polarisation 80—2708
- ferroelectric materials for dielectric power conversion, dielectric prop. anal. 80—80712
- ferroelectric semiconductor, magnetic field influence, ferroelectric transitions 80—55049
- ferroelectrics with hydrogen bonds, phase transition into coherent state, two-level proton calcs. *(Russian)* 80—71356
- film, thermodynamics in vicinity of second order phase transitions 79—91381
- glycine silver nitrate, and deuterated analogue, hydrostatic press. effects 77—36185

ferroelectric Curie temperature continued
- glycine silver nitrate, dielec. relax. in paraelec. and ferroelec. phases 80—29678
- Ising model, central peak with transverse field 80—7306
- lattice dynamics of ferroelectrics with impurities 79—37802
- liquid crystal, ferroelectric, review of props. 77—85667
- liquid crystals, temp. depend. of elec. susceptibility and spontaneous polarisation *(Japanese)* 78—68467
- methyl ammonium aluminium sulphate, ferroelec., proton spin-lattice relax. time anomaly 80—60440
- methylammonium alums, dielec. relax. near transition point 80—71301
- mixed crystals, CPA calc. 78—10855
- narrow-gap ferroelectric, phase transition due to strong mag. field 80—103924
- oxyfluoride ferroelectrics, chemical bonding, Curie temp., spontaneous polarisation 80—75981
- phase transition, by impurity carriers, electron-phonon interaction *(Russian)* 78—48134
- rare earth arsenates, $RAsO_4$, ferroelectricity, dielec. meas. 80—60515
- rare earth mixed molybdates, $R_2(MoO_4)_3$, $R_{2(1-x)}R'_{2x}(MoO_4)_3$, cryst. growth and crystallographic data, Curie temp. determs. 79—43132
- Rayleigh wave propag. near Curie temp., ferroelec. cryst. with piezoeffect 77—89630
- Rochelle salt, dehydration kinetics in ferroelec. and paraelec. phases, surface acoustic waves influence 80—97204
- Rochelle salt, dielectric props. near upper Curie pt. under hydrostatic press. 79—82935
- Rochelle salt, ferroelectric phase transition, external field induced 80—29700
- Rochelle salt, thermal expansion and spontaneous strain meas., −40 to 40°C, electrostrictive consts. 77—16262
- $(\text{Rochelle salt})_{1-x}(\text{ammonium Rochelle salt})_x$, phase transitions, hydrostatic press. effects 80—93246
- sodium benzoylacetonate, pyroelectric effect, peak near Curie temp. 79—8096
- tetramethyl ammonium cobalt chloride, ferroelec., Curie temp. determ. 79—38485
- TGFB, Curie point press. coeff. tensor 79—33635
- TGFB, deuterated, effects of deuteration on lattice parameters and Curie temp. 79—24422
- TGFB, high press. influence on anomalous specific heat, tricritical point 80—25322
- TGS:α-alanine, single crysts., pyro- and dielectric props. *(Russian)* 77—59520
- TGS:Cr single cryst., lattice defect influence on critical behaviour 80—25315
- TGS:nitroanilines, permittivity, elec. cond. and Curie temp. 80—25273
- TGS, autostabilised state, elec. second harmonic generation 80—103921
- TGS, complex dielec. permitt. near Curie temp., ferroelec. polarisation mechanism interpretation 78—43808
- TGS, Curie point press. coeff. tensor 79—33635
- TGS, deuterated, dielectric props., ageing 77—16257
- TGS, ferroelec. single crystal, low freq. nonlinear effects 80—84490
- TGS, light diffr. by US waves, increase in light scattering 78—19441
- TGS, monocrystalline, ferroelectric, domain boundary dynamics contrib. to permittivity near Curie point *(Russian)* 79—73875
- TGS, neutron diffraction enhancement near Curie point with DC field appl. *(Chinese)* 78—68462
- TGS, static crit. phenomena, lattice defect influence 80—71336
- TGS, thermoluminesc. near Curie temp., effect of DC elec. field 79—33848
- TGS, US relax. time constant 80—84257
- TGS type ferroelectric, US absorpt. anomalies near T_c 77—16264
- TGS-TGSe solid soln., phase transitions under hydrostatic press. 79—99840
- TGSe, behaviour under press. near tricritical point 79—95716
- TGSe, Curie point press. coeff. tensor 79—33635
- TGSe, deuterated, dielectric props., ageing 77—16257
- TGSe, deuterated, thermal and dielectric props. at high hydrostatic press. 80—34864
- TGSe, ferroelec. Curie temp. affected by strain, electrostriction 79—55832
- TGSe, low freq. dielec. dispersion near Curie point 79—38432
- TGSSe, autostabilised state, elec. second harmonic generation 80—103921
- tris-sarcosine calcium bromide and chloride solid solns., Mn^{2+} doped, EPR linewidths and ferroelec. behaviour 79—24213
- tris-sarcosine calcium chloride, US attenuation and vel., elastic consts., and permitt. near Curie temp. 79—37761
- vibronic theory of ferroelectricity 79—19854
- vinylidene fluoride-trifluoroethylene film, cryst. phase transition 80—66120
- $As_xSb_{1-x}SI$ mixed crystals, phonon coupling, ferroelectric phase transition, Raman study 80—108165
- $As_xSb_{1-x}SI$, solid solns., ferroelec. props. 78—23409
- $Ba_{0.92}Ca_{0.08}TiO_3$ ceramic, uniaxial stress effects, US dilatometric and dielec. meas. 78—52454
- $Ba_2NaNb_{5-x}Ti_xO_{15-x}F_x$ and $Ba_{2-x}Na_{1+x}Nb_5O_{15-x}F_x$, ferroelectric props., F substitution effect 77—12331
- $(Ba_xSb_{1-x})TiO_3$, ferroelectric films, dielectric and semicond. props. 79—91388
- $Ba_{0.725}Sr_{1.775}Li_xNb_{5-x}Ti_xO_{15}$, solid soln., prep., struct., dielec. props. *(French)* 77—69782
- $Ba_xSr_{1-x}Nb_2O_6$, struct. and dielec. props., isomorphic substitution effect 78—27165
- $Ba_{0.4}Sr_{0.6}TiO_3$, ferroelec. thin film, fabrication, props. 77—28521
- $BaTiO_3$, cubic-tetragonal phase transition, birefringence meas., surface distortion effects 78—95564
- $BaTiO_3$, electron exoemission unipolarity associated with phase transitions 80—97415
- $BaTiO_3$, exam. of anomalous pyroelectric effect above Curie point 79—33613
- $BaTiO_3$ films, effect of elec. field on dielec. props. 79—33642
- $BaTiO_3$, laminar domains, periodic motion under const. elec. field 78—15133
- $BaTiO_3$, OH^- impurity IR spectra meas. 80—20679
- $BaTiO_3$, paraelec. cryst., electro-optical absorpt. near Curie temp. 77—1657
- $BaTiO_3$, polycrystalline, X-ray diffraction, Curie temp., lattice defects, phase changes 79—99830

ferroelectric Curie temperature continued
$BaTiO_3$, single cryst., dielec. const., var. with applied AC field and temp. 78–2787
$BaTiO_3$, thermodynamic props. 77–39680
$BaTiO_3$, undoped and Cu doped, Γ_{15} phonon freezing, electronic instability, LCAO calc. 80–25318
$BaTiO_3$:Mn, polycrystn., annealing effect on transition temps. 80–3100
$BaTiO_3$-$BaNb_2O_6$ system, solid solns. of tungsten bronze struct. of type $BA_{5+x/2}Nb_{10-x}Ti_xO_{30}$ 77–52021
$BaTiO_3$-Ni(Co, Mn)Fe_2O_4, ceramic, exam. of prep. and physical props. 78–68655
$BaTiO_3$-type ferroelectrics, existence of noncommensurate phases due to gradient term in free energy 79–69792
$BiBi_4Ti_3FeO_{15}$, perovskite-like layer-type ferroelec. magnetic cpd., Mossbauer expts., 80-1200K 78–64329
Bi_2MoO_6 ceramic, permittivity, ferroelec. T_c and hysteresis 79–82932
$Bi_xSb_{1-x}SI$, atomic substitution and ferroelec. phase transition 78–68464
$Bi_2TiO_4F_2$, one-layer perovskite-like ferroelec., dielec. study 79–38486
$Ca_3(VO_4)_2$, new high temp. ferroelectric, Curie temp. 78–43811
CsD_2AsO_4, piezoelec. coupled soft modes, Brillouin scatt. near Curie temp. obs. 77–52109
CsH_2AsO_4, Mandelstam-Brillouin spectra and US vel. meas. near ferroelec. Curie point 79–38553
CsH_2AsO_4, piezoelec. coupled soft mode, Brillouin scatt. near Curie temp. obs. 77–52109
CsH_2AsO_4, pres. depend., LF dielec. response, ferroelec. props. 78–15120
$Cs(H_{1-x}D_x)_2PO_4$, dielec. props., temp. meas. 80–71335
CsH_2PO_4 and CsD_2PO_4, dielectric props. and ferroelec. transition temp. 77–12335
CsH_2PO_4, deuteration and press. effects 78–35101
CsH_2PO_4, lattice consts., temp. depend. of dielec. const. and birefringence, high temp. phase transitions 79–56746
$Cs_2KMO_3F_3$, (M=Mo, W), low temp. phase transitions *(French)* 78–92036
$Cs_2RbMO_3F_3$, (M=Mo, W), low temp. phase transitions *(French)* 78–92036
$Eu_{0.5}Ba_{0.5}TiO_3$, ferromag., ferroelec., ceramic, Curie temps. determ. 78–68230
$Gd_2(MoO_4)_3$, effect of ferroelec. ordering on refractive index 79–33653
$Gd_2(MoO_4)_3$, optical activity, gyration tensor determ. near Curie point 79–33660
KD_2PO_4, attenuation const. meas. by SHF dielec. resonance, Curie point 79–47406
KD_2PO_4, nonlinear electrooptic coeffs. near Curie temp. 80–11366
KH_2AsO_4, ferroelec., temp. broadening of hard mode Raman lines near Tc 78–88296
KH_2AsO_4, NQR of ^{75}As, press. and temp. depend., 77K to Curie temp. 80–71227
KH_2AsO_4, pres. depend., LF dielec. response, ferroelec. props. 78–15120
KH_2AsO_4, soft shear mode, Brillouin scatt. obs. 78–15176
$K(H_{1-x}D_x)_2PO_4$, polarisation relaxation time and Landau kinetic coeff. rel. to degree of deuteration 80–84251
$K(H_{1-x}D_x)_2PO_4$, pseudo-spin model calc., Curie temp. calc. 77–52024
$K(H_{1-x}D_x)_2PO_4$, static dielec. props., and Curie temp., press. depend. 79–87405
KH_2PO_4, and isomorphs, ferroelectric transition and Curie temp., soft mode effect, Green's function anal. 79–24269
KH_2PO_4, attenuation const. meas. by SHF dielec. resonance, Curie point 79–47406
KH_2PO_4, crit. behaviour, dilatometric study 80–92689
KH_2PO_4, ferroelec., temp. broadening of hard mode Raman lines near Tc 78–88296
KH_2PO_4, ferroelectric transition, order-disorder character of hydrogen bond 80–93251
KH_2PO_4, light diffr. by US waves, increase in light scattering 78–19441
KH_2PO_4, optical activity, gyration tensor determ. near Curie point 79–33660
KH_2PO_4 type ferroelectrics, Green's function theory of phase transitions with pseudo-spin-lattice coupled mode model 80–71354
KH_2PO_4-KD_2PO_4 mixed crystals, static and dynamic props., proton-lattice coupled mode model 78–64328
KH_2PO_4-type crystals, H bond in ferroelectricity, role of high pressure research, T_c press. depend. 79–15414
$K_{1-x}Na_xTaO_3$, quantum ferroelec., elastic compliance, impurity effects 79–99835
$K_{1-x}Na_xTaO_3$ quantum ferroelectric, dielec. susceptibility 80–103922
$KNbO_3$-$BaTiO_3$, ferroelec. Curie temp., theory 80–7313
$KNbO_3$-$PbTiO_3$, ferroelec. Curie temp., theory 80–7313
$K_2SbNb_5O_{15}$, dielec. and pyroelec. props. 79–99841
$KTa_{1-x}Nb_xO_3$, quantum ferroelectric, dielec. susceptibility 80–103922
$KTa_{1-y}Nb_yO_3$, quantum ferroelec., elastic compliance, impurity effects 79–99835
$KTaO_3$:Fe^{3+} local phase transition, EPR line temp. broadening *(Russian)* 80–54944
K_2ZnCl_4, ferroelec. props. 79–4772
$La_{0.003}Ba_{0.66}Sr_{0.34}TiO_3$ ceramic, positive TCR near Curie temp. rel. to charge dispersion *(Russian)* 80–16511
Li_2Gd_4 $(MoO_4)_7$, ferroelec. and paramag. props. 78–39517
$LiNbO_3$, Raman spectra and dielec. props. near Curie point 79–38530
$LiNbO_3$, Ti diffused optical waveguide, ferrolectric domain inversion 79–94338
$LiTaO_3$, Raman spectra and dielec. props. near Curie point 79–38530
$LiTaO_3$, single crysts., Czochralski growth, Curie temp. variations 79–33922
$LiTaO_3$-$CaZrO_3$, struct. and dielec. props. 78–80298
$Li_{1+y}Ta_{1.5y}Ti_{6y}O_3$ ($0\leq y\leq 0.028$), non-stoichiometric phase, crystallographic and dielec. props. 80–75212
$NH_4H_2AsO_4$-$NH_4H_2PO_4$ solid soln., Curie temp. and permittivity comp. depend. 77–59533
$NH_4H_2PO_4$, Mn^{3+} doping effect on Curie temp. and dielec. permittivity 77–59532
NH_4HSO_4, ferroelec., critical slowing down of dielec. relax. *(Japanese)* 77–90109
NH_4HSeO_4, ferroelec. props. rel. to struct. 80–71345
NH_4HSeO_4, ferroelec., phase transitions, permittivity and pyroelectricity meas. 80–71350
$(NH_4)_3H(SeO_4)_2$, press. effects, up to 8.5 kbar 78–23413
$(NH_4)_{2(1-x)}Rb_{2x}SO_4$, mixed crystal, dielectric and US meas. of ferroelec. phase transition *(Japanese)* 80–7305

ferroelectric Curie temperature continued
$(NH_4)_2SO_4$, ferroelec. dispersion in microwave region, transition to ferrielectric structure 80–45016
$(NH_4)_2SO_4$, static and dynamic dielec. behaviour 80–71337
$(Na,Li)NbO_3$, ceramics, electrophys. and struct. props. near morphotropic transition 78–2816
$Na_{0.5}Bi_{0.5}TiO_3$, dielectric const. thermal hysteresis, ferroelectric-antiferroelectric transitions 80–50281
$NaH_3(SeO_3)_2$, ferroelectric, electromechanical props. near Curie point 80–29690
$Na_{1-x}Li_xNbO_3$ mixture, ferroelec.-paraelec. transitions, dielec. props. meas. 80–66125
$NaNbO_3$, elec. and photoelec. props. near ferroelec.-antiferroelec. phase transition 80–15989
$NaNbO_3$-$BaTiO_3$, ferroelec. Curie temp., theory 80–7313
$NaNbO_3$-based solid solns., morphotropic transitions and elec. props., enhanced vacancy conc. 80–55048
$NaNbO_3$-$PbTiO_3$, ferroelec. Curie temp., theory 80–7313
$NaNbO_3$-$SrNb_2O_6$, phase diagram, props. meas. 79–11576
$(Na_{5-x}Nd_x)(W_{3-2x}Nb_{2x})O_9F_5$, ferroelastic-ferroelectric material *(French)* 79–99834
$Na_4R(WNb_2)O_9F_5$, (R=Y, Nd, Eu, Gd, Dy, Lu), synthesis, cryst.-chem. and dielec. study *(French)* 80–108164
$Na_3Sc_2(PO_4)_3$, ferroelectric props., X-ray diffr. study 79–69789
PLZT ceramics, modified by $Ca^{2+}(Sr^{2+})(Nd^{3+})(Y^{3+})$, dielec. behaviour 80–60519
PLZT film, growth by RF sputtering, struct. and ferroelec. props. 77–48340
PLZT modified high voltage dielectric, permittivity, Curie temp., loss meas. 80–80720
PLZT, thin film prep. by RF sputtering, struct. and ferroelec. props. *(Japanese)* 77–69992
$(Pb_{1-y}Ba_y)_{1-x}La_xNb_{2-x/5}O_6$, transparent ferroelec. ceramic, optical transmittance, electrooptic props. and Curie temp. 77–32395
$Pb_{2-x}Ba_xLi_{0.5}Nb_{1.5}O_6$, elec. resistivity, Curie temp., x=0-0.15, 50-350°C 78–2478
$(Pb_{1-x}Bi_x)_5Ge_3O_{11}$, spontaneous and induced electrogyration 79–42946
$PbBi_4Ti_4O_{15}$ ceramic, dielec. props., temp. depend. 78–95561
$Pb(Fe_{1/2}Nb_{1/2})O_3$-$La_2O_3(CeO_2)$ ferroelec. ceramics, electrophysical props. 78–35099
$Pb_5(Ge,Si)_3O_{11}$, dielec. and elec. props., 20 to 250°C 80–29697
Pb_3GeO_5, single crystal, props., grown by hydrothermal method 79–11504
$Pb_5Ge_3O_{11}$, photodielectric effects, Curie temp., permittivity and polarisation 80–40034
$Pb_5(Ge_{1-x}Si_x)_3O_{11}$, electrogyration, phase transition and dielectric props. 80–93269
$PbHAsO_4$, hydrostatic press. effect on ferroelec. transition 78–35102
$PbHPO_4$, hydrostatic press. effect on ferroelec. transition 78–35102
$Pb_2KNb_{5-x}Ta_xO_{15}$, ferroelastic-ferroelectric coupling, dielec. props. 79–38433
$Pb_{0.9}K_{0.1}(Zn_{1/3}Nb_{2/3})O_{2.95}$-$PbZrO_3$-$PbTiO_3$, morphotropic tetragonal-rhombohedral phase boundary 78–48129
$Pb(Mg_{0.5}W_{0.5})O_3$-$BiFeO_3$, dielec. props., cryst. struct. 78–84534
$PbNb_2O_6$, permittivity and elec. cond. meas., first order transition 79–24270
$PbNb_{0.5}Sc_{0.5}O_3$, ceramic, dielec. props. 79–11392
$Pb_{1-nx}R_xTiO_{3+x(1.5-n)}$, R=rare earth, ferroelec. Curie temp. comp. depend. 77–16258
$PbSc_{2/3}Te_{1/3}O_3$-$PbSc_{2/3}W_{1/3}0_3(PbFe_{2/3}Te_{1/3}O_3)$ ferroelec. props. and lattice consts. 80–60520
$Pb_{1-x}Sn_xTe$, mag. and kinetic props. near ferroelec. transition 80–11160
$Pb_{0.94}Sr_{0.06}(Ti_{0.47}Zr_{0.53})O_3$-NiO, modified, dielec. and piezoelec. props. 80–11342
PbTe-SnTe compound semiconductors, lattice instability by mm-wave magnetoplasma refl. 80–54336
$PbTiO_3$, anomalies in elec., photoelectric and mechanical props. 80–55051
$PbTiO_3$, X-ray interference intensity temp. depend., lattice ion vibr. *(Russian)* 80–20601
$PbTiO_3$-$CaFe_{2/3}W_{1/3}O_3$, solid solutions 78–43816
$PbTiO_3$-$La_2O_3.3TiO_2$, struct. and dielec. props. 80–54200
$PbTiO_3$-$Pb(Fe_{1/2}Nb_{1/2})O_3$-$PbZrO_3$, with additions, exam. of electrical characteristics 80–2698
$PbTiO_3$-$Pb(Ni_{1/2}W_{1/2})O_3$ system, solid soln. form., struct., dielec. props. and thermal expansion *(Japanese)* 78–27501
$Pb(Zn_{1/3}Nb_{2/3})O_3$, diffuse phase transition, electro-optical and dielec. obs. 79–82933
$Pb(Zr,Ti,Sn)O_3$ ceramics, ferroelec., doped with tri- and pentavalent oxides, piezoelectric props. 78–19413
$Pb(Zr,Ti)O_3$ film, ferroelec. and optical props. 77–85674
$Pb(Zr,Ti)O_3$, polarisation effect on deform. and strength, Curie pt. region 79–42902
$Pb(Zr,Ti)O_3$, thin film evaporated on stainless steel, photovoltaic effect 79–4580
$PbZrO_3$, ferroelec. solid solns., atom shifts, polarisation and Curie temps. 80–100636
$PbZr0_3$, X-ray interference intensity temp. depend., lattice ion vibr. *(Russian)* 80–20601
Rb_2CoBr_4, ferroelec., Curie temp. determ. 79–38485
Rb_2CoCl_4, ferroelec., Curie temp. determ. 79–38485
RbH_2AsO_4, attenuation const. meas. by SHF dielec. resonance, Curie point 79–47406
RbH_2AsO_4, pres. depend., LF dielec. response, ferroelec. props. 78–15120
RbH_2PO_4, attenuation const. meas. by SHF dielec. resonance, Curie point 79–47406
RbH_2PO_4, static dielec. props., and Curie temp., press. depend. 79–87405
$RbHSO_4$, acoustic and dielectric props. near phase transition 80–55053
$RbHSO_4$, ferroelec., dielec. dispersion 80–97179
$RbHSeO_4$, ferroelec. props. rel. to struct. 80–71345
$RbH_3(SeO_3)$, ferroelectric phase transition, Raman spectra meas. 79–19871
$RbH_3(SeO_3)_2$, dielec. relax. near ferroelec. Curie temp. 80–97207
$RbH_3(SeO_3)_2$, US vel. and absorpt. near ferroelec. Curie temp. 80–97206
$Rb_3KMO_3F_3$, (M=MO, W), low temp. phase transitions *(French)* 78–92036
Rb_2ZnBr_4, ferroelec., Curie temp. determ. 79–38485

ferroelectric Curie temperature continued
  Rb_2ZnBr_4, ferroelectricity, hysteresis loops and dielec. const. meas. 78—23416
  Rb_2ZnBr_4, incommensurate phases, neutron scattering study 79—15417
  Rb_2ZnCl_4, ferroelec., Curie temp. determ. 79—38485
  Rb_2ZnCl_4, ferroelectricity, hysteresis loops and dielec. const. meas. 78—23415
  Sb_5O_7I polytypes, cryst. growth, struct., ferroelastic and ferroelec. props. 78—31309
  Sb_2S_3, cond. anomalies at phase transition pts. 77—43604
  SbSI, aggregates of needle-like crystals, nonstoichiometric, ferroelectric properties *(Japanese)* 78—43821
  SbSI, free energy function, temp. depend. and anisotropy of dielec. const., ferro- and paraelec. phases 78—64330
  SbSI materials, piezoelectric props. rel. to use as electroacoustic transducers 78—52445
  SbSI-Sb_2S_3 system, ferroelec. phase transition temp. 79—78632
  $Sn_2P_2S_6$, ferroelec. and pyroelec. props. meas. 78—35107
  $Sn_2P_2S_6$, illumination effect on soft mode and dielectric props., luminesc. study *(Russian)* 80—50420
  $Sn_2P_2(S_{1-x}Se_x)_6$, solid solutions, ferroelectric soft mode freq., displacive transformations 80—29701
  $(Sn_{1-x}Pb_x)_2P_2S_6$, solid solutions, ferroelectric soft mode freq., displacive transformations 80—29701
  $Sr_2KNb_{5-x}Ti_xO_{15-x}F_x$ and $Sr_{2-x}K_{1+x}Nb_5O_{15-x}F_x$, ferroelectric props., F substitution effect 77—12331
  $Sr_2Ta_2O_7$:Nd,Na, SHG, effect of dopants on Curie temp. 79—24267
  $Sr_6Ti_2Nb_4O_{20}$, new class of layer ferroelectrics. X-ray anal. and permittivity meas. 77—16266
  $SrTiO_3$, thermodynamic props. 77—39680
  TGS, ferroelectric phase transition, high resolution NMR study 80—97214
  TGS-TGSe solid solution, temp. depend. of fundamental reflection spectra meas. 77—16337
  V_2O_5, ferroelec. semicond., dielec. and elec. meas. 80—60516
ferroelectric devices
  bimorph vibrator pump characts., using ferroelectric crystals 79—48182
  book, principles and appls. of ferroelectrics 77—90108
  ceramic films, resonant autothermostabilisation *(Russian)* 78—52451
  conference, Minneapolis, MN, USA (June 1979) 80—77535
  conformal transformation, allowing for spatial dispersion *(Russian)* 80—53183
  converters of shockwave mech. energy into elec. power 80—61429
  cylindrical thin shell, appl. of one-dimensional finite elements to normal mode anal. 77—31163
  electroacoustic transducer on 90° ferroelec. domain struct. theory 80—43585
  electrometer ferroelectric modulator temperature stabilisation 77—82550
  electrometer ferroelectric second-harmonic modulator design 77—82549
  ferroelectric-semiconductor structure, effect of potential relief of ferroelectric substrate on props. 79—11235
  ferroelectric-semiconductor system, illuminated, voltage redistrib. 77—40194
  finger length meas. by ferroelectric wedge thermal transducer 77—78001
  holographic recording materials and devices, book contrib. 78—25838
  information display technology, symposium, San Francisco (1978) 79—9209
  phase shifting at 94 GHz using bulk crystals, microwave electro-optic coeffs. determ. 80—71382
  photoconductor-ferroelectric ceramic structure, as optically controlled transparency 80—28343
  photoferroelectric image storage in antiferroelectric-phase PLZT ceramics 80—71353
  piezoceramic aperiodic transducer, mech. load study 80—87700
  piezoelectric ceramic plate energy trapping methods of thickness extension and thickness shear modes 80—15980
  pyroferroelectric energy convertor under thermocycling 78—15102
  radially polarised cylinders, electroacoustic sensitivity calc. by normal-mode methods 77—62131
  semiconductor-ferroelectric heterostruct. junction, nonvolatile polarised memory 79—78164
  thermometer based on ferroelectric capacitor *(Polish)* 80—31750
  $Gd_2(MoO_4)_3$, ferroelec., amorphous Si:H coating, domain wall motion, image scanning 80—83663
  $Gd_2(MoO_4)_3$, matrix-addressed analogue ferroelec. memory 80—103926
  In_2O_3 film, evaporated, on ferroelec. ceramic, switching characts. 78—19107
  PLZT ceramic photoferroelectric image storage device, characts. 77—55756
  PLZT ceramic photoferroelectric image storage and display systems 77—72084
  PLZT ceramics, optical information storage and spatial light modulation 78—83097
  PLZT ceramics, photoferroelectric effects, image storage device appl. 79—42924
  PLZT ceramics, photoferroelectric image storage in antiferroelectric phase 79—47404
  PLZT colour cell for real time two colour incoherent to coherent image convertor 78—38039
  PLZT pyroelectric detectors, delayed onset of piezoelec. oscills. 80—75953
  PLZT real time 2 colour incoherent to coherent image convertor 79—3805
  PLZT thermal, flash, ferroelectric protective goggles 80—81746
  SbSI single crysts., nonlinear dielec. effects and microelectronic applics. 77—43944
ferroelectric domains *see electric domains*
ferroelectric materials
  see also antiferroelectric materials; electric domain walls; ferroelectric semiconductors; ferroelectric thin films; ferroelectric transitions; lattice dynamics of ferroelectric crystals
  alkali metal double salts, $MB'BX_4$ (M=alkali; M'=alkali or NH_4^+; $BX_4=SO_4$, BeF_4, etc.), theory of phase transitions 79—99837
  alkali metal tungsten bronzes, enhanced supercond. T_c, possible explanation 78—14850
  alkali trihydrogen selenite: Mn^{2+} single crystal, EPR 78—72396
  alkaline trihydrogen selenites, ferroelec. phase transitions, Raman spectra 77—8525
  L-p-alkoxybenzylidene p′-amino 2 methylbutyl cinnamate chiral smectic liq. cryst., dielec. and ferroelec. props. 79—91394
ferroelectric materials continued
  L-p- alkoxybenzylidene p′-amino 2 methylbutyl-cinnamate, dielec. props. in ferroelec. smectic phase *(Japanese)* 79—82154
  aluminium methylammonium selenate alum, effect of hydrostatic pressure on dielec. props., near transition pt. 79—56712
  alums, dielec. behaviour and ferroelectricity 79—38431
  ammonia Rochelle salt, temp. depend. of optical axis angle, phase transitions *(Russian)* 80—97216
  ammonium double salts, MH_4 MBX_4, (M=alkali metal; $BX_4=SO_4$, SeO_4, BeF_4, etc.), theory of phase transitions 79—99837
  ammonium hydrogen chloracetate, order disorder type transition 79—47399
  ammonium Rochelle salt, cryst. with modulated struct., neutron scatt. obs. 79—95713
  ammonium Rochelle salt, first order phase transition 78—43818
  ammonium Rochelle salt, incommensurate ferroelectricity 79—61311
  ammonium Rochelle salt, incommensurate phase transitions under existence of Lifshitz invariant 79—15416
  ammonium Rochelle salt, thermodynamics of ferroelec. transition 80—84702
  arsenates, ferroelec. phase, E-mode splitting 78—15163
  bibliography, (Feb.-Aug. 1978) 79—82931
  bibliography, Jan-April 1976 77—48132
  bibliography, June 1977-Aug. 1977 79—19847
  bibliography, May-Sept. 1976 77—59529
  bibliography, Sept. 1977-Jan. 1978 79—19848
  bibliography 77—12326
  bibliography (Oct. 1976 to May 1977) 78—95557
  1,6-bis(2,4-dinitrophenoxy)-2,4-hexadiyne, obs. of apparent ferroelec. transition 80—66121
  book, principles and appls. of ferroelectrics 77—90108
  boracites, spontaneous birefr., meas. and appl., ferroelectric/ferroelastic phases 79—15434
  boracites, trigonal, spontaneous polarisation behaviour 77—43945
  bulk photovoltaic effect response coeff. 80—65631
  calcium strontium propionate, compressed powder, dielectric props., particle size effects 77—59503
  centrally-symmetric displacement type, dielec. losses, weak elec. field effect *(Russian)* 80—29683
  ceramic, axially loaded, nature of elec. field and resulting voltage 78—72468
  ceramic, elec. and thermoelec. props. of grains and grain boundaries 78—43382
  ceramic, microstructure and physical props. 78—72756
  ceramic, optical modulation by electrostriction during electron beam charging, spatial characts. 79—7224
  ceramic, polycryst., elasticity props., neutron bombardment effects 80—79856
  ceramic, shock induced polarisation 77—48133
  ceramic blocks, TsTS-23, TBk-3, TsTSNV-1, longit. piezoelec. effect and moduli 78—56430
  ceramics, ferroelec., dielec. losses due to domain wall oscill. 78—84541
  ceramics, materials and dielec. props., review 80—75957
  ceramics, Rochelle-type, controllable transparency *(Russian)* 77—630
  ceramics, transparent ferroelectric, composition selection for appl. in light modulators *(Russian)* 80—91869
  ceramics, with external inductive-resistive load, linear electromechanical responses 79—51909
  chemical reactions in plasma generated near ferroelectric surface, obs. 78—68931
  chiral smectic C, ferroelec. props., dielec. meas. 78—52463
  chiral smectic critical behaviour near phase transformation point between two ferroelectric phases *(Russian)* 80—44124
  chiral smectic liquid cryst., ferroelectric, flexoelectric effects, dielectric const. 80—33877
  complex oxides, AES investigation of corrosion and growth nature of surface layers 77—77330
  composite with nonferroelectric phase, permittivity calcs. 77—85659
  conference, ferroelectric materials and their applications, Kyoto, Japan, Nov. 17-19, 1977 79—19846
  conference, Leningrad, USSR (1977) 79—15406
  conference, Minneapolis, MN, USA (June 1979) 80—77535
  conference, Novosibirsk, USSR (Sep. 1976) 78—76393
  copper formate tetrahydrate, ice rule ferroelectric, polarisation correlations 80—97190
  copper formate tetrahydrate, model two-dimensional ferroelec., short-range order, neutron scatt. 78—68458
  coupled oscillation spectrum, phenomenological theory w.r.t. orientational transitions 79—8103
  crystals, miniature device for compressive stress anal. 79—93115
  Debye temperature, tabulation of calorimetric values 78—51639
  L-p-decyloxybenzylidene-p′-amino-2-methylbutyl-cinnamate, ferroelec. smectic liq. cryst., electro-optical effect 78—39527
  l-p-decyloxybenzylidene-p′-amino-2-methylbutylcinnamate, ferroelec. liq. cryst., pulsed pyroelec. effect 79—15405
  deformable, coupled acousto-optic modes 80—96093
  deformable, coupled electroacoustic eqns. 80—96092
  deuterated Rochelle salt, complex dielec. const., 5 MHz-24GHz, −45 to +45°, relax. mechanism 80—15983
  dialkyloxyazoxybenzenes, synthesis of ferroelec. smectic B, smectic C, and nematic phases 78—94969
  diazoxycinnamates, synthesis of ferroelec. smectic C and smectic A phases 78—94969
  dicalcium barium propionate, ferroelec. in press. induced phase VI 79—91393
  dicalcium barium propionate, press. induced ferroelectricity, dielectric meas. 79—51920
  dicalcium lead propionate, annealed, crit. exponents, dielec. const. temp. depend. 80—55050
  dicalcium lead propionate, effect of particle size on dielec. behaviour 79—38429
  dicalcium lead propionate, ferroelec., piezoelec. and elastic props. 78—84528
  dicalcium lead propionate, improper ferroelectric, dielectric props., IR radiation pyroelectric detection 80—80711
  dicalcium lead propionate, Raman scatt., order-disorder type transform 77—12373
  dicalcium strontium propionate, anomalous US attenuation near ferroelec. phase transition 79—91383
  dicalcium strontium propionate, cryst. symmetry in low temp. phase 79—37693

ferroelectric materials continued
dicalcium strontium propionate, effect of particle size on dielec. behaviour 79—38429
dicalcium strontium propionate, elastic stiffness consts., determ. in US freq. region 79—37752
dicalcium strontium propionate, ferroelec. domains, direct optical visibility 80—84704
dicalcium strontium propionate, Landau theory breakdown in ferroelec. transition 77—12344
dicalcium strontium propionate, Raman scatt., order-disorder type transform. 77—12373
dielectric aftereffect meas. with digital data acquisition 77—43952
dielectric constant meas. using automatic system *(German)* 80—90864
dielectric power conversion, dielectric prop. anal. 80—80712
dielectric props. meas. in vicinity of phase transition, microwave method 78—74022
diglycine nitrate, cryst. growth, dielec. and electromech. props. 80—2701
diglycine nitrate, dielec. relax. in paraelec. and ferroelec. regions 78—31149
dimethylammonium cadmium tetrachloride type compounds, structural phase transition model 79—37829
displacive ferroelectrics, model, fluctuation effects 79—33063
DOBAMBC, and DOBAMBCC, chiral smectic C liq. cryst., dielec. consts., electroclinic effect 78—94980
DOBAMBC, chiral smectic, ferroelec., press. and solute effects 80—103920
DOBAMBC, chiral smectic C-phase ferroelectric liq. crystal film, classical X-Y system, props. 80—44123
DOBAMBC, chiral smectic phases, pyroelectric and dielec. props. 79—91380
DOBAMBC, dielec. dispersion at ferroelec. smectic A-smectic C transition 79—91385
DOBAMBC, dielec. props. near ferroelec. smectic A to C transition 80—45015
DOBAMBC, ferroelec. liq. cryst., helical struct., elec. field depend. *(Japanese)* 80—38910
DOBAMBC, ferroelec. liq. crysts., elec. and optical props., appls. *(Japanese)* 80—88943
DOBAMBC, ferroelec. props. 79—32884
DOBAMBC, liquid crystal film, freely suspended, polarisation, elastic consts. and viscosity meas. 79—55663
DOBAMBC, polarized Raman scatt. and elec. field effects in aligned smectic phases 79—94873
DOBAMBC, smectic, ferroelec. transition mechanism obs. by X-ray scatt. 79—77515
DOBAMBC, smectic A and ferroelec. smectic phases, ^{13}C NMR study 80—75153
L-DOBAMBC, smectic liq. cryst., ferroelec. behaviour 77—43949
DOBAMBC, smectic liquid crystal, colour switching in elec. field 80—29719
doped displacive ferroelectrics, sound attenuation constant, Green's function technique 79—11397
DTGS:VO^{2+}, ENDOR 79—99791
electro-optical and nonlinear-optical materials, review 80—74450
electroacoustic echo 78—95549
electrogyration in ferroelec. crystals, appls. 78—76394
electron microscopy investigations, review *(Japanese)* 80—71366
electrooptic ceramics and ferroelec. glasses *(Japanese)* 79—65840
epitaxy, appl. of electron microprobe methods 80—44443
EPR, elec. field modulated 80—75841
ester, smectic C phase liq. cryst., ferroelectricity and spontaneous polarisation *(Russian)* 79—8102
esters, SLC, ferroelectric behaviour, specific heat, spontaneous polarisation 80—75958
extrinsic ferroelectrics, transition, polarisation, dielectric divergence 80—80718
ferroelec. crystal, Barkhausen effect study 79—38507
ferromagnet, ferroelectric, soft mode damping, temp. anomalies *(Russian)* 80—44284
glycine silver nitrate, and deuterated analogue, hydrostatic press. effects 77—36185
glycine silver nitrate, dielec. relax. in paraelec. and ferroelec. phases 80—29678
glycine sulphate:L-alanine, unirradiated, optical spectroscopy of scintillations 80—80863
guanidine aluminium sulphate hexahydrate, SEM obs. of ferroelec. domain struct. in single crysts. 80—97219
guanidine aluminium sulphate hexahydrate type ferroelectrics, ESR of Fe^{3+} exchange pairs 77—90022
guanidinium aluminium sulphate, domain wall energies and domain structures 78—92039
guanidinium aluminium sulphate hexahydrate:Cr^{3+} pressure meas. from ESR 79—38375
guanidinium aluminium sulphate hexahydrate:Mn^{2+}, NMR 78—91939
guanidinium aluminium sulphate hexahydrate, pyroelectric coeff., 1.8-300K, dynamic method *(French)* 79—19844
guanidinium aluminium sulphate hexahydrate, surface obs., SEM and AES expts. 80—71362
guanidinium aluminium sulphate hydrate, ferroelec., decoration patterns on cleavage surface, domain obs. 80—97218
guanidinium gallium sulphate hexahydrate:Cr^{3+} pressure meas. from ESR 79—38375
guanidinium uranyl sulphate hydrate, ferroelec., decoration patterns on cleavage surface, domain obs. 80—97218
guanidinium uranyl sulphate trihydrate, new ferroelec., dielec. props. 78—43824
guanidinium uranyl sulphate trihydrate, X-ray diffr., crystal struct. 78—14331
halide ferroelectrics, transitions, formulae, structural data 80—75980
heat capacity meas., by dynamic method at high hydrostatic pressures 80—47059
heterogeneous states, statistics *(Russian)* 80—80721
HOAB-DOBAMBC nonchiral-chiral smectic C mixture, spontaneous polarization and induced circular dichroism 79—27910
HOBACPC, chiral smectic C liq. cryst., dielec. consts., electroclinic effect 78—94980
hologram storage in ferroelec. crysts., book contrib. 78—25834
hydrogen bonded, low freq. lattice vibrs. and pseudospin modes, instabilities, struct. phase transitions 78—15108
hydrogen-bonded, incoherent and coherent inelastic neutron scatt. cross sections 77—59524
hydrogen-bonded, parametric reson., influence of lattice vibr. by parallel electric microwave pumping 77—48140
hysteresis loop sensing *(Czech)* 80—82792
improper, electro-opt. props. 78—76426
incommensurate phase transitions, symmetry aspects, structs., and phys. props. *(Japanese)* 79—65813
ion-ion interaction due to soft phonon modes 79—99838
large-gap type, vibronic theory and opt. props., anomalous bulk photovoltaic effect 80—103939
LF HV generator for studying properties *(French)* 77—41647
$^{6}LiH_3(SeO_3)_2$, absolute atomic arrangement rel. to spontaneous polarisation, neutron diffr. study 80—15067
liquid crystal ferroelec. phases, mag. material analogy 77—11467
liquid crystals, chiral smectic C phase, phys. props., review 80—75150
liquid crystals, kinetics of spontaneous polarisation *(Russian)* 79—8101
liquid crystals, soft mode dynamics 77—7852
liquid crystals, temp. depend. of elec. susceptibility and spontaneous polarisation *(Japanese)* 78—68467
lithium ammonium tartrate monohydrate, in paraelec. phase, Brillouin scatt. 78—64373
lithium ammonium tartrate monohydrate, Raman spectra, anomalous low-lying response 80—2746
lithium ammonium tartrate monohydrate, spontaneous shear strain, X-ray obs. 78—56433
lithium ammonium tartrate monohydrate elastic props., piezoelec. reson. method meas. 77—63370
lithium thallium tartrate, single cryst., thermal cond. at low temps. 79—33125
lithium thallium tartrate, sp. ht., 0.3 to 25K, second-order ferroelec. transition 80—59674
lithium thallium tartrate monohydrate, paraelectric phase structure by neutron diffraction data 79—19238
magnetic, mechanism of phonon relaxation *(Russian)* 79—90742
methyl ammonium aluminium sulphate, ferroelec., proton spin-lattice relax. time anomaly 80—60440
methylammonium aluminium sulphate dodecahydrate, single crysts., high-order EPR transitions of Cr^{3+} 80—108052
methylammonium aluminiumselenate:Cr^{3+}, EPR and linewidth anomaly 77—12191
methylammonium alums, dielec. relax. near transition point 80—71301
methylammonium chromium selenate, lattice consts. and ferroelec. props. 79—33641
methylammonium chromium selenate dodecahydrate crystals, dielectric relaxation 80—40043
methylammonium gallium selenate, lattice consts. and ferroelec. props. 79—33641
methylammonium-$Ga(SO_4)_2.12H_2O$, ferroelec. alum single crysts., dielec. dispersion and characts. 79—15408
methylammoniumgallium sulphate:Cr^{3+}, EPR and linewidth anomaly 77—12191
microferroelectrics, thermodynamics 77—59534
Mossbauer spectrum, isomer shift and quadrupolar splitting, internal elec. field effects 79—56648
neutron scattering in H-bonded materials, coherent crit. scatt. 79—56742
$(NH_4)_2SO_4$:Mn^{2+}, ferroelec. phonon driven phase transform., reduction of spin Hamiltonian consts. 78—92033
niobates, Lorentz elec. field, and short-range Nb-O interactions 77—43941
NOBAMBC, chiral smectic phases, pyroelectric and dielec. props. 79—91380
noncentrally symmetric phase identification using SHG 78—74947
Nyquist noise in mag. and dielec. materials 77—1569
one dimensional dynamic electromechanical constitutive relations of ferroelectric materials 79—56738
optical data storage material requirements and possibilities *(German)* 78—25937
optical recording media, review 78—71172
optically induced refr. index changes, holography appls. 77—50742
order-disorder ferroelectrics, phonon damping and freq. shift *(Russian)* 79—60471
order-disorder type, dynamic structure factor *(Russian)* 80—40068
oxide ceramic, perovskite structure type, cond. and polarisation 77—12325
oxide crystals for electrooptics and nonlinear optics, optical inhomogeneities, review *(Japanese)* 77—65613
oxyfluoride ferroelectrics, chemical bonding, Curie temp., spontaneous polarisation 80—75981
P- and T-nonconserving interactions, macroscopic effects 78—84532
$Pb_3M_gNb_2O_9$ crystals for optical radiation control 79—81554
$Pb_5Ge_3O_{11}$:Gd^{3+}, ESR spectra, electric-field effect and reversible permittivity 80—29614
perovskite, Re containing, new seignettomagnets and ferroelectrics 78—19425
perovskite crystals, static and dynamic aspects of PAC meas. 78—88241
perovskite oxides, single cryst., photocond. and TSC meas. 78—43436
perovskite type, transitions, bifurcation method of nonlinear eqn. system 77—12330
perovskites, Raman scatt. and ferroelec. soft modes 77—16300
photoelectretic states in real time spatial light modulators, photorefractive effect 80—80676
photorefractive effect, mechanisms 78—92045
photorefractive materials for optical data storage 78—79086
photovoltaic current, general formula *(Russian)* 80—39627
photovoltaic effect, photoelectron transport 79—4582
PLZT, diffuse phase transitions 79—33628
PLZT, optically induced birefr. change 78—43832
PLZT ceramic, ageing, dielec. props. 80—88940
PLZT ceramics, ferroelec., special props. 79—42916
PLZT coarse-grained solid solutions, electro-optical processes induced by longitudinal electric field *(Russian)* 80—80750
polar materials, appl. to SAW and other devices 80—66114
polydomain ferroelec. crysts., phys. consts., self consistent calcs. 80—88942
polyvinylidene fluoride, electro-optic and elasto- optic effects 80—80754
polyvinylidene fluoride, hysteresis phenomena under high elec. field 80—66134
polyvinylidene fluoride, piezoelec., pyroelec., and improper ferroelec. 80—7301
polyvinylidene fluoride, polycryst. ferroelec., microstruct., piezoelec. and pyroelec. props. 80—7303

ferroelectric materials continued
polyvinylidene fluoride, thermodynamical model, applications *(French)* 80−39315
polyvinylidene fluoride, X-ray diffr. evidence for ferroelectricity 78−60399
polyvinylidene fluoride film, hysteresis and dipolar orientation 80−97217
polyvinylidene fluoride-tetrafluoroethylene, ferroelectric props. 79−42929
pyroelectricity, primary and secondary, review 80−93243
PZT, ferroelec. ceramic, mechanical props. determ. by acoustic techniques 79−28685
PZT ceramics, ferroelec. energy conversion under shock loading 80−108163
Raman scattering, near phase transition point 78−76466
rare earth arsenates, $RAsO_4$, ferroelectricity, dielec. meas. 80−60515
rare earth mixed molybdates, $R_2(MoO_4)_3$, $R_{2(1-x)}R'_{2x}(MoO_4)_3$, cryst. growth and crystallographic data 79−43132
rare earth molybdates, cryst. growth, cryst. chem., and phys. props., book contrib. 80−44194
$(\text{rare-earth})_2\ Ti_2O_7$, (RE=La-Nd, Sm, Gd, Y), ferroelec., layer type struct., cryst. growth 80−108348
refractive index variation, fluctuative mechanism *(Russian)* 79−56755
relaxation effects, disorder excitations, LF dielectric const., spin lattice relaxation phonon-excitation coupled model 78−10852
relaxor ferroelectrics, electrostrictive effects 80−66112
Rochelle salt, ^2H NMR spectrum, correl. effects 78−76324
Rochelle salt, cryst., oriented intrinsic absorpt. edge shape 77−66505
Rochelle salt, dehydration kinetics in ferroelec. and paraelec. phases, surface acoustic waves influence 80−97204
Rochelle salt, depend. on mechanoluminescence on charge prod. during fracture 78−88370
Rochelle salt, dielec. relax., freq. and temp. depend., 10 kHz-1 MHz, 16-28°C 79−82930
Rochelle salt, dielectric props. near upper Curie pt. under hydrostatic press. 79−82935
Rochelle salt, electrogyration during phase transitions 79−19859
Rochelle salt, electromechanical behaviour, influence of ferroelec. phase transitions 77−8510
Rochelle salt, ferroelec. thin crysts., struct. investig. 79−27962
Rochelle salt, ferroelectric, Raman and IR study 80−71406
Rochelle salt, ferroelectric phase transition, external field induced 80−29700
Rochelle salt, high resolution heat capacity meas. *(Japanese)* 80−52218
Rochelle salt, layered domain struct. form., theory and expt. 77−52029
Rochelle salt, low temp. phase transition, dilatometric exam. 77−11691
Rochelle salt, paraelectric-ferroelectric phase transition, relaxing defects effects 79−61320
Rochelle salt, phase transition mechanisms by optical spectroscopy 79−15411
Rochelle salt, phase transitions, free energy in symm. group representation of parent phase 79−69790
Rochelle salt, phase transitions, high-resolution sp. ht. meas. 78−48128
Rochelle salt, polarisation echo, near ferroelec. transition 78−88266
Rochelle salt, polarisation echo in ferroelec. phase transition region 79−42920
Rochelle salt, polarisation relaxation, US vel. and attenuation meas. 77−28512
Rochelle salt, positron lifetime meas. during phase transitions 78−6644
Rochelle salt, refractive index, dispersion and temp. depend. 77−16275
Rochelle salt, thermal expansion and spontaneous strain meas., −40 to 40°C, electrostrictive consts. 77−16262
Rochelle salt, VO^{2+}-doped, EPR study 80−34762
Rochelle salt family, unified phenomenological theory, spherical system of transition parameters 77−31751
Rochelle salt ferroelectric surface creep discharge plasma channel and domain interactions 80−15996
Rochelle salt type cryst., dipole interaction symm. aspect 77−20805
Rochelle salt-type ferroelectrics, external field effect on phase transitions 79−73888
saccharose, single cryst. low-temp. pyroelectricity 79−42906
salicelidenanilines, SLC, ferroelectric behaviour, specific heat, spontaneous polarisation 80−75958
tris-sarcosine calcium chloride, elastic props., US damping 80−84229
schultenites, ferroelectric, sp. ht. 79−19853
SEM, polarisation contrast of cathodolum. for natural and synthetic ferroelecs. 79−7529
SHG determ. of ferroelec. and antiferroelec. props. 78−74947
siegnette magnets with hexagonal barium titanate structure 78−76397
smectic C liquid crystal, ferroelec. chiral, direct elec. meas. of permanent polarisation 77−32331
smectic C liquid crystals, ferroelec., fundamentals and display appl. 80−79676
smectic liquid crystal, ferroelec., two-dimensional X-Y crit. behaviour 79−77514
smectic liquid crystal, ferroelec. props., temp. depend. *(Russian)* 77−32332
smectic liquid crystal, linear electrooptic effect 80−11365
smectic liquid crystal, new ordered smectic phases 78−51407
smectic liquid crystals, piezoeffects and ferroelectric phenomena 79−32883
smectic liquid crystals, spontaneous polarisation meas. *(French)* 77−69765
smectic liquid crystals, symmetry and thermodynamic states, review 80−10493
smectic mesophases, viscoelastic properties and field instabilities 79−27904
smectic single domain C liquid cryst., electric field induced bend undulation instability 80−24351
smectic-C liquid crystal film, freely suspended, two-dimensional mol. orientation fluctuations, light scatt. meas. 78−47236
sodium acetylacetonate, anomalous dielec. behaviour, evidence for ferroelectricity 79−91390
sodium ammonium tartrate, crysts., temp. depend. of elastic compliances at phase transition 79−15409
sodium benzoylacetonate, dielec. props. and cryst. struct. 79−8099
sodium benzoylacetonate, pyroelectric effect, peak near Curie temp. 79−8096
specific heat, $T^{3/2}$ contrib. 77−59528
specific heat calc., soft mode contrib., near T_c 78−64338
squaric acid, cryst., neutron diffr., bond lengths and angles, vibr. modes 77−76384
squaric acid, hydrostatic press. effect on phase transition, dielec. and dilatometric meas. 78−55941
squaric acid and deuterated derivative, vibrational study, IR and Raman spectra 78−92076
$SrTiO_3$, second harmonic generation, bond charge theory 78−76395
stibiotantalite type structure ferro- and antiferroelectrics, props. and crit. points 79−38460
submillimetre monochromatic spectroscopic determination of dielec. props. of electro-opt. materials 78−76428
surface potential between domains, electron microscopy 78−15132
surface sound waves on domain boundaries, low temp. sp. ht. 78−71937
tanane, crit. behaviour near ferroelec.-ferroelastic transition 78−52459
Tanane, dielec. and electrooptic meas. near ferroelec. transition 79−33587
Tanane, ferroelec. ferroelastic transition, X-ray and optical expts. 78−15110
Tanane, ferroelec. mol. cryst., strong piezoelec. coupling 80−75942
TBACA, chiral, smectic C* and H* phases, mol. orientational ordering, ^{14}N NQR study 80−75152
TBK-3, ferroelectric ceramic, 90° electric domain processes, mech. stress, X-ray diffr. 78−72478
TDOBAMBCC, chiral smectic C liq. cryst., dielec. consts., electroclinic effect 78−94980
tetragonal ceramics, 90° domain processes in fixed elec. field 80−7315
tetragonal ceramics, 90° domain-rot. fraction after polarisation, X-ray determ. 80−75992
tetragonal ferroelectric irradiated by laser pulses, spatial temp. and bound-charge distrib. 80−103927
tetragonal tungsten bronze structure ferroelec. mech. for ferroelec. transition 79−38481
tetramethyl ammonium cobalt chloride, ferroelec., Curie temp. determ. 79−38485
tetramethylammonium cobalt tetrachloride, ferrielectricity, triple 60 Hz D-E hysteresis loops 80−71365
tetramethylammonium cobalt tetrachloride, Raman spectra near incommensurate phase transitions 80−76013
tetramethylammonium tetrachlorocobaltate, ferroelec., effects of hydrostatic press. on successive phase transitions 79−47402
tetramethylammonium tetrachlorocobaltate, ferroelec., pressure-temp. phase diagrams 80−97205
tetramethylammonium tetrachlorocobaltate, ferroelectricity 78−76408
tetramethylammonium tetrachloroferrate, press. induced ferroelectricity, dielec. and DTA meas. 80−80722
tetramethylammonium tetrachlorozincate, ferroelec., effects of hydrostatic press. on successive phase transitions 79−47402
tetramethylammonium tetrachlorozincate, ferroelec., incommensurate-commensurate transition, neutron scatt. study 80−40073
tetramethylammonium tetrachlorozincate, ferroelec., pressure-temp. phase diagrams 80−97205
tetramethylammonium tetrachlorozincate, ferroelectricity 78−39513
tetramethylammonium tetrachlorozincate, incommensurate phase transition, US propag. meas. 79−91382
tetramethylammonium tetrachlorozincate, incommensurate phase study, ferroelectric-paraelectric phases *(French)* 80−88318
tetramethylammonium tetrachlorozincate, low temp. phases, superstruct., X-ray study 80−39065
tetramethylammonium tetrachlorozincate, X-ray study of incommensurate phase 80−71351
tetramethylammonium zinc tetrachloride, ^{13}C NMR and PMR study of incommensurate phase transition 80−34863
tetramethylammonium zinc tetrachloride, ferrielectricity, triple 60 Hz D-E hysteresis loops 80−71365
tetramethylammonium zinc tetrachloride, incommensurate phase transitions, ^{13}C NMR study 80−75968
tetramethylammonium zinc tetrachloride, Raman spectra near incommensurate phase transitions 80−76013
TGFB:Cr^{3+}, polarisation reversal and ageing mechanisms, EPR meas. 79−8044
TGFB, Curie point press. coeff. tensor 79−33635
TGFB, deuterated, single cryst. growth and props. 79−24422
TGFB, dispersion and temp. depend. of refr. index *(Russian)* 77−66472
TGFB, ferroelec. and paraelec. phases, X-ray diffr. 79−86776
TGFB, high press. influence on anomalous specific heat, tricritical point 80−25322
TGFB, IR spectra and optical consts. *(French)* 79−95748
TGFB, optical props. in 5 to 22 eV region, reflectance spectra 79−33652
TGFB, refl. spectra 4-22 eV, optical consts. 79−4821
TGS:α-alanine, electro-optic props. *(Russian)* 79−78654
TGS:α-alanine, piezoelectric props., ferroelec. phase existence *(Russian)* 79−47387
TGS:α-alanine, single crysts., dielec. spectrum in RF range *(Russian)* 80−66097
TGS:α-alanine, single crysts., pyro- and dielectric props. *(Russian)* 77−59520
TGS:($CuSO_4$), internal friction 80−44257
TGS: nitroaniline, dielec. and pyroelec. props. 80−75916
TGS:Cr^{3+}, EPR and spontaneous polarisation stabilisation during annealing 77−4610
TGS:Cr^{3+}, EPR obs. of ferroelectric monocrystals, fine struct. EHT-SCCC-MO calcs. 79−19769
TGS:Cr^{3+}, EPR obs. of fluctuations near phase transition 78−43820
TGS:$Cr^{3+}(VO^{2+})$, polarization reversal, static hysteresis loops, switching processes, EPR 78−43633
TGS:Cr single cryst., lattice defect influence on critical behaviour 80−25315
TGS:$Fe^{3+}(Cu^{2+})(Mn^{2+})(Ni^{2+})$, dynamical props. using slowly varying elec. fields, hysteresis *(Spanish)* 77−69785
TGS:Fe^{3+} and aq. solns., optical absorpt. spectra 79−82997
TGS:L-alanine, unirradiated, optical spectroscopy of scintillations 80−80863
TGS:nitroanilines, permittivity, elec. cond. and Curie temp. 80−25273
TGS:VO^{2+}, single cryst. H^2 ENDOR investig. 79−99791
TGS, γ-irrad., lattice defect effects on ferroelec. dispersion 79−51904
TGS, acoustic emission, threshold electric field 79−60874
TGS, admixed with nitroanilines or L-alanine, US vel. and absorpt., ferroelec. transition 77−32333
TGS, alignment on domains of nematic liq. cryst. 79−38506
TGS, autostabilised state, elec. second harmonic generation 80−103921
TGS, Barkhausen jump, elec. pulse shapes 77−66465
TGS, Brillouin scatt. spectra, depolarisation field effect 78−15177

ferroelectric materials continued
TGS, calorimetry, sp. ht., 0-80°C 78—15122
TGS, capacitive bolometer effect in paraelectric phase 77—57389
TGS, cleavage surface, electron microscopy using shadow decoration technique 77—7955
TGS, complex dielec. permitt. near Curie temp., ferroelec. polarisation mechanism interpretation 78—43808
TGS, conditions for electret state 78—43773
TGS, correlation between domain struct. and dielec. props. 79—42927
TGS, crit. behaviour of thermal expansion, neutron diffr. study 80—75371
TGS, critical behaviour in thermal expsn. coeff. and dielectric const. 79—91334
TGS, critical region in sp. ht. 79—28106
TGS, cryst., vibr. bands, ferroelec. and paraelec. phase H bonds *(Russian)* 78—15172
TGS, cryst. struct. exam. after X-irradiation/field treatment 77—11531
TGS, cryst. struct. exam. at low radiation doses 77—11530
TGS, crystallisation by epitaxial germination *(French)* 77—21040
TGS, Curie point press. coeff. tensor 79—33635
TGS, deuterated, Brillouin spectra and elastic consts., behaviour near T$_c$ 78—15178
TGS, deuterated, dielectric props., ageing 77—16257
TGS, deuterated, ferroelec., dielec. nonlinearity 80—75959
TGS, deuterated, paraelec. phase, D atom positions 78—14334
TGS, deuterated, undoped and alanine-doped, growth by rotating disc method and elec. props. 79—47611
TGS, deuterated and undeuterated, pyroelectric, dielectric and thermal props., temp. depend. 78—43809
TGS, dielec. behaviour near transition temp. 78—15127
TGS, dilatometric study, examination of logarithmic connection to classical Landau-type theory 78—6642
TGS, dispersion and temp. depend. of refr. index *(Russian)* 77—66472
TGS, domain boundaries, X-ray topographic study 78—48136
TGS, domain boundaries, X-ray topography 78—60409
TGS, domain growth shapes 78—27168
TGS, domain nucleation in AC elec. fields 80—34867
TGS, domain wall dynamics and small signal permitt., loss mechanism absence 78—43825
TGS, domain wall thickness determ. from longit. US wave propagation meas. 77—66463
TGS, effect of aniline in aqueous crystal growing soln. on physical props. 78—43810
TGS, effect of edge dislocations on shapes of moving domain boundary 80—20602
TGS, effect of Fe^{3+} admixture on phys. props. 80—76052
TGS, elastic and dielec. consts. from Brillouin scatt. 77—48180
TGS, elastic vs. polarisation energy near transition 78—15118
TGS, electrogyration during phase transitions 79—19859
TGS, electromech. coupling of surface acoustic waves near ferroelec. transition 78—19415
TGS, electrooptic switching anomalies 78—52473
TGS, electrostrictive and dielec. coeffs., neutron diffr. study 80—75943
TGS, emission of free charge carriers in vacuum as symptom of pyroelec. props. 79—42908
TGS, epitaxial growth method from soln., on Ag layer 77—32536
TGS, eqn. of state near ferroelec. Curie temp., including tunnel effect 77—12342
TGS, exponential switching by sidewise domain wall motion 80—29703
TGS, ferroelec., domain wall orientations and domain shapes 79—38508
TGS, ferroelec., meas. of sp.ht. at constant elec. flux density by AC method 79—33098
TGS, ferroelec., negative ENDOR study of radiation damage 78—19373
TGS, ferroelec., phonon contributions to anomalous sp. ht. near phase transition temp. 77—52023
TGS, ferroelec., positron lifetime meas. during phase transitions 78—6644
TGS, ferroelec., spontaneous polarisation, 2.2-20K 79—19849
TGS, ferroelec., thermal expansion 79—37855
TGS, ferroelec., vacuum cleaved, charge compensation 80—60510
TGS, ferroelec. activation field change 80—71358
TGS, ferroelec. cleavage surface microscopic struct. by electron microscopy 79—51403
TGS, ferroelec. crystal, Barkhausen effect study 79—38507
TGS, ferroelec. domain struct., polarisation obs. *(Chinese)* 80—20603
TGS, ferroelec. single crystal, low freq. nonlinear effects 80—84490
TGS, ferroelec. transition, electrooptical hysteresis and crit. behaviour of electrooptical props. 78—2817
TGS, ferroelec. transition, struct. changes, ^{13}C NMR obs. 78—60344
TGS, ferroelectric, domain pattern using pyroelectric effect 77—40196
TGS, ferroelectric crystal, non-linear pyroelec. effect in phase transition region 79—47393
TGS, ferroelectric domain exam., decoration with auramine 77—16268
TGS, ferroelectric hysteresis, dielectric and pyroelectric props. *(Chinese)* 80—88938
TGS, ferroelectric transition, neutron diffr. obs. 80—25324
TGS, gamma irrad. effects on heat capacity, Curie temp., permittivity 78—67737
TGS, growth from solution containing aniline, dielec. and pyroelec. props. 78—6639
TGS, growth of large area, doped and undoped crysts.. by rotating disc method 78—19652
TGS, interaction of γ-irrad., induced defect electron microscope expts. 79—10876
TGS, internal bias field, hysteresis loops *(Chinese)* 80—84705
TGS, internal field prod. in layer periodical domain struct. by X-ray irrad. 80—71359
TGS, kinetics of domain formation during phase transition 80—66130
TGS, L-α-alanine disordered regions, dielec. prop. changes in transition region 80—108159
TGS, large scale inhomogeneity effect on ferroelectric transition *(Russian)* 78—76411
TGS, layered domain struct. form., theory and expt. 77—52029
TGS, monocrystalline, ferroelectric, domain boundary dynamics contrib. to permittivity near Curie point *(Russian)* 79—73875
TGS, morphology of Au and AgCl films on complementary cleavage planes 79—15031
TGS, neutron diffraction enhancement near Curie point with DC field appl. *(Chinese)* 78—68462
TGS, optical props. in 5 to 22 eV region, reflectance spectra 79—33652
TGS, orientation depend. of l-alanine incorporation 78—42938

ferroelectric materials continued
TGS, paraelec. phase, elastic and thermoelastic consts. 77—47503
TGS, perfect and imperfect, sp. ht. and sound vel., crit. anomalies 80—71331
TGS, photoelastic const. behaviour new ferroelectric transition 78—19441
TGS, piezoelec. RF reson. rel. to ferroelec. domain struct. 77—16269
TGS, polarisation reversal, cryst. defects effect 78—27156
TGS, positron annihilation and ferroelectric transition 78—19594
TGS, proper and improper ferroelec., direct meas. of figure of merit 79—95711
TGS, pure and Cu doped, growth from soln., dislocation density 79—52096
TGS, pure and deuterated, domain wall thickness and surface energy 79—87408
TGS, pure and doped, thermal diffusivity, domain wall thickness determ. 79—42324
TGS, pure and Fe^{3+}-doped, thermal diffusivity, 25°C 79—90833
TGS, pure and nitroaniline-admixtured, longit. US wave propag., domain struct. effects 77—55322
TGS, pure and with lattice defects, elec. cond. 79—42538
TGS, pyroelec. IR detectors, permanent polarisation due to X-rays, optimum non-ferroelec. behaviour 77—41684
TGS, pyroelec. signal, domain struct. determ. 77—43951
TGS, pyroelec. single cryst., elec. field meas., thermally stimulated charges 80—45012
TGS, pyroelectric coeff., 1.8-300K, dynamic method *(French)* 79—19844
TGS, pyroelectric coeff., polarising field effect 79—47391
TGS, pyroelectric figures of merit 77—59519
TGS, refl. spectra 4-22 eV, optical consts. 79—4821
TGS, SAW phase velocity in b-plane 77—85043
TGS, sound group vel. vector direction, temp. depend. 78—67774
TGS, spin-lattice relax. meas. of ^{1}H, ^{13}C, and ^{15}N near ferroelec. transition 77—1646
TGS, spontaneous polarisation, low temp. meas. 80—75921
TGS, spontaneous polarisation and coercive field from 30 to 1000 Hz 77—66464
TGS, static and dynamic crit. behaviour of uniaxial ferroelectrics 78—35103
TGS, static crit. phenomena, lattice defect influence 80—71336
TGS, substrate for PbTE film, induced elec. inhomogeneity 77—15909
TGS, surface alignment of nematic liq. cryst. controlled by domain struct. 79—99068
TGS, switching induced electrolum. 79—38669
TGS, tan δ depend. upon sample thickness 77—59510
TGS, temp. depend. and effect of Cr and α-alanine impurities 78—91448
TGS, temp. depend. of spontaneous polarisation, microscopic mechanism, NMR expts. 77—81070
TGS, temp. depend. of spontaneous polarization near ferroelec. transition 79—33597
TGS, thermal expsn. coeffs. log. anomaly 79—28112
TGS, thermoluminesc. near Curie temp., effect of DC elec. field 79—33848
TGS, US propag. and vel. rel. to growth defects 79—28049
TGS, US relax., just above T$_c$, velocity and attenuation coeffs. 77—35637
TGS, US vel. and absorpt. anisotropy and crit. anomalies, acousto-opt. obs. 78—95574
TGS, US vel. and absorpt. in ferroelec. transition region 77—66461
TGS, vacuum-cleaved cryst., charge compensation, ferroelec. field effect obs. 78—95556
TGS, with radiation defects, dielec. dispersion 79—42882
TGS, X-irrad., glycine radicals, geom. struct. by ENDOR and INDO calc. 79—24230
TGS γ-ray irrad. cryst., heat capacity anomalies near phase transition *(Russian)* 80—49375
TGS ($-$d$_x$), sp. ht. near ferroelec. phase transition 80—70420
TGS and deuterated cpd., ferroelec. US relax. time constant 80—84257
TGS cleavage faces, ferroelec., oriented growth of Te 79—38509
TGS crystal, generation of second acoustic harmonics 78—18711
TGS crystals, influence of domain struct. on pyroelec. props. 78—31159
TGS crystals, thermal props., γ-radiation defects and inhomogeneity of domain deposition 79—46810
TGS crysts., effects of radiation induced defects on internal bias field 80—88941
TGS deuterated, X-irrad., negative ENDOR, collective motion 79—47357
TGS family, change of order of phase transition under hydrostatic pressure 78—52452
TGS powder, complex dielectric const. temp. depend. 79—47379
TGS powders, dielec. dispersion 80—97180
TGS substrate, ferroelec. field effect in Te films 79—42675
TGS substrate, for AgCl epitaxial growth, model system for orientation mechanism determ. during epitaxy 79—11022
TGS substrate, influence of polarisation reversal on elec. cond. of CdTe thin film 80—65720
TGS type ferroelectric, US absorpt. anomalies near T$_c$ 77—16264
TGS X-irradiated, paramag. relax, spin-echo study 80—7168
TGS-TGSe solid soln., phase transitions under hydrostatic press. 79—99840
TGS-type crystals:Cr^{3+}, radiospectroscopic studies 79—15341
TGSe:Cu^{2+}, EPR ang. depend., coord. of Cu^{2+}, Cu-ligand bond obs. and ferroelec. transition anomaly 80—7156
TGSe, acoustic and thermal anomaly correlation near ferroelec. transition 79—4775
TGSe, behaviour under press. near tricritical point 79—95716
TGSe, Brillouin scatt. spectra, depolarisation field effect 78—15177
TGSe, cryst., US vel., crit. anomaly and electromech. effects 79—55832
TGSe, Curie point press. coeff. tensor 79—33635
TGSe, deuterated, dielectric props., ageing 77—16257
TGSe, deuterated, thermal and dielectric props. at high hydrostatic press. 80—34864
TGSe, deuterised, elec. field induced Merz double hysteresis loop obs. 78—31164
TGSe, dielectric const. near ferroelec. transition temp., effect of surface capacitance 78—56438
TGSe, domain growth shapes 78—27168
TGSe, ferroelec., dielec. nonlinearity 80—75959
TGSe, ferroelec., domain wall orientations and domain shapes 79—38508
TGSe, ferroelec., effect of gamma irradiation on dielec., piezoelec. and elastic props. 77—43943

- **ferroelectric materials** continued
  - TGSe, ferroelec., meas. of sp.ht. at constant elec. flux density by AC method 79—33098
  - TGSe, ferroelec. transition, electrooptical hysteresis and crit. behaviour of electrooptical props. 78—2817
  - TGSe, hydrostatic pressure and deuteration effects on order of phase transition 77—12334
  - TGSe, IR trichroism, epitaxial prop. process 77—63475
  - TGSe, low freq. dielec. dispersion near Curie point 79—38432
  - TGSe, pyroelectric coeff., 1.8-300K, dynamic method *(French)* 79—19844
  - TGSe, sp. ht. anomaly, AC calorimetric obs. 78—23414
  - TGSe, surface layers effect on coercive field, spontaneous polarisation, and dielec. const. 79—61321
  - TGSe, therm. strains, electrostriction, by combined two-beam and holographic interferometry 79—3650
  - TGSe, US vel. and absorpt. anisotropy and crit. anomalies, acousto-opt. obs. 78—95574
  - TGSe, US vel. and absorpt. in ferroelec. transition region 77—66461
  - TGSe, US velocity and absorpt., 10 MHz, crit. anomalies 77—15504
  - TGSSe, autostabilised state, elec. second harmonic generation 80—103921
  - thiourea, Brillouin scatt., Debye relax. 79—87453
  - thiourea, commensurate-incommensurate phase transition, X-ray diffuse scatt. meas. *(French)* 79—19856
  - thiourea, cryst. with modulated struct., neutron scatt. obs. 79—95713
  - thiourea, dielec. const. and IR spectra in ferroelec. and antiferroelec. phases 79—33589
  - thiourea, expansion coeffs. in phase transition range 78—76407
  - thiourea, ferroelec., soft mode and Debye relax., IR reflection spectra 77—90111
  - thiourea, ferroelectric, Raman and IR study 80—71406
  - thiourea, ferroelectric transition, X-ray scatt. 79—47398
  - thiourea, incommensurate phase, soft modes, condensation of even-order harmonics 80—103313
  - thiourea, incommensurate phase transition, X-ray and neutron scatt. study 80—75963
  - thiourea, IR reflectivity study of ferroelec. and antiferroelec. phases, dielec. function model 79—33686
  - thiourea, lattice vibrs. in incommensurate phase 79—28056
  - thiourea, lock-in phase transform. 80—29698
  - thiourea, phase transitions accompanied by noncommensurate superstruct. form. 77—32336
  - thiourea, pyroelectric coeff., 1.8-300K, dynamic method *(French)* 79—19844
  - thiourea, Raman scattering spectra, soft mode frequency 79—24305
  - thiourea, thermally stimulated depolarisation currents, peaks interpreted in terms of molecular relaxations 78—19407
  - thiourea, X-ray diffuse scattering studies using high-pressure and low-temp. cell 80—86336
  - thiourea crystal, ferroelec., i.r. reflection spectra meas., shift of soft mode obs. *(French)* 77—4635
  - thiourea monocrystals, γ-irrad. effects on dielec. props. 79—91391
  - thiourea single cryst., γ-irrad. effect on elec. permittivity 78—64311
  - titanates, Lorentz elec. field, and short-range TiO interactions 77—43941
  - triboluminescence on piezo-electrification of surfaces during fracture 80—29815
  - triglycine fluoberyllate, deuterated, dislocation line defect X-ray topographic analysis 80—59465
  - triglycine fluoberyllate, pyroelectric, dielectric and thermal props., temp. depend. 78—43809
  - triglycine fluoroberyllate, ferroelec. transition, electrooptical hysteresis and crit. behaviour of electrooptical props. 78—2817
  - triglycine fluoroberyllate, spin-lattice relax. meas. of ^{1}H, ^{13}C, and ^{15}N near ferroelec. transition 77—1646
  - triglycine fluoroberyllate, thermodynamic props. 78—15123
  - triglycine selenate, ferroelec. coercive field as function of impressing rate of field 79—8108
  - triglycine sulfate crystal, nematic liquid crystal behaviour on cleavage face 79—94899
  - triglycine sulphate, ferroelec., decoration patterns on cleavage surface, domain obs. 80—97218
  - triglycine sulphate, paraelec. phase, thermal expansion coeff. and dielec. constant 79—8100
  - tris sarcosine calcium chloride:VO^{2+}, EPR and absorpt. spectra 78—60330
  - tris-sarcosine calcium bromide and chloride solid solns., Mn^{2+} doped, EPR linewidths and ferroelec. behaviour 79—24213
  - tris-sarcosine calcium chloride:Mn^{2+} ferroelec. dynamics, EPR and ENDOR study 80—75972
  - tris-sarcosine calcium chloride:Mn(Fe), influence of cryst. defects on ferroelec. transition, EPR 79—38466
  - tris-sarcosine calcium chloride, ferroelec., ferroelasticity and hypothetical hexagonal to orthorhombic phase transition 77—63377
  - tris-sarcosine calcium chloride, ferroelec. transition, order parameter 77—1204
  - tris-sarcosine calcium chloride, ferroelec. transitions, soft modes, Raman scatt. spectra obs. 80—80763
  - tris-sarcosine calcium chloride, phase transition, hydrostatic press. effect, dielec. const. meas. 80—71327
  - tris-sarcosine calcium chloride, US attenuation and vel., elastic consts., and permitt. near Curie temp. 79—37761
  - trisarcosine calcium chloride crystals, ferroelec., electrooptic and ferroelastic props. 80—34865
  - trissarcosine calcium chloride:Mn^{2+}, ferroelec., electron spin-lattice relax. 78—80208
  - trissarcosine calcium chloride, ferroelec. phase transition, Raman and Brillouin scatt. studies 80—71340
  - TSCC:Mn^{2+}, microscopic, mechanism of ferroelectric transition, EPR fine struct. tensor calc. 78—35104
  - TSCC ferroelastic monodomain crysts., dielec. behaviour 79—42888
  - TsTS-23, ferroelectric ceramic, 90° electric domain processes, mech. stress, X-ray diffr. 78—72478
  - tungsten-bronze ferroelectrics, $A_5B_{10}O_{30}$- and $A_6B_{10}O_{30}$-type, phase relations 78—35100
  - twisted smectic C phase, mol. conformation and orientational order, NMR studies, review 80—75151
  - vibron ferroelectric, intrinsic anomalous photovoltaic effect *(Russian)* 80—44665
  - vinylidene fluoride trifluoroethylene copolymer, ferroelec. behaviour 80—50284

- **ferroelectric materials** continued
  - vinylidene-fluoride-trifluoroethylene copolymer, piezoelectricity 80—88930
  - volume phase holographic storage in ferroelec. crysts. 78—82929
  - $Zn_3B_7O_{13}Br$, ferroelec. 43m-mm2 phase transition, molar heat capacity meas. 80—93249
  - Ag_3AsS_3, proustite, ferroelec. with no 180° polarisation reversal, ferroelec. phase transition 79—38465
  - Ag_3AsS_3, proustite, ferroelectric transition, thermodynamic description 79—69787
  - Ag_3AsS_3, prustite ferroelectric order model in prustite type nonlinear crystals *(Russian)* 79—65807
  - $AgNaNO_2$, ferroelectric transitions, one-mode model 80—29702
  - $AgNa(NO_2)_2$, ^{23}Na elec. field gradient tensor from NMR satellite lines near phase transition 80—71191
  - $AgNa(NO_2)_2$, crit. dynamics, hydrostatic press. effect, dielec. props. meas. 80—71328
  - $AgNa(NO_2)_2$, crit. sp. ht. near ferroelec. transition 79—38474
  - $AgNa(NO_2)_2$, ferroelec. transition, ^{23}Na elec. field gradient tensor, NMR meas. 79—4777
  - $AgNa(NO_2)_2$, ferroelectric transitions, group theoretic comparison with $NaNO_2$ 80—7311
  - $AgNa(NO_2)_2$, ferroelec. cryst., Raman spectrum, phase transition, comparative anal. with $NaNO_2$ 80—88935
  - $AgNa(NO_2)_2$, Landau behaviour of sp. ht. close to nearly tricritical ferroelec. phase transition 78—10861
  - $AgNa(NO_2)_2$, order-disorder ferroelec., influence of hydrostatic press. on polarisation dynamics 80—103913
  - $AgNa(NO_2)_2$, Raman spectrum, NO_2 bending vibr. 79—28737
  - $AgNa(NO_2)_2$, triplet absorpt. polarised spectra, near ferroelec. phase transition 79—47473
  - $AgNa(NO_2)_2$, ultraslow crit. dynamics of order parameter, ^{23}Na spin relax. times obs. 78—76410
  - Ag_3SbS_3, NQR elec. field effect, temp. depend. near ferroelec. transition 77—77121
  - Ag_3SbS_3, pyrargyrite, order-disorder phase transition and elec. polarisation 79—38468
  - Ag_5SbS_4, dielec. and acoustic props. *(German)* 78—64335
  - $(AsO_4)_2H_2(UO_2)_2.8H_2O$, point group symmetry for ferroelec., antiferroelec. and paraelect. phases 78—42983
  - $As_{0.2}Sb_{0.8}SI$ cryst., ferroelec., soft mode Raman and IR spectroscopy 80—76016
  - $As_xSb_{1-x}SI$ mixed crystals, phonon coupling, ferroelectric phase transition, Raman study 80—108165
  - $As_xSb_{1-x}SI$, solid solns., ferroelec. props. 78—23409
  - $(Ba, Ca)(Ti, Zr)O_3$, segregation of $CaTiO_3$ and effect on dielec. props. 78—38849
  - $(Ba,Sr)TiO_3$, ferroelec. solid solution, dielec. nonlinearity in nonpolar phase *(Russian)* 77—32317
  - $(Ba, Sr)TiO_3$ ferroelectric film, phys. props. in weak elec. fields 78—35098
  - $(Ba,Sr)TiO_3$, ferroelec. props., press. depend., anharmonic oscillator model 80—80716
  - $(Ba,Sr)Nb_2O_6$ monocrystal optical homogeneity requirement for light beam control 79—82952
  - $Ba_{0.25}$ $Sr_{0.75}Nb_2O_6$, inhomogeneous ferroelec., photorefractive effect 79—42935
  - $Ba_2AgNb_5O_{15}$, $Ba_2AgTa_5O_{15}$, ferroelec. and ferroelastic props. *(French)* 79—24266
  - $BaBi_4Ti_4O_{15}$, SHG, temp. depend. ferroelec.-ferroelec. transition 78—15121
  - $Ba_{0.92}Ca_{0.08}TiO_3$ ceramic, uniaxial stress effects, US dilatometric and dielec. meas. 78—52454
  - $Ba_3Fe_2BO_9$ (B=Re, Te, W, Mo), siegnette magnets with hexagonal barium titanate structure 78—76397
  - Ba_2FeSbO_6, siegnette magnets with hexagonal barium titanate structure 78—76397
  - $BaHfO_3$, $BaSnO_3$ and $BaZrO_3$, high-density ceramics prep. and elec. props. 80—60812
  - $BaMgF_4$:Mn^{2+} ferroelec., EPR and ENDOR study, cryst. field tensor 80—71162
  - $BaMn_{0.99}Co_{0.01}F_4$, magnetoelec. phenomena, dielec. behaviour near Neel temp. 80—71151
  - $BaMnF_4$, dielec. anomaly, mechanism, spin canting 78—10744
  - $BaMnF_4$, ferromag. ferroelectrics *(Japanese)* 79—65804
  - $BaMnF_4$, incommensurate transition, Brillouin scatt. investigation 79—87406
  - $BaMnF_4$, low temp. dielec. props. and phase transitions 77—20790
  - $BaMnF_4$, pure and Co doped, ferroelec. antiferromag., dielec. anomalies 80—71288
  - $BaMnF_4$, spectroscopy near ferroelec. transition, dielec. anomalies near mag. ordering temp. 80—75965
  - $BaMnO_4$, ferroelectrically induced ferromagnetism 77—73067
  - Ba_2MoO_5, Ba_3MoO_6, electrophys. props., effects of thermophys. props. of medium in synthesis 77—48375
  - $Ba_2Na(Nb,Ti)_5O_{15}$, prep. and electro-opt. props. 78—76432
  - $Ba_2NaNb_3O_{15}$, struct. phase transitions, light scatt. meas. 79—95774
  - $Ba_2NaNb_5O_{15}$, cathodlum. spectral and temp. depend. 78—84665
  - $Ba_2NaNb_5O_{15}$, cryst. comp. effect on low temp. phase transition 80—71346
  - $Ba_2NaNb_5O_{15}$ crystal domains, amplitude modulation of light by diffr. 79—59832
  - $Ba_2NaNb_5O_{15}$, electrooptic coeffs. and refractive indices 79—33673
  - $Ba_2NaNb_5O_{15}$, electrooptical diffr. by periodic domain struct. 80—40090
  - $Ba_2NaNb_5O_{15}$, ferroelastic transition sequence, cooperative pseudo-Jahn-Teller model 77—35689
  - $Ba_2NaNb_5O_{15}$, ferroelec. conversion to single domain, elec. and photoelec. props. 78—88271
  - $Ba_2NaNb_5O_{15}$, Gd substitution, effect on linear thermal expansion, possible BSN replacement 78—43153
  - $Ba_2NaNb_5O_{15}$, growth layer form., crystallization conditions effect, light diffr., Curie temp. 80—100778
  - $Ba_2NaNb_5O_{15}$, high press. phase transitions, Raman scatt. studies 80—71402
  - $Ba_2NaNb_5O_{15}$, incommensurate refls. near ferroelastic transition, neutron and X-ray precession obs. 80—70395
  - $Ba_2NaNb_5O_{15}$, kinetics of low temp. conversion into single domain form 77—43953
  - $Ba_2NaNb_5O_{15}$, local states, thermoluminesc. study 80—60690
  - $Ba_2NaNb_5O_{15}$, low temp. ferroelectric transitions, birefr. and dielec. meas. 79—38499

ferroelectric materials continued

$Ba_2NaNb_5O_{15}$, Raman spectra, soft oscillations, temp. depend. 78—31203
$Ba_2NaNb_5O_{15}$, Raman spectra in elec. field 79—1763
$Ba_{2.09}Na_{0.72}Nb_{5.02}O_{15}$, photocond. and optical absorpt. spectra 77—8149
$Ba_{2.09}Na_{0.72}Nb_{5.02}O_{15}$, cryst. growth, monodomenisation, detwinning, optical homogeneity, composition, dielec., spectral props. 77—44151
$Ba_{4+x}Na_{2-2x}Nb_{10}O_{30}$, tetragonal tungsten bronze structure ferroelec. mech. for ferroelec. transition 79—38481
$Ba_2NaNb_{5-x}Ti_xO_{15-x}F_x$ and $Ba_{2-x}Na_{1+x}Nb_5O_{15-x}F_x$, ferroelectric props., F substitution effect 77—12331
$Ba_2NaNb_5O_{15}$, crystals for electrooptics and nonlinear optics, optical inhomogeneities, review *(Japanese)* 77—65613
$Ba_3Nb_{10}O_{28}$, diffuse ferroelec. phase transition, dielec. const. and X-ray diffr. meas. 78—23419
$BaNb_x{}^{V}Ti_x{}^{III}Ti_{1-x}{}^{IV}O_3$, A and C-domain crysts., elec. cond. and absorption spectra 77—47805
$BaNiF_4$, obs. of anomalous pyroelec. behaviour due to cooperative mag. singularity 77—59517
BaO-Nd_2O_3-TiO_2-Bi_2O_3 system ceramics, high stability low loss dielectric preparation 80—81008
$(Ba_xSb_{1-x})TiO_3$ 80—60514
$Ba_{1.35}Sr_{0.65}NaNb_5O_{15}$ crystals, struct., dielec. and pyroelectric characts. 79—51913
$BaSr_{1-x}Nb_2O_6$, with diffused phase transition, photoelectret states 80—20583
$Ba_{0.25}Sr_{0.75}Nb_2O_6$, anomalous photovoltaic effect and photocond. 79—38122
$Ba_{0.25}Sr_{0.75}Nb_2O_6$, ferroelec., influence of temp. on Raman scatt. spectra 77—69842
$Ba_{0.25}Sr_{0.75}Nb_2O_6$, photocond. and optical absorpt. spectra 77—8149
$Ba_{0.25}Sr_{0.75}Nb_2O_6$, photovoltaic current, temp. and spectral depend. 78—47828
$Ba_{0.25}Sr_{0.75}Nb_2O_6$, spontaneous electroopticabsorption effect 78—19443
$Ba_{0.25}Sr_{0.75}Nb_2O_6$, thermal and spectral variations in the photovoltaic current in ferroelectrics 78—91719
$Ba_{0.5}Sr_{0.5}Nb_2O_6$, temp. depend. of Raman spectra 78—72524
$Ba_{0.54}Sr_{0.46}Nb_2O_6$, line broadening effect in Rayleigh scatt. of Mossbauer radiation 80—50238
$Ba_{0.54}Sr_{0.46}Nb_2O_6$:Y(La)(Tm), dielectric and electrooptic props. 78—68466
$(Ba_{1-x}Sr_x)_{1-y}(Nb_2O_6)_y$:$CeO_2$ crystals, photoelectric and photorefractive props., hologram recording 80—53239
$Ba_xSr_{1-x}Nb_2O_6$ (x=0.27 to 0.54) exam. of freq. dependence of permittivity diffuse ferroelectric phase transition kinetics 80—2703
$Ba_xSr_{1-x}Nb_2O_6$ crystals, struct., dielec. and pyroelectric characts. 79—51913
$Ba_xSr_{1-x}Nb_2O_6$, ferroelec., cathodlum. spectral and temp. depend. 78—84665
$Ba_xSr_{1-x}Nb_2O_6$, struct. and dielec. props., isomorphic substitution effect 78—27165
$Ba_xSr_{1-x}Nb_2O_6$:Ce, pure and doped, photoelec. props. and photorefraction 80—60538
$(BaSr)TiO_3$ film, ferroelec., dielec. props. in strong elec. fields 78—27163
$Ba_xSr_{1-x}TiO_3$, disordered ferroelec., dielec. const. and spontaneous polarisation meas. 78—48130
$Ba_xSr_{1-x}TiO_3$, ferroelec. film, heteroepitaxial growth in cathode sputtering 80—93486
$Ba_xSr_{1-x}TiO_3$, thin ferroelec. layers 79—42912
$BaT{:}O_3$, surface microrelief revealed by ion irradiation 80—54485
$BaT{:}O_3$:Mn, ferroelec. domain stabilisation by bulk ordering of defects 79—42925
BaTiO, mosaic struct. charge at ferroelec. phase transition *(Russian)* 77—32335
$BaTiO_2$, Fe-Co-Ti-Ba-O, composites, magnetoelectric effects, idealised analysis *(Russian)* 80—20440
$BaTiO_3$, 90° electric domain processes, mech. stress, X-ray diffr. 78—72478
$BaTiO_3$, A_1 and E optical phonons obs. in temp. range 10 to 132°C 77—27963
$BaTiO_3$, A_1-modes reflectivity meas. 79—65875
$BaTiO_3$, A_1(TO) phonon spectrum, ferroelectric phase transition, Raman scatt. meas. 78—56478
$BaTiO_3$ a-domain crystals, domain struct. influence on physical consts. 79—69798
$BaTiO_3$, acoustic wave interaction with microwave radiation field 80—6913
$BaTiO_3$, anisotropic emission of exoelectrons ferroelec. phase transitions *(Russian)* 78—48291
$BaTiO_3$, anomalous photovoltaic effect and photocond. 79—38122
$BaTiO_3$, antireson. in EPR spectra of Fe^{3+} ions *(Russian)* 80—11257
$BaTiO_3$, automatic anomalous noise meas. for ferroelectric capacitor parameters, not in equilib. *(French)* 78—74029
$BaTiO_3$, band struct. calc., interpretation of XPS and UPS spectra 80—70597
$BaTiO_3$, broadening of ferroelec. transition, heterophase fluctuations theory 77—81073
$BaTiO_3$, c-domain cryst., HF dispersion of permittivity 78—60379
$BaTiO_3$ ceramic, degradation under high AC elec. field 80—60499
$BaTiO_3$, ceramic, effect of grain size on nonlinear dielec. props. 77—8522
$BaTiO_3$ ceramic, mech. strength 78—64332
$BaTiO_3$ ceramic dielectric capacitor, processing prop. relations, hysteresis, permittivity 80—80730
$BaTiO_3$ ceramics, grain boundary pot. barriers, cathodoluminesc., electron probe anal. 80—2864
$BaTiO_3$ ceramics, PTC-type, grain boundary study using TEM 80—107267
$BaTiO_3$, Clausius-Mossotti formula and irreducible susceptibility *(Japanese)* 79—65802
$BaTiO_3$, Co substituted, ferroelec., diffuse behaviour 79—38475
$BaTiO_3$, coherent excitation of soft polariton mode 79—15464
$BaTiO_3$, controlled surface layers 78—48120
$BaTiO_3$, crit. X-ray scatt. 79—33636
$BaTiO_3$, crystallisation from melt, nucl. and final cryst. sizes 77—24951
$BaTiO_3$ crystals, mechanically compressed, dielec. const. 79—56711
$BaTiO_3$, crystn. from melts, comparison of different prospective oxy-anion solvents 80—71583
$BaTiO_3$, cubic, optical modes meas. by neutron scatt. 79—69213
$BaTiO_3$, defect chem., elec. cond. obs. 77—4097
$BaTiO_3$, deform. and stress relax. of single crysts. 77—59542

ferroelectric materials continued

$BaTiO_3$, dielec. and elastic consts., temp. depend. *(Russian)* 78—64307
$BaTiO_3$, dielec. and optical props. using shell model 79—33654
$BaTiO_3$, dielectric const. and polarisation, fluctuations, catastrophes 77—8491
$BaTiO_3$, diffr. of Mossbauer radiation near Curie point *(Russian)* 79—8079
$BaTiO_3$, displacive type ferroelectric, SHG 79—36955
$BaTiO_3$, domain structure obs. using SEM 77—1647
$BaTiO_3$, domain struct., formation at phase transitions 79—38510
$BaTiO_3$, doped, loss mechanism and domain stabilisation 78—84542
$BaTiO_3$, doped-undoped ceramic composites, sintering behaviour 79—100094
$BaTiO_3$, Doppler-broadened positron annihilation 78—64428
$BaTiO_3$, dynamic Rayleigh light scatt. in region of ferroelectric-paraelectric transition 78—64371
$BaTiO_3$, effect of phase transformation on fracture behaviour 78—48507
$BaTiO_3$, elastooptic effect near ferroelec. transition, temp. depend. 80—97233
$BaTiO_3$, electron exoemission unipolarity associated with phase transitions 80—97415
$BaTiO_3$, electron microscopy investigs. of ferroelec. substances, review *(Japanese)* 80—71366
$BaTiO_3$, electronic props., SCF-MS-Xα calc. 80—54607
$BaTiO_3$, electronic struct., XPS and band struct. calc. 79—38708
$BaTiO_3$, epitaxial ferroelectric, appl. of electron microprobe methods 80—44443
$BaTiO_3$, epitaxial films and single domain crysts., exoelectron emission obs. of phase transition 79—74069
$BaTiO_3$, exam. of anomalous pyroelectric effect above Curie point 79—33613
$BaTiO_3$, exoelectron emission during phase transition, orientational depend. 79—69786
$BaTiO_3$ family, unified phenomenological theory, spherical system of transition parameters 77—31751
$BaTiO_3$, ferroelec., appl. of pseudo-ionic model for ionic cryst. 79—33049
$BaTiO_3$, ferroelec., elec. field in 90° domain walls 80—2713
$BaTiO_3$, ferroelec., nonlinear optical susceptibility calc. 78—9409
$BaTiO_3$, ferroelec., reduction of hysteresis losses 79—42926
$BaTiO_3$, ferroelec., susceptibility of eight site order-disorder model calcs. 77—8523
$BaTiO_3$, ferroelec., X-ray diffr. topographic study of polarisation reversal 79—38442
$BaTiO_3$, ferroelec. ceramic, 90° domain rot. in fixed elec. field 80—7315
$BaTiO_3$, ferroelec. cryst., IR and Raman spectra, mode coupling 80—66194
$BaTiO_3$, ferroelec. domain boundary struct., TEM 77—24806
$BaTiO_3$, ferroelec. domain form., X-ray topography 79—78638
$BaTiO_3$, ferroelec. phase transition, soft phonons, Raman scatt. obs. *(Japanese)* 79—65880
$BaTiO_3$, ferroelec. temp. depend. of broad A_1 (TO) phonon Raman linewidth 78—2857
$BaTiO_3$, ferroelec. thin films, r.f. sputtering, X-ray and microprobe obs. 79—47627
$BaTiO_3$, ferroelec. to paraelec. transform., influence of domain boundaries on interface struct. 79—95718
$BaTiO_3$, ferroelectric transitions rel. to Earth and planetary interiors 77—53045
$BaTiO_3$, ferroelectric ceramic, dielec., piezoelec. and elastic props., orientational contrib. 78—68468
$BaTiO_3$, ferroelectric polydomain crysts., piezoresonance effects, appl. as transducer 79—4779
$BaTiO_3$, ferroelectric domains, X-ray topography 79—65815
$BaTiO_3$, ferroelectric-paraelectric transform., basic struct. and characts. 79—95717
$BaTiO_3$, ferroelectric mechanisms, anharmonic couplings by scanning IR interferometry 80—75978
$BaTiO_3$, ferroic materials, fracture processes 80—79869
$BaTiO_3$ film, ferroelec., composition profiles by Auger electron spectra anal. 79—66391
$BaTiO_3$, film, ferroelectricity of vap. deposited coating 79—69781
$BaTiO_3$ film, sputtered, refr. index, 0.3-1.0 μm, substrate temp. effects 77—55840
$BaTiO_3$ film, struct. and dielec. props. 80—60514
$BaTiO_3$ film, surface layer nature, AES obs., and effect on permittivity 77—24498
$BaTiO_3$ film, unstable modulated struct. near ferroelec. phase transition 78—27164
$BaTiO_3$, film deposition by HF cathode sputtering 77—36398
$BaTiO_3$ films, ferroelec., effect of elec. field on dielec. props. 79—33642
$BaTiO_3$, head to head and tail to tail domains 78—43826
$BaTiO_3$, internal stress and strength, failure mechanism 80—66128
$BaTiO_3$, intrinsic luminesc. 80—71467
$BaTiO_3$, isotropic dielectric, US vel. and longit. elec. field *(Russian)* 78—38785
$BaTiO_3$, K-edge X-ray absorpt., cond. band states 80—97382
$BaTiO_3$, LF relaxational polarisation 78—68460
$BaTiO_3$, laminar domains, periodic motion under const. elec. field 78—15133
$BaTiO_3$, light scatt., Comes Lambert Guinier model 79—15471
$BaTiO_3$, line broadening effect in Rayleigh scatt. of Mossbauer radiation 80—50238
$BaTiO_3$, logarithmic velocity variations for longitudinal US waves near ferroelec. transition 78—72472
$BaTiO_3$, magnetochemical exam. of phase transition, mag. suscept. meas. 78—88265
$BaTiO_3$, martensite type phase transition 78—64326
$BaTiO_3$, mean square atomic displacement temp. depend., sublattice vibration anharmonicity 80—79890
$BaTiO_3$, melt grown, drift mobility meas. 79—19596
$BaTiO_3$, molecular field statistical model, ferroelectric materials, props. *(French)* 79—69793
$BaTiO_3$, monocrystalline, dielectric loss after superposition of unidirectional electric field time depend. *(Slovak)* 78—52435
$BaTiO_3$, Mossbauer spectrum, isomer shift and quadrupolar splitting, internal elec. field effects 79—56648
$BaTiO_3$, Mossbauer spectroscopy, sample prep. and results 80—66078
$BaTiO_3$, nonstoichiometry of vac. condensates, effect on dielectric props. 77—16260
$BaTiO_3$, O K_α X-ray emission band spectra *(Russian)* 79—15563
$BaTiO_3$ on Si substrate, prep. and elec. props., expt. 77—20460

ferroelectric materials continued

- $BaTiO_3$, para to ferroelec. transition, strong Rayleigh scatt. 78-76486
- $BaTiO_3$, paraelec. cryst., electro-optical absorpt. near Curie temp. 77-1657
- $BaTiO_3$, paraelec. phase, stabilisation of soft mode 80-75985
- $BaTiO_3$, paraelectric crystal, nonlinear props. 80-84699
- $BaTiO_3$, periodic domain struct. and opalescence at tetragonal to orthorhombic transition 80-66131
- $BaTiO_3$, permittivity, low freq. and lattice contribs. 78-15105
- $BaTiO_3$, photo-ferroelectric noise effect *(Russian)* 78-52450
- $BaTiO_3$, photocond. of doped single cryst., photoexcitable levels 77-4391
- $BaTiO_3$, photoferroelec., lighting effect on deform. and stresses 78-43802
- $BaTiO_3$, piezoceramic, nonlinear piezoeffect 79-42900
- $BaTiO_3$, piezoelectric ceramic, secondary electron emission yield 79-91546
- $BaTiO_3$, planar phase boundaries and domain struct. 79-69795
- $BaTiO_3$, polarisation reversal and surface neutralisation 78-27169
- $BaTiO_3$, polarisation switching, influence of charges arising from defects 79-69796
- $BaTiO_3$, polariton freq. meas. by Raman scattering and permittivity 78-76006
- $BaTiO_3$, polycryst., form. from coprecip. products 77-24997
- $BaTiO_3$, polycryst., prep. from coprecipitated $BaCO_3$-BaF_2-$TiO(OH)_2$ 77-24996
- $BaTiO_3$, polycryst., phase transition obs. in −170 to 220°C range *(Russian)* 80-103474
- $BaTiO_3$, polycrystalline, X-ray diffraction, Curie temp., lattice defects, phase changes 79-99830
- $BaTiO_3$, polycrystalline, dielec. nonlinearity coeffs. difference in free and clamped specimens *(Russian)* 80-25314
- $BaTiO_3$, polycrystalline ferroelectric, grain-size dependent props. 80-71352
- $BaTiO_3$ polydomain crystals, dielec. props. 78-43827
- $BaTiO_3$, polydomain ferroelec. crysts., phys. consts., self consistent calcs. 80-88942
- $BaTiO_3$ polymorph, hexagonal, low temp. and surface CO_3 adsorption and desorption 80-80713
- $BaTiO_3$, pot. functions of ions 80-19885
- $BaTiO_3$, powders, Bragg reflection integral intensities due to structural anomalies 80-107098
- $BaTiO_3$, pure, dielec. behaviour at ultralow freq. 79-38425
- $BaTiO_3$, pure, dielectric const. and elastic compliance temp. depend. for various phases 79-19830
- $BaTiO_3$, pure and doped, cryst. growth and chemical composition 77-40349
- $BaTiO_3$, pure and doped, photocurrent kinetics 79-42576
- $BaTiO_3$, pure and doped crysts., surface and domain struct., AES and SEM expts. 80-71363
- $BaTiO_3$, pure and Fe doped, ferroelec., switching and electrolum. 80-76079
- $BaTiO_3$, quadratic electro-optic effect, incident light wavelength depend. 80-16010
- $BaTiO_3$, Raman intensity analysis, symmetry coords., optical modes, electro-opt. consts. 79-95740
- $BaTiO_3$, reduction inhibition by impurity ions 80-101018
- $BaTiO_3$, secondary struct. periodic motion 80-15993
- $BaTiO_3$, single cryst., dielec. breakdown and electroluminesc. 78-2917
- $BaTiO_3$, single crysts., electron microscope study of domain and defect structs. 79-15425
- $BaTiO_3$, single crysts., dielec. spectrum 80-25275
- $BaTiO_3$, soft mode dielec., anomalous low temp. sp. ht. 78-14423
- $BaTiO_3$, soft mode exam. 79-37799
- $BaTiO_3$, soft mode spectroscopy IR refl. meas. 80-88982
- $BaTiO_3$, spontaneous polarisation, low temp. meas. 80-75921
- $BaTiO_3$, struct. changes due to cubic-tetragonal phase transition 78-60407
- $BaTiO_3$, struct. phase transitions, light scatt. meas. 79-95774
- $BaTiO_3$, surface layer exam. 78-43805
- $BaTiO_3$, surface microrelief after ion irrad. 80-59774
- $BaTiO_3$, surface study using AES and ion scatt. spectroscopy 80-65339
- $BaTiO_3$, tetragonal, model for temp. depend. of dielec. const., ferro-paraelectric transition 78-43771
- $BaTiO_3$, tetragonal, over-damped soft E-polariton and dielec. dispersion 78-15111
- $BaTiO_3$, thermodynamic props. 77-39680
- $BaTiO_3$ thin film microwave complex permittivity meas. 79-73879
- $BaTiO_3$, transform. of cryst. struct., at cubic-to-tetragonal phase transitions 79-37827
- $BaTiO_3$, transport and optical props., small polaron hopping theory 79-47096
- $BaTiO_3$, tricrit. point 77-63378
- $BaTiO_3$ type crystal, thermodynamic analysis of struct. phase transitions *(Russian)* 80-103473
- $BaTiO_3$ type crystals, determ. of phase transitions using symmetry breaking theory *(French)* 78-83950
- $BaTiO_3$ type ferroelectrics, surface acoustic waves on domain boundaries 79-90860
- $BaTiO_3$ type perovskite ferroelectric, neutron irradiated. amplification of freq. dispersion of permittivity *(Russian)* 78-52419
- $BaTiO_3$ type vibronic ferroelectric, light induced refractive index change *(Russian)* 79-91399
- $BaTiO_3$, undoped and Cu doped, Γ_{15} phonon freezing, electronic instability, LCAO calc. 80-25318
- $BaTiO_3$, unipolar cryst., topography of defect. and thermodepolarisation currents 77-43954
- $BaTiO_3$, vacuum UV spectra and electro-optical prop. *(Japanese)* 79-65900
- $BaTiO_3$, valence band UPS and partial p and d density of states 80-71560
- $BaTiO_3$, vibronic ferroelec., spontaneous birefringence calc. 78-68473
- $BaTiO_3$, vibronic theory and opt. props. 80-103939
- $BaTiO_3$, X-ray diffr. intensities, anomalous temp. depend. *(Russian)* 79-1484
- $BaTiO_3$, X-ray irrad. effect on dielec. props. 78-15082
- $BaTiO_3$:$BaTi_3O_7$, dielec. props. and microstruct. 80-60481
- $BaTiO_3$:C, solubility of C at low O_2 potentials, 800°C 80-100334
- $BaTiO_3$:Co, charact. behaviour of spontaneous polarisation and dielec. const. 78-60382
- $BaTiO_3$:Co, tricritical point, X-ray diffr. meas. 80-71341

ferroelectric materials continued

- $BaTiO_3$:Cu, photoferroelec. props., Jahn-Teller effect, laser irrad. effect on pyroelec. props. 78-60400
- $BaTiO_3$:Dy ceramic, sintering, grain size, characterisation and props. 77-55923
- $BaTiO_3$:Fe, photoinduced Rayleigh scatt. and bulk photovoltaic effect 79-38554
- $BaTiO_3$:Fe, short circuit photocurrent, depend. on polarization 79-38121
- $BaTiO_3$:Fe^{3+}, local position of Fe^{3+} in ferroelec. phases, EPR study 80-25196
- $BaTiO_3$:Fe^{3+}, local position determ. by EPR 80-108057
- $BaTiO_3$:Fe^{3+} bulk photovoltaic effect and photoinduced Rayleigh scatt. 77-77226
- $BaTiO_3$:Hf, crystal field distortion by stacking faults, PAC meas. 80-11306
- $BaTiO_3$:Mn, polycrystn., annealing effect on transition temps. 80-3100
- $BaTiO_3$:Mn^{2+}, electrooptical effect, charge transfer mechanism, defect. pair form. 79-38519
- $BaTiO_3$:Nb, ferroelec. and paraelec. phases, props. 79-42919
- $BaTiO_3$:X(X=Cr, Mn, Fe, Co, Ni, Zn, Ga), annealed in H_2 and O_2, valence change in phase stability 80-20600
- $BaTiO_3$:ZrO_2, dielec. loss tangent and const. 79-4769
- $BaTiO_3$-$BaNb_2O_6$ system, solid solns. of tungsten bronze struct. of type $BA_{5+x/2}Nb_{10-x}Ti_xO_{30}$ 77-52021
- $BaTiO_3$-$BaNbO_3$ system, solid solns., thermal ionic relaxation, vacancy form. 77-8499
- $BaTiO_3$-$BiFeO_3$ solid solns., ferroelec.-antiferromag., magnetoelectric effect at ferroelec. transition 80-100637
- $BaTiO_3$-KCl composite cryst., F-centres, thermoluminesc., DC field and X-irrad. effects 78-2926
- $BaTiO_3$-Ni ferrite, piezoelectric-piezomagnetic sintered two-phase composite, magnetoelec. conversion 77-12181
- $BaTiO_3$-type ferroelectrics, existence of noncommensurate phases due to gradient term in free energy 79-69792
- $BaTiO_{3-x}$, ferroelec., Auger spectroscopy of surface layers 79-42343
- $BaTiO_{3\ x}$, single cryst. and film, Auger spectra, surface comp. 78-27353
- $Ba_2Ti_9O_{20}$ single crysts., prep. and unit-cell parameters 80-103302
- $BaTi_{0.98}Sn_{0.02}O_3$, ferroelec. film, switching process 80-60518
- $Ba(Ti_{0.98}Sn_{0.02})O_3$ film, ferroelec., switching process in elec. field with rectangular impulses, domain wall nucleation and motion 80-2714
- $Ba(Ti_xSn_{1-x})O_3$ film, struct. and dielec. props. 80-60514
- $Be_4Ti_2O_{12}$ grain oriented ferroelectric ceramic, prep. by molten salt synthesis-tape casting method 80-40296
- $(Bi_{2/3},Sr)TiO_3$, ferroelec. solid solution, dielec. nonlinearity in nonpolar phase *(Russian)* 77-32317
- Bi complex oxides, antiferroelec. and ferroelec., pyrochlore struct., dielec. and structural study 79-38488
- Bi oxides containing perovskite layers, ferroelec. cryst., electron microscopy, dislocation and domain boundaries 77-52030
- $Bi_2Bi_4Fe_2Ti_3O_8$, dielec. and magnetoelec. props. 78-95562
- $BiBi_4Ti_3FeO_{15}$, perovskite-like layer-type ferroelec. magnetic cpd., Mossbauer expts., 80-1200K 78-64329
- $BiFeO_3$, ferroelec., antiferromag., cryst. and mag. struct., neutron diffr. study 80-65786
- $BiFeO_3$-$Pb(Fe_{0.5}Nb_{0.5})O_3$, ferroelec., magnetoelec. obs. temp. and conc. depend. 80-50156
- Bi_3GeVO_9, dielec. props. and twin struct. 77-12350
- Bi_2MoO_6 ceramic, permittivity, ferroelec. T_c and hysteresis 79-82932
- $Bi_xSb_{1\ x}SI$, atomic substitution and ferroelec. phase transition 78-68464
- $Bi_{12}SiO_{20}$, optical information recording, PROM device resolution 79-41443
- $Bi_9Ti_3Fe_5O_{27}$, combined hyperfine interaction 79-28663
- $Bi_4Ti_3O_{12}$ ceramics, ferroelectric, hot-forged, grain orientation and dielectric props. 80-40076
- $Bi_4Ti_3O_{12}$, elec. characts., phase transition obs. 80-60517
- $Bi_4Ti_3O_{12}$, IR refl. spectrum, 60-2000 cm^{-1} 77-69843
- $Bi_4Ti_3O_{12}$, thick single cryst. growth from Bi_2O_3-B_2O_3-TiO_2 77-8746
- $Bi_4Ti_3O_{12}$-CdS optical storage plane 77-39006
- $Bi_xTi_yO_z$, poling method 77-59544
- $Bi_2TiO_4F_2$, one-layer perovskite-like ferroelec., dielec. study 79-38486
- $Bi_7Ti_{2.5}Sn_{0.5}Fe_3O_{21}$, layered ferroelec. antiferromag., superparamagnetism, Mossbauer spectra obs. 77-51999
- Bi_2WO_6, ferroelectric, dielectric props., elec. cond. and relaxation phenomena obs. 80-80692
- Bi_2WO_6 grain oriented ferroelectric ceramic, prep. by molten salt synthesis-tape casting method 80-40296
- Bi_2WO_6, ionic cond. and relaxation polarisation, capacitance, losses 80-24657
- Bi_2WO_6, layer-like ferroelec., cryst. growth 78-23598
- Bi_2WO_6 layered ferroelectric, anomalous photovoltaic effect, photovoltaic current 80-75603
- Bi_2WO_6 single crystal, growth from flux in Bi_2WO_6-Na_2WO_4, below transformation temperature 78-72713
- $C(NH_2)_3Al(SO_4)_26H_2O$:Cr^{3+}, isotope effect, zero field splitting, vibr. coupling temp. depend. 78-6570
- $CaB_3O_4(OH)_3.2H_2O$, NMR of ^{11}B in crit. region 77-16199
- $Ca_2Nb_2O_7$, ferroelec., temp. depend. of SHG intensity 79-24267
- $CaSnO_3$ and $CaZrO_3$, high-density ceramics prep. and elec. props. 80-60812
- $Ca_{1-y}Sr_{y/2}Ba_{y/2}Zr_{1-x}Ti_xO_3$, ceramic system, dielectric props., microwave resonator application 80-80674
- $CaTiO_3$, O K_α X-ray emission band spectra *(Russian)* 79-15563
- $Ca_3(VO_4)_2$, new high temp. ferroelectric, Curie temp. 78-43811
- Cd-perovskites, $CdXO_3$ (X=Ti,Zr,Hf,Sn), electric field gradient temp. depend. 78-39454
- $Cd_2(NH_4)_2(SO_4)_3$, X-ray and optical studies of ferroelec. phase transition 79-38495
- $Cd_2Nb_2O_7$, ferroelec., sp. ht. and Debye temp. meas., 2-25K 79-73319
- $Cd_2Nb_2O_6S$, pyrochlore struct., ferroelec., dielec. and structural study 79-38488
- $Cd_{1.6}Pd_{0.4}Nb_2O_7$, ferroelec., sp. ht. and Debye temp. meas., 2-25K 79-73319
- $CdTiO_3$, perovskite, elec. quadrupole interactions, TDPAC meas. 78-31129
- $CdTiO_3$, single cryst. growth and props. 79-100046
- $CeTiNbO_6$, electrophys. props. 78-23388
- $Ce_2Ti_2O_7$, ferroelec., temp. depend. of SHG intensity 79-24267
- $Co_3B_7O_{13}Cl$, polydomain ferroelec., magnetoelec. effect below Neel temp. 78-10745

ferroelectric materials continued
$Co_3B_7O_{13}I$, intermediate phase between paraelectric and ferroelectric phase *(Russian)* 78-68465
$Co_3B_7O_{13}I$, neutron diffr. investig. of mag. and cryst. struct., ferro- and paraelec. phases 77-32170
$Co_3B_7O_{13}X$, X=Cl, Br, I, ferromag. ferroelectrics *(Japanese)* 79-65804
$Cr_3B_7O_{13}Cl$, ferroelec. 43m-mm2 phase transition, molar heat capacity meas. 80-93249
Cr_2BeO_4, magnetoferroelectricity, weak pyroelectric effect 79-42914
$Cs(B_xW_{3-x})O_9$ (B=Na, Ca, Co, Ni, Cd, Ga, Bi, Nb, Ta) cryst. struct., temp. dielec. anomalies 80-1998
Cs_2CdBr_4, struct. phase transitions, NQR study 80-71343
CsD_2AsO_4, ferroelec., elastic consts., HF meas. 77-8524
CsD_2AsO_4, ferroelect. phase transition, NMR study *(Chinese)* 79-33644
CsD_2AsO_4, shorted and free single crysts., piezoelec. coupled soft mode, Brillouin scatt. meas. 77-52109
$Cs(D_{1-x}H_x)_2AsO_4$, high temp. nondestructive phase transform. at 170°C 77-12337
$Cs(D_xH_{1-x})_2AsO_4$, cryst. struct. in ferroelec. and paraelec. phases neutron diffr. meas. 77-7694
$Cs(D_xH_{1-x})_2AsO_4$, isotope exchange during crystallisation from aqueous solns. 78-18569
$Cs(D_xH_{1-x})_2AsO_4$, phase transition exam. 77-12340
$Cs(D_xH_{1-x})_2PO_4$, isotope exchange during crystallisation from aqueous solns. 78-18569
CsD_2PO_4, dielec. props., press. and temp. depend. 80-25317
CsD_2PO_4, neutron scatt. study of ferroelectric phase transitions 77-59538
CsD_2PO_4, one dimens. ordering, ferroelec. transitions, neutron scatt. study 80-25316
CsD_2PO_4, pseudo-one-dimensional ferroelectric transition, ^{31}P chemical shift and relaxation study 80-66123
CsD_2PO_4, pseudo-one-dimens. ferroelec. transition, DMR and relax. study 80-71223
CsD_2PO_4, pseudo-one-dimensional ferrolec. and antiferroelec. transitions, phase diagram obs., soft modes 80-93245
CsH_2AsO_4 and $Cs(H_xD_{1-x})_2AsO_4$, acoustooptical and photoelastic props. 78-27181
CsH_2AsO_4, and deuterated derivative, attenuation of LF elastic oscills. 77-7791
CsH_2AsO_4, and deuterated isomorph, E-mode splitting in ferroelec. phase, Raman scatt. meas. 77-16296
CsH_2AsO_4, and deuterated isomorph., ferroelectric mode and molecular vibr. press. depend. 78-19424
CsH_2AsO_4, elastic props., photoelasticity near ferroelectric phase transition 80-29107
CsH_2AsO_4, ferroelec., temp. depend. of shear angle, neutron scatt. meas. 77-8524
CsH_2AsO_4, ferroelec., RF dielec. relax., loss mech. 79-38448
CsH_2AsO_4, Mandelstam-Brillouin spectra and US vel. meas. near ferroelec. Curie point 79-38553
CsH_2AsO_4, pres. depend., LF dielec. response, ferroelec. props. 78-15120
CsH_2AsO_4, pyroelectric investig. in ferroelec. phase 77-12321
CsH_2AsO_4, RF dielec. response close to transition temp. 77-90099
CsH_2AsO_4, shorted and free single crysts., piezoelec. coupled soft mode, Brillouin scatt. meas. 77-52109
$Cs(H_{1-x}D_x)_2PO_4$, dielec. props., temp. meas. 80-71335
CsH_2PO_4 and CsD_2PO_4, dielectric props. and ferroelec. transition temp. 77-12335
CsH_2PO_4 and CsD_2PO_4, pseudo one-dimens. ferroelec. ordering dynamics, ^{31}P NMR study 80-75971
CsH_2PO_4, dielec. props., press. and temp. depend. 80-25317
CsH_2PO_4, domain obs. in paraelectric phase 79-24277
CsH_2PO_4, ferroelec. transition, deuteration and press. effects 78-35101
CsH_2PO_4, ferroelec., press. induced antiferroelectricity 79-4774
CsH_2PO_4, ferroelec., X-ray and dielec. studies on phase transition 79-38477
CsH_2PO_4, ferroelec., critical behaviour of dielec. constant 80-34845
CsH_2PO_4, ferroelec. transition, electrooptic 80-76005
CsH_2PO_4, ferroelec., X-ray struct. study at room temp. 80-88113
CsH_2PO_4, ferroelec. transition, neutron diffr. study 80-93247
CsH_2PO_4, NMR of ^{133}Cs, elec. field gradient 78-15034
CsH_2PO_4, neutron-diffraction study of cryst. struct. in paraelectric phase 78-79592
CsH_2PO_4, one dimens. ordering, ferroelec. transitions, neutron scatt. study 80-25316
CsH_2PO_4, paraelectric phase, struct. exam. by neutron diffr. 79-37679
CsH_2PO_4, press.-induced antiferroelectricity *(Japanese)* 80-15992
$CsH_2PO_4(CsD_2PO_4)$, permittivity temp. depend., pseudo one-dimens. ferroelectric ordering and critical props., NMR 79-78635
$Cs_3MoO_3F_3$, ferroelec. and order-disorder phase transitions 78-92037
$Cs_3MoO_3F_3$, ferroelec., transition obs. 80-75989
$CsPbBr_3$, critical thermodynamic props. around successive phase transitions 79-33627
$CsPbCl_3$, critical thermodynamic props. around successive phase transitions 79-33627
$CsPbCl_3$, n.q.r. spin-lattice relax. near cubic-tetragonal transition, soft modes 77-1616
$CsR(MoO_4)$ R=Dy, Ho, Er, permittivity temp. depend., polymorphic transition 80-92670
$Cs_2RbMoO_3F_3$, and $Cs_2RbWO_3F_3$, ferroelec., transition obs. 80-75989
Cs_2SO_4-$(NH_4)_2SO_4$ mixed cryst., ferroelec. transition, structural and dielec. props., proton spin-lattice relax. 78-39512
$Cs_3WO_3F_3$, ferroelec. and order-disorder phase transitions 78-92037
$Cs_3WO_3F_3$, ferroelec., transition obs. 80-75989
Cu-Cl boracite, ferroelec., X-ray study on phase transition 79-33622
Cu-Cl boracite, pyroelec. coeff. meas. 80-75951
$Cu_3B_7O_{13}Cl$, ferroelec. 43m-mm2 phase transition, molar heat capacity meas. 80-93249
$Cu_3B_7O_{13}Cl$, Raman study of ferroelec. phase transition 79-38529
$Cu_3B_7O_{13}Cl(Br)$, piezoelectric, elastic and electromechanical coefficients *(French)* 78-39504
$Cu_3B_7O_{13}X$, X=Cl, Br, ferromag. ferroelectrics *(Japanese)* 79-65804
DBr(DCl), solid, ferroelec. and paraelec. phases, transitions, Raman scatt. 77-43980
dicalcium strontium propionate, electro-opt. props. 78-76426
$Dy_2(MoO_4)_3$, cryst. growth and props. 79-55727
$ErNbO_4$, ^{93}Nb NQR spectra, 77 to 450K 79-38401

ferroelectric materials continued
$Eu_{0.5}Ba_{0.5}TiO_3$, ferromag., ferroelec., ceramic, Curie temps. determ. 78-68230
Fe-I boracite, pyroelec. coeff. meas. 80-75951
$Fe_3B_7O_{13}Br$, $Fe_3B_7O_{13}Cl$, polydomain ferroelec., magnetoelec. effect below Neel temp. 78-10745
$Fe_3B_7O_{13}I$, electro-opt. props. 78-76426
$Fe_3B_7O_{13}I$, ferroelec., mag. ordering, neutron diffr. meas. 78-72331
$Fe_3B_7O_{13}I$, ferroelec. 43m-mm2 phase transition, molar heat capacity meas. 80-93249
$Fe_3B_7O_{13}I$, improper ferroelectric, dielectric props., IR radiation pyroelectric detection 80-80711
$Fe_3B_7O_{13}I$, spontaneous polarisation, dielec. const., d.c. resist., sp. ht. 77-1643
$Fe_3B_7O_{13}I$, twinning in orthorhombic phase, ferroelec. domain struct. with switching 78-19434
$Fe_3B_7O_{13}X$, X=Cl, Br, I, ferromag. ferroelectrics *(Japanese)* 79-65804
$(Fe_xCr_{1-x})_2O_3$ corundum-type solid solution single crystal growth, chem. vapour transport 80-93465
Fe_3O_4, ferromag. ferroelectrics *(Japanese)* 79-65804
Fe_3O_4, lattice parameters, NMR freqs., and magnetoelec. pots. near 12K 80-71146
$Gd_2(MoO_4)$, ferroelec., Raman scatt. from soft modes 77-85706
$Gd_2(MoO_4)_3$, and isotypes exam. of crystal growth, and defect generation 78-68617
β-$Gd_2(MoO_4)_3$, antiferromag., polarised ferroelec., ferroelastic, magnetothermodynamics 79-7996
$Gd_2(MoO_4)_3$, antiphase boundaries and phase transforms., electron microscope obs. 78-15134
$Gd_2(MoO_4)_3$, crysts., elastic props. during domain switching under mech. loading 79-55809
$Gd_2(MoO_4)_3$, domain structure obs. by GdF_3 decoration 78-84544
$Gd_2(MoO_4)_3$, domain wall motion dynamics 80-108030
$Gd_2(MoO_4)_3$, EM wave diffr. by domain walls 79-69799
$Gd_2(MoO_4)_3$, effect of ferroelec. ordering on refractive index 79-33653
$Gd_2(MoO_4)_3$, electro-opt. props. 78-76426
$Gd_2(MoO_4)_3$, electron microscope exam. of ferroelec. and ferroelastic props., domain walls and cryst. defects 77-69786
$Gd_2(MoO_4)_3$, electron microscopy investigs. of ferroelec. substances, review *(Japanese)* 80-71366
$Gd_2(MoO_4)_3$, ferroelastic, laser-induced twinning 77-76422
$Gd_2(MoO_4)_3$, ferroelec., anomalous damping of phonons, Raman spectra, stress and temp. effects 79-38503
$Gd_2(MoO_4)_3$, ferroelec., amorphous Si:H coating, domain wall motion, image scanning 80-83663
$Gd_2(MoO_4)_3$, ferroelec. and ferroelastic, electron microscopic study 77-85675
$Gd_2(MoO_4)_3$, ferroelec. ferroelastic, domain wall motion, crit. field var. 77-81075
$Gd_2(MoO_4)_3$, ferroelec.-ferroelastic, photolum. and photocond. meas. 80-84768
$Gd_2(MoO_4)_3$, ferroelectric domain decoration 78-10862
$Gd_2(MoO_4)_3$, nonlinear piezoelec. coeffs. near phase transition 79-95710
$Gd_2(MoO_4)_3$, one-dimensional ferroelectric image sensor with polymer photoconductor 80-80729
$Gd_2(MoO_4)_3$, optical activity, gyration tensor determ. near Curie point 79-33660
$Gd_2(MoO_4)_3$, optical activity *(Japanese)* 79-65832
$Gd_2(MoO_4)_3$, passivation of c surface against attack by HF by inert ion beam irradiation 78-35545
$Gd_2(MoO_4)_3$, photoelastic tensor components 77-48146
$Gd_2(MoO_4)_3$, prismatic domain exam. 78-56441
$Gd_2(MoO_4)_3$, spontaneous electrooptic effect, role of induced birefringence 78-68480
$Gd_2(MoO_4)_3$, surface study using AES and ion scatt. spectroscopy 80-65339
$Gd_2(MoO_4)_3$, temp. depend. of spontaneous biref. and electrooptic reponse 79-33662
$Gd_2(MoO_4)_3$, variable frequency SAW resonator on ferroelectric-ferroelastics 78-33977
$Gd_2(MoO_4)_3:Nd^{3+}$, optical spectrum, free ion wavefunctions, radiative transition probabilities 79-24339
$Gd_2Ti_2O_7$, ferroelec., temp. depend. of SHG intensity 79-24267
α-GeTe, diffraction contrast between inversion domains and at boundaries in TEM 77-62457
GeTe, heterophase state, plasma refl. spectra, twinning domain distrib. study 79-69845
HBr(HCl), solid, ferroelec. and paraelec. phases, transitions, Raman scatt. 77-43980
HCl and HCl-DCl, ferroelec. transition, ^{35}Cl NQR study 80-71233
HCl crystals, orthorhombic and cubic, CNDO calcs. 80-6383
HCl, ferroelec., helical system, energy band calc. 78-10329
HCl, infinite chain, ab-initio electronic band struct., MUNICH-CHAIN program 77-8017
HCl, solid, ferroelec., comparative calcs. 77-8529
HCl, solid, ferroelec. phase, spin-spin interactions, NQR meas. 77-85612
HF, ferroelec. helical system, energy band calc. 78-10329
HF, solid, ferroelec., comparative calcs. 77-8529
HF(Cl)(Br)(I), ferroelec. and paraelec. phases, elec. multipole interactions 77-59522
α-HIO_3, electrogyration coeff. meas. 79-19859
H_2SeO_3, IR overtone spectra and temp. depend. 79-47456
$(K,Na)NbO_3$ ceramic, hot pressed, dielec. props. 79-87375
$K(B_xW_{3-x})O_9$ (B=Na, Ca, Co, Ni, Cd, Ga, Bi, Nb, Ta) cryst. struct., temp. dielec. anomalies 80-1998
KCN-KCl mixed system, order-disorder transition, dielec. props. meas. 78-15112
KCN-KCl mixed system, order-disorder transition, Raman spectra obs. 78-15113
KCN_x-KCl_{1-x}, finite-freq. local field catastrophe with appl. to spectra 79-51491
KD_2, PO_4, polarisation echo, near ferroelec. transition 78-88266
KD_2AsO_4, ferroelec., high temp. phase transition, Raman spectra 80-71338
KD_2AsO_4, ferroelect. phase transition, NMR study *(Chinese)* 79-33644
KD_2AsO_4, high temp. phase transitions, proton dynamics 80-76023
KD_2AsO_4, LF dielectric dispersion near phase transition 77-59530
KD_2AsO_4, phase transition and Raman scattering 78-84540
$K(D_xH_{1-x})$ PO_4, ferroelectric, photovoltaic and photorefractive effects 78-72187

ferroelectric materials continued
$KD_{2x}H_{2(1-x)}PO_4$ crystals, $0<x<0.98$, light scatt. by polaritons 80—96802
$K(D_xH_{1-x})_2PO_4$, isotope exchange during crystallisation from aqueous solns. 78—18569
$K(D_xH_{1-x})_3(SeO_3)_2$, ferroelastic, anelastic and elastic infra-low freq. props. 80—70304
KDP, growth in soln., nucleation rate, supersaturation and temp. depend. 77—4728
KDP monocrystal, expansion and contraction coeffs., tricritical point, Landau theory explanation *(Russian)* 80—44340
KDP-type crystals, polarisation, dielec. const. thermodyn. props. 77—59527
KD_2PO_4, acoustic phonon dispersion, elastic stiffness, light scatt. obs. 80—103966
KD_2PO_4, attenuation const. meas. by SHF dielec. resonance 79—47406
KD_2PO_4, Brillouin spectrum and broad central component, depend. on scatt. wave vector direction 80—34931
KD_2PO_4, coexistence states during first order transition, optical obs. 80—75350
KD_2PO_4 crystals in D_2O, two phase stable zone *(Chinese)* 79—82937
KD_2PO_4, deuteron tunnelling, barrier height and energy level calc. 80—6482
KD_2PO_4, domain structure obs. using SEM 77—1647
KD_2PO_4, domain struct. obs. using TOF neutron diffractometer 79—51923
KD_2PO_4, electronic struct., UV reflection spectra 79—38558
KD_2PO_4, ferroelec. transition, ^{31}P chemical shift tensor meas. 77—28527
KD_2PO_4, ferroelec. transition, ^{31}P chem. shift obs. 78—76414
KD_2PO_4, ferroelect. phase transition, NMR study *(Chinese)* 79—33644
KD_2PO_4, ferroelectric transition obs. by ^{31}P chemical shift 77—59531
KD_2PO_4, ferroelectric, longit. and transverse props., Monte Carlo study 79—51912
KD_2PO_4, H-bonded phase transitions, SCF approach 78—92030
KD_2PO_4, high temp. phase transition, dielec. const., elec. cond. and IR refl. meas. 78—43118
KD_2PO_4, IR and Raman polarised spectra, rel. to crystal struct. 78—56489
KD_2PO_4, microwave spectra, temp. depend. mode rel. to proton subsystem 80—24548
KD_2PO_4, neutron scattering from coupled polar-elastic waves 80—92623
KD_2PO_4, nonlinear electrooptic coeffs. near Curie temp. 80—11366
KD_2PO_4, order-disorder type ferroelec., HF dynamics 77—39657
KD_2PO_4, para- and ferroelec. phases spatial distrib. during first order phase transitions 79—42923
KD_2PO_4, phase transitions study, role of cryst. struct. determ. 80—75197
KD_2PO_4, polarisation fluctuations, wavevector depend. 80—71295
KD_2PO_4, Rayleigh scatt. and narrow central component, depend. on scatt. wave vector direction 80—29747
KD_2PO_4, soft ferroelec. mode anisotropy 78—14430
KD_2PO_4, struct. at high press. in rel. to effect of press. on T_c 79—42915
KD_2PO_4, transverse dynamics, short-range interaction effects 78—14408
KD_2PO_4 type ferroelecs., distrib. functions and thermodynamic props. 78—76409
KD_2PO_4, X-irradiated, hysteresis effects obs. by ESR 80—103928
$KD_2PO_4:Fe^{3+}$, ESR, anomalous temp. depend. of D tensor 79—61205
$KD_2PO_4:Tl^{2+}$, EPR of ferroelec. and paraelec. phases 80—66012
KD_2PO_4-type crysts., photorefractive and photovolt. effects 79—15189
KD_2PO_4-type crysts., relax. processes in order-disorder transitions under short range correl. conditions 79—73889
KD_2PO_4-type ferroelectrics, parametric tunnelling-like reson. 80—66119
$KD_3(SeO_3)_2$, acoustic phonon softening and spontaneous strains 78—26652
$KD_3(SeO_3)_2$, D NMR above and below ferroelec. transition, H-bond behaviour 78—52460
$K_{0.5}Eu_{0.5}Nb_2O_6$, ^{93}Nb NQR spectra, 77 to 450K 79—38401
$K_4Fe(CN)_6.3H_2O$, C-N vibrs., Raman study 80—40106
$K_4Fe(CN)_6.3H_2O$, dynamic disorder and ferroelec. transition, Raman spectra obs. 77—81069
$K_4Fe(CN)_6.3H_2O$, effect of ordering on OH Raman bands 79—51959
$K_4Fe(CN)_6.3H_2O$ ferroelectric cryst., vibrational spectrum of $[Fe(CN)_6]^{4-}$ anion 77—69839
$K_4Fe(CN)_6.3H_2O$, ferroelec. and paraelec. phases, dielec. props. meas. 80—60494
$K_4Fe(CN)_6.3H_2O$, internal field and ferroelec. ordering 78—76406
$K_4Fe(CN)_6.3H_2O$, nature of phase transition 79—38470
$K_4Fe(CN)_6.3H_2O$, Raman spectrum and dielec. relax. 78—19476
$K_4Fe(CN)_6.3H_2O$, sp.ht. and spontaneous polarisation, −65 to 0 degrees C, mol. field model 78—64333
$K(H,D)_2PO_4$ crystals, effect of isotopic replacement on growth kinetics 78—95006
KH_2AsO_4, above T_c, ^{75}As NMR spectrum, correl. effects 78—76324
KH_2AsO_4, and deuterated isomorph, E-mode splitting in ferroelec. phase, Raman scatt. meas. 77—16296
KH_2AsO_4, and deuterated isomorph, ferroelectric mode and molecular vibr. press. depend. 78—19424
KH_2AsO_4, domain struct. formation, opt. polarisation obs. 77—63381
KH_2AsO_4, electronic struct., UV reflection spectra 79—38558
KH_2AsO_4, ferroelec. modes, polariton lineshape calc. 77—8585
KH_2AsO_4, ferroelec., temp. broadening of hard mode Raman lines near Tc 78—88296
KH_2AsO_4, ferroelec., RF dielec. relax., loss mech. 79—38448
KH_2AsO_4, ferroelec. phase transition under hydrostatic press., NQR spectra obs. 79—69785
KH_2AsO_4, ferroelec., electronic struct. study *(Japanese)* 79—87463
KH_2AsO_4, ferroelec., high temp. phase transition, Raman spectra 80—71338
KH_2AsO_4, ferroelectric phase transition under high hydrostatic press., mol. dynamics, NQR study 80—75880
KH_2AsO_4, γ-irradiated, free radicals, EPR and ENDOR study of consequences of ferroelec. transition *(French)* 80—93209
KH_2AsO_4, high temp. phase transition, dielec. const., elec. cond. and IR refl. meas. 78—43118
KH_2AsO_4, high temp. phase transitions, proton dynamics 80—76023
KH_2AsO_4, irrad. ferroelec., AsO_3H^- free radical localised near impurity, ENDOR 77—24762
KH_2AsO_4, KD_2AsO_4, slow dynamics from Cr^{5+} EPR 78—15126
KH_2AsO_4, LF dielectric dispersion near phase transition 77—59530
KH_2AsO_4, NQR of ^{75}As, press. and temp. depend., 77K to Curie temp. 80—71227
KH_2AsO_4, phase transition and Raman scattering 78—84540

ferroelectric materials continued
KH_2AsO_4, pres. depend., LF dielec. response, ferroelec. props. 78—15120
KH_2AsO_4, proton modes, dielec. spectroscopy 80—75915
KH_2AsO_4, Raman linewidth, isotope effect 77—8565
KH_2AsO_4, soft shear mode, Brillouin scatt. obs. 78—15176
KH_2AsO_4, transverse elec. susceptibilities 80—50273
$KH_2AsO_4:Cr^{5+}$, ferroelec. phase transition, EPR intensity and linewidth meas. 79—4721
KH_2AsO_4-KH_2PO_4, AsO_4^{4-} centre, EPR central peak dynamics 79—33523
$K(H_{1-x}D_x)_2PO_4$, for IR response exam. by asymmetric Fourier spectroscopy 77—28570
$K(H_{1-x}D_x)_2PO_4$, ferroelec., complex dielec. const., mm wave meas. 77—1633
$K(H_{1-x}D_x)_2PO_4$, ferroelec., dielec. susceptibility, pseudo-spin model 77—52024
$K(H_{1-x}D_x)_2PO_4$, polar mode softening and elastic anomaly temps. 79—28067
$K(H_{1-x}D_x)_2PO_4$, polarisation relaxation time and Landau kinetic coeff. rel. to degree of deuteration 80—84251
$K(H_{1-x}D_x)_2PO_4$, static dielec. props., and Curie temp., press. depend. 79—87405
$KH_{2(1-x)}D_{2x}PO_4$, proton modes, dielec. spectroscopy 80—75915
$KH_{2(1-x)}D_{2x}PO_4$, Raman spectra, effects of deuteration on proton tunnelling modes and coupled optic modes 77—59570
$KH_{2(1-x)}D_{2x}PO_4$, Raman spectra of overdamped mode 79—91427
$KH_{2x}D_{2(1-x)}PO_4$, domain struct. influence on switching processes 80—11355
$K(H_{1-x}D_x)_3(SeO_3)_2$, Brillouin spectrum central peak, soft acoustic mode 80—2777
KH_2PO_4, ^{39}K spin-lattice relax. time double NMR meas. 79—47358
KH_2PO_4, amplitude depend. of permittivity and losses 79—99842
KH_2PO_4 and deuterated derivative, attenuation of LF elastic oscills. 77—7791
KH_2PO_4, and isomorphs, phase transition 77—20807
KH_2PO_4, and isomorphs, dielec. props. and birefr., simultaneous obs. 78—15130
KH_2PO_4 and $K(H_xD_{1-x})_2PO_4$, acoustooptical and photoelastic props. 78—27181
KH_2PO_4 and related substances, electronic structures study *(Japanese)* 79—87463
KH_2PO_4, anharmonic phonons and central peaks at struct. phase transitions 79—95775
KH_2PO_4, appl. of γ-ray diffractometry to twinned crystals study 79—68987
KH_2PO_4, attenuation const. meas. by SHF dielec. resonance 79—47406
KH_2PO_4, Bloch equations 78—64324
KH_2PO_4, Brillouin-Rayleigh scatt. studies near ferroelec. transition temp. 80—76036
KH_2PO_4, central components in ferroelec. phase 78—56436
KH_2PO_4, central peak light scatt., scatt. centre props. 77—52108
KH_2PO_4, central peak susceptibility and US propag. near T_c 78—15125
KH_2PO_4, crit. behaviour near tricritical point, phenomenological interpretation 80—70389
KH_2PO_4, crit. behaviour, dilatometric study 80—92689
KH_2PO_4, critical and tricritical phenomena, susceptibility, exponents 80—75976
KH_2PO_4, cryst. regeneration of z-cut plates, effect of impurities 79—43120
KH_2PO_4 crystal, and deuterated cpd., optical meas. of phase transition point by domain obs. 77—40187
KH_2PO_4, crystal nonequilibrium thermodynamics, quasielastic light scatt., systematic anal. 79—61391
KH_2PO_4 crystals, mechanism of growth in presence of impurities 79—1403
KH_2PO_4, damping of transverse acoustic and ferroelec. modes 78—14413
KH_2PO_4, dendritic growth in silica gel 80—35072
KH_2PO_4, depolarised light scatt., dynamic central peak 78—10858
KH_2PO_4, dielec. functions above and below ferroelec. transition 79—33588
KH_2PO_4, dielectric const. and polarisation, fluctuations, catastrophes 77—8491
KH_2PO_4, dielectric const. at ultra low freq., domain wall relax. effects 77—12348
KH_2PO_4, differential γ-ray diffractometry, exam. of ferroelectric-ferroelastic cryst. in cyclic fields 79—38511
KH_2PO_4, dispersion of permittivity, 6 to 12 cm^{-1} 79—33616
KH_2PO_4, domain wall mobility, model 77—63385
KH_2PO_4, dynamic central peak in ferroelectric phase 78—84538
KH_2PO_4, E-mode splitting in ferroelec. phase, Raman scatt. meas. 77—16296
KH_2PO_4, E-symmetry Raman spectra 79—38535
KH_2PO_4, electro-optic props. near ferroelec. transition 78—19445
KH_2PO_4, electrogyration near transition pt. in nonenantiomorphic cryst. 79—61339
KH_2PO_4, electronic struct., UV reflection spectra and XPS 79—38558
KH_2PO_4, electrophotoluminescence obs. 79—47521
KH_2PO_4 family of crystals, proton modes, dielec. spectroscopy 80—75915
KH_2PO_4, far IR dispersive reflection spectra 77—36213
KH_2PO_4 far IR dispersive reflection obs. with asymmetric polarising interferometer 77—40249
KH_2PO_4, ferroelastic cryst., appl. of γ-ray diffractometry 77—8533
KH_2PO_4, ferroelec., tetragonal cryst. struct. determ., neutron diffr. meas. 77—7693
KH_2PO_4, ferroelec., Raman internal-mode line broadening by proton jumps 77—43981
KH_2PO_4, ferroelec., positron lifetime meas. during phase transitions 78—6644
KH_2PO_4, ferroelec., temp. broadening of hard mode Raman lines near Tc 78—88296
KH_2PO_4, ferroelec., RF dielec. relax., loss mech. 79—38448
KH_2PO_4, ferroelec., change of sign in pyroelec. coeff. 79—82929
KH_2PO_4, ferroelec. thin crysts., struct. investig. 79—27962
KH_2PO_4, ferroelec. phase transition, soft phonons, Raman scatt. obs. *(Japanese)* 79—65880
KH_2PO_4, ferroelectric phase transition exam. by spontaneous parametric light scatt. 78—19427
KH_2PO_4, ferroelectric-ferroelastic phase transition, γ-ray diffr. 78—43819

ferroelectric materials continued
KH_2PO_4, ferroelectric, crystal growth in silica gel, effect of pH and gel ageing 78—48301
KH_2PO_4, ferroelectric, photovoltaic and photorefractive effects 78—72187
KH_2PO_4, ferroelectric transition, press. induced tricrit. point 78—80301
KH_2PO_4, ferroelectric transition, neutron diffr. obs. 80—25324
KH_2PO_4, ferroelectric transition, order-disorder character of hydrogen bond 80—93251
KH_2PO_4, Green's function theory of ferroelec. phase transition 77—85669
KH_2PO_4, H-bonded phase transitions, SCF approach 78—92030
KH_2PO_4, high. press. tricrit. point rel. to zero press crit. point 78—15117
KH_2PO_4, IR overtone spectra and temp. depend. 79—47456
KH_2PO_4, initial dielec. const. in ferroelec. phase by thermal noise method 77—16267
KH_2PO_4, internal friction, torsion pendulum technique 78—72474
KH_2PO_4, KD_2PO_4, slow dynamics from Cr^{5+} EPR 78—15126
KH_2PO_4, KD_2PO_4, high-press. struct. rel. to dynamical models 78—80307
KH_2PO_4, kinetics of growth from aqueous soln. 78—6838
KH_2PO_4, Landau-Devonshire coeffs. 78—15116
KH_2PO_4, light scatt. in elec. field, ferroelec.-paraelec. transition 80—2707
KH_2PO_4, linear response function for tunnelling systems in polariton region 78—43799
KH_2PO_4, longit. sound attenuation, strain depend. pseudo spin coupling mechanism 77—85666
KH_2PO_4, one-dimensional Slater model, with random impurities due to partial deuteration 77—59537
KH_2PO_4, optical activity meas. 78—52466
KH_2PO_4, optical activity, gyration tensor determ. near Curie point 79—33660
KH_2PO_4, optical activity *(Japanese)* 79—65832
KH_2PO_4, paraelec., Raman scatt. spectra of B_2-polariton and B_2(LO) modes 79—28762
KH_2PO_4, paraelectric phase, forward and backward Raman scatt. 79—33681
KH_2PO_4, paraelectric, dynamic central peak depend. on deuterium content 79—65752
KH_2PO_4 paraelectric phase, solns. of Bloch-type eqns. 80—7304
KH_2PO_4, phase transitions study, role of cryst. struct. determ. 80—75197
KH_2PO_4, photoelastic const. behaviour new ferroelectric transition 78—19441
KH_2PO_4, photoelectric phenomena nonlinear optical rectification *(Russian)* 79—19628
KH_2PO_4, polarisation switching, influence of mobile point defects 78—31165
KH_2PO_4, polarisation echo in ferroelec. phase transition region 79—42920
KH_2PO_4, polycrystalline materials; pyroelec. temp. anal. as method for studying ferroelec. transitions 79—38502
KH_2PO_4 powder, dynamic polarisation echoes 79—4773
KH_2PO_4, powder sample, pyrocharge temp. depend. near phase transition 79—87399
KH_2PO_4, press. and deuteration effects on static ferroelec. props., four-particle cluster approx. 80—34861
KH_2PO_4, pressure effect on ferroelec. transitions *(Japanese)* 79—65814
KH_2PO_4, proton tunnelling, barrier height and energy level calc. 80—6482
KH_2PO_4, pyroelectric investig. in ferroelec. phase 77—12321
KH_2PO_4, pyroelectric coeff., 1.8-300K, dynamic method *(French)* 79—19844
KH_2PO_4, RF dielec. response close to transition temp. 77—90099
KH_2PO_4, Raman scatt. near T_c, search for soft modes 78—15114
KH_2PO_4, Raman scatt. for polaritons of mixed B_2-E symm. 79—56795
KH_2PO_4, shear angle and order parameter of ferroelec. transition by neutron diffr. 77—12339
KH_2PO_4, single cryst., thermal depolarisation current 79—51303
KH_2PO_4, single crystal neutron diffraction study at high pressure 80—92497
KH_2PO_4, soft mode behaviour, dispersive Fourier transform spectroscopy 77—7823
KH_2PO_4, spontaneous electrooptic effect in far IR 79—95734
KH_2PO_4, spontaneous polarisation, low temp. meas. 80—75921
KH_2PO_4, strong coupling of proton-phonon system 77—7822
KH_2PO_4, struct. at high press. in rel. to effect of press. on T_c 79—42915
KH_2PO_4, struct. memory effects in low temp. changes 79—28700
KH_2PO_4, struct. phase transitions, light scatt. meas. 79—95774
KH_2PO_4, supersaturated solution, nucleation rates meas. from induction period 79—23549
KH_2PO_4, transverse elec. susceptibilities 80—50273
KH_2PO_4, tricrit. point, γ-ray and neutron diffr. 78—39516
KH_2PO_4, tricrit. point, neutron diffr. study under high press. 79—33624
KH_2PO_4, tricritical point and tricritical exponent 79—33623
KH_2PO_4, two doublet model for ferroelec. phase transition 78—39510
KH_2PO_4 type, Raman spectra, coupled tunnel-phonon modes, isotope effect 79—69205
KH_2PO_4 type crystals, coupling between protonic E-mode and lattice vibrs. 77—7821
KH_2PO_4 type crystals, low lying ferroelec. modes, cluster dynamical theory 78—80305
KH_2PO_4 type crystal, H-bonded partially deuterated ferroelectrics, order parameter fluctuation spectra, central peak calcs. 79—61316
KH_2PO_4 type crysts., microhardness, expt. determ. 79—24603
KH_2PO_4 type crysts., evidence of non-linear behaviour of soft modes, Raman spectra 79—33639
KH_2PO_4 type ferroelectrics, isotopically disordered, collective modes, CPA 77—7825
KH_2PO_4 type ferroelectric, phase transition to spontaneous coherent state, theory *(Russian)* 78—6647
KH_2PO_4, vacuum UV spectra and electro-optical prop. *(Japanese)* 79—65900
KH_2PO_4, variational treatment of proton-photon system 78—88261
KH_2PO_4, X-irradiated, hysteresis effects obs. by ESR 80—103928
$KH_2PO_4:AsO_4^{4-}$, ESR, paraelectric phase, proton dynamics 77—81011
$KH_2PO_4:AsO_4^{4-}(SeO_4^{3-})$, ferroelec., low freq. fluctuations, isotope effects, EPR, ENDOR, ESCA 77—73118
KH_2PO_4:cation impurities, growth domains 79—99224

ferroelectric materials continued
$KH_2PO_4:CrO_4^{2-}(CrO_7^{2-})$, electrical cond., thermal depolarisation studies 79—95212
$KH_2PO_4:Fe^{3+}$, ESR, anomalous temp. depend. of D tensor 79—61205
$KH_2PO_4:SeO_4^{3-}$, slowing down of fluctuations near T_c, EPR obs. 78—60403
$KH_2PO_4:Tl^{2+}$, EPR of ferroelec. and paraelec. phases 80—66012
KH_2PO_4-KD_2PO_4 mixed cryst., dielec. polarisation, Green's function anal. 77—52011
KH_2PO_4-KD_2PO_4 mixed crysts., dielec. spectra, sub-mm wavelengths 80—80724
KH_2PO_4-type cpds., collective vibr. of protons, cluster approx. 79—51210
KH_2PO_4-type crystal, domain wall mobility, two-dimens. ordering effect 78—48137
KH_2PO_4-type crystals, H bond in ferroelectricity, role of high pressure research 79—15414
KH_2PO_4-type crysts., photorefractive and photovolt. effects 79—15189
KH_2PO_4-type ferroelectrics, inelastic neutron scatt. theory 78—48122
KH_2PO_4-type ferroelectrics, tunnelling integral 80—70156
KH_2PO_4-type ferroelectrics, dielec. props., four-cluster approx. 80—97202
$KH_2PO_4;Tl$, UV absorption bands obs. 78—27266
$KH_3(SeO_3)_2$, and $KD_3(SeO_3)_2$, anharmonic phonons and central peaks at struct. phase transitions 79—95775
$KH_3(SeO_3)_2$ and $KD_3(SeO_3)_2$, ferroelastic phase transition, mech. stress effect 80—70394
$KH_3(SeO_3)_2$, central peak obs. by light scatt. 77—32390
$KH_3(SeO_3)_2$, ferroelastic, lattice consts. and thermal expansion tensors, X-ray diffr. meas. 79—37856
$KH_3(SeO_3)_2$, ferroelastic transition under uniaxial press., EPR study 80—59562
$KH_3(SeO_3)_2$, phase transitions *(Japanese)* 79—65812
$KH_3(SeO_3)_2$, slightly deuterated, central peak obs. in Brillouin spectra 78—64374
KIO_3, temp. depend. Raman spectra and phase transitions *(Russian)* 78—15171
α-$KIO_3.HIO_3$, ^{127}I NQR study of ferroelec. phase transition 79—38400
$K_xLi_{1-x}NbO$ films, epitaxial growth by melting on $K_{1.5}Bi_{1.0}Nb_{5.1}O_{15}$ substrate 79—33204
$K_xLi_{1-x}NbO_3$, epitaxial growth of single-cryst. films on $K_2BiNb_5O_{15}$ substrate by RF sputtering 79—15041
$K_2Mn_2(SO_4)_3$, langbeinite type cryst., ferroelec., phase transitions, dielec., elastic and pyroelec. meas. 77—59535
$K_2Mn_2(SO_4)_3$, optical and dielectric props. 79—11403
$K_3MoO_3F_3$, ferroelec. and order-disorder phase transitions 78—92037
$K_3MoO_3F_3$, ferroelec., transition obs. 80—75989
KNO_2, NQR spectrum of ^{14}N at low temp., poss. ferroelec. transition 77—12223
KNO_3, and KNO_2, fused, electrolum. 79—99945
KNO_3, far IR study of dielec. function by asymmetric Fourier spectroscopy 79—51947
KNO_3, ferroelec. thin crysts., struct. investig. 79—27962
α-KNO_3, lattice dynamics, inelastic neutron scatt. 79—4383
KN_bO_3, single domain crystal growth, SHG with Nd:YAG laser 78—74954
$K_{1-x}Na_xTaO_3$, quantum ferroelec., elastic compliance, impurity effects 79—99835
$K_{1-x}Na_xTaO_3$ quantum ferroelectric, dielec. susceptibility 80—103922
$KNbO_3$, acoustic modes near orthorhombic-tetragonal phase transition, temp. depend. 79—28058
$KNbO_3$, anomalous scatt. and asymmetrical line shape in Raman spectra 77—20853
$KNbO_3$ catalysts, ferroelectric, for reactions involving CO and NO , and adsorption of NO 80—30282
$KNbO_3$, cubic, temp. depend. of intensity of X-ray interference 80—59613
$KNbO_3$, dielec. and optical props. using shell model 79—33654
$KNbO_3$, dielec. spectrum rel. to polarisation effects 80—15984
$KNbO_3$, domain struct. at transitions from twinned phase, appl. to tetragonal-orthorhombic transition 80—71360
$KNbO_3$, elec. and thermoelec. singularities due to small polaron hopping motion cond. transition 79—42565
$KNbO_3$, elec. and thermoelec. props., influence of O defects 80—29401
$KNbO_3$, electronic props., SCF-MS-Xα calc. 80—54607
$KNbO_3$, electronic struct., XPS and band struct. calc. 79—38708
$KNbO_3$, ferroelec., nonlinear optical susceptibility calc. 78—9409
$KNbO_3$, ferroelec. cryst., IR and Raman spectra, mode coupling 80—66194
$KNbO_3$, ferroelec. phase, phonon dispersion relations and lattice dynamics calcs., comparison with expt. 80—49319
$KNbO_3$, ferroelectric soft modes and order-disorder transition 77—47534
$KNbO_3$, ferroelectric transition, neutron diffr. obs. 80—25324
$KNbO_3$, growth from soln. in melt and characterisation of optical quality cryst. 77—8741
$KNbO_3$, one-dimens. ferroelectric, phonon dispersion surfaces 79—42180
$KNbO_3$, orthorhombic, anharmonic effects 78—79721
$KNbO_3$, photoferroelectric effects 78—92029
$KNbO_3$, photovoltaic current, temp. and spectral depend. 78—47828
$KNbO_3$, piezoelec. and electrostrictive coeffs. 77—85653
$KNbO_3$ reduced, phase hologram recording sensitivity, energy transfer, photovoltaic effects 80—78799
$KNbO_3$, single cryst., dielec. breakdown and electroluminesc. 78—2917
$KNbO_3$ single crystals, preparation of pure, Fe doped, and reduced crystals 78—60564
$KNbO_3$, spontaneous polarisation and pyroelec. effect meas. 77—90107
$KNbO_3$, thermoelec. effect and phase transitions 78—48123
$KNbO_3$ thick crystals, vol. nucleation of domains by impurities 77—73120
$KNbO_3$, X-ray diffr. before and after high temp. phase transition 77—11694
$KNbO_3:Al^{3+}(Ba^{2+})$, dopant effect on domain struct., etching study 79—56749
$KNbO_3$:Fe, large single domain cryst., growth and prep. for optical storage 77—1799
$KNbO_3$:Fe, optically induced refractive index changes 77—4612
$KNbO_3$:Fe, photovoltages, photocurrents and photorefractive effects 79—42580
$KNbO_3$:Fe, thermal and spectral variations in the photovoltaic current in ferroelectrics 78—91719
$KNbO_3$-$BaTiO_3$, ferroelec. Curie temp., theory 80—7313
$KNbO_3$-$PbTiO_3$, ferroelec. Curie temp., theory 80—7313

ferroelectric materials continued
$KNbW_2O_9$, crystallography, polymorphism and phys. props. 78—79599
K_2O-SrO-Nb_2O_5 system, selective delineation of dislocations by etching 77—72617
$K_2SbNb_5O_{15}$, dielec. and pyroelec. props. 79—99841
K_2SeO_4, anharmonic phonons and central peaks at struct. phase transitions 79—95775
K_2SeO_4, Brillouin scatt. at paraelectric-incommensurate phase transition, hypersonic waves 79—78690
K_2SeO_4, cryst. with modulated struct., neutron scatt. obs. 79—95713
K_2SeO_4, dielec. dispersion, 5-900 MHz, near incommensurate-commensurate transition 80—60522
K_2SeO_4, elastic compliance anomalies 80—45010
K_2SeO_4, ferrielectricity, triple 60 Hz D-E hysteresis loops 80—71364
K_2SeO_4, ferroelec., incommensurate struct., dynamic props. *(Russian)* 80—11373
K_2SeO_4, improper ferroelec., struct., phase transform. and lattice instability neutron scatt. meas. 77—63379
K_2SeO_4, incommensurate modulation along axis perpendicular to x-axis 78—6154
K_2SeO_4, incommensurate phase transitions under existence of Lifshitz invariant 79—15416
K_2SeO_4, incommensurate lattice instability, ferroelec. transition, neutron scatt. study 79—42210
K_2SeO_4, incommensurate and ferroelec., far IR and mm dielectric response 79—73955
K_2SeO_4, lower freq. soft-mode in ferroelec. phase 77—81065
K_2SeO_4, Raman scatt. and dielec. props. 80—11313
K_2SeO_4, Raman spectra, 77-300K *(Japanese)* 77—43988
K_2SeO_4, Raman spectra, effects of temp., substitutional cations, and stress 80—71405
K_2SeO_4, soft modes below incommensurate transition Raman and Brillouin scatt. meas. 79—91387
K_2SeO_4, symmetry determ. of commensurate and incommensurate phases by EPR of γ-irrad. crysts. 79—78525
K_2SeO_4, unpolarised-noncommensurate-polarised phase transition, phenomenological theory 79—15422
$K(Ta,Nb)O_3$ ceramic, prep. and electro-optical props. 80—25620
$KTa_{0.65}Nb_{0.35}O_3$, ferroelectric devices for optical systems 78—90473
$KTa_{0.9}Nb_{0.1}O_3$, dipolar behaviour, crit. exponent of dielec. const. 77—4604
$KTa_{1-x}Nb_xO_3$ film, RF sputtering, structural and electrical properties obs. 78—88426
$KTa_{1-x}Nb_xO_3$, holographic storage using photorefractive effect, dielectric const. 80—78800
$KTa_{1-x}Nb_xO_3$, local polarisability in quantum paraelec. and quantum ferroelec. phases 78—64325
$KTa_{1-x}Nb_xO_3$, paraelectric phase, defect induced fluctuations, Raman meas. 79—15423
$KTa_{1-x}Nb_xO_3$, quantum limit of ferroelec. transitions, dielec. and elastic consts. meas. 78—15128
$KTa_{1-x}Nb_xO_3$, quantum ferroelectric, dielec. susceptibility 80—103922
$KTa_{1-x}Nb_xO_3:Fe^{3+}$ ($0 \le x \le 0.16$), ferroelec., EPR meas. *(French)* 79—11337
$KTa_{1-y}Nb_yO_3$, quantum ferroelec., elastic compliance, impurity effects 79—99835
$KTaO_3$, complex refr. index meas. in far IR, by dispersive Fourier transform spectroscopy 78—92042
$KTaO_3$, crit. dielec. and optical props. and storage, 4K 77—24805
$KTaO_3$, dielec. response temp. depend. meas., dispersive Fourier transform spectroscopy 79—15449
$KTaO_3$, electronic props., SCF-MS-Xα calc. 80—54607
$KTaO_3$, electronic struct., XPS and band struct. calc. 79—38708
$KTaO_3$, ferroelec., local field determ., phase transition study by EPR 79—38471
$KTaO_3$, field depend. sp. ht. and soft modes at low temps. 79—8105
$KTaO_3$, freq. depend. of soft mode self-energy, for IR dielec. response meas. 79—33632
$KTaO_3$, incipient ferroelectric, mode-mode coupling 78—79717
$KTaO_3$, photoconduction in ferroelectrics 78—91720
$KTaO_3$ pseudodisplacive ferroelec., temp.-dependent dielectric response obs. 77—40247
$KTaO_3$, Raman scatt. and ferroelec. soft modes 77—16300
$KTaO_3$, second harmonic generation, bond charge theory 78—76395
$KTaO_3$, stress-induced ferroelectricity, Raman scatt. obs. 77—40190
$KTaO_3:Gd^{+}$, influence of external elec. field on EPR 78—15020
$KTaO_3$:Li, ferroelec. transition and atomic motions, ^{7}Li NMR study 80—75872
$KTaO_3$:Li, polarised cluster stabilisation by Li defects, polar glass form. 79—91342
$KTaO_3$:Li, susceptibility extrinsic peak, dielectric const. meas. 79—11394
$K_{0.5}Tm_{0.5}Nb_2O_6$, ^{93}Nb NQR spectra, 77 to 450K 79—38401
$K_3WO_3F_3$, ferroelec., transition obs. 80—75989
$K_3WO_3F_3$, ferroelec. and order-disorder phase transitions 78—92037
K_2ZnCl_4, cryst. with modulated struct., neutron scatt. obs. 79—95713
K_2ZnCl_4, ferrielectricity, triple 60 Hz D-E hysteresis loops 80—71365
K_2ZnCl_4, ferroelec. props. 79—4772
K_2ZnCl_4, incommensurate phases, neutron scatt. 79—38501
K_2ZnCl_4, incommensurate phase transitions, ^{35}Cl NQR study 80—75968
K_2ZnCl_4, modulated struct. in ferroelec. phase, X-ray obs. 80—64970
$K_2Zn_2(SO_4)_3$, langbeinite type cryst., ferroelec., phase transitions, dielec., elastic and pyroelec. meas. 77—59535
$kH_{2(1-x)}D_{2x}PO_4$, monoclinic, electro-optical props. 79—82951
$La_{0.003}Ba_{0.66}Sr_{0.34}TiO_3$ ceramic, positive TCR near Curie temp. rel. to charge dispersion *(Russian)* 80—16511
$LaNbO_4$, ^{93}Nb and ^{139}La NQR spectra 79—38401
$LaNbO_4$, room temp. phase exam. 78—26536
LaP_5O_{14}, ferroelastic transition, polarised Raman study 80—16035
$La_xPb_{1-x}Zr_yTa_{1-y}O_3$, ferroelec. with diffuse phase transition, electrostriction-optical props. 78—68457
$La_2Ti_2O_7$, ferroelecs., nonlinear optical props. 80—33086
$La_2Ti_2O_7$, layered ferroelectric anomalous photovoltaic effect, photovoltaic current 80—75603
(Li,Na,K) $(Nb,Ta)O_3$, pseudo-binary and ternary systems quenched metastable glassy and cryst. phases 80—29935
$Li_2B_4O_7$, ferroelectric glass, phase transition, permittivity, electrochromism, photochromism 80—80719
$(Li_2B_4O_7)_{1-x}(WO_3)_x$ dipolar glass, space charge injection, thermally stimulated depolarisation currents 80—66103
$Li_2B_4O_7.xWO_3$ (x=0 to 1 mol.) glass, random elec. dipole, cooperative phenomena 79—28693

ferroelectric materials continued
Li_2Gd_4 $(MoO_4)_7$, ferroelec. and paramag. props. 78—39517
$LiGd(MoO_4)_2$, defect struct. and phase transitions 79—28697
$LiGd_3(MoO_4)_5$, single crysts., cryst. growth, optical props. 80—60763
$LiH_3(SeO_3)_2$, ferroelec., absolute atomic arrangement and spontaneous polarisation, neutron diffr. study 80—59442
$LiH_3(SeO_3)_2:VO^{2+}$, ferroelectric, 298K, EPR 79—51846
α-$LiIO_3$, depolarisation current, dielectric const. relaxation behaviour *(Chinese)* 80—88905
$LiIO_3$, electrogyration coeff. meas. 79—19859
α-$LiIO_3$ single crystals, electrical conduction and dielectric behaviour *(Chinese)* 78—30783
α-$LiIO_3$ single crystals, research work, review *(Chinese)* 79—69782
α-$LiIO_3$, surface defect layer struct. due to mechanical working *(Russian)* 80—100238
$(Li_{0.5}La_{0.5})_xBa_{1-x}TiO_3$, cryst. struct., dielec. and IR spectral meas. 79—46614
$LiND_4SO_4$, ^{7}Li and ^{2}D NMR exam. of high-pressure phase 79—11396
$LiNH_4SO_4$ and $LiND_4SO_4$, dielec. pyroelec., and thermal props. 80—60509
$LiNH_4SO_4$, DC elec. cond. 80—88603
$LiNH_4SO_4$, ferroelect. and press. induced phase transitions 79—38473
$LiNH_4SO_4$, ferroelectric phase transition, lattice parameters and thermal expansion coeffs. 80—40074
$LiNH_4SO_4$, $LiNH_4SeO_4$, nonlinear opt. props. including SHG 78—76396
$LiNH_4SO_4$, nuclear spin lattice and effective proton relaxation, phase transitions 80—54965
$LiNH_4SO_4$, thermal props. near high temp. phase transition 78—19428
$Li(N_2H_5)SO_4$, thermal diffusivity exam. 78—63886
$LiNbO_3$, acousto-optic interaction, phase grating production 79—41454
$LiNbO_3$, amorphous ribbons, prep., electron and X-ray diffr. obs., dielec. const. temp. depend. 79—50993
$LiNbO_3$, anisotropy and phase velocities of prop. of elastic waves 79—1478
$LiNbO_3$, anomalous photovoltaic effect and photocond. 79—38122
$LiNbO_3$, appl. in sub-100 ps pyroelec. detectors, 10.6 μm damage threshold meas. 80—77859
$LiNbO_3$, asymm. phononlines, IR refl. analysis 78—27197
$LiNbO_3$, band struct. and spontaneous polarisation calcs. 78—95261
$LiNbO_3$, cathodlum. spectral and temp. depend. 78—84665
$LiNbO_3$, chemical, struct. and physical props., book contrib. 79—69783
$LiNbO_3$, comparative frustrated total refl. and Raman scatt., fundamental mode freq. and phonon dispersion 77—28579
$LiNbO_3$, crystal defects, X-ray diffr. topographic study *(Chinese)* 80—84173
$LiNbO_3$, crystal for electrooptics and nonlinear optics, optical inhomogeneities, review *(Japanese)* 77—65613
$LiNbO_3$, crystallisation from solution in borate, vanadate and tungstate melts 79—1820
$LiNbO_3$ crystals, activated by 3d^n ions, enhancement of polarisation echo 79—38439
$LiNbO_3$ crystals, low temp. polarisation reversal 79—61322
$LiNbO_3$, crysts., elec. field influence on hypersonic wave propag. 80—44668
$LiNbO_3$, damping of LF elastic vibrs., internal friction meas. 79—28043
$LiNbO_3$, diffusion of Ti, surface acoustic waveguide formation 77—79998
$LiNbO_3$, effect of spontaneous polarisation on thermionic emission 78—35245
$LiNbO_3$, ferroelec., displacive type phase transition, far IR reflection spectra 80—71339
$LiNbO_3$, ferroelec., phonon dispersion relations, neutron inelastic scatt. meas. 78—56435
$LiNbO_3$, ferroelec. glass *(Japanese)* 79—65840
$LiNbO_3$, ferroelec. phase, soft vibr. modes, far IR refl. meas. 79—87407
$LiNbO_3$, ferroelec. phase, phonon dispersion relations and lattice dynamics calcs., comparison with expt. 80—49319
$LiNbO_3$, ferroelectric devices for optical systems 78—90473
$LiNbO_3$, ferroelectric, anomalous photovoltaic effect 79—7861
$LiNbO_3$, ferroelectric transitions, thermally stimulated electron emission meas. 80—25534
$LiNbO_3$, Fourier transform Ir spectroscopy of vibr. states at high temp. 80—97256
$LiNbO_3$, guided wave devices, use of ferroelectric materials, review 78—38048
$LiNbO_3$, hologram storage depend. on envelope field, space charge field 80—78801
$LiNbO_3$, holographic storage at high temp., optical damage relax. 77—14677
$LiNbO_3$, holographic storage, expt. confirmation of theory for electro-optic crysts. in steady-state case 79—86136
$LiNbO_3$, holographic storage, beam coupling and light amplification, expt. compared with theory for electro-optic crysts. 79—86137
$LiNbO_3$, induced refl. and transparency increase *(Russian)* 78—59094
$LiNbO_3$, LF sound attenuation, internal friction 78—63804
$LiNbO_3$, laser induced optical damage, pyroelec. contrib., electrostatic obs. 78—37935
$LiNbO_3$, laser induced optical inhomogeneity in external electric field 79—95730
$LiNbO_3$, laser-induced optical damage, electrostatic obs. 78—18030
$LiNbO_3$, $LiNbO_3$:Fe, amplification of laser beams by ferroelectrics 78—90393
$LiNbO_3$, $LiNbO_3$:Fe, holography in ferroelectrics 78—90394
$LiNbO_3$, $LiNbO_3$-Fe, photorefraction in ferroelectrics rel. to electro-opt. effects 78—92048
$LiNbO_3$, light diffraction from volume phase holograms 79—36860
$LiNbO_3$, light emission from surface on heating or cooling 78—64416
$LiNbO_3$, light induced ultrasonic wave velocity change, refractive index 80—97236
$LiNbO_3$, microfabrication by ion-bombardment enhanced etching 78—76779
$LiNbO_3$, monodomain ferroelec. cryst., secondary electron emission coeff. 78—11032
$LiNbO_3$, OH^- groups effect on dielec. and optical props. of single crysts. 77—12327
$LiNbO_3$, optical damage effects 77—40186
$LiNbO_3$, optical damage in doped and undoped ferroelectric, mechanism 78—95570
$LiNbO_3$, optical phonon modes and anharmonic couplings 78—60466
$LiNbO_3$, partially clamped single cryst., secondary pyroelectricity, electrostatic meas. 79—82927

ferroelectric materials continued
$LiNbO_3$, partially clamped single cryst., tertiary pyroelectricity, electrostatic meas. 79—82928
$LiNbO_3$, photocond. induced by N_2 laser *(Japanese)* 78—2521
$LiNbO_3$, photorefractive effect sensitivity 78—43833
$LiNbO_3$, photorefractive sensitivity, dependence on impurity Fe^{2+}/Fe^{3+} ratio, EPR and APR data 79—73893
$LiNbO_3$, photovoltaic current, temp. and spectral depend. 78—47828
$LiNbO_3$, photovoltaic effect, latent-image formation kinetics, electrophotography appl. 78—84246
$LiNbO_3$, planar optical waveguide, SHG in angle-matched conditions 79—41422
$LiNbO_3$, polydomain, nonstoichiometric crysts., elastic, piezoelec., dielec. constants. 77—8513
$LiNbO_3$, powder, polarisation echo, repetitive read out effect 79—82913
$LiNbO_3$, pure and Fe doped, photorefraction kinetics under irradiation and heating 79—42934
$LiNbO_3$, pure and Fe doped, photorefraction, temp. and light intensity depend. 80—50288
$LiNbO_3$ pure and Fe doped, IR induced acousto-photorefractive memory effect 80—80746
$LiNbO_3$, pure and Fe doped, two-photon photorefractivity 80—80753
$LiNbO_3$, pyroelectric induced optical damage 78—52446
$LiNbO_3$, Raman spectra temp. depend. 77—40239
$LiNbO_3$, Raman spectra and dielec. props. near Curie point 79—38530
$LiNbO_3$, reduced, photovoltaic effect and holographic recording mechanisms 79—69556
$LiNbO_3$, reversed polarity layer at positive domain surface, heat-induced, etching investig. 77—63383
$LiNbO_3$, shock-wave compression, 2.4-44 GPa 80—34139
$LiNbO_3$, single cryst. growth and phys. props. *(Japanese)* 79—65018
$LiNbO_3$ single crystals, growth from melt, Czochralski method *(Chinese)* 80—76171
$LiNbO_3$ single crystals grown by automatic diameter control, power striations *(Chinese)* 80—81080
$LiNbO_3$, spontaneous elec. breakdown 77—66458
$LiNbO_3$, spontaneous polarisation, low temp. meas. 80—75921
$LiNbO_3$ sputtered layers, on $LiTaO_3$, optical waveguide props. 77—11012
$LiNbO_3$ substrate, struct. and morphology of VPE PbTe layer 80—54561
$LiNbO_3$, thermal and spectral variations in the photovoltaic current in ferroelectrics 78—91719
$LiNbO_3$, thermionic emission characts. 80—104034
$LiNbO_3$, Ti diffused optical waveguide, ferrolectric domain inversion 79—94338
$LiNbO_3$, transition metal doped, photoferroelectric phenomena and optical storage 79—42577
$LiNbO_3$, valence band UPS and partial p and d density of states 80—71560
$LiNbO_3$, vitreous, anomalous dielectric behaviour and reversible pyroelectricity 77—85658
$LiNbO_3$, wave front convolution in 4-wave interaction with nonlocal nonlinear media *(Russian)* 79—86205
$LiNbO_3$, X-ray determ. of piezoelec. coeff. 77—8511
$LiNbO_3$, X-ray diffr. study of lattice dynamics parameters *(Russian)* 79—65156
$LiNbO_3$, X-ray diffuse scatt., temp. depend., 20 to 750°C 79—37800
$LiNbO_3$, X-ray photovoltaic effect and its correl. with ESR 79—82639
$LiNbO_3$, XPS and UPS from surface defects 80—76136
$LiNbO_3$ Z-cut crystals, bit and holographic recording, electric field control *(Russian)* 77—42512
$LiNbO_3:3Li_2O.Nb_2O_5$ eutectic, dielectric props. 79—1743
$LiNbO_3:Cu^{2+}$, EPR and optical spectra 80—20453
$LiNbO_3$:Cu(Fe), light induced charge transport, photovoltaic effects, impurity states 80—80317
$LiNbO_3$:Fe, anomalous photovoltaic effect in polarised light *(Russian)* 80—34484
$LiNbO_3$:Fe, calc. of photorefraction *(Russian)* 78—92032
$LiNbO_3$:Fe, dynamic optical storage 78—33706
$LiNbO_3$:Fe, electron irrad., photoinduced charge transfer and hologram recording 79—36859
$LiNbO_3$:Fe, electron spin relaxation study, Mossbauer effect, mag. and crystal field effects 80—39902
$LiNbO_3$:Fe, impurity valence state charge on X-ray irrad., Mossbauer meas. 80—7235
$LiNbO_3$:Fe, impurity charge states after UV irradiation 80—60462
$LiNbO_3$:Fe, induced optical inhomogeneity, refr. index and short-circuit photocurrent meas. 79—69806
$LiNbO_3$:Fe, influence of anomalous photovoltaic effect on exoelectron emission 79—28374
$LiNbO_3$:Fe, laser induced optical damage 78—95572
$LiNbO_3$:Fe, local photodeformation 79—42932
$LiNbO_3$:Fe, local photodeform. and photorefraction 80—16003
$LiNbO_3$:Fe, Mossbauer spectra quadrupole doublet asymmetry 80—44960
$LiNbO_3$:Fe, optical damage, Fe ion conc., EPR and optical spectra evaluation 79—42933
$LiNbO_3$:Fe, optical damage depend. on temp., press., and applied elec. field *(Japanese)* 79—81498
$LiNbO_3$:Fe, photocond. and photorefractive effects 79—38124
$LiNbO_3$:Fe, photoinduced Rayleigh scatt. and bulk photovoltaic effect 79—38554
$LiNbO_3$:Fe, photorefractive recording of vol. holograms 77—637
$LiNbO_3$:Fe, photorefractive effect in a ferroelectric 78—92047
$LiNbO_3$:Fe, photovoltaic effect and charge transport mechanism 79—38123
$LiNbO_3$:Fe, polarization echo signals amplification *(Russian)* 78—43780
$LiNbO_3$:Fe, refractive index change induced by light irrad. *(Japanese)* 79—65824
$LiNbO_3$:Fe, spontaneous polarisation reversal and photorefractive effect 78—31163
$LiNbO_3$:Fe, treated in Li_2CO_3, formation of Fe^{2+} state, Mossbauer effect 78—92003
$LiNbO_3$:Fe, white-light image processing 80—87321
$LiNbO_3$:Fe (0.05%), hologram recording γ radiation effect 80—78812
$LiNbO_3$:Fe holographic information storage material 78—55321
$LiNbO_3:Fe^{3+}$, electrooptical effect, charge transfer mechanism, defect. pair form. 79—38519
$LiNbO_3$:Fe(Cu)(Co), pure and doped, nonlinear excitation, multiphoton photorefractive process 79—36950
$LiNbO_3$:Ni optical absorpt. spectra 80—71450

ferroelectric materials continued
$LiNbO_3$:Ti, planar optical waveguides, processing and props. 80—78965
$LiNbO_3$:Ti diffused optical waveguide, guided light scatt. sources 80—78966
$LiNbO_3$:Ti diffused optical waveguide, efficient tapered gap prism coupling 80—78967
$LiNbO_3$:Ti waveguide directional coupler switches, optically-induced cross-talk 80—48417
$LiNbO_3$-$Ca(NbO_3)_2$, cryst. growth in baked mixture, Seignettoelec. phase *(Russian)* 79—47395
$LiNbO_3$-CdSe layer structure, SAW absorpt., elec. field effects 80—65355
$LiNbO_4$, dispersion of vibrational excitations, Raman scatt. 78—84588
$LiNb_{1-y}Ta_yO_3$, Czochralski growth and basic props. 77—63556
$LiNd(MoO_4)_2$, defect struct. and phase transitions 79—28697
$LiTaO_3$, ^{181}Ta NQR spectra, 77K to room temp. 79—38401
$LiTaO_3$, anomalous polariton dispersion near Curie temp. 77—80743
$LiTaO_3$, appl. in sub-100 ps pyroelec. detectors, 10.6 μm damage threshold meas. 80—77859
$LiTaO_3$, asymm. phonon lines, IR refl. analysis in paraelec., ferroelec. phases 78—27197
$LiTaO_3$, crystallographic features and domain struct. 78—34498
$LiTaO_3$, crystals for electrooptics and nonlinear optics, optical inhomogeneities, review *(Japanese)* 77—65613
$LiTaO_3$ crystals for commercial SAW TV IF filters, fabrication 80—80961
$LiTaO_3$, crysts., elec. field influence on hypersonic wave propag. 80—44668
$LiTaO_3$, ferroelec., displacive type phase transition, far IR reflection spectra 80—71339
$LiTaO_3$, Fourier transform Ir spectroscopy of vibr. states at high temp. 80—97256
$LiTaO_3$ glass-ceramics, transparent fabrication by crystn. of aluminosilicate glasses 77—59734
$LiTaO_3$, guided wave devices, use of ferroelectric materials, review 78—38048
$LiTaO_3$ high-temp. ferroelec. transition, soft mode IR reflectivity spectroscopy 79—33692
$LiTaO_3$, multidomain cryst., birefringence, Tyndall cone struct. 77—4618
$LiTaO_3$, near ferroelec. transition, elasticity, photoelasticity 78—88268
$LiTaO_3$, optical phonon modes and anharmonic couplings 78—60466
$LiTaO_3$, paraelectric phase, soft vibr. modes, far IR refl. meas. 79—87407
$LiTaO_3$, Raman spectra and dielec. props. near Curie point 79—38530
$LiTaO_3$, single cryst. growth and phys. props. *(Japanese)* 79—65018
$LiTaO_3$, single crysts., Czochralski growth for SAW device appl. 79—33922
$LiTaO_3$, single crysts., temp. depend. of diffuse X-ray scattering intensity 79—61318
$LiTaO_3$, spontaneous elec. breakdown 77—66458
$LiTaO_3$, uniaxial ferroelec., polariton dispersion relations 77—20249
$LiTaO_3$, vitreous, anomalous dielectric behaviour and reversible pyroelectricity 77—85658
$LiTaO_3$, wave front convolution in 4-wave interaction with nonlocal nonlinear media *(Russian)* 79—86205
$LiTaO_3$, X-ray diffr. study of lattice dynamics parameters *(Russian)* 79—65156
$LiTaO_3$, X-ray diffuse scatt., temp. depend., 20 to 750°C 79—37800
$LiTaO_3$:Cu(Fe), light induced charge transport, photovoltaic effects, impurity states 80—80317
$LiTaO_3$:M, optical damage of transition-metal-doped ferroelectric 78—95571
$LiTaO_3$-$CaZrO_3$, struct. and dielec. props. 78—80298
$Li_{1+y}Ta_{1.5y}Ti_{6y}O_3$ ($0 \leq y \leq 0.028$), non-stoichiometric phase, crystallographic and dielec. props. 80—75212
$LiTuO_3$, light scatt. from ferroelec. domains 78—80310
$MNbO_3$, orthorhombic, electronic struct., SCF-MS-Xα calc. 80—70600
$MNbO_3$, tetragonal, electronic struct., optical anisotropy 80—70599
$Mn_3B_7O_{13}Cl$ improper ferroelec., orthorhombic phase, Raman spectrum, lattice vibrs. 78—43849
$(ND_4)_2BeF_4$ and $(NH_4)_2BeF_4$, incommensurate phase, ^{9}Be NMR study 80—75973
$(ND_4)_2BeF_4$, cryst. with modulated struct., neutron scatt. obs. 79—95713
$(ND_4)_2BeF_4$, incommensurate-commensurate phase transition and spontaneous polarisation 77—40192
$ND_4D_2PO_4$ type ferroelecs., distrib. functions and thermodynamic props. 78—76409
$(ND_4)_3D(SO_4)_2$, ferroelectricity and isotope effect on ferroelec. activity 77—85660
$(ND_4)_3D(SO_4)_2$, press.-temp. phase diagram 78—38834
$(ND_4)_3D(SeO_4)_2$, phase transitions, isotope effect, dielectric and dilatometric meas. 79—38500
$(ND_4)_2(SO_4)_3$, ferroelec. langbeinites, Raman scattering 80—34926
(NH_4), SO_4, nonclassical ferroelectricity, phase transitions 80—25320
$(NH_4)_2$,SO_4, ferrielectricity, triple 60 Hz D-E hysteresis loops 80—71364
$NH_4Al(SO_4)_2.12H_2O:Cr^{3+}$, zero-field fluctuations in Cr^{3+} near phase transition 77—28435
$(NH_4)_2BeF_2$, paraelec. phase, cryst. struct. 78—95025
$(NH_4)_2BeF_4$ crystal, macroscopic quadrupole moment anomalies in incommensurable phase *(Russian)* 79—65808
$(NH_4)_2BeF_4$ crystals, incommensurate-commensurate phase transitions, optical props. 79—95733
$(NH_4)_2BeF_4$, effect of surface layer on spontaneous polarisation 79—38445
$(NH_4)_2BeF_4$, elastic compliance, US attenuation and piezo-coeffis., 170 and 190K 79—51918
$(NH_4)_2BeF_4$, elastic props., US damping 80—84229
$(NH_4)_2BeF_4$, far-infrared and submillimetre dielectric response 80—80782
$(NH_4)_2BeF_4$, ferrielectricity, triple 60 Hz D-E hysteresis loops 80—71364
$(NH_4)_2BeF_4$, ferroelec. transition, Raman spectra obs. 77—85705
$(NH_4)_2BeF_4$, ferroelectric, Brillouin scattering study 79—15470
$(NH_4)_2BeF_4$, ferroelectric, cryst. struct., phase transition, X-ray study 79—28689
$(NH_4)_2BeF_4$, ferroelec., incommensurate struct., dynamic props. *(Russian)* 80—11373
$(NH_4)_2BeF_4$, γ-irrad., trapped H atoms, ferroelec. transition, EPR meas. 79—4724
$(NH_4)_2BeF_4$, improper ferroelec., incommensurate-commensurate transitions 78—60404

ferroelectric materials continued
$(NH_4)_2BeF_4$, incommensurate phase transitions under existence of Lifshitz invariant 79—15416
$(NH_4)_2BeF_4$, incommensurate phase, nonlinear optical props., SHG study *(Russian)* 80—33089
$(NH_4)_2BeF_4$, linear and nonlinear optical props. in incommensurate phase 80—69452
$(NH_4)_2BeF_4$, Mandelstam-Brillouin and US exam. of phase transitions 77—12347
$(NH_4)_2BeF_4$, paraelec. and ferroelec. phases, X-ray diffuse scatt. and superlattice struct. *(Japanese)* 77—43189
$(NH_4)_2BeF_4$, paraelec. phase, X-ray and neutron diffr. cryst. struct. anal. 80—84159
$(NH_4)_2BeF_4$, phase transition at 185K, X-ray scatt. obs. 77—36186
$(NH_4)_2BeF_4$, phase transitions, gamma-ray effects obs. *(Japanese)* 80—11349
$(NH_4)_2BeF_4$, polycrystalline, surface layer effects on dielec. behaviour 78—39494
$(NH_4)_2BeF_4$, powder, IR spectra, assignments, mol. libration, in paraelec. and ferroelec. phases 78—88299
$(NH_4)_2Cd_2(SO_4)_3$, dielec. and spontaneous polarisation, −195 to −180°C, particle size depend. 80—97200
$(NH_4)_2Cd_2(SO_4)_3$, ferroelec. langbeinites, Raman scattering 80—34926
$(NH_4)_2Cd_2(SO_4)_3{:}Mn^{2+}$, UO_2^{2+}, luminesc., vibr. modes 79—38629
$((NH_4)_{1-x}Cs_x)_2SO_4$ mixed cryst., EPR of NH_3^+ and SeO_3^- radicals 80—50190
$NH_4H_2AsO_4$, H positions, paraelectric phase 79—19210
$NH_4H_2AsO_4{:}Cr^{5+}$, ENDOR spectra 78—88224
$NH_4H_2PO_4$, acoustooptical and photoelastic props. 78—27181
$NH_4H_2PO_4$, electronic struct., UV reflection spectra and XPS 79—38558
$NH_4H_2PO_4$, ferroelec., electronic struct. study *(Japanese)* 79—87463
$NH_4H_2PO_4$, high temp. phase transition, IR spectra, differential 80—25319
$NH_4H_2PO_4$, IR overtone spectra and temp. depend. 79—47456
$NH_4H_2PO_4$, polycrystalline materials; pyroelec. temp. anal. as method for studying ferroelec. transitions 79—38502
$NH_4H_2PO_4$, powder sample, pyrocharge temp. depend. near phase transition 79—87399
$(NH_4)H_2PO_4{:}Cr^{3+}$, EPR exam. above and below T_c 78—68363
$NH_4H_2PO_4{:}CrO_4^{2-}$ $(Cr_2O_7^{2-})$, electrical cond., thermal depolarisation studies 79—95212
NH_4HSO_4, dielectric relax. in ferroelectric and paraelectric phases 77—16246
NH_4HSO_4, ferroelec., press.-temp. phase diagram 77—85663
NH_4HSO_4, ferroelec., critical slowing down of dielec. relax. *(Japanese)* 77—90109
NH_4HSO_4, ferroelectric powder dielectric behaviour particle size depend. 80—55046
NH_4HSO_4, movement of NH_4^+ in all phases over 77 to 388K, NMR study 77—28524
NH_4HSO_4, volume expansion, spontaneous strain, second order phase transitions 79—65224
$NH_4HSO_4{:}VO^{2+}$, ferroelastic, inernal strains, ferroelec. transitions, EPR 79—47400
NH_4HSO_4-type crystal, ferroelectric phase transform. model, SO_4 group ordering 77—77156
$(NH_4)_3H(SO_4)_2$, phase transitions, sp. ht. meas. 80—2157
$(NH_4)_3H(SO_4)_2$, press.-induced ferroelectricity, dielec. const. meas. 77—12328
$(NH_4)_3H(SO_4)_2$, press.-temp. phase diagram, dielec. and DTA meas. 77—81067
$(NH_4)_3H(SO_4)_2$, pressure-induced ferroelectricity, dielec. const. meas. 78—23412
$(NH_4)_3H(SO_4)_2$, room temp. phase, cryst. struct. 78—42965
$(NH_4)_3H(SO_4)_2$, successive phase transitions, dilatometric and X-ray expts. 80—11348
NH_4HSeO_4, cryst. struct., dielec. and ferroelec. props. 80—60528
NH_4HSeO_4, ferroelec. phase transition, pyroelec. props. 80—60513
NH_4HSeO_4, ferroelec. props. rel. to struct. 80—71345
NH_4HSeO_4, para- to ferroelectric transition obs. by permittivity meas. 79—51916
$(NH_4)_3H(SeO_4)$, ferroelec. transition, press. and temp. effects on dielec. props. 78—23413
$(NH_4)_3H(SeO_4)_2$, ferroelec. phase transition, dielec. meas. 77—63376
$NH_4H_3(SeO_3)_2$, Raman spectra meas. 78—10899
NH_4IO_3, effect of hydrostatic press. on ferroelec. phase transition 79—51917
NH_4IO_3, ferroelec., structural phase transition 80—7308
NH_4IO_3, new ferroelectric materials *(Japanese)* 77—28529
NH_4IO_3, static electrooptic coeffs., temp. depend. 77—28547
$((NH_4)_xK_{1-x})_2SO_4$, NH_4^+ dynamics, neutron scatt. study 79—42167
NH_4LiSO_4, ferroelec., phase transition points, hydrostatic press. effect 77—77155
NH_4LiSO_4, ferroelec., PMR line shape and spin-lattice relax. 78—88205
NH_4LiSO_4, high press. phase, point group symmetry 79—51039
NH_4LiSO_4, hydrostatic press. effect on I-II phase transition, dielec. meas. 79—38496
NH_4LiSO_4, I-II phase transition in improper ferroelec., hydrostatic press. effects 78—84533
NH_4LiSO_4, new ferroelectric materials *(Japanese)* 77—28529
NH_4LiSO_4, point group symm. at high press. phase 80—70150
$((NH_4)_{1-x}Rb_x)_2SO_4$, isomorphic impurity effect on dielec. and nonlinear optical props. 80—88911
$((NH_4)_{1-x}Rb_x)_2SO_4$ mixed cryst., EPR of NH_3^+ and SeO_3^- radicals 80—50190
$(NH_4)_{2(1-x)}Rb_{2x}SO_4$, mixed crystal, dielectric and US meas. of ferroelec. phase transition *(Japanese)* 80—7305
$(NH_4)_{2(1-x)}Rb_{2x}SO_4$, stoichiometry defects, electron probe microanal. 80—39143
$(NH_4)_2SO_4$, Brillouin scatt. from room temp. to −70°C 78—52517
$(NH_4)_2SO_4$, dielec. props., 210-250K, 1 MHz-25 GHz, ferroelec. transition obs. 77—59541
$(NH_4)_2SO_4$, ESR study of NH_3^+ radicals 79—38367
$(NH_4)_2SO_4$, e.s.r., of NH_3^+ and SeO_3^- radicals, ferroelec. transition obs. 77—16180
$(NH_4)_2SO_4$, ferrielec., dielec. behaviour and nature of phase transition 78—88262
$(NH_4)_2SO_4$ ferrielectric, X-ray anal. of sub-lattice order parameters 78—92035
$(NH_4)_2SO_4$, ferroelec., ion group reorientation temp. and press. depend., PMR obs. 78—72470

ferroelectric materials continued
$(NH_4)_2SO_4$, ferroelec. transition, EPR study 79—38472
$(NH_4)_2SO_4$, ferroelec. dispersion in microwave region, transition to ferrielectric structure 80—45016
$(NH_4)_2SO_4$, mechanically twinned, orthorhombic, search for antiphase boundaries 79—37715
$(NH_4)_2SO_4$, microscopic model for ferroelectric phase transition 78—6641
$(NH_4)_2SO_4$, NH_4^+ dynamics, neutron scatt. study 79—42167
$(NH_4)_2SO_4$, optical SHG expts. on microscopic origin of permanent dipoles 78—1299
$(NH_4)_2SO_4$, paraelec. phase, X-ray diffuse scatt., soft mode model 77—31744
$(NH_4)_2SO_4$, paraelectric to ferroelectric phase boundaries 78—19426
$(NH_4)_2SO_4$, paraelectric, N-quadrupole coupling meas. by proton-N double resonance 80—60459
$(NH_4)_2SO_4$, phase transition mechanisms by optical spectroscopy 79—15411
$(NH_4)_2SO_4$, phase transition theory 79—24275
$(NH_4)_2SO_4$, polycrystalline materials; pyroelec. temp. anal. as method for studying ferroelec. transitions 79—38502
$(NH_4)_2SO_4$, powder sample, pyrocharge temp. depend. near phase transition 79—87399
$(NH_4)_2SO_4$, pure and Rb doped, ferroelec. transition, light scatt. meas., dielec. and elastic props. 78—43822
$(NH_4)_2SO_4$, static and dynamic dielec. behaviour 80—71337
$(NH_4)_2SO_4{:}Cd^+$, ferroelec. transition, soft mode contrib., EPR obs. 78—72469
$(NH_4)_2SO_4{:}Cu^{2+}$, ESR, Cu^{2+} in trigonal bipyramidal coord. 78—23330
$(NH_4)_2SO_4{:}Cu^{2+}$, ESR parameters, effect of pH of mother soln., trapping sites 80—15791
$(NH_4)_2SO_4{:}Cu^{2+}$, ferroelec. transition, ESR study 79—91286
$(NH_4)_2SO_4{:}SeO_3^-$, γ-irrad., hyperfine interaction, ferroelec. transition effects, EPR expt. 78—15024
$(NH_4)_2SO_4{:}VO^{2+}$, EPR spectrum, temp depend. 110-300K 80—11249
$(NH_4)_2SO_4$-K_2SO_4 mixed crystal, ESR study of NH_3^+ radicals 79—38367
$(NH_4)_2ZnCl_4$, commensurate-incommensurate phase transition, ^{35}Cl NQR study 80—75966
$(NH_4)_2ZnCl_4$, ferroelectricity and incommunsurate-commensurate phase transitions 80—60523
$NaAl(MoO_4)_2$, domain struct., phase transition, and dielec. props. 79—56748
$Na_9(Al_6Si_6O_{24})(OH)_2.6H_2O$, hydrosodalite, ferroelec. transition, pyro- and piezoelec. activity 79—15421
$Na_{0.5}Bi_{0.5}TiO_3$, phase transition, hysteretic behaviour 80—71330
$Na_{0.5}Bi_{4.5}Ti_4O_{15}$, hot-forged ferroelec. ceramic with layer struct. 79—43175
$NaClO_3$, cryst. growth from soln., selective etching technique for observation of dislocations 79—19251
$Na(D_xH_{1-x})_3(Se_3)_2$, ferroelec. dispersion 80—40069
$NaD_{3x}H_{3(1-x)}(SeO_3)_2$, ferroelec. dispersion 80—66129
$Na(D_xH_{1-x})_3(SeO_3)_2$, Raman spectra and nature of phase transitions 78—80341
$NaD_3(SeO_3)_2$, ^{23}Na NQR. second-order quadrupole shift, temp. depend. 78—15055
$NaD_3(SeO_3)_2$, ^{23}Na resonance line temp. depend., of first order quadrupole shift and spontaneous polarisation 79—8069
$NaFe(MoO_4)_2$, domain struct., phase transition, and dielec. props. 79—56748
$Na(H_{1-x}D_x)_3(SeO_3)_2$, ferroelectric, dielectric behaviour at RF and microwave freq. 79—33640
$NaH_3(SeO_3)_2$, β to δ ferroelec. transition under press. Raman spectra study 80—80725
$NaH_3(SeO_3)_2$, domain struct. realignment and Barkhausen effect 80—71361
$NaH_3(SeO_3)_2$, dynamics of α-β transition, Brillouin scatt. meas. 77—8526
$NaH_3(SeO_3)_2$, electromechanical props. near Curie point 80—29690
$NaH_3(SeO_3)_2$, ferroelec. crystal, Barkhausen effect study 79—38507
$NaH_3(SeO_3)_2$, ferroelec., proton motion within H bonds, neutron scatt. study 80—75986
$NaH_3(SeO_3)_2$, high-pressure phase transform., ^{23}Na NMR obs. 77—63380
$NaH_3(SeO_3)_2$, phase transition, pyroelec. current meas. 79—82934
$NaH_3(SeO_3)_2$, proton behaviour in H-bonding, neutron spectroscopy obs. *(German)* 78—22816
$NaH_3(SeO_3)_2$, proton spin lattice relaxation 79—78557
$NaH_3(SeO_3)_2{:}VO^{2+}$, ESR spectra 79—4718
$(Na_{0.5}La_{0.5})_xBa_{1-x}TiO_3$, dielec. and IR spectra exam., ferroelec. transition 78—23418
$Na_{1-x}Li_xNbO_3$ mixture, ferroelec.-paraelec. transitions, dielec. props. meas. 80—66125
$NaND_4C_4H_2D_2O_6.4D_2O$, ferroelec. phase, incommensurate satellite refls. 78—84531
$NaND_4SeO_4.2D_2O$, nonlinear electromechanical props. above Curie temp. 79—33610
$NaNH_4SO_4.2H_2O$, $NaNH_4SeO_4.2H_2O$, nonlinear opt. props. including SHG 78—76396
$NaNH_4SO_4.2H_2O$, ferroelec. and thermal props. 78—83968
$NaNH_4SeO_4.2H_2O$ ferroelectric crystal optical SHG and pulse modulation *(Russian)* 77—14771
$NaNH_4SeO_4.2H_2O$, crystal struct. in ferroelec. phase, nature of transition 77—43946
$NaNH_4SeO_4.2H_2O$, model of ferroelec. phase transition 78—19433
$NaNH_4SeO_4.2H_2O$, ferroelectric phase transition mechanism 78—31162
$NaNH_4SeO_4.2H_2O$, atomic struct. exam. and phase transition 79—37678
$NaNO_2$, ^{23}Na elec. field gradient tensor from NMR satellite lines near phase transition 80—71191
$NaNO_2$, 163°C phase transition, thermal history effects on range of modulated struct. 78—95563
$NaNO_2$, ang. dispersion of internal phonon modes, Raman meas. 79—51211
$NaNO_2$, band struct., polarisation and piezoelec. consts. calc. 78—52448
$NaNO_2$, complex dielectric constant, sinusoidal phase in ferroelectric material 79—11376
$NaNO_2$, crit. X-ray scatt. 79—33636
$NaNO_2$, ferroelec., dielec. and thermal behaviour 80—80680
$NaNO_2$, ferroelec., electric field gradient *(Korean)* 79—15419
$NaNO_2$, ferroelec., electron distrib., X-ray and neutron diffraction study 80—24411

ferroelectric materials continued
$NaNO_2$, ferroelec., X-ray diffr. topographic study of polarisation reversal 79—38441
$NaNO_2$, ferroelec., X-ray obs. during polarisation reversal 79—51921
$NaNO_2$, ferroelec. thin crysts., struct. investig. 79—27962
$NaNO_2$, ferroelectric, NMR of ^{23}Na small particles 79—28629
$NaNO_2$, ferroelectric, second-order vibr. spectra and dispersion of phonon branches 79—69847
$NaNO_2$, ferroelectric transitions, based on model thermodynamic pot. 78—80295
$NaNO_2$, ferroelectric transitions, group theoretic comparison with $AgNaNO_2$ 80—7311
$NaNO_2$, ferroelectric transitions, one-mode model 80—29702
$NaNO_2$, fine struct. in luminesc. spectra in UV region 77—59607
$NaNO_2$, incommensurate phase transitions 78—26653
$NaNO_2$, incommensurate phase transition, Bethe-Peierls and mol. field approx. 80—20599
$NaNO_2$, lattice dynamics, two-phonon Raman scatt. and IR absorpt. 79—33684
$NaNO_2$, NQR of ^{14}N at ferroelec. transition, order-disorder fluctuations 77—63311
$NaNO_2$, nuclear quadrupole coupling const. and spontaneous polarisation 80—71229
$NaNO_2$, phase transitions accompanied by noncommensurate superstruct. form. 77—32336
$NaNO_2$, phonon side bands of triplet absorption 78—76488
$NaNO_2$, polarisation reversal by time-resolved X-ray diffr., NO_2 radical rot. 77—63382
$NaNO_2$, positron lifetimes, ferro-paraelectric transition 79—74017
$NaNO_2$ powder, surface layer effects on dielec. props. 77—1631
$NaNO_2$, rot. behaviour of NO_2 radicals in order-disorder transition, Fourier synthesis study of neutron data 79—56739
$NaNO_2$, second order phase transition prod. by strain 79—15420
$NaNO_2$, vacuum UV spectra and electro-optical prop. *(Japanese)* 79—65900
$NaNO_2$, X-ray crit. scatt. 78—52461
$NaNO_2{:}Mn^{2+}$, ferroelectric phase metastable struct., EPR obs. 78—60328
$NaNO_2{:}Mn^{2+}$, zero-field splitting, ferroelec. soft-mode contrib., phase transition, EPR obs. 79—15344
$NaNO_3$, press. induced ferroelec. transition, soft mode dynamics, Raman scatt. meas. 78—72475
$NaNbO_3$, birefr., temp. depend., behaviour at $P \rightleftarrows N$ struct. transition 78—64331
$NaNbO_3$, cubic to tetragonal transition, inelastic neutron scatt. study *(French)* 79—60469
$NaNbO_3$, elec. and thermoelec. props., influence of O defects 80—29401
$NaNbO_3$, ferroelec., local field determ., phase transition study by EPR 79—38471
$NaNbO_3$, hydrostatic press. effect on permittivity, phase transition, hysteresis 80—80670
$NaNbO_3$, memory effect, in ferroelec. phase, ESR meas. 79—28696
$NaNbO_3$, photoferroelectric effect 78—35108
$NaNbO_3{:}Mn^{2+}$, ESR, temp. depend., -269-750°C, fine splitting 77—51948
$NaNbO_3$-$BaTiO_3$, ferroelec. Curie temp., theory 80—7313
$NaNbO_3$-$BaTiO_3$, unidirectionally solidified transparent ceramics 80—25677
$NaNbO_3$-$BaTiO_3$ solid soln. form. and props. *(Russian)* 78—48378
$NaNbO_3$-based solid solns., morphotropic transitions and elec. props., enhanced vacancy conc. 80—55048
$NaNbO_3$-$PbTiO_3$, ferroelec. Curie temp., theory 80—7313
$(Na_{5-x}Nd_x)(W_{3-2x}Nb_{2x})O_9F_5$, ferroelastic-ferroelectric material *(French)* 79—99834
$Na_3Sc_2(PO_4)_3$, ferroelectric props., X-ray diffr. study 79—69789
$NaVO_3$, thermal expansion and ferroelec. phase transition 79—38482
$Nd(BrO_3)_3.9H_20$, single cryst. low-temp. pyroelectricity 79—42906
$NdNbO_4$, cryst. growth rel. to investig. of PbO-KF-B_2O_3-$PbNdTiNbO_7$ cross section 77—86004
NdP_5O_{14}, ferroelastic, spectroscopy, ferroelastic/ferroelectric coupling, soft optic mode frequencies 79—19845
$Nd_2Ti_2O_7$, ferroelec., temp. depend. of SHG intensity 79—24267
$Nd_2Ti_2O_7$, layered ferroelectric, anomalous photovoltaic effect, photovoltaic current 80—75603
$Ni_3B_7O_{13}Br$, ferroelec. 43m-mm2 phase transition, molar heat capacity meas. 80—93249
$Ni_3B_7O_{13}Cl$, boracite, on Cr-Cl boracite, gas phase synthesis of epitaxial layers 79—60650
$Ni_3B_7O_{13}Cl$, specific heat anomaly at $F43c \rightarrow Pca2_1$ transition 79—28690
$Ni_3B_7O_{13}I$, dynamics of ferroelec. phase transition, Raman spectra obs. 79—33630
$Ni_3B_7O_{13}I$, magnetoelectric tensor component detection 79—95625
$Ni_3B_7O_{13}I$, nonlinear magnetoelec. and dielec. props. 79—65704
$Ni_3B_7O_{13}X$, X=Cl, Br, I, ferromag. ferroelectrics *(Japanese)* 79—65804
$Ni_{0.6}Fe_{2.4}B_7O_{13}I$, boracite, mag. hyperfine interactions, Mossbauer study 80—39935
PLZT ceramic, bonded lens assembly manufacture 80—79018
PLZT ceramic, dielectric anisotropy, role of 90° domain processes 77—63384
PLZT ceramic, ferroelec., cathodlum. spectral and temp. depend. 78—84665
PLZT ceramic, photovoltaic effect 79—99585
PLZT ceramic, proton implanted, photoferroelectric effect for image storage and display devices 80—80315
PLZT ceramic, thin waver electrode slotting process 80—79017
PLZT ceramic, thin wafer production polishing process 80—81214
PLZT ceramic birefringence props., transverse electro-optical meas. 78—72487
PLZT ceramic photoferroelectric image storage device, characts. 77—55756
PLZT ceramic with memory, domain reorientation, alternating elec. field effect 79—47405
PLZT ceramic;, visible light scatt. depend. on photoferroelectric space charge fields 80—80806
PLZT ceramics, diffuse phase transitions and thermodynamics 80—29694
PLZT ceramics, electro-optic characts., w.r.t. future instrument applics. *(German)* 78—33792
PLZT ceramics, electro-optical props. *(Korean)* 79—11406
PLZT ceramics, electro-optic; defect struct. and prop. 79—42910
PLZT ceramics, elastooptic effect, stress induced birefr. 80—60543

ferroelectric materials continued
PLZT ceramics, ferroelectric and struct. transitions, crystallographic, thermal, and dielec. anal. 80—29693
PLZT ceramics, modified by $Ca^{2+}(Sr^{2+})(Nd^{3+})(Y^{3+})$, dielec. behaviour 80—60519
PLZT ceramics, photoferroelectric effects, image storage device appl. 79—42924
PLZT ceramics, photoinduced charge transfer process 79—50362
PLZT ceramics, phase transitions induced by elec. fields 80—29695
PLZT ceramics, SHG, anomalous phase transition 79—45996
PLZT ceramics, short circuit photocurrent, depend. on polarization 79—38121
PLZT ceramics, sp. ht., 2-25K, field depend., phonon modes 77—47586
PLZT ceramics, stress-induced ferrelec. transition, pseudoelasticity and shape memory, bending meas. 79—24274
PLZT ceramics, transparent ferroelec., photorefraction and photocond. study 79—42581
PLZT ceramics photosensitivity enhancement by H- and He-ion implantation 80—96934
PLZT composition, effect on its switching characts. 79—42917
PLZT, controlled light scatt. 78—10909
PLZT, deposition of transparent electrodes, opt. storage device applic. 78—74848
PLZT, diffuse phase transitions, Curie temp., dielectric props. 80—75979
PLZT, effect of ageing on temp. depend. of permittivity, for ferroelectric and antiferroelectric compositions 78—48121
PLZT, electrically polarised, size and conc. of light scatt. centres 77—28549
PLZT, electro-optical, physical elec. and optical props. and fabrication *(Polish)* 78—56458
PLZT, electrooptic systems *(Japanese)* 79—65840
PLZT ferroelec. ceramics, piezoelec. props. 79—42897
PLZT, ferroelectric domain struct. obs. by SEM and optical microscopy *(Japanese)* 78—15136
PLZT, ferroelectric devices for optical systems 78—90473
PLZT ferroelectric display electro-optical props. *(Russian)* 79—9211
PLZT, ferroelectric phase transitions, phase state identification 80—45018
PLZT film, epitaxial growth by RF sputtering, and characterisation 77—85937
PLZT, fine grained 90° electric domain wall movement, interpretation of dielectric losses *(German)* 79—33646
PLZT, light scatt., time depend., switching, memory modes 77—12362
PLZT, light scatt. under switching conditions, time characts. 77—52045
PLZT, mech. and elec. losses, correl., theory and expt. 80—66133
PLZT modified high voltage dielectric, permittivity, Curie temp., loss meas. 80—80720
PLZT, opt. spectra and luminesc. 78—76508
PLZT, phase transitions, permittivity, birefr. and light scatt. meas. 77—81074
PLZT, photorefractive effect and photoconductivity 78—92046
PLZT powder preparation, hyrolysis ball mixing 80—81006
PLZT, prep. by liquid phase sintering of oxides 79—38778
PLZT, RF sputtered thin film, ferroelectric props. 79—69780
PLZT, reduced, exam. of ageing phenomena, using dielectric hysteresis *(German)* 79—33647
PLZT, refr. index, 405-764 nm, surface layer 78—35110
PLZT slim-loop and linear ceramics, longit. electrooptic effects, display appl. 80—80751
PLZT slugs, powder hot pressing technique 80—81007
PLZT thermal, flash, ferroelectric protective goggles 80—81746
PLZT, thin, elec. cond. and pyroelectric behaviour 80—75954
PLZT, thin film epitaxial growth and characteris. 79—28918
PLZT, transparent, optical exam. of small signal behaviour, of 90° electric domain walls *(German)* 79—33645
PLZT, transparent, ceramics obtained by hot pressing, optimum conditions *(German)* 79—43176
PLZT, transparent ferroelec., RF sputtering and film characterisation 78—72727
PLZT type ceramics, variation of light scatt. during field induced $AF \rightarrow F$ transition *(French)* 77—90158
PLZT type ceramics, calorimetric meas. of energy of electrical polarisation 79—2770
PLZT, with broad phase transition, birefr., electro-optic and dielec. props. 77—16280
PLZT:Fe, enhancement of photochromic effect by multi-reflection scatt. 77—75632
PLZT/TFPD thermal/flash protective lens assembly, polarised delamination investigation 80—78929
(PLZT)(PLZN) system, ferroelec. transparent, prep. and study 79—42911
$(Pb,Ba)_5Ge_3O_{11}$ ferroelectric crystals, influence of Pb replacement by Ba on props. 79—87402
$(Pb,Ba)Nb_2O_6$, polycryst., orientational polarisation and phase comp. in strong field 78—27157
$(Pb,Ba)(Zr,Ti)O_3$, diffuse phase transitions, Curie temp., dielectric props. 80—75979
$(Pb,La)TiO_3$, soft E(TO) phonons, and phase transitions, Raman spectra, -200 to 400°C 78—15109
$(Pb,La)(Zr,Ti)O_3$, ferroelec. ceramic, polarisation distrib. obs. using electro-optic effect 80—25278
$(Pb, Sr)_5Ge_3O_{11}$, single crysts., growth and X-ray and dielec. investigations 80—88127
$(Pb,Sr)TiO_3$, ferroelec. solid solution, dielec. nonlinearity in nonpolar phase *(Russian)* 77—32317
Pb compounds, perovskites, polymorphic transformations possibility, mag. anal. elec. ordering effects 80—55389
Pb_z-$Sr_{1-z}(Zr_x$-$Ti_{1-x})O_3{:}Cr_2O_3$, ferroelec. ceramic, reversible characts. and dielectric losses *(Russian)* 78—84517
$Pb_2AgNb_5O_{15}$, $Pb_2AgTa_5O_{15}$, ferroelec. and ferroelastic props. *(French)* 79—24266
$(Pb_{1-x}Ba_x)_5Ge_3O_{11}$, ferroelec. phase transition, dielec. const. and quasi-elastic light scatt. 80—71289
$(Pb_xBa_{1-x})_5Ge_3O_{11}$, electrogyration, and dielectric props. 78—19444
$(Pb_{1-y}Ba_y)_{1-x}La_xNb_{2-x/5}O_6$, transparent ferroelec. ceramic, optical transmittance, electrooptic props. and Curie temp. 77—32395
$(Pb_{1-y}Ba_y)_{1-x}La_xNb_{2-x/5}O_6$, ferroelec., phase transitions 79—38487
$Pb_{2-x}Ba_xLi_{0.5}Nb_{1.5}O_6$, elec. resistivity, Curie temp., x=0-0.15, 50-350°C 78—2478
$Pb_{0.94-x/2}Ba_{0.6}Nb_xZr_{1-x}O_3$, Nb dopant morphology effect on microstructure 80—81005

ferroelectric materials continued
$Pb_{1-x}Ba_xZrO_3$, electric quadrupole interaction meas., by PAC 77—4591
$(Pb_{0.715}Ba_{0.285})_{0.991}(Zr_{0.707}Ti_{0.293})_{0.981}Bi_{0.019}O_3$, slim loop ferroelec. ceramic, shock wave compressed, elec. response 78—80293
$(Pb_{0.8}Ba_{0.2})(Zr_{0.8}Ti_{0.2})O_3$ ceramic, pulse-like voltage generation using polarisation reversal 78—2809
$PbBi_2Nb_2O_9$ ceramic, grain oriented, dielectric and piezoelectric props. 79—42896
$PbBi_2Nb_2O_9$, hot-forged ferroelec. ceramic with layer struct. 79—43175
$PbBi_4Ti_4O_{15}$ ceramic, dielec. props., temp. depend. 78—95561
$PbBi_4Ti_4O_{15}$, hot-forged ferroelec. ceramic with layer struct. 79—43175
$Pb_2Bi_4Ti_5O_{13}$, hot-forged ferroelec. ceramic with layer struct. 79—43175
$PbCo_{0.33}Nb_{0.66}O_3$, ferroelectric, exam. of permittivity and dielectric props. 79—1742
$Pb_{5-x}(Cs, Bi)_xGe_3O_{11}$ 80—75960
$Pb(Fe_{1/2}Nb_{1/2})O_3$-$La_2O_3(CeO_2)$ ferroelec. ceramics, electrophysical props. 78—35099
$2PbFe_{1/2}Nb_{1/2}O_3$-Pb_2FeReO_6, comp., struct., dielec. and mag. props. 80—2704
$Pb(FeTa)_{1/2}O_3$, Mossbauer spectra, 78-480K 79—51885
$2PbFe_{1/2}Ta_{1/2}O_3$-Ba_2FeReO_6, comp., struct., dielec. and mag. props. 80—2704
$2PbFe_{1/2}Ta_{1/2}O_3$-Pb_2FeReO_6, comp., struct., dielec. and mag. props. 80—2704
$PbFe_{2/3}W_{1/3}O_3$-$BaTiO_3$ system ferroelec., antiferromag., ESR and dielec. props. meas. 77—40172
$PbFe(_{2/3}W_{1/3})O_3$-$Pb(Co_{1/2}W_{1/2})O_3$ solid soln., crystallographic, dielectric, magnetic props., Mossbauer spectra 78—43807
$Pb_3Fe_2WO_9$, perovskite ferroelec., characts. of dielec. polarisation 77—8496
Pb_2GaTaO_6, transition from pyrochlore to imperfect fluorite struct. 80—19939
$Pb_3(Ge,Si)_2O$, growth from melt, struct. and dielec. props. 77—44148
$Pb_5(Ge,Si)_3O_{11}$, dielec. and elec. props., 20 to 250°C 80—29697
$PbGeO_3$, single cryst. films growth, temp. depend. of dielec. constant 79—100066
$Pb_3Ge_3O_{11}$, uniaxial ferroelec., thermal expansion and dielec. permittivity in vicinity of transition points 77—66459
Pb_5GeO_{11}, elastic nonlinearity and acoustic losses 80—59554
Pb_5GeO_{11}, induced and spontaneous optical activity, permittivity 79—33661
$Pb_5Ge_2O_{11}$ acoustic relax. assoc. with phase transition at hypersonic freq. 78—88267
$Pb_5Ge_3O_1$, anharmonic phonons and central peaks at struct. phase transitions 79—95775
$Pb_5Ge_3O_{11}$, acoustic emission, threshold electric field 79—60874
$Pb_5Ge_3O_{11}$ acoustic relaxation near ferroelectric transition 78—2814
$Pb_5Ge_3O_{11}$, anharmonic effects in low freq. symm. modes, Raman study 80—25365
$Pb_5Ge_3O_{11}$ crystal, ferroelec., luminesc. under pulse polarisation switching conditions 77—1735
$Pb_5Ge_3O_{11}$, dielec. behaviour, 60 Hz-100 kHz, particle size effects 79—33638
$Pb_5Ge_3O_{11}$, dielec. functions above and below ferroelec. transition 79—33588
$Pb_5Ge_3O_{11}$, dynamic central peaks and phonon interactions near structural phase transitions 78—83903
$Pb_5Ge_3O_{11}$, ESR of Fe^{3+} ions 79—95639
$Pb_5Ge_3O_{11}$, electrogyration during phase transitions 79—19859
$Pb_5Ge_3O_{11}$, electrostrictive interaction, mode damping 80—34862
$Pb_5Ge_3O_{11}$, ferroelec., surface capacitance effect on dielec. props., DC cond. and dielec. const. meas. 79—91333
$Pb_5Ge_3O_{11}$, ferroelec. phase transition, for IR transmission meas. 79—38478
$Pb_5Ge_3O_{11}$, ferroelectric transition exam. by Raman scatt. 78—56439
$Pb_5Ge_3O_{11}$, ferroelectric soft mode exam., Raman spectra 79—42202
$Pb_5Ge_3O_{11}$, freq. and damping of ferroelec. soft mode, permittivity meas. 77—52027
$Pb_5Ge_3O_{11}$, growth defects and polarisation switching 78—48132
$Pb_5Ge_3O_{11}$, lattice dynamics parameters anisotropy, X-ray diffr. study 80—59612
$Pb_5Ge_3O_{11}$, light scatt. meas., central peak dynamics at ferroelectric transition 77—4606
$Pb_5Ge_3O_{11}$, light scatt. obs. of unresolved central peak 77—4649
$Pb_5Ge_3O_{11}$, paraelectric and ferroelectric, Raman spectra near ferroelectric transition 80—55090
$Pb_5Ge_3O_{11}$, photodielectric effects, Curie temp., permittivity and polarisation 80—40034
$Pb_5Ge_3O_{11}$, pulsed polarisation switching process depend. on illumination 80—93253
$Pb_5Ge_3O_{11}$, Raman scatt., soft modes and damping near structural phase transition 79—28739
$Pb_5Ge_3O_{11}$, single crystal, ferroelec., Czochralski growth 78—3024
$Pb_5Ge_3O_{11}$ single crystals, switching behaviour and hysteresis 80—40077
$Pb_5Ge_3O_{11}$, ultrafine-grained crystallized from glass, ferroelectricity 78—39508
$Pb_5Ge_3O_{11}$, uniaxial displacive ferroelectrics, domain wall dynamics 79—73890
$Pb_5Ge_3O_{11}$, uniaxial ferroelectric, optical activity dispersion 78—48141
$Pb_5Ge_3O_{11}:Gd^{3+}$, displacive phase transition, S ion spin Hamiltonian parameter dependence on order parameter 80—70356
$Pb_5Ge_3O_{11}:Gd^{3+}$, ferroelec. transition, temp. depend., EPR study 80—66127
$Pb_5Ge_3O_{11}:Si$, switching velocity, increase over that of undoped crysts. 79—51922
$Pb_5(Ge_{1-x}Si_x)_3O_{11}$, dielec. spectra, ferroelec. behaviour 78—60406
$Pb_5(Ge_{1-x}Si_x)_3O_{11}$, electrogyration, phase transition and dielectric props. 80—93269
$Pb_5(Ge_{1-x}Si_x)_3O_{11}$ solid solutions, dielec. props., ferroelec. phase transitions 80—15988
$Pb_5Ge_{3-x}Si_xO_{11}$, ferroelec. soft mode, temp., press. and comp. depend. 78—80304
$Pb_5Ge_{3-x}Si_xO_{11}$, ferroelec., switching vel. and spontaneous polarisation 78—84543
$Pb_5Ge_{3-x}Si_xO_{11}$, ferroelec. phase transition, for IR transmission meas. 79—38478
$PbHAsO_4$, ($PbDAsO_4$), Raman spectra of ferroelec. transition proton tunnelling 78—23410
$PbHAsO_4$, ferroelec., far IR and submillimetre dielec. dispersion 79—38528
$PbHAsO_4$, hydrostatic press. effect on ferroelec. transition 78—35102

ferroelectric materials continued
$PbH(D)PO_4$, $PbH(D)AsO_4$, ferroelectric, sp. ht. 79—19853
$PbHPO_4$, crystals, ferroelec. phase transition, hydrostatic press. influence, dielec. meas. 80—88936
$PbHPO_4$, ferroelec. phase transition, Brillouin and Raman spectra obs. 79—33683
$PbHPO_4$, ferroelec., far IR and submillimetre dielec. dispersion 79—38528
$PbHPO_4$, hydrostatic press. effect on ferroelec. transition 78—35102
$PbHPO_4$, linear response function for tunnelling systems in polariton region 78—43799
$PbHPO_4$, microwave permitt. and far IR refl. spectra in paraelec. and ferroelec. phases 80—40033
$PbHPO_4$, neutron diffr. exam. of struct. at room temp. 79—38490
$PbHPO_4$, optical props. near ferroelec. transition 79—33663
$PbHPO_4$, phase transitions study, role of cryst. struct. determ. 80—75197
$PbHPO_4$, protonic order-disorder transition 78—26478
$PbHPO_4$, Raman spectra study of ferroelec. transition, proton tunnelling 78—23410
$PbHPO_4$, single cryst., growth, optical props., ferroelec. transition 78—35285
$PbHPO_4$, single cryst., dielec. props. 79—38426
$PbHPO_4$-type crystals, ferroelec. transition, statistical model 80—25321
$PbHfO_3$, elec. field gradient, crit. behaviour, DPAC meas. 78—80303
$PbHf_{1-x}Ti_xO_3$, phase diagram, influence of poling treatment, ferroelec. antiferroelec. transition *(French)* 77—63374
$PbIn_{0.5}Nb_{0.5}O_3$, ferroelectric, dielectric props. 80—103923
$Pb_{0.27}K_{0.56}Nb_{0.91}Ta_{4.15}O_{15}$, coupled ferroelastic-ferroelectric props. 77—59543
$Pb_{0.9}K_{0.1}(Zn_{1/3}Nb_{2/3})O_{2.95}$-$PbZrO_3$-$PbTiO_3$, morphotropic tetragonal-rhombohedral phase boundary 78—48129
$Pb_{0.97}La_{0.02}(Zr_{0.92}Ti_{0.08})O_3$, ferroelec. ceramic, stress effects 80—2119
$PbMg_{1/3}Nb_{2/3}O_3$, and its solid solns., low temp. phase transition obs. 79—69788
$PbMg_{1/3}Nb_{2/3}O_3$, carrier mobility and photoluminesc. near ferroelec. transition *(Russian)* 78—2813
$PbMg_{1/3}Nb_{2/3}O_3$, cathodlum. spectral and temp. depend. 78—84665
$Pb(Mg_{1/3}Nb_{2/3})O_3$, cation disordered perovskite, elastic consts. and thermal expansion 80—96587
$PbMg_{1/3}Nb_{2/3}O_3$, crit. electron-phonon phenomena and diffuse phase transition in elec. field 79—38497
$PbMg_{1/3}Nb_{2/3}O_3$, dielec. props. under high hydrostatic pressure near phase transition point 80—44997
$Pb(Mg_{1/3}Nb_{2/3})O_3$, electrostrictive effect 80—66113
$PbMg_{1/3}Nb_{2/3}O_3$, PMN, electro-opt., elasto-opt., opt. and photo-induced props. 78—95560
$PbMg_{1/3}Nb_{2/3}O_3$, photoinduced phenomena at diffuse phase transition 78—43814
$PbMg_{1/3}Nb_{2/3}O_3$, photolum. near ferroelec.-paraelec. phase transition 80—16100
$PbMg_{1/3}Nb_{2/3}O_3$ single cryst., electro-optical hysteresis curves and phase transitions *(German)* 79—28717
$PbMg_{1/3}Nb_{2/3}O_3$, vibr. spectrum and dispersion of optical consts., coexisting ferro- and paraelec. phases 77—63422
$PbMg_{1/3}Nb_{2/3}O_3$, with diffused phase transition, photoelectret states 80—20583
$PbMg_{1/3}Nb_{2/3}O_3$-$BiMg_{2/3}Nb_{1/3}O_3$, dielectric polarisation of solid solutions 78—43776
$Pb(Mg_{1/3}Nb_{2/3})O_3$-$Pb(W_{1/2}Mg_{1/2})O_3$, struct. and dielec. props. 80—25312
$Pb(Mg_{1/3}Nb_{2/3})O_3$-$Pb(Mg_{1/2}W_{1/2})O_3$, solid soln., electrostriction, strain gauge obs. 80—55043
$PbMg_xNb_{1-x}O_3$, ferroelec. with diffuse phase transition, electrostriction-optical props. 78—68457
$Pb_3MgNb_2O_9$, birefringence, pulse response of electro-optical effect 79—87417
$Pb_3MgNb_2O_9$, crystal growth procedure, meas. electro-optic and dielectric props. 78—88418
$Pb_3MgNb_2O_9$-$PbTiO_3$, relaxor ferroelectrics, electrostrictive effects 80—66112
$PbMg_{0.33}Ta_{0.66}O_3$, ferroelectric, exam. of permittivity and dielectric props. 79—1742
$Pb_3Mg_2Ta_2O_9$, crystal growth procedure, meas. electro-optic and dielectric props. 78—88418
$PbMoO_4$, electrogyration coeff. meas. 79—19859
$PbNb_2O_6$, cryst. struct., at. displacements, superstruct. *(French)* 77—72588
$PbNb_2O_6$, ferroelec., sp. ht. and Debye temp. meas., 2-25K 79—73319
$PbNb_2O_6$, ferroelectric thick crystals, domain formation and dislocation loops 78—60410
$PbNb_2O_6$ ferroelectric single crysts., domain struct., cryst. planes, twinning 78—64340
$PbNb_2O_6$, ferroelectric strain polarisation interaction, domain wall formation 79—56750
$PbNb_2O_6$, O defects and elec. props. anomalies 79—42898
$PbNb_2O_6$, permittivity and elec. cond. meas., first order transition 79—24270
$PbNb_2O_6$, surface (001), microstruct. obs. by optical, etching, and interferometric techniques 79—11399
$PbNb_2O_6$-$NaNbO_3$, DTA *(French)* 77—44234
$PbNb_{0.5}Sc_{0.5}O_3$, ceramic, dielec. props. 79—11392
$Pb_{0.99}Nb_{0.02}(Zr_{0.95}Ti_{0.05})_{0.98}O_3$, ferroelec. ceramic, stress effects 80—2119
$Pb_{5-x}Nd_xGe_3O_{11}$, ferroelec. props. 80—75960
$PbNdTiNbO_7$, cryst. growth rel. to investig. of PbO-KF-B_2O_3-$PbNdTiNbO_7$ cross section 77—86004
PbO-GeO system, pyroelec. and TSC props. 78—43798
PbO-MoO_3-MO and PbO-WO_3-MO systems, M=Ca, Ba, Mg, Sr, perovskite type cpds. detection 80—108404
PbO-TiO_2, phase equilib. determ. by mass-loss Knudsen effusion method 77—11668
PbO_x, photoconducting, phase transitions, occurrence of ferroelectricity, pyrocurrent obs. 79—11395
Pb_3O_4, IR and Raman study of structural phase transitions *(French)* 78—84582
$Pb_{1-\alpha x}R_xTiO_{3+x(1.5-\alpha)}$, R=La or Sm exam. of permittivity as function of temp. 79—33586
$Pb_{1-nx}R_xTiO_{3+x(1.5-n)}$, R=rare earth, ferroelec. Curie temp. comp. depend. 77—16258
$Pb_5S_2I_6$, ferroelec., synthesis and hydrothermal growth 79—38731
$PbSc_{0.5}Nb_{0.5}O_3$, single cryst., dielec. props. 80—66126

ferroelectric materials continued
$Pb(Sc_{0.6}Ta_{0.5})_3$ ceramics, ordering and diffuse phase transitions 80—29699
$PbSc_{2/3}Te_{1/3}O_3$, ferroelec., high-frequency permittivity, temp. depend. 80—71325
$PbSc_{2/3}Te_{1/3}O_3$-$PbSc_{2/3}W_{1/3}0_3(PbFe_{2/3}Te_{1/3}O_3)$ ferroelec. props. and lattice consts. 80—60520
$Pb_{0.56}Sn_{0.44}Te$, press. induced ferroelec. phase transition 79—65809
$Pb_{0.94}Sr_{0.06}(Ti_{0.47}Zr_{0.53})O_3$-NiO, modified, dielec. and piezoelec. props. 80—11342
$Pb_{0.95}Sr_{0.05}(Ti_xZr_{1-x})O_3$, solid solns., parameters of Curie Weiss law, permittivity meas. 78—15129
$Pb_{0.95}Sr_{0.05}(Zr_x, Ti_{1-x})O_3$-$Nb_2O_5$, phase coexistence range, lattice consts. 80—92680
$Pb_{0.95}Sr_{0.5}(Zr_{0.53}Ti_{0.47})O_3+Nb_2O_5$, optimum comp. for soft ferroelectric ceramic 77—43938
$(Pb_{0.97}Sr_{0.03})Zr_{0.51}Ti_{0.49}O_3$, ferroelec. phase transition under high press. 77—36188
$Pb_{0.95}Sr_{0.05}(Zr_{0.53}.Ti_{0.47})O_3$, low temp. internal friction in ferroelectric ceramic 77—21200
Pb_2TaMnO_6, reaction of form. from oxides, ferroder. props. 80—55326
$Pb(Ti,Zr,[Fe_{1/2}Ta_{1/2}])O_3$, pyroelec. props. at transition between ferroelec. phases 78—52447
$Pb(Ti, Zr)O_3$, piezoelectric-ferroelectric ceramic, polarisation processes, X-ray obs. 80—34847
$Pb(Ti,Zr)O_3$, polycryst., orientational polarisation and phase comp. in strong field 78—27157
$Pb(Ti,Zr)O_3$, pyroelectric props., addition effects 79—33608
$Pb(Ti,Zr)O_3$, soft E(TO) phonons, and phase transitions, Raman spectra, −200 to 400°C 78—15109
$Pb(Ti,Zr)O_3$:Fe(Mn)(Al), internal bias field and hysteresis relaxation 78—43823
$PbTiO_3$, $(PbTiO_3)_{0.9}(B_2O_3)_{0.1}$ amorphous ribbons, prep., electron and X-ray diffr. obs., dielec. const. temp. depend. 79—50993
$PbTiO_3$ ceramic, mech. strength 78—64332
$PbTiO_3$, cryst., polarisation and resistivity, elec. field effects 78—64313
$PbTiO_3$, damping of soft E-symmetry phonon, Raman scatt. meas. 78—67799
$PbTiO_3$, domain struct. formation during jump motion of phase front 78—64339
$PbTiO_3$, domain struct., formation at phase transitions 79—38510
$PbTiO_3$, domain struct. form. during jump-like motion of phase boundary 79—69794
$PbTiO_3$, ferroelec., nonlinear optical susceptibility calc. 78—9409
$PbTiO_3$, ferroelec. domain boundaries, rigid body displacement of lattice 80—40079
$PbTiO_3$, ferroelectric ceramic, dielec., piezoelec. and elastic props., orientational contrib. 78—68468
$PbTiO_3$ glass-ceramics, transparent, fabrication method by crystn. 77—59733
$PbTiO_3$, mechanical twinning, spontaneous polarisation shielding 79—42930
$PbTiO_3$, neutron powder profile refinement, temp. depend. 78—51476
$PbTiO_3$, O K_α X-ray emission band spectra *(Russian)* 79—15563
$PbTiO_3$, optical birefringence in low temp. region 80—93276
$PbTiO_3$, phase transform., different kinetic types 80—71347
$PbTiO_3$, phase transition study by X-ray powder structural refinement 80—40075
$PbTiO_3$, single cryst., He^+ backscatt. shoulder spectra struct., domain struct. 80—35048
$PbTiO_3$ single crystals, electroluminesc., elec. field, freq. and temp. depend. 78—80422
$PbTiO_3$ single crystal, channelling of He^+ ions, polarisation effects 79—99258
$PbTiO_3$ single crystals, dielectric permittivity meas. 79—99817
$PbTiO_3$, single crysts., lattice parameters and birefringence as function of temp. 79—38517
$PbTiO_3$, spontaneous polaris. shielding destruction by polishing and scribing 79—15427
$PbTiO_3$, switching, domain structure reorganisation and polarisation change 77—1645
$PbTiO_3$, tetragonal deform. of TiO_6 octahedron 77—55759
$PbTiO_3$, thermoelectric effect and ferroelectric transition 78—48123
$PbTiO_3$, vibronic theory and opt. props. 80—103939
$PbTiO_3$, X-ray interference intensity temp. depend., lattice ion vibr. *(Russian)* 80—20601
$PbTiO_3$-$PbZrO_3$-$PbNb_{2/2}Zn_{1/3}O_3(-PbNb_{2/3}Co(Mg)_{1/3}O_3)$ solid solutions, dielec. and piezoelec. props. 79—87393
$PbTiO_3$-$PbZrO_3$-based multicomponent ferroelec. solid solns., morphotropic transitions and comp.-temp. phase diagrams 80—55047
$PbTiO_3$-$Pb(Ni_{1/2}W_{1/2})O_3$ system, solid soln. form., struct., dielec. props. and thermal expansion *(Japanese)* 78—27501
$PbTi_{1-x}Zr_xO_3$, low freq. vibrational modes and ferroelec. transitions 79—33637
$Pb(Ti_{1-x}Zr_x)O_3$, thermodynamic anal. of phase transitions 78—19431
$PbTi_xZr_{1-x}O_3$, ferroelec., electric field depend. of contour mode reson. 77—12351
$Pb(Ti_{0.47}ZrO_{.53})O_3$, small polaron cond. mechanism, elec. cond. and thermopower meas. point defects 78—43380
$Pb(Zn_{1/3}Nb_{2/3})O_3$, diffuse phase transition, electro-optical and dielec. obs. 79—82933
$Pb(Zn_{1/3}Nb_{2/3})O_3$, electrostriction investigation, strain gauge method 79—87395
$PbZn_{1/3}Nb_{2/3}O_3$, PZN, electro-opt., elasto-opt., opt. and photo-induced props. 78—95560
$Pb(Zn_{1/3}Nb_{2/3})O_3$ single cryst., pyroelec. props., meas. under laser beam illum. 80—66117
$Pb(Zr,Ti,Ge)O_3$, antiferro-ferroelectric transition 78—95565
$Pb(Zr,Ti,Sn)O_3$ ceramics, ferroelec., doped with tri- and pentavalent oxides, piezoelectric props. 78—19413
$Pb(Zr, Ti)O_3$, ceramics in solid matrix, high pressure effect on dielectric props. 77—16259
$Pb(Zr,Ti)O_3$ ceramic, mech. strength 78—64332
$Pb(Zr,Ti)O_3$, ceramic, axially loaded, nature of elec. field and resulting voltage 78—72468
$Pb(Zr,Ti)O_3$ ceramic, substrate for In_2O_3 film, ferroelec. field effect 79—47177
$Pb(Zr, Ti)O_3$ ceramics for IR detectors, pyroelectric characts. 79—56736
$Pb(Zr,Ti)O_3$ ceramics, modified, measurement of electrical field-polarisation using automated system 79—67268

ferroelectric materials continued
$Pb(Zr,Ti)O_3$ ceramic/polymer, composite systems, piezoelec. props. 79—99823
$Pb(Zr,Ti)O_3$ ceramic, X-ray investigation before and after polarisation *(Chinese)* 80—2712
$Pb(Zr,Ti)O_3$ ceramics, space charge field meas. by ferroelec. domain switching current, piezoelec. reson. freq. ageing characts. 80—7296
$Pb(Zr, Ti)O_3$ ceramics, low temp. sintering, elec. and mech. props. 80—71616
$Pb(Zr,Ti)O_3$, dielectric response in solid-medium high-pressure device 78—43766
$Pb(Zr,Ti)O_3$, doped, Goldschmidt factors and ferroelec. antiferroelec. transition 77—12332
$Pb(Zr,Ti)O_3$, electrooptic ceramic *(Japanese)* 79—65840
$Pb(Zr,Ti)O_3$, excitation of mechanical vibr. by ionising radiation beams 77—24799
$Pb(Zr, Ti)O_3$, ferroelectric ceramic discs, axial-current-mode shock depoling 79—78631
$Pb(Zr,Ti)O_3$, ferroic materials, fracture processes 80—79869
$Pb(Zr,Ti)O_3$ film, by RF sputtering in PbO vapour 78—39689
$Pb(Zr,Ti)O_3$ film, ferroelec. and optical props. 77—85674
$Pb(Zr,Ti)O_3$ film, prep. by electron beam evaporation technique 77—1809
$Pb(Zr,Ti)O_3$, fracture and deform. 80—79870
$Pb(Zr, Ti)O_3$ internal struct., prep. effect, ionic shadowing obs. *(Polish)* 80—11612
$Pb(Zr,Ti)O_3$, order of ferroelec. paraelec. transition 77—12333
$Pb(Zr,Ti)O_3$ photovoltaic ferroelectric as optical memory storage medium 78—50877
$Pb(Zr,Ti)O_3$, piezoceramic, nonlinear piezoeffect 79—42900
$Pb(Zr,Ti)O_3$, polarisation effect on deform. and strength, Curie pt. region 79—42902
$Pb(Zr,Ti)O_3$, porosity-permittivity relations, depolarising factors determ. and pore effects *(Japanese)* 80—97189
$Pb(Zr,Ti)O_3$, shock depoling, for pulse chargingh of nanofarad capacitors 79—42913
$Pb(Zr,Ti)O_3$, shock depoled ferroelec. ceramic, anal. of ideal response 80—60511
$Pb(Zr,Ti)O_3$, shock wave compressed, dielec. props. 77—48139
$Pb(Zr,Ti)O_3$ solid solutions, elec. and thermoelec. props. appl. *(Polish)* 77—28203
$Pb(Zr,Ti)O_3$, temp. and hydrostatic press. depend of vibr. modes, rel. to phase transforms 77—89510
$Pb(Zr,Ti)O_3$, tetragonal ferroelec. ceramic, 90° domain-rot. fraction after polarisation, X-ray determ. 80—75992
$Pb(Zr,Ti)O_3$, thin film evaporated on stainless steel, photovoltaic effect 79—4580
$Pb(Zr,Ti)O_3$ thin films, fabrication and characterisation electron-beam deposition 80—16188
$Pb(Zr,Ti)O_3$ thin layers, tan δ temp. dependence obs. *(Bulgarian)* 78—88259
$Pb(Zr,Ti)O_3$, X-ray anal. of phase transform. at 163K *(Ukrainian)* 77—69082
$Pb(Zr,Ti)O_3$, X-ray study in tetragonal-rhombohedral phase-transition composition area 79—42921
$Pb(Zr,Ti)O_3$:Ba, paraelectric ceramic, giant electrostrictive effect 79—91378
$Pb(Zr,Ti)O_3$:Cr_2O_3 ceramics, reson. freq. comp. and temp. depend. 80—70413
$Pb(Zr,Ti)O_3$:Fe(Nb) ceramic, elec. and electromechanical props., depend. on dopants 80—81212
$Pb(Zr,Ti)O_3$:La(Cd,W), electro-optical ferroelec. ceramic, secondary electron emission yield 79—91546
$Pb(Zr,Ti)O_3$:Mn, crystal struct. and electrophysical props., piezotransformer props. 78—43806
$Pb(Zr,Ti)O_3$:Nb ceramic, stress effects on ferroelec. hysteresis, macroscopic strain, US vel. 79—4778
$Pb(Zr,Ti)O_3$:$Nb_2O_5(Sc_2O_3)$, elec. cond. investigation with and without various dopants and stoichiometry 79—11120
$Pb(Zr,Ti)O_3$:$PbTiO_3$ (up to 5%), dielec. props. and ferroelec. transitions 77—20806
$PbZr_{1-x}Ti_xO_3$, paraelec. phase, first-order phase transition 77—89540
$PbZr_{1-x}Hf_xO_3$, crystal field distortion by impurities, PAC meas. 80—11306
$PbZrO_3$ based ferroelec. ceramic, pressure-temp. phase diagrams 79—24273
$PbZrO_3$ crystal, structural phase transitions in very high elec. fields 80—15987
$PbZrO_3$, electric field induced phase transitions, 20 to 160°C 77—43947
$PbZrO_3$, ferroelec., crystallographic shear planes as nonstoichiometric defects 80—59484
$PbZrO_3$, ferroelec. solid solns., atom shifts, polarisation and Curie temps. 80—100636
$PbZrO_3$, structural phase transition in super high elec. fields 79—33626
$PbZrO_3$, thermoelec. effect and phase transitions 78—48123
$PbZrO_3$:La, appl. in sub-100 ps pyroelec. detectors, 10.6 μm damage threshold meas. 80—77859
$PbZrO_3$-monocryst., elec. cond., permittivity, polarisation, para- and ferro- to antiferroelec. phase transistions 78—60402
$PbZrO_3$-Pb_2FeNbO_6-$PbTiO_3$, pyroelectric props. of ferroelec. rhombohedral transition 77—12336
$Pb(Zr_{0.52}Ti_{0.48})O_3$, polycrystalline ferroelectric, grain-size dependent props. 80—71352
$PbZr_{0.9}Ti_{0.1}O_3$, neutron powder profile refinement, temp. depend. 78—51475
$PbZr_{0.95}Ti_{0.05}O_3$ ceramics, of ABO_3 type, dopant distrib. between A and B sites 79—42093
$PbZr_{0.95}Ti_{0.05}O_3$, impact loading, mech. and elec. response, elec. state effect 78—64317
$PbZr_{0.95}Ti_{0.05}O_3$:oxide doped, A and B site dopant distrib., antiferroelec.-ferroelectric transition 78—34532
$Pb(Zr_{1-x}Ti_x)O_3$, electrical conductivity and I-V charact., neutron effects 78—47781
$Pb(Zr_xTi_{1-x})O_3$, anomalous photovoltaic effect 79—19625
$PbZr_xTi_{1-x}O_3$ ceramics, morphotropic phase boundary 80—81035
$Pb(Zr_xTi_{1-x})O_3$, elec. props. effect of proportional composition, morphotropic phase boundary 78—35105
$Pb(Zr_xTi_{1-x})O_3$, elec. props. temp. and composition depend. 78—47817
$Pb(Zr_xTi_{1-x})O_3$, ferroelectric energy generation by shock compression, modes 77—55757
$PbZr_xTi_{1-x}O_3$, ferroelec. phase transition under high press. 79—99833

ferroelectric materials continued

$Pb(Zr_xTi_{1-x})O_3$, meas. of Hugoniot curve with commercial manganin stress gauges 80—70362

$Pb(Zr_xTi_{1-x})O_3$ solid solns., elec. props. near morphotropic phase boundary 79—42566

$Pb(Zr_{0.47}Ti_{0.43}Sn_{0.10})O_3{:}Cr_2O_3$, ferroelec. ceramic, reversible characts. and dielectric losses *(Russian)* 78—84517

$PbZr0_3$, X-ray interference intensity temp. depend., lattice ion vibr. *(Russian)* 80—20601

$Pr_2Ti_2O_7$, ferroelec., temp. depend. of SHG intensity 79—24267

$Pr_2Ti_2O_7$, layered ferroelectric, anomalous photovoltaic effect, photovoltaic current 80—75603

$Rb(B_xW_{3-x})O_9$ (B=Na, Ca, Co, Ni, Cd, Ga, Bi, Nb, Ta) cryst. struct., temp. dielec. anomalies 80—1998

$RbCdCl_3$, n.q.r. spin-lattice relax. near cubic-tetragonal transition, soft modes 77—1616

$Rb_2Cd_2(SO_4)_3$, ferroelec., X-ray study on phase transition 77—85665

$Rb_2Cd_2(SO_4)_3$, pyroelectric and dielectric props., ferroelectric transitions 79—38458

Rb_2CoBr_4, ferroelec., Curie temp. determ. 79—38485

Rb_2CoCl_4, ferroelec., Curie temp. determ. 79—38485

$Rb(D_xH_{1-x})_2PO_4$, isotope exchange during crystallisation from aqueous solns. 78—18569

$RbD_3(SeO_3)_2$, DMR, electric quadrupole coupling, ferroelec. transition 79—91312

$RbD_3(SeO_3)_2$, incommensurate nature of intermediate phase, neutron diffr. obs. 80—50276

$RbD_3(SeO_3)_2$, phase transform., inelastic neutron scatt. study 78—39514

$RbD_3(SeO_3)_2$, spontaneous polarisation meas. below T_c 77—24801

$Rb(H,D)_3(SeO_3)_2$, improper ferroelec. phase transition, anomalous elastic props. 79—33634

RbH_2AsO_4, acoustooptical and photoelastic props. 78—27181

RbH_2AsO_4, and deuterated isomorph, E-mode splitting in ferroelec. phase, Raman scatt. meas. 77—16296

RbH_2AsO_4, and deuterated isomorph, ferroelectric mode and molecular vibr. press. depend. 78—19424

RbH_2AsO_4, attenuation const. meas. by SHF dielec. resonance 79—47406

RbH_2AsO_4, ferroelec., attenuation of LF elastic oscills. 77—7791

RbH_2AsO_4, internal friction, torsion pendulum technique 78—72474

RbH_2AsO_4, phase transition, dielec. pyroelec. and internal friction meas. 77—16261

RbH_2AsO_4, pres. depend., LF dielec. response, ferroelec. props. 78—15120

RbH_2AsO_4, Raman scatt. near T_c, search for soft modes 78—15114

RbH_2PO_4, acoustooptical and photoelastic props. 78—27181

RbH_2PO_4, attenuation const. meas. by SHF dielec. resonance 79—47406

RbH_2PO_4, critical and tricritical phenomena, susceptibility, exponents 80- 75976

RbH_2PO_4, electro-optic props. near ferroelec. transition 78—19445

RbH_2PO_4, electrostrictive effects, US rel. 80—75941

RbH_2PO_4, ferroelec., attenuation of LF elastic oscills. 77—7791

RbH_2PO_4, ferroelec. phase transition, birefringence studies 80—108162

RbH_2PO_4, ferroelectric, US propag. near ferroelectric phase transition temp. 78—23417

RbH_2PO_4, ferroelectric-ferroelastic phase transition, γ-ray diffr. 78—43819

RbH_2PO_4, high temp. phase transition, dielec. const., elec. cond. and IR refl. meas. 78—43118

RbH_2PO_4, IR overtone spectra and temp. depend. 79—47456

RbH_2PO_4, internal friction, torsion pendulum technique 78—72474

RbH_2PO_4, longit. US wave propag. near ferroelectric phase transition temp. 78—84536

RbH_2PO_4 powder, phase transition in paraelectric (upper) phase by measuring damping const. and amplitude of phonon echoes 79—19855

RbH_2PO_4, proton modes, dielec. spectroscopy 80—75915

RbH_2PO_4, Raman scatt. near T_c, search for soft modes 78—15114

RbH_2PO_4, static dielec. props., and Curie temp., press. depend. 79—87405

RbH_2PO_4, transverse elec. susceptibilities 80—50273

RbH_2PO_4, X-irradiated, hysteresis effects obs. by ESR 80—103928

RbH_2PO_4, X-ray cryst. struct. refinement 79—14787

$RbH_2PO_4(AsO_4)$, pyroelectric investig. in ferroelec. phase 77—12321

$RbHSO_4$, acoustic and dielectric props. near phase transition 80—55053

$RbHSO_4$, anisotropy of US anomaly near ferroelec. phase transition 78—72473

$RbHSO_4$, compressed powder, dielectric const. and particle size, 77-335K 78—76371

$RbHSO_4$, Curie-Weiss behaviour, dielec. const. meas. *(Japanese)* 77—43940

$RbHSO_4$, dielec. dispersion near ferroelec. phase transition 80—2684

$RbHSO_4$, ferroelec., dielec. crit. phenomena, spontaneous polarisation meas. 77—85641

$RbHSO_4$, ferroelec. with small Curie-Weiss const., dielec. props. 78—39496

$RbHSO_4$, ferroelec. phase transition, US attenuation and velocity 78—39511

$RbHSO_4$, ferroelec., dielec. dispersion 80—97179

$RbHSO_4$, isotope effect, dielec. const. and spin polarisation investigation 80—20574

$RbHSO_4$, phase transition, sp. ht. and dielec. permittivity meas. 77—85672

$RbHSO_4$, volume expansion, spontaneous strain, second order phase transitions 79—65224

$RbHSeO_4$, ferroelec. props. and domain struct. 79—78637

$RbHSeO_4$, ferroelec. phase transition, X-ray study 80—7309

$RbHSeO_4$, ferroelec. props. rel. to struct. 80—71345

$RbHSeO_4$, ferroelec., far IR spectra 80—71404

$RbHSeO_4$, successive phase transitions 80—15985

$RbH_2(SeO_3)_2$, improper ferroelectric phase transformation, neutron scattering study 78—80302

$RbH_3(SeO_3)_2$, ^{87}Rb NMR, elec. field grad. temp. depend. 79—78536

$RbH_3(SeO_3)_2$ crystal, incommensurable phase, quadrupole moment study 80—97213

$RbH_3(SeO_3)_2$, crystal lattice monoclinic distortion determ. by phase transition from elec. meas. results 79—73887

$RbH_3(SeO_3)_2$, ferroelec., location of H atoms in cryst. struct., neutron diffr. meas. 78—2093

$RbH_3(SeO_3)_2$, ferroelec. phase transition, X-ray study 79—38479

$RbH_3(SeO_3)_2$, ferroelec. domain struct., obs. using dew method 80—50283

ferroelectric materials continued

$RbH_3(SeO_3)_2$, low temp. struct., neutron diffr. 78—38669

$RbH_3(SeO_3)_2$, paraelec. phase, H bonding, neutron diffr. 77—47420

$RbH_3(SeO_3)_2$, phase transitions *(Japanese)* 79—65812

$RbH_3(SeO_3)_2$, piezoelectric effect, near nonintrinsic ferroelectric phase transition 78—2815

$RbH_3(SeO_3)_2$, Raman spectra meas. 78—10899

$RbH_3(SeO_3)_2$, repolarisation in region of improper ferroelec. phase transition 77—8497

$RbH_3(SeO_3)_2$: VO^{2+}, EPR spectra, spin Hamiltonian parameters 80—100609

$Rb_2KMoO_3F_3$, and $Rb_2KWO_3F_3$, ferroelec., transition obs. 80—75989

$RbLiSO_4$, field induced ferroelec. phase 79—78633

$RbLiSO_4$, new ferroelectric materials *(Japanese)* 77—28529

$RbLiSO_4$, successive struct. transitions, X-ray diffr. 80—10521

$RbLiSO_4$, thermal and dielectric props., ferrielectricity 79—28688

$Rb_3MoO_3F_3$, ferroelec., phase transitions, crystallographic, DTA, dielec. and pyroelec. meas. *(French)* 77—85671

$Rb_3MoO_3F_3$, ferroelec. and order-disorder phase transitions 78—92037

$Rb_3MoO_3F_3$, ferroelec., transition obs. 80—75989

$RbNH_4SO_4$, ferroelec., ion group reorientation temp. and press. depend., PMR obs. 78—72470

Rb_2SO_4-$(NH_4)_2SO_4$ mixed cryst., ferroelec. transition, structural and dielec. props., proton spin-lattice relax. 78—39512

$Rb_3WO_3F_3$, ferroelec. and order-disorder phase transitions 78—92037

$Rb_3WO_3F_3$, ferroelec., transition obs. 80—75989

Rb_2ZnBr_4, dielectric const. and ferroelectric hysteresis 78—84535

Rb_2ZnBr_4, ferrielectricity, triple 60 Hz D-E hysteresis loops 80—71365

Rb_2ZnBr_4, ferroelec., Curie temp. determ. 79—38485

Rb_2ZnBr_4, ferroelec., photovoltaic and photorefractive phenomena 80—75598

Rb_2ZnBr_4, ferroelectricity, hysteresis loops and dielec. const. meas. 78—23416

Rb_2ZnBr_4, incommensurate phases, neutron scattering study 79—15417

Rb_2ZnBr_4, incommensurate and commensurate phases, neutron scatt. meas. 79—82936

Rb_2ZnBr_4, modulated struct., far IR transmission, temp. depend. 80—71408

Rb_2ZnBr_4, modulation phase transitions, neutron scatt. 79—95712

Rb_2ZnBr_4, Raman scatt., normal-incommensurate-commensurate phase transitions, soft modes 80—40071

Rb_2ZnBr_4, soft modes obs. by Raman scatt. 80—97283

$Rb_2ZnBr_4(Cl_4)$, Raman spectra near incommensurate phase transitions 80—76013

Rb_2ZnCl_4, ^{35}Cl NQR, incommensurate struct. phase transition 79—47401

Rb_2ZnCl_4, commensurate-incommensurate phase transition, crit. behaviour, sp. ht. meas. 80—71342

Rb_2ZnCl_4, commensurate-incommensurate phase transition, ^{35}Cl NQR study 80—75966

Rb_2ZnCl_4, dielec. dispersion, 5-900 MHz, near incommensurate-commensurate transition 80—60522

Rb_2ZnCl_4, ferrielectricity, triple 60 Hz D-E hysteresis loops 80—71365

Rb_2ZnCl_4, ferroelec., Curie temp. determ. 79—38485

Rb_2ZnCl_4, ferroelectricity, hysteresis loops and dielec. const. meas. 78—23415

Rb_2ZnCl_4, incommensurate phase form., domain struct. near phase transition, NQR obs. 79—33643

Rb_2ZnCl_4, incommensurate phases, neutron scatt. 79—38501

Rb_2ZnCl_4, incommensurate phase transition, ^{87}Rb NMR study 80—75967

Rb_2ZnCl_4, incommensurate phase transitions, ^{35}Cl NQR study 80—75968

Rb_2ZnCl_4, NQR exam. of noncommensurate superstructures produced by phase transitions 79—69791

Rb_2ZnCl_4, phase transitions, soft mode, Raman scatt. meas. 79—4389

Rb_2ZnCl_4, phase transition, Raman scatt. evidence 80—40116

Rb_2ZnCl_4, phase transitions, thermal expansion coeff. 80—100638

Rb_2ZnCl_4 single crystals, Raman scatt. spectra, temp. range covering two phase transitions 80—7340

Rb_2ZnCl_4 type ferroelectrics, phase transitions and physical props. *(Japanese)* 79—78636

Rb_2ZnCl_4, US vel. and attenuation at normal-incommensurate phase transition pt. 79—55833

Rb_2ZnCl_4, US velocity and attenuation, around normal-incommensurate phase transition 80—40072

$Rb_2ZnCl_4(Br_4)$, cryst. with modulated struct., neutron scatt. obs. 79—95713

$SC(NH_2)_2$, ferroelectric transitions, based on model thermodynamic pot. 78—80295

$Sb_{1-x}Bi_xSI$, mixed cryst., ferroelec. phase transition 79—33629

$SbNO_4$, ferro- and anti-ferroelec., crit. points and props. 79—38460

$SbNbO_4$, anomalous photovoltaic effect and photocond. 79—38122

$SbNbO_4$, ferroelec., synthesis and hydrothermal growth 79—38731

$SbNbO_4$ single crystals, pure and doped, growth and pyroelec. and ferroelec. props 80—40248

$SbNbO_4{:}CoO(Fe_2O_3)(TiO_2)$, growth, pyroelectric and ferroelectric props. 79—73886

Sb_5O_7I, polytype 2MA, ferroelectric, ferroelastic, Raman scattering and symmetry anal. 79—38550

Sb_5O_7I polytypes, cryst. growth, struct., ferroelastic and ferroelec. props. 78—31309

Sb_5O_7I, polytypes 2MC and 2MA, photoferroelastic phenomena 79—95447

Sb_2S_3, phase transitions and improper photoconductivity, effect of growth conditions *(German)* 78—39515

SbSBr, single crystals, birefringence meas., ferroelec. transition obs. 80—88933

SbSI, abrupt polarisation changes under influence of external forces 78—68459

SbSI, absorption edge, elec. field effect rel. to ferroelec. props. 80—97240

SbSI, aggregates of needle-like crystals, nonstoichiometric, ferroelectric properties *(Japanese)* 78—43821

SbSI, anharmonic at. pot. and temp. depend. of thermal vibrs. 80—39246

SbSI, Barkhausen effect, contrib. to repolarisation process *(Russian)* 77—32330

SbSI, birefr. and phase transitions 78—60405

SbSI, crystal struct. in ferroelec. phase, displacive type transition 77—11515

ferroelectric materials continued

SbSI, ferroelec., dielec. props. 79—38428
SbSI, ferroelec., phase transitions, birefringence meas. 78—56440
SbSI, ferroelec. transition critical phenomena *(Russian)* 80—7314
SbSI, ferroelectric, dark current and spontaneous polarisation, ferro-paraelectric transitions obs. 80—60521
SbSI, max. vel. of domain boundaries in polarisation reversal, Barkhausen effect meas. 78—60411
SbSI, reversible characts. of generation of second microwave harmonic 78—39509
SbSI, tricrit. point, NQR under press. 79—38469
SbSI, tricrit. point at 1.4 kbar and 235K 78—68463
SbSI, uniaxial displacive ferroelectrics, domain wall dynamics 79—73890
SbSI-Sb_2S_3 system, ferroelec. phase transition temp. 79—78632
SbSI-SbSBr system, ferroelec., anharmonic effects in far IR reflectivity spectra 80—76014
$SbTaO_4$, ferroelec., synthesis and hydrothermal growth 79—38731
$SbTaO_4$, X-ray and ESR study of phase changes 78—72476
$Sm_2Ti_2O_7$, ferroelec., temp. depend. of SHG intensity 79—24267
$SnCl_2.2H_2O$, ferroelec., Cl NQR study 79—38467
$Sn_2P_2S_6$, ferroelec., IR and Raman spectra, photocond., edge absorpt. spectra, spontaneous polarisation, forbidden gap 78—68514
$Sn_2P_2S_6$, ferroelec. and pyroelec. props. meas. 78—35107
$Sn_2P_2Se_6$, ferroelec. props. *(Russian)* 80—25313
$Sn_2P_2(Se_xS_{1-x})_6$, ferroelec. props. *(Russian)* 80—25313
Sr Nb_2O_6, crystallography, polymorphism and isomerism, X-ray diffr. and DTA study 80—100216
$Sr_2AgNb_5O_{15}$, $Sr_2AgTa_5O_{15}$, ferroelec. and ferroelastic props. *(French)* 79—24266
$Sr_{0.61}Ba_{0.39}Nb_2D_6$, photoinduced birefr. 80—7325
$Sr_{0.25}Ba_{0.75}Nb_2O_6$ film, growth and electrophys. props. 79—42928
$Sr_{0.5}Ba_{0.5}Nb_2O_6$ crystals, ferroelec., dislocation free, pyroelec. props. 79—42907
$Sr_{0.5}Ba_{0.5}Nb_2O_6$, ferroelec., primary pyroelectricity 77—63371
$Sr_{0.5}Ba_{0.5}Nb_2O_6$, ferroelec., dielec. behaviour 78—80309
$Sr_{0.5}Ba_{0.5}Nb_2O_6$:Fe(Mn)(Cr)(La), ceramic, additive effects on ferroelec. and pyroelec. props. 77—16256
$Sr_{0.61}Ba_{0.39}Nb_2O_6$, electromechanical props., permittivity, elastic compliance, piezoelectric moduli 80—29691
$Sr_{0.65}Ba_{0.35}Nb_2O_6$, internal field distrib. and photorefraction 79—99843
$Sr_{0.75}Ba_{0.25}Nb_2O_6$, ceramic ageing, dielec. props. 80—88940
$Sr_{0.75}Ba_{0.25}Nb_2O_6$, electrostriction 77—48130
$Sr_{0.75}Ba_{0.25}Nb_2O_6$, ferroelectric devices for optical systems 78—90473
$Sr_{0.75}Ba_{0.25}Nb_2O_6$, large cryst. growth, control of opt. defects 78—76595
$Sr_{0.75}Ba_{0.25}Nb_2O_6$ single cryst., electro-optical hysteresis curves and phase transitions *(German)* 79—28717
$Sr_{1-x}Ba_xNb_2O_6$, photorefraction in space charge field, phase transitions 80—97229
$Sr_{1-x}Ba_xNb_2O_6$, tetragonal tungsten bronze structure ferroelec. mech. for ferroelec. transition 79—38481
$Sr_xBa_{1-x}Nb_2O_6$, appl. in sub-100 ps pyroelec. detectors, 10.6 μm damage threshold meas. 80—77859
$Sr_xBa_{1-x}Nb_2O_6$, domain struct. influence on electrooptical props. 80—93283
$Sr_xBa_{1-x}Nb_2O_6$, high press. phase transitions, Raman scatt. studies 80—71402
$Sr_xBa_{1-x}Nb_2O_6$, neutron and light scatt. in phase transition region 78—64336
$Sr_{0.75}Ba_{0.25}O_6$, photorefractive effect, spectral characts. 78—43829
$SrBi_2Ta_2O_9$, SHG, temp. depend. ferroelec.-ferroelec. transition 78—15121
Sr_2CoReO_6, seignettomagnets with perovskite struct. 79—38459
$Sr_2KNb_{5-x}Ti_xO_{15-x}F_x$ and $Sr_{2-x}K_{1+x}Nb_5O_{15-x}F_x$, ferroelectric props., F substitution effect 77—12331
Sr_3MoO_6, electrophys. props., effects of thermophys. props. of medium in synthesis 77—48375
$Sr_x(Na_{0.5}Bi_{0.5})_{1-x}$ solid solutions, piezoelec. and ferroelec. props. *(French)* 80—108158
$Sr_x(Na_{0.5}Bi_{0.5})_{1-x}TiO_3$ ferroelec. ceramic, hot pressing, numerical simulation *(French)* 80—76220
$Sr_2Nb_2O_7$, ferroelec., temp. depend. of SHG intensity 79—24267
$Sr_2Nb_2O_7$, ferroelecs., nonlinear optical props. 80—33086
$Sr_2Nb_2O_7$, high press. phase transitions, Raman scatt. studies 80—71402
$Sr_2Nb_2O_7$, layered ferroelectric, anomalous photovoltaic effect, photovoltaic current 80—75603
$Sr_2Nb_2O_7$, normal-incommensurate phase transition, electron microscopy and diffraction study 80—39277
$Sr_2Nb_2O_7$, optical mode softening in incommensurate phase 80—7352
$Sr_2Nb_2O_7$, phase transition at 215°C, physical props. obs. 79—56744
$Sr_{1-x}Pb_xTeO_3$, ferroelec. soln., prep. at room temp. *(French)* 79—43190
$SrSnO_3$ and $SrZrO_3$, high-density ceramics prep. and elec. props. 80—60812
$Sr_2Ta_2O_7$, structural phase transition to superlattice, electron microscopy and diffraction study 80—39277
$Sr_2Ta_2O_7$:Nd,Na, SHG, effect of dopants on Curie temp. 79—24267
$SrTeO_3$, X-ray diffractional and optical studies, ferroelectric properties 79—65805
$Sr_6Ti_2Nb_4O_{20}$, new class of layer ferroelectrics. X-ray anal. and permittivity meas. 77—16266
$Sr_nTi_{n-4}Nb_4O_{3n+2}$ layer ferroelectrics, physical props. 78—10854
$SrTiO_3$, anharmonic phonons and central peaks at struct. phase transitions 79—95775
$SrTiO_3$, apparatus for biaxial stress production at low temp., appl. to ferroelectric 78—45609
$SrTiO_3$ based solid solns., ferroelec., US study 79—38476
$SrTiO_3$, calc. of matrix element effects in freq. dependent dielectric function 80—70632
$SrTiO_3$, cathodlum. spectral and temp. depend. 78—84665
$SrTiO_3$, central peak in spectrum of ferroelec. mode fluctuations and dielec. losses, 4.2K 78—19432
$SrTiO_3$ ceramic, electrocaloric effects for refrigeration at cryogenic temp. 80—77789
$SrTiO_3$, complex refr. index meas. in far IR, by dispersive Fourier transform spectroscopy 78—92042
$SrTiO_3$, crit. dielec. and optical props. and storage, 4K 77—24805
$SrTiO_3$, cubic, temp. depend. of X-ray reflection intensities 80—107021
$SrTiO_3$, dielec. nonlinearity and parametric interactions at low temps. 79—38430
$SrTiO_3$, dielec. props. in microwave region, 4.2-78K 77—16239
$SrTiO_3$, dielectric loss at microwave frequencies *(Russian)* 78—52440

ferroelectric materials continued

$SrTiO_3$, disorder manifestation, light scatt. spectra, high temp. 80—76017
$SrTiO_3$, doped, large gap ferroelectrics, phase transitions in mag. fields 79—33621
$SrTiO_3$, dynamic central peaks and phonon interactions near structural phase transitions 78—83903
$SrTiO_3$, EPR meas., Hamiltonians with quartic anharmonicities 78—27083
$SrTiO_3$, EPR of Fe^{3+}-V_O centre, above T_c 80—39870
$SrTiO_3$, electrooptic coeffs. 79—33673
$SrTiO_3$, energy band struct., two-photon absorption spectra study 80—15453
$SrTiO_3$, ferroelectric, first order structural phase transition, anharmonic oscillator model 80—86239
$SrTiO_3$ film, behaviour of ferroelecs. in strong elec. microwave field 79—42884
$SrTiO_3$ film, polycryst. dielec. losses, influence of amplitude of measuring microwave field 79—99829
$SrTiO_3$ film, sputtered, refr. index, 0.3-1.0 μm, substrate temp. effects 77—55840
$SrTiO_3$ film, surface layer nature, AES obs., and effect on permittivity 77—24498
$SrTiO_3$, forced thermal Rayleigh scattering 78—80371
$SrTiO_3$, freq. depend. of soft mode self-energy, for IR dielec. response meas. 79—33632
$SrTiO_3$ glass ceramics, polarisation and dielec. const., 4-77K 77—32319
$SrTiO_3$, heat capacity crit. behaviour 78—10857
$SrTiO_3$, heavily reduced, soft mode behaviour 80—71409
$SrTiO_3$, hyper-Raman scatt. spectra due to lattice vibr. 80—29732
$SrTiO_3$, impure, low temp. polarisation, thermoelectret state 77—12301
$SrTiO_3$, incipient ferroelectric, mode-mode coupling 78—79717
$SrTiO_3$, intrinsic quantum paraelec. below 4K, dielec. const. meas. 79—73877
$SrTiO_3$, low temp. phase, X-ray cryst. struct. anal. at 77K 79—37683
$SrTiO_3$, mean square atomic displacement temp. depend., sublattice vibration anharmonicity 80—79890
$SrTiO_3$, monodomain, O-D and O-H stretching vibrs., IR spectra 80—71449
$SrTiO_3$, Mossbauer spectroscopy, sample prep. and results 80—66078
$SrTiO_3$, neutron spectroscopy of central peak energy width 77—32334
$SrTiO_3$, O K_α X-ray emission band spectra *(Russian)* 79—15563
$SrTiO_3$, optical SHG near phase transition 80—71348
$SrTiO_3$, photoluminesc., thermoluminesc. and thermally stimulated currents 78—92121
$SrTiO_3$ pseudodisplacive ferroelec., temp.-dependent dielectric response obs. 77—40247
$SrTiO_3$, Raman scatt. and ferroelec. soft modes 77—16300
$SrTiO_3$, soft phonon and central peak coexistence, theory 78—14443
$SrTiO_3$, stressed, trigonal-to-tetragonal transition, EPR data, realisation of 3-state Potts model 77—28525
$SrTiO_3$, structural phase transition at 110K, theory 78—80300
$SrTiO_3$, structural phase transition, intrinsic and extrinsic central peak properties 80—34168
$SrTiO_3$, surface defects, electronic struct., LEED, AES, UPS study 78—84273
$SrTiO_3$, surface EM wave propag., IR refl. expts. 78—39553
$SrTiO_3$, surface microrelief revealed by ion irradiation 80—54485
$SrTiO_3$, surface microrelief after ion irrad. 80—59774
$SrTiO_3$, tetragonal, effect of impurities on Raman spectrum 80—2770
$SrTiO_3$, thermal expansion near displacive phase transition meas. 77—12345
$SrTiO_3$, thermal motion at room temp., anharmonic or disordered 79—37805
$SrTiO_3$, thermodynamic props. 77—39680
$SrTiO_3$, undispersive nonlinear dielectric, third harmonic generation *(Russian)* 80—95955
$SrTiO_3$, uniaxial stress induced ferroelectricity *(Japanese)* 79—65814
$SrTiO_3$, valence band UPS and partial p and d density of states 80—71560
$SrTiO_3$, X-ray and Mossbauer γ-ray scatt., near phase transition, energy width of central peak 78—79724
$SrTiO_3$:^{181}Ta, quadrupole interaction, γγ cascade PAC meas. 77—81042
$SrTiO_3$:Fe^{3+}, displacive struct. transition, order-disorder behaviour, phonon softening, EPR obs. 79—23695
$SrTiO_3$:Fe^{3+}, order-disorder and central peak behaviour, EPR study 80—75970
$SrTiO_3$:H(D), controlled doping, IR spectra 79—28007
$SrTiO_3$:V, Jahn-Teller impurity, V^{4+} EPR 80—29608
$SrTiO_{3-x}$, single cryst. and film, Auger spectra, surface comp. 78—27353
TBSe, crit. behaviour, electrostrictive coupling role 80—71329
TGFB, emission of free charge carriers in vacuum as symptom of pyroelec. props. 79—42908
TGS, crit. behaviour, electrostrictive coupling role 80—71329
TGS, deuterised, growth in form of oriented blocks, domain struct. obs. 77—90266
TGS, ferroelec., elec. SHG in autostabilised state 77—85661
TGS, ferroelec., temp. autostabilisation, impedance var. with DC bias 78—72467
TGS, ferroelec. cryst., complex permittivity at microwave freq. and high press. 80—2685
TGS, ferroelectric phase transition, high resolution NMR study 80—97214
TGS, temp. behaviour of optical phonons near T_c, evidence of non-linear pseudospin-phonon interaction 77—7824
TGS-TGSe solid solution, temp. depend. of fundamental reflection spectra meas. 77—16337
TGSe, deuterated, NMR investig. of ferroelec. and press. induced transition mechanisms 77—16189
TGSe, domain-wall orientations and wall energies 78—23420
TGSe, emission of free charge carriers in vacuum as symptom of pyroelec. props. 79—42908
TGSe, ferroelec. cryst., complex permittivity at microwave freq. and high press. 80—2685
TGSe, temp. behaviour of optical phonons near T_c, evidence of non-linear pseudospin-phonon interaction 77—7824
TGSe:Cu^{2+}, EPR studies 80—7153
TGSe:D,L-α-alanine crysts. with large unipolarity, dielec., piezoelec., elastic props. and internal friction 79—33615

ferroelectric materials continued

- $Tb(MoO_4)_3$ cryst. struct. in ferroelec., ferroelastic, antiferroelec. and paraelastic phases 80—75205
- $Tb_2(MoO_4)_2$, ferroelectric-ferroelastic crystal, room temp. crystal struct., X-ray scatt. 80—28978
- $Tb_2(MoO_4)_3$, crysts., elastic props. during domain switching under mech. loading 79—55809
- $Tb_2(MoO_4)_3$, elastic wave attenuation and velocity near ferroelec. transition 79—73257
- $Tb_2(MoO_4)_3$, first-order to continuous phase transition, crossover induced by symmetry-breaking fields 79—82312
- $Tb_2(MoO_4)_3$, hydrostatic press. effect on phase transition 78—27166
- $Tb_2(MoO_4)_3$, improper ferroelectric, dielectric props., IR radiation pyroelectric detection 80—80711
- $Tb_2(MoO_4)_3$, mode softening near ferroelec. transition, Raman and Brillouin spectra 79—33685
- $Tb_2(MoO_4)_3$, nonlinear elastic props. near phase transition 79—73244
- $Tb_2(MoO_4)_3$, nonlinear piezoelec. coeffs. near phase transition 79—95710
- $Tb_2(MoO_4)_3$, proper and improper ferroelec., direct meas. of figure of merit 79—95711
- $Tb_2(MoO_4)_3$, thermal expansivity and spontaneous strain temp. depend. 79—14943
- $Tb_{1-x}Sn_xTe$, ferroelectric transition calc., effect on carrier density 77—85673
- TeO_2, ferroelectric glass, phase transition, permittivity, electrochromism, photochromism 80—80719
- TeO_2-WO_2 glass, dipole correlations, capacitances and TSC meas. 79—28670
- thermogravimetric and X-ray phase investig., synthesis by solid-phase reactions 77—21067
- TiO_2, rutile, ferroelectric ceramic, dielec., piezoelec. and elastic props., orientational contrib. 78—68468
- $(Tl,NH_4)_2Cd_2(SO_4)_3$, langbeinite type mixed cryst., ferroelec. transitions, dielec. and elastic meas. 78—2810
- TlBr pseudodisplacive ferroelec., temp.-dependent dielectric response obs. 77—40247
- $Tl_2Cd_2(SO_4)_3$, langbeinites, symmetry limitations on choice of hypothetical protophase 80—33916
- $Tl_2Cd_2(SO_4)_3$, ferroelec. langbeinites, Raman scattering 80—34926
- TlH_2PO_4 and TlD_2PO_4, press. effect on dielec. props. 79—99832
- TlH_2PO_4, thermodynamics props. of solid phase transitions, heat capacity 79—10966
- Tl_2TaO_6, Tl I lone pair stereochem. activity rel. to ferroelectricity 78—15131
- WO_3, orthorhombic phase struct., rel. to struct. of other phases 77—24297
- $Y_2Ti_2O_7$, ferroelec., temp. depend. of SHG intensity 79—24267
- $YbNbO_4$, ^{93}Nb NQR spectra, 77 to 450K 79—38401
- Zn-Cl boracite, reinterpretation of EPR expt. on Cu^{2+} rel. to struct. 79—38372
- Zn-Cl boracite, X-ray powder spectra of structure 79—37828
- ZnF_2, elastic props., 4.2-300K, incipient ferroelec. transition 78—30691

ferroelectric phenomena *see ferroelectricity*

ferroelectric semiconductor materials *see ferroelectric semiconductors*

ferroelectric semiconductors

- band bending in surface layer 80—60061
- barrier capacitance of p-n junction in region of strong ferroelec. instability 79—11218
- book 80—82590
- cathodoluminescence, paraelec. phase transition *(Russian)* 78—23535
- conference, ferroelectric materials and their applications, Kyoto, Japan, Nov. 17-19, 1977 79—19846
- conference, Rostov-on-Don, USSR (1976) 78—43800
- degenerate narrow-gap semiconductors, ferroelec. phase transition, hybridization effect *(Russian)* 79—61319
- doped narrow gap semiconductor, two-channel vibronic mechanism of ferroelectric phase transitions *(Russian)* 79—56745
- electron theory 78—43801
- electronic density of states, effect of soft phonon-electron interaction *(Russian)* 77—80718
- ferroactive fluids, advanced appls. 80—80714
- ferroelectric transition, conductivity band theory rel. to vibronic theory of ferroelectricity 79—19854
- glass-ceramics, dielectric dispersion *(Russian)* 79—8097
- impurity carrier effects, vibronic theory 78—43803
- IV-VI compounds, dielec. props., elec. meas. 78—15119
- IV-VI compounds, mag.-field-induced displacive phase transition 80—50278
- IV-VI semiconductor, vibronic model of lattice instability 80—80723
- IV-VI semiconductors, crystal structure and symmetry of electron spectra, doping effects *(Russian)* 79—7696
- IV-VI semiconductors, mag. susceptibility near ferroelec. transition pt. *(Russian)* 79—95568
- magnetic field influence, ferroelectric phase transition 80—55049
- narrow band gap semiconductor, ferroelec. transition, quantising mag. field effect 79—87403
- niobates, anomalous bulk photovoltage effect, Jahn-Teller mechanism 77—28218
- perovskite oxides, ferroelec., point defects and elec. props. 79—42533
- perovskite oxides, point defects, elec. cond., and electron energy spectra 80—70706
- perovskite structure, semiconductor props., review *(Polish)* 78—56437
- phase boundary structure 79—11398
- phase transition temperature, rel. to free carrier conc. 78—10860
- phase transitions, self consistent approach 77—52028
- PLZT ferroelectric ceramic, anomalous bulk photovoltaic effect and cond. *(Russian)* 80—54733
- semiconductor, vibronic model, fluctuation effects 77—90113
- solid solution, phys. characts. nonlinearity near phase transition 78—43812
- spin susceptibility near ferroelectric transition 80—2710
- spontaneous polarisation field screening by free charge carriers *(Russian)* 80—50274
- thin films, ferroelectric properties, quantum size effect 80—97201
- V-VI-VII complex ferroelec. semiconductor monocrystalline film production 79—78905
- vibronic, interband light absorption 78—72555
- vibronic, mag. field effect on phase transition 77—40193
- vibronic, tunnel effect 78—10853
- vibronic ferroelectric semiconductor, mag. susceptibility calc. 80—2711

ferroelectric semiconductors continued

- vibronic theory of ferroelectricity, developments 79—33620
- zero-gap, ferroelec. phase transitions, effect of Coulomb interaction on RPA calc. 79—28691
- Ag_3AsS_3, proustite, cryst., new trigonally oriented ferroelec. semiconductor 79—61317
- Ag_3AsS_3, proustite, light effects on dielec. props., elec. resist. 80—49816
- Ag_3AsS_3, proustite, phonons and soft modes at ferroelec. transition 80—60524
- $(Ba,La)TiO_3$, defect chemistry and elec. cond., thermogravimetric meas. 77—39580
- $(Ba_xSb_{1-x})TiO_3$, ferroelectric films, dielectric and semicond. props. 79—91388
- $Ba_xSr_{1-x}Nb_2O_6$, anomalous photovoltaic effect and photocond. 78—52449
- $BaSrTiO_3$, excess noise characts. exam. 78—19110
- $BaSrTiO_3$, model for 1/f excess noise 79—99591
- $Ba_{0.4}Sr_{0.6}TiO_3$ films, DC conductivity, strong microwave field effect 80—65727
- $Ba(Ti,Sn)O_3$, thin film elec. and photoconductivity 79—33366
- $BaTiO_3$, acceptor doped, exam. of electrical conductivity 130 to 300°C 79—33286
- $BaTiO_3$, acceptor-doped defect equilibria, elec. cond. 77—39579
- $BaTiO_3$, adsorption of $O_2(H_2)$, effect on work function and spontaneous polarisation *(Russian)* 78—6211
- $BaTiO_3$, anomalous photovoltaic effect and photocond. 78—52449
- $BaTiO_3$, bulk photovoltaic effect in ferroelecs. 79—15181
- n-$BaTiO_3$, ceramic, expt. and theoretical investigation of grain-boundary resist. 79—56235
- $BaTiO_3$ ceramic, PTC-type, voltage contrast imaging for low and high Ti excess 77—28183
- $BaTiO_3$ ceramic, semiconductive sintering 77—36430
- n-$BaTiO_3$, ceramic, systematic expt. and theoretical investigation of grain-boundary resist. 79—56236
- $BaTiO_3$ ceramic semiconductors, principle and appl. *(Chinese)* 79—73523
- $BaTiO_3$ ceramic surface, neutralisation of bombarding ion beam 80—71528
- $BaTiO_3$, defect chemistry and elec. cond. improved positive temp. coeff. model 77—39859
- $BaTiO_3$, domain struct. characts. of unipolar ferroelec., photocarrier effects 78—19435
- $BaTiO_3$, donor doped, elec. props., effect of kinetic processes 78—64042
- $BaTiO_3$, doped, defect chemistry and elec. cond. kinetics of equilib. restoration 77—39700
- $BaTiO_3$, elec. and thermoelec. props. of grains and grain boundaries 78—43382
- n-$BaTiO_3$, elec. transport props., theoretical discussion and expt. 78—84215
- $BaTiO_3$ electrode, surface comp. changes during photoelectrolysis, XPS obs. 79—7894
- $BaTiO_3$, exam. of PTC effect as function of Ti excess *(German)* 79—23960
- $BaTiO_3$, ferroelec. inhomogeneous impurity distrib., distrib. of spontaneous induction 77—28530
- $BaTiO_3$, ferroelectric semicond. anomalous photovoltaic effect due to ionising radiation 80—29437
- $BaTiO_3$ film, sputtered, elec. props. 79—42676
- n-$BaTiO_3$, grain boundary resistivities 77—80782
- $BaTiO_3$, H_2-reduced, elec. cond. mechanism, EPR, resist. and Seebeck coeff. meas. 80—10976
- $BaTiO_3$, OH^- impurity IR spectra meas. 80—20679
- $BaTiO_3$, perovskite structure, semiconductor props. *(Polish)* 78—56437
- $BaTiO_3$, polycryst., elec. resist. anomaly in phase transition region 78—43381
- $BaTiO_3$, SCL currents, carrier mobility and trapping 77—15863
- $BaTiO_3$, semiconducting ceramic, AC thermopower measurement 80—44624
- $BaTiO_3$, thin film elec. and photoconductivity 79—33366
- $BaTiO_3$, XPS and UPS from surface defects 80—76136
- $BaTiO_3$:Co, trap recomb. consts., photocurrents 78—43435
- $BaTiO_3$:Co, voltaic current appearance on proton irrad. 80—104032
- $BaTiO_3$:Eu(Sm), absorption spectra, Ti^{3+} ion and Z-centre formation 77—24871
- $BaTiO_3$:La and undoped, defect chemistry elec. cond. at high temp. meas. 77—39858
- $BaTiO_3$:Nb, elec. props., contact material influence 80—70848
- $BaTiO_3$:SnO_2, transition temperature shift, resistivity anomaly obs. *(Korean)* 77—39856
- $BaTiO_3$-$BaNb_2O_6$, semiconducting ferroelectric ceramic, nonlinearity of dielectric layer capacitance 79—8098
- $Bi_xSb_{1-x}SI$, low freq. Raman spectroscopy 78—15162
- BiTeI-SbTeI, solid solns., phase diagrams, photocond., elec. props. 79—38125
- $Cd_2Nb_2O_7$, photolum. and carrier drift mobility at ferroelec. transition 80—71469
- $CuPbBiS_3$, aikenite, electrophysical props. 77—47822
- $FeSb_2S_4$, berthierite cryst., anomalies in elec. and dielec. props. 77—47821
- GeTe, ferroelec. with strong cubic anisotropy, phase transition 77—52026
- GeTe:I, ferroelectric transition exam. 78—88264
- n-InSb, ferroelec. semicond., transverse acousto-elec. effect *(Russian)* 78—30958
- $KNbO_3$ monocrystals, low freq. oscills. of elec. current 79—91053
- $KNbO_3$, perovskite structure, semiconductor props. *(Polish)* 78—56437
- $KNbO_3$, photovoltaic effect lux ampere characts., photoconductivity 80—15561
- $KNbO_3$, reduced, phase hologram recording, energy transfer and sensitivity 80—69338
- $KNbO_3$:Fe, anomalous photovoltaic effect and photocond. 78—52449
- $KNbO_3$:Fe, anomalously high photovoltage 77—69378
- $KTa_{0.7}Nb_{0.3}O_3$, pressure-induced resistance and colour change obs. 80—75608
- $KTaO_3$, electromech. props. and electron tunnelling 78—23403
- $KTaO_3$, pure and Gd_2O_3 doped, elec. cond. and sp. ht. 79—78097
- $KTaO_3$, quantum magnetoresist. results, using pulsed fields up to 35 T 79—73528
- $KTaO_3$, Shubnikov-de Haas effect, cond. band struct. 80—10875
- $LiNbO_3$, anomalous photovoltaic effect and photocond. 78—52449
- $LiNbO_3$, influence of spontaneous polarisation on photoelec. emission 79—28898

ferroelectric semiconductors continued
- $LiNbO_3$, monocryst., thermoemission, anomalous zone bending *(Russian)* 77—55860
- $LiNbO_3$, reduced, electron Hall mobility, photo-Hall meas. 77—8121
- $LiNbO_3$ surfaces, ion and electron bombard., photoelectron spectroscopy and electronic props. 80—71559
- $LiNbO_3$:Fe, anomalously high photovoltage 77—69378
- $LiNbO_3$:Fe, bulk photovoltaic effect in ferroelecs. 79—15181
- $LiNbO_3$:Fe, elec. resist., temp. and conc. depend. 80—80275
- $LiNbO_3$:Fe, electro-optic cryst., light induced charge transport, holographic obs. 80—70747
- $LiNbO_3$:Fe, exoelectron emission in pyroeffect regime 80—76158
- $LiNbO_3$:Fe, intensity enhanced bulk photovoltaic effects 79—19616
- $LiNbO_3$:Fe, intrinsic field effect, photoelectric emission study 79—69961
- $LiNbO_3$:Fe, pure and doped, photocond. and dark cond. 80—29439
- $LiNbO_3$:Fe, recording dynamical holograms in crystals with photovoltaic effect, nonstationary energy exchange *(Russian)* 79—31842
- $LiTaO_3$:Fe, electro-optic cryst., light induced charge transport, holographic obs. 80—70747
- $NaNbO_3$, elec. and photoelec. props. near ferroelec.-antiferroelec. phase transition 80—15989
- $NaNbO_3$, elect. cond. mech., resist., Hall coeff. and thermoelec. power meas. 80—65603
- $NaNbO_3$, perovskite structure, semiconductor props. *(Polish)* 78—56437
- $NaNbO_3$, thermoelec. power for small polaron 77—89784
- (Pb, Sn)Te-type semiconductors, displacive ferroelec. phase transitions, vibronic theory 80—11354
- $Pb_{1-x}Be_xTe$, anomalous resist. near ferroelec. phase transition 80—20196
- $(Pb_{1-x}Bi_x)_5Ge_3O_{11}$, spontaneous and induced electrogyration 79—42946
- $Pb_5Ge_3O_{11}$, ferroelec., elec. cond. meas. 79—65472
- $Pb_{1-x}Ge_xTe$, degenerate semiconducting ferroelectric, structural phase transition temp., mag. field effects 80—45017
- $Pb_{1-x}Ge_xTe$, dielec. const. determ. near ferroelec. transition 78—88269
- $Pb_{1-x}Ge_xTe$, electron-phonon interaction effect on ferroelec. transition 78—76416
- $Pb_{1-x}Ge_xTe$, ferroelec. phase transition, IR refl. and resist. meas. 80—11353
- $Pb_{1-x}Ge_xTe$, ferroelec. constants, C-V and C-T characts. of abrupt p-n junctions 80—25323
- $Pb_{1-x}Ge_xTe$, mag.-field-induced displacive phase transition 80—50278
- $Pb_{1-x}Ge_xTe$, p-n junctions, elec. characts., effect of ferroelec. phase transition 79—33338
- $PbMg_{1/3}Nb_{2/3}O_3$, electro-optical and elasto-optical props., appl. to optical storage *(Russian)* 80—80749
- $PbMg_{1/3}Nb_{2/3}O_3$, photolum. and carrier drift mobility at ferroelec. transition 80—71469
- $PbMg_{1/3}Ta_{2/3}O_3$ electro-optical and elasto-optical props., appl. to optical storage *(Russian)* 80—80749
- $Pb_{0.98}Nb_{0.02}(Zr_{0.95}Ti_{0.05})_{0.98}O_3$, PZT 95/5, ferroelec. ceramic, resist. meas. under shock wave compression 78—19031
- PbO, disordered photoconductor, dielec. props., temp. depend. anomalies 78—43765
- $Pb_6Sb_{14}S_{27}$, zinkenite, electrophysical properties 78—34834
- $Pb_{1-x}Sn_xTe$, anomalous resist. near ferroelec. phase transition 80—20196
- $Pb_{1-x}Sn_xTe$, ferroelec. phase transition, hybridization effect *(Russian)* 79—61319
- $Pb_{1-x}Sn_xTe$, mag. and kinetic props. near ferroelec. transition 80—11160
- $Pb_{1-x}Sn_xTe$, soft mode, ferroelec. phase transition crit. temp. and dielec. const. calcs. 77—8530
- $(Pb_{0.95}Sr_{0.05})(Zr_{0.53}Ti_{0.47})O_3$+3% mol PbO, Seebeck effect, meas. and interpretation *(Polish)* 79—4574
- PbTe, lattice permittivity determ. by magnetoplasma waves method 78—19075
- PbTe-SnTe compound semiconductors, lattice instability by mm-wave magnetoplasma refl. 80—54336
- $PbTiO_3$, crysts., X-ray investigation of 90° domain struct. 79—15426
- $PbTiO_3$, ferroelec. phase, photocond. and photovoltaic effect, temp. depend. 78—95309
- $PbTiO_3$, perovskite structure, semiconductor props. *(Polish)* 78—56437
- $PbTiO_3$, photolum. and carrier drift mobility at ferroelec. transition 80—71469
- $PbTiO_3$, thermoelec. power for small polaron 77—89784
- $PbZn_{1/3}Nb_{2/3}O_3$ electro-optical and elasto-optical props., appl. to optical storage *(Russian)* 80—80749
- $Pb(Zr,Ti)O_3$ solid soln., elec. cond. and Seebeck coeff. 79—51564
- $Pb(Zr,Ti)O_3$:Cr_2O_3 ceramic, electrical cond. and dielectric const. meas. 80—2389
- $PbZrO_3$, perovskite structure, semiconductor props. *(Polish)* 78—56437
- $PbZrO_3$, thermoelec. power for small polaron 77—89784
- $SbNbO_4$, anomalous photovoltaic effect and photocond. 78—52449
- $SbNbO_4$, anomalously high photovoltage 77—69378
- Sb_2S_3, cond. anomalies at phase transition pts. 77—43604
- Sb_2S_3, crystal, domain structure 78—43828
- Sb_2S_3, dielec. and acoustic nonlinearity 78—15107
- Sb_2S_3, effect of screening by conduction electrons on phase transitions 78—84537
- Sb_2S_3 type chain crystals, ferroelec. phase transitions 79—33625
- SbSBr glass, IR reflectivity spectra 80—71403
- SbSI, adsorption of $O_2(H_2)$, effect on work function and spontaneous polarisation *(Russian)* 78—6211
- SbSI, adsorption polarisation and depolarisation currents 77—43942
- SbSI, anomalous photovoltaic effect 79—38133
- SbSI, anomalous photovoltaic effect 80—70749
- SbSI, band gap photoreflectance spectra near ferroelec. transition 79—38559
- SbSI, cryst. and vitreous, nonlinear light absorpt., effect of temp. and phase transitions 77—75604
- SbSI, cryst. struct. and thermal vibr. parameters, neutron diffr. obs. at −185, 16 and 100°C 77—43180
- SbSI, crystal growth from SbI_3 flux 79—66000
- SbSI, crystallisation from vapour phase, morphology 77—4726
- SbSI, diffuse X-ray scatt., anisotropy in phonon dispersion relations 77—84866
- SbSI, domain struct. relaxation 78—48135
- SbSI, dynamic dielectric nonlinearity, in microwave band 78—35109
- SbSI, effect of screening by conduction electrons on phase transitions 78—84537
- SbSI, electrical cond. and acceptor level shift temp. depend., para- and ferroelec. phases 77—28181
- SbSI, electroreflectance exam. 78—48145
- SbSI, energy band struct. from modulation spectra 78—43892

ferroelectric semiconductors continued
- SbSI, ferroelec. phase transition and nonlinear props. 80—75988
- SbSI, ferroelec. semicond., laser-modulated reflectance near T_c 78—72552
- SbSI, ferroelec. semicond., influence of internal fields on polarisation reversal process 79—38443
- SbSI, ferroelec. semicond. near phase transition, anomalies of photocond. 79—42579
- SbSI ferroelectric, dielectric behaviour, particle-size dependence 78—2811
- SbSI, ferroelectric semicond. anomalous photovoltaic effect due to ionising radiation 80—29437
- SbSI, free energy function, temp. depend. and anisotropy of dielec. const., ferro- and paraelec. phases 78—64330
- SbSI materials, piezoelectric props. rel. to use as electroacoustic transducers 78—52445
- SbSI, nature of low-temp. phase transition 77—69784
- SbSI, nonlinear sound propagation in case of polarisation switching 79—27458
- SbSI, paraelec. phase, microwave reson. dielec. dispersion, near T_c 79—99839
- SbSI, paraelectric phase, nonlinear optical props. 78—10870
- SbSI, paraelectric phase, jump-like switching processes, ferroelec. surface layer 78—92038
- SbSI, paraelectric-ferroelectric transition, low freq. phonon branches, neutron scatt. obs. 79—61313
- SbSI, photoelectric current, modulated due to light intensity 79—19626
- SbSI, photolum. spectra in ferroelec. phase, 600-800 nm., 14-100K 80—71468
- SbSI, polarisation switching processes, effect of surface electron states 77—90115
- SbSI, Raman scatt., near tricritical point 78—15159
- SbSI single crysts., nonlinear dielec. effects and microelectronic applics. 77—43944
- SbSI, surface layer exam. 78—48119
- SbSI, vapour phase growth on seeds 78—11090
- SbSI-BiSI, solid solns., phase diagrams, photocond., elec. props. 79—38125
- SbSI(Br), transition possibility investig. for struct. coeff. calcs. of internal Lorentz field 77—73119
- $SbSI_{0.3}Br_{0.7}$, anomalous photovoltaic effect 80—70749
- $SbS_xSe_{1-x}I$ layer elec. and ferroelec. props., mech. stress effects *(Russian)* 80—50279
- $Sn_{0.9}Ge_{0.1}Te$, Mossbauer spectra, soft modes 80—20550
- $Sn_xGe_{1-x}Te$, ferroelec. semicond. structural phase transition, X-ray study 79—37836
- $Sn_2P_2S_6$, ferroelec. semicond., phase transition and lattice dynamics 80—60526
- $Sn_2P_2S_6$, investigation of p-T diagram near a singular point *(Russian)* 80—88937
- $Sn_2P_2S_6$ polarisation Raman scatt. spectra, X-ray struct. study 79—95778
- $Sn_2P_2S_6$, soft mode, temp. depend. of Raman spectra near phase transition 78—88263
- $Sn_2P_2S_6$, soft mode props., Raman scatt. study 80—60525
- $Sn_2P_2(S_{1-x}Se_x)_6$, solid solutions, ferroelectric soft mode freq., displacive transformations 80—29701
- $Sn_2P_2(Se_xS_{1-x})_6$, ferroelec. tricrit. phase transform., light transmission study 80—71355
- $(Sn_{1-x}Pb_x)_2P_2S_6$, solid solutions, ferroelectric soft mode freq., displacive transformations 80—29701
- SnSeI film, growth, effect of artificial nucleation centres 79—11032
- SnTe, displacive transform., interband electron-phonon interactions, phase diagram 80—93252
- SnTe, electron-phonon interaction effect on ferroelec. transition 78—76416
- SnTe, ferroelec. transition, quantising mag. field effect 79—87403
- SnTe, obs. of soft TO-phonon by Raman scatt. 77—69838
- SnTe, phase transition obs. by Mossbauer spectroscopy 77—55740
- SnTe, softening of TO phonon mode *(Japanese)* 78—2225
- SnTe:Mn, EPR as probe of phase transitions 80—15790
- $SrTiO_3$ (100) surface, struct. and electronic props., AES, LEED, EELS, and UPS study 80—24986
- n-$SrTiO_3$ electrode, flatband pot. determ. from differential stress meas. 80—75638
- $SrTiO_3$ ferroelectric modes, Raman spectra, neutron scatt. meas. 80—80727
- $SrTiO_3$, photolum. and carrier drift mobility at ferroelec. transition 80—71469
- $SrTiO_3$, semicond., free carrier optical absorption and scatt. *(Korean)* 78—23489
- $SrTiO_3$, semicond., structural phase transitions, US velocity meas. 79—28692
- $SrTiO_3$ semicond. electrodes, electroreduction process kinetics, cathodic dark current meas. 80—66807
- $SrTiO_3$, soft modes, zone boundary mode 80—71357
- n-$SrTiO_3$, surface electronic struct. calc. 78—88011
- $SrTiO_3$, transition metal doped anodes for water photoelectrolysis, response to visible and UV 79—74531
- $SrTiO_3$:B layers, ion implanted, conductive props. Hall mobility, defect energy levels 79—82693
- $SrTiO_3$:Eu(Sm), absorption spectra, Ti^{3+} ion and Z-centre formation 77—24871
- $SrTiO_{3-x}$-In contacts, differential capacitance, elec. field depend. permittivity effect 80—54779
- TlSe type crystals, possible second-order phase transitions, group-theoretical anal. 80—92672
- V_2O_5, ferroelec. semicond., dielec. and elec. meas. 80—60516

ferroelectric switching
- characteristics investigation using cct. containing bipolar square pulse generator 80—62687
- collinear ferroelectric, domain struct. changes on switching, liq. cryst. visualisation *(Russian)* 79—33648
- ferroelectric-semiconductor system, illuminated, voltage redistrib. 77—40194
- ferroics, secondary, polycryst., poling effects 77—16102
- film switching transition meas. instrument, operating principle 79—17443
- guanidine aluminium sulphate hexahydrate, ferroelec. cryst., growth, domain struct., dielec., switching props. 77—43950
- hysteresis loops and butterfly loops, macroscopic theory 80—66132

ferroelectric switching continued
α-quartz twinning and tailored domain patterns 77—40197
smectic liquid crystals, ferroelec., submicrosecond bistable electro-optic switching 80—84051
TGS:Cr^{3+}(VO^{2+}), polarization reversal, static hysteresis loops, switching processes, EPR 78—43633
TGS, effect of aniline in aqueous crystal growing soln. on physical props. 78—43810
TGS, electrooptic switching anomalies 78—52473
TGS, ferroelec. activation field change 80—71358
TGS, growth from solution containing aniline, dielec. and pyroelec. props. 78—6639
TGS, polarisation reversal, cryst. defects effect 78—27156
TGS substrate, influence of polarisation reversal on elec. cond. of CdTe thin film 80—65720
TGSe:Cr^{3+}, polarisation reversal and ageing mechanisms, EPR meas. 79—8044
$Ba_{0.92}Ca_{0.08}TiO_3$ ceramic, uniaxial stress effects, US dilatometric and dielec. meas. 78—52454
$(Ba_xSb_{1-x})TiO_3$ 80—60514
$(Ba_xSb_{1-x})TiO_3$, ferroelectric films, dielectric and semicond. props. 79—91388
$BaTiO_3$ film, struct. and dielec. props. 80—60514
$BaTiO_3$, polarisation switching, influence of charges arising from defects 79—69796
$BaTiO_3$, pure and Fe doped, ferroelec., switching and electrolum. 80—76079
$BaTi_{0.98}Sn_{0.02}O_3$, ferroelec. film, switching process 80—60518
$Ba(Ti_{0.98}Sn_{0.02})O_3$ film, ferroelec., switching process in elec. field with rectangular impulses 80—2714
$Ba(Ti_xSn_{1-x})O_3$ film, struct. and dielec. props. 80—60514
CsH_2PO_4, and deuterated phase, press. induced antiferroelec., switching behaviour 79—78634
$Fe_3B_7O_{13}I$, twinning in orthorhombic phase, ferroelec. domain struct. with switching 78—19434
$Gd_2(MoO_4)_3$, spontaneous birefringence, pulsed field switching, compression effect, domain movement 78—27187
KH_2PO_4, ferroelastic cryst., appl. of γ-ray diffractometry 77—8533
$LiNbO_3$:Fe, spontaneous polarisation reversal and photorefractive effect 78—31163
PLZT ceramics, photoferroelectric image storage in antiferroelectric phase 79—47404
PLZT ceramics, photoferroelectric effects, image storage device appl. 79—42924
PLZT composition, effect on its switching characts. 79—42917
PLZT, light scatt. under switching conditions, time characts. 77—52045
$Pb_5Ge_3O_{11}$, growth defects and polarisation switching 78—48132
$Pb_5Ge_3O_{11}$, pulsed polarisation switching process depend. on illumination 80—93253
$Pb_5Ge_3O_{11}$ single crystals, switching behaviour and hysteresis 80—40077
$Pb_5Ge_3O_{11}$:Si, switching velocity, increase over that of undoped crysts. 79—51922
$Pb_5Ge_{3-x}Si_xO_{11}$, ferroelec., switching vel. and spontaneous polarisation 78—84543
$Pb_{2.07}K_{0.56}Nb_{0.91}Ta_{4.15}O_{15}$, tetragonal tungsten bronze type, ferroelastic-ferroelectric coupling *(French)* 77—28522
$PbTiO_3$, domain structure reorganisation and polarisation change 77—1645
$Pb(Zr,Ti)O_3$ photovoltaic ferroelectric as optical memory storage medium 78—50877
SbSI, ferroelectric semiconductor, polarisation switching processes, effect of surface electron states 77—90115
SbSI, paraelectric phase, jump-like switching processes, ferroelec. surface layer 78—92038
$SrTiO_3$ ceramic, sp. ht and electrocaloric effects at low temps. 77—59518

ferroelectric thin films
anisotropy properties, thermodynamic anal. *(Russian)* 79—28686
application and properties at microwave frequencies 77—1632
ceramic, resonant autothermostabilisation *(Russian)* 78—52451
conference, ferroelectric materials and their applications, Kyoto, Japan, Nov. 17-19, 1977 79—19846
electrical hysteresis investigation, electronic system for loops display on CRO 78—89496
epitaxial film growth by sputtering, review 77—32521
ferroactive thin films, physical prop. optimisation 80—80698
ferroelectric thin film, pyroelectric radn. detector development *(Russian)* 79—47394
permittivity tensor at microwaves 79—42883
phase transitions, second order, thermodynamics *(Russian)* 78—52458
phthalocyanine metal free films, TSC, ferroelectric-semiconductor transition 80—66105
polyvinylidene fluoride, X-ray diffr. evidence for ferroelectricity 78—60399
pyroelectric effects, origin 78—88258
pyroelectric response to step radiation signals 80—7302
semiconducting, ferroelectric properties, quantum size effect 80—97201
smectic liquid cryst. film, ferroelec., two-dimens. X-Y crit. behaviour 79—77497
smectic-C liquid crystal film, ferroelec., freely suspended, two-dimensional mol. orientation fluctuations, light scatt. 78—47236
surface effects on phase transitions, local spontaneous polarisation 80—2708
switching transition meas. instrument, operating principle 79—17443
textured layered prep. by HF sputtering 77—85947
TGS epitaxial thin film, IR absorption spectra *(French)* 78—35129
thermodynamics, in neighbourhood of phase transition of second kind 80—45021
thermodynamics in vicinity of first order phase transition *(Russian)* 80—45014
thermodynamics in vicinity of second order phase transitions 79—91381
vacuum deposition method using RF sputtering technique 78—84712
$(Ba, Sr)TiO_3$ ferroelectric film, phys. props. in weak elec. fields 78—35098
$(Ba_xSb_{1-x})TiO_3$ 80—60514
$(Ba_xSb_{1-x})TiO_3$, dielectric and semicond. props. 79—91388
$(BaSr)TiO_3$ film, ferroelec., dielec. props. in strong elec. fields 78—27163
$Ba_{0.4}Sr_{0.6}TiO_3$, ferroelec. thin film, fabrication, props. 77—28521
$Ba_{0.60}Sr_{0.40}TiO_3$, sputtered film on Pt, pyro-effect for laser registration *(Russian)* 77—20804

ferroelectric thin films continued
$Ba_xSr_{1-x}TiO_3$, elec. characts. of HF cathode sputtered film *(Russian)* 78—23406
$Ba_xSr_{1-x}TiO_3$, ferroelec. film, heteroepitaxial growth in cathode sputtering 80—93486
$Ba_xSr_{1-x}TiO_3$, thin ferroelec. layers 79—42912
$Ba(Ti,Sn)O_3$, thin film elec. and photoconductivity 79—33366
$BaTiO_3$ and $BaTi_{0.08}Sn_{0.02}O_3$, pyroelectric response to step radiation signals 80—7302
$BaTiO_3$, deposition by HF cathode sputtering 77—36398
$BaTiO_3$, epitaxial films and single domain crysts., exoelectron emission obs. of phase transition 79—74069
$BaTiO_3$, ferroelec. thin films, r.f. sputtering, X-ray and microprobe obs. 79—47627
$BaTiO_3$, film, ferroelectricity of vap. deposited coating 79—69781
$BaTiO_3$ film, sputtered, elec. props. 79—42676
$BaTiO_3$ film, struct. and dielec. props. 80—60514
$BaTiO_3$ films, effect of elec. field on dielec. props. 79—33642
$BaTiO_3$, nonstoichiometry of vac. condensates, effect on dielectric props. 77—16260
$BaTiO_3$ on Si substrate, prep. and elec. props., expt. 77—20460
$BaTiO_3$, prep. by hydrolysis of organometallic cpds. 77—59702
$BaTiO_3$ RF sputtered ferroelectic film on Si substrate, ferroelectric props. 80—80697
$BaTiO_3$, RF-sputtered tetragonal films on Si, ferroelec. and insulating props. 79—78888
$BaTiO_3$, sputtered, refr. index, 0.3-1.0 μm, substrate temp. effects 77—55840
$BaTiO_3$, surface layer nature, AES obs., and effect on permittivity 77—24498
$BaTiO_3$, thin film elec. and photoconductivity 79—33366
$BaTiO_3$ thin film microwave complex permittivity meas. 79—73879
$BaTiO_3$, vacuum condensates on US irrad. substrates, props. 77—66466
$BaTiO_3/SiO_2$ charge storage memory films for IGFETs 80—11566
$BaTiO_{3-x}$, single cryst. and film, Auger spectra, surface comp. 78—27353
$BaTi_{0.98}Sn_{0.02}O_3$, ferroelec. film, switching process 80—60518
$Ba(Ti_{0.98}Sn_{0.02})O_3$, switching process in elec. field with rectangular impulses 80—2714
$Ba(Ti_xSn_{1-x})O_3$ film, struct. and dielec. props. 80—60514
$(BaZnSr)TiO_3$ parameters at upper end of centimetre waveband *(Russian)* 77—40185
$Bi_4Ti_3O_{12}$, ferroelec. film, on Si substrate, polarisation reversal and film struct. 79—91392
$Bi_4Ti_3O_{12}$ stoichiometric thin film prep. by DC sputtering with powder target 77—90273
$K_3Li_2Nb_5O_{15}$ films for optical waveguides epitaxial growth and characterisation 80—79016
$K_xLi_{1-x}NbO$ films, epitaxial growth by melting on $K_{1.5}Bi_{1.0}Nb_{5.1}O_{15}$ substrate 79—33204
$K_xLi_{1-x}NbO_3$, epitaxial growth of single-cryst. films on $K_2BiNb_5O_{15}$ substrate by RF sputtering 79—15041
$KTa_{1-x}Nb_xO_3$, preparation by RF sputtering, structural and electrical properties obs. 78—88426
$LiNbO_3$:Na structure field stability limits, LPE film growth, SAW velocity 80—80102
$LiNbO_3$:Na$^+$ (Co^{2+}, Zr^{4+}) film, improvement in temp. stability and SAW device appl. 80—75939
$Li(Nb_{1-x}Ta_x)O_3$, $0 \leq x \leq 1$, LPE thin film growth on $LiTaO_3$ substrate, lattice mismatches, meas. of temp. depend 79—56087
PLZT, electro-optic effects 78—6799
PLZT, epitaxial growth by RF sputtering, and characterisation 77—85937
PLZT ferroelectric thin films, epitaxial growth and optical props. 80—70543
PLZT, growth by RF sputtering, struct. and ferroelec. props. 77—48340
PLZT, RF sputtered thin film, ferroelectric props. 79—69780
PLZT, thin film epitaxial growth and characteris. 79—28918
PLZT, thin film prep. by RF sputtering, struct. and ferroelec. props. *(Japanese)* 77—69992
PLZT, transparent ferroelec., RF sputtering and film characterisation 78—72727
PZT, ferroelec. film, elec. props., composition anal., AES 78—84530
$PbGeO_3$, single cryst. films growth, temp. depend. of dielec. constant 79—100066
$Pb_3Ge_2O_7$, vacuum condensates on US irrad. substrates, props. 77—66466
$Pb_5Ge_3O_{11}$, sputtered ferroelec. films, prep. struct. and dielec. props. 80—75452
$PbTiO_3$ ferroelec. thin film, prep. by RF sputtering and dielec. props. 79—100052
$PbTiO_3$ thin films, fabrication by RF sputtering, characts. 80—40261
$Pb(Zr,Ti)O_3$, ferroelec. and optical props. 77—85674
$Pb(Zr,Ti)O_3$ film, by RF sputtering in PbO vapour 78—39689
$Pb(Zr,Ti)O_3$ film, prep. by electron beam evaporation technique 77—1809
$Pb(Zr,Ti)O_3$ films, ion beam sputtering, dielec. and ferroelec. props. 79—78881
$Pb(Zr,Ti)O_3$ films, ferroelec., ion beam deposition sputtered from multicomponent targets 80—80974
$Pb(Zr,Ti)O_3$, thin film evaporated on stainless steel, photovoltaic effect 79—4580
$Pb(Zr,Ti)O_3$ thin films, fabrication and characterisation electron-beam deposition 80—16188
$Pb(Zr,Ti)O_3$ thin film, ferroelec., fabrication by RF sputtering *(Japanese)* 80—25560
$Pb(Zr,Ti)O_3$ thin layers, tan δ temp. dependence obs. *(Bulgarian)* 78—88259
$Pb(Zr_xTi_{1-x})O_3$ films, ion beam deposition, struct., dielec. and ferroelec. props. 80—20788
$Pb(Zr_xTi_{1-x})O_3$ films, deposition by focused ion beam sputtering 80—76177
$SbNbO_4$, ferroelec. film characts. 77—48127
$Sr_{0.25}Ba_{0.75}Nb_2O_6$ film, growth and electrophys. props. 79—42928
$SrTeO_3$, ferroelec. vacuum condensates 77—40180
$SrTiO_3$ film, behaviour of ferroelecs. in strong elec. microwave field 79—42884
$SrTiO_3$, parameters at upper end of centimetre waveband *(Russian)* 77—40185
$SrTiO_3$, polycryst. dielec. losses, influence of amplitude of measuring microwave field 79—99829

ferroelectric thin films continued
- $SrTiO_3$, sputtered, refr. index, 0.3-1.0 μm, substrate temp. effects 77—55840
- $SrTiO_3$, surface layer nature, AES obs., and effect on permittivity 77—24498
- $SrTiO_3$, vacuum condensates on US irrad. substrates, props. 77—66466
- $SrTiO_{3-x}$, single cryst. and film, Auger spectra, surface comp. 78—27353

ferroelectric transitions
- *see also critical fluctuations; displacive transformations; ferroelectric Curie temperature; order-disorder transformations*
- absorption edge anomalies in phase transitions 80—2718
- acoustic activity near ferroelectric transition 77—90114
- acoustic properties at second-order phase transitions, effect of polarisation fluctuations 77—85664
- adiabatic and isothermal order-parameter susceptibilities and the thermal diffusion mode 80—36962
- β-Al_2O_3-Ag_2O, antiferroelectric transformation, Potts' model universality class 80—50277
- alkali metal double salts, $MB'BX_4$ (M=alkali; M'=alkali or NH_4^+; BX_4=SO_4, BeF_4, etc.), theory of phase transitions 79—99837
- alkali trihydrogen selenite: Mn^{2+} single crystal, EPR 78—72396
- alkaline trihydrogen selenites, ferroelec. phase transitions, Raman spectra 77—8525
- aluminium methylammonium selenate alum, effect of hydrostatic pressure on dielec. props., near transition pt. 79—56712
- ammonia Rochelle salt, temp. depend. of optical axis angle, phase transitions *(Russian)* 80—97216
- ammonium double salts, MH_4 MBX_4, (M=alkali metal; BX_4=SO_4, SeO_4, BeF_4, etc.), theory of phase transitions 79—99837
- ammonium hydrogen chloracetate, order disorder type transition 79—47399
- ammonium Rochelle salt, first order phase transition 78—43818
- ammonium Rochelle salt, incommensurate phase transitions under existence of Lifshitz invariant 79—15416
- ammonium Rochelle salt, incommensurate phases and ferroelectricity 78—52455
- ammonium Rochelle salt, thermodynamics of ferroelec. transition 80—84702
- anharmonic crystal, lattice dynamics and stability, self-consistent phonon theory 79—51209
- anharmonic crystal, lattice dynamics and stability 78—6129
- antiferroelectric ferrites, coupled magnetoelec. oscills. and high freq. susceptibility tensor *(Russian)* 80—93152
- antiferroelectric model dynamics, order-disorder transition, correl. functions and polarisation waves *(Russian)* 80—50282
- antiferroelectric transition, bias effect 77—81066
- antiferroelectric transition, phenomenological theory 79—4771
- antiferroelectrics, multicritical points in structural phase transitions, renormalisation 80—75982
- antiferromagnet, ferroelec., phase transformations *(Russian)* 80—93114
- barrier capacitance of p-n junction in region of strong ferroelec. instability 79—11218
- benzil, phase transition, far IR spectroscopy meas. 80—71407
- benzil, phase transition study be simultaneous Raman-scatt. and domain-struct. investigations 79—60504
- bifurcation of nonlinear integral eqns. 77—12330
- 1,6-bis(2,4-dinitrophenoxy)-2,4-hexadiyne, obs. of apparent ferroelec. transition 80—66121
- boracites, trigonal, spontaneous polarisation behaviour 77—43945
- Brillouin scattering spectroscopy, dynamical aspects 80—55115
- broadening of ferroelec. transition, heterophase fluctuations theory 77—81073
- calcium strontium propionate, compressed powder, dielectric props., particle size effects 77—59503
- classification of struct. transforms., using coupled double-well model 78—14443
- coexistence of ferroelectricity with ferromagnetism in systems with electron-hole pairing 80—7310
- commensurate ferroic phase, form. from prototypic phase, possibility of transition being second order 78—2223
- composite system, energy of formation of ferroelec. phase in inhomogeneous inclusion under press. 77—12338
- conference, Leningrad, USSR (1977) 79—15406
- converters of shockwave mech. energy into elec. power 80—61429
- cooperative model of dielec. behaviour, susceptibility amplitude, rel. to freq. of max. loss 80—2694
- copper formate tetradeuterate, deuterated, paraelec. and antiferroelec. phases, neutron diffr. obs. of struct. 79—87404
- copper formate tetrahydrate, dielec. anisotropy and dimer theory 79—38427
- copper formate tetrahydrate, ferrielectricity 80—2706
- copper formate tetrahydrate, short-range order, diffuse neutron scatt. 78—15124
- copper formate tetrahydrate, stress effect on antiferroelec. phase transition, dielec. meas. 79—38498
- critical dynamics at phase transitions and nuclear relaxation 78—75805
- critical indices in ferroelectric solid solns., admixture conc. 77—81064
- critical indices of primary and secondary order parameters using birefringence 77—28541
- critical points and transitions, in phase diagram, geometrical relation *(Japanese)* 80—24568
- critical points of infinite type 78—8374
- crystal classification by transition mechanisms *(Russian)* 78—60401
- crystalline phase transitions, symmetry determined phenomena 79—46800
- crystals with noncentral ions, ferroelec. transitions rel. to spontaneous polarisation 80—15991
- cubic crystal with dipole forces and anisotropic correlation function, phase transitions *(Russian)* 79—38504
- cubic ferroelectrics, crit. behaviour 79—33619
- cupric formate tetrahydrate, dielec. props. under hydrostatic press. 77—12343
- cupric formate tetrahydrate, uniaxial stress effect on dielec. props. 78—48125
- D_{2d} crystals, structural phase transitions, soft modes, group theory 80—92638
- de Gennes pseudospin model, lattice phonons tunnelling effects 79—73290
- defect structure near phase transition pt., effect on solid props. *(Russian)* 79—37838

ferroelectric transitions continued
- defect-containing crysts., US absorpt. near displacive phase transitions, anomalous temp. depend. 80—92612
- degenerate narrow-gap semiconductors, ferroelec. phase transition, hybridization effect *(Russian)* 79—61319
- Devil's staircase and harmless staircase, oscillating interactions through elastic stairs or other harmonic fields 80—88296
- diatomic linear chain, ferroelec. soft modes 80—70353
- dicalcium lead propionate, annealed, crit. exponents, dielec. const. temp. depend. 80—55050
- dicalcium lead propionate, effect of particle size on dielec. behaviour 79—38429
- dicalcium lead propionate, ferroelec., piezoelec. and elastic props. 78—84528
- dicalcium lead propionate, Raman scatt., order-disorder type transform 77—12373
- dicalcium strontium propionate, anomalous US attenuation near ferroelec. phase transition 79—91383
- dicalcium strontium propionate, effect of particle size on dielec. behaviour 79—38429
- dicalcium strontium propionate, elastic stiffness consts., determ. in US freq. region 79—37752
- dicalcium strontium propionate, Landau theory breakdown in ferroelec. transition 77—12344
- dicalcium strontium propionate, Raman scatt., order-disorder type transform. 77—12373
- dielectric props. meas. in vicinity of phase transition 78—74022
- dielectric spectroscopy, transitions, permittivity 80—75914
- diffuse phase transitions 79—33628
- dimethylammonium cadmium tetrachloride type compounds, structural phase transition model 79—37829
- dispersion of permittivity near N-phase point in $KTa_{1-x}Nb_xO_3$-type ferroelectrics 79—24276
- displacive, effect of strong cubic anisotropy of lattice anharmonicity, mol. field theory 77—52026
- displacive, unified theory, quantum limit, zero point energy 78—68461
- displacive and order-disorder type, thermal cond. at low temps. 80—75391
- displacive ferroelectric, inelastic neutron scatt. cross section 77—36187
- displacive limit, existence of phase transition for class of ferroelec. models 79—8104
- displacive phase transition, S ion spin Hamiltonian parameter dependence on order parameter 80—70356
- displacive transformations, ferroelectric, unified theory, quantum limit 78—27167
- displacive type, Ginzburg-Lavanyuk parameter 79—8106
- displacive type ferroelectric, thermal expansion and effect of press. on transition temp. 78—72471
- displacive type low-dimens. ferroelec., thermal cond. 79—61314
- DOBAMBC, dielec. dispersion at ferroelec. smectic A-smectic C transition 79—91385
- DOBAMBC, dielec. props. near ferroelec. smectic A to C transition 80—45015
- DOBAMBC, ferroelec. props. 79—32884
- DOBAMBC, smectic, ferroelec. transition mechanism obs. by X-ray scatt. 79—77515
- domain and thermal walls, kinetics of heterogeneous state *(Russian)* 80—45022
- domain structure as outcome state for poling procedure 80—80728
- domain wall struct., and stability under competitive phase transitions 79—78639
- doped displacive ferroelectrics, sound attenuation constant, Green's function technique 79—11397
- doped narrow gap semiconductor, two-channel vibronic mechanism of ferroelectric phase transitions *(Russian)* 79—56745
- dynamic critical phenomena 80—75962
- eight-site order-disorder model, influence of tunnelling 80—2709
- elastic moduli in ferroelectric transition region 78—6646
- elastic moduli near second order phase transition, temp. depend. 78—19429
- elastic nonlinearity near ferroelec. transition, effect of elec. field 77—24804
- electric field effect on first order phase transitions, double hysteresis loop criteria 79—65806
- electroacoustic echoes and long-time storage in piezo- and ferroelectrics 79—38454
- electrogyration in ferroelec. crystals, appls. 78—76394
- electron microscopy investigations, review *(Japanese)* 80—71366
- electron spin echo investigations 78—84476
- electron subsystem, crit. vibrs., order parameter 78—43813
- electron subsystem, steady-state statistical equilib. conditions, adiabatic approx. 78—87754
- electron-phonon interaction, structural transitions of antiferroelectric and displacive modulated type 78—43092
- entropy change, theoretical development of ferroelectrics and ferromagnets 78—43815
- EPR spectra above crit. temp., cluster theory for dynamic crit. phenomena 78—6566
- equilibrium configuration of ferroelectric domains near Curie temp. 78—88270
- exciton dielectric, inhomogeneous current state phase transition, free energy *(Russian)* 80—84703
- exciton insulators with spontaneous currents, impurity scatt. effect on phase transitions 80—80242
- extended defect system, phase transform., critical props. 80—103455
- extrinsic ferroelectrics, transition, polarisation, dielectric divergence 80—80718
- ferrodistortive, birefringence changes at phase transition 77—28541
- ferrodistortive and antiferrodistortive transforms., expt. results, book contrib. 77—89518
- ferrodistortive materials, dynamics of domain walls, theory 79—73282
- ferrodistortive structural phase transitions, exactly soluble model with tricritical points 77—7827
- ferroelastic, dislocation-phonon interactions, phase transition effects 80—59600
- ferroelectric antiferromagnetics, spin wave fluctuations in strong mag. fields *(Russian)* 79—82773
- ferroelectric films, surface effects on phase transitions, local spontaneous polarisation 80—2708
- ferroelectric materials, refractive index variation, fluctuative mechanism *(Russian)* 79—56755

ferroelectric transitions continued
ferroelectric materials for dielectric power conversion, dielectric prop. anal. 80—80712
ferroelectric semiconductor, phase transition temp., rel. to free carrier conc. 78—10860
ferroelectric semiconductors, vibronic, mag. field effect on phase transition 77—40193
ferroelectrics with hydrogen bonds, phase transition into coherent state, two-level proton calcs. *(Russian)* 80—71356
ferroic phase, second-order transition between prototypic and commensurate, thermal behaviour of soft modes 77—85662
ferroic phase transitions, non-mag., unified classification 80—70387
ferroics, nonmagnetic secondary and higher-order, order-parameter symmetries for the phase transitions 77—85668
ferromagnet, soft modes and ferromag. reson. 80—11275
ferromagnetic ferroelectric, soft mode damping, temp. anomalies *(Russian)* 80—44284
film, thermodynamics in vicinity of second order phase transitions 79—91381
films, ferroelec., phase transitions, second order, thermodynamics *(Russian)* 78—52458
fluctuons, calc. by method of parametric potential *(Russian)* 79—69784
geometric effects 79—38493
glass, microscopic model 77—40191
glycine silver nitrate, and deuterated analogue, hydrostatic press. effects 77—36185
gradient invariants and incommensurate phase transitions 78—22824
gyrotropic phase transitions 78—71852
gyrotropy, an implicity form of ferroicity 79—73286
halide ferroelectrics, transitions, formulae, structural data 80—75980
heat capacity meas., by dynamic method at high hydrostatic pressures 80—47059
helicoidal ferroelectric smectic A-smectic C phase transition, low freq. polarisation fluctuation spectrum 79—95714
heterogeneous states, statistics *(Russian)* 80—80721
high pressure solid state physics, review 79—90729
high pressure studies, rel. to Earth and planetary interiors 78—69334
hydrogen bond three-dimens. model with two critical points *(Chinese)* 79—24268
hydrogen-bonded ferroelectric, central peak, thermal cond. 80—93250
hydrogen-bonded ferroelectric, structural phase transition, intrinsic and extrinsic central peak properties 80—34168
hydrogen-bonded ferroelectrics, coherent crit. neutron scatt. 79—56742
hydrostatic press. effect on phase transitions in ferroelectrics 79—15413
hysteresis cycle computing during ferroelec. transition, statistical model *(French)* 79—11393
ice I_h, hexagonal, ferroelec. transition 79—91386
improper and incommensurate phase transitions, neutron scatt. studies 80—75974
improper ferroelectric nonferroelastic transition, order parameter symm. 77—4608
improper ferroelectrics, spontaneous polarisation, cryst. symm. in phase transitions 78—6645
impurity carriers, electron-phonon interaction *(Russian)* 78—48134
incipient ferroelectrics, mode-mode coupling 79—38464
incommensurate crystal phases, symm. props., superspace groups 80—75195
incommensurate phase transition, equivalent directions of modulation, unmodulated soft modes 79—24271
incommensurate phase transitions, symmetry aspects, structs., and phys. props. *(Japanese)* 79—65813
incommensurate phase transitions 80—75964
incommensurate phase transitions under existence of Lifshitz invariant 78—22822
incommensurate polar phase form. 80—71344
incommensurate-commensurate transitions in ferroelec., general approach 78—60404
inhomogeneous modulated phase, Landau theory analysis 77—8527
instability and phase transition in system with interband interaction 77—12346
introduction to ferroelectrics and their transitions *(Japanese)* 78—23407
Ising linear spin chains interacting with asymmetric pot. *(Russian)* 79—93074
Ising model, compressible, critical behaviour at marginal dimensionalities 79—69677
Ising model, relaxation processes, cluster approx., complex dielectric const. *(Russian)* 80—11352
Ising model, transverse, mean-field approach 77—28528
Ising model, with transverse field 77—77016
Ising system, ordering and phase transitions 79—91200
Ising type model, elastically coupled, effects of dipolar forces on crit. sound attenuation in uniaxial systems 80—50158
IV-VI compounds, dielec. props., elec. meas. 78—15119
IV-VI compounds, mag.-field-induced displacive phase transition 80—50278
IV-VI compounds, phase transitions induced by electron-phonon interaction 80—10656
IV-VI semiconductor, vibronic model of lattice instability 80—80723
IV-VI semiconductors, crystal structure and symmetry of electron spectra, doping effects *(Russian)* 79—7696
IV-VI semiconductors, mag. susceptibility near ferroelec. transition pt. *(Russian)* 79—95568
IV-VI semiconductors, structural phase transitions, anomalous resist., electron-soft phonon interactions 80—108167
Jahn-Teller crysts., elastic and dielec. anomalies, microscopic model 80—71332
kinetic Ising model with quenched relaxing impurities, crit. dynamics 78—10167
Landau theory, phase transitions, surface symmetry 79—56741
large gap ferroelectrics, phase transitions in mag. fields 79—33621
laser induced, centrosymmetric and noncentrosymmetric media 80—7312
laser light scatt. spectroscopy, phase transitions 78—10156
lattice dynamics of ferroelectrics with impurities 79—37802
lattice with local double-well pots., static susceptibility 77—8528
light generation at impurity atoms in ferroelectrics and LC, fluctuation effects *(Russian)* 80—91767
light scattering near phase transition points 79—15415
light scattering on central peaks *(Japanese)* 78—52522
lineal phase transitions, orders of 79—42206
liquid crystal, ferroelec., helicoidal, smectic-C, dynamics 79—1396
liquid crystal, soft modes 79—55653

ferroelectric transitions continued
liquid crystals, soft mode dynamics 77—7852
liquid crystals, temp. depend. of elec. susceptibility and spontaneous polarisation *(Japanese)* 78—68467
lithium ammonium tartrate, ferroelectric and ferroelastic transitions, Brillouin scatt. meas. 79—33716
lithium ammonium tartrate, piezoelec., proper ferroelastic transition 78—2812
lithium formate monohydrate, temp. depend. Raman spectra, H bonds 78—6673
lithium thallium tartrate, sp. ht., 0.3 to 25K, second-order ferroelec. transition 80—59674
low-lying vibrational modes and theory of local and transport props. at transitions 78—14425
macroscopic quadrupole effects as method of obs. of struct. transforms in crysts. 80—71321
magnetic field influence on ferroeelctric semiconductor, phase transition 80—55049
magnetoelectric effect at ferroelec. and antiferroelec. transitions 80—100637
methylammonium aluminium sulphate dodecahydrate, ferro to paraelectric transition, low freq. dielectric behaviour 79—4770
methylammonium chromium selenate, lattice consts. and ferroelec. props. 79—33641
methylammonium gallium selenate, lattice consts. and ferroelec. props. 79—33641
methylammonium-$Ga(SO_4)_2.12H_2O$, ferroelec. alum single crysts., dielec. dispersion and characts. 79—15408
MFA transition temp. for transverse Ising model, ferroelectric with dipolar interaction 78—31161
microferroelectrics 77—59534
mixed order-disorder displacive transition, model 77—59540
model theory of ferroelec. and first and second order struct. phase transitions 79—51915
modelling of ferroelectric-elastic transition, appl. to KH_2PO_4 and $LiNH_4C_4H_4O_6.2H_2O$ *(Russian)* 80—75961
modified F model, rel. to nearest-neighbour Ising model, crit. polarisation 79—93058
molecular dynamics results, for one-component displacement modeL 78—14424
Mossbauer spectroscopy study 80—39911
Mossbauer spectrum parameters, Fe^{3+} 4s shell polarisation by electric field 79—95698
narrow band gap semiconductor, quantising mag. field effect 79—87403
narrow-gap ferroelectric, phase transition due to strong mag. field 80—103924
neutron anomalous scatt., ferroelec. phase transitions 77—59539
neutron scattering obs. of ferroelec. crysts. with modulated struct. 79—95713
$(NH_4)_2SO_4:Mn^{2+}$, ferroelec. phonon driven phase transform., reduction of spin Hamiltonian consts. 78—92033
NMR, and soft collective lattice modes, spins and pseudospins, study 78—88208
noncentrosymmetric crystal with cooperative Jahn-Teller effect 77—8532
nonclassical ferroelectricity, phase transitions 80—25320
nonconducting linear chain systems, 3D Coulomb coupling and charge ordering 78—60075
noncritical fluctuations and temp. depend. of order parameter 77—1204
NQR studies 80—20489
order parameter fluctuation spectrum, central peaks near ferroelectric phase transitions, review 79—19851
order-disorder, dynamic structure factor *(Russian)* 80—40068
order-disorder, pseudo-one-dimens. kinetic Ising model 80—71333
order-disorder ferroelec., crit. dynamics, NMR data compared with dielec. data 78—76415
order-disorder ferroelectric, longitudinal phonon relax. *(Russian)* 79—55860
order-disorder ferroelectrics, exactly solvable model 77—32337
order-disorder ferroelectrics, phonon damping and freq. shift *(Russian)* 79—60471
order-disorder ferroelectrics, transverse Ising models, dipolar interaction and crit. behaviour 77—81071
order-disorder model, thermodynamic props. 78—10856
order-disorder phase transitions, thermodynamics in mean field approx. 79—33633
order-disorder transitions, static precursor nuclei, anomalies in high temp. superconductors, ferroelectrics, organic conductors 78—10165
order-disorder transitions in crystals with several orderly sublattices, model 77—59098
orthorhombic base centred lattices, Fourier transform of dipole-dipole interaction 78—76404
orthorhombic lattices, Fourier transform. of dipole-dipole interaction 78—64334
orthovanadates, centrosymmetric exhibiting cooperative Jahn-Teller effect, dielec. props. 79—28694
p-alkoxybenzylidene-p′-amino-2-chloropropyl-cinnamate, chiral smectic, dielec. props. 80—96441
paraelectric-ferroelectric-antiferroelectric phase transitions, electrostrictive effects 80—97209
$Pb_3M_gNb_2O_9$ crystals for optical radiation control 79—81554
perovskite crystals, static and dynamic aspects of PAC meas. 78—88241
perovskite ferroelectric, thermodynamic anal. of phase transitions 78—19431
perovskite-type ferroelectric crystals, calc. of domain wall motion 77—90117
perovskites, mechanisms of ferroelectric and structural phase transitions, structural distortions 79—15412
perovskites, Raman scatt. and ferroelec. soft modes 77—16300
perovskites, struct. phase transitions, octahedral tilt systems 77—11655
phase boundary fine struct. 80—45019
phenomenological theory of phase transitions with incommensurate phase formation 79—38491
photon condensation effect 77—68201
phthalocyanine metal free films, TSC, ferroelectric-semiconductor transition 80—66105
PLZT, diffuse phase transitions 79—33628
PLZT ceramics, ferroelec., special props. 79—42916
polaritons, appl. of IR reflectivity and Raman scatt. expt. 77—40237
polaron density of states near low temp. ferroelec. transition 78—60065
polaron state of electron near structural instability in ferroelectrics and antiferroelectrics 79—33245

ferroelectric transitions continued
polycrystalline materials; pyroelec. temp. anal. as method for studying ferroelec. transitions 79—38502
polyvinylidene fluoride, thermodynamical model, applications *(French)* 80—39315
Potts model, triangular, at transition temp., related models 78—8358
properties near phase transition point, influence of defects 79—42918
properties of phase transitions occurring when representations are reducible 78—35106
prototype temperature setting rel. to soft modes 78—63833
pyroelectric effect, non-linear in phase transition region 79—47393
pyroxene, ferroelectric-like phase transformation in mantle 78—61362
PZT ceramics, ferroelec. energy conversion under shock loading 80—108163
quantum transition suppression, pyroelectric, electrocaloric effects, specific heat 80—75984
random uniaxial systems with dipolar interactions, phase transitions 77—72677
refractive indices and electro-optics at ferroelectric and structural phase transitions 79—19850
Rochelle salt, cryst., oriented intrinsic absorpt. edge shape 77—66505
Rochelle salt, electrogyration during phase transitions 79—19859
Rochelle salt, electromechanical behaviour, influence of ferroelec. phase transitions 77—8510
Rochelle salt, ferroelec. phase transition, Raman scatt. study 80—97211
Rochelle salt, ferroelec. phase transitions in pseudo-spin lattice coupled mode model 80—108161
Rochelle salt, ferroelectric, Raman and IR study 80—71406
Rochelle salt, ferroelectric phase transition, external field induced 80—29700
Rochelle salt, high resolution heat capacity meas. *(Japanese)* 80—52218
Rochelle salt, optical characteristics in UV region *(Russian)* 78—84550
Rochelle salt, paraelectric-ferroelectric phase transition, relaxing defects effects 79—61320
Rochelle salt, phase transition mechanisms by optical spectroscopy 79—15411
Rochelle salt, phase transitions, free energy in symm. group representation of parent phase 79—69790
Rochelle salt, phase transitions, high-resolution sp. ht. meas. 78—48128
Rochelle salt, polarisation echo, near ferroelec. transition 78—88266
Rochelle salt, polarisation echo in ferroelec. phase transition region 79—42920
Rochelle salt, positron lifetime meas. during phase transitions 78—6644
Rochelle salt, refractive index, dispersion and temp. depend. 77—16275
Rochelle salt, spectra of absorption edge, low-temp. 79—4819
Rochelle salt, structural phase transitions 78—83938
Rochelle salt family, rectilinear system of transition parameters 78—48126
Rochelle salt family, unified phenomenological theory, spherical system of transition parameters 77—31751
Rochelle salt-type ferroelectrics, external field effect on phase transitions 79—73888
rotational phase transition in ferroelectrics and other crysts., Ising model 77—4605
tris-sarcosine calcium chloride, elastic props., US damping 80—84229
schultenites, ferroelectric, sp. ht. 79—19853
semiconductor, electronic density of states, effect of soft phonon-electron interaction *(Russian)* 77—80718
semiconductor, ferroelectric props., paraelec. phase transition, cathodoluminescence *(Russian)* 78—23535
semiconductor, phase boundary structure 79—11398
semiconductor, solid solution, phys. characts. nonlinearity near phase transition 78—43812
semiconductor, spin susceptibility near ferroelec., transition 80—2710
semiconductor, vibronic, interband light absorption 78—72555
semiconductor, vibronic model, fluctuation effects 77—90113
semiconductor thin films, ferroelectric properties, quantum size effect 80—97201
semiconductors, ferroelec., book 80—82590
semiconductors, self consistent approach 77—52028
semimetal-insulator ferroelectric phase transition due to interband electron-phonon interaction 77—8531
smectic liquid crystals, piezoeffects and ferroelectric phenomena 79—32883
SnTe, obs. of soft TO-phonon by Raman scatt. below phase transition temp. 77—69838
sodium acetylacetonate, anomalous dielec. behaviour, evidence for ferroelectricity 79—91390
sodium ammonium tartrate, crysts., temp. depend. of elastic compliances at phase transition 79—15409
sodium ammonium tartrate, improper ferroelec. transition anomalies 78—19430
sodium ammonium tartrate, polarisation, improper ferroelec. transition 78—72477
sodium ammonium tartrate, thermodynamic theory of phase transitions 77—90112
soft mode frequency and damping, temp. depend. 79—38484
soft mode in Jahn-Teller effect 79—69221
specific heat calc., soft mode contrib., near T_c 78—64338
spontaneous coherent state transition, chaotic phases approx. *(Russian)* 79—4776
squaric acid, ^{13}C chemical shift tensor study of antiferroelec. second order phase transition 78—52462
squaric acid, antiferrodistortive phase transition, proton chemical shift tensor determ. 77—63300
squaric acid, antiferroelec., struct. phase transition mechanism 80—75969
squaric acid, $C_4H_2O_4$ and $C_4D_2O_4$, theory 77—15585
squaric acid, critical slowing down of fluctuations at phase transition, ^{13}C spin-lattice relax. 80—44948
squaric acid, dielec. props., press. and temp. depend. 79—99815
squaric acid, layered, antiferroelec., phase transition mechanism 80—97210
squaric acid, sp. ht. near phase transition 79—91389
squaric acid, two-dimens. antiferroelec., temp. depend. of order parameter, birefr. obs. 80—11351
squaric acid, two-dimens. phase transition, Raman scatt. study 80—71401
squaric acid and deuterated derivative, vibrational study, IR and Raman spectra 78—92076
static critical behaviour, structural phase transitions 80—92640

ferroelectric transitions continued
stimulated emission from impurity atoms in ferroelectric, effect of phase transition 79—15490
structural phase transition at low temps. 80—75990
structural phase transition induced refractive index changes in crysts. 80—16000
structural phase transitions, applicability of thermodynamic theory 80—2139
structural phase transitions, ultrasonic velocity and attenuation meas. 80—75977
structural phase transitions in crystals, effect of high-power visible and IR laser radiation 78—71825
structural phase transitions in crystals of $D_{2d}{}^3$ symm. 80—15986
symmetry aspects of linear relations between anomalies at and near structural phase transitions 79—33618
system with strong electron-phonon interband interaction, phase transition and order parameter 77—66462
tanane, crit. behaviour near ferroelec.-ferroelastic transition 78—52459
Tanane, dielec. and electrooptic meas. near ferroelec. transition 79—33587
Tanane, ferroelec. ferroelastic transition, X-ray and optical expts. 78—15110
Tanane, ferroelec. mol. cryst., strong piezoelec. coupling 80—75942
temperature gradient effect on phase boundary 79—8107
tetragonal ferroelectric, crit. fluctuations, phase transition splitting *(Russian)* 78—48131
tetragonal tungsten bronze structure ferroelec. mech. for ferroelec. transition 79—38481
tetramethylammonium cobalt tetrachloride, Raman spectra near incommensurate phase transitions 80—76013
tetramethylammonium tetrachlorocobaltate, ferroelec., effects of hydrostatic press. on successive phase transitions 79—47402
tetramethylammonium tetrachlorocobaltate, ferroelec., pressure-temp. phase diagrams 80—97205
tetramethylammonium tetrachlorocobaltate, ferroelectricity 78—76408
tetramethylammonium tetrachlorozincate, ferroelec., effects of hydrostatic press. on successive phase transitions 79—47402
tetramethylammonium tetrachlorozincate, ferroelec., incommensurate-commensurate transition, neutron scatt. study 80—40073
tetramethylammonium tetrachlorozincate, ferroelec., pressure-temp. phase diagrams 80—97205
tetramethylammonium tetrachlorozincate, ferroelectricity 78—39513
tetramethylammonium tetrachlorozincate, incommensurate phase transition, US propag. meas. 79—91382
tetramethylammonium tetrachlorozincate, incommensurate phase study, ferroelectric-paraelectric phases *(French)* 80—88318
tetramethylammonium tetrachlorozincate, low temp. phases, superstruct., X-ray study 80—39065
tetramethylammonium tetrachlorozincate, X-ray study of incommensurate phase 80—71351
tetramethylammonium zinc tetrachloride, ^{13}C NMR and PMR study of incommensurate phase transition 80—34863
tetramethylammonium zinc tetrachloride, incommensurate phase transitions, ^{13}C NMR study 80—75968
tetramethylammonium zinc tetrachloride, Raman spectra near incommensurate phase transitions 80—76013
TGFB, high press. influence on anomalous specific heat, tricritical point 80—25322
TGFB, optical props. in 5 to 22 eV region, reflectance spectra 79—33652
TGFB, refr. index anomalies *(Russian)* 77—66472
TGS:α-alanine, piezoelectric props., ferroelec. phase existence *(Russian)* 79—47387
TGS:(CuSO$_4$), internal friction 80—44257
TGS:Cr^{3+}, EPR and spontaneous polarisation stabilisation during annealing 77—4610
TGS:Cr^{3+}, EPR obs. of ferroelectric monocrystals, fine struct. EHT-SCCC-MO calcs. 79—19769
TGS:Cr^{3+}, EPR obs. of fluctuations near phase transition 78—43820
TGS:Cr single cryst., lattice defect influence on critical behaviour 80—25315
TGS, admixed with nitroanilines or L-alanine, US vel. and absorpt., ferroelec. transition 77—32333
TGS, Brillouin scatt. spectra, depolarisation field effect 78—15177
TGS, calorimetry, sp. ht., 0-80°C 78—15122
TGS, characts. of dispersion of permittivity near phase transition 79—28695
TGS, crit. behaviour of thermal expansion, neutron diffr. study 80—75371
TGS, critical behaviour in thermal expsn. coeff. and dielectric const. 79—91334
TGS, deuterated, Brillouin spectra and elastic consts., behaviour near T_c 78—15178
TGS, dielec. behaviour near transition temp. 78—15127
TGS, dilatometric study, examination of logarithmic connection to classical Landau-type theory 78—6642
TGS, elastic vs. polarisation energy near transition 78—15118
TGS, electrogyration during phase transitions 79—19859
TGS, electromech. coupling of surface acoustic waves near ferroelec. transition 78—19415
TGS, eqn. of state near ferroelec. Curie temp., including tunnel effect 77—12342
TGS, ferroelec., meas. of sp.ht. at constant elec. flux density by AC method 79—33098
TGS, ferroelec., phonon contributions to anomalous sp. ht. near phase transition temp. 77—52023
TGS, ferroelec., positron lifetime meas. during phase transitions 78—6644
TGS, ferroelec., thermal expansion 79—37855
TGS, ferroelec. transition, electrooptical hysteresis and crit. behaviour of electrooptical props. 78—2817
TGS, ferroelec. transition, struct. changes, ^{13}C NMR obs. 78—60344
TGS, ferroelectric crystal, non-linear pyroelec. effect in phase transition region 79—47393
TGS, ferroelectric transition, neutron diffr. obs. 80—25324
TGS, gamma irrad. effects on heat capacity, Curie temp., permittivity 78—67737
TGS, kinetics of domain formation during phase transition 80—66130
TGS, L-α-alanine disordered regions, dielec. prop. changes in transition region 80—108159
TGS, large scale inhomogeneity effect on ferroelectric transition *(Russian)* 78—76411

ferroelectric transitions continued
TGS, layered domain struct. form., theory and expt. 77—52029
TGS, optical props. in 5 to 22 eV region, reflectance spectra 79—33652
TGS, perfect and imperfect, sp. ht. and sound vel., crit. anomalies 80—71331
TGS, positron annihilation and ferroelectric transition 78—19594
TGS, proton spin-lattice relax. time, temp. depend., near transition pt. 78—43668
TGS, pyroelec. effect in phase transition region *(Russian)* 79—87401
TGS, refr. index anomalies *(Russian)* 77—66472
TGS, spin-lattice relax. meas. of ^{1}H, ^{13}C, and ^{15}N near ferroelec. transition 77—1646
TGS, static and dynamic crit. behaviour of uniaxial ferroelectrics 78—35103
TGS, temp. depend. of spontaneous polarisation, microscopic mechanism, NMR expts. 77—81070
TGS, temp. depend. of spontaneous polarization near ferroelec. transition 79—33597
TGS, thermal expansion and dielec. const. near ferroelec. crit. temp. 77—40188
TGS, US relax., just above T_c, velocity and attenuation coeffs. 77—35637
TGS, US vel. and absorpt. in ferroelec. transition region 77—66461
TGS, X-irrad., glycine radicals, geom. struct. by ENDOR and INDO calc. 79—24230
TGS(Se), optical phonons near T_c, IR refl. and Raman spectra 77—48136
TGS(Se), optical phonons near T_c, nonlinear pseudospin-phonon interaction 77—48137
TGS γ-ray irrad. cryst., heat capacity anomalies near phase transition *(Russian)* 80—49375
TGS $(-d_x)$, sp. ht. near ferroelec. phase transition 80—70420
TGS family, change of order of phase transition under hydrostatic pressure 78—52452
TGS powder, complex dielectric const. temp. depend. 79—47379
TGS type crystal, phase transition model due to nonlinear reson. of lattice oscills. *(Russian)* 77—31746
TGS X-irradiated, paramag. relax, spin-echo study 80—7168
TGS-TGSe solid soln., phase transitions under hydrostatic press. 79—99840
TGS-type crystals:Cr^{3+}, radiospectroscopic studies, D parameter anomolies at phase transitions 79—15341
TGSe:Cu^{2+}, EPR ang. depend., coord. of Cu^{2+}, Cu-ligand bond obs. and ferroelec. transition anomaly 80—7156
TGSe, acoustic and thermal anomaly correlation near ferroelec. transition 79—4775
TGSe, behaviour under press. near tricritical point 79—95716
TGSe, Brillouin scatt. spectra, depolarisation field effect 78—15177
TGSe, deuterated, thermal and dielectric props. at high hydrostatic press. 80—34864
TGSe, deuterised, elec. field induced Merz double hysteresis loop obs. 78—31164
TGSe, dielectric const. near ferroelec. transition temp., effect of surface capacitance 78—56438
TGSe, ferroelec., domain wall orientations and domain shapes 79—38508
TGSe, ferroelec., meas. of sp.ht. at constant elec. flux density by AC method 79—33098
TGSe, ferroelec. transition, electrooptical hysteresis and crit. behaviour of electrooptical props. 78—2817
TGSe, hydrostatic pressure and deuteration effects on order of phase transition 77—12334
TGSe, sp. ht. anomaly, AC calorimetric obs. 78—23414
TGSe, US vel. and absorpt. in ferroelec. transition region 77—66461
TGSe, US velocity and absorpt., 10 MHz, crit. anomalies 77—15504
theory and dynamics, optical, acoustic electro-optical props., Brillouin zone struct. 80—11347
thermal conductivity, anomalies near structural phase transitions *(Russian)* 80—75394
thermal expansion of crystals, book 80—73115
thermodynamic potential of systems with size effects *(Russian)* 78—80297
thermoelectric conversion in ferroelectric ceramics during phase transitions *(French)* 78—76412
thin film, thermodynamics, in neighbourhood of phase transition of second kind 80—45021
thin film, thermodynamics in vicinity of first order phase transition *(Russian)* 80—45014
thiourea, Brillouin scatt., Debye relax. 79—87453
thiourea, commensurate-incommensurate phase transition, X-ray diffuse scatt. meas. *(French)* 79—19856
thiourea, dielec. const. and IR spectra in ferroelec. and antiferroelec. phases 79—33589
thiourea, expansion coeffs. in phase transition range 78—76407
thiourea, ferroelec., soft mode and Debye relax., IR reflection spectra 77—90111
thiourea, ferroelectric, Raman and IR study 80—71406
thiourea, ferroelectric transition, X-ray scatt. 79—47398
thiourea, incommensurate phase, soft modes, condensation of even-order harmonics 80—103313
thiourea, incommensurate phase transition, X-ray and neutron scatt. study 80—75963
thiourea, IR reflectivity study of ferroelec. and antiferroelec. phases, dielec. function model 79—33686
thiourea, lock-in phase transform. 80—29698
thiourea, phase transition into inhomogeneous modulated state, Landau theory 77—8527
thiourea, phase transitions accompanied by noncommensurate superstruct. form. 77—32336
thiourea, phonon modes near order-disorder transforms., hard-core modes due to pseudospin-phonon coupling 80—44285
thiourea, phonon modes near phase transitions, IR and Raman spectra 80—45084
thiourea, Raman scattering spectra, soft mode frequency 79—24305
thiourea monocrystals, γ-irrad. effects on dielec. props. 79—91391
triglycine fluoroberyllate, ferroelec. transition, electrooptical hysteresis and crit. behaviour of electrooptical props. 78—2817
triglycine fluoroberyllate, thermodynamic props. 78—15123
trigonal crystals, ferroelectric phase transition, renormalisation group theory 80—55052
tris-sarcosine calcium chloride:Mn^{2+} ferroelec. dynamics, EPR and ENDOR study 80—75972

ferroelectric transitions continued
tris-sarcosine calcium chloride:Mn(Fe), influence of cryst. defects on ferroelec. transition, EPR 79—38466
tris-sarcosine calcium chloride, ferroelec., ferroelasticity and hypothetical hexagonal to orthorhombic phase transition 77—63377
tris-sarcosine calcium chloride, ferroelec. transitions, soft modes, Raman scatt. spectra obs. 80—80763
tris-sarcosine calcium chloride, phase transition, hydrostatic press. effect, dielec. const. meas. 80—71327
tris-sarcosine calcium chloride, temp. depend. of order parameter 77—1204
trisarcosine calcium chloride crystals, ferroelec., electrooptic and ferroelastic props. 80—34865
trissarcosine calcium chloride:Mn^{2+}, ferroelec., electron spin-lattice relax. 78—80208
trissarcosine calcium chloride, ferroelec. phase transition, Raman and Brillouin scatt. studies 80—71340
trissarcosine calcium chloride, press. effect 80—84681
TSCC:Mn^{2+}, microscopic, mechanism of ferroelectric transition, EPR fine struct. tensor calc. 78—35104
tungsten bronze, tetragonal, type structure cpds, transition sequences *(French)* 77—89538
tungsten bronze structure ferroelectrics, tetragonal, model of ferroelec. transition 77—28526
tungsten-bronze ferroelectrics, $A_5B_{10}O_{30}$- and $A_6B_{10}O_{30}$-type, phase relations 78—35100
tunnelling concept in general theory 77—63375
tunnelling effects, self-consistent pseudospin-phonon formalism 79—55858
two order parameter systems, Landau-Ginzburg-Devonshire theory 78—10164
two-level electron system with electron-phonon interactions in field of strong EM wave 77—24524
uniaxial antiferroelectric, Ising model with dipole interaction, crit. behaviour 78—48133
uniaxial dipole system, order-disorder transition, computer expt. and high temp. expansion 79—38494
uniaxial ferroelectric, acoustic attenuation near transition point 80—11350
uniaxial ferroelectric, dipolar crossover effects 77—89961
uniaxial ferroelectric, static and dynamic crit. phenomena, Larkin-Khmelnitzkii theory 78—64327
uniaxial ferroelectric, US vel. and absorpt. anisotropy and crit. anomalies, acousto-opt. obs. 78—95574
uniaxial ferroelectrics, crit. behaviour, electrostrictive coupling role 80—71329
uniaxial ferroelectrics, domain formation during second order phase transition 79—38505
uniaxial ferroelectrics, microscopic theory, crit. behaviour and anomalous elastic consts. 79—38463
uniaxial ferroelectrics, static and dynamic crit. behaviour 78—35103
uniaxial ferroelectrics, Urbach rule and polarisation fluctuations, optical absorpt. edge 80—88910
unified theory 77—20808
unified theory for order-disorder and displacive types 77—12329
unit cell multiplication during phase transform., spontaneous polarisation 80—75983
vibrational modes, crit. behaviour of uniaxial materials 78—84539
vibronic ferroelectric semiconductor, mag. susceptibility calc. 80—2711
vibronic ferroelectric semiconductor, tunnel effect 78—10853
vibronic ferroelectrics, band struct. temp. depend. 80—70598
vibronic model, fluctuations of order parameter and anharmonic interaction 77—52022
vibronic theory, developments 79—33620
vibronic theory of antiferroelec. and struct. modulated transitions, soft modes 78—79719
vibronic theory of ferroelectricity 79—19854
vinylidene fluoride trifluoroethylene copolymer, ferroelec. behaviour 80—50284
vinylidene-fluoride-trifluoroethylene copolymer, piezoelectricity 80—88930
zero-gap semiconductor, ferroelec. phase transitions, effect of Coulomb interaction on RPA calc. 79—28691
$Zn_3B_7O_{13}Br$, ferroelec. 43m-mm2 phase transition, molar heat capacity meas. 80—93249
Ag_3AsS_3, proustite, cryst., new trigonally oriented ferroelec. semiconductor 79—61317
Ag_3AsS_3, proustite, ferroelec. with no 180° polarisation reversal, ferroelec. phase transition 79—38465
Ag_3AsS_3, proustite, ferroelectric phase transition under continuous illumination *(Russian)* 79—61315
Ag_3AsS_3, proustite, ferroelectric transition, thermodynamic description 79—69787
Ag_3AsS_3, proustite, phonons and soft modes at ferroelec. transition 80—60524
Ag_3AsS_3, proustite crystals, stoichiometric composition derivation influence on phase transition 79—95715
Ag_3AsS_3, prustite ferroelectric order model in prustite type nonlinear crystals *(Russian)* 79—65807
$Ag_2H_3IO_6$, antiferroelec. phase transition investig., Landau anal. 77—1644
$Ag_2H_3IO_6$ crystal, growth, specific heat, antiferroelec. transition 77—69781
$Ag_{26}I_{18}W_4O_{16}$, superionic conductor, order-disorder type transitions, ionic conductivity meas. 80—66122
$AgNaNO_2$, one-mode model 80—29702
$AgNa(NO_2)_2$, ^{23}Na elec. field gradient tensor from NMR satellite lines near phase transition 80—71191
$AgNa(NO_2)_2$, crit. dynamics, hydrostatic press. effect, dielec. props. meas. 80—71328
$AgNa(NO_2)_2$, crit. sp. ht. near ferroelec. transition 79—38474
$AgNa(NO_2)_2$, ferroelec. transition, ^{23}Na elec. field gradient tensor, NMR meas. 79—4777
$AgNa(NO_2)_2$, ferroelectric phase transition, theory 79—24272
$AgNa(NO_2)_2$, ferroelectric transitions, group theoretic comparison with $NaNO_2$ 80—7311
$AgNa(NO_2)_2$, ferroelec., Raman scatt. and phase transitions 80—71349
$AgNa(NO_2)_2$, ferroelec. cryst., Raman spectrum, phase transition, comparative anal. with $NaNO_2$ 80—88935
$AgNa(NO_2)_2$, Landau behaviour of sp. ht. close to nearly tricritical ferroelec. phase transition 78—10861
$AgNa(NO_2)_2$, Raman spectrum, NO_2^- bending vibr. 79—28737

ferroelectric transitions continued
$AgNa(NO_2)_2$, single cryst., specific heat anomaly, −90-55°C, ferroelec. transition entropy 77−77157
$AgNa(NO_2)_2$, triplet absorpt. polarised spectra, near ferroelec. phase transition 79−47473
$AgNa(NO_2)_2$, ultraslow crit. dynamics of order parameter, ^{23}Na spin relax. times obs. 78−76410
$AgNbO_3$, cryst. growth and phase transitions 80−40243
Ag_3SbS_3, NQR elec. field effect, temp. depend. near ferroelec. transition 77−77121
Ag_3SbS_3, pyrargyrite, order-disorder phase transition and elec. polarisation 79−38468
Ag_5SbS_4, dielec. and acoustic props. *(German)* 78−64335
$(AsO_4)_2H_2(UO_2)_2.8H_2O$, point group symmetry for ferroelec., antiferroelec. and paraelect. phases 78−42983
$As_{0.2}Sb_{0.8}SI$ cryst., ferroelec., soft mode Raman and IR spectroscopy 80−76016
$As_xSb_{1-x}SI$, solid solns., ferroelec. props. 78−23409
$(Ba,Sr)TiO_3$, ferroelec. solid solution, dielec. nonlinearity in nonpolar phase *(Russian)* 77−32317
$BaBi_4Ti_4O_{15}$, SHG, temp. depend. ferroelec.-ferroelec. transition 78−15121
$Ba(H_2PO_4)_2$, phonon spectra above and below transition temp. 77−62592
Ba_2MgTeO_6, ferroelec. behaviour, microwave dielec. props. meas. 77−43948
$BaMnF_4$, incommensurate transition, Brillouin scatt. investigation 79−87406
$BaMnF_4$, phase transitions, review 79−78378
$BaMnF_4$, spectroscopy near ferroelec. transition, dielec. anomalies near mag. ordering temp. 80−75965
$Ba_2NaNb_3O_{15}$, struct. phase transitions, light scatt. meas. 79−95774
$Ba_2NaNb_5O_{15}$, cryst. comp. effect on low temp. phase transition 80−71346
$Ba_2NaNb_5O_{15}$, ferroelec. conversion to single domain, elec. and photoelec. props. 78−88271
$Ba_2NaNb_5O_{15}$, high press. phase transitions, Raman scatt. studies 80−71402
$Ba_2NaNb_5O_{15}$, high-pressure phase transitions, ferroelastic phase 79−7687
$Ba_2NaNb_5O_{15}$, low temp. ferroelectric transitions, birefr. and dielec. meas. 79−38499
$Ba_2NaNb_5O_{15}$, optical mode softenings, Raman scatt. meas., 1.5 to 600K 79−33631
$Ba_2NaNb_5O_{15}$, transition with increasing symm. on cooling 77−16265
$Ba_{4+x}Na_{2-2x}Nb_{10}O_{30}$, tetragonal tungsten bronze structure ferroelec. mech. for ferroelec. transition 79−38481
$Ba_3Nb_{10}O_{28}$, diffuse ferroelec. phase transition, dielec. const. and X-ray diffr. meas. 78−23419
$Ba_{1.35}Sr_{0.65}NaNb_5O_{15}$ crystals, struct., dielec. and pyroelectric characts. 79−51913
$Ba_{0.25}Sr_{0.75}Nb_2O_6$, ferroelec., influence of temp. on Raman scatt. spectra 77−69842
$Ba_{0.25}Sr_{0.75}Nb_2O_6$, photoresponse in transition region 77−1451
$Ba_{0.25}Sr_{0.75}Nb_2O_6$, spontaneous electroopticabsorption effect 78−19443
$Ba_{0.5}Sr_{0.5}Nb_2O_6$, temp. depend. of Raman spectra 78−72524
$Ba_{0.54}Sr_{0.46}Nb_2O_6$, line broadening effect in Rayleigh scatt. of Mossbauer radiation 80−50238
$Ba_{0.54}Sr_{0.46}Nb_2O_6$:Y(La)(Tm), dielectric and electrooptic props. 78−68466
$Ba_xSr_{1-x}Nb_2O_6$ (x=0.27 to 0.54) exam. of freq. dependence of permittivity diffuse ferroelectric phase transition kinetics 80−2703
$Ba_xSr_{1-x}Nb_2O_6$ crystals, struct., dielec. and pyroelectric characts. 79−51913
$Ba_xSr_{1-x}Nb_2O_6$, ferroelec., cathodlum. spectral and temp. depend. 78−84665
$Ba_xSr_{1-x}Nb_2O_6$, nonequilibrium processes 78−48124
$Ba_{1-x}Sr_xTiO_3$ ceramic pyroelec. responsivity, −140° to +160°C obs. 78−23405
$Ba_xSr_{1-x}TiO_3$, disordered ferroelec., dielec. const. and spontaneous polarisation meas. 78−48130
BaTiO, mosaic struct. charge at ferroelec. phase transition *(Russian)* 77−32335
$BaTiO_3$, A_1(TO) phonon spectrum, ferroelectric phase transition, Raman scatt. meas. 78−56478
$BaTiO_3$, anisotropic emission of exoelectrons ferroelec. phase transitions *(Russian)* 78−48291
$BaTiO_3$, broadening of ferroelec. transition, heterophase fluctuations theory 77−81073
$BaTiO_3$, charges effect on form. of nucleation centres of ferroelec. phase 79−65810
$BaTiO_3$, Co substituted, ferroelec., diffuse behaviour 79−38475
$BaTiO_3$, crit. X-ray scatt. 79−33636
$BaTiO_3$, cubic-tetragonal phase transition, birefringence meas., surface distortion effects 78−95564
$BaTiO_3$, diffr. of Mossbauer radiation near Curie point *(Russian)* 79−8079
$BaTiO_3$, displacive ferroelectric, effective charge determ. 80−97212
$BaTiO_3$, domain struct., formation at phase transitions 79−38510
$BaTiO_3$, doped, loss mechanism and domain stabilisation 78−84542
$BaTiO_3$, dynamic Rayleigh light scatt. in region of ferroelectric-paraelectric transition 78−64371
$BaTiO_3$, effect of phase transformation on fracture behaviour 78−48507
$BaTiO_3$, elastic props., singularities near tetragonal-cubic phase transition 80−70303
$BaTiO_3$, elastooptic effect near ferroelec. transition, temp. depend. 80−97233
$BaTiO_3$, electron exoemission unipolarity associated with phase transitions 80−97415
$BaTiO_3$, epitaxial films and single domain crysts., exoelectron emission obs. of phase transition 79−74069
$BaTiO_3$, exoelectron emission during phase transition, orientational depend. 79−69786
$BaTiO_3$ family, unified phenomenological theory, spherical system of transition parameters 77−31751
$BaTiO_3$, ferroelec. phase transition, soft phonons, Raman scatt. obs. *(Japanese)* 79−65880
$BaTiO_3$, ferroelec. to paraelec. transform., influence of domain boundaries on interface struct. 79−95718
$BaTiO_3$, ferroelectric domain struct. and cryst. struct. changes, X-ray diffr. 77−24803

ferroelectric transitions continued
$BaTiO_3$, ferroelectric transitions rel. to Earth and planetary interiors 77−53045
$BaTiO_3$, ferroelectric-paraelectric transform., basic struct. and characts. 79−95717
$BaTiO_3$, ferroelectric mechanisms, anharmonic couplings by scanning IR interferometry 80−75978
$BaTiO_3$, ferroic materials, fracture processes 80−79869
$BaTiO_3$ film, unstable modulated struct. near ferroelec. phase transition 78−27164
$BaTiO_3$, internal stress and strength, failure mechanism 80−66128
$BaTiO_3$, light emission during repolarisation 77−36299
$BaTiO_3$, light scatt., Comes Lambert Guinier model 79−15471
$BaTiO_3$, line broadening effect in Rayleigh scatt. of Mossbauer radiation 80−50238
$BaTiO_3$, logarithmic velocity variations for longitudinal US waves near ferroelec. transition 78−72472
$BaTiO_3$, magnetochemical exam. of phase transition, mag. suscept. meas. 78−88265
$BaTiO_3$, martensite type phase transition 78−64326
$BaTiO_3$, nonstoichiometry of vac. condensates, effect on dielectric props. 77−16260
$BaTiO_3$, para to ferroelec. transition, strong Rayleigh scatt. 78−76486
$BaTiO_3$, paraelec. phase, stabilisation of soft mode 80−75985
$BaTiO_3$, periodic domain struct. and opalescence at tetragonal to orthorhombic transition 80−66131
$BaTiO_3$, perovskite structure, semiconductor props. *(Polish)* 78−56437
$BaTiO_3$, polariton and central mode softening 78−76006
$BaTiO_3$, polycryst., elec. resist. anomaly in phase transition region 78−43381
$BaTiO_3$, polycrystalline, X-ray diffraction, Curie temp., lattice defects, phase changes 79−99830
$BaTiO_3$, polycrystalline ferroelectric, grain-size dependent props. 80−71352
$BaTiO_3$, pure, dielectric const. and elastic compliance temp. depend. for various phases 79−19830
$BaTiO_3$, pure and Fe doped, ferroelec., switching and electrolum. 80−76079
$BaTiO_3$, single crysts., dielec. spectrum 80−25275
$BaTiO_3$, soft mode exam. 79−37799
$BaTiO_3$, soft mode spectroscopy IR refl. meas. 80−88982
$BaTiO_3$, struct. changes due to cubic-tetragonal phase transition 78−60407
$BaTiO_3$, tetragonal, model for temp. depend. of dielec. const., ferro-paraelectric transition 78−43771
$BaTiO_3$, tetragonal, over-damped soft E-polariton and dielec. dispersion 78−15111
$BaTiO_3$, thermodynamic props. 77−39680
$BaTiO_3$, thin film, polarisation reversal, electric field induced phase transform. 80−103925
$BaTiO_3$, transform. of cryst. struct., at cubic-to-tetragonal phase transitions 79−37827
$BaTiO_3$, tricrit. point 77−63378
$BaTiO_3$ type crystals, determ. of phase transitions using symmetry breaking theory *(French)* 78−83950
$BaTiO_3$, undoped and Cu doped, Γ_{15} phonon freezing, electronic instability, LCAO calc. 80−25318
$BaTiO_3$, X-ray diffr. intensities, anomalous temp. depend. *(Russian)* 79−1484
$BaTiO_3$:^{89}Zr, electron capture decay lifetime, struct. environment effects 77−28523
$BaTiO_3$:Co, charact. behaviour of spontaneous polarisation and dielec. const. 78−60382
$BaTiO_3$:Co, tricritical point, X-ray diffr. meas. 80−71341
$BaTiO_3$:La_2O_3 and $BaTiO_3$:$La_2O_3.3TiO_2$ capacitor, permittivity ageing obs. *(Korean)* 80−25325
$BaTiO_3$:Mn, polycrystn., annealing effect on transition temps. 80−3100
$BaTiO_3$:Nb, ferroelec. and paraelec. phases, props. 79−42919
$BaTiO_3$:SnO_2, transition temperature shift, resistivity anomaly obs. *(Korean)* 77−39856
$BaTiO_3$:X(X=Cr, Mn, Fe, Co, Ni, Zn, Ga), annealed in H_2 and O_2, valence change in phase stability 80−20600
$BaTiO_3$-$BiFeO_3$ solid solns., ferroelec.-antiferromag., magnetoelectric effect at ferroelec. transition 80−100637
$BaTiO_3$-type ferroelectrics, existence of noncommensurate phases due to gradient term in free energy 79−69792
$Ba(Ti_xSn_{1-x})O_3$ thick film, ferroelec., phase transitions and dielec. props. 80−97215
$(Bi_{2/3},Sr)TiO_3$, ferroelec. solid solution, dielec. nonlinearity in nonpolar phase *(Russian)* 77−32317
$Bi_2B'_xB''_{2-x}O_7$, pyrochlore-structured compounds, diffuse transition 77−36182
$Bi_2Bi_4Fe_2Ti_3O_8$, dielec. and magnetoelec. props. 78−95562
$BiBi_4Ti_3FeO_{15}$, perovskite-like layer-type ferroelec. magnetic cpd., Mossbauer expts., 80-1200K 78−64329
$BiFeO_3$, ferroelec., antiferromag., cryst. and mag. struct., neutron diffr. study 80−65786
$Bi_2O_3.2MoO_3$, at 300°C 77−89816
$Bi_xSb_{1-x}SI$, atomic substitution and ferroelec. phase transition 78−68464
$Bi_xSb_{1-x}SI$, low freq. Raman spectroscopy 78−15162
$BiTaO_4$, X-ray and ESR study of phase changes 78−72476
$Bi_4Ti_3O_{12}$, elec. characts., phase transition obs. 80−60517
Bi_2WO_6, ferroelectric, dielectric props., elec. cond. and relaxation phenomena obs. 80−80692
$CaB_3O_4(OH)_3.2H_2O$, NMR of ^{11}B in crit. region 77−16199
$Ca_2Nb_2O_7$, ferroelectric phase transitions, dielec. constant and thermal expansion rel. to temp. 80−88934
$CdFe_{1/2}Nb_{1/2}O_3$, high temp. X-ray exam. 77−11527
$Cd_2(NH_4)_2(SO_4)_3$, X-ray and optical studies of ferroelec. phase transition 79−38495
$Cd(NO_3)_2$, phase transition, SHG, optical and dielec. meas. 80−71334
$Cd_2Nb_2O_7$, photolum. and carrier drift mobility at ferroelec. transition 80−71469
$Cd_2Nb_2O_7$, Raman-scattering investigation of vibrational structure 78−76441
$Cd_2Nb_2O_6S$, pyrochlore struct., ferroelec., dielec. and structural study 79−38488
$CdTiO_3$, single cryst. growth and props. 79−100046
$Co_3B_7O_{13}I$, intermediate phase between paraelectric and ferroelectric phase *(Russian)* 78−68465

ferroelectric transitions continued
$Cr_3B_7O_{13}Cl$, cubic, approx. nonlinear optical susceptibility 80–78904
$Cr_3B_7O_{13}Cl$, ferroelec. 43m-mm2 phase transition, molar heat capacity meas. 80–93249
$CsBi(MoO_4)_2$, low temp. phase transition, permittivity meas. 79–28698
$CsCaCl_3$, birefringence, twinning and structural phase transitions 79–38480
$CsCaCl_3$:Co(Mn), EPR, 4.2 to 450K, ferroelec. transition 80–60414
Cs_2CdBr_4, struct. phase transitions, NQR study 80–71343
CsD_2AsO_4, ferroelect. phase transition, NMR study *(Chinese)* 79–33644
$Cs(D_xH_{1-x})_2AsO_4$, phase transition exam. 77–12340
CsD_2PO_4, dielec. props., press. and temp. depend. 80–25317
CsD_2PO_4, neutron scatt. study of ferroelectric phase transitions 77–59538
CsD_2PO_4, one dimens. ordering, ferroelec. transitions, neutron scatt. study 80–25316
CsD_2PO_4, pseudo-one-dimensional ferroelectric transition, ^{31}P chemical shift and relaxation study 80–66123
CsD_2PO_4, pseudo-one-dimens. ferroelec. transition, DMR and relax. study 80–71223
CsD_2PO_4, pseudo-one-dimensional ferrolec. and antiferroelec. transitions, phase diagram obs., soft modes 80–93245
CsH_2AsO_4, and deuterated derivative, attenuation of LF elastic oscills. 77–7791
CsH_2AsO_4, elastic props., photoelasticity near ferroelectric phase transition 80–29107
CsH_2AsO_4, ferroelec., temp. depend. of shear angle, neutron scatt. meas. 77–8524
CsH_2AsO_4, ferroelec., RF dielec. relax., loss mech. 79–38448
CsH_2AsO_4, RF dielec. response close to transition temp. 77–90099
CsH_2PO_4 and CsD_2PO_4, pseudo one-dimens. ferroelec. ordering dynamics, ^{31}P NMR study 80–75971
CsH_2PO_4, dielec. props., press. and temp. depend. 80–25317
CsH_2PO_4, ferroelec., press. induced antiferroelectricity 79–4774
CsH_2PO_4, ferroelec., X-ray and dielec. studies on phase transition 79–38477
CsH_2PO_4, ferroelec. transition, electrooptic 80–76005
CsH_2PO_4, ferroelec. transition, neutron diffr. study 80–93247
CsH_2PO_4, high press. phase diagram 78–52457
CsH_2PO_4, lattice consts., temp. depend. of dielec. const. and birefringence, high temp. phase transitions 79–56746
CsH_2PO_4, NMR of ^{133}Cs, elec. field gradient 78–15034
CsH_2PO_4, one dimens. ordering, ferroelec. transitions, neutron scatt. study 80–25316
CsH_2PO_4, press.-induced antiferroelectricity *(Japanese)* 80–15992
CsH_2PO_4, single cryst. growth, struct. and elec. props. 78–71693
CsH_2PO_4-d, antiferroelec. under hydrostatic press. 79–91384
$CsH_2PO_4(CsD_2PO_4)$, permittivity temp. depend., pseudo one-dimens. ferroelectric ordering and critical props., NMR 79–78635
$Cs_2KMO_3F_3$, (M=Mo, W), low temp. phase transitions *(French)* 78–92036
$Cs_3MoO_3F_3$, ferroelec. and order-disorder phase transitions 78–92037
$CsNO_2$, NQR spectrum of ^{14}N at low temp., poss. ferroelec. transition 77–12223
$CsPbBr_3$, critical thermodynamic props. around successive phase transitions 79–33627
$CsPbCl_3$, birefringence, twinning and structural phase transitions 79–38480
$CsPbCl_3$, critical thermodynamic props. around successive phase transitions 79–33627
$CsPbCl_3$, lattice thermal expansion, X-ray powder technique 80–19965
$CsPbCl_3$, n.q.r. spin-lattice relax. near cubic-tetragonal transition, soft modes 77–1616
$Cs_2RbMO_3F_3$, (M=Mo, W), low temp. phase transitions *(French)* 78–92036
Cs_2SO_4-$(NH_4)_2SO_4$ mixed cryst., ferroelec. transition, structural and dielec. props., proton spin-lattice relax. 78–39512
$CsSrCl_3$, birefringence, twinning and structural phase transitions 79–38480
$Cs_3WO_3F_3$, ferroelec. and order-disorder phase transitions 78–92037
Cu-Cl boracite, ferroelec., X-ray study on phase transition 79–33622
$Cu_3B_7O_{13}Cl$, cubic, approx. nonlinear optical susceptibility 80–78904
$Cu_3B_7O_{13}Cl$, dielec. const. and elec. resist. 77–69783
$Cu_3B_7O_{13}Cl$, ferroelec. 43m-mm2 phase transition, molar heat capacity meas. 80–93249
$Cu_3B_7O_{13}Cl$, Raman study of ferroelec. phase transition 79–38529
DBr(DCl), solid, ferroelec. and paraelec. phases, transitions, Raman scatt. 77–43980
$Dy_2(MoO_4)_3$, cryst. growth and props. 79–55727
$DyVO_4$, electric field influence on elastic props., electron state initial splitting 80–34123
$DyVO_4$ Jahn-Teller crystal, deform. induced transitions, elastic and dielectric characts. *(Russian)* 80–80726
$Fe_3B_7O_{13}I$, cubic, approx. nonlinear optical susceptibility 80–78904
$Fe_3B_7O_{13}I$, ferroelec. 43m-mm2 phase transition, molar heat capacity meas. 80–93249
$Fe_3B_7O_{13}I$, spontaneous polarisation, dielec. const., d.c. resist., sp. ht. 77–1643
$Gd_2(MoO_4)_3$, electro-optical properties 78–88281
$Gd_2(MoO_4)_3$, electron microscope exam. 78–15134
$Gd_2(MoO_4)_3$, electron microscopy investigs. of ferroelec. substances, review *(Japanese)* 80–71366
$Gd_2(MoO_4)_3$, nonlinear piezoelec. coeffs. near phase transition 79–95710
$Gd_2(MoO_4)_3$, temp. depend. of spontaneous biref. and electrooptic reponse 79–33662
$Gd_2(MoO_4)_3$, thin film, polarisation reversal, electric field induced phase transform. 80–103925
$Gd_2(MoO_4)_3$, uniaxial stress effect on ferroelec. transition, Raman scatt. 78–80360
GeTe:I, ferroelectric transition exam. 78–88264
H-bonded ferroelectrics, phonon relax. mechanism 80–79906
HBr(HCl), solid, ferroelec. and paraelec. phases, transitions, Raman scatt. 77–43980
HCl and HCl-DCl, ferroelec. transition, ^{35}Cl NQR study 80–71233
HCl, solid, ferroelec., comparative calcs. 77–8529
HF, solid, ferroelec., comparative calcs. 77–8529
H_2SeO_3, IR overtone spectra and temp. depend. 79–47456
$(K,Na)NbO_3$ ceramic, hot pressed, dielec. props. 79–87375
KCN, antiferroelectric phase, 83K phase transition based on model Hamiltonian 79–15418

ferroelectric transitions continued
KCN, dynamics of CN^- ions near phase transitions at 83K 80–80717
KCN, lattice dynamics and order-disorder transitions, neutron scatt. expts. 78–14434
KCN, mean field theory 80–92830
KCN, optical F centres and phase transitions 78–56504
KCN:H^-, U-centre, local mode meas. 77–1199
KCN-KCl mixed system, order-disorder transition, dielec. props. meas. 78–15112
KCN-KCl mixed system, order-disorder transition, Raman spectra obs. 78–15113
KCN_x-KCl_{1-x}, finite-freq. local field catastrophe with appl. to spectra 79–51491
KD_2, PO_4, polarisation echo, near ferroelec. transition 78–88266
KD_2AsO_4, ferroelec., high temp. phase transition, Raman spectra 80–71338
KD_2AsO_4, ferroelect. phase transition, NMR study *(Chinese)* 79–33644
KD_2AsO_4, high temp phase transitions, proton dynamics 80–76023
KD_2AsO_4, LF dielectric dispersion near phase transition 77–59530
KD_2AsO_4, phase transition and Raman scattering 78–84540
KDP monocrystal, expansion and contraction coeffs., tricritical point, Landau theory explanation *(Russian)* 80–44340
KDP type crystals, ferroelec. phase transition, Greens function theory *(Chinese)* 79–56740
KDP-type cryst., Raman scattering and phase transitions, deuteration effects 78–76400
KDP-type crystals, polarisation, dielec. const. thermodyn. props. 77–59527
KDP-type crystals, phase transitions, quadratic electrooptical coeff., electrostriction 78–76430
KD_2PO_4, ^{31}P chem. shift obs. 78–76414
KD_2PO_4, Cr^{5+} EPR, line shape and elec. field effect 79–11336
KD_2PO_4, electronic struct., UV reflection spectra 79–38558
KD_2PO_4, ferroelec. transition, ^{31}P chemical shift tensor meas. 77–28527
KD_2PO_4, ferroelect. phase transition, NMR study *(Chinese)* 79–33644
KD_2PO_4, ferroelectric transition obs. by ^{31}P chemical shift 77–59531
KD_2PO_4, H-bonded phase transitions, SCF approach 78–92030
KD_2PO_4, high press. phase diagram 78–52457
KD_2PO_4, microwave spectra, temp. depend. mode rel. to proton subsystem 80–24548
KD_2PO_4 monocrystal, electrooptical props. in paraelectric phase *(Polish)* 80–11368
KD_2PO_4, para- and ferroelec. phases spatial distrib. during first order phase transitions 79–42923
KD_2PO_4, phase transitions study, role of cryst. struct. determ. 80–75197
KD_2PO_4, polarisation fluctuations, wavevector depend. 80–71295
KD_2PO_4, struct. at high press. in rel. to effect of press. on T_c 79–42915
KD_2PO_4 type ferroelecs., distrib. functions and thermodynamic props. 78–76409
KD_2PO_4:Tl^{2+}, EPR of ferroelec. and paraelec. phases 80–66012
KD_2PO_4-type crysts., relax. processes in order-disorder transitions under short range correl. conditions 79–73889
$KD_3(SeO_3)_2$, acoustic phonon softening and spontaneous strains 78–26652
$KD_3(SeO_3)_2$, D NMR above and below ferroelec. transition, H-bond behaviour 78–52460
$KD_3(SeO_3)_2$, phase transition, neutron diffr. 80–2158
$K_4Fe(CN)_6.3H_2O$, dynamic disorder and ferroelec. transition, Raman spectra obs. 77–81069
$K_4Fe(CN)_6.3H_2O$ ferroelectric cryst., vibrational spectrum of $[Fe(CN)_6]^{4-}$ anion 77–69839
$K_4Fe(CN)_6.3H_2O$, freq. and bandwidth of OH spectrum, influence of paraelectric-ferroelectric transition 79–51959
$K_4Fe(CN)_6.3H_2O$, internal field and ferroelec. ordering 78–76406
$K_4Fe(CN)_6.3H_2O$, nature of phase transition 79–38470
$K_4Fe(CN)_6.3H_2O$, Raman spectrum and dielec. relax. 78–19476
$K_4Fe(CN)_6.3H_2O$, sp.ht. and spontaneous polarisation, −65 to 0 degrees C, mol. field model 78–64333
KH_2AsO_4, domain struct. formation, opt. polarisation obs. 77–63381
KH_2AsO_4, electronic struct., UV reflection spectra 79–38558
KH_2AsO_4, fast and slow dynamic reorientation 78–80306
KH_2AsO_4, ferroelec., RF dielec. relax., loss mech. 79–38448
KH_2AsO_4, ferroelec. phase transition under hydrostatic press., NQR spectra obs. 79–69785
KH_2AsO_4, ferroelec., high temp. phase transition, Raman spectra 80–71338
KH_2AsO_4, ferroelectric phase transition under high hydrostatic press., mol. dynamics, NQR study 80–75880
KH_2AsO_4, γ-irradiated, free radicals, EPR and ENDOR study of consequences of ferroelec. transition *(French)* 80–93209
KH_2AsO_4, high temp. phase transitions, proton dynamics 80–76023
KH_2AsO_4, KD_2AsO_4, slow dynamics from Cr^{5+} EPR 78–15126
KH_2AsO_4, LF dielectric dispersion near phase transition 77–59530
KH_2AsO_4, phase transition and Raman scattering 78–84540
KH_2AsO_4, Raman linewidth, isotope effect 77–8565
KH_2AsO_4, soft shear mode, Brillouin scatt. obs. 78–15176
KH_2AsO_4:Cr^{5+}, ferroelec. phase transition, EPR intensity and linewidth meas. 79–4721
KH_2AsO_4-KH_2PO_4, AsO_4^{4-} centre, EPR central peak dynamics 79–33523
$K(H_{1-n}D_n)_2PO_4$, degree of deuteration, depend. of Landau kinetic coeff. 77–85670
$K(H_{1-x}D_x)_2PO_4$ polarised impurity cluster effects in light scatt. expts. 80–29716
$K(H_{1-x}D_x)_2PO_4$, polarisation relaxation time and Landau kinetic coeff. rel. to degree of deuteration 80–84251
$K(H_{1-x}D_x)_2PO_4$, single cryst., 77K, γ-radiation damage centres, and EPR obs. 78–68379
$K(H_{1-x}D_x)_2PO_4$, static dielec. props., and Curie temp., press. depend. 79–87405
$KH_{2(1-x)}D_{2x}PO_4$, Raman spectra, effects of deuteration on proton tunnelling modes and coupled optic modes 77–59570
$KH_{2(1-x)}D_{2x}PO_4$, Raman spectra of overdamped mode 79–91427
$K(H_{1-x}D_x)_3(SeO_3)_2$, Brillouin spectrum central peak, soft acoustic mode 80–2777
KH_2PO_4 and deuterated derivative, attenuation of LF elastic oscills. 77–7791
KH_2PO_4, and isomorphs, phase transition 77–20807
KH_2PO_4, and isomorphs, ferroelectric transition and Curie temp., soft mode effect, Green's function anal. 79–24269

ferroelectric transitions continued
KH_2PO_4, anharmonic phonons and central peaks at struct. phase transitions 79−95775
KH_2PO_4, Brillouin-Rayleigh scatt. studies near ferroelec. transition temp. 80−76036
KH_2PO_4, central components in ferroelec. phase 78−56436
KH_2PO_4, central peak light scatt., scatt. centre props. 77−52108
KH_2PO_4, central peak susceptibility and US propag. near T_c 78−15125
KH_2PO_4, crit. behaviour near tricritical point, phenomenological interpretation 80−70389
KH_2PO_4, critical and tricritical phenomena, susceptibility, exponents 80−75976
KH_2PO_4 crystal, and deuterated cpd., optical meas. of phase transition point by domain obs. 77−40187
KH_2PO_4, D_2-impurities effect on Rayleigh central peak 77−81068
KH_2PO_4, depolarised light scatt., dynamic central peak 78−10858
KH_2PO_4, dielec. functions above and below ferroelec. transition 79−33588
KH_2PO_4, dynamic central peak in ferroelectric phase 78−84538
KH_2PO_4, electro-optic props. near ferroelec. transition 78−19445
KH_2PO_4, electrogyration near transition pt. in nonenantiomorphic cryst. 79−61339
KH_2PO_4, electronic struct., UV reflection spectra and XPS 79−38558
KH_2PO_4, ferroelec., positron lifetime meas. during phase transitions 78−6644
KH_2PO_4, ferroelec., RF dielec. relax., loss mech. 79−38448
KH_2PO_4, ferroelec. cryst., internal friction, torsion pendulum obs. 78−72474
KH_2PO_4, ferroelec. phase transition, soft phonons, Raman scatt. obs. *(Japanese)* 79−65880
KH_2PO_4, ferroelectric phase transition exam. by spontaneous parametric light scatt. 78−19427
KH_2PO_4, ferroelectric-ferroelastic phase transition, γ-ray diffr. 78−43819
KH_2PO_4, ferroelectric transition, press. induced tricrit. point 78−80301
KH_2PO_4, ferroelectric transition, neutron diffr. obs. 80−25324
KH_2PO_4, ferroelectric transition, order-disorder character of hydrogen bond 80−93251
KH_2PO_4, Green's function theory of ferroelec. phase transition 77−85669
KH_2PO_4, H-bonded phase transitions, SCF approach 78−92030
KH_2PO_4, high. press. tricrit. point rel. to zero press crit. point 78−15117
KH_2PO_4, IR overtone spectra and temp. depend. 79−47456
KH_2PO_4, KD_2PO_4, slow dynamics from Cr^{3+} EPR 78−15126
KH_2PO_4, KD_2PO_4, high-press. struct. rel. to dynamical models 78−80307
KH_2PO_4, Landau-Devonshire coeffs. 78−15116
KH_2PO_4, light scatt. in elec. field, ferroelec.-paraelec. transition 80−2707
KH_2PO_4, longit. sound attenuation, strain depend. pseudo spin coupling mechanism near T_c 77−85666
KH_2PO_4, low temp. transition, thermal hysteresis, Cr impurity effect on transition temp. 80−2705
KH_2PO_4, neutron critical scatt. in struct. transition due to homogeneous crystal deform. 79−42922
KH_2PO_4, one-dimensional Slater model, with random impurities due to partial deuteration 77−59537
KH_2PO_4 optical SHG and γ [quartz, struct. transitions, optical SHG and γ-ray diffr. results]-ray diffr. results 78−14459
KH_2PO_4, paraelectric, dynamic central peak depend. on deuterium content 79−65752
KH_2PO_4 paraelectric phase, solns. of Bloch-type eqns., soft mode freq. fluctuations 80−7304
KH_2PO_4, phase transitions study, role of cryst. struct. determ. 80−75197
KH_2PO_4, polarisation echo in ferroelec. phase transition region 79−42920
KH_2PO_4 powder, dynamic polarisation echoes 79−4773
KH_2PO_4, powder sample, pyrocharge temp. depend. near phase transition 79−87399
KH_2PO_4, pressure effect on ferroelec. transitions *(Japanese)* 79−65814
KH_2PO_4, RF dielec. response close to transition temp. 77−90099
KH_2PO_4, Raman scatt. near T_c, search for soft modes 78−15114
KH_2PO_4, shear angle and order parameter of ferroelec. transition by neutron diffr. 77−12339
KH_2PO_4, strong coupling of proton-phonon system 77−7822
KH_2PO_4, struct. at high press. in rel. to effect of press. on T_c 79−42915
KH_2PO_4, struct. phase transitions, light scatt. meas. 79−95774
KH_2PO_4, transition temp., transverse Ising model 77−90110
KH_2PO_4, tricrit. point, γ-ray and neutron diffr. 79−39516
KH_2PO_4, tricrit. point, neutron diffr. study under high press. 79−33624
KH_2PO_4, tricritical point and tricritical exponent 79−33623
KH_2PO_4, two doublet model for ferroelec. phase transition 78−39510
KH_2PO_4 type crystals, low lying ferroelec. modes, cluster dynamical theory 78−80305
KH_2PO_4 type crystal, H-bonded partially deuterated ferroelectrics, order parameter fluctuation spectra, central peak calcs. 79−61316
KH_2PO_4 type crysts., evidence of non-linear behaviour of soft modes, Raman spectra 79−33639
KH_2PO_4 type ferroelectric, phase transition to spontaneous coherent state, theory *(Russian)* 78−6647
KH_2PO_4, variational treatment of proton-photon system 78−88261
$KH_2PO_4:AsO_4^{4-}$ (SeO_4^{3-}), ferroelec., low freq. fluctuations, isotope effects, EPR, ENDOR, ESCA 77−73118
$KH_2PO_4:SeO_4^{3-}$, slowing down of fluctuations near T_c, EPR obs. 78−60403
KH_2PO_4:Tl, 5.76 eV absorpt. band, temp. effects on doublet struct. 79−78713
$KH_2PO_4:Tl^{2+}$, EPR of ferroelec. and paraelec. phases 80−66012
$KH_2PO_4:VO^{2+}$, EPR spectra, Hamiltonian parameters, ferroelec. transition 78−39387
KH_2PO_4-KD_2PO_4 mixed crystals, static and dynamic props., proton-lattice coupled mode model 78−64328
KH_2PO_4-KD_2PO_4 mixed crysts., dielec. spectra, sub-mm wavelengths 80−80724
KH_2PO_4-type crystals, H bond in ferroelectricity, role of high pressure research 79−15414
$K_3H(SO_4)_2$, and $K_3D(SO_{42})_2$, dielec. props. and phase transitions 80−60482
$KH_3(SeO_3)_2$, and $KD_3(SeO_3)_2$, anharmonic phonons and central peaks at struct. phase transitions 79−95775

ferroelectric transitions continued
$KH_3(SeO_3)_2$, central peak obs. by light scatt. 77−32390
$KH_3(SeO_3)_2$, ferroelastic, low-frequency elastic props., −190 to 50°C 79−37759
$KH_3(SeO_3)_2$, slightly deuterated, central peak obs. in Brillouin spectra 78−64374
KIO_3, temp. depend. Raman spectra and phase transitions *(Russian)* 78−15171
α-$KIO_3.HIO_3$, ^{127}I NQR study of ferroelec. phase transition 79−38400
$K_{0.75}Li_{0.25}TaO_3$, press. depend. of impurity soft modes, low energy Raman scatt. meas. 78−2852
$K_2Mn_2(SO_4)_3$, langbeinite type cryst., ferroelec., phase transitions, dielec., elastic and pyroelec. meas. 77−59535
$K_3MoO_3F_3$, ferroelec. and order-disorder phase transitions 78−92037
KNO_2, NQR spectrum of ^{14}N at low temp., poss. ferroelec. transition 77−12223
KNO_3, antiferroelec., press. induced II to IV phase transition, Raman scatt. 78−15161
KNO_3, far IR study of dielec. function by asymmetric Fourier spectroscopy 79−51947
$K_xNa_{1-x}TaO_3$, press. depend. of impurity soft modes, low energy Raman scatt. meas. 78−2852
$KNbO_3$, acoustic modes near orthorhombic-tetragonal phase transition, temp. depend. 79−28058
$KNbO_3$, anomalous scatt. and asymmetrical line shape in Raman spectra 77−20853
$KNbO_3$, displacive ferroelectric, effective charge determ. 80−97212
$KNbO_3$, domain struct. at transitions from twinned phase, appl. to tetragonal-orthorhombic transition 80−71360
$KNbO_3$, ferroelec. phase, phonon dispersion relations and lattice dynamics calcs., comparison with expt. 80−49319
$KNbO_3$, ferroelectric soft modes and order-disorder transition 77−47534
$KNbO_3$, ferroelectric transition, neutron diffr. obs. 80−25324
$KNbO_3$, perovskite structure, semiconductor props. *(Polish)* 78−56437
$KNbO_3$, thermoelec. effect and phase transitions 78−48123
$K_2SbNb_5O_{15}$, dielec. and pyroelec. props. 79−99841
K_2SeO_4, anharmonic phonons and central peaks at struct. phase transitions 79−95775
K_2SeO_4, Brillouin scatt. at paraelectric-incommensurate phase transition, hypersonic waves 79−78690
K_2SeO_4, dielec. dispersion, 5-900 MHz, near incommensurate-commensurate transition 80−60522
K_2SeO_4, elastic compliance anomalies 80−45010
K_2SeO_4, elastic props. at commensurate-incommensurate transition, Brillouin scatt. and US study 80−93248
K_2SeO_4, ferroelec., incommensurate struct., dynamic props. *(Russian)* 80−11373
K_2SeO_4, hexagonal-orthorhombic transition, Brillouin scatt. study 80−97208
K_2SeO_4, improper ferroelec., struct., phase transform. and lattice instability neutron scatt. meas. 77−63379
K_2SeO_4, incommensurate modulation along axis perpendicular to x-axis 78−6154
K_2SeO_4, incommensurate phase transition, stress depend. of T_c 79−4391
K_2SeO_4, incommensurate phase transitions under existence of Lifshitz invariant 79−15416
K_2SeO_4, incommensurate structure, IR and Raman activity of soft mode 79−28738
K_2SeO_4, incommensurate lattice instability, ferroelec. transition, neutron scatt. study 79−42210
K_2SeO_4, incommensurate to ferroelec. transition, hydrostatic press. effects, neutron scatt. study 80−108166
K_2SeO_4, lower freq. soft-mode in ferroelec. phase 77−81065
K_2SeO_4, phenomenological theory of transition sequence 77−76546
K_2SeO_4, Raman scatt. and dielec. props. 80−11313
K_2SeO_4, Raman scattering spectra and discovery of soft mode 78−76442
K_2SeO_4, Raman spectra, 77-300K *(Japanese)* 77−43988
K_2SeO_4, soft modes below incommensurate transition Raman and Brillouin scatt. meas. 79−91387
K_2SeO_4, symmetry determ. of commensurate and incommensurate phases by EPR of γ-irrad. crysts. 79−78525
K_2SeO_4, thermal expansion, phase transitions, 77-190K 77−16263
K_2SeO_4, unpolarised-noncommensurate-polarised phase transition, phenomenological theory 79−15422
$KTa_{0.9}Nb_{0.1}O_3$, dipolar behaviour, crit. exponent of dielec. const. 77−4604
$KTa_{1-x}Nb_xO_3$, paraelectric phase, defect induced fluctuations, Raman meas. 79−15423
$KTa_{1-x}Nb_xO_3$, quantum limit of ferroelec. transitions, dielec. and elastic consts. meas. 78−15128
$KTa_xNb_{1-x}O_3$, ferroelectric transition, US attenuation, elastic consts., soft modes 78−23411
$KTaO_3$, crit. dielec. and optical props. and storage, 4K 77−24805
$KTaO_3$, ferroelec., local field determ., phase transition study by EPR 79−38471
$KTaO_3$, field depend. sp. ht. and soft modes at low temps. 79−8105
$KTaO_3$, freq. depend. of soft mode self-energy, for IR dielec. response meas. 79−33632
$KTaO_3$, Raman scatt. and ferroelec. soft modes 77−16300
$KTaO_3$, stress-induced ferroelectricity, Raman scatt. obs. 77−40190
$KTaO_3:Fe^{3+}$ local phase transition, EPR line temp. broadening *(Russian)* 80−54944
$KTaO_3$:Li, ferroelec. transition and atomic motions, ^7Li NMR study 80−75872
$K_3WO_3F_3$, ferroelec. and order-disorder phase transitions 78−92037
K_2ZnCl_4, incommensurate phases, neutron scatt. 79−38501
K_2ZnCl_4, incommensurate phase transitions, ^{35}Cl NQR study 80−75968
$K_2Zn_2(SO_4)_3$, langbeinite type cryst., ferroelec., phase transitions, dielec., elastic and pyroelec. meas. 77−59535
$La_xPb_{1-x}Zr_yTa_{1-y}O_3$, ferroelec. with diffuse phase transition, electrostriction-optical props. 78−68457
$Li_2B_4O_7$, ferroelectric glass, phase transition, permittivity, electrochromism, photochromism 80−80719
$Li_2B_4O_7.xWO_3$ ($x=0$ to 1 mol.) glass, random elec. dipole, cooperative phenomena 79−28693
$LiGd(MoO_4)_2$, defect struct. and phase transitions 79−28697
$LiND_4SO_4$, ^7Li and ^2D NMR exam. of high-pressure phase 79−11396
$LiNH_4SO_4$ and $LiND_4SO_4$, dielec. pyroelec., and thermal props. 80−60509
$LiNH_4SO_4$, DC elec. cond. 80−88603
$LiNH_4SO_4$, ferroelect. and press. induced phase transitions 79−38473

ferroelectric transitions continued
  $LiNH_4SO_4$, ferroelectric phase transition, lattice parameters and thermal expansion coeffs. 80-40074
  $LiNH_4SO_4$, nuclear spin lattice and effective proton relaxation, phase transitions 80-54965
  $LiNH_4SO_4$, phase transitions and phys. props. 78-76399
  $LiNH_4SO_4$, press.-temp. phase diagram, NMR and SHG meas. 78-23690
  $LiNH_4SO_4$, thermal props. near high temp. phase transition 78-19428
  $LiNbO_3$, ferroelec., displacive type phase transition, far IR reflection spectra 80-71339
  $LiNbO_3$, ferroelec., phonon dispersion relations, neutron inelastic scatt. meas. 78-56435
  $LiNbO_3$, ferroelec. phase, soft vibr. modes, far IR refl. meas. 79-87407
  $LiNbO_3$, Fourier transform Ir spectroscopy of vibr. states at high temp. 80-97256
  $LiNbO_3$, single crystal, dielectric props., second order phase change 77-16245
  $LiNbO_3$, thermally stimulated electron emission meas. 80-25534
  $LiNbO_3$:Fe, calc. of photorefraction *(Russian)* 78-92032
  $LiNd(MoO_4)_2$, defect struct. and phase transitions 79-28697
  $LiTaO_3$, anomalous polariton dispersion near Curie temp. 77-80743
  $LiTaO_3$, displacive ferroelectric, effective charge determ. 80-97212
  $LiTaO_3$, ferroelec., displacive type phase transition, far IR reflection spectra 80-71339
  $LiTaO_3$, Fourier transform Ir spectroscopy of vibr. states at high temp. 80-97256
  $LiTaO_3$ high-temp. ferroelec. transition, soft mode IR reflectivity spectroscopy 79-33692
  $LiTaO_3$, near ferroelec. transition, elasticity, photoelasticity 78-88268
  $LiTaO_3$, paraelectric phase, soft vibr. modes, far IR refl. meas. 79-87407
  $LiTaO_3$, single crysts., temp. depend. of diffuse X-ray scattering intensity 79-61318
  $Mg_3B_7O_{13}Cl$, pyroelec. effect, spontaneous polarisation, domain struct. 77-8520
  $Mn_3B_7O_{13}Cl$ improper ferroelec., orthorhombic phase, Raman spectrum, lattice vibrs. 78-43849
  $(ND_4)_2BeF_4$ and $(NH_4)_2BeF_4$, incommensurate phase, ^{9}Be NMR study 80-75973
  $(ND_4)_2BeF_4$, ferroelec. transition, Raman spectra obs. *(Russian)* 78-23408
  $(ND_4)_2BeF_4$, incommensurate-commensurate phase transition and spontaneous polarisation 77-40192
  $ND_4D_2AsO_4$, protonic cond. near antiferroelec. Neel temp. 80-59703
  $ND_4D_2PO_4$ type ferroelecs., distrib. functions and thermodynamic props. 78-76409
  $(ND_4)_3D(SO_4)_2$, press.-temp. phase diagram 78-38834
  $(ND_4)_3D(SeO_4)_2$, phase transitions, isotope effect, dielectric and dilatometric meas. 79-38500
  $(ND_4)_2(SO_4)_3$, ferroelec. langbeinites, Raman scattering 80-34926
  $NH_4Al(SO_4)_2.12H_2O:Cr^{3+}$, zero-field fluctuations in Cr^{3+} near phase transition 77-28435
  $(NH_4)_2BeF_4$ crystal, macroscopic quadrupole moment anomalies in incommensurable phase *(Russian)* 79-65808
  $(NH_4)_2BeF_4$ crystals, incommensurate-commensurate phase transitions, optical props., at 177K 79-95733
  $(NH_4)_2BeF_4$, elastic compliance, US attenuation and piezo-coeffis., 170 and 190K 79-51918
  $(NH_4)_2BeF_4$, elastic props., US damping 80-84229
  $(NH_4)_2BeF_4$, far-infrared and submillimetre dielectric response 80-80782
  $(NH_4)_2BeF_4$, ferroelec. transition, Raman spectra obs. 77-85705
  $(NH_4)_2BeF_4$, ferroelectric, cryst. struct., phase transition, X-ray study 79-28689
  $(NH_4)_2BeF_4$, ferroelec., incommensurate struct., dynamic props. *(Russian)* 80-11373
  $(NH_4)_2BeF_4$, gamma-ray effects obs. *(Japanese)* 80-11349
  $(NH_4)_2BeF_4$, γ-irrad., trapped H atoms, ferroelec. transition, EPR meas. 79-4724
  $(NH_4)_2BeF_4$, incommensurate-commensurate transitions 78-60404
  $(NH_4)_2BeF_4$, incommensurate phase transitions under existence of Lifshitz invariant 79-15416
  $(NH_4)_2BeF_4$, Mandelstam-Brillouin and US exam. of phase transitions 77-12347
  $(NH_4)_2BeF_4$, phase transition into inhomogeneous modulated state, Landau theory 77-8527
  $(NH_4)_2BeF_4$, phase transition at 185K, X-ray scatt. obs. 77-36186
  $(NH_4)_2Cd_2(SO_4)_3$, ferroelec. langbeinites, Raman scattering 80-34926
  $(NH_4)H_2AsO_4$, $(NH_4)H_2PO_4$ and deuterated analogues, low temp. transition, thermal hysteresis, Cr impurity effect on transition temp. 80-2705
  $NH_4H_2AsO_4$, paraelec. phase, ^{75}As NMR linewidth, near transition temp. 77-36184
  $NH_4H_2AsO_4:Cr^{5+}$, fast and slow dynamic reorientation 78-80306
  $NH_4H_2AsO_4:Cr^{5+}$, antiferroelec. phase transition, EPR intensity and linewidth meas. 79-4721
  $NH_4H_2AsO_4$-$NH_4H_2PO_4$, AsO_4^{4-} centre, EPR central peak dynamics 79-33523
  $NH_4H_2PO_4$, ^{1}H spin-lattice relax. in paraelec. and antiferroelec. phases 79-33555
  $NH_4H_2PO_4$, antiferroelec., positron lifetime meas. during phase transitions 78-6644
  $NH_4H_2PO_4$, crystal, and deuterated cpd., optical meas. of phase transition point by domain obs. 77-40187
  $NH_4H_2PO_4$, electronic struct., UV reflection spectra and XPS 79-38558
  $NH_4H_2PO_4$, high temp. phase transition, IR spectra, differential 80-25319
  $NH_4H_2PO_4$, IR overtone spectra and temp. depend. 79-47456
  $NH_4H_2PO_4$, phase transition, phonon echo meas. *(French)* 78-6640
  $NH_4H_2PO_4$, powder sample, pyrocharge temp. depend. near phase transition 79-87399
  $NH_4H_2PO_4:AsO_4^{4-}(SeO_4^{3-})$, antiferroelec., low freq. fluctuations, isotope effects, EPR, ENDOR, ESCA 77-73118
  NH_4HSO_4, Brillouin shifts and linewidths 77-16322
  NH_4HSO_4, dielectric relax. in ferroelectric and paraelectric phases 77-16246
  NH_4HSO_4, ferroelec., press.-temp. phase diagram 77-85663
  NH_4HSO_4, ferroelec., critical slowing down of dielec. relax. *(Japanese)* 77-90109

ferroelectric transitions continued
  NH_4HSO_4, movement of NH_4^+ in all phases over 77 to 388K, NMR study 77-28524
  NH_4HSO_4, volume expansion, spontaneous strain, second order phase transitions 79-65224
  $NH_4HSO_4:VO^{2+}$, ferroelastic, inernal strains, ferroelec. transitions, EPR 79-47400
  NH_4HSO_4-type crystal, ferroelectric phase transform. model, SO_4 group ordering 77-77156
  $(NH_4)_3H(SO_4)_2$, movement of NH_4^+ in all phases over 77 to 388K, NMR study 77-28524
  $(NH_4)_3H(SO_4)_2$, phase transitions, sp. ht. meas. 80-2157
  $(NH_4)_3H(SO_4)_2$, phase transitions, dielec. study at low temps. 80-88902
  $(NH_4)_3H(SO_4)_2$, press.-temp. phase diagram, dielec. and DTA meas. 77-81067
  $(NH_4)_3H(SO_4)_2$, pressure-induced ferroelectricity, dielec. const. meas. 78-23412
  $(NH_4)_3H(SO_4)_2$, successive phase transitions, dilatometric and X-ray expts. 80-11348
  $((NH_4)_3H(SO_4)_2)_{1-x}[(ND_4)_3D(SO_4)_2]_x$ system, ferroelectric transitions 80-108160
  NH_4HSeO_4, cryst. struct., dielec. and ferroelec. props. 80-60528
  NH_4HSeO_4, ferroelec. phase transition, pyroelec. props. 80-60513
  NH_4HSeO_4, ferroelec., phase transitions, permittivity and pyroelectricity meas. 80-71350
  NH_4HSeO_4, para- to ferroelectric transition obs. by permittivity meas. 79-51916
  $(NH_4)_3H(SeO_4)_2$, ferroelec. phase transition, dielec. meas. 77-63376
  $(NH_4)_3H(SeO_4)_2$, press. and temp. effects on dielec. props. 78-23413
  NH_4IO_3, effect of hydrostatic press. on ferroelec. phase transition 79-51917
  NH_4IO_3, ferroelec., structural phase transition 80-7308
  NH_4IO_3, new ferroelectric materials *(Japanese)* 77-28529
  NH_4IO_3, phase transitions, SHG obs. 78-76398
  NH_4LiSO_4, ferroelec., phase transition points, hydrostatic press. effect 77-77155
  NH_4LiSO_4, hydrostatic press. effect on I-II phase transition, dielec. meas. 79-38496
  NH_4LiSO_4, I-II phase transition in improper ferroelec., hydrostatic press. effects 78-84533
  NH_4LiSO_4, new ferroelectric materials *(Japanese)* 77-28529
  NH_4LiSO_4, phase transforms., SHG obs. 78-76398
  NH_4NBeF_4, successive phase transitions, dielec. and optical props. obs. 80-50275
  $(NH_4)_{2(1-x)}Rb_{2x}SO_4$, mixed crystal, dielectric and US meas. of ferroelec. phase transition *(Japanese)* 80-7305
  $(NH_4)_2SO_4$, Brillouin scatt. from room temp. to −70°C 78-52517
  $(NH_4)_2SO_4$, dielec. props., 210-250K, 1 MHz-25 GHz 77-59541
  $(NH_4)_2SO_4$, e.s.r., of NH_3^+ and SeO_3^- radicals, ferroelec. transition obs. 77-16180
  $(NH_4)_2SO_4$ ferrielectric, X-ray anal. of sub-lattice order parameters 78-92035
  $(NH_4)_2SO_4$, ferroelec., ion group reorientation temp. and press. depend., PMR obs. 78-72470
  $(NH_4)_2SO_4$, ferroelec. transition, EPR study 79-38472
  $(NH_4)_2SO_4$, ferroelec. dispersion in microwave region, transition to ferrielectric structure 80-45016
  $(NH_4)_2SO_4$, microscopic model for ferroelectric phase transition 78-6641
  $(NH_4)_2SO_4$, paraelectric to ferroelectric phase boundaries 78-19426
  $(NH_4)_2SO_4$, paraelectric, N-quadrupole coupling meas. by proton-N double resonance 80-60459
  $(NH_4)_2SO_4$, phase transition mechanisms by optical spectroscopy 79-15411
  $(NH_4)_2SO_4$, phase transition theory 79-24275
  $(NH_4)_2SO_4$, powder sample, pyrocharge temp. depend. near phase transition 79-87399
  $(NH_4)_2SO_4$, pure and Rb doped, ferroelec. transition, light scatt. meas., dielec. and elastic props. 78-43822
  $(NH_4)_2SO_4:Cd^+$, ferroelec. transition, soft mode contrib., EPR obs. 78-72469
  $(NH_4)_2SO_4:Cr^{5+}$, EPR study of ferroelec. phase transition 78-64337
  $(NH_4)_2SO_4:Cu^{2+}$, ferroelec. transition, ESR study 79-91286
  $(NH_4)_2SO_4:SeO_3^-$, γ-irrad., hyperfine interaction, ferroelec. transition effects, EPR expt. 78-15024
  $(NH_4)_2SO_4:VO^{2+}$, ferrielectric phase transition, two-sublattice model, EPR of polar VO^{2+} probes 78-48127
  $(NH_4)_2SO_4$-type crystals, ferroelastic, ferrielectric, and incommensurate phase transitions *(Japanese)* 79-65811
  $(NH_4)_2ZnCl_4$, commensurate-incommensurate phase transition, ^{35}Cl NQR study 80-75966
  $(NH_4)_2ZnCl_4$, ferroelectricity and incommunsurate-commensurate phase transitions 80-60523
  $(Na,Li)NbO_3$, ceramics, electrophys. and struct. props. near morphotropic transition 78-2816
  $NaAl(MoO_4)_2$, domain struct., phase transition, and dielec. props. 79-56748
  $Na_9(Al_6Si_6O_{24})(OH)_2.6H_2O$, hydrosodalite, ferroelec. transition, pyro- and piezoelec. activity 79-15421
  $Na_{0.5}Bi_{0.5}TiO_3$, dielectric const. thermal hysteresis, ferroelectric-antiferroelectric transitions 80-50281
  $Na_{0.5}Bi_{0.5}TiO_3$, phase transition, hysteretic behaviour 80-71330
  NaCN, lattice dynamics and order-disorder transitions, neutron scatt. expts. 78-14434
  NaCN, optical F centres and phase transitions 78-56504
  $Na(D_xH_{1-x})_3(SeO_3)_2$, Raman spectra and nature of phase transitions 78-80341
  $NaD_3(SeO_3)_2$, ^{23}Na NQR, second-order quadrupole shift, temp. depend. 78-15055
  $NaD_3(SeO_3)_2$, polarised Raman spectra, lattice vibrs., ferroelec. transition 77-24851
  $NaFe(MoO_4)_2$, domain struct., phase transition, and dielec. props. 79-56748
  $Na(H_{1-x}D_x)_3(SeO_3)_2$, ferroelectric, dielectric behaviour at RF and microwave freq. 79-33640
  $NaH_3(SeO_3)_2$, β to δ ferroelec. transition under press. Raman spectra study 80-80725
  $NaH_3(SeO_3)_2$, dielec. props. 78-43764
  $NaH_3(SeO_3)_2$, dynamics of α-β transition, Brillouin scatt. meas. 77-8526

ferroelectric transitions continued
$NaH_3(SeO_3)_2$, ferroelec., proton motion within H bonds, neutron scatt. study 80—75986
$NaH_3(SeO_3)_2$, high-pressure phase transform., ^{23}Na NMR obs. 77—63380
$NaH_3(SeO_3)_2$, $NaD_3(SeO_3)_2$, IR and Raman spectral interpretation of ferroelectric phases 79—24312
$NaH_3(SeO_3)_2$, phase transition, pyroelec. current meas. 79—82934
$NaH_3(SeO_3)_2$, proton behaviour in H-bonding, neutron spectroscopy obs. *(German)* 78—22816
$NaH_3(SeO_3)_2$, proton spin lattice relaxation 79—78557
$NaH_3(SeO_3)_2{:}Cr^{3+}$, deuterated, phase transitions, EPR 77—48135
$(Na_{0.5}La_{0.5})_xBa_{1-x}TiO_3$, dielec. and IR spectra exam., ferroelec. transition 78—23418
$Na_{1-x}Li_xNbO_3$, dielec. const. and X-ray diffr., for Curie temp. and phase diagrams 78—72768
$Na_{1-x}Li_xNbO_3$ mixture, ferroelec.-paraelec. transitions, dielec. props. meas. 80—66125
$NaND_4C_4H_2D_2O_6.4D_2O$, ferroelec. phase, incommensurate satellite refls. 78—84531
$NaND_4SeO_4.2D_2O$, nonlinear electromechanical props. above Curie temp. 79—33610
$NaNH_4SeO_4.2H_2O$, crystal struct. in ferroelec. phase, nature of transition 77—43946
$NaNH_4SeO_4.2H_2O$, model of ferroelec. phase transition 78—19433
$NaNH_4SeO_4.2H_2O$, ferroelectric phase transition mechanism 78—31162
$NaNH_4SeO_4.2H_2O$, ferroelectric crystal, effect of hydrostatic pressure on phase transition 78—52453
$NaNH_4SeO_4.2H_2O$, atomic struct. exam. and phase transition 79—37678
$NaNO_2$, ^{23}Na elec. field gradient tensor from NMR satellite lines near phase transition 80—71191
$NaNO_2$, 163°C phase transition, thermal history effects on range of modulated struct. 78—95563
$NaNO_2$, adiabatic and isothermal elastic compliances, critical behaviour 78—92031
$NaNO_2$, complex dielectric constant, sinusoidal phase in ferroelectric material 79—11376
$NaNO_2$, compressed powder, dielec. props., surface layer effects 78—76413
$NaNO_2$, crit. dynamics, nuclear relax. 78—75805
$NaNO_2$, crit. X-ray scatt. 79—33636
$NaNO_2$, elastic constants and US attenuation coeffs., anisotropic charact. 78—63809
$NaNO_2$, electrostrictive constants, isothermal and adiabatic, in antiferroelec. transition region 77—12317
$NaNO_2$, ferroelec., dielec. and thermal behaviour 80—80680
$NaNO_2$, ferroelec., electric field gradient *(Korean)* 79—15419
$NaNO_2$, ferroelectric, second-order vibr. spectra and dispersion of phonon branches 79—69847
$NaNO_2$, ferroelectric transitions, based on model thermodynamic pot. 78—80295
$NaNO_2$, ferroelectric transitions, group theoretic comparison with $AgNaNO_2$ 80—7311
$NaNO_2$, incommensurate phase transitions 78—26653
$NaNO_2$, incommensurate phase transition, Bethe-Peierls and mol. field approx. 80—20599
$NaNO_2$, incommensurate-and-antiferroelectric phase transition, amplitude mode, ultrasonic study 80—39227
$NaNO_2$, lattice dynamics, two-phonon Raman scatt. and IR absorpt. 79—33684
$NaNO_2$, mechanism of ordering type ferroelec. transition, vibr. spectroscopy 78—76402
$NaNO_2$, mechanism of order-disorder transition, opt. spectra 78—76403
$NaNO_2$, NMR of ^{23}Na small particles 79—28629
$NaNO_2$, NQR of ^{14}N at ferroelec. transition, order-disorder fluctuations 77—63311
$NaNO_2$, one-mode model 80—29702
$NaNO_2$, optical harmonic generation near ferroelec. transition 80—91858
$NaNO_2$, phase transition into inhomogeneous modulated state, Landau theory 77—8527
$NaNO_2$, phase transitions accompanied by noncommensurate superstruct. form. 77—32336
$NaNO_2$, positron lifetimes, ferro-paraelectric transition 79—74017
$NaNO_2$, rot. behaviour of NO_2 radicals in order-disorder transition, Fourier synthesis study of neutron data 79—56739
$NaNO_2$, second order phase transition prod. by strain 79—15420
$NaNO_2$, X-ray crit. scatt. 78—52461
$NaNO_2{:}Mn^{2+}$, ferroelectric phase metastable struct., EPR obs. 78—60328
$NaNO_2{:}Mn^{2+}$, zero-field splitting, ferroelec. soft-mode contrib., phase transition, EPR obs. 79—15344
$NaNO_3$, press. induced ferroelec. transition, soft mode dynamics, Raman scatt. meas. 78—72475
$NaNO_3$, soft mode dynamics at ferroelec. transition 78—80308
$NaNbO_3$, antiferroelec., primary order parameter, X-ray scatt. 79—51919
$NaNbO_3$, birefr., temp. depend., behaviour at $P \rightleftarrows N$ struct. transition 78—64331
$NaNbO_3$, elec. and photoelec. props. near ferroelec.-antiferroelec. phase transition 80—15989
$NaNbO_3$, ferroelec., local field determ., phase transition study by EPR 79—38471
$NaNbO_3$, hydrostatic press. effect on permittivity, phase transition, hysteresis 80—80670
$NaNbO_3$, memory effect, in ferroelec. phase, ESR meas. 79—28696
$NaNbO_3$, perovskite structure, semiconductor props. *(Polish)* 78—56437
$NaNbO_3$, photoferroelectric effect 78—35108
$NaNbO_3$, thermoelec. effect and phase transitions 78—48123
$NaNbO_3$-based ferroelec. solid solns., morphotropic transitions and elec. props., enhanced vacancy conc. 80—55048
$Na_4R(WNb_2)O_9F_5$, (R=Y, Nd, Eu, Gd, Dy, Lu), synthesis, cryst.-chem. and dielec. study *(French)* 80—108164
$NaVO_3$, thermal expansion and ferroelec. phase transition 79—38482
$Na_5W_3O_9F_5$, single cryst., prep., optical and dielec. studies *(French)* 80—15994
$Nd(BrO_3)_3.9H_20$, single cryst. low-temp. pyroelectricity 79—42906
Ni-I single crystals, mag. and dielectric props. 80—93095
$Ni_3B_7O_{13}Br$, cubic, approx. nonlinear optical susceptibility 80—78904
$Ni_3B_7O_{13}Br$, ferroelec. 43m-mm2 phase transition, molar heat capacity meas. 80—93249
$Ni_3B_7O_{13}Cl$, specific heat anomaly at $F43c \rightarrow Pca2_1$ transition 79—28690

ferroelectric transitions continued
$Ni_3B_7O_{13}I$, dynamics of ferroelec. phase transition, Raman spectra obs. 79—33630
$Ni_3B_7O_{13}I$, Raman spectra in paraelec. phase 78—60434
$Ni_3B_7O_{13}I$, shear modulus anomalous temp. depend. 78—43061
$Ni_3B_7O_{13}I$, struct. and mag. transitions, light scatt. study 79—24308
O^{2-} polarisability rel. to ferroelec. phase transitions 80—71326
PLZT ceramic, ageing, dielec. props. 80—88940
PLZT ceramics, diffuse phase transitions and thermodynamics 80—29694
PLZT ceramics, ferroelectric and struct. transitions, crystallographic, thermal, and dielec. anal. 80—29693
PLZT ceramics, phase transitions induced by elec. fields 80—29695
PLZT ceramics, SHG, anomalous phase transition 79—45996
PLZT ceramics, stress-induced ferrelec. transition, pseudoelasticity and shape memory, bending meas. 79—24274
PLZT, diffuse phase transitions, Curie temp., dielectric props. 80—75979
PLZT, ferroelectric phase transitions, phase state identification 80—45018
PLZT, phase transitions, permittivity, birefr. and light scatt. meas. 77—81074
PLZT type ceramics, variation of light scatt. during field induced AF→F transition *(French)* 77—90158
PLZT type ceramics, calorimetric meas. of energy of electrical polarisation 79—2770
PLZT, with broad phase transition, birefr., electro-optic and dielec. props. 77—16280
$(Pb,Ba)(Zr,Ti)O_3$, diffuse phase transitions, Curie temp., dielectric props. 80—75979
$(Pb,La)TiO_3$, soft E(TO) phonons, and phase transitions, Raman spectra, −200 to 400°C 78—15109
(Pb, Sn)Te-type semiconductors, displacive ferroelec. phase transitions, vibronic theory 80—11354
$(Pb,Sr)TiO_3$, ferroelec. solid solution, dielec. nonlinearity in nonpolar phase *(Russian)* 77—32317
Pb ternary oxides, antiferroelec., growth and props. 79—38461
$(Pb_{1-x}Ba_x)_5Ge_3O_{11}$, ferroelec. phase transition, dielec. const. and quasi-elastic light scatt. 80—71289
$Pb_{5-x}Ba_xGe_3O_{11}$, Raman spectra, temp. depend. of ferroelec. soft A-mode 79—33682
$(Pb_xBa_{1-x})_5Ge_3O_{11}$, electrogyration, and dielectric props. 78—19444
$(Pb_{1-y}Ba_y)_{1-x}La_xNb_{2-x/5}O_6$, ferroelec., phase transitions 79—38487
$Pb_{0.94-x/2}Ba_{0.6}Nb_xZr_{1-x}O_3$, Nb dopant morphology effect on microstructure 80—81005
$Pb_{1-x}Be_xTe$, anomalous resist. near ferroelec. phase transition 80—20196
$(Pb_{1-x}Bi_x)_5Ge_3O_{11}$, spontaneous and induced electrogyration 79—42946
Pb_2CoWO_6, antiferroelectric substruct. 79—38489
Pb_2CrO_5, thermal X-ray and dielec. investigations, antiferroelec. phase transition 79—47403
PbF_2, phonon energy dispersion relations 78—79697
$2PbFe_{1/2}Nb_{1/2}O_3$-Pb_2FeReO_6, comp., struct., dielec. and mag. props. 80—2704
$Pb(FeTa)_{1/2}O_3$, Mossbauer spectra, 78-480K 79—51885
$2PbFe_{1/2}Ta_{1/2}O_3$-Ba_2FeReO_6, comp., struct., dielec. and mag. props. 80—2704
$2PbFe_{1/2}Ta_{1/2}O_3$-Pb_2FeReO_6, comp., struct., dielec. and mag. props. 80—2704
$Pb(Fe_{2/2}U_{1/3})O_3$-$PbZrO_3$ solid solns., phase transition 77—48138
$Pb(Fe_{2/3}W_{1/3})O_3$-$Pb(M_{3/2}W_{1/2})O_3$, (M-Mn, Co, Ni), ferroelec. phenomenological theory 79—99831
$Pb_3(Ge,Si)_2O$, growth from melt, struct. and dielec. props. 77—44148
$Pb_3Ge_3O_{11}$, uniaxial ferroelec., thermal expansion and dielec. permittivity in vicinity of transition points 77—66459
Pb_5GeO_{11}, induced and spontaneous optical activity, permittivity 79—33661
$Pb_5Ge_2O_{11}$ acoustic relax. assoc. with phase transition at hypersonic freq. 78—88267
$Pb_5Ge_3O_1$, anharmonic phonons and central peaks at struct. phase transitions 79—95775
$Pb_5Ge_3O_{11}$ acoustic relaxation near ferroelectric transition 78—2814
$Pb_5Ge_3O_{11}$, anharmonic effects in low freq. symm. modes, Raman study 80—25365
$Pb_5Ge_3O_{11}$ crystal, luminesc. under pulse polarisation switching conditions near ferroelec. transition 77—1735
$Pb_5Ge_3O_{11}$, dielec. behaviour, 60 Hz-100 kHz, particle size effects 79—33638
$Pb_5Ge_3O_{11}$, dielec. functions above and below ferroelec. transition 79—33588
$Pb_5Ge_3O_{11}$, dynamic central peaks and phonon interactions near structural phase transitions 78—83903
$Pb_5Ge_3O_{11}$, electrogyration during phase transitions 79—19859
$Pb_5Ge_3O_{11}$, ferroelec. phase transition, for IR transmission meas. 79—38478
$Pb_5Ge_3O_{11}$, ferroelec. transition, US and elasto-optic props. 80—60527
$Pb_5Ge_3O_{11}$, ferroelectric transition exam. by Raman scatt. 78—56439
$Pb_5Ge_3O_{11}$, ferroelectric soft mode exam., Raman spectra 79—42202
$Pb_5Ge_3O_{11}$, freq. and damping of ferroelec. soft mode, permittivity meas. 77—52027
$Pb_5Ge_3O_{11}$, lattice dynamics parameters anisotropy, X-ray diffr. study 80—59612
$Pb_5Ge_3O_{11}$, light scatt. meas., central peak dynamics at ferroelectric transition 77—4606
$Pb_5Ge_3O_{11}$, paraelectric and ferroelectric, Raman spectra near ferroelectric transition 80—55090
$Pb_5Ge_3O_{11}$, Raman scatt., soft modes and damping near structural phase transition 79—28739
$Pb_5Ge_3O_{11}$, Raman spectrum factor group anal., external and librational modes 77—36240
$Pb_5Ge_3O_{11}$, single crysts., photoemission anamoly during ferroelectric phase transitions 79—47599
$Pb_5Ge_3O_{11}$, struct. of paraelec. phase, neutron diffr. meas., rel. to phase transition mechanism 77—84720
$Pb_5Ge_3O_{11}{:}Gd^{3+}$, ferroelec. transition, temp. depend., EPR study 80—66127
$Pb_5(Ge_{1-x}Si_x)_3O_{11}$, dielec. spectra, ferroelec. behaviour 78—60406
$Pb_5(Ge_{1-x}Si_x)_3O_{11}$, electrogyration, phase transition and dielectric props. 80—93269
$Pb_5(Ge_{1-x}Si_x)_3O_{11}$, ferroelec. soft mode, temp. and Si impurity, effects Raman scatt. 79—1762
$Pb_5(Ge_{1-x}Si_x)_3O_{11}$ solid solutions, dielec. props., ferroelec. phase transitions 80—15988

ferroelectric transitions continued
$Pb_5Ge_{3-x}Si_xO_{11}$, ferroelec. soft mode, temp., press. and comp. depend. 78—80304
$Pb_5Ge_{3-x}Si_xO_{11}$, ferroelec. phase transition, for IR transmission meas. 79—38478
$Pb_{1-x}Ge_xTe$, degenerate semiconducting ferroelectric, structural phase transition temp., mag. field effects 80—45017
$Pb_{1-x}Ge_xTe$, dielec. const. determ. near ferroelec. transition 78—88269
$Pb_{1-x}Ge_xTe$, electron-phonon interaction effect on ferroelec. transition 78—76416
$Pb_{1-x}Ge_xTe$, ferroelec. phase transition, IR refl. and resist. meas. 80—11353
$Pb_{1-x}Ge_xTe$, ferroelec. constants, C-V and C-T characts. of abrupt p-n junctions 80—25323
$Pb_{1-x}Ge_xTe$, ferroelectric phase transition effect on forbidden band width 80—24794
$Pb_{1-x}Ge_xTe$, p-n junctions, elec. characts., effect of ferroelec. phase transition 79—33338
$Pb_{1-x}Ge_xTe$, phase transitions 78—60408
$PbHAsO_4$, ($PbDAsO_4$), Raman spectra of ferroelec. transition proton tunnelling 78—23410
$PbHAsO_4$, ferroelec., far IR and submillimetre dielec. dispersion 79—38528
$PbH(D)PO_4$, $PbH(D)AsO_4$, ferroelectric, sp. ht. 79—19853
$PbHPO_4$, crystals, ferroelec. phase transition, hydrostatic press. influence, dielec. meas. 80—88936
$PbHPO_4$, ferroelec. phase transition, Brillouin and Raman spectra obs. 79—33683
$PbHPO_4$, ferroelec., far IR and submillimetre dielec. dispersion 79—38528
$PbHPO_4$, microwave permitt. and far IR refl. spectra in paraelec. and ferroelec. phases 80—40033
$PbHPO_4$, neutron diffr. exam. of struct. at room temp. 79—38490
$PbHPO_4$, optical props. near ferroelec. transition 79—33663
$PbHPO_4$, phase transitions study, role of cryst. struct. determ. 80—75197
$PbHPO_4$, protonic order-disorder transition 78—26478
$PbHPO_4$, Raman spectra study of ferroelec. transition, proton tunnelling 78—23410
$PbHPO_4$, single cryst., growth, optical props., ferroelec. transition 78—35285
$PbHPO_4$-type crystals, statistical model 80—25321
$PbHfO_3$, antiferroelectric-ferroelectric phase transition in strong elec. field 80—15990
$PbHfO_3$, elec. field gradient, crit. behaviour, DPAC meas. 78—80303
$PbHfO_3$, elec. quadrupole interaction, temp. depend., DPAC meas. 79—51884
$PbHf_{1-x}Ti_xO_3$, phase diagram, influence of poling treatment, ferroelec. antiferroelec. transition *(French)* 77—63374
$PbIn_{0.5}Nb_{0.5}O_3$, ferroelectric, dielectric props. 80—103923
$Pb_{0.27}K_{0.56}Nb_{0.91}Ta_{4.15}O_{15}$, coupled ferroelastic-ferroelectric props. 77—59543
$Pb_{2.07}K_{0.56}Nb_{0.91}Ta_{4.15}O_{15}$, tetragonal tungsten bronze type, ferroelastic-ferroelectric coupling *(French)* 77—28522
$Pb_{0.9}K_{0.1}(Zn_{1/3}Nb_{2/3})O_{2.95}$-$PbZrO_3$-$PbTiO_3$, morphotropic tetragonal-rhombohedral phase boundary 78—48129
$Pb_{0.97}La_{0.02}(Zr_{0.92}Ti_{0.08})O_3$, ferroelec. ceramic, stress effects 80—2119
$Pb_2Li_{1/2}Nb_{3/2}O_6$, antiferroelec. cryst. growth and props. 77—36189
Pb_2MTeO_6, (M=Ca,Cd,Mg), ferroelec. behaviour, microwave dielec. props. meas. 77—43948
$PbMg_{1/3}Nb_{2/3}O_3$, and its solid solns., low temp. phase transition obs. 79—69788
$PbMg_{1/3}Nb_{2/3}O_3$, carrier mobility and photoluminesc. near ferroelec. transition *(Russian)* 78—2813
$PbMg_{1/3}Nb_{2/3}O_3$, cathodlum. spectral and temp. depend. 78—84665
$PbMg_{1/3}Nb_{2/3}O_3$, crit. electron-phonon phenomena and diffuse phase transition in elec. field 79—38497
$PbMg_{1/3}Nb_{2/3}O_3$, dielec. props. under high hydrostatic pressure near phase transition point 80—44997
$PbMg_{1/3}Nb_{2/3}O_3$, photoinduced phenomena at diffuse phase transition 78—43814
$PbMg_{1/3}Nb_{2/3}O_3$, photolum. near ferroelec.-paraelec. phase transition 80—16100
$PbMg_{1/3}Nb_{2/3}O_3$, photolum. and carrier drift mobility at ferroelec. transition 80—71469
$PbMg_{1/3}Nb_{2/3}O_3$ single cryst., electro-optical hysteresis curves and phase transitions *(German)* 79—28717
$PbMg_xNb_{1-x}O_3$, ferroelec. with diffuse phase transition, electrostriction-optical props. 78—68457
$Pb_3MgNb_2O_9$ diffuse phase transition, Brillouin scatt. and acoustic phonons 78—76401
$PbNb_2O_6$, permittivity and elec. cond. meas., first order transition 79—24270
$PbNb_2O_6$-$NaNbO_3$, DTA *(French)* 77—44234
$Pb_{0.99}Nb_{0.02}(Zr_{0.95}Ti_{0.05})_{0.98}O_3$, ferroelec. ceramic, stress effects 80—2119
PbO_x, photoconducting, phase transitions, occurrence of ferroelectricity, pyrocurrent obs. 79—11395
Pb_3O_4, IR and Raman study of structural phase transitions *(French)* 78—84582
$Pb_5S_2I_6$, ferroelec., synthesis and hydrothermal growth 79—38731
$PbSc_{0.5}Nb_{0.5}O_3$, single cryst., dielec. props. 80—66126
$Pb(Sc_{0.6}Ta_{0.5})_3$ ceramics, ordering and diffuse phase transitions 80—29699
$Pb_{0.56}Sn_{0.44}Te$, press. induced ferroelec. phase transition 79—65809
$Pb_{1-x}Sn_xTe$, anomalous resist. near ferroelec. phase transition 80—20196
$Pb_{1-x}Sn_xTe$, ferroelec. phase transition, hybridization effect *(Russian)* 79—61319
$Pb_{1-x}Sn_xTe$, soft mode, ferroelec. phase transition crit. temp. and dielec. const. calcs. 77—8530
$Pb_{0.95}Sr_{0.05}(Ti_xZr_{1-x})O_3$, solid solns., parameters of Curie Weiss law, permittivity meas. 78—15129
$(Pb_{0.97}Sr_{0.03})Zr_{0.51}Ti_{0.49}O_3$, ferroelec. phase transition under high press. 77—36188
$Pb_{0.95}Sr_{0.05}(Zr_{0.53}.Ti_{0.47})O_3$, low temp. internal friction in ferroelectric ceramic 77—21200
PbTe-SnTe compound semiconductors, lattice instability by mm-wave magnetoplasma refl. 80—54336
$Pb(Ti,Zr,[Fe_{1/2}Ta_{1/2}])O_3$, pyroelec. props. at transition between ferroelec. phases 78—52447
$Pb(Ti,Zr)O_3$, pyroelectric props., addition effects 79—33608
$Pb(Ti,Zr)O_3$, soft E(TO) phonons, and phase transitions, Raman spectra, −200 to 400°C 78—15109

ferroelectric transitions continued
$PbTiO_3$, anomalies in elec., photoelectric and mechanical props. 80—55051
$PbTiO_3$, damping of soft E-symmetry phonon, Raman scatt. meas. 78—67799
$PbTiO_3$, domain struct. formation during jump motion of phase front 78—64339
$PbTiO_3$, domain struct., formation at phase transitions 79—38510
$PbTiO_3$, perovskite structure, semiconductor props. *(Polish)* 78—56437
$PbTiO_3$, phase transition study by X-ray powder structural refinement 80—40075
$PbTiO_3$, photolum. and carrier drift mobility at ferroelec. transition 80—71469
$PbTiO_3$, tetragonal deform. of TiO_6 octahedron 77—55759
$PbTiO_3$, thermoelectric effect and ferroelectric transition 78—48123
$PbTiO_3$-$PbZrO_3$-based multicomponent ferroelec. solid solns., morphotropic transitions and comp.-temp. phase diagrams 80—55047
$PbTi_{1-x}Zr_xO_3$, low freq. vibrational modes and ferroelec. transitions 79—33637
$Pb(Ti_{1-x}Zr_x)O_3$, thermodynamic anal. of phase transitions 78—19431
$Pb(Zn_{1/3}Nb_{2/3})O_3$, diffuse phase transition, electro-optical and dielec. obs. 79—82933
$Pb(Zr,Ti,Ge)O_3$, antiferro-ferroelectric transition 78—95565
$Pb(Zr, Ti)O_3$, ceramics in solid matrix, high pressure effect on dielectric props. 77—16259
$Pb(Zr,Ti)O_3$, doped, Goldschmidt factors and ferroelec. antiferroelec. transition 77—12332
$Pb(Zr,Ti)O_3$, ferroic materials, fracture processes 80—79869
$Pb(Zr,Ti)O_3$, order of ferroelec. paraelec. transition 77—12333
$Pb(Zr,Ti)O_3$, shock wave compressed, dielec. props. 77—48139
$Pb(Zr,Ti)O_3$ solid solutions, elec. and thermoelec. props. appl. *(Polish)* 77—28203
$Pb(Zr,Ti)O_3$, temp. and hydrostatic press. depend of vibr. modes, rel. to phase transforms 77—89510
$Pb(Zr,Ti)O_3$, thin film evaporated on stainless steel, photovoltaic effect 79—4580
$Pb(Zr,Ti)O_3$ thin film, ferroelec., fabrication by RF sputtering *(Japanese)* 80—25560
$Pb(Zr,Ti)O_3$, X-ray study in tetragonal-rhombohedral phase-transition composition area 79—42921
$Pb(Zr,Ti)O_3$:$PbTiO_3$ (up to 5%), dielec. props. and ferroelec. transitions 77—20806
$PbZrO_3$ based ceramic, press. induced ferroelec. to antiferroelec. transition 79—24273
$PbZrO_3$ crystal, structural phase transitions in very high elec. fields 80—15987
$PbZrO_3$, electric field induced phase transitions, 20 to 160°C 77—43947
$PbZrO_3$, perovskite structure, semiconductor props. *(Polish)* 78—56437
$PbZrO_3$, phase transitions, X-ray, dielec., and thermal anal. 80—45020
$PbZrO_3$, struct. phase transition 79—61312
$PbZrO_3$, structural phase transition in super high elec. fields 79—33626
$PbZrO_3$, thermoelec. effect and phase transitions 78—48123
$PbZrO_3$-monocryst., elec. cond., permittivity, polarisation, para- and ferro-to antiferroelec. phase transistions 78—60402
$PbZrO_3$-Pb_2FeNbO_6-$PbTiO_3$, pyroelectric props. of ferroelec. rhombohedral transition 77—12336
$PbZrO_3$-$PbCd_{0.5}W_{0.5}O_3$, phase transitions 78—43817
1-x$PbZrO_3$-x$PbSc_{0.5}Nb_{0.5}O_3$, $0 \leq x \leq 1$, phase transitions, X-ray, dielec., and thermal anal. 80—45020
$Pb(Zr_{0.52}Ti_{0.48})O_3$, polycrystalline ferroelectric, grain-size dependent props. 80—71352
$PbZr_{0.95}Ti_{0.05}O_3$:oxide doped, A and B site dopant distrib., antiferroelec.-ferroelectric transition 78—34532
$PbZr_{1-x}Ti_xO_3$:Nb_2O_5 ceramic, ferroelec. transitions, polarisation meas. *(French)* 80—66124
$PbZr_xTi_{1-x}O_3$ ceramics, morphotropic phase boundary 80—81035
$Pb(Zr_xTi_{1-x})O_3$, elec. props. effect of proportional composition, morphotropic phase boundary 78—35105
$PbZr_xTi_{1-x}O_3$, ferroelec. phase transition under high press. 79—99833
$PbZr_xTi_{1-x}O_3$ solid solutions, tricritical behaviour 78—80296
$PrCl_3$, cooperative Jahn-Teller ordering of elec. dipoles in non-Kramers doublets 78—15115
$PrCl_3$, one and three dimensional antiferroelec. ordering 77—4607
$RbCaF_3$, sp. ht. anomaly at struct. transform. 78—14426
$RbCdCl_3$, birefringence, twinning and structural phase transitions 79—38480
$RbCdCl_3$, n.q.r. spin-lattice relax. near cubic-tetragonal transition, soft modes 77—1616
$Rb_2Cd_2(SO_4)_3$, ferroelec., X-ray study on phase transition 77—85665
$Rb_2Cd_2(SO_4)_3$, pyroelectric and dielectric props., ferroelectric transitions 79—38458
$RbD_3(SeO_3)_2$, DMR, electric quadrupole coupling, ferroelec. transition 79—91312
$RbD_3(SeO_3)_2$, incommensurate nature of intermediate phase, neutron diffr. obs. 80—50276
$RbD_3(SeO_3)_2$, phase transform., inelastic neutron scatt. study 78—39514
$Rb(H,D)_3(SeO_3)_2$, improper ferroelec. phase transition, anomalous elastic props. 79—33634
RbH_2AsO_4, ferroelec., attenuation of LF elastic oscills. 77—7791
RbH_2AsO_4 ferroelec. cryst., internal friction, torsion pendulum obs. 78—72474
RbH_2AsO_4, phase transition, dielec. pyroelec. and internal friction meas. 77—16261
RbH_2AsO_4, Raman scatt. near T_c, search for soft modes 78—15114
RbH_2PO_4, acoustic longit. mode coupling to order parameter and effect on ferroelec. phase transition 79—51914
RbH_2PO_4, critical and tricritical phenomena, susceptibility, exponents 80—75976
RbH_2PO_4, electro-optic props. near ferroelec. transition 78—19445
RbH_2PO_4, ferroelec., attenuation of LF elastic oscills. 77—7791
RbH_2PO_4, ferroelec. cryst., internal friction, torsion pendulum obs. 78—72474
RbH_2PO_4, ferroelec. phase transition, birefringence studies 80—108162
RbH_2PO_4, ferroelectric, US propag. near ferroelectric phase transition temp. 78—23417
RbH_2PO_4, ferroelectric-ferroelastic phase transition, γ-ray diffr. 78—43819
RbH_2PO_4, high press. phase diagram 78—52457
RbH_2PO_4, IR overtone spectra and temp. depend. 79—47456
RbH_2PO_4, longit. US wave propag. near ferroelectric phase transition temp. 78—84536

ferroelectric transitions continued
- RbH$_2$PO$_4$, phase transitions study, role of cryst. struct. determ. 80—75197
- RbH$_2$PO$_4$ powder, phase transition in paraelectric (upper) phase by measuring damping const. and amplitude of phonon echoes 79—19855
- RbH$_2$PO$_4$, Raman scatt. near T_c, search for soft modes 78—15114
- RbH$_2$PO$_4$, static dielec. props., and Curie temp., press. depend. 79—87405
- RbHSO$_4$, acoustic and dielectric props. near phase transition 80—55053
- RbHSO$_4$, anisotropy of US anomaly near ferroelec. phase transition 78—72473
- RbHSO$_4$, dielec. dispersion near ferroelec. phase transition 80—2684
- RbHSO$_4$, ferroelec. phase transition, US attenuation and velocity 78—39511
- RbHSO$_4$, phase transition, sp. ht. and dielec. permittivity meas. 77—85672
- RbHSO$_4$, volume expansion, spontaneous strain, second order phase transitions 79—65224
- Rb$_3$H(SO$_4$)$_2$, and Rb$_3$D(SO$_4$)$_2$, dielec. props. and phase transitions 80—60482
- Rb$_3$H(SO$_4$)$_2$, phase transitions at 56°C and 126°C, dielec. const. meas. 78—76405
- RbHSeO$_4$, ferroelec. props. and domain struct. 79—78637
- RbHSeO$_4$, ferroelec. phase transition, X-ray study 80—7309
- RbHSeO$_4$, ferroelec., far IR spectra 80—71404
- RbHSeO$_4$, successive phase transitions 80—15985
- RbH$_2$(SeO$_3$)$_2$, improper ferroelectric phase transformation, neutron scattering study 78—80302
- RbH$_3$(SeO$_3$), ferroelectric phase transition, Raman spectra meas. 79—19871
- RbH$_3$(SeO$_3$)$_2$, ^{87}Rb NMR, elec. field grad. temp. depend. 79—78536
- RbH$_3$(SeO$_3$)$_2$ crystal, incommensurable phase, quadrupole moment study 80—97213
- RbH$_3$(SeO$_3$)$_2$, crystal lattice monoclinic distortion determ. by phase transition from elec. meas. results 79—73887
- RbH$_3$(SeO$_3$)$_2$, dielec. relax. near ferroelec. Curie temp. 80—97207
- RbH$_3$(SeO$_3$)$_2$, ferroelec. phase transition, X-ray study 79—38479
- RbH$_3$(SeO$_3$)$_2$, order parameter 77—66460
- RbH$_3$(SeO$_3$)$_2$, phase transitions, elastic compliance temp. depend. 77—90116
- RbH$_3$(SeO$_3$)$_2$, piezoelectric effect, near nonintrinsic ferroelectric phase transition 78—2815
- RbH$_3$(SeO$_3$)$_2$, repolarisation in region of improper ferroelec. phase transition 77—8497
- RbH$_3$(SeO$_3$)$_2$, thermodynamic theory of phase transitions 77—90112
- RbH$_3$(SeO$_3$)$_2$, US vel. and absorpt. near ferroelec. Curie temp. 80—97206
- Rb$_3$KMO$_3$F$_3$, (M = MO, W), low temp. phase transitions *(French)* 78—92036
- RbLiSO$_4$, field induced ferroelec. phase 79—78633
- RbLiSO$_4$, new ferroelectric materials *(Japanese)* 77—28529
- RbLiSO$_4$, successive struct. transitions, X-ray diffr. 80—10521
- RbLiSO$_4$, thermal and dielectric props., ferrielectricity 79—28688
- RbMnCl$_3$, birefringence, twinning and structural phase transitions 79—38480
- Rb$_3$MoO$_3$F$_3$, ferroelec., phase transitions, crystallographic, DTA, dielec. and pyroelec. meas. *(French)* 77—85671
- Rb$_3$MoO$_3$F$_3$, ferroelec. and order-disorder phase transitions 78—92037
- RbNH$_4$SO$_4$, ferroelec., ion group reorientation temp. and press. depend., PMR obs. 78—72470
- RbNO$_3$, permittivity and dielec. cond. press. up to 5 kbar, antiferroelec. transition obs. 77—36183
- RbNO$_3$, single cryst., DC cond., dielec. and thermophys. props., temp. depend., transitions interpret. 78—26682
- RbNbW$_2$O$_9$ crysts., growth and props. 80—104054
- Rb$_2$SO$_4$-(NH$_4$)$_2$SO$_4$ mixed cryst., ferroelec. transition, structural and dielec. props., proton spin-lattice relax. 78—39512
- Rb$_3$WO$_3$F$_3$, ferroelec. and order-disorder phase transitions 78—92037
- Rb$_2$ZnBr$_4$, ferroelectricity, hysteresis loops and dielec. const. meas. 78—23416
- Rb$_2$ZnBr$_4$, incommensurate phases, neutron scattering study 79—15417
- Rb$_2$ZnBr$_4$, incommensurate and commensurate phases, neutron scatt. meas. 79—82936
- Rb$_2$ZnBr$_4$, modulated struct., far IR transmission, temp. depend. 80—71408
- Rb$_2$ZnBr$_4$, modulation phase transitions, neutron scatt. 79—95712
- Rb$_2$ZnBr$_4$, Raman scatt., normal-incommensurate-commensurate phase transitions, soft modes 80—40071
- Rb$_2$ZnBr$_4$, soft modes at phase transforms., far IR spectrum study 80—107398
- Rb$_2$ZnBr$_4$, soft modes obs. by Raman scatt. 80—97283
- Rb$_2$ZnBr$_4$(Cl$_4$), Raman spectra near incommensurate phase transitions 80—76013
- Rb$_2$ZnCl$_4$, ^{35}Cl NQR, incommensurate struct. phase transition 79—47401
- Rb$_2$ZnCl$_4$, commensurate-incommensurate phase transition, crit. behaviour, sp. ht. meas. 80—71342
- Rb$_2$ZnCl$_4$, commensurate-incommensurate phase transition, ^{35}Cl NQR study 80—75966
- Rb$_2$ZnCl$_4$, dielec. dispersion, 5-900 MHz, near incommensurate-commensurate transition 80—60522
- Rb$_2$ZnCl$_4$, ferroelectricity, hysteresis loops and dielec. const. meas. 78—23415
- Rb$_2$ZnCl$_4$, incommensurate phases, neutron scatt. 79—38501
- Rb$_2$ZnCl$_4$, incommensurate phase form., domain struct. near phase transition, NQR obs. 79—33643
- Rb$_2$ZnCl$_4$, incommensurate phase transition, ^{87}Rb NMR study 80—75967
- Rb$_2$ZnCl$_4$, incommensurate phase transitions, ^{35}Cl NQR study 80—75968
- Rb$_2$ZnCl$_4$, NQR exam. of noncommensurate superstructures produced by phase transitions 79—69791
- Rb$_2$ZnCl$_4$, phase transitions, soft mode, Raman scatt. meas. 79—4389
- Rb$_2$ZnCl$_4$, phase transition, Raman scatt. evidence 80—40116
- Rb$_2$ZnCl$_4$ single crystals, Raman scatt. spectra, temp. range covering two phase transitions 80—7340
- Rb$_2$ZnCl$_4$ type ferroelectrics, phase transitions and physical props. *(Japanese)* 79—78636
- Rb$_2$ZnCl$_4$, US vel. and attenuation at normal-incommensurate phase transition pt. 79—55833

ferroelectric transitions continued
- Rb$_2$ZnCl$_4$, US velocity and attenuation, around normal-incommensurate phase transition 80—40072
- SC(NH$_2$)$_2$, ferroelectric transitions, based on model thermodynamic pot. 78—80295
- Sb$_{1-x}$Bi$_x$SI, mixed cryst., ferroelec. phase transition 79—33629
- SbNbO$_4$:CoO(Fe$_2$O$_3$)(TiO$_2$), growth, pyroelectric and ferroelectric props. 79—73886
- Sb$_5$O$_7$I, polytype 2MA, ferroelectric, ferroelastic, Raman scattering and symmetry anal. 79—38550
- Sb$_2$S$_3$, crystal, domain structure 78—43828
- Sb$_2$S$_3$, ferroelectric semiconductor, effect of screening by conduction electrons on phase transitions 78—84537
- Sb$_2$S$_3$, phase transitions and improper photoconductivity, effect of growth conditions *(German)* 78—39515
- Sb$_2$S$_3$ type chain crystals, ferroelec. phase transitions 79—33625
- SbSBr, single crystals, birefringence meas., ferroelec. transition obs. 80—88933
- SbSI, anharmonic at. pot. and temp. depend. of thermal vibrs. 80—39246
- SbSI, band gap photoreflectance spectra near ferroelec. transition 79—38559
- SbSI, birefr. and phase transitions 78—60405
- SbSI, central mode, microwave freqs. 79—19852
- SbSI, cryst. and vitreous, nonlinear light absorpt., effect of temp. and phase transitions 77—75604
- SbSI, crystal struct. in ferroelec. phase, displacive type transition 77—11515
- SbSI, ferroelec., phase transitions, birefringence meas. 78—56440
- SbSI, ferroelec. phase transition and nonlinear props. 80—75988
- SbSI, ferroelec. semicond., nature of low-temp. phase transition 77—69784
- SbSI, ferroelec. semicond., laser-modulated reflectance near T_c 78—72552
- SbSI, ferroelec. semicond. near phase transition, anomalies of photocond. 79—42579
- SbSI, ferroelec. transition critical phenomena *(Russian)* 80—7314
- SbSI ferroelectric, dielectric behaviour, particle-size dependence 78—2811
- SbSI, ferroelectric, dark current and spontaneous polarisation, ferroparaelectric transitions obs. 80—60521
- SbSI, ferroelectric semiconductor, effect of screening by conduction electrons on phase transitions 78—84537
- SbSI, free energy function, temp. depend. and anisotropy of dielec. const., ferro- and paraelec. phases 78—64330
- SbSI, inelastic neutron scatt. 77—40189
- SbSI, paraelec. phase, microwave reson. dielec. dispersion, near T_c 79—99839
- SbSI, paraelectric-ferroelectric transition, low freq. phonon branches, neutron scatt. obs. 79—61313
- SbSI, Raman scatt., near tricritical point 78—15159
- SbSI, tricrit. point, NQR under press. 79—38469
- SbSI, tricrit. point at 1.4 kbar and 235K 78—68463
- SbSI-Sb$_2$S$_3$ system, ferroelec. phase transition temp. 79—78632
- SbSI-SbSBr system, ferroelec., anharmonic effects in far IR reflectivity spectra 80—76014
- SbSI(Br), transition possibility investig. for struct. coeff. calcs. of internal Lorentz field 77—73119
- SbSI$_x$Br$_{1-x}$, T-p-x phase diagram *(Russian)* 77—16241
- Sb$_2$S$_3$(Se$_3$), transition possibility investig. from struct. coeff. calcs. for internal Lorentz field 77—73119
- SbS$_x$Se$_{1-x}$I layer elec. and ferroelec. props., mech. stress effects *(Russian)* 80—50279
- SbTaO$_4$, X-ray and ESR study of phase changes 78—72476
- SnCl$_2$.2H$_2$O, crit. dynamics, nuclear relax. 78—75805
- SnCl$_2$.2H$_2$O, dielectric dispersion and absorpt. and proton spin-lattice relax. at phase transition 77—8437
- SnCl$_2$.2H$_2$O, ferroelec., Cl NQR study 79—38467
- SnCl$_2$.2H$_2$O, layered, dielectric anomaly calc. using Ising model, possibility of antiferroelectricity 77—12341
- SnCl$_2$.2H$_2$O-type layer cpds., two dimens. ferroelec. ordering sp. ht. obs. 78—92034
- Sn$_{0.9}$Ge$_{0.1}$Te, Mossbauer spectra, soft modes 80—20550
- Sn$_x$Ge$_{1-x}$Te, ferroelec. semicond. structural phase transition, X-ray study 79—37836
- Sn$_2$P$_2$S$_6$, ferroelec. and pyroelec. props. meas. 78—35107
- Sn$_2$P$_2$S$_6$, ferroelec. semicond., phase transition and lattice dynamics 80—60526
- Sn$_2$P$_2$S$_6$ ferroelectric semicond., polarisation Raman scatt. spectra, X-ray struct. study 79—95778
- Sn$_2$P$_2$S$_6$, illumination effect on soft mode and dielectric props., luminesc. study *(Russian)* 80—50420
- Sn$_2$P$_2$S$_6$, investigation of p-T diagram near a singular point *(Russian)* 80—88937
- Sn$_2$P$_2$S$_6$, soft mode, interaction of modes and crit. Rayleigh scatt. 79—99836
- Sn$_2$P$_2$S$_6$, soft mode, temp. depend. of Raman spectra near phase transition 78—88263
- Sn$_2$P$_2$S$_6$, soft mode props., Raman scatt. study 80—60525
- Sn$_2$P$_2$(S$_{1-x}$Se$_x$)$_6$, solid solutions, ferroelectric soft mode freq., displacive transformations 80—29701
- Sn$_2$P$_2$(Se$_x$S$_{1-x}$)$_6$, ferroelec. props. *(Russian)* 80—25313
- Sn$_2$P$_2$(Se$_x$S$_{1-x}$)$_6$, ferroelec. tricrit. phase transform., light transmission study 80—71355
- (Sn$_{1-x}$Pb$_x$)$_2$P$_2$S$_6$, solid solutions, ferroelectric soft mode freq., displacive transformations 80—29701
- SnTe, electron-phonon interaction effect on ferroelec. transition 78—76416
- SnTe, phase transition obs. by Mossbauer spectroscopy 77—55740
- SnTe quantising mag. field effect 79—87403
- SnTe, softening of TO phonon mode *(Japanese)* 78—2225
- SnTe:Mn, EPR as probe of phase transitions 80—15790
- Sr$_{0.75}$Ba$_{0.25}$Nb$_2$O$_6$, ceramic ageing dielec. props. 80—88940
- Sr$_{0.75}$Ba$_{0.25}$Nb$_2$O$_6$ single cryst., electro-optical hysteresis curves and phase transitions *(German)* 79—28717
- Sr$_{1-x}$Ba$_x$Nb$_2$O$_6$, photorefraction in space charge field, phase transitions 80—97229
- Sr$_{1-x}$Ba$_x$Nb$_2$O$_6$, tetragonal tungsten bronze structure ferroelec. mech. for ferroelec. transition 79—38481
- Sr$_x$Ba$_{1-x}$Nb$_2$O$_6$, domain struct. influence on electrooptical props. 80—93283

ferroelectric transitions continued

$Sr_xBa_{1-x}Nb_2O_6$, high press. phase transitions, Raman scatt. studies 80—71402
$Sr_xBa_{1-x}Nb_2O_6$, neutron and light scatt. in phase transition region 78—64336
$SrBi_2Ta_2O_9$, SHG, temp. depend. ferroelec.-ferroelec. transition 78—15121
$Sr_{1.8}Na_{0.1}Nd_{0.1}Ta_2O_7$, solid soln., ferroelectric phase transitions, dielec. constant and thermal expansion rel. to temp. 80—88934
$Sr_2Nb_2O_7$, ferroelectric phase transitions, dielec. constant and thermal expansion rel. to temp. 80—88934
$Sr_2Nb_2O_7$, high press. phase transitions, Raman scatt. studies 80—71402
$Sr_2Ta_2O_7$, ferroelectric phase transitions, dielec. constant and thermal expansion rel. to temp. 80—88934
$SrTeO_3$, X-ray diffractional and optical studies, ferroelectric properties 79—65805
$SrTiO_3$, anharmonic phonons and central peaks at struct. phase transitions 79—95775
$SrTiO_3$, apparatus for biaxial stress production at low temp., appl. to ferroelectric 78—45609
$SrTiO_3$ based solid solns., ferroelec., US study 79—38476
$SrTiO_3$, central peak in spectrum of ferroelec. mode fluctuations and dielec. losses, 4.2K 78—19432
$SrTiO_3$, crit. behaviour under stress 77—31745
$SrTiO_3$, crit. dielec. and optical props. and storage, 4K 77—24805
$SrTiO_3$, doped, large gap ferroelectrics, phase transitions in mag. fields 79—33621
$SrTiO_3$, dynamic central peaks and phonon interactions near structural phase transitions 78—83903
$SrTiO_3$, EPR meas., Hamiltonians with quartic anharmonicities 78—27083
$SrTiO_3$, forced thermal Rayleigh scattering 78—80371
$SrTiO_3$, freq. depend. of soft mode self-energy, for IR dielec. response meas. 79—33632
$SrTiO_3$, heat capacity crit. behaviour 78—10857
$SrTiO_3$, neutron spectroscopy of central peak energy width 77—32334
$SrTiO_3$, optical SHG near phase transition 80—71348
$SrTiO_3$, photolum. and carrier drift mobility at ferroelec. transition 80—71469
$SrTiO_3$, Raman scatt. and ferroelec. soft modes 77—16300
$SrTiO_3$, semicond., structural phase transitions, US velocity meas. 79—28692
$SrTiO_3$, semiconductor, soft modes, zone boundary mode 80—71357
$SrTiO_3$, specific heat near structural transition 77—81072
$SrTiO_3$, stressed, trigonal-to-tetragonal transition, EPR data, realisation of 3-state Potts model 77—28525
$SrTiO_3$, structural phase transition, intrinsic and extrinsic central peak properties 80—34168
$SrTiO_3$, thermal expansion near displacive phase transition meas. 77—12345
$SrTiO_3$, thermodynamic props. 77—39680
$SrTiO_3$, thin film, polarisation reversal, electric field induced phase transform. 80—103925
$SrTiO_3$, X-ray and Mossbauer γ-ray scatt., near phase transition, energy width of central peak 78—79724
$SrTiO_3$:Fe^{3+}, displacive struct. transition, order-disorder behaviour, phonon softening, EPR obs. 79—23695
$SrTiO_3$:Fe^{3+}, order-disorder and central peak behaviour, EPR study 80—75970
TGS, ferroelectric phase transition, high resolution NMR study 80—97214
TGS, temp. behaviour of optical phonons near T_c, evidence of non-linear pseudospin-phonon interaction 77—7824
TGSe, anomalous sound velocity near ferroelec. phase transition at high pressure 78—52456
TGSe, deuterated, NMR investig. of ferroelec. and press. induced transition mechanisms 77—16189
TGSe, domain-wall orientations and wall energies 78—23420
TGSe, temp. behaviour of optical phonons near T_c, evidence of non-linear pseudospin-phonon interaction 77—7824
$Tb(MoO_4)_3$ cryst. struct. in ferroelec., ferroelastic, antiferroelec. and paraelastic phases 80—75205
$Tb_2(MoO_4)_3$, elastic wave attenuation and velocity near ferroelec. transition 79—73257
$Tb_2(MoO_4)_3$, first-order to continuous phase transition, crossover induced by symmetry-breaking fields 79—82312
$Tb_2(MoO_4)_3$, hydrostatic press. effect on phase transition 78—27166
$Tb_2(MoO_4)_3$, mode softening near ferroelec. transition, Raman and Brillouin spectra 79—33685
$Tb_2(MoO_4)_3$, nonlinear elastic props. near phase transition 79—73244
$Tb_2(MoO_4)_3$, nonlinear piezoelec. coeffs. near phase transition 79—95710
$Tb_{1-x}Sn_xTe$, ferroelectric transition calc., effect on carrier density 77—85673
TeO_2, ferroelectric glass, phase transition, permittivity, electrochromism, photochromism 80—80719
$TiSe_2$, optical refl. spectra obs., suppression of antiferroelectricity by excess carriers 77—59536
$(Tl,NH_4)_2Cd_2(SO_4)_3$, langbeinite type mixed cryst., ferroelec. transitions, dielec. and elastic meas. 78—2810
$Tl_2Cd_2(SO_4)_3$, ferroelec. langbeinites, Raman scattering 80—34926
TlH_2PO_4 and TlD_2PO_4, press. effect on dielec. props. 79—99832
TlH_2PO_4 and TlD_2PO_4, dielec. props. under hydrostatic press. up to 7 kbar 80—29696
TlH_2PO_4, thermodynamics props. of solid phase transitions, heat capacity 79—10966
$TlMnCl_3$, birefringence, twinning and structural phase transitions 79—38480
TlSe type crystals, possible second-order phase transitions, group-theoretical anal. 80—92672
WO_3, ceramic, Raman spectra, 80-300K, inhibited ferroelectric phase transition 77—32378
WO_3, orthorhombic phase struct., rel. to struct. of other phases 77—24297
ZnF_2, elastic props., 4.2-300K, incipient ferroelec. transition 78—30691

ferroelectricity
see also antiferroelectricity; ferroelectric devices; ferroelectric materials; ferroelectric switching; ferroelectric transitions
acceleration waves in elastic dielectrics with internal state variables 79—47396

ferroelectricity continued
acoustic properties of ferroelectrics, at second-order phase transition, effect of polarisation fluctuations 77—85664
acoustic wave interaction with microwave radiation field 80—6913
anisotropic ferroelectric, ratios between critical indices of thermoelasticity *(Russian)* 77—1642
anomalous bulk photovolt. effect, quantum-mechanical theory of electron transport 79—69545
anomalous photovoltaic effect of ferroelectrics, review 80—65628
antiferroelectrics, multicritical points in structural phase transitions, renormalisation 80—75982
antiferromagnet, coupled ferroelec.-magnetoelastic waves 77—51935
antiferromagnet, energy gap in spin wave spectrum 78—91858
antiferromagnet, ferroelec., damping of spin waves and ‘hard’ excitation effect 79—28518
antiferromagnet, ferroelec., exchange enhancement of magnetoelec. coupling 78—88159
asbestos, piezoelec. and ferroelec. rel. to asbestosis and model of carcinogenesis 77—78075
automatic anomalous noise meas. for ferroelectric capacitor parameters, not in equilib. *(French)* 78—74029
band structure, calc. using Euwema PWG method with X_α approx. 78—15106
Barkhausen effect, contrib. to repolarisation process *(Russian)* 77—32330
bibliography, (Feb.-Aug. 1978) 79—82931
bibliography 77—12326
bibliography (Aug.-Dec. 1978) 80—62405
book, principles and appls. of ferroelectrics 77—90108
bose condensation, polar modes with elastic restoring forces, metastable ferroelec. state 77—81464
ceramic, mech. and elec. losses, correl., theory and expt. 80—66133
ceramics, 1-D linear dynamic electromechanical responses 79—47397
ceramics, elastic and piezoelec. eigenstate spaces 79—42901
chiral smectic C, distortion under shear, optical study 77—39536
commensurate ferroic, elucidation with model of ‘situations’ and ‘oriates’ 78—26651
conference, condensed matter physics, Sarajevo, Yugoslavia (Oct. 1976) 77—51629
conference, Krusevac, Yugoslavia, Sept. 1978 79—56104
conference, Leningrad, USSR (1977) 79—15406
conference, Portoroz, Yugoslavia (Sep. 1979) 80—73092
continual model, boundary conditions 80—93244
critical indices for systems with strong dipole interactions *(Russian)* 77—28390
critical parameters of ferroelec. cryst. meas. *(Polish)* 78—88272
de Gennes’ model sum rules, decoupling procedure in Green’s function method *(Russian)* 78—56434
deformable dielectric, model of interactions between material lattice and polarisation sub-lattices 77—59521
dielectric behaviour of materials undergoing dipole alignment transitions 80—88922
dielectric spectroscopy, transitions, permittivity 80—75914
diffraction of EM waves by domain walls in improper ferroelectric 79—69799
dipolar lattice, 2-D, Monte-Carlo calc., lattice energy 78—14308
dipole waves, low temp. sp.ht. and spontaneous polarisation calc. 79—33614
dispersion of permittivity near N-phase point in $KTa_{1-x}Nb_xO_3$-type ferroelectrics 79—24276
displacive ferroelectric, effect of elec. field on thermal cond. 77—85002
displacive ferroelectric, inelastic neutron scatt. cross. section determ. 77—31737
displacive ferroelectrics, connection between electron spectrum parameters and ferroelec. parameters 79—38483
displacive ferroelectrics, Curie temp., microwave absorption, elec. field depend. 80—50280
displacive type ferroelectrics with impurities, lattice dynamics 79—28061
domain boundaries, structure, light diffr. 78—15135
domain boundary quasielastic displacements 77—24807
domain wall, EM wave diffr. *(Russian)* 77—90118
domain wall, interaction energy with elec. charge 80—88939
domain wall shift, interaction with mobile point defects 77—32338
doped displacive ferroelectrics, sound vel. change 80—45013
double quadratic kink soln. to ferroelec. domain wall dynamic polarisability 80—66135
eight-site order-disorder model, influence of tunnelling 80—2709
electret effects in ferroelectrics, phenomenological theory 78—88260
electro-optical effects in ferroelec. crysts., polarimeter appl. *(Japanese)* 78—37045
electroacoustic echoes and long-time storage in piezo- and ferroelectrics 79—38454
electron beam, self-focusing in ferrodielectric channel, nonlinear eqn. anal. 77—61905
electron emitter with negative electron affinity 80—100762
electronic micropositioning with ferroelastic-ferroelectrics 79—17392
exchange integral, hydrostatic press. effect, H bonding *(Russian)* 78—35097
exciton insulator, coexistence of ferromag. and ferroelec. ordering 78—18973
ferrites, ferroelec., coupled ferroelec. and spin waves, exchange interactions 80—70995
ferroactive fluids, advanced appls. 80—80714
ferroelectric antiferromagnetics, spin wave fluctuations in strong mag. fields *(Russian)* 79—82773
ferroelectric crystals, polariton light scatt. freq.-angle spectra, nonlinear susceptibility interference *(Russian)* 80—92834
ferroelectric-magnetic coupled oscills., excitation by electron beam *(Russian)* 78—23257
ferroelectroantiferromagnetics, spin wave spectrum and exchange amplification of magnetoelectric correlation 79—38311
ferroic crystals, prototypic point group, physical props., model 80—80715
ferromagnet, energy gap in spin wave spectrum 78—91858
ferromagnet, soft modes and ferromag. reson. 80—11275
geometric effects 79—38493
glass, dielectric instabilities in high permittivity glass 78—52433
gyrotropy, an implicity form of ferroicity 79—73286
history of the development of subject 78—8208
homogeneous ferroelectrics; bulk photovoltaic effect 79—42578
hydrogen-bonded ferroelectric, Ising model in transverse tunnelling field and proton-lattice interaction 80—7307

ferroelectricity continued
hydrogen-bonded partially-deuterated cryst., coupled tunnelling-lattice modes 77—63372
hysteresis loops and butterfly loops, macroscopic theory 80—66132
ice model, triangular lattice 77—82463
improper ferroelectric, domain wall theory using simple one-dimens. model 77—12349
incommensurate crystals, first order Raman scatt. from unbounded phonons 80—88990
inelastic neutron scatt., one-phonon differential cross section 80—28883
introduction to ferroelectrics and their transitions *(Japanese)* 78—23407
Ising model, temp. depend. of domain wall parameters 79—69797
Ising model, transverse field dynamic behaviour 78—22814
Ising model, with transverse field 77—77016
isotopically disordered ferroelectric cryst., thermal cond. 77—76628
langbeinite-type crystals, phase transitions, dielec. props. obs. 78—6643
leaves of palmlike plant Encephalartos villosus, absence of ferroelec. 77—77876
liquid crystal, crit. exponents 77—80607
liquid crystal, ferroelectric, review of props. 77—85667
liquid crystals, theory 77—66018
local electric field, impurity centre dipole transitions *(Russian)* 78—34811
local potential approach *(Japanese)* 77—43939
low lying lattice vibrational modes, conf., San Juan, Puerto Rico, (Dec 75) 78—10131
magnetostatic waves in long rectangular bars, with domain struct. *(Russian)* 77—66383
Mossbauer spectrum parameters, Fe^{3+} 4s shell polarisation by electric field 79—95698
multistable self-wave media 80—86094
mutual compatibility with superconductivity 78—15104
negative capacitances, comparison with negative viscosities 80—66118
negative permittivity, existence in stable steady state 77—43937
nematic and smectic liquid crystals, ferroelectricity explanation *(French)* 78—83729
nematic-isotropic transition, permanent dipoles effect 77—20054
one-dimensional ferroelectric, quantum corrections to domain walls 77—4609
optical absorpt. coeff. calc., Green functions method 78—10851
optically induced internal fields in ferroelectrics 80—107855
order-disorder, displacive transformations, tunnelling, phonons 80—75975
order-disorder type ferroelectrics, piezoelec. and elastic props. 77—12318
order-disorder type ferroelectrics, static and dynamic electrostrictive props. 77—85652
orthophosphates, dynamics of ferroactive cryst. 79—37801
paraelectric reson. of H-bonds and related phenomena 77—28531
paraelectric state, Curie-Weiss law, anharmonic oscillator anal. 79—8087
permittivity, nonlinearity in ferroelec. cryst. with defects 78—27170
perovskite struct., review, Vegard's rule, Curie-Weiss law, spontaneous electro-optical effect *(Russian)* 77—48134
phonon echo in travelling and standing wave regimes in ferroelectrics 77—8521
photo-Hall effect in ferroelectric crystal without centre of symmetry *(Russian)* 78—60152
photoferroelectric phenomena, physical models derivation 79—15407
photoferroelectrics, book 80—2702
photogalvanic current in ferroelectrics 80—70748
photogalvanic effect in ferroelectrics, theory 79—42575
photoinduced changes in refractive index and spontaneous polarisation 78—43804
photostimulated processes in inorganic materials and optical information storage, review 78—82926
photovoltaic and photorefractive effects, fluctuation model interpretation 77—69369
photovoltaic current, bulk, in ferroelectrics, model calc. 78—84256
photovoltaic effect due to electron-phonon coupling 78—14757
piezoceramic complex composites near morphotropic phase boundary, dielec. and electromech. anomalies *(German)* 77—20800
piezomaterials, ferroelectric, pyrochlore struct., high sound-propag. velocity 78—43791
polarisation switching influence of mobile point defects 78—31165
polarised ferroelectric ceramic, acoustic vel. anisotropy 79—55835
polariton states in ferroelectrics of the order-disorder type 80—10894
polarized dielectric appl. *(French)* 79—51902
polydomain ferroelectrics, spontaneous polaris. screening *(Russian)* 79—91395
powders, origin of memory in echo phenomena 79—38440
powders, phonon electroacoustic echoes, storage mechanisms 80—75606
prototype and prototypic phase explained 78—38833
quantum transition suppression, pyroelectric, electrocaloric effects, specific heat 80—75984
quartz, ferroelastoelectricity, expt. 80—40078
random uniaxial systems with dipolar interactions, crit. dynamics 77—73034
Rayleigh wave propag. near Curie temp., ferroelec. cryst. with piezoeffect 77—89630
repolarisation of ferroelectric materials in SEM 79—15424
rotational domains, electric polarisation *(Chinese)* 79—56747
SAW propagation along domain boundaries, low temp. sp. ht. contrib. 77—77158
self-focusing of EM wave in crystal with anomalously high dielectric constant 80—14408
semiconductors, antiferromagnetic, magnetoelec. effect, magnetization and ferroelec. props. 80—25180
shallow impurity centres near Curie point, influence of dielec. nonlinearity on temp. depend. of ionisation energy 80—10916
shock compression of solids, review 80—24534
smectic C liq. crystal with induced helical struct., ferroelectric props. and spontaneous polarisation, C→A transition 80—54123
smectic liquid crystal, dipole ordering 78—2238
space modulated cryst. struct., theory of symmetry 79—38004
specific heat anomaly, Ising model, Monte Carlo calcs. 78—47989
stimulated emission from impurity atoms in ferroelectric, effect of phase transition 79—15490
structural phase transitions, ultrasonic velocity and attenuation meas. 80—75977
surface EM wave propag. along domain boundaries 77—40195
susceptibility, Raman line shape of overdamped mode 79—91426
theory and dynamics, optical, acoustic electro-optical props., Brillouin zone struct. 80—11347

ferroelectricity continued
thin ferroelec. layers 79—42912
transverse field ferroelec., lattice vibrs. effect on parametric ferroelec. reson. 77—59525
tungsten bronze, tetragonal, type structure cpds, transition sequences *(French)* 77—89538
tunnelling motion, phonon vibrs. and statistical disorder in unified theory 77—63373
tunnelling of atoms, phonon vibrs. and statistical disorder in unified theory 78—31160
uniaxial, critical behaviour studied via renormalisation group theory 78—8367
uniaxial ferroelectric-crystal, with one-dimensional inhomogeneity, fluctuations of order parameter 80—15995
uniaxial ferroelectrics, microscopic theory, crit. behaviour and anomalous elastic consts. 79—38463
uniaxial material domain struct., branching *(Russian)* 80—34868
unit cell multiplication during phase transform., spontaneous polarisation 80—75983
vibronic carrier, dependence of plasma frequency on spontaneous lattice distortions *(Russian)* 79—15410
vibronic ferroelectrics, band struct. temp. depend. 80—70598
vibronic theory, developments 79—33620
vibronic theory of ferroelectricity 79—38492
$Ca_2Mg(Co)(Zn)(Mn)(Cd)(Ca)TeO_6$, optical SHG study of acentricity, ferroelec. of low temp. phases 80—71324
$Cd_2Mg(Co)(Zn)(Mn)(Cd)(Ca)TeO_6$, optical SHG study of acentricity, ferroelec. of low temp. phases 80—71324
Cu-Zn-Al Marmem alloy, β_1 phase superstruct. obs., rel. to transform. mode 78—39776
$Gd_2(MoO_4)_3$, effect of ferroelec. ordering on refractive index 79—33653
KH_2PO_4-type crystal, domain wall mobility, two-dimens. ordering effect 78—48137
KH_2PO_4-type ferroelectrics, pseudospin-phonon models, consistency with expt. results 77—59523
$KTaO_3$, SHG and quadratic electrooptic effect 78—76429
$NH_4H_2PO_4$ crystal, ferroelectricity, spontaneous polarisation obs. 79—28687
$(NH_4)_2SO_4$, mechanically twinned, orthorhombic, search for antiphase boundaries 79—37715
Na_2CO_3, structural modulation, theory 77—35535
$Na_5W_3O_9F_5$, phase transitions obs. *(French)* 80—6516
$Pb(Zr_xTi_{1-x})O_3$, ferroelectric energy generation by shock compression, modes 77—55757
$Sr_2Mg(Co)(Zn)(Mn)(Cd)(Ca)(Sr)TeO_6$, optical SHG study of acentricity, ferroelec. of low temp. phases 80—71324
$SrTiO_3$, SHG and quadratic electrooptic effect 78—76429

ferrofluids *see magnetic fluids*

ferromagnetic-antiferromagnetic transitions
see also metamagnetism; Morin temperature
anisotropic magnet mixture, Heisenberg spin system by Monte Carlo simulation 79—78408
antiferromagnet, intermediate state, stability in HF mag. field *(Russian)* 79—95591
α-bis(N-methylsalicylaldiminato) copper II, dynamic behaviour of antiferro- to ferromagnetic transition 79—73715
dimethylammonium copper tetrahalide, layer compound $(CH_3NH_3)_2Cu(Cl_xBr_{1-x})_4$, antiferro- to ferromag. transition 80—108005
first kind PT1 transformations *(Russian)* 79—69670
Heisenberg ferromagnet, boson field anal. of crit. temp. region 77—51911
intermediate valence, mag. susceptibility and mag. instabilities 80—39532
Ising ferromagnet, 3-D critical behaviour in random mag. field 78—68250
Ising model, free energy and susceptibility inequalities, phase transition 78—43541
Ising model, spin glass state, mixed nearest-neighbour exchange interaction 78—39341
Ising system, Lifshitz points, phase diagram transition temp. determ. interface free energy vanishing 79—99716
Ising system, ordering and phase transitions 79—91200
magnetic material, fluctuational breakdown of metastable states at phase transitions *(Russian)* 78—52245
metamagnetic dielectrics, at finite temp. *(Russian)* 78—88118
metamagnetic transition in absence of mag. field, model 80—97092
metamagnetism, review 78—19248
microscopic model for the exchange-inversion transition 79—56548
nucleation of new phase, role of planar, linear and point defects 77—24695
rare earth alloys, RFe_4Al_8, mag. props., Mossbauer spectra, ordering effects 77—63179
rare earth compounds and alloys, spin-reorientation transitions, review 77—36073
rare earth cpds., RRh_4B_4 and RMo_6X_8 (X=S, Se), mag. order and supercond., neutron scatt. studies 80—44807
rare earth heavy binary alloys, press. effect on mag. props. *(Japanese)* 77—43835
rare earth metal, ferromagnet-simple helix transition, cond. electron spin polarisation *(Russian)* 79—7995
rhombic distortion of cryst. lattice at low temp. 78—2253
semiconductor, metamagnetic, magnetostriction ferrons 78—88160
soft phonons and mag. phase transitions 80—54889
TCNQ salts, $Mn(TCNQ)_2$ and hydrates, mag. and elec. props. 79—82767
temperature induced antiferromagnetic-ferromagnetic phase transition, s-f two-band Hubbard model 80—60253
two-sublattice magnetic substances, mag. transitions due to exchange-striction mechanism *(Russian)* 77—47995
CO, chemisorbed monolayer on Pt or Au, mag. phase transition, thermomagnetic study *(Russian)* 80—34319
$CdCr_2Se_4$-$ZnCr_2Se_4$, single cryst., mag. props. 79—28526
$Cd_{1-x}Zn_xCr_2Se_4$, synthesis Curie pt., photomag. effect 77—51937
$CeMn_2(Si_xGe_{1-x})_2$, $Ce(Mn_{1-x}M_x)_2Si_2$, (M=Fe, Cu), mag. props. 80—25134
$Ce_{1-x}Pr_xAl_2$, mag. struct., comp. depend., neutron diffr. and mag. susceptibility meas. 80—50054
CeSb, commensurate-commensurate transitions, devil's stairs theory 79—19740
CoMnSi, $CoMnSi_{0.85}Ge_{0.15}$, mag. props. 79—42758

ferromagnetic-antiferromagnetic transitions continued
$\mathrm{CoMnSi_{1-x}Ge_x}$, amg. props. 80—60270
Cr-Si (1.37 at.%), thermal and elec. props. 79—78071
$\mathrm{(Cr_{1-x}Fe_x)_{1+\delta}Sb}$, interstitial occupancy, Cr:Fe distrib., X-ray and neutron diffr. study 79—42012
$\mathrm{Cr_xMn_{1-x}As}$, antiferromagnetic-ferromagnetic transition, mag. moment and elec. resist. meas. 80—15718
$\mathrm{Cr_xMn_{1-x}As}$, antiferromag. to ferromag. transitions, superexchange-double exchange mag. coupling, susceptibility and resist. obs. 80—50070
$\mathrm{CsNiF_3}$, crit. exponent crossover, quasielastic neutron scatt. around Neel point 77—24693
$\mathrm{CsNiF_3}$, one-dimens. ferromag. far IR investig. of ferromag. reson., temp. and mag. field depend. 77—66427
$\mathrm{Cu_2MnAl}$-$\mathrm{Pd_2}$ MnAl mixed Heusler alloys, mag. props. 80—60269
$\mathrm{Cu_{1-x}Pd_xMnSb}$, mag. phase transition 80—60268
Dy, change in easy axis during magnetisation 77—8306
Dy, domain effects near order-disorder and order-order ferromagnetic transitions 80—65886
Dy, magnetic domain structure, hysteresis, thermal modulation study 80—71082
Dy, magnetic transitions and internal friction temp. depend. *(Russian)* 78—39317
Dy, magnetocaloric effect and mag. phase transitions, 80 to 300K 80—60279
Dy, US attenuation maxima in mag. field 77—16140
Dy-Sm alloys, elec. resist. singularities and mag. transitions *(Russian)* 79—47075
Dy-Sn alloy, hyperfine fields acting on diamag. impurities and anisotropic exchange, Mossbauer spectra 77—1625
$\mathrm{DyFe_{0.998}Co_{0.002}O_3}$; orthoferrite, domain struct. near mag. transitions 80—2599
$\mathrm{DyFeO_3}$, mag. field induced intermediate state, magneto-optical effect meas. 77—55672
$\mathrm{Dy_{0.5}Ho_{0.5}FeO_3}$, mag. transitions, influence of $\mathrm{Dy^{3+}}$, $\mathrm{Ho^{3+}}$ ground states 77—89955
$\mathrm{Dy_{0.7}La_{0.3}FeO_3}$, reorientational phase transitions, influence of $\mathrm{La^{3+}}$ ions 80—7108
$\mathrm{Dy_{1.2}Mo_6S_8}$, long-range mag. order and supercond., neutron diffr. obs. 79—78320
$\mathrm{DyVO_4}$, antiferromag.-ferromag. structural phase transition induced by elec. field *(Russian)* 79—46802
$\mathrm{ErCrO_3}$, magnetisation, NMR freq. temps. depend. weak ferromagnetic-antiferromagnetic spin reorientation transition 80—29631
Fe, fine particle dispersions, shock induced mag. effects 79—82832
Fe-based system, concentration ferro-antiferromag. transitions *(Russian)* 79—99699
Fe-Cr-Ni, mag. state at low temps. *(Russian)* 78—56298
Fe-Ni system, γ phase mag. struct. 79—91231
$\mathrm{FeCl_2}$, magnetic transition and sublattice mag. moment rotation nonequivalence *(Russian)* 80—100586
$\mathrm{Fe_xCu_{1-x}Cr_2Se_4}$, crystallographic and image props. 80—39049
$\mathrm{FeI_2}$, first order mag. phase transition, neutron scatt. study 80—50090
$\mathrm{Fe_xMn_{1-x}Pt_3}$, ferro-antiferromag. transform. at 4.2K *(Russian)* 78—88117
$\mathrm{(Fe_{1-x}Mn_x)_3Si}$, mag. phase diagram determ. 77—24697
$\mathrm{Fe_{65}Ni_{28}Mn_1}$, disordered, mag. struct. near ferro-antiferromagnetic transition 80—60211
α-$\mathrm{Fe_2O_3}$, antiferromag., muon spin rotation meas. 78—48106
α-$\mathrm{Fe_2O_3}$, H-T phase diagram 79—87258
α-$\mathrm{Fe_2O_3}$, haematite, linear mag. birefr., Morin transition 77—8309
$\mathrm{Fe_2O_3}$, haematite, Morin transition, Mossbauer expt. using selective excitation method 78—25375
$\mathrm{Fe_2O_3}$, haematite, optical indicatrix deform. and rot. during field induced phase transition 78—68482
α-$\mathrm{Fe_2O_3}$, haematite, substituted, Morin transition, neutron diffr. study 80—54897
α-$\mathrm{Fe_2O_3}$, Morin transition, Mossbauer spectra meas. 78—31071
α-$\mathrm{Fe_2O_3}$, muon spin rotation above and below Morin transition 78—43762
α-$\mathrm{Fe_2O_3}$, pure and Mn doped, characts. of Morin phase transition, linear mag. birefringence meas. 77—69560
α-$\mathrm{Fe_2O_3}$, X-ray diffr. exam. at phase transition from weakly ferromag. to pure antiferromag. state 77—51904
$\mathrm{Fe_{25}Pd_{50}Au_{25}}$, atomic ordering influence on mag. props. and elec. resistance *(Russian)* 80—7551
$\mathrm{FePt_3}$, metamagnetic transitions in external fields 80—60272
FeRh, antiferromag.-ferromag. transition, appl. of interacting virtual bound state picture 77—69464
FeRh, transition mechanism, interacting virtual state approach 77—72987
$\mathrm{Fe_{1-x}Rh_x}$, press. effects on mag. phase transition, resist. meas. 77—4516
$\mathrm{GdMg_3}$, mag. props. 78—72346
$\mathrm{Gd_2S_3}$, antiferromag. to ferromag. and semiconductor to metal transitions *(Russian)* 79—33485
$\mathrm{^3He}$, submonolayer on Grafoil, vacancy induced ferromag. 78—14536
$\mathrm{Hg_{1-x}Zn_xCr_2Se_4}$, magnetic struct., neutrongraphic and mag. investigation *(Russian)* 80—88726
$\mathrm{Ho_{0.5}Dy_{0.5}FeO_3}$ orthoferrite, domain wall struct., stability conditions, Morin transition, anisotropy const. 80—34684
$\mathrm{(La_{0.8}Ca_{0.2})MnO_{3+y}}$, mag. props., Faraday method meas. 80—103832
Mh-Rh-Cr, mag. transition, effect of press. 77—16077
Mn-Ga, mag. and cryst. struct. in conc. region of gamma phase, temp. depend. *(Russian)* 79—65649
$\mathrm{MnB_2}$, polycryst., magnetoresist. and mag. props. *(Russian)* 80—92907
MnCoSi, effect of press on mag. transition temp. *(Russian)* 80—25137
MnCoSi, mag. struct. *(French)* 78—39323
$\mathrm{Mn_{1-x}Cr_xP}$, mag. susceptibility and transitions 79—47256
$\mathrm{Mn_{1-x}Fe_xP}$, magnetisation, susceptibility and mag. transitions 79—47256
$\mathrm{Mn_{5-x}Fe_xSi_3}$, elec. resist. and mag. susceptibility, ferromag. to antiferromag. transition 80—80504
$\mathrm{Mn_3Ge}$, elec. and mag. props. *(Russian)* 77—76792
MnPt, disordered film produced by RF sputtering, ferromag. behaviour 78—68310
MnSi, mag. anisotropy exam., ferromag. to antiferromag. transition 79—73708
$\mathrm{Nd_xEu_{1-x}B_6}$ solid solution, mag. susceptibility, lattice parameters, Weiss temp. 80—29535
$\mathrm{NdFeTiO_5}$, magnetic props. and crystal growth 78—92185
$\mathrm{NiS_2}$, high press. effect on mag. transition temps. 78—91866
$\mathrm{(Pd_xPt_{1-x})_3Fe}$ atomically ordered alloy, thermoelectric power, carrier energy spin shift, mag. props. 80—29394

ferromagnetic-antiferromagnetic transitions continued
$\mathrm{(Pd_xPt_{1-x})_3Fe}$, magnetisation intensity and coercive force, antiferro- to ferromag. transition *(Russian)* 77—48008
Pt-Fe ordered alloy, multiply mag. phase transitions 80—60264
Tb, magnetisation intensity in antiferromag. state and mag. field induced phase transforms. *(Russian)* 80—65811
Tb-Cu-Zn(Al), mag. props. *(Russian)* 77—51905
Tb-Y, helicoid antiferromag. ferromag. transition, magnetostriction and magnetocaloric effect *(Russian)* 77—80937
Tb-Y alloy, mag. hysteresis in antiferromag.-ferromag. transition *(Russian)* 79—33508
$\mathrm{TbMg_3}$, mag. props. 78—72346
$\mathrm{Tb_{1.2}Mo_6S_8}$, long-range mag. order and supercond., neutron diffr. obs. 79—78320
$\mathrm{TbNi_{2-x}Cu_x}$, elec. resist. and mag. props. 78—72348
$\mathrm{Tb_{1-x}Y_x}$ alloy, helicoidal antiferromag. to ferromag. transition 78—10687
UAs, magnetic struct. in high mag. fields, neutron diffr. study 80—34597
$\mathrm{USb_{1-x}Te_x}$, mag. struct. and mag. phase diagram, neutron diffr. study 80—50059
$\mathrm{YCrO_3}$, magnetisation, NMR freq. temps. depend. weak ferromagnetic-antiferromagnetic spin reorientation transition 80—29631
$\mathrm{Y_{1-x}Th_xFe_3}$, saturation magnetisation, fields up to 120 kOe, comp. depend. 77—8283

ferromagnetic Curie temperature *see Curie temperature*

ferromagnetic-paramagnetic transitions
see also Curie temperature
alkylammonium copper halides, mag. sp. ht., two-dimens. S1/2 Heisenberg ferromag. behaviour 77—32206
amorphous magnet, random anisotropy axis model in the infinite-range limit 80—88761
anisotropic spin one ferromagnetic in Callen's decoupling approx. 77—8258
anisotropic system, libron interactions, transition temp. depend. *(German)* 78—76237
binary alloy, atomic and mag. ordering, critical slowing down 78—14915
binary alloy, atomic ordering and ferromagnetism 79—87278
Chromel, thermocouple alloy, heat treatment effects on thermo EMF and mag. flux 77—63235
critical behaviour, mag. moment fluctuations and sp. ht. 77—28388
critical dynamics above crit. temp., dipolar coupling 78—52286
critical dynamics above T_c, high freq. *(Russian)* 78—10718
cubic and tetragonal ferromagnets, crit. behaviour in mag. field 77—66329
dialkylammonium copper tetrachllride, ferromag., static and dynamic mag. props. 80—50074
diluted Ising and Heisenberg magnets with competing interactions, phase diagrams and mag. props. 80—34672
dysprosium ethylsulphate, pure dipolar Ising ferromag., critical thermodynamics 77—16095
education, renormalisation group theory, second order phase transitions, undergraduate statistical physics 78—62012
exciton migration in crit. region 79—73440
ferromagnet, disordered, phase transitions, mol. field and Landau-Ginzburg theories 80—93118
ferromagnet, triple dynamic magnetisation fluctuation correl. and feasibility of polarised neutron exam. *(Russian)* 78—88133
ferromagnetic Fermi-liquid model, electron-impurity system hydrodynamics, elec. cond. 80—103835
ferromagnetic instability in two-band Hubbard model 79—1653
Heisenberg film, spin-one isotropic, quadratic interactions, quadrupolar-paramag. T_c 78—64210
Heisenberg magnet, classical, with layer structure, mag. phase transitions, anisotropic lattice, theory 80—29557
hexagonal ferromagnet, nonlinear magnetoelastic effects and phase transforms. *(Russian)* 78—48015
inhomogeneous ferromagnets, Landau's theory of second-order phase transition 80—50092
inhomogeneous ferromagnets, phase transitions, micromagnetic theory 80—65942
intermediate-valence systems, magnetic-nonmagnetic transitions, heuristic model 79—73718
internal energy relationship to moment 77—16028
Ising ferromagnet, disordering, short-range mag. order 80—50119
Ising model, critical surface calc. 79—4692
Ising model, percolation points and critical point 77—20608
Ising model, random bond mixtures, triangular cactus tree, statistical theory 80—39790
Ising model, square lattice bond dilute, renormalisation group attempts to obtain transition line 80—44836
magnetic material, fluctuational breakdown of metastable states at phase transitions *(Russian)* 78—52245
magnetically ordered metals, possible first order phase transformation 79—95589
metallic ferromagnet above insulator-metal transition, s-d exchange interaction effects 78—2421
metals, ferromagnetic metals, resist. anisotropy, crit. behaviour and temp. depend. 80—96858
metals, magnetic, Seebeck coefficient anomaly near spin ordering temp. 77—20302
metals, uniaxial ferrogmagnetic, influence of anisotropic fluctuations on elec. resist. near T_c 79—91038
neutron polarisation, crit. scatt. above Curie pt. 78—43565
non-uniform ferromagnets, simple model with spontaneous magnetisation at T_c *(Chinese)* 77—8256
optical absorption of mag. impurity ion near Curie point 77—16355
quadratic magnetostriction, exactly soluble model 79—8030
rare earth alloys, $\mathrm{RAuNi_4}$, (R=Gd, Tb, Dy, Ho, Tm, Yb and Er), mag. props. 77—20595
rare earth cobalt intermetallics, $\mathrm{RCo_2}$, elastic moduli, 4.2-300K 78—52332
rare earth compounds, Curie constant rel. to valence bond strength 80—60251
rare earth cpds., $\mathrm{RMo_6S_8(Se_8)}$ and $\mathrm{RRh_4B_4}$, coexistence of supercond. and mag. ordering *(Russian)* 80—84542
rare earth heavy binary alloys, press. effect on mag. props. *(Japanese)* 77—43835
rare earth-transition metal alloys, $\mathrm{H_2}$ absorption, effect on mag. props. 78—68231

ferromagnetic-paramagnetic transitions continued
- semiconductor, magnetic phase transitions in impurity band *(Russian)* 80−50097
- site Ising model, spin glass phase, transition temps. 79−95592
- smectic liquid cryst. film, ferroelec., two-dimens. X-Y crit. behaviour 79−77497
- surface energy role in transition *(Russian)* 79−87260
- thermomagnetic recording singularities at Curie point, cylindrical domain form. *(Russian)* 77−8318
- thermopower near crit. point, metallic ferromags., inelastic scatt. processes 77−15836
- Au-Fe (22 at.%), ferromag. phase, AC susceptibility near T_c 78−43575
- Au-Ni, magnetisation and sp. ht., ferromag., paramag. and crit.-conc. regions 79−38330
- $Be_2Mn_{1-x}Fe_x$, mag. props., giant moment clusters 79−28508
- $CdCr_2S_4(Se_4)$, thermoreflectance, photoconductance, Raman scatt. near mag. phase transition 80−97298
- $CdCr_2Se_4$, Crit. relax. processes, mag. reson. expts. 80−60425
- p- $CdCr_2Se_4$, resistivity anomalies at mag. transitions, sp.ht. 80−39785
- $CdCr_2S_4(se_4)$, ferromag. semicond., band struct., EHT calc. 80−54608
- $Cd_{1-x}In_xCr_2Se_4$, electric, photoelectric and mag. props., metal-semicond. transition *(Russian)* 80−54738
- $Ce_{0.73}Ho_{0.27}Ru_2$:Co, spontaneous mag. order below superconducting transition temp., Mossbauer study 80−39701
- Co, diffusion of Mn, 860-1246°C, mag. transform. effects 77−24427
- Co, FCC, self-diffusion and isotope effect, influence of mag. order-disorder transition 80−29205
- Co, oxidation at Curie temp. 79−29279
- Co, small-angle crit. neutron scatt. 78−31087
- Co-Mn (5.22 at.%), Mn diffusion, 868-1200°C, mag. transform. effects 77−24427
- $Co_2Ga_{2-x}Fe_x$, elec. resist., temp. and mag. field depend., mag. contrib. 80−96846
- $(Co_{1-x}M_x)B$, M=Mn or Fe, paramag., spin echo NMR spectra, ferromag. transition, spin-lattice relax. 80−29645
- $Co(S, Se)_2$, metamagnetic transitions in external fields 80−60272
- CrO_2, optical conductivities and dielec. functions in 0.2-6 eV range, rel. to band struct., above and below $T_c=392K$ 79−42938
- $CuCr_2Se_4$, Crit. relax. processes, mag. reson. expts. 80−60425
- $Cu_yCr_2Se_{4-z}Br_x$, degenerate ferromag. semicond., resist. minimum 79−73517
- $Cu_yCr_2Se_{4-z}Br_x$, paramagnetic-ferromagnetic phase transition temp. depend. on element conc. 79−69672
- Cu_2MnAl superparamagnetic particles in Cu_3Al lattice, magnetic moment ferromagnetic ordering *(Russian)* 79−78444
- $Cu(NH_4)_2Br_4.2H_2O$ Heisenberg ferromagnet, mag. props. in mag. field 80−34637
- $Cu_{1-x}Ni_x$, mag. transition, NMR meas. by spin-echo technique 77−32267
- Dy, rel. to longitudinal galvanomag. effect in single crysts. *(Russian)* 78−56132
- $DyCo_2$, field induced vol. magnetostriction 78−91920
- $DyFe_2$, phonon softening below Curie temp., Mossbauer effect 77−4589
- $ErCo_2$, field induced vol. magnetostriction 78−91920
- $(Er_{1-x}Ho_x)Rh_4B_4$, superconductive and mag. interactions, hydrostatic press. effect 80−49973
- EuB_6, mag., transport and thermal props. 79−73738
- EuO, critical EPR spin dynamics, sample shape and temp. depend. 77−32244
- EuO, Heisenberg ferromagnet, static crit. props., neutron scatt. expts. 77−20618
- EuO, magnetic semiconductor, piezoresistance effect, 4.2 to 300K 80−34450
- EuO, microwave cond., influence of mag. ordering 79−69544
- EuO, Raman scatt. and phonon dispersion 77−55786
- $EuO_{1.05}$, specific heat, mag. phase transition 77−36077
- EuO(S), phase transition spectroscopy 77−63426
- EuO(S), spin order and fluctuations, Raman scatt. study 80−97273
- EuS, heat capacity near ferromag. transition 78−47986
- EuS, Heisenberg ferromagnet, static crit. props., neutron scatt. expts. 77−20618
- EuS, Raman scatt. and phonon dispersion 77−55786
- EuS, spin relaxation crit. behaviour 78−76251
- EuSe, Raman scatt. and phonon dispersion 77−55786
- EuTe, Raman scatt. and phonon dispersion 77−55786
- α-Fe, C drift velocity for electromigration temp. depend. in paramag., ferromag. phases 78−18835
- Fe complex, bis(N,N-diethyldithiocarbamato)-iron chloride, ferromag., sp. ht. meas., 0.4-20K 78−19258
- Fe complex, $Fe(Cl)[S_2CN(C_2H_5)_2]_2$, susceptibility near critical pt. 79−24147
- Fe, crit. fluctuations, Mossbauer obs. 78−43724
- Fe, mag. anisotropy in crit. region, neutron polarisation-vector analysis 78−31065
- Fe, magnetic moments, local short range order, high temp. effects 80−65902
- Fe, magnetisation process in high mag. fields in crit. region 77−85498
- Fe, Mossbauer energy shift near Curie temp. 78−52388
- Fe, neutron critical scatt., above T_c, polaris. asymmetry 78−34994
- Fe, oxidation at Curie temp. 79−29279
- Fe, oxidation kinetics near Curie temp. 79−66218
- Fe, resistivity anomalies at mag. transitions, sp.ht. 80−39785
- Fe, thermal cond., elec. resist., Lorenz number and magnetisation, crit. behaviour 77−4521
- Fe-Al, high temp. Mossbauer study of order-disorder transform. 79−100137
- Fe-Al, Mossbauer study of ordering *(Japanese)* 79−19822
- Fe-Cr, hyperfine magnetic fields, Mossbauer spectra 80−97165
- Fe-Mn (9 to 20 wt.%), ^{57}Fe Mossbauer spectroscopy in phase transformations 80−29948
- Fe-Ni, thermal expansion, ferromagnetic-paramagnetic transition *(Russian)* 80−54412
- Fe-Ni alloy near crit. conc., Mossbauer γ-rays small angle scatt. 80−7217
- Fe-Ni alloys, FCC, mag. props. calc. 79−65659
- Fe-Ni Invar alloy, mag. phase mixing effect on thermodynamic props. 80−54891
- Fe-Pd, anomalous elec. cond. near mag. phase transition point, α to γ phase transition 80−15722
- Fe-Pt, ordered single cryst., magnetisation in strong mag. field *(Russian)* 78−47954

ferromagnetic-paramagnetic transitions continued
- Fe-V alloy, elec. resist. between 78 and 1200K 77−8065
- Fe-V alloys, Mossbauer study, hyperfine field effect on formation of local moments 78−27134
- Fe_3B, mag. props., ^{57}Fe Mossbauer spectra meas. 79−95693
- Fe_xB_{100-x}, amorphous, mag. props., ^{57}Fe Mossbauer spectra and magnetisation meas. 79−95693
- $Fe_{65}(Ni_{1-x}Cr_x)_{35}$, mag. viscosity and anomalies near Curie temp. 79−73781
- Fe_2P, grown in liq. Cu medium, composition and mag. props. 79−11313
- Fe_2P:Cu, Mossbauer spectra, mag. transition 80−50240
- $Fe_{2-x}P$, first order ferro- to paramag. transition, 216K, susceptibility obs. 78−39322
- $Fe_{1-x}Rh_x$, press. effects on mag. phase transition, resist. meas. 77−4516
- $FrCr_2S_4$, second-order phase transition, Mossbauer spectra 80−20569
- Gd, AC susceptibility and temp. modulation near Curie point 77−4515
- Gd, coil noise due to permeability fluctuations at phase transition temp. 80−84598
- Gd, domain effects near order-disorder and order-order ferromagnetic transitions 80−65886
- Gd, EPR near Curie temp. 78−19321
- Gd, thermal conductivity critical behaviour near Curie point 80−75540
- Gd, thermal expansion, near ferromag. transition 78−31084
- Gd-Dy alloy, rel. to longitudinal galvanomag. effect in single crysts. *(Russian)* 78−56132
- Gd-La alloy, optical freq. cond. in 0.5-3.1 eV range, paramag.-ferromag. transition 80−29761
- Gd-Mn alloy, mag. props. and effect of H_2 absorpt. 78−19250
- $GdAl_2$-$GdCo_2$ system, EPR and mag. props. 79−33478
- ^3He in Grafoil, ultralow temp. NMR mag. susceptibility, surface magnetisation and transition 78−79843
- ^3He with C particles, pulsed NMR, mag. susceptibility surface induced ferromagnetism, antiferromagnetic exchange interaction 78−79844
- $Hf(Fe_{1-x}Co_x)_2$, mag. props., Mossbauer spectra and magnetisation meas. 80−39948
- $HgCr_2Se_4$, initial mag. permeability freq. depend. near Curie temp. 78−10729
- $HgCr_2Se_4$, thermorefl. near ferro- to paramagnetic transition 79−78660
- $HgCr_2Se_4$, thermoreflectance, photoconductance, Raman scatt. near mag. phase transition 80−97298
- $Hg_{1-x}Mn_xTe$, EPR investigation of ordering effects 79−47330
- $(Ho,Y)Co_2$, first order phase transitions 78−84426
- $HoCo_2$, field induced vol. magnetostriction 78−91920
- K_2CuF_4, layered, mag. sp. ht., two-dimens. $S^1/_2$ Heisenberg ferromag. behaviour 77−32206
- K_2CuF_4, layered spin system, planar rotator symmetry, phase transition 80−65951
- K_2CuF_4, spin relax:, crit. behaviour, high freq. susceptibility meas. 80−65936
- $(La_{0.8}Ca_{0.2})MnO_{3+y}$, mag. props., Faraday method meas. 80−103832
- $LaMnO_3$, ferromag.-paramag. phase transition, neutron diffr., calorimetric investigs. 78−31072
- $La_{0.71}Pb_{0.29}MnO_3$, metal-semicond. transition at Curie point, transport props. obs. 79−73554
- $LiTbF_4$, ferromag., spontaneous magnetisation at marginal dimensionality 77−24683
- $LiTbF_4$, mag. props., crit. behaviour at marginal dimensionality 80−54906
- Lu-Mn alloy, mag. props. and effect of H_2 absorpt. 78−19250
- $LuMn_2$, Lu_6Mn_{23}, H_2 absorption effect on mag. props. 77−89931
- MnAs, formation of nuclei in ferromag. paramag. transition, thermal hysteresis 79−73720
- MnAs, generalised P-T phase diagram, mag. and structural phase transition 80−39780
- MnAs, PTH phase diagram of mag. transitions, Curie point 80−44832
- MnAs pseudocrystals, magnetostriction, anisotropy 77−4537
- MnAs, relation between displacive and first order ferromagnetic-paramagnetic transition 79−10908
- MnAs, struct. and mag. props., temp. depend., neutron study 79−47246
- $MnAs_{0.96}P_{0.04}$, latent ferromagnetism 80−11197
- $Mn_xNi_{1-x}Sb$, spin glass state and synthesis in high temp. and press. atmospheres 78−23277
- MnP, Lifshitz point, transverse differential susceptibility meas. 80−84599
- MnP, US vel. and crit. attenuation, longit. waves, external mag. field 78−27035
- $Mn_{1-x}Ti_xAs$, effect of press. and isostructural increments 77−89954
- $(NH_4)_2CuBr_4.2H_2O$, ferromag., static and dynamic mag. props. 80−50074
- Ni, angular resolved photoemission 78−68603
- Ni, atomic layers, Pauli paramagnetism to band ferromagnetism transition thickness depend. 78−72377
- Ni, critical NMR obs. near mag. transition 77−81026
- Ni film, effects of finite size on crit. phenomena, resistivity anomaly 79−38192
- Ni film, few atomic layers thick, transition from Pauli paramag. to band ferromag. 80−44885
- Ni film, magnetooptic Kerr effect meas. near crit. point 77−69811
- Ni film, transition from Pauli paramagnetism to band ferromagnetism 79−61192
- Ni, hyperfine interactions on implanted ^{12}B, crit. behaviour near T_c 78−43663
- Ni, magnetisation process in high mag. fields in crit. region 77−85498
- Ni, oxidation at Curie temp. 79−29279
- Ni, oxidation kinetics near Curie temperature 78−88578
- Ni, photoemission near Curie temp. 79−78841
- Ni, thermal expansion, 300-1000K, and power law consts. near Curie temp. 78−38858
- Ni-Cr, low temp. sp. ht. near ferro-paramag. transition 77−63218
- Ni-Cu, hydrogenated, Curie point, cluster magnetism 78−14960
- Ni-Cu, Ni rich alloys, magnetic phase transition, elec. resistivity meas. 300-700K 79−82781
- Ni-Fe solid soln., precip. hardened, paramag.-ferromag. transition on ageing 78−52255
- Ni-Mn-Al-Si-Co, Alumel, Ettingshausen-Nernst coeff. and transport props. from 200 to 473K 80−44573
- Ni-P, amorphous magnetisation, NMR and coercive force meas. 77−32187
- Ni-Ta, dil., crit. behaviour, ^{181}Ta PAC expt. 78−43723
- Ni-Ti (0-1.5 at.%), elec. cond., mag. phase transition, 300-750K 78−2678

ferromagnetic-paramagnetic transitions continued
- Ni-V, low temp. sp. ht. near ferro-paramag. transition 77−63218
- $(Ni_{1-c}Co_c)_{0.78}P_{0.14}B_{0.08}$, amorphous, mag. props., local environment model 77−12119
- $Ni_{1-x}Cu_x$, phase transform. influence on surface chem. reaction 80−108737
- NiPB amorphous alloys, ^{31}P and ^{11}B NMR near paramag.-ferromag. transition 79−33558
- Pd based 3d metal alloys, mag. phase diagram calc. 78−80144
- Pd-Ni, thermal expansion and magnetostriction meas. near crit. conc. for ferromagnetism 80−65881
- $(Pd_{1-y}M_y)_{100-x}Fe_x$, M=Ag, Rh, exchange-enhanced alloys, mag. ordering 79−61050
- Pr_3Tl, exchange-coupled singlet-groundstate system, central model 77−77060
- Pr_3Tl, singlet-ground state system, central mode, in ferromag. transition, neutron scatt. obs. 77−66317
- $Rb_2CuBr_4.2H_2O$, ferromag., static and dynamic mag. props. 80−50074
- Rb_2CuCl_4, layered, mag. sp. ht., two-dimens. $S^1/_2$ Heisenberg ferromag. behaviour 77−32206
- Rb_2ZnCl_4, phase transitions, thermal expansion coeff. 80−100638
- Sm compounds, mixed valence, metals or small gap insulators, two-band Hubbard Hamiltonian 80−34399
- $Sr_{0.3}La_{0.7}MnO_3$, neutron-irrad. induced phase transition 77−89952
- Tb-Gd, elec. resistivity and thermopower critical behaviour 80−15499
- Tb-Gd, ferromag. monocrystalline, crit. behaviour of elec. resist. 77−62886
- TbG_3, uniaxial ferromagnet, logarthmic corrections to crit. behaviour 78−60294
- TbZn, elec. resist., behaviour at mag. crit. points 80−65901
- TbZn, ferromag. transition, transport coeffs. critical behaviour 80−15498
- Th-Mn alloy, mag. props. and effect of H_2 absorpt. 78−19250
- Th_7Fe_3, H induced change from supercond. to mag. ordered state 79−28525
- $ThMn_2$, Th_6Mn_{23}, H_2 absorption effect on mag. props. 77−89931
- $Ti(Fe_{1-x}Co_x)$, press. depend., weak itinerant ferromagnetism 77−73028
- TmSe, Curie constant rel. to valence bond strength 80−60251
- TmSe, mixed valence cpd., thermal, mag., and transport props. 79−61074
- TmZn, magnetic-ion-lattice interactions, cryst. elec. field 77−4540
- U_3As_4, ferromagnetic transitions and heat capacities from 5 to 950K 78−14955
- $U_3As_4(Bi_4)(P_4)(Sb_4)(Se_4)(Te_4)$, symmetry changes 77−20597
- UD_3, crystalline elec. field studies using neutron inelastic scatt. at NRCN 80−10931
- UMn_2-UCo_2, mag. props., ferromag. transition *(Russian)* 78−68148
- UMn_2-UFe_2, mag. props., ferromag. transition *(Russian)* 78−68148
- $U_{1-x}Nd_xS$, mag. phase diagram 80−71027
- $U_{1-x}Pr_xS$, mag. phase diagram 80−71027
- US, elastic consts. temp. depend. in para- and ferromag. regions 79−77666
- U_3Sb_4, ferromagnetic transitions and heat capacities from 5 to 950K 78−14955
- UTe, critical mag. fluctuations near T_c 80−7122
- U_3X_4, (X=P, As, Sb, Bi), molecular field approx. study of mag. ordering, Curie temp., paramagnetic susceptibility 79−78410
- Y-Mn alloy, mag. props. and effect of H_2 absorpt. 78−19250
- YCo_2, density of states, mag. props. 79−90936
- YFe_2, phonon softening below Curie temp., Mossbauer effect 77−4589
- $Y(Fe_{1-c}Al_c)_2$, mag. and Mossbauer study, local environment effects 78−27033
- $Y(Fe_{1-x}Mn_x)_2$, mag. order onset 80−25135
- $Y(Fe_{1-x}Mn_x)_2$, Mossbauer spectra and mag. props. 80−39952
- $Y_6(Fe_{1-x}Mn_x)_{23}$, press. depend. 77−73028
- $YFeO_3$ orthoferrite, weak ferromagnet domain struct. near Neel temp. 79−99739
- YIG, pure and Ga-substituted diffuse refl. and thermorefl. spectra near Curie point 80−40131
- YMn_2, Y_6Mn_{23}, H_2 absorption effect on mag. props. 77−89931
- $Zr(Fe_{1-x}Co_x)_2$, press. effects on ferromag. to paramag. transition 77−66302
- $ZrZn_2$, weak itinerant electron ferromagnet, resistivity 77−72850

ferromagnetic properties of substances
- *see also ferromagnetic relaxation; ferromagnetic resonance; ferromagnetism; magnetic semiconductors*
- 35KFN10 alloy, X-ray diffr. investig. after thermomech. treatment *(Russian)* 77−48457
- actinide compound, ferromag. with mag. axial symmetry, temp. depend. of magnetisation 77−40044
- actinide compounds, mag. and structural props. review 77−63132
- actinide elements and compounds, book contrib. 80−75727
- actinide intermetallic cpds., cubic, var. from localised to itinerant magnetism 77−20534
- actinide intermetallics, $AnFe_2$, (An=U, Np, Pu, Am), magnetisation, neutron diffr. and Mossbauer expts. 77−63137
- actinide systems, nearly ferromag., coupled d- and f-band model 77−63211
- agricultural soil and plant improvement by ferromagnetic additives *(Russian)* 77−66882
- alaninium copper tetrahalides, exchange, mag. anisotropy, and spin diffusion contribs. to EPR linewidth 80−80597
- alkali metal metastable magnetic crystal, aligned electronic spins, mag. props. 77−77035
- alkaline earth transition metal ternary and quaternary oxides, ATO_3, $ATi_{1-x}T_xO_3$, and $AZr_{1-x}T_xO_3$, prep., mag. props. and struct. 79−15277
- alkyl ammonium copper chloride, two-dimensional ferromag., low temp. lattice cond., phonon spectrum 77−4227
- alkylammonium compounds, $(C_nH_{2n+1}NH_3)_2CuCl_4$ and $(C_6H_5C_mH_{2m}NH_3)_2CuCl_4$, interlayer exchange field 77−20714
- alkylammonium copper chlorides, high-temp. susceptibility obs., 80-300K, ferromag. interactions 77−66274
- alkylammonium copper halides, mag. sp. ht., two-dimens. S1/2 Heisenberg ferromag. behaviour 77−32206
- alloy under microplastic strain, singular behaviour *(Russian)* 78−39838
- alloy with two ferromagnetic components, surface excitations 80−25179
- alloys, d-metal, magnetic susceptibility and Knight shift meas. 80−66055
- alloys, electrical resistance meas. *(Dutch)* 77−8066

ferromagnetic properties of substances continued
- alloys, ferromagnetic exam. of atomic ordering mech., when in mag. field *(Russian)* 79−11609
- alloys, itinerant electron model, spin wave stiffness const. calc. 80−34613
- alloys, surface spin waves, cluster Bethe lattice approach 80−70983
- Alnico, 5 and 8, spinel type permanent magnet, magnetic aftereffect 77−16118
- Alnico, domain struct., variation under influence of heat treatment *(Russian)* 78−23292
- Alnico, interaction domains after heat treatment in mag. field *(Russian)* 78−68286
- alnico, thermal magnetic hysteresis *(Russian)* 77−16119
- Alnico 5, thermal treatment in mag. field, mag. props. 78−91905
- Alnico 8, permanent magnetic alloy, topography of precipitate phase *(Chinese)* 80−66512
- Alnico 8 permanent magnet, magnetic props. rel. with crystallographic texture 78−95483
- Alnico alloy, C addition effects on struct. and mag. props. 78−23835
- Alnico alloys, effect of Ce addition on mag. props. 78−2699
- alumel, B versus H measurement from 25 to 180°C 78−23297
- aluminoborate glass, Fe and Cr ion interaction, mag. and spectral props. 80−103883
- amorphous alloys, at. order effects 77−73006
- amorphous alloys, sputter-deposited, soft mag. props., magnetostriction 80−34696
- amorphous alloys, temp. depend. of mag. hysteresis props. 79−61186
- amorphous alloys, thermal expansion anomaly near Curie temp. *(Japanese)* 77−85542
- amorphous alloys 77−16054
- amorphous ferromagnetic materials, deposition from vapour or liquid, uniaxial mag. anisotropy 78−10677
- amorphous ferromagnetic ribbon, HF mag. characts., magnetostriction role 77−66408
- amorphous ferromagnets, book contrib. 80−75743
- amorphous ferromagnets, itinerant electron model, Invar anomalies, review 78−95413
- amorphous ferromagnets, resist. and magnetoresist. 77−66148
- amorphous magnetic alloys, developments and appl. 80−50143
- amorphous materials, mag. fundamentals, props. and appl. *(German)* 79−28557
- amorphous materials status and appls. *(Japanese)* 79−15325
- amorphous metals, possibility of low temp. phase below ferromag. phase 79−4674
- amorphous ribbon, saturation magnetostriction, and electronically controllable delay line 79−1700
- amorphous substance, ferromag. or spin glass transitions 78−2690
- amorphous system, cluster effective lattice method, mag. and electron props. 77−66242
- anisotropy energy density 80−88742
- atomic order, interaction with localised ferromagnetism 77−72965
- austenitic stainless steel, heat conductivity, low temp. mag. susceptibility meas. *(Chinese)* 79−47080
- BCC magnetically ordered alloys, effects on at. ordering-spontaneous magnetisation reln. *(Russian)* 78−19261
- binary alloys, narrow band, with random hopping, spin wave stiffness const. 79−56524
- biotite, thermal decomposition, stability of ferromag. products 78−57195
- blast furnace magnetic structure of ferromagnetic metals and alloys, metallographic study *(Bulgarian)* 78−73008
- borosilicate glass, Fe and Cr ion interaction, mag. and spectral props. 80−103883
- ceramic suspension, ferromagnetic treatment, optimum system construction with FOL instruments 78−4666
- chalcogenide spinels, ACr_2X_4 (A=Zn, Cd, Hg), mag. exchange interactions 77−24690
- chromindur, origin of coercivity, Lorentz microscopy, magnetisation and Mossbauer effect 78−64219
- chromindur, phase separation, Mossbauer obs. 78−88116
- coal, mag. susceptibility and Mossbauer meas. 80−60464
- copper formate anhydrate, cryst. struct. and mag. props. 80−79768
- cubic ferromagnetic single crystal, magnetisation process 77−69622
- cyclo-hexyl-ammonium-copper-trichloride, specific heat, ferromagnetic chain system 80−103491
- cyclohexyl ammonium copper chloride, one dimensional spin $^1/_2$ ferromag., mag. props. 80−71000
- cylindrical ferromag. conductor, acoustic wave propag., EM field behaviour 80−88857
- demagnetisability of grain-oriented materials 78−84449
- demagnetisation level determination, ferromagnetic materials, after NDT 79−49261
- detecting faults, magnetic particle inspection, arc strikes and counter meas. *(German)* 77−4880
- di(alkyl ammonium)copper tetrachloride, two-dimens. magnon and phonon thermal cond. in high mag. fields 77−69123
- di(propylammonium) copper tetrachloride, mag. suscept. meas. 77−63131
- di-(2,2,6,6-tetramethyl-4-piperidinyl-1-oxyl) suberate, nitroxide radical polarised neutron study in paramag. phase 79−47231
- dialkylammonium copper chloride, nearly 2-D ferromag., low temp. NMR 77−28455
- dialkylammonium copper chloride, two-dimens. ferromag., energy transport by paramag. magnons 77−80909
- dialkylammonium copper chlorides, mag. and struct. transitions, IR absorption 77−52097
- dialkylammonium copper chlorides nearly two dimens. Heisenberg ferromagnet, NMR study of magnetisation 77−85586
- dialkylammonium copper tetrachllride, ferromag., static and dynamic mag. props. 80−50074
- dialkylammonium copper tetrachloride, ferromagnetic layer compound, magnetostatic mode excitation 80−29538
- dialkylammonium copper tetracholorides, quasi 2-dimens., lattice- and spin-dimens. crossovers 77−59416
- diamond-Co, sintered together, remanent magnetism 79−99731
- dibutylammonium copper chloride, parallel pumping of two-dimens. spin waves, spin wave bandwidth 77−66425
- diethylammonium copper chloride, Heisenberg ferromag., spin wave theory 77−89922
- diethylammonium copper tetrabromide, mag. struct., NMR meas. 80−71192
- dil. impurity hyperfine fields, comparison with models 78−14954

ferromagnetic properties of substances continued
  dimethyl ammonium copper chloride, nearly two-dimensional ferromag., nucl. transverse relax. rates meas. 77—81024
  dimethyl ammonium copper chloride, spin dynamics near crit. pt. 80—7112
  dimethylammonium copper chloride bromide, mag. props., pulsed NMR expts. 80—11292
  dimethylammonium copper manganese chloride, two-dimens. mixed magnet, EPR 80—66030
  dimethylammonium copper tetra(chlorobromide), mag. susceptibility, 1 to 30K, mag. phase transition 79—4675
  dimethylammonium copper tetrachloride, crit. slowing down and anomalous relax. near Curie temp. 80—71053
  dimethylammonium copper tetrachloride, ferromag., quasi two-dimensional, ordering temp., press. depend. 80—84601
  dimethylammonium copper tetrachloride-tetrabromide mixed cryst., mag. transition 80—65874
  dimethylammonium manganese tetrachloride-d$_6$, structural and mag. phase transitions, neutron scatt. and AC susceptibility meas. 80—44825
  dipropylammonium copper chloride, ferromag., low temp. magnetism *(Japanese)* 77—20748
  dipropylammonium copper chloride, nearly 2D ferromag., spin wave theory 77—85436
  dislocated crystal, mag. anisotropy *(Russian)* 77—8377
  dislocation effects on phys. props. at $T \neq 0$K *(Russian)* 77—8378
  disordered ferromagnetic alloys, even magneto-optical effects, light cond. tensor 79—4792
  dispersions for magnetic tapes, structural and magnetic characteristics, cinematography appl. *(Russian)* 78—16886
  DyNi$_{3.4}$, magnetisation data 77—32177
  dysprosium ethylsulphate, pure dipolar Ising ferromag., critical thermodynamics 77—16095
  eddy-current flaw detection of long ferromag. products, magnetizing device parameters 80—89447
  electromagnetic props. inspection by electromagnetic transducer with frequency output signal 78—53131
  electron gas, 2D, intermediate density region 79—60110
  electron spin-lattice relaxation *(Russian)* 80—103823
  Elinvar, Curie point, magnetisation and susceptibility, heat treatment effects *(Russian)* 78—47973
  ethylammoniumtetrachlorochromate, optical absorption intensity, short-range spin correlation 80—108185
  Eu-Ag alloy, amorphous, formation and mag. props. 79—91216
  exchange narrowing 77—85627
  γ-Fe$_2$O$_3$ acicular particles, remanent coercive force 80—44872
  Fe$_{40}$Ni$_{40}$P$_{14}$B$_6$, amorphous, tape wound core, fluctuations of driving field 78—10726
  Fe$_{40}$Ni$_{40}$P$_{14}$B$_6$, Fe$_{32}$Ni$_{36}$Cr$_{14}$P$_{12}$B$_6$, amorphous Hall effect, press. and temp. depends. 77—66155
  α-Fe, mag. ordering affecting homodiffusion coeff., 511-1200°C 79—73711
  α-Fe alloy, ferromagnetic, thermodynamic analysis of solubility and miscibility gap 79—60508
  Fe particles in glass-like C matrix, identification and props. 80—11229
  ferric solution ferromagnetic liquid insulation in redox flow battery, quantum parameters separation 80—61338
  ferromagnetic, EMF generation by pulsed laser irrad. 78—68021
  ferromagnetic cantilevered beam plate, magnetoelastic buckling 79—18761
  ferromagnetic semiconductors, dielectric function depend. on magnetisation, light absorpt. coeff. *(Russian)* 80—15467
  ferrous formate dihydrate, mag. sp. ht. 79—91235
  film, evaporated, galvanomag. and mag. props., thickness depend. 78—23181
  film, sinusoidal voltage prod., mag. field meas. 78—26972
  film, transverse Kerr magento-optical effect, thickness depend. 77—59559
  film developments, review *(Japanese)* 77—69635
  films, induced mag. anisotropy, temp. depend. *(Russian)* 79—42757
  fine particle systems, physical basis and applications 78—84457
  flaw detected hy high freq. magnetization, harmonic content in mag. field 80—71857
  fluid rotating about vertical axis, convective instability of layer 79—27698
  garnets, ferro- and paramag., gyromag. ratio determ. by magneto-optical method *(Russian)* 77—32356
  Gd-alloy, ferromagnetic, nuclear spins as probe for mag. coupling and crystallographic order 78—10799
  GdCo amorphous film, magnetic compensation walls 77—8375
  Gentalloy, in Fe-W system, damping capacity *(Japanese)* 79—20094
  group VIII and nearly related elements, cmpd. and superlattice form. 79—94955
  Heisenberg open finite chains, mag. and thermodyn. props. 77—72971
  Heusler alloy, Mn-containing hyperfine field and magnetic behaviour 79—78360
  Heusler alloy, Mn-containing theory of spin waves 79—78354
  Heusler alloy with nonmagnetic impurity, transferred hyperfine field using volume overlap model 79—78054
  Heusler alloys, ferromag. alignment rel. to conduction electron polarisation 80—60235
  Heusler alloys, hyperfine fields at sp sites, spin echo NMR meas. 78—19371
  intermetallic compounds, containing d-transition metal, hydrogenated, magnetism 80—34609
  interstitial compounds, electronic structure and useful phys. props. 77—89683
  Invar, anomalous magnetisation and magnetoresistance under high mag. fields 77—80764
  Invar, deformed, magnetism and temp. depend. of effective field on ^{57}Fe *(Russian)* 79—24234
  Invar, elec. resistivity temp. depend., 300-1300K *(Ukrainian)* 77—69290
  Invar, elec. transport props. and Invar features *(Russian)* 78—14710
  Invar, Fe-Ni and Fe-Pt, magnetoelastic contribs. to US vel., elastic consts., and susceptibility 80—75829
  Invar, Fe-Ni-C, spin pinning effect in RF collapse studies, Mossbauer spectroscopy 80—44971
  Invar, ferromagnetic, lattice dynamics 79—55838
  Invar, ferromagnetism and antiferromagnetism coexistance at low temp. 77—66320
  Invar, hysteresis loop displacement 78—52312
  Invar, influence of magnetoelastic effects on lattice vibrs., neutron scatt. meas. 78—2722

ferromagnetic properties of substances continued
  Invar, itinerant electron character 77—66240
  Invar, mag. inhomogeneity, ^{57}Fe and ^{61}Ni NMR 79—19803
  Invar, mag. phase transitions, linear expansion coeff. and mag. susceptibility meas. 77—69553
  Invar, mag. susceptibility in technical saturation region and internal stress 77—85429
  Invar, magnetic and thermal anomalies 80—34603
  Invar, magnetic structure, absorbed H$_2$ effect 80—20534
  Invar, magnetic structure, depend. on absorbed H, Stoner's band model calcs., Mossbauer spectra 80—65787
  Invar, magnetisation, effect of deform. by cold rolling 77—48556
  Invar, magnetisation curves in high mag. fields above Curie point 77—66386
  Invar, magnetisation reversal, fast, forced by external RF mag. field, Mossbauer obs. 78—52311
  Invar, magnetocryst. anisotropy rel. to magnetisation 77—16070
  Invar, magnetocrystalline anisotropy 77—63173
  Invar, magnetovolume contrib. to temp. variation of magnetoresist. 77—31999
  Invar, press. effects on mag. props. 77—66241
  Invar, RF collapse studies, skin depth effect, Mossbauer spectroscopy 80—39953
  Invar, specific heat, temp. depend. *(Russian)* 78—56341
  Invar, stainless, thermal expansion, elastic props. and Mossbauer effect 79—56502
  Invar, thermal expansion coeff. relationship to magnetisation 80—15269
  Invar, thermal expansion coefficient, origin of anisotropy 77—84951
  Invar, volume magnetostriction 79—56590
  Invar, XPS of valence electrons, temp. effects, 122-580K *(Russian)* 77—8727
  Invar alloys, mag. struct. small angle neutron scatt. study 79—47249
  Invar alloys elastic and magnetoelastic effects 79—56589
  Invar behaviour in crystalline and amorphous alloys 79—56489
  Invar film, mag. props. and elec. resist. 77—32221
  Invar film, superfine mag. struct. *(Russian)* 80—80572
  Invar films, exchange interaction depend. on lattice parameter, spin-wave reson. and magnetisation meas. *(Russian)* 79—42751
  Invar neutron small angle scatt. magnetocrystalline anisotropy 77—85420
  Invar problem, conf., Nagoya, Japan (Sept. 78) 79—56481
  Invar-type alloys, review of magnetomechanical effects and state of art of materials 78—52330
  irreversible magnetising processes, random propag. 80—88818
  isopermalloy, permeability stability calc. rel. to texture *(Chinese)* 80—65959
  itinerant ferromagnet, spin-wave dispersion and linewidth 79—4668
  Kovar, effect of magnetic electrons on atomic interactions 77—43820
  liquids for energy conversion devices, long term stability 77—29051
  Lorentz microscopy, mag. domain images resolution, computer calcs. 78—35004
  mag. props. after isothermal thermomag. treatment *(Russian)* 80—25159
  magnetic inhomogeneous struct. model 79—56503
  magnetic stray fields, optical detection 78—31602
  magnetisation and hysteresis losses, math. model *(Russian)* 78—88140
  magnetisation characts. approximation *(Russian)* 78—31094
  magnetisation noise and power loss 79—24197
  magnetizing device for inspection of products of ferromagnetic materials according to parameters of Barkhausen discontinuity 80—89457
  magnetocrystalline anisotropy meas., capacitance torquemeter 78—93743
  magnetoelastic effects in mag. ordered regime 78—15003
  magnetoresistance anisotropy, planar Hall effect 79—23947
  Magnico alloy, with Si, Nb, Ti and La, low-temp. thermomag. treatment 77—63812
  Magnico alloy, with Si, Nb, Ti effect of Ub on mag. props. and grindability 77—63811
  α-martensite, quenching in const. magnetic field, struct. peculiarities *(Russian)* 79—52204
  metal, electron-phonon interaction effects on spin susceptibility 80—93108
  metal, excitations in mag. field, theory *(Russian)* 77—8291
  metal, ferromagnetic, mechanically stressed, magnetic-inductive method of discontinuous vibration detection, theory *(German)* 79—20315
  metal, ferromagnetic, Nernst-Ettingshausen effect, rel. to Hall effect and thermoelec. power 79—56199
  metal, inhomogeneously magnetised, muon (μ^+) method, mag. struct. study 79—42739
  metal hydrides, rare earth and intermetallic, electronic and mag. props., Mossbauer study 80—34830
  metal-H systems, anelastic and plastic props., review 80—49298
  metallic, glasses, soft-magnetic properties *(German)* 80—71108
  metallic glass, annealing, struct. relax. and crossover effect 79—86715
  metallic glass, hyperfine field and spin wave excitations, T$^{3/2}$ depend. 78—10672
  metallic glass, isotropic and anisotropic magnetoelastic effects, review 78—68352
  metallic glass, magnetostrictive film, overlay for variable SAW delay line 78—63240
  metallic glass, micromag. calcs. and props. 80—80501
  metallic glass, splat cooled, mag. props. 80—80491
  metallic glasses, Brillouin-Mandelstam scattering from thermal and excited magnons 80—70980
  metallic glasses, characts. and appls. *(French)* 80—39815
  metallic glasses, mag. props., struct., and prep., book contrib. 79—65665
  metallic glasses, Mossbauer investigation of electronic struct. 78—92009
  metallic glasses, review *(German)* 79—41962
  metallic glasses quenched from melt, appl. as soft mag. materials *(German)* 78—10676
  metallic magnets investigation, present state *(Polish)* 80—107987
  metallic rare earths, conference, St. Pierre-de-Chartreuse, France (Sept. 1978) 80—12844
  metallic very small particles, mag. ordering temps., ferro- and antiferromag. spin structures 77—73027
  metals, electron spin-lattice relaxation *(Russian)* 80—103823
  metals, max. in acoustic attenuation at low mag. fields 80—93158
  metals, thermal oxidation rate determ. using nanowebermeters 80—61045
  metals, transport props., crit. behaviour 80—65522
  metals, ultrasound attenuation and EM generation 80—108046
  metals, uniaxial ferrogmagnetic, influence of anisotropic fluctuations on elec. resist. near T$_c$ 79—91038

ferromagnetic properties of substances continued
metals and alloys, coercive force, automatic meas. by remote means 79—24690
Metglas 2605, and 2605 A, transport props., resist. and magnetoresist. 79—1590
Metglas 2605 ribbon, saturation magnetostriction meas. by small-angle magnetisation rot. 80—60391
Metglas 2826 ribbon, saturation magnetostriction meas. by small-angle magnetisation rot. 80—60391
Metglas 2826-A, anomalous magnetisation, critical effects, superparamagnetism 77—8328
Metglas 2826A, Invar related system, high press. Mossbauer spectra 79—56642
methylammoniumtetrachlorochromate, optical absorption intensity, short-range spin correlation 80—108185
mild steel, effect of elastic stress on mag. props. *(Russian)* 77—8329
mischmetal-based magnets, $MM_{1-x}Sm_xCo_5$, demagnetisation, temp. depend., 175 to 425K 79—78440
mischmetal-Co system, thermomagnetic analysis of intermediate phases 80—93115
mischmetal-cobalt alloy, $MMCo_5$, polished, domain wall grooving, optical microscopy and SEM obs. 77—8334
$Mn_{1-x}Cu_xSb$ films, $0 \leq X \leq 0.3$, magneto-optical props. 79—51981
Mumetal, magnetization curve and Gaussian error function *(German)* 80—50137
NDT, magnetic inductive method appl. *(German)* 78—48581
NDT by external induction and field selective display 78—15618
$(Ni_{1-x}Co_x)_{0.98}Mn_{0.02}$, average mag. moment of Mn atoms 79—28509
non-oriented elec., internal oxidation and nitridation effects on mag. props. 79—83336
nuclear fuel shell inspection, mag. method for detecting ferromag. particles 80—66746
organic alternant molecules with conjugated bonds, ground state multiplicity, ferromag. 79—774
oxides, $RCu_3Mn_4O_{12}$, R=La to Lu, Y, synthesis and mag. props. 80—75717
oxides with perovskite struct., neutron diffr., ferri- and ferromag. props. 78—52214
palaeomagnetic record carriers synthetic analogues, preparation, characterisation and mag. props. 78—65276
particles, ferromag., flocculation effects during mag. beneficiation 77—77809
Pd_3Fe, ferromag. spin wave meas., inelastic scattering of polarised neutrons 78—2665
pearlite, coercivity temp. depend., −196 to 770°C 77—20637
pearlite in C steels (0.08 to 1.6 wt.%), exam. of temp. depend. of mag. coercivity 78—52304
Permalloy, 50NP, and 79NM, magnetic properties and structure, environment effect during annealing 80—60366
Permalloy, conductor crossing effect on bubble propagation margins 80—29588
Permalloy, corrosion resist. and mag. props., effect of Cr addition 77—86219
permalloy, cylindrical domain static performance in inhomogeneous external field *(German)* 77—63226
Permalloy, demagnetisation eigenfunctions anal. of linear transverse magnetisation in long, thin stripes 80—34687
Permalloy, electrodeposition, mag. props. *(French)* 78—64488
Permalloy, FCC, mag. anisotropy induced by cold rolling 80—11188
Permalloy, films, Faraday rotation effect dispersion 80—40092
Permalloy, high permeability, effect of hardening additions on mag. props. *(German)* 79—28566
Permalloy, high-permeability, influence of grain struct. and non-mag. particles on mag. props. *(German)* 77—16112
Permalloy, magnetic head wear resistance and surface charact. against magnetic tape *(Japanese)* 80—35335
Permalloy, magnetisation improvement through solid state refining 78—91893
Permalloy, magnetisation reversal, fast, forced by external RF mag. field, Mossbauer obs. 78—52311
Permalloy, magnetoconductivity modulation by substrate electrostriction 79—60908
Permalloy, order-disorder transform. and magnetic props. obs., by neutron diffraction method *(Slovak)* 79—4963
Permalloy, oxidised film, magnetic noise, low temp. depression *(Russian)* 79—99734
Permalloy, proton radiation effects, Mossbauer obs. 80—40008
Permalloy, reference materials characts. obs., temperature effect 80—80563
Permalloy, T- and I-shaped elements with cylindrical mag. domains, magnetisation distrib. 77—77074
Permalloy, thin film, oscillatory metallic field effect and surface magnetoelasticity 79—56282
Permalloy 51N, powder metallurgy product. and props. 78—60603
Permalloy barrier film, worm-like motion of domain boundaries *(Russian)* 78—39375
Permalloy cylindrical film, magnetisation in crossed steady/alternating fields, easy axis dispersion influence 79—8024
Permalloy ferromagnetic noise eval. 79—2799
Permalloy film, break-cross-tie domain walls, thickness depend. 78—43619
Permalloy film, coercive force associated with domain boundary displacement *(Russian)* 80—50151
Permalloy film, corrosion kinetics, mass and resist. change techniques, comparison 78—27675
Permalloy film, domain nucleation using low intensity US 80—34731
Permalloy film, domain wall mass and energy, wall vel. depend. calc. 80—2614
Permalloy film, domain walls, magnetisation components distrib. 79—87298
Permalloy film, domain walls streaming *(Russian)* 79—82842
Permalloy film, electrodeposition with zero magnetostriction composition, technological control 79—33955
permalloy film, Fe-overcoated, optical and magneto-optical characts., mag. preps. 79—82956
Permalloy film, galvanomag. rotation characts., under uniaxial stress 78—84466
Permalloy film, hysteresis loop meas. using magnetooptical system 79—69707
Permalloy film, in weak field, pulse mag. reversal mechanism *(Russian)* 77—80976

ferromagnetic properties of substances continued
Permalloy film, mag. microstruct. obs. in nonlinear ripple magnetis. case *(Russian)* 80—65971
Permalloy film, mag. susceptibility meas. anal. *(German)* 77—16133
Permalloy film, magnetic leakage fields above stripe domains 77—77077
Permalloy film, magnetoresistive determ. of anisotropy energy and its strain depend. 79—56575
Permalloy film, mobility of Bloch lines 77—28421
Permalloy film, movement of circular Bloch line in cross-tie wall 78—31099
Permalloy film, multi- and single-layer, reson. curves subjected to tangential mag. reversals *(Russian)* 80—50195
Permalloy film, obliquely deposited, mag. anisotropy, annealing and deposition parameter effects *(Russian)* 77—80971
Permalloy film, on quartz, two-layer disc, bending reson. vibrs. *(Russian)* 77—24797
Permalloy film, oxidation, quartz cryst. microbalance, AES and XPS obs. 78—27676
Permalloy film, perpendicular anisotropy, structural and thermal stresses *(Russian)* 79—4708
Permalloy film, quasistatic and pulsed mag. reversals of Neel domain walls *(Russian)* 78—39374
Permalloy film, stray fields arising during pulse reversal 77—80980
Permalloy film, stripe domain struct., distrib. of magnetisation *(Russian)* 77—66396
Permalloy film, submicroscopical magnetisation structs. induced by fields normal to film plane 79—1697
Permalloy film, two-layer, with magnetostatic coupling, creep of domain boundaries *(Russian)* 77—43857
Permalloy film, velocity of motion of nonequilibrium walls of edge domains *(Russian)* 79—1694
Permalloy film, with band domain struct., pulse mag. reversals *(Russian)* 79—38361
Permalloy film, with-small surface anisotropy, ferromag. reson. 77—69701
Permalloy film demagnetising field and magnetisation curve determ. 77—73059
Permalloy film magnetometer, mag. props. and LF noise 78—48005
Permalloy film strip, wall curvature calc. with in-phase magnetisation 78—2717
Permalloy films, domain propelling tunnel, domain struct. displacement *(Russian)* 79—99736
Permalloy films, domain struct., nonuniform rotation of magnetisation *(Russian)* 79—47313
Permalloy films, induced mag. anisotropy, temp. depend. *(Russian)* 79—42757
Permalloy films, RF sputtered on Au, coercivity 80—80575
Permalloy films, thickness depend. of Bloch line mobility 79—24204
Permalloy films with band domain struct., thermomag. recording, resolving power *(Russian)* 80—75769
Permalloy I bars, hysteretic props., Bitter soln. obs. and Kerr effect meas. 79—78439
Permalloy I-bar elements, magnetostatic effects, unifying overview of domain and continuum results 80—44853
Permalloy narrow stripes, permeability 77—89987
Permalloy overlay bars, bubble stray field effect on domain wall struct., interference contrast technique 79—78457
Permalloy RF sputtered films, O effects in mag. and elec. props. 80—100603
Permalloy RF sputtered films, struct.-sensitive mag. props. 80—34705
Permalloy thick film coercivity control 80—15764
Permalloy thin film cores, domain wall motion and flux patterns, Kerr magneto-optic effect obs. 80—34721
Permalloy thin films, Neel wall transitions into cross-tie walls 79—95619
Permalloy-Co film, domain walls, magnetisation ripple *(Russian)* 79—47314
Permalloy-Cu(Al) two-layer films, mag. anisotropy, grain boundary diffusion *(Russian)* 80—71122
Permalloy-Rh, film, influence of Rh on corrosion resist. and mag. props. 80—3235
Permalloy-SiO_2-Schott glass, bubble propagation struct. 80—34719
perovskite-like oxides, $ACu_3B_4O_{12}$ subseries, synthesis, struct. and mag. props. 77—68960
phenyl alkyl ammonium copper chloride, quasi-two-dimens. Heisenberg ferromag., mag. props. 77—66273
polarised neutrons in condensed matter [conference, Zaborow, Poland (Sept. 1979)] 80—22136
polycrystalline ferromagnets, demagnetisation and reptation (creep) anisotropy *(French)* 78—43616
polytwin ferromagnetic cryst., crystallite thickness effects on mag. struct. *(Russian)* 77—80913
positive muons as light isotopes of H, book contrib. 79—82907
precipitation-induced coercive field enhancement, analogy to precip. hardening 77—77490
1,3-Propanediammonium-$CuCl_4$, antisymmetric and anisotropic exchange, EPR linewidth 78—10761
random binary alloys, elastic neutron scatt. cross section 78—91845
rare earth$_{50}$$Ag_{50}$, amorphous, bulk mag. props., field, time and temp. depends. 77—89932
rare earth alloy, amorphous, ferromag. state, non-axial elec. field gradient effect 80—75728
rare earth alloy, heavy, mag. anisotropy *(Japanese)* 77—85444
rare earth alloy, $R(Co,M)_5$, magnetisation reversal and high coercive force, domain boundary pinning *(Russian)* 77—8345
rare earth alloys, amorphous, mag. props. rel. to struct., review 79—15298
rare earth alloys, amorphous, magnetoresistivity, exchange scatt. model 78—95287
rare earth alloys, amorphous random anisotropy ferromagnetism in pair approx. 79—47276
rare earth alloys, magnetic properties, impurity effects, CPA calc. 80—44784
rare earth alloys, R_2Co_{17}, formation of mag. anisotropy role of rare earth ions *(Russian)* 78—76238
rare earth alloys, R_3Pt_4, R=Nd, Gd, Tb, Dy, Ho, Er, Tm, mag. props., 4.2 to 160K 79—78343
rare earth alloys, $R_{69}Ni_{31}$, amorphous, Curie temp., mag. susceptibility and coercive force, 4.2 to 300K 80—93092
rare earth alloys, RCo_2 and R_2Fe_{17}, Invar props. 79—56593
rare earth alloys, RCoAl, mag. props. 78—2659

ferromagnetic properties of substances continued
  rare earth alloys, RFe_2, magnetostriction studies, book contrib. 80−39846
  rare earth alloys, RM_2, (M=Fe, Co, Ni), magnetism, review 80−20365
  rare earth alloys, vol. magnetisation, point charge cryst. field model 77−63254
  rare earth aluminium Laves phase cpds., RAl_2, anisotropic magnetostriction, temp. depend. 80−39841
  rare earth amorphous alloys, random anisotropy magnetism 80−65853
  rare earth amorphous alloys, transport props. 80−20152
  rare earth cobalt intermetallics, Cu or Ni-substituted, narrow Bloch walls, magnetisation, 4.2K 77−8333
  rare earth cobalt intermetallics, RCo_2, elastic moduli, 4.2-300K 78−52332
  rare earth cobaltides, R_2Co_{17}, ^{59}Co NMR obs. of hyperfine fields and mag. moments 77−20726
  rare earth compounds, Kramers, temp. renormalised spectrum of mag. excitations, cryst. field level ordering 77−20516
  rare earth compounds, $R_xMo_6S_8$ mag. susceptibility meas., 1.3-300K 78−14936
  rare earth compounds, RCo_2 metamagnetic transitions in internal fields 80−60272
  rare earth compounds, RMo_6X_8, (X=S, Se), supercond. and long range mag. order coexistence 80−15642
  rare earth compounds, RRh_4B_4, coexistence of supercond. and ferromag. order 79−65579
  rare earth compounds, ternary, superconductivity and ferromagnetism 79−69617
  rare earth cpds., $RMo_6S_8(Se_8)$ and RRh_4B_4, coexistence of supercond. and mag. ordering *(Russian)* 80−84542
  rare earth cpds., RRh_4B_4 and RMo_6X_8 (X=S, Se), mag. order and supercond., neutron scatt. studies 80−44807
  rare earth ferromagnet, mag. hyperfine field interaction, ^{197}Au Mossbauer effect 77−8463
  rare earth ferromagnet, polarisation in external mag. fields, TDPAC 77−8462
  rare earth ferromagnets, spin polarised electron tunnelling 78−68094
  rare earth germanides, RMn_2Ge_2, magnetisation, 4.2-1200K 77−8285
  rare earth hydrides, magnetic props., book contrib. 79−82754
  rare earth intermetallic, $R(Fe_{1-x}Mn_x)_2$, phase struct., mag. and Mossbauer meas. 77−20563
  rare earth intermetallic compounds, book contrib. 80−75726
  rare earth intermetallic RCu_4Ag (R=Dy,Ho), mag. props. and cryst. struct. 77−20562
  rare earth intermetallics, magnetocryst. anisotropy 77−8299
  rare earth intermetallics, R_2Fe_{17} and $R_2Fe_{17-x}Ni_x(Co_2)$, mag. anisotropy and hyperfine interactions 77−8298
  rare earth intermetallics, RAl_2, cryst. field volume magnetostriction calc. 79−8029
  rare earth intermetallics, RAl_2, exchange modification of cond. bands 79−82568
  rare earth intermetallics, RAl_2, orbital and spin polarisations of cond. electrons 80−65791
  rare earth intermetallics, RFe_2, spontaneous magnetoelastic distortion, X-ray diffr. expts. 77−63253
  rare earth intermetallics, $RFe_{5-x}Ni_x$, giant intrinsic mag. hardness 78−56354
  rare earth intermetallics, RGa, mag. props., 4.2-350K 77−63230
  rare earth intermetallics, RMg_2, cryst. and mag. props., ordering 78−68185
  rare earth intermetallics, $RNiSi_3$, susceptibility, 80-1200K *(Russian)* 77−66281
  rare earth intermetallics, RPt, (R=Gd, Tb, Dy, Ho, Er, Tm), structs. and mag. props. 80−50069
  rare earth iron intermetallics, RFe_2, (R=Sc, Lu, Y), mag. props., 80-1300K *(Russian)* 80−75750
  rare earth iron intermetallics, RFe_2, magnetostrictive, book contrib. 80−75838
  rare earth iron intermetallics, RFe_2 type, magnetostriction in polycryst. samples 77−73065
  rare earth magnetically hard materials, review 77−73051
  rare earth metal, anisotropy of magnetic component of electrical resistivity 79−69494
  rare earth metal, magnetic properties, nonlinear s-f exchange interaction effect 80−15711
  rare earth metal, spin polarisation of field-emitted electrons 77−40337
  rare earth metals, ferromag. ordering *(Russian)* 78−60262
  rare earth metals, ferromagnetic theory of low-temp. and freq. depend. of extraordinary kinetic effects *(Russian)* 79−91408
  rare earth metals, heavy, liq., mag. susceptibility meas. 80−75740
  rare earth metals, heavy, mag. anisotropy *(Japanese)* 77−85444
  rare earth metals, mag. and transport props. 79−69658
  rare earth metals, magnon dispersions in ferromag. and screw structs., nonlinear s-f exchange interaction effect 80−75746
  rare earth metals, narrow domain walls, magnetic aftereffect obs. 77−8364
  rare earth metals, RKKY interaction and conduction electron polarisation 78−91859
  rare earth metals and alloys, book contrib. 80−75725
  rare earth molybdenum sulphides, $R_{1.2}Mo_6S_8$, low temp. magnetisation meas., and supercond. props. 79−8018
  rare earth orthocobaltites, $R_{1-x}Sr_xCoO_3$, ferromag. reson., Lande g-factor 80−25215
  rare earth orthocobaltites, $R_{1-x}Sr_xCoO_3$ and $La_{1-x}M_xCoO_3$, itinerant electron ferromagnetism obs. 78−10660
  rare earth orthotitanites, unusual mag. props., role of mag. moments 78−84400
  rare earth permanent magnets, physics and technology 80−20433
  rare earth rhodium borides, RRh_4B_4, NMR and sp. ht. in supercond. and mag. ordered phases 80−7037
  rare earth silicides, RMn_2Si_2, magnetisation, 4.2-1200K 77−8285
  rare earth systems with singlet ground states, low freq. modes 78−68131
  rare earth ternary borides, RRh_4B_4, ferromag. Curie Temp., high supercond. transition temp. 77−89893
  rare earth ternary borides, RRh_4B_4, supercond., re-entrant magnetism, energy band calcs. 78−52140
  rare earth ternary borides, RRh_4B_4, supercond. and ferromag., cryst. struct., X-ray diffr. 77−89423
  rare earth transition metal intermetallic permanent magnets, props. and technology, book contrib. 79−65696

ferromagnetic properties of substances continued
  rare earth-$(Co_{1-x}Ni_x)_5$, single cryst., mag. props., mag. reversal 77−85489
  rare earth-$Al_2(Zn)$, mag. coupling mechanism 79−4655
  rare earth-Al, RAl_2, spontaneous cell distortion due to cryst. field, magnetoelastic consts. 77−63255
  rare earth-Al Laves phase intermetallics, RAl_2, R=Gd, Ho, Dy, Tb, cubic Laves phase compounds, exchange striction determ. 80−44895
  rare earth-Au(Cu), amorphous, mag. and transport props. 80−34605
  rare earth-Co_2-Al, dil., nonmag. impurities effect on ordering temp. 78−84427
  rare earth-Co, RCo_3 (R=Gd, Dy and Ho), effect of absorbed H_2 on mag. behaviour 79−33483
  rare earth-Co, RCo_5, high anisotropy origin, cryst. field contrib. 77−73020
  rare earth-Co, RCo_5, mag. moment orientation, anisotropic mol. field model 77−89950
  rare earth-Co alloy, mag. anisotropy origin 79−38319
  rare earth-Co alloy, RCo_5, mag. anisotropy, individual Co site contribution 79−78366
  rare earth-Co alloys, ferromagnetic intermetallic compounds, comminution charact. 77−12564
  rare earth-Co alloys, first and second order transitions 80−34631
  rare earth-Co alloys, R_2Co_{17}, substituted 77−89947
  rare earth-Co permanent magnets, generation mechanism of high coercive force *(Japanese)* 79−100269
  rare earth-Co permanent magnets, microstruct., TEM obs., magnetisation 78−91901
  rare earth-Co system, spin reorientation and sp. ht. anomaly *(Japanese)* 79−47287
  rare earth-Co-Ni alloys, $Pr(CoNi)_5$ type, mag. props. and mag. reversal phenomena *(Russian)* 77−51924
  rare earth-cobalt intermetallics, permanent magnet production and props. 78−52309
  rare earth-cobalt intermetallics, RCo_2, spontaneous vol. magnetostriction and thermal expansion meas. 77−12183
  rare earth-Cu intermetallic compds. single crysts., mag. props. 80−54892
  rare earth-Fe_2, mag. props. changes due to H_2 absorption, unit cell vol. 77−63178
  rare earth-Fe_2, magnetomech. coupling and Young's modulus 78−84472
  rare earth-Fe_2 Laves phase compounds, magnetostriction anisotropy 77−63250
  rare earth-Fe, intermetallic compounds, mag. props. *(Rumanian)* 78−92007
  rare earth-Fe alloys, highly magnetostrictive, isotropy breaking magnetoelastic behaviour 78−72386
  rare earth-Fe alloys, RFe_2, temp. depend of coercivity 79−61185
  rare earth-iron alloys, elastic vs. magnetoelastic anisotropy 78−68347
  rare earth-Mg, magnetisation and neutron diffr. meas. 77−63105
  rare earth-Sb(Zn), cubic ferromag. single crysts., mag. and magnetoelastic props. 79−15332
  rare earth-Tb-Fe alloys, $R_xTb_{1-x}Fe_2$, Laves phase type, magnetostriction *(Russian)* 77−51932
  rare earth-transition metal alloy, disordered, saturation mag. moment using CPA 77−20515
  rare earth-transition metal alloys, amorphous, struct. and mag. props., book contrib. 80−39818
  rare earth-transition metal alloys, disordered, magnetisation behaviour 80−71099
  rare earth-transition metal amorphous alloy films with single mag. species 77−16121
  rare earth-transition metal hydrides, magnetic props., book contrib. 79−82754
  rare earth-transition metal intermetallics, struct. and props. review 78−10668
  rare earth-transition metal Laves phase, thermodynamic exam. of formation 77−1241
  rare earth-Zn alloys, parastriction and magnetoelastic coeffs. 80−65996
  rare earths, heavy, mag., electronic struct., book 78−60259
  rare-earth-Ni alloy, RNi_2 (R=Gd, Tb, Dy, Ho or Er), Mossbauer effect of ^{57}Fe 77−69743
  Rayleigh constant meas., electronic technique 78−12732
  Recalloy, Fe-Nb, semihard magnetic alloy, magnetic props., hardness, microstruct. 78−56660
  remanence rel. to palaeomagnetic studies 77−33062
  remanent magnetisation, anomalous temp. depend. 77−33060
  ring ferromagnetic samples, remagnetisation dynamics *(Russian)* 78−19275
  round bar, high energy alternating field stray flux testing technique 80−100972
  semiconductor, magnon-plasmon system 79−69659
  semiconductor, optical transparency, photoferromag. effect, Curie temp. shift *(Russian)* 78−72387
  semiconductor, Raman scatt. due to magnon-spin flip of cond. electrons 77−20839
  semiconductor, red shift effect, optical absorpt. edge calc. 80−66140
  semiconductors, ferromagnetic multivalley anisotropic, electron autolocalisation *(Russian)* 80−92848
  semiconductors, magnetic, spin wave electron amplification theory 80−97083
  semiconductors, magnetic, static magnetic properties, mean field approach 80−7090
  semiconductors, nearly ferromag., spin fluctuation theory 79−65636
  Sendust alloy, magnetic head wear resistance and surface characts. against mag. tape *(Japanese)* 80−35335
  Sendust ribbon, mag. props. 80−15761
  siegnette magnets with hexagonal barium titanate structure 78−76397
  single crystal balls, portable instrument for axes of easy magnets. determ. 78−8424
  sintered permanent magnets, development history, magnetic and physical props., appl. 80−29901
  $Sm_{1-x}R_xCo_5$ (R=Y, La, Ce, Nd), mag. props., domain boundary pinning on statistical conc. heterogeneities *(Russian)* 79−99728
  soft magnetic material, analysis by means of Barkhausen noise cross spectra 79−24199
  soft magnetic materials, coercivity meas. 77−41659
  sol, relaxation of mag. birefr. and dichroism 79−57301
  spin glass-ferromag. alloys, high-field magnetisation 79−33488
  spinels, electron exchange between Fe^{2+} and Fe^{3+} on octahedral sites 77−69752

ferromagnetic properties of substances continued
spinodal alloys characterisation techniques, props. and appls., review 80—50588
steel, alloy, deep drawing sheet, annealing effect on coercive force *(German)* 80—29573
steel, alloy, YuNDK24, magnetisation direction in interaction domains *(Russian)* 79—99720
steel, austenitic, crack determ. using mag. permeability probe *(German)* 79—52549
steel, austenitic, magnetisation meas. of stability 77—1579
steel, austenitic, martensitic transform., mechanism and kinetics, TEM, X-ray and optical obs. *(Rumanian)* 78—19746
steel, austenitic, Mn-Al-V-F2, EM characts. after nitriding, aging, austenitizing, NDT of nitrided layer depth 79—11750
steel, austenitic, Ni-Ti, alloy N35T5, ageing, magnetisation and Curie temp. depend. on plastic deform., Mossbauer studies *(Russian)* 79—69669
steel, austenitic stainless, Cr-Ni, elec. resistivity and struct.-mag. transitions at low temp. 79—99527
steel, austenitic stainless, magnetic susceptibility and magnetisation, low temp. 80—25102
steel, austenitic stainless, neutron irrad., mag. props. 80—29067
steel, austenitic stainless, stress corrosion cracking in H_2SO_4-NaCl soln., Ni and N_2 effects *(Japanese)* 79—100289
steel, austenitic stainless type 304N, machining induced deformation transformation, mag. evaluation 79—83195
steel, B-Si, grain-oriented, high induction, Cu impurity effects 80—89366
steel, C, ferromagnetic rods, direct and inverse electromagnetic conversion 79—52569
steel, C, magnetomechanical acoustic emission for residual stress NDT 80—71149
steel, C, mech. property meas., method and instrument 80—35469
steel, C, residual stress induced by uniaxial deform., mag. meas. 77—73390
steel, C, resistivity, thermal and elec., spin disorder scatt. anal. 78—76063
steel, C, rotational hysteresis 78—91889
steel, C, texture effect on mech. props./magnetic props. relationship, NDT appl. 79—96274
steel, C (0.01 and 0.06 wt.%), rephosphorised, mag. props. and texture 77—20634
steel, coercive force determ. *(Russian)* 79—73764
steel, coercive force measurement method of quality inspection of heat and thermomechanically treated parts 79—5113
steel, cold-rolled, isotropic, specific magnetic loss meas. at high frequency 80—101808
steel, Cr-Ni-Mo-V, magnetic induction, struct. dependence *(Czech)* 80—50141
steel, Cr-Ni-Mo-V, Mossbauer austenitometry and mag. props. 80—40003
steel, elect., mag. props. determ. with Epstein hysteresis tester 80—60364
steel, electric generator, anisotropic mag. props. obs. using NDT 80—21212
steel, electrical, mag. hysteresis representation in numerical modelling of mag. fields 80—88813
steel, Fe-Ni-Cr mag. susceptibility and magnetoresistance, temp. depend. *(Ukrainian)* 77—73004
steel, ferritic, magnetomechanical acoustic emission for residual stress NDT 80—71149
steel, ferromagnetic, U8, magnetic method of martensite transform. study *(Russian)* 79—87631
steel, ferromagnetic round bar, eddy current crack detection *(German)* 79—91880
steel, high-speed, low temp. mag. cycling effects on ferromag. struct. 80—100928
steel, low alloy and C, hardened and tempered parts, nondestructive magnetic inspection 78—95889
steel, low alloy and C, hardened and tempered parts, nondestructive magnetic inspection 79—1929
steel, low C, Al-killed, effect of V on mag. props. 79—83339
steel, low C, mech. props. determ., NDT methods 79—29176
steel, magnetic field effect on retained austenite transformation 77—16580
steel, magnetisation transitions, Barkhausen noise 78—91894
steel, magnetostriction effect, depend. on magnetising field intensity *(Russian)* 79—51831
steel, martensitic, sp. ht. and magnetisation meas. 1.2 to 10K 80—71059
steel, mild, acoustic emission during magnetisation, stress effects 79—82854
steel, mild, fatigue softening and hardening detected from Barkhausen noise 80—76428
steel, mild, plastic deform. during fatigue, detection by Barkhausen noise meas. 79—43524
steel, mild, rotational hysteresis 78—91889
steel, Mn, type 35SGM, magnetic, electrical, and mech. props. after tempering and hardening 79—66086
steel, Mn-Mo-Nb-C, transform. charact. and struct. during continuous cooling 79—29057
steel, Mn-Si, mag. method of NDT of mech. props. 80—21211
steel, non-oriented, texture and mag. props., effect of Mn and S content 77—86047
steel, Si, grain-oriented, high permeability, dissoln. and precip. of AlN and MnS 80—89223
steel, Si, highly-oriented domain and grain obs. methods, using ferromagnetic colloid technique 80—11856
steel, Si, nonoriented elec. sheet, solute oxidation effect on mag. props. 79—83335
steel, Si, nonoriented sheet prod. with texture of {100} ⟨ovw⟩ 80—89246
steel, Si, permeability change due to stress variation after demagnetization in Rayleigh region 80—88854
steel, Si, with coating, grain-oriented, domain pattern measurements *(Japanese)* 79—38353
steel, Si(3 wt.%) grain oriented, high permeability obs. 77—1881
steel, Si (6.5 wt.%) Mn, Ni and Al additions influence obs., on mech. and magnetic props. *(Slovak)* 79—5064
steel, stainless, Cr-Ni, low temp. plastic deformation, in mag. field 79—83256
steel, stainless, Fecralloy, creep-rupture props., 650-800°C 80—97535
steel, stainless, Invar related system, high press. Mossbauer spectra 79—56642

ferromagnetic properties of substances continued
steel, structural, 34KhN3M, heat treatment effect on magnetostriction 80—104306
steel, structural, nondestructive method of struct. damage investig. using cyclic loading effects and mag. characts. 78—3275
steel, transformations, influence of type of cold plastic strain *(Russian)* 79—52232
steel, transformer, anisotropy of temp. depend. of mag. props. *(Russian)* 78—39362
steel, transformer, cold-rolled effect of uniaxial elastic stress on dynamic magnetostriction *(Russian)* 77—69651
steel, transformer, EM losses, influence of charact. of substruct. distrib. *(Russian)* 78—7058
steel, types 45 and U8, plastically deformed, magnetoelastic props. *(Russian)* 80—44893
steel, Zi, high permeability grain-oriented, AlN precip. study 79—83337
steel 40Kh2N20, paraprocess magnetostriction near martensitic point in mag. field *(Russian)* 79—82850
steel 42NKhTYuA wire, hysteresis loop and differential permeab. after US and conventional drawing 79—15818
steel plate, fundamental and harmonic flux, sinusoidal applied mag. field 78—2708
steel strips, elec., grain-oriented, effect on stress-relief annealing treatments on permeability and ageing 78—23832
steel struct. testing from anal. of Barkhausen noise statistics 77—77647
steel wire, magnetically hard Kh13N13M2-type, electroplastic drawing *(Russian)* 80—20967
steels, constructional and tool, heat treatment effects on elec., mag. and mech. props. expt. 77—77719
steels, tool, type U10A and R6M5, phase comp. and phys. props. after hydrostatic extrusion 79—96053
steels Kh18N(10-25), mag. susceptibility, 4.2 to 300K, and magnetoelasticity *(Russian)* 80—65812
stress determ. by portable magnetic equipment 78—53172
superconducting film, long reentrant, self-heating-induced phenomena 80—50013
superconductor, critical behaviour, coexistence near supercond.-ferromag. multicritical point 79—47197
superconductor, magnetic, shape effects 80—103773
Supermalloy, 24 GHz ferromagnetic antiresonance transmission 77—51957
supermalloy, foil, microwave transmission, parallel RF and mag. fields 77—59462
superparamagnetism, magnetisation vector diffusion coeff., anisotropy energy, vol. distrib. of particles by Mossbauer effect 78—48099
synthesis, struct. and mag. props. 77—89934
TCNQ salt, 1-methyl-3′-ethyl-2,2′-quinoselenacyanine-$[TCNQ]_2$, two-dimens. ferromag., EPR 77—16148
TCNQ salts, $Mn(TCNQ)_2$ and hydrates, mag. and elec, props. 79—82767
temperature modulation, phase sensitive detect., theory 77—12098
terbium ethyl sulphate, mag. and thermal props. 79—7971
ternary compounds, supercond., p-state pairing and magnetism 80—54819
tetramethylammonium copper chloride, $S=1/2$ Heisenberg 1-dimens. ferromag., mag. props. 79—82766
thin film, direct determ. of mag. domain wall profiles, using split detector STEM 80—103867
Ticonal, domain struct., variation under influence of heat treatment *(Russian)* 78—23292
Ticonal, effect of rare earth metals on mag. props., struct., and phase transformations 79—99732
Ticonal, interaction domains after heat treatment in mag. field *(Russian)* 78—68286
Ticonal strength, effect of thermal stresses and phase transforms. 79—87721
Ticonal with Sm, magnetic props., phase transform. after thermomagnetic treatment 78—3155
Ticonal-type alloys, struct. after quenching from 800-850°C *(Russian)* 77—59822
TMNB, ferromag. chains with easy-plane anisotropy, exchange const., anisotropy const. and g-value 77—80927
TMNB, linear $S=1$ ferromag., easy plane anisotropy, low-temp. mag. props. 78—23250
TMNC, ferromag. chains with easy-plane anisotropy, exchange const., anisotropy const. and g-value 77—80927
TMNC, linear $S=1$ ferromag., easy plane anisotropy, low-temp. mag. props. 78—23250
TMNC, quasi one dimensional planar ferromag., low temp. NMR study im mag. field 80—97157
Trafoperm N2, magnetization curve and Gaussian error function *(German)* 80—50137
transformer, EM losses, effect of degree of perfection of crystallographic texture *(Russian)* 78—60309
transformer steel magnetic loss variation due to nonuniform normal press. *(Russian)* 79—91250
transition metal, 3d, localised moments, detection by electron energy loss spectra 77—69949
transition metal, bulk modulus, effect of correlations and ferromag. order 78—34564
transition metal, chemisorption of H, effect of surface spin fluctuations 80—75613
transition metal, d-d electron correlations in cohesion and ferromagnetism 77—62810
transition metal, Fano effect and hyperfine field of non-transition impurity 80—25128
transition metal, mag. susceptibility, spin wave spectrum for improved itinerant-localised electron model 79—1654
transition metal, magnetic ground state props., simple one-electron theory 77—63063
transition metal, surface density of states, continued fraction method 77—20388
transition metal 3d, spin-orbital interaction effect on NMR, g-factor anisotropy *(Russian)* 77—24752
transition metal alloy, electronic structure, mag. props. 78—95254
transition metal alloy, H-impurity complex obs. by mag. aftereffect 78—72373
transition metal alloy ferromagnetic thin films, fabrication by sputtering, and mag. props. 78—91881
transition metal alloys, AFe_2 and ACo_2, Invar effect, magnetovolume meas. 79—56592

ferromagnetic properties of substances continued
transition metal alloys, amorphous, mag. props., chem. short-range order 80—75739
transition metal alloys, amorphous, mag. props., structure and preparation 80—75737
transition metal alloys, CPA appls. 77—72983
transition metal alloys, dilute, spin glasses, mag. ordering, book contrib. 80—75787
transition metal alloys, dilute ferromagnetic, itinerant d-electron(hole) degenerate, spin stiffness constant 80—70930
transition metal alloys, effects of order on electronic struct. 79—90938
transition metal alloys, electronic specific heat, near and weak ferromagnetics 78—80158
transition metal alloys, ferromag., with atomic short range order, local environment effects on electronic struct., Fe-V appl. 78—67936
transition metal alloys, ferromagnetic, BCC, spin wave stiffness constant 78—91851
transition metal alloys, high-field susceptibility 80—7083
transition metal alloys, local environment effect on magnetic states 79—56491
transition metal alloys, mag. props., review 80—44823
transition metal alloys, mag. props. *(Japanese)* 78—47935
transition metal alloys, magnetically ordered, effect of magnetic field on P-T diagram 78—52246
transition metal alloys, volume anomalies 79—56490
transition metal alloys and cpds., sp. ht. and electronic structure *(French)* 77—28400
transition metal based amorphous mag. alloys, elec. field gradient 78—39475
transition metal elements and alloys, spin distribution, neutron diffraction expts. 80—25097
transition metal ferromagnetic amorphous alloys, mag. props. 77—55690
transition metal halides, $M(Cl_2)(Br_2)(I_2)$ ferromag. ordering of cation spin ang. momenta due to 90° exchange interactions 79—69666
transition metal intercalates of Ni and Ta dichalcogenides, Hall coefficient and resistivity 80—39610
transition metal intercalates of Ni and Ta dichalcogenides, magnetic susceptibility, function of temp. 80—39756
transition metal intermetallic cpds., H absorption and mag. props. 80—60224
transition metal layer compounds, mag. model, 0K phase diagram, spin wave spectrum 79—87273
transition metal silicides, NMR and μSR, microscopic mag. props. *(Japanese)* 78—52368
transition metal symmetric clusters, higher-order isotropic exchange, Schrodinger exchange model 79—7955
transition metal vanadates, elec. and mag. props. 79—78094
transition metal-H systems under high H pressure, phase diagrams., electrical cond., mag. props. 80—29923
transition metal-metalloid amorphous alloys, mag. props. review 78—52300
3d-transition metal-metalloid cryst. and glassy alloys, electronic struct. from magnetisation and Mossbauer meas. 80—29363
transition metal-metalloid metallic glasses, deformed, mag. props., mag. screening 79—15287
transition metals, 3d, ferromag., itinerant electron magnetism, magnetic excitation props., theory 80—34581
transition metals, electronic structure and ordering of sp defects 78—91639
transition metals, energy of cohesion calc., Hubbard Hamiltonian with exchange interaction 77—69261
transition metals, ferromag., dil. H electronic struct. 80—70638
transition metals, ferromag., electronic struct. of interstitials 77—62867
transition metals, interstitial or substitutional sp impurity doped, electronic struct. 80—34384
transition metals, itinerant ferromagnetism theory 79—78301
transition metals, photoemission spectra, core-level satellite struct. 80—29855
transition metals, role of electron correlation 77—72974
transition metals and alloys, 3d, Hall effect, electron scatt. processes 80—34419
transition metals and alloys, magnetisation in high mag. field, Arrott-Noakes plot 80—54919
3d-transition-metal dichalcogenides, mag. props. rel. to Hubbard model 79—78373
trimethyl ammonium cobalt chloride, magnetisation temp. depend. 80—7128
trimethylammonium cobalt trichloride dihydrate, Ising-like system, nucl. spin-lattice relax. of ^1H and ^{35}Cl 80—29638
trimethylammonium copper chloride dihydrate, mag. props., evidence for lattice dimensionality 77—89967
trimethylammonium copper heptachloride, one-dimens. ferromag., mag. susceptibility, 2 to 300K 79—61077
TTF-bis-dithiolene metal complex compounds, donor-acceptor type, one-dimens. mag. variety and props. 77—66271
two-layer mag. structures, thermomag. recording 80—100588
US, large magnetic anisotropy exam. 77—20585
V-Fe (29-35 at%), ferromag., mag. props. near crit. conc. for ferromagnetism 78—19225
vicalloy-2, high heating rate effect on mag. props. *(Russian)* 77—81328
^{O}, Heisenberg ferromagnet, spin dynamics, neutron scatt. expts. 77—20619
Ag-Ni, composite, fibre and layer structs., anomalous props. caused by internal phase boundaries 78—72754
τ-Al-Mn-C, permanent magnetism and microstruct. 80—75811
Al-Mn-Fe(Co)(Ni)(Cu), permanent magnetic materials, grain struct. effect *(Rumanian)* 79—73773
$Al_2Mn_3Si_3O_{12}$, spin correlations and phase transitions, neturon diffr. exam. 78—84390
$AmFe_2$, high temp. mag. props., 300 to 1100K 79—51757
$AmFe_2$, mag. props. of Laves phases 77—27851
Au-Co, liquidus line determ. by mag. meas. 80—60250
Au-Co solid solution, mag. susceptibility 79—61081
Au-Co solid solution, mag. props., freq. depend. suscept. maximum 79—69655
Au-Fe, competing interactions in FCC alloys 78—95453
Au-Fe, finite mag. clusters near percolation conc. 78—72371
Au-Fe, long range mag. order 77—63215
Au-Fe, spin-glass, characteristic temps. 79—38348
Au-Fe, spin-orbit coupling and electron scatt. 80—2370

ferromagnetic properties of substances continued
Au-Fe (1-7 at.%), extraordinary Hall effect, near ferromag. percolation limit 79—19575
Au-Fe (22 at.%), ferromag. phase, AC susceptibility near T_c 78—43575
Au-Fe alloys, spin correlations, neutron diffr. meas. 80—80482
Au-Mn, spin-orbit coupling and electron scatt. 80—2370
Au-Mn-Cr(Pd) alloy, ferro- to non-mag. transform. 77—12117
Au-Ni, fast liq. quenched, anomalous sp. ht. near ferromag. crit. comp. 77—80947
Au-Ni, heat capacity, 1.5 to 15K 78—95452
Au-Ni, magnetisation and sp. ht., ferromag., paramag. and crit.-conc. regions 79—38330
AuFe, spin glass freezing above ferromag. percolation limit 78—52264
$Au_{1-x}Fe_x$, $0.14<x<0.28$, ferromagnetism study by specific heat meas. 80—7121
$Au_2(Mn,Z)_2$, Heusler alloy, (Z=Al, Cu, Ga, In or Zn), magnetic order and coupling 79—38303
Au_4Mn, magnetic anisotropy const., anomalous field depend. 77—12113
Au_4Mn, magnetocrystalline anisotropy temp. depend. 77—51900
Au_2MnAl, Heusler alloy, ferromag., NMR meas. 78—76320
Au_2MnIn, Heusler alloy, ferromag., NMR meas. 78—76320
AuMnSb, ferromag. Heusler alloy, mag. hyperfine fields at Au and Sb sites, Mossbauer spectra 77—32303
$(Au_xPb_{1-x})_{1-c}Fe_c$, ferromag. and spin glass ordering 78—56335
Au_4V, partially disordered, magnetisation distrib., polarised neutron diffr. study 79—47244
Au_4V single crystal, ordered, mag, props., domain models 80—39770
BMn, ferromag., ^{55}Mn magnon-induced pseudoquadrupole processes 79—19802
$Ba_2Co_{1.65}Fe_{0.35}{}^{2+}Fe_{28}{}^{3+}O_{46}$, temp.-mag. field phase diagram, torque method 80—60276
$Ba_3Fe_2BO_9$, (B=Re, Te, W, Mo), siegnette magnets with hexagonal barium titanate structure 78—76397
$Ba_3Fe_{2-x}Ho_xUO_9$, $O\leq x\leq1.2$, perovskites, struct. and mag. props. *(French)* 78—18612
Ba_2FeSbO_6, siegnette magnets with hexagonal barium titanate structure 78—76397
$Ba_xLa_{1-x}CoO_3$, x=0 to 0.5, structural, elec. and mag. props., Zener double exchange and Goodenough's model 79—65663
$BaMnF_4$, ferromag. ferroelectrics *(Japanese)* 79—65804
$BaMnO_4$, ferroelectrically induced ferromagnetism 77—73067
$BaVS_3$, exam. of ferromagnetic, antiferromagnetic behaviour, depending on stoichiometry 78—52233
$BaVS_3$, mag. and elec. props. 79—91214
$BaV_xTi_{1-x}S_3$, mag. and elec. props. 79—91214
$Be_2Mn_{1-x}Fe_x$, mag. props., giant moment clusters 79—28508
Bi-MnBi, mag. props. singularities, electron microscope exam. *(Russian)* 78—39363
Bi-MnBi directionally solidified eutectic alloys, struct. and mag. props. 79—51815
Bi-MnBi eutectic composites, microstructure and mag. props., annealing effect 79—82827
$Bi_2Bi_4Fe_2Ti_3O_8$, dielec. and magnetoelec. props. 78—95562
$BiCo_{1-x}Fe_xO_3$, $x\leq0.7$, ferromag., X-ray powder diffr. data, configuration 79—64956
BiMn, ferromag., nucl. orientation of Bi isotopes 78—13010
BiMn, with ferromag. inclusions, magnetisation changes by US pulses 80—34732
$Bi_{95.6}Mn_{4.4}$, magnetisation of ferromag. precipitates, effect of ultrasonic pulses 80—2121
$(CH_3)_3NHCoCl_3.2H_2O$, chain ferromag. two magnon bound state, nuclear spin-lattice relax. 78—88206
CO_4P, amorphous ferromag., spectral density functions calcs. 79—47269
$Ca(Cu_{0.78}Mn_{0.22})_3Mn_4O_{12}$, mag. structure, neutron diffr. powder data, 350K ferromag. T_c 77—69502
$(Ca_{1-x}Sr_x)RuO_3$, mag. props. 78—27027
$Cd_{1-x}Ag_xCr_2Se_4$, Ag acceptor states effect on exchange interaction 80—20397
$Cd_{1-x}Ag_xCr_2Se_4$, ferromag. semicond., influence of strong elec. field on microwave absorption 77—28207
$Cd_{1-x}Ag_xCr_2Se_4$, ferromag., magneto-resistance exam. *(Russian)* 78—84238
$CdCr_2S_4$, $Cd_{1-x}X_xCr_2Se_4$, (X=Zn, Hg), optical and magneto-optical surface effects 79—82953
$CdCr_2S_4$, EPR line profiles in paramag. and ferromag. phases 79—28602
$CdCr_2S_4$ ferromag. semicond. film, props. 78—76175
$CdCr_2S_4$, ferromagnetic semiconductor films, prep. and props. *(Japanese)* 79—47308
$CdCr_2S_4$, Heisenberg ferromag., obs. of dynamic dipolar crossover, ESR linewidths meas. 79—24209
$CdCr_2S_4$, magnetic semicond., resonance Raman scatt., mag. circular polarisation props. 80—50341
$CdCr_2S_4$, phonon Raman scatt., mag. circular polarization effects 79—8134
$CdCr_2S_4$, photothreshold changes below mag. ordering temp. 80—97406
$CdCr_2S_4$, polycrystalline films, mag. semicond., spinel-type, magneto-optical effects *(Japanese)* 79—47415
$CdCr_2S_4$, single crystal ferromagnetic semiconductor, vapour-liquid transport growth method 77—21013
$CdCr_2S_4$, single crysts., EPR linewidth near Curie point, temp. and susceptibility depend. 77—63272
$CdCr_2S_4$, spin dependent phonon Raman scatt., resonance effects 77—73145
$CdCr_2S_4$:Cu, magnetic microregions caused by s-d exchange 77—77050
$CdCr_2S_4$:Gd, ferromag. reson. and electrical cond. 79—28626
$CdCr_2S_4$:In(Ga), resist. and magnetoresist. meas., effect of donor impurities 79—19608
$CdCr_2S_4(Se_4)$, ferromagnetic semiconductors, spinel-type, resonance Raman scattering and electronic structure *(Japanese)* 79—47421
$CdCr_2S_4(Se_4)$, spontaneous magnetisation temp. depend., nuclear resonance freq. depend. *(French)* 80—80483
$CdCr_2(S_xSe_{1-x})_4$, mag. transition obs. *(Russian)* 77—4517
$CdCrSe_4$, ferromag. semiconductor, mag. props. near Curie pt., doping effects 79—1670
$CdCr_2Se_4$, crit. behaviour near Curie point 78—31068
$CdCr_2Se_4$, crit. behaviour of optical absorption edge 78—35143
$CdCr_2Se_4$, Crit. relax. processes, mag. reson. expts. 80—60425
$CdCr_2Se_4$, deviation from Kittel's mag. resonance formula near T_c 79—87322
$CdCr_2Se_4$, ferromag. semiconductor, light scatt. from magnons under strong fields 78—84554

ferromagnetic properties of substances continued
$CdCr_2Se_4$, ferromag. semicond., photoinduced mag. anisotropy 80—50086
$CdCr_2Se_4$, ferromag. semicond., conc. anomalies rel. to red shift of absorpt. edge 80—70732
$CdCr_2Se_4$, ferromagnetic semiconductor, P_{Se}-T phase diagram, where $Se=Se_2$, near peritectoid reaction temps. *(Japanese)* 77—52290
$CdCr_2Se_4$, ferromagnetic semiconductor, single cryst. growth *(Japanese)* 79—47612
$CdCr_2Se_4$, ferromagnetic low anisotropy semicond., spontaneous magnetisation RF determ. 80—22396
$CdCr_2Se_4$ film, absorpt. and Faraday effect 78—2936
$CdCr_2Se_4$ film, ferromag. semicond., prep. by vacuum condensation 77—28724
$CdCr_2Se_4$ film, mag. linear and circular dichroism and Faraday rot. 79—99966
$CdCr_2Se_4$, influence of Co ions on anisotropy and magnetostriction, ferromag. reson. meas. 77—69659
$CdCr_2Se_4$, influence of ferromag. ordering on phonon Raman scatt. 78—2853
$CdCr_2Se_4$, mag. semicond., photoinduced binding of domain walls *(Russian)* 78—80174
$CdCr_2Se_4$, mag. semicond., domain struct. by IR Faraday effect 79—95604
$CdCr_2Se_4$, magnetic red shift origin, specular reflectivity, band struct. 80—40127
$CdCr_2Se_4$ magnetic semiconductor, photoinduced centre kinetics 80—71110
$CdCr_2Se_4$, magnetisation, study of photoindduced charges 80—80567
$CdCr_2Se_4$, magnon instability, under intense EM field 77—40048
$CdCr_2Se_4$, Mott ferromagnetic semiconductor, optical absorption edge, critical behaviour 80—97226
$CdCr_2Se_4$, optical absorption due to transitions between bands and local levels 79—38537
$CdCr_2Se_4$, reactor radiation influence on ferromagnetic phase transform. *(Russian)* 80—75760
$CdCr_2Se_4$, reflectance magneto-circular dichroism 77—81120
$CdCr_2Se_4$, refr. index variation in strong alternating mag. field 80—23741
p- $CdCr_2Se_4$, resistivity anomalies at mag. transitions, sp.ht. 80—39785
$CdCr_2Se_4$, resonant Raman scatt. 79—4802
n-$CdCr_2Se_4$, single crystal, transport props. near Curie temp. *(Japanese)* 78—6406
$CdCr_2Se_4$, single crysts., mag. semicond., spinel-type, magneto-optical effects *(Japanese)* 79—47415
$CdCr_2Se_4$, spin dependent phonon Raman scat., resonance effects 77—73145
$CdCr_2Se_4$, spin system heating by drifting current carriers, magnon-phonon system energy transfer *(Russian)* 80—29541
$CdCr_2Se_4$:Ag, ferromag. reson. meas. 77—8415
$CdCr_2Se_4$:Ag, ferromag. reson. field and linewidth anisotropy, Se vacancy effects 78—60338
$CdCr_2Se_4$:Ag, ferromag. linewidth and eddy current losses 79—33541
$CdCr_2Se_4$:Ag, mag. anisotropy, effect of annealing in vacuum 77—80929
$CdCr_2Se_4$:Ag(Gd), doping effects on exchange interaction 78—43579
$CdCr_2Se_4$:Cu(In), ferromag. semicond., mag. and elec. props. 77—20588
$CdCr_2Se_4$:Ga(In), photoconductivity, photomagnetoresistance near Curie point *(Russian)* 80—100485
$CdCr_2Se_4$:In, ferromag. semicond., carrier mobility, electron-two magnon scatt. Hall effect 78—51992
$CdCr_2Se_4$:In, influence of Se-deficiency on props. 78—30921
$CdCr_2Se_4$:In, nondegenerate ferromagnetic semiconductor, positive magnetoresistance 78—2505
$CdCr_2Se_4$:In(Ga)(Cu), magnetic microregions caused by s-d exchange 77—77050
$CdCr_2Se_4$:Ir(Cu), mag. props. near Curie temp. *(Russian)* 77—63234
$CdCr_2Se_4$-$ZnCr_2Se_4$, single cryst., mag. props. 79—28526
$CdCr_2Se_4(S_4)$, ESR line intensity near Curie point 78—64269
$CdCr_2Se_4(S_4)$, thermoreflectance, photoconductance, Raman scatt. near mag. phase transition 80—97298
$CdCr_2Si_4$:Ga, negative magnetoresist. effects near Curie temp. 79—11152
$CdCr_2Sr_4$, press. depend. optical aborption edge shift and compressibility 79—28714
$CdCr_2S_4(se_4)$, ferromag. semicond., band struct., EHT calc. 80—54608
$Cd_{1-x}Cu_xCr_2S_4$, elec. resist., temp. depend., behaviour at Curie point 77—62929
$Cd_{1-x}Fe_xCr_2S_4$, single cryst., mag. semicond., spinel-type, magneto-optical effects *(Japanese)* 79—47415
$Cd_{1-x}Fe_xCr_2S_4$:Cu, effect of doping on elec. props. and Curie temp. 78—84214
$Cd_{1-x}Hg_xCr_2Se_4$, ferromag. semicond. surface magnetism, magneto-optical meas. 77—20831
$Cd_{1-x}Hg_xCr_2Se_4$, photoferromag. effect and photocond. obs. 79—28376
$Cd_{1-x}In_xCr_2S_4$, ferromagnetic spinel, Cr^{3+} exchange interaction mechanism, Cr^{2+} relaxation, EPR line width depend. 79—69715
$Cd_{1-x}In_xCr_2S_{4-x}P_x$, ferromagnetic spinel, Cr^{3+} exchange interaction mechanism, Cr^{2+} relaxation, EPR line width depend. 79—69715
$Cd_{1-x}In_xCr_2Se_4$, electric, photoelectric and mag. props., metal-semicond. transition *(Russian)* 80—54738
$Cd_{1-x}Mn_xTe$, magnetic behaviour of Mn 78—14938
$Cd_{1-x}Zn_xCr_2Se_4$, ferromag. semicond., surface magnetism, magneto-optical meas. 77—20831
Ce-Sm-Co-Fe-Cu alloy, permanent magnet props. 79—8013
CeAg, mag. and structural phase transition at hydrostatic press., elec. resist. meas. 79—61102
$CeAl_3$, sp. ht., Kondo effect and ferromag. order coexistence 80—65927
Ce_3Al_{11}, competition between ferro- and antiferromag. interactions 80—60258
Ce_3Al_{11}, sp. ht., Kondo effect and ferromag. order coexistence 80—65927
CeBi, phase diagram in mag. field, hydrostatic press. effect 80—25132
$CeCo_5$, magnetisation and coercive strength 77—55688
$CeCo_{5+x}$, Cu and Fe modified, coercive force *(Czech)* 79—42805
Ce_2Co_7, and ternary hydride, mag. props. 80—108007
$CeCo_3H_4$, mag. props. 80—108007
$CeFe_2$, ferromagnetic cpds., mean field exchange consts., Stoner itinerant model calcs. 80—50084
$CeFe_2$, H_2 absorption effect on mag. props. and struct. 77—40045
$CeFe_2$, magnetostriction and magnetisation 80—39844
$Ce_{1-x}Gd_xRu_2$, superconductivity and ferromagnetism coexistence, 60 mK-4.2K, spin echo NMR 78—84349
$CeMM_{0.8}Sm_{0.2}Co_5$, (MM=mischmetal), thermal props. *(German)* 77—8359

ferromagnetic properties of substances continued
$Ce_2Mg_3(NO_3)_{12}.24H_2O$, ground state with dipole-dipole and exchange interactions in external mag. field 80—84582
$CeMn_2(Si_xGe_{1-x})_2$, $Ce(Mn_{1-x}M_x)_2Si_2$, (M=Fe, Cu), mag. props. 80—25134
$CeNi_4Al$, mag. susceptibility, H adsorption-desorption cycle effects 80—107990
$Ce_{1-x}Pr_xAl_2$, mag. struct., comp. depend., neutron diffr. and mag. susceptibility meas. 80—50054
$Ce_{3-x}S_4$, mag. ordering and elec. cond. 78—10681
CeSb, commensurate-commensurate transitions, devil's stairs theory 79—19740
CeSb, commensurate-commensurate transitions and devil's staircase 79—78317
CeSb, mag. excitation spectrum, inelastic neutron scatt. obs. 79—78352
CeSb, mag. excitations dispersion 80—25121
CeSb, mag. phase diagram and mag. struct., neutron diffr. determ. 77—63182
CeSb, mag. phase diagram for mag. field applied along ⟨111⟩ direction 79—33458
$(Ce_xY_{1-x})Fe_2$, mag. susceptibility and Mossbauer meas., lattice parameters 80—97068
$(Co, Cu, Fe)_5Ce$, sintered permanent magnets, magnetic charact. 78—60608
$(Co,Cu,Fe)_5Ce$, sintered, mag. props. 78—68302
$(Co,Fe,M)_{78}Si_8B_{14}$ amorphous alloys (M=V,Nb,Ta,Cr,Mo,W,Mn or Ni), zero magnetostriction and low field mag. props. 80—34741
$(Co,Fe)_{80}B_{20}$ glass, induced anisotropy and time changes of permeability 80—75815
Co (0001), photoemission, exchange-split energy-band dispersions 80—35059
Co, acoustic nucl. spin echo obs. at 4.2K *(Russian)* 78—6599
Co alloys, amorphous, effects of metalloids on mag. props. 80—75738
Co alloys, ferromag., 4d and 5d impurities, hyperfine fields 78—31133
Co, amorphous and liquid, density of electronic states 79—23881
Co, amorphous ferromag. film, resist. anisotropy rel. to struct. 77—72926
Co, and alloys, ferromag. films, coercive force, ion plating prep. 77—28730
Co, anomalies in thermal expansion and heat capacity 79—73744
Co, atomic layers, Pauli paramagnetism to band ferromagnetism transition thickness depend. 78—72377
Co, atomic magnetic moments comparison to values of ferromagnetic metal 78—52244
Co based alloys, mag. interactions, effects on moments *(Rumanian)* 79—15296
Co based alloys, resistivity magnetoresistance, s,p impurities in ferromag. host 78—68008
Co based amorphous alloy, mag. ordered, hyperfine field distribs., NMR meas. 78—68409
Co based amorphous alloys, struct. and thermomag. meas. 77—16055
Co based Heusler alloys, ferromag., hyperfine fields meas. by NMR 77—63315
Co catalyst, magnetooptical investigation of mag. props. 79—69858
Co, Co alloys, electrical resistivity and specific heat meas., anomalies rel. to thermally excited states 80—6809
Co complex, $CoCl_2(indazole)_2$, linear chain ferromagnetism 79—56519
Co complex, $CoCl_2(pyrazole)_2$, linear chain ferromagnetism 79—56519
Co, crystal hyperfine fields and neutron scatt. 79—56172
Co, diffusion of Mn, 860-1246°C, mag. transform. effects 77—24427
Co, dipole field anisotropy, at interstitial sites, lattice-deformation effects 79—33584
Co, electrical resist. temp. depend. near Curie point *(Russian)* 77—31989
Co, electrical resistivity, effect of domain wall orientation at 4K 78—91662
Co, electrodeposited coating, struct. and magnetic props. 79—46985
Co, electron irradiated, mag. after-effect spectrum, 20-350K 77—1570
Co, energy band dispersion and mag. exchange splitting, angle-resolved photoemission meas. 80—71567
Co epitaxial films, even magneto-optical effects 80—76007
Co, FCC, ferromag. domains of fine particles, Lorentz electron microscopy obs. 78—27053
Co, FCC, itinerant ferromagnetism 78—23238
Co, FCC, mag. props. of single-domain powders after plastic deform. *(Russian)* 78—6554
Co, FCC, self-diffusion and isotope effect, influence of mag. order-disorder transition 80—29205
Co, FCC single-crystals, NMR freq. depend. on interatomic distances 79—69748
Co, Faraday rotation in X-ray region 79—82958
Co, Fermi surface under press., de Haas-van Alphen effect meas. 80—75499
Co, ferromag., domain struct., small-angle neutron scatt. 77—66382
Co, ferromag., energy band struct. X-ray emission spectra *(Russian)* 79—15564
Co, ferromag., hyperfine fields at positive muons 78—43758
Co, ferromag., spin subband level position determ. by de Haas-van Alphen meas. under press. *(Russian)* 79—90947
Co, ferromag. film, ion plating prep., coercive force and magnetoresist. 77—12546
Co, ferromag. film, magnetoresistance parameter meas. *(Spanish)* 80—2485
Co, ferromagnetic, calc. hyperfine fields and their press. derivations 80—6796
Co, ferromagnetic, EMF generation by pulsed laser irrad. 78—68021
Co, ferromagnetic micropowder, cryst. struct., coercivity, remanence, saturation 80—65967
Co, ferromagnetism, theory 80—2541
Co film, amorphous, magnetoresist. in fields up to 80 kG 77—39823
Co film, evaporated, uniaxial mag. anisotropy 77—51929
Co film, even magneto-optical transmission effects, 0.4-1.25 μm 77—32354
Co film, ion beam sputtering prep., struct. and mag. props. 80—35085
Co film, linear mag. birefr. dispersion 77—69807
Co film, low-angle grain boundary struct. *(Russian)* 79—42807
Co film, mag. anisotropy study using NMR spin echo method 80—60384
Co film, mag. domain wall obs. by electron holography 80—80582
Co film, magnetic domain wall width, shadow and interf. electron microscope exam. 79—11330
Co fine particles in Cu, interface magnetisation 80—88858
Co, flow stress, effect of mag. field 77—20673

ferromagnetic properties of substances continued
Co, fundamental and secondary mag. props., book contrib. 80−75724
Co, giant internal mag. press. and compressibility anomalies itinerant model 77−16034
Co, HCP, electronic struct. calcs., cohesive energy and exchange splitting 78−34791
Co, HCP, electronic struct. calcs., band props. 78−39012
Co, HCP, electronic struct. calcs., mag. hyperfine field 78−39080
Co, HCP, ferromag., anisotropic hyperfine interactions, NMR expt. 78−43658
Co, HCP, NMR and nucl. relax. meas. in domain walls 77−36146
Co, HCP to FCC transition, mag. domain nucleation 78−64218
Co, HCP-FCC transition, mag. domain behaviour, Lorentz electron microscopy 77−80958
Co host, dil. impurity hyperfine fields, comparison with models 78−14954
Co, hyperfine mag. fields at ^{67}Ge, TDPAC meas. 78−43701
Co, internal fields, positive muon investigation 78−68438
Co, interstitial site determ., μSR technique 80−71287
Co, itinerant ferromag., Fermi surface and single particle excitations 80−34350
Co, Kerr equatorial effect freq. spectra anisotropy, dielectric permeability tensor *(Russian)* 80−55072
Co, local mag. field at positive muon 77−12295
Co, local magnetic fields probed by μ^+ 78−48103
Co, mag. domain struct. determ., high resolution colloid-SEM method 77−43846
Co, magnetic aftereffects of H isotopes, book contrib. 79−82835
Co, magnetic anisotropy induced by magnetic and stress annealing 78−35010
Co, magnetic anisotropy induced by mag. annealing and cold rolling, expt. 80−7695
Co, magnetic anisotropy induced by mag. annealing and cold rolling, calc. 80−7696
Co, magnetic domain struct. temp. depend. 79−78436
Co, magnetic permeability, effect of ion implantation 77−28414
Co, magnetised to saturation, props., positive-muon study 78−6619
Co, magneto-volume effects calc., rel. to itinerant electron model 78−43621
Co, magnetocrystalline anisotropy consts. meas., 77-700K 78−43582
Co, modulus defect due to internal strain 78−76286
Co, muon spin rotation; freqs., and relax. rates 80−55006
Co, NMR enhancement of modulating field due to anisotropic component of hyperfine field 77−55729
Co, NMR spectra temp. depend. 78−52364
Co, NMR-ON meas., mag. hyperfine splitting const. of ^{60}Co, ^{52}Mn and ^{90}Nb 78−43651
Co, oxidation at Curie temp. 79−29279
Co, oxidation kinetics, effect of Curie temp. 77−48592
Co particles, ferromagnetic colloids in toluene, small-angle X-ray scatt., interparticle correlations 79−11831
Co, plated film, magnetisation and mag. interface anisotropy 77−85510
Co, positive muons as light isotopes of H, book contrib. 79−82907
Co, press. effects on mag. props. 77−66241
Co, random close packed, normal Hall effect meas. 77−35924
Co rod, spontaneous vibr. modes excited by reversible magnetostriction 79−56587
Co, small-angle crit. neutron scatt. 78−31087
Co, spin fluctuations above Curie temp., diffuse mag. neutron scatt. obs. 80−50102
Co, spin polarisation of field-emitted electrons 77−40337
Co, spin polarised photoemission, surface magnetism 79−52083
Co, sputtered film, high coercivity and high hysteresis loop squareness 79−91259
Co, Stoner model, mol. field coeff., temp. and field depends. 77−72975
Co, sublimation rate near Curie temp. 80−49351
Co surface, electron spin polarisation, electron capture spectroscopy 78−95645
Co, transient mag. field discontinuity seen by O(F) ions 80−24515
Co, UPS, single cryst. and polycryst. film, electronic struct. 78−11081
Co, ultrafine particles prepared by vacuum evap. on running oil substrate, mag. behaviour 79−28565
Co, uniaxial magneto-crystalline anisotropy, temp. depend. 79−42753
Co:^{129m}Xe, mag. hyperfine field determ. by Mossbauer effect 77−8460
Co:Ga(Ge)(As), temp. anomalies of hyperfine fields 78−23265
Co:Lu, nuclear orientation meas., hyperfine field 77−32308
Co:Ra, hyperfine field determ. 77−85622
Co-3d transition metal alloys, hyperfine field and mag. perturbation distrib., NMR spectra meas. 79−61263
Co-Al, mag. struct. of Co rich intermetallic cpd., neutron scatt., cluster model 78−80130
Co-B alloys, amorphous, mag. moment and exchange stiffness constant 79−1662
Co-B alloys, amorphous, saturation magnetisation, mag. moments, X-ray diffr. obs. 79−4704
Co-B-Si, mag. props. different in amorphous and cryst. phases 77−69617
Co-B(-Cr) thin film glasses, mag. props. and corrosion resist. 80−80576
Co-C, ferromag., prep. by splat-quenching, obs. of electronic struct. of interstitial C 77−62868
Co-Cd, dil. alloy, impurity hyperfine interactions 78−84416
Co-CoO films, evaporated, exchange anisotropy 80−88841
Co-Cr films, mag. props. in range of transition from thin-film to hypercritical state *(Russian)* 79−51824
Co-Cr mag. film, crystallographic texture formation effects on props. *(Russian)* 80−108471
Co-Cr recording films, perpendicular mag. anisotropy, hysteresis loop, microstruct., TEM obs. 78−95491
Co-Cu-Fe-Ce alloys, sintered permanent magnets, mag. characts. 77−43855
Co-Fe, dil., effective mag. field at ^{59}Co, impurity conc. depend., spin echo expts. 78−48080
Co-Fe, dil., hyperfine mag. fields, press. effect, Mossbauer meas. 80−71277
Co-Fe, film, mag. and hyperfine field exam. of uniaxial anisotropy 77−66391
Co-Fe, soft mag. props. rel. to metallurgical aspects 80−88810
Co-Fe (6 wt.%), alloy, operation at 850 to 1000°C range *(Slovak)* 79−4698
Co-Fe alloy, HCP and DHCP, magnetostriction consts. determ. 78−80184

ferromagnetic properties of substances continued
Co-Fe alloy, Invar characts. 77−1550
Co-Fe alloy films, magnetostriction and orientation of easy magnetisation axes *(Russian)* 79−19756
Co-Fe alloys, FCC structure, average mag. moment, conc. depend. 78−88099
Co-Fe alloys, mag. anisotropy induced by mag. annealing through to double h.c.p. 77−1552
Co-Fe alloys, mag. loss meas. 78−6558
Co-Fe amorphous alloys, worked, perminvar type mag. hysteresis loop, longit. Kerr effect obs. 80−65958
Co-Fe-B and Co-Fe-Cr-P-B sputtered amorphous films, mag. props. and corrosion resist. 79−28567
Co-Fe-B films, amorphous, mag. annealing behaviour 79−73782
Co-Fe-Mn, dil. ferromag. alloy, mag. moment, saturation magnetisation meas. 78−64195
Co-Fe-Nb, heavily cold worked, magnetic hardening 79−20073
Co-Fe-Nb alloys, effect of cold working on mag. props., and precipitation morphology 78−39803
Co-Fe-Nb semihard mag. alloy, mag. precip. hardening 77−8960
Co-Fe-Nb-Mo, semihard magnetic alloy, magnetic props. 78−95469
Co-Fe-Ni semi-hard mag. alloy, 3-D Barkhausen effect meas. 77−69623
Co-Fe-Ni semihard magnetic alloy, directional distrib. of magnetisation changes connected with Barkhausen effect 78−14985
Co-Fe-Ni-Si-B glasses, soft mag. props. 79−73774
Co-Fe-P film, ferromag., coercive force meas. 78−10737
Co-Fe-Si-B, amorphous alloys, substitution effect on mag. props. 79−69695
Co-Fe-Si-B, ferromag., magneto-optical spectra in amorphous and cryst. states *(Russian)* 80−84749
Co-Fe-Ti (12,6 wt.%), semihard permanent magnet, magnetic precipitation hardening 78−52830
Co-Fe-V-Ni, mag. and mech. props., heat treatment and stress effects 80−60363
Co-Fe(Ni), magnetic anisotropy induced by magnetic and stress annealing 78−35010
Co-Ga, binary alloy, small-angle neutron scatt. from superparamag. behaviour 78−19217
Co-Ga alloys, ferromag., local configuration studies, neutron scatt. and spin echo NMR 77−63114
Co-Ga-Fe, small-angle mag. neutron scatt., states of mag. order study rel. to Mn and Fe substitution 79−11292
Co-Gd(Ho) film, amorphous, stripe domains and mag. anisotropy by Lorentz microscopy 77−63243
Co-Gd(Nd)(Pr)(Sm), dilute, magnetic annealing effect, induced anisotropy 77−73054
Co-Gd(Tb)(Sm) film, magneto-optic coeff. and refr. index, ellipsometric determ. 80−71501
Co-H, solid soln., magnetisation curve 78−84452
Co-mischmetall system, phase relations, microstruct., mag. props. 80−104118
Co-Mn, permanent magnetic materials 78−8426
Co-Mn (5.22 at.%), Mn diffusion, 868-1200°C, mag. transform. effects 77−24427
Co-Mn alloys, FCC, mag. moments of Mn atoms 78−76226
Co-Mn alloys, ferromagnetic, high field mag. susceptibility meas. 80−75729
Co-Mn-Ni-Fe-Si-B amorphous alloys, mag. props., low magnetostriction 80−75832
β-Co-Mn-Sn Heusler alloy, constitution and magnetic props. *(German)* 79−34009
Co-Ni, dil., effective mag. field at ^{59}Co, impurity conc. depend., spin echo expts. 78−48080
Co-Ni, electrodeposition, mag. props. *(French)* 78−64488
Co-Ni, ferromag. film, ion plating prep., coercive force and magnetoresist. 77−12546
Co-Ni, magnetic anisotropy induced by mag. annealing and cold rolling, expt. 80−7695
Co-Ni, magnetic anisotropy induced by mag. annealing and cold rolling, calc. 80−7696
Co-Ni, magnetocrystalline anisotropy consts. meas., 77-700K 78−43582
Co-Ni-Fe, semi-hard magnet, irreversible magnetisation changes, directional distrib. 79−24196
Co-Ni-Fe-Si(B), amorphous ribbon, magnetostriction meas. 80−15778
Co-Ni-P electrolytic layers, partial anhysteretic remanent magnetisation, additivity prop. *(French)* 80−44882
Co-Ni(Ti)(Cu)(Mn), cryst. struct. and stacking fault influence on mag. props. *(Russian)* 80−25164
Co-P, amorphous, domain struct., mag. anisotropy origin 80−80554
Co-P, amorphous, ferromag. antireson. 24 GHz microwave transmission, mag. props. 80−34778
Co-P, amorphous, sound propagation 77−62586
Co-P, amorphous alloy, domain struct., effect of annealing 78−60304
Co-P, amorphous foil, complex permeability and eddy currents, annealing induced short-range order 77−8360
Co-P, cryst. and amorphous mag. films, ferromag. resonance line width *(Russian)* 78−88192
Co-P, electrodeposited amorphous alloy, mag. permeability 78−52310
Co-P amorphous alloy, domain struct. 78−10720
Co-P amorphous alloy, ferromagnetic reson. exam. 79−28620
Co-P amorphous alloy, mag. props. 78−10724
Co-P amorphous alloy film, mag. domain struct. 77−69604
Co-P amorphous alloys, electrodeposited, magnetic anisotropy 79−28568
Co-P amorphous alloys, electrodeposited, mag. anisotropy 80−15713
Co-P electroless film on Al base disc substrate, microstruct. rel. to mag. props. 78−68304
Co-P film, amorphous, spin wave dispersion law, spin wave reson. obs. *(Russian)* 78−88196
Co-P films, electrodeposited, magnetic recording media *(Japanese)* 80−29587
Co-P films with various preferred orientations, mag. props. 80−100604
Co-Pt, amplitude depend. of internal friction *(Polish)* 79−95627
Co-Pt, atomic ordering props. and domain growth in strong pulsed mag. field *(Russian)* 80−54918
Co-Pt, struct. and mag. props. rel. to degree of order 78−72368
Co-Pt ferromagnetic alloy, 6 T ultrasonic study of magnetoelastic coupling 80−93154
Co-Pt film, electrodeposited, saturation mag. induction, mag. anisotropy and coercive field meas. *(French)* 80−2610
Co-Pt films, mag. and magneto-optic props., appl. to holographic and bit-by-bit storage 79−33512

ferromagnetic properties of substances continued
Co-rare earth dilute alloys, mag. annealing, conc. depend. 78–35011
Co-rare earth permanent magnet, grain alignment, metallographic method using eutectoid transform, of Co_5R 77–9003
Co-Re, sputtered film, high coercivity and high hysteresis loop squareness 79–91259
Co-Si-B, amorphous ribbon, saturation magnetostriction meas. by small-angle magnetisation rot. 80–60391
Co-Si-B-Fe amorphous alloy, electron diffr., mag. anal. *(German)* 79–61182
Co-Sm permanent magnet, grain alignment determ., metallographic method using eutectoid transform. of Co_5Sm 77–9003
Co-Sm-Gd(Ho) magnets, prep. and characterisation 77–8351
Co-Sm-Sn-$Co_{17}Sm_2$ eutectic fibre composite, coercive force 77–40084
Co-Sn, dil., ferromag., temp. anomalies of Sn mag. hyperfine field and thermal expansion 79–33270
Co-Ti (9 at.%), decomp. kinetics, elec. resist., hardness, and saturation magnetisation during ageing *(Russian)* 80–50587
Co-transition metal, transition metal additives influence on struct., specific resistance, microhardness, mech. props., magnetic props. 79–29078
Co-V, Co rich, mag. moments, Curie temp., and NMR spectrum 80–70964
Co-V, ferromag. struct. in nucl. spin echoes 80–60453
Co-V (12.4-18.7 at.%), ferromag. behaviour 79–24163
Co-W alloy electrolytic coatings, heat treatment effects on coercivity, hysteresis and structure *(Russian)* 80–60381
Co-W(Mo) magnetic alloys for high temp. appl. 77–85503
Co(-Re) sputtered films, mag. props. and microstructures 79–82837
$Co_{1-x}Au_x$, amorphous, elec. resist., temp. depend., spin wave contrib. and resist. minimum 78–51961
$Co_{1-x}B_x$, polycrystalline and amorphous sputtered films, Brillouin spectra 80–2775
$Co_{100-x}B_x$, amorphous, mag. struct., mag. susceptibility meas. 80–80485
$Co_{100-x}B_x$, amorphous alloys, saturation magnetostriction and annealing behaviour 80–34739
$Co_{100-x}B_x$ glassy alloys, mag. props. 79–73689
Co_3B, glassy and cryst., hyperfine field distrib., ^{59}Co spin echo spectra 80–80635
$Co_3B_7O_{13}X$, X=Cl, Br, I, ferromag. ferroelectrics *(Japanese)* 79–65804
$CoBr_2$, magnetic excitations, neutron scatt. investigation 80–39761
$CoBr_2.2H_2O$, metamagnetic, relax. phenomena at phase transitions 79–24164
$CoCl_2$, spin orientation of mag. impurity atom 77–59403
$CoCl_2.2H_2O$, magnetisation temp. depend. 80–7128
$CoCl_2.2NC_5H_5$, 1-dimens. Ising ferromag., charact. EPR modes 79–91287
$CoCl_2.2NC_5H_5$, magnetisation temp. depend. 80–7128
$(Co_{0.83}Cu_{0.17})_6Ce$, cryst. struct. and mag. props., decomp. during ageing *(Russian)* 79–37661
$Co_4CuCe_{0.9}$, correl. of cryst. struct. and coercive force *(Russian)* 77–80962
$(Co_{1-x}Fe_x)$-B-Si, amorphous mag. props. *(Japanese)* 77–85433
Co_xFe_{1-x}, ferromagnetism and spatial long-range order 80–60159
$Co_{74}Fe_6B_{20}$, metallic glass, zero magnetostriction, magnetisation characts. 77–12158
$Co_{79}Fe_{6.5}B_{14.5}$ amorphous thin films, zero magnetostriction, high magnetisation 80–34708
$(CoFeB)_{100-x}Cr_x$ thin films, magnetic props. and corrosion resist. 80–34709
$(Co_{0.93}Fe_{0.07})_{75-x}Cr_xSi_{15}B_{10}$ amorphous alloy, thermal stability, Cr conc. effects, DTA expts. 80–59395
$(Co_xFe_{1-x})_5Ge_3$, Mossbauer investig. of hyperfine field at Fe nuclei 77–20776
$(Co_{0.89}Fe_{0.11})_{72}Mo_3Si_{15}B_{10}$, metallic glass, strain- and field-induced mag. anisotropy 80–108004
$Co_{57}Fe_5Ni_{10}(Si,B)_{28}$, amorphous, soft mag. props., switched-mode power supply appls. 80–88850
$Co_{70.4}Fe_{4.6}Si_{15}B_{10}$, amorphous, mag. aftereffect spectra and annealing props. 80–88831
$Co_{75-x}Fe_xSi_{15}B_{10}$, quenched ferromag. ribbon, Brillouin spectra 80–2776
CoGa, onset of ferromag., diffuse mag. neutron scatt. meas. 77–63113
β-$Co_{52}Ga_{48}$, negative TCR obs. 80–75543
Co_xGa_{100-x}, electrical resistivity anomaly, spin cluster model 79–99531
$Co_2Ga_{2-x}Cr_x$, ferromag., local configurational studies, neutron scatt. and spin echo NMR 77–63114
$Co_2Ga_{2-x}Cr_x$, ferromag., site selecting and moment distrib. 77–77031
$Co_2Ga_{2-x}Cu_x$, mag. and struct. phases from magnetisation, neutron, X-ray diffr. techniques 78–52253
$Co_2Ga_{2-x}Fe_x$, elec. resist., temp. and mag. field depend., mag. contrib. 80–96846
$Co_2Ga_{2-x}Fe_x$, mag. field depend. of resist., 5.80K 80–70676
$Co_2Ga_{2-x}M_x$ (M=V, Cr, Mn, Fe), mag. props. and order 77–12093
$Co_2Ga_{2-x}Ni_x$, mag. and struct. phases from magnetisation, neutron, X-ray diffr. techniques 78–52253
Co(GaTiV) alloys, ferromag. onset, electron conc. depend. 80–60203
$Co_2Ga_{2-x}V_x$, ferromag., local configuration studies, neutron scatt. and spin echo NMR 77–63114
$Co_2Ga_{2-x}V_x$, ferromag., site selectivity and moment distrib. 77–77031
Co_2HfSn-Fe, dil., Heusler alloy, Fe hyperfine fields, Mossbauer obs. 78–68424
$(Co_{1-x}M_x)B$, M=Mn or Fe, ferromag., internal fields meas. by NMR spin echo 80–29646
$(Co_{1-x}Mn_x)_2B$, $0\leq x\leq 1$, magnetisation, lattice consts., press. depend. of Curie temp. 80–7137
$(Co_{1-x}Mn_x)_2B$, magnetocrystalline anisotropy meas., 4.2-300K 80–71006
CoMn(Cr)(V)(Ti), dil., low temp. specific heat and magnetisation 80–65925
$Co_{50}Mn_xGa_{50-x}$, cryst. struct. transform. of B2 type *(German)* 79–91642
$Co_{50}Mn_xGa_{50-x}$, ordering and disordering phenomena, mag. study 80–70154
CoMnP, cryst. mag. struct., neutron diffr. study *(French)* 80–59439
CoMnP, ferromagnetism and metamagnetism, polarized neutron diffr. study 80–44809
CoMnSi, $CoMnSi_{0.85}Ge_{0.15}$, mag. props. 79–42758
Co_2MnSi, ferromag. Heusler alloy, spin echo NMR meas. 77–63319
$CoMnSi_{1-x}Ge_x$, amg. props. 80–60270
$Co_{73}Mo_2Si_{15}B_{10}$, metallic glass, strain- and field-induced mag. anisotropy 80–108004

ferromagnetic properties of substances continued
$Co(NH_4)_2(SO_4)_2.6H_2O$ Tutton salt, low-temp. spin orientation, mag. props. 0-0.1K 79–15286
$Co_{0.08}(Ni,Cu)_{0.92}Fe_2O_4$ sphere, rotational hysteresis, mag. field strength and orientation depend. *(Russian)* 77–16110
$Co_{2-x}(Ni,Fe)_xTiSn$, Heusler alloy, positive contribs. to hyperfine fields, magnetisation and NMR meas. 78–43654
$Co_{1-x}Ni_xAl$, Knight shift and mag. susceptibility study, electron struct. peculiarities *(Russian)* 80–15814
$Co_{50}Ni_{20}Fe_6Si_{12}B_{12}$, amorphous, mag. props., effects mech. deform. 80–39840
CoNiP film, amorphous, electrolytic, prep. and props. *(Slovak)* 79–51823
CoP, and CoNiP, cylindrical amorphous electrodeposited layers, mag. props., torsion influence 80–88848
CoP-NiCoP, composite ferromag. film, exchange coupling between soft and hard layers, FMR obs. 79–78448
$Co_{1-x}P_x$ glass, crystn., spin wave reson. 79–73104
$Co_{35}P_{15}$, amorphous, strip domains, anisotropy const. effects 80–29571
Co_4P, amorphous, mag. excitations and static struct., neutron scatt. obs. 78–68204
Co_4P, amorphous ferromag., mag. excitations calc. in Heisenberg model 77–1546
$Co_{80}P_{20}$ glass, mag. props. 77–63125
CoPd, single crysts., domain struct., temp. and field depend. 80–71085
$Co_xPd_{80-x}Si_{20}$, amorphous, low field susceptibility near transition temp. 77–66359
$CoPt_3$, electrolytic films, saturation mag. induction, coercive fields, thickness depend. *(French)* 80–44883
Co_5R-H(D) system, R=rare earth, mag. orientation aftereffect 80–50148
Co_2RhS_4, mag. semicond., mag. and elec. props. 80–93121
$Co(S, Se)_2$, metamagnetic transitions in external fields 80–60272
CoS_2, ferromagnet, elec. resist. and thermal expansion anomalies 80–15542
CoS_2, galvanomagnetic effect of single cryst. 80–96912
CoS_2, hyperfine parameters and quadrupole splitting determ., ^{57}Fe Mossbauer spectra 77–77131
CoS_2, itinerant ferromagnet, ferromag. reson. and EPR meas. 80–66044
CoS_2, microscopic mag. props., NMR meas. 79–91306
CoS_2, narrow-band ferromag., high press. effect on anomalous elec. resist. 80–70698
$CoS_{2-x}Se_x$, conc. and temp. effects on metamagnetic transition 80–15716
$Co(S_xSe_{1-x})_2$, $(0\leq x\leq 1)$, mag. props. and elec. resist. 79–65657
$Co(S_xSe_{1-x})_2$, galvanomag. effects, obs. and interpretation 80–70726
$Co(S_xSe_{1-x})_2$, high field magnetisation, metamag. 79–91253
$Co(S_xSe_{1-x})_2$, metamagnetic transition, ^{59}Co NMR 79–38322
$Co_{74}Si_{10}B_{16}$ amorphous toroidal core, switching characts. and domain structs. 78–95477
$Co_{74}Si_{10}B_{16}$, amorphous ferromagnetic alloy, isothermal annealing effect on static magnetic props. *(Japanese)* 79–52398
$Co_{75}Si_{25-x}B_x$ glass, mag. moment, Curie temp., and microhardness, metalloid comp. depend. 77–55665
Co_5Sm, coercive field temp. depend. 77–8358
Co_5Sm crystals, microstruct., homogeneous precip. and nucleation 80–104160
Co_5Sm, magnetic domains, nucleation and pinning, magneto-optical Kerr effect 80–39811
Co_5Sm sintered magnet, effect of surface conditions on mag. props. 79–28556
$Co_2(Ti,Mn)Sn$, Heusler alloy, mag. meas. 79–47261
$Co_{1-x}Ti_x$, ferromag. props., Ti conc. effect 80–54872
$CoTi_{1-x}Al_x$, form. of mag. moment of Co atom, X-ray diffr., mag. meas. and NMR 77–43819
$CoTi_{1-x}Al_x$, mag. and electronic props., ferromag. and paramag. state 80–65814
Co_2TiAl, ^{59}Co NMR, above and below Curie temp. 78–2760
Co_2TiSn, Heusler alloy, positive contribs. to hyperfine fields, magnetisation and NMR meas. 78–43654
Co_2TiSn-Fe, dil., Heusler alloy, Fe hyperfine fields, Mossbauer obs. 78–68424
CoU_2S_5, mag. struct., exchange energy, magnetisation and neutron diffr. expts. 78–68170
Co_2VGa. ferromag. Heusler alloy, spin echo NMR meas. 77–63319
$Co_{90}Zr_{10}$, ferromag. amorphous alloy, crystn. and domain struct. study 80–107056
Co_2ZrSn-Fe, dil., Heusler alloy, Fe hyperfine fields, Mossbauer obs. 78–68424
Cr-Co-Fe, chromindur alloy, field heat treatment, and mag. props. 80–35354
Cr-Co-Fe; for telephone receiver mag. use 80–45318
Cr-Co-Fe, low Co, phase separation, TEM and Mossbauer spectra obs. 80–71269
Cr-Co-Fe cold formable mag. alloys for use in telephone receiver 79–52227
Cr-Co-Fe permanent magnet anisotropic alloys, plastic deform., ageing, particle alignment temp. 80–35254
Cr-Co-Ni hard film on Mo substrate for magnetic recording 80–2608
Cr-Fe, dil., magnetisation, Fe local moments 80–60215
Cr-Fe, dil., spin correlations and neutron scatt. near crit. conc., theory 80–60327
Cr-Fe, disordered, polarised neutron diffuse scatt. meas., 4.6-110K 80–34592
Cr-Fe, spin-glass phase, magnetisation curve test for mag. ordering 80–11201
Cr-Fe, superparamagnetism and mag. order charact. near critical conc., neutron scatt. study 79–11293
Cr-Fe (20 to 30 at.%), Mossbauer spectra temp. var. and ferromag. props. 77–81037
Cr-Fe-Si alloy, sp. ht., 1.4-4.2K 77–20079
Cr-Ge system, phase anal. and physical props. 79–24160
Cr-Ge system, XPS, X-ray and neutron diffr. and mag. meas. to study chem. bonding and electronic struct. 80–60749
Cr-Pt alloy, mag. props., effect of atomic environment 78–23247
Cr-S system, mag. props. *(Japanese)* 77–43825
CrB_3, crit. spin-relax. in hard mag. direction 78–72390
$CrBr_2$, ferromag. domains, using liq. He mag. specimen stage 80–103855
$CrBr_3$ anisotropic ferromagnet. crit. mag. relax., field and temp. depend. 79–1717

ferromagnetic properties of substances continued
$CrBr_3$, HF spectra, susceptibility, spin waves in domain walls *(Russian)* 80—80909
$CrBr_3$, reflectance and thermoreflectance spectra in paramag. and ferromag. phases 79—56770
$CrBr_3$, thick crystal, magneto-optical imaging of domain struct., multiple diffr. 77—8552
$CrBr_3$, two-dimensional mag. insulators, cryst. field spectra, mag. circular dichroism 79—47058
$CrBr_3$, two-dimensional mag. insulator, cryst. field splitting, spectroscopic g-factors 79—47059
$Cr_2(CrO_4)_3$, ferromagnet, ESR spectra near Curie temp. 79—8042
CrFe, mag. correls. and onset of ferromag., neutron scatt. study 80—50105
$(Cr_{1-x}Fe_x)_{1+\delta}Sb$, interstitial occupancy, Cr:Fe distrib., X-ray and neutron diffr. study 79—42012
CrI_3, ferromagnetic, origin of magnetic hyperfine field transferred at iodine 78—92000
$Cr_xMn_{1-x}As$, antiferromagnetic-ferromagnetic transition, mag. moment and elec. resist. meas. 80—15718
CrO_2 and tetravalent Cr oxide derivatives, metallic, chem. and phys. props. review 78—31069
CrO_2, epitaxial growth on rutile, possible appl. as bit oriented mag. material 77—16127
CrO_2, epitaxial growth on sapphire in air 78—27414
CrO_2, oxidative prep. method, mag. props. 80—44863
CrO_2 powder, thermal-magnetic props. 79—51821
CrO_2 powders, print through values and mag. characts. 80—44871
CrO_2, single mag. particle, remanent coercive force and remanent loop meas. 78—95480
CrO_2, synthesis and morphology 79—24481
$Cr_{1-x}Rh_xO_2$, ferromag., new prep. method by high-pressure oxidation, SEM characterisation 79—43164
$Cr_{1-x}Rh_xO_2$, oxidative prep. method, mag. props. 80—44863
CrS_xTe_{1-x} ($x=0$ to 0.2), magnetic props. study 80—11194
$Cr_2Se_{3-x}Te_x$, mag. props. and lattice parameters, comp. depend. 77—66263
Cr_3SeTe_3, anomalous Hall effect 77—69351
$Cr_3Se_{4-x}Te_x$, mag. props. and lattice parameters, comp. depend. 77—66263
CrTe, effect of high pressures on magnetic properties 78—52238
CrTe, mag. ordering under high-press., ferromag. transition, ESR and neutron diffr. *(French)* 78—31053
Cr_5Te_6, high press. effects on magnetisation and mag. transitions, 77 to 360K 77—77057
Cr_5Te_6, magnetoresist. in region of mag. phase transforms. *(Russian)* 77—66299
Cr_7Te_8 film, optical and magneto-optical props., appl. as storage medium 78—23545
$CrTe_{1-x}Se_x$ (Sb_x), Curie temp., high press. and doping effects *(Russian)* 77—12125
$Cs_2CuCl_4.2H_2O$, Bloch-wall NMR, anisotropic hyperfine interaction 79—51864
$Cs_2CuCl_4.2H_2O$, ferromag., hyperfine and exchange interactions, NMR study 80—50208
$CsFeCl_3$, linear chain ferromag., optical absorpt. and dichroism in mag. field 77—77237
$CsFeCl_3$, pseudo-one-dimens. singlet ground state ferromag., mag. excitations, neutron scatt. study 80—97064
$CsFeCl_3$, single cryst. mag. susceptibility meas. 77—20560
$CsMnF_4$, planar ferromag., cryst. and mag. struct., Jahn-Teller effect 80—75715
$CsNiF_3$, ^{19}F NMR, spin fluctuation suppression 78—91970
$CsNiF_3$, 1-dimens. ferromag., evidence for solitons, inelastic neutron scatt. study 79—78430
$CsNiF_3$, 1D ferromag., optical absorption and spin dynamics 80—71417
$CsNiF_3$, anisotropic Heisenberg chain, nonlinear excitations 80—70927
$CsNiF_3$, double-excitonic optical transition intensity, exchange and dimensionality effects 77—69591
$CsNiF_3$, easy-plane ferromagnet, one-dimens., dynamic props., review 80—15737
$CsNiF_3$, ferromag., Heisenberg chains with easy plane, validity of classical statistical mechanics 80—44786
$CsNiF_3$, field depend. mag. behaviour, mag. linear dichroism 79—73903
$CsNiF_3$, in mag. field, spin wave dispersion, inelastic neutron scatt. 77—77046
$CsNiF_3$, linear $S=1$ ferromag., easy plane anisotropy, low-temp. mag. props. 78—23250
$CsNiF_3$, low frequency dynamics in external mag. field 80—108020
$CsNiF_3$, NMR and relax. exam. 78—52371
$CsNiF_3$, nonlinear excitations, 1D-ferromag., neutron scatt. 80—70949
$CsNiF_3$, one dimens. ferromag., spin wave dynamics, inelastic neutron scatt. study 79—47270
$CsNiF_3$, one dimensional ferromag., magnetisation, FMR, 2.61-20K 77—20719
$CsNiF_3$, one dimensional planar model with symm. breaking fields, thermodynamics, static props. 80—97111
$CsNiF_3$, one-dimens. ferromag. far IR investig. of ferromag. reson., temp. and mag. field depend. 77—66427
$CsNiF_3$, one-dimens. ferromag., solitons in external mag. field 79—19724
$CsNiF_3$, one-dimens. ferromag. phonon dispersion surfaces 79—42180
$CsNiF_3$, one-dimens. ferromag., solitons as gas of quasiparticles, inelastic neutron scatt. obs. 79—73679
$CsNiF_3$, one-dimens. ferromag., collective excitations in mag. field 80—44822
$CsNiF_3$, one-dimens. magnet, local magnon modes 80—65829
$CsNiF_3$, one-dimensional magnet, dynamics, mol. field theory approach 80—34614
$CsNiF_3$, one-dimensional ferromagnet, optical absorpt. and static spin correlation functions 80—71415
$CsNiF_3$, planar ferromagnet, US attenuation, spin-phonon coupling, magnons and magnetostriction contrib., calc. 80—34611
$CsNiF_3$, quasi one dimensional planar ferromag., low temp. NMR study im mag. field 80—97157
$CsNiF_3$, quasi-1D planar Heisenberg ferromag., thermal renormalisation of sine-Gordon soliton mass 79—54036
$CsNiF_3$, quasi-one-dimensional ferromagnet, subthreshold parallel pumping of magnons 80—75745
$CsNiF_3$, single cryst. mag. susceptibility meas. 77—20560
$CsNiF_3$, stochastic motion of Sine-Gordon-solitons, spin-correlation function 80—93105

ferromagnetic properties of substances continued
$CsNiF_3$, subthreshold parallel pumping of magnons and antiferromag. reson. 80—71185
$CsNiF_3$:Mg, ferromag. chain system, temp. depend. of correlation length, quasi-elastic neutron scatt. meas. 77—16046
Cu complex, $(CH_3NH_3)_2Cu(Cl_{1-x}Br_x)_4$, ferromag., Br NMR mas. 80—29642
Cu complex, $[C_6H_5(CH_2)_nNH_3]_2CuCl_4$, $n=1,2,3$, two-dimens. ferromagnet, NMR and mag. susceptibility 77—16058
Cu complex, chloride monodimethylsulfoxide, spin $^1/_2$ ferromag. Heisenberg linear chain, cryst. struct. and mag. susceptibility 80—15706
Cu complex, chloride tetramethylsulfoxide, spin $^1/_2$ ferromag. Heisenberg linear chain, cryst. struct. and mag. susceptibility 80—15706
Cu complex, halocuprates, ferromagnetic insulator, two-dimens. Heisenberg layers, mag. susceptibility 80—50068
Cu compounds, layered, anisotropic and dipolar interaction terms effect on mag. phase transition 77—63210
Cu HCP film, uniaxial, mag. domain struct. 80—60385
Cu:Co precipitates, mag. anisotropy, precipitate shape, coercive force 80—80500
Cu-Al-Mn, Heusler alloy, magnetic prop. investig. of struct. transitions *(German)* 77—8289
Cu-Au-Fe, ferromag. ordering in FCC γ-Fe precipitates, Mossbauer study 80—71267
Cu-Fe, composite, fibre and layer structs., anomalous props. caused by internal phase boundaries 78—72754
Cu-Fe, dil., internally oxidised mag. and electrical prop. 77—12100
Cu-Mn (7 at.%), magnetic susceptibility, clustering, band model of heterogeneous magnetics 77—43823
Cu-Mn-Al, constricted hysteresis loop rel. to microstruct. 78—19273
Cu-Mn-Al, Heusler alloys, ferromag. inclusions, mag. props. and struct. study *(Russian)* 80—80570
Cu-Mn-Al, mag. props. and atomic ordering 79—24139
Cu-Mn-Al alloys, displaced hysteresis loop and microstructure obs. 80—84613
Cu-Ni, disordered ferromag., spin density asphericity, neutron diffr. study 79—47251
Cu-Ni, mag. ordering temp. depend. on atomic short-range order from susceptibility meas. 79—61159
Cu-Ni, random ferromag. alloy, local mag. moment calc. 80—70974
Cu-Ni alloy, critical conc. for ferromagnetism 78—14969
Cu-Ni alloys, magnetic diffuse neutron scatt. 78—14931
Cu-Ni film, mag. susceptibility meas., 30-130°C 79—95615
Cu-Ni films, compositionally modulated, magnetic anisotropy, magnetisation curves 80—88840
Cu-Ni films, thickness depend. of Curie temp., resist. meas. 78—6545
Cu-Ni-Co, mag. props. of system of disperse ferromag. particles, 73 to 673K *(Russian)* 80—65968
Cu-Ni-Fe, magnetic properties, heat treatment and compressive stress effects 80—60367
Cu-Ni-Fe, permanent magnet, temp. effect 80—34701
Cu-Ni-Fe, spinodal alloy, heat treatments for improved mech. props. 79—5024
Cu-Ni-Fe (14, 7 wt.%), solid soln., decomposed, magnetostatic interaction between ferromag. particles *(Russian)* 77—80967
Cu-Ni-Fe alloy, quenched and aged, deformed, low-temp. elec. resist. meas. *(Russian)* 77—52514
Cu-Ni-Fe solid solution, after precip., susceptibility of interacting superparamag. grains 79—99733
Cu-steel composites for intense pulsed mag. field generation 80—42245
$Cu_3B_7O_{13}X$, $X=Cl$, Br, ferromag. ferroelectrics *(Japanese)* 79—65804
$CuCl_2$.TMSO, ferromag. spin $^1/_2$ linear chain, mag. susceptibility 78—68180
$CuCl_2.2H_2O$, submillimetre ESR meas. using pulsed high mag. field 80—44905
$CuCr_2S_4$, ferromag., spin wave contrib. to nucl. spin-lattice relax. time meas. 77—36147
$CuCr_2S_4$, mechanism for phase transition from ferromag.-ferrimag. state *(Russian)* 77—36075
$CuCr_2S_4$, neutron diffr. study of mag. struct. *(Russian)* 79—95580
$CuCr_2S_{4-x}Se_x$ spinels, NMR spin echo study 80—71238
$CuCr_2Se_4$, crit. behaviour near Curie point 78—31068
$CuCr_2Se_4$, Crit. relax. processes, mag. reson. expts. 80—60425
$CuCr_2Se_4$, electronic state, polarized neutron diffr. obs. 79—56501
$CuCr_2Se_4$, experimental obs. 78—76227
$CuCr_2Se_4$, mechanism for phase transition from ferromag.-ferrimag. state *(Russian)* 77—36075
$CuCr_2Se_4$ single crystal, magnetic props. *(Japanese)* 78—6520
$CuCr_2Se_{4-x}Br_x$, elec. resistance, Hall const., magnetoresistance singularities *(Russian)* 79—91078
$Cu_yCr_2Se_{4-x}Br_x$, ferromag. magneto-resistance exam. *(Russian)* 78—84238
$Cu_yCr_2Se_{4-x}Br_x$, Hall effect 80—60012
$Cu_yCr_2Se_{4-z}Br_x$, degenerate ferromag. semicond., resist. minimum 79—73517
$Cu_yCr_2Se_{4-z}Br_x$, paramagnetic-ferromagnetic phase transition temp. depend. on element conc. 79—69672
$CuCr_2Se_4(S_4)(Te_4)$, binary and ternary solid solns., mag. and elec. props. 80—2407
$CuCr_2Se_{4-x}Y_x$, ($Y=Cl$, Br), magnetisation, Curie const. 79—91225
CuFeCrMn spinel oxides, struct. determ., mag. states of Mn^{3+} ions *(Russian)* 78—19227
$CuFe_2S_3$, cubanite, spontaneous magnetisation, polarised neutron obs. *(French)* 78—23245
$CuK_2Cl_4.2H_2O$, 3-dimens. Heisenberg ferromag., crit. behaviour 77—20594
$CuK_2Cl_4.2H_2O$, Heisenberg ferromag., press. effect on Curie temp. and susceptibility 77—28386
$CuK_2Cl_4.2H_2O$, Heisenberg ferromagnet, spontaneous magnetisation under press. *(Russian)* 77—36058
$CuK_2Cl_4.2H_2O$, Heisenberg ferromag., mag. props. at high press. 77—69512
$CuK_2Cl_4.2H_2O$, Heisenberg ferromag., mag. field effect on susceptibility near crit. point 80—39758
Cu_2MnAl, dynamical mag. susceptibility, spin waves, calc. from band struct. 80—54871
Cu_2MnAl, ferromag. Heusler alloy, polarised neutron study of mag. moment density 78—84391
Cu_2MnAl, Heusler alloy, spin waves, neutron inelastic scatt. meas., Heisenberg Hamiltonian analysis 77—80921
Cu_2MnAl, Heusler alloy, decomposition at 360°C 80—7536

ferromagnetic properties of substances continued
Cu_2MnAl superparamagnetic particles in Cu_3Al lattice, magnetic moment ferromagnetic ordering *(Russian)* 79—78444
$Cu_2Mn(Al_{1-x}Sn_x)$, Heusler alloys, thermal effects, saturation magnetisation 77—85499
$Cu_2MnAl_{1-x}Sn_x$, Mossbauer effect study 80—60473
$Cu_2MnSn(In)$, Heusler alloy, hyperfine field at ^{111}Cd, TDPAC meas. 78—43705
$Cu(NH_4)_2Br_4.2H_2O$, 3-dimens. Heisenberg ferromag., crit. behaviour 77—20594
$Cu(NH_4)_2Br_4.2H_2O$, Heisenberg ferromag. press. effect on Curie temp. and susceptibility 77—28386
$Cu(NH_4)_2Br_4.2H_2O$, Heisenberg ferromag., corrections to scaling in sp. ht. 77—66328
$Cu(NH_4)_2Br_4.2H_2O$, Heisenberg ferromag., mag. props. at high press. 77—69512
$Cu(NH_4)_2Br_4.2H_2O$, uniaxial ferromag. insulator, influence of press. on magnetisation 77—69661
$Cu(NH_4)_2Br_4.2H_2O$, Heisenberg ferromagnet, phase transition in mag. field 79—7992
$Cu(NH_4)_2Br_4.2H_2O$ Heisenberg ferromagnet, mag. props. in mag. field 80—34637
$CuRb_2Br_1.2H_2O$, three-dimens. ferromag., crit. susceptibility exponents in Curie temp. region using relax. techniques 77—66304
$CuRb_2Br_4.2H_2O$, 3-dimens. Heisenberg, ferromag., crit. behaviour 77—20594
$Cu(Rh_{1-x}Cr_x)S_4$, spinel system, susceptibility and metallic resistivity, anomalies due to s-d interaction 80—70958
dibutylammonium copper chloride, two-dimens. spin wave spectrum, parallel pumping meas. 77—20715
Dy, basal plane mag. anisotropy constant, field depend. meas., 4.2-120K 77—63165
Dy, crystal hyperfine fields at positive muons 79—56662
Dy, domain wall dynamics, NMR 77—69614
Dy, elastic constants, magnetoelastic contrib. 80—15777
Dy, field induced transitions of helical state 78—72349
Dy film, magnetoelastic waves, GHz, excitation, field depend. 78—72378
Dy, internal fields, positive muon investigation 78—68438
Dy, interstitial site determ., μSR technique 80—71287
Dy, longitudinal galvanomag. effect in single crysts. *(Russian)* 78—56132
Dy, mag. anisotropy and susceptibility 77—69539
Dy, mag. characts. in strong mag. field 77—89936
Dy, magnetic domain structure, hysteresis, thermal modulation study 80—71082
Dy, magnetic phase transitions, field-induced, isothermal magnetisation meas. 79—24161
Dy, magnetic phases, US study 78—31101
Dy, magnetoplastic deform., 70-90 kOe, 4.2K 77—8376
Dy, magnetoresist., fields up to 75 kOe, 1-70K 77—20297
Dy, magnetostriction meas. re-analysis, domain effects corrected by phase theory 78—6555
Dy, muon spin rotation; freqs., and relax. rates 80—55006
Dy, μSR in ferro- and antiferromag. phases, local fields 78—43763
Dy, parasusceptibility meas., 4.2-130K, spin wave anal. 79—95583
Dy, spin wave exam. 78—56306
Dy, US attenuation in mag. field 77—40104
Dy:$^{111}Cd(^{177}Hf)$, polycryst. ferromag., impurity hyperfine field polarisation, TDPAC and IPAC 77—73106
Dy:^{181}Ta, ferro- and antiferromag. phases, temp. depend. of mag. hyperfine field, TDPAC obs. 77—36165
Dy-Fe, amorphous, random anisotropy effects 78—68223
Dy-Fe alloy film, amorphous, contact printing 77—73061
Dy-Fe_xNi_{1-x} system, mag. hyperfine field, influence of lattice struct. and substituent 77—8058
Dy-Fe-Al, pseudobinary alloys, mag. props. 77—59397
Dy-Fe-O system, O-stabilised intermetallic $Dy_{12}Fe_{32}O_2$, prep. and characterisation 77—8956
Dy-Sm alloys, elec. resist. singularities and mag. transitions *(Russian)* 79—47075
Dy-Sm(Eu), mag. props. at low temp. in high mag. fields 79—56570
Dy-Sn alloy, hyperfine fields acting on diamag. impurities and anisotropic exchange, Mossbauer spectra 77—1625
Dy-Th, single cryst., mag. susceptibility, transitions, anisotropy 80—54873
$DyAl_2$, first order transition and tricrit. points, three-state Potts model 78—43589
$DyAl_2$, magnetisation, three-state Potts model 79—42804
$DyAl_2$, sp. ht. and thermal props., 5 to 300K 77—43342
DyBi, mag. behaviour 80—71025
DyC_x, $0.28<x<0.53$, cryst. struct. and Curie temp. 79—86741
$Dy_xCe_{1-x}Ru$, supercond., mag. order 79—87189
$Dy_xCe_{1-x}Ru_2$, investig. of coexistence of supercond. and ferromagnetism 79—11267
$Dy(Co,Ni)_2$, intrinsic mag. aftereffect obs. 77—63237
$Dy(Co,Ni)_2$, intrinsic mag. aftereffect meas., domain wall motion 80—71121
$DyCo_2$, field induced vol. magnetostriction 78—91920
$DyCo_2$, magnetocryst. anisotropy props. by ^{57}Fe Mossbauer spectroscopy 77—63328
Dy_2Co_{17}, and $Y_{2x}Dy_{2(1-x)}Co_{17}$, magnetocryst. anisotropy, 77-383K 77—89949
Dy_2Co_{17}, domain wall behaviour, TEM expts. 77—4524
$DyCrO_4$, determ. of mag. struct. by neutron diffr. 79—51753
DyF_3, transferred hyperfine interaction, NMR study 78—68393
$Dy(Fe,Al)_2$, saturation and remanent magnetostriction meas. 77—63256
$Dy_2(Fe,Co)_{17}$, mag. anisotropy fields by singular pt. detection 79—24156
$Dy_2(Fe,Co)_{17}$, magnetic anisotropy meas. by singular point detection method 77—63170
$DyFe_2$, high field magnetostriction and magnetisation 78—84471
$DyFe_2$, magnetisation and magnetic anisotropy 78—91862
$DyFe_2$ powders, mag. and hysteresis props. *(Russian)* 79—42800
$DyFe_3$ and Dy_6Fe_{23}, magnetostriction, room temp. to 80K 80—65993
$DyFe_3$, effect of adsorbed H on mag. props. 77—63129
$DyFe_3$, Mossbauer spectra, easy magnetisation axis temp. rot. 80—15859
$Dy_{1-x}Fe_x$, mean mag. moment calc. 79—82761
Dy_2Fe_{17}, domain structures and anisotropy constant. 80—93136
$DyFe_2H_2$, mag. props., ^{57}Fe and ^{161}Dy Mossbauer spectra and magnetisation meas. 79—78579
$Dy_2(Fe_{1-x}Ni_x)_{17}$, Mossbauer spectra, hyperfine field interactions 78—6614

ferromagnetic properties of substances continued
$Dy_{1-x}Gd_xAl_2$, easy axis rot., ^{163}Dy NMR obs. 79—78562
$Dy_{1-x}Gd_xAl_2$, ordered alloys, ^{163}Dy NMR, hyperfine field 78—10801
DyM_3, M=Fe, Co, Ni, amorphous, mag. struct. and moments 77—66260
$Dy_2(MoO_4)_3$, mag. susceptibility, ferromagnetism, mol. field theory 78—34966
$Dy_{1.2}Mo_6S_8$, long-range mag. order and supercond., neutron diffr. obs. 79—78320
$DyNi_2$, single cryst. mag. props. 77—24684
$Dy(OH)_3$, Mossbauer spectra, cryst. field and mag. props. 80—15873
$Dy_{1-x}Sm_x$, magnetoresist. of polycryst. specimens in fields up to 44 kOe *(Russian)* 80—92880
$Dy_xTb_{1-x}Fe_2$, and $Ho_xTb_yDy_{1-x-y}Fe_2$, high magnetostriction cpd., mag. anisotropy origins 78—68217
$DyVO_4$, antiferromag.-ferromag. structural phase transition induced by elec. field *(Russian)* 79—46802
$Dy_2(WO_4)_2$, mag. props., 300 to 900K 79—28510
$Dy_{1-x}Y_xAl_2$, ordered alloys, ^{163}Dy NMR, hyperfine field 78—10801
$Dy_xY_{1-x}Al_2$, domain wall dynamics, NMR 77—69614
Er film, magnetoelastic excitations, phonon spectroscopy and forbidden transitions 79—82853
Er, magnetisation and susceptibility in basal plane in strong mag. field *(Russian)* 80—50145
Er, spin wave exam. 78—56306
Er-Fe amorphous alloys, mag. props. 79—90557
Er-Ta, dil., mag. hyperfine field determ., TOPAC meas. 79—91330
$ErAl_2$, sp. ht. and thermal props., 5 to 300K 77—43342
$ErCo_2$, field induced vol. magnetostriction 78—91920
$ErCo_2$, magnetocryst. anisotropy props. by ^{57}Fe Mossbauer spectroscopy 77—63328
Er_2Co_{17}, magnetisation, magnetocryst. anisotropy and magnetostriction 77—8303
Er_2Co_{17}, single cryst., magnetostriction const. temp. depend., 78 to 300K 79—51836
$ErCo_3B_2$, ferromag. ordering and saturation moments 77—24711
$(ErCo_2)_x(ErAl_2)_{1-x}$, mag. and struct. investigations of intermetallic systems 78—95440
$Er_2(Co_{1-x}Fe_x)_{17}$, mag. anisotropy and intersublattice exchange interactions 78—31066
$Er_2Co_{17-x}Fe_x(Mn_x)(Ni_x)$, saturation magnetisation, Curie temp., easy direction, and anisotropy field 77—8304
$Er_2Co_{17-x}M_x$, M=Cr, Ni, effect of substitution on mag. props. 79—78363
$Er_2(Co_{1-x}Ni_x)_{17}$, mag. anisotropy and intersublattice exchange interactions 78—31066
$ErFe_2$, Czochralski growth, and cryst. quality determ. 77—8742
$ErFe_2$, Laves phase, cryst. field effects on spin wave dispersion relations 78—84408
$ErFe_2$ powders, mag. and hysteresis props. *(Russian)* 79—42800
$ErFe_2$, spin excitations, neutron scatt. obs. 77—63153
$ErFe_2$-YFe_2, and $ErFe_2$-$LuFe_2$, mag. props., 80-1300K *(Russian)* 80—75750
$ErFe_3$ and Er_6Fe_{23}, magnetostriction, room temp. to 80K 80—65993
$ErFe_3$, mag. struct., powder neutron diffr. meas. 78—2651
Er_6Fe_{23}, magnetostriction, temp. depend., 20 to 350K 80—65994
$ErFe_4Al_8$, neutron diffr. exam., mag. struct. 78—10656
$Er_{1-x}Gd_xAl_2$, nuclear hyperfine field, quadrupolar splitting, NMR study 80—39888
$Er_{1-x}Gd_xRh_4B_4$, supercond. and mag. transitions at press. up to 19 kbar 79—38236
$Er_{1-x}Ho_xRh_4B_4$, mag. and supercond. transitions, cryst. field effects 80—107950
$(Er_{1-x}Ho_x)Rh_4B_4$, superconducting ferromag., Josephson effect, point contact junction meas. 80—7043
$(Er_{1-x}Ho_x)Rh_4B_4$, superconductive and mag. interactions, hydrostatic press. effect 80—49973
ErMg, mag. props., neutron diffraction and magnetisation meas. 77—16045
$Er_2(MoO_4)_3$, mag. susceptibility, ferromagnetism, mol. field theory 78—34966
$ErNi_5$, cryst. field parameters in ferromag., paramag. states, susceptibility meas. 77—63139
$Er(OH)_3$, Mossbauer spectra, cryst. field and mag. props. 80—15873
$ErRh_4B_4$, ferromag. superconductor, vortex phase 80—80441
$ErRh_4B_4$, long ferromag. supercond., metastable supercond. state 80—103771
$ErRh_4B_4$, reentrant supercond., mag ordering, neutron diffr. obs. 78—14879
$ErRh_4B_4$, superconducting and mag. transitions, alpha particle irradiation damage effects 79—60954
$ErRh_4B_4$, superconducting and normal state props. 79—73632
$ErRh_4B_4$, superconductor, neutron scatt. exam. of mag. phase 79—73680
$ErTiO_3$, magnetic structure determination, neutron scatt. study 80—65809
$Er_{1-x}Tm_xRh_4B_4$, mag. and supercond. transitions, cryst. field effects 80—107950
$Er_2(WO_4)_3$, mag. props., 300 to 900K 79—28510
$Er_xY_{1-x}Rh_4B_4$, supercond. phase transitions, recentering temp. to normal ferromag. state 80—7024
ErZn, preferred mag. domain orientation, and microstructural defects, magnetostriction meas. 79—73769
Eu chalcogenide, spin-disorder Raman scatt., mag. phase depend., theory 78—10887
Eu chalcogenides, anomalous Hall effect, spin correlations, analysis 77—20344
Eu chalcogenides, anomalous Hall effect, impurity scatt. 78—39131
Eu chalcogenides, cond. band spin struct. 80—71577
Eu chalcogenides, heavily doped mag. semiconductors, effect of carriers statistics on indirect exchange 77—69280
Eu chalcogenides, resonant Raman scatt. 77—55787
Eu chalcogenides, resonant Raman scattering model via magnetic exciton in ferromagnetic phase 80—93326
Eu chalcogenides, spin-dependent Raman scatt. from phonons 80—97274
$Eu(Al_{0.5}Ta_{0.5})O_3$, mag. props. 77—4587
EuB_6, correlation between mag. struct. and elec. props. 77—63192
EuB_6, elec. cond. under hydrostatic press. 79—7832
EuB_6, electronic struct., transport and mag. props. 80—96782
EuB_6, ferromag., mag. props. 80—2561
EuB_6, ferromag., spin-polarised energy band struct., APW calc. 80—96779

ferromagnetic properties of substances continued
EuB_6, ferromag. and antiferromag. sp. ht meas., 1.8-77K 80—65948
EuB_6, Hall effect and resistivity data, ferromagnetic ordering temp., pressure depend. 80—60010
EuB_6, low temp. nucl. spin-lattice and spin-spin relax. times meas. 77—90063
EuB_6, mag., transport and thermal props. 79—73738
EuB_6, pure single crystals, magnetic and electric props. 80—11260
EuB_6, single and bulk polycryst., EPR, temp. and freq. depend. 79—28606
$EuB_{6-x}C_x$, magnetisation, effects of C 80—25163
$EuB_{6-x}C_x$, Mossbauer spectra, cond. electrons effect 80—20545
$EuB_{6-x}C_x$, pure and doped, mag. and transport props. 80—54689
$Eu_{0.5}Ba_{0.5}TiO_3$, ferromag., ferroelec., ceramic, Curie temps. determ. 78—68230
$EuCu_5(Pt_2)(Pd_2)$, indirect exchange, spin echo NMR meas. 80—15822
$Eu_{1-x}Gd_xO$, specific heat, magnetocaloric effect 79—69688
$Eu_{1-x}Gd_xO_{1-x}N_x$, ferromag. semicond., prep., ferromag. props. *(French)* 77—69550
$Eu_{1-x}Gd_xS$, concentrated system with ferromag. and antiferromag. interactions, spin-glass props. 80—34639
$Eu_{1-x}Gd_xS$ films, mag. and elec. props. 80—15766
Eu_2IrH_5, prep., cryst. struct., mag. and elec. props. 80—88117
$EuLiH_3$, transferred hyperfine fields at Eu nuclei, NMR meas. 80—71195
$EuNi_xCu_{5-x}$, mixed valency of Eu, Mossbauer expts. 78—52407
$EuNi_xZn_{5-x}$, mixed valency of Eu, Mossbauer expts. 78—52407
EuO, ^{153}Eu spin-spin relax. time and Suhl-Nakamura interaction 77—69722
EuO (100), disordered, LEED and electron spectroscopy 79—28178
EuO, anti-Stokes luminesc., magnon assisted 78—31252
EuO, critical EPR spin dynamics, sample shape and temp. depend. 77—32244
EuO, Curie temp. raising by impurity addition *(Russian)* 77—47994
EuO, degenerate ferromag. semiconductor, mechanism of transition to insulating state *(Russian)* 77—8024
EuO, dynamic dipolar cross over 78—76339
EuO, electronic struct. and props., mol. cluster approx. 77—11852
EuO, Eu rich, insulator-metal transition, model Hamiltonian 78—2422
EuO, Eu-rich, IR absorpt. spectra, 4.2 to 300K, transitions assoc. with O vacancies 77—52142
EuO, excitation of spin waves by current carriers, magnetisation and elec. cond. reduction *(Russian)* 79—7981
EuO, ferromag. reson. and nonlinear phenomena 79—28627
EuO, ferromag. semicond., electronic spectrum, influence of finite carrier conc. 78—76220
EuO, ferromagnetic, mag. field effect on optical absorpt. edge, piezotransmission spectra 78—95578
EuO, ferromagnetic piezotransmission behaviour in magnetic field 80—97272
EuO, ferromagnetic resonance and dielectric losses 78—2748
EuO film, thermomag. effects for reversible holographic storage 77—34851
EuO film threshold characteristics in holographic and bit recording *(Russian)* 80—63944
EuO, Heisenberg ferromagnet, exchange interactions, neutron scatt. expts. 77—20579
EuO, Heisenberg ferromagnet, static crit. props., neutron scatt. expts. 77—20618
EuO, light absorpt. during ferromag. reson. *(Russian)* 79—28618
EuO, light scatt. by spin waves 80—45086
EuO, light scatt. from bulk and surface spin waves 78—19497
EuO, light scatt. from bulk and surface spin waves 79—28778
EuO, mag. form factor of Eu^{2+}, solid state effects 78—2653
EuO, mag. struct. and transition temp., indirect exchange 78—91860
EuO, magnetic semiconductor, piezoresistance effect, 4.2 to 300K 80—34450
EuO, magnetic susceptibility, quasiphase transition 79—65684
EuO, magnetic susceptibility critical exponent, corrections to scaling 80—103846
EuO, magnetocaloric effect in high magnetic fields 80—25140
EuO, microwave and DC cond., dielec. const., 1.7 to 300K 77—20347
EuO, microwave cond., influence of mag. ordering 79—69544
EuO, optical orientation of f-electrons, Curie temp. variation due to exchange interactions *(Russian)* 79—15431
EuO, origin of exchange interaction 78—10675
EuO, physical and physicochem. props., review 80—96875
EuO, quadrupole coupling due to lattice imperfections 78—76347
EuO, single crystal enriched in ^{17}O, growth from melt in sealed Mo crucible 77—4734
EuO, spin system heating by drifting current carriers, magnon-phonon system energy transfer *(Russian)* 80—29541
EuO, spin wave damping, theory compared with expt. 78—52237
EuO, spin wave lifetime, theory compared with expt. 80—60228
EuO, spin-dependent Raman scattering 79—95782
EuO, stoichiometric, crit. behaviour of piezotransmission at Curie temp. 77—85688
EuO, surface magnons and surface mag. struct. 77—36066
EuO, transmission and resistivity, stress modulation effect near Curie temperature 80—96874
EuO, transport properties at ferromag. reson. 78—68387
EuO, zero-field critical relax. rate, mode-coupling theory 77—69593
EuO, zero-wave vector kinetic coefficient near T_c 79—73714
EuO:Eu, doped ferromag. semicond., carrier density and mag. susceptibility rel. to M-S transition 77—72820
EuO:Gd, 4f-photoelectron spin polarization, temp. depend. 79—78842
EuO:Gd, critical specific heat depend. on doping, microwave cond. 79—95602
EuO:Gd, elec. cond. under hydrostatic press., Curie temp. 80—96881
EuO:Gd, electron mobility below Curie temp. 78—91696
EuO:Gd, ferromag. semicond., electron spin polarisation and conduction band struct. 80—65449
EuO:Gd, mag. props. and instability phenomena 79—1666
EuO:Gd, pure and doped, elec., mag., and optical props. rel. to electronic conc. 80—96880
EuO:Gd, surface depolarisation of photoelectrons 78—15286
EuO:Gd, surface mag. props. 80—71566
EuO:La, metallic, photothreshold, correl. and exchange energy of electron gas 77—62852
EuO:La, photothreshold reduction by mag. induced space charge layer 78—72692

ferromagnetic properties of substances continued
EuO:La(Gd), photoelectron spin polarisation, temp. depend. 77—69966
EuO:La(Gd), photothreshold changes below mag. ordering temp. 80—97406
$EuO:Sm^{3+}$, hyperfine field at Sm, TDPAC meas. 80—93215
EuO:Yb(Sm), electron transition and valence state of impurities, X-ray spectroscopy and structural anal. 78—39064
EuO-RN solid soln., (R=Nd,Eu,Gd), ^{151} Mossbauer spectroscopy 78—6610
$EuO_{1-\Delta}$, thin film, Faraday effect dispersion and transmission, 0.5-1.1 μ, 20.4 and 77K, anion vacancies 79—19945
$EuO_{1.05}$, specific heat, mag. phase transition 77—36077
$Eu_{1-x}O$, optical absorpt. spectra at metal insulator transition 78—10928
Eu_2O_3, large single crystals, production and props. rel. to structural anisotropy *(French)* 77—36396
$EuO_{1-x}N_x$, ferromag., temp. variation of EPR linewidth *(French)* 77—85547
$EuO_{1-x}N_x$, ferromag. semicond., elec. and mag. props. *(French)* 78—79993
EuO(S), cryst. and electronic struct., mag., elec., and optical props., book contrib. 80—39760
EuO(S), ferromagnetic electronic structure, absorption, thermoreflection and thermotransmission spectra *(French)* 80—97300
EuO(S), phase transition spectroscopy 77—63426
EuO(S), spin assisted Raman scatt. theory 78—43866
EuO(S), spin order and fluctuations, Raman scatt. study 80—97273
EuO(S), spin polarisation of field-emitted electrons 77—40337
EuO(S):Gd, indirect exchange 78—23264
EuO(S)(Se), exchange interaction mechanisms, theory compared with expt. *(Russian)* 78—39312
EuO(S)(Se), superexchange interaction parameters, many-electron model calc. 79—7988
EuO(S)(Se)(Te), Heisenberg ferromag. semicond., hyperfine and exchange interactions 77—69530
EuO(s), mag. semicond., s-f model, intermediate coupling theory 79—95326
$EuPt_x$ compounds, partial valence change, ^{151}Eu Mossbauer and magnetisation obs. 80—70167
$Eu_{1-x}{}^{2+}R_x{}^{3+}O_{1-x}N_x$ (R=Eu,Gd), lattice parameters, mag. and elec. props. 80—100578
EuS, conduction band density of states, redistrib. near ferromag. saturation 78—67939
EuS, electronic struct. and props., mol. cluster approx. 77—11852
EuS, ferromag., on W, electron field emission 79—8230
EuS, ferromag. semicond. film, Hanle effect, optical orientation time consts. meas. 77—40214
EuS, ferromag. semicond., high field susceptibility, spin waves 80—75735
EuS, ferromagnetic film, optically induced magnetisation amplification, Curie temp. increase *(Russian)* 77—24719
EuS film, influence of prep. on mag. props. 79—24201
EuS, film, intrinsic demagnetising fields 78—10735
EuS, film, mag. surface reconstruction, ferromag. reson. 78—10781
EuS film, magnetic props. using transverse Kerr and Voigt effects 77—52054
EuS films, mag. and elec. props. rel. to stoichiometry and defects 80—97122
EuS films, optical spectra and light scatt. from spin waves 80—16116
EuS, heat capacity near ferromag. transition 78—47986
EuS, Heisenberg ferromagnet, exchange interactions, neutron scatt. expts. 77—20579
EuS, Heisenberg ferromagnet, static crit. props., neutron scatt. expts. 77—20618
EuS, hyperfine field and magnetisation temp. depend., NMR meas. 77—8422
EuS, mag. phase depend. Raman scatt. 78—10886
EuS, mag. struct. and transition temp., indirect exchange 78—91860
EuS, optical spin orientation, Curie temp. increase 77—20627
EuS, pure and Gd doped, electronic struct., mag. exchange and elec. transport props. 78—87974
EuS, single cryst., high-field susceptibility meas., temp. range 2.5 to 16.5K 80—84589
EuS, spin polarised tunnelling and mixed spin states in conduction band 79—52085
EuS, spin relax. in crit. region 78—52270
EuS, spin relaxation crit. behaviour 78—76251
EuS thin film, Brillouin scattering from spin waves 80—65843
EuS, three dimens. Heisenberg ferromagnet, crit. relax. spectra mag. susceptibility 79—8000
EuS:Yb(Sm), electron transition and valence state of impurities, X-ray spectroscopy and structural anal. 78—39064
EuS-W interface, electron spin polarisation in field emission 78—35265
EuS(Se), surface magnons and surface mag. struct. 77—36066
EuSe, bound mag. polaron, temp. and field depend. of resist. 79—90976
EuSe, giant negative magnetoresist., anomalous carrier density mag. field depend. 80—49774
EuSe, mag. phase depend. Raman scatt. 78—10886
EuSe, mag. phase stability, theory 77—63183
EuSe, mag. struct. and transition temp., indirect exchange 78—91860
EuSe, spin structs., mol. field theory 78—31054
EuSe:Gd, mag. props. explained by band struct. 78—43324
$Eu_{1-x}Sm_xO$, mag. semicond., thermodynamics of mag. quasimols. 78—19266
$EuSm_2S_4$, mag. props. 78—68237
$Eu_{1-x}Sm_xS$, electronic transition in Sm impurity ions, rel. to exchange interactions, L absorpt. spectra 77—59644
$(Eu_{1-x}Sn_x)S$, high press. Mossbauer exam. of Curie temp. and transferred hyperfine field 79—56643
$(Eu_{1-x}Sn_x)Se$, high press. Mossbauer exam. of Curie temp. and transferred hyperfine field 79—56643
$Eu_xSr_{1-x}O$, ferromag. ordering and photoluminesc. 77—66313
$Eu_xSr_{1-x}S$, blocking of pairs and spin glass freezing 79—61174
$Eu_xSr_{1-x}S$, chalcogenide-like system, crit. conc. for ferromagnet-spin glass transition 80—34662
$(Eu_xSr_{1-x})S$, dilute, magnetic ‘blocking’ 79—78348
$Eu_xSr_{1-x}S$, ferromag. ordering and photoluminesc. 77—66313
$Eu_xSr_{1-x}S$, ferromagnet-spin glass transition, mag. ordering, mag. susceptibility and neutron scatt. meas. 80—50135
$Eu_xSr_{1-x}S$, Heisenberg spin glass system, excitations 80—84610
$Eu_xSr_{1-x}S$, insulating spin-glass, sp. ht. near ferromag. onset 80—34667
$Eu_xSr_{1-x}S$, insulating spin glass, sp. ht. near ferromag. onset 80—97106

ferromagnetic properties of substances continued
$Eu_xSr_{1-x}S$, magneto-optical redshift in absorpt. and photoluminesc., mag. short-range order 80—71388
$Eu_xSr_{1-x}S$, onset of ferromagnetism for x near 0.5 neutron diffr. obs. 79—24181
$Eu_xSr_{1-x}S$, spin glass to ferromag. transition, neutron scatt. and susceptibility meas. 80—60254
$Eu_3V_2O_7$, prep. and props. 77—15379
Eu_4Y_2X, (Y=pnictogen, X=chalcogen), anti-Th_3P_4 type struct. 79—65048
$Eu_{1-x}Yb_xO$, solid soln., ferromag. semicond., increase of exchange interaction 78—88109
$Eu_{1-x}Yb_xS$, solid soln., ferromag. semicond., increase of exchange interaction 78—88109
(Fe,Co,Ni)-Si(B), amorphous mag. alloy, magnetostriction rel. to soft mag. props. 80—84633
$(Fe,Mo)_{80}B_{20}$, glassy alloy, Curie temp. and crystn. temp., Mo additions effect, Mossbauer spectra 78—68428
$(Fe,Ni)_{83}B_{15}C_2$, amorphous alloy, mag. props., possible appl. to power transformers 79—28558
$(Fe,Ni)_{80}(P,B)_{20}$, quenched alloy ribbon, mag. moments, Curie temp. 77—40041
$(Fe,Ni)_{80}P_{14}B_6$ amorphous alloy, mag. props., possible appl. to power transformers 79—28558
Fe, 90° walls, stable orientations, theory and X-ray observations *(Japanese)* 80—60359
Fe (001) surface, spectral density of transfer matrix formalism 78—39185
Fe (111), photoemission, exchange-split energy-band dispersions 80—35059
Fe, [111] oriented whisker, mag. domain struct. and approach to saturation 79—82814
Fe ⟨100⟩ whiskers, inverse Wiedemann effect 77—90001
Fe alloy, low, (110)[001] oriented, mag. charact. 77—1879
Fe alloy wire, glassy, shape, energy, eddy current loss and relax. damping of mag. domain walls 77—89975
Fe alloy wires magnetisation, torsion stress influence obs. *(Slovak)* 77—90468
Fe alloy YuNDK35T5, mag., solidification, direct elec. current effect 79—78954
Fe alloy YuNDK35T5BA, thermomag. treatment, post-decomp. processes 79—87668
Fe alloys, amorphous, effects of metalloids on mag. props. 80—75738
Fe alloys, amorphous, mag. saturation, spin wave stiffness, temp. depend. 80—75741
Fe alloys, amorphous, room-temp. saturation induction 78—95476
Fe alloys, amorphous, saturation magnetisation, Curie temp. and size effect 80—65815
Fe alloys, anisotropic precipitation struct. in external mag. field *(German)* 78—72785
Fe alloys, BCC, Mossbauer spectra, local mag. moments 80—15861
Fe alloys, dilute, residual resist. in two-current model, impurity mag. moments 77—15818
Fe alloys, FCC, Invar effect, model 80—25105
Fe alloys, ferromag., 4d and 5d impurities, hyperfine fields 78—31133
Fe alloys, ferromagnetic, EMF generation by pulsed laser irrad. 78—68021
Fe alloys, magnetic resist. anisotropy, two-current model 77—20295
Fe alloys, magnetic sp. ht., Curie temp., alloying effects model 79—61116
Fe alloys, temperature-time instability of initial susceptibility meas., using bridge instrument with electronic demagnetiser *(Slovak)* 78—57989
Fe, amorphous film, Hall effect and magnetisation *(Russian)* 77—35922
Fe, and alloys, ferromag. films, coercive force, ion plating prep. 77—28730
Fe and Fe-Ni Metglas alloys, ohmic and Hall resist. 100-700K, mag. behaviour 80—80254
Fe, atomic layers, Pauli paramagnetism to band ferromagnetism transition thickness depend. 78—72377
Fe, atomic magnetic moments comparison to values of ferromagnetic metal 78—52244
Fe, atomized powder compacts for mag. cores, mag. props. *(Japanese)* 78—72751
Fe, BCC, high field Knight shift and hyperfine anisotropy of ^{57}Fe 80—71205
Fe, BCC, mag. relax. due to C and N meas., 210 to 410K 77—36102
Fe, band theoretic interpretation of neutron scatt. expts., spin wave modes 80—44791
Fe, Barkhausen effect, grain size depend. at 300K and 77K *(German)* 77—16113
Fe based alloys, amorphous toroidal core, switching characts. and domain structs. 78—95477
Fe based alloys, resistivity magnetoresistance, s,p impurities in ferromag. host 78—68008
Fe based amorphous alloy, mag. ordered, hyperfine field distribs., NMR meas. 78—68409
Fe based amorphous alloys, struct. and thermomag. meas. 77—16055
Fe based ternary alloys, Coulomb and exchange scatt. amplitudes, spin dependent residual resistivities 78—64033
Fe, bulk modulus and thermal expansion coefficient, mag. contributions 79—8039
α-Fe, C drift velocity for electromigration temp. depend. in paramag., ferromag. phases 78—18835
Fe, carbonyl powder, mangetic material 77—12160
Fe, carbonyl powder, particle size distrib. anal. by microscopy with statistical anal. of results 78—19691
Fe, cast, grey, pearlitic relationship of magnetic props. to condition of C 78—56353
Fe, chemisorption of H, spin-spin interactions, UPS spectra calc. 80—6630
Fe, cluster method, environmental effects 78—95405
Fe clusters, supported, Mossbauer spectra 80—7220
Fe, coercive force measurement method of quality inspection of heat and thermomechanically treated parts 79—5113
α-Fe, cold work aftereffects 80—88830
Fe, cold work stored energy effects on mag. moment vs. temp. curve 78—95419
Fe complex, bis(N,N-diethyldithiocarbamato)-iron chloride, ferromag., sp. ht. meas., 0.4-20K 78—19258
Fe complex, $Fe(Br)[S_2CN(C_2H_5)_2]_2$, 3-D Ising ferromag., cryst. susceptibility, 1.5-20K 80—20390

ferromagnetic properties of substances continued
Fe complex, $Fe(Cl)[S_2CN(C_2H_5)_2]_2$, single cryst. susceptibilities 78—31057
Fe complex, $Fe(Cl)[S_2CN(C_2H_5)_2]_2$, susceptibility near critical pt. 79—24147
Fe complex, $Fe(Cl)[S_2Cn(C_2H_5)_2]_2$, 3-D Ising ferromag., cryst. susceptibility, 1.5-20K 80—20390
Fe complexes, $FeOCl[Co(cyclopentadienyl)_2]_{0.16}$ and $FeOCl[Fe(cyclopentadienyl)_2]_{0.16}$, Mossbauer and mag. susceptibility meas. 80—44176
Fe, compression deformed single cryst., induced uniaxial anisotropy 78—52336
Fe, Compton profile of mag. electrons meas. 77—32461
Fe, conductive, eddy current and hysteresis losses anal. 77—12153
Fe, crit. fluctuations, Mossbauer obs. 78—43724
Fe, crystal hyperfine fields and neutron scatt. 79—56172
Fe, Curie point and A-γ transition to 53 kbar 79—56529
Fe, Curie temp. calc. using model containing five bands 79—56536
α-Fe, cyclically deformed, mag. props. 77—28412
Fe, damping during and after deformation 79—43344
Fe, de Haas-van Alphen effect and exchange splitting, effect of pressure *(Russian)* 78—95252
Fe, deformed, dislocation structure determ. from magnetic props. 78—55874
Fe, density of states, photoemission expts. above and below T_c, rel. to magnetism model 77—20536
Fe dilute alloys, with s-p elements of third or fourth periods, Mossbauer spectra meas. 77—63344
Fe discontinuous film, Mossbauer effect exam. of magnetic state 77—24769
Fe, domain wall-dislocation interaction, magnetoelastic damping 78—14980
Fe, double critical magnetic scattering in polarised neutron expts. 79—65652
Fe, dynamic exponent, crossover obs., TDPAC Meas. 80—108021
Fe, effect of pressure on electron struct. *(Russian)* 79—77987
Fe, elastic and magnon-inelastic spin polarised low energy electron scatt. 78—34970
Fe, elastoresistivity effect, meas. of resistance at 4.2K and 300K, using mag. field method 78—72132
Fe, electron tunnelling 80—60104
Fe, electron-phonon coupling, point contact spectroscopy obs. *(Russian)* 80—70342
Fe, electronic structure of nontransition element impurity atoms 77—73023
Fe, energy band dispersion and mag. exchange splitting, angle-resolved photoemission meas. 80—71567
Fe, energy bands, tight binding calc. *(Korean)* 79—51479
Fe, energy of mag. anisotropy, band calcs. *(Russian)* 77—20583
γ-Fe epitaxial film, ferromagnetism, spontaneous magnetisation and Curie temp. determ. 78—2711
Fe epitaxial film, Mossbauer effect, depth profiling of mag. hyperfine field 80—11295
Fe epitaxial film, Mossbauer effect, interface magnetism 80—11297
Fe epitaxial films, even magneto-optical effects 80—76007
γ-Fe, FCC film, epitaxial growth on CuAu (111) surfaces, strong ferromagnetism 80—70557
Fe, Fermi surface under press., de Haas-van Alphen effect meas. 80—75499
Fe, ferromag., Compton profile meas. with circularly polarised gamma rays from oriented nuclei *(Japanese)* 78—23548
Fe, ferromag., domain struct., small-angle neutron scatt. 77—66382
Fe, ferromag., evidence for itinerant electron model, angle resolved photoemission from surface 79—24414
Fe, ferromag., hyperfine fields at positive muons 78—43758
Fe, ferromag., spin wave energies and intensities calc. 77—8293
Fe, ferromag., transient mag. field for ^{13}C 79—47362
Fe, ferromag. film, magnetoresistance parameter meas. *(Spanish)* 80—2485
Fe, ferromag. film, surface states, surface magnetisation and electron spin polarisation 80—65648
Fe, ferromagnetic, calc. hyperfine fields and their press. derivations 80—6796
Fe, ferromagnetic, hyperfine fields; SCF calcs. 77—8061
Fe, ferromagnetic, partial circular polarisation of thermal emission in mag. field 80—71387
Fe, ferromagnetic, temp. depend. of hyperfine fields for F 80—20141
Fe, ferromagnetic micropowder, cryst. struct., coercivity, remanence, saturation 80—65967
Fe film, amorphous and polycrystalline, Hall effect, resistivity and mag. moment 78—91786
Fe, film, asymmetric 180° Bloch walls, Lorentz electron microscopy obs. 78—27063
Fe film, chemisorption induced mag. dead layers, ferromag. reson. obs. 79—91261
Fe film, coated, interface magnetism by Mossbauer spectroscopy 80—75890
Fe film, domain wall struct. obs. by Lorentz electron microscopy 77-85527
Fe film, effect of tensile stress on mag. domain struct. 78—68332
Fe film, enriched, NMR obs. 78—39443
Fe film, evaporated at oblique incidence, columnar grain struct. using anisotropy field meas. 77—59231
Fe film, evaporated at oblique incidence, optical and mag. anisotropies 80—7134
Fe film, even magneto-optical transmission effects, 0.4-1.25 μm 77—32354
Fe film, ferromag. reson., thermodynamical anal. 79—42840
Fe film, Hall resist., effect of N impurity codeposition 78—64146
Fe film, high rate deposition by sputtering from two facing targets 77—85938
Fe, film, ion beam sputtering prep., struct. and mag. props. 80—35085
Fe film, linear mag. birefr. dispersion 77—69807
Fe film, low-angle grain boundary struct. *(Russian)* 79—42807
Fe film, magnetoelastic excitations, phonon spectroscopy and forbidden transitions 79—82853
Fe film, nuclear magnetisation relax. at 77 to 500K 78—60352
Fe film, nuclear spin system dynamics Mossbauer study in FMR conditions *(Russian)* 80—80651
Fe film, on Cu and Ag substrates, mag. props., Mossbauer spectra meas. 80—11233

ferromagnetic properties of substances continued
Fe film, single crystal, less than 1000 Å thick, inclined 90° walls 78—72384
Fe film, transverse Kerr magneto-optical effect enhancement by surface magnetoplasma waves 77—52056
Fe film, ultra-thin Mossbauer spectroscopic studies of mag. props. 80—44970
Fe film, vacuum deposited, resist. minimum 80—44741
Fe film coated by MgO, MgF_2 and Sb, surface mag. 80—7196
Fe film coated by MgO, Mossbauer spectra, mag. hyperfine field 80—7221
Fe, film mag. structures and stresses, ferromagnetic resonance 78—72375
γ-Fe film on Cu (111) mag. props. 78—31098
Fe films, ferromagnetic reson., photoacoustic detection 80—80613
Fe films, thickness variations in extraordinary and spontaneous Hall coeffs. 80—97013
Fe, first order shock induced mag. transitions characts. and discrimination from TRM 78—64205
Fe, flow stress, effect of mag. field 77—20673
Fe foil, electrodeposited, phys. and mag. props. 79—91275
Fe foil, ferromag. domain-wall width, anisotropy depend. 78—19269
Fe, foil, ferromagnetic resonance detection by photoacoustic effect 80—20463
Fe foil, hyperfine interactions of implanted reaction products 78—48093
Fe, fundamental and secondary mag. props., book contrib. 80—75724
Fe garnets, sublattice magnetisation curves, Mossbaeur study 80—75808
Fe, giant internal mag. press. and compressibility anomalies, itinerant model 77—16034
Fe, grade EA, plastically deformed, magnetoelastic props. *(Russian)* 80—44893
Fe group, mol. Jahn-Teller reson. states as possible antecedents to magnetism 80—75701
Fe, H_2 embrittlement and H_2 adsorption 80—89401
Fe, high dispersion ferromagnet, magnetic powder defectoscopy material 80—35137
Fe, high purity, dislocation-magnetic domain wall interaction, magnetomechanical damping expts. 78—39360
Fe, high purity, mag. viscosity mechanism 78—19282
Fe, high purity, magnetomechanical damping, magnetic field variations 80—93156
α-Fe, high purity, neutron and electron-irrad., interstitial migration at 200K 79—55920
Fe, high-purity, low-temp. mag. relax. after thermal ageing and demagnetisation 77—85502
Fe, high-purity, magnetic 90° domain wall-dislocation tangle interaction, magnetomechanical damping expts. 79—78496
Fe, hyperfine field and diffusion of μ^+ 77—52006
Fe, hyperfine field at nonmagnetic impurities 80—25129
Fe, hyperfine fields at impurity sites 77—66297
Fe, hyperfine fields at impurities in ferromag. metal 78—52244
Fe, hyperfine mag. fields at ^{67}Ge, TDPAC meas. 78—43701
Fe, interband optical conductivity, self energy correction 80—2792
Fe, intercell exchange energy, Hartree-Fock approx. 80—60239
Fe, internal fields, positive muon investigation 78—68438
Fe, internal friction near Curie point 79—24567
α-Fe, interstitial or substitutional sp impurity doped, electronic struct. 80—34384
Fe, interstitial site determ., μSR technique 80—71287
Fe, irreversible magnetisation changes, directional distrib. 79—24196
Fe, itinerant electron model, spin quantization direction fluctuations, short range order. 80—34582
Fe, itinerant ferromag., Fermi surface and single particle excitations 80—34350
Fe, itinerant ferromagnet, neutron inelastic scatt. 79—7970
Fe, itinerant model of spin polarised field emission 78—95685
Fe, lattice vibrations, temp. depend. 78—95124
Fe, light scatt. by spin waves 80—45086
Fe, light scatt. from surface and bulk thermal magnons 80—45087
α-Fe, mag. aftereffect after neutron irrad. at 77K 78—2705
Fe, mag. aftereffect meas., phenomenological description 80—88835
α-Fe, mag. aftereffect spectrum after low temp. electron irrad. 78—2704
Fe, mag. anisotropy in crit. region, neutron polarisation-vector analysis 78—31065
Fe, mag. breakdown and Hall resist., theory and model calcs. 80—75552
Fe, mag. hyperfine field at ^{129}I, press. depend., nucl. gamma reson. 80—71256
Fe, mag. surface props., Mossbauer effect 77—69757
α-Fe, magnetic aftereffect correlations with internal friction after low temp. neutron irradiation 78—10733
α-Fe, magnetic aftereffect disaccommodation between 30 and 300K after low-temp. neutron-irrad. 80—29585
Fe, magnetic aftereffect of interstitial O 78—91903
α-Fe, magnetic aftereffect spectrum after low temp. neutron irradiation 78—10732
Fe, magnetic aftereffects of H isotopes, book contrib. 79—82835
Fe, magnetic disaccommodation, low temp. in neutron-irrad. sample, Bordoni relax. 77—4542
Fe, magnetic hyperfine fields of Zr, DPAD meas. 80—39901
Fe, magnetic moments, local short range order, high temp. effects 80—65902
Fe, magnetic susceptibility, lineshape and moment analysis, magnon excitations 79—99693
Fe, magnetisation curves in high mag. fields above Curie point 77—66386
Fe, magnetisation process in high mag. fields in crit. region 77—85498
Fe, magnetisation self-reversal, tensile stress effect 78—14982
Fe, magnetised to saturation, props., positive-muon study 78—6619
Fe, magnetism at high temps. 80—75721
Fe, magneto-optical near UV reflection-spectra, meridional and polar intensity effects *(Russian)* 78—39572
Fe, magneto-volume effects calc., rel. to itinerant electron model 78—43621
Fe, magnetoelastic excitations and ferromagnetic resonance 79—82879
Fe, magnetomechanical acoustic emission for residual stress NDT 80—71149
Fe monocrystal, neutron crit. scatt. anisotropy 77—66327
Fe, Mossbauer absorpt. spectrum, domain struct. effect 79—69758
Fe, Mossbauer effect at high press. in α-, ε- and γ-phases 80—15858
Fe, Mossbauer energy shift near Curie temp. 78—52388
Fe, Mossbauer spectra, demagnetising field effect on magnetic splitting 80—39932

ferromagnetic properties of substances continued
Fe, muon spin rotation; freqs., and relax. rates 80—55006
Fe, muon$^+$, 40 MeV, traversing magnetised plates, dynamic mag. fields 79—38422
Fe, muon$^+$ spin precession and relax., hyperfine field temp. depend. 77—63350
Fe, muon$^+$ spin rotation meas., local hyperfine field temp. depend. 77—63349
Fe, μ^+ hyperfine field and relaxation, temp. depend. 78—95538
Fe, neutron critical scattering, temp. shift 78—38589
α-Fe, neutron irradiated, low temp. mag. relax. 79—8022
α-Fe, neutron irradiated, mobile C atom trapping, anelastic and magnetic relaxations 80—100306
Fe, neutron magnetic critical phenomena, review of new effects 79—56534
Fe, nitrided wire, magnetic charact. and microstruct. *(Korean)* 78—19277
Fe, noncrystalline, mag. hyperfine data from Mossbauer spectra 78—39477
Fe, nonrelativistic LCAO energy band calc. 78—10343
Fe, oxidation at Curie temp. 79—29279
Fe, oxidation kinetics near Curie temp. 79—66218
Fe, oxidised powder, soft mag. props. oxide film-Fe composite material, magnetically soft, preparation, elec., mag. props. 77—8778
Fe particles, dispersed in Hg, mag. props., aggregate form. 80—60375
α-Fe particles, in fused SiO_2, g-values and anisotropy consts., FMR study 79—82876
Fe particles, lunar matter, FMR study, effective linewidth method 78—95523
Fe particles, spin collinearity, Mossbauer spectra study 80—71114
Fe, photoelectron spin polarisation and itinerant magnetism 78—68602
Fe, photoemission study of (100), (110) and (111) surfaces, ferromag. band struct. 79—38714
Fe, plastically deformed, dislocation arrangement exam. by ferromag. techniques 78—63774
Fe, plastically deformed, high field suscept. anisotropy and domain struct. 78—15002
Fe, point contacts between ferromag. metals, singularities depend. in d^2V/dI^2, phonon spectra 79—60457
Fe, polarised, ferromag., evidence for K-shell polarisation of ^{12}C ions via mol. orbital promotion 80—71273
Fe, polycryst., magnetostriction sign change under compressive stress 80—29596
Fe, polycryst., spectral thermal emission circular polarisation 79—77784
Fe polycrystal, temp. shift of neutron crit. scatt. max., test of dynamic scaling theory 79—50953
Fe polycrystalline, two ferromag. methods for eval. of fatigue limit 80—89438
Fe, positive muon diffusion, press. depend. 80—75907
Fe powder, BH_4 reduced, coercive force and remanence ang. variation 80—44879
Fe powder, Debye-Waller factor by neutron diffraction 79—95113
Fe powder, prep. by reducing iron phthalate in mag. field, mag. props. 77—40090
Fe powder, sintered and hot pressed, effect of porosity, grain size on magnetic props. 79—96159
Fe powder-plastic composite, soft mag. material, mag. and mech. props. 80—75812
Fe powders, Co- or Cu-plated, prep. by rad. and chem. plating, mag. props. 80—44867
Fe powders, prep. by BH_4 process, comp. and stability 80—44878
Fe, press. effects on mag. props. 77—66241
Fe, pure, magnetoelastic damping at low shear stress amplitudes *(French)* 77—59441
Fe, pure and doped, electron irrad., mag. aftereffect 80—88838
Fe pyrophoric powders, stabilising layer form. during passivation, saturation moment meas. 80—44865
α-Fe, quenching, C atom pair form., isothermal mag. permeability disaccommodation meas. 77—36540
Fe, remagnetisation processes, temp. and grain size depend. *(German)* 78—14987
Fe, residual stress induced by uniaxial deform., magnetic meas. 77—73390
Fe, resistivity anomalies at mag. transitions, sp.ht. 80—39785
Fe rod, spontaneous vibr. modes excited by reversible magnetostriction 79—56587
Fe, rotational hysteresis 78—91889
Fe sheet, surface magnetisation, ferromag. nucl. reson. meas. 78—60348
Fe single crystal frames, use in transient field meas., surface magnetisation meas. 79—59324
Fe single crystals (111), elasticity modulus variation, depend. on external mag. field *(Russian)* 79—82849
Fe, spectral thermal emission, partial circular polarisation 78—18806
Fe, spectral thermal emission, partial circular polarization 79—23751
Fe, spin correlation function 79—78334
Fe, spin dependent momentum distrib., APW calc. 78—2416
Fe, spin fluctuations above Curie temp., diffuse mag. neutron scatt. obs. 80—50102
Fe, spin polarisation in electron field emission, surface magnetism 78—68607
Fe, spin polarisation of field-emitted electrons 77—40337
Fe, spin polarised LEED, calc. 79—99686
Fe, spin polarised photoemission, surface magnetism 79—52083
Fe, spin susceptibility, high-field, spin-density functional formalism 80—70959
Fe, spontaneous magnetisation data up to 0.98 T_c, reanalysis 78—47959
Fe, spontaneous volume magnetostriction 80—65989
Fe sputtered film, amorphous, Mossbauer study and electron diffr. obs. 80—75897
Fe, Stoner model, mol. field coeff., temp. and field depends. 77—72975
γ-Fe, Stoner theory support for two-state hypothesis 77—69477
Fe, stray mag. fields above stripe domains, electron microscope and μ^*-tensor determ. 80—71089
Fe, stress fields and strains energies associated with closure domains 77—1563
Fe surface, spin orientation effect of shallow electrons by magnetization 79—65881
Fe, surface chemistry during annealing of soft magnet 78—48546
Fe, temp. depend. of spontaneous magnetisation 77—63141
Fe, theory of magnetism 79—78299
Fe, thermal acoustic magnons, Brillouin scatt. meas. 78—95424

ferromagnetic properties of substances continued
Fe, thermal cond., elec. resist., Lorenz number and magnetisation, crit. behaviour 77—4521
Fe thin film, Brillouin scattering from spin waves 80—65843
Fe thin layers, vacuum coated on PMMA, mag. behaviour during mech. stress cycles *(German)* 80—80581
Fe, transient mag. field, vel. and atomic number depend. 78—91999
Fe, transient mag. field discontinuity seen by O(F) ions 80—24515
Fe, UPS, density of states determ. 78—52623
Fe ultrafine particles, Fe$_3$O$_4$/γ-Fe$_2$O$_3$ surface layers, Mossbauer expts. 79—8081
Fe ultrafine particles prepared by vacuum evaporation, mag. props. 78—35007
Fe, ultrafine particles prepared by vacuum evap. on running oil substrate, mag. behaviour 79—28565
Fe, ultrathin film, mag. hyperfine field, temp. and thickness depend. 78—39478
Fe, var. in mag. moment of ferromags. during plastic deform. *(Russian)* 77—66401
Fe whisker, domain theory, quasi-dislocation theory appl. *(Japanese)* 80—60358
Fe, whisker, mag. crit. phenomena, size effects 78—68258
Fe whisker, magnetic aftereffect in 180° mag. bowed Bloch walls 79—78432
Fe whisker, magnetisation curve meas. using SQUID system 80—86347
Fe, whisker, magnetoresistance, deviations from Kohler's rule 80—70673
Fe whisker, optimisation of magnification of magneto-optic Kerr effect by interference layers 79—51808
Fe whisker crystals, domain walls, interaction with dislocation bundle, X-ray topography obs. 79—87282
Fe, whisker domain wall interaction with mobile impurities 77—12145
Fe, whisker single crystals, ferromag. reson. and surface anisotropy 80—71187
Fe whiskers, AC susceptibility, critical slowing down of mag. fluctuations 77—69594
Fe whiskers, dynamics of mag. freq. response near Curie point 80—34648
Fe whiskers, elastically and plastically deformed, mag. domain structs. 80—15752
Fe whiskers, mag. anisotropy, magnetisation and temp. depend. near T$_c$ 80—39766
Fe whiskers, magnetisation in small mag. fields, investigation using Kerr magneto-optic effect 80—2603
Fe, zig-zag 90° Bloch wall, magnetoelastic problem 77—4526
Fe:^{129m}Xe, mag. hyperfine field determ. by Mossbauer effect 77—8460
Fe:^{12}C($2_1{}^+$), PAC meas. of transient mag. fields 79—99800
Fe:^{169}Tm(^{175}Lu), radiation-damage evolution influence on hyperfine interaction 80—6793
α-Fe:C, electronic struct., Hartree-Fock calc. 78—14692
Fe:Lu, nuclear orientation meas., hyperfine field 77—32308
α-Fe:N, mag. field depend. of reverse permeability 77—80969
Fe:Ra, hyperfine field determ. 77—85622
Fe:Xe, isotope ion implantation control *(Flemish)* 78—79623
Fe-Al, dil., film, NMR spin echo, rel. to struct. inhomogeneities *(Russian)* 80—29644
Fe-Al, dil. alloy, temp. depend. of ^{27}Al hyperfine field 78—47972
Fe-Al, domain struct. and magnetostriction, heat treatment effect 80—60398
Fe-Al, equilibria of Fe, Al ordered phase *(Japanese)* 79—70042
Fe-Al, ferromag.-mictomag. transition, intermediate superparamag. 77—12140
Fe-Al, low energy Stoner excitations, spin wave obs. in neutron scatt. study 79—51770
α-Fe-Al, migration of C, mag. permeability disaccommodation meas. 77—36100
Fe-Al, Mossbauer spectra, local mag. moments 80—15861
Fe-Al, residual elec. resist., contrib. from static lattice distortions and short-range parameters *(Russian)* 79—51548
Fe-Al (16 wt.%), improvement of certain props. discussion *(Chinese)* 78—84826
Fe-Al (25 at.%), anomalous magnetic behaviour *(Japanese)* 77—48011
Fe-Al (25 at.%), double Curie point phenomena 77—73030
Fe-Al (25 at.%), long-range ordered, compression induced mag. anisotropy 77—69546
Fe-Al (4 wt.%) alloy, mag. anisotropy induced by cold rolling *(Russian)* 80—84595
Fe-Al (4 wt.%) single crystals, rolling induced mag. anisotropy and its removal by annealing treatment *(Russian)* 79—61746
Fe-Al alloys, rapidly quenched, mag. props. 80—29579
Fe-Al-C alloys, C migration and mag. aftereffect, mag. permeab. disaccommodation and long-range order meas. 79—8020
Fe-Al-Co-Ni, Alnico alloys, irreversible remagnetisation processes in rotating fields *(Russian)* 79—8015
Fe-Al-Fe, phase diagram, microscopic model 80—34630
Fe-Al-Ni-Co-Cu alloys, Ti alloying and deoxidising addition *(Russian)* 78—80181
Fe-Al-Si alloy, order-disorder transform. exam. by Mossbauer spectroscopy 77—63334
Fe-Al(Si)(Ga)(Ge)(As)(Sn)(Sb) dil. alloys, mag. hyperfine fields, Curie temps. and Mossbauer meas. 77—63190
Fe-Al(Ti), O containing, mag. aftereffect and disaccommodation meas., time depend., activation energy, and ageing props. 80—88836
Fe-Al(24.3 at.%)-C alloy, magnetic permeability disaccommodation, 260-400K 80—93144
Fe-Al(25 at.%), mag. anisotropy induced by plastic deform., dislocations, long-range order 77—4544
Fe-Al(4 wt.%), ferromag. alloy, mag. anisotropy induced by cold rolling 80—30114
Fe-alloy, FCC, Invar, thermally excited electron transitions 79—56559
Fe-Au layers, amorphous ferromag., elec. transport phenomena and reson. scatt. *(German)* 77—72847
Fe-B, (16.3 at.%) amorphous, coercive force temp. depend. 80—25158
Fe-B, amorphous, induced anisotropy, development by mag. annealing and under applied mech. stress 80—65868
Fe-B, amorphous, induced anisotropy by heat treatment in mag. field and under applied mech. stress 80—75758
Fe-B, amorphous, Invar-type alloy, mag. moment and high field susceptibility 78—34965
Fe-B, amorphous, mag. aftereffect, initial susceptibility time depend. 80—88829
Fe-B, amorphous alloy, mag. props. 80—84618

ferromagnetic properties of substances continued
Fe-B, amorphous ferromag., Invar type, magnetisation, elec. resist. and thermal expansion meas. 78—2663
Fe-B, amorphous ferromag., temp. depend. of resist., appl. of extended Ziman theory 80—59950
Fe-B, amorphous metallic glasses, high-temp. mag. anal. 78—91258
Fe-B, liq., mag. susceptibility meas. 80—75740
Fe-B, sputtered amorphous film, strong stripe domains, Kerr effect obs. and theory 79—91265
Fe-B (14-25 at.%), amorphous, saturation magnetisation, temp. and comp. depend. 77—85430
Fe-B (15-25 at.%) glass, quasicryst. struct. Mossbauer expts. 79—4255
Fe-B alloys, rapidly quenched metastable solid solns., prop. and mag. props. 78—92218
Fe-B amorphous alloy, annealed, microstruct. and mag. domain changes 80—75790
Fe-B amorphous alloy, mag. anisotropy temp. depend. 80—15846
Fe-B amorphous alloys, mag. aftereffect 80—65970
Fe-B amorphous alloys, Mossbauer spectra, soft ferromag. props. 80—11302
Fe-B amorphous alloys, Mossbauer spectra, mag. moment conc. depend. 80—15847
Fe-B amorphous Invar alloy, elastic props., Elinvar characts. and ΔE effect 79—56595
Fe-B ferromag. film, props. 79—4709
Fe-B films, amorphous, mag. annealing behaviour 79—73782
Fe-B metallic glass, role of Fe$_3$B in crystn., mag. and Mossbauer expts. 78—94997
Fe-B metallic glasses, struct., stability and crystn. 80—75173
Fe-B metallic ribbons, correl. between quenching temp. and mech. and mag. props. 80—89373
Fe-B metastable alloys, Mossbauer spectroscopy and electron microscopy 79—28653
Fe-B phase ferromag. amorphous alloys, stiffening below Curie temp., pole effect *(Japanese)* 80—84632
Fe-B ribbon, microhardness, and static coercive force, melt overheating effect 80—84978
Fe-B-C, amorphous, effects of replacement of B by C on mag. props. 80—84621
Fe-B-C alloys, amorphous, temp. depend. of magnetisation 79—73690
Fe-B-C amorphous alloy, formation, mag. props., thermal stability and density 80—75796
Fe-B-C amorphous alloys, room-temp. saturation induction over 17.5 kG 79—47300
Fe-B-C amorphous alloys, atomic struct., energy dispersive X-ray diffr. meas. 79—73100
Fe-B-C amorphous alloys, effect of Si addition on mag. props. 80—34694
Fe-B-C amorphous alloys for use in power transformers 80—88808
Fe-B-C amorphous alloys with high saturation induction 80—84617
Fe-B-Cr(Mo), metallic glasses, mag., struct., and elec. props. 80—88751
Fe-B-Cr(Si) thin film glasses, mag. props. and corrosion resist. 80—80576
Fe-B-Si, amorphous ferromag. alloys, mag. struct., Mossbauer study 80—39746
Fe-B-Si amorphous ribbon, strain induced anisotropy, and toroid diam. effect on mag. props. 80—34623
Fe-B-Si amorphous ribbons, effect of annealing conditions on magnetomechanical props. 80—34740
Fe-B-Si-C amorphous alloys, prep. and props. 80—88748
Fe-B(-Si), glassy, field-induced mag. anisotropy near eutectic comp. 80—93110
Fe-B(P) amorphous alloy, Invar effects, mag. props. meas. 79—56594
Fe-B(P) amorphous alloys, anomalous thermal expansion, ΔE effect, Invar and Elinvar characts., delay time 80—80589
Fe-based alloys, volume interactions between substitutional sp and 3d solutes 79—78069
Fe-based system, concentration ferro-antiferromag. transitions *(Russian)* 79—99699
Fe-C, electronic structure of interstitials 79—1583
Fe-c, Fe-Si-B, and Fe-Cr-P-C sputtered amorphous films, mag. props. and corrosion resist. 79—28567
Fe-C, ferromag., prep. by splat-quenching, obs. of electronic struct. of interstitial C 77—62868
α-Fe-C(N), containing substitutional atoms, mag. permeability disaccommodation *(Polish)* 79—95612
Fe-Ci, high permeability, mag. props., applied stress effects 80—34726
Fe-Ci (3 wt.%), commercially produced, grain-oriented, mag. props., stress coating effects 80—34727
Fe-Ci (3 wt.%), local magnetisation losses, grain orientation effect 80—88817
Fe-Co, 3d ferromagnet nuclear spin-lattice relaxation 80—80627
Fe-Co, amorphous alloy, stress effect on mag. domain struct. 79—33502
Fe-Co, BCC, ferromag., spin wave stiffness constant 78—91851
Fe-Co, dil., film, NMR spin echo, rel. to struct. inhomogeneities *(Russian)* 80—29644
Fe-Co, ferromagnetic micropowder, cryst. struct., coercivity, remanence, saturation 80—65967
Fe-Co, local environment effect on at. mag. moment 79—82763
Fe-Co, mag. moment of Cr and Mn atoms, polarised neutron scattering 79—11290
Fe-Co, partially ordered, elec. cond. 78—91663
Fe-Co, surface excitations 80—25179
Fe-Co (46%) film, evaporated, uniaxial mag. anisotropy 77—51929
Fe-Co alloy, diffusion of H$_2$, diffusion coefficient and permeability *(Russian)* 78—79819
Fe-Co alloy, local environment effect on atomic moments, itinerant model 78—68188
Fe-Co alloy, optical characts., 0.073-4.92 eV, quantum absorption 79—56814
Fe-Co alloy, order-disorder and α-γ transitions 77—25042
Fe-Co alloy particles for mag. tapes, mag. props. 78—95479
Fe-Co alloy ring samples, force fitting effect on mag. props. 77—40083
Fe-Co alloys, atomic valence states *(Ukrainian)* 78—2656
Fe-Co based alloys (52KF, 35KKh, 35KFN), effect of heat treatment and mech. working, on sensitivity of mag. props. to mech. stresses *(Russian)* 79—34161
Fe-Co based amorphous alloys, mag. props. *(Japanese)* 79—95971
Fe-Co based Laves phases, mag. saturation moment, Co conc. depend. 78—15037
Fe-Co film, magnetisation induced uniaxial anisotropy 77—48016

ferromagnetic properties of substances continued
- Fe-Co-B powders, synthesis and mag. props., appl. to mag. recording 80−20432
- Fe-Co-Cd(Sn), mag. hyperfine fields at Fe, Cd and Sn sites, Mossbauer and TDPAC meas. 78−60363
- Fe-Co-Cr, magnetic, phase transform. obs. *(French)* 79−47676
- Fe-Co-Cr alloys, atomic mag. moment, magnetisation, Mossbauer spectra and NMR spin echo spectra 77−63127
- Fe-Co-Cr-Si, structural transform. and mag. props. following heat treatment *(Russian)* 77−81274
- Fe-Co-Mn, BCC, mag. state of Mn, NMR and saturation magnetisation meas. 78−39442
- Fe-Co-Mn alloys, BCC, atomic mag. moment, magnetisation, Mossbauer spectra and NMR spin echo spectra 77−63127
- Fe-Co-Mo-Nb(Ta) semihard mag. alloy, mag. props., thermal expansion, elec. resistivity and hardness *(Japanese)* 80−88789
- Fe-Co-Ni, at. mag. moments, neutron scatt. and Mossbauer meas. 79−42744
- Fe-Co-Ni alloy powder, video recording appl. *(Russian)* 77−55910
- Fe-Co-Ni Perminvar, mag. props. singularities in region of mag. anisotropy *(Russian)* 80−84614
- Fe-Co-Ni-Al, Si alloying of mag. hard alloys *(Russian)* 79−73765
- Fe-Co-Ni-Al-Cu alloy, polycryst. hard mag., C diffusion 79−77827
- Fe-Co-Ni-Al-Zr magnetically hard alloys, reduction *(Russian)* 78−43614
- Fe-Co-Ni-Si-B amorphous alloy, magnetostriction and permeability, effect of annealing 79−1701
- Fe-Co-Si (4,1.5 wt.%), textured, mag. props. 80−35200
- Fe-Co-Si-B, amorphous soft ferromagnet with high mag. induction 80−84619
- Fe-Co-Si-B, zero magnetostrictive amorphous alloy with high saturation induction, mag. annealing 80−60362
- Fe-Co-Si-B alloy, amorphous, rapidly quenched, mag. heads appl. *(Japanese)* 80−54922
- Fe-Co-Si-B sputtered amorphous thin film, coercivity, galvanomagnetic props., resistivity 80−29578
- Fe-Co-Si(B), amorphous ferromagnet, mag. after effect on soft mag. props. 80−84626
- Fe-Co-Ta for semipermanent magnets *(French)* 79−47675
- Fe-Co-Ti(V)(Cr)(Mn), sp. ht. in ordered and disordered phases 80−71061
- Fe-Co-V, Vicalloy, magnetisation reversal by stretching and twisting 80−34733
- Fe-Co-V(-Ni), annealing effect on microstruct. rel. to mag. and mech. props. 80−89267
- Fe-Co-X alloys, semihard wires, creeping magnetisation reversal 77−16106
- Fe-Co(Si), determ. of chem. and magnetic interchange energies 77−80925
- Fe-Cr, BCC, ferromag., spin wave stiffness constant 78−91851
- Fe-Cr, disordered, mag. order, Mossbauer study 80−39992
- Fe-Cr, hyperfine magnetic fields, Mossbauer spectra 80−97165
- Fe-Cr, Invar alloy, explanation of phys. anomalies *(Russian)* 78−88112
- Fe-Cr, random ferromag. alloys, local mag. moment calc. 80−70974
- Fe-Cr, spin waves by neutron spectrometry 80−44819
- Fe-Cr (10 to 70 at.%), ferromag. reson., anisotropy const., and saturation magnetisation *(Russian)* 77−81013
- Fe-Cr (1.20, 3.63, 7.98 wt.%), Mossbauer spectra shape depend. on deformations 79−61272
- Fe-Cr (70-92 at.%), coexistence of ferro- and antiferromagnetism *(Russian)* 78−47955
- Fe-Cr alloy, mag. moments and Fe site hyperfine fields, magnetis. obs. 78−76276
- Fe-Cr alloys, crit. mag. props. near ferromag. Curie points 77−63216
- Fe-Cr alloys, mixed ferro-/antiferromag. interactions *(Russian)* 77−32173
- Fe-Cr-Al (12, 3 wt.%), internal friction and rigidity modulus, strain amplitude depend. *(Japanese)* 80−92606
- Fe-Cr-Al alloys, localised mag. moment determ. and electron struct. 77−66268
- Fe-Cr-Al alloys, low temp. sp. ht., resistivity and coercive force 78−63866
- Fe-Cr-B, amorphous, Elinvar and Invar charact. *(Japanese)* 80−11832
- Fe-Cr-B amorphous alloys, corrosion resistance, Invar and Elinvar characts. *(Japanese)* 79−96213
- Fe-Cr-Ce, decomposition of solid soln. in mag. field, neutron and X-ray diffr. study *(Russian)* 78−68694
- Fe-Cr-Co, anisotropic, spinel type permanent magnet, magnetic aftereffect 77−16118
- Fe-Cr-Co, heat treatment effect on strain gauge factor *(Japanese)* 78−6954
- Fe-Cr-Co, mag. props. of ductile permanent ductile alloys *(Chinese)* 79−19746
- Fe-Cr-Co, mechanism of coercive force 80−34674
- Fe-Cr-Co, permanent magnet, temp. effect 80−34701
- Fe-Cr-Co (28, 10.5 wt.%) ductile magnet alloy, humidity-induced H_2 embrittlement 80−89406
- Fe-Cr-Co (31 wt.%, 23 wt.%), microstruct. and mag. props., ageing and thermomag. treatment effects 78−76769
- Fe-Cr-Co alloy, coercive force mechanism 80−71103
- Fe-Cr-Co alloy, Mossbauer exam. of spinodal decomposition 77−69742
- Fe-Cr-Co alloys, (5-9 wt.% Co), obtained by slow cooling under mag. field, permanent magnet props. 80−75797
- Fe-Cr-Co alloys, mag. props., heat treatment effects *(Russian)* 78−39365
- Fe-Cr-Co alloys, permanent magnets, magnetic props. and heat treatment *(Russian)* 79−91809
- Fe-Cr-Co ductile magnet, with high $(BH)_{max}$, processing, mag. props., and microstruct. 77−8957
- Fe-Cr-Co ductile magnet alloys, phase diagram and mag. props., V or V+Ti addition effects 77−8959
- Fe-Cr-Co hard-mag. alloys, fine cryst. struct. *(Russian)* 77−66706
- Fe-Cr-Co permanent magnet system, miscibility gap, microstruct. and mag. props. obs. 80−76228
- Fe-Cr-Co-Al (27.5, 17.5, 0.5) alloy, magnetic props. and microstructure 78−72367
- Fe-Cr-Co-Al (27.5, 17.5, 0.5 wt.%) alloy, induced anisotropy 78−76239
- Fe-Cr-Co-Mo, melted in open induction furnace, microstruct. and magnetic props. 79−61626
- Fe-Cr-Co-Mo, microstruct., hardness, mag. props., influence of isothermal tempering and heat treatment 79−79129

ferromagnetic properties of substances continued
- Fe-Cr-Co-Mo alloys, struct. transform. and mag. props. *(Russian)* 77−76543
- Fe-Cr-Co-Mo high energy permanent magnets, mag. props. 80−97119
- Fe-Cr-Co-Si alloy, interaction domains after heat treatment in mag. fields *(Russian)* 78−68286
- Fe-Cr-Co-V alloy, microstruct. and mag. props. 78−68221
- Fe-Cr-Co-V-(Ti) hard magnets, V and V-Ti effects on mag. and mech. props. 79−91810
- Fe-Cr-Ni, cold-rolled foils, dilatometric study 80−21033
- Fe-Cr-Ni, Fe-Co-Mn, Fe-Cr-Co and Fe-Ni-Mn alloys, BCC, atomic mag. moments determ. 77−59396
- Fe-Cr-Ni, spin system, relaxation props. at low temp. 79−82758
- Fe-Cr-(Co), decomposition of solid soln. in mag. field, neutron and X-ray diffr. study *(Russian)* 78−68694
- Fe-Cr-b amorphous Invar alloy, elastic props., Elinvar characts. and ΔE effect 79−56595
- Fe-Cu, dilute, coercive field, initial permeability and relax. loss, non-mag. impurity effect 77−69628
- Fe-Cu alloys, mag. moment distrib., elastic neutron scatt. obs. 79−78340
- Fe-Cu metastable dil. alloy film, hyperfine interactions 78−52398
- Fe-Fe_3O_4, sintered two-phase soft mag. material, prep. and props. 77−63813
- Fe-Gd(Tb) film, magneto-optic coeff. and refr. index, ellipsometric determ. 80−71501
- Fe-Ge amorphous films, conversion electron Mossbauer spectra, mag. moments 77−16231
- Fe-La, Fe-rich alloys, mag. props. for bulk amorphous deposits *(Japanese)* 79−95971
- Fe-La(Zr) amorphous films, mag. props., Mossbauer effect and magnetisation meas. 79−69701
- Fe-Mn, BCC, ferromag., spin wave stiffness constant 78−91851
- Fe-Mn, dil. alloy, mag. moment distrib., temp. depend., diffuse polarised neutron scatt. study 79−47250
- Fe-Mn, electron redistrib. and BCC struct. stability, Mossbauer meas. *(Russian)* 79−42873
- Fe-Mn, Mossbauer spectroscopy of temp. hysteresis of phase transformations *(Czech)* 80−29949
- Fe-Mn (9 to 20 wt.%), ^{57}Fe Mossbauer spectroscopy in phase transformations 80−29948
- Fe-Mn alloy, magnetovolumetric anomaly *(Russian)* 78−64248
- Fe-Mn base alloy, mag. preferred directions 78−39370
- Fe-Mn-Ti-Al, magnetic texture rel. to annealing temp., Mossbauer investig. 77−28499
- Fe-Mo (0.54 to 2.50 wt.%) ferromag. ordering effect on Fe diffusion *(Czech)* 77−62665
- Fe-Mo(W), semihard magnetic alloys, magnetic, elec. mech. props. *(Japanese)* 79−70078
- Fe-N, hexagonal, ferromag. Mossbauer spectroscopy 77−63331
- Fe-N (10 at.%), structural transforms., expt. investig. *(Russian)* 77−12613
- Fe-N crystal, orienting $Fe_{16}N_2$ particles by external magnetic field *(German)* 77−25058
- Fe-Nb alloys, mag. and Mossbauer meas. 77−63133
- Fe-Nb(Ta)-Co, Recalloys, semihard mag. alloys, mag. and elec. props., hardness, thermal expansion *(Japanese)* 79−5066
- Fe-Ni, (35 wt.%), transport props. and Invar features *(Russian)* 78−51973
- Fe-Ni, BCC, ferromag., spin wave stiffness constant 78−91851
- Fe-Ni, coercive force depend. on grain struct. and inclusions 77−20635
- Fe-Ni, dil., point defect relax. after low temp. neutron irrad. 78−52316
- Fe-Ni, electrodeposition, mag. props. *(French)* 78−64488
- Fe-Ni, electrolytic film, coercive force depend. on electroplating conditions *(French)* 77−55691
- Fe-Ni, FCC, anomalous props. at high temp. and new phase *(Japanese)* 78−80520
- Fe-Ni, FCC alloy, magnetovolume instability 79−8031
- Fe-Ni, FCC alloy, thermoelec. power, anomalous conc. depend. at high temp. 79−4548
- Fe-Ni, fcc alloys, spin wave energy calc. 79−87247
- Fe-Ni, $Fe_{65}(Ni_{1-x}Cr_x)_{35}$, low-temp. elec. and galvanomag. props. rel. to mag. boundaries *(Russian)* 77−35910
- Fe-Ni, ferromagnetic films, domain boundary creep relaxation effects *(Russian)* 79−82840
- Fe-Ni, Invar, Curie point, annealing effects and time depend. 80−80508
- Fe-Ni, Invar alloy, explanation of phys. anomalies *(Russian)* 78−88112
- Fe-Ni, Invar problem, vibronic state model 79−56492
- Fe-Ni, local environment effect on at. mag. moment 79−82763
- γ-Fe-Ni, local magnetisation of Fe atoms, Mossbauer effect meas. 80−75891
- Fe-Ni, low frequency power losses 78−95466
- Fe-Ni, magnetic ordering, effect on diffusibility, penetrability and solubility of H_2 *(Russian)* 77−24435
- Fe-Ni, magnetisation calc. method based on moments of density of states 80−65770
- Fe-Ni, mechanisms of EM generation and detection of US Lamb waves 78−39382
- γ-Fe-Ni, Mossbauer exam. 79−56640
- Fe-Ni, quenched irreversible alloy, zero or negative thermal dilatation 79−4419
- Fe-Ni, secondary recrystn. and mag. props. 80−89247
- Fe-Ni, thermodynamic props., anomalous 80−39313
- Fe-Ni (23-35 at.%), cooled below 70K in mag. field, uniaxial anisotropy *(Russian)* 78−19244
- Fe-Ni (308-44.1 at.%) Invar alloys, anomalous mag. anisotropy and thermal expansion 80−75755
- Fe-Ni (32.3 at.%), mag. struct. in commensurable approx., neutron diffr. study 80−60212
- Fe-Ni (33-38 at.%), low-angle neutron diffr., anomalous crit. scatt. *(Russian)* 80−60193
- Fe-Ni (35 to 100%), magnetoelastic attenuation of torsional vibr. and shear modulus defect *(Russian)* 77−80982
- Fe-Ni (47 to 65 wt.%), soft magnetic alloy with crystallographic texture and field induced anisotropy, pulse permeability and excursion rate *(German)* 79−73779
- Fe-Ni (50 to 94 wt.%), FCC, form. and migration energy of vacancies, induced magnetic anisotropy *(French)* 78−2110
- Fe-Ni alloy, anisotropic hyperfine interactions, Mossbauer spectra 80−15854
- Fe-Ni alloy, cold work stored energy effect on mag. moment vs. temp. curve 78−95419

ferromagnetic properties of substances continued
Fe-Ni alloy, FCC, high-field susceptibility and spin wave spectrum 79—56493
Fe-Ni alloy, low-noise, for cores of ferromag. probes and mag. modulators 79—8017
Fe-Ni alloy, permeability and coercive force, effect of thermomag. treatment in rotating field *(Russian)* 77—21294
Fe-Ni alloy, surface decarburisation rate in dry H_2, soft mag. material manufacture 78—60882
Fe-Ni alloy near crit. conc., Mossbauer γ-rays small angle scatt. 80—7217
Fe-Ni alloy toroidal core, magnetic noise *(Russian)* 78—60308
Fe-Ni alloy type YuNDK25B, anomalous magnetocaloric effect 80—60278
Fe-Ni alloys, anomalous thermal expansion, Gruneisen eqn. 78—83980
Fe-Ni alloys, atomic valence states *(Ukrainian)* 78—2656
Fe-Ni alloys, electronic struct. by XPS obs. 79—33226
Fe-Ni alloys, FCC, mag. props. calc. 79—65659
Fe-Ni alloys, Invar effect explanation in localised moment model *(Russian)* 77—76580
Fe-Ni alloys, mag. state of austenite and $\gamma \rightarrow \alpha$ transform. *(Russian)* 80—40350
Fe-Ni base amorphous alloy, crystallisation 77—84660
Fe-Ni based alloy, amorphous rapidly quenched, mag. props. 77—66269
Fe-Ni based amorphous alloys, Hall and ohmic resistivities 79—91013
Fe-Ni based metallic glasses, hydrostatic press. effect on mag. props. 78—19300
Fe-Ni based metallic glasses, search for Invar-like magnetoelastic behaviour 79—56596
Fe-Ni based metallic glass, Metglas 2826 MB, Mossbauer study 80—75897
Fe-Ni FCC alloys, invar effect by local moment model 77—90006
Fe-Ni film, mag. and struct. props., effect of O_2 partial press. during deposition 79—90903
Fe-Ni films, dynamic domains and pulse mag. reversals *(Russian)* 79—28571
Fe-Ni films, lattice constants rel. to mag. moments *(Russian)* 77—32218
Fe-Ni Invar, magnetisation and high field susceptibility 79—56518
Fe-Ni Invar, magnetovolume coupling enhancement factor, temp. depend. 80—88851
Fe-Ni Invar, Mossbauer exam. 79—56639
Fe-Ni Invar alloy, bulk modulus anomaly, mag. effect 79—91728
Fe-Ni Invar alloy, Curie temp. and elec. resist., effect of press. 77—85449
Fe-Ni Invar alloy, effect of hydrogenation, Mossbauer spectra 79—56641
Fe-Ni Invar alloy, electron irrad. effects 79—56638
Fe-Ni Invar alloy, mag. phase mixing effect on thermodynamic props. 80—54891
γ-Fe-Ni Invar alloy, phase mixture produced by long annealing 79—5065
Fe-Ni Invar alloy, thermal expansion coeff. at low temp. 79—86911
Fe-Ni Invar alloys, Arrott plots rel. to itinerant electron characts. 77—73009
Fe-Ni Invar alloys, forced and spontaneous magnetostriction 78—48019
Fe-Ni Invar alloys, Mossbauer spectra, heat treatment effect 80—15855
Fe-Ni Invar alloys, splat quenched, mag. props. 80—75799
Fe-Ni Invar alloys, thermodynamic props. 79—56560
Fe-Ni Invar alloys of crit. conc., mag. props., flow theory methods *(Russian)* 80—65894
Fe-Ni Invar anomalies, explanation in terms of itinerant electron magnetism 80—75705
Fe-Ni Invar anomalies, low spin to high spin transition 79—56558
Fe-Ni metallic glass wide strips, low-field mag. props. 79—51822
Fe-Ni metallic glasses, crystallisation 77—43157
Fe-Ni ordered phase in meteorites, Mossbauer studies 80—41776
Fe-Ni/Fe, bimetal film, exchange const. determ. from hysteresis loops *(Russian)* 77—48015
Fe-Ni_3, hyperfine field, variation with atomic order 79—7953
Fe-Ni/pure Fe exchange coupled films, mag. reversals, hard layer thickness effects *(Russian)* 78—56359
Fe-Ni-Al, Curie temp. depend. on ordering, antiferromag. ordering *(Russian)* 79—61101
Fe-Ni-Al, magnetic anisotropy form. and struct. changes by annealing, Mossbauer obs. 80—39994
Fe-Ni-Al, type YuN14DK25BA, thermomag. treatment 80—16512
Fe-Ni-Al alloy, metastable equilib. in its high-coercivity state *(Russian)* 79—52161
Fe-Ni-Al alloys, phase diagram, miscibility gap, mag. props. 78—92237
Fe-Ni-Al-Co-Cu alloy, sintered single-crystal mag. prod., props. 77—66709
Fe-Ni-Al-Co-Cu-Sn alloy YuNDK35T5, Sn addition effects on physicomechanical and magnetic props. and workability *(Russian)* 77—70101
Fe-Ni-Al-Co-Cu-Ti, 38 to 40 wt.% Co, 8 to 8.5 wt.% Ti, alloy YuNDKT tempering and thermomagnetic treatments 78—3154
Fe-Ni-Al-Co-Cu-Ti magnetic alloy electrolytic treatment with programmed pulse current *(Russian)* 79—100282
Fe-Ni-Al-Co-Ti base alloys, highly coercive, phase comp., Mossbauer meas. 80—39996
Fe-Ni-Al-Cu (25, 14, 4 wt.%), alloy YuND4, effect of Ti addition on structure, mag. props. 80—15714
Fe-Ni-B-Si, amorphous, mag. props., heat treatment effects 80—89370
Fe-Ni-B(-P), ferromag., magneto-optical spectra in amorphous and cryst. states *(Russian)* 80—84749
Fe-Ni-C, Invar, coated, Mossbauer spectra, effect of applied RF mag. field 80—80645
Fe-Ni-Co, magnetic permeability, effect of ion implantation 77—28414
Fe-Ni-Co film, electron-nucl. mag. reson. 78—35063
Fe-Ni-Co foils, mag. reversals of mag. domains in low-coercivity channels *(Russian)* 79—42813
Fe-Ni-Co-Cu-Ti YuNDKT alloys, impaired mag. props. with C and S additions 80—60368
Fe-Ni-Co-Mo-Ge alloy 40NKM, excess mag. noise after various thermomag. treatments *(Russian)* 80—29575
Fe-Ni-Cr, at. distrib. effect on mag. props. *(Russian)* 78—2657
Fe-Ni-Cr, Elinvar, struct. and mag. props., singularities during tempering *(Russian)* 80—50627
Fe-Ni-Cr, Invar alloy, ^{57}Fe effective field distrib., Mossbauer obs. *(Russian)* 78—19381
Fe-Ni-Cr, mag. props. in weak mag. fields *(Russian)* 80—75771
Fe-Ni-Cr, vapour-deposited film, effect of condensation temp. on form. of metastable phases and mag. props. 79—65700

ferromagnetic properties of substances continued
Fe-Ni-Cr film, ferromag. reson. meas. *(Russian)* 77—1601
Fe-Ni-Cr vapour deposited film metastable phase formation *(German)* 78—38984
Fe-Ni-Cr-Ti-Al Elinvar alloys, dispersion-hardened, structural transform. *(Russian)* 79—1872
Fe-Ni-Mn, BCC, mag. state of Mn, NMR and saturation magnetisation meas. 78—39442
Fe-Ni-Mn, Invar, RF collapse and thermal effects, Mossbauer study 80—100624
Fe-Ni-Mn alloy, rel. to temp. coeff. of linear expansion *(Russian)* 77—80634
Fe-Ni-Mn-H, ferromag., magnetisation curves 78—88144
Fe-Ni-Mo, martensitic transformation, annealing, influence on struct. of austenite *(Russian)* 80—81057
Fe-Ni-P-B, amorphous ferromag. alloys, mag. struct., Mossbauer study 80—39746
Fe-Ni-P-B, metallic glasses, struct. relax., annealing effects on mag. props. 80—89261
Fe-Ni-P-B amorphous alloy, magnetically induced anisotropy 77—89948
Fe-Ni-Pt alloy, Invar behaviour 79—56531
Fe-Ni-Si-Mn-Cr(Co-Mo), effect of prolonged aging on mag. props. 80—16513
Fe-Ni-Te alloys, magnetisation 79—7975
Fe-Ni-Ti-Al-Nb, struct. mechanism for inverse $\alpha \rightarrow \gamma$ transform. *(Russian)* 80—40351
Fe-Ni(-Al)(Mn) Invar alloys, mag. heterogeneities *(Russian)* 77—66251
Fe-Ni(-Mn)(Cr)(V), concentration ferromag. antiferromag. phase transition and mag. state diagram. *(Russian)* 80—20401
Fe-Ni(Al), mag. aftereffect meas., phenomenological description 80—88835
Fe-Ni(Cr), Invar, exchange interactions between ferromag. and antiferromag. components 80—29545
Fe-Ni(Pt), Invar alloy, magnetic excitation exam. by neutron diffr. 79—56521
Fe-Ni(Pt) Invars, elastic and mag. props., magnetoelastic interaction effects *(Russian)* 80—84631
Fe-Ni(35.4 at.%) Invar alloys, T^2 term contribution to magnetisation 80—71096
Fe-nonmagnetic impurity, transferred hyperfine field using volume overlap model 79—78054
Fe-P, amorphous, temp. depend. of saturation magnetisation 78—19223
Fe-P alloys, amorphous, Mossbauer spectra 79—51886
Fe-P amorphous alloys, electrodeposited, mag. anisotropy 80—15713
Fe-P amorphous alloys, initial permeability, time depend. 80—15759
Fe-P electrodeposited foil, amorphous, mag. domains 80—75821
Fe-P film, amorphous, ion implanted, struct. and domain struct. obs. 79—91272
Fe-P-B, amorphous alloys, mag. props., conc. depend. 77—8314
Fe-P-B-Al, amorphous, magnetostriction as function of glass formers 78—19299
Fe-P-C, amorphous, struct. and mag. props., Mossbauer, X-ray diffr. and elec. resist. meas. 78—2009
Fe-P-C alloys, amorphous, mag. anisotropy, Mossbauer obs., prior cooling effects *(Russian)* 77—32300
Fe-P(Ga)(As)(Sb), dil., short range order, NMR study 80—71237
Fe-Pd, FCC, ferromag., spin wave stiffness constant 78—91851
Fe-Pd, magnetic after-effect of H isotopes 80—75817
Fe-Pd (47 at.%) alloy, powders and powder compacts, mag. props. rel. to heat treatment *(Russian)* 79—15816
Fe-Pd alloy, mag. struct. determ., neutron scatt., Mossbauer and mag. meas. *(Russian)* 78—2648
Fe-Pd alloy, uniaxial ferromag., anisotropic component of localised mag. field, Mossbauer meas. *(Russian)* 79—15382
Fe-Pd alloys, spin density radial distrib. determ. 79—73685
Fe-Pd crystalline alloy, positive large linear magnetostriction 80—25173
Fe-Pd Invar alloys, elec. and mag. props. and thermal expansion 80—75732
Fe-Pd-Pt alloy powders, coercive force and specific remanence *(Russian)* 79—47302
Fe-Pd(Pt), magnetic struct. changes assoc. with crystallite thickness increase *(Russian)* 77—80913
Fe-Pt, Invar alloy, strong ferromagnetism, magnetostriction and thermal expansion 79—8037
Fe-Pt, Invar alloy, thermodynamic properties, effects of forced magnetostriction 79—11331
Fe-Pt, Invar type, charact. magnetovolume effects 79—82855
Fe-Pt, Invar type, strong ferromagnetism, mag. props. 78—64197
Fe-Pt, ordered single cryst., magnetisation in strong mag. field *(Russian)* 78—47954
Fe-Pt, plastic deform. effect on struct. singularities and mag. props. *(Russian)* 80—44892
Fe-Pt films, mag. and magneto-optic props., appl. to holographic and bit-by-bit storage 79—33512
Fe-Pt Invar, magnetovolume effects 79—56597
Fe-Pt Invar alloy, bulk modulus anomaly, mag. effect 79—91728
Fe-Pt Invar alloy, homogeneous strong ferromagnet, thermal expansion and mag. props 79—91278
Fe-Pt Invar alloy, magnetocryst. anisotropy energy, itinerant electron model 80—54884
Fe-Pt Invar alloys, magnetocrystalline anisotropy const. determ. 80—65861
Fe-Pt-Ir, Mossbauer effect of ^{193}Ir and ^{57}Fe, hyperfine field, isomer shift 78—15072
Fe-Pu, dil., effective mag. fields, temp. depend. *(Russian)* 78—43587
Fe-rare earth alloys, amorphous, magnetoelasticity and moment rot., US vel. calc. and neutron scatt. meas. 80—65992
Fe-Rh, ferromag., spin wave stiffness constant calc. 79—38307
Fe-Rh, mag. phase transitions, triple point 79—1672
Fe-Rh alloy, nonmag. and mag., band theory 79—37973
Fe-Rh alloys, spin wave spectrum in antiferromag. and ferromag. phases, inelastic neutron spectrometry 77—63158
Fe-Sb-Ni(Cr), dil., short range order, NMR study 80—71237
Fe-Si, amorphous film, mag. props. 77—1575
Fe-Si, Bloch wall motion, irreversible processes 79—78431
Fe-Si, Bloch wall motion self-similarity *(French)* 79—82810
Fe-Si, coated, effective domain and grain obs. methods and Fe losses 80—34675
Fe-Si, domain struct., influence of insulating coating, high voltage SEM obs. 77—1565
Fe-Si, domain struct. obs. by high voltage SEM 77—1564

ferromagnetic properties of substances continued
Fe-Si, domain structure of Neel oriented samples 77—69601
Fe-Si, grain oriented, core losses *(Japanese)* 78—60303
Fe-Si, grain oriented, effect of tensile stress on domain struct. 78—95462
Fe-Si, grain oriented, misorientation effects on mag. props 80—88792
Fe-Si, grain oriented sheet, grain struct. by computer mapping 80—88168
Fe-Si, grain oriented sheet, AC hysteresis, surface struct. and elastic stress effects 80—88791
Fe-Si, grain oriented transformer sheets, permeability and magnetostriction, tensile stress effects 80—88843
Fe-Si, grain-oriented, AC magnetostriction at high temp., mag. annealing effects 77—20672
Fe-Si, grain-oriented, magnetostriction, and domain struct. 79—1703
Fe-Si, grain-oriented, surface coating effect on transverse magnetostriction 77—66402
Fe-Si, grain-oriented sheets, high permeability, low losses, review 80—88790
Fe-Si, hyperfine fields, Mossbauer meas. 80—40024
Fe-Si, hysteresis loops described by 180° Bloch wall *(French)* 79—15322
Fe-Si, internal friction, domain boundary area *(Russian)* 79—24562
Fe-Si, irreversible Barkhausen jumps *(French)* 77—1568
Fe-Si, loss meas. at high flux densities 80—88799
Fe-Si, low frequency power losses 78—95466
Fe-Si, low-texture patterns, X-ray examination 77—43109
Fe-Si, mag. losses, depend. on stress and orientation 77—1882
Fe-Si, mag. method for rapid analysis 77—44540
Fe-Si, mag. props., stress and reannealing effects 80—88844
Fe-Si, magnetic domain obs. by SEM 77—69606
Fe-Si, magnetic props., material for electrical engineering *(German)* 77—21293
Fe-Si, magnetisation in high fields, influence of internal field nonuniformity 79—51819
Fe-Si, magnetostatic couplings between 180° Bloch walls 77—69613
Fe-Si, maze domains upon appl. of horizontal mag. field or mech. tension 80—11218
Fe-Si, Mossbauer study of mag. ordering 79—24245
Fe-Si, non-oriented sheets, production and props. 80—88797
Fe-Si, power loss and permeability meas. by means of Hall probes and stochastic ergodic correl. 80—86350
Fe-Si, ribbon, prep. by rapid quenching 79—33957
Fe-Si, simple domain structs., magnetisation jumps 77—69624
Fe-Si, single cryst., mag. domain wall motion, X-ray topography study 80—65953
Fe-Si, stator core, grain-oriented and non-oriented, magnetic flux and loss distrib. 80—88798
Fe-Si, stress and plastic deform. effect on Barkhausen effect, instrumentation 78—52313
Fe-Si, strips and rods, spatial extent of flux due to irreversible changes of mag. polarisation 79—33506
Fe-Si, thermally activated motion of 180° Bloch wall 78—95457
Fe-Si, thin cryst., domain struct. behaviour during magnetisation *(Russian)* 78—2697
Fe-Si, type B_1 domain struct., Mossbauer exam. 77—51931
Fe-Si (1-5 wt.%), optimum sintering conditions and mag. props. 77—85958
Fe-Si (110)[001] sheet, normal stress effect on magnetostriction 77—40102
Fe-Si (2.4 wt.%), simulation of X-ray topographies of ferromag. domains *(French)* 77—77070
Fe-Si (2.5%), Bloch wall zig-zag struct., neutron small angle scatt. 77—16099
Fe-Si (2.5%), mag. stray fields above stripe domains, electron optic meas. 80—15755
Fe-Si (3 to 5 wt.%) sinters, mag. props., Si and Fe-Si additions effect 80—71104
Fe-Si (3 wt.%), Al-bearing, grain-oriented, N_2-H_2 annealing effect on texture, mag. props. 77—12714
Fe-Si (3 wt.%), AlN-inhibited, Se effect on primary grain recrystallisation 77—12715
Fe-Si (3 wt.%), anisotropy induced by rolling in (001) and (111) planes *(Russian)* 77—80931
Fe-Si (3 wt.%), Barkhausen effect meas. 77—85492
Fe-Si (3 wt.%), containing B, grain boundary segregation, AES evidence 77—86046
Fe-Si (3 wt.%), cube-on-edge oriented, high permeability, mill processing and mag. props. 77—86045
Fe-Si (3 wt.%), directional, power loss anomalies temp. depend., effect of intrinsic parameters 77—12156
Fe-Si (3 wt.%), domain struct. rel. to cryst. size *(Russian)* 80—29568
Fe-Si (3 wt.%), domain wall spacing and losses, orientation depend. 78—56343
Fe-Si (3 wt.%), domain wall spacing and core loss, forsterite and stress coatings effect 80—88780
Fe-Si (3 wt.%), EM losses, effect of bending of 180° domain boundaries *(Russian)* 78—39357
Fe-Si (3 wt.%), eddy current and hysteresis losses, role of domain struct. *(Russian)* 77—80961
Fe-Si (3 wt.%), effect of heating rate during primary recrystn. on props. after secondary recrystn. 78—84837
Fe-Si (3 wt.%), ferromag. domains, imaging by neutron interferometry 80—71087
Fe-Si (3 wt.%), Goss oriented, stress effects 78—91916
Fe-Si (3 wt.%), grain oriented tape-wound core, dynamic domain size var. and Fe losses 77—12146
Fe-Si (3 wt.%), grain oriented, MnS-AlN-inhibited, precipitate morphology 77—12648
Fe-Si (3 wt.%), grain oriented, lowest core loss 78—91887
Fe-Si (3 wt.%), grain orientated, negative magnetostriction, theory 78—91917
Fe-Si (3 wt.%), grain oriented, domain wall variation throughout magnetisation cycle 78—95459
Fe-Si (3 wt.%), grain oriented, power loss depend. on domain wall bowing 78—95460
Fe-Si (3 wt.%), grain oriented, mag. domain movements 79—82815
Fe-Si (3 wt.%), grain oriented, mag. props., effect of decarburizing *(Chinese)* 80—103821
Fe-Si (3 wt.%), grain-oriented, effect of forsterite coatings in domain struct. 78—23293

ferromagnetic properties of substances continued
Fe-Si (3 wt.%), grain-oriented, domain struct. regulation and power loss reduction 80—88779
Fe-Si (3 wt.%), grain-oriented, domain wall profiles throughout magnetisation cycle 80—88781
Fe-Si (3 wt.%), grain-oriented, stacking effect on power loss, mag. props. 80—88795
Fe-Si (3 wt.%), grain-oriented, power loss and domain wall variation with lamination thickness 80—88814
Fe-Si (3 wt.%), grain-oriented, energy loss reduction by lowering sheet thickness 80—88816
Fe-Si (3 wt.%), high induction grain oriented, metallurgical treatment and mag. props. 77—86044
Fe-Si (3 wt.%), high permeability, use in transformer cores 80—88793
Fe-Si (3 wt.%), hysteretic losses, domain struct. and cryst. defects 79—19747
Fe-Si (3 wt.%), internal friction, instantaneous, depend. on phase of torsional oscills. *(Russian)* 80—71142
Fe-Si (3 wt.%), loss contribs. from correlations among irreversible movements of Bloch walls 77—85483
Fe-Si (3 wt.%), losses, demagnetisation freq. and grain orientation depend. 80—88796
Fe-Si (3 wt.%), mag. anisotropy induced by rolling in (110) plane *(Russian)* 78—34978
Fe-Si (3 wt.%), mag. domain wall contrast in synchrotron X-ray topographs 80—75792
Fe-Si (3 wt.%), mag. loss and magnetostriction, DC flux alternation effects 80—88794
Fe-Si (3 wt.%), mag. props., stress coating effects 80—34728
Fe-Si (3 wt.%), magnetisation variation during bending oscills., rel. to ΔE effect *(Russian)* 80—65983
Fe-Si (3 wt.%), Mossbauer spectra, domain magnetisation vector rotations, domain struct. 79—69761
Fe-Si (3 wt.%), nonoriented sheets, magnetisation, tensile stress effects 80—88845
Fe-Si (3 wt.%), orientation distrib. in primary recrystallised textures, mag. permeability 77—12712
Fe-Si (3 wt.%), orientation development during secondary recrystallisation, primary matrix effect, magnetic props. *(Czech)* 78—60679
Fe-Si (3 wt.%), oriented, losses and domains, mech. stress effects 80—88852
Fe-Si (3 wt.%), polycrystal in mag. field, stress induced magnetisation, synchrotron Bragg refl. topography obs. 80—50139
Fe-Si (3 wt.%), power losses at extremely low freqs. 80—88815
Fe-Si (3 wt.%), prediction of magnetisation hysteresis loops for distorted waveforms 79—47303
Fe-Si (3 wt.%), rotational power losses, freq. depend. 78—91888
Fe-Si (3 wt.%), scratching effects on mag. losses in single crysts. with orientation near (110)[001] 79—51802
Fe-Si (3 wt.%), secondary recrystn., struct. inhibition, permeability improvement 77—12713
Fe-Si (3 wt.%), secondary recrystn., role of solutes 77—86043
Fe-Si (3 wt.%), square etch pit characts., subgrain misorientation and mag. domain patterns 77—25199
Fe-Si (3 wt.%), stripe domain structure, dynamic behaviour at high max. induction values *(Russian)* 80—80553
Fe-Si (3 wt.%), texture, Mossbauer expts. 80—71262
Fe-Si (3 wt.%), total losses under tensile stress, rel. to orientation near (110)[001] 78—76272
Fe-Si (3 wt.%), transformer steel, grain-oriented, magneto-optical domain obs., magnetisation mechanism 77—12364
Fe-Si (3 wt.%), transformer laminations, processing and props. 78—52325
Fe-Si (3 wt.%) (110), domain size depend. on crystal thickness *(Russian)* 79—69692
Fe-Si (3 wt.%) alloy, domain structure influence obs. and calc. *(Slovak)* 79—4693
Fe-Si (3 wt.%) alloy, mag. domain movements prod. by mech. stress 79—87284
Fe-Si (3 wt.%) alloy, mag. anisotropy induced by cold rolling *(Russian)* 80—84595
Fe-Si (3 wt.%) domain struct., tensile load effects *(Russian)* 78—47995
Fe-Si (3 wt.%) grain-oriented transformer sheet, effect of phosphate coating containing Cr_2O_3 and CaO 77—16135
Fe-Si (3 wt.%) laminations, orientation and stacking influence on losses obs. *(Slovak)* 79—4696
Fe-Si (3 wt.%) laminations, isotropic and cube-on-face, magnetostriction behaviour 80—39843
Fe-Si (3 wt.%) laminations, magnetostriction behaviour associated with closure domain spikes 80—75834
Fe-Si (3 wt.%) laminations, grain oriented, plastically deformed, anomalous losses 80—88853
Fe-Si (3 wt.%) layers, with ceramic coating, interface struct., electron microscopy and Mossbauer obs. *(Russian)* 79—28216
Fe-Si (3 wt.%) locally deformed, EM loss depend. on cryst. struct. and orientation *(Russian)* 80—7694
Fe-Si (3 wt.%) mag. domain motion quasi-lifetime topography using white synchrotron radiation, mag. field effects 79—42797
Fe-Si (3 wt.%) sheet, obs. through surface coating of domain struct., SEM 77—85482
Fe-Si (3 wt.%) single crysts., rolling-induced mag. anisotropy *(Russian)* 78—19243
Fe-Si (3 wt.%) steel, high permeability, grain oriented 78—91886
Fe-Si (3 wt.%) steel, high permeability, magnetostriction, stress inducing coating effects 80—34730
Fe-Si (3 wt.%) steel, oriented, stress depend. mag. props., coating effects 80—34729
Fe-Si (3% wt.) polycrystalline, short-range order and induced anisotropy *(Russian)* 79—51772
Fe-Si (3%), power loss, domain wall motion depend. 77—16100
Fe-Si (3%), spikn related contrast effect, visibility of 180° ferromag. domain walls 78—43612
Fe-Si (3%wt.), dynamics of 180° domain boundaries and electromag. losses *(Russian)* 79—51801
Fe-Si (3.2 wt.%), single cryst., prism-shaped closure domains on (110) surface 79—69690
Fe-Si (3.22 wt.%), topographic and type-2 magnetic contrast, effect of collector position in SEM 79—12909
Fe-Si (3.25 wt.%), mag. props., influence of struct. and chemical composition of surface oxide layer 78—2700

ferromagnetic properties of substances continued
Fe-Si (3.25 wt.%) alloy, single cryst. with (007) planes, domain struct. influence on mag. torque 80—108034
Fe-Si (3.5 wt.%), Barkhausen noise, strain depend., interaction of dislocations and domain walls 77—12155
Fe-Si (3.5 wt.%), dynamic neutron depolarisation meas. of ferromag. domain struct. 79—82812
Fe-Si (3.5 wt.%), magnetisation reversal and domain walls 78—84451
Fe-Si (3.5 wt.%), static neutron depolarisation meas. of ferromag. domain struct. 78—14978
Fe-Si (3.5 wt.%) picture frame cryst. , domain wall bowing dynamic neutron depolarisation 78—56344
Fe-Si (3.5 wt.%) picture frame, domain wall bowing, time-depend. neutron depolarisation 78—95458
Fe-Si (3wt.%), grain-oriented, secondary recryst., grain growth inhibition 80—89245
Fe-Si (4 at.%), Bloch wall thickness determ. by neutron small-angle scatt. 80—15754
Fe-Si (4 wt.%), freq. depend. of Fe losses in single crysts. with (100) [001] 79—51803
Fe-Si (4 wt.%), neutron crit. scatt., experimental anisotropy 78—38590
Fe-Si (4 wt.%) alloy, coercive force, influence of stabilisation of domain struct. on temp. depend. *(Russian)* 77—52513
Fe-Si (4%), (110)[001] and (100)[001], dynamic domain struct., AC excitation 77—16097
Fe-Si (6.5 wt%) filament, formation by modified Taylor technique, and mag. props. 80—75795
Fe-Si (6.5 wt.%), ductility and mag. props., Ni and Mn addition effects 78—76704
Fe-Si (6.5 wt.%), Ni, Al and Mn additions effect on mech. and mag. props. 77—12667
Fe-Si (6.5 wt.%) ribbon, splat-cooled, mag. props. 80—88805
Fe-Si (7.5, 14.3 at.%), mag. moments and form factors, neutron diffr. obs., d-band electron redistrib. 79—51751
Fe-Si (up to 8 wt.%), magnetostriction temp. and comp. depend. 77—66405
Fe-Si alloys, polycrystalline, domain struct. at grain boundaries *(Russian)* 77—51917
Fe-Si amorphous film, struct. and crystallisation, Mossbauer study 80—11300
Fe-Si amorphous films, mag. and magnetoelastic props. 79—99746
Fe-Si crystal, neutron depolarisation studies of ferromagnetic domain structures 80—25155
Fe-Si ferromag. film, props. 79—4709
Fe-Si plate, domain structure obs. by neutron diffr. topography 77—69645
Fe-Si sheets, grain oriented, with insulating coating, nondestructive grain identification methods *(Slovak)* 79—5090
Fe-Si single crysts., interaction of {110} 90° walls with lattice imperfections 80—39807
Fe-Si steel, high permeability, processing effect on recrystn. and deform. 77—12716
Fe-Si transformer steel, supplementary domain struct. of misoriented grains *(German)* 78—14979
Fe-Si-Al, Sendust, 12 μ thick film prep. by sputtering, mag. and other props. 77—55888
Fe-Si-Al, Sendust, ribbon-form, prep. by rapid quenching, mech. and mag. props. 80—71611
Fe-Si-Al (6,4 wt.%), Sendust alloy, effect of Ni content on mag. props. 78—72897
Fe-Si-Al (9.6, 5.4 wt.%), ribbon-form Sendust alloy, mag. props., annealing effects 80—88800
Fe-Si-Al ribbon-form Sendust alloy made by rapid roll quenching, mag. props., recording head appls. 80—81001
Fe-Si-Al Sendust alloy ribbon form, rapid quench prepared, elec. cond., coercive field, permeability 79—83151
Fe-Si-Al-Ni alloy, Super Sendust, Ni content and thermomag. treatment effects 77—4861
Fe-Si-B, high induction, hot rolling treatment 80—89266
Fe-Si-B, high induction alloy, improving mag. props. by adding B to coating 79—83338
Fe-Si-B, magnetic metallic glasses, mag. props. 80—84620
Fe-Si-B, melt C content effect on grain growth and induction 80—35351
Fe-Si-B amorphous films, mag. props. 80—34710
Fe-Si-B amorphous powder, production by spark erosion, and mag. props. 77—90290
Fe-Si-B ferromagnetic amorphous alloys, Young's modulus and delay time characts. *(Japanese)* 77—85543
Fe-Si-B glassy alloys, mag. props., comp. effects 80—88752
Fe-Si-B magnetic powder, amorphous, prep. by atomisation technique 78—92213
Fe-Si-B metallic glass, magnetisation meas. 78—23252
Fe-Si-B metallic glasses, mag. props., depend. on metalloid content 77—85485
Fe-Si-Mn, effect of Mn addition on mag. props. and elec. resist. 78—91890
Fe-Si-MnS-Al, Al effect on hot rolling struct., recrystallization, texture magnetic props. *(Chinese)* 78—11237
Fe-SiO multilayer film, interface magnetisation 80—7135
Fe-SiO multilayer films, interface magnetisation 80—88858
Fe-SiO_2, granular compund, superpara- to ferromag. transition temp. meas. 77—69633
Fe-$SiO_2(Al_2O_3)(ZrO_2)$ granular films, superparamag., Mossbauer effect 80—7131
Fe-Si(3 wt.%), ferromag. alloy, mag. anisotropy induced by cold rolling 80—30114
Fe-Si(4 wt.%), (110) and (100)[001] oriented, simulation of domain wall bowing 80—44854
Fe-Si(6.5 wt.%) ribbon, prep. by rapid quenching and mag. props. 80—45251
Fe-Si(6.5 wt.%) steel, core mat. development *(Korean)* 78—60852
Fe-Sn, dil., ferromag., temp. anomalies of Sn mag. hyperfine field and thermal expansion 79—33270
Fe-Ta alloy, mech. drawn and aged, exam. of electrical resistivity, hardness, microstruct., and mag. props. *(Japanese)* 78—48545
Fe-Tb, magnetoelastic hysteresis, elastic stress and mag. field depend. *(Russian)* 80—65982
Fe-Tb dilute alloy, amorphous, small angle mag. scatt. 78—27021
Fe-Ti, mag. permeability disaccommodation rel. to dissolved N migration *(Polish)* 79—95611
Fe-Ti, magnetic aftereffects of H isotopes, book contrib. 79—82835
Fe-Ti:H(D), isotope effects of diatomic TiH and TiD complexes 79—47259
α-Fe-Ti-N, mag. migrational relax., −60 to +200 degrees C 77—36099
Fe-V, conc. depend. of mag. moment distrib., polarised neutron diffr. meas. 78—19218
Fe-V, ferromag. struct. in nucl. spin echoes 80—60453
Fe-V, local environment effect on magnetic states 79—56491
Fe-V alloy, Curie temp. determ. using deviation from Mattheisen's rule 79—15306
Fe-V alloy, elec. resist. between 78 and 1200K 77—8065
Fe-V alloy, local environment effect on atomic moments, itinerant model 78—68188
Fe-V alloys, BCC, ferromag. polarised neutron diffr., appl. of multiband CPA theory 77—77033
Fe-V alloys, hyperfine fields at solute and solvent sites rel. to mag. moments 77—8461
Fe-V(Cr)(Mn), dil., local mag. moments, polarised neutron elastic diffuse scatt. 80—50088
Fe-W (5%), internal friction, mag. and nonmag. components *(Russian)* 78—48018
Fe-W system, damping capacity of Gentalloy, internal friction, mech. and mag. props. 79—77679
Fe-W-Cr-Mo system, mag. and mech. props. rel. to production methods *(Japanese)* 80—71107
Fe-W-Cr-Mo-Co with austenitic phase, magnetic and mech. props., cold working and ageing effects *(Japanese)* 78—60678
Fe-Zn alloys, coercive force anisotropy after cold plastic deform. *(Bulgarian)* 80—75809
Fe_3, effect of adsorbed H on mag. props. 77—63129
Fe_3 Pt, ordered ferromagnetic alloy, magnetic excitation obs. 80—70978
$(Fe\text{-}Co\text{-}Ni)_{78}Si_8B_{14}$, amorphous, low coercivity and zero magnetostriction 78—23299
$(Fe\text{-}Ni\text{-}Mo)_{80}(P\text{-}B)_{20}$, amorphous, mag. aftereffects and struct. instabilities 80—88833
FeAl-Pr (16 wt.%), for mag. heads, resist. depend. upon rolling process, thermal treatment *(Polish)* 80—39555
$FeAl_x$, ferromag. to mictomag. transition, Mossbauer meas. 77—24692
$Fe_{0.7}Al_{0.3}$, local environment effects and magnetic clustering 78—10658
Fe_2Al, mag. moment determ., role of local environment, self consistent calcs. 80—44815
Fe_3Al, containing C in solid solution., mag-permeability disaccommodation *(Polish)* 79—95613
Fe_3Al, magnetic form factor 78—76222
Fe_3Al, order-disorder transition effect on low energy spin waves 79—47271
Fe_3Al, ordered, magnetostriction and thermal expansion 80—39842
Fe_3Al, partly disordered B2 struct., spin wave dispersion relation 78—64201
Fe_3Al, roll magnetic anisotropy and dislocations *(Japanese)* 77—80930
Fe_3Al, super-lattice, band theory 77—15758
$Fe_3Al(Si)$, electronic structure, magnetic moments 80—107695
$Fe_{1-x}Au_x$, amorphous, elec. resist., temp. depend., spin wave contrib. and resist. minimum 78—51961
Fe_cAu_{1-c}, amorphous ferromagnetic, resistivity, anisotropic, field dependence 78—87960
FeB and Fe_2B, multiplet splitting of ESCA Fe 3s core levels 80—29847
FeB, thermophysical props., 296-2000K 78—14477
$Fe_{1-x}B_x$, amorphous, hyperfine fields and local mag. moments, Mossbauer study 80—75895
$Fe_{1-x}B_x$ amorphous films, mag. props. and thermal stability 79—78446
$Fe_{1-x}B_x$ film, optical and magneto-optical characts., mag. preps. 79—82956
$Fe_{1-x}B_x$ metallic glasses, struct. and cryst., Mossbauer spectra, DSC, and magnetisation meas. 79—94906
$Fe_{1-x}B_x$, polycrystalline and amorphous sputtered films, Brillouin spectra 80—2775
$Fe_{100-x}B_x$, amorphous, effect of metalloids on mag. props. 79—11304
$Fe_{100-x}B_x$, amorphous, mag. struct., mag. susceptibility meas. 80—80485
$Fe_{100-x}B_x$ amorphous alloys, magnetostriction meas. 79—19760
$Fe_{100-x}B_x$, amorphous alloys, saturation magnetostriction and annealing behaviour 80—34739
$Fe_{100-x}B_x$, crystalline and glassy, low temp. magnetisation study 79—95608
$Fe_{100-x}B_x$ glass, magnetostriction meas., temp. depend. 79—73792
$Fe_{100-x}B_x$, mag. and struct. props., comp. depend. 78—60314
$Fe_{100-x}B_x$ metallic glass, magnetisation meas. 78—80134
$Fe_{100-x}B_x$, quenched ferromag. ribbon, Brillouin spectra 80—2776
$Fe_{100-x}B_x$ ribbon, magnetostriction exam. 79—73794
Fe_3B, distinctness of magnetic hyperfine fields associated with structurally unique Fe sites 77—63330
Fe_3B, mag. props., ^{57}Fe Mossbauer spectra meas. 79—95693
$Fe_{80}B_{20}$, amorphous, Brillouin scatt. from magnons, ferromag. reson. 80—65844
$Fe_{80}B_{20}$, amorphous, deform. and annealing effects on mag. and mech. props. 77—12717
$Fe_{80}B_{20}$, amorphous, elec. and mag. hyperfine field distribs., Mossbauer study 80—39964
$Fe_{80}B_{20}$, amorphous, evaluation of complex Mossbauer spectra 78—43755
$Fe_{80}B_{20}$, amorphous, mag. permeability aftereffect during annealing 80—88834
$Fe_{80}B_{20}$, amorphous, transverse magnetoresist., stress effect 80—15501
$Fe_{80}B_{20}$ amorphous alloy, low field magnetic props. 77—55690
$Fe_{80}B_{20}$ amorphous alloys, domain struct. exam., magneto-optic Kerr effect 79—28550
$Fe_{80}B_{20}$, amorphous ferromag., temp. depend. of hyperfine field distrib. 78—43756
$Fe_{80}B_{20}$, amorphous ferromag. metallic glass, stress-induced rot. of magnetisation, Mossbauer study 80—20445
$Fe_{80}B_{20}$, amorphous ferromagnet, Mossbauer hyperfine fields, mag. struct. 80—75894
$Fe_{80}B_{20}$ amorphous ribbons, magnetomechanical coupling constant and Young's modulus, mag. annealing 79—15333
$Fe_{80}B_{20}$ amorphous ribbon, initial susceptibility time lag 80—100579
$Fe_{80}B_{20}$, binary amorphous ferromagnet, Mossbauer spectra 79—4749
$Fe_{80}B_{20}$, elastic, magnetoelastic and thermal props. 79—19759
$Fe_{80}B_{20}$, evaluation of complex Mossbauer spectra 78—60370
$Fe_{80}B_{20}$, ferromagnetic metallic glasses, Brillouin scattering 78—92085
$Fe_{80}B_{20}$ glass, low-field mag. props. 77—8380
$Fe_{80}B_{20}$ glass, magnetisation reorientation, Mossbauer effect 80—66092
$Fe_{80}B_{20}$, glassy, ferromag. anisotropy of resistivity 79—23939

ferromagnetic properties of substances continued
$Fe_{80}B_{20}$, METGLAS 2605, mag. anisotropy and electronic struct., Mossbauer meas. 77—28384
$Fe_{80}B_{20}$, metallic glass, mag. props. 77—16107
$Fe_{80}B_{20}$, metallic glass, Mossbauer spectroscopy 78—60365
$Fe_{80}B_{20}$ metallic glass, spin texture determ. 80—15842
$Fe_{80}B_{20}$ metallic glass, crystn. and struct. relax., Mossbauer effect study 80—75182
$Fe_{80}B_{20}$ metallic glasses, stability and transforms. 80—75174
$Fe_{80}B_{20}$ Metglass, Mossbauer spectra line broadening 78—52400
$Fe_{80}B_{20}$, sputter deposited amorphous, low field mag. props. 78—68335
$Fe_{81}B_{19}$ amorphous alloy, mag. anisotropy temp. depend. 78—14953
$Fe_{83.4}B_{16.6}$, amorphous, mag. props. and microstruct., cooling rate and melt overheating effects 80—65965
$Fe_{83.4}B_{16.6}$ amorphous, mag. props., melt overheating and cooling rate effects 80—89371
Fe_xB_{100-x}, amorphous, mag. props., ^{57}Fe Mossbauer spectra and magnetisation meas. 79—95693
$Fe_{80}(B_yC_{1-y})_{20}$, amorphous, saturation magnetostriction, comp. effects 80—34735
$Fe_{84}B_{16-x}C_x$, amorphous, hyperfine interaction and Curie temps., Mossbauer meas. 79—73858
$Fe_{84}B_{16-x}C_x$, amorphous alloys, short range order, Mossbauer and DSC study 80—39960
$Fe_{80}B_{20-x}M_x$ (X=Al, Si, Ge, C, P) and $(FeCo)_{80}B_{20}$ glass, magnetisation, Curie and crystn. temps. 79—87289
$FeBO_3$, crit. behaviour, Mossbauer and magnetisation meas. *(Russian)* 79—61106
$FeBO_3$, mag. linear dichroism and absorpt. spectra, Jahn-Teller effect 80—54662
$FeBO_3$, magnon dispersion by light scatt. and ferromag. reson. 77—55668
$FeBO_3$, polycrystalline, ferromagnetic resonance, crystallite orientation 78—15027
$Fe_3B_7O_{13}X$, X=Cl, Br, I, ferromag. ferroelectrics *(Japanese)* 79—65804
$Fe_{80}(B_{1-x}P_x)_{20}$ amorphous alloys, isothermal crystallisation kinetics 80—33895
$Fe_{78}B_{12}Si_{10}$, amorphous, Mossbauer study of hyperfine interaction and mag. anisotropy 80—40027
$Fe_{78}B_{12}Si_{10}$, amorphous ferromagnet, long and short range exchange interactions, Mossbauer spectra and interpretation 79—56526
$Fe_{80}B_{15}Si_5$ metallic glass, large uniaxial magnetostrictive anisotropy, magnetisation reversal 80—34736
$Fe_{80}B_{20-x}Si_x$, metallic glass, mech. and mag. props., depend. on metalloid content 79—91213
$Fe_{80}(B_ySi_{1-y})_{20}$, amorphous, saturation magnetostriction, comp. effects 80—34735
$Fe_{82}B_{18-x}Si_x$ glasses, soft mag. props. 79—73774
$Fe_{83}B_{16.5}Si_{0.5}$, amorphous, spin waves, inelastic neutron scatt. meas. 79—73701
$Fe_{100-x}Be_x$, amorphous ribbon, saturation magnetostriction, and electronically controllable delay line 79—1700
Fe_xC_{1-x} amorphous sputtered film, mag. props. 78—68311
$Fe(CO)_5$, R-10, R-20, optimum process parameters for mag. permeability temp. depend 78—35009
$FeCl_2$, magnetic excitation in presence of transverse field, ferromag. reson. 78—19335
$FeCl_2$, spin orientation of mag. impurity atom 77—59403
$FeCl_2.2H_2O$, metamagnetic, resonant magnon-optical phonon coupling 79—28773
FeCo disordered alloys, Mossbauer spectra, hyperfine mag. field distrib., Curie temp. 80—7198
FeCo, electronic structures, order effect 79—90938
FeCo molecules, matrix-isolation Mossbauer spectra 80—23448
$(Fe_{0.06}Co_{0.94})$-B, amorphous, mag. instability rel. to struct. 79—99729
$Fe_{68}Co_{32}$, ferromagnet, magnon heat cond. and lifetimes, 1-2 to 4.5K 77—16066
$Fe_{1-x}Co_xAl$, Knight shift and mag. susceptibility study, electron struct. peculiarities *(Russian)* 80—15814
$Fe_{3-x}Co_xAl$, site preference and local environment effects, Mossbauer and NMR meas. 80—71264
$(FeCo)_{80}B_{20}$, metallic glass, saturation moments and Curie temp. 77—1542
$(Fe_{0.5}Co_{0.5})_{1-x}B_x$, amorphous, hyperfine fields and local mag. moments, Mossbauer study 80—75895
$(Fe_{0.65}Co_{0.35})B$, crystalline disordered, evaluation of complex Mossbauer spectra 78—43755
$Fe_{0.65}Co_{0.35}B$, crystalline disordered, evaluation of complex Mossbauer spectra 78—60370
$Fe_5Co_{75}B_{20}$, amorphous, magnetisation reversal and domain boundary configs. 80—88809
$Fe_{71}Co_9B_{20}$, glassy ribbon, magnetostatic effects 79—73790
$Fe_{80-x}Co_xB_{20}$, ferromag. metallic glass saturation magnetostriction meas. 77—36108
$Fe_xCo_{80-x}B_{20}$, amorphous, mag. after-effect 79—61189
$Fe_{35}Co_{32}B_{20}Si_{10}Al_3$, stress-induced variation in magnetisation and dynamic magnetostrictive charact. 80—88855
$Fe_xCo_{1-x}Cl_2$, metamagnet, mag. phase diagram by mag. induced light scatt. 80—65883
$Fe_{0.5}Co_{0.5-x}Cr_x$ films, vacuum-deposited cryst. and mag. struct. *(Russian)* 80—93081
$(Fe_xCo_yNi_{1-x-y})_{78}Si_8Bi_{14}$ amorphous ribbons, saturation magnetostriction and vol. magnetostriction 77—85538
$(Fe_{100-x}Co_x)_{79}P_{13}B_8$, amorphous, hyperfine field distrib., ^{59}Co NMR spin-echo meas. 80—34818
$(Fe_{1-x}Co_x)_yPBAl$ metallic glasses, influence of composition and ageing on Curie temps. 77—85445
$Fe_{0.2}Co_{0.8}S_2$, narrow-band ferromag., high press. effect on anomalous elec. resist. 80—70698
$Fe_xCo_{1-x}S_2$, ferromagnetic solid soln., electronic props. 79—7990
$FeCo_2Si$, Heusler type materials, mag. props. 77—40042
$(Fe_{0.5}Co_{0.5})Si$, weak itinerant ferromag., polarised neutron scatt. exam. 77—4503
$Fe_{1-x}Co_xSi$, mag. props., sp. ht., n.m.r. and Mossbauer effect meas. 77—12129
$Fe_{3-x}Co_xSi$, structural, mag. moment, and hyperfine field behaviour, local environment model 79—65762
$Fe_xCo_{1-x}Si$ alloys, disordered, hydrostatic pressure effects on mag. props. 77—32175
$Fe_xCo_{1-x}Si$, mag. props., effect of hydrostatic press. 77—12101
$Fe_xCo_{1-x}Si$, mag. props. 79—56532

ferromagnetic properties of substances continued
$(Fe_{0.9}Co_{0.1})_xSi_yB_2$, $(Fe_{1-x}Co_x)_{78}Si_8B_{14}$ amorphous ribbons, magnetomech. coupling and saturation magnetostriction 78—68353
$(Fe_{1-x}Co_x)_{77}Si_{10}B_{13}$ alloys, amorphous, induced mag. anisotropy by mag. annealing 79—4671
$(Fe_{1-x}Co_x)_{77}Si_{10}B_{13}$, amorphous, mag. moments at 0K, Curie temp., mag. interactions 79—4670
$(Fe_{1-x}Co_x)_{78}Si_{10}B_{12}$, amorphous Hall effect and magnetoresist. *(Japanese)* 77—85199
$(Fe_{1-x}Co_x)_{78}Si_{10}B_{12}$, amorphous alloys, magnetic anisotropy meas. 80—2570
$(Fe_{1-x}Co_x)_{78}Si_{10}B_{12}$, amorphous, roll mag. anisotropy 80—75757
$(Fe_{1-x}Co_x)_{78}Si_8B_{14}$ ribbon, magnetostriction exam. 79—73794
$Fe_{4.7}Co_{70.3}Si_{15}B_{10}$, amorphous ferromag., roll mag. anisotropy 79—51773
$Fe_5Co_{70}Si_{10}B_{15}$ amorphous magnetic alloy, decrease of permeability after demagnetisation, disaccommodation 80—39814
$Fe_5Co_{70}Si_{15}B_{10}$ amorphous ferromag. ribbons, change of permeability by heat treatment 77—85493
$Fe_5Co_{70}Si_{15}B_{10}$, amorphous, change of mag. props. by low temp. annealing 78—27058
$Fe_5Co_{70}Si_{15}B_{10}$, amorphous ferromagnetic alloy, isothermal annealing effect on static magnetic props. *(Japanese)* 79—52398
$Fe_5Co_{70}Si_{15}B_{10}$, amorphous, crystn. effect on mag. props. *(Russian)* 80—44858
$(Fe_xCo_{1-x})_{78}Si_8B_{14}$, amorphous, saturation magnetostriction, strain modulated FMR obs. 80—75863
$(Fe_xCo_{100-x})_{100-(y+z)}Si_yB_z$ amorphous ribbon, mag. moment and Curie temp., comp. depend. 78—95421
$Fe_xCo_{1-x}Si(Ti)$, magnetic props., sp. ht. and resist. meas. 79—61120
$Fe_xCo_{1-x}Ti$, mag. props. 79—56532
$(Fe_{1-x}Cr_x)$-P-C, amorphous mag. props. *(Japanese)* 77—85433
Fe_xCr_{1-x}, spin-wave evolution crossing from ferromag. to spin-glass regime 80—97080
$Fe_{85-x}Cr_xB_{15}$ metallic glass, Curie temp., crystn. temp. and room temp. elec. resist., Cr content effect 79—91229
$Fe_{1-x}Cu_xCr_2S_4$, Hall effect and magnetoresist. 79—78119
$Fe_{1-x}Cu_xCr_2S_4$, mag. semicond., mag. props. and elec. cond. *(Japanese)* 79—47111
FeF_2, Mossbauer effect at high press. 80—15858
FeGe, cubic, spin reson., 4.2-300K, 3-35 GHz 79—38384
$Fe_{1.67}Ge$, Mossbauer and X-ray expts. 79—1734
Fe_3Ge, ^{119}Sn mag. hyperfine interaction, Mossbauer spectra *(Russian)* 79—38420
Fe_3Ge, mag. props. of cubic and hexagonal phases 77—8475
Fe_xGe_{1-x}, amorphous film, FMR meas. of mag. props., temp. and comp. depend. 77—69636
Fe_xGe_{1-x} amorphous film, low temp. conversion electron Mossbauer spectroscopy 78—48101
Fe_xGe_{1-x} amorphous film, XPS and Mossbauer exam. 79—56577
Fe_2Hf, ferromagnetism in hexagonal and cubic compounds 77—36074
$(Fe_{1-x}M_x)_2P$, (M=Co,Ni), magnetisation, susceptibility, thermal expsn. 79—11302
$Fe_xMg_{1-x}Cl_2$, metamagnetic transition, magnetooptic exam. of mag. phase diagram 77—63175
$Fe_xMg_{1-x}Cl_2$, metamagnet, mag. phase diagram by mag. induced light scatt. 80—65883
FeMn, dil., diffuse scatt. cross sections, polarized neutrons 78—43567
$(Fe_{1-x}Mn_x)_3Al$, mag. moments determ. from magnetisation and neutron and electron diffr. expts. 79—56520
$(Fe_{1-x}Mn_x)_{75}P_{16}B_6Al_3$, amorphous, spin-glass-ferromag. multicritical point, AC susceptibility meas. 80—50117
$(Fe_xMn_{1-x})_{75}P_{16}B_6Al_3$, amorphous, mag. ordering temp., hyperfine field distrib., elec. resist. 80—34633
$(Fe_{1-x}Mn_x)_{75}P_{15}C_{10}$, amorphous, mag. ordering, Mossbauer study 80—39747
$(Fe_{1-x}Mn_x)_{75}P_{15}C_{10}$, amorphous pair radial distrib. functions, neutron scatt. study 80—49128
$Fe_xMn_{1-x}Pt_3$, ferro-antiferromag. transform. at 4.2K *(Russian)* 78—88117
$(FeMn)_3Si$ alloys, ferromag. props. at low Mn concs. 77—59393
$(Fe_{1-x}Mn_x)Si$, US vel. rel. to mag. struct. and phase transforms *(Russian)* 77—47976
Fe_2MnSi, antiferro- and ferromag. props. 77—12104
$Fe_{3-x}Mn_xSi$, evidence for the ang. depend. of the hyperfine interactions 78—76241
$Fe_{3-x}Mn_xSi$, Mossbauer and NMR exam. of site substitution and mag. struct. 77—12092
$Fe_{3-x}Mn_xSi$, struct., magnetisation, and spin echo expts., rel. to local environment model 77—20518
$(Fe_{1-x}Mn_x)_2Y(B)$, Mn effect on Fe mag. moments, Mossbauer and mag. meas. 80—71016
$Fe_{76}Mo_4B_{20}$, quenched ferromag. ribbon, Brillouin spectra 80—2776
$Fe_{78}Mo_2B_{20}$, amorphous, transverse magnetoresist., stress effect 80—15501
$Fe_{78}Mo_2B_{20}$, amorphous ferromag., $T^{3/2}$ depend. of hyperfine field 78—39474
$Fe_{78}Mo_2B_{20}$, amorphous ferromag., mag. props. 79—38309
$Fe_{78}Mo_2B_{20}$, Elinvar-type behaviour 79—66091
$Fe_{78}Mo_2B_{20}$, glassy, ferromag. anisotropy of resistivity 79—23939
$(Fe_{93}Mo_7)_{80}B_{10}P_{10}$, amorphous, neutron scatt. investig. of spin waves, magnetisation 77—47984
$(Fe_xMo_{1-x})_{75}P_{16}B_6Al_3$, amorphous, effects of Mo on mag. props., Mossbauer meas. 79—73859
FeN alloy, coercive force, effect of $Fe_{16}N_2$, anisotropic model 77—85501
α''-$Fe_{16}N_2$ film, mag. mechanism, at. mag. moment *(Korean)* 79—7973
$Fe(Nb_{1-x}W_x)O_4$, mag. and elec. props. and Mossbauer effect 79—78590
FeNi, itinerant electron model, spin wave stiffness const. calc. 80—34613
FeNi-Cu, composite fibre and layer structs., anomalous props. caused by internal phase boundaries 78—72754
$Fe_{0.65}Ni_{0.35}$, UPS, density of states determ. 78—52623
$Fe_{0.66}Ni_{0.34}$ Invar alloy, magnetic form factor 79—56504
$Fe_{0.7}Ni_{0.3}$, Invar alloy, bulk moduli, pressure effect on lattice spacing 79—55805
$Fe_{1-x}Ni_x$, elec. resist., anomalies in temp. depend. 79—23942
$Fe_{1-x}Ni_x$, FCC, anomalies in sp. ht. and thermal expansion 79—19739
$Fe_{40}Ni_{38}$-Mo_4B_{18} amorphous alloys, compatibility of DC and AC mag. props. 80—34695
$Fe_{65}Ni_{35}$ ferromagnetic alloy, zero sound anomaly, inelastic neutron scatt. 79—46764
$Fe_{65}Ni_{35}$, ferromagnetic Invar alloy, lattice vibrations 78—91403

ferromagnetic properties of substances continued
$Fe_{65}Ni_{35}$, H-infused, internal mag. field determ., Mossbauer effect 78−23382
$Fe_{65}Ni_{35}$, quasi-localised spin system, neutron scatt. 78−68194
$Fe_{65}{}^{60}Ni_{35}$, electron irradiated, small angle neutron scatt. 78−52218
$Fe_{70}Ni_{30}$, short range order, diffuse elastic neutron scatt. study 78−52219
$Fe_{70}{}^{60}Ni_{30}$, small angle neutron scatt., magnetisation inhomogeneity 78−52218
$Fe_{1-x}Ni_xAl$, Knight shift and mag. susceptibility study, electron struct. peculiarities *(Russian)* 80−15814
$(FeNi)_{80}B_{20}$, metallic glass, saturation moments and Curie temp. 77−1542
$(Fe_{1-x}Ni_x)_{83}B_{17}$, amorphous alloys ferromagnetic resonance 80−108080
$Fe_{38}Ni_{38}B_{24}$, amorphous, magnetisation and FMR expts. 79−95607
$Fe_{40}Ni_{40}B_{20}$, amorphous, processing conditions effect on mag. props. 79−73775
$Fe_{40}Ni_{40}B_{20}$, amorphous, mag. loss meas. 79−73776
$Fe_{40}Ni_{40}B_{20}$, amorphous, high-field magnetisation curve, spin wave spectrum and microstructural inhomogeneities 80−15702
$Fe_{40}Ni_{40}B_{20}$, amorphous, casting conditions effect on mag. props. *(Japanese)* 80−34698
$Fe_{40}Ni_{40}B_{20}$, amorphous, RF annealing effects 80−108037
$Fe_{40}Ni_{40}B_{20}$, amorphous ferromag., resist. and galvanomagnetic props., rel. to magnetisation 78−14712
$Fe_{40}Ni_{40}B_{20}$, and $Fe_{40}Ni_{40}P_{14}B_6$, amorphous, mag. props., effects mech. deform. 80−39840
$Fe_{40}Ni_{40}B_{20}$ and $Fe_{40}Ni_{40}P_{14}B_6$, amorphous, mag. aftereffect spectra and annealing props. 80−88831
$Fe_{80-x}Ni_xB_{20}$ and $Fe_{80-x}Ni_xP_{14}B_6$ amorphous alloys, microhardness correl. with mag. props. 80−88826
$Fe_{80-x}Ni_xB_{20}$, $Fe_{80-x}Ni_xP_{14}B_6$, amorphous, microhardness meas., dependence on mag. props. *(Croatian)* 79−11688
$Fe_{80-x}Ni_xB_{20}$, ferromag. metallic glass, saturation magnetostriction meas. 77−36108
$(Fe_xNi_{1-x})_{80}B_{20}$, $(Fe_xNi_{1-x})_{80}P_{14}B_6$, new soft amorphous ferromagnetic glasses *(Croatian)* 79−11298
$(Fe_xNi_{100-x})_{80}B_{20}$, glassy, elec. resist. at elevated temp. 79−73484
$Fe_xNi_{80-x}B_{20}$, amorphous ferromag., low temp. resistivity 79−56181
$Fe_xNi_{80-x}B_{20}$ and $Fe_xNi_{80-x}P_{14}B_6$ metallic glasses, low temp. resist. and galvanomag. effects, mag. state influence 80−84461
$Fe_xNi_{80-x}B_{20}$, $Fe_xNi_{80-x}P_{14}B_4$, amorphous Hall effect voltage meas. *(Croatian)* 79−11102
$Fe_xNi_{80-x}B_{20}$, $Fe_xNi_{80-x}P_{14}B_6$, amorphous ferromag., galvanomag. props. 79−56196
$Fe_xNi_{80-x}B_{20}$ glass, resist., magnetoresist., and thermoelec. power 80−70681
$Fe_xNi_{80-x}B_{20}$, quenched ferromag. ribbon, Brillouin spectra 80−2776
$(Fe_yNi_{1-y})_{80}B_{20}$, mag. anneal anisotropy in amorphous alloys 77−16069
$(Fe_{1-y}Ni_y)_{0.8}B_{0.2-x}P_x$, amorphous, hyperfine fields and local mag. moments, Mossbauer study 80−75895
$Fe_{20}Ni_{60}B_{19}P_1$, amorphous, spin waves, inelastic neutron scatt. meas. 79−73701
$Fe_{80-x}Ni_xB_{20-y}P_y$, amorphous, Rayleigh region and coercive force 80−88806
$(FeNi)_{80}Bi_{17.5}Al_2Si_{0.5}$, stress-induced variation in magnetisation and dynamic magnetostrictive charact. 80−88855
$Fe_{40}Ni_{40}C_{14}P_6$ amorphous film, dislocation and mag. struct., neutron diffr. study 80−70956
$(Fe_{0.5}Ni_{0.5})_{1-x}Co_x$, paramag. susceptibility, 1000-1800°C, and T_c *(Russian)* 77−16040
$Fe_{0.65}(Ni_{1-x}Co_x)_{0.35}$, Mossbauer spectra, ${}^{57}Fe$ hyperfine field distrib. 80−20533
$Fe_{65}(Ni_{1-x}Cr_x)_{35}$, mag. viscosity and anomalies near Curie temp. 79−73781
$Fe_{65}(Ni_{1-x}Cr_x)_{35}$, remanent magnetisation, temp. depend., anomalies near Curie temp. *(Russian)* 78−60310
$Fe_{32}Ni_{36}Cr_{14}P_{12}B_6$, metallic glass, changes in Curie temp., physical dimensions and mag. anisotropy during annealing 77−85446
$Fe_{32}Ni_{36}Cr_{14}P_{12}B_6$, Metglas 2826A, Hall resistivity, effect of thermal cycling and annealing 78−56125
$Fe_{32}Ni_{36}Cr_{14}P_{12}B_6$, elastic, magnetoelastic and thermal props. 79−19759
$Fe_{32}Ni_{36}Cr_{14}P_{12}B_6$, amorphous ferromagnet, long and short range exchange interactions, Mossbauer spectra and interpretation 79−56526
$Fe_{32}Ni_{36}Cr_{14}P_{12}B_6$, amorphous mag. solids, Mossbauer exam. 79−61281
$Fe_{32}Ni_{36}Cr_{14}P_{12}B_6$, Metglass 2826A, mag. props. under high press., Mossbauer meas. 79−73860
$Fe_{0.5}(Ni_xMn_{1-x})_{0.5}$, ferromag. ground state, elec. resist., anomalies in temp. depend. 79−23942
$Fe_{0.65}(Ni_{1-x}Mn_x)_{0.35}$, Mossbauer spectra, ${}^{57}Fe$ hyperfine field distrib. 80−20533
$Fe_{65}(Ni_{1-x}Mn_x)_{35}$, anomaly of subcrit. neutron scatt. and depolarisation effects at antiferro- to ferromag. transition *(Russian)* 77−47996
$Fe_{65}(Ni_{1-x}Mn_x)_{35}$, H solid solutions magnetisation behaviour in pulsed mag. fields 79−65674
$Fe_{65}(Ni_{1-x}Mn_x)_{35}$, magnetic struct. and inhomogeneities by neutron scatt. and Mossbauer effect *(Russian)* 77−63122
$Fe_{66}Ni_{31}Mn_3$, H-infused, internal mag. field determ., Mossbauer effect 78−23382
$Fe_{40}Ni_{40}(Mo,Si,B)_{20}$, amorphous, soft mag. props., switched-mode power supply appls. 80−88850
$Fe_{40}Ni_{38}Mo_4B_{18}$, amorphous, mag. anisotropy, Mossbauer study 80−65864
$Fe_{40}Ni_{38}Mo_4B_{18}$ and $Fe_{78}Mo_2B_{20}$ amorphous ribbons, magnetoelastic effects in as-quenched and stress-relieved states 80−80588
$Fe_{40}Ni_{38}Mo_4B_{18}$ glassy alloy, high permeability, low field mag. characts. 78−68301
$Fe_{40}Ni_{38}Mo_4B_{18}$ metallic glass, reorientation kinetics of magnetization 79−24155
$Fe_{40}Ni_{38}Mo_4B_{18}$, metallic glass, mag. and transport props. 80−39752
$Fe_{40}Ni_{38}Mo_4B_{18}$ ribbon, magnetic characterisation 80−34680
$(Fe_{1-x}Ni_x)_2P$, Curie temp., press. depend. meas. 80−97091
$(Fe_{1-x}Ni_x)_{80}P_{20}$, amorphous, ferromagnetic alloys, mag. anomalies of Invar type *(Russian)* 80−93089
$(Fe_{0.04}Ni_{0.96})_{80}P_{10}B_{10}$, amorphous, mictomagnetic to ferromag. transition 78−34981
$(Fe_{0.04}Ni_{0.96})_{80}P_{10}B_{10}$, amorphous magnetisation, field and temp. depend. 80−39755
$(Fe_{1-x}Ni_x)_{80}P_{10}B_{10}$, amorphous, magnetostriction meas. by ferromag. reson., induced anisotropy 77−32232

ferromagnetic properties of substances continued
$(Fe_{1-x}Ni_x)_{80}P_{10}B_{10}$, amorphous microwires, magnetisation reversal and anisotropy 78−91885
$Fe_{20}Ni_{60}P_{14}B_6$, $Fe_{30}Ni_{50}P_{14}B_6$, amorphous ferromags., thermoelec. power and resistivity near Curie temp. 79−56200
$Fe_{27}Ni_{53}P_{14}B_6$, amorphous, Hall resist. and mag. props., short range order effects 80−34422
$Fe_{27}Ni_{53}P_{14}B_6$, metallic glass, changes in Curie temp., physical dimensions and mag. anisotropy during annealing 77−85446
$Fe_{40}Ni_{40}P_{14}B_{06}$, amorphous, strip domains, anisotropy const. effects 80−29571
$Fe_{40}Ni_{40}P_{14}B_6$, (Metglas 2826), ferromag. Curie temp. determ. 78−64206
$Fe_{40}Ni_{40}P_{14}B_6$, amorphous ribbon, cold rolling, annealing mag. props. 77−8958
$Fe_{40}Ni_{40}P_{14}B_6$, amorphous, deform. and annealing effects on mag. and mech. props. 77−12717
$Fe_{40}Ni_{40}P_{14}B_6$, amorphous, magnetoelastic props. 77−16136
$Fe_{40}Ni_{40}P_{14}B_6$, amorphous, thermal stress effect on mag. easy axis 77−80928
$Fe_{40}Ni_{40}P_{14}B_6$, amorphous, domain struct. 78−10719
$Fe_{40}Ni_{40}P_{14}B_6$, amorphous tape wound cores, mag. props. *(German)* 78−10727
$Fe_{40}Ni_{40}P_{14}B_6$, amorphous, mag. props. 78−10728
$Fe_{40}Ni_{40}P_{14}B_6$ amorphous ribbon, mag. anisotropy distrib. near surface 78−95430
$Fe_{40}Ni_{40}P_{14}B_6$, amorphous ferromagnet, domain struct., Rayleigh region and coercive field 79−28559
$Fe_{40}Ni_{40}P_{14}B_6$, amorphous, stress-induced mag. easy axis 79−33516
$Fe_{40}Ni_{40}P_{14}B_6$, amorphous, transverse magnetoresist., stress effect 80−15501
$Fe_{40}Ni_{40}P_{14}B_6$, amorphous ferromagnet, Mossbauer hyperfine fields, mag. struct. 80−75894
$Fe_{40}Ni_{40}P_{14}B_6$, amorphous, mag. polarisation in approach to ferromag. saturation 80−80560
$Fe_{40}Ni_{40}P_{14}B_6$, amorphous, mag. permeability aftereffect during annealing 80−88834
$Fe_{40}Ni_{40}P_{14}B_6$, amorphous ferromag., spin wave excitations 80−97079
$Fe_{40}Ni_{40}P_{14}B_6$ amorphous ribbon, mag. domains and anisotropy distrib. 80−108029
$Fe_{40}Ni_{40}P_{14}B_6$, and $Fe_{32}Ni_{36}Cr_{14}P_{12}B_6$, glassy, ferromag. anisotropy of resistivity 79−23939
$Fe_{40}Ni_{40}P_{14}B_6$, elastic, magnetoelastic and thermal props. 79−19759
$Fe_{40}Ni_{40}P_{14}B_6$, $Fe_{35}Ni_{32}Cr_{15}P_{12}B_6$, amorphous ferromagnets, Barkhausen noise and core losses 77−69618
$Fe_{40}Ni_{40}P_{14}B_6$, ferromagnetic metallic glasses, Brillouin scattering 78−92085
$Fe_{40}Ni_{40}P_{14}B_6$ glass, low temp. heat capacity meas., electronic, phonon contributions exam. 78−10689
$Fe_{40}Ni_{40}P_{14}B_6$ glass, crystn. kinetics, DSC expts. 78−26444
$Fe_{40}Ni_{40}P_{14}B_6$ glass, struct. relax., ferromag. reson. and X-ray scatt. 79−90566
$Fe_{40}Ni_{40}P_{14}B_6$, glassy, mag. props. and hyperfine interactions, Mossbauer obs., 4.2-1000K 78−10812
$Fe_{40}Ni_{40}P_{14}B_6$, hardness, elec. cond., photo emission, and mag. props. *(Norwegian)* 79−32909
$Fe_{40}Ni_{40}P_{14}B_6$, high-field suscept. and spin wave spectrum 78−10662
$Fe_{40}Ni_{40}P_{14}B_6$ metallic glass, ferromag. reson., spin waves, thermal ageing and long-range order effects 80−25214
$Fe_{40}Ni_{40}P_{14}B_6$, Metglas 2826, ferromag. antireson. transmission at 24 GHz, 26 to 270°C 77−69696
$Fe_{40}Ni_{40}P_{14}B_6$, Metglas 2826, magnetising processes 78−10725
$Fe_{40}Ni_{40}P_{14}B_6$, Metglas 2826, amorphous ribbon core, appl. in force transducer 78−93669
$Fe_{40}Ni_{40}P_{14}B_6$, metglas 2826, amorphous, Hall resistivity, thermal cycling and annealing effects 79−38050
$Fe_{40}Ni_{40}P_{14}B_6$ Metglass, spontaneous vibr. modes excited by reversible magnetostriction 79−56587
$Fe_{40}Ni_{40}P_{14}B_6$, quenched amorphous, high field susceptibility and microstructure 77−69506
$Fe_{40}Ni_{40}P_{16}B_6$, amorphous, kinetics of induced mag. directional order 80−44824
$Fe_{40}Ni_{40}P_{20-x(B)}B_{x(B)}$, ferromagnetic metallic glass, thermal and mech. stability 77−66698
$Fe_{40}Ni_{40}P_yB_{20-y}$, amorphous, mag. props. effect of metalloid elements 79−28658
$Fe_{46}Ni_{40}P_{16}B_6$, ferromagnetic amorphous alloy, even magneto-optic effects 77−55776
$(Fe_xNi_{1-x})_{80}P_{10}B_{10}$, amorphous, weak itinerant ferromag., Arrott plots 77−73007
$(Fe_xNi_{1-x})_{80}P_{10}B_{10}$, amorphous, magnetisation reversal and domain boundary configs. 80−88809
$(Fe_xNi_{1-x})_{80}P_{14}B_6$, amorphous, hyperfine field distrib., ${}^{57}Fe$ Mossbauer spectra 79−11367
$(Fe_xNi_{1-x})_{80}P_{14}B_6$, Mossbauer spectroscopy, mag. hyperfine interaction, Curie temps. 78−6617
$(Fe_xNi_{100-x})_{80}P_{10}B_{10}$, amorphous, elec. resist., 2 to 300K, composition depend. 80−44562
$Fe_xNi_{80-x}P_{14}B_6$ (x=0, 20, 40, 60, 80), metallic glass, low temp. sp. ht. 80−2588
$Fe_xNi_{80-x}P_{14}B_6$, amorphous ferromag., resistivity, mag. contrib., 1.5-50K 79−56182
$Fe_xNi_{80-x}P_{14}B_6$, amorphous ferromag., T^2 saturation in resist. below 0.3K 79−60785
$Fe_xNi_{80-x}P_{14}B_6$, and $Fe_xNi_{80-x}B_{20}$ glass, microhardness, correl. with mag. props. 79−57085
$Fe_xNi_{80-x}P_{14}B_6$ glass, resist., magnetoresist., and thermoelec. power 80−70681
$Fe_xNi_{80-x}P_{14}B_6$ metallic glasses, low temp. resistivities 78−91659
$(Fe_{0.3}Ni_{0.7})_{0.75}P_{0.16}B_{0.06}Al_{0.03}$, amorphous, spin wave spectrum, neutron scatt. 77−16064
$(Fe_{0.5}Ni_{0.5})_{75}P_{16}B_6Al_3$ glass, struct. relax. as origin of Curie temp. ageing 78−84418
$(Fe_{1-x}Ni_x)_{75}P_{16}B_6Al_3$, amorphous alloy, low temp. elec. resist. saturation 78−68005
$(Fe_{1-x}Ni_x)_{75}P_{16}B_6Al_3$, amorphous, saturation magnetisation, temp. depend., ferromag. reson. meas. 79−73818
$(Fe_{65}Ni_{35})_{75}P_{16}B_6Al_3$, amorphous ferromag., high temp. spin dynamics 78−47965
$(Fe_{65}Ni_{35})_{75}P_{16}B_6Al_3$, mag. excitations 79−7984

ferromagnetic properties of substances continued
$(Fe_xNi_{1-x})_{75}P_{16}B_6Al_3$, amorphous, spin wave excitations and low temp. magnetisation 79−33468
$(Fe_xNi_{1-x})_{75}P_{16}B_6Al_3$, magnetisation temp. depend., spin wave theory 80−44927
$Fe_{29}Ni_{49}P_{14}B_6Si_2$ glass, crystn. kinetics, DSC expts. 78−26444
$Fe_{29}Ni_{49}P_{14}B_6Si_2$, metallic glass, changes in Curie temp., physical dimensions and mag. anisotropy during annealing 77−85446
$Fe_{29}Ni_{49}P_{14}B_6Si_2$, Metglas 2826B, Hall, elec. resist., magnetisation and heat capacity meas. 78−68019
$Fe_{29}Ni_{49}P_{14}B_6Si_2$, Metglass 2826B, saturation magnetisation, temp. depend., ferromag. reson. meas. 79−73818
$(Fe_{1-x}Ni_x)_{80}PyB_{20-y}$, local struct. disorder and crystallisation, Mossbauer exam. 79−1728
$(Fe_{1-x}Ni_x)_{77}Si_{10}B_{13}$ amorphous alloy system, saturation mag. moment, Curie temp., mag. susceptibility 80−39753
$(Fe_{1-x}Ni_x)_{77}Si_{10}B_{13}$, amorphous, Landau-Ginzburg theory, magnetisation and Curie temp. 80−75700
$(Fe_{1-x}Ni_x)_{78}Si_{10}B_{12}$, amorphous, Hall effect and magnetoresist. *(Japanese)* 77−85199
$Fe_{62.4}Ni_{15.6}Si_7B_{15}$ amorphous ferromagnetic alloy, anomalous magnetisation possible reasons, Mossbauer spectra *(Russian)* 79−78441
$(Fe_{0.2}Ni_{0.8})_{1-y}(SiO)_y$, Permalloy material, magnetisation, temp. and impurity atom conc. depend., band model calcs. *(Russian)* 80−93088
$(Fe_yNi_{1-y})_{1-x}(SiO)_x$, dielec. effect on magnetisation and Faraday rot. *(Russian)* 78−39298
FeNiTe alloys, disordered, polycrystalline, elec. resist., temp. depend. 80−49692
α-Fe_2O_3, analysis of car exhaust by Mossbauer spectroscopy 78−92963
γ-Fe_2O_3, densified, rheological and mag. props. 80−44873
γ-Fe_2O_3, elongated particles, mag. struct. 78−88096
α-Fe_2O_3, hematite, field-induced domain struct., neutron diffr. meas. *(German)* 77−16101
γ-Fe_2O_3-organic interfaces, mag. struct., Mossbauer effect, IR absorpt., and magnetisation meas. 80−44869
Fe_3O_4 ferrofluid, mag. birefringence, estimation of particle size 79−33511
Fe_3O_4, ferromag. ferroelectrics *(Japanese)* 79−65804
Fe_3O_4 in suspension, ferromagnetic colloid, optical meas. 78−10906
Fe_3O_4, magnetoelectric effects from electric field depend. macroscopic mag. anisotropy energy 77−69656
Fe_3O_4:^{119}Sn, magnetic interactions, Mossbauer spectra 79−15301
Fe_xO_y epitaxial film, ferromag. reson. 77−51964
Fe_2P, grown in liq. Cu medium, composition and mag. props. 79−11313
Fe_2P, mag. moments and form factors, polarised neutron diffr. study 79−65650
Fe_2P, mag. struct., neutron diffr. study 78−23246
Fe_2P, magnetisation, susceptibility, thermal expansion and elec. resist. meas. 77−77037
Fe_2P, Mossbauer spectra and mag. props., Curie temp. dispersion 77−36162
Fe_2P, spin wave excitations meas. 80−65831
Fe_2P:Cu, Mossbauer spectra, mag. transition 80−50240
$Fe_{80}P_{20}$, binary amorphous ferromagnet, Mossbauer study 80−34829
$Fe_{80}P_{20}$ glass, mag. props. 77−63125
$Fe_{82}P_{18}$, amorphous, uniaxial mag. anisotropy 78−19246
$Fe_2P_{1-y}As$, mag. props., Mossbauer effect 77−40156
$Fe_{79}P_{13}B_8$ amorphous alloys, splat cooled, Mn, Cr and V substituted, mag. and transport props. 80−84593
$Fe_{80}P_{14}B_6$ glass, low temp. heat capacity meas., electronic, phonon contributions exam. 78−10689
$Fe_{83}P_{17-x(B)}B_{x(B)}$, ferromagnetic, metallic glass thermal and mech. stability 77−66698
$Fe_{75}P_{16}B_6Al_3$, aged metallic glass, Mossbauer effect 79−91318
$Fe_{80}P_{16}B_1C_3$, ferromag. metallic glass, Mossbauer spectra, crystn. 77−12276
$Fe_{0.75}P_{0.15}C_{0.10}$, amorphous, mag. excitations and static struct., neutron scatt. obs. 78−68204
$Fe_{75}P_{15}C_{10}$, amorphous, magnetoelastic props. 77−16136
$Fe_{75}P_{15}C_{10}$, amorphous, mag. excitations, inelastic neutron scatt. 78−10674
$Fe_{75}P_{15}C_{10}$ amorphous foil, ferromag. domain orientation, Mossbauer exam. 78−52402
$Fe_{75}P_{15}C_{10}$, amorphous spin echo NMR of ^{31}P 78−2770
$Fe_{75}P_{15}C_{10}$ foils, amorphous, ferromag. domain orientation, Mossbauer study 78−15000
$Fe_{75}P_{15}C_{10}$, glassy ferromag., crit. sp. ht. meas. 78−10716
$Fe_{80}P_{13}C_7$, amorphous, mag. domain struct. obs. 77−36091
$Fe_{80}P_{13}C_7$, amorphous ferromag. ribbons, US rel. meas. 77−80582
$Fe_{80}P_{13}C_7$ amorphous ferromag. ribbons, change of permeability by heat treatment 77−85493
$Fe_{80}P_{13}C_7$, amorphous ferromagnetic alloy, isothermal annealing effect on static magnetic props. *(Japanese)* 79−52398
$Fe_{80}P_{20-x}C_x(Si_x)(Ge_x)$, amorphous, size effect of metalloids on mag. props. 80−84594
$Fe_{75}P_{15}O_{10}$, amorphous, ferromag. domain-wall width, anisotropy depend. 78−19269
FePd epitaxial film, vacuum-deposited, for thermomag. recording, mag. and magneto-optical props. *(Russian)* 78−60319
$FePd_{1-x}Pt_x$, permanent magnet, coercive force increased by Pt 79−24157
$Fe_{1-x}Pd_x$ films, vacuum deposited, mag. and corrosion props. 79−56574
Fe_3Pd, quenched, or annealed exam. of magnetostriction, galvano- and thermomagnetic props. *(Russian)* 79−19757
$Fe_{50}Pd_{50}$, order-disorder transition, Mossbauer study 80−71268
$Fe(Pd_{1-x}Au_x)_3$, mag. struct. ferro-antiferromagnetism coexistence *(Russian)* 79−82759
$Fe(Pd_{1-x}Au_x)_3$ ordering alloys, mag. props., 4.2 to 500K *(Russian)* 79−47301
$Fe_{25}Pd_{50}Au_{25}$, atomic ordering influence on mag. props. and elec. resistance *(Russian)* 80−7551
$Fe_{34}Pd_{46}P_{20}$, amorphous, sp. ht. and resist. near ferromag. phase transition 78−56333
$Fe_xPd_{80-x}Si_{20}$, low field susceptibility near transition temp. 77−66359
$Fe_xPd_{82-x}Si_{18}$, amorphous, magnetisation, magnetoresist., spin glass and ferromag. phases 80−34697
FePt epitaxial film, vacuum-deposited, for thermomag. recording, mag. and magneto-optical props. *(Russian)* 78−60319
Fe_3Pt Invar alloy, anomalous Curie const., susceptibility meas. 80−75731

ferromagnetic properties of substances continued
Fe_3Pt, Invar alloy, elastically stressed, ^{57}Fe effective field, anomalous behaviour, Mossbauer obs. *(Russian)* 77−8485
Fe_3Pt Invar alloy, mag. props., martensitic transform. 79−78365
Fe_3Pt, Invar alloy, theory of elastic-anomalies 78−95505
Fe_3Pt Invar alloy, thermal expansion and spontaneous magnetisation, Invar anomalies, low spin model 80−71001
Fe_3Pt Invar alloys, elec. resist. anomalous crit. behaviour 79−78067
Fe_3Pt, premartensitic phenomena *(French)* 79−8297
Fe_3Pt, quasi-localised spin system, neutron scatt. 78−68194
$Fe_{3-x}Pt_{1+x}$, ordered and disordered, mag. props. at low temp. 79−56517
$Fe_{72}Pt_{28}$, ferromagnetic Invar alloy, lattice vibrations 78−91403
$Fe_{72}Pt_{28}$ Invar alloy, low temp. thermal expsn. 79−65221
$Fe_{76}Pt_{24}$ Invar alloy, ferromag., fine-powdered, Mossbauer effect 79−56634
$Fe_{48}Rh_{52}$, hyperfine mag. field at ^{57}Fe and ^{119}Sn nuclei, press. depend. *(Russian)* 78−80266
$FeRh_2S_4$, mag. semicond., mag. and elec. props. 80−93121
$Fe_7S_8(Se_8)$, magnetocrystalline nature 78−41337
$Fe_{1+x}Sb$-CoSb solid soln., mag. props., Mossbauer spectra, solubility limits, and lattice consts. *(Russian)* 77−59394
$Fe_{1+x}Sb$-NiSb solid soln., mag. props., Mossbauer spectra, solubility limits, and lattice consts. *(Russian)* 77−59394
$Fe_{1-x}Se$, phase relation 79−14926
FeSi, (110), Neel cryst., refr. of neutrons in Bloch walls using double cryst. arrangement 79−24191
FeSi, domain struct. and magnetisation reversal, time depend. neutron depolarisation 80−50138
FeSi, hyperfine fields about μ^+ 79−56664
FeSi, nearly ferromag. semicond. mag. and thermal props., spin fluctuation theory 79−65687
FeSi, single cryst., orientation of pieces of zigzag Block walls, neutron small-angle scatt. determ. 79−24190
FeSi, single crysts., domain struct., temp. and field depend. 80−71085
$Fe_{1-x}Si_x$ film, optical and magneto-optical characts., mag. preps. 79−82956
$Fe_{100-x}Si_x$ ribbon, magnetostriction exam. 79−73794
Fe_2Si-transition metal alloys, Heusler type materials, mag. props. 77−40042
Fe_3Si, 3d transition metal substituted, limits of solubility, mag. props. and electron conc. 78−10670
Fe_3Si, transition metal impurities, hyperfine fields 77−59365
Fe_3Si-based alloy, dil., cond. electron polarisation and moment perturbations 78−68224
$Fe_{3+x}Si_{1-x}$, electron transport 78−91669
η-Fe_5Si_3, thermal and mag. props. 77−36080
$Fe_{95}Si_5$, thermal and elec. cond., heat transport by spin waves 79−38047
Fe_xSi_{1-x}, amorphous, high field magnetisation meas. 78−39367
Fe_xSi_{1-x}, amorphous, struct. and mag. props., giant moment form. at mag. ordering 78−68192
Fe_xSi_{1-x} amorphous alloys, magnetisation meas. showing crit. conc. at $x=0.4$ 77−59429
Fe_xSi_{1-x}, amorphous film, magneto-optic Kerr effect 80−66158
$Fe_3Si_{1-x}Al_x$, hyperfine interactions and structural disorder, spin echo, X-ray and magnetisation meas. 77−32289
$Fe_xSi_yAl_z$ ribbon, magnetostriction exam. 79−73794
Fe_5SiB_2, Mossbauer spectra, 140-784K, spin rotation 78−52409
$Fe_{75}(Si_{0.5}B_{0.5})_{25}$ film, amorphous, sputtered, thermal stability 78−76280
$Fe_{75}Si_{15}B_{10}$, amorphous ferromag. ribbons, US rel. meas. 77−80582
$Fe_{75}Si_{15}B_{10}$, amorphous ferromagnetic alloy, isothermal annealing effect on static magnetic props. *(Japanese)* 79−52398
$Fe_{75}Si_{15}B_{10}$, duplex ferromag. alloy, thermoremanent magnetization 79−73778
$Fe_{75}Si_{15}B_{10}$, mag. behaviour rel. to magnetostatic interactions 80−11224
$Fe_{78}Si_{10}B_{12}$ amorphous ferromag. ribbons, change of permeability by heat treatment 77−85493
$Fe_{78}Si_{10}B_{12}$ amorphous ribbons, magnetomechanical coupling constant and Young's modulus, mag. annealing 79−15333
$Fe_{80}Si_5B_{15}$, amorphous, soft mag. props. and potential uses 80−88807
Fe_3Sn_2, mag. props., neutron diffr. and magnetisation meas. 79−11294
Fe_3Sn_2, Mossbauer effect and magnetisation meas. 78−31132
Fe_xSn_{1-x}, amorphous, mag. behaviour 78−95478
Fe_xSn_{1-x} amorphous alloy films, magnetisation meas. and Mossbauer spectra 78−95489
Fe_xSn_{1-x}, amorphous alloy, Mossbauer spectra, charge transfer and atomic vol. effects 80−39959
Fe_xSn_{1-x}, amorphous film, struct. and mag. props. 80−65972
Fe_xTaS_2, metallic, mag. susceptibility at low temp. 80−70972
FeTi, surface segregation and catalytic effect on hydrogenation, AES and XPS study 79−11626
$Fe_{1-x}Ti_x$, ferromag. props., Ti conc. effect 80−54872
$Fe_{2.6-x}Ti_{0.4}Al_x O_4$, $Fe_{2.4-x}Ti_{0.6}Al_xO_4$, titanomagnetite, monodomain, mag. props. 78−56346
Fe_2TiO_4, cooperative Jahn-Teller effect, neutron scatt. study 80−49678
Fe_2TiO_4 magnetisation, Mossbauer spectra 79−87244
Fe_2TiO_4-Fe_3O_4, titanomagnetite, prepared at different oxidation conditions, hysteresis props. 78−56352
$Fe_{2.4}Ti_{0.6}O_4$, TRM acquired by multi-domain single cryst. 80−36293
$Fe_{2.4}Ti_{0.6}O_4$, titanomagnetite, single-crystal, mag. props. of multidomain TRM 78−56345
FeU_2S_5, mag. struct., exchange energy, magnetisation and neutron diffr. expts. 78−68170
FeV (2 at.%), NMR spin echoes, domain wall effects 80−75883
$Fe_{0.85}V_{0.15}$ film, ^{51}V NMR, spin echo expts., 77 and 300K 77−69728
$(Fe_{1-x}V_x)_3Ge$, magnetic and X-ray studies 80−1966
$Fe_{3-x}V_xSi$, Fe hyperfine fields 79−78055
$Fe_{3-x}V_xSi$, selective site substitution and spin polarisation 79−78583
$Fe_{3-x}V_xSi$, struct., magnetisation, and spin echo expts., rel. to local environment model 77−20518
^{57}Fe powder, NMR excitation function, drumhead model of Bloch walls 80−15810
$Fe_{80}b_{20-x}C_x(Si_x)(Ge_x)$, amorphous, size effect of metalloids on mag. props. 80−84594
Fo-Fe-Nb, cold-worked and aged, mag. props. and microstruct. 80−34690
GaAs:Fe, static magnetis. rel. to doping method and heat treatment conditions 77−36092
$Ga_{1-x}Mn_xSb$, elec. cond., mag. susceptibility, Hall const., and thermo-EMF, 80 to 1000K *(Russian)* 80−88549
$GaMo_5S_6$, mag. and struct. transition temps., press. effects, 0-6 kbar *(Russian)* 77−89956

ferromagnetic properties of substances continued
$(Gd,Dy)Al_2$, spin adjustment, NMR spin echo obs. 78—15058
Gd, AC susceptibility, temp. modulation studies, domain property thermal relaxation 79—61072
Gd, AC susceptibility and temp. modulation near Curie point 77—4515
Gd alloys, amorphous, mag. props. and ferromag. reson. 80—54952
Gd alloys, Curie temp. and saturated mag. moment, nonmag. solute effects 78—39301
Gd alloys, ferromag., 4d and 5d impurities, hyperfine fields 78—31133
Gd, band structure and Fermi surface using KKR formalism 79—77993
Gd, cryst., elec. resist. meas., 4.2-600K 78—14706
Gd, crystal hyperfine fields at positive muons 79—56662
Gd, dipole field anisotropy, at interstitial sites, lattice-deformation effects 79—33584
Gd, easy axis of magnetisation as function of press. and temp. 77—63231
Gd, electron irradiated, relation of defect densities to Rayleigh parameters 77—62517
Gd, Fermi surface and band struct., press. effects, dHvA expts. 78—14656
Gd, ferromag., activation energies using transient enhancement of AC permeability 77—59431
Gd, ferromag., domain struct., small-angle neutron scatt. 77—66382
Gd, ferromag., hyperfine fields at positive muons 78—43758
Gd, ferromag., magneto-optical reson., optical consts. determ. 78—6657
Gd, ferromag., transient mag. fields at stopping nuclei, stopping power 78—34555
Gd, ferromag., transport props., crit. behaviour 80—65522
Gd, ferromag., vel.- and Z-depend. of transient mag. fields 78—43698
Gd ferromagnet, enhanced transient fields acting on fast Gd nuclei 77—90081
Gd, ferromagnetic, crit. sp. ht. and thermal expansion 80—60343
Gd, ferromagnetic, temp. depend. of hyperfine fields for F 80—20141
Gd film, magnetoelastic excitations, phonon spectroscopy and forbidden transitions 79—82853
Gd foil, domain and domain wall structure 77—69603
Gd, HCP, ferromag. band struct. and Fermi surface, KKR band calcs. 77—62815
Gd, high quality single cryst., mag. anisotropy 78—84413
Gd host, dil. impurity hyperfine fields, comparison with models 78—14954
Gd, hyperfine interaction of ^{197}Au, Mossbauer obs. 77—20773
Gd, hysteresis, departure from Rayleigh law in low mag. fields 77—40086
Gd, internal fields, positive muon investigation 78—68438
Gd, interstitial site determ., μSR technique 80—71287
Gd, local mag. field at positive muon 77—85637
Gd, local magnetic fields probed by μ^+ 78—48103
Gd, longitudinal galvanomag. effect in single crysts. *(Russian)* 78—56132
Gd, mag. domain obs. at 77K 77—69602
Gd, mag. domain struct., 77K 78—84447
Gd, mag. domain struct. obs. by wet and dry colloid techniques 78—6542
Gd, mag. domains, Lorentz microscopy obs. 78—84448
Gd, magnetic transient hyperfine fields, IMPAC obs. 77—8464
Gd, magneto-optical Kerr effect in UV region, 4f excitations and binding energy 77—52127
Gd, magnetocrystalline anisotropy, temp. and press. depend. 77—20586
Gd, magnetoelastic anomaly at 240K, spin reorientation region 77—40105
Gd, magnetoelastic excitations and ferromagnetic resonance 79—82879
Gd, magnetoresist., 4.2-220K, temp. depend. anisotropy 77—62903
Gd, meas. of easy direction of magnetisation with aid of phase theory 80—65963
Gd, muon spin rotation; freqs., and relax. rates 80—55006
Gd, nonmagnetic inclusions, effect on easy direction 77—77052
Gd, optical conductivity, direct interband transitions 80—15488
Gd, optical consts. polarimetric meas., mag. ordering effects 78—15184
Gd, positive muons as light isotopes of H, book contrib. 79—82907
Gd, RKKY interactions, anisotropic effects from spin-split bands 80—15712
Gd, self consistent relativistic ferromag. band struct. 78—91609
Gd, sp. ht. near T_c, scaling behaviour 77—66333
Gd, spin relax., ferromag. transmission reson. 78—31113
Gd, spin reorientation transition, crit. behaviour of elec. resist. 79—51787
Gd, spin wave exam. 78—56306
Gd, spin wave temp. depend., exchange coupling role 78—68199
Gd surface, spin polarised electron gas model 77—8034
Gd, temp. variation of absolute thermoelec. power 77—11900
Gd, thermal expansion, near ferromag. transition 78—31084
Gd, transient enhancement of AC susceptibility, domain wall pinning 77—20633
Gd, working medium in mag. Stirling cycle wheel, refrigerator and heat engine modes of operation 78—57964
^{160}Gd, ferromagnetic, isotopically enriched single crystals short-range order 79—4653
Gd:^{177}Hf, polycryst. ferromag., impurity hyperfine field polarisation, IPAC 77—73106
Gd:Ra, hyperfine field determ. 77—85622
Gd-Ag, vap. quenched alloys, struct. and mag. props. 78—84461
Gd-Ag (0-16 at.%), vapour-quenched, struct. and mag. props. 78—38980
Gd-Ag(Cu) alloy film, amorphous, struct. and mag. props. 78—52318
Gd-Al(C)(Cu)(Ga)(Ni)(Pd)(Rh) alloys, amorphous, mag. and elec. props. 80—80499
Gd-Al(Cu), amorphous alloy films, mag. phase diagram, spin glass and ferromag. regions 78—68234
Gd-Al(Cu)(Ga)(Rh)(Pd), amorphous alloys, mag. coupling of rare earth moments 78—88108
Gd-Co, disordered, saturation mag. moment calc., CPA 77—20515
Gd-Co amorphous film, mag. anisotropy 77—20649
Gd-Co amorphous film, sputtered perpendicular mag. anisotropy 79—56576
Gd-Co film, amorphous, magnetisation and anisotropy meas. 77—8370
Gd-Co film, with layer struct., mag. torque and anisotropy 77—63246
Gd-Co-Au amorphous magnetic films, domain wall obs. by Lorentz electron microscopy 77—80979
Gd-Co-Mo film, amorphous, bubble and stripe domain wall vel. meas. 77—40094

ferromagnetic properties of substances continued
Gd-Co-Ni series intermetallics, induced moments, magnetisation meas. 77—63138
Gd-Co(Ni)(Cu)(Rh)(Ru)(Pd)(Ga), amorphous, mag. props. and ferromag. reson. 80—75862
Gd-Cu sputtered amorphous films, ferromag. props. 77—66393
Gd-Cu(Fe) splat-cooled, internal friction exam. 77—20012
Gd-Dy alloy, longitudinal galvanomag. effect in single crysts. *(Russian)* 78—56132
Gd-Dy alloy, mag. anisotropy, magnetisation meas. 77—12115
Gd-Dy(Er)(Tb)(Tb), magnetic and electric hyperfine fields at Gd, NMR spin echo 77—77123
Gd-Er alloy, mag. anisotropy, magnetisation meas. 77—12115
Gd-Fe, disordered, saturation mag. moment calc., CPA 77—20515
Gd-Fe alloy film, amorphous, contact printing 77—73061
Gd-Fe amorphous alloys, mag. props. and crystn. 79—90557
Gd-Ho alloy, mag. anisotropy, magnetisation meas. 77—12115
Gd-Ir, dil., hyperfine interaction of ^{193}Ir, Mossbauer effect meas. 78—52413
Gd-Mn alloy, mag. props. and effect of H_2 absorpt. 78—19250
Gd-Mo-Mo amorphous film, domain drag effect obs. 78—91911
Gd-Ni, ferromag., elec. resist. temp. depend. 80—96843
Gd-Sc, dil. alloy, ferromag. hyperfine field determ. 77—43919
Gd-Sm(Eu), mag. props. at low temp. in high mag. fields 79—56570
Gd-Ta, dil., mag. hyperfine field and elec. field gradient at ^{181}Ta impurities, TDPAC meas. 79—47361
Gd-Ti(V)(Cr)(Mg)(Nb)(Ge)(Si)(Au) amorphous films, spontaneous Hall effect and elec. resist. 80—80251
Gd-Tm alloy, mag. anisotropy, from magnetisation meas. at 4.2K 78—68216
Gd-Y (40 wt.%) alloy, magnetic phase transitions, elastic consts. meas. 78—14957
Gd-Y alloys, mag. crit. temp. gap 80—60260
Gd-Yb(Ir), dil., ferromag., mag. hyperfine fields of ^{170}Yb and ^{193}Ir, Mossbauer effect meas. 79—24242
$Gd_{56}Ag_{46}$, amorphous, susceptibility and magnetisation, 6-300K *(French)* 77—36060
$GdAl_2$, anisotropy and magnetostriction 78—10741
$GdAl_2$, anomalous change of Curie temp. 78—47976
$GdAl_2$, extraordinary Hall effect 80—39560
$GdAl_2$, ferromag., spin reorientation 78—39334
$GdAl_2$, hyperfine fields, ferromagnetic coupling between rare earth spins, NMR study 80—39880
$GdAl_2$, spin reorientation 78—39335
$GdAl_2$, thermal expansion and heat capacity Curie temp. determ. 77—1559
$GdAl_2$-$GdCo_2$ system, EPR and mag. props. 79—33478
$GdAl_4$, mag. props., mag. exchange strength 77—85440
$Gd_{0.37}Al_{0.63}$, amorphous film, anomalous resonance field shift 79—73821
$Gd(Al_{1-x}Cu_x)_2$, C15 struct., elec. resist., comp. depend. 78—14705
$Gd(Al_{1-x}Cu_x)_2$, thermoelec. power, exchange interactions 80—24881
$Gd_{80}Au_{20}$, amorphous ferromag., critical phenomena and mag. props. 77—85469
$Gd_{80}Au_{20}$, amorphous ferromag., mag. and transport meas. 77—89930
$Gd_{1-x}Ca_xAl_2$, mag. props. and phase relations 80—107991
$Gd_xCe_{1-x}Ru_2$, magnetic ordering by ^{155}Gd Mossbauer spectroscopy 78—27139
$GdCl_3$, crystn. field parameter of Gd^{3+} 80—10930
$GdCo_2$, dilute ferromagnets, press. effect on Curie temp. 80—65873
$GdCo_5$, large Barkhausen discontinuities, effect of dynamic elastic stresses *(Russian)* 78—39364
$GdCo_5$, spin polarised energy band struct., APW calc. 78—10342
Gd_2Co, amorphous ferromag. obtained by splat cooling, local and bulk mag. props. 79—1685
$Gd_{2+x}Co_{17-x}$, magnetocryst. anisotropy, stoichiometry and temp. effects 77—8296
$Gd_{67}Co_{33}$, amorphous, elec. resist. and magnetoresist. 80—49693
$Gd_{67}Co_{33}$, amorphous ferromag., mag. and transport meas. 77—89930
Gd_xCo_{1-x} annealing amorphous film, ferromag. reson. 77—85580
$GdCo_3B_2$, ferromag. ordering and saturation moments 77—24711
$Gd(Co_xFe_{1-x})_2$, mag. props., composition and temp. depend. 79—15289
$Gd(Co_xIr_{1-x})_2$, struct. and mag. moments, comp. depend. 79—86743
$GdCo_{5c}Ni_{5-5c}$, intrinsic coercivity, anisotropy, exchange and cryst. field interactions 80—75806
$Gd(Co_xNi_{1-x})_2$, mag. props., composition and temp. depend. 79—15289
$Gd(Co_xNi_{1-x})_2$, Mossbauer spectra, mag. props. 80—20563
$Gd_xEr_{1-x}Rh_4B_4$, ferromag. and structural transitions, low temp. calorimetric meas. 79—55888
$Gd_xEr_{1-x}Rh_4B_4$, mag. ordering near supercond. region 79—73696
$Gd_2(Fe,Co)_{17}$, mag. anisotropy fields by singular pt. detection 79—24156
$Gd_2(Fe,Co)_{17}$, magnetic anisotropy meas. by singular point detection method 77—63170
$GdFe_2$, easy direction of magnetisation 80—20535
$Gd(Fe_{1-x}Al_x)_2$, magnetisation, Curie temps., and mean mag. moments 79—51817
$(Gd_{65}Fe_{35})_{90}B_{10}$, amorphous, mag. props., Mossbauer study 80—93093
$Gd_{18}Fe_{82-x}Ni_x$, amorphous film, mag. and galvanomag. props. 77—24715
$Gd_2(Fe_{1-x}Ni_x)_{17}$, Mossbauer spectra, hyperfine field interactions 78—6614
$Gd(Fe_xT_{1-x})_2$, Mossbauer spectra, mag. props. 80—20563
$Gd_{0.9}La_{0.1}Al_2$, ferromag., NMR of ^{139}La 78—52377
$Gd_{0.9}La_{0.1}Ni_2$, Ni contrib. to ordering, ^{139}La NMR spin echo 77—63317
$Gd_{1-x}La_xRh_2$, NMR, contribution of Gd neighbours to Gd hyperfine field 77—8423
$Gd_xLa_{1-x}Zn$, magnetisation and paramag. suscept. 78—88101
$Gd_{1-x}M_x$, M=Co, Ni, Fe, temp. depend. of magnetisation 77—77043
GdMg, noncollinear mag. struct., nonlinear band behaviour 80—75706
GdMg, sp. ht., magnetisation and stability of canted struct. 79—78412
$GdMg_3$, mag. props., Mg conc. depend. 78—84392
$GdMn_2$-$GdAl_2$ intermetallics, mag. props., 80-650K 78—60282
$(GdMn_2)_x(GdAl_2)_{1-x}$, mag. and struct. investigations of intermetallic systems 78—95440
$Gd_2(MoO_4)_3$, domain wall motion dynamics 80—108030
GdN, and $GdN_{1-x}O_x$, mag. interactions 80—60218
$GdN_{1-x}O_x$, magnetic interaction and carrier conc. 80—71005
$(Gd_{1-y}Nd_y)_{1-x}Fe_x$ amorphous bubble films with good temp. characts. 79—95616
$Gd_xNd_{1-x}Zn$, ferromag., mag. susceptibility and magnetisation, temp. depend. 80—70975
$Gd_{68}Ni_{32}$, amorphous ferromag., mag. and transport meas. 77—89930
$GdNi_2H_4$, effect of absorbed H_2 on struct. and mag. behaviour 78—2682

ferromagnetic properties of substances continued
$GdNi_2H_4$, effect of H_2 absorption on struct. and mag. behaviour 78—10685
$Gd(OH)_3$, dynamical effects of interaction between 4f electrons and optical phonons 80—108196
$GdPt_x$, $Gd_{1-x}A_xPt_2$ (A=Sc, La), Laves phase alloy, NMR, nonstoichiometry 77—63298
$Gd(Rh_{1-x}Fe_x)_2$, $x \leq 0.15$, magnetisation and EPR studies 80—34767
$Gd_{3-x}S_4$, ferromag., elec. props. near Curie temp. 80—107788
$Gd_{3-x}S_4$, mag. ordering and elec. cond. 78—10681
Gd_xS_y, nonuniform ferro-antiferromag. ordering, 1.6 to 300K range obs. *(Russian)* 77—69504
GdTb, ferromag., magnetisation and microwave absorpt. 80—65816
$Gd_{70}Tb_{30}$, magnetisation, AC susceptibility and microwave absorption meas. 80—60221
$(Gd_xY_{1-x})Al_2$, ferromag. and spin glass like behaviour, magnetisation meas. 80—75734
$(Gd_xY_{1-x})_4Co_3$, Curie temp. and resist.-temp. curves, comp. depend. 80—71020
$(Gd_{0.5}Y_{0.5})Ni$, FeB struct., cryst. field effects on mag. struct. 78—52226
$Gd_xY_{1-x}Zn$, ferromag., mag. susceptibility and magnetisation, temp. depend. 80—70975
$GdZrFe_2$, hyperfine field at Gd, TDPAC meas. 80—93214
$Gd_{3-x}\square_xS_4$, transport and mag. props., mag. Wigner localisation 80—97069
Ge-Se-Fe films, metallic and semicond., amorphous, mag. and elec. props. 78—52319
Ge-Si amorphous film, ferromagnetic interaction between spins 78—2710
$Ge_{1-x}Mn_xTe$, magnetic behaviour of Mn 78—14938
GeTe:Mn, thermoelec. power, 2.5-25K, magnon drag effect 78—56169
H_2, solid, with low ortho-fraction, ferrorotational transition *(Russian)* 79—60597
^{3}He A-phase, superfluid, ferromag. props. 78—14529
^{3}He admixed with C particles, surface induced ferromagnetism, pulsed NMR expts. 79—51362
^{3}He, HCP, and adsorbed ^{3}He with triangular lattice, exchange and mag. order 80—107606
^{3}He, liq., reinforcement of low temp. surface ferromag. instability due to ^{3}He-wall attraction 79—51373
^{3}He, liquid, surface ferromagnetic instability, attraction to solid substrate 79—46863
^{3}He, solid, mag. phases *(Russian)* 77—72743
^{3}He, solid, magnetic polarisation around vacancies, on two-dimens. lattice 79—51368
^{3}He, solid, struct. of vacancy induced spin polarons 79—95244
^{3}He, submonolayer on Grafoil, vacancy induced ferromag. 78—14536
^{3}He, superfluid, surface magnetism 79—51361
^{3}He, superfluid A-phase 79—42333
^{3}He, surface ferromagnetism, possibility in confined geometries 77—69137
^{3}He, vacancy relaxational phenomena *(Russian)* 78—95203
^{3}He, vacancy struct., neighbouring ferromag. domains *(Russian)* 77—20161
^{3}He with C particles, pulsed NMR, mag. susceptibility surface induced ferromagnetism, antiferromagnetic exchange interaction 78—79844
^{3}He-^{4}He, solid soln., struct. of vacancies 80—2242
^{3}He-A, superfluid, ferromagnetic orbital magnetisation 78—38902
$HfCo_6$, saturation magnetisation, Co mag. moment and electron transfer 77—73005
Hf_2Fe, moment form. on H_2 absorpt. 79—87343
$Hf(Fe_{1-x}Co_x)_2$, mag. props., Mossbauer spectra and magnetisation meas. 80—39948
$HfFe_{2-x}Si_x$, Mossbauer spectra, hyperfine interactions 80—15862
HfNi, hyperfine critical exponents, TDPAC meas. of bulk meas. 77—8465
Hg, liquid, containing Fe particles, time depend. magnetisation 80—44877
$HgCr_2S_4$, spinel, mag. struct., symmetry anal. in neutron diffr. studies 80—25091
$HgCr_2Sd_{4-x}Te_x$, ferromag. semicond., zero bandgap transition 80—96783
$HgCr_2Se_4$, crit. behaviour near Curie point 78—31068
$HgCr_2Se_4$, ESR line intensity near Curie point 78—64269
$HgCr_2Se_4$, ferromag. semicond., surface magnetism, magneto-optical meas. 77—20831
$HgCr_2Se_4$, ferromag. semicond., Raman spectra 78—52496
$HgCr_2Se_4$, ferromag. semicond., transport props. 78—68039
$HgCr_2Se_4$, influence of Co ions on anisotropy and magnetostriction, ferromag. reson. meas. 77—69659
$HgCr_2Se_4$, initial mag. permeability freq. depend. near Curie temp. 78—10729
$HgCr_2Se_4$, initial mag. permeab., 77 to 300K, domain wall motion and damped ferromag. reson. 79—28562
$HgCr_2Se_4$, n-type ferromag. semicond., galvanomagnetic props. 80—70727
$HgCr_2Se_4$, optical and magneto-optical surface effects 79—82953
n-$HgCr_2Se_4$, plasmon refl., 86 to 320K 80—50346
$HgCr_2Se_4$, Raman scattering, as function of temp. and incident photon energy 79—95781
$HgCr_2Se_4$, spontaneous magnetisation temp. depend., nuclear resonance freq. depend. *(French)* 80—80483
$HgCr_2Se_4$, thermorefl. near ferro- to paramagnetic transition 79—78660
$HgCr_2Se_4$, thermoreflectance, photoconductance, Raman scatt. near mag. phase transition 80—97298
$HgCr_2Se_4$, vapour growth using $AlCl_3+Cl_2$ as transport components 78—35282
$HgCr_2Se_{4-x}S_x$, temp. depend. of EPR line intensity 78—27074
$Hg_{1-x}Mn_xTe$, magnetic behaviour of Mn 78—14938
$Hg_xZn_{1-x}Cr_2Se_4$, absorption spectra near the absorption edge 78—80340
Ho, Hall effect, field and temp. depend., 4.2-150K, singularities *(Russian)* 80—29387
Ho, low field susceptibility and helical-ferromag. field induced phase transition 78—47975
Ho, magnetic phase diagrams, helicoid-ferromag. transform. *(Russian)* 80—50089
Ho, single cryst., transverse magnetoresist. 77—66154
Ho, sp. ht., using lattice dynamical model for HCP metals 79—51273
Ho:^{119}Sn, mag. hysteresis of hyperfine field, compensation in mag. field *(Russian)* 77—81039
Ho-Sm, magnetic phase diagrams, helicoid-ferromag. transform. *(Russian)* 80—50089

ferromagnetic properties of substances continued
Ho-Sm alloy, Hall effect, field and temp. depend., 4.2-150K, singularities *(Russian)* 80—29387
Ho-Sm(Eu), mag. props. at low temp. in high mag. fields 79—56570
Ho-Sn, dil. alloy, hyperfine interaction of ^{119}Sn, Mossbauer meas. 78—91998
Ho-Ta, dil., mag. hyperfine field determ., TOPAC meas. 79—91330
Ho-Zn, crystal field parameters from neutron spectra, rel. to mag. props. in ordered state 77—43546
$HoAl_2$, biquadratic pair coupling from mag. anisotropy 77—28383
$HoAl_2$, heat capacity, 1.5-12K, magnetocryst. anisotropy effects 78—68236
$HoAl_2$, Ho moment reorientation, polarized neutron diffr. study 79—42761
$HoAl_2$, magnetisation and neutron diffr. meas., cryst. field and exchange 77—63163
$HoAl_2$, magnetisation reorientation 79—87291
$HoAl_2$, spin reorientation, sp. ht. meas. 79—73724
Ho_2Au, mag. props., 4.2-300K 79—7972
$HoCo_2$, easy direction of magnetisation, Mossbauer data, 4.2K 78—43584
$HoCo_2$, field induced vol. magnetostriction 78—91920
$HoCo_2$, magnetisation reorientation 78—23300
$HoCo_2$, vol. magnetostriction, point charge cryst. field model 77—63254
Ho_2Co_{17}, magnetisation, magnetocryst. anisotropy and magnetostriction 77—8303
Ho_2Co_{17}, single cryst., magnetostriction const. temp. depend., 78 to 300K 79—51836
$HoCo_{5-x}Ni_x(Cu_x)$, lattice parameters and mag. props. 79—82817
$HoCo_2Si_2$, mag. props. 80—107988
$HoCu_5$, resist. and magnetoresist., mag. ordering obs. 80—70677
$Ho_xDy_yTb_{1-x-y}Fe_2$, Laves phase cpds., anisotropy and magnetostriction 77—63167
$HoFe_2$, Czochralski growth, and cryst. quality determ. 77—8742
$HoFe_2$, magnetostriction and magnetisation temp. depend. 79—73795
$HoFe_3$ and Ho_6Fe_{23}, magnetostriction, room temp. to 80K 80—65993
$HoFe_3$, effect of adsorbed H on mag. props. 77—63129
Ho_6Fe_{23}, magnetostriction, temp. depend., 20 to 350K 80—65994
$Ho_2(MoO_4)_3$, mag. susceptibility, ferromagnetism, mol. field theory 78—34966
$HoMo_6S_8$, reentrant supercond., direct. obs. of long range ferromag. order 78—76190
$HoMo_6S_8$, superconductor, neutron scatt. exam. of mag. phase 79—73680
$Ho_{1.2}Mo_6S_8$, re-entrant ferromag. supercond., heat capacity and AC mag. susceptibility 79—60948
$HoNi_5$, ferromag., magnetisation and paramag. susceptibility 80—25082
$HoNi_{0.7}Cu_{0.3}$, mag. behaviour 79—99688
$Ho(OH)_3$, Mossbauer spectra, cryst. field and mag. props. 80—15873
HoP, flopside mag. struct. to ferromag. transition, elastic neutron scatt. obs. 80—50058
$HoRh_4B_4$, low temperature magnetic properties 80—88728
$HoRh_4B_4$, mag. struct., neutron diffr. obs. 79—78323
$Ho_xTb_{1-x}Co_2$ lave phase compounds, elastic props., temp. and magnetic field dependence 80—60393
$Ho_{0.58}Tb_{0.20}Dy_{0.22}Fe_2$, magnetoelastic surface wave propagation, mag. field depend. 77—85535
$Ho_xTb_{1-x}Fe_2$, and $Ho_xTb_yDy_{1-x-y}Fe_2$, high magnetostriction cpd., mag. anisotropy origins 78—68217
$Ho_xTb_{1-x}Fe_2$, Laves phase, mag. anisotropy meas., cubic harmonic anal. 78—84410
$Ho_xTb_{1-x}Fe_2$, single cryst., spin orientations 78—84425
$Ho_xTb_{1-x}Fe_2$, single crystals, continuous spin orientations, magnetisation easy direction 78—84453
$Ho_2(WO_4)_3$, mag. props., 300 to 900K 79—28510
$Ho_{1-x}Y_xNi$, ferromag. behaviour, struct., Curie temp. 79—99677
$Ho_xY_{1-x}Sb$, mag. props. 80—34634
HoZn, mag. excitations near spin rot. temp., neutron scatt. study 79—19731
HoZn, magnetic excitations 80—25115
HoZn, spin wave spectrum, Green function analysis 78—2666
InSb:Mn^{2+} nondegenerate semicond., mag. impurity indirect interaction *(Russian)* 80—34591
Ir ternary and quaternary oxides, prep., cryst. struct., and mag. props. 79—14771
$Ir_{1.07}Mn_{1.07}Sn_{0.88}$, ferromag. Heusler alloy, ^{193}Ir and ^{119}Sn hyperfine fields 79—78581
K_2CrCl_4, ionic ferromag., temp. depend. intensity in optical absorption 77—12399
$K_2CuCl_4.2H_2O$, and isomorphous cpds., mag. interactions of H and D nuclei, NMR obs. 79—87251
$K_2CuCl_4.2H_2O$, Bloch-wall NMR, anisotropic hyperfine interaction 79—51864
$K_2CuCl_4.2H_2O$, ferromag., hyperfine and exchange interactions, NMR study 80—50208
$K_2CuCl_4.2H_2O$ structure compounds, 3-dimens. ferromag., exchange anisotropy by NMR 77—55714
$K_2CuCl_4.2H_2O$ structures, BCC Heisenberg ferromags., transferred hyperfine interactions of ^{1}H, ^{2}D and ^{17}O 77—69725
$K_2CuCl_4.2H_2O$ struct. Heisenberg ferromagnets, ^{17}O transferred hyperfine interactions 78—39439
$K_2CuCl_4.2H_2O$, thermal effects in mag. exchange interaction 77—16067
K_2CuF_4, 2-D ferromagnet, optical and magneto-optical props. 77—52062
K_2CuF_4, 2-dimens. ferromagnet, low-temp. mag. struct. *(Japanese)* 79—33461
K_2CuF_4, Curie temp. XY-like anisotropy effect, inter-layer exchange 77—59406
K_2CuF_4, ferromag., orbital ordering, review *(Japanese)* 78—76224
K_2CuF_4, layered, mag. sp. ht., two-dimens. $S^1/_2$ Heisenberg ferromag. behaviour 77—32206
K_2CuF_4, layered spin system, planar rotator symmetry, phase transition 80—65951
K_2CuF_4, magnon condensation 79—91220
K_2CuF_4, magnon condensation obs. in quasi-2D planar ferromag. phase 80—60232
K_2CuF_4, microwave excitation, optical detection of ferromagnetic reson. 80—50197
K_2CuF_4, nearly two-dimens. Heisenberg ferromag., renormalised spin wave theory 77—66285
K_2CuF_4, nearly two-dimensional ferromag. nucl. transverse relax. rates meas. 77—81024

ferromagnetic properties of substances continued

K_2CuF_4, obs. of magnon density of states by subthreshold steady-state absorption 77−12107
K_2CuF_4, quasi two-dimens. Heisenberg ferromag., spin wave spectrum lineshape, neutron scatt. obs. 77−66286
K_2CuF_4, spin relax., crit. behaviour, high freq. susceptibility meas. 80−65936
K_2CuF_4, spin wave meas. in low energy range, inelastic neutron scatt. 78−88105
K_2CuF_4, spin-wave relaxation, parallel pumping expt. 79−4729
K_2CuF_4, two-dimens. ferromagnet, nuclear spin-spin-relax. *(Japanese)* 77−48082
K_2CuF_4, two-dimens. ferromagnet, half-field EPR line 79−19765
K_2CuF_4, two-dimens. ferromag., magneto-optical props., absorpt., MCD and MLD 79−87419
K_2CuF_4, two-dimensional ferromag., spin-wave lineshape, neutron scatt. data 77−16065
K_2CuF_4, two-dimensional planar ferromagnet, giant fluctuation of spins *(Japanese)* 80−54894
$K_2Cu_{1-x}Mn_xF_4$ system, $(0 \leq x \leq 0.2)$, prep., cryst. chem., and ferromag. props., X-ray and neutron diffr. study 79−24162
$K_2Cu_{1-x}Zn_xF_4$, two-dimens., ferromag., spin wave excitations 78−80140
$K_2Cu_cZn_{1-c}F_4$, EPR, spin correlation decay rate 79−19772
$K_2Cu_xZn_{1-x}F_4$, Curie temp., Cu conc. depend. 80−60255
$K_2Cu_xZn_{1-x}F_4$, two-dimens. ferromag., spin correls. near percolation limit 80−44840
$KFeCl_3$, linear chain ferromag., optical absorpt. and dichroism in mag. field 77−77237
$KFeS_2$, magnetic reson. meas. 78−95524
$KNiF_3:Mn^{2+}$, isotropic Heisenberg ferromagnet, localised spin-wave modes, biquadratic exchange effects 77−51896
$K_2O-Al_2O_3-B_2O_3:Fe_2O_3$, glasses, liq.-liq. phase separation, Fe^{3+} ions rel. to mag., optical props. 77−15322
KTb_3F_{10}, mag., optical, magneto-optical behaviour 78−68484
$(La,Gd)Al_2$, reverse Kondo alloy, transport props. at finite mag. field 80−6812
La-Fe, amorphous alloy film, spin reson. meas. 78−68389
La-Fe alloy, amorphous, sputtered at high rate, mag. props. 80−75753
La-Fe bulk amorphous alloys, mag. props. *(Japanese)* 79−95588
La-Gd-Au alloys, amorphous, high Gd content, bulk mag. props. 77−59426
La_2Co_7, mag. saturation and anisotropy, density, lattice parameters 77−85426
$(La_{1-x}Gd_x)Al_2$, dil., reverse resistance anomaly 78−76054
$LaMnO_3$, monoclinic and cubic perovskite struct., mag. props., neutron diffr. meas. 78−27022
$LaMnO_3$, orthorhombic lattice distortions, mag. props. rel. to prep. conditions 77−20592
$LaMnO_3$, phase diagram, mag. moments, neutron diffr. study 80−108414
$LaNi_{1-x}Mn_xO_3$, ^{55}Mn NMR study, magnetisation meas., ferromag. and Pauli paramag. components 80−7191
$La_{1-x}Pb_xMn_{1-y}Fe_yO_3$, magnetically ordered, NMR, spin echoes and relax. 77−48087
$La_{0.71}Pb_{0.29}MnO_3$, metal-semicond. transition at Curie point, transport props. obs. 79−73554
$(La_{1-x}Pr_x)_3Tl$, mag. props., simple phenomenological model 77−16041
$La_{3-x}S_4$, mag. ordering and elec. cond. 78−10681
$La_{0.5}Sr_{0.5}CoO_3$, ferromagnetic phase transition obs. at 230K, heat capacity meas. *(Japanese)* 80−54898
$La_{1-x}Sr_xCoO_3$ $(0.5 \leq x \leq 1.0)$, mag. props. 79−24154
$La_{1-x}Sr_xCoO_3$, $(0.5 \leq x \leq 0.9)$, ferromag., elec. props., itinerant electron model 80−107785
LiH, mag. domains and nucl. mag. ordered phases, antiferromag. and ferromag. neutron diffr. obs. 80−50051
LiH, nuclear ordered ferromag. and antiferromag. phases, neutron diffr. study 80−50052
$LiHoF_4$, crit. behaviour of mag. suscept. 79−33465
$LiHoF_4$, dipolar-coupled Ising ferromag., submillimetre ferromag. and paramag. reson. 77−69697
$LiHoF_4$, EPR studies, lowest levels of rare-earth ions, submillimetre freq. 80−39865
$LiHoF_4$, uniaxial dipolar ferromag. crit. behaviour 79−61149
$LiHoF_4$, uniaxial dipolar ferromag., critical behaviour, mag. susceptibility meas. 80−80528
$Li_xMn_{1-x}Se$, anomalies obs. in mag. and elec. props. 77−69509
$Li_{0.04}Na_{0.1}Fe_{2.5}O_4$, $Li_{0.3}Na_{0.2}Fe_{2.5}O_4$, ferrites, form., X-ray, chem. and mag. anal. 77−36424
$LiRF_4$ (R=Tb,Ho,Er), cryst. field parameters, mag. susceptibility meas., 0.3 to 100K 80−60214
$LiRF_4$, R=rare earth, low-temp. magnetically ordered states 77−63098
$LiTbF_4$, dipolar-coupled Ising ferromag., submillimetre ferromag. and paramag. reson. 77−69697
$LiTbF_4$, EPR studies, lowest levels of rare-earth ions, submillimetre freq. 80−39865
$LiTbF_4$, Faraday rotation, optical absorpt. spectra and refr. index 78−72542
$LiTbF_4$, ferromag., spontaneous magnetisation at marginal dimensionality 77−24683
$LiTbF_4$, ferromag., susceptibility, sp. ht., renormalisation group theory test 77−16087
$LiTbF_4$, mag., optical, magneto-optical behaviour 78−68484
$LiTbF_4$, mag. props., crit. behaviour at marginal dimensionality 80−54906
$LiTbF_4$, magnetisation near crit. pt., temp. and field depend. 79−38337
$LiTbF_4$, optical study of spontaneous magnetisation at marginal dimensionality 79−73699
$LiTbF_4$, uniaxial dipolar ferromag., critical behaviour, mag. susceptibility meas. 80−80528
$LiTb_{0.5}Y_{0.5}F_4$, mag. susceptibility, dilution effect on critical behaviour of dipolar uniaxial ferromagnet 80−34635
$LiTb_{0.5}Y_{0.5}F_4$, uniaxial dipolar ferromag., critical behaviour, mag. susceptibility meas., effect of Y^{3+} dilution 80−80528
Lu-Fe, amorphous alloy film, spin reson. meas. 78 68389
Lu-Mn alloy, mag. props. and effect of H_2 absorpt. 78−19250
$LuAl_2$, sp. ht. and thermal props., 5 to 300K 77−43342
$LuCo_2$, anomalous high-field magnetisation 78−47958
$LuCo_2$, high-field magnetisation, Fermi liquid model 79−11303
Lu_2Co_{17}, single cryst., magnetostriction const. temp. depend., 78 to 300K 79−51836
$LuFe_2$, ferromag., magnetisation density, neutron diffr. study 80−60217

ferromagnetic properties of substances continued

$LuFe_2$, ferromagnetic cpds., mean field exchange consts., Stoner itinerant model calcs. 80−50084
$(Lu_{1-x}Ho_x)Rh_4B_4$, interaction between superconductivity and magnetism 79−38248
$Lu_2V_2O_7$, pyrochlore struct., mag. props. 78−72335
$MgFe_2O_4$, Faraday rotation in X-ray region 79−82958
δ-Mn, paramag., antiferromag. and ferromag., magnetic moment calcs. 80−60223
Mn ternary carbides, Mn_3MC, M=metal, mag. props. 77−63116
Mn-Al alloy, domain struct., cryst. defect effects 77−69609
Mn-Al permanent magnets, defect structure, mag. props. TEM obs. 78−91902
Mn-Al-C, ferromag., transform. kinetics 80−34627
Mn-Al-C, ferromag. alloy, transform. kinetics 80−76229
Mn-Al-C, fine-grained cast struct., remanence and coercive force 80−60365
Mn-Al-C (70, 29.5 wt.%) alloy magnet, Almax, anisotropic, mag. props. *(Japanese)* 80−60371
Mn-Al-C alloy, anisotropic, permanent magnet appl., properties and production *(German)* 79−8309
Mn-Al-C anisotropic permanent mag., cryst. orientation and form., X-ray diffr. anal. 79−82778
Mn-Bi, magnetically uniaxial, strongly anisotropic, discontinuous mag. reversal singularities *(Russian)* 77−48010
Mn-Bi alloy, melting and solidification under microgravity, mag. props. *(German)* 80−45296
Mn-Bi alloys, improvement study *(Japanese)* 78−43617
Mn-Bi eutectic alloy, mag. anisotropy 78−68220
Mn-Bi film, amorphous, form. and crystn. 79−28923
Mn-Bi film, negative transverse magnetoresist. in c-plane, domain wall effects 77−20465
Mn-Bi film, with perpendicular anisotropy, galvanomag. props., hysteresis loops 77−20464
Mn-Ga, mag. and cryst. struct. in conc. region of gamma phase, temp. depend. *(Russian)* 79−65649
Mn-H(D), ferromag., thermal, struct. mag. props. 78−88145
Mn-V-Al, magnetic props., heat treatment effects 79−29233
τ-MnAl, estimated theoretical limit of mag. moment 80−97072
$Mn_{1.11}Al_{0.89}$, crit. behaviour, neutron diffr. meas. 78−34982
$Mn_{1.11}Al_{0.89}$, neutron diffr. investig. of mag. struct., degree of order 77−55662
$Mn_{1.11}Al_{0.89}$, unit cell parameters, temp. depend. 79−55697
$Mn_{55}Al_{45}$ alloy, permanent mag. props., depend. on particle size 78−91899
MnAlGe film, mag. domains and amorphous to cryst. phase transition, electron microscopy obs. 80−71129
MnAs, estimation of ionic states through neutron form factor meas. 77−63115
MnAs, formation of nuclei in ferromag. paramag. transition, thermal hysteresis 79−73720
MnAs, generalised P-T phase diagram, mag. and structural phase transition 80−39780
MnAs, high spin state electron config. *(Japanese)* 77−43812
MnAs in suspension, ferromagnetic colloid, optical meas. 78−10906
MnAs, PTH phase diagram of mag. transitions, Curie point 80−44832
MnAs pseudocrystals, magnetostriction, anisotropy 77−4537
MnAs, second-order phase transition, elastic anomalies 79−10908
MnAs, struct. and mag. props., temp. depend., neutron study 79−47246
$MnAs_{0.88}P_{0.12}$, excitonic absorpt., derivative refl. spectra 80−25406
$MnAs_{0.925}P_{0.075}$, estimation of ionic states through neutron form factor meas. 77−63115
$MnAs_{0.96}P_{0.04}$, latent ferromagnetism 80−11197
$MnAs_{1-x}P_x$, double exchange ferromag. coupling, magnetisation meas. 80−75751
$MnAs_{1-x}P_x$, low temp. resistivity minimum 77−8122
$MnAu_4$, domain struct. exam. by powder method *(German)* 78−91883
MnB, NMR of ^{55}Mn 77−28468
MnBi, domain boundaries shift, mag. reversal processes 79−87286
MnBi, domain boundary inertia during mag. reversals *(Russian)* 80−88776
MnBi film, ferromag., diffr. efficiency of mag. holograms, Faraday effect 77−32355
MnBi film, magnetic reversal mechanism, hysteresis loops for polycryst. and single cryst. specimens *(Russian)* 78−60318
MnBi film, optical, magneto-optical and struct. props. 77−1664
MnBi film, optical radiation spectral conversion 79−64344
MnBi film anisotropy field intensity meas. by Faraday rotation *(Russian)* 77−12162
MnBi films, prep. by ionised-cluster beam deposition technique, magnetooptical props. 80−100790
MnBi films, stability of magneto-optical props. on pulse heating *(Russian)* 78−88282
MnBi, ionized-cluster beam and reactive ionized-cluster beam deposition 80−16202
MnBi, mictomag. alloys, elastic props. *(Russian)* 80−7141
MnBi particles, demagnetised, coercivity, remanence and magnetisation reversal 78−19281
MnBi particles, effect of grinding on coercivity 77−36098
MnBi, thin film, fine mag. domains, SEM obs. 79−24202
MnBi, thin film, struct. and mag. props. 79−47315
MnBi, two-phase coercive force for domain wall motion, mag. reversal nucleation mechanism *(Russian)* 77−48009
MnBi-Bi garnet film structure, thermomag. information recording appls. *(Russian)* 78−23305
$Mn_{1-x}Co_xSb$, ferromagnetic, NMR exam. 79−24228
$Mn_{1-y}Cr_yAs$, double exchange ferromag. coupling, magnetisation meas. 80−75751
$(Mn_{1-x}Cr_x(Fe_x))B$, Invar charact. 77−15602
$Mn_{2.5}Cr_{0.5}O_4$, mag. struct., neutron diffr. obs. 79−33460
$Mn_xCr_{3-x}O_4$, mag. struct. determ. by neutron diffr. 77−40035
$Mn_{1-x}Cr_xP$, mag. susceptibility and transitions 79−47256
$Mn_{2-x}Cr_xSb$ film, prep. and mag. props. 78−48009
MnCuBi film, coated with SiO layer Kerr readout characts. 77−85509
MnCuBi film, for mag. storage appl., prep. by RF sputtering, and props. 77−8369
MnCuBi film, optical and magneto-optical props. 77−4695
$MnCu_{1-x}Dy_xBi_{0.86}$ film, mag. and magneto-optical props., appl. as storage medium 77−8550
$Mn_{1-x}Cu_xSb$, ferromag., NMR exam. 77−12207
$Mn_{1-x}Cu_xSb$ film, ferromag. reson. 78−31114

ferromagnetic properties of substances continued
$Mn_{0.97}Fe_{0.03}As$, field induced ferromag. phase *(Russian)* 77—36070
$Mn_{1-x}Fe_xAs$, high-pressure phase, magnetic properties 78—52247
$Mn_{1-x}Fe_xAs$, magnetic transition under high press., exchange striction model calcs. *(Russian)* 80—50096
$Mn_{1-x}Fe_xP$, magnetisation, susceptibility and mag. transitions 79—47256
$Mn_{1-c}Fe_cPt_3$, noncollinear mag. structs., neutron diffr. anal. *(Russian)* 80—25087
$Mn_{5-x}Fe_xSi_3$, elec. resist. and mag. susceptibility, ferromag. to antiferromag. transition 80—80504
MnGaGe film, mag. domains and amorphous to cryst. phase transition, electron microscopy obs. 80—71129
$Mn_{0.6}Ga_{0.4}Sb$, eutectics, galvanomag. props., thermo EMF 77—15869
$Mn_{1-x}M_xAs$, M=V, Cr, Fe, Co, mag. props., phase diags. 77—66300
$Mn_{1/3}NbS_2$, intercalate, metallic cond., Hall effect and mag. props. 77—76789
$Mn_{3-x}Ni_xB_4$, mag. props. *(Russian)* 77—51923
$Mn_{3-x}Ni_xB_4$, with onset of spontaneous magnetisation below T_N, singularities of mag. props. *(Russian)* 77—59427
$MnNiSi_{1-x}Ge_x$, mag. props. 77—12118
MnP, anisotropic, ferromagnetic microwave resonance relations 80—15805
MnP, elec. resist. of different mag. phases, temp. depend. 80—54691
MnP, Lifshitz point, transverse differential susceptibility meas. 80—84599
MnP, magnetisation and spin waves temp. depend. 79—91221
MnP, noncubic ferromag., relax. times for domain and wall resonances 77—77119
MnP, sp. ht., 1.5-8.0K 79—91236
MnP, US vel. and crit. attenuation, longit. waves, external mag. field 78—27035
MnPt, disordered film produced by RF sputtering, ferromag. behaviour 78—68310
MnSb, electronic state, neutron diffr. study 78—87906
MnSb, hyperfine interactions, ^{119}Sn Mossbauer obs. 77—40160
MnSb, hyperfine interactions at ^{57}Fe and ^{119}Sn, Mossbauer spectroscopy 78—23375
MnSb, interstitial cations, mag. and crystallographic study 79—55698
MnSb-Mn_2Sn alloy system, continuous series of solid solns., homogeneity and ferromagnetic props. 79—52159
$Mn_{1+\delta}Sb$, ferromag., mag. disturbance around Mn interstitials 80—54868
$MnSb_{1-x}Sn_x$, zero-field NMR investig. of domains and domain walls 77—32271
$Mn_{1+x}Sb_{1-x}Sn_x$, magnetisation and Curie temp., prep. and comp. depends. 78—64200
$Mn_{1+x}Sb_{1-x}Sn_x$, nuclear Zeeman effect, Mossbauer meas. 79—28654
MnSi, itinerant electron system, helical spin structure 78—23234
MnSi, itinerant ferromag. spin dynamics field depend. 79—38315
MnSi, mag. anisotropy exam., ferromag. to antiferromag. transition 79—73708
MnSi, μ^+ Knight shift, temp. depend. 78—80270
$Mn_5(Si_{1-x}Ge_x)_3$, magnetic and cryst. struct., ferromag. props. 77—59391
$Mn_5(Si_xGe_{1-x})_3$ solid solution, mag. ordering, magnetisation and neutron scatt. meas. 78—27023
MnZn ferrite, polydispersive spin relax. near Curie temp., mag. susceptibility meas. 77—69513
MnZn ferrites, initial mag. permeabilities under low temp. reactor irrad. 77—36093
β_1-MnZn, ferromag., spin wave contrib. to nucl. spin-lattice relax. time meas. 77—36147
MnZn-ferroferrites, sintered, microstruct., TEM study *(Dutch)* 80—2036
Mo oxides, magnetic susceptibility meas., temp. effect 80—103822
Mo ternary chalcogenide, MMo_6X_8 (M=metal, X=chalcogen) Chevrel phase, supercond. and normal state props. 78—56267
Mo-Permalloy, galvanomag. props. 77—39822
Mo-permalloy, magnetic permeability and order form. kinetics under annealing, conc. depend. 77—8356
$(NH_4)_2Co(SO_4)_2.6H_2O$, submillimetre ESR meas. using pulsed high mag. field 80—44905
$(NH_4)_2CuBr_4.2H_2O$, ferromag., static and dynamic mag. props. 80—50074
$(NH_4)_2CuBr_4.2H_2O$, ferromag., hyperfine and exchange interactions, NMR study 80—50208
$(NH_4)_2CuCl_4.2H_2O$, Bloch-wall NMR, anisotropic hyperfine interaction 79—51864
$(NH_4)_2CuCl_4.2H_2O$, submillimetre ESR meas. using pulsed high mag. field 80—44905
$(NH_4)_2CuCl_4.2H_2O$, ferromag., hyperfine and exchange interactions, NMR study 80—50208
NI_3Al, structural order and homogeneity, X-ray, mag. susceptibility and Mossbauer meas. 77—63663
Nb, superconductor, deformational twinning, mag. props. *(Russian)* 79—95543
$NbMn_2Si_2$, Mossbauer and magnetisation expts. 78—31138
$Nb_{50}Ni_{50-x}Fe_x$, amorphous alloy, mag. interactions 78—95432
$Nb_{50}Ni_{50-x}Fe_x$, magnetically dil. glass, 3d moments, mag. susceptibility and magnetisation meas. 79—95574
$NbS_2(Se_2)$ intercalation complexes with 3d transition metals, mag. and metallic transport props. 80—44814
Nd, magnetic form factors, polarised neutron diffr. meas. 80—50057
$NdAl_2$, cryst. field excitations, neutron inelastic scatt. meas. 77—63154
$NdAl_2$, extraordinary Hall effect 80—39560
$NdAl_2$, mag. excitation spectrum, neutron inelastic scatt. 78—10673
$NdAl_2$, mag. form factor, diffuse moment density, polarised neutron meas. 77—63108
$NdAl_2$, magnetostriction in high mag. fields 79—99745
$NdCo_5$, ferromag., thermomag. charact. in mag. field *(Russian)* 78—23273
$NdCo_5$, single ion anisotropy consts. temp. depend. effect of spatial variation of mag. moment 78—91864
$NdCo_5$, spin reorientation, magnetisation and torque curves, 77-925K 77—4532
$Nd_{0.35}Co_{0.65}$ film, vac. evaporated, magnetisation ripple struct., TEM and defocused Lorentz microscopy 80—7136
Nd_2Co_7, mag. saturation and anisotropy, density, lattice parameters 77—85426
$Nd(Co_{1-x}Cu_x)_5$, coercive force temp. depend. 79—82823
$Nd_{1-x}Dy_xCo_5$, rotational type spin reorientation, appl. to thermomagnetic generator 77—85451

ferromagnetic properties of substances continued
$Nd_xEu_{1-x}B_6$ solid solution, mag. susceptibility, lattice parameters, Weiss temp. 80—29535
$NdFe_2$, amorphous, magnetization and neutron scatt. meas. 79—78314
$NdFe_2$, Curie temp., elec. quadrupole couplings, Mossbauer study 80—39949
$NdFe_2$, high field Mossbauer study 80—75893
$Nd(OH)_3$, dynamical effects of interaction between 4f electrons and optical phonons 80—108196
$Nd_xPr_ySm_zCo_5$ permanent magnets, coercive force, low-temp. annealing influence *(Russian)* 80—39812
Nd_3S_4 chem. and mag. structures, neutron diffr. obs., ferromag. long-range order *(German)* 78—10654
NdSi mag. struct. and mag. moments, neutron diffr. meas. 77—85424
Ni, 109° and 71° walls, stable orientations, theory and X-ray observations *(Japanese)* 80—60359
Ni (001) film, self consistent calc. of surface phenomena 79—73560
Ni, (001) surface, spin polarised photoemission theory 79—15584
Ni (100), Bloch wall meas. by enutron small-angle meas. 80—15753
Ni (100), electron field emission, positive spin polarisation and band model of magnetism 77—52226
Ni (100) films, spin density by self-consistent linear APW method 80—65710
Ni, (100) surface mag. props. 80—44861
Ni (110), polarised LEED study of magnetism 80—71102
Ni, (110) film, strain effects on mag. anisotropy 77—80972
Ni (110) surface, electron spin polarisation, effect of H_2 adsorption, electron capture spectroscopy 78—14933
Ni (110) surface, positive spin polarisation in field emission and demagnetisation by H_2 adsorption 78—52646
Ni (111), band struct. and temp.-depend. mag. exchange splitting, angle resolved photoemission obs. 78—60546
Ni (111), electron spin polarised photoemission spectrum 80—25525
Ni (111), Mossbauer effect emission spectroscopy and AES 79—91329
Ni (111), photoemission, exchange-split energy-band dispersions 80—35059
Ni (111), single crystal, spin polarisation of emitted photoelectrons 80—45215
Ni, (111) surface, VUV photoyield, electron spin polaris. enhancement 79—74054
Ni, APS and band theory of magnetism 77—40303
Ni, absorption of H_2, demagnetisation of surface due to absorption 77—80990
Ni, acoustic emission during magnetisation, stress effects 79—82854
Ni, alloying effect of magnetostriction and rolling texture *(Russian)* 77—32229
Ni alloys, at freq. up to 1 MHz *(Russian)* 77—8330
Ni alloys, ferromag., 4d and 5d impurities, hyperfine fields 78—31133
Ni alloys, mag. moment distrib. 77—32178
Ni alloys, magnetic resist. anisotropy, two-current model 77—20295
Ni alloys, normal Hall effect at 4.2K, two-spin current model interpretation 77—15829
Ni alloys, spontaneous resistivity anisotropy 77—39821
Ni, amorphous film, getter sputtered at 25K, resistivity, Curie temp. 78—52673
Ni, and its alloys, spin polarised tunnelling expts. 78—39372
Ni, and Ni alloys, rolling and oxidation, effect on magnetostriction and texture 77—36671
Ni and Ni alloys, tunnel currents, spin polarisation, simple band theory interpretation 79—78451
Ni, anisotropic magnetisation meas., 4-250K 80—65862
Ni, anisotropy consts., K_3 and K_1, determ. 77—4512
Ni, anisotropy energy in (100) plane, temp. dependence 78—2674
Ni, anomalies in thermal expansion and heat capacity 79—73744
Ni, anomalous resistivity near Curie temp., band theoretical calc. 78—56127
Ni, anomalous transmission of microwave power at FMR at 4.2K 79—82877
Ni, atomic layers, Pauli paramagnetism to band ferromagnetism transition thickness depend. 78—72377
Ni, atomic magnetic moments comparison to values of ferromagnetic metal 78—52244
Ni, band structure, μSR Knight shift meas. 79—56663
Ni, band theoretic interpretation of neutron scatt. expts., spin wave modes 80—44791
Ni based alloys, resistivity magnetoresistance, s,p impurities in ferromag. host 78—68008
Ni based ternary alloys, Coulomb and exchange scatt. amplitudes, spin dependent residual resistivities 78—64033
Ni catalyst, magnetooptical investigation of mag. props. 79—69858
Ni, chemisorption of H, spin-spin interactions, UPS spectra calc. 80—6630
Ni, chemisorption of H, surface magnetism 78—95510
Ni, creep, effect of AC mag. field, 1.5-4.2K *(Russian)* 79—11657
Ni, creep, mag. field effects, 30-250 Oe 77—16141
Ni, critical exponent β for hyperfine fields, PAD techniques 78—19403
Ni, critical exponent meas. by PAC in Ni-^{100}Rh 77—20774
Ni, critical NMR obs. near mag. transition 77—81026
Ni, crossover phenomena, stress induced above Curie point, neutron scatt. study 79—61113
Ni, crystal hyperfine fields and neutron scatt. 79—56172
Ni crystals, at mag. crit. temp., sp. ht. rounding 79—95595
Ni crystals in strong mag. field, EM excitation and vel. dispersion of sound *(Russian)* 80—39837
Ni Curie temp., press. depend., using press. cell developed for meas. with cubic-anvil press 80—13109
Ni, Curie temp. calc. using model containing five bands 79—56536
Ni, Czochralski-grown single crysts., domain walls, X-ray topography 77—20630
Ni, de Haas-van Alphen effect, press. effects *(Russian)* 78—2413
Ni, deformation in const. mag. field, 4.2K *(Russian)* 80—29591
Ni, deformed, coercivity and remanence anisotropy 78—31093
Ni, deformed, magnetic susceptibility anisotropic changes 78—27025
Ni, density of states, photoemission expts. above and below T_c, rel. to magnetism model 77—20536
Ni, diffusion and orientation aftereffects 80—88830
Ni dispersions, semi-amorphous, on Al_2O_3-graphite, mag. characterisation 80—44876
Ni dynamic exponent, crossover obs., TDPAC meas. 80—108021
Ni, dynamical spin susceptibility, noninteracting spin band model 78—31059

ferromagnetic properties of substances continued
Ni, effect of pressure on electron struct. *(Russian)* 79—77987
Ni, effective Coulomb interaction momentum depend. band model 79—78298
Ni, effective mag. anisotropy const., magnetoelastic contrib. 78—14951
Ni, effects of grain size on resist. anomaly near Curie point *(French)* 77—4318
Ni, elastic and magnon-inelastic spin polarised low energy electron scatt. 78—34970
Ni electrodeposit, mag. domain struct., neutron depolarisation 78—2716
Ni, electrodeposited film, saturation magnetisation and perpendicular anisotropy meas. 78—76277
Ni, electrodeposited sheet, mag. domain struct. obs. by neutron depolarisation 77—69605
Ni electrodeposits on (001)Cu films, growth and mag. anisotropy 79—42810
Ni, electromagnetically excited acoustic waves at low temp. 77—77081
Ni, electron field emission, spin polarisation positive sign 77—73220
Ni, electron tunnelling 80—60104
Ni, electron-phonon coupling, point contact spectroscopy obs. *(Russian)* 80—70342
Ni, electronic and magnetic props., spin split energy band dispersions 79—78829
Ni, electronic structure of nontransition element impurity atoms 77—73023
Ni, energy band dispersion and mag. exchange splitting, angle-resolved photoemission meas. 80—71567
Ni, energy bands, self-consistent calc. 77—39774
Ni, energy-band dispersions and exchange splitting, angle-resolved photoelectron spectroscopy 79—69402
Ni epitaxial films, even magneto-optical effects 80—76007
Ni, exchange integral maximisation, neutron scatt. obs. and ten-fold degenerate Hubbard model comparison 80—71004
Ni, exchange splitting of 3d bands, angle-resolved photoemission meas. 80—71568
Ni, Faraday rotation in X-ray region 79—82958
Ni, Fermi surface determ. 77—11843
Ni, Fermi surface under press., de Haas-van Alphen effect meas. 80—75499
Ni, ferromag., domain struct., small-angle neutron scatt. 77—66382
Ni, ferromag., exchange splitting, angle-resolved photoemission meas. 78—43985
Ni, ferromag., hyperfine fields at positive muons 78—43758
Ni, ferromag., hyperfine field of positive muon 79—47378
Ni, ferromag. film, ion plating prep., coercive force and magnetoresist. 77—12546
Ni, ferromag. film, magnetoresistance parameter meas. *(Spanish)* 80—2485
Ni, ferromag. film, surface states, surface magnetisation and electron spin polarisation 80—65648
Ni, ferromag. props., teaching expt. 80—82608
Ni, ferromag. reson., expt. data to explain asymmetry of reson. curves *(Russian)* 79—4728
Ni, ferromag. struct. in nucl. spin echoes 80—60453
Ni, ferromagnetic, calc. hyperfine fields and their press. derivations 80—6796
Ni, ferromagnetic, EMF generation by pulsed laser irrad. 78—68021
Ni, ferromagnetic, electron-magnon interactions 78—68205
Ni, ferromagnetic, electronic struct. by real space approach 80—65432
Ni, ferromagnetic, electronic struct. and hyperfine field of nonmag. impurities, calc. 80—70658
Ni, ferromagnetic, Fermi surface and band struct. 78—6267
Ni, ferromagnetic, Hall effect, anomalous, rel. to scatt. processes 80—44572
Ni, ferromagnetic, photoemission spectra and band struct., spin polarisation of bulk photoemission 79—78843
Ni, ferromagnetic, temp. depend. of μ^+ hyperfine field 78—43760
Ni, ferromagnetic, temp. depend. of hyperfine fields for F 80—20141
Ni, ferromagnetic antiresonance transmission at 24 GHz, temp. depend., g-factor and magnetisation 77—51959
Ni, ferromagnetic domain struct., static neutron depolarisation meas. 79—82812
Ni, ferromagnetic metals, ultrasound attenuation, EM generation 80—108046
Ni, ferromagnetic reson. determ. of first three anisotropy consts. 77—8414
Ni, ferromagnetic rods, direct and inverse electromagnetic conversion 79—52569
Ni, ferromagnetic state, energy bands, self-consistent calcs. 79—19509
Ni, ferromagnetic zero point motion effect on hyperfine field at interstitial positive muon site 80—2681
Ni fibres, magnetisation reversal 77—69625
Ni film, chemisorption induced mag. dead layers, ferromag. reson. obs. 79—91261
Ni film, effect of He ion implantation on domain struct., Lorentz electron microscopy 77—20654
Ni film, effects of finite size on crit. phenomena, resistivity anomaly 79—38192
Ni film, evaporated, for use as variable delay SAW device, magnetostrictive effects 80—71144
Ni film, evaporated, galvanomag. and mag. props. 78—23180
Ni film, evaporated, oscill. due to CO adsorption 77—1496
Ni film, evaporated, uniaxial mag. anisotropy 77—51929
Ni film, evaporated at oblique incidence, residual stress, mag. anisotropy meas. 78—22992
Ni film, even magneto-optical transmission effects, 0.4-1.25 μm 77—32354
Ni film, ferromag. reson., thermodynamical anal. 79—42840
Ni film, ferromagnetic (100) and (110), energy bands 79—1630
Ni film, granular, tunnelling of spin-polarised electrons and magnetoresist., exchange effects 77—12024
Ni film, ion beam sputtering prep., struct. and mag. props. 80—35085
Ni film, light scatt. from surface acoustic spin waves 79—33719
Ni film, linear mag. birefr. dispersion 77—69807
Ni film, low-angle grain boundary struct. *(Russian)* 79—42807
Ni film, mag. field depend. surface acoustic wave attenuation meas. 77—20674
Ni film, mag. structures and stresses, ferromag. resonance 78—72375
Ni film, magnetoelastic excitations, phonon spectroscopy and forbidden transitions 79—82853

ferromagnetic properties of substances continued
Ni film, microstructure of charged boundary between ferromag. domains 79—69705
Ni film, multi- and single-layer, reson. curves subjected to tangential mag. reversals *(Russian)* 80—50195
Ni film, polycrystalline, resist., conduction electrons and s-d exchange interaction 78—19021
Ni film, spin wave resonance 79—33542
Ni film, strained and strain-free, ferromag. reson. meas. 78—95525
Ni film, surface magnetisation, electric field effect 78—14991
Ni film, surface magnetoplasma waves, ATR meas. 77—69639
Ni film, temp. depend. of magneto-optical effects 77—81167
Ni film, thickness dependence of perpendicular mag. anisotropy 77—80974
Ni film, transverse Kerr magnet-optical effect enhancement by surface magnetoplasma waves 77—52056
Ni film, two-dimens. ⟨110⟩ domain wall 77—69648
Ni film, vac, deposited on liquid-He-cooled sapphire, galvanomag. props. 79—95519
Ni film (111), ferromag., energy bands and planar densities of states, LCAO calc. 79—4309
Ni films, electronic struct. calc., effects of chemisorption; contact pot. and surface magnetisation 80—103734
Ni films, evaporated, effect of CO adsorption on galvanomag. and mag. props. 79—33363
Ni films, evaporated, effect of CO adsorption on galvanomag. and mag. props. 79—33364
Ni films, Faraday rotation effect dispersion 80—40092
Ni films, ferromagnetic reson., photoacoustic detection 80—80613
Ni foil, critical exponent β determ. by microwave transmission 77—69575
Ni, foil, microwave transmission, parallel RF and mag. fields 77—59462
Ni foil, saturation magnetisation, during cathodic charging with H 78—71860
Ni, forbidden magnon scatt., polarized neutron meas. 79—78350
Ni, forced magnetostriction at 4.2K 80—50155
Ni, formed in decomposing β-NiH α-phase precipitate detection by Bitter powder pattern 79—28104
Ni fundamental and secondary mag. props., book contrib. 80—75724
Ni, giant internal mag. press and compressibility anomalies, itinerant model 77—16034
Ni, heat diffusivity and heat cond. near Curie point 77—24706
Ni, Hopkinson effect, mag. field depend. *(Russian)* 79—4657
Ni, hydrostatic press. effect on magnetisation Procopiu effect and hysteresis meas. 77—48023
Ni, hyperfine field and magnetisation, press. and temp. depend. 80—6795
Ni, hyperfine field of μ^+, calc. 77—40167
Ni, hyperfine fields on ^{12}B, NMR obs., near T_c 77—28476
Ni, hyperfine interactions on implanted ^{12}B, crit. behaviour near T_c 78—43663
Ni, hyperfine mag. fields at ^{67}Ge, TDPAC meas. 78—43701
Ni, in W-oxide-Ni high speed submicron junction, ferromagnetism, rel. to electron tunnelling 79—99635
Ni, interband optical conductivity, self energy correction 80—2792
Ni, intermodulation generation in RF mag. field, field interaction with domain walls 79—56600
Ni, internal fields, positive muon investigation 78—68438
Ni, internal friction, instantaneous, depend. on phase of torsional oscills. *(Russian)* 80—71142
Ni, internal friction and ridigity modulus, strain amplitude depend. *(Japanese)* 80—92606
Ni, internal friction near Curie temperature 78—44163
Ni, interstitial site determ., μSR technique 80—71287
Ni, itinerant electron model, spin quantization direction fluctuations, short range order. 80—34582
Ni, itinerant ferromag., Fermi surface and single particle excitations 80—34350
Ni, itinerant ferromagnet, spin-wave dispersion and linewidth 79—4668
Ni, Knight shift of hyperfine field at positive muon 77—43925
Ni, Landau-Lifshitz damping, wave no. and temp. depend. 80—34779
Ni, light scatt. from surface and bulk thermal magnons 80—45087
Ni, mag. anisotropy, $X_{2\text{spin down}}$ hole pocket in Fermi surface 78—39314
Ni, mag. anisotropy energy, symmetrical polynomials 77—66293
Ni, mag. densities, spin and orbital contrib., neutron diffr. meas. 79—78316
Ni, mag. domains, μ^*-tensor method, temp. and surface orientation depend. 77—16098
Ni, mag. excitations variation of de Haas-van Alphen frequency 79—8019
Ni, mag. field effect on creep, 4.2K *(Russian)* 77—90000
Ni, mag. props. of single-domain powders after plastic deform. *(Russian)* 78—6554
Ni, mag. surface anisotropy calc. 77—1553
Ni, magnetic aftereffect reactivation of single crystal by plastic deform. 79—65697
Ni, magnetic aftereffects of H isotopes, book contrib. 79—82835
Ni, magnetic anisotropy constants fitting to torque curves 79—7989
Ni, magnetic anisotropy energy 77—28382
Ni, magnetic hyperfine fields of Zr, DPAD meas. 80—39901
Ni, magnetic neutron scattering by dislocations, temp. depend. 80—103820
Ni, magnetic permeability, effect of ion implantation 77—28414
Ni, magnetic permeability, reversible, deform. and ion implantation effects 77—48013
Ni, magnetic surface anisotropy of transition metals, model calc. 80—34625
Ni, magnetic susceptibility, generalised, neutron scatt. meas. 80—34606
Ni, magnetically ordered state, softening with varying mag. field *(Russian)* 78—35017
Ni, magnetisation and relative vol. temp. depend. near Curie point *(Russian)* 78—14962
Ni, magnetisation curves in high mag. fields above Curie point 77—66386
Ni, magnetisation effect on channelling and blocking of proton beam 77—69022
Ni, magnetisation in pulsed field up to 320 kOe, 283 to 693K, band theory *(Russian)* 77—80920
Ni, magnetisation process in high mag. fields in crit. region 77—85498
Ni, magnetised mono- and polycryst., activation vol. var. during low temp. deform. *(Russian)* 78—3178
Ni, magnetised to saturation, props., positive-muon study 78—6619

ferromagnetic properties of substances continued

- Ni, magneto-optical Kerr effect in UV region, electronic struct. 77—52127
- Ni, magneto-optical near UV reflection-spectra, meridional and polar intensity effects *(Russian)* 78—39572
- Ni, magneto-volume effects calc., rel. to itinerant electron model 78—43621
- Ni, magnetocryst. anisotropy consts., determ. from magnetisation perpendicular to applied field 78—68219
- Ni, magnetocrystalline anisotropy energy in (100) plane, 13.8 to 258K 77—63171
- Ni, magnetocrystalline anisotropy energy, temp. and magnetisation depend. 78—6525
- Ni, magnetoelastic and magnetostrictive sensitivities, reversible and irreversible components *(Russian)* 80—25172
- Ni, magnetoelastic contribs. to US vel., elastic consts., and susceptibility 80—75829
- Ni, magnetoelastic effect on longitudinal compression, weak field spin rotation model 79—82851
- Ni, magnetoelastic effects, ΔE-effect and macroeddy current damping, internal friction meas. 78—64253
- Ni, magnetoelastic excitations and ferromagnetic resonance 79—82879
- Ni, magnetostriction, lattice parameter changes, direct X-ray obs. 78—15001
- Ni, magnetostrictive vibr. meas., appl. of laser interferometric technique 80—37059
- Ni, magnetostrictive vibr. obs. by laser interferometric technique 80—66000
- Ni, magnon relaxation, spin-orbit interaction, itinerant electron ferromagnets 80—11179
- Ni, Matteucci effect for tubular samples 78—43620
- Ni, modulus defect due to internal strain 78—76286
- Ni, muon hyperfine field, cluster calc. 79—56661
- Ni, muon probe expts. 77—63351
- Ni, muon spin rotation; freqs., and relax. rates 80—55006
- Ni, muon$^+$ spin rotation, hyperfine field determ., 0.12 to 300K 77—24775
- Ni, muon$^+$ spin rotation meas., local hyperfine field temp. depend. 77—63349
- Ni, neutron depolarisation near Curie point *(German)* 78—14934
- Ni, normal magnetisation meas. by rotating sample magnetometry 77—69514
- Ni, oblique mag. domain walls, obs. by X-ray topography 78—6540
- Ni, optical spectrum, anomalous temp. depend. around T_c, band struct. 80—40128
- Ni, oxidation, electron beam influence, disappearance potential spectroscopy obs., near T_c 77—1766
- Ni, oxidation at Curie temp. 79—29279
- Ni, phonon assisted magnon transmission at 24 GHz 79—82878
- Ni, phonon generation and attenuation at FMR 80—39875
- Ni, photoelectric effect in paramag. and ferromag. states, Auger spectra 78—95649
- Ni, photoelectron spin polarisation 77—32501
- Ni, photoemission near Curie temp. 79—78841
- Ni, plastically deformed, dislocation struct., mag. small angle scatt. of neutrons *(German)* 78—22730
- Ni plate, thin, helicon-Doppleron effect on spin wave prop. 77—66394
- Ni, plated film, magnetisation and mag. interface anisotropy 77—85510
- Ni, point contacts between ferromag. metals, singularities depend. in d^2V/dI^2, phonon spectra 79—60457
- Ni, polarised, ferromag., evidence for K-shell polarisation of ^{12}C ions via mol. orbital promotion 80—71273
- Ni, positive muon diffusion, press. depend. 80—75907
- Ni, positive muons as light isotopes of H, book contrib. 79—82907
- Ni, press. effects on mag. props. 77—66241
- Ni, pure and doped, mech., mag. relax. meas. dumb-bell self-interstitital reorientation *(German)* 78—52879
- Ni, rectilinear screw dislocation, magnetisation distrib., mag. moment anal. 80—44897
- Ni, resistivity, thermal and elec., spin disorder scatt. anal. 78—76063
- Ni rod, polycryst., demagnetising factor 77—73046
- Ni rod, spontaneous vibr. modes excited by reversible magnetostriction 79—56587
- Ni, secondary electron emission under Ar^+ ion bombard. near Curie point 80—29838
- Ni, Si ion projectile bound s electron polaris. rel. to transient mag. fields 79—33023
- Ni, simultaneous obs. of Barkhausen and magnetoplastic effect 79—28583
- Ni, single cryst., domain patterns in cyclically deform. cryst., behaviour during annealing 78—71740
- Ni, single cryst., magnetisation and US attenuation, mag. field depend. *(Russian)* 78—6559
- Ni, single crystal, structure of mag. domains 79—65695
- Ni single crystal near T_c, neutron transmission depolarisation 79—33479
- Ni, single-crystal films, spin wave reson. spectra 79—11350
- Ni, specific heat, temp. depend. *(Russian)* 78—56341
- Ni, spin polarisation in electron field emission, surface magnetism 78—68607
- Ni, spin polarisation of field-emitted electrons 77—40337
- Ni, spin polarisation of field-emitted electrons, theory 77—44134
- Ni, spin polarised electron emission, review 77—73215
- Ni, spin polarised photoemission, surface magnetism 79—52083
- Ni, spin-elastic wave three freq. interactions, parameters, excited wave amplitudes *(Russian)* 79—91276
- Ni, spontaneous magnetisation data up to 0.98 T_c, reanalysis 78—47959
- Ni, spontaneous magnetostriction determ. method, molecular field theory study *(Russian)* 80—50157
- Ni, Stoner model, mol. field coeff., temp. and field depends. 77—72975
- Ni, stray mag. fields above stripe domains, electron microscope and μ^*-tensor determ. 80—71089
- Ni surface, electron spin polarisation, electron capture spectroscopy 78—95645
- Ni surface, spin distribution of electrons, electron capture spectroscopy 78—14932
- Ni, surface decarburisation rate in dry H_2, soft mag. material manufacture 78—60882
- Ni, surface electronic structure, rigid exchange splitting model 77—11977
- Ni, temp. depend. of spontaneous magnetisation 77—63141
- Ni, temperature magnetic hysteresis near Curie temp. 79—56567

ferromagnetic properties of substances continued

- Ni, thermal acoustic magnons, Brillouin scatt. meas. 78—95424
- Ni, thermal expansion, 300-1000K, and power law consts. near Curie temp. 78—38858
- Ni, thermal expansion anomaly near Curie temp. 77—85474
- Ni, thermal softening, influence of alternating mag. field *(Russian)* 78—23312
- Ni, transient mag. field discontinuity seen by O(F) ions 80—24515
- Ni, transmission of 24 GHz radiation, effect of diffuse surface scatt. of carriers, calc. 80—34780
- Ni, twisted tubular polycryst. sample in axial mag. field, circular magnetisation 77—32230
- Ni, UPS, density of states determ. 78—52623
- Ni, US induced mag. reversals, stroboscopic electron microscope obs. 77—48026
- Ni, ultrafine particles prepared by vacuum evap. on running oil substrate, mag. behaviour 79—28565
- Ni, W-fibre reinforced, fabrication, heat treatment, and mag. and mech. props. 77—40408
- Ni wire, polycryst., inverse Wiedemann effect for low torsional stress 79—11332
- Ni wire, polycryst., magnetoelastic hysteresis with torsion, inverse Wiedemann effect *(Spanish)* 77—73064
- Ni wire in Ag matrix, coercivity meas. 77—20642
- Ni, XPS valence band spectra 77—21007
- Ni:^{129m}Xe, Mossbauer obs. of mag. hyperfine field 77—8460
- Ni:^{12}B, NMR, crit. slowing-down at Curie temp. 77—8418
- Ni:^{57}Fe, Mossbauer meas. near Curie temp. 78—10817
- Ni:B, impurity electronic struct. calc., ^{12}B NMR data anal., magnetisation decrease 79—47046
- Ni:C, H(D), isotope effects of C-H and C-D complexes 77—20129
- Ni:F, ion-implanted, mag. hyperfine field, anomalous temp. depend., PAC meas. 79—4754
- Ni:Lu, nuclear orientation meas., hyperfine field 77—32308
- Ni:Ra, hyperfine field determ. 77—85622
- Ni/Al_2O_3, sintered catalysts. mag. and catalytic props. for methanation reaction 79—79296
- Ni-Al, ferromag. solid sol., electronic struct., X-ray absorpt. spectra meas. 79—69653
- Ni-Al-Ti ferromagnetic non-homogeneous alloy, composition determination by Curie temp. meas. 80—11196
- Ni-alloy, anomalous Hall effect, contribution from skew scattering and side displacement of two-current model 79—56198
- Ni-alloys, spin polarised tunnelling 78—95494
- Ni-As, dil., temp. depend. of hyperfine field, TDPAD meas. 78—43700
- Ni-Au, amorphous film, anomalous Hall resist. 77—15832
- Ni-Au, local environment effects, magnetisation decrease 79—65664
- Ni-Au film, amorphous, magnetoresist. in fields up to 80 kG 77—39823
- Ni-b, hyperfine interactions from 6 to 730K, ^{12}B NMR 80—29372
- Ni-B alloy film, magnetisation-temp. characts., order-disorder transform. *(Japanese)* 78—76279
- Ni-B thin film glasses, mag. props. and corrosion resist. 80—80576
- Ni-C, ferromag., prep. by splat-quenching, obs. of electronic struct. of interstitial C 77—62868
- Ni-C, magnetic aftereffects of H isotopes, book contrib. 79—82835
- Ni-Cd, dil., ferromagnetic dynamic crit. exponent, hyperfine interaction vs. neutron scatt. expts. 78—84437
- Ni-Co, elementary excitations, exchange stiffness const., inelastic neutron scatt. study 79—47294
- Ni-Co, FCC, spin wave stiffness const., neutron scatt. study 79—51769
- Ni-Co, ferromag. films, magnetoresistance effect, crystal struct. 78—68017
- Ni-Co, ferromagnetic resonance, surface anisotropy 78—95526
- Ni-Co, high-field susceptibility, spin-wave spectrum, CPA calc. 80—65818
- Ni-Co, local mag. field on μ^+ 79—56665
- Ni-Co, mag. props. of single-domain powders after plastic deform. *(Russian)* 78—6554
- Ni-Co (25 wt.%), single crysts., mag. annealing effect on magnetostriction and magnetisation *(Japanese)* 80—34744
- Ni-Co (25 wt.%), single crysts., mag. annealing effect on magnetostriction and magnetisation at high temps. 80—108047
- Ni-Co alloys, FCC, spin wave stiffness, inelastic neutron scatt. 77—63156
- Ni-Co amorphous alloys, magnetostriction 80—34738
- Ni-Co film, magnetisation induced uniaxial anisotropy 77—48016
- Ni-Co film, spin wave resonance 79—33542
- Ni-Co film, spin-wave reson. exam. 78—2746
- Ni-Co plate, surface anisotropy from ferromagnetic reson. 78—48049
- Ni-Co-H, solid soln., Curie points and spontaneous magnetisation behaviour 80—50093
- Ni-Co-Mn, dil. ferromag. alloy, mag. moment, saturation magnetisation meas. 78—64195
- Ni-Co(Fe) film, anal. of main component by atomic absorpt. spectrophotometry 77—70381
- Ni-Cr, elementary excitations, exchange stiffness const., inelastic neutron scatt. study 79—47294
- Ni-Cr directional order anisotropy energy induced by neutron irradiation, temp. depend. 77—66294
- Ni-Cr-Mo-Mn alloy 02KhN40MB, corrosion-resist, heat-resist., phys. and mech. props. 80—35411
- Ni-Cu, directional order anisotropy energy induced by neutron irradiation, temp. depend. 77—66294
- Ni-Cu, ferromag., mag. moment, local environment effects, HF CPA cluster calc. 80—65817
- Ni-Cu, ferromagnetic, Hall effect, anomalous, rel. to scatt. processes 80—44572
- Ni-Cu, ferromagnetic and spin glass transition, DC magnetisation meas. 79—78369
- Ni-Cu, high-field susceptibility, spin-wave spectrum, CPA calc. 80—65818
- Ni-Cu, hydrogenated, Curie point, cluster magnetism 78—14960
- Ni-Cu, local environment effects, magnetisation decrease 79—65664
- Ni-Cu, local mag. field on μ^+ 79—56665
- Ni-Cu, low field magnetisation meas., mag. props. comp. depend. 78—91879
- Ni-Cu, mag. anisotropy, temp. and conc. depend. 77—63172
- Ni-Cu, Ni rich alloys, magnetic phase transition, elec. resistivity meas. 300-700K 79—82781
- Ni-Cu, Ni-rich, temp. depend. resist. 80—10943
- Ni-Cu alloy, magnetoresistance anisotropy, planar Hall effect 79—23947

ferromagnetic properties of substances continued
- Ni-Cu alloy, polarised neutron scatt., evidence for mag. environment effect 77—40039
- Ni-Cu alloys, spontaneous resist. anisotropy 77—89752
- Ni-Cu-H systems, Curie temp. during phase transitions under high press. H_2 80—71029
- Ni-Cu-Mn alloys, mag. and galvanomag. meas. 77—89928
- Ni-Cu(Pd)(Pt)(Rh), ferromag., press. effect on Curie temp. 79—51781
- Ni-Cu(Zn)(Ga)(Ge)(As)(Se)(Br)(Kr), dil., ferromagnetic, hyperfine field and relax. time obs. of impurity heavy nuclei 80—75533
- Ni-Fe, 79 NM alloy, gamma and neutron influence on mag. susceptibility comparative study *(Russian)* 80—39751
- Ni-Fe, dil., hyperfine mag. fields, press. effect, Mossbauer meas. 80—71277
- Ni-Fe, dil., temp. depend. of Mossbauer absorpt. near Curie point *(French)* 80—11305
- Ni-Fe, electronic struct. calc., effects of chemisorption; contact pot. and surface magnetisation 80—103734
- Ni-Fe, elementary excitations, exchange stiffness const., inelastic neutron scatt. study 79—47294
- Ni-Fe, epitaxial thin film, mag. structures and stresses, ferromag. resonance 78—72375
- Ni-Fe, FCC, Invar behaviour, spin waves stiffness consts., neutron scatt. study 79—51769
- Ni-Fe, film, anomalous Hall and Nernst-Ettingshausen effect, contribution of phonon and impurity scatt. *(Russian)* 78—64145
- Ni-Fe, film, domain struct., effect of biaxial stresses 78—88153
- Ni-Fe, film, magnetisation induced uniaxial anisotropy, substrate temp. depend. 77—8367
- Ni-Fe, film, magnetisation reversal, magnetoresistance meas. 77—16132
- Ni-Fe, high-field susceptibility, spin-wave spectrum, CPA calc. 80—65818
- Ni-Fe, magnetic aftereffects of H isotopes, book contrib. 79—82835
- Ni-Fe, magnetisation curling in superparamagnetic spheres 77—8363
- Ni-Fe, magnetostrictive vibr. meas., appl. of laser interferometric technique 80—37059
- Ni-Fe, new soft magnetic material for pulse transfer and choking in power electronics *(German)* 79—28555
- Ni-Fe, orientation aftereffect 80—88830
- Ni-Fe, power losses at extremely low freqs. 80—88815
- Ni-Fe, soft mag. props. rel. to metallurgical aspects 80—88810
- Ni-Fe, split bands rel. to sp. ht., g-factor and magnetostriction data 77—72977
- Ni-Fe, thermal fluctuation aftereffect meas. by pulse field method 80—88837
- Ni-Fe (15%) film, evaporated, uniaxial mag. anisotropy 77—51929
- Ni-Fe (19 wt.%) alloy, mag. anisotropy induced by cold rolling *(Russian)* 80—84595
- Ni-Fe (20 wt.%), thin film ferromagnetic band, magnetisation under domain creep conditions *(Russian)* 79—91262
- Ni-Fe (36 to 50 wt.%), initial permeability, domain struct. model 80—88811
- Ni-Fe (40%) (111) film with C coating, surface magnetism 77—73056
- Ni-Fe (50%), slow mag. domain wall motion 77—69597
- Ni-Fe alloy, atomic and mag. ordering, cluster variation calc. *(Russian)* 78—15391
- Ni-Fe alloy, extraordinary viscous magnetic wall motion 78—84465
- Ni-Fe alloy, W-fibre reinforced, fabrication, heat treatment, and mag. and mech. props. 77—40408
- Ni-Fe alloys, high-permeability, development trends *(Slovak)* 79—4694
- Ni-Fe alloys, pulse permeability and loss in toroidal core pulse current transformers 78—43615
- Ni-Fe based metallic glasses, Curie pt. anomalies 80—60256
- Ni-Fe conductor, EM pulse shielding, magnetisation curves 80—28143
- Ni-Fe film, differential susceptibility, struct. const. and losses 79—91271
- Ni-Fe film, domain struct., uniaxial stress effects 78—10740
- Ni-Fe film, effect of tensile stress on mag. domain struct. 78—68332
- Ni-Fe film, electrodeposition, role of buffers and anions 80—25583
- Ni-Fe film, ferromag. reson. under weak influence of eddy currents *(German)* 77—8412
- Ni-Fe film, Kerr magnetooptic effect, appl. to waveguide type optical modulator, theory 77—11015
- Ni-Fe film, low field domain wall mobility 80—25167
- Ni-Fe film, mag. and hyperfine field exam. of uniaxial anisotropy 77—66391
- Ni-Fe film, oligatomic, ferromag. reson. and torsion magnetometry, 123-373K 77—59461
- Ni-Fe film, relax. effects in domain boundary creep *(Russian)* 77—24723
- Ni-Fe film, thermally activated domain wall motion 80—88777
- Ni-Fe films, coercivity control for single-level masking bubble devices using surface modification and intermediate layers 79—51816
- Ni-Fe films, energy change of Bloch wall with angle to easy axis, calc. *(Slovak)* 80—103863
- Ni-Fe films, in state of undersaturation in perpendicular fields, micromagnetic struct. *(Russian)* 79—61193
- Ni-Fe films, magnetisation reversal in narrow strips, TEM study 80—34720
- Ni-Fe films, US generation by ferromag. reson. 78—88155
- Ni-Fe films, viscous magnetic domain wall motion anal. 79—95617
- Ni-Fe Invar, thermal expansion and spontaneous magnetisation, Invar anomalies, low spin model 80—71001
- Ni-Fe Invar alloy, thermoelectric power temp. and mag. field depend. 78—26849
- Ni-Fe multilayered films, mag. domain structures 79—82847
- Ni-Fe narrow stripes, mag. props. and domain struct. 79—82843
- Ni-Fe overlay, influence on bubble device performance 79—78466
- Ni-Fe oxidised film, extraordinary viscous wall motion at extreme vel. 78—14997
- Ni-Fe oxidised films, easy-axis switching 79—91266
- Ni-Fe soft magnetic alloys, developments and components *(Hungarian)* 78—48000
- Ni-Fe solid soln., precip. hardened, paramag.-ferromag. transition on ageing 78—52255
- Ni-Fe wire, hard-drawn, increased Barkhausen noise at low temps. 77—16114
- Ni-Fe/Mn interface, mag. surface effects, dead layers and exchange anisotropy 77—24718
- Ni-Fe-C, 20 at.% Fe, vacancy-C interaction, induced mag. anisotropy *(French)* 79—55775
- Ni-Fe-Co, alloy with step hysteresis loops *(German)* 79—42806

ferromagnetic properties of substances continued
- Ni-Fe-Co (17,3 wt.%), thin film ferromagnetic band, magnetisation under domain creep conditions *(Russian)* 79—91262
- Ni-Fe-Co alloy films for logic devices, mag. switching vel., anisotropy field and coercive force *(Korean)* 77—51930
- Ni-Fe-Co film, domain wall energy meas., by domain tip propag. method 77—55692
- Ni-Fe-Co film, magnetoelastic vibr. generation during high freq. mag. reversals *(Russian)* 78—60320
- Ni-Fe-Co film, nonmagnetostrictive, mag. props., effect of deposition parameters of Al underlayer 77—77078
- Ni-Fe-Co films, nonmagnetostrictive, magnetoresistance effects 78—35013
- Ni-Fe-Co films, saw tooth domains investigated 78—14994
- Ni-Fe-Co-Ti, electron microscopy and mag. meas. 80—71097
- Ni-Fe-Co(Mo) films, anal. of main component by atomic absorpt. spectrophotometry 77—70381
- Ni-Fe-Cr, extraordinary Hall effect, elec. and mag. meas. at 77 and 300K 80—34421
- Ni-Fe-Cr alloy, PE 16, coercivity of picture frame cryst. 78—14988
- Ni-Fe-Cr alloy, PE 16, thermally activated domain wall motion 79—95603
- Ni-Fe-Cr film, hysteresis loop meas. using magnetooptical system 79—69707
- Ni-Fe-Cr-Mo-Ti-Al, PE 16, thermally activated domain wall motion 80—88777
- Ni-Fe-H, Curie points, mag. props. of H solutions FCC metal sublattice parameter behaviour 79—69671
- Ni-Fe-Ho film strips, domain struct. and new rot. processes 77—85533
- Ni-Fe-Mn, ferromag. reson. linewidth and saturation magnetisation 78—72418
- Ni-Fe-Mn ferromagnetic alloy, magnetic state of Mn atom, local environment effect 77—66298
- Ni-Fe-Mo-Cu (79, 16, 4.3, 0.7 wt.%) K-state formation, physical props. exam. 78—47761
- Ni-Fe-Nb, hardperm alloy, effect of sheet thickness and heat treatment on magnetic props. *(Japanese)* 78—31095
- Ni-Fe-Nb (Mo), magnetic alloy, TEM and X-ray obs. *(Chinese)* 80—24401
- Ni-Fe-Nb alloys, mag. permeability and struct. *(Chinese)* 78—84450
- Ni-Fe-Nb-Al alloys, mag. permeability and struct. *(Chinese)* 78—84450
- Ni-Fe-Nb-Al(-Mo), wear resisting mag. head material, mag. props. and struct. 80—35350
- Ni-Fe-Nb-Mo (11.42, 6.92, 1.54 wt.%), Hardperm, high magnetic permeability alloys 77—8361
- Ni-Fe-Nb-Mo-Al, head material for mag. recording, DC and AC mag. props. 80—88812
- Ni-Fe-Pd thin films, mag., surface and corrosion props. 80—34707
- Ni-Fe-Rh films, mag. and corrosion props. 80—34702
- Ni-Fe(Co), local ordering effect on spin wave stiffness const. 77—66282
- Ni-Fe(Cr) alloy film, electron spin polarisation, meas. using supercond. tunnel junction 77—69637
- Ni-Fe(Pd)(Pt)(Cu), ferromag., influence of local ordering on spin wave stiffness const. 77—89937
- Ni-H, ferromag., H impurities and μSR, self-consistent calc. 80—84447
- Ni-H, ferromag. disappearance obs. 77—43824
- Ni-Mn, dil., mag. moment distribs. and environmental effects, neutron scatt. obs. 80—60247
- Ni-Mn, hydrogenation kinetics, magnetisation, interstitial H influence 80—35528
- Ni-Mn, low temp. kinetic props., 4.2-77.3K *(Russian)* 79—19568
- Ni-Mn, mag. moment and asphericity of spin density distrib., polarised neutron scatt. obs. 80—44813
- Ni-Mn, ordered and disordered, press. effect on Curie temp. 80—71148
- Ni-Mn, spin wave stiffness const., low temp. neutron scatt. meas. 79—51768
- Ni-Mn, temp.-resist. graph deflection points, mag. moment orientation rel. to magnetisation matrix *(Russian)* 79—60788
- Ni-Mn (17-27 at.%), low-angle neutron diffr., anomalous crit. scatt. *(Russian)* 80—60193
- Ni-Mn (5%), magnetisation curve reduction 78—31096
- Ni-Mn (up to 32 at.%), Curie temp., press. depend., using press. cell developed for meas. with cubic-anvil press 80—13109
- Ni-Mn alloy, disordered, exchange-anisotropy field, magnetisation curves 78—72365
- Ni-Mn alloy, disordered, mag. struct., high field twist deform. 78—68166
- Ni-Mn alloy, disordered FCC, stiffness const., single cryst. neutron inelastic scatt. meas. 77—20558
- Ni-Mn alloy film, heat treatment influence obs. *(German)* 77—56118
- Ni-Mn alloys, equilib. ordered, high field magnetisation 77—85491
- Ni-Mn alloys, ferromagnetism-to-spin glass phase transition and strong mag. field effect 80—75773
- Ni-Mn alloys, remanent magnetisation reversal, local environment model 79—33507
- Ni-Mn base polynary alloys, magnetic and elect. props. *(Japanese)* 78—15551
- Ni-Mn base polynary alloys, magnetic, and elec. props., composition and heat treatment effects 79—11710
- Ni-Mn ferromagnetic alloy, magnetic state of Mn atom, local environment effect 77—66298
- Ni-Mn-Al-Si-Co, Alumel, Ettingshausen-Nernst coeff. and transport props. from 200 to 473K 80—44573
- Ni-Mn-H, hydride phase form. and decomposition in hygh-press. gaseous H_2, magnetisation meas. 79—56953
- Ni-Mn-H solid solutions, mag. props. 80—88753
- Ni-P, amorphous alloys, low temp. mag. props., comp. depend. 77—66387
- Ni-P alloy, amorphous, NMR expts. and interpretation 79—8060
- Ni-P electrodeposit, magnetisation coercivity and magnetostriction 78—68338
- Ni-P film, amorphous, ion implanted, struct. and domain struct. obs. 79 91272
- Ni-Pd, directional order anisotropy energy induced by neutron irradiation, temp. depend. 77—66294
- Ni-Pd, FCC disordered polycryst. alloy, magnetisation, band ferromag. 78—80180
- Ni-Pd, high mag. field effects, mag. isotherms near Curie point, exchange splitting energies 80—60272
- Ni-Pd, mag. form. factor, polarised neutron diffr. meas. 80—29525
- Ni-Pd, mag. moment distrib., one-mag.-species model calc. 80—65788

ferromagnetic properties of substances continued
Ni-Pd alloy, disordered, local environment effects, neutron scatt. expts. 78—68172
Ni-Pd alloy, magnetostriction and mag. anisotropy meas. 79—4713
Ni-Pd alloys, mag. props., average and local density of states, CPA calc. 77—59242
Ni-Pd-Mn, ternary FCC solid soln., saturation magnetisation and Curie temp., medical appl. *(Japanese)* 79—61114
Ni-Pd-Mn ternary alloys, mag. characts., use for thermoseed 80—107995
Ni-Pd-P, Ni-Pt-P, amorphous and electronic structs., NMR Knight shifts and linewidths meas. 78—68400
Ni-Pd(Pt), renormalisation of spin wave stiffness 79—51764
Ni-Pt, itinerant ferromagnet. magneto-volume expts. 77—66404
Ni-Pt, magnetic moment distrib., diffuse neutron scatt. meas. 80—34593
Ni-Pt alloys, magnetic-moment distrib. neutron study 80—97066
Ni-Pt alloys, thermal expansion, mag. contribs. 77—43355
Ni-Pt disordered alloy, off-diagonal, T-matrix itinerant electron ferromagnetism calcs. 80—25067
Ni-Pu, dil., effective mag. fields, temp. depend. *(Russian)* 78—43587
Ni-Rh, mag. moment distrib., one-mag.-species model calc. 80—65788
Ni-Rh alloy, disordered, local environment effects, neutron scatt. expts. 78—68172
Ni-Rh alloys, ferromag., local-environment effects, mag. diffuse neutron scatt. cross-section meas. 77—55664
Ni-Rh alloys, thermal EMF, elec. resist., mag. susceptibility, mag. moment and Curie temps., 18-500°C *(Russian)* 77—20288
Ni-Rh ferromagnetic alloy, mag. moment spatial distrib. 77—66275
Ni-Ru, environmental effects and mag. moment distrib., magnetisation and neutron scatt. meas. 79—91211
Ni-Ru ($\leq$4 at.%), influence of alloying on mag. anisotropy 80—71010
Ni-SiO multilayer film, interface magnetisation 80—7135
Ni-SiO multilayer films, interface magnetisation 80—88858
Ni-Sn(Sb), dilute ferromagnetic alloy, resistivity and magnetoresist. anisotropy 79—11106
Ni-Ta, dil., crit. behaviour, ^{181}Ta PAC expt. 78—43723
Ni-Ti, mag. moment distrib. and environmental effects around Ti impurity 80—7092
Ni-Ti, Ni-rich, temp. depend. resist. 80—10943
Ni-Ti (2wt.%) alloy, polarised neutron diffuse scatt. 77—36057
Ni-Ti alloy, Curie temp. determ. using deviation from Mattheisen's rule 79—15306
Ni-Ti(Mn)(Cu), tunnelling electron spin polarisation 77—73058
Ni-V, del. alloy, anisotropy consts., K_3 and K_1, determ. 77—4512
Ni-V, elementary excitations, exchange stiffness const., inelastic neutron scatt. study 79—47294
Ni-V, magnetocryst. temp. and conc. depends., rel. to resistivity 77—40052
Ni_3Al, elastic moduli changes at Curie point 77—66406
Ni_3Al, electronic, mag., and cohesive props. 80—44491
Ni_3Al, itinerant ferromagnet, magneto-volume expt. 77—66404
Ni_3Al, itinerant ferromag., Fermi surface and single particle excitations 80—34350
Ni_3Al, thermal expansion, mag. contribs. 77—43355
Ni_3Al, unpaired spin density distrib., polarised neutron diffr. 78—10659
$Ni_3Al(Ga)$, off-stoichiometric alloy, inverse mag. susceptibility rel. to defect conc. 80—60216
$Ni_{1-x}Au_x$, amorphous, elec. resist., temp. depend., spin wave contrib. and resist. minimum 78—51961
$Ni_{100-x}B_x$, amorphous, mag. struct., mag. susceptibility meas. 80—80485
$Ni_3B_7O_{13}X$, X=Cl, Br, I, ferromag. ferroelectrics *(Japanese)* 79—65804
NiC, electronic structure of interstitials 79—1583
$NiCl_2$, spin orientation of mag. impurity atom 77—59403
NiCo, itinerant electron model, spin wave stiffness const. calc. 80—34613
$(Ni_{1-c}Co_c)_{0.78}P_{0.14}B_{0.08}$, amorphous, mag. props., local environment model 77—12119
NiCr, hyperfine fields about μ^+ 79—56664
$Ni_{1-x}Cu_x$+CO, $Ni(CO)_4$ form. activation energy, mag. phase depend. 80—3409
$Ni_{0.7}Cu_{0.3-x}Si_x$, magnetic props., 4.2 to 800K 77—8290
Ni(Fe,Cr) and Ni_3(Fe,Cr), electron states density model and mag. characts. calcs. *(Russian)* 80—92804
Ni_3(Fe,M), M=Cu, Cr, Mo, W, kinetic phenomena rel. to ordering and electron struct. *(Russian)* 78—76043
NiFe disordered alloys, Mossbauer spectra, hyperfine mag. field distrib., Curie temp. 80—7198
NiFe film, ferromag. reson., thermodynamical anal. 79—42840
NiFe film, stationarity and behaviour of Barkhausen noise 79—24198
NiFe, grain oriented, mag. domain wall slow motion, tunnelling mechanism 77—32210
NiFe, hysteresis, departure from Rayleigh law in low mag. fields 77—40086
NiFe, itinerant electron model, spin wave stiffness const. calc. 80—34613
NiFe, magnetic surface anisotropy of transition metals, model calc. 80—34625
NiFe soft magnetic alloys, magnetic props., effect of annealing and fabrication *(German)* 78—53004
NiFe stripes, mag. props. and domain struct. 80—44886
NiFe tape, rapid surface and vol. magnetisation, eddy-current-limited domain wall motion 77—12159
NiFe thin films, magnetoresistance, quasi-static characts. 80—107766
NiFe, US induced mag. reversals, stroboscopic electron microscope obs. 77—48026
$Ni_{0.75}Fe_{0.25}$, influence of atomic ordering on spin waves, inelastic neutron scatt. 77—69516
$Ni_{0.83}Fe_{0.17}$ films, reson. oscills. of mag. domain walls and Bloch lines, stroboscopic electron microscopy 80—54931
$Ni_{1-x}Fe_x$, short range order exam. allowing for formation of structural domains *(Russian)* 78—6888
Ni_3Fe alloys, low-temperature specific heat, long and short range order effects 80—100339
Ni_3Fe, compression induced mag. anisotropy and superlattice dislocations, annealing effect 78—31067
Ni_3Fe, compression induced magnetic anisotropy, annealing effect 80—93112
Ni_3Fe, disaccommodation meas. after low temp. electron and neutron irrad. 80—88832
Ni_3Fe disordered alloys, Mossbauer spectra, hyperfine mag. field distrib., Curie temp. 80—7198
Ni_3Fe, domain struct. after tensile deform., dislocation effects 80—71083
Ni_3Fe, electronic structures, order effect 79—90938
Ni_3Fe, roll magnetic anisotropy and dislocations *(Japanese)* 77—80930

ferromagnetic properties of substances continued
Ni_3Fe single crystals, longitudinal magnetoresist. meas. 80—70675
Ni_3Fe, superlattice dislocations, compression induced mag. anisotropy 77—85443
Ni_3Fe, transport props. and magnetisation, effect of alloying with Cr, Mo, W or Cu *(Russian)* 78—39095
Ni_3Fe:C, mag. anisotropy depend. on C content, magnetometric study *(Russian)* 80—54887
$Ni_{73}Fe_{27}$, order-disorder transition, Mossbauer study 79—95163
$Ni_xFe_yCr_{1-x-y}$ films, struct., mag. props., and corrosion resist. 80—34706
$Ni_{36}Fe_{32}Cr_{14}P_{12}B_6$ metallic glass, mech. props. and thermal stability 80—76362
$(Ni_{100-x}Fe_x)_{79}P_{13}B_8$, amorphous dil. alloys, spin glasses, magnetisation meas. 79—61178
$Ni_{40}Fe_{40}P_{14}B_6$, amorphous alloy, microstruct. study of crystallisation 77—86062
$Ni_{80-x}Fe_xP_{14}B_6$, amorphous alloy, resistivity variations near critical temp. 79—73488
$(Ni_xFe_{1-x})_{80}P_{10}B_{10}$, amorphous, Curie temp., press. effect 80—75833
NiH_x, magnetization, elec. resist., and non-occurrence of supercond. 79—56195
$Ni_{98}M_2$, M=impurity metal, formation of MH(D)-complexes 80—65236
NiMn, high field magnetisation 80—2557
Ni_3Mn, at. ordering during annealing, mag. field effect 78—15394
Ni_3Mn, mag. domains perpendicular to AC demagnetising field 77—20632
Ni_3Mn, magnetic phase exam. 77—20631
Ni_3Mn, neutron irradiated, disordering by replacement collision sequences, saturation magnetisation meas. 77—47492
Ni_3Mn, partially ordered, field induced uniaxial anisotropy at low temp. 77—40053
Ni_3Mn, partially ordered, spin-wave dispersion relation, inelastic neutron scatt. meas. 80—20394
Ni_xMn_{1-x} disordered alloy, mag. interactions exam. 77—24687
$Ni_2Mn_{0.9}Fe_{0.1}Sn$, Fe site hyperfine field and mag. moment, Mossbauer effect meas. 78—76365
$NiMnGe_{1-x}Si_x$, mag. props., neutron diffr. and magnetometric meas., 80-600K 80—65793
$Ni_2Mn_xM_{1-x}Sn$ (M=Ti,V) mag. hyperfine fields, ^{119}Sn Mossbauer spectra study 80—55003
NiMnSb, hyperfine mag. field at Cd impurity, TDPAC study 80—39906
$Ni_{1+x}MnSb$, mag. hyperfine field on ^{111}Cd, TDPAC obs. 78—43709
$(Ni_{0.75}Mn_{0.25})_{82}Si_{10}B_8$, amorphous, exchange anisotropy, mag. susceptibility meas., 4.2K to room temp. 80—11186
Ni_2MnSn, ferromag. Heusler alloy, electronic struct., spin polarisations, theory 80—54598
Ni_2MnSn, Heusler alloy, mag. interactions and cond. electron polarisation, spin echo NMR meas. 77—77125
$Ni_2MnSn(In)(Sb)$, Heusler alloy, hyperfine field at ^{111}Cd, TDPAC meas. 78—43705
$Ni_2Mn_xT_{1-x}Sn$, (T=Ti, V or Cr), Heusler alloy, mag. moment exam. 77—24682
$Ni_2Mn_xT_{1-x}Sn$, T=Ti(V)(Cr), ferromag., magnetisation, susceptibility 77—12102
$Ni_2Mn_xTi_{1-x}Sn$, Mossbauer spectra, mag. hyperfine field 80—15857
$Ni_{65}Mo_2Fe$, O_2 effect on secondary recrystallisation and mag. props. 80—35201
$Ni_{80}P_{20}$ glass, mag. props. 77—63125
$Ni_{0.98}Pd_{0.02}$, dil. ferromag., nucl. mag. relax. meas. 77—16198
Ni_xPt_{1-x} disordered alloy, itinerant system, induced magnetism 78—52191
$Ni(Rh_{1-x}Cr_x)_2S_4$, ferromag. spinel system with metallic conduction 79—56513
$(Ni_{1-x}Rh_x)_{99}Mn$, ferromagnetic, NMR study of local environment effect 80—7192
$Ni_{0.97}Ru_{0.03}$, mag. form factor and moment distrib., obs. using polarised neutrons 78—68171
$Ni_{0.97}Ru_{0.03}$, mag. moment distrib. polarised neutron study 79—42738
$(Ni_{1-x}Ru_x)_{99}Mn$, ferromagnetic, NMR study of local environment effect 80—7192
NiS film, electrolytically deposited, S content influence 80—44884
$NiSiF_6.6H_2O$, ferromag. ordering, susceptibility and heat capacity obs. 79—61080
$NiSnF_6.6H_2O$, ferromag. ordering, susceptibility and heat capacity obs. 79—61080
Ni_2(Ti,Mn)Sn, Heusler alloy, mag. meas. 79—47261
NiTi alloy single cryts., ferromag. reson., g-value and linewidth 80—71186
$Ni_{1-x}Ti_x$, ferromag. props., Ti conc. effect 80—54872
$NiTiF_6.6H_2O$, mag. and struct. transitions 78—68257
$(Ni_{1-x}X_x)_{99}Mn$, X=Rh, Fe, Mn, ferromagnetic, NMR study of local environment effect, relaxation mechanism 80—7193
$Ni_{0.8}Zn_{0.2}Fe_2O_4$, twisted tubular polycryst. sample in axial mag. field, circular magnetisation 77—32230
$(Ni_xZn_{1-x})_{0.5}Fe_2O_4$, spontaneous vibr. modes excited by reversible magnetostriction 79—56587
$NiZrF_6.6H_2O$, uniaxial ferromagnetism 78—80143
Ni(001) surface states, surface magnetisation, electron spin polarisation 80—88612
Ni(100) platelet surface optical and magneto-optic consts. 78—15151
Ni(110), ferromag., surface magnetisation, polarised LEED expt. 80—97118
Ni(110), mag. exchange splitting of electronic surface states 80—88610
$NpCu_2Si_2$, mag. struct., neutron diffr. determ. 80—93084
$NpFe_2$, high temp. mag. props., 300 to 1100K 79—51757
$NpFe_2$, lattice distortions in ferromag. phase, X-ray obs. 80—15774
$NpNi_2$, lattice distortions in ferromag. phase, X-ray obs. 80—15774
$NpOs_2$, band magnetism due to f-electrons, T_c 77—73039
$NpOs_2$, itinerant ferromagnet, sp. ht., 3-25K 77—63212
O single layer on Au, ferromag. props., thermomag. effect *(Russian)* 78—64256
$PbFe_{12}O_{19}$, Mossbauer spectra, domain magnetisation vector rotations, domain struct. 79—69761
$Pb_{1-x}Sn_xTe$, basic electrons energy spectrum near mag. phase transition *(Russian)* 79—90955
Pd based alloys, extraordinary Hall effect 78—76053
Pd, confined geometry, p-wave supercond. or itinerant ferromag. 80—11129
Pd, film with defects, field-induced resist. min. 80—11050
Pd, magnetic properties in para-process region *(Russian)* 78—2672

ferromagnetic properties of substances continued
- Pd-Ag-Fe, (0.5, 1.0, 2 at.% Fe), elec. resist. reduction near ferromag. and spin glass ordering 77—69299
- Pd-Co, dil., breakdown of ferromag. order, magnetoresist. obs. 80—71046
- Pd-Co, dil., local orbital moment evidence 77—20299
- Pd-Co, dilute, extraordinary Hall effect meas., 2-250K 80—34420
- Pd-Co, dilute alloy, ferromag. ordering, depend. on Co impurity at low temp. 79—61055
- Pd-Co, normal Hall effect *(Russian)* 80—103676
- Pd-Co, pressure effect on Curie point, Debye temp. in ferromag. state *(Russian)* 77—32194
- Pd-Co-P amorphous alloy, mag. an elec. props. 77—40043
- Pd-Fe, magnetic anisotropy near Curie point, quasi domain struct. *(Russian)* 80—65867
- Pd-Fe, magnetoresist., rel. to dil. ferromag. model 78—30907
- Pd-Fe, Mossbauer spectra, scatt. and transmission geometries, differences in crit. behaviour near T_c 78—76367
- Pd-Fe, normal Hall effect, temp. and conc. depend. *(Russian)* 77—80763
- Pd-Fe, normal Hall effect *(Russian)* 80—103676
- Pd-Fe, onset of ferromagnetism 78—23270
- Pd-Fe, scatt. and transmission Mossbauer spectra near Curie temp. 80—15864
- Pd-Fe (25-55 at.%) ^{57}Fe effective field and mag. struct., Mossbauer and magnetisation expts. *(Russian)* 77—90085
- Pd-Fe alloy, dil., cond. electron polarisation studied by positive muons 77—28397
- Pd-Fe alloy, IR absorpt. characts., 0.9 to 19 μm, mag. order effect 78—84577
- Pd-Fe alloy, NMR of ^{27}Al meas. 77—12215
- Pd-Fe alloys, dil., anisotropy of neutron polarisation near ferromag. phase transition 77—32234
- Pd-Fe alloys, dil., spin polarisation effect on hyperfine interactions, anal. of Mossbauer meas. *(Russian)* 79—47055
- Pd-Fe alloys, disordered FCC, exchange stiffness consts., temp. depend. of magnetisation 77—69528
- Pd-Fe alloys, H_2 absorption and mag. behaviour 78—35012
- Pd-Fe and Pd, muon$^+$ Knight shift, cond. electron polarisation, RKKY oscill. 77—66450
- Pd-Fe disordered alloy, Landau model for mag. props. 77—66276
- Pd-Fe type dil. ferromag. alloys, spin wave propag. *(Russian)* 77—12110
- Pd-Fe-Mn, differential susceptibility, spin glass and ferromag. transition 79—61169
- Pd-Fe-Mn, dil. alloy, high press. study 80—34600
- Pd-Fe-Mn, ferromag. and spin-glass props; comment 80—2591
- Pd-Fe-Mn, ferromagnet-spin glass, thermal expansion forced, magnetostriction and magnetisation under high press. 80—65255
- Pd-Fe-Mn, ferromagnetic-spin glass transition 78—39339
- Pd-Fe(Co)(Ni), dilute ferromagnets, press. effect on Curie temp. 80—65873
- Pd-Fe(Co)(Ni) dilute alloys, ferromag., magnetoresist. 78—91665
- Pd-Mn, ferromagnetism to spin glass behaviour transition 80—71062
- Pd-Mn, spin glass-ferromag. alloys, high-field magnetisation 79—33488
- Pd-Mn alloy, NMR of ^{27}Al meas. 77—12215
- Pd-Mn(Fe), mag. ordering phenomena, neutron scatt. obs. 80—44812
- Pd-Ni, dil., local orbital moment evidence 77—20299
- Pd-Ni, disordered alloy, onset of ferromagnetism, effect of press. 79—61111
- Pd-Ni, local susceptibilities, ^{61}Ni Mossbauer spectroscopy 78—95536
- Pd-Ni, normal Hall effect *(Russian)* 80—103676
- Pd-Ni, onset of ferromagnetism 78—23270
- Pd-Ni, thermal expansion and magnetostriction meas. near crit. conc. for ferromagnetism 80—65881
- Pd-Ni alloy, dil., ferromagnetism, local moments, susceptibility, magnetisation and Curie temp. *(Russian)* 78—88115
- Pd-Ni alloy, NMR of ^{27}Al meas. 77—12215
- Pd-Ni alloys, kinetic props., transverse magnetoresistance *(Russian)* 77—76790
- Pd-Ni alloys, kinetic props., anomalous Hall coefficient *(Russian)* 77—76791
- Pd-Ni alloys, onset of ferromag. 79—56533
- Pd-Ni disordered alloy, Landau model for mag. props. 77—66276
- Pd-Pt alloys, mag. props., average and local density of states, CPA calc. 77—59242
- PdAgFe, ferromag., Curie temp. depend. on susceptibility, non-mean field theory 80—44829
- PdCo, dil., nucl. mag. relax. 78—6590
- $(Pd_{0.996}Co_{0.004})_{1-x}Mn_x$ alloys, ferromag. and spin glass transition, NMR 79—65761
- PdFe alloy, magnetoresistance meas. below 295K 79—78070
- $Pd_{0.98}Fe_{0.01}$ $Gd_{0.01}$, Pd-Gd exchange const., neutron diffuse scatt. meas. 80—71002
- Pd_3Fe, ferromag., spin wave spectrum 77—69515
- Pd_3Fe, spin wave dispersion relation at 4.2K, neutron inelastic scatt. meas. 77—63157
- Pd_3Fe, spin wave dispersion, neutron inelastic scatt. meas. 78—14943
- $(Pd_{0.67}Fe_{0.33})_{1-x}Au_x$, ordering effects on mag. props. *(Russian)* 78—47942
- $Pd_{50}Fe_{37.5}Co_{12.5}$, elec. resist., cond. electron scatt. and heterogeneities of spin system *(Russian)* 79—56189
- $Pd_{0.98}Fe_{0.01}Gd_{0.01}$, ferromag., Pd-Gd exchange const. and Pd polarisation, neutron scatt. meas. 80—25122
- $(Pd_{0.9965}Fe_{0.0035})Mn_{0.05}$, ferromag. and spin-glass props. 80—2590
- $(Pd_{0.9965}Fe_{0.0035})_{1-x}Mn_x$, mag. behaviour at Fe sites, Mossbauer effect meas. 80—66085
- PdFeRh, ferromag., Curie temp. depend. on susceptibility, non-mean field theory 80—44829
- $Pd_{0.95}Gd_{0.05}$, mag. transition temp. determ., magnetisation data 77—12123
- $(Pd_{1-y}M_y)_{100-x}Fe_x$, M=Ag, Rh, exchange-enhanced alloys, mag. ordering 79—61050
- $Pd_2MnIn_{1-y}Sb_y$, Heusler alloy, mag. order obs. 80—29528
- $Pd_2MnIn_{1-x}Sb_x(Sn_x)$, Heusler alloy, Mossbauer effect exam., mag. coupling 79—69755
- $Pd_2MnIn_{1-x}Sb_x(Sn_x)$, Heusler alloy, Mossbauer effect exam., hyperfine interactions in ferromag. phase 79—69756
- $Pd_2MnIn_{1-x}Sn_x$-Cd, dil., Heusler alloy, hyperfine mag. field on Cd, TDPAC obs. 79—8075
- $Pd_2Mn_{1-x}Nb_xSn$, Heusler alloy, NMR and mag. coupling 78—43676

ferromagnetic properties of substances continued
- $Pd_{1+x}MnSb$ Heusler alloys, magnetic hyperfine fields on ^{111}Cd, TDPAC and magnetisation meas. 80—93219
- Pd_2MnSb and PdMnSb, Heusler alloy, hyperfine field at ^{111}Cd, TDPAC meas. 78—43705
- Pd_2MnSb, ferromag. Heusler alloy, mechanical and heat treatment effects 79—78582
- Pd_2MnSb, mag. hyperfine field of ^{129}I, Mossbauer spectra 78—43706
- Pd_2MnSb:^{119}Sn, mag. hyperfine structure, Mossbauer obs. 77—32309
- $Pd_{2-x}MnSb$, struct., appl. as improved neutron polariser 80—60199
- Pd_2MnSn, ferromag. Heusler alloy, electronic struct., spin polarisations, theory 80—54598
- Pd_2MnSn, Heusler alloy, mag. interactions and cond. electron polarisation, spin echo NMR meas. 77—77125
- Pd_2MnSn, Heusler alloy, NMR and mag. coupling 78—43676
- $Pd_2MnSn(Sb)$, Cd impurities, hyperfine field meas. 78—15074
- $Pd_2MnSn_{1-x}Sb_x$, Heusler alloy, Mossbauer effect exam., hyperfine interactions in ferromag. phase 79—69756
- $Pd_2MnSn_{1-x}Sb_x$, mag. order exam. 77—40036
- $Pd_2MnSn_{1-x}Sb_x$, Mossbauer spectra, mag. hyperfine field 80—15868
- $Pd_2Mn_xV_{1-x}Sn$, Heusler alloy, structural disorder, Mossbauer study 80—80650
- $(Pd_xPt_{1-x})_3Fe$ atomically ordered alloy, thermoelectric power, carrier energy spin shift, mag. props. 80—29394
- $(Pd_xPt_{1-x})_3Fe$, magnetisation intensity and coercive force, antiferro- to ferromag. transition *(Russian)* 77—48008
- $Pd_{95}Rh_5$, low-temp. spin-fluctuation resist., effect of pot. scatt., effect of Ni addition 77—15840
- $(Pd_{95}Rh_5)Co$, exchange enhanced system, AC susceptibility meas. 77—16096
- $Pd_{80-x}Si_{20}Fe_x$, amorphous, low x, hyperfine interactions and mag. ordering temp. 79—15303
- $Pd_{35}Zr_{65}$, mag. susceptibility meas. 80—75740
- Permalloy, domain struct., influence of planar anisotropy 79—78472
- Pr-Nd alloy, elec. resist. and magnetisation 77—66367
- $PrAg_x$, low temp. mag. meas. 80—107989
- $PrAl_2$, cryst. field interpretations of inelastic neutron scatt. meas. and mag. props. 79—56174
- $PrAl_2$, cryst. field splitting of Pr^{3+}, inelastic neutron scatt. exam. 77—20275
- $PrAl_2$, extraordinary Hall effect 80—39560
- $PrAl_{2-x}Ag_x$, cryst. field and exchange interactions 77—63076
- PrB_4 *(French)* 77—20566
- PrB_4, mag. and elec. props. 80—20386
- $Pr_{1-x}Ca_xAl_2$, mag. props. and phase relations 80—107991
- $Pr_{0.9}Ca_{0.1}MnO_3$, mag. struct. neutron diffr. and magnetisation study 79—61061
- $PrCo_2$, magnetocryst. anisotropy props. by ^{57}Fe Mossbauer spectroscopy 77—63328
- $PrCo_5$, heat treated, coercive force exam. 78—68298
- $PrCo_5$, uniaxial ferromag. cryst., irreversible rotation processes 80—39768
- Pr_2Co_7, mag. saturation and anisotropy, density, lattice parameters 77—85426
- $Pr(Co_{0.7}Cu_{0.3})_5$, anomalous magnetisation curves 80—15757
- $Pr(Co_{1-x}Cu_x)_5$, coercive force temp. depend. 79—82823
- $Pr(Co_{1-x}Cu_x)_5$, magnetocrystalline anisotropy exam. 78—39315
- $Pr(Co_{1-x}Cu_x)_5$, saturation magnetisation anisotropy 78—47960
- $Pr_2(Co_{1-x}Fe_x)_{17}$, hard direction magnetisation, 5-300K, and anisotropy field 77—12114
- $PrCu_5$, nuclear induced ferromagnetism 79—61069
- $PrCu_6$, nucl. mag. ordering, heat capacity and magnetisation obs. 79—87272
- $PrFe_2$, Curie temp., elec. quadrupole couplings, Mossbauer study 80—39949
- $PrFe_2$, high field Mossbauer study 80—75893
- $PrFe_2$, Laves phase, mag. props., Mossbauer spectra, crystalline field mag. anisotropy 80—65851
- $PrIr_2(Pt_2)(Rh_2)(Ru_2)$, hyperfine sp. ht. and magnetisation meas. at 4.2K 80—75775
- $Pr_{1-c}La_cAl_2$, mag. props. 79—65658
- PrP, nonstoichiometric, with singlet ground state, induced van Vleck ferromag. spin glass 77—66378
- Pr_3Se_4, induced ferromagnet, effect of press. on magnetisation 78—95422
- $Pr_3Se_4(S_4)$, induced ferromagnet, mag. props. under hydrostatic press. 80—60395
- PrSi, mag. struct. and mag. moments, neutron diffr. meas. 77—85424
- $Pr_xSm_{1-x}Co_5$, magnetisation and magnetocryst. anisotropy 78—68215
- Pr_3Tl, critical fluctuations temp. depend. 80—25160
- Pr_3Tl, exchange-coupled singlet-groundstate system, central model 77—77060
- Pr_3Tl, hyperfine interactions, sp. ht. and magnetisation meas. 79—28531
- Pr_3Tl, induced ferromag., mag. props. under hydrostatic press. 78—56315
- Pr_3Tl, microwave resist. meas., rel. to singlet ground state paramag. systems 77—20353
- Pr_3Tl, resistivity and sp. ht. near threshold 79—78399
- Pr_3Tl, singlet-ground state system, central mode, in ferromag. transition, neutron scatt. obs. 77—66317
- Pr_3Tl, thermal expansion and transverse elastic const. near mag. phase transition 80—60394
- Pr_3Tl, transition temp. and magnetisation 80—25161
- Pt-Co, magnetically hard, struct. and morphology, electron microscope study 79—82171
- Pt-Co alloys, crit. neutron scatt. in crit. conc. region for onset of ferromagnetism 78—72347
- Pt-Co system, low temp. susceptibility 80—65920
- Pt-Fe, competing interactions in FCC alloys 78—95453
- Pt-Fe, dil., breakdown of ferromag. order, magnetoresist. obs. 80—71046
- Pt-Fe alloy, low field AC susceptibility 79—73698
- Pt-Fe alloy, ordered, T-c phase diagram, antiferro- and ferromagnetism *(Russian)* 80—65871
- Pt-Fe ordered alloy, multiply mag. phase transitions 80—60264
- Pt-Fe(Co), dilute ferromagnets, press. effect on Curie temp. 80—65873
- Pt-Ni alloys, onset of ferromag. 79—56533
- Pt-Ni disordered alloy, Landau model for mag. props. 77—66276
- PtCr, AC susceptibility near percolation limit, ordered and disordered alloy 80—65900
- $Pt_{0.75}(Cr_{1-x}Mn_x)_{0.25}$, pseudobinary, magnon energy derivation 80—107996
- $Pt_{0.72}Fe_{0.28}$, isomer shift and effective mag. field at ^{57}Fe, press. depend. 77—16232

ferromagnetic properties of substances continued
$Pt_{50}Fe_{12.5}Co_{37.5}$, elec. resist., cond. electron scatt. and heterogeneities of spin system *(Russian)* 79−56189
Pt_3Mn, cryst. dynamics at 80K 79−23688
Pt_3Mn, mag. excitation dispersion relation 80−25090
Pt_3Mn, obs. of magnon sp. ht. 77−63217
$Pt_3Mn_xCr_{1-x}$ alloys, mag. props. 80−2562
PtMnSb, hyperfine mag. field at Cd impurity, TDPAC study 80−39906
PtMnSn(Sb), Cd impurities, hyperfine field meas. 78−15074
$Pt(NH_3)_4CuCl_4$, antisymmetric and anisotropic exchange, EPR linewidth 78−10761
$Pt_{0.7}Ni_{0.3}Fe$, magnetically hard, cryst. morphology and mag. domain struct. 77−69615
$Pt_{37.5}Pd_{12.5}Co_{50}$, elec. resist., cond. electron scatt. and heterogeneities of spin system *(Russian)* 79−56189
$Pt_{12.5}Pd_{37.5}Fe_{50}$, elec. resist., cond. electron scatt. and heterogeneities of spin system *(Russian)* 79−56189
$PuFe_2$, ferromag. mag. cross section, form factors, saturation magnetisation values, polarized neutron study 79−47245
$PuFe_2$, high temp. mag. props., 300 to 1100K 79−51757
PuP, electronic ground state, neutron diffr. 77−15789
PuP, ferromag. mag. cross section, form factors, saturation magnetisation values, polarized neutron study 79−47245
PuP, lattice distortions in ferromag. phase, X-ray obs. 80−15774
RFeAl, scatter order cpds., mag. props. 77−51891
rare earth-Tb-Fe alloys, $R_xTb_{1-x}Fe_2$, (R=Gd, Sm, Dy, He, Zr), props. of near magnetostrictive materials 77−51934
Rb_2CrCl_4, 2D-ferromag., renormalisation of long wavelength spin waves, neutron scatt. 80−60229
Rb_2CrCl_4, cryst. growth by Czochralski technique 77−28710
Rb_2CrCl_4, NMR of ^{53}Cr 78−10798
Rb_2CrCl_4, optical absorption intensity, short-range spin correlation 80−108185
Rb_2CrCl_4, planar ferromag., spin waves 80−65835
Rb_2CrCl_4, spin wave temp. depend. 79−4662
Rb_2CrCl_4, two-dimens. easy-plane ferromag., cryst. and mag. struct., temp. variation of moment 77−66255
Rb_2CrCl_4, zone centre magnon gap determ., exciton-magnon combination band meas. 79−61082
$Rb_2Cr_8O_{16}$, Hollandite type compound, synthesis, struct. and magnetic props. 79−11543
$Rb_2CuBr_4.2H_2O$, ferromag., static and dynamic mag. props. 80−50074
$Rb_2CuBr_4.2H_2O$, ferromag., hyperfine and exchange interactions, NMR study 80−50208
Rb_2CuCl_4, layered, mag. sp. ht., two-dimens. $S^1/_2$ Heisenberg ferromag. behaviour 77−32206
$Rb_2CuCl_4.2H_2O$, BCC Heisenberg ferromag., transferred hyperfine interactions of ^1H, ^1D and ^{17}O 77−69725
$Rb_2CuCl_4.2H_2O$, Bloch-wall NMR, anisotropic hyperfine interaction 79−51864
$Rb_2CuCl_4.2H_2O$, ferromag., hyperfine and exchange interactions, NMR study 80−50208
$Rb_2CuCl_4.2H_2O$, NMR spectra, second-order effects of mag. hyperfine interaction, pseudoquadrupole interaction 79−78540
$Rb_2CuX_4.2H_2O$, (X=Cl, Br), fine struct. due to indirect coupling of nuclear spins 79−78541
$RbFeCl_3$, linear chain ferromag., optical absorpt. and dichroism in mag. field 77−77237
$RbFeCl_3$, linear chain cryst., quadrupole and mag. reson., rel. to $CsFeCl_3$ 79−38403
$RbFeCl_3$, one-dimens. ferromagnet, lowest excitation, far IR study 80−66186
$RbFeCl_3$, pseudo-one-dimens. singlet ground state ferromag., mag. excitations, neutron scatt. study 80−97064
$RbFeCl_3$, singlet ground state 1-D ferromag., far IR Zeeman spectra 77−52098
$RbFeCl_3$, singlet ground state one-dimens. ferromag., 2-magnon excitation, far IR spectra obs. 77−69831
Rh based ferromag. Heusler alloys, peaks in low field AC susceptibility 80−50071
Rh-Fe, competing interactions in FCC alloys 78−95453
Rh-Ni alloy, onset of ferromag. 79−56533
Rh_2CoSn, crit. exponent of ^{119}Sn hyperfine field, Mossbauer obs. 78−92008
Rh_2CoSn, ferromag., mag. hyperfine fields of ^{119}Sn, Mossbauer meas. 78−10816
Rh_2CoSn, ferromag. Heusler alloys, hyperfine fields, spin echo meas. 77−63314
Rh_2CoSn, Heusler alloy, Sn hyperfine field, Mossbauer exam. 77−43920
Rh_2CoSn, hyperfine mag. fields at ^{119}Sn, under press., Mossbauer expts. 79−99812
Rh_2CoSn, metallic ferromagnet, hyperfine mag. field temp. depend. *(Russian)* 78−80265
Rh_2FeSn, ferromag., mag. hyperfine fields of ^{119}Sn, Mossbauer meas. 78−10816
Rh_2FeSn, ferromag. Heusler alloy, hyperfine fields, spin echo meas. 77−63314
Rh_2FeSn, Heusler alloy, Sn and Fe hyperfine field, Mossbauer exam. 77−43920
Rh_2FeSn, hyperfine mag. fields at ^{119}Sn and ^{57}Fe, under press., Mossbauer expts. 79−99812
Rh_2FeSn, metallic ferromagnet, hyperfine mag. field temp. depend. *(Russian)* 78−80265
Rh_2MnGe, ferromag. Heusler alloy, hyperfine mag. field meas. by TDPAC technique 79−78580
Rh_2MnPb, hyperfine fields, ferromag., NMR and Mossbauer effect studies 80−71259
Rh_2MnSb, hyperfine fields, ferromag., NMR and Mossbauer effect studies 80−71259
Rh_2MnSn, and related cpds., with Heusler and Heusler-related struct., mag. props. 77−8311
Rh_2MnSn, ferromag., mag. hyperfine fields, time differential PAC meas. 77−81040
Rh_2MnSn, ferromag. Heusler alloy, hyperfine fields, spin echo meas. 77−63314
Rh_2MnSn, ferromag. Heusler alloy, hyperfine mag. field meas. by TDPAC technique 79−78580
Rh_2MnSn, Heusler alloy, Sn hyperfine field, Mossbauer exam. 77−43920
Rh_2MnSn, mag. hyperfine fields at Rh and Sn sites, and their temp. depend. 78−43708

ferromagnetic properties of substances continued
Rh_2MnSn, Rh_2NiSn, Heusler alloys, hyperfine mag. field at Sn 78−39482
Rh_2MnX, (X=Al, Ga, In, Tl, Sn, Pb, Sb), Heusler and Heusler-related cpds., mag. and cryst. props. 77−20568
Ru based ferromag. Heusler alloys, peaks in low field AC susceptibility 80−50071
Ru ternary and quaternary oxides, prep., cryst. struct. and mag. props. 79−14771
Ru_2FeSn, ferromag. Heusler alloys, hyperfine fields at nonmagnetic atoms in various sites, Mossbauer effect and NMR meas. 80−66089
Ru_2FeSn, hyperfine mag. field, Mossbauer spectra 80−15865
Sc-Gd, dil., reverse resist. anomaly and negative magnetoresist. 80−84459
Sc_3In, itinerant electron ferromagnet, spin fluctuations 77−73096
Sc_3In, itinerant electron ferromag., NMR and relax. 78−6586
Sc_3In, itinerant electron ferromag., low temp. sp. ht., mag. field depend. 79−42765
$(Sc_xLu_{1-x})_2V_2O_7$ 80−29547
Si, amorphised by ion implantation, EPR obs. of mag. ordering 79−24186
Si, ferromagnetism induced by ion irrad., e.p.r. investig. *(Russian)* 77−1595
Si-Fe, domain and grain obs. using ferromag. colloid technique 80−11219
Si-Fe, ferromagnetic domains and their junctions, simulation of X-ray topographs 79−78434
Si-Fe, freq. spectrum of Barkhausen noise of moving 180° domain wall 77−16115
Si_xFe_{100-x} polycryst. ribbon, prep. by rapid quenching, and props. 80−75803
Sm,$(Co,M)_{17}$, (M=Fe, Mn, Cr), exchange and crystal field parameters, anisotropy meas. 77−69535
Sm intermetallics temp. depend. of Sm^{3+} magnetisation, exchange and cryst. field effects 77−8302
Sm-Al(Fe)(Co)(Pt), hyperfine field exam. by NMR spin echo 78−23365
Sm-Co, alloy powders and sintered magnets, effect of chem. treatment on mag. props. 78−60311
Sm-Co, amorphous, plasma-sprayed, role of Ar or H_2 atm. in mag. props. and crystn., rel. to H_2 storage 80−64898
Sm-Co, decomp. kinetics when aged, X-ray mag. props. and metallography study *(Russian)* 78−56644
Sm-Co base ternary alloy, mag. props. and cryst. struct. 77−8352
Sm-Co-Cu, with Sm_2Co_{17} struct., aged, TEM high coercivity material, TEM obs. of microstruct. 77−77073
Sm-Co-Cu-Fe, single phase 2-17 sample, hard mag. props. 77−8349
Sm-Co-Cu-Fe-Te magnets, comp. and sintering effects on coercivity 79−15326
Sm-Co-Cu-Fe-Zr alloy, reversible changes in coercive force and struct. state during heat treatment 400-800°C *(Russian)* 80−29574
Sm-Co-Cu-Fe-Zr magnet, production and mag. props. 77−40085
Sm-Hf-Co alloy, rare-earth electron transfer 77−40028
Sm-Pr-Co, added Fe_2Sn, permanent magnets, demagnetisation curves, X-ray obs. 78−91900
Sm-Pr-Co alloys, mag. props. and struct., comp. depend. *(Russian)* 80−20430
$SmAl_2$, hyperfine fields, ferromagnetic coupling between rare earth spins, NMR study 80−39880
$SmCO_5$ based permanent magnets, props. and cryst. orientation *(Russian)* 80−20431
$SmCO_5$, etched microparticles, Barkhausen discontinuity, nucleation, and domain wall pinning 79−87288
$SmCO_5$ magnets, sintering time effect on props. 79−95977
$Sm_2(Co, Cu, Fe, M)_{17}$, M=Nb, V, Ta, Zr, effect of M on mag. props. 77−89978
Sm(Co, Cu) alloys, coercivity mech. 80−44862
$Sm(Co,Cu)_5$, eutectoid transform. 77−8799
$Sm(Co,Cu)_z$, precip.-hardened, mag. and metallographic props. 77−8339
$SmCo_5$, amorphous, supermag.-ferromag. transition and directional crystallisation 80−65891
$SmCo_5$, and related alloys, nucleation and pinning at 360° domain walls 77−73042
$SmCo_5$, and $SmCo_{3.5}Cu_{1.5}$, anisotropy and coercivity, Kerr effect, magnetisation and aftereffect expts. 77−8300
$SmCo_5$ based permanent magnets with low reversible temp. coeff. 79−51814
$SmCo_5$ based solid soln., X-ray diffr. obs. of decomp. *(Russian)* 77−81264
$SmCo_5$ based ternary and quaternary permanent mag. materials with low reversible temp. coeffs. 79−82822
$SmCo_5$, Bloch wall energy determ. *(German)* 78−19271
$SmCo_5$, Cu-modified, magnetisation reversal mechanism 77−8350
$SmCo_5$, domain wall nucleation sites and magnetization reversal 79−56563
$SmCo_5$, exchange and cryst. field effects 80−24857
$SmCo_5$ films, struct. transformations effect on coercive force and mag. reversal *(Russian)* 80−20436
$SmCo_5$, heat treated, coercive force exam. 78−68298
$SmCo_5$, high coercivity isotropic plasma-sprayed magnet, eutectoid decomp. 80−68568
$SmCo_5$ hydride films, mag. props. 78−68306
$SmCo_5$, improvement of mag. domain contrast in SE-mode of SEM *(German)* 77−51920
$SmCo_5$, intrinsic coercivity losses, temp. depend. 78−95468
$SmCo_5$, intrinsic magnetic props. 79−82779
$SmCo_5$ isotropic plasma sprayed magnet, high coercivity 78−68295
$SmCo_5$, isotropic plasma-sprayed high coercivity magnet, eutectoid decomp. 80−75810
$SmCo_5$, mag. properties in low temp. range, obs. *(Russian)* 77−73050
$SmCo_5$, mag. props., effect of phase and struct. transforms. during liq.-phase sintering 79−100086
$SmCo_5$, magnetic aftereffect of H and D 79−56573
$SmCo_5$, magnetic anisotropy, Co contrib., ^{59}Co NMR Obs. 78−43583
$SmCo_5$ magnets, ageing at high temp. 80−7129
$SmCo_5$ magnets, effect of heat treatment on coercive force *(Russian)* 79−1684
$SmCo_5$ magnets, magnetisation and demagnetisation, heating effects 79−38357
$SmCo_5$ material for accelerator permanent magnets 79−6776
$SmCo_5$, nucleation of reversed domains at Co_7Sm_2 precips. 80−75791

ferromagnetic properties of substances continued

- $SmCo_5$ permanent magnet, liq. phase sintered, hysteresis loops, ageing, temp. depend. *(Chinese)* 77−51921
- $SmCo_5$, permanent magnet stability, during long-term ageing *(Chinese)* 80−55428
- $SmCo_5$, polished, domain wall grooving, optical microscopy and SEM obs. 77−8334
- $SmCo_5$, powder, comminution temp. effect on mag. props. 80−39819
- $SmCo_5$, powder, exam. of protective preps. of organic media against oxidation 79−96220
- $SmCo_5$, powder prod. by electroerosion mag. props. 77−59718
- $SmCo_5$, radial pulse magnetisation, magnetising and testing fixtures 77−8354
- $SmCo_5$, remanence and energy product, X-ray method of planar orientation 77−8342
- $SmCo_5$, single cryst., grown-in dislocations and stacking faults, TEM investigation 79−19253
- $SmCo_5$, single cryst. and liq. phase sintered, magnetostriction, field depend. 77−63245
- $SmCo_5$ single crystals subjected to shock waves, magnetisation, creation of high-coercivity state *(Russian)* 77−66384
- $SmCo_5$, single crysts., mag. props. study and role of anisotropy *(French)* 79−38356
- $SmCo_5$, single-cryst. and liq. phase sintered, elastic stiffness consts., US velocity obs. 77−73066
- $SmCo_5$, sintered, hard mag. material, magnetisation behaviour 80−75805
- $SmCo_5$, sintered, high coercivity, microstruct. and mag. props. 77−69629
- $SmCo_5$, sintered, mag. after-effect, expt. and model 80−75816
- $SmCo_5$, sintered, mag. props. *(German)* 77−43852
- $SmCo_5$, sintered, magnetic reversal processes *(German)* 77−32216
- $SmCo_5$, sintered, orientation of particle easy axes, statistical model 77−8305
- $SmCo_5$ sintered alloy magnetic properties *(Russian)* 78−72369
- $SmCo_5$, sintered alloy permanent magnets, temp. depend. of domain struct. *(Russian)* 77−66380
- $SmCo_5$ sintered magnets, periodic struct. and coercive force *(Russian)* 79−28554
- $SmCo_5$ sintered magnets, struct. and magnetic characts., sintering temp. influence *(Russian)* 79−52397
- $SmCo_5$, sintered permanent magnet, mag. props., 4.2-300K, fields up to 100 kOe 77−8341
- $SmCo_5$, sintered permanent magnet manufacture 80−20838
- $SmCo_5$, specific heat and kinetic props. at elevated temp. *(Russian)* 79−28530
- $SmCo_5$, spin polarised energy band struct., APW calc. 78−10342
- $SmCo_5$, sprayed magnet, microstruct. and mag. props. between 650°c and 800°C 79−82829
- $SmCo_5$, substituted alloy, low reversible temp. coeff. 78−68178
- $SmCo_5$, temp. depend. of Sm^{3+} magnetisation, exchange and cryst. field effects 77−8302
- $SmCo_5$, temp. depend. of Sm mag. form factor, polarized neutron expts. 79−78329
- $SmCo_5$ thin film, hydride form., kinetics, mag. monitoring 80−35571
- $SmCo_{5+x}$, Cu and Fe modified, coercive force, demagnetization curves *(Czech)* 79−42805
- Sm_2Co_{17}, coercive force depend. on annealing temp. 80−65964
- Sm_2Co_7 sintered magnets, coercive force and constitution, annealing temp. depend. *(Russian)* 80−88786
- Sm_xCo_y, mag. and struct. investigations of intermetallic systems 78−95440
- Sm_xCo_y, mag. props. 78−43568
- $Sm_2(Co_{1-x}Al_x)_{17}$ *(Russian)* 78−64202
- $SmCo_3B_2$, high coercive forces, ferromag. ordering and saturation moments 77−24711
- $Sm(Co_{0.65}Cu_{0.35})_{5.6}$, cryst. struct. and coercive force, heat treatment effects *(Russian)* 80−44170
- $Sm(Co_{0.84}Cu_{0.16})_{6.9}$, microstruct. and domain struct., mag. reversal *(Russian)* 80−20429
- $Sm(Co_{0.87}Cu_{0.13})_{7.8}$, coercivity and microstruct. 79−56569
- $Sm(Co_{1-x}Cu_x)_{7.8}$ alloys, coercive fields, domain wall energies, mag. and metallographic exam. 78−91897
- $SmCo_{3.5}Cu_{1.5}$, mag. aftereffects, coercive mechanism, magnetisation reversal 77−69634
- $SmCo_{3.5}Cu_{1.5}$, single cryst., domain wall motion and domain form. 78−39359
- $SmCo_{3.5}Cu_{1.5}$, single crysts., mag. props. study and role of anisotropy *(French)* 79−38356
- $SmCo_{3.5}Cu_{1.5}$, time dependent magnetisation 78−80176
- $SmCo_4Cu$, domain boundaries shift, mag. reversal processes 79−87286
- $SmCo_4Cu$, nonuniform comp., domain struct. and mag. reversals process *(Russian)* 79−1681
- $SmCo_{4.3}Cu_{0.7}$, highly anisotropic ferromag., mag. state after large Barkhausen jump *(Russian)* 79−4699
- $SmCo_{5-x}Cu_x$, giant intrinsic mag. hardness obs. 77−59432
- $SmCo_{5-x}Cu_x$, giant intrinsic mag. hardness 79−91255
- $SmCo_{5-x}Cu_x$ magnet alloy, metallurgical study *(Korean)* 77−8853
- $SmCo_{5-y}Cu_y$, giant intrinsic magnetic hardness, high field meas. 78−68289
- $Sm(Co_{0.86-x}Cu_{0.14}Fe_x)_7$, permanent magnet, sintering and heat treatment effects 80−39817
- $Sm_2(Co_{1-x}Fe_x)_{17}$, anisotropy consts., conc. and temp. depend. *(Russian)* 78−64202
- $Sm_2(Co_{1-x}Fe_x)_{17}$, magnetocryst. anisotropy, Tb, Mn or Cr substituent effects 77−8297
- $Sm(Co_{0.85}Fe_{0.05}Cu_{0.10})_z$, coercive force meas. 77−4530
- $Sm(CoFeCuMn)_7$, coercive force and anisotropy temp. depend. 78−68297
- $Sm_2(Co_{1-x}M_x)_{17}$, bulk magnetisation and magnetocryst. anisotropy, interpretation 77−40055
- $Sm_2(Co_{1-x}M_x)_{17}$, magnetocryst. anisotropy 77−40054
- $Sm_2Co_{17-x}M_x$, M=Cr, Ni, effect of substitution on mag. props. 79−78363
- $SmCo_2Ni_3$-Y(Pr)(Gd)(Tb)(Er), giant intrinsic magnetic hardness 78−56347
- $SmCo_{2.5}Ni_{2.5}$, mag. after effect *(Russian)* 78−6544
- $SmCc_{5-x}Ni_x$, giant intrinsic mag. hardness, temp. and time depend. 77−69627
- $SmCo_{5-x}Ni_x$, giant intrinsic magnetic hardness, high field meas. 78−68289
- $SmCo_{5-x}Ni_x$, giant intrinsic magnetic hardness analysis 78−88146

ferromagnetic properties of substances continued

- $SmCo_{5c}Ni_{5-5C}$, exchange fluctuations and giant intrinsic mag. hardness 78−56310
- $Sm_2Cu_{1.6}Zr_{0.16}Fe_{3.3}Co_{12}$, enhancement of mag. props. 79−82825
- $SmFe_2$, ferromagnetic-ferrimag. cpds., mean field exchange consts., Stoner itinerant model calcs. 80−50084
- $SmFe_2$ powders, mag. and hysteresis props. *(Russian)* 79−42800
- $SmFe_3$ and Sm_6Fe_{23}, magnetostriction, room temp. to 80K 80−65993
- $SmFe_2(Co_2)(Ni_2)$, hyperfine interactions and exchange fields acting on Eu^{3+}, Mossbauer obs. 77−63338
- $Sm_{1-x}Gd_xAl_2$, hyperfine fields, ferromagnetic coupling between rare earth spins, NMR study 80−39880
- $Sm_{2-x}Gd_xCo_{17-y}Mn_y$, saturation magnetisation and anisotropy field temp. depend., suitability for microwave/millimetre wave TWT 79−82824
- Sm_2M_{17}, sintered magnet, hard mag. props. optimisation 77−8340
- $Sm_{1-x}Nd_xCo_5$ alloys, magnetisation, magnetocrystalline anisotropy, 4.2 to 280K 78−91863
- $Sm_xNd_{1-x}Co_5$ powders, mag. props. *(Russian)* 79−51812
- $SmNi_{5-x}Cu_x$, giant intrinsic mag. hardness due to randomised cryst. field interactions 78−68208
- $SmNi_4M$, M=Fe, Cu, Al, intrinsic mag. hardness 77−85506
- $Sm_{0.5}Pr_{0.5}Co_5$, sintered alloy permanent magnets, temp. depend. of domain struct. *(Russian)* 77−66380
- $Sm_{0.5}Pr_{0.5}Co_5$ sintered magnets, periodic struct. and coercive force *(Russian)* 79−28554
- $Sm_{1-x}Pr_xCo_5$ single crystals, magnetocryst. anisotropy and stepwise mag. reversals *(Russian)* 77−66291
- SmS, physical and physicochem. props., review 80−96875
- SmZn, ferromag., cond. band antiparallel polarisation exceeding 4f moment 80−60207
- $SnCo_5$, magnetisation and cohesive strength 77−55688
- $Sn_{1-x}Mn_xTe$, $0.02<x<0.08$, transport and magnetic properties, low magnetic field 79−99569
- $Sn_{1-x}Mn_xTe$, electronic struct., transport props., mag. ordering effects 80−65441
- $Sn_{1-x}Mn_xTe$, IR reflectivity, elec. susceptibility mag. order effects 79−47433
- $Sn_{1-x}Mn_xTe$, magnetic behaviour of Mn 78−14938
- SnTe:Mn, ferromag.-ordering, transverse magnetoresist. and Hall effect meas. 77−85240
- $SrCoO_{2.70}$, growth and props. 78−48310
- $SrCoO_3$:Fe^{4+}, sign of Fe^{4+} hyperfine field, spin struct., Mossbauer study 80−39933
- $SrCoO_{3-\delta}$.$(0<\delta<0.5)$, ferromag., metallic elec. props. 80−70668
- $SrCoO_{3-\delta}$, crystal struct. and mag. props., O vacancy effect 79−95587
- $SrCoO_{3-x}$, mag. and neutron diffr. study 80−65805
- $Sr_{0.3}La_{0.7}MnO_3$, neutron-irrad. induced phase transition 77−89952
- $SrRuO_3$, mag. props., mag. torque meas. 78−23295
- $SrRuO_3$ single cryst., reduced ferromag. moment obs. 77−20564
- $SrRuO_3$ single cryst., magnetocryst. anisotropy and reduced ferromag. moment 77−24691
- steel, Cr-Ni, ferrite precip. *(Japanese)* 80−35187
- TaS_2 intercalation complexes with 3d transition metals, mag. and metallic transport props. 80−44814
- $(Tb,Dy)Fe_2$ alloys, giant magnetostriction *(Chinese)* 79−51830
- Tb, basal plane mag. anisotropy energy meas. at low temps. 77−63166
- Tb, conduction electron polarisation and high field magnetisation 78−72332
- Tb, critical magnetic studies 80−15745
- Tb, elastic constants, magnetoelastic contrib. 80−15777
- Tb, elastic modulus in mag. field, US meas. using CdS transducer 77−11151
- Tb, electron-magnon interaction and elec. resist., 1.5 to 50K 79−60790
- Tb, ferromag. domains obs. by cryogenic X-ray topography 77−39507
- Tb, ferromagnet, field depend. of elastic const. c_{66} 80−15181
- Tb, ferromagnetic domain structures down to 95K 80−71080
- Tb film, GHz magnetoelastic wave excitation, field depend. 78−52334
- Tb, high-precision elec. resist. meas., 1-4K 77−15817
- Tb, mag. characts. in strong mag. field 77−89936
- Tb, mag. dipole and elec. quadrupole hyperfine fields, NMR obs. 80−34791
- Tb, mag. domains, Lorentz microscopy obs. 78−84448
- Tb, magnetic phase diagram, US meas. of elastic const. 80−15721
- Tb, magnetisation, AC susceptibility and microwave absorption meas. 80−60221
- Tb, magnetisation in basal plane, calc. 80−70969
- Tb, magnetocaloric effect in high magnetic fields 80−25140
- Tb, magnon lifetimes at 4.2K 80−15710
- Tb, neutron elastic scattering, high-angle, anal. 80−80480
- Tb, single cryst., transverse magnetoresist. 77−66154
- Tb, small particles, disappearance of mag. order., mag. susceptibility and magnetisation meas. 77−16117
- Tb, sp. ht., using lattice dynamical model for HCP metals 79−51273
- Tb, spin wave exam. 78−56306
- Tb, spin wave resist., 1.5-50K 79−60813
- Tb/Mo, point contact spectroscopy of magnons 79−38312
- Tb-Fe, amorphous, random anisotropy effects 78−68223
- Tb-Fe, amorphous magnetism in bulk samples 77−66278
- Tb-Fe alloy film, amorphous, contact printing 77−73061
- Tb-Fe amorphous magnetic films, domain wall obs. by Lorentz electron microscopy 77−80979
- Tb-Gd, elec. resistivity and thermopower critical behaviour 80−15499
- Tb-Gd, spontaneous striction and phonon contributions to thermal expansion *(Russian)* 79−90800
- Tb-Gd alloy, single cryst., mag., magnetoelastic and elec. props. *(Russian)* 78−2677
- Tb-Gd alloy, spin orientation transition obs. 79−99714
- Tb-Gd alloys, ferromag. monocrystalline, crit. behaviour of elec. resist. 77−62886
- Tb-Ho, thermal expansion in vicinity of Curie temp. 79−28524
- Tb-Ho, US attenuation and elastic consts. in 3 mag. phases, 4.2 to 300K 77−72645
- Tb-Sc(Y)(La)(Lu)(Yb)(Mg)(Th), mag. ordering temps., susceptibility meas. 80−25136
- Tb-Sn, effective field at diamag. Sn impurities, 4.2 to 235K *(Russian)* 77−69549
- Tb-Y, Fermi surface topology var., mag. and elec. props. *(Russian)* 77−80723
- Tb-Y, helicoid antiferromag. ferromag. transition, magnetostriction and magnetocaloric effect *(Russian)* 77−80937
- Tb-Y, magnetostriction, mag. and elec. props. 78−27068

ferromagnetic properties of substances continued
Tb-Y-Zn, magnetic props. conc. and temp. depend. *(Russian)* 77—47989
Tb-Y(Gd), mag. anisotropy, contrib. from single-ion cryst. anisotropy and anisotropic exchange *(Russian)* 80—29546
Tb-Y(Gd), mag. ordering temp. and indirect exchange integrals *(Russian)* 79—95590
$Tb_{52}Ag_{48}$, amorphous, bulk magnetic props., evidence of strong local anisotropy 77—43830
$TbAl_2$, extraordinary Hall effect 80—39560
$TbAl_2$, hyperfine field exam. by NMR spin echo 78—23365
$TbAl_2$, origin of magnetostriction 79—78499
$TbAsO_4$, ferromag., static and AC susceptibility meas. 80—29533
TbAu, amorphous, magnetisation characts., 5 to 300K, hysteresis cycle *(French)* 77—80965
TbB_2, mag. props. and neutron diffr. 78—84401
TbB_2, mag. struct., ferromag. ordering, neutron diffr. study 80—15692
TbB_4, ferromag. ordering, neutron scatt. meas. 78—10655
$TbCo_2$, magnetocryst. anisotropy props. by ^{57}Fe Mossbauer spectroscopy 77—63328
$TbCo_2$, rhombohedral distortion at low temp. 80—34743
$TbCo_2$, spontaneous distortion, mag. props. due to cryst. field, exchange field, magnetoelastic energy 79—61096
$TbCo_5$, mag. state of Tb sublattice neutron diffr. meas. *(Russian)* 77—80915
$TbCo_{5.1}$, singularities of mag. transition *(Russian)* 77—77053
$TbCo_{5.1}$, sublattice magnetisation, temp. depend., neutron diffr. anal. *(Russian)* 80—103815
Tb_2Co_{17}, magnetisation, magnetocryst. anisotropy and magnetostriction 77—8303
$TbCo_2Si_2$, mag. props. 80—107988
$TbCrO_4$, mag. susceptibility and magnetis. meas., 1.7-1000K, Curie pt. positron 77—66266
$Tb_{0.26}Dy_{0.74}Fe_2$, temp. depend. of magnetomechanical coupling factor 77—90002
$Tb_{0.27}Dy_{0.13}Fe_{1.98}$, grain-oriented, permeability, magnetomechanical coupling and magnetostriction 79—78491
$Tb_{0.27}Dy_{0.73}Fe_2$, anomalous thermal expansion and magnetostriction 77—90003
$Tb_{0.27}Dy_{0.73}Fe_2$, magnetisation and magnetic anisotropy 78—91862
$(Tb_{0.27}Dy_{0.73})Fe_2$, magnetisation, ferromag. domains 80—25162
$Tb_{0.27}Dy_{0.73}Fe_2$, perpendicular suscept., magnetomechanical coupling and shear modulus 78—91918
$Tb_{0.27}Dy_{0.73}Fe_2$, vertically zoned, magnetomechanical coupling and magnetostriction 80—65999
$Tb_{0.3}Dy_{0.7}Fe_2$, elastic vs. magnetoelastic anisotropy 78—68347
$Tb_{0.3}Dy_{0.7}Fe_2$, magnetoelastic coupling meas. by US method 77—69652
$Tb_{0.3}Dy_{0.7}Fe_2$, magnetostrictive, resonant coupling of shear waves 79—33517
$Tb_{0.3}Dy_{0.7}Fe_2$, prep. by powder metallurgy, magnetostrictive props. 80—75826
$Tb_{0.3}Dy_{0.7}Fe_2$, sound velocity mag. field and temp. depend. elastic moduli calcs. 80—39839
$Tb_xDy_{1-x}Fe_2$, Laves phase alloy, magnetostriction depend. on powder orientation before sintering 78—76284
$Tb_{0.20}Dy_{0.22}Ho_{0.58}Fe_{1.95}$, grain-oriented, permeability, magnetomechanical coupling and magnetostriction 79—78491
$Tb_xDy_yHo_zFe_2$, temp. depend. of magnetomechanical coupling factor 77—90002
TbF_3, mag. phase diagram, crit. and tricrit. behaviour 78—14959
TbF_3, transferred hyperfine interaction, NMR study 78—68393
$TbFe_2$, amorphous, Mossbauer spectra *(French)* 80—25261
$TbFe_2$, amorphous, temp. depend. of mag. hystersis props. 79—61186
$TbFe_2$, high field magnetostriction and magnetisation 78—84471
$TbFe_2$, magnetisation, ferromag. domains 80—25162
$TbFe_2$, magnetisation and magnetic anisotropy 78—91862
$TbFe_2$, magnetoelastic props., magnetostriction hysteresis *(Russian)* 80—29590
$TbFe_2$ monocrystalline (111), under elastic compressive stresses, domain structure *(Russian)* 79—91247
$TbFe_2$ powders, mag. and hysteresis props. *(Russian)* 79—42800
$TbFe_3$ and Tb_6Fe_{23}, magnetostriction, room temp. to 80K 80—65993
$TbFe_4Al_8$, commensurate-incommensurate modulated mag. struct., neutron diffr. obs. 79—95576
$TbFe_4Al_8$, neutron diffr. exam., mag. struct. 78—10656
$TbFeO_3$, mag. susceptibility, temp. depend., effective field at Tb ion sites 80—75742
$TbFeO_3$, magnetisation exam. 77—24681
TbG_3, uniaxial ferromagnet, logarthmic corrections to crit. behaviour 78—60294
Tb_xGd_{1-x}, orientation phase transitions near Curie pt., magnetization and magnetocaloric effect meas. *(Russian)* 79—87261
$Tb_xGd_{1-x}Al_2$, magnetic anisotropy, magnetostriction 78—56364
$Tb_{0.5}Ho_{0.5}$, ferromag. and helical phase, spin wave dispersion relations 79—24149
$(Tb_cLa_{1-c})Be_{13}$, mag. struct., cryst. field effects, neutron diffr. study 80—65789
TbMg, mag. struct. and mag. props. 77—8275
$TbMg_3$, mag. props., Mg conc. depend. 78—84392
$Tb_{1.2}Mo_6S_8$, long-range mag. order and supercond., neutron diffr. obs. 79—78320
$TbNi_5$, ferromag., magnetisation and paramag. susceptibility 80—25082
$Tb(OH)_3$, dynamical effects of interaction between 4f electrons and optical phonons 80—108196
$Tb(OH)_3:Er^{3+}$, ferromag., anisotropic exchange effects in optical spectra 78—80141
$TbPt_5$, low temp. mag. susceptibility 80—93075
TbSc, basal plane magnetocrystalline anisotropy and ferromag. ordering 79—1667
$Tb_2(WO_4)_3$, mag. props., 300 to 900K 79—28510
$Tb_{0.76}Y_{0.24}$, spin waves rel. to cond. electron susceptibility 78—68195
$(Tb_{1-x}Y_x)_3Co$, mag. props. and transitions, conc. depend. *(Russian)* 78—10671
TbZn, ferromag., elec. resist., just below crit. temp., effect of mag.-domains 80—39557
TbZn, ferromag., thermoelec. power, temp. depend. and crit. behaviour 80—96852
TbZn, ferromag. transition, transport coeffs. critical behaviour 80—15498
TbZn, mag. excitations meas. 80—70979
Th-Mn alloy, mag. props. and effect of H_2 absorpt. 78—19250

ferromagnetic properties of substances continued
$ThCo_5$ itinerant electron metamagnetism, polarised neutron study 80—39742
$ThCo_5$, lattice consts., magnetisation, and anisotropy fields 79—78364
$ThCo_5$, mag. transition due to Co moment change, metamagnetism of 3d-band 77—63184
$ThCo_{5-x}Mn_x$, struct. and magnetisation exam., temp. depend. 78—2662
$ThFe_3$, H_2 absorption effect on mag. props. and struct. 77—40045
$Th_{1-x}Fe_x$ amorphous alloys, mag. props. and Mossbauer spectra 79—91326
Th_7Fe_3, H induced change from supercond. to mag. ordered state 79—28525
$Th_6Mn_{23}H_x$, H induced mag. ordering obs. 77—85423
$ThNi_{5-x}Mn_x$, struct. and magnetisation exam., temp. depend. 78—2662
$Th_{1-x}Y_xCo_{5-y}Fe_y$, lattice consts., magnetisation, and anisotropy fields 79—78364
Ti-Permalloy films, interdiffusion, Auger anal. and X-ray diffr. obs., degradation of mag. props. 80—34251
Ti-Permalloy thin film diffusion couples, low temp. interdiffusion interdiffusion 78—71889
$TiBe_{2-x}Cu_x$, C-15 lower phase, itinerant ferromagnetism 80—15723
$TiBe_{2-x}Cu_x$, high press. study of Curie temp. and mag. susceptibility 80—84600
Ti(Fe, Co), itinerant ferromagnet, magneto-volume expts. 77—66404
Ti(Fe, Co), off-stoichiometric alloy, inverse mag. susceptibility rel. to defect conc. 80—60216
$TiFe_{1-x}Co_x$, electronic struct. and mag. moment calcs. 80—65821
$TiFe_{1-x}Co_x$, mag. props., under high press. and in high mag. fields 78—95423
TiN-CrN systems, solid solns., mag. props. 77—12086
TiO_2-P_2O_5 glasses, reduced, mag. susceptibility, 1 to 400K, mag. exchange between Ti^{3+} ions 79—73691
$(Ti_{1-x}V_x)_2O_3$, spin-glass props., 0.05-300K 80—25149
$Tl_2Cr_2O_7$, $Tl_2Mn_2O_7$, pyrochlore type, synthesis and physical props. 80—33963
Tm ferrogarnet film, cylindrical mag. domain motions, domain boundary oscills. *(Russian)* 80—71140
Tm, magnetisation, uniaxial anisotropy, mean field model 78—2660
$TmAl_2$, ferromagnetic structs., elastic neutron scatt. obs. 80—50055
Tm_2Co_{17}, single cryst., magnetostriction const. temp. depend., 78 to 300K 79—51836
$TmFe_2$, magnetisation and magnetic anisotropy 78—91862
$TmFe_3$ and Tm_6Fe_{23}, magnetostriction, room temp. to 80K 80—65993
$Tm_2Fe_{17-x}Co_x$, and related cpds., easy magnetisation direction, Mossbauer spectra 77—63169
$TmRh_4B_4$, mag. and supercond. props., mag. susceptibility and sp. ht. meas. 79—78344
TmSe, mixed valence cpd., thermal, mag., and transport props. 79—61074
TmSe, mixed valence state, ferromag. alignment 80—20133
$Tm_xSe_yTe_{1-y}$, magnetic ordering studies *(German)* 80—54882
$Tm_2V_2O_7$, pyrochlore struct., mag. props. 78—72335
$Tm_2(WO_4)_3$, mag. props., 300 to 900K 79—28510
TmZn, magnetic-ion-lattice interactions, cryst. elec. field 77—4540
U sesquichalcogenides, mag. props. temp. depend. 77—8287
U-Ga system cpds., elec. resist. paramag. susceptibility, magnetis., temp. depend., mag. struct. 77—20559
UAL_2, band magnetism due to f-electrons, T_{sf} 77—73039
UAl_2, high field, high press. mag. props. 80—11172
UAl_2, inelastic neutron scatt. 80—11165
UAl_2, transport props., susceptibility and sp. ht. 80—11174
UAs, magnetic struct. in high mag. fields, neutron diffr. study 80—34597
U_3As_4 (110), (211) single crystal, Bitter figure obs. 79—65693
U_3As_4, elec. resist. in vicinity of Curie point, influence of mag. field 77—69314
U_3As_4, ferromag., mag. field induced phase transitions 80—65887
U_3As_4, ferromagnetic transitions and heat capacities from 5 to 950K 78—14955
U_3As_4, heat capacity, 5-300K, ferromag. transition obs. 80—88769
U_3As_4, high-field magnetisation, field-induced phase transition near hard (100) directions 77—28413
U_3As_4, high-field suscept. at He temp. 77—89935
U_3As_4, mag. anisotropy, magnetisation meas. 80—50085
U_3As_4, magnetisation in strong fields, 4.2 to 200K anisotropy and exchange forces 80—54886
U_3As_4, rhombohedral distortion of low temp. 77—7828
$U_3As_4(Bi_4)(P_4)(Sb_4)(Se_4)(Te_4)$, symmetry changes in mag. phase transitions 77—20597
UAsSe, strongly anisotropic ferromag., negative magnetoresist. meas., 77-135K 77—89774
UAs_xSe_{1-x}, lattice distortion below Curie temp. 77—63252
UAsTe, crit. behaviour, Ising-like props. 78—43605
$UCo_{5.3}$, mag. props., cryst. and domain struct. *(Russian)* 77—4529
$U(Co_{1-x}Fe_x)_2$, ferromag. onset, susceptibility and resist. meas. 80—70967
β-UD_3, electronic props., metallic character 80—6693
UFe_2, giant magnetoelastic deform. of cryst. struct. mag. props. *(Russian)* 80—93159
UFe_2, mag. anisotropy of single crysts. 79—56527
UFe_2, magnetisation meas. 79—51756
UFe_2, nonstoichiometry effects on Curie temp., susceptibility obs. 80—25131
$UFe_3B_2(B_4)$, Mossbauer effect of ^{57}Fe nuclei, mag. props. 80—103907
UGa_2, cryst. struct., mag. and magnetoelastic props. *(Russian)* 79—38364
UGa_2, mag. and magnetoelastic props. 80—15775
UH_3, hyperfine splitting of proton determ. by inelastic neutron scatt. 77—43814
$U_2N_2Bi(Sb)(Te)$, mag. props. 78—72333
U_2N_2Te, and related cpds., crit. behaviour 78—43605
U_2N_2Te, mag. struct. 77—63119
U_2N_2Te, powdered, high field magnetisation 78—35008
$UOCl_2$, crystal struct., IR spectra, and mag. meas. *(French)* 79—60331
U_3P_4, magnetocryst. anisotropy, torque meas. at 0.34, 0.65 and 0.91 T, 118K 78—47969
U_3P_4, press. effects on elec. resist. and Curie temp. 80—75559
U_3P_4, rhombohedral distortion of low temp. 77—7828
$UP_{1-x}S_x$, sp.ht. and electronic struct. 79—91240
UPTe, crit. behaviour, Ising-like props. 78—43605
US, ferromag., AC mag. susceptibility at high press. 80—7085
US, ferromagnet, electronic structure, reflectivity *(German)* 80—49567

ferromagnetic properties of substances continued
US, magnetisation, temp., mag. field and orientation depend. 77–63232
US, magnetisation temp. and field depend. 77–20565
US(Se)(Te), photoelectron energy distrib. and spin polarisation, electronic and mag. props. 80–16146
US(Se)(Te), spin polarisation and magnetism, photoelectron study 80–40219
U_3Sb_4, ferromagnetic transitions and heat capacities from 5 to 950K 78–14955
$USb_{0.8}Te_{0.2}$, magnetisation and polarised neutron studies 79–56515
$USb_{0.8}Te_{0.2}$, magnetisation and neutron meas., mag. moments 80–15703
$USb_{1-x}Te_x$, mag. struct. and mag. phase diagram, neutron diffr. study 80–50059
USe, anisotropic mag. moments 79–42754
USe, ferromag., spin polarisation of photoelectrons 79–78831
USn_3, inelastic neutron scatt. 80–11165
UTe, crit. exponents, neutron and magnetisation meas. 80–88823
UTe, critical mag. fluctuations near T_c 80–7122
UTe, ferromag., negative electron spin polarisation in photoemission 79–19967
UTe, magnetisation and neutron meas., mag. moments 80–15703
UTe, photoemission energy distrib. curve and electron spin polarisation 79–52074
UTe_xSb_{1-x}, photoemission, densities of states 80–16147
$U_{1-x}Th_xAl_2$, ferromag. spin fluctuation system, sp. ht. and elec. props. 77–20604
$U_{1-x}Th_xAl_2$, mag. susceptibility, low temp. depend. 80–11173
$(U_xTh_{1-x})S$, mag. props. rel. to elec. struct., 1.5-300K 77–1557
$(U_xTh_{1-x})Sb$, magnetisation, U valence change 80–7089
$U_xTh_{1-x}Sb$, valence change of U accompanied by singlet-ground-state ferromag. 80–70965
U_3X_4, (X=P, As, Sb, Bi), molecular field approx. study of mag. ordering, Curie temp., paramagnetic susceptibility 79–78410
V-Fe, ferromagnetism to mictomagnetism at low Fe conc. 78–91878
V-Fe, mag. ordering temp. depend. on atomic short-range order from susceptibility meas. 79–61159
V-Ni alloy, onset of ferromag. 79–56533
V-Pt, sp. ht. and mag. meas. in ordered and disordered phases 80–70422
$V(Ir_{1-x}Pt_x)_3$, mag. props., ferromagnetism, comp. depend. 77–77039
$V(Ir_{1-x}Pt_x)_3$, NMR study of ferromag. 79–65760
W/EuS field emitters, electron emission current depend. on annealing temp., mag. props. 80–16160
WC-Co hardmetals, heat-treated, single domain obs. 79–73771
Y alloys, pseudobinary Laves phases, mag. reson. 79–87323
Y-Co, amorphous alloy film, spin reson. meas., exchange stiffness 78–68389
Y-Co, first and second order transitions 80–34631
Y-Co, hyperfine fields, NMR spin echo 77–63318
Y-Fe, evap. amorphous alloys, thermomag. history effects 77–66389
Y-Fe alloys, mag. interactions, effects on moments *(Rumanian)* 79–15296
Y-Gd, dil., reverse resist. anomaly and negative magnetoresist. 80–84459
Y-Mn alloy, mag. props. and effect of H_2 absorpt. 78–19250
Y-Sm ferrogarnet *(Russian)* 80–71140
YCo_2, anomalous high-field magnetisation 78–47958
YCo_3, amorphous ferromagnet, exchange dominated surface modes 78–52359
YCo_3 amorphous films, ^{59}Co spin echo study 80–80636
YCo_3 film, amorphous, impurity like relaxation mechanism 79–73820
YCo_5, NMR enhancement of modulating field due to anisotropic component of hyperfine field 77–55729
YCo_5, spin polarised energy band struct., APW calc. 78–10342
YCo_5, substituted, magnetocryst. anisotropy, different contribs. of two Co sites 77–8301
$Y_{1-x}Co_x$, temp. depend. of magnetisation 77–77043
$Y_{2+x}Co_{17-2x}$ single crystal, magnetocrystalline anisotropy 79–38320
Y_2Co_{17}, and $Y_{2x}Dy_{2(1-x)}Co_{17}$, magnetocryst. anisotropy, 77-383K 77–89949
$Y_2(Co_{1-x}Al_x)_{17}$, electronic contrib. to sp. ht. at low temp. 79–56541
$Y_2(Co_{0.31}Fe_{0.69})_{19.2}$, statistical site occupancy deviations, effect on mag. anisotropy 77–7717
$Y_2(Co_{1-x}M_x)_{17}$, bulk magnetisation and magnetocryst. anisotropy interpretation 77–40055
$Y_2(Co_{1-x}M_x)_{17}$, M=Al, Cu, single crystal, mag. props. 77–47993
$Y_2(Co_{1-x}M_x)_{17}$, matnetocryst. anisotropy 77–40054
$Y(Co_{1-x}Ni_x)_5$, mag. heterogeneities and coercive force, neutron scatt. study 80–2553
$Y(Co_{1-x}Ni_x)_5$, spontaneous magnetisation mag. anisotropy, spin reorientation transformation *(Russian)* 80–7082
$Y_2Cr_2O_7$, $Y_2Mn_2O_7$, pyrochlore type, synthesis and physical props. 80–33963
$Y_2(Fe,Co)_{17}$, mag. anisotropy fields by singular pt. detection 79–24156
$Y_2(Fe,Co)_{17}$, magnetic anisotropy meas. by singular point detection method 77–63170
$Y_6(Fe, Mn)_{23}$, itinerant ferromagnet, magneto-volume, expts. 77–66404
YFe_2, amorphous, mag. order, cluster phenomena, hyperfine struct. 77–16079
YFe_2, amorphous, surface ferromag. layer, spin wave reson. Rutherford backscatt., and magnetisation meas. 79–73819
YFe_2, ferromagnetic cpds., mean field exchange consts., Stoner itinerant model calcs. 80–50084
$Y_{1-x}Fe_x$, amorphous, spin resonance exam. 79–51860
$Y_{1-x}Fe_x$, mean mag. moment calc. 79–82761
Y_6Fe_{23}, magnetostriction, temp. depend., 20 to 350K 80–65994
$Y(Fe_{1-x}A_x)_2$, A=Al or Ni, Laves phase, mag. props. and Mossbauer effect 77–85632
$Y(Fe_{1-c}Al_c)_2$, local model for mag. behaviour 77–63135
$YFe_{2-x}Al_x$, magnetisation behaviour, mag. scatter order 77–28373
$Y(Fe_cAl_{1-c})_2$, mag. props. 79–38308
$Y(Fe_xAl_{1-x})_2$, mag. order in pseudobinary systems down to millikelvin temps. 78–19251
$Y_6(Fe_{1-x}Al_x)_{23}$, cryst. struct. and mag. props. 79–82180
$Y(Fe_{0.022}Co_{0.978})_2$, ferromag. relax. model, Mossbauer spectra 80–15853
$Y(Fe_{0.022}Co_{0.978})_2$ mag. props., Mossbauer expts., 0.15-4.2K 78–43712
$Y(Fe_{1-x}Co_x)_2$, mag. hyperfine field, conc. depend., Mossbauer expts. 77–63337
$Y(Fe_{1-x}Co_x)_2$, NMR study 80–75882
$Y(Fe_xCo_{1-x})_2$, ferromag. reson. of pseudobinary cubic compounds 78–91961

ferromagnetic properties of substances continued
$Y(Fe_xCo_{1-x})_2$, $x \leq 0.2$, mag. props. and Mossbauer meas. 80–75798
$Y(Fe_{1-x}Mn_x)_2$, Mossbauer spectra and mag. props. 80–39952
$YFe_{2x}Mn_{2-2x}$, mag. props. and FMR 79–95581
$Y_6(Fe_xMn_{1-x})_{23}$, mag. order in pseudobinary systems down to millikelvin temps. 78–19251
$Y_2(Fe_{1-x}Ni_x)_{17}$, Mossbauer spectra, hyperfine field interactions 78–6614
$YFeO_3$, hydrothermal synthesis, mag. struct. 77–47972
$YFeO_3$ monocrystalline, mag. field depend. of magnetic domain *(Korean)* 78–68337
$Y(Fe_xT_{1-x})_2$, Mossbauer spectra, mag. props. 80–20563
$Y(Fe_1-xCo_x)_2$, electronic sp. ht. meas., rel. to mag. props. 77–63197
$Y_{3-x}Gd_xFe_5O_{12}$, mag. phase diagrams, mag. transitions, exchange interaction *(Russian)* 80–54896
$Y_{1-x}Gd_xRh_4B_4$, mag. supercond., anomalous temp. depend. of upper crit. fields 80–29510
$(YGdYbBi)_3(FeAl)_5O_{12}$ epitaxial garnet film, uniaxial ferromagnet domain struct., phase transition *(Russian)* 80–108044
YIG, distrib. of easy magnetisation axes near edge dislocation *(Russian)* 80–44891
YIG ferromagnetic film, quasi surface spin wave giant oscills. *(Russian)* 80–15767
YIG, heat transport by magnons, effect of magnon-phonon thermal relax., calc. 77–39705
YIG monocrystals, echo of magnetoelastic waves 77–55697
YIG, plastic deform. and mag. props 77–40087
YIG, spin-wave and magnetostatic mode attenuation, double-pulse echo method 79–82874
YIG, thin ferromagnetic film, exchange interaction constant, from paramag. resonance spectra of spin waves 79–42811
$(Y_xLu_{1-x})_2V_2O_7$ semiconducting ferromag. pyrochlore, mag. props. 80–29547
Y_6Mn_{23}, lattice consts. and mag. props. before and after H_2 absorption 77–36061
Y_6Mn_{23}, low temp. specific heat determ. 80–65896
$YMn_{2-x}Co_x$, mag. order in pseudobinary region 79–99689
$Y_6(Mn_{1-x}Fe_x)_{23}$, hydriding characts. and mag. props. 77–69527
YMn_2H_x, lattice consts. and mag. props. 77–36061
$Y_{0.25}Nd_{0.75}Co_5$, basal plane anisotropy 77–8295
YNi_3, loss of ferromagnetism after H_2 absorpt., Pauli paramag. props. 80–34588
YNi_3, magnetism resurgence, neutron diffr. and mag. props. study 80–65819
$Y_{0.22}Ni_{0.78}$ amorphous alloy, low temp. sp. ht. 79–65680
Y_2Ni_{17}, ferromag. struct., neutron diffr. expt., cryst. field calcs. 77–73001
Y_xNi_{1-x}, amorphous, high press. magnetisation and Curie temp. 80–20442
$Y(OH)_3$, dynamical effects of interaction between 4f electrons and optical phonons 80–108196
$Y_{1-x}Tb_xCo_5$, spontaneous magnetisation anisotropy, spin reorientation transforms. *(Russian)* 80–7082
$Y_{1-x}Th_xFe_3$, saturation magnetisation, fields up to 120 kOe, comp. depend. 77–8283
$(Y_{1-x}2Co_x)Co_5$, anisotropy fields, coercivities, annealing effects 78–91898
Yb-Eu alloys, mag. ordering, magnetisation meas. 80–7081
$YbFe_2$, cryst. elec. field and exchange interac., ^{170}Yb Mossbauer obs., magnetostriction contrib. 80–108124
$YbFe_2$, Curie temp., elec. quadrupole couplings, Mossbauer study 80–39949
$YbFe_2$, high field Mossbauer study 80–75893
$Yb_2V_2O_7$, pyrochlore struct., mag. props. 78–72335
$Yb_2(WO_4)_3$, mag. props., 300 to 900K 79–28510
$ZnCr_2Se_4$, electroconductivity, thermoelectromotive force, Hall effect *(Russian)* 80–70694
$Zn_{1-x}Ge_xFe_{2-x}{}^{3+}Fe_{2x}{}^{2+}O_4$, double exchange magnetism, Mossbauer study 80–66087
$Zn_xMn_{2-x}Sb$, anti-PbFCl type, cryst. struct. and ferromag. ordering 77–84723
Zr-Co(Fe), amorphous alloy film, spin reson. meas. 78–68389
$Zr_{40}Cu_{50}Fe_{10}$, magnetically dil. glass, 3d moments, mag. susceptibility and magnetisation meas. 79–95574
$Zr_{40}Cu_{60-x}Fe_x$, electronic and mag. props. 77–8271
$Zr_{40}Cu_{60-x}M_x$, (M=Gd, Tb, Fe or Mn), amorphous alloy, mag. interactions 78–95432
$Zr(Fe, Co)_2$, itinerant ferromagnet, magneto-volume expts. 77–66404
$Zr(Fe_{1-x}A_x)_2$, A=Al or Ni, Laves phase, mag. props. and Mossbauer effect 77–85632
$Zr(Fe_{1-x}Al_x)_2$, Curie temp., magnetisation, and cryst. struct., conc. depend. 80–75730
$Zr(Fe_{1-x}Co_x)_2$, low temp. sp. ht. and mag. props. 79–61153
$Zr(Fe_{1-x}Co_x)_2$, mag. props. and Mossbauer effects 79–91322
$Zr(Fe_{1-x}Co_x)_2$, magnetovolume effects, thermal expansion and forced vol. magnetostriction meas. 80–29595
$Zr(Fe_{1-x}Co_x)_2$, NMR study 80–75882
$Zr(Fe_{1-x}Co_x)_2$, thermal expansion and forced volume magnetostriction 80–75830
$Zr(Fe_xCo_{1-x})_2$, mag. order in pseudobinary systems down to millikelvin temps. 78–19251
$(Zr_{1-x}Nb_x)Fe_2$, magnetovolume effects and Invar characters 80–15773
$Zr_{1-x}Nb_xZn_2$, microscopic mag. props., NMR investigation 80–15807
$Zr_xTb_{1-x}Fe_2$, Laves phase alloys, magnetostriction *(Russian)* 77–51932
$Zr_xTb_{1-x}Fe_2$, props. of near magnetostrictive material 77–51934
$ZrZn_2$, high press. study of Curie temp. and mag. susceptibility 80–84600
$ZrZn_2$, itinerant electron ferromag., NMR exam. of effect of spin fluctuations 77–16192
$ZrZn_2$, itinerant electron ferromag., nucl. spin-lattice relax. time meas. 77–63308
$ZrZn_2$, phonon contrib. to Stoner enhancement factor, ferromag. and possible superconductivity 80–25070
$ZrZn_2$, weak itinerant magnetism as inhibited superconductivity 79–51715

ferromagnetic relaxation
see also ferromagnetic resonance
classical theory of superparamag. relaxation 77–8411
dynamics of ferromagnet in strong alternating mag. field *(Russian)* 78–88097
ferrofluid, relax. in external mag. field, cubic cryst. case 80–71113

ferromagnetic relaxation continued
ferromagnetic spin system, under quenched random mag. field, phase transition crit. dynamics 79—82798
impurity spin dynamics in rapid spin relax. ferromagnet *(Russian)* 77—51960
magnon relaxation, spin-orbit interaction, itinerant electron ferromagnets 80—11179
uniform precession of magnetisation, scatt. by pores *(Russian)* 78—6581
$Ca_{2x}Bi_{3-2x}Fe_{5-x-y}V_xIn_yO_{12}$, ferromagnetic relax. meas., 4.2-300K 80—44923
$CdCr_2Se_4$, Crit. relax. processes, mag. reson. expts. 80—60425
$CrBr_3$ anisotropic ferromagnet. crit. mag. relax., field and temp. depend. 79—1717
$Cr_2(CrO_4)_3$, ferromagnet, ESR spectra near Curie temp. 79—8042
$CuCr_2Se_4$, Crit. relax. processes, mag. reson. expts. 80—60425
$CuRb_2Br_1.2H_2O$, three-dimens. ferromag., crit. susceptibility exponents in Curie temp. region using relax. techniques 77—66304
EuO, zero-field critical relax. rate, mode-coupling theory 77—69593
EuS, three dimens. Heisenberg ferromagnet, crit. relax. spectra mag. susceptibility 79—8000
α-Fe, high purity, neutron and electron-irrad., interstitial migration at 200K 79—55920
$Fe_{80}B_{20}$ amorphous ribbon, initial susceptibility time lag 80—100579
Gd, spin relax., ferromag. transmission reson. 78—31113
Ni, cold-worked, rel. between dislocation and ferromag. damping 80—107369
$Y(Fe_{0.022}Co_{0.978})_2$, ferromag. relax. model, Mossbauer spectra 80—15853
YIG, homogeneous mag. relax. near phase transition *(Russian)* 78—23351
YIG, polycrystalline, microwave relax. at high power levels 79—61231
$Zn_xCu_{0.1}Fe_{2.9-x}O_4$, ferromag. relax. 80—60422

ferromagnetic resonance
see also ferromagnetic relaxation
alkylammonium compounds, $(C_nH_{2n+1}NH_3)_2CuCl_4$ and $(C_6H_5C_mH_{2m}NH_3)_2CuCl_4$, interlayer exchange field 77—20714
alloy, HTR material, oxidation and carburization in He 80—108645
alloys, ferromagnetic disordered, spin wave and ferromag. reson. linewidth 80—66045
anisotropic ferromagnet, magnon spectrum, FMR line intensity, Curie pt. behaviour *(Russian)* 77—69694
anisotropic Heisenberg model, ferromag. reson., magnon-magnon, phonon-magnon interactions *(Russian)* 80—11274
asymmetry of ferromag. reson. curve, theory and expt. data for Ni *(Russian)* 79—4728
bilayer compounds, spin-wave resonance, effect of random dilution 79—61236
Brillouin-Mandelstam scattering from thermal and excited magnons 80—70980
bubble collapse and stripout field, microwave meas. technique using mag. reson. apparatus 77—20661
bubble film, uniaxial anisotropy energy, effect of ion implantation 79—78476
chemisorption on metal films, use of external mag. field, review 78—72003
coaxial cylinders, two, magnetostatically coupled uniformly magnetised, ferromag. reson. 77—69702
composite garnet ferrite epitaxial film ferromag. resonance obs. 77—85578
detection by photoacoustic effect 80—20463
dibutylammonium copper chloride, parallel pumping of two-dimens. spin waves, spin wave bandwidth 77—66425
dimethylammonium copper tetrachloride, two-dimens. ferromag., saturation of parallel-pumped magnons 80—97147
dislocated ferromagnet, inhomogeneous magnetisation near dislocation effect on FMR linewidth 80—25213
dislocation broadening of uniform ferromag. reson. line at finite temps. 78—19334
disordered media, ferro- and antiferromag., and spin glasses, dynamic props. *(Russian)* 78—39350
dispersive props., effect of sample size of ferrimagnetic materials 80—39878
elliptical spin precession correction factor in spin-wave reson. theory 80—20464
elliptical spin precession in microscopic spin-wave resonance theory, validity 78—80224
ferrite, formulation of resonance, principal types of devices 78—88548
ferrite, microwave mag. props., grain size effect 78—10722
ferrite, polycrystalline, ferromagnetic reson. curves, theory and meas. method *(Russian)* 77—20713
ferrite, polycrystalline applicability limits of theory *(Russian)* 77—55709
ferrite, sphere, small anisotropic, excitation by pot. field 77—43890
ferrite film, magnetostriction const., mag. saturation and internal stress determ. *(Russian)* 77—16126
ferrite spinel films, LPE growth and props., SIMS, X-ray diffr., and spin wave reson. obs. 80—34323
ferrite with platelike domain struct., FMR absorpt. line intensity and shape 77—90041
ferrites, inhomogeneous exchange interaction influence on ferromagnetic resonance line moments 80—75864
ferrites, magneto-microwave Kerr effect *(German)* 78—2742
ferrites, polycryst., dynamic mag. susceptibility rel. to ferromag. reson. *(Russian)* 77—66267
ferrodielectrics, ferromag. reson., press. influence 78—88193
ferroelectric, soft modes and ferromag. reson. 80—11275
ferromagnet, cubic, magnetised along ⟨110⟩ with negative first anisotropy constant, stability of lamellar domain struct. 79—15323
ferromagnet, domain wall dynamic slowing down *(Russian)* 79—78438
ferromagnet, easy-axis, higher order corrections to spectrum 78—80222
ferromagnet, parallel pumping, in microwave field, magnon-photon interaction 79—51861
ferromagnet, spin wave resonance temp. depend., surface mode threshold conditions 77—28450
ferromagnetic conductor, plasma effects, selective transparency near antiresonance region 80—100476
ferromagnetic film, magnon avalanche under NMR saturation 78—10783
ferromagnetic insulator in weak mag. field, quasistationary eqn. of state 78—19333
ferromagnetic layer in perpendicular mag. field, ground state, spin wave reson. 77—85512

ferromagnetic resonance continued
ferromagnetic resonance absorpt. lineshape 24 GHz microwave transmission apparatus 77—49755
ferromagnetic thin film, with nearest neighbour and next nearest neighbour exchange interactions spin-wave excitations 79—73783
ferrometnatic metal slab, transmission of 24 GHz radiation, effect of diffuse surface scatt. of carriers, calc. 80—34780
film, electron-nuclear oscillations in conditions of strong coupling between electronic and nuclear subsystems *(Russian)* 79—19782
film, FMR in cylindrical mag. domains *(Russian)* 78—10780
film, nonlinear spin wave parametric resonance 80—2642
film, on antiferromag. backing, parametric reson. *(Russian)* 77—90043
film, resonance props. in network of cylindrical mag. domains *(Russian)* 80—50194
film, spin pinning and mag. surface reconstruction, effect on standing spin waves 77—1600
film, spin wave parametric reson. near phase transition 79—8053
film, surface spin waves and surface anisotropy effects at finite temp. 79—78452
film, surface state swapping effect 77—90040
film, tangentially magnetised, parallel pump spin wave instability 77—8294
film, tangentially magnetized spin wave instability 78—2712
film, with internal isotropically coupled impurity layer, spin wave reson. spectrum 78—80223
finite ferromagnets, dynamical props. of flat parallel domain struct. *(Russian)* 78—6499
garnet bubble film, high g, two resonant peaks 78—68388
garnet epitaxial film, damage prod. by multiple ion implantation, ferromag. reson. obs. 80—34703
garnet film, bubble, anisotropy field and nonmagnetic regions in implanted layers, ferromag. reson. study 79—99774
garnets, magnetic relaxation phenomena 79—99776
garnets, photoinduced phenomena 79—99718
garnets magnetic excitations 79—99695
Heisenberg anisotropic $S={}^1/_2$ ferromagnet, reson. susceptibility, statistical mech. theory 77—8413
Heisenberg ferromagnet, two-magnon reson. in absence of bound states, calc. 80—60423
high frequency, kinetic and thermodynamic props. *(Russian)* 78—19340
high pressure apparatus for ferromag. reson. expts. 77—51956
homogeneous, natural oscills. in ferromag. plate, subject to delay 79—28624
horizontally dipped LPE film, inhomogeneities, spin wave reson. meas. 79—91298
Invar films, exchange interaction depend. on lattice parameter, spin-wave reson. and magnetisation meas. *(Russian)* 79—42751
line broadening by dislocations 78—64275
line width, inhomogeneous broadening, magnon scatt. 78—35043
linear electric field effects 80—65854
linewidth meas. method and apparatus 80—22411
lunar samples, sample quality effects 79—70971
magnesioferrite precipitated particles in MgO, resonance anisotropy field 77—69541
magnetic excitations in amorphous ferromagnets 79—78356
magnetic semiconductors, magnetoelectric effect, classical and quantum theory, magnon drag effect 80—34746
magnetic surface states, theory, review 80—84654
magnetic thin films, pulse magnetic reversal in high freq. field in ferromag. reson. range *(Russian)* 80—11230
magnetodynamic resonance, microwave modulation of light appl. 80—71393
magnetoelastic surface wave attenuation in ferromag. conductor, loss bands near FMR 77—20667
magnetoresonance forces, comments *(Russian)* 79—1713
magnetoresonance forces, reply to comments *(Russian)* 79—1714
magnetostriction, meas. by means of strain modulated ferromag. reson. 78—76285
magnon coherent generation by optical technique using mag. Raman nonlinearity 78—68201
magnon splitting, photon effects 78—64276
magnon-photon interaction in ferromagnets, construct. and radiation effects 80—71188
metal, damping, one electron model 77—8409
metal, ferromagnetic resonance linewidth, interaction of spin waves with conduction electron current 80—25216
metal, metal, magnon and cond. electron relax. processes *(Russian)* 80—7102
metallic ferromagnet, antiresonance region, EM wave propag., Maxwells' eqns. soln. 80—66038
metallic ferromagnetics, two-magnon scatt. on dislocations, resonance linewidth broadening 77—20708
metallic multilayers, ferromag. reson. formal treatment 77—73083
metallic multilayers, ferromag. reson. numerical example and semiquantitative model 77—73084
metals, ferromagnetic transmission resonance, nonlinear phenomena 77—85577
metals, s-d exchange interactions, effect on attenuation of spin waves *(Russian)* 79—19730
Metglas 2826 ribbons, ferromagnetic resonance and SEM obs. 80—15804
multidomain ferromagnetic resonance anal., appl. to stripe and bubble arrays 79—78528
multidomain magnetic disc, ferromagnetic reson. 78—68386
multilayer thin films, spin wave resonance, model 78—76316
nonequilibrium electrons polarised opposite to magnetisation, HF magnon prod. *(Russian)* 78—23262
nonlinear phenomena 79—61232
normally magnetised disc, reson. modes of magnetostatic waves 77—81015
nuclear spin echo in the NMR and FMR overlap region 79—24229
parametrically excited waves, interaction with defects exhibiting internal structure 80—7173
Permalloy film, multi- and single-layer, reson. curves subjected to tangential mag. reversals *(Russian)* 80—50195
Permalloy film, with-small surface anisotropy, ferromag. reson. 77—69701
Permalloy platelet, transmission reson. meas. 77—20710
Permalloy platelets, mode positions, spin pinning 77—4562
phonon inelastic scattering by magnons 77—20570
phonon propagation 78—88194
polariton linewidths in ferromagnets, theory 78—87918

ferromagnetic resonance continued
quarter wave absorbers, C-band, NiZn ferrite appl. 79—38386
rare earth orthocobaltites, $R_{1-x}Sr_xCoO_3$, ferromag. reson., Lande g-factor 80—25215
rare earth-Co amorphous film, sputtered, in-plane anisotropy induced by rare gas annealing 78—84458
rare earth-transition metal alloys, amorphous, struct. and mag. props., book contrib. 80—39818
review of magnetic resonance, book contrib. 80—11242
saturable transformer, anal. using rectangular hysteresis-free approximation method *(Russian)* 77—55708
semiconductor, ferromag., parametric excitation of magnetoplasma reson. 79—28623
small gyromagnetic sphere, EM excitations 78—15030
spectrometer for wide resonant line meas. *(Slovak)* 79—12829
spin wave instability on approaching FMR *(Russian)* 78—76318
spin wave resonance, surface mode magnetisation, inhomogeneities effect 77—69710
spin wave resonance, surface modes, influence of inhomogeneities of magnetisation 77—12205
spin-orbit interaction effects on spin-wave resonance *(Russian)* 77—90039
standing spinwave resonance in film with nearest and next-nearest neighbour exchange 78—68390
stationary and transition processes in region of identical nucl. and electron mag. reson. freqs. *(Russian)* 78—80225
strip films, bulk and surface spin oscills., mag. reson. 80—97149
stripe domain structure, magnetostatic modes 78—68333
submillimetric spectroscopy appl. to mag. excitations 77—40135
Supermalloy, 24 GHz ferromagnetic antiresonance transmission 77—51957
Supermalloy, 9, 24 and 38 GHz ferromagnetic reson. absorpt., line shapes 77—51958
supermalloy, foil, microwave transmission, parallel RF and mag. fields 77—59462
superparamagnet, magnetodipole broadening of reson. line *(Russian)* 79—38385
superparamagnetic particles, resonance anisotropy field 77—69541
surface, freq. in semi-infinite cryst., theory 79—65742
surface spin waves, microscopic theory, mag. field effects 78—35044
tensorial permeability and conductivity medium, EM wave propag., ferromag. resonance, spin waves *(French)* 78—74820
thick ferromagnetic film, reson. transmission of EM energy via phonons 80—60382
thin ferromagnetic resonators, intermodulation distortion, spin waves 78—48048
thin film, with uniaxial-biaxial anisotropy, low freq. ferromag. reson. 79—8055
thin uniaxial platelet with stripe domain struct. magnetised along easy axis, FMR absorpt. 79—42841
transition phenomena in region of equal NMR and ferromag. reson. frequencies *(Russian)* 77—32272
unclamped specimen, magnetoreson. force effects *(Russian)* 77—32264
uniaxial antiferromagnet, mag. polaritons in spin-flop phase 78—23349
uniform precession of magnetisation, scatt. by pores *(Russian)* 78—6581
YIG, reson. magnetostatic modes, spectrum in inhomogeneous mag. field 79—28621
Ba ferrite, FMR in uniaxial crystal plate with bubble domain lattice 80—93182
Ba ferrite platelets in multidomain state and at saturation, FMR absorpt. 79—42841
$BaFe_{12-2x}M_xTi_xO_{19}$ (M=Co, Ni, Zn), mag. props. determ. 80—75759
$BaFe_{12}O_{19}$ plate, with cylindrical domain struct., ferromag. reson. at arbitrary magnetisation 77—81017
$Ba_2Mg_2Fe_{12}O_{22}$, hexagonal ferrite, with anisotropic g-factor, ferromag. reson. 77—69700
$Ba_3Zn_2Fe_{24}O_{41}$, ferromag. reson., low power nonlinear effects 80—75861
$Bi_{3-2x}Ca_{2x}Fe_{5-x-y}In_yV_xO_{12}$, single crystal by flux method ferrimag. garnet *(Chinese)* 77—40056
$CdCr_2S_4$:Ag, mag. semicond., ferromagnet resonance angular and temp. depend. 79—69730
$CdCr_2S_4$:Gd, ferromag. reson. and electrical cond. 79—28626
$CdCr_2Se_4$, Crit. relax. processes, mag. reson. expts. 80—60425
$CdCr_2Se_4$, influence of Co ions on anisotropy and magnetostriction, ferromag. reson. meas. 77—69659
$CdCr_2Se_4$:Ag, ferromag. reson. meas. 77—8415
$CdCr_2Se_4$:Ag, ferromag. reson. field and linewidth anisotropy, Se vacancy effects 78—60338
$CdCr_2Se_4$:Ag, ferromag. linewidth and eddy current losses 79—33541
$CdCr_2Se_4$:Ag, impurity contrib. to low temp. ferromag. reson. linewidth 79—65743
$CdCr_2Se_4$:Cu(Ag), ferromag. reson. and ESR line widths 80—60413
Co ferrite, crystalline anisotropy, FMR meas. 77—8408
Co, NMR spectra temp. depend. 78—52364
Co-P, amorphous, ferromag. antireson. 24 GHz microwave transmission, mag. props. 80—34778
Co-P, cryst. and amorphous mag. films, ferromag. resonance line width *(Russian)* 78—88192
Co-P amorphous alloy, ferromagnetic reson. exam. 79—28620
Co-P film, amorphous, spin wave dispersion law, spin wave reson. obs. *(Russian)* 78—88196
$(Co_{1-x}Fe_xNi_y)_{80}(Si_{1-z}B_z)_{20}$, amorphous films, spin wave spectra 80—34777
$Co_{0.25}Mn_{0.75}Fe_2O_4$, ferromag. reson. in frozen lattice model, anisotropy consts. 79—51859
$Co_x(Ni_{0.5}Cu_{0.5})_{1-x}Fe_2O_4$ ferrite, relation between elec. cond. and mag. anisotropy 80—75548
CoP-NiCoP, composite ferromag. film, exchange coupling between soft and hard layers, FMR obs. 79—78448
$Co_{0.9}P_{0.1}$ noncrystalline ferromagnet, electroless deposited, struct. and microscopic mag. props. 80—88063
$Co_{1-x}P_x$ glass, crystn., spin wave reson. 79—73104
$Co_xPd_{80-x}Si_{20}$, amorphous, structural and mag. heterogeneities 80—80484
CoS_2, itinerant ferromagnet, ferromag. reson. and EPR meas. 80—66044
$CsMnF_3$, parametric excitation of magnons, effect of RF modulation of mag. field 80—65842
$CsNiF_3$, one dimensional ferromag., magnetisation, FMR, 2.61-20K 77—20719
$CsNiF_3$, one-dimens. ferromag. far IR investig. of ferromag. reson., temp. and mag. field depend. 77—66427

ferromagnetic resonance continued
Cu-Fe, interface, ferromagnetic and cond. spin reson. mode coupling 79—78521
Cu-Ni, film, compositionally modulated, enhanced magnetisation density 78—84460
Cu-Ni, interface, ferromagnetic and cond. spin reson. mode coupling 79—78521
Cu-Permalloy, interafce, ferromagnetic and cond. spin reson. mode coupling 79—78521
$CuCr_2Se_4$, Crit. relax. processes, mag. reson. expts. 80—60425
$CuCr_2Se_4$, experimental obs. 78—76227
$CuCr_2Se_4$, mag. reson. and valence state of Cu and Cr ions 80—60413
$CuCr_2Se_4$ single crystal, magnetic props. *(Japanese)* 78—6520
dibutylammonium copper chloride, two-dimens. spin wave spectrum, parallel pumping meas. 77—20715
Er film, magnetoelastic excitations, phonon spectroscopy and forbidden transitions 79—82853
$(Eu,Lu)_3Fe_5O_{12}$:Ga(Al)(Ca,Ge), bubble material, dynamic characterisation, comparison between transport and FMR methods 80—39833
EuGaYIG film, bubble dynamics, anisotropy depend., ferromag. reson. expts. 77—63240
EuO, ferromag. reson. and nonlinear phenomena 79—28627
EuO, ferromagnetic resonance and dielectric losses 78—2748
EuO, light absorpt. during ferromag. reson. *(Russian)* 79—28618
EuO, transport properties at ferromag. reson. 78—68387
EuS, film, mag. surface reconstruction 78—10781
Fe, ferromagnetic transmission resonance, nonlinear phenomena 77—81016
Fe film, chemisorption induced mag. dead layers, ferromag. reson. obs. 79—91261
Fe film, ferromag. reson., thermodynamical anal. 79—42840
Fe film, mag. structures and stresses 78—72375
Fe film, magnetoelastic excitations, phonon spectroscopy and forbidden transitions 79—82853
Fe film, nuclear spin system dynamics Mossbauer study in FMR conditions *(Russian)* 80—80651
Fe films, ferromagnetic reson., photoacoustic detection 80—80613
Fe, foil, ferromagnetic resonance detection by photoacoustic effect 80—20463
Fe, magnetoelastic excitations and ferromagnetic resonance 79—82879
Fe, microwave subharmonic generation, transmission reson. expt. 77—20709
α-Fe particles, in fused SiO_2, g-values and anisotropy consts., FMR study 79—82876
Fe particles, lunar matter, FMR study, effective linewidth method 78—95523
Fe, polycryst., g-factor meas. 77—24748
Fe, static and dynamic magnetoelastic coupling 77—20665
Fe thin films, surface demagnetisation due to chemisorption, ferromagnetic reson. study 80—80616
Fe, whisker single crystals, ferromag. reson. and surface anisotropy 80—71187
Fe-Al_2O_3 granular films, superparamagnetism and relax. effects 80—71118
Fe-Cr (10 to 70 at.%), ferromag. reson., anisotropy const., and saturation magnetisation *(Russian)* 77—81013
Fe-MgO system, decomp. reactions, ferromag. reson. obs. 77—9058
Fe-Ni films, scatt. of homogeneous spin waves by anisomeric oriented plane, ferromag. reson. 78—19336
Fe-Ni-Co film, electron-nucl. mag. reson. 78—35063
Fe-Ni-Cr film, ferromag. reson. meas. *(Russian)* 77—1601
Fe-SiO_2, granular compund, superpara- to ferromag. transition temp. meas. 77—69633
$Fe_{80}B_{20}$, amorphous, Brillouin scatt. from magnons, ferromag. reson. 80—65844
$Fe_{80}B_{20}$, metallic glass, ferromag. props. 77—16107
$FeBO_3$, Brillouin scatt. from parametrically excited phonons 79—73956
$FeBO_3$, magnon dispersion by light scatt. and ferromag. reson. 77—55668
$FeBO_3$, polycrystalline, crystallite orientation 78—15027
$FeBO_3$, spin wave dispersion at small wavevectors, Brillouin scatt. and ferromag. reson. 78—47962
$FeBO_3$, weak ferromag., FMR instability, parametric excitation of phonons, Brillouin scatt. obs. 79—78529
$FeBO_3$, weak ferromagnet, spin wave band struct. and microwave props. 79—1661
Fe_3BO_6, weak ferromag. and antiferromag. reson. modes obs. 77—69706
$FeCl_2$, magnetic excitation in presence of transverse field, ferromag. reson. 78—19335
$(Fe_{0.06}Co_{0.94})$-B, amorphous, ferromag., mag. instability rel. to struct. 79—99729
$(Fe_xCo_{1-x})_{78}Si_8B_{14}$, amorphous, saturation magnetostriction, strain modulated FMR obs. 80—75863
Fe_xGd_{1-x}, $0.5>x>0.65$, amorphous film, FMR, spin wave spectra 77—16181
FeGe, cubic, spin reson., 4.2-300K, 3-35 GHz 79—38384
Fe_xGe_{1-x}, amorphous film, FMR meas. of mag. props., temp. and comp. depend. 77—69636
$(Fe_{1-x}Ni_x)_{83}B_{17}$, amorphous alloys ferromagnetic resonance 80—108080
$Fe_{38}Ni_{38}B_{24}$, amorphous, magnetisation and FMR expts. 79—95607
$Fe_{32}Ni_{36}Cr_{14}P_{12}B_6$, Metglas 2826 A, g-values and relax. parameters, 77 to 430K 77—63289
$Fe_{40}Ni_{38}Mo_4B_{18}$ ribbon, magnetic characterisation 80—34680
$(Fe_{1-x}Ni_x)_{80}P_{10}B_{10}$, amorphous microwires, magnetisation reversal and anisotropy 78—91885
$Fe_{40}Ni_{40}P_{14}B_6$ glass, struct. relax., ferromag. reson. and X-ray scatt. 79—90566
$Fe_{40}Ni_{40}P_{14}B_6$ metallic glass, ferromag. reson., spin waves, thermal ageing and long-range order effects 80—25214
$Fe_{40}Ni_{40}P_{14}B_6$, Metglas 2826, g-values and relax. parameters, 77 to 430K 77—63289
$Fe_{40}Ni_{40}P_{14}B_6$, Metglas 2826, ferromag. antireson. transmission at 24 GHz, 26 to 270°C 77—69696
$(Fe_{1-x}Ni_x)_{75}P_{16}B_6Al_3$, amorphous, saturation magnetisation, temp. depend., ferromag. reson. meas. 79—73818
$(Fe_xNi_{1-x})_{75}P_{16}B_6Al_3$, magnetisation temp. depend., spin wave theory 80—44927
$Fe_{29}Ni_{49}P_{14}B_6Si_2$, Metglas 2826 B, g-values and relax. parameters, 77 to 430K 77—63289
$Fe_{29}Ni_{49}P_{14}B_6Si_2$, Metglass 2826B, saturation magnetisation, temp. depend., ferromag. reson. meas. 79—73818

ferromagnetic resonance continued
Fe_3O_4, ultrafine particles in ferrofluid, superparamag. and ferromag. reson. 78—15026
Fe_xO_y epitaxial film, ferromag. reson. 77—51964
$Fe_xPd_{80-x}Si_{20}$, amorphous, structural and mag. heterogeneities 80—80484
$(Gd,Tm,Y)_3(Fe,Ga)_5O_{12}$ film, magnetocrystalline anisotropy 79—78450
Gd alloys, amorphous, mag. props. and ferromag. reson. 80—54952
Gd alloys, pseudobinary Laves phases, mag. reson. 79—87323
Gd, ferromag. reson. line width *(Russian)* 78—39406
Gd film, magnetoelastic excitations, phonon spectroscopy and forbidden transitions 79—82853
Gd, magnetoelastic excitations and ferromagnetic resonance 79—82879
Gd, spin relax., ferromag. transmission reson. 78—31113
Gd, static and dynamic magnetoelastic coupling 77—20665
Gd-Co, amorphous films, mag. props. ferromag. reson. meas., 20-520°C *(Russian)* 80—97144
Gd-Co, evap. amorphous film, mag. props. 77—24720
Gd-Co, evap. amorphous films, anisotropy, magnetisation and FMR meas. 77—66392
Gd-Co amorphous film, mag. anisotropy 77—20649
Gd-Co amorphous film, sputtered, FMR spectra 79—73822
Gd-Co amorphous films, mag. anisotropy, static and ferromag. reson. expts. 79—33477
Gd-Co(Ni)(Cu)(Rh)(Ru)(Pd)(Ga), amorphous, mag. props. and ferromag. reson. 80—75862
Gd-Fe amorphous films, anisotropy dispersion, FMR meas. 79—73824
$Gd_{0.37}Al_{0.63}$, amorphous film, anomalous resonance field shift 79—73821
$Gd_{37}Al_{63}$ amorphous film, spin glass, microwave mag. resonance, freq. dependence 80—39798
Gd_xCo_{1-x} annealing amorphous film, ferromag. reson. 77—85580
$(Gd_xCo_{1-x})_{1-y}Ar_y$ amorphous films, effective anisotropy field, ferromag. reson. obs. 80—71123
$Gd_{6.9}Co_{74.0}Mo_{12.8}Ar_{6.3}$, amorphous film, spin wave reson. 79—73823
$Gd(Fe_xCo_{1-x})_2$, ferromag. reson. of pseudobinary cubic compounds 78—91961
$Gd_{70}Tb_{30}$, magnetisation, AC susceptibility and microwave absorption meas. 80—60221
$Gd_xY_{1-x}Fe_2$, effective g-values, ferromag. reson. meas. 77—20720
$(Gd_xY_{1-x})Fe_2$, Fe mag. behaviour, FMR measurements, mag. props., Vangsness relation anal. 79—78336
$Gd_{0.9}YTm_{1.1}1Ga_{0.44}Fe_{4.56}O_{12}$, ion implanted, ferromag. reson. meas. 78—68385
Ge-Se-Fe phase system, amorphous films, mag. and elec. props. 79—51695
^3He, cryst., HF susceptibility, ferromag. reson. type *(Russian)* 77—59175
$HgCr_2Se_4$, influence of Co ions on anisotropy and magnetostriction, ferromag. reson. meas. 77—69659
$HgCr_2Se_4$, initial mag. permeab., 77 to 300K, domain wall motion and damped ferromag. reson. 79—28562
K_2CuF_4, microwave excitation, optical detection of ferromagnetic reson. 80—50197
K_2CuF_4, obs. of magnon density of states by subthreshold steady-state absorption 77—12107
K_2CuF_4, spin-wave relaxation, parallel pumping expt. 79—4729
K_2CuF_4, two-dimens. ferromag., saturation of parallel-pumped magnons 80—97147
$KFeS_2$, magnetic reson. meas. 78—95524
La-Fe, amorphous alloy film, spin reson. meas. 78—68389
Li ferrite, ferromag. reson., linear elec. field shift 79—1716
$Li_{0.5}Al_xFe_{2.5-x}O_4$ and $Li_{0.5}Ga_xFe_{2.5-x}O_4$, polycrystalline, ferromag. reson. theory *(Russian)* 77—55709
$Li_{0.5}Al_xFe_{2.5-x}O_4$, polycrystalline, ferromag. reson. absorpt. curves, stress effects *(Russian)* 77—20713
$Li_{0.5}Fe_{2.5-x}Cr_xO_4$, mag. anisotropy, ferromag. reson. meas. 77—69542
$Li_{0.5}Fe_{2.5}O_4$, linear elec. field shift of ferromag. reson. field 79—78530
$LiHoF_4$, dipolar-coupled Ising ferromag., submillimetre ferromag. and paramag. reson. 77—69697
$LiTbF_4$, dipolar-coupled Ising ferromag., submillimetre ferromag. and paramag. reson. 77—69697
Lu-Fe, amorphous alloy film, spin reson. meas. 78—68389
$MgFe_2O_4$, epilayer, perpendicular anisotropy 80—39769
$Mg_{0.5}Fe_{2.5}O_4$, ferrimag. epilayer, superparamag. interface, mag. props., FMR 78—95492
MgMn ferrite CVD epitaxial layers, bubble mobility, FMR meas. 77—85516
MgMn ferrite film, magnetostriction const., mag. saturation, and internal stresses determ. *(Russian)* 77—16126
Mn ferrite, monocrystalline epitaxial layers, surface spin-wave modes in ferromag. reson. 78—2743
$MnCO_3$, parametric excitation of magnons, effect of RF modulation of mag. field 80—65842
$Mn_{1-x}Cu_xSb$ film, ferromag. reson. 78—31114
MnFe ferrites, reson., effect of EM propagation 78—64277
$MnFe_2O_4$ film, bulk and surface spin waves, spin wave reson. expts. 79—73826
$Mn_{0.9}Fe_{2.1}O_4$ cylinder, low-resist., ferromag. reson. absorpt. 79—1718
$Mn_xFe_{3-x}O_4$ epitaxial films, mag. and reson. props. 80—50149
$Mn_xFe_{3-x}O_4$ film, spin wave reson., exchange const. 77—16183
MnP, anisotropic, ferromagnetic microwave resonance relations 80—15805
MnSb, magnetic losses, ferromagnetic resonance and antiresonance 80—100618
MnZn ferrite, high cond., magneto-microwave Kerr effect, ferromag. reson. linewidth determ. 77—43888
Ni, anomalous transmission of microwave power at FMR at 4.2K 79—82877
Ni, dispersed catalyst on Al_2O_3 and SiO_2, epitaxial and textural effects, ferromag. reson. 78—23963
Ni expt. data used to explain asymmetry of reson. curves *(Russian)* 79—4728
Ni ferrite with domain struct., FMR absorpt. line intensity and shape 77—90041
Ni, ferromagnetic antiresonance transmission at 24 GHz, temp. depend., g-factor and magnetisation 77—51959
Ni, ferromagnetic reson. determ. of first three anisotropy consts. 77—8414
Ni, ferromagnetic transmission resonance, nonlinear phenomena 77—81016
Ni film, adsorbed $H_2(CO)$, ferromag. reson. exam. 78—15028

ferromagnetic resonance continued
Ni film, chemisorption induced mag. dead layers, ferromag. reson. obs. 79—91261
Ni film, ferromag. reson., thermodynamical anal. 79—42840
Ni film, influence of H chemisorpt. on magnetism, ferromag. reson. spectroscopy 77—66395
Ni film, mag. structures and stresses 78—72375
Ni film, magnetoelastic excitations, phonon spectroscopy and forbidden transitions 79—82853
Ni film, multi- and single-layer, reson. curves subjected to tangential mag. reversals *(Russian)* 80—50195
Ni film, single cryst., domain width from ferromag. reson. 80—39879
Ni film, spin wave resonance 79—33542
Ni film, strained and strain-free, ferromag. reson. meas. 78—95525
Ni film, thickness dependence of perpendicular mag. anisotropy 77—80974
Ni films, ferromagnetic reson., photoacoustic detection 80—80613
Ni films, oriented, hypersound excitation at 8.9 GHz by exploiting mag. anisotropy 77—85541
Ni, foil, microwave transmission, parallel RF and mag. fields 77—59462
Ni, Landau-Lifshitz damping, wave no. and temp. depend. 80—34779
Ni, magnetoelastic excitations and ferromagnetic resonance 79—82879
Ni, phonon assisted magnon transmission at 24 GHz 79—82878
Ni, phonon generation and attenuation at FMR 80—39875
Ni, platelet, transmission reson. meas. 77—20710
Ni, single crystal, linewidth 78—2744
Ni, static and dynamic magnetoelastic coupling 77—20665
Ni, thin films, surface demagnetisation due to chemisorption, ferromagnetic reson. study 80—80616
Ni-Co, ferromagnetic resonance, surface anisotropy 78—95526
Ni-Co, platelets, FMR field and linewidth, room temp. 77—4563
Ni-Co film, spin wave resonance 79—33542
Ni-Co film, spin-wave reson. exam. 78—2746
Ni-Co plate, surface anisotropy from ferromagnetic reson. 78—48049
Ni-Co thin films, spin-wave reson. obs., exchange stiffness const. 80—44924
Ni-Fe, epitaxial thin film, mag. structures and stresses, ferromag. resonance 78—72375
Ni-Fe film, ferromag. reson. under weak influence of eddy currents *(German)* 77—8412
Ni-Fe film, oligatomic, ferromag. reson. and torsion magnetometry, 123-373K 77—59461
Ni-Fe films, US generation by ferromag. reson. 78—88155
Ni-Fe-Mn, ferromag. reson. linewidth and saturation magnetisation 78—72418
Ni-V, ferromag. reson. meas., anisotropy consts. determ. 78—39410
NiCo film, crit. angle meas., pinning mech. 79—1719
$Ni_{2-x}Co_xBaFe_{16}O_{27}$, ferromagnetic reson., anisotropy and g-factor, spin-orbit interactions 77—24749
$Ni_{50}Co_{40}P_{10}$ amorphous film, spin wave excitation, ferromagnetic resonance study 80—50198
NiFe film, ferromag. reson., thermodynamical anal. 79—42840
$NiFe_2O_4$ epitaxial film on NdGG, structural and ferromagnetic reson. meas. 77—1574
Ni_3Mn, ferromagnetic reson. field and line width temp. depend. 3-300K 79—95651
NiO, thin films with spinel-type defect structure, FMR study 80—39877
NiO, with spinel-type defect struct., ferromagnetic reson. meas. 78—43647
NiO:Fe, exchange anisotropy of Ni-ferrite precipitates 79—28520
NiTi alloy single cryts., ferromag. reson., g-value and linewidth 80—71186
$PbFe_{12-x}Ga_xO_{19}$ ferrite, single cryst., ferromag. reson. 80—50193
$PbFe_{12}O_{19}$ platelets, ferromag. reson. absorpt. of close-packed bubble lattice 77—69709
$RbFeCl_3.2H_2O$, pseudo-one-dimens. canted Ising antiferromag., spin-cluster reson. 79—61233
$RbFeCl_3.2H_2O$, pseudo-one-dimens. canted Ising antiferromag., spin cluster reson. 79—61235
$RbFeCl_3.2H_2O$, spin cluster excitation expts. 80—66039
Tb, magnetisation, AC susceptibility and microwave absorption meas. 80—60221
W, ferromagnetic layer coating, longitudinal conduction electron spin waves, Larmor wave 79—33543
$(Y,Ca)_3(Fe,Ge)_5O_{12}$ LPE layer, exchange stiffness coeffs., 30-300K 79—78464
$(Y,Ca)_3(Fe)_2(FeGe)_3O_{12}$ film, exchange const., ferromag. reson. meas. 79—8023
$(Y,Lu)_3(Fe,Sc)_5O_{12}$ LPE layer, exchange stiffness coeffs., 30-300K 79—78464
Y alloys, pseudobinary Laves phases, mag. reson. 79—87323
Y-Co, amorphous alloy film, spin reson. meas., exchange stiffness 78—68389
YCo_3, amorphous ferromagnet, exchange dominated surface modes 78—52359
YCo_3 film, amorphous, DC sputtered, easy axis and easy plane magnetisation 78—64237
YCo_3 film, amorphous, induced and surface anisotropies, ferromag. reson. and static meas. 77—85507
YCo_3 film, amorphous, impurity like relaxation mechanism 79—73820
$(YEuYbCa)_3(GeFe)_5O_{12}$ bubble film with ion-implanted layer, FMR study 80—2643
YFe_2, amorphous, surface ferromag. layer, spin wave reson. Rutherford backscatt., and magnetisation meas. 79—73819
YFe_x film, $(x \simeq 2)$, magnetoelastic excitations obs. 78—68307
$Y_{1-x}Fe_x$, amorphous, spin resonance exam. 79—51860
$Y(Fe_xCo_{1-x})_2$, ferromag. reson. of pseudobinary cubic compounds 78—91961
$Y_3Fe_{5-x-y}Co_xGe_yO_{12}$, anisotropy and magnetostriction, ferromag. reson. expts., 4.2-500K 78—27030
$Y_3Fe_{5-x}Co_{x/2}Si_{x/2}O_{12}$, spin reorientation, NMR and ferromag. reson. meas. 80—65890
$Y_3Fe_{4.2}Ga_{0.8}O_{12}$, LPE grown thin film, ferromag. reson. 78—35041
$Y_3Fe_{4.6}Ga_{0.4}O_{12}$ film, surface spin wave reson. 77—85576
$Y_3Fe_{5-x}Ga_xO_{12}$, inhomogeneous stress effect on ferromagnetic resonance 79—24219
$Y_3Fe_{5-x}Ga_xO_{12}$, substituted garnet, floating zone grown, FMR line width, saturation magnetisation 80—29626
$YFe_{2x}Mn_{2-2x}$, mag. props. and FMR 79—95581
$Y_3Ga_xFe_{1-x}O_{12}$, film growth conditions rel. to memory element props. 77—66399

ferromagnetic resonance continued
- $Y_{3-x}Gd_xFe_{5-y}Al_yO_{12}$, solid solns., IR absorpt. spectra, physical props. 80—55082
- $Y_{3-x}Gd_xFe_5O_{12}$, FMR, influence of Gd^{3+} substitution on linewidth 77—8416
- $Y_{3-x}Gd_xFe_5O_{12}$, solid solns., IR absorpt. spectra, physical props. 80—55082
- $Y_{1.3}GdYb_{0.7}GaO_{12}$, epitaxial film, ferromagnetic reson. exam. 77—85579
- YIG, anomalous subsidiary absorpt. butterfly curves at 9.16 GHz and 300K 79—82875
- YIG, diamagnetically substituted, annealing effects on cation distrib. 79—1455
- YIG, diffr. of laser radiation by parametrically excited elastic and magnetoelastic waves 78—19338
- YIG, ferromagnetic resonance and magnetostatic waves in inhomogeneous internal field *(Russian)* 80—54954
- YIG film, low field microwave excitations of mag. domain walls 79—78456
- YIG film, on GdGaG, mag. excitations, diffusion layer effects 78—31112
- YIG film, periodically corrugated, insertion loss, reson. linewidth effect 80—80614
- YIG, film, photoinduced mag. surface anisotropy spin wave reson. 77—4560
- YIG, film, spin wave reson., complex mag. surface energies 77—4561
- YIG, film, spin-wave spectra in terms of mag. boundary conditions 79—78532
- YIG film, surface effects in spin wave reson. 77—16182
- YIG, homogeneous crit. relax. in dipole region *(Russian)* 78—10782
- YIG, LPE and CVD films, boundary effects, spin wave reson. meas. 79—78447
- YIG, LPE grown, FMR linewidth, Pb incorporation effects 77—8407
- YIG, La- and Ga-substituted, inhomogeneous epitaxial films, spin wave reson. 79—99773
- YIG, light scatt. by parametric spin waves with longit. pumping *(Russian)* 78—43648
- YIG, localised high-Q ferromag. reson. in nonuniform mag. fields 77—85575
- YIG, magnetic domain wall motion in high drive fields 80—65955
- YIG, magnetostatic precession modes, optical investigation 78—19337
- YIG multilayered film, magnetostatic spectrum 78—23350
- YIG, normally magnetised disc, reson. modes of magnetostatic waves 77—81015
- YIG, open die hot pressing, spin wave and FMR line width 80—89170
- YIG, optical detection of scatt. of homogeneous precession of magnetisation by defects 79—69728
- YIG, optical spectroscopic exam. of ferromag. reson. *(Russian)* 77—48057
- YIG, parallel microwave pumping threshold, RF modulation of mag. field 78—88195
- YIG, parametric excitation of spin waves in single-domain and polydomain states 77—12206
- YIG, parametrically excited wave discrete structure obs., light diffr. and modulation *(Russian)* 79—95650
- YIG, perpendicular pumping, spin wave instabilities, laser probing 77—43889
- YIG, polycrystalline, microwave relax. at low power levels 78—39409
- YIG, porous, parallel-pump spin-wave instability temp. depend. 79—78531
- YIG, porous and fine grain polycrystalline, temp. depend. of effective linewidth 77—85574
- YIG, press. up to 6.5 kbar 77—51956
- YIG, relax. after spin wave excitation in ferrite *(Russian)* 79—19783
- YIG, single cryst. film, pinning effects on magnetostatic modes 78—31111
- YIG, single crysts. grown by floating zone method, quality eval. of etching and optical microscopy, ferromag. resonance linewidth meas. 79—19990
- YIG spheres, anomalously low saturation threshold of magnetostatic modes 79—69729
- YIG, spin and magnetoelastic waves on longit. mag. pumping, optical obs. *(Russian)* 80—29727
- YIG, spin wave and magnetostatic wave echo 77—43887
- YIG, spin wave instability theory 79—73825
- YIG, spin waves, nonlinear spectroscopy studies 79—99696
- YIG, spin-wave and magnetostatic mode attenuation, double-pulse echo method 79—82874
- YIG, subsidiary absorpt. spin-wave instability threshold, anomalous struct. 80—34776
- YIG, surface spin waves, microscopic theory, mag. field effects 78—35044
- YIG, thick epilayer, unpinned magnetostatic modes 77—63290
- YIG, thin ferromagnetic film, exchange interaction constant, from paramag. resonance spectra of spin waves 79—42811
- YIG thin film, metal film effect on mag. boundary conditions, spin wave reson. obs. 79—78527
- YIG, unclamped specimen, magnetoreson. force effects *(Russian)* 77—32264
- YIG: Ca,(Mg), films, microwave losses induced by Fe^{4+} ions, ferromag. reson. study 79—1715
- YIG:Be^{2+} LPE film, microwave relaxation props. 79—65741
- YIG:Ca, epilayer, reversible oxidation, ferromag. reson. 78—76781
- YIG:Ca eddy current damping 80—39876
- YIG:Ca film, strong mag. reson. of Fe^{4+} 78—48047
- YIG:Co LPE films, with rectangular bubble domains, prep. and props. 79—82848
- YIG:Fe^{2+}, magnetocrystalline anisotropy, effect of high hydrostatic press. 77—43831
- YIG:Fe^{2+}, magnetostriction const. temp. depend., ferromag. reson. meas. 77—40103
- YIG:La,Ga, film, LPE-grown, Ga incorporation, depend. of magnetisation on growth rate 80—84627
- YIG:La,Ga film, uniaxial anisotropy, variation along growth direction 77—28416
- YIG:La film, for microwave applics., growth and ferromag. reson. meas. 78—3008
- YIG:La(Ga) films, ferromagnetic resonance, ion implantation effect 80—97145
- YIG:Pb(Si) film, (111) LPE, in-plane mag. anisotropy and ferromag. reson. meas. 78—2706
- YIG:Pr^{3+} influence of Pr^{3+} ions on spin-wave damping 79—28625
- YIG:Si, thermomagnetic processing and illum. effects on mag. props. *(Russian)* 77—8410

ferromagnetic resonance continued
- YIG:Sm^{3+}, mag. anisotropy, effect of Sm^{3+} ferromag. reson. study 80—80615
- YIG:V, mag. anisotropy and magnetostriction, effect of V 78—27029
- YIG:Yb, magnetoelastic coupling of Yb ions, ferromag. reson. meas. 77—69698
- YIG-Ge layered struct., anisotropy of EMF under nonlinear ferromag. reson. conditions 77—8417
- $Y_{2.85}La_{0.15}Fe_{3.75}Ga_{1.25}O_{12}$ epitaxial film, magnetostriction consts., microwave reson. meas. 77—24716
- $Y_{2.85}La_{0.15}Fe_{3.75}Ga_{1.25}O_{12}$, inhomogeneous bubble film, spin wave reson. 77—32265
- $Y_{2.85}La_{0.15}Fe_{3.75}Ga_{1.25}O_{12}$ epitaxial film, spin wave reson. spectrum 77—69703
- $Y_{2.85}La_{0.15}Fe_{3.75}Ga_{1.25}O_{12}$ LPE films, ion implantation effect on spin waves 80—71124
- $Y_{3-x}La_xFe_{5-y}Ga_yO_{12}$ film, horizontally dipped LPE grown, FMR, anisotropy field obs. 79—78449
- $Y_{1.62}Sm_{0.21}$ $Lu_{0.27}Cu_{0.9}Ge_{0.9}Fe_{4.1}O_{12}$, implanted bubble garnet, anisotropy profile, FMR study 80—7103
- $(YSmCaLu)_3(FeGe)_5O_{12}$, bubble film inhomogeneity, spin wave reson. meas. 80—44439
- $Y_{3-x}Sm_xFe_5O_{12}$, cubic and induced anisotropy, temp. depend., 100-300K, ferromag. reson. obs. *(Russian)* 78—39313
- $(YSmLuCa)_3(FeGe)_5O_{12}$, bubble material, dynamic characterisation, comparison between transport and FMR methods 80—39833
- $Zn_xCn_{0.1}Fe_{2.9}O_4$, Cu, Zn substituted magnetite, domain wall resonance, mag. props. 80—15756
- $Zn_xCu_{0.1}Fe_{2.9-x}O_4$, ferromag. reson., g-factors, Jahn-Teller ion effects 80—66043
- $Zn_xFe_{3-x}O_4$, ferromag. reson., g-factors, Jahn-Teller ion effects 80—66043
- Zr-Co(Fe), amorphous alloy film, spin reson. meas. 78—68389

ferromagnetism
- *see also ferromagnetic properties of substances; ferromagnetic relaxation; ferromagnetic resonance; Ising model; spin waves*
- acoustic wave scatt. and reemission by moving domain walls 77—24713
- admixture of antiferromag. bonds, thermodynamic functions *(Russian)* 79—87224
- alloy, binary, with mixed ferro- and antiferromag. exchange, magnetisation, phenomenological theory *(German)* 78—56297
- alloy, binary random Heisenberg ferromagnet transition temp., crit. conc. RKKY model 78—52266
- alloy, FCC, binary, on Ising system, sublattice magnetisation, tricrit. point, simulation 79—33491
- alloy, ferromag., temp. depend. of mag. props. and sp. ht., mag. phase transition region 78—64207
- alloy, local density of one-magnon states, cluster-Bethe-lattice approximation 77—32181
- alloy, partially ordered, spin wave stiffness const. 79—24150
- alloy, pseudobinary, magnon energy derivation 80—107996
- alloy between ferromag. and antiferromag. species, competing order parameters, Bethe-Peierls approx. 77—48003
- alloys, binary, anomalous Hall effect *(Russian)* 79—42521
- alloys, binary, ferromagnetism and spatial long-range order 80—60159
- alloys, crystalline and amorphous mag. props. from Rhodes-Wohlfarth plot 78—52190
- alloys, disordered cryst. and amorphous, mag. dipolar field distrib., computer simulation 80—65790
- alloys, ferromag., hyperfine field systematics of nonmag. ions 78—60093
- alloys, hyperfine field 77—24537
- alloys, itinerant electron ferromag., magnon stiffness const. 77—63155
- alloys, Lifshitz point occurrence, review 78—52265
- amorphous, itinerant electron model 79—73664
- amorphous, Landau-Ginzburg theory, magnetisation and Curie temp. 80—75700
- amorphous, spin wave excitations, similarity to liquid metal electronic struct. 77—12109
- amorphous, structural instabilities and mag. permeability relax., 77 to 400K 80—80559
- amorphous alloy resistivity, contrib. of mag. ordering *(French)* 77—89746
- amorphous alloys, domain struct. and mag. microstruct., review 80—15751
- amorphous alloys, indirect exchange interaction and paramag. Curie temp. 80—75752
- amorphous alloys, micromagnetic eqns. for case of dipolar and magnetocryst. fluctuations 80—11171
- amorphous alloys, props. and appls. 79—8016
- amorphous and crystalline ferromagnet, evaluation of complex Mossbauer spectra 78—43755
- amorphous and crystalline ferromagnets, evaluation of complex Mossbauer spectra 78—60370
- amorphous and fine-crystalline ferromagnets, with dipole-dipole interaction, spin waves *(Russian)* 78—56308
- amorphous ferromag., law of approach to magnetic saturation, effect of precipitates 78—72334
- amorphous ferromagnet, effective-field distrib. and resistivity minima 79—73501
- amorphous ferromagnet, excitations, calc. using hard sphere models 77—66289
- amorphous ferromagnet, Ising model, Curie temp., exchange integral fluctuation effects 80—50121
- amorphous ferromagnet, localised spin and phonon excitations, theory 79—7979
- amorphous ferromagnet, mag. excitations 78—68204
- amorphous ferromagnet, magnetisation, temp. depend. effect of nonrandom anisotropy 80—39773
- amorphous ferromagnet, metastable states in random anisotropy model 79—19710
- amorphous ferromagnet, micromagnetic theory 78—10661
- amorphous ferromagnet, random anisotropy effects 78—68223
- amorphous ferromagnet, random model spin wave spectrum 77—89918
- amorphous ferromagnet, resist. 78—64021
- amorphous ferromagnet, spin wave spectra *(Chinese)* 79—91219
- amorphous ferromagnet, spin wave spectrum rel. to struct. 77—66290
- amorphous ferromagnet, spin waves 79—24148
- amorphous ferromagnet, thermal cycling and annealing, critical behaviour 79—42790

ferromagnetism continued
amorphous ferromagnet with random anisotropy, temp depend. of magnetisation 79—78442
amorphous ferromagnet with random uniaxial anisotropy, hysteresis, magnetisation 77—80963
amorphous ferromagnets, apparent spin wave stiffness, low temps. 79—82776
amorphous ferromagnets, asperomagnets and spin-glasses, spin waves, theory 80—75747
amorphous ferromagnets, classical-spin model 79—33446
amorphous ferromagnets, Curie temp. depend. on nearest neighbour fluctuations 80—50120
amorphous ferromagnets, dispersion rels. and spin-wave spectroscopy *(Russian)* 79—7983
amorphous ferromagnets, ferromag. saturation, spatially random magnetostatic, magnetocrystalline, magnetostrictive and exchange fluctuations 78—60277
amorphous ferromagnets, hidden excitations, theory 80—75748
amorphous ferromagnets, localised spin excitations 80—15708
amorphous ferromagnets, magnetic and phonon rotons 79—61087
amorphous ferromagnets, neutron scatt. rel. to elementary excitations, amorphons 80—39494
amorphous ferromagnets, spatial fluctuations of magnetisation 79—19727
amorphous ferromagnets with random anisotropy axes, spin waves 80—7096
amorphous Heisenberg and Ising chains, thermodynamics 80—108022
amorphous Heisenberg ferromagnet, spin disorder resist., force-force correl. function method 80—24918
amorphous Heisenberg ferromagnet, spin wave excitations and magnetization curve 79—15292
amorphous Heisenberg ferromagnet, spin waves, effective medium approx. 78—68203
amorphous Heisenberg ferromagnet, variational cluster method 80—39728
amorphous magnet, Bethe-Peierls-Weiss approx. 78—76263
amorphous magnet, random anisotropy axis model in the infinite-range limit 80—88761
amorphous magnetism, Curie temperature and mag. excitation spectrum 78—10693
amorphous magnetism, random-axis model, low temp. renormalisation group anal. 79—61137
amorphous system, directional order and induced anisotropy energy, theory 78—95431
amorphous systems with dense random packed hard sphere structure, density of states and itinerant ferromagnetism 78—34950
amorphous thin films, struct. and mag. props., review 80—93148
analogy with coalescence of strange particles 77—13951
anharmonic, one dimensional ferromagnet, magnon and lattice deformation, bound state 79—78357
anharmonic Heisenberg ferromagnet, renormalised magnons and phonons 77—59373
anisotropic, critical behaviour in external field, renormalisation group approach 77—20601
anisotropic, domain-wall struct. depend. on const. and oscillating mag. fields *(Russian)* 79—69691
anisotropic, uniaxial two-sublattice ferromagnet, thermodynamic and mag. props. 80—65866
anisotropic critical freq. depend. of spin correlation functions 78—56321
anisotropic exchange interaction, random phase and Callen approximations *(Japanese)* 79—95560
anisotropic Fermi liquid, mag. order and transitions, phenomenological theory *(Russian)* 77—36038
anisotropic ferromagnet, crit. line shape anomalies 78—10698
anisotropic ferromagnet, critical behaviour at field-induced transition at mag. displacive limit 77—66335
anisotropic ferromagnet, Green-function theory 77—16025
anisotropic ferromagnet, in random longitudinal field, multicrit. point, theory 80—54903
anisotropic ferromagnet, longitudinal correlation function 78—34948
anisotropic ferromagnet, magnon spectrum, FMR line intensity, Curie pt. behaviour *(Russian)* 77—69694
anisotropic ferromagnet, one-dimensional Landau-Lifshits eqn. multi-soliton solutions *(Russian)* 80—71014
anisotropic ferromagnet, one-magnon light scatt., temp. depend. 77—52063
anisotropic ferromagnet, theory of light scatt. 77—90161
anisotropic ferromagnet domain wall, solitary-wave solns. 79—58553
anisotropic ferromagnet with biquadratic exchange, crit. temp. 77—12124
anisotropic ferromagnet with biquadratic exchange, critical temp. 77—40075
anisotropic ferromagnet with external field, crit. pts. derivation 80—103837
anisotropic ferromagnets, HF magnon energy renormalisation, kinematic consistency 80—29539
anisotropic ferromagnets, influence of spatially varying field on phase transitions 80—60339
anisotropic ferromagnets, spin wave interactions *(French)* 77—69524
anisotropic Heisenberg chain, nonlinear excitations 80—70927
anisotropic Heisenberg ferromag., inhomogeneous dynamic susceptibility tensor 80—39729
anisotropic Heisenberg model, ferromag. reson., magnon-magnon, phonon-magnon interactions *(Russian)* 80—11274
anisotropic magnet, low-temperature properties 79—65633
anisotropic magnet in external mag. field, continuous phase transition existence 80—108011
anisotropic magnet mixture, Heisenberg spin system by Monte Carlo simulation 79—78408
anisotropic $S={}^{1}/_{2}$ ferromagnet, reson. susceptibility, statistical mech. theory 77—8413
anisotropic spin one ferromagnetic in Callen's decoupling approx. 77—8258
anomalous dimensions of composite operators near two dimens. for ferromag. with O(n) symm. 77—20532
antiferromagnetic heavily doped semiconductors, Faraday light depolarisation in mixed mag. states 80—29726
asperomagnetism, short-range order, in Heisenberg magnet 80—65941
atomic order, interaction with localised ferromagnetism 77—72965
atomically rough surfaces, mag. excitations 77—69664
axisymmetric stationary mag. field calc. on nonlinear ferromag. media by iterative method *(Ukrainian)* 79—94127
band model, origin of magnetostriction, review *(Rumanian)* 80—34747

ferromagnetism continued
band model, pseudodipolar theory of magneto crystalline anisotropy 77—36068
band theory, electron orbital ordering 77—89923
Barkhausen discontinuities in model of rigid domain boundaries *(Russian)* 77—51922
basic models, classification of theories *(Rumanian)* 78—91840
BCC and HCP crystals, anisotropy of dipole fields, at interstitial sites 79—33584
BCC Ising model with competing interactions, fluction-induced first-order transition 80—20424
Berthollides, chaotic mag. states 78—56330
biaxial Lifshitz point problem in 3-dimens., spin wave theory 80—88759
bilayer compounds, spin-wave resonance, effect of random dilution 79—61236
binary alloy, annealed Ising ferromagnet 78—47927
binary alloy, atomic and mag. ordering, critical slowing down 78—14915
binary alloy, atomic ordering and ferromagnetism 79—87278
binary alloy, electrical resist. temp. depend. *(Russian)* 79—1592
binary alloy, electron interactions and spin-wave stiffness const. 77—1548
binary alloys, concentration derivatives and correlation functions of intrinsic variables 77—17937
binary alloys, strictly regular, quasi chemical model 78—39316
binary ferromagnetic alloys, with itinerant electrons, magnon lifetime, theory 78—34949
binary ordered alloy, dynamic mag. susceptibility, spin wave stiffness const. 79—38307
biquadratic exchange systems, low temp. spectrum and elementary excitation damping 77—72969
biquadratic systems, spin 3/2, elementary excitations in antiquadrupolar, ferrimag. and ferromag. phases 79—51763
bitter technique, model calc. for colloid accumulation on surface in mag. field *(German)* 77—9139
Bloch and Neel stability, calcs. of solitary domains 80—25157
Bloch electrons, dynamic longit. spin susceptibility 79—19709
Bloch wall steady-state motion in ferromag. 78—68291
Bloch wall-Neel wall transformation in a mag. field *(Russian)* 79—1682
Blume-Capel model for plane-triangular and FCC lattices 78—80114
Blume-Emery-Griffiths-Potts model, 2-dimens., phase diagram and crit. props. 77—20620
Bravais lattice, ferromagnetic ground state conditions in Ising and Heisenberg models 80—50129
bubble film, domain wall mass, under large in-plane fields 79—95618
bubble lattice existence near compensation point *(Russian)* 77—80977
catastrophe theory, appl. to ferromag. mol. field, for teaching 79—35467
chain, isotropic, solitary waves 78—64180
chain ferromagnet with uniaxial exchange, localised one-magnon states in presence of impurity *(Russian)* 77—63143
chain with isotropic long range interaction, crit. behaviour 77—12137
chemical spin systems, n-component, upper bounds on transition temp. 79—61122
chiral connection with axisymmetric gravitational problem and SU(2) vacuum gauge field 78—70258
circular ring, ferromag., elastic buckling in radial mag. field 78—23314
classical ferromagnet systems, partition functions zeros, correl. inequalities 78—27008
classical planar rotor, crit. temp. and correl. functions 78—14974
classical vector model, extension of high temp. free energy series 80—7062
cluster expansion of random ferromagnets 78—10637
coaxial semi-infinite cylinders fitted on each other, mag. conducting capacity anal. *(Bulgarian)* 77—61891
coexistence of phases, equiv. of different order parameter 78—49772
coexistence with ferroelectricity in systems with electron-hole pairing 80—7310
competing interaction systems, R-S model, series expansion and rigorous results 78—19201
concentrated alloys, ferromag., spin fluctuations 78—64290
conducting cryst., dynamics of s-d model in alternating mag. field *(Russian)* 80—65825
conducting ferromagnets, magnon spectra and magnetoacoustic reson. singularities *(Russian)* 80—50154
conducting ferromagnets, surface impedance resonance depend. *(Russian)* 79—91089
conduction electron spin, EM wave propagation with discrete spectrum 80—92923
conduction electrons and s-d exchange interaction in ferromag. elements 78—19021
conductor, electric field response and electrofluctuation instability *(Russian)* 78—56083
conductor, ferromag., microscopic analysis of eddy current losses 77—85484
conductor, plasma effects, selective transparency near antiresonance region 80—100476
constitutive eqns. of ferromagnetic bodies *(Italian)* 78—72317
constitutive equations for ferromagnetic bodies *(Italian)* 78—84372
continuous EM-acoustic conversion, normal skin effect case, expt. *(Russian)* 77—59304
continuous-spin Ising ferromagnets phase transitions 78—60260
continuum Heisenberg spin system, stationary spherically and axially symm. spin waves 80—34615
correlation function near free surface of Ising ferromagnet 78—21076
correlation inequalities for continuous-spin Ising ferromagnets 77—16020
correlation inequalities for Ising ferromagnets with symm. 78—21073
critical behaviour, low temp. renormalisation group, case with long-range interactions 77—63206
critical behaviour, mag. moment fluctuations and sp. ht. 77—28388
critical dynamics, influence of static impurities *(Russian)* 78—10713
critical dynamics above crit. temp., dipolar coupling 78—52286
critical dynamics above Curie pt. 79—87262
critical dynamics of ferromag. with exchange-anisotropy and dipolar interaction 77—36086
critical dynamics under quenched random magnetic fields 79—4681
critical indices for systems with strong dipole interactions *(Russian)* 77—28390
critical phenomena, modern theory, graduate level text 77—102
critical spin dynamics, appl. of 3-D neutron polarimeter 79—18098
crossover, field-induced, in mag. chain, scaling theory 80—54904
crystal field model of Invar effects in weak and strong ferromagnets 79—56484

ferromagnetism continued
crystal with defects, domain boundary displacement and magnetisation discontinuities, statistical theory *(Russian)* 79—51800
cubic and tetragonal ferromagnets, crit. behaviour in mag. field 77—66329
cubic crystal, mag. and magnetoelastic props. 79—15332
cubic crystal, texture analysis, generalisation of dispersion theory 80—80556
cubic crystal with dipole forces and anisotropic correlation function, phase transitions *(Russian)* 79—38504
cubic ferromagnet, elastic props., group theoretical approach 80—29600
cubic ferromagnet, localised magnon modes in narrow domain walls 77—69523
cubic ferromagnet, magnetic crystal, semi-infinite, impurity states, Green's function method *(Russian)* 79—51647
cubic ferromagnet, magnetised along ⟨110⟩, stability of lamellar domain struct. 79—15323
cubic ferromagnet, magnetoelastic interaction energy, arbitrary coordinate system 78—52335
cubic ferromagnet, second magnetoacoustic harmonic generation *(Russian)* 79—42816
cubic Ising ferromagnet, three spin interaction effect on mag. props. 80—54910
cubic lattices, fully frustrated, phase transitions, Gaussian and spherical model, free energy calcs. 80—60281
cubic metals, ferromag., mechanisms for elec. field gradients 78—43340
Curie point determ. from saturation magnetisation-temp. charact. 78—60281
Curie temperature, effects of biquadratic exchange and uniaxial anisotropy 80—60329
Curie temperature of ferromag. with random anisotropy, constant coupling approx. 78—76264
Curie temperature variation with small uniaxial anisotropy 77—85448
current distributions calc. in presence of ferromagnetic bodies, integral equations solution 80—18958
cyclically remagnetised ferromagnets, discrete spectra of induction calcs., demagnetising factor 80—103859
cylinder in MHD liquid, drag coeff. *(French)* 79—72952
cylinders, sinusoidally varying end fields, eddy current phenomena numerical calcs. *(German)* 79—94131
degenerate d-electron alloys, dilute, local moment and ferromagnetic state formation 79—51748
degenerate Hubbard model 77—69479
degenerate semiconductor, ferrogmag., magnon spectrum near instability of homogeneous state 79—28516
degenerate semiconductor, homogeneous state, phase transition and stability 78—6528
degenerate semiconductors, Curie temp. 78—6529
dense neutron matter, ferromag. transition, pure hard core gas model 78—70478
dielectric, crit. behaviour of exciton relaxation consts. 78—84442
dil. classical, crit. props. Heisenberg ferromagnet 79—28536
dilute, two dimens., spin wave spectrum 77—66287
dilute alloy, localised magnon mode in extended Wolff-Clogston 79—61097
dilute alloys, ferromag. ordering, long-range interaction of mag. impurities 78—19216
dilute alloys, mag. ordering impurities, random phase approx. and conc. limits 79—24187
dilute ferromagnet, Ising model, crit. props. in percolation limit 79—1677
dilute ferromagnet, linear spin-wave theory, effective medium approach 80—20393
dilute ferromagnet, slow neutron inelastic scatt. by spin excitations, cluster approx. 80—11168
dilute ferromagnet, spin wave excitations, multicomponent CPA theory 78—68135
dilute ferromagnets, Curie temp. *(Japanese)* 79—33484
dilute ferromagnets, spin waves at surface 79—61089
dilute ferromagnets, with site and bond disorders, Curie temp. 77—59407
dilute Heisenberg magnet, cluster expansion 80—15734
dilute Heisenberg magnet excitations near percolation threshold 79—87270
dilute magnetic systems, with nearest-neighbor and next-nearest neighbour interactions, crit. temp. 79—61121
dilute system, antiferromag. impurity with arbitrary spin, ground state calc. *(Russian)* 78—43585
dilute two-dimensional ferromagnet, concentration expansion, derivation of series *(Japanese)* 77—16019
diluted classical Heisenberg ferromagnet, position space treatment 79—87268
diluted ferromagnetic systems, cluster theory, second-neighbour interaction 77—89965
diluted ferromagnets, mag. excitations, appl. of recursion method 78—23223
diluted two-dimensional magnet, with anisotropic exchange interaction, excitation spectra 77—43826
dipolar Ising renormalisation group appls. to critical phenomena 77—57296
dipolar uniaxial ferromagnet, equation of motion, nonlinear response near critical point 79—99717
dipole moment of nuclear state using transient mag. field from ion passing through ferromag. *(Dutch)* 78—29386
dipole-exchange spin waves in cylindrical ferromag. *(Chinese)* 78—6521
disaccommodation in ferromagnets, electronic device for automatic measurement *(Japanese)* 80—68227
dislocated ferromagnet, inhomogeneous magnetisation near dislocation effect on FMR linewidth 80—25213
dislocation dynamic deceleration by spin waves *(Russian)* 77—28379
dislocation motion, mag. moments around screw dislocations, spin waves retarding dislocations 78—87670
dislocations, dynamic slowing down near Curie point *(Russian)* 79—8036
disordered, phase transitions, mol. field and Landau-Ginzburg theories 80—93118
disordered alloy, electron correls. and ferromagnetism 78—43548
disordered alloy, magnetooptic effects, theory 77—12366
disordered binary alloy, CPA theory of magnetoabsorption, electron scatt. mechanisms *(Russian)* 77—8549
disordered binary alloy, mag., with mixed exchange interaction, crit. behaviour *(Russian)* 79—1675

ferromagnetism continued
disordered binary alloys of ferromag. crystals, mag. dipole fields at interstitial sites 80—97176
disordered Ising model on Cayley tree, mag. transition above percolation threshold 79—73757
disordered itinerant-electron ferromagnet, spin waves 78—95427
disordered magnet, effective field approx., Ising model Hamiltonian 77—8261
disordered media, ferro- and antiferromag., and spin glasses, dynamic props. *(Russian)* 78—39350
disordered substitutional alloy, mag. props., Heisenberg model 79—38342
disordered systems, ferromag., review 80—29513
dispersion relations for energy eigenvalues of two magnon bound state 78—47964
domain, ferromagnet, interaction with mag. monopole 77—40078
domain boundaries, rigid, displacement theory including demagnetising field random perturbations *(Russian)* 77—8344
domain boundary interaction with solute atoms, review *(Russian)* 79—42098
domain boundary parade motion, low freq. *(Russian)* 80—103852
domain drag effect in presence of variable mag. field or variable transport current 79—78433
domain struct. effects on dynamic props., review 80—34678
domain struct. near first-order phase transition resembling second-order transition 80—93139
domain struct. study by time depend. neutron depolarisation 80—50138
domain structure, band model 77—69608
domain structure, dynamics, and microeddy currents in HF fields *(Russian)* 77—80957
domain structure, effect of defects, electron microscopy 78—64214
domain structure, influence of rapidly oscillating mag. field *(Russian)* 77—43847
domain structure, Landau-Lifshitz, in appl. mag. field *(Russian)* 78—60305
domain structure, multiaxial ferromag. applied stress effect *(Russian)* 78—76267
domain structure, theory, band model of ferromagnetism approach 77—80954
domain structure anal. by neutron depolarisation 77—40081
domain structure dynamics, EM losses 79—87281
domain structure image obtained by SEM *(Polish)* 80—34682
domain structure obs. using dry colloid observation apparatus, 90K to 290K 80—73394
domain structure stability in ferromagnet. with itinerant electron 77—20629
domain structure under torsion of cubic ferromagnetic polycrystals *(Spanish)* 79—91246
domain theory, boundary conditions and surface tension *(Russian)* 77—69616
domain theory, quasi-dislocation theory appl. *(Japanese)* 80—60358
domain wall, freq. const. for thermal activation 77—89976
domain wall, soliton theory and dynamics 80—29569
domain wall crit. vel. of ferromagnet in external mag. field 79—38354
domain wall dynamic slowing down *(Russian)* 79—78438
domain wall dynamics, soliton theory appl. 79—82813
domain wall dynamics and soliton theory, coercive force determ. 79—42796
domain wall dynamics in cubic ferromag. 79—73770
domain wall interaction energy with spherical cavity 77—8335
domain wall mobility, damping, dipole-dipole interaction 80—93140
domain wall motion, effect of transverse mag. field 78—68292
domain wall motion, exact soln. 79—87283
domain wall motion, limiting velocity *(Russian)* 78—56342
domain wall motion in ferromag. metals, voltage generation 80—34679
domain wall pinning, planar defects, coercive force and correl. length, soliton theory 78—31092
domain wall pinning effect and intrinsic coercivity, computer simulation 78—64217
domain wall retardation by spin waves *(Russian)* 80—25154
domain wall width, comments on definition 79—24193
domain walls, hypersound effect *(Russian)* 79—51810
domains, dynamic behaviour, struct., rel. to ferromag., teaching appls. 78—86080
domains, ferromagnetic and antiferromagnetic, neutron techniques for obs., review 78—64213
domains, phase transition, mathematical bifurcation process 80—29572
double critical magnetic scattering in polarised neutron expts. 79—65652
double transition spin glass-ferromagnetic systems, differential susceptibility 78—88131
duality transform. of equilib. states, surface tension between phases 78—144
dynamic demagnetisation of relatively large ferromagnetic bodies 79—61184
dynamic magnetic field on fast charged particle traversing ferromagnet 79—38423
dynamic structure factor in scaling region to first order in $\varepsilon=6$-d 77—63208
dynamic susceptibility, effect of inter-atomic interaction 79—65662
dynamical critical exponent crossover, hyperfine interaction vs. neutron scatt. expts. 78—84437
dynamics of ferromagnet in strong alternating mag. field *(Russian)* 78—88097
easy plane amorphous wire, magnetisation, variational calc. 80—71098
easy plene ferromagnets, containing dislocations, static props. 79—95626
easy-plane anisotropy, HF magnon energies, kinematic consistency 80—93097
easy-plane ferromagnet, magnetic anisotropy, temp. and field depend., classical model 80—71008
eddy current losses, in ferromagnetic plate, due to currents in parallel conductors *(Polish)* 78—29877
eddy current losses in ferromag. media *(French)* 79—69697
eddy current phenomena in ferromagnetic plates, numerical computation *(German)* 80—65952
eddy currents in saturable solid Fe, calc. methods *(German)* 77—54644
eddy-current problems, including moving Fe parts, numerical soln. 78—90340
education, Heisenberg theory of ferromagnetism, const. coupling approx. 77—78919
elastic beam, prismatic ferromag. deform. by external mag. field 80—34749
elastic ferromagnets, higher order surface couplings 78—79212

ferromagnetism continued
elastic hard ferromagnets, relaxation effects, vectorial internal variables, rational thermodynamics 80—75828
elastic properties of magnetic materials, review 80—7142
elastic solid, ferromagnetic, two coplanar Griffith cracks, singular stresses 80—65985
electrical resistivity of ferromagnet just below crit. temp., effect of mag. domains 80—39557
electron capture spectroscopy, technique for surface science and ferromagnetism 80—92766
electron ferromagnet, longit. US attenuation due to spin fluctuations 79—56588
electron gas, ferromagnetic, short-ranged correlations 79—7798
electron gas, ferromagnetic response functions, lattice effects 80—10898
electron gas, two dimens. 78—60258
electron gas, two dimensional, mag. props. 78—56095
electron gas, two-dimensional, polarised, correl. energy, para- and ferromag. states 77—47757
electron liquid with any spin polarisation, correlation energy, local exchange-correlation pot. 79—65399
electron liquids, temp. mag. transitions 77—69563
electron pair, in one-dimens. pot. box, possible ferromagnetism 79—61020
electron scatt. from ferromagnet in presence of mag. surface reconstruction 79—1705
electron transport with arbitrarily oriented ellipsoidal Fermi surfaces for ferromagnets 78—23006
electron work function ferromagnetic anomaly at Curie point, Vonsovsky-Sokolov model 77—12142
electron-magnon interaction effects on Ward-Takahashi identities in itinerant electron ferromag. 80—39730
EM and acoustic energy attenuation in many-domain magnets 80—7140
EM energy distribution, between orthogonal loops *(Russian)* 80—37934
EM field arbitrary discontinuity disintegration 80—28141
EM field distribution, wave impedance, power loss derived, constructional steel appl. 77—23595
EM field penetration, perturbation calc. *(Russian)* 79—59617
EM losses in monocrystalline ferromagnetic plate, influence of 90° domain wall motion *(Russian)* 78—27052
EM wave, refracted, unattenuated propag., optical modulation appl. *(Russian)* 78—25774
EM wave in ferromag. medium with variable permeability and hysteresis loss *(Polish)* 77—79722
EM wave penetration, plane, penetration depth calc. *(Bulgarian)* 78—50679
EM wave propagation, nonlinear waves and discontinuities 79—81330
EM wave propagation, nonlinear waves and strong discontinuities *(Russian)* 78—74819
EMF in ferromag. material under torsion *(Rumanian)* 78—86986
exchange and dipoles coupled ferromags., light scatt. from mag. surfaces, response theory 79—42820
exchange interaction, ferromag., role in X-ray threshold 77—90219
exchange interaction, ferromag. interaction obeying Kanamori-Goodenough rules 78—39307
excitations of ferromagnets with liq.-like disorder 79—61084
exciton condensation effects on props., Hubbard model of ferromag. metal 80—60171
exciton ferromagnet, and Peierls antiferromagnet, two-parameter Landau expansion 79—23907
exciton ferromagnet, incommensurate mag. structs., inhomogeneous magnetisation *(Russian)* 80—29566
exciton ferromagnet, inhomogeneous state *(Russian)* 78—88132
exciton ferromagnet, spin-lattice relax., light and US absorption *(Russian)* 79—7960
exciton insulator, coexistence of ferromag. and ferroelec. ordering 78—18973
excitonic, zero-sound excitations, Fermi liq. model 80—93101
excitons, in magnetically ordered dielectric, review *(Russian)* 77—80943
extended Hubbard model, ferromag. solns. 80—80473
fast charged particle traversing ferromag., dynamic mag. field, RPA 79—73230
FCC alloy, long range mag. order 77—63215
FCC Ising ferromagnet., cluster variation approx. 78—68278
fermi crystal, mag. props. of vacancies *(Russian)* 79—46881
Fermi liquid, ferromag. stability conditions 79—47224
Fermi liquid, multicomponent ferromag., g-factor 77—80724
Fermi liquid, spin ordering 77—15779
Fermi liquid model in external mag. field *(Russian)* 77—47952
ferroelectric, soft modes and ferromag. reson. 80—11275
ferroelectric ferro- and antiferromagnet, energy gap in spin wave spectrum 78—91858
ferroelectric ferromagnet soft mode damping, temp. anomalies *(Russian)* 80—44284
ferroelectric-magnetic coupled oscills., excitation by electron beam *(Russian)* 78—23257
ferroic crystals, prototypic point group, physical props., model 80—80715
ferromagnet, Bloch walls correlation and magnetic loss 78—95456
ferromagnet, easy-axis, higher order corrections to spectrum 78—80222
ferromagnet, impurity spin critical dynamics 80—2593
ferromagnet, magnon drops and mag. solitons 79—61093
ferromagnet, nuclear magnetisation motion, hyperfine field microscopic inhomogeneity, NMR freq. shift *(Russian)* 80—80623
ferromagnet, refractive index, magnetic contribution 79—28727
ferromagnet magnetisation, influence of high intensity longitudinal sound waves 80—103875
ferromagnet-antiferromagnet alloys, phase diagrams and multicrit. points in random mixed magnets 79—73756
ferromagnet-semiconductor structure, surface wave gain, ang. depend. 77—51938
ferromagnetic alloys, disordered crystalline and amorphous, dipole field distribution 80—25101
ferromagnetic metal, impurity resist., band model calcs. 77—39830
ferromagnetic semicond., spin-helicon wave parametric amplification 79—69665
ferromagnetic semiconductor, spectral density approach for s-f model quasiparticle concept 80—80173
ferromagnetic superconductor, paramagnetic fluctuations, influence on superconductivity 80—70900
ferromagnetic superconductors, self-induced vortices, magnetisation, Gibbs free energy 80—70916

ferromagnetism continued
ferromagnetism, Bethe-Peierls-Weiss model, phase transition calc. 79—2585
ferromagnets, exchange and dipolar coupled, spin wave renormalisation, Damon-Eshbach surface spin waves 80—2564
ferromagnets and spin glasses, supercond. and mag. order 80—93029
fibre, trajectories of paramagnetic particle stream near fibre 79—86128
with field intensity-dependent permeability, eddy current anal. *(German)* 77—40088
field theory, critical exponents, Borel transform. 80—80541
filament, ferromag., motion of charged particle in mag. field 77—46675
film, ϕ^4 domain walls, magnetisation, occurrence of crit. point 78—95500
film, band model of domain struct. 77—36105
film, Bloch wall struct. and anisotropy, analytical representation 78—88151
film, bubble domain lattice, parametric excitation of oscillations 77—8374
film, crit. angle of external mag. field for surface spin waves 79—47309
film, cross tie domain wall struct. and energy 77—59438
film, depend. of Curie temp. and spontaneous magnetisation on film thickness 77—32222
film, domain wall width meas. with electron microscope, astigmatism effects 79—19753
film, dynamics near transition pt. from homogeneous to inhomogeneous magnetis. state 80—108038
film, electric-charge-induced magnetisation 79—69700
film, ferromag., of cubic symmetry, depend. of Curie temp. on thickness and boundary conditions 78—19287
film, ferromag., shift of ant. temp. as result of Raman scatt. 80—54909
film, Fourier optics, mag. struct. determ. *(Russian)* 78—39371
film, ground state, effect of surface and bulk anisotropy *(Russian)* 79—11328
film, heterogeneity influence on static and dynamic props. of domain walls *(Russian)* 80—65974
film, influence of interference field harmonics on mean magnetisation vector *(Polish)* 77—40092
film, mag. anisotropy and defect distrib. *(Russian)* 77—59434
film, mag. bubble, effect of propag. on shape 77—16134
film, mag. domain wall energy determ. 79—95620
film, mag. props., rel. to struct. 79—91270
film, mag. props. meas. using planar magnetoresist. effect 78—21186
film, magnetostatic surface wave propag. 79—4661
film, n-vector model with Kac-type interactions 77—59436
film, nonlinear spin wave parametric resonance 80—2642
film, on antiferromag. backing, parametric reson. *(Russian)* 77—90043
film, phenomenology of domain walls, review *(Rumanian)* 78—60324
film, resistivity anisotropy theory 77—59342
film, spin pinning and mag. surface reconstruction, effect on standing spin waves 77—1600
film, spin wave propagation near surface 78—68308
film, surface rearranged, spinwave spectrum, derivation from generalisation of Bogoliubov canonical transform. 79—69702
film, surface spin waves and surface anisotropy effects at finite temp. 79—78452
film, tangentially magnetized, spin wave instability 78—2712
film, transverse bioped susceptibility, two-dimens. micromagnetism 80—11231
film, two-layer exchange coupled, mag. reversal, exchange energy const. *(Russian)* 77—59435
film, uniaxial anisotropy, approx. determ. of anisotropy const. 78—2713
film, with domain struct., magnetostatic oscills. 78—48010
film, with nearest neighbour and next nearest neighbour exchange interactions spin-wave excitations 79—73783
film, with unidirectional anisotropy, domain struct., mag. field effect *(Russian)* 78—19289
film energy absorpt. by magnetisation vector forced oscill. *(Polish)* 77—80970
film spin wave parametric reson. near phase transition 79—8053
films, (111), macrostripe and microstripe domain structs. *(Russian)* 79—28572
films, perpendicularly magnetised, surface and vol. magnetoelastic waves *(Russian)* 80—93151
films, spin correl. functions, crit. indices 80—7133
fine particle systems, physical basis and applications 78—84457
fine particles, stability of magnetisation curling mode and magnetisation helicoid struct. 80—11227
fine particles, thermal fluctuations, Brownian motion theory 80—11226
finite ferromagnets, dynamical props. of flat parallel domain struct. *(Russian)* 78—6499
FKG inequalities and fluctuations, probabilistic approach 80—77712
flow stress, effect of magnon mechanism of dislocation drag 77—69662
fluid, molecule system eqn. of state, exchange interactions, spin independent forces 77—59412
fluid 1D Ising and 3D Heisenberg solns. 77—85478
flux density curve analysis, transverse magnetisation by variable mag. field *(Russian)* 79—69696
flux quantisation in ordered ferromagnetic substances 78—80136
fracture-induced magnetic effect 77—80986
free electron pair, possible ferromagnetism of triplet state 79—30272
fully symmetric nonlinear theories, Green's function methods, SCF theory 77—61180
Gaussian random field, ferromagnets in $4+\varepsilon$ space dimens. 78—73954
generator coordinate method for boson representation of energy of $S={}^1/_2$ ferromag. 80—25066
geomagnetic field sensitivity in animals, ferromag. coupling to muscle receptors as basis 80—72185
giant intrinsic magnetic hardness, review 78—48004
Goldstone mode singularities, eqn. of state of isotropic magnet 79—42803
Green function, contrib. of bubble graphs due to dynamic and kinematic spin wave interactions 77—51894
Green function theory, dipolar crit. temps. 77—89962
ground state of magnetic polaron in $S \geq 1$ ferromag. cryst. *(Russian)* 77—63142
ground state representation of infinite one-dimens. Heisenberg ferromagnet 77—66234
gyrotropy, an implicity form of ferroicity 79—73286
Hall conductivity, scattering-independent contribs. 78—51957
Hall effect, AC, ferromag., in electron-impurity system, itinerant electron model 77—47796

ferromagnetism continued
hard magnetic materials, demagnetisation curve, single function approx. using computer *(Hungarian)* 78—60307
hardening, of ferromagnets by non-magnetic inclusions 79—38841
harmonic rotator, Coulomb plasma and related model, two dimens. case 78—88137
harmonic rotator, Coulomb plasma and related models, case of dimensions $D<2$ and $D>2$ 78—88136
harmonic rotator, Coulomb plasma and related models, renormalisation group treatment 78—88135
harmonic rotor model, interactions, spirals and phase transitions with and without long range order 80—60350
Heisenberg, ferromagnet, classical, with dipole-dipole interaction, renormalisation group and crit. exponents 80—60351
Heisenberg, ferromagnet, nearly two-dimensional and nearly one-dimensional thermodynamic props., Green's function investigation 79—15275
Heisenberg, ferromagnet, spin-one, uni- and biaxial anisotropy, RPA and mol. field approx. 78—34989
Heisenberg, ferromagnet, three-dimens. solitons 79—82741
Heisenberg, spin $^1/_2$ dil. magnet, crit. props. 80—15733
Heisenberg amorphous ferromagnet, magnetisation and Curie temp., CPA calc. 80—75703
Heisenberg and biquadratic exchange, eigenstates of short chains of spin-1 atoms 77—55652
Heisenberg and planar ferromagnets, exact results for spin-wave renormalisation 79—69660
Heisenberg and X-Y models, inequalities 77—91
Heisenberg anisotropic ferromagnet, Bogoliubov inequalities, inhomogeneous dynamic susceptibility, single particle matrix Green's function 79—95564
Heisenberg anisotropic ferromagnet, collective Green function, longit. susceptibility *(Russian)* 79—65631
Heisenberg anisotropic ferromagnet, longit. correl. function, generating Green functions 78—6500
Heisenberg chain, classical, nearest-neighbour, low temp. dynamics 80—80524
Heisenberg chain, explicit Plancherel theorem for ground state representation 77—89921
Heisenberg chain, ferromagnetically coupled and in mag. field, second magnons 79—65666
Heisenberg chain, spin diffusion coeff. and static spin correlators *(Russian)* 77—80942
Heisenberg chain, weakly bound magnon states *(Russian)* 80—100591
Heisenberg chain with biquadratic exchange, spin correl. length, susceptibility and spin diffusion *(Russian)* 77—69568
Heisenberg chains with easy plane, validity of classical statistical mechanics 80—44786
Heisenberg classical nearest-neighbour chain, dynamics, exact perturbative results 78—10700
Heisenberg classical spins on triangular cactus tree, random ordered phase 79—87265
Heisenberg continuous ferromagnetic chain, finite amplitude spin wave, stability 80—20395
Heisenberg dilute systems, computer simulation, mag. conc. of clusters, linearised eqns. of motion 79—78409
Heisenberg exchange integral, in nonorthogonal basis, for anti- and ferromag. systems 78—2641
Heisenberg ferromag. localised magnons around surface impurity *(Russian)* 78—84376
Heisenberg ferromagnet, amorphisation, anisotropically distrib. exchange forces *(Russian)* 77—85408
Heisenberg ferromagnet, and quantum inverse scattering method 79—61029
Heisenberg ferromagnet, anharmonic, renormalised magnons and phonons 78—91837
Heisenberg ferromagnet, anisotropic, collective Green's function, dynamical RPA 80—70925
Heisenberg ferromagnet, anisotropic, with biquadratic exchange interaction and uniaxial anisotropy, Curie temp. 80—7118
Heisenberg ferromagnet, biquadratic exchange, Green's function method, Hamiltonian and Curie temp. 80—15675
Heisenberg ferromagnet, boson field anal. of crit. temp. region 77—51911
Heisenberg ferromagnet, classical one-dimensional, transfer integral and collective coordinate results for free energy 80—93067
Heisenberg ferromagnet, classical spin field model in mag. field, statistical mechanics in one dimens. 78—43544
Heisenberg ferromagnet, consistent linearised Green's function theory for $s=1/2$ 79—4685
Heisenberg ferromagnet, correlation functions in ferromagnetic and paramagnetic regions, RPA 80—71075
Heisenberg ferromagnet, crit. dynamics in $2+\varepsilon$ dimens., low temp. phase 78—76262
Heisenberg ferromagnet, critical dynamics of impurity spin below T_c 80—71076
Heisenberg ferromagnet, critical points and two-magnon spectrum 79—87274
Heisenberg ferromagnet, cubic, with next nearest neighbour interactions, two-magnon bound states 80—70977
Heisenberg ferromagnet, Curie temp., decoupling of Green functions 77—12133
Heisenberg ferromagnet, diagram techniques for Greens functions with spin operators 78—91836
Heisenberg ferromagnet, dil., CPA theory, spin-wave stiffness and Curie temp. 78—31080
Heisenberg ferromagnet, dil., localisation of excitations near percolation threshold 79—15271
Heisenberg ferromagnet, dil., mag. excitations, localisation, wavefunctions 78—60275
Heisenberg ferromagnet, dil., spin wave localisation near percolation threshold 80—25120
Heisenberg ferromagnet, dil. spin $^1/_2$, renormalisation group treatment 79—69679
Heisenberg ferromagnet, dipole-dipole interaction, quantisation axis, magnetisation and critical point effects 78—34946
Heisenberg ferromagnet, disordered, influence of inhomogeneity of effective field on props. 78—10701
Heisenberg ferromagnet, disordered, pair effects in bond model 79—78290

ferromagnetism continued
Heisenberg ferromagnet, disordered, two spin species, spin-wave spectra calc. 77—59375
Heisenberg ferromagnet, disordered two-dimens., CPA theory of bond model 80—60163
Heisenberg ferromagnet, equivalence of large biquadratic exchange to small uniaxial single ion anisotropy 79—78292
Heisenberg ferromagnet, FCC, two-magnon bound state 77—20575
Heisenberg ferromagnet, Gell-Mann and Low renormalisation group, eqn. of state 78—31033
Heisenberg ferromagnet, infinite, one-dimens., ground state representation 80—25065
Heisenberg ferromagnet, instanton contrib. to correlation function *(Russian)* 78—95412
Heisenberg ferromagnet, intermediate quadrupolar phase existence 79—51784
Heisenberg ferromagnet, isotropic, second-order Green's function theory 80—2578
Heisenberg ferromagnet, isotropic with biquadratic exchange 78—39344
Heisenberg ferromagnet, linear, with applied mag. field, second-magnon like excitations 80—65837
Heisenberg ferromagnet, local levels arising from spin wave kinematic interactions 77—59374
Heisenberg ferromagnet, localised magnons around impurity 78—39305
Heisenberg ferromagnet, localized magnons in a spin chain with two 'surface' impurities 79—38310
Heisenberg ferromagnet, longitudinal dynamic susceptibility 78—64181
Heisenberg ferromagnet, low temp. behaviour in spectral density method 80—50028
Heisenberg ferromagnet, low-dimens., crit. temp. *(Russian)* 78—23274
Heisenberg ferromagnet, magnon renormalisation, higher approx. 78—14945
Heisenberg ferromagnet, magnon renormalisation 80—65849
Heisenberg ferromagnet, n-layer, effects of dilution and bond randomness 79—78296
Heisenberg ferromagnet, nearly one- and nearly two-dimensional, long-range order, upper bound for magnetisation 78—34947
Heisenberg ferromagnet, one-dimens., symm. crossover 79—87269
Heisenberg ferromagnet, quasi-two-dimensional, EPR at high temp. *(Russian)* 80—11243
Heisenberg ferromagnet, quasi-two-dimensional $S={}^1/_2$, expt. susceptibilities compared with high-temp-series expansion analysis 77—4506
Heisenberg ferromagnet, randomly diluted, 2-dimens., dynamics calcs. 77—40024
Heisenberg ferromagnet, randomly noncollinear mag. struct. and spin waves *(Russian)* 79—42764
Heisenberg ferromagnet, $S=1/2$, two magnon bound states, redefinition 79—42725
Heisenberg ferromagnet, self-consistent renormalisation of spin waves 77—72966
Heisenberg ferromagnet, spin coherent state representation, spin waves excitation spectrum 78—80117
Heisenberg ferromagnet, spin configurations near singularities in micromagnetism 80—54908
Heisenberg ferromagnet, spin operator study by small angle mag. neutron scatt. 80—15700
Heisenberg ferromagnet, spin waves at low temp., method of variational derivatives 79—24152
Heisenberg ferromagnet, spin-one, with biquadratic and uniaxial anisotropy, Curie temp. 79—61123
Heisenberg ferromagnet, spin-wave renormalisation, $S\geq1$ 80—71070
Heisenberg ferromagnet, stepped surface, spin-wave modes calc. 77—73015
Heisenberg ferromagnet, strongly anisotropic with impurities, in transverse field, one-magnon states 77—69476
Heisenberg ferromagnet, structural disorder effects on Curie temp. 79—78417
Heisenberg ferromagnet, structurally disordered, variational method for cluster model 78—91839
Heisenberg ferromagnet, surface spin waves theory *(Russian)* 77—89939
Heisenberg ferromagnet, three-dimens., two magnon states, effect of next nearest neighbour interactions 78—64178
Heisenberg ferromagnet, transition temp., mean field upper bound 80—97048
Heisenberg ferromagnet, two-dimens., spin dynamics, renormalisation group calc. 78—47966
Heisenberg ferromagnet, two-dimensional, soln. 80—60166
Heisenberg ferromagnet, two-magnon reson. in absence of bound states, calc. 80—60423
Heisenberg ferromagnet, with biquadratic exchange interaction 78—34999
Heisenberg ferromagnet, with single-ion anisotropy, correlation functions calc. 78—31076
Heisenberg ferromagnet 80—25064
Heisenberg ferromagnet containing nonmagnetic impurity, local mean spin deviations 77—66236
Heisenberg ferromagnet eqn. equivalence to nonlinear Schrodinger eqn. 79—95563
Heisenberg ferromagnet in critical region, Bloch renormalised spin wave approx. 79—82784
Heisenberg ferromagnet system, temp. Green's function sum rules *(Chinese)* 80—31678
Heisenberg ferromagnet with biquadratic exchange 79—38338
Heisenberg ferromagnet with biquadratic interactions, Green's function approaches 77—55653
Heisenberg ferromagnet with higher-order exchange interactions, thermodynamic props. 79—42770
Heisenberg ferromagnet with resonant impurities, localised degrees of freedom *(Russian)* 79—87280
Heisenberg ferromagnet with s-d exchange interactions, Curie temp. 78—19255
Heisenberg ferromagnetic alloy, critical behaviour *(Russian)* 78—88127
Heisenberg ferromagnetic one-dimens. chain, solitary magnon solution 77—69473
Heisenberg ferromagnetic system with biquadratic exchange interactions, spin wave theory *(Chinese)* 80—88755
Heisenberg ferromagnets, entropy 79—65635
Heisenberg ferromagnets, surface effect on thermodynamic props. and excitation spectra 79—11282
Heisenberg Hamiltonian, ferromagnetic ground state, conditions for existence 79—73662

ferromagnetism continued
Heisenberg isotropic ferromagnet, first-order Green's function theory 77—36046
Heisenberg linear chain, dynamical correl. functions 77—63221
Heisenberg linear spin systems, dynamical spin correlation functions 78—31035
Heisenberg magnet, dil., renormalisation group calcs. 79—56550
Heisenberg magnet, with 180° domain walls, quantum mech. treatment 77—48007
Heisenberg magnet surface, spin behaviour, review 77—20527
Heisenberg magnets, with two kinds of exchange interactions, surface magnons and surface spin arrangements 77—36043
Heisenberg mixed crystal mag. props. 80—34579
Heisenberg model, 1- and 2-dimens., NMR line breadth 77—48064
Heisenberg model, anisotropic, quasicollective spin waves in paramag. region 77—43827
Heisenberg model, classical, low temp. spin wave dynamics 78—6501
Heisenberg model, classical, magnetisation, Monte Carlo calc. 78—23229
Heisenberg model, critical dynamics spin wave theory, dynamic scaling hypothesis failure 80—97082
Heisenberg model, density of states and heat capacity near percolation threshold 77—77021
Heisenberg model, disordered ferromag. states, random exchange integrals 80—80550
Heisenberg model, disordered spin system, commutator and anticommutator Green's functions 79—51792
Heisenberg model, elastic approximation, vibr. and mag. props. of interface and planar defect *(French)* 77—72767
Heisenberg model, eqn. of state, using modified Gell-Mann Low renormalisation group 77—63225
Heisenberg model, Faddeev eqns. for three-magnon T-matrix 77—36045
Heisenberg model, finite magnetisation assuming ferromag. coupling 78—43541
Heisenberg model, helical spin chains, static and dynamic props. 79—73661
Heisenberg model, mag. excitation near surface of high Miller indices 77—51871
Heisenberg model, magnetic excitations on ideas and atomically rough surfaces 78—14944
Heisenberg model, nearest-neighbour spin-spin correl. functions calc. 80—80537
Heisenberg model, nuclear spin quantum mechanical behaviour 77—51872
Heisenberg model, point singularities in micromagnetic systems with radial symmetry 80—107976
Heisenberg model, pseudoparticle solns. 79—47223
Heisenberg model, quasiclassical description, soliton solutions 78—39282
Heisenberg model, quasilow dimensional, small dilution perturbation theory at 0K 78—56281
Heisenberg model, random, thermodynamics, cluster approx. 77—16032
Heisenberg model, single site anisotropy, statistical mechanics 78—31034
Heisenberg model, specific heat, high-temp. expansions, numerical investigation *(German)* 77—59420
Heisenberg model, spin wave excitations at finite temp., CPA calc. 77—32142
Heisenberg model, structurally and chemically disordered, critical behaviour 77—43838
Heisenberg model, surface spin instabilities 77—20533
Heisenberg model, transition temp. calc., depend. on spin and coordination no. *(Russian)* 77—47997
Heisenberg model, two-dimensional dil., density of states near percolation threshold 77—1533
Heisenberg model, with anisotropic exchange, homogeneous relax., time const. calc. 77—16149
Heisenberg model, with biquadratic exchange, first-order quadrupolar transition 77—69571
Heisenberg model, with biquadratic exchange 77—63060
Heisenberg model, with uniaxial exchange anisotropy, cumulant expansion method 77—12076
Heisenberg planar model, two dimens., renormalisation vortices, and symmetry breaking perturbations 78—10638
Heisenberg random ferromag., cluster approx. 79—82807
Heisenberg randomly dil., ferromag., spin wave excitation exam. 77—24665
Heisenberg spin-$^{1}/_{2}$ ferromagnets, 1st order Green's function theory 78—72323
Heisenberg theory, spin wave exam. *(Dutch)* 79—1663
Heisenberg three-dimens. quantum models, ferromag. phase, conditions for $T_{c}=0$K 79—38345
Heisenberg two-dimensional ferromagnet, conformal symm. *(Russian)* 78—23232
Heisenberg-Ising magnets, random, critical temps., binary mixture, amorphous magnet and spin glasses 80—54911
Heisenburg ferromagnet, surface magnetisation profile and localised magnons 80—70985
helical order of spins, coexistence with superconductivity 79—65588
helical structures, magnetooptic light interaction 79—65843
helimagnetic-ferromagnetic transition for two-dimens. spins case 77—66349
helimagnetism, isotropic bilinear spin Hamiltonian on Bravais lattice 77—51866
hexagonal ferromagnet, nonlinear magnetoelastic effects and phase transforms. *(Russian)* 78—48015
hierarchical model, renormalisation group approach 80—34580
high-energy magnetic materials, development, props., treatment procedures and testing *(Italian)* 80—54914
higher harmonic method, ferromag. object inspection, difference schemes 80—89444
homogeneous ferromagnet, nuclear spin-lattice relaxation, magnon effects 79—51877
honeycomb lattice, real space renormalisation, ferromag. (antiferromag.) appls. 80—11200
Hubbard chain, half-filled band, strong coupling, low temp. absorpt. lineshape 77—59546
Hubbard III approximation, numerical results for arbitrary values of correlation energy and electron density 77—51874
Hubbard model, doubly degenerate, ferromag. instability 77—32151
Hubbard model, doubly degenerate, functional integral approach 79—99711
Hubbard model, doubly degenerate, long range order 80—50029
Hubbard model, extended, phase transitions 78—6531

ferromagnetism continued
Hubbard model, ferromag. phase transition 77—77062
Hubbard model, hybridised, absence of ferromagnetism 80—39731
Hubbard model, mag. susceptibility, modified Stoner criterion 79—51736
Hubbard model, narrow S-band with inclusion of intersite correlations 77—63066
Hubbard model, photoemission spectrum, effect of electron correlation 79—78828
Hubbard model, single band with infinite repulsion on 2×2×2 lattice, thermodynamic props. 79—87225
Hubbard model, single site approx., condition for ferromag. instability 78—2643
Hubbard model, static approx., mag. phase transitions 77—1558
Hubbard model, two band, mag., orbital and charge ordered states 78—27012
Hubbard model on 2×2×2 lattice, ground state energy and total spin 80—29518
Hume-Rothery alloys, magnetism 78—95417
hydroelastic instability of ferromagnetic plate in magnetic field 77—68483
hyperfine field at positive muon in ferromagnets 80—40029
hysteresis, departure from Rayleigh law in low mag. fields, expts. on Gd and NiFe 77—40086
hysteresis, static models 77—85490
hysteresis, swallow tail catastrophe anal. 78—56349
hysteresis loops, oscillography using ferroprobe transducers 79—87785
hysteresis loops, symmetric, polynomial expression *(Spanish)* 77—73044
hysteresis rel. to irreversible phase transition in soft ferromagnets 80—34693
ideal Heisenberg ferromagnet, phonon renormalisation and spin waves 80—88754
impurity relaxation in nonresonance field, phonon amplification *(Russian)* 80—100310
impurity uniaxial ferromagnet, thermodynamics below Curie point *(Russian)* 77—43801
inclusions in paramagnetic matrix, mag. susceptibility determ. 79—97407
induced moment systems, effect of spin fluctuations 80—2585
infinite ferromagnetic medium, energy and mobility of Bloch point singularities 78—68331
inhomogeneous ferromagnetic conductors, skin effect *(Russian)* 77—47847
inhomogeneous ferromagnets, Landau's theory of second-order phase transition 80—50092
inhomogeneous ferromagnets, phase transitions, micromagnetic theory 80—65942
inhomogeneous itinerant electron ferromagnet, mag. and thermal props. 79—7964
inhomogeneous systems, Ginzburg-Landau theory, free energy and Curie temp. 79—51789
instantons in anisotropic ferromagnets 80—7066
insulating solids, long-range ferromag., antiferromag. superexchange, limit function 80—54883
insulating systems, magnetic, review of expts. 78—68240
insulator, magnetoelastic wave dispersion rels. and normal modes 77—55694
insulator-metal transition, s-d exchange interaction effects 78—2421
insulators, spin waves and uniform transverse magnetization, oscillatory eigenstates *(Russian)* 80—11181
insulators at parallel pumping, nonlinear magnetisation dynamics 77—8288
interaction between localised moments in system with electron hole pairing *(Russian)* 78—88111
intermediate spherical model, critical temp. 77—63053
intermediate valence compounds, phonon produced instabilities, periodic Anderson model 78—79964
internal energy relationship to moment 77—16028
internal fields, positive muon investigation 78—68438
intrinsic semiconductors, indirect exchange interaction, finite temp., valence bands and energy gaps effect 80—59943
Invar alloys, bulk modulus anomaly, rel. to itinerant electron model of ferromag. 77—48025
invariant equilibrium states and surface tension in ferromagnetic systems 79—40491
ion implantation in ferromagnets *(Flemish)* 78—79623
irreversible and reversible magnetising processes, impressed propag. 80—88819
irreversible Bloch wall jumps and static losses 78—19276
Ising, correlation decay, zero-field susceptibility, mass gap 80—50116
Ising, high-freq. props. quantum theory, susceptibility tensor calcs. *(Russian)* 80—11143
Ising, kinetic chain relaxation, randomly signed exchange 80—70919
Ising, rectangular, susceptibility, determ. of critical indices 79—28537
Ising, spin $^{1}/_{2}$ dil. magnet, crit. props. 80—15733
Ising amorphous, crit. temp. 80—11207
Ising and Heisenberg ferromagnets with biquadratic exchange, uniaxial anisotropy, susceptibility calc. 79—99670
Ising and Heisenberg model, threshold inequalities for ground state 80—7064
Ising chains, metamagnet, absence of first-order transitions 79—51794
Ising disordered chains, ferromag., long-time relax. 80—34652
Ising ferro and antiferromagnet random bond mixture, on s.c. lattice, phase transition 77—12131
Ising ferro- and antiferromagnet, quenched random mixture, Bethe approx. for phase transition 77—16082
Ising ferromagnet, 2-D, boundary conditions and cluster property, translation-invariant correlation functions 80—54856
Ising ferromagnet, 2-D, with quenched bond disorder, critical temp. 78—56328
Ising ferromagnet, 4-D, correction to leading singularity of order parameter 80—25061
Ising ferromagnet, annealed, of binary alloys 77—59368
Ising ferromagnet, comparison with plane rotor 80—60348
Ising ferromagnet, correl. functions, boundary conditions 78—27009
Ising ferromagnet, crit. correlation-function approxs. 78—56324
Ising ferromagnet, crit. exponents in integral representation 78—56325
Ising ferromagnet, diamond lattice, phase transition, crit. props. 80—93127
Ising ferromagnet, diluted, theory generalisation 79—78283
Ising ferromagnet, disordered, approximate treatment 78—52262
Ising ferromagnet, disordering, short-range mag. order 80—50119

ferromagnetism continued
Ising ferromagnet, four-dimensional logarithmic correction to mean-field order parameter 79—73754
Ising ferromagnet, gaussian fluctuations of mol. field, magnetisation and free energy 80—70918
Ising ferromagnet, general, Lee-Yang theorem GHS inequality, spin-$^1/_2$ approx. 77—20524
Ising ferromagnet, linearisation assumption, crit. correlation function 80—60158
Ising ferromagnet, phase coexistence, translation invariance and stability 80—80513
Ising ferromagnet, randomly dilute, determ. of transition temp. by Monte Carlo simulations 77—12130
Ising ferromagnet, randomly dilute, with second neighbour interaction, concentration expansion study 77—85452
Ising ferromagnet, rectangular, n-point functions 77—63054
Ising ferromagnet, S=1, single-ion type uniaxial anisotropy, cluster-variation method appl. in pair approx. 78—68281
Ising ferromagnet, site diluted, crit. props. 78—72351
Ising ferromagnet, spin 1/2, integral representation 78—2639
Ising ferromagnet, spin S, integral representation 78—43543
Ising ferromagnet, spin-operator reduction relations, representation 78—95443
Ising ferromagnet, surface tension using real-space renormalisation group methods 79—73760
Ising ferromagnet, three-dimens., transition temp. with two- and four-spin interactions 79—42769
Ising ferromagnet, two-dimensional, with second-neighbour interaction, computer simulation, series-expansion method 77—63052
Ising ferromagnet, upper bounds for correlation functions 79—42718
Ising ferromagnet, with transverse single-ion anisotropy, phase transitions 78—19259
Ising ferromagnet and antiferromagnet, two-dimens. square, ground state, apparent 3-spin interactions 80—88709
Ising ferromagnet and spin glass systems, random, crit. dynamics 80—34666
Ising ferromagnet with two- and four-spin interaction, improved product average decomposition method 80—20406
Ising ferromagnetic half-plane, surface, pinned domain wall, free energy and magnetisation profile 80—60361
Ising ferromagnets, coexistence of phases, new inequalities 77—80946
Ising ferromagnets Ursell function inequality 79—4640
Ising ferromgnet, rectangular, n-point functions 78—76250
Ising magnet, one-dimens., with mag. impurity, one-magnon states 77—36042
Ising metamagnet, dilute tricritical point calcs. 80—50099
Ising mixed ferromagnetic-antiferromagnetic systems with arbitrary spin, critical temp. 79—78407
Ising mixture, quenched random, on Cactus tree 77—16081
Ising model, bond random, ferromagnetic-antiferromag. mixture, triangular cactus tree, statistical theory 80—75702
Ising model, bond-dil. two-dimens., phase transition 80—60320
Ising model, bond-diluted, first and second neighbour interactions 78—91870
Ising model, cluster size and percolation 79—65630
Ising model, constant-coupling approx., successive phase transitions 80—97108
Ising model, critical exponents for high temperature series expansion 79—99701
Ising model, Curie point in quenched bond model 78—56318
Ising model, disordered, thermodynamic pot., ferro-and antiferromagnetic bonds, mag. moment and entropy *(Russian)* 79—19714
Ising model, effective field theory 79—4684
Ising model, equivalence of different order parameters 77—36082
Ising model, exponent inequalities at roughening transition 77—32204
Ising model, FCC, cluster variation approx. 78—27049
Ising model, ferromag. and antiferromag. in mag. field, new perturbation approach 78—56336
Ising model, ferromagnetic, band-mixed square lattice, approx. crit. surface 80—70921
Ising model, free energy and susceptibility inequalities, phase transition 78—43541
Ising model, looped tree-like lattice, phase transition 80—7113
Ising model, mixed, renormalisation group calc. 79—56547
Ising model, nonuniform mag. field method, crit. correlation function approximations, calc. 80—20407
Ising model, one-dimens., with phase transition, thermodynamic props. calc. 80—80536
Ising model, percolation threshold, real-space rescaling approx. 77—40073
Ising model, phase boundary rigidity, Onsager Temperley model 77—28394
Ising model, random field instability of ferromag. state 77—40072
Ising model, randomly dilute, conc. expansion study 80—60315
Ising model, renormalised crit. behaviour 78—52272
Ising model, semi-infinite, with free surface, renormalisation group approach 78—14975
Ising model, spin-1, with random anisotropy, Curie temperature 77—28399
Ising model, spin-glass, renormalisation group calc. for two dimens. models 78—14968
Ising model, spin-one three dimensional, single-ion anisotropy, crit. behaviour 80—80540
Ising model, three-dimensional, two-spin correlation function, method for phase diagram 78—56323
Ising model, transition point calc. 80—20408
Ising model, tricritical phenomena, nearest neighbour and next nearest neighbour interactions 77—69566
Ising model, two dimensional, second neighbour interaction, Pade approximant, critical behaviour 79—4682
Ising model, two-dimens., ferromagnet-spin glass transition, Monte Carlo calc. 80—60287
Ising model, two-dimens., order parameter and induced susceptibility 80—71036
Ising model, two-dimens., surface tension of diagonal interface 77—59369
Ising model, with antiferromag. next-nearest-neighbour coupling, relative mag. scattering intensity and anomalous scatt. 77—69469
Ising model, with regularly spaced blocks of impurities, crit. temp. and sp. ht. 77—69576

ferromagnetism continued
Ising model, with transverse field, ferromagnetic and antiferromagnetic susceptibilities 80—60160
Ising model, with transverse field 77—77016
Ising model and P(ϕ) theories, correl. inequalities 77—51865
Ising model crit. props. of site and bond diluted model 79—42766
Ising model for annealed magnetic mixture with continuous distrib. of random bonds 77—16023
Ising model lattice, impurities and probe independence of hyperfine crit. exponents 79—87267
Ising model transition temperature in new mean-field theory 79—51785
Ising model with competing interactions, critical properties and exact results 80—93129
Ising model with mag. field and lattice gas 78—10703
Ising model with random exchange bonds, phase diagram 78—43604
Ising models, quenched, with random ferromag. interactions, magnetisation upper bound 77—66233
Ising or ϕ^4 ferromagnet, rigorous inequality for sp. ht. 79—78413
Ising planar ferromag. model, spinor algebra and odd operators 78—45570
Ising quadratic two-dimensional ferromagnet with three spin interactions 80—2542
Ising S=1, $^1/_2$ mixture, one-dimens., random, mag. props., spin distrib. 78—95407
Ising site model, random mixtures, Monte Carlo simulation 78—73935
Ising site model, random mixtures, Monte Carlo simulation 78—73936
Ising spin 1/2 three-dimensional model, transition temp. in integral representation 77—77059
Ising spin glass, d-dimensional, frustration effect 80—108019
Ising spin glass, d-dimensional, frustration effect and dilution problems 80—108018
Ising spin glasses, dual transformation into ferromagnetic models, critical temp. in frustrated models 79—73763
Ising spin glasses, in effective interaction approx. 80—60288
Ising spin-s model, crit. curve 79—4679
Ising spins randomly located, with oscillatory exchange interactions 79—42778
Ising system, Lifshitz points, phase diagram transition temp. determ. interface free energy vanishing 79—99716
Ising systems, finite thickness, renormalization-group transformation, real-space 80—15749
Ising two-dimensional spin systems, decimation transforms. 77—77017
Ising type model, elastically coupled, effects of dipolar forces on crit. sound attenuation in uniaxial systems 80—50158
Ising-Heisenberg linear ferromagnet, excitation spectrum and thermodynamic props. 80—50118
Ising-Heisenberg-XY crossover, bicritical point, partial differential approximants for susceptibility series 77—85466
isolated pores and brittle cracks in single domain ferromagnets *(Russian)* 78—39381
isotropic, dynamical spin-spin correl. function at Curie temp. in 6ϵ dimensions 77—4481
isotropic ferromagnet, critical behaviour in random uniaxial anisotropy model 79—38349
isotropic Heisenberg ferromagnet, localised spin-wave modes, biquadratic exchange effects 77—51896
isotropic Heisenberg ferromagnet, resistance inequalities, C*-algebra 77—4487
isotropic Heisenberg ferromagnet, with arbitrary spin, correlation functions 78—31075
isotropic magnet, Goldstone mode singularities eqn. of state, magnetisation curve, perturbation theory calcs. 78—43607
isotropic model ferromagnet, longitudinal magnetisation spectrum calc. 78—10627
isotropic two-dimensional magnetism, long range forces effect 78—52291
itinerant, effective Hamiltonian 80—11150
itinerant, local band theory, Fermi-liq. theory 78—31040
itinerant, local band theory, nonlinear Landau Lifshitz eqns. 78—31042
itinerant, local band theory, spin waves 78—31041
itinerant electron, surface spin waves, tight-binding Hubbard model 80—39763
itinerant electron ferro- and antiferromagnetism, spin fluctuations 79—7961
itinerant electron ferromag., spin fluctuation *(Japanese)* 78—47936
itinerant electron ferromag., Ward-Takahashi identities, zero temp. case 79—73669
itinerant electron ferromagnet, effective Lorentz force and Landau level 78—80120
itinerant electron ferromagnet, magnetoelastic contribs. to US vel., elastic consts., and susceptibility 80—75829
itinerant electron ferromagnet, magnetoresist. and anomalous Hall effect due to electron-phonon interactions 80—70680
itinerant electron ferromagnet, magnon spectrum just below T_c, theory 80—65833
itinerant electron ferromagnet, temp. depend. of angle-resolved photoemission 80—76142
itinerant electron ferromagnet, two magnon bound states 77—20537
itinerant electron ferromagnet with domain struct., spin waves 78—64182
itinerant electron ferromagnetic alloys, magnon energy, effect of ordering 79—7986
itinerant electron ferromagnetism, linear response theory 77—72989
itinerant electron ferromagnetism, local exchange model 77—72994
itinerant electron ferromagnetism, single-site functional integral approach 79—65637
itinerant electron ferromagnetism, spin fluctuation theory 78—80151
itinerant electron ferromagnetism, thermodynamic props. 79—91245
itinerant electron ferromagnetism at zero temp. 78—56285
itinerant electron ferromagnetism of two dimensional system 77—24666
itinerant electron ferromagnets, elastic props. 79—61035
itinerant electron ferromagnets, elastic props. and electronic struct. 80—66001
itinerant electron ferromagnets, magnetisation fluctuations, Landau-Lifshitz eqn. 79—73729
itinerant electron ferromagnets, magneto-volume effects 80—60397
itinerant electron magnetism, thermodynamic aspects 77—72992
itinerant electron magnetism in two dimensions 77—63065
itinerant electron model, contrib. of Conyers Herring in 1930s 80—57056
itinerant electron model, spin quantization direction fluctuations, short range order. 80—34582
itinerant electron model, spin wave stiffness temp. depend. 77—20535

ferromagnetism continued

- itinerant electron model, susceptibility, local exchange approx. calc. 80—60169
- itinerant electron model for ferro- and antiferromag. systems, dynamic susceptibility 77—72988
- itinerant electron system, coexistence of antiferro- and ferromagnetism 78—2645
- itinerant electron theory, local moment approach, review *(Japanese)* 80—25071
- itinerant ferromagnet, effect of planar defects on electronic struct. and mag. ordering 79—99672
- itinerant ferromagnet, Einstein temp. 79—24126
- itinerant ferromagnet, electron-magnon interactions 79—99673
- itinerant ferromagnet, inhomogeneity corrections to ground-state props. 78—14921
- itinerant ferromagnet, mag. props., temp. depend., functional integral approach 80—60170
- itinerant ferromagnet, magneto-volume ext. 77—66404
- itinerant ferromagnet, sloppy spin waves above T_c 77—72979
- itinerant ferromagnet, spin wave stiffness const., electron correl. effects 79—19733
- itinerant ferromagnet, spin waves, surface effects, RPA calc. 80—60226
- itinerant ferromagnet, spin-wave dispersion and linewidth 79—4668
- itinerant ferromagnet, surface spin waves 77—69480
- itinerant ferromagnet, thermodynamics 79—4645
- itinerant ferromagnet in disordered phase, energy band struct. 78—68141
- itinerant ferromagnet with helical spin struct., US attenuation 79—78497
- itinerant ferromagnetism, statistical mechanics of spin waves 79—82746
- itinerant ferromagnetism and density of states, off-diagonal disorder effects 77—28360
- itinerant ferromagnetism with at. ordering 78—14920
- itinerant ferromagnets, magnetoelastic props., thermodynamic aspects 80—66002
- itinerant ferromagnets, spin waves, appl. of self consistent many-body theory 79—73702
- itinerant magnetism, local-band theory, equivalent Heisenberg model 79—82745
- itinerant magnetism 79—73668
- itinerant strong ferromagnetism, effect of electron correlations 79—7962
- itinerant-electron, possible coexistence with itinerant-electron antiferromagnetism 78—39286
- itinerant-electron ferromagnet, US propag. and struct. instabilities, screening effects 77—69653
- kinetic exchange interaction, doubly degenerate narrow bands 78—23263
- kink excitations of anisotropic ferromagnetic chain, nonlinear model 80—54881
- Krieger-James approx. of short range order effects, antiferro- and ferromag. 78—56276
- Landau-Ginzberg model, static and dynamic correl. functions near magnetization curve 79—15318
- Landau-Lifschitz equation, nonlinear, exact integration 80—80495
- Landau-Lifshitz anisotropic ferromagnet, quasiclassical excitation spectra of nonlinear spin string *(Russian)* 80—15678
- Landau-Lifshitz eqn., two soliton solns. for nonlinear dynamics *(Russian)* 78—43646
- Landau-Lifshitz eqns., self-localised solns., accidental degeneracy *(Russian)* 79—33444
- Landau-Lifshitz equation, new conservation law *(Russian)* 79—95559
- Landau-Lifshitz nonlinear equation, N-soliton solutions *(Russian)* 79—24184
- lattice diffusion, Heisenberg ferromagnet 78—88090
- lattice spin model with multicrit. pt., soln. in spherical model limit 77—66338
- layer systems, mag. polaritons 78—31060
- layered ferromagnet, real space renormalization and the honeycomb lattice 80—11200
- layered system, coexistence of superconductivity and ferromagnetism *(Russian)* 79—7918
- LEED from ferromagnets, spin polarisation effects, calc. 79—99686
- Lifshitz point, critical behaviour, universal amplitude ratio calc. 79—33496
- Lifshitz point, ferromag., renormalisation-group anal. of crit. modes in cryst. systems 79—82806
- Lifshitz point, ferromag., symmetry derived crit. modes 79—73758
- light scattering by spin waves 80—45086
- light scattering from bulk and surface spin waves in ferromag. slab, theory 80—71389
- linear chain, disordered, q-depend. mag. susceptibility 78—27010
- linear chain, Heisenberg Hamiltonian, existence of isolated magnon 79—4666
- linear chain model system, ferromagnetic state 79—56483
- linear Ising-Heisenberg ferromagnet, spectrum of elementary excitations 79—61091
- linear Ising-Heisenberg ferromagnet, spin waves vs. bound states, exact soln. 78—68202
- linear mag. birefr. *(Russian)* 80—93284
- liquid ferromagnet, model calculation 78—88088
- liquids, mean-field criterion for ferromagnetism 79—42791
- local field at positive muon 78—92010
- localised model for systems with double-exchange coupling 79—38318
- localised nonlinear oscillations, unidimensional magnetisation soliton, analytic soln. *(Russian)* 79—78437
- localised topological solitons in ferromagnets *(Russian)* 79—69661
- long-range, low temp. series for magnetization, crit. exponents 79—61131
- Lorentz microscopy, thin film and bulk specimen, recent advances 78—35002
- Lorentz microscopy using STEM for domain wall profiles determ. 78—35003
- low temp. renormalisation group, critical behaviour 78—10688
- low temperature Heisenberg ferromagnet dynamical longit. correl. function, hydrodynamic regime 78—31039
- low-dimensional systems, infrared problems and phase transitions of continuous order 78—6286
- Lu-tinger-Tisza method generalisation, appl. to highly anisotropic dipole-dipole interactions 77—20514
- mag. excitations, atomically rough surfaces, isolated cluster of overlayer spin 78—31102
- magnetic aftereffects, review 80—88830
- magnetic anisotropy, local variations due to linear defects *(Russian)* 78—68214

ferromagnetism continued

- magnetic anisotropy energy, symmetrical polynomials, appl. to Ni 77—66293
- magnetic bubbles as tilted cylindrical magnetic domains 78—64246
- magnetic damping due to pinned domain wall motion 79—56598
- magnetic dipoles on a lattice, theory at low temps. 80—50082
- magnetic excitations within local exchange approx. 77—69517
- magnetic field asymmetry correction on fast moving ions 79—14862
- magnetic impurity ion in mag. ordered cryst., optical absorpt., exchange interaction effects 77—16355
- magnetic impurity levels, standard basis operator method *(Russian)* 80—11192
- magnetic materials, μSR meas. 79—56660
- magnetic order coexistence with charge density waves 80—97096
- magnetic oscillations, Fermi surfaces and high magnetic fields 79—73423
- magnetic reversal processes in ferromag. with narrow domain walls 79—87287
- magnetic semiconductor, light scatt. by magnons, appl. to $CdCr_2Se_4$ and EuTe 77—69805
- magnetic solitons propagating along anisotropy axis *(Russian)* 79—73798
- magnetic stability at 0K of simple cubic ferromag. array of pseudospin S=1/2, nearest neighbours anisotropic exchange 77—1547
- magnetic Stirling cycles, new appl. for mag. materials 77—85450
- magnetic structures, non-periodic, ferromagnetic spin wave propagation, interaction with domain walls 79—99692
- magnetic susceptibility, spin and charge density waves, Curie temp. *(Russian)* 80—100581
- magnetic system with cryst. field pots., Green's function theory and high temp. series expsn. 80—15673
- magnetic vortex as topological soliton in Landau-Lifshitz eqns. *(Russian)* 80—7097
- magnetically ordered cryst., indirect nuclear spin interactions 80—103847
- magnetically ordered substances, book 80—73112
- magnetically soft cylinders, micromagnetics of curling configurations 79—82826
- magnetically uniaxial ferromagnetic particles, high-anisotropy many domain, magnetisation, hysteresis *(Russian)* 79—91256
- magnetisation at low temp., disorder induced behaviour 78—52234
- magnetisation curve determ. by plane surface attachment *(Russian)* 79—63282
- magnetisation curved optimal analytical representation, automatic choice method *(Italian)* 78—47998
- magnetisation curves, spin reorientational phase transitions 79—82785
- magnetisation density waves, weakly linear 77—51888
- magnetisation distribution function, rigid boundary model *(Russian)* 77—80955
- magnetisation in ferromagnet with mag. axial symmetry 77—85487
- magnetisation in high fields, influence of internal field nonuniformity 79—51819
- magnetisation in unidirectional field, math. model *(Russian)* 77—24660
- magnetisation intensity, meas. method for ferromag. material in static mag. field 77—49751
- magnetisation of large ferromagnetic parts, by use of applied electromagnets 78—72999
- magnetisation of uniaxial ferromagnet with single-ion and exchange anisotropies in transverse mag. field 78—56277
- magnetisation of uniaxial ferromagnets with single ion anisotropy in transverse field 77—32143
- magnetisation reversal, stress indication by transverse and longitudinal internal induction 77—16138
- magnetisation stimulation by nonresonance AC mag. field *(Russian)* 80—65962
- magneto-dipole interaction influence on one dimensional magnetisation soliton *(Russian)* 80—54880
- magneto-optical effects and current operator form *(Russian)* 77—81084
- magneto-volume effect and Invar phenomena ferromagnetic metals, magneto-volume effect, Invar phenomena 80—66007
- magnetoacoustic singularities of sound propag., mag. with periodic domain struct. *(Russian)* 77—24727
- magnetoelastic properties of ferromagnet in low mag. field, simplified model 77—90004
- magnetoelastic transducer impedance calc., use of energy balance equation of dynamic magnetoelastic coupling 78—35019
- magnetomechanical effects, magnetostriction, hysteresis, stress, yielding, fatigue damage, crack growth *(Polish)* 80—71150
- magnetostatic modes of gyrotropic cylinder and bar 77—77048
- magnetostatic parametric mode coupling in amplification 77—4545
- magnetostatic theory of response functions for finite thickness ferromag. slab, appl. to Brillouin scatt. 79—61083
- magnetostatic volume wave dispersion relations, metal plate effects 78—47963
- magnetostriction, SHG in magnetoelastic media 77—36109
- magnetostriction effect on domain neighbourhood *(Russian)* 78—39356
- magnetostriction is magnetic field, sound-spin wave coupling 79—15334
- magnetostriction US vibrs., review of γ-reson. spectroscopy under HF excitation 77—48113
- magnetostrictive ferromagnet, conditions for stress induced bulk moments 79—78493
- magnetostrictive sensitivity, experimental study *(Bulgarian)* 77—55695
- magnetostrictive waves, mag. impulse produced in ferromagnet. polycrystalline materials *(Italian)* 78—2720
- magnetothermoelastic continua, macroscopic nonlinear theory 77—83775
- magnon, nonequilibrium state under nonresonance alternating mag. field 79—87248
- magnon bound state formation *(Russian)* 77—63162
- magnon density of states for ferromag. with screw dislocation 78—84402
- magnon drops in three-dimens. ferromagnet *(Russian)* 77—12111
- magnon edge modes localised at apex of semi-infinite right-angle wedge 77—63148
- magnon excitations in simple cubic ferromag. square bar 77—77047
- magnon gas of Heisenberg ferromag., transport eqn. 77—12112
- magnon kinetic eqns. in parametric ultrasonically excited frromagnets 80—44820
- magnon problem, anisotropic spin chain with exchange interaction 78—6502
- magnon relaxation, spin-orbit interaction, itinerant electron ferromagnets 80—11179
- magnon-phonon coupling, continuum approach, general eqns., background soln. 79—95622

ferromagnetism continued
magnon-phonon coupling, continuum approach, hexagonal symmetry, wave propagation 79—95623
magnon-phonon interactions, Heisenberg exchange red. 80—80494
magnons, nonlinear, multidomain ferromagnets with 180° Bloch walls 78—34967
magnons and lattice deformations, solitary bound states, Dyson-Maleev representation 78—91838
many-domain, indirect interaction of electrons via spin waves 77—85382
many-electron exchange Hamiltonian in theory of ferromagnetism 78—19199
material inspection by method of two harmonics 78—88608
Maxwell's equations in ferromagnetic materials, asymptotic solns. *(Italian)* 78—78860
mean spherical model, Langevin approach 78—72350
metal, amorphous ferromagnetic, paramagnetic Curie temp. determ. 78—76242
metal, anisotropic, spin-fluctuation resist. 78—56137
metal, anomalous Hall effect 79—87084
metal, anomalous magnetooptic effects near Curie temp., s-f exchange model 80—2736
metal, asymmetric electron scatt., anomalous Hall effect in ferromags. *(Slovak)* 78—79986
metal, band struct. contribs. to shear consts., deform. pot. formalism and Stoner model 79—91280
metal, dragging of domains by temp. gradient 80—34425
metal, dynamic scatt. effects on crit. transport props. 78—84239
metal, electron scatt. by fluctuations of mag. moment near Curie temp. 79—73502
metal, electron spin polarised tunnelling from superconductors 79—78263
metal, electron theory *(Japanese)* 77—66102
metal, electron-magnon mass enhancement 77—15748
metal, electron-phonon interaction, magnetism influence 77—73040
metal, ferromag., freq. depend. elec. cond. 77—66181
metal, hyperfine fields at rare earth impurity 78—87947
metal, itinerant electron model, for US propagation and structural instabilities 78—95508
metal, longitudinal spin susceptibility 79—61078
metal, magnetisation density in vacancies, μ^+ probe, theory 77—28504
metal, magnetoelastic coupling effect on magnetoelec. reson. 80—75837
metal, magnon and cond. electron relax. processes *(Russian)* 80—7102
metal, many-electron direct exchange interaction 79—69667
metal, RKKY oscills. in surface spin density, density functional formalism 77—20512
metal, spin wave propagation 79—7982
metal, spin-polarised field emission, many-body and spin-dependent surface pot. effects 79—74065
metal, superconductivity and ferromagnetism 79—73616
metal, temp. depend. of hyperfine fields at impurities 79—15300
metal, two-band model, ordinary Hall effect and spin-depend. phenomena 79—19577
metal, two-site interaction model 79—82744
metal, uniaxial ferromag. anisotropic spin fluctuations and anisotropic band struct. effects on resist. near T_c 80—65543
metal, with domain struct., resistivity 78—95285
metal polycrystals, model for EM generation of US guided waves 78—22236
metal slab, transmission of 24 GHz radiation, effect of diffuse surface scatt. of carriers, calc. 80—34780
metal surface, charged, magnetic moment and hyperfine splitting 77—20677
metallic, criterion for Fermi liq. picture 77—66231
metallic alloys, highly diluted, ferromag. ordering, long-range mag. impurity interactions 77—16043
metallic ferromagnet, antiresonance region, EM wave propag., Maxwells' eqns. soln. 80—66038
metallic ferromagnet, correl. of temp. anomalies of hyperfine field and thermal expansion of lattice 80—20400
metallic lamination, domain wall bowing, simulation using new spline model 79—51807
metals, crystalline, disordered ferromagnetism 78—19207
metals, dislocation drag by conduction electrons 80—24451
metals, elec. cond., review 77—31993
metals, electronic struct. and magnetism, review 80—70573
metals, ferromagnetic, point contact spectroscopy, electron-magnon interactions *(Russian)* 80—54766
metals, ferromagnetism quantitative criterion correlation calcs. *(Russian)* 80—2540
metals, itinerant electron ferromag., theory of crit. US propag. 77—69655
metals, narrow-band, magnetism and mag. excitations 77—69478
metals, nonmagnetic impurity hyperfine field temp. depend. 80—34402
metals, polar states and free electron gas, mag. moments *(Russian)* 80—84415
metals, resist. anisotropy, crit. behaviour and temp. depend. 80—96858
metals, simple theory of spin-wave relax. 78—19231
metals, spin fluctuation theory, Curie temp., mag. susceptibility 80—65937
metals, theory, unified picture *(Japanese)* 80—20366
metals, with domain struct., low-temp. resist. 77—47791
metals, X-ray photoelectron and absorpt. spectra, edge singularities in spin-depend. final-state interactions 78—6810
metals, zero temp., Fermi liquid effects 77—51897
metamagnetic dielectrics, at finite temp. *(Russian)* 78—88118
microcanonical high-temp. expansion 78—2638
microwave modulation of light using magnetodynamic reson. 80—71393
microwave radiation in parallel pumping ferromagnet, magnon-photon interaction 79—51861
Migdal's recursion relation, generalisation, appl. to O(n) symmetric spin systems, $n>2$ 78—91834
mixed, spin-$^1/_2$ Ising ferromagnet, crit. props. 80—34655
mixed ferromagnetic Heisenberg and Ising bonds, appl. of effective Hamiltonian method 80—50023
mixed magnets, competing spin glass and mag. order, phase diagrams, crit. points 80—39802
mixed valence compounds, dynamic susceptibility, RPA study of Anderson lattice 80—97075
mixed valence state, electronic structure 79—11092
model, spin wave stiffness, temp. renormalisation 77—85435
modulus defect due to internal strain 78—76286
Mossbauer effect at temp. close to Curie temp. *(Russian)* 79—87339

ferromagnetism continued
Mossbauer effect for impurity atoms *(Russian)* 77—48098
Mossbauer lineshape in ferromagnet 80—71251
Mott insulator, magnetism and charge ordering 79—60751
Mott insulators, excitonic spin polarons, appl. of Nagaoka's theorem for electron-Hole pair 80—107978
moving conducting ribbon, interaction with ferromag. inductor field *(Russian)* 78—94359
multidomain magnet with 180° Bloch walls, sound generation by RF field *(Russian)* 77—32235
muon$^+$ contact magnetic field in ferromags., μ^+ and muonium phys. and chem. review *(Russian)* 77—50566
n-vector lattice spin model near two-dimens., crit. temp. 77—8324
n-vector model, spherical limit and correlation inequalities 80—22298
narrow conduction bands, allowance for correl. effects 78—47933
narrow domain wall ferromagnets, localised modes 80—34681
narrow domain walls, lattice coercivity 79—28552
narrow-band s-d magnetic materials, ground state and thermodynamic parameters, cond. electron density depend. 78—47934
NDT, investigation of the through-transducer signal spectrum 80—35487
nearly ferromagnetic Fermi systems, spin-conserving approx. spin susceptibility 78—47982
neutron beam channelling and focusing in ferromagnets *(Russian)* 80—107351
neutron crit. scatt., temp. shift of max. in second Born approx. 78—34963
neutron depolarisation on passage through ferromag., statistical theory 78—87593
neutron depolarisation studies of ferromagnetic domain structures 80—25155
neutron diffr., integrated intensity heats, crystal and mag. struct. determ. 80—44079
neutron magnetic octupole scatt., quadrupole excitation creation 77—47977
neutron scattering, domain struct. and magnetisation determ., vector polarisation techniques 77—63117
NMR, microscopic theory for low conc. case, lineshapes 77—59467
NMR frequency, amplification and dynamic shift, rel. to local mag. props. *(Russian)* 77—20722
noise charact., applicability of physical similitude 79—4705
non-purely ferromagnetic systems, correlation inequalities 79—47219
non-uniform ferromagnets, simple model with spontaneous magnetisation at T_c *(Chinese)* 77—8256
nondestructive electromagnetic inspection, transducer for 79—87771
nondestructive inspection of ferromagnets, using magnetic noise method 78—72997
nonequilibrium superconductors, ferromag. ordering of quasi-particles and rise of domains 80—107958
nonexchange surface spin waves at interface between two ferromagnets 80—29544
nonlinear localised magnetisation wave as bound state of large no. of magnons *(Russian)* 77—89940
nonlinear localised wave of magnetisation as bound state of magnons *(Russian)* 77—63160
nonsymmetry distrib. of parametrically excited waves *(Russian)* 78—47967
nonuniform ferromagnet, spontaneous magnetisation, mean field theory *(Chinese)* 78—91865
nuclear magnetisation, temp. dependence 79—33462
nuclear magnetisation ground state 79—73703
nuclear magnetism 77—63124
nuclear secondary echo in ferromagnets and antiferromagnets 79—73852
nuclear spin waves, possible detection by inelastic neutron scatt. 77—85438
nuclear spin waves, surface and bulk, Green function formalism 80—70984
nuclear spin-lattice relaxation, possible magnon bottleneck 77—32283
Nyquist noise in mag. and dielec. materials 77—1569
one dimensional ferromagnets, effect of biquadratic exchange on solitary waves 80—65836
one dimensional randomly dilute Ising ferromagnet, dynamics 80—70922
one domain ferromagnetic insulators, spin wave and elastic wave interactions 79—73700
one magnon states in linear chains of spin 1/2 particles 78—14946
one-dimensional, localised nuclear magnon modes 80—93098
one-dimensional, thermodynamically stable long-range order *(Russian)* 79—27946
one-dimensional, with biquadratic exchange, solitary excitations 78—76232
one-dimensional chain, solitary magnon propag. 77—63146
one-dimensional dilute Heisenberg system, mag. props. 78—64179
one-dimensional disordered systems, magnetism 80—25152
one-dimensional ferromagnet, algebraic soliton in mag. field directed along anisotropy axis 80—75785
one-dimensional ferromagnet, characts. of soliton-like mag. excitations 80—39762
one-dimensional ferromagnet, quasiclassical approach to many-magnon bound states *(Russian)* 78—23222
one-dimensional ferromagnet with biquadratic exchange, solitary bound states of magnons and lattice deform. 79—19732
one-dimensional ferromagnet with long range interaction, correlation weakening 79—95561
one-dimensional Heisenberg magnet, in mag. field, dynamic correlations 80—70926
one-dimensional magnetic systems, sound attenuation at finite temp. 77—63247
one-dimensional quasiclassical spin wave model in mag. field, static and dynamical props. 77—66284
one-spin ferromagnet, high temp. series expansion for mag. susceptibility and sp. ht. 80—25148
optical excitation of spin complexes, bound-magnon states 77—28554
order parameter for exactly soluble model 78—76207
ordered Heisenberg ferromagnet/liq. ^{3}He system, mag. Kapitza cond. calc. 79—51415
ordered nonsingular systems, topology appls. 78—10166
ordered regions near macroscopic defects and percolation phase transform. in crystals *(Russian)* 80—92665
orthogonally magnetised materials, study of mechanism using digital computer *(Rumanian)* 77—55687
$P(\phi)_2$ Euclidean field theory, boundary conditions rel. to ferromagnetic spin systems 77—54036

ferromagnetism continued
paramagnet and ferromagnet, multiboson spin wave representation 79—4664
parametric excitation of sound near phase transition point 79—69710
parametric excitation on spin waves in the induced magnetoelastic crystals *(Russian)* 78—60272
parametric spin waves distrib. function *(Russian)* 79—87250
particle suspensions in non-conducting and metallic liqs., review 80—60372
particle system, micromagnetism and mag. reversal 79—82830
particles, quantum effects *(Russian)* 80—29584
Peierls condition and number of ground states 78—80150
percolation clusters, one dimens., crit. exponents 78—31082
percolation on 2-D lattices, Cayley tree, boundary problem 80—52138
periodic domain structures, micromagnetic theory, stability problem 77—69612
permeability, frequency dispersion determination using Kramers-Kronig relation 78—39355
phase transformation theory, easy axis anisotropy, quadrupole interaction, renormalisation method calcs. *(Russian)* 79—65671
phase transition of spin-one Ising system with biquadratic interaction 79—4683
phase transitions, nucl. spin dynamics in anisotropic systems 80—11205
phase transitions, nucl. spin dynamics in isotropic systems 80—11204
phase transitions in ferromag. spin systems at low temp. 79—56538
phenomenological theory 78—52184
phonon-magnon interaction, energy minimum excitation 79—61086
photoelectric effect rel. to saturation magnetisation 80—65618
photon magnon bound states in ferromag. 78—47711
photon-photon bond state via magnons in ferromagnet 79—61458
pinned domain wall motion, magnetic damping studies 80—65956
pinning and nucleation of mag. domain walls at antiphase boundaries 80—11216
planar chain, soliton dynamic struct. factors 80—7125
planar cyclic remagnetisation, of isotropic ferromagnet with two mutually orthogonal sinusoidal mag. intensities *(Russian)* 80—80561
planar cyclic remagnetisation of ferromagnet under sinusoidal induction *(Russian)* 78—80177
planar ferromagnet hydrodynamic mode microscopic theory 78—39280
planar ferromagnet with small basal plane anisotropy, crit. dynamics anal. 77—12116
planar Ising ferromagnet solvable model with roughening transitions 80—71069
plane rotator ferromagnetic model, equilib. state anal. 78—29055
plane rotator model, partition function and Gaussian inequality zeros 80—42158
plane rotator model lattice system, Euclidean Bose field approx. 77—28351
plate, domain struct. during spin reorientation, phase diagram *(Russian)* 78—52320
plate, EM wave diffr. by domain walls 79—99724
plate, magnetic hysteresis theory, singularities of magnetic reversals on industrial freq. *(Russian)* 78—39373
plate, nonlinear magnetostatic waves *(Russian)* 78—35014
plate, phase diagram in magnetic field *(Russian)* 77—48018
plate, with anisotropic surface discontinuities, spectrum and damping of quasi-surface spin waves 80—11185
plate of layered media, band domains *(Russian)* 77—12178
polarised photoelectrons from ferromagnets, review 77—32505
polaritons, asymmetrical guided mag., in ferromag. slab 80—88738
polycrystal, magnetisation law, Bloch wall motion *(French)* 79—95606
polycrystalline ferromagnetic material, magnetic texture anal. 80—108002
polycrystalline materials, law of approaching saturation, expt. study *(Chinese)* 79—24144
polydomain magnetic struct., excitation of sound 78—88162
porous ferromagnet, with Bloch walls and self-consistent magnetisation, energy and coercive field 80—15760
porous ferromagnet with Bloch walls, energy and coercive field 79—51818
porous material, coercive field 78—14984
positivity constraints for ferromag. Ising model 77—28348
Potts lattice gas, crit. and tricrit. exponents using Kadanoff transform. 80—101768
Potts model, 1st and 2nd order transitions, renormalisation group soln. 79—99706
Potts model, first-order phase transform., three-state model, Monte Carlo renormalisation group method 79—99709
powders, ferromag. and ferrimag., conc. characts. of magnetic props. 77—73052
Procopiu effect, harmonics generated in ferromag. sample 77—24729
pure and random uniaxial ferromagnets, with dipolar interaction, US attenuation 80—11239
quantum critical dynamics with mode coupling 80—108023
quantum Heisenberg ferromagnets and stochastic exclusion processes 80—88712
quantum mechanical theories of magnetism, review of properties and explanations 78—76215
quantum spin systems, renormalisation group transformation 78—47984
quantum theory of ferromagnets with double exchange 78—19204
quenched random system, dual relations 80—34664
random, relation between quenched and annealed systems 79—82794
random anisotropy amorphous ferromagnet, initial magnetisation, remanence and coercivity 77—80964
random anisotropy and random field models, textural singularities and frustration 79—24182
random anisotropy model in Ising model, Monte Carlo simulation 80—80546
random exchange interactions, and 'frustration effect' 78—68212
random ferromagnet, new inequality, proved using FKGP and correl. inequalities 77—51909
random ferromagnet, with long-range interactions, dynamics 77—89942
random ferromagnetic-antiferromagnetic alloy, elementary excitations 79—8001
random ferromagnets, crit. exponents 78—10694
random ferromagnets, Ginzburg criterion, critical fluctuations 80—71032
random ferromagnets, large exchange interaction, Green function theory 78—6537
random impurity effects on long range order 78—95061
random Ising ferromagnet, upper bounds 80—34663
random Ising magnet, phase diagrams 80—7065

ferromagnetism continued
random mixture of ferro- and antiferromag. exchange interactions, high temp. expansion 78—23280
random ordered phase in site model, statistical theory 79—47218
random quenched ferromagnet, crit. behaviour, effective exponents, renormalisation 80—60326
random quenched mixtures, ferro- and antiferromagnetic exchanges 77—51864
random quenched site model, competing exchange energies and competing anisotropy energies 80—29552
random site Ising model near percolation threshold 78—23282
random spherical model in nonzero mag. field 77—55677
random uniaxial ferromagnet, dipolar interactions, crossover behaviour, renormalisation group equations numerical soln. 80—50136
random uniaxial systems with dipolar interactions, crit. dynamics 77—73034
randomly anisotropic ferromagnet, long wavelength mag. excitations 78—84406
randomly dilute ferromagnet, essential singularities 77—20615
randomly disordered alloys, ferromagnetism onset, mag. inhomogeneity 80—75774
rare earth alloys, amorphous, study of hysteresis effects using Monte Carlo technique 79—1686
rectangular bodies surface charge distribution, meas. and calc. w.r.t. nonlinear field-dependent susceptibility *(Slovak)* 79—4656
rectilinear screw dislocation, magnetisation distrib. 80—44897
remagnetisation, hyperfine structure collapse, review of γ-reson. spectroscopy under HF excitation 77—48113
remanent magnetisation during thermal demagnetisation near a phase transition 78—88142
renormalisation group approach to critical phenomena, ferromagnetic example 78—8497
renormalisation group equations in critical dynamics, scaling far from equilib. 77—28395
resistance critical behaviour, temp. and mag. field depends. 77—73037
resistive anomalies at mag. crit. points, effect of inelastic scatt. 77—55675
resistivity anomalies of ferromag. metals near Curie temp., itinerant mag. electron theory 78—95292
resistivity of magnetic systems, critical behaviour 78—87955
resonance excitation of ultrasound in ferromagnetic fluids 78—95112
retarded EM modes in ferromag. slab 78—84405
reverse magnetostrictive effect in stressed ferromagnetic bar *(Rumanian)* 80—84630
rocks, E.Canada ophiolites, thermomagnetic evidence for native Fe 78—3760
rocks, ferromagnetic component indication by magnetic hysteresis 77—64271
rotating magnetometer appl. to ferromag. materials 77—49750
s-d model, electronic spectrum struct., moments method 80—97052
saturation, reactive power, and harmonics anal. *(Slovene)* 77—85488
scalar spin systems, wall and boundary free energies 78—155
scaling relations in mag., mechanical and superconducting pinning theory 77—76403
screw spin ordered state through dipole-dipole interaction 78—39337
second order phase transitions, superspace group description *(Chinese)* 80—8942
self-consistent field theory, diagrammatic review and implications 77—74313
semi-infinite ferromagnet, surface magnon-phonon interaction processes, scatt. and annihilation *(Russian)* 77—63144
semi-infinite Heisenberg ferromagnet, macroscopic theory of response functions and appl. to light scatt. 80—20410
semiconductor, absorpt. edge and cond. band width, temp. and mag. field depend. 77—36267
semiconductor, acoustic plasmons 80—7098
semiconductor, anomalous carrier density mag. field depend., EuSe appl. 80—49774
semiconductor, anomalous Hall effect, s-f model 78—10478
semiconductor, autolocalised electron states 78—51924
semiconductor, bound mag. polaron 79—90976
semiconductor, carrier-assisted magnon contrib. to phonon damping 77—20018
semiconductor, carrier-assisted radiation pumping of spin waves under strong mag. field 77—55667
semiconductor, CESR in strong alternating electric field 78—35038
semiconductor, CESR line width, two-magnon exchange splitting 80—29621
semiconductor, double exchange and small-polaron hopping 79—19591
semiconductor, electronic excitation spectrum 80—11149
semiconductor, electronic props., effect of electron-ion spin coupling 77—28359
semiconductor, electronic quasiparticle spectrum in sf-model 78—52188
semiconductor, electronic spectra, s-d model, method of moments 80—7070
semiconductor, electronic spectrum, influence of finite carrier conc. 78—76220
semiconductor, energy and mobility of spin polarons 80—70982
semiconductor, exciton ferromagnetism 79—28293
semiconductor, ferromag., doped, electron spin polarisation and conduction band struct. 80—65449
semiconductor, ferromag., electron mobility below Curie temp. calc. 78—51992
semiconductor, ferromag., localised magnon mode relax. theory 80—70986
semiconductor, ferromag., parametric excitation of magnetoplasma reson. 79—28623
semiconductor, ferromag., polaron solitary waves 80—70625
semiconductor, ferromag., short wavelength magnon generation 80—70987
semiconductor, ferromag., spin polaron props., effect on carrier scatt. 80—60233
semiconductor, ferromag., surface localised low energy electron-magnon states *(Russian)* 80—88734
semiconductor, ferromag., thermoelec. amplification of magnons 78—14748
semiconductor, ferromag. two-band s-d model hybridization 80—65446
semiconductor, ferromagnetic, theory review 80—20369
semiconductor, ferromagnetic, with doubly charged donors, quasiphase transition 79—65684

ferromagnetism continued
semiconductor, ferromagnetic, with mag. impurities, low-energy localised states *(Russian)* 79—19543
semiconductor, free carrier absorption below Curie temp. 79—47440
semiconductor, HF magnon generation by pumping *(Russian)* 77—24686
semiconductor, hot electron relax. *(Russian)* 79—51593
semiconductor, localised states on imperfections and red shift of absorpt. edge 77—66527
semiconductor, longitudinal response function 77—72831
semiconductor, mag. polaron stability 80—96803
semiconductor, magnon coupling to plasmons and LA phonons, s-d model 80—29536
semiconductor, magnon damping under intense radiation 77—63150
semiconductor, magnon instability, under intense EM field 77—40048
semiconductor, phase transition and instability of homogeneous state 77—28398
semiconductor, Raman scattering of light on plasmon excitations 80—2738
semiconductor, refr. index variation in strong alternating mag. field 80—23741
semiconductor, spectrum of quantum spin waves in field of strong EM wave 78—91857
semiconductor, spin polarons in s-d model with off-diagonal exchange 78—34784
semiconductor, wide-gap, nonlinear galvanomag. effects 77—39862
semiconductor, with impurities. semicond.-metal transition and instability phenomena 77—59257
semiconductor laser, ferromagnetic ordering, radiation polarisation *(Russian)* 78—9384
semiconductor narrow band gap, valence electrons in filled band, ferromagnetism *(Russian)* 79—78300
semiconductor s-d model, electronic struct. from lowest six momenta 80—39732
semiconductor with defects, exchange Hamiltonian 79—82777
semiconductor-ferromagnet contact, spin-depend. recomb. and scatt. on electron injection 80—65654
semiconductor-ferromagnet structure, periodic, surface magnetostatic waves 78—27070
semiconductor-ferromagnetic structure, thermal fluctuations during amplification of magnetoacoustic surface waves 78—88158
semiconductors, conduction electron heating, critical scatt. effects 79—91040
semiconductors, electronic quasiparticle spectrum 80—97051
semiconductors, ferromag., review of cryst. growth 77—85923
semiconductors, ferromagnetic, parametric amplification of coupled spin, helical and acoustic waves *(Russian)* 80—2621
semiconductors, ferromagnetic with hot electrons, instability of coupled spin-helical waves 80—107841
semiconductors, free carrier absorpt. of radiation 80—97227
semiconductors, nondegenerate, magnon drag thermoelec. power calcs. 78—80012
semiconductors, s-f interaction on conduction band, red shift effect theory 80—59872
separable many-particle interactions, free energy calcs. 77—9954
SH wave magnetostrictive generation model for ferromag. materials 79—55836
shear waves, horizontally polarised, generation in ferromagnets using magnetostrictively coupled meander-coil EM transducers 79—46144
simple ferromagnets, crit. behaviour 80—60331
sine Gordon theory, equivalence to z-dimens. ferromag. classical X-Y model low temp. behaviour 77—13873
sine-Gordon Hamiltonian, general soln., domain walls appl. 78—19198
single ion anisotropy consts. temp. depend., effect of spatial variation of mag. moment 78—91864
single site theories for systems with Goldstone modes 77—63145
singlet ground state ferromag., Heisenberg Hamiltonian model 79—11283
singlet state, theory 77—12073
singlet-doublet model of induced moment system, surface magnetism near Curie point 77—1530
singlet-triplet dynamics, spectral density method 79—73652
singlet-triplet ferromagnet, Dyson eqn. derivation 80—107974
singlet-triplet ferromagnet hydrodynamics 80—11142
singlet-triplet ferromagnetic systems, excitation spectrum, double-time Green's functions 80—84603
sintering theory and diffusion flow of ferromagnets 79—28977
slab, finite thickness, spin correl. functions 80—80522
smectic liquid cryst. film, ferroelec., two-dimens. X-Y crit. behaviour 79—77497
soft cylinder, point singularities and magnetisation reversal 80—11223
soft elastic-solid, ferromag., with finite crack, linear magnetoelastic problem 77—66410
soft ferromagnetic elastic solid, magnetoelastic interaction with penny shaped crack in const. mag. field 79—18829
solid plate, EM field induced by local lateral magnetic flux *(Polish)* 79—98259
solid state physics, 1933-40, contrib. of Sir Nevill Mott 80—57055
solitons near critical point, neutron scattering observation 80—34650
sound wave damping, due to phonon-magnon interactions 77—36107
spherical ferromagnetic models, Yang-Lee edge singularity density in thermodynamic limit 79—30378
spherical model, phase separation 79—44869
spin 1 Heisenberg ferromagnet with single ion anisotropy, collective modes 77—28354
spin correlation in ferromag. with random anisotropy 79—73722
spin dependent electron momentum distrib. by double Compton scatt. 78—35218
spin deviation states in spin-1 system with Heisenberg and biquadratic exchange 78—84378
spin excitation spectrum in mag. fields of arbitrary direction 77—24662
spin glass model, stability of Sherrington-Kirkpatrick soln. 78—56319
spin glass-ferromagnetic phase, mean field theory 80—103841
spin glasses, dilute, at zero temperature, low concentration series expansion 80—93131
spin glasses, dilute ferromagnets, ferromagnetic modes 80—93133
spin Hamiltonians, infinite-range, exact solns., singlet-ground-state ferromag. 79—78281
spin polarisation of emitted photoelectrons 80—45215
spin polarised electron emission from mag. materials, review 77—73215

ferromagnetism continued
spin polarons in narrow almost half-filled s-band, appl. to BCC ^{3}He 77—62703
spin reorientation and magnon-phonon hybridization in ferromagnet 78—19233
spin subsystem thermodynamics, spin-phonon interactions, mag. order parameter 80—103848
spin susceptibility for itinerant electrons with energy dependent effective interactions 78—19209
spin system, mag. susceptibility and correl. length crossover relationship 79—78395
spin system, under quenched random mag. field, phase transition crit. dynamics 79—82798
spin system, variable distrib., convergence to normal Gaussians, Lee-Yang theory 79—69681
spin systems with three-atom exchange, elementary excitations 78—84404
spin wave damping, magnetic materials with canted mag. struct., thermodynamic and high freq. props. 80—11184
spin wave damping, magnetisation relax. 78—88106
spin wave damping, theory, and comparison with expt. for EuO 78—52237
spin wave excitation, with moving domain wall *(Russian)* 78—88103
spin wave excitation due to parallel pumping, mag. impurity interactions *(Russian)* 80—80497
spin wave excitation in ferromag. films by antenna field 80—44816
spin wave nonresonant excitation by varying mag. field, nonequilibrium states *(Russian)* 80—34616
spin wave parametric excitation by noise pumping *(Russian)* 80—34617
spin wave relaxation due to dipole interactions, damping temp. depend. 79—69664
spin wave resonance temp. depend., surface mode threshold conditions 77—28450
spin wave spectrum, magnetoelastic gap *(Russian)* 77—59400
spin wave stiffness coefficient, spin density functional theory 78—76230
spin wave system, kinetic eqn. on parametric excitation *(Russian)* 79—87249
spin wave system, stationary weakly turbulent distrib. *(Russian)* 79—38316
spin wave theory in lower dimens., failure of dynamic scaling hypothesis in ferromag. chain 79—78284
spin wave theory in strongly anisotropic magnets 77—63151
spin wave theory of two-dimens. ferromagnet, magnetisation, susceptibility *(Japanese)* 77—47954
spin waves, appl. of surface problem expansion technique 77—4244
spin waves above Curie temp., Fisher's droplet model 78—56307
spin waves in absorptive mag. material, light scatt. lineshape 78—23476
spin waves in weak exchange field systems 78—43576
spin waves with moving domain wall 80—39764
spin X-Y, correl. functions 79—47221
spin-1 ferromagnet, susceptibility, appl. of high high-temp. series expansion for complicated level systems 77—51863
spin-1/2 cubic lattice, with anisotropic exchange, configs. 80—65926
spin-1/2 models on square lattice, sublattice renormalisation transform. 78—23225
spin-$^1/_2$ system, two-point correlations decay for decreasing pots. 78—19202
spin-glass and ferromagnetic behaviour induced by random uniaxial anisotropy 78—39338
spin-one Ising system, phase diagram 78—95441
spin-one system, quadrupolar to paramagnetic phase transition 77—80934
spin-orbit interaction effects on spin-wave resonance *(Russian)* 77—90039
spin-wave and magnetostatic mode attenuation by double-pulse echo method, in ferromag. crystals 79—82874
spin-wave spectrum in antiferromagnet Heisenberg 1-dimens. chain, external mag. field effect 77—89943
spinel structure ferromagnets, prediction of existence using cybernetic computer learning methods 80—108048
spinglass, ferromagnetic clusters, mean-field approx., static props. 79—4689
steady field penetration into ferromagnetic halfspace *(German)* 79—45878
Stoner ferromagnetism, criteria in doped semimetals, uncompensated metals, derivation 78—68145
stress measurement, ferromag. sample, by internal induction 77—62222
strong ferromagnetic 3d alloys, electron correls. 77—40030
subdominant critical indices for the ferromagnetic susceptibility of the spin-1/2 Ising model 80—100574
substitutionally disordered ferromagnet, spin dynamics, linear spin-wave approx. 77—40067
substrate, ferromagnetic transition, anomalies in adsorption equilib. near crit. point 78—79895
substrates, ferromag., propag. of surface magnetoelastic waves 77—55698
superconducting, magnetic ordering, spin wave dispersion *(Russian)* 80—54818
superconductivity coexistence, intersection lines 77—47924
superconductivity coexistence with mag. order 78—19177
superconductivity reentry behaviour, versus ferromagnetism 78—39247
superconductivity-ferromagnetism coexistence, transition temp., magnon freq., indirect exchange 80—44757
superconductivity-ferromagnetism coexistence in two-band model *(Russian)* 80—84539
superconductor, ferromag., new phase, crit. temp. and wave number determ. 79—82705
superconductor, ferromagnetic, mean-field theory 79—65586
superconductor, mag. domain struct., sample thickness effects 80—39704
superconductor, spin correls., effect on nonlocality 79—82708
superconductor, supercond. Bloch wall 80—20349
superconductor, uniaxial, domain struct. parameters 80—39705
superconductor, vortex structure 80—25055
superconductor, with domain struct. mag. induction vector 79—65585
superconductor to ferromagnetic transition, EM effects 79—51708
superconductor with magnetic impurities, coexistence of superconductivity and ferromag., BCS and Zener models 80—88676
superconductors, ferromagnetic, phase transitions, renormalisation group treatment 80—29505
superdiamagnetic and ferromagnetic state struct., gradient invariant free energy functional *(Russian)* 80—7143

ferromagnetism continued
- surface magnetisation profile, in crit. region by ε-expansion, Wilson perturbation theory calc. 80−50100
- surface magnetoelastic waves in the presence of exchange interactions and pinning of surface spins 78−80186
- surface magnetostatic wave excitation in ferromag. plate 80−25119
- surface spin fluctuations and light scatt. 80−84727
- surface spin waves, Brillouin light scatt. 80−93359
- surface spin waves and surface spin correlations in presence of mag. surface reconstruction 78−6522
- surface structure, adatoms, electron state at high coverages 79−28400
- susceptibilities of $S=1/2$ XY model on the square lattice at $T=0$ 80−88732
- susceptibility, parallel, ferromag. and anti-ferromag., graphical illustration, for teaching 78−41118
- susceptibility crossover 77−24680
- suspension of one-domain particles, birefringence in mag. field *(Russian)* 77−43979
- system with two parameters, Mott and ferromagnetic transitions, phase diagram of the extended Caron Pratt model 79−15083
- systems far from thermodynamic equilib., dissipative structures, broken symm. equilib. phase transition theory 80−65827
- TEM lens system with eucentric goniometer for ferromag. material obs. 77−72530
- ternary alloy, spin-disorder resist. in CPA weak scatt. limit 78−39100
- thermal conductivity of ferromagnets, crit. anomalies *(Russian)* 78−80159
- thermodynamic and dynamic properties of ferromagnetics with ferromag. impurities *(Russian)* 78−27032
- thermodynamic stability and crit. points, comparison with simple fluids 78−16766
- thick film, reson. transmission of EM energy via phonons 80−60382
- thin film, unipolar simple domain walls *(Rumanian)* 79−19752
- thin film alloys, surface magnetism props., Curie temp., Ising model 80−108039
- thin films, parametric oscill. with biaxial anisotropy 80−103861
- thin films, two dimens. spin-wave theory, spontaneous magnetisation parameter depend. 80−34714
- thin nonmetallic film, stand exchange mode determ. 80−2565
- three-component model, global phase diagram 77−37835
- tight-binding model ferromagnet, surface magnetisation 80−103807
- total spin distrib. in spherical model with long-range pot. 79−30383
- transition d element, hyperfine field on nucleus, mag. moment and electron struct. 77−62883
- transition metal, 3d, electron spin polarisation in field emission, state-of-the-art 77−69972
- transition metal, 3d and 4d, local density theory, mech. and mag. props. evaluation 78−91630
- transition metal, band theory of linear magnetostriction 80−71141
- transition metal alloy, ferromag., local environment effect on atomic moments, itinerant model 78−68188
- transition metal alloy, local ordering effect on spin wave stiffness const. 77−66282
- transition metal alloys, ferromagnetic, low temp. resist. calc. 80−24919
- transition metals, conf., Toronto, Canada (Aug. 1977) 78−91577
- transition metals, electron spin polarisation, review 78−76591
- transition metals, electron spin polarisation, review 78−76592
- transition metals, theory of ferromagnetism 80−2541
- transition to ferromagnetic state, theoretical development of ferroelectrics and ferromagnets 78−43815
- transition to spin glass ordering 80−34628
- transitions, first-order, intrinsic volume magnetostriction concept 80−29562
- translationally invariant ferromagnet, renormalisation group struct., crit. phenomena 77−51907
- transverse dynamical susceptibility within the local exchange approx. 78−76229
- triangular Ising lattice with small second neighbour interaction crit. temps. 78−56331
- triangular Ising model, anisotropic ferromag., corner transfer matrices, spontaneous magnetisation 78−10629
- triaxial ferromagnets, spontaneous magnetisation distrib., plane stress state influence *(Russian)* 79−61071
- triple dynamic magnetisation fluctuation correl. and feasibility of polarised neutron exam. near T_c *(Russian)* 78−88133
- tunnelling between ferromagnets 77−11986
- twin crystals, Bloch mag. struct., depend. on crystallite thickness and mag. field *(Russian)* 79−42792
- twisted domain wall dynamics in ferromag. plate 78−68340
- two-dimensional, magnetically dilute, concentration expansion, series anal. *(Japanese)* 77−20587
- two-dimensional, magnetisation, spin wave theory *(Japanese)* 77−20578
- two-dimensional heisenberg ferromagnet, open diffusion effects *(Russian)* 77−32201
- two-dimensional Heisenberg model, second order phase transition 77−16094
- two-dimensional planar ferromagnet dipole forces and phase transition *(Russian)* 79−51782
- two-dimensional spin model, Wilson renormalisation group theory appl. *(Norwegian)* 78−56275
- two-sublattice ferromagnet, biquadratic exchange effects 77−4502
- two-sublattice isotropic Heisenberg ferromagnet, impurity localised level theory 79−69471
- unaxial, random with dipolar interactions, crit. amplitude ratio change 78−31083
- unbounded n-component spin systems on lattice, statistical mech. 77−4477
- uniaxial anisotropy, first order magnetisation processes theory 80−60242
- uniaxial antiferromagnet, spin configuration in ferromag. phase, field and temp. depend. 79−38321
- uniaxial crystals, linear Cosserats theory description of magnetoelastic interactions 79−28576
- uniaxial dipolar ferromagnet, crossover behaviour, theory 80−29559
- uniaxial dipolar magnet, critical dynamics and statics 77−59422
- uniaxial ferromagentic with intrinsic mag. field, domain struct. 80−93141
- uniaxial ferromagnet, arbitrary spin and single-ion anisotropy of second order, Green's function 78−84379
- uniaxial ferromagnet, coercive force associated with domain boundary pinning on plane defects *(Russian)* 78−6543
- uniaxial ferromagnet, dipolar crossover effects 77−89961

ferromagnetism continued
- uniaxial ferromagnet, domain struct. in mag. field 80−103853
- uniaxial ferromagnet, dynamical behaviour near mag. transition point *(Russian)* 78−84431
- uniaxial ferromagnet, in transverse mag. field, quantum theory *(Russian)* 79−15297
- uniaxial ferromagnet, in weak mag. field, domain wall struct. transform. 77−59425
- uniaxial ferromagnet, neutron depolarisation calc. 78−64192
- uniaxial ferromagnet, NMR under magnon bottleneck conditions, eqns. of motion 77−66429
- uniaxial ferromagnet, phase front motion 79−82792
- uniaxial ferromagnet, quantum anomalies in susceptibility during second order phase tansitions *(Russian)* 78−19226
- uniaxial ferromagnet, remanent magnetisation from X-ray pole figure data 79−91252
- uniaxial ferromagnet, with flat-parallel domain struct., classical phenomenological description 78−56316
- uniaxial ferromagnet *(Russian)* 78−19270
- uniaxial ferromagnet with random exchange bonds of different signs, spin waves 78−76233
- uniaxial ferromagnetic crystal, irreversible rotation processes 80−39768
- uniaxial ferromagnetic superconductor, mag. domain struct. and mag. field penetration depth 79−65583
- uniaxial ferromagnets, negative magnetocaloric effect 79−82783
- uniaxial ferromagnets, nonuniversal props. in dipolar crit. region 77−24703
- uniaxial ferromagnets, US attenuation and kinetic coeffs. near crit. point, renormalisation group theory 79−4715
- uniaxial Lifshitz point, Monte Carlo calcs. 78−39353
- uniaxial one-dimens. ferromagnet, role of Bloch walls in statistical mechanics 77−40079
- uniaxial particles, domain struct, and crit. size *(Russian)* 80−25153
- uniaxial plates, domain struct. and magnetisation curves *(Russian)* 79−19743
- US attenuation, spin-phonon coupling, magnons and magnetostriction contrib., calc. in planar ferromagnets 80−34611
- US attenuation anomalies *(German)* 77−8381
- US spectrum, RF field in multidomain struct. 78−68056
- vacancy distribution along mag. sublattices in β-brass type ferro and antiferromagnetic alloys *(Russian)* 80−79783
- void in ferromagnet, Gibbs free energy, numerical calc. 80−29597
- vortex lines, Heisenberg model calc. 80−50026
- wavevector-dependent spin susceptibility, variational principle 78−91586
- weak magnetic samples, conduction of flux 79−28560
- weakly disordered uniaxial ferromagnet, phase transition *(Russian)* 78−23291
- wire, circular magnetisation meas. 78−70167
- X-Y ferromagnet, $S=1$, with uniaxial anisotropy, Curie temp. 79−78425
- X-Y magnetically dilute ferromagnet, two dimens. lattices 77−63056
- X-Y model, biquadratic, spin one, variation of Curie temp. 80−97102
- X-Y model, finite magnetisation assuming ferromag. coupling 78−43541
- X-Y model, $S=1/2$, on triangular lattice, ground state props. 80−60165
- X-Y model, zero temp. props. in 3 dimens. 79−61032
- X-Y model classical one-dimensional, free energy in mag. field 77−4484
- X-Y model for linear chain, struct. transition under external mag. field and stress 77−12126
- X-Y model of ferromagnet, one-dimensional planar, in external field, static props. 79−51735
- Yang-Lee edge singularity and ϕ^3 field theory 78−65882
- Fe ferromagnetism, transition metal valence electron struct. explanation 78−47932
- ^{3}He, liquid-ordered ferromagnet interface magnetic Kapitza conductance, surface spin wave effects 79−99406
- ^{3}He, solid mag., review 78−38906
- HoN type conducting magnets with singlet ground state, inhomogeneous ferromagnetism *(Russian)* 77−63118
- Pt-Ni (42 wt.%) relationship between mag. saturation flux and tensile strength 79−15819
- Y garnet, inhomogeneous collective magnon oscill. excited by RF field *(Russian)* 80−100582

ferromagnets *see ferromagnetic properties of substances; ferromagnetism*

ferrous alloys *see iron alloys*

Feshbach resonances *see atomic resonant states; molecular resonant states*

f.e.t. *see field effect transistors*

few-nucleon reactions *see nuclear reactions involving few nucleon systems*

few-nucleon scattering *see nuclear scattering involving few nucleon systems*

few-nucleon systems *see nuclei with mass number 1 to 5*

Feynman diagrams
- $\lambda\phi^4$ theory, dual string theory from Feynman graph expansion 78−54544
- $\lambda\phi^4$ theory, renormalised perturbation theory, Feynman graphs 78−54570
- $(\phi^3)_6$ field theory, deep inelastic lepton-headron scatt., cut vertex theory and reciprocity relation 80−57466
- Φ^3 field theory, Regge pole behaviour 78−66053
- ϕ^4 theory, Euclidean, local existence of Borel transform of Schwinger functions 80−77932
- Abelian spontaneously broken gauge model, perturbation expansions *(Chinese)* 78−8500
- amplitude circuit breakers 80−86558
- amplitudes in cross section calcs., computer code 79−13094
- applications in advanced quantum theory, book 80−22157
- asymptotic estimates of generical very high order Feynman diagram 77−61224
- asymptotic expansion, Feynman amplitudes, theorem 78−93790
- asymptotic limits of Feynman diagrams, discontinuities, d-lines 78−29233
- atom, heavy and superheavy, K-electron binding, self-energy correction 77−18802
- atom, many-electron, energy calc. by diagrammatic method *(Russian)* 77−14332
- atom with open shells, f_k and g_k coeffs. *(Russian)* 77−46480
- atomic fine structure calc. by Feynman diagrammatic technique 77−26981
- atomic ground state energy, relativistic and radiative corrections *(Russian)* 77−67991
- atomic interactions, retarded energy shift and pair polarisability, field theoretical perturbation theory 80−102560
- atoms, and ions, parity nonconservation effects 79−10086

Feynman diagrams continued
axion production, astrophys. implications of new light Higgs boson 79—22007
block diagrams, divergence cancellation in energy level perturbation theory 79—80751
causality and dynamical pictures in finite temp. Green's function 77—79219
chiral field, supersymmetric, 1/N perturbation theory and quantum conservation laws 80—68373
Compton effect on vector particle, differential cross section calc. *(Russian)* 78—12916
computer generation of Feynman graphs in QED 77—6065
Coulomb gas 2-D, interaction potential, screening length, critical temp. 80—62571
critical exponents, three dimensional system with short-range interaction, calc. 80—42348
cross sections, calc. using effective Feyman diagrams, in plasma 80—38566
crossed diagrams effect in Bethe Salpeter eqns. 77—2725
derivative-coupling model, 2 dimens., zero mass limit and induced interactions 79—49397
diagonal equiv. photon density matrix, appl. to lepton interactions 77—237
dimensional anal. in renormalised perturbation theory 78—24950
dual unitarisation and baryons 78—16999
effective potential anomalous behaviour 80—32023
eikonal theory, interacting Pomeron production by retaining Feynman graphs 78—8633
electron g-factor, sixth order contributions, anal. evaluation of graphs 77—6066
Euclidean 0^4 theory, simple Feynman graph evaluation 78—41404
Euclidean quantisation of gauge theories, Weinger integral and nonstandard analysis 80—68358
Euclidean quantum field theory, n-point functions, renormalised G-convolution 80—68341
Euclidean scalar field theory, asymptotic behaviour of Feynmann integrals 78—388
Fermi systems, review of methods in quantum field theory 78—8338
fermion scattering, comment on radiative corrections in large Higgs mass limit 79—67557
fermion-fermion scatt. in the eikonal limit, spin depend. 79—71662
fermion-fermion scattering in supersymm. field theory, high energy behaviour 77—13887
Feynman integrals, singularity struct. study using micro differential eqns. 78—74123
Feynman maps and the Wiener integral 78—77758
Feynman path integral and gauge invariance 80—82601
Feynmann path integral, cylindrical approx. 79—105
finite regularisation algorithm for relativistic field theories 79—93283
finite-range effects in the πNN, $\pi N\Delta$ and $\pi\Delta\Delta$ vertices 79—22129
$g\phi^3$ theory, ladder graph scatt. amplitudes, bounds at their boundary 77—71420
gauge theories, box diagrams with nonvanishing external four-momenta 80—22525
generic Feynman amplitudes, mass singularities 77—49820
gluon exchange diagrams, effect on parity violating weak interactions 79—97565
Green's functions, finite temp., dynamical picture and causality 79—63144
group theoretical weights attached to diagrams in non Abelian gauge theories 77—6004
group weight and vanishing graphs 80—57482
hadron total cross sections in quark parton model 78—45859
high energy behaviour of a double discontinuity and the bare Pomeron 78—82179
high-energy behaviour of a double discontinuity and the bare Pomeron 79—17696
high-energy behaviour of renormalised Feynman amplitudes 78—58114
holonomic character and local monodromy struct. of Feynman integrals 77—54038
inclusive processes, bremsstrahlung approx. 77—50033
incompressible viscous fluid, $(2-\varepsilon)$ dimens., long-wavelength non-equilibrium props. 77—61008
induced representations, reproducing kernels, conformal group, ladder representations, SU(2,2) 77—13882
integral representation for the dimensionally regularized massive Feynman amplitude 79—71592
interacting spin-1 field theories, anomalies, expansion of S-matrix into Feynman graphs 78—45798
inverse bremsstrahlung, high energy, nucl. mag. contribs. 78—74350
IR divergences in Yang-Mills theories, Feynman diagram labelling 78—54547
IR singularities for arbitrary Euclidean external momenta 79—58861
Ising model, convergence of Feynman diag. expansions 78—16750
Kerr-Schild's gravitational fields, quantisation 80—31653
Klein-Gordon particles, charged, quantum kinetic theory, Feynman rules and thermal eqn. 80—57177
Lagrangian, objective interpretation 78—24686
large order expansions in perturbation theory 78—54525
leading IR divergences in quantum chromodynamics, behaviour in axial gauge 77—13924
lepton-pion deep inelastic scatt. from composite particle in scale-invariant quark model *(Russian)* 77—22740
light-cone gauge, QCD calcs., non-singlet quark struct. function 80—57464
limit $\hbar \to 0$ in quantum field theory, rel. to scatt. amplitudes, differential cross section *(Russian)* 77—61202
magnetic critical phenomena, use of renormalisation group, review 77—20625
massive particle decoupling in field theory, scaled mass, Feynman amplitudes 79—71585
massless QED, calc. of Feynman integrals arising in $F_1(\alpha)$ 77—46001
meson-meson interactions, symmetry restoration in $\lambda\Phi^4$, and large NO(N) σ-models 77—5989
Molien function of a symmetric group 80—8857
multiloop dimensionally regularised Feynman diagram evaluation 80—86586
multiperipheral parton model, deep inelastic processes 80—82961
multiple direct exchange in Yang Mills theory, high energy behaviour of Feynman diagrams sum 77—34088

Feynman diagrams continued
multiple scattering of waves by particle ensembles, radiation transport 77—95
multiquark systems in Feynman's bremsstrahlung analogy, Regge intercepts 79—97590
n-component spin system, anisotropic Brillouin zone, Wilson-Feynman graph technique, universality 77—5764
N-particle system, many body correl. and scatt. amplitudes 79—30683
n-point functions, renormalised G-convolution, convergence in Euclidean case 80—77930
n-vertex loop diagrams in superstrong calc. field, calc. method 77—71472
nonAbelian gauge theory, construction of planar diagrams 77—6031
nonlinear optics, time evolution operators and Feynman diagrams appl. 78—18004
nonrelativistic, loop and triangular, existence of excited states of $A=3$ nuclei 79—9553
nonrelativistic ϕ^3 field theory in two spatial dimens., automation, FORTRAN system 78—8502
nuclear reaction diagram theory, nucleon identity effects 79—9530
numbers and weights of Feynman diagrams, ϕ^N, QED and non-Abelian theories 79—2937
$O(N)\psi^4$ interaction, strong coupling limit, rel. to renormalizability of chiral field 78—386
one-loop diagrams, reduction, scalar field theory *(Russian)* 80—62864
one-loop diagrams, reduction in scalar field theory *(Russian)* 80—27413
operator ordering, interaction Hamiltonian noncommuting operators, S-matrix expansion, Feynman rules 80—57472
orthopositronium decay rate, double-vertex contribution improved error estimate 77—6964
OZI rule violation, analyticity and duality 78—24978
pair production in slowly varying and constant fields, diagrammatic approach 80—374
path integrals on nonlinear phase space 78—37147
Pauli-Villars regularization for non-Abelian gauge theories 79—21956
perturbation expansion of quantised composite field theory, gauge invariance *(Chinese)* 78—82156
perturbation theory at large orders 80—32022
photon exchange between neutral neighbours and cooperative radiation 77—27141
physical operations, diagram operations 80—46846
planar diag. enumeration 79—26239
planar diagrams, SU(N) asymmetric model, semiclassical approach 80—77957
planar Feynman diagrams in perturbation theory 77—61189
points splitting and dimensional renormalisation for Feynman amplitudes 78—86402
proton-nucleus inclusive collisions, very large momentum transfer, cluster representation 79—93615
QCD_2, fermionic Green function and functional determinant, closed representation 80—13269
QCD, 2-dimens., confinement effects on analyticity meson inelastic form factor, scatt. amplitude 79—333
QCD, gauge independence of IR cancellation, fermion-fermion scatt. 78—50006
QCD, struct. functions, perturbation theory *(Russian)* 78—8595
QCD inside hadron, Feynman rules 79—63425
QED, near mass shell IR singularities, Feynman diagrams sum 78—37164
QED infrared singularities, Feynman diagram investigation for e^+e^- annihilation 79—71671
Reggeisation of meson trajectories quark-gluon gauge theories 78—25005
regularised diagrams without Feynman parameters 78—49970
regularization method 80—62844
renormalised Feynman amplitude, high energy behaviour 80—86555
S-matrix for interaction of gravitational and Yang-Mills fields 80—42315
scalar one-loop integrals, soft bremsstrahlung and radiative corrections 79—75682
scalar supersymmetric theory, α-representations 79—30680
scattering amplitudes, sixth-order, Yang-Mills fields, finite-diagram theory 80—73585
Schrodinger handbag model 78—427
sine-Gordon S-matrix, origin of double poles 78—70292
singularities of Feynman diagrams in the coordinate space 79—58884
space-time structure of the two-Reggeon exchange process 79—9311
stability and supersymmetry, general formalism, explicit two-loop appls. 77—79228
star-product representation of path integrals 79—97253
strings from field theory, statistical approach 78—25023
SU(6) exotic gauge model, lepton-quark symm., CP-violation and Feynman rules 78—12875
SU(N) symmetric quantum dynamical systems, $N \to \infty$, energy spectrum for singlet and adjoint states 80—62880
subtracted Feynman amplitudes, low energy asymptotic anal. 80—99040
subtraction procedure, algorithmic features 78—375
symbolic evaluation of dimensionally regularised Feynman diagrams 80—13259
two-particle system in QED, Dyson-Schwinger eqn. 79—2962
UV convergence and analytic properties of manifestly finite perturbation theory 79—71600
vertex functions of chronological exponential, renormalised system of equations 79—30661
virtual processes, Coulomb interaction, scope for experiments 79—9438
weakly coupled mixtures of charged particles at zero temperature 80—140
Yang-Mills 2-D theory in leading 1/N expansion 79—26242
Yang-Mills fields, finite, Feynman diagram theory, analogy with space-time approach 80—52400
zero-mass behaviour of Feynman amplitudes 80—68353
(α,α) scatt. on ^{12}C, ^{13}C, ^{15}N and ^{16}O, forward differential cross sections 78—25210
$e^-e^+ \to 2\gamma$, in neutron star mag. field 77—10236
$e^+e \to \pi^+\pi^-\gamma$, virtual electrons bremsstrahlung photon, Feynman diagrams, Weizsacker-Williams approx. 80—52484
$e^+e^- a\mu^+\mu^-\gamma$, virtual electrons bremsstrahlung photon, Feynman diagrams, Weizsacker-Williams approx. 80—52484
ep deep inelast. scatt., QCD perturbative corrections 78—74263
ep deep inelastic scatt., density matrix appl. to scaling props. 78—8673
$\gamma p \to \pi\Delta(1236)$, 744 to 1044 MeV, graphs of gauge invariant one pion exchange model *(Japanese)* 78—17032
$NN \to NN\pi$, lowest order Feynman diagram calc. 79—63508

Feynman diagrams continued
- ϕ^4 3-D field theory, IR behaviour and connection with critical phenomena 79—71601
- π EM form factor, asymptotic behaviour in scale-invariant quark model 78—37211
- π EM form factor factorisation and asymptotic behaviour in QCD 80—91090
- πNN form factor, $\Delta(1236)$ contrib., calc. 80—22609
- πNN form factor; relativistic calc. of $\Delta(1232)$ contribution to imaginary part *(Korean)* 80—47292
- ψ^{2N} field theory, asymptotic graphs counting techniques 79—17608
- W^{+or-} bosons, lowest order g-2 Weinberg-Salam model, Feynman diagrams 80—47291
- ^{9}Be(d,d'), 12.8 MeV, two stage mechanism described by square Feynman diagrams *(Russian)* 79—22299
- ^{9}Be(p,p'), 6.4 MeV, two stage mechanism described by square Feynman diagrams *(Russian)* 79—22299
- ^{13}C(d,d'), 12.8 MeV, two stage mechanism described by square Feynman diagrams *(Russian)* 79—22299
- ^{208}Pb(p,p'), 5 to 8 MeV, hyperfine reson. struct., Feynman diagrams 79—6589

f.h.p. motors *see fractional-horsepower motors*

fibre optics
- acoustic detection using single-mode fibres, sensitivity meas. 79—50542
- acoustic noise level meas. using optical fibre interometric hydrophone 80—87673
- acoustic sensing with single coiled monomode fibre 80—102826
- acoustic sensitivity of single-mode optical power dividers 80—5835
- acoustic sensor, fibre-optic, modulation processes 80—58771
- acoustic sensor, single multimode fibre, using mode-mode interf. 79—50553
- acoustic sensor using bending loss modulation mechanism 79—50564
- acoustic sensors with composite structure, analysis 80—19087
- acoustic sensors with increased sensitivity due to composite structures 80—5834
- acoustical detector probe 80—91916
- acousto-optic modulator for optical fibres 79—98499
- acousto-optic parallel channel wideband receiver 80—48447
- acousto-optical fibre interferometer for reflective surface motion meas. 80—13127
- acousto-optical multiplexer 77—27370
- active re-entrant Sagnac system, for inertial rotation sensing 80—10038
- analogue fibre optic data link, hardened, construction and analysis 78—30057
- anemometer, laser fibre-optic Doppler 78—30373
- asymmetric fiber power splitter 80—83661
- basic theory 79—32037
- bifurcated probe used in photo-optic measuring system 79—81569
- birefringent fibre interferometric secondary light source 80—105702
- birefringent single-model fibre reciprocity for optical gyros 79—81513
- bistable optical devices: an overview 80—58625
- boroscope 78—50938
- brain reflectance, mapping technique using optical fibres 80—72381
- Brillouin ring laser, fibre-optic, use for inertial sensing 80—87411
- bronchoscope, Kr laser, for early lung cancer detection *(German)* 79—12024
- bronchoscope system, localisation of small lung tumours by fluoresc. bronchoscopy 77—86580
- bundles and single fibres, appls. *(Japanese)* 80—78998
- butt-joined fibre component combination, resolution 78—30079
- cable design, testing and installation 79—37026
- cable design and installation, environmental considerations 79—94362
- catheter, for intravascular press. and sound meas. 78—44638
- catheter oximeter system, solid-state, using three single optical fibres 78—44637
- catheter tip pressure transducer, for intracardiac press. meas. 79—2150
- catheter transducer, side hole type, for intracardiac press. meas. *(Japanese)* 78—73272
- catheter-tip micromanometer as intracardiac press. transducer *(Japanese)* 78—73270
- channel-plate intensifiers for single-exposure photography 78—38036
- chart recorders using UV recording papers 77—18006
- choledochoscope, rigid optical-fibre, KhVS-1, bile duct inspection, surgical appl. 77—37071
- coherent fibre optics testing techniques 80—78992
- commercial developments, 1978 state of art 79—3776
- communication and integrated-optics sources *(Italian)* 79—94371
- communication technology, evaluation under normal telephone system conditions 78—30061
- component developments 80—1356
- component polished end degradation in storage 79—32064
- concentrated solar energy transmission, high-power lightpipe development 80—87481
- conference, Reston, VA, USA, (Mar 1976) 77—46811
- conference on laser and fibre-optics communications, San Diego, CA, USA, Aug. (1978) 79—86203
- connector manufacture and insertion loss 79—90035
- connectors and preparation procedures to minimise losses 77—14803
- contactless displacement/vibration meas. by fibre-optic and capacitive transducers 78—8400
- contactless photoelectric fibre-optic vibration transducers 77—57319
- coupled optical waveguides, coupling coeff. meas. by detuning 78—30066
- coupling loss investigations, scanning automatised optical bench 78—83124
- coupling of fibre optic data links 80—43450
- CRT face-plates for high efficiency photographic recording *(German)* 77—54801
- CRT recording oscilloscope, characts. 77—37911
- CRT recording technique, medicine and research appl. 79—27389
- curved graded index medium, aberration analysis 80—14295
- CW backward-wave generation, degenerate four-wave mixing in CS$_2$ filled optical fibres 79—27327
- cylindrical gradient index lens and array radiometric props. 80—14421
- damaged layer struct. after diamond grinding and polishing 79—7220
- dark field magnification microphotographic illumination system 78—58025
- data bus design and circuit miniaturisation 79—90034
- data bus system with planar access coupler, optimized layout 78—33823
- delay line signal processing devices 80—48443
- demand explosion, review 77—46812

fibre optics continued
- dermatological photobiology, fibre optic light guides for phototesting 78—53472
- diesel engine transient fuel jet droplet photography using light pipes 80—23784
- digital sensors appl. 80—19089
- diode laser wavelength monitoring using fibre interferometer 80—74413
- displacement transducer, fibre optic lever 80—5816
- diverse applications 79—27414
- dosimeter, for large area radiation monitoring 77—46423
- dosimeter on Navigational Technology Sattelite 2 79—22487
- electric field intensity meas., electro-optical sensor with fibre transmission line 80—69509
- electromechanical fibre optic sectional filter 78—13874
- electronics appl., components operation and technical data *(Hungarian)* 79—18514
- end forming of optical precision surfaces on fibre optic elements 77—50779
- endoscope, carrier directional control using magnetic clutches 77—2066
- endoscope, flexible, Soviet SVO1 sigmoidoscope, medical appl. 77—37067
- endoscope, image quality improvement 78—71219
- endoscope one-component objective dimensional design *(Russian)* 78—69228
- endoscope type OD-20Eh, internal surface inspection 79—79216
- endoscope with rigid to flexible imaging multifibre coupling, MTF 79—23052
- endoscopes, equipment for checking optical and illum. characts. 80—56157
- endoscopes, flexible, comparison with lens gastroscopes, gastrointestinal investigation, appl. 77—37070
- endoscopes, flexible optical fibre, comparative study, medical appl. 77—37068
- endoscopes, rod shaped elements improve luminosity 77—37069
- endoscopic laser photocoagulation, use of gas jet appositional pressurisation 78—53468
- endoscopic manometry in gastroenterology 78—92730
- endoscopic miniature camera with fibre-optic faceplate 80—77896
- esophagogastroscope, flexible fibre optic instrument, experience of use of 79—34622
- Faraday effect in lightguide, weak microwave field meas. 80—73463
- Faraday rotators in fibre Raman lasers 80—58775
- fibre laser high-power stimulated emission pulses, substruct. 80—9890
- fibre optic Mach-Zehnder interferometer, sensing of press. and temp. 79—72671
- fibrescopes using leached fibre image bundles, manufacture 80—83670
- filter fluorometer, for anal. of absorbing solns. 77—36813
- flame propagation in long tubes, ducts investig., fibre optic technique 77—31404
- flowmeter using optical-fibre transducer 79—98830
- fluorometric flow cell, using fibre optic system, design and evaluation 78—32879
- force transducer for isometric muscle contraction meas. 79—79715
- Fourier hologram recording using Selfoc-type optical fibres 80—95850
- fusion reactor, fibre optic telemetering for high voltage test stand 78—54939
- fusion reactor, pulser system, air-driven fibre-optic coupled for Los Alamos ZT-40 expt. 78—54943
- gas flow calibrator fibre-optic timing system 77—31408
- glass manufacture using polypropylene sump pumps 80—14410
- glass tubing dia. and wall thickness meas., P-329M instrum. 80—86262
- graded index fibre profile determ., interferometric method 80—14481
- graded-index, multimode, differential mode delay and attenuation meas., optimal excitation calc. 80—99842
- gradient index fibre array, illumination intensity unevenness, theory and expt. 80—14480
- gradient index fibre array, transmittance analysis 80—14478
- gradient index fibre array development and imaging props. 80—14483
- gradient index fibre array for photocopying machine 80—14482
- gradient index fibre image intensifier system 80—14484
- gradient index optical imaging systems, topical meeting, Rochester, USA (May 1979) 80—12851
- guided wave optical systems and devices, conf. Washington DC, USA, 1978, Mar. 79—37031
- gyroscope, fibre ring interferometer, nonreciprocity noise, fibre dispersion meas. 80—1346
- gyroscope, phase nulling 79—72719
- gyroscope, possible integrated optics soln. 80—10041
- gyroscope, Sagnac or Fizeau effect 79—72669
- heterodyne interferometer for vibr. meas. in biological systems 78—77101
- high-speed scanning laser diffractometer 79—68437
- histroy of development and markets 77—7194
- holographic interferometry with optical fibres, hearing mechanism obs. 80—76879
- hybrid optoelectronic modules for OEM fibre-optic data systems 79—86259
- hydrophone, fibre-optic, description and advantages 80—58770
- hydrophone, improved strain config. and environmental noise protection 79—98471
- hydrophone, interferometric fibre optic, static press. sensitivity amplification 80—38094
- hydrophone, moving fibre optic, based on intensity-modulation mech. 80—43455
- hydrophone, multimode fibre optic, frustrated total internal reflection, testing 80—38096
- hydrophone, noise-equivalent pressure 80—33387
- hydrophone, optical interferometric, with homodyne detection, signal stabilization by light source tuning 80—87477
- hydrophone, using single-mode and multimode fibres, sensitivity 78—13882
- hydrophone sensitivity, strain configs. 80—23771
- hydrophones, comments on mechanism of transduction 80—58882
- hydrophones, mechanism of transduction 80—10103
- IEEE International Microwave Symposium, Orlando (1979) 79—68356
- III-V semiconductor emitters and detectors for 1.0-1.6 μ fibre-optic communications 80—10007
- illuminating fibre bundles, improved characts. due to glasses type VS 1637 and VO 720 80—102844
- illuminator output speckle, smoothing methods 79—7209
- illuminators for hologram recording and reconstruction 79—41353
- image intensifier with fibre optic plates for astronomy *(Russian)* 79—40079

fibre optics continued
  - image quality at fibre laser amplifier output, comparative anal. under active, passive conditions 79—7225
  - image tube with fibre optics, cooling effect 78—96401
  - incoherent optical power launching limits, fibre endoscopic inspection appl. 78—63193
  - industrial IR thermometry using fibre-optic lightguides 80—86302
  - injection laser diodes for fibre optic communication 78—33751
  - integrated subsystems, progress in development and appls. 79—46068
  - interferometer, laser single-mode fibre 78—49892
  - interferometer, rotation-sensing fibre-ring, polarisation analysis 79—64333
  - interferometer, single mode optical fibre, small phase shift meas. 80—57366
  - interferometer gyro, thermally induced nonreciprocity 80—58665
  - interferometer gyroscope 80—1348
  - interferometers for length, temp., pressure and force meas. 80—98971
  - interferometric sensor for acoustic detect., thermally induced optical phase effects 80—74479
  - interferometry through single-mode fibres 80—73442
  - intravascular O_2 saturation continuous meas. using fibre optic catheter *(German)* 78—85411
  - introduction to theory and applications, book 80—90617
  - ion source light link control system 79—68093
  - Kohler illumination using fibre optics and quartz-halogen lamp 78—58027
  - laser amplifier and monomode optical fibre system *(German)* 79—81454
  - laser beam diffuser for uniform beam production 79—68436
  - laser bronchoscope for optical fluoresc. localisation of early lung cancer 78—48921
  - laser Doppler velocimeter, follow-up-type, using single-mode optical fibres 80—74476
  - laser endoscopy, associated ophthalmic hazards 79—79598
  - laser fusion reactor, NOVA, pulsed power control system, fibre-optic multi-tapped computer bus 80—95443
  - laser gyro applications 80—1345
  - laser gyro signal detection and processing technique 79—37037
  - laser inertial rotation sensors, conf., San Diego USA (Aug. 1978) 80—1265
  - laser plate for digital image processing, all-optical parallel logic operation 80—106463
  - laser plate for optical parallel processing 79—76695
  - laser radiation damage of fibre optic elements 80—102747
  - laser surgery, flexible fibre-optic beam-guiding system, oto-rhino-laryngology appls. *(German)* 79—83886
  - LED coupling fine adjustment *(French)* 79—94332
  - lens, gradient-index rod, aberrations in multimode optical fibre devices 80—69487
  - light guide for lighting inlet slit of metal spectroscope *(Russian)* 79—41456
  - light mode stripping reservoir 79—76835
  - light protecting shield 78—18066
  - light ray tracing through deformed glass rods with radially graded RI 79—64338
  - light shield, fibre selector with absorbing cladding, Fraunhofer diffr. 78—90521
  - light source for curved platen illumination 78—63163
  - liquid crystal thermometry, optically active binary mixture 79—42952
  - long distance communications, fibre optic developments *(Norwegian)* 80—1318
  - low-loss optical fibre evolution 80—69532
  - low-loss single-mode fibres, elliptical and circular core, laser gyro appl. 80—1344
  - magnetic field detection possibility through optical fibre magnetostrictive perturbation 80—53450
  - magnetic field sensors 80—69510
  - magneto-optic current measuring device using low-birefringence silicone-clad fused silica fibre 79—50425
  - magneto-optic current sensing with birefringent fibres 79—75544
  - market trends, worldwide 80—58699
  - marketing data for 1977-8, USA trends 79—18513
  - mass spectrometer electro-optical ion detector applic. 77—45915
  - mechanical vibration meas., using fibre optic laser Doppler probe 78—30248
  - medical application of monofibres *(French)* 79—39462
  - medical applications, diagnostic and therapeutic 79—39466
  - medical applications, review 77—48901
  - medical applications, review *(Italian)* 78—53540
  - micro-spectrophotofluorimeter for in vivo animals studies 77—60327
  - microfluorimeter for animal haemodynamic and pharmacokinetic meas. 79—92455
  - microinterferometer transducer, air-bearing, for use with universal inspection machines 78—57899
  - microphones and hydrophones compared with conventional devices 79—72717
  - microscopy, UV, with image intensification and TV image displays 77—5888
  - microtransducer for temperature and power density meas. appl. *(French)* 77—61084
  - microwave and satellite terminal fibre-optic links 77—27377
  - miniature probe microphone using optical fibre 80—48534
  - modulated fibre ring interferometer, laser appl. 80—74506
  - molecular beam detector, state-resolved 79—54999
  - monolithic component glasses and rigid sintered fibre-optic elements, microcrack form. during grinding 78—87175
  - monomode fibre selective excitation for differential group delay meas. 80—99876
  - moving-fibre panoramic camera, image motion velocity calc. 79—26168
  - multimode fibre bussing, active fail-safe terminal 78—55438
  - multimode fibre coupler-type acoustic sensor, optical intensity modulation 80—102945
  - multimode fibre optic interferometry, applications 80—86387
  - multiphase flow optical fibre sensors, appls. *(German)* 78—26215
  - multiplexing of scintillation detector arrays 77—54438
  - multiturn fibre Sagnac interferometer, shot-noise-limited inertial rotation meas. 80—1349
  - nanosecond hydrodynamic diagnostics, streaking camera, fibre optic probes 78—37096
  - near-IR fibre Raman oscillator, 1.07-1.32 μm tunable 79—72622
  - neonatal probe for oximetry and dye curves 79—70603

fibre optics continued
  - nitrobenzene-in-benzene optical fibre amplifier performance estimation 79—7217
  - nonlinear effects, appl. to active and passive device fabrication 80—58638
  - oil detection, in water, using combined GaAlAs laser and fibre optic bundles 78—96301
  - optical path meas. using fibre optics, theoretical investigations of path transducers *(German)* 80—106608
  - optical processing systems, seminar, Huntsville, USA (May 1979) 80—46732
  - optical time domain reflectometer 79—37036
  - opticomechanical anemometer for flow vel. meas. of optically transparent material 77—68718
  - opticomechanical pressure transducers, designing and testing 80—105662
  - parallel transmission of one-dimens. light distrib. by single optical fibre 78—30047
  - parametric oscillator, Brillouin, mode-locked optical fibre, bandwidth-limited operation 78—50851
  - parametric oscillator, sequence freq. generation 80—83636
  - passive optical rotation sensors using guided waves, developments 80—58781
  - PFM fibre-optic video transmission to and from undersea vehicles 80—46310
  - pH sensor, miniature, for physiological use 80—109074
  - phase-nulling fibre optical laser gyro 79—36949
  - phased array of optical fibres for laser beam scanning 79—81514
  - photocopier lens array design, Wood lens and gradient index fibre comparison 80—14479
  - photoelectric detection improvements 80—91919
  - pinhole light source, bright and inexpensive 78—83058
  - plastic fibre optic sheets fabricated by selective photopolymerization 79—55235
  - polarisation rotator, birefr. single mode optical fibre 79—76808
  - polarisation transformer, in-line 79—72667
  - polariser, in-line, formation and props. 80—106603
  - polychromator, rapid-scanning, for time-resolved temp. and radius meas. in 40 kA SF_6 arcs 79—50907
  - probe, angular position transducer, IR source 80—86257
  - probe for thermal profiling of liquids during crystal growth 79—68443
  - proximity transducer, evaluation for surface texture meas. 80—36985
  - quality of fibre optic glass pairs, effective aperture and light scatt. analysis 78—90522
  - radiation thermometer with fibre-glass bundle, up to 1000°C *(German)* 79—35745
  - Raman and Brillouin laser gains in fibres, polarisation effects 80—9887
  - Raman fibre laser oscillators, theory 79—81439
  - Raman laser, CW fibre, bandwidth reduction using prisms, gratings and etalons 80—53366
  - Raman lasers, fibre 80—102767
  - Raman oscillator, CW optical fibre, using two-mirror resonator config. 79—7152
  - Raman ring laser 79—22981
  - reactor safety and protection, electrical isolation devices employing fiber optic cable 79—59218
  - recorder, use in US imaging 77—5057
  - recorders for traces and images 79—67292
  - rectoscopes, optical fibre, unified design for adults and children, medical appl. 77—40827
  - refractometer for liquid chromatographic use 77—2683
  - relay device with metallic pads heated by light 78—18038
  - remote inelastic light scatt. probe, use of optical fibres 80—58769
  - research and development, advances, conf., Kingston, RI, USA (June 1978) 80—57005
  - research in USA 77—27363
  - resonant cantilevered fibre-optic scanner 80—53428
  - ring gyroscope, optimum sensitivity limits 80—10039
  - ring interferometer, Sagnac-effect, sensitivity analysis 79—50379
  - ring interferometer gyroscope, Fresnel drag effect 78—79142
  - rotating sensor, Sagnac interferometer preliminary results 80—10040
  - rotation rate sensors, Air Force appls. 80—9932
  - rotation sensor, all-waveguide configuration, key element tests 80—58796
  - rotation sensor, laboratory performance evaluation 80—1347
  - rotation sensor, signal detection and processing, inertial reference device 79—54111
  - rotation sensor (FORS), signal detection and processing 79—37034
  - rotation sensor construction and laboratory test 79—98497
  - rotation sensor with low drift 80—69530
  - ruby fibre laser, room temp. continuous operation without cooling, crystal growth, heating effects 78—66833
  - safety closure with deflector 80—53425
  - Sagnac effect fibre ring gyro with electronic phase sensing 80—1350
  - Sagnac fibre-ring interferometer gyro with electronic phase sensing 79—17472
  - Schlieren multimode fibre-optic hydrophone 80—102938
  - scintillation counter hodoscope 1 mm granularity 77—34515
  - scintillation counter hodoscope using fibre optic light guides 78—37514
  - Second European Conference on Optical Fibre Communication, September 1976, review *(Italian)* 78—5552
  - selector for Sun position sensors 77—49262
  - sensor for photoelectric recording, design 80—28338
  - sensors, appl. to basic variables meas. *(Norwegian)* 79—93121
  - sensors appl. *(Japanese)* 80—78997
  - sensors for measurement and control appls. 80—58780
  - sheet formation by selective photopolymerisation, appl. in image guiding equipment 78—42477
  - Shiva laser fibre-optic digital links 79—85804
  - signal processing activities of United States Army 80—48172
  - signal processing devices 80—58768
  - signal processing research programme of United States Air Force 80—48171
  - signal processing with fibre and integrated optical devices 80—33233
  - single mode CVD fibre, bend-induced birefringence obs. 80—58723
  - single mode fibre analysis and fabrication for low polarisation birefringence 80—58722
  - single mode fibre for current meas. system, birefr. induced by bends and twists 80—99832
  - single mode fibre polarisation stabilisation 80—58724
  - single mode optical fibre polarisation stabilisation 80—33154
  - single-mode fibres, fractional wave devices and polarisation controllers 80—106606

fibre optics continued
single-mode optical fibre phase modulators, pressure sensitivity meas. 79—7205
single-mode optical waveguides for ring interferometer, Fresnel drag 79—37035
single-mode sensors, polarisation effects 80—43426
sintered plates, micropore sealing, vac. tightness improvement 80—28333
slurry conc. and particle size determ., on-line light backscattering method, fibre optic appl. 79—58674
sonar, computerised system, geological and hydrographic survey applications 78—88947
sound detection, fibre-optic technique 78—13871
sound reading systems for cine projectors *(Russian)* 78—312
spatial coherence and index-profiling in optical fibres 80—1335
spectrophotometer dip probe bubble formation prevention 80—13154
spectrophotometer head with fibre-optic bundles 79—93201
spectrophotometer head with small-spot fibre-optic viewer 79—30525
spectroscopic cooled and intensified array detectors 78—65983
state-of-the-art and available equipment *(German)* 80—87484
statistically irregular focusing fibre, losses 77—46804
step-index fibre transmission system variable equaliser 79—55243
stereo-fibrescope with magnetic interlens bridge for laryngeal observation 79—44068
strain gauge, arbitrarily shaped path length meas. 78—70112
strain gauge 78—94426
streak camera, direct readout devices 78—38037
subnanosecond X-ray framing camera, fibre array technique 78—41394
switch, crossbar 80—74497
systems and field trials, review 80—58700
systems aspects of optical-fibre communications 77—7016
technical innovations and market development 80—10008
temperature meas. appl. using phosphors as sensors 80—73360
temperature probe with SiO_2 fibre guide 78—208
tension-coiled single-mode fibres, high birefr. 80—99858
theory, basic principles and equations, multimode and single-mode fibre characteristics 80—43457
tiltmeter, using optical fibres 80—8958
time-dispersion-tuned fibre Raman oscillator 77—42562
training, educational course status and effectiveness 80—62413
transmission characts. meas., Tektronix digital radiometer/photometer appl. *(French)* 79—89000
transmission system components *(Spanish)* 79—94348
triplet lens for fibre-optic bundle 80—14414
turbine blade surface temperature meas. IR pyrometer 77—17983
twisted single-mode fibres, polarisation optics 79—81524
units and terminology used in light meas. rel. to photometry and displays 79—21691
US pressure sensor 80—58878
vibration meter, high sensitivity, laser type using a fibre-optic probe 79—7351
viewing instrument appls., flexible fibre light-guides 80—87545
visible IR spin-scan radiometer 78—59160
vitreous surgery via pars plana, instrument design 78—81056
wavelength division multiplexer using optical fibre pieces 80—91917
welded optical fibre signal splitter 80—102814
West German developments 1978 survey *(Swedish)* 79—55209
white light, information processing and transmission 80—95833
X-ray image intensifier, large-area contrast 77—70534
X-ray streak camera, high time resolution, with X-ray microscope *(French)* 78—42823
AgBr single-crystal IR optical fibres, growth from melt 80—53449
$Al_xGa_{1-x}As$-GaAs LED design and characterisation for fibre-optic communications 78—46796
CsI:Tl, X-ray screens consisting of scintillating crystal fibers 79—6244
GaAs lasers, current research 80—83613
GaAs lasers, optical fibre coupled arrays 80—69393
Nd:glass conical fibre optics quantum amplifier parameters 78—59024
Nd:Y_2O_3 single crystal fibre laser, room temp. CW operation at 1.07 and 1.35 μm 78—63121
Nd:YAG single crystal fibre laser, self-contained LED pumped 79—59711
SiO_2 fibre near IR Raman laser, as universal fibre optic meas. system 79—23070
SiO_2, fused, fibre Raman laser emitting over very large spectral region *(French)* 78—55405

fibre reinforced composites
see also carbon fibre reinforced composites; glass fibre reinforced plastics
acoustic imaging 79—15918
adhesion between fibre and matrix, AE testing *(Japanese)* 77—70254
adhesive debonding, exam. 78—60773
AE monitoring review 79—11735
Ag-Cu fibre composites, highly deformed, lattice defects, X-ray interference lines anal. 80—10559
aircraft materials, design allowables 80—81204
Al-graphite composite, mech. props., effect of thermal exposure 77—36629
alloying effect on interphase interaction, thermodynamic calc. *(Russian)* 79—74134
analytical method of determ. 79—100201
anelastic behaviour using continuum theory of internal separation 77—46907
angle ply, delamination mechanics and failure mode 80—79236
angle ply laminate, fibre reinforced, interlaminar strength test for delamination 78—88523
angle-ply laminate, edge effects 78—19803
anisotropic elastic medium reinforced with thin tapes, model 80—38276
anisotropic reinforced resin laminate, cyclically reversing load, strain behaviour determ., approx. method *(German)* 79—5096
anisotropic two phase media, freq. depend. of elastic wave velocity and attenuation 79—50644
annular discs surrounding circular hole in flat plate, stress anal. 77—46912
apparent fibre spacing 78—79222
aramid fibre reinforced acrylic bone cement, tensile strength and fracture toughness, SEM study 79—29667
aramid fibre reinforced epoxy resin, shear props. 77—81354
asbestos fibre reinforced cement, strength and fracture props. 80—108533

fibre reinforced composites continued
asbestos fibre reinforced cement mortar, strength and fracture properties 79—100241
asbestos fibre reinforced Portland cement analytical fracture resistance curve expression 78—76756
B fibre reinforced Al, real-time NDT during fatigue loading 77—86264
B fibre reinforced Al alloys, new production method with continuous fibres 77—66610
bagasse fibre reinforced phenol formaldehyde, tensile strength and Young's modulus, SEM study 80—60952
bars, cylindrical, elastic-plastic torsion 80—33473
beam, rigid plastic, impulsive loading 79—3928
beams, vibration analysis 77—68482
bent thin-wall constructions, rupture 80—64472
biaxially fibre reinforced composites, two dimens. mixture theory, dynamic crack appl. 78—87301
bond stresses of isotropic body with elastic inclusions 78—30180
bone, model to explain anisotropy of Young's modulus 80—35944
bone tissue, compact, fracture 80—12178
borsic fibre reinforced Al, hot pressed forged, plasma sputtered *(Russian)* 78—35330
borsic fibre reinforced Ti, unidirectional, K-calibration and compliance curves 78—88518
brittle fibre reinforced alloys, anal. of fracture process and fibre strength, by Monte Carlo simulation *(Japanese)* 78—80634
brittle fibre reinforced composite, brittle reaction zones at interfaces, tensile strength 79—52306
brittle fibre reinforced composite, static strength depend. on component separation boundaries *(Russian)* 80—76304
brittle fracture, crack interactions 80—65149
brittle fracture, effect of cracks and imperfections on contact surfaces 80—10203
brittle interlayers influence on tensile strength *(Russian)* 80—21006
brittle zone on fibre surface deform. and fracture 77—56104
calculation of stress distrib. and X-ray elastic consts. *(German)* 78—52883
cement matrix, mech. and rheological props. *(German)* 79—20129
ceramic, matrix, design and prod. *(Polish)* 78—11188
ceramic matrix, strength and fracture 79—87723
ceramic-ceramic composites, high temp. high performance materials *(French)* 79—83166
chain of bundles probability model for fibrous material strength 78—67095
chain of bundles probability model for strength, numerical study of convergence 78—88496
characterisation by differential scanning calorimetry 80—71869
cheese cloth filled cellulose acetate film, diffusion and permeation of gases 79—55934
chopped high-modulus fibre reinforced polyurethane foam, morphology and fracture 77—36447
circular tube fibre reinforced sector, elastic deform. 77—72164
complex structural mouldings, accurate stretch data for reinforcement, deform. 80—11694
complex structural mouldings, accurate stretch data for reinforcement, deform. 80—16375
composite beams, effects of fibre orientations on free vibrations 80—87734
composite principle, further development *(German)* 77—36448
compound arbitrary anisotropic body, stress singularity, composites appl. *(Russian)* 80—33455
concrete, beam with mixed type of reinforcement, shear and bending strength 79—20124
concrete, fibre and polymer reinforced, commercial prospects 77—12592
concrete, lower bound anal. for torsion 78—35436
concrete, reinforced deep beams, with web opening, structural idealization 79—20125
concrete, review *(Japanese)* 78—31372
concrete, with glass or steel fibres, mechanical props., and drying shrinkage obs. 79—87706
concrete beam, load-deflection curves in flexure 78—35437
concrete curved beam, expt. investigation of collapse 77—90404
concrete matrix, flexural strength 78—11288
concrete matrix, strength calc. 78—11286
concrete reinforced members, limit index point and flexural capacity *(Japanese)* 79—83283
concrete structures, reinforcement position measurement 77—90534
conductive filler-polymer composite conductivity theory *(Japanese)* 78—11351
conference, Moscow, USSR (Nov. 1978) 80—8733
cord reinforced rubber laminate, interlaminar-shear-strain meas. 79—57043
cord-rubber laminates, two-ply balanced, interlaminar-shear strain study 80—97526
Cotac 74, directionally solidified composite, creep behaviour prediction *(French)* 78—68754
crack growth, effect of additional matrix toughening component 77—56076
crack growth, fracture mechanics 80—10212
crack growth due to creep *(Japanese)* 77—32702
crack propag. *(Russian)* 77—25147
crack-tip analysis for elastic materials reinforced with strong fibres 79—27594
cracking and fracture, review 78—60772
cracks, emanating from circular hole in unidirectional specimen, anal. 80—100301
cracks, energy release rate per unit length 77—66690
creep behaviour of fibre reinforced metals *(German)* 78—52931
cross-reinforced layered, moment effects in plane problem 80—64393
cylinder, stresses due to plane temp. distrib. 80—5935
cylinders, fibre-reinforced, singular stress layers 79—14268
cylindrical shells, stress strain state and stability 80—14598
damage tolerant fibre reinforced sheet metal composites, crack growth 77—81319
deformability, determ. by stiffness averaging method 80—3115
deformability characteristics, reinforcement scheme effect 80—58930
deformation, mathematical theory 77—68453
deformation and fracture in combined stress states 77—70106
deformation diagram construction method, based on statistical distrib. of strength of fibres 77—52437
deformation in incompress. material reinforced by nonextensible fibres *(German)* 79—87702

fibre reinforced composites continued
  densification in free forging, exam. of specific work and kinetics 80—16218
  dielectric properties of medium with regular struct. 80—20576
  discrete W fibre reinforced alloy, effect of microstruct. on impact strength 77—56099
  dispersed fracture of unidirectional composites 80—11768
  dispersive waves, phase and group vels. determ. 78—81848
  ductile-fibre composites, strengthening effects of brittle zones 77—8946
  dynamic model 77—68496
  dynamic testing discontinuous fibre reinforced composites 80—21235
  dynamic universal solns. for fibre-reinforced incompressible isotropic elastic material 77—14925
  dynamically induced interfacial stresses 79—18727
  elastic characteristics *(Russian)* 78—59304
  elastic constants calc., for randomly reinforced plastics *(Japanese)* 78—31437
  elastic fibre reinforced composites, wave guide-type propag., microstruct. theory 78—83279
  elastic fibre-reinforced continuum, wavefront motion *(German)* 77—35068
  elastic moduli, approx. formulae 77—66672
  elastic moduli, representative volume calcs. by photoelasticity method *(Russian)* 79—34094
  elastic moduli and shrinkage factors, calc. taking account of anisotropy 79—52291
  elastic modulus, estimate for composites isotropic on the average 78—51077
  elastic props. determ. *(Russian)* 77—19532
  elastic shear waves propagation 80—58963
  elastic slab subjected to axial loads, instability and buckling 80—64420
  elastic-plastic behaviour of fibrous composites 79—76985
  electric orthotropic cylindrical shell, axisymmetric contact problems, shell interaction with tires 78—1569
  epoxy laminates, interlaminar failure 80—81207
  epoxy matrix laminate, static and impact props. 77—63725
  epoxy resin composites, cooldown residual thermal stresses, viscoelastic response 80—60941
  epoxy resin reinforced by multilayer systems, exam. of stress states, using photoelastic method 79—41638
  epoxy-graphite laminate creep behaviour humidity effects 77—66682
  fabric reinforced laminates, stress-strain relationship *(Polish)* 79—91750
  failure, mathematical simulation 78—3221
  failure, probability bounds 79—87716
  failure, role of binding agent 79—1912
  failure analysis by acoustic emission 78—80691
  fatigue, conf., London, England June (1977) 78—15489
  fatigue 78—68767
  fatigue behaviour under random loadings, mathematical model and digital simulation *(Japanese)* 80—85032
  fatigue damage, early detection by NDT 77—28951
  fatigue damage under pulsating tensile stress 79—100237
  fatigue testing machine, materials in pure bending 77—1906
  fiberglass materials, fatigue damage effects on light scatt. 79—11706
  fibre composite structure, thermal field techniques for NDT 80—66737
  fibre glass laminate in tension, creep 80—71718
  fibre pull-out at high loading rate *(Japanese)* 80—45357
  fibre reinforced composites, surface wave propag., load transfer from reinforcement to matrix 78—46904
  fibre reinforced Ni, work hardening tendency, at elevated temps. 77—52353
  fibre reinforced plastic, fracture mechanism study, cumulative failure model 78—92315
  fibre reinforced plastic/Al/adhesive laminate, interlaminar behaviour under thermal loading 77—81309
  fibre reinforced silicone rubber composites, interfacial slip and damping 79—5010
  fibreglass, solar glazing hemispherical transmittance props. 79—52957
  fibreglass composite, oriented, model, conditions of monolithicity, exam. 78—67044
  fibrous composite models, photoelastic analysis of interlaminar matrix stresses 77—3799
  fibrous laminated composite, tensile failure, quantitative fault tree anal. 77—59891
  filament-wound pipe, microscopy of failure mechanisms 79—24604
  fixed-free generally orthotropic beam vibration finite-element models 79—68621
  flextensional transducer design trends 80—43588
  flexural strength, denture base appl. *(Japanese)* 78—40409
  flexural vibration of beam, forced vibration technique for meas. of material damping 78—19964
  fracture, fibre geometry and filler vol. influence on fracture stresses 80—45397
  fracture, mixed mode, in unidirectional samples 80—100302
  fracture, theory 80—89351
  fracture initiation prediction 80—11870
  fracture kinetics determ. 80—11770
  fracture mechanics, review 79—27597
  fracture mechanics appl. to failure 77—52453
  fracture processes modelling, digital computer appl. 80—65147
  fracture toughness, fibre bunching effects 79—61699
  fracture with bonding strength defects between components, computer simulation 80—11771
  FRC, reinforcement parameter 78—79223
  glass fabric, effect of phosphate binders on properties 78—44075
  glass fibre composite, shell, carrying capacity, heating effects 77—4865
  glass fibre reinforced cement, durability in wet and dry conditions, fibre length and content effect 80—71726
  glass fibre reinforced cement, glass content meas. by X-ray fluorescence anal. 79—52840
  glass fibre reinforced cement, glass fibre volume fraction determ., using photodiode 78—48578
  glass fibre reinforced cement, progress report 79—91905
  glass fibre reinforced cement, review of reinforcing theory, ageing, stress/strain relations 78—44165
  glass fibre reinforced composite, fatigue failure, role of shear deform. 78—15494
  glass fibre reinforced composite, shear fatigue 78—15493
  glass fibre reinforced composites, energy absorption during axial collapse 79—96112

fibre reinforced composites continued
  glass fibre reinforced Pb, production by infiltration, tensile strength 77—59720
  glass fibre reinforced plaster, glass fibre volume fraction determ., using photodiode 78—48578
  glass fibre reinforced polyester, photoelasticity, optical characts. 79—18709
  glass fibre reinforced shell of rotation, stability 78—13938
  glass reinforced brittle matrix, failure anal. by fault tree technique 79—29193
  glass reinforced fabric, tensile strength, low temp. testing, −196 to +20°C 79—61692
  glass-ceramic composite, internal stress effects on mech. props. 77—21250
  glass-fibre reinforced Al, highly deformed, microstruct. and mech. props. *(German)* 80—55489
  glass-fibre reinforced cement, strength study by reliability concept, fibre concept and temp. depend. *(Japanese)* 80—66586
  glass/C fibre reinforced plastic, hybrid effects between interlaminar and translaminar config., mech. props. 79—52351
  glass/epoxy composite, tensile test 80—11778
  glued microplastic threads, tensile strength 79—61670
  graphite, fibre reinforced Sn-Pb investment castings, tensile strength 77—48487
  graphite fibre epoxy composites, eutectic coating moisture barriers 80—81228
  graphite fibre epoxy laminates, low thermal expansivity, design considerations 80—81031
  graphite fibre filled phthalocyanine composites, cure cycle investigation 80—81030
  graphite fibre filled polyimide composite laminates, space environment, phys. and mech. response 80—81140
  graphite fibre filled polyimide composite prepreg laminates, room-temp. ageing effect 80—81093
  graphite fibre reinforced Al, mech. props., comparison with B-Al composite 77—52470
  graphite fibre reinforced composites, damage by moisture, diffusion anal. 80—81227
  graphite fibre reinforced composites, energy absorption during axial collapse 79—96112
  graphite fibre reinforced glass, impact damage tolerance and reliability 80—81177
  graphite fibre/epoxy laminates, free edge induced failure 80—11775
  graphite-Al composite development using liquid infiltration technology 77—24986
  graphite-epoxy composites, moisture profile meas. using nucl. reaction anal. 80—55760
  graphitised PAN fibre layered compounds with metal chlorides 79—91600
  gypsum plaster, plain and glass reinforced, fracture energy 77—36621
  heat conduction eqns. *(Russian)* 77—75767
  homogeneous isotropic composite, small vibr. propag. in static deformation 77—42775
  hybrid, tensile strength, statistical analysis 77—63624
  hybrid composite material beams, exam. of shear stress correction factors 78—46899
  hydrostatic states of stress, deformation 77—36602
  hygrothermal microstresses, in material exhibiting inelastic behaviour 77—84141
  hyperelastic composite reinforced by inextensible fibre, first- and second-order constitutive eqns. *(German)* 78—18174
  ideal, finite plane deformation and energy dissipation 78—79274
  ideal elastic fibre-reinforced slab, dynamic flexural deformations, flexural wave propag. 80—33510
  ideal fibre reinforced, rigid plastic cantilever beam, impulsive loading, subsequent motion 77—80096
  ideal fibre reinforced rigid plastic beams, impulsive transverse loading, control impact 77—80094
  ideal fibre reinforced rigid plastic beams with end supports, impulsive transverse loading 77—80095
  impact response analysis, perpendicular to fibres *(Japanese)* 79—43377
  imperfections, piezo- and elasto-optical effects under longitudinal shear *(Russian)* 78—56457
  inextensible elastic materials, general solns. in equilib. theory 79—12602
  initial yield surface, in plane stressed state 77—86106
  interface strength *(Japanese)* 78—15646
  interfacial interactions and bonding, fibre surface props. 80—80046
  intralaminar-shear charact., 10 deg off axis test 78—35422
  ionomer composites, fatigue strength, dynamic viscoelastic props. and fracture surface exam. *(Japanese)* 78—92339
  Kapron fibre reinforced phenolic resin, fracture kinetics, interface props. 80—66640
  Kevlar 49 fibre reinforced composite, shear fatigue 78—15493
  Kevlar aramid fibre reinforced composites, flexural strength 79—11671
  kevlar fibre reinforced composites, energy absorption during axial collapse 79—96112
  Kevlar fibre reinforced epoxy, fibre orientation effect on friction and wear 79—79125
  kevlar-epoxy composites pressure vessels, holographic nondestructive eval. 80—81275
  Kevlar-fibre-reinforced plastic laminates, US evaluation of hygrothermal effects 80—7730
  Kevlar/epoxy, unidirectional and bidirectional, thermal expansion behaviour 80—24622
  Kevlav fibre reinforced cement composites, cement boards, exam. of mech. props. 78—48499
  laminate, anisotropic layers, fibre reinforced, effective moduli of elasticity 77—4802
  laminate, elastic law for materials with different tensile and compressional moduli 80—11713
  laminate, fracture mode determ. by AE 79—57187
  laminate, moisture diffusion, 3-D Fick's law 78—10218
  laminate in combined stress state, fracture models 80—10211
  laminated, reliability anal. approach to fatigue life dispersion *(Japanese)* 79—61704
  laminated composite panels, flutter instability, shear deformation and damping effects 79—72841
  laminated fibre reinforced plastic cylindrical shell, coupling effect under internal press. *(Japanese)* 80—55449
  laminated hybrid, tensile first cracking strain and strength 80—81175

fibre reinforced composites continued
  laminated plate under tension, stacking sequence and lay up angle effect on free edge stresses round hole 78—88524
  laminates, optimum design under natural frequency restraints 80—53688
  lamination theory for failure envelope prediction under biaxial loading 79—38931
  layered, harmonic elastic waves, dispersion 78—63223
  layered or reinforced composites, elastic constants and stress-strain parameters *(Russian)* 79—46209
  leucosapphire single cryst., W grid reinforced, growth 77—16530
  lightweight solar array flexible substrates with anticharging layers 79—96456
  linen-cloth-reinforced phenolic resin, epoxy resin laminate, sliding behaviour against Cu or Al spheres at cryogenic 80—66671
  longitudinal shear of reinforced medium with a periodic system of cracks 80—35323
  Longitudinal wave behaviour at low and high frequencies 78—38246
  materials properties, unsolved problems, review 77—4843
  mechanical behaviour, axial residual stress effect 77—36573
  mechanical characterisation at low temps. 78—64611
  mechanical model 78—51105
  mechanical properties, physics of strength, kinetics of failure 78—3206
  mechanical strength, depend. on fibre morphology *(German)* 80—30043
  metal and alloy bases 77—21060
  metal clad, debonding risk 80—3132
  metal fibre filled polymer, mech. and cond. props. 79—91808
  metal gauze reinforced porous permeable mats. with prearranged struct., prep. 78—68652
  metal matrix, complex torsional and tensile loading 79—61669
  metal matrix, high temp. appl., creep, dislocation processes 77—48369
  metal matrix composites, thermal expansion effects, fibre length depend. 78—51708
  metal matrix-fibre composites, brittle interface layers and tensile strength 79—79039
  metal-based fibre-type, designing for structural integrity 79—83155
  metallic, electrical conductivity, fibre effects 80—100450
  metallic composite materials, stress redistrib. upon breakage of brittle fibres 78—48527
  metals, fibre reinforced, fatigue limit *(German)* 78—72859
  micro- and macrocracks 80—65148
  mineral wool fibre composites, mech. props., effects of thermally induced phys. and chem. changes 77—59884
  mineral-fibre composites that resist fracture and cracking 77—8798
  mixture theory for longitudinal waves in rectangular fibre arrays 78—9590
  models for composites with different props. in tension and compression 78—35417
  modulus of brittleness, crit. tensile span 78—92318
  moisture content under transient conditions 77—48598
  mullite fibre reinforced mullite, in vitro degradation, bending strength, Young's modulus, density meas. 78—85011
  multicomponent, mech. props. 79—52329
  multilayer fibre reinforced composite, alternate hybrid stress elements for anal. 77—50926
  new, physical props. 77—8797
  Nichrome/steel, porous metal-thread sheet materials, filteration, permeability and strength props. *(Russian)* 79—78915
  non-linear optimized fibre reinforced plates in bending 79—27550
  nonlinear response 77—70107
  nonlinear stress-strain behaviour 78—26035
  nonlinearly elastic in transverse direction, programmed winding of articles 79—86339
  notched, analytical method for predicting plastic flow 77—70114
  notched fibre reinforced composites, tensile fracture 78—52991
  nylon 6 block polyether amide blend fibres, fine struct. and elec. cond. *(Japanese)* 77—89769
  nylon fibre reinforced polypropylene, enhanced fracture strain 78—15503
  optimal composite sheets, fixed upper bound on number of layers 78—30177
  organic fibre composites, lifetime prediction, expt. verification of accelerated test 77—50993
  organic fibre reinforced plastics, failure 80—11774
  organic matrix composites, use of unidirectional flexural tests, to assess environmental behaviour 79—20301
  organic textolite, long-term strength in plane stressed state 80—60930
  organicfibre reinforced epoxy, temp. dependence of strength under plane stress state 80—7642
  organoplastics, fracture characts., effect on strength 80—66642
  oriented, statistical theory of fracture and scale factor effect in reliability 77—70171
  orthogonal fibre reinforced viscoelastic composites, wave propagation and dispersion 78—42558
  orthotropic cylinder, nonuniform, thermoelastic stresses 77—7312
  orthotropic materials design for stress optimisation 78—63291
  osteons with crossed lamellae, micromech. study 77—25493
  overall moduli, effect of fibre length, self-consistent method 79—76977
  paper strip reinforced paraffin, model composite, optimum reinforced plates, tension/compression tests 77—86124
  PET fibre reinforced polypropylene, enhanced fracture strain 78—15503
  plane stress state anal. in macroscopic model *(Russian)* 77—80069
  plastic, dynamic strains investigation using EM wave method 79—20321
  plastic, fatigue mech., charact. and defect detection 79—24687
  plastic, mech. damage, thermodynamic anal. *(Ukrainian)* 79—37186
  plastic laminate with circular holes, stress conc. and breaking strength *(Japanese)* 78—23816
  plastic matrix, fracture mechanism study, cumulative failure model 78—92315
  plastic matrix, optimum reinforcement laydown 80—38267
  plastic matrix, oriented fibre wear mechanism against mild steel 78—56782
  plastic matrix, preparation by pultrusion 79—95995
  plastic matrix, props., implications for structural design 80—81174
  plastic matrix, review *(Japanese)* 78—39733
  plastic matrix, stress distributions along short fibre 80—60913
  plastic matrix, tensile and compressive strengths, structural theory 77—52435
  plastic matrix, ultrasonic curing time investigation 79—83430
  plastic matrix shrinkage stress calc. in regular struct. composite 77—70125
  plastic matrix uniform plane bending fatigue test, temp. increase *(Japanese)* 78—44200

fibre reinforced composites continued
  plasticity, extension of theory for porous media *(Russian)* 77—68443
  plastics, failure of thin walled flexural structures 80—10209
  plastics, mech. props. stabilisation by PVA fibres modification 79—20022
  plastics, spread of strength rel. to stress conc. *(Japanese)* 79—24610
  plastics reinforcement theory, functional model *(German)* 77—58564
  plate, anisotropic, stress intensity factor for crack 80—48643
  plates, 3-layered, optimisation 80—20996
  plates, anisotropic skew, large amplitude vibrs., transverse shear and rot. inertia, numerical results 80—79208
  plates, orthotropic curved, bending behaviour, nonhomogeneity effects 80—23903
  plates, symmetrically laminated cross-ply rectangular, initial flexural failure anal. 80—64461
  polyester cloth reinforced epoxy resin, fatigue strength and reliability under repeated impact tensile load *(Japanese)* 79—61703
  polyester dough moulding compounds, fibre orientation and mech. props. 77—25116
  polyester fibres, thiuram and dithiocarbamate rubber accelerator degradation 79—78986
  polyethylene, high density, self-reinforced thermoplastic, extrusion 79—15699
  polyethylene, highly oriented, fibre composite model 78—3183
  polyethylene, highly oriented fibre composite, self-hardening, tensile props. 77—55939
  polyimide fibre reinforced polyamide-12 80—11754
  polymer matrix, fatigue and damage accumulation 78—15490
  polymer matrix, soaking, wetting and compounding of materials during production *(German)* 80—93535
  polymer matrix, space environmental effects 80—71721
  polymer matrix, US spectroscopy location of delaminations 77—81352
  polymer multilayer composites, wire-reinforced, dynamically loaded, crack propagation and arrest 80—97567
  polymer reinforcement, fracture mechanics 80—10207
  polymeric, thermal strain determ. 78—1560
  polymeric fibre-reinforced plastic, creep prediction from components props. 80—40448
  polypropylene fibre reinforced cement based beams, flexural strength, fibre pull-out 77—56020
  polypropylene fibre reinforced polyoxyethylene, fracture kinetics, interface props. 80—66640
  polypropylene fibrillated film reinforced cement, loading capacity, cracking 78—72759
  polypropylene fibrillated film reinforced cement matrix for low cost sheeting 80—80996
  polyvinyl alcohol fibre reinforced epoxy resin, fracture kinetics 78—3222
  porous composite anal. by US wave velocity meas. of fibre vol. and matrix porosity 78—95902
  porous matrix, densification kinetics in free hot pressing 80—25618
  powder, densification during hot pressing 77—12566
  preparation by crystallizing metallic and metal-ceramic eutectics *(Polish)* 79—20008
  pressurised wound tube, failure from longitudinal defects 77—16660
  prestressed elastic circular cylinder, stability 78—79234
  propagation of plane harmonic waves, infinite isotropic medium having embedded doubly periodic array of cylindrical fibres 80—87607
  protective coating effect on fibre-matrix bond strength 77—44195
  PTFE, expanded, use as grafts in haemodialysis 80—8211
  PVA-fibre-reinforced composites, thermal fluctuation dimensional effect on strength 80—16476
  quasi-one-dimensional heat conduction, nonlinear mixture theory 80—64335
  quasi-static crack propagation in single cells of fibre reinforced materials under tension *(German)* 80—106759
  radiographically opaque fibres, inspection aid by B fibre addition 78—95880
  random volume fractions in reinforced cylindrical shells 78—15352
  rational bonding of structures from composite materials, fracture resistance 80—5990
  refractory composites, fibre reinforced, directionally solidified tensile tests, in HVEM, deform. and fracture *(French)* 78—68785
  refractory compound fibre reinforced cpd. materials, diffusional reaction, effect of alloying calc. 80—20851
  reinforced epoxy angle-ply laminate wave propag. during transverse impaction 79—83295
  reinforcement scheme optimisation with respect to deformability at assigned stresses 80—69689
  reinforcing fibres for plastics, review 79—61506
  residual stress form. during hardening 78—1575
  rigid plastic fibre reinforced plates, impulsive loading, dynamic deformations theory 79—23222
  rings, ultimate load determ. by AE method 78—48604
  rods, rectangular, elastic wave propagation *(French)* 80—83749
  roving cloth fibre reinforced plastic, strength of fibre/matrix, matrix/matrix and FRP/FRP interfaces *(Japanese)* 78—27608
  rubber belt, cord reinforced, finite cylindrical deformation, stresses 78—38203
  sandwich composite beam, impact bending behaviour *(Japanese)* 80—55468
  sapphire fibre reinforced Mo, strength at rupture 80—104286
  secondary stresses associated with structures, exam. 78—67043
  shear props., test method eval. 77—81353
  sheet manufacture without fracturing on rolling *(Russian)* 77—55914
  sheet moulding compound, laminate, charge pattern influence on tensile strength *(Japanese)* 80—55513
  shell, cylindrical, axisymmetric damped vibrations calc. 79—14297
  shell, orthotropic cylindrical of reinforced plastic, axisymmetrical contact problems, theory 77—84147
  shell under external press., max. stability 78—94597
  shell-type structures, strength estimation using limit state method 79—18820
  short fibre distribution 80—71882
  short fibre reinforced polymers, expressions governing stress-strain curves 78—80592
  short steel wire reinforced (polymer impregnated) concretes, cracking and toughening 78—80626
  single fibre-brittle zone model, fracture behaviour 80—97570
  single ply, thickness effect of percolation and conductivity 80—92953
  sintered reinforced magnetically hard material, porosity and impact strength 77—55916

fibre reinforced composites continued
sintering of materials with undeformable inclusions, densification kinetics prediction 77—63601
sisal fibre reinforced cement, flexural strength 80—11692
slender fibre-reinforced materials, non-dilute, thermal and mechanical props. 80—103524
slender nearly-perfect conductors, dilute, bulk thermal properties 80—103525
stability of parallel cracks in solids reinforced by bars 80—43671
stainless steel wire reinforced Al sheet, prod. by explosive compaction, and mech. props. 77—32542
steel, C, hypoeutectoid based, strength characts. after deform. and quenching 80—35271
steel, C, natural reinforced composite 80—30039
steel, fibre reinforced Al, fracture mechanics under fatigue *(Czech)* 78—64629
steel, reinforced Al and Cu based composites, fatigue strength, surface layer effects 77—12697
steel, stainless, fibre reinforced Al, CC strengthened by lattice transformations, mech. props. study *(Japanese)* 79—43332
steel, stainless, fibre reinforced Al alloy, exam. of deformation, fracture and forging behaviour 80—11681
steel, stainless, fibre reinforced Al alloy, tensile props., cryogenic cooling effect 79—61623
steel, stainless, fibre reinforced porous coating, isostatically compressed for bone ingrowth 80—35134
steel, stainless, fibre reinforced wustite, strength and toughness 78—27602
steel, stainless brittle zone Al 3 component composites deform. and fracture 77—56104
steel, stainless wire reinforced Al-Zn-Mg system, resistance to crack propagation 79—43409
steel, wire, reinforced prestressed concrete, strain-tempering conductions and mech. props. *(Japanese)* 78—39816
steel core/steel tube duplex reinforced metal sheet, fatigue crack growth 77—28894
steel fibre reinforced Ag, exam. of recrystallisation behaviour *(German)* 78—84849
steel fibre reinforced Al_2O_3-Al, production and mech. props. 80—11619
steel fibre reinforced Al, fatigue strength *(Czech)* 78—60748
steel fibre reinforced Al, fibre orientation effect on strength *(Korean)* 80—30027
steel fibre reinforced Al, role of brittle layers at elevated temps. 79—96135
steel fibre reinforced Al, thermophys. props. 80—59745
steel fibre reinforced Al, vacuum hot pressing, strength *(Czechoslovakian)* 77—32543
steel fibre reinforced Al alloy, corrosion resistance, electrochemical characts. 80—11806
steel fibre reinforced Al alloy, new production method with continuous fibres 77—66610
steel fibre reinforced Al alloy, stressed state nondestructive testing method *(Russian)* 80—40631
steel fibre reinforced Al alloy D16T, sheet reinforced by Ti alloy butt straps, fatigue 79—100262
steel fibre reinforced cement based beams, flexural strength, fibre pull-out 77—56020
steel fibre reinforced cementitious material, radiographic anal. of fibre distribs. 78—52747
steel fibre reinforced concrete, accelerated corrosion test at high temps. *(Japanese)* 78—31553
steel fibre reinforced concrete, strength problems 77—4844
steel fibre reinforced concrete, tensile strength and ultimate strain *(Polish)* 80—21027
steel fibre reinforced concrete, vibr. compaction, pressure compaction and curing *(Japanese)* 80—89179
steel fibre reinforced concrete *(Japanese)* 77—4762
steel fibre reinforced Cu, exam. of creep behaviour, comparison with theory *(German)* 78—52931
steel fibre reinforced Cu, fatigue 79—29221
steel fibre reinforced Mg, fibre-matrix interfacial reactions 80—20043
steel fibre reinforced Pb, fabrication, mech. props. *(Korean)* 77—12579
steel fibre reinforced porous mat. prod., mat. props. 77—59723
steel reinforced concrete, computer expt. on slender beam columns 79—70127
steel reinforced concrete, local bond-stress/slip relationships under repeated loading 79—20123
steel reinforced concrete, steel corrosion *(Japanese)* 79—39038
steel reinforced concrete slabs, connected via shear connectors, exam. of fatigue in shear connectors, exam. of method 79—43539
steel reinforced epoxy, static tensile behaviour *(Japanese)* 78—15482
steel rod reinforced concrete, laterized columns, random axial loading, compressive strength to failure 78—27614
steel wire reinforced Al-Zn-Mg, tensile strength depend. on angle of reinforcement *(Russian)* 78—15452
steel wire reinforced polymer, crack growth matrix toughening effect of glass fibres 77—56076
steel wire reinforced Portland cement mortar, wire pull out, inelastic behaviour 78—56681
steel wires, reinforced Pb, deformation behaviour and effect of volume fraction and surface treatments *(Japanese)* 79—66118
stiffness and strength investig. 77—63874
stochastic three dimensional finite element structural anal. 78—30188
strain rate effect on AE 78—44193
strain-rate sensitive, toughness 77—16664
strength, Monte Carlo study 80—25844
strength, statistical struct. parameter effects *(German)* 77—56095
strength and deformation anisotropy, numerical characts. 80—38285
strength props., US method for evaluating 78—76796
stress boundary value problem for finite plane deform. 80—48583
stress measurement, IR spectroscopy 79—52559
stress redistribution dynamics during fibre rupture 80—64394
structure optimisation in stability problems 80—58947
symposium, USA-USSR, 1978, on composite materials fracture 80—11766
tape disc, chord winding, elastic props. 79—87679
tendon composite, structural hierarchies and interactions 77—86526
tensile strength, struct. parameters depend. 80—65134
tension stability, deformation up to failure *(Russian)* 80—75289
test methods, impetus of composite mechanics 80—11868
testing methods *(Japanese)* 78—39974

fibre reinforced composites continued
thermal and electrical conductivities *(German)* 77—28053
thermal cond., transverse, determ. of effective cond. 78—18146
thermal conductivity bound calculations, for short-fibre unidirectional composites 80—92727
thermal crack propagation anal. 80—10205
thermal cycling, elastoplastic strain calc. under action of external stresses *(Russian)* 79—38896
thermal diffusion, quasi-one-dimens., mixture theory 78—71271
thermal expansion coeff. 78—67836
thermal NDT using liquid crystals, fibreglass laminates 80—93709
thermal stress fracture in compound materials, exam. 78—75103
thermal stresses in unit cell 80—10160
thermoelastic anal. of finite orthotropic slab 79—1111
thermoelastic matrix materials, nonlinear thermodynamic continuum theory 80—14579
thick laminar reinforced plastics, deformation fixing in polarisation optics *(Ukrainian)* 78—90802
thin films on reinforcing fibres, morphological stability *(Russian)* 79—37928
thin walled cylinder, glass fibre reinforced tangential stress charact. during twisting 78—13911
Thornel reinforced epoxy laminates, strength and biaxial stress-strain response, analytical expt. correlation 79—29131
three-dimensional structure, mech. characts. 80—38266
three-dimensionally reinforced with short fibres, effective elastic consts. 80—58910
transverse impact of fibre-reinforced rigid-plastic plates 78—38211
transverse plane, elastic, failure behaviour *(Japanese)* 78—48510
transverse strength rel. to fracture mech., stress interactions 80—16421
two dimensional, reinforced concrete, finite element analysis of structures taking account of nonlinear physical behaviour and discrete crack development 79—57121
ultrasonic scanning, C-scan technique for fibre misorientations, delaminations, bond failures 78—95882
ultrasonic vibrs. propagation velocity, dependence on composites elastic props. 80—5975
undirectional fibre composites, anisotropic constituents, effect elastic moduli and other props. 80—58911
uniaxially reinforced powder, densification by dynamic hot pressing in rigid sheath 77—12568
unidirectional, fibre packing density study 77—70026
unidirectional, high-strength, tensile testing 80—40664
unidirectional, Saint-Venant effect 79—34121
unidirectional composites, appl. of linear elastic fracture mech. to longitudinal fracture 79—91784
unidirectional elastic solid, impact loading, numerical study of fibre orientation effects 79—57094
unidirectional fibrous composite, mixture theory for longitudinal wave propagation, formulation 79—50631
unidirectional fibrous composite, mixture theory for longitudinal wave propagation, computational procedure 79—50632
unidirectional model for longit. tensile strength prediction 78—95778
unidirectionally reinforced, deform., strength, and failure 80—3134
unidirectionally reinforced composite, plane strain deform. processing limits 77—55918
unidirectionally reinforced composites, large deflection, plastic constitutive relations 80—43624
uniform plane stress states, method for prod. 78—85064
US diagnosis of elastic characts. and struct. parameters 80—40663
US velocity and elastic consts., in void-containing composite, theory 77—89498
vegetable fibre reinforced cement sheets, strength 80—21024
vibration technique for NDT 79—57183
viscoelastic fibre-reinforced composites, wave propag. 79—76992
viscoelastic thermal shrinkage stresses 80—38287
viscoelasticity measurement using mech. drive viscoelastic tester *(Japanese)* 79—34232
viscous matrix, random stresses in components, laws of distrib. 79—23226
W, wire reinforced Cu 77—70114
W fibre reinforced Nb, plastic deform. and fracture 77—40438
wave propagations in orthogonally reinforced fibre composites 78—41168
waveguides, axisymm. elastic vibrs. 80—102995
wear mechanisms, quantitative model 79—47786
wire reinforced Al, stress-deformed state, elastic, strength props. *(Russian)* 80—76303
wood fibre reinforced cement, coupling agent effect on strength 80—35295
wood fibre reinforced Portland cement composite, strength 80—100822
yield surface 77—59871
yield surfaces, micromech. prediction of unidirectional composites 80—25777
zirconosilicate glass fibre, effect of cement environment on mech. props., rel. to composite strength 77—44335
zonal winding pattern analysis, thin spherical shells 80—38253
Ag composite, SiC whisker-reinforced, prep. aboard Skylab. 78—84741
Ag-Cu, anomalous props. caused by internal phase boundaries 78—72754
Ag-Ni, composite, fibre and layer structs., anomalous props. caused by internal phase boundaries 78—72754
Al 6061 alloy, B fibre reinforced, fracture 80—11773
Al alloy, formed by hot extrusion, mech. props., 77—24987
Al alloy, formed by hot extrusion, heat-treatment 77—24988
Al alloy matrix, reinforced with fibrous and particulate nonmetals, wear, friction 77—4758
Al-Al_2O_3 composite, brittle zone on fibre surface deform. and fracture 77—56104
Al-B fibre-D16 alloy welded composites, structure, strength and fracture props. *(Russian)* 80—108524
Al-matrix, composites preparation by Na-process, interface reactions 78—84742
Al-Mg/Al_2O_3 composites, interface phase, Auger and electron diffr. study 80—25646
Al-SiC, thermal stresses in unit cell 80—10160
AlN filamentary crystal reinforced mullite-corundum ceramics, filaments strength, eval. 80—104230
Al_3Ni fibre prep. by electrolysis of Al-Al_3Ni eutectic 80—100817
Al_3Ni-Al two-phase matrix, Al electrolytic etching in $AlCl_3$ molten salts 78—3280
α-Al_2O_3 fibre FP reinforced Al and Mg composites, fabrication and props. 80—81004

fibre reinforced composites continued
Al_2O_3 fibre reinforced Al-Mg(Mg-Cu)(Cu) exam. of interface interactions during fabrication 78—76616
α-Al_2O_3 filamentary crystal reinforced mullite-corundum ceramics, filaments strength, eval. 80—104230
Al_2O_3-SiO_2 fibre/mineral wool fibre composites, exam. of strength and shrinkage characts. rel. to Al_2O_3-SiO_2 fibre content effects 79—20105
B fibre reinforced, Al, hot pressed forged, plasma sputtered *(Russian)* 78—35330
B fibre reinforced Al, crack tip damage and fracture toughness 79—57093
B fibre reinforced Al, dynamic Young's modulus and internal friction 80—25754
B fibre reinforced Al, fracture toughness 77—70157
B fibre reinforced Al, fracture propag. 78—23823
B fibre reinforced Al, fracture mechanical study, unidirectional composites 78—88520
B fibre reinforced Al, fracture 79—57092
B fibre reinforced Al, hot reverse moulding of tubes, calc. of process optimum parameters *(Russian)* 78—15344
B fibre reinforced Al, impact behaviour under fatigue 80—7661
B fibre reinforced Al, impact damage tolerance and reliability 80—81177
B fibre reinforced Al, interaction between fibre and matrix 80—10712
B fibre reinforced Al, orthotropic elastic stiffness consts., US vel. meas. 80—49289
B fibre reinforced Al, prep. by reaction sintering 79—38769
B fibre reinforced Al, residual stress, internal friction anal. 80—45339
B fibre reinforced Al, stress redistrib. anal., upon brittle fibre breakage 78—48527
B fibre reinforced Al, strength determ. procedure in annular specimens *(Russian)* 78—95864
B fibre reinforced Al, stress redistribution in fibre elastic deformation failure *(Russian)* 79—47740
B fibre reinforced Al, stressed state nondestructive testing method *(Russian)* 80—40631
B fibre reinforced Al, tensile and compressive strength, prior thermal treatment effect 78—11264
B fibre reinforced Al, tensile strength and brittle fracture 80—11707
B fibre reinforced Al, thermal expansion 77—51525
B fibre reinforced Al, thermal degradation of tensile strength, due to fibre strength degradation 78—39861
B fibre reinforced Al, thermophys. props. 80—59745
B fibre reinforced Al, unidirectional, K-calibration and compliance curves 78—88518
B fibre reinforced Al, X-ray investigation of internal stresses *(Russian)* 77—73290
B fibre reinforced Al, yield strength parameter calcs. 80—25777
B fibre reinforced Al alloy 6061, cross plied laminate, tension-compression fatigue 79—38940
B fibre reinforced Al alloy, influence of bond strength on failure *(Russian)* 79—43387
B fibre reinforced Al alloys, hot compression moulding, optimum parameter calc. by pipe piercing *(Russian)* 79—66027
B fibre reinforced Al alloy D16T, sheet reinforced by Ti alloy butt straps, fatigue 79—100262
B fibre reinforced Al alloy, corrosion resistance, electrochemistry 80—11806
B fibre reinforced Al composites, corrosion, electrochem. behaviour 79—20225
B fibre reinforced Al composite, strength of fibre-matrix interface and tensile strength *(Russian)* 80—21005
B fibre reinforced Al laminate with discontinuities, fracture 78—19877
B fibre reinforced Al laminate, unidirectional, interlaminar shear strength exam. 78—35434
B fibre reinforced Al laminate, effect of ply by-up sequence on fracture toughness 78—35492
B fibre reinforced Al VKA-1 composite, fibre/matrix interface reaction during prep. 80—25619
B fibre reinforced Al-Cr(Mg)(Mn)(Si), calc. of thermodynamic interaction potential between B fibre and matrix 80—11627
B fibre reinforced Al-Mg, heat treatment effect on struct., tensile strength 80—55487
B fibre reinforced Al-Zn-Mg, packet rolling, thermodeform. process parameters *(Russian)* 80—55433
B fibre reinforced AlB_2 and TiB_2 fibre coating effect on strength *(Russian)* 80—40426
B fibre reinforced epoxy, tensile anal. of edge notch 77—70159
B fibre reinforced epoxy, eval. of tensor polynomial and Hoffman strength theories 78—19830
B fibre reinforced epoxy, fracture mechanical study, unidirectional composites 78—88520
B fibre reinforced epoxy, laminate, stress anal. finite element modelling 79—59924
B fibre reinforced epoxy, dynamic Young's modulus and internal friction 80—25754
B fibre reinforced epoxy, fracture mechanics 80—35294
B fibre reinforced epoxy and Al, cryogenic tensile, compressive and shear props. 78—6983
B fibre reinforced epoxy composites, notched, tensile strength and failure modes 80—81205
B fibre reinforced epoxy laminate, energy release approach for stable crack growth in free edge delamination problem 78—19878
B fibre reinforced epoxy resin, anisotropic laminate, effective modulus of elasticity 77—4802
B fibre reinforced epoxy resin, real-time NDT during fatigue loading 77—86264
B fibre reinforced epoxy resin laminate, fatigue damage, stiffness/strength comparison 77—90451
B fibre reinforced Mg, exam. of fatigue props. and corrosion 80—11751
B fibre reinforced Mg, fibre-matrix interfacial reactions 80—20043
B fibre reinforced W double coaxial composition rod, waveguide, normal mode US propag. 79—100317
B fibre reinforcement of thermoplastics, creep resist. and elastic moduli 80—55458
B fibres, prod. and phys. props. *(French)* 78—23647
B reinforced Al, double lapped composite joints, efficiency in bending with steel hub 78—68870
B reinforced Al laminates, applic. of linear elastic fracture mechanics 77—28893
B reinforced epoxy, double lapped composite joints, efficiency in bending with steel hub 78—68870

fibre reinforced composites continued
B-Al cast braid, crystallisation and structuring of Al matrix *(Russian)* 78—52725
B-Al composites, B filament CVD technology, book contrib. 78—48352
B-Al thermal and electrical conductivities *(German)* 77—28053
B-fibre reinforced Al, with imperfect separation boundary, material stability *(Russian)* 80—54307
B-reinforced Al, elastic props., 300-4K 77—86066
B-SiC fibres, tensile strength, influence of brittle layers 79—79039
B_4C-epoxy(C) fibre reinforced composite, prep., mech. props. 78—48365
B_4C-phenolic fibre reinforced composite for nuclear shielding appls. 80—102353
BN/BN composites, prep., mech. props. 77—21080
Be fibre reinforced Ti-Al-V (6.4 wt.%), synthesis and mech. props. 77—32544
β-epoxy composite, intermittently bonded, water and ice effects 77—12685
C fibre composite/metal joint, fatigue research 78—15497
C fibre reinforced composite, shear fatigue 78—15493
C fibre reinforced epoxy, fatigue strength 78—15495
C fibre reinforced epoxy phenol plastic, resistance to interlayer shear and elec. resistivity 78—68752
C fibre reinforced plastic, multi-directional reinforcement, fatigue 78—15491
C fibre reinforced plastic laminates, axial and short beam shear fatigue 78—15492
C-Al thermal and electrical conductivities *(German)* 77—28053
C-C composite, reinforcement scheme effect on mech. props. 77—66620
C-C thermal and electrical conductivities *(German)* 77—28053
$CaSiO_3$ fibrous crystal reinforced matrix, unidirectional crystallization, anisotropic properties 79—56969
Cr_3C_2 fibre reinforced Ni-based composite, oxidation and creep, Y additions effect 80—66685
Cu film on Mo substrates, film stability on reinforced fibre substrates *(Russian)* 80—39462
Cu/Cr-Ni-steel fibres, primary creep *(German)* 80—11734
Cu-Fe, composite, fibre and layer structs., anomalous props. caused by internal phase boundaries 78—72754
Cu-Nb multifilamentary composite, in situ formed, high temp. tensile strength 79—61602
Fe-Co heterogeneous alloys, fabrication by powder metallurgy, tensile strength 77—63600
Fe-P-Cu-SiO_2-$FeAl_3$-asbestos composite, thermal and elec. conds., temp. and composition depends. 77—66609
FeNi-Cu, composite fibre and layer structs., anomalous props. caused by internal phase boundaries 78—72754
$Fe_{29}Ni_{49}P_{14}B_6Si_{12}$, Metglas fibre reinforced mortar, fracture props. 79—70159
InSb, dislocations due to thermal stress, single and composite crysts. 78—2124
Mo fibre reinforced Al and Al alloys, SEM study *(Slovenian)* 78—84923
Mo fibre reinforced Cu, rule of mixtures of deform. parameters in stage III 80—97532
Mo fibre reinforced Cu with weak interfaces, stability of tensile deform. 80—97533
Mo fibre reinforced Ni-Cr, effect of fibre coatings on composite strength 78—56710
Mo reinforced Al and Cu based composites, fatigue strength, surface layer effects 77—12697
Nb fatigue strength, surface layer effects 77—12697
Nb fibre glass composites, new technique for producing fine metal fibres 80—108384
Nb-Ta fibre reinforced Cu, fatigue testing in normal and superconducting states 78—19959
NbC fibre reinforced Ni-Cr, eutectic, unidirectional solidification, thermal cycling, temp. range effect on microstruct. 80—89272
Nb_3Sn microfilamentary superconducting composite, critical currents, fracture props. 80—107970
Ni wire reinforced epoxy resin, and cement paste matrices, debonding and pull-out of wires 79—29142
Ni wire reinforced epoxy resin, crack propagation 79—29188
Ni-Al-Mo (12.7, 21.6 wt.%), directionally solidified eutectic composite, precipitation 80—108454
Ni-Cr-NbC eutectic composite, unidirectional solidification, thermal cycling, temp. range effect on microstructural degradation 80—89272
γ-Ni-γ'-Ni_3Al-TaC fibre reinforced eutectic, oxidation protection 77—40475
Ni-Nb_2O_5, fibrous composite, aligned in situ growth by preferential internal oxidation 78—6879
Ni-TaC, eutectic alloy, fibre reinforced, directionally solidified, anisotropic yielding behaviour 79—11675
NiTa C-13, advanced fibre reinforced eutectic superalloy, creep and rupture 77—63744
Pb(Zr,Ti)O_3 fibre arrays in epoxy cement, ferroelectric ceramic-plastic composites 80—81015
Si filler reinforced polyethylene, calc. of increase of shear modulus *(German)* 77—32613
Si/SiC ceramic composite, elastic moduli and bend strength meas., anisotropy 77—59838
Si-SiC composite, high temp. time depend. strength 77—56083
SiC coated B fibre Al-V-Ti, tensile and compressive strength, prior thermal treatment effect 78—11264
SiC fibre reinforced Al-Si alloy, liq. phase process prep. effect on mech. props. 79—70020
SiC fibre reinforced Al interaction between components and compatibility, mech. props. effect 80—11761
SiC fibre reinforced Al-Mg, heat treatment effect on struct., tensile strength 80—55487
SiC fibre reinforced Al, thermophys. props. 80—59745
SiC fibre reinforced Al, plasma-formed semifinished products, props. 80—84890
SiC fibre reinforced Al, synthesis by liquid pressing method 80—100816
SiC fibre reinforced Ni-Cr, alumina coated fibres, hot pressed, annealed, IR study 78—60623
SiC fibre reinforced Ti, effect of Al, Zr and Mo alloying additions on reaction rate of Ti with fibres 80—16249
SiC fibre reinforced Ti-Al-Mo-Zr composites, matrix selection *(Russian)* 80—35192
SiC fibre reinforced Ti-Al-Mo-Zr-Si (6.6, 3.3, 1.8, 0.3 wt.%) composite, component interaction kinetics *(Russian)* 80—55364

fibre reinforced composites continued

- SiC fibres, continuous, for metal-matric composites, elevated temp. strength props. 77—59885
- SiC fibres reinforced Ni complex alloy, influence of TiN coating on fibre matrix interaction *(Russian)* 78—95820
- SiC filament reinforced phosphate foam ceramics, bending strength 80—11716
- SiC reinforced alloy, prevention of interface reaction by CVD coating of filaments 78—15347
- SiC-Al thermal and electrical conductivities *(German)* 77—28053
- SiC-fibre reinforced glass, fabrication, thermal expansion, flexural and fracture toughness 80—40319
- SiO_2 fibre reinforced $CaSiO_3$, production from xonolite slurry 78—39730
- SiO_2 fibres, plastic deformation and Young's modulus *(French)* 78—23746
- SiO_2 reinforced Al, thermal degradation kinetics 77—44194
- Sn fibre reinforced Pb-Bi (12 at.%), type II superconductor, flux pinning *(German)* 77—85397
- Steel, C, fibre reinforced Cu matrix, deformation parameters controlling dislocation motion, flow stress, activation volume 79—57055
- Ti matrix, reinforced with B, borsic, SiC, Al_2O_3, Be, W, Mo, prep. and mech. props. *(Russian)* 78—35335
- TiO_2 based construction ceramics, fibre-like cryst. reinforced, mech. props. 80—55341
- W alloy wire reinforced stainless steel, fibre/matrix interaction, fabrication and heat treatment effect 79—91607
- W fibre reinforced Al, alloying element effect on interface form. *(Czech)* 77—85963
- W fibre reinforced Co powder alloys, reactions and recryst. 80—11603
- W fibre reinforced Cr alloy composites, reactivity of Y_2O_3 protective film 79—100297
- W fibre reinforced Cu, interface porosity formation, on thermal cycling 80—30092
- W fibre reinforced Cu composite, work hardening 77—52341
- W fibre reinforced Cu composite, hardening in two-phase material 77—52448
- W, fibre reinforced Cu composite, temp.-load depend. of time-to-rupture *(Russian)* 78—11299
- W fibre reinforced Cu composites, correl. between thermal cycling-induced microstructural changes at interphase boundaries and tensile behaviour *(Japanese)* 80—71674
- W fibre reinforced epoxy resin, strength of metal-polymer adhesive contact, time-temp. depend. 78—68753
- W fibre reinforced Ni, high temp. stability 77—48372
- W, fibre reinforced Ni, produced by liquid infiltration 77—48371
- W fibre reinforced Ni alloy, high temp. composite development 77—48370
- W fibre reinforced Ni composite, study at high temp. in O_2 and combustion gases 77—48567
- W fibre reinforced Ni composites, high temp. tensile and creep props. 77—52444
- W fibre reinforced Ni composite, prep. by hot isotactic pressing, mech. props. *(Slovak)* 78—19694
- W fibre reinforced Ni-Cr (20 wt.%), hot pressing kinetics 78—35334
- W fibre reinforced Ni-Cr alloys, Ni, Co, Co alloys, and Ni alloys, effect of alloying on structural stability, mech. props. 78—56600
- W fibre reinforced Ni-Cr steel, TiN coated fibre, protective props. *(Russian)* 79—66201
- W fibre reinforced Ni-Cu composite, liquid phase sintering under press. 78—19695
- W, fibre reinforced powder metal and alloy based composites, high temp. strength of W wire 79—70021
- W reinforced epoxy, static tensile behaviour *(Japanese)* 78—15482
- W wire reinforced Cu, exam. of thermal cycling induced deformation 79—5050
- W wire reinforced Cu, microfield, flow stress 78—27575
- W wire reinforced Ni alloy, heat resist. testing, specimen gripping arrangement 79—15895
- W-Cu fibre reinforced composites, interface shear strength, critical aspect ratio 77—4826
- W-Re fibre-reinforced Ni-base refractory alloy, struct. and props. *(Russian)* 77—59721
- W-reinforced Ni and Ni-Fe, fabrication, heat treatment, and mag. and mech. props. 77—40408
- W-ThO_2 (1 wt.%) reinforced alloy, prevention of interface reaction by CVD coating of filaments 78—15347
- W-ThO_2 fibre reinforced Ni base alloys, powdered matrices, fibre/matrix interaction above 1300°C, alloying effects *(Russian)* 78—95755
- ZnO fibre reinforced elastomer, X-ray diffr. exam. of filamentary crystal distrib. 80—7738
- ZrC coating on refractory metal fibre, diffusion barrier, deposition 77—4759

fibres

see also carbon fibres; composite materials; fibre reinforced composites; glass fibres; optical fibres

- acoustic absorber, numerical results for elementary cells model *(German)* 77—802
- acrylic fibre, oxidative stabilisation, O_2 takeup and general model 79—38998
- acrylic fibres, oxidative stabilisation, moisture sensitivity 80—16524
- acrylic fibres, oxidative stabilisation dynamics 79—38999
- Agave cantala natural fibre, small-angle X-ray scatt. of densely packed colloidal system, scatt. inhomogeneities 80—76565
- airborne fibre sampling method for pollution detection using separated deposition 77—82031
- albuminated Dacron prostheses as improved blood vessel substitutes 79—29669
- aliphatic polymer fibres, supermol. struct., X-ray diffr. and acoustic methods 78—75570
- amphibole fibre conc. in water, interlaboratory meas. by TEM 78—88590
- amphiboles, fibrous, hydrothermal crystn. from talcs in NaOH soln. 80—20810
- anatase fibres synthesis from K_2TiO_3 fibres, hydrothermal leaching *(Japanese)* 79—56949
- aromatic polyamide, sputter etching 80—21147
- aromatic polyamide fibres, evidence of radial and tangential morphology 79—73107
- aromatic polyamides, rigid and nonrigid, ultrahigh modulus fibres 79—95992

fibres continued

- aromatic polymer fibres, supermol. struct., X-ray diffr. and acoustic methods 78—75570
- asbestos, identification techniques 77—60018
- asbestos, selected area electron diffr. patterns in analytical TEM, optimum procedure using tilted specimens 78—24009
- asbestos aerosol electron microscopy and analysis *(French)* 77—37461
- asbestos fibres concentration meas., in air and liquid, analytical methods review 80—72120
- basalt, cement reinforcing fibre, alkali resist. 80—89377
- bundle time-dependent failure, probabilistic model 77—3798
- bundles, stochastic strength and fatigue 78—79262
- capillary and clad acoustic fibre delay line storage 78—9504
- cellulose, fibres crystallised from hydrazine, texture by X-ray diffr. 79—69030
- cellulose, surface aggregation of dispersed resin particles in elec. field 78—53262
- cellulose acetate fibre and film, stabilisation, post UV-irrad. mech. strength *(Russian)* 79—24778
- cellulose fibre, gamma-irrad., and storage effects on props. *(Russian)* 80—61121
- cellulose fibre, moist, dielec. props. 78—76380
- cellulose fibre formation in stirred dimethyl sulphoxide-paraformaldehyde soln. 80—104440
- cellulose fibres, elec. anisotropy 80—97220
- cellulose fibres, from jute, crystallinity percentage, estimation by X-ray methods 79—7553
- cellulose fibres, with planar crimp, tensile deformation 80—84235
- charging in electroflocculation, expt. *(Russian)* 79—83515
- chrysotile, cryst. struct. rel. to milling, X-ray diffr. 77—55278
- chrysotile asbestos, aggregation to form pseudocrystals 77—76310
- chrysotile asbestos fibres, texture rel. to mech. props. 77—81300
- chrysotile fibre conc. in water, interlaboratory meas. by TEM 78—88590
- collagen fibre electrode for peripheral neural activity recording *(Japanese)* 77—66879
- collagen fibres, mech. props., role of struct. organisation 80—72207
- collagen fibres, of dermis, structural and mech. charact. and natural interweaving 78—48824
- composite models, photoelastic analysis of interlaminar matrix stresses 77—3799
- cotton, otpical anisotropy, multiple-beam interferometric obs. 79—8115
- cotton, water drainage, by capillary flow *(Japanese)* 78—95208
- cotton fibre fineness and maturity comparison on air flow instruments 78—88591
- cotton fibres, specimen clamps for X-ray angle-tensile meas. 78—4603
- crocidolite fibre fine structure rel. to pulmonary tissue immunoresponse 79—74824
- crystallite shear deforms. rel. to small-angle X-ray scatt. pattern *(Russian)* 78—71690
- degummed silk fibres, mol. motion and fine struct., X-ray, thermal, mech., dynamic loss tangent meas. *(Japanese)* 78—59765
- discontinuous fibre orientation in high viscous liquid flow *(Japanese)* 78—34189
- drag reduction in fibre suspensions, fibre degradation effects 79—72918
- drop on fibre systems, contact angle, phase contact areas, drop vol. and Laplace excess press. meas. 77—7950
- elastic filaments, tensile test method, and treatment of expt. data 80—85111
- elastic moduli, automatic laboratory display unit 79—55349
- electrical contact, bridge transfer on electrodes with fibre struct. of heat-proof component 77—59325
- environmental, convergent beam electron microscopy obs. 80—108689
- equipment for testing elongation of high strength and high tensile fibres 78—56844
- failure charact. determ. by electrical simulation, feasibility study 77—52597
- failure kinetics, internal stresses, computer simulation *(Russian)* 80—40479
- fatigue properties, biaxial rotation over a pin 78—64699
- fatigue tester based on rot. over wire for use in different environments 77—44421
- fatigue testing, biaxial rotation, torque development 80—71840
- fatigue testing using biaxial rotation test 79—97381
- felt sound absorption rel. to airflow resistance, obs. 77—58506
- ferromagnetic fibre, trajectories of paramagnetic particle stream near fibre 79—86128
- fibre, metallisation by continuous casting in Al and Al alloys *(Russian)* 78—35538
- filament, thin, technical strength rel. to diameter environmental effects *(German)* 79—27529
- filament velocity measurement, during spinning, streak photography 78—41367
- filament yarn fatigue under cyclic tension, study *(Japanese)* 77—36701
- filter, fibrous, distrib. of fluid vels., flow resist., random flow model 80—79393
- finite fibre, fluctuation magnetocond. 80—24956
- fir-tree textures, possible existence 80—76269
- fluoramphibole fibres, synthesis by unidirectional crystn. 80—2941
- for regular fibre arrangements acoustic absorber, model theory *(German)* 77—801
- freeze and viscous coating of fibres 78—48350
- friction, apparent paradox for fibre passing over moving curved surface 77—31263
- glued microplastic threads, tensile strength 79—61670
- graphite Raman microprobe-microscope appl. 80—62737
- growth, flow induced form. of long fibres, engineering model 79—78927
- haemodialysis and haemoperfusion, joint system, evaluation of novel sorbent systems 78—7542
- haemoglobin S, fibres, discs having six-fold symmetry, electron microscopy 78—76989
- high modulus diffusion barrier appl. 77—77449
- high-strength alloy filamentary crystal prep. from brittle high-strength mats., mech. props. *(Russian)* 77—59712
- homogeneous elastic matrix containing short fibre, stress state *(Russian)* 77—68412
- humidity effect in flow resistance of loaded fibrous filters 77—29451
- industrial atmosphere submicroscopic asbestos fibre evaluation 79—74585
- inorganic, refractory behaviour testing 77—25204
- inorganic fibre, diameter measurement by microscopy *(French)* 79—93095

fibres continued
- interconnected fibre masses, precipitated from polymer solns. under sonic agitation 79—47655
- IR emittance of fibrous materials 79—95189
- IR laser for optical fibre communication 77—88745
- jute, cement reinforcing fibre, alkali resist. 80—89377
- jute filament, bending rigidity at various delignification stages 78—19817
- kaolin fibres, heat induced changes 79—83244
- Kevlar 29 and 49, aramid fibres, microvoid obs. 80—38960
- Kevlar 49, fibre, mech. props., environmental effects incl. sunlight, ionising rad. 77—36560
- Kevlar 49, macromol. struct., electron diffr. and dark-field electron microscope obs. 78—34446
- Kevlar 49 fibre, poly p-phenylene terephthalate, Raman spectroscopy, heat, stress, radiation effects 79—65871
- Kevlar 49 high modulus polyaromatic fibre, supramolecular struct. 78—55819
- Kevlar aramid fibre, regular fine bands obs. by polarization microscopy 80—107064
- Kevlar fibres, effect of crystallinity and orientation on mech. props. *(Japanese)* 79—38952
- Kevlar-29, flexural fatigue and surface abrasion 78—15504
- Kevlar-49, chemical characterisation 78—95725
- Kevler fibre, mech. props. in aq. H_2SO_4 soln. *(Japanese)* 79—47753
- leucosapphire fibres, multicapillary growth 80—44459
- light scattering from micron sized fibre 77—65571
- low-density structure, centrifugal method for mech. prop. obs. 80—71823
- macromolecules, flexible, flow-induced crystallisation, nonhomogeneous shear rates effect 80—38952
- mechanical props. meas. using automated direct reading dynamic viscoelastometer, Rheovibron 79—3980
- mechanical relaxation theory, of fibrous structs. 78—13916
- mechanical tensile test machine 77—40484
- metal, dendritic deposition of aerosol particles 80—40755
- metal, fibres, cubic struct., texture form. in uniaxial deform. theory 79—24532
- metal fiber permeable materials, struct. characts. 79—24464
- metal fibre materials, permeable, porous struct. parameters 79—100083
- metal fibre materials, thermal and elec. conductivities 78—10419
- metal fibre mats., porous, struct., hydraulic characts., liq. permeability 78—67848
- metal fibre wick for cryogenic heat pipes 80—4725
- metal fibre wicks, max. heat flux 80—19390
- metallic fibre knitted gauze permeable materials, mech. props. 80—66607
- metallic permeable materials, obliteration phenomenon 79—98799
- mineral fibre characterisation using energy dispersive X-ray spectrometry in TEM *(French)* 80—82857
- mineral fibre production with low dust and zero lubricant contents *(German)* 78—19678
- mineral wool fibre prod., anal. of jet diameter with Helmholtz instability 77—35191
- monofilament, substitute particles for optical single-particle-size spectrometer testing 80—58819
- multifilament bundles, slightly curved, eqns. of steady filtration flow 78—38397
- natural, Brillouin scatt. shifts, comparison with synthetic polypeptide obs. 80—55991
- nitrocellulose fibres, polarised light study 80—80736
- Nomex, fibre, mech. props., environmental effects, incl. sunlight and ionising rad. effs. 77—36560
- nylon 66, filament, heat setting and thermomechanical behaviour 78—15435
- nylon 6,6, drawn fibre, selective degradation, cryst. morphology 78—71683
- Nylon 6,6 fibres, birefringence determination, using backscattered light intensity distrib. 79—42939
- nylon 6, drawn yarn, origin of double melting peaks 78—3118
- Nylon 6, fibre, crystallite dimensions, effect on struct., mech. and diffusive props. 78—11273
- nylon 6, microfibril dimensions, from small-angle X-ray scattering 79—37574
- Nylon 6 fibre, shrinkage, influence of chain rupture during tensile deform. 79—34055
- nylon 6 fibres, chain rupture during tensile deform. 79—15740
- nylon 6 fibres, dynamic mech. props., interpretive nonlinear viscoelasticity 79—4994
- nylon 6 fibres, highly oriented, fatigue process, struct. changes 77—90447
- nylon 6 fibres, struct. changes due to strain annealing 79—15692
- Nylon 6 gut yarn, fine struct. change in twisting, annealing and untwisting, microbeam X-ray obs. 80—81026
- Nylon 6 gut yarn, fine struct. change in twisting, annealing and untwisting, X-ray and electron microscopy obs. 80—84904
- Nylon 6 yarns, NMR, fibre struct. rel. to annealing, drawing *(Japanese)* 77—32269
- Nylon-12, hydrostatic extrusion, struct. change *(Japanese)* 79—15693
- nylon-6 fibre, chain rupture and tensile deform. viscosity-av. mol. wt. obs. 78—76714
- Nylon-6 fibre, crystal struct., WAXS obs. 80—15015
- nylon-quartz fibre support for low temp. mag. suscept. meas. 78—65947
- orientation in paper, automation of real-time optical meas. of small structures 79—85115
- oriented, nonisothermal deform., thermomech. curves, statistical interpretation 77—32651
- osmosis, pressure-retarded, two-coeff. water transport eqn. 79—83509
- PA-6, polymer fibre, orientation changes during stretching, IR spectra 78—75568
- PAN, SO_2 treatment 79—52403
- PAN fibre, pre-oxidised, IR absorpt. 77—28561
- PAN fibres, heat treatment, structural changes *(Polish)* 77—28835
- paper, fracture behaviour, SEM investigation 79—34149
- para-polyamide based, struct. deform. props. 80—60928
- PBI fibre, mech. props., environmental effects, incl. sunlight and ionising rad. effs. 77—36560
- permeable, quantitative charact. of porous struct. 78—19683
- PET, fibre, crystallite dimensions, effect on struct., mech. and diffusive props. 78—11273
- PET, filament form. from gels 78—80508
- PET, irrad., radical yields 79—96343
- PET fibre, aminolyzed, dynamic viscoelasticity and thermal behaviour *(Japanese)* 79—38880

fibres continued
- PET fibre, anisotropy of dielectric relaxation 80—25297
- PET fibre, molecular orientation determ. by US propag. velocity 77—58961
- PET fibres, adhesivity improvement by plasma surface treatment 79—15823
- PET fibres, amorphous, exam. of birefringence 80—11360
- PET fibres, orientation distrib. of crystallites 79—86722
- plant fibre, fracture energy 79—52355
- plant fibres, fracture mechanism 80—35931
- poly(L-alanine) fibres, mol. motion and fine struct., X-ray, thermal, mech., dynamic loss tangent meas. *(Japanese)* 78—59765
- poly(p-phenylene terephthalamide) fibres, chain orientation distrib., and elastic props. 78—75566
- poly(p-phenylene terephthalamide) fibres, optical anisotropy determ. 79—4786
- poly-m-phenylene isophthalamide, precipitated from soln., morphology *(Japanese)* 79—14706
- poly-p-benzamide fibre, supermol. struct., X-ray diffr. and acoustic methods 78—75570
- poly-p-phenylene terephthalate, high modulus fibre, struct. obs. 78—75564
- polyacrylonitrile, new model for structure, small-angle X-ray scattering and TEM study 79—77531
- polyacrylonitrile, struct. of heat treated fibres, X-ray diffr. 78—83752
- polyacrylonitrile fibres, section cutting, technique *(Russian)* 80—7754
- polyamide, aromatic, fibre, high modulus, mol. and supramol. struct. 80—79710
- polyamide, differently matted, meas. of diffuse reflectance spectra, using SPEKOL spectrocolorimeter 80—77836
- polyamide, sputter etching 80—21147
- p-polyamide based organic fibres, effect of temp. and deform. time, on deform. strength props. 80—11720
- polyamide fibre, chain-segment orientation, US vel. meas., humidity effects *(German)* 78—75590
- polyamide fibres, crystallinity and crystallite size meas. 78—30549
- polyamides, extended chain aromatic, fibres, tensile strength and moduli 80—81021
- polycaprolactam, fibre, struct. change when used as resin reinforcement *(German)* 77—21091
- polycaprolactam, lifetime under load, in presence of UV radiation, stress depend. 78—48535
- polycarbonate fibre, highly-oriented, drawing behaviour and mech. props. 78—76708
- polydiacetylene fibre resonance Raman spectrum meas. 79—17507
- polyester, sputter etching 80—21147
- polyester fibres, crystallinity and crystallite size meas. 78—30549
- polyester fibres, orientation in drawn fibres, birefringence meas. 78—35344
- polyester fibres, plasma surface treatment, ESR detect. of free radicals 79—15824
- polyester fibres, thiuram and dithiocarbamate rubber accelerator degradation 79—78986
- polyester-hydrazide, aromatic, fibres and films, synthesis and props. *(Japanese)* 80—108387
- polyethylene, fibrous samples, struct. obs. by low-angle X-ray diffr. 78—34445
- polyethylene, flow-induced fibril form. from soln. 80—59402
- polyethylene, hard elastic fibres, deform. and struct., −196 to 80°C 78—51437
- polyethylene, high density extruded fibres, morphology effect on physical and mech. props. 79—83235
- polyethylene, high modulus filaments, form. from melt, cryst. nucleation effects 79—70034
- polyethylene, high-density fibres, extrusion conditions influence on thermal props. and morphology 79—61617
- polyethylene, high-density fibres, solid-state extruded, form. props. 79—70035
- polyethylene, lightly crosslinked, processed under mol. orient., boiling H_2O resist. fibres prep. 80—38957
- polyethylene, phase structure and molecular mobility, broad-line NMR spectroscopy 78—14290
- polyethylene, ultra-high-strength filaments, soln. spun/drawn, mech. and thermal props. 80—40440
- polyethylene, ultra-oriented, prep. technique, extreme moduli 77—21086
- polyethylene fibre, high-strength high-modulus, morphology and tensile prop. relations 80—103264
- polyethylene fibre, production by hot drawing 80—60894
- polyethylene fibre explosion, neutron and energetic ion emission 78—5927
- polyethylene fibre growth from flowing solns., kinetics 79—47654
- polyethylene fibre prod. by surface growth method, mech. props. 80—104108
- polyethylene fibres, electron microscope investig. of internal struct. 80—28926
- polyethylene fibres, high density, ultra oriented, physical, mech. props. 80—25649
- polyethylene fibres, X-ray diffraction-profile Fourier analysis, determ. of microstruct. parameters 80—49042
- polyethylene fibres radiation initiated graft polymerisation of acrylonitrile, initiation rate rel. to props. *(Russian)* 80—7531
- polyethylene filaments, ultrahigh-strength, from soln. spinning and hot drawing 80—45268
- polyethylene films modified by polyacrylonitrile grafting before, after orientating elongation, struct. *(Russian)* 77—32554
- polyethylene melt, drawing filaments, surface instabilities 78—71305
- polyethylene melt spinning, extensional flow induced crystallisation 78—55818
- polyethylene terephthalate, chain rupture and tensile deform., viscosity-av. mol. wt. obs. 78—76714
- polyethylene terephthalate, fibre, melting in crystn., intermediate and amorphous phases 77—84898
- polyethylene terephthalate, filament, heat setting and thermomechanical behaviour 78—15435
- polyethylene terephthalate, lifetime under load, in presence of UV radiation, stress depend. 78—48535
- polyethylene terephthalate, radiation grafting 79—96342
- polyethylene terephthalate fabric, surface struct., props. rel. to plasma surface treatment 78—95831
- polyethylene terephthalate fibres, elastic modulus 79—79019

fibres continued
polyethylene terephthalate fibres, high freq. US effects on physical and chem. structs. *(Polish)* 78—51446
polyethylene terephthalate fibres, interdependence between struct. and thermal contraction *(Rumanian)* 78—91259
polyethylene terephthalate monofilaments, friction and adhesion 79—52386
polyethylene terephthalate yarns, NMR, fibre struct. rel. to annealing, drawing *(Japanese)* 77—32269
polyethylene-paraffin wax, blends, rapid cooling processing techniques 80—84905
polyethylene/polypropylene blends, surface growth of fibres and films 80—66470
polyethylenes, linear, ultra-high modulus, tensile creep, recovery 78—95784
polyimides, oriented cycloaliphatic, thermomech. props., synthesis *(Russian)* 80—55443
polymer, lifetime under load, in presence of UV radiation, stress depend. 78—48535
polymer, oriented, elastic constants meas. 78—38261
polymer fibre, highly oriented, struct. and mech. props. 78—75563
polymer fibre formation, fibrous crystallisation and chain extension 78—75573
polymer fibres, ultra high modulus, prep. by soln. and melt spinning, review 79—11544
polymer lifetime under load, in presence of UV radiation stress depend. 78—48534
polymer melt mixtures, thermodynamically incompatible, flow, specific fibre formation mechanism 77—23926
polymer melt spinning, mechanics of nonisothermal process 77—51010
polymer solution elongational flow, wet spinning process for fibres 78—72760
polymeric fibres, cyclic tension endurance, Prevorsek-Lyons theory 78—52967
polymers, cryst., hard-elastic fibres, morphology mech. props., mechanisms, review 77—32612
polymers development, condensation (step-growth) 79—83168
polyoxymethylene-copolyamide melts, flow, fibrillation, mechanism 77—4765
polyoxymethylene-copolyamide mixture melt, plasticiser effect on props. and fibre form. during flow 77—27500
polypentamethylene terephthalate, oriented fibres, struct. anal. of two cryst. phases 79—73108
polypropylene, drawn fibres, SEM and US study 78—47249
polypropylene, film and fibre, chain rupture and tensile deform., viscosity-av. mol. wt. obs. 78—76714
polypropylene, hard elastic, macroscopic deforms. in lamellae 79—96097
polypropylene, hard elastic fibres, stress relaxation 77—36564
polypropylene, helically twisted, small-angle light scatt. 79—1765
polypropylene, monofilaments, drawing behaviour, melt-induced orientation effects 78—84922
polypropylene, oriented fibre drawing *(Russian)* 77—21088
polypropylene, with helical internal texture, SEM obs. of surface morphology 80—39394
polypropylene fibers, and films, and their hard elastic precursor small-angle X-ray diffr. studies 79—10815
polypropylene fibre, melt-spun with twist, helical orientation and mech. props. 78—75569
polypropylene fibres, EPR during glass transition, γ-irrad. 79—8445
polypropylene fibres, high strength, elastic 80—20992
polypropylene fibres, homologue mixtures, props. 78—76709
polypropylene film and fibre, plasma etching 78—95871
polypropylene monofilaments, draw rate effect on long period 79—47726
polypropylene nonfilaments, highly drawn, plastic deform. 78—44174
polypropylene-nylon 11 fibres, bimodal cryst. texture, X-ray diffr. and electron microscopy 78—75567
polystyrene fibre, ageing effects on elongation to fracture *(German)* 78—76750
polystyrene filament, melt spun, struct. and mech. props., effect of drawing, twisting, annealing, untwisting 80—45331
polystyrene monofilaments, uniaxial extension, strengthening 79—8334
polytetramethylene terephthalate, monofilaments, chain conform. rel. to strain 77—4055
polyurethane, elastic fibres, cross link density effect on mech. props. 77—70023
production, solid matter content radiometric meas. experience *(German)* 77—67488
PTE, polymer fibre, orientation changes during stretching, IR spectra 78—75568
PTFE, oriented fibre drawing *(Russian)* 77—21088
PTFE fibres, US effects on structure *(Polish)* 78—68702
PVC, chlorinated, fibres, radiation initiated graft polymerisation of acrylonitrile, initiation rate rel. to props. *(Russian)* 80—7531
quartz, ESR and IR obs. of microinhomogeneities 77—8401
quartz, polar orientation, stereospecific twisting 78—42930
quartz, torsion balance, sat up by welding fused quartz rods and fibres *(Japanese)* 80—31738
refractory, effect on high-temp. strength of refractory coatings *(Russian)* 77—52536
refractory, exam. of deform. behaviour and thermal cond. *(French)* 79—15719
refractory compounds, viscous-sheath filaments production 78—3077
refractory thermal insulation effective thermal cond., fibre diameter effects 80—104105
reinforcing, strength eval. by dry bundle method 79—100312
reinforcing for plastics, review 79—61506
sapphire fibres, meas. of bending strength 80—25964
sapphite, strength at rupture 80—104286
silk, lifetime under load, in presence of UV radiation, stress depend. 78—48535
silk, spider, tensile, fracture strength, elongation and ageing effects 80—41072
sintering, consolidation theory 77—73243
size measurement, using Fraunhofer diffraction 79—171
sizing using light scatt., error contour charts 80—4689
small particle spectral diffuse IR reflectivity meas. 80—68276
steel, austenitic Kh18N9T, porous fibres, oriented struct., strength props. 78—3199
steel, austenitic stainless, porous fibre, sintered and compacted, mech. props. 79—15623
steel, polycrystalline, Mossbauer spectroscopy 80—44959

fibres continued
steel, reinforcing wires, high strength, microstruct. obs. *(Czech)* 79—43342
steel, Si (6.5 wt.%) Mn, Ni and Al additions influence obs., on mech. and magnetic props. *(Slovak)* 79—5064
steel, stainless, filament produced by glass coated melt spinning, new metastable tetragonal struct. 79—20072
steel, stainless, filament produced by glass-coated melt spinning, tensile strength 78—31488
steel, stainless 12kh18N9T, wire, mechanical and heat treatment effect on static and cyclical strength *(Russian)* 78—35410
steel core/steel tube duplex reinforcing member, behaviour under cyclic loading, core element geometry effects 77—28894
steel wire reinforced Portland cement mortar, wire pull out, inelastic behaviour 78—56681
structure, interatomic forces calcs. 79—22875
suspension, dil., mechanistic aspects of drag reduction in turbulent pipe flow 80—6102
suspension, rheology, rel. to turbulent drag reduction 78—22315
suspension flow in pipes, transition regime analysis, drag reduction 77—89186
tensile strength, thread diameter depend. *(Russian)* 77—59852
textile, moving dielectric, measurement of electrical charge 79—75549
textile fibres, polymer treated, sectioning technique for SEM 79—2891
textile filaments, with planar crimp, tensile deformation 80—84235
textiles, fatigue testing, multistation apparatus using biaxial rotation over a pin 80—66726
texture, quantitative determ. of volume fraction, analytical method by pole figures 80—11863
thermal expansion coefficient, determ. using optical dilatometer 80—45454
viscose, solid porous film form. in electromagnetic field *(Russian)* 77—66595
water suspended solid analysis by single-particle scatt. 79—79435
wicks, metal fibres, in heat pipes, thermal resist. 80—43601
wool, diameter meas. for grade determ., truncated sequential sampling 79—87802
wool fibre, directional friction obs. by capstan method 78—19899
Ag, filament produced by glass coated melt spinning, mech. props. 77—86125
Ag-Cu alloy filaments, prod. by glass coated melt spinning, microstruct. and tensile strength 79—91667
Al wire, torsion fatigue strength and fibre texture 77—48549
α-Al_2O_3 fibre FP, manufacture, strength and modulus 80—81013
B, amplitude depend. of internal friction 80—20990
B, CVD, morphologies, influencing factors, temp. range 1390-1640K 80—89154
B, fibre, metallisation by continuous casting in Al and Al alloys *(Russian)* 78—35538
B fibre, prep. by closed CVD system, mech. props. and surface defects 79—52311
B fibres, plasticizing and wettability-enhancing coatings 79—29252
B fibres, quality evaluation from morphological and fractographic characteristics *(Russian)* 79—70150
B fibres, radial cracks 78—15505
B fibres of various diameters, tensile strength, elasticity, elongation 78—3189
B, filament, light emission during fracture 77—28896
B filament, uncoated and SiC coated, high temp. physicomech. props. 79—20140
B, filament CVD technology, book contrib. 78—48352
B, fracture, Griffith criterion appl. 77—12684
B, prep. 79—28983
B, prep. in closed CVD system 79—83129
B, prod. and phys. props. *(French)* 78—23647
B, proximate void origin and initial growth stages 77—80498
B, reinforced Al, strength determ. procedure in annular specimens *(Russian)* 78—95864
B, surface energy meas. from Griffith cracks 77—77563
B, surface morphologies rel. to mech. props. 80—11749
B, to graphite reinforced epoxy, radiographic inspection aid 78—95880
B_4C fibres, yarn prep. from C fibres, mech., chem. props., struct., book contrib. 78—48365
BN fibres, prep., struct., thermal, mech. and elec. props., appls., book contrib. 78—48360
$BaTiO_3$ fibres synthesised from $Ba(OH)_2+2K_2O.11TiO_2.3H_2O$ fibre hydrothermal reaction *(Japanese)* 80—93527
$CaSiO_3$, fibrous, controlled crystallisation and anisotropy 80—59425
Cu, coating with biphenyl, freeze and viscous coating technique 78—48350
Cu, fibre texture of filament produced by glass coated melt spinning 77—85966
Cu-Al_2O_3 dispersion hardened wires, drawn, substruct. and strength 78—35405
Fe, fibre texture of filaments produced by glass coated melt spinning 77—85966
Fe loss from asbestos fibres in pulmonary tissue, obs. 79—74825
Fe porous material, props. 79—98798
Fe-base fibres, extruded, heat treatment 78—35414
$(K_2O)_x.TiO_2$ fibres, flux growth reactions 80—16171
$K_2O.3MoO_3.3H_2O$, fibrillar crysts., morphology and struct. 78—63959
K_2TiO_3 use for anatase fibres synthesis, hydrothermal leaching *(Japanese)* 79—56949
$K_2Ti_3O_7$ fibres, synthesis by kneading, drying, calcination process *(Japanese)* 79—38779
$K_2Ti_6O_{13}$ fibre synthesis from melt reaction of TiO_2 and K_2CO_3 *(Japanese)* 78—44070
$K_2Ti_6O_{13}$ fibres, synthesis by the hydrothermal dehydration method 79—43121
$Li_2O.3MoO_3.5.7H_2O$, fibrillar crysts., morphology and struct. 78—63959
MgO, filamentary crysts., mech. props. 77—52402
Mo, fibre, brittle to tough transition, impact strength meas. 80—40527
Nb_3Sn, filamentary conductors, type-II, low temp. 30 GeV proton effects on critical props. 78—52178
Nb_3Sn, filamentary superconducting composite, TEM 77—80887
NbTi, filamentary conductors, type-II, low temp. 30 GeV proton effects on critical props. 78—52178
Ni, porous, permeable material production 77—12580
NiCr-AlY sintered fibre metal struct. abradable seal material, friction and wear 78—56785

fibres continued
Pb, filament production, ejection of molten metal through nozzle, jet stability *(Japanese)* 78—52719
Si, growth by thermal decomp. of SiH_4 79—69970
$Si-SiO_2-Mg-Cu$ powder compact, nitridation to form Si_2ON_2 whiskers *(Japanese)* 80—93674
SiC, continuous, tensile strengths and Young's moduli, 600-1400°C 77—59885
SiC, continuous fibre synthesis with high tensile strength and Young's modulus 79—15633
SiC continuous fibres, mech. props. depend. on testing conditions *(Russian)* 80—35297
SiC, fibre, metallisation by continuous casting in Al and Al alloys *(Russian)* 78—35538
SiC fibre development using organosilicon polymer precursor 78—60627
SiC, fibre growth kinetics in laser-heated system 77—81203
SiC fibres, microcrystalline state anomalous characts. 79—74122
SiC fibres, plasticizing and wettability-enhancing coatings 79—29252
SiC fibres obtained from polycarbosilane fibre 80—50582
SiC fibres with protective Al_2O_3 coatings in Ni-Cr alloy based composites, IR investigation 78—60623
SiO_2 fibre, characterisation of physical props., $CaSiO_3$ production from xonolite slurry 78—39730
SiO_2 fibres, freeze formed from polysilicic acid aq. soln. 80—71609
SiO_2 fibres, fused, load-elongation curves, elastic hysteresis, tensile testing machine 79—1891
SiO_2 fibres, LF optical phonons, Raman spectra 80—80789
SiO_2 fibres, plastic deformation and Young's modulus *(French)* 78—23746
SiO_2, fused, fibres, lifetime predictions, applicability of crack velocity date 77—52467
SiO_2 fused fibres, radii determ. by multiwavelength laser light scatt. 80—22321
Ti base alloys, melt-extracted polycryst., mech. props. 80—76360
Ti, high-temp. nitriding kinetics *(Russian)* 80—21166
TiO_2-SiO_2 fibre, prep. from metal alcoholates, prep. of spinnable soln. *(Japanese)* 78—44071
V_3Ga, filamentary conductors, type-II, low temp. 30 GeV proton effects on critical props. 78—52178
V_2O_5, amorphous semicond., solubility and fibrous texture 80—75162
W, deposition of ZrC coating acting as diffusion barrier in composite 77—4759
W, fibre, brittle to tough transition, impact strength meas. 80—40527
W fibres, dependence of fine struct., on processing parameters 79—34082
W, KAl, KSi, KSiAl and KSiGa, addition effects on workability *(German)* 78—64557
W, KSiAl doped, recrystallisation, Li diffusion effects, hardness, strength, microstructure meas. *(German)* 78—64644
W, spiral, brittle, densification of particulate materials, general law 78—19692
W wire, cold drawn, dislocation processes occurring during tensile testing *(Hungarian)* 77—48450
Zr, high-temp. nitriding kinetics *(Russian)* 80—21166

field, crystal internal *see crystal field interactions*

field effect devices
see also field effect integrated circuits; field effect transistors; metal-insulator-semiconductor devices
FET transducer, H^+, Ca^{++} and K^+-sensitive, biomedical appls. 78—28117
hybrid field-effect liquid crystal light valve, sensitometry control 80—23788
hybrid field-effect liquid-crystal light valve, optical data processing performance 80—99860
ion controlled chemically sensitive diodes 80—13066
junction field effect structures, 2-D subbanding 78—64125
liquid crystal light valve operation and appls. 78—46826
magnetodiode and magnetoconcentration effects, influence of field effect 80—107903
MNOS thin-oxide devices, effects of $Si-SiO_2$ interface states on memory characts. 79—82681
MOS, generation lifetimes from C-t transients 78—88036
pre-amplifier, use with HgI_2 as low energy X-ray spectrom. 78—37479
radiation effects, damage coeffs. for fission neutron and gamma-ray irrad. 80—34058
SOS, Si-sapphire interface charge trapping, effects of sapphire type and epi growth conditions 77—20447
SOS device structure, nonlinear B impurity redistrib., numerical soln. 79—1625
$AgBr-SiO_2$, field effect potentiometric sensors 78—35691
GaAs, epitaxial film, field effect struct., elec. breakdown, negative resist. 77—12030
GaAs, epitaxial layers, low freq. current noise between 4.4 and 300K 78—95388
In_2O_3 film, evaporated, on ferroelec. ceramic, switching characts. 78—19107

field effect integrated circuits
see also charge-coupled device circuits
blind person's rocking motion sensor and recorder 77—52921
CMOS 77—41653
CMOS analogue gate, small DC voltage meas., at low temp. 79—35776
CMOS ICM 7555 capacitance meter cct., using radio receiver indicator 80—62692
CMOS ICs electrically active stacking faults, anomalous leakage currents 79—78191
CMOS logic, basics 77—78925
CMOS microcircuit failure anal. by scanning electron microscope and mass spectrometry 78—21264
CMOS R wave inhibited threshold adaptive pacemaker 77—25610
cross-correlator for broad-band impedance meas. using high-speed CMOS switches 77—26324
CVD dielectric thin films, multiple internal refl. IR spectroscopy 80—11499
digital chronometer with seven-function selector *(French)* 78—12677
dual-gate depletion-mode FET/piezoelectric film transducer 79—50563
four-channel EEG amplifier 79—39535
ion sensitive FET, reference, for compensation, biomedical appl. 78—44642
ion sensitive FET micro pH sensor, for biomedical appl. 78—44643
ion sensor for physiological pH and pNa monitoring 78—44641

field effect integrated circuits continued
IR detector array of monolithic Si, design, processing and performance 77—74498
IR sensing, Si:In(Ga) MOSFET, characts. 3 to 5 and 8 to 14 μm 77—74503
MIS integrated stepped-sawtooth waveform generator 78—86376
monolithically integrated optical repeater, fabrication and characts. 80—28353
MOS, charge build-up due to radiation, mathematical model 79—19667
p-MOS, master slice, appl. of B diffusion into Si from CVD Bn covered with Si_3N_4 80—107564
MOS, photodiode sensor array circuits and performance 77—39077
MOS, properties of sputtered WSi_2 as gate electrode and interconnecting material 80—70831
MOS capacitors, radiation-induced increase of Na ions 78—26956
MOS compatibility of RF sputtered polySi films 78—6455
MOS governing SAW transducers, fast action commutators of analogue signals 78—33963
MOS LSI passivation using reactive plasma deposited Si-N films 78—56584
MOS processing, appl. of plasma etching techniques 80—40577
MOS RAM, influence of point like and extended defects 79—82679
MOS RAM, Siemens HYB 4116 16 384-bit, failure anal. using modified scanning electron microscope 79—21876
MOS-LSI organ circuits *(German)* 77—19493
MOSFET amplifier, fabrication on Si wafer, integrated acoustic transducer arrays 80—74683
MS'IS structure free carrier redistribution control 78—95384
PMOS, deep diffusion of B at solid solubility limits 78—10070
PMOS process with ion implanted threshold adjust, radiation hardening 79—46689
PMOS programmable sound generator, microprocessor-compatible, electronic music appls. *(German)* 80—79092
potentiometric sensor, for biomedical appl. 78—44644
sapphire substrate surface evaluation for SOS 77—76653
SAW convolver, MIS struct., basic characts. 77—23791
Schottky-barrier metal-thin oxide-semicond. structures, physical processes and microelectronics applications *(Russian)* 78—84307
solid-state imaging charge injection devices 77—39083
SOS, elec. investigation of Si-sapphire interface 80—11097
SOS, laser annealing to round edges of Si structures 80—25742
SOS capacitors, ion-implanted with negative charge gamma radiation effects 79—23645
SOS film, electron mobility 78—91792
SOS for LSI/VLSI technology *(German)* 79—95918
SOS MOST, electronic props. at Si-sapphire interface 80—96993
SOS substrate quality evaluation by X-ray rocking curve technique 77—76262
transducer research and development for biomedical appl. 78—44640
VMOS dynamic memory, 65536-bit, investigation of alpha-particle induced soft errors 80—88223
Si dry pressure-oxidation for low-temp. IC processing 78—7068
Si, polycryst. barrier layer formation, investigation *(Slovak)* 78—92196
ZnO/SOS monolithic SAW amplifier 78—6205

field effect transistor circuits
Used for general papers and papers where the use of field effect transistors is significant
autodyne detector of acoustic nuclear magnetic resonance 79—17457
burst-generating neuron electronic analogue 77—25411
charge sensitive preamplifiers, signal and noise response 78—33404
charge-sensitive preamplifier, universal, using FET, cct. 78—77932
digital integrator, for pulsed NMR spectrometer 77—26372
GaAs FET amplifier, varactor-tuned, for UHF SQUID magnetometer 80—31814
hybrid p-i-n photodiode-FET preamplifier design for digital optical receivers *(German)* 78—33878
laser beam profile monitor system using photodiode or pyroelec. array 77—58364
low-noise FETs, use in preamplifier for gravit. research 78—243
MESFET preamplifier in p-i-n/FET hybrid optical receiver for communication systems 80—33158
MOSFET electrometer amplifier, characts. 77—74446
MOSFET electrometer amplifier type MDM 77—79106
MOSFET preamplifier, liquid He-coooled, for use with astronomical bolometer 77—61123
oscillator, for quartz thermometer 78—81967
photodetector low-noise amplifiers using J-FETs for optical fibre receivers 78—37997
photodetector with automatically adjustable threshold level, design considerations 80—62724
photoreceiver system, photodiode-FET, achievable threshold limit calc. 79—49292
preamplifier, bioelectric measurements including intracellular potentials 77—40855
preamplifier, with drain feedback, X-ray spectrometer appl. 77—38074
Q-switch circuit for pulsed NMR 77—49760
six-channel MOSFET commutator, monopolar mass spectrometer appls. *(Russian)* 78—74099
spectrometric installation preamplifier modernisation by input FET operating regime control 80—32579
strain gauge blood pressure transducer, chopper preamplifier cct. 78—3659
temperature measuring bridge, using constant-current FET circuits 77—129
voltmeter with high input impedance *(Spanish)* 77—37934
GaAs antenna mounted FET for DC-RF conversion in solar power satellite 80—40870
GaAs FET preamplifier, cooled (4.2K), for use in UHF SQUID magnetometer 80—52282
GaAs, low-noise, FET preamplifier for low-temp. NMR and SQUIDs 78—4672

field effect transistors
see also field effect integrated circuits; insulated gate field effect transistors; junction gate field effect transistors; Schottky gate field effect transistors
chemically sensitive devices for trace level anal. 77—52720
computer simulation, student lab expt. 79—44673
continuous monitoring by ion-sensitive FET *(Spanish)* 79—83986
GaAs photo-FET high speed photoconductive integrated optical receiver 80—58816

field effect transistors continued
ion sensitive, mechanism 77−48741
ion sensitive FET theory based on membrane electrodes 80−41280
model, alloy scatt., high field transport 78−30929
MOS p-channel transistors, ion implantation effect on threshold voltage 78−34903
network, simulation of quasilinear parabolic equations 77−50854
neuron model of burst generation analogue 77−44630
noise at high elec. fields 77−8163
noise figure, measurement by connecting source resistance between input and output *(French)* 80−68214
probes for improving CRO meas. 78−93667
spectrum measurements of oscillatory data, appl. to de Haas-van Alphen effect 79−42434
static induction transistors, one-dimens. potential profile anal. 79−56290
thermogenesis, harmonic analysis and inverse filter 80−27304
GaAs, active layers produced by high energy Se^{++} implantation, FET appls. 77−39605
GaAs and related cpds., conf., Edinburgh, Scotland (Sep 1976) 78−3039
GaAs and related cpds., conference, St. Louis, MO, USA (Sept. 1978) 80−8737
GaAs, continuous growth of LPE double layers 78−64487
GaAs, epitaxial growth for microwave devices *(French)* 77−48360
GaAs, epitaxial layer, micron and submicron vap. phase growth, for FET 80−11577
GaAs, epitaxial layer uniformity and reproducibility, data 79−38744
GaAs FET buffers, high purity LPE growth by sliding boat method *(Japanese)* 79−28955
GaAs FET double layer production, study by sliding boat method *(Japanese)* 79−66014
GaAs, failure anal. using SEM electron beam 78−29216
GaAs, ion implantation, trends 80−39132
GaAs, LPE, residual impurities and deep levels, FET fabrication 79−28964
GaAs, MBE, semi-insulating growth and use as buffer layer 79−28946
GaAs Schottky-gate FET and GaAlAs injection DH laser, monolithic integration 80−58593
GaAs, sharp line photolum. spectra 78−72248
GaAs VPE layers for FET devices, impurity characterisation 80−29491
GaAs:Cr, FET, influence of Cr on mobility of electrons 80−92910
GaAs:Ge MBE power FETs with Sn surface impurities 80−80374
n-GaAs:Sn, nonalloyed and in situ Ohmic contacts for FETs 79−56307
GaAs-n-Al$_x$Ga$_{1-x}$As heterojunctions, selectively doped, FET 80−80364
GaInSb, Be ion implantation, device appl. 80−24478
Ge FET, fabrication on high purity substrate 79−45579
InAsSb, Be ion implantation, device appl. 80−24478
In$_{0.53}$Ga$_{0.47}$As p-i-n photodiode-FET photoreceiver for 1.0 to 1.7 μm wavelength optical fibre communications systems 80−58794
SiO$_2$ in FET, electron trapping due to electron beam deposited Al 78−80060
(W-Au)-SiO$_2$-Si:B MOS transistor, ion implantation effect on threshold voltage 78−34903
WSi$_2$ film, FET gate electrode, oxidation mechanism, SiO$_2$ overlayer formation 78−76773

field emission, electron *see electron field emission*

field emission electron microscopes
see also field emission electron microscopy
atomic resolution 78−32929
conference, Clermont-Ferrand, France (Jun 1976) *(French)* 77−26436
contrast transfer function, beam intensity influence 79−30621
electron gun, comparison of cold and thermal types used in the same electron microscope 80−101890
electron gun, for TEM, advantages in high resolution and in-line Fraunhofer holography *(French)* 77−34057
electron gun, noise and energy broadening 80−101889
electron gun *(Japanese)* 77−61162
electron gun equipped, description *(Japanese)* 80−47146
electron holography, off-axis 80−101905
electron holography, review of progress *(Japanese)* 80−52369
electron source geometry determination by computer assisted shadowgraph technique 77−87882
glass, for investigation of emission probs. of single cryst. faces 80−101879
gun, electron source size 79−71575
gun design *(French)* 77−26442
gun design for column with energy dispersive spectrometer *(French)* 77−26443
gun lenses, electrostatic for high-brightness field emitters 80−62809
high resolution electron holography 79−30614
high vacuum, modification for simultaneous meas. of local and integral emission characts. of electron emitters 79−9263
hydrocarbon vacuum gauge 77−18002
in-situ gas reaction cell, for field emission SEM 80−81415
local and integral emission meas., electron emission microscope adaptation 79−93258
magnification, rel. to emission from microprojections on W point 77−1789
metal-Al$_2$O$_3$-Au type uniformly emitting MIM thin film cathode with evaporated insulator *(German)* 79−19675
micro SEM, for UHV surface anal. 80−86519
monochromatic, with highly stabilized gun and illuminating system 80−18047
monochromator, telescopic, in CTEM, with cylindrical mirror analysers 80−87296
numerical field calc. in field emission devices 79−97478
probe size to current relationship, advantages for restricted divergence probe 80−68324
rotationally symmetric gun, theoretical investigation 80−99006
scanning, high resolution image 80−86520
scanning-transmission, for X-ray microanal. 80−85260
SEM, enhanced secondary electron detection at small working distance 78−21303
SEM, high resolution type HFS-2, development 77−18146
SEM field emission electron gun *(Czech)* 79−6240
SEM field emission gun column electron-optical performance obs. and model 80−68328
SEM with electron energies up to 5 MeV 79−80728
single-pole magnetic lens as condenser for field emission electron gun 80−68325
STEM, 100 kV, with energy dispersive X-ray spectrometer 77−26441

field emission electron microscopes continued
STEM, high resoln., 100 kV, (HB5) 77−26438
STEM, high resoln., 100 kV, AEI 77−26439
STEM, high resoln. ELMISKOP ST 100 F 77−26437
STEM, high resolution, design principles and practical advantages 77−49815
STEM, improved spatial resolution of X-ray microanalysis 80−104490
STEM, microanal. by energy loss spectrometry 78−53286
STEM, phase contrast characteristics 80−100153
STEM, with detector for phase and amplitude contrast 77−26440
thermocouple temperature controller for field emitter 78−24898
ultrahigh vacuum field-emission SEM 80−62812

field emission electron microscopy
see also field emission electron microscopes
AES, appl. of new integral field emission gun with small spot size 79−75663
asymmetric electrostatic lens for field-emission microprobe applications 79−75656
atomically clean surface environment, confirmation using field electron emission 80−52250
biopolymers, epitaxial sandwiching, electron microscopy specimen prep. 78−36080
crystal defects, obs. using SEM fitted with field emisson gun *(French)* 77−35452
early development 78−32644
electron backscattering patterns, in field emission gun SEM 80−100142
electron beam exposure system for semiconductor fabrication 79−30624
electron holography, review of progress *(Japanese)* 80−52369
electron holography appl. to micro-area electron diffr. 80−49055
electron lens spherical aberration correction by holography 79−85203
electron work function of individual cryst. faces 80−101879
ferritin particle visibility in SEM with field emission gun 79−25174
Fowler-Nordheim slope variation with cryst. plane size, FEM-FIM obs. 78−27383
haemoglobin S, fibres, discs having six-fold symmetry, electron microscopy 78−76989
imaging and diffraction techniques, (book) 79−67441
interference electron microscopy using electron holography 80−32929
interference electron microscopy using electron holography and Mach-Zehnder interferometry 79−54231
lipoprotein, low density, from human serum, STEM and FE-TEM obs. 79−100566
local field strength and work function rel. to field emitters, analogue simulation on Teledeltos paper 77−41731
magnetic domains obs. using Lorentz microscope with field emission gun 77−63228
metal tip profile change meas. for evaporation rate determ. 77−24403
microfield effects on spectrum of electrons emitted from surface 79−6227
micropoint field emitters, location, nanosecond UHV discharges 78−332
microscopic tip regeneration and cathode polishing by explosive emission 77−16472
phase contrast characteristics in bright field electron microscopy 79−89048
principles and applications, review 79−65982
SEM display, effects of field emission instability, electronic removal device 78−21279
STEM, Fresnel fringes 78−8476
surface microstructure determ. and microanalysis by ultrahigh vacuum field emission gun SEM 80−96423
surface studies, by field emission 79−67444
tip prep. from sheet and block metal 78−7155
transmission, sub-angstrom resolution 80−82851
virtual surface states, simple modelistic treatment 80−103739
W, field emission tip, microscopic protuberance formation, min. elec. field and temp. 78−6835
Ag, adsorption on W, substrate temp. effect on relation between work function and coverage, FEM obs. 80−2272
Au film, on W substrate, chemisorbed N$_2$ effect on crystallite growth, FEM obs. 79−46976
Au, lattice images, obs. with a field emission electron microscope 79−14659
Co film, mag. domain wall obs. by electron holography 80−80582
GaAs(P), adsorption and field-desorption of O$_2$ and Au, FEM studies 80−34304
p-Ge, adsorption of Au, effect on I-V characteristics field emission study 78−67925
Hg, condensation, two-dimensional, on W 80−107666
In, epitaxial layer, growth and desorption on W tips, high field microscopy obs. 79−69380
Mo (111) planes, adsorption of NH$_3$, preferential nitriding, FEM study 80−66877
Mo, adsorpt. of NH$_3$ and catalytic decomposition 78−14596
Ni, lattice images, obs. with a field emission electron microscope 79−14659
Pt, adsorption and decomp. of ethylene, 90 to 500K 79−46933
Pt, adsorption of H, face specificity, field emission probe-hole microscope obs. 77−11783
Pt, adsorption of water, H$_2$ and reaction between H$_2$ and adsorbed O 80−49514
Pt, Cs adsorption 78−51822
Pt tips, glass-coated, field emission microscopy Fowler-Nordheim emission regime and periodic current oscills. 79−95907
RE, adsorption of K, work function changes, FEM obs. 77−72772
Re, adsorpt. of Au, on low index planes 78−14597
Ta, adsorption of O$_2$, FEM obs. of work function changes 78−26771
Ti, surface struct., HCP to BCC type struct. transition, FEM obs. *(Japanese)* 78−22938
U, emissive props. 78−88409
W (100) surface, Pb and Fe adsorption, field emission microscopy study 79−15015
W (110) surface, adsorbed Pd, growth, struct., stability, desorption 80−59794
W, adsorpt. surface migration and thermal desorpt. of LaB$_6$, field emission microscopy 79−56075
W, adsorption of Au, field emission microscopy exam. of work function, correlation with LEED and RHEED meas. 78−35276
W, adsorption of Be, crystallites growth, FEM obs. 78−26799
W, adsorption of CO, FEM expt., pseudoclean pattern *(Japanese)* 78−34701

field emission electron microscopy continued
W, adsorption of Cu, FIM and FEM obs. of nucleation, epitaxial growth and interface form. 78−26800
W, adsorption of Cu 78−14612
W, adsorption of NO and NO_2 80−84390
W, chemisorption of NO, 80K, FEM obs. 77−39733
W, coadsorpt. of Ni and K, average work function change 79−28190
W, coadsorption of La and B, field emission meas. 78−47662
W, coadsorption of La and B, field emission and field ion microscopy 80−104049
W, dissociative adsorption of NO, FEM obs. 77−4258
W, methane adsorption on (111) and (100), work function 78−38963
W points, micro-size, change in shape and electron field emission 79−74067
W resistance temp. scale 77−45841
W, stacking faults, microstress relax. effects, field ion images 77−89453
W-Th, field ion specimen, contrast bands in elec. field induced evaporation 79−50967
W_2C, oxidation, oriented struct. transform. to W, FEM and TEM obs. 80−30124
W_2C, single cryst., decarburization, field emission microscopy and TEM 79−70368

field emission ion microscopes
see also field emission ion microscopy
atom probe time-of-flight microscope, computer-controlled, for metal defects study 77−82645
atom-probe field-ion microscope, using single time-gated channel plate 78−21276
atomic probe, field ion microscope with time-of-flight mass spectrometer, recording unit 80−73520
electric field distrib. near surface of field emitters 79−75658
high brightness ion sources, field effect contribs. 78−32930
imaging atom probe for surface studies 78−14555
ion trajectories for hyperboloidal and paraboloidal emitters 78−32924
low temperature rise heating of a field emission tip 80−52371
magnification 79−54228
metallic microscope for metal crystal radiation defect research 78−333
scanning ion microscope with field ionisation source 78−21289
time-of-flight atom probe for studying impurity atom or alloying element interaction with defects 78−45754
transmission microscope with spatial resolution 1-2 nm at 180000× magnification 79−49341
video recorder registration of unstationary images 78−24897
Ga ion source, emission characts. obs. 80−62810
Ga, liquid-metal high-intensity scanning ion probe with submicroscopic spot size 79−54225

field emission ion microscopy
see also atom probe field ion microscopy; field emission ion microscopes
atom-probe FIM data, quantification appl. to surface segregation of alloys 78−62263
atoms, direct obs., application to ultra-fine processing *(Japanese)* 79−7532
atoms on metal surfaces diffusion parameters, binding energy and dipole moment 79−51422
black chrome, electroplated layer, field ion microscopy study 79−28246
coatings, defects and their effect on props. 80−39474
detects in materials, direct observation and characterisation 78−88617
early development 78−32644
electrical contacts surface damage caused by closing voltages 78−64098
Faraday cup for simultaneous ion-beam current obs. and meas. 78−49865
FCC crystal, field-ion images, computer simulation of contrast of dislocation loops 77−11561
field emitter surface, elec. field empirical formula 80−97413
field ion microscopy, developments 79−67445
finite element determ., operational stress-state of field ion microscope specimen 78−32933
flavanthrene molecules, stationary stochastic adparticle flip-flop as a precursor to surface diffusion 80−15371
Fowler-Nordheim slope variation with cryst. plane size, FEM-FIM obs. 78−27383
gas supply function, expt. determ. from adsorption rate 80−100402
glass tip, surface and crystallographic struct. using field-ion and electron microscopy 80−10767
gnomonic method for indexing of micrographs 78−82078
grain boundary dislocations, appl. of field-ion microscopy 79−73170
grain boundary migration obs. using FIM 78−79617
image contrast, gas distrib., hypothesis reexamined 78−60552
image formation 78−35266
image intensifier, EMI T2001, performance 78−24896
imaging and diffraction techniques, (book) 79−67441
imaging practical surfaces 77−82653
ion current-voltage characts., field ionisation and field evaporation mechanisms 79−15594
local field strength and work function rel. to field emitters, analogue simulation on Teledeltos paper 77−41731
metal, direct obs. of individual atoms 77−62724
metal, direct obs. of surface diffusion and atomic interactions 78−34716
metal, grain boundary elements, FIM *(German)* 77−27894
metal adatom pair, on metal surface, effective interaction, from FIM expts. 78−22953
metallurgical problem studies, review 78−35620
metals, chemisorption of gases, book 79−69370
metals, radiation damage, FIM and atom probe FIM expts., review 78−35623
metals and alloys, defects and chemical inhomogeneities *(German)* 80−57431
metals and alloys, refractory, surface investigation by FIM and atom probe *(German)* 79−55623
microstructures digital simulation 80−19679
miscellaneous expts. survey, in PSU and NIT laboratories, (1960 to 1978) *(Japanese)* 80−4810
needle field emitter, ion bombardment effects, field emission microscope obs. 77−55869
plasma-wall interactions in Princeton Large Torus Tokamak, appl. of high-field surface and techniques 79−68942
projection geometry of field-ion image 78−66011
protein adsorbed layers on field-emitter tips, removal by UV radiation 80−104836
quantitative analysis of micrographs using Moire techniques 77−90259

field emission ion microscopy continued
ring counting in field-ion micrographs 79−17565
segregation of solute to planar imperfections, field ion microscopy investigation 77−8816
semiconductor, possible role of surface states, Kronig-Penney model 77−47883
shape of emitter from field-ion image 80−2930
steel, Ti (0.1 to 0.55 wt.%), strengthening by carbide precipitation 77−25062
surface characterisation, physical methods, review *(French)* 80−7889
surface states role, one-dimens. model 78−26399
tip prep. from sheet and block metal 78−7155
transition metal hydrides, occurrence in slow field evaporation 77−85903
Al alloy, FIM and microanalysis, developments 80−100155
Al alloys, FIM and microanalysis developments 78−35782
Al, atomistic images of field ion microscopy at high temps. 78−55792
Al imaging by FIM 78−30526
Au, atomistic images of field ion microscopy at high temps. 78−55792
Au-W interface struct., FIM obs. 80−65384
BaO, film, initial struct., field electron emission microscopy and LEED determ. 79−11033
Co-Nb alloys, segregation of Nb to stacking faults, field ion microscopy investigation 77−8816
Cs, VPE on W emitter, FEM obs. 80−70552
Cu alloy, internally oxidised, FIM 77−20074
Cu, atomistic images of field ion microscopy at high temps. 78−55792
Cu, cathode, ns voltage pulse breakdown of emitting sites, field emission microscopy obs. *(German)* 77−63547
Cu cementation on W substrate, field ion microscopy of cementation vs. substrate dissolution, pH effect 80−16206
Cu, electrochem. overgrowths, role of substrate dislocations and grain boundaries in nucleation and growth 79−51454
Cu film, on W substrate, cementation, vac. deposition, and electroplating, growth characts. 79−95291
Fe deposited W tip, FIM obs., epitaxial growth 78−79904
α-Fe, FIM specimens annealed at $0.5T_m$, surface energy anisotropy 77−20181
Fe, oxidation, FIM obs. 80−89388
Fe, VPE on W tip, depositing direction depend. 80−10812
Fe whisker, polycryst., FIM obs. of struct. 78−84111
Fe-Al (51 at.%), crystal vacancies, dilatometric and field ion microscopy exam. 78−47346
Fe-Cu (0.34 wt.%), neutron irradiated, field-ion microscope detection of ultra-fine defects 79−42116
$Fe_{80}B_{20}$ amorphous wire, crystn. by annealing at 780°C 80−100177
$Fe_{80}B_{20}$, metallic glass, triplet correlation, field-ion microscopy study 80−38921
$Fe_{78}Mo_2B_{20}$, metallic glass, triplet correlation, field-ion microscopy study 80−38921
GaAs, atom probe field ion microscopy 78−80460
GaAs, field penetration in FIM, band bending 79−87567
GaAs, GaP, surface struct. 78−19644
GaAs(P), adsorption and field-desorption of O_2 and Au, FEM studies 80−34304
GaP, atom probe field ion microscopy 78−80460
Ge, adsorption of O, enhancement by elec. field of polarity facilitating field-ion emission 79−65325
In, epitaxial layer on imperfect FEM/FIM W emitter 78−60037
Ir, adsorption of H_2 and O_2, surface reaction, thermal desorption and FEM obs. 79−52774
LaB_6 and $La_{0.58}Sm_{0.42}B_6$, FIM study 80−71578
LaB_6, field emission and FIM expts. 77−90255
Mo cathode, ns voltage pulse breakdown of emitting sites, field emission microscopy obs. *(German)* 77−63547
Mo surface, adsorbed Ga and Sn, struct., FIM obs. 80−103576
Mo wire, laser shock induced microstructural changes, rel. to explosive shock induced phenomena 78−67768
Nb-Zr (1.5 wt.%) alloy, field ion microscopy investigation, surface struct. 80−45220
Nb-Zr-Ti, needle field emitter, ion bombardment effects, field emission microscope obs. 77−55869
Ni, electrochem. overgrowths, role of substrate dislocations and grain boundaries in nucleation and growth 79−51454
Ni, electroplated layer, field ion microscope study 79−28246
Ni film on W (110), field ion microscope exam. 78−34731
Ni superalloy, cast, microstruct. and microanalysis 78−35393
Ni surface, single-atom self-diffusion FIM study 80−103548
Ni-Cu(5%), absolute composition depth profile, surface segregation, field-ion microscope obs. 79−33166
Ni-Ta (70, 30 wt.%) metallic glass, struct. and crystn. *(Russian)* 80−70136
Ni_4Mo, statistically homogeneous ordering, computer-simulated field ion images 78−9991
Os field ion microscope exam. *(German)* 77−36376
Pd film on W (110), field ion microscope exam. 78−34731
Pt film on W (110), field ion microscope exam. 78−34731
Pt, surface diffusion of single atoms of Pt, Ir and Au, FIM expts. and Morse potential calcs. 78−34717
Pt tips, glass-coated, field emission microscopy Fowler-Nordheim emission regime and periodic current oscills. 79−95907
Pt-Au, ion-irradiated, self-interstitial migration in stage II recovery, FIM obs. 77−59140
Pt-Ir, structural phase transform., ion field emission microscopy obs. *(Russian)* 80−50628
Pt-Ir solid solutions, investigation of field-ion micropattern contrast, selective evaporation and ionisation models 79−69962
Pt-Pt mechanical contact, FIM obs. of contact area 78−35527
Re, oxide formation and surface rearrangement, field ion microscope obs. 77−28936
Re_2, adsorbed on W (211) surface, dissoc., thermodynamics 78−87861
Ru, NO chemisorpt. and decomp. 78−18903
Ru surface, clean, oxidation, FIM study 79−47796
Si, field penetration in FIM, band bending 79−87567
SmB_6, FIM study 80−71578
Ta; adsorbed $CO(CO_2)$, FEM and flash filament method exam. 78−43245
Th, atomic struct. by field ion microscopy 80−59437
W (110) surface, adsorbed Pd, growth, struct., stability, desorption 80−59794
W (111), (211), and (311), adsorption of W single atoms, surface site geometry determ. by FIM 80−39447

field emission ion microscopy continued
W (112), adsorption of La, contact pot. difference, LEED and field emission microscopy *(Russian)* 78−14618
W (211) planes, of Mo, direct obs. of atomic processes by field ion microscopy 77−59219
W {123} plane, clean and H saturated, surface diffusion of single W atoms 80−80081
W, adsorption of Cu, FIM and FEM obs. of nucleation, epitaxial growth and interface form. 78−26800
W, adsorption of Ga, In and Sn, struct., work function, diffusion, binding energy 77−16470
W, adsorption of H_2, FEM study of binding states *(Japanese)* 78−2370
W and W alloys, ion-irradiated, recovery, behaviour 80−29074
W, coadsorption of La and B, field emission and field ion microscopy 80−104049
W, coadsorption of Th and H, FEM exam. 79−90869
W, collective field evaporation from (110) face, field ion microscopy *(Russian)* 79−61504
W, electron irrad., or ion irrad., stage II, point defect struct., FIM 77−80542
W, electron irradiated, or quenched, point-defect mechanism for Stage III recovery, field ion microscope study 79−60403
W emitter tip, surface shape changes, field ion microscopy meas. 78−26754
W FEM tips, Pd or C adsorbed layer conc. using nucl. microanal. *(French)* 80−29860
W, FIM study of lattice damage caused by low-energy He ion bombardment 78−95090
W, field evaporation, in FIM, computer simulation 77−69973
W, incoherent twin boundary microfaceting on annealing, field ion microscope determ. 79−77608
W, ion irradiated, defect clusters obs. 80−2089
W, low-energy ion bombardment, depth of sputtering damage obs. by FIM 80−60734
W, needle field emitter, ion bombardment effects, field emission microscope obs. 77−55869
W, neutron irrad., at thermal energies, annealing exam. of recovery 78−47355
W, neutron irradiated, FIM obs. of radiation damage 79−7632
W, stacking fault stability determ. 80−96548
W, stripe field-ion contrast form., dislocations effect 78−18652
W surface, adsorbed W, Ga, Sn, struct., FIM obs. 80−103576
W surface, atom zigzag chains obs. by field ion microscopy 78−84036
W, surface energy anisotropy and faceting behaviour, field ion microscope obs. 77−7961
W surface self-diffusion, ion impact induced, FIM study 80−103549
W, surface structure and topological modification during depth profiling, FIM obs. 79−78816
W tip, Cu covered, field ion microscopy study 78−23587
W, vacancy struct. of depleted zones after ion irrad. 79−73224
W wire, laser shock induced microstructural changes, rel. to explosive shock induced phenomena 78−67768
W:La, B coadsorption and work function, FEM and FIM obs. 79−52087
W-Cr alloys, segregation of Cr to gain boundaries, field ion microscope investigation 77−8816
W-Mo, refractory, surface investigation by FIM and atom probe *(German)* 79−55623
W-Pt mechanical contact, FIM obs. of contact area 78−35527
W-Re (3%) alloy, W adatom-substitutional Re atom interaction, FIM obs. 77−89626
W(100), atomic struct. using FIM 79−73384
W(211), Re adsorbed atoms and dimers, surface diffusion 77−20183
W{001} surface, clean, reconstructed, field-ion microsc. obs., 15-400K 80−15348
ZnO (000$\bar{1}$) and (0001), Ar field ion microscopy 79−47601
Zr, adsorbed on W(Ta)(Re), low-temp. mobility, surface struct. 77−20197
Zr, specimen prep. and results 77−11449

field evaporation
atom probe FIM evaporation pulse generator 78−78041
atomic-jug formalism 78−35268
desorption mass spectroscopy, new sample supply technique 77−56279
electrolyte, aq. soln., field-induced ion evap. from liq. surface at atm. press. 80−29859
field desorption microscopy investigations 77−21010
field ion image formation 78−35266
FIM, quantitative analysis of micrographs using Moire techniques 77−90259
hyperboloidal sample model, time of flight determ. by atom probe *(French)* 77−16469
ions, post-ionisation by tunnelling into substrate 80−80951
metals, highly charged ions in field evaporation 78−35269
semiconductor surface, field ionisation and field evaporation mechanisms 79−15594
standard field ion appearance energies, generalised theory 77−21011
transition metals, field evaporation rate meas. 78−76590
vacuum arc cathode spot dynamic models 78−75481
Ag, field desorbed ions, appearance pots. 79−24417
CeB_6, single cryst. work function, thermionic emission, evaporation 77−24922
Ga liquid metal ion source, energy distrib. meas. 80−95493
GaAs, atom probe field ion microscopy 78−80460
GaAs, field penetration in FIM, band bending 79−87567
GaP, atom probe field ion microscopy 78−80460
Ge surface, field penetration and band bending in high elec. fields 79−42613
He, field-ion appearance pot., theory 77−545
Ir, field evaporation end form at 4.2K 77−1790
Ir, multilayer field evaporation patterns 77−59675
LaB_6, single cryst. work function, thermionic emission, evaporation 77−24922
LaB_6, time of flight atom-probe FIM study 80−6652
Mo film, epitaxially grown on W tips, field evaporation, struct. obs. 77−28723
Mo, multilayer field evaporation patterns 77−59675
Ni_4Mo, ionisation states of field evaporated ions 77−81200
Ni_4W_9 ionisation states of field evaporated ions 77−81200
Pt, multilayer field evaporation patterns 77−59675
Pt-Ir solid solutions, investigation of field-ion micropattern contrast, selective evaporation and ionisation models 79−69962

field evaporation continued
Rh, multilayer field evaporation patterns 77−59675
Rh^+, Rh^{2+}, field evaporation, field ion mass spectra and field ion appearance spectra study 80−7479
Si, anomalous field evaporation 79−15596
Si, field penetration in FIM, band bending 79−87567
Si, photoillumination effect on field ion microscopy 79−78850
Si surface, field penetration and band bending in high elec. fields 79−42613
Si whisker, (111) oriented, FIM and atom-probe FIM obs. 80−10473
Si whisker field desorption ion source, Cu, Sn, Ag, Te, Cd and Sb isotope abundance ratios 80−11975
β-SiC, atom-probe FIM expts., field evaporation mechanism 78−35275
surface atoms, Debye temps. determ. during field evaporation and LEED 80−39406
Ta, multilayer field evaporation patterns 77−59675
W (110) surface, D depth profiles using imaging field desorption 77−59038
W, adsorption of Ga, In and Sn, struct., work function, diffusion, binding energy 77−16470
W, collective field evaporation from (110) face, field ion microscopy *(Russian)* 79−61504
W field desorption of K, from (001), (011) and (112) planes 78−34715
W, field evaporation end form at 4.2K 77−1790
W, gas-surface interaction in atom-probe FIM 77−40336
W, in FIM, computer simulation 77−69973
W, multilayer field evaporation patterns 77−59675
W^{3+} field ion evaporated from ionic bonding states, appearance energies 80−89125
W-Th, field ion specimen, contrast bands in elec. field induced evaporation 79−50967
ZnO surface layers, high-field electrolysis during field emission 79−52084

field intensity patterns (antenna) *see antenna radiation patterns*

field interactions (condensed matter)
see also crystal field interactions; hyperfine field interactions (condensed matter)
amorphous element, local fields, coeffs. for classical electrostatic pot. calc. 78−34808
amorphous ferrimagnet, molecular field theory, struct. fluctuations 77−40018
amorphous metals, mag. anisotropy, spin glass like phase 77−66295
rare earth alloys, magnetic amorphous, nonaxial elec. field gradients 78−39285
rare earth amorphous alloys, cryst. field, nonaxial elec. field gradient 80−20138
rare earth-Fe alloy, amorphous, random anisotropy model, generalised mol. field calcs. 77−28345
rare earth-transition metal alloy, disordered, model of localised spins d-band interaction 77−20515
transition metal halide-alkali halide binary melt, spectra by cryst. field theory 79−4820
BeF_2:Eu^{3+} glass, struct. and optical props. 80−84067
$Ce_{80}Au_{20}$, metallic glass, mag. ordering and cryst. field effects, speromagnetism 80−80531
(Fe, Ti) silicate glasses, optical absorption and Mossbauer spectra 80−55136
Na_2O-SiO_2:Cu^{2+} glass ESR and optical absorption 79−77526
Ni-rare earth intermetallics, RNi_3, amorphous alloys, mag. and transport props. 79−42513
PbO-SiO_2 glasses, high temp. ESR of Fe(III) 80−60410
$Pr_{21}Ag_{79}$, amorphous, sp. ht. at low temp. 80−75780
$Sm_{21}Ag_{79}$, amorphous, sp. ht. at low temp. 80−75780

field ion emission
adsorbed salt layers, field ion emission, field desorption and ionic cond. 77−16473
adsorption, correction to short-range binding energy, isolated dipole pair approx. 79−100027
atomic polarisability in SI system 77−58191
axisymmetric emitter, field-induced stresses, numerical analysis 78−35274
cathode flare, fast ion emission 77−62426
critical energy deficit of field emitted ions, theory 77−73221
dendrite growth on ion emitters for field desorption mass spectroscopy 79−2873
desorption mass spectrometry of salts, emitter characts. and production 77−63980
field calibration of emitter, using energy distrib. of free space field ionisation 77−69971
field emitter surface, elec. field empirical formula 80−97413
fine focus beams, field ionisation source appl. for microprobe 78−76589
image contrast, gas distrib., hypothesis reexamined 78−60552
inert gases, temp. effects on appearance potentials of gas phase field ions 79−19978
integral energy distributions of ions, evaluation method 79−38723
metal ion deposition sources 79−83127
metallic multi-point field emission source, prep. by cathodic growth 80−100758
metals, highly charged ions in field evaporation 78−35269
monopole-dipole interaction, field adsorption 79−19979
multipoint field ionisation source characts. 77−22606
nanosecond high-voltage pulse shapes, determ. at surface of needle emitters 77−12502
organic liquids, electrohydrodynamic ionisation, solvated ion mass spectroscopy, anal. appl. 78−73102
into plasma of electric arc, current density eqn. 79−43108
semiconductor of simple geometries, field penetration and band bending in high elec. fields 79−87106
shape of emitter from field-ion image 80−2930
surface plasmon excitation and Jason effect, comment 77−28699
surface plasmon interpretation, comment 77−28700
transition metal-Ne compound ions, slow field evaporation 77−48322
work function, absolute determ. method for metals and semiconductors 77−28697
Ag, crit. energy deficit of field emitted Ag^+, theory compared with expt. 77−73221
Ag vapour, field ion appearance potential spectroscopy, temp. effects 79−19978
Au, EHD emitted ions, energy distrib. 79−61503
Au, liq., field emitted ions, energy distrib. 79−61501

field ion emission continued
- Au-SiO_2-Si structures, electron and ion emission from MOS field cathodes *(German)* 77—12499
- Be, field ion appearance spectroscopy, ion generating processes at field emitter surface 79—52086
- Bi, liquid, field ion source emission characts. 80—74059
- Cu, electrodes, breakdown voltage, prebreakdown current in vacuum, crossed elec. mag. fields depend. 80—79604
- Cu, field ion appearance spectroscopy, ion generating processes at field emitter surface 79—52086
- Ga ionisation mechanism on W field emitter 80—76156
- Ga, liquid, field ion source emission characts. 80—74059
- Ga liquid metal field emission ion source, characts. 80—108326
- Ga liquid metal ion source, energy distrib. meas. 80—95493
- Ga, liquid point anodes, field-ion emission 80—2928
- Ga, liquid-metal high-intensity scanning ion probe with submicroscopic spot size 79—54225
- Ge-Au eutectic alloys, field ion sources 80—97414
- He, field-ion appearance pot., theory 77—545
- Ir, adsorbed gases, field desorption from field ion tips 80—59793
- Ni, field ion appearance spectroscopy, ion generating processes at field emitter surface 79—52086
- Si-Au eutectic alloys, field ion sources 80—97414
- W (111), field adsorption of He, array model 80—59800
- W, adsorbed gases, field desorption from field ion tips 80—59793
- W, adsorption of Ga, In and Sn, struct., work function, diffusion, binding energy 77—16470
- W, desorption of Cl(Br)(I), field ion microscope exam. 78—35270
- W, monolayer of Ga(In)(Sn), field ion image qualities and work function 78—35272
- W, multiple field ion emitters, props., ionisation efficiency improvement 78—76588
- W, stripe field-ion contrast form., dislocations effect 78—18652
- W surface, adsorbed K, field emission flicker noise power 80—59795
- W^{3+} field ion evaporated from ionic bonding states, appearance energies 80—89125
- ZnO, polar surfaces (0001), (000$\bar{1}$) specificity, field emission, H adsorption 77—21009
- ZnO surface layers, high-field electrolysis during field emission 79—52084

field ion microscopy, atom-probe *see atom probe field ion microscopy*

field ionisation
- adsorbed amines and hydrazines, identification on oxidised metal surfaces 77—21456
- alkali halides, cluster ions and mol. ions in salt field desorption 80—40238
- atom, highly excited, linearly polarised elec. field ionisation, freq. (amplitude) depend. 80—32630
- atom, microwave ionisation of highly excited states, and excitation 79—31482
- atom-surface impact, electron tunnelling in external electric field, atomic resonant ionis. and field ionis. 77—52208
- atoms, ionisation of Rydberg states, depend. on $|m_l|$ 78—58856
- calibration of field ion emitter, using energy distrib. of free space field ionisation 77—69971
- cryogenic liquid, ionic mobility measurement, pulsed spacecharge technique 77—74420
- cycloheptatriene, field ionis. to excited states 77—19002
- desorption mass spectrometry, analytical chem. uses 79—92015
- diethyl ether, field ionisation, thermal energy distribution and energy deposition 80—95732
- energy distributions, effect of cryst. struct. of field emitter 77—59676
- ethylene adsorbed on Ag, photon-induced field ionisation mass spectroscopy 80—6639
- evaporated ions, post-ionisation by tunnelling into substrate 80—80951
- excited atoms, field ionisation mechanisms 78—70761
- field desorption mass spectrometry, appl. to biochemistry, medicine, and environmental science 80—35592
- field ion image formation 78—35266
- gas-phase field ionisation source, ang. intensity 80—2929
- halogen intense negative ion source 78—66001
- 1-heptene, field ionisation mass spectra, surface processes 79—11503
- hexafluoro ethyl cation fragmentation, mass spectrometry 80—53070
- hexanes, isomeric, 80—95732
- hexanes, isomeric, unimol. decomp. processes following field ionisation, temp. depend. 80—95733
- 1-hexene-water(-D_2O), field-induced surface reactions, field ionis. mass spectra obs. 78—95949
- inert gas, field ionis. and proton capture, critical energy deficits 78—82853
- inorganic compounds, field ionisation mass spectrometry, review 78—35764
- ion source, of mass spectrometer, EI/FI modes pot. distrib. calcs. 77—74553
- ion source-quadrupole mass analyser interfacing, ferrite insert, repeller electrode 77—18125
- kinetic data acquisition and processing, computer controlled 78—2999
- mass spectrometry, field desorption and field ionis. kinetics, review 78—324
- mass spectrometry, review *(Japanese)* 79—66384
- metal surface, field desorption and field ionisation of Cs, H, and He 80—104047
- negative ion formation by field ionisation 80—89123
- negative ions, formation in high elec. fields 80—2927
- neutral particle detector, appl. to He^+ pulse height defect in Si 77—50330
- orbitron device, electronic injection, ionisation phenomena and space charge influence 79—40587
- organic compounds, field ionisation mass spectrometry, review 78—35763
- phenol, field ionis. to excited states 77—19002
- photon enhanced field ionisation, theory 79—56915
- photon stimulated, semicond. and insulator surface obs. 77—1787
- preactivated linear field ionisation source 77—5959
- propion-aldehyde ion, fragment/mol. ion current ratio, field ionis. mass spectrum, CNDO/BW calc. 77—65544
- Rydberg states, fine struct. splitting, quantum beat and double reson. spectroscopy 78—86979
- scanning ion microscope with field ionisation source 78—21289
- semiconductor, low temp. field ionisation of localised impurity levels 79—47600

field ionisation continued
- semiconductor, photo-field ionisation of deep centres allowing for Coulomb action *(Russian)* 78—27376
- semiconductor surface, field ionisation and field evaporation mechanisms 79—15594
- semiconductor surface, photon enhanced field ionisation 79—83109
- spherical particle with extremely high resistivity, corona charging 80—6944
- standard field ion appearance energies, generalised theory 77—21011
- surface anal. by photon-induced field ionisation mass spectroscopy 80—40780
- surface states role in FIM, one-dimens. model 78—26399
- surface-atom polarisability derivation from field-ion energy deficits 80—76155
- tetracyanoethylene molecule with high electronegativity on field polarisation, electron affinity determ. 79—27111
- thin film field ionisation source fabrication 80—52359
- toluene, field ionis. to excited states 77—19002
- transition metals, field emission and field ionisation, role in heterogeneous activation of gas molecules 78—35271
- Au, liq., ion source fabrication and emission characts. 80—68995
- CO, field ionis. to excited states 77—19002
- $CaCl_2$, cluster ions and mol. ions in salt field desorption 80—40238
- Cs Rydberg atom-blackbody radiation interactions 80—37761
- Ga, field ion microscopy using mag.-sector atom probe, ionisation characts. 79—43106
- Ga ion source, liquid, emission characts. obs. 80—62810
- Ga ionisation mechanism on W field emitter 80—76156
- Ga, ionisationj ionisation at field emitter, optical emission 80—93461
- Ga, liquid, field ionisation, surface temp. and elec. field depend. 79—78849
- GaAs, deep level, strongly anisotropic field ionisation 79—28317
- GaAs, field ionisation speed of shallow impurity levels, quantum-mechanical estimates 80—97412
- GaAs, field penetration in FIM, band bending 79—87567
- Ge surface, field penetration and band bending in high elec. fields 79—42613
- H, Stark spectrum and field ionisation, density of continuum states, normalised wavefunctions 80—83317
- H-like ions, critical ionisation, by electric fields, exact classical method 78—25731
- H_2 and rare gas field ion source with high angular current 80—68996
- H_2, field ionis. to excited states 77—19002
- $H_2(D_2)$, Rydberg states, nonadiabatic effects, elec. field ionis. 80—9528
- He, field-ion appearance pot., theory 77—545
- Ir, field depend. of spectral line energy of He-H_2 adsorbate 79—78853
- K, excited states field ionis., p states spin-orbit interaction 79—59592
- K, fine-struct. intervals, polarisabilities, highly excited d states 79—27100
- LaB_6, polycrystalline, negative surface ionisation of I atoms, negative ion desorption heat 79—78848
- Mo, field depend. of spectral line energy of He-H_2 adsorbate 79—78853
- NH_3, field ionis., critical energy deficits, field depend. 78—82852
- Na, diabatic field ionisation of highly excited at. states 80—43202
- Na, field ionisation of highly excited states 78—17814
- Na Rydberg atoms, selective field ionisation, 300K blackbody radiation detect. 79—58787
- Na, Rydberg levels mm resonances detected by field ionis., quantum defects, Stark shifts 77—42262
- Na, Rydberg states, elec. field ionisation, sensitive detection of multiple thresholds 79—7026
- Na, Rydberg states, millimeter spectra, quantum defect, fine struct., polarisability, field ionis. obs. 78—82672
- Na, Rydberg states, nd—(n+1)p intervals meas. 78—33629
- Na, Rydberg states, optically pumped, electric field ionis. *(Russian)* 79—27095
- Nb-Zr (1.5 wt.%) alloy, field ion microscopy investigation, surface struct. 80—45220
- Ni_4Mo, ionisation states of field evaporated ions 77—81200
- Ni_4W_9 ionisation states of field evaporated ions 77—81200
- O_3, at Ir surface 78—35273
- Pt-Ir solid solutions, investigation of field-ion micropattern contrast, selective evaporation and ionisation models 79—69962
- Rb, high lying Rydberg states, atomic beam laser spectra 79—94101
- Re, field depend. of spectral line energy of He-H_2 adsorbate 79—78853
- S_2 polymerisation, kinetics obs. by pulsed field ionis. time-of-flight mass spectrometer 77—63890
- Si, field penetration in FIM, band bending 79—87567
- Si surface, field penetration and band bending in high elec. fields 79—42613
- W, field depend. of spectral line energy of He-H_2 adsorbate 79—78853
- W filament, enhancement of field ionisation efficiency by carbide particle nucleation 77—90256
- W, potential of He atom above field adsorbed He or Ne atoms 78—35267
- W tip, photon assisted field ionisation 78—3000
- W wire, organic microneedle growth under intense elec. fields, X-ray diffr. and AES 80—54580
- Xe, Rydberg atoms, field ionisation, 300K background radiation effects 79—68271
- Xe(nf)+NH_3, at. Rydberg state further excitation by rot. transfer, field ionis. obs. 78—58795
- Yb, Rydberg states, optically pumped, electric field ionis. *(Russian)* 79—27095
- ZnO (000$\bar{1}$) and (0001), Ar field ion microscopy 79—47601
- ZnO surface layers, high-field electrolysis during field emission 79—52084

field measurement, electric *see electric field measurement*

field measurement, magnetic *see magnetic field measurement*

field plotting
- *see also field strength measurement*
- absolute ECG and clinical map curve experiences 79—39556
- biomagnetism, mag. fields of dipole in volume conductor shapes 77—81514
- biomedical surface mapping, interpolation methods, in FORTRAN 80—81750
- body surface mapping of cardiac field, computer-aided pattern recognition 79—39553
- cardiac acoustic model for computer-aided surface acceleration mapping 78—35791

field plotting continued
cardiac fields online body surface potential mapping 79—83992
cardioelectrical field, human, intraindividual variability obs. 79—39404
coronary artery disease diagnosis, exercise ECG, VCG and body surface mapping 79—44046
cutaneous receptors, on-line receptive field mapping technique 79—74797
ECG, isopotential surface map data reduction 79—39557
ECG, microprocessor-based body surface isopotential and topological maps 80—72361
ECG, surface isopotential and gradient maps 79—70670
ECG body surface potential mapping, improved diagnostic technique 80—26409
ECG body surface potential mapping project 80—104794
ECG map reconstruction computer system 79—39561
ECG potential distribution mapping instrumentation 80—21561
ECG surface mapping, gradient and potential data acquisition system 79—39555
ECG vector and isopotential maps, convertibility and comparison 79—39554
echo sounder transducer field plotter 78—59238
EEG, dyslexia detect. by computerised brain mapping 80—36185
EEG, simple computer-generated dot-density topogram 80—94407
electrophysiology, automated production of contour maps 80—72340
epicardial activation sequence rel. to body surface maps, right bundle branch block induced in dogs 79—39402
epicardial mapping, computerised display system *(Japanese)* 80—101279
epicardial mapping of ventricular arrhythmia onset by digital computer 79—70672
equipotential and mag. intensity contour line visualisation by SEM 79—6149
high-energy physics magnet meas. 79—31353
hyperthermia phantom for point by point temp. mapping 79—70698
LF and MF ground waves in realistic terrain, elec./mag. field ratios 78—88795
LF fields in linear media, two-dimensional finite element analysis 79—41297
magnetic field distrib. mapping of thin. mag. foils by holographic processing 79—89868
magnetic mapping system for particle spectrometers at Fermilab 77—10513
magnetic traces, observation technique 77—87616
optical fields using single-mode optical fibres 78—30097
pericardial potential simulation and mapping in dog 79—39399
permanent magnetic interpolar space uniform region conformal mapping *(Russian)* 77—53960
plasma, self-generated mag. fields, two-dimens. distrib., laser-plasma reson., mag. tape irradiation 79—41877
SEM potential distribution mapping technique 79—21857
skeletal muscle motor units, system for rapid acquisition of surface pot. maps 80—46077
supraventricular tachycardia, diagnosis and management, instrumentation and therapeutic techniques, review 79—39598
thoracic surface, human, heart potentials distrib. with left bundle branch blocks 79—39403
ventricular arrhythmias, intraoperative mapping system 80—56242

field strength measurement
see also electric field measurement; magnetic field measurement
100 kHz to 300 MHz radiation hazard probe requirements 77—44760
EM field, broadband antenna probes *(Polish)* 79—21722
EM fields using linear interferometric electro-optical modulator 80—58782
EM near field power density meas. *(Polish)* 79—21721
HF field distrib. in cavity resonators 80—98930
intensity meter calibration for 20 kHz to 300 MHz range 79—2786
international calibration cycles of field intensity and power density, measurements 80—82752
MF radiowave field strength digital measurement equipment *(Japanese)* 77—82051
MW broadcast field strength meas., sunset, night, ionospheric radiowave propagation appl. 77—67010
near-field radiation hazard and EMI meas. 77—44757
nonstandard atmosphere, arrival angle and echo delay meas. 77—64397
PAM microwave field dosimetric device 80—3818
particle beam, RF fields due to Schottky noise 77—88632
polyethylene surface field strength under DC stress 80—15967
RF environmental field intensity automated meas. system 77—37947

field theories, unified *see unified field theories*

field theory, classical *see classical field theory*

field theory, crystal *see crystal field interactions*

field theory, electromagnetic *see electromagnetic field theory*

field theory, meson *see meson field theory*

field theory, quantum *see quantum field theory*

fields, electric *see electric fields*

fields, magnetic *see magnetic fields*

filament lamps
beam type incandescent, tests using automated high-speed photometer 77—26379
calibration of incandescent lamps for spectral irradiance by absolute radiometers 80—102788
chromatic adaptation effects and colour appearance at various illum. levels *(Japanese)* 78—92628
cine-projector, performance obs. *(Russian)* 77—10129
framing spotlight, optimizing the compound reflector 79—3766
halogen, standard apparatus, to produce and meas. thermal radiation flux densities 80—62674
halogen doped, mass transfer model 77—32832
holographic displays, conventional light sources 79—50261
Kr-Ag-N gas mixture, thermal conduction coefficient calculational methods *(Russian)* 80—96335
radiant energy measurement, student expt. 78—8191
ribbon-filament temperature lamps, measurement of characts. 80—4720
slit lamp, hand-held, with lid opener for ocular exam. 80—67179
spatial image filter with noncoherent incandescent source, model and expt. *(Russian)* 79—7083
spectral irradiance scale comparison 77—106
standard temperature, with W ribbon filaments 80—95102
standard temperature-calibrated, spectral comparator method automatic testing 77—53907

filament lamps continued
temperature-calibrated, for radiation pyrometer calibration near IR region 77—53915
Mo, prep. by powder metallurgy technique, appl. in lighting industry 80—29904
W and W-Re alloy, prep. by powder metallurgy technique, appl. in lighting industry 80—29904
W, filament, incandescent lamps, creep, failure, life prediction 78—84927
W filament lamp, Stefan's law demonstration, student expt. 78—54125
W, for temp. scale representation in 1337.58-2200K range *(German)* 78—4621
W halogen lamp and mirror furnace at Czochralski growth 80—60766
W incandescent lamp, thermostatic control 79—36970
W ribbon-filament temperature lamps, radiation error estimation 80—64128
W strip, suitability as secondary standard sources below 1064 degrees C 80—27297
W, temp.-calibrated, standard, characts. 78—218
W wire, incandescent, motion and growth of K bubbles *(Hungarian)* 77—48460
W-Br regenerative cycle of linear quartz lamps, metallic impurity effects, thermochemical interpretation 80—3312
W-halogen quartz envelope lamp, polarization characteristics 80—95970
W-halogen quartz lamps with optical filters, solar simulator appls. 80—16838
Zr ribbon filament lamp, calibrated source for IR radiometer 80—83653

file management *see file organisation*

file organisation
see also data handling; data structures; database management systems; virtual storage
chemical data base, error detect. by text searching 77—37678
documented patient file concept and implementation 78—7498
EVOQ: a system configurable for automatic simulation and recording of mean evoked potentials on a minicomputer *(French)* 80—85507
experiment control parameters in distributed function computer network 77—57306
geodetic data base, basic entities definition 78—65392
INSITE system for nuclear site data storage and retrieval 78—5109
large file one dimensional search system 78—23977
main program and overlay manager subsystem within distrib. function lab. computer system 78—36980
mass storage directory entry repair for lost data retrieval 78—77954
memory system principles and descriptions *(German)* 78—29910
molecular formulae and homologous series, inverted file structure for searching large data bases 78—35738

filled polymers
ABS samples with 25 and 30% rubber, fracture toughness 80—16438
acoustic impedance and ultrasonic velocity calculation, simple approx. method 80—64314
acrylic bone cement improvement by addition of fillers 77—37109
acrylic cement, porous, sucrose filled, femoral tissue ingrowth in dogs 79—39611
adhesive joint contact layer, dried polymer dispersion intermol. interaction with substrate and filler *(German)* 79—8421
Aerosil-filled polyester, viscosity meas. under nonisothermal conditions with rotary viscometer 79—68664
agglomerated filler particles, dynamic mech. props. 80—66569
bis-acrylamide anilinefluorene polymerisation in thermostable card polyamide (polyimide) amorphous matrix *(Russian)* 79—57231
bisphenol-A polycarbonate, crystallization, spherulitic growth of plasticized polymer 80—19726
blends, viscoelastic props. *(Russian)* 78—72808
butadiene nitrile, soot filled, thermal treatment influence on mech. props. *(German)* 80—30000
butyl rubber, resin cured, filled, relaxation study *(German)* 80—35243
C black filled, DC conduction processes 79—56275
characterisation, by TEM 80—103270
combined packing of rods and spheres 79—52151
concrete-polymer modifications, unsolved materials properties problems 77—4763
cumulative internal damage, US assessment 79—57180
cumulative internal damage, US assessment 80—97653
dynamic shear modulus and acoustic velocity, filler content depend. 80—60900
elastic filler reinforced cylindrical shell, design optimisation under dynamic loading 79—59935
elastic moduli, effect of particle shape at finite conc. 79—15712
elastic moduli, interfacial slippage effect anal. 78—76688
elastic modulus, strength, rel. to crystallite shape 80—45335
elastic reinforcement theory, filler orientation distrib. anal. *(Japanese)* 78—39734
elastomer, role of particulate fillers, review 80—29921
elastomer reinforcement, carbon black-polymer interaction 79—83171
elastomers, filled, unfilled, Poisson ratio, dilatometric method 79—11733
elastomers, filler type, effect on concentration rel. to equilib. swelling in solvents 79—64979
elastomers, Mn-Zn ferrite filled, for elastic mag. materials, prep. and props. 79—52143
elastomers, network behaviour at high elongation 79—79049
elastomers, particle reinforced, network fracture mechanism 80—41928
elastomers, soot filled, mech. relax. behaviour *(German)* 80—84985
elastomers with inert fillers, swollen state, network density determ. from stress/strain meas. 79—34112
electrical conductivity of conductive filler polymer composites, theoretical study 79—19585
electrically conducting polymeric compositions, struct. effect on elec. props., review *(Russian)* 79—33317
electronic conductivity, electro-, photoresponsive effects, review 79—56261
epoxies, commercial powder-filled, measurement of thermal diffusivity, 1.5 to 15K 79—58729
epoxy, Al_2O_3-filled, shock-wave compression, 0.4-3.7 GPa 78—59856
epoxy, filled, adhesive, mech. props. 77—16638
epoxy, glass microsphere filled, low-cycle fatigue 80—40517
epoxy, mica filled, polishing by abrasive papers and lapping cpds. 80—108620
epoxy adhesive, A, filled, electrical cond. development by heat treatment 79—73559
epoxy based, creep and recovery under hydrostatic compression in programmed loading 80—100881

filled polymers continued
epoxy C plastics, under tensile stress, effect of whiskerization of polymer matrix on creep resist. 79—87699
epoxy composites, with different degrees of hardening, bulk-creep prediction 80—104223
epoxy material, filled, US props. for sonar transducers 78—59867
epoxy polyester, PE-933, metal-filled, elec. cond., theory and expt. 80—60057
epoxy polymer, glass microsphere-filled, glass transition temp. *(Russian)* 79—24489
epoxy polymer, with low thermal expansion coeff. 78—3094
epoxy polymers, unfilled and filled effect of specimen size on elec. strength expt. 77—8505
epoxy resin, filled, wear props., SEM obs. 80—16500
epoxy resin, glass bead filled, particle size effect on Young's modulus *(Japanese)* 78—60694
epoxy resin, glass bead filled, subjected to extensional creep, dynamic props. 80—71697
epoxy resin, powder filled, exam. of mech. props., thermal contraction 80—25821
epoxy resin based composites, superconducting magnet insulators, gamma-ray radiation effects 80—24495
epoxy resin composite, powder-filled, of adjustable thermal contraction, mech. props., for construction of superconducting magnets 79—61691
epoxy resin composite containing mica flakes, thermal depolarisation current, 20-190°C 77—90091
epoxy resin compositions, highly filled, influence of combined action of mechanical vibr. and ultrasound 79—56952
epoxy resin/particle composites, particle size effect in thermal expansion, filler effects on T_g 80—84305
epoxy-metal powder mixtures, cryo-tip refrigerator appl., heat transport 78—37013
epoxy-resin, Nomex or mica flake filled, thermal depolarisation currents and DC cond. studies 80—7282
epoxy-rubber glass transition rel. to filler, cooling rate 79—4403
equations of state, taking account of mech. damage 80—97553
fibre reinforced, space environmental effects 80—71721
fibre reinforced epoxy laminates, interlaminar failure 80—81207
filled, viscosity, anomalous conc. depend. at low filler concs. *(Russian)* 77—44287
filler materials, scanning microscopy, plasticiser absorpt. obs. *(German)* 79—39082
fillers for plastics 79—61507
fluid, rheology, characterised by mol. int. distrib., review 80—1504
furan resin, effect of silica fillers on compressive strength *(Polish)* 78—68740
furfuralacetone resin, filled, elastic modulus calc. 79—57030
glass bead epoxy resin, direct obs. of debonding at crack tips 80—3167
glass bead reinforced nylon, design parameters, fibre orientation effect 80—81141
glass bead reinforced polycarbonate, design parameters, fibre orientation effect 80—81141
glass fibre reinforced nylon, design parameters, fibre orientation effect 80—81141
glass fibre reinforced polycaproamide, viscoelastic, linearity conservation 80—108492
glass fibre reinforced polycarbonate, design parameters, fibre orientation effect 80—81141
glass transition temperature, internal stresses influence 80—10645
glassy, glass bead filled, crazing characts., slope-discontinuity method 79—11712
graphite fibre epoxy composites, eutectic coating moisture barriers 80—81228
graphite fibre epoxy laminates, low thermal expansivity, design considerations 80—81031
graphite fibre filled phthalocyanine composites, cure cycle investigation 80—81030
graphite fibre filled polyimide composite laminates, space environment, phys. and mech. response 80—81140
graphite fibre filled polyimide composite prepreg laminates, room-temp. ageing effect 80—81093
hollow spherical inclusions filler, elastic and strength props. 80—35245
hollow spherical particle filled, strength criterion 79—11682
hysteresis under uniaxial extension, test of Fitzgerald's concept *(Russian)* 77—86065
injection moulded GFRP distortion meas. by holographic interferometry 79—79020
isoprene rubber elastomers, thermal treatment influence on mech. props. *(German)* 80—30000
kevlar-epoxy composites pressure vessels, holographic nondestructive eval. 80—81275
light scattering in deformation 80—11718
lignocellulose polymer composites as γ-dosimeters in the kilorad range 80—95465
maleate-acrylate polyester resin, with phenol and glass microspheres, rheological behaviour 78—53267
mathematical model of strengthening *(German)* 78—63279
mechanical behaviour, filler effect 79—91729
mechanical properties, particle shape effect, review 80—100864
mechanical props. 79—29162
mechanical test unit, with intense high-temp. heating 80—100987
metal-composite rods, compressed, delamination 80—64396
metal-filled, elec. cond., theory and expt. 80—60057
metal-filled epoxy resin, temp. variation, current interruption appl. 78—76124
metallopolymer composite with var. elec. cond. 77—43676
microballoon reinforced plastics, acoustic and mech. props. rel. to hydrophone applic. *(Japanese)* 77—7793
mineral dispersed macromolecular matrix, holographic interferometric meas. of displacement vectors on boundaries 79—79015
mixture, particle size in dispersed phase, effect of component viscoelasticity 77—44514
natural rubber vulcanisate, network changes during physical testing 80—60936
nonuniform medium, model 80—38254
optical constants determ. 78—19472
optical transparency conditions, interparticle interference effects 78—23428
organic textolite, long-term strength in plane stressed state 80—60930
organoplastics, fracture characts., effect on strength 80—66642
pentaplast, plasticised, thermal treatment effect on props. 80—40324

filled polymers continued
PET, glass fibre filled, order-disorder transitions during extrusion 80—50633
phenol formaldehyde resin, (Novolak) with filler, mech. props. determ. *(German)* 78—84933
phenol formaldehyde resin (Novolak), with and without feldspar filler, mech. and thermal props. determ. *(German)* 78—84828
phenol resin (Resol), with and without feldspar filler, mech. and thermal props. determ. *(German)* 78—84828
phenolformaldehyde resin moulding compounds, dynamic testing *(German)* 78—76699
phenolic resin, Kapron fibre reinforced, fracture kinetics, interface props. 80—66640
phenolic resin, linen impregnated, abrasion, SEM obs. 78—64742
pitch-polymer polisher layer, durability 77—34969
plastic, elastic filler reinforced, cylindrical shell, design optimisation under dynamic loading 79—59935
PMMA, and hydroxides, heat resistant, electrically insulating, production methods 79—38787
PMMA, effect of fillers on molecular motions, dielectric relax. meas. 80—80691
PMMA, filled amorphous polymer, heat capacity meas. *(Russian)* 79—65211
PMMA, quartz- and glass-particle reinforced, abrasive wear 80—97594
PMMA glass, electron bombard. induced elec. discharge, electromech. effects *(Russian)* 77—32324
PMMA glasses, crosslinked, strips, sheets, compression, tensile testing, mech. props., plasticiser effects *(Russian)* 77—32621
PMMA-filled with SiO_2, degrading effect of filler on polymer fracture energy 78—52939
PMMA-spirobenzopyran mixed monolayers, photoresponsive effects 79—66316
poly(dimethylsiloxane) rubber, filled with modified silica, cross-linking 79—95990
poly-4-methyl pentene-1, long wave IR filters 77—75695
polyacetals with fusible alloy fillers, adhesive wear behaviour *(Japanese)* 79—70173
polyamide, Al_2O_3 filled, low temp. thermal and mech. props. 80—25816
polyamide-Cu(Ni) oxalate, oxalate decomposition kinetics, in polymeric medium, thermogravimetry and DTA 78—52749
polyamide-Cu system, antifrictional props., struct. 80—40552
polybutadiene, C black filled, positron annihilation and positronium form. 79—28856
polyester, unsaturated, glass bead filled, particle size effect on Young's modulus *(Japanese)* 78—60694
polyester based, creep and recovery under hydrostatic compression in programmed loading 80—100881
polyester polymer concrete, longitudinal deform. modulus study is creep conditions *(Bulgarian)* 80—71685
polyester polymer-C black composition, elec. cond. under press. 77—28224
polyester resin, unsaturated, $CaCO_3$ system, $CaCO_3$ addition effect on degradation in boiling water *(Japanese)* 78—11281
polyester resin, unsaturated, chalk filled, props. *(German)* 80—104228
polyester resin, unsaturated $CaCO_3$ system, $CaCO_3$ addition effect on water absorption in boiling water *(Japanese)* 78—11282
polyester resin-filler system, resistance to degradation in boiling water *(Japanese)* 78—11283
polyester-E glass composites, types SMC-25, SMC-65 and SMC-30EA, moisture absorpt. 80—93799
polyethylene, C filled, ultrathin films, photochemical props., transducer appl. 80—37020
polyethylene, filled, linear, struct., strength 79—29149
polyethylene, filled with glass particles, uniaxially drawn, elastic constants, filler addition effect *(Japanese)* 78—95780
polyethylene, filled with SiO_2, degrading effect of filler on polymer fracture energy 78—52939
polyethylene, high density, inorganic filled, calendered sheet, crystallisation in capillary viscometer *(Japanese)* 77—70112
polyethylene, high density, inorganic filler, calendered sheets, anisotropy of tear strength and crystalline texture *(Japanese)* 77—70110
polyethylene, high mol. wt., inorganic filler, calendered sheet, melt, flow props. *(Japanese)* 77—70111
polyethylene, high-density, effect of fillers and moulding process parameters on strength *(Russian)* 78—60640
polyethylene, high-density, mixed with gypsum, flow props. *(Japanese)* 77—7357
polyethylene, high-density, mixed with gypsum, flow props. *(Japanese)* 77—7358
polyethylene, mech. props., cyclic heating effect 80—55526
polyethylene, melt, low density, filler effect on viscosity and viscoelasticity 77—68546
polyethylene, model, effect of stiff fillers on elastic modulus 78—68720
polyethylene, with various antioxidant, stabilized and TiO_2 pigment additions, photo-yellowing and oxidation 79—16015
polyethylene based compositions, filled with Fe, Al_2O_3 powder, effect of filler particle size on wear resistance 78—44226
polyethylene glass sphere filled, crack form. and necking *(German)* 78—35452
polyethylene melt, low density, filler effect on viscosity and viscoelasticity 78—46919
polyethylene melts, low-density, viscosity and viscoelasticity, filler effect 80—10222
polyethylene with asbestos and glass wool fillers, thermal props. determ. *(Russian)* 77—43340
polyethylene-bone composites, fracture toughness 77—37108
polyhydroxyethyl methacrylate swollen network filled with polyhydroxyethyl methacrylate, viscoelastic and ultimate behaviour in rubbery region 79—83247
polyisobutylene solution in cetane, hyperelasticity, filler effect 80—10223
polymer concretes, hydrothermally stable, hydraulic cement-type fillers 80—85144
polymer-elastomer mixtures, temp.-time analogy 79—19317
polyolefines, struct.-mech. props. relation *(German)* 78—35451
polyorganosiloxane-talc composites, high-temp. transitions 79—52152
polyoxyethylene, polypropylene fibre reinforced, fracture kinetics, interface props. 80—66640
polyphenylquinoxaline cyclotriphosphazine hexaisothiocyanate networks, dynamic mech. props. *(Russian)* 78—72809
polyphenylquinoxalines, graphite filled, behaviour during friction 80—40553

filled polymers continued
- polypropylene, glass bead filled melt, velocity field rearrangement in stagnation flow leading to diverging radial flow between parallel plates 79—37360
- polypropylene, metallic glass filled, mech. props. rel. to temp., strain rate filler content *(Japanese)* 79—15742
- polypropylene, thermal stabilizer content effect on props., processing and ageing *(Polish)* 79—70099
- polypropylene melt, particle filled, blow moldability eval. by melt rheology *(Japanese)* 79—94578
- polypropylene systems, elastomeric impact modifiers rel. to morphology 79—66154
- polypropylene/peanut-hull flour composite, strength 79—8365
- polystyrene, γ-Fe_2O_3 powder filled, mag. films, packing and particle orientation *(Japanese)* 80—104115
- polystyrene, (-Kraton G blend), rubber toughened, charact. by SEM 79—14697
- polystyrene, filled amorphous polymer, heat capacity meas. *(Russian)* 79—65211
- polystyrene, improved impact strength by talc and $CaCO_3$ fillers 78—19846
- polystyrene, microcryst. cellulose filled, glass transition temp. shifts 78—95144
- polystyrene, plasticizer effect on electric strength 80—29688
- polystyrene, rubber-filled, mech. props. *(German)* 80—35320
- polystyrene, rubber-modified, fracture mechanics anal. of effect of rubber content, craze formation 79—29190
- polystyrene, wood filled exam. of reversible elastic deformation 78—48437
- polystyrene and cellulose particles, internal stresses influence on glass transition temperature 80—10645
- polystyrene melt, carbon-black filled, rheological study 80—48665
- polystyrene-SiO_2, glass transition rel. to filler, cooling rate 79—4403
- polystyrene-tetrachloroxylene(tetrachlorobenzene) glassy solns., additive morphology rel. to mech. props. 79—65007
- polystyrenes, rubber modified, mech. props., mol. orientation effects 79—52331
- polystyroles, struct.-mech. props. relation *(German)* 78—35451
- polyurethane, adhesive, mech. props. 77—16638
- polyurethane, relation between static and dynamic deform. characts. 80—3137
- polyurethane foam, SiO_2 particulate filled, mechanical props. 79—11666
- polyurethanes, crosslinked, effect of oligoglycol mol. wt. and SiO_2 filling on viscoelasticity and supermol. struct. *(Russian)* 79—34092
- polyvinyl acetate, γ-Fe_2O_3 powder filled, mag. films, packing and particle orientation *(Japanese)* 80—104115
- polyvinyl butyral, γ-Fe_2O_3 powder filled, mag. films, packing and particle orientation *(Japanese)* 80—104115
- polyvinyl furfural, CdO, MoS_2 and graphite filled, contact area, filler effect 79—57040
- PTFE, spacer material for supercond. cable, dielec. loss meas. using supercond. reson. cavity 77—8501
- PTFE based, nonlinear creep, compression bulk modulus 80—66593
- PTFE-Al, adhesion joints, effect of Cu and CuO 78—53183
- PVA, microcryst. cellulose filled, glass transition temp. shifts 78—95144
- PVC, antiplasticised, linear-nonlinear viscoelasticity transition 79—5015
- PVC, drawn, mol. orientation study by Raman spectroscopy 79—73919
- PVC, effects of mol. wt. and plasticiser on fatigue crack propagation rates 79—5044
- PVC, filler effect on adhesion to Cu 80—45476
- PVC, plasticised, processing-morphology-mech. props. relation 79—8264
- PVC, plasticised, thermomechanical and dielec. relax. props. rel. to degree of processing 79—70124
- PVC, rheology, viscoelasticity, panel discussion 79—3984
- PVC, rigid asbestos reinforced, stabilization and dynamic thermal stability 79—8270
- PVC, secondary relax., effect of different plasticisers 79—4995
- PVC, slightly plasticised, fracture toughness tests, impact tests 79—5037
- PVC, struct.-mech. props. relation *(German)* 78—35451
- PVC, viscoelasticity, plasticiser influence 79—52292
- PVC, waste soft, oil absorptive filler effect on heat distortion temp. *(Japanese)* 80—108389
- PVC, with varying plasticiser content, deformative props. in highly elastic state, temp. depend. 79—20099
- PVC cpds., rigid, plasticised, capillary flow 79—4046
- PVC extruded films, mech. props. *(Polish)* 79—70037
- PVC metal particle composite, effect of size, shape, and oxide content of metal particles, on segregated network form. 79—20021
- PVC mixture with processing aids, mech. props. and morphology 79—57047
- PVC plastisols, thermally hardened, rheological props. *(German)* 79—29154
- PVC with mineral fillers, mech. props. 80—21042
- PVC-C composite, fluctuation-induced tunnelling cond. 80—65516
- PVC-Cu composites, elec. resistivity rel. to compacting pressure 80—34495
- PZT/polymer composites, simplified fabrication 80—40323
- rheology, steady state shear flow and periodic deform., relaxation time, spectra, viscosity 79—96066
- rubber, C black filled, friction behaviour sliding against Al, applied voltage effects 79—74266
- rubber, filled, birefringence 78—68472
- rubber, graphite filled, performance assessed against steel structures under water lubrication conditions 80—21123
- rubber, natural, with furnace soot or acetylene black, natural ageing and dielectric props. *(German)* 78—19795
- rubber, styrene butadiene, dielectric const. and loss, lignin content depend. 80—29670
- rubber, with rigid filler, light scatt. by strains, theory and expt. 80—28162
- rubber filled epoxy, dense woven, fracture characts. 80—11757
- sheet moulding compound, material, process and performance 80—81032
- silica paricle filled epoxy resin, mech. props., fracture by slow crack growth 77—40443
- solution, rheology, normal stresses and hyperelasticity under simple shear flow 80—1506
- solution, structural strength 79—64973
- spherical inclusions, slope discontinuity prediction in stress/strain behaviour 78—94596
- spheroplastic, spherical shells, supporting capacity 80—87723
- spheroplastics, mech. characts. calc. 80—60931

filled polymers continued
- steel reinforced polycarbonate (epoxy resin), pull-out forces, effect of matrix stresses 77—21334
- styrene butadiene rubber-glass bead composites, network density determ. from stress/strain meas. 79—34112
- styrene-acrylic terpolymer surface tension rel. to temp., compatibility of external plasticiser 79—15834
- styrene-butadiene rubber, reinforcing effect of fillers, strain energy meas. *(Japanese)* 78—31468
- styrene-butadiene rubber, vulcanised $CaCO_3$ filled, stress/strain relations *(Japanese)* 80—40443
- tensile strength calc., rel. to fracture *(German)* 80—25795
- tetrafluoroethylene-vinylidene fluoride copolymer, exporide-diphenylolpropane resin filled, viscoelastic and strength parameters 79—91730
- thermal expansion, effect of particle shape at finite conc. 79—19384
- thermosetting, anisotropic structure on injection moulding *(German)* 78—76625
- toughened glassy, crazing within glassy occlusions in rubber particles, micromech. analysis 79—91824
- transducer, viscoelastic, in-situ, Duomorph, appl. to polymeric materials 79—30463
- urea-formaldehyde resin/wood materials, book 80—73114
- US study of internal damage, nonlinear elastic effects, theory 80—49307
- viscoelasticity measurement using mech. drive viscoelastic tester *(Japanese)* 79—34232
- viscoelasticity theory, appl. 80—64397
- Al_2O_3-Epon 828-Z, mixture, acoustic wave prop. characts., using differential-path US technique 79—42151
- Al_2O_3-loaded epoxy, shock-wave compressed, dielectric props. 78—80281
- B fibre reinforced epoxy composites, notched, tensile strength and failure modes 80—81205
- C fibre reinforced nylon, design parameters, fibre orientation effect 80—81141
- C fibre reinforced polycarbonate, design parameters, fibre orientation effect 80—81141
- $CaCO_3$ filled polymer melts, viscous props. 80—19311
- PVC-Cu, particulate composite, mech. props. effect of particle size 78—95799
- SiO_2 powder filled epoxy resin, flow props. during curing *(Japanese)* 78—59355

films
- *see also adsorbed layers; coatings; foils; helium films; Langmuir films; liquid films; monolayers; optical films; polymer films; replicas; thick films; thin films*
- black hydrocarbon, in aqueous medium, change in tension due to pot. diff. 77—25304
- diffusion-reaction produced layer growth rate, heat release effects *(Russian)* 77—55397
- DNA, sp. ht. in range 4.2-400K *(Russian)* 77—51511
- formaldehyde, normal and deuterated solid films, UV dissociation at 77K 77—29021
- glue, appl. in detaching single-stage C replicas 80—61038
- grease, on glass surfaces due to touching by hand, effect on optical transmittance 80—27329
- heat flux density and unsteady state temp. of surface film 78—75036
- lipid films, at fluid interfaces, phys. chem., review, book contrib. 77—39725
- multilayer orthotropic films, calc. of stability *(Russian)* 78—63281
- particle size measurement by monoparticulate film method *(Japanese)* 78—95874
- protein film, at liq. interfaces, dilatational props. 80—94255
- protein film, at liq. interfaces, shear rheologica props. 80—94256
- surface film phase transitions, conf., Erice, Sicily, Italy (Jun. 1979) 80—105429
- surface layer thickness measurement by kinetic method 77—24503
- testing, nondestructive, using electron spectroscopy 78—3430
- testing of film and fabric materials under cyclic loads, test unit design 78—7120
- thickness meas., various methods, critical assessment 80—47018
- thickness monitor, quartz crystal, based on SAW oscillator 78—3036
- two film struct., laser heating *(Russian)* 78—15259
- water cryofilm, on specular and diffusing surfaces, bidirectional reflectance 78—88274
- zinc dialkyldithiophosphate surface film, prep. and nature 80—104300
- Mn_3O_4, form. on glass surface from Mn^{2+} ions in water *(Japanese)* 80—45411

filtering and prediction theory
- *see also information theory; Kalman filters; random processes; Walsh functions*
- 2D linear prediction for freq. and bearing estimation 79—64409
- acoustic signal processing, influence of time- and space-varying random filters 78—5615
- acoustics, speech and signal processing, conf., Tulsa, USA, 1978, April 78—63242
- adaptive deconvolution, processing technique for time-varying seismic data 77—91287
- adaptive delay element for seismic noise cancellation 79—74994
- adaptive filter structures, for seismic signals deconvolution 80—98451
- adaptive laser beam control process, closed loop considerations 77—88660
- adaptive linear prediction filtering for airborne underwater acoustic signal processors 79—64388
- adaptive matched filters for the measurement of acoustically evoked potentials in the EEG *(German)* 78—88755
- adaptive model for flood warning system, on-line, desk-top computer appl. 79—34977
- adaptive predictive deconvolution of nonstationary seismic data 77—87096
- adaptive statistical filtering premature ECG monitoring and premature ventricular contraction detection 77—78022
- air pollutants spatial conc. estimation, new proposal for those which absorb optical energy 79—57533
- air pollution, statistical prediction by mixed order multi-variable AR scheme in Japan 79—57537
- air pollution, Venice region, real-time forecast, Kalman predictor 80—72103
- air pollution level prediction models based on Kalman filtering 77—29428
- air pollution levels, stat. prediction by Kalman filtering method 79—57535

filtering and prediction theory continued
air pollution prediction, based on observed data 79—57538
air pollution prediction via third order shaping filter modelling 79—57536
airborne radiometric data inversion, radioactive elements conc. mapping 78—77347
airborne target tracking filter configurations compared 80—96130
algorithms taking into account noise in input data, efficiency 79—25344
array algebra appls. 79—44702
astronomical images, coherent optical processing expts. *(Russian)* 80—12675
astronomical plates meas. via automatic microdensitometer, data compression filters 79—80230
atmosphere echo sounding, Doppler shift extraction hy adaptive linear-prediction filtering 77—64453
atmosphere spectral energetics, determ. via numerical filtering anal. 80—26577
atmosphere temperature field, spatial anal. from weather satellite meas. 78—20488
aural signal central spectral pattern anal. based on cochlear neural timing and freq. filtering 79—5300
automatic speaker recognition, cepstral/spectral and linear prediction techniques compared 80—91993
autoregression order selection 77—2270
average evoked potentials, a posteriori Wiener filtering theory and practice 78—96038
average visual evoked response estimation, predictor-subtractor-restorer filter 78—65143
biological n-compartment model, identification by filtering techniques 79—34507
biological signal time averaging, digital Wiener filtering and detection statistical aspects 78—35979
biomedical Doppler signal processing, swept-frequency transient signal filtering 78—48848
biomedical signals, development of common struct. for filters, correlators and Fourier analysers *(German)* 78—88748
blood-flow velocity estimation, Kalman filters for Doppler ultrasonic meas. 79—62325
brain activity EEG anal. using Parcor coeffs. 78—35822
C-CD transversal filter anal. in pattern recognition 78—71052
cardiovascular parameter estimation, nonlinear filter statistical parameters optimal choice 79—5308
chalcogenides of ABX_2 type comp., cybernetic prediction of form. possibility 80—101004
chemical analysis, multicomponent analysis computations based on Kalman filtering 80—40772
chemoreflex responses to hypercapnic stimuli models 79—34578
clock error with a Wiener predictor and by numerical calculation 80—82748
colour prediction model for multispectral imagery 77—71395
common depth point seismic data stacking, weighting coeffs. *(Russian)* 77—86816
composite signal anal., by cepstral inverse filtering, biomedical appl. 78—69243
continuous-time linear system, varying environment, state estimation methods 79—12581
deconvolution of seismic data using homomorphic filtering 77—81823
derivatives computation from equally spaced data, rainfall rate determ. 77—49125
digital filter for exptl. data anal. 79—17403
digital filtering of US data by deconvolution 80—106669
digital filters for long and short period seismic signal extraction from noise 77—81824
digital signal modelling and classification with the teleseismic data 78—73325
digital signal processing of radiographs for vessel edge detection in angiograms, appl. of Wiener filter, book contrib. 79—92357
digital speech processing, linear prediction parameter estimation using Kalman filtering *(German)* 80—96134
digital terrain modelling, reflexive prediction 79—2175
discrete time series spectral estimation novel aspects 77—91336
display-equalised filter for freq.-time anal. of seismic waves 77—73650
dosage population product in Venice, modelling and forecast 79—57546
dose reduction in X-ray computed tomography using a generalized filter 79—83946
earthquake model, nonstationary, identification, nonlinear filtering approach 79—5458
earthquake waves synthesis using prediction error filter 79—62630
ECG data analysis for data compression 77—40862
EEG analysis by all-pole model 80—41287
EEG cluster separation by nonlinear decision boundaries and linear filtering 77—56509
EEG epileptic transient detect., pattern recognition techniques 78—53542
EEG segment classification, usefulness of autoregressive models 80—30908
EEG signals with changing spectra, anal. using Kalman estimator 78—24167
EEG spectrum analysis, LF activity isolation by autoregressive filter 79—96672
EMG, rectified surface, time constant in low pass filtering 80—67266
EMG in moving finger muscle, pattern recognition by linear prediction 79—8555
environmental pollution regional distribution, pattern model for prediction 79—57501
European air temperature change patterns 78—92957
European air temperature series, band-pass filtering correls. and phases 80—26579
event location by recursive least squares prediction 80—96131
fast Walsh transform configuration program derivation, appl. to seismic data processing *(Chinese)* 80—21853
filter gain in reconstruction tomography 79—83919
flood event real-time predictors, stochastic model 80—67383
gamma-ray flaw detection, use of Kalman filter 79—5121
gamma-ray imaging stochastic distributed filtering approach 77—13026
geodesy, influence on window functions on prediction *(German)* 77—86749
geomagnetic D_{st} variations analyses, comparison using distortion free filter 80—17419
geomagnetic field microstructure separation, digital filtering methods 78—69480
geomagnetic fields space-time filtering 77—49178

filtering and prediction theory continued
geomagnetic Pc 1 pulsations, filtering rel. to spectral-temporal anal. 77—13188
geophysics, time series filtering with time variant operators, convolution and Fourier transform 77—87082
geopotential fields, filtering and transform. theory using information on input data noise 78—61584
Givens transformation techniques, appl. to Kalman filtering, orbit determ. 78—4473
gravitational-wave resonant antennas, optimum filtering and sensitivity 80—8545
gravity anomalies, second derivative method formulae evaluation by Fourier transform 79—100987
gravity antenna small perturbation meas., optimum strategy 77—82438
heat conduction, inverse nonlinear problems, simulation methods 78—94513
heterodyne interferometers, quasilinear filtration theory appl. to signal processing *(Russian)* 80—82807
hydrological prediction models, adaptive algorithm 79—53381
hydrophysical polygons, dynamic-stochastic approach to anal. of density field obs. *(Russian)* 79—8707
image multiplication using duplex spatial sampling filtering 79—7090
image processing, two-dimensional recursive digital filtering method, problems 78—58933
image processing, two-dimensional recursive filtering, system theory concept 78—58934
image processing algorithm for distortion anal. 79—88229
image processing and eigen representation 78—55312
image processing of additive-obtained moire patterns *(German)* 80—47017
image restoring with constrained optimisation filtering 79—39494
Infinite dimensional filtering problems in optical communication systems 78—66779
interpolation, multirate digital filtering approach appl. to common-depth-point stacking 79—29876
interpolation by linear least squares, numerical aspects of filtering *(German)* 77—9322
inverse filter which is optimum in error-distrib. sense, stability characts. 78—81424
inverse filter with optimum error distribution 77—81825
inverse filters rel. to recursive seismogram model *(Russian)* 77—86815
ionosphere electron content data, mixing freq. components identification by multiplicative homomorphic filtering 79—29929
ionosphere sounding, filtering effect on drift parameters determined by full correl. anal. 78—65450
iterative ρ-filter reconstruction from incomplete projections 77—25582
Kalman filter algorithms, use of Givens transformation techniques, for orbit determ. 78—4473
Kalman for nuclear reactor control system design *(Japanese)* 78—50278
Kalman-Bucy filters, extended, for passive microwave sounding of atmospheric temp. 79—21053
kinematic multiple wave analogues strongest families, parameter prediction algorithm *(Russian)* 79—39943
Kolmogorov-Wiener least-squares filters appl. to geophys. anomalies separation 78—61580
laser adaptive optical control with closed-loop estimation and predictive filtering 77—19298
left ventricular parameter meas., noninvasive radioisotope images with digital prefiltering and boundary detection 78—48887
local adaption effect simulation with nonlinear spatial filters 77—44657
lunar semidiurnal tidal line width in geomag. spectrum, filtering methods 77—21678
magnetotelluric probing in complex geoelec. conditions, data interpretation *(Russian)* 79—39932
Markov nonlinear filtering, stochastic differential eqns. *(French)* 77—17787
maximum entropy spectral analysis, prediction filter error length determ. for artificial samples 79—66829
maximum-likelihood estimation of source parameters from time-sampled outputs of linear array 77—75751
medical US, linear-filter model for signal transmission process 80—17026
multidimensional power spectral anal., new method, radioastron. appl. 77—17378
nerve field, isolated sciatic nerve in volume conductor 77—21505
nerve signal optimal filtering 77—73616
neural nonlinear system Wiener anal. using Poisson-Charlier crosscorrelation 78—24055
neuronal spike train data, adaptive filtering 80—67265
neuronal spike trains, simulation, multiple Markov sequences 77—25413
neuronal waveforms, optimal recognition 80—56003
noise intensity meas., nonstationary, using modulation radiometer 77—61048
nonlinear filtering equations for two parameter doubly stochastic Poisson processes *(French)* 80—17870
nonlinear inverse filtering technique, for glottal-area waveform estimation 77—56390
nuclear power system and fuel channels stochastic identification and parameter estimation 79—3201
nuclear reactor noise analysis, time series modelling methods, comparative eval. *(Japanese)* 80—13552
numerical weather forecasting, long-range, filtering method 79—84446
oil exploration seismic data processing, white noise estimators 78—3973
oil-bearing layer with input parameter correction, discrete dynamic model 80—83778
olfactory pattern recognition modelling by adaptive spatial filter 78—24080
optical differential operator processor, filter fabrication feasibility studies 78—58925
optimal multichannel filtering, simulated nerve signal appl. 79—48233
optimal multichannel filtering for nerve signals, modelling 79—48232
optimal numerical filters fitted for noise damping, atm. circulation simulation appl. 78—92997
optimal restoration filter for Poisson noise impaired and linearly blurred images 80—106481
orthogonal transforms program for medical scintigrams 80—72365
orthonormal lattice filter, multistage, multichannel estimation technique 79—84497
P wave detection and identification using statistical signal analysis 80—8202
partial spatial coherence blur correction by postdetection image processing 80—78792

filtering and prediction theory continued
passive tracking acoustic array evaluation, nonlinear filtering lower bound algorithms 80—96088
phase-matched filters appl. to Rayleigh waves from seismic sources 78—45010
phonocardiogram classification, linear prediction analysis appl. *(Japanese)* 78—36010
phonocardiogram pattern classification using linear prediction analysis 77—90950
pitch-synchronous coding, linear prediction coding, analysis frame position influence 80—14523
prediction error filter, quantitative evaluation 78—40496
prediction model of air pollution adapted to pattern of daily fluctuation 79—57539
preprocessing filter for enhancing linear predictive analysis/synthesis of noisy speech 79—64447
quasi-monochromatic incoherent optical image processing 79—76626
rainfall, Delhi, recursive prediction model 79—79998
rainfall variable infiltration, eqns. 79—53379
random data filtering, effects of detrending and smoothing 78—40685
random field fluctuations of near-water atm. layer and upper ocean layer, linear filtration errors 80—12425
random oscills., RMS level estimation, fast method 77—70857
random pulse train processing by linear filter *(Russian)* 78—46518
recursive filters for potential field data processing 77—2268
reflection seismograph data, maximum likelihood filtering 79—5453
related Hankel transforms, numerical integration by adaptive digital filtering 79—92599
road traffic noise abatement, noise propag. characts. identification under different conditions, Kalman filter theory appl. *(German)* 80—99896
satellite imagery, filtering to remove cloud cover 77—56744
scintigraphic image linear filtering, optimal compromise 80—36071
scintillation digital image processing, nonlinear filtering methods 77—81559
segmentation of band-limited speech signals using linear prediction 80—91970
seismic coda of local earthquakes, synthesis via narrow band pass filtering 77—73683
seismic data, optimal inverse filtering parameters in deconvolution correction *(Russian)* 77—86817
seismic data, optimum mixed delay spiking filters appls. 78—77346
seismic data, single-channel white-noise estimators for deconvolution 78—77345
seismic data deconvolution, overview 77—91060
seismic data deconvolution using homomorphic filtering 77—91063
seismic data filtering and smoothing, least-squared error, stationary and nonstationary 80—4158
seismic data filtering by sliding mean *(Russian)* 77—86821
seismic deconvolution and wavelet estimation 78—20542
seismic linear multichannel systems employed in regular waves separation, efficiency comparative anal. *(Russian)* 79—39922
seismic multiple waves, prediction filtering in non-ideal conditions *(Russian)* 79—44131
seismic signal filtering, distrib. theory appls. *(Rumanian)* 79—58122
seismic signals, optimal multichannel filtering evaluation taking account of amplitude and phase jitter *(Russian)* 78—40697
seismic signals deconvolution, adaptive filter structs. 80—98451
seismic spectra, least-squares inverse filtering and wavelet deconvolution 78—61339
seismic surface wave dispersion, digital processing *(Chinese)* 78—24374
seismic surface wave group vel. determ., optimum filter 77—56736
seismic surveys, optimum multichannel filters theory *(Russian)* 79—39921
seismic wavelet estimation using short-time homomorphic signal 78—88930
seismic waves with different velocities, separation using nonlinear interference systems 77—78438
seismology, multidimensional polarization analysis 78—73528
shape variation detection, two-component chromatographic peaks resolution 80—71971
short-pulse photodiode receiver quasioptimal filtering 79—26132
short-time homomorphic signal analysis, appls. to seismic wavelet estimation 78—81426
signal detection, definitions, normal distrib. for astronomers 80—17500
space filtering algorithm, influence on signal of optical system misalignment *(Russian)* 78—37815
space vehicle orbit determination optimization 79—8808
spectra differentiation, filtering props. of polynomial methods 80—66900
spectral anal., recursive multichannel max. entropy method 77—91338
spectral analysis using prediction methods based on autoregressive or maximum-entropy-method 79—55268
speech, linear prediction anal. based on pole-zero representation 79—10432
speech analysis, error evaluation for linear predictive using small anal. segment *(Japanese)* 78—31824
speech analysis, homomorphic filter in ARMA model *(Japanese)* 80—87666
speech signals, instantaneous value, statistical depend. represented as analytic signal *(German)* 79—94409
speech synthesis, linear prediction based system 79—90097
statistical error prediction in meas. of probability densities *(French)* 78—57885
stellar spectrograms smoothing by Whittaker method *(Russian)* 77—71008
stellar spectroscopy, appl. of linear filtering theory to line profiles *(Italian)* 80—90340
structural functions appl. to study of hydrophys. fields in ocean *(Russian)* 79—39901
surveying, interpolation via groups of triangulation data points of different statistical characts. *(German)* 77—9321
target discrimination methodology in remote sensing 80—58470
tectonomagnetic events, detect. using empirical transfer functions 79—16374
time-averaged areal mean of precipitation, estimation and network design 79—79901
time-domain finite length digital filter, exact wave-shaping, geophys. appl. 77—2266
time-domain wave-shaping filter weights computation 78—77351
two dimensional quasioptimal filtering, efficiency for separating geophysical fields *(Russian)* 77—70585
US image reconstruction processing limitations 78—73184

filtering and prediction theory continued
ventricular septal defect, prediction by non-invasive examination using interactive terminals 78—31954
vibroseis deconvolution 78—16171
volume-conductor fields of isolated axon, linear filtering problem 78—3463
vowel sound synthesis, autoregressive system, adaptive filter method *(Spanish)* 80—43556
water pollution, modelling, filtering and control 79—57520
weather radar matched filter criteria and range weighting 79—25341
Wiener filter and maximum entropy method, appl. to geophysics multichannel complex systems 79—92619
Wiener filtering, estimation of evoked potentials 79—48235
Wiener filtering appl. to nondestructive evaluation 79—11732
Wiener filtration versus averaging of evoked responses 78—3689
Wiener-filtering, a posteriori, statistical properties 79—88045
Wiener-Hopf method for resistivity sounding filter determ. 79—92621
wind, stochastic predictors, AR and ARMA models 80—67400
wind velocity estimation via optical signal processing 77—41107
X-ray reconstruction, Wiener filtering of successive overlapping sections 80—51214
He speech unscrambling by nonlinear power spectrum conversion 79—46134
U exploration, delayed fission neutron and prompt fission neutron logging, comparison of predicted signals 79—39879

filters
see also active filters; band-pass filters; crystal filters; digital filters; electromechanical filters; high-pass filters; Kalman filters; low-pass filters; matched filters; microwave filters; optical filters; passive filters; radiofrequency filters; spatial filters; switched filters
31st Annual Frequency Control Symposium, Atlantic City (1977) 78—57905
acoustic lens-filter plate, log-periodic, variation of props. with freq. 78—63256
acoustic signal processing equipment for ANSI standard psychoacoustic testing 78—83198
acoustic-band rejection filter, appl. of planar gratings of compliant cylindrical shells, scatt. anal. 77—31157
auditory filter, shape determ. from growth of masking 77—90806
auditory training apparatus, individual for persons suffering from severe hearing loss 79—39590
broadband radiometry, solar spectral distribution monitoring, error anal. 77—53163
C-filter: a method for filtering of biomedical specimens 79—20736
comb filter, use for describing time-varying biological rhythmicities 80—97852
computerised tomography, stochastic filter for transverse section reconstruction 79—66513
correlation filter, ECG P-wave detection *(Japanese)* 78—28119
double-pendulum vibration oscillator or seismograph, use as acoustic filter 78—16200
dust filtration, specimen prep. techniques for anal. of dust distrib. in fabrics 77—56191
DVMs measurement errors reduced by user-controllable filtering 78—77931
electric spatial filters, 2-D image formation, book 77—78906
electron filters as method of improving radiotherapy photon beam characts. 79—83939
electronic filter, for noise suppression in decrepitometric recorder *(French)* 79—48571
electrostatic energy filter, telescopic, with cylindrical mirror analysers 80—87296
energy, background current elimination in RF mass spectrometer, expt. results *(Japanese)* 80—82844
far IR interference filters 77—22592
Fourier transform spectrometer, SNR enhancement by elec. filter compensation of slide velocity errors 80—95151
frequency response plots for Savitzky-Golay filter functions 77—53741
harmonic current AC filters at KEK accelerator 78—33333
humidity effect in flow resistance of loaded fibrous filters 77—29451
ion optics, design of E×B filter with improved vel.-separating capability 77—41728
liner compression filter, for random values separation in geophysical data anal. *(Russian)* 79—74983
liquid crystal electrooptical filter, teaching expts. 77—41434
magnetic separation, particle capture and axial filters, theory 78—92516
magnetic sparation, particle capture in axial filters, theory and performance 78—92515
mechanical networks and applications *(Japanese)* 80—10072
mechanical notch filter, novel viscously damped dynamic absorbers design 77—62096
membrane filter inefficiencies for particulate collection under low loading conditions 77—70721
membrane filter mounts and quick-change device for aerosols and liq. suspensions 77—53873
membrane noise analysis by integral spectrum procedure 77—48958
mica nuclear track microfilters, prod. and props. 80—96574
micropore filters, preparation by bombarding lavsan film with Ar ions 78—3305
momentum filter for separation of electrons and negative ions 78—78034
MTI filter, with inherent A/D, for US blood flow velocimeter 79—16263
multichannel subtracting filters *(Russian)* 78—3969
multistage parallel-serial time averaging filters to reduce time jitter in scintillation counter time meas. 80—102405
narrowband, SAW resonators at 1.43 GHz appl. 80—87687
nomographs, basic theory and utilisation 77—17791
nuclear filters, prep. from polymers using Ar ions 78—86714
Nuclepore, characterization measurements 80—86324
nuclepore filters, amosite fibres collection efficiency 78—81341
octave filters, use in meas. of random noise spectral density 77—48957
optical fibre, analogue transmission system optimum receiver considerations 79—68449
optical fibre nonlinear equaliser, shaping filter 78—30052
optimal filter for photodiode detector, struct. and characts. 78—18067
optimum filter responses for liq. Ar total absorpt. detectors 78—46215
optimum filters, finite time width and area balance, for triangular or step current input waveforms 79—13610
optimum multichannel filters used in seismic surveys theory *(Russian)* 79—39921

filters continued
- polysulphone membrane, prep. and performance for ultrafiltration *(Japanese)* 78—31695
- proton filter, polarised, for polarisation of slow neutrons 79—63238
- quadrupole mass filter spectrum control, using PWM 77—61152
- radiotherapy dose compensation filter design using megavoltage radiography 80—3785
- resonance, influence on wave form of scanning signal *(Russian)* 79—55265
- SAW, asymmetric three-transducer configuration analysis 77—39165
- SAW, operator, transfer function *(French)* 77—54846
- SAW, use in communications equipment 78—38152
- SAW delay line filters, triplet-transit suppression technique 79—64453
- SAW device, fine frequency adjustment, by modifying propagating direction 78—18125
- SAW filter appl. to TV receiver *(Japanese)* 78—71247
- SAW filter using waveguide between input and output transducers, freq. response 77—39162
- SAW filter with low insertion loss using group-type unidirectional interdigital transducer *(Japanese)* 78—33980
- SAW filters with weighting of electrode overlap without beam integration *(German)* 78—51011
- SAW pulse compression filter using reflective dot array 77—75749
- SAW resonator filters with enhanced out-of-band rejection 80—19179
- SAW TV intermediate-frequency filter, 58 MHz, using ZnO sputtered film 77—80022
- scanning optoelectronic systems, optical and electrical filter simultaneous optimisation 79—72696
- seismology, multichannel subtracting filters synthesis *(Russian)* 78—49156
- self-adapting fan filters for seismic data 79—44265
- sleep EEG automatic K-complex detector 78—53557
- smoothing, for continouous radiometric monitoring, of material with fluctuating parameters 77—90553
- sonar signal processing, conf., London, England, 1978, Nov. 79—18618
- speech formant extraction, tracking loop filters 78—65051
- steam turbine lubricating oil, filter separators and centrifuges eval. for effects on props. 78—3283
- tone filters for electronic organs, tone spectra and source waveforms 80—106683
- transversal, for audio signal processing 79—64406
- water purification, granular charge inhomogeneity effect on head losses 77—75976
- whistler detection, multichannel filter and shift register obs. system 78—93031
- Wiener filter, evaluation and appl. to evoked EMG pots. 80—3747
- Wiener filters, effectiveness in evoked pot. estimation 80—61723
- X-ray, metal foil, electrolyte production method 79—95947
- Ge position sensitive γ-ray detectors using resistive charge division readout 77—54420
- Na film for expendable filter in VUV, use and preparation technique 80—33193
- SO_2 collection efficiency with 0.5 N KOH-impregnated filters 78—16168

filters, optical *see optical filters*

filtration
- aerosol, penetration through high efficiency filters 79—27690
- bile salt micelles as liquid membranes 80—21327
- blood microfilter materials and designs 79—48352
- blood purification methods and portable kidney machines *(German)* 79—5405
- cellulose acetate membrane, asymmetric, elec. and electroosmotic transport behaviour in hyperfiltration expts. 80—108746
- coal, permeability to methane, influence of temp., geostatic and stratal press. *(Russian)* 79—66695
- consolidation in compressible mixtures 79—46271
- constant pressure filtration, filter medium fast plugging, mathematical models 80—100030
- cryogens, porous solids, gradientless heat transfer, metallic thermal cond. theory 79—59902
- disperse systems, polymer-modified, filtration coeffs. 78—67264
- displacement reactor theory 80—7795
- dynamics, free boundary enclosure 78—55687
- efficiency, comparing particle-size distribution, in feed stream to filtrate 78—92417
- energy dispersive filtration for simultaneous energy and wavelength dispersive analysis 79—12918
- equations of motion of fluid in porous medium with stagnation zones 79—18951
- erythrocyte filtration through polycarbonate filter determ. method *(German)* 79—79708
- fibrous filter, distrib. of fluid vels., flow resist., random flow model 80—79393
- fibrous microfilter for blood, disposable 78—7527
- flow through heterogeneous earthen dam, problem solvability 80—90110
- flow through porous media, filtration theory problem soln. *(Russian)* 80—74970
- glomerular filtration rate meas., comparison of 4 commercial preps. of ^{99M}Tc(Sn)DTPA 80—81704
- granular bed, aerosol filtration efficiency, triboelec. effects 80—38487
- grid filters, collection efficiency, effect of Stokes and Reynolds numbers 78—61592
- groundwater dynamics in plane regions during time varying seepage and evaporation *(Russian)* 79—79878
- haemodialysis membranes, permeability and rejection coeffs. 80—26207
- haemodialysis with hollow fibre membranes, flow maldistribution effect on performance 80—26248
- haemofiltration control system *(German)* 79—5403
- haemofiltration experiments and application limits *(German)* 79—5402
- haemofiltration treatment, chronically intermittent, principles and results *(German)* 79—5404
- heat pipe, heat transfer agent flowrate through porous wick, approx. calc. method 78—75197
- hydrophobic and hydrophilic porous media, grain wettability, filtration coeff. 80—1676
- imperfect borehole, hydromechanics and stationary filtration *(Russian)* 79—88375
- liquid filtration by passing through partially saturated porous media 79—90326
- liquid hydrocarbon filtration, generation of charge 77—55082

filtration continued
- liquid suspension by deposited layers in filter device *(Russian)* 77—53872
- LMFBR, filtration of Na fire aerosols 79—30998
- LWR accidents, containment venting and filtration approaches 79—13465
- macromolecular soln., laminar ultrafiltration, limiting flux numerical calc., variable diffusion coeff. 78—40214
- macromolecular solution, gel conc. and diffusivity at gelling determ. by ultrafiltration 80—21325
- macromolecular solutions, laminar filtration under low polarization conditions 80—24056
- membrane, porous, filtration characts., pore and particle size distribs. correl. *(Japanese)* 80—3418
- membrane filters in air anal., review 79—79316
- membranes, hyperfiltration, outer phases composition 79—92003
- metal gauzes, porous, hydraulic resist. in laminar filtration 80—100034
- micro-perforated plates, collection efficiency of aerosols 79—64760
- microvascular filtration, comparison of characts. in isolated and intact lungs, dog expts. 80—97974
- mist filtration, press. drop in filter, model calcs. 78—44399
- multiway sorption filters, development and use for radioactive iodine removal from air 78—61543
- needle shaped particles, diffusion orientation on filtration surface in turbulent flow 80—33668
- New Waste Calcining Facility process filter remote handling 79—9820
- non-Newtonian liquid filtration eqn. 78—55690
- nonstationary filtration, source-type solns. 79—10608
- nuclepore filter, collection efficiency for asbestos fibres 78—57351
- Nuclepore filters, anomalous filtration of solid particles 79—12283
- oil, slurries, ultrasonic effects 78—94504
- optimal impulse control, separation theorem for classical filtering model *(French)* 80—90659
- ovalbumin aqueous soln., macromol. gel layer formed on ultrafiltration tubular membrane, charact. 80—14260
- plane filtration, of underground waters, convective mass transfer, boundary problems *(Russian)* 80—83793
- polymer membrane, transport of organic liqs., review 80—16720
- polyvinylalcohol, macromol. gel layer formed on ultrafiltration tubular membrane, charact. 80—14260
- porous medium with stagnation zones, hydrodynamical dispersion and sorption dynamics 80—6139
- pulse-jet fabric filter, high vel., dust retention effect on pressure drop 80—103072
- PWR, in-reactor loop expts. on corrosion product transport and water chemistry 78—58335
- Salts migration through porous media 79—90323
- soil, finite element method *(Russian)* 79—88374
- steel, stainless, porous sheet, pore dimensions, filtration and permeability *(Russian)* 80—76480
- suspension filtration, 2-component, conc. wave bifurcation *(Russian)* 78—22420
- suspensions, with a compressible residue, filtering, intensification by pulsation *(Russian)* 79—90324
- ultrafiltration, using membrane surface, slip vel. effects in channel flow system 79—60054
- ultrafiltration, using membrane surface, slip vel. effects in tube flow system 79—60055
- ultrafiltration apparatus, biopolymer appl. 78—7547
- unsteady filtration with unknown boundary, nonlinear integro-differential eqn. 80—43769
- $ClONO_2$ collection using impregnated filters, simulation 79—12257
- F, stack sampling apparatus for the collection of gaseous and particulate pollutants *(French)* 80—7986
- Fe fibre porous material, props. 79—98798
- MnZn ferrite particles, mag. filtration from air streams 77—4945
- Na-fire aerosol filtration in nuclear reactors 80—68853
- NaF filter material interaction mechanism with Al melt *(Russian)* 80—108743

FIM, atom-probe *see atom probe field ion microscopy*

financial ADP *see financial data processing*

financial data processing
- *see also accounts data processing*
- space research, computerised planning in ESA 80—4223

fine structure, atomic *see atomic fine structure*

fine structure, molecular *see molecular fine structure*

finite automata
- biological systems appls. of von Neumann cellular automata 78—31754
- cellular system growing, graph generation by parallel rewriting 79—66458
- Cytocomputer biomedical image analysis 79—92419
- stochastic cellular systems theory *(German)* 80—90661

finite element analysis
- 3-D cable networks, finite element study of free vibration 79—23197
- 3D nonlinear EM field anal. using computer program TOSCA 80—95765
- Abel's integral eqn., least squares finite element method appl. 79—25830
- accelerating fluid flow, finite-element soln. convergence 77—75873
- acoustic absorpt. in rigid porous materials 79—32114
- acoustic axisymmetric transmission system with sound absorbing wall 77—88974
- acoustic ducts, finite element simulation 78—38115
- acoustic field, equiv. circuit using finite element method *(Japanese)* 77—50790
- acoustic field, finite-element approach 79—7238
- acoustic filters, arbitrary profile, circular cross section, finite element simulation 77—11059
- acoustic filters with open end, finite element prediction of transmission characts. 80—33349
- acoustic propag. in nonhomogeneous, contiguous and discontinuous domains, numerical approx. of hyperbolic evolution problem and appl. to underwater propag. *(French)* 79—41489
- acoustic propagation in lined ducts with flow, finite element formulation of eigenvalue problem 80—23819
- acoustic streaming, multidimens., numerical anal. 77—962
- acoustic transmission system with radiation 79—3862
- acoustic transmission/radiation systems, appl. to horn and silencer design 80—87589
- acoustic wave propag. in shear flow with temp. gradient in rectangular duct 79—94379

finite element analysis continued
- acoustic wave propagation in anisotropic rods of rectangular cross-section 78—1463
- acoustic wave refl. from general surface, geometric props. 77—84026
- acoustics, sound-absorbing wall, finite element simulation of acoustic filters *(Japanese)* 77—84032
- adaptive approaches and reliability estimations in finite element analysis 79—49026
- adhesive bonded tubular lap jont, stress anal. 78—18253
- adhesively bonded metallic panels, 2-ply, finite element and integral eqns. anal. of fatigue crack growth 78—92347
- advection-diffusion equation, weighted-mean schemes for finite-difference approx. 78—34103
- advection-diffusion simulations, finite-element and finite-difference methods comparison 77—22424
- aerodynamics, high Reynolds number, global approach and coupling approach 80—48742
- aerofoil, oscillating, viscous incompressible flow, finite element anal. 80—38427
- aerofoil in unsteady viscous flow, numerical soln. procedures 78—75165
- Ahmad thick shell element, theoretically improved and easily implemented version 79—23205
- air cushion system, plenum, duct effects on heave stability 79—17202
- aircraft, deformable, dynamic model for natural vibration anal. by finite elements 78—46909
- airfoil optimisation, transonic flow finite element anal., book contrib. 80—1633
- algorithm for multipoint constraints 79—30206
- algorithms, unconditionally stable, elasto/visco-plastic finite element analysis 78—34030
- angiocardiogram computer analysis, pot. energy distrib. rel. to left ventricular efficiency 77—40757
- anisotropic axisymmetric solids, asymmetric stress anal. 78—26033
- anisotropic composite cantilever, bending and torsion, mathematical formulation 79—18708
- anisotropic plate symmetries, anisotropy and shear deformation 77—26174
- anisotropic shells symmetry considerations 77—11123
- anisotropic solid fluid flow with free or artesian surface, GROW1 program 78—92872
- anisotropic strip under tension, stresses round hole or annular inclusion 77—3726
- ANTRAS program system for structural anal. of shells of revolution *(German)* 79—46192
- aorta model, canine, soln. of Navier-Stokes eqn. 79—29550
- aortic valve human, stress analysis 77—44699
- aortic valve leaflets, stress anal. with smoothed geometrical data 77—52815
- approximation of Stokes problem, convergence of solutions 80—27138
- aquifer on sloping bed, steady state flow, finite element study 79—16531
- arc welding, temp. calc. 78—28930
- artificial hip joint construction compatible with femoral natural stress distrib. *(German)* 79—8576
- asymmetric impact of finite bars 77—75847
- AT quartz plate resonators and filters, discrete element model 79—55297
- AT-cut crystal resonance frequencies 79—56732
- atmosphere potential vorticity, conservation by finite difference eqns. in generalised vertical coordinates 80—26576
- atmosphere turbulent boundary layer, finite-element numerical modelling 80—77061
- atmospheric boundary layer, advection dominated flow, book contrib. 79—34934
- atmospheric transport from large area sources 80—16874
- atmospheric transport problems, contaminant movement, Galerkin finite element method 80—74902
- automatic mesh generation for thermal loading calcs. 77—3740
- automatic subdivision of 2-d region into finite elements, use of computer algorithm 78—81819
- automotive struct. analysis using hybrid stress finite elements 78—30176
- axial-flow compressor cascade flows computer simulation 78—79333
- axisymmetric bodies, semi-analytical finite element soln. of plastic and visco-plastic behaviour 79—90149
- axisymmetric elastic bodies subject to cyclic loadings *(Russian)* 77—75800
- axisymmetric elements, numerical comparison 78—89313
- axisymmetric large elastoplastic strain problems, natural finite element anal. 78—83259
- axisymmetric plasma, ideal MHD spectrum, finite hybrid elements method 78—42734
- axisymmetric shells, two noded straight element including shear deformation effects 78—47
- axisymmetric solids under nonsymmetric loads, structural analysis programme *(German)* 78—13896
- axisymmetric solids with material and geometric nonlinearities, finite element anal. 78—34037
- bar, circular, in tension, strain energy release rate for edge crack 79—18815
- bar with two natural freqs., minimum mass design 79—46246
- battered piles for nuclear power plant support, dynamic stiffness and seismic input motion 80—13954
- beam, cracked, dynamic weight function from finite element soln. 80—79234
- beam, double cantilever, dynamic crack propagation modelling, 1D anal. validation 79—72857
- beam, large displacement-small strain anal., finite elements with rot. degrees of freedom 78—86161
- beam, with attached concentrated mass, nonlinear vibrs. 77—19557
- beam deflection under moving loads, finite element anal. *(German)* 79—23204
- beam element in space, geometrical stiffness, virtual work approach 80—14567
- beam in transverse vibr., optimisation of higher order eigenfrequencies 77—78971
- beam inelastic bending including transverse shear 79—90148
- beam modelling, linear shape function for axial displacement approx., finite element anal. 80—69665
- beams, elastoplasticity, flexural motion, finite element anal. 79—46223
- beams, finite element soln. using element averaging technique 78—26079
- beams, frames, arches, axisymmetric shells, finite element anal., Newton Raphson method, nonlinear equilib. eqns. 78—22282

finite element analysis continued
- beams, isoparametric elements for cross sectional properties and stress anal. 79—44731
- beams, nonlinear bending 78—26068
- beams, nonlinear oscillation computation using space and time finite elements *(German)* 79—37213
- beams, plates and rings, refined finite element schemes based on moment scheme 79—53979
- beams, thin walls, stress-strain state determ., method of segments 80—28424
- beams with elastically restrained ends, large-amplitude vibrations 78—90747
- Benard convection, initial and boundary condition effects, book contrib. 80—1591
- bending, of plate, powerful finite element method for computing 78—1583
- bending, plates, bilinear and biquadratic quadrilaterals, variational principles, numerical convergence 80—48576
- bending analysis of nonuniform circular plates 77—7316
- bending of piezoelectric multilayer plates 80—40064
- bending of plates, finite difference variational method 80—92045
- bending of thick annular and sector plates 77—46950
- bending of thin plates, finite element anal., variational principle, simplified modified potential energy technique 80—52029
- biaxial strength tests, finite element anal. 80—89431
- biharmonic eqn. approx., dual iterative method 77—2524
- Bingham fluid, entrance flow through noncircular ducts, finite difference anal. 80—1684
- bladed disc vibration modes, finite element anal. 77—39250
- bladed discs, finite element dynamic anal. 79—37230
- blades in transonic flow, shocks and boundary layers, time marching method 79—4036
- blast waves, spherical, time-depend. energy deposition 78—9655
- blending function interpolants 78—24645
- block iterative finite element preprocessed scheme, large nonlinear problem simulation 79—53
- block-type fuel elements, stress calc. with finite element code *(German)* 77—71654
- blood flow through sclerotic arteries, numerical simulation 80—26246
- blood pulsative flow digital simulation 78—92670
- bodies in plane strain, stress-strain state calcs. 80—14574
- bodies of revolution, heat cond. during nonaxisymmetrical heating *(Ukrainian)* 79—98591
- bone, stress distrib. in long bone due to prosthesis positioning 77—36984
- bone compressive strength quantitation and effects on bone remodelling 78—31836
- bone remodelling beneath internal fixation plates of varying stiffness, parametric study 80—16990
- bone resonance, effects of geometrical parameters, shear deform. and rot. inertia 77—29165
- boudinage structures, displacement and stress distrib. 78—32078
- boundary element method for partial differential eqns. soln. 78—94634
- boundary integral eqn./finite element anal. of cracked solids 77—72178
- boundary layer, numerical soln. of linearised Navier-Stokes eqns., effect of cell Reynolds number 80—106780
- boundary layer flow equations, integral spline method 79—32450
- boundary layer flows, finite difference method 78—51155
- boundary layer flows in tilted square cavity, finite difference method 77—7385
- boundary layer problems, finite difference methods, nonuniform grid generation 80—83780
- boundary layers, laminar and turbulent, two-point finite difference method 77—19617
- boundary stresses, anal. by displacement of known element processes *(German)* 79—23203
- boundary-value problems, cf. boundary integrals 77—67250
- boundedness, definiteness of functional eqn. for nonconforming trial functions, finite element method, variational principle 79—2608
- Boussinesq equation of fluid dynamics 78—79292
- box beam anal. by finite strip method, performing element 79—80438
- brittle material, fast crack propagation, computer simulation 80—38331
- brittle materials, crack propagation under compression, finite element anal. *(Japanese)* 78—42567
- brittle rod, optimum specimen shape for compression tests, struct. and technological parameters 80—50798
- brittle solids, unstable growth of tension cracks 80—106756
- buckling, finite element analysis by ASKA program system 79—18753
- buckling and post-buckling analysis of structures, direct discrete method 77—68470
- buckling mode superposition, geometrically nonlinear finite element behaviour 80—1449
- buckling of pressure loaded rings and shells 77—42757
- buckling of simply supported skew plates 78—59319
- buckling strength of orthogonally stiffened plates under uniaxial compression 80—5964
- building two-dimensional heat load anal. 78—71336
- Burgers' nonlinear eqn. soln. 78—36835
- Burgers equations, in two dimens., finite element anal. 80—1532
- buttock deformations and stresses, sitting person 79—16241
- BWR, coupled vibrations of a structure and fluid excited by pressure shocks 80—13546
- BWR-II containment vessel, soil-struct. interaction for transient loads 78—29604
- C^0 efficient finite element for simply supported rhombic plate 77—80065
- C^1-class on tetrahedron 78—57759
- cable dynamics, nonlinear 77—2532
- cable problems, finite element approach 79—49041
- cambered helicoidal fan blades, vibr. anal. 79—3946
- cantilever beam, distorted isoparametric elements 79—27526
- cantilever column post-buckling, Galerkin finite element analysis 77—54907
- cantilever columns, spring hinged, post-buckling anal. 79—46235
- cantilever cones, buckling under external pressure, exptl. and numerical solns. 78—71287
- cantilever cylindrical shells, seismic design, appl. to nuclear steam system 78—58339
- capillary surfaces, calc. by finite element methods 80—20009
- capillary surfaces approx. in gravitational field 77—55415
- cardiac muscle stress/strain relationship determ. by computerised tomography 79—92262
- cascade flow, varying flow rate 78—90910

finite element analysis continued
- cascade flow in large distorted periodic flow, finite element soln. 78−87348
- casting, continuous, heat transfer anal. by finite element anal. 78−30167
- casting process, direct chill, semi-continuous, numerical heat transfer model 80−43592
- cat eardrum model as thin shell 78−65036
- cavity growth controlled by surface diffusion, numerical study 79−90668
- central difference approximations to the heat transport equation 79−3885
- centre cracked plate under quadratic thermal gradient, stress intensity factors analysis 80−43665
- ceramic, elastic behaviour, finite element anal. model, thermal props. 78−31449
- chemically induced spin polarisation, finite element method, stochastic-Liouville eqn. 79−64018
- CIDN(E)P, infinite elements, in variational soln. of stochastic-Liouville eqn. 79−94014
- circuit-breaker induction calc. using standard finite element software 79−41906
- circular arches, curved finite elements 78−5652
- circular cylinder in laminar incompressible viscous flow, finite element anal. 77−84216
- circular segment shaped plates vibration anal. 80−58957
- circumferentially notched tensile specimen 78−67150
- Clairaut eqn., connection to satellite geodesy and Jupiter 78−11795
- clamped plate, finite element anal. of secondary buckling, comparison with expt. 79−1120
- clamped skewed plates, elastic deformations by dynamic relaxation 78−34049
- clay, consolidation model, finite element anal. 79−18732
- cloud droplets, stochastic collection eqn., computational instability in numerical soln. 77−2211
- coal pillars, elastoplastic anal. of stresses, finite element method 79−66691
- coarse mesh methods for benchmark and realistic reactor problems 77−88191
- coastal aquifer water flow analysis 80−26654
- coiled multilayer shell, stress anal. of elastic and elastoplastic work 80−79156
- cold rolling of laminated composite sheet 78−39797
- collocation finite element method for potential problems in irregular domains 79−54072
- collocation for groundwater flow digital simulation 78−93018
- column, nonuniform, lower bound buckling load, finite difference scheme 78−18200
- columns and plates, lower bounds to fund. freq. and buckling loads 79−10469
- combinatorial approach to flexibility method 77−2528
- combined bend mode specimens, calc. of stress intensity factors 78−79284
- combined finite element and transfer matrix techniques, analysis of static and dynamic structural problems 80−53619
- combined mode bend specimens, calc. of stress intensity factors, 3 alternate methods 79−77025
- compact finite-difference methods and boundary conditions 77−49582
- compact tension specimen, J-integral eval. *(Japanese)* 78−9607
- compact tension specimens, stress intensity and crack openings 80−1474
- compact test pieces, optimization of electric potential technique for crack growth monitoring using finite element anal. 79−87799
- complementary and nonconforming finite elements relation *(German)* 78−12546
- complementary energy principle, finite elasticity solns., hybrid finite element anal. 79−32274
- complex aerofoils, compressible flows, isoparametric Hermite cubic element 80−1617
- complex part stress anal., photoelasticity and finite element methods 78−71279
- complex submerged structures, vibr. anal. by discrete element techniques 77−68520
- compliant bearing lubrication, finite element model minimisation algorithm 78−63400
- composite electrostrictive resonators, finite element simulation 78−59237
- composite laminates, transient moisture sorption induced stress field 78−34021
- composite material, plate, natural vibration investigation using finite element anal. 77−68495
- composite material crack tip fatigue behaviour and stress state study *(Japanese)* 80−28470
- composite material/metal sheet bonded, finite element anal. of patched cracks 80−10192
- composite materials, bimaterial plate, cracked, finite element anal. of stress distribution 78−75104
- composite materials, failure predictions 80−10200
- composite materials elastic characts. by vibr. tests and discrete conservative model calcs. *(French)* 80−45337
- composite piezoelectric US transducer, finite element simulation 79−41541
- composite piezoelectric US transducer, finite element simulation *(Japanese)* 79−68537
- composite systems, cracked, finite element microscopic stress anal. 78−34083
- compressed powder mixture electrical conductivity calc. *(German)* 80−10940
- compressible flow, conservation equations, characteristic method of lines soln. 80−59064
- compressible flow, inviscid, circular and elliptic, cylinders and airfoils, primitive variable least-squares finite element formulation 80−33623
- compressible flow, steady, thermodynamic consistency, finite difference scheme 80−48732
- compressible flow, subsonic numerical approx. *(French)* 77−47037
- compressible flow, two-dimens. subsonic, finite elements soln. by streamline perturbation 77−51077
- compressible flow, upstream-centred finite-difference scheme 77−27547
- compressible flow, variational principle and finite element method 79−46336
- compressional impulse interaction with slot normal to surface of elastic half space 79−50626
- computational methods, book 78−81820
- computer-aided analytic element analysis and similarities of tetrahedron 77−37749

finite element analysis continued
- concrete, reinforced, failed slabs, nonlinear analysis by finite element method *(Japanese)* 77−42785
- concrete, reinforced slabs, nonlinear statical props. anal. 80−25809
- concrete, stress distribs. under splitting loads *(Japanese)* 78−35495
- concrete, uniaxial compression, finite element failure anal. *(Japanese)* 80−35265
- concrete, unreinforced pavement slabs, environmentally induced stresses, computer experiments 78−35435
- concrete creep, unified concepts of constitutive modelling and numerical soln. 77−25093
- concrete creep under nonuniform temp. distrib., linear viscoelastic analysis 77−62172
- concrete reactor pressure vessels, finite element creep anal. 78−41813
- concrete slab, reinforcement optimisation by linear programming 77−89022
- concrete splitting test, nonlinear numerical analysis 77−7339
- concrete structures, nonlinear deform. and ultimate load behaviour 77−72163
- condensation for mixed dynamic FE analysis of rotational shells 79−32231
- conducting slab response to source fields, EM analogue model and finite difference calcs. 78−61329
- conductor, current carrying, finite element analysis of skin effect 77−83785
- conference, computation fluid dynamics, Rhode-Saint-Genese, Belgium (March 1977) 77−80134
- conference, computational methods in nonlinear problems in mechanics and engineering, Austin, Texas, USA (March 1979) 80−51945
- conference, computing methods in applied sciences, Le Chesnay, France (Dec. 1975) 77−33846
- conference, finite elements in nonlinear mechanics, Stuttgart, Germany (Aug.-Sept. 1978) 79−44727
- conformal mappings for curved boundary finite-difference problems 79−3912
- conforming crack tip element with quadratic variation in singular fields 78−38251
- conical shells, non-linear free vibrations 79−81795
- conjugate gradient solutions, finite element elastic problem with high Poisson ratio 78−90707
- connectivity theory for formally symmetric operators 78−49651
- connector choice in finite element anal. 78−45
- conservation equation, numerical soln. by variational approach, mass transfer problem appl. *(French)* 80−19317
- consistent conforming elements with singular derivative fields 79−30205
- constant strain triangle elements, efficient use 79−72798
- constrained finite element solns., convergence proof 78−54168
- constrained viscoelastic damping composites, noise and vibration insulation 80−83743
- contact problems involving friction, finite element soln. using nodal variables *(French)* 77−72183
- contact stress problems, counterformal, improved numerical method and program 79−41632
- contact with various frictional conditions 79−32388
- container subjected to forced pitching oscillation, liquid motion, nonlinear anal. 80−96270
- continuation method, adaptive step size selection 78−45476
- continuous bodies under gravity load, centrifugal force, optimum strength shape 79−98665
- continuous elements 78−24668
- convection, book contrib. 79−32523
- convection, creeping, finite-element thermal-mechanical model 77−7290
- convection, free, 2D flow, steady state, finite element anal. method 77−75910
- convection, natural, laminar, in open vertical channel, numerical soln. method 78−5799
- convection, upstream-centred finite-difference schemes 77−27548
- convection problems in fluid mechanics, book contrib. 79−32521
- convection-diffusion partial differential eqn. soln. 78−90889
- convective diffusion problems, finite element solns., Navier-Stokes eqns. 80−1583
- convective dispersive equation, movement of chemical pollutants in groundwater, numerical techniques 80−16855
- convective heat transfer anal. 78−18148
- convective heat transfer with diffusion 79−4011
- convective heat transfer with phase change 79−3887
- convective transport, stable finite element simulation 79−46317
- convective transport eqn., 2-D, upwind finite element scheme 77−13713
- convective-conductive transient heat transfer, finite-element method 79−3888
- convective-dispersion eqn., non-self-adjoint 77−27529
- convergence proof for constrained finite element solns. 79−21537
- convex analysis and variational inequalities *(Japanese)* 80−77606
- cooling bodies, thermal stresses and temps. determ. by finite elements 77−14881
- cooling fin with heat sink, design optimisation 79−1046
- cooling tower supporting columns and reinforcing rings, displacement analyses 78−38187
- cooling towers with column supports, free vibration analysis 78−83292
- cord-rubber laminates, two-ply balanced, interlaminar-shear strain study 80−97526
- corners and cracks, finite element approx., hybrid finite elements 79−64585
- corotational stretch theories, higher order, nonlinear finite element anal. appls. 79−32245
- Cosserat plate, Signorini problem, finite element anal. 80−1420
- coupled finite element-finite difference anal. of hydrodynamic and elastoplastic problems 77−71200
- coupled fluid-structure systems, vibr. anal. by displacement method 79−7323
- coupled fluid-structure systems, vibrations, substructure element variational anal. 79−55333
- coupled solid/fluid/surface wave dynamic interaction problem, improved fluid superelement 78−81108
- coupled structural-acoustic radiation system, appl. to loudspeaker charact. calc. 80−83691
- coupled thermomechanical phenomena, nonlinear transient anal. 79−32181
- coupled thermoviscoelastic structures, sustained periodic vibrs., finite element anal. 79−7315

finite element analysis continued
crack, elastodynamic anal. by finite element method using singular element 78—55603
crack, semi-elliptical, in finite plate, stress intensity factors *(Japanese)* 77—23914
crack, stable growth in antiplane shear, finite element investigation 79—3975
crack, virtual extension method for combined tensile and shear loading 78—67149
crack anal., three-dimens., finite element method 78—83332
crack edge stress field oval. using isoparametric elements 79—3973
crack energy release rates calc., inverse flexibility method 79—41617
crack extension forces in elasto-plastic stress fields 78—18250
crack extension process and nonlinear fracture criterion, finite element anal. 80—53702
crack growth, at rubber springs bonds, energy calc. and meas. 79—83316
crack growth, elastoplastic finite element anal. 79—46260
crack growth monitoring using finite element analysis, calibration of electric potential technique 79—32380
crack initiation notches, pure strain rate role, finite element computer program 77—70166
crack movement, isothermal conditions, heat liberation, finite element method *(Russian)* 79—27583
crack movement with fracture propagation *(Russian)* 79—77017
crack propag. simulation, using moving grid based finite difference scheme 78—83334
crack propagation, along non-straight path 80—1485
crack propagation in creep *(Japanese)* 77—8926
crack propagation through finite element mesh, nodal grafting method 77—75854
crack propagation under compression, finite element analysis 78—67148
crack tip elements, singularity reconsiderations 80—1479
crack tip finite element anals. 79—41624
crack tip opening displacement by finite element anal. *(Czech)* 78—59343
crack tip singularity analysis by global-local model of large finite elements 80—28466
crack tip singularity models, assessments for use with isoparametric elements 79—50652
crack tip stress intensity factor for stress singular problems, energy convergence and eval. by mixed finite element method 79—23276
crack-tip problems and quarter-point triangular elements 78—83333
cracked bodies, thermal anal. 77—3793
cracked elastic sheets, use of special tip elements 77—58605
cracked linear viscoelastic solid, dynamic anal. by finite element method 80—53706
cracked lug, test and analysis 78—67153
cracked thick walled cylinder, elastic plastic fracture anal. under displacement controlled loading 78—67119
cracking problem in timber 77—39261
cracks, branched, growth determ. by numerical methods 79—68649
cracks calc., power type singularities analysis 77—80106
creep, rapid cycling problems 78—63317
creep anal., variable stiffness method 78—22278
creep and fatigue fracture, of austenitic stainless steel plate with crack *(Japanese)* 80—50694
creep problems involving rapid cyclic loading, finite element soln. 77—3750
critical two-phase flow, multidimens. effects 79—14461
curved beams, nonlinear dynamic anal., finite element method 80—96213
curved finite elements, forbidden nodes 79—88796
curved macro-element for cracks and corners 80—33448
curved plate bending problem solved with nonconforming finite elements 79—37202
curved sandwich beam, finite elements for linear static elastic anal. 77—62153
cyclic elastic-plastic dynamic analysis 77—33864
cyclic thermoplasticity, by subvolume technique 77—42749
cylinder based bodies, turbulent boundary layers, three dimens., soln. method 79—1167
cylinder in incompressible flow, finite element anal., wake development and stability 79—14364
cylinder-to-cylinder structure, analytical and exptl. stress anal. 78—59308
cylinders, circular under end load, post-buckling anal. 79—98640
cylindrical punch, three-dimensional stress field, photoelastic studies 80—93272
cylindrical shell in fluid executing harmonic vibrations, determination of pressure of fluid on cylinder 79—64384
cylindrical shells, anal. of through cracks by quarter point elements 79—72856
cylindrical shells, vibr. anal. by finite element formulation 78—34048
cylindrical shells containing turbulent flowing fluid, numerical anal. 77—72291
cylindrical three layer pipe, stress-strain state, filler compressibility effects *(Russian)* 80—58901
dam porous media unsteady flow calc. 78—91012
dam unsteady compressible fluid flow digital simulation 78—90820
damped 3-layer plates, finite element analysis of harmonic response 80—53691
damped acoustic systems, finite element anal., reactive mufflers performance evaluation 77—14844
data struct. 78—16633
DEALS, demountable superconducting magnet system, for fusion reactors 80—52777
defect characterisation from magnetic leakage fields 77—12750
deformable solid, stress calc., finite element basis *(German)* 79—50602
delayed cracking by H_2 gathering simulations at plastically deformed notch, finite element anal. 78—31539
diaphragm supported cylindrical shells, static anal. using curved finite strip 79—27507
dielectric parts, stress patterns and deformation characts., computer anal. 80—17787
dielectric rib waveguide, propag. and radiation characts. 77—79933
difference methods for nonlinear two point boundary value problems 77—33849
difference scheme, appl. of second and third degree methods 77—5651
differential eqns. of mechanics, collocation and finite element methods 77—71198
diffusion, Galerkin finite element and finite difference anal. *(Japanese)* 79—30391
diffusion, nonlinear problem, integral soln. 78—36945

finite element analysis continued
diffusion equation, soln. by mixed finite elements *(French)* 77—71283
diffusion equations appl., linear and nonlinear *(French)* 77—78965
diffusion problems, two dimens., nuclear reactor structs., singularities in finite element approx. 77—6496
diffusion-convection, equation 1-D, finite elements method, weighted residuals 80—53775
diffusion-convection eqn. soln. 78—90888
diffusion-convection equation, stability of finite difference approximations 80—82730
diffusion-convection equations, finite difference scheme 78—42596
diffusion-type problems, mixed explicit implicit iterative finite element scheme, theory 77—22399
diffusion-type problems, mixed explicit-implicit iterative finite element scheme, soln. and examples 77—26155
direct radiator louspeaker model, vibrating shell and closed cavity radiating into semi-infinite acoustic space 80—69622
disc, thermal cycling endurance, finite element method calc. 80—48646
discrete angle finite element formulation of radiation transport 78—13197
discs, varying radial thickness, finite element dynamic anal. 79—37229
displacement hybrid finite element model of linear 3-D fracture mechanics 77—3792
displacements, strain and stress error nodal lines in finite elements 79—2606
dissipative mufflers with locally reactive lining, modelling 78—13849
dissociating turbulent gas flow around triangular rod bundle, heat and mass transfer *(Russian)* 79—68822
double cantilever beam, dynamic stress intensity factors computation and crack arrest stress intensity factors 78—34088
double edge notched specimen, elastoplasticity, curved boundary shape anal. 79—72823
double torsion fracture toughness test, 3-dimens. finite element anal. 80—30203
double torsion specimen, stress analysis 78—9567
drops, rotating, captive between co-rotating parallel faces, shapes and stability, capillarity eqns. 80—64592
duct, nonuniform, finite element method for acoustic transmission 78—83140
duct, thermal entrance region, laminar forced convection, finite-element soln. 80—10118
duct, vertical, laminar steady flow, combined forced-free convection, finite element anal. 79—27637
duct acoustic pressure distrib., Galerkin isoparametric finite element analysis 80—27144
duct entrance region, laminar heat transfer, finite element method 80—69836
duct flow, laminar, finite element methods compared to Doppler meas. 79—1253
ductile crack extension, hybrid displacement finite element model 80—28471
Dugdale model solution, of cracked bodies 78—67116
dynamic crack propagation and arrest 78—68758
dynamic destinations, removal of redundant operations in front algorithm 78—62064
dynamic finite element analysis of cracked bodies subjected to impact loading 80—69742
dynamic fracture toughness, influence on dynamic crack propag. 80—99966
dynamic problem of continua, reduction of stiffness, mass and damping matrices *(Polish)* 78—12565
dynamic response of a pressurized plane strain cylinder under impulsive distributed loading using finite elements 79—18788
dynamic stresses induced by moving cracks, numerical soln. 77—11146
dynamics analysis, rotationally periodic large space structures, transfer matrix combined method 80—74731
Earth crust deformation assoc. with fault form., finite element estimation *(Japanese)* 79—70759
Earth DC resistivity modelling for axially symmetric bodies via finite element method 79—5445
Earth electrical conductivity modelling technique 78—20357
Earth resistivity finite-difference modelling, practical approach 79—29878
Earth upper mantle, complex structures modelling by finite-element methods 77—5164
EBR-II 80—13598
ECG inverse problem solving method using finite element method *(Japanese)* 80—41272
eddy current nondestructive evaluation, finite element analysis appl. 80—35439
edge dislocation climb, numerical anal. 78—71736
edge-cracked plates subjected to transient thermal singularities, stress intensity factors 77—58612
eight node solid element for pure bending 79—44734
Einstein's gravitational field eqns., finite element method soln. 80—86177
elasti-plastic closed form stiffness matrix for axisymmetric finite elements 78—26048
elastic behaviour near an open circular hole *(Japanese)*. 80—74750
elastic circular cylindrical shells, axially compressed, stable postbuckling equilibria 78—38224
elastic compressibility, finite element displacement model 77—867
elastic contact problem with friction, solution using nodal parameters *(French)* 78—63401
elastic contact problems, in fracture mech., friction effects 78—67142
elastic contact problems, mixed approach *(Chinese)* 80—5995
elastic contact problems, soln. by finite element displacement method 77—31261
elastic contact problems with friction, nodal parameter soln. *(French)* 79—10475
elastic continuum, two-diemsional, side effects of discrete methods 79—58
elastic crack problem, soln. by superposition of finite elements and singular fields 78—38249
elastic cracked members, anal. by optimisation techniques 80—1470
elastic design problems, optimality, iterative solutions, finite element analysis and variational method 80—23887
elastic elbow, in-plane bending behaviour, finite element anal., pipeline design 78—18166
elastic flexible body dynamics, finite element anal., Hamilton's principle 78—24667
elastic half-space treatment 77—75793

finite element analysis continued
elastic incompressible body, contact problems involving forces and moments, rigid punch problems 80—53719
elastic lateral torsional buckling of unbraced and braced planar frames 79—46236
elastic massive designs, investigation of large deformations using finite-element moment system 79—41580
elastic material, finite element anal. of crack problems 78—67146
elastic mechanical systems, design sensitivity analysis, adjoint variable methods 78—90706
elastic plate, crack closure in bending, sixth order anal. 80—96231
elastic plate problems, novel finite element method 77—35063
elastic plates, cracked, buckling under tension, finite element anal. 80—53666
elastic ribbed plate, optimal design 80—14578
elastic sandwich plates, finite element anal. 78—67046
elastic shell, stable solutions of simplified problem *(French)* 79—5984
elastic shell problems, finite element anal. *(Ukrainian)* 80—69662
elastic shells, conforming finite element methods, convergence 80—53630
elastic shells, cylindrical, finite element anal., solid of rev., thin shell and interphase elements 80—74744
elastic shells, stable solutions, finite element and Newton-Raphson methods 80—14593
elastic shells, thin, doubly curved, numerical integration of triangular finite element 80—92044
elastic shells of revolution, finite-difference method *(Russian)* 79—10477
elastic shells of revolution, postbuckling finite-element analysis 77—62185
elastic solid, cracked or notched, general numerical method for three dimensional singularities 78—67137
elastic solid, difference and finite-element method for dynamical thermo-diffusion problem 77—62154
elastic stress analysis of constrained cylinders by special finite element method 80—106718
elastic structures, computer automated synthesis for minimum struct. weight 78—34015
elastic thermo-plasticity, approx., convergence 80—1435
elastic thin shells of revolution, finite element anal. of dynamics, and response to Earth motion *(Chinese)* 79—76965
elastic wave propag., one-dimens., finite element anal. *(Japanese)* 78—28961
elastic waves, spurious reflection in nonuniform finite element grids 79—14303
elastic-plastic analysis of shell structures 79—3926
elastic-plastic crack problem, comparison of finite element soln. 78—79263
elastic-plastic finite element analysis, interpolation vs. iterative soln. for Tresca yield condition 78—59312
elastic-plastic fracture mechanics, crack separation energy rates 78—46915
elastic-plastic impact problems involving severe distortions 77—17825
elastic-plastic incremental finite element anal. 78—34034
elastic-plastic initial value problem, iterative numerical integration 77—62170
elastic-plastic materials, finite deformation anal. of crack-tip opening 78—51126
elastic-plastic plane stress, direct soln. vs. quadratic programming 77—42740
elastic-plastic problems, supplementary strain method, appl. 80—96205
elastic-plastic solid containing holes in vicinity of crack tip, finite element anal. 78—67147
elastic-plastic torsion, variational inequality concept, finite element anal. 80—23907
elastic-plastic-creep-large strain analysis at elevated temperature by the finite element method 79—37185
elastic-viscoplastic analysis of plates by finite element method 78—34031
elasticity, beam bending on Pasternak foundation, reciprocal variational inequalities 80—92091
elasticity, finite element method, reduced integration 78—75066
elasticity, hybrid-stress finite element formulation for thick multilayer laminates 80—92043
elasticity, nonlinear two-point boundary-value problems 78—9566
elasticity, one-dimens. problems, diagonal mass matrices and finite element eqns. 78—73857
elasticity, thick orthotropic shell of revolution, stress-strained state, finite element method *(Russian)* 80—87713
elasticity, variational formulation of integral eqns. *(French)* 77—72181
elasticity problems, equilibrium finite element methods 80—28421
elasticity theory, finite element formulation 78—69985
elasto-plastic anal. of shallow shells *(Japanese)* 78—63323
elasto-plastic buckling of curved webs, Gauss-Seidel iterative procedure 78—34043
elasto-plastic contact problem 78—46917
elasto-plastic material, crack tip stress and strain fields and fracture behaviour, work hardening 78—22304
elasto-plastic stress and strain in cracked bars under torsion and shear calc. 79—68654
elasto-viscoplastic analysis of large deform. problems, natural finite element formalism 78—83258
elasto-viscoplastic flow, initial stress rate method 78—26047
elasto-viscoplastic thermal stress model, appl. to continuous casting of metals 79—18740
elastodynamic fields near running cracks 78—34066
elastodynamics, irregular finite element meshes, grading rules 80—68045
elastodynamics, linear, discrete time approx. of initial boundary value problems, error estimates 80—73175
elastomeric bearings, high-capacity, laminated, finite-element anal. 80—96197
elastoplastic anal. for large strains and displacement, natural factor displacement method 80—14580
elastoplastic bodies fracture, estimation of load required to start a crack *(Russian)* 79—14346
elastoplastic crack problems front soln. appl. 77—27493
elastoplastic fracture mechanics *(German)* 77—54935
elastoplastic strip or half-plane under moving load, residual stresses and plastic zones 80—53645
elastoplastic structures under cyclic loads 77—62171
elastoplastic structures with overlay materials during cyclic loading, finite element anal. 80—38280

finite element analysis continued
elastoplastic thermal stresses in axisymm. problems *(Japanese)* 78—51096
elastoplastic thick shell anal. by viscoplastic solid finite elements 78—38208
elastoplasticity, finite strain, rate problems, energy theorems, Lagrangians 80—74766
elastoplasticity, large deformation finite element formulation 77—75819
elastoplasticity, variational method using mixed finite elements *(French)* 79—72819
elastoplasticity algorithm, finite difference and variational methods in flow theory models 77—871
elastostatic end problems for finite cylinders 80—10143
elastostatics, combination of boundary and finite elements 79—92941
elastostatics, error estimates of finite element approx. 80—8793
electric and magnetic fields, 2D open boundary problems 78—94354
electric field, permittivity meas. through ponderomotive forces determ. 79—215
electric field automatic computation, three methods, comparative study *(French)* 79—68346
electric field calc. appl. *(Italian)* 79—94124
electric field computation by charge simulation and finite element methods 80—95759
electric fields, intensity, numerical calculation methods *(French)* 80—106413
electric- and mag.-fields with open boundaries, two-dimensional 78—22064
electrical and magnetic field problems, book 80—62399
electrochemical mechanisms, simplex fitting and finite difference simulation anal. 78—44381
electroelasticity problems, numerical soln. 80—80707
electromagnetic field anal., computer methods, MHD and finite elements method 80—32879
electromagnetism, stationary boundary value problems, finite element analysis *(Polish)* 79—98258
electron optical element computation 79—31785
electrostatic fields, element function shape, geometry matrix *(Polish)* 79—3609
electrostatic fields calc., finite element method using cubic potential distribution *(German)* 80—32872
elliptic boundary value problem, second order, hybrid finite element methods, Dirichlet problem 78—73835
elliptic problems with singularities 78—41140
elliptic variational equality, of Bingham type, approximation *(French)* 77—47048
elliptic-hyperbolic eqns. finite element soln. 77—33851
EM field laws integral forms, finite element method equations derivation 80—18961
EM fields, static and stationary, solving methods 79—36815
e.m. induction in Earth, two-dimens., finite difference soln. 77—2101
EM instruments for use in liquid sodium, theoretical anal. 78—54857
EM modelling, finite element program package 77—73874
EM NDT phenomena, fissile element modelling 80—40633
EM scattering calculations, boundary element method 78—90347
embedded semicircular surface crack, stress intensity factors, superposition methods 80—79217
endochronic plasticity, appl. to structural dynamic response of radioactive waste containers 80—16407
energy principles and finite element formulation *(Japanese)* 79—80437
engineering applications of finite-element and finite-difference methods 78—57765
engineering design, numerical, vital role of expt. stress anal. 79—32418
engineering problems, numerical anal. based on finite element method, wave propag. problems *(Japanese)* 78—28928
enriched isotope target preparation, design of quasi-hyperbolic electrostatic fields 80—23597
entrance flow, laminar, ducts of arbitrary cross-section 77—72351
environmental release prediction digital simulation 78—92880
environmental systems control, transient finite element and linear programming method 79—57497
epoxy adhesive layers, interlaminar stress distrib. in nonlinear range 79—39117
EPR spectral simulation via finite elements, variational method and stochastic-Liouville eqn. 79—85157
equilibrium and elastic stability problems, appl. of triangular facet shell element method, TRUMP 77—46946
equilibrium equations soln. for rapidly rot. stars 78—65601
equilibrium models in finite element elasto-plastic analysis 79—81742
error estimate for the approximation of Stokes problem by a conforming quadrilateral element *(French)* 79—49039
estuary water quality models, finite difference and finite element methods 78—77375
Euler equation in two dimens., numerical approx. *(French)* 80—48715
EURDYN, nonlinear transient dynamics programs for fast reactor safety 80—91234
EURDYN-1M, safety studies on LMFBR, computer program 80—99267
evaporation and condensation, BGK eqn., kinetic anal. 77—11683
even-parity transport eqn., complex trial functions 79—59108
evolution systems and convection-diffusion, stiffness and stability, Gershgorin theory 80—77626
evolutionary problems, error anal. of finite difference, finite element and spectral methods 80—46815
explicit finite difference method, anal. of dynamic crack and fracture 77—75860
extended plane fluid sheet, swelling finite element anal. 79—37277
exterior linear elliptic problem, numerical method, appl. to 2-dimens. wave resistance 80—28485
exterior regions containing moving conductors 79—41291
extrudate swell, thermally induced, Galerkin method 80—79312
F_2-layer, plasma continuity eqn., comparative anal. of numerical soln. methods 78—69578
fast fracture and crack arrest, finite difference anal., appl. to steel, epoxy resin 78—1607
fast ion Fokker-Planck code FIFPC 78—34342
fast reactor, dynamic elastic response of subassembly ducts to impact loading 80—18536
fast reactor energy excursion hydrodynamics, structural response 80—18537
fast reactor fuel pellets, crack pattern analysis 79—54497
fastener details, stress analysis hybrid finite element 77—54879

finite element analysis continued
fatigue crack, macroscopic residual stress at tip, X-ray obs. and finite element anal. *(Slovak)* 78—19885
fatigue crack closure, and delay effects under mode I spectrum loading, elastic-plastic anal. 80—19282
fatigue crack closure, influence of mech. factors 78—67100
fatigue crack closure and delay effect under variable amplitude loading, finite element anal. 77—73331
fatigue crack growth prediction methods, model development 78—34074
fatigue crack path prediction by finite element method *(Japanese)* 78—42568
fatigue crack propag., in deformable media with nonlinear characteristics, model 78—63393
fatigue growth of internal cracks 80—1472
fatigue growth of internal elliptic cracks in thick plate 77—80112
FEBIE—a combined finite element-boundary integral equation method 79—2633
femoral stress and strain calc. *(German)* 79—2089
femur, human, finite-element plane stress model 79—79590
femur, loaded, intact and with prostheses, strain gauge meas. 77—60228
ferroelectric cylindrical shells, appl. of one-dimensional finite elements to normal mode anal. 77—31163
ferromagnetic cantilevered beam plate, magnetoelastic buckling 79—18761
fetal head moulding, finite element model investigation 80—67129
fibre reinforced composite, hygrothermal microstresses, in material exhibiting inelastic behaviour 77—84141
fibre reinforced composite, stochastic three dimensional finite element structural anal. 78—30188
fibre reinforced composites, angle ply, delamination mechanics and failure mode 80—79236
fibre reinforced composites, transverse plane, elastic, failure behaviour *(Japanese)* 78—48510
fibrous composite, thermal crack propagation anal. 80—10205
field analysis computers, colloquium, London, England (March 1980) 80—94964
field problem inference-finite element model 78—81923
field problem structure, equilibrium, eigenvalue and propagation problems *(Rumanian)* 78—45520
field problems, multi-terminal representations appl., graph theoretical field model 80—90689
finite centre crack specimen, biaxial and nonlinear effects on energy release rate, J-integral 78—18232
finite difference and finite element relationships 77—26154
finite difference approx. of boundary conditions along irregular boundaries 78—36804
finite difference calc., campylotropic coords. for boundary value problems 78—65757
finite difference modelling, P-pulse propag. in elastic media 77—73868
finite difference technique, involving discontinuous derivatives, for flow problems 79—32435
finite elastic struct. immersed in acoustic medium 79—7254
finite elasticity solns. using hybrid finite elements, complementary energy principle, incompressible materials 79—63044
finite elements equivalence for nearly incompressible elasticity 77—68421
finite elements in fluids, book 79—32441
finite plate with circular hole, summary of SIF design graphs for cracks 79—23278
finite-difference scheme, elastic wave in vertically inhomogeneous media 77—73675
finite-difference/Galerkin finite element soln. for turbulent boundary layer 78—26104
finite-differential element nets, topological props. 77—67247
fission reaction fuel, kinematic hardening rule of plasticity 80—42764
fission reactor, effect of radiative heat transfer on thermal fluid behaviour of molten UO_2 79—93783
fission reactor, FAXMOD anal. of creep and sheath ballooning 80—42759
fission reactor, FEM anal. of pellet-clad bonding 80—42765
fission reactor fluid dynamic transient analysis using ASWR method with staggered meshes *(German)* 80—83176
fission reactor fuel pellet-cladding interaction, theoretical analysis 79—93699
fission reactor fuel performance anal. by finite element method 80—42750
fission reactor fuel rod deformation code FEMAXI-II and its application 80—37446
fission reactor Na pump, multimode heat transfer, computer codes 79—610
fixed-free generally orthotropic beam vibration finite-element models 79—68621
flames, premixed, laminar, time-depend. soln. determ. 78—67282
flange, rigid-plastic deformation in deep drawing process, finite element anal. 79—18735
flanges, elastic-plastic deform., thermal stress effects calcs. *(German)* 78—34029
flat skin-stringer structures, finite strip analysis 78—30220
flexible cylinder, structural-acoustic response of mech. excitation 79—3839
flexible plate, stress distrib. through crack 77—89074
flow, annulus entrance, heat transfer 79—4013
flow, curved (straight) channel entry, slender channel approx. 78—47042
flow, in channel array with interconnections, finite-difference scheme 79—4012
flow, incompressible and viscous, finite elements for numerical simulation, error estimates 79—1151
flow, multiply connected flow fields, numerically mapped macro-elements 79—1252
flow, optimum finite element mesh design 80—36867
flow, Ritz-Galerkin and least squares methods 79—1150
flow, rod cluster with blockage causing recirculation, finite difference method for temp. 79—3200
flow, separating, fluid-surface interface, static contact line, slip at wall and shape of free surface 80—53737
flow, subsonic and transonic, finite element formulation 80—28526
flow, turbulent, developing in circ. pipe 79—1164
flow, variational methods, book contrib. 79—32456
flow, viscous and inviscid, incompressible, computation methods 80—17806
flow and boundary layer development, finite difference and marching integration in straight core annular diffusers 80—53760

finite element analysis continued
flow between rotating discs, finite element anal. using exponentially weighted basis functions 78—16655
flow due to gravity, free surface, variable domain method 78—79294
flow field, multiply connected, curvilinear coords. and macro-elements 80—19318
flow in ducts, quasi-one-dimensional fluid, time depend. computations 77—84324
flow in pipe, laminar friction factor and heat transfer, finite-element technique 80—10247
flow in porous media, diphasic incompressible, diffusion-convection eqn., mixed finite element method, water flooding 80—74969
flow of recirculating type, numerical methods in Navier-Stokes eqns. 79—1202
flow problems in highly irregular domains, by finite-difference method 80—6166
flow through porous media, book contrib. 79—32665
flows with complex structure, numerical simulation, finite element methods 79—49055
fluid, superposed, stability, book contrib. 79—32467
fluid discontinuities, subgrid resolution in tracking methods 80—105506
fluid dynamics, 2-D incompressible Navier-Stokes flow, finite element MAC scheme 80—74824
fluid dynamics, axisymmetric Newtonian jets, die-swell, Galerkin finite element method 80—83830
fluid dynamics, boundary deform., Galkerkin finite element technique for multidimensional flow 80—86089
fluid dynamics, coarse mesh methods appl. *(German)* 77—88197
fluid dynamics, convection problems approx. 77—89115
fluid dynamics, groundwater flow, finite element eqns., Newton iteration and modified conjugate gradient method 80—77622
fluid dynamics, laminar flow, viscous fluid in toroidal tube, oscillations 80—79253
fluid dynamics, laminar flow in entrance region of ducts, marching technique 80—69761
fluid dynamics, lined ducts, eigenvalue problem, Hermitian elements 80—74983
fluid dynamics, Navier-Stokes equations, finite difference approx. with second-order accuracy 80—87756
fluid dynamics, Navier-Stokes equations, finite element soln., applied to blood flow 80—94269
fluid dynamics, Newtonian fluid, recirculating flow in rectangular cavity, free convective flow in enclosed container 80—74852
fluid dynamics, non-Newtonian, finite element routine using mixed method 80—103045
fluid dynamics, nonconventional methods, book contrib. 79—30257
fluid dynamics, partial differential eqns. 77—80135
fluid dynamics, partly elliptic flows, EMIT numerical procedure 80—79255
fluid dynamics, Poisson equation, non-uniform grid, finite-difference, matrix decomp. technique 80—69756
fluid dynamics, porous flow, new mathematical models 80—83837
fluid dynamics, pseudo-upstream finite difference scheme for advection 80—106773
fluid dynamics, small-disturbance transonic flow, nonlinear mixed elliptic hyperbolic eqn., finite element anal. 80—83814
fluid dynamics, stationary Navier-Stokes eqn., discretisation, splitting of linear operators, iterative methods 80—69755
fluid dynamics, transonic flow problems, modified FLIC method, finite element anal. 80—74911
fluid dynamics, two-phase flow with condensation, U enrichment by photochemical laser, mathematical model *(French)* 80—74029
fluid dynamics, unsteady compressible 3-D boundary layer flow 80—103011
fluid dynamics, viscous flow, unsteady, around elliptic cylinder, heat transfer, finite difference method *(Japanese)* 80—69831
fluid dynamics, viscous fluid, laminar flow, Navier-Stokes eqns., central difference scheme 80—69762
fluid dynamics, viscous-convective type flow, mixed finite element soln., discrete least squares approach 80—74851
fluid dynamics, water boundary layer along heated cylinder, buoyancy and variable viscosity effects 80—79256
fluid dynamics problems 77—26158
fluid flow, book 77—903
fluid flow, finite element method 79—9119
fluid flow, finite-difference schemes, comparative criteria 78—5720
fluid flow, hybrid finite element methods 79—9120
fluid flow, numerical methods comparison 79—9123
fluid flow analysis, in plasma centrifuges, third-order differential equation solution *(Japanese)* 80—53949
fluid flow problems 77—80138
fluid flow simulator, free boundaries, surface tension effects 80—82647
fluid flows with large density gradients, Eulerian finite difference technique 77—79424
fluid mechanics, book contrib. 77—45702
fluid mechanics, book contrib. 79—32446
fluid structure vibr. eigenvalue problems, finite elements, modal methods 80—96269
fluid-struct. interaction, added mass computation by boundary integral method 78—38228
fluid-structure coupling method in dynamic analysis of structs. 79—7322
fluid-structure systems, time integration, mixed methods 79—41568
fluid-structure systems, transient anal. 79—32232
fold propagation in rocks 77—53049
folding of single viscous layer, role of initial perturbs., finite element anal. 78—49003
FORTRAN subprograms for finite difference formulae 78—28927
fracture, appl. of continuum theory of dislocations fracture mechanics 78—67767
fracture, dynamic analysis with Lagrangrian finite difference method 77—35095
fracture, post-yield, numerical investigation 78—18249
fracture anal., symmetry and nonlinearity 77—3791
fracture analysis, 2D linear, elastic, finite element anal. vs. the edge function method 80—99963
fracture femur fixation device, optimum design 78—36050
fracture fixation, oblique, mechs. 77—52922
fracture initiation, strain velocity effects on critical crack opening displacement 79—18818
fracture initiation site prediction, idealized polycrystalline materials, stress and strain fields 78—34092

finite element analysis continued
fracture mechanics, appl. to nuclear reactor materials 77—42095
fracture mechanics, calc. of integral J_1 78—67129
fracture mechanics, conformal mappings to delete singularities, finite element anal. 77—72251
fracture mechanics, elastic-plastic, use of conventional and hybrid-displacement model 80—1489
fracture mechanics, plasticity, finite element anal., review 79—41612
fracture mechanics, self-adaptive finite element capability 79—14345
fracture mechanics, self-adaptive finite elements 77—72249
fracture mechanics appl. 77—3790
fracture problems, conic-section simulation anal. using finite elements 77—3773
fracture problems, finite element mesh optimisation 78—34070
fracture toughness, J-integral rel. to crack tip opening displacement *(Japanese)* 78—42569
fracture toughness parameters J and G^{Δ}, effect of load biaxiality 78—67128
frame nonlinear postbuckling behaviour 77—62183
free jet impingement calculations by finite element methods 80—28541
free shear, channel and turbulent flows, finite element anal. 79—68808
free surface flow digital simulation 78—90819
free vibrational analysis of frame structures 79—32329
free vibrations of antisymmetric laminated plates, including transverse shear deformation 80—53683
free vibrations of conical solid horn with flange *(Japanese)* 80—79045
free-surface flows, stream functions variational principle, finite element anal. appl. 79—64675
frequencies of orthotropic circular plates elastically restrained against rotation, large amplitude axisymmetric vibrations 80—83750
frequency anal. of unsupported structures 79—32333
frictionless elastic contact problems, approximate soln. 78—16646
frictionless tidal channel behaviour 78—92876
frontal method for structural mechanics, algorithm for excluding unknowns 80—79157
frontal solution algorithm for finite element frequency analysis 79—3942
fundamental ideas homework exercise 77—26157
fusion reactor, finite element anal. of structural response of superconducting magnet 77—3166
fusion reactor, magnetic confinement, structural anal., combined interactive/batch computer environment 80—91255
fusion reactor, PDX, toroidal field coil and frame struct., anal., finite element anal. 80—106165
fusion reactor, PDX power test results, struct. finite element anal. 80—91265
fusion reactor, PDX Tokamak, finite element anal. using computer graphics 80—95424
fusion reactor, PDX Tokamak, struct. anal. by finite element method 80—106166
fusion reactor, SLPX TF coil, stress anal. using COSMIC-NASTRAN 80—106168
fusion reactor, three-dimens. solid finite element anal. for simulating composite windings 78—55003
fusion reactor, Tokamak constant tension D-shaped coils, lateral support struct. 78—55013
fusion reactor anisotropic B_T-coil two-dimens. finite element anal. of laminate sliding 78—50382
fusion reactor B_T-coil stress anal., constraint finite element anal. for contact problem 78—55004
fusion reactor ceramics, Weibull probabilistic design approach 79—93822
fusion reactor design, dynamic analysis of electromagnetomechanical field by finite element method *(Japanese)* 78—8967
fusion reactor eddy current analysis, finite element circuit method 78—66373
fusion reactor JT-60, alternating mag. field, three dimens. finite element anal. 80—18663
fusion reactor solenoid, orthotropic, finite element stress anal. 78—55010
fusion reactor superconducting magnet magentoelastic energy calcs., finite element anal. 78—55002
fusion reactor TESPE coil, finite element method calc., winding package modelling 78—50376
fusion reactor toroidal field coil finite element stress anal. 80—91256
fusion reactor toroidal field coils, stress anal. by finite element method 80—13926
fusion reactor vacuum vessel, magnetic stress induced by plasma motion, 3-dimens. anal. 78—66370
fusion reactor vacuum vessel, stress anal. 78—66371
fusion reactors, high-energy water-cooled heat sink and 25 MW power tube 79—49838
Galerkin finite element analysis of harbour channels 79—2286
Galerkin finite element procedure for analyzing flow through random media 79—81967
Galerkin finite element-finite difference soln. of laminar boundary layer flows 78—42586
Galerkin for lakes or bays landslide wave generation simulation 78—92879
Galerkin method, fluid flow appl. 79—9118
Galerkin-finite element formulation in viscous flow 79—14367
Galerkin-finite element simulation of the effects of artificial recharge on flow and chemical quality in an alluvial aquifer 78—81263
gas-dynamics, non-stationary, one-dimens., computational methods *(Russian)* 77—19618
gas-liquid interaction in turbulent reacting flows, mathematical model 80—83862
gas-particle flow in shock tube, finite difference calc. *(Japanese)* 80—79390
general shell and axisymmetric shell elements, diagonal lumped mass matrix formulation 79—3911
general shell finite elements development 78—87274
generalised finite element method for magnetostatics 79—41270
geology, finite element models of folding 79—20788
geometrical nonlinear shell theory, continua with warped cross section *(German)* 79—23210
geometrically nonlinear anal., correlation of finite element notations 78—42527
geometrically similar elements 78—57760
geophysical prospecting, instability of finite difference schemes due to boundary conditions 77—21912
geophysics, interpretation of pulse neutron logging data in inhomogeneous beds *(Russian)* 79—44273

finite element analysis continued
geothermal heat, extraction by water circulation through crack in dry hot rock mass 79—57355
geothermal reservoir exploitation, finite difference modelling 80—55798
glacial isostatic adjustment and sea level, global finite element model 79—20800
glass, indentation process analysis using finite element method 77—12689
glass, ion-exchanged, anomalous stress profile, photoelastic meas. 78—90803
glass, narrow sandwich seals, shape factor, finite element anal. 78—75111
glass fibre reinforced plastic, cemented joint of cylindrical shell with cover, stressed state 80—69668
glass fibre reinforced plastic, laminate, stress anal. finite element modelling 79—59924
glass fibre reinforced plastic, strength dispersion, statistical anal. *(Japanese)* 79—61655
glass fibre reinforced polyester, plate struct., skeletal member effect on stiffness and strength, finite element anal. 79—91733
glass plate, stress analysis of large deflection by finite element method 77—7307
glass-metal seal, finite element anal. of stresses, photoelastic meas. 79—29197
global element method for elliptic partial differential equations 80—46805
global wavefunctions, appl. to scatt. theory 78—41179
graphite fibre reinforced epoxy, epoxy matrix, effect of material variability on predicted environmental behaviour, numerical anal. 78—90733
graphite fibre/epoxy laminates, free edge induced failure 80—11775
graphite-epoxy laminates, AS/3501-5, compressive fracture strength 79—43396
gravitational collapse, finite-particle scheme for three-dimens. gas dynamics 78—67218
gravity wave problem, upstream difference method 80—106806
gravity waves, one-dimens., finite-element and finite-difference techniques comparison 79—18902
gravity waves, two-dimens., finite-element and finite-difference techniques comparison 79—18903
groundwater, hillslope hydrographs using finite element method 77—70696
groundwater, two-dimens. contaminant transport simulation 77—78287
groundwater, unsteady flow through tunnel opening, reductive finite element/Crank-Nicolson anal. 78—92861
groundwater discrete kernel generator model 78—92873
groundwater flow, unconfined, tunnel opening, 2-D finite element anal. 78—11922
groundwater flow anal. 78—92875
groundwater flow calc. 78—89320
groundwater flow model 78—92874
groundwater flow systems, three-dimens. modelling 79—84318
groundwater singly dispersive convection, finite-difference simulation 77—37265
groundwater unsteady flow from tunnel opening *(Japanese)* 78—96251
groundwater unsteady flow in porous medium with sloping impervious bedrock 80—12459
groundwater with convective dispersion, book contrib. 79—34877
gyrating charged particle beam compression, modeling with finite circuit element code 80—14930
H-columns, local and member buckling finite strip method anal. 79—7306
Hastelloy-X, low cycle fatigue crack propagation at 25°C and 760°C 80—104270
head response to impact loading, parametric study 77—48826
heart, cross-sectional shape change during beats, simulation 77—44714
intact heart stress and strain three dimensional finite element anal. 77—66821
heat and mass transfer, finite element soln., for chemically reacting system 80—68153
heat and mass transfer in porous bodies, two-dimensional isoparametric finite element method 77—42708
heat and momentum transfer, viscous incompressible laminar flow, constricted duct 77—80155
heat conduction, fluid in contact with surface, transient temp. field, mesh refinement method 80—69825
heat conduction, transient problems, finite element and matrix methods calcs. 78—94515
heat conduction anal., stable explicit algorithm 77—46885
heat conduction anal., use of reduced eigenvalue method 77—3711
heat conduction and natural convection in phase change region 79—41563
heat conduction eqn., Crank-Nicolson noise control 77—75769
heat conduction equation, formulation in general orthogonal curvilinear coords. 77—14882
heat conduction equation with radiation boundary condition, implicit iterative soln. 78—5635
heat conduction in reactor solids 78—62593
heat conduction inverse problem 80—10112
heat conduction numerical soln. oscillations, nonlinearity allowance scheme effect *(Ukrainian)* 78—90625
heat conduction problems, method of finite elements 79—14204
heat conduction problems solution, quasilinear, time spacing selection *(German)* 80—33418
heat conduction transient, two-dimens., crit. time step for finite element solns. 78—71260
heat conduction with moving boundary *(Russian)* 80—38216
heat conductivity, temperature distrib. *(Russian)* 80—74701
heat equation, semilinear, blowing up of finite difference soln. 77—54854
heat exchanger tube, elastically constrained, forced vibration response 79—81786
heat exchanger tube, vibratory contact with support plate, forces produced 77—88211
heat transfer, calc. *(Japanese)* 78—89414
heat transfer, finite element nonlinear analysis, using an explicit stable method 77—89004
heat transfer, nonlinear, iterative-variational method 78—94511
heat transfer and flow through hydraulically induced fracturesin hot dry rock 79—34424
heat transfer calcs., finite element anal., HEATRAN, diffusion eqn. soln. 77—3710
heat transfer coeffs. determ., use of simplex direct search and finite element methods 77—3712

finite element analysis continued
heat transfer optimal control problem, finite element and conjugate grad. methods 80—19220
heat transfer simultaneous eqns. soln., matrix iterative substructuring 79—10564
helical compression springs, finite elements for dynamical anal. 80—96191
Helmholtz-eqn., eigenvalues by boundary integral eqn.-finite element method 77—71195
heterogeneous multiaquifer systems, iterative quasi-three-dimens. finite element model 79—79905
'heterosis' finite element for plate bending 79—3933
hierarchal elements and precomputed arrays 78—62063
hierarchical approx. 77—71197
high precision triangular laminated anisotropic cylindrical shell finite element 78—79206
higher order method for transient diffusion anal. 78—12653
hip bone stress analysis using finite element model 78—44518
hip prostheses femoral component biomechanics, bone cement stress 80—56285
hip prosthesis, analytical approaches to femoral stem stresses 77—44849
holed plates, stress and deformation, finite quadrilateral elements technique *(Rumanian)* 79—18707
Holmalite-100, dynamic photoelastic and dynamic finite-element analyses of dynamic-tear-test specimens 79—55348
Homalite-100 plate, fracturing, dynamic, energy release rates 77—7340
Homalite-100 plates, modified compact-tension specimens, dynamic anal. 80—97561
homopolar machine for fusion experiments, calc. of steady state mag. fields 77—23288
horizontal fluid layer in porous medium, convective instability, critical Rayleigh number 80—64564
horizontally curved beam finite element including warping, nodal displacement degrees-of-freedom 79—44735
horn loudspeaker, anal. of acoustic radiation by finite element method 80—96171
HTGR, annular fuel rod, contact viscoelastic stress anal. *(Japanese)* 78—54817
HTGR fuel and graphite structure stress analysis methods and programs *(Japanese)* 78—74434
human left ventricular wall finite element stress analysis 77—64079
human torso surface isopotential simulation using simple conduction-elec. field model with Neumann boundary 80—89706
hybrid, mathematical theory, accuracy, convergence and criteria for use 77—49581
hybrid displacement method, simplified, appl. of line integrals 78—89314
hybrid element method, calc. of vibr. freq. 77—26173
hybrid elements, historical note and definition 78—57761
hybrid-stress models for elastic-plastic analysis by the initial-stress approach 79—32288
hydraulic fracturing operations, material and structural simulations 78—31540
hydraulics, variational inequality approx. 77—13613
hydrocode convergence 78—36834
hydrodynamic model using smooth elements, estuarine appl. 80—98356
hydrodynamics codes, Eulerian and Lagrangian, pressure iteration, multigrid method 80—53738
hydrodynamics models, nonstationary gas flow, two dimens., variational approach to finite difference scheme 78—51147
hydrodynamics simulations, frontal solution method, finite element anal. 80—74825
hydrological system tracer digital simulation 78—92881
hyperbolic differential equations, difference and finite element anal. methods 79—49059
hyperbolic eqns. in one space dimens., finite-difference approx., method of lines 77—2525
hyperbolic initial boundary value problems with damping, Galerkin-Obrechkoff numerical methods 77—45686
hypervelocity impact initial stages 77—41
IGFET, simulation of semiconductor transport using coupled and decoupled solution techniques 80—65695
imbedded neutron flux calc., reconstruction of original material struct. of fuel bundle 77—88196
impact, high velocity, three dimens. anal. 77—65674
impact test, fracture toughness 78—68806
impacted pretensioned plate, dynamic finite element and photoelastic analyses 78—67111
impedance plethysmography and appl. of finite-element method, torso model and elec. potential distrib. 80—30958
implant design analysis 80—30932
implicit finite element algorithm for geometrically nonlinear problems of struct. dynamics, stability anal. 78—86157
implicit finite element algorithms for geometrically nonlinear problems of struct. dynamics, accuracy anal. 78—86158
implicit-explicit finite elements in nonlinear transient analysis 79—44729
implicit-explicit finite elements in transient analysis: implementation and numerical examples 79—17216
implicit-explicit finite elements in transient analysis: stability theory 79—17215
impression creep, digital simulation by finite element method 78—7142
in-stream settling basin sediment routeing, convective dispersion model 77—37272
incompatible basis functions in boundary value problems, variational techniques appl. to thin elastic plate 80—48587
incompatible quadrilateral basis functions 78—41146
incompletely integrated shape functions, numerical stability, finite element stiffness matrices 78—1567
incompressible elasticity, two dimens., conforming finite element method 79—63039
incompressible flow, high Reynolds no., book contrib. 79—32442
incompressible flow, Navier-Stokes eqn. soln. by integro-differential method 77—72266
incompressible flow, stream function-stress function approach 79—1146
incompressible flow fields, finite element dual variational anal. 79—40375
incompressible fluid flow past flat plate 77—13615
incompressible materials, approx. in displacement method 79—72801
incompressible solid, plane strain deformation, finite element anal. 79—1114
incompressible turbulent flow problems, appl. of mixed finite element methods 79—64638

finite element analysis continued
incompressible viscous flow, finite element-anal. by penalty function formulation 79—41651
incompressible viscous liquids, dynamic anal. 80—48729
Inconel, steam generator tubing, mag. probe inspection 80—85119
incremental, variational principles 77—50881
indentation of elastic half-space by rigid rectangular punch 78—18167
induction motor, polyphase, at no-load, nonlinear magnetostatic field determ. 78—33647
inelastic rate problems, improved soln. methods 79—18733
inelastic structural behaviour, finite element computational aspects 78—42546
infinite cracked isotropic sheet, under symmetric loads, Green's functions for stresses, stress intensity factors and displacements 80—99967
infinite elements 77—13590
infinite finite elements 77—71196
initial value problems, finite element, unconstrained variational approach 77—67256
initial value problems soln., unconstrained variational formulation 77—87637
initially stressed Mindlin plates, finite strip method, buckling anal. 78—26067
instability, dynamic, computation by finite element method 80—23927
insulating and semiconducting media, electric field numerical soln. *(Slovak)* 78—66710
integrated load increment method for finite elasto-plastic stress analysis 80—92072
integration of triangular elements containing corrective rational functions 77—13591
intensive finite element grading for stress concs. 78—55587
interblock hydraulic conductivity values for transient unsaturated flow problems, finite difference soln. 80—12460
internal fixation plate, effect on long bone remodelling 77—48935
internal fixation plates, evaluation of 1-, 2- and 3-dimens. finite element and exptl. models 77—48934
interpolation to boundary data in tetrahedra, appl. to finite elements 77—5645
intervertebral joint, systems identification for material props. 78—69125
inviscid barotropic vorticity eqn., soln. by finite difference, finite element and pseudospectral method 80—43687
inviscid fluid conservation law eqns., coeff. matrices for implicit finite difference soln. 78—42580
ion beam extraction, computer simulation, finite element method 80—96387
ionising shocks reflection in shock tube *(Japanese)* 78—42629
ionization-diffusion oscillations in glow discharge plasma, rel. to stepwise ionization 78—1927
irregular cavity acoustic impedance 78—42483
irrotational flow problems with free surface, inverse variable domain finite element anal. 77—68563
isochoric const. strain finite elements, modification of TRIM 3, TET 4, and TRIAX 3 elements 78—41144
isoparametric, integral equations variational, for three-dimensional fields 77—87635
isoparametric 2-D element based on Hermite bicubic interpolation scheme 78—24648
isoparametric cubic finite elements, curved edge eqn. 79—12584
isoparametric elements 78—45479
isoparametric elements flexible finite difference stencils 78—4472
isoparametric elements for linear elastic fracture mechanics 77—14957
isoparametric finite elements for free vibration analysis of shell segments and non-axisymmetric shells 80—23944
isoparametric Hermitian element for field problem solns. 78—24649
isoparametric linear bending element and one-point integration 79—3919
isoparametric nine-noded finite elements, accuracy 78—26039
isoparametric quadrilaterals, integration formulas 78—89317
isoparametric shell element moment balance 77—14903
isoparametric shell elements study *(Japanese)* 78—34016
isoparametric surface contouring algorithm 79—30215
isoparametric surfaces contouring 78—20948
isotropic plane sandwich plates, constant shear theory 80—99943
iterative algorithm for continuous stress and displacement solns. 79—1109
iterative algorithm for continuous stress field anal. 77—72179
iterative method using Kantorovich meth., appl. to MHD duct flow 77—74205
iterative methods in finite element anal. of reinforced concrete, convergence 78—38186
iterative procedures for penalty function solns. of algebraic systems 78—57770
iterative refinement method solving sparse matrix 77—2521
J-integral evaluation for CT specimen 78—67131
jet, buoyant, turbulent in cross flow, finite difference method 78—90907
jet flow with surface tension, viscous flow 78—79349
Kirchhoff plates and shells, conforming approx. 79—90129
Kirchhoff shells, static and dynamic anal. based on mixed finite element formulation 79—32328
Klein Gordon equation, equivalent variational integral, numerical soln. by finite element method 78—78064
Lagrangian method for barotropic fluids 77—68562
lake, wind-induced circulation and water level changes, two-dimensional finite difference model 78—77287
lakes, circulation, seiches, tides and storm surges, finite element methods, book contrib. 79—34876
laminar boundary layer flow with suction (blowing) and pressure gradient, finite element anal. 79—18866
laminar boundary layers, integral eqn. finite element soln. 80—10127
laminar flow, algorithm *(Chinese)* 79—72874
laminar flow, driven, in square cavity 80—23983
laminar flow in circular tubes, forced and combined convection, finite difference anal. 80—48711
laminar flows of viscoelastic fluids in concentric annuli with axially moving boundaries 78—79295
laminar incompressible boundary layer eqns. finite element soln. 78—79304
laminate, ±45°, multilayer hybrid-stress finite element analysis of through-thickness edge crack 77—54928
laminate, stress anal. finite element modelling 79—59924
laminated composite plates, stress/strain relation, finite element anal. 79—17219

finite element analysis continued
laminated composite shells, mixed isoparametric finite element models 77—78979
laminates, angle ply, 3D finite difference soln. of free edge effect 80—79152
laminates, cross-ply, edge effects, traction-free-edge condition satisfaction 80—79151
laminates, damage zone failure analysis 80—85059
laminates, symmetric, new results on edge effects 77—46971
large amplitude water wave digital simulation 78—92851
large defection anal., hybrid finite element and finite difference approach 77—72201
large deflection anal. of tail-wheel struct. of light aircraft 78—83272
large deformation elastoplastic analysis of arbitrary shells, triangular finite element 78—83257
large finite element method 77—78963
large strain applications of modified const. strain finite elements 79—2632
large strain inelastic analysis, quasi-static problems, finite element anal. 80—14568
large strains problem, formulation in terms of true stress and logarithmic strain 80—23901
large structural systems with local nonlinearities, finite element dynamic anal. 79—44711
large-scale lossy groove array finite difference analysis 77—27420
lateral tibial plateau, axisymm. finite element anal. 78—69127
leaky aquifer anal. 78—93017
leaky aquifiers, integrodifferential eqns., numerical method of unlimited appl. 78—11935
left ventricle active model deform., nonlinear finite element anal. 78—35877
left ventricular flow pattern index of pumping efficiency 79—96601
LF fields in linear media, two-dimensional finite element analysis 79—41297
light beam propagation through moving aqueous aerosol cloud containing medium 80—91750
limit analysis, complete static solns., appl. to vertical cut *(French)* 79—18702
limit torsion problems, finite element method, failure torque 79—72820
linear accelerator cavity anal., evaluation of LACC program 78—90000
linear accelerator cavity code, based on finite element method 78—33307
linear constraint eqns., soln. algorithm 78—24654
linear elastic continua, variational principles, finite element techniques *(German)* 79—9113
linear elastic half-space, frictional unloading problem, variational soln. for stress analysis 78—59350
linear elasticity, finite error approx., error estimates for continuous time approx. 80—52024
linear elasticity systems, finite equilibrium element models *(French)* 79—21550
linear equations systems solution, unsymmetric, sparse, computer program 77—80210
linear fracture mechanics using isoparametric finite element 77—22420
linear hydrodynamics exterior problems, variational formulation 79—32434
linear multipole, plasma simulation, finite element model 80—1837
linear plate bending, finite difference energy techniques 79—55330
linear strain triangular element solns. 78—90719
linear structures, complex, eigenvalues numerical bracketing *(French)* 80—42053
linear system solution by modified Stone finite element method *(French)* 79—41279
linear systems with sparse constraints, incompressible materials appl. 77—39224
linear viscoelastic bodies, approx. anal. using Legendre polynomials, finite element soln. *(Japanese)* 78—83266
linear viscoelasticity, finite element method variant 80—69692
liquid crystal laser self-focusing, effect of spatially dispersed nonlinearity 80—38908
LMFBR, comparison of neutron diffusion computer codes 77—88188
LMFBR, finite element formulation for thin reactor struct. thermal stress anal. 78—70613
LMFBR, large EM induction pump for high-temp. appl. 78—17291
LMFBR components, plastic dynamic anal., CEA-SEMT system 77—6506
LMFBR cores, numerical method for predicting subassembly seismic induced impact 78—74447
LMFBR DNB oscillatory temp. and thermal stress anal. 79—6767
LMFBR piping components, resistance to bending moments 77—6505
LMFBR shell structures, finite element elastic-plastic anal. 78—41804
LMFBR subassembly ducts dynamic response, comparison of finite element code with expts. 78—70614
LMFBR subassembly simulation, finite element computer model, safety anal. 78—70612
load increment analysis, elastic-plastic analysis of anisotropic materials by variable stiffness finite element method 77—7319
local mesh refinement with finite elements for elliptic problems 79—9091
LORA—an accurate four node stress plate bending element 79—27527
loudspeaker, cone, vibration analysis using finite element method *(Japanese)* 79—18660
loudspeaker cones, effect of voice-coil and surround on vibration and sound pressure level 80—96172
Love waves in 3-dimens. structures, propagation analysis 80—21631
low cycle fatigue and plasticity testing, specimen verification 80—30202
lubrication, point contact problem, finite element anal. 78—1613
lung, canine, strain variations in excised lobe 79—8517
lung, finite element model for macroscopic deform. 80—108945
lung, macroscopic deformation, finite element model 80—89781
LWR, 3D flux distrib. calc., axial continuous synthesis model with finite element trial functions 80—713
LWR, neutronic thermohydrodynamic interaction model *(French)* 79—89349
MacCormack finite-difference scheme, over-relax. procedure 77—26161
machine vibrations anal. and obs. block deformability influence *(Italian)* 78—51108
magnet coil for Tokamak device, finite element calc. 77—18058
magnetic field, AC, three-dimensional, Tokamak device appl. 79—50191
magnetic field, three dimensional finite element program 77—38769
magnetic field, three-dimens., determ. using scalar potential, finite element soln. 77—88616
magnetic field calc., Fourier anal. within finite elements 77—71903

finite element analysis continued
magnetic field calc. allowing for saturation and hysteresis 79—41278
magnetic field calc. from current distrib., finite element techniques 78—94358
magnetic field problems, numerical techniques 80—32878
magnetic fields, boundary-value problems, finite element and finite difference anal. 78—94353
magnetic fields, numerical analysis, fundamental equations and historical evolution *(Portuguese)* 80—78739
magnetic fields, quasi-stationary 78—94356
magnetic fields, two-dimensional graph-theoretical model 80—87260
magnetic lens design, finite element program improvement 80—69316
magnetic problems, grid and metric optimisation, finite difference and finite element methods 78—94352
magnetic problems appl., nonlinear, using scalar magnetic potential 77—38773
magnetostatic problems, soln. by MAGGY2 problem package 80—28134
magnetostatic problems, two-dimens., numerical soln. by augmented Lagrangian methods 78—1119
magnetotelluric fields, calc. in horizontally-inhomogeneous media using finite differences method *(Russian)* 79—44102
mandible, human, in vitro, math. model 77—52816
mantle convection model, finite element method 80—67354
math. and phys. models, fundamental differences and future possibilities 79—25844
Maxwell's eqns. in electromech., numerical resolution by finite element anal., eddy current effects *(French)* 79—30269
Maxwell eqn. finite difference soln., perfect conductor simulation 77—74236
Maxwell equations, boundary value approx. using finite element anal. *(German)* 80—91718
Maxwell fluid, die swell, finite element anal. 80—83822
mechanical dished supports, oscillation and stability conditions based on mixed finite elements *(German)* 78—87299
medullary implants with porous coating, stress distrib. 78—69256
medullary shaft implant, effects of material and geometric parameters 77—44850
meniscus, three-dimens., numerical simulation 77—59183
mesh generation-optimisation, for partitioning of intricate biological struct. for 3-D finite element anal. 77—40630
metal, axisymmetric drawing simulation, numerical method development 78—30206
metal, plastic flow, finite element approach to axisymmetric problems, METFLO 78—31490
metal, polycryst., elastic deform., free surface influence on mutual restriction between grains 77—51431
metal bicrystal, mech. behaviour, continuous theory of dislocations appl. 78—67717
metal ductile fracture, void growth stress/strain relations *(French)* 80—19280
metal forming processes, finite element anal. appl. 79—50606
metal structures, inelastic anal. 78—70586
metalforming processes, finite element anal., introduction of friction, appl. to ring compression 79—81818
metals, high temp. stress anal. by finite element method 80—96203
metals, residual stress and deformation, due to quenching, elastic-plastic anal. *(Japanese)* 78—83268
metals with mixed hardening, finite element anal. of elastic-plastic materials 79—27543
meteorology short-range numerical forecasts using finite element models 77—86962
MHD, nonsimilar incompressible laminar boundary layers, finite-difference scheme 78—79386
MHD codes, linear and nonlinear, plasma instabilities, PL1 program 77—76040
MHD equilibria numerical analysis *(Japanese)* 79—41760
MHD flow, time-independ. coupling analysis between mag. and vel. fields *(Japanese)* 78—30362
MHD generator, Faraday type, current profile optimisation, electrode cond. profile 78—94939
MHD generator duct potential and current distribution, two- and three-dimensional analysis, appl. 80—24259
MHD spectrum of straight plasma column with arbitrary cross section, finite element calc. 77—11327
micropolar elasticity, 3-D finite element approach to static and dynamic problems 78—34014
micropolar plate bending, stress concentration around hole 77—3731
Mindlin plate, transient and pseudotransient anal. 80—36850
Mindlin plate elements, free vibration anal. 79—46244
Mindlin plates, displacement formulation 80—10154
mixed finite element method, appl. to fourth order partial differential eqns. 77—33848
mixed finite element method for elasto-plastic plates 78—28929
mixed finite element method for the Navier-Stokes equations 79—50693
mixed mode crack tip finite element 77—14962
modal superposition method for computationally economical nonlinear structural analysis, seismic impact appl. 79—81004
modelling design process 80—28414
modified crack closure integral, finite element calc. of stress intensity factors 78—18235
Moire method effects modelling using finite element method 78—38259
moist atmospheric boundary layer, finite element model, eqns. 79—5585
moist atmospheric boundary layer, finite element model, soln. method 79—5586
'moment schema', structural design computing appl. *(German)* 80—14563
Mooney-Rivlin rubber-like materials, finite element anal. 78—46894
moving boundary computation with adaptige mesh 79—35536
moving interfacial cracks, dynamic stresses, finite difference approx., iterative process 77—46966
moving thermal contact problems, finite element soln. 78—26019
multi-axial stress states, elasto-plastic stress-strain relationships 79—1115
multiconfiguration Hartree Fock problem, finite-difference Newton-Raphson soln., He $1s2s^1S$ state appl. 77—6663
multigroup diffusion equation, synthesis-finite element method 80—27699
multigroup neutron diffusion eqn. finite element soln., appl. of natural coordinate system 77—54278
multigroup transfer cross-sections for elastic and discrete level inelastic neutron scatt. 80—42732
multilayer fibre reinforced composite, alternate hybrid stress elements for anal. 77—50926

finite element analysis continued
multiphase heat conduction problem, finite-element free boundary formulation 77—62133
multiphase materials, props. determ. from computer simulation 77—3717
multiple fuel failure resolution with gas tagging, barycentric coordinate technique 79—13485
myocardium of human left ventricle, stiffness distrib. rel. to shape change in diastole 80—41095
natural boundary conditions satisfaction 79—2610
natural convection in enclosed cavities, finite element numerical soln. 80—1557
Navier Stokes eqns., block iterative finite element algorithms 78—20971
Navier-Stokes eqns., finite difference methods, recent advances 77—80136
Navier-Stokes eqns., incompressible, finite-element soln. procedures using equal order variable interpolation 80—10226
Navier-Stokes eqns., numerical soln., vector and scalar pot. method 77—68558
Navier-Stokes eqns., thermal and buoyancy effects 79—9125
Navier-Stokes eqns., transient finite element soln. method 79—3986
Navier-Stokes eqns. for viscous and potential flow about arbitrary 2-D bodies 77—65730
Navier-Stokes eqns. stability techniques improvement 77—72263
Navier-Stokes equation soln. method, finite element anal., 2D unsteady viscous flow 77—89088
Navier-Stokes equation solution, smoothing techniques 78—90823
Navier-Stokes equations, comparison of schemes 79—1149
Navier-Stokes equations, finite element and finite difference methods, efficiency comparison 79—1148
Navier-Stokes equations, finite-difference methods 79—1145
Navier-Stokes equations, Hermitian finite-difference method 79—1144
Navier-Stokes equations, laminar flow through cylinder array, finite difference method 78—42585
Navier-Stokes equations, modal analysis of finite element soln. 77—54958
Navier-Stokes equations, primitive variables versus stream function 79—32443
Navier-Stokes equations, stream function-vorticity formulation incorporating no-slip conditions, variational principle 78—38267
Navier-Stokes equations, theory and numerical analysis, book 78—77721
Navier-Stokes equations, vel.-press. formulation, mixed-interpolation finite elements comparison 78—45486
Navier-Stokes formulation, incompressible viscous flow 79—1147
nearshore circulations finite element modelling 78—77270
network constructions, large strain anal., simplex membrane elements 79—32220
neutron diffusion, finite element soln. technique for 2-D equations 79—89347
neutron diffusion, mixed-lattice multidimensional reactor calcs., coarse mesh finite difference method 77—34375
neutron diffusion and P_1 eqns. soln. by iteration 77—50188
neutron diffusion calc. with space depend. cross sections 77—82986
neutron diffusion calcs., appl. to reactor design and anal. 77—79427
neutron diffusion eqns., finite difference method approx. by coarse mesh method 77—88185
neutron diffusion equation, three dimens., MULTIPOL code for coarse mesh approx. *(German)* 77—88186
neutron diffusion equations, finite element soln. tech. using imaginary nodal points and element subdivision 80—68721
neutron diffusion in 2-D, finite element energy depend. method 77—82987
neutron diffusion multigroup three dimensional calcs. with finite element method *(German)* 77—88189
neutron flux computation, finite element code 78—50449
neutron flux spatial approximation using coarse mesh methods QUABOX and CUBBOX, and higher order polynomials *(German)* 77—88192
neutron flux synthesis, single channel, finite element trial functions for 3-D reactor calcs. 80—42734
neutron flux synthesis program KASY, consideration and appl. to reactor design problems 77—88184
neutron kinetics, two-dimens. calc. 78—665
neutron transport, finite element method, theoretical considerations 79—13372
neutron transport, multi-group two-dimensional eqn., cylindrical geometry, finite element method appl. 78—29522
neutron transport, transverse buckling effects in 2-D calcs. 80—32318
neutron transport, two-dimensional, appl. of constrained finite elements 79—22360
neutron transport, variational coarse-mesh method based on constrained ang. trial functions 77—65245
neutron transport, ZEPHYR code for general two-dimensional geoms. 77—65249
neutron transport eqn., appl. to strong heterogeneities 77—26820
neutron transport eqn., response matrix finite element soln. 80—13527
neutron transport eqn. anal. using modified method 80—47529
neutron transport finite element method, two-dimens., one-group test problems 80—37412
neutron transport theory, buckling approximation inclusion in finite element calcs. 78—17276
neutron transport theory, constrained finite elements and response matrices 77—61475
neutron transport theory, nonuniform lattice problems, 2-D constrained finite element anal. 80—86952
Newtonian die swell eval. for axisymm. tube exits using finite element anal. 78—1741
nodal expansion method and depletion program MEDIUM-2, validation by benchmark calcs. and comparison with expts. for PWR design appls. 77—88194
non-linear field problem solution *(Russian)* 78—46485
non-Newtonian flow, method for memory effect fluids 79—60016
non-Newtonian flow in pipe, finite difference methods 78—94770
nonconforming, solving clamped plate with ribs 77—22418
nonconservative mechanical systems, variational principles, finite element approach 79—49027
nondeterministic thermal deformations of structures temp.-dependent material props. 77—65679
nonlinear, solution techniques, review 79—3914
nonlinear anal. of deep arches, using mixed curved-beam finite elements 78—18161
nonlinear beam structures, finite element method for deformation, kinematic functions *(German)* 79—37167

finite element analysis continued
nonlinear diffusion eqns., finite difference methods *(French)* 77—5654
nonlinear dynamics, finite element anal., accuracy versus computational efficiency 79—40362
nonlinear elastic stability problems using a finite difference perturbation method 78—83273
nonlinear elasticity, boundary value problems, finite element anal., recent developments 79—44737
nonlinear elasticity, two-point boundary-value problems 77—75804
nonlinear elasticity for nearly incompress. rubber like materials, large strains, finite element anal. 80—19238
nonlinear elastodynamics which conserve energy, finite element methods 79—18723
nonlinear field eqns., time discretisation and mixed finite element methods 79—40384
nonlinear field problems, variable basis functions *(Russian)* 80—37160
nonlinear finite element anal. ADINA program for stress anal. 78—41148
nonlinear fluid dynamic problems, least squares and finite element method soln. 79—49054
nonlinear fluid dynamics, spectral decomposition in advection-diffusion analysis by finite element methods 79—49053
nonlinear fluid problems, adaptive mesh refinement for finite element anal. 79—49052
nonlinear heat cond. problem with phase change, finite element anal. 78—75030
nonlinear heat transfer 79—23189
nonlinear hyperbolic conservation laws, finite difference methods 78—49649
nonlinear magnetostatic fields, three-dimens. anal. in saturable reactor 79—13860
nonlinear material and structural behaviors, soln. procedure, theoretical basis for program composite—III 78—30204
nonlinear materials, Mode I fracture behaviour, finite element anal. 80—84237
nonlinear mathematical model of the propagation of tides in interlacing channels 79—39720
nonlinear optics, finite element method appl. 80—9941
nonlinear panel flutter, finite element anal. 79—7316
nonlinear physical media, boundary valve problem soln. by finite element anal. 79—17214
nonlinear plate problems, unconditional stability of finite element scheme, nonlinear vibrs. *(Japanese)* 79—77004
nonlinear post-buckling anal., perturbation approach to imperfect structs. and snap-buckling 78—79244
nonlinear problem, partial differential eqn. soln. method, appl. to estuarine flow *(Japanese)* 78—8233
nonlinear problems anal. using combined finite element-boundary integral eqn. method 77—72156
nonlinear shell analysis via mixed isoparametric elements 78—1566
nonlinear shell problems, hybrid stress finite element model 79—14251
nonlinear static and dynamic response 77—27469
nonlinear structural dynamics, direct time integration methods 79—44730
nonlinear variation eqns., convergence of finite element solns. 78—86127
nonlinear wave propagation and unsteady transonic flow, variational formulations 78—55660
nonNewtonian flow, plane and axisymm., mixed finite element method 79—60017
nonrectangular reverberation chamber design and construction 78—83196
nonstationary heat conduction problem in presence of mass exchange, finite element anal. *(Russian)* 79—27492
nonuniform finite element lattice, automatic construction variant *(Russian)* 79—25829
nonuniform grids in finite difference approximations, application to fluid flow problems 80—105507
North Sea water circulation simulation 77—2162
notch fatigue cracks, propag. and initiation, elastic-plastic fracture mechanics 80—38329
notched bar design for creep-rupture testing under tri-axial stresses 77—62165
notched bars, creep stress redistrib. 77—62164
notched bars, elastic plastic stress and strain conc. factor *(Japanese)* 78—26052
notched flat tensile specimens, deform. zone *(German, English)* 78—64603
nozzle-to-cylinder structures subjected to internal pressure, finite plate method 78—34007
nuclear cross-section adjustment and evaluation, finite element basis in data adjustment 80—68612
nuclear fuel can designs for Safety Test Facility, structural analysis 77—46310
nuclear fuel element behaviour in transients 77—88202
nuclear fuel pellets, cracked, thermal stress anal. 78—82462
nuclear fuel pin inelastic modelling and stress analysis using FULMOD code 77—46233
nuclear fuel rod anal. program CYGRO-4 78—41805
nuclear fuel-cladding interaction between cracked surfaces, mechanical and temp. contact 78—66341
nuclear reactor, dynamic response of ducts to press. pulse, finite element calcs. using STRAW 77—3124
nuclear reactor, fluid-structure finite element method for anal. of reactor safety problems 77—3128
nuclear reactor, linearized, stability anal. by finite element method 78—29543
nuclear reactor, LMFBR, struct. response to HCDA, coupled Euler Lagrange computer program 77—71671
nuclear reactor, LOCA thermal shock in nuclear containment wall, computer code for safety anal. 77—3135
nuclear reactor 3-D calcs. 80—13566
nuclear reactor calcs., multidimensional, interface current techniques 77—88193
nuclear reactor coarse-mesh nodal method based on response matrix considerations 77—65262
nuclear reactor core pin power distribution det. based on nodal coarse mesh calcs. 77—88195
nuclear reactor cylindrical models, diffusional approx., finite element anal. *(Russian)* 80—18414
nuclear reactor flow boiling anal., numerical standards 77—79448
nuclear reactor fuel rod bowing, finite element computer model 77—46260
nuclear reactor structural mechanics, conf. 78—41874

finite element analysis continued

- nuclear reactor subassembly response to simulated accident conditions, finite element anal. 77—3123
- nuclear reactor transient heat conduction, soln. by hybrid method 78—681
- nuclear reactor turbulent flow in fuel rod bundles 78—37400
- nuclear reactor upper internal structures, finite element structural model appl. 80—32362
- nuclei, axially symm., soln. of HF eqns. in coord. space 77—88060
- numerical method for computing the electrical stress in dielectrics 79—4767
- numerical realization, appl. to two dimensional thermoelasticity problems 77—84132
- numerical simulation of fluid motion, conf., Melbourne, Australia (1976) 79—9116
- numerical solutions of three dimensional dynamic crack problems and simulation of dynamic fracture phenomena by a ‘non-standard’ finite difference method 79—41613
- numerical stability of complex finite elements 78—32659
- numerical surface integration, expressions for element base area unified with integration formulas 79—53967
- numerical weather prediction, finite element method appl. 80—12526
- ocean circulation driven by wind 80—56487
- operational stress-state of field ion microscope specimen 78—32933
- optical fibre, single-mode, single-polarisation, with refractive-index pits on both sides of core 80—99846
- optical fibre cable structure design *(Japanese)* 79—59821
- optical fibre cables, structure design, compressive loads and internal stress determination 79—59829
- optical fibre connector, using resilient alignment method 78—71230
- optical fibres, radially inhomogeneous, vectorial wave anal. using finite elements method 78—37999
- optical waveguide, single-mode, with inhomogeneous index variations 79—76804
- optical waveguide, trapezoidal cross-section ridge design, propag. characts. 78—55436
- optical waveguide, trapezoidal-cross-section ridge, dispersion characts. 77—88909
- optical waveguides, finite element anal. 80—87558
- optical windows at high-press. chamber, strain determ. by holographic interferometry and finite element anal. 77—26323
- optimal choice of finite element grids 78—77698
- optimal design of bending elements 79—10470
- optimal design of dynamically loaded continuous structs. 78—38185
- optimum machine element shape finite element technique 77—62152
- Orr-Sommerfeld flow problems, soln. using factorisation method, book contrib. 80—1688
- orthodontic adhesive joints, adherend topography effects 77—52916
- orthodontic appliances, 3-dimens. large displacement anal. 77—29228
- orthogonal base functions and consistent diagonal mass matrices for two-dimensional elements 79—90125
- orthotropic bridge decks with closed stiffeners, anal., behaviour 78—18164
- orthotropic cylinders under initial stress, natural vibrations 79—14318
- orthotropic plates, nonlinear vibration anal. by finite element method 77—7237
- orthotropic shallow spherical shells under concentrated central load, nonlinear flexural oscillations 79—37234
- oscillation rods in viscous fluids, added mass and damping, finite element anal. 80—58967
- oscillatory subsonic piecewise continuous kernel function method 78—5763
- otolith membrane, finite element model, computer soln. of differential eqns. 77—40636
- out-of-core assembly in FORTRAN IV subroutines, linear eqns., with nonsymm. coeff. matrix 79—30213
- overheated water reactor pin rewetting, effect of thermal diffusion from fuel pellets 77—46212
- overland flow equations soln., comparison of finite element methods 79—12152
- p-convergent finite element approx. in fracture mechanics 78—38252
- parabolic isometric plate element, laminated composites flexural analysis 77—14921
- parabolic partial differential eqns., finite difference methods, comparison of accuracy 79—72796
- parabolic partial differential eqns., finite element methods 79—72797
- parabolic problem exact control collocation method 77—26156
- parallel elastically-coupled flat plates, supersonic flutter analysis 77—75838
- parallel flows, stability anal. by finite element anal. 79—81843
- partial differential eqn. soln., preservation of conservation props., under local mesh refinement 78—16628
- partial differential eqns. reduction by Galerkin, collocation, and method of lines 78—77693
- partial differential equations, conference, Bethlehem, PA, USA (June 1979) 80—86039
- partial differential equations, time depend., Method of Lines compared to finite difference scheme 78—79291
- particulate systems, dynamic eqn., numerical soln., finite element anal. 79—5185
- patch test and general convergence criteria 77—31210
- patch test for nonconforming finite elements, conditions for piecewise polynomial functions 78—77697
- penalty function solution of steady-state Navier-Stokes equations 80—14648
- perforated plates, finite element elasto-plastic anal. 80—10168
- perforated plates, limit analysis 77—27471
- peristaltic flow, Navier-Stokes eqns., implicit finite difference method using orthogonal curvilinear coords. 77—39346
- Petrov-Galerkin finite element method, boundary layer problem 78—69989
- photoelastic fringe pattern analyzer, computer aided 80—38359
- piezoelectric transducers, farfield angular radiation pattern 80—33401
- pipe, axial crack, elastic-plastic dynamic finite element anal. 77—3795
- pipe, layered, support layer thickness effect on stress-strain state *(Russian)* 80—43614
- pipe bends, flexibility and stress factors, finite ring method 77—75828
- pipe bends, stress anal. by ring elements 79—10483
- pipe elbow element, linear anal., bending axial and torsional displacements, ovalisation 80—79177

finite element analysis continued

- pipe flow, finite element wall model for high Reynolds number flow 80—28565
- pipelines, installation, nonlinear finite element anal. 79—46183
- piping systems, structural performance characts., dynamic anal. 77—6508
- plain strain contained plastic deformation, elastic-plastic laws, finite element anal. 80—92073
- planar shear specimen with V-notch, anal. of stress and strain conc. factor using finite element method *(Japanese)* 78—38212
- plane elasticity, mixed finite element method, convergence and performance 80—38258
- plane elastoplasticity, subject to large strains, finite element anal. *(Japanese)* 80—96207
- plane jet propagation in incompressible liquids, numerical solution *(Russian)* 80—43753
- plane Newtonian jet with surface tension, computer solns. by finite element anal. 79—64722
- plane notch and crack problems, appl. of displacement and hybrid stress methods 78—63375
- plane strain, spurious modes in two-dimensional isoparametric elements 80—52
- plane strain deformation of strain rate sensitive materials, finite element anal. 80—1441
- plane strain shear cracks, rupture vel., rel. to earthquakes 77—17043
- plane stress crack geometries, comparison of finite element and expt. studies 77—89069
- plane triangular element, stress-strain finite dynamic element, FORTRAN IV program 80—53
- plane V-notched specimen, elastic-plastic limit load anal. 80—69684
- plasma diffusion in low-beta devices 77—80277
- plasma MHD, nonlinear time-dependent hydromagnetic model, spatial and temporal finite-difference techniques 80—59192
- plasma MHD, stability code, ERATO, convergence of solns. 80—83906
- plasma time-dependent diffusion in toroidal geometry, finite element code 77—84410
- plasma turbulence, finite element anal. of wave-particle interaction 77—39422
- PLASTEF code, numerical simulation of thermoelastoplastic behaviour using finite element method 78—90731
- plastic anal. of thin-walled beams of open cross section, finite-element model 80—74767
- plastic deformation, necked bar, void growth, finite element anal. 80—64383
- plastic dynamics discrete structural models, const. stress finite elements 77—35056
- plastic flow, isotropic body, finite element method for volume integration 80—74770
- plastic flow theory problems, convergence *(Russian)* 77—58569
- plastic instability during tensile deform., numerical calc. 78—30203
- plastic strain conc. in perforated struct. 77—75825
- plastic straining multiple mode, finite element convergence 77—62166
- plasticity, materials with convex yield criterion *(French)* 79—10501
- plasticity anal. with nonconforming plane element 78—38209
- plasticity and creep anal. fraction model, finite element description 77—3743
- plasticity and viscoplasticity problems *(French)* 78—63334
- plasticity theory, unifying concepts 78—42545
- plasticity theory for porous metals 80—83738
- plasticity with hardening, error estimate for incremental method 78—9577
- plate, circular arc aerofoil shaped, vibrational characts. 79—10516
- plate, inelastic thick, dynamic response, rectangular finite element development 79—94520
- plate, multilayer sandwich, stability and buckling analysis by finite strip method 78—26069
- plate, obliquely stiffened, subjected to uniform compression, buckling strength *(Japanese)* 78—67067
- plate, optimal design under dead weight and surface loading 79—3915
- plate, orthotropic, transient response to uniformly distributed transverse load, computer calcs. 77—68503
- plate, rectangular, variable thickness, stability and vibr. anal., finite element method 77—54918
- plate, rib stiffened, studies on vibrations 78—83297
- plate, thick, vibration anal. using Mindlin plate elements 80—38305
- plate and shell bending, finite elements by mixed formulations 78—38217
- plate bending, finite element anal. 78—46
- plate bending, penalty finite element method 77—35062
- plate bending, reduced and selective integration techniques 78—42552
- plate bending and plane elasticity 77—35033
- plate bending elements, quadrilateral, finite element anal. with reduced integration 78—75071
- plate bending elements, quintic triangle 78—77716
- plate boundary and extension problems, stress intensity factors, finite element anal. 79—55341
- plate buckling, variational formulation for hybrid finite element method 78—18205
- plate element, 2nd order *(German)* 79—10466
- plate problems, biharmonic oscill., finite element discretisation, preconditioned conjugate grad. method 79—72795
- plate structure, crack simulation computer program *(Japanese)* 80—79218
- plate structures, two-dimensional cracks, computer program based on superposition method *(Japanese)* 78—51123
- plate theory, nonlinear elasticity model, asymptotic expansion method anal. 79—44738
- plate-spring struct., dynamic characteristic determ. by rigid finite element method *(Polish)* 78—18220
- plates, dynamic instability anal. by finite element method 77—3769
- plates, elastic viscoplastic, transient dynamic large deflection anal., finite element method 80—69683
- plates, equil. finite element model of buckling 78—5675
- plates, isoparametric finite elements, variational formulation of plate equilib. problem *(French)* 80—43608
- plates, laminated anisotropic composite, penalty plate bending element 80—96200
- plates, open and loaded holes, exam. of part elliptical cracks 80—10195
- plates, plastic dynamic flexure 78—30196
- plates, ridigity matrix, triangular finite elements *(Russian)* 80—74739
- plates, thin and moderately thick, serendipity cubic displacement hybrid stress element 80—96202

finite element analysis continued
- plates, thin rectangular, with arbitrarily oriented stiffeners, free vibrs. 78—1591
- plates and shells, dynamic plastic anal. using stress resultant finite element formulation 79—37191
- plates on elastic foundation, simplified finite element soln. 78—26041
- PMMA plates with flawed fastner holes, static fracture testing 80—97651
- point loaded beam, stress distrib., analysis using symmetric/antisymmetric loading 79—41641
- point-loaded centre cracked plates, fracture studies 78—19884
- Poisson's eqn., finite-difference soln. in rectangular of arbitrary proportions 77—64939
- Poisson's eqn. triangular finite elements compact representation 77—26176
- Poisson's equation solution, using curvilinear finite differences 78—28923
- Poisson eqn. on surface of sphere, shooting method for finite-difference soln. 77—2527
- Poisson equation over complex domain, finite difference method, Neumann boundary conditions 78—79189
- pollutant transport eqn., 3-D, numerical algorithm 80—106811
- polycarbonate plates, modified compact-tension specimens, dynamic anal. 80—97561
- polycrystal, elastic deform., effect of Young's modulus, shear modulus, Poisson's ratio 77—24344
- polycrystalline materials, effect of grain boundary sliding on anelasticity 80—96592
- polycrystalline metals, effect of grain boundary sliding on steady creep 80—96590
- polycrystals, elastic stress and strain microinhomogeneity, finite element method 80—79155
- polycrystals, large elastic-plastic deform. anal. 78—26049
- polygonally bounded optical waveguides 77—27358
- polyhedral sandwich domes, elastic behaviour, failure, practical investigation and numerical simulation 78—59309
- polymer, amorphous, injection moulded, residual thermal stress calc. by FEM 79—55322
- polymer film elasto-plastic deformation calc. in re-drawing stretched film *(Japanese)* 80—7621
- polymers, glassy, craze surface displacements, model 80—93651
- pool type reactor, dynamic response of in tank component 79—85663
- porous bodies, stresses induced by drying, elastoviscoplastic model, finite element anal. 80—23904
- porous materials, fracture behaviour estimation using simulation model and finite element method 77—42777
- porous media, heat and mass transfer, numerical soln. 77—7441
- porous media one-dimensional unsteady drainage digital simulation 78—91011
- post-buckling behaviour of structures using a finite element-nonlinear eigenvalue technique 80—92078
- postbuckling analysis of elastic structures by the finite element method 80—96209
- potential energy with iterative correction or deterioration 78—89315
- potential flow, 3-D, about arbitrarily shaped bodies, direct matrix embedding technique 80—64511
- potential flow, mixed hybrid finite element methods, book contrib. 79—32445
- potential unbounded flows 79—88813
- Prandtl punch problem, finite element model for plane-strain plasticity 80—58940
- pre-twisted beam vibrs., elements based on approximation of displacements in fixed directions 77—75843
- press fitting thick cylinder into outer housing of octagonal form, finite element anal. 79—50603
- pressure vessel, elasto-plastic analysis, appl. *(Japanese)* 79—21555
- pressure vessel, reinforced concrete, stress anal. of cracked shell 78—44213
- pressure vessel and nozzle junction, optimum shape design 78—89941
- pressure vessel dynamic response to impulsive loading in nonlinear range 77—3191
- pressure vessel heads, torispherical, elastic instability and with triangular thin shell finite elements 77—58576
- pressurized pipeline, double cantilever beam, dynamic crack growth, finite element method 78—34080
- prestressed cablenets, 3-D, finite element anal. 78—5650
- prestressed concrete pressure vessels design, finite element anal., computer programs 77—23183
- prestressed concrete reactor vessel, 3-D nonlinear failure anal. 77—50268
- prestressed concrete reactor vessels, construction movements, finite element anal. 79—621
- prestressed concrete reactor vessels, perforated plate ligaments, time varying stress 79—49679
- prismatic bars, elastoplastic torsion by quadratic programming, finite element scheme 79—32251
- prismatic beams, element stiffness matrix 78—5653
- problems with non-removable singularities 77—72250
- propagation of plane harmonic waves, infinite isotropic medium having embedded doubly periodic array of cylindrical fibres 80—87607
- prosthesis, hinged knee, influence of dynamic loading on mech. loosening 78—48938
- prosthetic aortic valve, Reul-Ghista optimal tri-leaflet Avcothane design performance 78—44736
- prosthetic aortic valve stress analysis using finite element compute program 78—48930
- pulmonary regional electroaerosol deposition model 79—83842
- pulsating turbulent flow onto elastic surface, finite difference method *(Russian)* 78—75153
- punch stretching, localised necking, finite element anal. 80—102971
- PWR fuel pin transient heat conduction and open hot channel DNBR evaluation 79—9679
- PWR internals, vibration mode shape computation and expts. 79—13444
- PWR pressure vessel nozzle, comparison of 3-D and axisymm. finite element anal. 79—13423
- quadratic finite element schemes for 2-D convective transport 78—21084
- quadratic isoparametric elements, calc. of stress intensity coeff. *(Russian)* 77—58548
- quadrature rule for conforming quadratic crack tip elements 79—27587
- quadrilateral shell element utilising isoparametric principles 78—34012
- quarter elliptical cracks in irregular bodies, exam. using finite element alternating method 78—90796
- quarter plate support, planar flexibility depend. on fillet radius 80—5944

finite element analysis continued
- quartz rectangular AT-cut plates with patch electrodes, vibration modes 79—55295
- quasi static crack growth, in sheet materials 78—67106
- radial rotating beams, natural freqs. 78—59326
- radial turbomachine, meridian plane characts. for subsonic and transonic flow, finite element calcs. *(French)* 80—38418
- radiation absorbing bodies, temp. fields, Julich reactor expts., finite element calcs. *(German, English)* 77—82998
- radiation problem simplified boundary elements 78—86226
- radiation transport, appl. finite element methods 78—13196
- radiative heat transfer, integral eqn. finite element soln. 80—10127
- radio meteor wind data, anal. using finite element approximation 78—81475
- radioactive waste vault, temp. distrib. anal. 79—636
- Rayleigh-Jeffreys convective stability problem with temp. and salinity gradients *(Russian)* 78—14012
- reactive scattering, anal. methods 78—92453
- reactor dynamics, finite element analysis for two dimensional eqn. *(German)* 77—88190
- reactor fuel cladding tube mech. props., ring compression test, finite element anal. 77—83037
- reactor pressure vessel, bimetallic, composite geometry, subjected to thermal shock, temp. decay, 2-D soln. 77—88209
- reactor pressure vessels, 3D finite element anal. of surface cracks 79—10535
- recirculating flows, review of computing methods 79—10565
- rectangular bars and plates, thick, HF flexural vibr. 79—18779
- rectangular plate static stability soln. with fully conforming element 77—62184
- rectangular plates, moderately thick, free flexural vibr., effect of geometric nonlinearity 79—3940
- rectangular plates with rectangular inserts 77—23876
- rectilinear anisotropic material hybrid crack element 77—27492
- red blood cell elastic deforms. 77—56400
- reflector surface design by numerical method, bivariate beamshaping in elliptic case 77—27225
- reformulation of method 77—67255
- refractory, thermal stresses produced by temp. gradient, finite element anal. *(Japanese)* 80—33538
- reinforced concrete containment model behaviour under thermal gradients and internal pressure 80—42837
- reinforced concrete structures, nonlinear finite element anal. 79—41569
- reinforced plastic cylindrical shells, optimal design under dynamic constraints 80—102996
- residual correction applied to a sequence of block tridiagonal matrices 79—72800
- resonance frequencies of non-rectangular reverberation chambers, calculation by numerical methods 80—64324
- resonator vibration analysis, combined plate eqn. and finite element method 79—55296
- RF plasma torch, temp. distribution and EM field, one dimensional analysis, using finite element method 80—24264
- ribbed plates with large openings, design optimisation, finite element anal. appl. 80—87724
- rigid work hardening structures optimum design 78—13917
- rimming flow, numerical simulation of free-surface flow with surface tension 78—22353
- ring, axially cracked, numerical anal. of residual stress effect on crack closure 79—77012
- river tidal computations, explicit-implicit water level model 78—44886
- rock, soft, vibrating wire stress gauge 77—84199
- rock melting drills, thermal analysis 77—17258
- rocks, fold propagation in viscous layer 78—32083
- rocks asymmetric folding, finite-element simulation 78—77222
- rods with thin perforated walls, bending, finite element method *(German)* 80—14591
- rolling disc, elastic-plastic anal. of stress distrib. 77—68444
- rooms, field anal. by finite element method *(Japanese)* 79—27465
- rotating beam with tip mass, vibration 80—58960
- rotating flexible structures, modal anal. 77—31235
- rotating flow, Navier-Stokes eqns., upwind scheme 79—1201
- rotating liquid drops, asymmetric shapes and stability 80—87796
- rotational shells, geometric stiffness matrices *(French)* 77—68464
- rotationally periodic large space structures, finite element transfer matrix dynamic analysis, 100 m parabolic dish 80—74731
- rotor dynamics analysis using tapered beam finite element 80—38316
- rubberlike materials, finite plane strain deformations, finite element anal. 80—28438
- salt dome dynamics 79—20789
- San Fernando earthquake, California, 1971 Feb. 9, static and dynamic finite elements anal. 77—49010
- SAW interaction with discontinuities, computer model 79—68461
- scalar Helmholtz eqn. in 3-D, finite element soln. 77—30002
- Schrodinger eqn., mixed local-global variational approach and its application to a discontinuous potential 79—58564
- Schrodinger equation, finite element formulation in space-time continuum 77—67333
- Schrodinger equation, generalisations of finite element and R-matrix methods 78—24676
- Schrodinger equation, nonlinear time-depend., one dimens. wave packet soln., Fortran prog. 77—9897
- Schrodinger equation, two dimens., finite element package MANFEP 78—36870
- sclerotic arteries, shear stresses in pulse flow *(French)* 79—92249
- sea model, hydrodynamic, 3-D, variable vertical eddy viscosity, finite element anal. 80—85661
- seal ring deflection, finite element anal., reactor appl. 77—6502
- second order boundary value problem, variational Green's function 77—71193
- seepage flow variational inequalities by finite element method 77—68688
- seepage in porous elastic media, numerical performance of finite element schemes 77—91162
- seismic depth migration after stack, finite-difference method 80—98254
- seismic depth migration before stack, finite-difference method 80—98255
- seismic SH-waves propag. in stratified medium with local inhomogeneities, finite element treatment *(Russian)* 79—34763
- seismic surface waves in three-dimens. struct. 80—61765
- semicircular plate of variable thickness, finite element stress anal. 79—37180
- shallow spherical shell, parametric anal. of creep buckling 77—46938

finite element analysis continued
shallow spherical shells, deflections and internal forces, finite element anal. *(Chinese)* 79—68583
shallow thin shell finite element, stiffness matrix development 78—90705
shallow water wave equation model, finite element tidal computations 79—84282
shallow water with moving boundaries digital simulation 78—92847
shear lag problem, finite element anal. 79—32246
sheet metal, finite element anal. of hydrostatic bulging 77—72186
sheet metal stamping, finite element anal. 79—7344
shell, cylindrical, effect of material orthotropy on stress state around circular hole 78—34023
shell, cylindrical, semi-infinite, with end plate subjected to centrifugal force, large deflection analysis *(Japanese)* 79—1104
shell, cylindrical in supersonic flow, vibration, finite element anal. 80—5973
shell, spherical, glass, with metal insert, design strength parameters 80—14576
shell, thick, finite element study of large deflections 77—3725
shell calc., parabolic, shallow, thin, elastic behaviour calc. 79—57
shell design by finite element method, deformation and elasticity theory 80—74747
shell of rotation exposed to vibrs., optimum shape and reinforcing struct. 79—18792
shell problems, finite element methods, numerical integration *(French)* 77—74206
shell stability anal., finite element representation and pressure stiffness 79—90160
shell stress, efficient high order finite elements 77—35044
shell structure analysis, new stress finite element 78—18165
shell structures, appl. of new stress finite element 77—72157
shell structures, hood-shaped, membrane solution *(German)* 78—46891
shell structures, new high-precision stress finite element 77—62156
shell structures, thin, curved finite element 78—79205
shell surfaces calc., thick-walled, with axisymmetrical load *(Russian)* 80—48569
shells, axisymmetric multilayer, finite element technique for thermal and press. loading, vibr. modes *(French)* 77—50973
shells, curvilinear tubular, elastic equilib., finite element anal. *(Russian)* 80—79148
shells, cylindrical, diaphgragm-supported, static analysis using curved finite strip 77—89027
shells, cylindrical, mixed finite element approx. convergence 80—33450
shells, free-form, nonlinear anal. by flat finite elements 79—14247
shells, laminated, high-precision ring element used in vibration analysis 79—81789
shells, large inelastic deformations for arbitrary shape, TRUMP element appl. 80—92068
shells, paraboloid, elliptic, computerised stress analysis 78—59294
shells of arbitrary geometry, finite element anal. 78—34044
shells of resolution, ring-stiffened, dynamic nonlinear anal. by finite element program DYNAPLAS 77—3766
shells of resolution, transient dynamic and inelastic anal., survey of programs 77—3767
shells of revolution, bending, physical and geometrical nonlinearity, finite element method *(Russian)* 80—33471
shells of revolution, computer program for linear and geometrically nonlinear static analysis *(Japanese)* 80—64500
shells of revolution, finite element anal. of statics *(Chinese)* 79—76964
shells of revolution, mixed finite element formulation for geom. nonlinear anal. 78—38189
shells of revolution, rigid-plastic limit anal. under rotationally symmetric loading *(French)* 79—14276
shells of revolution, ring type finite element method *(German)* 79—14250
shells of revolution under axisymmetric and asymmetric loadings, linear elastic dynamic analysis program using finite element analysis *(Japanese)* 80—106719
shells of revolution with variable geometry, optimisation of mass 78—67030
shells with internally attached structures, transient response 79—3941
ship oscillation, wave-generated, numerical methods *(French)* 78—30216
shock capturing application of the finite element method. 79—27665
shock propagation, nonlinear hydrodynamic field equations, finite element anal. and method of weighted residuals 80—53813
shock wave ionisation in transverse magnetic field, finite-difference methods 78—51249
shock wave propagation in inhomogeneous medium using finite differences 77—7414
simpler elements of C^0 continuity with varying polynomial degrees 77—13589
simplified hybrid displacement method, critical assessment 77—14920
simply supported plates, finite element anal. and Babuska paradox 79—81720
simulated diffusion bonded lap joints, finite element stress analysis 78—18254
simulation appl. to materials, conf., Gaithersburg, USA (April 1976) 78—27387
single-pole electron lens 80—69315
singular finite elements, improvement of convergence *(French)* 77—49579
singular functions for convergence improvement 77—26152
singular integral eqns. of first kind 77—64935
singular isoparametric elements properties 77—13592
singularities in harmonic elements, elimination methods 77—45685
sintered carbide tips stress distribution anal. 78—5663
skew conditions, specification 78—62057
skirt-supported pressure vessel free vibrations 79—68632
slab criticality and Milne problem for neutron transport 77—57700
slab reactor neutron transport, finite element method, practical considerations 79—76046
slab with temp. depend. thermal cond., convective boundary, transient cond., finite difference method 78—75031
slab with temp. depend. thermal cond., optimal heating, finite element anal. 80—23863
slender channel laminar flows, numerical soln. 77—78985
sliding interfaces and impact, numerical treatment 79—41631
slip model for finite element plasticity 79—32301
smearing of material props. in axisymm. structural anal., appl. to GCFR steam generator cavity closure plug 77—14222

finite element analysis continued
smoke-motion, numerical anal. by finite-element method *(Japanese)* 80—69910
smooth interfacing of finite element models 79—72799
smooth spline-like finite-element differentiation, of full field experimental data over arbitrary geometry 80—62454
smoothing techniques for finite element anal. solns. of Navier-Stokes eqn. 80—17804
softwoods, transverse Poisson's ratio and Young's modulus *(Japanese)* 80—2111
soil, freezing processes, finite element simulation 79—16527
soil, two phase with viscoelastic skeleton, finite element anal. of consolidation 77—11138
soil, unsaturated, coupled heat and water movement prediction, math. model 78—61446
soil filtration problems, finite element method *(Russian)* 79—88374
soil mechanics, optimal lower bounds 77—72262
soil-struct., interaction initial stress finite element method 78—59313
soil-structure interaction anal. by finite elements 78—41879
soil-structure interaction for nuclear power plant design 77—3173
soil-structure interaction parameters, power plant design 77—3175
soil-structure systems, time integration, mixed methods 79—41568
solar energy compound parabolic concentrator, natural convection, finite element soln. 78—90634
solar energy thermal processes, appl. 79—24890
solid mechanics, natural mode technique, review 79—44728
solid transient dynamic problems, finite element formulations using explicit time integration 78—18162
solid-state convection in planetary interiors, numerical methods 79—84693
solids of revolution, stressed state 77—14910
solute transport in a saturated-unsaturated porous medium 79—23362
solute transport in soils, two-site adsorption-desorption model evaluation 77—41101
spherically symmetric elasticity problems, finite element soln. 78—63293
spinal cord electrical stimulation, 2D anal. 80—98054
spine, human, finite element model for in vivo freq. response anal. 80—104623
spring, complex arch type, movable, snap-through action characts., appl. to microswitches 78—63339
spring, complex arch type, movable, snap-through action characts., microswitch appls. 78—63340
square cantilever plate immersed in water, finite element method for dynamic behaviour 79—37224
square cavity, recirculating flow, finite element results 79—64764
square plate with parabolic thickness variation 79—68628
stability analysis of skew orthotropic plates by the finite strip method 78—79235
stable crack extension and nonlinear fracture criteria, finite element anal. *(Chinese)* 80—10184
stable crack-growth, fracture criteria, numerical approach 78—67104
stagnation point flow, least square finite element soln. 77—14981
stamp problem, elastic layer or half space, variational formalism, numerical soln. 79—1106
state determinants method *(Russian)* 78—77695
static condensation stress recovery algorithms, cost comparison 78—41145
static geometric and elastic stiffness matrices of finite element hybrid displacement models 78—18173
stationary heat cond. using successive overrelaxation and conjugate gradients 78—83206
stationary Stokes eqns. approx. using penalty-extrapolation method 77—14976
steady state convection-diffusion eqn., quadratic finite element solns. 80—92019
steady state creep analysis of a cracked body using the superposition method 79—94507
steady state shallow water equations, unified treatment, finite element penalty function approach 79—49056
steady viscous flows, finite element formulations 80—36859
steady viscous incompressible flow, two dimens., finite element anal. 79—23297
steam generator rupture disks, dynamic instability anal. 79—85662
steel, brittle fracture, J-integral fracture criterion *(Japanese)* 77—48597
steel, CrMoV, compact tension specimen, thickness effect 78—68764
steel, heat treated, residual stress calc. with finite element program *(German)* 79—66075
steel, high strength sheets, finite element anal. of crack propag. expts. 80—40498
steel, mild, bar stress wave propagation *(Japanese)* 79—79030
steel, mild, ductile fracture of cracked plates, nonlinear boundary-value problem 77—81318
steel, mild, Luders bound front, elastoplastic anal. by finite element method 78—3169
steel, Ni, cross girder connections, fatigue strength, design stress 78—64700
steel, parts, stress calcs. during cooling, program system THEPLA *(German)* 80—35237
steel, stainless, 316, nuclear fuel cladding, crack nucleation 78—72864
steel, stainless, type 304, elastoplastic fracture mechanics for reactor piping 78—68777
steel bridges, higher order horizontally curved beam finite element 78—26028
steel case hardened cylinders, heat treated, residual stress fields 80—3102
steel compact specimens, finite element analyses of dynamic stress intensity factors, and crack arrest stress intensity factors 79—61732
steel for nuclear pressure vessels, transient finite element crack propag. model 77—3106
steel-Al-steel plate, fatigue damage analysis and life predictor 77—25120
Stefan problem, one-dimens., third order accurate discontinuous finite element method calc. 79—81701
Stefan problem, two dimens., space-time finite element computation of free boundary 78—1556
Steiner surface, piecewise surface approx., finite element calcs., isoparametric method 80—12881
stiff bending plates, stress-strain states, finite element effectiveness, polynomial approx. *(Russian)* 80—58921
stiffened layered structs., dynamic large-deflection inelastic and thermal stress anal. 77—3752

finite element analysis continued
- stiffened plate struct., nonlinear anal. by combined Rayleigh-Ritz-finite element method 77—72162
- stiffened plates, constraint method anal. 78—26066
- stiffened plates, structural and by finite element and integration methods 77—3753
- stiffness, exact straight line element calc. 80—79138
- stiffness matrix for sandwich beams with thick anisotropic laminated faces 79—46182
- stiffness matrix softening, artificial 77—80067
- Stirling cycle analysis, accuracy evaluation 79—48170
- Stoke's problem in velocity pressure formulation, mixed finite element approx. *(French)* 78—86164
- Stokes eqns., num. soln. using finite element anal. 79—92947
- Stokes flow, stress-hybrid finite element method 80—99985
- Stokes problem with conforming Lagrangian finite elements, soln. error estimates *(French)* 78—62085
- strain displacement equations of thin shallow axisymmetric shells, incremental anal. 80—53628
- strain-hardening material, ductile fracture, J-integral estimates 77—89064
- stratified environmental flow, book contrib. 79—34875
- stratified turbulent flow digital simulation 78—90964
- stream function-vorticity finite element solns. for Navier-Stokes eqns. 79—14368
- strength of axisymmetric body, optimum shape calc., finite element technique 78—51060
- strength of materials and mechanical systems dynamics computing, based on three-dimensional models *(German)* 80—58976
- stress anal. in two dimensions, expt.-numerical hybrid technique 77—50910
- stress analysis, connection between finite element and integral equation methods *(French)* 77—87649
- stress analysis, energy methods, book 78—1571
- stress analysis, improved equilibrium finite elements 78—75067
- stress analysis by finite element program 79—64522
- stress analysis of cracks, elastoplastic range 78—67144
- stress analysis of human femur, three-dimensional 78—7379
- stress analysis of human left ventricle, computerised procedure 77—86518
- stress and displacement fields, continuous, algorithm for finite element anal. 78—30178
- stress calc. equilibrium method using finite element displacement models 77—23875
- stress corrosion test specimen-fixture interaction for slow crack-growth 77—56166
- stress deformation states in 3-layer cylindrical shells *(Russian)* 79—14256
- stress distribution, calc. for glassware after quenching 79—66087
- stress fields, discretisation 77—50879
- stress inteisity factors, time depend., singular finite element 80—1471
- stress intensity factor determ., accurate finite element method 77—54878
- stress intensity factors, UNCLE finite element system calcs., appls. in fracture mechanics 78—67098
- stress intensity factors calc., 3-D 77—27491
- stress intensity factors calc. using special 3-D elements 79—94556
- stress state of structural elements of vessels under external hydrostatic press. 77—14908
- stress-equilibrium membrane elements with holes 77—78980
- stress-strain states, 3-D elasticity, finite element method *(Russian)* 80—74728
- stress-strain stiffness matrix calc. in inelastic material 78—34032
- structural anal., axisymmetric solid of revolution elements based on assumed stress hybrid model 79—3917
- structural anal., underlying concepts 78—66337
- structural analysis, combined finite element-transfer matrix method 77—62201
- structural analysis, dynamic condensation method 79—3943
- structural analysis, nonlinear theory of shells 79—30230
- structural analysis of toroidal field coil struct. response 78—50396
- structural dynamics, finite element reduction scheme, variational theorem 77—890
- structural engineering problems, finite element analysis 79—2607
- structural mechanics, boundary soln. procedures 77—26175
- structural network and continua, critical features rel. to simulation 77—50882
- structural plasticity problems, nonlinear finite element anal., mathematical programming 79—46224
- structural stiffness matrix eqn., algorithms for direct access Gaussian soln. 78—57766
- structural systems with internal gaps, dynamic and under axial impact loading 77—3092
- structures of discontinuous shape, finite element analysis of bending behaviour *(Japanese)* 78—83238
- structures under impact loading, finite element modelling as tool for noise analysis and control 80—43535
- structures with rotational degrees of freedom, large displacement-small strain anal. 78—89310
- Sturm-Liouville, error estimation 78—81818
- sub-structure analysis for elastic fields with stress singularities, hybrid formulation 77—3730
- subsonic aerodynamics, finite element approach 79—55399
- subsonic aerodynamics, finite element method appl. 77—47038
- subsonic compressible flow, past symmetric profile, num. soln. method *(French)* 77—58720
- subsonic plane pot. flows, least squares finite element anal. *(Chinese)* 80—59063
- subsurface hydrology, finite element method using mixed explicit-implicit scheme 79—79900
- successive overretardation processes, estimation of optimum accelerator when applied to finite element anal. 78—16629
- Suhara-Fukuda method of network generation, modifications 78—24646
- SUPERB general isoparametric finite element program 77—42682
- superconducting composites, stress-induced heating, finite element calc. 77—28342
- superconducting dipole magnets for high energy accelerators, stress and strain distribs. 79—31250
- supersonic lifting surface, finite element anal. and collocation method 78—1687
- supersonic potential flow, panel flutter, finite element calc. 78—26152
- supersonic three-dimens. flow, finite difference method 78—51190

finite element analysis continued
- surface waves, long period, explicit-implicit method 79—4026
- surface waves, over submerged obstacle, finite-difference method 79—4027
- surface-fluid-shell system, finite element anal. of dynamically coupled motion 77—19536
- surface-wave dispersion in inhomogeneous medium, investigation by finite difference method 79—66631
- symbolic generation of finite element stiffness matrices 79—32244
- synthetic seismograms using finite difference techniques 78—73326
- tapered beams and beams carrying mass, vibrations, finite element formulation, comments and reply 78—13950
- tapered cantilever columns, post buckling finite element anal. 79—1119
- tapered circular plates elastically restrained against rotation at edges, nonlinear vibs. 79—18791
- tectonic visco-elastic system modelling 80—104930
- tectonics, finite element modelling of Nazca plate stresses 79—20802
- tectonics, Zagros collision orogeny, finite element modelling of lithosphere deformation 79—20803
- temperate lakes, finite element analysis of one dimensional thermocline problem 78—49042
- temperature field analysis using boundary value problem procedure *(Polish)* 79—94448
- temperature field equations, steady-state and transient case, 2-D, 3-D, finite element anal. 79—23182
- temperature field in hot rolled T-section finite element anal. *(Russian)* 79—29101
- temperature stress-state of internal combustion engines finite element study 77—80073
- tensile test specimen contour, expt. and calc. comparison *(German)* 77—86233
- tension creep, finite element anal. of void growth 79—18739
- thermal analysis, finite element method for temp. depend. parameters 79—32184
- thermal characteristics of finite element and finite difference calcs. for transient problems, comments 80—69633
- thermal elastoplastic stress analysis based on initial strain method *(Japanese)* 80—77620
- thermal loads in elastoplastic stress finite element anal. 79—46225
- thermal reactor containment, finite element anal. of luid-structure interactions 80—22998
- thermal stress anal., finite element variational method 77—7310
- thermal stress cracks, J-integral appl. for stress intensity factors 79—81811
- thermal stress simulation in continuous casting, finite element method 78—30170
- thermal stress variational anal. 77—7311
- thermal stresses computing rel. to uncoupled thermoelasticity *(Italian)* 79—18719
- thermal stresses in rectangular plates, variational and finite element solns. 78—51082
- thermally buckled finite element panel, flutter anal. 77—11143
- thermally expandable fluid transients, finite difference method 77—79418
- thermoelasticity in solid symmetrical bodies of revolution, thermal transients calc., appl. *(Spanish)* 79—23208
- thermoelectric cooler, single stage, finite element thermal stress anal. 80—108807
- thermomechanical interaction effect by finite-element method 80—42067
- thermoviscoelastic transient responses, stability and accuracy of finite element solns. 80—5951
- thick circular plates, sector finite element for dynamic anal. 79—72845
- thick cylinder under non-axisymmetric loads, computer stress analysis 77—54880
- thick multiply connected plates, stress state investigation by finite element methods 77—11132
- thick plate, reduced integration, function smoothing, and nonconformity 77—50880
- thick spherical shell under thermal loading, numerical anal. 77—68445
- thick walled tube in tension, stress intensity factor of annular cracks 77—62214
- thick-walled shells of revolution, axisymmetric problems soln. by design and exptl. methods *(Russian)* 78—73853
- thin elastic plate, bending problem soln. in fracture mech. using specialized finite element technique 79—77011
- thin film eddy current integro-differential eqns. soln. 78—90343
- thin orthotropic plates, bending stability and free vibration 79—3961
- thin plate Semiloof element for structural anal. 79—3913
- thin plates, bending anal. hybrid stress finite element model 80—96201
- thin plates, limit load and elasto-plastic bending, finite element anal. 79—27544
- thin rectangular plates, stability and vibration anal. by simplified mixed finite elements 78—34058
- thin shell, 9-node Lagrangian element 80—23888
- thin shell by mixed method formulation 77—9872
- thin shell mixed method formulation, large displacement and dynamic analysis 77—35032
- thin shell structs. mixed elements, theory, criticism, examples *(German)* 79—27506
- thin shells, algebraic constraints for weak C^1 continuity 78—4458
- thin structures, large displacement anal. 79—27514
- thin-walled structures, elastoplastic analysis by finite strip method *(Japanese)* 77—42753
- thorax, human, elastic finite element anal. models 78—3542
- thorax impedance finite element model for cardiovascular and respiration meas. 77—40887
- threaded connections, load transfer modelling 79—90195
- three dimensional computer code for stress anal. 77—49586
- three dimensional stationary supersonic flow fluid, progonka process calcs. 79—7383
- three dimensional structures, finite element technique for stress intensity factor computing 79—72854
- three dimensional structures, system of mathematical calc. 79—98623
- three-dimensional field modelling, finite-element interactive computer methods *(French)* 79—41294
- three-dimensional stress anal., transition finite elements 80—92042
- throughflow between rotating and stationary disk calc., laminar *(Japanese)* 80—6064
- tidal estuary two-dimensional hydrodynamic digital simulation 78—92846
- tidal flow, finite element analysis model, flow in rectangular channel example *(German)* 78—96233
- tidal flow, interlacing channels, nonlinear computer model 79—34828

finite element analysis continued
tidal flow, periodic, anal. by finite element perturbation method 78—24290
tidal flow, periodic Galerkin finite element method 78—28239
tidal flow, shallow water eqns., semi-implicit approach 79—34829
tidal motion on sphere, geodesic finite-difference method for curved domains 80—109153
tidal periodic flow anal. by finite element perturbation method 77—70690
tidal waves in estuaries, explicit finite-element formulation *(German)* 78—94755
tidal waves in rivers and estuaries, finite element models 79—53370
tidal waves spectral modelling *(French)* 80—21782
tides, oceanic and shallow water, spectral method of computation *(French)* 78—28321
tides, spectral modelling, finite element method, appl. to M_2 tide in English Channel 78—61579
time domain finite element solns., accuracy and stability 79—37232
time-dependent equations, multistep finite difference methods, boundary conditions 78—36829
time-dependent Navier-Stokes eqn. soln. 78—92956
time-varying magnetic field problems, finite element formulations 79—41265
Timoshenko beams, finite element eigenvalue anal. 78—59327
Timoshenko beams, finite element for vibr. anal. 79—18774
Timoshenko beams, resting on elastic foundation, dynamic stability 79—18775
Timoshenko rod, straight axis, free bending oscillations investigation *(Hungarian)* 80—89327
Tokamak, Texas exptl., homopolar generator, eddy currents, EM forces (torques), due to misalignment 78—54953
Tokamak devices, toroidal pinch systems using programs in FORTRAN-D *(Japanese)* 78—5910
Tokamak plasma equilib. by finite elements, book contrib. 79—32805
Tokamak reactors, supercond. toroidal magnets, max. mag. fields, mech. stress calcs. 79—36405
tooth-jaw system, mech. anal. 77—40703
toroidal reactor primary containment vessels, consistent mass matrix anal. of hydrodynamic effects 79—76066
trabecular bone-porous coating-hip prosthesis interface, mechanical behaviour 79—39436
transient and unconfined groundwater flow analysis 78—92871
transient creep analysis, finite-element and analytical soln. superposition 77—75820
transient diffusion with n-order irreversible chem. reaction, finite element method 78—85122
transient flow, split band Cholesky eqn., strategy for finite element anal. 78—46923
transient nonlinear mechanics problems, finite element anal., computational aspects 79—41565
transient thermal problems, finite difference and finite element calcs., suddenly cooled boundary 80—14554
transition finite elements for axisymmetric stress analysis 80—92048
transition from fine to coarse grid 78—26043
transitions elements for use with quarter point crack-tip elements 78—63376
transonic aerodynamics, finite element method, book contrib. 79—32556
transonic aerodynamics, variational formulation and finite element anal., book contrib. 79—32555
transonic airfoil problem, variational principles 78—42626
transonic flow, finite element and finite difference calcs., book contrib. 79—32558
transonic flow, num. simulation by finite element method using optimal control theory 77—55025
transonic flow, orthogonal finite element method 80—28529
transonic flow, wind tunnel wall and viscous effects, numerical simulation 77—27552
transonic flow field, discontinuous trial functions 77—68619
transonic flow simulation by finite element method via optimal control, book contrib. 79—32557
transonic flow with shocks, finite element method appl., shock-fitting 80—14730
transonic potential flow, partial differential equatn. solutn. 80—24045
transport eqn., unsteady convective diffusive, upwind finite element scheme 79—97320
transport eqn. soln., dispersion corrected numerical schemes 78—36946
transport equation, anal. of numerical soln. 77—64358
transversally nonhomogeneous waveguide EM wave propagation, using variational methods *(Czech)* 80—33155
Tresca yield condition usage in finite element plane strain anal. 78—83263
triangles, numerically integrated matrices and quadrature formulas 78—24644
triangular finite difference scheme for large deflection problems 79—32233
triangular finite element universal matrices construction 78—36805
triangular finite elements and numerical integration 78—33
triangular plate bending element, fast calc. algorithm 79—72830
triangular plate elements, numerical investigation using variation principles with relaxed continuity conditions *(German)* 79—10465
triangular quarter point element as elastic and perfectly-plastic crack tip elements 77—14956
Trombe wall channel, free convective laminar flow 79—86397
truncated conical shells, thermal buckling 77—68467
tsunami, island of Hawaii, 1979 November 25, numerical anal. by finite-element method 80—72449
tsunami long wave propagation anal. at Hawaiian Islands and Long Beach and Los Angeles harbours 78—92849
tsunami simulation, Hawaii, open boundary reflection interference 80—17232
tsunami wave propagation anal., 2-step explicit finite element method 78—40503
tsunami wave propagation anal. 78—92848
tsunamis interaction with Hawaiian Islands, finite element numerical model 78—69361
tubular joints stress anal., finite element anal., computer programs 78—41808
tuning fork for HF operation, second-mode, finite element anal. and expts. 80—102980
tuning forks, quartz crystal, finite element analysis of displacement at base portion 79—68470

finite element analysis continued
tunnel lining, bedding model using matched elastic springs *(German)* 77—35039
turbulence of air intake, calc. in 2-dimens. 79—3999
turbulent channel flow, secondary current numerical simulation 78—94828
turbulent flow, computational modelling by finite elements 79—1163
turbulent flow, Navier-Stokes eqns. 79—1162
turbulent flow, one-eqn. models, finite element soln. 79—7371
turbulent flow in pipes, numerical anal. by finite element method 78—18341
turbulent jet flow, mixing length calc., two-equation model solution 78—38295
turbulent recirculating flows in general orthogonal coordinates 78—38297
turbulent shear flow behind prolate spheroid, numerical model 79—23304
two dimensional, reinforced concrete, finite element analysis of structures taking account of nonlinear physical behaviour and discrete crack development 79—57121
two dimensional bound state problems, finite element method comparison with spectral method 80—47856
two dimensional flow with singularities formulation 78—90822
two dimensional steady flow problems, numerical soln., finite element method 79—23296
two-dimens. structs., finite dynamic element for free vibr. anal. 78—83287
two-dimensional hydrodynamics and water quality digital simulation 78—92877
two-dimensional nonlinear magnetostatic fields, isoparametric Hermite finite element program 79—41275
two-dimensional potential fields in complex media *(Slovak)* 78—94351
two-dimensional turbulent flow past rectangular cylinder 78—1645
two-phase flow, nonlinear test case 80—96293
two-phase flow soln. technique 78—79366
two-phase flow through porous media, simulation by finite elements 79—41752
two-phase flow through porous media, starting algorithm for numerical simulation 78—38388
ultracentrifuge, flow, isotope conc. field, numerical model 79—1199
unbounded field problems, flanged and unflanged open-ended waveguide 80—23600
UNCLE finite element scheme, input specification 80—95512
underground nuclear power plant fission product containment after accident 80—27768
unidirectional composites, two component finite element for determining transverse loads *(German)* 79—49043
unidirectional fibrous composite, mixture theory for longitudinal wave propagation, computational procedure 79—50632
unidirectional loaded rectangle disc with circular hole, estimation of error arising from Lagrange's reference system 79—50587
Unimoment method, simplified matrix element representation 77—74207
unmagnetised plasma column, anomalous skin effect, finite element calc. 79—14552
unsaturated porous media flow 78—92869
unsaturated soil simultaneous heat and moisture transport anal. 78—92868
unstable crack propag., in 2-dimensional geometries, transient finite element analysis 78—67151
unsteady boundary layer over an impulsively started flat plate using finite elements 79—14366
unsteady gas dynamics, least squares finite element approach 78—26134
unsteady heat cond. in domains of irregular boundary, numerical expts. 78—51039
unsteady subsonic and supersonic pot. aerodynamics for complex config. aircraft 77—72320
upwind finite elements development 78—89312
upwind scheme, reply to comments 78—24651
upwind schemes, spatial oscillations 78—24650
upwindings of high order Galerkin methods in conduction-convection problems 79—3886
urban flooding rel. to land use change, stormwater management model 77—37280
US exponential solid horn 78—94496
uterine muscle penetration by flexible IUCD shield 79—29556
vacuum vessel for ASDEX fusion reactor, finite element stress anal. 80—18655
variable thickness, curved beam and shell stiffening element with shear deformations 79—44733
ventricular myocardium plastic cast global Young's mod., calc. from angiograms 77—48827
vertebral model, computer-aided technique for 3-D finite element model generation 78—92591
vertebral response to laminectomy, finite element model 80—41090
vibrating beams, calc. of higher freqs. by simultaneous iteration technique 79—23258
vibrating hemispherical shells partially filled with liquid 79—81792
vibrating panels, support location influence on flutter, Galerkin method 78—1598
vibrating plate, variable thickness, spline technique method 80—79195
vibrating plates, 3-layered damped sandwich composites 79—81794
vibrating thin rectangular plates, influence of thermal grad. on natural freq. 79—32353
vibration anal. by combined holographic interferometry and finite element anal. *(German)* 78—90806
vibration of Mindlin plates, finite strip models 79—3966
vibration of viscoelastic orthotropic layered cylinderical shell in acoustic medium, numerical anal. 77—54828
vibration problems, element spaces and separation for determining bounds to eigenvalues 79—14317
vibration problems, solns. using high precision finite elements, comments and reply 77—72224
vibrations of shaft-supported plates, finite element formulation 77—68485
virtual crack extension method, nonlinear material behaviour 78—18230
visco plastic torsion, prismatic bar 80—38282
visco-plastic steady-state flow finite element solns. 77—5670
visco-plasticity problem with hardening, finite element anal. *(French)* 79—46222
viscoelastic body eigenfrequency determ. *(German)* 79—23270
viscoelastic fluid, creeping flow through tapered contraction 77—55050
viscoelastic fluid flow, die swell problems with free surface, collocation and Galerkin finite element 80—14751

finite element analysis continued
- viscoelastic fluid flow, mixed finite element anal. 77—39315
- viscoelastic fluid flow in fixed geometry, collocation and Galerkin finite element methods 80—14750
- viscoelastic isotropic linear material characteristics, finite element method *(German)* 78—32681
- viscoelasticity equations, finite element formulation for numerical solns. 77—89042
- viscoelasticity equations, stability of numerical soln. 78—16647
- viscoplastic flow, finite element anal. *(Russian)* 78—18195
- viscoplastic flow, finite element method with added boundary terms 78—42543
- viscoplastic limit load problem, kinematic soln. method *(French)* 78—30195
- viscoplasticity with singular yield surfaces, side and corner flow rules, finite element applications 80—48594
- viscosity by capillary rheometer, end correction for power-law fluids 78—91037
- viscous compressible liquid, bubble behaviour analysis by finite method 77—55072
- viscous flow calcs., polynomial interpolation methods 77—65729
- viscous fluid anal., book contrib. 79—32522
- viscous fluid mixture with thermomolecular diffusion, new variational-Lagrangian thermodynamics 79—49185
- viscous fluid unsteady periodic flow, Galerkin finite element method 77—75872
- viscous gas equations, numerical solution, difference schemes, moving grids 80—48730
- viscous incompressible flow 77—68561
- viscous incompressible flow problems, two-dimens., Navier-Stokes eqns. soln. and contaminant effects 77—58638
- viscous incompressible non-Newtonian flow, finite element method, Bingham fluid 80—92184
- void growth, coalescence, ahead of moving crack tip, finite element anal. 78—1609
- von Karman plate bending equations approx. 79—50598
- von Mises' eqn., finite element solution to eqns. of laminar boundary layer *(French)* 77—72268
- vortex flows, between rotating cylinders, axisymmetric Navier-Stokes equations 80—59044
- vortex wakes, implicit finite-difference procedure 78—14018
- water pollution prediction 78—93019
- water resources, conf. at London, England 1978 78—92867
- water seepage through porous medium 78—38401
- water wave diffraction by 3-D bodies, hybrid element method 78—38344
- water wave propag., long-period, finite difference-element integration scheme 78—75157
- water waves, hybrid element method appl. 80—10258
- wave equation, finite element Laplace transform. soln. 78—4488
- wave equations, finite difference approx. using cubic spline technique 79—49
- waves in shallow water, improved finite difference scheme 79—4028
- weakly coupled linear systems, block iterative LU solution technique 77—60941
- weather forecasting *(Chinese)* 77—87024
- weather forecasting and general circulation, 5-level global model 80—51504
- weather forecasting nonlinear evolutionary problems 80—21865
- weather prediction by finite difference scheme *(Chinese)* 80—46234
- weighted residuals, improved finite element formulation by using least squares fit 79—52
- weldbonded joint deform., finite element simulation 78—35636
- welded joints, low cycle fatigue anal. 77—3789
- welding, thermal stresses and metal movement, computer simulation 78—34002
- wells, large diameter bottom entry flow anal. 78—92870
- world ocean, normal modes, finite-element barotropic model 79—16489
- yield zone form., fracture resistance, influence of specimen configuration 78—68817
- yielding of plates with hardening and large deformations 78—59311
- Zircalloy in thermal gradient, calc. of supercharging effect of H_2 and hydride distrib. 78—21639
- Al alloy, crack opening displacement, expt. and FEM study 78—68811
- Al alloy 2024-0, work hardened circular plates, theoretical predictions of nonlinear-finite element computer code, deflection and strain data 79—38893
- Al high strength alloy bar stress wave propagation *(Japanese)* 79—79030
- Al sheet alloy, type 2036-T4, in-plane deformation, correlation with Hill's theory 79—83260
- Al, single cryst., latent hardening *(Japanese)* 78—44135
- Al single crysts., elastoplasticity, dislocation model, work hardening, tensile tests, stress/strain curves *(Japanese)* 77—52410
- Al-Cu-Si-Mn, type 2017S-T4, crack initiation at root of circumferential notch of round bar specimens *(Japanese)* 80—60947
- Al-CuAl_2 lamellar eutectic, computer simulation of two dimensional Zn diffusion 78—30799
- Al_2O_3, elastic behaviour, finite element anal. model, thermal props. 78—31449
- B fibre reinforced epoxy composites, notched, tensile strength and failure modes 80—81205
- B fibre reinforced epoxy laminate, energy release approach for stable crack growth in free edge delamination problem 78—19878
- C fibre reinforced plastic, stress analysis of butt strap joint 79—43300
- C fibre-reinforced plastic joints, fatigue life, stress distrib. analysis 80—55497
- Cr-Mo-V steel, creep rupture tests on notched cylindrical specimens at 600°C 77—32670
- Cu, continuum representation of computer simulated dislocations 78—30623
- Fe, cast, spherical, mech. behaviour, continuous theory of dislocations appl. 78—67717
- Fe, cast flake and nodular, rupture strength, circumferential notch *(Japanese)* 80—93649
- Fe-Ni-Co, diffusion controlled phase growth 78—30782
- H atom in box, 2-D Schroedinger equation, influence of constant elec. field, finite-element method 80—31544
- H bound states in strong mag. field 80—99438
- H_2^+ bound states in strong mag. field 80—99438
- He underground rippled dewar system for 10000 MWh superconductive energy storage magnets 79—58705

finite element analysis continued
- He$^+$, electron scatt., reson. state assoc., incomplete spectrum of Hamiltonian matrix 80—99568
- $LiNbO_3$ acoustic conversion, piezoelect. surface wave behaviour at discontinuities 77—31198
- NaCl, rock salt, progressively mined soln. cavities, struct. behaviour 78—61409
- O silent discharge, numerical simulation 78—63629
- Si-Ge thermoelectric generators, approximation errors when using averaged properties solutions for required heat rates estimation 80—108808
- Th-PuO_2 kernels, effect of fuel particle size on power excursions, Doppler feedback mechanism 79—30911
- Ti, diffusion of H_2, nonisothermal, in temp. field of instantaneous plane heat source *(Russian)* 77—20123
- Ti, integral composite joints, finite element and expt. eval. 79—11670
- Ti-Al-V (6,4 wt.%), alloy plate, fatigue crack propag. under in-plane loading, anal. 79—52338
- α-β Ti-Mn (8 wt.%), calc. of stress-strain curves by finite element method, comparison with expt. curve 78—84924
- WC-Co sintered carbide tips, microscopic stress anal. 78—5663

finite state automata *see finite automata*

Finlay-Freundlich red-shift hypothesis *see gravitational red shift*

fireproofing *see flameproofing*

fires
- *see also accidents; combustion; flames; safety*
- brush fires, influence on W.African atmospheric aerosols *(French)* 79—34883
- buoyant flow, thermally driven, equations of motion 79—23334
- convection plume over fire in polytropic atmosphere *(Russian)* 78—96262
- enclosure fire, static pressure meas. 78—90871
- extinguishing, experience in laboratory safety course 79—48995
- fast breeder reactor, Na pool fire, aerodynamic props. of Na aerosols 80—23011
- fire whirl phenomenon, model 79—72958
- flameproof coating for PVC insulated cables, composition, tests *(Russian)* 78—68828
- forest fire mapping using pyroelectric vidicon 77—65635
- forest fire survey application of microwave radiometry 77—87127
- human use of fire, history and effects on Earth albedo and climate 80—81893
- incipient fire detector, based on detection and size analysis of submicrometre particulates 79—75672
- intense fires, convection-diffusion coupling model, O_2 conc. enhancement 77—7481
- IR forest fire alarm system 80—86429
- Japan, fire tornadoes, max. wind speed estimation 78—36255
- LMFBR, expts. on extinguishing large quantities of burnina Na 79—41016
- LMFBR accident consequences, H_2 jet ignition and extinguishment 78—8932
- materials flammability testing, problems, language and scientific basis 79—5092
- Microwave radiation spectra of forest fire sources 80—52314
- microwave radiometric methods and the problem of forest and peat fires 80—31877
- nuclear power plant, fire hazard 78—50269
- nuclear power plant, startup and operating experience including cable tray fire 77—65284
- nuclear power plant fire frequency and core damage probability estimation 79—13461
- nuclear power plant fire protection policy 77—46356
- nuclear power plant fire risk assessment 80—23002
- nuclear power plants, fire occurrences, Bayesian prediction model 80—18527
- nuclear power stations, fire barriers, analytical hazards analysis 80—18534
- nuclear power stations, industrial activities nearby causing hazards 80—78408
- nuclear reactor secondary containment response to Na and H 80—27769
- nuclear safety exercises carried out in French industrial facilities *(French)* 78—55051
- pyrocumulus cloud over North Canterbury, New Zealand, 1878 April 10, obs. 80—109240
- radiation augmented fires within enclosures 79—32206
- smoke cloud plumes from forest fires in Canada, satellite obs. 78—24367
- smoke plume associated with intense local fire, obs. 77—49148
- spark discharges from body, electrostatic, nature and incendiary behaviour obs. 80—72406
- spent-fuel rail cask system, high-speed impact and fire test 79—59206
- sterilisers, ethylene oxide, evaluation of effectiveness and hazards 77—60269
- timber fires caused by lightning in Alaska, NOAA-5 images of smoke 78—49079
- turbulent fire plume, reaction rate, air entrainment, radiation 78—35682
- United States, synoptic weather situations assoc. with major wildland fires 78—61499
- wood burning, atm. CO_2 input 78—81368
- Na aerosols and fires, expts., LMFBR safety anal. data 77—71650
- Na fire in nuclear reactor, anal. with SPOOL-FIRE code 77—46322
- Na fires, origination and mechanism, form. and sedimentation of Na aerosols, review *(Czech)* 79—30956
- Na fires suppression in fission reactor, installations 80—27770
- Na spray fires, nucl. reactor containment 80—32369
- Na spray fires in nucl. reactors 80—32365
- O_2 index test, measurement and appl. 79—79337

fission
- *see also fission of plutonium; fission of uranium; photofission; spontaneous fission*
- ^{209}Bi(α,f), search for near threshold asymmetrical fission *(Russian)* 78—33233
- ^{298}114, high spin pot. energy surfaces, fission barrier, α-, γ-decay half lives, yrast spectrum 80—73764
- (α,f) on preactinide nuclei Hf-Bi 30-50 MeV, ang. anisotropy 77—18637
- Γ_n/Γ_f determ., 12 to 20 MeV excitation, from evaporation-residue cross sections 77—61451
- $\bar{\nu}(Z,A,E_n)$, prediction method developed 77—26792
- σ-model appl. to nuclear physics in one dimension, fission, Hartree approx. 79—80890

fission continued
A=170-212 nuclei, 20-60 MeV ^{3}He ion induced fission, effective momenta of inertia *(Russian)* 77−34360
A=200 region, macroscopic fission barriers, isospin depend., liquid drop model 80−57811
A=225-253, fission probability, applicability of conventional systematics *(Russian)* 79−54464
A=80-240 nuclei, capture of stopped π^-, spallation, fission, new isotope synthesis 77−6459
A=88 to 99, fission probability, applicability of conventional systematics *(Russian)* 79−54464
absolute cross section meas. using fixed energy neutron sources 79−13365
absolute fission ratio measurement, semiconductor fission chambers *(Japanese)* 77−67948
absolute fission-rate distribution in graphite-reflected lithium oxide blanket assembly 80−9317
actinide fission, statistical anal. of gamma emission 78−17255
actinide fission product X-rays in micas, comparison with superheavy elements K- and L-shell ionisation estimates 77−50581
actinide muonic atoms, n emission from radiationless muonic transitions and μ capture 79−3599
actinide nuclei, fission width calc. using doorway state approach 79−13278
actinide nuclei, photo- and electro-fission cross sections and yields, giant resonances 80−5187
actinide nuclei, statistical aspects in fission mechanism 77−14097
actinide series neutron-induced-fission systematics in MeV region 77−67778
actinides, fast reactor recycle as waste management alternative, performance calcs. 78−13269
actinides, fragment shell effects determ. from ^{32}S many nucleon correlations 78−41690
actinides, neutron fission cross section meas., fragment ang. distrib. using solid state track detector 79−76300
anisotropy of fragment emission, effect of spin of target nucleus *(Russian)* 77−22992
asymmetric, nuclear mass parameter 78−13053
asymmetric, statistical theory explanation, association with higher quantum state density 78−70509
barrier calculations, effect of simple consistency condition 77−67732
barrier calculations, experimental data, review 77−26661
barrier props., expt. studies and statistical anals. review 80−102216
beta strength function, half life and delays, nuclear- and astro-physics consequences 80−102149
beta strength function structures, nuclear- and astro-physics consequences 80−99152
binary fission saddle pints, shape parametrization for liquid-drop studies 80−106086
carbonaceous chondrites, fission Kr and Xe origin 79−35199
carbonaceous chondrites, superheavy element fission hypothesis for Xe origin 77−78726
chain reaction demonstration model 80−46774
charge division, droplet model 78−17173
collective modes in fission and deep inelastic scatt., ang. momenta equilib. statistical treatment 80−42688
compound nuclei prod. in (HI, xn), lifetimes with account of fission process *(Russian)* 78−25233
conference, natural fission reactors, Paris, France, 1977 80−17716
conference on heavy ion reaction dynamical props., Johannesburg, S.Africa (Aug. 78) 80−17715
conference on nuclear interactions, Canberra, Australia (Aug.-Sep. 1978) 80−4476
conference on nuclear physics, Mikolajki, Poland (2-14 Sept. 1979) 80−101662
conservation, Japan, molten-salt reactor strategies, LMFBR, HTGR, utilisation, coexistence *(Japanese)* 77−50257
Coulomb fission prompt component, model including rot. states and vibr. motion 79−67783
cranking model, all orders solution, appl. to nuclear fission 77−82838
cranking model anal., validity 77−18517
criticality safety of large facility, neutron interaction anal. 79−63822
deep inelastic processes, large scale collective motion in nuclear matter 80−5087
deeply inelastic heavy ion collisions, ang. momentum transfer from sequential fission 80−18333
deformation energies for nuclei with different charge-to-mass ratio for fusion or binary fragmentation 79−80869
deformation energy surfaces for U, Pu, Cm, two centre shell model 77−71559
deformation process mass parameter, liquid drop model 80−102221
deformations described by density moments 77−41883
delayed fission neutron technique, review 79−1979
delayed fission produced in synthesis induced by heavy-ion beams and neutron currents *(Russian)* 79−89341
delayed neutron emission probabilities, simple statistical model calcs. 77−50103
dipole giant resonance in fissioning nuclei, microscopic calcs., excitation energies, dipole strengths, transition densities 78−29442
discovery, research of 1930's, '40's, Otto Hahn 80−57063
discovery of fission 79−26418
double core model for fission 77−30546
double humped fission barrier concept, neutron induced fission 78−29443
double humped fission barrier using biharmonic oscillator pot., penetrability calcs. 78−86524
double well-cluster shell model, spurious states of cm motion during fission *(Chinese)* 77−14045
dynamic excitation model of fission process, scission, ^{240}Pu appl. 77−14095
dynamical interpretation of the statistical theory of fission 79−45311
dynamics, effects of shell struct. and pair correl. 79−6560
EAS, atomic nuclei fragmentation, analytical method *(Russian)* 78−65472
electrofission of light nuclei, recent obs. 79−3185
electron-collision cross-section data for atom or molecule, rel. to radiation physics 80−63829
even-even actinide nuclei, fission barriers, Strutinsky method with dynamic fission paths 77−71602
excitation during collective deformation, time depend. Hartree Fock Bogolyubov method, fission process 78−58229

fission continued
excited nuclei, state density renormalisation as function of deformation 77−6201
explosive r process cooling process 78−69791
fast reactor parameters, influence of fission spectra uncertainties 80−22928
Fermi system particle distrib., nuclear matter, heavy ion collisions and fission 79−36183
first order adiabatic approx., fission fragment excitation energy 80−32312
fission, ATDHF validity 78−50149
fission barrier determ. in region Z=82, N=126, using polycarbonate thin film and electron linac 78−55104
fissionability, target mass depend. for π, γ, α, p, cascade-evaporation and liquid drop calcs. *(Russian)* 80−106089
fissionable nuclei A=232 to 252, systemization of relative yields of retarded neutrons 79−40974
fragment excitation, prompt neutron distrib., renormalised gas model calcs. 80−99169
fragment formation as clustering effect, many-nucleon correl. 79−6561
fragment KE, viscosity effects for spontaneous and induced fission 77−18639
fragmentation theory, two body breakup channels in fission, fusion, heavy ion scatt. 78−46037
fragments, mass-yield curves, topological classification *(French)* 79−76043
frictional effects in nuclear reactions with large scale collective motion, review 78−78336
frictional effects on post-scission dynamics and fission fragment kinetic energies 79−36225
Gamow Teller giant resonance struct., consequences for delayed neutron spectra and nucleosynthesis 77−2950
generator coordinate method with conjugate parameters 80−47413
hadron induced fission, low energy evaporative particle emission from emulsion nuclei *(Russian)* 80−86943
Hauser-Feshbach calculation of the fission neutron spectrum 80−22801
heavy fissile nuclei, nuclear constants estimation *(Russian)* 79−30779
heavy ion collision induced fission, fragment ang. distrib., reaction mech. 78−74412
heavy ion collisions, resonance states in two-body breakup channels, theory of fragmentation 79−9619
heavy ion deep inelastic collisions, reln. to quasi-fission 78−13144
heavy ion reactions, dynamical properties, field overview 80−18327
heavy ion reactions, fission fragment angular distrib., shape of saddle point of compound nucleus *(Chinese)* 78−78427
heavy ion reactions, potential energy surface topography 77−330
heavy ion reactions, potential energy surfaces, binary fission, fusion, liquid drop model *(Rumanian)* 78−86547
heavy ion reactors, neutron ang. distrib., compound nucleus decay, fission fragment anisotropy *(Russian)* 80−5160
heavy ion reacts., cross-sections for fusion, quasifission and deep inelastic collisions *(Russian)* 78−54801
heavy ions collision, liquid drop model generalisation *(Rumanian)* 78−58260
heavy isotope reactivity coeffs., in fast neutron critical assemblies 79−63742
heavy nuclei, fission process gamma ray analysis *(Rumanian)* 79−40973
heavy nuclei meson induced fission, statistical relaxation process 79−59098
heavy-ion induced fusion reaction products, statistical and liquid drop model anal. 78−66312
heavy-ion reactions, collective pot. energy surfaces, appl. to Ar+Ag, Kr+Cu, and Xe+Bi 78−41748
high amplitude oscillatory states and external fields, in heavy ion interaction and fission *(Russian)* 79−97650
high-energy fission in astrophysics, comparison of methods for cross sections calc. 78−28505
independent fission-product yields to isomeric states, distrib. 77−50106
inertia matrix elements of highly deformed nuclei *(French)* 79−71838
isobaric widths, frozen quantal fluctuations, charge equilibration 80−37365
isomeric states population via isobaric analogue resonances 77−34231
isomers, spectrosc. props. 80−105966
JWKB approximation for multiple-humped fission barriers, ^{234}Th appl. 78−585
large deformations and dissipation in a random-matrix model approach for fission or colliding nuclei 80−18162
large-amplitude collective nuclear motion in fission and heavy ion reactions 80−22675
lifetime distribution and probability estimates 78−659
light-particle accompanied fission, 3-centre shell model 77−41941
liquid drop model, calc. of Coulomb energy of distorted nuclei 79−63654
low energy fission, charge distrib., quantum mechanical phenomenon of GDR 80−86945
Mandelstam-Sommerfeld-Watson transformation *(Rumanian)* 80−47463
mass asymmetry due to valley fragmentation 77−71616
mass distribution widths in statistical theory of fission, nucleon tunnelling *(Russian)* 80−5121
mean field theory of nuclear dynamics, time depend. 78−12986
mechanisms, recent progress *(French)* 80−78274
medium-heavy nuclei, fissility behaviour *(Russian)* 77−23121
mesoatoms, prompt fission internal γ-ray conversion, fragment radiative transitions *(Russian)* 80−86944
miniexplosion, critical masses in fission-fusion hybrid systems 77−3158
modern atomic and nuclear physics (book) 80−11
modified one body nuclear dissipation 78−50071
most probable charge, shell and deform. effects 78−29440
multi-chance high-spin fission, fragment anisotropy, stat. model anals. 80−57812
multidimensional barrier penetration and fission-widths, barrier resonance 80−13454
multifragment decay reactions induced by heavy ions, mica track detector study 78−17234
multiparticle, bubble chamber for expts. *(Russian)* 77−6640
muon induced, response tail to high threshold reaction 80−83075
muonic atoms, prompt fission, muon entrainment by fission fragment, probability *(Russian)* 80−37911
(n,2n) reaction, induced in fission neutron spectrum, effective threshold energies 78−25181

fission continued
natural nuclides from meteorites, spontaneous fission neutron multiplicity *(Russian)* 79—40977
neck rupture in nuclear fission, fragment kinetic energies 78—25169
neutron detection, pulse separation spectrum for fission neutrons and single neutron events 77—6651
neutron evaporation and fission widths, statistical formula correction *(Russian)* 79—13281
neutron induced, role of double humped barrier, review 77—26659
neutron induced fission resonances, spin determ. using polarised beam and target, review 77—26796
neutron interactions with nuclei, conf. 77—23015
neutron irradiation, multi-step, transuranium production in reactor, nuclear transformation chains, yields *(Japanese)* 80—52729
neutron kinetics of fissionable highly-compressed pellets 77—38315
neutron standards and appl., conference, Gaithersburg, MD, USA (March 1977) 79—9581
neutron transport theory, anisotropy of scatt. and fission 78—8865
neutrons with binding energy >40 MeV search in fission reactor spectrum *(Russian)* 79—89515
Nilsson potential, fission isomer props. investigation 78—29403
noble gases, fission yield meas. with Los Alamos on-line mass anal. facility 77—14301
nucleon exchange between fission fragments in two centre oscillatory pot. below threshold *(Russian)* 78—89847
one body dissipation and super viscidity of nuclei, nuclear fission, collisions and deformation 78—86501
pair excitation lifetime in nuclear fission, model 79—521
pairing effects on distrib. of fission-product yields 77—50107
partial fission channel characts. influence on fission phenomena, ^{239}Pu(n,f) calcs. 78—29515
polar emission in fission, nuclear orbiting, three-body trajectory classical calc. 79—3131
polarisation, order-disorder model of balance neutron distribution 79—13279
polarised nucleus fission, parity nonconservation mechanism, rot. state mixing *(Russian)* 80—37408
pre-actinide nuclei, fission barriers, level density collective effects *(Russian)* 80—106092
pre-actinide nuclei, level density and fission probability collective effects *(Russian)* 80—13455
pre-equilibrium neutron distribution *(Russian)* 77—26658
preactinide nuclei, fission excitation functions and fission barrier height, liquid drop model 80—47513
prompt fission neutron spectra calc., nucl. evaporation theory 80—22870
prompt fission neutron spectra for ENDF/B-V 80—22869
proton-induced fission, 70 to 200 MeV compound nucleus formation, fragment ang. anisotropy *(Russian)* 79—13359
PWR, fluctuation anal. of apparent malfunction, frequency and time domains 77—54313
quasi-fission, focusing effect, large energy loss, classical dynamic model 77—57689
quasi-fission reaction, mass-yield distrib. theory 77—42001
r-process, astrophysical, implications of fission mass distrib. 78—93204
r-process and r-cooling process, nuclear fissions 79—16816
radiative capture and fission cross sections ratio meas. in reson. region 77—50175
rate analysis from point of view of Brownian motion *(Chinese)* 80—52657
reaction rate standards and applications 79—9650
reaction valleys, two-centre shell model, fission and heavy-ion reactions *(Russian)* 77—82947
reactor materials, fission cross sections meas. in YAYOI reactor, fast neutron spectrum 77—42013
reference fission foils preparation by fluoride deposition, characterisation 80—23218
relaxation phenomena, collective deformation, and internal excitation energy *(Russian)* 79—80920
review of recent progress, barrier crossing, static and dynamical aspects *(French)* 79—520
rotating liquid drop model calc. of deformation energy surfaces, fission barriers 79—93603
saddle point, statistical fluctuations, Suzuki's scaling limit 80—86946
scission configuration determ., incorrect use of ternary fission data 79—36224
scission mechanism, statistical model, partial equilib. model 77—18631
scission of deformed nucleus, review of fission process 77—14096
scission point model based on deformed shell effects 77—10455
scission region, nascent fragment bending and wriggling modes, quantum numbers 80—18285
short lived α-emitters, cross section meas., spherical plate ionisation chamber 77—23380
slope constant of the exponential prompt-neutron yield formula 80—22806
Sommerfeld-Watson transformation *(Rumanian)* 78—86526
spatial parity nonconservation *(Russian)* 78—25170
spectrum-averaged cross section, integral meas. in standard neutron fields 79—13364
spontaneously fissioning isomers, probabilities of α-, β- and γ-transitions accompanied by changes in nuclear shape *(Russian)* 78—89820
standard neutron fields, integral meas. 79—13363
statistical fission parameters, ang. momentum depend. in statistical/rotating liquid drop model 78—89846
statistical fission parameters mass depend. 77—57696
statistical model de-excitation calcs. of compound nuclei 78—50146
statistical model of fission through double-humped barrier excitation energy 10-35 MeV 78—583
statistical theory, critical evaluation 78—70508
stopped pion induced nuclear fission, two-step model anal. 79—59097
sub-barrier (n,f) reactions, intermediate structure, cross sections, widths 77—34357
supercritical multiplying systems, extinction problem, point model approx., models for neutron multiplicity 80—22883
superdense nuclei in active zone of reactor *(Russian)* 78—33230
superdense nuclei production *(Russian)* 78—58310
superheavy elements in Allende meteorite, search for fission tracks 78—32415
superheavy nuclei, ^{300}120, effect of nuclear force finite range on fission and heavy-ion reactions 78—13180
superheavy region, neutron drip line, energy density mass formula extrapolation 78—93932

fission continued
symmetric, macroscopic potl. energy surfaces 77—14150
ternary fission, three-centre shell model 79—36226
thermal parameters of fissile isotopes, proposed reevaluation 77—23135
three humped fission barrier transmission including vibrational damping 78—41689
time-dependent variational approach to heavy ion reaction, appl. to fission 78—50193
trajectory calcs. basis for α-α accompanied fission 77—34352
trans-uranium nuclei, fission barrier and (neutron width-fission width), nucleon contents depend. *(Russian)* 80—106093
transuranics, neutron yields, estimation by compound nucleus formation 77—50108
two peaked pot. barrier, quasi-stationary state decay, semiclassical approx. *(Russian)* 80—37366
two spherical nuclei system, pot. energy calcs. for fission and fusion 79—13326
two-dimens. fission model with complex trajectories 78—37384
unified description of fission and nuclear collisions *(Russian)* 78—33163
unified nuclear pot. for heavy ion elastic scatt., fission, fusion, masses and deformations 80—5189
unified pot. from liquid drop model, description of nuclear props. 79—22213
Volterra kernel estimation of bilinear systems, cross correlation algorithm 79—80919
width distribution, statistical properties, effect on cross-section calcs. *(Russian)* 80—518
Z=73-85, preactinide nuclei, fission barriers in droplet model, isospin depend. *(Russian)* 80—5120
(α,f) 140, 150 MeV, fission cross sections and probabilities, isomeric yield ratio 79—45308
μ^- induced instantaneous fission, mesoatomic X-ray radiation *(Russian)* 79—30869
(n,f), 3-5 MeV, cross section predictions 78—29513
(n,f), cross sections, semi-empirical formula 80—22864
(n,f), integral data meas. in ΣΣ neutron field 78—70537
(n,f), near thermal, effects of phonon transfer on cross sections 78—50221
(n,f), parity violation in compound nuclei 80—47368
(n,f), themal, parity violation from opposite parity rot. states 80—95303
(n,f) cross sections from (^{3}He,df) and (^{3}He,tf) reactions 77—23128
(n,f) simulated cross sections for exotic actinide nuclei 80—544
(n,$\gamma\alpha$), (n,γf), low energy γ-transitions between compound states, statistical theory 80—57737
(p,f) on pre-Actinide nuclei targets, 24-30 MeV range, fission barriers *(Russian)* 77—82978
(p,X), 0.6-21 GeV, ^{A}Rb, A=83,84,86 prod. cross sections and recoil props. 80—9295
p induced reactions at intermediate energy, nuclear fissility anal. 78—70579
(π,f), emulsion nuclei, prod. cross section for ^{1}H, ^{2}H, ^{3}H *(Russian)* 79—67801
(π^-,f), at rest, exciton model 78—94042
^{232}U(α,f), 640MeV 80—95329
^{227}Ac, review of expt. data *(Russian)* 79—49641
Ag, proton-induced fission at 400 GeV, ternary to binary event ratio 78—13170
Ag(Fe,f), central collisions, nucleon characteristics, nuclear pionisation in complete fission *(Russian)* 79—80963
Ag(K$^-$,f), 1.8 GeV, ternary, quaternary and cascade fission 79—63708
^{107}Ag(α,f), 640MeV 80—95329
Ag(α,f), fission fragments tracklength and ang. distribs., fission moment of inertia 77—50182
Ag(p,f), 1 GeV, binary fission, possible mass instability of correlated fragments 80—83133
Ag(p,f), 600 MeV, binary fission process 77—3060
Ag(p,f), 600 MeV, fragment energies, cross sections level density and barrier heights 80—42723
Ag(p,f), 600 MeV, mass yields in binary fission 78—8819
^{27}Al+^{20}Ne, 120 MeV, strongly damped collisions 77—34332
Am (A-241, 243), neutron induced fission rate meas. in Zebra 77—57698
Am, A=244, 5, fission probabilities and barrier parameters calc. 77—79409
^{A}Am(n,f), thermal, sub-barrier fission fragment energy correlations for A=241, 243 80—42715
^{241}Am, fission cross section meas. 79—85569
^{241}Am, neutron cross sections, 1 keV to 15 MeV, optical and stat. model calcs. 77—57655
^{241}Am, neutron emission probability in Np(^{4}He,nx), fissionability energy depend. determ. 78—655
^{241}Am, thermal cross sections and resonance integrals of fission and capture 77—71629
^{241}Am, total and fission cross sections in resonance region, resonance parameters 77—23160
^{241}Am(n,f), 14.8 MeV, cross-section meas. using mica track detectors 80—95330
^{241}Am(n,f), 14.8 MeV, mass yield distrib., and absolute fission yield, isomer ratios 80—18352
^{241}Am(n,f) 100 eV to 5.3 MeV, fission cross-section meas. rel. to ^{235}U 79—85567
^{241}Am(n,f)/^{239}Pu(n,f), 0.13 to 7.0 MeV neutrons, fission cross section ratio meas. 79—97738
^{243}Am, thermal cross sections and resonance integrals of fission and capture 77—71629
^{243}Am(^{40}Ar,f), product mass distribs., shell effect manifestation 79—93673
^{243}Am(α,f), fragment mass distrib., and yield, statistical anal. *(Russian)* 80—5183
^{243}Am(n,f), low energy, far-out asymmetric mass distrib. 80—83132
^{243}Am(n,f), thermal neutron induced fission cross section 80—37403
(^{40}Ar,X), 222-340 MeV, A=116-197, charged particle emission, early collision evolution, fission and evaporation cross sections 80—106072
^{40}Ar, fission by 1 GeV protons, ang. distrib. of products *(Russian)* 77—46200
^{40}Ar+^{109}Ag, 170-340 MeV, fission barriers at high ang. momenta 77—26786
^{205}At mass distribution width for fission and quasifission from Re+^{20}Ne and ^{165}Mo+^{40}Av 79—63707
Au, binary fission characts. induced by α-particle bombardment of 0.65 to 4.12 GeV 78—13169

fission continued
Au, proton-induced fission at 400 GeV, ternary to binary event ratio 78−13170
Au(Ar,X), 227 MeV, ang. momentum transfer in deep inelastic collisions 79−45281
Au(^{63}Cu,X), 365 and 443 MeV, ang. momentum transfer in deep inelastic collisions 79−45281
Au(K$^-$,f), 380 MeV, binary decay 79−93671
^{147}Au(^{40}Ar, f), 340 MeV, H and He emission, rapid energy equilib., to ang. distribs. 80−86936
^{196}Au, proton induced, 1 GeV, cross section *(Russian)* 78−94041
^{197}Au+^{136}Xe, 979 MeV, quasi-fission, charge and ang. distribs., secondary fission of products 77−46193
^{197}Au+^{63}Cu quasifission, strongly damped collisions, kinetic energies, ang. distribs. 77−34337
^{197}Au(^{22}Ne, f), 178 MeV, α-particles and fission fragments, spectra and cross sections *(Russian)* 80−91203
^{197}Au(^{40}Ar,X), 222, 340 MeV, fusion cross sections, direct and evaporative p and α prod., evaporation, fission 80−13518
^{197}Au(^{40}Ar,X) 259 MeV, differential recoil range distributions, large contrib. of deep inelastic processes 78−70565
^{197}Au(^{63}Cu,X), 9.6 MeV/A, quasi elastic, deep inelastic and fission like ang. distribs. 80−18334
^{197}Au(^{84}Kr,X), 9.6 MeV/A, quasi elastic, deep inelastic and fission like ang. distribs. 80−18334
^{197}Au(^{86}Kr, X), 730 MeV, heavy fragment coincidences, sequential fission probability 79−22316
^{197}Au(^{86}Kr, Z_3f), 618 MeV, ang. momentum depolarisation, sequential fission 78−62585
^{197}Au(α,f), 640MeV 80−95329
^{197}Au(d,f), 2.1 GeV, binary and ternary fission kinetics *(French)* 78−70577
^{197}Au(d,f), 80 MeV, post neutron emission fission products 80−83136
^{197}Au(p,f), 1 GeV, fission fragment ang. correlation, kinematically different events search *(Russian)* 79−59103
^{197}Au(p,x) ^{22}Na-^{196}Au, 1-100 GeV radionuclide recoil props., fission, fragmentation and spallation 79−3149
Au(α,f) 0.65, 1.74, 4.12 GeV, and using polycarbonate detector 78−13178
Au(α,f), fission fragments tracklength and ang. distribs., fission moment of inertia 77−50182
^{8}Be fission mode, large amplitude collective motion, adiabatic TDHF calcs. 80−86786
Bi, binary fission characts. induced by α-particle bombardment of 0.65 to 4.12 GeV 78−13169
^{201}Bi (α,f), 23-140 MeV, l_{crit} from fragment ang. distribs. anal. 80−106087
^{208}Bi(d,f), 2.1 GeV, binary and ternary fission kinetics *(French)* 78−70577
^{209}Bi (n, xnf), fission high energy neutrons *(Russian)* 80−106091
^{209}Bi+p, nucleon losses on high-energy fission *(Russian)* 78−46120
^{209}Bi(^{136}Xe,X), 940 MeV bombarding energy depend., fragment deformation, sequential fision 80−86938
^{209}Bi(^{86}Kr, f), 610 MeV, deeply inelastic, Q and Z depend. of ang. momentum transfer 79−67786
^{209}Bi(α,X), 69.2, 140 MeV, scatt. and fission reaction mechanisms, cross sections 80−18350
^{209}Bi(α,f), 640MeV 80−95329
^{209}Bi(e,f), 110 MeV electrons, mass and kinetic energy distribs. 79−93672
^{209}Bi(p,X) *(Russian)* 79−80964
Bi(α,f), 0.65, 1.74, 4.12 GeV, and using polycarbonate detector 78−13178
Bk, A=245-9, fission probabilities and barrier parameters calc. 77−79409
^{A}Bk, A=240, 242, electron capture, delayed fission prob. and fission barrier height *(Russian)* 80−42722
^{249}Bk, thermal cross sections and resonance integrals of fission and capture 77−71629
^{249}Bk(n,f) cross section between 0.7 and 3.0 MeV 77−50170
Br(Fe,f), central collisions, nucleon characteristics, nuclear pionisation in complete fission *(Russian)* 79−80963
Br(K$^-$,f), 1.8 GeV, ternary, quaternary and cascade fission 79−63708
^{40}Ca+^{16}O, fusion cross section calc. in boundary condition model 79−9656
Cf, N=152 to 154, resonances, fission probabilities and thresholds 78−46119
Cf, splitting of cold and hot nuclei *(Russian)* 78−29516
^{A}Cf, A=244, 248, fission barrier heights from β-delayed fission, β-strength functions struct. 80−5184
^{249}Cf, thermal cross sections and resonance integrals of fission and capture 77−71629
^{249}Cf(n,f), separation, identification of Ru, Rh isotopes 78−89924
^{249}Cf(n,f), thermal., yields of isotopes of Nb, I and Cs, charge distrib. 78−41789
^{249}Cf(n,f) thermal n, ^{139}Ba and ^{142}La fractional independent yield and γ-activity 79−89337
^{252}Cf fission, isotopic mass dispersion discontinuity, neutron shell effect 79−45312
^{252}Cf fission, n angular distrib., 0 to 30° *(Russian)* 78−86564
^{252}Cf fission, scission point config., α-particle trajectories 77−82974
^{252}Cf fission fragment hard β-radiation 79−45306
^{252}Cf scission point configuration, α-ang. distrib., trajectory calcs. for LRA fission 80−83134
^{252}Cf spontaneous fission, prompt neutrons and fission fragments *(Russian)* 79−40976
^{252}Cf(n,f), fast reactor neutrons, effective cross section meas. 77−23119
^{A}Cm, A=246,248, fission isomer rot. spectra $I^2(I+1)^2$ correction 80−18229
^{A}Cm(n,f), A=224,246, 0.3-45 MeV, near threshold fission cross section, energy depend. *(Russian)* 80−37406
^{240}Cm, fission barrier heights from β-delayed fission, β-strength functions struct. 80−5184
^{243}Cm(n,f), thermal neutron fission cross section and fission-resonance integral 80−86942
^{244}Cm, neutron induced fission rate meas. in Zebra 77−57698
^{245}Cm (n,f), thermal, charge distrib., ^{135}I and ^{190}Ba fractional cumulative yields 80−63074
^{245}Cm, thermal cross sections and resonance integrals of fission and capture 77−71629
^{245}Cm(n,f), cross section, 0.01 to 35 eV 78−21612

fission continued
^{245}Cm(n,f), neutron yield dependence on fragment mass 79−67787
^{245}Cm(n,f), thermal neutron fission, kinetic energy distribs. determ. 78−658
^{245}Cm(n,f), thermal neutron induced fission, mass yield obs. 80−32309
^{248}Cm, Xe and Kr induced fission at Coulomb energies 77−61467
^{248}Cm(^{238}U,X), 7.5 MeV/amu, three particle exclusive meas. for exit channels fission fragment ang. distrib. 80−13513
^{63}Cu+^{197}Au system, quasi-fission at 443 MeV, γ-ray multiplicity 77−34330
^{243}Cu, thermal neutron capture and fission cross sections, resonance integrals 77−67744
^{164}Dy(^{40}Ar,X) 222, 340 MeV, fusion cross sections, direct and evaporative p and α prod., evaporation, fission 80−13518
^{162}Er compound nucleus fission at high ang. momentum, fragments from ^{30}Si(^{132}Xe,f) 80−99196
Es, A=249-51, fission probabilities and barrier parameters calc. 77−79409
^{A}Es, A=244, 246, 248, electron capture, delayed fission prob. and fission barrier height *(Russian)* 80−42722
^{A}Es, A=255,256, fission barrier first peak height, pot. energy surface struct. 80−42720
^{254}Es fission coincidence data from d, t, and ^{3}He induced reactions 80−42720
^{254}Es(n,f), neutron yield dependence on fragment mass 79−67787
Fe assembly, meas. of absolute fission rates/source neutron using solid state track detectors 78−58559
^{55}Fe(^{52}Cr, X), entrance channel mass asymmetry effects on reaction mechanism, fission and fusion 80−106077
^{A}Fm(n,f), A=253, 255, 257, 259, fission mass distrib. transition, liquid drop and shell model calcs. 80−32310
^{248}Fm, fission barrier heights from β-delayed fission, β-strength functions struct. 80−5184
^{255}Fm, fission barrier first peak height, pot. energy surface struct. 80−42720
^{258}Fm, nuclear pressure and fission fragment mass distrib. 80−18356
^{3}H, production in fission and fusion reactors 79−71874
(^{3}He,^{3}He), 12-51.3 MeV, ang. distribs., S-matrix formalism frame anal., fission ingoing channel *(Russian)* 80−5152
(^{4}He,xnf)^{239}Am, statistical model anal. of fission isomer production 78−66326
^{A}Hg(α,f) (A=198 to 204), 41 and 65 MeV, cross section, fragment mass distrib. 77−38307
^{194}Hg compound nucleus, fission, ^{1}H and ^{4}He emission 78−50220
^{194}Hg compound nucleus, fission and, n, p, ^{4}He emission ang. momentum and energy depend. 79−76045
^{128}In yield from symmetrical fission at 15 MeV, delayed neutron yield *(Russian)* 79−22266
^{139}La(p,f), 600 MeV, fragment energies, cross sections level density and barrier heights 80−42723
La(p,f), 600 MeV, mass yields in binary fission 78−8819
^{175}Lu(^{12}C,f), fission probability calc., α emission and evaporation effects 78−657
^{A}Md, A=248, 250, electron capture, delayed fission prob. and fission barrier height *(Russian)* 80−42722
^{24}Mg (α,α^{1} ^{12}C), 120 MeV, symmetric fission, resonances and average partial widths 80−42714
^{24}Mg giant isoscalar quadrupole fission/fusion doorway states from ^{12}C(^{12}C, ^{12}C) 80−37410
^{24}Mg+e, 21 to 32 MeV, E0 and E2 excitations, fission into two ^{12}Cg.s. nuclei 78−54744
^{92}Mo(^{16}O,X), entrance channel mass asymmetry effects on reaction mechanism, fission and fusion 80−106077
^{24}Na prod. in proton induced fission reactions 78−598
^{150}Nd+^{20}Ne, 175 MeV, cross sections and energy spectra 78−41760
^{A}Ni+^{35}Cl, A=58, 62, 155-170 MeV, fission prod. yields, ang. distribs. and mean kinetic energies 78−41790
^{58}Ni+^{208}Pb(^{238}U), 7.5 MeV/amu, ang. momentum transfer in deeply inelastic collisions from exclusive sequential-fission expts. 79−76044
^{62}Ni(^{32}Cl,f), statistical anal. of excitation functions, Bohr-Wheeler and liq. drop model 78−13181
^{252}No, high mass asymmetry distribs. in fissioning nuclei, shell effects 79−3186
^{A}Np(n,f), A=234, 235, low energy, far-out asymmetric mass distrib. 80−83132
^{227}Np damage track detectors, effects of subthreshold fission on neutron dose meas. 78−33375
^{237}Np (n,f), 3 eV to 2 MeV, cross-section meas. 77−3058
^{237}Np, absolute fast neutron fission cross sections 79−13366
^{237}Np absolute fission rate in spherical fusion blanket assemblies 77−67871
^{237}Np, appl. as neutron dosimeter for personnel 79−13539
^{237}Np fission and capture cross sections in GCFR neutron spectra 80−37404
^{237}Np, fission rates measured in graphite-reflected lithium assembly, nonelastic neutron anisotropy effect 78−29511
^{237}Np muonic, prompt fission, fragment atomic muon capture 80−95312
^{237}Np, muonic atom lifetimes from muon induced fission 80−69269
^{237}Np threshold detector, subthreshold phenomena effects on nondestructive assay of reactor fuel 79−22409
^{237}Np(^{4}He,f), (^{4}He,n), (^{4}He,2n), E=17.5-22.5 MeV excitation function meas. 78−656
^{237}Np(α,f), fragment mass distrib., and yield, statistical anal. *(Russian)* 80−5183
^{237}Np(e,e′f), 20-120 MeV, electrofission cross section, E1, E2 strengths 78−13174
^{237}Np(e,f), 10-34 MeV, electrofission cross section, E2 transition mode and giant resonances 80−106084
^{237}Np(e,f), 110 MeV electrons, mass and kinetic energy distribs. 79−93672
^{237}Np(n,f), 14.7 MeV, Xe relative cumulative yields, fine struct. peak *(Russian)* 79−30868
^{237}Np(n,f), ave. no. of neutrons/fission meas. 78−41792
^{237}Np(n,f), cross section, barrier heights, widths, intermediate structure theory 77−34357
^{237}Np(n,f), fission cross sections, use as standards in MeV region 79−13362
^{237}Np(n,f), intermediate struct. line fitting, subthreshold fission resonances 80−102214
^{237}Np(n,f), thermal neutron sub-barrier fission ^{134}I and ^{135}Xe yields 80−86935

fission continued
^{237}Np(n,f), thermal to 14.7 MeV, statistical theory calcs. 77—23137
^{237}Np(n,f), thermal-neutron sub-barrier fission 77—74891
^{237}Np(n,f) cross section in ^{252}Cf spectrum, integral test for evaluated data 77—23134
^{237}Np(n,f) cross section standard, status 77—23040
^{237}Np(n,f) integral cross section ratio meas. using ^{235}N(n_{th},f) neutron spectrum 77—23130
^{237}Np(n,f)/^{239}Pu(n,f), 0.13 to 7.0 MeV neutrons, fission cross section ratio meas. 79—97738
^{237}Np(nth, f), sub-barrier fission, fragment energy correl. meas. 78—21614
^{237}Np(p,f), 11-26 MeV, product yield 80—91197
^{238}Np(n,f), subthreshold fission, fine struct. resonances anal. 78—652
^{238}Np(n,f) near threshold cross-sections 77—65240
O ion induced fission of nuclei from Ag to U, fragment ang. distribs. *(Russian)* 78—17264
^{A}Pa, A=236, 238, β strength function struct., influence on β-delayed fission 78—89826
^{231}Pa, calc. of critical mass and radius by three group diffusion theory 79—13419
^{231}Pa(n,f), fission spectrum averaged cross section 78—70576
^{231}Pa(n,f), thermal to 14.7 MeV, statistical theory calcs. 77—23137
^{231}Pa(n,f), thermal-neutron sub-barrier fission 77—74891
^{231}Pa(n,f) sub-barrier fission, fragment mass and kinetic energy distribs. 79—17942
^{231}Pa(n,f) thermal neutron-induced fission cross-section 79—30859
^{233}Pa(n,f), cross sections, semi-empirical formula 80—22864
Pb, A=206, 208, proton induced, 1 GeV, cross section *(Russian)* 78—94041
Pb, binary fission characts. induced by α-particle bombardment of 0.65 to 4.12 GeV 78—13169
Pb(K$^-$,F), 380 MeV, binary decay 79—93671
^{A}Pb(n,γ), A=204, 206-8, sub- and super-barrier fission, results interpretation 79—67784
^{207}Pb(α,f), 640MeV 80—95329
^{208}Pb (^{16}O, X), 84, 92 MeV, total reaction cross section fragmentation 79—67775
^{208}Pb, closed-shell effect on fission barriers at Z=82 and N=126 77—309
^{208}Pb+^{58}Ni(^{90}Zr), fission phenomena in deep inelastic collisions 80—5186
^{208}Pb(^{16}O,f), 80-102 MeV, cross sections, optical model parameters 77—54246
^{208}Pb(^{208}Pb, HI), 7-7.5 MeV/N, product energy and element distrib., fission probab., energy losses 80—86916
^{208}Pb(^{48}Ca,γ), nuclear pressure and fission fragment mass distrib. 80—18356
^{208}Pb(^{86}Kr,X), 610 MeV, deep inelastic ang. momentum transfer from sequential fission fragments 80—18325
Pb(α,f), 0.65, 1.74, 4.12 GeV, and using polycarbonate detector 78—13178
Pb(α,f), 0.65, 1.74, 4.12 GeV, fission fragment recoil characts. 78—89925
Pb(e,e′f), 28-44 MeV, anomalous reson. struct. obs. 77—82972
^{207}Pd(d,f), 2.1 GeV, binary and ternary fission kinetics *(French)* 78—70577
^{210}Po, excited, deformed, fission or neutron emission, shell-correction approach to nuclear densities 77—30483
^{212}Po, fission excitation functions anal., shell effects at saddle point, nuclear shape 78—54737
^{141}Pr+^{35}Cl, 155-170 MeV, fission prod. yields, ang. distribs. and mean kinetic energies 78—41790
^{141}Pr(^{35}Cl,f), statistical anal. of excitation functions, Bohr-Wheeler and liq. drop model 78—13181
Pu, N=150 and 152, fission probabilities and thresholds 78—46119
^{239}Pu(n,f), statistical model anal. mass yield 77—26797
^{240}Pu, hexadecapole shape isomeric state, shell correction method fission barrier calcs. 80—545
^{226}Ra (n_{th},f), upper bound to cross-section determ. *(Russian)* 77—14201
^{226}Ra, review of expt. data *(Russian)* 79—49641
^{226}Ra(p,f), 12 MeV, prompt neutron energy distrib. meas. 78—13182
^{226}Ra(p,f), 12 MeV, prompt γ-ray spectra meas. 78—13183
(^{32}S,X), 153-184 MeV, fission like processes around A_{CN}=100, mass distrib. strong change 80—9318
^{28}Si (e,f), K=2 symmetry intermediate state 80—47514
^{28}Si electrofission, decay to ^{12}C($2_1{}^+$)+^{16}O($0_1{}^+$) fragments 78—41793
^{28}Si(e,e′^{16}O)^{12}C^{2+}, 23-34 MeV, ^{12}C yields and ang. distrib. meas. 77—61466
^{28}Si(e,f), alpha cluster model approach, intermediate state to ^{12}C+^{16}O 79—40972
^{28}Si(p,^{14}N)^{14}N, Q=−27.2 MeV 79—6717
Sm, proton induced, 1 GeV, cross section *(Russian)* 78—94041
^{154}Sm(^{40}Ar,X), 222, 340 MeV, fusion cross sections, direct and evaporative p and α prod., evaporation, fission 80—13518
^{A}Sn+^{35}Cl, A=112, 116, 120, 124, 155-170 MeV, fission prod. yields, ang. distribs. and mean kinetic energies 78—41790
^{116}Sn(^{32}Cl,f), statistical anal. of excitation functions, Bohr-Wheeler and liq. drop model 78—13181
^{116}Sn(^{40}Ar,X) 187, 222, 340 MeV, fusion cross sections, direct and evaporative p and α prod., evaporation, fission 80—13518
^{181}Ta, proton induced, 1 GeV, cross section *(Russian)* 78—94041
^{181}Ta(^{16}O,f), 77-102 MeV, cross sections, optical model parameters 77—54246
^{149}Tb compound nucleus, statistical model de-excitation calcs. 78—50146
^{153}Tb, fission barrier at 28.5 MeV 80—91202
^{159}Tb(^{14}N,αxn)$^{169-x}$Yb, 95 MeV, γ-ray identification 77—57697
^{159}Tb(p,f), 600 MeV, binary fission process 77—3060
^{159}Tb(p,f), 600 MeV, fragment energies, cross sections level density and barrier heights 80—42723
Tb(p,f), 600 MeV, mass yields in binary fission 78—8819
Te(α,f), fission fragments tracklength and ang. distribs., fission moment of inertia 77—50182
Th, K$^-$ meson induced fission at 700 MeV/c, fragment mass distrib. 78—13168
^{232}Th fission 14 MeV neutrons, rare gas yields measured by emanation method *(French)* 77—30640
Th+π^-, neutron multiplicity distrib. *(Russian)* 78—41783
Th(^{40,44,48}Ca,f), isotope and mass distribs. of fragments *(Russian)* 77—74897
Th(K$^-$,f), 380 MeV, binary decay 79—93671

fission continued
^{A}Th (A=230,232), fission penetrabilities, three-hump model of fission barrier 79—26419
^{212}Th(n,f), 1 eV-100 keV, subthreshold fission widths 77—26798
^{230}Th(n,f), 0.68-1.10 MeV, fission fragment ang. distribs., resonance and moment of inertia 80—102219
^{230}Th(n,γ), 680-1050 keV, fission barriers and cross sections, fragment ang. distribs. 80—18357
^{230}Th(n,γ) 720 keV, fission barrier third minimum, ^{231}Th, asymmetrically deformed, rot. bands 79—3068
^{232}Th, ^{4}He ion-induced fission, ^{148m}Pm, ^{148g}Pm independent form. cross-sections 78—33228
^{232}Th (e, f), 7-65 MeV, absolute electrofission cross sections, fragment ang. distribs. 80—5185
^{232}Th absolute fission rate in spherical fusion blanket assemblies 77—67871
^{232}Th, delayed neutron parameters selection, for nuclear reactor calc. *(Slovak)* 78—21534
^{232}Th fast fission yield of tritium, implications for FBRs 77—46195
^{232}Th fission, isotopic mass dispersion discontinuity, neutron shell effect 79—45312
^{232}Th, fission barrier heights from β-delayed fission, β-strength functions struct. 80—5184
^{232}Th, fission rates measured in graphite-reflected lithium assembly, nonelastic neutron anisotropy effect 78—29511
^{232}Th fuel, conversion and fission yield, irradiation expt. 78—86609
^{232}Th, induced fission in natural systems, radiochem. obs. 78—4966
^{232}Th, muonic, μ induced prompt fission, fate of the μ 78—86557
^{232}Th muonic atom, n emission, bound μ influence on fission barrier 78—89845
^{232}Th, μ capture rate in the fission mode, μ lifetime 78—89827
^{232}Th, proton induced, 1 GeV, cross section *(Russian)* 78—94041
^{232}Th, subCoulomb fission induced by Xe and Kr, excitation functions 77—3061
^{232}Th, Xe and Kr induced fission at Coulomb energies 77—61467
^{232}Th+^{16}0, fission following transfer below Coulomb barrier 79—22346
^{232}Th+^{19}F, fission following transfer below Coulomb barrier 79—22346
^{232}Th+α, 19.8 to 27.2 MeV, elastic scatt. or capture and fission, optical model pots. 77—88181
^{232}Th(^{16}O,γ), transfer induced fission, excitation functions and cross sections 80—13515
^{232}Th(^{19}F,γ), transfer induced fission, excitation functions and cross sections 80—13515
^{232}Th(α,α’f), total kinetic energy release 80—27682
^{232}Th(α,f), 19-27 MeV, integral and differential cross sections, anisotropy energy depend. *(Russian)* 80—37407
^{232}Th(α,f), 25.8-41.4 MeV, fragment ang. momentum determ. 77—82975
^{232}Th(α,x), 140 MeV, spallation and fission product yields 80—13512
^{232}Th(d,f), 2.1 GeV, binary and ternary fission kinetics *(French)* 78—70577
^{232}Th(e,e′f), 20-120 MeV, electrofission cross section, E1, E2 strengths 78—13174
^{232}Th(e,f), 110 MeV electrons, mass and kinetic energy distribs. 79—93672
^{232}Th(n,f), 0.1-30 MeV, subthreshold cross-section meas. 77—74894
^{232}Th(n,f), 1 eV to 20 keV, cross section meas. 79—67794
^{232}Th(n,f), 14.8 MeV, peak to valley ratio of mass distribs. 77—26801
^{232}Th(n,f), 1.35-2.1 MeV, $\bar{\nu}$p values 77—74893
^{232}Th(n,f), 1.35-5.3 MeV, yields and kinetic energies, vibrational states 79—45307
^{232}Th(n,f), 1.55-3 MeV, mass asymm., ang. anisotropy of fragments *(Russian)* 78—17265
^{232}Th(n,f), 2-8 MeV, fission product yields and mass distribs. 80—86939
^{232}Th(n,f), 35 to 1500 keV, near equilib. delayed neutron energy spectra 77—34354
^{232}Th(n,f), barriers of emitted fragments, fission asymm. *(Russian)* 77—10459
^{232}Th(n,f), cross sections, semi-empirical formula 80—22864
^{232}Th(n,f), fast neutrons, delayed neutron spectra, reactor calcs. 77—34355
^{232}Th(n,f), fission fragment ang. distribs., triplet-humped fission barrier 77—74892
^{232}Th(n,f), fission spectrum averaged cross section 78—17253
^{232}Th(n,f), Kr and Xe isotope yields 78—74410
^{232}Th(n,f), prompt-neutron ang. distrib. 77—65238
^{232}Th(n,f), studied with intense neutron spectrometer 77—23364
^{232}Th(n,f), thermal to 14.7 MeV, statistical theory calcs. 77—23137
^{232}Th(n,f), thermal-neutron sub-barrier fission 77—74891
^{232}Th(n,f), yield meas. of Kr, Xe, Sn, Sb, proton odd-even and neutron shell effect 77—82976
^{232}Th(n,f), yields of ^{131,132}Sn, $^{131\text{-}133}$Sb isotopes determ. 78—89923
^{232}Th(n,f) cross section up to 6 MeV 77—23161
^{232}Th(n,f) cross-section meas., rotational bands 77—26803
^{232}Th(p, f), 35-85 MeV, light mass nuclide charge dispersion curves for A=76-79 80—18349
^{232}Th(p,X), 10-100 MeV, spallation residue excitation functions, fissionability 80—18353
^{232}Th(p,f), 28 GeV, charge dispersion, mass yields 77—3062
^{232}Th(p,f), 29-97 MeV, Rb, In and Cs relative independ. yields, charge division 80—102218
^{232}Th(p,f), 4-7 MeV, cross sections *(Russian)* 78—41794
^{232}Th(p,f), 9.5-17 MeV, symmetric to asymmetric mass ratios for fragments 80—5178
^{232}Th(p,p′f), 52.5 MeV, fission probability 80—99195
^{232}Th(π^-, f), resting pions, delayed fission search *(Russian)* 80—52704
^{233}Th(α,α') 120 MeV, isoscalar giant quadrupole resonance fission decay channel inhibition 79—54419
^{233}Th(n,f), 1.2-2.3 MeV, transition state effect on fragment KE *(Russian)* 78—661
^{234}Th, anomaly in fission penetrability through a triple humped pot. barrier 79—3132
^{234}Th fission, three-hump pot. barrier 77—18635
^{234}Th, penetration through three peaks barrier, semiclassical approx. *(Russian)* 79—9544
Th(α,f), 0.65, 1.74, 4.12 GeV, fission fragment recoil characts. 78—89925
Th(α,f), 0.65-4.11 GeV, cross sections for binary and ternary fission 77—3055
^{50}Ti+^{32}S, diffusion model anal. of energy depend. of fission like mass distrib. 77—82949
^{50}Ti+^{32}S composite system, fission characts., fragment correls. 77—332

fission continued
^{50}Ti(^{32}S,f), 121 to 166 MeV, heavy fragments ang. distribs., mass distribs., excitation functions 77—30642
U+^{12}C, 25.2 GeV, large collision residues and fission 77—71618
U+^{136}Xe, 1080 MeV, reaction mechanisms obs. with mica detectors 77—79399
U+^{84}Kr, 800 MeV, reaction mechanisms obs. with mica detectors 77—79399
U(Xe,f), Coulomb fission problem, uniform semi-classical approach to forbidden transitions 79—36287
^{236}U fission path, zero point energies in two centre shell model 78—93952
^{238}U+^{40}Ar, 220 MeV, fissionability of target-like fragments in deep inelastic collisions, reaction mechanism 79—54455
^{238}U+^{40}Ar; cross-sections for fusion, quasifission and deep inelastic collisions *(Russian)* 78—54801
^{238}U(^{48}Ca,γ), nuclear pressure and fission fragment mass distrib. 80—18356
^{238}U(^{56}Fe,X), 538 MeV, binary coincident fragments, fragment mass and energy, fission following fusion 80—548
^{238}U(e,p), 40 MeV, p spectra, deduced ternary fission cross section 79—9549
^{239}U second-chance fission decay times from crystal blocking in ^{238}U(n,f) 79—85568
^W(^{12}C,f), A=182, 183, 184, 186, 80 to 115 MeV, lifetime meas. by crystal-blocking tech. 80—91198
^W(^{16}O,f), A=182, 183, 184, 186, 80 to 115 MeV, lifetime meas. by crystal-blocking tech. 80—91198
^W(α,f) (A=182 to 186), 41 and 65 MeV, cross section, fragment mass distrib. 77—38307
^W(e,f), A=182,184,186, 35-55 MeV, fission barriers, pairing strength deformation depend., stat. anal. 80—57810
^{182}W(^{12}C,X) 77-167 MeV, fusion cross sections, direct and evaporative p and α prod., evaporation, fission 80—13518
^{182}W(^{12}C,f), fission probability calc., α emission and evaporation effects 78—657
^{186}W+^{86}Kr, cross-sections for fusion, quasifission and deep inelastic collisions *(Russian)* 78—54801
$^{260}X_{105}$, prod., L X-ray spectra, decay 78—8780
Yb, proton induced, 1 GeV, cross section *(Russian)* 78—94041
^{174}Yb(^{12}C,f), fission probability calc., α emission and evaporation effects 78—657
Yb(p,f), 1 GeV, analysis of angular correlations between complementary fission products 79—76311
^{90}Zr+^{208}Pb(^{238}U), 7.5 MeV/amu, ang. momentum transfer in deeply inelastic collisions from exclusive sequential-fission expts. 79—76044

fission counters
activation detector ave. cross sections in ^{252}Cf benchmark field 78—82598
DC fission chamber, reactor control applications 77—54326
discharge counter for U in water determ. by fission track method 78—5108
fissile resistors, appl. to intense neutron flux pulse meas. 79—31326
fission counters of high sensitivity for use, in high gamma fields 78—8883
fission track spark counting method for neutron monitoring 80—58080
hemispherical fission ion chamber designed for $\leq 1\ \mu g$ samples 80—27900
high sensitivity neutron spectroscopy and dosimetry appl. *(French)* 80—58078
HTR, fission chamber development 79—76112
ionisation chamber, multiplate, with intrinsic background reduction, response to photofission 80—37685
ionisation chamber with intrinsic suppression of α-background, for fission fragment detection 78—78581
LMFBR high-temp. neutron detector test results 77—74909
miniature, for neutron field meas. in critical assemblies 78—82422
multiplicity detectors, seldom exploited props. 77—46468
neutron counter development, electron drift vel. simulation 80—48843
neutron dosimetry system, based on fission counter for fuel processing plant 80—57981
neutron fluence meas. using fission foils of ^{235}U, ^{238}U, ^{237}Np, optical microscopy counting after etching 78—13177
neutron flux monitor at BWR power plants 77—14240
neutron response of solid state nuclear track detector 80—27876
neutron self-powered detector with fissile emitter, theoretical evaluation 78—74533
neutron spectrometry in range 0.4 eV to 10 MeV 77—42210
performance optimisation algorithm 80—47828
position sensitive parallel plate avalanche fission detector, particle induced fission coincidence measurements 80—63485
position-sensitive ionization fission chamber 79—26819
pulse fission chamber, reactor control applications 77—54326
PWR, system for internal neutron meas. *(French)* 79—76113
reactor neutron flux meas., high temp. neutron rad. detectors and cables 79—76111
reactor neutron flux meas., integrated cable detectors for use under flux and/or at high temperature *(French)* 79—76114
rem-dose measurement of mixed p-n radiation using solid state detectors of fission fragments 80—36137
scintillator containing U, inorganic solid-soln. single-cryst., prototype fission detector, performance 77—54445
self-powered neutron detector with enriched-U emitter 79—76115
semiconductor fission chamber, absolute fission ratio measurement *(Japanese)* 77—67948
solid state, absolute neutron flux meas. and ^{239}Pu(n,f) resonance integral 80—5453
solid state track detector meas. of fine struct. of fission density distrib. in UO$_2$ fuel rod 77—57715
thin-film fission thermocouple detectors for reactors safety expts. 80—22987
BF$_3$ detector assembly for photofission and photoneutron studies 80—63484
chamber for surface multiplication meas. in cubic assemblies 77—42024
D-D neutron meas. on 40 kV, 60 A neutral beam test facility 80—37710
^{227}Np damage track detectors, effects of subthreshold fission on neutron dose meas. 78—33375
^{237}Np dosimeter and spark counting system, for routine personnel monitoring 78—89984

fission counters continued
^{237}Np threshold detector, subthreshold phenomena effects on nondestructive assay of reactor fuel 79—22409
^{239}Pu loaded, neutron flux absolute meas. at fast pulse reactors, calibration against ^{252}Cf source 77—23389
^{235}U content in enriched samples, fission track registration technique, solid state detectors 77—56291
Xe proportional scintillation detector, energies and angles of emission of ^{252}Cf fission fragments 80—63488

fission of plutonium
^{239}Pu(n,f), thermal, fission product yield 80—27678
$\sigma_f(^{239}Pu)/\sigma_f(^{235}U)$ meas., neutron energies 0.27-9.85 MeV 78—660
actinide series neutron-induced-fission systematics in MeV region 77—67778
average cross section trend, 3-5 MeV, statistical model description 77—23126
criticality of U-Pu aqueous solns., oxides and nitrates, effect of Gd, Gd-B neutron absorbers 77—34393
cross section calculations 77—26661
delayed-neutron yield 79—67798
determination system by passive neutron counting 79—40985
energy autocorrel. of fission cross-section data in resonance region, probability table method 79—36284
fallout observation, Chinese A-tests 80—27820
fast pulse reactor ^{237}Np/^{238}U and ^{239}Pu/^{237}Np spectral index meas. and calc. 79—9804
FBR fission yield, burnup determ. in mixed oxide fuels 77—23138
fine structure of yields of Xe isotopes, A=131-135 78—86560
fission probabilities and thresholds, N=150 and 152 78—46119
fragment recoil mass spectrometer HIAWATHA 79—9940
laser induced fission, Monte Carlo anal., critical mass and radius for bare spheres 78—62583
LMFBR fuelling requirements rel. to Pu isotopic composition, core design 79—9738
multigroup time-dependent delayed γ-spectra from fission and activation 78—13184
nonequilibrium fission bubble behaviour during fast transients in oxide fuel 78—8916
P-odd asymmetry accompanying fission by polarised thermal neutrons *(Russian)* 77—82977
prediction of fission-product mass yields and related parameters 79—30862
product ENDF/B data, processed, rapid spectral and decay heat calcs. 79—67797
prompt fission neutron spectra for ENDF/B-V 80—22869
prompt fission spectrum uncertainties, implications for integral data testing 80—22871
PWR, Pu isotope calcs. for steady-state core anal. 79—59126
reactivity reaction rate method for capture-fission ratio determ., spectral fine struct. effects 78—46136
recoil mass spectrometer, HIAWATHA, thermal neutron fission fragments of U, Pu 78—16892
spontaneously fissioning material, assay using neutron correl. counting 79—85605
ZPPR-4 control rod worth meas. and calc. 79—9803
ZPPR-5 Source Level Flux Monitor expt. analysis 79—9705
(n,f), integral data meas. in $\Sigma\Sigma$ neutron field 78—70537
(n,f) simulated cross sections for exotic actinide nuclei 80—544
^{241}Am(n,f)/^{239}Pu(n,f), 0.13 to 7.0 MeV neutrons, fission cross section ratio meas. 79—97738
DT-Pu plasma, neutron induced fission, fission fragment slowing down 79—26749
DT-Pu plasma, neutron induced fission, enhancement of neutron prod. and fusion rate 79—26750
DT-Pu plasma, neutron induced fission, plasma heating effect 80—27800
(^{4}He,2nf), statistical model anal. of fission isomer production Pu, A=235, 237 78—66326
^{237}Np(n,f)/^{239}Pu(n,f), 0.13 to 7.0 MeV neutrons, fission cross section ratio meas. 79—97738
Pu (A=239-242), neutron induced fission rate meas. in Zebra 77—57698
Pu (n,F) thermal, rare gas yields, odd-even effect *(French)* 77—50172
Pu, A=238, 239, neutron emission probability in U(^{4}He,xn), fissionability energy depend. determ. 78—655
Pu, A=239, 241, fission probability, Γ_n/Γ_f ratio struct. 78—37382
Pu^{239}, product separation asymmetry in fission by slow polarised neutrons *(Russian)* 80—106088
Pu+U mixed oxide aqueous solns., limiting critical concs., multiplication factor 77—26859
PuO$_2$, assemblies, fission and explosive energy releases 77—83108
PuO$_2$/UO$_2$ fuelled assemblies, integral meas. of effective delayed neutron fraction in FTR SNEAK 77—6497
PuO$_2$-UO$_2$ assemblies, fission and explosive energy releases 77—83108
^{4}Pu(n,f) A=239,242,244, 14.8 MeV, cross-section meas. using mica track detectors 80—95330
^Pu, A=238,240, fission isomer rot. spectra I^2(I+1)^2 correction 80—18229
^Pu, A=239, 240, 241, LMFBR 300 MWe, burnup characts. 3-D numerical anal. 79—22371
^Pu, A=239, 241, 2200 m/s and 20°C Maxwellian neutron data 79—9651
^Pu, A=239, 241, thermal neutrons, review of meas. of average number of neutrons emitted per fission 79—9652
^Pu, A=239,242, muonic, prompt fission, fragment atomic muon capture 80—95312
^Pu, A=239,242, muonic atom lifetimes from muon induced fission 80—69269
^Pu/^{235}U, A=240, 242, fission cross section ratio meas. 0.127 to 7.4 MeV 80—5180
^Pu(n,f), A=239, 242, 0.1 to 10 MeV fission cross section rel. to ^{235}U 79—13354
^Pu(n,f), A=239.241, nuclear constants eval. for heavy fissile nuclei using nuclear models *(Russian)* 79—59100
^Pu(n,f), A=240, 242, 244, 0.1 to 30 MeV, cross-sections rel. to ^{235}U 78—50217
^Pu(n,f), fission product decay heat calc. by summation method, appl. to FBR 79—30863
^Pu(n,f) A=240,241, 14.8 MeV, meas. of reaction parameters using solid state nuclear track detectors 80—91201
^{230}Pu(n,f), fission-fragment yields of neutron fission in FBR 80—83102

fission of plutonium continued
- ^{232}Pu, fission barrier determ., from β-delayed fission 78−29518
- ^{232}Pu, fission barrier heights from β-delayed fission, β-strength functions struct. 80−5184
- ^{236}Pu, 40 ps fission isomer quadrupole moment 77−50053
- ^{238}Pu, spontaneous fission decay const. meas. 77−23149
- ^{238}Pu(n,f), intermediate struct. line fitting, subthreshold fission resonances 80−102214
- ^{239}Pu, ^{241}Pu, third IAEA evaluation of 2200 m/s, 20°C Maxwellian neutron data 77−23136
- ^{239}Pu (n,f), 10 eV-100 keV, fission cross section 80−27681
- ^{239}Pu, absolute fission yield meas. by track-etch-cum-γ-spectrometry method 80−27859
- ^{239}Pu, capture/fission cross-section ratio meas., 0.007 eV-12 keV 77−54266
- ^{239}Pu, cross sections for α-decay and neutron induced fission *(Russian)* 79−17944
- ^{239}Pu, delayed neutron parameters selection, for nuclear reactor calc. *(Slovak)* 78−21534
- ^{239}Pu, e and $\bar{\nu}$ energy spectra from fission fragments *(Russian)* 77−23120
- ^{239}Pu, fast fission, product decay-heat calc. 77−61464
- ^{239}Pu, fast reactor dosimetry using zero-power facility ZEBRA 79−3219
- ^{239}Pu fission, isotopic mass dispersion discontinuity, neutron shell effect 79−45312
- ^{239}Pu fission isomers produced in ^{240}Pu(n,2n), half lives 77−30641
- ^{239}Pu, fission product beta decay, $\bar{\nu}$ spectra 80−102150
- ^{239}Pu fission products γ-ray and photoneutron spectra 77−23127
- ^{239}Pu, fission rate, absolute meas. 79−63678
- ^{239}Pu, infinite multiplication factors, neutron captures and fission, rel. to GCFR parameters 78−33245
- ^{239}Pu, irradiated in BOR-60 reactor, fission yields 79−17971
- ^{239}Pu muonic atom, n emission, bound μ influence on fission barrier 78−89845
- ^{239}Pu neutron data evaluation for ENDF/B-V 78−25288
- ^{239}Pu neutron data reevaluation for Nuclear Data Library KEDAK-3 77−23042
- ^{239}Pu, prompt fission neutron spectra 79−9654
- ^{239}Pu, prompt-neutron fission spectrum, Maxwellian and Watt distribs. 77−50177
- ^{239}Pu seeded DT plasma, neutron induced fission 79−71946
- ^{239}Pu, σ_c/σ_f ratio meas. in BFS critical assemblies 79−97737
- ^{239}Pu, $\sigma(n,\gamma)/\sigma(n,f)$ estimate based on expt. data up to 1977 79−89312
- ^{239}Pu, testing of ENDF/B-IV Th data in GCFR lattice 79−67836
- ^{239}Pu thermal fission, prompt neutrons and fission fragments *(Russian)* 79−40976
- ^{239}Pu thermal fission afterheat, sensitivity to errors in fission product data 77−26841
- ^{239}Pu, thermal neutron-induced fission, ^{96}Nb and ^{98}Nb yields 78−54807
- ^{239}Pu to ^{235}U fission cross-section ratio from 0.001-30 MeV 77−26807
- ^{239}Pu/^{235}U, (n,f) ratio meas. in range 1 keV-30 MeV 78−46118
- ^{239}Pu+n, 13.9, 14.6 MeV, absolute neutron fission cross sections, associated particle method 78−89926
- ^{239}Pu+n, ratio between capture and fission cross sections up to 30 keV 78−70538
- ^{239}Pu(α,α), 19-27 MeV, differential cross section, transmission coeffs. for fission cross section *(Russian)* 79−67800
- ^{239}Pu(α,f), 19-27 MeV, integral and differential cross sections, anisotropy energy depend. *(Russian)* 80−37407
- ^{239}Pu(γ,f), 15-55 MeV, photofission symmetric and asymmetric yields 80−83135
- ^{239}Pu(γ,f), asymmetry depend. on bremsstrahlung energy maxima 77−23117
- ^{239}Pu(n, f), 0.024 to 7.4 MeV fission cross section ^{235}U/^{239}Pu ratio 79−40975
- ^{239}Pu(n, f), undisturbed resonance integral determ., and neutron flux meas. 80−5453
- ^{239}Pu(n,X), thermal n, gamma spectra from capture, fission and fission products 80−37352
- ^{239}Pu(n,f,), 0.10-2.07 MeV, meas. of prompt fission neutron spectra 77−23146
- ^{239}Pu(n,f), 0.005-0.4 eV, fission fragment average kinetic energies in resonance region 80−18358
- ^{239}Pu(n,f), 0.1-1 Mev, light charged particle emission, saddle point states 79−22343
- ^{239}Pu(n,f), 0.3 eV resonance energy, mass distrib. of products 78−70578
- ^{239}Pu(n,f), 1 keV to 1 MeV, cross-section meas., ratio to ^{235}U 77−23144
- ^{239}Pu(n,f), 100 keV-1 MeV, light charged particle yields 77−71631
- ^{239}Pu(n,f), 2-144 keV, cross-section meas. 77−26813
- ^{239}Pu(n,f), 2-144 keV, cross-sections meas. 77−26814
- ^{239}Pu(n,f), 35 to 1500 keV, near equilib. delayed neutron energy spectra 77−34354
- ^{239}Pu(n,f), abs. meas. of fission cross-sections with photoneutron sources 79−30860
- ^{239}Pu(n,f), absolute yields and group constants of delayed neutrons in fast fission using Viper 77−54261
- ^{239}Pu(n,f), comparison exptl. cross section meas. methods 77−23157
- ^{239}Pu(n,f), cross section, parameter testing in statistical model *(Russian)* 80−52653
- ^{239}Pu(n,f), cross sections for ^{252}Cf neutrons 78−25258
- ^{239}Pu(n,f), cross-section, 2, 24, 55, 144 keV neutrons 78−17262
- ^{239}Pu(n,f), cumulative yields of Ru and Pd isotopes 79−576
- ^{239}Pu(n,f), effective cross section dependence on thermal neutron temp. 80−547
- ^{239}Pu(n,f), far-out asymmetric mass distrib. 80−83132
- ^{239}Pu(n,f), fission cross-section averaged over ^{252}Cf neutron spectrum 79−30861
- ^{239}Pu(n,f), fission neutron spectra, TOF meas. 78−17476
- ^{239}Pu(n,f), low energy, fission widths, channel characts. 78−29515
- ^{239}Pu(n,f), mass distribution of fragments *(Russian)* 78−29517
- ^{239}Pu(n,f), meas. of α-values in BOR-60 reactor core 79−97830
- ^{239}Pu(n,f), polarised thermal neutrons, parity nonconservation *(Russian)* 78−33232
- ^{239}Pu(n,f), separation, identification of Ru, Rh isotopes 78−89924
- ^{239}Pu(n,f), sub MeV neutrons, equilib. delayed neutron energy spectra meas. 77−38308
- ^{239}Pu(n,f), thermal, correlation for independent fission prod. yield uncertainties 78−50216
- ^{239}Pu(n,f), thermal, isotopic distrib. of rare gases, proton parity effect *(French)* 77−3054

fission of plutonium continued
- ^{239}Pu(n,f), thermal n, fission fragment energy correlation meas., fine struct. and deformation 79−13355
- ^{239}Pu(n,f), thermal n, reactor $\bar{\nu}$ and e spectra calc. 79−67791
- ^{239}Pu(n,f) 80−37405
- ^{239}Pu(n,f) 0.009-0.6 eV cross-section, Westcott factor 80−546
- ^{239}Pu(n,f) cross section in ^{252}Cf spectrum, integral test for evaluated data 77−23134
- ^{239}Pu(n,f) cross section meas., fragment ang. distrib. using solid state track detector 79−76300
- ^{239}Pu(n,f) integral cross section ratio meas. using ^{235}U(n_{th},f) neutron spectrum 77−23130
- ^{239}Pu(n,γ), thermal, fission product $\bar{\nu}_e$ spectrum, β-decay characts. 80−78340
- ^{239}Pu(n,t), absolute yields of ^{99}Mo, ^{111}Ag, ^{140}Ba, ^{147}Nd, ^{153}Sm 77−50167
- ^{239}Pu(n_{th},f), fission product mass distribs. 77−74896
- ^{239}Pu(n_{th},f), yields of Cd and Sn isotopes, symm. region 77−34358
- ^{240}Pu at very high spins, double-humped fission barrier anal. 78−4970
- ^{240}Pu, dynamic excitation model of fission process, scission 77−14095
- ^{240}Pu, effect of spontaneous fission on energy release in a nuclear explosive 80−95464
- ^{240}Pu fission, dynamic excitation and collective energy, quasiparticles 79−67792
- ^{240}Pu fission barrier, deformation energy curve; constrained HF calc. 80−83053
- ^{240}Pu fission total kinetic energy release, excitation energy depend., scission point anal. of ^{241}Pu(^{3}He,αf) 80−18351
- ^{240}Pu, mass distribution of fragments *(Russian)* 78−29517
- ^{240}Pu, moments of inertia of fissioning isomers, cranking model 78−74299
- ^{240}Pu, P-odd neutron emission asymmetry *(Russian)* 78−74413
- ^{240}Pu, reson. in isomeric and prompt fission probabilities 78−78429
- ^{240}Pu subbarrier resonances and fission probabilities from ^{239}Pu(d,pf) 79−13266
- ^{240}Pu(n,f), 14.8 MeV, products from ^{66}Ni to ^{169}Er, mass distrib., total chain yields 78−25255
- ^{240}Pu(n,f), 500-10000 eV, subthreshold fission structure 77−23143
- ^{240}Pu(n,f), cross section, barrier heights, widths, intermediate structure theory 77−34357
- ^{240}Pu(n,f), mass yield distrib. and absolute fission yields 79−13356
- ^{240}Pu(n,f) 10 to 250 keV, subthreshold neutron fission cross section meas. 79−22344
- ^{241}Pu (n, f), 0.02-7.4 MeV, fission cross section ratio to ^{235}U 79−45313
- ^{241}Pu compound nucleus lifetime by the shadow effect in ^{238}U(^{3}He,f) *(Russian)* 78−86562
- ^{241}Pu, delayed neutron parameters selection, for nuclear reactor calc. *(Slovak)* 78−21534
- ^{241}Pu, evaluation of neutron cross sections in region 10^{-5} eV to 15 MeV 78−17254
- ^{241}Pu, multilevel resonance parameters for 0.01 to 100 eV neutrons 79−36154
- ^{241}Pu, neutron capture and fission cross sections, 0.01 eV-30 keV 78−29512
- ^{241}Pu, statistical anal. of reson. neutron fission cross section 77−38305
- ^{241}Pu(n, f) thermal-neutron fission, determ. of cumulative fission yields 79−54462
- ^{241}Pu(n,f), 0.01-50 eV, fission cross-section, Westcott g_f factors 77−23153
- ^{241}Pu(n,f), thermal neutron fission, kinetic energy distribs. determ. 78−658
- ^{241}Pu(n,f) 1 keV to 30 MeV neutrons, cross section meas. rel. to ^{235}U 79−36286
- ^{241}Pu(n,f) fission cross section meas., 8 eV to 70 keV 77−50168
- ^{241}Pu(n,f) thermal, correlation for independent fission prod. yield uncertainties 78−50216
- ^{242}Pu(α,f), fragment mass distrib., and yield, statistical anal. *(Russian)* 80−5183
- ^{242}Pu(μ,f), radiationless muonic transition induced fission, fission dynamics probe, friction coeff. 80−78336
- ^{242}Pu(n,f), cross section, barrier heights, widths, intermediate structure theory 77−34357
- ^{243}Pu(n,f) near threshold cross-section calcs. 77−65240
- ^{244}Pu fast neutron fission cross-section 77−18636
- ^{244}Pu, fossil fission tracks in Allende meteorite 77−29663
- ^{244}Pu, in minerals, haloes prod. by fission alpha particles 77−29300
- ^{244}Pu, Xe and Kr induced fission at Coulomb barrier energies 77−61467
- Pu(n,f), 0-18 MeV, prompt neutron spectrum, evaporation model *(Chinese)* 80−42721
- Pu(n,f), A=240, 241, 242, cross-sections meas. in range 0.001-30 MeV 77−26809
- Pu(n,f), A=241, 243, subthreshold fission, fine struct. resonances anal. 78−652
- Pu(n,f), delayed neutron spectra from thermal- and fast-neutron fission, reactor calcs. 77−34355
- Pu(n,f), thermal to 14.7 MeV, statistical theory calcs. 77−23137
- Ru, fission product, isotope anal., U and Pu fission investig. *(German)* 77−63996

fission of uranium
- ^{238}U(n,f), reactor n, shoulders in very asymmetric mass distrib., cumulative yields 79−59005
- $\sigma_f(^{239}$Pu$)/\sigma_f(^{235}$U$)$ meas., neutron energies 0.27-9.85 MeV 78−660
- absolute fission rate distrib. in standard U shell, comparison with ANISN code 78−62584
- actinide series neutron-induced-fission systematics in MeV region 77−67778
- average cross section trend, 3-5 MeV, statistical model description 77−23126
- borehole logging by prompt fission neutron technique, log interpretation 79−53567
- borehole logging system, delayed neutron activation anal. method using ^{252}Cf source 79−53569
- breeder reactor, with circulating liquid-salt fuel, fission product radioactivity reduction and residual heat release 79−26490
- Breit-Wigner single-level formula for cross sections, multilevel correction 78−29441
- criticality of U-Pu aqueous solns., oxides and nitrates, effect of Gd, Gd-B neutron absorbers 77−34393
- cross section calculations 77−26661

fission of uranium continued
delayed fission neutron method for rapid U anal. in porcelain dentures 78—15907
delayed neutron probe characts. for uranium exploration, field meas. 79—53568
delayed-neutron yield 79—67798
energy autocorrel. of fission cross-section data in resonance region, probability table method 79—36284
exploration, delayed fission neutron and prompt fission neutron logging, comparison of predicted signals 79—39879
fast pulse reactor ^{237}Np/^{238}U and ^{239}Pu/^{237}Np spectral index meas. and calc. 79—9804
FBR fission yield, burnup determ. in mixed oxide fuels 77—23138
FFHR, tailoring the breeding-fission ratio by neutron moderation with iron 78—21677
fine structure of yields of Xe isotopes, A=131-135 78—86560
fission track annealing characteristics of epidote, appls. to geochronology, geol. 78—94038
fission track dating and estimation of U in garnets 78—94039
fission track dating using U glasses, error analysis 80—95503
fission track determ. of U abundance in Himalayan plants 80—101305
fission track determ. of U content in whole rock samples 77—73880
fragment recoil mass spectrometer HIAWATHA 79—9940
fusion-plasma neutron fission and activation of U fuels 79—13521
inert gas plasmas, prod. by U fission fragments in nucl. reactor props. 77—76147
K$^-$ meson induced fission at 700 MeV/c, fragment mass distrib. 78—13168
laser induced fission, Monte Carlo anal., critical mass and radius for bare spheres 78—62583
mass and charge division, asymmetry, order-disorder model 80—22866
mineral deposits, criticality study using ore model *(Spanish)* 77—70655
most probable charge, shell and deform. effects 78—29440
multigroup time-dependent delayed γ-spectra from fission and activation 78—13184
(n,f), 1 to 7 MeV, ratio of ^{238}U and ^{235}U cross sections 79—30867
nonequilibrium fission bubble behaviour during fast transients in oxide fuel 78—8916
nuclear power progress review (1939-79) *(French, English)* 80—18590
Oklo natural nuclear reactor, discovery and reactor parameters, geological formation 79—2240
ore grade direct determ. by photoneutron assay method 79—53570
ores, estimation of ratio of induced to spontaneous fission 78—53234
plasmas, fissioning, for space vehicle power, propulsion, terrestrial appls. 77—3145
product ENDF/B data, processed, rapid spectral and decay heat calcs. 79—67797
prompt fission neutron logging technique, computer modelling 79—53566
prompt fission neutron spectra for ENDF/B-V 80—22869
prompt fission spectrum uncertainties, implications for integral data testing 80—22871
quasistatic scission configurations obtained from long range particle accompanied fission distributions 78—74411
reactivity reaction rate method for capture-fission ratio determ., spectral fine struct. effects 78—46136
recoil mass spectrometer, HIAWATHA, thermal neutron fission fragments of U, Pu 78—16892
rocks, fission/α technique for U and Th determ. 77—29497
solid-state nuclear track detectors, review of appls. in fission physics 80—91396
Weale expt. calc. using modified ENDF/B-IV cross sections 79—17908
K$^-$ induced binary decay, 380 MeV 79—93671
(n,f), integral data meas. in $\Sigma\Sigma$ neutron field 78—70537
(n,f) simulated cross sections for exotic actinide nuclei 80—544
^{235} U(n,f), thermal to 1.75 MeV, energy spectra and yields of alpha-particles 77—26805
Ba fragments, differential ranges and ang. distribs. from ^{238}U(p,X) 79—67790
^{56}Fe+^{238}U, 538 MeV, quasifission dominance with projectile A and Z 77—74869
Pb+U, 750 MeV, classical model, kinetic energy, ang. distribs., instantaneous fission fragments 78—13185
Pu+U mixed oxide aqueous solns., limiting critical concs., multiplication factor 77—26859
^{240}Pu, moments of inertia of fissioning isomers, cranking model 78—74299
^{240}Pu, thermal neutron induced, average angular momenta of even-even fragments 78—86525
Ru, fission product, isotope anal., U and Pu fission investig. *(German)* 77—63996
Th/^{233}U fuel cycle in FBR and thermal convertors 79—9745
^{235,238}U(n,f), fast neutrons, fission product mass distribs. fission product mass distribs. 77—74896
U (M,f), muon excitation probabilities, muonic atoms, Schrodinger eqn. 80—47515
U anal. of natural waters by fission tracks 78—82587
U, proton-induced fission at 400 GeV, ternary to binary event ratio 78—13170
U solution systems, high-enriched benchmark critical expts. 79—63748
U spontaneously fissionable isomers, excitation by K shell e$^+$ annihilation, shape isomery model *(Russian)* 79—30802
U^{233}, product separation asymmetry in fission by slow polarised neutrons *(Russian)* 80—106088
U^{235} in pegmatites, homogenised fission track anal. using solid state track detector 80—97719
^{238}U fission by 14 MeV neutrons, rare gas yields measured by emanation method *(French)* 77—30640
U(^{40,44,48}Ca,f), isotope and mass distribs. of fragments *(Russian)* 77—74897
U(^{3}He, f), 530 MeV, cross section meas. by glass solid state track detectors 78—13179
UN ceramic fuel, fission enhanced creep, in-pile meas. 77—67807
UO$_{2.3}$ assemblies, fission and explosive energy releases 77—83108
UO$_2$, equilib. conc. of fission products, ^{235}U induced fission and ^{238}U spontaneous fission *(Spanish)* 78—44823
UO$_2$, equilib. conc. of fission products, calc. comparison with expt. values *(Spanish)* 78—44824
UO$_2$/PuO$_2$ fuelled assemblies, integral meas. of effective delayed neutron fractions in FTR SNEAK 77—6497
U(^{208}Pb, f), 1535 MeV, direct evidence for multiple sequential fission 79—30866

fission of uranium continued
U(^{238}U, f), 1785 MeV, direct evidence for multiple sequential fission 79—30866
^{A}U, A=233, 235, 2200 m/s and 20°C Maxwellian neutron data 79—9651
^{A}U, A=233, 235, thermal neutrons, review of meas. of average number of neutrons emitted per fission 79—9652
^{A}U, A=235, 236, 238, determ. of neutron multiplicities 80—32311
^{A}U, A=235,238, fission product beta decay, $\bar{\nu}$ spectra 80—102150
^{A}U, A=235,238, muonic atom lifetimes from muon induced fission 80—69269
^{A}U, A=236, 238, strength function of β-transitions, probability of delayed fission 80—22764
^{A}U, A=236,238, fission isomer rot. spectra $I^2(I+1)^2$ correction 80—18229
^{A}U fission, A=233,235,238, isotopic mass dispersion discontinuity, neutron shell effect 79—45312
^{A}U^{m}, A=236,238, isomeric to prompt fission ratios; fission fragments from (d,pf), (d,pnf) 80—86940
^{A}U(^{4}He,xn) A=233-235, x=1-4, cross sections, fission evaporation competition in Pu isotopes 78—66325
^{A}U(α,f), A=235,238, 19-27 MeV, integral and differential cross sections, anisotropy energy depend. *(Russian)* 80—37407
^{A}U(d,f), A=235, 238, 2.1 GeV, binary and ternary fission kinetics *(French)* 78—70577
^{A}U(γ,X), A=235, 236, 238, 5-18.3 MeV, photoneutron and photofission cross sections, giant resonance and deformations 80—68712
^{A}U(γ,f), A=235, 236, 238, deep subthreshold photofission, double humped fission barrier anal., shape isomer 80—5179
^{A}U(γ,f), A=235,238, 15-55 MeV, photofission symmetric and asymmetric yields 80—83135
^{A}U(μ,f), A=235,238, prompt and delayed fission, absolute yields and lifetimes 80—78337
^{A}U(n,X), A=233, 235, thermal n, gamma spectra from capture, fission and fission products 80—37352
^{A}U(n,f), A=233,235, ejection fission products angular depend. on thermally polarised neutron capture *(Russian)* 80—86941
^{A}U(n,f), A=235, 238, fission-fragment yields of neutron fission in FBR 80—83102
^{A}U(n,f), A=235, 238, low energy, far-out asymmetric mass distrib. 80—83132
^{A}U(n,f), A=235, 238, meas. of α-values in BOR-60 reactor core 79—97830
^{A}U(n,f), A=235,7,8, cross section meas., fragment ang. distrib. using solid state detector 79—76300
^{A}U(n,f) A=232 to 236, 238, prediction of fission-product mass yields and related parameters 79—30862
^{A}U(u,f), A=233, 235, cumulative yields of Ru and Pd isotopes 79—576
^{232}U production and decay, nonproliferation aspect of ^{233}U-Th fuel cycle 80—57839
^{232}U(n,f), fission product mass distrib. 79—67789
^{232}U(n,f), reactor neutron fission, kinetic energy distribs. determ. 78—658
^{233}U, ^{235}U, ^{238}U fission products γ-ray and photoneutron spectra 77—23127
^{233}U, ^{235}U, third IAEA evaluation of 2200 m/s, 20°C Maxwellian neutron data 77—23136
^{233}U, delayed neutron parameters selection, for nuclear reactor calc. *(Slovak)* 78—21534
^{233}U fission by polarised neutrons, P odd asymmetry of emitted fragments *(Russian)* 80—18354
^{233}U neutron-induced reaction, data eval. including $\bar{\nu}_p$ and fission spectrum 79—67795
^{233}U, prompt-fission-neutron spectra 79—67793
^{233}U solution, criticality anal. using KENO and SU-HAMMER codes 78—89949
^{233}U, statistical anal. of reson. neutron fission cross section 77—38305
^{233}U, thermal neutron fission with alpha-particle emission *(Russian)* 77—46198
^{233}U, thermal neutron-induced fission, ^{96}Nb and ^{98}Nb yields 78—54807
^{233}U/^{235}U, (n,f) ratio meas. in range 1 keV-30 MeV 78—46118
^{233}U-Th fuel cycle, fast reactor system, sensitivity anal. 79—67835
^{233}U-Th fuel cycle, review of fast integral data 79—67834
^{233}U(α,X), 28-140 MeV, scatt. and fission reaction mechanisms, cross sections 80—18350
^{233}U(d,pf), fission fragment energy-velocity correlation meas. 79—45309
^{233}U(γ,f) asymmetry depend. on bremsstrahlung energy maxima 77—23117
^{233}U(n, f), 0.02-7.4 MeV, fission cross section ratio to ^{235}U 79—45313
^{233}U(n,f), ^{148m}Pm, ^{148g}Pm and ^{146}Pm independ. yields 77—79407
^{233}U(n,f), effective cross section dependence on thermal neutron temp. 80—547
^{233}U(n,f), energy depend. of η^{233}U in 0.02 to 1.00 eV region 77—23118
^{233}U(n,f), fission neutron spectra, TOF meas. 78—17476
^{233}U(n,f), statistical model anal. of mass yield 77—26797
^{233}U(n,f), thermal, correlation for independent fission prod. yield uncertainties 78—50216
^{233}U(n,f), thermal polarised neutrons, neutron emission P-odd asymmetry *(Russian)* 80—78338
^{233}U(n,f) polarised thermal neutrons, P-odd asymm. *(Russian)* 78—33231
^{233}U(n,t), thermal, Mn bath meas. of η_{2200}, Monte-Carlo anal. 77—23142
^{233}U(n$_{th}$,f), fission neutrons per absorption, Monte Carlo anal. of meas. 77—23141
^{233}U(ρ,f), alpha-particle angular and energy spectra, cross-section anisotropy 80—57809
^{234}U subbarrier resonances and fission probabilities from ^{233}U(d,pf) 79—13266
^{234}U, thermal neutron induced, average angular momenta of even-even fragments 78—86525
^{234}U(n, f), 3 eV to 8.9 MeV, intermediate struct. 77—74895
^{234}U(n,f), cross section rel. to ^{235}U in 2-3 MeV region 78—21613
^{234}U(n,f), intermediate struct. anal. 77—79408
^{234}U(n,f), intermediate struct. line fitting, subthreshold fission resonances 80—102214
^{235}U, ^{238}U, absolute fast neutron fission cross sections 79—13366
^{235}U (n, f), thermal neutron fission, time-depend. delayed neutron group yields 79—54463
^{235}U (n,f), fission by fast neutrons, fragment K X-ray spectra, $\bar{\nu}$ energy depend. in heat balance method 78—17260

fission of uranium continued
^{235}U absolute fission rate in spherical fusion blanket assemblies 77—67871
^{235}U, absolute fission yield meas. by track-etch-cum-γ-spectrometry method 80—27859
^{235}U, capture to fission ratio determ. from low energy gamma-ray meas. 77—23152
^{235}U, capture to fission ratio in range 10-500 keV 77—26804
^{235}U, cross section for Na-Be photoneutrons 77—23159
^{235}U, cross sections for α-decay and neutron induced fission *(Russian)* 79—17944
^{235}U, cross-section from anal. of BNL exponential expts. with ENDF/B-IV data 78—13218
^{235}U, delayed neutron groups from thermal fission 79—30864
^{235}U, delayed neutron parameters selection, for nuclear reactor calc. *(Slovak)* 78—21534
^{235}U, e and $\bar{\nu}$ energy spectra from fission fragments *(Russian)* 77—23120
^{235}U, fission and activation by fusion plasma neutrons 79—13521
^{235}U, fission foil used for neutron fluence meas., optical microscopy counting after etching 78—13177
^{235}U fission fragment angle meas. with gridded ionisation chamber 79—85865
^{235}U fission fragment thermonuclear superheavy nuclei synthesis, prod. cross sections 80—95331
^{235}U, fission probability, Γ_n/Γ_f ratio struct. 78—37382
^{235}U, fission product mass. distrib. from 25 MeV bremsstrahlung irradiation 78—13175
^{235}U, fission rates measured in graphite-reflected lithium assembly, nonelastic neutron anisotropy effect 78—29511
^{235}U, fission recoils, chem. effects, energy deposition efficiencies, surface conditions depend. 78—80776
^{235}U, fission to capture ratios in range 0.2-15.0 keV 77—3057
^{235}U, fragmentation, HF calcs., neutron multiplicities and fragment KE 77—30635
^{235}U, in Oklo natural reactor, characts. from rare earth elements behaviour 78—49019
^{235}U, internal conversion cascading fission fragments 78—94036
^{235}U, irradiated in BOR-60 reactor, fission yields 79—17971
^{235}U, mass distribution of fragments *(Russian)* 78—29517
^{235}U, muonic, target preparation 80—23217
^{235}U, neutron induced fission cross section, 0.008 eV to 30 keV 77—50165
^{235}U, prompt fission neutron spectra 79—9654
^{235}U, prompt-fission-neutron spectra 79—67793
^{235}U, proton induced, 1 GeV, cross section *(Russian)* 78—94041
^{235}U solution, criticality anal. using KENO and SU-HAMMER codes 78—89949
^{235}U, spontaneous to induced ratio, B and Li impurity effects 79—45305
^{235}U, statistical anal. of reson. neutron fission cross section 77—38305
^{235}U, sublimation separation of ^{99}Mo from neutron irrad. UO_2 77—9257
^{235}U, subthreshold photofission 78—66323
^{235}U, σ_c/σ_f ratio meas. in BFS critical assemblies 79—97737
^{235}U, thermal fission, product decay-heat calc. 77—61464
^{235}U thermal fission afterheat, sensitivity to errors in fission product data 77—26841
^{235}U thermal fission product long-term activity meas. and calc. 79—9644
^{235}U, thermal n induced ternary fission, α energy and ang. distribs. 79—22345
^{235}U, thermal neutron fission with alpha-particle emission *(Russian)* 77—46198
^{235}U, thermal neutron fission, fission product decay energy release rates, effect on LWR LOCA 80—57894
^{235}U, thermal neutron induced fission, nuclear charge distribution in fission products 80—57808
^{235}U, thermal neutron irrad., fission product decay power calc. 80—22868
^{235}U, thermal neutron-induced fission, ^{96}Nb and ^{98}Nb yields 78—54807
^{235}U, thermal-neutron induced fission, scission point configuration determ. 77—82973
^{235}U, thermal-neutron-induced microscopic approach to statistical theory *(Chinese)* 78—86559
^{235}U to ^{239}Pu fission cross-section ratio from 0.001-30 MeV 77—26807
^{235}U/^{238}U fission ratio, Makrofol solid-state track recorder for fission rate meas. 78—13396
$^{235}UO_2$, visualisation of fissionable radionuclides in rat lung using neutron-induced autoradiography 78—28055
^{235}U+n, 13.9, 14.6 MeV, absolute neutron fission cross sections, associated particle method 78—89926
^{235}U(α,α), 19-27 MeV, differential cross section, transmission coeffs. for fission cross section *(Russian)* 79—67800
^{235}U(d,pf), 23 MeV, total KE release 78—78426
^{235}U(e,f), 110 MeV electrons, mass and kinetic energy distribs. 79—93672
^{235}U(γ, f), 12-70 MeV bremsstrahlung, product yields and γ-spectra 80—42716
^{235}U(γ,f), 25 MeV bremsstrahlung, neutron emission curve 77—10457
^{235}U(γ,f), ang. distrib. of fragments *(Russian)* 78—54808
^{235}U(n, f) 0.024 to 7.4 MeV fission cross section ^{235}U/^{239}Pu ratio 79—40975
^{235}U(n, f) thermal 3 MeV, ^{136}I isomeric ratio *(French)* 80—68709
^{235}U(n, γf), X-ray prefission yield depend. on fission width 77—10453
^{235}U(n,8), fission cross-section for 2200 m/s neutrons 79—17943
^{235}U(n,α), thermal fission neutron spectrum 80—42712
^{235}U(n,f), ^{148m}Pm, ^{148g}Pm and ^{146}Pm independ. yields 77—79407
^{235}U(n,f), 0.001-25 keV, polarised n, spin separated cross sections, resonance struct. 79—3126
^{235}U(n,f), 0.1 to 10 MeV fission cross section rel. to ^{239}Pu and ^{242}Pu 79—13354
^{235}U(n,f), 0.1-20 MeV neutron fission cross section 79—9655
^{235}U(n,f), 0.10-2.07 MeV, meas. of prompt fission neutron spectra 77—23146
^{235}U(n,f), 0.2 to 1.4 MeV, average number of prompt neutrons 77—23140
^{235}U(n,f), 0.3-10 MeV, cross-section meas. 77—26806
^{235}U(n,f), 0.3-12.5 MeV, fission cross-sections meas. 78—46117
^{235}U(n,f), 0.3-1.4 MeV, energy depend of fission fragment anisotropy 79—80962
^{235}U(n,f), 0.5 MeV, prompt neutron spectrum meas., TOF techniques 77—34356
^{235}U(n,f), 0.52 MeV, prompt neutron spectra meas. 77—23158

fission of uranium continued
^{235}U(n,f), 0.6, 7 MeV, fission neutron spectra meas. 80—22872
^{235}U(n,f), 1 keV to 30 MeV neutrons, cross section meas. rel. to ^{241}Pu 79—36286
^{235}U(n,f), 2-144 keV, cross-section meas. 77—26813
^{235}U(n,f), 2-144 keV, cross-sections meas. 77—26814
^{235}U(n,f), 550 keV, correlated fragments, 4-param. (E,v) meas. 77—26802
^{235}U(n,f), 6-9 MeV, fission product yields 78—66324
^{235}U(n,f), abs. meas. of fission cross-sections with photoneutron sources 79—30860
^{235}U(n,f), absolute yields and group constants of delayed neutrons in fast fission using Viper 77—54261
^{235}U(n,f), ang. distrib. of fission fragments 78—37383
^{235}U(n,f), cross section sensitivity anal. of fission rates in graphite reflected Li assembly 78—46166
^{235}U(n,f), cross sections for ^{252}Cf neutrons 78—25258
^{235}U(n,f), cross-section, 2, 24, 55, 144 keV neutrons 78—17262
^{235}U(n,f), cross-section below 1 keV 78—4969
^{235}U(n,f), energy depend. of cross section, 0.8-20 MeV 77—23156
^{235}U(n,f), fission cross-section averaged over ^{252}Cf neutron spectrum 79—30861
^{235}U(n,f), fission fragment average kinetic energies in resonance region 80—18358
^{235}U(n,f), fission fragments with high KE, mass separation based on TOF spectra 78—46209
^{235}U(n,f), fission neutron spectra, TOF meas. 78—17476
^{235}U(n,f), intermediate struct. in keV cross-section 77—23154
^{235}U(n,f), light particle yields and spectra 77—50173
^{235}U(n,f), neutron spectrum of thermal fission 79—97736
^{235}U(n,f), nuclear constants eval. for heavy fissile nuclei using nuclear models *(Russian)* 79—59100
^{235}U(n,f), polarised thermal neutrons, parity nonconservation *(Russian)* 78—33232
^{235}U(n,f), quantum numbers of low-lying resonances 77—23148
^{235}U(n,f), reconciliation of $\bar{\nu}_p$ meas. 77—67776
^{235}U(n,f), sensitivity of decay power to uncertainties in estimated decay data 80—22932
^{235}U(n,f), separation, identification of Ru, Rh isotopes 78—89924
^{235}U(n,f), spins of resonances below 150 eV 77—23147
^{235}U(n,f), statistical model anal. of mass yield 77—26797
^{235}U(n,f), subthreshold fission, fine struct. resonances anal. 78—652
^{235}U(n,f), symmetric fission, proton scatt. by fission fragments in neck area 80—83130
^{235}U(n,f), thermal, appl. of $\bar{\nu}$ constraint to fission product yields 80—22874
^{235}U(n,f), thermal, α-particle spectra 78—78425
^{235}U(n,f), thermal, charge and mass yields of light fission products 77—23122
^{235}U(n,f), thermal, charge distrib. of fission products 77—23123
^{235}U(n,f), thermal, correlation for independent fission prod. yield uncertainties 78—50216
^{235}U(n,f), thermal, determ. of high temp. diffusion of U in refractory metals 77—89587
^{235}U(n,f), thermal, discrete neutron emission probability 78—25257
^{235}U(n,f), thermal, fission product decay spectra calcs., comparison with expt. results 79—93674
^{235}U(n,f), thermal, fragment ionisation, charge distribs., stat. and instant perturbation theory *(Russian)* 80—63219
^{235}U(n,f), thermal, Rb and Cs relative and independ. fission yields 80—27679
^{235}U(n,f), thermal fission, fission product decay heat evaluation by least-squares method 79—30865
^{235}U(n,f), thermal n, fission fragment energy correlation meas., fine struct. and deformation 79—13355
^{235}U(n,f), thermal n, fission product isobaric charge distrib., parity effects 79—17791
^{235}U(n,f), thermal n, max. energy dissipation 79—89338
^{235}U(n,f), thermal polarised n capture, P-odd asymmetry meas. *(Russian)* 80—13452
^{235}U(n,f), thermal to 15 MeV, total delayed neutron yield calcs., energy depend. 77—34353
^{235}U(n,f), time correlated associated particle method, CAMAC experiment 80—52702
^{235}U(n,f) 3.5 MeV fragment X-rays 77—18638
^{235}U(n,f) absolute cross section, ^{252}Cf neutron source 77—23133
^{235}U(n,f) cross section, 1 keV to 1 MeV 77—23139
^{235}U(n,f) cross section, thermal normalization technique for meas. of neutron cross section vs. energy 79—9590
^{235}U(n,f) cross section in ^{252}Cf spectrum, integral test for evaluated data 77—23134
^{235}U(n,f) cross section in range 0.2-8.2 MeV 78—654
^{235}U(n,f) cross section standard, status 77—23040
^{235}U(n,f) fission cross section standard, propagation of uncertainties, critical benchmark meas. 79—13361
^{235}U(n,f) fission rates, interlaboratory comparison in Mol-ΣΣ field 77—23131
^{235}U(n,f) half-lives and γ-ray energies of short-lived isotopes of Mo 78—17137
^{235}U(n,f) integral cross section ratio meas. using ^{235}U(n_{th},f) neutron spectrum 77—23130
^{235}U(n,f) isomer yield ratios of ^{132m}I and ^{134m}I 77—38306
^{235}U(n,f) near threshold cross-section calcs. 77—65240
^{235}U(n,f) self-shielded fission rates, 0.464-2150 eV 79—59096
^{235}U(n,f) standard reaction, Monte Carlo simulation of cross section fluctuations 77—61461
^{235}U(n,f) sub-barrier fission, fragment mass and kinetic energy distribs. 79—17942
^{235}U(n,f) thermal n, reactor $\bar{\nu}$ and e spectra calc. 79—67791
^{235}U(n,f) up to 36 keV, statistical anal., cross sections, intermediate struct. 78—653
^{235}U(n,γ), 10-500 keV, capture to fission ratio, double humped fission barrier parameters 79—89336
^{235}U(n,γ), thermal, d, t, He emission probabilities from stable core model *(Russian)* 80—68713
^{235}U(n,γ), thermal, fission product $\bar{\nu}_e$ spectrum, β-decay characts. 80—78340
^{235}U(n,γf), X-ray yield fluctuations, γ-transitions in ^{236}U 80—106085
^{235}U(n,t), thermal, Mn bath meas. of η_{2200}, Monte-Carlo anal. 77—23142

fission of uranium continued
^{235}U(n$_{th}$,f), charge distrib. of products in mass chains 79 to 100 77—10456
^{235}U(n$_{th}$,f), decay power of fission products, sensitivity to uncertainty in yields 77—6494
^{235}U(n$_{th}$,f), fission fragment yield distribs., excitation energy depend. 78—50218
^{235}U(n$_{th}$,f), fission neutrons per absorption, Monte Carlo anal. of meas. 77—23141
^{235}U(n$_{th}$,f), fragment-mass depend. of fission neutron spectrum, TOF method 78—82398
^{235}U(n$_{th}$,f), investigation of conversion electrons in range 150 to 1500 keV *(Russian)* 77—10458
^{235}U(n$_{th}$,f), Maxwellian reference description of fission spectrum shape 77—23129
^{235}U(n$_{th}$,f), neutrons ang. correl., multiplicity 79—3187
^{235}U(n$_{th}$,f), statistical approach to scission mechanism 77—18631
^{235}U(n$_{th}$,f), yields of Cd and Sn isotopes, symm. region 77—34358
^{235}U(n$_{th}$,f) ionic charge distrib., effect of internal conversion 78—78428
^{235}U(n$_{th}$,f) mass yields, direct physical meas. using recoil mass spectrometer 77—50178
^{235}U(n$_{th}$,f) nuclide yields, direct physical meas. 79—9641
^{235}U(nth, f), above-the-barrier fission, fragment energy correl. meas. 78—21614
^{235}U(p,f), 13.7-14.2 MeV, isobaric analogue resonances, fission width 78—21616
^{236}U compound nucleus, lifetime meas. by means of shadow effect 77—50171
^{236}U, effect of nuclear force finite range on fission and heavy-ion reactions 78—13180
^{236}U fission, two parameter study, fragment mass and energy, thin film scintillators 79—13357
^{236}U fission as multi-dimensional Brownian motion, Fokker-Planck soln. *(Chinese)* 80—99197
^{236}U fission fragment kinetic energies, wall and window one body dissipation model 80—52703
^{236}U fission isomer produced in ^{238}U(γ,2n) prod. cross sections, half life 78—46045
^{236}U fission shape isomer, γ-decay from ^{238}U(γ,2n) 80—18230
^{236}U fission total kinetic energy release from ^{235}U (d,pf) 80—27682
^{236}U formation in ^{118}Pd+^{118}Pd, time depend. Hartree-Fock-Bogoliubov calc. 79—36265
^{236}U, giant E2 isoscalar resonance determ. 80—27607
^{236}U, induced fission dynamics 78—66261
^{236}U isomeric and prompt fission, nuclear superfluidity evidence from ^{235}U(d,pf) 80—68711
^{236}U nuclear instability and fission in strong mag. field energy level deformation *(Russian)* 79—13360
^{236}U, nuclear pressure and fission fragment mass distrib. 80—18356
^{236}U, photofission, deep sub-barrier anomalies 77—65241
^{236}U, potential energy surface depend. on neck-in and asymmetric fragmentation 77—54262
^{236}U shape isomer populated in ^{235}U(n$_{th}$,γ), isomeric/prompt fission ratio 77—323
^{236}U, subbarrier resonances and fission probabilities from ^{235}U(d,pf), 11-17 MeV, ^{236}U 79—13266
^{236}U, thermal neutron induced, average angular momenta of even-even fragments 78—86525
^{236}U two-peaked fission barrier penetrability, quasiclassical approximation *(Russian)* 79—13280
^{236}U* (6.4 MeV) ternary fission, fragment-mass yield curve, nucleon-parity type distribs. 77—67774
^{236}U(α,α'f), 50 MeV, total KE release 78—78426
^{236}U(α,α'f), total kinetic energy release 80—27682
^{236}U(γ,f), 5.2-6.4 MeV, ang. distrib. and yields of fission fragments 77—3059
^{236}U(n,f), cross section rel. to ^{235}U in 2-3 MeV region 78—21613
^{236}U(n,f), fast n, fragment mass and kinetic energy distribs. *(Russian)* 80—5181
^{236}U(n,f), P-odd asymmetry in neutron emission *(Russian)* 79—89339
^{236}U(p,t), cranking model anal., validity 77—18517
^{238}U, 14 MeV neutron induced, neutron emission and energetics 77—46192
^{238}U (^{6}Li, ^{6}Li'f), 150 MeV, isoscalar giant resonance struct. 79—89275
^{238}U (^{84}Kr, X), 522 MeV, heavy reaction product ang. distribs. and integral cross sections 79—49638
^{238}U (e, f), 7-65 MeV, absolute electrofission cross sections, fragment ang. distribs. 80—5185
^{238}U (μ^-,f), fission product mass distrib., fission probability, radiochem. investigation 78—29514
^{238}U, (p,f), 1 GeV, fission fragment ang. correlation, kinematically different events search *(Russian)* 79—59103
^{238}U absolute fission rate in spherical fusion blanket assemblies 77—67871
^{238}U, anal. of Rb and Cs isotopic distrib. in ^{11}B and ^{22}Ne-induced fission 77—18634
^{238}U asymmetrical fission, consistent two-centre model *(Russian)* 77—2974
^{238}U, deep subthreshold photofission using 3.8 to 5.7 MeV γ-rays 78—41787
^{238}U delayed fission cross-section for 14 MeV neutrons, shape isomer excitation 77—26808
^{238}U, delayed neutron parameters selection, for nuclear reactor calc. *(Slovak)* 78—21534
^{238}U Doppler effect obs. in advanced fuels critical assemblies 79—9739
^{238}U, E$_n$=14.9 MeV, effect of Fe shielding, hybrid reactor situation 77—50122
^{238}U electrofission, 6-60 MeV, relative E1 contrib. 77—6471
^{238}U, evaluation for ENDF/B-V 78—25289
^{238}U, fast fission, product decay-heat calc. 77—61464
^{238}U fast fission yield of tritium, implications for FBRs 77—46195
^{238}U, fast reactor dosimetry using zero-power facility ZEBRA 79—3219
^{238}U fast-neutron fission, calculated fission product yields 79—67796
^{238}U fission, pot.-energy surface calc. 77—61465
^{238}U, fission and activation by fusion plasma neutrons 79—13521
^{238}U, fission foil used for neutron fluence meas., optical microscopy counting after etching 78—13177
^{238}U, fission product mass. distrib. from 25 MeV bremsstrahlung irradiation 78—13175
^{238}U, fission rates measured in graphite-reflected lithium assembly, nonelastic neutron anisotropy effect 78—29511

fission of uranium continued
^{238}U, high mass asymmetry distribs. in fissioning nuclei, shell effects 79—3186
^{238}U, infinite multiplication factors, neutron captures and fission, rel. to GFR parameters 78—33245
^{238}U, meas. of Rb and Cs isotopic distrib. in ^{11}B and ^{22}Ne-induced fission 77—18633
^{238}U, mirror hybrid reactors 80—42860
^{238}U, muonic, μ induced prompt fission, fate of the μ 78—86557
^{238}U, muonic, target preparation 80—23217
^{238}U, muonic fission and electron decay 77—38754
^{238}U, μ capture rate in the fission mode, μ lifetime 78—89827
^{238}U, natural spontaneous fission, Xe prod., determ., extraction from granite 78—96216
^{238}U neutron data reevaluation for 77—23042
^{238}U, neutron induced fission rate meas. in Zebra 77—57698
^{238}U, neutron induced fission, ^{99}Mo and ^{111}Ag absolute yields 79—49642
^{238}U photofission, 20-60 MeV, relative E1 contrib. 77—6471
^{238}U, photofission, deep sub-barrier anomalies 77—65241
^{238}U, photofission products, ang. distrib., isomeric shelf region *(Russian)* 77—6475
^{238}U, photofission with bremsstrahlung, charge distrib., fractional independent yields 79—36283
^{238}U prompt fission, prompt neutron multiplicity distribs. *(Russian)* 77—340
^{238}U, proton induced, 1 GeV, cross section *(Russian)* 78—94041
^{238}U, proton-induced fission, asymm. region, nucl. charge distrib. 78—4967
^{238}U pulsed sphere meas., neutron emission spectra, rel. to fusion-fission blanket calcs. 77—23298
^{238}U source enhancement of ^{252}Cf spontaneous fission neutrons, determination of $\nu\sigma_f$ 77—6594
^{238}U, spontaneous fission, constant of disintegration meas. *(Portuguese)* 79—36282
^{238}U, spontaneous fission, half life and fragment kinetic energy meas. using cylindrical ionisation chamber 78—86555
^{238}U, subCoulomb fission induced by Xe and Kr, excitation functions 77—3061
^{238}U, subbarrier photofission, differential cross section 78—41796
^{238}U subbarrier photofission, cross section and half-life, double hump model 80—102217
^{238}U, Xe and Kr induced fission at Coulomb barrier energies 77—61467
^{238}U, Xe-induced Coulomb fission, rotation-vibration model for target nucleus 79—13367
^{238}U/^{235}U (n,f) cross-section ratio meas., 600 keV-22 MeV 77—23145
^{238}U/^{235}U fission cross section ratio, 2 to 25 MeV, high resolution meas. 77—50176
^{238}U/^{235}U fission ratio, Makrofol solid-state track recorder for fission rate meas. 78—13396
^{238}U+^{A}Xe, A=129, 132, 136, sub-Coulomb transfer and fission, cross sections 79—67802
^{238}U+^{136}Xe, 4.5-5.9 MeV/N excitation functions and ang. distrib. meas. 77—82965
^{238}U+^{238}U, 1785 MeV, cross sections, charge and mass distribs. of products 78—78408
^{238}U+^{238}U, 7.42 MeV/nucleon, charge, energy and ang. distribs. of prods. 78—8846
^{238}U+^{58}Ni(^{90}Zr), fission phenomena in deep inelastic collisions 80—5186
^{238}U+^{84}Kr, 605 MeV, quasi-fission reaction, mass-yield distrib. theory 77—42001
^{238}U+n, 13.9, 14.6 MeV, absolute neutron fission cross sections, associated particle method 78—89926
^{238}U+n, 2.47 MeV, energy spectra and ang. distrib. of neutrons 79—40927
^{238}U+p, 1-300 GeV, production props. of Sc nuclei 77—6389
^{238}U+p, nucleon losses on high energy fission *(Russian)* 78—46120
^{238}U(^{12}C,f), (^{18}O,f), (^{22}Ne,f), effective widths of excited state meas. by shadow effect *(Russian)* 77—46196
^{238}U(^{12}C,f), mass distrib. of fission fragments determ. *(Chinese)* 78—86558
^{238}U(^{16}O,f) 20 MeV/N, light particle spectra in central and peripheral collisions 80—5177
^{238}U(^{184}W, f), Coulomb fission excitation function, cross section 80—5176
^{238}U(^{238}U,X), 7.5 MeV/amu, three particle exclusive meas. for exit channels fission fragment ang. distrib. 80—13513
^{238}U(^{238}U,X), 7.5 MeV/A, 3-dimens. TDHF-BCS model calcs., possible fission 80—52694
^{238}U(^{238}U,f), 1785 MeV, exam. of multiprong events due to multiple sequential fission using solid state track detectors 80—91199
^{238}U(^{27}Al,f) 169, 190, 227 MeV, Z=105 compound nucleus lifetime using shadow effect *(Russian)* 78—86563
^{238}U(^{3}He,f), ^{241}Pu compound nucleus lifetime by the shadow effect *(Russian)* 78—86562
^{238}U(^{40}Ar,X), 237, 250 MeV, differential recoil range distributions, large contrib. of deep inelastic processes 78—70565
^{238}U(^{40}Ar,f), 212-340 MeV, I prod. relative thresholds from fusion and transfer induced fission 79—9640
^{238}U(^{48}Ca,X), 276 MeV, differential recoil range distributions, large contrib. of deep inelastic processes 78—70565
^{238}U(^{84}Kr,f), 806 MeV, exam. of multiprong events due to multiple sequential fission using solid state track detectors 80—91199
^{238}U(^{86}Kr,X), 730 MeV, transferred ang. momentum for fission and projectile like fragments 79—93675
^{238}U(HI,f), Coulomb fission cross sections from coupled channel calcs. 80—9319
^{238}U(Xe,f), depend. of Coulomb fission on nucl. struct. 78—13173
^{238}U(α,f), 100-1000 MeV, resonance production 80—52658
^{238}U(α,f), 140 MeV, fission cross sections and probabilities, isomeric yield ratio 79—45308
^{238}U(α,f), 23 to 115 MeV, interpretation of fragment anisotropies 77—30644
^{238}U(α,f), 640MeV 80—95329
^{238}U(α,f), fragment mass distrib., and yield, statistical anal. *(Russian)* 80—5183
^{238}U(α,xnf), 50 MeV, post and prefission neutron meas. 79—76042
^{238}U(d,pf), E$_d$=12 MeV, fission probability, energy depend. 77—71628
^{238}U(e,e'f), 20-120 MeV, electrofission cross section, E1, E2 strengths 78—13174
^{238}U(e,e'f), 5.5-9 MeV, fission fragment ang. distribs. DWBA anal., low lying fissioning levels 80—42713

fission of uranium continued
^{238}U(e,f), 110 MeV electrons, mass and kinetic energy distribs. 79—93672
^{238}U(γ,f), ^{135}Xe, direct meas. of absolute and fractional independ. yields 80—78341
^{238}U(γ,f), 12-70 MeV bremsstrahlung, cumulative and fractional product yields for A=128-136 79—36288
^{238}U(γ,f), 12-70 MeV bremsstrahlung, fragment mass and energy distribs. 80—27680
^{238}U(γ,f), 15 to 1300 MeV, cross sections meas. *(Russian)* 77—6473
^{238}U(γ,f), 20 MeV, fission product yields, charge distrib. 80—42533
^{238}U(γ,f), 25 MeV bremsstrahlung neutron emission curve 77—10457
^{238}U(γ,f), BF$_3$ detector assembly for photofission and photoneutron studies 80—63484
^{238}U(γ,f), bremsstrahlung of 600 MeV fragment energy correl. meas. max. energy 77—71630
^{238}U(γ,f), delayed neutron energy spectrum 77—23155
^{238}U(γ,f) 20 MeV, computer program for yield determ. of short-lived products 80—102215
^{238}U(γ,f) fission-neutron and fragment ang. distrib. 77—65239
^{238}U(n,2nf), 13.5-17.5 MeV, fragment anisotropy 77—54263
^{238}U(n,f), 0.10-2.07 MeV, meas. of prompt fission neutron spectra 77—23146
^{238}U(n,f), 0.3-10 MeV, cross-section meas. 77—26806
^{238}U(n,f), 0.3-12.5 MeV, fission cross-sections meas. 78—46117
^{238}U(n,f), 14.5 MeV, neutron emission, mass distrib. and energetics 80—47512
^{238}U(n,f), 1.5-7.7 MeV, mass yield curves 78—41788
^{238}U(n,f), 1.52 MeV, mass yield distrib. meas. 77—67777
^{238}U(n,f), 1.8-16.8 MeV, fission fragment energy spectra using glass sandwich detectors 78—82399
^{238}U(n,f), 5 eV-2.5 MeV, fission cross section, fission barrier second well parameters, resonances 80—63217
^{238}U(n,f), 5 eV-5 keV, sub-barrier fission 77—23151
^{238}U(n,f), 6-9 MeV, fission product yields 78—66324
^{238}U(n,f), 7 MeV, fission neutron spectra meas. 80—22872
^{238}U(n,f), absolute yields and group constants of delayed neutrons in fast fission using Viper 77—54261
^{238}U(n,f), cross section sensitivity anal. of fission rates in graphite reflected Li assembly 78—46166
^{238}U(n,f), fission cross sections, use as standards in MeV region 79—13362
^{238}U(n,f), fission product decay heat calc. by summation method, appl. to FBR 79—30863
^{238}U(n,f), prompt-neutron ang. distrib. 77—65238
^{238}U(n,f), second well gamma decay if subthreshold fission resonances 77—26800
^{238}U(n,f), separation, identification of Ru, Rh isotopes 78—89924
^{238}U(n,f), studied with intense neutron spectrometer 77—23364
^{238}U(n,f), subthreshold cross-section, high resolution meas. 77—26799
^{238}U(n,f) cross section in ^{252}Cf spectrum, integral test for evaluated data 77—23134
^{238}U(n,f) cross section meas., 3 eV-100 keV 77—26793
^{238}U(n,f) cross section up to 6 MeV 77—23161
^{238}U(n,f) fast neutron fission yield determ. 79—40970
^{238}U(n,f) fission rates, interlaboratory comparison in Mol-ΣΣ field 77—23131
^{238}U(n,f) integral cross section ratio meas. using ^{235}U(n_{th},f) neutron spectrum 77—23130
^{238}U(n,f) subthreshold fission cross section, 0.6 to 100 keV, barrier parameters 77—50169
^{238}U(p,X), 0.8-11.5 GeV, formation of A=131 isobaric nuclides 80—9293
^{238}U(p,X) *(Russian)* 79—80964
^{238}U(p,2n), production of ^{237m}Np fission isomer, statistical model anal. 78—25256
^{238}U(p,f), 11-29 GeV, three dimens. charge dispersion curves, isobaric yields 80—102111
^{238}U(p,f), 11.5 GeV, He and heavy fragment energy and ang. correlation 79—45310
^{238}U(p,f), 30-98.6 MeV, independ. yield of In and Ga isotopes 78—13171
^{238}U(p,f), 35-85 MeV, nuclear charge dispersion in light mass region 78—8864
^{238}U(p,f), 4-7 MeV, cross sections *(Russian)* 78—41794
^{238}U(p,f), 9.5-17 MeV, symmetric to asymmetric mass ratios for fragments 80—5178
^{238}U(p,f) 12 MeV, estimation of neutron yield from individual fragment in medium-excitation fission 80—542
^{238}U(p,nf), multiple scatt. effect due to filling in of blocking patterns 78—21617
^{238}U(p,t), 1 GeV, meas. of total fission cross-section *(Russian)* 77—341
^{238}U(p,t), 400 GeV, ang. distrib. of Sc fragments in thick targets 77—6472
^{238}U(p,xnf), lifetime of second chance fission at threshold, in UO$_2$ single cryst. 78—17259
^{238}U(π^-, f), resting pions, delayed fission search *(Russian)* 80—52704
^{239}U, induced by ^{238}U(d,p), subthreshold cross section meas., 2-centre shell model calc. 79—6719
^{240}U, fission probability, fragment ang. distrib. meas. in ^{238}U(t,pf) *(Russian)* 77—46199
U(α,f), 0.65, 1.74, 4.12 GeV, fission fragment recoil characts. 78—89925
U(α,f), 0.65-4.11 GeV, cross sections for binary and ternary fission 77—3055
U(γ,f), 5.2-6.4 MeV, A=234, 236, 238, doubly even isotopes, ang. distribs., fragment yields 78—50219
U(γ,f) A=235,238, 25 MeV bremsstrahlung, prod. yields, mass chains, charge distribs. 77—6470
U(γ,f), max. energy 580 MeV, track detector anal. 77—18640
U(μf), emission of conversion μ in radiation free fission *(Russian)* 78—62587
U(n,f), 0-18 MeV, prompt neutron spectrum, evaporation model *(Chinese)* 80—42721
U(n,f), A=233,235,238, 35 to 1500 keV, near equilib. delayed neutron energy spectrum 77—34354
U(n,f), A=233-238, cross-sections meas., 0.1-30 MeV 77—23150
U(n,f), A=234,6,8, 0.1-30 MeV, fission cross-sections relative to ^{235}U 77—61463
U(n,f) A=235,238, sub MeV neutrons, equilib. delayed neutron energy spectra meas. 77—38308

fission of uranium continued
U(n,f), delayed neutron spectra from thermal- and fast-neutron fission, reactor calcs. 77—34355
U(n,f) fission cross section ratio of ^{235}U to ^{238}U for 0.1 to 25 MeV neutrons 79—36285
U(n,f), heavier rare earths separation by radiochem. method 79—67785
U(n,f), thermal to 14.7 MeV, statistical theory calcs. 77—23137
U(n_{th},f), A=233,5, isomeric yield ratio of ^{148}Pm meas. 77—82975
U(p,f), 1 GeV, analysis of angular correlations between complementary fission products 79—76311
U(p,f) 300 to 660 MeV protons, neutron multiplication 79—59099
U(p,f), 600 MeV, fragment energies, cross sections level density and barrier heights 80—42723

fission products
^{262}[105] spontaneous fission, fragment mass distrib., total kinetic energy release 78—17256
β-radiation from fission products mean energy calcs. *(Russian)* 78—561
γ-spectrographic anal. of neutron fluxes and depleted fuel fission products 79—97933
A=116-140 fission products far from β-stability, Q_β-values 77—22949
A=134-144, fission yields from spectroscopic meas., γ-branching and half-lives 80—78213
A=135-143, odd A fission products, delayed n, decay studies and Q_β meas. 80—78227
A=144 to 147 short-lived fission products, β-decay energies 77—22948
A=90 to 101 short-lived fission products, β-decay energies 77—22948
A=90 to 160, neutron capture cross-section adjustment based on integral meas. 79—9578
A=97 and 99, nuclear structs. *(German)* 78—29395
absolute yield measurements by track-etch-cum-γ-spectrometry 80—27859
absorption cross section of fission product aggregate, energy dependence 79—76075
actinide elimination by fissioning in generic actinide burner reactor 79—93756
actinide fission product X-rays in micas, comparison with superheavy elements K- and L-shell ionisation estimates 77—50581
actinide nuclei, statistical aspects in fission mechanism 77—14097
actinides, fast reactor recycle as waste management alternative, performance calcs. 78—13269
adsorption on silica gel, for urinary gross α activity determ. 79—88155
aerosol products, bioindication using needles of common pine tree 79—100550
air over N.Atlantic, obs. of radioactivity and source region identification 80—77074
airborne short-lived radionuclides of unknown origin in Sweden (1976) 78—32219
alpha-particle energy spectrum, fission-emitted, fission-fragment shape and orientation depends. 78—74346
anisotropy of fragment emission, effect of spin of target nucleus *(Russian)* 77—22992
backscattering from Au, Cu and Al 80—16138
binary fission fragments of ^{209}Bi, ^{197}Au, ^{184}W, Yb, ^{165}Ho, ^{159}Tb, Sm, mass and energy distribs. meas. 77—71627
boric acid solutions, extractive purification from radioactive corrosion and fission products 80—18458
breeder reactor, with circulating liquid-salt fuel, fission product radioactivity reduction and residual heat release 79—26490
bubble nucleation modelling, and fission-induced re-soln. 79—71891
BWR spent fuel safeguarding, nondestructive assay using gamma spectrometry 80—68802
BWR-6 computer anal. of fission product release to containment via press. suppression pool 79—59223
carbide fuels, effect of burn-up and temp. on appearance of optically visible fission gas bubbles 80—63251
ceramic fuels, effect of gas composition on thermal conductivity 79—93733
ceramic nuclear fuels, irrad. induced rare gas diffusion 80—59524
charge and slope polarisation of nuclei, liquid drop model anal. 79—9543
charge distrib. in fission products, statistical calc. 77—18632
Chinese explosion 1977 Sept. 18, time distrib. and anal. fallout particles 79—25796
Chinese nuclear explosion, Jan. 1976, anal. of fission products 77—26884
clustering, fine struct. and mass distrib. 77—26660
coated fuel particles, metallic fission product migration 77—50231
complementary, ang. correlations anal. 79—76311
concentration profile in coating layers of irradiated fuel particles 77—50237
conference on nuclear spectroscopy of fission products, Grenoble, France (May 1979) 80—77546
confinement in glass, stability characts. *(French)* 77—61556
consensus and subsidiary yields, integral meas. in standard neutron fields 79—13364
conversion electron spectra, 150 to 1500 keV, in ^{235}U(n_{th},f) *(Russian)* 77—10458
correlated fragments from 550 keV neutron induced fission, 4-param. (E,v) meas. 77—26802
decay energy release rates following ^{235}U fission, effect on LWR LOCA 80—57894
decay heat, development of revised ANS standard 79—49742
decay heat anal., summation method, fast and thermal reactor systems 77—23195
decay heat calc. by summation method, appl. to FBR 79—30863
decay heat calcs. for ^{235}U and ^{239}Pu 79—76083
decay power in reactor, sensitivity to uncertainties in fission product yields, errors 77—6494
decay power of fission products in reactors, effects of neutron capture 77—6500
decay props. meas. at recoil separator using many-capillary gas jet system 77—88364
decontamination by Purex solvent extraction process 79—36387
decoupling model for fission fragment transitional nuclei, odd-odd and even mass 80—78174
deexcitation, statistical model anal. of spin effects 79—17941
delayed fission product γ spectra following short neutron irrad. 79—9645
delayed neutron emission probabilities, semi-empirical formula 77—22976
delayed neutron parameters selection, for nuclear reactor calc. *(Slovak)* 78—21534
delayed neutron spectra from precursors with A=79-130 77—82884
delayed neutrons and P_n values 80—78339

fission products continued
 delayed-n precursors in various mass chains half lives and P_n values 78−70497
 delayed-neutron spectra characterisation 77−79345
 delayed-neutron yield calcs. from ENDF/B-VC 79−67798
 density distribution of fission traces, meas. by tracer's method in dielectrics, fuel meas. appl. *(Rumanian)* 78−90033
 desorption fission fragment induced, method for correlated events in TOF mass spectrometry 78−58089
 EBR, dissolver soln. fission product determ. by spark source mass spectroscopy 80−32422
 EBR II, fission product source identification using Xe tag 78−70588
 EBR-II delayed neutron monitor, response to tramp uranium and fission prod. test source 79−67919
 EBR-II fission product control, cover-gas cleanup system and graphite trap 79−9791
 EBR-II primary system fission gas behaviour 79−9692
 ENDF/B data, processed, rapid spectral and decay heat calcs. 79−67797
 energy deposition kinetics into Ar and Ar-N_2 mixture 77−23652
 even-even neutron-rich fission products, de-excitation spectra, β-decay, deformation 80−78203
 fallout nuclide determination for 19th Chinese nuclear test 79−54601
 fallout observation, Chinese A-tests 80−27820
 fast reactor, operative monitoring of fission products in Na coolant 78−677
 fast reactor fission gas behaviour, eqn.-of-state of Xe at high temp. and pressure 79−67860
 fast reactor hypothetical accidents, review of fission gas effects 79−67900
 fast reactor whole core accidents, fission products role 78−54854
 FBR, role of fission gas swelling and release in reactor accidents 80−57854
 FBR, UO_2 and (U, Pu)O_2 fuel, gaseous and solid fission product behaviour, swelling 77−34396
 FBR LOF accident, role of fission gas and fuel melting on transient fuel response 79−59191
 FBR oxide fuels, dynamic response of grain boundary cavities to stress and temperature changes under conditions of continuous gas generation 80−66544
 FBR safety anal. modelling of fission gas behaviour 80−748
 FEBIAD ion source for fission fragment isotope separation 80−78483
 first order adiabatic approx., fission fragment excitation energy 80−32312
 fission gas, modelling transient behaviour 79−97826
 fission gas behaviour model, intragranular, nonequilibrium behaviour, numerical integration 80−32345
 fission gas bubble distribs. in mixed oxide fast reactor fuel pin, anal. of TEM obs. 78−58358
 fission gas effects in irradiated fuel rods operated in film boiling at high power 79−49744
 fission gas re-solution, comparison of single knock on and complete bubble destruction models 78−82455
 fission oxide fuels, in-pile densification of intergranular porosity, model 79−73345
 fissioning plasma from gas phase nucl. reactor, appl. 80−64794
 fragment recoil mass spectrometer HIAWATHA 79−9940
 frictional effects on post-scission dynamics and fission fragment kinetic energies 79−36225
 fuel pin modelling, Dutt fission gas release correl. 79−67826
 fuel reprocessing waste ^{137}Cs, ^{90}Sr and rare earth radioisotope separation by cation exchange 78−78486
 fuel transient heating conditions, mobility of fission gas bubbles 79−59189
 gamma peaks, appl. to burn up determ. of irrad. fuel samples *(Hungarian)* 78−82458
 gamma-ray and half life data tables 78−50134
 gamma-ray energy meas. at high precision 79−93865
 gamma-ray energy release rate, response matrix of NaI scintillation spectrometer *(Japanese)* 80−42888
 gamma-ray spectra analysis of fission products, automatic general-purpose program GSAP *(Chinese)* 80−69013
 gamma-spectra, estimation using nucl. systematics 78−70587
 gas, release from Na-bonded carbide fuel pins in OSIRIS *(French)* 80−73916
 gas bubble distribution, in fuel, anal. of TEM obs. 79−71890
 gas jet recoil transport system for fission products, appl. to chemical separation in gas phase 78−17459
 gas release from high burn-up oxide fuel, predictions in ELESIM code 80−57864
 gas release from ThO_2 and ThO_2-UO_2 fuel 78−86651
 gas release from UO_2 fuel, microstruct. depend. model 80−665
 gas release from UO_2 pellet reactor fuel rods 80−635
 gaseous fission product retention in fuel reprocessing 79−31153
 gaseous release, inclusion in AVR fuel cycle strategy program *(German)* 79−74576
 gases in HTGR fuel particles, content meas. apparatus 80−68793
 GCFR, Pu fuelled, fission products and secondary gamma-ray spectra 78−676
 GCFR fuel column, effect of Cs migration on fission gas permeability 79−67824
 heavy ion reactions, fission fragment angular distrib., shape of saddle point of compound nucleus *(Chinese)* 78−78427
 heavy ion track lengths in solid dielectric track detectors 79−59319
 high-level, fixation in glass ceramics 77−61558
 high-level, leaching of radioactivity from glass blocks buried below water table 77−65312
 HTGR, fission product plateout in primary cooling system, in situ meas. using Ge(Li) spectrometer 80−73881
 HTGR, gas release from fuel particles and rods 77−74938
 HTGR, inert gas release core-survey calc. 79−67908
 HTGR, metallic fission product retention 77−79443
 HTGR, multicomponent time depend. diffusion with radioactive decay 79−85588
 HTGR, release of metallic fission products from multilayered coated particles 77−79442
 HTGR coated fuel particles, behaviour of fission products *(Japanese)* 78−54830
 HTGR coated-particle fuel performance charact. by fission gas pressure meas. 79−54584

fission products continued
 HTGR core, γ-spectroscopic exam. of fission product distrib. after shutdown 79−67909
 HTGR core during transient temp. excursion, fission product release, computerised analysis *(Japanese)* 78−82467
 HTGR fission product release following LOCA 79−13457
 HTGR fuel element failure mechanisms and fission product release 80−13586
 HTGR fuel particles, influence of pyrocarbon props. on as-produced gas permeability of coatings 79−54511
 HTGR irradiation expts., fission product release 77−74939
 HTR, expt. JAERI, safety anal. of fission product behaviour and hypothetical accident *(Japanese)* 78−66330
 HTR, gas release by coated oxide fuel particles 77−74937
 HTR, spherical fuel elements, determ. of fission product release 80−647
 HTR oxide fuel, retention of solid fission products 79−54507
 inert gas plasmas, prod. by U fission fragments in nucl. reactor props. 77−76147
 inert gases, separation of ^{85}Kr from Xe for storage by distillation *(German, English)* 77−61516
 ion source fission product separators 80−78479
 ionisation by He jet rapid transport technique 79−63831
 ISOLDE as a source of neutron-rich nuclei 80−78480
 isotope separation using OSIRIS on-line separator 77−23352
 kinetic energies and fly-off angles, ionisation method of meas., online numerical processing *(Russian)* 80−52838
 kinetic energy distrib. of fission fragments, thermal fluctuation influence 80−22865
 kinetic energy of fragments at small excitation energies *(Russian)* 77−74830
 light ternary fission product charge distributions and fission probabilities 79−9643
 liquid fuel-fission gas bubble mixtures, equation of state 80−47568
 LMFBR, borosilicate glass and glass ceramics with highly radioactive waste 80−5271
 LMFBR, fission gas release and microscopic swelling in highly rated advanced fuels 80−52739
 LMFBR, fuel and fission gas response to simulated thermal transients 78−74453
 LMFBR, fuel motion pot. due to volatilisation of metallic fission product inclusions 79−49746
 LMFBR, HCDA, attenuation of airborne debris 80−13650
 LMFBR, pin plenum fission gas release model to describe fission gas effects in voided channel 79−31042
 LMFBR, yield characts. of short-lived fission products in Na heat-transfer agent 78−66338
 LMFBR advanced MX-type fuels, fission gas swelling, temp. depend. 80−57842
 LMFBR advanced MX-type fuels, low-temp. microscopic swelling, phenomenological model 80−57851
 LMFBR advanced MX-type fuels, swelling mechanism anal. 80−57850
 LMFBR core disruptive accident, fission gas bubble modelling 79−31043
 LMFBR failed-fuel detection using gaseous fission-product detectors 79−97856
 LMFBR fuel, fission gas behaviour during overpower transient, calcs. using COREF-1 code 80−57853
 LMFBR fuel behaviour during HCDA, intragranular fission gas behavior under isothermal conditions 80−102236
 LMFBR MX-type highly rated advanced fuels, fission gas release and correl. with fuel restructuring 80−642
 LMFBR transient fission gas behaviour modelling, bubble equilibration effects FRAS 2 code 79−59168
 LMFBR transient fuel behaviour, effect of grain boundary fission gas 79−54532
 long-lived fission product waste transmutation by spallation and neutron reactions using linear accelerator 78−13268
 LWR, borosilicate glass and glass ceramics with highly radioactive waste 80−5271
 LWR, dissolver soln. fission product determ. by spark source mass spectroscopy 80−32422
 LWR, fission product activities, fuel survey 80−736
 LWR core meltdown, release of fission and activation products 80−13667
 LWR fuel, mechanistic prediction of transient fission gas release 80−47571
 LWR fuel cycle costs, sensitivity to fission product data 80−23102
 LWR fuel elements, burnable poison management for high burnup reactivity compensation 80−707
 LWR fuel performance calcs., effect of Cs and I_2 release 79−31054
 LWR fuel rods, power cooling mismatch induced failure, meas. fission product release 79−93772
 LWR fuel rods, power ramp induced I and Cs redistrib. 80−32343
 LWR fuel rods containing fission gas, grain growth 79−67866
 LWR LOCA, fission product gamma-ray energy absorption in emergency cooling solns. 79−31052
 LWR LOCA, fission product release from defected fuel rods 80−23031
 LWR ruptured fuel rods in LOCA, fission product release, computer modelling 79−49780
 LWR spent fuel, non-destructive anal. using inherent and induced neutron radiation *(Russian)* 80−68805
 magic and doubly magic nuclei, A=129, 131, 133 chains, 0^+ states, spectroscopy 80−78165
 mass, charge, kinetic/distribs. in scission point model based on deformed shell effects 77−10455
 mass and charge distributions, determ. at Lohengrin mass separator *(German, English)* 78−16891
 mass distribution 78−17261
 mass spectra meas. with recoil separator Lohengrin 77−22607
 mass-yield curves, topological classification *(French)* 79−76043
 mesoatoms, prompt fission internal γ-ray conversion, fragment radiative transitions *(Russian)* 80−86944
 metallic product migration in reactor oxide fuels 77−74926
 mineral fission fragment track annealing characteristics for geochronology 79−100827
 mixed oxide fuel, retained fission gas determ., new instrumental method 79−54477
 mixed oxide fuels, SEM obs. of gas bubble morphology 80−57843
 mixed-oxide fuel, irradiated, microstruct. charact. and radial distrib. of retained fission gas 79−59188
 monitoring in gaseous CO_2 coolant by gamma spectrometry 79−89374

fission products continued
multi-chance high-spin fission, fragment anisotropy, stat. model anals. 80—57812
muonic atom fission, distribution of muons among fragments *(Russian)* 78—94040
muonic atoms, prompt fission, muon entrainment by fission fragment, probability *(Russian)* 80—37911
neutron capture cross sections in fast-thermal critical facility STEK, adjustment methods, error evaluation 77—6498
neutron cross sections for 27 nuclides important in fast reactor calcs. 77—67741
neutron cross-sections data for ENDF/B-IV library 78—25290
neutron dosimetric meas. using mica and pyrex, fission fragment track technique 78—13347
neutron fluence meas. using mica and plastic as fission fragment track detectors 78—13346
neutron induced fission prod. yields, tabulation 78—25253
neutron rich fission fragments, excited state spin assignment, various methods 80—78506
neutron rich nuclei, beta decay half lives, expt. techniques 80—78224
neutron rich transitional fission fragments, spectroscopy, 0^+ states and octupole vibrs. 80—78204
neutron-rich, gas-filled on-line separator *(German)* 77—18708
neutron-rich nuclei in $A \sim 100$ region, decay props. 77—22961
nonequilibrium fission gas behaviour 78—86626
NRX and process effluents, gamma ray spectrometric anal. 78—29656
nuclear data evaluation, cross sections up to 15 MeV, resonance parameters 77—23044
nuclear decay heat of short lived products 77—71594
nuclear energy, nonconventional conversion systems *(Rumanian)* 78—86705
nuclear far from β-stability, delayed neutron energy spectra, structure effects 80—78226
nuclear fuel, use of gamma active spikants for proliferation deterrence, effect on fusion product buildup 79—93716
nuclear fuel reprocessing by fluoride volatility process, distrib. of Ru contaminants 80—13743
nuclear fuel swelling, fission gas precipitation into intra- and intergranular porosity, theory 80—57849
nuclear fuels fission gas behaviour, conf. Karlsruhe, Germany (Oct. 1978) 80—56992
nuclear materials safeguards, collection and analysis of measured fission product data 80—95354
nuclei far from stability, β-decay energies, γ-rays, Q_β values and masses 80—78225
nucleon exchange between fission fragments in two centre oscillatory pot. below threshold *(Russian)* 78—89847
odd nuclei, soft and deformed, rotor plus quasiparticle approach, moments, transition probabilities 80—78214
odd-odd fission products, level schemes, rot. bands, shell model states 80—78167
on-line gas phase separations of ^{252}Cf fission products 77—14615
on-line mass spectrometer for obtaining nuclear data 77—22616
PBHTR, fission product retention in ultimate accidents 80—13647
post-scission motion of fission fragments 79—26420
power burst facility fission product detection system 79—54536
prediction of fission-product mass yields and related parameters 79—30862
Purex process, concs. of U, Pu, HNO_3, fission products, in LMOM2 extractor, expt., graphical determ. 78—41843
PWR defective fuel rod, effect of thermal cycling on fission product release 80—13669
PWR fuel clad failure characterisation based on fission product activity, PROFIP 3 code 80—95365
PWR irradiated fuel, monitoring by gamma spectrometry nondestructive meas. *(French)* 80—63288
pyrocarbon coated particles, influence of fast neutrons on transport behaviour of solid fission products *(German)* 79—13427
RA reactor fuel, gamma-spectrometric determ. of fission product activity ratio 78—33269
radioactive fallout in air and rain, results to end of 1977 78—82535
radioactive rare gas, removal from fuel reprocessing plant *(Japanese)* 79—93747
radiochemical continuous analysis of reactor coolant water, fission product identification 77—71652
radioiodine release from U_3O_8 in O_2 and inert gas atm., chem. identities 77—57712
radioisotopes in cooling system, prod., transfer, life cycle, radiation calcs. using program system TIBSO 78—54821
radiolysis in ethane-ammonia system, ethylamine and n-butane formation using fission fragments 77—56236
radionuclide corrosion and fission products, ion exchange separation 80—18460
radionuclide corrosion and fission products, liquid-liquid extractions with metal diethyldithiocarbamates 80—18459
rapid automated nuclear chemistry, short lived fission products, reactor safety 80—81353
rapid automated nuclear chemistry facility for the study of short lived fission products 79—71978
rare earths, isotopic separation after recoil in Ta foil 77—14614
rare-earth fission product isotopes, separation in thin-films chromatography *(German)* 80—37635
reactor fuel, fission product migration, FIPMIGR program 80—37453
reactor fuel, gamma-ray spectrometric determ. of fission product activity and activity ratios 78—37430
reactor fuel burn-up and cooling time determ. using gamma spectrometry 80—63289
reactor fuel burn-up determination using gamma spectrometric nondestructive assay for IAEA safeguards 80—68806
reactor fuel burn-up determination using gamma spectrometry, IAEA safeguards experience in Czechoslovakia 80—63292
reactor fuel burn-up measurement using spatial power distrib. eval. and gamma spectrometry 80—68803
reactor neutrino expts., fission fragment ν radiation, neutral currents, inverse β-decay, $\bar{\nu}$ scatt. *(Russian)* 80—42736
reactor primary coolant contamination, contribution from U impurities in fuel cladding 79—63751
reactor shutdown, decay heat, effects of depletion, buildup and fast fission 79—81041
reactor spent fuel safeguards verification using gamma spectrometry 80—63290

fission products continued
recoil characteristics, fission fragments due to high-energy α bombardment of U, Th, Pb 78—89925
recoil mass spectrometer for fission fragments, HIAWATHA, thermal neutron fission of U, Pu 78—16892
release and distrib. in coated particles, development and testing of laser system *(German)* 78—82403
review of recent progress, barrier crossing, static and dynamical aspects *(French)* 79—520
saddle point, statistical fluctuations, Suzuki's scaling limit 80—86946
scattering kinematics of fission fragments, multiparametric anal. TDF instrument with semiconductor detectors 78—78550
scattering kinematics of fission fragments, multiparametric anal., electronic meas. system, semiconducting detectors 78—78551
scission α-particles, emission mechanism 77—18516
scission region, nascent fragment bending and wriggling modes, quantum numbers 80—18285
separated fission products with $A=88$-144, delayed neutron spectra 77—34268
separation of Zr, Nb, Tc, Sb, rapid chem. methods 77—16856
separation performance of Kr, Xe, Ar fission products by thermal diffusion column 77—42192
separation using Lohengrin mass separator high flux reactor in Grenoble 78—17436
short lived light fission products, beta decay energies using online mass separator 78—8783
short-lived, rapid paper electrophoretic separation, γ-rays and half-lives determ. 77—44498
short-lived, spectroscopy, gas-jet recoil transport 77—23338
SIRIUS facility for neutron rich fission fragment studies 80—78484
SISAK 2, chemical separation method for short lived fission products in spectroscopic studies 80—74068
solid, effect on oxide fuel element behaviour in fast overpower transient 80—623
solid fission products, effect on swelling and fission gas release during fast overpower transient 78—8917
solid track detectors, efficiency 77—71726
solvent extraction kinetics 79—26685
spectroscopy, use of Buechner magnet-position sensitive counter system 77—23360
Sphere-Pac mixed carbide fuel, effect of early gas release in temp. calcs. 80—102235
spin distrib., statistical theory predictions, asymmetric fission explanation 78—70509
spontaneously fissioning nuclides, content anal. by neutron counting 79—72206
sputtering of Au foil by fission fragments 78—2968
sputtering of insulators 80—40207
superdense nuclei, search for neutrons with binding energy >40 MeV *(Russian)* 79—89515
superheavy elements in Fe meteorites, fission rel. to trace element abundances 79—48742
surface barrier detector, pulse height response to mass and energy separated fission fragments 77—57812
thermal and fast fission yields, meas. techniques and data status 79—9649
total neutron cross section meas. on gross fission products, 1 eV-240 eV 77—23064
track registration in crysts., development efficiencies, etchant (etching conditions) depend. 78—66454
transient fission gas behaviour, exptl. and analytical results 79—59190
transient fuel behaviour, modelling of grain boundary fission gas effects 79—59169
transient fuel fission gas behaviour, NEFIG model calcs., bubbles and swelling 80—618
transmutation of fission product waste using DT neutrons 80—32383
transport and deposition in primary coolant circuit of HTR, filter *(German)* 77—74915
transuranics, spontaneous fission, (3Z-A) depend. of prompt-neutron yield 79—67799
TRISTAN II mass separator, ion source, beam optics, computer system 80—78481
TRISTAN II mass separator at Brookhaven HFBR, research programme for fission products 80—78482
underground nuclear power plant, accidents, containment of fission products, finite element anal. 80—27768
unslowed fission product separators, gas filled JOSEF, parabola LOHENGRIN 80—78478
viscosity effects for spontaneous and induced fission fragment KE 77—18639
vitrification of fission product solutions at Marcoule [description and hot operation results] 80—5270
volatile fission product atmospheric release from nuclear reactors and fuel reprocessing plants 79—34461
volatile fission products from nuclear fuel cycle and power stations, pollution effects *(Russian)* 79—31152
waste, comparison of USA military and civilian inventories 78—4995
waste solidification, high-level, for final storage *(German)* 80—22958
whitlockite from Bjurbole chondrite, origin of fission fragment tracks 78—81595
$Z=37$-43, neutron rich fission products, mass energy surface, decay props. 80—78228
$Z>103$ transactinides, method for rapid separation and identification 77—26952
Zircaloy-2, tritium diffusion 80—32341
γ-radiation intensity in short operation nuclear reactors 79—67823
γ-ray and photoneutron spectra, fission of U and Pu 77—23127
(n,f), actinide nuclei, influence of isomeric states on independ. fission prod. yield 78—4968
(n,γ) cross sections for fission product nuclides in fast reactors *(Japanese)* 80—521
(n,γ) cross sections from anal. of integral meas. 77—23032
$\bar{\nu}$ energy distrib. from fission product decay in nucl. reactor 79—75924
^{87}Br, delayed neutron carrier, sorption parameter determ., appl. to fuel element leak detection 79—97828
^{111}Ag, absolute yields in ^{238}U neutron induced fission 79—49642
^{111}Ag, production by ^{239}Pu fission, absolute yields 77—50167
^{110m}Ag fission product, release from coated fuel particles in HTR, diffusion process 77—88228
^{110m}Ag release from coated particle fuel in HTR 77—74936

fission products continued
Ag(p,f), 1 GeV, binary fission, possible mass instability of correlated fragments 80−83133
Ag(p,f), 600 MeV, fragment energies, cross sections level density and barrier heights 80−42723
Ag(p,f), product event cross-sections at 14, 18, 23 GeV 77−10411
^{A}Am(γ,δ) 7-26 MeV, A=241,243, photofission cross section in E1 giant resonance region *(Russian)* 80−5182
^{A}Am(n,f), thermal, sub-barrier fission fragment energy correlations for A=241, 243 80−42715
^{241}Am(n,f), 14.8 MeV, mass yield distrib., and absolute fission yield, isomer ratios 80−18352
^{243}Am(^{40}Ar,f), product mass distribs., shell effect manifestation 79−93673
Ar+Au, 285 MeV, ang. distrib. of fission and deep inelastic products 77−82964
^{40}Ar, fission by 1 GeV protons, ang. distrib. of products *(Russian)* 77−46200
^{40}Ar+^{243}Am, 214-300 MeV, fusion-fission reaction, asymm. mass distrib. 77−82963
^{41}Ar dose distributions due to atm. release from HWR, including wind effects 77−14271
^{205}At mass distribution width for fission and quasifission from Re+^{20}Ne and ^{165}Mo+^{40}Av 79−63707
^{147}Au(^{40}Ar, f), 340 MeV, H and He emission, rapid energy equilib., to ang. distribs. 80−86936
^{197}Au(^{22}Ne, f), 178 MeV, α-particles and fission fragments, spectra and cross sections *(Russian)* 80−91203
^{197}Au(HI,X), 60-120 MeV complete fusion cross sections from fission fragment ang. distrib. 80−13516
^{197}Au(d,f), 80 MeV, post neutron emission fission products 80−83136
^{197}Au(p,f), 1 GeV, fission fragment ang. correlation, kinematically different events search *(Russian)* 79−59103
Ba, A=144, 145, short lived fission product, Q_{β}-value 78−37317
Ba fragments, differential ranges and ang. distribs. from ^{238}U(p,X) 79−67790
Ba isotopes, uptake and retention of ^{133}Ba and ^{140}Ba-^{140}La in mouse tissues, eye and skeleton doses 77−9276
^{A}Ba, A=134 to 138, 135, sensibility anal. of effect of key parameters of fission prod. conc. 79−30870
^{139}Ba, fractional independent yield and γ-activity from ^{249}Cf(n,f) 79−89337
^{140}Ba, fission product, γ-ray emission probability 77−82862
^{140}Ba, fractional cumulative yield from ^{245}Cm(n,f) 80−63074
^{140}Ba, production by ^{239}Pu fission, absolute yields 77−50167
^{141}Ba, gaseous fission products, β-decay energies 79−9519
^{145}Ba, fission product, β-decay anal. 78−78323
^{201}Bi $(\alpha$,f), 23-140 MeV, l_{crit} from fragment ang. distribs. anal. 80−106087
^{209}Bi+^{12}C reaction, fission product charge distrib., 40 to 66 MeV 77−79406
^{209}Bi+p, nucleon losses on high-energy fission *(Russian)* 78−46120
^{209}Bi(^{12}C,f), mass distrib. of fission fragments determ. *(Chinese)* 78−86558
^{209}Bi(HI,X), 60-120 MeV complete fusion cross sections from fission fragment ang. distrib. 80−13516
Br, isomer ratios in fission fragments at high excitation 80−32261
Br series isotopes, sensitivities to various parameters, analytical evaluation 78−82424
^{A}Br A=84-88, fission products, rapid electrophoretic separation technique 79−54982
^{A}Br, A=85 to 89, total β-decay energies and atomic masses of neutron-rich isotopes 79−40889
Cd stable isotopes, yields in ^{235}U(n_{th},f) and ^{239}Pu(n_{th},f) in symm. region 77−34358
Ce, A=145, 147, 148, short lived fission product, Q_{β}-value 78−37317
^{144}Ce, errors in activity ratio determ. in reactor RA used fuel element 79−41061
^{144}Ce/Pr, CANDU fuel, burnup determ. by γ-scanning 79−9825
^{145}Ce, fission product, β-decay anal. 78−78323
^{A}Cf, A=250, 252, 254, spontaneous fission fragment kinetic energy and neutron multiplicity meas. 80−42717
^{250}Cf, spontaneous fission, mass distrib., radiochem. and γ-ray spectrometric meas. 77−67775
^{252}Cf, empirical limitations for spontaneous fission energy dissipation, fragment deformation 79−3188
^{252}Cf fission, neutron deficient fragments, search for positron activity *(Russian)* 80−63218
^{252}Cf fission, search for abnormal energy release reln. to superdense nuclei *(Russian)* 79−89340
^{252}Cf fission fragment hard β-radiation 79−45306
^{252}Cf fission fragment implantation for wear meas. 79−87765
^{252}Cf fission fragment tracks in quartz glass, electron microscope obs. 78−17526
^{252}Cf fission fragment track soda lime glass, etchant conditions effect 80−52815
^{252}Cf fission products, g-factors of isomeric states 77−22890
^{252}Cf fission products, masses, β decay energies, halflives, He Jet TOF mass spectrometer meas. 77−23355
^{252}Cf fission source, ionisation characts. of electron oscillating ion source coupled to He-jet skimmer system 78−70661
^{252}Cf, positron activity of fission fragments *(Russian)* 77−6474
^{252}Cf spontaneous fission, element yields from X-ray multiplicities meas. 77−26812
^{252}Cf spontaneous fission, element yields from meas. X-ray multiplicities 77−50179
^{252}Cf, spontaneous fission, fragment ranges and kinetic energies in Al 78−94037
^{252}Cf, spontaneous fission, fragment slowing in gases 80−22875
^{252}Cf spontaneous fission, fission product β spectra *(Russian)* 80−91204
^{252}Cf spontaneous fission, prompt neutrons and fission fragments *(Russian)* 79−40976
^{252}Cf spontaneous fission, prompt γ-ray differential angular distrib. 80−102220
^{252}Cf spontaneous fission fragments, neutron emission fine struct. 77−26794
^{252}Cf, spontaneous fission fragment energy meas. using phosphate glasses 77−67932
^{252}Cf spontaneous fission neutron spectrum meas. 79−9653
^{254}Cf spontaneous fission, neutron-rich fragments, even-even products 80−78342

fission products continued
^{256}Cf, spontaneous fission, fission barriers and products 80−18355
^{245}Cm(n,f), thermal neutron fission, kinetic energy distribs. determ. 78−658
^{248}Cm, spontaneous fission, mass distrib., radiochem. and γ-spectrometric meas. 77−67775
Cs, A=134, 137, distrib. in Peach Bottom HTGR primary coolant circuit 78−13275
Cs desorption from graphite, release in nucl. reactor coolant 80−18431
Cs, fission fragment, delayed neutron branches from γ-spectroscopy 80−78230
Cs, ground state spins, moments, charge radii by laser spectroscopy 80−78147
Cs isotopic distrib. anal., for ^{11}B and ^{22}Ne-induced fission of ^{238}U 77−18634
Cs isotopic distrib. meas. for ^{11}B and ^{22}Ne-induced fission of ^{238}U 77−18633
Cs, isotopic yield in ^{249}Cf(n,f) 78−41789
Cs migration effects on fuel-cladding mech. interaction in $(U,Pu)O_2$ fuel pins 80−102250
Cs relative and independ. fission yields from ^{235}U(n,f) 80−27679
Cs, release and distribution in coated particles *(German)* 78−25298
Cs release and transport in coated HTGR fuel particles 77−74935
Cs release in Biso-coated HTR fuel particles 77−79441
Cs, sorption and fixation props. of shale, radioactive waste repository implications 80−32354
Cs-O system, phase diagram and O_2 potential 80−3011
^{A}Cs, A=133 to 137, sensibility anal. of effect of key parameters of fission prod. conc. 79−30870
^{A}Cs, A=139-144, beta endpoint energy measurements 78−93975
^{A}Cs, A=147, 148, $T_{1/2}$ determ. 79−9524
^{134}Cs, in low-enriched $(Pu,U)O_2$ fuel assemblies, profiles of activity ratios 77−57713
^{134}Cs/^{137}Cs activity ratio for LWR fuel burn-up determ. *(Russian)* 80−68804
^{135}Cs, error in activity ratio determ. in reactor RA used fuel element 79−41061
^{136}Cs, fractional independent yield form ^{238}U photofussion with bremsstrahlung 79−36283
^{137}Cs concentration determ. in LMFBR Na heat carrier 79−41043
^{137}Cs, distrib. in fuel elements of Peach Bottom HTGR 78−13274
^{137}Cs, errors in activity ratio determ. in reactor RA used fuel element 79−41061
^{137}Cs, fast neutron influence on fission product transport in UO_2 pyrocarbon-coated HTR fuel particles 80−42777
^{137}Cs, ground waste disposal, sorption and migration studies 79−54523
^{137}Cs in coated particle fuel conc. determ. using YAG:Nd^{3+} laser 80−18416
^{137}Cs, in low-enriched $(Pu,U)O_2$ fuel assemblies, profiles of activity ratios 77−57713
^{137}Cs, separation from nucl. waste using sodium zirconate 80−27760
^{137}Cs to ^{131}I fractional release ratio from breached fission fuel elements 78−21713
^{138}Cs, independent isomeric yield ratio from spontaneous fission of ^{252}Cf 79−22342
^{164}Dy+n, capture cross section meas. in Triton reactor *(French)* 80−18308
^{162}Er compound nucleus fission at high ang. momentum, fragments from ^{30}Si(^{132}Xe,f) 80−99196
^{153}Eu+n, capture cross section meas. in Triton reactor *(French)* 80−18308
^{A}Fm, A=258, 259, spontaneous fission, fission barriers and products 80−18355
^{A}Fm(n,f), A=253, 255, 257, 259, fission mass distrib. transition, liquid drop and shell model calcs. 80−32310
^{A}Fm(sf), A=254, 256, 258, 260, fission mass distrib. transition, liquid drop and shell model calcs. 80−32310
^{254}Fm spontaneous fission, distrib. of mass, KE and neutron yield 78−17257
^{257}Fm, spontaneous fission fragment kinetic energy and neutron multiplicity meas. 80−42717
^{258}Fm, nuclear pressure and fission fragment mass distrib. 80−18356
Ga isotopes, independ. yield in ^{238}U(p,F) 78−13171
^{158}Gd+n, capture cross section meas. in Triton reactor *(French)* 80−18308
He release from UO_2-Zr high burnup nuclear fuel rods 80−57846
^{3}He-Xe, nucl. pumped laser plasma, distrib. functions 79−36880
I, isotopic yield in ^{249}Cf(n,f) 78−41789
I, radioactive, air sampling system, separation into gaseous and particulate fractions 80−57962
I, sorption and diffusion in concrete and containment uptake 79−67898
^{A}I, A=127, 129, 130, 131, sensibility anal. of the effect of key parameters on fission prod. conc. 79−36290
^{A}I, A=133, 135, sensibility anal. of effect of key parameters of fission prod. conc. 79−30870
^{127}I$(n,\gamma)^{128}$I in fast reactors, effective cross sections calc., from expt. results *(Dutch)* 79−537
^{131}I, behaviour during rinsing in in-pile loop after fission product release expt. 80−73879
^{131}I, probability distrib. for release in PWR steam generator tube rupture 80−13668
^{131}I release from sintered ThO_2 pellets 78−21650
^{131}I, separation from water by ion exchange *(Japanese)* 77−60099
^{131}I spiking phenomenon in accidents involving coolant leakage, expt. *(Japanese)* 77−54320
^{134}I fractional independ. yield from ^{238}U$(\gamma$,f) 80−57814
^{134}I yield from ^{237}Np(n,f) 80−86935
^{135}I, fractional cumulative yields in ^{252}Cf SF 78−41791
^{135}I, fractional cumulative yield from ^{245}Cm(n,f) 80−63074
^{136}I, isomeric ratio, γ-spectra thermal neutron and 3 MeV fission of ^{235}U *(French)* 80−68709
^{132m}I, ^{134m}I, isomer yield ratios in ^{235}U(n,f) 77−38306
In isotopes, independ. yield in ^{238}U(p,f) 78−13171
Kr, A=90, 91, ^{232}Th fission products, yields, γ-ray spectra 78−74410
Kr, anomalous isotope composition at Oklo natural reactor site 77−56630
Kr, cryogenic distillation from gaseous effluents in fuel reprocessing 80−5309
Kr, fission gas atoms, diffusion into UO_2 79−6746
Kr, from ^{248}Cm and ^{250}Cf in meteorites 80−63215
Kr, gaseous, continuous determ. of content in reactor loop 79−30905

fission products continued

Kr, release from spherical fuel elements in HTGR 77−74940

Kr release from UO_2-Zr high burnup nuclear fuel rods 80−57846

Kr series isotopes, sensitivities to various parameters, analytical evaluation 78−82424

Kr yield from ^{238}U and ^{232}Th emanation method *(French)* 77−30640

^{84}Kr+n, capture cross section meas. in Triton reactor *(French)* 80−18308

^{85}Kr conc. determ. at high pressures using β-ray count, CaF_2 scintillation counter activated with Eu 78−13385

^{85}Kr, gaseous, absolute counting, calibration of well-type NaI(Tl)-detector 78−9036

^{85}Kr waste management, strategy anal. 80−37531

^{85}Kr/Xe separation from nucl. engineering off-gases, low temp. distillation *(German, English)* 77−18671

La, A=144, 145, 147, short lived fission product, Q_β-value 78−37317

^{139}La(p,f), 600 MeV, fragment energies, cross sections level density and barrier heights 80−42723

^{140}La, fission product, γ-ray emission probability 77−82862

^{142}La, fractional independent yield and γ-activity from ^{249}Cf(n,f) 79−89337

^{145}La, fission product, β-decay anal. 78−78323

Mo, A=103-5, half-lives and γ-ray energies of short-lived isotopes following ^{235}U fission 78−17137

^{99}Mo, absolute yields in ^{238}U neutron induced fission 79−49642

^{99}Mo effective activation cross section from (n,γ) reaction *(Japanese)* 79−97702

^{99}Mo, production by ^{239}Pu fission, absolute yields 77−50167

^{99}Mo separation from neutron irradiated ^{235}U, HNO_3 soln., S collector 77−42161

^{102}Mo fission product decay, ^{102}Tc decay scheme and γ-intensities 80−78229

Nb isotopes, A=95, 97, 99, beta-decay schemes, level struct. 77−26631

Nb, isotopic yield in ^{249}Cf(n,f) 78−41789

Nd isotopes, determ. in nuclear fuels as burnup indicator, separation, mass spectrometric method 77−44553

^{A}Nd+n, A=143,145, capture cross section meas. in Triton reactor *(French)* 80−18308

^{147}Nd, production by ^{239}Pu fission, absolute yields 77−50167

^{252}No spontaneous fission, fragment mass and kinetic energy distribs. 77−46194

^{237}Np muonic, prompt fission, fragment atomic muon capture 80−95312

^{237}Np(nth, f), sub-barrier fission, fragment energy correl. meas. 78−21614

O ion induced fission of nuclei from Ag to U, fragment ang. distribs. *(Russian)* 78−17264

^{231}Pa(n,f) sub-barrier fission, fragment mass and kinetic energy distribs. 79−17942

Pb+U, 750 MeV, classical model, kinetic energy, ang. distribs., instantaneous fission fragments 78−13185

^{208}Pb+^{48}Ca mass distribs. of fission fragments meas. 77−71621

^{208}Pb(^{136}Xe,X)Y, 470 MeV, search for delayed fission products from superheavy nuclei 78−70562

^{208}Pb(^{48}Ca,γ), nuclear pressure and fission fragment mass distrib. 80−18356

Pd, corrosion of SiC coating of HTGR coated particle fuels 80−102237

Pd isotope cumulative yields, from fission of U and Pu 79−576

^{107}Pd fission product neutron capture and total cross-section obs. 79−9573

^{107}Pd(n,γ) and transmission meas., level parameters 78−58277

^{148}Pm, isomeric yield ratio in fission of ^{236}U compound nucleus 77−82975

^{150}Pm, fractional independent yield from ^{238}U photofission with bremsstrahlung 79−36283

^{141}Pr, neutron capture cross section and transmission TOF meas. 79−67752

^{148}Pr, short lived fission product, Q_β-value 78−37317

Pt alloy, fission-fragment-induced He blistering 78−86601

Pu (n,F) thermal, rare gas yields, odd-even effect *(French)* 77−50172

Pu, fission fragments, thermal reactor, fragment capture cross section 78−17296

Pu^{239}, product separation asymmetry in fission by slow polarised neutrons *(Russian)* 80−106088

^{A}Pu, A=239,242, muonic, prompt fission, fragment atomic muon capture 80−95312

^{236}Pu, 40 ps fission isomer quadrupole moment 77−50053

^{239}Pu, e and $\bar{\nu}$ energy spectra from fission fragments *(Russian)* 77−23120

^{239}Pu, fast fission, product decay-heat calc. 77−61464

^{239}Pu, fission product beta decay, $\bar{\nu}$ spectra 80−102150

^{239}Pu, irradiated in BOR-60 reactor, fission yields 79−17971

^{239}Pu thermal fission, prompt neutrons and fission fragments *(Russian)* 79−40976

^{239}Pu(n,f), 0.005-0.4 eV, fission fragment average kinetic energies in resonance region 80−18358

^{239}Pu(n,f), 0.1-1 Mev, light charged particle emission, saddle point states 79−22343

^{239}Pu(n,f), 0.3 eV resonance energy, mass distrib. of products 78−70578

^{239}Pu(n,f), thermal n, fission fragment energy correlation meas., fine struct. and deformation 79−13355

^{239}Pu(n,γ), thermal, fission product $\bar{\nu}_e$ spectrum, β-decay characts. 80−78340

^{239}Pu(n_{th},f), fission product mass distribs. 77−74896

^{240}Pu(n,f), 14.8 MeV, products from ^{66}Ni to ^{169}Er, mass distrib., total chain yields 78−25255

^{241}Pu(n, f) thermal-neutron fission, determ. of cumulative fission yields 79−54462

^{241}Pu(n,f), thermal neutron fission, kinetic energy distribs. determ. 78−658

^{226}Ra, neutron fission fragment energy meas. using phosphate glasses 77−67932

Rb, fission fragment, delayed neutron branches from γ-spectroscopy 80−78230

Rb, fission products, precise Q_β values *(German)* 80−37354

Rb, ground state spins, moments, charge radii by laser spectroscopy 80−78147

Rb isotopic distrib. anal., for ^{11}B and ^{22}Ne-induced fission of ^{238}U 77−18634

Rb isotopic distrib. meas. for ^{11}B and ^{22}Ne-induced fission of ^{238}U 77−18633

Rb relative and independ. fission yields from ^{235}U(n,f) 80−27679

fission products continued

^{A}Rb, A=88-94, beta endpoint energy measurements 78−93975

^{A}Rb, A=96 to 100, half-lives and neutron emission probabilities in neutron rich isotopes 79−17864

^{90}Rb, independent isomeric yield ratio from spontaneous fission of ^{252}Cf 79−22342

Rh, A=108-111, prod. by fission of ^{235}U, ^{238}U, ^{239}Pu, ^{249}Cf, separation, identification 78−89924

^{103}Rh(n,γ), cross-sections above 2.6 keV 80−32276

Ru, fission product, isotope anal., U and Pu fission investig. *(German)* 77−63996

Ru isotope cumulative yields, from fission of U and Pu 79−576

Ru isotopes, A=107-113, prod. by fission of ^{235}U, ^{238}U, ^{239}Pu, ^{249}Cf, separation, identification 78−89924

Ru isotopic axial distributions in EBR II (U, Pu)O_2 failed fuel pins, γ-scanning determ. 78−687

^{A}Ru(n,γ), A=100-104, cross-sections above 2.6 keV 80−32276

^{106}Ru, errors in activity ratio determ. in reactor RA used fuel element 79−41061

^{106}Ru, in low-enriched (Pu,U)O_2 fuel assemblies profiles of activity ratios 77−57713

Sb, A=127-33, fission fragments, partial level schemes determ. 78−29392

Sb, A=131, 133 prod. by ^{232}Th reactor induced fission, yield, radiochem. separation, anal. 78−89923

Sb, isomer ratios in fission fragments at high excitation 80−32261

Sb isotopes, fission product conc., sensitivity anal. of various key parameter effects 78−82428

Sb, neutron rich isotopes, half-lives, fission yields, and neutron emission probabilities 77−67721

^{127}Sb, sensibility anal. of the effect of key parameters on fission prod. conc. 79−36290

Sc, ang. distrib. in thick targets following ^{238}U(p,t) 77−6472

Se series isotopes, sensitivities to various parameters, analytical evaluation 78−82424

Si surface barrier detector, pulse height defect of fission products 77−18741

Si surface barrier detector, fission fragment pulse height defect 79−76292

SiC-fission product reactions in HGTR TRISO UC_2 and UC_xO_y fuel under isothermal conditions 80−42744

SiC-fission product reaction kinetics in HTGR TRISO UC_2 and UC_xO_y fuel in thermal gradient 80−47570

^{90}Si transmutation in fusion reactors 79−26559

Sm decay chain expansion significance 79−9712

^{147}Sm+n, capture cross section meas. in Triton reactor *(French)* 80−18308

^{149}Sm poisoning calc., of KS-150 reactor, using spatial models *(Slovak)* 78−54850

^{153}Sm, production by ^{239}Pu fission, absolute yields 77−50167

Sn, A=131, 132 prod. by ^{232}Th reactor induced fission, yield, radiochem. separation, anal. 78−89923

Sn isotopes, fission product conc., sensitivity anal. of various key parameter effects 78−82428

Sn stable isotopes, yields in ^{235}U(n_{th},f) and ^{239}Pu(n_{th},f) in symm. region 77−34358

^{132}Sn levels, isomers, lifetimes and transition probabilities from fission 80−78163

Sr, fission products, precise Q_β values *(German)* 80−37354

Sr isotopes, A=95, 97, 99, beta-decay schemes, level struct. 77−26631

^{89}Sr and ^{90}Sr, radiochem. determ., error anal. comparison of methods 77−16873

^{89}Sr, soil analysis using total sample decomp. 80−35808

^{90}Sr, diffusion coeffs. determ. in HTGR fuel element graphite 79−67869

^{90}Sr, fast neutron influence on fission product transport in UO_2 pyrocarbon-coated HTR fuel particles 80−42777

^{90}Sr, ground waste disposal, sorption and migration studies 79−54523

^{90}Sr, release from irrad. reactor fuel elements *(German)* 79−67871

^{90}Sr, soil analysis using total sample decomp. 80−35808

^{159}Tb(p,f), 600 MeV, fragment energies, cross sections level density and barrier heights 80−42723

Tc decay, ^{104,106,108}Ru level scheme and transitions, collective model anal. 80−78166

^{99}Tc accumulation by plants 77−56489

^{99}Tc, neutron capture cross section meas. up to 80 keV 78−25197

^{99}Tc, reduction and sorption in granitic bedrock, biological hazard estimation 79−79415

^{99}Tc+n, capture cross section meas. in Triton reactor *(French)* 80−18308

Te isotopes, fission product conc., sensitivity anal. of various key parameter effects 78−82428

^{A}Te, A=127m, 128, 129m, 130, 131m, 132, sensibility anal. of the effect of key parameters on fission prod. conc. 79−36290

^{134}Te, fractional cumulative yields in ^{252}Cf SF 78−41791

Th, K$^-$ meson induced fission at 700 MeV/c, fragment mass distrib. 78−13168

^{230}Th(n,f), 0.68-1.10 MeV, fission fragment ang. distribs., resonance and moment of inertia 80−102219

^{230}Th(n,γ), 680-1050 keV, fission barriers and cross sections, fragment ang. distribs. 80−18357

^{232}Th (e, f), 7-65 MeV, absolute electrofission cross sections, fragment ang. distribs. 80−5185

^{232}Th (γ, f), deep subbarrier photofission ang. anisotropy from fragment ang. distrib. *(Russian)* 79−97739

^{232}Th(γ,f), 9, 15, 38 MeV peak bremsstrahlung 78−33229

^{232}Th(γ,f), fission-neutron and fragment ang. distrib. 77−65239

^{232}Th(n,f), 14.8 MeV, peak to valley ratio of mass distribs. 77−26801

^{232}Th(n,f), 1.38 MeV, prediction of fission-product mass yields and related parameters 79−30862

^{232}Th(n,f), 1.55-3 MeV, mass asymm., ang. anisotropy of fragments *(Russian)* 78−17265

^{232}Th(n,f), 2-8 MeV, fission product yields and mass distribs. 80−86939

^{232}Th(n,f), fast neutrons, fission product mass distribs. 77−74896

^{232}Th(n,f), prompt-neutron ang. distrib. 77−65238

^{232}Th(n,f), yield meas. of Kr, Xe, Sn, Sb, proton odd-even and neutron shell effect 77−82976

^{232}Th(n,f) cross section up to 6 MeV, fragment ang. anisotropy 77−23161

^{232}Th(p,f), 29-97 MeV, Rb, In and Cs relative independ. yields, charge division 80−102218

fission products continued
^{233}Th(n,f), 1.2-2.3 MeV, transition state effect on fragment KE *(Russian)* 78—661
(U, Pu) C, nuclear fuel, irradiation induced creep meas. 80—93605
(U,Pu)C FBR fuel pins, fission gas release 80—57847
(U,Pu)O$_2$ 80—63252
(U,Pu)O$_2$, fission gas release and retention in irrad. nuclear fuels 80—57841
^{235,238}U(n,f), fast neutrons, fission product mass distribs. fission product mass distribs. 77—74896
U anal. of natural waters by fission tracks 78—82587
U analysis, in geological samples, delayed neutrons method *(Rumanian)* 79—88507
U, assay of natural samples, meas. of gamma- or neutron activity of short-lived fission products 80—61179
U assay using continuous fast-neutron source 79—52849
U, K$^-$ meson induced fission at 700 MeV/c, fragment mass distrib. 78—13168
U^{233}, product separation asymmetry in fission by slow polarised neutrons *(Russian)* 80—106088
U-Ni dilute alloy fission product source design and use at EBR-II 79—9932
UC, nuclear fuels, irrad. induced kinetics, diffusion and fission gas resoln. 80—59523
UO$_2$ 80—63252
UO$_2$, cumulative diffusional release of fission product gases from an equivalent sphere, generalised anal. 80—47569
UO$_2$ equiaxed grain growth modelling 80—13589
UO$_2$, equilib. conc. of fission products, ^{235}U induced fission and ^{238}U spontaneous fission *(Spanish)* 78—44823
UO$_2$, equilib. conc. of fission products, calc. comparison with expt. values *(Spanish)* 78—44824
UO$_2$, fission gas release and retention in irrad. nuclear fuels 80—57841
UO$_2$ fuels, in-pile meas. of fission gas release 79—93697
UO$_2$, gases from fuel at high temp. in organic cooled reactor 78—25292
UO$_2$, high burnup nuclear fuels, relation between fission product release and fuel microstruct. 80—57845
UO$_2$ irradiated fuel, unstable fission product release 80—617
UO$_2$ irradiation, fission product cold trapping in stainless steel Na loop 77—61514
UO$_2$, microstruct. depend. model for fission product gas release and swelling 80—42757
UO$_2$ nuclear fuels, distribution and size of intragranular fission gas bubbles 80—57840
UO$_2$ nuclear fuels, fission gas release at high burn-ups 80—57852
UO$_2$ nuclear fuels, irrad. induced kinetics, diffusion and fission gas resoln. 80—59523
UO$_2$ volatization pot. of metallic inclusions in irrad. nuclear fuel during LOF overheating transients 80—57895
UO$_2$:Cr$_2$O$_3$, fission gas release and swelling 80—47567
UO$_{2\pm x}$, model of response of fission gas bubbles to dynamic behaviour of point defects 79—37735
^{A}U, A=235,238, fission product beta decay, $\bar{\nu}$ spectra 80—102150
^{A}U^m, A=236,238, isomeric to prompt fission ratios; fission fragments from (d,pf), (d,pnf) 80—86940
^{A}U(γ, f), A=236, 238, deep subbarrier photofission ang. anisotropy from fragment ang. distrib. *(Russian)* 79—97739
^{A}U(n,f), A=233,235, ejection fission products angular depend. on thermally polarised neutron capture *(Russian)* 80—86941
^{A}U(n,f) A=232 to 236, 238, prediction of fission-product mass yields and related parameters 79—30862
^{232}U(n,f), fission product mass distrib. 79—67789
^{232}U(n,f), reactor neutron fission, kinetic energy distribs. determ. 78—658
^{233}U neutron-induced reaction, data eval. including $\bar{\nu}_p$ and fission spectrum 79—67795
^{233}U(d,pf), fission fragment energy-velocity correlation meas. 79—45309
^{233}U(n,f), ^{148m}Pm, ^{148g}Pm and ^{146}Pm independ. yields 77—79407
^{234}U under barrier photofission, 4-5.7 MeV, fragment ang. distribs. *(Russian)* 80—106090
^{235}U (n,f), fission by fast neutrons, fragment K X-ray spectra, $\bar{\nu}$ energy depend. in heat balance method 78—17260
^{235}U decay heat meas. and calcs., review 80—13732
^{235}U, e and $\bar{\nu}$ energy spectra from fission fragments *(Russian)* 77—23120
^{235}U fission fragment angle meas. with gridded ionisation chamber 79—85865
^{235}U fission fragment thermonuclear superheavy nuclei synthesis, prod. cross sections 80—95331
^{235}U fission fragments, internal conversion cascading 78—94036
^{235}U, fission fragments, thermal reactor, fragment capture cross section 78—17296
^{235}U fission fragments and fission neutrons, reliability of use in simulating neutron irradiation 79—42113
^{235}U fission product γ radiation for short irrad. times, energy distrib. 80—73929
^{235}U, fission product mass distrib. from 25 MeV bremsstrahlung irradiation 78—13175
^{235}U, fission recoils, chem. effects, energy deposition efficiencies, surface conditions depend. 78—80776
^{235}U, irradiated in BOR-60 reactor, fission yields 79—17971
^{235}U, neutron fission fragment energy meas., using phosphate glasses 77—67932
^{235}U products, β-spectra and total β-energy 78—25158
^{235}U, thermal fission, product decay-heat calc. 77—61464
^{235}U thermal fission product long-term activity meas. and calc. 79—9644
^{235}U, thermal n induced ternary fission, α energy and ang. distribs. 79—22345
^{235}U, thermal neutron irrad., fission product decay power calc. 80—22868
^{235}U(N,f), theoretical β-spectra from fragmentation in secular equilib. 80—500
^{235}U(γ, f), 12-70 MeV bremsstrahlung, product yields and γ-spectra 80—42716
^{235}U(n,f), ^{148m}Pm, ^{148g}Pm and ^{146}Pm independ. yields 77—79407
^{235}U(n,f), 0.3-1.4 MeV, energy depend of fission fragment anisotropy 79—80962
^{235}U(n,f), 550 keV, correlated fragments, 4-param. (E,v) meas. 77—26802
^{235}U(n,f), 6-9 MeV, fission product yields 78—66324

fission products continued
^{235}U(n,f), fission fragment average kinetic energies in resonance region 80—18358
^{235}U(n,f), light particle yields and spectra 77—50173
^{235}U(n,f), symmetric fission, proton scatt. by fission fragments in neck area 80—83130
^{235}U(n,f), thermal, charge and mass yields of light fission products 77—23122
^{235}U(n,f), thermal, charge distrib. of fission products 77—23123
^{235}U(n,f), thermal, fission product decay spectra calcs., comparison with expt. results 79—93674
^{235}U(n,f), thermal, fragment ionisation, charge distribs., stat. and instant perturbation theory *(Russian)* 80—63219
^{235}U(n,f), thermal fission, fission product decay heat evaluation by least-squares method 79—30865
^{235}U(n,f), thermal n, fission product isobaric charge distrib., parity effects 79—17791
^{235}U(n,f), thermal n, fission fragment energy correlation meas., fine struct. and deformation 79—13355
^{235}U(n,f), thermal neutron induced fission, nuclear charge distribution in fission products 80—57808
^{235}U(n,f) 3.5 MeV fragment X-rays 77—18638
^{235}U(n,f) sub-barrier fission, fragment mass and kinetic energy distribs. 79—17942
^{235}U(n,γ), thermal, d, t, He emission probabilities from stable core model *(Russian)* 80—68713
^{235}U(n,γ), thermal, fission product $\bar{\nu}_e$ spectrum, β-decay characts. 80—78340
^{235}U(n$_{th}$,f), charge distrib. of products in mass chains 79 to 100 77—10456
^{235}U(n$_{th}$,f), fission fragment yield distribs., excitation energy depend. 78—50218
^{235}U(n$_{th}$,f), fragment-mass depend. of fission neutron spectrum, TOF method 78—82398
^{235}U(n$_{th}$,f) ionic charge distrib., effect of internal conversion 78—78428
^{235}U(n$_{th}$,f) nuclide yields, direct physical meas. 79—9641
^{235}U(nth, f), above-the-barrier fission, fragment energy correl. meas. 78—21614
^{236}U fission, two parameter study, fragment mass and energy, thin film scintillators 79—13357
^{236}U fission fragment kinetic energies, wall and window one body dissipation model 80—52703
^{236}U, nuclear pressure and fission fragment mass distrib. 80—18356
^{236}U* fission fragment charge distrib. in statistical model *(Russian)* 79—59102
^{236}U(n,f), fast n, fragment mass and kinetic energy distribs. *(Russian)* 80—5181
^{238}U (e, f), 7-65 MeV, absolute electrofission cross sections, fragment ang. distribs. 80—5185
^{238}U, (p,f), 1 GeV, fission fragment ang. correlation, kinematically different events search *(Russian)* 79—59103
^{238}U, fast fission, product decay-heat calc. 77—61464
^{238}U fast-neutron fission, calculated fission product yields 79—67796
^{238}U, fission product mass. distrib. from 25 MeV bremsstrahlung irradiation 78—13175
^{238}U+^{238}U, 1785 MeV, cross sections, charge and mass distribs. of products 78—78408
^{238}U+p, nucleon losses on high-energy fission *(Russian)* 78—46120
^{238}U(^{12}C,f), mass distrib. of fission fragments determ. *(Chinese)* 78—86558
^{238}U(^{16}O,f) 20 MeV/N, light particle spectra in central and peripheral collisions 80—5177
^{238}U(^{48}Ca,γ), nuclear pressure and fission fragment mass distrib. 80—18356
^{238}U(^{86}Kr,X), 730 MeV, transferred ang. momentum for fission and projectile like fragments 79—93675
^{238}U(e,e'f), 5.5-9 MeV, fission fragment ang. distribs. DWBA anal., low lying fissioning levels 80—42713
^{238}U(γ,f), 12-70 MeV bremsstrahlung, cumulative and fractional product yields for A=128-136 79—36288
^{238}U(γ,f), 12-70 MeV bremsstrahlung, fragment mass and energy distribs. 80—27680
^{238}U(γ,f), 20 MeV, fission product yields, charge distrib. 80—42533
^{238}U(γ,f) 20 MeV, computer program for yield determ. of short-lived products 80—102215
^{238}U(γ,f) fission-neutron and fragment ang. distrib. 77—65239
^{238}U(n,f), 14.5 MeV, neutron emission, mass distrib. and energetics 80—47512
^{238}U(n,f), 1.52 MeV, mass yield distrib. meas. 77—67777
^{238}U(n,f), 1.8-16.8 MeV, fission fragment energy spectra using glass sandwich detectors 78—82399
^{238}U(n,f), 6-9 MeV, fission product yields 78—66324
^{238}U(n,f), prompt-neutron ang. distrib. 77—65238
^{238}U(n,f) cross section up to 6 MeV, fragment ang. anisotropy 77—23161
^{238}U(p,f), 11-29 GeV, three dimens. charge dispersion curves, isobaric yields 80—102111
^{238}U(p,f), 11.5 GeV, He and heavy fragment energy and ang. correlation 79—45310
U(γ,f), 5.2-6.4 MeV, A=234, 236, 238, doubly even isotopes, ang. distribs., fragment yields 78—50219
U(p,f), 600 MeV, fragment energies, cross sections level density and barrier heights 80—42723
XE bonded fission gas, radial distrib. in mixed carbide fuel pins, electron probe anal. 79—36318
Xe, A=131-135, fine structure of yields for heavy nuclei fission 78—86560
Xe, A=139, 140, ^{232}Th fission products, yields, γ-ray spectra 78—74410
Xe, anomalous isotope composition at Oklo natural reactor site 77—56630
Xe, cryogenic distillation from gaseous effluents in fuel reprocessing 80—5309
Xe fission gas release and microscopic swelling in LMFBR highly-rated MX-type fuels 80—57848
Xe, from ^{248}Cm and ^{250}Cf in meteorites 80—63215
Xe, from ^{248}Cm spontaneous fission, rel. to origin of carbonaceous chondrite fission Xe 77—37581
Xe, gaseous, continuous determ. of content in reactor loop 79—30905
Xe, HTGR, pebble-bed, computational procedure for xenon stability 77—61501

fission products continued
- Xe ions measurement, Si surface-barrier detectors for fission fragments 78–78571
- Xe oscillations, program for optimal control in 1-D slab reactor *(German)* 77–61529
- Xe poison in nuclear reactor, optimal control *(Korean)* 77–54323
- Xe, radial distribution of bonded fission gas in mixed carbide fuel pins 80–57844
- Xe release from $(U,Pu)C_{1-x}N_x$ LMFBR MX-type fuels 80–73921
- Xe release from spherical fuel elements in HTGR 77–74940
- Xe release from UO_2-Zr high burnup nuclear fuel rods 80–57846
- Xe yield from ^{238}U and ^{232}Th emanation method *(French)* 77–30640
- ^{A}Xe, A=128 to 132, 129m, 131m, 133m, sensibility anal. of the effect of key parameters on fission prod. conc. 79–36290
- ^{A}Xe, A=133 to 136, sensibility anal. of effect of key parameters of fission prod. conc. 79–30870
- ^{132}Xe+n, capture cross section meas. in Triton reactor *(French)* 80–18308
- ^{133}Xe, gaseous, absolute counting, calibration of well-type NaI(Tl)-detector 78–9036
- ^{133}Xe, probability distrib. for release in PWR steam generator tube rupture 80–13668
- ^{135}Xe, control of space-time distrib. in reactors 79–36364
- ^{135}Xe, determ. of fission gas degassing constant from liquid Na to cover gas 79–41009
- ^{135}Xe, direct meas. of absolute and fractional independ. yields from ^{238}U(γ,f) 80–78341
- ^{135}Xe isotopes, production by ^{135}I decay in liq. Na in fission reactor, degassing behaviour 77–34410
- ^{135}Xe poisoning calc., of KS-150 reactor, using spatial models *(Slovak)* 78–54850
- ^{135}Xe yield from ^{237}Np(n,f) 80–86935
- ^{135}Xe-induced core instabilities, extended λ-mode linear anal., CANDU appl. 78–82494
- Y, fission products, precise Q_β values *(German)* 80–37354
- Y isotopes, A=95, 97, 99, beta-decay schemes, level struct. 77–26631
- ^{96}Y from ^{235}U fission, spectroscopic meas. *(German)* 77–67726
- ^{98}Y from ^{235}U fission, spectroscopic meas. *(German)* 77–67726
- Zr isotopes, A=95, 97, 99, beta-decay schemes, level struct. 77–26631
- ZrC CVD coated fuel particles, diffusion of ^{137}Cs, ^{90}Sr and ^{144}Ce 80–13582

fission reactor cooling and heat recovery
- *see also cooling; fission reactor core control and monitoring*
- 7-pin bundle simulation during flow rundown transient 80–68879
- 61-tube bundle with wire wrap, heat transfer, momentum losses, and flow mixing 80–32329
- accelerator-breeder systems for regeneration of reactor fuel assemblies, thermal hydraulics 80–5299
- adiabatic discharge of saturated water, from cylindrical channels, critical flow 77–84299
- AGR, Central Inertial Collector for removal of spalled oxide particles from coolant 80–5231
- AGR, commercial protection system, safety logic system 77–54325
- AGR, heat transfer to accel. gas flows, expt. and calcs. 78–54823
- AGR, helical monotube vapour generator, density wave instability, experimental-stochastic and theoretical anal. 80–47539
- AGR, moderator corrosion problems, soln. 77–18688
- AGR boiler tube, serpentine geometry at high press., two phase heat transfer 78–94077
- AGR design for Heysham II and Torness 80–23108
- AGR development and exploitation prospects 80–23109
- AGR for nuclear process heat appl., evaluation of high-temp. alloys 78–13237
- AGR fuel elements, heat transfer characteristics with rough surfaces 77–54283
- AGR helical coil boilers, analogue 77–58763
- AGR line development status and performance *(German)* 78–86568
- AGR once-though nuclear boiler at 14.5 MPa, hydrothermal and chemical conditions 80–63232
- AGR once-through high press. boiler feedwater solutes behaviour 80–63233
- AGR system, screening studies of materials for appl. to nucl. process heat systems 78–13236
- AGR system for nuclear process heat, primary circuit component materials 78–13233
- annular cooling channels, heat exchange crisis *(Russian)* 77–54301
- annular flow model, critical heat flux 78–94090
- axial flow in bare rod bundle, turbulence modeling 80–32338
- axial momentum altered transverse transport in coolant flows during oscillatory instabilities 79–17964
- axial pressure variations of two communicating parallel flows 77–42040
- benchmark rod-bundle thermal-hydraulic analysis using boundary-fitted coordinates 80–47548
- Bilibinsk atomic plant, gravity coeff. of coolant reactivity 80–32333
- blowdown, fluid behaviour in pressure vessel *(Japanese)* 79–17999
- blowdown expt., TRAC-P1A calcs. 80–18383
- blowdown from horiz. pipe 78–94093
- blowdown heat transfer experiment, nonstationary velocity tracking by adaptive cross-correl. algorithm 78–14074
- blowdown process, bubble growth by expansion and dissolution in variable pressure field 78–15723
- BN-350, design and experimental testing of intermediate heat exchangers *(Russian)* 79–97785
- BN-600, design and experimental testing of intermediate heat exchangers *(Russian)* 79–97785
- BN-600 reactor first loop, MHD phenomena 80–37421
- boiler water conditions, chemical monitoring development in UK *(Russian)* 77–88217
- boiling, forced convection type, in uniformly heated vert. tube, generalised crit. heat flux correlation 79–27498
- boiling crisis, nuclear reactor safety and performance, state of the art review 80–63312
- boiling curves for fission reactor core reflooding after LOCA 79–67814
- boiling flow instabilities, expt. and theoretical review of density-wave oscillations 80–18369
- boiling heat transfer during rewetting, one-dimens. cond. model 79–598
- boiling mixing studies in water loops, BWR, PWR reactors 79–26502
- BOR 60 fast reactor, primary coolant circuit radioactivity effects 79–63737
- BOR-60 reactor, boiling Na tests 79–97832

fission reactor cooling and heat recovery continued
- boric acid management in VVER reactor power plants *(Russian)* 79–30896
- boric acid solutions, extractive purification from radioactive corrosion and fission products 80–18458
- breeder reactors, SNR300, cooling system failure, effects *(German)* 78–695
- Browns Ferry BWR, load following test 80–68892
- buoyancy effects on pressure loss in rod arrays under laminar flow 80–27735
- BWR, ^{14}C production and discharge 79–52979
- BWR, axial distrib. of void fraction in subcooled boiling 77–46217
- BWR, boiling-channel stability, nonlinear math. model calc. of coolant-vel. perturbations 79–89353
- BWR, bypass flow distrib. 77–42017
- BWR, calc. of shutdown dose rate around recirculation pipes, radioactive corrosion products in primary cooling water 80–68734
- BWR, condensate feedwater system dynamics anal. 80–23025
- BWR, containment system coolant flows, LOCA modeling 79–54476
- BWR, control of Fe feed rate into feedwater system to reduce shutdown radiation level 80–5384
- BWR, coolant flowrate in evaporative channel, self-oscillation parameters investigation 80–37572
- BWR, core flow fluctuations, noise source, expt. study 79–13386
- BWR, coupled vibrations of a structure and fluid excited by pressure shocks 80–13546
- BWR, design and operation, review of water chemistry, in feed water, coolant and steam systems 79–36311
- BWR, dryout/post-dryout heat transfer, low flow, single tube 77–61498
- BWR, fast moderator feedback effects during severe press. transients 78–4990
- BWR, feedwater and recirculation control system coordination 80–73880
- BWR, global noise identification by spectral and parametric methods 79–63730
- BWR, heating, ventilation and air conditioning systems *(Japanese)* 80–91212
- BWR, high temp., high press. water circuit, NiOH injection effect on ass transfer 80–13533
- BWR, iron oxide deposition on heated surfaces, model 80–73902
- BWR, Kernkraftwerk Muehleburg special turbine trip tests 80–18513
- BWR, KKM turbine trip simulation with a one-dimensional transient model 80–18510
- BWR, LOCA, scaling of RPI parallel channel effects expt. 80–18381
- BWR, method for detecting bypass coolant boiling 80–571
- BWR, Millstone Unit No. 1, augmented off gas system experience 80–22919
- BWR, momentum coupled transient thermal-hydraulic model 80–13565
- BWR, multivariable autoregressive model of the dynamics 78–25307
- BWR, neutron noise field, two-group diffusion theory 80–18461
- BWR, off-gas recombiner operating experience at Chin-Shan 80–22920
- BWR, primary containment vessel, spray heat removal characteristics 80–73972
- BWR, primary coolant piping, Co deposition into corrosion films, model 80–13532
- BWR, radiochemical management, reactor cooling system, gamma spectroscopy of radionuclides 79–9731
- BWR, safety evaluation, experiments and analytical analysis, emergency core cooling system 80–13703
- BWR, safety relief valve discharge loads, dynamic effects on structures and eqpt. 80–99236
- BWR, shutdown dose rate of primary cooling system, prediction by empirical formula 79–22408
- BWR, simulation of cooling system conditions, stress corrosion cracking test 78–80696
- BWR, steam chugging during LOCA, general transient anal. 80–73903
- BWR, Tarapur, one-loop model, dynamics anal., power transient response 78–46131
- BWR, thermal-hydraulic technology, university contrib. opportunities 79–49652
- BWR, TRAB transient analysis program for pressure vessel and subsystems 80–73978
- BWR, transition boiling under forced convective conditions, reactor accident condition 78–89961
- BWR, vacuum relief valve sizing in condensing steam situations, analytical model 79–54545
- BWR, void fraction meas. by fast neutron moderation 77–34380
- BWR, water chemistry characterisations 78–21635
- BWR at PNC Japan, stability anal. of boiling loop in low-pressure operation 78–8894
- BWR augmented off-gas system flame arrester at Oyster Creek nuclear station 80–22918
- BWR benchmark calcs. with MEKIN code 80–18385
- BWR blowdown, [Thermal reactor safety.] Comparison of quasi-steady blowdown models with recent experiments 80–22999
- BWR boiling noise, local and global component obs. and calc. 78–94066
- BWR bundles, countercurrent flow limitation correl. during LOCA 79–31057
- BWR Channel, two-phase flow fluctuations and continuity 80–14786
- BWR channel stability, problem anal. 79–13387
- BWR cluster geometry, enthalpy and mass flow distribution 80–78359
- BWR condensate feedwater system, dynamic model 80–73883
- BWR containment system, effect of torus wall flexibility on hydro-structure interaction 80–83195
- BWR coolant, H_2-O_2 recombiner, appl. of Pd/Ni/Cr layered catalyst 80–18504
- BWR coolant oscillatory flow perturbations, altered transverse momentum transport 79–608
- BWR coolant pipes, integranular stress cracking, in-service inspection influences 80–68887
- BWR core flow fluctuation and neutron noise obs. 78–94060
- BWR critical heat flux density, heat transfer with boiling and burnout phenomenon *(German, English)* 78–58330
- BWR decay heat removal systems, probabilistic risk assessment, fault and event tree anal. 80–63333
- BWR fuel assembly, radiant heat transfer 78–17287
- BWR licensing basis transients, computer anal. of turbine without bypass transient 80–42814
- BWR LOCA, bubble collapse and fluid struct. interaction 80–689
- BWR LOCA, computer prediction of loading conditions on pressure suppression system 80–764

fission reactor cooling and heat recovery continued
BWR LOCA, containment dynamic loadings 80—763
BWR LOCA, hydrodynamic lead characteristics of primary containment vessel 80—73972
BWR LOCA, phased mission analysis of ECCS failures 80—68851
BWR LOCA, power channel thermal transients during reflooding 79—63755
BWR LOCA, press. drop across tieplate during countercurrent flooding 80—18530
BWR LOCA, press. oscill. phenomena induced by steam condensation, in containment with press. suppression system 80—68848
BWR LOCA, RELAP4 (MOD7/Version 1) core spray cooling calcs. compared with data 79—49730
BWR LOCA, some considerations in small-scale pool swell simulations 79—49740
BWR LOCA, steam fraction determ. in flowing air/stream mixtures by meas. of IR rad. attenuation 80—75010
BWR LOCA, vapour velocity in two-phase mixture during blowdown period 80—42821
BWR LOCA analysis, jet pump modelling using RELAP4 80—68850
BWR LOCA analysis, RELAP4/MOD7 calc. cf level swell test data 80—23003
BWR LOFA conditions, transition flow boiling heat transfer to water in verticle annulus 77—23182
BWR long-term cooling, closed form analytical model 80—78355
BWR loss-of-coolant accident, peak-clad temp. probability distribs. 77—74952
BWR multirod critical power reproducibility tests at different facilities 78—13211
BWR neutron noise local component meas., two phase flow study 78—94059
BWR noise, response of neutron detector to local coolant void distribs. 80—683
BWR NSSS structural integrity programs at GEC 80—99230
BWR off-gas systems, design considerations to prevent H_2 ignition 80—22917
BWR off-gas systems operating problems 80—22916
BWR plant, heat drain deaeration under forward conditions 77—88212
BWR power distribution analysis, three-dimensional calc. program 79—9674
BWR power stations, operating record and reliability, reviews 79—22403
BWR pressure suppression system, concrete condensation chamber, dynamic loading due to steam condensation 79—97754
BWR pressure-suppression system, steam chugging anal., heat transfer and fluid mechanics characts. 80—95339
BWR pressurisation effects of bypass streamline transient modelling 79—89408
BWR pressurisation transient anal. using MEKIN neutronics/thermal-hydraulic code 80—47626
BWR radioactive corrosion products behaviour 78—21661
BWR rapid transients, direct coolant heating and moderator temp. reactivity feedback effect 79—89442
BWR RELAP4 jet pump model 80—18380
BWR rod bundles, combined radiation and convection under emergency cooling conditions 77—14249
BWR rod drop accident, effect of thermal-hydraulic feedback, computer anal. 80—42815
BWR safety relief valve, remote set pressure verification 79—54487
BWR steam condensation pressure variations 78—46134
BWR stochastic neutron flux fluctuation obs. and modelling, thermohydraulic parameters 78—94065
BWR subchannel code with drift flux and vapor diffusion transport 79—59149
BWR suppression pool, role of Taylor instability during vent cleaning 79—31046
BWR suppression pool temperature transients following LOCA, computer anal. 80—762
BWR thermal hydraulics 80—27721
BWR transient anal., iterative procedure for predicting critical power ratio 80—42816
BWR transient anal. model for pressurisation transients 80—18509
BWR turbine trip transient analysis using ALMOS plant model *(German)* 80—83177
BWR turbine trip transients, additional separator modelling considerations 80—18511
BWR vent clearing hydrodynamics, numerical simulation using SOLA-VOF code 79—49659
BWR vertical separator superheater tube bundles, condensation heat transfer, noncondensing gas effects 80—47535
BWR void effects, stochastic point model and zero-power reactor simulation 78—94061
BWR with forward-pumped heater drains, water quality performance 79—67918
BWR with graphite channels, safety of nuclear power stations 79—26561
BWR-4 neutron noise analysis spectra, instrument tube flow-induced vibr. 78—94063
BWR-4 neutron noise analysis spectra characterisation 79—13482
BWRs, natural circulation of water by hydrodynamic models 79—93684
calorimeters for in-core nucl. heating rates meas. 78—25279
CANDU, energy, water, tritium budgets for Perch Lake 1975 78—29563
CANDU cooling with supercritical fluids, feasibility study 79—76064
CANDU fuel channels, power rundown, computer programs for fuel and struct. element decay heat 77—57711
CANDU nuclear power reactors, automated chemistry control system development 80—42738
CANDU nuclear power station safety, Atomic Energy Control Board guidelines 79—22425
CANDU PHWR heat transport network, SOPHT computer model 77—83025
CANDU power plant deaerator dynamics 79—93708
CANDU power plants, automated anal. system for control of secondary coolant chemistry 80—18446
CANDU reactor, heat exchanger tubing materials 78—29583
Candu reactor moderator effectiveness as LOCA heat sink 79—81021
CANDU secondary coolant circuit chemistry control, automated system development 78—66359
CANDU type 19 rod bundle, velocity distrib. in peripheral subchannel 80—32328
CANDU-PHW reactors, primary and secondary water chemistry, review 79—22382
CDFR secondary cct. design from PFR operations 79—97788

fission reactor cooling and heat recovery continued
Chalk Point cooling tower, salt emission and deposition 80—40941
channel array with interconnections, finite-difference scheme 79—4012
circular channel with rod clusters, heat transfer characts. 78—75140
circular cylinders and spheres, fluid flow and convective heat transfer *(German)* 79—94624
circular rods with regular polygonal concentric inner bore, heat flow shape factors 78—51048
circulating pump development, PWR appl. 77—82993
CIRENE, heavy water moderated BWR, LOCA simulation of recirculation circuit rupture 79—30949
civil AGR multistart helically ribbed fuel pin development 80—23111
cladding temp. fields in critical regions of rod bundles with Na flow 78—94084
Clinch River Breeder Reactor primary coolant pipe chaseway neutron streaming analysis 79—9661
combined cold and hot leg injection efficiency 78—21633
combined convection heat transfer in rod arrays, numerical anal., FBR cooling appl. 78—90898
composite fuels, heat conduction 77—42101
composite prismatic bars, doubly connected cross section, heat flow shape factors, anal. determ. 79—1068
compressible two-phase flow dynamics, distributed parameter model 80—24086
computer safety analysis, verification of the TRAC code on RSR standard problem 5 79—49724
condensation heat transfer, nonequilib. temp. profiles, mass transfer engineering calc. 80—63227
condensation heat transfer of steam flow on ice surface 78—94099
condensation-driven fluid motions, nuclear reactor safety 80—63228
condenser cooling by seawater, radiation monitoring programmes at Point Lepreau nuclear power station 78—29552
condensible vapour source expt. modelling 80—18542
conduction centrifugal EM pump for nuclear reactor coolants, characts., operation 78—86246
conduction controlled surface rewetting, general 1-D model 77—83011
conduction MHD systems, feedback and self-excitation threshold calcs. *(Russian)* 77—47108
conference, Berlin, Germany (Aug. 1979) 80—77539
containment blowdown following LOCA, press. and temp. transients and COPDA results 78—13303
containment heat transfer following LOCA, anal. 77—54314
containment main steam line break equipment qualification. [nuclear reactor safety] over 422K 80—42831
containment negative pressure evaluation 78—50275
containment of coolant during LOCA, ZOCO VI program appl. *(German)* 78—21668
containment spray droplet heat transfer, effect of internal circulation 77—83026
containment subcompartment flow, film entrainment determ. 79—49657
containment systems, critical flow mode for air-steam-water mixtures 80—18502
containment tightness, integral leakage rate tests 78—89956
convection with volumetric heat sources, fluid layer in spherical segment 79—614
coolant activity monitoring, automatic on-line system 80—684
coolant boiling crisis in rod assemblies 78—94087
coolant circuit contamination 78—21666
coolant circuits, fracture mech. appl. 79—43430
coolant flow in triangular rod bundles, turbulent-laminar transition 77—26838
coolant flow rate determ. using ^{16}N decay activity meas. 80—73955
coolant interchannel interaction for prolonged flow around bunches of rods 80—73888
coolant piping, relative rupture probabilities 78—21632
coolant pump, seismic anal. by response spectrum method 77—3183
coolant state, determ. by local temp. fluctuation anal. *(Russian)* 79—67845
coolant unsteady flow, with discharge from high-pressure vessel *(Russian)* 79—89448
cooling pipes, safety anal. for prestressed concrete reactor vessels 80—32370
cooling water chemical reagent pyrogallic acid, radiation effects *(Russian)* 79—43603
core heat transfer during reflooding, modelling 80—27781
core hydraulics fast neutron reactors *(French)* 79—63723
core internal coolant flow distrib., probabilistic evaluation 77—46250
core thermal performance assessment, acceptance of statistical techniques 80—18394
core-melt model, transient natural convection in single-phase heat-generating pool 80—9350
core-retention bed, horizontal heat transfer from molten fuel 77—46317
corrosion product transport, high temp. water loops 79—91840
countercurrent flow limitation, heater rod dynamics effects 80—73906
CRBR, heat transfer and thermal losses in above-core regions 80—32363
CRBR piping, structural reliability uncertainties 77—46350
CRBR primary piping reliability, stress-strength overlap method 77—46349
CRBR upper internal structure, thermal oscillations 77—46269
CRBRP mixing-tee model, vibration studies of perforated plates 79—49665
Creys-Malville station, nuclear boiler studies and construction, Super Phenix 1 *(French)* 79—36301
critical energy in heat transfer channels of complex shape, fuel rod assembly 78—78453
critical heat flux, review of data 77—57708
critical heat flux in boiling channels, BURN-2 computer program 77—54863
critical heat flux in tube, Freon-12 and water coolant 77—83020
critical heat transfer in Freon-12 cooled 3-rod bundle, orientation effects, meas. 79—93709
critical two-phase flow, bubble nuclei 80—64615
critical two-phase flow models, nuclear reactor safety 80—63229
DC electromagnetic pump using supercond. magnet, performance characts. 77—82994
decay power of fission products, sensitivity to uncertainty in yields 77—6494
decay power of fission products in reactors, effects of neutron capture 77—6500
defects of fuel elements calc. of MMI-2 nuclear power station (Harrisburg) *(German)* 80—23105

fission reactor cooling and heat recovery continued
density wave instability in once-through boiling flow system, distrib. parameter model 79—67815
density wave oscillations, linear stability anal. 80—19327
departure from nucleate boiling ratio safety limit to modelling parameters in COBRA IIIC/MIT 80—73901
depressurisation studies, transient density, press., temp. variations, during discharge 80—57833
direct contact condensation of flowing steam onto injected water 78—94097
directional integration method for 2-D fluid transients 78—683
dissociating coolant reactor core dynamics, modelling *(Russian)* 80—52732
dissociating turbulent gas flow around triangular rod bundle, heat and mass transfer *(Russian)* 79—68822
DISTAV calc. code for temp. determ. of Na and pile cladding *(French)* 78—94085
diversion cross flow between two parallel channels with lateral slot, axial press. variations 77—88201
diversion cross-flow between two parallel channels communicating by lateral slot 77—88200
diversion cross-flow between two parallel channels communicating by a lateral slot 79—30901
domains of complicated boundary shape, Helmholtz eqn. soln., GCR appl. 80—13540
Dounreay fast reactor, overheating, prevention by natural circulation, experimental investigation report 80—47598
Dounreay test reactor, fast breeder test experience 80—86961
drag disk dynamic anal. in transient two phase flow 80—73907
dryout, premature in conventional and nuclear power station evaporators, model 78—94120
dryout heat fluxes in debris beds cooled at the bottom and having subcooled liquid at the top 80—13652
dryout in an SGHWR rod bundle, exptl. and calc. comparison 79—3192
ducts, one-dimensional models for transient gas-liquid flows 80—64614
ducts and pipes intricately shaped cross section, heat transfer, Laplace and structural method 78—83477
dynamics of nuclear power facilities upon deterioration of heat exchange 80—63234
EBR II, Cs control by C getter 80—13648
EBR II primary heat transport cct., steady state natural circulation performance 77—38326
EBR-II, comparison of XX08 steady-state temp. meas. with anal. predictions 80—579
EBR-II, duct dilation expts. 79—93702
EBR-II, whole core thermal-hydraulic phenomena, experimental study 77—88206
EBR-II primary system fission gas behaviour 79—9692
EBR-II primary system piping evaluation for safety research modification 79—9785
EBR-II secondary Na network anal. for press. pulses from leaks of water or steam 77—54328
EBR-II sodium systems, control of oxygen, hydrogen and tritium impurities 79—93696
EBR-II steam generator duplex tubing, US inspection 80—32379
ECC reflood characts., effect of bottom injection location, SUNYAB/EPRI program 79—49726
ECC system, treatment of water packing effects [in fission reactors] 79—89401
ECCS, flooding phenomena with condensation 79—89429
ECCS analysis with decay-heat generation and inlet subcooling 79—89434
ECCS top spray, restrictive effect of ascending steam on falling water 79—49704
effluent dispersion, thermal and radioactive, math. model *(Spanish)* 77—74908
electrical system design for future AGR power stations 80—57935
electrochemical O_2 meter for meas. in liquid Na 78—58337
EM instruments for use in liquid sodium, theoretical anal. 78—54857
EM pumps for liquid metal fast breeder reactor, review 78—94074
emergency cooling model validation by Loss of Fluid Test Facility 79—80981
emergency cooling of a reactor with coolant dissociation *(Russian)* 79—59157
emergency cooling systems, transient thermal stresses, appl. to circuit integrity 77—6544
emergency core coolant injection, alternative concepts 78—21694
emergency core cooling system, unreliability estimates, comp. programs 77—54280
emergency core cooling system motor operated valves, failure mode anal. 78—54866
emergency core cooling system motor operated valves, failure criteria 78—70592
emergency reactor cooling, mathematical models and methods *(Russian)* 79—17975
EURDYN-1M, safety studies on LMFBR, computer program 80—99267
evaporator, vertical U-tube type, premature bend dryout phenomena, wall temps. 77—61499
experimental reactor loop construction, high-pressure and temp. type, Hungary *(Hungarian)* 77—3074
falling film rewetting 78—75906
fast breeder test reactor operator training simulator model development 80—91219
fast power reactor circuit activity, activation cross-sections 80—13614
fast power reactors, fuel pin viability in LOCA 79—76090
fast reactor, EM temp. sensor in liquid sodium, performance 78—700
fast reactor, operative monitoring of fission products in Na coolant 78—677
fast reactor, time series analysis and forecasting for ANL TREAT expts. 78—13289
fast reactor coolant blockages, detection by temp. noise tech. 79—30899
fast reactor fuel, thermohydraulic performance for low duct dilation 80—73893
fast reactor fuel assembly, turbulent laminar flow characteristics *(Czech)* 80—68738
fast reactor fuel rods, burnup-dependent heat transfer from fuel to cladding 79—36323
fast reactor safety, thermohydrodynamics code TWOPOOL, modelling and numerical methods 79—59195
fast reactors, Na purification system for primary and secondary loops 79—45344

fission reactor cooling and heat recovery continued
fast reactors, track detector determ. of fuel contamination of primary Na coolant 80—32394
fast reactors employing dissociating N_2O_4, thermophysical anal. *(Russian)* 79—30909
fast-neutron gas reactors, dissociating nitrogen tetroxide as coolant 80—13536
FBR, attenuation of HCDA work potential by heat transfer 79—93773
FBR, debris bed dryout, effect of particle size distrib. and segregation 79—49668
FBR, development in Japan, fuel, materials coolants and design *(Japanese)* 80—22888
FBR, experimental, math. model for control system design in FBR plants 79—17990
FBR, HCDA, 2Z 79—49669
FBR, molten fuel interaction with Na in active zone 77—54333
FBR, SAS3D prediction of intrasubassembly boiling incoherence, multipin boiling model 79—49662
FBR, sodium-cooled, blocking of cooling channels monitoring, simulation tests *(German)* 77—34372
FBR, thermal-hydraulic flow fields, stochastic processes 79—30991
FBR, types, cooling and safety aspects *(German)* 79—54587
FBR containment response to HCDA, effect of struct. components, Eulerian hydrodynamic anal. 80—23014
FBR core thermal and hydraulic design, effect of subassembly bowing *(Japanese)* 79—67816
FBR meltdown, post accident heat removal anal., turbulent convection and interfacial freezing 79—49670
FBR meltdown, post-accident heat removal, heat transfer mechanism associated with immersed melting surfaces 79—49671
FBR post-accident heat removal anal., convective heat transfer correlations for molten-core debris pools growing in concrete 80—47559
FBR power stations, development of modular steam generators 79—76058
FBR safety and economics, leak detection, cooling, waste disposal 80—63303
FBR safety calculations, numerical mixing errors in Eulerian calculations of coupled thermohydrodynamic motions 80—47553
FBR secondary cooling system, H behaviour *(Japanese)* 79—93688
FBR sphere-pac fuel, prediction of thermal conductivity 79—59174
FBR thermal hydraulics, sensitivity theory for general systems of nonlinear equations 80—86954
FBR TOP accident porous fuel blockage in core, theoretical anal. 79—49673
feedwater systems, auxiliary, fault tree anal. 80—63332
FFTF, interassembly flow redistribution at natural circulation conditions 79—85654
FFTF, natural-circulation testing 79—49676
FFTF, potential gas entry after postulated pipe rupture 79—85657
FFTF, simple models, HCDA expts., LMFBR safety evaluation programme 77—3130
FFTF, thermal-hydraulic anal. of air dump heat exchangers 79—59146
FFTF, transient overpower accidents, effect of intrasubassembly incoherencies 80—32373
FFTF design studies, simulation of hot-leg piping ruptures and loss-of-flow events 79—49677
FFTF heat transport system, design construction and testing 79—97783
FFTF loss-of-electric-power transient response, natural circulation tests, pre-test simulation using SSC-L code 80—42836
FFTF upper-plenum mixing and stratification, comparative studies 80—583
film boiling, contact heat transfer meas. 77—42037
film boiling and rewetting heat transfer during bottom flooding of a hot tube 78—94094
film boiling and vapour explosions from small spheres 80—18543
film region flow boiling dynamics 79—59145
fission energy generation in vol. boiling pool systems, microwave heating simulation 80—18386
fission products in primary coolant, possible contribution from U impurities in fuel cladding 79—63751
flow, 3-dimensional, in bundle of rods *(Russian)* 78—37408
flow anomaly diagnosis, autoregressive model appl. *(Japanese)* 80—83146
flow blockage anal., triangular edge-subchannel wire wrap ϕ-functions 80—580
flow boiling crisis, tube diameter effect 79—85603
flow boiling dynamics in film region 80—83142
flow rate meas., correlation with thermocouple random signals 78—17297
flow structure for critical discharge conditions of boiling water through cyl. channels 80—83145
flow-induced structural vibrations anal. 80—42795
flowmeter calibration, Na-cooled reactor, signal anal. method 78—38425
fluid dynamic transient analysis using ASWR method with staggered meshes *(German)* 80—83176
fluid dynamics, coarse mesh methods appl. *(German)* 77—88197
fluid dynamics, prospects for accurate computer simulation 77—79422
fluid dynamics eqns., asymmetric weighted residual method 77—79421
fluid flows with large density gradients, Eulerian finite difference technique 77—79424
fluid piping systems, transient cavitation effects 78—29554
fluid-elastically coupled coaxial cylindrical shells, response to external flow 77—89063
fluid-saturated porous layer with heat source, thermal convection onset 79—13406
fluid-structure system dynamics, reactor safety anal., computational algorithms 77—71669
FMSR, He-cooled, thermal-hydraulic design anal. 80—18408
forced convection in annuli and rod bundles with variable heat flux distribution 78—94082
Fort St. Brain HTGR, He circulator auxiliaries 79—67822
Fort St. Vrain HTGR, He circulators, development and testing 79—67821
Fort St. Vrain HTGR, He circulators for primary coolant cycle, developmental and performance tests 80—597
four-rod bundle burnout and heat removal intensification with water and freon-12 flows 80—18413
free convection flow between two containers at different temperature *(German)* 79—81984
FRJ-2 research reactor, elimination of flow rate fluctuations in core 77—67798

fission reactor cooling and heat recovery continued
fuel assemblies in vertical flow channels, computer dynamic model 79—22379
fuel cladding, three-regions rewetting model with decay heat generation and inlet subcooling 80—22965
fuel element array, temp. distrib. for turbulent liq. metal flow 78—13203
fuel element bundles, temp. field calc. 79—591
fuel element bundles at coolant boiling, fuel exchange enhancement 78—94086
fuel element centering system, flow through narrow sphere-cylinder channel 79—17962
fuel element gap conductance, heat transfer over range of Knudsen number 78—13213
fuel element modeling rod bundle in longit. air flow, heat transfer expt. 78—82415
fuel element nonlinear transient heat conduction, variational calc. 79—93685
fuel element surface roughness, turbulent convective heat transfer 77—46208
fuel elements, control rods, transient thermal stress anal. 79—599
fuel elements, cracked, gas-filled, temp. distribs. calc. 78—78446
fuel elements, with cladding, thermal shock *(Italian)* 80—27774
fuel failure detect., UO_2-loaded Na in-pile loop 78—37417
fuel pin heat transfer, digital transfer matrix 78—29548
fuel pins, eccentrically placed pellets, finite difference method for heat transfer 78—82419
fuel pins with eccentric pellets, two-dimensional temp. profile calc. 79—9677
fuel rod arrays, radiative heat transfer, Monte Carlo method, temp. distrib. 78—78447
fuel rod ballooning prevention 78—17290
fuel rod bundle, cross flow heat transfer via the fuel elements 80—63226
fuel rod bundle, dry patch spreading, post dryout temps. 80—42741
fuel rod dynamic response soln. by state space method 79—49647
fuel rod thermal behaviour, relocated gap width estimation for gap conductance calcs. 80—589
fuel rod thermal characteristics, on-line simulation by elec. heated rod 77—46209
fuel rod vibration induced by coolant water and air/water flow *(Japanese)* 78—74429
fuel rod with cladding, time depend. temp. distribs. 78—17288
fuel thermocouples and liquid-level probes for core monitoring 80—99239
fuel-to-cladding heat transfer coefficient in a reactor fuel element *(German)* 80—610
gamma densitometer meas., anal. of dynamic bias 80—27730
gamma densitometry, static error evaluation 80—27729
gamma-ray densitometry, dynamic bias 80—27728
gamma-ray spectrometer, wide range Ge, for on-line meas. of reactor cooling water activity 77—65381
gas cooled fast neutron reactors, He and CO_2 coolant comparison 77—42046
gas cooled reactor development 77—23184
gas cooled reactors, internal insulation 80—47537
gas cooled reactors, velocity flow field near moving cascade, meas. using hot wire technique 77—50195
gas cooled rough rod bundles, thermofluid dynamic expts., evaluation with code SAGAPO 80—24002
gas-cooled porous fuel elements, thermal design 78—94100
gas-solid turbulent suspension flow, frictional pressure drop Prandtl's mixing length anal. 79—14458
gaseous fission products, continuous determ. of content in reactor loop 79—30905
GCFR, 1000 MW(e), reliability anal. of decay heat removal system 77—14223
GCFR, 300 MW(e), gamma-ray heating in core and blanket 77—61486
GCFR, borax ($Na_2B_4O_7$) internal core catcher 78—58372
GCFR, core thermal hydraulics and pumping power anal. code JUPITER 80—73889
GCFR, design criteria for 300 MW(e) demonstration plant 79—97759
GCFR, dissociating gas cooled, integrated student design problem 77—46224
GCFR, effect of accidental steam entry on reactor parameters 78—33277
GCFR, heat transfer expts. on artificially roughened fuel rod bundle 77—18651
GCFR, nuclear heating in B_4C control rod 77—42115
GCFR, pressure drop of spacer grids in smooth and roughened rod bundles 77—42022
GCFR, Pu fuelled, fission products and secondary gamma-ray spectra 78—676
GCFR, thermohydraulic performance of ribbed surfaces 77—50200
GCFR blanket assembly, hydraulic and thermal performance 80—27731
GCFR configuration, simulated, evaluation of full-core steam flooding worth 78—33276
GCFR core-element and press. equalisation system, seal development 77—46271
GCFR cores, heat transfer with He and Na coolants, review 79—45331
GCFR fuel assembly thermal-hydraulic anal., modification of COBRA code 80—588
GCFR fuel rod roughness elements, pressure drop meas. 80—581
GCFR fuel rod roughness elements, surrounding flow visualisation technique 79—59141
GCFR He system, development programmes 77—18648
GCFR lattice, Monte Carlo and diffusion theory calcs. of steam worth 79—80991
GCFR residual heat removal system, safety features 77—14244
GCFR with N_2O_4 dissociating working substance, optimisation *(Russian)* 79—59159
generalized pressure drop correlation, in two-phase flow 79—9664
Gentilly-1 steam mains, hydrodynamic oscills., acoustic anal. 79—97771
grid spacers, effect on post critical heat flux heat transfer 80—27732
HDR, numerical investigation of radial mixing capabilities in strongly buoyancy-influenced vertical, turbulent channel flows 79—93751
heat conduction and fluid flow, local Green's function method for initial value problems 79—89359
heat exchange component vibrations in liquid and two-phase cross-flow 78—90770
heat exchange problems of power plants 80—18372
heat exchanger, potassium type, based on heat pipe principle 77—46210
heat exchanger materials, oxide protective layer formation meas. by hydrogen permeation 78—8895

fission reactor cooling and heat recovery continued
heat exchanger tube banks, crossflow induced vibr. 78—50245
heat exchanger tubes, US inspection by rotating search units method 79—9667
heat flux in liquids in annular channels, critical density *(Russian)* 78—37407
heat generating fluids, one-dimens. flow, thermal unsteady regimes, nuclear reactor appl. 79—1179
heat rate improvement, design modifications to condenser air-removal system 79—67830
heat transfer, finite element nonlinear analysis, using an explicit stable method 77—89004
heat transfer around circular cylinder in liquid Na crossflow *(Japanese)* 77—57706
heat transfer downstream of blockage with discrete permeability in rectangular channel 80—69915
heat transfer finite difference computer programs 79—14221
heat transfer from round-bottom pool with internal heat generation, expt., LMFBR appl. 79—13470
heat transfer problems, safety aspects 78—41842
heat transfer simulation using analogue computer elements *(Russian)* 80—52733
heat transfer tube failure propagation due to Na-water reaction in steam generator 79—6748
heavy water concentration meas. by neutron thermalisation method *(Japanese)* 79—93746
heavy water production, Canadian experience 79—30929
hermetic metallic thick-walled vessel, cooling by nitrine coolant *(Russian)* 79—59158
hermetically sealed valve for the safety systems of a nuclear power station *(Russian)* 78—89952
heterogeneous Gas Core Reactor power plants 79—9671
HGTR core, multiregional coupled conduction-convection model 78—94083
high flux test reactor, MARIA, nuclear power research programs *(Polish)* 79—93693
high temperature heat exchanger test plant for nuclear energy steel making process R and D *(Japanese)* 79—67817
Hinkley Point B AGR commissioning and three years' operational experience 80—23107
hockey stick heat exchanger, elbow centroid 80—9329
homogeneous nuclear reactor, water pool boiling, produced by distrib. internal heat sources 78—90685
hot water leakage from first loop, 22.8 MPa initial pressure, flow characts. 78—66357
HTGCR, downstream water flow steam generator 80—5223
HTGR, Brayton-Rankine binary cycles optimisation 80—22904
HTGR, consequence anal. of hypothetical accidents, core heatup and afterheat removal 78—58381
HTGR, coolant chemistry, design implications 79—67832
HTGR, dynamic characts., primary loop characts. *(Japanese)* 80—57832
HTGR, fission product plateout in primary cooling system, in situ meas. using Ge(Li) spectrometer 80—73881
HTGR, Fort St. Vrain, operation of safety features 78—21717
HTGR, fuel failure anal. following LOCA, post-accident temp. response 78—13276
HTGR, heat transfer effects in annular passages of heat exchangers *(Japanese)* 77—23239
HTGR, heated vertical pipe, gas buoyancy effect on downward flow and heat transfer 78—74427
HTGR, hydrogen secondary cooling system, construction and performance tests *(Japanese)* 80—91210
HTGR, Peach Bottom site, radionuclide distrib. in primary coolant circuit 78—13275
HTGR, T contamination of product gas 80—13590
HTGR, thermal insulation media, transient behaviour of gas 80—27701
HTGR, thermodynamic correlations for accident anal. *(German)* 78—25315
HTGR, US R and D programs for steam supply plant, fuel and materials 79—97757
HTGR containment, layering and combustion following depressurization accident 78—13277
HTGR core auxiliary cooling system, failure analysis 80—22964
HTGR Core Auxiliary Cooling System mathematical simulation 78—29570
HTGR core heatup, PCRV integrity, thermal anal. model 79—49735
HTGR fission product diffusion through core materials during LOFC, exact analytical soln. 80—47554
HTGR hypothetical accidents, consequences following breach of primary circuit and safeguard failure *(German)* 78—58390
HTGR multihole fuel, equivalent thermal conductivity calc. *(Japanese)* 79—45346
HTGR piping, heat transfer characts. of horizontal annular insulation layer *(Japanese)* 79—26520
HTGR primary circuit components, metallurgical eval. of structural materials 79—67867
HTGR primary coolant system depressurisation accident, expt. and numerical anal. 80—775
HTGR radiative gas heat exchangers, radiation effects at high temps. 80—95338
HTGR steam generator or heat exchanger materials, compatibility with coolant circuit media 77—57721
HTGR thermal hydraulics 80—27719
HTR, admissibility of Co as alloy constituent in primary cooling circuit components *(German)* 78—25294
HTR, design criteria of elec. generating plant with the turbine in a direct cycle 79—97758
HTR, hydrogen and tritium permeation through He heated tube walls 77—50250
HTR, metallurgical problems of intermed. heat exchanger 77—65256
HTR coal gasification plant, development of He-He intermediate heat exchanger 80—5222
HTR core, radiant heat transfer following failure of afterheat removal system 80—773
HTR pebble bed heat transport, particularly radiation, in hypothetical accidents *(German)* 79—49791
HTR vessel, thermodynamic calc. of cooling and design *(German)* 78—4982
HWR, safety research and development 78—29614

fission reactor cooling and heat recovery continued
HWR, shutdown heat removal systems, reliability fault tree anal. and β-factor method 80—63331
hydraulic pressure wave propagation in plastically deforming pipe, rel. to reactor HCDA 78—8876
hydrodynamic motions, value of distributed particle in cell techniques 79—59196
hydrodynamic oscillations in Gentilly-1 reactor steam mains, GISMO program 78—54824
hydrodynamic testing equipment with gravitational channel for reactor core meas. *(Slovak)* 78—21625
impurity monitoring in liquid Na, electrochemical meters 80—22886
in-core measuring system for VVER-440 and VVER-1000 type reactors 'INCORMER' *(Russian)* 79—30965
in-pile post accident heat removal facility, feasibility study 79—49774
Inconel 600, stress corrosion cracking in primary water 79—93728
inlet coolant temp. fluctuations transfer function, space-depend. global component 79—30887
integrated safe shutdown heat removal system for LWRs 77—54330
interchannel heat and mass transfer, wire-spaced fuel pins effect 78—94080
inverted annular film boiling heat transfer formulation 80—73899
IRT-2M reactor with loop channels in active area, physical parameters *(Russian)* 79—31067
Isar BWR power station, transient expts. during startup and initial operation *(German)* 80—83187
jet pump cavitation with ambient and high temperature water 79—76071
JPDR primary piping cracks, coolant pressure boundary weld joint in service inspection 79—49706
Kohlestein insulation, influence of high axial press. gradients *(German)* 79—13414
Krsko, construction, architecture and reactor system cooling *(Croatian)* 80—37416
Kyoto University reactor, airborne radioactivity from primary coolant 80—22959
laminar heat transfer data with step-varying wall heat flux 77—50210
lattice cell meas. in 36 element natural UO_2 fuel, stopping effect of coolant 78—58347
Leidenfrost temperature for spherical fuel particles, appl. FCI anal. 78—17371
lightly damped tubular arrays, damping props, flow induced vibr. tests 80—68760
liquid freon II, saturated and subcooled, two-phase critical flow 77—68678
liquid level detector based on level sensitive transducer for PWR environment 80—57874
liquid metal coolant pumping and stirring by thermoelectric MHD 79—50806
liquid metal cooling, gas bubble effect calculating method *(German)* 77—23238
liquid metal heat transfer in closed conduits 77—47016
liquid metal heat transfer in regular fuel element arrays, Nusselt no. calc. 78—89932
liquid metal turbulent heat fluxes, channel flow 77—42035
liquid metals, flow at high temperatures through circular pipes, connection mechanism *(Spanish)* 79—37315
liquid Na, thermocouple transfer function and flow velocity meas. by temp. noise 79—13394
liquid Na cooling pressure meas. using differential recorder *(German)* 77—88270
liquid Na crossflow, heat transfer round circular cylinder 79—86429
liquid pools, vol. heated, transient boiling, convex flux relations, fission reactor safety 77—31340
liquid pools, vol. heated, transient boiling non-convex flux relations, fission reactor safety 77—31341
liquid to vapour transformations, mechanics of two phase flows 77—89532
liquid-metal-cooled reactors, radionuclide trap in primary circuit 79—93768
liquid-vapour critical flow, two-fluid model 78—90973
LMFBR, accident anal., radiative transfer treatment 78—94573
LMFBR, acoustic anal. from Na boiling tests using THORS bundle 6A 79—31033
LMFBR, acoustic anal. of TREAT safety test R8 78—13290
LMFBR, acoustic anal. on Na boiling expt. in FFM Bundle 3B, Test 4 78—13291
LMFBR, acoustic surveillance of anomalous events 78—37397
LMFBR, attenuation of temp. oscillations by liquid metal boundary layers 77—83013
LMFBR, behaviour of H in liquid Na *(Japanese)* 79—49649
LMFBR, boiling stability tests on THORS Na loop 78—37396
LMFBR, BR-2, UO_2 behaviour for local cooling disturbances in in-pile Na loop 80—13542
LMFBR, calc. vs. exptl. temp. distrib. behind six-channel central blockage 79—31028
LMFBR, chemical comp. of Na coolant and Ar atmos. 79—71893
LMFBR, chemical leak detection, effects of NaOH in Na 80—63326
LMFBR, cladding meltdown phase for loss-of-heat-sink event during shutdown 78—8923
LMFBR, Clinch River, consequences of boiling in radial blanket due to hypothetical major pipe leak 78—8922
LMFBR, Clinch River, humidity effect on burning rate of Na droplets, Fick's eqn. anal. 78—13297
LMFBR, Clinch River, LOCA in one heat transport loop without reactor trip 78—8924
LMFBR, Clinch River Plant, pipe rupture simulation using DEMO code 78—8927
LMFBR, cluster of core assemblies, CORA transient anal. 80—18389
LMFBR, cold impurity trap regeneration in Na purifier 79—76091
LMFBR, computation studies of cladding relocation dynamics after transient undercooling accident 78—13255
LMFBR, computer control system for Na test loops 79—26550
LMFBR, containment codes appl., response predictions in HCDA conditions 77—71670
LMFBR, containment pressurisation by Na spray fires 80—32365
LMFBR, coolant cavitation in dynamic containment loading 80—32326
LMFBR, coolant pumping using accelerating devices on piston-driven gas-liq. flows 78—25261
LMFBR, coolant start of boiling detection by acoustic method 78—86646

fission reactor cooling and heat recovery continued
LMFBR, coolant thermodynamics and fluid dynamics *(Spanish)* 79—6726
LMFBR, core restraint systems, interassembly heat transfer model 80—567
LMFBR, core-disruptive accidents, neutronic and fuel element behaviour 80—32357
LMFBR, Creys-Malville boiler construction and features *(French)* 80—47542
LMFBR, design and function of thermal barriers in core outlet plenum 79—97765
LMFBR, design and thermohydraulic characts. of fuel and blanket subassemblies of a large core 80—711
LMFBR, design for near zero value of Na void reactivity 78—13205
LMFBR, detection of fuel assembly flow reduction in heterogeneous core 79—31032
LMFBR, diffusion type H_2 meter in Na loop 80—68728
LMFBR, dynamic response of containment vessel and coolant wave propag., REXCO-EUR code manual 78—58349
LMFBR, EBR II, Na purification by cold trapping, effectiveness 77—14225
LMFBR, effective conduction mixing lengths for subchannel anal. of finite hexagonal bundles 78—13210
LMFBR, effects of Na entrainment and heat transfer with two-phase UO_2 80—47596
LMFBR, effects of Na entrainment and heat transfer with UO_2 vapour during HCDA 79—93775
LMFBR, equipment design, Na-NaK engineering handbook 79—97815
LMFBR, establishment of buoyancy induced natural circulation, CURL-L code anal. 79—49663
LMFBR, failed fuel pin debris forming heat-generating blockage, heat transfer anal. 80—47648
LMFBR, flow behaviour of vol. heated boiling pools 80—13545
LMFBR, flow in Na circuit surge tank *(Czech)* 77—67792
LMFBR, flow instabilities of molten core debris pool following accidents 78—8931
LMFBR, fluid-to-struct. heat transfer effects on structural damage pot. 79—81023
LMFBR, fuel pin coolability in low power voiding, SAS3A computer code anal. 79—49661
LMFBR, H impurity conc. in liquid Na, meas. method 79—81030
LMFBR, HCDA, dryout in porous bed of nuclear fuel debris, heat transfer regimes 77—46316
LMFBR, HCDA, in react. expts. on debris cooling 80—13543
LMFBR, HCDA containment, current perspectives 80—32360
LMFBR, hydrodynamics of large-scale fuel-coolant interactions 80—78409
LMFBR, hypothetical LOCA, fission gas role in transition phase development 78—8935
LMFBR, intermediate heat exchangers in Phenix and SuperPhenix 80—5225
LMFBR, intersubassembly heat transfer effects during natural circulation 80—584
LMFBR, large carbide-fueled, press. drop constraint on breeding performance and pin diameter optimisation 77—50270
LMFBR, large EM induction pump for high-temp. appl. 78—17291
LMFBR, leak detection in steam generator, by acoustic spectra meas. *(Czech)* 78—54849
LMFBR, liq. Na natural convection from vertical plate 79—3202
LMFBR, local boiling calculations in subchannel geometry, feasibility study using CLAYMORE code 78—25280
LMFBR, localised boiling in radial blanket due to hypothetical major pipe leak 79—22376
LMFBR, LOFT for loss-of-piping-integrity transient, expt. data and COBRA-3M comparison 78—17370
LMFBR, loop-type, effect of pumped stored kinetic energy on natural circulation decay heat removal 80—23010
LMFBR, loop-type, transition to natural convection from low temp., low flow conditions 80—18533
LMFBR, low sodium void cores 80—13549
LMFBR, low temp. saturated cycle pool type 80—13574
LMFBR, maximum wake temp. and Nusselt number behind blockages in Na-cooled bundles 79—31026
LMFBR, modular steam generators, breakdown protection 79—76059
LMFBR, molten fuel coolant interaction *(Japanese)* 79—17997
LMFBR, molten fuel downward streaming through axial shield struct. 77—42020
LMFBR, molten UO_2 fuel-Na coolant thermal interaction, characterisation of fragmented fuel 80—68774
LMFBR, multichannel cladding relocation model for loss-of-flow accident 78—17366
LMFBR, Na boiling, acoustic detection using pulsed system 79—97839
LMFBR, Na boiling detection, power spectral density surveillance systems 80—68740
LMFBR, Na boiling under low heat flux condition during loss-of-heat sink accident 80—47636
LMFBR, Na circuit with high parameters *(Czech)* 77—46303
LMFBR, Na coolant transient flow and heat transfer in outlet plenum 79—26472
LMFBR, Na flow meas. in main pipes, application aspects 80—22884
LMFBR, Na flow transient anal. using NATOF-2D code 80—47633
LMFBR, Na incipient boiling under forced convection in seven pin bundle 79—22401
LMFBR, Na liquid coolant, determ. of saturated temp. with automatic plugging indicator 79—97747
LMfBR, Na loop temp. control using 100 kW elect. heater *(Czech)* 80—5203
LMFBR, Na ML-3 circuit for testing mech. props. of structural materials *(Spanish)* 80—55595
LMFBR, Na pump, multimode heat transfer, computer codes 79—610
LMFBR, Na pumps for Phenix and SuperPhenix 80—5228
LMFBR, Na purification system, cold traps and plugging indicator 80—99209
LMFBR, Na spillage due to slug impact on reactor cover 80—32364
LMFBR, Na spray fires 80—32369
LMFBR, Na void and Doppler reactivities 78—8891
LMFBR, Na void reactivity reduction for U-Pu-Zr fuel 79—85655
LMFBR, Na void reactivity sensitivity to design 78—8890
LMFBR, Na-H_2O steam generator, calc. local heat fluxes in circular channels 79—36312

fission reactor cooling and heat recovery continued
LMFBR, Na-H$_2$O steam generators, safety problems and their solution in the USSR 80−63318
LMFBR, natural circulation decay heat removal 79−31010
LMFBR, natural convective cooling of fuel debris bed following HCDA 78−8929
LMFBR, neutron streaming through control rod followers, diffusion coeff. by numerical integration 80−13636
LMFBR, once through boiling flow system, density wave instability 79−9666
LMFBR, plugging indicator, measuring accuracy 79−63732
LMFBR, pool type, natural circulation cooling 80−102289
LMFBR, pool-type, design effect on natural circulation establishment 77−6487
LMFBR, pool-type, PLOOP code for primary loop coolant flow and heat transfer anal. 79−31012
LMFBR, possible cleaning of Na using fully denatured ethanol 78−21689
LMFBR, post accident heat removal technology review 78−41839
LMFBR, pressure transient analysis in piping systems including the effects of plastic deformation and cavitation 80−74775
LMFBR, primary circuit contamination, release transport and removal of radioactive products 80−13631
LMFBR, primary containment response with upper internal struct. 80−32361
LMFBR, primary cooling circuits, Na loop system, anal. of radioactive corrosion product transfer 78−78464
LMFBR, probabilistic evaluation of core-internal coolant flow distrib., correl. among fuel subassemblies 77−88210
LMFBR, radial blanket assembly, flow split meas. 78−13209
LMFBR, red. of two-phase thermal cond. and heat transfer by entrained inert gases 79−30897
LMFBR, rod bundle, static press. meas. 80−73969
LMFBR, safety c.f. thermal reactors 79−26562
LMFBR, SAS-3D analysis of natural-convection boiling behavior in the sodium boiling test facility 80−47635
LMFBR, scaled down model of SNR-300 inlet plenum, convection effects on temp. distribs. during emergency cooling 77−26839
LMFBR, secondary containment response to Na and H 80−27769
LMFBR, selection of steam conditions 80−18404
LMFBR, shutdown heat removal systems, reliability fault tree anal. and β-factor method 80−63331
LMFBR, simulated LOFT, fuel response, role of fission gas and fuel melting 80−37475
LMFBR, soln. of COBRA energy equations during natural circulation conditions 79−89354
LMFBR, space time dynamics for localized disturbances 78−21674
LMFBR, squeeze flow between two adjacent subassemblies, discrete model 78−86634
LMFBR, statistical anal. of interaction coolant channels 79−59137
LMFBR, steam cycles checklist 80−22899
LMFBR, steam generator LOCA signalling by EM flowmeter *(Czech)* 79−6751
LMFBR, surface temp. distrib. of peripheral fuel elements, approx. thermal modelling 80−63237
LMFBR, temp. distrib. of subassembly including intersubassembly heat transfer 77−83014
LMFBR, thermal conditions controlling subassembly failure propag. during transition phase 79−49758
LMFBR, thermal mixer mixing correlations for Na and water 80−27733
LMFBR, thermal performance anal. of multiplate insulation 78−8888
LMFBR, thermal-hydraulic core anal., interassembly heat transfer, TRITON computer code 79−59153
LMFBR, thermal-hydraulic transients anal. with forced diversion model 78−29553
LMFBR, TOP, thermal hydraulic anal. of fuel blockages 80−13659
LMFBR, transient boiling of Na in 7-pin fuel bundle under loss-of-flow conditions 79−41007
LMFBR, transient boiling of sodium in seven-pin bundle under transient overpower conditions 79−76056
LMFBR, two-phase flow calculations in low-pressure systems 80−103068
LMFBR, unified model for fission gas release and Na boiling in reactor coolant channel 78−8921
LMFBR, US flowmeter *(Japanese)* 78−78455
LMFBR, W-ARD air flow tests, COBRA-IV comparison 80−27734
LMFBR, wastage effects in small leak Na+water reactions, safety considerations 78−82418
LMFBR, water leaks in secondary cooling circuit boilers 78−86572
LMFBR, whole core thermal hydraulic transient code 80−18387
LMFBR, wire wrapped assemblies, subchannel flow rates, meas. using turbulent flow split expt. 79−59140
LMFBR, wire wrapped rod bundles, coolant mixing, peripheral flow prediction 80−73891
LMFBR, yield characts. of short-lived fission products in Na heat-transfer agent 78−66338
LMFBR 1200 MW(e) performance rel. to core height reduction 79−9684
LMFBR 19-pin simulated fuel assembly, dynamic boiling tests 79−31029
LMFBR accident, Na$_2$O aerosol behaviour in closed chamber under thermal convection flow 77−57723
LMFBR accident anal., noncondensible void fraction effect on freezing of flowing fluids 79−31013
LMFBR coolant, decontamination by low-pressure distillation 80−13694
LMFBR coolant, simple multichannel thermal-hydraulic model for transient behaviour anal. 79−49660
LMFBR coolant and cladding temp. distrib., PACT probabilistic method 77−46256
LMFBR coolant flow, flux distortion flowmeter meas. 79−68858
LMFBR coolant flow monitoring by balanced outlet temp. signals 79−13393
LMFBR coolant flow rate meas. suing electromagnetic convertor 80−73887
LMFBR coolant scram transients, thermohydraulic behaviour 79−67889
LMFBR cooling channels blockages, simulation testing *(German)* 78−94044
LMFBR cooling circuit, calibration of EM flowmeters by average frequency method 80−570
LMFBR cooling systems, reliability 80−57838

fission reactor cooling and heat recovery continued
LMFBR core, partial failure expts., Na boiling in heated annular channel with blockage 77−42108
LMFBR core assemblies, interassembly heat transfer, using CORTEMP code 79−59154
LMFBR core design for Na void effect minimisation 79−9683
LMFBR core disruptive accidents, flow regime obs. in two-phase volume heated boiling pools 79−31014
LMFBR core meltdown accident anal., radiation-cond. problems 80−19381
LMFBR core meltdown accidents, void distribution in volume-heated boiling pools 77−46318
LMFBR core orificing, optimised method 78−8881
LMFBR core orificing computer code 79−9681
LMFBR core restraint transient responses, CORTAC 3-D thermal hydraulic model 80−18390
LMFBR coupled fluid-struct. problems, advanced Eulerian method 78−682
LMFBR deck insulation, thermal radiation transfer, through non opaque insulator 79−59147
LMFBR design requirements to alleviate thermal transient effects 79−97767
LMFBR evaporator tube, critical heat flux meas. 80−591
LMFBR finite hexagonal bundles, laminar mixed-convection heat transfer 79−607
LMFBR finite hexagonal bundles, three-dimensional coupled coolant cell heat transfer anal. 80−586
lMFBR fuel and blanket transient thermal performance characteristics 80−68880
LMFBR fuel assemblies with wire-wrapped rods, thermal-hydraulic anal. 80−47549
LMFBR fuel assembly, 19 pin, simulation of flow blockage 80−582
LMFBR fuel assembly, 3-D numerical simulation, thermal-hydraulic behaviour anal. 79−59143
LMFBR fuel assembly, anal. of loss of piping integrity accident 80−27783
LMFBR fuel assembly, coolant mixing, subchannel vels., electrolytic tracer, isokinetic sampling techniques 77−18653
LMFBR fuel assembly, edge blockage in 19-pin Na-cooled bundles 78−13292
LMFBR fuel assembly, thermal consequences of plenum fission gas release, TRUMP thermal anal. 80−47646
LMFBR fuel expansion, nonequilibrium evaporation and condensation 77−42021
LMFBR fuel intra-assembly flow mixing uncertainty, statistical determination methodology 80−73890
LMFBR fuel rod, hydraulic anal. of turbulent fluid flow by Galerkin method 79−30893
LMFBR fuel rod subassembly, thermal-hydraulic anal. as distrib. parameter system *(Japanese)* 80−68736
LMFBR fuel subassembly, approach for treating two-dimensional coolant boiling 79−31030
LMFBR fuel subassembly temp. noise prediction, Monte Carlo approach 79−13392
LMFBR generator, SWRP deposition from testing and cleaning 80−22924
LMFBR HCDA, containment response anal. to PAHR failure 79−49672
LMFBR HCDA, energetics of bubble expansions, potential attenuation mech. 80−83197
LMFBR HCDA, heat transfer from pool of molten UO$_2$ to concrete slab 78−8930
LMFBR HCDA, I-D compressible coolant dynamics, numerical anal. using EULFCI code 80−68733
LMFBR HCDA, Na interaction with basalt concrete and silaceous firebrick 80−47638
LMFBR HCDA, nonlinear dynamic anal. of piping system 80−5290
LMFBR HCDA, potential for plugged core pressurisation following LOF accident 79−76084
LMFBR HCDA, radiological consequences, attenuation due to radiative cooling 78−13296
LMFBR HCDA, vapour bubble-liquid slug heat transfer, Taylor instability mechanism 78−8939
LMFBR HCDA radiological consequences, attenuation by thermal radiation 77−46321
LMFBR heat exchangers, liquid metal temps. in pipes with wall fast flow discontinuities *(Spanish)* 77−74907
LMFBR inherent secondary shutdown assembly, hydraulic tests 79−49666
LMFBR intersubassembly transient heat transfer code, TCLUST1 80−63231
LMFBR large cores with interassembly heat transfer, flow orificing 78−13208
LMFBR LOCA, dynamics of natural circulation 80−57836
LMFBR LOCA, use of temperature variance to detect sodium boiling 79−54527
LMFBR meltdown conditons, molten fuel+coolant interaction, expts. 77−23225
LMFBR mesh-packed cold traps, O$_2$ impurity deposition, computational program 80−57824
LMFBR ML-3 Na circuit, electrical and control installations *(Spanish)* 80−57819
LMFBR modular steam generator tube plates, stress anal. 79−71883
LMFBR modular steam generators, heat transfer intensification using helically-ribbed tubes *(Czech)* 80−560
LMFBR molten oxide fuel layer, effect of radiation heat transfer on maximum nonboiling thickness 80−47558
LMFBR Na heated steam generator tubes, transition boiling characts. 79−81006
LMFBR Na loop computer control system based upon TOSBAC-40 multicomputer 80−47662
LMFBR Na-cooled 7-rod bundle acoustic and temp. noise obs. 79−13391
LMFBR outlet plena, stratification criteria 80−73892
LMFBR outlet plenum, air flow model, interferometric meas. of fluctuating temp. using FFTF 78−89943
LMFBR outlet plenum mixing, 3-D numerical simulation 78−8880
LMFBR outlet plenum transients, expt. and anal. using PLENUM-2 code 79−49664
LMFBR overpower excursions, mechanistic model of fuel freezing, channel plugging and continued coolability 78−58371

fission reactor cooling and heat recovery continued
LMFBR pin bundle, model to correlate wake residence time meas. behind blockages 79—31027
LMFBR piping tee, multiple jet thermal mixing 78—8879
LMFBR plant, modelling thermal hydraulic transients 77—88207
LMFBR pool type, study results 80—13575
LMFBR post accident containment response, effects of evaporation and condensation, using CONAN code 80—47637
LMFBR postulated core meltdown, onset of foam flow regime in volume heated boiling pool 79—31015
LMFBR primary heat transport pipe rupture and hydraulic response 79—9784
LMFBR primary pool, transient buoyancy induced flow stratification 79—612
LMFBR reactor vessel, buoyancy induced flow redistrib. 78—8887
LMFBR rotating shield plug annulus, Na vapour deposition rates and gas flow patterns 80—68732
LMFBR safety, collocation method soln. of radiation-conduction problems 80—13720
LMFBR safety, KNK II driver zone, Na boiling in 7-pin bundle 77—88246
LMFBR safety, local blockage formation and growth in grid spaced fuel elements, model 77—88243
LMFBR safety, local cooling disturbances, in-pile Na loop investigation 78—674
LMFBR safety anal., sAS-3D evaluation of boiling at decay-heat levels in FFTF 80—47634
LMFBR safety testing, scram signal generator for fluid motion monitoring 80—18551
LMFBR secondary cct. components 79—97793
LMFBR secondary Na ccts., design, construction and operating experience *(French)* 79—97789
LMFBR six channel subassembly blockages, max. Na temp. correlation 79—85656
LMFBR sodium-water heat exchangers, design of expansion pipe-bend 77—30648
LMFBR steam cycle conditions, comparison 80—18406
LMFBR steam cycle selection 80—18403
LMFBR steam cycles, thermal efficiency of saturated cycle and superheated Benson cycle 80—18407
LMFBR steam cycles comparison, PLBR design 80—18405
LMFBR steam generator, dryout characts. 78—90990
LMFBR steam generator, few-pressure model for transient two-phase flows in networks 79—59136
LMFBR steam generator, small leak detection by surface oscillation meas. during Na-water reaction 77—67789
LMFBR steam generator, small-leak Na+water reaction, dissolution rate of hydrogen 78—29545
LMFBR steam generator heat exchange doublex tube element, design and development 79—71882
LMFBR steam generator stability, STMFREQ code 80—73908
LMFBR steam generator tube thermal oscillation obs. 79—9672
LMFBR steam generators, behaviour of heat exchange tubes in Na-water contact 80—13670
LMFBR steam generators, leak detection of steam or water into sodium 79—13434
LMFBR steam generators, leak detection of water into sodium, magnetic flowmeter bubble noise monitor 80—9000
LMFBR steam generators, water leakage detection systems, development 80—37546
LMFBR subassemblies, coolant boiling calc., using Claymore code 78—82473
LMFBR subassemblies, TCLUST1 transient code 80—18391
LMFBR subassembly, central blockage wake anal. 78—29556
LMFBR subassembly, multichannel model for fuel coolant interaction 80—13653
LMFBR subassembly local boiling detection by outlet temp. fluctuation analysis 79—13390
LMFBR subassembly pressure loss, expt. study and evaluation 80—73894
LMFBR subchannel coolant flow behind blockage, temp. noise obs. 79—13389
LMFBR system design requirement to accommodate Na spillage 79—97845
LMFBR thermal hydraulics 80—27718
LMFBR thermal transients, impact of bypass flow 79—9680
LMFBR thermohydraulic transient simulation, appl. of multiple time-step integration in Super System Code 80—47552
LMFBR transient behaviour, effect of steam cycle 79—49678
LMFBR transient thermal hydraulic anal. in forced convection regime using TRANSENERGY 80—18393
LMFBR transition to natural circulation from an initial isothermal state 79—85653
LMFBR triangular rod array, flow resistance wall shear stress in interior subchannel 80—63244
LMFBR UO_2 pin meltdown simulation by direct electrical heating 77—88215
LMFBR vented assembly cores, appl. to nonlinear network anal. to hydraulic modelling 78—13207
LMFBR vented assembly hydraulic modeling and testing, vent flow discharge coeff. determ. 79—59148
LMFBR vented fuel assembly, thermodynamic modelling and testing 80—83144
LMFBR whole core transient anal., COBRA subchannel anal. code 80—18388
LMFBR whole core transient thermal hydraulic anal. with CORTRAN code 80—18392
LMFBR wire wrap spaced rod bundles, laminar, transition, and turbulent parallel flow press. drop 79—26478
LMFBR wire wrapped rods, 3-D thermal-hydraulic anal. 77—79425
LMFBR wire-wrapped assemblies, turbulent mixing expt. and model 80—590
LMFBR wire-wrapped blanket bundles, pressure drop meas. 80—587
LMFBR wire-wrapped subassemblies, Na boiling behaviour 79—31031
LMFBRs, mixed Na convection problems, digital model simulation *(French)* 80—42737
LMFRB steam generator design and development 80—5224
LMRBR, interchangeable core assessment, coolant orifice zoning 80—102229
LOCA, 3-dimens. flow with multiple interfaces 79—41024
LOCA, anal. of containment heat transfer 77—46248

fission reactor cooling and heat recovery continued
LOCA, anal. of secondary coolant system influence on LOCE 79—89431
LOCA, blowdown phase separation mechanics effect on containment pressure response 79—93771
LOCA, CHF expts. on effect of heated-wall press./temp. history on blowdown heat transfer 80—23005
LOCA, computer simulation of reflood heat transfer and hydrodynamics 79—67891
LOCA, condensing heat transfer 78—21684
LOCA, condensing heat transfer coeff. based on mass condensation 78—13304
LOCA, cooling mechanism during transient reflooding 77—88208
LOCA, creation and persistence of mist-laden containment atmospheres 79—89421
LOCA, data analysis using computer-aided models *(Czech)* 80—73949
LOCA, effect of entrance conditions on countercurrent flooding limits in the restricting upper tieplate region 80—18529
LOCA, experimental and theoretical study of the blowdown of the secondary side of a steam generator 80—761
LOCA, extreme loads and associated safety aspects, review 79—22405
LOCA, flow boiling dryout, transient heat transfer investigation 80—32359
LOCA, gravity-driven reflood hydrodynamics, EFLOD code 79—89426
LOCA, heat removal by passive heat sinks, model anal. 77—42019
LOCA, international standard problem exercises in nuclear safety 80—756
LOCA, modelling two-phase hydrodynamic phenomena, pipe blowdown with Freon-12 80—5267
LOCA, models for estimation of critical flow in two-phase systems 79—36361
LOCA, pressure oscillation in subcooled decompression under temperature gradient 80—559
LOCA, quench phenomena correlation for bottom flooding 79—54520
LOCA, rewetting of hot surface, development of cooling wave 80—27767
LOCA, straight pipe blowdown tests and code verification [of reactor LOCA] 80—759
LOCA, thermal hydraulic phenomena resulting in early critical heat flux 79—81005
LOCA, transient flow boiling anal. method 79—26549
LOCA anal., 1-D model of vapour generation in steady flashing flow 80—23004
LOCA anal. program TECAR 77—88250
LOCA analysis in small compact reactors uisng RELAP4/MOD5 thermal hydraulic code 80—68852
LOCA capability code for utility appl. 78—21690
LOCA codes, characteristics of two-phase one component flow with slip 77—83019
LOCA consequences, hydrodynamics mass method anal. 80—73909
LOCA containment anal., new condensation mass removal model 79—89423
LOCA in containment with press. suppression system, anal. of press. oscill. phenomena 79—67878
LOCA in PWR, critical two-phase flow, nonequilibrium vapour production model 80—52719
LOCA in water reactors, reversal of laminar flow in circular pipe 78—50271
LOCA quench front model for Transient Analysis Reactor Code 80—47550
LOCA reflood phase, thermo-hydrodynamic behaviour, REFLA-1D code 80—47592
LOCA rewetting, investigation in Freon-113 vapour environment 80—32358
LOCA simulation, armature testing *(German)* 80—42785
LOCA-generated drop size perdiction, thermal fragmentation model 79—89422
local Green's function method for heat conduction and fluid flow problems 77—79420
LOCE blowdown flow meas., improved spool piece 80—27727
LOFA, transient crit. heat flux, Freon 12 coolant 79—30954
LOFT, contribution to nuclear reactor safety 80—106139
LOFT, requalification following LOCE 80—57904
LOFT core fluid conditions during blowdown and refill 79—89440
LOFT drag disc turbine meter rakes for two-phase flow measurement 80—102260
LOFT facility, commercial PWR systems safety 80—37548
LOFT facility, PWR LOCA anal., system blowdown, core thermal response, emergency core cooling 80—37549
LOFT facility, PWR LOCE, two phase flow meas. instrumentation 80—37550
LOFT fuel design and operating experience, exposure to LOCA 79—89438
LOFT instrumented fuel design and operating experience during PWR LOCE 80—37551
LOFT LOCE fuel module structural response, computer code prediction 79—89439
LOFT reactor secondary cooling system, waterhammer phenomena 80—57905
longitudinal convective fins, internal heat generation, optimization 80—9333
loss of coolant effect on resonance escape probability 80—22963
loss-of-coolant accidents, German Risk Study *(German)* 80—57866
low temp. heat extraction from nuclear power plants for district heating 78—37456
LPWR, postulated LOCA, de-entrainment phenomena from droplet cross flow in vertical bundles 79—89430
LPWR fuel cladding temp. predictions for LOFT LOCE L1-5 79—89446
LWR, B and W cross-flow anal. by LYNX codes 80—22906
LWR, boiling heat transfer anal. 80—27724
LWR, chemical factors controlling γ radiation fields around coolant circuits 80—5371
LWR, decay heat power evaluation in shutdown reactors 80—5257
LWR, effect of district heat prod. on reactor operation and safety 79—85624
LWR, fission product decay heat, revised ANS standard 80—13649
LWR, fuel rod microstruct. changes associated with post-DNB operation during power-cooling-mismatch 78—21688
LWR, generalized theory for predicting mass effluence during reactor reflooding 79—36352
LWR, heat transfer model of quenching in reflooding phase *(Japanese)* 78—8874

fission reactor cooling and heat recovery continued
LWR, I spiking, release mechanism and its verification in plant operation 79−59229
LWR, interfacial mass and momentum transfer in two-phase flow 80−27725
LWR, loss of coolant accident, behaviour of Zircaloy fuel cladding *(Japanese)* 79−71889
LWR, NRC safety research programs, fuel behaviour, operational safety, metallurgy and materials 80−13705
LWR, pipe system failure characts., effects on plant availability and capacity 78−17375
LWR, post-LOCA γ-ray energy redistrib. and effects 78−13280
LWR, post-LOCA containment anal., space-dependent condensing heat transfer coeffs. 80−47630
LWR, power cooling mismatch accident, molten fuel radial motion and cladding melting 80−13638
LWR, solar-assisted heating, SOAR power system concept 80−55820
LWR, spray droplet heat transfer in LOCA 80−32380
LWR, stationary boiling front in liquid film cooling of a vertical heated rod 79−45341
LWR, system design for transfer of heat decay to external environment *(Italian)* 77−38320
LWR, two-phase critical flow phenomena 80−27723
LWR, two-phase flow, analytic simulation 80−13551
LWR anal., pressure-crossflow soln. method, COBRA-III codes 78−82417
LWR anal., verification of the RETRAN computer code with measured reactor coolant pump coastdown data 79−89406
LWR austenitic stainless steel coolant tubing, bending props. *(Czech)* 79−67851
LWR circulator auxiliaries system modelling 77−88221
LWR core, thermal and hydraulic behaviour, modelling in HOTRAN-3 *(Hungarian)* 80−32401
LWR core blowdown, dynamic behavior of valves, computer simulation 80−5288
LWR core transient anal. using coupled neutronics and thermal hydraulic models 80−715
LWR cores, single-fluid thermal hydraulic anal. 80−18410
LWR critical heat flux calc., anal. of empiric relations using CRISIS code *(Bulgarian)* 80−68766
LWR ECC, UCFLOOD code for bottom reflooding heat transfer 79−49728
LWR emergency core cooling component experience data, defect anal. programme 79−18010
LWR fuel assemblies, coolant channel closure modelling using pattern recognition techniques 80−42835
LWR fuel rod under power transients, CRATER code calc. *(French)* 80−42789
LWR fuel rods, power cooling mismatch induced failure, meas. fission product release 79−93772
LWR LOCA, analysis, role of LOFT program 80−18531
LWR LOCA, assessment of the RELAP4/MOD6 reactor transient thermal-hydraulic code 80−42826
LWR LOCA, fission product decay energy release rates following ^{235}U fission 80−57894
LWR LOCA, fission product release from defected fuel rods 80−23031
LWR LOCA, heat transfer in the inverted annular flow regime during reflooding 79−49731
LWR LOCA, modelling of press. and temp. changes in two-phase, two-component flow *(Bulgarian)* 80−68904
LWR LOCA, operating contractor's view of LOFT 80−23007
LWR LOCA, rewetting front axial and radial heat conduction 80−18528
LWR LOCA, rewetting models, review and comparison 80−83194
LWR LOCA, TRAC calculations of ECC bypass phenomena in a 1/15-scale experimental facility 79−49725
LWR LOCA, two-phase flow instrumentation for safety anal. 80−102259
LWR LOCA, utilisation of LOFT information for licensing 80−18532
LWR LOCA analysis, TRAC-1D code for Standard Problem 2 78−13288
LWR LOCA reflooding, prediction of quench fron velocities for constant inlet flooding rates 80−23000
LWR LOCA safety analysis, thermohydraulic phenomena, review *(German)* 79−13430
LWR materials of primary-circuit components, safety concepts, quality *(German)* 80−73914
LWR NRC safety research programs, thermo-hydraulics and computer code development, loss-of-coolant accident, emergency cooling core event 80−13704
LWR PCM transient, UO_2 fuel melting and Zircaloy cladding thermal failure 80−42834
LWR piping, intergranular stress-corrosion cracking 80−81234
LWR power plant, radioisotope activity meas. in secondary loop coolant 80−5345
LWR primary circuit component production, metallurgical aspects 79−36330
LWR primary coolant leakage detection using acoustic monitoring system 80−700
LWR safety, condensation heat transfer in stably stratified systems 80−63311
LWR safety, critical flow of two-phase one-component mixtures *(Italian)* 79−71880
LWR safety concerns, future possibilities 80−13702
LWR safety research programs by US NRC, review 80−42796
LWR steam generator behaviour during core blowdown tests 80−772
LWR steam generator tube integrity in KWU nuclear power plants 80−5287
LWR thermohydraulics, safety aspects 80−5266
magnetite particles, deposition from high velocity water onto isothermal tubes 77−67801
Magnox reactors, moderator graphite corrosion protection, H_2 injection into Wylfa reactor I coolant gas 77−6490
Magnox reactors, moderator graphite corrosion protection coolant comp. effect on radiolytic graphite/CO_2 reaction 77−6489
Maine Yankee reactor, thermal performance 80−22907
MARIA research reactor, dynamics model for fast transients anal., code TOTEM 80−37419
marine reactor systems, Monte Carlo reliability anal. of power and heat removal systems *(Japanese)* 78−58396
mass exchange rates in ^{16}N tagged slug flow 80−73911

fission reactor cooling and heat recovery continued
mass transfer model in high temp. high press. water circuits 79−67813
materials interfaces, thermal radiation props. 79−80980
melt fragmentation, initiation in fuel-coolant interactions 80−13537
mesh-packed cold traps, impurity interaction anal. 78−25262
methods review *(Italian)* 78−4978
MHD, Hall effect on unsteady flow due to rotating infinite disc 78−18354
MHD channel flow, effects of couple stresses 78−18353
MHD chemically reactive channel flow, effect of external circuit on dispersion of soluble matter 79−1267
mixing tees, thermal phenomena, flow visualisation studies 77−42039
mobile He cooling loop system for post-accident heat removal expts. 79−13403
molten fuel-coolant interaction, simulation experiment 79−17991
molten fuel-coolant interaction studies, simulated reactor accident, windscale shock tube rig 78−58363
molten metal-reactor coolant interaction, vapour film collapse expts. 79−13474
monitoring of boiling water and of steam content using Cherenkov radiation 80−73957
Monju heat transport system design and related R & D work 79−97791
Monte Carlo anal. of time depend. heat conduction with convective boundary conditions 78−680
multichannel low flow, boiling thermal hydraulic anal. 79−67885
multiphase processes, density-wave oscillations, linear stability anal. 80−48775
multiple volume blowdown expt. and prediction comparison 79−93814
multiple-jet thermal mixing in a piping tee 79−81938
MWR feedwater and recirculation flow, minicomputer-based digital control 80−23027
Na loop safety facility expts., disassembly at HFEF/N 79−45444
natural-circulation steam generator model for optimal steam generator water level control 80−68876
Navier Stokes eqns. for fluid flow and heat transfer anal., treatment of cylindrical co-ord. singularities 79−90213
neutron and photon, heat deposition, rate in nuclear reactor 78−29565
neutron diffusion equation, multigroup theory 80−27695
neutronic noise, relations with coolant temp. fluctuation and control rod vibr. at KUR 78−58327
nonequilibrium transient flow boiling, method of characts. soln. 80−14789
nonlinear surface absorption activity in primary circuits *(Russian)* 80−9340
NSSS, computerised simulator 80−22914
nuclear heating in thick iron slabs at the ORR pool side facility 80−63241
nuclear power station PWR, ice condenser system *(Japanese)* 80−91214
nuclear power station with HTR and He turbine, dry closed circuit cooling, principles and advantages *(German)* 78−74426
nuclear power stations, accumulation ponds cooling possibility analysis *(Slovenian)* 80−91208
nuclear power stations, transport process models for dissociative cooling *(Russian)* 79−13410
nuclear power stations, unsteady state processes for dissociative coolant *(Russian)* 79−13411
nuclear reaction flow boiling nucleate region, dynamics 77−88205
nuclear steam superheating, design tests of Zr channels 80−5211
OGL-1 high temp. in-pile gas loop, construction and performance tests *(Japanese)* 79−71881
once through steam generator, Na-heated, stability anal. nuclear reactor systems model 80−91218
once-though boiling flow system, density wave instability 79−22367
orthotropic circular cylinders, steady and unsteady solutions 80−10110
overheated water reactor pin rewetting, effect of thermal diffusion from fuel pellets 77−46212
oxide fuel transient gas release and swelling, generalised parametric model 77−83039
parallel channel forced convection boiling upflow system, instabilities 80−9327
parallel channel of forced convection boiling upflow system, instabilities 77−61494
passive containment system 77−42138
PBHTGR, core behaviour following massive air ingress, graphite corrosion eval. *(German)* 80−83181
PBHTGR, natural convection after heat removal 77−46245
PBHTR, afterheat removal anal. in accidents 77−46244
PBHTR, afterheat removal system failure, radiant heat transfer anal. 80−95364
PBHTR, depressurisation in primary circuit after failure of main coolant duct, analysis 78−25316
PBHTR, primary coolant purification by Ti gettering *(German)* 79−3204
PBHTR, source of nuclear process heat, development of power plant, overall time and cost estimates 77−3089
PBHTR, steady state coolant gas activity, STADIF-II code 78−29569
PBR, LOCA, evaluation code NAKOGAS-1 79−13492
PBR core, coolant flow predictions using PEBBLE computer code 79−54474
pebble bed HTR, delayed after heat removal *(German)* 80−106102
pebble-bed high-temp. reactor as a source of nuclear process heat 77−10479
PFR, electrical supplies and Na pumping system 80−52723
PFR primary cct., operating experience and CDFR design intentions 79−97870
Phenix and Super-Phenex, primary ccts. *(French)* 79−97780
PHENIX reactor exchanger, gas natural convection effect in annular spaces *(French)* 79−613
pin bundle, two-phase flow, eqns. of motion 78−86570
pipe bends with flanged tangents, bending and pressurising 79−94516
pipework analysis using code PACE 2 79−93707
piping conveying swirling liquid, free harmonic wave propagation 77−84187
piping system design, rationalisation of power plant pipe break criteria 80−99205
plant efficiency at Beaver Valley power station number 1, anal. of generating capability deficiency 79−67828
PNP-3000, prototype nuclear process heat reactor, core temp. transients, heat transfer calc. *(German)* 80−83180
pool swell dynamics during depressurisation, exact anal. soln. by method of characteristics 78−29555

fission reactor cooling and heat recovery continued
- pool swell dynamics during depressurization 79—30900
- pool-type reactor noise analysis and expt. 79—3195
- porosity correction of conductivity using spherical pore geom. 77—42722
- porosity correction to thermal conductivity based on analytical temperature solutions 79—59173
- power burst facility loop modification, appl. of RELAP4 code 79—89432
- power burst facility low pressure CHF in closely packed rod bundle 79—59144
- power plant cooling system design, optimal system synthesis, tower, pond 77—14260
- power reactor, water cooled and moderated, tube film boiling heat transfer coeffs. 80—73877
- power station performance evaluation by thermal hydraulic anal. 79—67831
- power system equipment and components, multiphase flow prediction 80—64616
- pressure boundary leakage detection system 80—63306
- pressure tube explosive rupture anal. using scaled-down model of CIRENE reactor 80—18449
- pressure tube type reactors, SENHOR-IV computer code for small pipe break anal. 79—89397
- pressure vessel, subjected to thermal shock, temp. decay, 2-D soln. 77—88209
- pressure vessel blowdown two-phase level swell calc. using drift flux correl. 79—89428
- pressure vessels, water pressure testing, test method and anal. *(German)* 78—25260
- pressure-induced diversion cross flow for rod bundle subchannel interconnection geometry 78—13215
- pressure-suppression systems, direct heat transfer 78—94096
- pressuriser, multiple surges pressure transients 77—26836
- primary circulator pressure vessel, structural representation in stress anal. 80—27703
- primary coolant circuit filter for fission products, HTRs *(German)* 77—74915
- primary coolant circuit service life, working condition effects *(Czech)* 80—73885
- primary coolant flow rate determ. using gamma/neutron ratio near primary line 77—65254
- primary coolant flowmeter 80—73912
- process heat from nuclear steam supply systems, appl. to prod. and treatment of liquid and gaseous prime movers *(German)* 79—87944
- prompt burst energetics experiments, UC series, fuel cladding coolant systems 79—49768
- prompt burst excursion experiments, fuel pin modelling 79—49769
- propagating physical quantity transit time estimation, improved correl. method, coolant bubbles appl. 78—94067
- Prototype Large Breeder Reactor pool concept 79—9670
- pulsed-neutron sources for flow measurement 79—93695
- pump coolant tests, computerised monitoring 78—70585
- PWR, 1300 MW, emergency core cooling system probabilities design 77—38365
- PWR, 450 MWe, noise obs., analysis and interpretation 78—94072
- PWR, alternative ECCS concepts, verification study 80—13539
- PWR, CIRENE reactor, zircaloy calandria tubes, stress evaluation using strain data *(Italian)* 77—50204
- PWR, computer program for accident anal. *(German)* 79—85623
- PWR, control and effects of pressure vessel failure in steam-water cycle 80—770
- PWR, control of fission products activity in primary coolant, computer code 80—32537
- PWR, control systems for selectively inhibiting protection system functions 78—37418
- PWR, coolant pump motors, max. freq. decay rate determ. 79—45337
- PWR, core reflooding, progress of hardening front *(French)* 80—91211
- PWR, crit. and transient heat flux exam. *(Hungarian)* 78—86580
- PWR, critical heat flux in fuel bundles at low mass vel. 80—73900
- PWR, data acquisition system for high press. water loop *(Hungarian)* 78—82432
- PWR, DNB is coldwall thimble cell geometry, partially bowed heated rod effect 79—54470
- PWR, dynamic pressure, scale flow modelling of random press. power spectral density 80—83143
- PWR, ECC performance during LOFT expts. 78—21709
- PWR, emergency core cooling, alternative injection configurations 78—21696
- PWR, European Community Italian Centre activities *(Italian)* 80—785
- PWR, evaluation of emergency conc. cooling systems 78—21697
- PWR, evaluation of environmental and in-plant effects of T recycle and build-up 78—33273
- PWR, fatigue crack growth in steel in reactor coolant 77—77584
- PWR, fluid, structure interactions, numerical anal. method 80—73884
- PWR, fluid-structural interactions, one-dimensional networks, MULTIFLEX code 80—13535
- PWR, German, U-tube steam generators, inspection findings 79—9849
- PWR, heat transfer equations for boiler tubes *(Rumanian)* 79—3189
- PWR, I spiking in coolant for defective fuel rod operation 78—33272
- PWR, in-reactor loop expts. on corrosion product transport and water chemistry 78—58335
- PWR, LOCA, anal. of LOFT semiscale test *(Japanese)* 79—17998
- PWR, LOCA, cold leg break during blowdown, ROSA II study *(Japanese)* 79—6750
- PWR, LOCA, one-dimensional network for multidimensional pressure wave propagation with hydrostructural interactions 79—89403
- PWR, LOCA, RELAP4/MOD6 program, test prediction for German PKL test K5A 80—13642
- PWR, LOCA, steam-water mixing 80—13651
- PWR, LOCA anal. for consolidated nuclear steam system 79—49729
- PWR, LOCA test, effect of LOFT pressurizer on RELAP4/MOD5 modelling 78—13286
- PWR, modification of subcooled boiling calc. in COBRA-3/KFKI program *(Russian)* 78—82434
- PWR, MULTIFLEX code, anal. of hydraulic force with hydro-structural interactions during LOCA 78—58373
- PWR, Oconee station, steam generator availability 80—22921
- PWR, operational dynamics, digital simulation model 80—27751
- PWR, peak cladding temp. sensitivity to LOCA reflood parameters 78—86639
- PWR, power distrib. comparison of U and Pu fuel in KWO core 77—14224

fission reactor cooling and heat recovery continued
- PWR, primary cct. leakage simulation, safety aspects *(German)* 78—33239
- PWR, primary coolant leak *(French)* 79—63724
- PWR, primary coolant leakage accident, flow models *(French)* 79—63725
- PWR, pump operation with two-phase water-steam flow *(French)* 79—63726
- PWR, radionuclide surface activities meas. 80—13941
- PWR, reactor coolant pump failure investig. at Arkansas Nuclear One 80—9336
- PWR, RETRAN simulation of the Three Mile Island Unit 1 turbine trip test 80—18512
- PWR, rod bowed to contact departure from nucleate boiling tests in coldwall thimble cell geometry 79—30892
- PWR, ROSA-II UHI tests in JAERI 78—21695
- PWR, scaling air-water flooding 80—73904
- PWR, sensitivity of LOCA heat transfer anal. 78—50246
- PWR, shutdown heat removal systems, reliability fault tree anal. and β-factor method 80—63331
- PWR, small scale ECC bypass data anal. 80—18505
- PWR, steady-state and transient CHF meas. in Freon-11 79—49732
- PWR, steam generators, design, subcooled and bulk boiling correls. 79—611
- PWR, thermal and hydraulic design considerations 79—49651
- PWR, thermohydraulic processes in high press. water loop, constructional details of loop *(Hungarian)* 78—82431
- PWR, thermohydraulic processes study, models and expt. instrumentation *(Hungarian)* 78—82433
- PWR, Three Mile Island, Pennsylvania, USA LOCA 79—89398
- PWR, Trojan reactor, net free containment vol. 78—21679
- PWR, two circuit system, licensing and design, European view 80—57930
- PWR, two phase flow modelling for LOCA *(French)* 80—78349
- PWR, two-phase critical flow in long nozzles 80—13550
- PWR, velocity and press. distrib. at core inlet 77—83018
- PWR and rod bundle cores, thermal-hydraulic THINC-IV computer program 77—46216
- PWR blowdown, pressure field and core barrel loadings, computer codes 80—13665
- PWR boiler steam generators, two-phase flow problems in low press. transients *(French)* 80—78350
- PWR boiler tubes, denting type corrosion, control by use of neutralisers 80—106109
- PWR CANDU, corrosion product transport, deposition on fuel bundles, press. tubes 77—61492
- PWR components subject to thermal shock, heat transfer coeffs. 80—32332
- PWR constructional elements vibrations, due to cooling medium flow, meas. and evaluation *(Hungarian)* 80—63304
- PWR coolant system, pipe rupture motion, time-history excitations 80—47602
- PWR coolant system corrosion product composition and significance 79—9689
- PWR coolant system under seismic and LOCA loads, dynamic anal. 77—6512
- PWR coolant water pumps, cavitation detection, brief review *(German)* 77—74906
- PWR core, steady-state single stage thermal anal. of hot assembly subchannels 78—13212
- PWR core, thermal analysis, Monte Carlo method 80—47603
- PWR core barrels with and without holes, various edge conditions, hydrodynamic vibrations 80—78406
- PWR core thermal-hydraulic response during steam line break accident 80—18384
- PWR critical heat flux in rod bundles using round tube correlation 80—73898
- PWR crud descriptive model 79—9691
- PWR depressurisation, hydraulic analogy 78—50243
- PWR differential rod worth and feedback coeff. online estimation system 79—9798
- PWR downcomer annulus model, correl. for penetration of ECC water 79—76085
- PWR dynamical behaviour modelling in FORTRAN 80—91217
- PWR dynamics, lumped parameter model, eval. of assumptions 80—585
- PWR ECC system performance, best-judgement anal. 77—57728
- PWR emergency core cooling system, design for higher reliability using fault-tree anal. and probabilistic evaluation methods 77—74976
- PWR experimental rig, high pressure loop cooling circuits safety aspects *(German)* 80—32397
- PWR flow transients, critical heat flux predictions using CODA 1-D coolant dynamics code 80—42817
- PWR fluctuation analysis, detection and meas. of echoes 77—61488
- PWR fuel anal. and testing, contrib. of LOFT 79—89437
- PWR fuel assemblies, LOCA behaviour in multirod burst tests 80—27739
- PWR fuel assembly, thermohydrodynamic process, obs. 79—30902
- PWR fuel clad failure characterisation based on fission product activity, PROFIP 3 code 80—95365
- PWR fuel pin transient heat conduction and open hot channel DNBR evaluation 79—9679
- PWR fuel rod failure during film boiling, power cooling mismatch test 79—89445
- PWR fuel rods, I spiking, cause and effects 79—59227
- PWR fuel rods, I spiking, general model of origin and behaviour 79—59228
- PWR heat rate improvements, controllable loss system 79—67827
- PWR hypothetical LOCA, best estimate evaluation model 79—89435
- PWR hypothetical LOCA sensitivity to fuel rod material props. 79—89436
- PWR internals, effect of water flow on behaviour and safety *(Czech)* 77—50258
- PWR internals, flow induced random vibr. anal. 77—83016
- PWR LOCA, average void fraction estimate in vertical two phase flow channel 80—73878
- PWR LOCA, blowdown fluid loadings, anal. of structural deformations 80—766
- PWR LOCA, blowdown hydraulic influence on core thermal response in LOFT nuclear experiment L2-3 80—42827
- PWR LOCA, coolant channel blockage during reflood phase influence of blockage shape 80—765

fission reactor cooling and heat recovery continued
  PWR LOCA, determ. of 3-D props. of pressure wave propagation by method of characts. 79—89402
  PWR LOCA, droplet cross-flow phenomena in a large PWR upper plenum 80—47627
  PWR LOCA, effect of cold-leg injection of low press. coolant, ROSA-II study *(Japanese)* 78—17334
  PWR LOCA, effect of rod external thermocouple simulators on steady-state and transient CHF for LOFT reactor 79—49734
  PWR LOCA, effect of steam generator tube rupture, computer simulation 80—23006
  PWR LOCA, effects of downstream geometry on blowdown of subcooled liquid 79—31063
  PWR LOCA, high-pressure Freon blowdown studies with inlet break 79—36367
  PWR LOCA, licensing evaluation calcs. at LOFT 80—23008
  PWR LOCA, LOFT post-test anal. using RELAP4/MOD5 blowdown model 80—42825
  PWR LOCA, LOFT safety anal. calc., carryover rate fraction correl. 80—42822
  PWR LOCA, LOFT tests, TRAC-P1A pre-test calculations 80—42824
  PWR LOCA, opening and extension of circumferential cracks in pipe 80—78364
  PWR LOCA, pressure vessel hydrodynamic loads, effect of subcooled critical flow discharge model 79—49733
  PWR LOCA, pump behaviour conveying two-phase flow *(French)* 80—78351
  PWR LOCA, refill and reflood phase, expt. results of combined injection using PKL test facility 80—760
  PWR LOCA, ROSA-II severe hot leg break for core cooling during blowdown *(Japanese)* 79—9769
  PWR LOCA, subcooled decompression, multidimensional wave prop. with FLASH-genre codes 79—59194
  PWR LOCA, upper plenum LPIS injection in the Semi-scale MOD-1 system 79—49727
  PWR LOCA reflood, effect of low containment press. on peak cladding temp. 80—57897
  PWR LOCA reflooding phase, two-phase flow and heat transfer at and near quench front 80—757
  PWR LOCA Standard Problem 5, TRAC-P1A anal. 80—42823
  PWR LOCA systems transient response, scaling conclusions from the LOFT nonnuclear experimental series 80—758
  PWR LOCE at LOFT facility, instrument calibration for mass flow rate meas. in two-phase flow 80—37552
  PWR main circulation pipe breakdown, mathematical model for primary circuit processes *(Russian)* 77—38368
  PWR main coolant system components, safety assessment 77—71661
  PWR modular steam generator, application possibilities 79—76057
  PWR natural circulation U-tube steam generator, digital code UTSG 78—50242
  PWR neutronic calcs., subcooled boiling and open channel effects 80—23053
  PWR non-LOCA transient anal. using IRT code 80—42819
  PWR nuclear power station, heating, ventilating and air conditioning systems *(Japanese)* 80—91213
  PWR once-through steam generators, operating reliability 80—13558
  PWR power plants, safety technical problems, core cooling *(Russian)* 79—31085
  PWR power station secondary water chemistry study, progress report 80—106108
  PWR pressuriser behaviour during operational transient, math. model 80—63230
  PWR primary and secondary water chemistry, European experience 80—106110
  PWR primary circuit, delayed neutron meas., influence of photoneutrons *(Czech)* 80—5205
  PWR primary circuit, in-service inspection *(French)* 79—22385
  PWR primary circuit component exam., development of automatic equipment 80—13559
  PWR primary circuit constituent materials, design features verification *(French)* 79—17976
  PWR primary coolant system, in-service inspection programs 79—22384
  PWR reactor, steam generator accidents, rel. to impurity enrichment in boiling on surface coated with porous struct. 78—2365
  PWR reflood, analytical treatment, computer code 79—89425
  PWR reflood simulation of FLECHT-SET system using RELAP4/MOD6 78—13285
  PWR rod bundles, radiative heat transfer calc. method 80—33602
  PWR scaled expts., ECC delivery and distrib. 79—89424
  PWR scaled expts., ECCS accumulator performance 79—89427
  PWR steady state thermal anal., single-pass procedure using simplified nodal layout 78—50244
  PWR steam generator, design and development 80—9335
  PWR steam generator blowdown review of international handling procedures 80—690
  PWR steam generator corrosion problems and design implications 79—93812
  PWR steam generator degradation, operating experience, regulatory considerations 79—93817
  PWR steam generator repair options 80—22923
  PWR steam generator tube rupture accident, radio-I behaviour 79—59230
  PWR steam line break, pipe rupture probability 80—18526
  PWR surface boiling, heat transfer with boiling and burnout phenomenon *(German, English)* 78—58330
  PWR thermal-hydraulic design 80—27720
  PWR transient anal. methods, qualification with plant startup meas. 80—18508
  PWR twin header bore welded steam generator design 79—93813
  PWR vessel and primary circuits estimation of reliability, probabilities and adaptive models 80—106125
  quench front in 2-D, difference method 77—79419
  quenching rates on hot surfaces, wetting of outer tube walls by water 77—82996
  radiation heat transfer in a 19-pin sodium-voided bundle 79—85596
  radiative heat release measurements, accuracy of exposure ionisation chambers 79—76070
  radioactive corrosion product accumulation in nuclear steam generators 80—13579
  radiochemical control of reactor cooling water *(Korean)* 78—54820

fission reactor cooling and heat recovery continued
  radiochemical management, reactor cooling system, gamma spectra of radioactive I from direct fission 79—9732
  radiochemical management, reactor cooling system, rapid determ. of radioactive I contamination 79—9733
  radioisotopes in cooling system, prod., transfer, life cycle, radiation calcs. using program system TIBSO 78—54821
  RAGRAF: temp. distrib. calc. code, multi-pin fuel assemblies in stagnant gas atmos. 79—85604
  reactor containment expts., Fourier transform anal. of transient condensation heat transfer coeff. 79—22410
  reactor coolant, automated system for radioiodine anal. 78—35768
  reactor small pin bundles, thermal-hydraulic anal. using COBRA-3M computer code 79—76067
  reactor suppression pool, acceleration forces generated by an oscillating air bubble 79—54546
  redflood heat transfer correlation 80—13548
  reflood heat transfer mechanisms 77—46241
  remote heat supply from nuclear power stations *(German)* 77—352
  residual heat removal system, reliability calc., importance sampling and Monte Carlo advantages 79—606
  RETRAN two-phase flow model, comparison with expt. 80—32330
  rewetting model using generalised boiling curve 79—9675
  rewetting of very hot vertical and horizontal channels by flooding 78—94095
  rewetting process, exptl. and numerical anal. 77—46243
  rewetting temperature in vertical channel coolant flow 79—59117
  rocket reactors, laminar flow, temp.-viscosity induced instabilities in gaseous heated channel 77—18689
  rod bundle critical heat flux at low pressure 80—13547
  rod bundle dryout, liq. film, droplet entrainment and deposition 78—13204
  rod bundle thermal-hydraulic anal., commix-1 program 80—13645
  rod bundle void fraction in two phase flow, fast neutron scatt. technique calibration 79—82017
  rod bundle with helical spacers, air distrib. in water flow 79—30894
  rod bundles, transient critical heat flux 78—94089
  rod bundles with flow sweeping, SIMPLE-2 code for single phase thermal-hydraulic calcs. 77—46215
  rod cluster, recirculating flow due to blockage, finite difference method for temp. 79—3200
  rod cluster assembly, forced convection heat transfer, Poisson eqn. by finite difference scheme 78—79189
  rod thermal response during isothermal loss of coolant expt. 79—89447
  rod thermal response during isothermal loss-of-coolant experiments 79—85651
  rod-bowing effects on critical heat flux, exptl. anal. 77—83015
  rod-bundle in nuclear fuel element, mathematical model for transient subchannel analysis 77—79430
  rod-type fuel elements in gas-cooled reactor, ribbing efficiency 77—42011
  rod-type fuel elements in regular lattice, thermal fields for streamline heat exchange 77—42010
  rough surface heat transfer, turbulent flow in annular channels, result anal. 80—24003
  roughening characts. of surfaces for improved heat transfer 77—18650
  safety, fault tree anal. using Monte Carlo and anal. methods *(Spanish)* 80—57870
  safety rel. to heat transfer problems 77—65276
  safety testing, LOFT (loss-of-fluid) project at INEL 80—32386
  saturated steam parameters in reactor containments with escape of coolant, simplified calc. 80—68764
  SECURE district heating reactor, core design and dynamics 78—37424
  self pressurised systems, thermohydraulic feedbacks 77—50197
  semiopen channel vel. distrib. 77—54303
  semiscale isothermal blowdown, appl. of self-initialized RELAP4 momentum eqn. 78—13287
  SGHWR, particulate corrosion product transients in primary coolant 80—47540
  shell-and-tube heat exchanger, flow distrib. anal., rel. to CRBRP-IHX 77—42052
  shutdown heat removal system failure, fault tree, common-cause anal. 80—63334
  single core subassembly model, coupling of struct. and coolant response 78—8934
  small bore piping, field support to ASME Section III rules 80—63346
  small PWR containment complex and coolant system 79—13402
  SNR 2 LMFBR, design of auxiliary systems 79—97768
  SNR 300, pumps, heat exchangers and manipulator systems 79—97784
  SNR 300 LMFBR steam generators 79—97792
  SNR-300, coolant outlet duct design from neutron transport experiments *(German)* 78—29566
  SNR-300 LMFBR, accidents in tertiary system, dynamic behaviour of steam generators *(German)* 80—83141
  SNR-300 LMFBR, ECCS, decay heat removal during heat sink failure, accident anal. using NOTUNG code *(German)* 80—83185
  SNR-300 LMFBR, hydrodynamic characteristics of shutdown systems 80—5289
  SNR-300 LMFBR steam generator transients, computer simulation 80—23012
  solidification of sphere with internal heat generation and surface convective cooling 77—61496
  spacer pressure losses prediction, analytical model 80—577
  spent fuel pool natural convection, multichannel analysis 79—9786
  spherical element surface boiling dynamics 80—27736
  spray cooling, heat and mass atmospheric transfer 78—94078
  spray ponds as large ultimate heat sink, thermal performance 78—13214
  stability analysis and characts. for two-phase flow eqn. systems with viscous terms 80—59103
  steam content, calculation of the true volume proportion of steam in the driving section of a natural-circulation loop 80—86957
  steam generating channels, volumetric steam content determ. by slow neutron method 79—30903
  steam generation, single-pass, heat exchange intensification in tubular fuel elements 77—61497
  steam generator, flow distribution anal., computer code 79—49653
  steam generator, integral economiser U-tube, mathematical model 77—74911
  steam generator, Na heated, dynamic instabilities 78—17281
  steam generator deactivation of Novovoronezhskya plant 79—71921
  steam generator leakage in the AVR nuclear power station 80—596
  steam generator thermal hydraulics 80—95342

fission reactor cooling and heat recovery continued
steam generator tube performance in water cooled reactors in 1978 80−78399
steam generator tube survey, causes of failures, repair procedure 78−54826
steam generator tubes testing and evaluation, using CIS/DASIO system *(Czech)* 80−63301
steam generators, linearised transient anal. 80−18378
steam generators, once-through, flow dynamics stability *(Czech)* 77−38386
steam generators, thermohydraulics *(French)* 79−63727
steam generators in fast neutron reactors, Na+water reaction *(French)* 79−63756
steam generators of water cooled nuclear power plants, corrosion phenomena, Review 80−558
steam supply system, design developments of Combustion Engineering System 80 79−97755
steam-generating pipe with internal ribbing, heat exchange 78−4979
steam-water flow, mass vel. meas. by Pitot tubes 77−79411
steam-water systems, two-phase press. drop correlations 77−82995
steam/air mixtures, instrument for steam fraction meas. 80−52724
steel 12X18H10T, microdefect behaviour at point of contact of coolants *(Russian)* 80−19793
Stellite-6 in liquid Na, tribology 79−26525
structure-fluid interaction between vibrating wall and channel flow 77−38325
subchannel void drift model, analytic derivation 80−68759
subchannel void drift model, analytic derivation 80−73905
subchannel void fraction by gamma scattering 80−27726
subcooled blowdown thrust force calculation using RELAP4/REPIPE 80−18382
subcooled blowdown transients, wave diagram solns. 80−13564
subcooled boiling flow, vapour bubble growth and recondensation 79−93692
subcooled film boiling heat transfer from spheres 78−51047
subcooled nucleate pool boiling, intensity and power spectral density of acoustic emission 78−17282
submerged cooling-water discharge structures for power plants at coastal waters 80−607
Superphenix internal shells, vibr. anal. *(French)* 78−50247
SuperPhenix nuclear boiler, design and construction 79−97761
temperature dist. in cylindrical fuel pins with gap and cladding *(Italian)* 79−13397
temperature field, generalised Duhamel integral 80−22943
temperature noise in one-phase heat transfer: stochastic models 80−68726
tensor formulation of the fluid-solid interaction force for multi-dimensional, two-phase flow within tube arrays 80−92211
terphenyl, partially hydrogenated, neutron thermalisation spectrum 77−67812
thermal channel heat transfer gap calc. by numerical methods 78−21630
thermal emission crisis onset determ. via acoustic emission *(Russian)* 77−54302
thermal hydraulic anal., of rod bundle fuel elements, COBRA-3C/KFKI digital computer program 78−54822
thermal hydraulic analysis of a wire-wrapped 19-rod bundle with edge blockage 79−59142
thermal hydraulic analysis of a wire-wrapped 19-rod bundle with edge blockage 79−71887
thermal hydraulic calculation *(Hungarian)* 78−25282
thermal hydraulics anal., teaching appl. of computer graphics 80−36824
thermal hydraulics analysis, differential sensitivity theory for nonlinear equations with nonlinear responses 80−47551
thermal mixer, advanced design, performance 80−63243
thermal mixer, state-of-art, development and testing 80−576
thermal mixer temp. fluctuation and pressure loss, scale model tests 79−9673
thermal reactor, rapid decomposition effects on bubble transition 80−73897
thermal reactor containment, finite element anal. of luid-structure interactions 80−22998
thermal reactor convective heat transfer coefficient enhancement in two-phase nonboiling flow 80−73895
thermal reactors, film boiling destabilisation due to pressure shock arrival 80−73896
thermal-hydraulic anal., COBRA IIIP/MIT code 77−79423
thermal-hydraulic conservation eqns., analytic integration 77−83012
thermal-hydraulic effects of pipe ruptures 79−97846
thermal-hydraulics, quality influence on the departure from nucleate boiling in cross flows through bundles 80−95340
thermally expandable fluid transients, finite difference method 77−79418
thermodynamic activity of C in Na 77−83045
thermohydraulic tests on 18-pin gridded subassembly in Na loop 77−46254
thermomechanical instability of a heat releasing granular layer, GCR model 80−92134
three-dimensional analogue reactor simulation with allowance for heat transfer 79−63739
Tokamak-driven hybrid breeder reactor, liquid metal coolant, MHD effects 79−17974
transient 1-D two-phase flow eqns., finite difference approx. 78−51229
transient critical heat flux; fluid modelling 77−42038
transient heat conduction, soln. by hybrid method 78−681
transient heat transfer, COMETHE code 80−42761
transient heat transfer between hot metal spheres and subcooled water 77−26832
transient nonboiling heat transfer in cooling channel during flow coast-down 77−46267
transient overpower, comparison of EPIC and PLUTO fuel-coolant interaction codes 78−8920
transient safety anal. using RETRAN computer code 80−18506
transient temp. field in nuclear fuel rod, calc. by variational procedure 79−9772
transient temperature distribution in cylindrical tubes, heating and cooling of high-vacuum furnace 80−47573
transient temperature distribution in the reactor vessel wall after cooling system failure 79−54473
transient two phase thermal hydraulics in channel, model 78−94091
transient two-phase flow, analytical modelling 80−27722
transient two-phase flow system, three-dimensional numerical simulation 80−687

fission reactor cooling and heat recovery continued
transient two-phase level swell, appl. of drift flux model 79−49656
transverse momentum eqn. for COBRA-IV-I, improved version 80−578
tREAT TOP test H6−preliminary results 79−49763
triangular rod bundles with flat or corrugated casing, longitudinal hydrodynamic characts. 77−34373
Trino power plant, in-service inspection and operating experience, main coolant circuit *(Italian)* 79−17992
tube arrays in cross-flow, flow induced vibrs. 78−46984
tube banks, flow-induced vibrs. 78−46929
tube banks, in-line, with pyramidal roughness, flow and heat transfer 78−18152
tube bundle in water, freq. response 77−83028
tube frettings in steam generators and heat exchangers, expt. study 79−81003
tube rows and arrays, fluid elastic whirling 78−46928
tubes with nonuniform axial heat distrib., heat transfer burnout 78−94088
turbulent convective heat transfer from rough surfaces 79−27638
turbulent diffusion, connected flow passages, computer prediction using k-ε turbulence model 80−9331
turbulent diffusion of heat between connected flow passages 80−9330
turbulent flow in fuel rod bundles, finite element anal. 78−37400
turbulent flow through wall subchannel of rod bundle 78−41802
turbulent heat transfer in annulus, transient, heating element, reactor cooling theory 78−86569
turbulent interchange in triangular array bare rod bundles 78−94081
turbulent-laminar flow transitions in rod bundles, Reynolds numbers determ. 77−42036
two phase flow induced vibrations in fuel pin model 79−13388
two phase flow instability, classification by density wave oscill. model 79−63731
two phase flow modelling, theoretical foundation, appl. to fission reactor fluid flow and heat transfer 80−103065
two-fluid thermohydraulics computer program, RELAP/SLIP 78−94092
two-phase annular flow, flooding and flow reversal 78−51230
two-phase annular flow, multifluid modelling of adiabatic and boiling flows 79−1233
two-phase annular flow through orifices, modelling 80−28555
two-phase flow, frictional energy dissipation, appl. to nuclear fuel assemblies *(Japanese)* 77−55074
two-phase flow, method of characteristics anal. 78−21628
two-phase flow characterisation by neutron noise techniques 78−94058
two-phase flow equation systems, characteristics, stability and short wavelength phenomena 78−38395
two-phase flow in pin bundle, two fluid model 80−91209
two-phase flow instability, programme for heat removal expt. at low power 78−54814
two-phase flow models, macroscopic balance eqns., appl. to steam supply systems 80−9332
two-phase flow operating conditions *(French)* 80−78348
two-phase flow patterns, high pressure water in heated four rod bundle 78−89938
two-phase flow system, local density measurements, side-scatter gamma technique 80−569
two-phase flow void fraction determ., simulation of neutron scatt. method 79−90321
two-phase flows, high-intensity X-ray system for stochastic measurements 79−93791
two-phase stratified horizontal flow, averaged and local instantaneous formulations, stability 80−64613
two-phase-flow instrumentation development at Brookhaven National Laboratory 80−102261
U-tube steam generator transient simulation using extend implicit continuous-fluid Eulerian method 79−89356
UKAEA Prototype fast reactor control system, commissioning and performance assessment 79−89459
underground nuclear power plant, accidents, containment of fission products, finite element anal. 80−27768
underwater shock at a free surface, refl. effects, rel. to fast reactor safety 79−68751
vapour phase heat transfer in post critical heat flux region 79−9668
vent clearing in pressure suppression pools 78−94098
VHTR, high-temperature nuclear heat source for hydrogen production 79−93686
VHTR heat exchangers, material criteria and selection 78−13232
VHTR system, material requirements for intermediate heat exchanger, rel. to creep-rupture tests 78−13235
vibration analysis of heat exchanger and steam generator designs 78−66333
VK-50 boiling reactor, characts. at reduced steam pressure 80−32337
void fraction determ. by slip ratio correlations 79−81955
void fraction for subcooled boiling, different heat flux distribs. along channel *(Russian)* 77−34381
void fraction meas. in water-steam mixtures by neutron gauge 79−80982
void fraction measurement, RF local probe development 80−568
void fractions in the phase flow, hydrodynamic and hydraulic studies for reactors 79−55411
void-distribution effects in void measurements using scattered/uncollided neutrons 80−73910
volumetric steam content determ. by noncontact neutron sensor 79−30904
vortex diodes in post accident heat removal systems 80−106100
VVER, T buildup estimation with allowance for ^{6}Li conc. 79−97833
VVER plant, gamma emitting radioactivity in heat transfer agent meas. *(Hungarian)* 77−26833
VVER-440 reactors, emergency operating conditions following main circulation pipe failure, computer-aided analysis 79−9823
walls, permeable, cooling characts., heat exchange, rad. emitter design 80−64535
waste heat storage, convection onset in horizontal water layer, with max. density effects 79−46164
waste heat utilisation at University of Missouri, USA 80−13562
water chemistry of reactor coolant *(Japanese)* 80−68737
water cooled, water moderated reactor, coolant tritium content in first loop 80−32334
water cooled and moderated reactors in Soviet Union nuclear power generation 79−642
water cooled reactor, RBMK, safety margin optimisation 80−37481
water cooled reactors, subcooled and low quality flow film boiling of water at atmospheric pressure 80−32324

fission reactor cooling and heat recovery continued
water critical flow states through pipe, modified Bernoulli theory 78—30345
water depressurisation, early response 79—30908
water droplets react. with molten Na 78—71263
water flow instability in Na heated once through steam generators 80—27737
water radiolysis, mathematical modelling for kinetics in operating reactors 78—61036
water reactor fuel elements under accident conditions, conf. 77—42159
water steam, boiling and nonboiling vertical two phase flow in tube, void fraction correl. 77—55073
water-cooled nuclear reactors, coolant circuit decontamination method 80—22885
water-cooled reactor core coolant flow calcs., computer code 77—74914
water-cooled reactor systems, water chemistry 79—93694
water-steam separators, operation anal. *(French)* 79—63728
water/Na temp. fluctuation correlation mixing tee expts. 78—8878
West German nuclear power plant liquid radioactive effluent control 79—13550
Westinghouse upper head injection system 78—21634
Windscale AGR, high pressure fuel test loops design, installation, commissioning 77—6491
wire-wrap model 77—46255
wire-wrapped 61-rod bundle edge subchannel flow distrib. 79—9676
with He turbine, (HHT), HTGR, heat exchangers *(German)* 80—5198
WWER fuel assembly, thermohydraulic evaluation, program module BIPR-5K *(Bulgarian)* 79—85695
WWER-1000 main cooling system solutions for different steam generators *(Russian)* 79—26480
Zircaloy heated surface, FeO deposition in boiling water 78—58353
Zircaloy-2 tube, external pressure creep behaviour 79—57083
Na leakage in reactor steam generators, solution kinetics of solid NaOH in Na 79—36365
Ar loaded K heat pipe performance characteristics 78—89934
B-thermal regeneration system using anion exchange resins 79—80972
CO oxidation in AGR coolants 77—54282
CO_2 fundamental condensation cycles in steam and nucl. power plants, performance characts. 80—63368
CO_2, gaseous reactor coolant, monitoring of U, Pu and fission products by gamma spectrometry 79—89374
Cl ion conc. in loop waters, potentiometric method 79—85599
Co radioactive release from reactor cooling water, fixation by sandy soil *(Japanese)* 78—74443
^{58}Co dissolution during PWR refuelling shutdown, control with H_2O_2 78—21698
^{60}Co distribution in N_2O_4 condensate cooling circuit *(Russian)* 79—13491
^{60}Co, shutdown dose rate prediction in BWR primary coolant circuit 78—74445
EBR-II Na system cold traps for control of O_2, H_2, T impurities 80—78411
H_3BO_3 concentration in primary circuit coolant, method and device for determ. *(Russian)* 77—38331
^{3}H formation in water cooled, water moderated reactors, role of nuclear reactions 79—17970
^{3}H meter for Na coolant systems 79—9690
^{131}I spiking phenomenon in accidents involving coolant leakage, expt. *(Japanese)* 77—54320
^{54}Mn distribution in N_2O_4 condensate cooling circuit *(Russian)* 79—13491
N_2O_4 circular channel hydraulic resistance and heat transfer expts. *(Russian)* 79—14213
N_2O_4 coolant, dissociating system, dynamic sorption of ^{131}I from gas phase *(Russian)* 78—58356
N_2O_4 coolant action on stainless steel, TEM study of intergranular corrosion *(Russian)* 78—58357
N_2O_4 corroded annular channels, heat transfer and pressure drop 80—1569
N_2O_4 dissociating coolant, chemical reaction kinetics in transient regimes *(Russian)* 78—58344
N_2O_4 dissociating coolant, O_2 generation time constant, enthalpy change *(Russian)* 78—58345
N_2O_4, dissociating in vertical tube, boiling heat transfer 80—1568
N_2O_4, dissociating turbulent convection on horizontal plate *(Russian)* 80—1587
N_2O_4, fission reactor coolant, heat transfer on condensation *(Russian)* 80—57860
N_2O_4 flow in axisymmetric channels, heat transfer calc. *(Russian)* 79—14214
N_2O_4 flowing in axisymmetric channels, mass and heat transfer calcs. 80—1570
N_2O_4, reactor coolant, stability in two-phase flow *(Russian)* 80—609
N_2O_4, turbulent dissoc. flow, along heated tubes, heat transfer 80—63225
$2NO_2 \rightleftarrows N_2O_4$, condensation, heat transfer and aerodynamics *(Russian)* 80—19932
$N_2O_4 \rightleftarrows 2NO_2 \rightleftarrows 2NO+O_2$, precipitation of corrosion products in a fractionating column *(Russian)* 80—25707
Na boiling acoustic emission burst detection in parasitic noise 79—3214
Na boiling detection technique tests, FFTF capabilities 79—13395
Na boiling in tubes, heat transfer and pressure drop 80—28408
Na coolant, effect of high reactivity with air and water on reactor design *(French)* 79—26526
Na cooled power reactor noise analysis for malfunction diagnosis 79—13450
Na evaporation into forced AR flow, critical supersaturation model predictions 79—54493
Na, fast reactor coolant, boiling in circular pipe, single-bubble model 77—10466
Na fire anal. with SPOOL-FIRE code 77—46322
Na fires suppression in fission reactor, installations 80—27770
Na, fission reactor coolant, meas. accuracy of plugging indicators 78—54813
Na, fuel element transient heat transfer, temp. distrib. 78—17280
Na heated steam generator, flow instability 77—46214
Na heated steam generators, tube degradation induced by dryout instability 77—46213
Na, impurity conc. meas. by automatic plugging indicator 78—17283
Na, liq., coolant in fission reactor, degassing of Xe invest. using Na loop 77—34410

fission reactor cooling and heat recovery continued
Na, liquid, heat transfer characteristics of flow field *(Japanese)* 78—54815
Na, liquid, local boiling behind local flow blockage, simulated LMFBR fuel subassembly 78—54842
Na, liquid, molten chlinak extraction of I_2 80—27702
Na, liquid, natural convection from plane surfaces, LMFBR design, review 80—37417
Na, liquid coolant, effect of O_2 on H_2 permeability, partial pressure 80—614
Na, liquid coolant loop, H bubbles, mathematical modelling 77—42042
Na liquid flowing in close cylinder, heat transfer *(Russian)* 77—67799
Na, liquid metal slug flow, transfer function of temp. fluctuations 78—46133
Na loop, plugging meter behaviour obs., hydride and oxide deposition analysis 80—5207
Na loop safety facility, molten fuel containment capability assessment 80—47605
Na, plugging indicator measuring accuracy, impurity conc. 78—54813
Na, pool boiling heat transfer, liq. head effects 78—89951
Na, superheated flow in pipe, single bubble slug expulsion 78—672
Na system cold trap temperature control using resistance heater 77—57710
Na temperature fluctuation in single-pin-heated blocked annular channel 78—78439
Na transient boiling in single-pin annular channel under loss of flow 78—89933
Na valves for advanced reactors, reliability data collection at CREDO 80—22897
Na, vapour, viscosity meas., 1101-1186K, 0.2-0.8 bar 80—1723
Na vapour condensation from rising bubble, effects of internal circulation velocity and noncondensable gas 78—50258
Na/water steam generator problems, soln. in USSR *(Russian)* 79—97876
Na-cooled fast reactor, structural steel properties 80—22942
Na-filled stainless steel heat pipes, with long adiabatic sctions, performance limits 80—38236
Na-H_2O reaction jets, material wastage experimental data anal. 80—27705
Na-H_2O reaction jets, metal wastage production prediction 80—27704
Na-H_2O reaction testing in large leak test rig 78—86577
Na-NaK engineering handbook, purification, heaters, coolers, radiators 80—27045
O_2 deposition in a mesh-packed cold trap 80—22905
Pb-Bi eutectic alloy flow rate meas. apparatus 77—79412
^{35}S content of coolant gas in Windscale AGR, gas chromatographic and radiochemical anal. 78—73125
SiC ceramic heat exchanger, cost-effective design 80—95341
T buildup in D_2O of CANDU reactors, due to ^{3}He(n,p)^{3}H reaction 79—22389
Th-U alloy fuel behaviour in organic-cooled reactor 78—86605
Ti condenser for power stations with seawater cooling 80—595
UF_4-CF_4 mixture, gas core fission reactor, fission based plasma engine 80—63366
UO_2 fuel element/sheath, heat transfer meas. 78—29580
UO_2 fuel-coolant interaction, film boiling and vapor explosion phenomena 80—95363
UO_2, LMFBR, boiling pools with internal heat generation, void distrib. 78—21626
UO_2 molten pool prod. by internal heating, heat transfer meas. 77—88214
UO_2, thermal cond. meas. under simulated in-reactor conditions 78—94079
UO_2 vapour condensation from rising bubble, effects of internal circulation velocity and noncondensable gas 78—50258
UO_2/Na, fuel/coolant thermal interaction in FBR, out of pile preliminary tests *(Italian)* 78—54828

fission reactor core control and monitoring
see also fission reactor safety; fission research reactors; nuclear engineering; nuclear reactor instrumentation
absorber rod vibr. induced neutron density fluctuations, QMC reactor expt. 80—37469
absorption cross section of fission product aggregate, energy dependence 79—76075
absorption resonance controlled reactor *(Spanish)* 78—8872
accelerator-driven breeding blankets, neutron-return effects, implications for fuel reenrichment without reprocessing 80—57914
acoustic wave propagation *(Russian)* 80—5292
adaptive control and parameter identification of nonlinear loosely coupled core reactor 80—672
adaptive control and parameter identification of two temp. feedback model 80—13635
advanced control room design 79—45362
advanced fuels program oxide zone assembly 80—22975
advanced reactor cycles, total core analysis 79—9782
annular control rods in press.-tube-type heavy water reactor 77—26850
annular core pulse reactor, advanced operating mode capabilities 79—93777
anticipated transients without reactor scram and other safety devices for PWR and LWR 79—18002
Argonaut reactors, coupled core, neutron wave propagation, Be, graphite and D_2O as internal reflectors 80—27752
Arkansas Nuclear One, refueling shuffle movement sequencing program 80—9357
at-power reactivity dynamic perturbation meas. 79—76081
ATR, power distrib. and control element reactivity changes, Be reflector redesign effect 80—9363
automatic diagnosis of abnormal phenomena, theory and computer simulation 78—17330
automatic power control of IRT-M reactor using in-core detector system 77—50264
automatic reactor regulator and xenon oscillations 79—41015
automatic stochastic data processing system for reactor monitoring 79—97962
axial momentum altered transverse transport in coolant flows during oscillatory instabilities 79—17964
B&W integrated control system improvement 78—8946
Biblis core protection and German safety regulations 77—88260
Biblis Nuclear Power Station, meas. and control system, fault statistics evaluation *(German)* 79—97819

fission reactor core control and monitoring continued
Bilibinsk atomic plant, gravity coeff. of coolant reactivity 80—32333
BN-350, physical characteristics study *(Russian)* 79—97898
BN-350 fast power reactor, reactivity, temp. and power effects, fuel depletion effect 78—17342
Bohunice A-1 reactor, type E2 instrumented fuel elements *(Slovak)* 77—50260
BOR-60, meas of α-values for ^{235}U, ^{238}U, ^{239}Pu 79—97830
BOR-60, operational characteristics of core and irradiated fuel parameters 79—97877
BOR-60 experimental fast reactor, safe operation in power plant conditions *(Russian)* 79—97865
boric acid solutions, extractive purification from radioactive corrosion and fission products 80—18458
BR2 BWR, densification of (U,Pu)O_2 fuel 79—49685
BR3 reactor, instrumentation for continuous monitoring of primary water B content *(French)* 80—32408
breached element location from mixture of Xe tags, MIXTAG code 78—33274
breached fuel element diagnosis, use of fractional release ratio ^{137}Cs to ^{131}I 78—21713
breeder reactor piles, instantaneous neutron kinetics in cavities 80—32393
Browns Ferry BWR, load following test 80—68892
BRUCE A Unit 1 reactor, flex distrib. meas. for various reactivity control configurations 78—25317
Bruce core, ZED-2 mockup, responses of Pt, V and Co self powered flux detectors 78—58391
Buffalo PULSTAR reactor refuelling 79—9793
burnup calcs., perturbation anal. of sensitivity 80—22936
burnup control problem considering fuel failure probability 77—67844
BWR, alternate refueling schemes 79—49723
BWR, appl. of warm water injection method to in-core wet sipping for leaker detection 78—78450
BWR, ASEA-ATOM, core supervision system 80—68883
BWR, Bilibino power station, internal power-distribution monitor system 78—17341
BWR, block-monitoring index for diagnosis of power station operating characts. 79—59185
BWR, condensate feedwater system dynamics anal. 80—23025
BWR, control blade worth depletion meas. 80—719
BWR, control rod programming using heuristic and mathematical methods 80—52766
BWR, control rod sequence exchanges utilizing an off-line predictive code 78—21725
BWR, core flow fluctuations, noise source, expt. study 79—13386
BWR, Dodewaard reactor, power control using Gd absorbers *(Dutch)* 78—50277
BWR, Doppler and void reactivity feedback 80—13661
BWR, effect of multiple boiling channels on void fluctuation spectra 80—18464
BWR, expt. reactor, design of control systems using Horowitz method 79—45338
BWR, fast moderator feedback effects during severe press. transients 78—4990
BWR, feasibility study of core management system by data communication 78—13254
BWR, fuel element positioning and control patterns, optimisation system 80—733
BWR, grey nose control rod design 80—5264
BWR, H_2 and O_2 monitoring in containment and off-gas systems 80—32414
BWR, Hatch-1, core management data magnetic tape transfer to central office 78—21719
BWR, improved fuel utilisation 80—732
BWR, in-core investigation of two-phase flow using neutron-noise techniques 79—54530
BWR, in-core neutron detector noise, local component modelling 80—68866
BWR, in-service inspection and external base-line tests, instrumentation 80—784
BWR, multivariable autoregressive model of the dynamics 78—25307
BWR, neutron image anal. by one-dimens. core model 77—61478
BWR, neutron noise field, two-group diffusion theory 80—18461
BWR, O_2 monitoring and control 78—25309
BWR, on-line core performance evaluation and operating guidance system 79—97859
BWR, ONDA-3 system for in-reactor fuel management 80—735
BWR, operating reactivity and power distrib. data base for nuclear methods qualification 79—89404
BWR, operational stability monitoring by reactor noise polar correlation 79—93761
BWR, optimal fuel pin enrichment distribs. 77—83008
BWR, optimal in-core fuel management using OPTLWR computer code 78—17363
BWR, optimum fuel loading and operation planning, FAPMAN model 80—47606
BWR, Oskarshamn I, Gd-loaded fuel: benchmarking CASMO program 79—81039
BWR, pellet-cladding interaction related failures during manoeuvring operations 78—21743
BWR, prediction model for shutdown margin reactivity 79—26476
BWR, pressure ATWS, γ and n heating, pressure wave propag. effects 80—13640
BWR, quasioptimum fuel assembly loading, hierarchical level scheme 78—29609
BWR, reln. between channel void and LPRM noise 77—42142
BWR, safety evaluation, experiments and analytical analysis, emergency core cooling system 80—13703
BWR, scram reactivity characteristics 78—29607
BWR, spent fuel γ-ray spectrometry and chemical analysis 78—54841
BWR, stability of radial and azimuthal energy distrib. 79—97749
BWR, startup control rod programming code system 80—13688
BWR, vacuum relief valve sizing in condensing steam situations, analytical model 79—54545
BWR, Vermont Yankee, effects of non-Haling power operation 78—21723
BWR, void and Doppler feedback eval. 80—22976
BWR, void fraction profile determ. by neutron noise anal. 78—46150
BWR, void reactivity feedback, space-time anal. 79—22414

fission reactor core control and monitoring continued
BWR capacity factor increase by anticipatory preconditioning with peripheral rods 80—23049
BWR computer based control systems 80—83211
BWR condensate feedwater system, dynamic model 80—73883
BWR control blade homogenization, influence on nodal coupling parameters 79—26563
BWR control blades, modelling for nodal calcs. 79—81040
BWR control cell core design concept 80—68763
BWR control cell core improved design 79—85593
BWR control rod drive hydraulic return nozzle repair 80—23043
BWR control rod programming, heuristic and mathematical approaches 79—9779
BWR core, moderator temp. coeff. and neutron leakage, DIFFUSION-ACE calc. 78—54844
BWR core calcs., void iteration convergence and accel. 77—83009
BWR core calculations using improved coarse mesh methods 80—68849
BWR core concept, WNS-type fuel, equilibrium cycle performance 80—68762
BWR decay heat removal systems, probabilistic risk assessment, fault and event tree anal. 80—63333
BWR diagnostic anal. using multivariate autoregressive processes 77—23220
BWR Dresden-3 fuel rods, pellet/cladding interaction induced stress corrosion cracking 79—67899
BWR dynamics, imbedded flux calc. 80—714
BWR fuel management anal., consistent modelling procedure 80—23052
BWR fuel management improvements for once-through fuel cycles 80—37505
BWR fuel preconditioning, initial pressurisation, fuel temps., fission product release 80—63357
BWR fuel preconditioning 80—63360
BWR fuel rod relocation, gap conductance anal. 80—83192
BWR in-core instrument tube vibration obs. by reactor noise techniques 78—94064
BWR in-core neutron detector sensitivity to control rod vibr. using neutron noise anal. 80—57910
BWR island-design Pu recycle fuel assemblies, nuclear fuel performance meas. 79—30907
BWR load following plant, low sensitivity design fo controller 78—78473
BWR LOCA, phased mission analysis of ECCS failures 80—68851
BWR LOCA, pool swell modelling and small-scale expts., comparative eval. 80—95362
BWR LOCA, pool swell reduced scale simulations, scaling law limitations 80—99238
BWR neutron noise local component meas., two phase flow study 78—94059
BWR neutron noise source identification, stochastic model data anal. 78—94106
BWR neutron noise source identification from existing instrumentation 79—13483
BWR noise, response of neutron detector to local coolant void distribs. 80—683
BWR noise anal., identifiability of dynamics using autoregressive modelling 79—45340
BWR nuclear plant nonlinear digital simulator, optimal digital control methods appl. 79—9826
BWR of Hamaoka nuclear power station, operating experience *(Japanese)* 78—17333
BWR once through fuel cycle optimisation 79—85590
BWR operating experience at Millstone I with the control cell core improved design 80—22925
BWR optimal control, regulator problem, feedback control laws 77—54315
BWR parameter estimation, multivariate anal. of neutron noise signals 80—18465
BWR plants, O_2 monitoring and control 78—21656
BWR power distrib. prediction system, on-line performance test 80—13689
BWR power distribution analysis, three-dimensional calc. program 79—9674
BWR power distribution changes, online prediction evaluation 79—9780
BWR power fluctuations, noise source estimation by autoregression 78—78476
BWR power plant, computerised core component accounting system shortens shuffling time 80—699
BWR power plant, direct cycle, low sensitivity optimal controller study 78—8947
BWR power plant, neutron noise meas. and analysis 78—94105
BWR power plant appl. of computer based systems 77—88264
BWR power plants, neutron flux monitor 77—14240
BWR power reactor, in-core startup system with neutron flux monitor 80—32405
BWR reflectors, effective albedo parameter determination 80—68756
BWR rod drop accident, effect of thermal-hydraulic feedback, computer anal. 80—42815
BWR simulation diagnosis by noise analysis 78—94062
BWR split void assembly benchmark verification of SIMULATE models 80—22938
BWR stability monitoring using time series anal. of neutron noise 80—47625
BWR stochastic neutron flux fluctuation obs. and modelling, thermohydraulic parameters 78—94065
BWR transient anal., iterative procedure for predicting critical power ratio 80—42816
BWR turbine trip test, computer anal. 80—692
BWR-4 neutron noise anal. of incore instrum. tube vibr. and impacting 79—36353
BWR-4 neutron noise analysis spectra, instrument tube flow-induced vibr. 78—94063
BWR-4 neutron noise analysis spectra characterisation 79—13482
BWR/6 axial reflectors, Monte Carlo modelling 80—22939
Calvert Cliffs power manoeuvring control strategy 79—9863
Canadian power reactor programme, role of Chalk River research reactors 79—81073
CANDU, development of irrad. fuel bundle counters for reactor safeguards systems 78—94119
CANDU, digital computer control 77—54324
CANDU, feasibility study for use as a breeder 78—25311
CANDU, feedback coeff. anal. 80—27716
CANDU, LOCA, space-time neutronic anal. 80—13663

fission reactor core control and monitoring continued
CANDU, optimum burnup distribution in a continuously fueled reactor 79—36305
CANDU, Th-fueled, axial fuel management strategies 79—26586
CANDU advanced BLWR with enriched fuel, controllability studies 77—71683
CANDU distributed computer control systems 79—76105
CANDU fuels, nondestructive determ. of burnup by gamma scanning, fission monitor appl. 78—94076
CANDU nuclear power station safety, Atomic Energy Control Board guidelines 79—22425
CANDU PHWR heat transport network, SOPHT computer model 77—83025
CANDU plant DDC, dual redundant minicomputer system max. utilisation 79—36375
CANDU power plants, automated anal. system for control of secondary coolant chemistry 80—18446
CANDU power stations, reduction, control and prediction of radioactivity transport 80—18448
CANDU pressurised HWR fuel, bundle end neutron flux peaking effects, plenum use 78—58385
CANDU reactor, shutdown system design, performance during commissioning 78—25319
CANDU reactor, Th-fuelled, importance of ^{233}Pa in neutron economy 80—22980
CANDU secondary coolant circuit chemistry control, automated system development 78—66359
CANDU self-powered flux detectors, response characts. 80—32404
CANDU simulated core in ZED-2, transient meas. anal., CERKIN code exam. 78—58386
CANDU simulated cores, transient expts., validation of computer codes 78—54825
CANDU-BLW reactor spatial power control 78—89962
CANDU-PHW, neutron flux regulation by two-phase flow absorber system 79—93799
CANDU-PHW, thermal neutron flux-mapping system 80—792
CANDU-PHW 600 MWe reactors, channel power mapping and calibration routing 80—57892
CANDU-PHW reactor online spatial control, flux mapping appl. 77—88266
CANDU-PHWR, low enriched U, channel power peaking 80—37509
cavity geometry impact on power distrib. meas. with multisection ex-core detectors 79—93794
channel reactors, automatic control system design for energy distrib. 78—82475
characterisation and quality control of nuclear fuels, conf. Karlsruhe Germany (June 1978) 79—49794
CIRENE core, design criteria and anal. 77—14213
CIRENE LWCHW reactor, two-phase flow rods for neutron flux control, computer anal. 79—59217
CIRENE reactor control, two phase flow rods, BUANA and TICO codes 79—17994
CIRENE reactor power channel, fuel string dynamics and pressure tube fretting corrosion 79—30950
Clinch River Breeder Reactor Project ex-vessel transfer machine design and development 79—9787
closed-loop control system synthesis 77—3117
colloqium on nucl. instrumentation, London, England 1979 80—4480
commercial reactor, control rod material behaviour 78—8918
computer applications, information processing, control, monitoring, data acquisition and evaluation 80—47595
computer modules appl. *(German)* 79—49788
computer safety analysis, verification of the TRAC code on RSR standard problem 5 79—49724
constrained feedback control system design 77—88257
continuous noisy signal analysis by autoregression time-series model 79—3209
control and instrumentation designs beyond the 1980s 80—57872
control and protection system future trends justification 77—88263
control assembly frequency anal. using standing wave methods 77—46263
control design procedure for depletion analysis 77—65292
control guidelines 80—106119
control instrumentation, commissioning and maintenance experience at Rajasthan 79—89455
control rod drive system penetration assemblies for Caorso Mark 2 primary containment 78—58368
control rod drop damping and velocity meas. instrumentation *(German)* 80—5248
control rod reactivity meas. error analysis 79—9783
control rods, influence of neutron trap on critical loading and efficiency *(Russian)* 80—37474
control room and desk design, alarm system, information displays 79—89462
control room and desk design, alarm system, information displays 79—89464
control systems for loop channel parameters 79—97835
control theory, steady-state accuracy of neutron field regulation 80—63319
coolant flow rate determ. using ^{16}N decay activity meas. 80—73955
coolant interchannel interaction for prolonged flow around bunches of rods 80—73888
core bowing history computer program 79—9688
core hot spot temperature, probabilistic evaluation *(Japanese)* 79—13440
core hydraulics fast neutron reactors *(French)* 79—63723
core meltdown, acoustic meas. of penetration of molten metallic pool into concrete 80—13544
core meltdown, contribution of collapsing vapor bubbles to the fragmentation of melts 80—755
core monitoring system accuracy, effect of inoperable in-core detectors 79—93790
core motion monitoring, exptl. methods 79—81025
core operating limit supervisory system stochastic simulation 79—630
core physics parameter meas. uncertainty 79—9801
core power distribution calc., FLAME3 nodal code accuracy 79—9703
core power transients without scram, calc. of moderator reactivity feedback 77—42152
core protection and surveillance system 79—9811
core system, bowed, NUBOW-3D program for static anal. including irrad. creep and swelling 80—5215

fission reactor core control and monitoring continued
core-wide fuel performance assessment 79—93766
coupled core reactor, space depend. neutron fluctuation spectra, HF struct. 80—37468
coupled core reacts., asymptotic stability 80—564
coupled core system, noise sources in coupling medium, stochastic study 80—22962
coupled cores, neutron transit time determ. by noise anal. method 78—37413
coupled-core nuclear reactor, distributed parameters identification, pseudorandom perturbation and correlation anal. 80—86966
coupled-core nuclear reactors, irreversible circulation of fluctuation 80—27700
CRBR, analysis of transient overpower accidents in BOL core using comp. code 77—46326
CRBR, calcs. of ex-vessel monitoring for initial fuel loading 80—27778
CRBR, primary control rod drive system 77—38397
CRBR core, recriticality potential of boiling pool 77—46332
CRBR shutdown system, Markovian reliability anal. 80—27761
CRBRP, fuel failure monitoring system 79—93795
CRBRP with radial parfait core, analysis of unprotected loss-of-flow accidents 77—46327
critical assembly, neutron spectra meas. by activation method • 80—32390
critical assembly fuel elements, apparatus for determ. of relative fission density release *(Russian)* 80—73973
critical facility, fast neutron spectrum meas. using (n, α) and (n, p) reactions 80—78403
critical heat transfer to flowing cooling water 77—74910
criticality calc. by Monte Carlo methods *(Czech)* 77—50259
criticality control of intermediate U enrichments, computer calcs. 80—37435
criticality criterion for core with pointwise concentration of control rods 77—38328
criticality search techniques for low and high switched systems 80—37494
cross section adjustment in anal. of benchmark expts. 79—63718
cross-section adjustments, sensitivity to uncertainties 80—47531
CRT man-machine communication system in nuclear power stations 79—45364
damaged fuel element detection and location at Atucha nuclear power station 79—89460
data acquisition program for research reactor 78—86679
data processing system of Dungeness 'B' power station 77—67831
data sheets for Stade Nuclear Power Station, West Germany *(German)* 78—58366
decentralized instrumentation and control system with bus transmission in nuclear power plants 79—97847
development of maneuvering strategies using optimal control theory 79—30959
DFR special experiments 79—97779
diagnostic system tasks and installation *(Hungarian)* 80—18452
diffusion theory calcs., fuel swelling and cladding shrinkage effects 80—22926
digital computer applications in reactor instrumentation and control 80—106134
digital computer control in Canadian nuclear plants, past performance and future outlook 78—58383
digital control using linear quadratic Gaussian regulator 80—37554
digital load-follow control concept, simulation in FRG-2 reactor *(German)* 77—50249
direct digital control of the WWR-SM research reactor 80—696
directional γ-ray detector for in-core fuel motion monitoring 78—37448
directional fully encapsulated gamma detector for in-core reactor meas. 80—63307
distributed parameter optimal control methods 78—54858
distributed parameter reactor system pointwise control and observation problems 78—54859
DNB open core algorithm for on-line thermal margin evaluation 80—27782
Dodewaard BWR, reactivity of core loaded and Gd poisoned fuel 78—41840
Doppler feedback use in control rod drop transients, Maine Yankee expt. 80—68895
dosimetry standards 79—9824
doubly heterogeneous cores, fine-energy cross section space shielding 80—22894
Dounreay Fast Reactor surveillance, noise analysis development 79—3215
Dounreay test reactor, fast breeder test experience 80—86961
Dragon reactor zero energy expts., further n energy group and transport calcs. 78—78445
dynamic characteristics meas. in power reactors using reactance oscillator 79—89400
dynamic measurements of a nuclear reactor using low-peak-factor excitation signals 79—36349
dynamic response characts., empirical modelling appl. 78—25284
dynamics identification by dynamic data system methodology 78—25321
EBR II, transient testing and simulation for LMFBR plant dynamic modelling 79—54558
EBR II gas-tagging anal., isotopic weighting factors 79—59221
EBR-II, $(U,Pu)O_2$ fuel burnup, effect of time varying power level 80—13719
EBR-II, exptl. determ. of decay power 79—85652
EBR-II, in-reactor measurement of neutron absorber performance, He release of B_4C 80—73951
EBR-II, radial-reactivity-coefficient weighting schemes 79—80998
EBR-II, whole core thermal-hydraulic phenomena, experimental study 77—88206
EBR-II cover gas, second Xe tag identification, code MIXTAG 77—42145
EBR-II delayed neutron concentrations, computer modelling 80—27717
EBR-II delayed neutron monitor, response to tramp uranium and fission prod. test source 79—67919
EBR-II fission product control, cover-gas cleanup system and graphite trap 79—9791
EBR-II loadings, correls. of calculated reactivities 80—22891
EBR-II primary system fission gas behaviour 79—9692
EBR-II reactor shutdown system upgrading, safety features 79—9796
EBR-II reflector assembly irrad. induced bowing, implications for core restraint design 80—104234
EBR-II slow transient tests, environmental tailoring 80—23009

fission reactor core control and monitoring continued
- educational module, in-core fuel management computer system 80−36826
- EM instruments for use in liquid sodium, theoretical anal. 78−54857
- emergency core cooling system, unreliability estimates, comp. programs 77−54280
- emergency monitoring procedures at CEGB stations, UK 77−54322
- ENDF/B-IV, absorption effects on decay heat and spectral pulse kernels 80−22931
- ENDF/B-IV benchmark analyses with full spectrum three-dimensional Monte Carlo models 79−9701
- energy distrib., discrete monitoring error 78−82476
- energy distribution, algorithm for extremal control 80−83209
- enrichment zoning and control rod programming for reactivity and power shape control 79−18003
- ex-core detector neutron noise to core barrel amplitude scale factor 80−27779
- experimental reactors channels, independent control of neutron flux using gaseous absorbers 79−71918
- failed fuel element detection, delayed neutrons meas. *(Polish)* 80−73952
- failed fuel element detection by delayed neutrons using solid state track-etch technique 80−5249
- failure location algorithm for complex networks 80−99228
- Fast Breeder Blanket Facility reaction rate and neutron energy spectrum meas. 80−68865
- fast breeder core with internal blanket 80−68870
- fast commercial reactor, hypothetical disruptive accidents in the core *(Spanish)* 79−45357
- fast metal assemblies, prompt alpha and reactivity meas., review 78−21685
- fast mixed spectrum reactor, fuel management and reactor physics 80−27715
- fast pulse reactor $^{237}Np/^{238}U$ and $^{239}Pu/^{237}Np$ spectral index meas. and calc. 79−9804
- fast reactor, effects of reactivity of materials 78−86575
- fast reactor, EM flowmeters, review 78−21686
- fast reactor, Eu_2O_3 control rod material, irrad. behaviour 78−37409
- fast reactor, large, multiple control rod worths, effective estimation method 78−29544
- fast reactor, multiple control rod worth estimation, strong interaction effect 77−46302
- fast reactor analysis, composition self shielding factors 80−73965
- fast reactor boiling detection by noise analysis 79−13449
- fast reactor burnup, correlation of $^{134}Cs/^{137}Cs$ 80−677
- fast reactor control, range of absorber materials 78−8919
- fast reactor core and shielding, performance calc. improvement by data adjustment 79−9698
- fast reactor core operation, safety aspects *(French)* 79−97864
- fast reactor dosimetry using zero-power facility ZEBRA 79−3219
- fast reactor integral expt. anal., appl. of uncertainty and sensitivity theory 78−50239
- fast reactor neutron noise analysis, energy-dependent formalism 79−13489
- fast reactor parameters, influence of fission spectra uncertainties 80−22928
- fast reactor pulsed neutron die-away dispersion laws, modelling method 80−68867
- fast reactor SDX cell homogenization code, validation results for pin geometry 79−80997
- fast reactors, fission product nuclides, $(n\gamma)$ cross sections *(Japanese)* 80−521
- FBR, anal. of exposure depend. heterogeneous spectra 80−22937
- FBR, effects of material properties on the dynamic response of pressure-loaded core subassembly wrappers 79−49756
- FBR, experimental, math. model for control system design in FBR plants 79−17990
- FBR, failed-fuel detection system *(French)* 79−97858
- FBR, fuel melt down, fragmentation requirements for detonating vapor explosions 79−49753
- FBR, in-pile testing, nonprototypic effects due to fuel length and number of pins 79−30988
- FBR, Monte Carlo benchamrk program for anal. of critical assemblies 79−89405
- FBR, neutron spectra in the MeV range in fast critical assemblies 80−83210
- FBR, optimisation of burnup characteristics, nonlinear programming method 77−14239
- FBR, SAS3D prediction of intrasubassembly boiling incoherence, multipin boiling model 79−49662
- FBR, some lessons drawn from operation of Phenix and Rapsodie cores 80−639
- FBR, space dependent simulation of transient behaviour using KINTIC-2 code *(German)* 80−83182
- FBR, zero-power neutron noise expt. anal., power spectral density and subcritical reactivity 80−57911
- FBR blanket facility, gamma-ray heating rate meas. in stainless steel and Pb 80−57912
- FBR containment code, structural deform., SEURBNUK-2 80−78404
- FBR containment code validation program, SEURBNUK 80−78405
- FBR core seismic anal. by assumed-mode math. modelling 79−89357
- FBR core surveillance and protection systems *(French)* 79−76099
- FBR film boiling destabilisation, thermodynamic prediction of temp., and rel. to vapour explosion phenomena 79−49667
- FBR fuel pin safety expts. at SLSF, centerline fuel thermocouple performance 80−102283
- FBR HCDA, convective heat transfer correlations for molten core debris pools growing in concrete 80−83196
- FBR LOF accident, first visual in-pile fuel disruption experiments 79−49747
- FBR mixed oxide fuel columns, irradiated, dimensional stability 79−67858
- FBR TOP accident porous fuel blockage in core, theoretical anal. 79−49673
- FBR transient fuel behaviour maps, fuel response to thermal transients 80−57926
- FBR transient fuel behaviour maps, fuel response to thermal transients 80−68874
- FDR type reactors, transient anal., neutron power and temp. form factors, depend. on time and power level 80−83178

fission reactor core control and monitoring continued
- FFHR, tailoring the breeding-fission ratio by neutron moderation with iron 78−21677
- FFTF, critical expts., with solid neutron absorbers 80−52727
- FFTF, fast reactor, He release correlation from B_4C during fast-neutron irradiation 78−8965
- FFTF control rod anal. with SCRAM program 77−46355
- FFTF core component measuring system 79−45446
- FFTF element measuring system 79−9729
- FFTF fuel, neutron source strength as function of irradiation 80−22929
- FFTF fuel element measuring system 79−45447
- FFTF fuel failure, cover-gas monitoring system 78−4998
- FFTF Interim Examination & Maintenance cell equipment mock-up testing 79−9816
- first power emergence, pressure excursion in fuel elements with compact UO_2 78−82477
- fission gas effects in irradiated fuel rods operated in film boiling at high power 79−49744
- fission product γ-radiation intensity in short operation nuclear reactors 79−67823
- fission product activity ratios in RA used fuel element, γ-ray spectroscopy 79−41061
- fission product decay heat, effects of depletion, buildup and fast fission in shutdown 79−81041
- fission product decay heat calcs. for ^{235}U and ^{239}Pu 79−76083
- fission products, solubility rules based on lattice parameter differences 78−59953
- fission products in primary coolant, possible contribution from U impurities in fuel cladding 79−63751
- fission rates and ratios in, intermediate energy standard neutron field 78−21687
- fission reaction rate standards and applications 79−9650
- fission reactor fuel performance modelling, pellet-cladding interaction 80−63264
- flooding system, reliability analysis *(German, English)* 77−38346
- flow-induced control element movement, expt. investigation using noise analysis 80−788
- flowmeter calibration, Na-cooled reactor, signal anal. method 78−38425
- flux distortion flowmeter for core monitoring, tests using analogue rig to simulate flow with boundary layer 78−38420
- flux distribution adjustment suboptimal control using functional anal. 77−71636
- Ford reactor, equilibrium core calcs. with reduced enrichment fuel 80−68885
- Ford reactor, neutronic anal. using low enrichment fuel 80−68886
- Ford reactor, reduced enrichment fuel effects on performance and utilisation 80−63344
- Fort St. Vrain HTGR, low power physics tests 79−67887
- FPR neutron spectrum in presence of experimenter's tahle 78−21676
- FRR-II, upper-plenum acoustic expts. 77−46362
- FTR, control rod failure detection 77−42144
- FTR, criticality expts. with concrete reflected fuel pins in water 80−78410
- FTR fuel pins with solid neutron absorbers, criticality expts. 80−18476
- FTR-type fuel motion in TREAT transient overpower test E6 79−36366
- fuel assembly power distrib. calc. by albedo method 79−93762
- fuel assembly spectrum code verification based on integral transport theory 79−80996
- fuel bundle thermal-hydraulic anal., comparison of computational techniques in COBRA-IIIC and COBRA-IIIP *(Japanese)* 80−95374
- fuel burnup determ., irrad. samples, from γ-peak analysis of fission products *(Hungarian)* 78−82458
- fuel burnup measurement and analysis methods *(Japanese)* 78−29592
- fuel cycle optimization with nonproliferation objectives 80−730
- fuel element centering system, flow through narrow sphere-cylinder channel 79−17962
- fuel element rod bundle, neutron field calc., surface pseudosource method 80−27772
- fuel elements during irradiation, thermal state study using contactless method 80−32392
- fuel failure detect., UO_2-loaded Na in-pile loop 78−37417
- fuel handling system availability, minimum requirements 78−41820
- fuel management optimization, influence of poison management 79−26585
- fuel management scheme for high burnup at VEPCO 80−37436
- fuel management schemes for extended fuel burnup in C-E operating reactors 80−37504
- fuel management with extended burnup fuels 80−37503
- fuel performance data base EPRI 79−93731
- fuel power detector for CANDU power reactors 79−41022
- fuel preconditioning, power shock anal. and sipping 80−63358
- fuel preconditioning, TVA Browns Ferry Nuclear Plant, in-core management and core manoeuverability 80−63359
- fuel rejuvenation based on in situ re-enrichment and fission product removal 80−37561
- fuel rod pellet-clad gap thermal conductances, exptl. results, anal. correl. 78−70606
- fuel rods, defect detection 78−86640
- fuel temp. feedback coeff. meas. using small excursion techniques 77−42045
- fuel thermocouples and liquid-level probes for core monitoring 80−99239
- FUGEN, 165 MWe prototype HW moderated BW cooled reactor, zero-power startup tests *(Japanese)* 79−26553
- FUGEN LWR, reactor physics tests 80−68893
- FUGEN plant dynamic tests 80−68894
- full m-core instrumentation system, calculational verification 77−42149
- full-range reactor power meas., pulsed ion chamber methodology 79−13480
- gamma-ray spectrum meas. inside reactor, calorimetric method 78−17293
- gamma-ray threshold self-powered detector, use as reactor power monitor 77−65280
- gas core reactors, temp. profile and power calcs., uniform density diffusion model 80−37553
- gas tagging, analytical design for optimization of tag gas isotopic compositions 80−23026
- gas tagging of fuel failure, simultaneous identification of multiple failures using barycentric-coords. tech. 80−83191
- gas tap system for fuel element failure anal. 79−85627
- GCFR, 300 MW(e), gamma-ray heating in core and blanket 77−61486
- GCFR, nuclear heating in B_4C control rod 77−42115

fission reactor core control and monitoring continued
GCFR core-element and press. equalisation system, seal development 77−46271
GCFR fuel column, effect of Cs migration on fission gas permeability 79−67824
GCFR lattice, Monte Carlo and diffusion theory calcs. of steam worth 79−80991
GCFR lattice, PROTEUS central ThO_2 zone expts. 80−22984
GCFR LOF accident, natural convection effects in blocked fuel assembly 79−49755
GCFR rodded lattice, axial UO_2 blanket meas. 79−81037
GCFR simulation central Doppler worth evaluation 79−9814
GCR He primary coolant impurity monitor 80−32413
graphite core components, design 78−41807
guard line circuits dual microprocessor system, decision-making and self-testing 80−57901
Harrisburg nuclear power station failure, safety and control *(Norwegian)* 79−81017
HCDA, bubble worth variation in molten cores 80−68854
HCDA, neutronics and hydrodynamics equations, energy release, DISCAL code 80−68842
HCDA condition, fuel motion measurement, time-resolved coded aperture imaging system 78−45764
heat release distribution random component determ. method 77−54289
heavy water, US velocity experimental determ. using freq. pulse method 78−21734
heavy water concentration meas. by neutron thermalisation method *(Japanese)* 79−93746
heavy water production, Canadian experience 79−30929
heterogeneous critical assemblies with strongly blocked absorber, reactivity temp. effects 80−32395
heterogeneous reactor, physical characts. optimisation 80−32335
HFBR, detection and identification of failed fuel elements 78−21708
HFR, graphite irradiation damage, correlation data, from GAMIN dosemeter 78−29657
HFR test reactor, HIP-TEDDI code for neutron flux calcs. 79−3223
high-power reactor, conditions for nonuniform field production 78−37405
highly enriched U plates, assay in random driver, absorption modified multiplication effects 80−32399
Horowitz method of reactor control system design, BWR appl. 79−45338
hot pellet nuclear reliability factors 80−68754
HTGR, Brayton-Rankine binary cycles optimisation 80−22904
HTGR, consequence anal. of hypothetical accidents, core heatup and afterheat removal 78−58381
HTGR, control rod ejection accident, comparison of one- and two-dimens. models 78−13279
HTGR, critical expts. on enriched-U graphite moderated cores, power, reactivity, control rods *(Japanese)* 80−47594
HTGR, dimensional stability of irradiated B_4C-graphite control materials 78−8905
HTGR, driver fuel elements, power profile meas. and in-pile thermocouple readings 79−67907
HTGR, Fort St. Vrain, nonlinear subcritical multiplication 78−21701
HTGR, inert gas release core-survey calc. 79−67908
HTGR, large pebble bed, Xe oscillations detection 80−22988
HTGR, medium enriched U fuelled, optimisaton 80−37512
HTGR, nonlinear dynamic anal. of prismatic graphite fuel elements, response to seismic excitation 80−99237
HTGR, pebble-bed, computational procedure for xenon stability 77−61501
HTGR, startup test techniques 78−21706
HTGR coated-particle fuel, irrad. performance determ. by irradiated microsphere gamma analyzer (IMGA) 79−54543
HTGR core, γ-spectroscopic exam. of fission product distrib. after shutdown 79−67909
HTGR Core Auxiliary Cooling System mathematical simulation 78−29570
HTGR core heatup, PCRV integrity, thermal anal. model 79−49735
HTGR cores, graphite oxidisation analysis computer program *(Japanese)* 79−81018
HTGR fuel cycle summary and recent developments 80−728
HTGR fuel elements, reactivity of multiplying systems determ., kinetic methods, pulsed neutron method 79−3220
HTGR graphite elements, transverse flow theory 79−67888
HTGR hypothetical accidents, consequences following breach of primary circuit and safeguard failure *(German)* 78−58390
HTGR instrumentation, special needs 78−734
HTGR pebble bed core, initial heterogeneous poisoning by B and HF 80−22981
HTGR refuelling, equipment safety, gamma dose meas. 80−47668
HTGR with closed-cycle gas turbine, technological assessment 79−54490
HTPBR, neutron and physical aspect calcs. *(German)* 80−22941
HTR, fission chamber development 79−76112
HTR, Fort St. Vrain core performance 78−17408
HTR, Xe dynamics, 2D reactor models, axially collapsing methods *(German)* 80−68731
HTR critical facility, KAHTER, reactivity meas. using neutron noise anal. *(German)* 77−83031
HTR power plant control 77−14262
HWGCR, KS-150, in-core instrumentation, neutron flux, temp. distrib. 77−83050
HWR, charact. of Pt self-powered flux detectors 77−65282
HWR, safety research and development 78−29614
HWR dynamics modelling for digital control system design 79−9829
HWR TV-O, active core neutron spectrometry using Bonner spheres *(Czech)* 80−73948
IBR-30 fast neutron spectrum, activation threshold detector readings, statistical regularisation method 78−37483
identification, test inputs review 78−41819
in-core fuel management educational module 80−36804
in-core meas. of energy release, computerised *(Czech)* 78−86637
in-core measuring system for VVER-440 and VVER-1000 type reactors 'INCORMER' *(Russian)* 79−30965
in-core movable neutron flux mapping computerised console development 78−13308
in-core neutron detection using mag. focused electrons, appl. to fast and thermal reactors 77−50271
in-reactor fuel temperature, transient response of centreline thermocouples, appl. to fuel modelling 80−95372

fission reactor core control and monitoring continued
in-reactor performance of surface-mounted and embedded thermocouples 79−93704
in-reactor small high temp. ionisation chamber 79−18087
in-reactor temp. meas. accuracy, thermometer construction effects 79−17969
instrumentation and control test loop diagrams 80−68890
instrumentation for protection and control of reactors, reliability improvements 80−32416
integral parameter correlations, reactor performance using data covariances 80−68869
integrated PWR, anticipated transients without scram, calc. of dynamical behaviour 80−5250
integration method for reactor systems analysis 78−78438
interactive fuel management using a CRT 79−85594
intermediate energy standard neutron field, ENDF/B-V cross sections 80−63325
International Electrotechnical Commission standards for reactor instrumentation and controls 79−45366
irradiated fuel, nondestructive devices for on-site examination 80−13699
irradiated fuel visual inspection, design of compact, portable stand 79−67912
irradiated nuclear fuels, characterisation by precision gamma scanning 79−49688
irradiated nuclear fuels, passive neutron assay, burnup determination 80−32398
IRT 2000 reactor in Sofia, neutron spectra and doses in exptl. canals *(Bulgarian)* 78−82489
IRT WWER, use of thermometric fuel assembly in safety anal. 79−97837
IRT-2M reactor with loop channels in active area, physical parameters *(Russian)* 79−31067
IVV-2 research reactor, thermal neutron flux distribs. using neutron probes 80−32391
JEN-2 reactor, kinetic parameters determ. by p_0 method *(Spanish)* 77−67819
Kalman filtering theory appl. *(Japanese)* 78−50278
KEMA Suspension Test Reactor neutron flux and Dodewaard BWR temp. noise 79−3193
kinetic param. meas. of Univ. of Maryland reactor by interval distrib. method 78−29598
KNK shutdown systems 79−97866
Kyoto University Critical Assembly, water moderated core, group consts. 80−22960
laser-based pin profilometry, noncontact gauging systems appl. 79−2745
lattice cell meas. in 36 element natural UO_2 fuel, stopping effect of coolant 78−58347
leakage neutron spectrum meas. in light water using time of flight technique 78−62592
lifetime fissile fuel requirement 80−37424
linear extrapolation distance for a black cylindrical control rod with the pulsed neutron method 80−68839
LMCBR, heterogeneous, core power distrib., sensitivity to localised reactivity insertion 80−68881
LMFBR, 300 MWe, ^{A}Pu, A=239, 240, 241, burnup characts. 3-D numerical anal. 79−22371
LMFBR, acoustic resonances as means of blockage detection 79−93752
LMFBR, alternative core disruption accidents 79−9774
LMFBR, analysis of in-pile MFCI experiments with carbide fuel 79−49754
LMFBR, anisotropic diffusion effect on criticality of plate lattice fast assembly 79−26463
LMFBR, ANL high temp. microphones 77−46361
LMFBR, appl. of EuB_6 to neutron absorbing control materials 78−8904
LMFBR, behaviour of H in liquid Na *(Japanese)* 79−49649
LMFBR, breeding ratio and fissile inventory for homogeneous and heterogeneous cover 80−32374
LMFBR, Clinch River, in-core instrumentation 78−29608
LMFBR, cluster of core assemblies, CORA transient anal. 80−18389
LMFBR, compact Na cooled reactor, KNK-1, total and fast neutron flux meas. *(German)* 78−62591
LMFBR, components and fuel handling systems, Italian industry contrib. 79−97875
LMFBR, computer control system for Na test loops 79−26550
LMFBR, core flow distrib., analytical prediction, using CATFISH hydraulic code 80−23018
LMFBR, core-disruptive accidents, neutronic and fuel element behaviour 80−32357
LMFBR, correl. meas. of Na flow rate using mag. detectors 79−71924
LMFBR, design and thermohydraulic characts. of fuel and blanket subassemblies of a large core 80−711
LMFBR, effect of mag. field on operating characts. 79−71885
LMFBR, effects of Th breeder material on Na-void reactivity 80−22982
LMFBR, effects on noncondensable gas bubbles on propag. of boiling acoustic noise 77−46364
LMFBR, enrichment and control optimization for reactivity losses during burnup 78−21692
LMFBR, establishment of buoyancy induced natural circulation, CURL-L code anal. 79−49663
LMFBR, fast integral model for the transient analysis of a melting fuel pin 79−54552
LMFBR, flow behaviour of vol. heated boiling pools 80−13545
LMFBR, fuel motion diagnostics instrumentation, evaluation with PARKA 79−45360
LMFBR, fuel motion pot. due to volatilisation of metallic fission product inclusions 79−49746
LMFBR, fuel pin coolability in low power voiding, SAS3A computer code anal. 79−49661
LMFBR, fuel pin deform. within wire-wrap fuel assembly, computer code anal. 79−71915
LMFBR, fuel pin optimal design for large scale testing 79−76065
LMFBR, full power rod drop calibration appl. to kinetics expts. 77−42151
LMFBR, gas tag identification of failed assemblies, anal. methods 80−95369
LMFBR, HCDA, evaluation and prevention of local core accidents 80−749
LMFBR, HCDA, role of radiative heat transfer in post-disassembly fuel self-mixing 79−49759
LMFBR, HCDA, two-phase momentum exchange experiment and analysis, using SIMMER code 79−49751

fission reactor core control and monitoring continued
LMFBR, heterogeneous, breeding performance improvements 80–68882
LMFBR, heterogeneous, physics performance with internal axial blankets 80–5218
LMFBR, heterogeneous, Th blanket zones study in ZPPR Assembly 8 80–22983
LMFBR, hydrodynamics of large-scale fuel-coolant interactions 80–78409
LMFBR, JOYO, fast reactor, experimental, functional and operational test results 79–93796
LMFBR, large carbide-fueled, press. drop constraint on breeding performance and pin diameter optimisation 77–50270
LMFBR, LOF accident, evaluation of incoherency effect on cladding motion in R-series test 79–49749
LMFBR, low sodium void cores 80–13549
LMFBR, meas. of T retention of fast-neutron-irradiated absorber elements of B_4C 78–8903
LMFBR, Na boiling, acoustic detection using pulsed system 79–97839
LMfBR, Na loop temp. control using 100 kW elect. heater *(Czech)* 80–5203
LMFBR, neutron flux distrib. on core support grid plate 78–21675
LMFBR, neutron streaming through control rod followers, diffusion coeff. by numerical integration 80–13636
LMFBR, pool-type, design effect on natural circulation establishment 77–6487
LMFBR, probabilistic evaluation of core-internal coolant flow distrib., correl. among fuel subassemblies 77–88210
LMFBR, procedures for meas. of bowing/expansion reactivity parameters 79–81038
LMFBR, props. of Eu_2O_3 as control material 78–50261
LMFBR, reactivity variations ass. with randomly distributed bubbles in molten core 77–46331
LMFBR, recriticality considerations for the loss-of-heat-sink accident with scram 79–49760
LMFBR, rod bundle, static press. meas. 80–73969
LMFBR, safeguards system for monitoring of fissile material inventory 80–63293
LMFBR, self actuated shutdown system for reactor protection 77–42106
LMFBR, simulated radial parfait core, control rod worth 78–33280
LMFBR, SNR-300, criticality prediction 79–40989
LMFBR, space time dynamics for localized disturbances 78–21674
LMFBR, system and in-core interactions for thermohydraulic transients 80–18545
LMFBR, thermal conditions controlling subassembly failure propag. during transition phase 79–49758
LMFBR, thermal expansion worths inferred from small sample reactivity meas. 78–29596
LMFBR, TOP, fuel pins and core response 80–13671
LMFBR, transient boiling of Na in 7-pin fuel bundle under loss-of-flow conditions 79–41007
LMFBR, whole core thermal hydraulic transient code 80–18387
LMFBR, yield characts. of short-lived fission products in Na heat-transfer agent 78–66338
LMFBR 91-pin subassembly, fuel displacement diagnostic facilities 79–49776
LMFBR (SNR 300), design of core catcher system 78–89937
LMFBR advanced fuels critical assemblies, integral alpha and point conversion ratio meas. 79–81012
LMFBR blanket assembly cooling, flow regulating device 80–23029
LMFBR blankets, comparative breeding potential of ^{232}Th and ^{238}U 80–22948
LMFBR boiling acoustic detection sensitivity, PFR commissioning expts. 79–13452
LMFBR control material, integral capture cross section meas. in CFRMF 77–26760
LMFBR coolant, simple multichannel thermal-hydraulic model for transient behaviour anal. 79–49660
LMFBR coolant flow, flux distortion flowmeter meas. 79–68858
LMFBR coolant flow monitoring by balanced outlet temp. signals 79–13393
LMFBR coolant temp. meas. using high integrity coaxial thermocouples 80–32410
LMFBR core, stochastic void models for bubble worth calcs. 80–22940
LMFBR core compaction, nonuniform interassembly gap effects 79–9682
LMFBR core instrumentation, approach based on IR television, on-line computing, pattern recognition 77–54310
LMFBR core melt-down protection system *(Russian)* 79–76101
LMFBR core restraint transient responses, CORTAC 3-D thermal hydraulic model 80–18390
LMFBR core simulation, Na loop safety facility, P2 expt., LOCA, acoustic meas. 78–33264
LMFBR core structural analysis codes verification/qualification 79–89407
LMFBR core subassembly cluster dynamic response to an accidental pressure rise 79–54551
LMFBR cores, 3-D mechanics anal. of structural reactivity effects 80–710
LMFBR data multiplexing system 79–76102
LMFBR demonstration plant, design, construction and operating experience 79–97887
LMFBR failed-fuel detection using gaseous fission-product detectors 79–97856
lMFBR fuel and blanket transient thermal performance characteristics 80–68880
LMFBR fuel handling experience 79–97873
LMFBR fuel pin failure monitoring, cumulative mech. damage function from materials data 78–13262
LMFBR fuel pin power calibration prediction, transient correction factor analysis 79–9719
LMFBR fuel pins, reactor illuminated, coded aperture imaging 79–30989
LMFBR fuel rod, hydraulic anal. of turbulent fluid flow by Galerkin method 79–30893
LMFBR fuel subassembly, effect of bundle insulation degradation on boiling stability tests 79–54548
LMFBR HCDA, damage potential of core disassembly, sensitivity study 79–54531
LMFBR HCDA, energetics of bubble expansions, potential attenuation mech. 80–83197

fission reactor core control and monitoring continued
LMFBR HCDA, potential for plugged core pressurisation following LOF accident 79–76084
LMFBR HCDA, US meas. of penetration of liquid Na into limestone concrete 80–78412
LMFBR HCDA aerosol behaviour, kinetic corrections to aerosol gravitational collisional efficiency 80–95386
LMFBR heterogeneous core, sensitivity anal. 80–22935
LMFBR heterogenous, control rod interactions in benchmark assembly 79–81035
LMFBR in HCDA transition phase analysis, material relocation and freezing 77–46329
LMFBR inherent secondary shutdown assembly, hydraulic tests 79–49666
LMFBR inherent shutdown system, expts. and analyses 79–31041
LMFBR LOCA, use of temperature variance to detect sodium boiling 79–54527
LMFBR LOF accident, analysis of in-pile fuel disruption experiments 79–49748
LMFBR LOF transient, sodium voiding dynamics and cladding motion 79–49750
LMFBR LOF-HCDA, solidification dynamics of flowing two-phase mixtures 79–49757
LMFBR meltdown cores, exptl. study of integral physics parameters 80–13664
LMFBR mockup, reactivity determ. from power spectral density meas. with ^{252}Cf 78–37421
LMFBR multipin bundles, eval. of hodoscopes for fuel motion meas. 79–93780
LMFBR Na flow meas. using US flowmeter 80–32412
LMFBR Na loop computer control system based upon TOSBAC-40 multicomputer 80–47662
LMFBR Na vapour bubble collapse detection by acoustic emission 79–13451
LMFBR Na-heated steam generator, flow instability detection by noise anal. 79–97854
LMFBR PHENIX vibration-induced neutron noise obs. 79–13453
LMFBR reactivity surveillance using ex-core detectors 79–9802
LMFBR refueling force limits criteria, testing, and evaluation 79–67913
LMFBR rot. shield plug annulus, Na vapour, deposition rate, controlling factors 80–47591
LMFBR safety testing, scram signal generator for fluid motion monitoring 80–18551
LMFBR spectrum, Doppler reactivity worth of UO_2 and ThO_2 meas. 80–27776
LMFBR subassembly fault detection, microprocessor-based distributed system appl. *(Japanese)* 79–41002
LMFBR surveillance technique development 79–13448
LMFBR TOP accident, implications of in-channel fuel plugging 80–78414
LMFBR transient behaviour, effect of steam cycle 79–49678
LMFBR whole core transient anal., COBRA subchannel anal. code 80–18388
LMFBR-subassembly outlet computerised temp. monitoring based on estimation theory 78–8948
LOCA, blowdown phase, two-phase mass flow rate meas. using true mass flowmeters 80–778
LOCA, pressure oscillation in subcooled decompression under temperature gradient 80–559
LOCA, reflooding phase, flow film boiling, void fraction meas. 80–92207
LOCA, spray cooling of hollow rod cladding 78–50262
LOFT fuel design and operating experience 80–18411
LOFT reactor advanced instrumented center fuel bundle, in-reactor meas. devices for LOCA expts. 80–23024
loose parts monitoring, USA technology status and recommendations 79–623
loose parts monitoring techniques and experience 79–3211
LWBR, calculational model used for nuclear anal. 79–67842
LWBR, unique thermal and hydraulic design features 79–54483
LWBR at Shippingport, expected nuclear performance and initial physics testing 79–67931
LWBR detection of thermal shield motion using ex-core neutron detectors 79–59220
LWR, 3D flux distrib. calc., axial continuous synthesis model with finite element trial functions 80–713
LWR, actinide decay power 80–22930
LWR, alternative fuel cycles containing Th 80–37510
LWR, automated procedure for selection of optimal refueling policies 79–67892
LWR, calc. of optimum power profiles using pattern search techniques, PROFILE code 80–47557
LWR, core reload optimisation 79–85642
LWR, failed fuel rod identification by gas tagging 80–23021
LWR, fission product activities, fuel survey 80–736
LWR, fission product decay heat, revised ANS standard 80–13649
LWR, fuel temp. correl. for power feedback and reactivity coeff. appl. 80–22979
LWR, fuel utilisation, spectral shift control methods 80–47586
LWR, generalized theory for predicting mass effluence during reactor reflooding 79–36352
LWR, in-service inspection, a critical assessment 79–63762
LWR, initial fuel loading problems 78–21741
LWR, interpretation of in-core measurements by semianalytical approach 80–712
LWR, multigoal fuel cycle optimization including nonproliferation objectives 80–52764
LWR, NRC safety research programs, fuel behaviour, operational safety, metallurgy and materials 80–13705
LWR, operation planning, optimum fuel loading and generation planning, comp. code FAPMAN8 80–47673
LWR, optimal power profile fuel management 78–37411
LWR, optimum fuel loading and coastdown operation 79–30970
LWR, optimum fuel loading and operation planning, FAPMAN model 80–47607
LWR, ore conservation by routine coastdown 80–37507
LWR, power distrib. monitoring using gamma thermometers 79–45368
LWR, power modulation testing of pre-irradiated fuel pins 78–70607
LWR, process monitoring and parameter estimation, multivariate signal analysis algorithms 80–47585
LWR, Pu recycling, CEA-EdF studies 80–722

fission reactor core control and monitoring continued

- LWR, Pu recycling, storage before use in breeders 80−37513
- LWR, Pu recycling, technical and economic study 80−720
- LWR, refuelling with natural U 80−679
- LWR, stationary boiling front in liquid film cooling of a vertical heated rod 79−45341
- LWR, thermal neutron disadvantage factors for PuO_2-UO_2 and UO_2 lattices 80−73945
- LWR, thermal-margin methodology improvements 80−23022
- LWR, two near-term alternatives to improved nuclear fuel utilization 80−37506
- LWR, UO_2 fuel, critical expts. supporting close packed water storage 80−37434
- LWR, zero power coupled core, cross power spectral densities, core separation distance effects 79−54469
- LWR alternative fuel cycles, sensitivity to data uncertainties 80−22934
- LWR code analysis, qualification of SIMULATE against the Hatch-1 end-of-cycle 1 gamma scan 80−57921
- LWR computer code package for core following and in-core fuel management benchmarking and operating experience 80−704
- LWR cones, computation of cell group consts. 80−566
- LWR controlled porosity fuels, short term irradiation behaviour 79−49686
- LWR core, few group 2-D diffusion eqns. in hexagonal geometry, HEXAB-II-30E code *(Bulgarian)* 80−68765
- LWR core, minimisation of energy distrib. inhomogeneities 80−63321
- LWR core, power shape determ., gain stabilized NaI(Tl) γ-ray detector system 78−33284
- LWR core, thermal and hydraulic behaviour, modelling in HOTRAN-3 *(Hungarian)* 80−32401
- LWR core flux distrib. using CETRA core simulator 80−716
- LWR core meltdown, accident anal. using computer system KESS 80−752
- LWR core meltdown, activity release and aerosol characts. 78−82469
- LWR core meltdown, materials behaviour 80−751
- LWR core meltdown, metastable state preceding entrapment explosions 80−771
- LWR core meltdown and containment anal., computer code solns. 80−753
- LWR core meltdown risk anal., penetration of hot melts into concrete structures 80−750
- LWR core performance studies in the UK, review of computer codes for static reactor physics anal. and kinetic anal. 80−703
- LWR core transient anal. using coupled neutronics and thermal hydraulic models 80−715
- LWR cores anal., experience with MEKIN code 80−23054
- LWR critical heat flux calc., anal. of empiric relations using CRISIS code *(Bulgarian)* 80−68766
- LWR ECC, UCFLOOD code for bottom reflooding heat transfer 79−49728
- LWR effect of fabrication variables on fuel in-core performance 79−63798
- LWR fuel, feasibility of accelerator driven rejuvenation 80−27780
- LWR fuel, future trends to improve U utilisation 79−85634
- LWR fuel elements, burnable poison management for high burnup reactivity compensation 80−707
- LWR fuel failure under reactivity initiated accident condition *(Japanese)* 78−25305
- LWR fuel management, power distrib. calcs. by nodal one-group simulators 80−706
- LWR fuel management decision analysis with fuel integrity prediction 79−9781
- LWR fuel performance, fabrication related effects 79−59238
- LWR fuel rods containing fission gas, grain growth 79−67866
- LWR fuel utilisation in US, historical survey 80−37460
- LWR gamma-scanning meas. of spent fuel elements, appl. to reactor simulation *(German)* 79−67874
- LWR hydrogen formation during core melt accident 78−50267
- LWR in-core fuel management techniques, review *(Italian)* 80−18447
- LWR irradiated fuel assemblies, nondestructive exam. using γ-ray and neutron techniques 80−66760
- LWR lattices, temp. effects, reactivity levels 80−22893
- LWR lattices of UO_2 and Gd_2O_3 rods, critical expt. 79−26474
- LWR LOCA, heat transfer in the inverted annular flow regime during reflooding 79−49731
- LWR LOCA, two-phase flow, horizontal stratified, 1-D two-fluid eqns. 80−91226
- LWR LOCA occurrence of critical heat flux during blowdown with flow reversal 79−54529
- LWR NRC safety research programs, thermo-hydraulics and computer code development, loss-of-coolant accident, emergency cooling core event 80−13704
- LWR nuclear power plant with passive containment system, surveillance system importance 80−795
- LWR plant control, linear quadratic theory appls. 77−88265
- LWR primary coolant leakage detection using acoustic monitoring system 80−700
- LWR protection system 79−97844
- LWR refueling outage times, effect on plant availability 79−67910
- LWR refuelling shutdown, multiple controlled-cell removal 80−99252
- LWR safety research programs by US NRC, review 80−42796
- LWR steam explosion pressure buildup estimation 79−13473
- LWR version of URANUS integral fuel rod code 78−17278
- magnetoacoustic rod position monitoring transducer system for nuclear power plant 78−33262
- Magnox reactors, moderator graphite corrosion protection coolant comp. effect on radiolytic graphite/CO_2 reaction 77−6489
- Magnox reactors, Trawsfynydd, computerised monitoring and control system 80−86965
- Maine Yankee reactor protection system setpoint calc. 79−13479
- malfunction detection by Dynamic Data System methodology 79−622
- MARIA research reactor, dynamics model for fast transients anal., code TOTEM 80−37419
- material safeguards, unirradiated fuel control in BOR-60 fuel assemblies *(Russian)* 80−68809
- materials safeguarding, fuel assembly identification using US signatures, statistical aspects 80−69620
- materials safeguarding, remote-controlled and long-distance unique identification of reactor fuel elements or assemblies 80−63296
- materials safeguards, in situ verification techniques for fast critical assembly cores 80−78390

fission reactor core control and monitoring continued

- maximum power limits with classical discrete control *(Russian)* 79−67920
- melting pool surfaces, temp. meas. by ratio pyrometers 78−82471
- metallic fuel cladding eutectic formation during postirradiation heating in EBRII 80−102241
- microcomputer based safety system 77−67845
- microprocessor based operator independent reactor power monitor 79−85644
- microprocessor controlled multipoint recorder with graphical video output for reactor core temperatures 80−57873
- microprocessor controlled reactivity meter for real time monitoring of reactors 78−33263
- microprocessor-based flux wire evaluation and anal. system 80−63353
- MIT research reactor, flux synthesis techniques for routine core physics calcs. 80−68868
- MITR-II research reactor, power and neutron flux distribs. 77−42043
- mixed oxide fuels, irradiation-induced densification and PuO_2 particle behaviour 79−49684
- modal control based on nonlinear model 77−38339
- molten metal-coolant interactions minimum film boiling temp. 79−54524
- molten salt breeder reactor, reactivity control capability of fuel-salt processing system 79−22399
- monitoring of boiling water and of steam content using Cherenkov radiation 80−73957
- monitoring system for energy liberation fields of Beloyarsk power station reactors 77−23232
- monitoring system improvement due to improved computer technology 80−57882
- Monte Carlo, radiation transport code, comparison of electron transport models 80−23030
- MSBR, transient Xe anal. 78−54843
- MSBR-1000 liquid salt reactor, operating characts. under variable loads 79−71886
- Muehleberg BWR, core simulation by fuel Management System, expt. verification 80−705
- multichannel low flow, boiling thermal hydraulic anal. 79−67885
- multicomponent noise signal decomposition 79−3210
- multicore reactor, optimal control determ. from energy release profile *(Russian)* 80−73974
- multilayered reflector region, neutron diffusion codes, analytic treatment 79−93683
- multiple fuel failure resolution with gas tagging, barycentric coordinate technique 79−13485
- multiple-core reactors, canonical decoupling and control 77−26837
- multiplex systems, reliability, reliability with repair and availability 79−41012
- multizonal absorbing rod, effectiveness in albedo and diffusion studies *(Russian)* 80−556
- multizone reactor, reactivity and power shape control, optimisation method 77−6529
- MWR feedwater and recirculation flow, minicomputer-based digital control 80−23027
- NBS standard neutron fields, average fission cross-section meas., error anal. 80−68857
- negative reactivity reactor expts. using controlled intensity neutron sources 79−17967
- neutron absorption, control poison optimisation, depletion calcs. 80−57906
- neutron beta-emission cable-type detector with Ag emitter, sensitivity during long service in reactor 78−86644
- neutron counting statistics in subcritical cyclo stationary multiplying system 80−32323
- neutron detector efficiency estimation, variational techniques 78−62601
- neutron detector response in water moderated reactor, influence of air bubbles 80−18442
- neutron detector telecontrol device with direct loading in reactor core and vertical channels of IRT-2000 *(Russian)* 80−52770
- neutron detectors for in-core flux monitoring 80−5297
- neutron detectors for reactor control 77−54326
- neutron distrib., approx. mathmatical models, core control 77−54290
- neutron field fluctuations, energy distrib. and reactor power 80−32396
- neutron field in fast reactor, spectral charact. *(Japanese)* 78−46222
- neutron fluence and reactor core centre flux mapping, mica and plastic detectors 78−13346
- neutron fluence meas. using solid state nuclear track detectors with Au and In foils 80−69035
- neutron flux, density measurements for reactor control *(German, English)* 78−17335
- neutron flux density distribution meas., azimuthal-axial, at fuel element surface *(Czech)* 79−36344
- neutron flux detection using self-powered Inconel-Inconel coaxial cable 80−42842
- neutron flux distrib., optimal allocation of in-core detectors 78−54839
- neutron flux instrumentation commissioning, EM compatibility 79−89466
- neutron flux level CRT state indicator 77−79444
- neutron flux meas., calculation of target and detector size in determination of 14-MeV neutron energy flux 79−97829
- neutron flux meas., counting-Campbelling channel for in-core and out of core meas. 80−32406
- neutron flux meas., high temp. neutron rad. detectors and cables 79−76111
- neutron flux meas., integrated cable detectors for use under flux and/or at high temperature *(French)* 79−76114
- neutron flux meas., self-powered neutron detector with enriched-U emitter 79−76115
- neutron flux monitoring during reactor refuelling and start-up, instrum. *(Polish)* 80−42792
- neutron flux optimum control during nuclear station load following 79−9761
- neutron flux peaking anal., nuclear fuel bundle ends, program PEAKAN 78−82493
- neutron flux regulation, dynamic simulation of two-phase control absorber 80−13731
- neutron importance meas. by dynamic method in subcritical reactor core 79−17956
- neutron instrumentation for protection and control of nuclear reactors *(French)* 80−32407
- neutron noise, diagnostic method of mech. vibrs. of VVER type reactor core *(Czech)* 77−3120

fission reactor core control and monitoring continued
neutron noise anal. techniques, unified theory 79−30886
neutron noise analysis in PWR and BWR power reactors 80−86964
neutron noise as information carrier for early detection of fuel rod malfunction 77−14242
neutron noise theory, role of factorial cumulants 79−63711
neutron self-powered detector with fissile emitter, theoretical evaluation 78−74533
neutron spectra in fast neutron systems using ^{6}Li sandwich counter 80−27884
neutron spectroscopy using miniature detectors and preamplifiers 80−47669
neutron spectrum evaluation in SR-0 reactor using activation method *(Czech)* 77−65288
neutron transport finite element method, two-dimens., one-group test problems 80−37412
neutron transport theory, collision probability method, development and applications 80−27706
neutron transport theory, homogenization methods to obtain group-diffusion parameters for reactor calculations 80−670
neutron-physical characteristics of Soviet BABETs reactors, startup experience 80−73953
neutronic noise, relations with coolant temp. fluctuation and control rod vibr. at KUR 78−58327
new load-follow strategy for improved return-to-power capability 79−9794
noise analysis of power reactor, simulation using nucleate boiling noise generator 78−54840
noise diagnostics and surveillance, experience of Babcock and Wilcox company 78−17346
noise experiments with delayed neutrons, general theory 77−54316
noise measurements for plant surveillance and anomaly detection in nuclear power stations 79−97853
non-destructing testing of reactor components using acoustic emission *(Spanish)* 80−57871
nondestructive burnup meas. by incore and out-of-core methods 79−17987
nondestructive gamma-ray spectrometry method for fuel burn-up control *(Slovak)* 78−21672
nondestructive neutron assay for nuclear materials accountability and criticality control 80−66759
nonlinear control system, relative stability anal. 77−3116
nonlinear coupled core reactor, computer simulation of decoupling theory appl. to power control 78−54845
nonlinear reactor noise anal., appl. of Langevin eqn. with system-size expansion 80−68727
normal and abnormal behaviour nonparametric recognition 79−81044
NRU, NRX reactors, homogeneous cell parameters for 2-D reactor codes by axial averaging of 3rd parameter 79−54577
nuclear fuel, radial distribution of nuclides, exam. during irrad. by gamma spectrometry *(French)* 78−78467
nuclear fuel management via fuel quality factor averaging 79−30943
nuclear power plant control and instrumentation. [conf. Cannes, France (Apr. 1978)] 79−76096
nuclear power plant performance improvement by Reactor Power Cutback System 79−9795
nuclear power station model validation and automatic control 77−88261
nuclear reactor, two-phase flow characterisation by neutron noise techniques 78−94058
nuclear reactor kinetics and control, book 79−26461
NWR, CANDU-type, at Bruce Nuclear Generating Station A, reactor physics meas. 78−21707
OGL-1 high temp. in-pile gas loop, construction and performance tests *(Japanese)* 79−71881
on-line alarm analysis in the hierarchical control system of the WWR-SM research reactor 79−76104
on-line reactivity meter, comparison between direct and polarity correlation techniques for projected Gauss Markovian process 79−54528
on-off zonal reactor control systems, analysis 77−71680
on-power measurements of reactor parameters using dynamic meas. methods, computer system description 79−89467
one zone fast reactors, reactivity measurement by pulsed neutron method 79−45377
online digital core protection calculator, thermal margin routine 79−9777
online Reactor Noise, Vibration and Loose Parts Monitor 79−3212
operational and reliability experience with ractor instrumentation for AGR and magnox reactors, review 79−89453
optical instrumentation methods for two-phase reactor flows 80−63313
optimal conditions for reactor shutdown for known period 78−86642
optimal control of distributed parameter reactor core by function space method, numerical experiences 77−54317
optimal control of nuclear reactor using Walsh function variational synthesis technique 77−38347
optimal shutdown control, quasilinearisation and numerical soln. *(Korean)* 79−89395
optimisation of spatial flux distrib. and Xe fluctuations by differential dynamic programming 79−45358
optimization of energy distribution in active region of large functional power reactor 79−59186
optimum trip level of m-out-of-n reactor temperature trip-amplifier systems 79−93741
oscillation techniques in power reactor dynamic characteristics study *(Czech)* 80−52755
output monitoring by neutrino detection 79−67897
Palisade PWR, physics model verification 80−63322
parameter identification and adaptive control, applic. to nuclear reactor systems 80−22970
parameter monitoring system, microcomputer-based *(Hungarian)* 80−18451
parameter tracking, via recursive nonlinear estimators 77−14253
pattern recognition methods, fission reactor surveillance appls. *(French)* 80−37477
pattern recognition system for abnormal behaviour monitoring 78−698
pattern recognition systems, ORNL expts. 80−63351
PB-HTGR, control-rod induced flux perturbations, numerical anal. using out-of-force instrumentation *(German)* 80−83179
PBF, temp. sensitivity of Co self-powered neutron detectors under PWR conditions 78−33275
PBHTGR, core behaviour following massive air ingress, graphite corrosion eval. *(German)* 80−83181

fission reactor core control and monitoring continued
PBHTR, afterheat removal system failure, radiant heat transfer anal. 80−95364
PBHTR, closed Th cycles, computational reactor lifetime simulation 79−85643
PBHTR, design accidents, exam. of temp. coeff. and short time dynamics 79−63781
PBHTR, out-of-core instrum. for detection of spatial flux irreg. *(German)* 78−82430
PBHTR, Th fuel cycle performance 78−41841
PBR, simulated THTR, spline anal. of dynamic transit reactivity meas. for pebbles *(German)* 78−66339
PBR, use of turning rods and its influence on coated particle failure 80−702
PBR axisymmetric core, thermal-hydraulic anal. techniques 79−71884
PBR core, coolant flow predictions using PEBBLE computer code 79−54474
PBR power distrib. and Xe oscillations control concept *(German)* 78−29612
PFR, fuel and component handling, CDFR intentions 79−97872
PFR core meas. rel. to safety and importance 79−97897
Phenix fuel assembly and core performance anal., CAPHE code system *(French)* 79−97878
Phenix reactor, characts. and operating behaviour of fuel element *(French)* 78−66349
PHWR valve bellows, effect of service parameters on fatigue life and fracture 78−58348
PHWR-1000, uniformity factor maximisation, nonlinear programming 80−739
Pickering reactor, simulation of wire activation expts. with SORGHUM code 78−25310
PIRK 2 program, inverse reactor kinetic eqn. solns. 79−76095
plant condition monitoring in nuclear power generating industry, review 80−47612
plant diagnostics−the integrated approach 80−68899
plant information measures selection criteria nuclear reactor monitoring appl. 79−41006
PNP-3000, prototype nuclear process heat reactor, core temp. transients, heat transfer calc. *(German)* 80−83180
point model nuclear reactor heuristic approach to reinforcement learning control 78−46144
point reactor population model using neutron and fuel cycle kinetics analogy 80−47556
pool-type reactor noise analysis and expt. 79−3195
post-accident filtration design for PWR and BWR containments 79−49739
power coefficient measurement based on reactor coolant system average temp. 80−57909
power coefficients and isothermal temp. coeffs., at-power meas. 78−21704
power density limitation system development 80−68884
power distrib. flattening, burn up optimisation *(Japanese)* 78−17397
power distribution control, multivariable control system theory appl. 77−67832
power measurement by continuous calorimetry, automated system 78−17336
power peak-to-average ratio minimisation analysis 77−65293
power plant availability improvement by acoustic emission surveillance 79−3213
power plant control problems survey 77−88258
power plant diagnostic instrumentation experience 79−3218
power reactor, Calvert Cliffs, power level manoeuvring experience 78−21718
power reactor, computational method of approximating discrete power distrib. meas. 78−17340
power reactor, Fort Calhoun, operation with reduced complement of in-core detectors 78−21716
power reactor, modal control 77−14252
power reactor in-core fuel management, computer programs 79−71914
power reactor noise anal. *(Bulgarian)* 78−82488
power reactor noise analysis, nonlinear kinetics effects and new techniques 79−13454
power reactor operational control algorithms 79−67896
power reactor parameter identification in Xe oscillation model using maximum likelihood method 80−18466
power reactor resonance determ. by rod-drop method, Fourier anal. 79−22407
power reactors, loose parts and neutron noise monitoring and diagnostics 78−21712
power reactors, min. unit generation cost 80−734
power shape control, reactor fuel reliability constraints 77−83057
power spectral density measurements with ^{252}Cf for a light-water-moderated research reactor, determ. of reactivity of far-subcritical systems 80−57913
power spectral density signature analysis, statistical algorithm 79−624
pressure and temp. sensors, reactor time const. determ. by dynamic data system method 79−93750
pressure tube-type reactors, moderator temp. coeffs. of reactivity meas. 80−57893
pressure vessel, crack initiation during thermal shock, warm pre-stress 78−41816
pressure vessel, Oconee nuclear station, surveillance capsule results 79−18019
pressure vessels, acoustic equipment for leak detection during hydraulic tests *(French)* 80−789
primary coolant flow rate determ. using gamma/neutron ratio near primary line 77−65254
primary-circuit components, surveillance of vibr. behaviour 80−790
prompt fission neutron spectra for ENDF/B-V 80−22869
prompt neutron yield calcs. from neutron induced fission 80−68858
propagating physical quantity transit time estimation, improved correl. method, coolant bubbles appl. 78−94067
protection system software validation, quality assurance experience 80−57886
Prototype Fast Reactor, instrumentation and control systems 77−67830
PURINAMA, PuO$_2$-fueled zero-energy fast reactor 79−40988
PURNIMA 1 fast reactor, k$_{eff}$ variation during core insertion into reflector 78−74438
PWR, 450 MWe, noise obs., analysis and interpretation 78−94072
PWR, appl. of moderator temp. for enhancement of operating flexibility 80−695

fission reactor core control and monitoring continued

- PWR, behaviour of previously failed fuel rods under power ramp and film boiling operation 79−49745
- PWR, benchmarking of ARMP system against large-scale mockup expts. 80−13696
- PWR, changes in group constants due to burnup, role of fuel nuclides *(German)* 78−17277
- PWR, clad free pellet recriticality possibilities 80−68863
- PWR, comparison of temp. coeff. calcs. and meas. 80−22977
- PWR, computerised axial power distrib. monitoring system 77−65279
- PWR, control of fission products activity in primary coolant, computer code 80−32537
- PWR, control systems for selectively inhibiting protection system functions 78−37418
- PWR, core control optimisation for scheduled load changes 79−71911
- PWR, core flux meas. by microprocessor based automatic flux mapping system 79−45359
- PWR, core physics measurements versus prediction at Fessenheim nuclear plant 80−718
- PWR, critical B concs. and cycle lifetime predictions 80−9365
- PWR, data acquisition system for high press. water loop *(Hungarian)* 78−82432
- PWR, digital rod position indicator system for control rod drive line dynamic characts. study 78−33265
- PWR, dynamic pressure, scale flow modelling of random press. power spectral density 80−83143
- PWR, effect of electrical network frequency control on equipment 80−698
- PWR, effect of measurement conditions on the design of delayed-neutron detector units *(French)* 79−97855
- PWR, equipment for the limitation of power density 80−697
- PWR, eval. of annular fuel economic benefits 80−57919
- PWR, evaluation of fuel performance *(Japanese)* 80−99226
- PWR, ex-core neutron detectors, calc. of spatial weighting func. 79−36351
- PWR, extended inverse kinetics for monitoring reactor feedback design parameters 78−33279
- PWR, fault tolerant multiplexed control rod position detection and system 77−65281
- PWR, fixed in-core gamma thermometer for neutron flux meas. 80−717
- PWR, flux monitoring startup and safety system, ex-core, design and qualification 77−65286
- PWR, french R and D development program 79−97843
- PWR, Fromatome's DMA plant control system 79−97842
- PWR, fuel monitoring, by delayed-neutron detectors 80−737
- PWR, HERMITE coupled neutronic thermal hydraulic code 80−23051
- PWR, high-speed in-core fuel management system 79−30971
- PWR, I spiking in coolant for defective fuel rod operation 78−33272
- PWR, improved instrumentation and computer control systems 78−29601
- PWR, improved load follow strategy for return-to-power capability 79−41010
- PWR, improved water density feedback model for neutron diffusion calc. 79−67890
- PWR, LOCA, RELAP4/MOD6 program, test prediction for German PKL test K5A 80−13642
- PWR, LOCA performance test of upper heat injection system 79−81028
- PWR, materials corrosion, steam generator operations, influence of water chemistry 79−54555
- PWR, neutron noise diagnostics of 2-D control rod vibrs. 80−68840
- PWR, Obrigheim nuclear power plant, inservice inspection, nondestructive testing, primary components *(German)* 77−34406
- PWR, on-line meas. of B concentration in water using neutron absorption method *(French)* 80−32409
- PWR, operational dynamics, digital simulation model 80−27751
- PWR, optimal fuel loading and operation planning 78−50276
- PWR, oxide fuel rods, computer program for mechanical and thermal anal. *(Korean)* 78−86571
- PWR, physics design of reload with nodal code system 80−723
- PWR, power distrib. comparison of U and Pu fuel in KWO core 77−14224
- PWR, power monitoring, direct charge detectors appl. 78−17344
- PWR, Pt-resistance thermometers, in-pile response time testing 79−59219
- PWR, Pu recycling, CEA-EdF studies 80−722
- PWR, Rancho Seco, feed and bleed operation for intermediate-rate reactivity transients 78−21722
- PWR, r.m.s. ex-core detector signal to core barrel amplitude scale factor 80−52767
- PWR, rod bowed to contact departure from nucleate boiling tests in cold-wall thimble cell geometry 79−30892
- PWR, rod ejection accident anal. by reactivity weighting method 79−22419
- PWR, sensitivity of emergency core coolant bypass and lower plenum refill to scale size and plenum press. 79−97827
- PWR, sensor response monitoring, time series modelling 79−26659
- PWR, spatial Xe oscillation time-optimal control 79−628
- PWR, steady-state and transient CHF meas. in Freon-11 79−49732
- PWR, Surry Units 1 and 2, impact of reduced hot channel factor limits on operation, reload core design, licensing 78−21720
- PWR, system for internal neutron meas. *(French)* 79−76113
- PWR, temp. coeff. meas. and eval. in at. power condition 80−22978
- PWR, Th cycle core characteristics 77−42123
- PWR, three loop, simulation in advanced recycle methodology program 80−68856
- PWR, Tihange-type, Pu recycling, physics and safety anal. 80−724
- PWR, two-point Xe oscillation model, variational technique 77−42044
- PWR, welded control rod drive mechanism, automated removal/installation 80−9358
- PWR, Westinghouse, neutron flux mapping at low power 78−21703
- PWR, Xe oscillations control using first overtone control method *(Japanese)* 77−57725
- PWR, Xe-induced spatial flux transient, anal. and control, parameter identification 80−18441
- PWR 18 month fuel cycles, core design operation and economics 79−85591
- PWR and BWR hot channel factors, nuclear, thermohydraulic and technological factors *(Spanish)* 79−36336
- PWR anticipated transients, coupled core system approach to DNB 77−42154

fission reactor core control and monitoring continued

- PWR assemblies, spectral and density components of moderator temp. coeff. 80−9356
- PWR automated optimal multiple cycle fuel management code 79−85641
- PWR barrel motion, bandwidth related errors from ex-core neutron detector signals 77−42141
- PWR CANDU, thermal neutron flux distribution, meas. and simulation 78−82492
- PWR control, computer program *(German)* 79−59249
- PWR control and monitoring during load-follow 80−793
- PWR control elements, Decontic control system appl. and features *(German)* 79−26548
- PWR control rod digital position indicating system *(Japanese)* 80−63314
- PWR control system design model 77−88262
- PWR core, finite cylindrical synthesis program soln. of flattest power density 77−50202
- PWR core, thermal analysis, Monte Carlo method 80−47603
- PWR core analysis, effects of improved UO_2 once-through fuel cycle 80−57917
- PWR core analysis, methods and data validation 80−57924
- PWR core analysis, steady-state core physics and thermal-hydraulic reload design calcs. 80−57923
- PWR core analysis, transport-to-diffusion theory for gadolinia-loaded fuel pins 80−57908
- PWR core analysis using EPRI ARMP program, calc. and meas. reactor physics parameters 80−57925
- PWR core analysis verification, reactivity rundown and power distrib. accuracy 80−57922
- PWR core barrel motion from neutron noise spectral density using scale factor 78−74450
- PWR core barrel motion quantification using scale factor and statistical noise parameters 78−74451
- PWR core barrels with and without holes, various edge conditions, hydrodynamic vibrations 80−78406
- PWR core control, multistage mathematical programming 80−91227
- PWR core Doppler spatial weight factor 79−9713
- PWR core mathematical model specification 79−71931
- PWR core meltdown accident, computer simulation of second phase 80−754
- PWR core power manoeuvres, fuel duties and fuel preconditioning, FLAIR-CENSOR 80−63337
- PWR core support barrel motion monitoring by ex-core detectors 79−13446
- PWR core support barrel motion monitoring using excore detectors 78−25320
- PWR core thermal hydraulic calculation *(Hungarian)* 78−25282
- PWR cores, thermohydrodynamic computer programs *(Polish)* 79−81031
- PWR differential rod worth and feedback coeff. online estimation system 79−9798
- PWR downcomer annulus model, correl. for penetration of ECC water 79−76085
- PWR engineered safety features actuation system follow-up system logic 80−57879
- PWR extended burnup fuel cycles, benefits of cycle stretchout 80−37508
- PWR fast transients, CRONOS code development 80−23055
- PWR first core design with Gd burnable poison for excess reactivity compensation 80−708
- PWR fuel assembly test instrumentation at LOFT facility 80−37551
- PWR fuel cycle alternatives, reactor physics anal. 80−57918
- PWR fuel induced cladding deformation, Zircaloy creep correl., in-pile meas. 80−97547
- PWR fuel rod, parametric study on influence of prepressurisation 80−13643
- PWR fuel rod behaviour under power-cooling-mismatch conditions 80−42818
- PWR fuel rod meltdown behaviour during LOCA 80−42832
- PWR fuel stored energy FRAP-S3 calc., response surface method of uncertainty anal. 80−9349
- PWR gas tagging, prooftest for Ne, Ar, Kr, Xe isotopes 79−59222
- PWR high-power-density core control and protection 80−47661
- PWR in-core fuel management, nonequilib. fuel cycle for reload optimisation 79−30942
- PWR instrumentation operating experience during start-up and operation 79−89456
- PWR internal vibrations, neutron noise monitoring 79−13445
- PWR internals, vibration mode shape computation and expts. 79−13444
- PWR LOCA, effect of rod external thermocouple simulators on steady-state and transient CHF for LOFT reactor 79−49734
- PWR LOCA, ROSA-II severe hot leg break for core cooling during blowdown *(Japanese)* 79−9769
- PWR manoeuvring strategy optimisation 79−629
- PWR multisection ex-core detector spatial weighting functions 79−13481
- PWR neutron flux detectors, reliability tests *(French)* 80−32403
- PWR neutron noise increase with operating time 79−13447
- PWR neutron noise meas. and modelling 79−13443
- PWR neutronic calcs., subcooled boiling and open channel effects 80−23053
- PWR noise analysis using multivariate autoregressive time series modelling 80−23028
- PWR once through fuel cycle improvements 79−85637
- PWR once through fuel cycles, improvement of fuel utilisation 79−85636
- PWR operation and controls concept 77−88259
- PWR overpower detection for conrol element assembly ejection transients 80−42820
- PWR pin power peaking factor prediction 79−9714
- PWR plant simulator, load-follow methods computer design anal. 79−67917
- PWR power plant, primary cct. leakage simulation, safety aspects *(German)* 78−33239
- PWR power plant, vibr. and press. signals, information for online vibr. monitoring system 77−18674
- PWR power plant modelling and simulation 79−9828
- PWR power plant self-tuning control and simulation 79−9827
- PWR power station operation in France, monitoring and control equipment eval. 79−89454

fission reactor core control and monitoring continued
PWR power unit, automatic control and meas. system design lines *(Russian)* 79—30964
PWR primary coolant after fuel failure, dynamic behaviour of tag gas isotopes 77—46363
PWR reactivity control systems, flexibility during load follow operations 78—21721
PWR reactor core barrel, vibrations, influence of boundary conditions and co-vibrating liquid obs., using model 79—36302
PWR reactor with reactivity perturbations, accident anal., methodical approach *(Czech)* 79—22402
PWR steam generator, γ-dose rate distrib. meas. 80—5382
PWR steam generators, remote controlled TV for detection of leaking tubes *(French)* 80—791
PWR steam supply control system optimisation 78—50251
PWR surveillance, empirical and physical models 77—42150
PWR temp. sensor response time characts., estimation by noise anal. method 79—59216
PWR through fuel cycle improvements 79—85635
PWR tight-pitch cores, reactor physics of fuel cycles 80—57920
PWR two-loop system with spherical containment and integrated air locks 77—46358
PWR VVER-1000 type reactors, operating state parameters, Skoda calcs. *(Czech)* 79—67818
PWR with wide vessel to concrete air gaps, ex-core detector sensitivity studies 80—73970
R-A reactor fuel burnup, gamma-spectrometric determ. 78—50265
RA fuel burnup determ. from γ-ray spectrometry of ^{106}Ru, ^{134}Cs, ^{137}Cs 78—54848
RA reactor fuel, gamma-spectrometric determ. of fission product activity ratio 78—33269
radial reactor stability, effect of automatic regulator 79—97838
radionuclides in reactor circuits, continuous meas. techniques *(French)* 79—97857
Rapsodie control plug replacement *(French)* 79—97871
RCP01 Monte Carlo program, neutron capture and photon heating rates 79—71912
reactimeter, microprocessor based, nucl. engineering lab. class enhancement 80—36825
reactivity calcs., Monte Carlo perturbation source method 78—37398
reactivity changes, influence of axial flux distrib. 77—46365
reactivity coefficient charges in Soviet RBMK reactors 80—73954
reactivity coefficients, perturbation effects from point-kinetics model *(Hungarian)* 80—78346
reactivity determination, pulsed neutron source technique, ZR-4 reactor appl. *(Hungarian)* 78—21673
reactivity determination, real time program 79—45379
reactivity due to bubble collapse, probability table method 78—37399
reactivity effect of cross-section processing for moist bulk-oxide criticals 80—37493
reactivity insertion, unexpected, rapid detection 78—58370
reactivity measurement by inverse kinetic method 79—63752
reactivity measurement by pulsed neutron technique, Sjostrand method foundations 78—17329
reactivity measurements of St. Lucie shims at swimming-pool MTR fuel-type reactor 78—21705
reactivity meter for LMFBR 80—32415
reactivity of compact core with two absorpt. reflector, pulsed neutron method *(German)* 77—61500
reactor control by asymmetric regularity system with external feedback 80—32389
reactor core examination for failed fuel elements following high fission product emission *(German)* 79—85622
reactor core gamma dosimetry, solid state nucl. track detector appl. 80—95466
reactor core melt frequency, probabilistic model using prob. of rare events 79—54526
reactor diagnosis by acoustic meas. methods, magnetostrictive and piezoelec. high-temp.-resistant sensors 80—32411
reactor dynamics optimal control, exact closed-form soln. for terminal cost problem 79—54472
reactor lifetime fuel logistics, fissile fuel doubling time characteristics 78—46135
reactor neutrino expts., fission fragment ν radiation, neutral currents, inverse β-decay, $\bar{\nu}$ scatt. *(Russian)* 80—42736
reactor neutron distribs. spectral characts., relative meas. by activation ratios method 77—34411
reactor noise, AR-MA anal. hidden state variables 80—73944
reactor noise, neutron multigroup theory, calc. of second order correl. functions *(German)* 79—89390
reactor noise analysis, Polish developments 79—3216
reactor noise monitor, real time calc. of RMS values, av. freq. and peak freq. 79—76079
reactor operation and control simulator ROCS, extension to two energy groups 79—81034
reactor optimal shutdown problem algorithm by branch and bound method *(Japanese)* 79—36341
reactor physics considerations in design for improved BWR fuel cycles 80—57916
reactor plant mathematical modelling, dynamic model verification by comparison with recorded plant transients 79—89468
reactor protection system, in-core power distribution synthesis from three-segment ex-core detectors 79—9865
reactor small pin bundles, thermal-hydraulic anal. using COBRA-3M computer code 79—76067
reactor trip system, design of internal architecture for Westinghouse microprocessor-based [nuclear reactor] integrated protection system 79—76100
reflected reactors, two-group theory of noise, appl. to vibr. absorbers 79—26468
refractory metals, work function, ionising radiation effects meas. method 80—6951
refueling, underwater fuel handling techniques 79—67911
refueling and fuel handling, ALARA occupational radiation exposure 79—67914
refuelling frequency, economic optimisation 80—731
reload core design optimisation 79—604
remote and continuous inspection of nuclear plants, safety requirements 80—5295
remote multiplexing appl., functional and cost analyses review 80—52752

fission reactor core control and monitoring continued
remote multiplexing for nuclear reactor instrumentation and control circuits 80—57885
research reactor, core and console, long term service and reliability investig. 80—9359
research reactor, IRT-2000, algorithms for direct digital control of neutron field 78—86643
research reactor, recovery from obsolescence programs 80—9360
research reactor, self-protection criteria for reactor fuel elements 80—9361
resonance absorption calculations in thermal reactors 80—86955
ribbed core shroud, ex-core detector shape annealing functions 79—93792
risk tree analysis in criticality control 79—85632
rocket propulsion using nuclear reactor, optimisation problem, calculus of variation 80—27694
rod bundle thermal-hydraulic anal., commix-1 program 80—13645
rod response coeffs., end effect depend. 79—30888
rod worth meas., improved rod drop method *(Japanese)* 78—54846
safety aspects of core power distribution surveillance and control 79—97860
safety research experiment facility, conceptual design, LMFBR safety testing needs 77—3129
SECURE district heating reactor, core design and dynamics 78—37424
self absorption factor of gamma radiation in reactor fuel assemblies 80—63320
self-powered detector responses, detailed analysis by Monte Carlo methods 77—46360
self-powered detectors, reactor in-core monitoring *(Slovak)* 79—31322
self-powered detectors for in-core reactor neutron flux meas., detector signal composition 80—32402
self-powered detectors for incore monitoring 79—45367
self-powered neutron and gamma-ray detectors, review 79—45558
self-powered neutron detectors for incore meas., comparative performance 79—45369
self-powered threshold gamma-ray detector, appl. for estimation of reactor kinetic parameters 79—59306
SGHWR fuel pins, fuel cladding ratchetting study 78—54855
shape factors of non-critical small fast assemblies and their use in k_{eff} calculations 79—89351
SIMULATE code for startup test predictions 80—18558
small-leak sodium-water reactions, effect of nozzle-to-target distance 77—46359
SNR 300 shutdown systems 79—97866
SNR-300 LMFBR control and load following performance *(German)* 80—83184
space craft thermionic reactors, reflector drum control mechanism, fuel and moderator 79—17988
space craft thermionic reactors, reflector drums as control mechanism 80—42784
space dependent stochastic neutron kinetics with Gaussian parametric excitation 80—63223
space independent low power model, multigroup energy formalism for reactor stochastic eqns. 80—63224
spacecraft thermionic reactors, neutron leakage control using boronated reflector drums leading to lower shielding mass 80—47663
spatial control during nuclear station load cycling, multivariable control algorithm 79—13490
spatial control optimisation methods 78—54860
spatial fluctuations of neutron and powder distribution in critical reactor 79—71917
spectral fine-structure effects on material and Doppler reactivity worths 79—26473
spectral shift controlled reactor, SSCR, Pu fuel cycles 80—47608
spent fuel measurements using high resolution gamma systems 80—32400
stability analysis of chemical fine-control reactor in state space 79—97822
Stade nuclear power station, dual 305 computer system 77—353
startup tests, comparison of expt. data and calc. for circuit overpressurisation, boiling, fuel failure 80—691
steady-state fuel centreline thermocouple data confirmation from transient response 79—93767
steam generator tubes testing and evaluation, using CIS/DASIO system *(Czech)* 80—63301
STF 3/4 critical assembly, worth and reaction rate calcs. 80—68864
stochastic point reactor kinetics eqn. soln., 79—63719
subchannel void fraction by gamma scattering 80—27726
subcritical cyclostationary nuclear reactor, neutron counting statistics, sinusoidally modulated neutron source 80—99203
subcritical reactivity determ., more direct method 79—9717
subcriticality meas. in power stressed reactors with analog reactimeter 79—97834
suboptimal control of reactors with distributed parameters, singular perturbation theory, computer model 77—6530
Super Phenix core design and development, fuel assembly behaviour *(French)* 79—30889
Super Phenix fuel fabrication for Creys-Malville station, core controls *(French)* 79—31089
Super-Phenix FBR, data processing and collection *(French)* 79—76107
Super-Phenix FBR control system evaluation *(French)* 79—76106
tagged assembly failure location analysis program 79—13486
temperature meas., automatic system using platinum resist. thermometers 79—89399
temperature measurement, in-core, ionic sensors *(Czech)* 78—32820
temperature monitoring, can thermocouple distribution procedure 78—54856
temperature sensors, response time testing by noise anal. 78—13300
test rods, directly heated, influence of thermocouples in wall 79—93706
thermal benchmark lattice expts., quantitative consistency testing 79—9700
thermal conduct. of gas mixture under fuel element jacket during burnup 78—82478
thermal neutron flux meas. method *(Rumanian)* 78—21670
thermal neutron scatt. in water, cylindrical graphite-water system with temp. discontinuity 79—71925
thermal power determ. using neutron flux density meas. 80—73955
thermal reactor assemblies, effective neutron diffusion parameters 80—73874
thermionic spacecraft reactors with ^{233}U as fuel, reflector drums as control mechanism 80—47686
thermocouples, 2200°C fuel centerline for LOFT program 80—57877

fission reactor core control and monitoring continued
- thin film fission thermocouples for energy deposition meas. in FBR safety expts. 80—47658
- Three Mile Island incident, operator/instrumentation interactions 80—57890
- THTR, core rod drive *(German)* 78—54837
- TIPSY program, thermal information processing system 79—67883
- TMI-2 accident, analysis of high readings by startup channel neutron detectors 80—102265
- TMI-2 accident, nuclear reactor safety, role of instrumentation and control *(Japanese)* 80—73947
- TR-1 reactor, thermal spectrum using neutron radiography of wedge shaped absorber 78—74439
- TR-O reactor, neutron spectrum meas., oscillation techniques *(Czech)* 80—52754
- track-etch monitor for reactor power anal., evaluation 80—78418
- training course for fuel cycle facilities design 80—36801
- transient temp. field in nuclear fuel rod, calc. by variational procedure 79—9772
- transport lag, stability effect on reactor control 80—57891
- TREAT, fast neutron hodoscope perform. tests on 91-pin fuel bundle 79—41005
- TREAT facility, pinhole imaging of test fuel element 78—21627
- TREAT fast-neutron hodoscope, time and mass resolution of fuel motion, data acquisition system 79—41003
- TREAT reactor, acoustic monitoring of IRT-10 test 78—8944
- TREAT reactor, computational method for predicting neutron hodoscope performance 79—80995
- triaxial chamber use and experience at V.I. Lenin Leningrad nuclear power station 79—22377
- TRIGA core, gamma dose meas. by plastic detectors 80—9381
- TRIGA III reactor, anal. of standard and FLIP fuel mixed loading patterns 80—57855
- TRIGA Mk.II reactor core, thermal neutron spectra parameters meas. 80—9348
- TRIGA reactor, kinetic parameters determ. by interval distrib. method 77—42146
- TRIGA-FLIP failed fuel element examination at HFEF 80—9383
- two phase control absorber, results from out-reactor static tests 78—58389
- two-different-core system, neutron transit time meas. 78—37414
- two-phase control absorber, horizontal absorber elements, expt. study 80—42841
- two-phase control absorber development, closed-loop control and noise meas. in ZED-2 test reactor 79—85697
- two-phase control absorber development program for CANDU reactors 80—42839
- two-phase flow instability, programme for heat removal expt. at low power 78—54814
- two-phase reactor control, neutron absorber development program 79—97852
- UKAEA Prototype fast reactor control system, commissioning and performance assessment 79—89459
- unattended surveillance, multivariate statistical pattern recognition system 78—29621
- US temp. profiling system for critical heat flux meas. of nuclear reactor fuel assembly 80—37032
- US thermometry appls. 80—73365
- US viewing system for reactor fuel assemblies under liquid Na 80—57875
- vibrations caused by flow, indirect meas. methods *(Hungarian)* 80—18453
- VVER, fuel burnup determ. by exact methods 79—41014
- VVER anal. of relative motion between pressure vessel and its internals 79—67882
- VVER reactors, neutron fields in ionisation chamber channels 79—71878
- VVER reactors, relative accumulation of ^{232}U and ^{233}U during ^{232}Th irrad. 79—71923
- VVER-440, role of IAEA *(Hungarian)* 79—13435
- VVER-440 reactor, use of CdTe detector for spent fuel γ-ray meas. 79—76094
- water cooled and moderated reactors in Soviet Union nuclear power generation 79—642
- water cooled channel reactor, electrical energy cost of change in fuel component 80—37480
- water cooled channel reactor, RBMK, deform, of energy release field 80—37422
- water moderated reactor, local and global effects of gas bubbles 78—17328
- water reactor fuel, power ramping performance assessment methods 80—23065
- water-moderated water-cooled reactor, local control of loop channel energy release profile and magnitude 78—86645
- weakly-coupled-core reactor, optimal power and distribution control *(Japanese)* 78—25306
- West German LWR primary system online surveillance 79—3217
- Westinghouse nuclear training reactor fuel inventory reduction plan 80—23115
- Westinghouse PWR, reduced temp. return-to-power 79—54559
- Westinghouse reactors, secondary neutron source, benefit of early removal 80—63343
- wire-wrapped core assemblies, turbulent flow split modelling and expts. 80—95370
- WWER 1000 reactor fuel element temp. determ. *(Bulgarian)* 79—85694
- WWER fuel assembly, thermohydraulic evaluation, program module BIPR-5K *(Bulgarian)* 79—85695
- Yankee reactor physics method verification 80—63323
- YAYOI, reactivity pulse operation, core displacement meas. *(Japanese)* 77—54321
- Zebra multi-chamber scanning system, fission distribs. in prototype fast reactor mock-up 77—42181
- ZED II reactor lattice parameter calcs. using LATREP CYCLE 4 80—27787
- zero-power control rod group reactivity worth, computerized determ. method 78—21702
- zone power control, three dimens. system 79—63764
- zone regulation system, power reactor, intra- and extrareactor sensors 77—61525
- ZPPR, critical experiments for 600-700 MW LMFBRs 80—68859
- ZPPR, loading error simulations and control worth meas. 80—27777

fission reactor core control and monitoring continued
- ZPPR pin geometry, SDX cell homogenisation code validation 80—86962
- ZPPR-4 control rod worth meas. and calc. 79—9803
- ZPPR-5 Source Level Flux Monitor expt. analysis 79—9705
- ZPPR-7 heterogeneous core expts., pin zone reaction rates 80—9334
- ZPPR-9, control rod interaction meas. 80—63324
- ZPPR-9, stimulated hodoscope slot effect in STF critical assembly 80—68860
- ZPR noise anal., interpretation of quadratic approx. 79—76082
- ^{87}Br, delayed neutron carrier, sorption parameter determ., appl. to fuel element leak detection 79—97828
- B, borides, neutron absorbing props., reactor control system, appls., review, book contrib. 78—46154
- B-thermal regeneration system using anion exchange resins 79—80972
- B_4C absorber pin in-reactor rupture test 79—93701
- B_4C-Al composite moderator rods, production and props. *(Russian)* 79—18006
- BWR, primary containment vessel, spray I_2 removal characteristics 80—73972
- C resistors as low temp. sensors in low temp. reactors, gamma, neutron irrad. investig. 77—45848
- CANDU fuel, burnup determ. by γ-scanning of ^{144}Ce/Pr and ^{134}Cs/^{137}Cs 79—9825
- CF_4-UF_4 mixture, gas core fission reactor, fission based plasma engine 80—63366
- $CaSO_4$:Dy TLD meas. of reactor thermal neutrons 78—78441
- ^{252}Cf shuttling source for nuclear fuel reactivity monitoring 79—9813
- ^{58}Co dissolution control by H_2O_2 addition in PWRs 78—21657
- ^{58}Co dissolution during PWR refuelling shutdown, control with H_2O_2 78—21698
- ^{137}Cs distributions effects on γ-intensity in γ scan method for reactor fuel bundle *(Japanese)* 79—36342
- ^{A}Eu (n,X), A=153, 154, 155, total neutron cross sections, effect on reactor characts. 80—32284
- ^{A}Eu(N, γ), A=151, 153, cross sections, time of flight spectra, scintillation detectors 80—27634
- Gd_2O_3-UO_2 fuel pins in cluster type fuel assembly, meas. of reactivity charge 80—27775
- ^{3}H formation in water cooled, water moderated reactors, role of nuclear reactions 79—17970
- LWR, sensitivity of fuel rod behaviour on as-fabricated characteristics 79—49805
- Mo-Mb, thermoelectric alloy for in pile temp. meas. *(French)* 79—67894
- Na boiling detection technique tests, FFTF capabilities 79—13395
- Na cooled power reactor noise analysis for malfunction diagnosis 79—13450
- ^{237}Np threshold detector, subthreshold phenomena effects on nondestructive assay of reactor fuel 79—22409
- O_2 activity meas. in liquid Na, development of electrolytic probes 80—18550
- platinum self-powered in-core detectors for PWR core power distrib. monitoring 80—73971
- Pt resistance thermometers, response time estimation by noise anal. technique 79—93742
- Pt resistance thermometers, in-situ response-time testing for safety systems 79—93743
- $Pu(NO_3)_4$ in light water, reactivity predictions using discrete ordinates transport theory 78—89957
- PuO_2-UO_2, light water moderated lattices, critical expts. 79—6728
- Rh self-powered neutron detectors, reliability anal. 79—41078
- Sa poisoning transient anal. using XESAMO code *(Spanish)* 80—52749
- Sn, solid and liquid, neutron cross sections, Doppler effect meas. 80—22933
- Th based cycles, relative worth of ^{233}U and ^{235}U 80—37511
- Th critical assembly, reactivity meas. 79—80976
- Th-PuO_2 kernels, effect of fuel particle size on power excursions, Doppler feedback mechanism 79—30911
- ThO_2, isolated rod, exptl. and calculated resonance integrals 80—22986
- $(U,Pu)O_2$ fuel, criticality control, critical mass meas., fission rate distrib. by solid state dosimetry 80—13723
- $(U,Pu)O_2$ fuel pin behaviour during FFTF 3c/s reactivity insertion event, TREAT expt. anal. 80—102240
- U hot loop, irradiator yield at steady state power level 79—97836
- U-Pu-Np fuel cycle to produce isotopically denatured Pu 80—729
- UF_6, high temp. fissioning plasma core reactors, fluid mechanical confinement 80—63248
- UO_2, ^{235}U enriched fuel rods in water, critical expts. 79—80977
- UO_2, ^{235}U enriched lattices, effect of soluble neutron absorbers on criticality 79—80978
- UO_2 fuels, in-pile meas. of fission gas release 79—93697
- UO_2, isolated rod, exptl. and calculated resonance integrals 80—22986
- UO_2, nuclear doppler effects, hybrid static dynamic heating technique 78—25308
- UO_2 rods in water with U or Pb reflecting walls, critical expts. 80—32331
- UO_2/Zircaloy pellet/cladding interaction, eval. of lubrication of graphite 79—67857
- UO_2-Na interaction, thermophysical behaviour of type 304 stainless steel impacted by jet of molten core debris 77—46319
- UO_2-PuO_2 fuelled lattice, reactivity predictions using multigroup transport theory 78—89957
- UO_2-water tightly-packed lattices, ENDF/B-IV data evaluation 79—9805
- $UO_2(NO_3)_2$ highly enriched soln. with $Cd(NO_3)_4.4H_2O$ neutron poison, criticality expts. 80—13724
- ^{233}U, symbiotic fast thermal fuel cycles, economic implications 80—726
- ^{233}U-^{235}U fuel, nondestructive isotopic meas. using fission neutron counting 80—32385
- $^{233}UO_2/ThO_2$ water-moderated lattice analysis with ENDF/B-IV data 79—9800
- ^{235}U decay heat meas. and calcs., review 80—13732
- ^{235}U+BeO nearly homogeneous multiplying systems, pulsed neutron study, age-diffusion model 80—37442
- ^{235}U(n,α), thermal fission neutron spectrum 80—42712
- ^{235}U(n,f), sensitivity of decay power to uncertainties in estimated decay data 80—22932
- ^{238}U in UO_2, Doppler effect in GCFR critical assemblies, 300-1100K 78—29574
- ^{238}U, neutron capture self-indication meas., shape anal. 80—68753

fission reactor core control and monitoring continued
Xe oscillation control anal. 80—674
Xe oscillation suppression, reactor system reciprocity props. 80—27773
Xe oscillations, program for optimal control in 1-D slab reactor *(German)* 77—61529
Xe oscillations, servo-anal. and stabilisation in large thermal nucl. plants 78—46148
Xe oscillations optimal control problem for large power reactor *(German)* 78—46153
Xe poisoning transient anal. using XESAMO code *(Spanish)* 80—52749
Xe processes, simultaneous optimisation of power plant reactors 78—37427
Xe spatial oscillations, optimal control by lambda mode anal. 77—42147
Xe stability, mu-mode and lambda-mode methods 77—42148
Xe transient processes optimisation, interrelation of various problems 78—17295
Xe-I induced spatial power oscillations, integration method 80—13567
^{135}Xe, control of space-time distrib. in reactors 79—36364
^{135}Xe, determ. of fission gas degassing constant from liquid Na to cover gas 79—41009
^{135}Xe-induced core instabilities, extended λ-mode linear anal., CANDU appl. 78—82494

fission reactor fuel
see also claddings; fission of plutonium; fission of uranium; fission reactor fuel preparation and reprocessing; isotope separation; radioactive waste
1 GW(e) mixed fuel cycle LMFBR performance, effect of ^{233}U in core 79—9868
^{252}Cf based nondestructive assay system for fissile material 78—73119
γ-spectrographic anal. of neutron fluxes and depleted fuel fission products 79—97933
accountability, U and P NDA of crated waste by gamma-ray and neutron coincidence counting 80—83166
accountability and control, use of novel data collection and processing techniques 79—85749
accountability control system in plutonium fuel facility *(Japanese)* 79—71909
accounting and rate making, regulatory issues 78—13242
accounting and safeguarding, spent fuel bundle counter for 600 MW CANDU reactor 80—63269
accounting practices at Duke Power Company 78—13244
accounting system, nuclear inventory and management system program 78—13245
actinide aqueous ions, chemical thermodynamics, book 77—60108
actinide carbides, lattice defects and rel. to phys. props., review 77—27874
actinide dioxides, dioxides, low temp. lattice parameters, Neel pt. behaviour 77—27867
actinide elements, chemical thermodynamics, book 77—60107
actinide oxide/rare earth oxide system, high temp. vaporization, valence effects 79—99309
actinide oxides, electronic props., review 77—28115
active spent fuel storage, replacement of underwater storage racks 80—23035
advanced ceramic nuclear fuels, mech. props. at compressive deformation 80—651
advanced FBR fuel, behaviour at high power density 79—30935
advanced fuel restructuring heated in radial temp. gradient 77—74928
advanced fuels, Xe retention, microprobe anal. meas. 79—40997
advanced fuels programme carbide benchmark critical assembly, nuclear data sensitivity 79—9707
advanced fuels with 3d transition metals, equilib. compatibility studies 77—74930
advanced high U-density reduced-enrichment plate-type fuel development for test and research reactors 80—23101
advanced nuclear energy systems, emerging concepts, conf., Graz, Austria (March 1978) 79—13381
advanced reactors, materials and design 78—78452
AGR fuel, material aspects 80—47577
AGR fuel neutron radiography 77—81452
AGR fuel pins, carbon deposits reduction, soln. 77—18688
AGR fuel pins, pellet-clad interactions, comparison of expts. and SLEUTH-SEER code results 80—42755
AGR fuel plug maintenance facility, corrosion product contamination control 80—5388
alpha waste production and proliferation hazard of different fuel cycles 80—83214
Alpha-Gamma Hot Cell Facility at Argonne-East 80—68779
alternative fuel cycles, $(U,Pu)O_2$ and $(^{233}U,Th)O_2$ and FBR development 80—47565
alternative fuel cycles, relative diversion resistance 80—37438
alternative reactor fuel cycles under consideration and their design ramifications 79—54516
analytical modeling of fuel rod ramp experiment 78—86590
apparatus to meas. thermophysical props. at high temps. 80—37458
assembly design features 78—89939
assessments of nuclear systems and use of nuclear power, review 79—45334
asymmetric fuel-cladding gap conductance and fuel pin thermal performance 80—42768
automatic evaluation of isotope anal. of nuclear fuels, isotope dilution, mass and α spectrometry 78—55120
automatic surface flaw inspection of nuclear fuel pellets 79—30939
autoradiograph techniques for rapid inventory of reactor fuel 78—82066
autoradiographic inventory methods for nondestructive assay of reactor fuels and fuel assemblies 80—71875
availability, FBR development *(German)* 77—18685
benchmarking results of the COMETHE code 80—37452
block-type fuel elements, stress calc. with finite element code *(German)* 77—71654
BN-600 type elements, irrad. in BOR-60 reactor to different burnups 77—23208
Bohunice A-1 reactor, long-run test of improved R II-U spare-type fuel element *(Czech)* 78—8875
Bohunice A-1 reactor, type E2 instrumented fuel elements *(Slovak)* 77—50260
boiling flow regimes for carbide fuel and steel 79—85617
book, advances in nuclear science and technology (vol.9) 77—14202
BOR-60, nuclear oxide fuel anal., coulometry, emission anal., chromatography, X-ray anal. 80—18420

fission reactor fuel continued
BOR-60, operational characteristics of core and irradiated fuel parameters 79—97877
breeder reactor system, rel. between nucl. growth rate and breeder doubling times 78—17323
breeder reactors, current status in Europe 80—27796
breeding, using independ. neutron sources, Th utilisation 77—26840
breeding using fusion-fission hybrid reactors 79—71950
bubble nucleation modelling, and fission-induced re-soln. 79—71891
burn-up, chemical separation, ion exchange 80—42746
burn-up determination using gamma spectrometric nondestructive assay for IAEA safeguards 80—68806
burn-up determination using gamma spectrometry, IAEA safeguards experience in Czechoslovakia 80—63292
burn-up measurement using spatial power distrib. eval. and gamma spectrometry 80—68803
burnup calcs. in LASER code 79—59119
burnup calculation code for cluster-type fuel lattices, BUNDLE 78—33246
burnup calculations for KWO reactor, critical B concs. 77—23199
burnup codes for calc. of fuel depletion and fission product poisoning 77—67800
burnup control problem considering fuel failure probability 77—67844
burnup determ., irrad. samples, from γ-peak analysis of fission products *(Hungarian)* 78—82458
burnup determination using Aragonit γ detector 80—63262
burnup measurement and analysis methods *(Japanese)* 78—29592
burnup meter for fast reactor fuels using γ-ray spectrometer with minicomputer *(Japanese)* 77—50206
burnup spatial nonuniformity in VVER reactors 77—30650
burnup verification, nondestructive, by gamma-ray spectrometry 77—3137
BWR, Dodewaard, fuel pin failures 77—67834
BWR, FFM anal. of pellet-clad bonding 80—42765
BWR, fuel element positioning and control patterns, optimisation system 80—733
BWR, improved fuel utilisation 80—732
BWR, ONDA-3 system for in-reactor fuel management 80—735
BWR, optimal in-core fuel management using OPTLWR computer code 78—17363
BWR, spent fuel γ-ray spectrometry and chemical analysis 78—54841
BWR, technology transfer experience 77—65349
BWR, transactinide buildup in nuclear fields, sensitivity anal. rel. to neutron flux and spectra *(Italian)* 79—45356
BWR core operation flexibility for improved fuel cycles 80—57915
BWR Dresden-3 fuel rods, pellet/cladding interaction induced stress corrosion cracking 79—67899
BWR fuel cycle improvements, reactor physics considerations 80—57916
BWR fuel integrity limits and criteria 80—575
BWR fuel management improvements for once-through fuel cycles 80—37505
BWR fuel preconditioning, initial pressurisation, fuel temps., fission product release 80—63357
BWR fuel preconditioning 80—63360
BWR fuel rod relocation, gap conductance anal. 80—83192
BWR fuel rods irradiated in Quad Cities 1, isotopic and burnup meas. 80—9342
BWR multirod critical power reproducibility tests at different facilities 78—13211
BWR once through fuel cycle optimisation 79—85590
BWR physics methods compared with ^{232}Th lattice benchmarks 79—9711
BWR rods, gadolinia spatial depletion meas. 79—67844
bWR servicing and refueling improvement program 80—9390
BWR spent fuel, post irrad. study, burn-up data and isotopic composition 80—667
BWR spent fuel element storage, neutron physical aspects 80—68841
BWR spent fuel safeguarding, nondestructive assay using gamma spectrometry 80—68802
BWR spent fuel storage and refueling La Crosse 80—23034
BWR with graphite channels, safety of nuclear power stations 79—26561
CAMEL seven-pin fuel sweepout tests 79—85669
can designs for Safety Test Facility, structural analysis 77—46310
Canadian power reactor programme, role of Chalk River research reactors 79—81073
CANDU, economic aspects 77—38382
CANDU, Pu-topped Th fuel cycle characts. 79—36322
CANDU, stress anal. of fuel channel interaction with end shields 79—59161
CANDU, Th fuel cycle utilisation 77—46305
CANDU 600 MW, spent fuel bundle counter, safeguard design 79—13495
CANDU advanced BLWR with enriched fuel, controllability studies 77—71683
CANDU design features that influence fuel modelling for transients 80—42740
CANDU fuel, 15 years' power reactor experience 79—30928
CANDU fuel, post-irradiation test facilities at Chalk River 80—30206
CANDU fuel behaviour under transient conditions 79—71930
CANDU fuel bundles, outline of Canadian R and D programme on fuel behaviour in transients 78—94102
CANDU fuel cycles, future prospects, advanced fuel cycles 79—81065
CANDU fuel cycles, future prospects 77—74975
CANDU fuel management principles and problems 77—50251
CANDU fuel pellet stacking, mathematical model of automatic assembler 80—37464
CANDU fuel performance and development 79—49701
CANDU fuel performance in NPD reactor with two-phase coolant 78—89950
CANDU fuel radioactive decay props., natural uranium fuel cycle 77—71655
CANDU fuel radioactive decay props., Pu product and high level waste 77—71656
CANDU fuels, nondestructive determ. of burnup by gamma scanning, fission monitor appl. 78—94076
CANDU irradiated fuel bundles, sheathed in Zircaloy-4, long-term stability investig. 80—13774
CANDU irradiated fuels, NDT anal. techniques 79—59177
CANDU PHW fuel elements, mechanistic strain rate eqn. verification 80—42760

fission reactor fuel continued
CANDU PHWR, Wolsung nuclear power plant, fuel cost anal. 78−54832
CANDU pressurised HWR fuel, bundle end neutron flux peaking effects, plenum use 78−58385
CANDU reactor core, materials and design criteria for fuel, cladding, and fuel channel 78−13238
CANDU Th cycle fuels, review of potential for actinide redistrib. 78−66347
CANDU-PHW, neutron group cross sections in resolved resonance region calcs. 80−13573
CANDU-PHW thorium convertor, study of running-in period 78−25313
CANDU-PHWR, low enriched U, channel power peaking 80−37509
CARAMEL, a sheeted fuel of UO$_2$ pellets for LWR 80−630
CARAMEL, Zircaloy-clad UO$_2$ fuel, cladding burst follow-up test 80−776
Caramel fuel cladding rupture, development and detection at OSIRIS experimental reactor *(French)* 80−95371
carbide, nitride and oxide fuel element performance modelling using LIFE-III, UNCLE-I and LIFE-LWR codes 77−46229
carbide fuel, deform. mech. map appl. to in-reactor deform. 77−18662
carbide fuel element development advances, fast reactor appl. 79−31138
carbide fuel element testing in fast reactor BOR-60 78−86582
carbide fuel elements, response to fast thermal transients, UNCLE-T-BUBE code 79−93715
carbide fuel pins, mixed, radial distrib. of Xe bonded fission gas, electron probe anal. 79−36318
carbide fuel-coolant interactions, PLUTO code 79−85613
carbide fueld pins, Na-bonded, fission gas release studies *(French)* 80−73916
carbide fuels, effect of burn-up and temp. on appearance of optically visible fission gas bubbles 80−63251
carbide fuels, vibro-compacted, initial stages of sintering and hot-pressing 80−16254
ceramic, effect of gas composition on thermal conductivity 79−93733
ceramic, porosity characterization, optical and electron microscope exam. 78−44302
ceramic *(Polish)* 79−17985
ceramic fuel, irradiation device for creep and swelling study 77−42063
ceramic fuels, vibro-compacted, initial stages of sintering and hot-pressing 80−16254
ceramic materials, irradiation creep model, based on nonstationary creep in out-pile tests, neutron flux and stress depend. 78−17316
ceramic nuclear fuels, irrad. induced rare gas diffusion 80−59524
ceramic nulcear fuel, irradiation induced creep 77−42056
ceramic reactor fuel, nonsteady radiational creep, theoretical-experimental model 80−35282
ceramic type *(Polish)* 79−22394
ceramics, grain boundary energy to surface energy ratio, as determ. from pore geometry 80−34291
ceramics, quantitative image anal. using light and SEM obs. 79−12912
ceramics, utilisation in nuclear industry 80−9341
characterisation and quality control of nuclear fuels, conf. Karlsruhe Germany (June 1978) 79−49794
characterisation by precision gamma scanning 79−49688
characteristic fuel element temps. calcs., statistical treatment of defects 79−45351
clad failure prediction during FBR overpower transiency, JANE code 80−78363
cladded reactor fuel rods, thermo-irradiation induced creep, stress analysis 80−35275
cladding failure due to I stress corrosion cracking 77−3100
cladding performance during power changes on fuel element model, strain defects 78−58359
cladding tensile testing, diametral meas. by precision laser extensometer 78−57896
Clinch River Breeder Reactor Project ex-vessel transfer machine design and development 79−9787
Clinch River Breeder Reactor Project fuel core design advances 79−9686
Clusius-Dickel effect in fuel rod 79−67820
cluster tests in NSRR 79−22369
coated fuel particles, failure statistics 77−74945
coated fuel particles, metallic fission product migration 77−50231
coated nuclear fuel particles, mech. design concept 77−18670
coated particle fuel, ^{137}Cs fission product conc. determ., crack simulation, YAG:Nd^{3+} laser 80−18416
Colgate fission plasma reactor, high temp., gaseous fissionable material, design, technical problems *(Dutch)* 78−50249
commercial LMFBR spent fuel shipping system 79−9821
commercial Tokamak hybrid reactor, fissile fuel and power prod. 80−13808
compacts for HTR, irrad.-induced creep 78−44168
components review *(Spanish)* 77−79429
composite fuels, heat cond. parametric anal. 77−6523
composite fuels, heat conduction 77−42101
composition calculation errors in nondestructive testing 79−71939
computer modelling of fuel element behaviour 78−86617
computer system for automatic inspection of fuel pellets 80−68795
computerised tomography appl. for fuel-element inspection 80−73927
computerized axial tomography for neutron radiography of nuclear fuel 78−82529
concentric-sphere design for spacing of tag-gas isotopic ratios 79−80983
conference, Berlin, Germany (Aug. 1979) 80−77539
Conference, nuclear materials, safeguards and accountability meas., Williamsburg, USA (May 1978) 79−81045
conference, nuclear power plant construction, operation and development, Tokyo, Japan (Sept. 78) 78−86672
conference, San Diego, Calif., USA (June 1978) 79−17972
conference, San Diego, Calif., USA (June 1978) 79−49650
conference in Salzburg report *(German)* 78−8896
conference on nuclear power and fuel cycle, Salzburg, Austria, (May 77) 79−26503
conservation, Japan, molten-salt reactor strategies, LMFRR, HTGR, utilisation, coexistence *(Japanese)* 77−50257
containment and surveillance techniques for the IAEA 79−85645
converter reactors, fuel supply enhancement by use of non-fission neutrons 79−17960
core burnup props., modified one-group calc. method for 3-d anal. of fast breeder reactors *(Japanese)* 79−49645
core materials development for water cooled reactor systems 77−46296

fission reactor fuel continued
core-wide fuel performance assessment 79−93766
crack formation, effect on fuel behaviour, semiquantitative anal. of crack patterns 80−650
CRBR simulated fuel pins, fuel freezing tests 79−85671
CRBRP, fuel failure monitoring system 79−93795
CRBRP fuel rod design analysis, life limiting criteria on ductility limited strain and cumulative damage function 80−102252
CRBRP LMFBR, effect of alternative fuel cycles on design 79−54484
creep, irradiation induced, transient state, kinetic eqn. treatment 80−88251
critical arrays, effects of packaging materials 79−26567
critical consts., review 78−59931
criticality in arrays of fissile materials, anal. 77−26844
criticality safety, fuel cycle education module 80−36798
criticality safety anal., determ. of Dancoff factor for cubic arrays of sphercial fuel particles 80−13725
criticality safety anal., reactivity effects in U-H$_2$O systems due to spherical fuel particles 80−13570
criticality safety analysis in nuclear fuel cycle *(Japanese)* 80−99225
criticality safety broadgroup library validation using uranium systems 79−26564
criticality search techniques for low and high switched systems 80−37494
CRNL experimental fuel element postirradiation exam. hot cell facility 79−9749
cycle, quality criteria, performance requirements for mass produced fuel elements *(German)* 79−49795
cycle management, interdisciplinary approach in education and research activities 77−38433
cycles, global optimisation, resource utilisation and non-proliferation 80−42783
cylindrical element, analytical soln. to mass transport eqn. 78−21643
damage impact on plant operations 80−686
damaged fuel element detection and location at Atucha nuclear power station 79−89460
debris bed and sacrificial materials interactions at high temperatures 79−85612
debris bed dryout obs. during D-3 expt. 79−85597
defect test loop remote handling system design 79−9730
defective fuel detection using vac. slipping technique 80−9389
defective fuel pin fission product release and detection 77−83061
defective fuel rods, behaviour under continued reactor operation 79−30915
defective fuel rods ultra sensitive detection with low core burn-up, method 79−45374
defects, loss of cladding tightness, anal. of fuel element exploitation *(Czech)* 80−52736
defects caused by power ramping, CANDU fuel performance data 77−57720
delayed neutron probe characts. for uranium exploration, field meas. 79−53568
delayed-neutron spectra characterisation 77−79345
denatured fuel cycles for international safeguards 79−41011
denatured Th cycle in symbiotic systems, potential role 79−26484
denatured Th fuel cycle evaluation 79−13421
denatured Th fuel cycle safeguards against proliferation 79−13422
density distribution of fission traces, meas. by tracer's method in dielectrics, fuel meas. appl. *(Rumanian)* 78−90033
depletion chain eqns., FORTRAN program for solns. using analytical methods 78−74423
depletion effect, reactivity, fast power reactor 78−17342
diametral evolution meas. during irradiation, medina service 77−42062
diffusion theory calcs., fuel swelling and cladding shrinkage effects 80−22926
DIMCO system for mechanical calculations on nuclear fuels *(Spanish)* 79−6727
disposal, in vault, preliminary assessment of temp. distrib., model simulation 79−636
disposal safety in Switzerland *(German)* 78−74455
distribution of speculative uranium resources 80−78369
Dounreay contribution to fast reactor development 80−27798
dry spent fuel cask handling system and transport 78−17348
dry spent fuel storage installation, design and operation 80−23036
dynamic materials accounting for LWR fuel cycle 79−36325
EBR II, metallic driver fuel, irrad. perform. at high burn-up, fuel-cladding interactions 80−95348
EBR II driver fuel, irradiation behaviour 80−32346
EBR II failed (U, Pu)O$_2$ fuel pins, Ru isotopic axial distributions, γ-scanning determ. 78−687
EBR-II, (U,Pu)O$_2$ fuel burnup, effect of time varying power level 80−13719
EBR-II, mixed-oxide fuel pins, results from expt. F11A after cladding break 79−67861
EBR-II, possible metal and oxide fuel loadings utilising ^{232}Th/^{233}U 80−13563
EBR-II breached fuel element experience, safe reactor operation 79−9736
EBR-II driver fuel lifetime, cumulative damage anal. and Weibull statistical anal. 80−13601
EBR-II Mark II metallic driver fuel, performance to 10 at.% burnup, cladding breaches 79−67863
EBR-II subassemblies, 61-pin wire-spaced, exptl. confirmation of design to minimize vibr. and wear 79−67825
economic analysis of 18 and 12 month fuel cycles at Vermont Yankee 80−22957
education, energy from nuclear sources, outline for secondary school students 79−80975
educational module, nucl. fuel design 80−36800
element, turbulent flows in tubes, Nu-number determ. *(German)* 77−38432
element cladding, corrosion product deposition, heat transfer model *(Bulgarian)* 80−71818
element modelling at CNEA 80−37449
elements for steam-superheating channels of Beloyarsk nuclear power station reactor 77−50217
ELESIM computer code for fuel element performance prediction 79−81007
EM breeding, at TRIUMF meson factory 78−21792
enriched U, lower costs 80−106111
exploration and production increase, 1977 survey *(Czech)* 77−83035

fission reactor fuel continued
failed fuel element detection, delayed neutrons meas. *(Polish)* 80—73952
failed fuel element detection by delayed neutrons using solid state track-etch technique 80—5249
failure, performance modelling, pellet-cladding interaction 80—63264
failure prediction using POSHO model 77—46226
fast breeder reactors, fuel rod behaviour, influence of design, materials and operation *(Spanish)* 79—36314
fast molten chloride reactor on Th cycle 79—67839
fast power reactor fuel, physical characts., effect on fuel cycle *(Russian)* 79—30936
fast power reactor fuels, physical props. and fuel cycle effects 79—31097
fast reactor burn-up determ., automated techniques *(German)* 77—14236
fast reactor burnup, correlation of ^{134}Cs/^{137}Cs 80—677
fast reactor disassembly, fuel vapour expansion work energy calcs., effect of eqn. of state uncertainties 78—8940
fast reactor fuel, thermohydraulic performance for low duct dilation 80—73893
fast reactor fuel development, safety considerations 79—26649
fast reactors, programme and state of work in the Soviet Union 79—643
FBR, development and production survey *(German)* 77—34391
FBR, development in Japan, fuel, materials coolants and design *(Japanese)* 80—22888
FBR, failed-fuel detection system *(French)* 79—97858
FBR, fission product decay heat calc. by summation method 79—30863
FBR, fuel melt down, fragmentation requirements for detonating vapor explosions 79—49753
FBR, fuel resources and reactor technology developments in India 78—733
FBR, HCDA, 2Z 79—49669
FBR, neutron/physical behaviour of thorium, expt. *(German)* 78—94109
FBR, refuelling process and doubling time calc. *(Czech)* 78—29593
FBR, role of fission gas swelling and release in reactor accidents 80—57854
FBR, some lessons drawn from operation of Phenix and Rapsodie cores 80—639
FBR carbide fuel, Sphere-Pac form, performance evaluation using computer code SPECKLE-I 80—637
FBR carbide fuels, comparative irradiation tests of pellet and sphere-pac fuels 80—643
FBR current status and development trends, review 79—22374
FBR fuel, accuracy and computational time of hierarchy of growth rate definitions 79—80979
FBR fuel clusters, Na boiling, corrective action 79—71913
FBR fuel development, international development programs 80—102248
FBR fuel growth rate, derivation of consistent measures 77—23174
FBR fuel handling, radiation safety 80—73985
FBR fuel pin safety expts. at SLSF, centerline fuel thermocouple performance 80—102283
FBR fuel subassemblies under nominal and non-nominal operation conditions, thermodynamics *(Japanese)* 79—93689
FBR LOF accident, first visual in-pile fuel disruption experiments 79—49747
FBR LOF transient, molten fuel containment anal., for sodium loop safety facility expts. 80—47651
FBR meltdown, post accident heat removal anal., turbulent convection and interfacial freezing 79—49670
FBR meltdown, post-accident heat removal, heat transfer mechanism associated with immersed melting surfaces 79—49671
FBR mixed oxide fuel burnup determ., fission yields for U and Pu 77—23138
FBR mixed oxide fuels, determ. of total H_2 content *(German)* 79—49809
FBR mixed-oxide fuel crusts, thermal fracturing and the effect of creep 79—49698
FBR oxide fuel, review of technological problems related to design, fabrication, operation and fuel cycle 80—636
FBR oxide fuels, dynamic response of grain boundary cavities to stress and temperature changes under conditions of continuous gas generation 80—66544
FBR R and D programs in Europe, basic objectives 80—47566
FBR Sphere-Pac carbide fuels, SPECKLE-I, computer modelling of thermal aspects of fuel response 80—18427
FBR sphere-pac fuel, prediction of thermal conductivity 79—59174
FBR TOP accident porous fuel blockage in core, theoretical anal. 79—49673
FBR transient fuel behaviour maps, fuel response to thermal transients 80—57926
FBR transient fuel behaviour maps, fuel response to thermal transients 80—68874
FBR UO_2-fuelled blanket assembly design considerations 80—102254
FFTF, instrumented fuel test at the fuels open test assembly 80—102247
FFTF driver fuel pins, updated temp. integrity limit 77—42089
FFTF element measuring system 79—9729
FFTF fuel and other core components, NDT 77—12757
FFTF fuel failure monitoring, in-core gas release capsule development 80—13681
FFTF fuel quality control, inspection techniques and processes 79—85610
FFTF fuel systems design criteria 80—102251
FFTF fuels and materials exam. facility and materials handling systems design 80—18421
financing and accounting, effects of Pu uncertainty 78—13243
finite element code MIPAC, fuel performance anal. 80—42750
fissile and fusion fuel exchange between fusion hybrid reactor, tritium producer reactor, and fission reactors 80—13811
fissile fuel breeding using electron beam 78—8992
fissile fuel dynamics of breeder/converter reactors 79—13385
fissile fuel prod. using hybrid reactors 79—76123
fissile material assay, cyclic method of neutron activation and delayed-neutron counting 77—34395
fissile material spallation breeding by high power accelerators 77—83162
fissile materials safeguards, quantity and isotopic comp. meas. *(Russian)* 80—63287
fission gas, steady state behaviour in carbide fuels, modelling 78—78469
fission gas behaviour, conf. Karlsruhe, Germany (Oct. 1978) 80—56992
fission gas behaviour in fast reactor fuel, model, steady state and transient conditions 77—67809
fission gas behaviour in fuel pins prior to transient testing 79—30921

fission reactor fuel continued
fission gas bubble distribs. in mixed oxide fast reactor fuel pin, anal. of TEM obs. 78—58358
fission gas effects in irradiated fuel rods operated in film boiling at high power 79—49744
fission gas re-solution, comparison of single knock on and complete bubble destruction models 78—82455
fission product activity ratios in RA used fuel element, γ-ray spectroscopy 79—41061
fission product decay heat, effects of depletion, buildup and fast fission in shutdown 79—81041
fission product migration in fuel pin, FIPMIGR program 80—37453
fission product release, enhanced by grain boundary diffusion 78—4986
fission product release and distrib. in coated particles, laser system *(German)* 78—82403
fission products decay heat, development of revised ANS standard 79—49742
fission products in primary coolant, possible contribution from U impurities in fuel cladding 79—63751
fission reactor fuel rod deformation code FEMAXI-II and its application 80—37446
Ford Nuclear reactor, reduced enrichment fuel element loading, calcs. 80—9394
Fort St. Vrain HTGR power station, review of design and operation 79—45353
French contribution to reduced enrichment research and test reactor program 80—68931
FTR, criticality expts. of fuel pins in water, computer calcs. 79—59162
FTR subassembly failure pattern under transient overpower accident 79—31006
fuel adjustment clause for collecting nuclear fuel costs 79—31105
fuel cycle, national and international aspects *(German)* 78—86665
fuel cycle alternatives for power reactors 77—42107
fuel cycle cost sensitivity anal. of alternative reactor fuel cycles 79—89368
fuel cycle industry development, limiting factors *(French)* 78—66430
fuel cycle optimization with nonproliferation objectives 80—730
fuel cycle options without Pu separation 79—26676
fuel defect test loop, design of remote handling system 78—82436
fuel defect test loop, remote handling system design 79—45395
fuel design limit for post-DNB operation 80—572
fuel disassembly experiments using the capacitor discharge vaporization (CDV) technique 79—85598
fuel element basics, text book 77—351
fuel element modelling, interpreting and predicting irradiation creep 77—42058
fuel element performance modelling, IAEA specialists meeting, 1978 80—36769
fuel elements, with cladding, thermal shock *(Italian)* 80—27774
fuel elements during irradiation, thermal state study using contactless method 80—32392
fuel failure behaviour of unirradiated fuel rods under reactivity initiated accident conditions *(Japanese)* 79—30955
fuel failure criteria, uncertain benefits 80—574
fuel form and cladding carbide distrib. on fuel-clad interaction during irrad. 79—85618
fuel management calc. procedures, applicability 78—58341
fuel management scheme for high burnup at VEPCO 80—37436
fuel management with extended burnup fuels 80—37503
fuel performance data base EPRI 79—93731
fuel pin profilometry adaptation, cutoff saw 79—45452
fuel pin rupture detection system using meas. of time differential of acoustic emissions 80—102282
fuel pins, eccentrically placed pellets, finite difference method for heat transfer 78—82419
fuel pins, fast breeder, fuel-cladding mech. interaction, obs. and anal. 80—86959
fuel rejuvenation based on in situ re-enrichment and fission product removal 80—37561
fuel rod, heat transfer code for calc. effect of asymmetric geometries 79—49743
fuel rod anal., statistical version of URANUS programme 80—42749
fuel rod bowing due to internally applied load 77—46257
fuel rod deformation, precision in-reactor meas. techniques 79—26542
fuel rod deformation code FEMAXI-II and its application 80—37446
fuel rod modelling, uncertainty 78—21629
fuel rod pellet clad interaction failures, I stress corrosion cracking tests 78—58351
fuel rod sealing by high pulsed magnetic fields using capacitor bank 78—8910
fuel rod structural anal. criticism 78—82441
fuel rod thermal stored energy, calculational uncertainty anal. 80—47609
fuel services, analysis, costing and economics of cooperative facilities 77—57772
fuel structure characterisation methods, review 79—49802
fuel-cladding chem. interactions at high burnup 78—86584
fuel-cladding interaction between cracked surfaces, mechanical and temp. contact 78—66341
fuel-coolant interactions, role of Rayleigh-Taylor flow instabilities 79—17983
fuel-sodium interactions, effects of finite mixing time and noncondensable gas 78—17331
fuel-to-cladding heat transfer coefficient in a reactor fuel element *(German)* 80—610
Fuels and Materials Examination Facility, design features and objectives 79—45448
Fuels and Materials Examination Facility, equipment design and development 79—45449
Fugen fuel clusters, pin gap stat. eval., reliability levels 80—13583
fusion-driven symbiotic energy systems, economic anal. of fuel cycle and power costs 80—23141
fusion-fission hybrid reactor, laser driven, fuel breeding and power prod. 79—22473
fusion-fission hybrid reactor energy research program 79—22471
fusion-fission hybrid reactor fuel cycle considerations 79—22474
fusion-fission hybrid reactors, fissile fuel breeding potential 77—50287
fusion-fission symbionts, nuclear fuel trajectories, fissile and fusile fuel characterisations 80—68947
future nuclear power technology, impact of nuclear research in India 80—95345

fission reactor fuel continued
gadolinia-based fuel pins, efficient diffusion theory parameterization 79—67840
gap conductance, heat transfer over range of Knudsen number 78—13213
gas bubble adhesion to heat transfer surfaces 79—89375
gas bubble distribution, in fuel, anal. of TEM obs. 79—71890
gas bubbles, nonequilibrium intragranular, role during transient heating of fuel 79—6740
gas cooled reactor experience and programs in France, reviews 79—45332
gas release, calc. fo diffusive flow to spherical boundary 80—47574
gas release and swelling, operational model, grain boundary gas 80—95346
gas swelling, physical processes and mechanisms 79—97808
gas tagging of fuel failure, simultaneous identification of multiple failures using barycentric-coords. tech. 80—83191
gas-discharge reactor, fuel element component conc., plasma temp. profile instabilities 80—63253
gas-phase composition in rods at Novyi Voronezh power station, burnup factors, ^{3}H, ^{85}Kr levels 77—30649
gaseous core reactor nonproliferation features 79—9740
gaseous core reactor U plasma radiative temp. calc. 79—9807
GCFR, design criteria for 300 MW(e) demonstration plant 79—97759
GCFR, fission gas release and molten fuel motion for slow overpower transient 78—17369
GCFR 300 MW(e) fuel element design 77—18649
GCFR cermet cylindrical core swelling *(Russian)* 79—13425
GCFR fuel bundle irrad. in BR2 He loop 77—18652
GCFR fuel column, effect of Cs migration on fission gas permeability 79—67824
GCFR fuel pin design, anal. of temp. distrib. using HELM test facility 80—18409
GCFR fuel rod roughness elements, pressure drop meas. 80—581
GCFR fuel rod roughness elements, surrounding flow visualisation technique 79—59141
GCFR grid spaced bundle for F-5 (X317) irradiation expt., fabrication 79—81058
GCFR lattice, PROTEUS central ThO$_2$ zone expts. 80—22984
GCFR lattice, testing of ENDF/B-IV Th data 79—67836
GCFR LOF accident, natural convection effects in blocked fuel assembly 79—49755
GCFR pressure-equalised fuel irradiation program 80—648
GCFR programmes, status 77—18647
GCFR proliferation-resistant heterogeneous fuel cycles, computer neutronic anal. 80—18435
GCFR rodded lattice, axial UO$_2$ blanket meas. 79—81037
GCFR simulation central Doppler worth evaluation 79—9814
Go-ri nuclear power plant, fuel cycle schemes, economic comparison 78—54831
grain boundary loss terms, use in fission gas release and swelling models 80—63257
graphite-matrix pulsed reactor fuels, characteris. including thermal stress fracture 77—46294
HCDA, natural convection heat transfer in fuel debris bed cooled at top and bottom 79—93785
HCDA condition, fuel motion measurement, time-resolved coded aperture imaging system 78—45764
heterogeneity effects on reaction rates in advanced fuels program oxide zone assembly 80—22975
heterogeneous fuel pin cells, nodal method in 2-D calcs. 78—21631
heterogeneous Gas Core Reactor power plants 79—9671
hexcans, elastoplastic anal. 77—83027
HFEF/N irradiated fuel element eddy-current exam., cladding performance 79—9750
HFR Petten Materials Test Reactor, reduced enriched fuels, utilisation and management schemes 80—9343
high flux beam reactor using medium-enriched uranium, feasibility study 80—23113
high flux test reactor, MARIA, nuclear power research programs *(Polish)* 79—93693
high power accelerators for spallation breeders of fissile materials *(Japanese)* 79—26517
high temp. (2300-2500°C) treatment, metallographic cross sections, microradiographic anal. *(German)* 78—29586
high U density fuel for test and research reactors 80—68801
high-pressure capsule for irradiation of fuel swelling specimens in FR2 reactor 77—46218
highly enriched U plates, assay in random driver, absorption modified multiplication effects 80—32399
hot cell extension optical profilometer 80—68789
hot fuel examination, neutron radiography facility 79—9725
hot fuel examination, sodium loop safety facility, loop disassembly system 79—9727
hot fuel examination facility, air cell decontamination and refurbishment 79—9910
hot fuel examination facility, air sampling system 79—13541
hot fuel examination facility/north, equipment repair room modifications 79—9723
hot fuel examination facility/north, wall feedthrough removal, portable glove box system 79—9724
HTGCR, determ. of defective particle fraction, Cl leach method 77—42165
HTGR, alternative fuel cycles using low- and middle enriched U, impact on core design 79—49674
HTGR, Cs release and transport in coated fuel particles 77—74935
HTGR, driver fuel elements, power profile meas. and in-pile thermocouple readings 79—67907
HTGR, fuel failure anal. following LOCA, post-accident temp. response 78—13276
HTGR, fuel optimization, symbiotic combinations, comparative evaluations 78—29605
HTGR, fuel particle failure fraction determ. by hot-Cl leaching 79—67868
HTGR, gas release from fuel particles and rods 77—74938
HTGR, inert gas release core-survey calc. 79—67908
HTGR, irradiation performance of fuel in capsule F-30 77—74934
HTGR, medium enriched U fuelled, optimisaton 80—37512
HTGR, metallic fission product retention 77—79443
HTGR, nonlinear dynamic anal. of prismatic graphite fuel elements, response to seismic excitation 80—99237

fission reactor fuel continued
HTGR, Peach Bottom site, distrib. of ^{137}Cs and other fission products in fuel elements 78—13274
HTGR, release of metallic fission products from multilayered coated particles 77—79442
HTGR, release of rare fission gases 77—74940
HTGR, stoichiometric effects on fuel performance 77—74933
HTGR, US R and D programs for steam supply plant, fuel and materials 79—97757
HTGR Biso coated fuel particles, neutron induced permeability 77—42100
HTGR Biso-coated fuel particles, defective fraction during in-block carbonisation 79—67922
HTGR block fuel elements, fuel zone location meas. using gamma scanning *(German)* 79—67847
HTGR coated fuel particles, behaviour of fission products *(Japanese)* 78—54830
HTGR coated particle fuels, SiC coating corrosion by fission product Pd 80—102237
HTGR coated particles, failure rate prediction during neutron irradiation 77—79466
HTGR coated-particle fuel, irrad. performance determ. by irradiated microsphere gamma analyzer (IMGA) 79—54543
HTGR fuel and graphite structure stress analysis methods and programs *(Japanese)* 78—74434
HTGR fuel assemblies, two-dimens. modelling 80—32351
HTGR fuel cycle summary and recent developments 80—728
HTGR fuel element failure mechanisms and fission product release 80—13586
HTGR fuel element graphite, determ. of ^{90}Sr diffusion coeffs. 79—67869
HTGR fuel particle, computer code for anal. of transient behaviour 78—8964
HTGR fuel particle failure, chemical aspects 77—42099
HTGR fuel particles, fission gas content meas. apparatus 80—68793
HTGR fuel particles, inert gas intrusion as charact. procedure for pyrocarbon coatings 79—54512
HTGR fuel particles, influence of pyrocarbon props. on as-produced gas permeability of coatings 79—54511
HTGR fuel particles, SiC corrosion 77—67817
HTGR fuel performance for hypothetical core heatup conditions 80—47579
HTGR fuel refabrication plant, nondestructive fissile assay technique 80—37562
HTGR fuel rod fabrication, estimation and control 80—83215
HTGR fuel rods with diluted thermosetting matrices, irradiation performance 77—83038
HTGR fuel selection 79—54504
HTGR irradiation expts., fission product release 77—74939
HTGR multihole fuel, equivalent thermal conductivity calc. *(Japanese)* 79—45346
HTGR pre-breeder and near-breeder symbiotic systems, U resource utilization 78—17321
HTGR proliferation-resistant MEU fuel design and qualification 80—42779
HTGR pyrocarbon coated fuel, neutron effects in range 1273-1773K 77—79434
HTGR pyrocarbon coated particles, neutron induced permeability 77—79435
HTGR spent fuel elements, ^{14}C determination, chemical anal. 80—42745
HTGR spherical fuel assemblies, resonance integral meas. *(German)* 78—29568
HTLTR, neutron multiplication factors, temp. depend., fuel lattices, comparative evaluation with HTGR 78—29557
HTR, ^{110m}Ag release from coated particle fuel 77—74936
HTR, Cs release in Biso-coated particles 77—79441
HTR, development and performance of spherical fuel elements 80—646
HTR, fuel temp. coeff. of k_∞, determ. by null reactivity oscillator method 79—30890
HTR, gas release by coated oxide fuel particles 77—74937
HTR, pyrocarbon coated fuel, C density determ. by X-ray absorpt. 80—5301
HTR, spherical fuel elements, determ. of fission product release 80—647
HTR, spherical fuel elements, fabrication, fuel loading and exposed heavy metal 80—599
HTR advanced system, materials for core-specific and primary circuit components 77—26842
HTR fuel, high neutron flux, high temp., post irradiation exam. 78—58360
HTR fuel cycle program in the Federal Republic of Germany 80—644
HTR fuel of low/medium enrichment 80—645
HTR fuel specimens, neutron irradiated, post irradiation exam., microradiography, metallography, burn-up determ. 78—58361
HTR fuel spheres, ice cleavage and subsequent examinations 79—36319
HTR fuels, SiC coating characterisation by small-angle X-ray scatt. 80—44451
HTR individual coated fuel particles, gas anal., optimum heating and crushing 77—56294
HTR individual coated fuel particles, mass spectrum. determ. of Xe, Co and Kr gases 77—56293
HTR irradiated fuel, anal. of α-emitting isotopes through laser microboring 80—37444
HTR oxide fuel, retention of solid fission products 79—54507
HTR particles, surface anal. by XPS 78—33252
HTR power station, design development, operation and appl., review *(German)* 79—76088
HTR system materials developments 77—46297
HTR Th closed fuel cycle, U resource conservation 80—727
HWR, CIRENE prototype reactor, fuel, fabrication performance *(Italian)* 77—10467
HWR, fuel cycle cost anal. using computer code HWRCOST on-power refuelling 77—83051
HWR, gas cooled, effect of fuel enrichment on transuranium isotope formation 78—17292
hybrid reactors, materials implications for reactor design 80—32430
hybrid Tokamak reactor, for prod. of Pu fuel and elec. energy, preliminary design 79—76122
image enhancement and mensuration algorithms 78—37395
in-cell weighing system at HFEF 77—54298
in-core fuel management educational module 80—36804
in-core irradiation facilities, development and expt. using JRR-2 and JMTR research reactors, Japan *(Japanese)* 80—63256

fission reactor fuel continued
- in-core molten fuel pool expt., heat flux and struct. ablation 79—13407
- in-core visual inspection of irradiated fuel, design of compact, portable stand 79—67912
- in-reactor fuel temperature, transient response of centreline thermocouples, appl. to fuel modelling 80—95372
- in-reactor fuel-to-sheath heat transfer meas. 79—13408
- inspection by neutron radiography, review 78—60890
- integral rods, anal. with COMETHE III-J programme 80—37448
- integrated reactor systems fuel strategy, review of future nuclear energy options 79—49696
- internal pressurisation in solid-mixed-oxide fuel due to fission gas release 77—83058
- international fuel cycle centres, economies and financing 77—46374
- international fuel exchange agreement, economic benefits 80—37462
- International Nuclear Fuel Cycle Evaluation, midterm assessment *(German)* 79—89370
- international resources assessment 80—99215
- inventory checks, accounting data optimal linear combinations for nonconstant loss detection 79—81057
- irradiated, α-autoradiography, effect of β-radiation *(German)* 78—78466
- irradiated, conc. profile of fission products 77—50237
- irradiated, highly radioactive, safe transportation 77—74956
- irradiated, nondestructive assay methods *(Slovenian)* 80—27744
- irradiated fuel, nondestructive devices for on-site examination 80—13699
- irradiated fuel, safe transport 77—79445
- irradiated fuel assemblies, burn-up and cooling time determ. using gamma spectrometry 80—63289
- irradiated fuel rod NDT using encircling and probe eddy-current systems 79—9751
- irradiated fuel rods, computer-controlled gamma scanning 79—9753
- irradiated LWR fuel, European transport experience 80—63309
- irradiated nuclear fuel, determ. of one group cross-section ratio from meas. isotopic comp. 80—612
- irradiated nuclear fuel, transport, packaging, UK experience 79—26782
- irradiated nuclear fuels, passive neutron assay, burnup determination 80—32398
- irradiated nuclear reactor fuel rod components, EM separation, feasibility 80—99224
- irradiated rods, assembly for power burst facility testing 77—54300
- irradiation expt. 78—86587
- irradiation test facility for high U-loaded fuel plates as part of reduced enrichment program 80—68932
- isotope correl. ratios, analytical capabilities for accurate prediction 79—85620
- isotopic correlations in irradiated fuel from VVER power reactors *(Russian)* 80—68838
- isotopic correlations in irradiated nuclear fuel, fissile material accounting 79—40994
- large-bundle LOCA expts., fuel rod ballooning probabilistic analysis 79—13462
- laser boring for material sampling of coated fission fuel particles 78—55399
- laser pulse heating, high speed pyrometry and spectroscopy, review of techniques 80—52225
- lattice cell meas., natural UO_2 fuel in ZED-2 hot loop facilities 78—58347
- lattice eigenvalue as function of buckling, perturbation theory correction 79—59118
- Leidenfrost temperature for spherical fuel particles, appl. FCI anal. 78—17371
- lifetime fissile fuel requirement 80—37424
- light water reactor fuel, Pu determ. by γ-ray spectrometry 79—11872
- liquid fuel-fission gas bubble mixtures, equation of state 80—47568
- LMBFBR overpower accidents, mechanistic model of fuel flow regimes and fuel plateout 79—85615
- LMFBR, 1500 MW, breeding perfomrance optimisation of He-bonded carbide fuel 78—17325
- LMFBR, analysis of in-pile MFCI experiments with carbide fuel 79—49754
- LMFBR, axial parfait heterogeneous core design, fuel cycle anal. 79—59156
- LMFBR, BR-2, UO_2 behaviour for local cooling disturbances in in-pile Na loop 80—13542
- LMFBR, breeding ratio and fissile inventory for homogeneous and heterogeneous cover 80—32374
- LMFBR, CAMEL single-pin fuel sweepout test C2 79—30983
- LMFBR, Clinch River, material release for advanced fuels following hypothetical core disruptive accident 79—31065
- LMFBR, combined fuel and coolant motion under high-ramp transient overpower conditions 79—31003
- LMFBR, core-disruptive accidents, neutronic and fuel element behaviour 80—32357
- LMFBR, demonstration, design, construction and operating experience 79—97796
- LMFBR, design of fuel rods *(Spanish)* 77—74918
- LMFBR, development and Pu allocation, optimal policies 80—725
- LMFBR, effect of alternative fuel cycles on reactor design 79—49675
- LMFBR, effect of design charges on fuel cycle cost and breeding performance 80—18436
- LMFBR, effective conduction mixing lengths for subchannel anal. of finite hexagonal bundles 78—13210
- LMFBR, effects of Na entrainment and heat transfer with UO_2 vapour during HCDA 79—93775
- LMFBR, effects of Th breeder material on Na-void reactivity 80—22982
- LMFBR, enrichment and control optimization for reactivity losses during burnup 78—21692
- LMFBR, fast integral model for the transient analysis of a melting fuel pin 79—54552
- LMFBR, feasibility of conducting a low ramp rate TOP experiment in TREAT 80—47655
- LMFBR, feasibility of using denatured ^{233}U diluted with ^{238}U 78—17324
- LMFBR, fission gas release and microscopic swelling in highly rated advanced fuels 80—52739
- LMFBR, fuel and fission gas response to simulated thermal transients 78—74453
- LMFBR, fuel cycle cost optimisation anal. of core design modifications 80—22900
- LMFBR, fuel failure propagation reliability assessment 79—49785
- LMFBR, fuel motion diagnostics instrumentation, evaluation with PARKA 79—45360

fission reactor fuel continued
- LMFBR, fuel motion pot. due to volatilisation of metallic fission product inclusions 79—49746
- LMFBR, fuel pin coolability in low power voiding, SAS3A computer code anal. 79—49661
- LMFBR, fuel pin deform. within wire-wrap fuel assembly, computer code anal. 79—71915
- LMFBR, gas tag identification of failed assemblies, anal. methods 80—95369
- LMFBR, HCDA, role of radiative heat transfer in post-disassembly fuel self-mixing 79—49759
- LMFBR, heterogeneous, fuel element performance, impact of design and operating parameters 80—102249
- LMFBR, heterogeneous, Th blanket zones study in ZPPR Assembly 8 80—22983
- LMFBR, heterogeneous and homogeneous core designs, performance characteristics 79—59123
- LMFBR, heterogeneous carbide-fueled reactors, thermal and economic performance 79—93703
- LMFBR, heterogeneous core concept studies, sensitivity to fuel cycle, design and cross section changes 78—13225
- LMFBR, hydrodynamics of large-scale fuel-coolant interactions 80—78409
- LMFBR, hypothetical LOCA, fission gas role in transition phase development 78—8935
- LMFBR, idealised equilibrium expansion of mixtures calc. for UO_2 vapour bubbles in Na 79—22390
- LMFBR, LOCA, fuel pin failure mechanisms 80—13587
- LMFBR, LOF accident, evaluation of incoherency effect on cladding motion in R-series test 79—49749
- LMFBR, LOFA, fuel assembly boiling and voiding, THARC-S code 80—13646
- LMFBR, modeling ejection of fresh fuel into sodium under prompt-burst conditions 79—85668
- LMFBR, molten fuel coolant interaction *(Japanese)* 79—17997
- LMFBR, molten UO_2 fuel-Na coolant thermal interaction, characterisation of fragmented fuel 80—68774
- LMFBR, natural convective cooling of fuel debris bed following HCDA 78—8929
- LMFBR, nonlinear structural dynamics of fuel elements, press. pulses, struct. models, expt. verification 77—3125
- LMFBR, nuclear fuel utilization factor 77—71647
- LMFBR, performance characts. in US nucl. energy system. rel. to breeding ratio, sp. power, discharge exposure 78—17404
- LMFBR, pin diam. optimisation in heterogeneous vs. homogeneous core 78—8892
- LMFBR, post-test anal. of transient overpower TREAT test R9 for BOL FFTF-type fuel 79—30985
- LMFBR, preirradiated mixed oxide fuel, EOS series of expts. in TREAT 79—30986
- LMFBR, Pu isotope prod., perturbation theory calcs. 77—23176
- LMFBR, radiative heat transfer in horizontal molten fuel layer with volumetric heating 79—93786
- LMFBR, recriticality considerations for the loss-of-heat-sink accident with scram 79—49760
- LMFBR, refuelling scheme optimisation using heuristic enumeration method 77—46301
- LMFBR, SAS3A simulations for a 19-pin dryout experiment 79—54547
- LMFBR, simulated LOFT, fuel response, role of fission gas and fuel melting 80—37475
- LMFBR, SNR-300, fuel rod performance and modelling at high burnup 78—58336
- LMFBR, SNR-300, HCDA anal. by failure incoherence modelling, HOPE computer code 77—88237
- LMFBR, spent fuel valuation, procedure appls. and analysis 80—738
- LMFBR, terminated transient overpower performance, fuel design and material effects 80—22902
- LMFBR, TOP, fuel pins and core response 80—13671
- LMFBR, transient fuel solidification and relocation from core during transition-phase conditions 79—85616
- LMFBR, uranium-thorium based fuels, breeding performance potential 79—59175
- LMFBR, wire wrap driver fuel assembly, development and testing at FFTF 79—59152
- LMFBR 91-pin subassembly, fuel displacement diagnostic facilities 79—49776
- LMFBR advanced fuel elements, Na bonded, wire wrap-cladding interaction 79—93734
- LMFBR advanced fuels critical assemblies, integral alpha and point conversion ratio meas. 79—81012
- LMFBR advanced MX-type fuels, fission gas swelling, temp. depend. 80—57842
- LMFBR advanced MX-type fuels, low-temp. microscopic swelling, phenomenological model 80—57851
- LMFBR advanced MX-type fuels, swelling mechanism anal. 80—57850
- LMFBR assembly, fuel pin deformations, analytical method, computational code (SHADOW) 78—54829
- LMFBR blanket fuel management anal., PUMA technique 80—13557
- LMFBR blankets, comparative breeding potential of ^{232}Th and ^{238}U 80—22948
- LMFBR claddings with axial fins, stress anal. including creep effects 77—88224
- LMFBR core and fuel design in Halian fast reactor programme 79—97795
- LMFBR demonstration plant, design, construction and operating experience 79—97887
- LMFBR design with the composite fuel assembly 79—54489
- LMFBR failed-fuel detection using gaseous fission-product detectors 79—97856
- LMFBR for maintenance of fuel reserves 77—67862
- LMFBR fuel, fission gas behaviour during overpower transient, calcs. using COREF-1 code 80—57853
- LMFBR fuel assembly, 19 pin, simulation of flow blockage 80—582
- LMFBR fuel assembly, 3-D numerical simulation, thermal-hydraulic behaviour anal. 79—59143
- LMFBR fuel behaviour during HCDA, intragranular fission gas behavior under isothermal conditions 80—102236
- LMFBR fuel bundles transient testing, operating experience 80—827
- LMFBR fuel disruption following LOF accident, in-pile expt. using high-speed cinematography 80—78366
- LMFBR fuel element design. overview 79—85584

fission reactor fuel continued
LMFBR fuel element model, dynamic characts., meas. of amplitudes and press. fluctuations 79−67852
LMFBR fuel expansion, nonequilibrium evaporation and condensation 77−42021
LMFBR fuel failure dynamics, appl. of Larson-Miller parameter 79−31002
LMFBR fuel pin behaviour, computer code FRUMP, stress, strain, temp. distribs., displacements 77−14235
LMFBR fuel pin bundle, wire-spaced, three-dimens. deflection modes 78−13301
LMFBR fuel pin failure monitoring, cumulative mech. damage function from materials data 78−13262
LMFBR fuel pin power calibration prediction, transient correction factor analysis 79−9719
LMFBR fuel pin transient behaviour, effect of shutdown cracks in TREAT tested pins 79−31001
LMFBR fuel pins, assay with Pb spectrom. 80−37461
LMFBR fuel pins, computer anal. and control for nondestructive gamma scanning 79−9754
LMFBR fuel rod enhanced thermal creep deformation, secondary stress cycling conditions, elastic region 77−4832
LMFBR fuel rod subassembly, thermal-hydraulic anal. as distrib. parameter system *(Japanese)* 80−68736
LMFBR fuel storage facilities, criticality calcs. 79−26568
LMFBR fuel subassembly, effect of bundle insulation degradation on boiling stability tests 79−54548
LMFBR fuel subassembly, pin bundle deflection anal. 78−78449
LMFBR fuel subassembly temp. noise prediction, Monte Carlo approach 79−13392
LMFBR fuelling requirements rel. to Pu isotopic composition, core design 79−9738
LMFBR heterogeneous core design with interchangeable oxide/carbide fuel, CDS development program 80−102253
LMFBR heterogeneous oxide reference, transmuter, denatured core designs 80−22901
LMFBR heterogenization, breeding and fissile inventory changes 80−13556
LMFBR hexagonal ducts, cracking, effect on safety and fuel pin failure 78−17318
LMFBR highly-rated MX-type fuels, fission gas release and microscopic swelling 80−57848
LMFBR LOF accident, analysis of in-pile fuel disruption experiments 79−49748
LMFBR LOF accident tests at TREAT on preirradiated mixed oxide fuel 80−47657
LMFBR LOF transient, sodium voiding dynamics and cladding motion 79−49750
LMFBR low power, high burnup carbide fuel elements, performance 77−42087
LMFBR metal fuel elements, development and performance 80−57856
LMFBR metal fuel elements, development and performance evaluation 80−598
LMFBR mixed oxide fuel pins, proposed mechanism for internal cladding corrosion 79−8384
LMFBR mixed-oxide fuel aggregates, dynamic shape factors 79−67853
LMFBR molten oxide fuel layer, effect of radiation heat transfer on maximum nonboiling thickness 80−47558
LMFBR multipin bundles, eval. of hodoscopes for fuel motion meas. 79−93780
LMFBR MX-type highly rated advanced fuels, fission gas release and correl. with fuel restructuring 80−642
LMFBR oxide elements, predicting serviceability, efficiency 77−23209
LMFBR oxide fuel analysis system 77−46227
LMFBR performance of Th-based fuel cycles 79−9744
LMFBR refueling force limits criteria, testing, and evaluation 79−67913
LMFBR refuelling scheme optimisation by man machine interactive method 77−67826
LMFBR safety, coded aperture imaging in many-pin fuel bundles 79−49777
LMFBR safety, international cooperation, progress 80−826
LMFBR safety analysis, effect of fuel rod bundle geometry on liquid solidification rates 80−47632
LMFBR simulated LOF transients in 37-pin subassemblies at SLSF, interpretation of voiding dynamics data 80−47656
LMFBR single component and mixed oxide fuel solidification anal. 78−74435
LMFBR test fuel element, appl. of nonredundant pinhole array 79−93781
LMFBR TOP accident, fuel pin failure, anal. 79−49699
LMFBR TOP accident, implications of in-channel fuel plugging 80−78414
LMFBR transient fission gas behaviour modelling, bubble equilibration effects FRAS 2 code 79−59168
LMFBR transient fuel behaviour, effect of grain boundary fission gas 79−54532
LMFBR type mixed oxide fuel pins, composition of corrosion product oxide phases in pin gaps 78−70599
LMFBR universal core layout, interchangeability of hetero(homo)geneous cores and oxide/carbide fuels 80−102228
LMRBR, interchangeable core assessment, coolant orifice zoning 80−102229
LMRBR interchangeable core assembly design 80−102230
LOCA, fuel element behaviour during high-temp. transients, ELOCA code 79−81043
LOCA, strain in Zircaloy clad of fuel pins 78−699
local burn-up rel. to construction material presence *(Russian)* 78−41812
LOFT, contribution to PWR fuel behaviour 80−106139
LOFT fuel design and operating experience, exposure to LOCA 79−89438
LOFT fuel design and operating experience 80−18411
LOFT LOCE fuel module structural response, computer code prediction 79−89439
LOFT test L2-2, fuel rod response 80−18520
low-enriched fuel particle performance review 79−13426
LWBR, unique thermal and hydraulic design features 79−54483
LWBR delayed-neutron pellet assay gauge 79−54590
LWR, alternative fuel cycles containing Th 80−37510
LWR, computer code package for core following and in-core fuel management benchmarking and operating experience 80−704

fission reactor fuel continued
LWR, ENDF/B-IV eigenvalue calcs. for UO_2 and mixed oxide critical lattice expts. 78−25272
LWR, failed fuel rod identification by gas tagging 80−23021
LWR, fission gas release high-burnup fuel during transient heating 78−13283
LWR, fission product activities, fuel survey 80−736
LWR, fuel rod microstruct. changes associated with post-DNB operation during power-cooling-mismatch 78−21688
LWR, fuel utilisation, spectral shift control methods 80−47586
LWR, fueld management optimisation *(Czech)* 77−42112
LWR, HCDA, behaviour of concrete in contact with molten corium 80−13584
LWR, I spiking, release mechanism and its verification in plant operation 79−59229
LWR, irradiated fuel assemblies, burn-up meas. for nuclear material safeguards, IAEA experience 80−68807
LWR, mixed oxide fuel, suitability of spent fuel shipping casks 80−27757
LWR, optimal power profile fuel management 78−37411
LWR, ore conservation by routine coastdown 80−37507
LWR, pellet-clad interaction modelling 80−37445
LWR, power cooling mismatch accident, molten fuel radial motion and cladding melting 80−13638
LWR, Pu recycling, CEA-EdF studies 80−722
LWR, Pu recycling, storage before use in breeders 80−37513
LWR, quality assurance of fuel and fuel elements *(German)* 79−49810
LWR, refuelling with natural U 80−679
LWR, spent fuel valuation, procedure appls. and analysis 80−738
LWR, two near-term alternatives to improved nuclear fuel utilization 80−37506
LWR, UO_2 fuel, critical expts. supporting close packed water storage 80−37434
LWR, vitrified high-level radioactive waste, rail transportation, fault tree anal. and accidental release 78−17358
LWR accidents, in-reactor expts. on fuel behaviour review *(Japanese)* 79−63760
LWR and HWR, anal. of UO_2-ThO_3 fueled exponential expts. with WIMS-D code and data 79−81000
LWR controlled porosity fuels, short term irradiation behaviour 79−49686
LWR core, power shape from irrad. fuel meas., gain stabilized NaI(Tl) γ-ray detector system 78−33284
LWR core meltdown, chemical reacts. between core melt and concrete 80−13588
LWR design modification for in-core Pu utilisation improvement 79−9709
LWR failed fuel expts., improved method 80−13595
LWR fuel, feasibility of accelerator driven rejuvenation 80−27780
LWR fuel, future trends to improve U utilisation 79−85634
LWR fuel, mechanistic prediction of transient fission gas release 80−47571
LWR fuel, pellet clad interaction failures 80−16441
LWR fuel, performance and reliability 79−26540
LWR fuel, power ramp failure propensity, exptl. investigations 79−26543
LWR fuel burn-up determ. from $^{134}Cs/^{137}Cs$ activity ratio *(Russian)* 80−68804
LWR fuel cycle resource requirements, implications of data uncertainties 80−18437
LWR fuel design, Italian progress in manufacturing, testing and management 79−26539
LWR fuel elements, behaviour under accident conditions 79−26545
LWR fuel elements, burnable poison management for high burnup reactivity compensation 80−707
LWR fuel elements, fault behaviour *(German)* 78−696
LWR fuel elements, Pacific Northwest Lab. Experimental Criticality program 80−37429
LWR fuel failure under reactivity initiated accident conditions, NSRR experiments *(Japanese)* 79−36340
LWR fuel management, power distrib. calcs. by nodal one-group simulators 80−706
LWR fuel management decision analysis with fuel integrity prediction 79−9781
LWR fuel performace anal., WAFER-2 code 80−37447
LWR fuel performance calcs., effect of Cs and I_2 release 79−31054
LWR fuel regeneration by linear accelerator reactor 80−32336
LWR fuel reliability, experience and future assessment, failure modes 79−26541
LWR fuel rod, transient pellet-cladding interaction, ISUNE-4 computer anal. 80−91228
LWR fuel rod behavior in a nine-rod bundle tested in film boiling 80−18500
LWR fuel rod failure probability, comparison of FRAP T4 and meas. 80−13644
LWR fuel rod mechanical performance predictor, SPEAR code 79−93730
LWR fuel rod quenching, two-dimensional heat conduction model 79−93815
LWR fuel rods containing fission gas, grain growth 79−67866
LWR fuel safety, failure thresholds, NSRR programme 79−26595
LWR fuel supply utilising hybrid reactors 80−42867
LWR fuel utilisation improvement 79−59160
LWR fuel utilisation in US, historical survey 80−37460
LWR fuel-cladding gap, Cs-U-Zr-H-I-O system, chemical thermodynamics 78−82440
LWR gamma-scanning meas. of spent fuel elements, appl. to reactor simulation *(German)* 79−67874
LWR high-power rods under irradiation, chemical state 79−97809
LWR in-core fuel management techniques, review *(Italian)* 80−18447
LWR irradiated fuel assemblies, nondestructive exam. using γ-ray and neutron techniques 80−66760
LWR lattices of UO_2 and Gd_2O_3 rods, critical expt. 79−26474
LWR LOCA, fission product release from defected fuel rods 80−23031
LWR LOCA, two-dimensional temperature distributions in fuel rods under blowdown conditions 80−774
LWR metallic U properties 78−8911
LWR mixed oxide fuels, determ. of H_2O, Hz content by hot extraction methods *(German)* 79−49808
LWR mixed oxide fuels, safety aspects of PuO_2 micro-heterogeneities 79−49798

fission reactor fuel continued
LWR oxide fuel, specification rel. to operational behaviour *(German)* 79—49797
LWR plant availability rel. to refuelling cycle duration 79—22440
LWR power stations, incremental fuel cost calcs. using FAPMAN-IC program module 80—95356
LWR Pu isotopics, Advanced Recycle Methodology Program calc. 79—9710
LWR reference fuel rods, acquisition and safeguards verification 80—68813
LWR refueling outage times, effect on plant availability 79—67910
LWR ruptured fuel rods in LOCA, fission product release, computer modelling 79—49780
LWR safety research programs by US NRC on fuel behaviour 80—42796
LWR spent fuel, alpha spectrometric meas. for SNM verification 80—78424
LWR spent fuel, non-destructive anal. using inherent and induced neutron radiation *(Russian)* 80—68805
LWR spent fuel, nondestructive meas. and verification for materials safeguards 80—78420
LWR spent fuel elements, gamma spectrometric meas. of burnup U/Pu ratio and cooling time for materials safeguards 80—78423
LWR Sphere-Pac oxide fuel, eval. of thermal conductivity 80—102234
LWR version of URANUS integral code for fuel rod mechanical calculations *(Spanish)* 79—36315
management and accounting, need for amortization 78—13241
management methods, validated computer codes for nuclear electric utility 78—17403
management schemes for extended fuel burnup in C-E operating reactions 80—37504
meaningful chemical analysis for nuclear fuels and reactor materials *(Japanese)* 79—26519
mechanical design, DIMCO system 80—37418
melting of finite steel slabs in flowing nuclear reactor fuel 79—54494
metallic fuel cladding eutectic formation during postirradiation heating in EBRII 80—102241
metallic product migration in reactor oxide fuels 77—74926
metallographic anal., quantitative, computer program, QMA 79—15951
MEU/Th fuel for HTGR-GT, core physics and performance anal. 80—22903
mixed carbide fuels, radial distrib. of bonded fission gas 80—57844
mixed oxide, in Phenix reactor, characts. and operating behaviour of fuel element *(French)* 78—66349
mixed oxide, microscopic depletion calc. with MICBURN code 78—25276
mixed oxide, retained fission gas determ., new instrumental method 79—54477
mixed oxide fast reactor fuel pin, fission gas bubble distrib. 78—78459
mixed oxide fuel columns, irradiated, dimensional stability 79—67858
mixed oxide fuel cycles, cost sensitivity anal. 79—89369
mixed oxide fuel pellets, close coupled X-ray anal. 79—11876
mixed oxide fuels, burnup-dependent fission gas release 80—42767
mixed oxide fuels, irradiation-induced densification and PuO_2 particle behaviour 79—49684
mixed oxide fuels, SEM obs. of gas bubble morphology 80—57843
mixed oxide rods, high burnup irrad. performance 77—3099
mixed-carbide sphere-pac fuel, irradiation behaviour 77—42091
mixed-carbide sphere-Pac fuel, thermal conductivity during initial stage reconstructuring 80—810
mixed-oxide, FBR LOF accident, role of fission gas and fuel melting on transient fuel response 79—59191
mixed-oxide fuel, cladding breaches 78—82450
mixed-oxide fuel, in-pile homogenisation 78—86576
mixed-oxide fuel, irradiated, microstruct. charact. and radial distrib. of retained fission gas 79—59188
mixed-oxide fuel, irradiation expt. 78—86586
mixed-oxide fuel, performance in EBR-II anal. 78—86585
mixed-oxide fuel, two-component gas transport within interconnected porosity 79—617
mixed-oxide fuel pellets, remote encapsulation for transient testing 80—18422
mixed-oxide fuel pin, cladding breaches 78—82451
mixed-oxide fuel-cladding interaction at high burnup effect of initial stoichiometry 79—67859
mixed-oxide thermal reactor parameters, sensitivity and uncertainty analysis 80—13553
modelling techniques, best-estimate calc. 79—17984
molten fuel containment capability of Na loop safety facility, freezing and melting in finite media 80—47605
molten fuel-coolant interaction, simulation experiment 79—17991
molten fuel-coolant interaction studies, simulated reactor accident, windscale shock tube rig 78—58363
monitoring and development of fuels for LWR Framatome R&D program 80—633
MSR strategies, fuel conservation effect, utilisation of convertors starting with Pu *(Japanese)* 77—50207
Muehleberg BWR, core simulation by fuel Management System, expt. verification 80—705
multigroup time-dependent delayed γ-spectra from fission and activation 78—13184
multiple fuel failure resolution with gas tagging, barycentric coordinate technique 79—13485
MX type nuclear fuels, self diffusion in- and out-of-pile 78—82457
MX type reactor fuels, microscopic swelling meas., effects of grain boundary migration 78—66348
MX-type fuel, porosity and stability obs. 78—86629
natural U fuel with improved performance, CANDU experience 79—71894
NDT using LASL 3.75 MV Van de Graaff 77—83182
neutron flux peaking anal., nuclear fuel bundle ends, program PEAKAN 78—82493
neutron induced diffusion in solids *(Japanese)* 77—59048
neutron interrogation of spent fuel 80—5307
neutron noise as information carrier for early detection of fuel rod malfunction 77—14242
neutron radiography, reson. energy techniques 78—82528
neutron radiography facility handling equipment 79—9726
neutron radiography of irrad. fuel pins, coupled fast reactivity measurement facility 79—93720

fission reactor fuel continued
ngutron detector for determ. of transuranic element comp. of nuclear fuel cladding hulls 80—63471
nine-rod cluster, film boiling behaviour 79—89444
nondestructive assay, by ^{237}Np threshold detector, subthreshold phenomena effects 79—22409
nondestructive assay method by detection of spontaneous neutrons 80—668
nondestructive assay of nuclear fuel cycle materials 80—18426
nondestructive assay technique for mixed samples using neutron activation anal. 80—18423
nondestructive burnup meas. by incore and out-of-core methods 79—17987
nondestructive element and isotope assay of Pu and U in nuclear materials 80—71870
nondestructive gamma-ray spectrometry method for fuel burn-up control *(Slovak)* 78—21672
nondestructive measurement of U and Th conc. and quantities using XFA and gamma spectrometry 80—71877
nondestructive surface exam. 80—21246
nonproliferation and safeguards systems 79—81102
nonproliferation characteristics 80—5304
nuclear energy materials, anal. techniques 80—93834
nuclear facility safeguards meas. systems analysis controllable unit approach appl., multiple closure equations effectiveness determ. 79—85746
nuclear fuel, coated HTR particles, failure statistics calc., effect of SiC fracture stress and kernel porosity 80—73920
Nuclear fuel and materials *(Japanese)* 78—46141
nuclear fuel cycle, core design optimisation 78—82420
nuclear fuel cycle, demand and supply estimates, U supply 79—26694
nuclear fuel management via fuel quality factor averaging 79—30943
nuclear fuel performance and radiation enhanced neutron diffusion *(Japanese)* 79—30914
nuclear fuel processing plant operation, critical safety criteria *(German)* 78—74440
nuclear fuel sheath deform. following fuel power transients, simulation 78—33258
nuclear fuel standard materials, analytic chemistry of trace impurities, and standard sample preparation 79—26521
nuclear material accounting, decision anal. 79—81049
nuclear material control for safeguard purposes in Czechoslovakia, anal. methods 79—26546
nuclear materials, mechanisms for assuring accurate meas. 79—81048
nuclear raw materials prospecting, isotopic dating methods *(Russian)* 79—30925
nuclear symbiosis, development of FBR and thermal spectrum near breeder reactors, review 79—45335
one-dimensional coded apertures, applications, fuel pin imaging 78—45746
optimised nuclear fuel rod array design for PWRs 80—106118
optimized once-through cycle and international nonproliferation objectives 79—85633
optimum location of reactor fuel assemblies 79—17968
oxide crust thermal stress effect in LMFBR accident 79—13471
oxide fuel, effect of solid fission products and dislocations on swelling and fission gas release during fast overpower transient 78—8917
oxide fuel, eqn. of state and nonequilib. fission bubble behaviour during fast transients 78—8916
oxide fuel, irradiated, physical processes, review *(Japanese)* 80—27742
oxide fuel, solubility and migration of fission product Ba 79—19373
oxide fuel behaviour under accident conditions *(German)* 79—49692
oxide fuel classification, quality criteria for fuel elements *(German)* 79—49812
oxide fuel element behaviour in fast overpower transient, effect of solid fission products and dislocations 80—623
oxide fuel in reactor creep, LMFBR design aspects 77—42057
oxide fuel pins, irradiation behaviour, effect of chemical factors *(German)* 79—49692
oxide fuel response to simulated thermal transients 79—22391
oxide fuel restructuring and relocation under irrad., COMETHE code calcs. 77—46235
oxide fuel rod behaviour modelling using LIFE-III code 77—46234
oxide fuel rods, steel-coated, effect of impurities on clad-corrosion *(German)* 79—49693
oxide fuel transient gas release and swelling, generalised parametric model 77—83039
oxide fuels, chemical props. and performance, O_2 potential and transport mechanism 80—13761
oxide fuels, in-pile densification by vacancy boil-off and vacancy knockout, model 79—8259
oxide fuels, intergranular densification, model 79—73345
oxide fuels and cladding in LWR or FBR, irrad. behaviour, chemical process, densification, corrosion *(Japanese)* 77—83033
oxide nuclear fuel, fission gas release and swelling, simple operational model 80—92565
p-cell homogenization, transient flux effects, incorporation into 2-D iteration scheme 78—17301
PBF, cladding temperature, deform., and failure threshold 78—13281
PBF, irradiated fuel rods, behaviour following film boiling operation 78—13282
PBHTR, 'once through' cycles for enriched fuels, breeding variations 78—58382
PBHTR, closed Th cycles, computational reactor lifetime simulation 79—85643
PBHTR, fuel cycle costs, bred fuel value of ^{233}U 77—42125
PBHTR, particle and fuel element design, props. and behaviour 80—47578
PBHTR, Th fuel cycle performance 78—41841
PBR, use of turning rods and its influence on coated particle failure 80—702
PBR using OTTO scheme, numerical anal. of fuel cycle including ^{236}U isotope separation *(German)* 77—83030
PCI-resistant fuel rod designs 80—102239
Peach Bottom 1, HTGR nuclear power station, review of design and operation 79—45327
pebble bed prebreeder reactor, conservation of U resources 79—49697
pebble-bed HTR thermal breeding 79—9715
pellet-cladding interaction, irradiation tests 78—86588
pellet-cladding interaction, theoretical analysis 79—93699

fission reactor fuel continued
pellet-cladding interaction induced by radiation-induced dilation, mech. anal. 78—13302
pellet-cladding interaction phenomenon investig. 77—46299
performance aspects of low-enriched oxide fuel for HTRs, review 80—42780
periphotography of fuel element surfaces 79—17512
Phenix FBR fuel cycle, breeding gain 80—709
Phenix fuel assembly and core performance anal., CAPHE code system *(French)* 79—97878
Phenix plant operations and modifications *(French)* 80—47615
Phenix reactor, fuel behaviour and characts. *(French)* 79—31162
PHWR, fuel cycle anal. 79—89387
PHWR-1000, uniformity factor maximisation, nonlinear programming 80—739
pin bundle tomographic visualisation, maximum entropy method 79—63883
pin diameter meas., sectioning cutoff saw adaptation 79—9748
pin gaps, probabilistic distrib. within wire-spaced fuel subassembly 78—78448
pin inelastic modelling and stress analysis using FULMOD code 77—46233
pin modelling, Dutt fission gas release correl. 79—67826
pin modelling principles and developments 77—46232
pin performance modelling codes for overpower performance analysis 77—46230
pin-cell burnup code BETTY 78—89946
pins, computer controlled meas. 80—5300
pins with eccentric pellets, two-dimensional temp. profile calc. 79—9677
plastic deformation, kinematic hardening rule finite element formulation 80—42764
plate type fuel, reduced enrichment, status report on high-U-density development 80—9393
plate-type research and test reactors, near-term reduced enrichment conversions 80—22951
point reactor population model using neutron and fuel cycle kinetics analogy 80—47556
portable comprehensive irradiated-fuel inspection stand 79—9836
post-irradiation examination, hot cell complex test facilities in Japan *(Japanese)* 80—63255
power burst facility low pressure CHF in closely packed rod bundle 79—59144
power of fuel element/power of critical assembly ratio, semistatistical determ. *(Russian)* 77—67815
power reactor in-core fuel management, computer programs 79—71914
power reactors, min. unit generation cost 80—734
preconditioning, power shock anal. and sipping 80—63358
preconditioning, TVA Browns Ferry Nuclear Plant, in-core management and core manoeuverability 80—63359
preparation and reprocessing, aspects 77—88267
pressure drop along longitudinally-finned seven-rod cluster nuclear fuel elements 80—83149
production process, fuel rods for HTGR 78—86614
production using commercial Tokamak hybrid reactor 80—13798
production using tandem mirror hybrid reactor 80—13799
proliferation resistance, Th-U cycle *(Dutch)* 80—27740
proliferation-resistant fuels development 80—13759
PWR, All-Zircaloy fuel assemblies, design and performance evaluation 80—13560
PWR, behaviour of previously failed fuel rods under power ramp and film boiling operation 79—49745
PWR, coated particle fuel element 77—74943
PWR, core-state models for fuel management of equilib. and transition cycles 77—67833
PWR, depressurisation accident, CUPIDON anal. of fuel rod behaviour *(French)* 80—42791
PWR, design, manufacture and marketing in France *(French)* 80—627
PWR, development and Pu allocation, optimal policies 80—725
PWR, eval. of annular fuel economic benefits 80—57919
PWR, evaluation of fuel performance *(Japanese)* 80—99226
PWR, fuel cycle anal. 79—89387
PWR, fuel monitoring, by delayed-neutron detectors 80—737
PWR, oxide fuel rods, computer program for mechanical and thermal anal. *(Korean)* 78—86571
PWR, performance, anal. and development of fuel by KWU, Germany 80—632
PWR, performance evaluation from I isotope concentrations in primary coolant *(Japanese)* 77—65272
PWR, physics of U-Pu fuel cycle 77—50278
PWR, power distrib. comparison of U and Pu fuel in KWO core 77—14224
PWR, Pu isotope calcs. for steady-state core anal. 79—59126
PWR, Pu recycling, CEA-EdF studies 80—722
PWR, quality study, production *(French)* 77—3110
PWR, Tihange-type, Pu recycling, physics and safety anal. 80—724
PWR, U-Pu, mixed oxide fuel, physical props. 77—67814
PWR 18 month fuel cycles, core design operation and economics 79—85591
PWR assembly, MAC code model of fuel rod behaviour *(French)* 80—37451
PWR core analysis, effects of improved UO$_2$ once-through fuel cycle 80—57917
PWR core power manoeuvres, fuel duties and fuel preconditioning, FLAIR-CENSOR 80—63337
PWR dynamical behaviour modelling in FORTRAN 80—91217
PWR extended burnup fuel cycles, benefits of cycle stretchout 80—37508
PWR fuel anal. and testing, contrib. of LOFT 79—89437
PWR fuel assemblies, LOCA behaviour in multirod burst tests 80—27739
PWR fuel assembly, lumped subchannel model anal. of enthalpy transfer 79—76063
PWR fuel assembly design, optimisation 80—821
PWR fuel assembly design, stress, temp., radiation and chem. environment effects on performance 78—13310
PWR fuel clad failure characterisation based on fission product activity, PROFIP 3 code 80—95365
PWR fuel cycle alternatives, reactor physics anal. 80—57918
PWR fuel dissolution, Idaho processing plant remote systems 79—45455
PWR fuel mangement program 80—18434

fission reactor fuel continued
PWR fuel pin transient heat conduction and open hot channel DNBR evaluation 79—9679
PWR fuel rod, parametric study on influence of prepressurisation 80—13643
PWR fuel rod failure during film boiling, power cooling mismatch test 79—89445
PWR fuel rod failure during film boiling operation 80—18501
PWR fuel rod meltdown behaviour during LOCA 80—42832
PWR fuel rods, I spiking, cause and effects 79—59227
PWR fuel rods, I spiking, general model of origin and behaviour 79—59228
PWR fuel rods. unirradiated and irradiated, pellet-cladding interaction phenomena 79—31053
PWR fuel storage criticality evaluation, expt. program 80—657
PWR fuel storage pool, safety calcs. and benchmarking 79—26565
PWR fuel stored energy FRAP-S3 calc., response surface method of uncertainty anal. 80—9349
PWR hypothetical LOCA sensitivity to fuel rod material props. 79—89436
PWR in-core fuel management, nonequilib. fuel cycle for reload optimisation 79—30942
PWR irradiated fuel, monitoring by gamma spectrometry nondestructive meas. *(French)* 80—63288
PWR neutron noise interpretation by vibration analysis 78—94073
PWR once through fuel cycle improvements 79—85637
PWR once through fuel cycles, improvement of fuel utilisation 79—85636
PWR rods subjected to simulated LOCA in PBF 79—89443
PWR shutdown, fission I increased release from defective fuel rods 79—49710
PWR spent fuel storage pools, graphic method for neutron multiplication factor comparison 79—26566
PWR steam generator tube rupture accident, radio-I behaviour 79—59230
PWR through fuel cycle improvements 79—85635
PWR tight-pitch cores, reactor physics of fuel cycles 80—57920
pyrocarbon, HTGR fuel particle coatings, struct. charact. 77—83034
pyrocarbon coated particles, influence of fast neutrons on transport behaviour of solid fission products *(German)* 79—13427
pyrocarbon coating of Biso fuel, neutron effects on stress and strain 77—79437
pyrocarbon coating of Biso fuel, neutron effects on stresses and strains 77—79436
pyrocarbon coating on fuel particles by spouted bed *(Japanese)* 77—350
pyrocarbon coatings, quantitative chemical method to determ. disordered C component 77—79462
pyrocarbon fuel coating, irradiation tests 78—86594
Quad City 1, fuel performance meas. following third irrad. cycle 80—68778
quality inspection by eddy currents, unit 79—100315
R-A reactor fuel burnup, gamma-spectrometric determ. 78—50265
RA fuel burnup determ. from γ-ray spectrometry of ^{106}Ru, ^{134}Cs, ^{137}Cs 78—54848
RA reactor fuel, gamma-spectrometric determ. of fission product activity ratio 78—33269
radial blankets, economic anal. for LMFBR and GCFR 79—59163
radial distribution of nuclides, during irrad., gamma spectrometry exam. *(French)* 78—78467
radiation enhanced kinetics in the fuel lattice 80—59522
radiation protection, ALARA, reactor inplant design, a regulatory viewpoint 80—23016
radioactive fuel and waste, review of treatment handling, storage and disposal *(Italian)* 79—63753
radioactive materials, reactor fuel transport requirements, Poland 79—31232
radioactive waste management, closed nuclear fuel cycle, W.Germany 79—619
radioactive waste recycling, prospects 77—71657
radiocolloids and pseudoradiocolloidal states of uranyl acetate solns. 78—44390
radiological implications of Pu recycling in HTGR fuels 80—68777
Rapsodie Fortissimo standard fuel, high burn-up behaviour *(French)* 79—97816
RBMK-1000 channel U-graphite reactor, fuel assembly and fuel element design 79—40991
RBMK-1000 reactor, U utilization efficiency increase 80—27747
reactor core examination for failed fuel elements following high fission product emission *(German)* 79—85622
reactor fuel anal. using radioactive thermal neutron capture gamma rays 80—61214
reduced enrichment program, fuel demonstrations, for test and research reactors 80—9392
reduced enrichment program for research and test reactors, generic studies 80—9391
refueling, underwater fuel handling techniques 79—67911
refueling and fuel handling, ALARA occupational radiation exposure 79—67914
refuelling frequency, economic optimisation 80—731
removal from irrad. cladding, eval. of methods 77—54306
reprocessed nuclear fuel transportation 79—30918
reprocessing and waste disposal, public issues 77—46375
reprocessing and waste management, review 80—5315
reprocessing implementation 77—42162
research activities in OECD Halden Reactor Project *(Japanese)* 79—30913
research reactor, core and console, long term service and reliability investig. 80—9359
research reactor, recovery from obsolescence programs 80—9360
research reactor, self-protection criteria for reactor fuel elements 80—9361
research reactor Caramel UO$_2$ fuel, proliferation resistant fuel service 80—27746
research reactor fuel element loadings with reduced U enrichment 80—68933
research reactors, safeguards requirements for highly enriched uranium and reduced enrichments 80—22952
resonance escape probability meas., U-graphite subcritical assembly example 77—71632
resource potential, geochemical surveys of large areas in USA and Alaska 79—30924

fission reactor fuel continued
review, worldwide variation of energy production, future Hungarian energy requirements *(Hungarian)* 78−70580
review of nuclear fuel cycles and waste management 78−54863
Rocky Flats Plant Critical Mass Lab., exptl. programs 80−37430
rod bundle subchannel interconnection geometry, press.-induced diversion cross flow 78−13215
rod gap conductance uncertainties deduced from fuel centreline temps. 77−46308
rod hairline cracks, effect on thermoelastic stress in surrounding can, iterative method of determ. 77−54285
rod modelling, utility requirements 78−21747
rod modelling complexities 77−46231
rod ramp tests analysis using SAFE-2D program 77−46228
rod thermal characteristics, on-line simulation by elec. heated rod 77−46209
rod thermal response during isothermal loss of coolant expt. 79−89447
rod vibration induced by coolant water and air/water flow *(Japanese)* 78−74429
rod-bundle in nuclear fuel element, mathematical model for transient subchannel analysis 77−79430
rod-type fuel elements in gas-cooled reactor, ribbing efficiency 77−42011
rod-type fuel elements in regular lattice, thermal fields for streamline heat exchange 77−42010
rods, defect detection 78−86640
safeguarding; 80−68835
safeguarding, determ. of U and Pu content of fuels using isotope correl. tech. 80−68834
safeguarding, fuel assembly identification using US signatures, statistical aspects 80−69620
safeguarding, remote-controlled and long-distance unique identification of reactor fuel elements or assemblies 80−63296
safeguarding, resonance neutron radiography using a position-sensitive proportional counter 80−13597
safeguarding fast critical facilities 79−85611
safeguarding on-power-fuelled reactors—instrumentation and techniques 79−26657
safeguards, materials accounting in a LWR fuel reprocessing plant 80−83173
safeguards, nondestructive, energy-dispersive, X-ray fluorescence analysis of product-stream concentrations from reprocessed nuclear fuels 80−83163
safeguards, sensitivity anal. of the MUF variance for large HEU fabrication plant 80−83169
safeguards and transportation 77−34400
safeguards control, integrated fuel cycles 78−82446
safeguards planning in plant design process 78−82423
safeguards problem, alternate fuel cycles and reactor types 78−736
safeguards scheme for 600-MW CANDU generating stations 80−63291
safeguards surveillance at reprocessing plants, fuel history anal. *(French)* 80−68837
safeguards verification of spent fuel using gamma spectrometry, burn-up, cooling time and fission product conc. determ. 80−63290
safety aspects of solvent nitration in HTGR fuel reprocessing 78−86650
scanning, Ge(Li) gamma spectroscopy, ANGEL computer program 79−9755
security, aggregated systems model for decision making 80−37535
security, fault tree and reliability relationships for analyzing noncoherent two-state systems 80−47600
security, integrated safeguards system, fuel labelling and perimeter monitors 80−37536
security, sabotage and terrorist attack, statistical anal. of threat reality and consequences 80−13727
SGHWR fuel performance, safety and reliability 79−36333
SGHWR fuel pins, fuel cladding ratchetting study 78−54855
SGHWR fuel pins, pellet-cladding interactions and length changes 80−42763
shell inspection, mag. method for detecting ferromag. particles 80−66746
shipping cask for irradiated nuclear fuel, design 77−79483
Si-alloyed C coatings for fuel particles 77−74942
simulated rods for HTGR, pre- and postirradiational thermal transport and thermal expansion 79−6742
simulation in COMETHE III-J, code improvements 80−42754
simulation in COMETHE III-J computer code 80−42752
simulation of performance with BACO computer code 80−37450
slab tanks for criticality control, neutron multiplication calc. 80−13606
slowing down spectra, Placzek discontinuities 77−51423
SNR fuel design, critical aspects from experimental evidence 79−30910
SNR-300 fuel element design, expts. on rod bundle fluid dynamics and thermodynamics 79−97794
SNR-300 fuel rods, postirradiation examinations of RAPSODIE-1 expt. 77−46219
SNR-Mk. II, Rapsodie-II expt. 77−46292
solid mixed-oxide, internal pressurisation due to fission, gas release 77−83058
solvent extraction and ion exchange learning module 80−36803
solvent extraction in HTGB fuel reprocessing 78−86667
space craft thermionic reactors, reflector drum control mechanism, fuel and moderator 79−17988
specification and characterisation methods for nuclear fuels *(German)* 79−49796
spectra shift controlled reactor, effect of alternative fuel cycles on reactor design 79−54482
spectral shift controlled reactor, SSCR, Pu fuel cycles 80−47608
spent fuel, nondestructive burnup determ. calibration using destructive radiochem. anal. 79−89372
spent fuel assembly, gamma dose rate distrib. meas. with TLD 80−47735
spent fuel assembly storage racks, dynamic anal. 80−13639
spent fuel bundle counters for CANDU reactors, appl. of safeguards design principles 80−63347
spent fuel burnup determ., U, Pu, Nd, isotopic comp. and conc. determ. by mass-spectrometric isotope dilution 79−89373
spent fuel casks under extreme accident conditions, behaviour prediction 77−71663
spent fuel cooling time determ. utilising gamma-ray meas. 80−63268
spent fuel elements, salt mine waste disposal, experience in West Germany 78−41828
spent fuel measurements using high resolution gamma systems 80−32400

fission reactor fuel continued
spent fuel overheating in pool drainage accident, protection 79−85639
spent fuel pool natural convection, multichannel analysis 79−9786
spent fuel safeguards, containment and surveillance at fuel reprocessing facilities 80−95351
spent fuel storage, benchmark subcritical meas. at Hanford N reactor 80−37433
spent fuel storage, supercriticality through optimum moderation 80−57896
spent fuel storage, US licensing and regulation 80−23039
spent fuel storage, use of poisoned racks at Point Beach 80−23038
spent fuel storage and transportation, operators experience 80−23037
spent fuel storage at independent installations, comparative risk assessment of external source damage 80−23041
spent fuel storage at independent installations, licensing considerations 80−23042
spent fuel storage expansion planning, site preparation, and installation 79−9819
spent fuel storage pool reracking, licensing experience at Trojan 80−23040
spent fuel storage vault, criticality safety determ. *(Korean)* 80−37478
spent fuel subassemblies, nondestructive assay, comparison of calcs. and meas. 80−78421
spent fuel transportation, commercial experience in US 80−63310
spent fuel verification by gamma-ray spectroscopy for materials safeguards 80−78422
spent fuel waste products, delayed neutron nondestructive assay instrumentation, Monte Carlo calculational design 80−81271
spent multicomponent fuel mixtures, comp. anal. by delayed-neutron decay 79−71899
spent nuclear fuel burn-up level determ., computerised equipment *(Polish)* 80−32582
spent nuclear fuel decay heat production, prediction by nomogram 77−38358
spent nuclear fuel elements, intermediary storage, stationary temp. level determ. calc. method 80−91223
spent nuclear fuel re-enrichment without reprocessing, calculation simulation 79−26660
spent nuclear fuel storage in HI-CAP high-capacity fuel rack, design considerations 78−17349
spent reactor fuel burnup determ. using anal. chem. [conf. Piestany, Czechoslovakia (Sept. 1978)] 79−89371
spent-fuel safeguards, surveillance instrumentation 79−85679
Sphere-Pac carbide fuel, model of swelling and gas release 80−13768
Sphere-Pac mixed carbide fuel, effect of early gas release in temp. calcs. 80−102235
spikants, gamma active, for proliferation deterrence, practical aspects 79−93716
square array rod bundles, shear stress distribution, axial flow 80−47679
SSCR, fuel cycle anal. 79−89387
stainless steel, 316, mechanical behaviour, 760 to 1204C 78−86604
statistical fuel model, FRP 80−42748
steady-state fuel centreline thermocouple data confirmation from transient response 79−93767
steam-gas system, joint use of nucl. and organic fuels 80−40807
steel, stainless, clad oxide fuel pin, thermodynamic model for attack 79−97807
steel, stainless, neutron irradiated, stress effects on microstruct. 77−47490
stoichiometry effects on cladding attack on mixed oxide fuel 78−86583
storage of fissile materials, use of neutron absorber for enhanced criticality safety 80−13609
storage of spent fuel, maximisation of pool size 79−67915
storage options compared, dry, shallow pool and deep pool 79−9843
storage pool criticality calc., transport-consistent diffusion algorithm 79−9721
stress analysis of fuel pins, internal and external press. effects *(Czech)* 80−5233
stresses in fuel rod cladding, effect of fuel-pellet chips 78−86589
structural anal. of reactor fuel elements 78−41814
structural analysis of fuel element codes 80−78362
Super Phenix core design and development, fuel assembly behaviour *(French)* 79−30889
supervision, safety measures review *(German)* 78−684
supervision in West Germany, by Euratom and IAEO *(German)* 80−18415
sweepout in HTOP accident, system hydraulic effects 79−85670
swelling, depend. of evolving cavity distrib. functions on cavity growth kinetics 79−3206
swelling, fission gas precipitation into intra- and intergranular porosity, theory 80−57849
synthetic and fissile fuel prod. by Cat-D fueled SAFFIRE reactors 80−99280
tandem mirror hybrid reactor, gas cooled blanket 80−37608
teaching, computer code for fuel management analysis course 78−4449
temperature dist. in cylindrical fuel pins with gap and cladding *(Italian)* 79−13397
temperature feedback coeff. meas. using small excursion techniques 77−42045
temperature field, generalised Duhamel integral 80−22943
test and research reactors, enrichment reduction 80−22953
test rods, directly heated, influence of thermocouples in wall 79−93706
testing, General Electric Test Reactor appls. 80−565
tFTR blanket module experiments 80−37609
TFTR breeding modules, neutronics 80−37611
TFTR exptl. blanket modules, mechanical design 80−37610
thermal and irradiation environment influences and material responses 80−52737
thermal behaviour, relocated gap width estimation for gap conductance calcs. 80−589
thermal breeding with mixed denatured fuel 79−67838
thermal conductivity, corrections for porosity entrainment using analytical temp. solns. 79−59173
thermal hydraulic analysis of a wire-wrapped 19-rod bundle with edge blockage 79−59142
thermal hydraulic analysis of a wire-wrapped 19-rod bundle with edge blockage 79−71887
thermal hydraulics, sensitivity theory development 79−17963
thermal near-breeder reactor, effect on future U utilization 78−17322
thermal reactor, integral testing of Th-^{233}U data 79−67833

fission reactor fuel continued
thermal reactor, reuse of power Pu and U, neutron regeneration 78-82421
thermal stress calc., cracked fuel pellets 78-82462
thermal-hydraulic anal., comparison of computational techniques in COBRA-IIIC and COBRA-IIIP *(Japanese)* 80-95374
thermionic reactor, ^{233}U fuel and Be moderator, neutron physics analysis 77-50281
thermocouple readings verification by transient response analysis 77-46309
thermographic imaging of fuel rods 77-42085
thermohydraulic code verification by rod bundle expts. 79-97769
THTR fuel element, irradiation testing in DRAGON reactor *(German)* 78-25295
Tokamak demonstration hybrid reactor, fissile fuel breeding and blanket power prod. 79-22470
Tokamak fusion-fission breeder, blanket fuel selection 79-22468
Tokamak-type thermonuclear hybrid reactor for the production of fission fuel and electric energy preliminary evaluation 79-71954
training course for fuel cycle facilities design 80-36801
transient fission gas behaviour, exptl. and analytical results 79-59190
transient fission gas release effects on carbide fuel failure dynamics 79-49762
transient fuel behaviour, modelling of grain boundary fission gas effects 79-59169
transient fuel fission gas behaviour, NEFIG model calcs., bubbles and swelling 80-618
transient heat conduction problem in composite region, simulation capability of elec. heater *(Japanese)* 80-68772
transient heat transfer, COMETHE code 80-42761
transient heating conditions, mobility of fission gas bubbles 79-59189
transient overpower accident, transient press. field of gas in MOX fuel porosity 79-36348
transport by air, feasibility and economics 78-94154
transport phenomena under severe temp. gradient 80-615
transportation of irradiated nuclear fuel, in Canada, emergency planning 78-50411
transportation SABRE II combat simulation model 80-37542
transportation security, railroad cask appl. 77-74948
TREAT, fast neutron hodoscope perform. tests on 91-pin fuel bundle 79-41005
TREAT facility, pinhole imaging of test fuel element 78-21627
TREAT fast-neutron hodoscope, time and mass resolution of fuel motion, data acquisition system 79-41003
tribology study reactor fuel element, PEC type, in Na at high temps. *(Italian)* 78-58362
TRIGA fuel, low-enrichment U, neutronic and heat transfer charact. 80-9397
TRIGA fuel rods, crack detection by neutron radiography 77-50229
TRIGA III reactor, anal. of standard and FLIP fuel mixed loading patterns 80-57855
TRIGA Mk.III fuel options, U-ZrH high density and highly enriched fuels 80-5235
TRIGA pulsing reactor without coolant loss, safety assessment for fuel and cans 80-52773
TRIGA reactor fuel, long-distance transfer 79-67929
TRIGA reactor fuel rods water-quench safety tests 80-42811
TRIGA-FLIP failed fuel element examination at HFEF 80-9383
underwater solution to nuclear fuel storage problem 80-86963
University of Missouri research reactor, fuel and productivity 80-9396
URANUS and EPRI code evaluation 80-42756
US inspection of end cap welds in thin walled fuel elements 77-32740
US thermometers, nuclear fuel temp. profile meas., TRESON expts. 78-57955
USA Reduced Enrichment Research and Test Reactor Program, current status 80-68930
used fuel shipment, risk assessment 79-81013
Venezuelan research reactor reload fuel optimisation 79-9737
VVER, fuel burnup determ. by exact methods 79-41014
VVER and RBMK power reactors, combined fuel use, transuranic nuclide formation 80-32352
VVER reactors, relative accumulation of ^{232}U and ^{233}U during ^{232}Th irrad. 79-71923
VVER-440, limit of fuel stay time, operation of nuclear power station with reduced utilisation of power *(Russian)* 77-65274
waste, long-term risk assessment of waste disposed in geologic formation 78-17361
waste material transportation, risk anal. 78-17357
water cooled reactors, main causes of fuel element failure 79-67872
water moderated water cooled reactors, rod bundle burnout characteristics, statistical analysis 77-74969
water reactor fuel, Federal Republic of Germany technology, development and experience 79-26703
water reactor fuel, power ramping performance assessment methods 80-23065
water reactor Pu wire 77-50277
wet chemical analytical methods, impurity specifications *(German)* 79-49690
wetted-wall ICF fissile fuel factory studies 80-13806
Windscale AGR, high pressure fuel test loops design, installation, commissioning 77-6491
wire-wrapped core assemblies, turbulent flow split modelling and expts. 80-95370
world resources, technological status 77-67911
world resources up to year 2020, review 78-685
YN-UN, solid soln., decomp. press.-temp. relations 78-52780
Zircaloy;UO$_2$ fuel design, LOWI 78-70600
Zircaloy-4 clad UO$_2$ fuel, long term storage in water and stress corrosion cracking 79-93737
(γ,f), non-destructive testing of fissile and fertile material 77-74917
^{233}U-Th, optimisation and growth potential in LMFBR 80-73930
^{239} Pu sample irrad. in EBR-II, calc. and exptl. anal. 80-22947
(Am,Cm)O$_2$ solid soln., struct. changes under self- and reactor irrad. 77-27927
AmO$_2$-UO$_2$, target possibilities for waste incineration, simulation study 80-32419
Am(VI) formation in molten salts 77-29039
^{241}Am, gamma ray spectra of reactor fuels 80-42577
Be$_2$C-graphite-UC$_2$ fuel development for pulsed reactors 79-67856
BeO-UO$_2$ fuel testing, annular core pulse reactor 78-86593

fission reactor fuel continued
CANDU fuel, burnup determ. by γ-scanning of ^{144}Ce/Pr and ^{134}Cs/^{137}Cs 79-9825
CANDU spent fuel, containment in concrete canisters, UO$_2$ oxidation 77-6539
^{252}Cf neutron assay system for nondestructive assay of enriched U 79-81067
CmO$_2$, struct. changes under self- and reactor irrad. 77-27927
Cs concentrations, mixed-oxide fuel 78-82452
Cs transport and isotopic fractional in fuel rods 78-82453
^{134}Cs/^{137}Cs activity ratio, spent fuel assembly 78-82487
^{137}Cs gamma-ray spectra of spherical reactor fuel elements, burn-up determ. *(German)* 78-25299
F$_2$+UO$_2$, reaction kinetics, molecular beam study 78-46157
Gd$_2$O$_3$-UO$_2$ fuel pins in cluster type fuel assembly, meas. of reactivity charge 80-27775
LMFBR, U-Pu-Zr fuelled breeding potential assessment 79-9685
LMRBF, ^{233}U-Th fuelled pin diameter optimisation 79-9687
LWR, sensitivity of fuel rod behaviour on as-fabricated characteristics 79-49805
Na bonded carbide fuel assemblies, anal. of structural members 77-46261
Na bonded mixed carbide fuel, unirradiated, behaviour during mild overpower transients 79-49761
Na pool fuel vapour and aerosol transport in HCDA 79-13455
NpC$_{1-x}$, nonstoichiometric, atomic short-range order obs. by diffuse neutron scatt. 77-24315
NpO$_2$/NpO$_3$, in fused salts, redox and chem. props. 77-29038
Np(V)/Np(IV) catalytic redox reactions, kinetics and mechanisms 77-29006
Np(VII) formation in molten salts 77-29039
^{237}Np, criticality anal., possible utilisation in fission reactors 80-621
^{237}Np, gamma ray spectra of reactor fuels 80-42577
O$_2$ getters for LMFBR fuel pins 78-74437
^{231}Pa, calc. of critical mass and radius by three group diffusion theory 79-13419
(Pu,U)O$_2$, <5 wt.% PuO$_2$, criticality data generated by SU-HAMMER 79-3198
(Pu,U)O$_2$, criticality data generation using SU-HAMMER code 78-29581
(Pu,U)O$_2$ fuel rods, in island design BWR, performance meas. 79-30907
(Pu,U)O$_2$, low-enriched fuel assemblies, profiles of activity ratios of ^{134}Cs, ^{137}Cs and ^{106}Ru fission products 77-57713
(Pu,U)O$_2$ mixed oxide pellet assay, using automated X-ray spectrometer 79-81066
(Pu,U)O$_2$, reactivity meas. under typical fuel element dissolution conditions, use of pulsed neutron source 77-3083
Pu accountability, nondestructive assay using neutron counting, calorimetry and gamma spectrometry 80-63266
Pu accountability and control, field nondestructive assay measurements as applied to process inventories 80-63265
Pu and other actinides, conf., Baden-Baden, Germany (Sept. 1975) 77-19807
Pu and radioactive waste management, Swedish approach 79-31075
Pu as energy resource, availability, health hazards, nuclear weapon proliferation 77-46286
Pu, assay of large samples using portable neutron coincidence counter 80-69041
Pu assembly, stainless steel clad, postirradiation examination 77-42090
Pu binary alloys, periodical depend. of equilibrium distrib. coeffs. of Pu admixtures on atomic number of admixture 80-18419
Pu, β to α, phase transformation kinetics anal. 77-70044
Pu, calorimetric nondestructive assay for in-field meas. 80-71874
Pu charging of VVER-440 water-cooled water-moderated reactor 77-50214
Pu compounds 18B packagings for transportation 80-37544
Pu content in nuclear fuels, appl. of isotopic safeguards tech. 80-99210
Pu, determination by volumetric and coulometric methods, effect of Am on accuracy 79-52826
Pu diffusion in pyrocarbon in HTGR 78-29578
Pu, elastic constants at elevated temps., noncontact meas. tech. 80-104405
Pu, elemental and isotopic conc. anal. using nondestructive assay 79-49691
Pu extraction-spectrophotometric determination in spent fuel of first Czechoslovakian nuclear power station *(Czech)* 77-3105
Pu, fabrication, use and handling anal. *(Japanese)* 77-349
Pu, fission products γ-ray and photoneutron spectra 77-23127
Pu fuel and fuel elements for fast and power reactors 79-616
Pu fuel cycles in spectral shift control reactor 79-89386
Pu fuel lattice, cluster-type, thermal-neutron behaviour 77-61477
Pu, fume aerosols, aerodynamic and dissolution behaviour of laser-ignited droplets 79-13438
Pu, general survey of possible use 77-34399
Pu, generation, recycling and storage problems 77-67813
Pu, hazards and nuclear fuel reprocessing 79-45387
Pu, high burnup fuels, shielding and handling problems 80-27833
Pu in irradiated reactor fuel, microamounts meas. by radiometric method *(Czech)* 77-42111
Pu in United Kingdom 77-50280
Pu, input accountability in reprocessing plants, tracer tech. using Mg and Pb 80-73919
Pu inventory verification of ANL, IAEA safeguards 78-821
Pu isolation, neutron irrad. of natural U in Japan Material Testing Reactor *(Japanese)* 80-52730
Pu, isotope compositon, determ. using gamma spectrometry 80-66915
Pu isotopes, ENDF/B-4 cross sections, integral data 77-23200
Pu, isotopic analysis by resin-bead mass spectrometry for materials safeguards 80-78392
Pu, isotopic composition, determ. using thermal ionisation spectrometry with automatic data eval. 80-66913
Pu, isotopic composition, determ. using precise absolute gamma spectroscopic meas. 80-66916
Pu, isotopically denatured, diversion resistance 79-89385
Pu, large samples, thermal-neutron coincidence counting 78-82444
Pu, liq., enthalpy and heat capacity meas. using neutron heating 77-20078
Pu loaded on TBP, reduction stripping 77-6548
Pu, mixed oxide fuels, development status, Japan 79-31130

fission reactor fuel continued
Pu, multigroup time-dependent delayed γ-spectra from fission and activation 78–13184
Pu nondestructive analysis, calibration by calorimetric assay 80–71878
Pu nondestructive assay, gamma-spectrometric method 79–81068
Pu, nondestructive assay of large samples 80–71871
Pu, nondestructive assay reference materials 79–49702
Pu nondestructive rapid isotopic anal. gamma-ray spectrometric method 79–81069
Pu oxide fuels, recycling in thermal reactors and fast breeders 79–31129
Pu passive assay using Euratom variable dead-time neutron counter 80–69042
Pu, power reactor fuel and fuel elements *(Russian)* 79–30933
Pu, production and availability, uses, reprocessing, fast reactor fuel cycles 80–68767
Pu, production by neutron irrad. of ^{241}Am Japan Material Testing Reactor *(Japanese)* 80–52731
α-Pu, production difficulties 78–50252
Pu proliferation, comparison thermal, FBR reactors, nuclear power stations appl. 78–86641
Pu, recycle facilities in Foratom countries, status and prospects 79–31131
Pu, recycle fuel experience in LWR in West Germany 79–30932
Pu, recycle options in USA, benefit/cost anal. 79–31132
Pu redistribution in outer regions of hyperstoichiometric mixed oxide fuel 77–42096
Pu, safe working, safety measures 79–41040
Pu safeguarding, automated ion-exchange system for rapid Pu separation from impurities 80–78383
Pu safeguarding, computer-assisted controlled potential coulometric determ. 80–78384
Pu safeguarding using resin bead mass spectroscopy 80–73984
Pu, safeguards, eval. of thermography 79–93719
Pu safeguards, fissile material accountancy using controlled potential coulometry 80–63298
Pu safeguards, fuel reprocessing product soln. accounting, using K-edge densitometer 80–95352
Pu safeguards, nondestructive assay using automated in-line instrumentation 80–95353
Pu safeguards, product soln. gamma-ray NDA using K-absorption edge densitometer 80–83162
Pu safeguards accountability, gamma-ray meas. of Pu and Am in molten salt residues 80–83165
Pu safeguards assay, isotopic meas. by gamma ray spectrometry using two-detector method 80–83161
Pu safeguards verification methods for input-accountability meas. at reprocessing plant 80–95349
Pu, source and availability of fuel for breeder reactor programme 77–61625
Pu, steady state isotopic composition for nuclear power industry model 79–59166
Pu storage, international scheme 79–67848
Pu, U, and Th, metal separation by column extraction chromatography 78–44421
Pu use, present status and prospects, use in fast and breeder reactors 79–26533
Pu, use in FBR in UK 77–67860
Pu use within German Federal Republic 77–54350
Pu, utilisation in fast breeder and light water reactors, Italy 79–30931
Pu utilisation in France 77–50279
Pu, utilisation in thermal and fast reactors in Japan 79–26534
Pu, utilization in reactors *(French)* 79–30930
Pu vapour pressure determ. 1724 to 2219K by Knudsen effusion technique 80–654
Pu-containing fuel, safety training program 79–18053
Pu-Ga (1-8.56 at.%) alloys, enthalpy sp. ht. determ. at elevated temp. 78–78458
Pu-island element, B304, gamma scanning of power and burnup distrib. 80–721
Pu-Re-C and Pu-Tc-C systems, phase relationships 77–21127
Pu-Th, optimisation and growth potential in LMFBR 80–73930
Pu-U anal., in-line evaluation of nondestructive assay instruments 79–85589
Pu+U mixed oxide aqueous solns., limiting critical concs., multiplication factor 77–26859
Pu(C,N), lattice parameter variation, 50 to 300K 78–51709
$PuC_{0.82(1.49)}$, high temp. enthalpies 80–49384
PuC_x (x=0.8, 1.44, 1.67), low temp. sp. ht., mag. ordering obs. 80–49372
PuC(N), lattice parameter variation, 50 to 300K 78–51709
$Pu(C_2O_4)_2$ precipitator, dynamic process model for nuclear materials safeguards 80–83150
Pu(IV) catalytic redox reactions, kinetics and mechanisms 77–29006
Pu(IV) oxide polymer, potential pollutant from fuel reprocessing, IR spectrum 78–76456
PuN, fabrication, high-temp. thermodynamic and transport props. 77–28774
$Pu(NO_3)_4$ in light water, reactivity predictions using discrete ordinates transport theory 78–89957
$Pu(NO_3)_4$ solution concentrator equipment for criticality safety 80–18432
PuO_2 air transportable package PAT-1, dose rate and criticality calcs. 80–13938
PuO_2, alpha radiation damage, point defect ingrowth and annealing behaviour 77–27926
PuO_2 assemblies, fission and explosive energy releases 77–83108
PuO_2, eqn. of state and thermodynamic props. 80–13592
PuO_2 heat sources, ave. total decay power meas. using Bunsen ice calorimeter 77–6547
PuO_2, particle size meas. in UO_2-PuO tablets, image analysis by LEITZ-TAS with process computer 80–68773
PuO_2 powder, leak rate determ. 80–42808
PuO_2 refractory, dissolution in HNO_3-HF-H_2O at 100°C 77–18683
PuO_2, release from contaminated burning Na, LMFBR safety evaluation 77–23224
239PuO_2, stoichiometric, high-temp. deformation 80–81111
PuO_2, struct. changes under self- and reactor irrad. 77–27927
PuO_2, substoichiometric, unified model for defects, thermodynamic functions 77–20094
PuO_2, substoichiometric, high temp. thermodynamic parameters 77–21125

fission reactor fuel continued
PuO_2, thermal and transport props., electronic contrib. 80–15432
$^{239}PuO_2$, hypostoichiometric, high temp. deformation rel. to cryst. microstruct. 79–79041
PuO_2/PuO_3, in fused salts, redox and chem. props. 77–29038
PuO_2-UO_2, actinide redistribution in the outer regions of mixed-oxide fuel 79–36321
PuO_2-UO_2, light water moderated lattices, critical expts. 79–6728
PuO_2-UO_2 assemblies, fission and explosive energy releases 77–83108
PuO_2-UO_2 critical clusters in D_2O perturbation anal. of buckling 78–29573
PuO_2-UO_2 mixed oxide fuel, plutonia particle behavior during sintering in Ar-H_2 (8%) atmosphere 79–8258
PuO_{2-x}, O_2 chem. diff., dilatometry and thermogravimetry study *(French)* 79–73339
$PuO_{(2)}$, spectroscopic data rel. to thermodynamic functions 80–34208
δ-PuSc (5, 12, 18 at.%), f.c.c., contraction by self irradiation at 4.2K *(French)* 77–4129
Pu(VII) formation in molten salts 77–29039
^{A}Pu, A=238 to 241, gamma ray spectra of reactor fuels 80–42577
^{A}Pu, A=239, 240, 241, LMFBR 300 MWe, burnup characts. 3-D numerical anal. 79–22371
^{238}Pu production from ^{237}Np, optimisation techniques 79–71936
^{239}Pu (n,f), 10 eV-100 keV, fission cross section 80–27681
^{239}Pu aerosol, characterisation inside safety enclosures of mixed oxide fuel fabrication facility 79–13501
^{239}Pu, anal. by cyclic activation of delayed neutrons 78–53296
^{239}Pu and ^{233}U droplets burning in air, aerosol generation investig. rel. to inhalation hazards 79–67959
^{239}Pu critical sphere, k_{eff} sensitivity to fission and inelastic scatt. spectra 77–23198
^{239}Pu, criticality of thin flat foils versus spherical shells, two-group diffusion anal. 79–26530
^{239}Pu, evaluation of portal monitors for the detection of nuclear materials 80–63406
^{239}Pu fuel cycles, potential radiological impacts 80–42799
^{239}Pu, integral neutron capture cross sections in GCFR lattices 78–13246
^{239}Pu, irradiated in BOR-60 reactor, fission yields 79–17971
^{239}Pu neutron data evaluation for ENDF/B-V 78–25288
^{239}Pu neutron data reevaluation, effect of k_{eff} for various critical assemblies 77–23042
^{239}Pu production, FBR, optimisation of burnup characteristics, nonlinear programming method 77–14239
^{239}Pu production in fusion-fission hybrid reactor, mirror confinement, fuel design consideration 79–22472
^{239}Pu(n,f), 35 to 1500 keV, near equilib. delayed neutron energy spectra 77–34354
^{239}Pu(n,f), sub MeV neutrons, equilib. delayed neutron energy spectra meas. 77–38308
^{240}Pu, coincidence counting of thermal neutrons, detector and calcs. 80–37716
^{240}Pu resonance capture in reactor cell codes, parametric description 79–13384
^{240}PuO, assay by neutron coincidence counting, Monte Carlo removal of multiplication effects 80–37715
^{241}Pu (n, f), 0.02-7.4 MeV, fission cross section ratio to ^{235}U 79–45313
^{241}Pu, multilevel resonance parameters for 0.01 to 100 eV neutrons 79–36154
^{241}Pu, neutron capture and fission cross sections, 0.01 eV-30 keV 78–29512
^{241}Pu(n,f) 1 keV to 30 MeV neutrons, cross section meas. rel. to ^{235}U 79–36286
Pu(n,f), delayed neutron spectra from thermal- and fast-neutron fission, reactor calcs. 77–34355
SiC coated fuel particles, failure during thermal excursion above 2000°C 79–36317
SiC corrosion in HTGR fuel particles 77–74932
^{90}Sr, release from irrad. reactor fuel elements *(German)* 79–67871
T and fissile fuel exchange between hybrids, fission power reactor and T prod. reactors 80–47703
TH reaction rate meas. in GCFR lattice 80–656
(Th, U) fuel, burnup determ., using ^{148}Nd 78–82459
$(Th,U)_2$, chemical form of solid fission product simulating high burnup 80–616
(Th,U)C advanced FBR fuels, radiological assessment of reprocessing 80–73983
$(Th,U)O_2$, burnup simulated, high O_2 pot., chem. state 80–91220
$(Th,U)O_2$, D_2O cooled, relative conversion ratio 78–29582
$(Th,U)O_2$ microspheres, fabrication 80–801
$(Th,U)O_2$, thermal conductivity model for temps. to melting 79–93732
Th advanced fuel cycle in HWR 77–67864
Th alloys, irradiation effects 78–86606
Th based cycles, relative worth of ^{233}U and ^{235}U 80–37511
Th blanket pellets, grain growth kinetics 78–86613
Th, CANDU-PWR, comparison of three axial fuel management strategies 78–94075
Th cycle, potential use in PWRs, parametric anal. 79–26467
Th cycles for HWRs 77–34401
Th, diffusion of fission products 77–4220
Th exploitation in Candu reactors 80–32344
Th, fast neutron total cross section, 0.1 to 5.0 MeV 78–58278
Th fuel cycle, CANDU reactors 78–86620
Th fuel cycle, feasibility study, CANDU system 78–86619
Th fuel cycle, nucl. strategy and recycle technology 78–86662
Th fuel cycle, U cycle comparison, use in LWRs *(Spanish)* 80–32420
Th fuel cycle and technology 79–31114
Th, fuel cycle for HTGR, merits 77–46385
Th fuel cycle performance in CANDU reactors and LMFBR 79–9742
Th fuel cycle role in thermal and fast reactors 79–13420
Th fuel cycles in CANDU 78–86661
Th fuel cycles in power reactors, anal. of waste hazards 79–30941
Th fueled CANDU, axial fuel management strategies 79–26586
Th fuelled FBR performance characteristics 79–9815
Th, HTGR fuel, French, fabrication, irrad. performance *(French)* 79–30934
Th, HTGR systems development 79–93717
Th metal, diffusion and electrotransport of Th metal 78–86611
Th, metal rods, neutron capture, effective resonance integral meas. 77–71653
Th metallic, heat capacity from 80 to 1000K 80–34201

fission reactor fuel continued
Th, nondestructive assay reference materials 79—49702
Th, resources and process technology 79—59170
Th, selective separation from lanthanides on sulphonic ion exchangers 78—58860
Th solid fuel utilisation in power reactors *(Japanese)* 78—74433
Th, use as breeder material in CANDU reactor 78—25311
Th use in LMFBR blankets 79—9743
Th/^{233}U cycle, arguments against 77—54305
Th/^{233}U fuel cycle in FBR and thermal convertors 79—9745
Th-^{233}U cycle, in molten-salt reactor, efficient fuel utilization without Pu separation 79—26499
Th-20 U metal fuel, compatibility with candidate cladding alloys 80—13769
Th-based, fuel cycles, nonproliferation aspect of ^{232}U presence in ^{233}U-Th fuel cycle 80—57839
Th-based fuel development for breeder reactor appl. 79—54502
Th-based fuel for LWR and LMFBR 78—86624
Th-based fuel pellets, fabrication 78—86669
Th-based metal alloy fuels for FBRs, determ. of solidus temperature 80—104124
Th-based Pu burner for improved fuel utilisation 78—13240
Th-Pu (20 wt.%) metal fuels, compatibility with cladding alloys for FBR appls. 80—102242
Th-Pu-U-Zr (20, 4, 8 wt.%) metal fuels, compatibility with cladding alloys for FBR appls. 80—102242
Th-PuO$_2$ kernels, effect of fuel particle size on power excursions, Doppler feedback mechanism 79—30911
Th-U (20 wt.%) metal fuels, compatibility with cladding alloys for FBR appls. 80—102242
Th-U alloy fast reactor fuel element, design basis considerations 79—54503
Th-U alloy fuel behaviour in organic-cooled reactor 78—86605
Th-U metal alloys, LMFBR appl. 77—83040
Th-U metallic fuel, irradiation performance 78—86608
Th-U Na-bonded metal fuel, transient heating test 78—86607
Th-U non-oxide compounds, use as refractory breeder fuels 78—86612
Th-U spent fuel, disposal of long lived α-emitters 77—26855
Th-U-C-O system, HTGR fuel system, thermodynamic assessment 78—70598
Th-U-Pu metal alloys, LMFBR appl. 77—83040
Th-U-Pu-C-O-N, kernel migration for HTGR fuel 77—38335
Th-U(Pu) fast breeder fuels, chemical, thermodynamic and selected transport props. 79—54505
Th-U(20 wt.%) alloy fuel, compatibility performance of candidate cladding alloys 79—54509
ThC$_x$, $0 \lesssim x \lesssim 2.0$, nonstoichiometric, statistical mechanical model for C activity 79—71892
ThC$_x$, interface with Cr-Fe-Ni alloys, basic chemical compatibility, thermodynamic calcs. 79—93727
ThC$_{1-x}$, nonstoichiometric, atomic short-range order obs. by diffuse neutron scatt. 77—24315
ThF$_4$, spallation cross section and recoils, range calcs. computer code MARLOWE 79—93736
Th(IV), selective separation from rare earth elements on chelate ion exchangers 78—58861
ThN-rare earth nitride mixed system, quasibinary existence *(German)* 80—91221
ThO$_2$ a once-through cycle for BWRs 80—18433
ThO$_2$ and Th$_{0.81}$U$_{0.19}$O$_2$, irradiated fuel particles, meas. and interpretation of CO and Kr-Xe content 78—25287
ThO$_2$ and ThO$_2$-UO$_2$ fuel, fission gas release 78—86651
ThO$_2$ base low burnup fuels, densification-related pellet diameter shrinkage 79—54510
ThO$_2$, Doppler reactivity worth meas. in LMFBR spectrum 80—27776
ThO$_2$, Gruneisen coeff., lattice vibrational frequencies in range 298-2300K 78—79712
ThO$_2$, HTR fuel particles, fission product behaviour anal. using gamma spectrometry 80—42778
ThO$_2$ in HTGR fuel design 78—86622
ThO$_2$, isolated rod, exptl. and calculated resonance integrals 80—22986
ThO$_2$ kernel migration in HTGR 77—79440
ThO$_2$, lattice defects and irrad. effects, review 77—27873
ThO$_2$ microspheres, coated, coating permeability meas. 80—95343
ThO$_2$, nucl. Doppler effect in fast and intermediate spectra measured by direct flux depression in neutron beam expt. 77—50232
ThO$_2$, simultaneous freezing and melting in finite media 80—620
ThO$_2$ sintered pellets, ^{131}I release at low temps. 78—21650
ThO$_2$, spherical pile, neutron spectrum meas. and analysis 78—17311
ThO$_2$, thermal and transport props., electronic contrib. 80—15432
ThO$_2$-^{233}U exponential expts. anal., cross section library sets, resonance integral correls. 77—23215
ThO$_2$-Biso (propene), high temp. (2300-2500°C) treatment, metallographic cross sections, microradiographic anal. *(German)* 78—29586
ThO$_2$-UO$_2$ (0.1 wt.%), ^{133}Xe release after low dose irradiation 77—74919
ThO$_2$-UO$_2$ fuel performance after irradiation 78—86621
ThO$_2$-UO$_2$ in PWR fuel rod, LIFE-THERMAL computer code anal. 78—86623
ThO$_2$-UO$_2$ solid solns., props. of importance for use as nuclear fuels 79—54506
ThO$_{2-x}$ phase, high temp. vaporisation behaviour 79—54508
ThO$_{(2)}$, spectroscopic data rel. to thermodynamic functions 80—34208
^{232}Th fast fission yield of tritium, implications for FBRs 77—46195
^{232}Th fuel, conversion and fission yield, irradiation expt. 78—86609
^{232}Th, mirror hybrid reactors 80—42860
^{232}Th/^{238}U neutron capture cross section ratio, direct determ. for reactor lattices 77—50137
^{232}Th-^{238}U containing lattices, direct meas. of relative capture rates 77—61403
^{232}Th(n,f), 35 to 1500 keV, near equilib. delayed neutron energy spectra 77—34354
^{232}Th(n,f), fast neutrons, delayed neutron spectra, reactor calcs. 77—34355
^{232}Th(n,γ), ratio to (n,2n) in fast reactor, direct meas. 80—102233
(U,Gd)O$_2$ sintered pellets, homogeneity determ. by ceramographical method *(German)* 79—49804
(U,Pn)O$_2$, LMFBR fuel pin lattices, calcs. of k$_{eff}$ valves 80—13569
(U,Po)O$_2$, liq., v.p. meas. at 5000K 77—20077
(U, Pu) C, nuclear fuel, irradiation induced creep meas. 80—93605

fission reactor fuel continued
(U,Pu) O$_2$, pore struct., characterisation for gas exchange anal. *(German)* 79—49687
(U,Pu)-oxide nuclear fuel, near and non-stoichiometric, O$_2$ potential, thermogravimetric and galvanic cell meas. comparison 79—63744
(U,Pu)$_{2+x}$, elec. cond., pure state and Mo addition influence, 350 to 750°C 77—20320
(U,Pu)(C,N) and (U,Pu)N, high burn-up simulated, Pu self diffusion 80—92712
(U, Pu)C, ceramic fuel, plastic deform. behaviour at stress changes 80—35261
(U,Pu)C, controlled oxidation for head-end step reprocessing 80—5308
(U,Pu)C FBR fuel pins, irrad. behaviour 80—57847
(U,Pu)C, fracture and crack healing, SEM study 79—79080
(U,Pu)C fuel, interaction with molten stainless-steel shroud 78—86592
(U, Pu)C, LMFBR carbide fuel cladding damage anal. at TREAT 80—13602
(U,Pu)C LMFBR fuel elements, transient overpower test results 77—46334
(U,Pu)C LMFBR fuel, Na-bonded, consequences of rapid Na loss on fuel behaviour 80—102238
(U,Pu)C, pellet and sphere-pac nuclear fuels, comparative irrad. tests 80—78367
(U,Pu)C possibility for GCFR fuel 77—18667
(U,Pu)C, self-diffusion meas. 80—6544
(U,Pu)C$_{1\pm x}$, evap. behaviour, 1500-2458°C 77—27994
(U,Pu)C$_{1-x}$N$_x$ LMFBR MX-type fuels, fission gas release and microscopic swelling 80—73921
(U,Pu)CNO irradiated fuel, electron microprobe anal. 78—70601
(U,Pu)N, self-consistent normal fluid eqn. of state, press., density, and enthalpy of vaporisation calc. 78—8909
(U,Pu)N, self-diffusion meas. 80—6544
(U,Pu)O$_2$ 80—63252
(U,Pu)O$_2$ 316 stainless steel clad rods for GCFR high temp. fast flux irrad. tests 77—18666
(U,Pu)O$_2$ (30 wt.%), oxidation behaviour 79—66210
(U,Pu)O$_2$, anal. of densification in BWR 79—49685
(U,Pu)O$_2$, autoradiographic anal. of PU distrib. 79—49811
(U,Pu)O$_2$, build-up and decay of actinide nuclei in fuel cycle of BWR, PWR, HWR, HTGR and LMFBR 78—17314
(U,Pu)O$_2$, ceramographic exam. of Dounreay PFR fuels, data bank storage 79—49811
(U,Pu)O$_2$, close coupled O-to-metal ratio anal., rapid thermogravimetric method 79—11878
(U,Pu)O$_2$ FBR fuel pin thermal design, effect of fuel stoichiometry 80—18570
(U,Pu)O$_2$, fission gas release and retention in irrad. nuclear fuels 80—57841
(U,Pu)O$_2$ fuel, criticality control, critical mass meas., fission rate distrib. by solid state dosimetry 80—13723
(U,Pu)O$_2$ fuel performance, effect of O$_2$-metal ratio 80—13762
(U,Pu)O$_2$ fuel pin behaviour during FFTF 3c/s reactivity insertion event, TREAT expt. anal. 80—102240
(U,Pu)O$_2$ fuel pins, Cs migration effects on fuel-cladding mech. interaction 80—102250
(U,Pu)O$_2$ fuel-cladding chemical interaction, effect of O$_2$-metal ratio 80—13763
(U,Pu)O$_2$ fuels, eqn. of state up to 5000K, high-temp. laser technique 77—27971
(U,Pu)O$_2$ fuels, O distrib. during irradiation, calc. using CODIF program 78—70604
(U,Pu)O$_2$ GCFR fuel behaviour, effect of O$_2$-metal ratio 80—18569
(U,Pu)O$_2$, hyperstoichiometric, oxygen potentials determ., 1500-1850K 77—20095
(U, Pu)O$_2$, hypostoichiometric fuels for FBR, effect of O$_2$ pot. on fuel props. *(German)* 79—49800
(U,Pu)O$_2$, in pile creep 77—42060
(U,Pu)O$_2$, irradiated fuel, O$_2$ pot. meas. using galvanic cell 79—49689
(U,Pu)O$_2$, lattice defects and irrad. damage, review 77—27873
(U,Pu)O$_2$, liq., v.p. up to 5000K 77—1239
(U,Pu)O$_2$, microsphere fabrication, hydrolysis process 77—23204
(U,Pu)O$_2$, mixed oxide fuel elements, lenticular pore movement 78—78460
(U,Pu)O$_2$, mixed oxide fuel elements, Pu redistribution 78—78463
(U,Pu)O$_2$, nondestructive active assay of ^{235}U and ^{239}Pu 80—71873
(U,Pu)O$_2$, substoichiometric, unified model for defects, thermodynamic functions 77—20094
(U,Pu)O$_2$, substoichiometric high temp. thermodynamic parameters 77—21125
(U,Pu)O$_2$, thermal creep in 40 to 100 N/mm^2 stress range 77—28881
(U,Pu)O$_2$, vapour press. eqn. of state, VENUS-II code studies 78—8908
(U,Pu)O$_{2-x}$, chemical diffusion of O *(French)* 79—42300
(U,Pu)O$_{2-x}$, mixed oxide fuel, final stage densification 79—49681
(U,Pu)O$_{2-x}$, O$_2$ thermomigration described by cluster model 78—22888
(U,Pu)O$_{2\pm x}$, cluster model approach to thermodynamic props. 77—20093
(U, Pu)O$_{2\pm x}$, gradient of U, Pu and O at surface 77—18665
(U, Pu)O$_{2\pm x}$, O chemical diffusion coeff. 79—10977
(U,Pu)O$_{2\pm x}$, solid state transport as mechanism of O thermomigration 79—19395
(U,Pu)0$_2$, prod., recycling for use in LWR *(Spanish)* 79—63786
(U,Th)O$_2$, γ-active pellet fuels fabrication, conceptual design of remotely operated plant 80—32340
(U,Th)O$_2$-Biso (methane), high temp. (2300-2500°C) treatment, metallographic cross sections, microradiographic anal. *(German)* 78—29586
U, aerial radiometric data anal. using line-intensity estimation code MAZAS 79—62627
U and Th, resources and prospecting techniques and equipment development in India 79—30923
U assay by passive gamma-ray spectrometry 78—92576
U assay in boreholes using Ge gamma spectrometers 79—53571
U, Australian reserves, development program 78—4983
U, autoionic images of dislocation struct., computer interpretation 77—62453
U blanket management, effects of power and irradiation behaviour 78—86595
U borehole logging by prompt fission neutron technique, log interpretation 79—53567
U borehole logging system, delayed neutron activation anal. method using ^{252}Cf source 79—53569
U boreholes, in situ assay using prompt fission neutron technique 77—37441

fission reactor fuel continued
U core fuel elements, of A-1 reactor, volume growth *(Czech)* 80—27745
U, D migration and trapping during D^+ implantation 80—34243
U demand of symbiotic reactor strategies 77—42120
U, deposit distribution patterns and formation investigation *(Russian)* 79—30926
U deposits, Canadian Uranium Reconnaissance Program 77—37439
U deposits, in situ assay logging system using delayed fission neutrons 77—37440
U determ. in safeguards materials, automated gravimetric titrator 80—622
U, determination of microamounts of Pu for burning estimation *(Czech)* 77—6521
U, elemental and isotopic conc. anal. using nondestructive assay 79—49691
U enriching gas centrifuge cascade, computer program for performance anal. 79—85805
U enrichment, asymmetric process, separative power, resoln. of inconsistencies 78—29622
U, enrichment, Italian activities 79—31126
U enrichment, market survey *(German)* 78—4999
U, enrichment, separation nozzle process 79—31124
U, enrichment by gas centrifuge, Japan 79—31123
U, enrichment by gaseous diffusion process *(French)* 79—31120
U, enrichment by gaseous diffusion, Japan, research and development, economic evaluation 79—31121
U enrichment by laser isotope separation 77—38418
U enrichment by laser isotope separation *(Japanese)* 80—68960
U enrichment for power reactors, laser isotope separation 77—6953
U enrichment induction in test and research reactors, US program 80—22949
U enrichment plants in France 77—14257
U, enrichment processes in France *(French)* 79—31127
U exploration, airborne phoswich detector system 79—53576
U, exploration, radiation transport anal. for borehole logging probes 79—53565
U, exploration and assessment technology survey 79—53564
U, exploration and evaluation techniques for ore bodies 79—26536
U exploration and international cooperation 78—86628
U, exploration in Australia, Alligator Rivers Uranium Province 79—30922
U exploration in Egypt, exploration under arid conditions 79—26538
U extraction from seawater using magnetic adsorbents 80—37563
U extraction from seawater, feasibility 80—37564
U, field emission microscopy, emissive props. 78—88409
U, fission products γ-ray and photoneutron spectra 77—23127
U, foil and powder, oxidation kinetics in CO_2, 375 to 602°C 77—50240
U fuel, burnup determ., using ^{148}Nd 78—82459
U fuel, correlation of U and Pu isotope compositions with burn-up 79—63746
U, fuel for HWR, radiation stability *(Russian)* 79—13424
U future demands estimate, 1976 to 2000 77—14232
U, future requirements, planning amidst uncertainty 79—63792
U gamma abundances 77—65270
U, gaseous fueled reactor use as power supply for nuclear pumped laser system 80—63247
U, γ- and β-hardened, recrystallisation, effect of impurity distrib. 78—70602
U, HTGR fuel, French, fabrication, irrad. performance *(French)* 79—30934
U hot loop, irradiator yield at steady state power level 79—97836
U, impact of fusion-fission hybrid reactors on world demand 80—95404
U, in situ mining, Wyoming State regulations and environmental monitoring 79—88510
U, irradiation growth during fission fragment and proton bombard. 80—92568
U, isotope separation, new processes 79—31128
U isotope separation appl. to nucl. fuel cycle, teaching module 80—36805
U isotopes, ENDF/B-4 cross sections, integral data 77—23200
U, isotopic analysis by resin-bead mass spectrometry for materials safeguards 80—78392
U, isotopic composition, determ. using thermal ionisation spectrometry with automatic data eval. 80—66913
U, isotopic compostion, determ. using thermal ionisation mass spectrometry 80—66914
U, isotopic X-ray fluorescence anal., apparatus construction and testing *(Czech)* 77—50244
U, liq., enthalpy and heat capacity meas. using neutron heating 77—20078
U, liq., O_2 solubility and comp. of lower phase boundary of UO_2 at 1950K 80—49366
U, low-enriched, appl. of Raschig Ring Standard 79—26528
α-U, martensitic behaviour 79—29058
U, meas. of ^{222}Rn concs. in Earth using nuclear track technique 79—53574
U meas. with automated gravimetric titrator 79—85609
α-U, mech. behaviour, strain rate influence, 300 to 550°C 79—38907
α-U, mech. props. at very high strain rates, double-notch shear test use 80—85131
U metallic, heat capacity from 80 to 1000K 80—34201
U minerals, fissile nuclide concentration ratios *(Spanish)* 77—33067
U minerals, Pu content, ore model calcs. comparison with expt. *(Spanish)* 77—70654
U mining, CEA and Cogema activities *(French)* 80—626
U mining, processing and transportation, in Western US, impact 80—45621
U, modern prospecting techniques evaluation, Athabaska sandstone deposits 79—26537
U, natural, lattice param. for rod clusters in D_2O, buckling anal. 77—6484
U neutron criticality, solid angle computations using computer code 80—13726
U, nondestructive assay reference materials 79—49702
U ore, solution mining, appl. of solution flow prediction computer models 79—88013
U ore, solution mining, effect of Environmental Protection Agency requirement for underground injection 79—92101
U ore, solution mining, environmental impact, groundwater restoration 79—88012

fission reactor fuel continued
U ore costs, optimisation of LWR and FBR power prod. strategy 80—99253
U ore detection, using trace detection sensitive to ^{222}Rn α-particles *(Hungarian)* 78—77339
U ore grade direct determ. by photoneutron assay method 79—53570
U ore treatment plants and techniques *(French)* 79—26699
U ore zone logging, corrections for prompt fission neutron data 79—88353
U, oxidation in air and CO_2, Al content effect 77—50236
U plasma fueled reactor, use as power supply for nuclear pumped laser system 80—63247
α-U, polycrystalline, compressive deform. at low temps. 77—28856
U production in New Mexico, constraints 80—42843
U, prompt fission neutron logging technique, computer modelling 79—53566
U prospecting, ^{222}Rn and ^{210}Pb meas. 79—53573
U, reactivity meas., determination method *(Russian)* 80—664
U, reactor fuel supply, exploration and production capacities, review 79—22388
U recovery as byproduct from manufacture of phosphatic fertilisers 78—17398
U removal from P_2O_5 in Spain, pilot plants *(Spanish)* 79—30927
U requirements for advanced fuel cycles in nuclear power systems 79—18027
U requirements for fuel cycles in expanding nuclear power systems 78—17320
U reserves, technological status 77—34398
U resource utilisation and antiproliferation reactor concept 79—9735
U resources, consumption and 30 year fuel commitments for Canada and the world, 1975-2025 78—82456
U resources, production and demand, report 80—30323
U resources and accessibility, reliability of nuclear fuel supply 80—99216
U, resources and future demand 77—10468
U, resources and supply outlook for 1985 79—63795
U safeguarding, 5 to 20 mg determ. by constant current coulometric titration 80—78381
U safeguarding, determ. of trace amounts by pulsed laser fluorometry 80—78382
U safeguarding, management information system at BWR fuel fabrication plant 79—85750
U, safeguarding using resin bead mass spectroscopy 80—73984
U safeguards, fissile material accountancy using controlled potential coulometry 80—63298
U, selective separation from lanthanides on sulphonic ion exchangers 78—58860
α-U, single crystal, thermal expansion coeff. and cones of zero expansion 78—34635
U, solution mining, in situ leach method 79—87983
U, solution mining facilities, operational and environmental aspects 79—87984
U solution systems, high-enriched benchmark critical expts. 79—63748
U sphere, enriched, water-reflected, critical measurements 79—26569
U supplies, United States industry and restrictive measures 78—686
U, supplies security, up to year 2000 *(French)* 80—3480
U supply, Canada's role 78—86627
U, supply and demand for reactor fuel, industrial and commercial considerations 79—26535
U supply and enrichment and irradiated fuel reprocessing developments *(French)* 80—18565
U, supply situation in the Federal Republic of Germany 79—30916
U supply study in Western world *(German)* 78—8960
U system-wide feed and enrichment requirements of expanding nuclear economy with advanced reactors 77—61624
U utilisation improvement, DOE objectives and projects 80—37459
U, vacancy formation and phase transformation by positron annihilation 80—49215
α-U, variable low temp. martensitic behaviour 78—41818
U waste, burning in three phase pellet for inertial confinement fusion systems 77—61600
U well logging, gamma-ray spectra calc. using discrete ordinates transport code 79—53572
U, world resources, effect on development of nuclear power 80—55826
U/Pu fuel reprocessing solutions, NDA using X-ray L-edge densitometer for materials safeguards 80—83167
U-^{238}Pu-^{237}Np GCRF fuel cycle to produce isotopically denatured Pu for LWR 80—78427
U-Al, storage of unirradiated fuel in borated concrete, criticality safety anal. 80—13608
U-Al, transform. and struct. changes, cooling, cooling rate effect *(Korean)* 77—63660
U-Al (0.78 at.%), behaviour of metastable phases under neutron irrad., application of model 78—48408
U-Al fuel elements in light water, neutron multiplier, criticality studies for ^{252}Cf source 78—25367
U-Al plate type, reduced fuel enrichment utilisation, design variations 80—9395
U-Ba-C FBR nuclear fuels, phase anal., 1400°C 80—66487
U-C system p-T diagram, 1000-2600°C, 0-10^{-16} atm. 77—73265
U-C-N system, high temp. X-ray diffr. exam. of structure *(French)* 78—72765
U-Cr-Al (0.2, 0.1 at.%) fuel elements with high swelling resistance for KS-150 reactor 78—78471
U-graphite subcritical assembly, resonance escape probability meas. 77—71632
U-Mo (1.5 wt.%), superplastic behaviour 450 to 720°C *(French)* 79—74203
U-Mo-Nb-Zr-Ti (0.75, 0.75, 0.75, 0.5 wt.%), heat treatment effect on microstruct. and mech. props. 78—23729
U-Mo-(Zr), ductile-brittle transition *(French)* 77—66693
U-Mo(Nb)-(Zr), gamma stabilised, internal H_2 embrittlement 77—28883
U-Mo(Re), high temp. phase diagram, thermodynamic props. of refractory metal solutes in liquid U 77—25022
U-Mo(Ti)(Q^4)(Q^5), Q^4-quad, Q^5-quint, stress corrosion cracking in moist air, salt water, salted moist air 78—35562
U-Mo(2 wt.%), mech. props., effect of ageing 77—8914
U-Nb (4.5 wt.%), correlation between oxidation and stress corrosion cracking 79—20253
U-Nb-Zr (7.5, 2.5 wt.%), elastically bent, ageing induced shape instability 77—16622
U-Nb(2-3, 4.5, 6.0 and 8.0 wt.%), SCC in air 77—73363

fission reactor fuel continued
U-Ni dilute alloy fission product source design and use at EBR-II 79–9932
U-O system, infrared spectroscopy 77–8573
U-O system, phase equilibrium, thermal, X-ray and cond. meas. 78–35371
U-Pr-C FBR nuclear fuels, phase anal., 1400°C 80–66486
U-Pu aqueous solutions of oxides and nitrates, criticality, effect of Gd, Gd-B neutron absorbers 77–34393
U-Pu carbide based fuel simulating high burnup 77–74929
U-Pu carbides, advanced LMFBR fuels, equilib. thermodynamics 79–67862
U-Pu mixed oxide fuel pin performance investigation *(German)* 77–88223
U-Pu mixed oxides, impurities, emission spectrometric anal., single carrier method 78–68944
U-Pu radial redistrib., effect of fuel rod parameters and fuel porosity *(German)* 79–49799
U-Pu-C system, segregation and v.p. obs. 77–28793
U-Pu-C-N system, phase relationships and equil., effects of oxygen, review 77–21126
U-Pu-Np fuel cycle to produce isotopically denatured Pu 80–729
U-Re-C, crystalline struct. of a compound 77–25023
U-Re-C and U-Tc-C systems, phase relationships 77–21127
U-Si-Al fuel rods, Zr-Nb cladding, irradiation behaviour with peripheral voidage 78–54835
U-Sr-C FBR nuclear fuels, phase anal., 1400°C 80–66487
U-Ti (0.75 wt.%), quench rate sensitivity, effect on microstruct., mech. props., ageing 77–70077
U-Ti(0.75 wt.%), mech. props., effect of ageing 77–8914
U-V (0.2 wt.%), mech. and struct. props., effect of internal H *(French)* 77–21253
U-Y-C FBR nuclear fuels, phase anal., 1400°C 80–66485
U-ZrH low enrichment fuel for TRIGA and plate-type reactors 80–22950
U-ZrH_x fuel for pulse reactor use from 900-1300°C 80–13770
(U-Pu)C, new CRBRP reload core design 79–59155
(U-Pu)O_2 interaction with stainless steel cladding, corrosion products, electron microprobe anal. 79–26524
(U-Th) oxide, carbide, nitride and metal fueled LMFBR breeding performance 79–59175
(U-Th)C fueled reactor system, large plant, performance parameters 79–26500
UAl_2-Al dispersion fuel, effect of reactions on Young's modulus and rupture strength *(German)* 78–62596
UAl_x dispersion nuclear fuels, development and irrad. performance 80–78368
UAl_x fuel, development, irrad. performance in test reactors 80–68799
UAl_x plate-type reactor fuel element fabrication 79–49822
UAl_x-Al dispersion fuel for thermal high flux reactors, irradiation 77–18660
UAsSb, prep. and struct. 77–68951
UBC, crystallographic relationship with with CrB, α-MoB, ThBC 79–42025
UC, chemical compatibility with Cr-Fe-Ni cladding alloys, thermodynamic model 80–63263
UC, compatibility with transitions metals used in stainless steel 77–46293
UC, effect of porosity on fission-gas-induced swelling 78–8959
UC, fission dose depend. of lattice parameter changes 77–24333
UC, fuel element performance anal. with UNCLE-I 77–42086
UC, irrad. induced kinetics, diffusion and fission gas resoln. 80–59523
UC, low temp. reactor irradiation 80–39168
UC, MX-type LMFBR fuels, TEM exam. of microscopic swelling 78–70596
UC, miscibility with rare earth nitrides *(German)* 80–96654
UC, polycrystalline, creep mechanism interpretation 78–8898
UC, quenched-in defects, formation, migration and resistivity 80–64990
UC response to transient heating 77–46333
UC, transient capillary wave generation on laser irradiated surface 78–21653
UC, vapour, thermal conductivity, theoretical prediction 77–72402
UC-based nuclear fuel materials, influence of parameters on sintering behaviour and properties 79–100100
UC-NbC, UC-ZrC and UC-ZrC-NbC, solid soln. strengthening rules, physicomech. prop. changes 77–28826
UC-PuC, carbothermal synthesis *(German)* 77–18661
UC-UN, in equilibrium with UC_2 and/or C, relationship between N_2 pressure and composition, phase relationships 79–43223
UC+UC_2, neutron irradiation, U_2C_3 deposition 78–33253
$UC_{1\pm x}$, C diffusion 80–49428
$UC_{1.5}$, creep behaviour and phase change under compression stress 78–35432
UC_2 and (8Th, 1U)O_2 fuel kernel, experimental containing CVD ZrC coatings, irradiation behaviour 77–3103
UC_2 fissile fuel, SiC-fission product reaction kinetics in thermal gradient 80–47570
UC_2, fission fuel, HTGR TRISO, SiC-fission product reaction under isothermal conditions 80–42744
UC_2, high temp. thermal diffusivity, thermal conductivity, spectral emissivity 77–28052
UC_2-Triso (propene), high temp. (2300-2500°C) treatment, metallographic cross sections, microradiographic anal. *(German)* 78–29586
UC_x, computer simulation of C activity and transport 78–86618
U_2C_3+UC, MX-type LMFBR fuels, TEM exam. of microscopic swelling 78–70596
UCN, quenched-in defects, formation, migration and resistivity 80–64990
$UC_{1-x}N_x$, NMR of ^{13}C and ^{15}N, 5f electrons nature, mag. susceptibility, spin fluctuations 77–20736
$UC_{1-x}N_x$, nonstoichiometric, atomic short-range order obs. by diffuse neutron scatt. 77–24315
UC_xN_{1-x}, self diffusion processes 78–50259
UC_xO_y, fissile fuel, SiC-fission product reaction kinetics in thermal gradient 80–47570
UC_xO_y fission fuel, HTGR TRISO, SiC-fission product reaction under isothermal conditions 80–42744
UCr_2O_6, hydrothermal cryst. growth, 40 kbar, 873K, cryst. struct. *(French)* 78–35342
UF_4-LiF(KF) molten binary mixtures, viscosity meas. 80–65270
UF_6, advantages 78–8912

fission reactor fuel continued
UF_6 conversion and its role in the 1980s 80–99266
UF_6 conversion to UO_2, review 80–23099
UF_6, emission and absorpt. spectra at 80 to 600 nm, decomp. products 77–23212
UF_6 gas, development for space and earth-bound appl., NASA-sponsored program 79–49829
UF_6, gaseous fuel reactor research 78–21736
UF_6, gaseous fuel reactor applications 80–63367
UF_6, plasma confinement expts. appl. to plasma core reactor 77–23190
UF_6, present technology status for gas core reactors 78–33254
UF_6, RF heated for gaseous nucl. reactor, handling technology 77–23189
UF_6, safeguarding of enriched UF_6 bulk transfers 80–68814
UF_6-He circulating gas critical expts. 79–13488
UFe_2, thermodynamic props., agreement with Campbell correlation of laves phase compounds 78–15370
UFe_2O_6, hydrothermal cryst. growth, 40 kbar, 873K, cryst. struct. *(French)* 78–35342
UH_3 critical mass calc. by Monte Carlo methods as function of ^{238}U enrichment 79–36320
$UMnNiO_6$, hydrothermal cryst. growth, 40 kbar, 873K, cryst. struct. *(French)* 78–35342
UMn_2O_6, hydrothermal cryst. growth, 40 kbar, 873K, cryst. struct. *(French)* 78–35342
UN, compatibility with transitions metals used in stainless steel 77–46293
UN, fission enhanced creep and swelling, in-pile meas. 77–42061
UN fission enhanced creep, in-pile meas. 77–67807
UN form. by UO_2 reaction with C in NH_3 and N_2-H_2 mixture 79–47914
UN formation, mechanism and kinetics, reaction of UO_2 with C and N_2 78–48649
UN, fuel element performance anal. with UNCLE-I 77–42086
UN, HTR fuel, X-ray phase anal. of thermodynamic stability 79–59165
UN, lattice parameters determ. by X-ray diff. 79–19212
UN, synthesis from UO_2 through carbide 80–73980
UN, UP and $UC_{1-x}N_x$, low temp. elec. resist., temp. depend., 3 to 90K 77–20321
UN, vapour, thermal conductivity, theoretical prediction 77–72401
UO_2 80–57852
UO_2 80–63252
$UO_{2\ \mathrm{and}\ 2.11}$, temperature factor determ. by powder elastic neutron diffraction 78–10152
UO_2, ^{235}U enriched fuel rods in water, critical expts. 79–80977
UO_2, ^{235}U enriched lattices, effect of soluble neutron absorbers on criticality 79–80978
UO_2, alpha radiation damage, point defect ingrowth and annealing behaviour 77–27926
UO_2 and (U, Pu)O_2, vapour pressure meas. for fast reactor safety anal. by laser techniques to 5000K 80–13591
UO_2 and (U, Pu)O_2 in FBR, gaseous and solid fission product behaviour, swelling 77–34396
UO_2 and U_4O_9 single crysts., optical props. rel. to chem. bonding 77–28598
UO_2 and UC, creep props. under irradiation 77–42059
UO_2 and UC drops, fragmentation on entering Na pool in LMFBR 79–3225
UO_2 and UO_2-Ni, surface, grain boundary and interfacial energies 78–21649
UO_2 BWR fuel rod design to remedy fuel-cladding interactions 80–42766
UO_2, boundary heat transfer from volumetrically boiling pools following LMFBR HCDA 80–47654
UO_2, build-up and decay of actinide nuclei in fuel cycle of BWR, PWR, HWR, HTGR and LMFBR 78–17314
UO_2, burnup determ. in PWR and BWR using NDA of neutron emission rates 80–83148
UO_2, closed boiling system, effect of condensation on dispersion following LMFBR HCDA 78–8936
UO_2, cluster-type fuel for ATR, lattice parameter meas. and neutron behaviour 77–46282
UO_2, clustering phenomena effect, anal. based on shock wave model 78–21652
UO_2 coated particle fuel, amoeba endurance parameters 77–79439
UO_2 collapsible clad elements, PECITIS-II program 80–42751
UO_2, commercial fuel pin, irradiation induced volume changes, comparison with model 78–78465
UO_2 compact, density distrib. determ. using autoradioagraphy 77–25234
UO_2 compact, first power emergence, pressure excursion in fuel elements 78–82477
UO_2, compressed, dislocation substructure obs. *(French)* 78–78461
UO_2, computer model of Young's modulus 78–31450
UO_2, condensate solidification onto steel struct. in above-core region of LMFBR after HCDA 78–17364
UO_2, condensed vapour following core disruptive accident, particle-size distribs. using first-generation model 78–13295
UO_2, config. and climb rate of dislocation links, contrib. to anelastic creep 77–52431
UO_2, controlled porosity reactor fuel 77–23205
UO_2 critical clusters in D_2O, perturbation anal. of buckling 78–29573
UO_2, crystn., specific heat anomaly 80–84299
UO_2, cumulative diffusional release of fission product gases from an equivalent sphere, generalised anal. 80–47569
UO_2 cylindrical fuel rods, thermal neutron flux depression meas. 79–81010
UO_2, D migration and trapping during D^+ implantation 80–34243
UO_2, dense solid reactor fuel particle preparation by sol-gel technique 79–31136
UO_2, desintering of unrestructured UO_2 fuel during film boiling testing, grain boundary separation 80–22997
UO_2, diffusion of Kr and Xe fission gas atoms 79–6746
UO_2, dislocation creep, creep deform. predictions 78–19815
UO_2, Doppler reactivity worth meas. in LMFBR spectrum 80–27776
UO_2 dynamic vaporisation, rate effects rel. to fast reactor safety anal. 79–31034
UO_2 effect of Be impurity on Pu breeding control 78–21740
UO_2, effect of pellet density and axial restraint on failure threshold 78–17367
UO_2, effect of point defects on nonequilibrium bubble behaviour 79–93722

fission reactor fuel continued
UO_2 effective eqn.-of-state meas. to determ. vapour pressure, rel. to LMFBR safety 79—31036
UO_2, elastic props. at high press., US meas. 77—4141
UO_2, electronic contribution to thermodynamics, sp. ht. 79—7699
UO_2, electronic struct. contribs. to excess enthalpy at 3000K and in liq. phase 80—15265
UO_2, energy depend. Doppler factor meas. using lead slowing-down time spectrometer 78—17310
UO_2 epitaxial films, epitaxial, channelling studies 79—49683
UO_2, eqn. of state and thermodynamic props. 80—13592
UO_2 equiaxed grain growth modelling 80—13589
UO_2 filled Zircaloy tube, effects of gas gap on rewetting 77—46212
UO_2 film, vacuum evaporated, He$^+$ ion energy loss parameter 78—50253
UO_2, fine grained, low-stress creep study, metallographic obs. 79—43312
UO_2, fission gas bubble, equilib. index 78—17368
UO_2, fission gas bubble distrib. from high temp. irradiated SGHWR fuel pins 77—46284
UO_2 fission gas release and swelling in irradiation, quantitative model 77—6488
UO_2, fission gas release and retention in irrad. nuclear fuels 80—57841
UO_2, fission product gas release, microstruct. depend. model 80—665
UO_2 fission vapourised fuel, aerosol close in sampling, accident safety 79—49779
UO_2 fracture strength meas. of sintered specimens by diametral compression testing, effect of temp. and deformation rate 79—79074
UO_2 fragmentation by capacitor discharge 77—88227
UO_2, fragmentation gas thermodynamics 79—13458
UO_2 fuel, density, thermal conductivity, specific heat, thermal diffusivity, flash method 77—55362
UO_2 fuel, dynamic intragranular fission gas behaviour model, DIGRAS computer code 80—32345
UO_2 fuel, fission product gas emission measurement 79—17980
UO_2, fuel, Zircaloy-2 cladding bonding mechanisms determ. by SEM and EPMA 78—17317
UO_2 fuel crust, submerged, mechanical stability 77—46323
UO_2 fuel element/sheath, heat transfer meas. 78—29580
UO_2 fuel melting and Zircaloy cladding thermal failure during LWR PCM transient 80—42834
UO_2 fuel modelling *(Japanese)* 77—71648
UO_2 fuel pellet, bending strength, fabrication and microstruct. effect 80—2986
UO_2 fuel pin specifications 79—97812
UO_2 fuel rod, fill-gas comp. and eccentric gap geometry effects 78—13284
UO_2 fuel rod, fine struct. meas. of fission density distrib. using solid state track detector 77—57715
UO_2 fuel rod, Zircaloy clad, chemical activity determ. of fission product 79—49682
UO_2 fuel vapour, condensation on vertical steel substrate 77—46330
UO_2 fuel-coolant interaction, film boiling and vapor explosion phenomena 80—95363
UO_2 fuels, in-pile meas. of fission gas release 79—93697
UO_2, gas bubble mobility 80—91222
UO_2, gas evolution kinetics, direct meas. of gaseous fission products 77—46291
UO_2, Gd bearing rods, magnetic and passive scanning system 80—37463
UO_2, grain boundary diffusion, sintering and creep correlation, reinterpretation of creep mechanism 79—66111
UO_2, grain growth, in-reactor and lab. testing 79—74184
UO_2 grain growth studies, grain size and activation energy meas., rel. to nuclear fuel evaluation 79—93808
UO_2, Gruneisen coeff., lattice vibrational frequencies in range 298-2300K 78—79712
UO_2, γ attenuation coeffs. meas. for burn-up determ. correction *(Russian)* 78—82597
UO_2, high burnup nuclear fuels, relation between fission product release and fuel microstruct. 80—57845
UO_2, high density, fuel kernel, burn-up swelling *(German)* 77—46283
UO_2, high temp. irradiation, effect on microstruct. and unstable fission products 78—33250
UO_2, hyperstoichiometric, O_2 chemical diffusion coefficient 79—85608
UO_2, in reactor densification 78—21648
UO_2 in UO_2-PuO_2, fast reactor fuel pins, Cs interaction 79—6743
UO_2, in-reactor meas. of modulus of elasticity, US spectroscopic method 77—23210
UO_2, interaction with Na, dropping experiments and subassembly test 78—82460
UO_2 interaction with water, in-pile meas. 77—42097
UO_2, interconnected grain edge porosity 79—17979
UO_2, intragranular fission gas bubbles, size and distrib. 80—57840
UO_2, ionic model partial struct. factors, radial distribs. 77—84617
UO_2 irrad. induced kinetics, diffusion and fission gas resoln. 80—59523
UO_2 irradiated, grain edge porosity growth 79—19285
UO_2, irradiated, intergranular fission gas bubbles 78—21651
UO_2, irradiated, spacing of intergranular fission gas bubbles 78—66340
UO_2, irradiated, T loss during oxidative processing in air 79—97831
UO_2 irradiated fuel, densification algorithm 79—78913
UO_2 irradiated fuel, unstable fission product release 80—617
UO_2, irradiated sample, 1000 to 2100K, swelling and fission gas obs. 78—78462
UO_2, irradiation induced lattice defects 78—33251
UO_2, irradiation induced vol. change 78—67740
UO_2, isolated rod, exptl. and calculated resonance integrals 80—22986
UO_2, LMFBR, boiling pools with internal heat generation, void distrib. 78—21626
UO_2, LMFBR fuel, mechanical response to transient heating, HCDA conditions 77—14237
UO_2, LWR fuel, microstruct. and chemical props. of powder and pellet 80—629
UO_2, LWR fuel, prep. and advantages of CARAMEL, a sheeted fuel of UO_2 pellets 80—630
UO_2, lattice defects and irrad. effects, review 77—27873
UO_2, lenticular void migration rate in thermal gradient 78—21642
UO_2, liq., splashed on Na, no evidence of entrapment 79—41000
UO_2, liquid, eqn. of state 79—14910
UO_2, liquid, pressure generated by encapsulated Na *(Italian)* 78—82454
UO_2, liquid, reactor safety research, laser experiments *(German)* 80—42787
UO_2, liquid, struct. differences between ionic and molecular fluid models 78—26423

fission reactor fuel continued
UO_2, liquid, surface tension 79—7733
UO_2, low enriched coated fuel particles for HTGR, anal. of O_2 partition equilibrium 80—68769
UO_2 low enriched fuel rods, storage and transportation, critical separation in water with fixed neutron poisons 80—73918
UO_2, matrix swelling rate 78—8900
UO_2 micropore sintering, irradiated below 1100°C, in Winfrith SGHWR 80—5255
UO_2 microspheres, prep. from UO_3 $(NH_3)_2$, exam. of mech. and physical preps. 79—6758
UO_2, microstruct. depend. model for fission product gas release and swelling 80—42757
UO_2, microstructure in rods operated above critical heat flux 77—42098
UO_2 minimum particle size to survive thermal stress fragmentation by fuel-coolant interaction 79—67886
UO_2, mobility of intergranular gas bubbles 80—15310
UO_2, mobility of intragranular bubbles during irradiation 77—6520
UO_2, modified Ashby's computer method for constructing sintering diagrams 79—43165
UO_2, molecular geometry determ. from IR spectra vibr. assignments 77—50437
UO_2, molten, effect of radiative heat transfer on thermal fluid behaviour 79—93783
UO_2, molten, fragmentation in flowing Na under TOP accident conditions 79—30978
UO_2 molten, interactions with steel and graphite 79—49700
UO_2, molten, interaction with stainless steel claddings during LMFBR TOP accident 79—54515
UO_2, molten fuel freezing in shield plug following LMFBR HCDA 78—8941
UO_2 molten fuel radial motion during a LWR high temp. transient 80—42833
UO_2, molten pool, heat transfer to concrete slab following LMFBR HCDA 78—8930
UO_2 molten pool prod. by internal heating, heat transfer meas. 77—88214
UO_2, monocrystalline, fission gas release charact. during irradiation 78—4985
UO_2, neutron and electron irradiated, imperfect dislocation loops *(French)* 79—7606
UO_2, neutron irradiated, diffusion of fission product T 78—67866
UO_2, neutron irradiated, thermal recovery of defects 79—45348
UO_2 neutron transmission temp. depend. 79—82265
UO_2, non-stoichiometric, oxidation reactions and dopants 79—42087
UO_2, nonstoichiometric, surface and interfacial props. 77—69161
UO_2, nucl. Doppler effect in fast and intermediate spectra measured by direct flux depression in neutron beam expt. 77—50232
UO_2, nuclear doppler effects, hybrid static dynamic heating technique 78—25308
UO_2 nuclear fuel, exam. of neutron yield on $O(\alpha,n)$ reaction 80—86912
UO_2 nuclear fuel element, lenticular pore movement 78—21644
UO_2, O diffusion during UO_2-Zircaloy interaction 79—10986
UO_2, O diffusion mechanism 78—33249
UO_2 pellet, interaction between cladding in water reactor fuel pins 78—25286
UO_2 pellet compliance model based on out-of-pile simulation 80—42753
UO_2 pellet fuel, radiation induced densification 77—6519
UO_2 pellet reactor fuel rods, fission gas release in high burnup range 80—635
UO_2 pellet surfaces, β-$UO_{2.33}$ formation in air at 229 to 275°C, X-ray diffr. study 80—35362
UO_2 pellets, irrad., ^{129}I, ^{3}H distrib., radiochem. anal. *(German)* 77—16880
UO_2, pellets, pore size distrib. for optimisation of dimens. behaviour *(German)* 79—49801
UO_2 pellets, quantitative characterisation of structural parameters *(German)* 79—49803
UO_2 pellets, sinterability, particle size effect 80—104098
UO_2 pellets, thermal densification *(Korean)* 78—44065
UO_2 pellets-graphite-Zircaloy cladding, evaluation of graphite lubrication 80—32342
UO_2, performance in organic-cooled reactor 78—25292
UO_2 phase, thermodynamic props. 80—13594
UO_2 pin meltdown simulation by direct electrical heating 77—88215
UO_2 pins, electrical resistance meas. at high temp. 77—15848
UO_2, point defects and electronic props., theoretical survey 77—31657
UO_2, polycrystalline, oxidation in air at room temp. 77—23206
UO_2 porous HTGR kernels, restoration of CO_2 equilibrium 77—79438
UO_2 powder, characterisation and quality control 79—49806
UO_2 powder, sintering charact. 78—35341
UO_2, powder, sintering effect of compaction 80—20874
UO_2 powder, temp. depend. of atomic thermal displacements, Rietveld profile-refinement procedure 80—49190
UO_2, powder and pellets, determ. of f and metal impurities *(German)* 79—49807
UO_2 powders, sintering characterisation 79—43189
UO_2 pressurised rods, He fill-gas absorpt. during irradiation 80—37454
UO_2, quantitative spectrographic anal. of rare earth and other impurities 79—59232
UO_2, quenched and neutron irrad., recovery processes, vacancy migration 77—28048
UO_2, radioactive gas release during irradiation 77—74922
UO_2 rate-dependent heat capacity, rel. to fast reactor safety 79—31035
UO_2 reactor fuel, high burnup performance in LWR 80—634
UO_2, reanal. of neutron diffr. data 80—15084
UO_2, relative growth rates of fission-gas bubbles on grain faces 79—6739
UO_2, resolution of fission gas from grain edge bubbles, porosity effect 79—85607
UO_2, review of diffusion coeff. of fission product rare gases 78—33248
UO_2 rods, dissolution and storage exptl. program 80—37432
UO_2 rods, microscopic depletion calc. with MICBURN code 78—25276
UO_2 rods in water with U or Pb reflecting walls, critical expts. 80—32331
UO_2, simultaneous freezing and melting in finite media 80—620
UO_2, single crysts., nucl. neutron diffr. intensity meas. analysis, extinction 79—27957
UO_2, single-cryst. neutron diffr. data, reanal. using third cumulants 80—100130
UO_2, sintered pellet, isothermal grain growth kinetics 77—18663

fission reactor fuel continued
- UO_2, sintered pellets, relationship between intercept length and grain diameter 78—52743
- UO_2 sintering, effect of impurity 79—33962
- UO_2, sintering, initial stage kinetics 80—2987
- UO_2 sintering, thermal anal., hexavalent uranium xerogel drying, thermal treatment modelling *(Czech)* 79—36378
- UO_2 sol-gel particles, low temp. sintering and props. 79—100101
- UO_2, solid state diffusion of Pu 79—7711
- UO_2 spectral emissivity meas. up to 3800K 80—24625
- UO_2, sputtering by thermal neutrons, depend. of ejection coeff. on neutron flux 80—83157
- UO_2, steel clad, contact conductance, heat transfer between solid surfaces, expt. data 78—46888
- UO_2, stoichiometric, sintering diagram *(Rumanian)* 79—87602
- UO_2, strain rate and temp. depend. of yield stress 77—46281
- UO_2, strength recovery and crack healing 77—8918
- UO_2, superplastic creep 79—15730
- UO_2, surface energy, determ. by Hertzian indentation 80—93641
- UO_2, surface energy *(German)* 79—7742
- UO_2, swelling and gas release at low and intermediate temps. 77—50241
- UO_2, thermal and in-reactor densification 78—66364
- UO_2, thermal cond. meas. under simulated in-reactor conditions 78—94079
- UO_2, thermal creep in 40 to 100 N/mm^2 stress range 77—28881
- UO_2, thermodynamics, defect props. 77—67810
- UO_2, transfer of fission gas between grain faces and edges 78—79815
- UO_2, unrestructured fuel, intergranular fracture during film boiling 80—3169
- UO_2 vapour, saturated, thermodynamic state and gas kinetic relaxation to 5000K 80—13593
- UO_2 vapour, thermal conductivity prediction 77—68733
- UO_2 vapour condensation from rising bubble, effects of internal circulation velocity and noncondensable gas 78—50258
- UO_2, vapour press. meas. up to 500K, critical point data prediction, present state of art 79—45347
- UO_2, vapour press. meas. up to 5000K, appl. of laser pulse heating 80—52230
- UO_2 volatization pot. of metallic inclusions in irrad. fuel during LOF overheating transients 80—57895
- UO_2 volume boiling pools, meas. and calc. of average void fraction for LMFBR HCDA anal. 80—47653
- UO_2 waste material, dry recovery 79—63787
- UO_2, Y_2O_3 stabilised, O self diffusion 79—28135
- UO_2, Zircaloy sheathed, CEA expt. on transient behaviour *(French)* 80—18417
- UO_2:Cr_2O_3, fission gas release and swelling 80—47567
- UO_2/Na, fuel/coolant thermal interaction in FBR, out of pile preliminary tests *(Italian)* 78—54828
- UO_2/UO_3, in fused salts, redox and chem. props. 77—29038
- UO_2/Zircaloy pellet/cladding interaction, eval. of lubrication of graphite 79—67857
- UO_2-20CeO_2 mixed powder, X-ray and microprobe exam. of homogenisation 80—25609
- UO_2-(Ni), surface, grain boundary and interfacial energies 78—71905
- UO_2-Gd_2O_3, interfacial energy meas. 77—59763
- UO_2-graphite interaction in operating reactor fuel elements 77—18669
- UO_2-loaded Na in-pile loop, fuel failure detect. 78—37417
- UO_2-Mg reactor fuel, U potentiometric and mass spectrometric determ. 79—97811
- UO_2-P-uO_2 rods, isotopic anal., gamma-ray spectrometric meas. calibration appl. 77—81440
- UO_2-PO_2, swelling in mixed-oxide fuel pins 79—22393
- UO_2-PuO_2, ceramic fuel, plastic deform. behaviour at stress changes 80—35261
- UO_2-PuO_2, effects of stoichiometry on cladding attack 79—26523
- UO_2-PuO_2, irradiated fuel pins with various initial stoichiometries, radial O_2 distrib. *(German)* 77—46285
- UO_2-PuO_2, mixed oxide fast reactor-fuel pin, fission gas bubble distrib. 78—78459
- UO_2-PuO_2, possible Pu particle detection by neutron radiography, simulated fuel expts. 77—71637
- UO_2-PuO_2, reaction with Zircaloy-2 79—17982
- UO_2-PuO_2 fast reactor fuel rods, burnup-dependent heat transfer from fuel to cladding 79—36323
- UO_2-PuO_2 fuel, O_2 diffusion at low temps. 78—8899
- UO_2-PuO_2 fuel pellets, porosity meas. methods *(German)* 80—73915
- UO_2-PuO_2 fuel pin, hyperstoichiometric, post irradiation examination 80—63258
- UO_2-PuO_2 fuelled lattice, reactivity predictions using multigroup transport theory 78—89957
- UO_2-PuO_2 powder compacts, homogenization kinetics study by X-ray diffr. technique 79—37883
- UO_2-Triso (propene), high temp. (2300-2500°C) treatment, metallographic cross sections, microradiographic anal. *(German)* 78—29586
- UO_2-U_4O_9, thermal cond., effect of microstruct. and microcracking 79—97810
- UO_2-UC microspheres, coated, coating permeability meas. 80—95343
- UO_2-Zircaloy fuel element behaviour in PWR power plants 80—631
- UO_2-zircaloy-4, reaction kinetics at high temps., O_2 diffusion 80—16667
- UO_2-Zr BWR type fuel rods, fission gas release 80—42758
- UO_2-Zr fuel performance evaluation in power ramp tests 79—26544
- UO_2-Zr fuel pins, high burnup pellet and Vipac type, overpower performance analysis 77—46230
- UO_2-Zr fuel pins, ramp testing 78—86591
- UO_2-Zr high burnup nuclear fuel rods, Xe, Kr, He release 80—57846
- UO_2+Na, fuel-coolant interaction, UO_2 fragmentation by thermal stress and pressurisation 77—88226
- UO_{2+x}, C coated particles, variation of O/U ratio and $CO+CO_2$ press. 77—61504
- UO_{2+x}, corrosion of austenitic steel effect on tensile props. *(German)* 77—70216
- UO_{2+x} dissolution in MgO, shell model calcs. of enthalpy, computer program for formation energies 79—42251
- UO_{2+x}, elect. cond. and thermoelectric power 78—52020
- UO_{2+x}, sintering mechanism 77—21071
- UO_{2+x}-ThO_2-MgO system, in air, phase rel., X-ray diffr., electron probe and metallography anal. 79—74137
- $UO_{2\pm x}$, model of response of fission gas bubbles to dynamic behaviour of point defects 79—37735
- $UO_{2\pm x}$, O self and chem. diff. coeff. 78—71879

fission reactor fuel continued
- $UO_{(2)(3)}$, spectroscopic data rel. to thermodynamic functions 80—34208
- U_2O_8, radioiodine release in O_2 and inert gas atm., chem. identities 77—57712
- U_3O_8, ^{235}U enriched aerosol, characterisation by solid state track recorders 78—17538
- U_3O_8 demand projections using a diaggregated market penetration model 80—99214
- U_3O_8 enrichment standards, gamma-ray spectra 80—78378
- U_3O_8, λ-type heat capacity anomalies 77—20080
- U_3O_8 maximal fabricable conc. in Al base fuel elements 80—68800
- U_3O_8 preparation from ammonium diuranate, thermal anal. 79—81009
- U_3O_8 recovery from seawater, R and D program 80—99217
- U_3O_8 two near-term alternatives for improved nuclear fuel utilization in PWR 80—95347
- U_3O_8-Al cermet fuel for research reactors 79—9835
- U_3O_{8-z}, therm. cond. from 200 to 750K using scanning temp. method 79—37886
- U_4O_{9-y}, doped, phase transitions, heat capacity meas. 77—18664
- U_4O_{9-y}, thermal conductivity and diffusivity, 250 to 415K 77—50234
- UO_2F_2 powder, F elimination kinetics 77—50235
- UO_2(II), selective separation from rare earth elements on chelate ion exchangers 78—58861
- UO_2(Li) pellets, T release on heating after neutron irradiation 78—40071
- $UO_2(NO_3)_2$ highly enriched soln. with $Cd(NO_3)_4.4H_2O$ neutron poison, criticality expts. 80—13724
- $UO_2(NO_3)_4$, secondary criticality control, use of chlorinated PVC piping 80—13607
- $UO_2(-Nb_2O_3)$, kinetics of initial state of sintering stoichiometric and nonstoichiometric oxide 79—91609
- $(U_{1-y}P_y)O_{2-x}$, thermodynamics 78—70594
- $(U_{0.8}Pu_{0.2})C$, enthalpy, 1039 to 2421K 77—74920
- $U_{0.8}Pu_{0.2}C_xN_{1-x}(0\leq X\leq 1)$, MX-type LMFBR fuels, TEM exam. of microscopic swelling 78—70596
- $U_{0.8}Pu_{0.2}N$, self diffusion of ^{238}Pu 78—78457
- $(U_{0.8}Pu_{0.2})N$, self diffusion of ^{238}Pu 78—82461
- $(UPu)O_{2-x}$, thermal expansion as a function of deviation from stoichiometry *(French)* 78—21645
- $U_{0.75}Pu_{0.25}O_{2-x}$, variation in O_2 potential with simulated burnup 78—70597
- $U_{0.77}Pu_{0.23}O_{2\pm x}$, oxygen potential in temp. range 1523 to 1822K 80—106113
- $(U_1Pu)O_2+x$, O_2 chem. diffusion *(French)* 80—49427
- $(U_{1-y}Pu_y)O_{2-x}$, thermodynamics 78—70593
- $U_xPu_{1-x}O_2$, theoretical study of electronic thermodynamic and valence props. 79—37655
- US-UC_2, solution studies 77—21120
- US-UC-UC_2 system, potential nuclear fuels, phase solid soln. studies, prep. and props. exam. 79—40996
- U_3Si, heat capacity and thermodynamic props., 1 to 1203K 77—72697
- $U_{1-x}Th_xO_2$, solid solution, single crystal growth by chemical transport reactions 78—72708
- U(VI) gel, prep. by internal gelation, determ. of region of existence 77—9136
- UZrH fuels, development for TRIGA reactors 80—68798
- UZrH low enrichment fuels, test programs and analysis 80—9398
- ^AU, A=234, 236, minor isotope concentration meas. for safeguarding U enrichment cascade 80—63283
- ^AU, A=235, 238, fission and activation by fusion plasma neutrons 79—13521
- $^AUO_2(NO_3)_2$, a=233, 235, slab tanks for criticality control, neutron multiplication calc. 80—13606
- ^{233}U and Pu fuels, relative occupational hazards 78—94101
- ^{233}U cross sections, evaluation of ENDF/B-IV and Hansen-Roach cross sections 78—29550
- ^{233}U, enhanced fuel prod. using Th-Li hybrid reactor blanket with UO_2 multipliers 80—13810
- ^{233}U enriched fuel for PWR 79—26513
- ^{233}U factories based on D-T and D-D cycles 80—37630
- ^{233}U fissile fuel FBR physics parameters 79—9722
- ^{233}U fuel cycles, potential radiological impacts 80—42799
- ^{233}U prod. in tandem mirror hybrid reactor 80—47708
- ^{233}U safeguards, expt. nondestructive assay using a random driver 80—83164
- ^{233}U, symbiotic fast thermal fuel cycles, economic implications 80—726
- $^{233}U/^{232}Th$ metal fuel, irradiation expt. 78—86610
- ^{233}U-^{232}Th fuel cycle alternatives to LMFBR 79—9741
- ^{233}U-^{235}U fuel, nondestructive isotopic meas. using fission neutron counting 80—32385
- ^{233}U-Th fuel cycle, fast reactor system, sensitivity anal. 79—67835
- ^{233}U-Th fuel cycle, review of fast integral data 79—67834
- $^{233}UO_2/ThO_2$ water-moderated lattice analysis with ENDF/B-IV data 79—9800
- $^{233}U(n, f)$, 0.02-7.4 MeV, fission cross section ratio to ^{235}U 79—45313
- ^{235}U, ^{235}U systems, criticality anal. using KENO and SU-HAMMER codes 78—89949
- ^{235}U, anal. by cyclic activation of delayed neutrons 78—53296
- ^{235}U, depleted fuel, reactivity worths of fixed neutron absorbers 78—21654
- ^{235}U fission product γ radiation for short irrad. times, energy distrib. 80—73929
- ^{235}U, fission to capture ratios in range 0.2-15.0 keV 77—3057
- ^{235}U, irradiated in BOR-60 reactor, fission yields 79—17971
- ^{235}U isotope separation, laser photochemistry appl., LASL developments 79—31719
- ^{235}U, nondestructive determ. of content in fuel elements using passive gamma ray spectrometry 80—18418
- ^{235}U thermal fission product long-term activity meas. and calc. 79—9644
- ^{235}U-Al castings in water, pulsed reactivity meas., Monte Carlo anal. 79—26522
- ^{235}U-Al castings in water moderated lattices, pulsed reactivity meas. 79—26529
- ^{235}U+Be subcritical bare assemblies, pulsed n study, age-diffusion model 79—76055
- ^{235}U+BeO nearly homogeneous multiplying systems, pulsed neutron study, age-diffusion model 80—37442
- $^{235}U(n,2n)$, threshold to 13 MeV, cross section meas. by Gd loaded liquid scintillator 80—52669
- $^{235}U(n,f)$, 0.5 MeV, prompt neutron spectrum meas., TOF techniques 77—34356

fission reactor fuel continued
^{235}U(n,f), 1 keV to 30 MeV neutrons, cross section meas. rel. to ^{241}Pu 79−36286
^{235}U(n,f), thermal to 15 MeV, total delayed neutron yield calcs., energy depend. 77−34353
^{235}U(n_{th},f) mass yields, direct physical meas. using recoil mass spectrometer 77−50178
^{238}U Doppler effect obs. in advanced fuels critical assemblies 79−9739
^{238}U, energy-depend. Doppler effect calc. using collision probability method 77−57714
^{238}U, evaluation for ENDF/B-V 78−25289
^{238}U fast fission yield of tritium, implications for FBRs 77−46195
^{238}U in UO$_2$, Doppler effect in GCFR critical assemblies, 300-1100K 78−29574
^{238}U, meas. of Cd ratio of neutron capture rates in slightly ^{235}U enriched fuel, systematic errors 78−8901
^{238}U, mirror hybrid reactors 80−42860
^{238}U neutron data reevaluation, effect of k_{eff} for various critical assemblies 77−23042
^{238}U, neutron resonance parameters, time-of-flight spectroscopy 80−47375
^{238}U total neutron cross section, ENDF/B-IV representation 77−2983
^{238}U vapour, hollow-cathode generator, energetic yield 80−47724
^{238}UO$_2$ grains distrib. in graphite matrix, effect on resonance integral 80−68768
^{238}U+n, Doppler effect meas. at 24 and 144 keV 79−97704
U(n,X), Japan Material Testing Reactor, U and Pu isolation and isotopic ratios *(Japanese)* 80−52730
U(n,f), 1 to 7 MeV, ratio of ^{238}U and ^{235}U cross sections 79−30867
U(n,f), A=233,235,238, 35 to 1500 keV, near equilib. delayed neutron energy spectrum 77−34354
U(n,f) A=235,238, sub MeV neutrons, equilib. delayed neutron energy spectra meas. 77−38308
U(n,f), delayed neutron spectra from thermal- and fast-neutron fission, reactor calcs. 77−34355
U(n,f) fission cross section ratio of ^{235}U to ^{238}U for 0.1 to 25 MeV neutrons 79−36285
Uo$_2$, thermal and transport props., electronic contrib. 80−15432
^{233}Uo$_2$-ThO$_2$ fuelled core, spent fuel rod assay, reactivity perturbation method 77−18654
Zr, fuel element sheathing, reliability, including hydration process, probabilistic model *(Russian)* 80−52742
Zr sheet, elasticity coefficient computation by use of pole figure data 77−77521
ZrC CVD coated fuel particles, diffusion of ^{137}Cs, ^{90}Sr and ^{144}Ce 80−13582
ZrC, CVD on reactor fuel elements 77−74941

fission reactor fuel preparation and reprocessing
see also isotope separation; radioactive waste
accelerator breeder, burner reactor, and reprocessing plant system, net energy and fissile material balance 79−85722
accelerator breeders appl. in nuclear fuel cycle 79−49814
accelerator-breeder, ^{233}U, ^{239}Pu 77−83065
accelerator-breeder concept, preliminary design 79−81059
accelerator-breeder systems for regeneration of reactor fuel assemblies, thermal hydraulics 80−5299
accelerator-breeder target neutronics, neutron leakage 79−81060
accelerator-driven breeding blankets, neutron-return effects, implications for fuel reenrichment without reprocessing 80−57914
accelerator-driven reactor fuel cycle 79−26678
accountability enhancement in first solvent extraction cycle, state estimation technique 80−83216
accounting and rate making, regulatory issues 78−13242
actinide aqueous ions, chemical thermodynamics, book 77−60108
actinide elements, chemical thermodynamics, book 77−60107
actinide elements, solvent extraction by trilaurylammonium nitrate carboxylic acid mixtures 79−22444
actinide elimination by fissioning in generic actinide burner reactor 79−93756
actinide incineration strategies, UK 79−85704
actinide nuclear transmutation, photon and neutron surface dose rates for actinide containing fuel 78−66428
actinide nuclei build-up and decay in fuel cycle of BWR, PWR, HWR, HTGR and LMFBR 78−17314
actinide partitioning from high-level radioactive wastes, arguments against 77−61570
actinide partitioning in LWR fuel reprocessing, conceptual methods 79−85810
actinide partitioning-transmutation, technological impacts on fuel cycle 79−85751
actinide production in different HTR fuel cycle concepts 79−85753
actinide radioactive waste, biological hazards, consequences for LMFBR fuel recycling 80−86960
actinide recycling, neutron multigroup cross sections 77−23237
actinide recycling in power reactor fuel cycle *(French)* 79−85714
actinide removal for reprocessing wastes by solubilisation and solvent extraction 79−36384
actinide removal from HNO$_3$ waste streams, bidentate organophosphorous extractants 77−26861
actinide sensitivity studies and nuclear data requirements 79−85710
actinide separation from high-level waste, nuclear transmutation 77−61569
actinide separation in nuclear fuel and wastes, hazard assessment 79−85806
actinide transmutation, nuclear fuel cycle impact studies 79−85752
actinide transmutation in fission reactors 79−26584
actinide transmutation in nuclear power reactors, neutron physical feasibility 79−85701
actinides, chemical separation from PUREX raffinates using organic solvents 78−66676
actinides, decay heat estimation, summation calcs. and Standard eqns., review 80−63317
actinides, fast reactor recycle as waste management alternative, performance calcs. 78−13269
actinides, nuclear incineration feasibility study 79−85705
actinides, recycling and recovery in fission reactor wastes 79−85699
actinides, separation from high level radioactive fuel reprocessing waste 79−85809
actinides, short lived, neutron cross sections for transmutation, Van de Graaff accel. study 79−85713

fission reactor fuel preparation and reprocessing continued
actinides in aqueous solutions, oxidation state and complex formation *(French)* 77−26858
active reprocessing plant, decommissioning and rebuilding 79−71932
advanced converter reactors with proliferation-resistant single fuel cycle 79−41026
advanced fuel reprocessing, remote operation anad maintenance demonstration facility 80−18568
advanced high U-density reduced-enrichment plate-type fuel development for test and research reactors 80−23101
advanced MX fuels, Pu depletion by vapour-phase transport in carbothermic reduction processes 80−815
AGR fuel element design improvement 80−23112
Al-Mg-Zn pyrometallurgical process for U-Pu fuel cycles 79−85735
aliphatic short chain compounds, oxidation and degradation by hypeeazeotropic nitric acid 78−37431
alkaline radioactive waste decontamination by ion exchange 78−50263
alpha waste production and proliferation hazard of different fuel cycles 80−83214
alpha-active waste production calcs. for various fuel cycles 79−59209
alternative fuel cycles, chemical problems 79−93803
alternative fuel cycles, reprocessing and fuel fabrication systems 79−49818
alternative fuel cycles and fast breeders 80−27791
alternative fuel cycles and processes, an overview 79−49817
American Nucl. Soc. winter meeting 1977 78−58315
American Nucl. Soc. Winter Meeting 1977 78−82408
analytical procedure and training material development at ICPP 80−37569
anion-exchange refinement of Pu and Np separated during extraction refinement of spent fuel elements 78−70624
aqueous wastes from reprocessing plants, long term planning for management 77−61532
aspects 77−88267
asymmetric separation processes, two types of ideal cascade 79−36377
availability calculations for nuclear material processing facilities 80−73988
Babcock & Wilcox hot cell facility 80−68910
BABCOCK-205 NSS fuel assembly units, advanced design 77−46386
Barnwell Nuclear Fuel Plant, remote handling systems, overview 80−68920
Barnwell nuclear fuel reprocessing plant, remote sampling and on-line anal. system 79−13511
Battelle Hot Cell Laboratory 80−68913
behaviour of coated fuel particles and spherical fuel elements in accident temperatures *(German)* 79−3228
benefit-cost analysis in nuclear fuel cycle 78−8957
Bohunice A-1 reactor, long-run test of improved R II-U spare-type fuel element *(Czech)* 78−8875
borated concrete use in Hanford N-reactor spent fuel basin 77−42128
breeder reactor, effect of cladding coating and internal pressurization on fuel-cladding interaction, rod overall length change 79−54581
breeder reactor fuel pin end closures, pulsed magnetic welding 79−93806
breeder reactor fuel remote fabrication program in UK 80−13747
breeder reactor pellet fuel remote fabrication program in USA 80−13746
breeder reactor spent-fuel shipping cask design 79−9834
breeding characteristics, comparison of hybrid fission-fusion plant and fast breeder 77−88269
British Nuclear Fuels' thermal oxide, reprocessing plant at Windscale, Development programme 78−82497
Brookhaven accelerator-reactor breeder concept 77−54294
Brookhaven National Laboratory Linear accelerator reactor, system study *(Japanese)* 79−93801
BWR, 770 MWe, ^{235}U enrichment staggering of initial fuel charge *(German)* 77−61582
BWR, fuel cycle cost sensitivity anal. 79−31104
BWR, fuel element positioning and control patterns, optimisation system 80−733
BWR, pellet-cladding interaction related failures during manoeuvring operations 78−21743
BWR, quasioptimum fuel assembly loading, hierarchical level scheme 78−29609
BWR fuel preconditioning, initial pressurisation, fuel temps., fission product release 80−63357
BWR fuel preconditioning 80−63360
BWR high density fuel storage 78−726
bWR servicing and refueling improvement program 80−9390
BWR spent fuel cask handling problems and solns. 79−9799
BWR Th cycles with improved performance 79−59138
Canadian program for storage and disposal of spent fuel and high-level waste 77−61535
CANDU, Th-U^{233} fuel cycle, future development 77−38381
CANDU−Canadian experience and expectations with the heavy-water reactor 79−26593
CANDU fuel cycles, future prospects, advanced fuel cycles 79−81065
CANDU fuel pellet stacking, mathematical model of automatic assembler 80−37464
CANDU fuel storage in pods and air-cooled concrete canisters 78−89963
CANDU irrad. fuel bundles, sheathed in Zircaloy-4, long term stability investig. 80−13774
CANDU irradiated fuel, monitoring for sheath defects in shipments 78−54864
CANDU irradiated fuel storage, concrete canister programme, heat transfer and shielding effectiveness 78−58388
CANDU reactor, Pu-topped Th cycle characts. 79−31101
CANDU reactor core, materials and design criteria for fuel, cladding, and fuel channel 78−13238
CANDU reprocessed fuel and high level waste radioactive decay props. 77−71656
CANDU Th advanced fuel cycle, accelerator breeder concept 79−45393
CANDU-PHW, advanced fuel cycles 78−89968
CANDU-PHW, once-through, slightly ^{235}U enriched U cycle 79−93711
CANDU-PHW, once-through natural U cycle 79−93710
CANDU-PHW, waste management and its role in Canadian fuel cycle 79−89393
CANDU-PHW operating on Th cycle 79−93712
carbide fuel element development advances, fast reactor appl. 79−31138
centrifugal extractor appl., mixing and separation obs. *(Japanese)* 80−52775

fission reactor fuel preparation and reprocessing continued
- centrifugal extractor for mass transfer examination by single drop method 77−67848
- characterisation and quality control of nuclear fuels, conf. Karlsruhe Germany (June 1978) 79−49794
- chemical analysis, appls., conf., Gatlinburg, USA (Oct. 1977) 79−9847
- chemical reprocessing, H_2NNH_2, HNO_3, $NaNO_2$, $Fe(NH_2)SO_3$ 78−78487
- chemical reprocessing, status review 77−67852
- chemical reprocessing, technical status review 77−34420
- chemical technology development in nuclear power generation fuel cycle factories 79−31096
- chop-leach fuel hulls, chemical decontamination and melt densification 77−65319
- Civex, a diversion resistant nuclear fuel cycle, historical developments 79−9832
- Civex, flow diagram for diversion resistant nuclear fuel cycle 79−9833
- civil AGR multistart helically ribbed fuel pin development 80−23111
- CMEA reactor development, fuel cycle aspects *(Russian)* 79−26505
- coated fuel particles, automatic size anal. 77−79460
- colloqium on nucl. instrumentation, London, England 1979 80−4480
- commercial LMFBR fuel handling and storage system 79−9845
- commercial nuclear capacity and spent-fuel accumulation, US projection 80−18574
- composition calculation errors in nondestructive testing 79−71939
- computer-aided fuel cycle management, w.r.t. economics 77−14241
- concrete canister spent fuel storage facility, conceptual design study 79−45378
- conference, actinide nuclear transmutation, Ispra, Italy (April 1977) 79−85698
- Conference, nuclear materials, safeguards and accountability meas., Williamsburg, USA (May 1978) 79−81045
- conference, San Diego, Calif., USA (June 1978) 79−17972
- conference, San Diego, Calif., USA (June 1978) 79−49650
- conference on nuclear engineering remote systems technology, San Francisco, USA (Nov.-Dec. 1977) 79−45438
- conference on nuclear power and fuel cycle, Salzburg, Austria, (May 77) 79−26503
- conference on nuclear power and its fuel cycle, Salzburg, Austria (May 1977) 79−26504
- control system for remote operation 80−18571
- COPRECAL conversion of $(Pu,U)NO_3$ to mixed oxide 80−37570
- coprocessing, chemical reprocessing without Pu separation, technical feasibility 79−18023
- coprocessing, partial Pu-U separation 79−89419
- coprocessing as an alternative fuel cycle, evaluation 79−49819
- criticality accidents, fission and explosive energy releases of PuO_2 and PuO_2-UO_2 assemblies 77−65295
- criticality accidents at facilities processing fissile material, characts., detect. and action procedures *(French)* 78−55054
- criticality analysis of dry fuel in ANO-2 fuel storage pool 79−26672
- criticality aspects of fuel storage and transport in UK 79−63791
- criticality control and long-term storage of spent fuel 79−26712
- criticality safety, fault tree logic anal. of violations 79−22445
- criticality safety analysis in nuclear fuel cycle *(Japanese)* 80−99225
- criticality safety of reprocessing equipment, neutron poisons appl. *(German)* 77−34407
- crossed progeny and other non-standard fuel cycles 79−26498
- cycle management, interdisciplinary approach in education and research activities 77−38433
- decommissioning of a nuclear fuel reprocessing plant 79−49821
- decommissioning of fuel reprocessing facility, nondestructive assay of ^{235}U content of materials 80−81269
- decontamination and waste management at shutdown reprocessing plant, experience 78−66354
- defective fuel detection using vac. slipping technique 80−9389
- denatured fuel cycles for international safeguards 79−41011
- denitration of aqueous waste solns. 80−5313
- density measuring meter, digital, remotely operated 80−68927
- design safety principles and safety assessment techniques for nuclear chemical plants 80−820
- direct enrichment and self-protected fissile fuel prod. using hybrid reactors 80−95390
- displacement re-extraction of U, Pu and Np, math. simulation 77−61586
- dodecane-tributyl phosphate solns., radiolysis, liquid products 80−40723
- dodecane-tributylphosphate solns. radiolysis 78−74459
- Dounreay contribution to fast reactor development 80−27798
- drum storage capacity computation via inventory model 79−9776
- dry storage pit for radioactive sources 78−13248
- dynamic materials accounting for LWR fuel cycle 79−36325
- EBR, dissolver soln. fission product determ. by spark source mass spectroscopy 80−32422
- EBR-II, possible metal and oxide fuel loadings utilising $^{232}Th/^{233}U$ 80−13563
- EBR-II, remote fuel fabrications experience 79−89476
- EBR-II, remote reprocessing of metal fuel 80−13767
- EBR-II remote fuel fabrication facility, review 80−13745
- ecological problems solution nuclear plant fuel cycle closing *(German)* 77−54344
- economic indices improvement for LWR power stations and fuel cycles *(Russian)* 79−26744
- EEC Commission, role in nuclear fuel industry *(French)* 79−31117
- effluent monitoring programme design and organisation principles 79−13548
- electrochemical processes for power reactor fuel aqueous reprocessing 79−85718
- electronuclear fuel producer, linear accelerator driven design 79−81063
- electronuclear fuel production, medium-energy nucleon-meson transport calcs. 79−81061
- energy analysis of nuclear power plants and their fuel cycle 79−26746
- energy extraction without reprocessing to separate Pu, alternative methods 79−26675
- energy-dispersive X-ray fluorescence analysis of highly radioactive samples with small tubes and pyrographite crystals 78−92578
- enrichment by centrifuge, Urenco/Centec project 79−31122
- enrichment by isotope separation, HAGA radial-separating-nozzle centrifuge process 79−67954
- enrichment facility, at Savannah River Plants, diversion path analysis 79−85739
- enrichment testing with CdTe detectors *(Czech)* 77−50276
- enrichment using linear accel. 79−67980

fission reactor fuel preparation and reprocessing continued
- environmental impact of nuclear fuel cycle, monitoring and control 79−57504
- environmental problems, nuclear power stations prospects *(Hungarian)* 80−13742
- European irradiated fuel transport, future trends 77−71662
- exhaust air, environmental radiation exposure *(German)* 80−57940
- extraction processing of nuclear fuel fluxes, effect of flux oscill. on Pu accumulation, math. simulation 80−63355
- extraction reprocessing of VVER fuel elements, apparatus for solns. clarification 77−54348
- extractor design data and flowsheets, comparison of selected reprocessing plants *(German)* 80−57938
- Exxon nuclear fuel recovery and recycling center, safety analysis 79−36389
- exxon nuclear fuel recovery and recycling center facility description 79−36388
- Exxon nuclear fuel recovery centre, maintenance philosophy 79−45459
- fast neutron reactor fuel cycle *(French)* 80−47681
- fast power reactor fuel, physical characts., effect on fuel cycle *(Russian)* 79−30936
- fast power reactor fuels, physical props. and fuel cycle effects 79−31097
- fast reactor, advanced fuel cycles 78−89968
- fast reactor, denatured fuel, symbiotic system 79−26682
- fast reactor fuel, handling system for inspection of fuel pellets 79−49824
- fast reactor fuel cycle, safety considerations 79−36396
- fast reactor fuel cycle closure 80−800
- fast reactor fuel cycle cost, sensitivity anal. 79−26501
- fast reactor fuel design and development 79−31133
- fast reactor fuel element regeneration by gas-fluoride method, highly active waste product behaviour 78−37425
- fast reactor fuel fabrication using high temp., low-power furnace 79−49823
- fast reactor fuel recovery, basic problems *(Russian)* 79−31144
- fast reactor fuel reprocessing, Dounreay plant progress 79−89473
- fast reactor fuel reprocessing, French technology *(French)* 79−31146
- fast reactor fuel reprocessing, UK experience 79−31145
- fast reactor fuel reprocessing plant at Dounreay, Scotland 79−71934
- fast test reactor fuel pins in water, critical expts. 79−85726
- FBR, alternative fuel recycling technology search 80−5303
- FBR, Clinch River, design and fabrication of ex-vessel storage tank 79−30973
- FBR, role in nuclear nonproliferation environment 79−26681
- FBR, status and programme in UK, out-of-pile fuel cycle 79−26736
- FBR carbide fuels, remote fabrication of mixed sphere-Pac fuels, Swiss developments 80−13750
- FBR carbide/nitride fuels, potential radiation doses from released ^{14}C 77−40799
- FBR driver fuel pins, integrated quality status and inventory tracking system 80−78431
- FBR fuel, development of secure automated fabrication systems 80−102287
- FBR fuel, U-Pu extraction by equilibrium water systems with 0.15 to 1 M HNO_3 acidity 79−71940
- FBR fuel cycle, experience 79−59233
- FBR fuel development, international development programs 80−102248
- FBR fuel fabrication using advanced secure automated system 80−102286
- FBR fuel handling, radiation safety 80−73985
- FBR fuel reprocessing, radiological protection problems 80−5376
- FBR fuel reprocessing plant, radiation protection, containment and shielding 80−23179
- FBR international development, influence on German policy *(German)* 80−18586
- FBR mixed oxide fuel pellet fabrication, control of O_2-to-metal ratio 80−13760
- FBR mixed oxide fuels, determ. of total H_2 content *(German)* 79−49809
- FBR oxide fuel, review of technological problems related to design, fabrication, operation and fuel cycle 80−636
- FBR/Civex diversion resistant nuclear fuel cycle 79−9831
- ferrous sulphamate radiolytic instability in nuclear process solns. 77−70314
- FFTF fuel element measuring system 79−45447
- FFTF fuel storage facility design 78−715
- financing and accounting, effects of Pu uncertainty 78−13243
- fissile fuel breeding with spallation breeder 78−25322
- fissile material conc. in high-activity solns., in-line determ. 77−83066
- fission product release, inclusion in AVR fuel cycle strategy program *(German)* 79−74576
- fission products, decay heat estimation, summation calcs. and Standard eqns., review 80−63317
- fissionable isotopes, in aq. soln., pulsed neutron interrogation method assay 79−11874
- fissionable isotopes in aq. soln., assay by pulsed neutron interrogation 78−68966
- fissionable material, assay by neutron methods in presence of fission products 79−13513
- fluoride volatility process, distrib. of Ru contaminants 80−13743
- fluoride-volatility processes, form. of Ru compounds 79−31090
- fluoride-volatility processes, separation of Ru from PuF_4 79−31091
- Foratom member countries, nuclear power programme financial aspects 79−26697
- Ford Nuclear reactor, reduced enrichment fuel element loading, calcs. 80−9394
- French contribution to reduced enrichment research and test reactor program 80−68931
- French nuclear fuel cycle activities and companies *(German)* 79−81054
- French private nuclear fuel cycle industries *(German)* 79−81055
- fuel breeding using proton linear accelerator 78−29630
- fuel cycle, extraction, concentration, UF_6 conversion, isotope separation *(French)* 80−63354
- fuel cycle, industrial integration, Argentina *(Spanish)* 79−31154
- fuel cycle, national and international aspects *(German)* 78−86665
- fuel cycle, quality criteria, performance requirements for mass produced fuel elements *(German)* 79−49795
- fuel cycle, radioactive material release, cost/benefit anal. 79−26605
- fuel cycle, transportation status and problems 79−59236
- fuel cycle and material international safeguards, current technical issues 79−26714

fission reactor fuel preparation and reprocessing continued
- fuel cycle and nuclear power plant development in USSR, economic aspects 79—644
- fuel cycle and radioactivity, regulatory control in Canada 79—26620
- fuel cycle back-end services, utility optimization model 79—30906
- fuel cycle cost sensitivity to data uncertainties, interactive graphic computation 79—9837
- fuel cycle environmental assessment methodology 78—94112
- fuel cycle evaluation in Korea *(Korean)* 79—6757
- fuel cycle facilities, advantages of on-site facilities 79—31118
- fuel cycle options without Pu separation 79—26676
- fuel cycle plants, accident anal., special completeness proof for licensing 80—817
- fuel cycle plants, radioactive discharges, limits 79—26779
- fuel cycle services, international cooperation 79—31116
- fuel cycle strategies, simulation using FISS computer program 80—5317
- fuel cycles, bibliography of AECL publications 80—5
- fuel cycles principle and state of art, critical review *(German)* 77—34408
- fuel design, manufacture and development in France *(French)* 79—26705
- fuel element, thermocentrifugal opening technique 79—76093
- fuel element fabrication *(French)* 80—73979
- fuel element in-cell laser profilometer 80—22955
- fuel elements recycling and thermal re-irradiation, technical, economic and safety problems *(German)* 80—99269
- fuel fabrication and reprocessing plants, Pu neutron emission checks *(French)* 79—26720
- fuel fabrication in 1980s changes in process equipment and facilities 79—63797
- fuel industry minimum size, India's integrated planning 79—26704
- fuel irradiation, German-Brazilian co-operation 79—31155
- fuel kernel coating in fluidised beds *(German)* 79—71941
- fuel particle coating, gas distrib. system optimisation in fluidised bed *(German)* 80—23104
- fuel pellet inspection system for remote operation and maintenance 79—89480
- fuel pellets, computerised fabrication and inspection for SNM accountability 80—78432
- fuel pins, computer controlled meas. 80—5300
- fuel recycling remote manipulation systems design and performance 77—67854
- fuel rejuvenation based on in situ re-enrichment and fission product removal 80—37561
- fuel reprocessing and waste treatment at Karlsruhe nuclear research centre 79—31143
- fuel reprocessing in India 79—31142
- fuel reprocessing plant safety aspects 79—26708
- fuel reprocessing plants, economic anal. of alternate location strategies 79—59235
- fuel reprocessing streams, remote anal. techniques 79—13510
- fuel reprocessing technology, development up to current status 78—58393
- fuel storage, close spaced racks 78—728
- fuel storage basin water, chloride ion removal 79—30975
- fuel storage pools, local distrib. of temp., cooling design *(German)* 79—49816
- fuel structure characterisation methods, review 79—49802
- Fuels and Materials Examination facility, design and construction 80—73986
- fusion-fission hybrids, trade-offs between fuel and power prod. 80—37605
- fusion-fission reactor symbiotic design, simple fuel reprocessing 78—66365
- fusion-fission reactors, performance parameters, design and fuel cycle anal. 79—17973
- fussion-triggered fusion pellets design, review 79—13519
- gas centrifuge, numerical anal. of weakly compressible rotating flows 80—47726
- gas centrifuges, shock-induced pressure recovery at high Mach number rotation 79—22480
- gas centriguge, effect of compressible flow on max. separating power 78—70644
- gas graphite reactor, and oxide fuels, technology of large reprocessing plants 77—65318
- gaseous effluents from LWR and reprocessing plants, treatment and control 77—61589
- gaseous effluents from reprocessing plants, treatment *(French)* 77—61588
- gaseous effluents reprocessing, radionuclide management 79—76078
- gaseous fission product retention in fuel reprocessing 79—31153
- gaseous fuel reactor applications 80—63367
- gaseous isotope separation by supersonic acceleration 79—22482
- gaseous waste, adsorptive removal of rare gases 79—31094
- GASP IV simulation model 78—41847
- GCFR core element fabrication technology 77—18682
- GCFR F-5 (X317) irrad. expt., fabrication of grid-spaced bundle 79—67925
- GCFR fuel assembly testing in BR-2 helium loop, Mol 79—67924
- GCFR grid spaced bundle for F-5 (X317) irradiation expt., fabrication 79—81058
- gel-Sphere-Pac technology, remote fabrication 79—89482
- geologic isolation for fuel cycle wastes, management perspective 77—42172
- German Government responsibility w.r.t. storage facility, legal aspects *(German)* 78—86701
- German nuclear fuel cycle centre 79—31109
- German Waste Management Centre, technical project design phase status *(German)* 79—13432
- glove box for sealed manipulator maintenance 80—18684
- graphite powder, characterisation, use in HTR fuel compact matrices 78—29631
- graphite-gas and fast neutron reactors, French policies at COGEMA *(French)* 80—808
- Hanford hot cell facility 80—68911
- Harwell inactive vitrification pilot plant 77—61543
- HFEF/N, equipment repair room modifications 79—45439
- HFR Petten Materials Test Reactor, reduced enriched fuels, utilisation and management schemes 80—9343
- high current DC injector for accelerator breeding systems, future developments 79—93846
- high level liquid waste evaporation and storage, lab. simulation 79—89409

fission reactor fuel preparation and reprocessing continued
- high level radioactive liquid waste, disposal options, fuel reprocessing 79—49703
- high level waste reprocessing, management in France *(French)* 79—26598
- high power accelerators for spallation breeders of fissile materials *(Japanese)* 79—26517
- high-burnup fuel reprocessing, hot cell facilities and techniques 79—9841
- high-level calcined waste solid spillage, recovery of U, erosion in solids transport system 78—13264
- high-level nuclear waste management from nuclear fuel reprocessing 77—65309
- high-level radioactive waste disposal on seabed following reprocessing, feasibility study 78—13271
- high-level-waste disposal on ocean floor, prospects of international cooperation 78—13272
- high-speed slitter for irradiated stainless-steel tubing 79—45450
- HLLW, safety analysis of tank storage 80—740
- homogeneous fluid-fueled reactors capable of in-situ fuel reprocessing nitride-liquid Sn concept 80—57834
- hot cell facilities and techniques, Karlsruhe 79—45458
- hot cell for reprocessing of spent nuclear fuel samples 78—58364
- hot fuel examination facility, auxiliary equipment for remote handling systems 80—18686
- Hot Fuel Examination Facility Complex, history and status 80—68909
- hot laboratories, post irrad. work, trends and prospects 78—41844
- hot laboratory design and construction *(Japanese)* 78—29623
- HTGCR, determ. of defective particle fraction, Cl leach method 77—42165
- HTGCR fuel, electrostatic transport system for spherical particles *(German)* 77—67847
- HTGR, coated fuel particles, fabrication technology 77—79456
- HTGR, electrolytic feed adjustment for separation of Np, Pu *(German)* 79—3229
- HTGR, LMFBR fuel reprocessing technology, USA 79—31148
- HTGR, Pu-containing coated particle fuels, irradiation performance 79—54583
- HTGR, solids handling and fluidised-bed combustion techniques development, pilot plant 79—45397
- HTGR, spherical fuel elements, coated particles, material development *(German)* 78—25297
- HTGR, weak and resin derived fuel microspheres 77—79454
- HTGR Biso-coated fuel particles, defective fraction during in-block carbonisation 79—67922
- HTGR coated particle development in UKAEA fuel element labs. 77—79457
- HTGR coated particles, failure rate prediction during neutron irradiation 77—79466
- HTGR coated-particle fuel performance charact. by fission gas pressure meas. 79—54584
- HTGR fuel, French, fabrication, irrad. performance *(French)* 79—30934
- HTGR fuel, remote fabrication technology 79—89483
- HTGR Fuel, SiC decladding by F_2-fluorination, feasibility study 79—89471
- HTGR fuel and fuel cycle technology 79—31134
- HTGR fuel cycle, reprocessing technology, West Germany 79—31147
- HTGR fuel cycle summary and recent developments 80—728
- HTGR fuel element component quality control 77—6550
- HTGR fuel element preparation, effluent monitoring using mass spectrometry 77—46376
- HTGR fuel fabrication equipment, criticality safety criteria 80—13771
- HTGR fuel particle coating, improved gas distributor 77—79455
- HTGR fuel particles, coating using improved gas distributor design 78—13311
- HTGR fuel particles irrad., performance from capsules HRB-11 and -12 79—54582
- HTGR fuel recycle technology 79—59246
- HTGR fuel refabrication plant, nondestructive fissile assay technique 80—37562
- HTGR fuel reprocessing, high-level solid waste, long term isolation from environment 79—26576
- HTGR fuel reprocessing, radioactive waste streams 77—42173
- HTGR fuel reprocessing off gases, simulated, efficiency of CO_2 removal 79—26577
- HTGR fuel reprocessing plant, cost and environmental impact of radioactive waste treatment 77—46380
- HTGR fuel rod fabrication, estimation and control 80—83215
- HTGR fuel rod length meas. and control microcomputer system 79—71942
- HTGR fuel rods, carbon-carbon composites designed for high weight and low strength 77—71684
- HTGR globular pile once through fuel cycle *(German)* 78—8913
- HTGR near-breeder cycles 79—59139
- HTGR pre-breeder and near-breeder symbiotic systems, U resource utilization 78—17321
- HTGR pyrocarbon coated fuel, neutron effects in range 1273-1773K 77—79434
- HTGR pyrocarbon coated particles, neutron induced permeability 77—79435
- HTGR reprocessing plant off-gas streams, ^{85}Kr removal 79—30972
- HTGR U by graphite fuel element and C fluidised bed combustion 78—13314
- HTPBR, gas injector to reduce pyrocarbon deposits *(German)* 78—29633
- HTR, actinide production reduction by use of Th-U fuel cycle *(German)* 80—9386
- HTR, pebble bed, closed Th/U fuel cycle 79—63799
- HTR, pebble bed, once-through cycles 79—31100
- HTR, pyrocarbon coated fuel, C density determ. by X-ray absorpt. 80—5301
- HTR, U/Th and U/Pu cycles, alpha-radiation production comparison *(German)* 77—6546
- HTR feed and breed particles, dry mechanical procedure for two grain fraction separation 79—93807
- HTR fuel element reprocessing plant, head end aspects *(German)* 79—93800
- HTR fuel elements, chem. prod. processes *(German, English)* 77—14256
- HTR fuel particle coating with pyrocarbon by pyrolysis in fluidised beds *(German)* 79—59247

fission reactor fuel preparation and reprocessing continued
HTR spent fuel reprocessing facility, real-time data acquisition and processing system *(German)* 80—106148
HTR Th closed fuel cycle, U resource conservation 80—727
hybrid reactors, fuel production for fission reactors, fuel cycle options 80—27812
hybrid tandem mirror reactors, design, fissile fuel production 80—27811
in-line monitors for fuel reprocessing plant 79—13509
in-process inventory dynamic measurement, computer simulation 77—38371
Incoloy 825, corrosion resistance as structural material for denitrification vessel 77—36685
inertial confinement fusion reactor, appl. PWR fuel rod reenriching 80—106174
input analysis, verification *(German)* 78—70623
instrumentation for international safeguards at fuel reprocessing plant 78—721
international arrangements for spent-fuel reprocessing—the view from developing countries 80—18583
International Fuel Service Centres for U resource conservation and proliferation resistance 80—57941
international market development 77—33821
international reprocessing business, small countries view 77—46373
intrinsic spiking with beta emitters during fuel reprocessing 79—85732
inventory checks, accounting data optimal linear combinations for nonconstant loss detection 79—81057
Iodox process for iodine removal from air with hyperazeotropic nitric acid 79—31107
irradiated CANDU fuel, long-term storage under water 79—41020
irradiated fuel element can removal from core, gas-thermal treatment 78—37432
irradiated fuel elements recycling plant design modifications and safety of used nuclear fuel during storage and disposal *(German)* 80—99219
irradiated fuel inspection station 80—68917
irradiated fuel pond at Trawsfynydd power station, management techniques 80—23072
irradiated fuel regeneration, laboratory line *(Czech)* 78—33283
irradiated fuel rods, in-cell welding techniques 80—22956
irradiated fuel rods, storage options, comparisons 79—45383
irradiated fuel sipping, inspection and repair 79—9844
irradiated fuels reprocessing, French and European policies *(French)* 80—809
irradiated nuclear fuel storage, waste management implications 79—31079
irradiation test facility for high U-loaded fuel plates as part of reduced enrichment program 80—68932
isotope centrifuge, effect of thermal convection on separative power, numerical anal. 78—58500
isotope separation, asymmetric process, separative power, resoln. of inconsistencies 78—29622
isotope separation, combined laser gas centrifuge technique 77—74946
isotope separation, ideal cascades, 2-up 1-down, separative power and interstage flow anal. 78—58499
isotope separation by H_2-Pd system, effect of isotopic conc. on separation coeff. of H-T, H-D and D-T mixtures 79—71979
isotope separation by laser, 1970-77 development and future prospects *(Japanese)* 78—5048
Italian nuclear power programme, fuel cycle industry development 79—31069
Japanese nucl. fuel cycle for LWRs 78—86670
Japanese reactor fuel reprocessing plant remote maintenance 79—9840
JEN, Spain, work on nuclear fuel cycle *(Spanish)* 77—38376
JUPITER experimental facility, engineering aspects of chemical process components 79—36379
lanthanides (III), extraction with di-isodecyl phosphoric acid from HNO_3 soln. 79—22398
large facility, neutron interaction anal. 79—63822
large fuel reprocessing plant, anticipated chem. emissions 78—5004
large pools for spent fuel, LUSH code cf with design methods for struct. load calc. 78—17337
large scale nuclear facilities and reprocessing plants, international safeguards 79—26715
large-scale, safety consideration 78—8961
large-scale fuel cycle centres, USA 79—31150
laser appl. to reprocessing 79—31719
laser beam appl., LASL developments 79—31719
laser isotope separation, principles and developments 79—76148
laser methods for fuel reprocessing, isotope separation 77—38378
laser-fission-fusion systems, coupled nuclear-thermohydrodynamic anal. 79—13520
leaching, design criteria for criticality safety of dissolution vessel 80—13772
linear accelerator driven and regenerative systems, U and Th fuel cycle 79—81064
linear accelerator driven fuel breeding 79—81062
linear accelerator fuel enricher regenerator and fission product transmutor 80—63365
liquid high level waste solidification 78—21669
liquid high-level waste at reprocessing plants, very long term storage of fission products *(French)* 77—61534
liquid waste from nuclear reprocessing, vitrification, durability 78—54852
liquid waste handling facilities for LWR fuel reprocessing plant 79—36390
liquid-liquid extraction column online control by modal control techniques 78—54865
LMFBR, borosilicate glass and glass ceramics with highly radioactive waste 80—5271
LMFBR, development and Pu allocation, optimal policies 80—725
LMFBR, development areas 77—57737
LMFBR, elimination of transuranium elements by neutron absorpt. 78—29628
LMFBR, fuel characterization pilot plant based on X-ray fluoresc. chem. anal. 78—5006
LMFBR, fuel cycle cost optimisation anal. of core design modifications 80—22900
LMFBR, fuel handling and storage system 79—45394
LMFBR, performance characts. in US nucl. energy system. rel. to breeding ratio, sp. power, discharge exposure 78—17404
LMFBR, radiological assessment, carbide and nitride fuel reprocessing 78—29627
LMFBR, spent fuel shipping system 79—45385

fission reactor fuel preparation and reprocessing continued
LMFBR core and fuel design in Halian fast reactor programme 79—97795
LMFBR fuel handling experience 79—97873
LMFBR fuel preirradiation for improved proliferation resistance 79—49826
LMFBR safety and fuel cycle, accident anal. 79—26650
LMFBR spent fuel coprocessing to ameliorate proliferation and waste management problems 79—26677
LMFBR spent fuel shipping cask designs, subcriticality guidelines, Monte Carlo calcs. 78—82470
LMFBR spent fuel transportation 78—711
LMFBR unirradiated assemblies, shipping containers 78—723
LMRBR spent fuel shipping casks, subcriticality design 78—706
low level radioactive liquid wastes, chem. treatment, clay numerals, cation exchange capacity 78—33270
low level radioactive waste solns. containing NH_4NO_3, spray tower treatment *(German)* 79—93798
low-decontamination approach to proliferation-resistant fuel cycle 79—26679
low-enriched fuel particle performance review 79—13426
LWHR, feasibility of Pu separation-free nuclear power economy 78—13313
LWR, alternative fuel recycling technology search 80—5303
LWR, borosilicate glass and glass ceramics with highly radioactive waste 80—5271
LWR, dissolver soln. fission product determ. by spark source mass spectroscopy 80—32422
LWR, fuel enrichment by linear accelerator 79—13497
LWR, fuel reprocessing plant, NDT control methods 80—5314
LWR, initial fuel loading problems 78—21741
LWR, laser fusion fissile-enrichment fuel factory, three-dimensional neutronics anal. 79—85794
LWR, optimum fuel loading and coastdown operation 79—30970
LWR, problems and solutions in W.Germany *(German)* 78—8952
LWR, Pu recycling, technical and economic study 80—720
LWR, quality assurance of fuel and fuel elements *(German)* 79—49810
LWR, review of alternative fuel schemes *(Italian)* 79—63784
LWR, Scale system cross-section validation with shipping-cask critical experiments 80—37559
LWR, system inception and fuel cycle in France *(French)* 79—26689
LWR, Tokai reprocessing plant in Japan, experience 78—89967
LWR, UO_2 fuel, critical expts. supporting close packed water storage 80—37434
LWR, use of recycle Pu in mixed oxide fuel, generic environmental statement *(Japanese)* 78—54862
LWR effect of fabrication variables on fuel in-core performance 79—63798
LWR fuel, feasibility of accelerator driven rejuvenation 80—27780
LWR fuel, partial partitioning of U and Pu by coprocessing solvent extraction 79—36382
LWR fuel, population dose calc. 80—46073
LWR fuel bundles, direct enrichment in laser fusion hybrid SOLASE-H 79—85793
LWR fuel containing Pn, waste treatment cost/benefit anal. 77—46378
LWR fuel cycle, back end, projecting 1985 fuel cycle impact of government action 79—59237
LWR fuel cycle, diversion anal. for material safeguarding 80—63274
LWR fuel cycle, high level waste, management 77—359
LWR fuel cycle, past and future in the Federal Republic of Germany 79—26688
LWR fuel cycle costs, future trends, waste disposal and reprocessing 79—26696
LWR fuel cycle costs, sensitivity to fission product data 80—23102
LWR fuel cycle effluent model for ENFORM system 78—94111
LWR fuel design, Italian progress in manufacturing, testing and management 79—26539
LWR fuel element regneration using linear accelerator reactor, anal. of AIROX process 80—23103
LWR fuel fabrication plant, cost of controlling inorganic chemical releases 78—5003
LWR fuel fabrication plant, Japanese national safeguards system 79—26717
LWR fuel performance, fabrication related effects 79—59238
LWR fuel regeneration by linear accelerator reactor 80—32336
LWR fuel reprocessing, hot cell studies 77—42169
LWR fuel reprocessing and mixed oxide fuel fabrication plant safety 79—26710
LWR fuel reprocessing plant, intermediate and high level waste management 77—42171
LWR fuel reprocessing plant, radioactive waste treatment costs and environmental impact 77—46379
LWR fuel researches, safety oriented, Japan *(Japanese)* 80—803
LWR fuels, actinide removal from high level wastes 77—26860
LWR high burnup fuels, chemical reprocessing problems 77—34420
LWR mixed oxide fuels, determ. of H_2O, Hz content by hot extraction methods *(German)* 79—49808
LWR mixed oxide fuels, safety aspects of PuO_2 micro-heterogeneities 79—49798
LWR multigoal fuel cycle optimization including nonproliferation objectives 80—73982
LWR oxide fuel, specification rel. to operational behaviour *(German)* 79—49797
LWR radioactive solid waste management 77—42130
LWR reprocessed fuel, EPMA 80—5306
LWR reprocessing solns., instabilities and solids formation 77—42170
LWR spent fuel, economics of away-from-reactor water storage basin 79—59201
LWR spent fuel, head-end part of fuel reprocessing facility, unloading installations, handling and transfer techniques *(German)* 80—57939
LWR spent fuel, receiving and shearing system 80—68928
LWR spent fuel containing ^{236}U, recycling in enriching plant 77—18684
LWR spent fuel coprocessing to ameliorate proliferation and waste management problems 79—26677
LWR spent fuel reprocessing plant, integrated safeguards assessment 79—89418
LWR spent fuel storage, B&W critical facility utilisation 80—37558
LWR spent fuel storage benchmarking expts. 79—63776
LWR spent fuel storage pools, k(∞) meter development 80—37560
LWR spent fuel transportation 78—724

fission reactor fuel preparation and reprocessing continued
LWR spent fuel water storage basins, away-from-reactor design comparisons 79−59200
LWR spent-fuel heatup following loss of water during storage 79−59202
LWR spent-fuel processing and packaging options, for disposal in geologic repository 80−18485
LWR stowaway fuel cycle effluent projections 78−94110
LWR ThO_2 fuel enrichment in laser fusion-fission reactor 79−81088
LWR-HWR tandem fuel flow concept 79−26496
LWR-type fuel element shipping casks and storage facilities, criticality assessment 79−63789
LWRs, Pu, commercial recycling assessment 79−71935
mass diffusion cascade, effectiveness increase using asymmetric schemes for combining stages 79−45392
material diversion, probability of detection, optimisation of safeguards 77−14258
material safeguarding, tamper and radiation resistant instrumentation 77−61584
material security, near-real-time accounting of strategic nuclear materials 79−85755
materials, safeguarding; 80−68835
materials, safeguarding, material accountability control automation at fuel reprocessing plant 80−68832
materials, safeguarding, meas. of fissile materials entering a reprocessing plant *(French)* 80−68828
materials, safeguarding, verification of reprocessing plant input and output analyses 80−68830
materials accounting and control system 79−13507
materials safeguard techniques capability in nuclear fuel facilities 80−63279
materials safeguarding, advanced accountability techniques for breeder fuel fabrication facilities 80−73939
materials safeguarding, advanced detection systems to prevent LWR spent fuel diversion 80−68822
materials safeguarding, advanced instrumental systems and techniques for fuel reprocessing plant 80−68821
materials safeguarding, determ. of U and Pu content of fuels using isotope correl. tech. 80−68834
materials safeguarding, dynamic materials accounting in chemical separations, conversion, and fuel fabrication facilities 80−73938
materials safeguarding, nondestructive measurements of irradiated fuel assemblies at a reprocessing facility 80−95392
materials safeguarding, possible ways of verifying the input of a reprocessing facility 80−68826
materials safeguarding, tracer techniques for Pu input accountability in reprocessing plants 80−68827
materials safeguarding at fuel reprocessing plant to prevent materials diversion 80−68824
materials safeguarding at reprocessing plants, inspection of hulls at La Hague *(French)* 80−68831
materials safeguarding at U fuel fabrication facility US/IAEA system 80−63284
materials safeguards, appl. of semidynamic material control in spent-fuel reprocessing plant 80−83174
materials safeguards, deviations from mass transfer equilibrium and mathematical modeling of mixer-settler contactors 80−83171
materials safeguards, dynamic materials accounting for solvent-extraction systems 80−83172
materials safeguards, microscopic process monitoring [for nuclear materials safeguards] of fuel reprocessing facilities to prevent material diversion 80−83153
materials safeguards, model for the application of IAEA safeguards at mixed-oxide fuel fabrication facilities 80−63286
materials safeguards, nondestructive, energy-dispersive, X-ray fluorescence analysis of product-stream concentrations from reprocessed nuclear fuels 80−83163
materials safeguards, sensitivity anal. of the MUF variance for large HEU fabrication plant 80−83169
materials safeguards and materials control, meas. tech. conf. Charleston, SC, USA (November 1979) 80−77544
materials safeguards procedures in fuel reprocessing plant 80−68823
materials safeguards surveillance at reprocessing plants, fuel history anal. *(French)* 80−68837
materials safeguards system for highly enriched U fuel fabrication plant 80−63285
materials safeguards system of back-end facilities with emphasis on waste management 80−83175
materials safeguards techniques appl. to Eurodif gas diffusion plant *(French)* 80−63281
materials safeguards techniques at Tokai fuel reprocessing plant 80−68833
materials testing reactors, low enriched fuel cycle 79−31095
methylradioiodide, catalytic trapping by beds of impregnated charcoal 78−21681
microsphere handling techniques and equipment 80−68924
MILLI test facility, operating experiences *(German)* 79−89470
Minch waters and sediments, Windscale effluent 77−91158
mixed oxide fuel fabrication, radiation protection and shielding 77−46417
mixed oxide fuel fabrication plant, operating conditions, general description 79−41028
mixed oxide fuel fabrication plant decommissioning, public radiation exposure 80−42800
mixed oxide fuel pellet fabrication using gel microspheres 80−42844
mixed oxide fuel production plant, safety aspects 80−819
mixed oxide fuel reprocessing, head-end steps, technological study 80−5305
mixed-oxide fuel, particle cavitation during reduction by H_2 78−8958
mixed-oxide fuel fabrication plant, large commercial, accident radiological risk assessment 78−17401
moderation control, risks and benefits evaluation 79−26671
moderation control in large-capacity process unit 77−65316
moderation control of ^{235}U enriched UF_6 77−65315
moderation controlled low-enrichment uranium systems, regulatory perspective 77−65317
molten salt breeder reactor, reactivity control capability of fuel-salt processing system 79−22399
MOX fuel, remote fabrication experience in FRG 80−13753
MOX fuel fabrication, safeguards systems alternatives 79−89474
MSR for efficient fuel utilisation without Pu separation 80−678
multiservice utility plug for remote fuel processing 80−68926

fission reactor fuel preparation and reprocessing continued
multistage counter current extraction with HDEHP, rare earth distrib. ratios calc. 79−49705
MX-type fuel and fuel pin swelling, 1973-76, fabrication and characterisation 79−41001
national energy programme of USA, nuclear power, fuel enrichment and waste disposal 79−26686
national waste terminal storage program waste packaging criteria 78−708
neutron dosimetry system, based on fission counter for fuel processing plant 80−57981
neutron monitors for process and safety control 80−5458
neutron shielding materials for spent fuel storage racks. radiation effects 80−9413
NFS reprocessing plant, radiation protection and shielding 77−46415
nitrate solutions, highly active, precipitation of Mo compounds during evaporation 78−37426
non-destructive assay technology and automated 'real-time' materials control 79−26721
nondeliverable fabrication plant fuel material with various enrichment, determ. of optimal comp. 78−13312
nondestructive assay of irradiated nuclear fuel for safeguards, review 78−82495
nondestructive assay of leached Zr-hulls in reprocessing plant 79−81070
nondestructive gamma-ray spectrometry method for fuel burn-up control *(Slovak)* 78−21672
nondestructive materials assay system for LASL's U recovery plant 77−42167
nonproliferation, nuclear fuel cycles and radiation damage 80−68934
nuclear energy, technical economic and safety aspects *(Hungarian)* 78−82465
nuclear energy centres, power development, economic and ecological problems, USSR *(Russian)* 79−31149
nuclear energy synergetics, characts. of integrated systems 79−13382
nuclear fuel, management and accounting, need for amortization 78−13241
nuclear fuel centre, fuel and waste facilities, safety, protection and socioeconomic aspects 78−58395
nuclear fuel cycle, demand and supply estimates, U supply 79−26694
nuclear fuel cycle facilities in USSR, nuclear material control and accounting *(Russian)* 79−26718
nuclear fuel cycle safeguards techniques development and appl. in European Community 79−26719
nuclear fuel cycles, U enrichment and nonproliferation safeguards *(French)* 79−26698
nuclear fuel processing plant operation, critical safety criteria *(German)* 78−74440
Nuclear Fuel Recovery & Recycling Center maintenance design criteria 79−9842
nuclear fuel reprocessing in West Germany, case against suspension *(German)* 80−32418
nuclear fuel technology project, implementation, Rumania 79−31156
nuclear material accounting, decision anal. 79−81049
nuclear material transport, West Germany, status future aspects 79−31234
nuclear materials, actinide determ. review of procedures at Rockwell Hanford Operations 79−81050
nuclear materials, nondestructive assay instruments for DYMAC program 79−11875
nuclear materials safeguards technology based on separation nozzle process for U enrichment facility 80−63280
nuclear power in Czechoslovakia, review *(Czech)* 79−31157
nuclear power plant spent fuel element reprocessing, basic problems *(Russian)* 79−26692
nuclear power programme, Philippines, prospects, problems 79−31175
nuclear power project management, book 79−30875
nuclear power stations, fuel circuit review, radioactive conditioned waste final storage *(German)* 80−799
nuclear safeguards, anal. chem. in nucl. fuel reprocessing 79−13505
nuclear safety aspects at power and fuel cycle plants in USSR *(Russian)* 79−26709
nuclear safety in France, reactors, waste, and fuel cycle installations 79−71908
nuclear waste disposal, geological aspects 79−9759
[Nuclear] fuel components QC reports 79−97883
occupational radiological exposure at nuclear fuel prep. plants, UK regulatory control 80−18708
on-line control *(Russian)* 78−74460
on-line nuclear materials accounting and control 78−29629
on-line radiation monitoring at a nuclear fuel reprocessing plant 80−95469
on-line radiation monitoring at fuel reprocessing plant 79−85731
organ-specific radiological impact of airborne effluents from model PWR and FBR reprocessing plants 80−3825
organic effluent toxicity from nuclear fuel reprocessing, rel. to carcinogenecity 78−5005
ORNL Transuranium Processing Plant, current status 80−68915
oxide fuel classification, quality criteria for fuel elements *(German)* 79−49812
oxide fuel pins, irradiation behaviour, effect of chemical factors *(German)* 79−49692
oxide fuel reprocessing plant at Windscale works, UK public inquiry 78−719
oxide fuels, chemical props. and performance, O_2 potential and transport mechanism 80−13761
oxide pellets, ammonium polyuranate precipitation, continuous, particle size distrib. and agglomeration control 79−93804
oxides fuels, introduction of spikes for diversion resistance, effect of recycling 80−13756
particle fuel prep. from U, Pu and Th nitrates, wet chem. process, for LWR, FBR and HTR *(German, English)* 77−65314
partitioning of high level radwaste, separation of transplutonium and rare earth elements 79−97881
partitioning of high level waste from fuel reprocessing *(Japanese)* 79−81019
PBHTR, Th fuel cycle performance 78−41841
Peach Bottom 1, HTGR nuclear power station, review of design and operation 79−45327
pellets, automated inspection 80−13766
personnel exposure minimisation at waste calcining factory 77−50312
PFR, fuel and component handling, CDFR intentions 79−97872

fission reactor fuel preparation and reprocessing continued
Phenix fast breeder reactor fuel dismantling hot cell 77—50274
photochemical modification of purex process, commercial benefits 77—79453
pilot reprocessing plants, Italian experience 79—31140
pin bowing in AGR fuel elements, meas. by camera device 80—106146
plant, Guard Tactics Simulation exercise 79—85742
plate type fuel, reduced enrichment, status report on high-U-density development 80—9393
PNC Pu fuel and reprocessing facilities, safety aspects 79—26711
political, ecological, social and economic aspects of nuclear fuel reprocessing, closed fuel cycle *(Dutch)* 80—106147
polyuranate gels, changes in pore structure during reduction and sintering 77—71685
post irradiation test equipment *(German)* 78—29632
postirradiation examination facility 80—18682
pot vitrification of fully radioactive fuel reprocessing wastes 77—61547
powder batching system development 80—68922
powder transfer in fuels refabrication by negative pressure pneumatic transport 80—68923
power plant fuel management, fuel cycle and in-core management 79—26702
power reactor, St. Lucie I, on-site reconstitution of 108 fuel assemblies 78—21742
power reactor design and fuel cycles, COMECON members' collaboration 79—603
power reactor fuel cycles, Pu, Th and U evaluation 79—26706
power reactor fuel manufacture, technological aspects 79—640
power reactors, fuel preparation, technological aspects *(Russian)* 79—31137
preconceptual accelerator-breeder design for fissile material and energy production 79—71933
preconditioning, power shock anal. and sipping 80—63358
preconditioning, TVA Browns Ferry Nuclear Plant, in-core management and core manoeuverability 80—63359
problems and cost in W.Germany *(German)* 77—79452
process control analysis of ^{235}U in U-Al alloy components, neutron absorpt. method 79—85720
process control in fuel reprocessing, destructive and nondestructive physical testing appls. 79—13512
production process, fuel rods for HTGR 78—86614
production process improvements 80—83213
programme in Switzerland *(German)* 78—8953
proliferation and Pu recycling, effects of future nuclear power 79—18021
proliferation resistant fuel cycle based on low decontamination approach 79—18022
proliferation-resistant method of recycling fissile-rich spent fuel, size classification of dry pulverised fuel 80—18581
proliferation-resistant reprocessing methods 80—27792
Pu holdup in glove-gox exhaust filter, in-line monitoring by gamma ray detection 80—78458
Pu recycling in LWR $(Th,Pu)O_2$ fuels, economic viability 80—18576
public issues concerned with reprocessing 77—33822
public issues of reprocessing and waste disposal, public issues 77—46375
pulsating solvent extraction columns, computation and simulation methods 79—97882
Purex kinetics, U extraction with tributylphosphate *(German)* 80—57937
Purex process, adaptation of centrifuge technology to active conditions 79—26684
Purex process, concs. of U, Pu, HNO_3, fission products, in LMOM2 extractor, expt., graphical determ. 78—41843
PUREX process, equipment testing for electrolytic methods 80—5311
Purex process, first extraction, Pu accumulation, computer simulation, SEPHIS code 80—68907
Purex process, radiolytic degradation of extractant-diluent systems 77—70313
Purex reprocessing plant, chemical separation of actinides from aqueous high level waste 77—26862
Purex solvent extracting system, monitoring and control instrumentation 80—37566
Purex solvent extraction process for fuel recovery and recycling 79—36387
Purex-type reprocessing plants, schematic flowsheet comparison *(German)* 80—57936
PWR, design, manufacture and marketing in France *(French)* 80—627
PWR, development and Pu allocation, optimal policies 80—725
PWR, economics of fuel cycle options 79—31102
PWR, planned cycle stretchout 79—31103
PWR, Point Beach Nuclear Plant, spent fuel storage modification 79—30974
PWR, Tihange-type, Pu recycling, physics and safety anal. 80—724
PWR advanced type fuels, dissolution process 80—37568
PWR and BWR systems and fuel cycle in USA 79—26687
PWR assemblies, pool-site fuel inspection and exam. techniques 80—18567
PWR core power manoeuvres, fuel duties and fuel preconditioning 80—63337
PWR fuel dissolution, Idaho processing plant remote systems 79—45455
PWR fuel storage, criticality eval. of low-density moderation 79—26667
PWR irradiated fuel assemblies, remote operations 80—68918
PWR refuelling fuel shuffle scheduling 79—9866
pyrocarbon, agglomerate model 77—79458
pyrocarbon, coating process and model 77—79459
pyrocarbon, HTGR fuel particle coatings, struct. charact. 77—83034
pyrocarbon, microstructure of coatings on fuel particles, TEM study 78—25293
pyrocarbon, quality control techniques 77—79461
pyrocarbon, X-ray anal. of porosity, effect on radiation stability 77—79464
pyrocarbon coating of Biso fuel, neutron effects on stress and strain 77—79437
pyrocarbon coating of Biso fuel, neutron effects on stresses and strains 77—79436
pyrocarbon coating of fuel element, hydrocarbon pyrolysis *(German)* 80—18585
pyrocarbon coating permeability effect on U redistrib. in HTGR fuel 77—40460
pyrocarbon coatings, gas permeable isotropic, fluidised bed prep. 77—46381

fission reactor fuel preparation and reprocessing continued
pyrocarbon coatings, quantitative chemical method to determ. disordered C component 77—79462
pyrocarbon coatings, TEM anal. 77—79463
pyrocarbon coatings for Biso fuel, the permeability meas. 77—79433
pyrocarbon deposition in fluidised bed, qualitative model, investigation with Stromungsrohr 78—56595
pyrochemical process chemistry 80—18578
pyrochemical processing for purification and recovery of spent reactor fuels 80—18577
pyrochemical reprocessing, evaluation of proliferation-resistant process 80—18580
pyrochemical reprocessing, process technology for Zn distillation, melt refining and salt transport 80—18579
quality control in nuclear fuel reprocessing and refabrication 79—13506
RA reactor fuel, gamma-ray spectrometric determ. of fission product activity and activity ratios 78—37430
radiation protection design 77—46416
radiation protection features of waste calcining facility 80—5377
radiation protection in nuclear power plants and the fuel cycle, conf., Bristol, England (Nov. 1978) 80—4471
radioactive effluent discharges, European Community, 1972-76, radiological aspects 79—41019
radioactive fission products formation and behaviour, Kr and Xe separation and processing *(Czech)* 79—49707
radioactive fuel, nonproliferation characts. 80—5304
radioactive fuel and waste, review of treatment handling, storage and disposal *(Italian)* 79—63753
radioactive particulates in gaseous effluents at nuclear fuel reprocessing facility 79—9848
radioactive rare gas, removal from fuel reprocessing plant *(Japanese)* 79—93747
radioactive reprocessing, comprehensive system of major hazard control 80—818
radioactive slagging pyrolysis incinerator, off gas treatment system 80—37514
radioactive solution sampling, vacuum-bottle system 80—18688
radioactive waste, final disposal possibilities, waste conditioning, storage and safety, review 79—26554
radioactive waste, report on 1977 IAEA conference *(Dutch)* 77—79446
radioactive waste, reprocessing, solidification vitrification of liquid waste, review 79—9762
radioactive waste, vitrification, industrial scale plant, under construction in France 78—78478
radioactive waste calcination and vitrification 77—61546
radioactive waste calcining at Idaho Chemical Reprocessing plant, design criteria 77—61549
radioactive waste elimination by nuclear transmutation *(Spanish)* 80—5298
radioactive waste in fuel cycle *(Japanese)* 79—9766
radiographic control of MTR fuel production, use of X-ray paper 78—5001
radionuclide corrosion and fission products, ion exchange separation 80—18460
radionuclide corrosion and fission products, liquid-liquid extractions with metal diethyldithiocarbamates 80—18459
radwaste denitration with organic reductants, effect of nitrate addition 79—97880
Rapsodie fast reactor, closed fuel cycle *(French)* 79—31161
re-extraction of U and Pu with weak acid, math. simulation 77—61587
reactor fuel cycles and proliferation, resource conservation and waste management *(German)* 79—13500
reactor operation and control simulator ROCS, extension to two energy groups 79—81034
recovery of byproduct U from manufacture of phosphatic fertilisers 78—17398
recycle facility, utility ownership 79—31099
recycle fuel plant layout, remote systems requirements 79—89481
recycle nitric acid, trace contaminants removal 79—85733
reduced enrichment program, fuel demonstrations, for test and research reactors 80—9392
reduced enrichment program for research and test reactors, generic studies 80—9391
refabrication technology development program 80—13759
refueling outage, planning and scheduling, flexibility problems 79—63793
regional fuel cycle centres for South and South-East Asia 79—31151
regional nuclear fuel cycle centres, IAEA study project 78—37429
regional nuclear fuel cycle centres. IAEA study project 79—31119
remote fabrication of nuclear fuel pellets 79—89478
remote fabrication of urania and thoria-urania fuels for HTGRs 80—13752
remote fuel fabrication, role of the Inst. of Nuclear Materials Management 80—13758
remote fuel refabrication laboratory concepts 80—68925
remote handling experience, Windscale 79—45456
remote radiation monitoring apparatus for processes of extractive separation of transuranium elements 79—71983
remote system mock-up testing for Idaho Chemical Reprocessing plant 80—73987
remote systems and maintenance, Japanese reprocessing plant 79—45457
remotely controlled computer-guided preparation facility for X-ray fluoresc. anal. *(German, English)* 78—17399
reprocessed nuclear fuel transportation 79—30918
reprocessing, status and prospects 79—26693
reprocessing and enrichment plants, IAEA safeguards 78—33282
reprocessing deferment policy anal., Pu recycle and nuclear proliferation 79—26680
reprocessing fast reactor fuel in Britain 78—89966
reprocessing plant, optimal installation program 77—46370
reprocessing plant for spent fuel, construction experience, Japan 79—31141
reprocessing plant off-gas, abatement techniques, control of ^{128}I, ^{85}Kr, ^{14}C, T 79—3221
reprocessing plant safety and protection anal. *(French)* 79—26713
reprocessing plants, design, construction, operation, maintenance *(French)* 79—31139
reprocessing plants, general characteristics, review 79—85717
reprocessing plants in International Fuel Service Centers, design concepts 80—18573
reprocessing solvent tributyl phosphate 77—65320
reprocessing solvents, decontamination and clean-up process 80—5254

fission reactor fuel preparation and reprocessing continued
reprocessing technology, research and development, review 79—26662
reprocessing technology status, large plants 78—21735
research programmes of Swiss Federal Institute for Reactor Research 80—52722
research reactor, Missouri University, fuel cycle optimisation 79—67930
research reactor fuel element loadings with reduced U enrichment 80—68933
review of nuclear fuel cycles and waste management 78—54863
risk analysis of the fuel cycle in the Netherlands 79—26624
risk assessment for potential accidental releases from nuclear fuel cycle operations 78—17353
risk estimation, evaluation, and management 78—17350
ROVER fuel, nondestructive anal. using isotopic source assay system 79—11873
safeguard application to Italian nuclear power plants and fuel cycle 79—26716
safeguarding a gas centrifuge pilot plant in Japan 80—63282
safeguarding fast critical facilities 79—85611
safeguarding of materials and facilities, effect on fuel cycle facility design 80—13757
safeguards, fuel reprocessing product soln. accounting, using K-edge densitometer 80—95352
safeguards, materials accounting in a LWR fuel reprocessing plant 80—83173
safeguards and transportation 77—67837
safeguards containment and surveillance concepts at fuel reprocessing plant 80—95350
safeguards instrumentation for Pu processing facility 80—63362
safety, materials management technique based on dynamic accounting methods 79—85738
safety, physical security assessment results synthesis, using decision analysis 79—85740
safety aspects of solvent nitration in HTGR fuel reprocessing 78—86650
safety exercises carried out in French industrial facilities *(French)* 78—55051
safety problems re environment and operating staff 80—816
Sandia solidification process for high level aqueous wastes 77—61551
Savannah River Plant, Purex process, 25 years of remote handling 80—68921
security, advanced safeguards system as proliferation deterrent 79—89383
security, fault tree and reliability relationships for analyzing noncoherent two-state systems 80—47600
security, integrated safeguards system, fuel labelling and perimeter monitors 80—37536
separation of Kr and Xe from dissolver off-gas in fuel reprocessing plant 77—61590
separation performance of Kr, Xe, Ar fission products by thermal diffusion column 77—42192
separation technologies, review 78—89965
separative power functions for enriched and depleted streams 80—47678
SHIELD computational system, nucl. fuel cycle appl. 80—37517
shielded cubicle and equipment for examination of coated fuel particles 80—68929
shipping cask criticality safety, SCALE system, correl. with expt. 79—63775
sintering furnace for remote fuel fabrication 79—89479
SNM safeguards, assay of dissolver solns. by totally sampled wavelength dispersive X-ray fluorescence 80—83160
SNR spent fuel element storage tank *(French)* 79—97884
solid neutron shield development, materials eval. for spent fuel shipping cask 80—13939
solidification of fission product solns. using a drum drier, FIPS method 77—61548
soluble neutron absorber use at ICPP 79—85730
soluble neutron poison use for criticality control at ICPP 79—85727
solvent extraction and ion exchange learning module 80—36803
solvent extraction equilibria, fast reactor fuel reprocessing 79—71937
solvent extraction in HTGB fuel reprocessing 78—86667
solvent extraction processing of mixed actinide residues, air sparge batch contactor 77—46369
solvent wash process to minimise radioactive waste volume 77—18681
South African isotope enrichment project, development and progress 79—31125
spallation breeder, parametric anal. 77—61585
specification and characterisation methods for nuclear fuels *(German)* 79—49796
spent fuel, neutron interrogation 80—5307
spent fuel assembly, gamma dose rate distrib. meas. with TLD 80—47735
spent fuel assembly storage racks, dynamic anal. 80—13639
spent fuel bundle counter, performance study 80—23064
spent fuel disassembly and Canning at Barnwell Fuel Plant 80—68919
spent fuel disposal in Germany *(German, English)* 79—9771
spent fuel element reprocessing, fundamental problems 79—26665
spent fuel elements storage in large pools, seismic load anal. 78—17400
spent fuel integrity in water pool storage 79—30976
spent fuel overheating in pool drainage accident, protection 79—85639
spent fuel reprocessing facilities continuous criticality control, dynamic approach 78—50291
spent fuel safeguards, containment and surveillance at fuel reprocessing facilities 80—95351
spent fuel storage, benchmark subcritical meas. at Hanford N reactor 80—37433
spent fuel storage 78—714
spent fuel storage basins 78—725
spent fuel storage expansion, planning, site preparation, installation considerations 79—45381
spent fuel storage facilities, design and operational characts. 79—36355
spent fuel storage facilities, methods of criticality anal. 79—63777
spent fuel storage in USA 78—713
spent fuel storage in water pools, technology assessment 79—36357
spent fuel storage optimisation 77—42129
spent fuel storage racks, design, safety calcs. and benchmarking 79—22416
spent fuel transportation logistics 79—89416
spent fuel transportation R and D in ERDA 78—710
spent fuel valuation, nation-nation transfer 79—89484
spent fuel valuation, procedure appls. and analysis 80—738
spent fuel zero leakage storage pool design 77—42139

fission reactor fuel preparation and reprocessing continued
spent LWR fuel, prospects for storage and reprocessing 78—5002
spent nuclear fuel, storage alternatives 78—74456
spent nuclear fuel re-enrichment without reprocessing, calculation simulation 79—26660
spent THTR fuel, in-line and off-line destructive chem. anal. 79—13508
spent-fuel shipping casks, Monte Carlo radiative heat transfer 79—59193
spent-fuel storage, time-integrated toxicity index 79—59203
spent-fuel storage, utility perspective 79—63794
spent-fuel storage facilities, capabilities for processing shipping casks 79—59199
spent-fuel storage program, US Dept. of Energy 79—63778
Sphere-Pac carbide fuel, model of swelling and gas release 80—13768
Sphere-Pac carbide fuels, temp. distrib. during restructuring 80—18572
sphere-Pac fuel, thermal conductivity during initial stage reconstructuring 80—810
Sphere-Pac fuel rods, techniques for quality assurance 79—93805
Sphere-Pac remote fuel fabrication process 80—13765
spherical carbide containing UO_2 pellets, fabrication by hydrolysis *(German)* 80—9399
spherical fuel particle porosity, testing equipment 80—27795
spikants, gamma active, for proliferation deterrence, practical aspects 79—93716
spouted bed, temp. distrib. meas., heat transfer characts. for appl. to PyC use *(Japanese)* 77—50275
storage of Candu fuel, air-cooled, Canadian canister program 80—5253
storage of irradiated Magnox fuel, dry, with air cooling 80—675
storage of spent nuclear fuel, design studies, cost estimates 78—29615
subsurface storage of commercial spent nuclear fuel 79—36356
Super Phenix fuel fabrication for Creys-Malville station, core controls *(French)* 79—31089
T immobilisation, possible solid mats., 80—27755
teaching, computer code for fuel management analysis course 78—4449
technical safety rules, catalogue and classification for reactors and fuel cycle plants 78—58384
technologies of preparation modification, w.r.t. unified production basis *(Czech)* 80—9388
technology assessment and nuclear waste management 79—89392
temp. distrib. in irradiated fuel pin bundle, analytical method of prediction 79—89472
tFTR blanket module experiments 80—37609
TFTR breeding modules, neutronics 80—37611
TFTR exptl. blanket modules, mechanical design 80—37610
Th-based nuclear fuels, pyrometallurgical reprocessing using Al alloys for proliferation resistance 80—18582
thermal reactor fuel cycles, actinide wastes toxicity limitations *(German)* 80—99220
thermal reactor stations in USSR, fuel reprocessing and waste disposal *(Russian)* 79—26592
thoria sol-gel processes 79—13503
THTR, Pu and Np separation from aqueous soln. *(German)* 77—83067
THTR fuel reprocessing, dibutyl phosphoric acid form. by degradation of TBP-n-paraffin extractant 77—70316
THTR fuel reprocessing, doses received by TBP-n-paraffin extractant 77—70315
Tokai reprocessing facility start-up *(Japanese)* 78—74457
toxicity reduction in Augean fusion reactor 80—106175
trans Cm isotope build-up in thermal reactors 79—85709
transmutation of waste actinides in thermal reactors 80—18491
transplutonium element symposium, Baden-Baden, Germany (September 1975) 77—28974
transport of nuclear material, especially nuclear fuel *(German)* 78—25314
transport package design, criticality evaluation, appl. of SCALE system 79—63774
transportation containers, struct. technology programs 78—707
transportation regulations 78—709
transportation status at fuel cycle end 78—712
transuranic element separation from radioactive waste and fuel reprocessing *(French)* 79—85811
transuranium element elimination *(French)* 77—26857
TRIGA fuel, low-enrichment U, neutronic and heat transfer charact. 80—9397
TRIGA Penn State Beazeale reactor, fuel management 80—63361
Trino Vercellese PWR, Am and Cm build-up in fuel rods 79—85754
tritium concentration in liquid waste by vacuum freeze distillation 77—14255
Trombay nuclear facilities, effluent release monitoring procedures 78—89993
UK reactor fuel reprocessing plant remote handling experience 79—9839
UK standards and procedures 79—81032
ultrasonic density meas., online system 78—718
underground solidified high-level radioactive waste retrieval system development 79—9818
United Reprocessors in Europe, present status review *(Dutch)* 77—14254
United States nuclear industry, new energy policy, review 78—5061
University of Missouri research reactor, fuel and productivity 80—9396
US decontamination system for reactor fuel transfer pool, remotely operated 80—68916
US nuclear fuel cycle, review 79—54585
USA nuclear policy, fuel supply, fuel cycle services 79—31115
USA policy in fuel reprocessing analysis, w.r.t. social costs, Pu recycle and nuclear proliferation 79—85737
USA Reduced Enrichment Research and Test Reactor Program, current status 80—68930
USA requirements for spent fuel processing industry 77—42166
Vallecitos Nuclear Center Hot Cells 80—68912
vapour-liq. equilib. data for gas mixtures *(German)* 77—84915
ventilation control of reprocessing plant 80—5318
VHTR fuel research, status in Japan 79—31135
virtual impactor aerosol separators, analytical study 80—42874
vitrified high-level waste, calcs. of radioactivity release due to leaching in final disposal 78—17360
vitrified waste, effects of post-devitrification leaching rel. to microstruct. 79—22417
volatile fission product atmospheric release from nuclear reactors and fuel reprocessing plants 79—34461
volatile fission products from nuclear fuel cycle and power stations, pollution effects *(Russian)* 79—31152
VVER, proposals for increasing power station efficiency 79—26491

fission reactor fuel preparation and reprocessing continued
VVER 365 reactor spent fuel, V isotope and transuranium element conc. 79−71938
VVER and RBMK power reactors, combined fuel use, transuranic nuclide formation 80−32352
VVER fuel elements, T and ^{85}Kr content obs. 77−54349
WAK reprocessing plant, a design basis for large-scale reprocessing plant 80−5310
WAK reprocessing plant, chemical decontamination of highly active process cell 80−5312
waste, high-level and actinide contaminated, from fuel reprocessing, long-term radiotoxicity problems 77−61571
waste ^{137}Cs, ^{90}Sr and rare earth radioisotope separation by cation exchange 78−78486
waste decontaminability, low level long lived radioactive liquids, chem. treatments 77−54351
waste disposal and storage management 77−10476
waste disposal rel. to fuel reprocessing 77−67853
waste management centre, features 77−88229
waste management in the Federal Republic of Germany. A survey of policy and research and development 79−26599
waste management problem *(German)* 79−13499
waste storage and reprocessing of fuels, nuclear burning and types of reactor *(French)* 80−91235
water pool spent fuel storage units, neutron anal., criticality state *(Spanish)* 80−32517
water reactor fuel, Federal Republic of Germany technology, development and experience 79−26703
water reactor fuel, reprocessing, waste disposal 79−36395
West German nuclear fuel element factory licensing legislation *(German)* 79−89469
Westinghouse high-density spent fuel rack design 78−727
Whiteshell Nuclear Research Establishment Hot Cell facility 80−68914
Windscale nuclear fuel reprocessing, shielding and radiation protection 80−18714
Windscale power station, possibilities and implications 77−79451
wiped-film evaporators for evaporating alkaline light water reactor radioactive wastes 79−36391
Zircaloy;UO_2 fuel design, LOWI 78−70600
Zircaloy cladding fabrication, review, characts. which impact fuel manufacture 79−59241
Zircaloy hulls, conversion to zirconate ion exchange materials for waste stabilisation 78−702
Zircaloy solid wastes from fuel reprocessing plant, management 77−61591
Al capsule dissolution and solidification from neutron irrad. UO_2 fuel rod 80−73981
AmO_2-UO_2, target possibilities for waste incineration, simulation study 80−32419
Ar-N_2 and Xe-Kr, evaporation equilibrium data method *(German)* 77−67846
Be_2C-graphite-UC_2 fuel development for pulsed reactors 79−67856
^{14}C, formation, distrib. in nuclear fuel cycle *(Russian)* 80−5316
$^{14}CO_2$ meas. in Karlsruhe Reprocessing Plant exhaust air 79−3231
^{252}Cf neutron assay system for nondestructive assay of enriched U 79−81067
$Gd(NO_3)_3$, use in fuel dissolution criticality control 79−85728
I, radioactive, adsorption on charcoal filter, safety evaluation *(Japanese)* 78−33267
I removal from fuel solns. as insoluble PdI_2 77−42164
^{129}I and organic compound determ. in LWR irradiated fuel solns. *(French)* 79−3230
Kr, cryogenic distillation from gaseous effluents 80−5309
Kr, immobilisation by incorporation into metallic matrix by ion implantation and sputtering 80−27794
Kr, separation in fission fuel reprocessing plants *(German)* 79−85719
^{85}Kr absorption in liquid CO_2 (KALC process), mass transfer efficiencies of packed columns 79−36354
^{85}Kr recovery system using cryogenic distillation 77−54331
^{85}Kr/Xe separation from nucl. engineering off-gases, low temp. distillation *(German, English)* 77−18671
LWR, sensitivity of fuel rod behaviour on as-fabricated characteristics 79−49805
^{99}Mo separation from neutron irradiated ^{235}U, HNO_3 soln., S collector 77−42161
^{99}Mo, separation regeneration of breeder reactor fuel *(Czech)* 78−82496
^{237}Np fission and capture cross sections in GCFR neutron spectra 80−37404
^{237}Np, neutron activation anal., determ. of small amounts in solns. containing U, Pu and fission prod. 78−21682
$(Pu,U)O_2$ mixed oxide pellet assay, using automated X-ray spectrometer 79−81066
Pu accountability, computerised gamma spectrometer system for meas. isotopic and total Pu conc. in solns. 80−63363
Pu accountability and control, field nondestructive assay measurements as applied to process inventories 80−63265
Pu accountancy by ceric oxidation, ferrous reduction and dichromate titration for nuclear materials safeguards 80−63364
Pu aerosols, charge distribution, from mixed-oxide reactor fuel fabrication lab. 79−5181
Pu, analysis, in fuel fabrication facility 79−16115
Pu analysis in irradiated fuel reprocessing solns., spectrophotometric determ. in near IR 80−78433
Pu and radioactive waste management, Swedish approach 79−31075
Pu as energy resource, availability, health hazards, nuclear weapon proliferation 77−46286
Pu assemblies in reload-1 of Dodewaard BWR 77−42018
Pu breeder reactor fuel, remote fabrication program, France 80−13748
Pu computerised inventory control system 79−36386
Pu concentration in irrad. fuel dissolver solns., determ. by isotope dilution alpha spectrometry 80−78428
Pu contamination of soil near Rocky Flats plant 80−42803
Pu content in nuclear fuels, appl. of isotopic safeguards tech. 80−99210
Pu ecological export from reprocessing waste pond 78−53533
Pu extraction, solvent choice effect 80−106149
Pu, FBR fuel remote fabrication development at PNC 80−13749
Pu, fuel and fuel elements for fast and power reactors 79−616
Pu fuel cycle back end services, utility optimisation model 78−41845
Pu fuel facility damage from high winds, risk anal. 80−63356

fission reactor fuel preparation and reprocessing continued
Pu fuel research facility for advanced LMFBR fuel *(Japanese)* 78−29624
Pu H_2O solns., Gd poisoned, calc. of sub-critical limits 79−85724
Pu, hazards and nuclear fuel reprocessing 79−45387
Pu, input accountability in reprocessing plants, tracer tech. using Mg and Pb 80−73919
Pu, LWR recycling in the European Communities 78−58394
Pu, mixed oxide fuels, development status, Japan 79−31130
Pu nondestructive assay, gamma-spectrometric method 79−81068
Pu nondestructive rapid isotopic anal. gamma-ray spectrometric method 79−81069
Pu oxide fuels, recycling in thermal reactors and fast breeders 79−31129
Pu, power reactor fuel and fuel elements *(Russian)* 79−30933
Pu processing for fast reactor fuel cycle 80−27793
Pu, production and availability, uses, reprocessing, fast reactor fuel cycles 80−68767
α-Pu, production difficulties 78−50252
Pu, programme in W.Germany *(German)* 78−8954
Pu radiation protection device based on neutron detection *(French)* 78−66362
Pu, reactivity effects of reflecting and interspersed concrete, composition effects 79−63788
Pu reclamation, precipitation-ion exchange scheme for actinide removal from salt waste soln. 79−49820
Pu recovery from nitric acid waste, comparison of anion exchange resins 80−681
Pu recovery from solid combustible waste 80−5274
Pu recycle, indecisiveness, impact on nuclear utilities 77−46384
Pu recycle and nuclear proliferation, economic analysis 80−5302
Pu, recycle facilities in Foratom countries, status and prospects 79−31131
Pu, recycle options in USA, benefit/cost anal. 79−31132
Pu recycle programme fuel cycles with reduced proliferation characteristics, review 79−18024
Pu recycling, influence on US future nuclear power developments 79−36394
Pu recycling by chemical process 78−58367
Pu recycling in LWR 79−45391
Pu, recycling in LWRs and environmental impact 78−89969
Pu, recycling in mixed oxide fuel for LWR 79−36385
Pu recycling in PWR reactors, VVER-440 reactor operation *(Czech)* 79−31093
Pu, reprocessing and recycle, economic and environmental benefits 77−46372
Pu reprocessing and safeguards in water reactors 77−67838
Pu reprocessing from spent fuel for LWR in Federal German Republic 77−67839
Pu, safe working, safety measures 79−41040
Pu safeguarding using resin bead mass spectroscopy 80−73984
Pu safeguards, fuel reprocessing product soln. accounting, using K-edge densitometer 80−95352
Pu safeguards, product soln. gamma-ray NDA using K-absorption edge densitometer 80−83162
Pu safeguards verification methods for input-accountability meas. at reprocessing plant 80−95349
Pu, source and availability of fuel for breeder reactor programme 77−61625
Pu transport, environmental impact 80−779
Pu, transportation, effect on environment, evaluation study *(French)* 80−27785
Pu, unmoderated, criticality safety practices for handling in glove boxes 79−26669
Pu use, decision making 77−42168
Pu, utilisation in thermal and fast reactors in Japan 79−26534
Pu-contaminated solid waste, operational techniques for minimisation, segregation and accounting 77−61567
Pu-contaminated waste management techniques 77−61568
Pu-enriched LWR fuels, remote fabrication at Belgonucleaire 80−13754
Pu-polyethylene system, min. critical mass calc. 77−42163
Pu-U anal., in-line evaluation of nondestructive assay instruments 79−85589
Pu+U mixed oxide aqueous solns., limiting critical concs., multiplication factor 77−26859
$Pu(C_2O_4)_2$ precipitator, dynamic process model for nuclear materials safeguards 80−83150
$Pu(NO_3)_4$-nitric acid soln., direct denitration in screw calciner 80−37567
PuO_2 air transportable package PAT-1, dose rate and criticality calcs. 80−13938
PuO_2, dissolution in HNO_3-HF soln., effects of metal ion impurities 77−70295
PuO_2 fuel, reproducible fabrication 77−77452
PuO_2 pellets, control of microstructural damage caused by He release 79−67926
PuO_2, rare earth, Y impurities separation, at. emission anal. 77−52723
PuO_2 refractory, dissolution in HNO_3-HF-H_2O at 100°C 77−18683
PuO_2 storage unit, design 79−41027
Pu(VI) reduction to Pu (IV) with NO_2 and NO gases 79−31108
^{236}Pu conc., prediction for mixed-oxide fuel 77−42121
^{238}Pu fuel form facility, Savannah River 79−45396
^{238}Pu fuel form facility at Savannah River Plant 79−9846
^{238}Pu production from ^{237}Np, optimisation techniques 79−71936
^{239}Pu aerosol, characterisation inside safety enclosures of mixed oxide fuel fabrication facility 79−13501
^{239}Pu direct enrichment of LWR assemblies in a fusion hybrid 80−37604
^{239}Pu, fissile fuel preparation by spallation of ^{238}U *(Russian)* 79−22441
^{239}Pu in aqueous soln., limiting critical conc. and thermal value of eta 79−63773
^{239}Pu in organic media, survey of criticality parameters 79−26670
^{222}Rn release from U ore crushing, grinding and leaching 78−89970
Ru, hazards and control in nuclear fuel cycle, review 79−36392
RuO_x, confinement of oxides volatilised during nucl. fuel reprocessing 80−47680
SiC coatings, CVD on microspheres in fluidised bed, parametric investig. 77−40457
SiC, pyrolitic coating for nuclear fuel particles 77−79465
SiC pyrolytic coatings for HTGR fuel particles, props. rel. to deposition conditions 79−31088
Tc, radiochemical characts. and role in nuclear fuel reprocessing, review *(Czech)* 78−82496

fission reactor fuel preparation and reprocessing continued
^{99}Tc separation regeneration of breeder reactor fuel *(Czech)* 78−82496
(Th,U) carbide fuel, radiological assessment 80−52776
(Th,U)C advanced FBR fuels, radiological assessment of reprocessing 80−73983
(Th,U)O_2 fuel conversion to (Th,U)C_2 for reprocessing 79−54579
(Th,U)O_2 fuel kernel prep. by external gelation of Th 79−93802
(Th,U)O_2 microspheres, fabrication 80−801
(Th,U)O_2 reactor fuel, dissolution in HNO_3-HF mixtures, fuel reprocessing study 78−59951
(Th,U)O_2 recycled fuel elements, composition calc. 79−13504
Th alternative fuel cycles, waste management aspects 79−59204
Th, ceramic recycle fuels, metal-clad, fabrication technology 79−59244
Th, continuous solvent extraction feed prep. 80−13773
Th fuel cycle, CANDU reactors 78−86620
Th fuel cycle, U cycle comparison, use in LWRs *(Spanish)* 80−32420
Th, fuel cycle, utilisation in light and heavy water reactors 79−26690
Th fuel cycle and technology 79−31114
Th, fuel cycle in water moderated reactor systems 79−26691
Th fuel cycle overview, DUTH fuels 79−59242
Th fuel cycle strategies in Canada 79−54586
Th fuel cycles, Savannah River Plant processing experience 79−59243
Th metal fuels, recycle technology 79−59245
Th nuclear fuel element reprocessing, avoidance of third phase *(German)* 79−6756
Th reprocessing by Thorex solvent extraction process at Savannah River Plant 79−36381
Th, resources and process technology 79−59170
Th sulphito complex ion precipitation with hexammine Co(III) chloride cation 78−92495
Th-20 U metal fuel, compatibility with candidate cladding alloys 80−13769
Th-based fuel pellets, fabrication 78−86669
Th-containing nuclear fuel, reprocessing, proliferation-resistant fuel cycles *(German)* 79−639
Th-U fuel reprocessing facility, computerised analytical process control system for material safeguards 80−78429
ThC_2 reaction with Zn and $ZnCl_2$ in KCl-LiCl fused salt mixture in 500-800°C range 79−54580
ThO_2 and (Th,U)O_2 fuel kernels, simplified preparation 78−86668
ThO_2 fuel kernel prep. by external gelation of Th 79−93802
ThO_2 nuclear fuel production, economic and environmental anal. 80−18575
ThO_2, sol-gel, for nucl. applics., sorption of water, CO_2 and N_2 77−4940
^{232}Th, assay in phosphate containing materials by solvent extraction-liquid scintillation method 79−22447
^{232}Th cycle, review of low cost fuel cycles using two separate fuels 79−45389
^{232}Th enrichment by linear accelerator for LWR 79−13497
^{232}Th enrichment by proton accelerator 79−13498
^{232}Th utilisation in reactor fuel cycles, review 79−45390
(U,Gd)O_2 sintered pellets, homogeneity determ. by ceramographical method *(German)* 79−49804
(U,Pu)C, controlled oxidation for head-end step reprocessing 80−5308
(U,Pu)O_2, ceramographic exam. of Dounreay PFR fuels, data bank storage 79−49811
(U,Pu)O_2 FBR fuel cycle, review 80−47682
(U,Pu)O_2, FBR fuel pellets, gel-supported precipitation conversion and prep. 80−813
(U,Pu)O_2 FBR fuel pin thermal design, effect of fuel stoichiometry 80−18570
(U,Pu)O_2 fuel performance, effect of O_2-metal ratio 80−13762
(U,Pu)O_2 fuel-cladding chemical interaction, effect of O_2-metal ratio 80−13763
(U,Pu)O_2 GCFR fuel behaviour, effect of O_2-metal ratio 80−18569
(U, Pu)O_2, hypostoichiometric fuels for FBR, effect of O_2 pot. on fuel props. *(German)* 79−49800
(U,Pu)O_2 LWR high burnup fuels, remote fabrication and performances 80−13755
(U,Pu)O_2, neutron activation determ. of O_2 coeff. 80−37457
(U,Pu)O_2, oxidation rates 80−37557
(U,Pu)O_2 powder, FBR fuel prep. by Au/PuC coprecipitation process 80−814
(U,Pu)O_2 rare earth, Y impurities separation, at. emission anal. 77−52723
(U,Pu)0_2, prod., recycling for use in LWR *(Spanish)* 79−63786
(U,Th)O_2 fuel rods, analytical stressing in hot cell 80−18566
U (VI) extraction from sea water, by adsorption on gel particles containing $Ti(OH)_4$ *(Japanese)* 77−54347
U and fission products, solvent extraction kinetics 79−26685
U and Pa decontamination, sorption and distillation methods, review *(Czech)* 78−82496
U and UF_6, mining, manufacture and purification processes, safety and waste disposal *(Spanish)* 79−63785
U, assay in phosphate-containing materials by solvent extraction-liquid scintillation method 79−22447
U concentration in fuel reprocessing streams, acid-compensation dual-wavelength spectrochem. anal. 80−78430
U, diffusion enrichment plant by Eurodif and Coredif, France 77−358
U enriching gas centrifuge cascade, reflux effect, enrichment enhancement control 77−54346
U enrichment, centrifuge, URENCO facilities at UK and Netherlands *(German)* 78−86666
U enrichment, centrifuge process, LWR fuel *(German)* 80−68905
U enrichment, commercial centrifuge plants in UK and Netherlands, prospects 78−5000
U enrichment, critical status report 77−34419
U enrichment, demonstration centrifuge plants at Capenhurst and Almelo, progress report 78−29626
U enrichment, HAGA radial separating nozzle centrifuge process, cost 78−46155
U enrichment, industrial processes 77−67851
U, enrichment, Italian activities 79−31126
U enrichment, jet membrane process 79−26683
U enrichment, layout of gas centrifuge cascades 79−26587
U enrichment, market survey *(German)* 78−4999
U enrichment, project using gas centrifuge at Centar, USA 77−357
U enrichment, random-walk model of holdup time of gas mols. in separation process 79−22481
U, enrichment, separation nozzle process 79−31124
U enrichment, US 1978 policy and future recommendations 79−36393

fission reactor fuel preparation and reprocessing continued
U enrichment, using advanced gas centrifuge technology, for commercial use 77−356
U enrichment by electrostatic filtration *(French)* 77−18707
U, enrichment by gas centrifuge, Japan 79−31123
U enrichment by gaseous diffusion process *(French)* 78−70622
U, enrichment by gaseous diffusion, Japan, research and development, economic evaluation 79−31121
U, enrichment by gaseous diffusion process *(French)* 79−31120
U enrichment by photochemical laser, two-phase flow with condensation, mathematical model *(French)* 80−74029
U enrichment calcs. and fuel requirements, basic information 77−74959
U enrichment changes, impact on utility fuel management, 1978-1985 period 79−63796
U enrichment facilities, cause analysis algorithm using cause consequence method 79−97823
U enrichment facility, based on separation nozzle process, materials management w.r.t. safety 79−85747
U, enrichment methods, efficiencies and costs *(Dutch)* 80−37634
U enrichment plant criticality analysis *(Japanese)* 78−46156
U, enrichment plants, general world situation, survey 77−355
U, enrichment processes in France *(French)* 79−31127
U enrichment prospects for 1980's 77−46368
U, enrichment services availability 79−26695
U enrichments that minimise blending consequences 78−13309
U, extraction from natural water *(Russian)* 79−31112
U extraction from sea water in Japan 79−31113
U extraction from seawater *(Japanese)* 78−36199
U extraction from seawater using magnetic adsorbents 80−37563
U extraction from seawater, feasibility 80−37564
U extraction from UO_2 minerals, underground leaching by H_2SO_4 of explosion crushed rock 77−61626
U extraction process for systems, with 2 extractable macrocomponents, graphical calc. 79−31098
U fuel, reprocessing of highly active fast reactor fuel 79−26666
U fuel enrichment, flow profile meas. of gas in rotating cylinder 77−46382
U fuel fabrication facility, integrated US/IAEA safeguards exercise 79−85736
U, future requirements estimates, 1976 to 2000 77−14232
U isotope separation, influence of flow field struct. in the separation nozzle 78−82498
U, isotope separation, new processes 79−31128
U isotope separation by Redox chromatography 80−37565
U isotope separation in countercurrent vortex tube, energy consumption *(German)* 79−27099
U, isotope separation in Fe^{3+}(III) water-glycerine solution-U(IV) cationic resin 79−41025
U isotope separation processes development *(French)* 78−66361
U isotope separation processes, w.r.t. economics, reliability and safety *(French)* 80−806
U isotope separation using ion exchange chromatography, U(IV)-U(VI) exchange isotope effects 79−36376
U isotopic enrichment, 1979 status *(French)* 80−807
U kernels preparation by external gelation process 79−26663
U laser 79−54578
U, laser enrichment, implications for nucl. weapons proliferation 77−67849
U loaded cation exchange resin, fabrication for HTGR fuel kernels, processing variables effect 78−8951
U, mass analysis for accountability in nucl. fuel processing 79−16112
U mill radiological effluent and environmental monitoring guidelines 78−94153
U mill tailings, meas. of surface Rn flux, effect of moisture content 78−5056
U milling, radioactive waste treatment costs and environmental impact 77−46377
U, milling waste management in USA 79−31077
U, mining and milling radioactive waste management N.Australia 79−31076
U, Mo and V, complex recovery from sedimentary ores 79−26701
U, nuclear fuel conversion plant, nondestructive assay 80−66761
U nuclear fuel particle prep. by ion exchange resin loading *(German)* 78−82499
U ore processing by filtration-free sorption method 79−26664
U ore processing plant development in Spain review *(Spanish)* 79−59231
U ore processing using nonfiltration sorption method *(Russian)* 79−31110
U ore treatment, in France and African countries *(French)* 80−805
U ore treatment plants and techniques *(French)* 79−26699
U ores, lower grade, cost saving techniques 77−34418
U, poor ore radiometric enrichment, plant flow scheme *(Russian)* 79−26700
U production from low grade Swedish shale 79−31111
U production in New Mexico, constraints 80−42843
U, recovery in slags containing calcium and magnesium *(Spanish)* 78−8955
U requirements for advanced fuel cycles in nuclear power systems 79−18027
U requirements for fuel cycles in expanding nuclear power systems 78−17320
U, safeguarding using resin bead mass spectroscopy 80−73984
U, selected enrichments for minimisation of blending losses, optimal set 78−17402
U, separation, gas centrifuge 79−3227
U solns., criticality safe tank design 78−722
U supplies in 1980s, trends 78−720
U supply and enrichment and irradiated fuel reprocessing developments *(French)* 80−18565
U, using gas centrifuge 79−49815
U utilisation, improved fuel cycles 80−787
U water flooded rod lattices, effect of soluble neutron absorbers in criticality prevention 79−85725
U/Pu coprocessing, impact on ore, conversion and enrichments costs 79−89475
U/Pu fuel reprocessing solutions, NDA using X-ray L-edge densitometer for materials safeguards 80−83167
U/Pu separation, use of carboxylic acids 77−38377
U/Pu systems, criticality control by Gd 79−85729

fission reactor fuel preparation and reprocessing continued
U-^{238}Pu-^{237}Np GCRF fuel cycle to produce isotopically denatured Pu for LWR 80–78427
U-Al plate type, reduced fuel enrichment utilisation, design variations 80–9395
U-Mo (1.5 wt.%) metallurgical study of forging *(French)* 78–21737
U-Pu aqueous solutions of oxides and nitrates, criticality, effect of Gd, Gd-B neutron absorbers 77–34393
U-Pu partitioning column, state of the art simulation 79–85734
U-Pu radial redistrib., effect of fuel rod parameters and fuel porosity *(German)* 79–49799
U-Pu-Np fuel cycle to produce isotopically denatured Pu 80–729
U-Pu-Zr metal fuel remote alloying and casting 79–89477
U-ZrH_x fuel for pulse reactor use from 900-1300°C 80–13770
UAl_x dispersion nuclear fuels, development and irrad. performance 80–78368
UAl_x fuel, development, irrad. performance in test reactors 80–68799
UAl_x plate-type reactor fuel element fabrication 79–49822
UC FBR fuel fabrication by reaction sintering of UO_2 and UC_2 80–812
UC:O, sample prep. method importance in O determ. *(Japanese)* 80–23100
UC-(PuC), ceramic fission reactor fuels, fabrication and performance, review 78–58392
UC_n-PuCn, refabricated fuel for breeder reactor, C determ. 79–11877
UF_4-CF_4 mixture, gas core fission reactor, fission based plasma engine 80–63366
UF_6 anal. with in-line gas chromatograph 77–63982
UF_6 centrifuge cascade, power supply loss accidents anal. 79–13502
UF_6 continuous gas flow control simulation *(German)* 80–78416
UF_6 conversion to UO_2 by fluid bed 79–97879
UF_6 conversion to UO_2, review 80–23099
UF_6, gaseous fuel reactor research 78–21736
UF_6 in gas centrifuge, fluid flow anal., computer calcs. 77–75924
UF_6 laser isotope separation for fuel enrichment 77–54618
UF_6, non-equilibr. condensation calcs. for laser isotope separation 80–10132
UF_6, temp. and density profiles in freely expanding gas for laser enrichment 78–74458
UF_6 vapor release in postulated accident 79–22442
UF_6-MF_5(MF_6), dil. solns., (M=Te, Mo, W, V, Sb, Ta), liq.-vapour equilib. 77–62632
UHg prep. from uranyl ion using two-compartment electrolyser 80–802
U(IV) photochem. prod. for use as reductant for Pu(IV) 79–36383
UN form. by reaction of C in NH_3 and H_2-N_2 mixture 78–21738
UN formation, mechanism and kinetics, reaction of UO_2 with C and N_2 78–48649
UN microspheres, prep., effect of process variables 78–8956
UN, synthesis from UO_2 through carbide 80–73980
UN-(PuN), ceramic fission reactor fuels, fabrication and performance, review 78–58392
UO_2 $(NO_3)_2$, establishing traceability to standard reference material 79–81052
UO_2 $(NO_3)_2$, preparation of uranium nitrate standards for X-ray fluoresc. anal. 79–81053
UO_2 ceramic fuel fabrication, simulation of thermal processes by emanation thermal anal. 80–811
UO_2 dense microsphere production by sol-gel technique *(Czech)* 80–68906
UO_2, dense solid reactor fuel particle preparation by sol-gel technique 79–31136
UO_2 effect of Be impurity on Pu breeding control 78–21740
UO_2, effect of H_2O vapour during sintering by sol-gel process *(Czech)* 79–31092
UO_2 fuel elements cores, electrically conducting inclusions detection, using eddy current flaw detector 77–90560
UO_2 fuel fabrication by AUC powder process 79–59240
UO_2 fuel fabrication by the AUC powder process 80–13744
UO_2, Gd bearing rods, magnetic and passive scanning system 80–37463
UO_2 grain growth studies, grain size and activation energy meas., rel. to nuclear fuel evaluation 79–93808
UO_2, green pellet with zinc stearate as additive, effect on sintering 80–68908
UO_2, irradiated, T loss during oxidative processing in air 79–97831
UO_2, LWR fuel, microstruct. and chemical props. of powder and pellet 80–629
UO_2, LWR fuel, prep. and advantages of CARAMEL, a sheeted fuel of UO_2 pellets 80–630
UO_2 low temp. fluorination in 3-inch diam. fluoridised beds *(Japanese)* 79–81056
UO_2 microspheres, Gel-Sphere-Pac process 80–13764
UO_2 microspheres, prep. from UO_3 $(NH_3)_2$, exam. of mech. and physical preps. 79–6758
UO_2, microwave heating in nuclear fuel preparation 80–37556
UO_2, oxidation rates 80–37557
UO_2 particle preparation by deposition on a fluidised bed 79–26707
UO_2 pellet storage facility, large dry, criticality eval. 79–26668
UO_2, pellets, pore size distrib. for optimisation of dimens. behaviour *(German)* 79–49801
UO_2 pellets, quantitative characterisation of structural parameters *(German)* 79–49803
UO_2 pellets, retention and release of water 79–67923
UO_2 powder, characterisation and quality control 79–49806
UO_2 powder, precompaction effect on compressibility 78–41846
UO_2 powder, sintering charact. 78–35341
UO_2, powder and pellets, determ. of f and metal impurities *(German)* 79–49807
UO_2 powder and pellets, fabrication by integrated dry route process 79–59239
UO_2 powder prep., effect of ammonium uranate props. 78–66363
UO_2 powders, cond. between sintering and agglomeration phenomena 79–9830
UO_2 preparation, emanation thermal anal. for characterisation of uranyl gel microspheres 80–95391
UO_2 preparation, thermal treatment of U^6 xerogels during calcination 79–49813
UO_2, preparation by sol-gel technique, intermediate products characterisation *(Czech)* 79–67921
UO_2, quantitative spectrographic anal. of rare earth and other impurities 79–59232
UO_2, removal of T and ^{85}Kr in O_2 medium 77–67850

fission reactor fuel preparation and reprocessing continued
UO_2 rods, 2.35 wt.% ^{235}U enriched, in water with fixed neutron poisons, critical separation between subcritical clusters 79–26673
UO_2 rods, 2.35 wt.% ^{235}U enriched, in water with fixed neutron poisons, benchmark calcs. for subcritical clusters 79–26674
UO_2 rods, 4.75 wt.% ^{235}U enriched, in lattices in water, critical expts. 79–63790
UO_2 rods, dissolution and storage exptl. program 80–37432
UO_2, sintered, fuel manufacturing technology *(Czech)* 78–50290
UO_2 sintered dense spheres from sol-gel technique intermediate products, characterisation *(Czech)* 79–22443
UO_2, sintered pellets, relationship between intercept length and grain diameter 78–52743
UO_2 sintering, thermal anal., hexavalent uranium xerogel drying, thermal treatment modelling *(Czech)* 79–36378
UO_2, sintering, use of NH_3, grain size changes 77–55920
UO_2, thermal and in-reactor densification 78–66364
UO_2 waste material, dry recovery 79–63787
UO_2-(PuO_2)(BeO), ceramic fission reactor fuels, fabrication and performance, review 78–58392
UO_2-UC_2-C, HTGR fuel microspheres, carbothermic conversion process 80–42845
UO_2-UC_2-C microspheres, carbothermic prep., rate-controlling preps. 80–45257
UO_2+F_2, reaction kinetics, molecular beam study 78–46157
$UO_{2+\alpha}$, ternary sintering diagram, grain boundary diffusion 79–59234
UO_3, microwave heating in nuclear fuel preparation 80–37556
U_3O_8 maximal fabricable conc. in Al base fuel elements 80–68800
U_3O_8, microwave heating in nuclear fuel preparation 80–37556
U_3O_8, oxidation rates 80–37557
U_3O_8 recovery from phosphoric acid *(Spanish)* 78–37428
U_3O_8-Al cermet fuel for research reactors 79–9835
UO_2(II), Th(IV), Cu(II), Ni(II), Fe(III), selective separation from rare earth elements on chelate ion exchangers 78–58861
$UO_2(NO_3)_2$ highly enriched solns., benchmark critical expt. calc. study, KENO-IV code 79–18026
$UO_2.(NO_3)_2$, highly enriched solution systems, benchmark critical expts. 79–18025
US-UC-UC_2 system, potential nuclear fuels, phase solid soln. studies, prep. and props. exam. 79–40996
U_3Si production, arc melting and hydrogenation methods comparison *(Chinese)* 79–85721
U(VI), extraction from sea water using polyacrylamide gel containing metal hydroxides 78–54861
U(VI) peroxo complex ion precipitation with Co(III) complex cation 78–80728
UZrH low enrichment fuels, test programs and analysis 80–9398
^{A}U, A=234, 236, minor isotope concentration meas. for safeguarding U enrichment cascade 80–63283
^{233}U, fissile fuel preparation by spallation of ^{232}Th *(Russian)* 79–22441
^{233}U, production by ^{232}Th cycle, review 79–45388
(^{233}U, Th)O_2 pellet-type fuels for CANDU reactors, remote fabrication plant design 80–13751
^{233}U/Th fuel recycle plant, materials safeguarding, control and accountability system 80–73942
^{235}U, conc. in $UO_2(NO_3)_2$ aq. soln., pulsed NMR determination 80–2658
^{235}U enrichment, separation nozzle process 79–31106
^{235}U enrichment, using double deflection separation nozzle *(German)* 77–46383
^{235}U enrichment, using laser based two-phase photoionisation and photodissociation methods *(Czech)* 77–61583
^{235}U enrichment analyzer based on interference spectroscopy, fabrication and performance *(Japanese)* 78–29625
^{235}U enrichment by chemical exchange process *(Japanese)* 79–26661
^{235}U enrichment by laser isotope separation 77–19113
^{235}U enrichment by laser isotope separation process, cost anal. 77–42160
^{235}U enrichment by separation nozzle systems with dynamic flow deflection 79–49825
^{235}U enrichment processes, flow profile measurements of gas in a rotating cylinder [^{235}U enrichment] 79–49793
^{235}U fuel enrichment, nondestructive determination by Ge(Li) spectrometer *(Czech)* 77–46371
^{235}U isotope separation, efficiency improvement by nuclear excitation by electron transition 78–55039
^{235}U isotopic content determ. of nuclear materials using gamma spectrometry 79–85756
^{235}U, low enriched, use of borosilicate glass Raschig rings 79–22446
^{235}U, recovery from enrichment plant tailings by laser isotope separation 80–83212
^{235}U, separation nozzle process for enrichment 78–21739
^{235}U to ^{238}U enrichment, ultracentrifuge, gas diffusion and nozzle separation techniques comparison, w.r.t economics 77–18680
^{235}U-Al castings in water, pulsed reactivity meas., Monte Carlo anal. 79–26522
^{235}U-H_2O solns., B poisoned, subcritical limits calc. 79–85723
$^{235}UF_6$ enrichment equipment, running-belt and rotary-disc concentrators, transient Knudsen diffusion 80–32421
^{238}U enrichment by linear accelerator for LWR 79–13497
^{238}U enrichment by proton accelerator 79–13498
V, extraction from seawater using Ti based composite hydrous oxides *(Japanese)* 80–804
Xe, cryogenic distillation from gaseous effluents 80–5309
Zr, PWR fuel dissolution process remote maintenance cell 79–9838
Zr-Nb (1 at.%) fuel element shells, high-temp. nitriding effects 79–24668

fission reactor instrumentation *see nuclear reactor instrumentation*

fission reactor materials
see also claddings; fission reactor fuel; fusion reactor materials; materials handling; moderators; radioactive waste
1200 MW, containment description *(German)* 77–42102
absorbed elements poisoned by Hf and B, KAHTER tests *(German)* 80–27749
accountability, dynamic materials control development and demonstration program 79–85745
accountability, fuel burn-up measurement using spatial power distrib. eval. and gamma spectrometry 80–68803
accountability, in-tank measurement of solution density 80–78391
accountability, tank volume calibration algorithm 80–83159
accountability tanks, automated calibrator 80–83158

fission reactor materials continued
- actinide waste burning in laser fusion driven hybrid reactor 79—22421
- activation cross-sections, rel. to fast power reactor circuit activity 80—13614
- advanced nuclear energy systems, emerging concepts, conf., Graz, Austria (March 1978) 79—13381
- advanced reactors, materials and design 78—78452
- aerodynamic and thermodynamic effects on environment of nuclear power plants *(German)* 80—61469
- ageing at high temp., effect on creep props. SEM 80—97516
- AGR, fuel cladding performance obs., biaxial creep meas. of 20/25/Nb stainless steel 78—82442
- AGR fuel, material aspects 80—47577
- AGR fuel cladding, development of high strength, ductile stainless steel alloys 80—45367
- AGR system for nuclear process heat, primary circuit component materials 78—13233
- alkali metal, liq., reactions with refractory metals and oxides, relevance to reactor technology 80—85173
- alkali metal technology development, high-temperature experimental plants *(German)* 77—10461
- alkali metals, liquid, O_2 pot. and O_2 distrib. coeffs. between alkali and struct. metals 80—65231
- alloy, order strengthening as method of reducing irradiation creep 77—48485
- alloy, solid soln. strengthening, HTR appl. 79—15688
- ALLOY 713LC, corrosion kinetics and products under low oxygen partial pressures *(German)* 79—87764
- alloy 800 for LMFBR steam generators 77—3108
- alloys, austenitic, neutron irradiation induced embrittlement, review 79—65120
- alloys, FBR components, in-reactor creep measurements 79—57082
- amine process for heavy water, design 79—615
- ANS annual meeting, 1977 78—663
- apparatus to meas. thermophysical props. at high temps. 80—37458
- Argonaut reactors, coupled core, neutron wave propagation, Be, graphite and D_2O as internal reflectors 80—27752
- assay and accountability of special nuclear materials using neutron correlation meas. tech. 80—69015
- austenitic alloys in hot water, low cycle fatigue, appl. to PWR 77—4871
- austenitic and ferritic steel in contact with liq. Na, C transfer 80—22945
- austenitic stainless steel, corrosion and creep in liquid Na, 873 and 973K 77—57722
- automated record keeping system 79—93759
- automated ultrasonic testing system for piping in nuclear power plant *(Japanese)* 80—71839
- ball bearing surface CVD coating expts. 79—83366
- behaviour during RBMK reactors start up and shutdown, investigation 79—9822
- biaxial creep behaviour, ribbed GCFR cladding at 650C 78—86597
- boiling flow regimes for carbide fuel and steel 79—85617
- BOR-60, operational characteristics of core and irradiated fuel parameters 79—97877
- BOR-60 reactor, boiling Na tests 79—97832
- BOR-60 reactor shim-rod sockets, Kh18N9 steel neutron irradiation 79—46716
- boral, reactivity worths of fixed neutron absorbers 78—21654
- borosilicate glass, behaviour as control rod in commercial reactor 78—8918
- borosilicate glass Raschig rings, appl. to low enriched ^{235}U fuels 79—22446
- α-brass, electron irradiated, defect production and interdiffusion 78—67739
- breeder reactor, with circulating liquid-salt fuel, fission product radioactivity reduction and residual heat release 79—26490
- bubble boundary layer formation over inclined porous plate 80—19504
- bubble nucleation, He-assisted, computer simulation 78—86625
- burnup anal., depletion pertubation theory for coupled neutron-nuclide field 79—45339
- BWR, Dodewaard reactor, power control using Gd absorbers *(Dutch)* 78—50277
- BWR, water chemistry characterisations 78—21635
- BWR containment vessels of prestressed concrete, pressure tests 80—81254
- BWR fuel rods, cladding, failure propensity, Studsvik Inter Ramp Project 80—13534
- BWR gamma ray field emitted by radioactive corrosion products, investigation 78—21661
- BWR LOCA, numerical simulation of hydrodynamic impact loads on cylinders 79—36350
- BWR piping cracks, relation between crack and stress 79—40995
- BWR power stations, operating record and reliability, reviews 79—22403
- BWR stainless steel piping, corrosion film charact. 79—54498
- BWR water chemistry characterisation 78—21658
- BWR with graphite channels, safety of nuclear power stations 79—26561
- CANDU, stress anal. of fuel channel interaction with end shields 79—59161
- CANDU, transuranium elements isotopic composition data tables 78—29564
- CANDU reactor, heat exchanger tubing materials 78—29583
- CANDU reactor core, materials and design criteria for fuel, cladding, and fuel channel 78—13238
- CANDU secondary side materials, selection and chemical specifications 80—613
- CANDU-PHW reactors, primary and secondary water chemistry, review 79—22382
- Caorso BWR power station, structural acceptance tests of primary containment *(Italian)* 79—30951
- carbide fuel-coolant interactions, PLUTO code 79—85613
- carbonaceous matrix materials for HTGK fuel rods, irradiation-induced dimensional changes 80—65052
- ceramic utilization in fission reactors 79—93718
- ceramics, TEM study of radiation damage, review 79—86816
- ceramics utilization, review 80—32350
- ceramics utilization in nuclear industry, current status and future trends, review 79—45349
- charged-particle-producing reactions of 15 MeV neutrons, cross section, ang. distrib. 80—13626
- chemical thermodynamic data of fission product compounds in irradiated nucl. fuels *(Japanese)* 79—22387
- CIRENE reactor, technological aspects, materials *(Italian)* 77—14214

fission reactor materials continued
- CIRENE reactor power channel, fuel string dynamics and pressure tube fretting corrosion 79—30950
- clad failure prediction during FBR overpower transiency, JANE code 80—78363
- clad material, C transfer *(German)* 77—50230
- clad strain, power history effect, in-reactor meas. 80—78357
- cladding, corrosion product deposition, water chemistry effect 80—106116
- cladding, cracks under stainless steel cladding of pressure vessel, detection, causes, danger 80—52760
- cladding, eddy-current integrity testing at HFER 80—68788
- cladding, irrad., fuel removal methods eval. 77—54306
- cladding, stainless steel, cold-worked Type 316, transient mechanical behaviour 78—86598
- cladding, strain ratcheting during power cycling 80—16442
- cladding, three-regions rewetting model with decay heat generation and inlet subcooling 80—22965
- cladding alloys, compatibility with Th-20 U fuel 80—13769
- cladding and oxide fuel in LWR, FBR, irrad. behaviour, chemical process, densification, corrosion *(Japanese)* 77—83033
- cladding dilatation, influence of radial temp. gradient 77—46287
- cladding motion in 37 pin loss of flow expt. 80—18541
- cladding performance during power changes on fuel element model, strain defects 78—58359
- cladding strain, effect of fuel density and fuel relocation, in-reactor meas. 80—104408
- cladding tube, effective temp. for expanding tube 77—74931
- claddings for AGR nitrided stainless steel alloy, struct. and prop. 79—54496
- coatings for nuclear fuel particles, irradiation performance, additives effects *(German)* 80—27748
- comparability study of fission and fusion reactors w.r.t. safety, costs and development time 79—59114
- component reliability, non-destructive testing and flaw evaluation *(French)* 79—24711
- component-support impact dynamics, elastic anal. by model expansion method 79—45343
- components review *(Spanish)* 77—79429
- composition changes in neutron-irradiated materials, calculation methods 77—62565
- computer assisted accountancy and control system *(German)* 79—13415
- computerised control system, real-time, generalised concept 79—89449
- computerised inventory and criticality control system, on-line, INMACS 79—89486
- concrete, 1-D penetration of UO_2 molten fuel debris, following FBR HCDA 80—47640
- concrete, behaviour in contact with molten corium 80—13584
- concrete, containment material, development of different types to overcome various problems 80—52738
- concrete, creep under combined shear and compression stresses *(Japanese)* 77—40511
- concrete, dynamic loading due to steam condensation, in BWR pressure suppression system 79—97754
- concrete, effect of liner on heat and mass transfer characts. 78—17388
- concrete, Eisenhauer-Simmons γ-ray build-up factors, Taylor coeffs. 77—34394
- concrete, finite element creep anal. 78—41813
- concrete, gamma-ray buildup factors, Tchebycheff-fitted Berger coeffs. 79—31226
- concrete, interaction with molten core material, heat flux determ. 78—17385
- concrete, large-scale steel melt/concrete interactions test for meltdown accident 78—17387
- concrete, neutron reflection characteristics 77—71633
- concrete, plastic-brittle behaviour, hardening and softening constitutive eqns. 77—21270
- concrete, reactor shielding thermal stress cracking anal. *(German)* 80—5232
- concrete, thermal decomposition, empirical model for kinetics and stoichiometry 78—17386
- concrete pressure vessel, uniaxial compressive strength, 450-1033K 78—44299
- concrete reactor vessels, behaviour of perforated slabs under temp. and external load 79—30917
- concrete shields containing iron, two dimens. cross section sensitivity anal. of Fe 77—23311
- concrete-Na interactions, high-temp. nuclear materials consideration 77—50243
- concrete-paraffin shielding, fast neutron leakage, use of Monte Carlo method 77—23309
- concretes, normal and ilmenite, neutron attenuation 77—23308
- conference, San Diego, Calif., USA (June 1978) 79—17972
- conference, San Diego, Calif., USA (June 1978) 79—49650
- consistent creep and rupture properties for creep-fatigue evaluation of nuclear components 80—35329
- containment liner seismic reliability under statistical uncertainty, cracking 78—89948
- containment of special nuclear materials for storage, transfer and nondestructive assay meas. 80—63267
- control and accountability system (DYMCAS), prototype terminal 79—89485
- control with VACOSS variable coding seal system 78—82491
- controllable unit approach to material control 78—82445
- coolant, continuous radiochem. anal., fission product identification from γ spectra 77—71652
- core debris interaction with concrete, LMFBR, HCDA anal. 77—71676
- core materials, plastic deform. constitutive eqns. 80—35259
- core materials development for water cooled reactor systems 77—46296
- core melt in hydrodynamic fragmentation, acoustic cavitation mechanism 79—85650
- core reactivity and space-domain noise effects of randomly dispersed materials 78—94071
- Corium-E simulants, effect of pressure on steam explosion triggering 79—49752
- corrosion damage, overview of water chemistry 79—54553
- corrosion damage, water chemistry influence on nuclear power stations 79—54517
- corrosion fatigue crack growth rate data, appl. to integrity anal. 80—32353

fission reactor materials continued
- corrosion in water-cooled reactors, control in CIRENE plant *(Spanish)* 77−34392
- corrosion problems and prevention in nuclear industries *(Japanese)* 80−42711
- corrosion product reduction program 78−21665
- corrosion products in main technological systems of atomic power plants with an RBMK-1000 reactor during operation 80−5236
- corrosion research in FBR and PWR nuclear power plants, review of problems *(Czech)* 78−62598
- crack propag., fracture, and ductile-brittle transition *(Spanish)* 79−36316
- crack-front tunnelling, investigated by single specimen compliance technique 80−70300
- creep, cyclic plasticity, recovery, unified approach to interaction prediction 79−8329
- creep, irradiation induced, correlation of theory with expt. evidence 80−88255
- creep capsules, multiaxially stressed, remote pressurization and laser closure welding 79−54514
- creep testing, extensometric method, for inside nuclear reactor channels 80−100998
- creep testing machine using torsion, in radiation zone of nuclear reactor 78−11480
- criticality calculations, random geometry model of fissile solns. containing borates Raschig rings 79−36310
- Croloy steel for LMFBR steam generator, meas. of T permeation 80−68775
- cyclic creep, enhnaced, high temp. theory for polycrystalline materials 78−7018
- cylinders, eigenload formulation of thermoelastic stress 79−46213
- cylindrical rods, anal. of self-equilibrating end stresses by Lanczos-Chebyshev method 79−46212
- data acquisition shelf monitor system for special nuclear material real-time inventory 79−45426
- debris bed and sacrificial materials interactions at high temperatures 79−85612
- debris bed dryout obs. during D-3 expt. 79−85597
- decision analysis in safeguarding special nuclear material 78−82485
- decommissioned structural materials, long-lived activity and implications for containment 80−13739
- decommissioning of fuel reprocessing facility, nondestructive assay of ^{235}U content of materials 80−81269
- defectoscopy of gamma-active objects in their natural radiation *(Bulgarian)* 80−71867
- depth profiling of H and He using ion beams 78−7300
- deuterium distillation at desalination plants 77−67894
- dilute alloys, defect trapping and solute segregation in irradiated alloys 80−13603
- dimensional instability of CF8 stainless-steel castings at elevated temperatures 78−82448
- diversion and weapon proliferation, use of MEU/Th fuel for HTGR-GT 80−22903
- double-wall piping welded joint residual stress study *(Russian)* 78−27541
- Dragon HTR project, review 79−45326
- dynamic buckling of shells 78−18210
- dynamic materials accounting for LWR fuel cycle 79−36325
- EBR-II, fabrication of in-reactor creep capsules using previously irradiated cladding tubes 79−54478
- EBR-II, multiaxial in-reactor creep in presence of significant void swelling 79−55818
- EBR-II 80−13598
- EBR-II preparation for breached-element operation, safety concerns 79−9792
- EBR-II sodium systems, control of oxygen, hydrogen and tritium impurities 79−93696
- elastic creep fatigue rules fo ASME B&PV code case 1592 78−44211
- elastic-plastic linear hardening material for thin-walled pressure vessels, stability and yield stress anal. 80−92075
- elastic-plastic struct. cyclic thermomech. loading 79−7299
- elastic-plastic-creep response of high-temp. nucl. components 77−3112
- elastomer compound O-rings for service in hot water, evaluation 79−29257
- engineering materials certification for safety and reliability testing 80−78360
- European Nuclear Conf., Hamburg, Germany, May 1979 79−97841
- evaporative removal of Na from components 79−93735
- failure analysis by remote fatigue crack growth meas. system 80−68790
- fast heterogeneous reactor, Na-voiding reactivity coeff. 80−52713
- fast power reactors, fuel pin viability in LOCA 79−76090
- fast reactor, assessment of struct. material Doppler effect 78−33255
- fast reactor ceramic fuel-steel system, freezing of flowing liquid in melting tube, simulation expt. 79−30981
- fast reactor cladding material, transient burst tests 79−93770
- fast reactor fission gas behaviour, eqn.-of-state of Xe at high temp. and pressure 79−67860
- fast reactor fuel pellets, crack pattern analysis 79−54497
- fast reactor materials, fast neutron damage 78−10093
- fast reactor peripheral fuel element shells, radiational swelling circumferential nonuniformity 79−19289
- fast reactor safety, Na boiling expts. *(Italian)* 79−9764
- fast reactor steels and alloys, neutron damage development, irradiation conditions, chemical composition 80−34082
- fast reactor structural material neutron data, conference, Geel, Belgium (December 1977) 80−13610
- fast reactor structural materials, energy-averaged neutron cross sections 80−13628
- fast reactor subassemblies, irrad. swelling induced bow 79−93724
- fast reactors Na cooled, core component material irradiation induced void swelling and creep, technological consequences summary 79−36327
- FBR, anal. of reactor component fluence limits, damage function methods 77−18668
- FBR, development in Japan, fuel, materials coolants and design *(Japanese)* 80−22888
- FBR, HCDA, retention of molten core debris pools in composite sacrificial beds 80−47643
- FBR, rigorous and efficient struct. Doppler effect calcs. 78−33256
- FBR, simultaneous freezing and melting in finite media 80−620
- FBR, some lessons drawn from operation of Phenix and Rapsodie cores 80−639

fission reactor materials continued
- FBR cladding dilatation, effect of radial temp. gradient 80−68776
- FBR containment code, structural deform., SEURBNUK-2 80−78404
- FBR containment code validation program, SEURBNUK 80−78405
- FBR containment materials interaction following HCDA, simulation 80−47642
- FBR core disruptive accident, response of upper internal structures, finite element computer anal. 80−47645
- FBR core materials studies for improving reactor performance, trends 80−102232
- FBR fuel cladding alloys, phase instabilities and swelling behaviour 79−54500
- FBR fuel element structural materials, consequences of improved behaviour under irradiation 80−640
- FBR fuel pin failure, fuel porosity and crack effects on transient overpower analysis 80−71760
- FBR fuel pins, cladding attack model 80−45446
- FBR materials, finite element fracture mechanics 77−42095
- FBR R and D programs in Europe, basic objectives for cladding and struct. materials 80−47566
- FBR safety analysis, expts. on hydrodynamic aspects of volumetric boiling of molten fuel-steel mixture 80−47652
- FBR structural materials, design appl. of irrad. creep and swelling data 79−59167
- ferritic alloy DT02, oxidation behaviour in CO_2 or Ar with H_2O and H_2, 823-123K 80−3249
- ferritic steel, mechanical property characterisation in support of HTR design 78−29577
- FFTF Fuels & Materials Examination Facility design features and objectives 79−9746
- FFTF Fuels & Materials Examination Facility equipment design and development 79−9747
- FFTF fuels and materials exam. facility and materials handling systems design 80−18421
- finite steel slabs, melting by flowing fast reactor fuel 79−54494
- firebricks for concrete floor protection from molten UO_2 80−18438
- fission cross sections meas. In YAYOI reactor, fast neutron spectrum 77−42013
- fission product cold trapping in stainless steel Na loop 77−61514
- fission product release and distrib. in coated particles, laser system *(German)* 78−82403
- fission products, neutron cross-sections data for ENDF/B-IV library 78−25290
- fission products, solubility rules based on lattice parameter differences 78−59953
- fission reactor, FAXMOD anal. of creep and sheath ballooning 80−42759
- flow induced vibrations and fretting wear damage 80−95357
- flow-induced vibration anal. of nuclear reactor components 79−22380
- Fort St. Vrain HTGR, He circulators, development and testing 79−67821
- Fort St. Vrain HTGR power station, review of design and operation 79−45353
- fracture mechanics analysis, Pilgrim I nozzle-to-press. vessel weld discontinuities 77−80110
- fracture mechanics of reactor primary system under operating and accident conditions 78−66342
- fracture problems in reactor technology 78−78472
- fracture zone analysis of fission reactor elastoplastic materials *(Spanish)* 79−66139
- Freon-11, reactor coolant, steady-state and transient CHF meas. 79−49732
- FTR, criticality expts. of fuel pins in water, computer calcs. 79−59162
- FTR, strain rate effects in transient overpower cladding failure analyses 79−85660
- fuel cladding, in-reactor creep testing 77−23211
- fuel cladding, slightly oval cylindrical shells, creep anal. 78−78468
- fuel cladding tube deformation monitoring, photodiode image scanning technique 79−30938
- fuel cladding tube mech. props., ring compression test, finite element anal. 77−83037
- fuel cycle and material international safeguards, current technical issues 79−26714
- fuel element distortion during irrad., meas. methods 79−63747
- fuel element in-cell laser profilometer 80−22955
- fuel element low meas. and data reduction at HFEF/N 80−22954
- fuel form and cladding carbide distrib. on fuel-clad interaction during irrad. 79−85618
- fuel pellet-cladding axial interactions, computer anal. of fuel pin performance 80−13605
- fuel pin claddings, fission gas driven creep calcs. 79−26531
- fuel pin profilometry adaptation, cutoff saw 79−45452
- fuel pin rupture in FBR, implicit compact difference method for solving linearized fuel sweepout equations 79−89355
- fuel pin tubes, obtaining material properties from the ring compression test 79−47755
- fuel pins, fast breeder, fuel-cladding mech. interaction, obs. and anal. 80−86959
- fuel sheath in boiling water, corrosion product deposition and release 79−91839
- fuel sheathing strain at high temp., steam oxidation effect 77−6525
- fuel sheaths, neck growth during high temp. transients in steam 80−78396
- fuel-coolant interactions, role of Rayleigh-Taylor flow instabilities 79−17983
- fuel-coolant interactions in a shock tube geometry 80−13660
- Fuels and Materials Examination Facility, design features and objectives 79−45448
- Fuels and Materials Examination Facility, equipment design and development 79−45449
- fusion and fast breeder reactors, a comparison, book 78−78430
- fusion-fission hybrids, mag. mirror blankets and drivers 79−13517
- gamma heating-effects, meas. using calorimetric and dosimetric techniques 80−658
- gamma-heating effects, calorimetric validation of TLD measurements 80−63254
- gas atoms per bubble of inert gas in solid 77−76468
- gas cooled reactors, background and status in UK, review 79−45333
- gas core reactor, high temp., wall stabilisation, possible use of graphite 79−3190

fission reactor materials continued
GCFR advanced alloy cladding, oxidation behaviour in the environment 80—104350
GCFR cladding motion simulation in concurrent flow 79—85614
GCFR claddings, neutron-induced He implantation, calc. of total flux 80—42773
General Atomic Hot Cell modification and refurbishment 80—68786
glass, ion bombardment, electromigration as deterioration mechanism 78—26601
graphite: Ba impregnated, sorption of Cs, thermodynamic modelling of multicomponent sorption behaviour 80—102243
graphite, CH_4 release, desorption study 79—51420
graphite, CO_2 permeability meas. up to 41 bars 80—29176
graphite, coarse grained, fracture toughness *(German)* 80—76358
graphite, corrosion by CO_2, CO production radiolytically induced gas pressure effects 80—106115
graphite, Cs sorption kinetics modelling 80—102244
graphite, cyclic fatigue, influence of stress cycle and neutron irrad. 79—52335
graphite, development and irradiation program for PBHTR appls. 80—5245
graphite, diffusion of Sr, lab. determ. 77—7900
graphite, electron-spectroscopic analysis of neutron-irradiated pyrographite 80—63261
graphite, failure criterion, J-integral critical value 78—84999
graphite, fast neutron flux effect on irradiation damage 78—22768
graphite, fracture mode criterion, combined, disk test study *(Japanese)* 79—66153
graphite, fracture toughness up to 2600°C 78—68760
graphite, heat strength calc. for power reactors 79—36331
graphite, irradiated, stored at room temp., neutron damage annealing and C_{44} shear modulus 80—2080
graphite, irradiation testing of reference grades with greater dimens. stability 80—42776
graphite, irradiation-induced temp.-change effects, semiempirical model calc. 80—42775
graphite, isotropic nuclear, neutron irrad. behaviour 78—18683
graphite, material properties, neutron irrad. effects, model 79—10880
graphite, neutron irradiation effects on thermal shock resist. and fracture toughness *(Japanese)* 80—66622
graphite, neutron-irradiated, EPR, rel. to electronic struct. *(Japanese)* 78—19326
graphite, nuclear, change in ratio of thermal expansion coeffs. at elevated temps. 79—42283
graphite, pyrolytic, ion bombard., flaking, stress fields around penny-shaped cracks 78—52946
graphite, pyrolytic, neutron irrad. at low temp., thermal cond. recovery *(French)* 77—62566
graphite, pyrolytic, numerical discussion of flaking mechanism from ion bombard. 78—52947
graphite, pyrolytic C coating within pores 79—41035
graphite, pyrolytic doped with B^{11}, neutron irrad. damage at 60°C 79—90702
graphite, quantitative microanalysis by laser emission spectroscopy 80—81384
graphite, radiation alteration over wide range of neutron flux and irradiation temp. 80—29072
graphite, radiational size stability, effect of technological factors 79—26527
graphite, reactor grade, irrad. creep, 850 to 1100°C 78—44167
graphite, reactor material, ultrasonic nondestructive testing *(Japanese)* 79—43520
graphite, stress and strain determ. depend. of mech. characts. on temp. and fluence 79—40998
graphite, synergistic effect of electrons on atomic H activity 80—106112
graphite, thermal conductivity, effect of porosity 80—65314
graphite, thermal shock fracture toughness eval. by arc discharge heating 78—72835
graphite, uniaxial tensile creep capsules with continuous strain registration 77—42071
graphite, unirrad. and neutron irrad., compressive stress effect on Young's modulus 77—61503
graphite, use as ISSEC in Tokamak reactor 78—41860
graphite core, of fission reactor, impurity migration, proton microprobe obs. 79—52803
graphite corrosion in PBHTGR process heat reactor following massive air ingress *(German)* 80—83181
graphite cylindrical thin shell, thermal shock, fundamental heat cond. soln. 78—29575
graphite elements in HTGR, transverse flow theory 79—67888
graphite high temp. bulk, B poisoned, thermal neutron spectra meas. 79—54465
graphite oxidation and coolant chemistry of CEGB gas-cooled reactors 80—42774
graphite permeability, effect of neutron irradiation 79—71900
graphitic reactor materials, determ. of macro and mesoporosity by stereometric anal. *(German)* 79—3205
haematite particles, crud deposition on heat transfer surface, surface chemistry 80—35376
Hastelloy, corrosion behaviour in simulated HTGR He environment 79—54495
Hastelloy C-276/Bi_2Te_3 contacts, elevated temp. compatibility, appl. to radioisotopically powered thermoelec. generator 79—49680
Hastelloy X, carburisation and dimens. stability in HTGR, He environment 80—45366
Hastelloy X, creep and creep rupture props. in air and helium at 900°C *(Japanese)* 77—52405
Hastelloy X, crevice corrosion by water vapour and methane in Ar at 1 and 25 atm. 77—25203
Hastelloy X, heat resistant superalloys, for nuclear plants in He, creep props. *(Japanese)* 79—83263
Hastelloy X, high temp. low cycle fatigue strength *(Japanese)* 77—59910
Hastelloy X, high temp. low cycle fatigue tests, ductility, fracture 77—90523
Hastelloy-X, carbonization and carburisation in high press. He environment *(Japanese)* 79—26516
Hastelloy-X, electron irrad., void swelling 79—14822
heat resisting alloys in various gas environments, high temp. props. *(Japanese)* 77—71649

fission reactor materials continued
heavy ion bombardment damage, comparison of analytical and Monte Carlo computer codes 80—102245
heavy water, process simulation of production plants 79—22396
heavy water, US velocity experimental determ. using freq. pulse method 78—21734
heavy water dielectric constant meas. over temp. range 473K to 643K 80—103912
heavy water dynamic viscosity coefficient in supercritical region of parameters of state, experimental investigation 78—67845
heavy water enrichment using amine process 79—49695
heavy water prod. plants, Girdler-Sulphide process, developments 79—22397
heavy water production, asymmetric process, separative power, resoln. of inconsistencies 78—29622
heavy water production, Canadian experience 79—30929
heavy water production, Girdler-sulphide process phys. props., computer program 78—25300
heavy water production, using laser isotope separation 77—83106
heavy water purification by deuterated ion exchange resins 78—8897
HFEF, irradiated fuel examination by eddy currents 79—45461
hot cell complex for post irradiation exam. in Japan, O-arai Engng. Centre *(Japanese)* 80—47536
hot cell measurement and test equipment, calibration control 80—68787
HRF at Petten, expt. facilities for high flux materials testing 79—63749
HTBFR, constitutive equations of structural austenitic steels 79—6730
HTGR, material development for reactor core and primary gas circuit *(German)* 78—25297
HTGR, T contamination of product gas 80—13590
HTGR, thermodynamic correlations for accident anal. *(German)* 78—25315
HTGR, US R and D programs for steam supply plant, fuel and materials 79—97757
HTGR fission product diffusion through core materials during LOFC, exact analytical soln. 80—47554
HTGR fuel particles, inert gas intrusion as charact. procedure for pyrocarbon coatings 79—54512
HTGR fuel particles, influence of pyrocarbon props. on as-produced gas permeability of coatings 79—54511
HTGR piping, heat transfer characts. of horizontal annular insulation layer *(Japanese)* 79—26520
HTGR plant materials developments 77—46298
HTGR primary circuit components, metallurgical eval. of structural materials 79—67867
HTGR steam generator or heat exchanger materials, compatibility with coolant circuit media 77—57721
HTR, ^{110m}Ag fission product, release from coated fuel particles 77—88228
HTR, failure processes, life prediction, elevated temp. codes 79—6745
HTR, long term mech. props. of alloy components, tensile failure prediction 80—5241
HTR, metallurgical problems of intermed. heat exchanger 77—65256
HTR advanced system, materials for core-specific and primary circuit components 77—26842
HTR annular compacts, creep strain limit expt. 77—42069
HTR compact and matrix material, uniaxial creep meas. under tensile load at 900°C 77—42068
HTR components, design implications of inelastic structural anal. 79—6729
HTR individual coated fuel particles, gas anal., optimum heating and crushing 77—56294
HTR individual coated fuel particles, mass spectrum. determ. of Xe, Co and Kr gases 77—56293
HTR material developments, Dragon Project 77—65273
HTR primary component materials, properties, advantages, and limitations 79—36329
HTR system materials developments 77—46297
In 519 high temp. low-cycle fatigue behaviour for nuclear process heat appl. 80—628
in-core irradiation facilities, development and expt. using JRR-2 and JMTR research reactors, Japan *(Japanese)* 80—63256
Incoloy, 800 and 807, heat resistant superalloys, for nuclear plants in He, creep props. *(Japanese)* 79—83263
Incoloy, evaluation for use in nuclear process heat appl. 78—13234
Incoloy 600 vacuum heat treatment for improved corrosion resistance of PWR steam generator tubing 80—5246
Incoloy 800, 600 and 718, press. vessel, fatigue design criteria 78—60758
Incoloy 800, chem. behaviour and mech. performance in HTR He at high temps. 79—47842
Incoloy 800, contamination and decontamination of samples from KFA experimental duct of DRAGON reactor 79—45600
Incoloy 800, corrosion and carburization in liquid Na up to 973K 79—47841
Incoloy 800, corrosion resist. props. in high temp. steam, review 79—47839
Incoloy 800, creep and fatigue props. in high temp. gas cooled reactor He environment 79—47776
Incoloy 800, design codes and lifetime prediction aspects for nuclear and non nuclear appls. 79—47778
Incoloy 800, design problems in steam generators of high temp. reactors 79—45352
Incoloy 800, eddy current testing *(German)* 79—96257
Incoloy 800, from KFA experimental duct at 700°C and 480 d in DRAGON reactor, mech. props. before and after contamination 79—47777
Incoloy 800, high temp. corrosion and mech. props. in Na environment 79—47840
Incoloy 800, mechanical props., heat treatment and appl., conf., Petten, Netherlands (March 1978) 79—43296
Incoloy 800, nuclear grade boiling tubing superalloy, Co and C content anal. 80—78397
Incoloy 800, oxidation resistance, alloy depletion effect 77—8989
Incoloy 800 for HTR appls., correlation of carburization behavior, mechanical property degradation, and exposure conditions 80—5244
Incoloy 800 H, 617, high temp. low-cycle fatigue behaviour for nuclear process heat appl. 80—628
Incoloy 800H, carburisation and dimens. stability in HTGR, He environment 80—45366
Incoloy-800, annealed, mech. behaviour anal. for elevated-temp. LMFBR appl. 80—18428

fission reactor materials continued
  Incoloy-800, meas. of H and D permeation for reactor safety anal. 79—77822
  Inconel, 617 and 625, heat resistant superalloys, for nuclear plants in He, creep props. *(Japanese)* 79—83263
  Inconel, corrosion behaviour in simulated HTGR He environment 79—54495
  Inconel, fatigue crack growth rate in high temp., high purity oxygenated water 80—40622
  Inconel, steam generator tubing, mag. probe inspection 80—85119
  Inconel 600, atomic S diffusion *(French)* 79—74307
  Inconel 600, nuclear grade boiling tubing superalloy, Co and C content anal. 80—78397
  Inconel 600, nuclear reactor boiler corrosion, XPS 80—66709
  Inconel 600, nuclear reactor boiler corrosion, XPS 80—71816
  Inconel 600, PWR primary corrosion products 80—13578
  Inconel 600, S penetration leading to sulphide form. *(French)* 79—74306
  Inconel 600, stress corrosion cracking in primary water 79—93728
  Inconel 600 and 718 in liquid Na environment, fatigue crack propag. 80—40624
  Inconel 600 safe-end cracking failure at Duane Arnold reactor 80—104295
  Inconel 606, discontinuous creep process 79—66124
  INCONEL 617, corrosion kinetics and products under low oxygen partial pressures *(German)* 79—87764
  Inconel 625, creep rupture strength and corrosion in HTC in He *(German)* 77—77557
  Inconel 625, surface treatment of plane and hollow components in glow discharges 79—1923
  Inconel 718 cladding possibility for GCFR fuel 77—18667
  Inconel 82, discontinuous creep process 79—66124
  Inconel alloys for VHTR heat exchangers, material criteria and selection 78—13232
  Inconel X750 springs, in-reactor stress relaxation 78—11256
  Inconel-718, blistering by 2 MeV He$^+$ ions, optical microscopy and SEM obs. 79—42119
  inelastic structural anal., thermomech. constitutive eqns. 79—6731
  inelasticity and the ASME code 78—41815
  influence function method, fracture mechs. and residual fatigue life anal. of power station cracked components 77—80109
  inspection by acoustic emission *(German)* 79—45373
  insulation for cables, deterioration test *(Japanese)* 80—27743
  intrareactor facility for physicomechanical props. investig. by pulsed US spectroscopic method 78—70591
  inventory differences interpretation, game theory appl. 79—85744
  irradiated cladding, in-cell facility for mechanical testing 80—21244
  irradiated fuel element can removal from core, gas-thermal treatment 78—37432
  irradiated fuel rods, examination by eddy currents 79—45464
  irradiated fuel rods, in-cell welding techniques 80—22956
  irradiated fuel sipping, inspection, and repair at Point Beach Nuclear Plant 79—45384
  irradiated reactor component fracture testing facility 79—79201
  irradiation creep, conf., Petten, Netherlands, (May, 1976) 77—42055
  irradiation creep facility, materials testing for fast and fusion reactors 79—57192
  irradiation creep mechanisms, theoretical assessment 79—55817
  irradiation effects, precipitation in pile, rel. to void swelling 78—70595
  kohlestein insulation for use in HTR systems, further investigations *(German)* 78—66346
  lamellar graphite in cast iron, tensile strength, reactor appl. 77—57718
  laser fusion driven actinide waste burner, neutronics anal. 78—58459
  laser fusion pellets, microradiographic characterization 78—745
  light water, cold neutron interactions, total cross-section meas. 77—67786
  liquid metal fragmentation following reactor core meltdown accident, contribution of collapsing vapour bubbles 80—755
  liquid radioactive waste, treatment system at CAMEN *(Italian)* 79—30952
  liquid-metal valves, materials selection 78—82449
  LMFBR, 1200 MW(e), ^{232}U prod. 78—29597
  LMFBR, analysis of in-pile MFCI experiments with carbide fuel 79—49754
  LMFBR, behaviour of H in liquid Na *(Japanese)* 79—49649
  LMFBR, demonstration, design, construction and operating experience 79—97796
  LMFBR, elimination of transuranium elements by neutron absorpt. 78—29628
  LMFBR, equipment design, Na-NaK engineering handbook 79—97815
  LMFBR, exam. of material requirement 78—50255
  LMFBR, failed fuel pin debris forming heat-generating blockage, heat transfer anal. 80—47648
  LMFBR, fission gas release and microscopic swelling in highly rated advanced fuels 80—52739
  LMFBR, fuel-steel mixtures, basic collapse criteria for HCDA 77—3107
  LMFBR, H burden from steam side corrosion in Na heated steam generators 78—58355
  LMFBR, H impurity conc. in liquid Na, meas. method 79—81030
  LMFBR, HCDA, Eulerian computer code anal., primary system response 77—3127
  LMFBR, HCDA conditions, PuO$_2$-UO$_2$-Na aerosol formation, aerodynamic and chem. behaviour 78—94104
  LMFBR, in-reactor irrad. creep expt., thermal anal. 79—67854
  LMFBR, incipient boiling press. signal and evaporation coeff. meas. of liquid metals 79—77734
  LMFBR, liquid Na-limestone concrete interaction following HCDA, US meas. 80—78412
  LMFBR, LOCA, fuel pin failure mechanisms 80—13587
  LMFBR, LOF accident, evaluation of incoherency effect on cladding motion in R-series test 79—49749
  LMFBR, Na incipient boiling under forced convection in seven pin bundle 79—22401
  LMFBR, Na ML-3 circuit for testing mech. props. of structural materials *(Spanish)* 80—55595
  LMFBR, Na purification system, cold traps and plugging indicator 80—99209
  LMFBR, Na test of bellows expansion joints, metallographic study *(Japanese)* 79—67850
  LMFBR, physics problems of fast reactor shielding 79—67873

fission reactor materials continued
  LMFBR, post-accident containment, high-temp. behaviour of concrete 79—31000
  LMFBR, primary circuit contamination, release transport and removal of radioactive products 80—13631
  LMFBR, radionuclide trap 80—52725
  LMFBR, red. of two-phase thermal cond. and heat transfer by entrained inert gases 79—30897
  LMFBR, safety c.f. thermal reactors 79—26562
  LMFBR, solubility of Li$_2$O in liq. Li by neutron activation anal. 78—11601
  LMFBR, thermal conditions controlling subassembly failure propag. during transition phase 79—49758
  LMFBR, transient boiling of Na in 7-pin fuel bundle under loss-of-flow conditions 79—41007
  LMFBR, UK, AISI 316 and 9Cr-1Mo steels assessment 78—86581
  LMFBR accident, large scale Na/concrete reactions 79—30999
  LMFBR accident material compatibility studies for PAHR in-core molten pool expt. 78—8933
  LMFBR blankets, simple representation of spectrum-averaged cross sections 80—22892
  LMFBR components, materials anal. 78—82447
  LMFBR components, plastic dynamic anal., CEA-SEMT system 77—6506
  LMFBR coolant, simple multichannel thermal-hydraulic model for transient behaviour anal. 79—49660
  LMFBR core, transient deform. from local failure, fuel-coolant interactions 77—88245
  LMFBR core design, benchmark tests of JENDL-1 for structural materials 80—13616
  LMFBR core materials, effect of swelling and creep on performance 78—13261
  LMFBR cores, performance of advanced alloys 77—42092
  LMFBR fuel channels, measurement of irradiation creep in bending 80—104406
  LMFBR fuel elements, remote exam. of shroud tubes 80—18470
  LMFBR fuel pin bundles in flowing Na, design and operation of SLSF test trains for safety tests 80—102281
  LMFBR fuel pin failure monitoring, cumulative mech. damage function from materials data 78—13262
  LMFBR fuel rod cladding tubes, effect of rod bowing on measured local temp. distrib. 80—638
  LMFBR heat exchangers, liquid metal temps. in pipes with wall fast flow discontinuities *(Spanish)* 77—74907
  LMFBR hexagonal ducts, cracking, effect on safety and fuel pin failure 78—17318
  LMFBR LOF accident, surface ablation in impingement region of liquid jet 79—54549
  LMFBR LOF transient, sodium voiding dynamics and cladding motion 79—49750
  LMFBR LOF-HCDA, solidification dynamics of flowing two-phase mixtures 79—49757
  LMFBR LOF-TOP, axial propagation of fuel failure, SAS3D-EPIC anal. 80—47650
  LMFBR materials, electron transport method, expt. verification, energy deposition 79—22386
  LMFBR materials, exam. of material requirement 78—50256
  LMFBR materials, interstitial loop nucleation and growth during irradiation, Fokker-Planck equation, numerical soln. 80—57857
  LMFBR materials, interstitial loop nucleation and growth during irradiation, Fokker-Planck equation, numerical soln. 80—68796
  LMFBR meltdown conditons, molten fuel+coolant interaction, expts. 77—23225
  LMFBR Na/basalt concrete interactions following accident, chemical phenomenology 80—47639
  LMFBR performance, effects of irradiation creep and swelling 78—78482
  LMFBR permanent reactor structures, design, irradiation effects 78—21623
  LMFBR post-accident containment, time-resolved penetration of liquid Na into limestone concrete 79—93787
  LMFBR primary and secondary circuit materials development, review 77—46295
  LMFBR program, simulation of void swelling and radiation-induced creep 78—8907
  LMFBR rot. shield plug annulus, Na vapour, deposition rate, controlling factors 80—47591
  LMFBR slow overpower transient, simplified computing method for cladding and fuel strain 79—31005
  LMFBR steam generators, behaviour of heat exchange tubes in Na-water contact 80—13670
  LMFBR steam generators, mass transfer props. of steel, test *(Japanese)* 77—348
  LMFBR structural materials, development of an instrumented materials irradiation test for FFTF 80—57858
  LMFBR structural materials, development of an instrumented materials irradiation test for FFTF 80—68797
  LMFBR structure materials in liquid Na, capsule type creep tester *(Japanese)* 80—108653
  LMFBR transient undercooling accident, molten stainless steel, wetting of UO$_2$ cracked fuel pellets 78—4993
  LOCA, fuel element behaviour during high-temp. transients, ELOCA code 79—81043
  low and intermediate energy radiation physics 80—19845
  LPWR fuel cladding temp. predictions for LOFT LOCE L1-5 79—89446
  lubrication, friction system in liquid Na and Ar 79—59176
  LWHR, source driven, Li-free neutron sources, feasibility and comparisons 79—13383
  LWR, HCDA, behaviour of concrete in contact with molten corium 80—13584
  LWR, pellet-clad interaction modelling 80—37445
  LWR, plates and forgings *(Japanese)* 77—54352
  LWR, power cooling mismatch accident, molten fuel radial motion and cladding melting 80—13638
  LWR, press. vessel and piping design, plasticity-related damage prevention 79—6735
  LWR, quality assurance of fuel and fuel elements *(German)* 79—49810
  LWR, risk-sensitive Markovian policies for detection and maintenance of fatigue cracks in pressure vessels 79—54534

fission reactor materials continued
LWR, stress conc. in cladding produced by cracked fuel pellets 78—50260
LWR, structural integrity of pressure boundary 78—66334
LWR austenitic stainless steel coolant tubing, bending props. *(Czech)* 79—67851
LWR concrete shielding, ANS coupled cross-section standards 79—59281
LWR coolant chemistry, developments to reduce pipe cracking 79—54554
LWR core materials, thermal-mechanical energy conversion in large scale steam explosions 79—85648
LWR core meltdown, chemical reacts. between core melt and concrete 80—13588
LWR core meltdown, materials behaviour 80—751
LWR core meltdown risk anal., penetration of hot melts into concrete structures 80—750
LWR core-concrete interfacial heat transfer and molten pool dynamics 80—47641
LWR fuel element reliability, materials science aspects 79—67855
LWR fuel rod failure associated with power changes 80—16525
LWR fuel rod failure probability, comparison of FRAP T4 and meas. 80—13644
LWR fuel rods, power ramp induced I and Cs redistrib. 80—32343
LWR fuel-cladding gap, Cs-U-Zr-H-I-O system, chemical thermodynamics 78—82440
LWR lattices of UO_2 and Gd_2O_3 rods, critical expt. 79—26474
LWR materials, pressure boundary problems, corrosion, cracking and radiation embrittlement props. 78—46142
LWR materials of primary-circuit components, safety concepts, quality *(German)* 80—73914
LWR piping, intergranular stress-corrosion cracking 80—81234
LWR primary circuit component production, metallurgical aspects 79—36330
LWR spent fuel reprocessing plant, integrated safeguards assessment 79—89418
LWR steam explosion triggering expts. with oxidised Corium-E simulants 79—13472
LWR wastes, treatment and disposal methods *(German)* 80—57868
MAGNOX fuel canning material, corroded, F conc. profiles determ. using $^{19}F(p,\alpha\gamma)^{16}O$ reaction 79—92035
magnox fuel cladding, surface struct. data acquisition and processing system 80—898
management, safeguarding and accounting, conf. Albuquerque, NM, USA (July 1979) 80—62382
mass transfer model in high temp. high press. water circuits 79—67813
material irradiation facility in the WR-1 research reactor, structural material development 78—54868
meaningful chemical analysis for nuclear fuels and reactor materials *(Japanese)* 79—26519
medium-mass nuclei, mechanisms for radiative capture at low neutron energies 80—13627
melting clad temperature distribution in fission reactor, Pekeris-Slichter series expansion method 77—88238
mesh-packed cold traps, impurity interaction anal. 78—25262
metal, anisotropic, inelastic deform. under complex loading conditions and high neutron flux, equation 78—80598
metal, heavy irradiation damage at high temps., void swelling problems *(Japanese)* 77—59049
metal, microstructural evidence supporting SIPA creep mechanism 79—61679
metal, refractory, BCC, free migration of self-interstitials 78—47574
metal containment, system safety anal. 78—41817
metal surface, He implantation lateral stress, role in bluster form. mech. 78—95068
metal surface radioactive waste chemical decontamination 80—37530
metal surfaces, radioactive contamination 80—68771
metallic fuel cladding eutectic formation during postirradiation heating in EBRII 80—102241
metallic material choice based on high energy neutron irradiation *(French)* 78—8902
metallic materials, radiation induced creep, fundamental mechanisms, review *(Italian)* 80—55457
metallic surfaces, radioactive waste electrodecontamination using a basic electrolyte 80—37529
metals, He behaviour 79—17981
metals, irradiated, general rate theory model of void swelling 79—23655
metals, irradiated, validity of rate theory, point defect diffusion eqns. 79—55777
metals, vacancy porosity kinetics at high irradiation doses of fast neturons 79—28018
metals and alloys, stress relaxation, in-reactor study at low temps. 80—93588
metals in nuclear reactors, thermo-elasto-visco-plasticity and neutron irradiation 77—3111
metals under stress, thermally and radiation induced creep, constitutive relns. 77—90413
methyl iodide, dissolution into aqueous NaOH solns., fission reactor accident conditions 77—88236
methylradioiodide, catalytic trapping by beds of impregnated charcoal 78—21681
MHSS, material handling system simulator 77—38337
molten core debris pools, PAHR anal., hot liquid pool penetration 80—18544
molten core materials, interactions with structural concrete 80—22946
molten Fe oxides, steam explosions 79—85649
monitoring, computerised, VACOSS electronic sealing system appl. 79—85687
multiaxial creep-fatigue damage, determ. of strain range 79—7650
MX-type fuel and fuel pin swelling, 1973-76, fabrication and characterisation 79—41001
natural reactors, at Oklo (Gabon), origin hypotheses *(Dutch)* 78—33261
NDT of special nucl. materials 78—82443
neutron and heavy ion damage correlation, predicted temp. shift on swelling with radiation dose rate change 79—7630
neutron capture cross sections, expt. determ., fast reactor materials *(Italian)* 78—82355
neutron effects in pressure vessels for PWR, BWR, safety calcs., design, operation control *(German)* 77—34404
neutron irrad., low temp., materials research *(Japanese)* 77—72637

fission reactor materials continued
neutron radiation damage simulation, effect of He preinjection on swelling of stainless steel 80—44236
neutron radiation effects, energy spectrum depend., damage function *(German)* 77—34386
neutron radiography at HFEF/N 79—45442
Ni-base alloy 713LC, creep rupture strength and corrosion in HTR in He *(German)* 77—77557
Nimonic, ageing, role of quenched-in vacancies 77—52363
Nimonic 75, crevice corrosion by water vapour and methane in Ar at 1 and 25 atm. 77—25203
NIMONIC 80A, corrosion kinetics and products under low oxygen partial pressures *(German)* 79—87764
Nimonic 80A, creep rupture strength and corrosion in HTR in He *(German)* 77—77557
Nimonic PE16, fatigue crack growth rate, temp. effect 77—77568
Nimonic PE16, irradiation creep data obtained in fast and thermal neutron spectra correlation with displacement cross-sections 80—84993
Nimonic PE16, Ni ion irradiated, Ni segregation to voids 79—28020
Nimonic PE16, oxidation in Ar-H_2O-H_2 atmosphere 78—35584
Nimonic PE 13, mass spectrometric study, high temp. reactor system appl. 79—43663
Nimonic PE-16, electron irrad. in HVEM, void growth, vacuum environment influence 80—107323
Nippon Nuclear Fuel Development Co. hot laboratory, present status 80—68781
non-destructive assay techniques for irradiated fissile material in extended configurations 80—71872
non-destructive assay technology and automated 'real-time' materials control 79—26721
non-destructive control and verification techniques 79—87813
nondestructive analysis, results of international collaboration in the ESARDA working group 80—71879
nondestructive analysis development, for EURATOM (CEC) Safeguards Directorate 79—85693
nondestructive assay equipment, calibration using reference materials for fissile material assay 80—71880
nondestructive neutron assay for nuclear materials accountability and criticality control 80—66759
nondestructive surface exam. 80—21246
nonequilibrium fission gas behaviour 78—86626
nonfissile metals and alloys, irradiation creep 77—42072
nonproliferation treaty safeguards implementation, nuclear facilities in USA 78—820
nuclear energy materials, anal. techniques 80—93834
nuclear energy synergetics, characts. of integrated systems 79—13382
Nuclear fuel and materials *(Japanese)* 78—46141
nuclear fuel processing plant operation, critical safety criteria *(German)* 78—74440
nuclear fuel reprocessing plant, material diversion, probability of detection, optimisation of safeguards 77—14258
nuclear material international safeguards 79—97817
nuclear materials management, design of minicomputer system 79—22395
nuclear power stations, nuclear materials, safeguarding experiences *(German)* 80—611
nuclear reactor components, NDT using acoustic emission *(Spanish)* 80—57871
nuclide inventory calculation code, FISPIN 80—42781
O-arai Engineering Centre post irradiation examination facilities 80—68780
O-ring compounds, resistance to heat and ionizing radiation 78—29584
Oak Ridge, hot cell facilities, history 80—68784
Oak Ridge National Laboratory Ceramic Fuels Alpha Facility 80—68783
on-line radiation monitoring at a nuclear fuel reprocessing plant 80—95469
ORNL Radioactive Materials Analytical Laboratory 80—68785
oxidation and corrosion induced deformation effects 80—3211
oxide fuel classification, quality criteria for fuel elements *(German)* 79—49812
oxide fuel pins, irradiation behaviour, effect of chemical factors *(German)* 79—49692
oxide fuel rods, steel-coated, effect of impurities on clad-corrosion *(German)* 79—49693
oxyanions, in nuclear waste materials, laser Raman spectrometric determ. 78—35743
Ozhennite, yield point, effect of ageing stress 77—21223
PBF blowdown tests, thermal hydraulic and mechancial deformation 79—81024
Peach Bottom 1, HTGR nuclear power station, review of design and operation 79—45327
pellet cladding interaction failures, stress corrosion of fission reactor cladding tubes 80—16526
pellet-cladding interaction, theoretical analysis 79—93699
performance of safeguards technology 78—82484
physical protection safeguards for nuclear materials and facilities 78—82483
pipe bends with flanged tangents, bending and pressurising 79—94516
pipeline system Cr-Ni alloyed austenitic steel, Ti stabilised, corrosion props. *(Hungarian)* 77—18658
piping components, fracture mech. methods, safety anal. 79—11698
piping components, safety anal., fracture mechanics methods 79—11699
piping fracture testing, impact loading *(Japanese)* 79—43373
plastics, applications in nuclear power industry 79—6744
Plate Inspection Steering Committee project, historical review 80—52744
pneumatic system for transferring radioactive samples at Savannah River Laboratory 80—68794
point defect nucleation and growth, rate theory model for simultaneous clustering 80—13604
polyatomic materials, damage energy functions 80—49264
polymers, dose rate effect on degradation behaviour 79—99239
postirradiation examination facility 80—18682
power conference, Lausanne, Switzerland (Oct. 1977) 79—36326
power ramp investigations, clad hoop strain and pellet clad interaction 80—16440
precipitation stability under irradiation, point defect effects 77—21148
pressure testing of structural materials *(Spanish)* 80—52735
pressure vessel, A508 C1 2 steel, microcrack formation during stress-relief annealing of a weldment 78—80629

fission reactor materials continued
pressure vessel, crack initiation during thermal shock, warm pre-stress 78—41816
pressure vessel, Oconee nuclear station, surveillance capsule results 79—18019
pressure vessel brittle fracture, safeguards, American and German ductility requirements *(German)* 79—41017
pressure vessel components reliability, conf. Vienna, Austria, 1977 79—17986
pressure vessel material, radiation embrittlement, current regulation assessment 78—52966
pressure vessel material surveillance capsule, neutron radiation, limiting condition 80—47572
pressure vessel reliability, sensitivity to material and other factors 79—18018
pressure vessel supports, fracture-safe design in neutron environment 79—93700
pressure vessels, brittle fracture probability using reactor surveillance capsule data 78—80641
pressure vessels, exam. for compliance with safety regulations 78—89954
pressure vessels, pre-stressed concrete, historical review 79—601
pressure vessels, strain measurements 80—79865
pressure vessels, use of prestressed cast steel for HTGR *(German)* 79—3196
pressurized tubes, creep measurement by laser interferometry *(German)* 77—74925
prestressed concrete reactor vessels, construction movements, finite element anal. 79—621
prestressed concrete reactor vessels, perforated plate ligaments, time varying stress 79—49679
primary circuit coolant, H_3BO_3 concentration determ., method and device *(Russian)* 77—38331
primary circuit structural materials, phase comp. of corrosion products by Mossbauer spectroscopy 80—5237
probabilistic fracture mechanics anal., nuclear power station structural components 77—81317
protection, tamper-indicating seal program development and implementation 79—85689
PWR, availability of pressure vessel after small LOCA 79—30967
PWR, critical B concs. and cycle lifetime predictions 80—9365
PWR, H_2-assisted fatigue-crack growth model 80—71745
PWR, in-reactor loop expts. on corrosion product transport and water chemistry 78—58335
PWR, materials corrosion, steam generator operations, influence of water chemistry 79—54555
PWR, metals and alloys *(Spanish)* 80—95344
PWR, spatial Xe oscillation time-optimal control 79—628
PWR cast materials, low-angle fatigue and fatigue crack growth rates 80—5240
PWR core barrels with and without holes, various edge conditions, hydrodynamic vibrations 80—78406
PWR dismantling, management of radioactive waste 80—27756
PWR fuel assembly design, stress, temp., radiation and chem. environment effects on performance 78—13310
PWR fuel cladding, long ballooning deformation following LOCA 80—660
PWR fuel rod behaviour during LOCA, probabilistic anal. using response surface method 80—663
PWR piping, circumferential cracks, opening and extension, MARC finite element program 80—78364
PWR power station secondary water chemistry study, progress report 80—106108
PWR power stations, operating record and reliability, reviews 79—22404
PWR pressure vessel nozzle, comparison of 3-D and axisymm. finite element anal. 79—13423
PWR primary and secondary water chemistry, European experience 80—106110
PWR steam generators, corrosion resistance of tubes 77—79432
PWR VVER-1000 type reactors, operating state parameters, Skoda calcs. *(Czech)* 79—67818
PWR-type, pressure component manufacture, new materials, technologies and equipment development 78—74436
pyrocarbon, Ag diffusion 77—24441
pyrocarbon, deposition from fluidised bed, quantitative aspects 77—50239
pyrocarbon, diffusion coeff. of Cs and Ag by post irradiation annealing of coated 78—13247
pyrocarbon, diffusion of Pu in HTGR 78—29578
pyrocarbon, fuel particle coating, strength and Young's modulus meas., brittle ring test 77—8868
pyrocarbon, low temp., isotropic, permeability study *(French)* 79—7549
pyrocarbon, microstructure of coatings on fuel particles, TEM study 78—25293
pyrocarbon, quality control techniques 77—79461
pyrocarbon cladding, gas permeability *(French)* 77—14234
pyrocarbon coating, isotropic, gas permeability, neutron irradiation effect *(French)* 80—63260
pyrocarbon coating, isotropic, gas permeability meas. *(French)* 80—63259
pyrocarbon coatings, mass spectrom. determ. of fission gas permeabilities 78—12785
pyrocarbon coatings, production *(German)* 80—18585
pyrocarbon coatings on HTGR fuel particles, Bacon anisotropy factors meas. technique 79—13418
pyrocarbon nuclear fuel coating, props. and neutron irrad. behaviour *(German)* 77—67816
quality control systems by acoustic emission 79—93758
radial blankets, economic anal. for LMFBR and GCFR 79—59163
radiation creep due to stress-induced preferential absorpt., theoretical model 79—89379
radiation damage, heavy ion beams application to modelling 77—55310
radiation damage, ion penetration distance calculations with multigroup transport computer codes 80—102246
radiation damage, review *(Japanese)* 79—81011
radiation damage problem, systematic approach 78—4984
radiation physics and nuclear technology 77—54373
radiation protection in nuclear power plants and the fuel cycle, conf., Bristol, England (Nov. 1978) 80—4471
radiation shielding materials, benchmark radiation transport data, air-over-ground neutron and gamma spectroscopy 80—23161
radiation-induced embrittlement and swelling due to void form, ASTM research 78—13231

fission reactor materials continued
radiational growth due to diffusional anisotropy 79—71897
radiational swelling of fast reactor materials modelling by inert gas ion irradiation 79—40999
radioactive corrosion product accumulation in nuclear steam generators 80—13579
radioactive effluent gases from nuclear power industry, ambient contamination *(Spanish)* 78—61540
radioactive materials transportation, safety anal. 79—63814
radioactive waste, final disposal possibilities, waste conditioning, storage and safety, review 79—26554
radiographic testing, sensitivity using 10 MeV microtron 78—70603
radioisotopes in cooling system, prod., transfer, life cycle, radiation calcs. using program system TIBSO 78—54821
radiolytically formed chelating agents, corrosion prevention appls. 78—64745
reactivity worths of neutron absorbing materials, critical expts. 77—42023
reactor cladding waste, spent fuel contamination, composition and amounts arising in EC 78—66360
reactor protection system performance, impact of ageing mechanism 79—18000
reactor radiation damage, neutron metrology for irradiation parameters 79—46717
reactor safety, materials science contribution *(German)* 78—58352
refractories, swelling on proton, deuteron and He ion bombardment 78—67750
refractory materials for GCFR core catcher crucible 79—59171
refractory metals and oxides, reactions of liq. alkali metals, relevance to reactor technology 80—85173
reinforced concrete structs., initial stress approach to nonlinear dynamic anal. 77—83036
reinforced concrete structures, under missile loading, finite difference code 80—13956
remote maintenance at Fuels and Materials Examination Facility 80—68792
review of fission reactor design, development and commercialisation of 17 types *(Japanese)* 79—80974
review of LMFBR and LWR materials 77—26843
safeguard role of standard reference materials in achieving measurement traceability 80—78371
safeguard systems, human performance charact. 79—85741
safeguard systems effectiveness, SNAP network analysis technique 79—26658
safeguard techniques capability in nuclear fuel facilities 80—63279
safeguarding; 80—68835
safeguarding, advanced accountability techniques for breeder fuel fabrication facilities 80—73939
safeguarding, advanced detection systems to prevent LWR spent fuel diversion 80—68822
safeguarding, advanced instrumental systems and techniques for fuel reprocessing plant 80—68821
safeguarding, appl. of mobile nondestructive assay system 80—71876
safeguarding, application of an improved volume calibration system to the calibration of accountability tanks 80—68829
safeguarding, containment and surveillance devices 80—63349
safeguarding, determ. of U and Pu content of fuels using isotope correl. tech. 80—68834
safeguarding, development of containment and surveillance measures for IAEA safeguards 80—63350
safeguarding, diverse forms of fissile material, large stocks verification 80—73932
safeguarding, dynamic material accountancy in an integrated safeguards system 80—73940
safeguarding, dynamic materials accounting in chemical separations, conversion, and fuel fabrication facilities 80—73938
safeguarding, dynamic materials control, development, test and eval. program 80—73936
safeguarding, dynamic materials control 80—68819
safeguarding, gamma spectrometric techniques and standards *(French)* 80—68811
safeguarding, isotopic correl. tech., R and D by ESRADA 80—68836
safeguarding, isotopic inventory prediction employing a Monte Carlo Dancoff factor 80—73924
safeguarding, judging the results of analytical verification meas. 80—68817
safeguarding, material accountability control automation at fuel reprocessing plant 80—68832
safeguarding, material control and accountability for ^{233}U/Th fuel recycle plant 80—73942
safeguarding, meas. of fissile materials entering a reprocessing plant *(French)* 80—68828
safeguarding, measurement errors 80—73935
safeguarding, measurement standardisation 80—68812
safeguarding, nondestructive measurements of irradiated fuel assemblies at a reprocessing facility 80—95392
safeguarding, nuclear materials control system in the THTR-300 high-temperature pebble-bed reactor 80—73941
safeguarding, optimal estimates of inventory and losses using nuclear material accountancy data 80—68818
safeguarding, possible ways of verifying the input of a reprocessing facility 80—68826
safeguarding, SNM control and accounting, role of certified reference materials 80—68815
safeguarding, SNM dynamic materials control and accountability system 80—73937
safeguarding, statistical anal. of materials accountability, computer simulation 80—73933
safeguarding, stratification of nuclear materials for control and accountability 80—68816
safeguarding, survey assay meter developments at BNL for nuclear materials safeguarding appls. 80—69038
safeguarding, tracer techniques for Pu input accountability in reprocessing plants 80—68827
safeguarding, two-stage sampling for detection of SNM diversions 80—73934
safeguarding, unirradiated fuel control in BOR-60 fuel assemblies *(Russian)* 80—68809
safeguarding, use of automated electromanometer at fuel processing facility 80—99211
safeguarding, VACOSS electronic sealing system 80—63348

fission reactor materials continued
safeguarding, verification of reprocessing plant input and output analyses 80−68830
safeguarding a gas centrifuge pilot plant in Japan 80−63282
safeguarding at fuel reprocessing plant to prevent materials diversion 80−68824
safeguarding at reprocessing plants, inspection of hulls at La Hague *(French)* 80−68831
safeguarding at U fuel fabrication facility US/IAEA system 80−63284
safeguarding isotopic correlations in irradiated fuel from VVER power reactors *(Russian)* 80−68838
safeguarding of critical facilities to detect diversion of nuclear materials 80−68808
safeguarding of materials from U/Th fuel cycle, nondestructive meas. 80−76457
safeguarding SNM control and accountability, reliability of nondestructive assay techniques 80−76456
safeguards, accountancy system for nuclear materials control in research centres 80−63499
safeguards, accounting and control in BOR-60 FBR *(Russian)* 80−63295
safeguards, appl. of semidynamic material control in spent-fuel reprocessing plant 80−83174
safeguards, burn-up meas. of irradiated LWR fuel assemblies 80−68807
safeguards, collection and analysis of measured fission product data 80−95354
safeguards, computerised nondestructive assay for materials management 80−78388
safeguards, definition and objectives of IAEA safeguards 80−83155
safeguards, deviations from mass transfer equilibrium and mathematical modeling of mixer-settler contactors 80−83171
safeguards, diversion anal. of LWR fuel cycle 80−63274
safeguards, diversion protection using personnel portal detectors 80−78389
safeguards, dynamic materials accounting for solvent-extraction systems 80−83172
safeguards, experience at the International Atomic Energy Agency in processing safeguards information 80−63497
safeguards, experience gained with Euratom's nuclear materials accounting and reporting system 80−63271
safeguards, experience in the application of IAEA inspection practices 80−63270
safeguards, facility design features relevant to improved IAEA safeguards 80−63277
safeguards, IAEA, containment and surveillance systems 79−85676
safeguards, IAEA, technical criteria for design, operation and evaluation 80−63272
safeguards, IAEA containment and surveillance measures 80−68810
safeguards, IAEA quantitative goals for measurement systems 80−83168
safeguards, improvement of material accountability verification procedure 80−63273
safeguards, in situ verification techniques for fast critical assembly cores 80−78390
safeguards, integrated quality status and inventory tracking system for FBR driver fuel pins during manufacture 80−78431
safeguards, inventory verification methods in DOE safeguards inspections 80−78386
safeguards, inventory verification using high resolution gamma spectroscopy 80−69016
safeguards, isotopic measurements on Kr and Xe, behaviour of the quadrupole mass-spectrometer towards various noble gases 80−63300
safeguards, LASL analytical chemistry program 80−78380
safeguards, mathematical simulation of calorimeters used for rapid nuclear fuel assay 80−95355
safeguards, meas. of fissile material in accounting tanks 80−68825
safeguards, microscopic process monitoring [for nuclear materials safeguards] of fuel reprocessing facilities to prevent material diversion 80−83153
safeguards, model for the application of IAEA safeguards at mixed-oxide fuel fabrication facilities 80−63286
safeguards, Monte Carlo simulation of MUF distrib. 80−83170
safeguards, nuclear materials analysis using plasma desorption mass spectrometry isotope ratio determ. using TOF mass spectrometry 80−78375
safeguards, performance and eval. of international analytical intercomparison expt. 80−78374
safeguards, performance goals and criteria 80−83154
safeguards, perimeter monitors as supplement to materials accounting 79−89509
safeguards, prototype, reference materials for nondestructive assay 80−78372
safeguards, quantitative determ. of unauthorised removal of nuclear materials, using changes in spectral indices *(Russian)* 80−63294
safeguards, reference materials and meas. traceability 80−78370
safeguards, simulated neutron tomography for nondestructive assays 80−99218
safeguards, systems design for materials accountability 80−78393
safeguards, ultrasonically identified security seals for CANDU safeguard systems 80−63297
safeguards, uniform data description for a generalized real-time nuclear materials control system 80−63498
safeguards, verification and control, instrument requirements in static locations 80−63299
safeguards against theft or diversion 77−23213
safeguards and materials control, meas. tech., conf. Charleston, SC, USA (November 1979) 80−77544
safeguards applications of far infrared radiometric techniques for the detection of contraband 80−73925
safeguards applications of far infrared radiometric techniques for the detection of contraband 80−83156
safeguards approaches and evaluation methods 80−73923
safeguards containment and surveillance concepts at fuel reprocessing plant 80−95350
safeguards for avoiding diversion of fissile materials using quasi-total containment *(French)* 80−63276
safeguards for control and accounting, NRC program 79−85619
safeguards in LWR power stations, design features and instrumentation *(Russian)* 80−63278
safeguards in Th-U, fuel reprocessing facility, computerised analytical process control system 80−78429
safeguards measurement system anal., appl. of controllable unit approach to materials control 80−68820

fission reactor materials continued
safeguards procedures in fuel reprocessing plant 80−68823
safeguards reference measurement system utilizing resonance neutron radiography for nondestructive assay meas. 80−78377
safeguards spectrochemical anal. of U, Pu, Th by alpha spectrometry using liquid scintillation methods 80−78379
safeguards surveillance at reprocessing plants, fuel history anal. *(French)* 80−68837
safeguards system for highly enriched U fuel fabrication plant 80−63285
safeguards system for LMFBR, monitoring of fissile material inventory 80−63293
safeguards system in Japan 80−83152
safeguards system of back-end facilities with emphasis on waste management 80−83175
safeguards systems, directed graph and fault tree anal. of material theft detection 80−13728
safeguards systems parameters for IAEA 80−63275
safeguards techniques appl. to Eurodif gas diffusion plant *(French)* 80−63281
safeguards techniques at Tokai fuel reprocessing plant 80−68833
safeguards technology, conf. Vienna, Austria (Oct. 1978) 80−62391
safeguards technology based on separation nozzle process for U enrichment facility 80−63280
safeguards within Euratom framework, NUMSAS data processing system for statistical accountancy 80−73926
safety, dynamic materials accounting data analysis 79−85684
safety, IAEA safeguards appl., technical criteria survey 79−85678
safety, material control system simulator 79−85685
safety, use of electronic self-monitoring seal 79−85690
safety analysis of reinforced concrete containments, thermal shock, LOCA, computer code 77−3135
safety and protection, measures *(German)* 77−42158
safety assessment, of material control and accounting system, using directed graph and fault tree techniques 79−85673
seawater distillation, heavy water concentration, numerical model calc. 79−26514
security, and management, Conf., Cincinnati, OH., USA, (June 1978) 79−85672
security, material control and accounting systems assessment 79−85675
security, near-real-time accounting of strategic nuclear materials during reprocessing 79−85755
security, on-line diversion detection safeguard concepts [for nuclear materials security] 80−13729
security, proliferation risk assessment of alternative nuclear energy system strategies 79−89384
security, use of US identified seals 79−85677
security of nuclear research facilities, inventory verification 79−85600
seismic response of flexible cylindrical liquid storage tanks 79−31241
seismically qualified piping, failure probability, ASME code limits 80−78365
selection and manufacture of materials for power plants with N_2O_4 coolant *(Russian)* 77−83043
shielding cross section test, integral meas. 77−23305
shipment, computerised transportation model 79−85743
sieve tray froths occurring in heavy water plants, expt. and anal. 78−82438
sieve trays for heavy water plants, development 78−82437
silicate glasses, swelling on proton, deuteron and He ion bombardment 78−67750
single core subassembly model, coupling of struct. and coolant response 78−8934
SIPA irradiation creep, material with preferred direction for dislocation Burgers vector, cold worked 79−20118
SNM, nondestructive assay techniques for control and accountability 80−81270
SNM accountability, computerised fabrication and inspection of fuel pellets 80−78432
SNM safeguards, assay of dissolver solns. by totally sampled wavelength dispersive X-ray fluorescence 80−83160
SNM safeguards, IAEA Meas. requirements and experience 80−78385
SNM safeguards, LASL DYMAC accountability system, software development 80−99212
SNM safeguards, US NRC material control and accountability inspection program 80−78387
solid analysis by secondary ion mass spectroscopy 79−30602
solid solutions, ordering and disordering under irradiation 79−87626
solidified melts, shape anal., appl. to water entrapment capability 79−54550
special nuclear materials, computer-based in-plant nondestructive assay instrumentation 79−9752
specimen preparation for TEM by ion beam thinning *(German, English)* 80−11861
spectral analysis of dissolved materials using plasma jets 80−19624
spherical carbide containing UO_2 pellets, fabrication by hydrolysis *(German)* 80−9399
spontaneously fissioning material, assay using neutron correl. counting 79−85605
spontaneously fissioning material, Monte Carlo neutronic and electronic model for thermal-neutron coincidence counting 80−23165
stainless steel, 18Cr-11Ni, mech. props., neutron effects 77−34383
stainless steel, 304, tensile stress effects on high-cycle fatigue 78−86603
stainless steel, 316, simulation of radiation damage and phase stability 78−86602
stainless steel, (n,α) cross sections importance for radiation damage prediction 80−13625
stainless steel, cladding void swelling obs. by HV electron microscope *(Japanese)* 79−42108
stainless steel, design fix for vibr. induced wear in fuel pin bundles 77−42094
stainless steel, He production by neutron effects, cross section determ. 79−22282
stainless steel, integral neutron capture cross sections in GCFR lattices 78−13246
stainless steel, neutron dose determ., from isotope abundance ratio, mass spectra obs. 80−61220
stainless steel, neutron group constants, meas. of energy and space distribs. 77−26829
stainless steel, structural material, integral expts. 80−13612
stainless steel, type 304, deformation behaviour for high temp. structural design 77−54287

fission reactor materials continued
stainless steel, type 304, stress free swelling at high neutron fluences 77—42093
stainless steel, type 304-L, reactivity worths of fixed neutron absorbers 78—21654
stainless steel, type 316, clad fuel rods for GCFR, high temp. fast flux irrad. tests 77—18666
stainless steel, type 316, deform. meas. on mixed oxide nuclear fuel 77—42088
stainless steel, type 316, irradiated cladding, second-phase precipitation 79—54501
stainless steel, type 316, updated temp. integrity limit for FFTF driver fuel pins 77—42089
stainless steel, types 304 and 308, fatigue crack growth at elevated temps. 77—46288
stainless steel claddings, interaction with molten UO_2 during LMFBR TOP accident 79—54515
stainless steel in FBRs, correl. between void swelling and thermodynamic stability 80—641
stainless steel in reactor cladding, const.-load creep curves 77—7322
stainless steel oxides, absorption of Cs, meas. of contamination using washing test 78—62597
stainless steel rod adaptor, failure anal. in Fast Burst Reactor 77—54307
stainless steel type 316 weld metal with controlled residual elements, creep behaviour 77—8902
stainless steels, type 304, fast-neutron swelling behaviour 79—67864
steam generator thermal hydraulics 80—95342
steam generator tube perform. anal., corrosion failure 79—59178
steam generator tube performance in water cooled reactors in 1978 80—78399
steam generator tubes testing, and evaluation using CIS/DASIO system *(Czech)* 80—63301
steam generator tubes with dented and wastage configurations 79—36332
steam generators, Na-heated, material consideration 78—82503
steam generators, Na-heated, material selection 78—82504
steel, 0Kh16N15M3B, irradiation effects on resistance to cyclic elastoplastic deformation 79—91767
steel, 0Kh16N15M3B type, He ion irradiation effect on struct. and mech. props. 78—19848
steel, 3.5% Ni neutron irrad. effects on tensile props., microstructure effects 77—69005
steel, 6 MeV γ penetration, bremsstrahlung in reactor shielding calcs. 78—58350
steel, A302B, neutron damage, ductile-brittle transition temp. 77—3109
steel, A516-60, press. vessels, fatigue crack growth rate 77—77585
steel, A533 B, fatigue crack propagation, grain size and temp. effects 78—56727
steel, A533 grade B, class 1, in PWR coolant, fatigue crack growth 77—77584
steel, A533B alloy, fatigue crack growth of irradiated pressure vessel steels in simulated, reactor-grade water environment 80—97582
steel, A-533 B, J_{Ic}-testing, statistical eval. of different techniques 78—56828
steel, AISI 316, fast reactor irradiated, solution treated, struct. 77—69008
steel, alloy A533B1, neutron irrad., flow growth characts. by acoustic monitoring 80—100918
steel, alloy cladding, oxidation behaviour in GCFR He environment 80—16594
steel, API 5LX-X60, pipe fatigue strength under cyclic internal pressure, inner surface defects 79—38980
steel, austenite, γ and neutron irradiation, Mossbauer spectra anal. 78—692
steel, austenite, effect of neutron irradiation on intercrystallite corrosion 78—688
steel, austenitic, alloy and stainless, fuel-element cans, deform., failure, rigid loading scheme 79—91765
steel, austenitic, approx. method for high-temp. cracking resistance estimation 78—23914
steel, austenitic, ASTM A533B and A542, H_2 embrittlement behavior of unirrad. steels for nuclear reactor press. vessels 79—8340
steel, austenitic, cold worked, derivation of simple void-swelling equation 79—7631
steel, austenitic, neutron irrad., He release kinetics 78—79638
steel, austenitic, neutron irradiated, He absorption 77—51414
steel, austenitic, Ni-Cr, neutron-irradiated solute segregation and void swelling 79—60407
steel, austenitic, Ni-Cr, precipitation strengthened, anelasticity, plastic creep limit, 823K 79—1899
steel, austenitic, stainless, life prediction of high temp. low cycle fatigue, strain rate effect 79—8360
steel, austenitic, type 316, void swelling, role of bulk point-defect recombination 79—42105
steel, austenitic, type En58B, martensite formation and reversion, effect on void swelling 80—11641
steel, austenitic, type FV548, irradiated, Ni and Si rich phase, energy dispersive X-ray anal. 79—66063
steel, austenitic, type M316, martensite formation and reversion, effect on void swelling 80—11641
steel, austenitic, types A533B and A508, acoustic emission and deformation processes during tensile tests 79—74212
steel, austenitic, types M316, FV548, 304, irradiation creep data obtained in fast and thermal neutron spectra correlation with displacement cross-sections 80—84993
steel, austenitic, X6CrNi1811 and X6CrNiMo1713, crack growth under Na cooled fast breeder reactor conditions *(German)* 78—56798
steel, austenitic 316, displacement energy determ., HVEM obs. and electron bombardment 78—6100
steel, austenitic (03KH18N10T), heat treatment for fission reactor appls. 80—66454
steel, austenitic AISI 310, creep damage and rupture 79—20127
steel, austenitic cladding stability of fuel element for gas-cooled fast reactors *(Russian)* 77—83042
steel, austenitic stainless, 304, solution annealed, tensile flow behaviour after exposure to flowing Na, in temp. range 550 to 700°C 78—35463
steel, austenitic stainless, AISI 316, irradiation effects on phase stability 79—11566
steel, austenitic stainless, cladding, stress-corrosion cracking 79—20293
steel, austenitic stainless, Cr-Ni (16, 16 wt.%), in-pile rupture strength, cold work and soln. annealing effects 77—63687

fission reactor materials continued
steel, austenitic stainless, creep, effect of temp. and dose rate variations, Dounreay fast reactor 80—93603
steel, austenitic stainless, DIN 1.4970, influence of He on high temp. mech. props. 79—7636
steel, austenitic stainless, effect of irrad. and other factors on fatigue crack propagation 79—20194
steel, austenitic stainless, effect of Soviet BR-5 reactor operating conditions on vacancy porosity 79—32990
steel, austenitic stainless, electron transmission microscopy, microstructural zones *(Spanish)* 79—39059
steel, austenitic stainless, embrittled by α-particle irrad. 77—69015
steel, austenitic stainless, fatigue crack propagation, effect of neutron irradiation 80—97583
steel, austenitic stainless, fatigue crack propagation, influence of neutron irradiation 80—97584
steel, austenitic stainless, for primary and auxiliary reactor systems 77—3102
steel, austenitic stainless, HVEM irrad., point defect trapping influence on void swelling 79—23652
steel, austenitic stainless, influence of steel comp. on corrosion in high temp. Na 78—80675
steel, austenitic stainless, irradiation induced creep, AISI 316, 20% cold worked effect of temp. change 78—72816
steel, austenitic stainless, irradiation induced creep by alpha particles, in type 316 steels *(French)* 78—72791
steel, austenitic stainless, multiaxial creep equations for nonlinear and volume-nonconservative in-reactor creep 79—59164
steel, austenitic stainless, neutron dose rate depend. of swelling in fission reactors 80—104233
steel, austenitic stainless, neutron irradiated OKh16N15M3B, low-cycle fatigue 79—91793
steel, austenitic stainless, neutron-irradiated, gamma-alpha transformation 79—96027
steel, austenitic stainless, postirradiation mechanical props. of honeycomb spacer grids 79—36324
steel, austenitic stainless, radiation-induced swelling in BOR-60 reactor 79—97814
steel, austenitic stainless, stress corrosion cracking, factors influencing susceptibility 80—97617
steel, austenitic stainless, thermal fatigue of sodium mixer *(French)* 79—91789
steel, austenitic stainless, type 304 with He distrib., foil, effect of momentum transfer, damage energy gradient, on He distrib. 78—71773
steel, austenitic stainless, type 316, irrad. induced creep 80—93606
steel, austenitic stainless, type 316, irradiated with 46.5 MeV Ni^{6+} ions, soluble C effect on void swelling and low dose dislocation structs. 80—49280
steel, austenitic stainless, type FV 548, 20% cold worked irradiated with 22 MeV C^{2+} ions or 46 MeV Ni^{6+} ions, study of void swelling 79—37744
steel, austenitic stainless AISI 321, Cr tracer diffusion coeffs. 80—2193
steel, austenitic stainless appl., props. 77—3101
steel, austenitic stainless FV548, neutron irradiated, Si-rich phase occurrence of M_6C phase 80—15156
steel, austenitic stainless in liq. Na, mechanical props., review 79—20150
steel, austenitic stainless oxide film morphology, irradiation effects in N_2O_4 *(Russian)* 79—33209
steel, austenitic stainless type 316, corrosion mechanism in hot flowing Na, computer simulation 80—3251
steel, C, pressure vessel and piping, factors affecting notch toughness 79—61730
steel, C transfer between structural steels and Na in LMFBR 79—97805
steel, C-Mn, pressure vessel usage, elevated temp. mech. beahviour 78—35462
steel, C-Mn-V and Cr-Mo-V, fracture toughness and fatigue characts. 79—20192
steel, CC Cr-Mo (2.25, 1 wt.%) effect of heat treatment on tensile props. 78—23745
steel, cold worked FV548, electron irradiated, void swelling after 10 ppm He preinjection 77—19989
steel, corroding surface in nuclear reactor, mixed cation spinel form. 78—35565
steel, corrosion, Na loop system, analysis of radioactive corrosion product transfer 78—78464
steel, corrosion behaviour in simulated HTGR He environment 79—54495
steel, Cr (13 wt.%), sintered, organometallic complex addition effects on mech. props. 80—25595
steel, Cr (9 wt.%), oxidation in CO_2, early stages study by AES 78—7080
steel, Cr-Mo, annealed, microstructural effects on creep-rupture behaviour 79—57120
steel, Cr-Mo, constitutive eqn. model for high temp. behaviour of fast reactor structural alloys 78—66343
steel, Cr-Mo, high-temp. props. and constitutive equations 79—34146
steel, Cr-Mo, Mn-V, V, fracture toughness, pressure vessel appl. *(Czech)* 79—79094
steel, Cr-Mo, press. vessel material, yield surface behaviour, investigation techniques 79—61658
steel, Cr-Mo (2.25, 1.00 wt.%), bainitic, strain rate effects on elevated temp. tensile behaviour 78—35461
steel, Cr-Mo (2.25, 1.0 wt.%), thermally aged and Na decarburised, stress-rupture props. 80—21102
steel, Cr-Mo (2.25, 1 wt.%), annealed, heat treatment effect on tensile props. 78—11243
steel, Cr-Mo (2.25, 1 wt.%), annealed, tertiary creep behaviour 79—43326
steel, Cr-Mo (2.25, 1 wt.%), corrosion behaviour in simulated HTGR He environment 79—54495
steel, Cr-Mo (2.25, 1 wt.%), corrosion in molten NaOH, rel. to reactor boiler wastage 77—90497
steel, Cr-Mo (2.25, 1 wt.%), creep-fatigue testing from thermal transient effects in CRBRP reactor 78—21660
steel, Cr-Mo (2.25, 1 wt.%), decarburization, carbide effects in high temp. Na *(Japanese)* 78—15403
steel, Cr-Mo (2.25, 1 wt.%), in high temp. Na, heat treatment and metallurgical struct. effects 77—16619
steel, Cr-Mo-Nb-Ni, low alloy, material selection for LMFBR steam generator tubes 78—54834

fission reactor materials continued
steel, Cr-Mo-Nb-Ti low alloy, material selection for nuclear steam generator tubes 78—54834
steel, CT specimens, irradiated in FRJ-1 research reactor, neutron flux densities, temp. fields meas. 77—83029
steel, development for FBR, low swelling and creep at high neutron fluences 79—22374
steel, effect of B on radiation embrittlement 78—691
steel, fast reactor structural materials, meas. and calcs. of integral capture cross-sections 80—13613
steel, fatigue crack growth rate in high temp., high purity oxygenated water 80—40622
steel, ferritic, Cr-Mo (2.25, 1 wt.%), annealed, time depend. strain controlled fatigue, nuclear steam generator appl. 77—8915
steel, ferritic, Cr-Mo (2.25, 1 wt.%), C and Nb influence on structural transformations *(French)* 80—84925
steel, ferritic, FV607, void swelling, theory 78—71763
steel, ferritic, FV607, void swelling in 1 MeV electron irradiation 78—71762
steel, ferritic, screening studies for evaluation for nucl. process heat system 78—13236
steel, ferritic, void swelling during irradiation, suppression mechanisms 80—6441
steel, ferritic alloy and martensitic stainless, void swelling response after fast reactor irradiation 80—6437
steel, ferritic and austenitic, corrosion in NaOH contaminated Na *(French)* 77—52541
steel, ferritic nuclear pressure vessel, methodology for fracture props. variability evaluation 78—33257
steel, ferritic stainless, radiation induced creep, fundamental mechanisms *(Italian)* 80—55457
steel, for pressure component, fracture charact., implications for reliability 79—20199
steel, for PWR press. vessels, RT_{NDT} shift of ductile-temp. curve, correl. with neutron dose *(German)* 77—34388
steel, fracture toughness of nuclear pressure vessels 80—81172
steel, He liberation during tempering 77—46290
steel, heat-exchanger alloys for use in nuclear steam coal gasification plant 78—15589
steel, heavy section, pressure vessel rupture tests 78—44212
steel, high purity, low S content, for tough semi-finished products in nuclear power plant *(German)* 80—45393
steel, hydrogen embrittlement, model including reversible and irreversible processes 77—25155
steel, I_2 adsorption on steel in HTGR He environment 80—44233
steel, irrad. effects, neutron energy depend., damage model *(German)* 77—34385
steel, irrad. effects at high temp., simulation by HV electron microscope 77—1153
steel, irradiation by neutrons, damage function for mech. props. 78—13228
steel, low alloy, 15Kh2MFA and 15Kh2NMFA, neutron irrad. embrittlement, effect of P, Sb and Sn impurities 80—85055
steel, low alloy, press. vessel, fracture toughness in post yield regime 77—16671
steel, low alloy, pressure vessel and piping, factors affecting notch toughness 79—61730
steel, low alloy, reactor pressure vessel, effect of Mn and C content on irrad. response 79—20196
steel, low-C, kinetics of void development in fracturing A533B tensile bars 80—76357
steel, LWR pressure vessel, neutron radiation effects on material props., review *(German)* 77—34382
steel, martensitic, delayed fractures suppression, by neutron irradiation *(Czech)* 78—67743
steel, mass spectrometric analysis of S content by remote meas. technique 78—23994
steel, materials specifications for AGR steam generators 80—42772
steel, metallurgical stability and corrosion in He atmos., HTR appl. 79—36329
steel, mild, biaxial fatigue, data compilation and anal. 77—4856
steel, mild, bolt thread strain meas. 78—60972
steel, mild, ductile fracture of cracked plates, nonlinear boundary-value problem 77—81318
steel, mild, yield point, effect of neutron irrad. and N_2 conc. 80—45365
steel, Mn(0.9 wt.%), hydrogen embrittlement resist. evaluation *(Czech)* 80—35308
steel, Mn (1.10 to 1.55 wt.%), reactor vessel material, assessment of weld heat affected zone mech. props. 79—29217
steel, Mn-Mo-Ni, embrittling effects of residual elements 80—66655
steel, Mn-Mo-Ni (A533 B), ductile-brittle transition, material fracture temp. depend., Gauss distrib. function 80—97574
steel, Mn-Ni-Mo, hydrogen embrittlement resist. evaluation *(Czech)* 80—35308
steel, Mn-Ni-Mo, PWR pressure vessel, irrad. induced embrittlement, chemical composition effect *(French)* 79—20195
steel, Mn-Ni-Mo low alloy steels for nuclear appl., toughness and heat treatment 80—5239
steel, Mn-V and Cr-Mo, for pressure vessels, hydrogen embrittlement evaluation *(Czech)* 79—38950
steel, neutron activation anal. in VVER reactor *(Czech)* 80—5234
steel, neutron irrad., additivity deviations in thermal and radiation induced embrittlement 77—73348
steel, neutron irradiated, liberation of He in uniform heating 77—50248
steel, neutron irradiated press. vessel material, small angle neutron scatt. meas. 79—13428
steel, neutron irradiation induced swelling, empirical relationship with dose and temp. 77—50247
steel, Ni-Cr, corrosion on N_2O_4 flow 520-890K and 8-9 MPa *(Russian)* 80—3256
steel, Ni-Mo-Cr, embrittling effects of residual elements 80—66655
steel, NiMoCr waterquenched, for BWR press. vessel, fast neutron fluence evaluation, irrad. behaviour *(German)* 77—34369
steel, non-irradiated and irradiated specimens, autoclaves for fatigue crack growth tests *(German)* 80—45467
steel, nuclear bolts, heat treatment for structural retraction prevention *(French)* 79—91713
steel, nuclear pressure vessel, SA533B-1 and SA302B, fracture toughness prediction using crit. fracture stress and strain models 80—25855
steel, nuclear pressure vessel, type A533B-1, three point bending, yield stress, exam., Charpy V-notch and precracked specimens 78—92310

fission reactor materials continued
steel, nuclear pressure vessel time A533 grade B class 1, thermal shock fracture toughness at elev. temp. *(Japanese)* 79—83304
steel, nuclear reactor press. vessel, neutron exposure, safety limitations *(German)* 77—34405
steel, nuclear reactor pressure vessel materials, AE assessment 79—83422
steel, pressure vessel, ASME SA-387 grade D, fatigue crack growth, liquid Na environment effects 77—8997
steel, pressure vessel, fracture toughness at elevated temps. 79—20193
steel, pressure vessel for light water reactors, corrosion fatigue, data review 79—79169
steel, pressurised tubes under dynamic bending and torsional loading, inelastic deform. 77—77549
steel, prestrained pressure vessel, dynamic toughness characts., expt. correlations 79—15783
steel, PWR pressure components, mechanical factors affecting reliability *(French)* 79—20198
steel, reactivity meas., determination method *(Russian)* 80—664
steel, reactor pressure vessel failure and radiation damage *(Czech)* 80—619
steel, reactor pressure vessels, positron annihilation as nondestructive monitor of radiation damage 77—4130
steel, reactor vessel, neutron irrad. effect on brittle fracture characts. *(Slovak)* 78—50254
steel, role of ASTM in providing standards 79—22435
steel, rolled 15 MND 6, nuclear reactor cell material, determination of non-cracking threshold *(French)* 79—52367
steel, RPV type, toughness values compilation, temp.-range validity 77—48611
steel, SA540, fracture toughness props. for nuclear bolting appl. 78—35514
steel, stabilised, pressurised capsules in-pile creep meas. 77—42077
steel, stainless, 20% cold worked, type 316, creep failure time 78—19894
steel, stainless, 20% cold worked 316, in-reactor stress relaxation in bending 77—42079
steel, stainless, 20% coldworked 316, irradiation creep, depend. on temp. and atom displacements 77—42075
steel, stainless, 304, beam, elastic-plastic response to impulse loads 79—34118
steel, stainless, 304, bend test ductility of irrad. specimens for LMFBR appls. 80—104235
steel, stainless, 304, thermal fatigue and strength estimation, creep fatigue interaction 79—11708
steel, stainless, 304, void form., effect of sequential and simultaneous He implantation 78—71719
steel, stainless, 304 and 316, fatigue crack growth in PWR environment 79—66170
steel, stainless, 304L, irrad. induced creep and swelling 79—93723
steel, stainless, 304L, T grainboundary diffusion and trapping, autoradiographic exam. 78—51738
steel, stainless, 316, 304, LMFBR primary piping materials, mech. props. review 77—25151
steel, stainless, 316, neutron irradiation embrittlement, pre-irradiation treatment and composition modification 80—3171
steel, stainless, 316, nuclear fuel cladding, crack nucleation 78—72864
steel, stainless, 316, oxidation behaviour in the environment, appl. to GCFR fuel claddings 80—104350
steel, stainless, air contamination effect on compatibility with liquid Li in stainless steel vessels at 600°C 78—25285
steel, stainless, AISI 316, irrad. creep in bending at low fluence, LMFBR fuel duct deform. 79—61680
steel, stainless, AM-350, enhanced in-reactor stress relaxation 79—93725
steel, stainless, annealed type 304, LMFBR, creep rupture mode of failure, reliability anal. 77—3113
steel, stainless, attack by liquid and vaporised CsOH 78—68840
steel, stainless, austenitic, dynamic uniaxial and biaxial stress-strain relationships 80—81122
steel, stainless, austenitic, type 316, high velocity tensile test at elevated temp. 80—35194
steel, stainless, basic corrosion studies 77—34402
steel, stainless, boiling water reactor, corrosion and oxidation potentials monitoring 79—20252
steel, stainless, BWR cooling system pipes, stress corrosion cracking 78—23880
steel, stainless, carbonisation and carburisation in high press. He environment *(Japanese)* 79—26516
steel, stainless, cc Cr-Ni (20, 18 wt.%), effect of tensile stress on growth of He bubbles 79—55796
steel, stainless, cladding, irradiation enhanced creep 77—42074
steel, stainless, cladding dimensional changes in FBR $(U,Pu)O_2$ fuel pins due to swelling and inelastic strain 80—104296
steel, stainless, cold worked, 316, prior stress history effect on irradiation creep 79—87648
steel, stainless, cold-worked, 316, chem. comp. effects on rupture life, tensile props. 77—25152
steel, stainless, corrosion behaviour in simulated HTGR He environment 79—54495
steel, stainless, corrosion in nonisothermal Li flow 79—79177
steel, stainless, corrosion spectrochem. anal. using luminesc. discharge *(Spanish)* 79—92029
steel, stainless, Cr-Ni-Nb stabilised, Te vapour effect on creep and tensile props. 79—24583
steel, stainless, Cr-Ni-Nb-Ti, effect of I_2 vapour on creep fracture props. 78—72814
steel, stainless, creep behavior of ribbed cladding in prototypic GCFR coolant environment 80—16480
steel, stainless, Cs enhanced corrosion, Te influence 78—23866
steel, stainless, D implanted, thermal desorption 78—71750
steel, stainless, diffusion bonding in presence of Fe intermediate layer 79—10987
steel, stainless, diffusion of Cs study using ion beams 77—20125
steel, stainless, dilation and bowing in EBR II ducts and cladding 80—625
steel, stainless, dose rate and cascade collapse effects on swelling 79—23656
steel, stainless, EBR-II fuel pin cladding, obs. of in-reactor creep and swelling 80—13600
steel, stainless, EBR-II reactor components, creep and swelling 79—54499
steel, stainless, EBR-II reflector assembly irrad. induced bowing, implications for core restraint design 80—104234

fission reactor materials continued
  steel, stainless, effects of material properties on the dynamic response of pressure-loaded core subassembly wrappers 79—49756
  steel, stainless, electron irrad. in HVEM, radiation damage obs. 77—50233
  steel, stainless, failure analysis at elevated temperatures 80—55499
  steel, stainless, fast neutron irradiated, solution annealed tubing, residual stress behaviour 80—65054
  steel, stainless, fast reactor cladding tubes subjected to thermal transients, rupture behaviour 80—37465
  steel, stainless, fatigue crack growth behaviour in air and high-C liquid Na, carburization studies 80—40625
  steel, stainless, fatigue props. of low-fluence neutron irrad. samples 80—97585
  steel, stainless, FBR blanket facility, gamma-ray heating rate meas. 80—57912
  steel, stainless, FBR cladding stress distrib., effect of irradiation-induced swelling 80—19850
  steel, stainless, FBR fuel pin cladding, burst strength eval. 79—89378
  steel, stainless, FBR fuel pin cladding, in-reactor endurance and rupture life 80—13599
  steel, stainless, FBR fuel pin cladding strain under transient testing 80—18425
  steel, stainless, FBR fuel rod cladding damage correl. for rod perform. predictions 80—18424
  steel, stainless, Fecralloy, creep-rupture props., 650-800°C 80—97535
  steel, stainless, ferritic, Fecralloy, with and without Y, oxidation in Ar-H_2O-H_2 atmosphere 78—35584
  steel, stainless, fuel cluster sheath of LMFBR, steel-coolant interaction effect on porosity development 77—71651
  steel, stainless, GCFR ribbed cladding, post-irradiation creep rupture tests 80—18430
  steel, stainless, in N_2O_4 medium physico-chemical effects *(Russian)* 77—83044
  steel, stainless, in-pile creep measuring rig 77—42083
  steel, stainless, in-pile irrad. effect simulation by Ni ion bombardment, dislocation density, swelling 77—347
  steel, stainless, in-reactor deformation and fracture behaviour of EBR-II driver fuel cladding 80—42769
  steel, stainless, ion irradiated, carbide precipitation *(French)* 77—16585
  steel, stainless, irradiated, vacancy loop effect on swelling 79—14852
  steel, stainless, irradiation creep in bending 77—42078
  steel, stainless, irradiation induced creep in BR2 reactor using resonant cavity method 77—42080
  steel, stainless, LMFBR fuel pin cladding long-term in-reactor corrosion by liquid Na 80—16593
  steel, stainless, LMFBR subassembly response to simulated accident conditions, finite element anal. 77—3123
  steel, stainless, low-cycle fatigue characteristics of neutron irrad. samples 80—97586
  steel, stainless, LWR fuel cladding material evaluation 80—99213
  steel, stainless, Na exposed, corrosion in chloride containing aq. soln. 79—57151
  steel, stainless, Nb, oxidation in Ar-H_2O-H_2 atmosphere 78—35584
  steel, stainless, neutron irrad., pore annealing kinetics 77—72638
  steel, stainless, neutron irrad., solution-annealed and cold-worked, swelling 78—13229
  steel, stainless, neutron irradiation and N_2O_4 corrosion effects *(Russian)* 80—52741
  steel, stainless, oxidised, adsorption and absorption of Cs 78—84061
  steel, stainless, phase instability effect on cladding deform. profile of LMFBR fuel elements 77—74921
  steel, stainless, PWR primary corrosion products 80—13578
  steel, stainless, radiation-thermal treatment, N_2O_4 coolant action, intergranular corrosion *(Russian)* 78—58357
  steel, stainless, sintered Kh18N10T, friction and corrosion props. for frictional units of nuclear plants 78—60845
  steel, stainless, solution annealed 304L, in-reactor deform. 77—42076
  steel, stainless, solution treated, irradiated to low doses with 22 MeV C^{2+} and 46.5 MeV Ni^{6+} ions, interstitial loops 79—14855
  steel, stainless, solution treated FV 548, irradiated with 22 MeV C^{2+} and 46.5 MeV Ni^{6+} ions void swelling 78—22771
  steel, stainless, sputtering of Cr^+ by 10 keV H_3^+ angular effects 79—52058
  steel, stainless, stabilised with Cr-Ni-Nb, reaction with Te vapour 77—8986
  steel, stainless, stress corrosion susceptibility in high purity water, O_2 and temp. effects 80—61002
  steel, stainless, tensile props. of GCFR ribbed claddings at 650°C 80—45364
  steel, stainless, Ti modified 316, uniaxial tensile behaviour, Na environment effect 78—52916
  steel, stainless, type 304, BWR coolant pipe, critical strength under stress corrosion cracking 80—52743
  steel, stainless, type 304, description of deformation induced plastic anisotropy 79—43268
  steel, stainless, type 304, elastoplastic fracture mechanics for reactor piping 78—68777
  steel, stainless, type 304, piping cracks, metallurgical exam., failure anal. 79—67849
  steel, stainless, type 304, solution-annealed and thermally aged, correl. of high- and low-cycle fatigue data 78—15532
  steel, stainless, type 304, void swelling 200 keV C^+ bombardment, dose and temp. depend. 77—55309
  steel, stainless, type 304L, neutron irradiated, in-reactor precipitation and ferritic transformation 79—77644
  steel, stainless, type 304L, neutron irradiated, TEM study of ferrite formation 79—42112
  steel, stainless, type 316, blistering by 2 MeV He^+ ions, optical microscopy and SEM obs. 79—42119
  steel, stainless, type 316, cold worked effect of prior neutron induced creep on burst strength 78—62599
  steel, stainless, type 316, electron irradiated, void swelling 78—55891
  steel, stainless, type 316, influence of preirrad. thermal-mechanical treatment on phase stability and swelling 79—55792
  steel, stainless, type 316, irradiated, numerical simulation of void nucleation 79—73208
  steel, stainless, type 316, LMFBR and P1 cladding tubes, burst tests 78—44210
  steel, stainless, type 316, low cycle fatigue props. in vac., fracture mode 80—85021

fission reactor materials continued
  steel, stainless, type 316, modelling effects of fast neutron irradiation in mech. behaviour 80—84234
  steel, stainless, type 316, neutron flux and irrad. temp. dependence of swelling 78—79636
  steel, stainless, type 316, neutron irrad. damage simulation using HVEM, surface effect on void swelling 78—29572
  steel, stainless, type 316, neutron irradiated, ferrite formation, study by mag. meas. and TEM 79—37742
  steel, stainless, type 316, stress-free swelling at high neutron fluence, rel. to LMFBR core environment 78—13239
  steel, stainless, type 316 20% cold worked fission reactor fuel cladding, axial stress effects on transient mech. response 80—71743
  steel, stainless, Type 316 and 321, irradiation-induced creep following 4 MeV H^+ bombardment 78—14390
  steel, stainless, type 316 cladding, Ti-modified, performance in mixed-oxide fuel pins 79—67865
  steel, stainless, type AISI 316, carburisation of crevices by impure liquid Na 78—80680
  steel, stainless, weld overlaid, creep-rupture props. 78—13230
  steel, stainless 304, previously irradiated, irradiation induced stress relaxation in fast flux environment 77—25104
  steel, stainless 304, secondary ion emission due to H ion bombardment 79—8216
  steel, stainless 304 and 308 and weld material, fatigue crack propag. in neutron irradiation 78—23815
  steel, stainless 316, 20% cold worked, swelling increase due to inreactor temp. reduction 78—34547
  steel, stainless 316, carbide precipitation rel. to in-reactor deform. 79—8302
  steel, stainless 316, cladding failure during thermal transients 79—8316
  steel, stainless 316, Fokker-Planck eqn. describing evolution of interstitial loop microstruct. during irradiation 80—107215
  steel, stainless 316, irradiated void swelling incubation period, stress effects 78—6105
  steel, stainless 316, irradiation induced swelling, stress effects 78—34545
  steel, stainless 316, soln. annealed, cavity alignment and precipitation during dual ion bombardment 80—70273
  steel, stainless AISI 316, fast neutron void swelling simulation dose and dose rate effects 77—15457
  steel, stainless AISI 316, neutron irradiated, rel. between irradiation induced swelling and shear modulus 80—15157
  steel, stainless AISI 316, Si and Ti effect in phase stability and swelling behaviour 79—78972
  steel, stainless and C, radioactive contamination under applied potential in high temp. water 79—24646
  steel, stainless austenitic, neutron irrad., swelling due to gamma prime and $M_{23}(C_1Si)_6$ form. 78—51590
  steel, stainless austenitic type 304, corrosion by molten Cs_2O_3-CsO_2 79—57141
  steel, stainless cold-worked austenitic, fatigue and creep crack growth at elevated temp. 78—48524
  steel, stainless FBR fuel pin cladding, failure stress and strain 811 to 1644K 79—89377
  steel, stainless LMFER fatigue in elevated temp. Na environment 79—24666
  steel, stainless M316, neutron irradiated, occurrence of ordered FCC phase 77—51411
  steel, stainless tubing 316, attack by $Te/O_2/Cs$ corrodents 80—50770
  steel, stainless type 304, radiation induced outgassing 80—624
  steel, stainless type 304, rupture of tubes, appl. of fracture mechanics 77—3794
  steel, stainless type 316, effect of damage rate on void growth, point defect conc., microstruct. development 79—73209
  steel, stainless type 316, irrad. induced nuclear cladding swelling, empirical development of design equation 80—59527
  steel, stainless type 316, irradiation induced creep under 60 MeV alpha irradiation 80—92597
  steel, stainless type 316, monotonic and cyclic biaxial loading at room temp. 78—52928
  steel, stainless type 316, neutron irradiated, or themally aged diamond-cubic η phase formation, TEM study 79—99249
  steel, stainless type 316, neutron irradiated, transient mech. response prediction 79—74207
  steel, stainless type 316, set of master curves for creep ductility 79—66112
  steel, stainless type 316, temp. effects on swelling 80—32347
  steel, trace element anal., spectra of laser plasma 78—88691
  steel, tubular, type 0Kh16N15M3B, reactor irradiated, creep resist. *(Russian)* 80—25762
  steel, type 12X18H10T, defect development in contact area with coolant *(Russian)* 80—57859
  steel, type DIN 1.4970, tensile creep rupture at cyclic load variation at 700°C 79—66143
  steel, type FV548, 1 MeV electron irradiated, influence of pre-injected He on void nucleation and growth 80—34054
  steel, type X16H15M3B, radiation swelling, predictions for conditions in fast reactors *(Russian)* 79—67870
  steel, voids and swelling following $^{56}Fe^{3+}$ bombardment, fast neutron effects simulation 77—30651
  steel 12X18H10T, microdefect behaviour at point of contact of coolants *(Russian)* 80—19793
  steel A533A, review of data in reln. to fracture toughness at upper shelf temp. 79—15797
  steel ablation and fuel-steel mixing phenomena following LMFBR accident 80—47649
  steel AISI 304 tubes, fatigue crack growth under mixed loading conditions 77—3114
  steel austenitic stainless, Cr-Ni 316 type, electron irradiated, void swelling 79—42104
  steel cladding, 8 distrib. after Na exposure and high-temp. 77—57719
  steel Cr-Mo (2.25, 1 wt.%), duplex LMFBR steam generator tubing, US equipment for NDT 78—11469
  steel Cr-Mo low-alloy, material selection for nuclear steam generator 78—54834
  steel for nucl. reactors, trace element anal., implications for decommissioning 78—54833
  steel for press. vessel, neutron flux densities, neutron spectra and temp. fields in large specimens 77—74924
  steel for pressure vessels, criteria for brittle fracture, neutron effects *(German)* 77—34389

fission reactor materials continued
steel for pressure vessels, irrad. and post-irrad. examination equip. and techniques *(German)* 77—36696
steel for pressure vessels, slow neutron small angle scatt. study of radiation induced embrittlement *(German)* 77—34390
steel pearlitic, statistical anal. of joint effect of Ni, Cu, P on irradiation embrittlement 78—71770
steel piping components, incremental collapse tests, structural behaviour 77—6526
steel plate for nuclear reactor containment, brittle fracture meas. 77—3115
steel plates for reactor pressure vessels prod. by basic oxygen process 77—74944
steel pressure vessel, notched, acoustic emission meas. during pressurisation 78—21638
steel pressure vessel, reliability aspects 79—22430
steel pressure vessel plates, destructive examination, PISC trial 80—52745
steel pressure vessel plates, PISC trials result 80—52746
steel pressure vessel plates, US examination, PISC project 80—57861
steel pressure vessel surveillance capsule exam., appl. of ASTM standards 79—22436
steel pressure vessel US examination, PISC trials result anal. scheme 80—57863
steel products for nuclear power stations, research and development *(Russian)* 79—34080
steel stainless capsules, soln. annealed He pressurised, type 304L, neutron irradiation-induced creep 79—42111
steel vessels, internal pulsed loads, effect of scale, geometry and filler on strength 78—21659
steels, austenitic and type 316, neutron irradiation induced embrittlement, review 79—65120
steels, dynamic material props. for FBR safety anal., testing devices 78—60966
steels, irradiated pressure vessel, reference fracture toughness curves 80—100921
steels, mass spectrometer system for He assay 77—34397
steels, nuclear reactor pressure vessel steels, optimum chem. comp. rel. to props. 80—93517
steels, oxidation of structural steels in gas-cooled reactors 80—45447
steels, radiational swelling of two-phase austenitic-ferritic stainless steels 80—65063
steels, wave propag. effects on dynamic loading of pressure vessels 77—3090
steels for nuclear pressure vessels, transient finite elememt crack propag. model 77—3106
steels for pressure vessels, neutron irrad. embrittlement, temp. effects, annealing *(German)* 77—34384
steels for PWRs, props. and development 77—38336
Stellite-6, XPS obs. of aqueous oxidation, surface comp. and gaseous oxidation effect 80—81238
Stellite-6 in liquid Na, tribology 79—26525
strain measurement, extensometric method, for inside nuclear reactor channels 80—100998
stress corrosion cracking, prediction in 10% NaOH soln. at 315°C 80—97616
stress corrosion cracking avoidance by improved welding in BWR pipes 80—42838
stress intensity factors for reactor vessel nozzle cracks 79—15796
stress rupture regression lines in reactor materials, statistical determination 80—30106
structural, alloy phase thermochemical stability, calc. of radiation effects 79—60406
structural alloys, constituent segregation during irradiation 79—55791
structural alloys, time-depend. fatigue behaviour 79—1909
structural anisotropic domes, deformation anal., fission reactor appl. *(Slovenian)* 80—48577
structural graphite, radiation dimensional stability, variations 79—71896
structural material, semi-integral transmission expts. using spherical shell 80—13615
structural material transmission meas. using TOF spectrometer 80—18440
structural materials, corrosion resistance in liquid metals *(Czech)* 77—50245
structural materials in nuclear power stations with RBMK reactors, corrosion monitoring 79—9756
structural reliability, conference, Berlin, Germany (Aug. 1979) 80—105422
structural reliability in reactor technology *(Japanese)* 78—17315
sulphonated cool, gamma radiation breakdown 78—693
surface analysis by SIMS, SEM AND ESCA 79—52825
surfaces, formation of hydrocarbons 80—21322
swelling, depend. of evolving cavity distrib. functions on cavity growth kinetics 79—3206
swelling during self-ion bombardment, effect of implanted interstitials 78—10099
tandem mirror hybrid reactor, nucl. performance sensitivity of Be/molten salt blanket 80—37606
tank support ring design *(German)* 77—42103
terphenyl, partially hydrogenated, neutron thermalisation spectrum 77—67812
testing, General Electric Test Reactor appls. 80—565
thermal and irradiation environment influences and material responses 80—52737
thermal bowing of wire-wrapped fuel pins in the fast test reactor 80—42770
thermal hydraulics, sensitivity theory development 79—17963
thermal properties at elevated temps., determ. method, appl. to Mo, W 77—73402
thermally orthotropic plates, determ. of unsteady temp. distrib. by conformal mapping 79—55310
thermodynamic activity of C in Na 77—83045
thermomechanical transient anal., strain-rate dependent plasticity 80—79864
thermophysical properties at high temp., conference, Moscow, USSR (May 1976) 77—28012
thermophysical property measurements at RFL Springfields 77—14230
THTR-300 PBR, nuclear material safeguards system 79—22427
trace diffusion of nuclear reaction products, lanthanides, in polycryst. Ta 78—22896

fission reactor materials continued
TRIGA pulsing reactor without coolant loss, safety assessment for fuel and cans 80—52773
TRIGA reactor at HFER, neutron radiography studies 80—68758
tritides, He behaviour 79—17981
tube flaw detection by annular US transducers 78—60971
tubular joints stress anal., finite element anal., computer programs 78—41808
TZM, air contamination effect on compatibility with liquid Li in stainless steel vessels at 600°C 78—25285
UMFBR molten core debris and core containment material interactions 79—13469
undersaturated alloys, irradiated, solute segregation kinetics, via drift and defect-solute complexes 80—60872
USA fission energy R&D redirection, weapon material utilization 79—26510
VHTR system, material requirements for intermediate heat exchanger, rel. to creep-rupture tests 78—13235
void, nucleation rate determ. from size distrib. 78—10035
void densities, interpretation from critical radius arguments 79—23657
void swelling, nucleation theory 80—65038
void swelling, transition from gas bubbles 78—14383
void swelling and dislocation loop growth on fast particle irrad. *(Russian)* 77—59047
void swelling calculations using FACSIMILE VSI 80—42782
void swelling depth distribution produced by 5 MeV Ni ions 77—7771
void swelling simulation, review 78—8906
VVER, T buildup estimation with allowance for ^{6}Li conc. 79—97833
water, ^{16}N activity from ^{16}O(n,p)^{16}N, nuclear powered ship 78—13192
water, superheated, specific heat estimation 77—24413
water, transition boiling under forced convective conditions, reactor accident condition 78—89961
water coolant decontamination *(Spanish)* 79—45345
water droplets react. with molten Na 78—71263
water phase diagrams, spline representation, for PWR programs 77—23207
water-moderated-water-cooled reactor VVER-1000, power plant technology 78—82501
water/Na temp. fluctuation correlation mixing tee expts. 78—8878
weld metal, submerged arc irradiated, reference fracture toughness curves 80—100921
welded pressure components, effect of material property changes on operating conditions 79—20197
Winfrith Hot Cells—1964-1979 80—68782
β-Zircalloy, creep charact. 79—8317
Zircalloy in thermal gradient, calc. of supercharging effect of H_2 and hydride distrib. 78—21639
Zircalloy-4 fuel sheathing, inverted primary creep 78—86615
Zircaloy, accelerated corrosion in BWR and high temp. high press. steam, correlation 77—3104
Zircaloy, cladding in fuel rods, stress corrosion fracture on power increase 79—47818
Zircaloy, deposits on inside surface in LWR cladding, SEM obs. 79—6741
Zircaloy, effect of dispersion and spheroidisation treatment of δ ZrH 79—76073
zircaloy, effect of reactor irradiation on H diffusion 77—14231
Zircaloy, H absorption, Sn(Fe)(Cr)(Ni) effect 80—49527
Zircaloy, H diffusion, neutron scatt. and absorpt. study 79—60556
Zircaloy, hydriding reaction kinetics, oxidised specimens 78—26728
zircaloy, in-pile creep measuring rig 77—42083
Zircaloy, in-reactor creep meas. appl. in design of PWR fuel 77—42073
Zircaloy, irradiated spent fuel cladding, annealing effects 79—89382
Zircaloy, irradiation growth in annealed and cold worked samples 77—88225
Zircaloy, LWR cladding, I_2 stress corrosion cracking 79—89380
Zircaloy, LWR fuel rod cladding, damage accumulation during I_2-induced stress corrosion cracking 80—71810
β-Zircaloy, O_2 diffusion 78—6181
Zircaloy, O diffusion during UO_2-Zircaloy interaction 79—10986
Zircaloy, post irradiation recovery of growth 79—46711
Zircaloy, PWR fuel induced cladding deformation, creep correl., in-pile meas. 80—97547
Zircaloy, PWR primary corrosion products 80—13578
Zircaloy, steam oxidised, partitioning behaviour of O_2 78—68839
Zircaloy, textured, interactive creep and growth, upper-bound evaluation 80—89293
Zircaloy, unirrad., stress corrosion cracking, I_2-induced, effect of test temp., alloy comp. and heat treatment 80—97632
Zircaloy 2 and 4, oxidation kinetics appl. to loss of coolant accidents, data review 78—19958
Zircaloy 2 irradiation creep strain meas. technique 77—42084
Zircaloy 2/I_2 system, stress corrosion crack growth for short cracks 78—80685
Zircaloy 4, creep anal. and appl. in prediction of residual stress relaxation 79—43325
Zircaloy 4, stress relaxation in bending 78—68719
Zircaloy 4 tubing, cold-worked and annealed, stress relaxation behaviour 77—57717
zircaloy calandria tubes in CIRENE PWR, stress evaluation using strain data *(Italian)* 77—50204
Zircaloy clad defective fuel rods, behaviour under continued reactor operation 79—30915
Zircaloy clad fuel rod burst behaviour in simulated PWR LOCA 79—36337
Zircaloy clad UO_2 fuel elements, irrad. effects 80—666
Zircaloy cladding, crud deposition 80—106117
Zircaloy cladding, embrittlement and failure during reactor power-cooling-mismatch 78—21688
Zircaloy cladding, enhanced steam oxidation by deformation under LWR LOCA 80—73917
Zircaloy cladding, stress corrosion cracking, inner surface texture effect 80—66695
Zircaloy cladding, stresses due to pellet cladding interaction 80—42762
Zircaloy cladding ballooning, analytical model for transient gas flow in LWR 80—18499
Zircaloy cladding fracture due to pellet-cladding in water reactor rods 77—74927
Zircaloy cladding stress corrosion cracking due to I *(Japanese)* 80—78361

fission reactor materials continued
Zircaloy cladding thermal failure and UO_2 fuel melting during LWR PCM transient 80—42834
Zircaloy cladding tubes, under internal and external overpressure in FRG-2 in-pile creep 77—42082
zircaloy cladding tubes of irrad. fuel, flattening test *(Japanese)* 77—42054
zircaloy corrosion, in-reactor, effects of water radiolysis 77—12817
Zircaloy corrosion in water reactors, comparison of uniform and nodular forms 79—47817
Zircaloy creep collapse, hot cell examination 78—86596
Zircaloy for reactor fuel pin cladding, metallurgical processing, transient temperature distribution 80—47573
Zircaloy fuel cladding, azimuthal temp. distrib. during LOCA 80—662
Zircaloy fuel cladding, behaviour during loss of coolant accident in LWR *(Japanese)* 79—71889
Zircaloy fuel cladding, irrad. capsule design for continuously monitoring creepdown 79—54513
Zircaloy fuel cladding, irradiation-induced in-reactor corrosion in CANDU reactors 80—104352
Zircaloy fuel cladding, O embrittlement obs. 78—89947
zircaloy fuel cladding tubes, prod. and inspection *(Japanese)* 79—26518
Zircaloy fuel claddings, multirod burst tests following PWR LOCA 80—777
Zircaloy fuel sheathing, NIRVANA high temp. creep model 79—87704
Zircaloy heated surface, FeO deposition in boiling water 78—58353
Zircaloy hulls, conversion to zirconate ion exchange materials for waste stabilisation 78—702
Zircaloy LWR cladding, modeling of deform. and fracture in SPEAR code system 79—93729
Zircaloy oxidation, improved evaluation model 80—32349
Zircaloy pressure tubes, effect of microstruct. on irradiation creep 79—74208
Zircaloy PWR cladding, deformation in LOCA 80—106114
Zircaloy PWR fuel cladding, balloon deformation during LOCA 80—659
Zircaloy PWR fuel cladding deformation tests under mainly convective cooling conditions 80—57862
Zircaloy reactor fuel cladding tubes, high temp. deformation model with nonlinear temps. 80—661
Zircaloy sheath, fission gas absorpt. following irrad., power history effects 80—78395
Zircaloy sheath tube, oxidation calc. *(German)* 77—346
Zircaloy sheaths, oxidation rate calc. method 80—78394
Zircaloy solid wastes from fuel reprocessing plant, management 77—61591
Zircaloy spacer grid design for PWR 80—18412
Zircaloy tubing, I_2 stress corrosion cracking, pellet cladding interaction mechanism *(German)* 80—16565
Zircaloy-2, anisotropic irradiation creep 79—8333
Zircaloy-2, annealed, neutron irradiation growth 79—42109
Zircaloy-2, anodic oxidation kinetics, in 0.05M oxalic acid (aq. and alcoholic) 80—104331
Zircaloy-2, Cd metal embrittlement in 300-340°C 77—16747
Zircaloy-2, cold worked, temp. cycling effects on irradiation growth 80—2079
Zircaloy-2, deformation and fracture behaviour, uniaxial tension test in I_2 environment 80—13580
Zircaloy-2, effect of simulated fission products on elongation fractography and metallography 80—649
Zircaloy-2, effects of simulated fission products on mechanical props. 80—52740
Zircaloy-2, elastic const. determ. 78—11257
Zircaloy-2, exposed to I_2 vapour, stress corrosion crack initiation sites 78—92324
Zircaloy-2, fretting corrosion in water-cooled nucl. reactor 77—79431
Zircaloy-2, hot-pressed, influence of diffused C on structure and oxidation 80—61016
Zircaloy-2, I_2 stress corrosion cracking, Cs_2O and Cs influence, in- and out-of-pile 80—3252
Zircaloy-2, iodine environment, plane strain tension test 80—22944
Zircaloy-2, irradiation creep under H^+ bombardment at 5.5 MeV 78—14392
Zircaloy-2, irradiation growth, reaction rate theory calcs. 80—88212
Zircaloy-2, irradiation growth, shape and volume changes 80—92562
Zircaloy-2, irradiation induced creep in reactor claddings under biaxial stress conditions 79—30912
Zircaloy-2, irradiation-induced creep following 4 MeV H^+ bombardment 78—14390
Zircaloy-2, mech. props. after exposure to I_2-methanol solutions, SEM study 80—93689
Zircaloy-2, neutron irrad. damage, TEM characts. 80—107332
Zircaloy-2, neutron irradiated, inhomogeneous deformation behaviour 80—50679
Zircaloy-2, neutron irradiation damage characterization by TEM 79—42110
Zircaloy-2, oxide coating thermal cond. meas. 80—80009
Zircaloy-2, polycrystn., thermal history effect on tensile props. 79—74204
Zircaloy-2, polycrystn., thermal history effect on tensile props., comment 79—74205
Zircaloy-2, pressure tube, fragmentation on failure 78—72863
Zircaloy-2, pressure tubes, irrad. creep and growth, anisotropy factors 80—97536
Zircaloy-2, radiation and isotope effects on corrosion in H_2O/D_2O mixture 77—21314
Zircaloy-2, radiation induced creep, yielding creep theory, time depend. of irrad. growth 77—26845
Zircaloy-2, reaction with UO_2-PuO_2 79—17982
Zircaloy-2, reactor cladding, delta-wrinkly zone near crack edge obs. 79—3203
Zircaloy-2, TEM and SEM of anodically formed oxides 77—21313
β-Zircaloy-2, tensile creep and creep rupture props. under vacuum 78—52915
Zircaloy-2, tritium diffusion 80—32341
zircaloy-2 and 4, tubing, rel. between contractile strain ratio R and texture 79—61607
Zircaloy-2 and -4, ⟨c⟩ component dislocations from TEM contrast expts. 80—6412
Zircaloy-2 and associated oxide layers, thermal property meas. 77—8063
Zircaloy-2 anodisation for claddings 77—81341

fission reactor materials continued
Zircaloy-2 cladding, bonding to UO_2 fuel, mechanisms determ. by SEM and EPMA 78—17317
Zircaloy-2 cladding, fracture in iodine environment 78—31581
Zircaloy-2 cladding, stress corrosion cracking in iodine vapour, 250-450°C 78—17313
zircaloy-2 cladding tube, fission cutting *(Japanese)* 77—67808
Zircaloy-2 cladding tubes, heat treatment influence on texture and mech. anisotropy 79—91694
Zircaloy-2 claddings, oxidation reaction kinetics in steam environment in temp. range 1273-1673K 80—35401
Zircaloy-2 fuel tube, thermal conductivity of oxide deposit 79—63745
Zircaloy-2 fuel tubes, cumulative damage fatigue tests at room temp. and 300°C 80—93638
Zircaloy-2 fuel tubes, low cycle fatigue studies at room temp., 300 and 350°C 80—93637
Zircaloy-2 irradiation growth at 353 and 553K, texture and temp. cycling effect 79—46709
Zircaloy-2 pressure tube, elongation in Douglas Point CANDU reactor 80—78398
Zircaloy-2 pressure tube elongation, neutron induced creep and growth, meas. and anal. 80—93628
Zircaloy-2 thin walled large diam. tubes in CANDU reactors 79—13429
Zircaloy-2 tube, external pressure creep behaviour 79—57083
Zircaloy-2 tubing, quantitative charact. of crystallographic texture 78—21647
Zircaloy-4, ^{51}Cr bulk diffusion 79—73347
Zircaloy-4, β-transformed, flow stress and dynamic strain ageing 80—3101
Zircaloy-4, creep damage at LWR temp. 79—52312
Zircaloy-4, creep rupture at monotonous stress and temp. ramp loading 79—74241
Zircaloy-4, creep rupture at superimposed non-stationary stress and temp. loading 80—66630
Zircaloy-4, cyclic nature of corrosion in 633K water, optical and electron microscope study 79—66207
Zircaloy-4, elastic props., O additions effect 80—66565
Zircaloy-4, exam. of plastic props. at elevated temps. in air 77—4811
Zircaloy-4, failure strain prediction under non-stationary loading conditions 80—93640
Zircaloy-4, fuel cladding, burst criteria under LOCA conditions 80—73931
Zircaloy-4, fuel cladding, steady-state creep from 940 to 1873K 79—74206
Zircaloy-4, in-pile PWR creep meas., comparative eval. of 10 creep correl. 80—652
Zircaloy-4, interdiffusion with Ni 79—42320
Zircaloy-4, microstrain and particle size meas. by Warren-Averbach method 80—55420
zircaloy-4, Nb additions, corrosion behaviour 77—40469
Zircaloy-4, oxidation at 900 and 1100°C in high pressure steam 79—66208
zircaloy-4, oxidation in high temp. steam atm. effect on cladding ductility 79—26515
Zircaloy-4, oxidation in steam, 900-1500°C, kinetics 80—3241
Zircaloy-4, oxidation in steam, 900-1500°C, O diffusion in oxide and α-phases 79—100288
Zircaloy-4, plain strain ductility dependent of struct. and texture 77—8885
Zircaloy-4, Poisson's ratio determ. at several temp. levels 78—52874
Zircaloy-4, polytype struct. of intermetallic precipitates, electron microscope obs. 79—43250
Zircaloy-4, PWR tubes, ZrO_2 scales formed in steam, microstruct. 77—6524
Zircaloy-4, quenched, strain ageing behaviour, ageing time and temp. effects 78—56657
Zircaloy-4, quenched and annealed, strain ageing 77—25071
Zircaloy-4, resistance-welded, microstruct. of weld region 80—66549
Zircaloy-4, strain rate sensitivity parameter measurement, from expt. load vs. time curves, superplastic range 79—8406
Zircaloy-4, stress relaxation specimens, thermally induced strain recovery causing microstruct. changes 77—25057
Zircaloy-4, stress-relieved and cold-worked, stress relaxation in bending at 673K 80—93609
Zircaloy-4, tensional stress cycling 80—3168
Zircaloy-4 BWR channels, corrosion resistance 80—104351
Zircaloy-4 clad UO_2 fuel, long term storage in water and stress corrosion cracking 79—93737
Zircaloy-4 cladding, creep transients, plastic hoop strain meas. 79—57068
Zircaloy-4 cladding, steady-state creep, 940 to 1873K 79—15759
Zircaloy-4 cladding deformation under LOCA transient heating conditions, analytical modelling 80—104236
Zircaloy-4 cladding rubes, burst strain and stress corrosion cracking, I influence 80—3248
Zircaloy-4 cold worked, strain ageing behaviour with varying O_2 content 77—48455
Zircaloy-4 diffusion bonding with 304 stainless steel 78—34658
Zircaloy-4 fuel cladding axial deform. in PWR LOCA 80—13585
Zircaloy-4 fuel sheaths, ballooning behaviour at heating rate 0.5°C s^{-1} 79—24593
Zircaloy-4 PWR cladding, effect of oxide coating on ductility 79—89381
Zircaloy-4 spent fuel cladding, tensile props. and annealing characts. 79—22392
Zircaloy-4 tubes, I stress corrosion cracking *(Korean)* 79—34195
Zircaloy-4 tubes, texture influence on anal. of thermoelastic/plastic anisotropy and initial yielding 80—35260
Zircaloy-4 tubing, unirradiated, under internal pressurisation, threshold conditions for I-induced stress corrosion cracking 79—66206
Zircaloy-4/stainless steel type 304 diffusion junction, hydriding behaviour 79—65200
Zircaloy-clad UO_2 fuel elements, stability during long-term storage 79—26588
Zircaloy-O_2 phase diagram 80—3003
Zircaloy-UO_2 fuel rods, eddy-current testing of claddings using encircling and probe coils 80—21245
Zircaloys, fractographic distinction between hydride cracking and stress corrosion cracking 78—92363
Zircaloys, I_2 induced stress corrosion cracking 79—8381
zirconium alloys, cladding strain reduction by changing pellet configurations 79—81008

fission reactor materials continued
Zirconium-4, oxidation reaction kinetics in unlimited steam environment 77−8988
(α,n), mixture and compound neutron yield from separate component thick target yields 80−37414
Na leakage in reactor steam generators, solution kinetics of solid NaOH in Na 79−36365
Ag, cascade energy density effect on isochronal recovery 78−47431
Ag, Doppler factor, comparison between calculated values and measured results 78−54811
Ag-Zn (30 at.%), electron irrad. exam. of defect supersaturation by elasticity, and creep meas. 78−47366
Ag-Zn(Cd), production and annealing of radiation defects 78−47362
^{108}Ag^{m}, prod. in nuclear reactors by thermal neutron capture in stainless-steel structure 80−42747
Al alloy, dil., neutron irradiation 78−22766
Al alloys, basic corrosion studies 77−34402
Al alloys, neutron irradiation effects, on microstruct., mech. props. and swelling 79−65121
Al film, He$^+$ irrad., overpressurised bubble obs. 79−51165
Al fuel tubes, proton activation determ. of impurities 80−27741
Al, He injected, tracing bubble evolution by positron annihilation 77−19992
Al, neutron damage, positron annihilation 80−65056
Al, pure, electron irradiation damage 77−19988
Al, quenched, vacancy-Fe interactions 78−47412
Al, stabiliser for fusion reactor supercond. mag., neutron irrad. effects on magnetoresistance 80−34062
Al, stress induced ordering of self-interstitial clusters 78−47358
Al, struct. metal, effective damage levels in neutron radiation environment 79−36236
Al-Cu (4 wt.%) alloy, neutron irrad., weak-beam dark-field obs. of dislocations near θ' precipitates 80−107333
Al-Ge (0.2 at.%), exam. of interstitial trapping by X-ray diffuse scatt. 78−47363
Al-Ge alloy, Ge precip., ion irrad., dose rate and temp. depend. 78−79642
Al-graphite two-dimensional shield, neutron penetration meas. 79−3245
Al-Mg (0.1 at.%), neutron damage, positron annihilation 80−65056
Al-Si alloys, neutron irrad., precip. processes, neutron small-angle scatt. obs. 77−4131
Al-Zn alloy cladding materials, corrosion behaviour under vacuum heating *(Japanese)* 79−91845
Al_2O_3-B_4C, behaviour as control rod in commercial reactor 78−8918
Al_2O_3-BaO-SiO_2 glass coatings in fission and fusion reactors, permeation, elec. cond. and dielectric breakdown 80−18439
^{241}Am(α,n), neutron yield in AmO_2 79−17912
^{241}Am(n,X)Cm, Japan Material Testing Reactor, separation of transuranium elements from fission products and cladding *(Japanese)* 80−52731
^{244}Am decay, relative probability of electron capture 78−17153
Ar binary mixtures, separation performance of Kr and Xe by thermal diffusion column 77−42192
Au, Doppler factor, comparison between calculated values and measured results 78−54811
B, borides, neutron absorbing props., reactor control system, appls., review, book contrib. 78−46154
B burnable poison in reactor fuel side plates, identification by neutron radiography 79−54492
B, laser photochemical isotope separation using Ti catalyst 77−61612
BC, physical and chemical interaction with energetic T 79−97902
B_4C, absorber material for fast reactor control appl. 78−8919
B_4C absorber pin in-reactor rupture test 79−93701
B_4C absorber rods, nondestructive exam. with dual-energy gamma gauge and multigauge scanners 79−93721
B_4C, behaviour as control rod in commercial reactor 78−8918
B_4C, behaviour in spent fuel storage pools 80−42771
B_4C, effect of fast neutron irradiation on struct. 78−26597
B_4C, FBR control rod elements, neutron damage and post-irrad. annealing 80−13581
B_4C, He release correlation during fast-neutron irradiation in fast reactor 78−8965
B_4C, LMFBR control material, integral capture cross section meas. in CFRMF 77−26760
B_4C, meas. of T retention of fast-neutron-irradiated absorber elements 78−8903
B_4C neutron absorber for EBR-II, He release, in-reactor meas. 80−73951
B_4C, neutron absorber material for FBR, in-reactor performance meas. 80−18429
B_4C rings, Al bonded, exam. of fabrication techniques 78−72748
B_4C rods, epithermal 1/V self-shielding of reactor poisons using Nordheim integral method 78−17306
B_4C, thermophysical props. and neutron absorpt. 80−103488
B_4C, used as control rods in FBR, irradiation effects 78−67742
B_4C-304 stainless steel cermet for nuclear shielding appls. 80−102352
B_4C-Al composite moderator rods, production and props. *(Russian)* 79−18006
B_4C-Cu cermet fabrication for neutron shielding appls. 80−102354
B_4C-graphite, irradiation-induced dimens. changes, rel. to HTGR conditions 78−8905
B_4C-phenolic fibre reinforced composite for nuclear shielding appls. 80−102353
BN, hexagonal, parallel to basal planes, thermal conductivity 78−22907
^{10}B separation using anion exchange resin, isotopic plateau holding displacement chromatography *(Japanese)* 78−56886
Be, ion bombarded, D trapping 79−19291
Be, irradiated with He$^+$ at 20 keV, surface damage and gas trapping profile meas. *(French)* 80−84218
Be, neutron irradiated, annealed, tensile props. and swelling, effect of He bubbles 78−22765
Be, two group calcs. for neutron wave propagation across an absorption discontinuity 78−89931
Bi and Bi:Te, neutron radiation defects 78−47430
C, activated adsorption of 0.98 mol.% Ar, vol. adsorption capacity 78−75933
C, automatic image analysis, variables and errors, definition and quantitative description *(German)* 78−25296
C, heat-treatment and neutron irrad. effects on US atten. and Young's modulus 79−11644
C materials, conf., Baden-Baden, Germany (June 1976) 78−43990

fission reactor materials continued
C, pyrolytic, tritium diffusion coeffs. and deuterium solubilities 80−37443
C steel containers for nuclear process liquid waste, stress corrosion 77−46311
C-graphite materials for HTR and fusion reactors 80−73928
CC Fe-Ni-Cr (35, 15 wt.%): Nb(Ti)(Mo), corrosion in HTGR He environment 80−61021
CO_2, gaseous reactor coolant, monitoring of U, Pu and fission products by gamma spectrometry 79−89374
CO_2, supercritical fluid coolant for CANDU reactors, feasibility study 79−76064
CO_2-$H_2O(D_2O)$-mineral oils, radiolysis products form. in nucl. reactor 78−689
^{14}C production by nuclear power industry 77−54367
^{14}C production in reactors and explosions, population dose, health impact 77−14274
Ca impurity, ^{37}Ar form., ^{40}Ca(n,α)^{37}Ar reaction 77−83048
Cd, reactivity worths of fixed neutron absorbers 78−21654
Cd, recovery after 6.1 MeV α-particle irradiation at 4.2K 78−47441
Cd thermal neutron filter, in-cell US inspection 80−68791
Cd-B(W) particulate composite, dispersion hardening, grain size and texture strengthening 77−8840
$CdAl_2O_4$, LWR burnable poison, irradiation and corrosion beahviour *(German)* 79−67846
Ce, gettering of H, mass spectrometry and microgravimetry study, rel. to HTGR gas purification 80−73374
Cm, production by neutron irrad. of ^{241}Am, Japan Material Testing Reactor *(Japanese)* 80−52731
Co^{2+} ion removal in high temp. water using TiO_2 79−89376
Co-Cr-W-C, hardfaced coating for high temp. liquid Na service, deposition and wear 77−32724
^{58}Co dissolution control by H_2O_2 addition in PWRs 78−21657
^{58}Co dissolution during PWR refuelling shutdown, control with H_2O_2 78−21698
^{60}Co, shutdown dose rate prediction in BWR primary coolant circuit 78−74445
Cr, 1 keV-1 MeV activation cross sections, rel. to fast reactor design 80−13624
Cr, fast reactor structural materials, nuclear data 80−13611
Cr, neutron capture cross sections in intermed. energy region, method and exptl. facility 78−21637
Cr, reactor structural material s-wave resonance parameters from capture cross section data 80−13629
Cr, resonance data eval. below 300 keV, Doppler effect calc. 80−13618
Cr structural material, integral expts. 80−13612
Cr, structural material data eval. for JENDL-1 80−13617
Cr-Fe-Ni alloys, claddings, chemical compatibility with UC nuclear fuels, thermodynamic model 80−63263
Cr-Fe-Ni alloys, interface with Th carbide fuels, basic chemical compatibility, thermodynamic calcs. 79−93727
Cr-Mo (2.25, 1 wt.%) steel, T permeation rate at 400 to 500°C, rel. to LMFBR conditions 78−17319
Cr-Mo low C steel forgings, material capabilities 77−42105
Cr-Mo steel for pressure vessels, improvement through electroslag remelting 77−42104
Cr_xC_y-(Ni-Cr) sprayed coatings, for gas cooled reactor heat exchangers, factors affecting performance 80−40609
Cs desorption from graphite, release in nucl. reactor coolant 80−18431
Cs-Cr-O system, phase equilibrium 80−3012
Cs-O system, phase diagram and O_2 potential 80−3011
$CsAlSiO_4$, prep. and X-ray characterisation 78−39728
Cu, cascade energy density effect on isochronal recovery 78−47431
Cu, defect clusters, electron microscope exam. 78−47380
Cu foi.foil, interstitial impurity interaction investigation by stage II isochronal recovery expts. 78−47423
Cu, He conc. profile meas. rel. to blistering 78−95089
Cu, irradiated with 20 keV He$^+$, surface damage and gas trapping profile meas. *(French)* 80−84219
Cu, neutron irrad., replacement sequences, calcs. using ADDES and COMENT codes 79−46714
Cu, proton-irradiated, H_2 gas-bubble struct., study at 300K 80−92569
Cu, stress induced ordering of self-interstitial clusters 78−47358
Cu-Ag (Au), dil., dose depend. of impurity detrapping stages after electron irradiation 78−51582
Cu-Al (2, 6.8 and 15 at.% Al), electron irrad. at 300 and 575 kV, exam. of damage rate 78−47425
Cu-Be (0.0182 at.%), radiation induced Be segregation 78−23710
Cu-Fe (1.5 wt.%), precipitation-effect on void formation during electron irradiation 80−84211
Cu-Fe (1.5 wt.%) alloy, void form. during irrad. in HVEM, reactor irrad. simulation and ageing effects 80−107327
Cu(II), selective separation from rare earth elements on chelate ion exchangers 78−58861
D isotope effect, corrosion stability in high temp. aqu. soln. 78−9091
D_2O leak detection, on-line infrared analyzers, CANDU report 78−82038
D_2O, neutron scatt. cross section determ. by DEUKER computer code 79−54468
D_2O, production in Fe/S/H_2O system 80−27750
depth distrib. of self-ion damage, TEM 77−51419
EuB_6, absorber material for fast reactor control appl. 78−8919
EuB_6, synthesis and hot pressing fabrication for appl. to neutron absorbing core control material 78−8904
Eu_2O_3, absorber material for fast reactor control appl. 78−8919
Eu_2O_3, appl. to LMFBR control 78−50261
Eu_2O_3, C→B transformation 77−11688
Eu_2O_3, for controlling fast reactor, irrad. behaviour 78−37409
Eu_2O_3, LMFBR control material, integral capture cross section meas. in CFRMF 77−26760
Eu_2O_3, thermophysical props. and neutron absorpt. 80−103488
Eu_2O_3-Ta_2O_5, microcracking, elastic props., internal friction 78−92326
Fe, 1 keV-1 MeV activation cross sections, rel. to fast reactor design 80−13624
Fe alloy, crevice corrosion by water vapour, CO, methane in HTR coolants, model 77−25202
Fe, amorphous, radiation damage simulation 80−34045
Fe and Fe alloys, fast neutron irradiated at high temps., mech. props. 79−51157
Fe base superalloy, type A-286, elevated temp. fracture toughness testing of thin section irrad. materials 80−61063

fission reactor materials continued
Fe, fast neutron penetration, cross section characts. effect, Monte Carlo study 77—23216
Fe fast neutron spectra, an assessment of ENDF/B-IV based on integral meas. 77—50194
Fe, fast reactor structural materials, nuclear data 80—13611
Fe, fast reactor structural materials, meas. and calcs. of integral capture cross-sections 80—13613
Fe, gamma fields induced by ^{252}Cf neutrons 78—50240
Fe, group consts., neutron spectra of small pile surrounded by Pb reflector 79—6738
Fe, high resolution fast neutron gamma-ray prod. cross sections 77—67745
Fe, integral neutron capture cross sections in GCFR lattices 78—13246
Fe, irradiation softening in single crystal, temp. and orientation depend. 77—86113
Fe, neutron capture cross sections in intermed. energy region, method and exptl. facility 78—21637
Fe, neutron group constants, meas. of energy and space distribs. 77—26829
Fe, ns. slowing down time, expt. obs. 78—58319
Fe, pure, corrosion in Na loop systems 77—48576
Fe, pure, neutron irrad. and H_2 absorption effects on mech. props. 78—34546
Fe, radiation induced defects, annealing exam. using channelling tech. 78—47316
Fe, radiation-induced swelling in BOR-60 reactor 79—97814
Fe, reactor structural material s-wave resonance parameters from capture cross section data 80—13629
Fe, resonance data eval. below 300 keV, Doppler effect calc. 80—13618
Fe, resonance parameters below 650 keV, self shielding coeffs. 80—13619
Fe struct. metal, effective damage levels in neutron radiation of environment 79—36236
Fe structural material, integral expts. 80—13612
Fe, structural material data eval. for JENDL-1 80—13617
α-Fe, void swelling during irradiation, suppression mechanisms 80—6441
α-Fe, void swelling response after fast reactor irradiation 80—6437
Fe:Xe(Te), interaction of impurities with point defects, Mossbauer spectroscopy exam. 78—47414
Fe-(Mo)-CaF_2, sintered, friction and corrosion props. for frictional units of nuclear plants 78—60845
Fe-Al (40 at.%) and Fe-Al (50.5 at.%) ordered alloys, 20K neutron irrad. effects, stoichiometry depend., resist. obs. *(French)* 80—84215
Fe-C-Cu (0.21, 0.2 wt.%), neutron irradiated, torsional props. effect of Cu additions and annealing temp. 78—56699
Fe-Co(Al), B_2 superlattices, point defect investigations 78—47357
Fe-Cr-Ni, solid soln. strengthened and precipitation hardened, in-reactor creep 79—43327
Fe-Cr-Ni (12, 15 wt.%) austenitic alloy, Ni^{6+} irradiated, void swelling and phase stability, Si and Ti effects 80—65055
Fe-Cr-Ni alloy, dual-ion-irradiated, swelling anal. 78—86600
Fe-Cr-Ti-Mo ferritic alloy, annealed, cold rolled, fast reactor material, mech. props. 78—21646
Fe-Cr-Ti-Mo-TiO_2 (13, 3.5, 1.5, 2 wt.%) dispersion hardened, void swelling 80—65046
Fe-Cu-Ti, improvement of irradiation-enhanced Cu embrittlement by Ti addition 79—43393
Fe-N, neutron irrad. effects on mech. props. 79—4338
Fe-Ni alloy, disordered, short-range order study by time-depend. PAC method 78—6618
Fe-Ni-Cr (35, 15 wt.%), high temp. alloys, for HTR primary components, alloying additions for carburisation protection 80—5243
Fe-Ni-Cr alloys in FBRs, correl. between void swelling and thermodynamic stability 80—641
Fe-Ni-Cr-base superalloy, characterization for PNP components 80—5242
Fe+H shield, neutron flux meas., comparison with Monte Carlo calcs. 77—23349
Fe(III), selective separation from rare earth elements on chelate ion exchangers 78—58861
$Fe_{40}Ni_{38}Mo_4B_{18}$, amorphous, crystallization, heat treatment and irradiation effects *(French)* 79—90558
Fe_2O_3 deposition on Zircaloy heated surfaces in pressurised boiling water 79—93714
Gd, use as burnable poison in PWRS 80—13662
Gd_2O_3-UO_2, behaviour as control rod in commercial reactor 78—8918
H permeation in HTR *(German)* 79—3204
H-related materials problems, in situ anal. using Li nuclear microprobe method 78—7299
H_2 permeation reduction using Pd foil in liquid metal *(Japanese)* 80—68770
H_2 permeation through HTGR heat exchanger tubes, reduction using calorising method *(Japanese)* 80—100360
$H_2(D_2)$ pumping by Ti film, pumping speed comparison 78—51819
H_2O-graphite system, neutron rethermalisation 79—97806
H_2O_2 monitoring and control in BWR plants 78—21656
^{3}H, production in fusion research reactors to fuel CTR expts., feasibility 80—18632
He coolant in GCFR cores, heat transfer props., review 79—45331
He corrosion test facility at Springfields nucl. power development lab. 79—29327
He fill gas absorpt. in UO_2 pressurised rods during irradiation 80—37454
He prod. in materials, integral meas. comparison with ENDF/B calcs. 77—23214
Hf and Zr, trace elements, simultaneous determ. in soln. using X-ray fluorescence anal. 80—97752
Hf, calciothermic, electrorefining 78—68647
Hg, volatilisation losses during neutron irradiation in a reactor 80—13596
I, PWR core, nonlinear balance eqns. and distribs. 78—58322
I partition equilibrium between air and NaOH aq, effect of CO_2 conc. 78—78474
I radioactive waste, solidification in concrete, leach rates 78—703
^{131}I, separation from water by ion exchange *(Japanese)* 77—60099
^{131}I spiking phenomenon in accidents involving coolant leakage, expt. *(Japanese)* 77—54320
Ir-W (0.3 wt.%), polycrystn., brittle fracture TEM study 79—61715
^{85}Kr waste encapsulation, in amorphous alloy 80—47589

fission reactor materials continued
Li liquid coolant, N contaminated, grain boundary grooving of pure Fe, corrosion mech. 77—6522
Li, solubility of Fe, Cr, and Ni, effects of nonmetallic impurities 79—77760
LiF tile and sheet for thermal neutron shielding *(Japanese)* 78—74510
$LiNbO_3$, ion bombardment, electromigration as deterioration mechanism 78—26601
Li_2O blanket assembly, absolute fission rate determ. 80—9317
Li_2O, C atom conc. profile determ. by proton backscattering 78—10079
Li_2O pellets, sintered, reaction with Mo and Ho alloys 79—47913
Mg alloy, texture of cladding tubes 79—87655
Mg alloy scales, F conc. profiles determ. using $^{19}F(p,\alpha\gamma)$ 78—88678
Mg alloys, neutron irradiation effects, on microstruct., mech. props. and swelling 79—65121
Mg, defect solute atom interaction investigation using channelling techniques 78—47442
Mg-Be, reactor fuel element cladding, corrosion resistance in $K_2Cr_2O_7$ aq. soln. 79—76074
$MgAl_2O_4$, faulted defect aggregates prod. by neutron-irrad. 80—107331
MgO, GCFR shielding material, anal. of shielding effectiveness 80—47746
Mo, 14 MeV neutron damage 77—15460
Mo alloy, metallurgical stability and corrosion in He atmos., HTR appl. 79—36329
Mo, annealing in stage I, dose depend. and radiation doping defects 78—47422
Mo, gas driven blister growth on He ion bombardment, SEM obs. 77—76473
Mo, He ion irradiated, TEM 77—19994
Mo, high-temp. neutron irradiated, annealing study by positron lifetime 77—51413
Mo, in structural steel, stable isotope eval., 5 keV-5 meV neutrons 80—13620
Mo, irradiation temp. determ. by electrical resistivity meas. 78—58354
Mo, natural and stable isotopes, radiative capture cross section eval. 80—13621
Mo, neutron irradiation induced voids, irrad. temp. determ. from void lattice const. 77—46289
Mo, neutron irradiation induced length change, 40 to 450 degrees C 78—47433
Mo, polycrystn., 2 keV Ne^+ ion bombard., dose and microstruct. effects on surface topography and sputtering yield 79—65124
Mo, sputtering yield meas. by AES 78—95633
Mo, use as ISSEC in Tokamak reactor 78—41860
Mo-Ti-Zr alloy TZM, fatigue and plastic flow, irradiation effects 77—52466
Mo-V alloys, corrosion in high purity liquid Na containing ≈ 1 ppm O, at 700°C for 500 h 79—8383
Mo-Zr-B, porosity and mech. props. after neutron bombard., 780-1080°C *(Russian)* 80—24502
Mo+n, 1.6×10^{-3} to 10 eV, total cross section, raactor structural material 78—46052
N_2O_4 coolant, dissociating system, dynamic sorption of ^{131}I from gas phase *(Russian)* 78—58356
N_2O_4 dissociating coolant, chemical reaction kinetics in transient regimes *(Russian)* 78—58344
N_2O_4, fission reactor coolant, heat transfer on condensation *(Russian)* 80—57860
N_2O_4, viscosity and thermal cond., approx. polynomials *(Russian)* 80—59739
$N_2O_4 \rightleftharpoons 2NO_2 \rightleftharpoons 2NO+O_2$, working fluid for power-producing thermodynamic cycles 80—13536
Na aerosols and fires, expts., LMFBR safety anal. data 77—71650
Na boiling, LMFBR safety, flow rundown expts. in seven pin bundle 77—88240
Na, boiling, LMFBR safety, seven pin bundle expts., flow patterns, two-phase press. drop 77—88241
Na boiling in 7-pin bundle, LMFBR safety, KNK II driver zone 77—88246
Na boiling in heated annular channel with blockage FBR, core, partial failure 77—42108
Na boiling in LMFBR, acoustic detection using pulsed system 79—97839
Na burning, aerosol release, temp., O conc. depend., LMFBR safety anal. 77—83049
Na, cleaning from LMFBR components using fully denatured ethanol 78—21689
Na coolant, effect of high reactivity with air and water on reactor design *(French)* 79—26526
Na coolant and Ar atmos., chemical comp. in LMFBR 79—71893
Na coolant in EBR II, purification by cold trapping, effectiveness 77—14225
Na coolant in GCFR cores, heat transfer props., review 79—45331
Na cooled, structural materials and elements, thermal cycling strength calc. 78—31534
Na droplet, preignition oxidation process, rel. to LMFBR accident 79—30996
Na evaporation in Ar atm., fog formation, expt. theory comparison 77—55352
Na evaporation into forced AR flow, critical supersaturation model predictions 79—54493
Na evaporative removal from LMFBR components 80—32348
Na, fast reactor coolant, boiling in circular pipe, single-bubble model 77—10466
Na fire in LMFBR accident condition, theoretical anal. using SPOOL-FIRE code 77—14248
Na fires, origination and mechanism form. and sedimentation of Na aerosols *(Czech)* 79—30956
Na, impurity conc. meas. by automatic plugging indicator 78—17283
Na interaction with basalt concrete and silaceous firebrick following LMFBR HCDA 80—47638
Na interactions with refractories and control materials at 850°C 77—83041
Na, LMFBR coolant transient boiling in seven-pin bundle under transient overpower conditions 79—76056
Na, large pool combustion in LMFBR, determ. of burning rate and flame struct. 80—47644
Na, liq., impurity removal by molten salt extraction 79—63743
Na, liq., O_2 content determ. by ceramic probes, manufacture and props. 77—54308

fission reactor materials continued
- Na, liq., thermodynamic activity of C, continuous method of determ. 77−56306
- Na liquid, contaminated, release of Pu compounds during burning, LMFBR safety evaluation 77−23224
- Na, liquid, effect on atomistic diffusion in alloys 77−7899
- Na, liquid, effect on corrosion and creep of stainless steels, 873 and 973K 77−57722
- Na liquid coolant, determ. of saturated temp. with automatic plugging indicator 79−97747
- Na, liquid coolant, effect of O_2 on H_2 permeability, partial pressure 80−614
- Na, liquid metal slug flow, transfer function of temp. fluctuations 78−46133
- Na, molten chlinak extraction of K_2, in LMFBR 80−27702
- Na, neutron cross sections, ENDF/B-IV assessment and evaluation 78−25291
- Na, neutron flux integral meas., interactive graphic techniques 78−62590
- Na, plugging indicator measuring accuracy, impurity conc. 78−54813
- Na, pool boiling heat transfer, liq. head effects 78−89951
- Na slug kinetic energy behaviour for varying HCDA energetics 79−85665
- Na, splashing of liq. UO_2, no evidence of entrapment 79−41000
- Na, superheated, LMFBR safety, formation of critical boiling nuclei 77−88242
- Na temperature fluctuation in single-pin-heated blocked annular channel 78−78439
- Na vapour bubble growth in superheated liquid, numerical anal. 78−29576
- Na vapour condensation from rising bubble, effects of internal circulation velocity and noncondensable gas 78−50258
- Na vapour diffusion in Ar(He), diffusion coeffs. meas. by Stefan method 79−41785
- Na void reactivity anal., applicability of Benoist's diffusion coeff. 77−14218
- Na, wetting, at high temps. in pure vapour atmos. 77−76645
- Na/water steam generator problems, soln. in USSR *(Russian)* 79−97876
- Na-cooled fast reactor, structural steel properties 80−22942
- Na-cooled fast reactors, material corrosion problems 79−36328
- Na-NaK engineering handbook, purification, heaters, coolers, radiators 80−27045
- Na-NaOH-Na_2O-NaH, reciprocal ternary system 77−73263
- Na-V-O system, low O_2 potential 77−50238
- Na+UO_2, fuel-coolant interaction, UO_2 fragmentation by thermal stress and pressurisation 77−88226
- $Na_2B_4O_7$, borax, internal core catcher for GCFR 78−58372
- β Na_4PuO_5 release from contaminated burning Na, LMFBR safety evaluation 77−23224
- Nb CVD coatings on graphite, grain struct. depend. on temp. 80−25574
- Nb, He implanted tensile specimens, TEM 77−51398
- Nb, neutron irrad. effects on mech. props. 78−91361
- Nb, O_2 getters for LMFBR fuel pins 78−74437
- Nb_3Sn, filamentary conductors, type-II, low temp. 30 GeV proton effects on critical props. 78−52178
- NbTi, filamentary conductors, type-II, low temp. 30 GeV proton effects on critical props. 78−52178
- Ni alloy, crevice corrosion by water vapour, CO, methane in HTR coolants, model 77−25202
- Ni alloy, metallurgical stability and corrosion in He atmos., HTR appl. 79−36329
- Ni alloy, radiation-induced swelling in BOR-60 reactor 79−97814
- Ni base alloys, oxidation reaction investigation by X-ray diffr. and fluorescence *(German)* 79−57345
- Ni, creep, irrad. induced with 17 MeV deuterons 80−93607
- Ni, effect of 2 MeV Xe^+ ion irradiation on pore distribution and size 79−71898
- Ni, fast reactor structural materials, nuclear data 80−13611
- Ni, fast reactor structural materials activation (n,p), (n,α) cross sections 80−13624
- Ni, He liberation during tempering 77−46290
- Ni, irradiation-induced creep following 4 MeV H^+ bombardment 78−14390
- Ni, irradiation-induced creep, mechanism for large transient strains 78−14391
- Ni neutron and heavy ion damage correlation, dose rate and He injection effects 79−7629
- Ni, neutron capture cross sections in intermed. energy region, method and exptl. facility 78−21637
- Ni, permeability and diffusivity of hydrogen *(Japanese)* 78−66345
- Ni, radiation-induced swelling in BOR-60 reactor 79−97814
- Ni, resonance data eval. below 300 keV, Doppler effect calc. 80−13618
- Ni structural material, integral expts. 80−13612
- Ni, structural material data eval. for JENDL-1 80−13617
- Ni, thermal neutron cross sections for He prod. 77−23079
- Ni, void swelling caused by neutron and self-ion bombardment, 573 to 873K 78−14387
- Ni, voids and swelling following $^{56}Fe^{3+}$ bombardment, fast neutron effects simulation 77−30651
- Ni-Al (6.35 wt.%) precipitate coarsening, redistribution and renucleation during ion irradiation 78−23709
- Ni-base alloy, screening studies for evaluation for nucl. process heat system 78−13236
- Ni-base alloys, creep, corrosion, and fatigue testing for appl. in nucl. process heat system 78−13237
- Ni-Cr, ERNiCr-3 weld metal, strain-rate effects on high temp. behaviour 79−93726
- Ni-Cr-Al-Ti, stress corrosion cracking, factors influencing susceptibility 80−97617
- Ni-Cr-Fe, stress corrosion cracking, factors influencing susceptibility 80−97617
- Ni-Cr-Fe Alloy 600, stress corrosion cracking in high purity water, effect of microstruct. 77−66713
- Ni-Cr-Fe alloys, radiation enhanced precip. and dissolution of precipitates, point defect kinetics and dislocation obs. 80−108467
- Ni-Cr-base superalloy, characterization for PNP components 80−5242
- Ni-Mo-Cr steel, elastic-plastic material characterisation 78−72854
- Ni-Si (1 at.%), dose depend. of ion irradiation induced segregation 79−42123
- Ni-ThO_2, irradiated with 5 MeV Ni^{++}, ThO_2 redistrib. 78−71771

fission reactor materials continued
- $Ni_xFe_{3-x}O_4$, solubility in high-temp. aqueous soln., appl. to PWR 78−4987
- Ni(II), selective separation from rare earth elements on chelate ion exchangers 78−58861
- Ni_3Mn, fission neutron disordering at 5K, exam. 78−47434
- Np, production by neutron irrad. of ^{241}Am Japan Material Testing Reactor *(Japanese)* 80−52731
- $^{237}NpO_2$ powder, oxalate based, prep. and charact. 78−11166
- O_2 deposition in a mesh-packed cold trap 80−22905
- O_2 monitoring and control in BWR plants 78−21656
- Pb, 6 MeV γ penetration, bremsstrahlung in reactor shielding calcs. 78−58350
- Pb, FBR blanket facility, gamma-ray heating rate meas. 80−57912
- Pb, reactivity worths of fixed neutron absorbers 78−21654
- Pb, reactor radiation-induced hardening, computer modelling *(Russian)* 79−37738
- $Pd_{0.8}Si_{0.2}$, amorphous, He^{2+} ion irradiation effect on structure 79−42120
- Pt alloy, fission-fragment-induced He blistering 78−86601
- Pt, boiling water reactor, corrosion and oxidation potentials monitoring 79−20252
- Pt, Frenkel defect migration and reactions, by subthreshold recoil events, exam. 78−47364
- Pt, neutron damage, positron annihilation 80−65056
- Pt, point defect properties, damage curve anal. 78−47359
- Pt, thermal and fission neutron produced defect configurations 78−47432
- Pt-Rh-W alloy corrosion by radioisotopic power system insulating and thermoelec. materials 78−7094
- Pt(Au), ion irradiated alloys, stage II recovery 78−47440
- Pu, energy autocorrel. of fission cross-section data in resonance region, probability table method 79−36284
- Pu fuelled LMFBR need, nuclear proliferation, W.German perspective 79−71895
- Pu safeguards, preparation of ^{244}Pu standard reference material 80−78373
- Pu-bearing materials, environmental impact of transportation, linear regression anal. 80−85308
- Pu-Ga (3.3 at.%) alloy, oxidation in air, 250-400°C 77−44401
- PuC_{1-x} and Pu_2C_3, sp. ht., 10 to 300K, mag. ordering 77−28403
- PuO_2, conversion to $PuC_{0.88}$, thermodynamic assessment 77−70293
- PuO_2/UO_2 fuelled assemblies, integral meas. of effective delayed neutron fraction in FTR SNEAK 77−6497
- ^{241}Pu(n, f) thermal-neutron fission, determ. of cumulative fission yields 79−54462
- ^{242}Pu, isotope form. calc., effect of reactor characts. 79−26489
- ^{222}Rn in biologically produced gas from reactor cooling pond 78−80976
- Si compounds in Na system, deposition and effects 78−86599
- Si, neutron induced binary and tertiary reactions, energy distribs. of secondaries 77−23043
- SiC cladding possibility for GCFR fuel 77−18667
- SiC corrosion in HTGR fuel particles 77−67817
- SiC, diffusion behaviour of fission products, 1650 to 1850°C 78−79814
- SiC, diffusion coeff. of Cs and Ag by post irradiation annealing of coated 78−13247
- SiC, energetic H and Ar ion sputtering, AES-SIMS-FDS combined obs. 78−80444
- β-SiC, fluidised bed deposited coatings for nucl. fuel granules, microstructural obs. by SEM 77−14233
- SiC, fuel particle, coating meas. of strength and Young's modulus, brittle ring test 77−8868
- β-SiC, oxidation in CO-CO_2 mixture *(German)* 78−23844
- SiC, pellet, rise in temp. involving reaction sintering 77−12555
- SiC protective coatings, on graphite for HTR, corrosion *(German)* 78−3248
- SiC, pyrolytic particles for high temp. reactor fuel, X-ray and SEM study *(French)* 78−22734
- SiC+CeO_2(Pd), high temp. chem. reactions, products obs. by X-ray diffr. 78−17312
- SiO_2, vitreous, radiation behaviour of optical props. 78−21655
- Sn melt fragmentation on quenching in n-pentadecane and water 79−15706
- Sn, neutron cross section, filtered neutron beam technique, Doppler effect 80−52670
- SrO, heated on W, vaporisation behaviour, mass spectrometric thermal anal. 77−56277
- steel, Cr-Mo-V, hydrogen embrittlement resist. evaluation *(Czech)* 80−35308
- steel, stainless, He cavitation, rel. to TiC precipitation 80−45399
- T buildup in D_2O of CANDU reactors, due to ^{3}He(n,p)^{3}H reaction 79−22389
- T permeation in HTR *(German)* 79−3204
- T production and distrib. in Peach Bottom HTGR 80−47581
- T, release from CTR, radiological dose calc. 78−78511
- T storage and monitoring, CANDU heavy water reactors 80−5291
- Ta, ion irradiated, ordered void arrays 78−34553
- Ta LMFBR control material, integral capture cross section meas. in CFRMF 77−26760
- Ta, neutron irradiated, microstruct. and swelling 77−69006
- Ta, thermophysical props. and neutron absorpt. 80−103488
- Th-Mo(Re), high temp. phase diagram, thermodynamic props. of refractory metal solutes in liquid Th 77−25022
- Th-Zr(Nb)(Ru)(Rh)-C, phase diagrams *(German)* 77−48413
- ThBC, crystal struct. 78−55853
- $Th_3B_2C_3$, crystal struct. 79−14772
- ThO_2, O_2 self-diffusion and intrinsic p-type electronic conduction 79−90821
- ^{232}Th utilisation in reactor fuel cycles, review 79−45390
- Ti alloys, corrosion in saline radioactive waste isolation environments 80−104349
- Ti condenser for power stations with seawater cooling 80−595
- Ti, gettering of H, mass spectrometry and microgravimetry study, rel. to HTGR gas purification 80−73374
- Ti, in fast reactor structure, (n,p) cross section eval. from threshold to 20 meV 80−13623
- Ti, natural, in fast reactor structure, capture cross section eval. 10^{-5} eV to 200 keV 80−13622
- Ti, neutron effects on thermally activated tensile props. 77−62567
- Ti, O_2 getters for LMFBR fuel pins 78−74437
- Ti, reactor structural material s-wave resonance parameters from capture cross section data 80−13629

fission reactor materials continued

- Ti-Al (14.4 at.%), void form. and solute segregation under Ni ion irradiation 79−42122
- Ti-Al-V alloys, 17.5 MeV Cu ion irradiation, resistance to void damage 79−55795
- TiB_2, low-temp. neutron irrad., electrical resistance and stored energy 78−67744
- TiC, low-temp. reactor irrad., calorimetric investig. 77−80547
- (U, Me)C, Me=Hf, Ti, Zr, Nb or Ta, effects of alloying and interaction with C 79−45350
- (U,Pu)C FBR fuel pins, fuel/clad compatibility 80−57847
- (U,Pu)C, sintering, role of Ni as sintering additive 80−84892
- U, energy, autocorrel. of fission cross-section data in resonance region, probability table method 79−36284
- U, European nuclear industry situation, review (*Dutch*) 77−3973
- α-U, martensitic behaviour 78−29059
- α-U, strain rate effect on tensile flow and fracture 80−84992
- U, Magnox fuel element materials performance 80−47580
- U-alloys, thermal creep and swelling, characterisation 79−74226
- U-ZrH system, neutron spectrum in critical pile 79−45322
- $U-H_2O$ lattice, number of fission neutrons emitted per thermal neutron absorbed, simple calc. 77−71644
- U(C,N), N vapour pressures and thermodynamic props. 80−84918
- UC, sintering, role of Ni as sintering additive 80−84892
- UC:Y(Zr)(La)(Ce), U self-diffusion 80−92711
- UCl_4 molten mixtures with alkali metal chlorides, physicochemical props. 78−30915
- UCl_5, mag. susceptibility, ESR and g-value, crystal field model anal. 79−91292
- UN, N vapour pressures and thermodynamic props. 80−84918
- $U_3Ni_3Sb_4$, and related compounds, X-ray diffr. cryst. struct. determ. 79−42005
- UO_2, contact conductivity between core and cladding, statistical processing of experimental data 80−5238
- UO_2, fission gas release during irradiation 79−17978
- UO_2, heat-generating, molten, interaction with MgO brick 79−13468
- UO_2, isothermal crack healing and strength recovery, thermal shock effects 77−36625
- UO_2, molten, interactions with steel and graphite 79−49700
- UO_2, molten fuel debris, 1-D penetration into concrete following FBR HCDA 80−47640
- UO_2 pellets-graphite-Zircaloy cladding, evaluation of graphite lubrication 80−32342
- UO_2 pyrocarbon-coated HTR fuel particles, fast neutron influence on fission product transport 80−42777
- UO_2 rods in water with U or Pb reflecting walls, critical expts. 80−32331
- UO_2^{2+}, aq. soln., ionic mobility meas., conductivity method 77−31791
- UO_2^{2+}, n-propanol soln., ionic mobility and assoc. consts. 77−31792
- UO_2-Nb_2O_5 additions on elec. cond. 80−49712
- UO_2-(Zr+Nb) system, high-temp. reaction 78−66344
- UO_2-fission products-Zircalloy system, thermodynamics 80−47576
- UO_2-graphite interactions, effect of stainless steel, temperature on reaction rate 79−59172
- UO_2-Na contact interface temp., effect of internal radiation 79−13477
- UO_2-PuO_2, fast reactor fuel rods, burnup-dependent heat transfer from fuel to cladding 79−36323
- UO_2-Zircaloy fuel element behaviour in PWR power plants 80−631
- UO_2-Zircaloy-4 reaction kinetics at high temps., O_2 diffusion 80−16667
- $UO_2(NO_3)_2$, highly enriched solns., benchmark critical expt. calc. study, KENO-IV code 79−18026
- $UO_2(NO_3)_2$, highly enriched solution systems, benchmark critical expts 79−18025
- $(U_{1-x}Pu_x)O_{2-x}$ fuel pin, post-irrad. examinations 80−78400
- U_3Si, interaction with ZrI_4, 700 to 800°C, exam. using metallographic and local X-ray spectral anal. 79−90831
- U_3Si, reversible twinning, in-situ obs. 80−104241
- ^{235}U, gamma ray spectra of reactor fuels 80−42577
- ^{235}U (n, f), thermal neutron fission, time-depend. delayed neutron group yields 79−54463
- $^{235}U/^{238}U$ isotope ratio determ. in UF_6 samples using gas quadrupole mass spectroscopy 80−78976
- $^{235}U-Be$ subcritical bare assemblies, pulsed n study, age-diffusion mode 79−76155
- $^{235}U-BeO$ nearly homogeneous multiplying systems, pulsed neutron study, age-diffusion model 80−37442
- UF_6, mass spectrometric determ. of ^{235}U content 80−68961
- V, H_2 permeability, surface impurity layer effect 77−24440
- V, He preinjected, void swelling on neutron irradiation 77−7765
- V, neutron irradiated, void swelling, O_2 effect 78−6106
- V, O_2 getters for LMFBR fuel pins 78−74437
- V surface, particle release by neutrons 80−25493
- V, use as ISSEC in Tokamak reactor 78−41866
- V-Nb, mech. props., −196-1000°C, comp. depend. 78−39847
- V-Nb-Mo(Cr), corrosion in liquid Na, O_2 effects 77−8987
- V-Ti (20wt.%), corrosion in liquid Na, O_2 effects 77−8987
- V_3Ga, filamentary conductors, type-II, low temp. 30 GeV proton effects on critical props. 78−52178
- W and welds, fatigue crack growth behaviour in air and high-C liquid Na, carburization studies 80−46625
- W, irradiation temp. determ. by electrical resistivity meas. 78−58354
- W, neutron irradiated, FIM obs. of radiation damage 79−7632
- W, radiation shielding material, integral tests of ENDF/B-IV high-energy neutron cross-section data 80−23162
- W, structural defect recovery after irradiation and cold work 78−47429
- W, thermal neutron irradiated, radiation damage and stage III defect annealing 78−51586
- W, use as ISSEC in Tokamak reactor 78−41866
- Xe oscillation model for PWRs, neutron diffusion eqn., nonlinear system 78−58322
- ^{135}Xe, control of space-time distrib. in reactors 79−36364
- ^{135}Xe, poisoning of IRT reactor, optimisation of operation regime (*Russian*) 80−37473
- YN, decomp. press.-temp. relations 78−52760
- Zircalloy-2, annealed, neutron irradiated, 573 to 923K, damage struct. 79−99247
- Zircaloy, dispersion and spheroidisation treatment of δ ZrH, effect on corrosion resistance 79−76072
- Zircaloy, foil, dislocation loop nucleation and growth during 1 MeV electron irrad. 80−88152

fission reactor materials continued

- Zircaloy, I_2 stress corrosion cracking, temp. and stress depend., threshold press. determ. 80−16595
- Zircaloy-2, effect of simulated fission products on mech. props. 80−73922
- Zircaloy-2, electron irradiation damage, direct obs. 80−84212
- Zircaloy-4, deformation behaviour between 77 and 900K 80−71686
- Zn, recovery after 6.1 MeV α-particle irradiation at 4.2K 78−47441
- $ZnSO_4$, LMFBR, boiling pools with internal heat generation, void distrib. 78−21626
- Zr alloy, cladding, new material development 77−50242
- Zr alloy, creep, steady state creep rate, stress depend. at low stress (*Czechoslovakian*) 77−32640
- Zr alloy, neutron irradiated, in-pile dimensional changes 77−24331
- Zr alloy pressure tubes, cracking due to high residual tensile stresses 78−29585
- Zr alloys, corrosion resistance and mech. parameters of sheaths and tubes for nuclear power appl. 79−97813
- Zr alloys, creep and growth, irradiation induced, rate theory approach 80−89294
- Zr alloys, diffusion coeff. of O, 675-1800°C, α and β alloys 77−62680
- Zr alloys, effect of steel presence on corrosion stability 77−56162
- Zr alloys, factors affecting anisotropy of irradiation creep and growth, calcs. from crystallographic texture 79−83255
- Zr alloys, irradiation growth, influence of microstructure and test conditions 80−92561
- Zr alloys, neutron irrad., yield strength changes and radiation hardening, damage annealing (*Italian*) 77−65269
- Zr alloys, reactor fuel sheath mat., thermophys. props. 77−46280
- Zr alloys, thermal capture cross-section var. with time, calc., mech. and corrosion props. var. 77−61505
- Zr and alloys, basic corrosion studies 77−34402
- Zr and alloys, neutron irrad. at 573 to 923K, damage struct. 80−107334
- Zr and Hf, reactor cooling and heat recovery appl. (*Italian*) 78−4978
- Zr and Hf, trace elements, simultaneous determ. in soln. using X-ray fluorescence anal. 80−97752
- Zr and Zircaloy, polarisation in high temp. water 77−52540
- α-Zr and Zircaloy 2, fatigue, 20 to 700°C 77−70154
- Zr and Zircaloy-4, damping, amplitude dependent, at high temp. 77−52383
- α-Zr and Zircaloy-4, O stabilized, O diffusion using ^{18}O tracer 78−51737
- Zr and Zircaloy-4, tensile props., room temp. to 900K 77−70104
- α-Zr, anelastic relaxation and O_2 diffusion 77−4219
- Zr, annealed, neutron irradiated, 573 to 923K, damage struct. 79−99247
- Zr base alloys, irradiation growth, dislocation model 78−51595
- Zr, blistering by 2 MeV He^+ ions, optical microscopy and SEM obs. 79−42119
- Zr, breakaway oxidation at 573K, SEM study 79−74305
- Zr, breakaway oxidation kinetics at 623K, SEM study 80−97633
- β-Zr, Cr diffusion rates in temp. range 914 to 1240°C 80−15304
- Zr, crept single crystal, nature of γ-hydride 77−21147
- Zr, defect solute atom interaction investigation using channelling techniques 78−47442
- Zr, deformed at 77K, effect of fast-neutron irradiation on deformation twinning, TEM and optical microscopy obs. 79−37741
- α-Zr, diffusion of O, 290 to 1500°C 77−76613
- Zr, dissolution of γ-ZrH, in situ study, HVEM obs. 78−55951
- α-Zr, electrolytic polishing optimal condition determ. from anodic impedance meas. (*French*) 80−3250
- Zr, electron irradiated, interaction of self interstitials with O_2 atoms 79−65118
- Zr, electron irradiation damage, direct obs. 80−84212
- Zr, foil, dislocation loop nucleation and growth during 1 MeV electron irrad. 80−88152
- Zr, foil bending by in situ ion irrad., neutron damage simulation, room temp. oxide growth 80−107342
- Zr, gettering of H, mass spectrometry and microgravimetry study, rel. to HTGR gas purification 80−73374
- Zr, γ attenuation coeffs. meas. for burn-up determ. correction (*Russian*) 78−82597
- α-Zr, H terminal solid solubility, optical metallographic study 80−34195
- Zr, irradiation growth, influence of microstructure and test conditions 80−92561
- Zr, irradiation growth, reaction rate theory calcs. 80−88212
- α-Zr monocrystal perfection using Berg method and diffractometer with omega device (*French*) 80−2035
- Zr, neutron induced displacement damage anal., program DISPKAN 79−14854
- Zr, neutron irradiated, dislocation loop nature 77−47489
- Zr, neutron irradiated, faulted loops 78−19694
- Zr, neutron irradiated, yield point phenomenon 79−52304
- Zr, nuclear steam superheating channels, design testing 80−5211
- Zr, oxide film texture determ., corrosion in air and water vapour 77−56163
- α-Zr, point defect props., effect on irradiation behaviour of Zr alloys 78−30609
- α-Zr, positron annihilation 77−68999
- Zr, radiation induced creep, yielding creep theory, time depend. of irrad. growth 77−26845
- Zr, single crystal, irradiation creep 77−42081
- Zr, TEM obs. of irradiation damage, critical review 79−10879
- Zr, tensile deformation behaviour, neutron irrad. effects, dislocations, twinning inhibition 77−90393
- Zr, thin film, trace element determ. by X-ray fluoresc. anal. 78−40107
- Zr, void swelling during electron irrad., HVEM study 80−92559
- Zr-Al (4.6 wt.%) martensite, precipitation of Zr_3Al_2, TEM study 79−74156
- Zr-Al (8.6 wt.%), dimensional stability struct. and mech. props, effects of neutron irrad. 80−92563
- Zr-Al (8.6 wt.%), effect of fast neutron irradiation on irradiation growth of Zr_3Al 78−55896
- Zr-Al (8.6 wt.%), neutron irradiation effect on tensile props., swelling 77−7768
- Zr-Al intermetallic compounds in SAES ST101 getter, surface anal. during stimulated pumping 79−67945
- Zr-Al(8.6 wt.%), mech. props., corrosion and fast neutron irrad. influence 78−84948
- Zr-Al(8.6 wt.%), neutron irradiated, irradiation growth and recovery, annealing 80−15162

fission reactor materials continued
Zr-Au (0.3 and 0.2 wt.%), irradiated, backscattering meas. of Zr self-interstitial atom trapping by Au 77−69014
Zr-base alloy as reactor core material, microstruct., deform. and fracture 78−4988
Zr-base alloys, annealed specimens, irradiation growth 80−49276
Zr-Cr-Fe, irradiation damage, metallurgical struct. effect 77−51412
Zr-H system, δ and ε phases, neutron irrad., radiation swelling investigation 78−18685
Zr-Hf (2.2 wt.%), high temp. oxidation in flowing O_2, 873-1173K 80−93687
Zr-Hf (2.2 wt.%), oxidation kinetics in flowing CO_2, 873 to 1173K 80−16596
Zr-Hf(2.2 wt.%), oxidation kinetics in flowing CO_2 at high temp. 80−47575
Zr-Nb, (2.5 wt.%), cold-worked pressure tubing for CANDU reactors, slit burst testing 79−26532
Zr-Nb, fracture resistance, atomic reactor material *(Russian)* 77−25140
Zr-Nb, pressure tube alloy, initiation COD as fracture criterion 78−72862
Zr-Nb (0.1, 2.5 wt.%), foil, dislocation loop nucleation and growth during 1 MeV electron irrad. 80−88152
Zr-Nb (1 wt.%), corrosion in water at 285°C 77−56161
Zr-Nb (1 wt.%), static strain ageing between 295 to 773K, TEM obs. of plastic strain 79−38855
Zr-Nb (1 wt.%), TEM study on intermetallics in Zr alloys 79−11622
Zr-Nb (1 wt.%), tensile props., 295 to 773K 79−8318
Zr-Nb (1 wt.%) exam. of creep behaviour, 373 to 773K 78−80599
Zr-Nb (2.25 wt.%), oxidation kinetics in flowing CO_2, 873 to 1173K 80−16596
Zr-Nb (2.3 and 5.5wt.%) martensite, precipitation 77−8836
Zr-Nb (2.5 wt.%), annealed, irradiation growth at 353K 79−46710
Zr-Nb (2.5 wt.%), annealed and quenched-and-aged, neutron irradiated, 573 to 923K, damage struct. 79−99247
Zr-Nb (2.5 wt.%), channel tubes, in-reactor creep and irrad. growth 80−93604
Zr-Nb (2.5 wt.%), cold worked, in reactor oxidation of crevices and cracks 78−23865
Zr-Nb (2.5 wt.%), cold worked, press. tubes, secondary cracking obs. 78−80630
Zr-Nb (2.5 wt.%), cold-worked, pressure tubing, metallography and mech. props. 80−89269
Zr-Nb (2.5 wt.%), crack resistance, influence of ZrH_x fracture toughness 80−16444
Zr-Nb (2.5 wt.%), effect of irradiation on stability of precipitates 77−69007
Zr-Nb (2.5 wt.%), fuel cladding, anisotropy after creep and irradiaton 78−7001
Zr-Nb (2.5 wt.%), high temp. oxidation in flowing O_2, 873-1173K 80−93687
Zr-Nb (2.5 wt.%), hydride TEM obs. in pressure tubing 79−8338
Zr-Nb (2.5 wt.%), memory effect in hydride precipitation 78−11227
Zr-Nb (2.5 wt.%), nuclear fuel channels, neutron effects on ultimate fracture strength, 293 to 573K 80−85054
Zr-Nb (2.5 wt.%), oxidation kinetics appl. to loss of coolant accidents, data review 78−19958
Zr-Nb (2.5 wt.%), pressure tubes, irrad. creep and growth, anisotropy factors 80−97536
Zr-Nb (2.5 wt.%), strain ageing 77−77511
Zr-Nb (2.5 wt.%), tensile specimen, stress corrosion cracking by stray contamination 77−70215
Zr-Nb (2.5 wt.%) neutron effects on oxidation kinetics 78−690
Zr-Nb (2.5 wt.%) pressure type rel. between stess intensity factor, crack opening displacement and J-integral 80−100920
Zr-Nb (97.5, 2.5 wt.%) nuclear reactor pressure tube material, H embrittlement study by TEM 80−76363
Zr-Nb-Sn (3,1 wt.%), corrosion resist. depend. on mech. and heat treatments 80−653
Zr-Nb-Sn (3.0, 1.0 wt.%), oxidation kinetics in flowing CO_2, 873 to 1173K 80−16596
Zr-Nb-Sn (3.0, 1.0 wt.%), high temp. oxidation in flowing O_2, 873-1173K 80−93687
Zr-Nb-Sn(3 wt.%, 1 wt.%), oxidation kinetics in flowing CO_2 at high temp. 80−47575
β-Zr-Nb(Cb) alloys, anneal hardening and flow softening 79−78993
Zr-Nb(2.5 wt.%), oxidation kinetics in flowing CO_2 at high temp. 80−47575
Zr-Nb(2.5 wt.%), tensile props., strain rate and temp. effects 77−73307
Zr-O(2.85 at.%), Pr effect on internal friction of single crystal 77−4155
Zr-Sn, grain-boundary migration during fatigue at 600 to 775°C 80−16443
Zr-Sn, oxide film texture determ., corrosion in air and water vapour 77−56163
Zr-Sn (1.5 wt.%), electron irradiation damage, direct obs. 80−84212
Zr-Sn alloys, mathematical models for transient deform. 78−86616
Zr-Sn-Fe-Ni (1.5, 0.1, 0.15 wt.%), electron irradiation damage, direct obs. 80−84212
Zr-Sn-Mo (6, 1 wt.%), creep and creep rupture 78−23778
Zr-Sn(Fe)(Ni) (0.15 wt.%), electron irradiation damage, direct obs. 80−84212
Zr-Ti, oxide film texture determ., corrosion in air and water vapour 77−56163
Zr_3Al, Ar^+ ion and electron irradiation, irradiation swelling, lattice parameter changes 79−65123
Zr_3Al base alloy, forming press. tubes 77−8784
Zr_3Al, deformed and irrad., lattice defects obs., superlattice dislocations and defect clusters 80−107261
Zr_3Al, disordering by 1 MeV electron irradiation 78−51583
Zr_3Al, hyperperitectoid, tensile strength, effect of fast neutron irrad. 77−52408
Zr_3Al, irradiation 78−6111
Zr_3Al, neutron irrad. effect on tensile props. 80−3156
Zr_3Al, ordered, exam. of Young's modulus and thermal expansion coeff. 78−72805
Zr_3Al, ordered, notch sensitivity, neutron suppression 78−23779
Zr_3Al, ordered, review of physical metallurgy 78−15419
Zr_3Al, tensile props., surface preparation depend. 80−3155
ZrC, factors affecting CVD 77−8760
ZrC, low-temp. reactor irrad., calorimetric investig. 77−80547
ZrC, solubility, diffusion and permeation of Cs 78−51684

fission reactor materials continued
ZrC-C, CVD, microhardness and microstruct. 77−8916
$ZrC+CeO_2(UO_2)(SrO)$, high temp. reactions 80−3320
$ZrH_{1.9}$, neutron irrad. induced defects, nature and thermal stability 77−50246
ZrNb, pressure tube, fragmentation on failure 78−72863
ZrO_2 films on Zr alloys, model of stress distrib. 79−49694
^{91}Zr, 292.4 eV neutron resonance parameters, radiative and neutron widths, spin assignments 77−6369
$^{94}Zr(n,\alpha)^{91}Sr$, fast n, fission spectrum averaged cross section 80−63177

fission reactor operation
see also fission reactor cooling and heat recovery; fission reactor core control and monitoring; fission reactor safety
1 GW(e) mixed fuel cycle LMFBR performance, effect of ^{233}U in core 79−9868
acoustically induced vibration of circular cylindrical rods 77−62098
ACR, fuel cycle evaluation, decision anal. and probability assessments 80−47587
advanced reactor development in Japan 78−86663
AGR, fossil-fired steam conditions, commissioning experience 78−17406
AGR line development status and performance *(German)* 78−86568
ANS annual meeting, 1977 78−663
ARBUS, operational experience with ditolylmethane coolant/moderator 78−41836
assessments of nuclear systems and use of nuclear power, review 79−45334
at-power reactor noise, second-order coherent functions 78−94070
Belleville springs as energy storage devices on packed valve stem seals 77−18679
Beloyarskaya Atomic Electric Power Plant, channel reactors, permissible power operating calculations 79−80984
BN-350 fast reactor, operating experience (1972-77) *(Russian)* 79−97868
BN-350 reactor, development, design and operating experience *(Russian)* 79−26511
Bohunice A-1 reactor, long-run test of improved R II-U spare-type fuel element *(Czech)* 78−8875
boron thermal regeneration system, operating experience 80−13683
BR-5 Soviet reactor, effect of operating conditions of vacancy porosity of austenitic stainless steel 79−32990
Brunswick plant post-startup optimization 80−23048
burn up in AVR spherical fuel elements, ^{137}Cs γ-ray spectroscopy *(German)* 78−25299
burnup determ., accuracy requirements for fuel cycle design, reactor operation and safety 78−58342
BWR, ASEA-ATOM supplied, operating experience 80−9375
BWR, block-monitoring index for diagnosis of power station operating characts. 79−59185
BWR, Brunswick Steam Electric Plant, radwaste system operating experience 78−17392
BWR, Brunswick Unit No.1, startup test experience 80−9353
BWR, design and operation, review of water chemistry, in feed water, coolant and steam systems 79−36311
BWR, Dodewaard, fuel pin failures 77−67834
BWR, dynamic loading of press. suppression containment, blowdown, power station expt. data 77−3133
BWR, Enrico Fermi Unit 2, temporary non-nuclear steam supply for preoperational testing 80−9354
BWR, Enrico Fermi-2, system turnover, test and startup program 80−63338
BWR, Finland's TVO 1, commissioning and startup 80−68888
BWR, fuel cycle cost sensitivity anal. 79−31104
BWR, Fukushima Daiichi power station, preoperational test, start-up test, operating experience *(Japanese)* 78−29635
BWR, grid freq. and control capability 77−46396
BWR, individual-tank fast shut down system, reliability anal. *(German)* 77−54311
BWR, KRB reactor press. vessel, fast neutron fluence evaluation, operational consequences *(German)* 77−34369
BWR, noise sources of neutron flux, coherence anal. 77−88199
BWR, power upgrading, feasibility, benefit, cost anal. 80−68877
BWR, preoperational tests, start up tests and operating experience of Japanese power station *(Japanese)* 79−67881
BWR, radioactive waste management 78−17389
BWR, radiochemical management, reactor cooling system, gamma spectroscopy of radionuclides 79−9731
BWR, shutdown dose rate of primary cooling system, prediction by empirical formula 79−22408
BWR, startup control rod programming code system 80−13688
BWR, sustaining improved plant operation 80−9374
BWR, TVO I, startup principles 80−9372
BWR, vent clearing transients calc., press. suppression system, digital computer simulation 77−3132
BWR, Wm. H. Zimmer station, startup and testing 80−9373
BWR and PWR, 1973-7 West European experiences *(Czech)* 79−36345
BWR core operation flexibility for improved fuel cycles 80−57915
BWR core simulation, few group coarse mesh diffusion scheme, expt. verification 77−23223
BWR designed for improved operation at Grand Gulf 80−106121
BWR dynamics, multivariable autoregressive identification 78−94107
BWR irradiated fuel channel disposal 78−21730
BWR island-design Pu recycle fuel assemblies, nuclear fuel performance meas. 79−30907
BWR of Hamaoka nuclear power station, operating experience *(Japanese)* 78−17333
BWR operating experience and outage services 77−46397
BWR operating experience at Millstone I with the control cell core improved design 80−22925
BWR plant, LOCA capability code for utility appl. 78−21690
BWR plant diagnosis system, on line process computer appl. 78−46146
BWR plants, I-131 airborne emission data for environmental impact evaluation 77−38391
BWR power plant, routine checks and radiation protection 78−74462
BWR power plant reactor operation and management using minicomputer 79−81042
BWR power plant turbine building, radiation protection, calc. and obs. 78−74461
BWR power stations, operating record and reliability, reviews 79−22403
BWR refuelling schedule, minimisation of power peaking 77−61513

fission reactor operation continued
BWR steam turbine, blast cleaning to remove radioactive deposits 80−18554
BWR with fracture live steam line, isolating valve loading *(German)* 77−38340
CANDU, feasibility study for use as a breeder 78−25311
CANDU, nuclear quality high pressure valve bellows, development, report 78−82490
CANDU, Pu-topped Th fuel cycle characts. 79−36322
CANDU, Th fuel cycle utilisation 77−46305
CANDU, Th fuel cycles 78−86661
CANDU fuel management principles and problems 77−50251
CANDU fuel performance in NPD reactor with two-phase coolant 78−89950
CANDU generating stations, reliability of performance 79−18029
CANDU operation for electricity prod. and district heating 78−41835
CANDU PHW commercial nucl. elec. stations, commissioning and operating experience 78−86656
CANDU PHWR, Wolsung nuclear power plant, fuel cost anal. 78−54832
CANDU-PHW, advanced fuel cycles 78−89968
CANDU-PHW, neutron group cross sections in resolved resonance region calcs. 80−13573
CANDU-PHW, once-through, slightly ^{235}U enriched U cycle 79−93711
CANDU-PHW, once-through natural U cycle 79−93710
CANDU-PHW, valve maintainability, design, application, layout, administrative factors 78−25318
CANDU-PHW operating on Th cycle 79−93712
CANDU-PHW thorium convertor, study of running-in period 78−25313
characterisation and quality control of nuclear fuels, conf. Karlsruhe Germany (June 1978) 79−49794
code implantation, technology transfer 77−65307
complex repairable systems, Karlsruhe computer program for availability and reliability evaluation 77−88249
conference, Arlington, Texas, USA (Aug. 1979) 80−8735
conference, Chattanooga, Tennessee, USA, August 1977 78−17266
conference, nuclear power quality assurance, Knoxville, USA (Oct. 1978) 79−97773
conference, San Diego, Calif., USA (June 1978) 79−17972
conference, San Diego, Calif., USA (June 1978) 79−49650
conference on nuclear power and its fuel cycle, Salzburg, Austria (May 1977) 79−26504
control by neutron flux, expt. investigation of optimal processes 77−3139
control rooms, human factors design approaches, improvement of man-machine interface, error reduction 80−63327
CRBR upper internal structure, thermal oscillations 77−46269
CRBRP ex-vessel transfer machine 78−8943
CRBRP steam generator, thermal transient and inelastic screening for Cr-Mo steel components 78−21660
Creys-Malville centre, siting, operation, safety, containment and waste *(French)* 79−30945
critical point reactor, response to inherent reactivity noise input 79−45336
criticality safety, pitfalls in calcs. and experiences in operation 79−63769
CRNL NOS/BE 1.3 system, dynamic core allocation 80−78425
Crystal River Unit 3, startup experience 80−13684
data retrieval and evaluation system RECORDS 80−13690
DC power failure following AC power failure 78−78483
decay power sensitivity to uncertainties in fission product yields, errors 77−6494
decontamination by liquid waste elimination without reactor defuelling, CAN-DECON process 80−73943
defective fuel rods ultra sensitive detection with low core burn-up, method 79−45374
denatured fuel cycles for international safeguards 79−41011
dense plasma focus devices matching with fission reactors 78−37436
design parameters, effect of ENDF/B-IV cross sections 78−13219
digital simulator software development, kinetic equations integration, numerical solution method 80−68901
Dounreay contribution to fast reactor development 80−27798
Dounreay FBR, post-operational improvements in plant design and operational techniques 79−63736
Dragon HTR project, review 79−45326
Dresden-1 chemical cleaning, radioactive waste treatment 78−17394
dynamic simulation of the Gentilly-1 reboiler system 78−82439
EBR-II, dynamic response of ducts to press. pulses, expts., finite element calcs. 77−3124
EBR-II, obs. of amplitude modulated 12 Hz effect in upper plenum acoustic expt. 78−33241
EBR-II, operating limits for subassembly deformation 78−21714
EBR-II breached fuel element experience, safe reactor operation 79−9736
EBR-II operating experience 78−17410
EBR-II preparation for breached-element operation, safety concerns 79−9792
EBR-II reactor components, creep and swelling 79−54499
EDF graphite-gas reactors, role of nuclear calculations in operation *(French)* 80−95373
electric heaters for nucl. applic. 78−86649
electronics in nuclear science and technology 80−9347
emergency monitoring procedures at CEGB stations, UK 77−54322
energy balance of nuclear power plant *(French)* 79−63729
European Nuclear Conf., Hamburg, Germany, May 1979 79−97841
failure probability distrib. from observed failure data, beta distrib. 80−63335
fast, prototype, scaling up, UK experience 78−5010
fast metal assemblies, prompt alpha and reactivity meas., review 78−21685
fast neutron source reactor (YAYOI), pulsed operation improvements, with POS5 as reactivity injector *(Japanese)* 80−9328
fast overpower transient, effect of solid fission products and dislocations on swelling and fission gas release 78−8917
fast reactor, advanced fuel cycles 78−89968
fast reactor, partly blocked fuel subassembly, turbulence meas. in air model 77−74965
fast transient, nonequilib. fission bubble behaviour and eqn. of state 78−8916
FBR, fuel cycle evaluation, decision anal. and probability assessments 80−47587
FBR, interpretation of the isotopic breeding worth 79−49655
FBR, neutron/physical behaviour of thorium, expt. *(German)* 78−94109

fission reactor operation continued
FBR, nuclear data needs 77−23248
FBR, refuelling process and doubling time calc. *(Czech)* 78−29593
FBR, Th fuelled, performance characteristics 79−9815
FBR components, in-reactor creep measurements 79−57082
FBR core materials studies for improving reactor performance, trends 80−102232
FBR fuel clusters, Na boiling, corrective action 79−71913
FBR fuel cycle, experience 79−59233
FBR neutron energy spectrum controlled blanket 77−23236
FBR power prod., optimised strategy rel. to U ore costs 80−99253
FBRs, testing full-scale components for sodium reactors 80−828
FFTF startup, instrument calibration program 80−9337
FFTF startup plan 78−17411
fissile fuel dynamics of breeder/converter reactors 79−13385
fixed end-point problem suboptimal control, singular perturbation theory appl. *(Japanese)* 78−33259
fluid systems, program for initial cleaning 80−23047
forced-convection boiling upflow system, instabilities in parallel channel, nonlinear model 77−57724
Forschungs- und Messreaktor Braunschweig, operating experience *(German)* 77−61527
Fort St. Vrain HTGR power station, review of design and operation 79−45353
fuel, rod modelling, utility requirements 78−21747
fuel adjustment clause for collecting nuclear fuel costs 79−31105
fuel conservation, Japan, molten-salt reactor strategies, LMFBR, HTGR, utilisation, coexistence *(Japanese)* 77−50257
fuel cycle alternatives for power reactors 77−42107
fuel cycle cost sensitivity anal. of alternative reactor fuel cycles 79−89368
fuel cycle costs 77−6575
fuel cycle economics, tutorial paper 78−17446
fuel cycle length flexibility in C-E reactors 77−42116
fuel cycle strategy in Korea, probabilistic anal. 77−57726
fuel cycles principle and state of art, critical review *(German)* 77−34408
fuel damage impact on plant operations 80−686
fuel element defects caused by power ramping, CANDU fuel performance data 77−57720
fuel elements for steam-superheating channels of Beloyarsk nuclear power station reactor 77−50217
fuel failure prediction using POSHO model 77−46226
fuel management analysis core, computer code for teaching assistance 78−4449
fuel outage management and quality assurance 79−97862
fuel pellet-cladding interaction phenomenon investig. 77−46299
fuel savings by 'stretch out' operation *(German)* 78−86632
fuel thermocouple readings verification by transient response analysis 77−46309
fuel-cladding bonding mechanisms in irradiated fuel rods 78−17317
fuelling of Atucha reactor, transition to burnup equilib., 3D code TRISIC *(German)* 77−61506
FUGEN, 165 MWe prototype HW moderated BW cooled reactor, zero-power startup tests *(Japanese)* 79−26553
fusion and fast breeder reactors, a comparison, book 78−78430
fusion-fission hybrid reactors, fissile fuel breeding potential 77−50287
gas cooled reactor experience and programs in France, reviews 79−45332
gas cooled reactors, background and status in UK, review 79−45333
gas phase cavity reactor design and operation with MHD generators and turbogenerators *(Russian)* 78−37435
gaseous core reactor U plasma radiative temp. calc. 79−9807
gaseous fuel reactor applications 80−63367
GCFR, economic anal. of radial blanket of LMFBR 79−59163
GCFR, He-cooled, 300 MWel and 1500 MWel plants, development trends *(Czech)* 78−29636
GCFR, sensitivity of reactivity effects to reactor model choice in safety anal. 78−13305
GCFR, transient analysis of closed gas turbine cycles, TUGSIM-10 computer code 77−18675
GCFR, venting system of fuel element, activity release anal., operating and accident conditons 77−23226
GCFR critical assemblies, ^{238}U Doppler reactivity worth meas. 77−54336
GCFR depressurisation transients without scram, anal. 77−14246
GCFR radial blanket, optimum management scheme 77−42126
GCFR reactivity insertion mechanisms 77−14245
GCR, primary circuit of CHINON 3 reactor, vibr. studies 77−6545
Genkai PWR plant operating experience 78−86655
Go-ri nuclear power plant, fuel cycle schemes, economic comparison 78−54831
Gosgen pressurized-water nuclear plant *(German)* 79−63763
Hamaoka BWR plant, operational experience 78−86654
Health Physics Research Reactor, operating history and recent improvements 80−9382
health risks of nuclear power, for teachers 79−35506
HFEF/N, equipment repair room modifications 79−45439
HFIR, dimensionality reduction of reactor noise signatures, improved automated noise anal. 77−6499
HFR test reactor, HIP-TEDDI code for neutron flux calcs. 79−3223
Hinkley Point B, AGR, construction, commissioning and early operation 80−694
Hinkley Point B AGR commissioning and three years' operational experience 80−23107
HTGR, 330 MWe nuclear power station, start-up and operating experience since 1975 80−830
HTGR, AVR, operational experience at gas outlet temp. of 950°C 78−17405
HTGR, Fort St. Vrain, operating experiences during power ascension 80−13778
HTGR, low temp. heat prod., energy transport systems 78−41837
HTGR, Peach Bottom, decommissioning and component removal 78−21756
HTGR, Peach Bottom site, radionuclide distrib. in primary coolant circuit 78−13275
HTGR, performance assessment of Peach Bottom Unit 1 prototype 79−67906
HTGR, prebreeder fuel optimization, symbiotic combinations, comparative evaluations 78−29605

fission reactor operation continued

- HTGR, surveillance robot for fuel and reflector element inspection 80—68873
- HTGR fuel particle, computer code for anal. of transient behaviour 78—8964
- HTGR low power startup model development and use 77—88220
- HTPBR, gas injector to reduce pyrocarbon deposits *(German)* 78—29633
- HTR, Fort St. Vrain startup experience 78—17407
- HTR, hydrogen and tritium permeation through He heated tube walls 77—50250
- HTR, modified RB-2 reactor, null reactivity oscillator method on fuel lattices, expt. feasibility 77—57703
- HTR, primary coolant circuit filter for fission products *(German)* 77—74915
- HTR power station, design development, operation and appl., review *(German)* 79—76088
- HTR Th closed fuel cycle, U resource conservation 80—727
- HTRs, large, shutdown system strategy *(German)* 79—97818
- human errors in high stress situations, data and assessment 78—17374
- human factors in nuclear power plants, review 79—89463
- HWR, characts., effect on U consumption *(Dutch)* 77—71658
- HWR, fuel cycle cost anal. using computer code HWRCOST on-power refuelling 77—83051
- HWR, MIT research reactor renovation 78—21753
- HWR, Th advanced fuel cycle 77—67864
- HWR reboiler hybrid computer dynamic simulation 78—8949
- IAEA international symposium on design, construction and operating experience with demonstration liquid metal fast breeder reactors (Bologna, Italy, April 10 to 14, 1978) 79—49646
- identification method, appl. to nucl. reactor plant *(Japanese)* 77—3118
- Ikata Power Station Unit I, operating experience *(Japanese)* 79—36397
- inservice examinations, effective quality assurance 79—97861
- IRT reactor, optimisation of operation regime *(Russian)* 80—37473
- JOYO experimental fast reactor, test and operational experience 79—97867
- JOYO MK II, design and related R and D experience *(Japanese)* 80—5201
- KNK II, first German LMFBR, power startup experience 79—97848
- Kori power plant unit I, startup and operating experience *(Korean)* 79—76080
- LMFBR, 1200 MW(e), ^{232}U prod. 78—29597
- LMFBR, 1500 MW, breeding perfomrance optimisation of He-bonded carbide fuel 78—17325
- LMFBR, BOR-60, reactivity rate of change during operation 77—71681
- LMFBR, buoyancy-induced flow stratification in cylindrical plenum during reactor scram 77—46366
- LMFBR, computer control system for Na test loops 79—26550
- LMFBR, control rel. to operational safety aspects 77—14251
- LMFBR, decommissioning of Na reactor expt. 78—8942
- LMFBR, development and Pu allocation, optimal policies 80—725
- LMFBR, economic anal. of radial blanket of GCFR 79—59163
- LMFBR, effect of finite plant life on doubling time 78—41809
- LMFBR, enrichment and control optimization for reactivity losses during burnup 78—21692
- LMFBR, failed fuel pin performance 78—21680
- LMFBR, heterogeneous carbide-fueled reactors, thermal and economic performance 79—93703
- LMFBR, instantaneous fuel growth rates 80—561
- LMFBR, integral concepts for fuel breeding description 80—562
- LMFBR, JOYO, fast reactor, experimental, functional and operational test results 79—93796
- LMFBR, large, performance parameter uncertainties 78—13216
- LMFBR, neutronic and engineering characts. during long-time operation 77—71660
- LMFBR, operational safety issues 77—67818
- LMFBR, performance characts. in US nucl. energy system. rel. to breeding ratio, sp. power, discharge exposure 78—17404
- LMFBR, Phenix plant, three years operating experience 78—17409
- LMFBR, refuelling scheme optimisation using heuristic enumeration method 77—46301
- LMFBR 1200 MW(e) performance rel. to core height reduction 79—9684
- LMFBR advanced fuel elements, Na bonded, wire wrap-cladding interaction 79—93734
- LMFBR core materials, effect of swelling and creep on performance 78—13261
- LMFBR demonstration plant, design, construction and operating experience 79—97887
- LMFBR design, construction and operating experience 80—32424
- LMFBR experimental reactor JOYO, construction and function tests *(Japanese)* 78—33266
- LMFBR fuel cycle characts., effects of nuclear data uncertainties 77—23197
- LMFBR fuel pin behaviour, computer code FRUMP, stress, strain, temp. distribs., displacements 77—14235
- LMFBR fuel pin bundle, wire-spaced, three-dimens. deflection modes 78—13301
- LMFBR fuel pin failure monitoring, cumulative mech. damage function from materials data 78—13262
- LMFBR maximum critical accident, assessment using theory of aerosols coagulation 77—3121
- LMFBR performance, effects of irradiation creep and swelling 78—78482
- LMFBR power stations, electric power generation and fuel fabrication 80—57928
- LMFBR refuelling scheme optimisation by man machine interactive method 77—67826
- LMFBR secondary shutdown, absorber balls test 78—41821
- LMFBR steam generator, T permeation rate through Cr-Mo steel 78—17319
- LMFBR subassembly response to simulated local press. loadings, accident conditions, finite element anal. 77—3123
- LOCA, thermal shock in nuclear containment wall, computer code for safety anal. 77—3135
- LWBR, startup and initial operating experience 80—13682
- LWR, commercial, evaluation of human errors and operator reliability 78—17373
- LWR, commercial, volume reduction system design and operation 78—21699

fission reactor operation continued

- LWR, design meas. to reduce radiation dose to reactor personnel 79—3199
- LWR, dynamics simulation, using hybrid computer system *(Czech)* 77—54309
- LWR, fuel cycle economics *(French)* 80—682
- LWR, fuel cycle evaluation, decision anal. and probability assessments 80—47587
- LWR, fuel cycle sensitivity anal. system 77—42119
- LWR, fuel rod microstruct. changes associated with post-DNB operation during power-cooling-mismatch 78—21688
- LWR, high-level radioactive waste prod. 77—26851
- LWR, LOCA separated air-water two-phase flow, mathematical anal. *(Japanese)* 79—36334
- LWR, molten fuel coolant interaction during HCDA 77—3136
- LWR, props. of core melts in LOCA, viscosity, thermal cond., specific heat 77—14247
- LWR, refuelling with natural U 80—679
- LWR, reliability demonstration test *(Japanese)* 79—26552
- LWR, scram experience for shutdown system reliability anal. 77—46347
- LWR, sensitivity of fuel cycle cost to uncertainties in nucl. data 80—680
- LWR at Genkai nuclear power plant, Japan, operating experience *(Japanese)* 77—79447
- LWR diversion resistant processes and cycles 78—86677
- LWR in Europe, operating experience 77—50282
- LWR maintenance problems for remote technology appl. 80—68871
- LWR operation and maintenance 78—86653
- LWR plant, decommisioning 78—29603
- LWR plant availability rel. to refuelling cycle duration 79—22440
- LWR plants in Japan, safety aspects and operating experience 79—26628
- LWR power prod., optimised strategy rel. to U ore costs 80—99253
- Magnox reactors, remote corrosion monitoring, laser based instrument 78—41822
- Maine Yankee power station uprate history 80—73967
- maintenance optimization through trend monitoring 80—18552
- master-slave manipulators and remote maintenance in nuclear research 77—71682
- Millstone power plant, Unit 3 design 80—22922
- mixed oxide fuel cycles, cost sensitivity anal. 79—89369
- molten clad relocation during unprotected undercooling transient in LMFBR 77—38348
- molten salt fusion-fission symbiotic systems, nuclear performance calcs. of catalysed D-D and D-T reactors 80—57948
- MSR for efficient fuel utilisation without Pu separation 80—678
- multidimensional reactor dynamics equation, fast factorization and exponential transform. procedures 78—17303
- multizone reactors, coupling, kinetics, appls. to Argonaut-ARK reactor *(Rumanian)* 77—46220
- neutron noise in presence of vibrating control plate, at-power measurement 77—61491
- new load-follow strategy for improved return-to-power capability 79—9794
- noise anal. *(Japanese)* 79—93749
- noise diagnostics appl., research programme in Poland *(Polish)* 77—88231
- nonequilibrium fuel management policies at San Onofre unit 1 77—42117
- nuclear energy complexes, economic and ecological problems of nuclear power development 79—645
- nuclear energy synergetics, characts. of integrated systems 79—13382
- nuclear merchant ship propulsion, operation experience 79—26745
- nuclear power conf., Chicago, United States, July 1979 80—794
- nuclear power project management, book 79—30875
- nuclear power station with VVER-400 reactor, primary circuit coolant pressure and quantity control *(Polish)* 80—91231
- nuclear power stations, gross operator error rates, evaluation of operator reliability 79—45371
- nuclear power stations, load factors and availability achieved with light water and heavy water reactors *(Slovenian)* 80—68843
- nuclear symbiosis, development of FBR and thermal spectrum near breeder reactors, review 79—45335
- nuclear technology transfer, Iran conf. 77—57757
- on-line surveillance of nuclear reactors based on decision theory 79—9775
- operating margin optimisation 79—85592
- operator reliability, Weibull distrib. model 80—63336
- operator reliability modelling for nuclear power stations 79—85621
- optimal cycle coastdown at San Onofre unit-1, reduced enrichment requirements 77—42118
- optimized once-through cycle and international nonproliferation objectives 79—85633
- optimum power reduction cycle, num. investig. 77—50265
- OTTO-HTR, Pu utilisation 77—42127
- overpressurized fission gas bubble form. in temp. transient, equilib. index 78—17368
- parametric REXCO H calcs., comparison with bare charge expt. results 77—3190
- PBF, irradiated fuel rods, behaviour following film boiling operation 78—13282
- PBF, temp. sensitivity of Co self-powered neutron detectors under PWR conditions 78—33275
- PBHTR, 'once through' cycles for enriched fuels, breeding variations 78—58382
- PBHTR, closed Th cycles, computational reactor lifetime simulation 79—85643
- PBHTR, design operation and applications, review 79—45328
- PBHTR, fuel cycle costs, bred fuel value of ^{233}U 77—42125
- PBHTR, Julich, 10 year operation *(German)* 78—54838
- PBHTR, performance of Th fuel cycles 77—42124
- PBHTR, Th fuel cycle performance 78—41841
- PBHTR net-breeding reactor system 79—3197
- PBR, flow of individual pebbles in cylindrical vessels 77—83017
- PBR using OTTO scheme, numerical anal. of fuel cycle including ^{236}U isotope separation *(German)* 77—83030
- Peach Bottom 1, HTGR nuclear power station, review of design and operation 79—45327
- pebble bed prebreeder reactor, conservation of U resources 79—49697
- pebble bed reactor emergency shut down system *(German)* 77—10480
- pellet-cladding gap conductance of UO_2, fuel rod, fill-gas comp. and eccentric gap geometry effects 78—13284

fission reactor operation continued
pellet-cladding interaction induced by radiation-induced dilation, mech. anal. 78—13302
performance analysis of power plants from operating experience data 78—21757
PFR primary cct., operating experience and CDFR design intentions 79—97870
Phenix and Super-Phenex, primary ccts. *(French)* 79—97780
Phenix FBR fuel cycle, breeding gain 80—709
Phenix LMFBR, operating experience since criticality 79—97849
Phenix plant operations and modifications *(French)* 80—47615
PHWR, CANDU reactor system, appropriate technology 78—58338
PHWR, fuel cycle anal. 79—89387
plant efficiency, and heat rate improvement program 79—67829
poisoning with fission products, ^{135}Xe and ^{149}Sm, spatial calc. *(Slovak)* 78—54850
power distrib. flattening, burn up optimisation *(Japanese)* 78—17397
power plant, Browns Ferry, startup and operating experience including cable tray fire 77—65284
power plant, Trojan, operating and startup experience 77—65283
power plant control appls., problems and trends 78—70609
power plant pathology 78—17345
power plants, diagnostic system using noise anal. 78—50279
power reactor with multiple transport lags and nonlinear controller characts., stability, parameter plane method 77—14217
power reactors in elec. utility system, short range system analysis method 77—50252
power station, modification during plant startup and operation 78—21758
power station, operator training, simulator 77—367
power station, Three Mile Island, operating experience with control, instrumentation and electrical system 77—65285
power station forced outages, statistical data anal. 80—13776
power stations, computer control systems for data acquisition and process control 79—22426
power stations in combined energy system, operating conditions *(Russian)* 77—38367
power upgrading, combustion engineering Inc. experience 80—73968
power upgrading, regulatory perspective 80—73966
power uprating, hardware and safety aspects 80—63342
pressure vessel dynamic loading, wave propagation effects 77—3090
pressure vessel dynamic response to impulsive loading in nonlinear range 77—3191
Project Manager organisation in nuclear plant turnover and startup 80—63339
prototype fast reactor steam generators, commercial size design 77—46393
PURINAMA, PuO_2-fueled zero-energy fast reactor 79—40988
PWR, 836 MWe nuclear power station, operating experience since 1974 80—831
PWR, 900 MW, probabilistic determ. of operating rules 77—46345
PWR, CANDU, operation, status and prospects of nuclear power in Canada 78—86664
PWR, commissioning and start-up procedures *(Slovak)* 79—36346
PWR, computer code for the study of migration and deposition of corrosion products 80—13700
PWR, construction and operation experience in Japan 77—57732
PWR, core-state models for fuel management of equilib. and transition cycles 77—67833
PWR, development and Pu allocation, optimal policies 80—725
PWR, economic and feasibility analysis of 18-month fuel cycles 80—18495
PWR, evaluation of environmental and in-plant effects of T recycle and build-up 78—33273
PWR, fluctuation anal. of apparent malfunction, frequency and time domains 77—54313
PWR, fuel cycle anal. 79—89387
PWR, N_2 bubble appl. to eliminate solid water plant evolutions 80—18557
PWR, Na leakage from condensate polishers 77—54357
PWR, normal operating radiation levels 77—88290
PWR, Oconee, occupational exposures, radiation levels and waste levels during operation 78—21726
PWR, planned cycle stretchout 79—31103
PWR, potential of Th cycle 77—42122
PWR, pressure tubes cracking, Zr-Nb alloy, Pickering power station experience 78—82472
PWR, quality assurance during operation, France 77—61526
PWR, reactor coolant pump failure investig. at Arkansas Nuclear One 80—9336
PWR, Salem Unit No.1, startup and operating experience 80—13685
PWR, startup, secondary-side corrosion product transport 80—9377
PWR, tritium control strategies, cost effectiveness 77—38360
PWR, Univ. of Missouri research reactor, ten-megawatt upgrade, exptl. use 78—21754
PWR and BWR pressure vessels, safety calcs., design, operation control, neutron effects *(German)* 77—34404
PWR fuel performance evaluation from I isotope concentrations in primary coolant *(Japanese)* 77—65272
PWR load factor statistical analysis 79—9789
PWR neutron noise increase with operating time 79—13447
PWR neutron noise interpretation by vibration analysis 78—94073
PWR neutron noise sources 78—94108
PWR occupational radiation exposure reduction techniques 79—9901
PWR operation, statistical analysis *(French)* 78—58374
PWR plant, dynamics, digital simulation 78—8882
PWR plant, LOCA capability code for utility appl. 78—21690
PWR plant control loop development model *(French)* 77—23218
PWR power plant dynamics, math. model *(Polish)* 79—63800
PWR power plant flow pressure fluctuations as vibration source, relationships *(Hungarian)* 80—47685
PWR power stations, operating record and reliability, reviews 79—22404
PWR radwaste systems design, factoring operating experience 78—17390
PWR reactivity changes, influence on transient processes *(Slovak)* 79—36343
PWR steam generator tubing, corrosion problems 79—24683
PWRs, auxiliary feedwater system, fault tree anal. 78—54867
quality assurance, cost effective programs 79—97863
quality assurance program for nuclear plant operations 80—783
quality assurance standards in USA, present status and appl. 80—781
radiation doses to equipment inside containment of power reactors 77—88253

fission reactor operation continued
radioactivity release, air monitoring, emergency procedures 78—70610
radiochemical management, reactor cooling system, gamma spectra of radioactive I from direct fission 79—9732
radiochemical management, reactor cooling system, rapid determ. of radioactive I contamination 79—9733
RBMK, startup and shutdown, H_2O_2 and Fe compounds behaviour investigation 79—9822
reactivity and neutron density noise excited by random rod vibr. 77—50203
reactivity determinations for performance of reactor safety, economics, operability *(Japanese)* 78—17332
reactivity meas. by Sjostrand method, on-line device *(Italian)* 77—38321
reactivity measurement by pulsed neutron technique, Sjostrand method foundations 78—17329
reactor heat and hydrogen energy utilisation *(Japanese)* 77—50253
reactor physics experiment using Kyoto University Critical Assembly *(Japanese)* 80—5202
reactor safety, quantifying plant availability, ALARA, and occupational radiation exposure relationships 79—59183
reactor vessel inspection techniques *(Dutch)* 80—27758
refueling outage, planning and scheduling, flexibility problems 79—63793
research and training reactor, ALARA program review at Texas A and M University 80—9362
residual power after shutdown. afterheat estimation *(Slovak)* 77—82997
residual reactivity role in plant transients 77—50228
rocket engine, gaseous-fuelled, reactivity effects 77—54354
rod swap test results, VEPCO analytical methods for Surry 1, cycle 5 80—9338
safety, regulatory problems, fuel cycle 77—50263
Sandia Pulsed Reactor III operational history 79—9790
SGHWR, 600 MWe, design and experience, UK 77—18686
SGHWR, UO_2 micropore sintering, irradiated below 1100°C 80—5255
SGHWR fuel performance under power ramp operation 77—74963
Shimane nuclear power plant, Japan, operating experience *(Japanese)* 77—71659
shutdown system reliability, effect of operator performance 78—29611
signal noise, characts. and benefits, results from CANDU-BLW reactor 77—65310
SNR-300 fuel element design, expts. on rod bundle fluid dynamics and thermodynamics 79—97794
sodium reactor experiment decommissioning, radiation protection 80—9432
spatial reactor control methods 77—83056
spectral shift controlled reactor, 1300 MW(e), conceptual design and performance 79—85595
spent fuel pools, regulatory aspects of structural evaluation for high-density storage 78—21727
spent fuel storage, high-density, economic evaluation of alternatives 78—21732
spent fuel storage, remote underwater rack removal and installation 78—21729
spent fuel storage, structural design problems with backfitting fuel racks to existing pools 78—21728
spent fuel storage racks, decontamination and disposal 78—21731
SSCR, fuel cycle anal. 79—89387
stable adaptive schemes, parameter identification nonlinear point reactor 79—9765
start-up experience of IBR-2 pulsed research reactor 80—73956
startup, benefits of standardisation 80—13686
startup, conduct of operations, organisation and personnel 80—63340
startup, RBMK reactor of Lenin Nuclear Power Station second unit 77—23231
startup, staffing program, scope, tasks, resources, constraints, anal., implementation 80—63341
startup planning, domestic Westinghouse plant and PWR comparison 80—9371
startup scheduling 80—13687
steel, AGR boilers, gas side corrosion, breakaway oxidisation treatment 78—48558
structural mechanics of PWR 78—41806
symbiotic reactor strategies, U demand 77—42120
Takahama power station, operation records *(Japanese)* 78—25304
teaching laboratory, computer modules for calculation of prompt-neutron generation time 78—4447
teaching project management as part of international technology transfer 78—4428
teleoperator systems for reactor maintenance, technology assessment 80—68872
testing pressure vessel, safeguarding containment *(German)* 79—13433
thermodynamics and fluid dynamics, photographic techniques *(Spanish)* 77—71635
Three Mile Island accident anal., observations and recommendations 80—18370
THTR 300 MW(e) Schmehausen station, anal. of non-central neutron source 77—67802
training simulator, design characteristics *(Spanish)* 80—58007
transient boiling heat transfer in vertical flow 77—354
TREAT, fission gas non-equilib. behaviour during fast thermal transients, simulation 78—41831
TRIGA-reflector regions, spatial variation of fast neutron spectra 77—46422
Trino power plant, in-service inspection and operating experience, main coolant circuit *(Italian)* 79—17992
underwater repair, innovative technique 79—3226
university type reactors, economic success, project update 80—68900
US reactor operating experience, qualitative assessment 79—26627
utilisation factors, economics, operating experience, Swedish nuclear power stations *(Swedish)* 77—79472
utility use of NSSS supplier reactor analysis code for operational support 78—21724
Vermont Yankee radwaste system 78—17391
void fraction for subcooled boiling, different heat flux distribs. along channel *(Russian)* 77—34381
VVER, optimisation of the cyclical operating regime 79—71916
VVER-440, limit of fuel stay time, operation of nuclear power station with reduced utilisation of power *(Russian)* 77—65274
VVER-440 reactor power stations, design and operation 79—59127
water cooled reactor, gas stripping in two-phase flow 79—638
water reactor decontamination, recirculating regenerable reagent appl. 78—46158

fission reactor operation continued
- water-cooled water-moderated reactor cooling system faults, hybrid simulation *(Russian)* 78—5008
- water-graphite reactors, optimisation study for power stations 79—76089
- water-moderated water-cooled reactor operational mode anal. by computer *(Russian)* 78—21760
- water-moderated-water-cooled reactor VVER-1000, power plant technology 78—82501
- Westinghouse plant availability anal. with operating data base 80—23050
- Westinghouse power plants, uprating capacity 80—68878
- Westinghouse steam generators, operations update 78—21683
- workers' protection against radiation hazards 79—59267
- YAYOI, fast reactor, pulse operation by reactivity insertion with R-pulser *(Japanese)* 78—8914
- ZPPR mockup critical assembly for Clinch River reactor, source level flux monitor expts. 77—54337
- CO_2 fundamental condensation cycles in steam and nucl. power plants, performance characts. 80—63368
- Cs fission product release and diffusion in fuel elements *(German)* 78—25298
- He cooled reactor turbine control experiences Fort St. Vrain HTGR *(German)* 80—57927
- N_2O_4 gas-liquid cycle anal. *(Russian)* 77—38366
- Na cooled fast reactor, partly blocked fuel subassembly, heat transfer meas. in air model 77—74964
- Na, liquid, purification by mesh-packed cold traps, effect of shape on perform. 79—40986
- Na system cold trap temperature control using resistance heater 77—57710
- Pu recycling in LWR 79—45391
- Th fuel cycle, nucl. strategy and recycle technology 78—86662
- Th fuel cycle role in thermal and fast reactors 79—13420
- UF_4-CF_4 mixture, gas core fission reactor, fission based plasma engine 80—63366
- UF_6-He circulating gas critical expts. 79—13488
- UO_2-Zircaloy fuel element behaviour in PWR power plants 80—631
- Xe spatial oscillations, time optimal control 80—32320

fission reactor safety
- *see also fission reactor cooling and heat recovery; fission reactor core control and monitoring*
- 7-pin bundle simulation during flow rundown transient 80—68879
- 1300 MW nuclear reactor steam isolating valve blowdown tests *(German)* 80—22967
- 1979 ANS/ENS International Meeting, Seattle, USA, overview 80—27764
- 2056 MW nuclear reactor pressure tubes cracking 78—82463
- absorption cross section of fission product aggregate, energy dependence 79—76075
- accelerator-breeder concept, preliminary design 79—81059
- accident at Three Mile Island, lessons learned in maintenance and reliability 80—57929
- accident consequences, estimated, effect of appl. of surface depletion model 80—30622
- accident dispersion model, direction depend. probability limits consistent with NRC practice 78—17372
- accident dosimetry, report on fourth IAEA intercomparison expt. at Harwell 77—38426
- accident dosimetry calcs., comparison with expt. data 79—36422
- accident dosimetry system *(Japanese)* 77—3119
- accident features affecting emergency measures 78—55055
- accident handling, conf., Vienna, Austria (Feb.-Mar., 1977) 78—53518
- accident health effects, incorporation of plume trajectories in CRAC code 80—47617
- accident management, automated notification of reactor data to off-site personnel 80—95388
- accident risk calcs., models and data 80—47613
- accidents, effects on public, casualty management 78—53519
- accidents, meas. of crit. environmental exposure by I radioisotopes 78—57081
- accidents, struct. shielding against gamma-ray sources, dose reduction factors 78—13251
- accidents, Three Mile Island nuclear power station, viewpoint of member of Commission of Enquiry 80—83190
- accidents due to loss of coolant, multiple-element model and computer solution 78—66358
- accidents in power stations of Electricite de France, protection organisation *(French)* 78—55049
- accountability control system in plutonium fuel facility *(Japanese)* 79—71909
- acoustic monitoring equipment for nuclear power plants: research, development and industrial production 79—76076
- acoustic wave attenuation meas. in air-water two phase medium 77—58513
- acoustically induced vibration of circular cylindrical rods 77—62098
- ACPR upgrade, criticality and preliminary characterization 80—13555
- actinide waste burning in laser fusion driven hybrid reactor 79—22421
- activity release, effect of meteorological parameters 80—17142
- advanced reactor Centralised Reliability Data Organisation 79—13463
- aerosol, radioactive charging, transient mean particle charge 78—23973
- aerosol behavior in nuclear accidents for LWR and LMFBR 80—746
- AGR, commercial protection system, safety logic system 77—54325
- AGR, moderator corrosion problems, soln. 77—18688
- AGR, radiation protection during operation and maintenance of irradiated fuel route 80—5375
- AGR fuel plug maintenance facility, corrosion product contamination control 80—5388
- AGR pressure vessel, safeguards for man-access 80—27790
- AGR pressure vessels, radiation protection for shutdown man-access 80—5374
- AGR shutdown sequence equipment, use of computer based training simulator 79—89461
- AGR system for nuclear process heat, primary circuit component materials 78—13233
- AGRs, principal technical features and advantages *(French)* 80—18375
- airborne and liquid releases from nuclear facilities, radiation monitoring systems 78—37450
- airborne radiactivity in reactor containment building, ^{133}Xe and ^{131}I activity following shutdown 80—47749
- aircraft impact, structural response, reaction-time and impact area-time curves 80—78407

fission reactor safety continued
- aircraft impact on reactor containment structures 78—29660
- ALARA, effectiveness of design modifications 80—18546
- ALARA, is it being achieved, utility and navy records 80—68898
- ALARA, reactor inplant design, a regulatory viewpoint 80—23016
- ALARA objectives, reactor design for occupational exposure 80—23017
- ALARA occupational radiation exposure, utility design viewpoint 80—18548
- alternative containment designs, value/impact comparison, containment failure and safety aspects 79—13464
- alternative fuel cycles, relative diversion resistance 80—37438
- annular core pulse reactor, advanced operating mode capabilities 79—93777
- anticipated transients without reactor scram and other safety devices for PWR and LWR 79—18002
- antiseismic supports of reinforced elastomer blocks *(French)* 79—54535
- ARMP model appl. to Beaver Valley Unit 1 80—68862
- aRMP reload safety evaluation methods for application to Kewaunee 80—68861
- artificial earthquake generation for dynamic anal. of nuclear power stations 79—97850
- aseismic bearing foundation system for power station earthquake protection 80—83206
- aseismic design, using rubber mounts 77—79470
- aseismic design and testing of equipment and components, Japan 80—52763
- atmospheric dispersion calcs. for nuclear plants, EFFAIR code 79—18007
- atmospheric emissions from nuclear plants, applications related concept for radiation exposure calc. *(German)* 78—82531
- atmospheric pollutant dispersion 80—47621
- atmospheric pollution, effects of wind shift and cross-plume concentration models on calculated accident consequences 80—3555
- atmospheric pollution following nuclear reactor accident, German consequence model 80—741
- ATWS, US NRC views and plans 80—47664
- ATWS analysis, moderator coefficient, impact on plant operation 80—47666
- ATWS considerations relative to the BWR 80—47665
- ATWS risk anal. of B and W PWRs 80—47667
- Austrian research and participation 77—10470
- automated approach to nuclear facility safeguards effectiveness evaluation 78—82486
- automatic diagnosis of abnormal phenomena, theory and computer simulation 78—17330
- availability of redundant safety systems with common-mode and undetected failures 80—91230
- AVR reactor steam generator leakage, meas. of activities and their origin in leakage water 80—693
- axisymmetric seismic response of thick circular plate supporting many rods, nuclear power plant appl. 80—1458
- BABEL, multigroup neutron library for fast reactor, shielding design studies 80—68745
- bare charge expts., parametric REXCO H calcs. 77—3190
- BEHAVE-SST interpretation of TREAT experiments HUT 5-5A and HUT 5-5B 79—85659
- Berger coeffs. for Eisenhauer-Simmons γ-ray buildup factors in concrete 78—78510
- Biblis B nuclear power station risk study, results and conclusions *(German)* 80—68902
- Biblis core protection and German safety regulations 77—88260
- Bilibinsk atomic plant, gravity coeff. of coolant reactivity 80—32333
- biological consequences of human exposure to radiation following reactor accident 78—7407
- biological protection in water-moderated, water-cooled nucl. reactors 78—818
- biological shield wall for Caorso nuclear plant, design, construction and erection 78—86694
- blast effects due to gas cloud explosions 77—38350
- blast effects from accidental explosions, US regulatory requirements 78—41877
- blowdown, fluid behaviour in pressure vessel *(Japanese)* 79—17999
- blowdown expt., TRAC-P1A calcs. 80—18383
- blowdown tests, effects of dissolved gas 77—42137
- BN-350, primary cct. and component design *(Russian)* 79—97781
- BN-350 reactor, radiation safety assessment at design stage *(Russian)* 79—97869
- BN-350 reactor shielding studies 78—21667
- BN-600, primary cct. and component design *(Russian)* 79—97781
- boiling crisis, nuclear reactor safety and performance, state of the art review 80—63312
- boiling flow regimes for carbide fuel and steel 79—85617
- boiling heat transfer during rewetting, one-dimens. cond. model 79—598
- boilup threshold for bottled-up transition phase pool 79—93776
- Boltzmann equation, P_1 approx. in presence of delayed neutron emission 80—78347
- BOR 60 fast reactor, primary coolant circuit radioactivity effects 79—63737
- BOR-60 experimental fast reactor, safe operation in power plant conditions *(Russian)* 79—97865
- BOR-60 reactor, boiling Na tests 79—97832
- breached element location from mixture of Xe tags, MIXTAG code 78—33274
- breached fuel element diagnosis, use of fractional release ratio ^{137}Cs to ^{131}I 78—21713
- breakdown in Three Mile Island power plant *(Hungarian)* 80—18454
- breakdown in TMI-2 power plant, consequences *(Hungarian)* 80—18455
- breeder reactors, current status in Europe 80—27796
- breeder reactors, SNR300, cooling system failure, effects *(German)* 78—695
- Browns Ferry BWR, load following test 80—68892
- Bruce core, ZED-2 mockup, responses of Pt, V and Co self powered flux detectors 78—58391
- bubble boundary layer formation over inclined porous plate 80—19504
- building walls, differential press. during tornadoes, computer program 77—38349
- buoyancy effects on pressure loss in rod arrays under laminar flow 80—27735
- burnup determ., accuracy requirements for fuel cycle design, reactor operation and safety 78—58342

fission reactor safety continued
- BWR, air clearing in H_2O-type press. suppression systems, scaling laws 79—54563
- BWR, air clearing in H_2O-type press. suppression systems, scaling laws 79—54564
- BWR, appl. of warm water injection method to in-core wet sipping for leaker detection 78—78450
- BWR, automatic protection system *(German)* 78—4989
- BWR, beta dose in skin from gaseous radioactive reactor effluents 80—26364
- BWR, block-monitoring index for diagnosis of power station operating characts. 79—59185
- BWR, calc. of shutdown dose rate around recirculation pipes, radioactive corrosion products in primary cooling water 80—68734
- BWR, containment system coolant flows, LOCA modeling 79—54476
- BWR, control blade worth depletion meas. 80—719
- BWR, control of Fe feed rate into feedwater system to reduce shutdown radiation level 80—5384
- BWR, coupled vibrations of a structure and fluid excited by pressure shocks 80—13546
- BWR, Doppler and void reactivity feedback 80—13661
- BWR, Dresden 1 plant, prototype operation for decontamination of primary system 79—54538
- BWR, dryout/post-dryout heat transfer, low flow, single tube 77—61498
- BWR, dynamic loading of press. suppression containment blowdown, power station expt. data 77—3133
- BWR, effect of multiple boiling channels on void fluctuation spectra 80—18464
- BWR, HDR reactor, design of blowdown loading expts., dynamic response of PWR-vessel internals 77—88204
- BWR, iron oxide deposition on heated surfaces, model 80—73902
- BWR, Kernkraftwerk Muehleburg special turbine trip tests 80—18513
- BWR, KKM turbine trip simulation with a one-dimensional transient model 80—18510
- BWR, LOCA, scaling of RPI parallel channel effects expt. 80—18381
- BWR, Millstone Unit No. 1, augmented off gas system experience 80—22919
- BWR, nuclear cores safety calc., microscopic and macroscopic layout *(German)* 77—10472
- BWR, off-gas explosions, minimisation procedures 80—9369
- BWR, pipe rupture, effect on reactor internals, analysis 78—29606
- BWR, pressure ATWS, γ and n heating, pressure wave propag. effects 80—13640
- BWR, primary containment vessel, spray heat removal characteristics 80—73972
- BWR, Quad Cities 1, localized cold critical expt. 79—81001
- BWR, reactor safety anal., sensitivity assessments, plant risk 77—18676
- BWR, revised Inservice Inspection program, implementation at Millstone Unit 1 80—23020
- BWR, safety evaluation, experiments and analytical analysis 80—13703
- BWR, safety models, systems engineering appl. 77—38359
- BWR, safety relief valve discharge loads, dynamic effects on structures and eqpt. 80—99236
- BWR, shield design against neutron streaming in pressure vessel vicinity 80—13678
- BWR, shutdown dose rate of primary cooling system, prediction by empirical formula 79—22408
- BWR, simulation of cooling system conditions, stress corrosion cracking test 78—80696
- BWR, steam chugging during LOCA, general transient anal. 80—73903
- BWR, surface inspection methods, in-service inspection of reactor pressure vessel 80—27759
- BWR, thermal-hydraulic technology, university contrib. opportunities 79—49652
- BWR, TRAB transient analysis program for pressure vessel and subsystems 80—73978
- BWR, vacuum relief valve sizing in condensing steam situations, analytical model 79—54545
- BWR, vent clearing transients calc., press. suppression system, digital computer simulation 77—3132
- BWR, void and Doppler feedback eval. 80—22976
- BWR, void reactivity feedback, space-time anal. 79—22414
- BWR 1/5 scale Mk.1 toroidal wetwell, induced vertical forces under LOCA 78—41832
- BWR airborne ^{131}I releases during operation 80—23033
- BWR augmented off-gas system flame arrester at Oyster Creek nuclear station 80—22918
- BWR benchmark calcs. with MEKIN code 80—18385
- BWR blowdown, [Thermal reactor safety.] Comparison of quasi-steady blowdown models with recent experiments 80—22999
- BWR building, soil-struct. interaction behaviour damping effects, expt. anal. 77—38434
- BWR bundles, countercurrent flow limitation correl. during LOCA 79—31057
- BWR containment, influence of safety relief valve discharge loads 80—42793
- BWR containment struct., appl. of frequency domain anal. 79—93753
- BWR containment system, effect of torus wall flexibility on hydro-structure interaction 80—83195
- BWR control rod drive hydraulic return nozzle repair 80—23043
- BWR coolant, H_2-O_2 recombiner, appl. of Pd/Ni/Cr layered catalyst 80—18504
- BWR coolant pipes, integranular stress cracking, in-service inspection influences 80—68887
- BWR decay heat removal systems, probabilistic risk assessment, fault and event tree anal. 80—63333
- BWR decontamination, research and development program 79—54539
- BWR Dresden-3 fuel rods, pellet/cladding interaction induced stress corrosion cracking 79—67899
- BWR feedwater nozzle cladding removal ALARA approach 79—59224
- BWR fuel assembly, radiant heat transfer 78—17287
- BWR fuel integrity limits and criteria 80—575
- BWR licensing basis transients, computer anal. of turbine without bypass transient 80—42814
- BWR LOCA, bubble collapse and fluid struct. interaction 80—689
- BWR LOCA, computer prediction of loading conditions on pressure suppression system 80—764
- BWR LOCA, containment dynamic loadings 80—763
- BWR LOCA, hydrodynamic lead characteristics of primary containment vessel 80—73972

fission reactor safety continued
- BWR LOCA, numerical simulation of hydrodynamic impact loads on cylinders 79—36350
- BWR LOCA, phased mission analysis of ECCS failures 80—68851
- BWR LOCA, pool swell modelling and small-scale expts., comparative eval. 80—95362
- BWR LOCA, pool swell reduced scale simulations, scaling law limitations 80—99238
- BWR LOCA, power channel thermal transients during reflooding 79—63755
- BWR LOCA, press. drop across tieplate during countercurrent flooding 80—18530
- BWR LOCA, press. oscill. phenomena induced by steam condensation, in containment with press. suppression system 80—68848
- BWR LOCA, RELAP4 (MOD7/Version 1) core spray cooling calcs. compared with data 79—49730
- BWR LOCA, some considerations in small-scale pool swell simulations 79—49740
- BWR LOCA, vapour velocity in two-phase mixture during blowdown period 80—42821
- BWR LOCA, vent clearing, downward forces effects 79—49741
- BWR LOCA anal. using homogeneous critical flow model, expt. determ. of blowdown flow rate 80—106120
- BWR LOCA analysis, jet pump modelling using RELAP4 80—68850
- BWR LOCA analysis, RELAP4/MOD7 calc. cf level swell test data 80—23003
- BWR LOFA conditions, transition flow boiling heat transfer to water in verticle annulus 77—23182
- BWR loss-of-coolant accident, peak-clad temp. probability distribs. 77—74952
- BWR Mk.I pressure suppression system, vent clearing during simulated LOCA 80—13657
- BWR nozzle corner, part circular cracks stress intensity factor 80—30105
- BWR NSSS structural integrity programs at GEC 80—99230
- BWR off-gas systems, design considerations to prevent H_2 ignition 80—22917
- BWR off-gas systems operating problems 80—22916
- BWR passive containment system, LOCA safety features 79—13466
- BWR pipe assemblies, stress corrosion cracking avoidance by improved welding methods 80—42838
- BWR piping cracks, relation between crack and stress 79—40995
- BWR plant, SOPRE 1, press. suppression containment system 77—38342
- BWR plant diagnosis system, on line process computer appl. 78—46146
- BWR plant in Japan, aseismic design 77—65267
- BWR plants, O_2 monitoring and control 78—21656
- BWR plants in Japan, seismic design and tests 78—86652
- BWR power plant, earthquake-proof design criteria 78—21733
- BWR power plant, neutron noise meas. and analysis 78—94105
- BWR power plant availability improvement by acoustic emission monitoring 79—9809
- BWR power plant shielding concept 80—18712
- BWR power stations, operating record and reliability, reviews 79—22403
- BWR pressure suppression pool, use of orificing to accomplish small scale representation 79—31051
- BWR pressure suppression systems behaviour during LOCA condensation phase 77—50269
- BWR pressurisation effects of bypass streamline transient modelling 79—89408
- BWR pressurisation transient anal. using MEKIN neutronics/thermal-hydraulic code 80—47626
- BWR primary steam circuits, decontamination procedures *(German)* 79—89389
- BWR radioactivity releases reported to Licensee Event Report file 80—68889
- BWR rapid transients, direct coolant heating and moderator temp. reactivity feedback effect 79—89442
- BWR rod bundles, combined radiation and convection under emergency cooling conditions 77—14249
- BWR rod drop accident, effect of thermal-hydraulic feedback, computer anal. 80—42815
- BWR safety relief valve, remote set pressure verification 79—54487
- BWR scram reactivity characteristics 77—46342
- BWR shield wall penetrations, radiation shielding 80—13679
- BWR shutdown dose rate prediction, calc. code 80—23061
- BWR shutdown margin prediction, multidimensional linear regression model 79—9778
- BWR stainless steel piping, corrosion film charact. 79—54498
- BWR steam condensation pressure variations 78—46134
- BWR steam discharge piping, acceleration forces exerted on finite cylinders by an oscillating air bubble 80—18503
- BWR suppression pool, role of Taylor instability during vent cleaning 79—31046
- BWR suppression pool temperature transients following LOCA, computer anal. 80—762
- BWR thermal hydraulics 80—27721
- BWR transient anal., iterative procedure for predicting critical power ratio 80—42816
- BWR transient anal. model for pressurisation transients 80—18509
- BWR turbine trip, RELAP/RETRAN steam line models, accuracy considerations 79—59197
- BWR turbine trip test, computer anal. 80—692
- BWR turbine trip transient analysis using ALMOS plant model *(German)* 80—83177
- BWR turbine trip transients, additional separator modelling considerations 80—18511
- BWR turbine valve closure, pressure transients 79—89441
- BWR vent clearing hydrodynamics, numerical simulation using SOLA-VOF code 79—49659
- BWR vent clearing hydrodynamics, SOLA VOF simulation 80—32356
- BWR with fracture live steam line, isolating valve loading *(German)* 77—38340
- BWR with graphite channels, safety of nuclear power stations 79—26561
- BWR-6 computer anal. of fission product release to containment via press. suppression pool 79—59223
- BWR-EM LOCA anal. with WRAP-EM system 80—18523
- BWR-II containment vessel, soil-struct. interaction for transient loads 78—29604
- cable tests to IEEE standards 80—57884
- cables, damage mechanisms in LOCA environment 80—13658

fission reactor safety continued
California underground siting study, effectiveness in mitigating health consequences 80—18402
California underground siting study, selection and analysis of accident sequences 80—18401
CAMEL seven-pin fuel sweepout tests 79—85669
CANDU, development of irrad. fuel bundle counters for reactor safeguards systems 78—94119
CANDU, digital computer control 77—54324
CANDU, LOCA, space-time neutronic anal. 80—13663
CANDU—Canadian experience and expectations with the heavy-water reactor 79—26593
CANDU 600 MW, spent fuel bundle counter, safeguard design 79—13495
CANDU 600 MW(e) station, man-rem expenditures 79—13493
CANDU design features that influence fuel modelling for transients 80—42740
CANDU design program for exposure minimisation 77—6570
CANDU distributed computer control systems 79—76105
CANDU fuel behaviour under transient conditions 79—71930
CANDU fuel channels, power rundown, computer programs for fuel and struct. element decay heat 77—57711
CANDU irradiated fuels, NDT anal. techniques 79—59177
CANDU nuclear power station safety, Atomic Energy Control Board guidelines 79—22425
CANDU power reactor, pressure tubes, design and development 79—36372
CANDU power stations, reduction, control and prediction of radioactivity transport 80—18448
CANDU reactor, shutdown system design, performance during commissioning 78—25319
Candu reactor moderator effectiveness as LOCA heat sink 79—81021
CANDU reactor safety, AECL publication bibliography 80—36797
CANDU reactor safety anal., types 77—74972
CANDU reactor safety and reliability requirements 79—26634
CANDU reactors, Atomic Energy of Canada report to Royal Commission on Electric Power Planning 78—25312
CANDU reactors, seismic design criteria and requirement 80—78358
CANDU simulated core in ZED-2, transient meas. anal., CERKIN code exam. 78—58386
CANDU-PHW, decommissioning cost, environmental impact hazards and size 77—61598
Caorso BWR power station, structural acceptance tests of primary containment *(Italian)* 79—30951
CARAMEL, Zircaloy-clad UO_2 fuel, cladding burst follow-up test 80—776
Caramel fuel cladding rupture, development and detection at OSIRIS experimental reactor *(French)* 80—95371
carbide fuel elements, response to fast thermal transients, UNCLE-T-BUBE code 79—93715
carbide fuel-coolant interactions, PLUTO code 79—85613
cavity geometry impact on power distrib. meas. with multisection ex-core detectors 79—93794
CEGB nuclear power station emergency arrangements 78—55050
CEGB nuclear power station emergency monitoring procedures 78—55053
channel-type reactors, γ-ray dose rate spatial distrib. over entire thickness of side shield 78—86697
characterisation and quality control of nuclear fuels, conf. Karlsruhe Germany (June 1978) 79—49794
chemical explosion induced, nuclear power plant protection 77—38351
CIRENE, heavy water moderated BWR, LOCA simulation of recirculation circuit rupture 79—30949
cladding, cracks under stainless steel cladding of pressure vessel, detection, causes, danger 80—52760
cladding loading by gas pressure during TOP accident, modelling 77—42030
class 1E electronic equipment qualification, ageing evaluation using Arrhenius techniques 79—45361
Clinch River breeder reactor, ALARA nature of design effluents 79—22420
Clinch River Breeder Reactor Plant reliability and safety methodology 78—29617
co-utilization of life safety systems in nuclear power plant facilities 80—47671
coastal nuclear power stations, gaseous release dilution meas. 79—52981
colloqium on nucl. instrumentation, London, England 1979 80—4480
column section seismic design subjected to three components of earthquake 77—38355
combined cold and hot leg injection efficiency 78—21633
common-mode failure analysis 78—29618
comparability study of fission and fusion reactors w.r.t. safety, costs and development time 79—59114
component improved reliability, design consideration 79—22383
component reliability, non-destructive testing and flaw evaluation *(French)* 79—24711
component unavailability and failure intensity 77—83063
component vibration investigation using fast Fourier transform analysers 80—63315
composite geometry reactor vessel, steady temp. distrib., thermal shock 77—54286
Compton recoil gamma-ray spectroscopy, current status 80—47808
computer appl. to reactor scram system *(German)* 78—86635
computer applications, information processing, control, monitoring, data acquisition and evaluation 80—47595
computer control, development of a reliable single-channel direct-digital reactor-control system 79—89458
computer organisation solution 80—669
computer safety analysis, verification of the TRAC code on RSR standard problem 5 79—49724
computerised reactor protection systems, reliability anal. using Markov methods 80—91229
computerised reactor safety systems, design, specification and implementation 79—63783
concrete, neutron number and dose albedo 79—93681
concrete reinforced walls, local behaviour under missile impact *(French)* 78—44180
concrete reinforced walls, local response to missile impact 78—44181
concrete slab perforation by missiles, nuclear plant appl. 77—38352
concrete slab perforation by missiles, nuclear plant appl. 77—38353
concrete slab perforation by missiles, nuclear plant appl. 77—38354

fission reactor safety continued
condensation-driven fluid motions, nuclear reactor safety 80—63228
condensible vapour source expt. modelling 80—18542
conduction controlled surface rewetting, general 1-D model 77—83011
conference, Berlin, Germany (Aug. 1979) 80—77539
conference, design, safety requirements, London, UK (Apr. 1980) 80—57013
conference, San Diego, Calif., USA (June 1978) 79—17972
conference, San Diego, Calif., USA (June 1978) 79—49650
conference on nuclear power and fuel cycle, Salzburg, Austria, (May 77) 79—26503
connector specification, performance, design and testing 77—23233
consistent creep and rupture properties for creep-fatigue evaluation of nuclear components 80—35329
containment, primary, modular electrical penetration assembly 78—716
containment air contamination, sampling and measurement techniques *(French)* 78—89997
containment analysis by ALICE code after HCDA 79—49736
containment and surveillance techniques for the IAEA 79—85645
containment blowdown following LOCA, press. and temp. transients and COPDA results 78—13303
containment building, Mark III, advantages, Grand Gulf Nuclear Station project 80—106122
containment buildings, integrated leak rate testing *(Spanish)* 79—54518
containment heat transfer following LOCA, anal. 77—54314
containment leak rate test duration time, acceptability of eight hour test 78—21700
containment leakage from Na fire anal., response surface method, SPOOL-FIRE code 79—18004
containment liner seismic reliability under statistical uncertainty, cracking 78—89948
containment main steam line break equipment qualification. [nuclear reactor safety] over 422K 80—42831
containment negative pressure evaluation 78—50275
containment of coolant during LOCA, ZOCO VI program appl. *(German)* 78—21668
containment pressure transients, anal. of evaporation rate effects 77—38363
containment response to accidents, comparison of CONTEMPT-LT calculations with Marviken experiments 79—49737
containment spray droplet heat transfer, effect of internal circulation 77—83026
containment structure design and service loads 80—106138
containment structures, design and construction, ACI-ASME code of practice impact 80—798
containment structures, integrity and safety aspects *(Spanish)* 79—93738
containment subcompartment flow, film entrainment determ. 79—49657
containment systems, critical flow mode for air-steam-water mixtures 80—18502
containment testing by TVA 80—68897
containment tightness, integral leakage rate tests 78—89956
containments, in-service leakage tests 79—67895
contaminated live steam release into turbine hall at Brunsbuttel *(German)* 79—89388
control and protection system future trends justification 77—88263
control instrumentation, commissioning and maintenance experience at Rajasthan 79—89455
control room and desk design, alarm system, information displays 79—89464
control systems for loop channel parameters 79—97835
convection with volumetric heat sources, fluid layer in spherical segment 79—614
convolution integral calculations for neutron transport in reactors 80—47561
coolant activity monitoring, automatic on-line system 80—684
coolant circuit contamination 78—21666
coolant circuits, fracture mech. appl. 79—43430
coolant depressurisation studies, transient density, press., temp. variations, during discharge 80—57833
coolant loss expt., LOFT project at INEL test facility 80—32386
coolant piping, relative rupture probabilities 78—21632
coolant pressure boundary leakage detection system 80—63306
coolant pump, seismic anal. by response spectrum method 77—3183
coolant unsteady flow, with discharge from high-pressure vessel *(Russian)* 79—89448
cooling pipes, safety anal. for prestressed concrete reactor vessels 80—32370
core disassembly calculations, vapour press. eqn. of state, VENUS-II code studies 78—8908
core flooding system, reliability analysis *(German, English)* 77—38346
core heat transfer during reflooding, modelling 80—27781
core melt in hydrodynamic fragmentation, acoustic cavitation mechanism 79—85650
core meltdown, acoustic meas. of penetration of molten metallic pool into concrete 80—13544
core meltdown, contribution of collapsing vapor bubbles to the fragmentation of melts 80—755
core meltdown accident, radioactive pollution consequences from liquid pathways 80—104778
core motion monitoring, exptl. methods 79—81025
core power distrib. surveillance and control, safety aspects 79—97860
core power transients without scram, calc. of moderator reactivity feedback 77—42152
core protection and surveillance system 79—9811
core temp. monitoring, can thermocouple distribution procedure 78—54856
core-melt model, transient natural convection in single-phase heat-generating pool 80—9350
core-retention bed, horizontal heat transfer from molten fuel 77—46317
corrosion damage, overview of water chemistry 79—54553
corrosion fatigue crack growth rate data, appl. to integrity anal. 80—32353
corrosion problems and prevention in nuclear industries *(Japanese)* 80—42711
corrosion product reduction program 78—21665
count-doubling time monitor, new reactor safety circuit for low-power-level operation 79—41004
coupled problems in transient fluid and structural dynamics 77—71646
CRBR, analysis of transient overpower accidents in BOL core using comp. code 77—46326

fission reactor safety continued
CRBR, heat transfer and thermal losses in above-core regions 80−32363
CRBR, primary pipe rupture accident anal. with DEMO code 78−70621
CRBR carbide reload design, comparison with reference oxide design during TUC 79−85658
CRBR core, recriticality potential of boiling pool 77−46332
CRBR mild transient overpower accidents with advanced fuels 80−18539
CRBR piping, structural reliability uncertainties 77−46350
CRBR primary piping reliability, stress-strength overlap method 77−46349
CRBR shutdown system, Markovian reliability anal. 80−27761
CRBR simulated fuel pins, fuel freezing tests 79−85671
CRBRP, fuel failure monitoring system 79−93795
CRBRP mixing-tee model, vibration studies of perforated plates 79−49665
CRBRP with radial parfait core, analysis of unprotected loss-of-flow accidents 77−46327
Creys Malville station, Super Phenix project safety *(French)* 79−30948
Creys-Malville centre, siting, operation, safety, containment and waste *(French)* 79−30945
Creys-Malville FBR power plant, main safety features 80−747
Creys-Malville station, safety arrangements *(French)* 79−30946
critical consts., review 78−59931
critical facility earthquake design criteria 79−88286
critical heat flux, review of data 77−57708
critical heat flux in tube, Freon-12 and water coolant 77−83020
critical two-phase flow models, nuclear reactor safety 80−63229
criticality accident dosimetry system 77−88288
criticality accidents, fission and explosive energy releases of PuO_2 and PuO_2-UO_2 assemblies 77−65295
criticality calculations, random geometry model of fissile solns. containing borates Raschig rings 79−36310
criticality incident detect. with γ dose rate alarm 79−36423
criticality safety, fuel cycle education module 80−36798
criticality safety, misleading assumption in array analysis 79−63772
criticality safety, obs. on problem solving 79−63768
criticality safety, pitfalls in calcs. and experiences in operation 79−63769
criticality safety, uncertainties in K-effective calcs. 79−63771
criticality safety anal., determ. of Dancoff factor for cubic arrays of sphercial fuel particles 80−13725
criticality safety anal., quality assurance for computer programs 79−63766
criticality safety analysis in nuclear fuel cycle *(Japanese)* 80−99225
criticality safety analysis using solid-angle method and Monte Carlo program 77−65294
criticality safety broadgroup library validation using uranium systems 79−26564
criticality safety calcs. quality assurance plan 79−63767
criticality safety program, role of computers in quality assurance 79−63765
criticality safety quality assurance, need for exptl. studies 79−63770
criticality safety research, regulatory history and status 80−37492
criticality safety workshop for graduate students 77−37699
current nuclear power plant safety issues, 1980 conf. preview 80−95360
cylindrical shells, transient response to localised heat sources, thermal displacement and stresses 80−13538
Czechoslovak Research Institute activities, safety, waste disposal and personnel training *(Slovak)* 80−83188
damaged fuel element detection and location at Atucha nuclear power station 79−89460
DC power failure following AC power failure 78−78483
debris bed and sacrificial materials interactions at high temperatures 79−85612
debris bed dryout obs. during D-3 expt. 79−85597
decision analysis in safeguarding special nuclear material 78−82485
decommissioning, alternative methods and regulations 79−54573
decommissioning, cost anal. for complete removal 79−67904
decommissioning, French experience rel. to safety *(French)* 80−13965
decommissioning, main problems 80−676
decommissioning nuclear reactors to safe condition, Windscale AGR work 79−26547
decommissioning of commercial power reactors, environmental, economic and sociological effects 79−67901
decommissioning of commercial power reactors, technical feasibility, cost, environmental effects 79−67902
decommissioning of power reactor, NRC regulations 79−67905
decommissioning of PWR power station, safety, cost and occupational radiation exposure estimates 79−67903
decontamination by liquid waste elimination without reactor defuelling, CAN-DECON process 80−73943
defective fuel rods, behaviour under continued reactor operation 79−30915
defective fuel rods ultra sensitive detection with low core burn-up, method 79−45374
departure from nucleate boiling ratio safety limit to modelling parameters in COBRA IIIC/MIT 80−73901
design and construction, safety and reliability criteria, especially pressure boundary components 79−18009
detection of flaws in metal during operation, review 78−17343
differential pressure, local void fraction probe, design and operational evaluation 79−49778
digital computer applications in reactor instrumentation and control 80−106134
digital radiation monitoring, plant-wide systems, design alternatives 79−41082
digital radiation monitoring system, signal processing by distributed microcomputer data modules 79−59279
dispersal mechanism test facility, Doppler coeff. optimisation 77−46339
dispersal mechanism test facility, fuel dispersal anal. 77−42136
dissociating N_2O_4 power plants, safety and accident response *(Russian)* 79−31066
district heating, safety study for BWR heating and power station 78−62600
district heating plant, safety 80−767
DNB open core algorithm for on-line thermal margin evaluation 80−27782
Doppler effect measurement technique 77−50232
Doppler feedback use in control rod drop transients, Maine Yankee expt. 80−68895
DOT 3.5, use in fast power reactor shield configuration calcs. 80−68749

fission reactor safety continued
Dounreay fast reactor, overheating, prevention by natural circulation, experimental investigation report 80−47598
Dounreay PFR, plant improvements 80−57933
Dounreay test reactor, fast breeder test experience 80−86961
downtime distrib. in reliability theory for single repairable component, time structs. 78−89959
dryout, premature in conventional and nuclear power station evaporators, model 78−94120
dryout heat fluxes in debris beds cooled at the bottom and having subcooled liquid at the top 80−13652
Dungeness A, radiation and contamination control 80−5386
Dutch reactor safety studies, Rasmussen report eval. *(Dutch)* 79−81016
dynamic response to earthquake, aircraft impact, soil structure interact. 79−3208
dynamic safeguards accounting and material control via modern estimation methods 77−34417
dynamic simulation of the Gentilly-1 reboiler system 78−82439
earthquake computations, reactor installations 78−25336
earthquake frequency/magnitude prediction for selected surface regions 79−16415
earthquake response spectra 78−41871
earthquake response spectrum amplitudes, probabilistic computation 79−8610
earthquake response spectrum estimation from stimulated spectrum 79−686
earthquake site response anal., construction of smooth site dependent spectra 79−76086
earthquakes, records, optimal digitisation 77−91044
earthquakes, structural anal. of lifting-off 79−596
EBR II, Cs control by C getter 80−13648
EBR II, transient testing and simulation for LMFBR plant dynamic modelling 79−54558
EBR-II, duct dilation expts. 79−93702
EBR-II, dynamic response of ducts to press. pulses, expts., finite element calcs. 77−3124
EBR-II, exptl. determ. of decay power 79−85652
EBR-II, mixed-oxide fuel pins, results from expt. F11A after cladding break 79−67861
EBR-II, Na-water, leak detection system 78−78484
EBR-II, neutronics design of safety research modification 79−30990
EBR-II, operating limits for subassembly deformation 78−21714
EBR-II, wake and dispersion models rel. to released material 77−91186
EBR-II anomalous reactivity meter 77−42114
EBR-II breached fuel element experience, safe reactor operation 79−9736
EBR-II cover-gas cleanup system 79−97874
EBR-II fast transient facility, physics design 77−46336
EBR-II preparation for breached-element operation, safety concerns 79−9792
EBR-II primary system piping evaluation for safety research modification 79−9785
EBR-II reactor shutdown system upgrading, safety features 79−9796
EBR-II secondary Na network anal. for press. pulses from leaks of water or steam 77−54328
EBR-II slow transient tests, environmental tailoring 80−23009
EBR-II steam generator duplex tubing, US inspection 80−32379
EBR-II transient facility, thermal anal. of driver subassemblies 77−42134
ECC reflood characts., effect of bottom injection location, SUNYAB/EPRI program 79−49726
ECC system, treatment of water packing effects [in fission reactors] 79−89401
ECCS, flooding phenomena with condensation 79−89429
ECCS analysis with decay-heat generation and inlet subcooling 79−89434
ECCS top spray, restrictive effect of ascending steam on falling water 79−49704
education at Northwestern Univ. 78−58376
educational courses at UCLA 78−58377
educational module on nuclear reactor safeguards and waste management 80−36802
educational programme at Purdue 78−58380
elastomeric seals for nuclear service, selection 78−46152
electrical and mechanical equipment, improved seismic tests, research needs 78−94053
electrical auxiliary systems, safety design for AGR's 80−57934
electrical equipment, qualification concept 80−57883
electrical power supply, safety requirements, emergency supplies 80−52762
electrical supply system performance, reliability of protection and control systems 80−52761
electrical system design for future AGR power stations 80−57935
electricity supplies for safety system, German Regulation KTA 3701.1 *(German)* 80−37466
electronic system of power-station control with modules and distributed software based on controbloc elements *(French)* 79−76110
electronics in nuclear science and technology 80−9347
elementary catastrophe theory modelling of Duffing's equation for seismic excitation of nuclear power facilities 79−31240
EM instruments for use in liquid sodium, theoretical anal. 78−54857
emergency cooling model validation by Loss of Fluid Test Facility 79−80981
emergency cooling of a reactor with coolant dissociation *(Russian)* 79−59157
emergency cooling systems, transient thermal stresses, appl. to circuit integrity 77−6544
emergency core coolant injection, alternative concepts 78−21694
emergency core cooling system motor operated valves, failure mode anal. 78−54866
emergency core cooling system motor operated valves, failure criteria 78−70592
emergency medical assistance programmes for nucl. power reactors 78−53532
emergency monitoring procedures at CEGB stations, UK 77−54322
emergency planning and preparedness 80−57887
emergency protection drive, optimum ratio between operational component times 78−82474
emergency reactor cooling, mathematical models and methods *(Russian)* 79−17975

fission reactor safety continued
Emergency Response Planning and Preparedness Training Programmes, USA 78—57079
environmental effects from nuclear energy, effects of small radiation doses 79—2312
environmental impact of nuclear fuel cycle, monitoring and control 79—57504
environmental protection, radioactive waste from power plants in USSR 79—26601
environmental protection, reactor safety and waste handling *(Hungarian)* 80—91224
environmental protection in Hungary *(Hungarian)* 80—91225
equipment qualification for dynamic loads 80—99233
EURDYN, nonlinear transient dynamics programs for fast reactor safety 80—91234
EURDYN-1M, containment and fuel subassembly analyses for fast reactor safety studies 80—52772
EURDYN-1M, safety studies on LMFBR, computer program 80—99267
European in-pile investigations of fast breeder reactor safety *(French)* 79—26653
European Nuclear Conf., Hamburg, Germany, May 1979 79—97841
evaporative removal of Na from components 79—93735
evaporator, vertical U-tube type, premature bend dryout phenomena, wall temps. 77—61499
event tree construction by AUTOET 1 computer code 78—17379
fail-safe logic elements for use with safety-channel trip comparator 77—65277
failure analysis and failure prevention in nuclear elec. power plants 77—79450
failure location algorithm for complex networks 80—99228
failure probability distrib. from observed failure data, beta distrib. 80—63335
failure rates of components, plant specific risk studies, data specialisation, Bayes' theorem 80—47601
failures modes of alternative containment designs following postulated core meltdown 77—54329
Farley Nuclear Plant Data Link System 79—9797
fast breeder reactor generating station, engineering technology aspects *(German)* 79—54567
Fast Burst Reactor, failure analysis of burst stainless steel rod adaptor 77—54307
fast commercial reactor, hypothetical disruptive accidents in the core *(Spanish)* 79—45357
fast neutron criticality monitor, response to prompt critical bursts 80—63398
fast neutron source reactor (YAYOI), pulsed operation improvements, with POS5 as reactivity injector *(Japanese)* 80—9328
fast power reactors, fuel pin viability in LOCA 79—76090
fast reactor, effect of radiative heat transfer on thermal fluid behaviour of molten UO_2 79—93783
fast reactor, EM temp. sensor in liquid sodium, performance 78—700
fast reactor, HCDA, heat conduction calc., method of weighted residuals 79—635
fast reactor, time series analysis and forecasting for ANL TREAT expts. 78—13289
fast reactor, UO_2 dynamic vaporisation, rate effects 79—31034
fast reactor, UO_2 rate-dependent heat capacity 79—31035
fast reactor boiling detection by noise analysis 79—13449
fast reactor ceramic fuel-steel system, freezing of flowing liquid in melting tube, simulation expt. 79—30981
fast reactor cladding material, transient burst tests 79—93770
fast reactor containment, COVA program for computer code validation 78—41833
fast reactor containment safety, study using computer code SEURBNUK-2 78—33260
fast reactor coolant blockages, detection by temp. noise tech. 79—30899
fast reactor core operation, safety aspects *(French)* 79—97864
fast reactor disassembly, fuel vapour expansion work energy calcs., effect of eqn. of state uncertainties 78—8940
fast reactor fuel development, safety considerations 79—26649
fast reactor hypothetical accidents, review of fission gas effects 79—67900
fast reactor safety, Na boiling expts. *(Italian)* 79—9764
fast reactor safety, thermohydrodynamics code TWOPOOL, modelling and numerical methods 79—59195
fast reactor shields, neutron transport 77—61481
fast reactor test loop anal. of severe accidents 77—3142
fast reactor transient overpower accident, cladding loading by two component gas 79—31038
fast reactor whole core accidents, fission products role 78—54854
fast reactors, calc. of core burnup effect on dynamic behaviour 77—23173
fast reactors, programme and state of work in the Soviet Union 79—643
fast reactors, track detector determ. of fuel contamination of primary Na coolant 80—32394
fatigue life prediction, defn. of safety factors 79—6732
fatigue loading, growth of underclad flaws 79—22429
fault tree anal., modular representation 78—78480
fault tree anal. code SUPKIT *(Japanese)* 78—54847
fault tree anal. using Monte Carlo and anal. methods *(Spanish)* 80—57870
fault tree analysis, development of DICOMICS-TWIN self-adaptive algorithm for minimal cut sets determ. 78—17380
fault tree and reliability analysis, modular decomp., PL/1 program 78—17381
fault tree and reliability relationships for analyzing noncoherent two-state systems 80—47600
fault trees, methodology for computer-aided construction, nuclear system appl. 78—37412
FBR, above-core structural response to molten core disassembly 79—30992
FBR, attenuation of HCDA work potential by heat transfer 79—93773
FBR, Clinch River, computer anal. and models 78—13260
FBR, commercial demonstration reactor, radiation damage shielding 80—23178
FBR, comparison of computer code predictions with COVA expts. under postulated accident conditions 79—30995
FBR, debris bed dryout, effect of particle size distrib. and segregation 79—49668
FBR, designers' viewpoints 77—14243

fission reactor safety continued
FBR, dispersive potential of irradiated fuel during thermal transient 79—31037
FBR, dynamic elastic response of subassembly ducts to impact loading, finite element anal. 80—18536
FBR, effects of material properties on the dynamic response of pressure-loaded core subassembly wrappers 79—49756
FBR, energy increase from bubble collapse following recriticality in large molten pools 79—31023
FBR, failed-fuel detection system *(French)* 79—97858
FBR, fuel melt down, fragmentation requirements for detonating vapor explosions 79—49753
FBR, HCDA, 2Z 79—49669
FBR, HCDA, retention of molten core debris pools in composite sacrificial beds 80—47643
FBR, in-pile testing, nonprototypic effects due to fuel length and number of pins 79—30988
FBR, modelling molten fuel-coolant interaction, INTER and CEFRA *(Czech)* 78—66352
FBR, molten fuel interaction with Na in active zone 77—54333
FBR, N_2O-Na leak detection system 77—38374
FBR, neutron shielding, integral expt. and data correlation 78—5057
FBR, potential accident anal., design implications 77—23234
FBR, role of fission gas swelling and release in reactor accidents 80—57854
FBR, safety strategies of the different phases of a hypothetical accident *(Italian)* 79—63754
FBR, SAS3D prediction of intrasubassembly boiling incoherence, multipin boiling model 79—49662
FBR, simultaneous freezing and melting in finite media 80—620
FBR, slug impact and coolant spillage anal. using hybrid Lagrangian Eulerian method 79—30993
FBR, space dependent simulation of transient behaviour using KINTIC-2 code *(German)* 80—83182
FBR, thermal-hydraulic flow fields, stochastic processes 79—30991
FBR, types, cooling and safety aspects *(German)* 79—54587
FBR, US development, safety aspects 78—86671
FBR, void reactivity effects on hypothetical core disruptive accident excursion energy 79—31024
FBR accident, TRANSIT computer code for mechanistic analysis of transition phase 77—46328
FBR containment response to HCDA, effect of struct. components, Eulerian hydrodynamic anal. 80—23014
FBR core disruptive accident, response of upper internal structures, finite element computer anal. 80—47645
FBR core seismic anal. by assumed-mode math. modelling 79—89357
FBR core surveillance and protection systems *(French)* 79—76099
FBR current status and development trends, review 79—22374
FBR development and safety program in UK 80—47564
FBR excursion model, ICECO predictions 77—42028
FBR film boiling destabilisation, thermodynamic prediction of temp., and rel. to vapour explosion phenomena 79—49667
FBR fuel clusters, Na boiling, corrective action 79—71913
FBR fuel pin failure, fuel porosity and crack effects on transient overpower analysis 80—71760
FBR fuel pin safety expts. at SLSF, centerline fuel thermocouple performance 80—102283
FBR HCDA, convective heat transfer correlations for molten core debris pools growing in concrete 80—83196
FBR HCDA, fluid-struct. interaction anal., evaluation of computer code 80—23015
FBR HCDA, one-dimensional penetration of molten UO_2 into substrate limestone concrete [following FBR HCDA] 80—47640
FBR HCDA, simulation of containment materials interaction 80—47642
FBR HCDA, structural response of the upper internals, finite element anal. 80—18537
FBR international development, influence on German policy *(German)* 80—18586
FBR LOF accident, first visual in-pile fuel disruption experiments 79—49747
FBR LOF accident, role of fission gas and fuel melting on transient fuel response 79—59191
FBR LOF transient, molten fuel containment anal., for sodium loop safety facility expts. 80—47651
FBR meltdown, post accident heat removal anal., turbulent convection and interfacial freezing 79—49670
FBR meltdown, post-accident heat removal, heat transfer mechanism associated with immersed melting surfaces 79—49671
FBR mixed-oxide fuel crusts, thermal fracturing and the effect of creep 79—49698
FBR post-accident heat removal anal., convective heat transfer correlations for molten-core debris pools growing in concrete 80—47559
FBR probabilistic accident anal. 77—83054
FBR R and D, conf., Lucerne, Switzerland (Oct. 1979) 80—46735
FBR safety, applicability of Safety Research Expt. Facilities to alternative fuels 79—49773
FBR safety anal. modelling of fission gas behaviour 80—748
FBR safety analysis, expts. on hydrodynamic aspects of volumetric boiling of molten fuel-steel mixture 80—47652
FBR safety analysis, multicomponent hydrodynamics, implicit Eulerian technique 79—634
FBR safety and economics, leak detection, cooling, waste disposal 80—63303
FBR safety calculations, numerical mixing errors in Eulerian calculations of coupled thermohydrodynamic motions 80—47553
FBR safety expts., thin film fission thermocouples for energy deposition meas. 80—47658
FBR safety related slowing down problems 78—678
FBR safety test facility, conceptual design 77—46337
FBR safety test facility, kinetic performance 77—42135
FBR SNR 300, design information, risk factors *(German)* 79—26727
FBR TOP accident porous fuel blockage in core, theoretical anal. 79—49673
FBR transient fuel behaviour maps, fuel response to thermal transients 80—57926
FBR transient fuel behaviour maps, fuel response to thermal transients 80—68874
FDR type reactors, transient anal., neutron power and temp. form factors, depend. on time and power level 80—83178
Federal radiological emergency response planning and preparedness activities 78—46147

fission reactor safety continued
feedwater systems, auxiliary, fault tree anal. 80−63332
FFTF, containment response to postulated core meltdown accidents 80−32381
FFTF, HCDA, NASTRAN nonlinear dynamic transient accident anal. 77−42133
FFTF, interassembly flow redistribution at natural circulation conditions 79−85654
FFTF, natural-circulation testing 79−49676
FFTF, potential gas entry after postulated pipe rupture 79−85657
FFTF, TOP anal. using Los Alamos failure model 80−13672
FFTF, transient overpower accidents, effect of intrasubassembly incoherencies 80−32373
FFTF containment building integrated leak-rate test 80−13680
FFTF design studies, simulation of hot-leg piping ruptures and loss-of-flow events 79−49677
FFTF fuel failure, cover-gas monitoring system 78−4998
FFTF fuel failure monitoring, in-core gas release capsule development 80−13681
FFTF loss-of-electric-power transient response, natural circulation tests, pre-test simulation using SSC-L code 80−42836
FFTF loss-of-flow accident, integrated FUMO/SAS3A (FUSS) neutronics update system 79−31009
FFTF TOP analysis, uncertainty in accident consequences calculated by large codes due to uncertainties in input 80−78413
FFTF upper-plenum mixing and stratification, comparative studies 80−583
FGR, water-vapour velocity transient meas. by cross-correlation anal. *(German)* 77−62312
fifth international conference on reactor shielding, review 78−29599
film boiling and vapour explosions from small spheres 80−18543
fire barriers, analytical hazards analysis 80−18534
fire hazard assessment 78−50269
fire occurrences, Bayesian prediction model 80−18527
fire protection policy 77−46356
fire risk assessment 80−23002
firebricks for concrete floor protection from molten UO_2 80−18438
fission energy generation in vol. boiling pool systems, microwave heating simulation 80−18386
fission gas, modelling transient behaviour 79−97826
fission gas behaviour in fuel pins prior to transient testing 79−30921
fission gas bubbles, nonequilibrium, relaxation times 77−46239
fission gas effects in irradiated fuel rods operated in film boiling at high power 79−49744
fission gas re-solution, comparison of single knock on and complete bubble destruction models 78−82455
fission gas release in charcoal spill accident 77−50262
fission product γ-radiation intensity in short operation nuclear reactors 79−67823
fission product release, evaluation of population hazards 77−14250
fission product release, inclusion in AVR fuel cycle strategy program *(German)* 79−74576
fission product release calcs. from reactor containment building 77−79449
fission products decay heat, development of revised ANS standard 79−49742
fission products in primary coolant, possible contribution from U impurities in fuel cladding 79−63751
fission reactor, FAXMOD anal. of creep and sheath ballooning 80−42759
fission reactor safety, two-phase flow, analytical simulations for safeguards design 78−46143
flaw detection probability estimation from inspection data 79−24712
flexible dual-containment approach design and licensing 79−13400
floating nuclear plant, shield design features 78−21777
floating power plant, environmental and safety aspects 78−21750
flow boiling anal., numerical standards 77−79448
flow-induced control element movement, expt. investigation using noise analysis 80−788
flow-induced structural vibrations anal. 80−42795
fluid dynamic transient analysis using ASWR method with staggered meshes *(German)* 80−83176
fluid surrounding structural members, dynamic behaviour 80−48667
fluid surrounding structural members, dynamic behaviour 80−48668
fluid velocity meas. by radiation intensity correlation 77−75996
fluid-saturated porous layer with heat source, thermal convection onset 79−13406
fluid-structure finite element method for anal. of reactor safety problems 77−3128
fluid-structure system dynamics, reactor safety anal., computational algorithms 77−71669
fluidised bed oven criticality for HTR fuel elements *(German)* 77−18656
Forsmark 3 plant, reactor safety study 80−18516
Fort St. Vrain HTGR, afterheat predictions and meas. 80−68891
fracture mechanics of reactor primary system under operating and accident conditions 78−66342
fracture safe design, appl. of elastic-plastic fracture mechanics params. 78−30241
French regulatory requirements and administrative practices in nuclear installation safety *(French)* 79−26623
French safety reliability methods for power plants *(French)* 79−26644
FTR, control rod failure detection 77−42144
FTR, criticality expts. with concrete reflected fuel pins in water 80−78410
FTR, mechanical failure of subassembly ducts and its effects on transition-phase analysis 79−85667
FTR, strain rate effects in transient overpower cladding failure analyses 79−85660
FTR fuel pins with solid neutron absorbers, criticality expts. 80−18476
FTR subassembly failure pattern under transient overpower accident 79−31006
FTR TOP accident, effect of power skew, computer code development 79−54481
FTR-type fuel motion in TREAT transient overpower test E6 79−36366
fuel accounting and safeguarding, spent fuel bundle counter for 600 MW CANDU reactor 80−63269
fuel can designs for Safety Test Facility, structural analysis 77−46310
fuel cladding, three-regions rewetting model with decay heat generation and inlet subcooling 80−22965
fuel cluster tests in NSRR 79−22369

fission reactor safety continued
fuel cycle, radioactive material release, cost/benefit anal. 79−26605
fuel cycle and radioactivity, regulatory control in Canada 79−26620
fuel cycle facilities, advantages of on-site facilities 79−31118
fuel cycle plants, radioactive discharges, limits 79−26779
fuel cycles, safeguards 78−82446
fuel damage impact on plant operations 80−686
fuel design limit for post-DNB operation 80−572
fuel disassembly experiments using the capacitor discharge vaporization (CDV) technique 79−85598
fuel element damage at Three Mile Island Nuclear Power Station, thermodynamic aspects *(German)* 79−93739
fuel elements, cracked, gas-filled, temp. distribs. calc. 78−78446
fuel elements, with cladding, thermal shock *(Italian)* 80−27774
fuel energy extraction without reprocessing to separate Pu, alternative methods 79−26675
fuel failure, relating uncertainty allowance in operating limits 80−13721
fuel failure behaviour of unirradiated fuel rods under reactivity initiated accident conditions *(Japanese)* 79−30955
fuel failure criteria, uncertain benefits 80−574
fuel failure detect., UO_2-loaded Na in-pile loop 78−37417
fuel pin imaging, appl. of one-dimens. coded apertures 78−45746
fuel pin rupture detection system using meas. of time differential of acoustic emissions 80−102282
fuel pin rupture in FBR, implicit compact difference method for solving linearized fuel sweepout equations 79−89355
fuel pins, computer controlled meas. 80−5300
fuel power detector for CANDU power reactors 79−41022
fuel reprocessing in HTGR, safety aspects of solvent nitration 78−86650
fuel rod, heat transfer code for calc. effect of asymmetric geometries 79−49743
fuel rod anal., statistical version of URANUS programme 80−42749
fuel rod arrays, radiative heat transfer, Monte Carlo method, temp. distrib. 78−78447
fuel rod ballooning prevention 78−17290
fuel rod bundle, dry patch spreading, post dryout temps. 80−42741
fuel rod gap conductance uncertainties deduced from fuel centreline temps. 77−46308
fuel rod gas pressure meas. during LOFT, sensor description 80−57876
fuel rod geometry changes, mech. interactions calcs. 79−40993
fuel rod modelling techniques, best-estimate calc. 79−17984
fuel rod rewetting following LOCA, analytical model 77−46240
fuel rod thermal characteristics, on-line simulation by elec. heated rod 77−46209
fuel rod thermal stored energy, calculational uncertainty anal. 80−47609
fuel rods, defect detection 78−86640
fuel security, use of gamma active spikants for proliferation deterrence, effect on fission product buildup 79−93716
fuel sweepout in HTOP accident, system hydraulic effects 79−85670
fuel thermocouples and liquid-level probes for core monitoring 80−99239
fuel-coolant interactions, role of Rayleigh-Taylor flow instabilities 79−17983
fuel-coolant interactions in a shock tube geometry 80−13660
fuel-sodium interactions, effects of finite mixing time and noncondensable gas 78−17331
fuels vapour pressure measurement UO_2 and $(U, Pu)O_2$, for safety anal. by laser techniques to 5000K 80−13591
FUGEN plant dynamic tests 80−68894
full-scale reactor safety experiments performed in the Marviken power station, Sweden 79−26633
fusion and fast breeder reactors, a comparison, book 78−78430
fusion-fission hybrid blanket designs, accidental criticality 78−778
fusion-fission hybrid power reactor, blanket cooling under LOCA conditions 78−775
fuzzy set theoretic approach to systems analysis 78−17352
gamma exposure rate, real time simulation by puff model 80−47618
gamma rays, 6 MeV, penetrating shielding materials, energy and ang. flux density spectra 80−63393
gas bubble adhesion to heat transfer surfaces 79−89375
gas cloud explosion pressure loading for reactor secondary containment 79−49789
gas discharge from failed fuel pin, model for calc. of press. in duct 78−675
gas tap system for fuel element failure anal. 79−85627
gas-cooled fast reactor safety 79−26654
gas-cooled reactors, importance of development 80−5214
gaseous fission products, continuous determ. of content in reactor loop 79−30905
gassy two-liq. pool., hollow sphere formation, LMFBR simulation 77−61518
gate values for nuclear facilities, high leak tightness and large diameter 79−36347
GCFBR, seismic model of core support structure 77−3184
GCFR, 1000 MW, calc. of depressurisation and flow coast down accidents 78−50274
GCFR, 1000 MW(e), design and safety aspects 77−18672
GCFR, 1000 MW(e), reliability anal. of decay heat removal system 77−14223
GCFR, borax ($Na_2B_4O_7$) internal core catcher 78−58372
GCFR, effect of accidental steam entry on reactor parameters 78−33277
GCFR, fission gas release and molten fuel motion for slow overpower transient 78−17369
GCFR, He-cooled, state of art and development trends *(Czech)* 78−29636
GCFR, prototypic grid-plate shield confirmation experiment 79−54562
GCFR, sensitivity of reactivity effects to reactor model choice in safety anal. 78−13305
GCFR, thermal radiation effects on subassembly wall failure 78−8938
GCFR, transient anal., systems simulation methods, development and validation 79−54486
GCFR, transient analysis of closed gas turbine cycles, TUGSIM-10 computer code 77−18675
GCFR, venting system of fuel element, activity release anal., operating and accident conditons 77−23226
GCFR benchmark shielding expts. 79−9902
GCFR cladding motion simulation in concurrent flow 79−85614
GCFR configuration, simulated, evaluation of full-core steam flooding worth 78−33276
GCFR core and core support struct., seismic model test 78−41869

fission reactor safety continued
- GCFR core support structural assembly, seismic response via modal synthesis 78−89942
- GCFR critical assemblies, ^{238}U Doppler reactivity worth meas. 77−54336
- GCFR critical assembly, reactivity worth of steam flooding 77−54335
- GCFR demonstration plant reactor shielding system design 80−47560
- GCFR fuel assembly thermal-hydraulic anal., modification of COBRA code 80−588
- GCFR grid-plate shield design experiment 79−59226
- GCFR inherent and design related safety features 77−14244
- GCFR LOF accident, natural convection effects in blocked fuel assembly 79−49755
- GCFR programmes, status 77−18647
- GCFR reactivity insertion mechanisms 77−14245
- GCFR with N_2O_4 coolant, power plant nuclear and chemical safety 79−30969
- generation HCDA model for particle-size distribs. for condensed UO_2 vapour 78−13295
- German power stations, assessment of accident risks 80−18517
- German reactor safety study, consequence model 80−18524
- German Reactor Study review 80−37479
- German Risk Study; social risk assessment *(German)* 80−57866
- globe main steam isolation valve unbalanced forces and novel actuator design 78−50288
- Go-ri nuclear power plant, containment integrated leak rate test *(Korean)* 78−54851
- graphite, failure criterion, J-integral critical value 78−84999
- grid spacers, effect on post critical heat flux heat transfer 80−27732
- guard line circuits dual microprocessor system, decision-making and self-testing 80−57901
- Harrisburg nuclear power station failure, safety and control *(Norwegian)* 79−81017
- Harrisburg reactor accident in 1979, lessons to be learned *(German)* 80−91233
- hazard management, aspects of the historical, philosophical and mathematical background to the statutory management of nuclear plant risks in the United Kingdom 80−5293
- HCDA, bubble worth variation in molten cores 80−68854
- HCDA, coupled hydrodynamic and struct. response, splitting method 77−74958
- HCDA, debris transport in horizontal piping 79−93784
- HCDA, exptl. anal. of internally heated liquid pool in solid bed 78−29549
- HCDA, natural convection heat transfer in fuel debris bed cooled at top and bottom 79−93785
- HCDA, neutronics and hydrodynamics equations, energy release, DISCAL code 80−68842
- HCDA, radiological consequences, attenuation due to radiative cooling 78−13296
- HCDA, REXCO code, comparison with flexible vessel expts. 78−70618
- HCDA, vapour condensation from rising bubble, effects of internal circulation velocity and noncondensable gas 78−50258
- HCDA condition, fuel motion measurement, time-resolved coded aperture imaging system 78−45764
- HCDA due to transient overpower, model for prediction of press. in core and upper plenum 78−8926
- HCDA experiments on simple FFTF models, LMFBR safety evaulation programme 77−3130
- HDR, numerical investigation of radial mixing capabilities in strongly buoyancy-influenced vertical, turbulent channel flows 79−93751
- health hazards, for teachers 79−35506
- heat exchanger tube, oval straight, plastic collapse under external pressure 79−10508
- heat exchanger tubes, US inspection by rotating search units method 79−9667
- heat transfer finite difference computer programs 79−14221
- heat transfer from round-bottom pool with internal heat generation, expt., LMFBR appl. 79−13470
- heat transfer problems 77−65276
- heat transfer problems 78−41842
- heat transfer tube failure propagation due to Na-water reaction in steam generator 79−6748
- hermetically sealed valve for the safety systems of a nuclear power station *(Russian)* 78−89952
- HFBR, detection and identification of failed fuel elements 78−21708
- HFR test reactor, HIP-TEDDI code for neutron flux calcs. 79−3223
- high efficiency particulate air filters, efficiency testing at large pressure transients rel. to nuclear facility safety 79−81020
- high flux test reactor, MARIA, nuclear power research programs *(Polish)* 79−93693
- high heat fluxes associated with interaction of concrete with molten core material 78−17385
- Hinkley Point B, AGR radiation protection, design criteria and operating experience 80−27832
- Hinkley Point B AGR station computer control system, performance review 79−89457
- hot fuel examination, sodium loop safety facility, loop disassembly system 79−9727
- hot water leakage from first loop, 22.8 MPa initial pressure, flow characts. 78−66357
- HTGR, consequence anal. of hypothetical accidents, core heatup and afterheat removal 78−58381
- HTGR, control rod ejection accident, comparison of one- and two-dimens. models 78−13279
- HTGR, critical expts. on enriched-U graphite moderated cores, power, reactivity, control rods *(Japanese)* 80−47594
- HTGR, Fort St. Vrain, operation of safety features 78−21717
- HTGR, fuel failure anal. following LOCA, post-accident temp. response 78−13276
- HTGR, inert gas release core-survey calc. 79−67908
- HTGR, maximum pot. hazard of ultimate accident sequence initiated by PCRV leak 78−13278
- HTGR, nonlinear dynamic anal. of prismatic graphite fuel elements, response to seismic excitation 80−99237
- HTGR, Peach Bottom site, distrib. of ^{137}Cs and other fission products in fuel elements 78−13274
- HTGR, Peach Bottom site, radionuclide distrib. in primary coolant circuit 78−13275
- HTGR, startup test techniques 78−21706
- HTGR, T contamination of product gas 80−13590

fission reactor safety continued
- HTGR, thermodynamic correlations for accident anal. *(German)* 78−25315
- HTGR, unlimited core heatup, fission product release, hypothetical accident anal. 79−6754
- HTGR coated-particle fuel, irrad. performance determ. by irradiated microsphere gamma analyzer (IMGA) 79−54543
- HTGR containment, layering and combustion following depressurization accident 78−13277
- HTGR core, 2-D vibr. test and simulation anal. for vertical slice model *(Japanese)* 78−58328
- HTGR core, seismic anal. 80−32327
- HTGR core auxiliary cooling system, failure analysis 80−22964
- HTGR core during transient temp. excursion, fission product release, computerised analysis *(Japanese)* 78−82467
- HTGR core heatup, PCRV integrity, thermal anal. model 79−49735
- HTGR core seismic response, analytical model 80−13953
- HTGR cores, transient thermal hydraulic anal., RETSAC code 77−46246
- HTGR fission product diffusion through core materials during LOFC, exact analytical soln. 80−47554
- HTGR fission product release following LOCA 79−13457
- HTGR fuel cycle summary and recent developments 80−728
- HTGR fuel element failure mechanisms and fission product release 80−13586
- HTGR fuel performance for hypothetical core heatup conditions 80−47579
- HTGR hypothetical accidents, consequences following breach of primary circuit and safeguard failure *(German)* 78−58390
- HTGR monitoring and control instrumentation, special needs 78−734
- HTGR nonlinear core struct. with constrained reflector blocks, dynamic response 77−46247
- HTGR PCRV depressurisation accident, anal. of gas circulation using HAZARD code 79−54561
- HTGR primary coolant system depressurisation accident, expt. and numerical anal. 80−775
- HTGR refuelling, equipment safety, gamma dose meas. 80−47668
- HTGR risk assessment, operator actions, event and fault tree anal. 80−63330
- HTGR with closed-cycle gas turbine, technological assessment 79−54490
- HTR, actinide production reduction by use of Th-U fuel cycle *(German)* 80−9386
- HTR, admissibility of Co as alloy constituent in primary cooling circuit components *(German)* 78−25294
- HTR, direct cycle, radiation exposure during maintenance and repair of He turbine 80−18563
- HTR, expt. JAERI, safety anal. of fission product behaviour and hypothetical accident *(Japanese)* 78−66330
- HTR, hypothetical depressurisation accident, environmental consequences 80−744
- HTR core, radiant heat transfer following failure of afterheat removal system 80−773
- HTR core cavity, accessibility and in-service inspection 80−18562
- HTR pebble bed heat transport, particularly radiation, in hypothetical accidents *(German)* 79−49791
- HTR power plant control 77−14262
- HTRs, large, shutdown system strategy *(German)* 79−97818
- human error, characterisation and quantification, probabilistic analysis staff program 80−47660
- human errors in high stress situations, data and assessment 78−17374
- human factors, normal operation and emergency procedures, errors, safety, maintenance, working conditions 80−63328
- human factors, safety system problems and risk assessment 80−22968
- human factors engineering 78−21711
- human factors in nuclear power plants, review 79−89463
- human health and safety, nuclear energy industry 77−25508
- HWR, accident prevention, effect on environment 78−29613
- HWR, charact. of Pt self-powered flux detectors 77−65282
- HWR, explosive rupture of power channel pressure tube 78−70605
- HWR, pressure tube reactor safety 77−67842
- HWR, safety research and development 78−29614
- HWR, shutdown heat removal systems, reliability fault tree anal. and β-factor method 80−63331
- hydraulic pressure pulses with structural flexibility 77−50266
- hydrodynamic motions, value of distributed particle in cell techniques 79−59196
- hypothetical meltdown accident, large-scale steel melt/concrete interactions test 78−17387
- IAEA's activities in safety codes and nuclear safeguards 77−65347
- IAEA nuclear safety standards program for protection, electric, instrumentation systems 79−45365
- IAEA safety codes and guides for thermal neutron power plants 79−26616
- ICEPEL code comparisons for flexible pipe elbow loop 79−49772
- ignition and extinguishment in simulated LMFBR accident conditions 78−8932
- impulse-initiated gas release triggering vapour explosion 78−17384
- in-core molten fuel pool expt., heat flux and struct. ablation 79−13407
- in-house safety analysis capability at nuclear utilities 80−23013
- in-pile post accident heat removal facility, feasibility study 79−49774
- Inconel, pressure vessel bottom, subcritical crack growth in ligament between instrumentation rods 79−22428
- Inconel 600, stress corrosion cracking in primary water 79−93728
- Indian Point Unit No.2 reactor vessel, detection and identification of loose object 80−18553
- industrial accident involving radiation exposure in Washington State, worldwide impact 77−3122
- industrial activities nearby causing hazards, deterministic and probabilistic studies 80−78408
- inelasticity and the ASME code 78−41815
- infinite cylinders, critical and subcritical, n multiplication factor, nuclear criticality safety 78−78442
- information at Nuclear Safety Information Center, products and available services 78−17545
- inservice inspection, power plant design and fabrication 78−78451
- inservice inspection of nuclear power plants in Japan, appl.; problems *(Japanese)* 77−50255
- inspection practices and decisions for safety and availability 77−46304
- instructional programs at RPI, LWR and FBR appl. 78−58375
- instrumentation, EM compatibility and protection against EM interference 79−89465

fission reactor safety continued
- instruments qualification, impact of IEEE Std. (323-1974) 80–52753
- integrated PWR, anticipated transients without scram, calc. of dynamical behaviour 80–5250
- integrated safe shutdown heat removal system for LWRs 77–54330
- integrated safeguards system, fuel labelling and perimeter monitors 80–37536
- internal pressurisation in solid-mixed-oxide fuel due to fission gas release 77–83058
- international co-operation in nuclear safety in the framework of the OECD nuclear energy agency 79–71905
- international cooperation incentives in safety practices and standards *(French)* 79–26618
- International Electrotechnical Commission standards for reactor instrumentation and controls 79–45366
- international safeguards, research 78–82482
- intragranular fission gas behaviour model, dynamic, numerical integration, DIGRAS computer code 80–32345
- IRAN-1,2, plants, calc. of radioactive releases 79–18056
- irradiated fuel sipping, inspection, and repair at Point Beach Nuclear Plant 79–45384
- irradiation sources and units, fundamentals *(German)* 78–46180
- IRT WWER, use of thermometric fuel assembly in safety anal. 79–97837
- IRT-2000 fission research reactor, personnel radiation monitoring and reactor radiation charact. 79–71927
- Isar BWR power station, transient expts. during startup and initial operation *(German)* 80–83187
- isolation and relief valve/piping transient force anal. program 78–50287
- Ispra Research Centre activities, w.r.t. EEC policy 79–97770
- JAERI program, probabilistic risk assessment techniques in Japan 80–18515
- Japan Atomic Energy Research Institute, reactor safety research 77–65305
- JEN, Spain, nuclear power development *(Spanish)* 77–38343
- Joint Research Centre of the Commission of the European Communities in safety research 77–65299
- JOYO experimental fast reactor, radiation protection monitoring programme 80–57992
- JOYO experimental fast reactor, test and operational experience 79–97867
- JPDR primary piping cracks, coolant pressure boundary weld joint in service inspection 79–49706
- KNK II fast breeder, construction and aseismic design 79–97778
- KNK shutdown systems 79–97866
- KWU-LWR safety systems design 79–31086
- Kyoto University reactor, airborne radioactivity from primary coolant 80–22959
- large fast neutron reactor, safety requirements and options *(French)* 79–26647
- large-bundle LOCA expts., fuel rod ballooning probabilistic analysis 79–13462
- large-water reactor, TRAC-P1 post-test anal. of US standard problem 7 79–89433
- laser system for determ. of fission product release and distrib. in coated particles *(German)* 78–82403
- leak detection system operating experience 79–9808
- leakage rate testing of containment structures *(Spanish)* 80–47582
- LIMITS–a fast Monte Carlo code for system reliability 79–49783
- liquid cooled fast reactor HCDA, fluid filled vessel response to internal explosions 79–49771
- liquid level detector based on level sensitive transducer for PWR environment 80–57874
- liquid pools, vol. heated, transient boiling, convex flux relations, fission reactor safety 77–31340
- liquid pools, vol. heated, transient boiling non-convex flux relations, fission reactor safety 77–31341
- liquid-metal-cooled reactors, radionuclide trap in primary circuit 79–93768
- LMBFBR overpower accidents, mechanistic model of fuel flow regimes and fuel plateout 79–85615
- LMFBR, 1200 MW(e), comparison of SAS3D LOF transient anal. for conventional and nonconventional core designs 79–31039
- LMFBR, accident conditions, theoretical anal. of Na fire using SPOOL-FIRE code 77–14248
- LMFBR, accident progression for loss-of-heat-sink with scram 79–81022
- LMFBR, accident progression within secondary containment boundary 80–32368
- LMFBR, acoustic anal. from Na boiling tests using THORS bundle 6A 79–31033
- LMFBR, acoustic anal. of TREAT safety test R8 78–13290
- LMFBR, acoustic anal. on Na boiling expt. in FFM Bundle 3B, Test 4 78–13291
- LMFBR, acoustic resonances as means of blockage detection 79–93752
- LMFBR, acoustic surveillance of anomalous events 78–37397
- LMFBR, alternative core disruption accidents 79–9774
- LMFBR, analysis of in-pile MFCI experiments with carbide fuel 79–49754
- LMFBR, behaviour of H in liquid Na *(Japanese)* 79–49649
- LMFBR, boiling stability tests on THORS Na loop 78–37396
- LMFBR, BR-2, UO_2 behaviour for local cooling disturbances in in-pile Na loop 80–13542
- LMFBR, bubble collapse reactivity increases in boiling fuel/steel pools 79–31025
- LMFBR, bubble worth calcs. using probability table method 78–13306
- LMFBR, buoyancy-induced flow stratification in cylindrical plenum during reactor scram 77–46366
- LMFBR, calc. vs. exptl. temp. distrib. behind six-channel central blockage 79–31028
- LMFBR, CAMEL single-pin fuel sweepout test C2 79–30983
- LMFBR, chemical leak detection, effects of NaOH in Na 80–63326
- LMFBR, cladding meltdown phase for loss-of-heat-sink event during shutdown 78–8923
- LMFBR, Clinch River, assessment of containment response to hypothetical core melt-through accident 78–8928
- LMFBR, Clinch River, consequences of boiling in radial blanket due to hypothetical major pipe leak 78–8922
- LMFBR, Clinch River, humidity effect on burning rate of Na droplets, Fick's eqn. anal. 78–13297
- LMFBR, Clinch River, LOCA in one heat transport loop without reactor trip 78–8924

fission reactor safety continued
- LMFBR, Clinch River, material release for advanced fuels following hypothetical core disruptive accident 79–31065
- LMFBR, Clinch River Plant, pipe rupture simulation using DEMO code 78–8927
- LMFBR, Clinch River Plant, sensitivity for radiological consequences to var. in aerosol parameters 78–13294
- LMFBR, Clinch River Plant, system damage potential 79–31019
- LMFBR, cluster of core assemblies, CORA transient anal. 80–18389
- LMFBR, cold impurity trap regeneration in Na purifier 79–76091
- LMFBR, combined fuel and coolant motion under high-ramp transient overpower conditions 79–31003
- LMFBR, combustion of large Na pools, determ. of burning rate and flame struct. 80–47644
- LMFBR, commercialisation 77–38380
- LMFBR, comparison of REXCO and ICEPEL code calcs. with tests of plastically deformable pipes filled with compressible fluids 79–30994
- LMFBR, computation studies of cladding relocation dynamics after transient undercooling accident 78–13255
- LMFBR, computer model for ^{3}H transport and release 79–36371
- LMFBR, computer modelling of piping components for transient hydrodynamic structural response 78–74449
- LMFBR, condensation from large HCDA vapour-gas bubble onto structures 79–93774
- LMFBR, containment, safety anal., conf., San Francisco (Aug. 1977) 77–71664
- LMFBR, containment building response to HCDA, risk assessment, computer anal. 77–71678
- LMFBR, containment codes appl., response predictions in HCDA conditions 77–71670
- LMFBR, containment pressurisation by Na spray fires 80–32365
- LMFBR, control rel. to operational safety aspects 77–14251
- LMFBR, coolant cavitation in dynamic containment loading 80–32326
- LMFBR, coolant start of boiling detection by acoustic method 78–86646
- LMFBR, core meltdown event, transient containment response, inherent retention capability 77–71677
- LMFBR, core-disruptive accidents, neutronic and fuel element behaviour 80–32357
- LMFBR, detection of fuel assembly flow reduction in heterogeneous core 79–31032
- LMFBR, determ. of ^{137}Cs conc. in Na heat carrier 79–41043
- LMFBR, development areas 77–57737
- LMFBR, dynamic core deform. during local failure propag., subassembly expts., CORE-1 code 77–88244
- LMFBR, dynamic response of reactor vessel to HCDA 77–71674
- LMFBR, effect of cracks in fast neutron embrittled hexagonal subassembly ducts 78–74446
- LMFBR, effects of Na entrainment and heat transfer with two-phase UO_2 80–47596
- LMFBR, effects of Na entrainment and heat transfer with UO_2 vapour during HCDA 79–93775
- LMFBR, establishment of buoyancy induced natural circulation, CURL-L code anal. 79–49663
- LMFBR, expts. on extinguishing large quantities of burnina Na 79–41016
- LMFBR, failed fuel pin debris forming heat-generating blockage, heat transfer anal. 80–47648
- LMFBR, fast integral model for the transient analysis of a melting fuel pin 79–54552
- LMFBR, fast integral modelling of HCDA 79–26555
- LMFBR, feasibility of conducting a low ramp rate TOP experiment in TREAT 80–47655
- LMFBR, feasibility of using denatured ^{233}U diluted with ^{238}U 78–17324
- LMFBR, filtration of Na fire aerosols 79–30998
- LMFBR, filtration of Na-fire aerosols 80–68853
- LMFBR, finite element formulation for thin reactor struct. thermal stress anal. 78–70613
- LMFBR, flow behaviour of vol. heated boiling pools 80–13545
- LMFBR, flow instabilities of molten core debris pool following accidents 78–8931
- LMFBR, fluid-to-struct. heat transfer effects on structural damage pot. 79–81023
- LMFBR, fragmentation dynamics of molten UO_2 in Na under TOP conditions 79–30978
- LMFBR, fuel and coolant motion following pin failure, EPIC code 77–83055
- LMFBR, fuel and fission gas response to simulated thermal transients 78–74453
- LMFBR, fuel failure propagation reliability assessment 79–49785
- LMFBR, fuel freezing and drainage in shield plug following HCDA 78–50270
- LMFBR, fuel motion diagnostics instrumentation, evaluation with PARKA 79–45360
- LMFBR, fuel motion pot. due to volatilisation of metallic fission product inclusions 79–49746
- LMFBR, fuel pin coolability in low power voiding, SAS3A computer code anal. 79–49661
- LMFBR, fuel-coolant interaction, pressure waves in compressible liquid, one-dimens. anal. 77–88235
- LMFBR, fuel-coolant interaction, UO_2 fragmentation by thermal stress and pressurisation 77–88226
- LMFBR, fuel-steel mixtures, basic collapse criteria for HCDA 77–3107
- LMFBR, gas tag identification of failed assemblies, anal. methods 80–95369
- LMFBR, generic, gas tag design for failed core assembly identification 79–31040
- LMFBR, H impurity conc. in liquid Na, meas. method 79–81030
- LMFBR, HCDA, accident energetics assessment 77–71667
- LMFBR, HCDA, attenuation of airborne debris 80–13650
- LMFBR, HCDA, core debris behaviour, interaction with concrete 77–71676
- LMFBR, HCDA, dryout in porous bed of nuclear fuel debris, heat transfer regimes 77–46316
- LMFBR, HCDA, Eulerian computer code anal., primary system response 77–3127
- LMFBR, HCDA, evaluation and prevention of local core accidents 80–749
- LMFBR, HCDA, in react. expts. on debris cooling 80–13543
- LMFBR, HCDA, role of radiative heat transfer in post-disassembly fuel self-mixing 79–49759

fission reactor safety continued

LMFBR, HCDA, structural response calcs., methods, codes development 77−3126
LMFBR, HCDA, two-phase momentum exchange experiment and analysis, using SIMMER code 79−49751
LMFBR, HCDA anal., effects on reactor struct., radiological consequences 77−71666
LMFBR, HCDA conditions, PuO$_2$-UO$_2$-Na aerosol formation, aerodynamic and chem. behaviour 78−94104
LMFBR, HCDA conditions, UO$_2$ mech. response to transient heating 77−14237
LMFBR, HCDA containment, current perspectives 80−32360
LMFBR, HCDA exptl. modelling 80−32366
LMFBR, HCDA or Na-water interactions, primary containment integrity, design, tests 77−71673
LMFBR, heat and mass transfer behind heated reactor cell liner following hot Na spill 78−17388
LMFBR, hydrodynamics of large-scale fuel-coolant interactions 80−78409
LMFBR, hypothetical core disruptive accident, molten fuel relocation dynamics, simulant fluids 79−30980
LMFBR, hypothetical LOCA, fission gas role in transition phase development 78−8935
LMFBR, hypothetical loss of flow accident, computer simulation 79−3222
LMFBR, inherent safety features 80−106145
LMFBR, inservice inspection methods, NDT 77−38357
LMFBR, intermediate Na activation, Monte Carlo anal. 78−4997
LMFBR, intersubassembly heat transfer effects during natural circulation 80−584
LMFBR, JOYO, fast reactor, experimental, functional and operational test results 79−93796
LMFBR, large, systematic method for constructing low Na void heterogeneous cores 78−13220
LMFBR, leak detection in steam generator, by acoustic spectra meas. *(Czech)* 78−54849
LMFBR, liquid metal to gas leak detection system 77−38375
LMFBR, LOCA, fuel pin failure mechanisms 80−13587
LMFBR, local heat flux density reduction by highly cond. liner 79−637
LMFBR, localised boiling in radial blanket due to hypothetical major pipe leak 79−22376
LMFBR, LOF, molten fuel cladding relocation, multichannel model 79−26556
LMFBR, LOF accident, evaluation of incoherency effect on cladding motion in R-series test 79−49749
LMFBR, LOF-driven TOP, FCI related material movements 80−73946
LMFBR, LOFA, fuel assembly boiling and voiding, THARC-S code 80−13646
LMFBR, LOFT for loss-of-piping-integrity transient, expt. data and COBRA-3M comparison 78−17370
LMFBR, loop-type, effect of pumped stored kinetic energy on natural circulation decay heat removal 80−23010
LMFBR, loop-type, transition to natural convection from low temp., low flow conditions 80−18533
LMFBR, maximum wake temp. and Nusselt number behind blockages in Na-cooled bundles 79−31026
LMFBR, modeling ejection of fresh fuel into sodium under prompt-burst conditions 79−85668
LMFBR, modelling in prompt burst HCDA calcs. 78−74454
LMFBR, modular steam generators, breakdown protection 79−76059
LMFBR, molten cladding film relocation following HCDA, large wave dynamics 78−17365
LMFBR, molten fuel coolant interaction *(Japanese)* 79−17997
LMFBR, molten fuel downward streaming through axial shield struct. 77−42020
LMFBR, molten fuel pins, Sandia's safety research program, United States 77−10484
LMFBR, molten UO$_2$ fuel-Na coolant thermal interaction, characterisation of fragmented fuel 80−68774
LMFBR, multichannel cladding relocation model for loss-of-flow accident 78−17366
LMFBR, Na boiling detection, power spectral density surveillance systems 80−68740
LMFBR, Na boiling hazard *(French)* 80−78402
LMFBR, Na boiling under low heat flux condition during loss-of-heat sink accident 80−47636
LMFBR, Na burning, aerosol release, temp., O conc. depend. 77−83049
LMFBR, Na circuit with high parameters *(Czech)* 77−46303
LMFBR, Na droplet, preignition oxidation process 79−30996
LMFBR, Na fire, statistical parametric anal. 79−30997
LMFBR, Na fires and aerosols expts. for safety anal. data 77−71650
LMFBR, Na flow transient anal. using NATOF-2D code 80−47633
LMFBR, Na incipient boiling under forced convection in seven pin bundle 79−22401
LMFBR, Na pool fire, aerodynamic props. of Na aerosols 80−23011
LMFBR, Na spillage due to slug impact on reactor cover 80−32364
LMFBR, Na spray fires 80−32369
LMFBR, Na void and Doppler reactivities 78−8891
LMFBR, Na void reactivity reduction for U-Pu-Zr fuel 79−85655
LMFBR, Na void reactivity sensitivity to design 78−8890
LMFBR, Na-H$_2$O steam generators, safety problems and their solution in the USSR 80−63318
LMFBR, natural circulation decay heat removal 79−31010
LMFBR, natural convective cooling of fuel debris bed following HCDA 78−8929
LMFBR, neutron and gamma transport, direct coupled-ray method for design oriented 3-D anal. 77−83111
LMFBR, nonlinear structural dynamics of fuel elements, press. pulses, struct. models, expt. verification 77−3125
LMFBR, nucl. design and economic comparison of conventional and bullseye core 78−13222
LMFBR, nucl. performance of reactor designed to preclude energetic HCDAs 78−13307
LMFBR, operational safety issues 77−67818
LMFBR, parametric safety analyses for reduced energetics in PLBR-sized core 78−13298
LMFBR, penetration of turbulent jet with negative buoyancy into upper plenum, safety evaluation 77−23221
LMFBR, physics problems of fast reactor shielding 79−67873
LMFBR, pin plenum fission gas release model to describe fission gas effects in voided channel 79−31042

fission reactor safety continued

LMFBR, pool type, natural circulation cooling 80−102289
LMFBR, pool-type, PLOOP code for primary loop coolant flow and heat transfer anal. 79−31012
LMFBR, post accident heat removal technology review 78−41839
LMFBR, post HCDA aerosols, gravitational collision efficiency 80−32375
LMFBR, post-accident containment, high-temp. behaviour of concrete 79−31000
LMFBR, post-test anal. of transient overpower TREAT test R9 for BOL FFTF-type fuel 79−30985
LMFBR, post-test eval. of SLSF loss-of-flow safety expt. P2 79−30984
LMFBR, preirradiated mixed oxide fuel, EOS series of expts. in TREAT 79−30986
LMFBR, pressure transient analysis in piping systems including the effects of plastic deformation and cavitation 80−74775
LMFBR, primary circuit contamination, release transport and removal of radioactive products 80−13631
LMFBR, primary containment response with upper internal struct. 80−32361
LMFBR, primary cooling circuits, Na loop system, anal. of radioactive corrosion product transfer 78−78464
LMFBR, probabilistic accident anal. with deterministic codes 78−37420
LMFBR, prompt critical excursion, disassembly energy release for mech. damage evaluation 77−71668
LMFBR, Pu release from contaminated burning Na, safety evaluation 77−23224
LMFBR, radiative heat transfer in horizontal molten fuel layer with volumetric heating 79−93786
LMFBR, radionuclide trap 80−52725
LMFBR, reactivity variations ass. with randomly distributed bubbles in molten core 77−46331
LMFBR, recriticality considerations for the loss-of-heat-sink accident with scram 79−49760
LMFBR, response to abnormal events, applied mechanics in design and safety review 78−70611
LMFBR, role of scale model tests in structural dynamics 77−3141
LMFBR, safety and related design and engineered safeguards 80−47676
LMFBR, safety c.f. thermal reactors 79−26562
LMFBR, safety research and development, review 79−36362
LMFBR, SAS3A simulations for a 19-pin dryout experiment 79−54547
LMFBR, SAS-3D analysis of natural-convection boiling behavior in the sodium boiling test facility 80−47635
LMFBR, scaled down model of SNR-300 inlet plenum, convection effects on temp. distribs. during emergency cooling 77−26839
LMFBR, scram and nonlinear system seismic anal. 77−3185
LMFBR, secondary containment response to Na and H 80−27769
LMFBR, seed-blanket-type modular assembly design with favorable safety parameters 78−17308
LMFBR, self actuated shutdown system for reactor protection 77−42106
LMFBR, shutdown heat removal systems, reliability fault tree anal. and β-factor method 80−63331
LMFBR, simulated LOFT, fuel response, role of fission gas and fuel melting 80−37475
LMFBR, SNR-300, HCDA anal. by failure incoherence modelling, HOPE computer code 77−88237
LMFBR, SNR-300, HCDA expt. simulation, theory reliability test 77−71675
LMFBR, space time dynamics for localized disturbances 78−21674
LMFBR, squeeze flow between two adjacent subassemblies, discrete model 78−86634
LMFBR, steam generator LOCA signalling by EM flowmeter *(Czech)* 79−6751
LMFBR, struct. response to HCDA, appl. of coupled Euler Lagrange computer program 77−71671
LMFBR, system and in-core interactions for thermohydraulic transients 80−18545
LMFBR, terminated transient overpower performance, fuel design and material effects 80−22902
LMFBR, thermal conditions controlling subassembly failure propag. during transition phase 79−49758
LMFBR, thermal profile development and inversion, analytic prediction for safety expt(s) 79−93754
LMFBR, thermal radiation effects on subassembly wall failure 78−8938
LMFBR, thermohydraulic transients, numerical simulation using SSC-L code 79−54485
LMFBR, thermomechanical loading of adjacent hexcan 78−8889
LMFBR, TOP, fuel pins and core response 80−13671
LMFBR, TOP, thermal hydraulic anal. of fuel blockages 80−13659
LMFBR, transient boiling of Na in 7-pin fuel bundle under loss-of-flow conditions 79−41007
LMFBR, transient boiling of sodium in seven-pin bundle under transient overpower conditions 79−76056
LMFBR, transient fuel solidification and relocation from core during transition-phase conditions 79−85616
LMFBR, transient simulation code CURL 79−31011
LMFBR, U-Pu-Zr fuelled, study of core disruptive accidents 80−18540
LMFBR, unified model for fission gas release and Na boiling in reactor coolant channel 78−8921
LMFBR, UO$_2$ effective eqn.-of-state meas. to determ. vapour pressure 79−31036
LMFBR, UO$_2$ minimum particle size to survive thermal stress fragmentation by fuel-coolant interaction 79−67886
LMFBR, UO$_2$ vapour bubble characts. determ. for core disruptive accident 79−22390
LMFBR, W-ARD air flow tests, COBRA-IV comparison 80−27734
LMFBR, wastage effects in small leak Na+water reactions, safety considerations 78−82418
LMFBR, water leaks in secondary cooling circuit boilers 78−86572
LMFBR 19-pin simulated fuel assembly, dynamic boiling tests 79−31029
LMFBR 91-pin subassembly, fuel displacement diagnostic facilities 79−49776
LMFBR (SNR 300), design of core catcher system 78−89937
LMFBR accident, contained radioactive suspension behavior anal. 80−99227
LMFBR accident, heat transfer from liquid Na sphere to infinite UO$_2$ medium 77−75783
LMFBR accident, large scale Na/concrete reactions 79−30999
LMFBR accident, Na$_2$O aerosol behaviour in closed chamber under thermal convection flow 77−57723

fission reactor safety continued
LMFBR accident anal., noncondensible void fraction effect on freezing of flowing fluids 79−31013
LMFBR accident consequences, probabilistic anal. by response surface techniques 78−29595
LMFBR accident material compatibility studies for PAHR in-core molten pool expt. 78−8933
LMFBR accidents, licensing decisions and safety research 79−26651
LMFBR accidents, steel ablation and fuel-steel mixing phenomena, LEVITATE code anal. 80−47649
LMFBR aerosols, size dependent density, gravitational collision efficiency 79−93789
LMFBR assembly, fuel pin deformations, analytical method, computational code (SHADOW) 78−54829
LMFBR component decontamination, glycolic-citric acids process 79−93769
LMFBR containment, anal. of nonlinear fluid-struct. interaction, improved ICECO code 78−70615
LMFBR containment performance studies with simple computer code 79−93788
LMFBR containment response anal., Eulerian computer code MICE for multifield fluids 78−70616
LMFBR containment response to postulated Na spills and fires, computer anal. 79−54480
LMFBR containments, post-accident conds., gravitational agglomeration of aerosols 79−36369
LMFBR containments, severe post-accident conds., approx. in aerosol behaviour models for source-term calcs. 79−31064
LMFBR coolant, simple multichannel thermal-hydraulic model for transient behaviour anal. 79−49660
LMFBR coolant scram transients, thermohydraulic behaviour 79−67889
LMFBR cooling channels blockages, simulation testing *(German)* 78−94044
LMFBR cooling systems, reliability 80−57838
LMFBR core, modelling of fluid struct. coupling for seismic anal. 79−89358
LMFBR core, partial failure expts., Na boiling in heated annular channel with blockage 77−42108
LMFBR core, transient deform. from local failure, fuel-coolant interactions 77−88245
LMFBR core design anal., initiating phase energetics in core disruptive accidents 79−22415
LMFBR core design guidance, generic transient limit curves 80−5217
LMFBR core designs to preclude energetic HCDA 79−59125
LMFBR core disassemblies, damage potential sensitivity in prompt critical excursion 79−49766
LMFBR core disruptive accident, effect of internal circulation vel. and noncondensible gas on vapour condensation from rising bubble 79−31017
LMFBR core disruptive accident, fission gas bubble modelling 79−31043
LMFBR core disruptive accident, SIMMER-VENUS II comparison for mechanical disassembly 79−31018
LMFBR core disruptive accident anal., heat transfer effects 77−74949
LMFBR core disruptive accidents, flow regime obs. in two-phase volume heated boiling pools 79−31014
LMFBR core disruptive accidents, SIMMER-I accident consequence calcs. 79−31020
LMFBR core melt-down protection system *(Russian)* 79−76101
LMFBR core meltdown accident anal., radiation-cond. problems 80−19381
LMFBR core meltdown accidents, void distribution in volume-heated boiling pools 77−46318
LMFBR core simulation, Na loop safety facility, P2 expt., LOCA, acoustic meas. 78−33264
LMFBR core subassembly cluster dynamic response to an accidental pressure rise 79−54551
LMFBR cores, numerical method for predicting subassembly seismic induced impact 78−74447
LMFBR coupled fluid-struct. problems, advanced Eulerian method 78−682
LMFBR data multiplexing system 79−76102
LMFBR debris bed simulation expt., in-reactor expt. 79−13404
LMFBR demonstration plant, design, construction and operating experience 79−97887
LMFBR design, reliability, risk assessment, power plant safety anal. 77−71665
LMFBR design requirements to alleviate thermal transient effects 79−97767
LMFBR diagnosis, electrochemical and physical methods 79−97787
LMFBR failed-fuel detection using gaseous fission-product detectors 79−97856
LMFBR finite hexagonal bundles, laminar mixed-convection heat transfer 79−607
LMFBR fuel, fission gas behaviour during overpower transient, calcs. using COREF-1 code 80−57853
LMFBR fuel and blanket transient thermal performance characteristics 80−68880
LMFBR fuel assembly, anal. of loss of piping integrity accident 80−27783
LMFBR fuel assembly, edge blockage in 19-pin Na-cooled bundles 78−13292
LMFBR fuel assembly, thermal consequences of plenum fission gas release, TRUMP thermal anal. 80−47646
LMFBR fuel bundles transient testing, operating experience 80−827
LMFBR fuel disruption following LOF accident, in-pile expt. using high-speed cinematography 80−78366
LMFBR fuel elements, remote exam. of shroud tubes 80−18470
LMFBR fuel elements, transient overpower test results 77−46334
LMFBR fuel failure dynamics, appl. of Larson-Miller parameter 79−31002
LMFBR fuel pin bundles in flowing Na, design and operation of SLSF test trains for safety tests 80−102281
LMFBR fuel pin transient behaviour, effect of shutdown cracks in TREAT tested pins 79−31001
LMFBR fuel pins, assay with Pb spectrom. 80−37461
LMFBR fuel pins, reactor illuminated, coded aperture imaging 79−30989
LMFBR fuel subassembly, approach for treating two-dimensional coolant boiling 79−31030

fission reactor safety continued
LMFBR fuel subassembly, effect of bundle insulation degradation on boiling stability tests 79−54548
LMFBR generator, SWRP deposition from testing and cleaning 80−22924
LMFBR HCDA, appl. of acoustic agglomerators for suppression of Na-fire aerosols 79−54525
LMFBR HCDA, boundary heat transfer from volumetrically boiling pools 80−47654
LMFBR HCDA, containment response anal. to PAHR failure 79−49672
LMFBR HCDA, damage potential of core disassembly, sensitivity study 79−54531
LMFBR HCDA, energetics of bubble expansions, potential attenuation mech. 80−83197
LMFBR HCDA, fuel condensate solidification onto steel struct. in above-core region 78−17364
LMFBR HCDA, fuel motion during in reactor TOP test H4 77−46335
LMFBR HCDA, heat transfer from pool of molten UO_2 to concrete slab 78−8930
LMFBR HCDA, I-D compressible coolant dynamics, numerical anal. using EULFCI code 80−68733
LMFBR HCDA, molten fuel freezing in shield plug 78−8941
LMFBR HCDA, Na_2O aerosol gravitational fallout rate, validation of computer code 80−18535
LMFBR HCDA, Na interaction with basalt concrete and silaceous firebrick 80−47638
LMFBR HCDA, nonlinear dynamic anal. of piping system 80−5290
LMFBR HCDA, pipe rupture following earthquake, accident course 78−8925
LMFBR HCDA, potential for plugged core pressurisation following LOF accident 79−76084
LMFBR HCDA, simulation of fuel-speed pool during transition to transition phase 78−8937
LMFBR HCDA, US meas. of penetration of liquid Na into limestone concrete 80−78412
LMFBR HCDA, vapour bubble-liquid slug heat transfer, Taylor instability mechanism 78−8939
LMFBR HCDA, wave propagation ICECO code predictions in rigid 2-dimens. vessel 79−49770
LMFBR HCDA aerosol behaviour, kinetic corrections to aerosol gravitational collisional efficiency 80−95386
LMFBR HCDA anal. with FUTURE and FRUMP codes 79−85661
LMFBR HCDA analysis, effect of condensation on dispersion of closed boiling UO_2 78−8936
LMFBR HCDA analysis, meas. and calc. of average void fraction in volume-boiling pools with inclined boundaries 80−47653
LMFBR HCDA analysis, uncertainty in accident consequences calculated by large codes due to uncertainties in input 80−78413
LMFBR HCDA containment response productions, validation of computer code 80−18538
LMFBR HCDA radiological consequences, attenuation by thermal radiation 77−46321
LMFBR head closures, dynamic struct. response to HCDA 78−70617
LMFBR heterogeneous core designs with axial internal blankets 78−13227
LMFBR heterogeneous oxide reference, transmuter, denatured core designs 80−22901
LMFBR hexagonal ducts, cracking, effect on safety and fuel pin failure 78−17318
LMFBR hypothetical accident, use of hodoscopes to obtain tomographic resoln. of fuel motion 79−54537
LMFBR hypothetical accident, use of sonic agglomerators for aerosol particle suppression 79−36370
LMFBR hypothetical core disruptive accident, simplified multicomponent phase transition model 79−31016
LMFBR hypothetical overpower accident, intersubassembly incoherencies and grouping techniques 79−31008
LMFBR in HCDA transition phase analysis, material relocation and freezing 77−46329
LMFBR inherent secondary shutdown assembly, hydraulic tests 79−49666
LMFBR inherent shutdown system, expts. and analyses 79−31041
LMFBR LOCA, use of temperature variance to detect sodium boiling 79−54527
LMFBR LOF accident, analysis of in-pile fuel disruption experiments 79−49748
LMFBR LOF accident, surface ablation in impingement region of liquid jet 79−54549
LMFBR LOF accident tests at TREAT on preirradiated mixed oxide fuel 80−47657
LMFBR LOF transient, integral model for voiding phase conditions 77−42032
LMFBR LOF transient, sodium voiding dynamics and cladding motion 79−49750
LMFBR LOF-HCDA, solidification dynamics of flowing two-phase mixtures 79−49757
LMFBR LOF-TOP, axial propagation of fuel failure, SAS3D-EPIC anal. 80−47650
LMFBR loss of flow transient anal., soln. of COBRA energy equations during natural circulation conditions 79−89354
LMFBR loss of piping integrity expt. 77−42027
LMFBR loss-of-flow accident, 28-pin cladding relocation simulation expt. 79−30979
LMFBR loss-of-flow accident, empirical fuel motion model for TREAT test F1 79−30977
LMFBR maximum critical accident, assessment using theory of aerosols coagulation 77−3121
LMFBR meltdown conditons, molten fuel+coolant interaction, expts. 77−23225
LMFBR meltdown cores, exptl. study of integral physics parameters 80−13664
LMFBR molten oxide fuel layer, effect of radiation heat transfer on maximum nonboiling thickness 80−47558
LMFBR multipin bundles, eval. of hodoscopes for fuel motion meas. 79−93780
LMFBR Na-cooled 7-rod bundle acoustic and temp. noise obs. 79−13391
LMFBR Na/basalt concrete interactions following accident, chemical phenomenology 80−47639
LMFBR outlet plenum mixing, 3-D numerical simulation 78−8880

fission reactor safety continued
LMFBR outlet plenum transients, expt. and anal. using PLENUM-2 code 79−49664
LMFBR outlet plenums, transient anal. with PLENUM-2A program 80−32378
LMFBR overpower excursions, mechanistic model of fuel freezing, channel plugging and continued coolability 78−58371
LMFBR performance of Th-based fuel cycles 79−9744
LMFBR pin bundle, model to correlate wake residence time meas. behind blockages 79−31027
LMFBR plant, preaccident modelling 77−46324
LMFBR post accident containment response, effects of evaporation and condensation, using CONAN code 80−47637
LMFBR post-accident containment, time-resolved penetration of liquid Na into limestone concrete 79−93787
LMFBR postulated accident, aerosol behaviour within containment, Na_2O agglomerate props. 79−36368
LMFBR postulated core meltdown, onset of foam flow regime in volume heated boiling pool 79−31015
LMFBR prestressed concrete reactor vessels, analytical model and code applications 78−74448
LMFBR primary heat transport pipe rupture and hydraulic response 79−9784
LMFBR probabilistic accident anal., stochastically variable parameters 79−31021
LMFBR prompt burst calcs., FX2-TWOPOOL code for hydrodynamics, thermodynamics and neutronics 79−49767
LMFBR prompt burst excursion expt., hydrodynamic anal. 79−30987
LMFBR reactivity surveillance using ex-core detectors 79−9802
LMFBR rot. shield plug annulus, Na vapour, deposition rate, controlling factors 80−47591
LMFBR safety, coded aperture imaging in many-pin fuel bundles 79−49777
LMFBR safety, collocation method soln. of radiation-conduction problems 80−13720
LMFBR safety, comparison of ICECO code with flexible vessel expts. 78−70619
LMFBR safety, comparison of ICEPEL code with straight flexible pipe expts. 78−70620
LMFBR safety, flow rundown expts. in seven pin bundle, Na boiling 77−88240
LMFBR safety, formation of critical boiling nuclei in superheated Na 77−88242
LMFBR safety, international cooperation, progress 80−826
LMFBR safety, KNK II driver zone, Na boiling in 7-pin bundle 77−88246
LMFBR safety, local blockage formation and growth in grid spaced fuel elements, model 77−88243
LMFBR safety, local cooling disturbances, in-pile Na loop investigation 78−674
LMFBR safety, review 78−13257
LMFBR safety, review of computer code packages 77−83053
LMFBR safety, scale modelling 80−32367
LMFBR safety, seven pin bundle expts., flow patterns, two-phase press. drop, Na boiling 77−88241
LMFBR safety against propagation of local subassembly failures, CDA conditions 77−18673
LMFBR safety anal., sAS-3D evaluation of boiling at decay-heat levels in FFTF 80−47634
LMFBR safety anal., theoretical interpretation of SCARABEE single pin in-pile boiling expts. 77−88239
LMFBR safety analysis, computational techniques 78−66355
LMFBR safety analysis, computer code for determ. of aerosol attenuation in leakage paths 78−13293
LMFBR safety analysis, design features to prevent and terminate plant accidents 80−47677
LMFBR safety analysis, pipe-break model 77−46325
LMFBR safety analysis, solidification in a fuel rod bundle 80−47632
LMFBR safety and fuel cycle, accident anal. 79−26650
LMFBR safety application of US thermometry 79−45400
LMFBR safety testing, scram signal generator for fluid motion monitoring 80−18551
LMFBR safety testing needs, conceptual design of safety research experiment facility 77−3129
LMFBR shock-induced fragmentation and detonating thermal explosions 79−13475
LMFBR simulated fuel subassembly, local Na boiling behind flow blockage 78−54842
LMFBR simulated LOF transients in 37-pin subassemblies at SLSF, interpretation of voiding dynamics data 80−47656
LMFBR simulated meltdown configs., integral physics parameter meas. 80−13698
LMFBR simulated meltdown configs., reactivity worths 79−81036
LMFBR simulation, parameter estimation 80−47597
LMFBR single component and mixed oxide fuel solidification anal. 78−74435
LMFBR six channel subassembly blockages, max. Na temp. correlation 79−85656
LMFBR slow overpower transient, simplified computing method for cladding and fuel strain 79−31005
LMFBR small core disruptive accidents, transport/diffusion comparisons 79−31022
LMFBR spectrum, Doppler reactivity worth of UO_2 and ThO_2 meas. 80−27776
LMFBR steam generator, acoustic detection of small leak Na-water reaction 78−29589
LMFBR steam generator, small-leak Na+water reaction, dissolution rate of hydrogen 78−29545
LMFBR steam generator leak, meas. of sound produced during steam injection into Na 79−93782
LMFBR steam generator rupture disks, dynamic instability anal. 79−85662
LMFBR steam generators, behaviour of heat exchange tubes in Na-water contact 80−13670
LMFBR steam generators, leak detection of steam or water into sodium 79−13434
LMFBR steam generators, leak detection of water into sodium, magnetic flowmeter bubble noise monitor 80−9000
LMFBR steam generators, reliability considerations 79−22437
LMFBR steam generators, safety alarm system, water leakage detection *(Czech)* 78−33268

fission reactor safety continued
LMFBR steam generators, water leakage detection systems, development 80−37546
LMFBR subassemblies, coolant boiling calc., using Claymore code 78−82473
LMFBR subassembly, fuel coolant interaction anal.model and computer code SAMI 80−106136
LMFBR subassembly, multichannel model for fuel coolant interaction 80−13653
LMFBR subassembly, thermal hydraulics anal. 79−89396
LMFBR subassembly ducts dynamic response, comparison of finite element code with expts. 78−70614
LMFBR subassembly fault detection, microprocessor-based distributed system appl. *(Japanese)* 79−41002
LMFBR subassembly response to simulated local press. loadings, accident conditions, finite element anal. 77−3123
LMFBR subassembly simulation, finite element computer model, safety anal. 78−70612
LMFBR subchannel coolant flow behind blockage, temp. noise obs. 79−13389
LMFBR surveillance technique development 79−13448
LMFBR system design requirement to accommodate Na spillage 79−97845
LMFBR test facility, exptl. determ. of reliability data of sodium components 79−18015
LMFBR test fuel element, appl. of nonredundant pinhole array 79−93781
LMFBR thermal explosion hazards, review of present understanding and simulation expts. 78−82464
LMFBR thermohydraulic transient simulation, appl. of multiple time-step integration in Super System Code 80−47552
LMFBR TOP accident, effect of transient power histories on intrasubassembly failure incoherencies 80−47647
LMFBR TOP accident, fuel pin failure, anal. 79−49699
LMFBR TOP accident, implications of in-channel fuel plugging 80−78414
LMFBR TOP accident 79−54515
LMFBR transient behaviour, effect of steam cycle 79−49678
LMFBR transient fission gas behaviour modelling, bubble equilibration effects FRAS 2 code 79−59168
LMFBR transient fuel behaviour, effect of grain boundary fission gas 79−54532
LMFBR transient over power accident, plateout and thermal loading of ejected fuel 79−30982
LMFBR transient overpower accident anal. using PLUTO2 code 79−31004
LMFBR transient undercooling accident, molten stainless steel, wetting of UO_2 cracked fuel pellets 78−4993
LMFBR transition to natural circulation from an initial isothermal state 79−85653
LMFBR unprotected loss-of-flow accidents, boiling incoherency effects 79−31007
LMFBR UO_2 pin meltdown simulation by direct electrical heating 77−88215
LMFBR vessel structural response to HCDA, model tests *(Japanese)* 77−67829
LMFBR wire-wrapped subassemblies, Na boiling behaviour 79−31031
LMFBR-type steam generator, consequences of intentional steam tube failure 79−54544
LMFBRs, tritium control, sources and removal 79−36335
LMFBRs evaluation of local accidents out-and in-pile expts. 79−26652
LOCA, 3-dimens. flow with multiple interfaces 79−41024
LOCA, anal. of containment heat transfer 77−46248
LOCA, anal. of secondary coolant system influence on LOCE 79−89431
LOCA, blowdown phase, two-phase mass flow rate meas. using true mass flowmeters 80−778
LOCA, blowdown phase separation mechanics effect on containment pressure response 79−93771
LOCA, CHF expts. on effect of heated-wall press./temp. history on blowdown heat transfer 80−23005
LOCA, cocurrent two-phase downflow in tubes, flow pattern, void fraction and press. drop 79−77229
LOCA, computer simulation of reflood heat transfer and hydrodynamics 79−67891
LOCA, condensing heat transfer 78−21684
LOCA, condensing heat transfer coeff. based on mass condensation 78−13304
LOCA, cooling mechanism during transient reflooding 77−88208
LOCA, counter-current flow limiting phenomena with vapour condensation, model 77−61519
LOCA, crack extension limiting, warm prestress for small ΔT 80−27784
LOCA, creation and persistence of mist-laden containment atmospheres 79−89421
LOCA, data analysis using computer-aided models *(Czech)* 80−73949
LOCA, effect of drop evaporation rate on containment pressure transients 79−22413
LOCA, effect of entrance conditions on countercurrent flooding limits in the restricting upper tieplate region 80−18529
LOCA, evaluation of unavailability of the containment spray system by use of a cause-consequence chart 80−52756
LOCA, experimental and theoretical study of the blowdown of the secondary side of a steam generator 80−761
LOCA, extreme loads and associated safety aspects, review 79−22405
LOCA, flow boiling dryout, transient heat transfer investigation 80−32359
LOCA, fuel element behaviour during high-temp. transients, ELOCA code 79−81043
LOCA, fuel performance, HOTROD code 80−42790
LOCA, gravity-driven reflood hydrodynamics, EFLOD code 79−89426
LOCA, heat removal by passive heat sinks, model anal. 77−42019
LOCA, international standard problem exercises in nuclear safety 80−756
LOCA, modelling two-phase hydrodynamic phenomena, pipe blowdown with Freon-12 80−5267
LOCA, models for estimation of critical flow in two-phase systems 79−36361
LOCA, pressure oscillation in subcooled decompression under temperature gradient 80−559
LOCA, quench phenomena correlation for bottom flooding 79−54520
LOCA, reflood heat transfer and entrainment expts. 79−31060

fission reactor safety continued
LOCA, reflooding phase, flow film boiling, void fraction meas. 80−92207
LOCA, reflooding phenomena in single heated tool 80−27754
LOCA, response of reactor containments 79−30958
LOCA, results from LOFT PWR expts. 77−42016
LOCA, rewetting of hot surface, development of cooling wave 80−27767
LOCA, rewetting temp. in vert. channel 79−59117
LOCA, spray cooling of hollow rod cladding 78−50262
LOCA, straight pipe blowdown tests and code verification [of reactor LOCA] 80−759
LOCA, strain in Zircaloy clad of fuel pins 78−699
LOCA, stratified cocurrent flow of gas-liquid mixtures in horizontal pipes 79−77214
LOCA, thermal hydrualic phenomena resulting in early critical heat flux 79−81005
LOCA, thermal shock in nuclear containment wall, computer code for safety anal. 77−3135
LOCA, transient flow boiling anal. method 79−26549
LOCA, Zircaloy fuel cladding, azimuthal temp. distrib. 80−662
LOCA 79−633
LOCA anal., 1-D model of vapour generation in steady flashing flow 80−23004
LOCA anal. in Federal Republic of Germany, computer models 79−26642
LOCA anal. program TECAR 77−88250
LOCA analysis in small compact reactors uisng RELAP4/MOD5 thermal hydraulic code 80−68852
LOCA capability code for utility appl. 78−21690
LOCA causing core meltdown, vapour explosion caused by water entrapment with melt 78−17382
LOCA codes, characteristics of two-phase one component flow with slip 77−83019
LOCA conditions, transient two-phase flow reversal prediction 78−94811
LOCA consequences, hydrodynamics mass method anal. 80−73909
LOCA containment anal., new condensation mass removal model 79−89423
LOCA in containment with press. suppression system, anal. of press. oscill. phenomena 79−67878
LOCA in PWR, critical two-phase flow, nonequilibrium vapour production model 80−52719
LOCA in water reactors, reversal of laminar flow in circular pipe 78−50271
LOCA mathematical models for PWR safety analysis *(Russian)* 79−30963
LOCA quench front model for Transient Analysis Reactor Code 80−47550
LOCA reflood phase, hydrodynamics of water cooled reactor, moving control vol. method 78−704
LOCA reflood phase, thermo-hydrodynamic behaviour, REFLA-1D code 80−47592
LOCA rewetting, investigation in Freon-113 vapour environment 80−32358
LOCA simulation, armature testing *(German)* 80−42785
LOCA-generated drop size perdiction, thermal fragmentation model 79−89422
local and general coincidence schemes assuming two failure modes 79−49787
LOCE blowdown flow meas., improved spool piece 80−27727
LOF overheating transients, volatization pot. of metallic inclusions in irrad. UO$_2$ fuel 80−57895
LOFA, transient crit. heat flux, Freon 12 coolant 79−30954
LOFT, contribution to nuclear reactor safety 80−106139
LOFT, requalification following LOCE 80−57904
LOFT core fluid conditions during blowdown and refill 79−89440
LOFT drag disc turbine meter rakes for two-phase flow measurement 80−102260
LOFT facility, commercial PWR systems safety 80−37548
LOFT facility, PWR LOCA anal., system blowdown, core thermal response, emergency core cooling 80−37549
LOFT facility, PWR LOCE, two phase flow meas. instrumentation 80−37550
LOFT fuel design and operating experience, exposure to LOCA 79−89438
LOFT instrumented fuel design and operating experience during PWR LOCE 80−37551
LOFT L2-4 test and FLOOD4 code, PWR reflood behaviour anal. *(Japanese)* 79−97824
LOFT LOCE fuel module structural response, computer code prediction 79−89439
LOFT non nucl. test L1-4, TRAC anal. 80−13655
LOFT nucl. test L2-2, TRAC pre-test and post test calcs. 80−18519
LOFT program, recent results *(Japanese)* 80−673
LOFT project, design and results *(Dutch)* 80−42735
LOFT reactor L2-2 expt., pre-LOCE thermal safety anal. 80−22896
LOFT reactor secondary cooling system, waterhammer phenomena 80−57905
LOFT start-up program, unique features 80−23116
LOFT test L2-2, fuel rod response 80−18520
LOFT test L2-2, pre-test calc. using RETRAN code 80−18518
logic protection system using a redundant computer struct., self-checking procedures *(French)* 79−76103
loop disposal system of sodium loop safety facility 80−18467
loose parts monitoring, USA technology status and recommendations 79−623
loss of coolant effect on resonance escape probability 80−22963
loss of coolant studies, gamma densitometer detector comparison 80−57881
Loviisa-1 Nuclear Power Station, in Finland, safety during design, building, and operating stages *(Russian)* 80−106128
LPWR, postulated LOCA, de-entrainment phenomena from droplet cross flow in vertical bundles 79−89430
LPWR fuel cladding temp. predictions for LOFT LOCE L1-5 79−89446
Lucens reactor accident, alarm and surveillance 78−50283
LWFBR, neutron balance in chain reaction, delayed neutrons role, reactor safety *(German)* 79−26726
LWPR, radiological emergency monitoring and instrumentation, Federal guidance 80−57961
LWR, accidents, effects and damages 80−22961

fission reactor safety continued
LWR, anticipated transients without trip, dependence of results on core kinetic parameters 77−50273
LWR, boiling heat transfer anal. 80−27724
LWR, commercial, evaluation of human errors and operator reliability 78−17373
LWR, condenser tube failures 78−21715
LWR, core reactivity changes, influence of axial flux distrib. 77−46365
LWR, decay heat power evaluation in shutdown reactors 80−5257
LWR, design meas. to reduce radiation dose to reactor personnel 79−3199
LWR, deterministic criteria vs. probabilistic analyses 80−32377
LWR, Dutch nuclear safety requirements 80−768
LWR, effect of district heat prod. on reactor operation and safety 79−85624
LWR, effect of small pipe weld types on personnel exposure 78−4996
LWR, fission gas release high-burnup fuel during transient heating 78−13283
LWR, frequency of anticipated transients 80−18525
LWR, generalized theory for predicting mass effluence during reactor reflooding 79−36352
LWR, heat transfer model of quenching in reflooding phase *(Japanese)* 78−8874
LWR, human operator errors, analytical model 80−63329
LWR, I spiking, release mechanism and its verification in plant operation 79−59229
LWR, in-service inspection, a critical assessment 79−63762
LWR, initial fuel loading problems 78−21741
LWR, interfacial mass and momentum transfer in two-phase flow 80−27725
LWR, LOCA, fission product source terms 80−13654
LWR, LOCA, safety methodology *(French)* 80−52751
LWR, LOCA conditions, fuel rod behaviour, code system SSYST-Mod 1 calcs. 77−88248
LWR, LOCA separated air-water two-phase flow, mathematical anal. *(Japanese)* 79−36334
LWR, loss of coolant accident, behaviour of Zircaloy fuel cladding *(Japanese)* 79−71889
LWR, molten fuel coolant interaction during HCDA 77−3136
LWR, NRC safety research programs, fuel behaviour, operational safety, metallurgy and materials 80−13705
LWR, pipe system failure characts., effects on plant availability and capacity 78−17375
LWR, plutonium fuelled, control and safety investigations 78−89969
LWR, post-LOCA γ-ray energy redistrib. and effects 78−13280
LWR, post-LOCA containment anal., space-dependent condensing heat transfer coeffs. 80−47630
LWR, power cooling mismatch accident, molten fuel radial motion and cladding melting 80−13638
LWR, press. and temp. loads on containment after LOCA, scale model expts. 77−3134
LWR, props. of core melts in LOCA, viscosity, thermal cond., specific heat 77−14247
LWR, Pu recycling, CEA-EdF studies 80−722
LWR, reliability demonstration test *(Japanese)* 79−26552
LWR, reliability of piping 79−18017
LWR, rem reduction plan for standard 1100MW(e) plant designs 80−745
LWR, risk-sensitive Markovian policies for detection and maintenance of fatigue cracks in pressure vessels 79−54534
LWR, safety, research needs 79−49711
LWR, safety of Pu use in Federal German Republic 77−67839
LWR, scram experience for shutdown system reliability anal. 77−46347
LWR, seawater levels of radioactive ^{54}Mn, ^{59}Fe, ^{58,60}Co 78−85608
LWR, spray droplet heat transfer in LOCA 80−32380
LWR, stationary boiling front in liquid film cooling of a vertical heated rod 79−45341
LWR, steam explosion parametric study during core melt accidents *(German)* 77−6527
LWR, stress conc. in cladding produced by cracked fuel pellets 78−50260
LWR, structural integrity of pressure boundary 78−66334
LWR, system design for transfer of heat decay to external environment *(Italian)* 77−38320
LWR, technical safety rules, catalogue and classification for reactors and fuel cycle plants 78−58384
LWR, thermal interaction of molten core materials with water 78−17383
LWR, two-phase critical flow phenomena 80−27723
LWR, two-phase flow, analytic simulation 80−13551
LWR, Zircaloy cladding, ballooning, analytical model for transient gas flow 80−18499
LWR, Zircaloy cladding, internally pressurized, effect of temp. nonuniformity on diametral expansion during transient heating in steam 79−30920
LWR 1300 MWe system, design of containment to withstand core melt 78−66335
LWR accidents, containment venting and filtration approaches 79−13465
LWR accidents, in-reactor expts. on fuel behaviour review *(Japanese)* 79−63760
LWR anal., verification of the RETRAN computer code with measured reactor coolant pump coastdown data 79−89406
LWR assessment and licensing requirements, EEC-JRC research 80−42786
LWR blow down accident, French studies, assessment codes *(French)* 79−26641
LWR chemical decontamination and cleaning for radiation control 79−54554
LWR containment vessel, I removal by spray after LOCA, MIRA-PB code 80−47593
LWR core barrel model, circular cylindrical shell, dynamic response to nonaxisymm. loading 77−88247
LWR core blowdown, dynamic behavior of valves, computer simulation 80−5288
LWR core meltdown, accident anal. using computer system KESS 80−752
LWR core meltdown, activity release and aerosol characts. 78−82469
LWR core meltdown, chemical reacts. between core melt and concrete 80−13588

fission reactor safety continued
- LWR core meltdown, core-concrete interfacial heat transfer and molten pool dynamics 80−47641
- LWR core meltdown, materials behaviour 80−751
- LWR core meltdown, metastable state preceding entrapment explosions 80−771
- LWR core meltdown, release of fission and activation products 80−13667
- LWR core meltdown accident simulation using MELSIM-1 code 80−18507
- LWR core meltdown and containment anal., computer code solns. 80−753
- LWR core meltdown risk anal., penetration of hot melts into concrete structures 80−750
- LWR core transient anal. using coupled neutronics and thermal hydraulic models 80−715
- LWR ECC, UCFLOOD code for bottom reflooding heat transfer 79−49728
- LWR emergency core cooling component experience data, defect anal. programme 79−18010
- LWR emergency core cooling system, effects of pressure and materials on quenching of solids 79−31061
- LWR failed fuel expts., improved method 80−13595
- LWR fuel, mixed oxide, suitability of spent fuel shipping casks 80−27757
- LWR fuel, power ramp failure propensity, exptl. investigations 79−26543
- LWR fuel assemblies, coolant channel closure modelling using pattern recognition techniques 80−42835
- LWR fuel elements, behaviour under accident conditions 79−26545
- LWR fuel elements, fault behaviour *(German)* 78−696
- LWR fuel failure under reactivity initiated accident condition *(Japanese)* 78−25305
- LWR fuel failure under reactivity initiated accident conditions, NSRR experiments *(Japanese)* 79−36340
- LWR fuel melt accident, effects of pressure on steam explosion triggering in Corium-E simulants 79−49752
- LWR fuel performance calcs., effect of Cs and I_2 release 79−31054
- LWR fuel researches, safety oriented, Japan *(Japanese)* 80−803
- LWR fuel rod, transient pellet-cladding interaction, ISUNE-4 computer anal. 80−91228
- LWR fuel rod behavior in a nine-rod bundle tested in film boiling 80−18500
- LWR fuel rod failure probability, comparison of FRAP T4 and meas. 80−13644
- LWR fuel rod quenching, two-dimensional heat conduction model 79−93815
- LWR fuel rod under power transients, CRATER code calc. *(French)* 80−42789
- LWR fuel rods, power cooling mismatch induced failure, meas. fission product release 79−93772
- LWR fuel safety, failure thresholds, NSRR programme 79−26595
- LWR hydrogen formation during core melt accident 78−50267
- LWR hypothetical core meltdown, vapour explosion potentials at high interface temp. 79−13476
- LWR kinetic anal. with feedback, hypothetical accident transients 80−13697
- LWR LOCA, analysis, role of LOFT program 80−18531
- LWR LOCA, analysis of shapes of solidified melts from entrapment experiments 79−54550
- LWR LOCA, assessment of the RELAP4/MOD6 reactor transient thermal-hydraulic code 80−42826
- LWR LOCA, enhanced steam oxidation of Zircaloy cladding by deformation 80−73917
- LWR LOCA, fission product decay energy release rates following ^{235}U fission 80−57894
- LWR LOCA, fission product gamma-ray energy absorption in emergency cooling solns. 79−31052
- LWR LOCA, fission product release from defected fuel rods 80−23031
- LWR LOCA, heat transfer in the inverted annular flow regime during reflooding 79−49731
- LWR LOCA, Ispra studies 77−42156
- LWR LOCA, modelling of press. and temp. changes in two-phase, two-component flow *(Bulgarian)* 80−68904
- LWR LOCA, operating contractor's view of LOFT 80−23007
- LWR LOCA, rewetting front axial and radial heat conduction 80−18528
- LWR LOCA, rewetting models, review and comparison 80−83194
- LWR LOCA, TRAC calculations of ECC bypass phenomena in a 1/15-scale experimental facility 79−49725
- LWR LOCA, two-dimensional temperature distributions in fuel rods under blowdown conditions 80−774
- LWR LOCA, two-phase flow, horizontal stratified, 1-D two-fluid eqns. 80−91226
- LWR LOCA, two-phase flow instrumentation for safety anal. 80−102259
- LWR LOCA, utilisation of LOFT information for licensing 80−18532
- LWR LOCA anal., errors in decay heat function 77−26841
- LWR LOCA analysis, TRAC-1D code for Standard Problem 2 78−13288
- LWR LOCA occurrence of critical heat flux during blowdown with flow reversal 79−54529
- LWR LOCA reflooding, prediction of quench fron velocities for constant inlet flooding rates 80−23000
- LWR LOCA safety analysis, thermohydraulic phenomena, review *(German)* 79−13430
- LWR maintenance problems for remote technology appl. 80−68871
- LWR mixed oxide fuels, safety aspects of PuO_2 micro-heterogeneities 79−49798
- LWR NRC safety research programs, thermo-hydraulics and computer code development 80−13704
- LWR nuclear power plant with passive containment system, surveillance system importance 80−795
- LWR operation and maintenance 78−86653
- LWR PCM transient, UO_2 fuel melting and Zircaloy cladding thermal failure 80−42834
- LWR piping, intergranular stress-corrosion cracking 80−81234
- LWR plant, plume exposure monitoring system 80−42875
- LWR plants in Japan, safety aspects and operating experience 79−26628
- LWR post-accident aerosol removal, steam condensation expt. 79−13456

fission reactor safety continued
- LWR power plant, radioisotope activity meas. in secondary loop coolant 80−5345
- LWR power plant human errors 79−13459
- LWR power plants, inservice inspection 79−30944
- LWR power plants, protection of maintenance personnel 80−5368
- LWR power plants, radioactivity release in LOCA uncertainties 79−26639
- LWR power station radioactive unplanned dischage meas. 78−89995
- LWR power stations, R and D for improving seismic safety 80−99231
- LWR pressure boundary failure and LOCA studies 79−26640
- LWR pressure vessel, unstable fracture *(Japanese)* 79−9767
- LWR pressure vessels testing, using ultrasonic probe 78−17339
- LWR primary circuit, austenitic stainless steel cladding, stress-corrosion cracking 79−20293
- LWR protection system 79−97844
- LWR radiation control techniques 79−59184
- LWR radiation dose minimization during operation, maintenance and inspection 80−5294
- LWR radwaste, gas processing with low temp. rectification for quasi-null release 79−67877
- LWR refuelling shutdown, multiple controlled-cell removal 80−99252
- LWR ruptured fuel rods in LOCA, fission product release, computer modelling 79−49780
- LWR sabotage risk modelling 80−23001
- LWR safety, condensation heat transfer in stably stratified systems 80−63311
- LWR safety, critical flow of two-phase one-component mixtures *(Italian)* 79−71880
- LWR safety, Monte Carlo calc. of gamma ray heating 77−50272
- LWR safety anal., appl. of advanced neutron physics models 77−42153
- LWR safety concerns, future possibilities 80−13702
- LWR safety considerations in Sweden, reactor design for power plants 79−26631
- LWR safety criteria, radioactive waste disposal 80−18472
- LWR safety practices in Europe, harmonisation 80−27765
- LWR safety research in Japan, status *(Japanese)* 77−67827
- LWR safety research in the Federal Republic of Germany 79−26638
- LWR safety research in USA 79−26645
- LWR safety research programs by US NRC, review 80−42796
- LWR safety technology, US DOE man-machine interaction program 80−47659
- LWR spent fuel reprocessing plant, integrated safeguards assessment 79−89418
- LWR spent-fuel heatup following loss of water during storage 79−59202
- LWR steam explosion pressure buildup estimation 79−13473
- LWR steam explosion triggering expts. with oxidised Corium-E simulants 79−13472
- LWR steam generator behaviour during core blowdown tests 80−772
- LWR steam generator tube integrity in KWU nuclear power plants 80−5287
- LWR thermohydraulics, safety aspects 80−5266
- LWR UO_2 molten fuel radial motion during a high temp. transient 80−42833
- LWR utility, development of non-LOCA safety anal. methods 78−21691
- LWR with superheated steam isolation valve, blowdown expts. 79−625
- LWRs, accident prevention study 78−66356
- LWRs, safety strategy and principles *(German)* 78−37410
- LWRs at Harrisburg and Mulheim-Karlich, safety systems comparison *(German)* 80−22966
- Magnox reactors, influence of design and operation on personnel radiation dose meas. 80−5385
- Magnox reactors, remote corrosion monitoring, laser based instrument 78−41822
- main steam isolating valves, back pressure light, PWR appl. 78−29602
- Maine Yankee reactor, thermal performance 80−22907
- Maine Yankee reactor protection system setpoint calc. 79−13479
- maintenance optimization through trend monitoring 80−18552
- MARIA, Polish high flux test reactor, leakage rate meas. in reactor containment 79−18001
- mass effluence during FLECHT forced reflood expts. 77−46242
- materials, automated record keeping system 79−93759
- materials control with VACOSS variable coding seal system 78−82491
- materials science contribution to safety, components failure probabilities *(German)* 78−58352
- materials security, on-line diversion detection safeguard concepts [for nuclear materials security] 80−13729
- melt fragmentation, initiation in fuel-coolant interactions 80−13537
- melting clad temperature distribution in fission reactor, Pekeris-Slichter series expansion method 77−88238
- melting of finite steel slabs in flowing nuclear reactor fuel 79−54494
- melting pool surfaces, temp. meas. by ratio pyrometers 78−82471
- metal containment, system safety anal. 78−41817
- metalwork fault monitoring, US flaw detection system *(Russian)* 78−25302
- meteorological information system for response to nuclear power station accidental release of radioactivity 80−16888
- methyl iodide, dissolution into aqueous NaOH solns., fission reactor accident conditions 77−88236
- microcomputer based system 77−67845
- microprocessor controlled multipoint recorder with graphical video output for reactor core temperatures 80−57873
- mirror fusion-fission reactor, safety 79−22461
- mixed-oxide fuel, irradiated, microstruct. charact. and radial distrib. of retained fission gas 79−59188
- mixed-oxide fuel, two-component gas transport within interconnected porosity, during melting 79−617
- mixed-oxide fuel pellets, remote encapsulation for transient testing 80−18422
- MO200 model for evaluating safeguards in mixed-oxide fuel-rod fabrication plant 77−38372
- mobile He cooling loop system for post-accident heat removal expts. 79−13403
- modal superposition method for computationally economical nonlinear structural analysis, seismic impact appl. 79−81004
- molten core debris contact with Na, particulate debris bed formation expt. 79−13405
- molten core debris pools, PAHR anal., hot liquid pool penetration 80−18544
- molten Fe oxides, steam explosions 79−85649
- molten fuel-coolant interaction, simulation experiment 79−17991

fission reactor safety continued
molten fuel-coolant interaction studies, simulated reactor accident, windscale shock tube rig 78—58363
molten glass thermal interaction with H_2O, fuel-coolant simulation 77—46320
molten glass/water thermal interaction 78—46149
molten metal-coolant interactions minimum film boiling temp. 79—54524
molten metal-reactor coolant interaction, vapour film collapse expts. 79—13474
MSBR, locked rotor accident anal., point reactor model 79—54521
MSBR safety anal. using one point kinetics model 79—22400
MSR for efficient fuel utilisation without Pu separation 80—678
multichannel low flow, boiling thermal hydraulic anal. 79—67885
multiple reactor sites, simultaneous accidents, concept of exclusion area 77—46346
multiple volume blowdown expt. and prediction comparison 79—93814
multiple-support excitation piping problems, automated anal. 79—9773
multiplex systems, reliability, reliability with repair and availability 79—41012
N-reactor, radiation source control, chemical decontamination 80—23058
national programmes, aspects 78—697
natural-circulation steam generator model for optimal steam generator water level control 80—68876
NDT of special nucl. materials 78—82443
near plume impingement press., method of characteristics 77—38362
near-stack dose calc., diffusion model applicability 78—94147
network computations using a transient two-phase velocity difference model 79—26477
neutron detector telecontrol device with direct loading in reactor core and vertical channels of IRT-2000 *(Russian)* 80—52770
neutron dosimetry, standardized techniques for appl. beyond reactor core 79—9920
neutron exposure of reactor press. vessel steel, safety limitations *(German)* 77—34405
neutron flux instrumentation commissioning, EM compatibility 79—89466
neutron instrumentation for protection and control of nuclear reactors *(French)* 80—32407
neutron leakage spectra from critical assemblies, depth dose, dose equiv. and quality factor 78—58504
neutron radiography appl. *(Slovak)* 80—76430
neutron radiography of irrad. fuel pins, coupled fast reactivity measurement facility 79—93720
neutron-physical characteristics of Soviet BABETs reactors, startup experience 80—73953
nine-rod cluster, film boiling behaviour 79—89444
noise measurements for plant surveillance and anomaly detection in nuclear power stations 79—97853
non-destructing testing of reactor components using acoustic emission *(Spanish)* 80—57871
nondestructive analysis applications in the nuclear industry 80—13706
nondestructive assay of irradiated nuclear fuel for safeguards, review 78—82495
nonlinear systems, nonparametric system identification, damage assessment of nuclear reactors 80—32325
nonproliferation and safeguards systems 79—81102
nonproliferation treaty safeguards implementation, nuclear facilities in USA 78—820
NORHAV—a Nordic reactor safety evaluation project 79—26619
NRC Reactor Safety Study (the Rasmussen Report), review 79—63750
NRX and process effluents, gamma ray spectrometric anal. 78—29656
N.S. Mutsu, primary shield, mock-up experiments, analysis 78—21782
N.S. Mutsu, radiation streaming, repair plan 78—21781
nuclear accident dosimetry systems, comparison 79—22496
nuclear accident dosimetry systems, Czechoslovak-Hungarian comparison 79—45437
nuclear accident dosimetry systems, neutron and gamma-ray dose meas. 77—38425
nuclear accidents, review 79—618
nuclear accidents, review 79—3207
nuclear containment vessel with attached masses, seismic anal. 77—3181
nuclear energy, technical economic and safety aspects *(Hungarian)* 78—82465
nuclear energy complexes, economic and ecological problems of nuclear power development 79—645
Nuclear Energy Research Centre, Mol, Belgium, emergency plan organisation in event of major accident *(French)* 78—53527
nuclear facility safety requirements and experience in Federal Republic of Germany 79—26621
nuclear fuel, irradiated, transportation by railroad cask 77—74948
nuclear fuel cycle, safeguards implementation technology 78—86660
nuclear fuel movement monitoring, using dosimeter 77—67899
nuclear heating in thick iron slabs at the ORR pool side facility 80—63241
nuclear industry safety criteria 77—65302
nuclear industry value of reliability analysis 78—29619
nuclear installation safety assessment criteria in UK 79—26615
nuclear installations safety, report on 1977 IAEA conference *(Dutch)* 77—83047
nuclear material and facilities, physical protection, IAEA first training course, report 79—76077
nuclear material international safeguards 79—97817
nuclear material security, aggregated systems model for decision making 80—37535
nuclear plant safety system redundancy, cable routine inspection 78—735
nuclear power conf., Chicago, United States, July 1979 80—794
nuclear power in developing countries, regulatory capability transfer 80—13634
nuclear power plan in Holland, a *(Dutch)* 78—13252
nuclear power plant, aircraft impact, simplified derivation of reaction-time history 78—89958
nuclear power plant, class 1E auxiliary power systems, degraded or loss of voltage protection 79—45363
nuclear power plant, quality systems standards comparison 79—22439
nuclear power plant, safety-related induction motor appls. 77—3144
nuclear power plant, seismic design requirements in Japan 79—26747
nuclear power plant control and instrumentation. [conf. Cannes, France (Apr. 1978)] 79—76096
nuclear power plant cost reduction by containment elimination 79—13467

fission reactor safety continued
nuclear power plant design and operation, new security regulations in United States, impact 80—796
nuclear power plant equipment electromagnetic interference and RFI effects 80—57880
nuclear power plant equipment response to airplane crash 77—3186
nuclear power plant fire frequency and core damage probability estimation 79—13461
nuclear power plant in developing countries, safety problems 77—67825
nuclear power plant piping systems under seismic motion, method of residues 77—3182
nuclear power plant safety systems, common mode failures, investigation *(German)* 78—694
nuclear power plant structure probable risk assessment, improved safety system research plan 80—797
nuclear power plants, seismic safety, review 77—374
nuclear power project management, book 79—30875
nuclear power station, safety, USSR basic approaches 79—627
nuclear power station, seismic anal., slab modelling 78—50414
nuclear power stations, ambiental radiology, equipment and methods, review *(Spanish)* 79—45425
nuclear power stations, gross operator error rates, evaluation of operator reliability 79—45371
nuclear power stations, management *(French)* 77—3154
nuclear pressure vessel surveillance capsule remote dismantling and testing 79—9817
nuclear reactor kinetics and control, book 79—26461
nuclear reactor pressure vessels, stress analysis program, STANSAS *(Japanese)* 80—22969
nuclear reactors, computer modules appl. *(German)* 79—49788
nuclear risks, energy source health effects 79—85696
nuclear safety and licensing, OECD member country cooperation 79—26617
nuclear safety aspects at power and fuel cycle plants in USSR *(Russian)* 79—26709
Nuclear Safety Chain concept development to increase operator awareness 80—57931
nuclear safety in France, reactors, waste, and fuel cycle installations 79—71908
nuclear safety issues in Japan *(Japanese)* 79—9894
nuclear safety research reactor, pulsing characts., expt. capability, meas. and evaluation 77—67790
nuclear simulation programme based on a quality system *(German)* 80—57902
nuclear structures, probabilistic design, state of art, research needs 78—94055
NWR, CANDU-type, at Bruce Nuclear Generating Station A, reactor physics meas. 78—21707
occupational doses in Ontario Hydro nucl. power program 77—88285
occupational exposure at Millstone 2 PWR, long-term man-rem meas. program 80—5383
occupational radiation exposure at nuclear power plants, meas. and prediction 79—59182
occupational radiation exposure reduction techniques 79—9898
off-site emergency monitoring systems 78—46178
on-line alarm analysis in the hierarchical control system of the WWR-SM research reactor 79—76104
online digital core protection calculator, thermal margin routine 79—9777
online inform. retrieval system, development 79—26551
operating reactor data retrieval and evaluation system RECORDS 80—13690
operator reliability, Weibull distrib. model 80—63336
operator reliability modelling for nuclear power stations 79—85621
optical instrumentation methods for two-phase reactor flows 80—63313
optimisation with regard to design, materials and testing *(German)* 80—42739
optimized once-through cycle and international nonproliferation objectives 79—85633
optimum trip level of m-out-of-n reactor temperature trip-amplifier systems 79—93741
overpressure conditions in isolated piping section 77—74955
oxide crust thermal stress effect in LMFBR accident 79—13471
oxide fuel behaviour under accident conditions *(German)* 79—49692
oxide fuel element behaviour in fast overpower transient, effect of solid fission products and dislocations 80—623
oxide fuel transient gas release and swelling, generalised parametric model 77—83039
parametric model of transient fission gas release and swelling in oxide fuels 77—42031
partial differential equatn. finite difference solutn. 80—18564
passive containment system 77—42138
pattern recognition methods, fission reactor surveillance appls. *(French)* 80—37477
PBF, cladding temperature, deform., and failure threshold 78—13281
PBF, irradiated fuel rods, behaviour following film boiling operation 78—13282
PBF blowdown tests, thermal hydraulic and mechancial deformation 79—81024
PBHTGR, core behaviour following massive air ingress, graphite corrosion eval. *(German)* 80—83181
PBHTGR, natural convection after heat removal 77—46245
PBHTR, afterheat removal anal. in accidents 77—46244
PBHTR, afterheat removal system failure, radiant heat transfer anal. 80—95364
PBHTR, depressurisation in primary circuit after failure of main coolant duct, analysis 78—25316
PBHTR, design accidents, exam. of temp. coeff. and short time dynamics 79—63781
PBHTR, fission product retention in ultimate accidents 80—13647
PBHTR, space-shielding cross sections 78—25274
PBR, LOCA, evaluation code NAKOGAS-1 79—13492
pebble bed HTR, delayed after heat removal *(German)* 80—106102
pebble bed reactor emergency shut down system *(German)* 77—10480
performance of safeguards technology 78—82484
personnel dosimetry 77—42195
personnel dosimetry and access monitoring by process computers in nucl. power station *(German, English)* 78—17440
personnel dosimetry monitoring, use of evaluation device for rod and process computer at power station *(German, English)* 78—17441
personnel radiation minimisation in nuclear power plants 78—21663

fission reactor safety continued
PFR core meas. rel. to safety and importance 79—97897
PFR Dounreay, radiation and contamination control 80—27834
PFR Dounreay, utilisation of neutrons meas. for shielding calcs. 80—32538
PHWRs in India, reactivity requirements and safety systems 79—26635
physical protection safeguards for nuclear materials and facilities 78—82483
Pilgrim power station, radiation source control activities 80—23059
pipe blowdown, expts. and nonequilib. anal. 79—30960
pipe ruptures, blowout panel considerations in subcompartment pressure analyses 79—67884
pipe whip behaviour, 4B sch-80 pipe under BWR conditions, parametric study *(Japanese)* 79—97825
pipework integrity assessment 79—22431
piping components, fracture mech. methods, safety anal. 79—11698
piping components, safety anal., fracture mechanics methods 79—11699
piping system, crack initiation and propagation, fracture mechanics 80—83193
piping systems under seismic excitation, modal anal. 80—33512
PL-MODT: a modular fault tree analysis and transient evaluation code 79—49784
plant component design, dynamic analysis, nonlinear effects, research status and needs 79—593
plant condition monitoring in nuclear power generating industry, review 80—47612
plant diagnostics—the integrated approach 80—68899
PNP-3000, prototype nuclear process heat reactor, core temp. transients, heat transfer calc. *(German)* 80—83180
pollutant release assessment, JEREMIAH computational system environmental transport and dose calcs. 78—94150
pool heated volumetrically, reactor accident condition, phase change, free surface, thermal instability 78—89960
pool swell dynamics during depressurization 79—30900
pool type reactor, dynamic response of in tank component 79—85663
Pool type reactor, Livermore, safety channel system with on-line testing capability 77—65278
population doses from reactor operation, compliance with appendix I 77—46410
population exposure doses from USSR power plants, evaluation, prediction, regulation *(Russian)* 79—26776
population exposure standards, determination problems *(Russian)* 79—26778
population radiation exposure, radioactive effluent from nuclear facilities in West Germany 79—26781
population risk, implication of WASH-1400 in FRG 77—46351
post LOCA doses, effect of I plateout 77—88254
post-accident filtration design for PWR and BWR containments 79—49739
post-accident heat transfer Leidenfrost temperature for spherical fuel particles 78—17371
post-LOCA containment atmospheres, physical state 79—76087
potential radiation exposure, West German nuclear installations 79—26603
power burst facility fission product detection system 79—54536
power burst facility loop modification, appl. of RELAP4 code 79—89432
power burst facility low pressure CHF in closely packed rod bundle 79—59144
power burst facility testing, assembly of irrad. fuel rods 77—54300
power density limitation system development 80—68884
power plant, contrib. of quality assurance to safety and reliability 79—22438
power plant, failure probability of battery system following loss of AC power 78—17376
power plant, fire protection research 78—21710
power plant availability improvement by surveillance techniques 79—9812
power plant control appls., problems and trends 78—70609
power plant decommissioning, technical and economic aspects 79—26602
power plant design for underground rock cavity location, safety aspects 79—13398
power plant emergencies, prevention of excessive irrad. of staff and population *(Russian)* 78—50286
power plant licensing procedures in the UK 80—27708
power plant machinery monitoring and online diagnostic systems 79—9810
power plant operation, standardised international guide *(Czech)* 77—38383
power plant operational diagnostics and control computerisation 79—3233
power plant safety, merits of separation against multiple failures 79—26626
power plant safety in USSR *(Russian)* 79—26614
power plant safety requirements in rapidly industrialising countries 77—65304
power plant safety rules and standards 77—65301
power plant safety systems, reliability criteria 79—18014
power plants, channel type, graphite BWR, safety problems in USSR *(Russian)* 79—26637
power reactor, off-site power loss probability estimation 79—13460
power reactor, seismic trip system, risk assessment 78—17377
power reactor, water cooled and moderated, tube film boiling heat transfer coeffs. 80—73877
power reactor noise anal. *(Bulgarian)* 78—82488
power reactor resonance determ. by rod-drop method, Fourier anal. 79—22407
power reactor safety and technology, world-wide standardisation by ISO 79—22434
power reactor underground siting feasibility, Californian programme 79—13399
power reactors, loose parts and neutron noise monitoring and diagnostics 78—21712
power station siting safety criteria *(Spanish)* 79—59179
power stations in Italy, district emergency exercises 78—55052
pressure components, common cause failures 79—18012
pressure pulses generated by gas released from a breached fuel element 79—26557
pressure transducer response verification, testing unit and test methodology 78—13253
pressure tube explosive rupture anal. using scaled-down model of CIRENE reactor 80—18449

fission reactor safety continued
pressure tube type reactors, SENHOR-IV computer code for small pipe break anal. 79—89397
pressure tube type reactors, small scale pipe rupture anal. 77—42034
pressure vessel, crack initiation during thermal shock, warm pre-stress 78—41816
pressure vessel, defect detection, strain evaluation laser holographic and speckle photography methods 77—81365
pressure vessel, failure risk due to manufacturing defect 79—22432
pressure vessel, Oconee nuclear station, surveillance capsule results 79—18019
pressure vessel, safeguarding containment *(German)* 79—13433
pressure vessel, ZR-6M rupture test using scaled simulation *(Hungarian)* 78—89964
pressure vessel blowdown two-phase level swell calc. using drift flux correl. 79—89428
pressure vessel brittle fracture, safeguards, American and German ductility requirements *(German)* 79—41017
pressure vessel cracks and elastic fracture mechanics 77—67843
pressure vessel gradient stress fields, stress intensity factor determ., nuclear safety appl. 78—34089
pressure vessel material surveillance capsule, neutron radiation, limiting condition 80—47572
pressure vessel nozzle under internal press. safety against bursting *(German)* 78—17326
pressure vessel prestressed concrete model, gas press. testing *(Dutch)* 79—13436
pressure vessel reliability, sensitivity to material and other factors 79—18018
pressure vessel reliability and sfaety, in-service inspection, surveillance specimens 79—18020
pressure vessel safety and reliability evaluation, two-criteria approach 79—18016
pressure vessel safety technology and accident analysis 77—67840
pressure vessel steel, fracture toughness at elevated temps. 79—20193
pressure vessel steels, fracture toughness 80—81172
pressure vessel surveillance capsule exam., appl. of ASTM standards 79—22436
pressure vessel surveillance capsules, remote disassembly and examination 79—45463
pressure vessel walls, ultrasonic inspection reliability 79—24713
pressure vessels, 3D finite element anal. of surface cracks 79—10535
pressure vessels, acoustic equipment for leak detection during hydraulic tests *(French)* 80—789
pressure vessels, exam. for compliance with safety regulations 78—89954
pressure vessels, prestressed concrete, safety and reliability 79—22412
pressure vessels, remote controlled US pre-service and in-service inspections 78—89955
pressure vessels, thick steel sections, inspection by US nondestructive examination 80—102258
pressure vessels, unconditioned probability of brittle fracture 78—78479
pressure vessels, warm prestressing effects, fracture mechanics during severe thermal shock 79—22411
pressure vessels for LWRs, brittle fracture initiation, propagation and arrest, investigation 79—22422
pressurised heavy water Candu nuclear power plants, safety aspects *(French)* 80—18463
pressurized systems reliability, influence of codes, standards and practices 79—22433
prestressed concrete reactor vessel, 3-D nonlinear failure anal. 77—50268
prestressed concrete reactor vessels, construction movements, finite element anal. 79—621
prestressed concrete reactor vessels, perforated plate ligaments, time varying stress 79—49679
prestressed concrete safety containments, calc. and constructional problems *(Russian)* 79—30961
prestressed concrete vessels, transient anal. for HCDA loads 79—85666
prestressed secondary containments, explosive characts. near ultimate load,, review 79—30968
primary coolant circuit service life, working condition effects *(Czech)* 80—73885
primary coolant inlet of PWR vessel, fracture mech. exam. of integrity *(German)* 78—17327
primary piping loop response to HCDA, fluid dynamics, shell deformation 77—6509
principles underlying IAEA nuclear safety programme 80—95361
probabilistic anal., 1978 American Nuclear Society meeting, overview 78—82468
probabilistic analysis, review of ANS symposium 79—45354
probabilistic approach *(French)* 77—18677
probabilistic assessment of risks, of accidents and normal operation 78—50281
probabilistic methods, reliability and risk analysis, Fed. Rep. Germany 80—106124
probabilistic methods for risk assessment and safety standard 78—21693
probabilistic methods in safety analysis and regulations in France 80—106123
probabilistic methods in the field of reactor safety in Germany 79—71907
probabilistic risk assessment, methodology and appls. 80—63352
probabilistic risk assessment 77—46344
probabilistic siting analysis, atmospheric releases, health effects 80—106130
probabilistic structural design, component level, Monte Carlo simulation approach 78—94056
probability approach to reactor safety, Safety and Reliability Directorate 79—71904
prompt burst energetics experiments, UC series, fuel cladding coolant systems 79—49768
prompt burst excursion experiments, fuel pin modelling 79—49769
protection system, development of integrated numerical protection system *(French)* 79—76097
protection system and engineered safeguard system separation review program 80—57820
protection system design criteria 80—68935
protection system design using microcomputers 77—67823
protection system equipment, class 1E, qualification requirement 77—67822
protection system performance, impact of ageing mechanism 79—18000
protection system software validation, quality assurance experience 80—57886

fission reactor safety continued
protection systems, treatment, analysis and presentation of information on component faults and [nuclear power] plant disturbances 79—76098
protective coating, for components in contact with HTR-He, CVD W coatings 79—626
protective system, optimum supervision intervals and order of supervision 78—37419
protective systems, proability level of readiness anal., four-state Markov process 80—27762
pulsed-neutron sources for flow measurement 79—93695
pump-induced acoustic pressure distribution in an annular cavity bounded by rigid walls [pressurised water reactor] 79—72848
PURINAMA, PuO$_2$-fueled zero-energy fast reactor 79—40988
PWR, 1300 MW, emergency core cooling system probabilities design 77—38365
PWR, 900 MW, probabilistic determ. of operating rules 77—46345
PWR, accident with loss of coolant, computer-aided calc. *(Slovak)* 78—29594
PWR, alternative ECCS concepts, verification study 80—13539
PWR, availability of pressure vessel after small LOCA 79—30967
PWR, behaviour of previously failed fuel rods under power ramp and film boiling operation 79—49745
PWR, calcs. of neutron environment inside containment 80—13676
PWR, cavity streaming problem, shield config. optimisation 80—9352
PWR, choice of vent flow formulation for subcompartment anal. 79—31047
PWR, clad free pellet recriticality possibilities 80—68863
PWR, combined injection reflood studies 79—31062
PWR, comparison of containment leak rate data analysis methods 77—42143
PWR, computer code for the study of migration and deposition of corrosion products 80—13700
PWR, computer program for accident anal. *(German)* 79—85623
PWR, computerised axial power distrib. monitoring system 77—65279
PWR, control and effects of pressure vessel failure in steam-water cycle 80—770
PWR, control of fission products activity in primary coolant, computer code 80—32537
PWR, control systems for selectively inhibiting protection system functions 78—37418
PWR, coolant pump motors, max. freq. decay rate determ. 79—45337
PWR, core reflooding, progress of hardening front *(French)* 80—91211
PWR, depressurisation accident, CUPIDON anal. of fuel rod behaviour *(French)* 80—42791
PWR, determ. of typical accidents and consequences, rel. to emergency planning *(French)* 78—50285
PWR, ECC performance during LOFT expts. 78—21709
PWR, effects of early core flow predictions and CHF correl. characts. in RELAP4/MOD5 best estimate blowdown calcs. 79—31059
PWR, emergency core cooling, alternative injection configurations 78—21696
PWR, engineered safeguards, human failure 80—42788
PWR, European Community Italian Centre activities *(Italian)* 80—785
PWR, evaluation of emergency conc. cooling systems 78—21697
PWR, evaluation of environmental and in-plant effects of T recycle and build-up 78—33273
PWR, fast-neutron dose rate meas. inside containment shell 80—13674
PWR, fluid-structural interactions, one-dimensional networks, MULTIFLEX code 80—13535
PWR, flux monitoring startup and safety system, ex-core, design and qualification 77—65286
PWR, French, cracks in containment vessels *(French)* 80—32387
PWR, french R and D development program 79—97843
PWR, French safety studies 80—5265
PWR, generic safety issues rel. to use as commercial power plant in UK 78—21662
PWR, German, U-tube steam generators, inspection findings 79—9849
PWR, I spiking in coolant for defective fuel rod operation 78—33272
PWR, improved instrumentation and computer control systems 78—29601
PWR, internal vibration calc. rel to operational safety condition *(Czech)* 78—8915
PWR, JAERI, test of LOCA/ECCS anal., code verification, by participation in LOFT program *(Japanese)* 77—50256
PWR, LOCA, anal. of LOFT semiscale test *(Japanese)* 79—17998
PWR, LOCA, anal. of simulated small break in semiscale system 80—13656
PWR, LOCA, cold leg break during blowdown, ROSA II study *(Japanese)* 79—6750
PWR, LOCA, one-dimensional network for multidimensional pressure wave propagation with hydrostructural interactions 79—89403
PWR, LOCA, phase-change front propagation during reactor transients 79—631
PWR, LOCA, RELAP4/MOD6 program, test prediction for German PKL test K5A 80—13642
PWR, LOCA, steam-water mixing 80—13651
PWR, LOCA anal., turbulent flow in fuel rod bundle with partial flow blockages 79—30898
PWR, LOCA anal. for consolidated nuclear steam system 79—49729
PWR, LOCA performance test of upper heat injection system 79—81028
PWR, LOCA test, effect of LOFT pressurizer on RELAP4/MOD5 modelling 78—13286
PWR, loss of coolant accident, mathematical model *(Czech)* 77—3072
PWR, low-pressure drop reactor cavity shield system 80—13677
PWR, meas. of transient steam/air fraction in vent pipes 79—31044
PWR, meltdown accident risk-analysis 79—45375
PWR, MULTIFLEX code, anal. of hydraulic force with hydro-structural interactions during LOCA 78—58373
PWR, new design procedure for DNB limits 80—573
PWR, normal operating radiation levels 77—88290
PWR, Obrigheim nuclear power plant, inservice inspection, nondestructive testing, primary components *(German)* 77—34406
PWR, occupational radiation exposure 78—21664
PWR, Oconee, occupational exposures, radiation levels and waste levels during operation 78—21726
PWR, operational dynamics, digital simulation model 80—27751
PWR, peak cladding temp. sensitivity to LOCA reflood parameters 78—86639
PWR, post LOCA accident doses to equipment 77—88255
PWR, power stations containing VVER-440 reactors, radiation safety of personnel and local population 77—71700

fission reactor safety continued
PWR, primary coolant leak *(French)* 79—63724
PWR, primary coolant leakage accident, flow models *(French)* 79—63725
PWR, probabilistic anal. of interfacing system in LOCA 78—21678
PWR, Pu recycling, CEA-EdF studies 80—722
PWR, pump operation with two-phase water-steam flow *(French)* 79—63726
PWR, quality assurance by Framatome 80—782
PWR, radionuclide surface activities meas. 80—13941
PWR, reactor cavity shield system, design and anal. 79—59225
PWR, reactor coolant pump failure investig. at Arkansas Nuclear One 80—9336
PWR, reactor safety anal., sensitivity assessments, plant risk 77—18676
PWR, release of radioactive material, ability to meet appendix I to 10CFR50 77—46306
PWR, releases of radioactivity reported in the LER file (1971-1977) 79—85647
PWR, reliability assessment of containment 78—78481
PWR, RETRAN simulation of the Three Mile Island Unit 1 turbine trip test 80—18512
PWR, rod ejection accident anal. by reactivity weighting method 79—22419
PWR, ROSA-II UHI tests in JAERI 78—21695
PWR, safety aspects of using Gd as burnable poison 80—13662
PWR, selection of events for probabilistic safety assesssment 80—742
PWR, sensitivity of emergency core coolant bypass and lower plenum refill to scale size and plenum press. 79—97827
PWR, sensitivity of LOCA heat transfer anal. 78—50246
PWR, sensor response monitoring, time series modelling 79—26659
PWR, shielding against neutron and gamma streaming, computational methods 78—21783
PWR, shutdown heat removal systems, reliability fault tree anal. and β-factor method 80—63331
PWR, small scale ECC bypass data anal. 80—18505
PWR, souces of ^{131}I airborne release 80—17138
PWR, St. Lucie 850 MWe, neutron streaming meas. and shielding recommendations 78—70608
PWR, steady-state and transient CHF meas. in Freon-11 79—49732
PWR, subcompartment pressure-temp. response comparison between anal. and exptl. results 79—31050
PWR, superheated containment atmosphere heat/mass transfer to passive heat sinks, analytical model 79—49658
PWR, survey of neutrons inside containment 80—13675
PWR, T sources, releases, monitoring, management and environmental impact 80—18690
PWR, thermal and hydraulic design considerations 79—49651
PWR, Three Mile Island, Pennsylvania, USA LOCA 79—89398
PWR, Tihange-type, Pu recycling, physics and safety anal. 80—724
PWR, Tritium transport at nuclear power stations 80—23032
PWR, Trojan reactor, net free containment vol. 78—21679
PWR, two circuit system, licensing and design, European view 80—57930
PWR, two phase flow modelling for LOCA *(French)* 80—78349
PWR, two-phase blowdown from horizontal pipe, unequal phase vel. and temp. theory appl. 77—39335
PWR, two-phase critical flow in long nozzles 80—13550
PWR, welded control rod drive mechanism, automated removal/installation 80—9358
PWR, w.r.t siting in densely populated areas *(Czech)* 77—50261
PWR, WWER-440 type, piping structural anal. after large pipe break 77—6511
PWR accident prevention, extra instrumentation for Ringhals 2 station, Sweden 80—63369
PWR and BWR hot channel factors, nuclear, thermohydraulic and technological factors *(Spanish)* 79—36336
PWR and BWR pressure vessels, safety calcs., design, operation control, neutron effects *(German)* 77—34404
PWR and PHWR-Candu types, qualitative comparison of nuclear safety features *(Slovenian)* 80—95358
PWR anticipated transients, coupled core system approach to DNB 77—42154
PWR assemblies, spectral and density components of moderator temp. coeff. 80—9356
PWR blowdown, pressure field and core barrel loadings, computer codes 80—13665
PWR blowdown processes, homogeneous nonequilibrium model 79—632
PWR boiler steam generators, two-phase flow problems in low press. transients *(French)* 80—78350
PWR boiler tubes, denting type corrosion, control by use of neutralisers 80—106109
PWR CANDU, corrosion product transport, deposition on fuel bundles, press. tubes 77—61492
PWR containment, effect of separation of steam and air in blowdown transients 79—31045
PWR containment air monitoring system 80—57965
PWR containment building, design and anal. of cavity shield system 80—18713
PWR containment design margins *(German)* 78—717
PWR containment isolation using butterfly valves 78—13256
PWR containment pressure-temp. transients eval., nonequilibrium states 79—31048
PWR containment vessel optimisation 80—106137
PWR containment vessel wall electrical penetration tests *(Japanese)* 79—6747
PWR containments following LOCA, heat transfer coefficient 80—86958
PWR control, computer program *(German)* 79—59249
PWR control elements, Decontic control system appl. and features *(German)* 79—26548
PWR coolant pH effect on radiation field buildup 80—23060
PWR coolant system, pipe rupture motion, time-history excitations 80—47602
PWR coolant system under seismic and LOCA loads, dynamic anal. 77—6512
PWR core meltdown accident, computer simulation of second phase 80—754
PWR core thermal-hydraulic response during steam line break accident 80—18384
PWR damage calculations using CASK and EPR multigroup libraries 80—47670

fission reactor safety continued
PWR defective fuel rod, effect of thermal cycling on fission product release 80—13669
PWR depressurisation, hydraulic analogy 78—50243
PWR design and plant layout, safety criteria 80—102288
PWR downcomer annulus model, correl. for penetration of ECC water 79—76085
PWR ECC system performance, best-judgement anal. 77—57728
PWR engineered safety features actuation system follow-up system logic 80—57879
PWR experimental rig, high pressure loop cooling circuits safety aspects *(German)* 80—32397
PWR flow transients, critical heat flux predictions using CODA 1-D coolant dynamics code 80—42817
PWR for commercial electricity generation in Britain 77—79468
PWR fuel anal. and testing, contrib. of LOFT 79—89437
PWR fuel assemblies, LOCA behaviour in multirod burst tests 80—27739
PWR fuel clad failure characterisation based on fission product activity, PROFIP 3 code 80—95365
PWR fuel rod, parametric study on influence of prepressurisation 80—13643
PWR fuel rod behaviour under power-cooling-mismatch conditions 80—42818
PWR fuel rod failure during film boiling, power cooling mismatch test 79—89445
PWR fuel rod failure during film boiling operation 80—18501
PWR fuel rod meltdown behaviour during LOCA 80—42832
PWR fuel rods, I spiking, cause and effects 79—59227
PWR fuel rods, I spiking, general model of origin and behaviour 79—59228
PWR fuel rods testing at power burst facility 77—38361
PWR fuel rods. unirradiated and irradiated, pellet-cladding interaction phenomena 79—31053
PWR fuel storage, criticality eval. of low-density moderation 79—26667
PWR fuel storage pool, safety calcs. and benchmarking 79—26565
PWR hypothetical LOCA, best estimate evaluation model 79—89435
PWR hypothetical LOCA sensitivity to fuel rod material props. 79—89436
PWR ice condenser plant, dominant accident sequences 79—85646
PWR instrumentation operating experience during start-up and operation 79—89456
PWR internal vibrations, neutron noise monitoring 79—13445
PWR internals, effect of water flow on behaviour and safety *(Czech)* 77—50258
PWR internals, vibration mode shape computation and expts. 79—13444
PWR LOCA, average void fraction estimate in vertical two phase flow channel 80—73878
PWR LOCA, balloon deformation of Zircaloy fuel cladding 80—659
PWR LOCA, blowdown fluid loadings, anal. of structural deformations 80—766
PWR LOCA, blowdown hydraulic influence on core thermal response in LOFT nuclear experiment L2-3 80—42827
PWR LOCA, cavity pressurization relief with rotating neutron shield tanks 79—31049
PWR LOCA, containment accident analysis using CONTEMPT4/MOD2 compared with experimental data 79—49738
PWR LOCA, coolant channel blockage during reflood phase influence of blockage shape 80—765
PWR LOCA, determ. of 3-D props. of pressure wave propagation by method of characts. 79—89402
PWR LOCA, drift flux appl. to transient two-phase level swell 79—81027
PWR LOCA, droplet cross-flow phenomena in a large PWR upper plenum 80—47627
PWR LOCA, effect of cold-leg injection of low press. coolant, ROSA-II study *(Japanese)* 78—17334
PWR LOCA, effect of rod external thermocouple simulators on steady-state and transient CHF for LOFT reactor 79—49734
PWR LOCA, effect of steam generator tube rupture, computer simulation 80—23006
PWR LOCA, effects of downstream geometry on blowdown of subcooled liquid 79—31063
PWR LOCA, fuel rod behaviour, probabilistic anal. using response surface method 80—663
PWR LOCA, generalized model for predicting mass effluence during reflooding 79—31056
PWR LOCA, high-pressure Freon blowdown studies with inlet break 79—36367
PWR LOCA, licensing evaluation calcs. at LOFT 80—23008
PWR LOCA, LOFT post-test anal. using RELAP4/MOD5 blowdown model 80—42825
PWR LOCA, LOFT safety anal. calc., carryover rate fraction correl. 80—42822
PWR LOCA, LOFT tests, TRAC-P1A pre-test calculations 80—42824
PWR LOCA, long ballooning deformation of fuel cladding 80—660
PWR LOCA, multirod burst tests of Zircaloy fuel claddings 80—777
PWR LOCA, opening and extension of circumferential cracks in pipe 80—78364
PWR LOCA, pressure vessel hydrodynamic loads, effect of subcooled critical flow discharge model 79—49733
PWR LOCA, pump behaviour conveying two-phase flow *(French)* 80—78351
PWR LOCA, refill and reflood phase, expt. results of combined injection using PKL test facility 80—760
PWR LOCA, ROSA-II severe hot leg break for core cooling during blowdown *(Japanese)* 79—9769
PWR LOCA, subcooled decompression, multidimensional wave prop. with FLASH-genre codes 79—59194
PWR LOCA, upper plenum LPIS injection in the Semi-scale MOD-1 system 79—49727
PWR LOCA, Zircaloy-4 fuel cladding axial deform. 80—13585
PWR LOCA best estimate anal. using TRAC 80—18521
PWR LOCA reflood, effect of low containment press. on peak cladding temp. 80—57897
PWR LOCA reflooding phase, two-phase flow and heat transfer at and near quench front 80—757
PWR LOCA Standard Problem 5, TRAC-P1A anal. 80—42823
PWR LOCA systems transient response, scaling conclusions from the LOFT nonnuclear experimental series 80—758

fission reactor safety continued
PWR LOCE at LOFT facility, instrument calibration for mass flow rate meas. in two-phase flow 80—37552
PWR main coolant system components, safety assessment 77—71661
PWR neutron noise meas. and modelling 79—13443
PWR non-LOCA transient anal. using IRT code 80—42819
PWR overpower detection for conrol element assembly ejection transients 80—42820
PWR plant, cut-and-cover construction, feasibility and safety *(German)* 78—82429
PWR power plant, assessment of underground siting as engineered safety factor 78—13316
PWR power plant, development trends *(German)* 78—50282
PWR power plant, primary cct. leakage simulation *(German)* 78—33239
PWR power plant, radiation protection *(French)* 78—82521
PWR power plant, safeguard system, diagnosis of fault conditions using fault trees 77—6549
PWR power plant, vibr. and press. signals, information for online vibr. monitoring system 77—18674
PWR power plant steam dump valve stability anal. 78—50289
PWR power plants, design concepts to facilitate dismantling 80—13577
PWR power plants, safety technical problems, core cooling *(Russian)* 79—31085
PWR power stations, operating record and reliability, reviews 79—22404
PWR pressure components reliability and residual life evaluation and precipitation 79—20191
PWR pressure transients, sensitivity anal. 80—769
PWR pressure vessel availability after small LOCA 79—31055
PWR pressure vessel failure probability from pressure transients, OCTAVIA computer code 79—18011
PWR pressure vessel reliability, simplified model extension and appl. 80—27786
PWR pressure vessel safety, term paper from course at Georgia Tech 78—58379
PWR pressure vessel vibration excitation, noise correlation and modelling 79—13442
PWR pressuriser behaviour during operational transient, math. model 80—63230
PWR primary cct., corrosion product transport and radiation field growth 77—88256
PWR primary circuit, in-service inspection *(French)* 79—22385
PWR primary circuits NDT 80—5268
PWR primary coolant after fuel failure, dynamic behaviour of tag gas isotopes 77—46363
PWR primary coolant system, in-service inspection programs 79—22384
PWR reactivity changes, influence on transient processes *(Slovak)* 79—36343
PWR reactor, steam generator accidents, rel. to impurity enrichment in boiling on surface coated with porous struct. 78—2365
PWR reactor core barrel, vibrations, influence of boundary conditions and co-vibrating liquid obs., using model 79—36302
PWR reactor with reactivity perturbations, accident anal., methodical approach *(Czech)* 79—22402
PWR reflood, analytical treatment, computer code 79—89425
PWR reflood simulation of FLECHT-SET system using RELAP4/MOD6 78—13285
PWR refuelling shutdown 80—23066
PWR rod bundles, radiative heat transfer calc. method 80—33602
PWR rods subjected to simulated LOCA in PBF 79—89443
PWR safety analysis, hybrid method of void fraction prediction, depressurization of diabatic systems 77—23222
PWR safety considerations in USA 79—26630
PWR scaled expts., ECC delivery and distrib. 79—89424
PWR scaled expts., ECCS accumulator performance 79—89427
PWR shield configs., concrete attenuation effectiveness, numerical studies 77—38356
PWR shutdown, fission I increased release from defective fuel rods 79—49710
PWR steam generator, γ-dose rate distrib. meas. 80—5382
PWR steam generator blowdown review of international handling procedures 80—690
PWR steam generator chemical cleaning 79—93819
PWR steam generator degradation, operating experience, regulatory considerations 79—93817
PWR steam generator force anal. during LOCA 80—13666
PWR steam generator operations, Westinghouse, benefits of contaminant control 79—93818
PWR steam generator tube rupture, probability distrib. for releases of ^{131}I and ^{133}Xe 80—13668
PWR steam generator tube rupture accident, radio-I behaviour 79—59230
PWR steam line break, pipe rupture probability 80—18526
PWR surveillance, empirical and physical models 77—42150
PWR transient anal. methods, qualification with plant startup meas. 80—18508
PWR transients, safety research by CEA and EdF 77—42155
PWR two-loop system with spherical containment and integrated air locks 77—46358
PWR vessel and primary circuits estimation of reliability, probabilities and adaptive models 80—106125
PWR West German risk evaluation study, interim report 77—74960
PWR with combined ECC injection, TRAC anal. of LOCA 80—18522
PWR with reactivity perturbations, accident anal. by FATRAP code, logic construction *(Czech)* 79—30957
PWRs, auxiliary feedwater system, fault tree anal. 78—54867
PWRs, fault analysis and calcs., FORTRAN program *(German)* 79—41018
qualification of class 1E transmitters 77—65287
quality assurance, effects on reactor safety 80—47628
quality assurance, need for sensible interpretation 80—57932
quality assurance criteria, international standardisation 80—780
quality assurance program for nuclear plant operations 80—783
quality assurance programs, development, application and results 80—42830
quality assurance requirements, impact on reactor safety 80—42828
quality assurance requirements and reactor safety, public utilities viewpoint on regulations and their implementation 80—42829
quality assurance requirements in Western Europe and the USA 80—47629
quality assurance standards in USA, present status and appl. 80—781
quality control systems by acoustic emission 79—93758

fission reactor safety continued
quantifying plant availability, ALARA, and occupational radiation exposure relationships 79—59183
quantitative methods of assessing risks 80—57903
quantitative risk anal., limitations 77—46354
quantitative risk evaluation, risk projection and human factors as related to nuclear systems 80—13722
quasi-redundant protective systems, optimal design 79—17996
quasilinear reactor system subject to white Gaussian multiplicative noise, moment stability anal. 79—22373
radiation doses to equipment inside containment of power reactors 77—88253
radiation exposure ALARA concept 80—32388
radiation exposure and protection 78—25301
radiation field functional calc. method for shielding parameters 79—71928
radiation field reduction, several techniques 77—6572
radiation heat transfer in a 19-pin sodium-voided bundle 79—85596
radiation heating in stainless steel and Na shield 79—9903
radiation monitor for nuclear power station radioactivity meas. *(German)* 79—67876
radiation monitoring, digital data collection and display 79—59278
radiation monitoring, distributed processor-based system for large scale power plant monitoring 79—59280
radiation monitoring, in-plant standards 79—59276
radiation monitoring, on-line computer appl. 80—5391
radiation prediction around out-core components 77—6571
radiation protection, ALARA inplant design for occupational radiation exposure, cost-benefit anal. 80—18547
radiation protection, regulatory control, implications of ICRP publication 26 80—18706
radiation protection estimation of individual and collective equivalent dose *(Spanish)* 80—5336
radiation protection/shield design, systematic approach 78—21779
radiation qualification of reactor components 77—88252
radiation risks in nuclear industry, comparison to other jobs 80—18680
radiation safety in nuclear power stations, doses to personnel, local population 77—71701
radiation safety monitoring instrumentation complex at the USSR nuclear power plants *(Russian)* 79—76108
radiation shielding, cross section sensitivity analysis 78—21778
radiation source control programs at EPRI 80—23056
radiation source reduction, potential benefits of occupational radiation exposure reduction 80—23057
radiation streaming, shield design problems 78—21780
radioactive aerosol dispersiveness in main ventilation system 78—70650
radioactive effluent release reduction, Japanese LWRs 79—31078
radioactive material leakage, accident risk 77—67820
radioactive plume in atmosphere, depletion calc., and exposure from deposited activity 79—66561
radioactive pollution from nuclear power stations, accident anal. 79—63782
radioactive products transport, model, air concentration in working rooms *(Russian)* 77—42110
radioactive release following PWR LOCA with an initially breached containment 80—47631
radioactive releases and waste disposal, CEGB Research Division report 78—46145
radioactive releases from nuclear installations, eval. of accidental atmos. discharges 79—39529
radioactive waste, final disposal possibilities, waste conditioning, storage and safety, review 79—26554
radioactive waste hazards due to Th fuel cycle use in power reactor systems 79—30941
radioactive waste management, influence on standardised plant design 77—46307
radioactivity at nuclear installations, standards rel. to dose and radioactive waste limits *(Spanish)* 80—52789
radiochemical control of reactor cooling water *(Korean)* 78—54820
radioisotope relays, operation, construction and appl. *(Polish)* 80—106129
radionuclides in reactor circuits, continuous meas. techniques *(French)* 79—97857
rapid automated nuclear chemistry, short lived fission products, reactor safety 80—81353
Rasmussen report on reactor safety, retrospective and prospective view 79—26632
reactivity determinations for performance of reactor safety, economics, operability *(Japanese)* 78—17332
reactivity worths of neutron absorbing materials, critical expts. 77—42023
reactor accidents and the environment 79—30940
reactor components inspection by acoustic emission *(German)* 79—45373
reactor containment, nonlinear dynamic response, seismic analysis 77—3180
reactor containment development for PWRs, BWRs and HWRs 79—26643
reactor containment expts., Fourier transform anal. of transient condensation heat transfer coeff. 79—22410
reactor containment response to HCDA anal. with MICE code 77—42029
reactor core melt frequency, probabilistic model using prob. of rare events 79—54526
reactor incident duct plugging by aerosol deposits, simple model 79—49782
reactor loop, experimental, hazard and protection from tritium 79—36420
reactor portal monitors, evaluation and vulnerability anal. 79—49722
reactor protection computer systems, statistical verification of reliability 80—32417
reactor protection system, electrical isolation devices employing fiber optic cable 79—59218
reactor protection system, in-core power distribution synthesis from three-segment ex-core detectors 79—9865
reactor radiation damage, neutron metrology for irradiation parameters 79—46717
Reactor Safety Study (Wash-1400) and implications for radiological emergency response planning 78—50284
reactor shielding, current status and future prospects 78—25328
reactor shielding methods, development in USA 78—21776
reactor shielding methods, evolution, data 78—21775

fission reactor safety continued
reactor trip system, design of internal architecture for Westinghouse microprocessor-based [nuclear reactor] integrated protection system 79—76100
reactor vessel design-basis-accident presure-pulse prediction using SPIRT code 79—89361
redflood heat transfer correlation 80—13548
redundancy systems, common mode failures 80—13641
reflood heat transfer mechanisms 77—46241
refueling and fuel handling, ALARA occupational radiation exposure 79—67914
regional nuclear fuel cycle centres. IAEA study project 79—31119
regulations in Japan 80—47599
regulatory activities and their research and developmental support in the CSSR 79—26625
regulatory control ot nuclear power stations in the United Kingdom 80—18707
regulatory problems, fuel cycle, safety management 77—50263
reinforced concrete, nonlinear dynamic response under loading, research status and needs 78—94054
reinforced concrete containment model behaviour under thermal gradients and internal pressure 80—42837
reinforced concrete containment structures, improved design, research requirements 78—94049
reinforced concrete structs., missile impact loading, nuclear power plant appl. 79—31237
reinforced concrete structures, under missile loading, finite difference code 80—13956
reliability analysis, unavailability of systems under periodic test and maintenance 80—95368
reliability appl., nuclear station safety estimation 77—10471
reliability improvements of nuclear reactor instrumentation 80—32416
reliability in design of reactor safety equipment 80—37555
reliability technology, role of ASTM in providing standards 79—22435
reliability technology 78—701
remote and continuous inspection of nuclear plants, safety requirements 80—5295
remote inspection system, for nuclear power stations 79—45386
remote multiplexing control and safety systems evaluation 79—76109
remote US inspection unit for piping and vessel inspection 80—104394
reprocessing equipment, neutron poisons appl. *(German)* 77—34407
reprocessing in-process inventory dynamic measurement computer simulation 77—38371
research and training reactor, ALARA program review at Texas A and M University 80—9362
research needs, standards improvement, nuclear power plant design 78—94046
research programmes of Swiss Federal Institute for Reactor Research 80—52722
residual power after shutdown. afterheat estimation *(Slovak)* 77—82997
response surface of fuel-cladding gap conductance determ. by power oscillations 77—50267
review and research 77—61510
review of accident prevention and control *(French)* 80—52747
review of safety, proliferation and theft 77—74953
rewetting process, exptl. and numerical anal. 77—46243
ribbed core shroud, ex-core detector shape annealing functions 79—93792
risk acceptability criteria development 78—29616
risk analysis, computer role 77—38373
risk analysis of nuclear systems, anal. of human performance 80—18475
risk analysis of the fuel cycle in the Netherlands 79—26624
risk assessment, role in nuclear regulatory processes 79—71906
risk assessment in absence of complete data, freq.-consequence model 77—83062
risk assessment in European Community 80—106135
risk assessment of necessary functions for protection against external accidents 80—743
risk Assessment Review Group report to the US Nuclear Regulatory Commission 79—97821
risk estimates, communication techniques 80—18514
risk estimation, evaluation, and management 78—17350
risk estimation methods and wider applications *(French)* 79—89492
risk evaluation model, on-site meteorological data, environmental consequences 80—36155
risk-benefit evaluation of nuclear power plant siting, comparison with coal-fired power station *(Czech)* 78—50266
rod bundle blowdown heat transfer instrumentation, transient two-phase flow meas. 80—685
rod bundle critical heat flux at low pressure 80—13547
rod thermal response during isothermal loss of coolant expt. 79—89447
rod thermal response during isothermal loss-of-coolant experiments 79—85651
routine operation, importance of personnel training 77—34415
routine reactor operation safety 77—67841
against sabotage and natural catastrophes, measures *(German)* 77—42158
safeguard systems effectiveness, SNAP network analysis technique 79—26658
safeguarding of nuclear facilities, methodology to aid decision-making 80—18477
safeguarding on-power-fuelled reactors—instrumentation and techniques 79—26657
safeguards for control and accounting, NRC program 79—85619
safeguards network anal. procedure, SNAP, appl 80—47672
safeguards planning in plant design process 78—82423
safeguards systems, directed graph and fault tree anal. of material theft detection 80—13728
safeguards technology, present status *(Japanese)* 79—26783
Safety and Reliability Directorate, development and work 79—71902
safety in nuclear power stations, statutory requirements 77—79485
safety test facility configurations, performance 77—46338
San Jaoquin site, Bakersfield, California, palaeomagnetic study of faulting history rel. to safety 78—40487
SAREF test fuel motion reactivity feedback, experimentally based limits 79—49775
scram system, appl. of three-valued logic 77—46348
secondary system fission product transport study at the Oconee Nuclear Station 79—49781
secondary system radioactivity monitoring 80—18445
SECURE district heating reactor, core design and dynamics 78—37424
SECURE nucl. district heating plant, safety evaluation 78—37422

fission reactor safety continued
- security, sabotage and terrorist attack, statistical anal. of threat reality and consequences 80—13727
- seismic amplification factors of reactor components 79—597
- seismic anal. 78—41834
- seismic anal. of nuclear plant, multicountry application 77—65306
- seismic areas, nucl. power plant siting 78—82481
- seismic design, automated generation of spectrum compatible artificial time histories 78—29661
- seismic design, probable simultaneous response by response spectrum method 77—83060
- seismic design of power plants 77—3179
- seismic design standardised spectra for plant equipment 78—41870
- seismic effects in secondary containments: research needs 78—94050
- seismic input through rigid foundation filtering 78—29659
- seismic instrumentation for nuclear power plants in Germany, review 79—620
- seismic load effects on structures, R and D requirements 78—94051
- seismic load studies on nuclear power plants, research needs 78—94052
- seismic qualification of Class 1E eqpt. 80—99234
- seismic qualification of safety-related instrumentation cabinets 80—23063
- seismic qualification of systems, structures, equipment and components 78—41878
- seismic qualification tests of elect. eqpt., damage severity factor concept 80—99235
- seismic response, modal response method 77—83059
- seismic response of flexible cylindrical liquid storage tanks 79—31241
- seismic response spectrum normalisation 78—50415
- seismic safety margins research program of the US Nuclear Regulatory Commission 80—99229
- seismic safety of mechanical eqpt., R and D program 80—99232
- seismic testing for class 1E equipment 78—78475
- seismic testing motions anal. with instantaneous response spectra 79—22498
- seismically qualified piping, failure probability, ASME code limits 80—78365
- semi-elliptical fault fatigue propagation, three-dimensional anal. *(French)* 79—23283
- semiscale isothermal blowdown, appl. of self-initialized RELAP4 momentum eqn. 78—13287
- SGHWR, radiation protection and plant maintenance 80—27789
- SGHWR fuel performance, safety and reliability 79—36333
- SGHWR safety design and evaluation 79—26636
- shielding, 6 MeV gamma photons penetration through Al, concrete and graphite determ. 80—5256
- shielding, reactor types review and appl. *(German)* 78—29638
- shielding benchmark calcs. by Discrete Ordinates and Monte Carlo methods 80—73886
- shielding design, two-dimensional discrete ordinates calc. characts. *(Japanese)* 79—93744
- shock absorbing reactor auxiliary building for aircraft impact loading, design criteria *(German)* 79—89348
- shut-down control, optimal, of unconstrained bilinear systems 77—10464
- shutdown heat removal system failure, fault tree, common-cause anal. 80—63334
- shutdown system reliability, effect of operator performance 78—29611
- Shutdown System Reliability Duty Cycle generation method 78—29620
- SIMMER II results, statistical anal. for postdisassembly in vessel dynamics 79—49786
- simulated meltdown experiment, modified diffusion coeffs. for neutron streaming 78—33278
- single core subassembly model, coupling of struct. and coolant response 78—8934
- siting of power plant, geological and seismology surveys of US midcontinent 78—85501
- Sizewell power station, radiation and contamination control 80—5387
- skyshine dose due to gamma-rays from nucl. power plant *(Japanese)* 79—29917
- SLSF P3, cladding motion in 37 pin loss-of-flow expt. 80—18541
- small bore piping, field support to ASME Section III rules 80—63346
- SNR 300 shutdown systems 79—97866
- SNR-2, design studies for heterogeneous core concept 78—13226
- SNR-300, coolant outlet duct design from neutron transport experiments *(German)* 78—29566
- SNR-300 LMFBR, accidents in tertiary system, dynamic behaviour of steam generators *(German)* 80—83141
- SNR-300 LMFBR, ECCS, decay heat removal during heat sink failure, accident anal. using NOTUNG code *(German)* 80—83185
- SNR-300 LMFBR, hydrodynamic characteristics of shutdown systems 80—5289
- SNR-300 LMFBR, response to reactivity insertions *(German)* 80—83183
- SNR-300 LMFBR steam generator transients, computer simulation 80—23012
- snubber evaluation program 80—63345
- snubber operability criteria for increased seismic safety 80—9364
- society effects of nuclear power developments 80—47590
- software coding for reliable data communication in reactor safety system 79—13496
- soil-structure interaction anal. by finite elements 78—41879
- solid state trip system 79—6753
- solid state trip system 79—63758
- Spanish research is radiological protection *(Spanish)* 77—38419
- spent fuel bundle counter, performance study 80—23064
- spherical element surface boiling dynamics 80—27736
- stability analysis and characts. for two-phase flow eqn. systems with viscous terms 80—59103
- stack gas monitor, β scintillation detector+Ge(Li) detector system, environmental γ dose *(Japanese)* 79—3246
- standardisation, of plant design, General Electric standard safety anal. report for licensing 80—22908
- standards and regulations in USA and Germany 77—65298
- standby component unavailability with inspection and repair 80—13637
- standby diesel units behaviour on load takeover 77—46341
- startup tests, comparison of expt. data and calc. for circuit overpressurisation, boiling, fuel failure 80—691
- statistical fuel model, FRP 80—42748
- steady-state fuel centreline thermocouple data confirmation from transient response 79—93767
- steam explosion propagation phenomena, multidimensional aspects 79—89420

fission reactor safety continued
- steam explosions, energy conversion, efficiency of LWR core materials 79—85648
- steam generating system, seismic design, math. model 78—58339
- steam generator, modular, liquid Na heated, pressure and temp. loading in breakdown situation *(Czech)* 78—50264
- steam generator, multiple tube rupture, radiological consequences 78—74452
- steam generator deactivation of Novovoronezhskya plant 79—71921
- steam generator inspection by photographic and visual methods 79—54557
- steam generator leakage in the AVR nuclear power station 80—596
- steam generator life evaluation, safety features in stress anal. for some accidents 79—54560
- steam generator repair, influence of water chemistry 79—54556
- steam generator tube perform. anal., corrosion failure 79—59178
- steam generator tube performance in water cooled reactors in 1978 80—78399
- steam generators in fast neutron reactors, Na+water reaction *(French)* 79—63756
- steam supply system, German licensing conditions 77—46340
- steam/air mixtures, instrument for steam fraction meas. 80—52724
- steel, for pressure components, fracture charact., implications for reliability 79—20199
- steel, PWR pressure components, mechanical factors affecting reliability *(French)* 79—20198
- steel, stainless, fast reactor cladding tubes subjected to thermal transients, rupture behaviour 80—37465
- steel lining as containment sealing layer *(Russian)* 79—30962
- steel pressure vessel, reliability aspects 79—22430
- steels, dynamic material props. for FBR safety anal., testing devices 78—60966
- stress rupture regression lines in reactor materials, statistical determination 80—30106
- structural design and analysis, research survey, nuclear power plants 78—94048
- structural design and analysis research programme for nuclear power stations 78—94047
- structural integrity assessment, mat. prop. variations 78—89953
- structural integrity in postulated accidents, scaling laws for contained explosions 80—47604
- structural mechanics of PWR 78—41806
- structural protection measures, against disruptive accidents *(German)* 78—94118
- structural reliability, conference, Berlin, Germany (Aug. 1979) 80—105422
- structural reliability, time-depend. nature modelling 79—18013
- structural shock tests, prototype FBR MONJU scale models, computer code verification 77—3131
- structural wall test results, applicability to seismic design, review 79—592
- structure loading and response studies, testing philosophies, simulation techniques 77—71672
- structure-fluid mesh partitions of explicit-implicit integration 77—46238
- subcompartment anal., inclusion of momentum flux 77—50224
- subcompartment pressurisation anal. 77—38364
- subcooled blowdown thrust force calculation using RELAP4/REPIPE 80—18382
- subcooled nucleate pool boiling, intensity and power spectral density of acoustic emission 78—17282
- subcritical assemblies, interaction parameter method 77—54334
- subcritical limits, validity of calculation methods 79—59198
- subcritical limits in mixed oxide criticality safety standards 77—74950
- Super Phenix reactor vessel research and development *(French)* 79—30947
- Super-Phenix FBR, data processing and collection *(French)* 79—76107
- Super-Phenix FBR control system evaluation *(French)* 79—76106
- Superphenix internal shells, vibr. anal. *(French)* 78—50247
- supervised protective systems, availability maximisation 79—59180
- suppression pool, acceleration forces generated by an oscillating air bubble 79—54546
- surface coating materials in nuclear generating stations, ionising radiation protection *(German)* 80—18681
- surface decontamination efficiency, influence of carrier *(Czech)* 79—31222
- surface multiplication meas. with fission chamber 77—42024
- surveillance testing feedback to improve plant availability 80—9384
- surveillance testing safety system unavailability 80—9385
- Swedish project *(Swedish)* 77—38341
- Swedish State Power Board nuclear power stations, training of emergency organisation 78—50412
- Swedish underground nuclear reactor containment studies, review 79—600
- Swiss Federal Institute for Reactor Research emergency organisation 78—55047
- TAPIRO fast research reactor, computerised protection system 80—63308
- teaching, MIT nucl. engineering dept. courses, USA 78—58378
- technical safety control during normal reactor operation 79—26646
- technology transfer, role of nuclear standards 77—65296
- technology transfer to developing countries 77—65303
- technology transfer to developing countries on radiation protection and nuclear safety 77—65297
- test facilities at AEE, Winfrith, UK 77—6528
- test gauge, operation at low multiplication 78—82526
- test rods, directly heated, influence of thermocouples in wall 79—93706
- Thailand's first nuclear power plant, radiation monitoring programme 80—57996
- thermal hydraulics, sensitivity theory development 79—17963
- thermal power reaction, 3-dimens. transient anal., finite difference and spacetime synthesis methods 79—17989
- thermal reactor containment, finite element anal. of luid-structure interactions 80—22998
- thermal reactor station safety requirements UK experience 79—26622
- thermal response of safety related equipment under high superheat conditions 77—46343
- thermal-hydraulic effects of pipe ruptures 79—97846
- thermal-hydraulic margin analysis, appl. response surface methodology 78—17378
- thermocouples, 2200°C fuel centerline for LOFT program 80—57877
- THERMOS reactors, district heating and desalination appl. 78—41853

fission reactor safety continued
thin plates perforated by hard missiles, energy dissipation prediction 79−8361
thin-film fission thermocouple detectors for reactors safety expts. 80−22987
Thre Mile Island, Unit 2 accident, noble gas releases 80−47616
Three Mile Island, accident, malfunction development, prevention *(Hungarian)* 80−68846
Three Mile Island, accident account and status of nuclear security *(French)* 79−81033
three mile island, accidents *(Korean)* 80−32355
Three Mile Island, Japan Safety Commission preliminary report *(Japanese)* 80−22972
Three Mile Island accident, commission report 80−32372
Three Mile Island accident anal., observations and recommendations 80−18370
Three Mile Island accident anal. 80−18457
Three Mile Island accident conclusions and recommendations *(German)* 80−47588
Three Mile Island incident, Atmospheric Release Advisory Capability, response and support 80−57889
Three Mile Island incident, operator/instrumentation interactions 80−57890
Three Mile Island incident, Pennsylvania's emergency preparedness and response 80−57888
Three Mile Island initial recovery programme 80−27766
Three Mile Island malfunction, monitoring, radiation exposure 80−57960
Three Mile Island reactor accident, radiological consequences 80−27771
THTR 300 MW(e) prototype reactor, safety anal. under extreme accident conditions 79−31087
THTR-300 PBR, nuclear material safeguards system 79−22427
time dependent flow area problems, conservation eqns. in control vol. form= form., reactor safety and anal. appl. 77−72264
time dependent unavailability anal., FRANTIC computer code 78−29588
TMI, Kemeny Commission report, conclusions and recommendations, summary 80−63302
TMI, role of analytical chemistry in accident control, assessment and recovery 80−95389
TMI-2 accident, analysis of high readings by startup channel neutron detectors 80−102265
TMI-2 accident, cause, radiological consequences, NRC action 80−102262
TMI-2 accident, nuclear reactor safety, role of instrumentation and control *(Japanese)* 80−73947
TMI-2 accident, preliminary study report (May 28, 1979) *(Japanese)* 79−93748
TMI-2 accident analysis, ^{131}I release, steam explosions and molten fuel-concrete interactions 80−102264
TMI-2 accident analysis using two-loop RETRAN model 80−102263
tornado missile hazard, synthesized windfield model 79−31239
tornado missile impact full scale tests 78−41876
tornado missile transport analysis 79−12205
tornado vortex model, appl. to nuclear plant design 78−17444
transfer of nuclear regulatory and safety technology 77−65300
transient analysis, appl. of statistical methods to sensitivity anal. of Problem 2 79−31058
transient analysis, imposed space-time kinetics method 79−59130
transient fission gas behaviour, exptl. and analytical results 79−59190
transient fission gas release effects on carbide fuel failure dynamics 79−49762
transient fluid and structural dynamics problems, flow singularity methods 78−86633
transient fuel behaviour, modelling of grain boundary fission gas effects 79−59169
transient fuel fission gas behaviour, NEFIG model calcs., bubbles and swelling 80−618
transient heating conditions, mobility of fission gas bubbles 79−59189
transient overpower, comparison of EPIC and PLUTO fuel-coolant interaction codes 78−8920
transient overpower accident, transient press. field of gas in MOX fuel porosity 79−36348
transient process dynamics in reactor with dissociating coolant *(Russian)* 77−42050
transient safety anal. using RETRAN computer code 80−18506
transient state initialization of quasi-static neutronics treatment 79−59192
transient temp. field in nuclear fuel rod, calc. by variational procedure 79−9772
transient temperature distribution in the reactor vessel wall after cooling system failure 79−54473
transient two-phase flow system, three-dimensional numerical simulation 80−687
transient two-phase level swell, appl. of drift flux model 79−49656
transportation and safeguards 77−67837
TREAT, behaviour of unirradiated He bonded carbide during mild TOP test 77−46237
TREAT, fast neutron hodoscope perform. tests on 91-pin fuel bundle 79−41005
TREAT, fission gas non-equilib. behaviour during fast thermal transients, simulation 78−41831
TREAT experiments, fuel pin failure, statistical analysis 79−97840
TREAT loss of flow safety test R8 with pressurised FTR fuel pins 77−42131
TREAT test AX-1, safety anal. of mark II CB loop 79−85664
TREAT test H6, TOP HCDA 79−93755
TREAT test R12, acoustic data anal. 79−93778
TREAT test results on fuel, cladding and coolant motion 77−3070
TREAT tests, statistical model to identify boiling inception 79−93779
TREAT TOP experiments, applicability to post failure dynamics 79−49765
TREAT TOP expt. R9 77−42025
TREAT TOP test E8, fuel motion 77−42132
tREAT TOP test H6−preliminary results for transient overpower 79−49763
tREAT transient overpower experiment R12 79−49764
TRIGA pulsing reactor without coolant loss, safety assessment for fuel and cans 80−52773
TRIGA reactor fuel rods water-quench safety tests 80−42811
TRIGA-FLIP failed fuel element examination at HFEF 80−9383

fission reactor safety continued
Trino power plant, in-service inspection and operating experience, main coolant circuit *(Italian)* 79−17992
Trino PWR pressure vessel in service inspection, planning and organisation *(Italian)* 79−17993
Tsuruga power station anal. of corrosion products 80−23062
tube frettings in steam generators and heat exchangers, expt. study 79−81003
turbulent convection in fluid layer with internal and external heating, reactor safety anal. 79−32514
tVA pipe rupture evaluation and typical mitigation fixes 80−18549
two-phase flows, high-intensity X-ray system for stochastic measurements 79−93791
two-phase systems, high-temperature optical void probe 79−93705
two-phase-flow instrumentation development at Brookhaven National Laboratory 80−102261
UK standards and procedures 79−81032
UKAEA Prototype fast reactor control system, commissioning and performance assessment 79−89459
underground nuclear power plant, accidents, containment of fission products, finite element anal. 80−27768
underground nuclear power station design, safety and economic considerations 79−76068
underground siting, conceptual design and estimated cost of nuclear power plants in mined caverns 80−688
underwater repair, innovative technique 79−3226
underwater shock at a free surface, refl. effects, rel. to fast reactor safety 79−68751
upper internal structures, finite element structural model appl. 80−32362
urban-sited heating reactor, risk assessment 78−37423
US decontamination system for reactor fuel transfer pool, remotely operated 80−68916
US holography for defect size meas. at inservice inspections of nuclear components 79−45372
US reactor operating experience, qualitative assessment 79−26627
US reactor safety principle evolution, accidents and safety systems 79−26613
US temp. profiling system for critical heat flux meas. of nuclear reactor fuel assembly 80−37032
US test results, data evaluation problems 79−9770
US testing in power plant *(German)* 80−13730
US testing to ensure safety, trends *(German)* 77−26847
US viewing system for reactor fuel assemblies under liquid Na 80−57875
validated computer codes for nuclear electric utility 78−17403
vapour bubble collapse model for fragmentation of melts in melt/water reactions *(German)* 77−61507
vapour phase heat transfer in post critical heat flux region 79−9668
vent clearing analysis of a mark III pressure suppression containment 80−32371
vent filtered containment, feasibility and effectiveness issues 80−68875
vibration analysis of heat exchanger and steam generator designs 78−66333
VK-50 boiling reactor, characts. at reduced steam pressure 80−32337
vortex diodes in post accident heat removal systems 80−106100
VVER, Czechoslovak legislation and practices *(Slovak)* 80−13632
VVER, nuclear power station safety 79−26560
VVER, T buildup estimation with allowance for ^{6}Li conc. 79−97833
VVER type nuclear reactors, in Soviet Union, biological shielding problems 80−106127
VVER-440, nuclear fuel control, role of IAEA *(Hungarian)* 79−13435
VVER-440 reactor power stations, design and operation 79−59127
VVER-440 reactors, emergency operating conditions following main circulation pipe failure, computer aided anal. 79−9823
VVR-SM reactor, neutron flux and dose meas. and evaluation *(Czech)* 80−5252
WAK reprocessing plant, a design basis for large-scale reprocessing plant 80−5310
WASH 1400 report, safety evaluation in France 77−46353
WASH-1400 study, implications 77−46352
water, neutron number and dose albedo 79−93681
water, transition boiling under forced convective conditions, reactor accident condition 78−89961
water cooled, water moderated reactor, coolant tritium content in first loop 80−32334
water cooled reactor, RBMK, safety margin optimisation 80−37481
water cooled reactors, main causes of fuel element failure 79−67872
water cooled reactors, safety technology R&D 77−34416
water cooled reactors, technology for accident anal. and consequences mitigation, pressure vessel types 77−34414
water cooled reactors 77−34413
water moderated reactor, 10 W, construction, student project *(German)* 78−33238
water reactor decontamination, recirculating regenerable reagent appl. 78−46158
water reactor fuel, power ramping performance assessment methods 80−23065
water reactor fuel elements under accident conditions, conf. 77−42159
weld seam inspection, nuclear steam supply system, quality assurance *(German, English)* 77−83052
welded pressure components, effect of material property changes on operating conditions 79−20197
West German policy *(German)* 80−57865
Westinghouse nuclear training reactor fuel inventory reduction plan 80−23115
Westinghouse PWR, radiation levels 80−5296
Westinghouse upper head injection system 78−21634
worldwide ISO standards for nuclear technology safety 80−102266
WWER reactor safety problems, LOCA prevention *(Russian)* 79−26629
WWER reactors for district heating appl. 78−41854
Zircaloy clad fuel rod burst behaviour in simulated PWR LOCA 79−36337
Zircaloy cladding, effects of stress biaxiality on ballooning behaviour 79−30919
Zircaloy fuel cladding, O embrittlement obs. 78−89947
Zircaloy LWR cladding, modeling of deform. and fracture in SPEAR code system 79−93729
Zircaloy PWR cladding, deformation in LOCA 80−106114
Zircaloy-2 cladding, reactor accident conditions, creep and creep rupture props., 1000 to 1500°C 78−78470

fission reactor safety continued
  zircaloy-4, oxidation in high temp. steam atm. effect on cladding ductility 79–26515
  zirconium alloys, cladding strain reduction by changing pellet configurations 79–81008
  ZPPR-9, stimulated hodoscope slot effect in STF critical assembly 80–68860
  Na leakage in reactor steam generators, solution kinetics of solid NaOH in Na 79–36365
  ^{87}Br, delayed neutron carrier, sorption parameter determ., appl. to fuel element leak detection 79–97828
  B_4C absorber pin in-reactor rupture test 79–93701
  BWR, primary containment vessel, spray I_2 removal characteristics 80–73972
  $Bi_4Ge_3O_{12}$ scintillators, appl. as high energy gamma detectors 80–47827
  ^{14}C activity and distrib. in gaseous effluents from PWRs 79–85829
  Co radioactive release from reactor cooling water, fixation by sandy soil *(Japanese)* 78–74443
  ^{60}Co, shutdown dose rate prediction in BWR primary coolant circuit 78–74445
  D_2O leak detection, on-line infrared analyzers, CANDU report 78–82038
  EBR-II Na system cold traps for control of O_2, H_2, T impurities 80–78411
  FBR, safety, research needs 79–49711
  Fe, neutron number and dose albedo 79–93681
  H permeation through Incoloy-800 reactor material 79–77822
  ^{3}H behaviour in pebble bed reactors, numerical calc. *(German)* 80–9387
  ^{3}H concentration measurements in nuclear power plant atmosphere, instrumentation 79–26765
  ^{3}H distribution between gas and liquid in isotope equilibrium in H_2O-H_2S and D_2O-D_2S systems 79–45376
  I partition equilibrium between air and NaOH aq, effect of CO_2 conc. 78–78474
  I, radioactive, air sampling system, separation into gaseous and particulate fractions 80–57962
  I radioactive isotopes, nuclear fuel cycle radiation safety problem, *(Russian)* 80–18560
  I radioisotopes, high efficiency mixed species air sampling, readout and dose assessment system 78–57074
  ^{129}I, dose to world population from nucl. power industry 80–47619
  ^{131}I, behaviour during rinsing in in-pile loop after fission product release expt. 80–73879
  ^{131}I filters, design against weathering 80–32524
  ^{131}I spiking phenomenon in accidents involving coolant leakage, expt. *(Japanese)* 77–54320
  Lif-TLD, nuclear reactor mixed radiation field, ambient atm. effect 79–13537
  N_2O_4 gas cooled fast reactor power stations, nuclear and chemical safety *(Russian)* 79–26655
  ^{16}N activity from $^{16}O(n,p)^{16}N$, nuclear powered ship, computer code and expt. comparison 78–13192
  Na bonded mixed carbide fuel, unirradiated, behaviour during mild overpower transients 79–49761
  Na coolant, effect of high reactivity with air and water on reactor design *(French)* 79–26526
  Na cooled fast reactors, safety aspects *(Russian)* 79–26648
  Na evaporation into forced AR flow, critical supersaturation model predictions 79–54493
  Na fire anal. with SPOOL-FIRE code 77–46322
  Na fires, origination and mechanism, form. and sedimentation of Na aerosols, review *(Czech)* 79–30956
  Na fires suppression in fission reactor, installations 80–27770
  Na loop safety facility, molten fuel containment capability assessment 80–47605
  Na pool fuel vapour and aerosol transport in HCDA 79–13455
  Na slug kinetic energy behaviour for varying HCDA energetics 79–85665
  Na test loop boiling, acoustic detection expts. 79–13487
  Na thermodynamic props. for reactor safety analysis 79–13478
  Na transient boiling in single-pin annular channel under loss of flow 78–89933
  Na valves for advanced reactors, reliability data collection at CREDO 80–22897
  Na/water steam generator problems, soln. in USSR *(Russian)* 79–97876
  Pb shield, effects of thickness and geometry var. on neutron spectra 78–33300
  Pt resistance thermometers, response time estimation by noise anal. technique 79–93742
  Pt resistance thermometers, in-situ response-time testing for safety systems 79–93743
  Pu, fume aerosols, aerodynamic and dissolution behaviour of laser-ignited droplets 79–13438
  Pu, reactivity effects of reflecting and interspersed concrete, composition effects 79–63788
  Pu reactor facility, zero power, continuous controllable containment, West German safeguards system 79–85683
  Pu reprocessing and safeguards in water reactors 77–67838
  Pu safeguards, eval. of thermography 79–93719
  PuO_2, assemblies, fission and explosive energy releases 77–83108
  PuO_2-UO_2 assemblies, fission and explosive energy releases 77–83108
  ^{236}Pu conc., prediction for mixed-oxide fuel 77–42121
  ^{239}Pu fuel cycles, potential radiological impacts 80–42799
  ^{239}Pu in aqueous soln., limiting critical conc. and thermal value of eta 79–63773
  ^{239}Pu, use in weapons and energy prod., radiological hazards, security 77–10492
  ^{240}Pu, coincidence counting of thermal neutrons, detector and calcs. 80–37716
  ^{88}Rh releases, continuous air monitor appl. 77–46411
  SO_2, downwind conc. from Four Corners Generating Station 80–47620
  T buildup in D_2O of CANDU reactors, due to $^{3}He(n,p)^{3}H$ reaction 79–22389
  T monitoring at nuclear power stations 80–18691
  T release behaviour and chem. forms on heating neutron irradiated UO_2(Li) pellets 78–40071
  T, role in radiation safety in nucl. fuel cycle *(Russian)* 80–56227
  (U,Pu)O_2 fuel, criticality control, critical mass meas., fission rate distrib. by solid state dosimetry 80–13723
  (U,Pu)O_2 fuel pin behaviour during FFTF 3c/s reactivity insertion event, TREAT expt. anal. 80–102240
  U meas. safeguards materials, automated gravimetric titrator 80–622
  U neutron criticality, solid angle computations using computer code 80–13726
  U solution systems, high-enriched benchmark critical expts. 79–63748
  UC response to transient heating 77–46333
  UF_4-CF_4 mixture, gas core fission reactor, fission based plasma engine 80–63366
  $UO_{2,3}$ assemblies, fission and explosive energy releases 77–83108
  UO_2, ^{235}U enriched fuel rods in water, critical expts. 79–80977
  UO_2, ^{235}U enriched lattices, effect of soluble neutron absorbers on criticality 79–80978
  UO_2 and UC drops, fragmentation on entering Na pool in LMFBR 79–3225
  UO_2, desintering of unrestructured UO_2 fuel during film boiling testing, grain boundary separation 80–22997
  UO_2 fission vapourised fuel, aerosol close in sampling, accident safety 79–49779
  UO_2 fuel, fragmentation gas thermodynamics 79–13458
  UO_2 fuel crust, submerged, mechanical stability 77–46323
  UO_2 fuel vapour, condensation on vertical steel substrate 77–46330
  UO_2 fuel-coolant interaction, film boiling and vapor explosion phenomena 80–95363
  UO_2 heat-generating, molten, interaction with MgO brick 79–13468
  UO_2, interaction with Na, dropping experiments and subassembly test 78–82460
  UO_2, LMFBR, boiling pools with internal heat generation, void distrib. 78–21626
  UO_2, liq., splashed on Na, no evidence of entrapment 79–41000
  UO_2, liquid, pressure generated by encapsulated Na *(Italian)* 78–82454
  UO_2, liquid, reactor safety research, laser experiments *(German)* 80–42787
  UO_2 molten, interactions with steel and graphite 79–49700
  UO_2 molten pool prod. by internal heating, heat transfer meas. 77–88214
  UO_2 pellet storage facility, large dry, criticality eval. 79–26668
  UO_2 rods, dissolution and storage exptl. program 80–37432
  UO_2-Na contact interface temp., effect of internal radiation 79–13477
  UO_2-Na interaction, thermophysical behaviour of type 304 stainless steel impacted by jet of molten core debris 77–46319
  UO_2-Zr fuel performance evaluation in power ramp tests 79–26544
  $UO_2(NO_3)_2$ highly enriched soln. with $Cd(NO_3)_4.4H_2O$ neutron poison, criticality expts. 80–13724
  ^{233}U fuel cycles, potential radiological impacts 80–42799
  ^{238}U Doppler effect obs. in advanced fuels critical assemblies 79–9739
  Xe poison in nuclear reactor, optimal control *(Korean)* 77–54323

fission reactor theory and design
  see also fission reactors; fission research reactors; neutron transport theory
  1 GW(e) mixed fuel cycle LMFBR performance, effect of ^{233}U in core 79–9868
  $\bar{\nu}(Z,A,E_n)$, prediction method developed 77–26792
  A-1 power reactor, Pu isotope form. calc., effect of reactor characts. 79–26489
  absolute fission rate distrib. in standard U shell, comparison with ANISN code 78–62584
  absorption resonance controlled reactor *(Spanish)* 78–8872
  accelerator breeder, burner reactor, and reprocessing plant system, net energy and fissile material balance 79–85722
  accelerator-based spallation breeder for fuel enrichment 79–13498
  accelerator-driven reactor fuel cycle 79–26678
  ACPR upgrade, criticality and preliminary characterization 80–13555
  ACR, development, influence of nuclear power growth rates on introduction date 80–18379
  actinide burning very hard spectrum reactors 79–89414
  adjoint space, functions, formulations 77–3071
  advanced continuous fluid Eulerian comput. scheme for flows with large density gradients 77–46236
  advanced fuel performance, definitions of breeding ratio and doubling time 78–25271
  advanced fuels programme carbide benchmark critical assembly, nuclear data sensitivity 79–9707
  advanced nuclear energy systems, emerging concepts, conf., Graz, Austria (March 1978) 79–13381
  advanced reactor and fuel cycle systems, potentials and limitations for United States utilities 80–106106
  advanced reactor development, goals, near and mid-term opportunities 77–34377
  advanced reactors, materials and design 78–78452
  AGR, advantages of downward flow config. over conventional design 78–70584
  AGR, internal radiation shields, design and performance evaluation 80–5373
  AGR, radiation protection during operation and maintenance of irradiated fuel route 80–5375
  AGR design for Heysham II and Torness 80–23108
  AGR pressure vessels, radiation protection for shutdown man-access 80–5374
  AGRs, principal technical features and advantages *(French)* 80–18375
  air-water, two-phase mixtures, vertical downward flow, void fraction 77–11235
  alternative containment designs, value/impact comparison, containment failure and safety aspects 79–13464
  alternative fuel cycles, relative diversion resistance 80–37438
  alternative reactor fuel cycles under consideration and their design ramifications 79–54516
  AMPX code, operating experience 80–68743
  AMPX code for coupled multigroup n-γ cross section sets 80–68741
  AMPX code implementation problems at KFA Julich 80–68742
  annular core pulse reactor upgrade physics and core design calc. 79–13409
  Argonaut reactors, coupled core, neutron wave propagation, Be, graphite and D_2O as internal reflectors 80–27752
  Argonaut research reactors, effect of atmos. press. variation on reactivity *(German)* 80–5199
  aseismic design and testing of equipment and components, Japan 80–52763

fission reactor theory and design continued
assessments of nuclear systems and use of nuclear power, review 79−45334
asymptotic expansion method 77−23181
asymptotic solutions in neutron transport theory 77−23179
at-power reactor noise, second-order coherent functions 78−94070
ATWS risk anal. of B and W PWRs 80−47667
automatic diagnosis of abnormal phenomena, theory and computer simulation 78−17330
BABEL, multigroup neutron library for fast reactor, shielding design studies 80−68745
basic nuclear engineering, book 78−54810
benchmark computation 77−79417
benchmark testing of anisotropic diffusion coefficients, void-worth calcs. for finite lattices 80−47546
bidimensional transport coeff. N_H, influence of transverse flow *(Spanish)* 78−8873
bilinear functionals, upper-bound estimations 77−67796
bilinear system Volterra-kernel estimation 79−26512
block-type fuel elements, stress calc. with finite element code *(German)* 77−71654
blowdown anal., two-phase crit. flow models 77−6531
BN-350, design and experimental testing of intermediate heat exchangers *(Russian)* 79−97785
BN-350, primary cct. and component design *(Russian)* 79−97781
BN-350 reactor, development, design and operating experience *(Russian)* 79−26511
BN-350 reactor, radiation safety assessment at design stage *(Russian)* 79−97869
BN-600, design and experimental testing of intermediate heat exchangers *(Russian)* 79−97785
BN-600, primary cct. and component design *(Russian)* 79−97781
boiling mixing studies in water loops, BWR, PWR reactors 79−26502
Boltzmann equation, P_1 approx. in presence of delayed neutron emission 80−78347
BOR-60 fast reactor, reactivity balance calc. statistical error 79−17966
boundary-value problems, method of imbedded elements, construction of coordinate functions 79−59128
breeder reactor, with circulating liquid-salt fuel, fission product radioactivity reduction and residual heat release 79−26490
breeder reactor system, rel. between nucl. growth rate and breeder doubling times 78−17323
breeder reactors, current status in Europe 80−27796
breeding ratio and doubling time definitions 78−25266
Breit-Wigner single-level formula for cross sections, multilevel correction 78−29441
Brookhaven accelerator-reactor breeder concept 77−54294
buckling design rules for power plant components 77−3096
buckling of structural elements, high temp. environment, nonlinear effects 77−3756
building walls, differential press. during tornadoes, computer program 77−38349
burnup, anal. of sources of errors in calculational and experimental methods 78−58343
burnup anal., depletion pertubation theory for coupled neutron-nuclide field 79−45339
burnup calcs., perturbation anal. of sensitivity 80−22936
burnup calculation code for cluster-type fuel lattices, BUNDLE 78−33246
burnup calculations, time dependent generalised perturbation theory 77−23176
burnup calculations for KWO reactor, critical B concs. 77−23199
burnup codes for calc. of fuel depletion and fission product poisoning 77−67800
burnup determ., accuracy requirements for fuel cycle design, reactor operation and safety 78−58342
burnup equations, determination of neutron flux and isotopic changes in reactor cell 78−58340
burst reactor, spatial kinetics *(Russian)* 77−38329
BWR, anal. of occupational radiation exposure, design implications 80−5380
BWR, axial distrib. of void fraction in subcooled boiling 77−46217
BWR, benchmarking ARMP system against Quad Cities Unit 1 Cycle 1 meas. 80−27712
BWR, boiling-channel stability, nonlinear math. model calc. of coolant-vel. perturbations 79−89353
BWR, bypass flow distrib. 77−42017
BWR, containment system coolant flows, LOCA modeling 79−54476
BWR, coupled problems in transient fluid and structural dynamics 77−71646
BWR, design, construction and organisation of Caorso nuclear power station, Italy *(Italian)* 79−26471
BWR, design and operation, review of water chemistry, in feed water, coolant and steam systems 79−36311
BWR, Dodewaard, Pu assemblies in reload-1 77−42018
BWR, Doppler and void reactivity feedback 80−13661
BWR, effect of multiple boiling channels on void fluctuation spectra 80−18464
BWR, expt. reactor, design of control systems using Horowitz method 79−45338
BWR, fast moderator feedback effects during severe press. transients 78−4990
BWR, flow oscills, with random excitations 77−6486
BWR, fuel element sheaths construction and operation *(German)* 77−10460
BWR, grey nose control rod design 80−5264
BWR, improved core design 80−68761
BWR, min. critical power ratio thermal limit 80−18398
BWR, multivariable autoregressive model of the dynamics 78−25307
BWR, neutron image anal. by one-dimens. core model 77−61478
BWR, noise anal. model 78−50237
BWR, noise sources of neutron flux, coherence anal. 77−88199
BWR, nuclear cores safety calc., microscopic and macroscopic layout *(German)* 77−10472
BWR, optimal fuel pin enrichment distribs. 77−83008
BWR, optimal in-core fuel management using OPTLWR computer code 78−17363
BWR, Oskarshamn I, Gd-loaded fuel: benchmarking CASMO program 79−81039
BWR, prediction model for shutdown margin reactivity 79−26476

fission reactor theory and design continued
BWR, process monitoring and parameter estimation, multivariate signal analysis algorithms 80−47585
BWR, Quad Cities 1, localized cold critical expt. 79−81001
BWR, scram reactivity characteristics 78−29607
BWR, shutdown dose rate of primary cooling system, prediction by empirical formula 79−22408
BWR, stability of radial and azimuthal energy distrib. 79−97749
BWR, Swiss 942 MWe project, Dutch (NUCON) development *(Dutch)* 79−3191
BWR, Tarapur, one-loop model, dynamics anal., power transient response 78−46131
BWR, thermal-hydraulic technology, university contrib. opportunities 79−49652
BWR, UO_2, Gd bearing rods, magnetic and passive scanning system 80−37463
BWR, vacuum relief valve sizing in condensing steam situations, analytical model 79−54545
BWR, vent clearing transients calc., press. suppression system, digital computer simulation 77−3132
BWR, void and Doppler feedback eval. 80−22976
BWR augmented off-gas system flame arrester at Oyster Creek nuclear station 80−22918
BWR boiling noise, local and global component obs. and calc. 78−94066
BWR condensate feedwater system, dynamic model 80−73883
BWR containment struct., appl. of frequency domain anal. 79−93753
BWR control blade homogenization, influence on nodal coupling parameters 79−26563
BWR control blades, modelling for nodal calcs. 79−81040
BWR control cell core design concept 80−68763
BWR control cell core improved design 79−85593
BWR core, moderator temp. coeff. and neutron leakage, DIFFUSION-ACE calc. 78−54844
BWR core, three dimens. calcs., new brief neutron diffusion scheme 77−42014
BWR core calcs., void iteration convergence and accel. 77−83009
BWR core calculations using improved coarse mesh methods 80−68849
BWR core concept, WNS-type fuel, equilibrium cycle performance 80−68762
BWR dynamics, multivariable autoregressive identification 78−94107
BWR fluctuations, in neutron flux, due to steam bubbles 80−47534
BWR fuel integrity limits and criteria 80−575
BWR fuel management anal., consistent modelling procedure 80−23052
BWR in-core neutron detector sensitivity to control rod vibr. using neutron noise anal. 80−57910
BWR island-design Pu recycle fuel assemblies, nuclear fuel performance meas. 79−30907
BWR lattice geometries, comparative study of two-dimens. transport methods 77−61484
BWR load following plant, low sensitivity design fo controller 78−78473
BWR LOCA, some considerations in small-scale pool swell simulations 79−49740
BWR LOCA anal. using homogeneous critical flow model, expt. determ. of blowdown flow rate 80−106120
BWR neutronics, computational benchmark problems review 77−79413
BWR noise anal., identifiability of dynamics using autoregressive modelling 79−45340
BWR off-gas systems, design considerations to prevent H_2 ignition 80−22917
BWR once through fuel cycle optimisation 79−85590
BWR operating experience at Millstone I with the control cell core improved design 80−22925
BWR parameter estimation, multivariate anal. of neutron noise signals 80−18465
BWR physics methods compared with ^{232}Th lattice benchmarks 79−9711
BWR plant in Japan, aseismic design 77−65267
BWR plants in Japan, seismic design and tests 78−86652
BWR power fluctuations, noise source estimation by autoregression 78−78476
BWR power plant, earthquake-proof design criteria 78−21733
BWR reactivity feedback modelling effects 80−22927
BWR reflectors, effective albedo parameter determination 80−68756
BWR simulation diagnosis by noise analysis 78−94062
BWR split void assembly benchmark verification of SIMULATE models 80−22938
BWR stochastic neutron flux fluctuation obs. and modelling, thermohydraulic parameters 78−94065
BWR Th cycles with improved performance 79−59138
BWR turbine trip, RELAP/RETRAN steam line models, accuracy considerations 79−59197
BWR vent clearing hydrodynamics, numerical simulation using SOLA-VOF code 79−49659
BWR void effects, stochastic point model and zero-power reactor simulation 78−94061
BWR void reactivity feedback, statistical weight factor 79−9702
BWR with graphite channels, safety of nuclear power stations 79−26561
BWR WNS, a new core design with improved performance 79−59151
BWR/6 axial reflectors, Monte Carlo modelling 80−22939
California underground siting study, anal. 80−18400
California underground siting study, effectiveness in mitigating health consequences 80−18402
California underground siting study, selection and analysis of accident sequences 80−18401
can temp. and thermoelastic stress perturbations, conjugate heat transfer effects 77−54284
CANDU, feasibility study for use as a breeder 78−25311
CANDU, feedback coeff. anal. 80−27716
CANDU, optimum burnup distribution in a continuously fueled reactor 79−36305
CANDU advanced BLWR with enriched fuel, controllability studies 77−71683
CANDU design evolution 79−13417
CANDU design features that influence fuel modelling for transients 80−42740
CANDU design program for exposure minimisation 77−6570
CANDU fuel bundle design with reduced void effect 78−25277
CANDU fuel bundles, outline of Canadian R and D programme on fuel behaviour in transients 78−94102
CANDU fuel performance and development 79−49701

fission reactor theory and design continued

- CANDU power reactor, pressure tubes, design and development 79−36372
- CANDU pressurised HWR fuel, bundle end neutron flux peaking effects, plenum use 78−58385
- CANDU reactor, integral transport code PEAKAN for flux peaking anal. 79−59135
- CANDU reactor, shutdown system design, performance during commissioning 78−25319
- CANDU reactor, Th-fuelled, importance of ^{233}Pa in neutron economy 80−22980
- CANDU reactor core, materials and design criteria for fuel, cladding, and fuel channel 78−13238
- CANDU reactor kinetics benchmark activity 77−79416
- CANDU reactors, seismic design criteria and requirement 80−78358
- CANDU simulated core in ZED-2, transient meas. anal., CERKIN code exam. 78−58386
- CANDU-PHW, once-through, slightly ^{235}U enriched U cycle 79−93711
- CANDU-PHW, once-through natural U cycle 79−93710
- CANDU-PHW, valve maintainability, design, application, layout, administrative factors 78−25318
- CANDU-PHW operating on Th cycle 79−93712
- CANDU-PHWR, low enriched U, channel power peaking 80−37509
- CANDU-PWR, comparison of three axial fuel management strategies 78−94075
- CDFR secondary cct. design from PFR operations 79−97788
- centralised heat supply and central heating, reactor design and development 79−26730
- ceramic reactor fuel, nonsteady radiational creep, theoretical-experimental model 80−35282
- characteristic fuel element temps. calcs., statistical treatment of defects 79−45351
- checkerboard pool core, series of two group calcs. 78−74424
- circular cylinder under intermittently sudden heat generation, transient thermal stresses 77−3728
- CIRENE core, design criteria and anal. 77−14213
- cladding loading by gas pressure during TOP accident, modelling 77−42030
- cladding tube, effective temp. for expanding tube 77−74931
- Clinch River breeder reactor, ALARA nature of design effluents 79−22420
- Clinch River Breeder Reactor Plant, role and progress in LMFBR development 80−13781
- Clinch River Breeder Reactor Plant containment concept 79−13401
- Clinch River Breeder Reactor Project ex-vessel transfer machine design and development 79−9787
- Clinch River Breeder Reactor Project fuel core design advances 79−9686
- Clusius-Dickel effect in fuel rod 79−67820
- cluster-type fuel for ATR, lattice parameter meas. and neutron behaviour 77−46282
- CMEA reactor development, fuel cycle aspects *(Russian)* 79−26505
- coarse mesh methods for benchmark and realistic reactor problems 77−88191
- coarse-mesh nodal method based on response matrix considerations 77−65262
- coarse-mesh nodal methods, generalized approach 79−80987
- Colgate fission plasma reactor, high temp., gaseous fissionable material, design, technical problems *(Dutch)* 78−50249
- column section seismic design subjected to three components of earthquake 77−38355
- component improved reliability, design consideration 79−22383
- component unavailability and failure intensity 77−83063
- component-support impact dynamics, elastic anal. by model expansion method 79−45343
- composite fuels, heat cond. parametric anal. 77−6523
- composite geometry reactor vessel, steady temp. distrib., thermal shock 77−54286
- composite prismatic bars, doubly connected cross section, heat flow shape factors, anal. determ. 79−1068
- compound system doubling time, expression including approach to equilibrium 78−25270
- computational uncertainty anal. methods, comparison 77−79426
- concentric-sphere design for spacing of tag-gas isotopic ratios 79−80983
- concrete structs., steady-state stresses under sustained and cyclic temp. 77−83024
- condenser air-removal system, design modifications for heat rate improvement 79−67830
- conference, design, safety requirements, London, UK (Apr. 1980) 80−57013
- conference on nuclear power and its fuel cycle, Salzburg, Austria (May 1977) 79−26504
- consistent homogenization procedure to obtain few-group cell parameters 79−85586
- containment analysis by ALICE code after HCDA 79−49736
- containment heat transfer following LOCA, anal. 77−54314
- containment pressure transients, anal. of evaporation rate effects 77−38363
- containment response to accidents, comparison of CONTEMPT-LT calculations with Marviken experiments 79−49737
- containment subcompartment flow, film entrainment determ. 79−49657
- containment vessels, dynamic large-deflection inelastic and thermal stress anal. 77−3752
- continuous slowing down theory params. in highly absorbing media 78−29559
- contribution transport, deterministic approaches 80−555
- control and instrumentation designs beyond the 1980s 80−57872
- control assembly frequency anal. using standing wave methods 77−46263
- control design procedure for depletion analysis 77−65292
- control rod drive system penetration assemblies for Caorso Mark 2 primary containment 78−58368
- control system, nonlinear, relative stability anal. 77−3116
- control theory, steady-state accuracy of neutron field regulation 80−63319
- converter reactors, fuel supply enhancement by use of non-fission neutrons 79−17960
- convolution integral calculations for neutron transport in reactors 80−47561
- coolant axial flow in bare rod bundle, turbulence modeling 80−32338

fission reactor theory and design continued

- coolant flow in triangular rod bundles, turbulent-laminar transition 77−26838
- cooling system, flow around obstacles determ. *(Czech)* 78−66331
- core and fuel element design at National Bureau of Standards reactor 78−21636
- core and shield calc., radiation transport program benchmark tests 78−78440
- core bowing history computer program 79−9688
- core design, utility use and requirements 78−17299
- core heat transfer during reflooding, modelling 80−27781
- core internal coolant flow distrib., probabilistic evaluation 77−46250
- core physics parameter meas. uncertainty 79−9801
- core pin power distribution det. based on nodal coarse mesh calcs. 77−88195
- core power and flux distribs., BITNOD large-mesh code appl. 78−17304
- core power distribution calc., FLAME3 nodal code accuracy 79−9703
- core reactivity and space-domain noise effects of randomly dispersed materials 78−94071
- core system, bowed, NUBOW-3D program for static anal. including irrad. creep and swelling 80−5215
- core thermal performance assessment, acceptance of statistical techniques 80−18394
- core transient thermal-hydraulic anal., computer code 77−83022
- core-wide fuel performance assessment 79−93766
- correlation technique for resonance calculations 79−71875
- coupled core reacts., asymptotic stability 80−564
- coupled core system, noise sources in coupling medium, stochastic study 80−22962
- coupled cores, calc. of buckling variation and neutron flux, Green's function method 78−74421
- coupled cores, neutron transit time determ. by noise anal. method 78−37413
- coupled neutron-nuclide problems, time depend. generalised perturbation theory 80−32322
- coupled-core kinetics, research review *(Japanese)* 79−63733
- coupled-core nuclear reactors, irreversible circulation of fluctuation 80−27700
- coupled-core reactor, optimal control by two level scheme based on decomposition principle *(Japanese)* 79−17961
- coupled-core reactors anal. with method of moderator region response function 78−58331
- cover gas seals for breeder reactors, design approach 80−47562
- CRBR, calcs. of ex-vessel monitoring for initial fuel loading 80−27778
- CRBR carbide reload design, comparison with reference oxide design during TUC 79−85658
- CRBR steam generator design 79−97790
- CRBRP, breeding ratio and doubling time definitions 78−25268
- CRBRP, future design and construction of LMFBRs in USA 79−97804
- CRBRP arrangement engineering considerations 79−97764
- CRBRP LMFBR, effect of alternative fuel cycles on design 79−54484
- CRBRP reload core designs, using (U-Pu)C fuel 79−59155
- Creys-Malville FBR power plant, main safety features 80−747
- critical assemblies, bare homogeneous, anal., interrelating differential and integral nuclear data 80−68739
- critical assemblies, comparison of nuclear physics parameters 77−50219
- critical energy in heat transfer channels of complex shape, fuel rod assembly 78−78453
- critical facility earthquake design criteria 79−88286
- critical fast test reactor fuel pin lattices, calcs. of k_{eff} valves 80−13569
- critical point reactor, response to inherent reactivity noise input 79−45336
- critical reactor calc., AGA two-sweep iterative methods 79−36298
- criticality calcs., Monte Carlo algorithm *(Czech)* 77−50209
- criticality calculations, Monte Carlo MONK code 77−14226
- criticality calculations, random geometry model of fissile solns. containing borates Raschig rings 79−36310
- criticality calculations by source-collision iteration technique for cylindrical system 77−65268
- criticality control of intermediate U enrichments, computer calcs. 80−37435
- criticality criterion for core with pointwise concentration of control rods 77−38328
- criticality data, computerised bibiliographic data base at LLL 80−13568
- criticality in arrays of fissile materials, anal. 77−26844
- criticality safety, misleading assumption in array analysis 79−63772
- criticality safety, obs. on problem solving 79−63768
- criticality safety, uncertainties in K-effective calcs. 79−63771
- criticality safety anal., determ. of Dancoff factor for cubic arrays of sphercial fuel particles 80−13725
- criticality safety anal. at Oak Ridge 80−37431
- criticality safety broadgroup library validation using uranium systems 79−26564
- criticality search techniques for low and high switched systems 80−37494
- cross-section probability tables generation in unresolved resonance energy range 79−80986
- cross-section self shielding factors, analytic bounds 80−37426
- crossed progeny and other non-standard fuel cycles 79−26498
- CTR fusion-fission blanket calcs. ^{238}U pulsed sphere meas. 77−23298
- cylinder-to-cylinder shell models, expt. anal. comp. with theory 77−42748
- cylinders coupled by fluid gap, generalised hydrodynamic mass for beam mode vibr. 77−68515
- cylindrical models, diffusional approx., finite element anal. *(Russian)* 80−18414
- cylindrical shells, transient response to localised heat sources, thermal displacement and stresses 80−13538
- cylindrical source shielding eqns. including buildup, lateral dose rate, compact function use 78−89982
- cylindrical transient inverse heat cond., numerical soln. 77−6501
- damage effect on power plant with dissociating coolant *(Russian)* 77−42051
- data adjustment iteration procedure 79−9696
- data evaluation using lognormal distribs. in least squares algorithm 79−93902
- decay heat anal., summation method, fast and thermal reactor systems 77−23195
- decay heat uncertainties estimate 78−25263
- decay power of fission products in reactors, effects of neutron capture 77−6500

fission reactor theory and design continued

- delayed neutron parameter selection for reactor calcs. *(Slovak)* 78—21534
- departure from nucleate boiling ratio safety limit to modelling parameters in COBRA IIIC/MIT 80—73901
- depletion chain eqns., FORTRAN program for solns. using analytical methods 78—74423
- design basis R and D of power stations to cut costs and schedules 80—99204
- design mangement, plant replication for low-cost nuclear power, Philippines National Power Corp. 80—63242
- development, secrecy and simultaneous discovery, 1938-45 78—12523
- diffusion problems, two dimens., nuclear reactor structs., singularities in finite element approx. 77—6496
- diffusion theory calcs., fuel swelling and cladding shrinkage effects 80—22926
- DIMCO system for mechanical calculations on nuclear fuels *(Spanish)* 79—6727
- discrete angle finite element formulation of radiation transport 78—13197
- discrete multiplicative processes in Markovian environments, long run growth rates 79—75453
- discrete neutron decay constants above Corngold limit for infinite slabs 77—50212
- dispersal mechanism test facility, Doppler coeff. optimisation 77—46339
- dispersal mechanism test facility, fuel dispersal anal. 77—42136
- distributed parameter nuclear reactor three-point model, neutron and delayed-neutron emitter behaviour, describing differential equations *(Spanish)* 80—22889
- diversion cross-flow between two parallel channels communicating by a lateral slot 79—30901
- DNB open core algorithm for on-line thermal margin evaluation 80—27782
- Dodewaard BWR, reactivity of core loaded and Gd poisoned fuel 78—41840
- domains of complicated boundary shape, Helmholtz eqn. soln., GCR appl. 80—13540
- Doppler effect calcs., resonance data set choice in unresolved resonance region, sensitivity study 80—52651
- DOT 3.5, use in fast power reactor shield configuration calcs. 80—68749
- double criticality of uniform-power-reflected reactors 80—57828
- doubly heterogeneous cores, fine-energy cross section space shielding 80—22894
- Dounreay FBR, post-operational improvements in plant design and operational techniques 79—63736
- Dragon HTR project, review 79—45326
- ducts and pipes intricately shaped cross section, heat transfer, Laplace and structural method 78—83477
- DWR core global power distrib. calcs. equivalent, Homogenized, and condensed nuclear parameters 80—655
- dynamic model evolution eqns. freq. domain conditions *(French)* 77—67201
- dynamic response characts., empirical modelling appl. 78—25284
- dynamic simulation, design anal. tool 77—88222
- dynamic structural anal., comparative evaluation of numerical methods 77—3091
- dynamics identification by dynamic data system methodology 78—25321
- earthquake computations, reactor installations 78—25336
- earthquake response spectrum estimation from stimulated spectrum 79—686
- earthquake site response anal., construction of smooth site dependent spectra 79—76086
- earthquakes, structural anal. of lifting-off 79—596
- EBR-II, comparison of XX08 steady-state temp. meas. with anal. predictions 80—579
- EBR-II, fabrication of in-reactor creep capsules using previously irradiated cladding tubes 79—54478
- EBR-II, neutronics design of safety research modification 79—30990
- EBR-II, possible metal and oxide fuel loadings utilising ^{232}Th/^{233}U 80—13563
- EBR-II, radial-reactivity-coefficient weighting schemes 79—80998
- EBR-II delayed neutron concentrations, computer modelling 80—27717
- EBR-II energy depositions by nuclear recoil from neutron inelastic scatt. 77—46277
- EBR-II fast transient facility, physics design 77—46336
- EBR-II irradiation subassembly and creep specimen container design 79—54479
- EBR-II loadings, correls, of calculated reactivities 80—22891
- EBR-II mixed-oxide subassemblies, bundle duct clearance at HEDL 77—46270
- EBR-II reflector assembly irrad. induced bowing, implications for core restraint design 80—104234
- EBR-II subassemblies, 61-pin wire-spaced, exptl. confirmation of design to minimize vibr. and wear 79—67825
- education, energy from nuclear sources, outline for secondary school students 79—80975
- education, nuclear reactor dynamics, theory and computer simulation 77—45636
- educational module, nucl. fuel design 80—36800
- effective neutron resonance cross sections, calc. in energy and space 79—17954
- eigenvalue spectrum of homogeneous multiplying systems for monoenergetic neutrons with anisotropic scattering 79—22353
- elastic-removal cross sections, spectral corrections 77—46278
- electrical and mechanical equipment, improved seismic tests, research needs 78—94053
- electrical auxiliary systems, safety design for AGR's 80—57934
- electrical system design for future AGR power stations 80—57935
- empirical modelling using time series anal. 78—25265
- ENDF/B-IV, absorption effects on decay heat and spectral pulse kernels 80—22931
- ENDF/B-IV benchmark analyses with full spectrum three-dimensional Monte Carlo models 79—9701
- ENDF/B-V uncertainty data processing into multigroup covariance matrices 80—68752
- energy autocorrel. of fission cross-section data in resonance region, probability table method 79—36284
- energy dependent transport theory, exact solns. 80—32319
- energy distrib., discrete monitoring error 78—82476
- energy distribution, algorithm for extremal control 80—83209

fission reactor theory and design continued

- engineering test facility as a test device for inertially confined fission 80—57831
- epithermal 1/V self-shielding of reactor poisons using Nordheim integral method 78—17306
- epithermal neutron flux distrib., effect on neutron activation anal. 79—52833
- ESSOR heterogeneous reactor, calc. of reactivity, flux distrib. and power by CART loop 79—30891
- experimental reactor loop construction, high-pressure and temp. type, Hungary *(Hungarian)* 77—3074
- explicit iterative technique for FX2 reactor analysis computer code 78—17302
- failures modes of alternative containment designs following postulated core meltdown 77—54329
- fast breeder core with internal blanket 80—68870
- fast breeder reactors, fuel rod behaviour, influence of design, materials and operation *(Spanish)* 79—36314
- fast burst reactor, WSMR, thermal shock stress anal. for enlarged irradiation cavity 78—33242
- fast burst reactors, thermal shock effects stress anal. 77—79428
- fast critical expts., effective delayed neutron fractions and central reactivity worths 78—62602
- fast heterogeneous reactor, Na-voiding reactivity coeff. 80—52713
- fast high-power reactor calcs. using ZELVA program *(Czech)* 77—6493
- fast mixed spectrum reactor, fuel management and reactor physics 80—27715
- fast molten chloride reactor on Th cycle 79—67839
- fast power reactor, material distrib. optimisation by nonlinear programming method 77—14210
- fast power reactor circuit activity investigation, activation cross-section meas. 80—13614
- fast reactor, assessment of struct. material Doppler effect 78—33255
- fast reactor, effective cross section preparation from multigroup cross sections *(Rumanian)* 80—47543
- fast reactor, effective cross sections of fission products calc. *(Dutch)* 79—537
- fast reactor, large, multiple control rod worths, effective estimation method 78—29544
- fast reactor, multiple control rod worth estimation, strong interaction effect 77—46302
- fast reactor, nuclear data and benchmark test *(Japanese)* 78—29634
- fast reactor, physical studies of large heterogeneous core concept 78—17307
- fast reactor, physics performances of heterogeneous core concept, MASURCA expts. 78—13223
- fast reactor, plate lattice heterogeneity effect with course group consts. 77—3075
- fast reactor, single-group approach to neutron characts. calc. *(Russian)* 78—46161
- fast reactor adjoint neutron spectrum calc. using bilinear weighted cross sections 77—83003
- fast reactor benchmark anal., appl. of FORSS sensitivity and uncertainty methodology 77—46276
- fast reactor design, desirable accuracy eval. for nucl. data using optimisation method 77—57704
- fast reactor design data adjustments 79—9695
- fast reactor finite difference diffusion theory codes, optimised iteration strategies and data management 77—83005
- fast reactor fission gas behaviour, eqn.-of-state of Xe at high temp. and pressure 79—67860
- fast reactor fuel cycle cost, sensitivity anal. 79—26501
- fast reactor fuel design and development 79—31133
- fast reactor integral expt. anal., appl. of uncertainty and sensitivity theory 78—50239
- fast reactor models, iterative methods comparison 79—97752
- fast reactor parameters, influence of fission spectra uncertainties 80—22928
- fast reactor physics, assessment of JAERI fast group constants set version 2 80—602
- fast reactor plant, future design and construction plans, review of national papers SM 225/81-87 79—97797
- fast reactor power distribution calc., effective one-group coarse mesh method 79—63717
- fast reactor safety, thermohydrodynamics code TWOPOOL, modelling and numerical methods 79—59195
- fast reactor SDX cell homogenization code, validation results for pin geometry 79—80997
- fast reactor space-depend. depletion anal. continuous slowing down theory 79—80990
- fast reactor spectrum, Wigner-type continuous slowing down theory 77—50190
- fast reactor spectrum calculation by space-depend. continuous slowing down theory 77—54293
- fast reactor system, eval. of variational method for estim. of neutron detection efficiency 79—80992
- fast reactor system, sensitivity anal. including ^{232}Th and ^{233}U 79—67835
- fast reactor three-dimensional hexagonal-Z systems anal. using THREETRAN (hex,z) 79—80994
- fast reactor transfer functions determ. 77—3082
- fast reactors, ^{239}Pu decay heat evaluation 80—63239
- fast reactors, calc. of core burnup effect on dynamic behaviour 77—23173
- fast reactors, criticality and reproduction I-D calculational model (Baker Model) for comparative anal. 79—97753
- fast reactors, delayed neutron effective fraction sensitivity to basic data uncertainties 77—46207
- fast reactors, effect of neutron reflection from walls of room on pulse parameters 77—23187
- fast reactors, error anal. of computational models 79—97750
- fast reactors, generalized treatment of heterogeneity effects for the shielding factor method 79—40990
- fast reactors, impact of ENDF standards 79—9734
- fast reactors, neutron cross sections for 27 fission product nuclides 77—67741
- fast reactors, one-dimens. anal., improved response matrix method 77—14215
- fast reactors, programme and state of work in the Soviet Union 79—643
- fast reactors employing dissociating N_2O_4, thermophysical anal. *(Russian)* 79—30909

fission reactor theory and design continued
- fast spectrum reactor core design for nuclear electric spacecraft propulsion 80−37440
- fast spectrum reactor space power system with thermoelec. conversion, baseline design 80−37441
- fast systems, stochastic method for calc. of Rossi-α parameter 77−61502
- fast systems with cylindrical geometry, Monte-Carlo method anal. 78−46132
- fatigue life prediction, defn. of safety factors 79−6732
- fatigue loading, growth of underclad flaws 79−22429
- FBR, 2-D power distrib. calc. by appl. of Askew coarse mesh method 79−22372
- FBR, anal. of exposure depend. heterogeneous spectra 80−22937
- FBR, anal. of reactor component fluence limits, damage function methods 77−18668
- FBR, core design for UK commercial demonstration reactor 80−603
- FBR, delayed neutron spectra from neutron induced fission of U, P and Th, calcs. 77−34355
- FBR, development, influence of nuclear power growth rates on introduction date 80−18379
- FBR, development in Japan, fuel, materials coolants and design *(Japanese)* 80−22888
- FBR, electric power generation, research, development and demonstration, risk and timing 80−57837
- FBR, experimental, math. model for control system design in FBR plants 79−17990
- FBR, few group constants for reactivity calcs. errors *(Czech)* 77−71639
- FBR, fission product decay heat calc. by summation method 79−30863
- FBR, French fast reactor physics program 80−601
- FBR, heterogeneous active zone, development trends *(Czech)* 79−36303
- FBR, interpretation of the isotopic breeding worth 79−49655
- FBR, methods of condensing efficient cross sections *(Spanish)* 78−58325
- FBR, multigroup 1-D diffusion program MED 78−78456
- FBR, multiplication factor evaluation of bare and reflected small fast assemblies using variational method 79−85583
- FBR, neutron capture cross sections for Fe, Ni and Cr, intermed. energy region, method and exptl. facility 78−21637
- FBR, neutron physical characts. calcs. *(Bulgarian)* 79−85602
- FBR, neutron shielding, integral expt. and data correlation 78−5057
- FBR, neutron-physical calc., multi-group diffusion equation solution *(Czech)* 78−66332
- FBR, nonstationary prompt-neutron diffusion, multigroup treatment 80−86956
- FBR, programme and development status in France *(French)* 79−26509
- FBR, rigorous and efficient struct. Doppler effect calcs. 78−33256
- FBR, some lessons drawn from operation of Phenix and Rapsodie cores 80−639
- FBR, spatial mesh effect in 3-D burnup calcs. *(Japanese)* 80−47544
- FBR, Th cycle, reactor physics parameters 79−26482
- FBR, Th fuelled, breeding ratio determ. 79−26483
- FBR, three-dimens. diffusion calcs., spatial mesh effects 79−13515
- FBR, zero-power neutron noise expt. anal., power spectral density and subcritical reactivity 80−57911
- FBR alternative fuelled core designs, physics parameters 79−9722
- FBR analysis, general multigroup nodal procedure based on response matrix principles [for FBR analysis] 80−57827
- FBR blanket design, integral meas. in FBBF facility 80−22887
- FBR core seismic anal. by assumed-mode math. modelling 79−89357
- FBR core thermal and hydraulic design, effect of subassembly bowing *(Japanese)* 79−67816
- FBR current status and development trends, review 79−22374
- FBR development and safety program in UK 80−47564
- FBR excursion model, ICECO predictions 77−42028
- FBR film boiling destabilisation, thermodynamic prediction of temp., and rel. to vapour explosion phenomena 79−49667
- FBR fuel, accuracy and computational time of hierarchy of growth rate definitions 79−80979
- FBR fuel growth rate, derivation of consistent measures 77−23174
- FBR fuel subassemblies under nominal and non-nominal operation conditions, thermodynamics *(Japanese)* 79−93689
- FBR neutron fields, spectral charact., expts. and calcs. *(Japanese)* 78−46222
- FBR R and D, conf., Lucerne, Switzerland (Oct. 1979) 80−46735
- FBR R and D programs in Europe, basic objectives for fuels and materials 80−47566
- FBR radial blanket, comparison of economic perform. for LMFBR and GCFR 79−49654
- FBR safety related slowing down problems 78−678
- FBR safety test facility, conceptual design 77−46337
- FBR structural materials, design appl. of irrad. creep and swelling data 79−59167
- FBR thermal hydraulics, sensitivity theory for general systems of nonlinear equations 80−86954
- FBR transitory fuel growth rates 78−679
- FBR UO_2-fuelled blanket assembly design considerations 80−102254
- FDR type reactors, transient anal., neutron power and temp. form factors, depend. on time and power level 80−83178
- few-group diffusion theory, one-group coarse mesh technique 79−26495
- few-group diffusion theory model for VO_2 and MO_2 assembly anal. 77−46273
- few-nucleon data needs 77−18657
- FFTF, delayed-neutron parameters 79−80999
- FFTF, fast reactor, He release correlation from B_4C during fast-neutron irradiation 78−8965
- FFTF, future design and construction of LMFBRs in USA 79−97804
- FFTF, HCDA, NASTRAN nonlinear dynamic transient accident anal. 77−42133
- FFTF, quality assurance appl. to design procurement and construction 79−97786
- FFTF control rod anal. with SCRAM program 77−46355
- FFTF design studies, simulation of hot-leg piping ruptures and loss-of-flow events 79−49677
- FFTF dynamic modelling and sensitivity analysis 79−605
- FFTF fuel, neutron source strength as function of irradiation 80−22929
- FFTF heat transport system, design construction and testing 79−97783
- FFTF reactor shielding anal., spatial channel theory 77−6569
- field problem structure, neutron field *(Rumanian)* 78−45520
- fifth international conference on reactor shielding, review 78−29599
- finite element heat cond. in reactor solids, review and TEMPEL computer program 78−62593

fission reactor theory and design continued
- finite element thermal transient problems, use of reduced eigenvalue method 77−3711
- finite short circular cylinder with arbitrary heat supply, unsteady thermal stress length effects 80−13541
- fissile fuel dynamics of breeder/converter reactors 79−13385
- fission, slope constant of the exponential prompt-neutron yield formula 80−22806
- fission gas, steady state behaviour in carbide fuels, modelling 78−78469
- fission gas behaviour in fuel pins prior to transient testing 79−30921
- fission gas bubbles, nonequilibrium, relaxation times 77−46239
- fission gas release and swelling in irradiated UO_2, model 77−6488
- fission product decay heat, effects of depletion, buildup and fast fission in shutdown 79−81041
- fission product decay heat calcs. for ^{235}U and ^{239}Pu 79−76083
- fission product sensitivities, analytic evaluation 78−82424
- fission products decay heat, development of revised ANS standard 79−49742
- fission reaction rate standards and applications 79−9650
- flexible dual-containment approach design and licensing 79−13400
- floating nuclear plant, shield design features 78−21777
- floor response spectra direct calc., appl. to SUPERPHENIX fast breeder project 77−38327
- flow blockage anal., triangular edge-subchannel wire wrap ϕ-functions 80−580
- flow-induced vibration anal. of nuclear reactor components 79−22380
- fluctuating cross sections in Monte Carlo calcs. 77−65265
- fluid coupled concentric cylindrical vessels, normal mode solution 79−37157
- fluid dynamics, coarse mesh methods appl. *(German)* 77−88197
- fluid-elastically coupled coaxial cylindrical shells, response to external flow 77−89063
- fluidised bed concept, diffusion theory 80−68729
- fluidised bed oven criticality for HTR fuel elements *(German)* 77−18656
- flux calculation in complex heterogeneous reactor cells by imbedding element method *(Russian)* 78−58321
- flux control system design, optimal control theory 77−3138
- flux interpolation for elastic down scatt. 78−29560
- flux synthesis, single channel, finite element trial functions for 3-D reactor calcs. 80−42734
- flux synthesis program KASY, consideration and appl. to reactor design problems 77−88184
- FMSR, He-cooled, thermal-hydraulic design anal. 80−18408
- FMSR, physics performance of a centrally moderated fast reactor concept 80−99208
- formal logic appl. 78−33247
- Fort St. Vrain HTGR, He circulators, development and testing 79−67821
- Fort St. Vrain HTGR power station, review of design and operation 79−45353
- fracture safe design, appl. of elastic-plastic fracture mechanics params. 78−30241
- frequency domain stability for a class of equations arising in reactor dynamics 79−54475
- FTR, calc. of resonant reaction rates near region interface 79−80993
- FTR TOP accident, effect of power skew, computer code development 79−54481
- fuel, rod modelling, utility requirements 78−21747
- fuel assemblies in vertical flow channels, computer dynamic model 79−22379
- fuel assembly design features 78−89939
- fuel assembly power distrib. calc. by albedo method 79−93762
- fuel assembly spectrum code verification based on integral transport theory 79−80996
- fuel bearing rectangular plates, flow-induced bending 77−80088
- fuel burnup calcs. in LASER code 79−59119
- fuel burnup computer codes, physical simplifications 77−6483
- fuel can designs for Safety Test Facility, structural analysis 77−46310
- fuel cell temp. distrib., statistical variance 77−83021
- fuel cycle and nuclear power plant development in USSR, economic aspects 79−644
- fuel cycle back-end services, utility optimization model 79−30906
- fuel cycle cost sensitivity anal. of alternative reactor fuel cycles 79−89368
- fuel design limit for post-DNB operation 80−572
- fuel element behaviour in transients 77−88202
- fuel element finite element thermal loading calcs., automatic mesh generation 77−3740
- fuel element gap conductance, heat transfer over range of Knudsen number 78−13213
- fuel element modeling rod bundle in longit. air flow, heat transfer expt. 78−82415
- fuel element modelling at CNEA 80−37449
- fuel element performance modelling, IAEA specialists meeting, 1978 80−36769
- fuel element performance modelling using LIFE-III, UNCLE-I and LIFE-LWR codes 77−46229
- fuel element spacers, structural anisotropic plates composed of cylindrical shells 78−89940
- fuel element surface roughness, turbulent convective heat transfer 77−46208
- fuel elements, control rods, transient thermal stress anal. 79−599
- fuel elements, cracked, gas-filled, temp. distribs. calc. 78−78446
- fuel elements for steam-superheating channels of Beloyarsk nuclear power station reactor 77−50217
- fuel failure criteria, uncertain benefits 80−574
- fuel failure prediction using POSHO model 77−46226
- fuel growth rate anal. 78−25269
- fuel management analysis core, computer code for teaching assistance 78−4449
- fuel management reactor calcs., educational aspects 78−17298
- fuel management scheme for high burnup at VEPCO 80−37436
- fuel management with extended burnup fuels 80−37503
- fuel pellet-cladding interaction phenomenon investig. 77−46299
- fuel performance data base EPRI 79−93731
- fuel pin claddings, fission gas driven creep calcs. 79−26531
- fuel pin gaps, probabilistic distrib. within wire-spaced fuel subassembly 78−78448
- fuel pin heat transfer, digital transfer matrix 78−29548

fission reactor theory and design continued

- fuel pin inelastic modelling and stress analysis using FULMOD code 77—46233
- fuel pin modelling, Dutt fission gas release correl. 79—67826
- fuel pin modelling principles and developments 77—46232
- fuel pin performance modelling codes for overpower performance analysis 77—46230
- fuel pin rupture in FBR, implicit compact difference method for solving linearized fuel sweepout equations 79—89355
- fuel pin-cell burnup code BETTY 78—89946
- fuel restructuring and relocation under irrad., COMETHE code calcs. 77—46235
- fuel rod arrays, radiative heat transfer, Monte Carlo method, temp. distrib. 78—78447
- fuel rod behaviour modelling using LIFE-III code 77—46234
- fuel rod bowing, finite element computer model 77—46260
- fuel rod bowing due to internally applied load 77—46257
- fuel rod dynamic response soln. by state space method 79—49647
- fuel rod geometry changes, mech. interactions calcs. 79—40993
- fuel rod hairline cracks, effect on thermoelastic stress in surrounding can, iterative method of determ. 77—54285
- fuel rod mechanical design, DIMCO system 80—37418
- fuel rod modelling, uncertainty 78—21629
- fuel rod modelling complexities 77—46231
- fuel rod ramp tests analysis using SAFE-2D program 77—46228
- fuel rod rewetting following LOCA, analytical model 77—46240
- fuel rod structural anal. criticism 78—82441
- fuel rod thermal behaviour, relocated gap width estimation for gap conductance calcs. 80—589
- fuel rod with cladding, time depend. temp. distribs. 78—17288
- fuel rods, thermal and mechanical anal. with URANUS code 78—41803
- fuel storage, in-plant facilities, design considerations 79—67916
- fuel storage pool criticality calc., transport-consistent diffusion algorithm 79—9721
- fuel-assembly dynamic response 77—46265
- fuelling of Atucha reactor, transition to burnup equilib., 3D code TRISIC *(German)* 77—61506
- functional anal. of multigram neutron diffusion problem 78—58317
- fusion and fast breeder reactors, a comparison, book 78—78430
- fusion-fission breeder reactor, supercond. poloidal field coil design 78—70640
- fusion-fission hybrid reactor, laser driven, fuel breeding and power prod. 79—22473
- fusion-fission hybrid reactor, mirror confinement, fuel design consideration 79—22472
- fusion-fission hybrid reactor fuel cycle considerations 79—22474
- fusion-fission hybrids, mag. mirror blankets and drivers 79—13517
- fusion-fission reactor, pulsed high-density linear confinement 77—74983
- fusion-fission reactor symbiotic design, simple fuel reprocessing 78—66365
- fusion-fission reactors, performance parameters, design and fuel cycle anal. 79—17973
- fusion-fission system, basic characts., breeding ratio, thermal power ratio 77—50283
- fusion/fission reactors, inertial confinement systems, review 79—13519
- gadolinia-based fuel pins, efficient diffusion theory parameterization 79—67840
- GAM library data formation in energy groups, PWR appl. 80—68746
- gamma spectra of fission products, estimation using nucl. systematics 78—70587
- gamma-power of hot circuit, calc., effect of flow hydrodyanmics of process materials 80—63235
- gas cooled reactor experience and programs in France, reviews 79—45332
- gas cooled reactor technology *(Japanese)* 77—71638
- gas cooled reactors, background and status in UK, review 79—45333
- gas cooled rough rod bundles, thermofluid dynamic expts., evaluation with code SAGAPO 80—24002
- gas core, fission-fragment-generated plasma from interaction in neutral gas 78—34345
- gas core reactor, high temp., wall stabilisation, possible use of graphite 79—3190
- gas core reactors, temp. profile and power calcs., uniform density diffusion model 80—37553
- gas discharge from failed fuel pin, model for calc. of press. in duct 78—675
- gas phase cavity reactor design and operation with MHD generators and turbogenerators *(Russian)* 78—37435
- gas-cooled reactors, current development status, review 79—22375
- gas-cooled reactors, importance of development 80—5214
- gaseous core reactor, basis for direct nucl. pumped gas laser 78—33725
- gaseous core reactor, electron energy distrib. in radiation-induced U-He plasma 77—24054
- gaseous core reactor, UF$_6$ technology 78—33254
- gaseous core reactor neutronics, proliferation potential, and resource utilisation 79—9716
- gaseous core reactor nonproliferation features 79—9740
- gaseous core reactor with U-fuelling, preliminary expts. 78—33243
- gaseous-core reactor fission fragment effect on electron energy distrib., radiative transport 77—24062
- GCFBR, seismic model of core support structure 77—3184
- GCFR, 1000 MW(e), design and safety aspects 77—18672
- GCFR, 300 MW(e), gamma-ray heating in core and blanket 77—61486
- GCFR, Argonne, calc. of void streaming in critical expts. 77—83007
- GCFR, core thermal hydraulics and pumping power anal. code JUPITER 80—73889
- GCFR, design and development, review *(Italian)* 79—63721
- GCFR, design and operation, review 79—45325
- GCFR, design criteria for 300 MW(e) demonstration plant 79—97759
- GCFR, dissociating gas cooled, integrated student design problem 77—46224
- GCFR, mass-energy anals., fuel and power prod. 79—81085
- GCFR, nuclear heating in B$_4$C control rod 77—42115
- GCFR, Pu fuelled, fission products and secondary gamma-ray spectra 78—676
- GCFR, roughening characts. of surfaces for improved heat transfer 77—18650
- GCFR, sensitivity of reactivity effects to reactor model choice in safety anal. 78—13305
- GCFR, thermohydraulic code SAGAPO for roughened fuel rods 77—18651

fission reactor theory and design continued

- GCFR, thermohydraulic performance of ribbed surfaces 77—50200
- GCFR, transient anal., systems simulation methods, development and validation 79—54486
- GCFR 300 MW(e) fuel element design 77—18649
- GCFR component development programmes 77—18648
- GCFR core support structural assembly, seismic response via modal synthesis 78—89942
- GCFR demonstration plant reactor shielding system design 80—47560
- GCFR design studies, review 79—45330
- GCFR fuel assembly thermal-hydraulic anal., modification of COBRA code 80—588
- GCFR fuel pin design, anal. of temp. distrib. using HELM test facility 80—18409
- GCFR fuel rod-spacer mechanical interaction 77—46264
- GCFR grid plate shield design, anal. of confirmation expt. 80—23166
- GCFR lattice, integral neutron capture cross sections of steel, Fe, and ^{239}Pu 78—13246
- GCFR lattice, Monte Carlo and diffusion theory calcs. of steam worth 79—80991
- GCFR lattice, testing of ENDF/B-IV Th data 79—67836
- GCFR lattice with K_∞ close to 1, meas. and calc. integral data 78—33245
- GCFR programmes, status 77—18647
- GCFR radial blanket velocity and temp. distrib., buoyancy effect 79—9678
- GCFR shield anal., neutron-coupled γ-ray cross section requirements 77—23310
- GCFR thermohydraulic design codes, expt. verification 77—14221
- German nuclear data library KEDAK-3, evaluation 77—23042
- global reactor calcs. review, practical calc. for reactor burnup 78—58341
- graphite, radiation damage and its relevance to reactor design 79—33016
- graphite core components, design 78—41807
- graphite high temp. bulk, B poisoned, thermal neutron spectra meas. 79—54465
- grid plenum assembly stress anal., appl. to EBR-II 77—54288
- HCDA, coupled hydrodynamic and struct. response, splitting method 77—74958
- HCDA, REXCO code, comparison with flexible vessel expts. 78—70618
- heat conduction moving boundary problems, collocation method using B-splines, bubble expansion and collapse 77—7288
- heat conduction problems with internal sources, Monte Carlo soln. 77—65259
- heat release distribution random component determ. method 77—54289
- heat transfer coeffs. determ., use of simplex direct search and finite element methods 77—3712
- heat-pipe nuclear power plants for reliable space power 80—18377
- heating, nuclear, approx. method, direct energy balance calc., γ transport, accuracy 77—6495
- heavy element decay data, reactor related calcs., current status 79—97772
- helical wire subassemblies, mechanical behaviour anal. with SWAMB code 77—46259
- heterogeneity effects on reaction rates in advanced fuels program oxide zone assembly 80—22975
- heterogeneous computer program for square fuel rod lattices in cylindrical tank 78—58346
- heterogeneous fuel pin cells, nodal method in 2-D calcs. 78—21631
- heterogeneous Gas Core Reactor power plants 79—9671
- heterogeneous lattices, unified theory 80—37428
- heterogeneous LMFBR power distribution sensitivity reduction 79—9704
- heterogeneous reactor, homogenization, finite difference eqns. of neutron distrib. 79—40992
- heterogeneous reactor, neutron distrib. determ. by 1-D multiregion cylindrical cell 79—26488
- heterogeneous reactor, neutron importance function 77—50216
- heterogeneous reactor, neutron thermalisation effects on physical characts. 79—26487
- heterogeneous reactor, physical characts. optimisation 80—32335
- heterogeneous reactor eqns., difference eqn. approach to soln. 77—61485
- heterogeneous reactors, thermodynamic improvement *(Russian)* 77—42048
- heterogeneous-reactor eqns., difference-scheme soln. 78—37404
- hexcans, elastoplastic anal. 77—83027
- HFR test reactor, HIP-TEDDI code for neutron flux calcs. 79—3223
- HHV high-temp. test plant for design of HTGR with the turbine 79—97760
- high flux test reactor, MARIA, nuclear power research programs *(Polish)* 79—93693
- high temperature heat exchanger test plant for nuclear energy steel making process R and D *(Japanese)* 79—67817
- high-power reactor, conditions for nonuniform field production 78—37405
- higher order perturbation methods, implicit and explicit, for reactor anal. 78—78444
- Hinkley Point B, AGR radiation protection, design criteria and operating experience 80—27832
- HITREX 1 reactor expt. anal. using several codes 77—6503
- homogeneous fluid-fueled reactors capable of in-situ fuel reprocessing nitride-liquid Sn concept 80—57834
- homogenised diffusion theory parameters, rigorous calc. 79—85587
- homogenized group parameter computation 79—26493
- homogenized-cell diffusion parameters from transport codes 78—17300
- Horowitz method of reactor control system design, BWR appl. 79—45338
- hot pellet nuclear reliability factors 80—68754
- HTBFR, constitutive equations of structural austenitic steels 79—6730
- HTGCR, downstream water flow steam generator 80—5223
- HTGCR, fuel with double heterogeneity, resonance absorpt. 80—32321
- HTGR, acoustic environment determ. 79—89352
- HTGR, alternative fuel cycles using low- and middle enriched U, impact on core design 79—49674
- HTGR, annular fuel rod, contact viscoelastic stress anal. *(Japanese)* 78—54817
- HTGR, Brayton-Rankine binary cycles optimisation 80—22904
- HTGR, component characts. anal. *(Japanese)* 80—37439
- HTGR, coolant chemistry, design implications 79—67832
- HTGR, critical expts. on enriched-U graphite moderated cores, power, reactivity, control rods *(Japanese)* 80—47594
- HTGR, design and development, review *(Italian)* 79—63721

fission reactor theory and design continued
HTGR, dimensional stability of irradiated B_4C-graphite control materials 78—8905
HTGR, dynamic characts., primary loop characts. *(Japanese)* 80—57832
HTGR, inert gas release core-survey calc. 79—67908
HTGR, material development for reactor core and primary gas circuit *(German)* 78—25297
HTGR, multicomponent time depend. diffusion with radioactive decay 79—85588
HTGR, pebble-bed, computational procedure for xenon stability 77—61501
HTGR, perspectives, problems and programmes 79—26508
HTGR, rational approximations for cross-section space shielding 77—3079
HTGR, US R and D programs for steam supply plant, fuel and materials 79—97757
HTGR 900-MW(e) steam cycle plant design 80—592
HTGR core, effect of clearance on resonant frequency 77—46249
HTGR core, seismic anal. 80—32327
HTGR Core Auxiliary Cooling System mathematical simulation 78—29570
HTGR core heatup, PCRV integrity, thermal anal. model 79—49735
HTGR cores, graphite oxidisation analysis computer program *(Japanese)* 79—81018
HTGR cores, transient thermal hydraulic anal., RETSAC code 77—46246
HTGR development and its process heat, steam-cycle and gas turbine appls. 80—63250
HTGR fuel assemblies, two-dimens. modelling 80—32351
HTGR fuel elements, reactivity of multiplying systems determ., kinetic methods, pulsed neutron method 79—3220
HTGR fuel particles, coating using improved gas distributor design 78—13311
HTGR low power startup model development and use 77—88220
HTGR near-breeder cycles 79—59139
HTGR nonlinear core struct. with constrained reflector blocks, dynamic response 77—46247
HTGR nuclear power and technological plant for H prod. and others non-elec. appls. 80—42742
HTGR plant, reoptimisation using nonproliferation fuel cycle 80—13576
HTGR pre-breeder and near-breeder symbiotic systems, U resource utilization 78—17321
HTGR prestressed concrete pressure vessels, design of removable closures for large cavities 80—78356
HTGR steam generator, construction and development *(German)* 77—369
HTGR steam power plant, nonlinear dynamic model, digital simulation 78—78437
HTGR thermal hydraulics 80—27719
HTGR with closed-cycle gas turbine, technological assessment 79—54490
HTGR-GT core with MEU/Th fuel, core physics and performance anal. 80—22903
HTLTR, neutron multiplication factors, temp. depend., fuel lattices, comparative evaluation with HTGR 78—29557
HTPBR, neutron and physical aspect calcs. *(German)* 80—22941
HTR, admissibility of Co as alloy constituent in primary cooling circuit components *(German)* 78—25294
HTR, design criteria of elec. generating plant with the turbine in a direct cycle 79—97758
HTR, development and performance of spherical fuel elements 80—646
HTR, expt. multipurpose, status of core design studies at JAERI *(Japanese)* 78—66330
HTR, failure processes, life prediction, elevated temp. codes 79—6745
HTR, fuel temp. coeff. of k_∞, determ. by null reactivity oscillator method 79—30890
HTR, inelastic structural anal. for component design 79—6734
HTR, metallurgical problems of intermed. heat exchanger 77—65256
HTR, modified RB-2 reactor, null reactivity oscillator method on fuel lattices, expt. feasibility 77—57703
HTR, reactor types, design, uses *(French)* 77—67857
HTR, spherical fuel elements, fabrication, fuel loading and exposed heavy metal 80—599
HTR, Xe dynamics, 2D reactor models, axially collapsing methods *(German)* 80—68731
HTR coal gasification plant, development of He-He intermediate heat exchanger 80—5222
HTR components, design implications of inelastic structural anal. 79—6729
HTR cores, comparison of energy group models for Xe transients determ. 77—67803
HTR design, mechanical property characterisation 78—29577
HTR power station, design development, operation and appl., review *(German)* 79—76088
HTR vessel, thermodynamic calc. of cooling and design *(German)* 78—4982
HTR-PRCV development of a removable closure for large cavities 80—5221
human resources, quality assurance, reliability in nuclear power plant construction 79—97776
Hungarian research reactor, reconstruction and modifications *(Hungarian)* 77—50205
HWAGR, 1800 MWt, cylindrical geometry, CECAS modeling code 78—41811
HWR, gas cooled, effect of fuel enrichment on transuranium isotope formation 78—17292
HWR, multidimens. space time kinetics studies 78—29547
HWR, multidimensional space time kinetics, TRIMHX code 80—47538
HWR, safety research and development 78—29614
HWR, Wolsung power reactor, D_2O moderated, temp. coeff. of reactivity, numerical calcs. 78—54818
HWR lattices, depend. of material buckling and k_∞ on structure 77—50198
HWR neutronics, computational benchmark problems review 77—79413
hybrid fusion, fission blanket, ^{238}U fueled, data deficiencies, weighting functions, neutron source effects 77—23295
hybrid reactor analysis, separation technique for transport eqn. and sensitivity theory 80—57823
hybrid reactors, laser induced photonuclear and fusion-fission reactions 77—61599

fission reactor theory and design continued
hydraulic pressure wave propagation in plastically deforming pipe, rel. to reactor HCDA 78—8876
hydrodynamic motions, value of distributed particle in cell techniques 79—59196
hydrodynamic/neutronic coupled code FX2-POOL for HCDA anal. 77—23219
IAEA international symposium on design, construction and operating experience with demonstration liquid metal fast breeder reactors (Bologna, Italy, April 10 to 14, 1978) 79—49646
identification, plant responses 77—88213
identification, test inputs review 78—41819
identification technique for reactor system 77—65266
imbedded neutron flux calc., reconstruction of original material struct. of fuel bundle 77—88196
implicit nonstationary iteration, appl. to 3D neutron diffusion 79—63712
Inconel, pressure vessel bottom, subcritical crack growth in ligament between instrumentation rods 79—22428
inelastic structural anal., thermomech. constitutive eqns. 79—6731
inelasticity and the ASME code 78—41815
inertial confinement hybrid reactor design with flowing Li/molten salt 80—95405
infinite cylinders, critical and subcritical, n multiplication factor, nuclear criticality safety 78—78442
infinite homogeneous multiplying system, joint factorial moments of neutron and count bivariate distrib. 79—76062
infinite plate with two holes, stress concentration reduction by interference fits 79—37158
inlet coolant temp. fluctuations transfer function, space-depend. global component 79—30887
inservice inspection, power plant design and fabrication 78—78451
integral and differential expt. interplay in uncertainty identification 79—9699
integral and integro-differential transport theory 78—50228
integral coarse mesh diffusion method appl. to reactor transients with feedback 79—85585
integral experiments for testing Th and ^{233}U data 80—27707
integral parameter correlations, reactor performance using data covariances 80—68869
integrated nuclear power system, mathematical model *(Rumanian)* 79—41013
integrated safe shutdown heat removal system for LWRs 77—54330
integration method for reactor systems analysis 78—78438
integro-differential coupled-core reactor models, asymptotic stability 80—13531
interacting breeding assemblies, analytical soln. for reactivity matrix eqn. 77—23186
interactive fuel management using a CRT 79—85594
intermediate resonance method for heterogeneous media, new formulation 77—61490
internal pressurisation in solid mixed-oxide fuel due to fission gas release 77—83058
international symbiotic nuclear energy parks using breeders and advanced convertors, economic feasibility 80—57825
inverse perturbation theory 79—93691
irradiation effects, precipitation in pile, rel. to void swelling 78—70595
irradiation loop containing nonfissile material, optimality criterion based on γ-ray flux losses 80—63236
iterative method acceleration procedure 79—63722
Japanese Evaluated Nuclear Data Library, first version evaluation *(Japanese)* 78—74428
Japanese Evaluated Nuclear Data library, use of nuclear data *(Japanese)* 79—9982
JEN experimental reactor design, development and construction in Spain *(Spanish)* 77—38384
joints, review of design and anal. techniques 77—3098
JOYO MK II, design and related R and D experience *(Japanese)* 80—5201
k_{eff} of metallic assemblies, sensitivity to fission and inelastic scatt. spectra 77—23198
Kalman filtering theory appl. *(Japanese)* 78—50278
kinetics, higher order prompt jump approx. 78—50238
kinetics, quasistatic solutions, nonlinear system, iterative procedure 80—52711
kinetics, smoothing and extrapolation techniques 77—83002
kinetics eqns., appl. of third-order Hermite polynomials 78—46138
kinetics eqns., piecewise polynomial approx. 78—4981
kinetics two-node model, delayed differential system, stable state domain of attraction 77—34374
KNK II fast breeder, construction and aseismic design 79—97778
large core hexagonal assembly, triangular-mesh neutron transport calc. 79—9720
large LMFBRs, balance-of-plant design considerations 80—106107
laser-driven fission-fusion microexplosions, nuclear and thermohydrodynamic calcs. 80—47696
laser-fission-fusion systems, coupled nuclear-thermohydrodynamic anal. 79—13520
lattice cell diffusion coefficients, unified derivation of definitions 78—58332
lattice eigenvalue as function of buckling, perturbation theory correction 79—59118
lattice param. for natural U rod clusters in D_2O, material buckling anal. 77—6484
lattice parameters for CANDU-type reactor, correction to HAMBUR resonance integral 77—46275
lattices, uniform, homogenisation, small buckling approx. 80—52721
leakage effects in self-shielding factor methods, consistent treatment 77—50227
lifetime fissile fuel requirement 80—37424
linear acceleration reactors, anal. of neutron yield produced by high-energy protons 80—22895
linear model symmetry reduction of reactor systems 77—83010
linearized reactor, stability anal. by finite element method 78—29543
liquid metal flow, inert gas bubble dynamics, simplified model 77—15098
LMFBR, 1000 MW(e), selection of reactor cover seals and bearings 80—5219
LMFBR, 1000 MW(e) pool plant, fabrication and construction 80—5213
LMFBR, 1200 MW(e), comparison of SAS3D LOF transient anal. for conventional and nonconventional core designs 79—31039
LMFBR, 1200 MWe, Na-cooled, superphenix *(Norwegian)* 77—74913

fission reactor theory and design continued
LMFBR, 1500 MW, breeding perfomrance optimisation of He-bonded carbide fuel 78—17325
LMFBR, 300 MWe, ^{A}Pu, A=239, 240, 241, burnup characts. 3-D numerical anal. 79—22371
LMFBR, 700 MW(e), use of ZPPR Assembly 9 as benchmark 80—22890
LMFBR, advanced, core design methods 78—8885
LMFBR, anisotropic diffusion effect on criticality of plate lattice fast assembly 79—26463
LMFBR, appl. of BWR simulator to neutronics calc. tool 79—40987
LMFBR, axial parfait heterogeneous core design, fuel cycle anal. 79—59156
LMFBR, benchmark calc., neutronics codes validation 77—79415
LMFBR, benchmark calcs. by diffusion methods 77—79414
LMFBR, breeding ratio and fissile inventory for homogeneous and heterogeneous cover 80—32374
LMFBR, breeding ratio and multiplication factor uncertainties 80—86953
LMFBR, bubble worth calcs. using probability table method 78—13306
LMFBR, commercial plants, French development program 79—97762
LMFBR, comparison of neutron diffusion computer codes 77—88188
LMFBR, components and fuel handling systems, Italian industry contrib. 79—97875
LMFBR, computer modelling of piping components for transient hydrodynamic structural response 78—74449
LMFBR, consideration of data uncertainties, COROPT code 80—27714
LMFBR, core design optimisation, simplified reactor physics model 78—8886
LMFBR, core designs, loss of flow transient anal. for 1200 MWe reactor 79—22415
LMFBR, core restraint systems, interassembly heat transfer model 80—567
LMFBR, Creys-Malville boiler construction and features *(French)* 80—47542
LMFBR, current developments in nuclear breeder technology 80—57835
LMFBR, demonstration, design, construction and operating experience 79—97796
LMFBR, design and construction of roof slab 80—5229
LMFBR, design and function of thermal barriers in core outlet plenum 79—97765
LMFBR, design and thermohydraulic characts. of fuel and blanket subassemblies of a large core 80—711
LMFBR, design for near zero value of Na void reactivity 78—13205
LMFBR, design of fuel rods *(Spanish)* 77—74918
LMFBR, dynamic response of containment vessel and coolant wave propag., REXCO-EUR code manual 78—58349
LMFBR, effect of alternative fuel cycles on reactor design 79—49675
LMFBR, effect of cracks in fast neutron embrittled hexagonal subassembly ducts 78—74446
LMFBR, effect of design charges on fuel cycle cost and breeding performance 80—18436
LMFBR, effect of finite plant life on doubling time 78—41809
LMFBR, effect of mag. field on operating characts. 79—71885
LMFBR, effective conduction mixing lengths for subchannel anal. of finite hexagonal bundles 78—13210
LMFBR, enrichment and control optimization for reactivity losses during burnup 78—21692
LMFBR, equipment design, Na-NaK engineering handbook 79—97815
LMFBR, feasibility of using denatured ^{233}U diluted with ^{238}U 78—17324
LMFBR, finite element formulation for thin reactor struct. thermal stress anal. 78—70613
LMFBR, flow behaviour of vol. heated boiling pools 80—13545
LMFBR, fuel and coolant motion following pin failure, EPIC code 77—83055
LMFBR, fuel cycle cost optimisation anal. of core design modifications 80—22900
LMFBR, fuel pin optimal design for large scale testing 79—76065
LMFBR, fuel-steel mixtures, basic collapse criteria for HCDA 77—3107
LMFBR, future design and construction in USSR *(Russian)* 79—97803
LMFBR, future design and construction plans in Federal Republic of Germany 79—97799
LMFBR, future design and construction plans in Italy 79—97800
LMFBR, future design and construction plans in Japan 79—97801
LMFBR, future design and construction plans in UK 79—97802
LMFBR, HCDA or Na-water interactions, primary containment integrity, design, tests 77—71673
LMFBR, heterogeneous, fuel element performance, impact of design and operating parameters 80—102249
LMFBR, heterogeneous, physics performance with internal axial blankets 80—5218
LMFBR, heterogeneous and homogeneous core designs, performance characteristics 79—59123
LMFBR, heterogeneous carbide-fueled reactors, thermal and economic performance 79—93703
LMFBR, heterogeneous core concept studies, sensitivity to fuel cycle, design and cross section changes 78—13225
LMFBR, heterogeneous core design, neutron and γ-transport effects 78—8893
LMFBR, high power, optimisation by nonconvex programming mathematical model 78—41810
LMFBR, idealised equilibrium expansion of mixtures calc. for UO_2 vapour bubbles in Na 79—22390
LMFBR, instantaneous fuel growth rates 80—561
LMFBR, integral concepts for fuel breeding description 80—562
LMFBR, intermediate heat exchangers in Phenix and SuperPhenix 80—5225
LMFBR, large, performance parameter uncertainties 78—13216
LMFBR, large, systematic method for constructing low Na void heterogeneous cores 78—13220
LMFBR, large heterogeneous design, power distrib. sensitivity 78—13217
LMFBR, LOF, molten fuel cladding relocation, multichannel model 79—26556
LMFBR, low sodium void cores 80—13549
LMFBR, low temp. saturated cycle pool type 80—13574
LMFBR, modelling in prompt burst HCDA calcs. 78—74454
LMFBR, Na flow meas. in main pipes, application aspects 80—22884
LMFBR, Na pumps for Phenix and SuperPhenix 80—5228
LMFBR, Na void and Doppler reactivities 78—8891
LMFBR, Na void reactivity sensitivity to design 78—8890

fission reactor theory and design continued
LMFBR, Na-H_2O steam generator, calc. local heat fluxes in circular channels 79—36312
LMFBR, neutron elastic removal cross sections, interference effect of strong scattering resonances 80—68658
LMFBR, neutronic and engineering characts. during long-time operation 77—71660
LMFBR, nonrefuelling reactor design 80—37437
LMFBR, nucl. design and economic comparison of conventional and bullseye core 78—13222
LMFBR, nucl. performance of reactor designed to preclude energetic HCDAs 78—13307
LMFBR, nuclear fuel utilization factor 77—71647
LMFBR, performance characts. in US nucl. energy system. rel. to breeding ratio, sp. power, discharge exposure 78—17404
LMFBR, physics problems of fast reactor shielding 79—67873
LMFBR, pin diam. optimisation in heterogeneous vs. homogeneous core 78—8892
LMFBR, pool type, French RAMSES design rules for elevated temp. appl. 79—97763
LMFBR, pool-type, dried hot concrete vessel design 78—50248
LMFBR, pool-type, engineering design and construction 80—5212
LMFBR, pool-type, natural circulation establishment 77—6487
LMFBR, potential and limitations of heterogeneous core concept 78—13221
LMFBR, primary loop components, design and testing *(French)* 79—97782
LMFBR, reactor closure assembly, rotating plug size 80—5227
LMFBR, red. of two-phase thermal cond. and heat transfer by entrained inert gases 79—30897
LMFBR, reproduction characteristics 80—37423
LMFBR, response to abnormal events, applied mechanics in design and safety review 78—70611
LMFBR, review of worldwide R and D 80—63249
LMFBR, rotating plug size study 80—52726
LMFBR, safety and related design and engineered safeguards 80—47676
LMFBR, scram and nonlinear system seismic anal. 77—3185
LMFBR, seed-blanket-type modular assembly design with favorable safety parameters 78—17308
LMFBR, significance of breeding ratio and doubling time definitions 78—25267
LMFBR, simulated radial parfait core, control rod worth 78—33280
LMFBR, SNR-300, criticality prediction 79—40989
LMFBR, SNR-300, fuel rod performance and modelling at high burnup 78—58336
LMFBR, soln. of COBRA energy equations during natural circulation conditions 79—89354
LMFBR, statistical anal. of interaction coolant channels 79—59137
LMFBR, terminated transient overpower performance, fuel design and material effects 80—22902
LMFBR, thermal performance anal. of multiplate insulation 78—8888
LMFBR, thermal-hydraulic core anal., interassembly heat transfer, TRITON computer code 79—59153
LMFBR, thermal-hydraulic transients anal. with forced diversion model 78—29553
LMFBR, thermohydraulic transients, numerical simulation using SSC-L code 79—54485
LMFBR, thermomechanical loading of adjacent hexcan 78—8889
LMFBR, uranium-thorium based fuels, breeding performance potential 79—59175
LMFBR, value function, reson. struct., reactivity coeff. 79—76069
LMFBR, water leaks in secondary cooling circuit boilers 78—86572
LMFBR, wire wrap driver fuel assembly, development and testing at FFTF 79—59152
LMFBR, wire wrapped rod bundles, coolant mixing, peripheral flow prediction 80—73891
LMFBR 1200 MW(e) performance rel. to core height reduction 79—9684
LMFBR (SNR 300), design of core catcher system 78—89937
LMFBR annealed type 304 stainless steel, creep rupture mode of failure, reliability anal. 77—3113
LMFBR assembly, fuel pin deformations, analytical method, computational code (SHADOW) 78—54829
LMFBR beam-type core components separated by thin fluid layers, transverse impulsive motion, Timoshenko beam anal. 77—88203
LMFBR benchmark calcs., effects of recent changes in ENDF/B 77—23177
LMFBR benchmark calcs. by 2 and 3 dimens. diffusion methods 78—74432
LMFBR blanket fuel management anal., PUMA technique 80—13557
LMFBR blankets, simple representation of spectrum-averaged cross sections 80—22892
LMFBR bullseye core, performance, design characts. and economic anal. 79—59121
LMFBR burnup calc., allowance for ^{239}Np 78—89936
LMFBR claddings with axial fins, stress anal. including creep effects 77—88224
LMFBR commercial plant design 78—8877
LMFBR containment, anal. of nonlinear fluid-struct. interaction, improved ICECO code 78—70615
LMFBR containment response anal., Eulerian computer code MICE for multifield fluids 78—70616
LMFBR containment response to postulated Na spills and fires, computer anal. 79—54480
LMFBR control rod bowing, CRPBOW program 77—46262
LMFBR coolant and cladding temp. distrib., PACT probabilistic method 77—46256
LMFBR core, impact of design constraints on selection of feasible design 80—5216
LMFBR core, modelling of fluid struct. coupling for seismic anal. 79—89358
LMFBR core, stochastic void models for bubble worth calcs. 80—22940
LMFBR core, transient deform. from local failure, fuel-coolant interactions 77—88245
LMFBR core and fuel design in Halian fast reactor programme 79—97795
LMFBR core assemblies, interassembly heat transfer, using CORTEMP code 79—59154
LMFBR core compaction, nonuniform interassembly gap effects 79—9682
LMFBR core design, advanced oxide fuel system 77—46268

fission reactor theory and design continued
LMFBR core design, benchmark tests of JENDL-1 for structural materials 80—13616
LMFBR core design for Na void effect minimisation 79—9683
LMFBR core design guidance, generic transient limit curves 80—5217
LMFBR core design optimisation, COROPT code 77—42041
LMFBR core designs to preclude energetic HCDA 79—59125
LMFBR core orificing, optimised method 78—8881
LMFBR core orificing computer code 79—9681
LMFBR core structural mechanics, fuel element duct design *(Czech)* 77—65255
LMFBR cores, numerical method for predicting subassembly seismic induced impact 78—74447
LMFBR coupled fluid-struct. problems, advanced Eulerian method 78—682
LMFBR critical assembly, neutron diffusion calc., DB^2 transverse leaking predictions 80—13529
LMFBR demonstration plant, design, construction and operating experience 79—97887
LMFBR design, construction and operating experience 80—32424
LMFBR design, risk-based approach 77—88198
LMFBR design codes, multigroup diffusion, current weighted total cross section determ. in unresolved energy region 80—18365
LMFBR design concept validation, EEC-JRC research 80—42786
LMFBR design implications of sodium-void worths from ZPPR critical expts. 77—54295
LMFBR design limits *(Spanish)* 80—52714
LMFBR design requirements to alleviate thermal transient effects 79—97767
LMFBR design with the composite fuel assembly 79—54489
LMFBR development, significance of nuclear data 77—26865
LMFBR experimental reactor JOYO, construction and function tests *(Japanese)* 78—33266
LMFBR finite hexagonal bundles, laminar mixed-convection heat transfer 79—607
LMFBR finite hexagonal bundles, three-dimensional coupled coolant cell heat transfer anal. 80—586
LMFBR fuel assembly, 19 pin, simulation of flow blockage 80—582
LMFBR fuel assembly channel cross section optimisation 77—46258
LMFBR fuel assembly decay heat anal., ENDF/B-IV data 77—23201
LMFBR fuel cycle characts., effects of nuclear data uncertainties 77—23197
LMFBR fuel cycles that reduce nuclear weapon material proliferation 80—106105
LMFBR fuel element design, overview 79—85584
LMFBR fuel element model, dynamic characts., meas. of amplitudes and press. fluctuations 79—67852
LMFBR fuel handling experience 79—97873
LMFBR fuel intra-assembly flow mixing uncertainty, statistical determination methodology 80—73890
LMFBR fuel pin bundle, wire-spaced, three-dimens. deflection modes 78—13301
LMFBR fuel subassembly, pin bundle deflection anal. 78—78449
LMFBR fuel subassembly temp. noise prediction, Monte Carlo approach 79—13392
LMFBR fuelling requirements rel. to Pu isotopic composition, core design 79—9738
LMFBR head closures, dynamic struct. response to HCDA 78—70617
LMFBR heterogeneous carbide-fueled cores, nuclear design 80—593
LMFBR heterogeneous core, sensitivity anal. 80—22935
LMFBR heterogeneous core design, performance characts. and computer calcs. 79—59124
LMFBR heterogeneous core design with interchangeable oxide/carbide fuel, CDS development program 80—102253
LMFBR heterogeneous core designs with axial internal blankets 78—13227
LMFBR heterogeneous oxide reference, transmuter, denatured core designs 80—22901
LMFBR heterogenization, breeding and fissile inventory changes 80—13556
LMFBR heterogenous, control rod interactions in benchmark assembly 79—81035
LMFBR large cores with interassembly heat transfer, flow orificing 78—13208
LMFBR LOF transient, integral model for voiding phase conditions 77—42032
LMFBR LOF transient, sodium voiding dynamics and cladding motion 79—49750
LMFBR metal fuel elements, development and performance evaluation 80—598
LMFBR oxide elements, predicting serviceability, efficiency 77—23209
LMFBR oxide fuel analysis system 77—46227
LMFBR permanent reactor structures, design, irradiation effects 78—21623
LMFBR plant, thermohydraulic transient simulation 77—83001
LMFBR plant components *(Japanese)* 79—63734
LMFBR plant system design, review *(Japanese)* 79—80973
LMFBR power reactor, objective function optimisation *(Russian)* 78—70590
LMFBR prestressed concrete reactor vessels, analytical model and code applications 78—74448
LMFBR primary piping system components, fracture mech. review 79—595
LMFBR reactor closure assembly, seals for rotating plugs 80—5226
LMFBR reactor vessel, buoyancy induced flow redistrib. 78—8887
LMFBR safety, comparison of ICECO code with flexible vessel expts. 78—70619
LMFBR safety, comparison of ICEPEL code with straight flexible pipe expts. 78—70620
LMFBR safety analysis, design features to prevent and terminate plant accidents 80—47677
LMFBR secondary cct. components 79—97793
LMFBR secondary Na ccts., design, construction and operating experience *(French)* 79—97789
LMFBR shielding calculations, accuracy of ENDF/B-IV cross sections 78—13401
LMFBR simulation, parameter estimation 80—47597
LMFBR single component and mixed oxide fuel solidification anal. 78—74435
LMFBR spectrum, Doppler reactivity worth of UO_2 and ThO_2 meas. 80—27776

fission reactor theory and design continued
LMFBR steam generators, design developments *(Czech)* 80—5206
LMFBR subassembly, thermal hydraulics anal. 79—89396
LMFBR subassembly ducts dynamic response, comparison of finite element code with expts. 78—70614
LMFBR subassembly simulation, finite element computer model, safety anal. 78—70612
LMFBR system design requirement to accommodate Na spillage 79—97845
LMFBR transient behaviour, effect of steam cycle 79—49678
LMFBR transient fission gas behaviour modelling, bubble equilibration effects FRAS 2 code 79—59168
LMFBR universal core layout, interchangeability of hetero(homo)geneous cores and oxide/carbide fuels 80—102228
LMFBR vented assembly cores, appl. to nonlinear network anal. to hydraulic modelling 78—13207
LMFBR vented fuel assembly, thermodynamic modelling and testing 80—83144
LMFBR vessel cavity and cell liners, elastic/plastic design 80—52728
LMFBR wire wrapped fuel assemblies, temp. distrib., approx. method based on porous body model 77—18646
LMFBR wire wrapped rods, 3-D thermal-hydraulic anal. 77—79425
LMFBR with U-Pu-Zr alloy fuel, 1000 MW(e), design and perform. characts. 80—604
LMFBRs, national development programmes, status assessment 80—106104
LMFISR, in France, Future design and construction plans *(French)* 79—97798
LMFRB steam generator design and development 80—5224
LMRBR, interchangeable core assessment, coolant orifice zoning 80—102229
LMRBR interchangeable core assembly design 80—102230
LOCA codes, characteristics of two-phase one component flow with slip 77—83019
local burn-up rel. to construction material presence *(Russian)* 78—41812
LOFT, contribution to nuclear reactor safety 80—106139
LOFT, zero power physics testing, meas. vs. calcs. 80—27713
LOFT fuel design and operating experience, exposure to LOCA 79—89438
LOFT fuel design and operating experience 80—18411
Los Alamos density exponent formula, integral version, comparisons using multigroup theory 78—74425
low-decontamination approach to proliferation-resistant fuel cycle 79—26679
LWBR, calculational model used for nuclear anal. 79—67842
LWBR, symbiotic system using ^{238}U-Pu and ^{233}Th-^{233}U fuel cycles 80—57822
LWBR, unique thermal and hydraulic design features 79—54483
LWHR, energy multiplication and T breeding 78—5031
LWR, 3D flux distrib. calc., axial continuous synthesis model with finite element trial functions 80—713
LWR, actinide decay power 80—22930
LWR, anal. of BNL exponential expts. with ENDF/B-IV data 78—13218
LWR, analysis of operating reactors with the SIMULATE nodal program 79—59150
LWR, automated procedure for selection of optimal refueling policies 79—67892
LWR, B and W cross-flow anal. by LYNX codes 80—22906
LWR, boiling heat transfer anal. 80—27724
LWR, calc. of optimum power profiles using pattern search techniques, PROFILE code 80—47557
LWR, core reactivity changes, influence of axial flux distrib. 77—46365
LWR, core reload optimisation 79—85642
LWR, critical heat flux data for uniformly heated tubes, validity of appl. to rod bundles 79—97756
LWR, design meas. to reduce radiation dose to reactor personnel 79—3199
LWR, effect of pellet cracking on fuel temp. 77—3085
LWR, ENDF/B-IV eigenvalue calcs. for UO_2 and mixed oxide critical lattice expts. 78—25272
LWR, feasibility of reactivity determ. from neutron noise spectral density with ^{252}Cf in initial loading 79—81002
LWR, first order perturbation methods in sensitivity anal. 80—37425
LWR, fuel temp. correl. for power feedback and reactivity coeff. appl. 80—22979
LWR, large cores, anal. of space-time effects using coarse mesh flux expansion method 77—67794
LWR, molten fuel coolant interaction during HCDA 77—3136
LWR, NEPTUNE reactor calc. system, development and assessment 80—600
LWR, neutronic thermohydrodynamic interaction model *(French)* 79—89349
LWR, nodal expansion method for reactor calcs., treatment of 3-D effects 80—605
LWR, NRC safety research programs, fuel behaviour, operational safety, metallurgy and materials 80—13705
LWR, operation planning, optimum fuel loading and generation planning, comp. code FAPMAN8 80—47673
LWR, outgoing neutron spectrum from H_2O in H_2OV interface 80—27697
LWR, press. vessel and piping design, plasticity-related damage prevention 79—6735
LWR, rem reduction plan for standard 1100MW(e) plant designs 80—745
LWR, statistical techniques for core thermal hydraulic design 80—18399
LWR, structural integrity of pressure boundary 78—66334
LWR, thermal neutron steady state spectra in pure and poisoned water 79—36306
LWR, water props. modelling using splines 77—42033
LWR, zero power coupled core, cross power spectral densities, core separation distance effects 79—54469
LWR 1300 MWe system, design of containment to withstand core melt 78—66335
LWR alternative fuel cycles, sensitivity to data uncertainties 80—22934
LWR anal., CASMO fast transport theory assembly depletion code 78—25278
LWR anal., pressure-crossflow soln. method, COBRA-III codes 78—82417

fission reactor theory and design continued
- LWR and HWR, anal. of UO_2-ThO_3 fueled exponential expts. with WIMS-D code and data 79—81000
- LWR blowdown transient, implicit computational scheme 78—34038
- LWR cell depletion code EPRI-CELL 77—50225
- LWR cones, computation of cell group consts. 80—566
- LWR containment vessels, dynamic nonlinear anal. 77—3766
- LWR core, few group 2-D diffusion eqns. in hexagonal geometry, HEXAB-II-30E code *(Bulgarian)* 80—68765
- LWR core, minimisation of energy distrib. inhomogeneities 80—63321
- LWR core analysis, qualification of SIMULATE against the Hatch-1 end-of-cycle 1 gamma scan 80—57921
- LWR core power distrib. calc., convergence of reiterating process *(French)* 80—5200
- LWR cores, single-fluid thermal hydraulic anal. 80—18410
- LWR cores anal., experience with MEKIN code 80—23054
- LWR design codes EPRI-CELL and CPM, implementation 80—68751
- LWR design modification for in-core Pu utilisation improvement 79—9709
- LWR efficiency improvement utilising OTEC technology 80—52734
- LWR fuel, future trends to improve U utilisation 79—85634
- LWR fuel assembly, lattice calculation by double sampling Monte Carlo approach 80—606
- LWR fuel cycle costs, sensitivity to fission product data 80—23102
- LWR fuel cycle resource requirements, implications of data uncertainties 80—18437
- LWR fuel design, Italian progress in manufacturing, testing and management 79—26539
- LWR fuel enrichment by linear accelerator, accelerator-target design 79—13497
- LWR fuel performance, fabrication related effects 79—59238
- LWR fuel pin modelling 77—74916
- LWR fuel regeneration by linear accelerator reactor 80—32336
- LWR gamma-scanning meas. of spent fuel elements, appl. to reactor simulation *(German)* 79—67874
- LWR in Japan, improvements and standardisation *(Japanese)* 78—17285
- LWR kinetic anal. with feedback, hypothetical accident transients 80—13697
- LWR lattices, Monte Carlo radiation transport program for reactor bundle gamma transport and energy deposition analysis 80—22915
- LWR lattices, temp. effects, reactivity levels 80—22893
- LWR neutron flux distrib. in hexagonal geom., appl. of transmission probability method 79—93680
- LWR nuclear data needs 77—23194
- LWR parameter sensitivity to neutron scatt. kernel models and data 80—63240
- LWR parameter sensitivity to uncertainties in thermal neutron data 78—29561
- LWR plant, economic effect of increased seismic load on design and construction costs 78—66432
- LWR power plant, general design philosophy *(Japanese)* 78—54816
- LWR power stations, design features and instrumentation for materials safeguards *(Russian)* 80—63278
- LWR pressure vessels, radiation embrittlement, allowable crack size, unstable fracture 77—10465
- LWR Pu isotopics, Advanced Recycle Methodology Program calc. 79—9710
- LWR safety anal., appl. of advanced neutron physics models 77—42153
- LWR safety considerations in Sweden, reactor design for power plants 79—26631
- LWR sensitivity coeffs. depend. on macroscopic spatial flux variation 79—80988
- LWR spectral effects, corrected one-group coarse-mesh representation 79—59132
- LWR systems analysis, validated computer codes for nuclear electric utility 78—17403
- LWR transient anal., improved nodal method 79—59131
- LWR version of URANUS integral code for fuel rod mechanical calculations *(Spanish)* 79—36315
- LWR version of URANUS integral fuel rod code 78—17278
- LWR-HWR tandem fuel flow concept 79—26496
- LWRs in Japan, design improvement and standardisation 78—86579
- Magnox reactors, influence of design and operation on personnel radiation dose meas. 80—5385
- maintainability, human factors engineering review of design, c.f. fossil plant 80—22913
- MARIA, Polish high flux test reactor, leakage rate meas. in reactor containment 79—18001
- MARIA research reactor, dynamics model for fast transients anal., code TOTEM 80—37419
- materials safeguards, facility design features relevant to improved IAEA safeguards 80—63277
- maximum power limits with classical discrete control *(Russian)* 79—67920
- metal structures, inelastic anal. 78—70586
- metallic fuel rod heat conduction and thermal stress anal. 77—7295
- MFBR, design and development, review *(Italian)* 79—63721
- microscopic depletion in UO_2 and mixed oxide fuel rods, MICBURN code 78—25276
- Millstone power plant, Unit 3 design 80—22922
- minimum critical mass problem, slipping conditions 77—23188
- mixed oxide fuel cycles, cost sensitivity anal. 79—89369
- mixed-mesh method description of highly anisotropic scattering 79—26494
- mixed-oxide fuel-cladding interaction at high burnup effect of initial stoichiometry 79—67859
- mixed-oxide thermal reactor parameters, sensitivity and uncertainty analysis 80—13553
- modal superposition method for computationally economical nonlinear structural analysis, seismic impact appl. 79—81004
- model of developing industry, estimation of Pu steady-state isotopic composition 79—59166
- molten core-vessel system, heat transfer steady state anal. 77—83023
- molten salt reactors, work in United States and France *(French)* 80—18376
- molten-salt reactor, efficient fuel utilization without Pu separation 79—26499
- Monju heat transport system design and related R & D work 79—97791
- Monte Carlo calc., energy contribs. of absorbed fast neutrons *(Russian)* 77—42049

fission reactor theory and design continued
- Monte Carlo code, RISO, for resonance integral calc. in reactor cell lattice 77—3088
- Monte Carlo heat conduction solution using transport theory approx. 77—65260
- Monte Carlo importance sampling with parametric depend. 80—13013
- Monte Carlo infinite cell calculations for TRX-1 and TRX-2 benchmarks 80—27711
- Monte Carlo recursive methods, optimal strategies for appl. 80—13014
- Monte Carlo tracking technique for slab cells 79—85580
- Monte Carlo transport calcs., second moment functionals for last event and collision estimators 80—13012
- MORSE continuous weights code 80—68748
- MSBR safety anal. using one point kinetics model 79—22400
- MSBR-1000 liquid salt reactor, operating characts. under variable loads 79—71886
- MSR, design and development, review *(Italian)* 79—63721
- multicore reactor, optimal control determ. from energy release profile *(Russian)* 80—73974
- multidimensional neutron transport equation, spherical harmonics soln. by finite Fourier transform. 78—17269
- multidimensional reactor calcs., interface current techniques 77—88193
- multidimensional reactor dynamics equation, fast factorization and exponential transform. procedures 78—17303
- multigroup calculations for TRIGA-type reactor analysis 79—30876
- multigroup charged-particle transport calcs., temp. effects on cross sections 80—57818
- multigroup cross section calculation, self-shielding, subgroup method *(Rumanian)* 78—46140
- multigroup diffusion program EMA-II-30, two dimens., flux distrib. *(Russian)* 77—38318
- multigroup neutron diffusion eqn. finite element soln., appl. of natural coordinate system 77—54278
- multigroup neutron flux calcs. with MURLAB program 78—29541
- multigroup scattering matrices, processing of ENDF/B data 79—26464
- multigroup time-dependent delayed γ-spectra from fission and activation of U and Pu 78—13184
- multigroup transfer cross-sections for elastic and discrete level inelastic neutron scatt. 80—42732
- multigroup-multipoint diffusion operator spectrum with delayed n 78—74430
- multigroup-multipoint diffusion operator with delayed neutrons, spectrum 77—54274
- multiple-core reactors, canonical decoupling and control 77—26837
- multiple-rod worth estimation by single-rod expts. 78—17284
- multiplex systems, reliability, reliability with repair and availability 79—41012
- multiplication coeff. calc. by quotient matrix method *(Russian)* 77—42047
- multizone reactor, reactivity and power shape control, optimisation method 77—6529
- multizone reactor neutron flux profile optimisation program *(Russian)* 79—13412
- multizone reactors, coupling, kinetics, appls. to Argonaut-ARK reactor *(Rumanian)* 77—46220
- national energy and nuclear power system plans of the Federal Republic of Germany 79—26506
- NBS standard neutron fields, average fission cross-section meas., error anal. 80—68857
- near plume impingement press., method of characteristics 77—38362
- network computations using a transient two-phase velocity difference model 79—26477
- neutron, kinetics digital simulation 77—88216
- neutron 2-D integral transport eqn. approx. soln. by collision probability methods 77—82984
- neutron absorption, control poison optimisation, depletion calcs. 80—57906
- neutron and photon, heat deposition, rate in nuclear reactor 78—29565
- neutron bursts in matter, time-depend. linear transport eqn. 79—26462
- neutron capture cross sections for fission products, statistical adjustment method, error evaluation 77—6498
- neutron collision probability program for uniform slab lattices 79—89350
- neutron counting statistics in subcritical cyclo stationary multiplying system 80—32323
- neutron cross section needs 77—23193
- neutron cross sections, U and Pu isotopes, ENDF/B-IV library, integral data 77—23200
- neutron cross sections for ^{232}Th, ^{233}Th, ^{233}U, optical and statistical model calcs. 77—54227
- neutron data importance, review 77—23192
- neutron density fluctuations, statistical anal. by Fokker-Planck method 77—26818
- neutron density fluctuations in on-off controlled reactor, exact stochastic anal. 79—36308
- neutron diffusion, homogeneous reactor cells, few-group cell parameters 80—27696
- neutron diffusion, linear eqns., soln. by method of implicit non-stationary iteration 78—70581
- neutron diffusion, mixed-lattice multidimensional reactor calcs., coarse mesh finite difference method 77—34375
- neutron diffusion, multidimens. calcs. using a nodal Green's function method 80—47547
- neutron diffusion, multidimensional, nodal Green's function method 79—59106
- neutron diffusion, multigroup equation, synthesis-finite element method 80—27699
- neutron diffusion, relationship among the various anisotropic diffusion coefficients for periodic lattices 80—57826
- neutron diffusion 3-D coarse mesh code, ROCS 77—46252
- neutron diffusion and transport, GGTC-ENEL computer code for multigroup cross sections 78—58323
- neutron diffusion calcs., appl. to reactor design and anal. 77—79427
- neutron diffusion eqn., grid coupling methods for the multigrid soln. 80—47555
- neutron diffusion eqns., channel power meas. correlation with lattice consts. 79—13380
- neutron diffusion eqns., param. adjustment with DELILAH correlation code 79—13413
- neutron diffusion equation, multigroup theory 80—27695
- neutron diffusion finite element anal. with space depend. cross sections 77—82986

fission reactor theory and design continued
neutron diffusion in 2-D, finite element energy depend. method 77—82987
neutron diffusion in reactor core, uniform infinite lattice eigenvalue as function of buckling 79—609
neutron diffusion multigroup three dimensional calcs. with finite element method *(German)* 77—88189
neutron diffusion synthetic acceleration methods for diamond differenced discrete ordinates eqns. 77—82983
neutron distrib., approx. mathmatical models, core control 77—54290
neutron dosimetry, standardized techniques for appl. beyond reactor core 79—9920
neutron drift, complex buckling modes in asymmetric cell lattices 79—30881
neutron evaluated nuclear data files in unresolved resonance region, data representation 78—29459
neutron fast flux, approximated space-energy resolution 77—82991
neutron flux distortion in 3-D reactors due to plane absorbers *(German)* 77—6478
neutron flux distrib., optimal allocation of in-core detectors 78—54839
neutron flux distribution, transmission probability method 80—106101
neutron flux distributions, improved response matrix method calcs. 77—34363
neutron flux regulation dynamic simulation algorithm 80—27738
neutron flux spatial approximation using coarse mesh methods QUABOX and CUBBOX, and higher order polynomials *(German)* 77—88192
neutron gas, nonequilibrium thermodynamics *(Japanese)* 78—62595
neutron importance function distrib. in reactor with trap 78—17294
neutron information at National Neutron Cross-Section Center 78—13403
neutron irradiation, multi-step, transuranium production in reactor, nuclear transformation chains, yields *(Japanese)* 80—52729
neutron leakage in presence of voids, Monte Carlo anal. 77—38324
neutron noise, space-depend., induced by vibr. absorber 77—74900
neutron noise analysis techniques 77—3069
neutron point kinetics, smoothing and extrapolation method 77—65252
neutron pulse behaviour in multizone breeder system, two-zone system pulse method 78—86574
neutron resonance heterogeneity effect in vicinity of gross region interface 77—82992
neutron shields, homogeneous slabs, computer calcs. of transmitted, reflected spectra 77—3067
neutron spectra, overlapping, multigroup collision prob. method 80—52718
neutron spectrum calculating module of pin-cell burnup code BETTY 77—71634
neutron spectrum evaluation in SR-0 reactor using activation method *(Czech)* 77—65288
neutron spectrum structure near a resonance absorption line 77—50221
neutron thermalisation, THERMOS spectrum code, accurate reduced mesh model 80—57829
neutron thermalisation in heavy water, meas. and calc. of spectra using TOF methods 79—85582
neutron transport, 3-D integral transport code SHETAN 80—63238
neutron transport, contribution Monte Carlo, exponential biasing model 80—5195
neutron transport, contribution Monte Carlo technique, variational derivation 80—5194
neutron transport, eigenvalue eqns., appl. to fast and thermal neutron systems 78—50231
neutron transport, multigroup, Monte Carlo game, moments method 80—52720
neutron transport, multiregion problems in plane geometry 78—17274
neutron transport codes, linear continuous triangular-mesh difference scheme 79—59134
neutron transport during transients, approximation methods, range of validity 77—54304
neutron transport eqn. soln. singularities in cylindrical symm. 77—23162
neutron transport equation, perturbation method to estimate functionals 80—27698
neutron transport theory, ω mode transport eqn., asymptotic soln. 80—102231
neutron transport theory, collision probability method, development and applications 80—27706
neutron transport theory, constrained finite elements and response matrices 77—61475
neutron transport theory, P_N-value of asymptotic decay constant 80—57830
neutron transport theory, reduced three-dimensional transport equation with anisotropic scattering 80—18368
neutron two-group diffusion calc. by spatial synthesis algorithm 78—13200
neutron wave expts. in subcritical assemblies, transport calcs. 77—82990
neutron-field control system in power reactor, stability anal. 77—3086
neutron-induced cross sections at 14 MeV for reactor and shield design 78—13103
neutron-noise theory, adiabatic model 77—61489
neutronic analysis of the NBS intermediate-energy standard neutron field (ISNF) 80—27692
neutronic data base generation for transient reactor calcs. 77—83004
neutronics code, CONIFERS for reactors with channels 78—25281
nodal codes, efficient coarse mesh rebalancing method 77—14211
nodal equations, numerical approach to numerical anal. 80—13554
nodal expansion method and depletion program MEDIUM-2, validation by benchmark calcs. and comparison with expts. for PWR design appls. 77—88194
nodal fluxes determination using approx. analytical method 77—65261
nodal methods for solving time depend. group diffusion eqns. 77—82988
nodal reactor simulation code, response matrix approach 77—83000
noise, nonMarkovian formulation, hidden state-variables 77—54281
noise anal., system size expansion method 77—26830
noise analysis, irreversible circulation parameter 78—94069
noise analysis, time series modelling methods, comparative eval. *(Japanese)* 80—13552
noise analysis of power reactor, simulation using nucleate boiling noise generator 78—54840
noise theory, adjoint space applic. 78—13202
noise theory, fluctuation coarse-graining and normality preservation 78—94068
nonanalogue Monte Carlo games, conditions concerning nonanalogue transition kernels and estimators 78—62594

fission reactor theory and design continued
nonfissile nuclei, inherent inaccuracy in capture cross section calc. reactor appl. 80—22836
nonlinear coupled core reactor, computer simulation of decoupling theory appl. to power control 78—54845
nonlinear diffusion system in reactor dynamics, bifurcation anal. 79—97741
nonlinear dynamic response of containment, seismic analysis 77—3180
nonlinear reactor noise anal., appl. of Langevin eqn. with system-size expansion 80—68727
nonlinear reactor problems. appl. of successive overrelaxation method 79—59133
nonlinear systems, nonparametric system identification, damage assessment of nuclear reactors 80—32325
Nordheim integral treatment for resonance processing, proper use 80—37427
NRU, NRX reactors, homogeneous cell parameters for 2-D reactor codes by axial averaging of 3rd parameter 79—54577
nuclear data files of UK Chemical Committee, summary of data, available in ENDF/B format 78—82425
Nuclear Energy Centre, Th-based Pu burner for improved fuel utilisation 78—13240
nuclear energy synergetics, characts. of integrated systems 79—13382
nuclear engineering design, one term vs. one year projects 77—45632
nuclear engineering design at Idaho State Univ. 77—45631
nuclear engineering design course at Ohio State Univ. 77—45630
nuclear engineering design curriculum at Univ. of Illinois 77—45628
nuclear engineering design education of Mississippi State Univ. 77—45629
nuclear fuel cycle, core design optimisation 78—82420
nuclear fuel management via fuel quality factor averaging 79—30943
nuclear plant mix with minimum natural fuel requirement, optimum theory 79—26469
[nuclear plant] construction sequence scale model an aid to productivity and quality assurance 79—97777
nuclear power engineering appl. 77—18645
nuclear power plant identification methods 77—88219
nuclear power project management, book 79—30875
nuclear power reactor systems, dynamical behaviour modelling 80—91216
nuclear reactor dynamics, qualitative anal. of simplified model 79—26486
nuclear reactor kinetics and control, book 79—26461
nuclear reactor types, past and future *(French)* 80—18373
Nuclear Safety Chain concept development to increase operator awareness 80—57931
nuclear steam superheating, design tests of Zr channels 80—5211
nuclear structures, probabilistic design, state of art, research needs 78—94055
nuclear symbiosis, development of FBR and thermal spectrum near breeder reactors, review 79—45335
nuclide concentrations, time-depend. generalised perturbation theory 77—23180
offshore floating plants, design and anal. methodologies 78—66336
on-off fission reactor zonal control systems, analysis 77—71680
one-group model, convergence acceleration in perturbation theory problems 78—37406
one-group neutron transport equation and angular flux separability 79—17952
one-group transport theory, benchmark solns. of multimedia problems 79—85581
operating margin optimisation 79—85592
operating plant experience utilisation in plant design 77—65325
operating reactor data, effect of ENDF/B-IV cross sections on design parameters 78—13219
operating reactor data retrieval and evaluation system RECORDS 80—13690
operation and control simulation code 77—83006
operator eqn. model of reactor with delayed neutrons 77—50213
optimal arrangement of effective absorber 77—50223
optimal control of distributed parameter reactor core by function space method, numerical experiences 77—54317
optimal iteration strategies, geometric interpretation 79—22358
optimisation of spatial flux distrib. and Xe fluctuations by differential dynamic programming 79—45358
optimisation with regard to design, materials and testing *(German)* 80—42739
optimization of energy distribution in active region of large functional power reactor 79—59186
optimized once-through cycle and international nonproliferation objectives 79—85633
p-cell homogenization, transient flux effects, incorporation into 2-D iteration scheme 78—17301
parameter identification applying stochastic approx. 78—17279
parameter identification using the irreversible circulation of fluctuation 80—73882
parametric model of transient fission gas release and swelling in oxide fuels 77—42031
particle collision method in spherical geometry by escape probabilities, flux transport eqn. 78—78433
PBF reload core cell calc., failure of Wigner Seitz approx. 78—25264
PBHTR, closed Th cycles, computational reactor lifetime simulation 79—85643
PBHTR, depressurisation in primary circuit after failure of main coolant duct, analysis 78—25316
PBHTR, design accidents, exam. of temp. coeff. and short time dynamics 79—63781
PBHTR, design operation and applications, review 79—45328
PBHTR, space-shielding cross sections 78—25274
PBHTR net-breeding reactor system 79—3197
PBR, cylindrical upper cavity, diffusion theory simulation *(German)* 79—93713
PBR, fast power excursions, DYN and COSTANZA programs 78—50241
PBR, neutron flux distribs. in multisphere configs., diffusion-theoretical model *(German)* 80—73875
PBR, simulated THTR, spline anal. of dynamic transit reactivity meas. for pebbles *(German)* 78—66339
PBR axisymmetric core, thermal-hydraulic anal. techniques 79—71884
PBR using OTTO scheme, numerical anal. of fuel cycle including ^{236}U isotope separation *(German)* 77—83030

fission reactor theory and design continued
PBR with OTTO fueling, graphite reflectors, neutron effects, stress anal., cooling measures *(German)* 77−34368
Peach Bottom 1, HTGR nuclear power station, review of design and operation 79−45327
pebble bed HTR, heterogeneity effects in temp. coeff. calcs. 80−68757
pebble-bed high-temp. reactor as a source of nuclear process heat 77−10479
pebble-bed HTR thermal breeding 79−9715
pebble-bed HTRs, stability analyses using λ-modes 77−50226
pellet-cladding interaction, theoretical analysis 79−93699
pellet-cladding interaction induced by radiation-induced dilation, mech. anal. 78−13302
performance calc. improvement by data adjustment 79−9698
performance uncertainty anal., effects of uncertainties in cross sections 77−23196
perturbation computation with correlated sampling, nuclear reactor neutron transport 79−588
perturbation higher order time depend. theory, appl. to nuclear reactors 78−58333
perturbation method, convergence criterion and error estimate 77−14216
perturbation theory developments, review 77−14227
perturbation theory for ratios, linear and nonlinear problems 77−23175
PFR primary cct., operating experience and CDFR design intentions 79−97870
Phenix fuel assembly and core performance anal., CAPHE code system *(French)* 79−97878
photon production nuclear data for reactor design *(Japanese)* 79−93687
PHWR, struct. optimisation at burnup equilib. by nonlinear programming 79−6736
PHWR design, integration into power stations, small plant role in developing countries 79−31170
PHWR valve bellows, effect of service parameters on fatigue life and fracture 78−58348
Pickering reactor, simulation of wire activation expts. with SORGHUM code 78−25310
pin bundle, two-phase flow, eqns. of motion 78−86570
pipe bend in-plane bending, shell theory anal. 77−6516
pipe blowdown, expts. and nonequilib. anal. 79−30960
pipe ruptures, blowout panel considerations in subcompartment pressure analyses 79−67884
pipe whip behaviour, 4B sch-80 pipe under BWR conditions, parametric study *(Japanese)* 79−97825
pipes, straight, fracture under large deflection conditions, structural deformation 77−58615
pipework analysis using code PACE 2 79−93707
pipework integrity assessment 79−22431
piping system design, rationalisation of power plant pipe break criteria 80−99205
piston engine concept involving pulsed quasisteady-state gaseous-core reactor 77−34423
planning and construction of nuclear power plant *(Korean)* 78−54819
plant component design, dynamic analysis, nonlinear effects, research status and needs 79−593
plasma core nuclear reactors based on fissioning U 78−33244
plates and shells, elastic-plastic, cyclic loading anal. variational method 79−37198
point kinetics equation, integration with improved steady-state behaviour 79−22378
point kinetics on asymptotic representation of space-, energy-, angle-depend. reactor kinetics 79−80985
point reactor, time depend. probability distrib. *(German)* 77−6485
point reactor kinetic eqn. with Gaussian reactivity fluctuation, exact soln. 80−68735
point reactor kinetics equations soln. using Taylor series methods 78−13201
point reactor population model using neutron and fuel cycle kinetics analogy 80−47556
point reactor without delayed neutrons, moments of probability distrib. calc. 77−57705
point-like nuclear reactor neutron kinetics solns. using numerical method *(Italian)* 78−58324
polarity correlations in nuclear reactor anal. using noise techniques 77−14219
polynomial solns. to tensorial differential eqns. for monoenergetic neutrons in slab and sphere geom. 78−50232
pool heated volumetrically, reactor accident condition, phase change, free surface, thermal instability 78−89960
pool swell dynamics during depressurization 79−30900
porosity correction of conductivity using spherical pore geom. 77−42722
postirradiation examination facility 80−18682
power and temp. fluctuations for reactor with temp. feedback, exact statistical anal. 79−36309
power coefficient measurement based on reactor coolant system average temp. 80−57909
power distribution calcs., nodal methods, unified analysis 77−46274
power increase of water-cooled, water-moderated reactor by reconstruction of active zone 77−71642
power peak-to-average ratio minimisation analysis 77−65293
power plant cooling system design, optimal system synthesis, tower, pond 77−14260
power plant design for underground rock cavity location, safety aspects 79−13398
power plant licensing procedures in the UK 80−27708
power reactor, neutron density fluctuations, stochastic nonlinear model, Fokker-Planck eqn. 78−58316
power reactor design and fuel cycles, COMECON members' collaboration 79−603
power reactor nodal anal., albedo conditions 79−80989
power reactor parameter identification in Xe oscillation model using maximum likelihood method 80−18466
power reactor resonance determ. by rod-drop method, Fourier anal. 79−22407
power reactor underground siting feasibility, Californian programme 79−13399
power reactor with multiple transport lags and nonlinear controller characts., stability, parameter plane method 77−14217
power station steam generators, Na-water type 77−50215
power system and fuel channels stochastic identification and parameter estimation 79−3201

fission reactor theory and design continued
pressure tube type reactors, SENHOR-IV computer code for small pipe break anal. 79−89397
pressure tube type reactors, small scale pipe rupture anal. 77−42034
pressure vessel and circuit development, conf. report 80−47541
pressure vessel and nozzle junction, optimum shape design 78−89941
pressure vessel design, brittle fracture criteria for steel, neutron effects *(German)* 77−34389
pressure vessel supports, fracture-safe design in neutron environment 79−93700
pressure vessels, exam. for compliance with safety regulations 78−89954
pressure vessels, pre-stressed concrete, historical review 79−601
pressure vessels, shearing stress minimisation by automated design optimisation 78−17289
pressure vessels, use of prestressed cast steel for HTGR *(German)* 79−3196
prestressed concrete pressure vessels design, finite element anal., computer programs 77−23183
prestressed concrete reactor vessels, construction movements, finite element anal. 79−621
prestressed concrete safety containments, calc. and constructional problems *(Russian)* 79−30961
prestressed secondary containments, explosive characts. near ultimate load,, review 79−30968
probabilistic structural design, component level, Monte Carlo simulation approach 78−94056
probability-based design criteria for nuclear structures 80−99207
prompt fission neutron spectra calc., nucl. evaporation theory 80−22870
prompt fission neutron spectra for ENDF/B-V 80−22869
prompt fission spectrum uncertainties, implications for integral data testing 80−22871
prompt neutron yield calcs. from neutron induced fission 80−68858
protection system and engineered safeguard system separation review program 80−57820
protective systems, proability level of readiness anal., four-state Markov process 80−27762
prototype fast reactor steam generators, commercial size design 77−46393
Prototype Large Breeder Reactor pool concept 79−9670
pulsed neutron die-away in fast multiplying assemblies 80−18366
pulsed neutron reactivity meas., approx. of kinetic distortion correction factor 77−54268
pulsed neutron source, use of perturbation theory for exptl. study 78−66328
PURINAMA, PuO_2-fueled zero-energy fast reactor 79−40988
PURNIMA 1 fast reactor, k_{eff} variation during core insertion into reflector 78−74438
PWR, 1300 MW, emergency core cooling system probabilities design 77−38365
PWR, All-Zircaloy fuel assemblies, design and performance evaluation 80−13560
PWR, anal. of occupational radiation exposure, design implications 80−5381
PWR, benchmarking of ARMP system against large-scale mockup expts. 80−13696
PWR, changes in group constants due to burnup, role of fuel nuclides *(German)* 78−17277
PWR, CIRENE reactor, zircaloy calandria tubes, stress evaluation using strain data *(Italian)* 77−50204
PWR, comparison of temp. coeff. calcs. and meas. 80−22977
PWR, core control optimisation for scheduled load changes 79−71911
PWR, core-state models for fuel management of equilib. and transition cycles 77−67833
PWR, effects of probabilistic design methods on operating characteristics 80−18397
PWR, extended inverse kinetics for monitoring reactor feedback design parameters 78−33279
PWR, HERMITE coupled neutronic thermal hydraulic code 80−23051
PWR, high-speed in-core fuel management system 79−30971
PWR, improved load follow strategy for return-to-power capability 79−41010
PWR, improved water density feedback model for neutron diffusion calc. 79−67890
PWR, internal vibration calc. rel to operational safety condition *(Czech)* 78−8915
PWR, KWU 1300 MWe facility, neutron flux computer calcs., radiation damage 77−34370
PWR, LOCA anal., turbulent flow in fuel rod bundle with partial flow blockages 79−30898
PWR, LOCA anal. for consolidated nuclear steam system 79−49729
PWR, Markov model for quantitative systems interactions anal. of system unavailability 80−22898
PWR, modification of subcooled boiling calc. in COBRA-3/KFKI program *(Russian)* 78−82434
PWR, neutron streaming in upper reactor cavity, dose rate calc. 79−89365
PWR, new design procedure for DNB limits 80−573
PWR, operational dynamics, digital simulation model 80−27751
PWR, oxide fuel rods, computer program for mechanical and thermal anal. *(Korean)* 78−86571
PWR, physics design of reload with nodal code system 80−723
PWR, probabilistic anal. of interfacing system in LOCA 78−21678
PWR, process monitoring and parameter estimation, multivariate signal analysis algorithms 80−47585
PWR, Pu charging of VVER-440 water-cooled water-moderated reactor 77−50214
PWR, Pu isotope calcs. for steady-state core anal. 79−59126
PWR, quality assurance by Framatome 80−782
PWR, reactor cavity shield system, design and anal. 79−59225
PWR, release of radioactive material, ability to meet appendix I to 10CFR50 77−46306
PWR, reliability assessment of containment 78−78481
PWR, safety aspects of using Gd as burnable poison 80−13662
PWR, superheated containment atmosphere heat/mass transfer to passive heat sinks, analytical model 79−49658
PWR, Th cycle, parametric anal. 79−26467
PWR, thermal and hydraulic design considerations 79−49651
PWR, thermohydraulic processes study, models and expt. instrumentation *(Hungarian)* 78−82433
PWR, two circuit system, licensing and design, European view 80−57930

fission reactor theory and design continued
PWR, two-point Xe oscillation model, variational technique 77—42044
PWR, use of ^{233}U enriched fuel 79—26513
PWR, velocity and press. distrib. at core inlet 77—83018
PWR, Zircaloy spacer grid design 80—18412
PWR 18 month fuel cycles, core design operation and economics 79—85591
PWR and BWR hot channel factors, nuclear, thermohydraulic and technological factors *(Spanish)* 79—36336
PWR and BWR pressure vessels, safety calcs., design, operation control, neutron effects *(German)* 77—34404
PWR and rod bundle cores, thermal-hydraulic THINC-IV computer program 77—46216
PWR anticipated transients, coupled core system approach to DNB 77—42154
PWR assemblies, spectral and density components of moderator temp. coeff. 80—9356
PWR automated optimal multiple cycle fuel management code 79—85641
PWR balance-of-plant design standardisation 80—22911
PWR CANDU, corrosion product transport, deposition on fuel bundles, press. tubes 77—61492
PWR cavity shield design, radiation streaming, calc., appl. of Monte Carlo and discrete-coordinates technique 79—89364
PWR containment safety design margins *(German)* 78—717
PWR containments following LOCA, heat transfer coefficient 80—86958
PWR core, appl. few-group diffusion-theory computer calcs. in teaching course 78—4448
PWR core, finite cylindrical synthesis program soln. of flattest power density 77—50202
PWR core, large, appl. of coarse-mesh finite difference eqns. for k_{eff} and peak power factors 78—17305
PWR core, steady-state single stage thermal anal. of hot assembly subchannels 78—13212
PWR core, Xe oscillation model, neutron diffusion eqn., nonlinear system 78—58322
PWR core anal. using 3-D spatial neutronics codes 79—89360
PWR core analysis, effects of improved UO$_2$ once-through fuel cycle 80—57917
PWR core analysis, methods and data validation 80—57924
PWR core analysis, steady-state core physics and thermal-hydraulic reload design calcs. 80—57923
PWR core analysis, transport-to-diffusion theory for gadolinia-loaded fuel pins 80—57908
PWR core analysis using EPRI ARMP program, calc. and meas. reactor physics parameters 80—57925
PWR core analysis verification, reactivity rundown and power distrib. accuracy 80—57922
PWR core barrel motion from neutron noise spectral density using scale factor 78—74450
PWR core barrel motion quantification using scale factor and statistical noise parameters 78—74451
PWR core Doppler spatial weight factor 79—9713
PWR core thermal hydraulic calculation *(Hungarian)* 78—25282
PWR cores, thermohydrodynamic computer programs *(Polish)* 79—81031
PWR damage calculations using CASK and EPR multigroup libraries 80—47670
PWR design, higher order nodal depletion program MEDIUM-2, exptl. verification 79—26492
PWR design and plant layout, safety criteria 80—102288
PWR dynamical behaviour modelling in FORTRAN 80—91217
PWR dynamics, lumped parameter model, eval. of assumptions 80—585
PWR fast transients, CRONOS code development 80—23055
PWR first core design with Gd burnable poison for excess reactivity compensation 80—708
PWR fuel assembly, lumped subchannel model anal. of enthalpy transfer 79—76063
PWR fuel assembly design, optimisation 80—821
PWR fuel assembly design, stress, temp., radiation and chem. environment effects on performance 78—13310
PWR fuel dissolution, Idaho processing plant remote systems 79—45455
PWR fuel storage, criticality eval. of low-density moderation 79—26667
PWR internal vibrs., multiple noise source model 77—26831
PWR LOCA, subcooled decompression, multidimensional wave prop. with FLASH-genre codes 79—59194
PWR main circulation pipe breakdown, mathematical model for primary circuit processes *(Russian)* 77—38368
PWR manoeuvring strategy optimisation 79—629
PWR neutron noise interpretation by vibration analysis 78—94073
PWR neutron noise sources 78—94108
PWR neutronic calcs., subcooled boiling and open channel effects 80—23053
PWR neutronic predictions with improved water density evaluation model 77—46272
PWR neutronics and thermal hydraulics, computational benchmark problems review 77—79413
PWR once through fuel cycle improvements 79—85637
PWR once through fuel cycles, improvement of fuel utilisation 79—85636
PWR pin power peaking factor prediction 79—9714
PWR plant, cut-and-cover construction, feasibility and safety *(German)* 78—82429
PWR plant, dynamics, digital simulation 78—8882
PWR plant simulator, load-follow methods computer design anal. 79—67917
PWR power plant, assessment of underground siting as engineered safety factor 78—13316
PWR power plant, dynamic model 77—46266
PWR power plant dynamics, math. model *(Polish)* 79—63800
PWR power plants, design concepts to facilitate dismantling 80—13577
PWR pressure vessel reliability, failure anal. 77—74962
PWR primary circuit constituent materials, design features verification *(French)* 79—17976
PWR reactor cavity shield system, design and anal. 79—89366
PWR reliability prediction in design, empirical and Monte Carlo techniques 78—54827
PWR steady state thermal anal., single-pass procedure using simplified nodal layout 78—50244
PWR steam generator, design and development 80—9335
PWR steam supply control system optimisation 78—50251

fission reactor theory and design continued
PWR system nonlinear model comparison with test results 78—29571
PWR thermal-hydraulic design 80—27720
PWR thermodynamic design calcs., using iteration system based on secondary circuit system model *(German)* 80—13571
PWR three unit 1300 MW(e) plant, engineering and design 78—86578
PWR tight-pitch cores, reactor physics of fuel cycles 80—57920
PWR VVER-1000 type reactors, operating state parameters, Skoda calcs. *(Czech)* 79—67818
PWR with D$_2$O in primary circuit, preliminary physics design 79—67837
quality assurance criteria, international standardisation 80—780
quality assurance program for nuclear plant operations 80—783
quality assurance standards in USA, present status and appl. 80—781
quality control program in design planning for reliability, availability and maintainability 79—97774
quasi stationary regimes of nuclear reactor calc. *(Russian)* 80—13572
quasi-redundant protective systems, optimal design 79—17996
quasilinear reactor system subject to white Gaussian multiplicative noise, moment stability anal. 79—22373
quench front motion, heat transfer coeff., surface approx. using boundary layer anal. 79—45342
radiation protection, ALARA, effectiveness of design modifications 80—18546
radiation protection, ALARA, reactor inplant design, a regulatory viewpoint 80—23016
radiation protection, ALARA inplant design for occupational radiation exposure, cost-benefit anal. 80—18547
radiation protection, ALARA objectives, reactor design for occupational exposure 80—23017
radiation protection, ALARA occupational radiation exposure, utility design viewpoint 80—18548
radiation protection in nuclear power plants and the fuel cycle, conf., Bristol, England (Nov. 1978) 80—4471
radiation streaming anal. using spherical harmonics expansion of albedo data 79—89367
radiation transport calc., Monte Carlo approach for engineers 79—585
radiative heat release measurements, accuracy of exposure ionisation chambers 79—76070
radioactive atoms in critical reactor, fluctuation in numbers, anal. 77—3076
radioactive nuclide decay data for reactor calcs., activation products and related isotopes 78—82426
radioactive waste management, influence on standardised plant design 77—46307
radioisotopes in cooling system, prod., transfer, life cycle, radiation calcs. using program system TIBSO 78—54821
RBMK-1000 channel U-graphite reactor, fuel assembly and fuel element design 79—40991
RBMK-1000 reactor, U utilization efficiency increase 80—27747
RCP01 Monte Carlo program, neutron capture and photon heating rates 79—71912
reaction rate Monte Carlo estimators, unified definition 78—58334
reactivity and neutron density noise excited by random rod vibr. 77—50203
reactivity calc., cross-section library inadequacy 79—9697
reactivity calcs., correlated sampling Monte Carlo methods 79—22368
reactivity calcs., Monte Carlo perturbation source method 78—37398
reactivity coefficient charges in Soviet RBMK reactors 80—73954
reactivity determ., independ. of reactor fuel 77—3078
reactivity determination, pulsed neutron source technique, ZR-4 reactor appl. *(Hungarian)* 78—21673
reactivity due to bubble collapse, probability table method 78—37399
reactivity effect of cross-section processing for moist bulk-oxide criticals 80—37493
reactivity effects in U-H$_2$O systems due to spherical fuel particles 80—13570
reactivity increase due to compaction of unmoderated fissile materials 78—70589
reactivity insertion, unexpected, rapid detection 78—58370
reactivity perturbation calc. by difference iterations in the Monte Carlo method 80—5210
reactivity reaction rate method for capture-fission ratio determ., spectral fine struct. effects 78—46136
reactivity reserve and K_{eff} estimation *(Russian)* 80—73913
reactivity variation factors, calc. 77—26834
reactor boundary changes, generalised perturbation theory 78—4980
reactor cavity radiation streaming, albedo Monte Carlo methods 79—89363
reactor containment response to HCDA anal. with MICE code 77—42029
reactor core melt frequency, probabilistic model using prob. of rare events 79—54526
reactor decay power, model of fission prod. capture effect 78—37403
reactor dynamics, finite element analysis for two dimensional eqn. *(German)* 77—88190
reactor dynamics, numerical integration using real integrating factors 80—68730
reactor dynamics optimal control, exact closed-form soln. for terminal cost problem 79—54472
reactor fuel assemblies, optimum location 79—17968
reactor kinetics, computational methods and computer codes for space-dependent transient analysis 80—52716
reactor kinetics, computer assisted learning package 77—33809
reactor kinetics eqns., appl. of higher order prompt-jump approx. 78—74422
reactor lattice epithermal neutron spectra, spherical harmonics anal. 78—21619
reactor lifetime fuel logistics, fissile fuel doubling time characteristics 78—46135
reactor neutron noise anal. techniques, unified theory 79—30886
reactor noise theory as a Markov process 78—74420
reactor operation and control simulator ROCS, extension to two energy groups 79—81034
reactor parameter estimation using empirical criticality eqn. 79—17965
reactor physics, review 80—63245
reactor physics considerations in design for improved BWR fuel cycles 80—57916
reactor physics considerations of PWR fuel cycle alternatives 80—57918
reactor plant mathematical modelling, dynamic model verification by comparison with recorded plant transients 79—89468
reactor point model, kinetic eqns. anal. soln., starting mode 80—27709

fission reactor theory and design continued
- reactor shielding computation methods and programs in Poland *(Russian)* 79—26767
- reactor small pin bundles, thermal-hydraulic anal. using COBRA-3M computer code 79—76067
- reactor space time kinetics, quasi-static synthesis method 79—26479
- reactor spatial dynamics, hybrid computer simulation 78—29567
- reactor struct. seismic response, modal response method 77—83059
- reactor vessel design-basis-accident presure-pulse prediction using SPIRT code 79—89361
- reactors with delayed temp. feedback, linear stability anal. 78—29551
- reflected critical reactor problem, slab geometry, improved P-L soln. 77—23178
- reflected critical slab, asymptotic soln. using invariant embedding principle 80—27683
- reflected cylindrical reactor, eigenfunction and numerical solns. to critical problem 78—58326
- reflected reactors, two-group theory of noise, appl. to vibr. absorbers 79—26468
- reflected systems, neutron generation time 80—563
- reflecting boundary conditions for diffusion coefficient calculations in Wigner-Seitz cells 80—27710
- regulatory activities and their research and developmental support in the CSSR 79—26625
- reinforced concrete, nonlinear dynamic response under loading, research status and needs 78—94054
- reinforced concrete containment structures, improved design, research requirements 78—94049
- RELAP-4 code, self initialisation of momentum eqn. 79—36307
- reliability and maintainability symposium, Los Angeles (1978) 78—50250
- reload core design optimisation 79—604
- removal-diffusion shielding code SHREDI, bidimensional, fundamentals and results 78—70645
- research criteria, economical nuclear power plant structs. and components 78—94045
- research needs, standards improvement, nuclear power plant design 78—94046
- residual power after shutdown. afterheat estimation *(Slovak)* 77—82997
- residual reactivity role in plant transients 77—50228
- resonance absorption calculations in thermal reactors 80—86955
- resonance $J(\Theta,\beta)$ function evaluation, comparison of various computational models 77—61483
- resonance reaction rates, group averaged, correl. technique 79—59129
- response matrix doubling equations for particle distribs. calcs. improved formulations 77—6480
- response matrix eqns., properties 77—67795
- response surface of fuel-cladding gap conductance determ. by power oscillations 77—50267
- review of fission reactor design, development and commercialisation of 17 types *(Japanese)* 79—80974
- RFIT, data evaluation program, theoretical background 78—29562
- rock cavity construction of a nuclear power plant—a case study 79—26485
- rocket engine, gaseous-fuelled, reactivity effects 77—54354
- rocket propulsion using nuclear reactor, optimisation problem, calculus of variation 80—27694
- rod bundles with flow sweeping, SIMPLE-2 code for single phase thermal-hydraulic calcs. 77—46215
- rod response coeffs., end effect depend. 79—30888
- rod-bundle in nuclear fuel element, mathematical model for transient subchannel analysis 77—79430
- rotating components, design to probabilistic criteria 77—3716
- rough surface heat transfer, turbulent flow in annular channels, result anal. 80—24003
- safeguards planning in plant design process 78—82423
- safety and reliability criteria, especially pressure boundary components 79—18009
- safety design, risk assessment of necessary functions for protection against external accidents 80—743
- safety problems analysis by fluid-struct. finite element method 77—3128
- safety research experiment facility, conceptual design, LMFBR safety testing needs 77—3129
- scaling laws for modelling 79—93690
- seal ring deflection, finite element anal. 77—6502
- seawater desalination plants using simplified nucl. reactor 78—13315
- seed-blanket calcs., 2-D, one-channel synthesis method, transport and diffusion 80—73876
- seismic amplification factors of reactor components 79—597
- seismic anal., Bell ring. vibr. of vessels with attached masses 77—3181
- seismic anal. of nuclear plant, multicountry application 77—65306
- seismic design, automated generation of spectrum compatible artificial time histories 78—29661
- seismic design, probable simultaneous response by response spectrum method 77—83060
- seismic design of power plants 77—3179
- seismic design standardised spectra for plant equipment 78—41870
- seismic effects in secondary containments: research needs 78—94050
- seismic instructure response spectra, development and use 77—3080
- seismic instrumentation for nuclear power plants in Germany, review 79—620
- seismic load effects on structures, R and D requirements 78—94051
- seismic load studies on nuclear power plants, research needs 78—94052
- seismic response, artificial time history generation 77—3172
- seismic response anal. of structures, new discrete models 78—67081
- self-shielded cross-section generation in complex multiregion cells 79—9718
- self-shielding factors, discrepancies between ETOX and TIMS codes 80—68744
- semi-elliptical fault fatigue propagation, three-dimensional anal. *(French)* 79—23283
- SGHWR, 600 MWe, design and operational experience, UK 77—18686
- SGHWR fuel performance under power ramp operation 77—74963
- SGHWR safety design and evaluation 79—26636
- shape factors of non-critical small fast assemblies and their use in k_{eff} calculations 79—89351
- shell, finite circular cylindrical, rate formulation for elastic-plastic creep anal. 77—58568
- shells, internally pressurised 2:1 ellipsoidal, elastic and elastic-plastic buckling 79—37206

fission reactor theory and design continued
- shielding, multigroup libraries from radiation shielding information centre 78—13399
- shielding, sensitivity-based cross-section data assessment 78—9048
- shielding benchmark calcs. by Discrete Ordinates and Monte Carlo methods 80—73886
- ship propulsion, standardised nuclear reactor system, US development program 80—5230
- shock absorbing reactor auxiliary building for aircraft impact loading, design criteria *(German)* 79—89348
- shut-down control, optimal, of unconstrained bilinear systems 77—10464
- SIMULATE code for startup test predictions 80—18558
- simulated meltdown experiment, modified diffusion coeffs. for neutron streaming 78—33278
- singularly perturbed fixed end pt., problem, asymptotic series soln. 79—22370
- slab reactor with finite reflectors, criticality 79—26475
- slowing down spectra, Placzek discontinuities 77—51423
- small bore piping, field support to ASME Section III rules 80—63346
- small PWR containment complex and coolant system 79—13402
- SNR 300, pumps, heat exchangers and manipulator systems 79—97784
- SNR 300 LMFBR steam generators 79—97792
- SNR fuel design, critical aspects from experimental evidence 79—30910
- SNR-2, design studies for heterogeneous core concept 78—13226
- SNR-2, future design and construction plans in Federal Republic of Germany 79—97799
- SNR-300, coolant outlet duct design from neutron transport experiments *(German)* 78—29566
- sNR-300, strategy and state of the elevated temperature design 79—6733
- SNR-300 fuel element design, expts. on rod bundle fluid dynamics and thermodynamics 79—97794
- soil-structure interaction anal. by finite elements 78—41879
- solar assisted LWR nuclear reactors, SOAR power system concept 80—55820
- solar-assisted LWR hybrid power plant 80—13561
- solidification of sphere with internal heat generation and surface convective cooling 77—61496
- source importance factor in reactor kinetics, adiabatic approx. 78—46137
- source-driven systems, second-order generalised perturbation theory 79—36304
- space dependent stochastic neutron kinetics with Gaussian parametric excitation 80—63223
- space electric power systems, nuclear power plant elements 80—32339
- space independent low power model, multigroup energy formalism for reactor stochastic eqns. 80—63224
- space-depend. reactor transients, early time anal. 77—3077
- spacer pressure losses prediction, analytical model 80—577
- spatial kinetics approx. techniques, computational problems 77—38334
- spectra shift controlled reactor, effect of alternative fuel cycles on reactor design 79—54482
- spectral fine-structure effects on material and Doppler reactivity worths 79—26473
- spectral shift control reactor reevaluation 79—26497
- spectral shift controlled reactor, 1300 MW(e), conceptual design and performance 79—85595
- spherical shell with circular elastic inclusion, thermal stresses 77—3727
- stable adaptive schemes, parameter identification nonlinear point reactor 79—9765
- standard neutron fields, integral meas. 79—13363
- standard variance reduction techniques in Monte Carlo transport problems, leakage estimator 78—78443
- standardisation, of plant design, General Electric standard safety anal. report for licensing 80—22908
- standardisation, scoping anal., and early site review for 1980's generation 80—22912
- standardisation of balance-of-plant design and final design evolution 80—22909
- standardisation of design, licensing experience at Palo Verde 80—22910
- state-space splitting in Monte Carlo calcs. 77—65264
- statistical aspects of uncertainty anal. 80—18395
- steam system, seismic design study using cantilever cylindrical shells 78—58339
- steel pressure vessel, reliability aspects 79—22430
- stochastic point reactor kinetics eqn. soln., 79—63719
- stochastic point reactor kinetics with Gaussian parametric noise, Novikov Furutsu formula appl. 80—37415
- stress and failure anal. of reactor components 77—3095
- stressed state in reactor pressure vessels, model studies by polarised optics 78—78454
- structural alloys, time-depend. fatigue behaviour 79—1909
- structural anal., underlying concepts of finite element analysis 78—66337
- structural analysis, inelastic response, constitutive modelling 77—3093
- structural analysis technology, high-temp. design 77—3094
- structural analysis technology for high temp. design 77—54287
- structural anisotropic domes, deformation anal., fission reactor appl. *(Slovenian)* 80—48577
- structural design and analysis, research survey, nuclear power plants 78—94048
- structural design and analysis research programme for nuclear power stations 78—94047
- structural material data eval. for JENDL-1 80—13617
- structural reliability in reactor technology *(Japanese)* 78—17315
- structural reliability of mech. components and subassemblies of nuclear power plants, conf. 79—594
- structural reliability under time varying multi-parameter loading 77—3715
- structural response to dynamic loads, simulation of dynamic environments for design verification 80—99206
- structural systems with internal gaps, dynamic and under axial impact loading 77—3092
- structural wall test results, applicability to seismic design, review 79—592
- structure-fluid interaction between vibrating wall and channel flow 77—38325
- structure-fluid mesh partitions of explicit-implicit integration 77—46238
- sub-structure analysis for elastic fields with stress singularities, hybrid formulation 77—3730
- subcompartment anal., inclusion of momentum flux 77—50224
- subcompartment pressurisation anal. 77—38364
- subcritical assemblies, interaction parameter method 77—54334

fission reactor theory and design continued
subcritical cyclostationary nuclear reactor, neutron counting statistics, sinusoidally modulated neutron source 80—99203
subcritical limits, validity of calculation methods 79—59198
subcritical limits for special fissile actinides 80—52708
subcritical reactivity determ., more direct method 79—9717
subcritical reactor, neutron joint factorial moments and count bivariate distribs. 79—59120
submerged cooling-water discharge structures for power plants at coastal waters 80—607
suboptimal control of reactors with distributed parameters, singular perturbation theory, computer model 77—6530
Super Phenix core design and development, fuel assembly behaviour *(French)* 79—30889
supercritical multiplying systems, extinction problem, point model approx., models for neutron multiplicity 80—22883
Superphenix internal shells, vibr. anal. *(French)* 78—50247
Superphenix LMFBR, design and construction of the nuclear boiler 80—47563
Swedish underground nuclear reactor containment studies, review 79—600
symmetric SOR and SIP methods, numerical soln. of multigroup diffusion eqn. 78—74431
symmetrised neutron transport eqn., fast Fourier transform method solns. 78—78435
synthesis finite element method for three-dimensional reactor calculations 80—13566
system reliability prediction, appl. of Bayes eqn. 77—67797
systems reliability analysis, cost effective quality control program 79—97775
tandem mirror fusion-fission system studies 80—37607
tandem mirror hybrid reactor, nucl. performance sensitivity of Be/molten salt blanket 80—37606
teaching, reactor analysis 80—36806
temperature-dependent resonance integral evaluation by HAMMER code 79—9708
TESHOM computer code, data format input data for lattice codes 79—22381
thermal, homogeneous, critical size calc. 77—23171
thermal benchmark lattice expts., quantitative consistency testing 79—9700
thermal breeding with mixed denatured fuel 79—67838
thermal channel heat transfer gap calc. by numerical methods 78—21630
thermal fission afterheat, sensitivity to errors in fission product data 77—26841
thermal hydraulic anal., of rod bundle fuel elements, COBRA-3C/KFKI digital computer program 78—54822
thermal hydraulics, sensitivity theory development 79—17963
thermal hydraulics anal., teaching appl. of computer graphics 80—36824
thermal lattice leakage calcs. using modified B_1 method 80—47545
thermal near-breeder reactor, effect on future U utilization 78—17322
thermal neutron reactor, possibility of decreasing minimum critical mass 79—63740
thermal neutron research reactor-2000, mathematical model of dynamics *(Russian)* 77—38330
thermal power reaction, 3-dimens. transient anal., finite difference and spacetime synthesis methods 79—17989
thermal power reactor, operations research 79—13396
thermal reactor, fission fragment heat prod. and capture cross-section 78—17296
thermal reactor, integral testing of Th-^{233}U data 79—67833
thermal reactor, reuse of power Pu and U, neutron regeneration 78—82421
thermal reactor benchmark calculations with the MCNP Monte Carlo code 80—68755
thermal-hydraulic calcs., effect of variable thermal conductivity 77—3084
thermal-hydraulic conservation eqns., analytic integration 77—83012
thermal-hydraulic numerical calculations for VVER reactor cores *(Russian)* 79—26481
thermionic reactor, ^{233}U fuel and Be moderator, neutron physics analysis 77—50281
thermionic reactors with ^{233}U fuel and $ZrH_{1.7}$ moderator, neutronics anal. 77—6482
thermohydraulic code verification by rod bundle expts. 79—97769
Thor, a thorium-reflected plutonium-metal critical assembly 79—76061
Three Mile Island, accident account and status of nuclear security *(French)* 79—81033
Three Mile Island accident anal., observations and recommendations 80—18370
THTR 300 MW(e) Schmehausen station, anal. of non-central neutron source 77—67802
THTR-300 PBR, nuclear material safeguards system 79—22427
tilted neutron flux distrib., influence of small and large absorb. rods 77—79410
time-varying reactivity reconstruction via Walsh functions 78—671
Tokamak demonstration hybrid reactor, blanket neutronics analysis 79—22469
Tokamak fusion-fission hybrid reactor, beam-driven, design parameters 77—34459
Tokamak-driven hybrid breeder reactor, liquid metal coolant, MHD effects 79—17974
toroidal reactor primary containment vessels, consistent mass matrix anal. of hydrodynamic effects 79—76066
track length type estimators, general formulation 78—37401
training course for fuel cycle facilities design 80—36801
transfer function by parameter estimation *(German)* 77—74905
transient analysis, appl. of statistical methods to sensitivity anal. of Problem 2 79—31058
transient analysis, imposed space-time kinetics method 79—59130
transient conditions anal. with FLAME-3 nodal code 77—46251
transient critical flow analysis in nodalised system 77—65258
transient fuel behaviour, modelling of grain boundary fission gas effects 79—59169
transient overpower, comparison of EPIC and PLUTO fuel-coolant interaction codes 78—8920
transient process dynamics in reactor with dissociating coolant, computer simulation *(Russian)* 77—42050
transient state initialization of quasi-static neutronics treatment 79—59192
transient thermal hydraulic analysis, RELAP4 transform. into fully implicit iterative code 77—65257

fission reactor theory and design continued
transient two-phase flow, analytical modelling 80—27722
transient two-phase level swell, appl. of drift flux model 79—49656
transplutonium multigroup neutron cross-sections 77—26754
transport calculations, two-dimensional, comparison of rebalance stabilization methods 80—5220
transport codes DOT and TWOTRAN as standards for diffusion in pebble bed reactors 80—68750
transport effects on nodal coupling parameters 78—29558
transport equations for contributons 79—22354
transport theory, P_N approx., modified form with exact asymptotic roots, change in Marshak free surface boundary conditions 80—52717
transverse momentum eqn. for COBRA-IV-I, improved version 80—578
TREAT reactor, computational method for predicting neutron hodoscope performance 79—80995
TRX-2 lattice param. sensitivity anal., ^{238}U capture cross-section representation 78—25275
turbulent flow in fuel rod bundles, finite element anal. 78—37400
turbulent heat transfer in annulus, transient, heating element, reactor cooling theory 78—86369
two-dimensional fast reactor model, space-time synthesis 78—89935
two-dimensional reactor sensitivity analysis using discrete-ordinates transport theory 79—9706
two-dimensional response matrix doubling eqns. for currents calc. in infinite rod 77—65263
two-phase flow, analytical simulations for safeguards design 78—46143
two-phase flow patterns, high pressure water in heated four rod bundle 78—89938
two-phase reactor control, neutron absorber development program 79—97852
U isotopes, sensitivities to cross sections, decay constants flux and time, analytical evaluation 78—82427
UK standards and procedures 79—81032
uncertainty analysis and stored-energy calcs. 79—93698
underground containment, dynamic anal. for design criteria 77—3170
underground nuclear power station design, safety and economic considerations 79—76068
underground siting, cut-and-cover technique 77—3171
unified neutron transport theory for reactor analysis 80—63246
upper bound estimation method 78—37402
upper internal structures for liquid-metal fast breeder reactors 79—97766
USA fission energy R&D redirection, weapon material utilization 79—26510
variable direction method, choice of optimal variant for 2-D reactor models 79—97751
vent clearing analysis of a mark III pressure suppression containment 80—32371
VHTR, high-temperature nuclear heat source for hydrogen production 79—93686
vibration analysis of heat exchanger and steam generator designs 78—66333
void coefficient for tight water lattices, dependence of moderator type 79—26470
void fraction for subcooled boiling, different heat flux distribs. along channel *(Russian)* 77—34381
void fractions in the phase flow, hydrodynamic and hydraulic studies for reactors 79—55411
VVER, fuel burnup determ. by exact methods 79—41014
VVER, proposals for increasing power station efficiency 79—26491
VVER-1000 reactor, neutron axial field stabilisation 79—63741
VVER-100 LWR reactor core theory, calc. of physical parameters 79—63735
VVER-440 reactor power stations, design and operation 79—59127
VVR-S, Bucharest, IRT-M expt. bundle power distrib., obs. and computer anal. 77—18655
water cooled and moderated reactors in Soviet Union nuclear power generation 79—642
water cooled channel reactor, RBMK, deform, of energy release field 80—37422
water cooled reactors, epithermal few-group cross sections, unit cell with neutron leakage 77—50199
water cooled reactors, main causes of fuel element failure 79—67872
water phase diagrams, spline representation, for PWR programs 77—23207
water shield, neutron transport, 2-D benchmark expt. 78—58318
water steam, boiling and nonboiling vertical two phase flow in tube, void fraction correl. 77—55073
weakly-coupled-core reactor, optimal power and distribution control *(Japanese)* 78—25306
Weale expt. calc. using modified ENDF/B-IV cross sections 79—17908
Westinghouse plant, hardware considerations for new DNB design procedure 80—18396
WIMS-D performance in cell parameters calculation for UO_2-D_2O systems 80—68747
Windscale AGR, high pressure fuel test loops design, installation, commissioning 77—6491
wire-wrap model 77—46255
Wolsung-1 CANDU-PHW generating station, nuclear computer design anal. 79—76060
WWER light water cores inserted in heavy water zero power TR-0 reactor *(Czech)* 80—5204
WWER-440 reactors, neutron-physical characts. calc. by BIPR 5K programme *(Bulgarian)* 79—85601
ZEBRA-8 series of zero-leakage test zones, calcs. using ENDF/B-IV data 77—54296
zone regulation system, power reactor, intra- and extrareactor sensors 77—61525
ZPPR, reactor kinetics of heterogeneous design core 79—59122
ZPPR critical expts. for radial parfait heterogeneous reactor concept 78—13224
ZPPR measurements use in criticality prediction for SNR-300 77—54297
ZPPR pin geometry, SDX cell homogenisation code validation 80—86962
ZPPR-7 heterogeneous core expts., pin zone reaction rates 80—9334
ZPR, neutron power spectral density with injection of air bubbles *(French)* 77—10463
ZPR noise anal., interpretation of quadratic approx. 79—76082
(α,n), mixture and compound neutron yield from separate component thick target yields 80—37414
(n, p) absolute cross section at excitation function maximum 79—45272

fission reactor theory and design continued
- ^{239}Pu sample irrad. in EBR-II, calc. and exptl. anal. 80−22947
- Am isotopes, sensitivities to cross sections, decay constants flux and time, analytical evaluation 78−82427
- Br series fission product isotopes, sensitivities to various parameters, analytical evaluation 78−82424
- Cd cutoff energies, Monte Carlo calcs. 77−50211
- D_2O, neutron scatt. cross section determ. by DEUKER computer code 79−54468
- D_2O systems, finite medium age-diffusion kernels in source-sink theory 77−67782
- ^{3}H behaviour in pebble bed reactors, numerical calc. *(German)* 80−9387
- ^{3}He(n,p)^{3}H, plasma form by reaction prods. in nuclear reactor 77−76146
- Kr series isotopes, sensitivities to various parameters, analytical evaluation 78−82424
- LMFBR, U-Pu-Zr fuelled breeding potential assessment 79−9685
- LMRBF, ^{233}U-Th fuelled pin diameter optimisation 79−9687
- Na bonded carbide fuel assemblies, anal. of structural members 77−46261
- Na coolant, effect of high reactivity with air and water on reactor design *(French)* 79−26526
- Na, liquid, natural convection from plane surfaces, LMFBR design, review 80−37417
- Na, liquid coolant loop, H bubbles, mathematical modelling 77−42042
- Na, liquid metal slug flow, transfer function of temp. fluctuations 78−46133
- Na void reactivity anal., applicability of Benoist's diffusion coeff. 77−14218
- Np isotopes, sensitivities to cross sections, decay constants flux and time, analytical evaluation 78−82427
- O cross section data test using n spatial distrib. in water 78−74417
- $(Pu,U)O_2$, <5 wt.% PuO_2, criticality data generated by SU-HAMMER 79−3198
- Pu isotopes, sensitivities to cross sections, decay constants flux and time, analytical evaluation 78−82427
- $Pu(NO_3)_4$ in light water, reactivity predictions using discrete ordinates transport theory 78−89957
- ^{230}Pu(n,f), fission-fragment yields of neutron fission in FBR 80−83102
- ^{239}Pu, criticality of thin flat foils versus spherical shells, two-group diffusion anal. 79−26530
- ^{240}Pu resonance capture in reactor cell codes, parametric description 79−13384
- ^{242}Pu+n, 10 keV-20 MeV, ENDF/B-V cross sections 80−22837
- Sb isotopes, fission product conc., sensitivity anal. of cross section effects 78−82428
- Se series fission product isotopes, sensitivities to various parameters, analytical evaluation 78−82424
- Sn isotopes, fission product conc., sensitivity anal. of cross section effects 78−82428
- Sn, solid and liquid, neutron cross sections, Doppler effect meas. 80−22933
- T and fissile fuel exchange between hybrids, fission power reactor and T prod. reactors 80−47703
- $(Th,U)O_2$, thermal conductivity model for temps. to melting 79−93732
- Th critical assembly, reactivity meas. 79−80976
- Th fuelled thermal reactor, model for estimating flux distribs. 77−61482
- Th-PuO_2 kernels, effect of fuel particle size on power excursions, Doppler feedback mechanism 79−30911
- Th-U alloy fast reactor fuel element, design basis considerations 79−54503
- ThO_2, isolated rod, exptl. and calculated resonance integrals 80−22986
- ^{232}Th+n, 0.1-18 eV, neutron total cross section determ. 80−22838
- U gas mixture plasmas, electron energy distrib., radiation source 77−46225
- U neutron criticality, solid angle computations using computer code 80−13726
- U plasma fission reactor, for space vehicle power, propulsion, terrestrial appls. 77−3145
- U radiation contour, effect of neutron flux distrib. in active zone 77−54291
- U requirements for fuel cycles in expanding nuclear power systems 78−17320
- U resource utilisation and antiproliferation reactor concept 79−9735
- U utilisation improvement, DOE objectives and projects 80−37459
- U-graphite channel power reactors, development in USSR *(Russian)* 79−26507
- U-graphite channel reactor development in the USSR 79−602
- U-ZrH system, neutron spectrum in critical pile 79−45322
- U+H_2O lattice, number of fission neutrons emitted per thermal neutron absorbed, simple calc. 77−71644
- (U-Th)C fueled reactor system, large plant, performance parameters 79−26500
- UF_6, high temp. fissioning plasma core reactors, fluid mechanical confinement 80−63248
- UO_2 fuel modelling *(Japanese)* 77−71648
- UO_2, isolated rod, exptl. and calculated resonance integrals 80−22986
- UO_2 rods in water with U or Pb reflecting walls, critical expts. 80−32331
- UO_2/Na, fuel/coolant thermal interaction in FBR, out of pile preliminary tests *(Italian)* 78−54828
- UO_2-PuO_2 fuelled lattice, reactivity predictions using multigroup transport theory 78−89957
- UO_2-water tightly-packed lattices, ENDF/B-IV data evaluation 79−9805
- ^{A}U(n,f), A=235, 238, fission-fragment yields of neutron fission in FBR 80−83102
- ^{233}U cross sections, evaluation of ENDF/B-IV and Hansen-Roach cross sections 78−29550
- ^{233}U-Th fuel cycle, review of fast integral data 79−67834
- $^{233}UO_2/ThO_2$ water-moderated lattice analysis with ENDF/B-IV data 79−9800
- ^{235}U+Be subcritical bare assemblies, pulsed n study, age-diffusion model 79−76055
- ^{235}U+BeO nearly homogeneous multiplying systems, pulsed neutron study, age-diffusion model 80−37442
- ^{235}U(n,f), sensitivity of decay power to uncertainties in estimated decay data 80−22932
- ^{235}U(n,f), thermal, appl. of $\bar{\nu}$ constraint to fission product yields 80−22874
- ^{235}U(n,f), thermal fission, fission product decay heat evaluation by least-squares method 79−30865
- ^{235}U(n,f) fission cross section standard, propagation of uncertainties, critical benchmark meas. 79−13361
- ^{238}U, neutron capture self-indication meas., shape anal. 80−68753
- ^{238}U, neutron resonance parameters, time-of-flight spectroscopy 80−47375
- ^{238}U+n, Doppler effect meas. at 24 and 144 keV 79−97704
- Xe decay chain expansion significance 79−9712
- Xe oscillations, program for optimal control in 1-D slab reactor *(German)* 77−61529
- Xe oscillations, servo-anal. and stabilisation in large thermal nucl. plants 78−46148
- Xe spatial oscillations, time optimal control 80−32320
- Xe transient processes optimisation, interrelation of various problems 78−17295
- Xe-I induced spatial power oscillations, integration method 80−13567
- ^{135}Xe, control of space-time distrib. in reactors 79−36364

fission reactors
- *see also fission reactor materials; fission reactor operation; fission reactor theory and design; fission research reactors; hybrid reactors; nuclear engineering; nuclear physics; nuclear power stations*
- 440 MW water-moderated water-cooled reactors type VVER-440, description 77−18691
- 1100 MWe, MARK-II type, primary containment vessel design and fabrication 77−18659
- 1200 MwE FBR, nuclear steam boiler system Super Phenix 79−93816
- 1200 MWe FBR steam generators, Creys-Malville in France, manufacture 80−27797
- 4150 MW nuclear power station with PWRs, at Bugey, in France, commissioning report *(French)* 80−37571
- accident and failure probability, reliability technique appl. 77−30653
- acoustic background noise of liquid metal fast breeder reactor 79−81622
- acoustic wave propag. and damping, in ducts with flow, section discontinuity effects *(French)* 77−6576
- actinide burning very hard spectrum reactors 79−89414
- advanced, report on 1977 IAEA conference *(Dutch)* 77−83069
- advanced converter reactors with proliferation-resistant single fuel cycle 79−41026
- advanced nuclear energy systems, emerging concepts, conf., Graz, Austria (March 1978) 79−13381
- advanced power reactor development strategies in Japan, overview 77−3149
- advanced systems, possible development trends 77−34376
- aerospace appl., energy conversion Conf., San Diego, CA, USA (Aug 1978) 79−48038
- AGR, commercial designs 77−71687
- AGR, commercial protection system, safety logic system 77−54325
- AGR, future energy generation prospects 78−729
- AGR, Hinkley B type, construction and design experience 77−30655
- alternative fuel cycles and fast breeders 80−27791
- American Nucl. Soc. winter meeting 1977 78−58315
- American Nucl. Soc. Winter Meeting 1977 78−82408
- American Nuclear Society 25th Annual Meeting (Atlanta, GA, USA (June 1979)) 80−12847
- American Nuclear Society proceedings (conf. Las Vegas, NV, June 1980) 80−94920
- Aquitaine 1 loop for studies of crack growth rate and propagation in piping 77−3796
- AVR graphite pebble bed system, meas. of neutron wave propagation *(German)* 77−6481
- AVR PBR, Julich, continuation store for burned up fuel elements *(German, English)* 77−65289
- benchmark experiments for thermal and fast reactor testing 77−23203
- BFS-1 fast critical assemblies, expt. results on homogeneous and heterogeneous insertions 77−46221
- BN-350, physical characteristics study *(Russian)* 79−97898
- BN-350 reactor shielding studies 78−21667
- book, advances in nuclear science and technology (vol.9) 77−14202
- BOR 60 fast reactor, primary coolant circuit radioactivity effects 79−63737
- breeder nuclear power stations, introductory outline *(German)* 79−26731
- breeder reactor development, survey *(German)* 78−5007
- breeder reactor programme in United States, near term objective 78−5009
- breeder reactors, current status in Europe 80−27796
- breeder reactors, fast Na cooled, operational system *(Dutch)* 80−5320
- breeder reactors, French commitment and European cooperation *(French)* 80−47690
- breeder reactors, long term economic forecast and place in French and worldwide energy needs *(French)* 80−47687
- breeder reactors introduction, essential conditions 80−829
- breeder United States nuclear industry, new energy policy, review 78−5061
- breeder-convertor association characts. 77−61487
- breeding characteristics, comparison of hybrid fission-fusion plant and fast breeder 77−88269
- BWR, 770 MWe, ^{235}U enrichment staggering of initial fuel charge *(German)* 77−61582
- BWR, ^{14}C production and discharge 79−52979
- BWR, advanced reactor, characteristics design and economics *(French)* 77−74968
- BWR, boilers and pressure vessels, in-service inspection, General Electric's code 77−3152
- BWR, containment system coolant flows, LOCA modeling 79−54476
- BWR, global noise identification by spectral and parametric methods 79−63730
- BWR, HDR reactor, design of blowdown loading expts., dynamic response of PWR-vessel internals 77−88204
- BWR, heavy water moderated, manufacture and installation experience 77−83070
- BWR, input neutron noise, stochastic variables quantisation 79−85573
- BWR, KRB reactor press vessel, fast neutron fluence evaluation, operational consequences *(German)* 77−34369
- BWR, neutron noise studies 80−557
- BWR, noise sources of neutron flux, coherence anal. 77−88199
- BWR, optimal in-core fuel management using OPTLWR computer code 78−17363

fission reactors continued
- BWR, pipe system failure characts., effects on plant availability and capacity 78–17375
- BWR, reactor safety anal., sensitivity assessments, plant risk 77–18676
- BWR, surface inspection methods, in-service inspection of reactor pressure vessel 80–27759
- BWR, Swiss 942 MWe project, Dutch (NUCON) development *(Dutch)* 79–3191
- BWR, thermal-hydraulic technology, university contrib. opportunities 79–49652
- BWR availability improvement 77–38379
- BWR computer based control systems 80–83211
- BWR core, three dimens. calcs., new brief neutron diffusion scheme 77–42014
- BWR core simulation, few group coarse mesh diffusion scheme, expt. verification 77–23223
- BWR designed for improved operation at Grand Gulf 80–106121
- BWR dynamics, multivariable autoregressive identification 78–94107
- BWR feedwater and reactor water specifications 77–54355
- BWR LOFA conditions, transition flow boiling heat transfer to water in verticle annulus 77–23182
- BWR power stations, operating record and reliability, reviews 79–22403
- BWR pressure vessels, safety calcs., design, operation control, neutron effects *(German)* 77–34404
- BWR technical parameters in Italian power plant Caorso 77–38388
- BWR turbine, simulation 78–737
- BWR Vermont Yankee power station, external radiation field meas. 77–54368
- CANDU, Canadian nuclear power programme 77–10481
- CANDU, decommissioning 80–95394
- CANDU, economic aspects 77–38382
- CANDU, future developments 77–38381
- CANDU, future routes for Canada's effort 77–46388
- CANDU, initial fissile U requirements for fuel cycle, computer simulation 78–17320
- CANDU, political and economic uncertainties 79–85758
- CANDU, T buildup in D$_2$O due to ^{3}He(n,p)^{3}H reaction 79–22389
- CANDU, thermal near-breeder reactor, effect on future U utilization 78–17322
- CANDU, unique characts. 77–74971
- CANDU and HTGR thermal reactors, principles and charac. review *(Dutch)* 80–68847
- CANDU reactors, present state and future development 77–74970
- CANDU system, general review 80–95393
- CANDU-OCR power station options and costs 80–73989
- CANDU-PHW decommissioning, costs, environmental impact, radioactive waste management 80–13964
- CANDU-PHW program, status and prospects *(Czech)* 77–38387
- CAS medium-size nuclear plants 79–31169
- catalysed D fusion-fusion hybrid reactors 78–58436
- channel-type uranium-graphite, of Leningrad Atomic Power Station, construction experience 77–23241
- CIRENE core, design criteria and anal. 77–14213
- CIRENE reactor, technological aspects, materials *(Italian)* 77–14214
- Colgate fission plasma reactor, high temp., gaseous fissionable material, design, technical problems *(Dutch)* 78–50249
- comparability study of fission and fusion reactors w.r.t. safety, costs and development time 79–59114
- component failure prevention by NDT *(German, English)* 79–52560
- components and vessels, underwater plasma arc and explosive cutting 79–9922
- components review *(Spanish)* 77–79429
- conference, nuclear cross sections and technology, Washington, USA (March 1975) 77–22826
- conference, San Diego, Calif., USA (June 1978) 79–17972
- conference, San Diego, Calif., USA (June 1978) 79–49650
- conference, world nuclear energy, Washington, D.C., USA (Nov. 1976) 77–34361
- containment vessel, response to impact using PISCES finite difference codes 77–3097
- converter reactors, fuel supply enhancement by use of non-fission neutrons 79–17960
- cost comparison of PWR and PHWR nuclear power plants in Korea 80–57821
- CRBRP, ex-vessel storage tank design and fabrication 78–17347
- CRBRP steam generator, thermal transient and inelastic screening for Cr-Mo steel components 78–21660
- creep, rupture of structures subjected to variable loading and temp. 77–3786
- Creys-Malville plant, installation, design and construction planning *(French)* 80–47691
- Creys-Malville plant worksite and progress *(French)* 80–47692
- current status, USA, as of 31/12/1977 78–58398
- decommissioning, conf., Vienna, Austria (Nov. 1978) 80–12855
- decommissioning, criteria for the management of redundant nuclear facilities 80–13975
- decommissioning, deform. of acceptable residual radioactive contamination levels 80–13973
- decommissioning, dismantling of French-type fast-neutron power reactors *(French)* 80–13968
- decommissioning, disposition planning system for engineered approach 80–13963
- decommissioning, establishment of activity limits for items to be released for unrestricted use 80–13972
- decommissioning, experience gained with the decontamination of a shutdown reprocessing plant 80–13981
- decommissioning, Halian experience 80–13967
- decommissioning, industrial experience gained in the decontamination and partial dismantling of a shut-down reprocessing plant 80–13985
- decommissioning, legal aspects 80–13961
- decommissioning, main problems 80–676
- decommissioning, national policies and international aspects 80–13959
- decommissioning, radioactive waste disposal *(French)* 80–13736
- decommissioning, radioactivity limits for release of liquid radwaste, math. model 80–13737
- decommissioning, residual activity levels allowing radioactive waste to be considered inactive 80–13735
- decommissioning, state-of-the-art handbook 80–824
- decommissioning, summary of US DOE handbook 80–13969
- decommissioning, treatment of contaminated metallic wastes by smelting 80–13741

fission reactors continued
- decommissioning, US policy and standards 80–13960
- decommissioning and dismantling projects at Idaho National Engineering laboratory 80–13984
- decommissioning and reconstruction of the fast reactor fuel reprocessing plant, Dounreay 80–13983
- decommissioning and total dismantling of PWR power plant 80–13982
- decommissioning aspects of a nuclear chemical plant 80–13986
- decommissioning nuclear facilities, criteria, standards, policies 79–31166
- decommissioning of a ^{239}Pu contaminated incinerator facility 80–13987
- decommissioning of LWR power plants by German utilities 80–13962
- decommissioning of LWR power station, radioactive waste decay behaviour 80–13738
- decommissioning of nuclear facilities 79–31165
- decommissioning of nuclear installations in the preliminary safety report *(French)* 80–13966
- decommissioning of PWR and fuel reprocessing plant 80–13970
- decommissioning quantitative anal. of radioactive waste development 80–13974
- denatured Th cycle in symbiotic systems, potential role 79–26484
- desalination, THERMOS reactor energy source *(French)* 80–47684
- development and role in national economy of USSR 77–23314
- DFR special experiments 79–97779
- district heating reactor with heat exchanger, 70 MW, transportable 78–46159
- Dounreay contribution to fast reactor development 80–27798
- Dounreay Fast Reactor, instrumentation developments since 1972 80–23118
- Dounreay PFR, plant improvements 80–57933
- Dounreay test reactor, fast breeder test experience 80–86961
- earthquake response of nonlinear plates 80–13955
- entry-control system, computerised, design 79–85688
- European Nuclear Conf., Hamburg, Germany, May 1979 79–97841
- European nuclear industry situation, review *(Dutch)* 77–3073
- experiments, control and data processing by Siemens-301 computer *(German)* 77–83032
- explosive materials detectors evaluation 79–89451
- fast, Na-cooled, 600 MWel, Soviet BN-600, design and construction *(Czech)* 78–21746
- fast, prototype, scaling up, UK experience 78–5010
- fast breeder, using uranium-plutonium cycle, Na-cooled, technical and economic viewpoints of application *(German)* 80–99202
- fast breeder comparison to fission reactor *(German)* 79–93832
- fast breeder reactor generating station, safety engineering technology aspects *(German)* 79–54567
- fast breeder reactors, French national program 80–99271
- fast breeder reactors, Na cooled, Phenix, Super Phenix, SWR2, development survey *(Dutch)* 79–49827
- fast heterogeneous reactor, Na-voiding reactivity coeff. 80–52713
- fast neutron reactor development, European electricty producers cooperation, Creys-Malville plant *(French)* 80–47689
- fast neutron reactor development, French and other programmes *(French)* 80–47688
- fast pulse reactor, standardisation of neutron dosimetry 79–13543
- fast pulsed reactors, development and utilisation *(Japanese)* 77–61495
- fast reactor, commercial, sodium test rigs, in UK 78–732
- fast reactor control, range of absorber materials 78–8919
- fast reactor developments in various countries *(French)* 80–86967
- fast reactor electricity generation, experience and future development 80–18587
- fast reactor fuel design and development 79–31133
- fast reactor program in UK, progress on PFR, CFR, and associated fuel cycle 77–3150
- fast reactor projects, progress report 79–85757
- fast reactor role in limitation and control of Pu prod., waste disposal 79–9758
- fast reactors, ^{239}Pu decay heat evaluation 80–63239
- fast reactors, glossary of terms 79–85760
- fast reactors, Na components, test facility 77–46394
- fast reactors Na cooled, core component material irradiation induced void swelling and creep, technological consequences summary 79–36327
- fast-core experimental power station KNK II 79–81074
- fault conditions diagnosis based on tree logic and probabilistic importance, appl. to nuclear power plant 77–6549
- FBR, 1200 MWe Super Phenix, construction work in France 77–46391
- FBR, 1200 MWe Super Phenix, steam generators design, France 77–46392
- FBR, 1300 MW demonstration commercial fast reactor CFR 1, economic assessment, UK 77–3168
- FBR, anal. of reactor component fluence limits, damage function methods 77–18668
- FBR, appl. in Spanish electricity supply system, review *(Spanish)* 79–59115
- FBR, development, fuel cycle, hazards and alternatives, review 79–63715
- FBR, development of LMFBR and GCFR and alternative fuel cycles 80–47565
- FBR, few group constants for reactivity calcs. errors *(Czech)* 77–71639
- FBR, fuel development and prod. survey *(German)* 77–34391
- FBR, fuel resources and reactor technology developments in India 78–733
- FBR, gas-cooled, 600 MWe, progress in Europe 78–5012
- FBR, Na-cooled, for 250 MWe Phenix-250 station, France *(Dutch)* 77–71686
- FBR, optimisation of burnup characteristics, nonlinear programming method 77–14239
- FBR, oxide fuels and cladding, irrad. behaviour, chemical process, densification, corrosion *(Japanese)* 77–83033
- FBR, programme and development status in France *(French)* 79–26509
- FBR, Pu use in France 77–67859
- FBR, radiological hazards, security, of ^{239}Pu 77–10492
- FBR, refuelling process and doubling time calc. *(Czech)* 78–29593
- FBR, review 80–57943
- FBR, status and development in Japan 79–26737
- FBR, status and development in the Federal Republic of Germany 79–26738
- FBR, status and programme in UK, out-of-pile fuel cycle 79–26736
- FBR, types, cooling and safety aspects *(German)* 79–54587
- FBR, UO$_2$ and (U, Pu)O$_2$ fuel, gaseous and solid fission product behaviour, swelling 77–34396
- FBR, US 1977 policy and future prospects 79–49828

fission reactors continued
FBR, US development, safety aspects 78—86671
FBR accidental releases, implications of dose-mortality relationships 80—46064
FBR and HWR, in-service inspection, Japanese practices 77—366
FBR blanket design, Conf., Chicago, Il, USA, Nov. (1978) 80—23123
FBR development, importance of nuclear data programs 77—23248
FBR development and importance 78—46160
FBR development in the USSR 80—47695
FBR for electricity generation in UK 78—730
FBR international development, influence on German policy *(German)* 80—18586
FBR power stations, plutonium waste treatment, comparison with thermal reactors 78—86641
FBR programme in USSR, present status *(Russian)* 79—26735
FBR prototype, MONJU, mockup critical expts. *(Japanese)* 77—50208
FBR R and D, conf., Lucerne, Switzerland (Oct. 1979) 80—46735
FBR R and D program in USA 80—47694
FBR SNR 300, design information, risk factors *(German)* 79—26727
FBR solution to world energy problem *(French, English)* 80—18591
FBR technical and economic prospects *(German)* 77—18685
FBR technology and strategies, role of nuclear power in world energy supply 80—50948
FFTF, fast reactor, He release correlation from B_4C during fast-neutron irradiation 78—8965
fissioning plasma from gas phase nucl. reactor, appl. 80—64794
fluid-structure system dynamics, reactor safety anal., computational algorithms 77—71669
fuel rod bowing effect on critical heat flux 77—46253
fuel rod radiography, feature extraction via least squares fit to model 77—14229
FUGEN LWR, reactor physics tests 80—68893
fusion and fast breeder reactors, a comparison, book 78—78430
fusion-fission hybrid reactor, laser driven, fuel breeding and power prod. 79—22473
fusion-fission hybrid reactor, mirror confinement, fuel design consideration 79—22472
fusion-fission hybrid reactor energy research program 79—22471
fusion-fission hybrid system using divertored Tokamak, optimisation 78—798
fusion-fission reactor, hybrid, Fe shielding thickness effect on (n,2n) reactions and fission rates in ^{238}U 77—50122
fusion-fission reactors, performance parameters, design and fuel cycle anal. 79—17973
fusion-fission Tokamak, T breeding, optimisation with geom. program 78—74477
future nuclear power technology, impact of nuclear research in India 80—95345
future prospects, technical, economic and political review *(Spanish)* 79—59116
gas cooled breeder reactors, development status and performance comparison 79—26741
gas cooled fast neutron reactors, He and CO_2 coolant comparison 77—42046
gas cooled fast reactors with dissociating coolant, 1200-1500 MW, problems and prospects *(Russian)* 79—26742
gas turbine-HTGR system heat exchanger design 78—739
gaseous core reactor neutronics, proliferation potential, and resource utilisation 79—9716
gaseous core reactor power production with minimal transuranic wastes 79—9806
gaseous fuel reactor for earth-based electricity generation appl., USA 77—79469
gaseous hydrocarbons pyrolysis in fluidised beds, quantitative model conceptions *(German)* 77—73448
GCFBR, research and development, current status *(Hungarian)* 79—6759
GCFBR symbiosis with thermal reactors 77—57738
GCFR, 1000 MW(e), reliability anal. of decay heat removal system 77—14223
GCFR, He-cooled, state of art and development trends *(Czech)* 78—29636
GCFR, need, performance and comparison with LMFBR 77—57731
GCFR, Pu fuelled, fission products and secondary gamma-ray spectra 78—676
GCFR, venting system of fuel element, activity release anal., operating and accident conditons 77—23226
GCFR benchmark lattices, reaction rate ratios, neutron spectra 77—23202
GCFR critical expts., physics parameters 77—14220
GCFR development in United States, 'Helium Breeder Associates' activities 79—49830
GCFR steam generator cavity closure plug, smearing in axisymm. finite element anal. 77—14222
GCFR technology *(Japanese)* 77—71638
GCHTR, steam gasification of coal using fluidised bed gasifier 77—83071
heat supply, district heating, nuclear reactors, applicability *(Russian)* 79—31173
heating, nuclear, approx. method, direct energy balance calc., γ transport, accuracy 77—6495
heating plants, big cities, industrial complexes, nuclear reactor applicability *(Russian)* 79—31174
high temperature, economy, ecology and technology 77—38389
high temperature, He gas behaviour anal. *(German)* 77—67855
high-level radioactive waste management 80—37470
HRF at Petten, expt. facilities for high flux materials testing 79—63749
HTGR, a high-temperature nuclear heat source for hydrogen production 80—45803
HTGR, appl. development in United States, 1979 prospects 80—5321
HTGR, Brayton-Rankine binary cycles optimisation 80—22904
HTGR, control rod ejection accident, comparison of one- and two-dimens. models 78—13279
HTGR, dimensional stability of irradiated B_4C-graphite control materials 78—8905
HTGR, economies in U reserve use 77—42175
HTGR, European Community Italian Centre activities *(Italian)* 80—785
HTGR, fuel failure anal. following LOCA, post-accident temp. response 78—13276
HTGR, He-cooled, prospects and status 77—79467

fission reactors continued
HTGR, heat transfer effects in annular passages of heat exchangers *(Japanese)* 77—23239
HTGR, maximum pot. hazard of ultimate accident sequence initiated by PCRV leak 78—13278
HTGR, nonelec. appl., prod. of H_2 and synthetic hydrocarbons, review 79—45329
HTGR, passage walls heat transfer performance study *(Japanese)* 77—18687
HTGR, Peach Bottom site, distrib. of ^{137}Cs and other fission products in fuel elements 78—13274
HTGR, Peach Bottom site, radionuclide distrib. in primary coolant circuit 78—13275
HTGR, process heat source for synthetic liquid fuel production 80—55781
HTGR and alternative nuclear strategies *(Chinese)* 80—78353
HTGR containment, layering and combustion following depressurization accident 78—13277
HTGR development 77—34379
HTGR development of 330 MW(e) Fort St. Vrain reactor, status report 80—47565
HTGR fuel particle, computer code for anal. of transient behaviour 78—8964
HTGR fuel particles, coating using improved gas distributor design 78—13311
HTGR heat exchanger, factors affecting performance of Cr_xC_y sprayed coatings 80—40609
HTGR operating experience and advancement potential 77—67863
HTGR pre-breeder and near-breeder symbiotic systems, U resource utilization 78—17321
HTGR steam generator, construction and development *(German)* 77—369
HTGR technology *(Japanese)* 77—71638
HTGR utilisation in technological processes and electric power generation, review 79—97886
HTPBR, neutron and physical aspect calcs. *(German)* 80—22941
HTR, ^{110m}Ag fission product, release from coated fuel particles 77—88228
HTR, characteristics, status and future prospects 77—54353
HTR, coal gasification appl. 80—11996
HTR, He-cooled, advantages and prospects 80—5322
HTR, in West Germany 77—61594
HTR, near breeder concepts *(German)* 77—26863
HTR, reactor types, design, uses *(French)* 77—67857
HTR, Th fuelled, 300 MWe, status report, W. Germany *(Dutch)* 77—14259
HTR in nuclear power generation programme, factors stimulating development 77—23242
HTR plants components development and testing *(German)* 77—10482
HTR primary component materials, properties, advantages, and limitations 79—36329
HTR process steam for coal gasification 78—78488
HTRs, current development and commercial advantages *(German)* 78—37433
HTRs, experimental and operational *(French)* 80—18374
HWGCR, KS-150, in-core instrumentation, neutron flux, temp. distrib. 77—83050
HWR, ^{41}Ar dose distributions due to atm. release 77—14271
HWR, CIRENE prototype reactor, fuel, fabrication performance *(Italian)* 77—10467
HWR, fuel cycle cost anal. using computer code HWRCOST on-power refuelling 77—83051
HWR, option for technology transfer 77—46387
HWRS, characteristics and prospects, CIRENE venture *(Italian)* 77—46205
HWRs, Th fuel cycles 77—34401
hybrid fusion reactors, problems 77—38403
hybrid fusion-fission energy systems prospects 79—49831
hybrids, fissile fuel breeding, development 78—5047
IAEA safeguards, instruments and techniques for nondestructive assay 78—33302
important types used in West, survey *(German)* 78—74463
in-service inspection, using acoustic emission technique 77—34409
integrated nuclear energy complex system of CMEA member countries *(Czech)* 80—52715
IPWR, appl. to district heating and desalination 78—41852
Iranian nuclear power reactor concept 79—93809
irradiation expts., Cd jacket for pneumatic tube 77—63991
IRT-2M reactor with loop channels in active area, physical parameters *(Russian)* 79—31067
isotope producing reactor, accumulation losses of transuranium isotopes 77—61595
ITR-2000, neutron tangential channel for nucl. gamma-reson. spectroscopy *(Russian)* 79—67819
JEN nuclear power industry, uses of isotopes *(Spanish)* 77—50313
JET vacuum vessel, mechanical reliability in disruptive instability 80—18643
laser fusion-fission hybrid reactor design 78—802
light water hybrid breeding reactors, source driven, blanket design and perform. 79—13518
liquid-cooled, reactor safety rel. heat transfer problems 77—65276
LMFBR, 1500 MW, breeding perfomrance optimisation of He-bonded carbide fuel 78—17325
LMFBR, accident conditions, theoretical anal. of Na fire using SPOOL-FIRE code 77—14248
LMFBR, acoustic anal. of TREAT safety test R8 78—13290
LMFBR, acoustic anal. on Na boiling expt. in FFM Bundle 3B, Test 4 78—13291
LMFBR, appl. of EuB_6 to neutron absorbing control materials 78—8904
LMFBR, BOR 60, modular Na heated steam generators, performance, specifications *(Czech)* 77—3147
LMFBR, cladding meltdown phase for loss-of-heat-sink event during shutdown 78—8923
LMFBR, Clinch River, assessment of containment response to hypothetical core melt-through accident 78—8928
LMFBR, Clinch River, consequences of boiling in radial blanket due to hypothetical major pipe leak 78—8922
LMFBR, Clinch River, humidity effect on burning rate of Na droplets, Fick's eqn. anal. 78—13297
LMFBR, Clinch River, LOCA in one heat transport loop without reactor trip 78—8924

fission reactors continued
- LMFBR, Clinch River Plant, sensitivity for radiological consequences to var. in aerosol parameters 78—13294
- LMFBR, containment, safety anal., conf., San Francisco (Aug. 1977) 77—71664
- LMFBR, containment building response to HCDA, risk assessment, computer anal. 77—71678
- LMFBR, containment codes appl., response predictions in HCDA conditions 77—71670
- LMFBR, core meltdown event, transient containment response, inherent retention capability 77—71677
- LMFBR, design of fuel rods *(Spanish)* 77—74918
- LMFBR, dynamic core deform. during local failure propag., subassembly expts., CORE-1 code 77—88244
- LMFBR, dynamic response of reactor vessel to HCDA 77—71674
- LMFBR, EBR II, Na purification by cold trapping, effectiveness 77—14225
- LMFBR, energy investment 78—78512
- LMFBR, enrichment and control optimization for reactivity losses during burnup 78—21692
- LMFBR, equipment design, Na-NaK engineering handbook 79—97815
- LMFBR, experience with Rapsodie and Phenix in France *(French)* 79—97892
- LMFBR, fast neutron streaming through grid plate shield 77—3081
- LMFBR, feasibility of using denatured ^{235}U diluted with ^{238}U 78—17324
- LMFBR, for elec. power generation, advantages 77—23244
- LMFBR, fuel characterization pilot plant based on X-ray fluoresc. chem. anal. 78—5006
- LMFBR, fuel handling and storage system 79—45394
- LMFBR, fuel-coolant interaction, pressure waves in compressible liquid, one-dimens. anal. 77—88235
- LMFBR, fuel-coolant interaction, UO_2 fragmentation by thermal stress and pressurisation 77—88226
- LMFBR, HCDA, accident energetics assessment 77—71667
- LMFBR, HCDA, core debris behaviour, interaction with concrete 77—71676
- LMFBR, HCDA, Eulerian computer code anal., primary system response 77—3127
- LMFBR, HCDA anal., effects on reactor struct., radiological consequences 77—71666
- LMFBR, HCDA conditions, UO_2 mech. response to transient heating 77—14237
- LMFBR, HCDA or Na-water interactions, primary containment integrity, design, tests 77—71673
- LMFBR, He leak testing of pressure vessels of subassemblies 77—67791
- LMFBR, initial fissile U requirements for fuel cycle, computer simulation 78—17320
- LMFBR, inservice inspection methods, NDT 77—38357
- LMFBR, insulations 77—83068
- LMFBR, Japanese development program 80—47693
- LMFBR, meas. of T retention of fast-neutron-irradiated absorber elements of B_4C 78—8903
- LMFBR, mixed oxide rods, high burnup irrad. performance 77—3099
- LMFBR, N contaminated liquid Li on pure Fe, grain boundary grooving. mech. 77—6522
- LMFBR, Na breeder reactors, French and Soviet programme survey *(French)* 79—41029
- LMFBR, Na fires and aerosols expts. for safety anal. data 77—71650
- LMFBR, nuclear energy strategy, Japan, possibility of FFHR 80—42868
- LMFBR, nuclear fuel utilization factor 77—71647
- LMFBR, parametric safety analyses for reduced energetics in PLBR-sized core 78—13298
- LMFBR, past and present role in Federal Republic of Germany 79—97891
- LMFBR, past and present role in Italy 79—97895
- LMFBR, past and present role in UK 79—97894
- LMFBR, past and present role in USSR *(Russian)* 79—97893
- LMFBR, penetration of turbulent jet with negative buoyancy into upper plenum, safety evaluation 77—23221
- LMFBR, performance characts. in US nucl. energy system. rel. to breeding ratio, sp. power, discharge exposure 78—17404
- LMFBR, possible cleaning of Na using fully denatured ethanol 78—21689
- LMFBR, prompt critical excursion, disassembly energy release for mech. damage evaluation 77—71668
- LMFBR, Pu release from contaminated burning Na, safety evaluation 77—23224
- LMFBR, safety anal., Na burning, aerosol release, temp., O conc. depend. 77—83049
- LMFBR, safety c.f. thermal reactors 79—26562
- LMFBR, scaled down model of SNR-300 inlet plenum, convection effects on temp. distribs. during emergency cooling 77—26839
- LMFBR, SNR-300, HCDA anal. by failure incoherence modelling, HOPE computer code 77—88237
- LMFBR, SNR-300, HCDA expt. simulation, theory reliability test 77—71675
- LMFBR, spent fuel shipping system 79—45385
- LMFBR, struct. response to HCDA, appl. of coupled Euler Lagrange computer program 77—71671
- LMFBR, survey of French national reports SM-225/73-79 *(French)* 79—97896
- LMFBR, two dimens. diffusion problems, singularities in finite element approx. 77—6496
- LMFBR, US breeder reactor programme 78—731
- LMFBR annealed type 304 stainless steel, creep rupture mode of failure, reliability anal. 77—3113
- LMFBR beam-type core components separated by thin fluid layers, transverse impulsive motion, Timoshenko beam anal. 77—88203
- LMFBR components, plastic dynamic anal., CEA-SEMT system 77—6506
- LMFBR cooling system, flow in Na circuit surge tank *(Czech)* 77—67792
- LMFBR core, partial failure expts., Na boiling in heated annular channel with blockage 77—42108
- LMFBR core, transient deform. from local failure, fuel-coolant interactions 77—88245
- LMFBR design, reliability, risk assessment, power plant safety anal. 77—71665
- LMFBR development design, economy, safety 77—34378
- LMFBR evaporator tubes, corrosion and heat transfer 79—1088
- LMFBR for maintenance of fuel reserves 77—67862

fission reactors continued
- LMFBR fuel assembly, coolant mixing, subchannel vels., electrolytic tracer, isokinetic sampling techniques 77—18653
- LMFBR fuel assembly, edge blockage in 19-pin Na-cooled bundles 78—13292
- LMFBR fuel pin behaviour, computer code FRUMP, stress, strain, temp. distribs., displacements 77—14235
- LMFBR fuel rod, enhanced thermal creep deformation, secondary stress cycling conditions, elastic region 77—4832
- LMFBR HCDA, pipe rupture following earthquake, accident course 78—8925
- LMFBR HCDA, radiological consequences, attenuation due to radiative cooling 78—13296
- LMFBR HCDA, study of natural convection in porous media with heat generation 77—51114
- LMFBR heat exchangers, liquid metal temps. in pipes with wall fast flow discontinuities *(Spanish)* 77—74907
- LMFBR high-temp. neutron detector test results 77—74909
- LMFBR in Italian electric power program *(Italian)* 77—10483
- LMFBR interlaboratory reaction rate program, evaluated decay scheme data 77—22928
- LMFBR maximum critical accident, assessment using theory of aerosols coagulation 77—3121
- LMFBR meltdown conditons, molten fuel+coolant interaction, expts. 77—23225
- LMFBR piping components, resistance to bending moments 77—6505
- LMFBR primary piping materials, types 316, 304, stainless steel, mech. props., review 77—25151
- LMFBR principles and potential advantages 79—81072
- LMFBR program, simulation of void swelling and radiation-induced creep 78—8907
- LMFBR programme, economic issues 77—38392
- LMFBR prospects, reln. to world energy resources 79—97888
- LMFBR safety, flow rundown expts. in seven pin bundle, Na boiling 77—88240
- LMFBR safety, formation of critical boiling nuclei in superheated Na 77—88242
- LMFBR safety, KNK II driver zone, Na boiling in 7-pin bundle 77—88246
- LMFBR safety, local blockage formation and growth in grid spaced fuel elements, model 77—88243
- LMFBR safety, local cooling disturbances, in-pile Na loop investigation 78—674
- LMFBR safety, seven pin bundle expts., flow patterns, two-phase press. drop, Na boiling 77—88241
- LMFBR safety against propagation of local subassembly failures, CDA conditions 77—18673
- LMFBR safety anal., theoretical interpretation of SCARABEE single pin in-pile boiling expts. 77—88239
- LMFBR safety analysis, computer code for determ. of aerosol attenuation in leakage paths 78—13293
- LMFBR shielding calculations, accuracy of ENDF/B-IV cross sections 78—13401
- LMFBR steam generators, design developments *(Czech)* 80—5206
- LMFBR steam generators, flow induced vibr., review 77—23240
- LMFBR transient undercooling accident, molten stainless steel, wetting of UO_2 cracked fuel pellets 78—4993
- LMFBR type EBR-II, 10 years' operation experience 77—42176
- LMFBR use of plated thermocouple in notched well, response time 78—29546
- LMFBR vessel, US testing of austenitic steel welds 77—1903
- LMFBRs in Japan, past and present role 79—97889
- LMFBRs in USA, past and present role 79—97890
- LMFBRs in West Germany, current status and prospects 77—61593
- LOCA reflood phase, hydrodynamics of water cooled reactor, moving control vol. method 78—704
- long-term nuclear energy strategies, role of fission and fusion 80—78354
- LWFBR, neutron balance in chain reaction, delayed neutrons role, reactor safety *(German)* 79—26726
- LWHR, feasibility of Pu separation-free nuclear power economy 78—13313
- LWHR, source driven, Li-free neutron sources, feasibility and comparisons 79—13383
- LWR, ^{3}H, formation and elimination *(French)* 79—31164
- LWR, advanced reactor development 77—67861
- LWR, fission gas release high-burnup fuel during transient heating 78—13283
- LWR, heavy water moderated, prototype, pressure tube monitoring with US devices 77—88268
- LWR, incorporation of wastes into heat-hardened resins *(French)* 77—61566
- LWR, initial fissile U requirements for fuel cycle, computer simulation 78—17320
- LWR, LOCA, safety methodology *(French)* 80—52751
- LWR, LOCA conditions, fuel rod behaviour, code system SSYST-Mod 1 calcs. 77—88248
- LWR, occupational radiation exposure problems 77—18711
- LWR, oxide fuels and cladding, irrad. behaviour, chemical process, densification, corrosion *(Japanese)* 77—83033
- LWR, post-LOCA γ-ray energy redistrib. and effects 78—13280
- LWR, props. of core melts in LOCA, viscosity, thermal cond., specific heat 77—14247
- LWR, safety, research needs 79—49711
- LWR, system inception and fuel cycle in France *(French)* 79—26689
- LWR, waste production, yearly average 80—23067
- LWR, W.German guidelines and regulations 77—30656
- LWR and coal power stations, effects on ambient media from mining to waste disposal *(Spanish)* 77—75005
- LWR and LMFBR, intermediary system alternative *(French)* 77—18690
- LWR at Genkai nuclear power plant, Japan, operating experience *(Japanese)* 77—79447
- LWR core barrel model, circular cylindrical shell, dynamic response to nonaxisymm. loading 77—88247
- LWR designs, US nuclear policy 78—5011
- LWR fossil fired superheater technical and economic assessments 78—8966
- LWR fuel element reliability, materials science aspects 79—67855
- LWR fuel fabrication plant, cost of controlling inorganic chemical releases 78—5003
- LWR fuel regeneration by linear accelerator reactor 80—32336

fission reactors continued
- LWR in Japan, improvements and standardisation *(Japanese)* 78—17285
- LWR LOCA analysis, TRAC-1D code for Standard Problem 2 78—13288
- LWR local corrosion causes and preventive methods *(French)* 78—8963
- LWR pressure vessels, radiation embrittlement, allowable crack size, unstable fracture 77—10465
- LWR spent fuel containing ^{236}U, recycling in enriching plant 77—18684
- LWR steel pressure vessel, neutron radiation effects on material props., review *(German)* 77—34382
- LWR unit sizes, development trends *(German)* 80—32423
- LWRs, installation in small developing countries 79—31167
- LWRs, status of technology in West Germany 77—61592
- Magnox power station, decommissioned, rad. levels, neutron activation, waste disposal 80—13976
- medical applications *(Japanese)* 79—83913
- modern atomic and nuclear physics (book) 80—11
- molten salt breeder reactor technology, recent progress *(Japanese)* 80—91236
- MR research reactor, fast neutron space-energy distrib. 79—40983
- MSR (Pu converters) and MSBR's in commercial nuclear power stations 79—26740
- MSR strategies, fuel conservation effect, utilisation of convertors starting with Pu *(Japanese)* 77—50207
- natural reactor at Oklo, anomalous Xe and Kr isotope composition 77—56630
- natural reactor in Oklo, isotopic composition 77—56628
- natural reactor theory, Oklo and Sudbury phenomena *(Japanese)* 77—73735
- natural reactors, at Oklo (Gabon), origin hypotheses *(Dutch)* 78—33261
- NBS reactor, summary of activities, (July 1976 to June 1977) 78—82435
- negative reactivity determ. by rod-drop, correction for time of fall 77—46222
- neutron flux dice games to illustrate probability, teaching 78—12515
- neutron skyshine from nucl. facilities *(Japanese)* 79—18054
- nitrided stainless steel alloy 79—54496
- noise, specialists' meeting, Gatlinburg, USA, Sept. 1977 78—94057
- noise analysis by multivariate statistical pattern recognition system 77—14228
- nonlinear optimisation algorithms 80—18623
- nuclear energy, appl. and processes *(Portuguese)* 77—3189
- nuclear energy options, for future, fusion-fission concepts, accelerator breeding 80—13838
- nuclear power conf., Chicago, United States, July 1979 80—794
- nuclear power development, in Soviet Union, present trends *(Russian)* 79—97885
- nuclear power programme, Philippines, prospects, problems 79—31175
- nuclear power reactor systems, dynamical behaviour modelling 80—91216
- nuclear power station with VVER, for semi-peak load generation, mathematical model 80—68936
- nuclear waste incineration for destroying actinides, costs and risks 78—41825
- OCR, WR-1, UO$_2$ fuel performance 78—25292
- Oklo fossil reactor, review 77—60377
- Oklo natural reactor, rare earth elements behaviour 78—49019
- Oklo phenomenon, isotopic abundances, long-term radioactive waste storage information 80—52769
- oxide thickness monitor, mild steel structures, ferrite appl. 77—67806
- paint coatings in radiation fields of reactors and accelerators, and after contamination by radionuclides 77—75006
- pattern recognition systems, ORNL expts. 80—63351
- PBHTR, source of nuclear process heat, development of power plant, overall time and cost estimates 77—3089
- PBR graphite structures, neutron radiation damage, mech. props., stress fields *(German)* 77—34387
- PBR with OTTO fueling, graphite reflectors, neutron effects, stress anal., cooling measures *(German)* 77—34368
- PFR, sodium-cooled, 250 MWe, British development 77—71689
- PFR, UK operation and influence on CFR I design 77—23243
- PFR core meas. rel. to safety and importance 79—97897
- Phenix LMFBR, radioactive effluent release, operating team irrad. results *(French)* 79—31163
- Phenix reactor, fuel behaviour and characts. *(French)* 79—31162
- PHWR, CANDU reactor system, appropriate technology 78—58338
- PHWR design, integration into power stations, small plant role in developing countries 79—31170
- pipe bends, short radius, creep bending 77—6517
- pipe whip anal. modelling techniques, FRUSTRA code 77—6515
- pipe whip analysis procedure 77—6514
- pipe whip restraints, conceptual design using interactive computer anal. 77—6513
- piping system anal. to nuclear standard regulations 77—6504
- piping systems, structural performance characts., dynamic anal. 77—6508
- piping systems under blowdown conditions, simplified dynamic anal. 77—6510
- plasma, nucl. reactor-induced, simulation by accel. ion beam plasma creation *(French)* 80—10407
- power conference, Lausanne, Switzerland (Oct. 1977) 79—36326
- power plant dynamics and control, conf. Hyderabad, India (Feb. 1979) 80—91215
- power reactors worldwide, review 77—67856
- pressure vessel, in-service inspection and automatic US testing equipment 77—1892
- pressure vessel, stress intensities for nozzle cracks 78—70583
- pressure vessel design advances 77—71640
- pressure vessels, high temp. design system *(Japanese)* 78—673
- propulsion system for planetary exploration 77—87235
- pulsed measurements with low absorpt. reflector crit. assembly 77—50201
- pulsed neutron reactivity meas., approx. of kinetic distortion correction factor 77—54268
- PWR, 1300 MWe units, construction work in Brazil 77—46390
- PWR, CIRENE reactor, zircaloy calandria tubes, stress evaluation using strain data *(Italian)* 77—50204
- PWR, core reflooding, progress of hardening front *(French)* 80—91211
- PWR, direct bituminisation of spent effluents *(French)* 77—61562
- PWR, French, cracks in containment vessels *(French)* 80—32387
- PWR, french R and D development program 79—97843
- PWR, fuel element gap conductance, heat transfer over range of Knudsen number 78—13213
- PWR, German, U-tube steam generators, inspection findings 79—9849
- PWR, JAERI, test of LOCA/ECCS anal., code verification, by participation in LOFT program *(Japanese)* 77—50256
- PWR, KWU 1300 MWe facility, neutron flux computer calcs., radiation damage 77—34370
- PWR, LOCA performance test of upper heat injection system 79—81028
- PWR, LOCA test, effect of LOFT pressurizer on RELAP4/MOD5 modelling 78—13286
- PWR, neutron noise studies 80—557
- PWR, Obrigheim nuclear power plant, inservice inspection, nondestructive testing, primary components *(German)* 77—34406
- PWR, pipe system failure characts., effects on plant availability and capacity 78—17375
- PWR, power distrib. comparison of U and Pu fuel in KWO core 77—14224
- PWR, power stations containing VVER-440 reactors, radiation safety of personnel and local population 77—71700
- PWR, pressure vessel steel, RT$_{NDT}$ shift of ductile-temp. curve, correl. with neutron dose *(German)* 77—34388
- PWR, pressure vessel US inspection *(Czech)* 78—29658
- PWR, reactor safety anal., sensitivity assessments, plant risk 77—18676
- PWR, small, electricity and steam supply, technical and economic studies 79—31171
- PWR, small, for industrial use, study 77—23246
- PWR, Spanish nuclear power program, technology transfer 77—65353
- PWR, St. Lucie 850 MWe, neutron streaming meas. and shielding recommendations 78—70608
- PWR, Th cycle, parametric anal. 79—26467
- PWR, thermal and hydraulic design considerations 79—49651
- PWR, three loop, simulation in advanced recycle methodology program 80—68856
- PWR, transient state studies 77—14263
- PWR, two dimens. diffusion problems, singularities in finite element approx. 77—6496
- PWR, use of ^{233}U enriched fuel 79—26513
- PWR and BWR systems and fuel cycle in USA 79—26687
- PWR, CANDU, corrosion product transport, deposition on fuel bundles, press. tubes 77—61492
- PWR core, appl. few-group diffusion-theory computer calcs. in teaching course 78—4448
- PWR core, large, appl. of coarse-mesh finite difference eqns. for k$_{eff}$ and peak power factors 78—17305
- PWR development 79—93811
- PWR development in France *(French)* 78—8962
- PWR power plant, assessment of underground siting as engineered safety factor 78—13316
- PWR power plant, dynamic testing for model validation 77—3087
- PWR power plant, vibr. and press. signals, information for online vibr. monitoring system 77—18674
- PWR power stations, operating record and reliability, reviews 79—22404
- PWR pressure vessel, novel design, advantages 77—79471
- PWR pressure vessel design *(German)* 77—42180
- PWR pressure vessel reliability, failure anal. 77—74962
- PWR pressure vessels, safety calcs., design, operation control, neutron effects *(German)* 77—34404
- PWR radioactive gaseous effluents, relase trends in US 1977 80—95481
- PWR reactor dismantling, model scheme to meet West German regulations 80—825
- PWR reflood simulation of FLECHT-SET system using RELAP4/MOD6 78—13285
- PWR safety analysis, hybrid method of void fraction prediction, depressurization of diabatic systems 77—23222
- PWR secondary water chemistry, EPRI program 77—54356
- PWR system, fluctuating mechanical forces of a pipe-bend 77—54279
- PWR vendor water chemistry specifications, for secondary systems 77—54355
- PWR with straight tube steam generator, 1300 MW, characts. *(German)* 78—50292
- PWR/BWR power stations, waste-water treatment plants, engineering experience 77—6543
- PWRs in Framatome plants, manufacture of pressure vessels and steam generators 77—38323
- Quad City 1, fuel performance meas. following third irrad. cycle 80—68778
- radioactive waste, high level, disposal in deep-sea bed, New Zealand 78—705
- radioactive waste disposal 77—74954
- radioactive waste management practices in selected European countries 80—37471
- radioactive wastes, disposal in sea 80—37472
- Rapsodie fast reactor, closed fuel cycle *(French)* 79—31161
- reactivity functions generation by use of Cd rod 77—57709
- reactivity meas. under typical fuel element dissolution conditions, use of pulsed neutron source 77—3083
- reactor hybrid-organic Rankine cycle power system for spacecraft power supply 78—8993
- reactor physics development by BSSR Nuclear Energy Institute *(Russian)* 79—36313
- refrigeration system design for low temp. irrad. facility 77—42009
- reliability, NATO Advanced Study Institute, Liverpool, England (Jul. 1973) 77—38396
- research and development in Japan 80—47701
- research reactor in Noril'sk mining-metallurgical complex, experience in use 77—23185
- review of types and appl. *(German)* 78—29638
- rocket reactors, laminar flow, temp.-viscosity induced instabilities in gaseous heat channel 77—18689
- Rocky Flats Plant Critical Mass Lab., exptl. programs 80—37430
- safety, physical protection system, role of barriers 79—85686
- safety, vital area identification, fault tree analysis appl. 79—85691
- safety policies in West Germany, physical protection program review 79—89450
- sea water desalination appl. 77—38385
- seawater desalination, evaluation of single purpose fission reactor 80—5319
- seawater desalting, reactors coupled to multieffect distillation plants, feasibility 79—31172
- SGHWR, Britain's controversial program 77—368

fission reactors continued
SGHWR preliminary work at Winfrith, UK *(German)* 77—14261
shale oil extraction using nucl. heat sources, feasibility 77—34422
ship, streaming neutron meas. by two-detector method 77—46408
small and medium power reactors, problems, prospects 79—31168
small nuclear reactors for power production and ship propulsion appl., prospects 77—10485
spent fuel rod assay, $^{233}UO_2$-ThO_2 fuelled core, reactivity perturbation method 77—18654
spent LWR fuel storage in Pacific Basin at Palmyra Island, decision making methods 80—27763
SSCR, Pu fuel cycles 79—89386
standardisation of power stations w.r.t. plant rating, plant engineering and system engineering 80—594
steam generator channel, once-through, flow dynamic stability, influence of press. loss components *(Czech)* 77—3148
steel piping components, incremental collapse tests, structural behaviour 77—6526
steels, nuclear reactor pressure vessel steels, optimum chem. comp. rel. to props. 80—93517
structural systems modelling for transient response anal. 77—6507
subcritical systems, heterogeneity effect on integral parameter meas. 77—50218
suboptimal control, param. imbedding method appl. 77—34421
Super Phenix nuclear reactor containment vessel, stress anal. *(French)* 79—41023
Super-Phenix fast reactor power station, in France *(French)* 80—86967
Superphenix full-scale breeder reactor construction in France 77—65324
systems reliability, computer programs *(Slovak)* 78—82416
thermal breeding, status and prospects, preliminary report 79—26739
thermal reactor choice, Britain 77—74961
thermal reactors, trans Cm isotope build up 79—85709
Thermos pool reactor, characteristics, environmental effects and economics *(French)* 77—74967
theta-pinch reactor, first wall environment 77—30661
THTR-300, continuation store for burned-up fuel, absorber and moderator elements *(German, English)* 77—65289
Tokamak, physical properties 79—6765
Tokamak hybrid breeder blanket, liq. metal coolant, MHD effects 78—74481
Triga Mark III nuclear reactor, as intense gamma radiation source *(Spanish)* 80—83232
Trino Vercellese PWR, Am and Cm build-up in fuel rods 79—85754
two-component Torus hybrid system, pressure tube convertor for hybrid blanket 78—74478
types and development in Europe and USA *(German)* 78—29647
unbiased core magnetic flux direct component calc. *(Russian)* 77—61493
undergraduate reactor laboratory course 77—37697
USA, reactors built, being constructed, or planned Dec. 1978 79—54491
USA facilities, IAEA inspections effect, (1960s to 1978) 79—85680
USA fission reactor sites as of 30th June 1977 78—25334
utilisation, factors affecting choice of type and power *(French)* 80—52712
very high temp., graphite moderated He cooled for H_2 production 77—23247
VHTR, gas-cooled graphite-moderated, for industrial process heating, assessment 77—23245
VHTR heat exchangers, material criteria and selection 78—13232
volatile fission product atmospheric release from nuclear reactors and fuel reprocessing plants 79—34461
VVER, proposals for increasing power station efficiency 79—26491
VVER 440, design and engineering props., production and assembly 80—91207
VVER type reactor physics, ZR-6 critical assembly *(Russian)* 79—31159
VVER-1000 reactor, neutron axial field stabilisation 79—63741
VVR-M reaction channel slow neutron field, parameter meas. 79—31325
WWER reactors for district heating appl. 78—41854
YAYOI FBR, prod. of epithermal neutron field for ^{10}B neutron capture therapy 80—61692
CO-N_2-^3He, nucl. reactor active zone, plasma and sustained discharge props. 80—5729
^{14}C production in reactors and explosions, population dose, health impact 77—14274
D-D catalytic fusion-fission breeder, synergetics 79—22460
D-D fusion-fission hybrid reactor, energy multiplication and fissile prod. 79—36409
FBR, safety, research needs 79—49711
H_2 production using high temp. reactors 80—97814
N_2O_4 dissociating coolant reactors, power stations and radiation sterilization in Belorussia *(Russian)* 79—36398
Na test facility for LMFBR core components 77—50196
Na-cooled fast reactors, material corrosion problems 79—36328
Pu reactor facility, zero power, continuous controllable containment, West German safeguards system 79—85683
T storage and monitoring, CANDU heavy water reactors 80—5291
Th breeder, US nuclear policy 78—5011
U, gaseous fueled reactor use as power supply for nuclear pumped laser system 80—63247
U plasma fueled reactor, use as power supply for nuclear pumped laser system 80—63247
U-graphite channel power reactors, development in USSR *(Russian)* 79—26507
UF_6 gas fuel appl., space and earth-bound appl., NASA-sponsored program 79—49829
^{233}U-^{232}Th reactor as burner of actinide wastes 77—23235

fission research reactors
see also fission reactor core control and monitoring; fission reactor theory and design; nuclear reactor instrumentation
advanced high U-density reduced-enrichment plate-type fuel development for test and research reactors 80—23101
advanced reactor development in Japan 78—86663
AGR, heat transfer to accel. gas flows, expt. and calcs. 78—54823
ALARA program review at Texas A and M University 80—9362
annular core pulse reactor upgrade physics and core design calc. 79—13409
ARBUS, operational experience with ditolylmethane coolant/moderator 78—41836

fission research reactors continued
Argonaut research reactors, effect of atmos. press. variation on reactivity *(German)* 80—5199
Army pulse radiation facility reactor, expt. radiation transport to large distances 79—59275
ATR, power distrib. and control element reactivity changes, Be reflector redesign effect 80—9363
AUWARM, H- and T-permeation in HTR reactors *(German)* 79—3204
BER II research reactor, transport capsule separation from sample containers at fast pneumatic transport systems for neutron activation analysis 77—74966
BNL high flux beam reactor, neutron beams 77—30693
boiling mixing studies in water loops, BWR, PWR reactors 79—26502
BOR-60, operational characteristics of core and irradiated fuel parameters 79—97877
BOR-60 experimental fast reactor, safe operation in power plant conditions *(Russian)* 79—97865
BR2 BWR, densification of $(U,Pu)O_2$ fuel 79—49685
Braunschweig research and measurement reactor, work report for 1977 *(German)* 79—6737
breeder reactors, SNR300, cooling system failure, effects *(German)* 78—695
Brookhaven High Flux Beam Reactor capability enhancement 79—9694
Bruce core, ZED-2 mockup, responses of Pt, V and Co self powered flux detectors 78—58391
Buffalo PULSTAR reactor refuelling 79—9793
BWR, steady state reactor plasma in $CO_2+N_2+{}^3He$ gas mixture 79—10279
BWR 1/5 scale Mk.1 toroidal wetwell, induced vertical forces under LOCA 78—41832
BWR at PNC Japan, stability anal. of boiling loop in low-pressure operation 78—8894
BWR Mk.I pressure suppression system, vent clearing during simulated LOCA 80—13657
C-E System 80^{tm} reactor, Th-based Pu burner for improved fuel utilisation 78—13240
Canadian power reactor programme, role of Chalk River research reactors 79—81073
Caramel UO_2 fuel, proliferation resistant fuel service 80—27746
carbide fuel element testing in fast reactor BOR-60 78—86582
CIRENE, pressure tube explosive rupture anal. using scaled-down model 80—18449
CIRENE LOCA, power channel thermal transients during reflooding 79—63755
CIRENE reactor control, two phase flow rods, BUANA and TICO codes 79—17994
computer controlled neutron irrad. system 80—19851
core and console, long term service and reliability investig. 80—9359
core and fuel element design at National Bureau of Standards reactor 78—21636
CRBRP, effect of pumped stored kinetic energy on natural circulation decay heat removal 80—23010
CRBRP, gas tag identification of failed assemblies, anal. methods 80—95369
CRBRP, transition to natural convection from low temp., low flow conditions 80—18533
CRBRP arrangement engineering considerations 79—97764
CRBRP LMFBR, effect of alternative fuel cycles on design 79—54484
CRBRP reload core designs, using (U-Pu)C fuel 79—59155
critical assembly, Big Ten, ^{235}U enriched U (10%) 80—823
critical fast test reactor fuel pin lattices, calcs. of k_{eff} valves 80—13569
cryostat for low temp. expts. in reactor pile *(Japanese)* 79—54471
Czechoslovak Rez Nuclear Research Institute airborne radioactive release monitoring 78—89991
data acquisition program for reactor control 78—86679
decommissioning, partial dismantling of the Avogadro RS-1 materials testing reactor *(French)* 80—13980
decommissioning, progress and plans at Ames Laboratory 80—13971
decommissioning, progress report on dismantling of the Sodium Reactor Experiment 80—13978
decommissioning of the Lucens experimental nuclear power plant *(French)* 80—13979
Demokritos, fast neutron irrad. facility 80—99270
Demokritos reactor irradiations facility, 70-400°C 80—6439
Demonstration Tokamak Hybrid Reactor, design of advanced bundle divertor 80—13834
DFR special experiments 79—97779
DIDO, three-dimensional SNAP diffusion theory calc., including upscattering 80—5208
digital control of a nuclear reactor using optimal control and state estimation methods 80—37554
dispersal mechanism test facility, Doppler coeff. optimisation 77—46339
dispersal mechanism test facility, fuel dispersal anal. 77—42136
dosimetric intercomparison using chem. dosimeters and Ni foil threshold detector 77—57753
Dounreay fast reactor, overheating, prevention by natural circulation, experimental investigation report 80—47598
Dounreay FBR, post-operational improvements in plant design and operational techniques 79—63736
DRAGON, irradiation testing of THTR fuel element *(German)* 78—25295
Dragon HTR project, review 79—45326
Dragon reactor zero energy expts., further n energy group and transport calcs. 78—78445
dynamic measurements of a nuclear reactor using low-peak-factor excitation signals 79—36349
EBR II, $^{238}U(n,f)$ fast neutron fission yield determ. 79—40970
EBR II, Cs control by C getter 80—13648
EBR II, fission product source identification using Xe tag 78—70588
EBR II, metallic driver fuel, irrad. perform. at high burn-up, fuel-cladding interactions 80—95348
EBR II, reactor subassembly removal using gripper device 80—57942
EBR II, transient testing and simulation for LMFBR plant dynamic modelling 79—54558
EBR II driver fuel, irradiation behaviour 80—32346
EBR II ducts and cladding, obs. of dilation and bowing 80—625
EBR II failed (U, Pu)O_2 fuel pins, Ru isotopic axial distributions, γ-scanning determ. 78—687
EBR II gas-tagging anal., isotopic weighting factors 79—59221
EBR-II, $(U,Pu)O_2$ fuel burnup, effect of time varying power level 80—13719

fission research reactors continued
EBR-II, breached element location from mixture of Xe tags, MIXTAG code 78—33274
EBR-II, comparison of XX08 steady-state temp. meas. with anal. predictions 80—579
EBR-II, dynamic response of ducts to press. pulses, expts., finite element calcs. 77—3124
EBR-II, exptl. determ. of decay power 79—85652
EBR-II, fabrication of in-reactor creep capsules using previously irradiated cladding tubes 79—54478
EBR-II, in-reactor measurement of neutron absorber performance, He release of B_4C 80—73951
EBR-II, meas. of T retention of fast-neutron-irradiated absorber elements of B_4C 78—8903
EBR-II, Na-water, leak detection system 78—78484
EBR-II, neutronics design of safety research modification 79—30990
EBR-II, obs. of amplitude modulated 12 Hz effect in upper plenum acoustic expt. 78—33241
EBR-II, operating limits for subassembly deformation 78—21714
EBR-II, possible metal and oxide fuel loadings utilising $^{232}Th/^{233}U$ 80—13563
EBR-II, remote fuel fabrications experience 79—89476
EBR-II, remote reprocessing of metal fuel 80—13767
EBR-II, whole core thermal-hydraulic phenomena, experimental study 77—88206
EBR-II 80—13598
EBR-II active calorimeter design improvement 79—9967
EBR-II anomalous reactivity meter 77—42114
EBR-II cover gas, second Xe tag identification, code MIXTAG 77—42145
EBR-II cover gas clean-up system, transient anal. 77—46357
EBR-II cover-gas cleanup system 79—97874
EBR-II delayed neutron concentrations, computer modelling 80—27717
EBR-II driver fuel lifetime, cumulative damage anal. and Weibull statistical anal. 80—13601
EBR-II fast transient facility, physics design 77—46336
EBR-II fuel pin cladding, obs. of in-reactor creep and swelling 80—13600
EBR-II grid plenum assembly stress anal. 77—54288
EBR-II irradiation subassembly and creep specimen container design 79—54479
EBR-II mixed-oxide subassemblies, bundle duct clearance at HEDL 77—46270
EBR-II primary system piping evaluation for safety research modification 79—9785
EBR-II reactor shutdown system upgrading, safety features 79—9796
EBR-II reflector assembly irrad. induced bowing, implications for core restraint design 80—104234
EBR-II secondary Na network anal. for press. pulses from leaks of water or steam 77—54328
EBR-II slow transient tests, environmental tailoring 80—23009
EBR-II steam generator tube bore side inspection probe and drive 79—9850
EBR-II transient facility, thermal anal. of driver subassemblies 77—42134
effluent monitoring programme design and organisation principles 79—13548
engineering test facility as a test device for inertially confined fission 80—57831
epithermal neutron radiation field development for cerebral tumour therapy *(Japanese)* 78—88742
experimental reactor loop construction, high-pressure and temp. type, Hungary *(Hungarian)* 77—3074
experimental reactors channels, independent control of neutron flux using gaseous absorbers 79—71918
Fast Breeder Blanket Facility reaction rate and neutron energy spectrum meas. 80—68865
fast breeder test reactor operator training simulator model development 80—91219
Fast Burst Reactor, failure analysis of burst stainless steel rod adaptor 77—54307
fast burst reactor, research into nucl. pumped lasers 78—33726
fast burst reactor, WSMR, thermal shock stress anal. for enlarged irradiation cavity 78—33242
fast burst reactor neutron leakage, scattering materials effect on average neutron energy, spectral index, hardness parameter 77—26816
fast burst reactor neutrons damage in Si transistors, Pb, paraffin shields 77—23172
fast burst reactors, thermal shock effects stress anal. 77—79428
fast critical expts., effective delayed neutron fractions and central reactivity worths 78—62602
fast flux reactor tests, neutron radiography facility 80—18371
fast neutron facility in CP-5 reactor, neutron flux, energy spectrum, primary recoil distribution 79—41056
fast neutron pulse reactor, IBR-2, 4 MW 79—699
fast neutron source reactor (YAYOI), pulsed operation improvements, with POS5 as reactivity injector *(Japanese)* 80—9328
fast pulse reactor at APRF, absolute neutron flux meas., dosimetry, calibration against ^{252}Cf source 77—23389
fast reactor parameters, influence of fission spectra uncertainties 80—22928
fast reactor test loop anal. of severe accidents 77—3142
fast-thermal critical facility STEK, neutron capture cross sections for fission products 77—6498
FBR, experimental, math. model for control system design in FBR plants 79—17990
FBR, generation of a neutron reference field by B_4C filtering of a reactor spectrum 80—42884
FBR, IBR-30 at Dubna, characts. of mixed neutron-gamma beam *(Russian)* 77—67793
FBR, large critical facilities, inventory verification 79—85600
FBR, spatial mesh effect in 3-D burnup calcs. *(Japanese)* 80—47544
FBR, types, cooling and safety aspects *(German)* 79—54587
FBR safety test facility, conceptual design 77—46337
FBR safety test facility, kinetic performance 77—42135
FFTF, bundle-duct interaction characts. of LMFBR wire-wrap driver fuel assembly 79—59152
FFTF, containment response to postulated core meltdown accidents 80—32381
FFTF, critical expts., with solid neutron absorbers 80—52727

fission research reactors continued
FFTF, development of an instrumented materials irrad. test for LMFBR structural materials 80—57858
FFTF, development of an instrumented materials irrad. test for LMFBR structural materials 80—68797
FFTF, future design and construction of LMFBRs in USA 79—97804
FFTF, gas tag identification of failed assemblies, anal. methods 80—95369
FFTF, HCDA, NASTRAN nonlinear dynamic transient accident anal. 77—42133
FFTF, HCDA or Na-water interactions, primary containment integrity tests 77—71673
FFTF, interassembly flow redistribution at natural circulation conditions 79—85654
FFTF, natural-circulation testing 79—49676
FFTF, operator training simulator 78—5013
FFTF, potential gas entry after postulated pipe rupture 79—85657
FFTF, quality assurance appl. to design procurement and construction 79—97786
FFTF, simple models, HCDA expts., LMFBR safety evaluation programme 77—3130
FFTF, thermal-hydraulic anal. of air dump heat exchangers 79—59146
FFTF, TOP anal. using Los Alamos failure model 80—13672
FFTF control rod anal. with SCRAM program 77—46355
FFTF core component meas. system 79—9728
FFTF design studies, simulation of hot-leg piping ruptures and loss-of-flow events 79—49677
FFTF dynamic modelling and sensitivity analysis 79—605
FFTF element measuring system 79—9729
FFTF fuel, neutron source strength as function of irradiation 80—22929
FFTF fuel and other core components, NDT 77—12757
FFTF fuel failure, cover-gas monitoring system 78—4998
FFTF fuel quality control, inspection techniques and processes 79—85610
FFTF fuel storage facility design 78—715
FFTF heat transport system, design construction and testing 79—97783
FFTF irradiation test program 79—67928
FFTF loss-of-electric-power transient response, natural circulation tests, pre-test simulation using SSC-L code 80—42836
FFTF reactor shielding anal., spatial channel theory 77—6569
FFTF startup, instrument calibration program 80—9337
FFTF status update 79—67927
FFTF upper-plenum mixing and stratification, comparative studies 80—583
FFTF-type eddy-current flowmeter performance in SLSF P-series test trains 79—9669
Ford Nuclear reactor, reduced enrichment fuel element loading, calcs. 80—9394
Ford reactor, equilibrium core calcs. with reduced enrichment fuel 80—68885
Ford reactor, neutronic anal. using low enrichment fuel 80—68886
Ford reactor, reduced enrichment fuel effects on performance and utilisation 80—63344
Forschungs- und Messreaktor Braunschweig, operating experience *(German)* 77—61527
FR2 reactor, high-pressure capsule for irradiation of fuel swelling specimens 77—46218
French contribution to reduced enrichment research and test reactor program 80—68931
FRJ-1, steel irrad. expts., neutron flux densities, temp. fields 77—83029
FRJ-2, elimination of flow rate fluctuations in core 77—67798
FTR, control rod failure detection 77—42144
FTR, mechanical failure of subassembly ducts and its effects on transition-phase analysis 79—85667
FTR, SNEAK, effective delayed neutron fractions, integral meas. on PuO_2/UO_2 77—6497
FTR, strain rate effects in transient overpower cladding failure analyses 79—85660
FTR fuel pins with solid neutron absorbers, criticality expts. 80—18476
FTR TOP accident, effect of power skew, computer code development 79—54481
fuel element loadings with reduced U enrichment 80—68933
fuel elements, self protection criteria 80—9361
fuel enrichment reduction program, for plate type reactors, generic studies 80—9391
gamma radiation spectrum, measurement inside reactor, calorimetric method 78—17293
gas core, fission-fragment-generated plasma, theory of spectroscopic diagnostics 78—34374
gas core, fission-fragment-generated plasma from interaction in neutral gas 78—34345
gas-cooled reactors, current development status, review 79—22375
gaseous core reactor, expt. for generation of fissioning high press. gas. 77—23191
gaseous core reactor, UF_6 technology 78—33254
gaseous core reactor with U-fuelling, preliminary expts. 78—33243
gaseous nuclear reactor with RF heated UF_6 fuel 77—23189
GCFR, design criteria for 300 MW(e) demonstration plant 79—97759
GCFR, prototypic grid-plate shield confirmation experiment 79—54562
GCFR demonstration plant reactor shielding system design 80—47560
GCFR grid-plate shield design experiment 79—59226
General Electric test reactor for neutron transmutation doping 80—15140
General Electric Test Reactor fuel and materials testing 80—565
GLEEP reactor neutron thermal and epithermal flux calibration 79—93856
Grenoble high flux reactor, neutron physics expts., methodical aspects *(German)* 80—554
Health Physics Research Reactor, operating history and recent improvements 80—9382
heat-pipe nuclear power plants for reliable space power 80—18377
HELM test facility for GCFR fuel pin design anal. 80—18409
HFBR, detection and identification of failed fuel elements 78—21708
HFBR, safety features of cold neutron moderator 80—23114
HFIR, appl. to fusion reactor materials evaluation 78—13324
HFIR, dimensionality reduction of reactor noise signatures, improved automated noise anal. 77—6499
HFR at Grenoble, neutron beam installations 77—26864
HFR Petten Materials Test Reactor, reduced enriched fuels, utilisation and management schemes 80—9343
HFR test reactor, HIP-TEDDI code for neutron flux calcs. 79—3223

fission research reactors continued
- HHV high-temp. test plant for design of HTGR with the turbine 79—97760
- HIFAR materials testing reactor, spent fuel safeguards verification using gamma spectrometry 80—63290
- high flux beam reactor using medium-enriched uranium, feasibility study 80—23113
- high flux reactor in Grenoble, fission product separation using Lohengrin mass separator 78—17436
- high flux test reactor, MARIA, nuclear power research programs *(Polish)* 79—93693
- high temperature heat exchanger test plant for nuclear energy steel making process R and D *(Japanese)* 79—67817
- high U density fuel for test and research reactors 80—68801
- HTGR, perspectives, problems and programmes 79—26508
- HTLTR, neutron multiplication factors, temp. depend., fuel lattices, comparative evaluation with HTGR 78—29557
- HTR, design criteria of elec. generating plant with the turbine in a direct cycle 79—97758
- HTR, modified RB-2 reactor, null reactivity oscillator method on fuel lattices, expt. feasibility 77—57703
- HTR critical facility, KAHTER, reactivity meas. using neutron noise anal. *(German)* 77—83031
- HTR experimental reactors in West Germany, progress report *(German)* 80—23106
- HTR nuclear long distance energy system, heat transport by chemical circuit 80—7905
- HTR plant with methane reformers for long distance energy system 80—7906
- Hungarian research reactor, reconstruction and modifications *(Hungarian)* 77—50205
- HWR, MIT research reactor renovation 78—21753
- IAEA international symposium on design, construction and operating experience with demonstration liquid metal fast breeder reactors (Bologna, Italy, April 10 to 14, 1978) 79—49646
- IBR-2 pulsed research reactor, start-up experience 80—73956
- ILL HFR, Grenoble, fundamental phys. expts. with neutrons and ν 79—67932
- in-pile post accident heat removal facility, feasibility study 79—49774
- intermediate-energy secondary spectrum system, determ. of neutron characteristics, ΣΣ-ITN *(Rumanian)* 79—22355
- irradiation test facility for high U-loaded fuel plates as part of reduced enrichment program 80—68932
- IRT 2000 reactor in Sofia, neutron spectra and doses in exptl. canals *(Bulgarian)* 78—82489
- IRT WWER, use of thermometric fuel assembly in safety anal. 79—97837
- IRT-2000 fission research reactor, personnel radiation monitoring and reactor radiation charact. 79—71927
- Ispra Research Centre activities, w.r.t. EEC policy 79—97770
- IVV-2 research reactor, thermal neutron flux distribs. using neutron probes 80—32391
- Japan, reactor fuel and material development and expt. using JRR-2 and JMTR research reactors *(Japanese)* 80—63256
- JASON low power reactor, nuclear engineering education and training 77—41431
- JEN experimental reactor design, development and construction in Spain *(Spanish)* 77—38384
- JEN research facility *(Spanish)* 77—38322
- JOYO experimental fast reactor, test and operational experience 79—97867
- JPDR, stainless steel type 304, piping cracks, metallurgical exam., failure anal. 79—67849
- Karlsruhe research centre, neutron installations and facilities 77—23317
- KEMA suspension test reactor, 1976 May tests *(Dutch)* 78—37434
- KEMA Suspension Test Reactor neutron flux and Dodewaard BWR temp. noise 79—3193
- KEMA suspension test reactor postoperative examination *(Dutch)* 80—42846
- KNK II fast breeder, construction and aseismic design 79—97778
- KNK shutdown systems 79—97866
- KS-150 reactor, radial shielding model, neutron and γ-ray spectra meas. *(Slovak)* 78—21624
- Kyoto University Critical Assembly, water moderated core, group consts. 80—22960
- Kyoto University reactor, airborne radioactivity from primary coolant 80—22959
- Kyoto University reactor, He-type on-line isotope separator 80—23152
- laser reactors utilising UF_6 and CO_2 laser 80—23117
- linear acceleration reactors, anal. of neutron yield produced by high-energy protons 80—22895
- LMFBR, 700 MW(e), use of ZPPR Assembly 9 as benchmark 80—22890
- LMFBR, BOR-60, reactivity rate of change during operation 77—71681
- LMFBR, Clinch River, HCDA or Na-water interactions, primary containment design tests 77—71673
- LMFBR, demonstration, design, construction and operating experience 79—97796
- LMFBR, fuel pin optimal design for large scale testing 79—76065
- LMFBR, heterogeneous and homogeneous core designs, performance characteristics 79—59123
- LMFBR, JOYO, fast reactor, experimental, functional and operational test results 79—93796
- LMFBR bullseye core, performance, design characts. and economic anal. 79—59121
- LMFBR core designs to preclude energetic HCDA 79—59125
- LMFBR core simulation, Na loop safety facility, P2 expt., LOCA, acoustic meas. 78—33264
- LMFBR experimental reactor JOYO, construction and function tests *(Japanese)* 78—33266
- LMFBR fuel handling experience 79—97873
- LMFBR outlet plenum, air flow model, interferometric meas. of fluctuating temp. using FFTF 78—89943
- LOFT, effect of rod external thermocouple simulators on steady-state and transient CHF 79—49734
- LOFT, licensing calcs. for PWR LOCA 80—23008
- LOFT, PWR LOCA tests TRAC-P1A pre-test calculations 80—42824
- LOFT, PWR LOCE L2-3, blowdown hydraulic influence on core thermal response 80—42827
- LOFT, requalification following LOCE 80—57904
- LOFT, utilisation for LWR LOCA analysis and licensing 80—18532

fission research reactors continued
- LOFT, zero power physics testing, meas. vs. calcs. 80—27713
- LOFT facility, commercial PWR systems safety 80—37548
- LOFT facility, PWR LOCA anal., system blowdown, core thermal response, emergency core cooling 80—37549
- LOFT facility, PWR LOCE, two phase flow meas. instrumentation 80—37550
- LOFT facility PWR LOCE, instrument calibration for mass flow rate meas. in two phase flow 80—37552
- LOFT for LWR LOCA anal., operating contractor's view 80—23007
- LOFT fuel design and operating experience 80—18411
- LOFT instrumented fuel design and operating experience during PWR LOCE 80—37551
- LOFT nucl. test L2-2, TRAC pre-test and post test calcs. 80—18519
- LOFT project, design and results *(Dutch)* 80—42735
- LOFT PWR LOCE post test anal. using RELAP4/MOD5 blowdown model 80—42825
- LOFT reactor advanced instrumented center fuel bundle, in-reactor meas. devices for LOCA expts. 80—23024
- LOFT reactor L2-2 expt., pre-LOCE thermal safety anal. 80—22896
- LOFT reactor secondary cooling system, waterhammer phenomena 80—57905
- LOFT role in LWR LOCA evaluation 80—18531
- LOFT safety anal. calc., carryover rate fraction correl. for PWR LOCA reflooding phase 80—42822
- LOFT start-up program, unique features 80—23116
- LOFT test facility for PWR LOCA systems transient response 80—758
- LOFT test L2-2, fuel rod response 80—18520
- LOFT test L2-2, pre-test calc. using RETRAN code 80—18518
- Lucens reactor accident, alarm and surveillance 78—50283
- LWR ECC, UCFLOOD code for bottom reflooding heat transfer 79—49728
- LWR LOCA, TRAC calculations of ECC bypass phenomena in a 1/15-scale experimental facility 79—49725
- MARIA, dynamics model for fast transients anal., code TOTEM 80—37419
- MARIA, Polish high flux test reactor, leakage rate meas. in reactor containment 79—18001
- MARIUS III critical facility, prompt-neutron lifetime meas. 79—67841
- MASURCA LMFBR heterogeneous core design, performance characts. and computer calcs. 79—59124
- materials testing reactors, low enriched fuel cycle 79—31095
- metallic fuel cladding eutectic formation during postirradiation heating in EBRII 80—102241
- MIT reactor modifications 77—42179
- MIT research reactor, flux synthesis techniques for routine core physics calcs. 80—68868
- MITR-II research reactor, power and neutron flux distribs. 77—42043
- MTR fuel, radiographic control of fuel prod., use of X-ray paper 78—5001
- NBS reactor, activity summary July 1978 to June 1979 80—106103
- near-stack reactor effluent dispersion studies, SF_6 tracer technique 78—11992
- neutron, tomography investigation using research reactor 78—23915
- neutron automated irrad. facility for Si doping 80—15141
- neutron importance function distrib. in reactor with trap 78—17294
- neutron irradiation facility in WR-1 organic-cooled research reactor, corrosion testing 78—89945
- neutron irradiation techniques for Si doping 80—19827
- neutron radiography facility on IRT-2000 reactor 78—17286
- neutron radiography using research reactors 79—11757
- neutron scatt. techniques in applied research, medium-flux research reactors 79—13514
- NISUS facility, sensitivity anal. for secondary intermediate energy standard neutron field 79—36451
- noise analysis, Polish developments 79—3216
- noise analysis of power reactor, simulation using nucleate boiling noise generator 78—54840
- noise experiments with delayed neutrons, general theory 77—54316
- North Carolina State Univ., PULSTAR reactor utilisation 79—9856
- NRU, NRX reactors, homogeneous cell parameters for 2-D reactor codes by axial averaging of 3rd parameter 79—54577
- NRU analysis support expts. performed in ZED-2 79—93820
- NRX anal. support expts. performed in ZED-2 79—13416
- nuclear heat appl. to space heating at Karlsruhe Nuclear Research Centre *(German)* 79—87943
- nuclear medicine growth, contribution of research reactors 79—11998
- nuclear safety research reactor, pulsing characts., expt. capability, meas. and evaluation 77—67790
- Orphee, new experimental reactor *(French)* 79—45399
- ORR fission reactor for simulation of neutron environment in fusion reactor first-wall studies 78—8973
- OSIRIS, Caramel fuel cladding rupture, development and detection *(French)* 80—95371
- PBF, temp. sensitivity of Co self-powered neutron detectors under PWR conditions 78—33275
- PBHTGR process heat reactor, core behaviour following massive air ingress *(German)* 80—83181
- PBHTR, Julich, 10 year operation *(German)* 78—54838
- PBHTR, out-of-core instrum. for detection of spatial flux irreg. *(German)* 78—82430
- Peach Bottom 1, HTGR nuclear power station, review of design and operation 79—45327
- Peach Bottom 2 BWR pressurisation effects of bypass streamline transient modelling 79—89408
- Peach Bottom BWR turbine trip test, computer anal. 80—692
- Peach Bottom HTGR, coolant chemistry, design implications 79—67832
- Peach Bottom HTGR, driver fuel elements, power profile meas. and in-pile thermocouple readings 79—67907
- Peach Bottom HTGR, fuel particle failure fraction determ. by hot-Cl leaching 79—67868
- Peach Bottom HTGR, inert gas release core-survey calc. 79—67908
- Peach Bottom HTGR core, γ-spectroscopic exam. of fission product distrib. after shutdown 79—67909
- Peach Bottom HTGR fuel element graphite, determ. of ^{90}Sr diffusion coeffs. 79—67869
- Peach Bottom HTGR primary circuit components, metallurgical eval. of structural materials 79—67867
- Peach Bottom Unit 1 HTGR, performance assessment 79—67906
- Peach Bottom-2 turbine trip, computer anal. 80—47626
- pebble bed prebreeder reactor, conservation of U resources 79—49697

fission research reactors continued
Penn State Breazeale Reactor, D_2O thermal column irradiation facility 80—9339
personnel dosimetry intercomparison studies at the ORNL Health Physics Research Reactor 80—9427
PFR Dounreay, radiation and contamination control 80—27834
PFR Dounreay, utilisation of neutrons meas. for shielding calcs. 80—32538
PFR operation, CDFR secondary cct. design 79—97788
PFR primary cct., operating experience and CDFR design intentions 79—97870
plasma core reactor, laboratory scale UF_6 plasma confinement expt. 77—23190
plate type fuel, reduced enrichment, status report on high-U-density development 80—9393
plate-type research and test reactors, near-term reduced enrichment conversions 80—22951
PNP-3000, prototype nuclear process heat reactor, core temp. transients, heat transfer calc. *(German)* 80—83180
PNP-3000 PBHTR, design accidents, exam. of temp. coeff. and short time dynamics 79—63781
pool type, medium powered, research reactor for governmental funding in Australia 78—41848
power burst facility, fuel rod microstruct. changes associated with post-DNB operation during power-cooling-mismatch 78—21688
power burst facility, PWR fuel rods testing 77—38361
power burst facility low pressure CHF in closely packed rod bundle 79—59144
power spectral density measurements with ^{252}Cf for a light-water-moderated research reactor, determ. of reactivity of far-subcritical systems 80—57913
pressure tube type reactors, small scale pipe rupture anal. 77—42034
primary coolant flow rate determ. using gamma/neutron ratio near primary line 77—65254
protection system design criteria 80—68935
pulse reactor, U-ZrH$_x$ fuel testing from 900-1300°C 80—13770
pulsed reactor, fast neutron spectra meas. 77—50222
PURINAMA, PuO_2-fueled zero-energy fast reactor 79—40988
PWR, emergency core cooling, alternative injection configurations 78—21696
PWR, LOCA anal. for consolidated nuclear steam system 79—49729
PWR, LOFT, emergency core cooling results 77—42016
PWR, Missouri University, fuel cycle optimisation 79—67930
PWR, Univ. of Missouri research reactor, ten-megawatt upgrade, exptl. use 78—21754
PWR experimental rig, high pressure loop cooling circuits safety aspects *(German)* 80—32397
RA reactor, fuel burn-up measurement using spatial power distrib. eval. and gamma spectrometry 80—68803
RBT-6 swimming pool research thermal reactor 79—18028
reactivity measurements of St. Lucie shims at swimming-pool MTR fuel-type reactor 78—21705
reactor loop, experimental, hazard and protection from tritium 79—36420
reactor physics experiment using Kyoto University Critical Assembly *(Japanese)* 80—5202
reactor sharing program for expanded reactor utilization, experience report 78—21755
recovery from obsolescence programs 80—9360
reduced enrichment program, fuel demonstrations activity, status report 80—9392
research reactor, IRT-2000, algorithms for direct digital control of neutron field 78—86643
Rossendorf ECH-1 irradiated fuel assemblies, burn-up and cooling time determ. using gamma spectrometry 80—63289
safeguards requirements for highly enriched uranium and reduced enrichments 80—22952
safety research experiment facility, conceptual design, LMFBR safety testing needs 77—3129
safety test facility configurations, performance 77—46338
safety testing, LOFT (loss-of-fluid) project at INEL 80—32386
Sandia Laboratories nuclear weapon neutron environment simulation, hardening tests 79—22448
Sandia Pulsed Reactor III operational history 79—9790
semiscale MOD-1, steam generator behaviour during core blowdown tests 80—772
semiscale MOD-1, upper plenum low-pressure injection ECC 79—49727
SLSF P3, cladding motion in 37 pin loss-of-flow expt. 80—18541
SNR 300 shutdown systems 79—97866
SNR-2, design studies for heterogeneous core concept 78—13226
SNR-300, LMFBR, HCDA, evaluation and prevention of local core accidents 80—749
SNR-300 fuel rods, postirradiation examinations of RAPSODIE-1 expt. 77—46219
SNR-300 LMFBR, hydrodynamic characteristics of shutdown systems 80—5289
SNR-300 LMFBR steam generator transients, computer simulation 80—23012
SNR-Mk. II, Rapsodie-II expt. 77—46292
STF 3/4 critical assembly, worth and reaction rate calcs. 80—68864
SuperPhenix nuclear boiler, design and construction 79—97761
swimming pool, neutron noise measurement technique *(French)* 77—10462
teaching laboratory, development at Ecole Polytechnique 78—4444
test and research reactors, enrichment reduction 80—22953
Texas A and M Nuclear Science Centre, neutron radiography facility, development and utilisation 80—9401
thermal neutron flux density, working standard based on F-1 reactor 78—82410
thermal-neutron-driven 14-MeV neutron generator 80—95496
thermionic reactors with ^{233}U fuel and $ZrH_{1.7}$ moderator, neutronics anal. 77—6482
THORS, transient anal. of fuel subassembly boiling test results 79—54548
THTR 300 MW(e) prototype reactor, safety anal. under extreme accident conditions 79—31087
Tower Shielding Facility, ORNL, GCFR shielding expts 80—47739
TR-1 reactor, thermal spectrum using neutron radiography of wedge shaped absorber 78—74439
training, main features and commercial types *(Czech)* 78—21745

fission research reactors continued
TREAT, behaviour of unirradiated He bonded carbide during mild TOP test 77—46237
TREAT, fast neutron hodoscope perform. tests on 91-pin fuel bundle 79—41005
TREAT, fission gas non-equilib. behaviour during fast thermal transients, simulation 78—41831
TREAT, LMFBR LOF accident tests on preirradiation mixed oxide fuel 80—47657
TREAT, low ramp rate TOP expt. feasibility in 2 to 10 cent/s range 80—47655
TREAT, new hodoscope collimator 77—42026
TREAT experiments, fuel pin failure, statistical analysis 79—97840
TREAT facility, pinhole imaging of test fuel element 78—21627
TREAT fast-neutron hodoscope, time and mass resolution of fuel motion, data acquisition system 79—41003
TREAT loss of flow safety test R8 with pressurised FTR fuel pins 77—42131
TREAT reactor, acoustic monitoring of IRT-10 test 78—8944
TREAT test AX-1, safety anal. of mark II CB loop 79—85664
TREAT test H6, TOP HCDA 79—93755
TREAT test R12, acoustic data anal. 79—93778
TREAT test results on fuel, cladding and coolant motion 77—3070
TREAT tests, statistical model to identify boiling inception 79—93779
TREAT TOP expt. R9 77—42025
TREAT TOP test E8, fuel motion 77—42132
TRIGA, instrumental neutron activation analysis pulsed irradiations 79—36450
TRIGA fuel, low-enrichment U, neutronic and heat transfer charact. 80—9397
TRIGA III reactor, anal. of standard and FLIP fuel mixed loading patterns 80—57855
TRIGA mark III reactor expt., source enhancement of ^{252}Cf spontaneous fission neutrons by ^{238}U 77—6594
TRIGA Penn State Beazeale reactor, fuel management 80—63361
TRIGA reactor, kinetic parameters determ. by interval distrib. method 77—42146
TRIGA reactor at HFER, neutron radiography studies 80—68758
TRIGA reactor fuel, long-distance transfer 79—67929
TRIGA reactor technical specifications, comparative study 80—13777
TRIGA-FLIP failed fuel element examination at HFEF 80—9383
TRIGA-II Musashi reactor, neutron irradiation facility for medical purposes *(Japanese)* 77—56459
Trombay nuclear facilities, effluent release monitoring procedures 78—89993
two-component torus hybrid reactor, double wall for first wall, struct. anal. 78—66409
two-phase control absorber development, closed-loop control and noise meas. in ZED-2 test reactor 79—85697
ultrahigh flux reactor, Grenoble, neutron-physical expts. *(German)* 80—5209
University of Lowell Reactor utilisation 79—9857
University of Missouri research reactor, fuel and productivity 80—9396
university type reactors, economic success, project update 80—68900
US National Bureau of Standards reactor, review of activities July 1977 to June 1978 79—85761
USA National Bureau of Standards reactor utilisation 79—9693
USA Reduced Enrichment Research and Test Reactor Program, current status 80—68930
Venezuelan research reactor reload fuel optimisation 79—9737
VHTR, high-temperature nuclear heat source for hydrogen production 79—93686
Viper, absolute yields and group constants of delayed neutrons in fast fission ^{235}U, ^{238}U, ^{239}Pu 77—54261
VIPER reactor, neutron leakage spectrum and dose meas. 79—3243
water moderated, 10 W, construction, student project *(German)* 78—33238
water resource research using Pennsylvania State Univ. reactor 79—12159
water trap, polarised-neutron beam shut-off 80—87004
Weapons Neutron Research Facility initial target/moderator configuration 79—9933
West German nuclear plant airborne radioactive effluent monitoring 78—89990
Westinghouse Nuclear Training Reactor, NRC physical security controls 80—9400
Westinghouse nuclear training reactor fuel inventory reduction plan 80—23115
Westinghouse Zion PWR plant simulator, load-follow methods computer design anal. 79—67917
with He turbine, (HHT), HTGR, heat exchangers *(German)* 80—5198
WR-1 organic reactor, material irradiation facility 78—54868
WWR-SM research reactor, direct digital control system 80—696
WWR-SM research reactor computerised control system, on-line alarm anal. 79—76104
YAYOI core absorbed dose meas. by chemical dosimeters *(Japanese)* 78—86695
Zebra 8 assemblies, neutron spectra meas. with proton recoil counters 77—38393
Zebra multi-chamber scanning system, fission distribs. in prototype fast reactor mock-up 77—42181
Zebra Pu fuelled assembly, neutron TOF spectra meas. 77—38333
ZED-2, simulated CANDU cores, transient meas. anal. 78—58386
ZED-2 hot loop, lattice cell meas. in 36 element natural UO_2 fuel, stopping effect of coolant 78—58347
ZERLINA zero energy thermal reactor, meas. of prompt neutron lifetime using γ-γ correlation 77—14212
zero power reactor simulation of BWR void effects 78—94061
zero-power plutonium reactor gamma-ray counting system, computer processing code for large numbers of spectra 79—9942
ZPPR, critical experiments for 600-700 MW LMFBRs 80—68859
ZPPR, generalized treatment of heterogeneity effects for the shielding factor method 79—40990
ZPPR, loading error simulations and control worth meas. 80—27777
ZPPR, reactor kinetics of heterogeneous design core 79—59122
ZPPR at Argonne, gamma-ray response calc. for encapsulated solid-state dosimeters 77—46420
ZPPR critical expts. for radial parfait heterogeneous reactor concept 78—13224
ZPPR meas., criticality prediction of SNR 300 79—40989
ZPPR modification (1977), neutron diffusion calcs. 79—9662

fission research reactors continued
ZPPR study of simulated radial parfait LMFBR core, control rod worths 78—33280
ZPPR-5 Source Level Flux Monitor expt. analysis 79—9705
ZPPR-9, control rod interaction meas. 80—63324
ZPPR-9, stimulated hodoscope slot effect in STF critical assembly 80—68860
ZPR, noise analyses, determination of kinetic parameters *(Rumanian)* 78—46139
ZPR noise anal., interpretation of quadratic approx. 79—76082
EBR-II Na system cold traps for control of O_2, H_2, T impurities 80—78411
^3H, production in fusion research reactors to fuel CTR expts., feasibility 80—18632
T monitoring methodology using SiO_2 desiccant, appl. to research reactor facility 80—21434
Th critical assembly, reactivity meas. 79—80976
U enrichment induction in test and research reactors, US program 80—22949
U-Al plate type, reduced fuel enrichment utilisation, design variations 80—9395
U-ZrH low enrichment fuel for TRIGA and plate-type reactors 80—22950
UAl_x fuel, development, irrad. performance in test reactors 80—68799
UAl_x plate-type reactor fuel element fabrication 79—49822
UF_6, high temp. fissioning plasma core reactors, fluid mechanical confinement 80—63248
U_3O_8 maximal fabricable conc. in Al base fuel elements 80—68800
U_3O_8-Al cermet fuel for research reactors 79—9835
UZrH fuels, development for TRIGA reactors 80—68798
UZrH low enrichment fuels, test programs and analysis 80—9398

fissures *see cracks*

flame sprayed coatings
adhesion, ASTM test 80—50812
applications to design 78—35588
metal hot sprayed deposit adhesion quality factors 79—83365
oxidation protective coating for Ni base TaC eutectics 77—40475
AL, thermal sprayed coating on steel substrate, cavitation and corrosion resist. in sea water 80—35427
Fe alloy casting, surface alloy layer by flame spraying technique *(Japanese)* 77—48586
Fe-Si gas-flame spray deposited protective coating, for C steel heat exchanger 80—61025
Mo flame sprayed coatings, comp., microstruct. and mech. props. 80—16598
Zn, thermal sprayed coating on steel substrate, cavitation and corrosion resist. in sea water 80—35427
Zn-Al (15 wt.%), thermal sprayed coating on steel substrate, cavitation and corrosion resist. in sea water 80—35427

flame spraying
coating for aircraft, process 79—83115
metal flame spray coating acceptance factors and tests in steelworks environment 79—83397
steel, ferritic, base material for powder flame spraying process, intercrystn. corrosion *(Czech)* 80—30158
surface alloy layer on casting by flame spraying technique *(Japanese)* 77—48586

flameproofing
see also fires
cables, flame resistant, for nuclear power stations, develop. and qualification tests 79—687
ceramic materials, for use in direct energy conversion *(Czech)* 79—70455
flameproof coating for PVC insulated cables, composition, tests *(Russian)* 78—68828
International wire and cable symposium, Cherry Hill USA (Nov. 1978) 79—37018
plastics, materials testing, application-oriented test standardisation *(French)* 78—85061
PMMA fracture toughness, flame-retardant additive effect obs. 80—16470
Mo-containing formulations 77—77761

flames
see also chemically reactive flow; combustion; fires
AAS with discrete nebulization, automatically triggered digital integrator 80—35610
acetylene flame, Na and MgO concs. meas. by laser saturation spectroscopy 79—29425
acetylene-air, Ba and Sr reson. lines, emission and absorpt. core profiles 77—50389
acetylene-air, eddy entrainment and combustion in depth process, three-region model 79—100384
acetylene-air, energy transfer from laser excited Na, Li, optoacoustic pulses 78—25490
acetylene-air, local temp. profiles and at. fluoresc. intensity profiles meas. 77—52680
acetylene-air flame, Li(Na)(K)(Mg)(Ca) damping consts., Lorentz collisions, mag. field effect 80—66805
acetylene-N_2O flame, chem. equilib. rel. to AAS 77—4957
acetylene-O_2, H_2O form., higher ro-vibr. levels, high resolution flame spectra 77—58033
acoustic noise from turbulent diffusion gaseous flames 78—38135
acoustic radiation rel. to flame loudspeakers 78—59227
advection and propagation in fluid 80—59097
air-acetylene flame, atom form., theory 78—7208
air-acetylene flame, multichannel apparatus detect. limits using atomic absorpt. spectra 80—76586
air-H_2 flame, temp. profile, two-line at. fluoresc. method meas. 77—71328
alkaline earth flame chemistry, photometric meas. of $H_2+O_2+N_2$ flames with/without Ca, Sr, Ba additions 79—8439
analytical, small vol. temp. meas. by two-line at. fluoresc. 77—40594
atmospheric pressure flame, ion sampling aerodynamic disturbance by sampling system 77—60142
atmospheric pressure flame, supersonic sampling, boundary layer cooling 77—60143
atom distribution, in flame spectrometry, moving point source model 78—61084
atomic absorption anal. in solid sample, method for anal. in flames 80—35614

flames continued
atomic absorption spectrometry, spectral interference by lithium salts in air-acetylene and Ar-H_2 flames *(Japanese)* 79—48018
atomic absorption spectrometry, spectral interference by potassium salts in air-acetylene and air-Ar-H_2 flames *(Japanese)* 79—48019
atomic absorption spectroscopy, flame atom trap for increased sensitivity 77—9148
atomic fluorescence and emission measurements with image dissector echelle spectrometer 80—11993
atomic fluorescence flame spectrometry using CW dye laser 78—3409
atomiser chamber electrode-diffusion flame, atoms distrib. in absorpt. zone, convection currents role *(Russian)* 79—34420
atoms, absorpt. spectra, flame and discharge laser irrad., opto-galvanic spectroscopy 80—42272
axisymmetric confined flame, aerodynamic and heat transfer, finite difference scheme, program 78—94689
axisymmetric laminar jet diffusion flame, split operator finite difference solns. 78—51252
bluff body configuration and its effect on flame stabilization 79—94719
bluff-body flame-stabiliser flow modelling 77—72367
bluff-body stabilised diffusion flame, CARS meas. 79—85964
buoyancy dominated wall diffusion flames, numerical model 77—68710
CARS spectrometer for gases and flames 80—95154
coaxial burner flame, struct., holographic interferometry determ. *(Russian)* 78—94851
collisional processes, coherent optical transient spectroscopy 79—39147
combustion bomb microwave cavity, electrically loaded with propagating flame front electron plasma, theory and expt. 79—20369
combustion diagnostics, laser Raman and fluoresc. techniques 78—88635
combustion front, laminar stability model 78—42680
combustion front thermal propagation and thermodiffusional instability 80—7796
combustion noise, flow induced, suppression using appl. of DC elec. field 80—38176
composite materials, surface, flame propagation velocity rel. to thermal props. *(Russian)* 80—7797
compressible ideal medium, flame front instability analysis *(Russian)* 79—27711
condensed fuel, combustion and extinction in stagnation pt. boundary layer 79—29356
confined burning jet, droplet vaporisation, expt. and theory 78—94855
constant density approx., asymptotic derivation of two models 80—30240
convection-diffusion coupling near flames, model 77—7481
cool flame explosion, during piston compression, time predicted by Livengood-Wu integral method 78—15675
counterflow diffusion flame struct. in transverse elec. field, interferometric investig. 80—16685
deflagration waves, heterogeneous, flame model for gas phase, nonlinear differential eqn. 80—81326
deflagration waves, heterogeneous, flame model for gas phase, partial differential eqn. 80—85177
detectors, using gas-filled photoelec. UV sensors 77—168
diagnosis, CARS appls. 80—16689
diagnostics using multichannel pulsed Raman spectroscopy 80—30237
diffuse flame extinction conditions with two component gas mixture 79—91956
diffusion, radiation-convection interaction 77—80231
diffusion flame, oppositely directed jets, elec. props. 78—56896
diffusion flame gas-phase ignition, in stagnation point fuel boundary layer 77—58803
diffusion flames, appl. of quasi-linearisation techniques 79—20368
diffusion flames, laminar and planar, large activation energies, asymptotic development *(German)* 78—91035
diffusional thermal instability, acceleration effects 80—30239
disc-stabilised diffusion flames, vel. characts. 79—34309
Doppler velocimetry within turbulent phase boundaries 77—11289
duct confined turbulent flames, laminar burning vel. effect on struct. and propagation 79—90351
dust clouds, ignition and flame quenching 80—28577
dust explosion, flame propag. vel., uniform dispersion of single sized particles 80—66803
education, plasma-laser beam self focusing using paint stripper flame 79—9066
electric field effect on propagation rate, precombustion Joule heating 78—53207
electron and noise temps. relationship for nonMaxwellian electron vel. distrib. *(Russian)* 78—35686
electron attachment to O_2 and H_2O in flames, kinetics 80—3349
electron energy distribution function in flame plasma, probe meas. 79—60190
electron-neutral energy exchange in AC field 77—42519
emission spectroscopy, use of plasma jet and aerosol desolvation system 77—86425
fires on flat terrain, photographic flame size determination 77—67516
flat diffusive flame, with low press. counterflow, spectrosc. and probe obs. *(Russian)* 77—36755
flow velocity field induced by flame spreading over fuel, laser velocimeter meas. 78—59529
flows induced by flames propagating over condensed fuels, two-component LDV meas. 79—23380
formyl radical, lower electronic states, ab initio calc. of pot. energy surface, hydrocarbon flame band 79—68287
free diffusion flame, length *(Russian)* 78—3334
free-jet diffusion type, ionis. meas. and combustion progress 80—30238
fuel droplet, burning anal., quasisteady model *(Japanese)* 79—32712
fuel droplet, deflagration and extinction in weakly reactive atoms. 78—64840
fuel mixture stream, regular reflection of shock wave from solid wall 79—77291
fuel-air mixtures, ignition and flame quenching 80—14847
furnace-flame atomiser, decrease in absorption changing from H-air to C-containing flame *(Russian)* 77—29082
gas breakdown thresholds induced by ruby laser 79—1951
gas jets, laminar homogeneous, combustion process *(Russian)* 78—94850
gas temperature measurement, spectral technique *(Chinese)* 79—35749
gas velocity measurement by cross correlation of random thermal fluctuations 77—58812
gaseous chemiexcited mol., modulated transmission spectra 77—86316
gasoline-air flame, laser induced fluorescence spectra obs. 80—91587
halogenated compounds, CH and C_2 flame emission *(German)* 79—52668

flames continued
heat exchangers, combustion 78—27761
n-heptane, cool flame stabilised by turbulence *(French)* 79—1952
n-hexane, tank flame, turbulence, holographic interferometric synchronous photography *(German)* 78—51255
and hot gas flows, similarity criteria *(Italian)* 79—27714
hydrocarbon diffusional combustion in air, finite activation energy anal. 78—95930
hydrocarbon fuel flame, electron density determ. by Michelson interferometry 78—1890
hydrocarbon turbulent diffusion flame, flame-zone model anal. 80—16684
hydrodynamic discontinuity model of distorted flame front 77—58802
hydrolysis reaction control for glass OH content reduction in vapour axial deposition 80—48474
ignition and flame quenching in flowing gaseous mixtures 77—80230
ignition and propagation, self-consistent 2-dimens. hydrocode 78—47066
impinging jet flames, stabilizing limit 77—89177
industrial flare flames, smoke detection and control by electric fields 78—81360
inverted flames, blowoff phenomena, explanation by area increase concept 80—14845
ion sampling system, characts. and calibr., atm. press. flame 77—56270
ion-molecule thermochemistry 80—55664
ionisation, mass spectrometric and mobility analyses for flame ionisation detector 78—40050
ionisation and Massey's adiabatic criterion, review 78—33563
IR flame radiation 77—19513
isothermal flame problem, 2-dimens., combustion limits and rates 79—100369
jet, premixed, impinging on plane surface, turbulent heat transfer 79—4054
jet, turbulent diffusion flames, statistical props. *(Japanese)* 79—81939
jet diffusion flames, blowout and attachment mechanisms 79—72957
jet flame, props. and mixing process in recirculation zone 78—91025
jet flame stabilisation in subsonic and supersonic flows 78—34206
kerosene-air flame laser induced fluorescence spectra obs. 80—91587
laminar, rise velocity meas., spectroscopic method 78—74064
laminar and turbulent, normal vels. of propag. calc. 77—84342
laminar diffusion flames, struct. and extinction by suppressive agents 79—32705
laminar flame, diffusion-thermal instability, boundary-value calc. 78—42682
laminar flame, front, hydrodynamic instability, numerical solns. 78—51254
laminar flame front, diffusion-thermal stability *(Russian)* 77—7477
laminar flame front, hydrodynamic instability, nonlinear integro-differential eqn. 78—51253
laminar flame in tube, diffusion-thermal instability 79—86320
laminar flame propagation, asymptotic anal., review and extension 79—47926
laminar flames, premixed, non-adiabatic, nonlinear theory 80—93757
laminar highly ionised flame, elec. props. *(Russian)* 77—32788
laminar jet diffusion flame size prediction, Burke-Schumann theory extension 78—14096
laminar jet diffusion flame size prediction from diffusion coeff. 78—14097
laminar mixed-mode forced-free diffusion type, on vert. burning fuel slab 78—91033
laminar premixed, two-dimens. elliptic partial differential eqns. soln. 79—94738
laminar premixed gaseous, amplification of propagating acoustic signal 79—29357
Langmuir probe technique for flame temp. meas. 77—24181
laser Doppler anemometry of high-temp. industrial gas flow *(German)* 79—10618
laser Doppler velocity measurements in turbulent flames using spark discharge particle generator 80—59139
laser excitation, rate eqns. 77—86327
laser fluorescence temperature measurements in flames 80—11892
laser induced fluoresc. spectroscopy in flames, detectability limit 78—73096
laser Raman diagnostics using coherent antiStokes scattering *(French)* 77—35280
liquid fuel flames in open air, noise from jet and flames *(French)* 77—19476
local temperature measurement, by two-line at. fluoresc. and photon counting method 79—71447
local turbulence props., Raman spectroscopy meas. 80—64648
low temperature, atomic absorption element determ. 80—30307
luminescing flame, propag. limit with respect to pressure 79—100376
luminous flares, heat of radiation calcs. *(German)* 80—68154
mass streamline, vel. and density fluctuations correlation *(Japanese)* 80—6164
metal combustion, laser-initiated, time-resolved spectroscopy 77—77765
methane-air, OH conc., temp. and rot. temp., laser absorption spectroscopy 78—76862
methane-air flame, Raman scattering diagnostics of turbulent flow field 78—18328
methane-air flame, reactions, radical overshoot 79—34308
methane-air flame, stimulated Raman scatt. obs. 80—53003
methane-air flames, meas. of temp. and OH conc. 80—16687
methane-air flames, OH conc. profile 80—35534
methane-air flames, temp. meas. by laser Raman spectroscopy 80—13074
methane-O_2-N_2, OH radical conc., hook method meas. 77—77762
methane-O_2-N_2 mixtures, prediction of propagating laminar flames 79—52663
methanol-O_2 flame, combustion and ionisation 79—20357
mixture preheating effect on flame propag. in semi-open tube 78—47067
molecular absorption spectra of complex matrices in premixed flames 79—92021
molecule, absorpt. spectra, flame and discharge laser irrad., opto-galvanic spectroscopy 80—42272
multi-diffusion configurations 77—51134
multicomponent nonequilibrium chemically reacting boundary layers, transport coupling theory 79—77294
multidimensional unsteady laminar flames, scaling transformations for numerical computations 80—19522
multiple turbulent, struct., operating conditions rel. to characts. *(Russian)* 77—7476
mutual ion neutralisation 80—35537

flames continued
Na-coloured intracavity flame, in dye laser, mode competition 78—46594
noise generation by laminar flames in tubes 79—86422
noise sources, in open turbulent pre-mixed flames 77—51127
nonadiabatic flames, linear stability anal., diffusional-thermal model 80—14846
nonlinear acoustic phenomena related to combustion zones 80—38156
optical properties and temp. measurement of light scatt. particles containing flame *(Russian)* 78—56894
oxy-acetylene flame, $C_2\ {}^3\pi_u$ conc. meas., saturation spectroscopy 77—77832
periodic cold flames, autooscillatory model, Lotka-Franck-Kamenetskii kinetic scheme *(Russian)* 78—35685
photometers with automatic dilutor 78—49878
plane flame, flameholder influence on static stability 80—101020
plasma, with rectangular cross section, prod. by nozzle *(Japanese)* 78—47108
plasma flow velocity measurement, Langmuir probe method 79—46475
plasma microwave-emission diagnostics, propane-O_2 flame obs. 80—45503
plume behind bluff body with fuel injection, elec. cond. mechanism 79—39150
plumes in cocurrent flow, analysis by method of superimposition momentum fields 77—58805
polymer surface, flame propagation velocity rel. to thermal props. *(Russian)* 80—7797
pool flames, convective mass transfer, appl. to air pollutants distrib. *(German)* 79—52662
pool flames, heat and mass transfer *(German)* 78—94677
premixed burning in diffusion flames, Libby Economos flame zone model 79—60093
premixed flame regime, Linan's linear stability anal. 79—52666
premixed gaseous flame noise, influence of combustion substrate parameters 79—74384
premixed H_2-O_2-N_2 laminar flames, temp. profiles, Raman, absorpt. and line reversal obs. 80—42227
premixed laminar, multiplicity and stability, bifurcation theory applic. 80—16681
premixed laminar flame, time-depend. soln. determ. 78—67282
premixed turbulent flame combustion, heat transfer obs. and calc. *(French)* 78—94688
premixed turbulent flame struct. 79—86515
premixed turbulent flame structure investig. by light intensity distrib. meas. 80—16680
premixed turbulent flow, spectral interpretation of the propag. vel. *(French)* 79—4090
probe sampling, flow patterns at probe sampling pt. *(Russian)* 78—35687
propagation, natural convection effects 80—53882
propagation in flowing turbulent combustible mixture *(Russian)* 77—27624
propagation in long tubes, ducts investig., fibre optic technique 77—31404
propagation limits, mixture turbulence effects 80—16679
propagation of premixed flame, in supersonic airstream 77—84339
propagation of premixed flame in large-scale turbulence 79—50813
propagation through media with slightly perturbed initial temp. distrib. 77—60067
propagation through stratified charge combustion channel, model 79—64795
propane, diffusion flame, coherent spectral interference from C_2, CARS spectra 80—43404
propane flame, wake stabilized, response to sudden accel. or deceleration of free stream 80—61096
propane flame plasma, Langmuir probe teaching expt. 78—12456
propane-air, eddy entrainment and combustion in depth process, three-region model 79—100384
propane-air flame, chem. anal. of reaction zone by Raman spectra 78—64837
propane-air flame, effect of EHD boundary layer on heat transfer 77—80228
propane-air flame, premixed turbulent, three region model 79—100383
propane-air flame premixed turbulent, three region model 79—100382
propane-air flame-generated turbulence, approach stream turbulence effects 79—64793
propane-air flat flame, high resolution spectroscopy on CO 77—81434
propane-air mixtures, combustion limits in large vols. 79—100368
propane-O_2-air flame, temp. meas. by laser Raman spectroscopy 77—5833
pyrolising slab, laminar wake flame heights 80—76513
pyrometer, 3 wavelength for flame temp. meas. 79—93141
quenching, by narrow cylindrical passage 78—15674
radiation, in IR porous perforated gas radiators 78—3335
radiation measurement techniques 78—94506
Raman scattering and laser Doppler velocimetry techniques for turbulent flow field investigs. 78—34224
Raman scattering diagnosis, laser modulated particulate incandescence effects 78—20117
Raman spectroscopy, remote spontaneous, new trends in recording of signals 80—73485
rare earth elements, and monoxides flame absorption spectra, dye laser amplified absorption method 77—29075
rate constants for $A+X\rightleftarrows A^++X^-$ and $AX+M\rightleftarrows A^++X^-+M$ (A=metal, X=halogen, M=flame species) 79—34310
reaction rate coefficients, for flame calcs. 78—85160
reaction rates in diffusion flames 78—35637
round jet type, mass exchange between recirculation zone and outer flows, stabilisation 80—14842
Rubens flame tube demonstration of standing sound waves 80—8760
saturated fluorescence excitation, transition probabilities and particle density determ. 78—58871
semiautomated thin-layer chromatography with scanning flame ionisation detector 79—74466
singing, struct. investig. by holographic interferometry *(Russian)* 79—29361
single-beam absorption-emission flame spectrophotometer design *(Russian)* 78—27866
small volume flames, temp., temporal meas., two line at. fluoresc. technique, Raman scatt. 80—42226
soot-gas mixture, in luminous flames and smoke, IR mean absorption coeffs. calc. procedure 78—91061

flames continued
sooting flame, absorpt. spectrosc. using tunable diode laser 80−55660
sooty diffusion flame, CARS obs. 80−16690
sound measurement in flames, microphone probe design 77−62114
spectrometry, senisitivity and detection limit, review *(Japanese)* 80−11990
spectroscopic flame temperature measurements, role of transition probability factors 77−1925
spectroscopic temperature and OH concentration measurement 77−32853
spherical blast waves generated by spherical flames, anal. 80−16686
spherical drop combustion, asymptotic, drop shrinkage and flame movement, heat and mass transfer 77−81405
spread over PMMA sheets in laminar forced oxidising gas flow 80−35535
stabilisation behind bluff-body flame holder *(Japanese)* 78−67284
swirled gas flame aerodynamics, empirical results 77−58804
swirling, temp. distrib. 80−61098
synergy in flame-propagation processes 79−100370
temperature, concentration, and velocity in jets, flames, and shock tubes 79−68778
temperature, meas. using unresolved rot. struct. of mol. spectra 80−86300
temperature, specie conc. meas., CARS and laser induced saturation fluoresc. spectroscopy obs. 80−45617
temperature and conc. meas. by rot. Raman scatt. 79−31530
temperature and OH concentration, simultaneous determ. by high-resolution laser absorpt. spectroscopy *(German)* 78−35776
temperature determ. by laser Raman optical multichannel analyser 78−73098
temperature meas., spectral remote sensing 78−32818
temperature meas., using nonlinear inversion techniques 79−85140
temperature meas. by Raman scattering 77−16822
temperature measurement, 5 laser-excited fluoresc. methods, theoretical basis 80−101793
temperature measurement, laser Raman spectroscopy method *(German)* 78−32900
temperature measurement, spatially resolved, spectroscopic method 79−71446
temperature measurement by suction pyrometer, corrections to local values 77−22551
temperature measurement using laser induced fluoresc. spectrosc. of OH 80−90839
thermal, temp. field meas., buoyant vortex bubbles and turbulent thermals 78−34232
thermal diffusion flame, two dimens. cellular struct. formation 80−69947
thermochemical gas analyzer, porous flame barrier, reagents, reaction products, conc. diffusion *(Russian)* 79−29359
turbulence, real time study by Raman scatt. 77−72368
turbulence effects on wrinkled flame speed and struct. 80−26015
turbulent, acoustic noise *(Russian)* 79−32708
turbulent, calc. in one-dimensional approach 80−30236
turbulent, combustion model and calc. 78−35684
turbulent, flow pulsation effect on chem. reaction 77−35260
turbulent, interaction of flow pulsation and chem. reaction 77−58801
turbulent, temp. and conc. calcs. *(Russian)* 79−32707
turbulent combustion, premixed, effects of finite reaction rate and molecular transport 80−3348
turbulent combustion of mixed gases, thermal exchange effect on reaction rate 78−7205
turbulent diffusion, flames, high Reynolds number, rocket exhaust appl., chem. processes theory 80−45504
turbulent diffusion, mass entrainment, momentum flux and temp. 79−32704
turbulent diffusion, mean flow props. 78−1753
turbulent diffusion, transport eqn. for probability density function, closure 80−1585
turbulent diffusion flame, analytic incorporation of probability density functions 78−75232
turbulent diffusion flame, burning vel. *(Russian)* 77−7475
turbulent diffusion flame, visible length of vertical free flames 78−85163
turbulent diffusion flame jet, anal., pulsations of conc. and Archimedian forces *(Russian)* 77−51130
turbulent flame theory, probabilistic approach 77−24034
turbulent flames, statistical theory 79−70329
turbulent flames and isothermal free jets, mathematical model *(German)* 79−74387
turbulent jet flame, stabilisation using thick burner rim *(Japanese)* 77−68706
turbulent premixed flame, interaction effects 77−11279
turbulent premixed flame, sequential chemistry, closure model 78−35683
turbulent premixed flame, theoretical predictions *(French)* 78−94853
turbulent premixed flame, variable density effects 78−5824
turbulent reactive gas flows, two-dimens., nonequil. processes analysis 77−51129
turbulent-jet-diffusion flame, effect of mol. gas radn. 77−80232
unsteady, propagation, numerical modelling 79−64794
V-gutter stabilised flame, laser anemometry and schlieren photography meas. 77−35263
vibrating flames in tubes, dynamical props. 77−31388
wake of blunt body with chemical reaction, flow field meas. using laser Doppler anemometry 77−35262
Ar-H flame, Se trace amount determ. by hydride generation-nondispersive flame at. fluoresc. spectroscopy 80−89553
Ba compounds in flame, laser excited fluoresc. 79−68260
$Ba+CO(CO_2)$, flame spectra, 500-1150 nm mechanism 77−48646
$Ba+N_2O$, chemiluminescent flame, BaO states population 79−39153
$Ba+O_2$ flame, chemilum. from three-body recombination reactions 77−77759
$BaO+Ar(CO_2)$, in Ar flame, rot. and translational relax. by sub-Doppler optical-optical double reson. 80−95583
C particles in flame, laser heating and sublimation 78−61012
C_2, conc. meas. in oxyacetylene flame rel. to saturation spectroscopy 77−60148
C_2 resonance fluoresc. technique for transient flame investigs. 77−30894
CH, in low pressure flame, laser-excited fluoresc. 78−90199
CO, background-free CARS technique 79−94288
CO, detectability levels for CARS species sensitivity 80−43404
CO flame rise vel. meas. by particle track method 80−89489
CO, output spectra from CS_2-O_2-$CO_2(N_2O)$ flame lasers 80−83601

flames continued
$CO+O+M \rightarrow CO_2+M$, time-resolved and flame-band emissions in shock tube expts. 77−36729
CO_2 conc. and temp. in flames, Raman spectroscopy 80−32720
CS_2-O_2 flame, rate of population of CO vibr. levels, CO emission intensity 78−7186
Ca, flame luminesc., laser irrad. effects 77−77766
Ca, laser saturation broadening in flames, fluoresc. excitation profile obs. 80−95568
$Cs+F_2$, electronic excited states, chemiluminesc. in flame, spectra 77−52643
CuF, from gas phase reaction, photon yields, chemi- and photo-luminesc., excitation spectra 79−5157
DF repetitively pulsed subsonic chem. laser, flameout using fluidic switching 78−29943
F_2-H_2 mixture, parameters influence on flame propag. velocity, rej to HF chem. laser 80−50855
$GeCl_4$ hydrolysis and oxidation kinetics for graded-index fibre vapour phase axial deposition 80−48477
H supersonic flames, chemical kinetics and unmixedness effects on burning 80−64649
H-air, laminar diffusion flames, chem. nonequilib. effects model 78−48654
H-air flame, premixed turbulent, three region model 79−100382
H-Br systems, thermokinetic oscillations in flame propagation, stability diagram 79−79253
H_2, atm. press., heat and mass transfer meas. using Ir/Ir-Rh alloy thermocouple 77−86314
H_2 diffusion flame, Rayleigh temp. profiles meas. 80−16692
H_2 laminar diffusion flame in air, Raman spectra diagnostics 79−47928
H_2-air jet diffusion flames with finite chemical reaction rates 79−81992
H_2-N_2-Na jet, ignition and extinguishment in simulated LMFBR accident conditions 78−8932
H_2-O_2, H_2O form., higher ro-vibr. levels, high resolution flame spectra 77−58033
H_2-O_2-Ar, excitation profiles of Na D-doublet 77−88436
H_2-O_2-N_2 flame, photochem. reactions involving Na*, laser saturated conditions 78−80762
H_2-O_2-N_2 flames, diffusion coeff. meas. for CO, Br, I and Tl 78−51272
H_2-O_2-N_2:K, P, electron attachment, compound form. 79−11794
HCl, dissoc. electron attachment kinetics in flame, mass spectra obs. 78−68872
HF repetitively pulsed subsonic chem. laser, flameout using fluidic switching 78−29943
H_2O in flames, coherent anti-Stokes Raman spectrum 79−36652
H_2O, vibr. Raman scatt. signature in flames 78−25539
HX (X=Cl,Br,I) dissoc. attachment, negative ion form. and removal kinetics in flame 77−52642
He-O_2-acetylene flame atom cell, for at. spectrometry, characterisation 78−32876
In, laser saturation broadening in flames, fluoresc. excitation profile obs. 80−95568
$K+Cl \rightleftarrows K^++Cl^-$, $KCl+M \rightleftarrows K^++Cl^-+M$, rate consts. in at. press. flames 77−60036
Li, seeded flames, excitation, laser radiation absorpt., sound vel., opto-acoustic effects obs. 80−43345
$Li(2^2P_{1/2,3/2})$, laser induced flame chemistry, saturated mode fluoresc. meas. 80−89491
Mg, flame luminesc., laser irrad. effects 77−77766
N_2, atm. press., heat and mass transfer meas. using Ir/Ir-Rh alloy thermocouple 77−86314
N_2, flame temp., CARS spectra diagnostic investigation 80−43404
N_2 in premixed laminar methane-air flame, Raman scatt. meas. of vibr. temp. 79−80622
N_2, rot. temps. determ. in diffusion flames using CARS 79−29358
N_2H_4-F_2 flame, chemiluminesc., HNF A-X emission spectrum 79−50033
NO-H_2 flame, OH form., collisional broadening parameter, curve of growth method 80−53052
$NO^++e^- \rightarrow N+O$, recombination rate const. determ. in flames 78−48632
$NO^++X^- \rightarrow NO+X$ (X=Cl, Br, I), rate const. determ. in flames 78−48633
NO_2 laser fluoresc. meas. in flames 78−56923
N_2O-acetylene flame, background compensation in differential atomic emission spectrometry *(French)* 78−7296
N_2O-acetylene flame, spectral source using Reticon photodiode array 77−63999
N_2O-CO, flame, alkaline earth atom catalysed combustion 77−9081
N_2O-CO flame, alkaline earth catalyzed chain reaction chemiluminesc. 77−40548
N_2O-CO flame, Mg catalyzed chain reaction chemiluminesc. 77−36758
N_2O-H_2 flame, appls. to Mn determ. in gasoline by AAS 78−15729
Na, 5890/96 Å resonance emission lines, wing profile meas. 77−46534
Na combustion in LMFBR, determ. of flame struct., temp. and position 80−47644
Na concentration profiles saturated fluoresc. meas. 77−79571
Na, excitation temperature meas. with spatial resolution, hook method 77−58200
Na, fluoresc. in flame, saturation curves with pulsed tunable dye laser 79−36579
Na in flames, laser-induced fluoresc. temp. meas. 80−11893
Na, laser saturation broadening in flames, fluoresc. excitation profile obs. 80−95568
Na, near-resonant Rayleigh scattering and atomic flame fluorescence spectroscopy 79−92033
Na, Rayleigh scatt. from vap. in flames with N_2 and Ar diluents 79−22627
Na, reson. line, laser excitation, combustion Rayleigh scatt., at. flame fluoresc. spectroscopy 80−42972
Na seeded, gain probing by intracavity dye laser spectroscopy 77−7092
Na seeded flames, excitation, laser radiation absorpt., sound vel., opto-acoustic effects obs. 80−43345
Na, spin polarisation in flames by optical pumping, mag. reson. transitions 78−29762
Na, two-photon excitation in flame, saturation broadening, fluoresc. obs., broad-band excitation 78−74625
Na, wing profiles in flames with N_2 and Ar diluent 79−22660
Na-seeded H_2-O_2-Ar, population inversion, two-photon laser excitation 79−34307

flames continued
- NaCO$_3$+ZrC, flame, optical and temp. characts. meas. method, light scatt. ZrO$_2$ particles *(Russian)* 78−56894
- Na(3^{2}P$_{1/2,3/2}$), laser induced flame chemistry, saturated mode fluoresc. meas. 80−89491
- O$_2$, atm. press., heat and mass transfer meas. using Ir/Ir-Rh alloy thermocouple 77−86314
- O$_2$-H$_2$-Ar, atm. press., Na(3^{2}P) lifetime obs. 79−39149
- O$_2$+Be(Mg)(Ca)(Sr)(Ba), reaction kinetics in diffusion flame 77−90579
- O$_3$, decomposition flame, flat, laminar, vel., struct. 78−51256
- OH A$^2\Sigma^+$ state, laser excited, vibr. energy transfer, flame thermometry appls. 80−58349
- OH concentration in flame, local and instantaneous meas. by laser induced fluoresc. obs. *(French)* 79−15999
- OH in flames, laser excitation dynamics 80−74201
- OH local concentration in flame, direct meas. from single laser pulse induced fluoresc. 79−39229
- OH radical in premixed laminar methane-air flame, fluoresc. meas. of rot. temp. 79−80622
- Pb, chemiexcitation of ^{3}P metastable states, during combustion of acetylene and C$_2$H$_2$ 78−3339
- S containing aerosols, continuous meas. and speciation by flame photometry 78−95974
- S$_2$ in flames, laser induced fluoresc. meas: 78−61132
- SH, in flames, laser induced fluoresc. meas. 78−61132
- SO, SO$_2$ in flames, laser induced fluoresc. meas. 78−61132
- SeH$_2$, atomisation in cool H$_2$-O$_2$ flame burning in quartz tube atomiser 80−76581
- Si+F$_2$, chemilum., at. absorption, and laser-induced fluoresc. obs. 80−3315
- Si+N$_2$O, chemiluminesc., SiO emission, A$^1\Pi$, b$^3\Pi$ and a$^3\Sigma$ states, and effect of CO and N 77−77767
- SiCl$_4$ hydrolysis and oxidation kinetics for graded-index fibre vapour phase axial deposition 80−48477
- SiH$_4$(SiD$_4$)+F$_2$, chemilum., at. absorption, and laser-induced fluoresc. obs. 80−3315
- Sn+O$_2$(NO$_2$), chemiluminescence and photon yields 77−29012
- Sr, 4607 Å resonance emission line, wing profile meas. 77−46534
- Sr, 4607.33 Å resonance line, spectral width depend. on at. density in flame 77−46535
- Sr, laser saturation broadening in flames, fluoresc. excitation profile obs. 80−95568
- TiO, (C$^3\Delta$-X$^3\Delta$) system, radiative lifetimes, oscillator strengths, flame spectroscopy 78−42136
- TiO, emission spectra in chemiluminesc. flames 77−38689
- TiO, photoluminesc. of α(C$^3\Delta$-X$^3\Delta$) system in chemiluminesc. flames 77−38690

flare stars *see stars*

flares, solar *see solar flares*

flash lamps
- ablative flashlamps for high peak power dye lasers 77−79836
- air surrounding bulb, optical inhomogeneity due to light absorpt. 79−64299
- alkali metal vapour flash lamp, absolute spectral distrib. and radiant output 78−66510
- ballast volume effect on solid laser pumping efficiency 77−707
- coaxial flashlamp pumped dye laser *(Chinese)* 79−55144
- cooling fluid interaction of high-power flash lamp radiation 78−13718
- correcting absorber selection for Si photodiodes, luminous meas. in flash photometry 79−72699
- current and voltage distrib. of flashlamp array, supplied from storage inductor 77−83940
- discharge-channel development, effect of reflected shock waves, photographic obs. 77−43093
- drive circuit discharge currents, Fourier anal. 80−23695
- dye laser, reliable thyratron switched flashlamp pumped 79−31930
- dye laser, simmer-enhanced flashlamp-pumped, efficiency improvement 79−64240
- dye laser, small-bore coaxial flashlamp pumped, negative effect of cyclooctatetraene 77−14708
- dye laser, tunable, flashlamp pumped, ultra-narrow bandwidth 80−9897
- dye laser pump, construction and performance of laser and pumping source *(Japanese)* 77−58341
- dye ring laser, flashlamp pumped, injection of N$_2$ laser excited oscillator beam 80−5754
- dye solutions, flashlamp-pumped, thermal effects 77−10917
- electro-optical pyrometer single-pulse calibration flash tube 78−12702
- excimer, initiation of pulsed HF-DF chem. laser 77−88754
- flashlamps, coaxial and preionised linear, comparison as pumping sources for high power dye lasers 80−102730
- flowing gas vortex stabilised lamp, for dye laser pumping 77−19334
- fused quartz flashlamps, correlation between static stress distrib. and explosion energy 77−10931
- high energy flash tube, enhancement of luminous efficiency using high power pre-ionisation 78−37958
- high-energy, short-pulse, operating characts. in ablation regime 77−23724
- IFP-1200 flash lamps, performance under different discharge conditions 79−94313
- inert gas flash lamp, absolute spectral distrib. and radiant output 78−66510
- laser, tunable organic-dye, detachable pumping lamp 79−36907
- laser pump source, discharge brightness radial profile, laser illuminator effects 77−692
- laser pumping, discharge development effects on pumping efficiency 78−71114
- laser pumping, optimal lamp filling, review *(Russian)* 78−63123
- laser pumping by pulsed lamp *(Russian)* 78−22138
- laser pumping lamp ignition pulse semiconductor shaper 79−72585
- laser pumping of rectangular cross section active elements, efficiency 77−695
- laser pumping optimisation of flash lamp drive circuit 77−75534
- light-time characts. *(Russian)* 79−32012
- macrophotography, simple flash equipment 79−17513
- nomogram for load conditions calc. 77−58411
- ocular photography, accessory fill-in flash for the Nikon photo-slit lamp 80−36056
- photodissociation laser, flashtube-pumped 79−76712
- photoflash units, chemical and electronic, temporal spectral characts., meas. method 80−95171

flash lamps continued
- photographic flash light meas. instruments development *(Hungarian)* 80−57411
- photographic flash sequencer, using thyristor control 80−62749
- photographic flash units, basic types 79−71548
- photographic flashlamp trigger circuit 80−62750
- plasma-wall interaction, spectroscopic meas. 79−77421
- power supply with volt. and capacitance control 77−67518
- prepulsed, anomalous plasma resistivity in discharges 78−87508
- pulsed lamps for laser systems, bulb transmittance changes 80−5740
- pulsed laser operation, flashlamp technology and design requirements 79−36912
- pulsed Xe spectrophotometer with parallel wavelength sensing 78−54427
- pumping source for lasers, expendable flash lamp with Zr foil 77−50679
- quadraxial high repetition rate adapter for coaxial flashlamp pumping of laser dyes 79−45949
- shell transparency changes and dynamic colour *(Russian)* 79−10370
- silhouette photography, high-speed, of small biological subjects 78−44743
- slave triggers for photographic flash 80−95168
- sound triggered electronic photo flash unit; using variable time delay 80−57407
- sound triggered flash cct., using variable time delay 80−57414
- sound-controlled flashlamp trigger circuit *(Spanish)* 80−13175
- temperature jump and photochem. studies, fast flashlight appl. 78−22588
- triggered light pulse generator for recording fast processes 80−105727
- tubular, gas-discharge expansion rate 79−82110
- unconfined discharge channel, spatial instability 78−38571
- vortex stabilised, pumping of high average power dye laser 77−14749
- wall ablation lamps for high energy dye laser pumping 78−29961
- Ar for vacuum UV spectral region 79−93236
- H$_2$ flashlamp light pulse shape calibration, using synchrotron radiation excitation standard 79−72642
- Hg capillary lamp, pulsed high pressure, as efficient pumping source for dye laser 77−14710
- I$_2$, flashlamp excited photodissociation laser 79−72558
- Nd^{3+}:YAlO$_3$ laser double-pulse flashlamp trigger cct. 78−55378
- Xe and Ar flashlamps for vacuum UV radiation 80−106590
- Xe flashlamp discharge channel evolution 77−84559
- Xe flashlamp efficiency for photoinitiation of HF pulsed laser 80−69403
- Xe flashlamps with interf. coatings, laser pumping efficiency improvement 79−10316
- Xe Kh-122-PM pumplamp module operating conditions, for Nd laser system 80−91815
- Xe miniature flash lamp, excitation of NdP$_5$O$_{14}$ laser 77−88779
- Xe, thermally assisted flash annealing of ion-implanted Ge and Si 79−10881
- Xe ultrahigh-pressure, Soviet-made DKSSh lamp spectral characts., in pulsed regime 80−48371

flash photolysis *see photolysis*

flashover
- air, positive/negative leader breakdown process, problems 77−11427
- air, rod-to-plane gap, space charges, impulse voltage meas. *(Japanese)* 80−87970
- air gap corona pulse delay obs. and HV insulation design 79−19117
- air gaps impulse flashover characteristics, at varying humidity conditions, Indian standards 78−22585
- arc quenching system for transient and statistical flashover, fusion reactor systems 78−75455
- back corona, sparkover voltage 79−50909
- back discharge, flashover meas., streamer or steady glow mode, dust layer effects 78−59708
- breakdown voltage of air, effect of sand particle pollution 78−81363
- cathode initiated surface flashover, propag. vel. 78−14233
- contaminated insulators, flashover under DC conditions 79−68967
- dielectric materials spacecraft, surface discharge arc propag. and damage 80−71314
- dielectric stimulated arcs in lighting-arrestor connectors, substantial lowering of breakdown voltage 79−99013
- dielectric surface creep discharge flash intensity and time distrib. obs. 78−67562
- discharge in positive point-to-plane air gaps, obs. 77−35414
- electric machines, volts-per-bar and flashover, causal mechanisms and preventive measures 80−92408
- electrically stressed insulator-vacuum interface, secondary electron avalanche 77−81185
- electrodes, space charge effects *(Japanese)* 79−50917
- electrolyte surface discharge development and influence on model reactions *(Russian)* 79−96320
- electron beam propagation in dielectric guide due to space charge neutralisation, surface flashover 80−18716
- electrostatic precipitator voltage meas. method principle and results *(Polish)* 77−67471
- fast insulator surface flashover, investigation using electro-optical elec. field meas. 80−64820
- fast insulator surface flashover in vacuum, mechanism, electro-optical investig. 80−103206
- insulating oils elec. breakdown at solid-liquid interface with EHD motion, expt. 77−76226
- insulator flashover in HV vacuum transmission line, mag. effects 77−24236
- insulator surface, in liq. He, elec. discharge 77−84558
- insulator surface flashover in vacuum, electro-optical meas. 80−38823
- insulator surface in vacuum mag. inhibition 77−11411
- insulators, HV, influence of air pollution on dielectric rigidity *(Slovenian)* 80−64801
- insulators, HV for transmission lines, power arcs occurring in networks and laboratories, comparisons 80−87983
- lightning stroke onto tower, calc. *(Russian)* 77−55180
- polycarbonate plate, impulse surface flashover in vacuum, effect of normal elec. stress 79−4199
- polymers, flashover behaviour, of spacers at low temps. 80−25882
- porcelain, flashover behaviour, of spacers at low temps. 80−25882
- probability dependence and Weibull distribution *(Czech)* 78−67449
- pulsed surface flashover mechanism involving electron-stimulated desorption 80−70055
- rod-to-plane air gap breakdown under negative impulse voltage 78−67563

flashover continued
sliding spark at switching-wave on rod-plate arrangement *(Czech)* 77—47278
solid dielectric bridged vacuum gap microparticle collection and analysis 78—5964
solid insulator surface flashover in vacuum streak photography 78—59700
solid-liquid interfaces, permittivity matching effect 78—1945
spark gaps, long air, disruptive voltage calc. with positive switch voltages *(German)* 80—87964
switching surge, long spark modelling, conversion factors *(Czech)* 77—15254
vacuum flashover due to thermal breakdown or streamer discharge 78—38570
vertical single-pole earth sphere gap, voltage measurement influence of neighbouring surfaces *(German)* 78—29880
SF_6 dielectric strength, conductor surface irregularities influence 80—14946
SnO_2 coated glass, surface elec. breakdown 80—25303
TiO_2-polycarbonate laminate, impulse surface flashover in vacuum, effect of normal elec. stress 79—4199

flaw detection *see crack detection*

flexoelectricity
bilayer lipid membranes, flexoelectric polarisation at blocked flip-flop 79—100582
biomembranes, liquid-protein interactions, flexoelec. effects 78—92600
chiral smectic liquid cryst., ferroelectric, flexoelectric effects, dielectric const. 80—33877
cholesteric liquid cryst., shear electricity, symm. considerations 78—60394
p,p′-dihexyloxytolan, flexoelec. coeff. in nematic phase, thermal depend. 80—79685
DOBAMBC, chiral smectic, flexoelectric effect and polarisation props. *(Russian)* 80—15002
ferroelectric smectic single C liquid cryst., electric field induced bend undulation instability 80—24351
liquid crystals, microscopic interpretation of flexoelec. 77—32339
MBBA, flexoelec. coeff. in nematic phase, thermal depend. 80—79685
MBBA, flexoelectricity and surface polarisation 77—89376
MBBA, nematic, flexoelec. and dielec. relax. behaviour 78—94979
MBBA, one-dimens. dielectric-flexoelectric deforms. 78—38616
nematic liquid cryst., flexo-electric domains 78—43792
nematic liquid cryst., flexoelec. domains in thin layers 78—18549
nematic liquid cryst., flexoelec. polar deform. and second order elasticity 78—1979
nematic liquid cryst., one-dimens. dielectric-flexoelectric deforms. 78—38616
nematic liquid crystal, parallel and cross-like domains due to DC and LF electric fields 79—46557
nematic liquid crystal, total internal reflection, review 80—96445
nematic liquid crystal wedgelike layer 79—60264
nematic liquid crystals, paramagnetic, flexomagnetoelec. effects 80—75158
nematic liquid crystals 79—77495
nematogen, flexoelectricity in isotropic phases 78—63672
p,p′-octyloxycyanobiphenyl, flexoelec. coeff. in nematic phase, thermal depend. 80—79685
4-n-pentyl phenyl-4(4-pentyl benzoyloxy)3-chlorobenzoate, flexoelec. and dielec. relax. behaviour 78—94979
4,n-pentylphenyl (pentylbenzoyloxy)-3-chlorobenzoate, flexoelec. coeff. in nematic phase, thermal depend. 80—79685
smectic liquid crystals, piezoeffects and ferroelectric phenomena 79—32883
smectic mesophases, viscoelastic properties and field instabilities 79—27904
LC-440, flexoelec. charact. of longitudinal domains 79—46570
MBBA, flexoelec. charact. of longitudinal domains 79—46570
PAA, flexoelec. charact. of longitudinal domains 79—46570

flexural strength *see bending strength*

flicker noise *see random noise*

flip-chip devices
see also thin film circuits
No entries

flip-flops
bistable optical devices: an overview 80—58625
digital phase shift for meter calibration 79—44898
electro-optical multivibrator operation, in optical bistable device 80—58674
frequency differences indicated on CRO 79—88919
gas, Stark tunable, mirrorless optical bistability and optical limiting, obs. 80—38056
integrated bistable optical multivibrator using electro-optically controlled directional coupler switches 80—19111
optical, for bistable TV-optical feedback system 80—53354
optical image processing, analogue and digital, feedback, review 80—102639
semiconductor laser two-resonator systems as multivibrators and flip-flops 77—79839

floating zone method (crystal growth) *see zone melting*

floating zone refining *see zone refining*

flocculation
see also colloids; sedimentation
agglomeration, computer simulation *(Japanese)* 78—95706
book, scientific basis of flocculation 78—92520
colloidal suspensions, coagulated, expt. props. of flow curve parameters 77—938
colloidal suspensions, coagulated, flow props., elastic floc model 77—939
colloidal suspensions, coagulated, flow props., energy dissipation in flow units 77—3862
depletion stabilisation and depletion flocculation, theory 80—89534
disperse systems, coagulation, slow, turbulent 78—53259
dispersion, sterically-stabilised, reversible flocculation 78—44411
dissolved Fe, Mn, Al, Cu, Ni, Co and Cd flocculation during estuarine mixing 79—29774
emulsion, oil-in-water, electrolyte flocculation of stabilised potassium 79—43638
estuarine environment, natural suspended matter flocculation and electro-kinetic pot. *(French)* 80—61817

flocculation continued
estuarine particle dynamics, math. model, phys. and chem. processes 77—21793
ferromagnetic particles, mag. flocculation effects during mag. beneficiation 77—77809
fibre charging in electroflocculation, expt. *(Russian)* 79—83515
floc settling velocity, rel. to permeability 79—43636
flocs, physical characts., floc density function and Al floc 79—100454
flocs physical characts., floc strength determ. 79—100455
Graphon, colloidal dispersion in butanol, stability ratio 79—29413
heterosteric stabilization and selective flocculation 79—24836
kaolin, -flint mixtures, polyethylene oxide additive effect on plastic strength after tempering 79—24568
latex+free polymer, dispersion flocculation, equilib. anal. 80—45574
latex particles, kinetics of flocculation under effect of protein 80—11958
α methyl styrene-acrylonitrile, molecular mass determ., solubility studies *(German)* 80—23590
mixed sterically-stabilised dispersions, equilib. aspects of heteroflocculation 80—45570
physical aspects, contact flocculation 79—100457
physical aspects of flocculation process 79—100456
pigment dispersion rheology, kinetic model, expt. results 79—7361
polymer flocculation and stabilisation, concentration effects 80—45569
polymerisation, from emulsion, homogeneous nucleation 79—29354
polystyrene, colloidal dispersion in butanol, stability ratio 79—29413
polystyrene dispersion, sterically-stabilised, reversible flocculation 78—44411
polystyrene latex dispersions, aqueous, in presence of poly(vinyl alcohol), stability, crit. flocculation temp. 78—85207
polystyrene particles flocculation, light scatt. for close range struct. determ. 78—53273
prolate spheroidal primary particles, floc simulation 79—79302
protein, dimensions of disperse forms of cross-linked polyelectrolytes 80—11957
sediments, agglomerated, in N.Chesapeake Bay estuary, microstruct. rel. to electrochemical flocculation 79—53336
sterically stabilised dispersions, critical flocculation temperature, effect of dipolar substituent groups 78—61061
sterically stabilised dispersions, under better-than-theta conditions 77—77810
surface chemistry effects in particle deposition 77—60134
suspension, polymer aided flocculation, shear effect 79—52779
suspensions, sedimentation, review 80—35577
turbulent, mathematical model *(Japanese)* 80—79389
Fe_2O_3, flocculated suspension in ethylene glycol, intrinsic viscosity rel. to shear rate 80—1502
SiO_2-water system, inorg. polymer struct. form., globular crystn. 80—101042
TiO_2 in non-aqueous liquids, effects of mol. architecture of long chain fatty acids on dispersion props. 80—40751

floodlighting
photo flood dimming, thyristor circuit, to reduce heating and extend life of lamps *(German)* 78—29193
urban and rural, large orbiting mirrors for night illumination 80—45632

flow
see also chemically reactive flow; compressible flow; Couette flow; external flows; flow instability; flow measurement; flow through porous media; Knudsen flow; laminar flow; magnetohydrodynamics; multiphase flow; non-Newtonian flow; plasma flow; Poiseuille flow; pulsatile flow; rotational flow; shear flow; stratified flow; supersonic flow; transonic flow
ablation, transient, with time-depend. heat flux, integral solns. 79—60088
accelerating fluid flow, finite-element soln. convergence 77—75873
N.Adriatic Sea, bora driven circulation 78—40556
advection processes, finite difference method, balanced expansion technique 78—77719
axisymmetric potential, past sphere near plane wall, virtual mass of sphere 77—68560
benthic ocean, flow structs. 80—72532
Bernoulli force, coffee cup demonstration, for teachers 79—35482
bifurcating flow in channel with branch 79—55418
bifurcation and nonequilibrium phase transitions of limit cycles and multiperiodic flows in continuous media 78—81937
book, for undergraduates 78—59358
boundary elements method appl. 78—90821
boundary-value problems three-dimensional region elliptic transformation 78—55624
Boussinesq equation, finite element anal. 78—79292
Brownian motion in flowing incompressible fluid, diffusional mass flux, eqns. of motion in large friction limit 79—93043
channel, approx. rectangular cross section, long wave eqns. approx. 77—35111
channel, distributed injection of gas or combustible gas mixture from walls 79—68810
channel, straight (buckled), two-dimens. flow, stability anal. 78—59490
channel, variational methods, book contrib. 79—32456
channel array with interconnections, finite-difference scheme 79—4012
channel flow, analytical soln. 79—32672
channel flow, Navier-Stokes eqns. by semidirect method 79—7413
channel flow, upstream interactions 77—35240
channel flow, wall heat transfer, thick wall case, difference method 79—37129
channel flow of viscous gas, heat exchange 77—80218
channel flow of viscous media, heat transfer 78—1662
channel flow with injection through walls *(Russian)* 78—34197
channel flow with longitudinal press. gradient, friction meas. 77—58792
channel streamlines, second-order-smooth plane sign-alternating contours 79—32678
channel variable-viscosity flow, temp. effects 78—9716
channel with 90° bends, controlled flow expts. 79—32677
channel with rough walls, developed flow, viscosity transfer coeff. soln. *(Russian)* 78—47036
Charles' law, low-speed incompressible gas flow model 77—46982
cholesteric liquid crystal flow between two parallel hot plates in relative motion 80—49097
collapsible tubes, oscills. 78—59488
complex structure flows, numerical simulation, finite element methods 79—49055
condensation, flow of vap. over cylinder, two-phase boundary layer eqns. 79—46306

flow continued
condensation on inner tube wall, laminar film condensation 79—46388
containment dyke, flow over wall 78—71412
continuous medium eqns. of motion, fluid flow, vol. viscosity, Hamilton Jacobi eqn. *(Russian)* 77—46984
continuum mechanics, non-local, at atomic scale 78—12563
curved channel, energy stability limit 77—47094
cylinder array, wall attached and with tip clearance, heat transfer and press. drop 79—14394
cylinder in incompressible flow, finite element anal., wake development and stability 79—14364
cylindrical straight pipe, reorganisation criteria *(French)* 77—75980
dense liquid flow around deforming contour *(Russian)* 78—67178
discrete flow modelling, general discrete time compartmental model 78—1625
dispersion eqn., solns. 79—41649
distorting duct, restoration of turbulent energy, evidence *(French)* 78—90841
diversion cross flow between two parallel channels with lateral slot, axial press. variations 77—88201
diversion cross-flow between two parallel channels communicating by lateral slot 77—88200
drop, spherical or cylindrical, flow produced by uniform translation along cylinder vertical axis *(French)* 78—90967
duct flow, quasi-one-dimensional fluid, boundary conditions on time depend. computations 77—84324
ducts, axisymmetric potential flow 79—14480
ducts, design for specified press. distrib., unbranched, branched ducts 78—9713
ducts, noncircular straight, steady and unsteady flow 77—65795
Earth mantle, two-dimensional flow beneath rigid accreting, lithosphere 79—12102
education, irreversible processes, linear coeff. calc., kinetic and Onsager reciprocity theorems, gas flow appl. 79—9053
electroslag refining, mathematical formulation for EMF, fluid flow, and heat transfer 78—52722
elementary gasdynamics of real fluids, similarity principle 77—75876
enclosure fire, static pressure meas. 78—90871
entrance region flow in a vertical cooled pipe with variable viscosity 79—7409
expansion process, initial value problem, two step difference method *(German)* 78—57877
finite element analysis, Ritz-Galerkin and least squares methods 79—1150
finite element methods for viscous and inviscid incompressible flow 80—17806
finite elements for numerical simulation, error estimates, Stokes problem 79—1151
flames and hot gas flows, similarity criteria *(Italian)* 79—27714
fluid computations using infinitesimal functionals, variational approach 79—14365
fluid flow equations, solns. 78—90817
fluid in tubes, tube vibrs. and flow parameters 78—1492
fluids with memory, simple, thermodynamics of linear flows 78—90812
free liquid surface, nonstationary flow vel. from open vessel 77—80133
free surface, digital simulation by finite element method 78—90819
gas, flow through aperture into vacuum 78—9621
gas, nonsteady flow in parallel pipelines, asymptotic anal. 77—39350
gas diffusion in pipe, wall sticking probability from diffusion penetration meas. 77—51149
gas escape from vessel into vacuum 79—86394
gas flow, Monte Carlo simulation, book contrib. 78—59365
gas flow, one-dimens., non-steady, invariant transformation of eqns. 77—39270
gas flow in pipes, unsteady, nonisothermal, group props. and invariant solns. *(Russian)* 77—31390
gas flow in plane-parallel channel, irreversible thermodynamics *(Russian)* 77—84382
gas flow in smooth and rough channels, heat transfer efficiency comparison 78—51243
gas flows, particle-bearing, probe measurement of electrostatic fields 79—75552
gas motion in channel with cryogenic walls 78—59487
gas nonisothermal stationary motion in pipe anal., solution by iterative mthod 77—89086
gas pipe flow, appl. to press. and density in users of gas wells 79—68811
gas pipe lines, decompression waves following rupture 79—68807
gas to vacuum flow through capillary, geom. of capillary 79—7411
gas turbine exhaust gas diffuser, anal. 77—75884
gas unsteady expansion into nonuniform near-vacuum 77—72265
Gauss-Hertz principle for fluid flow, Poisson eqn. and nonlinear flow 77—84212
gravity current head dynamics, mixing and Kelvin-Helmholtz billows 79—37368
groundwater, calc. by boundary element method 78—94634
groundwater, unsteady flow from tunnel opening, reductive finite element anal. *(Japanese)* 78—96251
groundwater calc. by finite element Galerkin method 78—89320
groundwater flow pathways determ. from satellite altitudes, apparent radiance data appl. 79—16522
groundwater migration during soil freezing, obs. *(Japanese)* 78—88862
groundwater two-dimensional flow digital simulation using finite element method 78—93018
heat exchanger check calculations with parallel/mixed flow, standard expressions 78—67199
heat transfer, separated flow over triangular prisms 78—87339
heat transfer bibliography 79—32503
heavy fluid, surface tension forces effect on unilateral overflow characts. *(Russian)* 77—55416
high Reynolds no. flows, finite element method, book contrib. 79—32442
high viscosity fluids in circular tubes *(German)* 77—15124
homogeneous mixtures, flow, theory *(Russian)* 78—87326
hydraulic equivalent of generalized one-dimensional flow 78—94627
hydrodynamic flow modelling by AC induced electric fields *(German)* 77—57200
hyperbaric Fano flow of Newtonian fluids, device 78—94863
ice, dynamics of late Wurm Arctic Ice Sheet 77—45132
ideal fluid flow, pseudo three-dimens. model, generalisation for stream function *(French)* 77—51025
immiscible liquid replacement, in capillary tube, moving contact line 77—55414

flow continued
implicit divergent difference formulation *(Russian)* 77—51022
incompressible flow, losses due to direction change, investigation 79—18896
incompressible flow, three-dimens. problems 77—84211
incompressible flow influenced by gravitation, hydrodynamic soln. 79—41648
incompressible irrotational axisymmetric flow about body of revolution and the inverse problem 78—94630
incompressible Newtonian fluid flow through sinusoidal tube 80—14816
incompressible three-dimensional internal flows, finite difference soln. of Navier-Stokes eqns. 77—58795
incompressible viscous flow, finite element-anal. by penalty function formulation 79—41651
induced by torsionally oscillating wavy cylinder 79—64772
inertial motion of fluid, shock formation 78—13985
infrasonic flow noise, meas. by H-58 omnidirectional hydrophone 77—47119
instationary, in incompressible micropolar fluids, existence theorems 78—63465
internal viscous flow problems for circle integral methods 77—31387
irrotational symmetric steady flow in channel, soln. by variational method *(French)* 79—18954
isentropic compression, initially uniform medium, time reverse method *(French)* 79—23295
isentropic flow, exact and approx. eqns. 80—1512
isolated liquid volume motion 79—46280
kinetic and basic energy equations *(Bulgarian)* 77—23931
linear equation solution, out-of-core assembly in FORTRAN IV subroutines 79—30213
linear viscoelastic fluids in channel and pipe, unsteady flow 78—79375
liquid, rate calc. *(Russian)* 79—32436
liquid flow blockage in circular tube below freezing point, theory and expt. 78—94830
liquid leveling, numerical soln. 77—14974
liquid of constant mass and vol. during barotropic processes, average press. increase 79—64620
liquid potential flow with elliptical form free boundary, viscosity effect 78—42581
liquid slip inside channel exit 79—10612
local velocity variations in open flow cross sections *(Bulgarian)* 78—18268
lunar lavas, effusion rates and rheology 77—60654
manifolds, flow rates and press. distrib., anal. and expt. 77—51122
Mars fretted terrain, erosional debris flow 78—65537
mass continuity eqn., soln. obtained by change of variable 79—27613
mean residence times in continuous flow systems 78—13984
E.Mediterranean Sea, T conc. and flow rate of Levantine Intermediate Water core 80—17298
micropolar fluids, initial boundary value problems 79—14373
mixing in finite channel 79—90336
modelling, subgrid scale 80—17808
modelling of viscous flow, over mobile base, Navier-Stokes eqns. 78—46921
moisture transfer in annular vertical channels 77—15119
Monte Carlo and Bayesian probability techniques, flow prediction 78—30256
mountain streams, channel roughness coeffs., Chezy-Manning relation 78—49045
multiperiodic flow and limit cycles bifurcation and nonequilibrium phase transitions 78—24759
multiply connected flow field, curvilinear coords. and macro-elements 80—19318
narrow channels, effect of surface induced gradual viscosity increase 78—83488
Navier-Stokes equation solution, smoothing techniques 78—90823
Navier-Stokes initial value problem approx. soln., incompressible boundary-free flow 78—57788
Newtonian creeping flow through periodically constricted tubes 78—42662
Newtonian fluid, secondary flow in cone-and-plate viscometer 78—42692
non-steady fluid actions, derivatives and functional representation 77—62232
nonlinear fluid dynamics, spectral decomposition in advection-diffusion analysis by finite element methods 79—49053
nonlinear fluid motion, order and disorder 78—94629
nonlinear fluid problems, adaptive mesh refinement for finite element anal. 79—49052
nonlinear free surface, anal. by boundary integral eqn. method 78—92850
nonlinear singular perturbation problem on a semi-infinite interval 78—94631
nonstationary flows, slowly varying, calc. via method of characteristics with fixed net *(German)* 79—5515
nonsteady flow through the ports of a hydrodynamic siren 78—94824
nonsteady gas flow through annular pipeline, asymptotic anal. 77—68692
nozzle, vibr. nonequilib. flow, computational methods comparison 79—60073
nucleate boiling in horizontal tube, heat-transfer correl. for refrigerants 79—59911
numerical downstream continuation, sufficiency 79—77053
numerical modelling appls., conf., Southampton, England (July 1977) 78—77285
ocean, current vel. and temp. oscills. with periods to inertial oscills. *(Russian)* 77—33088
ocean, nearshore currents off Long Island rel. to sea level slope 77—45014
ocean currents and temp. field, transformation after passage of tropical cyclone *(Russian)* 77—53069
one-dimens. unsteady non-equilib. flows, method of characts., exponential fitting 78—49648
open channel flow with side discharge, recirculation zone, depth-averaged model 78—63499
oscillations in duct 77—35241
oscillatory flow through axisymmetric pipes and two dimens. channels 78—94823
oscillatory secondary flow, simple fluid between torsionally oscill. cylinders 77—57202
Oseen, unsteady three dimens., applied conc. force 78—67167
outflow from finite container into vacuum *(Russian)* 78—46922

flow continued
paraboloid wholly immersed in infinite inviscid, thrust due to source at point on axis 78—59360
Parana river basin, moisture flow field rel. to water balance *(Russian)* 77—53090
passive scalar, effective long-time diffusivity in Gaussian model fluid flow 79—32439
perforated shell, escape of liquid *(Russian)* 79—77324
periodic flow of simple fluids *(German)* 79—86396
permanent one-dimens. flow, small unsteady perturbations *(French)* 77—51024
pipe, complex quadratic eigenvalue soln. 77—13614
pipe, flow onset *(Russian)* 78—38406
pipe discharging liq. into gas-filled spcae, conditions to run full 77—84326
pipe flow, nonaxisymmetric wave 79—46390
pipe flow, smooth- and rough-walled, turbulence struct. asymptotic similarity 77—35242
pipe flow, thermal entry length problem, numerical soln. *(German)* 78—83494
pipe flow, turbulent, in rough circular pipe, vel. and heat transfer calc. 79—60065
pipe flow with high viscosity, acoustical streaming and thermal effects 77—15122
pipe mode characteristics determination, pipe flow conditions effects *(French)* 78—79246
pipe resistance with ball packing, calc. 77—72356
pipe with fluid flow, sound wave reflection at end *(Japanese)* 79—68457
piped fluids in motion, turbulent flow, direct analytical soln. 78—87393
pipes, variable cross-section, potential axisymmetrical motion 78—59489
potential flow, approx. numerical solns. 78—79293
potential flow, mixed hybrid finite element methods, book contrib. 79—32445
potential flow, transient state, Liesegang rings demonstration 78—63408
potential flow of an ideal liquid past a periodic system of bodies 80—6018
potential flow with directional variation of source mass flow singularity 77—35109
pressure reflection ratio in ducts with flow 77—72354
pressure surge propagation in thick-walled conduits of rectangular cross section 77—35243
quasi-one-dimensional flow equations, exterior differential form represent. *(Japanese)* 78—8243
rarefied gas flow induced by thermal stress, imperfect accommodation at boundary 78—87362
rectangular catchment basin downflow and infiltration, kinematic wave models 78—81235
recycle systems, limiting forms of residence time distribution 78—9620
rewetting temperature in vertical channel coolant flow 79—59117
Reynolds eqn., one-dimensional, with slip boundary conds., perturbation soln. 79—14372
rib-roughened surface, heat transfer and friction 79—46308
rivulets, flowing down vertical solid surface, contact angles, roughness effect 79—27731
rod cluster, recirculating flow due to blockage, finite difference method for temp. 79—3200
sand, flow law, limiting condition 77—54948
secondary flow in channel, determ. from Reynolds eqn. 77—35237
secondary flow in oscill. torus 77—15121
single and two phase flow over rough surfaces, heat transfer effects 78—30297
sinusoidal flow, theoretical study of stability *(French)* 79—27619
slender streams with gravity, outer asymptotic expansions 78—13986
slender streams with gravity, outer asymptotic expansions 78—13987
slender-body theory, at low-Reynolds number 79—3992
slow flow of viscous fluid, inhomogeneity finite deform. 77—7425
slow unsteady flow in axisymmetric tube of varying radius 79—7410
sluice gate problem, fluid-sheet approach 77—7361
sluice gate problems with gravity 77—39349
solar receiver, fluid flow in helical channel *(French)* 79—24910
sound generation and transmission in flow ducts with axial temperature gradients 78—90551
spatial free-boundary flow, boundary-value pattern 79—46279
square plate in oblique airflow, local heat transfer 79—41684
static electrification effects, progress up to 1979 80—69292
steady and non-steady flow through IC engines inlet valve with heat transfer 78—59390
steady flow of incompressible fluid through axisymmetric constriction *(French)* 77—58789
steady flow past cylinder, num. calc. method 77—54956
steady flows, fully stalled, flow computation in two dimens. passages 78—94826
steady plane isochoric flows, acceleration and pressures 78—81845
steady viscous incompressible flow, two dimens., finite element anal. 79—23297
steam condensation in annular duct flow, heat transfer to condensate film 78—94709
Stefan and dam problems, free boundary convexity 78—83356
step-backward flow, with surface discontinuity, flow separation 79—77078
Stoke's problem in velocity pressure formulation, mixed finite element approx. *(French)* 78—86164
Stokes, round smooth body with attached vortex 77—14984
Stokes flow, analogy to incompressible nonviscous plasma flow *(Italian)* 79—19008
Stokes flow, stress-hybrid finite element method 80—99985
Stokes flow due to a Stokeslet in a pipe 78—67268
Stokes flow edge and biharmonic problems, convergence of biorthogonal series 78—81847
Stokes flow separation, local boundary geometry depend. 77—54949
Stokes flow surface integral representation, note 77—54951
Stokes stream function, direct soln. method 80—64
stopped flow kinetic studies, problems concerning mixers and detectors 79—8585
stream function-stress function approach incompressible flow 79—1146
streamline geometry, anholonomic co-ordinate system anal. 80—1510
streamlines in permanent flow, separation and division *(French)* 78—34102
subcritical to supercritical flow transition in channel 77—24024
surface run off models, two dimens., kinematic wave approx. 79—4099
symmetric gas jet, flow computation *(Russian)* 79—37374

flow continued
three dimensional flow in bundle of rods heat exchanger *(Russian)* 78—37408
three dimensional flow in controlled atmosphere, mathematical model *(German)* 79—64636
tidal flow, finite element analysis model, flow in rectangular channel example *(German)* 78—96233
time dependent flow area problems, conservation eqns. in control vol. form. 77—72264
transient and periodic flows through cascades, blade oscillation 78—22318
transient and steady symmetric flow in rectangular cavities 78—46924
transient and unconfined groundwater flow analysis by finite element method 78—92871
transient liquid flow, variable time steps for simulation by method of characteristics 77—65732
tube, symmetrically constricted, upstream separation 79—4083
tubes flow with periodic step changes in diameter, numerical soln. 78—22423
turbine blades, subsonic gas flow integral eqn. method *(Russian)* 79—27662
turbulent homogeneous fields, spectral modelling *(French)* 77—75890
two-dimensional gas flow model, comparison of two methods of computation *(Russian)* 78—59413
two-dimensional torus, first order quasilinear partial differential eqns. *(French)* 78—89345
two-dimensional with singularities, anal. by finite element method 78—90822
unsteady efflux from vessel with time dependent inflow *(German)* 77—35110
unsteady flow in open channels, num. analysis method, teaching aid paper 77—29972
unsteady flow in radial channel, incident shock wave 78—1744
unsteady pipe friction coefficients *(Japanese)* 78—14086
valve connected to pipe, acoustic oscills. from flow 78—59491
variable viscosity channel flow with high heat generation 78—9717
vibrational relaxation, sudden-freezing analysis 77—58806
vibrationally relaxing gas flow, eqns. and transport coeffs. 77—89084
viscogravitational flow in vertical channel, vel. meas. 79—32671
viscous, computational methods of treating nonlinear and special linear problems 77—74226
viscous, downstream boundary conditions 77—35108
viscous, time-dependent, integral representation approach to simulation 80—38375
viscous flow part cylinder, singular perturbation of an Exterior Dirichlet problem 79—12613
viscous fluid unsteady periodic flow, Galerkin finite element method 77—75872
viscous free flowing media in tubes 79—14479
viscous gas, in cylindrical channel of finite length, nonlinear acoustic effects 79—18958
viscous gas flow computation, grid point condensation, high-order schemes 80—36866
viscous incompressible flow, integral eqn., soln. by function-theoretic method 78—69990
viscous incompressible inhomogeneous fluid flow, uniqueness and existence of soln. of initial value problem 77—51019
viscous incompressible Newtonian fluid, hyperbolic flow 77—46983
viscous incompressible Stokes flow, primitive eqns. solns., variational models 79—18857
viscous-gravitational flow in tubes, thermogravitation effect 78—42663
water cooling system, fluid relay responding to flow rate 77—37879
water flow rate through cylindrical channels, determ. 79—90339
Al alloy, sheets, type 7004, asymmetrical solidification structures, fluid flow, in W arc welds 78—84794
^{3}He-^{4}He II, pulsed NMR investig. of ^{3}He flow vel. 77—59171
U isotope separation, influence of flow field struct. in the separation nozzle 78—82498

flow birefringence
aqueous solution charact. relations, transmitted radiation 78—56453
p-aromatic poly(amide hydrazide), dimethyl sulphoxide solvent, dynamic birefringence, conform., viscosity *(Russian)* 78—39525
arterial bifurcations, glass models, pressure meas. 79—25021
atmosphere, boundary layer turbulence, birefringence, ellipsometric meas. 78—69453
cell birefringence change during action pot., Nitellopsis obtusa internodal cell 79—100585
coefficient, polyatomic gases, spherical tensors methods 79—55436
colloidal solution, flow alignment, transition from isotopic to nematic phase 80—84060
critical fluids under flow, large flow birefringence 80—103938
drag reducing polymer solns., dynamical behaviour, mol. conformation and optical props., expt. and rheological model 79—60034
elliptically polarised light, analysis of flow birefringence and extinction angle using U-shaped glass modulator 79—63293
equilibrium birefringence for weakly ionised molecular gas in strong mag. field 80—83881
gas mixtures, conc. depend. 77—84394
gases, heat flow birefringence, improved meas. apparatus 80—10355
gases of linear and symmetric top mols. 77—84393
hydrodynamic boundary conditions and flow birefringence for molecular transport properties 80—45030
liquid, coupling of vel. gradients to molecular orientation, light scatt. and flow birefringence anal. 80—25398
liquids, molecular, depolarised light scatt., flow birefringence and local order 80—45094
liquids under shear, Couette cell for birefringent, viscous and dielectric props. meas. 78—37034
localized, induced behind obstacles in polymer soln. *(French)* 80—93275
macromolecular solution, local flow birefr. in double roller mill *(French)* 78—80315
macromolecule, semirigid, dynamo-optic const. MW depend. *(Russian)* 77—20821
magnetic liq. birefringence and dichroism kinetics, Brownian diffusion *(Russian)* 78—5806
Maxwell stress, deformable surface, general case 78—59501
MBBA, nematic mesophase, struct. of flow in cylindrical capillary 77—7671
measurement using circularly polarised laser beam 79—35813

flow birefringence continued
milling yellow colloidal water soln. flow birefr. props. for US visualisation 80—53585
molecular liqs., Maxwell effect relax. timeand light scatt. line broadening 80—76040
organic homologous series, mol. orientational interaction, Maxwell effect 79—65833
poly-m-phenylene-isophthalamide in dimethylacetamide, flow birefringence *(Russian)* 80—66148
poly-N-vinyl imidazole solution, light scatt., viscosity and dynamic birefringence, mol. wt. obs. *(Russian)* 79—33665
poly-p-aminobenzhydride terephthalamide in dimethyl sulphoxide soln., rheological study 80—43683
polyacrylamides-water-glycerol, streaming birefringence in extensional flow 80—6013
polyatomic gas, plane Couette flow in Knudsen regime, wall induced polarisation 80—19443
polycaprolactam, and copolymers, optical anisotropy and rigidity 80—88959
polycarbonate, secondary flow and stress birefringence patterns in pressure hole 80—64590
polycyclohexanamide, and copolymers, optical anisotropy and rigidity 80—88959
polydichlorophenylsiloxane, cyclolinear, flow birefringence and orientation angles in soln. *(Russian)* 79—65835
polyethylene, melt, shear flow birefringence meas. using cone-and-plate apparatus 77—36197
polyethylene glycol, conformation in liq. state from flow birefringence 78—76423
polyethyleneoxide dilute solns., flow birefringence at high rates 79—81834
polymer flow, birefringence meas. of normal and tangential stresses 77—58625
polymer melt, flow birefringence, in shear flow, rel. to time depend. rheological props. 77—36198
polymer melt, flow birefringence meas., influence of parasitic birefringences 80—88963
polymer melt, flow-induced orientation freezing-in by vitrification, appl. to processing 79—23531
polymer melt in intermittent shear flow, transient birefringence 78—63457
polymer melts, vel. and temp. profiles calc. in cone and plate rheometer 77—54945
polymer solutions, flow birefringence, in time dependent field 80—7323
polymer solutions, high mol. wt., birefringence lines in elongational flow *(French)* 80—25337
polymer solutions, intrinsic stress, birefringence tensor, bead/spring model, freq. depend. 78—42574
polymer solutions, liquid cryst., rheo-optics of shear and elongational flow, quiescent and flow birefringent characts. 80—83773
polymer solutions, rigid-chain, flow birefr., hydrodynamic and dynamic-optical props. 79—24286
polyphenylquinoxaline, soln., conform., equilib. rigidity *(Russian)* 79—55643
polystyrene, melt, shear flow birefringence meas. using cone-and-plate apparatus 77—36197
polystyrene in chlorinated biphenyl, flow birefringence on appl. of step-shear strain 80—25335
polystyrene solution, constitutive models, exptl. tests based on birefringence data 80—100015
polystyrene-Aroclor 1254, streaming birefringence in extensional flow 80—6013
polysytrene melts, stresses and birefringence in intermittent shear flows 80—19308
Raman-Krishnan theory, for simple liq. 79—8116
Rayleigh-Gans-Debye approx. c.f. exact calcs. 77—58255
rigid chain polymer solns., flow birefringence rel. to mol. wt. and chain length *(Russian)* 79—33664
scattered radiation charact. 78—60418
shared polymer melt, birefringence build up and relax. Lodge's rubberlike liquid model 77—54946
superfluids, flow birefringence, depend. on normal-superfluid component relative motion *(Russian)* 80—45032
As-S, melt struct., orientation birefr., viscosity, refr. index, and density 80—84713

flow charts *see flowcharting*

flow control
anaesthesia delivery system, microprocessor controlled 77—44832
artificial heart, automatic control system 77—44841
atrial and/or arterial blood pressure servo control in expt. animals 78—31986
axial flowmeter aperture ratio calc. method *(Dutch)* 78—67285
blood flow/pressure relationships, when to meas. flow or hold flow const. 77—77926
blood pressure or flow control system for unanaesthetised animal 77—48983
blood pump regulation electropneumatic servo operation *(German)* 79—8579
bottom flow control of liquid around sphere with peripheral annular jet *(Russian)* 79—77204
cardiac assist system, intrathoracic, self-sufficient instantaneous haemodynamic control 77—44842
cooling water flow control in continuous casting process, vortex flowmeters 80—64655
diffuser, wide-angled conical, various techniques and characts. 77—51145
drip feed unit microprocessor control development 78—53563
drying, heat and mass transfer, optimal control 78—67006
DTA and scanning calorimetry cell flow control system 79—67303
ferrofluid seal, for blood flow statis during surgery, hydrostatic loading 77—13031
flood prevention device for laboratory procedures 78—179
flow rate convertor, EM, optimal mag. system design 79—77313
fusion reactor, TFTR, T gas injection system transient response 80—102337
gas chromatograph, self-monitoring high-performance instrument 77—36823
gas stripping column, periodically cycled, feedback control, simulations 79—1231
hydrological system, state space modelling and identification 79—79908

flow control continued
jet, axisymmetric, modelling of large eddies, harmonic forcing effect 78—90957
left ventricle prosthesis, pneumatically regulated, in-vitro/in-vivo performance 78—3681
liquid metal flow redistribution using const. inhomogeneous mag. fields 79—77285
liquid metal systems, mechanical or MHD flow rate regulators *(Russian)* 78—75229
liquid oscillations in cavity in solid body, effect on solid body control device motion *(Russian)* 78—14031
mass gas flow stabiliser, expt. 77—75960
molecular flow measurement, precision, and control for single and multi-gas systems 78—70135
multidimensional gas chromatography, advantages of pressure balancing 79—70408
Newtonian and non-Newtonian fluids in flow regulation systems *(German)* 80—1535
non-Newtonian fluid in roll clearance 79—41718
nuclear fuel production, continuous gas flow control simulation *(German)* 80—78416
orifice, cavitating, under reattached flow conditions, noise and vibration characteristics 80—83829
plastic fluids, under aggressive, toxic or radioactive conditions 77—7488
PWR power plant steam dump valve stability anal. 78—50289
RF sputtering gas flow regulation with vacuum press. controller 77—28720
rotametric device with Hall transducer, flow meas., recording and control *(Rumanian)* 80—48826
rotating channel flow, hydraulic control theory 77—56642
separate-bubble cavitation tests, nucleation meas. by Venturi tube *(French)* 79—55402
solar heating and cooling systems, optimisation, feedback control strategies design 79—62127
solar water heating systems, entering water control, by thermal operated mechanical device 79—62138
tank water, digital IC pneumatic bubbler probe system appl. 77—41569
thermal regenerator, with variable mass flow rate, computer model 78—75047
transducer for automated gas flow control 78—59508
urethral occlusive techniques for restoration of urinary continence, development 78—7543
vortex flowmeter for student laboratory use 79—7424
wall reattachment device, loading effects on switching *(Japanese)* 79—10548
H_2O vapour under point corona discharge, microprocessor control for vapour generator and EHD phenomena 80—106852
^{4}He pumping lines, low press. safety value 78—32822
NO, combustion gas sampling system and valves for sampling during engine expansion process 78—24380
O_2 regulator, solid-state, high-temperature 80—57301

flow diagrams *see flowcharting*

flow instability
ablation front, laminar, stability model 78—42680
absolute and convective instabilities, distinction and appl. to interstellar medium 80—98539
aerofoil, dynamic forces acting, subsonic instabilities *(French)* 78—67213
aerofoil, in transonic cascade, choking flutter 77—75885
aerosol impactors, fluid jet impinging upon void 78—63472
air flow near Earth's surface and structures models, perturbations due to flow measuring devices *(Italian)* 80—6180
air flow over water surface instability 79—46290
air-water flow, periodic instability related to continuity waves 78—1716
aircraft dynamics, unsteady airloads prediction, aeroelastic anal. 78—71346
algebraic disturbances in stratified shear flows 79—50766
annular flow, linear stability 78—63497
annulus, tall, vertical, conduction regime of natural convection stability 80—99987
arc, axial flow stability, cathode emission mechanism change effect 78—83638
arterial blood, incompressible flow, stability *(French)* 77—5023
asymptotic stability of unsteady inviscid stratified flows 80—83832
atmosphere, African waves generation 77—37299
atmosphere, dissipative effects, convective instability *(French)* 80—77058
atmosphere, exchange stabilities principle *(French)* 78—88871
atmosphere, finite amplitude Kelvin-Helmholtz billows, evolution 78—81293
atmosphere, preferred mode of Ekman conditional instability of second kind (CISK) 80—72617
atmosphere, Rossby waves stability *(Russian)* 78—44923
atmosphere, stably stratified, resonant parallel shear instability 77—2200
atmosphere, trapeze instability modified by mean shear flow 77—5301
atmosphere, turbulent shearing layers, growth, limiting thickness, dominant eddy scale 78—92955
atmosphere asymmetric jets, instability 80—56537
atmosphere baroclinic instability, numerical modelling *(Russian)* 78—44922
atmosphere shearing instability mechanism model, effect of horizontal differencing 80—26578
atmosphere short internal waves, nonlinear instability *(Russian)* 77—49107
atmosphere unstable baroclinic waves, downstream and upstream development 80—56540
autocatalytic kinetic system, asymmetric multiple steady states 79—86527
autooscillations, azimuthal wave type, rot. Couette flow stability loss 77—75882
axial flow between cylinders, stability to asymmetric disturbances 78—38294
axial flow in annuli, instability 78—55631
axial flow in annulus, numerical stability anal. 78—83363
axisymmetric annular fluid interfaces, stability at zero contact angle 79—94697
axisymmetric convection, stability, solar granulation appl 79—77093
axisymmetric cylinder-flare body, turbulent boundary layer response to lateral divergence 79—90236
axisymmetric jet of magnetisable fluid, stability 80—14835
axisymmetrical wakes, velocity fluctuation probability distrib. 79—98804

flow instability continued
backflow appearance conditions for rot. fluid in channel, stability *(Russian)* 79—86439
baroclinic, in rot. eccentric annulus 77—11197
baroclinic finite amplitude instabilities, book contrib., review 80—19328
baroclinic instabilities of deep fluid 78—79307
baroclinic instability, finite amplitude model, supercriticality 77—17166
baroclinic instability in three-layer fluid 78—16099
baroclinic two-layer flow in channel, instability, geophys. appl. 79—55420
baroclinic unstable wave field modulation 77—33144
Benard convection, in heat conducting media *(German)* 78—79308
Benard convection, stability of horizontal layer of fluid heated from below 80—87767
Benard convective instability, anomalies in sound propag. 77—34975
Benard convective instability threshold, seed particle motion 77—11172
Benard instability, critical fluctuation, slowing, optical and acoustic study 79—77075
Benard instability, depolarised light scatt. from fluid 77—7371
Benard Karman street of vortices generated in asymmetric fluid field *(Italian)* 78—83406
Benard system, convective instability, hydrodynamic fluctuations 77—35143
Benard-Rayleigh convection, finite amplitude, nonlinear stability anal. 79—46311
Benard-Rayleigh problem, experimental system for measurement of equivalent thermal conductivity 80—33711
Benjamin-Ono equation, internal wave solitons, linear stability 80—53802
Bernard convection, and linear fluctuation theory, Markovian processes and irreversibility 80—87766
Bickley's jet, nonparallel effects on stability 79—46356
bifurcation in steady flows of viscous fluid, expt. 78—30267
bifurcation in steady flows of viscous fluid, theory 78—30266
binary alloy indirectional solidification, convective and interfacial instabilities 80—60851
binary fluid layer, heated from below or above, stability anal. 80—33563
binary gas mixtures, convective instabilities in closed vertical cylinder heated from below 79—72880
binary liq. layer, microgravity, thermoconvective stability 80—74866
binary liquid mixture, horizontal layer, surface tension driven instability in presence of Soret effect 80—10227
binary liquid mixture heated from above, convective instability, optical meas. 77—42823
Blasius boundary layer, non-parallel flow stability 79—41668
bluff body, boundary layer separation, control method 79—72881
blunt slender cones at high Mach numbers, stability derivatives, nose bluntness effects 80—19438
boiling, sustained and transient, inlet subcooling effect on flow instabilities 78—94809
boiling in channel, thermally induced two-phase flow instabilities, thermal nonequilib. 78—51240
boiling loop in low-pressure operation of BWR at PNC Japan, stability anal. 78—8894
book, fluid motion stability, part II 77—3811
boundary layer, high viscous eigenstates 77—907
boundary layer, nonstationary, with self-induced press. 78—34164
boundary layer, transition, stability theory 78—38274
boundary layer, transitional, natural convection instabilities effect *(French)* 78—38333
boundary layer flow, laminar, over porous flexible surface, oscillatory flow 80—92107
boundary layer instabilities, Mach number 7 77—65760
boundary layer perturbations, three freq. wave resonance *(Russian)* 79—32538
boundary layer stability, nonlinear effects 78—1636
boundary layer stability of catalytically recombining gas 79—41768
boundary layer transition on a flat plate 79—41676
boundary layer turbulence, burst cycle and drag reduction 77—15003
boundary layers, Navier-Stokes eqns., finite difference model 77—14991
boundary-layer flows, neutral stability calcs., Taylor-series expansion of dispersion relation 80—53744
bounded axial flow, stability of cluster of flexible cylinders 78—38292
Boussinesq fluid, porous media, convective instabilities 77—80213
Boussinesq fluid, Rayleigh-Benard instability in nonreactive binary fluids, results 79—90226
Boussinesq fluids, Rayleigh-Benard instability in nonreactive binary fluids, theory 79—90225
buoyancy boundary layer, supercritical solns. 79—55384
buoyancy effects in entraining turbulent boundary layers: a second-order closure study 80—21815
buoyancy induced flow over inclined heated porous surface, vortex instability 80—33601
buoyancy-thermocapillary convection layers with free surface, energy stability theory 80—87768
BWR Channel, two-phase flow fluctuations and continuity 80—14786
BWR channel stability, problem anal. 79—13387
BWR suppression pool, role of Taylor instability during vent cleaning 79—31046
cambered blade, unsteady aerodynamic force due to nonuniform amplitude gusts 80—19418
cantilever pipes, internal flow induced instabilities 78—63496
capillary jets, flow and instability of jets interacting with surrounding medium 80—6110
capillary stability in circular containers with convex spheroidal bottom 79—32462
cascade static stability and critical velocity *(German)* 78—79306
cavitation bubble, dynamic instability phenomenon, governing eqn. 78—59434
cavitation bubbles, linear stability of growth or collapse, slightly viscous liquid 78—90947
cavity type geometries, self sustaining cavity oscills., review 78—94645
cellular flow wavelength selection, convection and turbulence 80—38380
centrifugal instabilities in finite containers, periodic model 80—106783
centrifugal instabilities of circumferential flow in finite cylinders, nonlinear theory 80—99989
centrifugally stratified helical Couette flow, stability 77—89183
channel, vertical, round, in nonuniform mag. field, steady-state MHD convection 80—33696
channel bottom, kinematic characts. of nonuniform flow, limiting stability, erosion 80—94547

flow instability continued
channel flow, plane, shear rate dependent viscosity, effect on stability *(German)* 80—87809
channel flow stability, influence of nonparallelism 80—83845
channel flow stability, moving boundary, mould filling problem 77—58793
chaotic circular Couette flow, reemergent order 79—27651
chaotic Taylor vortex flow, dynamic instabilities and transition 79—94630
chemically active liquid in horizontal porous bed, convective instability 79—41769
chemically driven convection of dissociating Navier Stokes fluid, instabilities 80—59128
chemically reacting turbulent shear layer between two streams obs. 80—6163
cholesteric liquid crystals, oscillatory convective instabilities, caused by heating from below 80—103239
circular Couette flow, centrifugal instabilities in cylindrical annulus 79—18956
circular semi-infinite liquid jet, harmonically forced at nozzle, instability and wave propagation 79—32618
clumping instability of falling horiz. lattice 77—3866
cocurrent flow, jet initial zone, boundary mixing layer turbulisation, fluctuations 80—1657
cohesionless bottom sediments, limiting stability in turbulent channel flow, erosion 80—94546
cold fluid displacement by hot fluid in porous medium, stability 79—27691
collapse and flutter in thin tubes conveying fluid 77—42919
collapsible tube subjected to external pressure or body forces, unsteady flow 80—14822
collisional drift waves, nonlinear evolution, bifurcations to chaotic state 80—14666
colloidal dispersions, stability in flow fields, trajectory anal. 78—5782
combined convection flow along vertical surface, fluctuating boundary layers 80—96254
combustion front, laminar stability model 78—42680
combustion-driven oscillations in small tube 79—52664
comet tails, Kelvin-Helmholtz instability 80—46493
complex unsteady flow, convective modelling procedure based on quadratic upstream interpolation 79—68694
composite mixture, flow through porous medium, Rayleigh-Taylor instability 80—69912
compressible and incompressible flows, recent theoretical and expt. developments, book 80—1620
compressible axisymmetric jet sound radiation by instability waves 80—69792
compressible boundary layers, unsteady two-dimens. and axisymm. 79—27616
compressible finitely conducting rotating fluid in mag. field, Rayleigh-Taylor instability 80—10228
compressible flow fields, two-dimensional, computation by modified local stability scheme 78—1681
compressible fluid layer through porous medium, thermal instability 80—92114
compressible fluid with free boundary, nonsteady flow 80—6078
compressible fluids, thermal instability in presence of mag. field and rotation 77—89204
compressible time depend. flow, numerical soln., first order local stability scheme 77—72318
compression shock stability in streams of spontaneously condensing vapour 80—28563
computational algorithms construction for hydrodynamic stability problems 80—19329
computational fluid mechanics, book 80—1517
concentration fluctuations, chem. species in unsteady flow, Raman spectrosc. obs. 79—66379
concentric rotating cylinders, temp. gradient effect on stability 80—79263
concentric spheres, unstable motion of viscous fluid *(Russian)* 78—55649
conducting fluid, finite amplitude overstable convection, stability *(German)* 79—41751
conducting fluid, heated below, stability in parallel mag. and gravit. fields 77—7472
conducting fluid in porous box, thermohydromag. stability and onset of convection 77—62308
conducting liq., heated layer in mag. field, convection stability numerical calc. *(Russian)* 78—47053
conducting liq. in mag. field, convective flow stability *(Russian)* 78—47052
conducting liq. layer, surface tension effects, MHD convection stability and thermocapillarity *(Russian)* 78—47054
conducting liquid in crossed electric and mag. fields, instability *(Russian)* 78—26211
conference on dynamical critical phenomena, Geneva (Apr. 1979) 80—27040
conference on nonlinear nonequilibrium statistical mechanics, Kyoto, Japan, (Jul. 78) 79—75441
confined jet, instability modes, visualisation using laser-induced fluoresc. 77—35283
continuity equation, 1-dimens., for unsteady flow 80—82598
convection, instability, crit. slowing, config. inversion acoustic obs. 78—34133
convection, nonlinear, in anisotropic porous media 79—55414
convection, past marginal state, amplitude determ., Landau's conjection 79—55311
convection, time dependent, double diffusive, stability in inclined slot 78—5744
convection, vertical fluid layer 78—14007
convection in fluid layer, turbulence from Rayleigh-Bernard instability 78—42605
convection in Hele-Shaw cell, nonlinear 79—41685
convection in horizontal layer, crit. slowing near Rayleigh-Benard convective instability 79—18889
convection in vibr. layer of fluid, stability limit *(Russian)* 78—46960
convection in vibr. layer of fluid heated from above 79—86424
convection of vertical layer, flow stability, boundary thermal props. effect 78—55644
convection onset, natural, in heated water-saturated porous cylinder 78—59478

flow instability continued
convection roll instability in moderate Prandtl no. fluid 79—50727
convection rolls in inclined layer 77—58674
convection-rolls, two-dimens., stability, temp. depend. viscosity 79—32507
convective flow over horizontal plate, laminar, wave instability 79—32499
convective flow stabilisation in vertical layer by permeable partition 80—14699
convective flows in spherical shell, bifurcation and stability 80—28507
convective heat transfer augocentation thermal entrance regions using thermal instability 79—81887
convective instability, review 77—84226
convective instability and heat transfer in plane Poiseuille flow, viscous dissipation effects 77—31295
convective instability in thermal entrance region of heated channel 77—42812
convective instability of self-similar spherical expansion into vacuum 80—28490
convective instability-MHD instability analogy, AC and DC fields *(Russian)* 77—65807
convective motion due to nonuniformly distributed heat sources *(Russian)* 77—80154
convective motion in fluid due to internal heat sources 79—77091
convective motion in two-dimens. vertical fluid layer with permeable boundaries 77—55086
convective motion of liquid caused by internal heat sources *(Russian)* 79—14390
convective stability of medium containing heavy particles 77—80203
Cosserat fluid, flow stability 78—51203
Cosserat fluid layer heated from below, stability 79—50702
Cosserat fluid with heat transfer, universal stability and uniqueness of unsteady motions 79—50705
Couette cylindrical flow 79—46288
Couette flow, finite amplitude instability 78—13993
Couette flow, instability of longitudinal convection rolls 78—26122
Couette flow, spherical, in thick layer, with revolving inner sphere, stability, review 79—81969
Couette flow, unsteady, Hall effects 77—15127
Couette linearised stability, Green's functions 77—31279
Couette MHD flow instability, cond. liq., finite disturbances effect *(Russian)* 77—65808
Couette modulated circular flow, energy stability 77—31313
Couette modulated flow, stability 77—3810
Couette-Taylor flow, laser Doppler velocimetry obs. of transition to turbulence 80—92163
Coulomb fluid, hydrodynamic instabilities in applied thermal and pot. gradients 77—31397
counter-current two-phase flow, annuli, rod bundles, liq. film behaviour, flooding 78—59452
critical dynamics far from equilibrium 80—27258
critical fluids under shear flow, nonequilib. steady state, renormalisation group approach 80—6026
critical mixtures, shear and critical fluctuations, instantaneous mapping of velocity gradients 80—79420
critical Reynolds number in pipe Poiseuille flow 78—94644
curved free streamline, inviscid stability criterion 78—46937
p-cyanobenzilidene p-octyl oxyaniline, nematic, new type of hydrodynamic instability 77—43142
cylinder array in cross-flow, potential flow interactions 77—51029
cylinder in incompressible flow, finite element anal., wake development and stability 79—14364
cylindrical spaces, liquid filled, natural convection development, transients 80—1563
Czochralski growth, fluid flow changes, depth depend. 77—69981
dam porous media unsteady flow calculation, combined finite element/characteristics methods appl. 78—91012
deep water waves, instabilities, review, book contrib. 80—96274
deformable tubes, unsteady flow of incompressible fluids 80—1682
deformational instability of plane interface with transfer of matter 77—46994
density stratification as catalyst for instability 80—48676
density wave instability in once-through boiling flow system, distrib. parameter model 79—67815
density wave oscillation in boiling channels *(Japanese)* 79—14400
density wave oscillations, linear stability anal. 80—19327
die entry flow, kinematics and stability 79—60026
dielectric liquid, stationary EHD instability, charge carrier mobility temp. induced variations effects 79—77269
dielectric polar liq., electroviscosity rel. to cond. process, EHD model 78—1750
diffusive instabilities in rotating elec. conducting compressible layers 80—38379
digital processing of unsteady periodic signals around oscillating airfoils 80—10340
discharging gas reservoir, thermal instability obs. 77—15016
discontinuity surface stabilisation in magnetisable media by mag. field 80—48806
dissipative open system, dynamical transitions 79—64629
dissociating fluid layer, heated, effect of rot. on Benard convection 79—4020
double diffusive convection, influence of third diffusing component, stability anal. 79—72889
double injection with recombination, EHD linear and nonlinear stability 78—87412
double row of moving vortices near a wall, stability condition *(Italian)* 78—83407
driven mixing layer of circular jet, turbulent static pressure fluctuations spectra 79—77195
dry ice sublimation, Taylor instability 78—90689
duct, horizontal, slugging onset 80—10296
duct with rough walls, turbulent shear flow, stability anal. 80—38496
duct with sudden expsns., asymmetric flows and instabilities 78—22425
dust-gas flows, steady and oscill., mean heat transfer 80—89536
dusty gas, unsteady flow in channel with annular sector cross section 79—77247
dusty viscous flow through a cylinder of elliptic section under time-dependent pressure gradient 79—77248
dusty viscous liquid, laminar flow through tube 79—37399
dusty viscous liquid, unsteady flow through elliptic ducts 79—50703
early nonperiodic transitions in Couette flow 80—59056
Earth asthenosphere, frictionally heated shear flows stability 79—44164
EDH, surface waves, nonlinear stability 79—50810

flow instability continued
EHD, convective instability in dielectric fluid between two coaxial cylinders 80—74994
EHD, liq. dielectrics interface equilib. and instability, curved wall effects *(Russian)* 78—5807
EHD instabilities of nematics, successive transitions 79—77287
EHD mixing and instability induced by colinear fields and conductivity gradients 77—72362
Ekman boundary layer, incompressible, nonlinear stability, numerical soln. 80—38378
Ekman layer, mechanically induced unsteady compressible, theory 80—24033
elastic liquids, stability of plane Poiseuille flow 78—9662
elastic viscous fluid, unsteady flow past infinite porous plate 79—68794
elastico-viscous flow, due to oscillating plate 79—4043
elasticoviscous capillary jet stability 79—90303
elastoplastic flow, stability 79—14442
electrically conducting rarefied gas, oscill. flow, past vertical porous plate, free convection 78—90830
electroconvective instabilities overstable 79—27706
electrodiffusion method for turbulent boundary layers in adverse pressure gradients 80—10321
electrohydrodynamic stability in rigid cylinder, dielectric viscous fluids, eigen wavenumbers 78—59497
electrolytic gas evolution, hydrodynamic instabilities 78—48660
energy stability for the flow between rotating, coaxial disks 80—14712
energy stability of a natural convective flow in a horizontal annular space 79—68815
energy stability of the Eulerian-mean motion in the upper ocean to three-dimensional perturbations 80—92149
ethane, flow continuity in arterial capillary systems in cryogenic heat pipes 80—64536
ethanol-water mixture, saturated, min. film boiling temp. on horiz. stainless steel and Cu surfaces 78—90692
evaporating interface, Marangoni instability 77—908
explosion, spherical, Rayleigh-Taylor instability, boundary between products and surrounding atm. *(Russian)* 78—26135
external noise effect on transition to turbulent convection 80—96263
extragalactic radio sources, relativistic Kelvin-Helmholtz instabilities 78—45419
extruded polymer soln. through capillary, flow instability and electrostatic effects 79—60035
falling film, equivalence of spatial and temporal formulations for linear stability 77—19589
falling film, linear stability theory, applicability 77—23938
falling film, vol. profiles in hydrodynamic stabilisation zone from non-parallel sided slot 80—53748
falling film flow, spatially growing three dimens. wave, annular-froth flow transition 78—14071
FBR, HCDA, 2Z 79—49669
ferrofluid, convective stability of horizontal layer in mag. field *(Russian)* 77—3885
ferroliquid in annular channel, hydromag. stability, thermomagnetic effect 79—94593
ferromagnetic fluid, stability in vertical magnetic field, variational approach *(German)* 80—96316
ferromagnetic fluid rotating about vertical axis, convective instability of layer 79—27698
fibre suspension in water, turbulent jet, analogous behaviour to polymer solns. 78—1732
film, falling, wave struct., linear stability problem and Orr-Sommerfeld eqn., expt. 78—38343
film, liq., flowing down inclined plane with heat transfer, interfacial shear, stability 79—37290
film boiling destabilisation, liq. drop falling onto hot liq. surface 78—94588
film flow, down vertical cylinder, linear hydrodynamic stability 77—19588
film flow down cone, stability, non-parallel flow effect 80—33561
fingers in fluid surfaces, stability to instability transition 80—79260
finite amplitude stability, perturbative and iterative methods 78—38293
finite difference scheme solution of physical instability and weather prediction problems 77—53763
finite-amplitude thermal convection and geostrophic flow in a rotating magnetic system 80—87813
fission reactor fuel-coolant interactions, role of Rayleigh-Taylor flow instabilities 79—17983
fission reactor multiphase systems, expt. and theoretical review of density-wave oscillations 80—18369
fission reactor safety, stability analysis and characts. for two-phase flow eqn. systems with viscous terms 80—59103
flame, laminar, diffusion-thermal instability, boundary-value calc. 78—42682
flame, laminar long wave stability, EHD problem anal. 80—53866
flame, premixed laminar, multiplicity and stability, bifurcation theory applic. 80—16681
flame, round jet type, mass exchange between recirculation zone and outer flows, stabilisation 80—14842
flame front, laminar, hydrodynamic instability, nonlinear integro-differential eqn. 78—51253
flame front, laminar, hydrodynamic instability, numerical solns. 78—51254
flame front instability analysis in compressible ideal medium *(Russian)* 79—27711
flames, unsteady, propagation, numerical modelling 79—64794
flames, vibrating, in tubes, dynamical props. 77—31388
flat insulated plate, supersonic laminar boundary layer stability 79—98749
flat plate, MHD unsteady flow of Maxwell fluid, relaxation parameter 80—24101
flow under a sluice gate, instability 79—86403
flowmeters, stabilizing liquid flows 80—103084
fluctuating boundary layer, at horizontal plate, free and forced convection 78—30277
fluctuating flow, mass transfer near front stagnation point of axisymmetric body 80—48675
fluctuating flow of viscous fluid through a porous medium bounded by a porous plate 80—24088
fluid dynamic transient analysis using ASWR method with staggered meshes *(German)* 80—83176

flow instability continued
fluid flow along heated inclined wall, double diffusive instability 79—55405
fluid flow past sphere, anomalous separation, wake formation 77—51091
fluid in inclined slender slot, stability depend. on rad. and convective boundary conditions 79—86513
fluid interfaces, isothermal and deformable, mass transfer and surface tension, review 80—33564
fluid interfaces, Marangoni instability, dissipative structures and nonlinear kinetics 80—33565
fluid interfaces dynamics and instability, conf., Lyngby, Denmark (May 1978) 80—31423
fluid layer, two-component, Soret effect on thermal instability 77—11185
fluid layer, under general convective boundary conditions 78—94683
fluid layer between co-axial cylinders, instability of natural convection 80—64558
fluid layer heated from below, thermal disturbance propag. 79—32464
fluid motion within ellipsoidal cavity, Coriolis force field rel. to instability regions *(Russian)* 78—81296
fluidisation, stability, lift force effect 77—11259
fluidised bed reactor, solid-circulation model, steady-state multiplicity 79—86524
fluidised beds, heated, operation depend. on temp., investig. 80—19502
fluidised beds, instability waves and bubble origin, two-fluid eqns. 80—92205
foam stability relation to structure, criteria derivation w.r.t. drainage stage 80—69904
forced oscillations of separated shear layer, appl. to cavity flow-tone effects 80—64256
forced standing wave instability in viscous stratified fluid, stratosphere quasibiennial oscill. simulation 79—55396
forced-convection boiling upflow system, instabilities in parallel channel, nonlinear model 77—57724
free conducting shear layers in transverse mag. field *(German)* 77—15132
free convection flow past infinite plate with constant suction and heat sources 79—81868
free convection mass transfer from horizontal surface, electrochemical and holographic interferometric obs. 78—87344
free convective flow in porous medium, longit. vortices, onset, linear stability anal. 78—94813
free oscillation of liquids through a tube with abrupt changes in flow sections, damping ratio calc. 79—77149
free shear layer, compressibility effect on stability 80—33562
free shear layer in viscous critical layer regime, nonlinear stability 80—33576
free shear layer tone phenomenon, probe interface 78—71324
freon-114 boundary layer, stability, press. gradient and heating effects 79—18891
fully developed laminar flow with internal heat generation between horizontal parallel plates, thermal instability 78—90899
fundamental problems in general fluid dynamics and hydromag. dynamo theory, book contrib. 77—84213
galaxies, global instability of polytropic gaseous discs with Toomre density distrib. 80—98725
galaxies, spiral disturbances caused by Kelvin-Helmholtz instability *(Russian)* 77—74142
galaxies flat, with double-peaked rot. curves, spiral struct. generation in gaseous component 80—46679
gas, horizontal layer, oscillatory instability of convective motion 77—54974
gas, rotating, convective instability in gravitational field 79—27642
gas bubble in acoustic field, effect of diffusion on evolution, stability 77—15105
gas bubbles in vibrating liq., localisation and translational motion *(Russian)* 79—14455
gas column response to destabilising boundary condition, nonlinear self excited acoustic oscillations 79—41492
gas filled tube, radial resonances excitation, boundary layer considerations 79—98808
gas flow, plane and helical, restrictions on instabilities 79—98745
gas flow instability, nonlinear stabilization of unstabel acoustical vibrations in a bounded heat-evolving medium 80—6028
gas flow through pipelines, asymptotic anal. 77—72357
gas stream, supersonic, stationary, conical flow about plane wedge and circular cone 80—74912
gas-liquid film interface stability behind slipping shock wave front *(Russian)* 78—55630
gas-liquid pipe flow, stability at slugging onset 77—11237
gasdynamics of explosions, reactive systems, conf., Stockholm, Sweden (Aug. 1977) 79—64690
generalised Benard problem for stratified fluid, rotation effects 80—24031
generalised biharmonic eqn., appl. to hydrodynamic stability using homogeneous boundary conditions 78—90834
Gortler stability at rigid and elastic plane plates *(Russian)* 80—79261
Gortler vortex type perturbation profiles in boundary layers problem on curved surface *(Russian)* 80—74834
granular bed fluidised by gas flow, instability 78—5795
granular bed in conical system, fluidisation 79—90327
graphite-air mixture steady and oscill., mean heat transfer 80—89536
gravitating medium, non-Jeans instability 77—75889
gravitational cylinder, hydrodynamic instabilities 77—78628
gravitational instability in presence of suspended particles and rot. 79—64633
gravitational instability of two fluids in EM field *(Russian)* 77—27602
gravity current head dynamics when advancing over no-slip horizontal surface 80—6036
groundwater, instability of horizontal thermohaline flow in a porous medium layer 79—77239
Hamel flow in channel with permeable walls, stability *(Russian)* 78—34108
Hamel flow through permeable walled channel, stability 79—68679
Hartmann flow, evolution of resonance disturbances 79—90220
Hartmann flow, nonlinear stability, monoharmonic analysis 80—83850
Hartmann flow between nonconducting walls, commencement 79—18962
Hartmann flow in heated channel, thermal instability 77—7461
heat conducting fluid motion, two. temp. theory stability 78—18303
heat conducting simple fluid with memory, nonsteady helical flow 79—81900

flow instability continued
heat exchange component vibrations in liquid and two-phase cross-flow 78—90770
heat flux-flow coupling effects in the stability of vapour generators *(German)* 80—74967
heat transfer and flow instability of natural convection over upward-facing horizontal surfaces 78—94698
heat transfer conditions, free convection-film boiling transition 78—14006
heated turbulent jet, local isotropy and large structs. 80—6116
heavy liquid, free surface equilibrium and stability between charged and bent vertical surfaces 80—48812
Hele-Shaw cell, supercritical convective motions, equilib. stability boundary, porous flow simulation 80—33583
helical flow of gas, steady and inviscid, stability condition 79—32465
helical instabilities of slowly divergent jets 79—68776
helical velocity and magnetic fields, stability 78—73624
helicopter rotor, nonlinear mathematical simulation of unsteady flow past rotor 79—86442
Helmholtz instability of vortex sheet, effect of background vorticity *(Japanese)* 80—10254
high free stream turbulence, turbulent boundary layer characts., fluctuations 80—14674
high subsonic nozzle flows, pressure waves from convection of temp. disturbances 80—6125
highly separated transonic flow, first vel. and RMS vel. fluctuation meas. 79—77166
homeotropic nematic films heated from below, overstability and inverted bifurcation 79—77501
homogeneous isotropic turbulence, Heisenberg's decay eqn., stability anal. 78—30272
horizontal fluid layer, internally heated, heat transfer and stability props. of convection rolls 78—14015
horizontal fluid layer in porous medium, convective instability, critical Rayleigh number 80—64564
horizontal layers with volumetric energy sources, hydrodynamic stability 79—55356
horizontal liquid layer, convective instabilities, single mode dynamics 80—23987
horizontal liquid layer, convective instabilities dynamics 79—4008
horizontal parallel plates, unsteady laminar flow of viscous fluid, Navier-Stokes eqn. solns. 80—1683
horizontal porous layer, with internal heat sources, thermal convection 77—84247
horizontal porous layer with timewise periodic boundary conditions, stability and convection 79—81965
hot layer, hydromagnetic stability, effect of non-uniform elec. cond. 79—14485
hot-wire direction sensitive probe for flow reversal detection in unsteady flow 80—10333
hydraulic jumps with waves, kinematic approach, extension of Rayleigh's method 80—69854
hydrodynamic instabilities, transition to turbulence, Couette flow, vertex streets, Rayleigh-Benard instability 78—83362
hydrodynamic instabilities and turbulence, flow states, examples and meas. methods 80—92116
hydrodynamic instability in isotropic fluids, review, book contrib. 77—89098
hydrodynamic stability, open disc theorem, upper bound of eigenvalues 78—59370
hydrodynamic stability of liquid films and jets, effect of soluble surface-active substances 80—6027
hydrodynamic stability of structurally viscous medium, effect of elastic factor 80—19303
hydrodynamic stability problems, computer program for testing linear stability of vel. profiles 77—54975
hydrofoil profile for accelerating cascade, surface press. distribs. 78—18321
hydromagnetic capillary instability of a liquid jet with an axial flow 80—74990
hydromagnetic convection, thermally driven, in rapidly rotating sphere 80—14548
hydromagnetic convection post marginal state, amplitude determ., Landau's conjecture 79—77286
hydromagnetic flow, stability in temp. field 80—92231
hydromagnetic generalised Benard problem, mag. field character, stratified layer stability 79—77267
hydromagnetic penetration in a rotating fluid 80—14839
hydromagnetic stability of a vortex sheet in compressible, perfectly conducting fluids 80—14831
hydromagnetic stability of compressible fluid 79—32689
hydromagnetic thermal convection instability, effect of suspended particles 79—53709
hydromagnetic thermal instability of rotating fluid layer, Hall current effects 79—27699
hydromagnetic thermal shear flow stability 79—32690
hyperbolic system, simple wave growth, charact. shock instability, fluid appl. *(French)* 77—68623
ideal fluid with free surface, laminar flow instability, reson. surface wave buildup 78—34106
ideal fluids in uniform motion, perturbation effects, fundamental solns. 79—50704
immiscible fluids interface, conditions for viscous displacement in homogeneous porous medium 80—10301
immiscible incompressible fluids, interfacial convective instability, diffusional exchanges, adsorption-desorption processes 80—70504
immiscible liquid horizontal layer, convective stability 77—7392
immiscible liquid two-phase flow in porous media, unstable displacement 80—92213
impinging free shear layers, self sustained oscillations, book contrib., review 80—19466
inclined air layers, heat transfer, secondary instability 80—38397
inclined fluid layer, double diffusive instability, linear stability anal. 80—92113
inclined fluid layer, double diffusive instability, secondary convecting layers 80—92112
inclined open channel, stability of permanent roll waves 80—64629
inclined surfaces, wave instability of laminar mixed convection flow 80—69837
incompressible flow, stability of partially 2-dimens. surfaces 80—28489
incompressible fluid flow along mag. flux tubes, stability 77—53488
incompressible simple fluid with fading memory, stability 80—43741

flow instability continued
incompressible viscoelastic fluid, Rayleigh-Taylor instability 80—79363
incompressible viscous flow, numerical methods *(Chinese)* 77—82395
inertial oscills. in rot. fluid, DuFort-Frankel difference scheme 77—51035
inertial wave and flow struct. for disturbances at low Rossby number 78—22360
infinite vertical fluid layer, transverse rolls transition from conduction regime, power series soln. 79—94611
infinite vertical porous plate, unsteady free convective elastica-viscous flow, viscous dissipation heat 80—24012
ink jet nozzle flow, 100:1 scaled-up model 77—75957
instability and convection in fluid layers: a report on Euromech 106 79—68783
instability zones due to acoustic pulse striking a vortex sheet on a supersonic stream 79—64689
insulating liquid subject to unipolar injection, EHD stability, nonlinear phenomena 78—87411
interface, mechanical, chem. and elec. constraints, review 80—34278
interface, miscible fluids, internal electrohydrodynamic instability in collinear field-cond. gradients 78—26199
interface, stability problem, diffusion, reaction and convection 80—33567
interface between conducting liq. and insulating atm., destabilising effect of alternating mag. field *(French)* 77—62306
interface between immiscible liquids, convection induced by chem. react.-hydrodynamic coupling *(French)* 79—41682
interfacial EHD instability, viscous dominated in polar geometry 80—38501
interfacial EHD instability in normal electric field 77—72363
interfacial instability, mass transfer under high press. 79—94601
interfacial stability with heat and mass transfer, appl. to Rayleigh-Taylor and Kelvin-Helmholtz cases 78—67253
interstellar radiative shocks, thermal instability rel. to maser condensations form. 80—67821
inviscid, rotating, compressible fluid, linear stability 80—92161
inviscid centrifugal instability, Rayleigh's criterion for slowly varying flow 79—59966
inviscid flow over elastic medium, surface waves generation 77—49603
inviscid linearly-sheared parallel flow, characterisation of acoustic disturbances 80—69848
inviscid shear flow over flexible membranes, stability 80—14658
ionosphere turbulent polar cusp, Kelvin-Helmholtz instability in low-energy proton flow 78—96343
isothermal self-similar blast waves, one-dimensional flow and its stability 78—45214
isothermal self-similar blast waves, two-dimensional flow and its stability 78—49307
jet, controlled break-up, droplet prod. by imposed flow perturbation 77—68667
jet, horizontal five-layer, instability 78—79348
jet, liq., breakup, 3rd perturbation Cosserat soln. 79—32615
jet, liq. cylindrical, flowing into pulsating stream of immiscible liq., stability 78—83444
jet, magnetisable liquid, stability 80—83831
jet, round, helical disturbances amplification 77—68655
jet, round, instabilities, cocurrent flow effects 79—60045
jet, supersonic, noise, Reynolds number depend. 78—14053
jet, turbulent, slowly diverging, linear instability modes 77—3856
jet, two-dimensional, effect of density and cond. discontinuities on MHD stability 77—31396
jet exhaust noise, role of shear-layer instability waves 77—47054
jet exhaust noise, shear layer instability effect 78—94791
jet flame, props. and mixing process in recirculation zone 78—91025
jet flows, linear stability 78—38379
jet noise and large scale instability waves, effect of upstream tones 80—69790
jet streaming, planar and cylindrical, instabilities rel. to glassy alloy casting 80—35129
jets, axisymmetric, spatial viscous instability 77—11228
jets, electrically conducting plane and annular, in axial mag. field, instability 77—35247
jets, elliptical, stability and noise 78—38377
jets, nonlinear capillary instability, satellite drop formation and control 80—33646
jets, nonlinear capillary instability, theory 80—33644
jets, nonlinear capilllary instability, behaviour effects before droplet formation 80—33645
jets, quasi-parallel, MHD instability 78—83495
jets, viscous and inviscid, circular and elliptical, breakup and instability 80—48763
jets undergoing mass transfer, break-up effect of nonlinear concentration profiles 80—79371
Jupiter atmosphere zonal flow, baroclinic instabilities 80—31245
Kelvin instability development in unstationary flow 77—7405
Kelvin-Helmholtz billow cloud obs. 77—70730
Kelvin-Helmholtz billows in Loch Ness, rel. to thermocline fine struct. 77—66935
Kelvin-Helmholtz hydromagnetic instability, of streaming layer in unbounded self-gravitational field 80—53878
Kelvin-Helmholtz instability, nonlinear wave packets, amplitude eqn., formulation and soln. 79—46289
Kelvin-Helmholtz instability in stellar winds, influence on turbulent mixing with interstellar gas 80—67701
Kelvin-Helmholtz instability in supersonic and super-Alvenic fluids 80—87816
Kelvin-Helmholtz instability waves and breaking gravity-waves 79—81847
Kelvin-Helmholtz waves, aircraft obs. of life cycle in low level inversion 79—53417
Kutta condition, unsteady 78—90917
laminal flowing liquids, concurrent, in horizontal cylindrical channel 80—79397
laminar, subcrit. Re, nonlinear stability, small disturbance asymptotic theory 77—84223
laminar boundary layer, elongational viscosity and secondary instability 77—23997
laminar boundary layer, heated, stability 78—9626
laminar boundary layer, hydrodynamic stability over flexible surface with constant suction 79—77070
laminar boundary layer, local wall deform. effect on evol. of natural instabilities *(French)* 78—30263

flow instability continued
laminar boundary layer, small amplitude oscillation development, stability characts. 80—48674
laminar boundary layer with separation and reattachment, unsteady 79—59963
laminar boundary layers on concave curved walls, heating effect on stability 77—65745
laminar compressible boundary layers, Taylor-Gortler instability 78—26140
laminar Couette flow in rot. fluid between coaxial cylinders, Taylor instability 77—51066
laminar eddy motion, in flat horizontal fluid layers, resulting from thermal lift *(German)* 77—11171
laminar flame front, diffusion-thermal stability *(Russian)* 77—7477
laminar flame in tube, diffusion-thermal instability 79—86320
laminar flow, gaseous heated channel, temperature-viscosity induced, nuclear rocket reactor appl. 77—18689
laminar flow in 2-D nonlinear perturbations, secondary flow existence *(Russian)* 78—22326
laminar flow in multiple channels 79—90217
laminar jet, axisymmetrical, with and without buoyancy *(German)* 78—83450
laminar natural convection along cylinder, stability 78—1663
laminar to turbulent boundary layer shear flow, three-dimens., stability eqns. 78—38284
laminar to turbulent boundary layer transition prediction, linear stability theory 78—38279
laminar to turbulent transition, laser Doppler velocimetry expt. 79—77073
laminar unsteady viscous plane stagnation flows, incompressible boundary layer, heat transfer 80—1584
laminar vapour flow in film boiling, stability limits 78—90832
laminar wing flow, tip vortex stability 77—19611
large eddies in wake and turbulent boundary layer, vel. fluctuations 80—24036
large wavelength convection rolls low Prandtl number fluids 79—27643
large-scale coherent structures in the wake of axisymmetric bodies, unsteady flow 79—77121
laser velocimetry appl. for unsteady transonic flow meas. 80—10341
linear boundary layer, heated, stability 78—38332
linear induction MHD machines, instability *(Russian)* 78—94841
linear stability of flat Stokes layers 78—13994
liquid, motion instability in vessels of elliptical cross-section *(Russian)* 77—51062
liquid, viscous incompressible, heat transfer and flow stabilisation problem *(Russian)* 77—80165
liquid convective stability in electrostatic field *(Russian)* 77—27601
liquid crystal, EHD instabilities, director relax. time depend. on wave number near WD pt. *(Japanese)* 79—32700
liquid crystal, EHD instabilities, electric Nusselt no. *(Japanese)* 78—18356
liquid crystal, nematic, oscill. convective instabilities 78—9943
liquid crystal, nematic, Poiseuille flow, instabilities 77—1073
liquid crystal, nematic, Poiseuille flow, uniform instability 77—1074
liquid crystal shear flow instability, model eqns. 79—41664
liquid crystals, hydrodynamic instabilities and neutron scattering 79—50990
liquid drop collisions 78—38396
liquid filled spinning spheroids, stability via Liapunov's second method 80—48677
liquid film, gas entrained, combined plane parallel flow, linear and nonlinear stability 80—33655
liquid film, instability on surface of rot. sphere 80—59006
liquid film, laminar, stability, mass exchange and heterogeneous chem. reaction effects 77—75990
liquid film, ripple flow, stat. characts. 77—7408
liquid film condensation on vertical wall, linearised stability anal. 79—55381
liquid film flow down inclined plane, stability, anal. quadrature by differentiation method 79—90219
liquid film on rotating surface, hydrodynamics and heat exchange, entrance section influence, interface frictional forces 79—86433
liquid film on vertical plate, hydrodynamic stabilisation *(Russian)* 77—35117
liquid film stability adjacent to supersonic boundary layer 77—930
liquid flow in-rotating spherical layers, stability and nonuniqueness 79—77135
liquid jet, capillary instability, effect of harmonics 78—71378
liquid jet, instability, one-dimens. Cosserat theory 78—42638
liquid jet satellite droplet formation 77—75953
liquid layer flow down plane, stability *(Russian)* 78—9627
liquid layer flowing down inclined plane, heating and cooling effects on stability 80—79254
liquid layer on inclined plane, stability 79—64631
liquid metal, in elec. field, new surface instability 79—64634
liquid metal electrode, polarographic max. current theory, electrochem. and hydrodynamic instability 79—24750
liquid metal electrode, polarographic max. current theory, hydrodynamic instability 79—24749
liquid metal film in elec. field, instability 79—64780
liquid metal film in electric field, instability *(Russian)* 77—89203
liquid mixture, binary, oscillatory convective instability, thermodynamic anal. 78—94753
liquid sheet, thin, instability and its break-up 77—11205
liquid sheet sprayed by air stream, aerodynamic stability 80—1528
liquid spiral flow, self-oscills., loss of stability 77—80171
liquid system, turbulent flow, drag reduction, neutral stability 77—7380
liquid with fine particles, flow instability 79—64745
liquid-liquid disperse systems, Taylor instabilities rel. to drop fragmentation and thermal explosions 78—71368
liquid-liquid interface, with temp. discontinuity, shock wave generation 78—51197
liquid-liquid system interfacial instability and longitudinal waves 80—33566
liquids in longwave limit, static and dynamic stability, heat diffusion 80—92138
LMFBR, once through boiling flow system, density wave instability 79—9666
LMFBR Na-heated steam generator, flow instability detection by noise anal. 79—97854

flow instability continued
- local mass-transfer coeffs. meas. by holographic interferometry, vortex instability effect 78—75234
- longitudinal instabilities in exit flow from a slit, surface tension origin 79—98684
- longitudinal vel. fluctuations and zero crossings in turbulent flows, maxima universal trends 79—77076
- Lorentz equation derivation for unstable dispersive physical systems 80—83786
- Lorentz model of convective instabilities, 1-D dynamics of particle in pot. well 79—4007
- Lorenz model dynamics for convective instability 80—59007
- low-conductivity liquid, electroconvective stability 80—48814
- lower critical Reynolds number, pipes and annuli, Newtonian and non-Newtonian flow, stability parameter anal. 78—87363
- magnetic field, flow stability of thin layer *(Russian)* 78—9721
- magnetic fluid, thermoconvective instability, with mag. field perturbations 78—94847
- magnetic fluid boundary layer, flow stability 79—64782
- magnetic fluid layer, thermocapillary instability with thermally insulated boundary 80—33595
- magnetic fluid layer in mag. field, instability *(Russian)* 78—26210
- magnetic fluids, instabilities, leading to rupture of continuity 80—59003
- magnetic instabilities of rot. gas in presence of radial gravit. force and azimuthal mag. field 78—47046
- magnetisable liquid, thin layer instability 79—41762
- magnetisable liquid layer, with solid boundaries, convective stability 79—94592
- magnetised fluids, surface instability in nonisothermal layer *(Russian)* 78—94834
- magnetised liquids, separated by thin elastic film, surface stability 79—94727
- magnetizable liq., convective stability depend. on mag. field *(Russian)* 78—47051
- magnetoatmospheric flow, aligned, stratified, compressible, shear 78—26197
- magnetogasdynamic parallel flows, inviscid stability 80—69933
- Magnus method appl. to nonlinear eqns. near stability boundaries *(Russian)* 78—87331
- main-sequence stars envelopes, hydrodynamical instabilities constraints from Li, Be and B obs. 78—93202
- mass gas flow stabiliser, expt. 77—75960
- Maxwell fluid, Rayleigh-Taylor instability 80—33631
- MBBA, electrohydrodynamic instabilities, flow patterns and phase diagrams 77—68915
- MBBA, electrohydrodynamic instabilities, power spectra and autocorrel. in flow transitions 77—68914
- MBBA, liq. crystal, hydrodynamic instabilities and elastic deformation created by US 77—19873
- MBBA, nematic, EHD flow patterns, analogy of instabilities with classical fluid behaviour 77—84335
- MBBA, nematic, EHD instabilities, director-fluctuation autocorrelation and power spectrum 79—41944
- MBBA, nematic, EHD instabilities, director-fluctuation second moment 79—41943
- MBBA, nematic liq. cryst., acoustohydrodynamic instability 77—4036
- MBBA, nematic liq. cryst., dynamic scatt. mode due to electrohydrodynamic instability *(Japanese)* 77—43133
- MBBA, nematic liquid crystals, wave number spectrum of dissipative structures 80—38904
- MBBA nematic crystal, EHD instability, damped oscill. of current and flow patterns 79—46562
- mechanical model using Orr-Sommerfeld eqn. 79—81856
- melting, of substrate into different miscible liq. layer, hydrodynamic instability, heat transfer 78—90695
- metastable flows of water, spontaneous boiling 80—106709
- MHD, mag. liq. in travelling mag. field perturbation development *(Russian)* 78—5811
- MHD, non-isothermal, asymptotic stability anal. 79—97197
- MHD, steady, diffusive instability, rel. to geomagnetism 79—50807
- MHD, unsteady convection in vertical cylinder 79—77271
- MHD channel flow, thermally radiative, stability 78—55695
- MHD convection in rapidly rot. fluid layer, stability, rel. to geomagnetism 79—50808
- MHD convection with rot. spatial heat source, stability 79—4085
- MHD Couette flow stability in presence of mag. field 79—23373
- MHD Couette flow with Hall currents, stability, numerical soln. 77—72360
- MHD equilibria, by secondary bifurcation, rectangular boundary conditions 78—42673
- MHD flow, surface instability of nonisothermal layers 79—77272
- MHD flow in temp. and conc. field 78—30360
- MHD fluid layer, stability in rot. frame of reference with temp. and conc. gradients 77—27600
- MHD fluid layer, thermal instability in transverse field 80—87812
- MHD forced flow through horizontal channel, Hall effect, buoyancy force effects 80—53871
- MHD helical flow, linear and nonlinear stability 79—37408
- MHD instability, helical symmetry, linear theory 79—94729
- MHD laminar flow, suspended particle motion stabiity *(Russian)* 78—5808
- MHD liq. liquid axisymmetric flow in rot. mag. field, stationary instability *(Russian)* 78—5813
- MHD nonlinear stability, perturbations resonant interaction *(Russian)* 78—26204
- MHD oscillatory flow past flat plate, Hall current effects 79—98816
- MHD rotational flow, stability in axial and toroidal mag. fields 77—31394
- MHD rotational stability sufficiency conditions 79—10616
- MHD sausage instability growth time, current-carrying liq. cond. 78—67279
- MHD shear flow stability 78—51244
- MHD shear invisual flow, vortex sheet stability 80—28571
- MHD shift flow, in strong field, of viscous fluid 80—28576
- MHD stability of laminar boundary layer flow along flat plate with transverse mag. field 79—27709
- MHD turbulence stream with 2-dimens. struct. perturbation, shear region momentum transfer *(Russian)* 78—5812
- MHD viscous flow, stability in curved channel 78—9720
- micropolar fluid flow, stability problem 80—14662

flow instability continued
- micropolar fluid layer between rigid boundaries, thermal instability, numerical soln. 79—68692
- micropolar fluid layer subject to magnetic field, thermal instability 80—64585
- micropolar fluid with stretch, convection, appl. to Earth mantle 78—51202
- micropolar fluids, stability of laminar flows between parallel walls 79—1160
- micropolar viscoelastic fluid motions, universal stability 77—11165
- microstretch fluid flow eqns., periodic solns., stability 79—77069
- microstretch fluid motion, stability 79—35566
- miscible non-isothermal vertical displacement stability through homogeneous porous medium *(French)* 80—43771
- mixture, stability conditions and wave speeds 78—30344
- mixture of two fluids at different temp., stability theorem 77—51034
- mode crossing stability, Lagrangian nondegenerate fluid or Vlasov plasma 78—42735
- molten reactor core debris pool, hydrodynamic instabilities and convective mixing 78—8931
- monocomponent gases, convective instabilities in closed vertical cylinder heated from below 79—77072
- moving surface layer, flow structure in front *(German)* 78—1712
- multi-layered liquid films, instability 79—1158
- multicomponent flow through porous media from underground nuclear explosion, flow stability 80—53857
- natural convection, between nonuniformly heated plates, stability 77—58668
- natural convection flow above heat source, instability 79—90252
- natural convection in vertical fluid layer, anal. by linear stability theory 78—34180
- Navy vessel fracture mechanics and flow separation 80—99971
- nebulae ionisation-shock fronts hydrodynamic linear theory 80—17625
- nematic cell, EHD instability limits under action of sinusoidal electric fields 77—47342
- nematic crystal, subjected to elliptical shear, instability 79—1393
- nematic film, phase grating produced by shear flow induced instability 78—9945
- nematic liq. cryst., nonlinearities and fluctuations at hydrodynamic instability threshold 78—87614
- nematic liquid, oscillatory convective instability *(French)* 79—1279
- nematic liquid crystal, hydrodynamic instability phenomena and mechanisms, book contrib. *(French)* 77—84229
- nematic liquid crystal, nonlinar stability of motion, stability criteria *(French)* 77—80410
- nematic liquid crystal, stability 79—32526
- nematic liquid crystal, Williams domain mode, non-linear analysis 77—62472
- nematic liquid crystals, homogeneous instabilities 78—63674
- nematic liquid crystals, nonlinear stability of motion 80—83784
- nematic liquid crystals, oscillatory instabilities in elec. and mag. fields 80—24361
- nematic liquid of positive dielec. anisotropy, electrohydrodynamic instability 77—7659
- nematic-cholesteric binary mixture, EHD instability, phase diagram 78—1980
- nematics, Poiseuille flow instabilities 79—77499
- nematics, thermoconvective instabilities 79—77500
- neutral stability curves, analytic approach, book contrib. 80—1529
- non-equilibrium thermodynamics of hydrodynamic instabilities 80—42184
- non-linear hydrodynamic stability, unipolar injection of insulating liquid, Galerkin method 80—74835
- non-Newtonian fluid, convection, stationary, vibr. instability 79—94683
- non-Newtonian fluid, Hartmann flow, hydrodynamic stability, viscous core effects *(Russian)* 77—27611
- non-Newtonian fluid, hydrodynamic stability of free convection in vertical layer 78—59430
- non-Newtonian fluid, rot. liq. film, free surface instability 79—37294
- non-Newtonian liquid, convective stability, energy method 80—38455
- non-Newtonian plane jet, stability to infinitely small perturbations 78—51211
- non-Newtonian Poiseuille flow in cooled channel, hydrodynamic stability 79—14441
- non-Newtonian third grade fluids, thermodynamics and stability 80—33638
- nonequilibrium thermally-induced flow fluctuations 80—14661
- noninertial deformable rot. coordinate system, unsteady gasdynamic flow eqns. 80—43726
- nonisothermal magnetisable fluid, thermal convective stability, modulated mag. field effects 80—64646
- nonlinear axisymmetric flow between concentric rot. spheres, numerical anal. 80—19412
- nonlinear convection in elasticoviscous layer heated from below 77—68634
- nonlinear effects in laminar stability theory *(French)* 80—103012
- nonlinear focusing and Kelvin-Helmholtz instability 80—83785
- nonlinear instabilities, filtering in fluid dynamic eqns. 79—41667
- nonlinear interactions in turbulent and convective flows, barotropic and baroclinic instability 79—98706
- nonlinear Rayleigh-Taylor stability with mass and heat transfer 79—90224
- nonlinear stability of boundary layers for disturbances of various sizes 80—6025
- nonlinear stability of motion of viscous liquid between concentric rotating cylinders 79—14409
- nonlinear viscoelastic fluid, steady shearing flow instability 79—32461
- nonlinear wave propagation and unsteady transonic flow, variational formulations 78—55660
- nonlinear waves and solitons, stability in three dimens. 79—97211
- nonNewtonian flow between rotating porous cylinders, stability wide gap case 79—68761
- nonparallel stability of two-dimensional nonuniformly heated boundary-layer flows 80—38401
- nonsteady flow in one-dimens. pipe systems, boundary condition based anal. 80—1685
- nonsteady one-dimensional liquid flow, analytic method calcs. 80—59009
- nonsteady two-dimens. transonic flow, numerical solns., shock waves 80—53808
- nonuniformly heated horizontal surface, convection and Rayleigh-Benard instability 77—39296
- Norwegian Current, evidence for baroclinic instability 77—60385

flow instability continued
  nuclear reactor, AGR, helical monotube vapour generator, density wave instability, experimental-stochastic and theoretical anal. 80—47539
  oblique instability of periodic waves in shallow water 78—63418
  ocean, exptl. study of nonlinear baroclinic instability and mode selection in large basin 80—85669
  ocean, hydrodynamic friction layer instability rel. to Langmuir circulation 78—92840
  ocean, stably stratified, convective instability 77—86913
  ocean, turbulence generation by flow instability *(Russian)* 78—16022
  ocean circulation modelling expts., baroclinic instabilities obs. 79—57952
  ocean internal short-period waves generation by shear flow instability 79—2273
  ocean large-scale density anomalies, non-linear evolution and instability *(Russian)* 79—16479
  ocean near-surface mixing layer, Kelvin-Helmholtz instability in stable heating conditions 78—85568
  ocean solitary Rossby waves over variable relief, analytical theory rel. to stability 80—101371
  ocean solitary Rossby waves over variable relief, numerical expts. rel. to stability 80—101372
  ocean surf zone, hydrodynamic instability as mechanism for horizontal gyres form. 79—2244
  ocean upper layer, hydrodynamic instability rel. to equilib. Langmuir circulation model 80—101381
  oil, multi-dimens. simulation of flow nonuniformities in fissured porous media 80—28559
  oil shale retort dispersion, effect of particle size distrib. and flow nonuniformities 80—28560
  oil shale retort flow nonuniformities c.f. numerical predictions 80—28492
  oil-water interface, chem. and hydrodynamic instabilities *(French)* 80—7789
  open channel thermally stratified flow, eddy diffusivity buoyancy effects, obs. 78—90904
  Orr-Sommerfeld eqn., continuous spectrum and eigenfunctions 78—67176
  Orr-Sommerfeld eqn. for laminar flow stability, accurate soln., Blasius profile neutral curve 80—33559
  Orr-Sommerfeld flow problems, soln. using factorisation method, book contrib. 80—1688
  Orr-Sommerfeld problem, approx. to eigenvalue reln. 79—3995
  Orr-Sommerfeld problem, orthogonal expansions 77—58646
  oscillating two-stream instability, exact soln. 80—92115
  oscillations in water outflow from collapsible tube 77—89202
  oscillatory airfoil, vel. and incidence large amplitude fluctuations, unsteady flow features 80—23986
  oscillatory flow around the edge of a flat plate 79—72879
  oscillatory flow of electrically conducting fluid past porous plate, free convection currents 79—55428
  oscillatory flow past infinite, porous plate, free convection current effects 78—14079
  overstability in horizontal layer of binary liq. mixture with Soret effect 80—106782
  PAA, nonlinear soft mode at Rayleigh-Benard instability, neutron cond. spectrosc. obs. 80—79266
  panels in incompressible flow, nonlinear stability 78—13992
  parallel channel forced convection boiling upflow system, instabilities 80—9327
  parallel compressible flows, stability inviscid theory 77—72277
  parallel flow, role of negative energy waves in some instabilities 79—59967
  parallel flow between concentric cylinders, stability, heat transfer 77—11190
  parallel flow in concentric annulus, linear stability 77—80142
  parallel flow stability, numerical calc. 79—32460
  parallel flows, stability anal. by finite element anal. 79—81843
  parallel hydrodynamic flow, stability against wall disturbances *(German)* 77—14977
  parallel viscous compressible flows, linearised disturbances, asymptotic anal. 79—27618
  parametric instabilities in internal gravity waves 77—19615
  partially ionised fluid, thermal instability, compressibility and collisional effects 78—55693
  particle array, falling through fluid, clumping instability 77—42906
  particulate sedimentation, stability, two-dimens. anal. 80—69768
  perfect gas unsteady flow, sonic discontinuity propag. 77—14989
  periodic helical flow in pipe, linear stability, Hermitian forms and eigenvalue bounds 79—37401
  periodic MHD oscillations, stability, perturbation theory 80—83858
  periodic secondary motions in plane channel, num. soln. method 77—55092
  permeable boundary, stability of flow, velocity slip effects 77—68571
  permeable surface, injection, laminar to turbulent transition, heat and mass transfer 78—83361
  perturbations at interface between two liqs. 79—64630
  pipe, circular, time-periodic flow stability 77—84225
  pipe, turbulent velocity profiles from stability criteria 79—50717
  pipe, unstable phase following turbulent flow past sudden enlargement *(French)* 79—1157
  pipe flow, finite amplitude stability theory 78—63498
  pipe Poiseuille flow, hydrodynamic stability including viscous dissipation, temp. fluctuation *(French)* 79—32466
  pipelines with liquid, stability and oscillations 80—14612
  pipes with regular artificial wall roughness, laminar flow stability, turbulence 79—98803
  plane channel flow, subcrit. turbulence transition 80—106787
  plane channel with parallel walls, turbulent flow stability *(Russian)* 79—37295
  plane Couette flow, critical Reynolds number 79—81931
  plane Couette flow, finite amplitude, instability shear layer parallel flow, cellular motion 80—1601
  plane Couette flow, stability, Orr-Sommerfeld eqn. exact soln. 79—98685
  plane Couette flow hydrodynamic stability rel. to finite amplitude perturb. *(Russian)* 79—37291
  plane interface between two viscoelastic superposed cond. fluids, instability in mag. field 80—1694
  plane jet, stability and autooscillations from channel anal. 80—100018
  plane parallel incompressible inviscid, Lyapunov functionals in linear stability 77—14990
  plane periodic flow, post-critical regime construction *(Russian)* 78—34109

flow instability continued
  plane plate with roughness element, nonsteady flow, numerical calc. *(German)* 78—94663
  plane Poiseuille flow, instability caused by nonlinear, nonperiodic and three-dimensional disturbance 78—38291
  plane Poiseuille flow, nonlinear stability by high order amplitude expansions 80—74975
  plane Poiseuille flow, stability numerical computation 79—10549
  plane Poiseuille flow in channel, stability, orthogonal expansion method *(Russian)* 78—5730
  plane turbulent jet, outer intermittent turbulent motion structural characts. 79—77208
  plane two-layer flows, effect of fluid microstructure on stability 79—77212
  plane wall jet, nonlinear stability *(Russian)* 80—24066
  plane-parallel flow instability with coordinate depend. viscosity *(Russian)* 78—22328
  plasma flame, with rectangular cross section, prod. by nozzle *(Japanese)* 78—47108
  plasma focus, pinch column form. and stability 80—96380
  plastic non-Newtonian fluids in circular pipes, laminar flow stability loss 78—79342
  plate, flat, attached subsonic and transonic turbulent boundary layers, press. fluctuations effect 79—94642
  point vortices in regular polygons, reson. instability of steady states 77—62262
  Poiseuille channel flow, finite amplitude, instability shear layer parallel flow, cellular motion 80—1601
  Poiseuille flow, effect of external forcing on stability 78—22327
  Poiseuille flow, horizontal plane, heated from below, axial heat cond. effects on thermal instability 77—42825
  Poiseuille flow, nonlinear Tolmin-Schlichting waves, self-excited oscillation stability 79—90263
  Poiseuille flow, plane, horiz., rot., stability, effect of Coriolis force 78—67203
  Poiseuille flow, rot. modified, energy stability limit 78—30268
  Poiseuille flow, subcrit. Re, nonlinear stability, finite axisymmetric disturbances 77—84224
  Poiseuille flow, tube elasticity effect on stability 77—72278
  Poiseuille flow in circular pipe, linear stability 80—79399
  Poiseuille flow in elastic channel 78—90835
  Poiseuille flow in elastic tubes, stability to axisymm. disturbances 77—65796
  Poiseuille flow in elliptic pipe 78—71397
  Poiseuille flow in elliptic pipe with large aspect ratio 78—1745
  Poiseuille flow with flexible boundaries, MHD stability 77—11277
  Poiseuille pipe flow, hydrodynamic stability *(French)* 78—18347
  Poiseuille pipe flow linear instability 79—90223
  Poiseuille pipe flow of incompressible second order fluid *(German)* 78—87395
  Poiseulle flow, thermally stratified plane, linear differential eqn., asymptotic fundamental system construct. *(German)* 77—902
  Poisseuille pipe flow transitional behaviour, effect of inlet flow disturbances 79—90216
  polyethylene melt, oscillatory flow through capillary 80—103046
  polymer soln., buoyancy-driven instability 78—10206
  polymer solns., unstable flow, reservoir to capillary, jet instability onset and flow patterns, obs. 78—87364
  polymer solution, dil., rotating Couette flow, elongational viscosity and stability 79—27669
  polymer solution, flow singularities, polymer chain extension and hydrodynamic instabilities 78—71376
  polymer solution, highly elastic, vel. meas. in die entry region of capillary rheometer 80—99988
  polymer solution, stability in Couette flow *(German)* 77—47047
  polymer solution, turbulent jet behaviour 78—1732
  polymer solution, viscoelastic, in annular die entry, upstream flow characts., instability onset 79—60036
  polymeric liquids in pipes, non-steady two-phase stratified laminar flow 79—81832
  porous cermet, heat transfer and stability for moving evaporating coolant 80—64563
  potential, unsteady flow around arbitrary system of K profiles 80—14660
  potential subsonic and transonic cascade flow, stability anal., finite area methods 80—48737
  power law non-Newtonian liquid, stability of laminar boundary layer 77—55048
  Prandtl-Meyer expansion with access of heat *(German)* 79—86484
  propane-air flame, premixed turbulent, three region model 79—100383
  propane-O_2 system with Ar, N_2 diluents, detonation wave instabilities 78—5762
  pseudo-periodic flow in U-shaped tube, stability anal. 79—98809
  pulsating air bubbles in water, stability using optoelectrical method *(German)* 77—27578
  radial wall jet, linear stability anal. 80—19458
  radiative thermal instabilities in relativistic flows, rel. to compact synchrotron sources variability 80—105369
  radio sources, extragalactic, pinching and fluting modes rel. to jets configuration and propag. 80—31374
  rapidly rotating fluid bodies, struct. and stability in general relativity beyond ang. vel. peak 79—101139
  Rayleigh method, modification for nonlinear and three-dimens. problems 77—84227
  Rayleigh stability of shear flow in relaxing media 77—80141
  Rayleigh-Benard convection, crit. effects 78—71328
  Rayleigh-Benard convection, induced, pretransitional 79—55374
  Rayleigh-Benard convection, randomly forced, initial value problem 80—79314
  Rayleigh-Benard convection, turbulence and intermittency, expt. 80—99998
  Rayleigh-Benard instability, n-component reactive fluids 80—69945
  Rayleigh-Benard instability, reactive binary fluids 80—69944
  Rayleigh-Benard instability, transition to turbulence 80—28491
  Rayleigh-Benard instability, vel. field, transition to turbulence 80—6029
  Rayleigh-Benard instability and the evolution of turbulence 79—77074
  Rayleigh-Benard instability in p-azoxyanisole, fluctuations, real time obs. by neutron scatt. 80—59390
  Rayleigh-Benard system, turbulence near onset of convection 80—48686
  Rayleigh-Benard-Marangoni instability, exptl. results 80—14700
  Rayleigh-Bernard convection, forced phase diffusion 80—103019

flow instability continued
- Rayleigh-Jeffreys convective stability problem with temp. and salinity gradients *(Russian)* 78—14012
- Rayleigh-Taylor, general oblique mag. field effect 79—94591
- Rayleigh-Taylor instability, method of generalised coords. 78—65771
- Rayleigh-Taylor instability, thermal cond. and compressibility effects 80—79262
- Rayleigh-Taylor instability, turbulent stage anal. 79—41669
- Rayleigh-Taylor instability, two superposed cond. fluids, with suspended particles 78—87399
- Rayleigh-Taylor instability, unstable normal mode 78—26100
- Rayleigh-Taylor instability at interface of two heavy liquids 80—14663
- Rayleigh-Taylor instability in inverted shallow water 79—64635
- Rayleigh-Taylor instability in oscillating mag. field 80—59008
- Rayleigh-Taylor instability in presence of rot. 77—19591
- Rayleigh-Taylor instability in presence of rotation 80—53749
- Rayleigh-Taylor instability of a conducting viscous fluid in a magnetic field 80—43785
- Rayleigh-Taylor instability of viscous fluids, initial value problem 79—1159
- Rayleigh-Taylor modes in fluid accelerated by radn. pressure 77—51133
- Rayleigh-Taylor stability of radiation-supported surfaces and slabs, appl. to QSO clouds 77—53697
- reactor two phase flow instability, classification by density wave oscill. model 79—63731
- reactors, chem., relaxation oscills. 79—39120
- reattaching laminar and turbulent separated flow, three-dimens. heat and mass transfer 77—65759
- rectangular pipe with large aspect ratio, plane Poiseuille flow nonlinear instability 78—59492
- rectilinear flow, pressure error upper and lower bounds with pressure gradient 80—6010
- regime of combined buoyancy mode driven flow, stability 78—18302
- relativistic fluids flow through channels, self similar solns. and stability rel. to radio galaxies 80—62006
- relaxation autooscillations of granular bed 78—59472
- relaxing gas in neighbourhood of equilib. position, flow stability 79—77071
- resonance tube, jet flow and heating, unsteady complex shock struct. 80—6115
- ripple and dune formation on erodible bed by low Froude number flow 80—106784
- rivers, meandering, braiding, sediment transport mechanisms 78—36212
- rivulets, static, moving contact lines and rivulet instabilities 80—79264
- roll-cell instability, rot. laminar and turbulent channel flows 77—946
- roll-wave stability on thin laminar flow down inclined plane wall 80—28488
- Rossby small amplitude wave stability in channel 77—56684
- Rossby wave flow, finite-amplitude stability 79—16579
- Rossby wave interactions and stability in rot. two-layer fluid on β-plane 80—10257
- Rossby waves, barotropic, instabilities 78—55654
- Rossby waves in parallel flow, nonlinear critical level evolution 79—27621
- Rossby waves in rot. two-layer fluid on β-plane, reson. interactions 79—77145
- rotating Boussinesq viscous fluid, inertial instability, appl. to atm. 80—90131
- rotating conducting fluid in horizontal mag. field, Rayleigh instability 77—15126
- rotating cylinder flow, effect of thermal diffusion on flow stability 78—18308
- rotating cylindrical annulus, transition to Taylor vortices, Ekman layers 80—87776
- rotating disc boundary layer transition regime, spiral vortices 80—59040
- rotating flow, nonstationary eqns. soln., appl. to flow between discs 80—28516
- rotating flow, numerical simulation methods, review 80—19411
- rotating fluid, spin-up and spin-down, vel. meas., stability 77—11196
- rotating fluids, convective modes and convective stability 79—16818
- rotating gaseous masses, secular stability and points of bifurcation 77—42843
- rotating horizontal fluid layer, thermal instability 78—63438
- rotating liquid shell, Rayleigh-Taylor stability 79—14381
- rotating self-gravitating fluid sphere with uniform distrib. of heat sources, MHD convective instability 77—29264
- rotating square cavity, laminar flow, flow problems with body forces soln. 79—68715
- rotating stratified flow, in horizontal mag. field, stability 78—67246
- rotating stratified fluid, hydromagnetic stability 78—55692
- rotating stratified fluid, parallel shear flow, baroclinic and barotropic instability 80—98328
- rotating superposed fluids, MHD instability, flow through porous medium 78—14089
- rotating two-layer fluid, barotropic and baroclinic Rossby waves interactions and instabilities 79—57955
- rotating viscoelastic fluid layer heated from below, MHD convective instability 77—58800
- rotational symmetric flow between concentric spheres *(German)* 80—1609
- rotatory Couette flow, amplitude steady secondary flow past marginal state, Landau's conjecture 79—77128
- salt fingers, rot. effects 79—50767
- saturated porous layer, sudden temp. rise, stability, linear and energy methods, convection 80—74972
- Schwarzschild black hole stationary spherical accretion, stability 80—51800
- secondary flows and stability study of rotating spherical layers at arbitrary Rossby numbers 79—18899
- secondary flows of viscous liquid in unbounded space *(Russian)* 77—35119
- sedimentation, settling instability, horizontally homogeneous suspension 78—42652
- self-gravitating fluid column, modulational instability 80—85848
- self-similar spherical expansion, Rayleigh-Taylor instability., astrophysical appls. 79—8823
- semi-infinite porous medium bounded by horizontal surface, mixed convective flow, vortex instability 80—79304
- separation flow over a disc, accel. influence 79—86443
- separation of flow along line of regular surface *(French)* 79—41661
- sessile drops, equilib., stability 77—31376

flow instability continued
- shaped charge jet stability 78—13919
- shear flow, non-parallel, stability and mixing 79—10547
- shear flow, thermal, stability 78—34110
- shear flow instability problem, Howard's semi-circle reduction 78—90833
- shear flow stability, modified Tietjens function for asymptotic anal. 77—65733
- shear flows, heterogeneous, infinitesimal stability 78—30262
- shear flows, inviscid and parallel, instability 80—79265
- shear instability, vortex nutation, amplitude oscill. 78—51171
- shear layer, instability and edgetone 78—94672
- shear layer, thermally stratified, turbulence structure and stability *(Japanese)* 79—41731
- shear layer, weakly nonlinear stability 77—35118
- shear layer instability noise produced by various jet nozzle configurations 80—69791
- shear layer instability of compressible fluid 77—80177
- shear-induced instabilities in stratified fluids, modal struct. 77—68662
- shell, uniformly imploded ablatively driven, fluid instabilities 80—92111
- shock tube wall boundary layer instability, transition evolution 79—64642
- shock waves, converging, stability calcs. by computer 79—41715
- shock waves, metagalactic, thermal instability due to rapid cooling 80—46678
- shock waves, stability of an ionizing shock wave in an electromagnetic field 80—6076
- shock waves instability in a relaxing medium 80—100013
- shock waves of arbitrary strength, with viscosity and heat conduction, stability 80—59076
- silicone oil, Newtonian, vel. meas. in die entry region of capillary rheometer 80—99988
- simple fluid, energy stability method 79—27629
- singularities in unsteady boundary layers 80—14651
- sinusoidal flow, stability in circular tube *(French)* 79—23363
- slender bodies and wings, vortex asymmetries 78—9644
- slender body, axisymmetric wake, transition and instability 79—32524
- slow liquid combustion, evaporation and combustion front stability 80—53884
- slowly spreading jets, MHD instability 80—87818
- slowly varying wavetrains, dissipation and dispersion effects 80—64573
- slug formation, wave instability effects 78—14085
- small body in nonuniform flow 79—18873
- small inviscid disturbance, evolution to marginally unstable stratified shear flow 78—83453
- smectic mesophases, viscoelastic properties and field instabilities 79—27904
- smectic-A liquid crystals, oscillatory convective instabilities, caused by heating from below 80—103239
- smooth circular pipe, turbulent wall flows, velocity fluctuation probability distrib. 79—98804
- solar atmosphere, penetrative instabilities theory in presence of thermal dissipation 80—109406
- solid body progressive motions in liquid, stability *(Russian)* 77—31281
- solid particle bed fluidisation characts. from hydrodynamic instability 80—6140
- solid-gas flow, fluctuation damping 80—19478
- soluble flat surface in turbulent flow 80—14676
- solution branching in wavy flow problem of viscous liquid with free boundary 80—14760
- Soret driven instability, secondary effects 80—6062
- Soret driven instability, transient and steady state behaviour, analogy with laser instability 79—55413
- Soret-driven convective instability in two-component liq. layer heated from below, phase transition picture 79—77110
- Soret-driven convective instability with rotation 78—46968
- spatially periodic convective flow, stability and fluctuations 80—19394
- spherical Couette flows, loss of stability between two rotating spheres 80—1527
- spherical gas bubble in unsteady viscous flow, unsteady boundary layer 79—55357
- spherical rot. fluid shell with non-uniform heating, thermal stability 77—31314
- spherical symmetry stability in general relativity, virial theorem consequences 79—21593
- spherically symmetric flow stability 78—83456
- spinning, isothermal, of Newtonian and viscoelastic liq., draw reson. instability 79—60027
- spiral flow between coaxial cylinders, branching and stability loss 80—19406
- spiral modes in gaseous cylindrical systems 79—66914
- spiral vortex flow characteristics at high Taylor numbers 80—1598
- spiral vortex flow stability, experimental investigation 80—79327
- spontaneous fluctuations, far from equilib. 78—42590
- spray nozzles, stability of thin, radially moving liquid sheets 78—71381
- stability of viscous flow between rotating concentric cylinders with an axial flow 79—59989
- stabilization of flows through porous media 79—72944
- stable surface chemical reactions, interfacial hydrodynamic instability 80—66874
- stagnation counterflow, interface perturbations growth and decay 78—30264
- stagnation flow, nonlinear stability 78—90831
- stagnation flow, stability to three-dimens. disturbances 78—30265
- stagnation flow, two-dimens., stability, longit. vortices, perturbation method 78—75146
- steady flows, stability criteria of perfect incompressible fluid with a free boundary 80—69767
- steady state flow in coaxial channel, with scanning mag. field, approx. model *(Russian)* 77—3877
- steady-state MHD convection in a vertical annular duct in a radial magnetic field 80—48809
- steam generator, Na heated, dynamic instabilities 78—17281
- steam generator channel, once-through, flow dynamic stability, influence of press. loss components *(Czech)* 77—3148
- steam jet condensation, dynamical pressure pulse effects 78—94549
- steam-generating channel hydraulic characts., two phase flow instability effects 79—90333
- steam-generating tube, bubble/plug flow boiling regimes, elevated press., drift vel. and void fraction determs. 78—87379
- stellar atmosphere, thermal-convective instability, finite Larmor radius effect 78—32438

flow instability continued
stellar penetrative atmosphere, instabilities 79—84783
Stewartson layer, stability in a rapidly rot. compressible fluid 78—46979
Stokes' problem for vertical infinite plate with variable temp. 79—23301
Stokes layer, centrifugal instability and asymmetric disturbances 79—98686
Stokes layer centrifugal instability, nonlinear theory 77—31280
Stokes wave, high wavenumber instabilities 79—81907
straight alluvial streams, unsteady flow, dune modification 79—62535
stratified boundary layers, stability calc., numerical integration *(German)* 80—53834
stratified flow, boundary conditions imposed on instability 79—55404
stratified flow, two-layer, entrainment at interface *(Japanese)* 78—9671
stratified flow of two fluids between vertical planes, interface stability *(French)* 78—38382
stratified fluid, duct, equilibrium breakdown, thermosiphon work *(French)* 80—59114
stratified fluid, sugar soln., cellular convection, effect of inclination of heated wall 77—39323
stratified fluid in sheared motion, over-reflection instabilities 79—60048
stratified fluid layer, heated from below, thermal instability 78—63476
stratified fluid with shear, instability and turbulence 79—77216
stratified fluids in open channel, critical flow conditions 80—74956
stratified inviscid Boussinesq fluid, instability of internal gravity wave 77—68663
stratified shear flow, wave breakdown 77—31358
stratified shear flow, weakly nonlinear stability theory 78—18331
stratified viscous plane Couette flow, stability, const. buoyancy freq. 77—47059
stratified viscous plane Couette flow, stability, variable buoyancy freq. 77—47060
streamwise vortex separation and stability *(German)* 80—6069
structural stability in evolving flow fields 80—8802
subsonic flow, diverging, stability aspects, time-dependent method 80—74906
subsonic gasdynamic flow, stability anal. for gas in varying cross-section channel *(Russian)* 78—46992
subsonic gasdynamic flow stability 79—86451
suction controlled boundary layer flow, perturbation caused stability loss 77—75886
supercritical steam generators, conditions determination 78—46936
superheating-convective instability, effect of boundaries 77—35137
superimposed miscible liquids, dynamic stabilization, turbulent transport through diffuse boundary layer 80—74844
superposed conducting fluids, hydrodynamic and hydromagnetic stability 79—18969
superposed flow, interfacial instability 79—4057
superposed fluid stability, finite element anal., book contrib. 79—32467
superposed fluids, Taylor instability nonlinear theory for wavenumbers near linear cutoff value 79—55355
supersonic and hypersonic flight, longitudinal stability conditions *(German)* 77—31330
supersonic boundary layer on plate with leading edge blunting, stability 79—64688
supersonic compressed boundary layer on two-dimens. plate, unstable localised disturbance characts. 77—55031
supersonic flow over deep cavity, flow disturbances, laser appl. 79—98748
supersonic quasihomogeneous flow, turbulence in presence of density and vel. fluctuations 80—1638
surface tension driven instability of liq. film flow down heated incline 79—27620
surface-boiling, in pipe, high-frequency pressure oscillations 77—35239
surge and rot. stall, flow instabilities 80—106803
suspension, macroscopic transport coefficients *(French)* 78—35729
suspension, wave motion in flow down inclined plane *(Ukrainian)* 79—77220
suspension of slender fibres, Poiseuille flow stability 78—71388
swirling water bells 79—50733
tangential discontinuity on fluid interface, two-dimens. perturbation development 80—96245
Taylor 80—59044
Taylor cells hydrodynamics instability and vortex currents in Couette flow 80—64571
Taylor column irregularity in rapidly rotating MHD fluid, mag. field effects 80—43786
Taylor instability, superposed fluids of different densities, three dimens., nonlinear theory 77—75888
Taylor instability, transition to turbulence 80—28491
Taylor instability in flow between rot. cylinders *(German)* 78—79308
Taylor vortex flow, finite difference transient implicit method, stability 79—14404
Taylor vortices near instability point, amplitude, mode-coupling theory 77—68598
Taylor vortices near oscillating cylinder, subharmonic destabilisation 80—92162
Taylor-Couette flows at very high Taylor number, marginal instability 80—1599
Taylor-Gortler instability in turbulent shear flows and boundary layer transitions 78—90836
Taylor-Gortler instability of boundary layer with suction and blowing 77—27512
Taylor-Helmholtz instability, jet diameter, appl. to mineral wool fibre prod. 77—35191
Taylor-vortex flow between rot. cylinders, amplification rates and torques 77—42848
thermal diffusion and convective stability; role of rotating container 79—68725
thermal diffusion flame, two dimens. cellular struct. formation 80—69947
thermal fluctuations, effect on turbulent flow 79—77079
thermal hydrodynamic instability, heating condition effect 78—18288
thermal instability anal. for horizontal liq. layers with a density max. 78—67193
thermal instability of an internally heated fluid layer in a magnetic field 80—53875
thermal instability of stochastically modulated flow 78—14011
thermally driven shear flow heated from below, stability 78—67177
thermoacoustic pressure oscillations in heated channel 79—46319
thermoconvective instabilities of confined fluids, review 80—38399

flow instability continued
thermoconvective waves in stratified compressible fluid, stability criterion contradiction 80—19414
thermoelastic fluids, stability of motion anal. 80—10221
thermohaline convection, past marginal state, determ. amplitude and freq., Landau's conjecture 79—55312
thermosyphon steady flow, existence in open curved heated ducts *(French)* 80—43689
thin cylindrical shell, compression dynamics, nonlinear evolution of Rayleigh-Taylor instability 78—79243
thin falling liquid films in tubes, 'dry patch' stability 80—53747
thin laminar flow down inclined plane wall, roll wave form. 80—48673
thin liquid film, instability and rupture 80—34279
three dimensional growing boundary layers, linear stability 80—74833
three dimensional incompressible boundary layer flow, temporal and spatial stability relation 80—14659
three dimensional parallel shear flows, stability and transition for rot. disc 80—74887
three-dimensional disturbances, instability, turbulence generation *(Russian)* 77—27511
three-wave decay interaction, steady-state turbulence spectrum 80—96249
time dependent flows, stability criteria 78—79305
Timoshenko bar, aerodynamic stability, time- and space-harmonic balance *(German)* 80—83812
Tollmien Schlichting secondary instability, in boundary layer flows 79—64632
Tollmien-Schlichting wave packet formation and nonlinear evolution in unstable parallel flow *(French)* 79—50739
tornado, simulated, instability rel. to flow meas. via three-dimensional anemometers 77—17244
toroidal thermosyphon, transient and stability behaviour 80—38408
transient boundary layer on porous plate, coolant injection, laminar flow stability and heat transfer 78—83389
transient convective turbulent heat transfer in tubes, thermal and hydrodynamic instability 78—83485
transient flow in porous media, Green's function appl. 79—72935
transient free convection from an isothermal horizontal circular cylinder *(German)* 79—77115
transitory stall in plane wall diffusers, flow unsteadiness 80—48678
translational-rotational flow stability, Rayleigh method generalisation 77—58702
transonic flow over airfoil, steady and unsteady, shock-induced separation 79—59999
transonic flow over body of revolution, perturbation theory and numerical body 79—60000
transonic potential flows past cascades, in nozzles and channels, pseudo-unsteady method 80—14727
transonic two-phase vapour-drop flow in channel, stability singular point 77—55078
transonic unsteady flows calc. using integral eqn. method, aerodynamics 79—32554
transportation flows in pipes, energy comparison for steady, unsteady flow 78—91017
triple correlation of the pressure in subsonic circular jets and nonlinear interaction of instability waves 80—69893
tube array, whirling instability, phase relationships 78—51175
tubes, viscous liquid turbulent unsteady flow, pressure drop in transition region 80—74978
tubes with inclined terminal nozzle, stability boundaries for flow induced vibrations 80—19512
tubes with variable cross-section, difference equations solution *(German)* 80—6155
tubular film blowing, expt. 77—42804
turbulence, free-stream, in air and water, control by means of honeycombs 77—35122
turbulence, onset, fluctuation spectrum calc., appl. to Rayleigh Benard flow 80—23989
turbulence transition, predictability 78—87332
turbulent channel flow, mixing length from max. stability principle 80—53859
turbulent channel flow wall region, fluctuating vel. components 79—77250
turbulent flow, interaction of external disturbance, stability 77—54977
turbulent jet, large scale struct. and vortices, linear stability theory 78—26179
turbulent jets, wakes, and shear layers, marginal instability principle rel. to power laws 79—32458
turbulent shear layer, instability waves, radiation of sound 80—79341
two coaxial cylinders, fluctuating flow and heat transfer for incompressible fluid 80—24013
two coaxial rotating discs, viscous fluid unsteady motion and heat transfer 79—94633
two dimensional flows stability, Eckhaus and Benjamin-Feir resonance mechs. 78—55632
two layer flow stability *(Russian)* 79—14380
two phase chemically reactive flow, dynamic stability, numerical anal. *(Russian)* 79—68823
two temperature fluid layer heated from below, stability 77—65741
two viscous incompressible fluids in parallel uniform shearing motion, hydrodynamic stability 80—59010
two-dimensional boundary layer, fluctuations in external vel. 77—51043
two-dimensional shear layer, instability wave excitation by sound 79—32541
two-layer film flow stability down inclined plane 79—90222
two-phase, programme for nucl. reactor heat removal expt. at low power 78—54814
two-phase channel flow, hydrodynamic crisis 78—14066
two-phase flow, an.. of induced vibral in horizontal piping system 77—80215
two-phase flow, horizontal stratified, 1-D two-fluid eqns. for LWR LOCA 80—91226
two-phase flow, nonequilib. subsonic/supersonic, acoustic vel. obs. 78—42642
two-phase flow, pressure drops and hydraulic losses w.r.t. local resistances 79—77221
two-phase flow equation systems, characteristics, stability and short wavelength phenomena 78—38395
two-phase flow instability in parallel channels 78—94810
two-phase flow instability in parallel multichannels 79—90221

flow instability continued
two-phase stratified horizontal flow, averaged and local instantaneous formulations, stability 80—64613
two-phase systems, thermally induced flow oscillations investig. 77—42907
uniqueness and drag for fluids of second grade in steady motion 79—32584
unstable boundary layer, streamwise vorticity growth 77—58700
unstable flow past cavities, shear layer oscill. freqs. 77—84228
unstable flow past cavity, three-dimens. nature, obs. 80—59053
unstable laminar boundary layer, response to acoustic excitation 79—98681
unstable laminar boundary layers, nonlinear evolution and breakdown 80—92109
unsteady 3-dimens. compressible flow, implicit finite difference simulations, transonic appl. 80—64576
unsteady 3-dimens. incompressible viscous flows in vessels with moving boundaries 79—98682
unsteady axisymmetric 1-dimens. motions of ideal incompressible liquid, small perturbations 80—59004
unsteady boundary layer flow, past suddenly cooled vertical plate 79—32480
unsteady boundary layer of a plate with a time-interrupted suction *(Russian)* 80—23988
unsteady boundary layer separation, mathematical criterion 80—69884
unsteady buoyant plumes in neutral surroundings, time similarity anal. 79—81870
unsteady combined free and forced convection in flow in narrow channel 79—60061
unsteady compressible boundary layer equations, generalised soln. 79—32463
unsteady convection study, simultaneous velocity and interferometric meas. 79—98839
unsteady flow arising from rotating fluid above a fixed plane 80—24029
unsteady flow velocity meas. using hot-film sensors 79—98828
unsteady gas and liquid flow, through throttling elements, effect on pressure equation parameters *(German)* 80—1670
unsteady hydromagnetic thermal boundary layer problem, numerical treatment 80—92227
unsteady hypersonic gas flow past thin finite-span wing 79—86457
unsteady imcompressible laminar boundary layers around impulsively started cylinders *(French)* 79—72876
unsteady incompressible laminar boundary layer, eqn. soln. for 2-dimens. flow 80—48672
unsteady inviscid 2-D flow analogy using stretched membrane and moire fringes 80—64658
unsteady Lagally theorem for multipoles and deformable bodies 80—33560
unsteady laminar boundary layers, collision at equator of rotating sphere 79—72896
unsteady laminar boundary layers in an incompressible three-dimensional stagnation flow 79—81848
unsteady laminar boundary layers in an incompressible three-dimensional stagnation flow, book contrib. 80—1525
unsteady laminar flow through porous media in presence of transverse mag. field 79—37394
unsteady laminar separation and stall from aerodynamic surfaces 80—59090
unsteady motion of finite mass of fluid 80—59005
unsteady pipe flows, finite difference scheme 80—6146
unsteady separated flow, aerodynamic characts., vorticity field 80—38457
unsteady transonic flow, freq. effects 80—14728
unsteady viscous flow near axisymmetric stagnation point on circular cylinder 79—23302
unsteady viscous MHD flow, through porous channel with constant suction 79—72951
vapour bubble-liquid slug heat transfer, Taylor instability mechanism for LMFBR HCDA 78—8939
vapour generator, two-phase flow dynamics 78—94808
Vela supernova remnant, Rayleigh-Taylor and thermal instabilities rel. to turbulent struct. 80—51836
vertical circular channel, convective stability relative to periodical disturbances *(Russian)* 80—43711
vertical flat plate, wave instability of liminar mixed convection flow 80—10245
vertical plane turbulent buoyant jet in confined depth channel, stability and mixing 79—90302
vibrations and stability in nonlinear systems with one degree of freedom, book contrib. 80—1530
viscoelastic capillary jets, stability 79—46352
viscoelastic fluid, flow stability in converging channel against perturbations *(German)* 80—1654
viscoelastic fluid, stability of laminar boundary layers *(German)* 77—72335
viscoelastic fluid, stability of steady shearing flows, energy method and parabolic maximum principle 80—74926
viscoelastic fluid, unsteady flow through long circular ducts 79—77249
viscoelastic fluid layer, convective instability, boundary thermal cond. independence 78—9659
viscoelastic fluid layer heated from below, vertical periodic oscillations, convection, overstability 80—48755
viscoelastic fluids, unstable tubular entry flow 79—90218
viscoelastic layer, flow down inclined plane, finite amplitude long wave stability 79—37365
viscoelastic liquid, horizontal layer, thermal instability 77—68545
viscoelastic liquid layer, electrohydrodynamic instability 80—14832
viscoelastic Maxwell fluid, unsteady flow between parallel planes, in transverse mag. field 78—38411
viscoelastic unsteady flow through tubes 80—14753
viscoplastic conducting liq., finite perturbations, Hartman flow instability *(Russian)* 78—47049
viscoplastic liquid film on vertical vibr. wall, with slip, shaking loose 78—59371
viscosity stratified fluid layer, heated from below, thermal instability 77—58762
viscous axial flow in annulus with rot. cylinder, instability 77—7404
viscous binary mixture in porous medium, thermal conc. instability 77—35231
viscous capillary jet, oscills., investigation of axisymmetric perturbation 79—37370
viscous film, nonlinear stability w.r.t. side-band disturbances 77—75887

flow instability continued
viscous film on inclined plane, nonlinear stability, finite 3-D disturbances 78—26101
viscous flow between rot. coaxial cylinders, hydrodynamic instability 77—72307
viscous flow between two revolving spheres, unstable motion *(Russian)* 79—32530
viscous fluid, stability of steady vertical flow 80—64520
viscous fluid drop, induced flow field in oscillating fluid 78—90980
viscous fluid in porous annulus, exact soln. for unsteady motion 80—19499
viscous fluid layer with heat source, stability in presence of inclined mag. field 77—89206
viscous heating at low Reynolds number, stability anal. 77—72280
viscous incompressible heat generating flow past porous plate with free stream oscillations, laminar free convection 79—37311
viscous incompressible heat generating flow past porous plate with free stream oscillations, laminar free convection 79—37312
viscous liquid, neutral curves of linear fluctuations, analytic method 80—14664
viscous liquid boundary layer, nonlinear wave growth in perturbed flow, stability 78—34107
viscous liquid film instability under the influence of an adjacent gas flow 80—92110
viscous liquid in tube with arbitrary press. distrib., unsteady motion 79—14478
viscous liquid unsteady flow in annular channel 78—75205
viscous stratified flow in an oscillating cylinder 79—98782
viscous stratified shear flow, stability eqns., completeness obs. 80—64519
viscous two-layer flow, stability to small perturbations, neutral stability curve 80—33652
vortex flow and breakdown, disrupted states 77—89131
vortex ring, constant vorticity, instability to short azimuthal bending waves 78—22354
vortex shedding flowmeter, stabilisation in low Reynolds number range 80—83865
vortex sheet, Helmholtz instability in uniform shear flow 79—37328
vortex sheet, plane, in ideal fluid 78—63437
vortex sheet 79—10567
vortex sheet discretised evolution with buoyancy and surface tension effects 77—27579
vortex sheets, calculation of three-dimensional unsteady flows *(French)* 78—14025
vortex sheets, instability mechanism of rolled sheets *(French)* 79—81901
vortex stretching, due to shear layer instability 77—65776
vortex system, stable solns. 79—98735
vortex systems, stable solns. 80—33613
vortex with top-hat jet core, stability 77—19612
vortex-induced wake buffeting and its suppression 80—103030
vortices, body-centred polygonal configs. 78—71341
vorticity streets stability on curved surfaces with reflection symmetry 80—46810
wake, axisymmetric, instability and laminar to turbulent transition 78—38337
wall jet, radial, linear stability 78—22392
wall jet, two-dimens., linear stability 78—22391
wall reattachment device, loading effects on switching *(Japanese)* 79—10548
wall turbulence struct., adverse pressure gradients effects, fluctuations and separation 80—10231
water, apparent Weissenberg effect 80—83787
water, horizontal layer, convection onset with max. density effects, nucl. plant waste heat storage 79—46164
water, MHD free convection flow past infinite porous plate 80—33703
water, non-Boussinesq convective struct. near 4°C 79—18886
water, thermoconvective instabilities, 0 to 4°C *(French)* 78—18300
water boundary layers, Tollmien-Schlichting waves and transition 79—81845
water flow instability in Na heated once through steam generators 80—27737
water in cavity heated from below, convective instability *(Russian)* 79—14391
water jets, waves 78—5775
water jets sensitive to sound, two-dimensional, velocity fluctuations behaviour *(Japanese)* 80—100020
water near 4°C, plane-parallel convective flow instability 80—92137
water wave stability, linear theory approach 77—51068
water waves, nonlinear, instability to infinitesimal long-wave perturbations 78—5757
water waves in closed channels approaching Kelvin-Helmholtz instability 77—89136
water-air two phase flow, oscillatory flow instabilities 80—83833
wave interactions, explosive, reson., in three-layer fluid flow 79—64680
wave propagation, gravit. instability, rot. and streaming effects 79—37293
wavefronts in reaction-diffusion systems, instability and turbulence 80—106855
wavelets, initial generation by coupled shear flow instability wind wave evolution 79—94635
waves, deepwater, nonlinear, evolution of continuous wave train 78—5756
weakly amplified modes, interaction in nonlinear convectible instability *(French)* 79—64650
weakly compressible gas flow, stability in pipe of model roughness 80—28562
wings, low aspect ratio, computation of nonlinear characts. 79—41690
WKB approx., flow stability between concentric cylinders 77—51120
Ar, ionising shock waves, stability, H impurities effect 78—22371
CO_2-N_2-H_2O mixture, unstable-oscillatory expansion *(Russian)* 78—1637
H_2-O_2 system with N_2, O_2 diluents, detonation wave instabilities 78—5762
He, liq., Rayleigh-Benard expt., freq. locking and turbulence onset 79—90255
He, liq., time depend. effects above convection, Rayleigh-Benard expt. using local probe 79—7718
He-I, liquid, Taylor vortex instability in Couette flow 79—98683
^{3}He-^{4}He mixture, Benard instability near λ-temperature 80—34268
^{3}He-A, hydrodynamic stability of ^{3}He-A uniform superflow, truncated variational approx. 78—67881
^{4}He, liq., heat transport and critical slowing down near Rayleigh-Benard instability in cylindrical containers 77—84253

flow instability continued
^{4}He, superfluid, capillary flow props., instabilities and vortex motion 77−55408
^{4}He, superfluid, hydrodynamic stability of vortex ring in counterflow 79−86944
^{4}He, superfluid film, saturated, oscills. induced by persistent circulation 77−47637
K, boiling, in tubes, superheat and instability 77−35136
Li thin films on inclined surface 79−22458
N_2, liq., thermosiphon, flow oscills. 77−23960
N_2, liquid, in thermosiphon, effects of heater geometry on flow stability 79−58728
N_2O_4, dissociating, nonsteady flow in steam-generating channel 79−37422
N_2O_4, reactor coolant, stability in two-phase flow *(Russian)* 80−609
$N_2 \rightleftharpoons 2N$ layer, hydrodynamic stability anal. 77−75993

flow measurement
see also anemometers; flow visualisation; flowmeters; laser velocimeters
1st normal stress difference meas., water rel. to polymer solns. 79−98829
acoustic characteristics of low through duct systems, transfer function technique 79−18650
acoustic flowmeter, for open channels, accuracy 79−68876
acoustic flowmeters for pipelines 80−43808
acoustic techniques principles *(German)* 79−82019
acoustic velocimetry, corrected ray theory 79−41774
adhesive forces, between solid particles in liq., hydrodynamic method of meas. 79−68826
aerosol measurement, particle deposition in sampling lines 78−81472
aerospace instrumentation, conference, Las Vegas, Nev., USA, (May 1977) 78−12075
aerospace simulation facilities, conf., Shrivenham, England, (Sept. 1977) 77−80251
air, indirect methods 80−53892
air, using hot-wire anemometer, calibration at low vels. 79−27724
air and water flows, measurement of skin friction using viscosity balance 79−64811
air flow, low velocity, pulsed-wire anemometer appl. *(Japanese)* 77−62319
air flow consumption meas., respiratory process parameters determ. using electric model *(Bulgarian)* 80−76867
air flow meas. in tunnel using anemometers and pitot tubes 79−41779
air flow near Earth's surface and structures models, perturbations due to flow measuring devices *(Italian)* 80−6180
air tightness inspection by gas anal. method 78−41323
air transported dust concentration, annular Venturi tube meas. *(Polish)* 79−72971
air vel. meas. using triple hot-wire probe 79−27718
air velocity meas. by triple hot-wire probe 77−62315
air/water mixture mass flow meas. by drag devices and γ densitometer 80−79385
airflow measurement in speech using mask-type wire screen pneumotachograph 77−52808
airflow rate, with electrical indication and automatic data logging system 80−75014
airflow through cascade of turbine blades, laser anemometry 80−59146
airflowmeter using wire-mesh element 77−39388
airfoils, transonic testing at high Reynolds number in shock tube 80−14852
airtightness inspection, standard conditions, flow through through-defects 79−50801
anemometer, cond.-type, with external mag. field, turbulence spectrum correction 78−1766
anemometer, constant resistance hot wire, flow average temp. variations effect on reading *(Russian)* 78−88925
anemometer, hot film, calibration and use in fluids at varying background temp. 78−1767
anemometer, hot wire technique for simultaneous nonisothermal flow vel. and temp. meas. *(Japanese)* 78−38421
anemometer, hot-wire, computerised, for vel.-and temp.-meas. in heat turbulent flow 78−91040
anemometer, hot-wire linearised type, with bridge cct., characts. 77−55118
anemometer, inside-out type, constructional details 78−59516
anemometer, rotating hot wire single inclined type, characts. anal. and obs. 77−51146
anemometers, for indoor climate research, modification and calibration 77−3897
anemometers, three dimensional feasibility of use in simulated tornado flow meas. 77−17244
anemometrical technique for flow rate meas. in liq. N_2 77−31409
annular flow, vel. distrib., expt. determ. 80−38510
annular-averaging flow sensor, error in averaging technique and discharge coeff. 80−38509
arterial bifurcations, glass models, pressure meas. 79−25021
arterial flow velocity, Doppler US vascular diagnostic system 77−29190
arterial haemodynamics evaluation using venous US catheter-tip technique 77−44730
arterial pulse wave vel. meas. by Doppler shifted US and EM flowmetry 78−69229
arterial stenosis detection by transcutaneous pulsed Doppler method 77−44732
arterial system, forward and backward wave calc. 79−57697
artificial heart, pneumatically driven, cardiac output meas. 78−44729
axial flow fans, noise and aerodynamic characts. 80−43536
axisymmetric jets, coherent structs. using optical technique, convection vel. 80−69888
backswept centrifugal impeller, laser-Doppler investigation of flow 79−77304
ballistic device, hypersonic wake, anomalous dispersion meas. 79−82014
bell type volume dynamic systems for gas flow meas., error anal. 78−75239
bidirectional fluidic flowmeter, respiratory meas. appl., tests 78−35993
biological flows, plethysmograph with servo-control of hydrostatic press. 77−5118
blood, implantable telemetery using CW Doppler US vel. meter, IC 77−86565
blood, in capillary beds, two-regime model of heated thermocouple probe 77−5110
blood, in fish, use of laser Doppler velocimeter *(Japanese)* 79−84052

flow measurement continued
blood, limb, using cylindrical crossed-coil NMR flowmeter, for noninvasive measurement 79−62328
blood, measurement using NMR and flat crossed-coil detector 78−40284
blood, multiple noncritical stenoses, fluid dynamics ext. 77−90844
blood, plethysmography using Hg-in-rubber strain gauge, temp. drift error and compensation 77−52900
blood, quantitative flow meas. by constant infusion of short-lived isotopes 80−17088
blood, real-time US carotid arteriography system 78−24108
blood, true volumetric US technique 77−90824
blood, using implantable pulsed Doppler flowmeter, dogs 77−90966
blood flow, future appls. and prospects 77−78010
blood flow, in objective determ. of human $+G_z$ accel. tolerance, ultrasonic method 78−3619
blood flow, radiotracer meas., automatic bolus injector 77−9238
blood flow, regional, assessment by intravenous injection of ^{99m}Tc pertechnetate 80−104732
blood flow, renal, using externally monitored ^{131}I-hippurate uptake 77−2036
blood flow, transcutaneous EM flowmetry meas. using steady mag. fields 80−41158
blood flow, US Doppler signal LF spectral analysis 79−62312
blood flow, using indocyanine green and microspheres 77−77925
blood flow by laser Doppler system *(Swedish)* 80−51199
blood flow calc. by indicator dilution, pulsatile error analysis 77−60225
blood flow disturbance detect. using pulsed US Doppler method 77−40724
blood flow evaluation in peripheral circulation, noninvasive techniques 80−56163
blood flow meas., cerebral, using NMR 77−40730
blood flow meas., instantaneous, X-ray imaging using cine/video densitometric data 79−34598
blood flow measurement by CW Doppler technique using implanted transducers, accuracy 77−25537
blood flow measurement by US Doppler method, computer-aided determ. of angles *(German)* 78−80931
blood flow measurement from freq. analysed US Doppler signal 78−44573
blood flow measurement in dynamic phantom using ^{81}Rb-^{81m}Kr and NaI detector 77−66843
blood flow measurement using NMR flat crossed-coil detector 79−83880
blood flow measurements by NMR of the intact body 80−81680
blood flow sensing in conscious rats, multichannel pulsed Doppler technique 78−44577
blood flow speed and quantity determ. from digital angiograms *(German)* 78−92690
blood flow telemetering system using implantable CW Doppler US flowmeter, IC appls. 78−11749
blood flow values in iliac artery, angiocinedensitometry meas. in conscious humans 79−25022
blood flow vel. meas. in microvessels using video correl. system 78−53543
blood flow velocity estimation, Kalman filter for Doppler ultrasonic meas. 79−62325
blood flow velocity meas. by hot-film anemometer *(Japanese)* 79−29678
blood flow velocity waveform freq. anal., invasive and noninvasive meas. near stenosis 77−56417
blood flow-velocity meas. by US techniques, Kalman filter appls. 79−100686
blood flow/pressure relationships, when to meas. flow or hold flow const. 77−77926
blood flowmetry, noninvasive, in upper limbs of patients with arteriovenous dialysis fistulas 80−21562
blood turbulent flow measurement with pulsed Doppler US 77−40871
blood US correlation technique for blood flow meas. 77−36968
blood velocimeters, US transesophageal meas. of human haemodynamic parameters 80−41146
blood velocity, catheter meas., cross correl. technique 78−80943
blood velocity analysis during pulsed Doppler US imaging of carotid artery disease 77−29189
blood velocity noninvasive meas. in large vessels, broadband pulsed Doppler US system 78−61224
blood vessel bubble detection and flow evaluation 79−34612
blood volume flow quantitative estimation with transcutaneous Doppler US 80−36052
bone blood flow determ., comparative study of $^{99m}TcO_4$ and ^{131}I-iodoantipyrine 78−28046
borehole flow, instrument for simultaneous meas. of axial and radial components 79−80051
boundary layer transition, detection using holography 78−14101
boundary layer transition region, IR emission meas. 78−38438
boundary layer turbulence, meas. of microstruct. with hot and cold wires 80−24109
boundary layer turbulence at subsonic speed, coherent structure meas., minicomputer appl. 80−10338
boundary layer velocity measurement by single-beam laser time-of-flight method 79−77298
brachial artery blood flow measurement, noninvasive ultrasonic Doppler technique 77−86570
brewing industry flow metering 77−84368
bubble dynamics, laser schlieren meas. 79−41773
bubble size spectra, appl. of acoustical cross-sections technique 78−9735
bubble-flow regime, two-phase laser Doppler anemometry 77−39366
bubbles, acoustical meas. of gas bubble volumes and gas flow rates 80−62633
bubbly, laser meas. of local liquid velocity and void fraction *(Japanese)* 78−9693
bubbly flows, simultaneous meas. of local liq. vel. and void fraction using gas laser *(Japanese)* 77−42947
bubbly flows, simultaneous meas. of local liquid vel. and void fraction by gas laser, accuracy *(Japanese)* 78−67295
BWR core flow fluctuation and neutron noise obs. 78−94060
capillary blood flow, dual beam laser velocimeter anal. 80−75015
capillary blood volume flow determ. by improved photoplethysmograph, Hemorheograph 78−31934
capillary rheometer, viscous heating from power law fluid, perturbation expansion anal. 78−63519
cardiac blood flow meas., computerised system 80−36051
cardiac output meas. by US transoesophageal probe 79−92315

flow measurement continued
- cardiac output measurement, in vitro comparison of six commercially available thermodilution systems 78—77135
- cardiocirculatory computer-aided monitoring after open-heart surgery, appl. to adrenaline effects meas. 78—81059
- cardiology, pulsed Doppler velocimetry, clinical appls. 80—46003
- cardiovascular changes associated with age, US obs. in dogs 77—25504
- cardiovascular flow disturbance detection by pulsed US Doppler velocimeter autocorrelograms 77—25526
- carotid artery imager, CW Doppler US and spectrum analyser 79—57731
- carotid-vertebral circulation exam. by variable range-gated directional Doppler technique 77—29188
- catheter flow probe for left ventricular source parameters meas. 79—92324
- cavitation nuclei in liquid flows, size distrib. determ. technique 77—68716
- cavitation tunnel, for high-temp. operation 78—63521
- cerebral blood flow, atraumatic meas. by ^{133}Xe *(French)* 77—37039
- cerebral blood flow, confidence limits with positron emission 79—11994
- cerebral blood flow, meas. in pig by ^{133}Xe clearance technique 80—94421
- cerebral blood flow, tissue pO$_2$ and pCO$_2$, continuous and simultaneous meas. 79—57829
- cerebral blood flow computer for use in angiogram theatres 78—73227
- cerebral blood flow determination, computer assisted method for multi-exponential curve fitting 78—20246
- cerebral blood flow meas., lateral counting corrections 79—8536
- cerebral blood flow meas. in animals using ^{14}C-ethanol 80—41205
- cerebral blood flow noninvasive regional meas. and computer analysis 78—35948
- cerebral blood flow system using H_2 clearance method 78—40457
- cerebral cortial blood flow transients in cat. meas. technique using tissue heat transfer 79—92457
- cerebral regional blood flow and vol. meas., intravenous isotope method 77—86610
- cerebral regional blood flow assessment by continuous carotid infusion of ^{81m}Kr 78—20254
- cerebral regional blood flow meas., ^{133}Xe inhalation method with on-line computer 77—40734
- cerebral regional blood flow meas. by ^{133}Xe inhalation, anal. method comparison 78—44604
- cerebral regional blood flow meas. with ^{133}Xe, functional landscapes in brain 78—85356
- cerebrospinal fluid flow meas. 80—17165
- channel, 2-dimens. rectangular, vel. profiles and fluctuations, laser Doppler anemometry 80—53864
- chemical industry, VDI and DIN 1952 standards and correction factors *(German)* 77—42946
- choroidal blood flow, non-invasive meas. 77—40704
- circular cylinder near wake in turbulent crossflow, expt. techniques 80—14705
- coal dust mass flow meas. methods *(German)* 80—92242
- coal slurry, flow meas., activation method 79—48015
- coherent anti-Stokes Raman scattering for local and continuous density meas. in gas flow *(French)* 77—35281
- coherent structure in flow fields anal. using laser Doppler anemometry 80—10339
- combination pressure-sensing probes, flow direction meas. error 78—22436
- combustion flow, laser Doppler velocimetry 77—80255
- COMECON standard for measuring volumetric and mass flow of fluids 80—43809
- compensation method for volume flow meas. at air sluices *(German)* 79—98842
- computerised, based on velocity distribution curves *(Polish)* 78—34221
- conditional sampling, detection and data signal phase relation, turbulent boundary layer appl. 78—24772
- conduction flowmeter, weighting function, mag. field distrib. effects *(Russian)* 77—47121
- conduction flowmeter with calculable and controlled calibration characteristics *(Russian)* 79—7428
- conductive liquids, flow rate meas. using EM velocimeters 79—68859
- through conduits, quadrant-edged orifice meter standardisation 77—51138
- conference, flow meas. techniques, Brighton, England (April 1977) 77—84358
- conference, fluid flow research instrumentation, Saint-Louis, France, May 1976 77—35271
- contactless, transit time determ. by pick-up *(German)* 80—14862
- convection, natural, on inclined surface, transition, vortex system, meas. method 79—27632
- convective and pressure-driven fluid flow profiles, meas. using pulsed NMR 78—14109
- convective mass transfer measurement methods, review *(German)* 78—46959
- coronary blood flow meas., precordial counting collimator 77—77967
- correlator, Malvern, based on photon correlation and laser scattering spectroscopy, development and appl. 80—5741
- counter current extraction column, efficiency, using nonlinear PD model *(Russian)* 79—64808
- critical flow venturi nozzles, primary calibration in high pressure gas 80—53832
- cross correlation flow meas. system 77—84376
- cross correlation techniques for low vel. flue gases 77—84377
- cross-correlation flow meas. error estimation and reduction 79—3194
- cross-correlation system operation 78—1760
- crossed beam technique for characterisation of noise sources in hot jet *(French)* 77—35284
- cryogenic flow meas. using NMR double-tuned pickup 77—13756
- cryogenic flow measurement, transfer standards 79—68888
- curve correction by FORTRAN program *(German)* 78—79394
- custody transfer measurements, accuracy 79—68845
- cutaneous blood, laser beam Doppler shift method, instrument 78—28030
- CW Doppler bloodflow meas., perivascular transducer effect on accuracy 77—90825
- CW NMR to determine volume fractions and flow rates of component mixtures 80—33710
- cylindrical, convergent flowmeter, medium expansion correction factor determination 78—67296

flow measurement continued
- cylindrical nozzles with sharp upstream edges, critical flowmetering appl. 80—28546
- data reduction technique for flow angle and mass flow rate meas. in unknown flowfield 79—77306
- deep ocean current meas. system 77—5382
- densitometer with resonating twin tube for ethane/propane, calibration and sampling techniques 77—38052
- desorption-permeation time lags of permanent gases through microporous plugs 80—59137
- diaphragm and Venturi tube appl. *(Bulgarian)* 78—47077
- dielectric, by electrohydrodynamic means *(Russian)* 78—26216
- dielectric flows, EM method for flowrate and velocity meas. 80—53893
- differential, digital technique 78—38424
- differential pressure, inductive, ultrasonic methods, charact., appls. 78—83507
- differential pressure flowmeter appl. 78—38422
- differential pressure flowmeters 78—38423
- differential pressure method, using pad and quad resistors 78—42688
- differential pressure transmitter, electronic, design and appls. 79—17435
- diffusion coefficient determination, using Stefan cell 77—51136
- digital data filtering in continuous wind tunnels 80—10336
- digital loss meter in mechanical oscillating systems *(Russian)* 79—60079
- dilution method for discharge meas. in pipes 78—30396
- dilution method with incomplete mixing 79—50821
- dimensionless slippage coefficient of flow over wall, meas. method *(Japanese)* 79—94582
- direction, pressure probes, yaw meter sensitivity for null reading technique 80—69954
- direction meas., liquid flow velocimeter using single type probe *(Japanese)* 80—1713
- direction probes for turbomachine technology 80—87824
- directional Doppler flowmeter, implantable, pulmonary artery flow meas. after lung homograft in dogs 77—90823
- disc-stabilised diffusion flames, vel. characts. 79—34309
- discharge coefficient of orifice plates, effects of bends 79—68865
- discharge from partly filled pipes, EM and US flowmeter meas. 79—68857
- dispersed phase of two-phase flow, holographic anal. 80—103061
- Doppler anemometry, velocity and photomultiplier bias effects 80—59140
- Doppler difference signals, struct., autocorrel. function anal. rel. to laser anemometry 79—50830
- Doppler microscope for flow velocity meas. in areas <10 μ dia., signal-analysing system *(Japanese)* 78—22441
- Doppler sonographic flow meas. over small cross-sections in vitro and in vivo *(German)* 78—88729
- Doppler velocimetry within turbulent phase boundaries 77—11289
- drag sphere velocity probe, miniature, development and testing 78—55705
- drop size distributions in nozzle flows current pulse method 77—42904
- drop size measurement, spherical mirror method 79—64806
- dual-scatter laser velocimeter, appl. to transonic flow wind tunnel 77—39376
- dust trajectory photography for compressible flow velocity meas. 79—82008
- dye dilution method for large open and closed channel flows, validation 78—30395
- dye-dilution laser induced fluoresc. meas. on turbulent jet 78—30397
- dynamic flow characteristic determ. of electro-hydraulic servo-valve using laser velocimeter 79—32719
- dynamic measurements of liquid quantities, international harmonisation 79—68840
- echocardiography, pulsed Doppler, variable sample vol. dimension 80—76816
- eddy-current flowsensor, model 78—5829
- elbow meters for flow monitoring, description 79—37426
- electrochemical shear-stress pickup, freq. characts. 80—10322
- electroconductivity technique for holdups meas. in fluidised beds 78—67286
- electrodiffusion method for convective heat transfer characts. in various liquids 79—94746
- electrodiffusion method for turbulent boundary layers in adverse pressure gradients 80—10321
- electrodiffusion velocity sensor, freq. characts. calcs. 80—96675
- electrodiffusive flow and shear transducer electrical anal. 80—48824
- electrolyte soln. flow, transducer-electrode freq.-ampl. characts. 77—76001
- electrolytic method of mass transfer meas., advantages and disadvantages 79—68827
- electron beam diagnostics of rarefied gas flow, intensity fluctuations 77—55104
- electron beam fluorescence technique for hypersonic turbulent flow 77—35282
- electronic equipment, legal aspects 79—68841
- electronic measurements for small quantities *(German)* 80—1708
- electrostatic precipitator, particle velocity, laser Doppler anemometry study 80—59144
- EM devices, theoretical aspects *(Dutch)* 78—22442
- EM flowmeter type ERO-1, calibration use 80—43812
- EM flowmeter with rectangular wave excitation, operational principles *(Japanese)* 77—80237
- EM flowmeters, dry calibration methods 80—43811
- EM meas. methods, theoretical aspects *(Dutch)* 78—14113
- EM pressureless flowmeter with linear output signal description *(Russian)* 77—89213
- EM transducer for conducting liquid flow meas., testing 78—1768
- EM velocity transducer with a multipole mag. 80—83868
- end effects in a flow-rate transducer with a cylindrical magnet 80—83869
- energy balance technique *(German)* 79—82019
- equivalent flow, through through-defects 79—50801
- errors due to plate buckling in orifice meter 77—84371
- ethylene, supercritical, mass-flow meter inaccuracy 79—68842
- ethylene gas-density meter, calibration method 77—84356
- expansion tunnel performance with and without an EM opened tertiary diaphragm 77—89211
- facts and fiction 77—84361
- fast flowing wet steam, electrical meas. of droplet size 80—64659
- ferrofluid constitution examination by rotating test tube method 80—33693

flow measurement continued
fine particles in gas flow, Doppler laser velocimeter meas. of motion 77−27583
fire gas velocity measurement by cross correlation of random thermal fluctuations 77−58812
fiscal metering 77−84369
fission reactor coolant, natural circulation, correlation with thermocouple random signals 78−17297
fission reactor coolant flow rate determ. using ^{16}N decay activity meas. 80−73955
fission reactor research, pulsed-neutron sources for flow measurement 78−93695
flame, V-gutter stabilised, laser anemometry and schlieren photography meas. 77−35263
flame induced flows propagating over condensed fuels, two-component LDV meas. 79−23380
flame ionisation detector, meas. fluctuating conc., in turbulent flows 80−92240
flame propagation in long tubes, ducts investig., fibre optic technique 77−31404
flames, laminar, rise velocity meas., spectroscopic method 78−74064
flames, local turbulence props., Raman spectroscopy meas. 80−64648
float method for measuring liquid levels 79−77310
flow over cone, dual-plate holographic interferometry 78−63512
flow rate transducer dynamic error determ. 77−72386
flow separation experiments, galloping and vortex induced oscillations 80−43750
flow statistics derived from laser anemometry, retrieval via photon correl. 77−3896
flowfield diagnostics using lasers 80−14853
flowmeter calibration methods with liquids, comparative survey 77−68720
flowmeter for small gas consumption, construction principles *(Russian)* 77−72393
flowmeter generators for calibration and checking of standard flowmeters 80−43814
flowmeter reading, viscosity change influence compensation *(Russian)* 77−65823
flowmeter repeatability testing, calibration system 77−84357
flowmeter selection guidelines 78−71404
flowmeters, low liquid flow rate, automatic testing by dynamic weighing 77−55111
flowmeters operational principles and appl. 78−47073
flowpath velocity meas., semiconductor hot element anemometer 80−48823
fluid flow discharge, laser Doppler vel. meas. in open and closed conduits 79−68882
fluid section flow pattern speckle photography 80−103096
fluid slippage meas. over annular walls *(Japanese)* 78−1774
fluid velocity distribution meas. by speckle photography, expt. 79−86543
fluidic amplifier, using laser Doppler anemometer *(German)* 77−961
fluidic flow rate, metrological model appl. *(Russian)* 77−62318
fluidised bed, chaotic motion of particles, statistical characteristics determ. 77−51140
fluidised bed, gas motion, statistical characts., expt. determ. method 77−65790
fluidised bed, particle motion 80−24090
fluidised bed bubble observation using probes and X-rays 80−79379
fluids, conf., Groningen, Netherlands (Sept. 1978) 79−68839
fluorescence polarimeter for flow cytometry 78−73191
fluorometer for underwater detection of rhodamine dye tracer 78−36313
flush-mounted hot film probe, shear stress meas. in laminar and Taylor vortex flows 80−28486
four wire probe for turbulent flow temp. and vel. meas. 78−67290
free binding liquid film, mean velocity distrib. meas. by laser Doppler velocimeter 80−38508
free jet mixing region, conditional coherence of hot-wire signal with far field microphone 77−19497
free shear layer tone phenomenon, probe interface 78−71324
fringe mode fluorescence velocimetry, organic dye appl. 77−39380
fundamentals and techniques, book 78−81941
gamma densitometer meas., anal. of dynamic bias 80−27730
gamma densitometry, static error evaluation 80−27729
gamma-ray densitometry, dynamic bias 80−27728
gas, critical nozzle profile effect on unchoking back-pressure ratio *(Japanese)* 77−65779
gas, flowmeter calibration, gravimetric standard method *(German)* 77−55112
gas, low speed, constant gas flow production *(Hungarian)* 80−1702
gas, standard methods review 78−94864
gas and air flows, low velocities measurement 78−47078
gas and fluid, using four-wire case thermocouple elements *(German)* 78−14111
gas binary mixtures, flowing, probe for conc. meas. 79−4098
gas conc. fluctuation meas., laser schlieren technique 80−3444
gas cooled reactors, velocity flow field near moving cascade, meas. using hot wire technique 77−50195
gas dynamics diagnostics by glow discharge-generated high-power pulsed electron beam 78−83515
gas flow, two dimensional, laser streak velocimetry or streak velocimetry of two dimens. gas flow 77−42937
gas flow dust content, temp. and speed meas. method 78−34216
gas flow generator transient process anal., controlled plunger movement method 77−72384
gas flow meas. using cryogenic method 78−34245
gas flow measurement techniques, rel. to significance and treatment of phys. quantities *(German)* 78−1775
gas flow rate in pipe, by flow parameter finite increment calc. 77−72355
gas flow rate meas. by multiple electric breakdown method 77−39371
gas flow rates up to 2.5 m^3/sec, dynamic volumetric method 77−72380
gas flow temp. meas. by two thermocouples 78−34218
gas flow turbulent press. and vel. fluctuations meas. by condensation method 78−34217
gas in rot. cylinder, velocity profile meas. 79−50737
gas in rotating cylinder, profile meas., rel. to ^{235}U enrichment processes 79−49793
gas permeability measurement in high polymers, techniques and detectors 80−14354
gas volumetric flow rate meas., automatic system 78−38427
gas with fluctuating pressures and temperatures, transit time of spark charged plasma cloud determ. *(German)* 80−14861

flow measurement continued
gas-liquid annular flow, wire probe meas. of liq. film thickness 79−64805
gas-liquid bed, flow props. and bubble vel. determ. method and instrument 77−72374
gas-liquid flow, hydrodynamics and transport processes, electrodiffusion modelling method, convection and boiling 79−90309
gas-liquid system, unsteady state determination of mass transfer coefficients 78−14106
gas-liquid two-phase flow, response of small pitot tubes 80−92209
gasdynamic flow diagnostics by laser interferometry 77−51137
gases, cryogenic technique 79−4093
gases binary diffusion coeffs., appl. to two-bulb cells calibration 77−76019
granular material in channel, vel. profile from fibre optics obs. 79−64753
haemodynamic function of heart valves, resistance to flow 77−48830
haemodynamic properties of beagle puppies, effects of growth, US obs. 77−25505
haemodynamics, directional Doppler flowmeter, stroke prevention appl. 77−52823
head meters appl., flow effects and calcs. *(German)* 77−55116
heat bridge flowmeter description *(Russian)* 79−7429
heat flow birefringence measuring apparatus for gases 80−10355
heat waves, appls. in flow metrology 79−68879
heated circular jet, outer part, temp. and vel. simultaneous meas. errors 80−87830
heated flows, fine scale turbulence, hot and cold wire sensitivity corrections 80−69956
heated turbulent flows, cct. for instantaneous temp. meas. 78−21137
high integrity metering 79−81999
high pressure gas, critical flow venturi nozzle calibration 79−68844
high pressure piston flowmeter with digital readout *(Polish)* 80−64661
high speed photography, in aeroballistic range, track facilities of von Karman gas dynamics facility 78−37094
high temperature aggressive solutions, phase shifter with Hall effect transducer appl. 79−8459
high velocity gas flow, tunable dye laser meas. 77−68719
high-pressure gas flow test facilities, EEC intercomparison campaign, transfer standards 79−72979
high-resolution blood flow imaging system using binary phase coded pseudonoise sequences 79−57703
high-temperature gas flow, electric-arc heater apparatus *(Russian)* 77−39368
high-velocity gas jets, interaction, photographic study 78−42695
highly separated transonic flow, first vel. and RMS vel. fluctuation meas. 79−77166
highly viscous fluid emerging from slit onto plate, flow development and meas. 80−59142
holographic interferometry, 3D flow field, separate reference and scene holograms 77−89210
holographic interferometry, for displacement or flow velocity distrib. meas., fringe analysis 78−25820
holographic interferometry, two reference beam, for aerodynamic flow meas. 78−34226
holographic interferometry *(French)* 78−5833
holographic interferometry appl. in turbulence effects on optical wavefront 78−82936
holographic interferometry measurements for supersonic flow *(Russian)* 78−14108
holographic interferometry with wide field angle of view, air flow meas. around heated wire 79−76637
horizontal gas-liquid stream, flow vel. meas. 80−96301
hot film in reversing shear flow, heat transfer 77−15014
hot film probe, heat transfer to substrate *(French)* 79−23381
hot gas flows, X-ray diagnostics of density distrib. *(Russian)* 77−19647
hot wire and hot film temperature compensating circuits, temp. probe appl. 78−59510
hot wire anemometry of turbulent compressible gas flows 79−46408
hot wire probes perpendicular to flow velocity vector, interaction 79−68825
hot wire readings, wall proximity effects heat transfer, laminar and turbulent boundary layers 80−48822
hot wire signal analysis method, book contrib. 80−1716
hot wire signal conditional sampling techniques for transition intermittency studies *(French)* 79−77066
hot wire transducer, use for vel. meas. in fluids of variable press. and temp. *(Rumanian)* 78−34212
hot-film sensors for unsteady flow velocity meas. 79−98828
hot-film velocity sensors, cylindrical, low Reynolds number calibration 79−64815
hot-wire anemometry in transonic flow, fluctuation anal. 77−65817
hot-wire direction sensitive probe for flow reversal detection in unsteady flow 80−10333
hot-wire measurement errors in shear flows 77−55119
hot-wire measurements in the wall vicinity, anal. of errors 78−34220
hot-wire probe, simultaneous, instantaneous, temp. and vol. component meas. in turbulent flow 78−34236
hot-wire probe measurements on flow field, effects of cooling law and probe adjustment 79−27721
hot-wire sensor, effect of centrifugal and Coriolis forces on rotating probe 78−94862
hot-wire signal analysis, flow field determ. with high/low turbulence intensity 80−1719
human retinal blood flow meas. by laser Doppler velocimeter 79−79623
hydrodynamic factors, calibration of flowmeters, meas. errors 80−96322
hydrodynamic instabilities and turbulence, flow states, examples and meas. methods 80−92116
hydroresistor thermoanemometer, empirical heat exchange eqn. 80−21852
hypersonic ballistics experiment, application of laser light source 78−38433
impedance plethysmography, influence of erythrocyte vel. 78−61238
impringement flow, skin friction and heat transfer meas., hot and cold-film sensors 77−27629
impulse flowmeters accuracy, survey of flowmeters *(German)* 79−98843
inclined hot-wire response equations, for flow field having dominant tangential velocity component 78−14105
inclined surface, natural convection flow, transition, vortex system, meas. method 79−27632

flow measurement continued

- indicator dilution measurements of flow parameters in curved tubes and branching networks 77—66824
- indicator dilution methods appl. to flow rate meas. 77—65825
- individual realisation laser anemometry, sampling bias evaluation 77—58810
- induction flow-meas. theory for poorly conducting fluids 78—38429
- initial flowmeter for critical gas flow rate meas., principle 77—72382
- instrumentation calibration for mass flow rate meas. in PWR coolant two-phase flow 80—37552
- instrumentation for localised meas. in PWR coolant two-phase flow conditions 80—37550
- intact circulation, X-ray filming, video techniques, haemodynamics appl. 77—52822
- integrating float, lag effects on water flow vels. integration 78—93012
- interference measurement using monochromatic light 78—32867
- intermittency coefficient measurement circuit 78—9733
- internal combustion engine, measurement of pulsating temp. and vel. using US flowmeter 80—1704
- internal interfacial wave motions, IR optical sensor meas. 79—18981
- international standards, adequacy of supportive data base 78—34247
- international standards organisations, review 78—34246
- intracardiac blood flow measurement, noninvasive ultrasonic technique 77—86569
- ions in laser-excited metal vapour, flow vel. meas. 79—82002
- IR camera for separated flow regions diagnosis in wind tunnels 80—10335
- isothermal annular jets, vel. characts. 79—34309
- jet, air, subsonic, fully pulsed, near field vel. meas. 80—19540
- jet, axisymmetric, coherent struct. obs. using new optical technique 80—10282
- jet, nonisothermal axisymmetric turbulent transfer, vel. and temp. fluctuations, correl. coeffs. 78—83445
- jet, turbulent, axisymmetric, spatial correlations 80—19539
- jet displacement transducers, relation between dynamic and precision characts. 80—64660
- journal bearing rheometer, experimental investigations *(German)* 80—6014
- Kovasznay type vorticity probe, influence of fluctuating vel. components 79—72973
- laboratories, comparison using transfer-standard flowmeters for calibration 79—23389
- laboratory measurement methods and problems, book contrib. *(French)* 77—84355
- laer Doppler anemometry meas. in water flows 77—58818
- lakes, vertical automatic profiling system for temp. and current meas. 78—36327
- laminar channel flow, mass transfer electrochem. meas. 77—58794
- laminar fluid flow measurements employing white light fringe image velocimeter 79—64816
- laser anemointerferometer, for simultaneous velocity and density meas. 79—18976
- laser anemometer, appl. to investigation of supersonic shock-wave boundary-layer interaction 77—35275
- laser anemometer Doppler system, optics and signal processor for turbulent low speed flows *(French)* 78—59521
- laser anemometry, fringe-type, review of high-speed wind tunnel appl. in France and Germany 77—35272
- laser anemometry, fundamental limitation and accuracy 80—87829
- laser anemometry meas. in gas-solid suspension flow 77—35268
- laser beam propagation, thermal turbulence effects *(French)* 77—24038
- laser cavitation meter, design and testing 77—68715
- laser Doppler anemometer, two-component, using rotating radial diffr. grating 77—3898
- laser doppler anemometer feasibility assessment method *(Russian)* 79—98832
- laser Doppler anemometer measurement, effect of finite-size probe vol. 77—24036
- laser Doppler anemometer with microscopic intersection volume 79—94750
- laser Doppler anemometer-computer system, for flow rate meas. 79—68881
- laser Doppler anemometery digital data acquisition system 77—80253
- laser Doppler anemometry, instrumentation, appls., explanation using Moire patterns 77—7490
- laser Doppler anemometry, practical considerations 79—27725
- laser Doppler anemometry 78—34227
- laser Doppler anemometry principles and status survey *(German)* 78—9738
- laser Doppler correlation technique for meas. of periodic flows 77—35278
- laser Doppler flowmeter, LADO 1, non-contact meas. of liquid and gas flow rate 79—77305
- laser Doppler techniques 79—68883
- laser Doppler velocimeter, appl. to meas. in subsonic and supersonic flows 77—35273
- laser Doppler velocimeter, for turbulent flow velocity meas., redesign 78—1245
- laser Doppler velocimeter, optical system with multifrequency shifting for simultaneous meas. of several flow velocities 80—43805
- laser Doppler velocimeter, spatial resolution and accuracy 77—24043
- laser Doppler velocimeter direction-sensitive simultaneous multivelocity component 78—94857
- laser Doppler velocimeter two-dimens. meas. of flow induced by flames 78—59529
- laser Doppler velocimeter with double passage of beam through flow 77—19652
- laser Doppler velocimeter with high resolution Fabry-Perot interferometer for supersonic vel. meas. 77—39377
- laser Doppler velocimeter with variable frequency shift for combustion flow meas. *(Japanese)* 78—67294
- laser Doppler velocimetry in turbulent flow meas. *(French)* 77—35276
- laser Doppler velocity meter, operating principles, optical configs., appls. *(Dutch)* 78—1769
- laser dual-focus flow velocimeter 77—39381
- laser fringe anemometry, association with photographic particle tracking 80—38512
- laser induced fluorescence of complex reacting gas flow 77—76011
- laser interference velocimeter, features, appls. 77—80254
- laser interferometry appl. 80—75018
- laser light scatt. meas. of turbulent flow 77—35288

flow measurement continued

- laser Raman diagnostics of aerodynamic flows and flames *(French)* 77—35280
- laser scanner sensor for stratified flow meas. *(Japanese)* 78—9671
- laser scattered light intensity, recurrence rate correl. 78—66760
- laser shearing interferometer appl. to supersonic flow field meas. *(Chinese)* 79—32715
- laser speckle photography for fluid flow vel. meas. 78—14112
- laser velocimeter, appl. to aerodynamics, operating principle *(Spanish)* 80—53902
- laser velocimeter, flow over dam, appl. *(Chinese)* 79—64804
- laser velocimeter for wind tunnel meas. appl. 77—80252
- laser velocimeter for wind tunnel measurements, principles 78—71405
- laser velocimeter optical scanning system 77—58481
- laser velocimeters, optical design and signal processing advances 77—19655
- laser velocimetry, flow velocity at olfactory organ nares of fishes *(German)* 78—69262
- laser velocimetry appl. for unsteady transonic flow meas. 80—10341
- laser velocimetry in transonic and supersonic aerodynamics 77—35274
- laser velocimetry principles and aerodynamic appls. *(French)* 78—63518
- laser-Dopper anemometry, microprocessor-based signal processing system 77—89218
- laser-Doppler anemometry and photon correlation for turbulence length scales 80—87828
- leak detector pickups, halide, optimal flow rate determ. 80—48825
- light beating spectroscopic instrument for continuous meas. of tissue blood flow 80—41160
- light scattering in dynamical props. study, principles spectra derivation and applics. 80—53218
- light scattering techniques, digital correlation appl. 78—57916
- limb blood flow automated monitoring system using venous occlusion admittance plethysmography 78—31937
- limb blood flow meas. by elec. admittance plethymography, evaluation of theory and accuracy 78—31936
- liquid, energy approach reproduction method 80—96321
- liquid, incompressible, electro-hydrodynamic analogy, design 77—27627
- liquid, laser sources and cinematography appl. *(Italian)* 78—14107
- liquid, using chemotronic transducer, features 78—9739
- liquid calibration, weighing method, accuracy 79—68891
- liquid crystal indicator, for the velocity of fluids 77—55108
- liquid film, wave parameter meas., local electrical cond. method 77—51141
- liquid film flow down inclined plane, polarographic velocity meas. method *(French)* 78—34214
- liquid flow meas., flowmeter principles in outline 79—86533
- liquid flow rates through pipes, applicability of experimental meas. methods 80—100044
- liquid in pipes, continuity determ., gamma-ray appl. 79—94748
- liquid metal flow rate meas. method 80—43793
- liquid metals, flow rate measurement for metals with poor contact resistance 79—41778
- liquid metals, MHD rot., vel. meas. by vane type sensor *(Russian)* 77—47123
- liquid Na, thermocouple transfer function and flow velocity meas. by temp. noise 79—13394
- liquid stream vel. profile meas. by laser Doppler velocimeter *(Russian)* 78—9731
- liquid streams vel. profiles using laser Doppler velocimeter 79—64807
- liquid vortex flowmeter appls. and principle 77—89209
- liquid-borne solids monitoring, optical instrument general principles 79—37424
- liquid-flow measurement system using positron active tracer, microcomputer-controlled 80—24113
- liquids, rotating, two-dimensional velocity measurement by automatic analysis of trace particle motion 79—64810
- liquids, volumetric flow rates meas. via hot wire sensors combination 77—17966
- LMFBR, correl. meas. of Na flow rate using mag. detectors 79—71924
- LMFBR, radial blanket assembly, flow split meas. 78—13209
- LMFBR, US flowmeter *(Japanese)* 78—78455
- LMFBR coolant flow, flux distortion flowmeter meas. 79—68858
- LMFBR coolant flow monitoring by balanced outlet temp. signals 79—13393
- LMFBR coolant flow rate meas. suing electromagnetic convertor 80—73887
- LMFBR outlet plenum, air flow model, interferometric meas. of fluctuating temp. using FFTF 78—89943
- load ring equipment for testing and calibrating flow rate equipment of noncorrosive gases 80—43813
- local circulatory system characterisation by CW Doppler US flow meas. 78—57109
- local void fraction in two phase flow, Raman effect measurement technique 79—64813
- localised optical heating, principle of meas. on flows *(French)* 77—31406
- low and high turbulence flows, hot wire measurement based analysis 78—59511
- low flow generator and calibrator development 77—30125
- low flow rate, Flo-Tron microflow meter appl. 78—14118
- low liquid flow measurement, using turbine transmitter with radial rotor 79—68849
- low speed, hot-wire probes 79—82010
- low vel. airflow calibration and research facility 80—1718
- low-intensity flows, turbulence meas. 79—50826
- Ludwieg tube, steady flow duration extension, reservoir orifice method, variable opening area effect 80—64579
- Mach-Zehnder heterodyne interferometer, RF phase reference 77—26390
- magnetic field as a tool for investigating transition and turbulence 80—1696
- magnetic flow meas. devices, mains supplied, elimination of transformer strayvoltage *(German)* 79—82018
- magnetic induction flowmeter principles and applics. *(German)* 77—39374
- magnetically suspended cones, laminar near wake meas. probe interference 77—84257
- magneto-inductive flowmeters, installation *(German)* 80—64662
- magneto-inductive technique *(German)* 79—82019
- marine dynamics and current meas. transducers 78—32260
- mass flow instrumentation performance, during LOFT nonuclear test series 80—69952

flow measurement continued
  mass flow measurements of single-phase and multi-phase flows using radionuclide methods *(German)* 79—86532
  mass flow meter using Coriolis principle, electro-optical force sensing techniques 80—103094
  mass flow rate measurements, estimates of probability characts. 80—73302
  mass transfer by forced convection, at rough surfaces in annuli, rate meas. 77—27532
  material method technique *(German)* 79—82019
  mean velocity very close to a wall, hot-wire anemometer meas. errors 80—79413
  methane jet, turbulent conc. field meas. by Raman spectrum, data interpretation 79—32609
  methane jet flow, average conc. meas. by Raman scatt. 79—98827
  methods and appls. for optimum reliability 79—81998
  metrological assurance in petroleum-gas industry, Soviet standardisation 77—76004
  metrological provisions, development of programme 79—14503
  metrological services in Soviet Union, economic evaluation 77—80239
  MHD flow, compressible, subsonic, use of Pitot tube probe 77—84347
  MHD flow parameter determ. by holographic interferometry *(Hungarian)* 78—22433
  microcirculation flow dynamics meas. using video microscope 77—78009
  microcirculation semiquantitative demonstration using US noninvasive meas. method *(German)* 78—85348
  microkymography, flow vel. meas. in microvascular bed after exdotoxin administration *(German)* 78—77173
  microwave Doppler-effect flowmeter, particle moisture content effects 78—9732
  mid-radius flow, US meas. 79—68852
  minicomputer-based scheme for turbulence measurements with pulsed Doppler ultrasound 80—26435
  mixing length determination, from turbulence characts. meas., in tubes and boundary layers *(Russian)* 78—83371
  mixtures and suspensions, flow rate meas., ultrasound propagation and scatt. approach 80—43806
  molar flow rates in dilution refrigerators, determ. method 77—10032
  molecular flow measurement, precision, and control for single and multi-gas systems 78—70135
  multiframe shadow photography using optical delay like 77—764
  multiparameter anal., flow injection anal. for using unsegmented flowing streams 80—53896
  multiphase pipeline flows, measurement of component ratios using γ-ray attenuation 80—38513
  natural convection air flows, vel. meas. using laser velocimeter 79—82016
  natural convection flows, hot wire measurements, fluid temp. and mixed convection effects 79—64817
  natural convection patterns in inclined box, three-dimensional photography 77—19600
  natural waters, low vel. meas. with submerged floats 78—7813
  Navy liquid flow correl. program 78—30380
  near wall vel. meas. for wall shear inference in turbulent flow 78—34234
  neonatal peripheral circulation, human, characterisation by US pulsed Doppler technique 80—76815
  Newtonian liquid between coaxial cylinders, end-effect correction of Margules eqn. 78—79399
  NMR diffusion and flow meas., spin phase graphing 78—47074
  NMR flowmeter for automatic liquid dosage systems 80—43815
  NMR flowmeters, vortex meters, and mass flowmeters, calibration 80—92239
  NMR spin-echo difference meas. method, plug and laminar flow, appl. to plant stem 78—14110
  NMR with nonuniform RF field, appl. to self diffusion and liq. flow meas. 78—60343
  non-isothermal flow, turbulence measurement, laser Doppler velocimetry appl. 79—41776
  non-Newtonian fluids, capillary and slit methods of normal stress measurements 80—43807
  non-Newtonian shear flow, transient viscosity determination method 80—43746
  non-Newtonian tube flow, small internal press. meas. 78—51260
  nonisothermal flow, two-wire probe, simultaneous vel. and temp. meas. 78—91042
  nonisothermal streams, turbulent velocity pulsations meas., procedure 80—19514
  nonstationary flow rates, use of electrofluidic analogy *(Bulgarian)* 80—28583
  nozzle flowmeter instantaneous flow rate meas. in pulsating water flow *(Japanese)* 80—59133
  nozzles, quarter circle and combined, investigation *(Russian)* 78—42689
  nuclear reactor, hydrodynamic testing equipment with gravitational channel for reactor core meas. *(Slovak)* 78—21625
  nuclear reactor, two-phase flow characterisation by neutron noise techniques 78—94058
  nuclear reactor LOCE blowdown flow meas., improved spool piece 80—27727
  nuclear reactor pressuriser, multiple surges pressure transients 77—26836
  numerical digital filter for on-line processing of wind tunnel data *(French)* 80—19537
  ocean, mobile sand grains underwater detect. 78—96192
  ocean current meter using SeaTrak Data Processor surface data reduction system 78—45042
  ocean currents, data collection via drifting 79—5668
  oil, US flow measurement in laminar-turbulent transition region 79—68850
  oil films, thickness meas. by neutron imaging, and scattering, exam. of flow props. 79—15815
  omnidirectional wall shear stress meter 80—106860
  on-axis velocity component measurement with laser velocimeters 80—19526
  open channel, standardisation in Soviet Union 77—80241
  open channel acoustic flowmeters, design, calibration and errors 78—55701
  open channel acoustic flowmeters, design, meas. errors and operation 78—63516
  open channel and closed conduit flows, conf., Gaithersburg, USA (Feb. 77) 78—30378
  open channel flow, monitoring or metering 78—30383
  open channel flow meas. instrument errors 78—30384
  open channel flow measurement, fundamentals 77—84366

flow measurement continued
  open channel flows, meas. via plexiglas HS flumes 77—62321
  open channels with weirs and flumes, discharge measuring structs. 79—68874
  optical crossed beam correlation method, localised turbulence props 78—34223
  optical instrument for measuring fluctuating velocities in highly turbulent flows 78—83500
  optical instrumentation methods for two-phase reactor flows 80—63313
  optical interferometry, gas dynamic meas., review 77—35286
  optical measurement techniques of thermodynamic props. in flow fields, review 77—35279
  optical pseudo-colour processing of height and flow velocity *(Japanese)* 80—9826
  opticomechanical anemometer for flow vel. meas. of optically transparent material 77—68718
  organ blood flow determ. using radioactive microsphere technique, PDP-11 interactive program 78—20247
  organ blood flow measurements, effect of instantaneous partition coeff. of Xe 80—101256
  orifice meters, relative error in nonstandard approach conditions 78—79398
  orifice plate calibration, interlaboratory comparison 79—68866
  orifice plates, discharge coeffs., calc. eqn. 79—68890
  oscillating ball device measures ultra low flows 80—6171
  oscillations in isochronous containers 80—53899
  oscillatory boundary layer, on bed beneath gravity waves, laser Doppler anemometry 78—90929
  otpical probe for fluidised bed meas. 79—82000
  parallel hot wire probes, flow direction meas. error 78—22436
  parallel-plate plastometer, appl. to rheology of filled polymer melts 79—77036
  particle meas. concentration in turbulent jet, laser scatt. technique 77—39372
  particle motion in gas stream, motion parameters determ. with photographic system 78—5837
  particulate, using microwave Doppler effect 77—27628
  particulate materials, dynamic shear strength and flow behaviour, shear cell meas. 78—53048
  passive remote crosswind sensor 78—7773
  perfusion rate in biological tissue meas. by dynamic thermal dilution 77—40883
  periodic fluid flows by laser anemometry, periodic sampling 80—64657
  photon correlation anemometer, differential Doppler system, appl. supersonic flow 77—35277
  photon correlation technique, appl. to sinusoidally perturbed flow characts. meas. 77—42945
  photon correlation techniques in fluid mech., conf., Cambridge, England (March 1979) 80—56998
  physics field course, for school pupils 77—87612
  piezometer ring design 77—15142
  pipe, slanting hot-wire anemometer appl. 77—62313
  pipe flow, linear and nonlinear resistors, two new methods 77—65818
  pipe flow, spatial cavitation-nuclei-measurements by means of laser velocimeter 80—64593
  pipeline film flow speed, electromagnetic system 80—79417
  pipeline gas and liquid, double orifice plate appl. *(Polish)* 77—72392
  pipeline networks, flow rates distrib. *(Japanese)* 78—91015
  pitot, orifice and static drop element flow and span calcs. 78—1763
  pitot static tube, errors in flow rate meas. 79—68886
  placental blood flow evaluation, comparison of ^{113m}In and ^{133}Xe intravenous injection methods 78—28043
  plane mixing layer, two-point LDV meas., vorticity distrib. 80—38506
  plasma flow, meas. method for solid particles *(Russian)* 78—94903
  plastic fluids, under aggressive, toxic or radioactive conditions 77—7488
  plethysmograph, automatic venous occlusion device 80—17176
  plethysmography, deep vein thrombosis detect. 77—40884
  pneumotachograph, for flow and vol. meas. in normal and dense atm. 77—5120
  polarisation interferometer, appl. to ballistic expt. 79—55435
  polydispersed flows, Doppler signal spectrum 80—103081
  polymer liquids, elastic and Newtonian, vel. distrib. determ. in channel terminals 79—77046
  polymer melts, rheological properties at low shear stresses, meas. using sandwich type creep rheometer 80—59153
  polymer soln. highly elastic, vel. meas. in die entry region of capillary rheometer 80—99988
  polymer solution, second normal stress difference, meas. 80—43747
  polymer solution, turbulent flow investig. using laser Doppler velocimeter 77—58822
  porous carbonaceous materials, transient diffusion coeff. meas. 78—38400
  positive displacement measurement system for diesel pump and injector performance testing, microcomputer-controlled 80—24112
  powder, flow measurement by gravimetric method *(Polish)* 78—9740
  powder, temperature effect on flow and tensile strength 79—61668
  powder electrodeposition process, laser anemometer appl. 78—18364
  powder stream mean flow rate meas. by Doppler scatt. null enumeration *(Russian)* 78—47071
  power station dust-laden gas, cylindrical hot wire anemometer appl. 77—27632
  prepolymer, two-phase, US flowmeter optimisation 77—31410
  pressure difference devices for fluid flow, accuracy limitations *(German)* 79—98841
  pressure difference methods, for flow at submerged control sections 79—68873
  pressure losses across fluid metering nozzle, anal. and reduction method 77—51144
  pressure probe, meas. of complete velocity vector in subsonic flow 79—77316
  pressure vessels two-phase unsteady flow, meas. problems 77—27633
  pressure-difference meter measurement of swirling or axisymmetric flows 80—10330
  Preston tube calibration in transpired turbulent boundary layer 78—79397
  probe, 4-hole cylindrical cantilever, for 3D flow meas. 80—87833
  probe, spherical Pitot, construction and calibration *(Italian)* 80—69957
  probe, three parallel wire type, characts., appl. 77—62314
  prosthetic cardiac valve, concave-convex pivoting disc two-dimensional model 79—84028

flow measurement continued
- pulmonary blood flow, method for noninvasive bedside determ. 80−81762
- pulmonary capillary blood flow in dogs, atraumatic meas. 78−7552
- pulmonary haemodynamics meas. using US oesophageal probe 78−35902
- pulmonary vascular response to hypoxia, online impedance analysis system 77−52943
- pulsatile air flow, time-averaged stagnation pressure probe design 78−14116
- pulsating air bubbles in water, stability using optoelectrical method *(German)* 77−27578
- pulsating flow facility, design and evaluation 79−68863
- pulsating turbulent pipe flow, velocity field and press. gradients 80−64641
- pulse-compensation method of meas. liquid flow-rate based on NMR 80−103088
- pulsed extraction column, with perforated plates, efficiency 79−64809
- pulsed neutron measurement of single and two phase flow 79−50771
- pulsed-neutron activation anal., asymmetry effects 78−83508
- quasi-Lagrangian technique for mesoscale coastal studies 77−39386
- radiolabelled microspheres, use in meas. of regional blood flows during $+G_z$ stress 80−81786
- radionuclide mean clearance time transverse section imaging 78−73222
- radiotracer methods for laminar flow in small channels, liq. tracer method 77−58816
- radiotracer methods for laminar flow in small channels, response model 77−58814
- radiotracer methods for laminar flow in small channels, tracer-sphere method 77−58815
- Raman scattering diagnostics of turbulent flow field in coaxial jets 78−18328
- random, statistics analysed by photon correlation anemometry 80−64522
- rarefied flow of N_2, electron beam-body interactions 80−6186
- rarefied free jet, N_2^+ UV spectra for rot. temp. 80−6184
- Rayleigh-Benard flow, equal velocity fringes by speckle photography 80−75005
- reactor primary coolant flow rate determ. using gamma/neutron ratio near primary line 77−65254
- recent progress *(Japanese)* 79−98833
- reciprocating pumps, control system, high performance liquid chromatographic detectors appl. 78−92559
- rectangular cavity walls, shear stress by electrodiffusion method 80−10308
- regional myocardial perfusion determ. from H_2 washout curve 79−92459
- remote level and velocity measurement by random signal anal. from surface waves 79−72976
- renal diagnosis by blood circulation angiocinedensitometry *(German)* 79−2127
- renal function studies, combined in vitro-in vivo radionuclide procedure, technical aspects 77−90884
- reproducibility conditions analysis and obs. 77−80240
- resonant hydraulic circuit pulsatile water flow meas. using laser Doppler velocimeter 80−103091
- respiratory, improved vane respirometer *(German)* 77−40826
- respiratory flow telemetering with mag. type flowmeter 77−86654
- respiratory flow-volume integrator 77−48914
- respiratory function telemetering using combined receptor 77−86657
- respiratory gas flow meas., constant-temp. hot-wire anemometer evaluation 79−83967
- respiratory system, freq. characts. determ. 77−5093
- respiratory system forced perturbation, traditional model 79−83815
- respiratory total compliance non-invasive meas. in free-breathing rabbits 78−28123
- reverse flow sensing hot-wire probe 79−98838
- review of thermal and optical methods 78−34233
- Reynolds number characteristic curves, adjustable valves selection *(German)* 78−22439
- Reynolds stress tensor, turbulent flow in rectangular channel, use of laser anemometry *(Italian)* 79−4094
- rheometer, rot., inertial normal force correction 78−63520
- river flows, transverse mixing coeffs., evaluation from slug tests 77−21806
- river volumetric flow gauging, electronic methods 77−73891
- rivers and open channels, by anal. of random signals from surface waves 77−45205
- rod bundle void fraction in two phase flow, fast neutron scatt. technique calibration 79−82017
- rolling bottle device, for measuring flow of liqs. and powders 80−6174
- rotametric device with Hall transducer, flow meas., recording and control *(Rumanian)* 80−48826
- rotannular weight meters, for gas flow meter calibration 79−68843
- rotary gas flowmeter error anal. *(Russian)* 78−71407
- rotating annular jets, velocity distrib. and profile meas. 79−50829
- rotating flow around circular cylinder, azimuthal velocity in gas centrifuge 80−74890
- rotating turbulent flow, method for meas. vel. vector and stress tensor components *(Russian)* 80−83867
- rotation viscosimeters, real flow curve determ., with wall effects *(Russian)* 79−64714
- rotational rheometry, edge effects and related error sources 80−19536
- rotors, 2-probe synchronized sampling technique, calibration 80−14865
- saline containing dissolved O, velocity magnitude transducer 79−21733
- schlieren instruments threshold sensitivity to turbulent inhomogenities 78−79134
- sea water, current vel. determ. via neutron-activation method *(Russian)* 78−77358
- seawater, surface current probes, rapid method for data recovery 79−84518
- separate-bubble cavitation tests, nucleation meas. by Venturi tube *(French)* 79−55402
- shadow instrument with photoelec. recording, signal characts. rel. to turbulence spectrum characts. 77−35267
- shear flow, flow direction meas. and error 78−22436
- shear force instrument, force-balance 78−51263
- shock flow, time analysis using dual microwave and dual schlieren systems 77−15143
- shock front precursor, probe meas. 79−64701
- shock tube, flow parameter meas. *(Chinese)* 79−37336
- shock wave diagnostics using laser interferometer, appl. to Al plate 79−64814
- simple linearised hot wire anemometer, performance characts. 80−53904

flow measurement continued
- single scattering particle laser Doppler measurements of turbulence, data reduction 77−39379
- sinusoidal pressure response method for determ. of flow props. in porous medium 77−68713
- size distribution, reduced function, determ. from local meas. 77−68717
- skin blood flow meas. by ^{133}Xe, radiation dose 77−16994
- skin friction, meas. by viscosity balance method, appls. to three dimensional flow 77−19645
- skin friction in turbulent boundary layers, meas. techniques 78−1770
- skin friction measurement, comparison of viscosity balance and Preston tube methods 77−55109
- skin friction variation with Reynolds number, viscosity balance meas. compared with Preston tubes 77−72377
- skin-friction balance measurement, error sources 77−65828
- slurry measurement, by press. differential devices 77−35265
- small liquid flow rate monitor using displacement transducer and float 79−68836
- solar energy collector array flow imbalance detection by thermography 79−83634
- solid particles into hot high pressure gas flow, dispensing and meas. system 79−37430
- solid-liquid pipe flow, cross correlation method anal. 79−32638
- solids velocity in air by laser Doppler systems 77−84379
- sonic venturi nozzle, for volume or mass flow, differential interferometric meas. 79−68872
- Spacelab optical techniques for liquid flow and temp. meas. 79−82007
- Spar Buoy Oceanographic Telemetry System 80−46307
- spatial flow field determination, hot wire anemometry based analysis 78−59512
- spatial vorticity distrib. meas. technique 78−67289
- speckle photography, flow velocity distrib. meas. 78−67288
- speckle photography and interferometry 78−26221
- spectrometric analysers, error charact. reduction method *(Russian)* 77−42944
- spermatozoa, human, motility evaluation, photon correlation meas. 80−61745
- spherical probe appl., pressure and velocity gradients influence obs., computer-aided calc. *(Polish)* 78−34222
- spray, droplet vel. meas. using laser Doppler velocimeter *(German)* 79−50818
- standards, primary, Soviet, for mass and volume flows, of liquid and gas 77−76002
- standards for units of flow rate of water 80−43810
- standing sound waves, particle vel. detect. via hot wire anemometer 77−62124
- state-of-the-art review, special features and appls. 80−64654
- static pressure probe, laminar limiting boundary layer *(French)* 77−31402
- static pressure probe, yaw insensitive, development and testing 78−94869
- steady-state flow boiling curve, meas. using temp. controllers 79−32720
- steam, wet, supersonic flow, total- and static-press. probe characts. 77−84353
- steam turbine flow holographic interferogram processing by minicomputer 77−19656
- steam-water flow, mass vel. meas. by Pitot tubes 77−79411
- steam/air mixtures, instrument for steam fraction meas. 80−52724
- stirred vessel, velocity measurement and flow trajectory, using image sensor 80−69950
- stress transient meas. in cone and plate flow, geometry effects 77−31407
- structure-forming solutions, double light refraction and viscosimetry 79−94745
- subsonic airflows, interpretation of hot-wire probe signals 80−14857
- sudden enlargement in circular pipe, downstream flow reorganisation, spatio-temporal study *(French)* 80−38497
- supersonic, using computerised laser transit anemometer system 80−10332
- supersonic flow, meas. turbulence, using hot-film and modified hot-wire sensors 79−90356
- supersonic flow, optical method for measuring intensity of fluctuations of conc. of inert impurity 77−80234
- supersonic stream flow in vacuum, by electron diffr. instrument 78−75235
- supersonic thin turbulent layer, hot-wire anemometry, error reduction 78−34235
- survey of classic methods, range of appl. and limits *(German)* 79−77317
- swirling flow hydrodynamic parameters in flow transducer input, expt. 77−72390
- swirling or asymmetric flow meas., review 77−84360
- tachometric sensors with levitating sphere *(Russian)* 77−41586
- tachygraph, appls. to flow velocity and positional meas. 79−72977
- tank depletion flow detection by pneumatic purge probes 77−80236
- tank water, digital IC pneumatic bubbler probe system appl. 77−41569
- temperature fluctuation measurement in turbulent channel, sensor wire-supports cond. influence *(French)* 79−94751
- tensoresistive transducer for flow velocity vector meas. in gas with low spontaneous comb. temp. *(Russian)* 77−11286
- thermal, temp. field meas., buoyant vortex bubbles and turbulent thermals 78−34232
- thermal measurement systems for flow rate and flow composition *(Russian)* 80−69953
- thermal method technique *(German)* 79−82019
- thermal plume, vel. meas. by electrochem. probe *(French)* 78−9728
- thermistor-respiratory flow sensor, shunted, characts. *(German)* 78−28097
- thermoanemometer, influence of probe filament aspect ratio and diameter 80−19532
- thermoanemometry, systems of linear eqns., numerical method of soln. 77−84352
- thermocouple hot-wire anemometer for boundary layer meas. with free convection in liquids *(German)* 80−10329
- thermocouple-anemometer, mass flow meas. in shock tube 79−77300
- thermosyphon solar water heaters, transient flow meas. using laser doppler anemometer 80−61413
- thin film shear-stress gauge for three dimensional flow 78−55702
- thin fluid layers under centrifugal forces, wave flows, obs. 79−23335
- thin-wall cylinder method for heat transfer studies in tubes and channels 77−24045
- three-dimens. fluid vel. vector and temp. fields from acoustic transmission meas. 78−30394

flow measurement continued
three-dimensional characts., using five-hole probes, calibration and appl. 80—69951
three-dimensional flow field graphic representation 77—27636
three-dimensional flow structure in circular cylinder *(French)* 77—23941
thrombophlebitis diagnosis, reliability of Doppler and impedance techniques 78—77144
thrombosis detection by US, plethysmography and phlebography 78—7435
throughflow recording and measuring equipment, survey *(German)* 80—1707
tissue characteristion, static and moving, high spatial resolution US meas. techniques 80—51187
tissue perfusion measurements made with thermal diffusion probe, effect of probe geometry 80—104802
torsion-weighing effusion vapour pressure measurements, appl. to organic compounds 77—89530
total, using auxiliary pipe line *(Japanese)* 78—79395
total head/static probe meas. of skin friction and surface pressure 77—62311
transfer standards 79—68892
transient gas density meas. using neutron radiography 78—47076
transient jet experiment, multiple-laser light source 78—14114
transient-flow parameter meas. and computing set, features 77—72389
transit time correlation, appl. to flow meas. 79—68880
transit-time technique *(German)* 79—82019
transonic axial compressor rotor, anal. by laser velocimetry 79—4009
transonic flow, hot-wire anemometry and boundary layer turbulence 78—14103
transonic flow, quantitative holographic interferometry *(French)* 77—65826
transonic gas flow, holographic interferometry appl. 79—86542
transversal study, corresponding to flow characteristics *(Japanese)* 79—98834
trapezoidal profile weirs, 2-dimens., discharge characts. 79—68875
traverse methods, integration techniques comparison *(French)* 77—75871
triple-sensor probes for turbulent flow-field investigations 80—100043
true mass flow meas. theory and systems 77—11284
true volume steam content in thin channels at high pressures 79—13585
truncated autocorrelation functions, numerical inversion 80—57097
tubes with ball seatings, basic groups, appl. in flowmeters *(Russian)* 78—67287
tumour blood flow, meas. by photon activation, ^{15}O decay technique 80—104755
turbine and vortex meter comparison, theory of operation 77—84350
turbulence analysis, recurrence rate techniques 79—50831
turbulence characts. meas. using 45° slant hot-wire probe 79—72967
turbulence meas. by hot-film anemometry in two-phase flow *(German)* 77—11254
turbulence meas. in stirred vessels, scaling rules 79—23303
turbulence spectra, meas. with randomly triggered pulsed-wire anemometer 77—15141
turbulence spectrum reconstruction from light propag. time correlation function 77—19178
turbulence structure around oscillating airfoils, digital processing of unsteady periodic signals 80—10340
turbulent, optical Doppler instrument, small flow velocities appl. 78—90838
turbulent boundary layer, wall interference effects of static pressure probes 78—1762
turbulent channel flow, meas. of vorticity and turbulence prod., pattern recognition method 78—26194
turbulent flow, developing, in rectangular duct, laser Doppler anemometer obs. 77—14995
turbulent flow, hot wire meas., conduction error in probe 79—7423
turbulent flow, meas. in vicinity of cation-selective membrane using scatt. laser radiation Doppler shift 79—46301
turbulent flow fields, multidimensional, analysis 79—27720
turbulent flow meas., light beam coherence effect on optical method information capacity 80—1709
turbulent flow meas. by pulse luminescence method using N pulse laser 77—24041
turbulent flow measurement by laser Doppler anemometry, concentration and size of tracer particles, theoretical limits 78—59514
turbulent free jets, subsonic and supersonic, laser velocimeter meas. 79—77307
turbulent intensity, mean velocity, for plane turbulent mixing layers 79—50716
turbulent medium, US imaging system using random phase mask and stationary point receiver 77—80035
turbulent mixing flow, simultaneous laser measurements of instantaneous vel. and conc. 77—35287
turbulent mixing flow, velocity biasing resulting from non-uniform seeding 80—59143
turbulent mixing meas., laser light scatt. technique 77—11285
turbulent pipe flow, mass transfer, electrochem. meas. 78—5830
turbulent shear flow using hot-wire probe, effects of orientation 79—27722
turbulent shear in pipe flows, trace particle method 77—3872
turbulent structure determ. using thermoprobe unit *(Bulgarian)* 80—28584
turbulent supersonic flows, freq. response of constant temp. hot-wire anemometers 80—59149
turbulent wake, meas. with pulsed-wire and hot-wire anemometers 77—11288
two flat plates, fluid flow anal. for fluid control meas. *(Chinese)* 79—81997
two phase diffuse flow, investigation 78—59513
two phase flow, computerised tomography meas. technique 80—59135
two phase flow, indirect meas., methodological error anal. and reduction 78—34241
two phase flow continuity measurement by radioisotope method, error 79—32723
two phase flow pattern characterisation by electrical conductance probe 80—106857
two phase one component, single substance flows, probe method for phase concentration determ. 80—74954
two-dimensional space isothermal and nonisothermal turbulent flow *(German)* 80—28505
two-phase, gas-liquid mixtures, standard system design principles 77—76005

flow measurement continued
two-phase, through sharp edge orifices, correlations evaluation 78—26223
two-phase flow, digital signal processor for real-time anal. 77—80235
two-phase flow, isotopic computerised tomography meas. 80—59136
two-phase flow, local vels. of particles, using mag. markers *(German)* 77—42939
two-phase flow, measurement techniques, recent progress *(French)* 80—79411
two-phase flow, nonequil., true mass steam content meas. by diffusion indicator method 79—86538
two-phase flow, nonstationary velocity tracking by adaptive cross-correl. algorithm 78—14074
two-phase flow, time-of-flight laser anemometer 77—39383
two-phase flow, transient and statistical meas. techniques, review 77—11287
two-phase flow, with orifice-couple in horizontal pipeline 79—94744
two-phase flow instrumentation for safety anal. of LWR LOCA 80—102259
two-phase flow meas. in nuclear reactors, LOFT drag disc turbine meter rakes 80—102260
two-phase fluid velocity meas. by radiation intensity correlation 77—75996
two-phase mass flow measurement, ^{16}N tagging 79—93793
two-phase mass flow rate meas. in fission reactors using true mass flowmeter 80—778
two-phase systems, high-temperature optical void probe 79—93705
ultramicroscope anemometer for three-dimens. flow meas. in models of arterial branchings 78—35876
ultrasonic flow transmitter 80—1710
ultrasonic flowmeters 79—50832
ultrasonic meters *(Spanish)* 80—6181
underwater, significance of beam pattern side lobes 80—19136
unsaturated water flow within porous materials, obs. by NMR imaging 79—98840
unsteady gas stream temperature determ. using slow-response thermocouple 77—24046
unsteady inviscid 2-D flow analogy using stretched membrane and moire fringes 80—64658
urethral resistance and mural tension, using programmable modules 77—2067
US, microcomputer-controlled 80—24111
US blood flow imaging model eqns. and implications 79—48308
US blood flow meas. using random noise, target model and optimal receiver 77—21589
US blood flow spectral anal. using coherent optics 78—53459
US correlation flow metering for liqs. and gases 77—84378
US detectors for contactless techniques *(Italian)* 80—53891
US Doppler blood flow meas., effects of geometrical spectrum broadening 77—40725
US Doppler velocimetry for 3D blood flow meas. 78—88730
US Doppler-shift arterial flow signals, Fourier anal. 77—29187
US flowmeter, multichannel time-freq. type, operating principle 77—72387
US flowmeter *(French)* 79—1274
US flowmeter for small time-interval meas., methods *(Russian)* 77—65824
US flowmeter interface development 78—38426
US flowmeter metrological properties *(Polish)* 78—51265
US flowmeter performance anal. 79—14500
US pulsed Doppler techniques for cardiovascular meas. 77—77947
US range-gated echo Doppler techniques for cardiac output and aortic flow meas. 78—40276
US synchronized pulsed Doppler blood flow and dimension meas. in conscious dogs 79—62318
vaneless diffuser of centrifugal compressor, flow velocity meas. using laser Doppler anemometer 80—59147
variable press. drop method, flowmeter designs comparative anal. *(Russian)* 79—7427
vascular stenosis detection using flow continuity and turbulence, US Doppler method 77—40723
vascular system, US Doppler imaging, book contrib. 80—36045
velocimeter for fluctuating temp. and vel. meas. in combustion field 80—14856
velocity and direction of water flow, meas. method 80—96318
velocity and turbulence meas. by image sensor 79—77297
velocity correlation functions, direct measurement using Erdmann-Gellert correlation technique 79—27728
velocity gradients and laminar and turbulent diffusion, direct optical meas. 80—59132
velocity meas. in capillary using pulsed NMR 78—83506
velocity measurement, repetitive pulse NMR technique 80—31829
velocity measurement using Doppler laser velocitometer, fluctuation of meas. values of a constant velocity *(Japanese)* 80—6179
velocity measurements inside a rotating cylindrical cavity with a radial outflow of fluid 80—96275
velocity perturbation meas., comparison of dynamic and static hot wire anemometer calibrations 77—19644
velocity probes for non-uniform gas flow in large ducts 80—48829
velocity sensor, calibration equipment and technique, oceanographic appls. 80—8447
velocity sensor, optical *(Russian)* 78—1759
velocity vector, meas. via novel three-tube probe arrangement 77—72378
velocity vector and temp. fields, three-dimens. reconstruction from acoustic transmission meas. 78—51261
viscous flow, between concentric rot. spheres, visualisation and meas. 77—15038
viscous fluids in pipeline, optimum flowrate meas. zone 79—7425
visualisation, in environmental and technical systems *(German)* 79—86540
visualisation by foreign particle or energy optical tracing 80—96329
void fraction and phase distrib. meas. in transient flow boiling by neutron scatt. 78—94870
void traction, rotating electric field conductance gauge 77—80250
volume, integrating pressure tubes, theory, method and experimental results *(German)* 80—33712
vortex flow rotational speed meas. instrument 77—80247
vortex shedding and precession techniques 77—84373
vortex shedding flowmeter characts. improvement in low Reynolds number *(Japanese)* 78—79396
vortex shedding flowmeter for liquids 77—42934
vortex shedding flowmeter principles and potential 78—22432

flow measurement continued
vortex shedding principle appl. *(German)* 80—79419
vortices, merging, in wind tunnel, laser velocimeter surveys 79—32718
vortices in wind tunnel expts. meas. using US pulses 80—10334
vorticity, in unsteady flow, meas. technique and data acquisition 80—19525
vorticity indicators, vane-type, construction, calibration, streamwise vorticity meas. in swirling flows 79—60074
wake, of heated cylinder, turbulent temp. and thermal flux characts. using four-wire probe 80—19541
wall flow direction probe for turbulent separating and reattaching flows 80—53903
wall shear stress meas. with hot film device in var. temp. flow 77—51142
water, cavitation expts. using shock tube 80—87789
water, flow through circular pipe, pulsed NMR study 80—28566
water channel with wall cut-out, laser Doppler anemometer flow meas. 79—46403
water industry, current and new techniques 77—84367
water jet, turbulence fine struct., polymer addition effects, high speed photography 78—26178
water streams in wide channels, by laser Doppler method *(Russian)* 78—30370
water tunnel for multilayered stratified flow investigation *(Russian)* 80—1703
water-vapour velocity transient meas. by cross-correlation anal. *(German)* 77—62312
weighing techniques 77—84365
weirs and flumes, book 80—1717
Weissenberg rheogoniometer, computerised calib. and meas. of Newtonian fluids 78—87323
wide rivers, acoustic flow meas. 79—72975
wind generated waves, using submerging hot-wire probes 77—7483
wind tunnels, laser velocimeter appl. 78—46467
wind-tunnel laser anemometer photon correlation techniques 77—80256
Winter-Kennedy method, research 79—68864
Wirbelrespirometer dynamic response improvements *(German)* 78—28099
wire-wrapped 61-rod bundle edge subchannel flow distrib. 79—9676
worldwide flow meas. calibration facilities list 77—62322
x-array hot wire probe, prong config. 78—75243
X-hot wire probe method for two-dimensional nonsteady air flow *(Japanese)* 80—59134
X-ray diagnostics, temp. field determ. *(Russian)* 77—19648
xerographic cascade flow, carrier bead velocity distribution meas. probe 80—47136
zero-mean-shear mixed layer, turbulence meas. 80—1705
$Fe_{40}Ni_{40}P_{14}B_6$, metallic glass, glass transition, viscous flow and differential scanning calorimetry meas. 80—96635
HF chemical laser, 10 kW CW arc-driven, diagnostic system for supersonic free jets 77—23667
H_2O, low density flow temp. and density meas. by submillimetre spectroscopy 80—43816
He, liq. in forced-flow Nb_3Sn conductors for toroidal-field coils, flow characts. 79—58741
Hg, acoustic streaming meas. 79—64380
NO_2, real time method using tapered variable area flowmeter 78—71410
^{16}N tag for water transient flow meas. 79—14504
Na flow meas. in main pipes of LMFBR, application aspects 80—22884
Na flowmeter principles *(Japanese)* 80—28585
Na, liquid, anal. of temp. fluctuations for local flow velocity determ. *(Spanish)* 79—46405
O_2 molecule reduction flow probe for cerebrospinal fluid 79—100777
^{133}Xe washout curve discriminant analysis for lower extremity vascular impairment 78—35949

flow process charts *see flowcharting*

flow resistance *see viscosity*

flow separation
aerodynamic interaction between two spheres at Reynolds numbers around 10^4, induced forces 79—81946
aerofoil, dynamic forces acting, subsonic instabilities *(French)* 78—67213
aeronautics, infinite swept attachment line boundary layer, turbulence 80—74840
air flow over rearward facing step, flow separation meas. 80—69885
air flow separation over water waves 77—11208
air intake, at high incidence, finite element anal. 79—3999
air scoops at supersonic and hypersonic vels., throttling, separation and central body cooling 80—14739
air-conditioning systems, acoustical characts. of certain flow-spoiling devices 77—50832
airfoil, leading-edge separation bubbles, shear layer and transitional reattaching flow 77—27580
annular diffuses with conical walls, swirling flow and separation 80—43715
aortic arch principle separation region, depend. on freq., amplitude and rate of flow 77—52831
arbitrary body, unsteady separated inviscid incompressible flow, numerical soln. 80—28509
axisymmetric afterbodies, separated turbulent flows, wakes, exhaust plume effects 80—74885
axisymmetric bluff body flows, near wake props. 77—58694
axisymmetric starting vortices, visualisation using laser-induced fluoresc. 77—35283
axisymmetric transonic turbulent base pressures 80—19425
axisymmetry jet, inblow parameter effect on separation, boundary layers and heat transfer *(Russian)* 80—24064
Baylor left ventricular bypass pump, calf expts. 78—73295
bibliography, 1975-76 77—27526
bibliography, 1975-76 77—84250
bibliography 77—58671
bifurcation on refl. from shock tube end wall 79—46346
bluff body, boundary layer separation, control method 79—72881
blunt circ. cylinder, separated, reattached, redeveloped air flow, heat transfer characts. 77—58692
blunt flat plates, air flow, 2-D, thermal boundary layer characteristics, nose shape effects 80—92121
body of revolution with heating and cooling, boundary layer transition and separation 80—64518
boundary layer, laminar, subsonic, strong slot injection, triple deck theory 80—74831

flow separation continued
boundary layer flow past circular cylinder, rapidly convergent series soln. 80—96244
boundary layer form. in inviscid flow with vorticity 78—14022
boundary layer separation, on moving walls, use of integral theory 77—58640
boundary layer separation, transverse surface curvature effect 79—64644
boundary layer separation from wall, nature of reversed flow 77—75956
boundary layers, laminar, compressible, Prandtl = 0.72, sharp pressure rise effect 80—83782
boundary-layer flows from fixed to moving surfaces, gap effects 79—14377
cavity flow about slender body of revolution in tube 80—33641
cavity flow at high Reynolds numbers 77—31276
channel, two-dimens., turbulent flow with separation 80—19356
channel flow stability, influence of nonparallelism 80—83845
channel flows, severe nonsymmetric constriction, curving or cornering, separation 80—92222
circular cylinder in liquid Na crossflow, local heat transfer, numerical study 80—64539
circular cylinders, surface-roughness effects on mean flow, turbulent boundary layers 80—92128
circular cylinders and spheres, fluid flow and convective heat transfer *(German)* 79—94624
closed stationary separation zone formation as $Re \rightarrow \infty$ 79—81846
compressible laminar boundary-layer, 2D eqn., near separation, numerical soln. 77—46989
compressible supersonic turbulent boundary layers, compressible press. gradient effects 79—60001
convection in channel downstream of constriction, local transfer coeffs. augmentation 78—5800
corner, three-dimens., Navier-Stokes eqn. soln., numerical code 78—30314
corner boundary layer, press. gradient and leading edge effects 80—14652
corner interaction of boundary layer and shock wave, flow separation 80—96287
critical flow separation, modified Stratford method 77—15000
curvature and displacement effects on separation of accelerated flow past cylinder 80—10272
cylinder, axisymmetric, with slanted base, near-wake flow 80—74886
past cylinder and plane 77—68567
cylinder in rotating system, flow separation 79—68720
cylinder on β-plane, prograde and retrograde rot. flows, boundary layer separation 80—92189
cylinder wakes, vortex periodicity criterion, separated flow region 80—19399
cylinders, eccentric rot., Newtonian flow inertial effects 77—919
dense ionised gas, MHD flow with viscous stress relax., similarity anal. 78—22427
detached flow around bodies with local vortex sheets 80—87778
detached flows past a cylinder with a flat end, subsonic and transonic vels. 80—92187
die swell problem, free surface separation 79—90295
diffuser, self-similar MHD flows with induced mag. fields 78—34205
in diffuser 77—84221
disc, accel. influence on separation flow 79—86443
disc normal to wall, turbulence intensities and local mean vels.; separated flow 80—64531
discrete vortex method for flow representation including separated regions 77—80172
dispersion in porous media, pore distrib. and flow segregation effects 80—10302
duct, plane, with sudden expansion, aerodynamics 79—94722
expansion corner effect on shock-wave and boundary layer interactions 80—14737
external supersonic flow, turbulent boundary layer interaction on concave corner and spherical intake 77—55032
extraction columns, perforated plate, operation under jetting conditions, design 79—90299
ferrofluid droplet, interphase boundary hydrostatic characts. in uniform mag. field 80—33692
film condensation, along vertical plate in enclosed chamber, effect of non-condensable gas 77—80703
flow past circular disc, appl. of Hess' surface source model 77—11167
flows with heat addition, review 77—916
fluid flow past sphere, anomalous separation, wake formation 77—51091
fluid-particle separation, chainlike form. of particle deposits 77—77813
fluid-surface interface, static contact line, slip at wall and shape of free surface 80—53737
forced and free convection in laminar flow over plate 80—24005
forward facing step, neutrally stable atmospheric flow, shear layer, separation, vortices 80—48685
free shear layer behavior in rotating systems 80—1545
furrowed channels with pulsatile flow, Navier-Stokes soln. flow patterns, separation 80—33672
furrowed channels with pulsatile flow, observed flow patterns, separation and vortices 80—33673
gas, perfect, vortex sheet, separation from smooth body at large Reynolds number *(French)* 80—74908
gas centrifuge, fluid flow anal., computer calcs., appl. to UF_6 77—75924
gas jet blowing into supersonic flow without 3-dimens. boundary layer separation, nozzle shape 80—100009
gas-film cooling efficiency in supersonic axisymmetric nozzles 79—98715
gas-liquid pipe flow, influence of return bends on velocity ratio 80—74962
gas-solid turbulent shear channel flow, particulate motion, numerical simulation 80—53863
gaseous microbubble growth in laminar separation bubbles 80—106821
geostrophic adjustment in sea straits and wide estuaries, two-layer system 79—48503
high Reynolds number supersonic flow, compression corner flowfields, turbulent boundary layer separation 80—14735
highly separated transonic flow, first vel. and RMS vel. fluctuation meas. 79—77166
horizontal circular cylinder, mixed convection, boundary layer effects 77—15011
hydraulic resistance of channels with separation or merging of incompressible flows 77—68669
hydrodynamic eqns. formulation 77—68682

flow separation continued
hydrofoil cavitation noise and inception, boundary layer development 77−55057
hydrofoil profile for accelerating cascade, surface press. distribs. 78−18321
hydrofoils, two-dimens., with massive turbulent separation, press. distrib. prediction 77−7377
hypersonic conical nozzle, boundary layer separation from compression shock 80−48766
hypersonic flow, separation behind aerofoil 77−42864
hypersonic laminar boundary layer, shock wave interactions 77−89151
ideal fluid flow round body with formation of tangential separation *(Russian)* 77−35124
ideal fluid separated flow, turbulent wakes and vortices locations 79−98732
impulsively started circular cylinder, initial flow, separation, vortices, wakes and boundary layers 80−19401
impulsively started flow about circular cylinder, two-dimens. vortex shedding, inviscid model 80−19400
incompressible boundary layer separation, review, book contrib. 77−51033
incompressible separated boundary layer prediction, including viscous-inviscid interaction 80−1548
incompressible separated boundary layers including viscous-inviscid interaction, transition bubble 80−64515
interacting boundary layers in high Reynolds number laminar separated flow 77−42865
internal flow computation using coupled boundary layer-inviscid core, elliptic representation 80−1549
internal separated flows at large Reynolds number, Poiseulle flow development in channel 80−53755
laminar boundary layer, separating, incompressible, over smooth step of small height 80−19325
laminar boundary layer flow, three-dimens., soln. using method of integral relations 77−58645
laminar boundary layer with separated bubble 77−23935
laminar boundary layer with separation and reattachment, unsteady 79−59963
laminar flow, direct finite difference calc. of through separated regions 77−35115
laminar flow with separation, successive approx. algorithm, convergence *(Russian)* 78−75117
laminar forced convection between concentric spheres, num. soln. 77−42831
laminar separated flow between periodically varied walls, num. simulation using perturbated primitive variables method 77−54971
laminar separation bubbles, airfoil performance effects, turbulent shear layer reattachment 80−48774
laminar separation of incompressible fluid streaming past smooth surface 77−75897
laminar swirled flow in annular channel 79−90260
laminar viscoelastic boundary layers, role of fluid relaxation time 79−81829
Lavrentiev wake model and cascade 77−35145
leading edge bubble formation, peaky airfoil *(French)* 80−64524
liquid dielectrics between charged coaxial cylinders, separation boundary equilib. 79−64781
longitudinal blunt circular cylinder, axisymmetric separated and reattached flow, turbulence 80−79285
MHD boundary layer flow, on flat plate, effects of varying velocity 78−67275
MHD generator, compressible laminar boundary layer separation from segmented electrode wall 77−27598
micropolar fluid, nonsimilar incompressible laminar boundary-layer flow 77−35184
Newtonian flow between rotating cylinders 77−80186
non-Newtonian flow between rotating cylinders 77−80186
nonlinear stern wave production in pot. flow past flat bottomed body 80−38425
nose separation for laminar boundary layers on body of revolution 80−59091
open pipe exits, flow during acoustic resonance, vortices and boundary layers 80−92224
periodic wavy surface, laminar boundary layer, nonlinear anal. for long waves, separation 80−87759
permeable contour in flow with jet separation, impulses and impact effects 80−92196
plane converging duct, separation zone for turbulent boundary layer and oblique shock interaction 80−14759
plane symmetric sudden expansion over backward step, turbulence and separation 80−53752
plate, Kirchhoff-Rayleigh flow, separation, wakes and vortices 80−69839
plate, thick, parallel flow, with separation and reattachment, local and average mass transfer *(German)* 78−22339
plate at angle to flow, heat loss meas. for boundary turbulence and separation 78−90846
plate leeside, viscous hypersonic flowfield boundary layer separation 80−48743
polymer flow on inclined plane, edge effects 80−19451
polystyrene solution, drag reduction, mean vel. profile 78−22384
porous medium, saturated, mixed convection boundary layer flow on vertical surface 80−106798
post shock expansion behind normal shock on curved wall, flow separation, book contrib. *(German)* 80−1628
potential theory model for separation regions behind shock waves *(German)* 80−1636
pseudo-shocks in cylindrical duct 77−58722
pseudoshock, friction in channel 77−27546
pulsatile flow in channel of small exponential divergence, flow separation 77−86528
rarefied binary gas mixture, two-dimens. channel flow, separation phenomena, num. soln. 77−58740
real gas laminar boundary-layer separation prediction methodology 80−19322
rearward facing step, turbulent incompressible reattaching flow, adverse press. gradient effects 80−69773
rectangular body, laminar flow, separation bubble and stagnation line 80−64514
rectangular body in forced convection, heat transfer study, flow separation 80−74874
along regular surface line *(French)* 79−41661

flow separation continued
rigid circular cylinder in confined flow, fluctuating lift and drag forces 77−15118
rivers, stable numerical model of local scour 77−21809
roll of slender wings at incidence in separated flow 77−3840
rotating sphere, small yaw ang., laminar boundary layer *(Japanese)* 78−38272
second-order fluid, flow separation at straight edge 77−15079
semi-infinite body, two-dimensional linear and nonlinear stern waves, separation point 80−69852
separated boundary layer flow, vel. characts. and recirculation 80−38456
separated flow around flat plate, influence of vortex diffusion 77−19613
separated flow behind double step at duct entrance, turbulent fluctuations and heat transfer 77−42829
separated flow types over slotted wings 80−38458
separated flows, three-dimens., with vortex filaments, num. simulation 77−58706
separated flows, upwind and central difference schemes 80−28539
separated flows around circular cylinder, numerical solns. 77−3815
separated high Reynolds number flow past a corner, numerical solns. 79−81855
separated region experiments, galloping and vortex induced oscillations 80−43750
separated turbulent boundary layer, laser velocimetry meas. 77−35274
separated turbulent boundary layer at compression corner, mean flow meas. 77−42867
separating boundary-layer flow calculations 79−68678
separating laminar boundary layer, horsehoe vortex 80−19405
separating layer with airfoil-type press. distrib. 77−31290
shaped edge cylinders in oscillatory flow, separation and vortex shedding forces 80−53825
shock separated boundary layer, suction effects, compressible Navier-Stokes eqn. solns. 80−24050
shock wave interaction with turbulent boundary layer disturbed by injection 80−74916
shock-wave boundary-layer interaction, appl. laser anemometer 77−35275
short plane diffuser, wall turbulence meas. 80−38384
singularity at free streamline separation pt., capillary modification 80−1655
solution branching in wavy flow problem of viscous liquid with free boundary 80−14760
spheres falling in viscoelastic fluid, interactions along line of centres 77−15106
spheroid at incidence, flow separation, laminar separation lines, turbulent separation 79−72878
spiked bodies in supersonic flow, nonstationary separation 80−38460
square prism separation-reattachment wall press. 79−98704
static pressure probe, laminar limiting boundary layer *(French)* 77−31402
statistical characteristics of pressure fluctuations on plate behind spoiler 80−14761
steady separation from curved surfaces 77−75879
steady viscous flow past circular cylinder, numerical study, vortices and separation 80−92108
step-backward flow, with surface discontinuity, flow separation 79−77078
Stokes flow, attached and free eddies 80−48679
Stokes flow, effect of separation on drag and torque 80−106818
Stokes flow, in wedge-shaped trench, separation of variables theory 77−47093
Stokes flow, past spherical caps, visualisation of separation 79−60076
Stokes flow, viscous wake development for spherical particle near large obstacle 77−89126
Stokes flow between two spheres, flow separation 77−11176
Stokes flow past circ. arc, separation 79−90214
Stokes flow past plane with cylindrical ridge or trough, separation 78−55653
Stokes flow separation, local boundary geometry depend. 77−54949
Stokes flow visualisation 79−77064
Stokes flows, eddy motions between fluid spheres 80−48680
stratified flow, averaged formulation, high order dispersion effects in separated flow models 80−74960
streamwise vortex separation and stability *(German)* 80−6069
sub and transonic flow over wing, flow separation, vortex struct., shock wave shape *(French)* 80−14733
subsonic, flow separation downstream of stepped rod in wind tunnel 77−58718
subsonic, three dimensional flow transverse to circular cylinder 77−58719
subsonic turbulent flow past a downstream facing annular step, flow separation 80−43696
subsonic turbulent flow past a planar fence, separation bubbles 80−53807
supersonic, flare-induced separation 77−3843
supersonic, leeside flowfields of planar delta wings, Reynolds number 79−60003
supersonic and hypersonic flow, turbulent boundary layer separation and reattachment on flat plate with ramp 77−23990
supersonic boundary layer, moderate injection with reattachment, shear layer 79−32562
supersonic flow, jet injection, separation zone, boundary layer thickness and transverse curvature effects 80−48745
supersonic flow field meas. of slender cone at high angle of attack 79−77177
supersonic flow over compression ramp, laminar separation, second order asymptotic soln. 80−83828
supersonic laminar boundary layers, strong slot injection, flow separation 80−48738
supersonic laminar boundary-layer separation by slot injection 79−98747
supersonic laminar viscous flow, partial differential eqns., separation 80−24062
supersonic rarefied gas flow at low Reynolds no., heat transfer 79−98713
supersonic self-excitation of acoustic oscillations 77−7411
supersonic separation flow, 2- and 3-dimens., turbulent boundary layer and shock wave 80−100017
supersonic stream, laminar separation, Reynolds no. effect 80−19432
suppression by sequential wall jets 77−31354
surface orientation effects in air flow 79−98709

flow separation continued
- suspensions, settling, accelerated by addition of buoyant particles 79—96369
- thermal boundary layers in gradient flow around nonisothermal surfaces, temp. depend. of fluid thermophys., props. influence *(Ukrainian)* 77—51054
- three dimensional separated turbulent flows at supersonic speeds 80—19435
- three-dimensional boundary-layer separation 80—92188
- three-dimensional flow over wings with leading-edge vortex separation 80—74927
- transonic flow over airfoil, steady and unsteady, shock-induced separation 79—59999
- transonic turbulent boundary layer, shock wave causing separation *(French)* 79—77186
- triple deck problem for supersonic and subsonic flow, numerical technique for separation 80—14757
- tube, round, vortex streams, radius of separation *(Russian)* 80—69841
- tube bank heat transfer in air crossflow at high Reynolds nos. *(Russian)* 78—14010
- turbulence measurements in a constricted tube, haemodynamic appl. 80—53860
- turbulent boundary layer separation at curved wall with shock 79—46343
- turbulent boundary layer separation near step 79—64646
- turbulent boundary layer separation prediction *(Chinese)* 80—6035
- turbulent boundary layer with separated flow, integral method 80—1547
- turbulent flow separation, review 80—1543
- turbulent heat transfer measurements in axisymmetric external separated and reattached flows 80—10234
- turbulent pipe flow, segmented blockage, downstream flow and pressure characts. 80—43778
- turbulent separating boundary layer, subsonic, integral prediction method 80—1623
- turbulent separating flow 79—98703
- two dimensional shockwave—turbulent boundary layer interaction, flow separation 80—14758
- two tandem circular cylinders, flow at very high Reynolds numbers 80—19341
- two-dimensional shear flow, viscosity effects, microscopic model 77—89085
- two-phase flow, energy dividing props. in discharge from supersonic jet *(Russian)* 77—39332
- two-phase stratified horizontal flow, averaged and local instantaneous formulations, stability 80—64613
- unsteady, behind normal plate, discrete-vortex model, modified velocity-point scheme *(Japanese)* 80—79331
- unsteady, behind normal plate, discrete-vortex model, velocity-point scheme *(Japanese)* 80—79330
- unsteady boundary layer separation, mathematical criterion 80—69884
- unsteady comp. laminar boundary layer flow, num. anal. 79—94586
- unsteady laminar separation and stall from aerodynamic surfaces 80—59090
- unsteady separated flow, aerodynamic characts., vorticity field 80—38457
- UVUTUP two-phase separated flow models 80—48793
- variational methods, book contrib. 79—32456
- viscid-inviscid interaction of incompressible separated flows 77—19593
- viscous two-dimens. incomp. flow with separation at cascade inlet edge, num. calc 79—90232
- vortex free downflow, in vertical drain 77—51098
- vortex shedding from smooth and roughened cylinders in crossflow near plane surface 79—81911
- vortex tube input parameters, effect on rate of rotation of flows *(Russian)* 80—96264
- vortices formation in mixing layer downstream of a separation in near wake of body *(French)* 80—48716
- wake of circular cylinder with boundary layer suction 80—53785
- wall flow direction probe for turbulent separating and reattaching flows 80—53903
- wall turbulence struct., adverse pressure gradients effects, fluctuations and separation 80—10231
- wave-induced flow, through sharp-edged orifice, starting mechanism 77—75925
- wedge impulsively set into motion, boundary layer development 80—79259
- wedge like sharp edge starting vortex, flow visualisation expts. 80—59046
- wedges, high Reynolds number flow, base pressure in near wake 80—59038
- wind turbines, compact shroud theory 77—72373
- yawed cone, anal. of compressible laminar boundary layer 77—23973

flow through porous media
- accelerated flow, at permeable graphite burning surface, turbulent heat/mass transfer 78—38417
- acoustic absorption in flexible porous materials 79—32115
- aerosol, penetration through high efficiency filters 79—27690
- aerosol particle deposition in fibrous media with dendritic pattern 77—60124
- aerosol particle deposition in flow through model filters 78—1740
- aerosol particles, dendritic deposition in fibrous, inertial impaction and interception 80—74945
- air, outflow from porous materials and noise reduction theory of porous diffuser *(Chinese)* 79—50785
- air injected through porous surface, shock wave interaction with turbulent boundary layer 80—74916
- air-H_2O injection into permeable bed for underground coal gasification, numerical model 80—30359
- anisotropic porous media, degrees of anisotropy of fluid flow and diffusion (elec. conduction) 77—51109
- annular conduit, wall suction, turbulent flow *(French)* 78—18343
- annular region, steady flow 78—75201
- annulus with porous walls, temperature distrib. 77—15112
- aquiferous phreatic media, porous, filtration parameters of polluting miscible fluids 80—53855
- axisymmetric body, skin friction of turbulent boundary layer 78—9630
- Barenblatt's problem, flow through media with double porosity, anal. using continuum theory of mixtures 80—83841
- between porous walls of different permeability, quasilinearisation soln. 79—55415
- binary mixtures flowing through activated C, adsorpt. interference 80—107635

flow through porous media continued
- Blasius type boundary layer subject to blowing or suction, transition behaviour 79—18869
- blast furnace, simulated, interaction between gas and liq. flow 80—10300
- blob mechanics visualisation in flow through porous media 79—4076
- blood, red cell flexibility, whole blood filtration technique using 5 μm pores *(German)* 78—57030
- blood plasma filtration from whole blood, effect of various parameters 78—48826
- body immersed in fluidised bed, max. drag forces 80—14808
- boiling, from porous coated surface 79—76946
- boiling and evaporating liq. heat transfer, on capillary and porous surfaces 78—94526
- boiling in steam generating pipe with Fe oxide deposits on wall, steam bubble growth 79—76947
- botany, transpiration from plant leaf, simulation expts. 79—48279
- boundary layer, porous plate, vel. and friction stress distribs. 77—84243
- boundary layer, wall shear stress with mass transfer 78—47032
- boundary layer extraction through a system of slots of finite width *(Russian)* 79—27692
- boundary layer flow on vertical surface, mixed convection 80—106798
- boundary layer on porous plate with suction and blowing, hydrodynamic and MHD flow 78—34201
- boundary layer with blowing, numerical exponential box scheme 79—1240
- boundary layer with hard suction 78—26097
- bubble boundary layer formation over inclined porous plate 80—19504
- bubble distribution, eruption diam. in fluidised bed with horizontal tube bundle 80—14781
- bubble Reynolds number effect on heat transfer of forced convection subcooled boiling *(Japanese)* 80—19365
- bubbling gas, liq. repulsion effect 77—58784
- building with porous walls for air ventilation, heat transmission 79—4016
- buoyancy induced flow over inclined heated porous surface, vortex instability 80—33601
- butane, condensation in porous bulk media 78—47510
- capillary equilibrium, theory 80—24091
- capillary equilibrium at surface of porous body 79—60059
- capillary mass transfer of porous solids based on pore distrib. curves 77—7443
- capillary penetration problem, refined mathematical anal. 80—24713
- capillary porous bodies, boiling heat transfer to liquid N_2 or He 80—1575
- capillary porous body, drying, X-ray absorption obs., radiometry, temp. control 78—67023
- capillary system, interconnected, analysis of flow and flow resist. 77—47080
- capillary system, isolated and interconnected, rate of liq. uptake 77—47081
- capillary-porous bodies, heat and moisture transfer, analytical formulae 78—67013
- capillary-porous bodies, internal mass transfer, influence of inhomogeneous elec. and mag. fields 80—6138
- capillary-porous body, slit model 78—47031
- capillary-porous structs., heat transfer and max. heat flux with boiling 80—33600
- capillary-porous submerged coating, boiling model 77—65792
- cascade wake pattern with trailing-edge slot or surface suction 78—90909
- cascaded blade surface, appl. turbulent boundary layer with suction or injection 77—31377
- catalyst, simultaneous forced convection, diffusion and reaction 77—35254
- catalyst granular bed, static, flow transfer processes 80—45554
- catalysts, heterogeneous, gas phase diffusion and reaction calcs., viscous flow importance 79—47970
- catalytic reaction in porous solid with boundary layer flow 78—31684
- cellulose acetate membrane water permeab. at low press., nature of flow 77—73467
- cellulose acetate membrane water permeab. at low press., temp. var. 77—73466
- ceramics, frost action under one dimens. heat flow *(Japanese)* 79—79140
- channel, axisymmetric, with axial press. gradient injection, turbulent boundary layer characts. 79—37304
- channel, packed with spherical elements, hydrodynamics heat exchange 79—94712
- channel and tube flow with mass transfer and vel. slip 77—84322
- channel bounded by confocal porous elliptic walls, steady viscous incompressible flow 80—43776
- channel flow, nonerodible porous lining thickness effects 77—58788
- channel with periodically varying diameter, model for randomly packed beds 78—63493
- channel with porous walls, convective diffusion and mass transfer *(French)* 80—79305
- channels with porous walls, turbulence development *(Russian)* 77—27590
- charging current generated during liquid hydrocarbon filtration 77—55082
- chemical gas-liquid reactions in packed trickle bed, extended crossflow model implications 79—46399
- chemical pollutant, hydrodynamic dispersion in soil *(Italian)* 77—41071
- chemically active liquid in horizontal porous bed, convective instability 79—41769
- chemically reacting flows in porous media, numerical solns. 80—43801
- chemically reactive flow, stiff boundary valued problems in kinetics and diffusion, numerical methods 79—86525
- chemically reactive flow in porous catalyst, conc. and temp. profiles, computation method 79—86523
- coal, permeability to methane, influence of temp., geostatic and stratal press. *(Russian)* 79—66695
- cocurrent two-phase downflow through packed beds, multiple hydrodynamic states 79—18942
- cold fluid displacement by hot fluid in porous medium, stability 79—27691
- column drainage, moving boundary problems, theory and numerical analysis 78—81252
- composite mixture, flow through porous medium, Rayleigh-Taylor instability 80—69912
- compressible flow past profile set between permeable walls 79—46335

flow through porous media continued
compressible fluid layer through porous medium, thermal instability 80—92114
condensable rarefied gas flow through porous media, heat and mass transfer 78—59473
condensation on rotating disc in presence of const. axial suction 77—42839
conducting fluid, finite amplitude overstable convection, stability *(German)* 79—41751
conducting fluid, uniform current, flow past conducting porous sphere 78—34204
conducting fluid film drainage over permeable wall in transverse mag. field 79—41761
conducting fluid in porous box, thermohydromag. stability and onset of convection 77—62308
conducting liquid flow on moving porous plate with Hall effect 79—18964
conical flow of non-Newtonian elastic power law fluid with injection/suction, similarity solns. 79—14439
consolidation in compressible mixtures 79—46271
constant pressure filtration, filter medium fast plugging, mathematical models 80—100030
constricted unit cell model, isotropic granular media, creeping Newtonian flow 78—30350
convected heat loss, forced or free, through porous insulation filled cavity wall 77—75909
convection, effect of temp. depend. viscosity and thermal expansion 79—32662
convection, finite amplitude, three-dimensional, in cubic box of fluid-saturated porous material 79—55373
convection, free, in saturated porous medium boundary layer with lateral mass flux 79—27689
convection, free, unsteady, flow past vertical plate with const. suction and mass transfer 78—18290
convection, free, unsteady, flow past vertical plate with variable suction and mass transfer 78—18291
convection, infinite media with compact heat source 79—32659
convection, mixed forced/free, from horizontal plate, in porous medium 77—75908
convection, mixed free/forced, about inclined surfaces in porous medium 77—75973
convection, natural, in horizontal porous medium subjected to end-to-end temp. difference 78—91010
convection, nonlinear, in anisotropic porous media 79—55414
convection, past hot porous circ. cylinders, of 2nd-order liq. 79—14476
convection about permeable cylinder, numerical anal. 79—98723
convection fluid dynamics in a model of a fault zone in the Earth's crust 79—34778
convection in confined porous medium 78—34136
convection in porous cavity, Darcy medium, 2-dimens. solns. 78—91007
convection in porous layer flows 77—39343
convection in rectangular box containing saturated porous material 78—71393
convection natural, in porous medium, singular perturbation problem 79—94715
convection onset, natural, in heated water-saturated porous cylinder 78—59478
convection onset, porous elastic matrix, variable prop. effects 77—84321
convective dispersive equation, movement of chemical pollutants in groundwater, model 80—16855
convective heat transfer in porous layers by integral methods 79—7408
convective heat transfer in porous media 80—6053
convective heat transfer in porous medium *(French)* 77—72298
convective instabilities 77—80213
convective motion in a porous medium near equilibrium instability threshold 79—14398
convergent shock wave in ideal elastic nonhomogeneous medium 77—55036
coolant flow rates through porous media, heat and mass transfer *(Russian)* 78—59479
cooled porous wall, temp. state, numerical soln. 80—14693
cooling, by liq. boiling in capillary porous layer, statistical model 77—89196
Couette flow, permeable wall layer, heat transfer and temp. distrib. 78—51165
Couette flow, plane, past permeable bed, buoyancy effect 80—92215
countercurrent capillary saturation of porous media by active impurity solution 80—38489
crude oils, heavy, and solvents, flow of mixtures *(Spanish)* 79—98800
curtain cooling, behind permeable surface section, effect of injected gas flow distrib. 78—42657
cylinder, flow past at small Reynolds no. 79—7407
cylinder, perforated, circ., finite-aspect-ratio, drag coeff. 79—23360
cylinder, permeable, in viscous fluid, friction coeff. 79—46385
cylinder immersed in porous medium, unsteady heat transfer, Darcy flow 80—83794
cylindrical porous medium, free convection boundary conditions, mean heat transfer 80—79302
dam porous media unsteady flow calculation, combined finite element/characteristics methods appl. 78—91012
dam seepage, variational inequality appl. to flow through porous media 80—100028
Darcy's law, theor. deriv. 77—68683
Darcy's law generalisation for nonuniform flows 80—10305
Darcy flow, chilled pipe freezing zone, finite difference method 78—94734
deformable media, nonequilib. thermodynamic theory 79—27688
diffusers, 2-dimens., with suction through porous parallel side walls, characts. *(Japanese)* 78—83492
diffusion, 2-D, transient, along high-diffusivity lamina bisecting half-space 80—106841
diffusion coeff. meas., transient tech. for carbonaceous materials 78—38400
diffusion in porous system in crossed electric and mag. fields 78—34202
diffusion of immiscible fluids in porous media 79—90329
diffusion problem, nonlinear, soln. with const. flux boundary conditions 77—75782
diffusional extraction, effect of entrapped gas and resaturation 79—37392
disc packed column with falling liquid film, gas phase mass transfer involving vap. diffusion 78—94815

flow through porous media continued
disk, fluctuating flow induced by periodic suction 77—68592
dispersion coefficients, longit. and transverse, in unsaturated Plainfield sand 79—53382
dispersion in porous media, pore distrib. and flow segregation effects 80—10302
dispersion resulting from flow through spatially periodic porous media 80—92216
drag on bodies of revolution, effect of distributed boundary layer suction 77—46998
ducts with porous walls, Navier-Stokes exact eqns. 78—67266
dusty-gas equation modification to predict mass transfer in porous media 79—46377
dynamic behaviour of a porous medium saturated by a Newtonian fluid 80—83840
dynamic theory, hydrodynamic eqns. and thermodynamic transfer eqns. eddy motion characts. 80—6136
Earth crust, implications of dilatancy-fluid diffusion theory for aftershock sequences 80—85604
Ekman and Hartman layers on plate with variable suction or blowing 78—38416
elastic liquid flow past porous plate 77—15078
elastic porous media, acoustic phenomena 78—25997
elastic porous media, transient compressible liq. flow, linearisation of nonlinear partial differential eqn. 78—63490
elastic viscous fluid, unsteady flow past infinite porous plate 79—68794
elastic-viscous fluid, steady flow through annulus of porous rotating coaxial cylinders 77—72349
elasticoviscous flow along plane wall with periodic suction 79—10594
elastoviscous liquid, combined free and forced convection flow through porous channel 80—103073
electrically conducting rarefied gas, oscill. flow, past vertical porous plate, free convection 78—90830
electrically conducting rarefied gas near accelerated porous plate, MHD flow 80—14836
electrokinetic measurements with submicron particles and pores by the resistive pulse technique 77—86384
electroosmotic transport, of nonaqueous media, in strong electric fields 77—29043
elliptic porous slider, fluid dynamics 79—18952
equations of motion of fluid in porous medium with stagnation zones 79—18951
Ergun equation, accuracy and applicability study 80—19498
erythrocyte, flow resistance into pores 80—61609
ethane, condensation in porous bulk media 78—47510
evaporation from capillary pore, mass transfer kinetics 78—51233
evaporative cooling of porous wall, thermal state of vapour zone *(Russian)* 79—64763
external condensation problem, with suction (blowing), self-similar soln. 79—94705
ferrofluid, helical flow with heat cond. between coaxial porous tubes 79—23371
fibre bundle, centrifugal flow, fluid vel. and press. distribs. *(Polish)* 78—51236
fibrous filter, distrib. of fluid vels., flow resist., random flow model 80—79393
fibrous metallic material, flow and internal heat transfer 77—35228
Fick's law validity for transient diffusion through porous medium 80—13003
film cooling, by injection from porous section 77—51041
filter beds, axially symmetric, water flow using conducting paper analogue 77—80211
filtering gases, mixing zone in different porous media *(Russian)* 77—51112
filtration, nonlinear nonstationary, flow inhomogeneity effects 79—68799
filtration, nonlinear nonstationary *(Russian)* 78—38399
filtration, pressureless nonlinear 79—81960
filtration in heterogeneous earthen dam, problem solvability 80—90110
filtration of immiscible liqs., model 79—68800
filtration problem, free boundary enclosure 78—55687
filtration problem, smoothness of free surface in porous dam 77—47079
filtration theory problem soln. *(Russian)* 80—74970
fingero-imbibition phenomena with varying phase density, two parameter singular perturb. soln. 79—29789
finite element anal. of free boundary problems, book contrib. 79—32665
finite element methods, book contrib. 79—32446
fixed and fluidised beds, heat transfer from particle to fluid, stochastic model 78—51234
fixed porous beds under isothermal conditions, velocity distrib. flow model *(German)* 79—77242
fixed swarm of permeable spheres, appl. of self-consistent model 78—67260
flame radiation, in IR porous perforated gas radiators 78—3335
flat plate boundary layer in porous medium, free convection, similarity solns. 78—75199
flat porous plate with suction, unsteady heat transfer, boundary layers 79—77105
flow normal to perforated plates, heat transfer and friction loss 78—94733
flow through thin porous layer *(Russian)* 79—14469
fluctuating flow of viscous cond. fluid on porous plate in rot. medium with transverse mag. field 79—90340
fluctuating flow of viscous fluid through a porous medium bounded by a porous plate 80—24088
fluctuating flow past an infinite plate with suction and constant heat flux, heat transfer analysis 79—50724
fluid filled porous medium, thermal behaviour, thermoconsolidation eqns. for elastic lattice 79—72933
fluid motion stability, book, part II 77—3811
fluid saturated porous elastic solid, tensorial eqns. of motion 79—40366
fluid saturated porous media, 3-dimens. and multicellular steady and unsteady convection 79—94615
fluid saturated porous solid, eqns. of motion 78—79208
fluid saturated porous solid, fundamental solns., deformation, pore-fluid diffusion, soil mechs. 77—84160
fluid-infiltrated elastic materials, deformation of cavities and inclusions 78—51073
fluid-saturated porous layer with heat source, thermal convection onset 79—13406
fluidisation of fine powders, bubbling behaviour rel. to particle size 77—31362

flow through porous media continued
- fluidised bed, fluidisation uniformity, disturbance criterion with uniform coding medium flow distrib. 80—43772
- fluidised bed of porous particles, liq. removal from porous particles 79—72942
- fluidised bed reactor, gas flow anal. 78—83468
- fluidised bed reactor discrete cut particle size distributions, calc. 80—14812
- fluidised bed reactors, gas flow, anal. 79—94703
- fluidised bed wall-to-liquid mass transfer, local particle influence 79—94713
- fluidised beds, combustion facility, radiation heat transfer, particle size and flow parameter effects 80—69641
- foaming, liquid and gas relative permeabilities 80—33669
- forced convection flow and heat transfer of compressible fluid in porous medium *(French)* 78—30354
- forced convection heat transfer in porous medium with Joule-Thomson effect 77—89198
- fractured porous media, fluid flow 77—91173
- free air flows with perforated walls, permeability laws study *(French)* 79—10607
- free and forced convection flow in rot. channel bounded by permeable bed 79—23366
- free convection boundary layer on arbitrary shaped bodies in saturated porous media 80—24009
- free convection effects on oscillatory flow past infinite porous vertical limiting surface 79—92751
- free convection flow past vertical porous plate set in impulsive motion 80—69818
- free convective flow, longit. vortices, onset, linear stability anal. 78—94813
- free convective heat transfer in liq. saturated porous bed at high Rayleigh number *(German)* 80—33605
- free molecular vapour flow, mass transfer during condensation in channel 78—51198
- free water surface behaviour, appl. to earth dam seepage 80—8349
- freezing of saturated porous media, effect of seepage flow 79—1241
- friction factor for isothermal and nonisothermal flow 78—91008
- frozen soil, self-similar soln. of water infiltration eqns. 77—70713
- frozen soils hydraulic conductivity 77—45035
- fully developed pipe flow, turbulence struct., suction effects 79—50799
- Galerkin finite element procedure for analyzing flow through random media 79—81967
- gas, circulating, forced convection through porous cavity, solar heating *(French)* 80—69626
- gas, combined press. and diffusional transition region flow 78—42655
- gas, low-viscosity, incompressible flow in perforated tube *(Russian)* 77—39351
- gas, nonsteady flow through semipermeable screen to vacuum 80—100029
- gas, transient high speed flow through porous media, similarity 77—35232
- gas absorption, plastic packed column, mass transfer characteristics, proposal of packed column blood oxygenator 80—74968
- gas behaviour in closed porosity body, exam. 80—24642
- gas blow through, exothermal reaction wave propagation 79—79222
- gas diffusion (slow) through pore, gas influence during sintering 80—40281
- gas diffusion in porous bodies with press. changes 77—62662
- gas distribution in a deep granular bed injected by flat jets 80—19501
- gas filled porous media, free convection heat transfer 79—98796
- gas filtration, in centrifugal field 77—51113
- gas flow, diffusion eqn., continuity of soln. in n space dimensions 78—95130
- gas flow, recirculating, in packed columns, mass transfer and mixing, cell model 80—69913
- gas flow, transient, non-Darcy, in finite porous bed 78—47033
- gas flow characteristics through fibrous filter with supercrit. press. drops 78—1738
- gas flow in thermal insulation media, transient behaviour at rapid depressurisation 80—27701
- gas flow round porous axisymm. body with injection, vorticity *(Ukrainian)* 77—75923
- gas flow through multilayered regions 80—59108
- gas flow through porous materials, pressure loss 80—64623
- gas in porous sorbent, initial impurity content 80—64624
- gas injection into liquid through porous plate, squeezing out of liq. 80—64622
- gas injection through loose layered material, heat transfer, free convection effects *(Russian)* 79—18953
- gas jet, heat transfer to porous baffle 79—98776
- gas screen, subsonic turbulent boundary layer, friction behind permeable section 80—92127
- gas screen region behind permeable plate, heat transfer and friction laws 79—1250
- gas-liquid cocurrent downflow in fixed bed in pulsed regime, mass transfer fluctuations 80—19485
- gas-liquid countercurrent packed column, with intermittent voids, residence time distrib. studies 80—19483
- gas-liquid flow, hydraulic resistance 80—24077
- gas-liquid fluidised beds, axial and radial dispersion in dispersed plug flow model 80—10290
- gas-liquid fluidised beds, axial liq. dispersion in plug flow model 80—10289
- gas-saturated porous media, deform. theory *(Russian)* 77—41483
- gas-solid packed column, gas and solid phase axial dispersion at trickel flow 80—14807
- gaseous mixture separation, with asymmetric dense polymeric membranes 78—9696
- Gauss' equation, plane motions with free and wet surfaces in homogeneous porous media 80—53854
- gels for extended wear contact lenses, water flow cond. 78—81062
- geosphere transport model for WIPP site, radioactive waste repository 80—16854
- geothermal energy extraction, liq. flow pattern in system with three-dimens. filtration zone 77—49037
- geothermal reservoir, effect of magma dike intrusion on free convection 78—7599
- geothermal reservoir simulation, math. models 80—12446
- geothermal reservoir simulation, numerical soln. techniques 80—12447

flow through porous media continued
- geothermal reservoirs, mathematical modelling of heat and mass transfer 80—55802
- glass, free molecule flow and interdiffusion 79—32658
- glass bead sintered pellets, pore struct. and diffusibility *(Japanese)* 78—14509
- glass sintered powder porous bodies, liq. penetration mechanism *(Japanese)* 80—53853
- glasses, porous, thermoosmotic flow, filtration, of water 78—53248
- granites, fluid transfer in metamorphism rel. to microcracking and healing 80—51391
- granular bed, valve effect when stream compresses bed 79—72938
- granular layer, bubble coalescence for jet injection under constrained flow conditions 77—89197
- granular material fillings, pressure drops evaluation *(German)* 77—35234
- granular materials, heat and mass transfer with low Peclet number flow *(German)* 78—42656
- granular materials, particle density measurement by pycnometry 80—69903
- granular media, nonuniform, nonlinear flow analysis 77—58779
- Green and Ampt infiltration eqn. parameters depend. on initial water content 79—79899
- grid flow, exact hydrodynamic formulation 79—77236
- ground water, stochastic analysis of one- and three-dimens. subsurface flows 79—5520
- groundwater, instability of horizontal thermohaline flow in a porous medium layer 79—77239
- groundwater, macroscopic dispersion in porous media, controlling factors 78—11938
- groundwater, nonlinear laminar flow into well in porous aquifer 78—7670
- groundwater, saturated-unsaturated flow in deformable porous media, numerical model 77—91181
- groundwater, thermal convection in porous medium 77—33109
- groundwater, unsteady flow through tunnel opening, reductive finite element/Crank-Nicolson anal. 78—92861
- groundwater dynamics in plane regions during time varying seepage and evaporation *(Russian)* 79—79878
- groundwater filtration characteristics, multiple functions of filters in thermistor meas. *(Polish)* 78—40716
- groundwater flow, free boundary problem 77—66933
- groundwater flow in deformable porous media, algorithm 79—2323
- groundwater flow models for statistically homogeneous porous formations 80—12448
- groundwater modelling, hydrogeologic conditions at radioactive waste burial sites 80—21550
- groundwater nonlinear laminar flow into eccentrically placed well 77—66929
- groundwater two-dimensional flow, calculation methods 79—100875
- groundwater unsteady flow in porous medium with sloping impervious bedrock 80—12459
- Hamel flow in channel with permeable walls, stability *(Russian)* 78—34108
- Hamel flow through permeable walled channel, stability 79—68679
- heat and mass transfer, numerical soln. 77—7441
- heat and mass transfer during phase and chemical transformations 77—42917
- heat and mass transfer in capillary-porous body, kinetic eqns. 78—5796
- heat and mass transfer in porous media subject to fires 79—86507
- heat exchange on porous surface, optimal control 79—32661
- heat exchanger, porous cylindrical board temp. field, heat transfer efficiency 78—5793
- heat pipe, filled with porous material, glycol water circulation 80—66986
- heat pipe, heat transfer agent flowrate through porous wick, approx. calc. method 78—75197
- heat pipe, turbulent vapour stream gasdyanmics 79—90335
- heat pipe with capillary struct., thermal characts. 80—14558
- heat storage in porous medium with circulating heat transfer fluid, solar system appl. *(French)* 80—40916
- heat transfer, adiabatic wall temp., downstream of gas injection, mainstream accel. effect 79—1251
- heat transfer, capillary porous media with variable parameters 78—83471
- heat transfer, forced convection in low-porosity media 78—83472
- heat transfer, Nusselt no., temp. distrib. permeable bed boundary layer flow 78—51166
- heat transfer bibliography 78—63425
- heat transfer characts., saturated media, internal heat generation with cooling from above 77—51114
- heat transfer downstream of blockage with discrete permeability in rectangular channel 80—69915
- heat transfer from porous sphere in low Reynolds number flow 78—59482
- heat transfer in channel with permeable wall 78—63426
- heat transfer in gaseous screen with longitudinal press. gradient 80—23998
- heat transfer in porous sintered materials, expt. data correlation 77—42915
- heat transfer in turbulent boundary layers on porous plate, gas cooling film 79—98714
- heat transfer to porous cylinder with intense injection 78—79370
- heat transfer with liquid filtration into shattered rocks 79—81962
- heat waves moving through porous bed, heat transfer coeffs. determ. 77—42914
- heated porous body, impregnation with viscous liquid 80—79392
- Hele-Shaw cell, permeability determ., geothermal modelling appl. 78—59466
- Hele-Shaw cell, supercritical convective motions, equilib. stability boundary, porous flow simulation 80—33583
- heterogeneous flows of multi-component mixtures in porous media—review 78—59471
- heterogeneous porous medium, two-phase flow, multidimensional problem *(Chinese)* 80—64608
- highly dispersed porous body, kinetic theory of transfer in heterogeneous chem. reactors 77—15136
- hodograph method, use of reference function 79—84323
- horizontal circular cylinder bounded by a porous medium, flow 80—48798
- horizontal fluid layer in porous medium, convective instability, critical Rayleigh number 80—64564

flow through porous media continued
  horizontal porous layer of two different media flow patterns and convection 80—10303
  horizontal porous layer with timewise periodic boundary conditions, stability and convection 79—81965
  horizontal tubes in fluidised beds, local heat transfer coeffs. 80—74875
  hydraulic characts. of liqs. flowing through porous metal fibre mats., permeability laws 78—67848
  hydraulic conductivity of unsaturated porous media 79—5526
  hydrodynamic calculations, porous struct. parameters, theory 79—98797
  hydrodynamical dispersion and sorption dynamics in porous medium with stagnation zones, hydrodynamical dispersion and sorption dynamics 80—6139
  hydrologic behaviour of forested mountian soil, coastal British Columbia 79—84320
  hydromagnetic flow near oscillating porous flat plate 78—51250
  hydromagnetic free convection flow in Stokes problem, for porous vertical limiting surface with const. suction 80—90328
  hydromagnetic free convection past infinite porous flat plate in rot. system, slip effects 79—81989
  hydromagnetic squeeze film between porous circular disks with velocity slip 80—74997
  hydrophobic and hydrophilic porous media, grain wettability, filtration coeff. 80—1676
  hydrothermal convection, theoretical study rel. to Cyprus ophiolitic sulphide ore deposits origin 79—29761
  hydrothermal flows, two-phase, in permeable media, struct. 80—85693
  hysteretical models for prediction of hydraulic conductivity of unsaturated porous media 77—41088
  imbibition equation, similarity solutions, wetting abilities of immiscible fluids 80—43773
  imbibition in 2-phase flow through porous medium with capillary pressure 79—20884
  immiscible fluids in one dimensional porous medium, regularity and asymptotic behaviour 79—72936
  immiscible fluids interface, conditions for viscous displacement in homogeneous porous medium 80—10301
  immiscible fluids with capillary pressure, similarity soln. 77—72350
  immiscible liquid two-phase flow in porous media, unstable displacement 80—92213
  immobile fluid model 77—75979
  imperfect borehole; hydromechanics and stationary filtration *(Russian)* 79—88375
  incompressible Newtonian fluid, flow past wall with small particle injection *(French)* 79—46384
  incompressible viscous fluid, constitutive equations 79—32660
  inductively-heated particle bed, water-cooled, natural convection heat transfer 78—71396
  infiltration, parameter estimation of Green and Ampt eqn. 78—61473
  infiltration in homogeneous isotropic porous medium, moisture profiles and wetting 78—18336
  infinite porous plate, heat and mass transfer 78—30352
  infinite vertical porous plate, unsteady free convective elastica-viscous flow, viscous dissipation heat 80—24012
  interblock hydraulic conductivity values for transient unsaturated flow problems, finite difference soln. 80—12460
  interlayers between horizontal coaxial cylinders, flow field, natural convection and heat transfer 80—28558
  internally energised flat shaped porous element, non-Darcy flow with phase change 79—94709
  ion-selective membrane, flicker noise and turbulent convection in depleted layer 78—48692
  isobutane, condensation in porous bulk media 78—47510
  isobutane-air, in packed bed, heat and mass transfer, axial mass dispersion 78—75200
  isolated porous tube with nonuniform wall thickness, generated flow, jets 80—24087
  isotope separation, laser stimulation-filtering diffusion method *(Russian)* 77—555
  isotope separation by gaseous diffusion, aerodynamic effects 78—59469
  isotropic porous media flow, longitudinal dispersion 79—14470
  jet entering fluidised bed, aerodynamics and mass transfer 80—14809
  jet flow in porous layer 77—39341
  Knudsen diffusion, effect of cross sectional pore shape 77—24021
  Knudsen diffusion through noncircular pores 78—14076
  Knudsen flow, through periodically constricted pores *(Japanese)* 79—72911
  Knudsen flow in random networks, capillary model 77—80212
  Knudsen to Poiseuille flow transition, capillary model 78—55689
  lamina, porous, generalised boundary conditions, heat and moisture transfer Prudnikov problem soln. 78—1551
  laminar boundary layer, flow stagnation with suction 79—68676
  laminar boundary layer, on permeable surface, in crossed elec. and mag. fields *(Russian)* 78—75118
  laminar boundary layer, optimal control by wall suction or blowing 79—1242
  laminar boundary layer, with suction or injection, parametric calc. method 78—22323
  laminar boundary layer flow with suction (blowing) and pressure gradient, finite element anal. 79—18866
  laminar boundary layer over porous flat plate, recovery factor, general soln. 77—46987
  laminar film condensation from moving vapour, with suction 78—59459
  laminar flow, electrokinetic effects, analysis *(Russian)* 78—1748
  laminar flow along porous vertical wall 78—90825
  laminar flow between parallel plates, reactant injection effects 78—34208
  laminar flow between porous plates, heat transfer 79—68708
  laminar flow in a channel variable cross-section with movable and porous walls *(Polish)* 79—64768
  laminar flow in channel with mass transfer across porous walls 79—41759
  laminar flow in rotating porous annuli, Navier-Stokes eqns. 77—68687
  laminar flow over porous flexible boundary, oscillatory flow 80—92107
  laminar flow through porous tube or channel, nonunique solns. 78—94816
  laminar isothermal flow of two immiscible compressible fluid phases 80—69919
  laminar mass transfer, tubes and plates with wall resistance 79—60053
  laminar MHD pipe flow with heat transfer 79—14482
  laminar non-Newtonian flow in porous annulus 77—72333

flow through porous media continued
  laminar semi-infinite jet on porous surface, initial part calc. *(Russian)* 79—77203
  laminar source flow between parallel porous discs with equal suction and injection, in mag. field 77—84331
  laminar steady free surface flow past a permeable bed, buoyancy effects *(German)* 79—41665
  laminar sublayer on permeable surface with injection 79—64645
  laminar viscous flow down an open inclined channel with naturally permeable bed 80—69764
  laser, elec. discharge type, flow generated by an array of eccentric porous tubes 79—965
  law of the wall, appl. to turbulent boundary layer calc. with injection or suction 78—67187
  layered porous medium heated from below, onset of convection 80—33593
  layered transversely isotropic media, directional dispersion coeffs., vel. and ang. depends. 78—30348
  leaching from model porous bodies by reflection spectroscopy 80—100031
  limestone, groundwater seepage, $^{18}O/^{16}O$ in central Kentucky karst 80—8370
  linear equations systems solution, unsymmetric, sparse, computer program 77—80210
  liquid coolant, porous evaporative cooling for subcritical, critical, supercritical coolant parameters 79—55372
  liquid crystal, reentrant nematic, oriented, capillary shear flow 80—49344
  liquid elimination from porous body by fluidised porous particles system, kinetics 79—86510
  liquid evaporation in circulating gas, porous channel temp. determ., obs. 79—72943
  liquid fileed porous medium, linear thermoconsolidation eqns. 79—98601
  liquid filtration by passing through partially saturated porous media 79—90326
  liquid filtration US enhancement 78—59526
  liquid flow, 20 kHz US stimulation 77—31385
  liquid motion in channels with permeable walls, hydraulic resistance 78—5797
  liquid-filled porous solid, first strain gradient theory of thermoelasticity 77—53783
  liquid-saturated porous media theory with account of simultaneous deform. of structure and liq. *(Russian)* 77—41482
  longitudinal dispersion in saturated porous media 79—4080
  loose material forced displacement processes in pipes, gas flow filtration effect 77—58783
  low-density gas, motion and absorption in porous medium, stochastic calcs. 77—7449
  macromolecular dilute aqueous solns., flow in various geometries 79—41757
  macromolecular solutions, laminar filtration under low polarization conditions 80—24056
  magnetic fluid, penetration through porous medium with uniform mag. field oblique to interface 80—59107
  magnetic fluids, response to mech., mag. and thermal forces 80—59122
  magnetohydrodynamic flow between rotating and stationary porous coaxial discs 80—43799
  marine sediments diffusion coefficients determ., resistivity techniques validity 79—92601
  mass transfer correlations for flow between fluidised spheres and liquid 80—14805
  mass transfer of dissolved gases through tubular membranes 77—35225
  mass-diffusion element, anal. of separative power 79—41039
  mathematical model 80—83837
  mechanics equations for porous medium saturated by a two-phase liquid 79—94699
  medium with low initial water saturation, end effect in two-phase flow 80—33656
  melting heat transfer in steady laminar flow over flat plate 77—15027
  membrane, filtration characts., pore and particle size distribs. correl. *(Japanese)* 80—3418
  membrane, heteroporous, permeab. to pluridisperse soln. of ^{125}I-polyvinylpyrrolidone 77—12890
  membrane, passive transport through open membrane, multicomponent system, statistical-mech. theory 78—67261
  membrane, porous, hydrophobic, anomalous gas mixture flow into liqs. 80—40744
  membrane fluid flux, Kedem-Katchalsky eqns., flow limits 77—1979
  membranes, linear laminated media, permeation, sorpt. 79—1966
  membranes with low porosity, diffusional boundary layer resistance 77—58778
  metal fibre materials, permeable, obliteration phenomenon 79—98799
  metal gauze materials, struct. and hydraulic characts. 80—11729
  metal gauzes, hydraulic resist. in laminar filtration 80—100034
  metals, liq., infiltration in medium with interconnected pores, during passage of elec. current 80—100033
  methane and N_2 counter diffusion through porous solids 77—80649
  methane-H_2, in packed bed, heat and mass transfer, axial mass dispersion 78—75200
  methane-hydrogen mixture, flow through glass bead bed, axial dispersion coefficients 79—46378
  MHD, of turbulent boundary layer flow at porous surface, in crossed inhomogeneous fields 79—77274
  MHD boundary layers, unsteady on porous plate in rot. system 77—24027
  MHD convection, forced horizontal flow between moving porous walls 77—68695
  MHD convective viscous flow past porous plate with suction, mass transfer effects 78—87398
  MHD Couette flow with porous boundary 80—53876
  MHD Ekman layer, near accelerated porous media, flow anal. 77—75987
  MHD Ekman layer on porous flat plate, heat transfer, steady asymptotic soln. 78—79385
  MHD film flow, porous-walled squeeze film, slip effect in transverse field 79—77262
  MHD flow around porous plate with time-varying motion 78—51251
  MHD flow between rotating parallel porous walls 79—64779
  MHD flow near a time-varying accelerated porous plate 79—23372
  MHD flow near oscillating porous flat plate under body force action 80—24102

flow through porous media continued
  MHD flow over oscillating porous plate, Hall current and rot. effects 78—5803
  MHD flow over porous plate, Hall effect 78—51246
  MHD flow through porous straight channel 80—69932
  MHD forced convection in channel bounded by plate and permeable bed, Hall effects 80—69934
  MHD free and forced convective flow between porous plates with Hall effect 79—41763
  MHD of elec. cond., incompressible, viscous fluid, unsteady flow 78—59496
  MHD oscillatory flow past impulsively started porous limiting surface, variable suction 79—86518
  MHD viscoelastic free convection boundary layer flow past porous plate 80—10317
  MHD viscous flow through porous channel, exact soln. 77—31393
  micro-perforated plates, collection efficiency of aerosols 79—64760
  microporous graphite compact, anomalous diffusion of N_2, time-lag and transient-state kinetic analysis 78—34655
  microporous plugs, measurement of desorption-permeation time lags of permanent gases 80—59137
  midocean ridge hydrothermal systems, hot water egress thermal constraints 79—39700
  migration of salts in a porous medium allowing for their crystallisation *(Russian)* 78—87388
  miscible non-isothermal vertical displacement stability through homogeneous porous medium *(French)* 80—43771
  miscible or immiscible displacements, identification and modelling 78—69392
  moist dispersed solid, local Rebinder criterion determ. 77—89199
  moist material, external heat transfer, calc. methods, drying kinetics 78—59467
  moist porous material subject to sudden heating, mass transfer, press. rise 77—58787
  moisture transfer, multiphase, in porous media with temp. gradient 80—19497
  Monte Carlo models for water circulation study *(Rumanian)* 80—69917
  moving bed solid flow in inclined pipe leading to fluidised bed., gas leakage 80—64619
  moving bed solids flow in inclined pipe leading to fluidised bed 80—64620
  moving boundary problems, weak soln. 80—179
  multi-layer soils, state vector approach to one dimens. consolidation 78—3757
  multicellular free convection flow, in spherical porous layer *(French)* 79—46375
  multicomponent flow through porous media from underground nuclear explosion, flow stability 80—53857
  multifilament bundle, eqns. of steady flow of viscous incompressible fluid 77—51111
  multifilament bundles, slightly curved, eqns. of steady filtration flow 78—38397
  multiperforate laminae, mass transfer of chem. species by diffusion, plate and associated boundary layer case 80—40736
  multiphase systems, local vol. averaging and distrib. function 77—58780
  natural convection in a slightly slanted rectangular box filled with a porous medium *(French)* 80—19378
  natural convection in a vertical cylindrical well filled with porous medium 80—79297
  natural convection in box of water-saturated porous media 77—31384
  natural convection in porous layer with permeable boundary *(Russian)* 79—18941
  natural convection in porous media and geothermal systems, r eview 79—1194
  natural convection in porous media bounded by concentric spheres and horizontal cylinders 79—68699
  natural convection mass transfer along porous vertical plate 78—90876
  natural thermoconvectional filtration in circular porous interlayers 78—94817
  needle shaped particles, diffusion orientation on filtration surface in turbulent flow 80—33668
  non-Darcy flow with phase change in internally heated cylindrical porous cylinder 79—37393
  non-isothermal liquid flow and heat transfer in sintered metallic porous media 79—86506
  non-Newtonian flow through porous media, fluidised beds, solid-fluid interaction *(Portuguese)* 80—38454
  non-Newtonian fluid, forced convection, on circular cylinder, suction and slip velocity effects 78—34169
  non-Newtonian fluid, heat transfer by fluctuating flow past porous plate 78—38309
  non-Newtonian liquid filtration eqn. 78—55690
  non-steady flow problem in two-layer porous medium 78—81260
  noncoaxial rotations of porous disc and fluid at infinity, Navier-Stokes eqns. soln. 77—68600
  nonisothermal filtration, 2-D numerical anal. 80—6137
  nonisothermal mixture motion through porous media, sorption dynamics and heat exchange kinetics 77—7447
  nonlinear diffusion eqn., perturbation soln. 77—41087
  nonlinear heat and mass transfer in porous media 80—1577
  nonlinear heat/mass transfer problem, soln. using invariant groups 78—55688
  nonlinear laminar flow of fluid into fully penetrating cylindrical well 78—75198
  nonNewtonian flow between rotating porous cylinders, stability wide gap case 79—68761
  nonstationary filtration, source-type solns. 79—10608
  nonstationary flow between rotating coaxial porous discs, porosity effects 79—32657
  nonsteady filtration of two immiscible liquids alternative to kdV-Burgers eqn. 80—6019
  nonsteady multiphase flow through porous media, struct. determ. 78—51237
  nonsteady problem, existence and uniqueness of weak solns. 78—47028
  nonswelling porous body, moisture-retaining capacity and struct. 77—12773
  nuclear reactor mixed-oxide fuel, two-component gas transport within interconnected porosity 79—617
  numerical analysis, flow parameters, potential distrib. *(German)* 77—11260
  numerical methods for flows through porous media. II 80—69914

flow through porous media continued
  oblique high-drag heat exchangers, turbulent flow and pressure losses 79—94710
  oil shale retort dispersion, effect of particle size distrib. and flow nonuniformities 80—28560
  oil shale retorts, multi-dimens. simulation of flow nonuniformities in fissured porous media 80—28559
  Oldroyd B-fluid flow between porous plates with fluctuating vel. 78—26168
  Oldroyd liquid, unsteady flow between two porous walls 78—63452
  one-dimensional moisture migration caused by temp. gradients 80—96305
  oscillating porous flat plate, MHD flow with variable suction 77—65802
  oscillatory convection, in porous medium heated from below 78—79320
  oscillatory flow of electrically conducting fluid past porous plate, free convection currents 79—55428
  oscillatory flow past infinite, porous plate, free convection current effects 78—14079
  oscillatory flow past infinite vertical plate with variable suction and constant heat flux 78—38324
  oscillatory flow past porous bed, boundary layer characts. 80—48797
  oscillatory flow past vertical porous plate with constant suction, free convection effect, correction to earlier paper 77—27594
  packed bed, flow conditions, examination by local meas. 80—14806
  packed bed, mass transfer time domain evaluation from chromatograph peaks 80—19496
  packed bed, regular, of equally-sized spheres, local voidage, local equiv radius, tortuosity *(Japanese)* 79—50793
  packed bed flow, particle-to-fluid heat transfer rel. to fluid dispersion 79—68795
  packed bed wall-to-liquid mass transfer, local particle influence 79—94714
  packed beds, low Peclet number particle-to-fluid heat and mass transfer 78—94799
  packed beds, particle-to-fluid transfer coeffs., fluid diffusivities 77—31378
  packed beds, pressure drop in low Knudsen number regime 79—50792
  packed beds, thermal response at low Reynolds number 78—87386
  packed beds of cylindrical bodies, press. drop *(German)* 79—72945
  packed bubble columns, holdup profiles, elec. cond. meas. 77—35201
  packed column, trickle and two-phase flow, tracer dispersion obs. 79—86502
  parallel porous discs of different permeability, laminar flow heat transfer 80—14810
  parallel porous tube array, flowfield struct., turbulence and vorticity distribs. 77—27589
  paramagnetic fluid flow through an annulus with porous walls 79—41748
  partial differential eqn., strong soln. existence and uniqueness *(French)* 78—62084
  particle sizing by capillary hydrodynamic chromatography 79—64759
  particulate beds, sheared, mass transport kinetics, Markov chains appl. 79—60057
  particulate solid, reactions, viscous flow and Knudsen diffusion 77—4937
  PBR, flow of individual pebbles in cylindrical vessels 77—83017
  penetration gas cooling, porous wall with external heat appl., stability determ. 79—64761
  penetration of fluid into a Hele-Shaw cell: the Saffman-Taylor experiment 80—53852
  percolation processes, critical contact number 80—14811
  percolation theory, bond problem, critical probabilities, bond clusters 78—86224
  percolation threshold, asymptotic method—diagram technique calcs. 78—79374
  perfect fluid motion in presence of inhomogeneous porous body 78—22422
  perforated surfaces, heat exchanger cores, three forms of heat transfer augmentation 78—38402
  permeability, unsteady state meas. method 80—53895
  permeability calc. from Navier-Stokes eqns. 77—27593
  permeable boundaries in multidimensional unsteady flow 80—38490
  permeable contour in flow with jet separation, impulses and impact effects 80—92196
  permeable cylinder in sheet of viscous fluid, translational frictional coeff. 80—19500
  permeable plate, numerical anal. of turbulent boundary layers 78—67186
  permeable plate, turbulent boundary layer at different free stream turbulence levels, injection 80—10233
  permeable polymer mol. in soln., intrinsic viscosity and friction coeff. 78—30353
  permeable shells with pole hole, pot. nonseparational inviscid flow *(Russian)* 77—75972
  permeable spheres in incompressible fluid, hydrodynamic interaction, mobility tensors 78—71395
  permeable spheres in incompressible fluid, hydrodynamic interaction vel. fluid, friction consts. 78—75202
  permeable surface, injection, laminar to turbulent transition, heat and mass transfer 78—83361
  permeable tube with wall injection, transient turbulent boundary layer 78—83486
  pipe, porous, uniform air outflow, turbulent momentum flow and friction coeffs. formula 78—1737
  pipe outflow, turbulent, with wall suction, dynamic and thermal fields *(French)* 79—4082
  pipes, porous, complementary variational principles for steady and unsteady Poiseuille flow 80—92225
  plane flow of fluids in piece-wise homogeneous porous media 79—18945
  plane stationary flow, temp. field calc. using Lauwerier formula analogue 80—38485
  plasmatron, discharge stabilised, by gas blown through porous wall 80—75105
  plate, flat, with suction, boundary layer eddy viscosity, mixing length, Von Karman's constant 80—1680
  plate, flat, with suction, boundary layer turbulence and momentum props. 80—1679
  plate, permeable, turbulent boundary layer with injection, heat transfer 79—1247
  plate, with suction, three-dimens. fluctuating flow, heat transfer, skin friction 78—87389
  plate with simultaneous injection and suction, turbulent layer friction and vel. profile 78—83469
  platelet interaction with vessel surface, blood rheological factor influences 80—61612

flow through porous media continued
Poiseuille flow between porous flat plates, transpiration cooling, variable viscosity 77—47082
polyacrylamide, aq. soln. viscoelastic effect in flow through porous media 79—94684
polydisperse filter bed, immobile, heat and mass transfer eqns. soln. 77—7446
polymer dilute soln., polymer effect onset and saturation limit in porous media 78—26190
polymer membrane gas permeation, pore size distrib. *(Japanese)* 78—79372
polymer solns., rheological props. in flow through porous media 80—53819
polymer solution, semidilute, hydrodynamic interaction of two permeable spheres, method of reflections 78—71394
polymer solution elongational flow through porous bed, drag increase 78—22419
polymer solution flow in porous media, oil extraction appl. 79—68802
polymer solution flow through porous media *(French)* 79—46376
polymer solution laminar capillary flow, excess press. drop 79—60038
polymer solution one- and two-phase flow through porous media 78—42659
polymer solutions, flow behaviour in porous media *(German)* 78—55666
polymer solutions, flow through sand filters, flow resistance 80—79395
polyox dilute aqueous solns., flow resistance mechanisms in porous media 79—41747
pore geometry effect on pressure drop, systematically packed sphere assemblies *(German)* 80—10304
pore geometry effects on pressure loss, model channels with varying diameter *(German)* 80—1677
pore size determ. of powder and wire gauge filter materials 77—12776
poroelastic material dynamic characterisation, complex, modulus meas. 80—14640
porosity and pore size measurement using soln. of luminescent material flowing around sorbent granules 80—53850
porous bed with permeable boundary, natural convection 79—77238
porous body drying in heated gas flow 79—90328
porous cermet, heat transfer and stability for moving evaporating coolant 80—64563
porous channel inlet region, second order fluid flow, injection effects 79—68804
porous ducts, fully developed laminar flow 78—47038
porous elastic fluid filled spherical shell, radial vibr. 79—18771
porous element under phase conversion and vap. superheat, steady and transient operation 77—7442
porous flow through rectangular dam, proof of free boundary convexity using maximum principle 80—69916
porous medium being dried, moisture flow, generalised model *(Hungarian)* 80—83839
porous oxide pellet, spherical, reduction by gas flow *(French)* 79—27713
porous pipe in a pipe heat exchanger, laminar flow, vel. changes 80—64512
porous sphere in stream of small Reynolds no., heat transfer 78—42608
porous structures for cooling laser reflectors, theoretical study 80—91809
porous thermoelastic matrix, slow fluid flow theory 79—7406
porous wall evaporation cooling system, liquid component temperature state *(Russian)* 79—32664
powder, Knudsen diffusion, gas diffusion relationship of Knudsen flow permeametry 77—55087
powder, Knudsen diffusion, pore size distrib. effect on surface areas obtained by diffusion meas. and Hg porosimetry 77—55088
powders, surface area measurement using Knudsen diffusional flow of gas 79—40536
power law fluids, laminar flow through granular beds 80—38488
power-law fluid, fluctuating flow past porous flat plate 77—68639
pressure gradients generated during the drying of porous shapes 79—68801
Preston tube calibration in transpired turbulent boundary layer 78—79397
propane, condensation in porous bulk media 78—47510
pseudocontinuum mass transfer in media with spatially periodic boundaries 79—86500
pulsatile flow in porous channel, heat transfer 77—19604
radioactive gas, convective diffusion and adsorption in porous media, inverse problem 79—90322
radioactive gas adsorpt. in porous medium, convective diffusion *(Russian)* 78—87387
radioactive gas diffusion, adsorpt. in porous media *(Russian)* 77—27591
radioactive gas distrib. in porous medium, diffusion and sorption effects 79—81964
radionuclide migration from low-level waste burial site 78—21671
radionuclide migration through soils 80—16849
radionuclide movement from hypothetical nuclear waste repository, groundwater modelling 80—16853
rainfall variable infiltration, eqns. 79—53379
random bed, porosity estimation based on Lichtenstein Liapunov expansion functional 78—14078
random capillary networks, Knudsen to gaseous diffusion transition, struct. factor calc. 78—14080
reactive gas flow through porous barrier, exit flux, composition depend. 77—31383
rectangular cavity packed with porous media, heat transfer 78—71392
rectangular cavity with porous filling, steady convection and boundary layers 80—79309
reflection, of obliquely incident waves, at permeable quaywall with reservoir *(Japanese)* 79—32546
residual phases flow, percolation theory 77—75978
resin flow between roller and absorbent compressible paper 79—41749
Reynolds eqn., generalised form for porous boundaries 80—87803
rheologically anomalous fluids, flow in porous media 80—53851
rigid shell, oscillatory flow through perforated surface, sound generation 79—18950
rock, subjected to water jet, drag force on grains in permeable medium 78—55691
rocks, microporous, movement of solutes through aqueous fissures 80—94553
rocks, of water, shear thinning and shear thickening polymer additives 80—72100
rocks, permeability from resistivity and pore shape 77—86866
rotating channel in porous medium, heat transfer 79—72932

flow through porous media continued
rotating channel with porous walls, heat transfer and temp. distrib. 78—30355
rotating disc and porous disc. fluid flow 80—64569
rotating disc with suction and stationary disc, flow between 78—46975
rotating porous cylinder, lift, torque, appl. to wind power generation 78—46987
rotating superposed fluids, MHD instability, flow through porous medium 78—14089
Salts migration through porous media 79—90323
sand column, migration of non-ionic ^{90}Y *(Japanese)* 77—944
saturated medium, macroscopic behaviour *(French)* 78—51235
saturated porous layer, sudden temp. rise, stability, linear and energy methods, convection 80—74972
saturated porous medium, completely confined, onset of thermal convection 78—83387
saturated porous medium, free convection boundary layers, lateral mass flux effects 77—27592
saturated porous wedge with impermeable boundaries, heat and mass transfer 80—19375
saturated-unsaturated flow in deformable porous media, numerical model, appls. 79—81966
saturated-unsaturated media, hysteresis effect influence on transient flows 78—59481
screen, fine-mesh square weave, low Reynolds no. loss coeff. 77—55089
screens, book contrib. 78—59483
second order fluid, natural convection flow from porous plate, suction and injection effects 80—59029
second order liquid porous parallel walled channel flow with free and forced convection 78—42635
seepage flow variational inequalities by finite element method 77—68688
seepage in porous elastic media, numerical performance of finite element schemes 77—91162
semi-infinite porous medium bounded by horizontal surface, mixed convective flow, vortex instability 80—79304
semibounded compressible stream, optimal suction at heat-cond. porous surface *(Russian)* 80—79346
semifluidised bed, mass transfer rate 80—59105
separation method, flow field-flow fractionation 77—960
sieve plate column without downcomers, anal. and NH_3 stripping expt. 78—22430
sintered composite-liq. metal interaction, mass transfer eqn. approx. soln. 78—67262
sintered metal, heat transfer in forced convection of fluid 77—55084
skin friction at porous plate, injection or removal from boundary layer due to turbulent wall jet 78—47029
slender permeable profile, cavitation flow 80—38466
slip flow, MHD, over porous plate, with variable suction, heat transfer 78—79337
slip flow in porous medium, effective diffusion coeff., variational method 79—90325
slip flows, analogy for viscous incomp. flows 79—64707
slow injection of fluid into a porous medium, general laws *(French)* 79—50791
smectic-A liquid crystal, permeative flow around obstacle, extended boundary layers 78—67644
soil, blocked air pore volume meas. based on volume-weight relns. 78—57231
soil, filtration with partial saturation *(Russian)* 77—60433
soil, heat and mass transfer with phase change 79—1093
soil, nonsaturated, water infiltration, positive head effect *(French)* 79—2296
soil, pore size distrib. estimation from moisture charact. 80—12454
soil, two-dimens. infiltration and redistrib., numerical anal. 78—11942
soil, water infiltration into uniformly packed soil 77—2152
soil, with initial gradient, water flow 78—32127
soil filtration problems, finite element method *(Russian)* 79—88374
soil hydraulic properties, empirical eqns. 79—53385
soil hydraulic properties, scaling of field meas. using similar media concept 77—78278
soil moisture, capillary hysteresis model 79—53386
soil moisture movement in liquid phase, model 79—79894
soil water, flow regimes near porous cup water samplers 77—66942
soil water flow model with two-dimens. automatic γ-ray attenuation scanner 79—53387
soils, hillside, N.Yorkshire, England, pedological features affecting permeability 77—45021
solid particle bed fluidisation characts. from hydrodynamic instability 80—6140
solid soluble phase extraction from mixture of polydisperse porous particles 79—14475
soluble flat surface stability in turbulent flow 80—14676
solute dispersion in porous medium in MHD flow between parallel plates, homo- and heterogeneous reaction effects 78—55697
solute transport in a saturated-unsaturated porous medium 79—23362
solute transport in porous media, statistical theory 80—28899
sorption dynamics, nonisothermal multicomponent, with widely differing mass-transfer coeffs. 77—65793
space above inhomogeneous fluidised bed, heat transfer 77—55085
species transport eqn., space-averaging formalism 77—3868
sphere approaching permeable wall, hydrodynamic force 79—46383
spheres, porous, in a linear flow field, motion and rupture 79—64755
spherical permeable shell motion at axis of rotating viscous incompressible fluid 79—18944
spouted beds of spherical particles, spout termination, parameters 80—64621
stability of convective motion in two-dimens. vertical fluid layer with permeable boundaries 77—55086
stability of flow down permeable boundary, velocity slip effects 77—68571
stabilization of flows through porous media 79—72944
stationary flow between porous rotating cylinders in a radial magnetic field 80—83857
stationary flow between water reservoirs separated by non-homogeneous dam, free boundary problem 79—10606
steady flow between a rotating and a porous stationary disc in the presence of transverse magnetic field 78—79382
steady flow between rotating disc and stationary naturally permeable disc 79—72934
steady flow in porous region between two rot. spheres 79—46382
steady flow prod. by rot. disc, series soln. anal. 78—71308

flow through porous media continued
- steam-generating pipe, containing porous deposits, mass transfer (impurities) 78—38398
- steam-water counterflow in porous media, model, geothermal systems appl. 79—79879
- steel, permeability, deform. effects 79—100229
- steel, stainless, porous sheet, pore dimensions, filtration and permeability *(Russian)* 80—76480
- Stokes flow through channel and tubes with sinusoidal boundaries as model for porous media 78—18337
- Stokes problem, effects of free convection on oscillatory flow past infinite porous vertical limiting surface 80—109348
- stream distribution in channel with porous wall, energy eqn. soln. 77—7445
- Streaming potential and noncreeping flow in porous beds 77—84317
- subcritical rotational stationary symmetric plane flows for profile set between porous walls *(French)* 79—50786
- sublimation, heat, mass transfer from parallel capillaries 79—37395
- subsurface nuclear waste disposal, groundwater modelling 80—16852
- suction effects on shock wave-boundary layer interaction, numerical Navier-Stokes soln. 79—1243
- suction or blowing flows through openings in the wall of a boundary layer *(French)* 79—18947
- suction-induced asymptotic boundary layers, exptl. and predicted props. 80—1553
- superfluid ^{4}He, critical superflow through Grafoil, two-dimens. random bond model 80—15319
- superfluid turbulence, penetration through porous filters 79—46855
- supersonic flow, heat transfer on flat porous wall with alternating injection and suction zones 79—98719
- supersonic flow, surface blowing, fluid injection and suction 77—27554
- supersonic flow around a cone, power-law injection, bease influence 80—100010
- supersonic jet, thermogasdynamic interaction with inclined permeable baffle 79—98773
- supersonic Mach 6 hydrodynamic flow past permeable wedge, holographic interferometry meas. *(Russian)* 78—14108
- surface flow of dilute gas in model pores, free mol. flow calc. in adsorbent force field 80—6100
- surface friction dependence on compressible fluid injection and removal by suction from wall jet 77—47052
- surface suction effect on condensation in presence of noncondensable gas 78—90691
- surfaces covered with capillary-porous structures, heat transfer with boiling, approximate theory 78—94537
- suspension, conc., of aggregable particles, viscosity calc. 79—7362
- suspension, movement in porous solid interior *(French)* 80—43770
- suspension filtration, 2-component, conc. wave bifurcation *(Russian)* 78—22420
- suspensions, with a compressible residue, filtering, intensification by pulsation *(Russian)* 79—90324
- sweat cooled porous hollow cylinder, heat transfer from hot fluid 79—18943
- synthetic oil in unconsolidated medium, sinusoidal press. response method 77—68713
- tensor formulation of the fluid-solid interaction force for multi-dimensional, two-phase flow within tube arrays 80—92211
- thermal convection, two-phase, in porous layer, flow visualisation study 79—72930
- thermal convection in Hele-Shaw cell 77—31301
- thermal convection in porous media, dispersion effects 80—103027
- thermal convection in saturated heat generating porous layer 79—77113
- thermal storage by sensitive, latent heat,, dynamic model *(French)* 80—40917
- thermal-convective instability through porous medium 80—53769
- thermochemical gas analyzer, porous flame barrier, reagents, reaction products, conc. diffusion *(Russian)* 79—29359
- thermomigration, capillary diffusion coeffs. *(French)* 77—89006
- thermoosmosis, liq. in capillary pore media 79—41750
- thick capillary-porous structure, mass exchange during boiling 80—19503
- three dimensional free convection flow and heat transfer along a porous vertical plate 78—90866
- three-dimensional natural convection in a confined porous medium heated from below 79—72937
- torsionally oscillating impermeable disc and stationary naturally permeable disc, flow streamlines 80—24030
- transient boundary layer on porous plate, coolant injection, laminar flow stability and heat transfer 78—83389
- transient boundary layers between porous plates 77—46990
- transient diffusion of gas in highly dispersed sorbing porous solid 77—15114
- transient filtration in porous elastic cylinder 77—47088
- transient flow in porous media, Green's function appl. 79—72935
- transient natural convection in rectangular enclosures, numerical anal. 79—77111
- transient vertical flow 78—34194
- transient waves in fluid-filled porous media, refl. and refr. 77—49604
- transpiration, thermal, effect of gas-surface interaction, dusty gas theory 77—19634
- transpiration-cooled system, thermal response in radiative and convective environment 78—32323
- transverse force on a spinning porous sphere at small Reynolds number 79—77243
- tube entrance segment, heat transfer anal. with initial flow swirl and transverse injection 77—24025
- tube inlet zone, flow and heat transfer with injection into swirled flow 79—98717
- tube of elliptic cross-section, steady viscous flow, generalised momentum eqn. 78—75203
- turbulent axisymmetric boundary layer, weak and strong disturbances effect 78—90857
- turbulent boundary layer, at permeable surface, in crossed elec. and mag. fields *(Russian)* 78—94836
- turbulent boundary layer, fully rough, accelerated stability conditions 77—84240
- turbulent boundary layer, wall suction and heating *(French)* 77—19595
- turbulent boundary layer at permeable plate, with strong injection 79—81963
- turbulent boundary layer at permeable plate with shock waves, heat transfer 79—81922
- turbulent boundary layer on permeable plate 79—1169

flow through porous media continued
- turbulent boundary layer on permeable surface with intensive blowing 77—84241
- turbulent boundary layer on porous plate, suction *(French)* 78—51156
- turbulent boundary layer on rough surface with blowing, heat transfer behaviour 78—71334
- turbulent boundary layer on surfaces with porous section 79—86412
- turbulent boundary layer with wall suction, thermal and dynamic fields analogy *(French)* 79—1249
- turbulent boundary layers at low Reynolds number 77—31288
- turbulent boundary layers near separation point, adverse press. gradients and injection 77—72287
- turbulent compressible boundary layer on permeable rough surface with heat transfer 79—1176
- turbulent flow in channel with porous walls 78—67179
- turbulent flow into homogeneous porous media on inclined bedrock 79—10609
- turbulent jet in concurrent stream at permeable surface 77—7444
- twisted air flow in permeable tube, local heat transfer 78—71338
- two immiscible liquids, flow inbibition due to differential wettability 80—87802
- two moderately rotating porous discs, heat transfer 80—103028
- two phase convection driven by phase change instability mechanism 77—86834
- two phase natural convection in permeable medium adjacent to vertical heated surface 79—68790
- two-dimensional infiltration in unsaturated soils, nonlinear diffusion eqn. numerical soln. 80—69918
- two-dimensional isoparametric Hermitian element for field problem soln. 77—60914
- two-dimensional laminar flow between porous walls 79—14477
- two-phase, finite element simulation 79—41752
- two-phase, starting algorithm for numerical simulation 78—38388
- two-phase convection in a sandbox rel. to geological porblems 77—64238
- two-phase flow, fingero-imbibition, composite expansion soln. 78—79373
- two-phase flow through cracked porous media in mag. field, imbibition 78—34200
- two-phase flow through packing, with longit. dispersion 79—68796
- two-phase flow through porous media, perturbation soln. due to differential wettability 78—59470
- two-phase flow through underground porous medium, similarity anal. of fingero-imbibition 78—18338
- two-phase flow with end effect allowance, numerical simulation 80—33659
- two-phase incompressible flow, diffusion-convection eqn., mixed finite element method, water flooding 80—74969
- two-phase interface and free surface equations in groundwater flow 79—48527
- two-phase porous cooling system, hydrodynamic and thermal characteristics 77—10012
- two-phase porous cooling system development 78—59477
- two-phase reacting flow, heterogeneous, balance eqns. and soln., interior ballistic phenomena modelling 79—94737
- two-phase stratified flow through fractures in porous media 78—5792
- two-phase transpiration cooling system 78—22418
- ultrafiltration, using membrane surface, slip vel. effects in channel flow system 79—60054
- ultrafiltration, using membrane surface, slip vel. effects in tube flow system 79—60055
- underground cable system, convectively cooled, temp. distribs., heat transfer correlations 78—71262
- underground cable system, convectively cooled, vel. distribs., press. drop correlations 78—71330
- underground nuclear explosion, gas flow in permeable Earth formation with crack 78—61372
- unsaturated porous media, one dimens. flow, two parameter singular perturbation soln. 79—23361
- unsaturated porous media flow anal. by finite element method 78—92869
- unsaturated water flow within porous materials, obs. by NMR imaging 79—98840
- unstable displacement problem for porous media with different permeability layers, developed stage anal. 80—14813
- unsteady Couette flow through porous wall in presence of mag. field 80—53856
- unsteady drainage, one-dimens., digital simulation, finite element method appl. 78—91011
- unsteady filtration with unknown boundary, nonlinear integro-differential eqn. 80—43769
- unsteady flow past porous plate, theory for incompressible fluid 79—86499
- unsteady free convection flow past a vertical porous plate with variable suction and transverse magnetic field 79—32691
- unsteady laminar flow of elastic viscous fluid through porous channel, applied mag. field effects 80—38499
- unsteady laminar flow through porous media in presence of transverse mag. field 79—37394
- unsteady rotating boundary layer flows between porous plates 77—47112
- unsteady viscous MHD flow, through porous channel with constant suction 79—72951
- vapor-liquid energy transport in a porous medium 79—64762
- vapour dynamic diffusion batcher with porous partition 78—79404
- vapour permeability mechanism of porous bodies 77—58782
- variational irreversible thermodynamics of heat and mass transfer in porous solids 79—4081
- velocity and longitudinal dispersion, deterministic model 80—83842
- vertical cavity with saturated porous filling, asymptotic Nusselt number *(French)* 80—43700
- vertical channel flow, heat convection, fluid injection problem, Newton-Raphson method solns. 79—10556
- vertical enclosure, convective heat transfer, boundary layer 79—59908
- vertical plane surface, suction and injection effects on liq. film flow 80—53849
- vertical porous stratum, natural convection, modified Poiseuille flow distrib. 78—5794
- vertical surface with suction, oscillatory flow, free convection effects 80—53865
- vertical wall, laminar flow integral approach to flow 79—77059
- visco-elastic liquid, flow past hot porous circular cylinder, free and forced convection 78—83386
- viscoelastic, test particle approach to flow classification 77—23996
- viscoelastic Ekman layer on porous plate 77—72336

flow through porous media continued
viscoelastic fluid, fluctuating flow in a porous channel 79—64774
viscoelastic fluid, oscillatory flow past infinite porous plate with variable suction 78—38373
viscoelastic fluid fluctuating flow past infinite porous wall in slip flow regime 79—18917
viscoelastic free convection boundary layer flow past infinite plate with constant suction 78—90936
viscoelastic liquid, flow through porous channel, free and forced convection effects 80—53861
viscoelastic liquid steady flow about porous rotating disc 79—32586
viscoplastic liquid, steady filtration with variable initial gradient, exact solns. of two-dimensional problems 77—58786
viscous binary mixture in porous medium, thermal conc. instability 77—35231
viscous displacement, immiscible, stability anal. 80—48799
viscous drainage, over permeable wall, Navier-Stokes eqn. 77—31278
viscous flow, slow, through rigid porous medium, macroscopic fied eqns. 79—94711
viscous flow between rotating discs with injection on the porous disc 80—14713
viscous flow in a rotating channel bounded below by a permeable bed 78—91013
viscous flow in porous solid, relaxation phenomena *(French)* 78—87385
viscous flow of variable viscosity between porous bed and moving impermeable plate 78—90962
viscous fluid, incompressible, hydromagnetic free convective flow past vertical porous wall, mass transfer 80—64645
viscous fluid in porous annulus, exact soln. for unsteady motion 80—19499
viscous fluid in straight porous tube, annular effect 79—77240
viscous heat generating fluid, convective flow and heat transfer near moving porous plate 80—14703
viscous incompressible flow, past porous sucking vertical plate, free convection 78—30283
viscous incompressible fluid, laminar divergent flow through porous cone *(French)* 80—83838
viscous incompressible heat generating flow past porous plate with free stream oscillations, laminar free convection 79—37312
viscous incompressible heat generating flow past porous plate with free stream oscillations, laminar free convection 79—37311
viscous incompressible laminar flow entry problem in porous ducts, anal. 77—62302
viscous-inviscid flow interaction method, using blowing and suction flows 79—1154
wall, perforated, relative effects of external and internal convection *(French)* 79—1248
walled dam, water table shape near boundaries 77—78275
walls, permeable, cooling characts., heat exchange, rad. emitter design 80—64535
water, at 4°C, free convective flow, past infinite porous plate with const. suction 78—42606
water, deep evaporation characterisation *(French)* 78—59468
water, MHD free convection flow past infinite porous plate 80—33703
water bearing bed, pressure field determ. during pumping and injection of water 79—77237
water flow through inhomogeneous porous media, analytical theory 77—62301
water flow through rock specimen, average pore vel. meas. 79—5473
water impurity concentration in steam-generating channels with capillary-porous structure 80—103071
water infiltration equations for simple soil systems 77—78282
water infiltration into frozen soils, numerical modelling 79—39772
water infiltration into horizontal sand column, flow characts. 77—78280
water purification, granular charge inhomogeneity effect on head losses 77—75976
water saturated porous box with conducting walls, convection onset anal. 79—18949
water seepage, confined, finite element method 78—38401
water transport in soils, review, book contrib. 80—96308
water transport through unsaturated soil, Buckingham-Darcy flux law, statistical mechanical theory 79—16541
water transport through unsaturated soil, conservation laws derived from statistical mechanical methods 79—16540
water transport towards ice front in porous media 77—945
water vertical infiltration in dry soil 77—78279
water-free oil yield, inhomogeneous inclusions effect on permeability 79—86504
water-water vapour flow through packed bed 80—38484
waves, travelling, gravity-capillary, on liq. film surface falling past permeable bed 78—87351
wedge, intense supersonic gas blowing through wall, dividing static press. determ. 77—84273
wettability dependent permeability in porous media 79—98795
wetting, capillary rise, contact angle effect *(German)* 78—84033
wind tunnel, wall interference, two-dimens., correction method, examples *(French)* 78—67293
wire gauzes resistance coefficient measurement at low air velocity *(Japanese)* 80—106843
wood chip disc refiner, steam flow anal. 79—50787
Ar, viscosity, meas. up to 2000K by percolation through porous medium 78—1781
BCl_3, gas, isotope separation, laser stimulation-filtering diffusion method *(Russian)* 77—555
CO_2 chemisorbed molecules, surface flow through $MgCr_2O_4$ 77—47083
CO_2 laser amplifiers, porous tube generated flow field, heat and mass diffusion 80—63969
Fe fibre, props. 79—98798
He II, flow through porous plugs, space cooling system appl., plug characts. 78—49842
He, liq., superflow into a solid superleak 80—39372
^{4}He, adsorpt. and sp.ht. in 0.2 μm Nuclepore filters 77—35773
^{4}He superfluid, acoustic vibration field density of states in piecewise const. parameter media 80—6483
^{4}He, superfluid, density in submicrometer diameter channels, Helmholtz resonator meas. 79—77852
^{4}He superfluid, evaporation through narrow channels 79—60578
^{4}He, superfluid, flow, thermally-driven, in two coupled capillaries 79—86950
^{4}He, superfluid, flow through porous Vycor glass under small press. gradient 80—49442

flow through porous media continued
^{4}He, superfluid, self-diffusion of turbulence through porous media 79—55961
Hg penetration, in porous materials, pore size determ. 78—43165
MHD flow and heat transfer, porous disc eccentric rotations at infinity 79—18965
Mo, permeability, deform. effects 79—100229
N_2, flow, cold gas, through porous-tube, heat-transfer, suction effect 78—59474
Na, vaporisation from capillary-porous structs. (heat tubes, vap. chambers) crit. heat flux 78—90631
Pb-Sn(20 wt.%), partially remelted interdendritic fluid flow 77—4771
Rn concentration variation, temporal (spatial), rel. to Earth crust 80—33671
UO_2 low temp. fluorination in 3-inch diam. fluoridised beds *(Japanese)* 79—81056

flow visualisation
aerodynamic, methods *(French)* 77—62317
aerofoil at high angle of incidence in longitudinal oscillations 79—72969
airfoil, wave drag in transonic flow, shear interferometry obs. 79—77165
aortic and mitral valve prostheses, in vitro flow visualisation 77—86703
artificial heart blood pump ventricle, mech. driven, visual study of flow field 77—56539
blob mechanics visualisation in flow through porous media 79—4076
blood analogue in curve tube 78—44546
blood flow in branching vessels, water model 77—25477
bluff bodies, cylindrical, flow visualisation investig. of wakes at low Reynolds number 78—83405
blunt cone hypersonic and supersonic flow, near wake Reynolds number effects, interferometric obs. 80—43733
body of revolution with heating and cooling, boundary layer transition and separation 80—64518
boiling, nucleation centres interaction, obs. technique 78—14065
boundary layer turbulence, press. fluctuation meas. by optical interferometry 78—26222
boundary layer visualisation in shock tube, book contrib. 80—1715
bounded turbulent shear flow mechanism obs. 78—90854
brain blood flow display on colour TV using computerised picture processing technique *(Swedish)* 77—44780
bubble condensation, in subcooled liquid, high-speed photographic study 78—42654
bubble formation during gas injection into liq. through orifice, interfacial area, press. *(German)* 79—18937
bubble motion and bubble-droplets in immiscible liq., photographic obs. method *(German)* 79—72931
bubbles, fluid flow in Newtonian and non-Newtonian fluids *(French)* 79—46374
bubbles for flow visualisation in wind tunnel around bluff body 77—80238
buoyant surface jet, 2-D flow props. *(Japanese)* 80—48762
bursting, spanwise struct. obs., in turbulent channel wall region 78—90855
CANDU type 19 rod bundle, velocity distrib. in peripheral subchannel 80—32328
cardiovascular flow visualisation methods for in vitro studies 77—56409
carotid bifurcation tomographic scanner, US Doppler colour coded vel. display 77—25529
cascade shock loss location and magnitude by high speed smoke visualisation 80—24051
cathodic diffusion boundary layer, free convective flow obs. with shadow Schlieren method 78—68894
cavitation bubble collapse, shadowgraph study 80—48827
cavitation in water jets, flow visualisation using holography 80—106862
channel, two-dimens., turbulent flow with separation 80—19356
channel, with varying cross section, shock wave proag. 79—23339
chemically reacting turbulent shear layer between two streams obs. 80—6163
coaxial jet drop generator for holographic flow visualisation in water tunnels 78—5836
convection, free, laminar, three-dimens., about surface, numerical anal., visualisation *(French)* 78—87343
convection measurement, differential interferometer with achromatic $\lambda/2$ compensation 78—87419
convective mass transfer measurement methods, review *(German)* 78—46959
corrugated wall, exptl. study of flow *(French)* 78—90844
Couette-Taylor flow, laser Doppler velocimetry obs. of transition to turbulence 80—92163
critical mixtures, shear and critical fluctuations, instantaneous mapping of velocity gradients 80—79420
curved wall power fluidics characts. 80—103053
cylinder, circ., inclined, laminar 3-dimens. free convection, stability *(French)* 79—18884
cylinder, circular, with slit, flow characts., control, patterns, wake flow, vortices 78—83404
cylinder, perforated, circ., finite-aspect-ratio, drag coeff. 79—23360
cylindrical tube rows downstream flow, complex struct. 79—64812
diffuser, stream struct. meas. by laser Doppler anemometer 79—86477
disc-stabilised diffusion flames, vel. characts. 79—34309
discrete particles dispersion in turbulent fluid field 80—33580
dispersion profiles in porous bed, non-destructive method using dye 78—26214
double-exposure holographic interferometry of flow vel. distrib. 78—5831
EHD flow intensity and efficiency, low voltage liq. conductivity depend. 80—33699
electrochemical reactors with three-dimensional electrodes, characterisation using electrochemical tracer method 80—76520
film cooling, use of cholesteric liquid crystals 79—186
films, thin fluid, optical method of meas. velocity profiles *(French)* 80—6170
flame, counterflow diffusion, struct. in elec. field, interferometric obs. 80—16685
flapper-valve flow characts., interferometry appl. 77—24040
floating zone melting, microgravity simulation of Marangoni convection 79—28911
flow visualisation holography, generalised phase control during reconstruction 79—50246
fluid flow visualisation techniques 79—90352
fluidised bed probing using optical fibres 80—19533

flow visualisation continued

free convection mass transfer from horizontal surface, electrochemical and holographic interferometric obs. 78—87344
free shear layer behavior in rotating systems 80—1545
gas flow application of shearing interferometers 78—55706
gas-jet visualisation by laser induced I_2 molecular fluorescence 77—80257
GCFR fuel rod roughness elements, surrounding flow visualisation technique 79—59141
glycerin-water solns., visualization of standing vortices behind cylinder 80—59151
glycerine-water drops, collision dynamics, ang. of incidence influence *(Russian)* 78—83461
haemofoil mitral valve, results of flow visualisation expts. 80—104632
haemorheograms for Couette-type transient blood flow 79—79582
heart valve element, artificial, visual representation of flow *(Russian)* 77—32926
Helmholtz resonators with grazing flow, dye streamlines 78—63511
holocinematography of cavitation bubbles 77—46704
hologram interferometer 77—55117
holographic interferometry, multiple exposure, fringe form. anal., appl. to flow vel. distrib. meas. 80—9831
holographic shearing interferometer for recording of pulsed gasdynamic processes 77—47117
holographic shearing interferometer with narrow ref. beam for flow investig. in reflecting nozzle of shock wave 77—47118
holography, appl. of generalised phase control during reconstruction 79—94742
holography, use of photopolymer 80—6176
holography for cavitation and flow research 78—38436
hot wire in liquid, heat transfer, transverse oscills. effects, holographic interferometry 77—15013
hypersonic sphere in air, obs. with open microwave resonator 79—77301
injection of the He for visualisation of air flow patterns past models 77—58813
jet, 3-dimens., at wall, two-point statistical props. 79—1223
jet, circ., controlled perturbation, smoke visualisation 78—90956
jet, circ., free shear layer transition wave development 78—94643
jet, cross stream injection boundary layer, flow and temp. field 79—1225
jet, subsonic, of gas, vortices, flow visualisation patterns 78—63471
jets, radial turbulent, flow, attachment to disc plate, flow patterns, nozzle dimension effects 78—83443
jets and wakes, coflowing, coherent struct., strobing laser beam visualisation 79—32610
laboratory measurement methods and problems, book contrib. *(French)* 77—84355
Lagrangian turbulence characteristics meas. using photographic techniques 77—58811
laminar and turbulent flow around free and surface-mounted obstacles, topology, flow visualization 78—51157
laser Doppler anemometry on transparent turbulent electromagnetically driven flow 80—103090
laser induced breakdown, high speed holography 78—18360
laser velocimetry and visualisation, two-phase supersonic streams, gas-dust 79—68830
laser-induced fluorescence, spatially-resolved meas. 77—35283
liquid, tracer techniques eval. 77—58817
liquid crop falling into still liq., vortex ring formation 78—90946
liquid film, falling, 3-dimens. wave characts., laser beam refraction obs. 79—27654
liquid flow through diffuser, gas bubble motion study *(French)* 77—42940
liquid wave-fronts in free-flow transients, position fixing method based on Ti memory property *(Italian)* 80—43723
liquid/vapour flows in steam generating equipment, instrumentation 79—46404
local mass-transfer coeffs. meas. by holographic interferometry, vortex instability effect 78—75234
low density flow visualisation, capability of holographic phase-shift interferometric technique *(Chinese)* 79—72964
low density gas flows, multipass hologram interferometry 79—32724
multi-vortex ring interaction *(Japanese)* 77—42846
natural convection in liqs. between sphere and cubical enclosure 77—23953
natural convection in narrow vertical cavity 78—34130
nozzle, heat transfer of transonic air flow 79—1230
ozone tracer using UV absorption, for qualitative and quantitative flow visualisation 79—72972
particle mobility in liqs., meas. by optical and elec. transients 79—77303
pattern study *(Japanese)* 79—98835
photochromic tracer film, measurements using POLLY, film reading computer system 78—42696
photochromic tracer technique, for nondisturbing flow measurement 78—38435
photochromic visualisation, effect of turbulence on precision of vel. and vel. fluctuation data 77—68714
pipe-exit flow visualisation using high-speed photography 80—106863
pipeline gas non-steady state flow linearisation coeffs. calc. using finite difference method 77—72395
Pitot sphere appl. *(Polish)* 77—55113
plane mixing layer vortex digital image processing 80—103095
PMMA latex particles, laser light scatt. for visualisation in EHD 78—75236
polyethylenoxide additive mixing, turbulent drag reduction, schlieren obs. 78—26163
polymer flow, birefringence meas. of normal and tangential stresses 77—58625
polymer solution, flow visualization near rot. disc 79—72914
pool barbotage, heat transfer coeffs., high-speed cine-photography and oscillography 78—90982
potential flow, transient state, Liesegang rings demonstration 78—63408
power spectra for chaotic transitions in Rossler dynamical system 80—53898
prosthetic heart valve flow pattern visualisation by laser technique 78—44734
prosthetic ventricle and valve evaluation, flow visualisation data anal. 78—40425
pulsed nozzle jet struct., direct shadow method and streak photography 80—10323
quasiperiodic flow between rot. cylinders, second charact. mode visualisation 80—28519

flow visualisation continued

resonant Doppler velocimeter, direct flow visualisation 77—35285
rheometer, analytical, optical sliding contact, for flow visualisation at articular surface 80—104847
scale model flow testing, in pollution studies 77—3901
seeding method for high-temp. laser Doppler velocimetry 78—9730
separated unsteady flows around bodies, streamline and steakline photographs 78—1634
separating Stokes flow 79—77064
shadow optical method for turbulent flow microstruct. investig., stat. analysis problems 80—19534
shadow photometry of high vel. gas flow, complex diaphragm shape 77—35270
shear flow, stratified, free-turbulent, buoyancy effects on large scale struct. 78—90849
sieve plate column without downcomers, anal. and NH_3 stripping expt. 78—22430
smoke flow visualisation combined with hot-wire anemometry, technique, appl. to turbulent boundary layer 78—91044
smoke tunnel, school and undergraduate use 78—16614
soap bubbles technique for air flow visualisation *(Japanese)* 78—9737
spark tracing, high frequency, application in engineering and aerodynamics 78—38434
speckle interference fringes 77—84346
sphere, external laminar boundary layer vel. profile, photographic-tracer film anal. 79—50698
stagnation flow turbulence about circular cylinder, visual study 80—96248
Stokes flow, past spherical caps, visualisation of separation 79—60076
stroboscopic, flow structure in immediate vicinity of wall 79—1215
stroboscopic flow imaging method, three coordinate technique 80—38507
supersonic chemical laser flowfield, laser induced I_2 fluorescence meas. 80—38008
supersonic flow over hemisphere-cylinder at incidence up to 19° 78—59419
supersonic flow pattern around sphere, using broad light source holographic interferometry 80—19008
surface patterns using O quenching of dye fluorescence 80—79422
tall-form spray chamber, residence-time distribution of air 78—9679
thermal convection, two-phase, in porous layer, flow visualisation study 79—72930
thermal energy storage material cylinders, heat transfer during melting 79—3894
thermal markers for liq. vel. field meas., error reduction 78—91036
thermal turbulent wake studied by 3-beam holographic interferometry *(French)* 77—62316
thymol blue method for visualising high Prandtl number convection 80—6182
tracer dispersion in annular climbing film flow 79—64751
tube bundle beds, photographic observation 77—84315
tubes, single horizontal and bundles, vibr. fluidised disperse medium flow 80—33658
turbine nozzle steam under periodic perturbations, Topler method appl. 77—80249
turbomachine combustor, analysis and modelling of flow *(French)* 79—46401
turbulence diagnostics by holographic interferometry 79—60078
turbulence separation, subsonic and supersonic, ultra-short duration visualisation *(French)* 78—75128
turbulent convection in liquid, laser beam propagation 79—98831
turbulent core of boundary layer 79—1168
turbulent flow fields, evaluation of stereoscopic trace particle records 78—1648
turbulent flow relaminarisation, flow visualisation 78—75244
turbulent free convection in fresh and salt water, characts., visualisation 79—18888
turbulent horseshoe vortex 80—103016
turbulent shear flow, coherent structure, stereoscopic camera obs. 79—32485
turbulent spot, entrainment behaviour, flow visualisation and laser Doppler velocimetry 78—26102
two phase flow method 80—33714
two-dimensional random field model for image structural analysis *(Russian)* 80—63932
two-dimensionalism condensed system axisymmetric channel, mathematical model 77—76010
two-phase, structure in critical cross section 77—65827
unsteady airfoil, Kutta condition *(Japanese)* 80—92155
unsteady airfoil stall in laminar boundary layer, water tunnel visualisations 80—53745
unsteady convection study, simultaneous velocity and interferometric meas. 79—98839
unsteady inviscid 2-D flow analogy using stretched membrane and moire fringes 80—64658
unsteady quasiperiodic flows, self-synchronising Schlieren flow visualisation, near wake 80—19527
velocity measurements inside a rotating cylindrical cavity with a radial outflow of fluid 80—96275
venous blood flow visualisation using dynamic leg scintigraphy with large field-of-view scintillation camera 78—73215
viscous flow, between concentric rot. spheres, visualisation and meas. 77—15038
viscous sublayer and near wall turbulence struct., stroboscopic visualisation 80—19349
vortex breakdown regimes, in rot. cylindrical cavity, identification 79—50731
vortex flow, motion of near buoyant tracer particles 77—89216
vortex ring visualisation, smoke wire technique appl. *(Japanese)* 77—35264
vortex-excited vibration mechanism of cylindrical struct., photographic evidence 79—46406
wake core recirculation bubbles, adverse press. gradient, wind tunnel visualisation *(French)* 77—54997
wake vortices, flow visualisation *(Japanese)* 77—89128
water, convective heat transfer, free, with density inversion, in confined rectangular vessel *(German)* 79—18671
water fog generation system, for subsonic flow visualisation 77—24037
water jet, penetration through water surface, high-speed photography 78—42693
water-in-oil emulsion, boiling, bubble formation, cinemicrophotography 80—74961

flow visualisation continued
- wedge like sharp edge starting vortex, flow visualisation expts. 80—59046
- wind tunnels with adapted walls for reducing wall interference *(German)* 79—77320
- Al plastic flow in plain strain extrusion, photographic appl. 80—7626
- He hypersonic flow, Na vapour seed, quantitative flow visualisation 78—47072
- He hypersonic flow, Na vapour seeded, velocity profile visualisation 78—59530
- He, liq., flow boiling in vertical channels, visualisation 77—42938
- N_2 vapour columns, cryogenic, complex flow 78—34119
- Na vapour, reson. refr. and dispersion, appl. to flow visualisation 79—41790

flowcharting
- *see also programming; systems analysis*
- DC corona discharges in coaxial cylinder electrode 80—33837
- dilute solutions, Monte Carlo algorithm for preferential sampling near solutes 77—51287
- elastic structures, computer automated synthesis for minimum struct. weight 78—34015

flowmeters
- *see also anemometers; flow measurement; laser velocimeters*
- 4 MHz range-gated US Doppler flowmeter design and application 78—59527
- 90° elbow flow meter, effect of inaccuracy of curvature *(Japanese)* 77—89215
- Aanderaa current meter, shallow-water meas. accuracy 77—5378
- accurate meas., special flow meter *(Croatian)* 80—53890
- acoustic, multiple and single path, sources of error, accuracy, appls. 79—94749
- acoustic flowmeter, for use with hydraulic models 79—68878
- acoustic flowmeters for pipelines 80—43808
- analogue output device for Rotameter flow rate measurements, photoelectric cells appl. 78—75237
- anemometer, const.-temp. hot-wire, for respiratory gas flow meas. 79—83967
- animal research, totally implantable directional Doppler flowmeters 80—67293
- annular-averaging flow sensor, error in averaging technique and discharge coeff. 80—38509
- area type flowmeter, flow coefficient *(Japanese)* 80—1711
- arterial haemodynamic transfer function calc. from Doppler US flowmeter waveforms 78—61235
- automotive air-intake flowmeter using corona discharge principle 80—33716
- axial, aperture ratio calc. method *(Dutch)* 78—67285
- axial flow gasmeter, 10″, rotor thrust meas. 79—68848
- bidirectional fluidic, respiratory meas. appl., tests 78—35993
- blood, cylindrical crossed-coil NMR, for noninvasive measurement 79—62328
- blood, ultrasonic, design considerations 80—23853
- blood flow detection in human heart, US pulsed Doppler flowmeter system, microcomputer based 80—104690
- blood flowmeter, implantable bidirectional pulsed Doppler, for animal research 78—44749
- blood flowmeter US implantable bidirectional pulsed Doppler device, timing and signal processing ICs 80—76812
- Borda inlet a-r flowmeters, performance characts. 78—22437
- borehole flow, instrument for simultaneous meas. of axial and radial components 79—80051
- boundary layer acoustic monitor for hypersonic turbulence transition determ. 78—34237
- CAD, standard orifice plate calc., for meas. flowrate of liquids, gases and vapours 80—1714
- calibrating devices, accuracy 79—68846
- calibration, design advancements, microcomputer-controlled flow rigs 80—10320
- calibration, dynamic, for liquid flow 77—76006
- calibration and profile effect on unchoking back-pressure ratio *(Japanese)* 77—65779
- calibration at low flow rates 79—68847
- calibration by electronic weighing 78—55700
- calibration method using sonic nozzles *(Japanese)* 77—65821
- calibration methods with liquids, comparative survey 77—68720
- calibration of permanent magnet Na flowmeter, signals anal. method 78—38425
- calorimetric and heat-label, with IR or UHF sources, calibration 77—80243
- closed-loop EM flowmeter with power conserving ccts. 80—38511
- Coanda fluidic digital gas flowmeter 80—59138
- conducting flow vel. meter, characts., freq. depend. calibration *(Russian)* 77—65819
- conduction flowmeter, weighting function, mag. field distrib. effects *(Russian)* 77—47121
- conduction flowmeter with calculable and controlled calibration characteristics *(Russian)* 79—7428
- conductive fluids local induced voltage velometry *(German)* 79—86517
- cone and plate rheometer, vel. and temp. profiles, flow birefringence polymer melts 77—54945
- conference, flow meas. techniques, Brighton, England (April 1977) 77—84358
- constricting device for flowmeters of viscous liquids and gases 78—75241
- constriction meter orifice, swirling flow component effect on discharge coeffs. 78—63514
- contact-type flowmeter working in thermal boundary layer, temp. error determination 80—103093
- contactless, construction principles *(Russian)* 80—87823
- contactless thermal, calibration characts. 80—103085
- converging devices, effect of aeration on error 80—10327
- cooling water flow control in continuous casting process, vortex flowmeters 80—64655
- correction factor appls. for blunting of diaphragm input rim 78—75240
- corrosive liquid flowmeter with UHF heater *(Russian)* 78—59523
- critical venturi type, discharge coeff. meas. 79—68871
- cross-correlation system operation 78—1760
- cryogenic, three-year experience at NBS 77—27637
- cryogenics, dynamic flow rate meas. 79—60075
- CW Doppler, implanted, for renal/iliac bloodflow telemetering from exercising dogs 77—90822

flowmeters continued
- cylindrical, convergent flowmeter, medium expansion correction factor determination 78—67296
- cylindrical nozzles with sharp upstream edges, critical flowmetering appl. 80—28546
- design types for gas throughput meas. in vacuum gauge calibration apparatus, review 77—26319
- diaphragm and Venturi tube appl. *(Bulgarian)* 78—47077
- differential, for large flow rate meas., tracer calibration 79—68885
- differential, for ultrafiltration dialysis meas. and control 77—21657
- differential digital type, operations 78—38424
- differential pressure, distorted profile effects 79—68860
- differential pressure flowmeters, errors due to pressure fluctuations 79—68862
- differential pressure fluid meter, loss coeff. 77—65829
- differential pressure type, appl. 78—38422
- differential pressure type, using pad and quad resistors 78—42688
- differential pressure type 78—38423
- differential producer flowmeter, statistical improvement 77—65830
- digital, planar Si diode sensor long-term stability anal., 70-420K *(Czech)* 77—67435
- digital 2D full range Doppler velocity meter for cardiovascular diagnosis 78—88731
- discharge coefficient based on boundary layer parameters 80—48828
- discharge coefficients for 360 degree bend flowmeters 79—27717
- Doppler beat signals, freq. error, due to extended scatt. particles, theory and expt. 77—7487
- Doppler signal centre freq. estimation using quadrature zero-crossing counter, US blood flowmeters 78—31879
- Doppler ultrasonic, operating principle 79—50817
- Doppler ultrasonic flowmeter 79—68889
- Doppler US blood velocity meas., phase-locked loop technique 78—61234
- Doppler US flowmeters, optimum vel. resolution 77—957
- double-chambered thermal type, operational principles *(Polish)* 78—42686
- drag plate flowmeter, for pulsating flow, design and evaluation 79—68863
- drag sphere velocity probe, miniature, development and testing 78—55705
- drift detection, repeatability testing technique 77—84357
- DUS 20 US flowmeter for liquids, operation *(French)* 79—50819
- dynamic errors, mobile weighing system 80—96326
- eddy-current flowsensor, model 78—5829
- elbow, wall curvature inaccuracies rel. to discharge coeffs. 78—83501
- elbow meters for flow monitoring, description 79—37426
- electrohydrodynamic for dielectric media flow meas. *(Russian)* 78—26216
- electrokinetic with automatic temp. compensation for dielectric liquid, description *(Russian)* 77—3894
- electromagnetic, anal. in ducts and open channels 78—59524
- electromagnetic, calibration using a flow simulator 79—68854
- electromagnetic, distorted profile effects 79—68860
- electromagnetic, effect of electrode processes on transmission coefficient of transducer 79—7426
- electromagnetic, mag. circuits for special appls. 79—68861
- electromagnetic, with ultra-stable zero, description 77—956
- electromagnetic flow meters, recent developments *(Japanese)* 79—98836
- electromagnetic flowmeter with moving field, fluid flow and moving field equations *(Rumanian)* 80—64663
- electromagnetic flowmeters, design considerations *(German)* 80—38514
- electronic, for determining low gas pressures 79—37427
- electrostatic, effect of arrangement of electrodes on accuracy 80—103087
- EM, accuracy, influence of velocity profile 79—68856
- EM, appl. to meas. of discharge from partly filled pipes 79—68857
- EM, for blood flow and vel. meas. 77—78008
- EM, for fast reactors, review 78—21686
- EM, for industrial appl. 80—1701
- EM, non-flow test method *(Russian)* 77—3899
- EM, testing without using liquids 77—80244
- EM, ultra-stable zero, installation 77—39389
- EM, vel. profile invariance, sensitivity, error *(Russian)* 77—24042
- EM, water supply monitoring appl., Japan 77—53877
- EM, with large-area electrodes, performance anal. of three models 80—1706
- EM, with non-uniform mag. field, liquidless calibration 77—72385
- EM blood, comparison of dynamic calibration methods 78—40362
- EM devices, theoretical aspects *(Dutch)* 78—22442
- EM flowmeter, performance with mag. slurry 78—26219
- EM flowmeter, with nonuniform mag. field, for liq. metals *(Russian)* 77—47122
- EM flowmeter dynamic calibration device 80—43817
- EM flowmeter theory and application 80—96328
- EM flowmeter variant system 78—18359
- EM pressureless with linear output signal, description *(Russian)* 77—89213
- EM pump and plant with liq.-metal working fluid, review *(Russian)* 77—19639
- EM type, optimal mag. system design *(Russian)* 79—1275
- EM velocity transducer with a multipole mag. 80—83868
- EM water current nonlinearity and sensitivity 77—5383
- EM with rectangular wave excitation, operational principles *(Japanese)* 77—80237
- end effects in a flow-rate transducer with a cylindrical magnet 80—83869
- estuarine current meter data acquisition microcomputer system 80—46265
- FFTF-type eddy-current flowmeter performance in SLSF P-series test trains 79—9669
- fission reactor primary coolant flowmeter 80—73912
- flange tap orifice flowmeters, Stolz and ASME-AGA orifice eqns., lab. data comparison 80—64604
- float type, with US meas. of float position *(Russian)* 77—42943
- float-area-type, jumping instabilities of float 80—14855
- flowpath velocity meas., semiconductor hot element anemometer 80—48823
- fluid, metrological characts. determ. *(Russian)* 77—62318
- fluidic, state of art and semiconductor tensometric membrane based design *(Czech)* 78—26213
- flume, two-dimens. numerical modeling 78—30388
- flumes and weir, construction error compensation, computer anal. 78—30387

flowmeters continued
flux distortion, tests using analogue rig to simulate flow with boundary layer 78—38420
flux distortion flowmeter, for LMFBR coolant flow meas. 79—68858
gas, calibration, gravimetric standard method *(German)* 77—55112
gas, certification of convergent nozzles by comparison with standard 80—6126
gas, checking by standard throttle system 77—80242
gas, comparison of calibration methods *(Japanese)* 79—72970
gas, low speed, constant gas flow production *(Hungarian)* 80—1702
gas, movable L-tube, with density meter *(Japanese)* 77—3900
gas discharges, flowmeter 77—76000
gas flow calibrator fibre-optic timing system 77—31408
gas flow meas. with vortex meter and microcomputer *(German)* 80—92241
head meters appl., flow effects and calcs. *(German)* 77—55116
heat bridge flowmeter description *(Russian)* 79—7429
high integrity metering 79—81999
high pressure piston flowmeter with digital readout *(Polish)* 80—64661
hot wire tachometric probes, calibration instrument features *(Italian)* 79—72966
hot-film anemometer for cylinder wake pattern with spray cooling 78—34238
hot-film probe, in reversing flow, forced convection, finite difference soln. 80—12177
hot-wire anemometer, static and total press. probes turbulence effects 78—34240
hydrodynamic factors, calibration and meas. errors 80—96322
IC, direction sensitive, small size, wide range flow speed *(Dutch)* 77—55120
implantable bidirectional blood flowmeter, micropower ICs 77—13038
implantable directional Doppler type, pulmonary artery flow meas. after lung homograft in dogs 77—90823
implantable Doppler design with phase-locked loop 78—31873
impulse flowmeters accuracy, survey of flowmeters *(German)* 79—98843
induction flowmeter, large cross-section pipe, calc. method 79—7422
inductive, unsymmetrical flow velocity profile, hydraulic transport appl. *(German)* 79—77318
inductive type, features, drainage flow meas. appl. *(German)* 77—84354
initial, for critical gas flow rate meas., principle 77—72382
integrated direction sensitive flowmeter 77—7484
interference compensation in chemotronic flowmeter for electrically conducting liquids 77—19650
Karman vortex flowmeter *(Japanese)* 80—10325
laboratory practice, repair and checking *(German)* 78—32803
laser Doppler flowmeter, LADO 1, non-contact meas. of liquid and gas flow rate 79—77305
linear digital orifice plate with turbinemeter 77—84364
linear pad resistor type, calibration 79—68868
liquid, design nomogram 80—96323
liquid, low flow rate, automatic testing by dynamic weighing 77—55111
liquid flow rates through pipes, applicability of experimental meas. methods 80—100044
liquid flowmeter calibration automated secondary standard 77—37841
liquid vortex, appls. and principle 77—89209
LMFBR, correl. meas. of Na flow rate using mag. detectors 79—71924
LMFBR, steam generator LOCA signalling by EM flowmeter *(Czech)* 79—6751
LMFBR cooling circuit, calibration of EM flowmeters by average frequency method 80—570
looped receiver impinging jets flowmeter with circular and rectangular jets, respiration meas. 77—40878
low and high turbulence flows, hot wire measurement based analysis 78—59511
magnetic, bubble noise effects on output signal, Na loop test 78—91038
magnetic, with capacitative signal pick-off 79—72978
magnetic flowmeter, enhanced performance with pulsed DC excitation 79—68855
magnetic flowmeter construction and reliability 79—23386
magnetic flowmeters, with keyed DC field, appls. and developments 79—68887
magnetic induction, principles and applics. *(German)* 77—39374
magnetic type, respiratory flow telemetering appl. 77—86654
magneto-inductive flowmeters, installation *(German)* 80—64662
mass, meas. Coriolis effect on mols., electro-optical sensing 80—96327
mass flow meas. by means of heat flowmeter 79—68833
mass flow meter using Coriolis principle, electro-optical force sensing techniques 80—103094
measurement methods and appls. for optimum reliability 79—81998
mechanical, engineering meas., conf., Johannesburg, South Africa, (Feb. 1979) 80—75016
mechanical, readout conversion to electrical output 80—75012
metrological assurance in petroleum-gas industry, Soviet standardisation 77—76004
metrological services in Soviet Union, economic evaluation 77—80239
MHD flowmeter, with circ. cross section, inhomogeneous mag. field effect on signal 80—33709
MHD flowmeter, with circ. cross section, symmetry conditions effect on signal, arbitrary vel. profile 80—33708
microflow meter, Flo-Tron, for low flow rate meas. 78—14118
microwave Doppler-effect type, particle moisture content effects 78—9732
movable L tube gas flowmeter, momentum type *(Japanese)* 77—39373
movable orifice type, meas. principle, design and trial meter results *(Japanese)* 80—59148
movable throttle flowmeter for meas. flow rate and quantity of a gas condensate 79—68834
movable tube mass flowmeter with single const. vol. flow apparatus *(Japanese)* 77—65820
multipole field EM velometers 79—18977
nasal flowmeter for preterm infants, self-retaining 80—98158
NMR flowmeters, vortex meters, and mass flowmeters, calibration 80—92239
NMR limb blood flowmeter, clinical appls. 80—17178
nonstationary flow rates, meas., use of electrofluidic analogy *(Bulgarian)* 80—28583
nozzle, instantaneous flow rate meas. in pulsating water flow *(Japanese)* 80—59133
nozzle, long radius, rel. to quadrant edged orifice 79—68869
nuclear reactor 80—99268
oil, differential, mechanical to electrical readout conversion 80—75013

flowmeters continued
open channel, standardisation in Soviet Union 77—80241
open channel acoustic flowmeter, error sources and calibration 78—30389
open channel acoustic flowmeters, design, calibration and errors 78—55701
open channel acoustic flowmeters, design, meas. errors and operation 78—63516
operational principles and appl. 78—47073
optical-fibre flowmeter using transducer 79—98830
orifice meter, plate buckling, flow meas. errors 77—84371
orifice meter, pulsating incompressible flow, anal. and expt. 78—34230
orifice metering installations for natural gas 77—84372
orifice meters, influence of bends *(Italian)* 78—94859
orifice meters, quadrant-edged, standardisation 77—51138
orifice plate meters, appl. to gas flow under high press. 79—68884
particle, microwave Doppler effect, approx. signal theory 79—94747
pipe bends as flowmeters *(Italian)* 80—69958
piston type meter prover specifications *(Japanese)* 77—62320
Pitot tube meas. in large pipe flow, uncertainties 78—34228
positive displacement, linear and nonlinear specific gravity digital compensation 78—34242
positive displacement measurement system for diesel pump and injector performance testing, microcomputer-controlled 80—24112
precision, commercial instruments survey *(French)* 80—83871
pressure differential devices for slurry meas. 77—35265
Price and Pygmy current meter traverses, error sources 78—30385
probe type EM flowmeter, sensitivity 79—68853
propeller Vector Measuring Current Meter development 80—46313
pulse-compensation method of meas. liquid flow-rate based on NMR 80—103088
pulsed Doppler, implantable, for bloodflow meas. in dogs 77—90966
pulsed Doppler flowmeter, development and cardiac appls. *(Japanese)* 80—36037
quadrant edged orifice, rel. to nozzle type 79—68869
radioisotope steady gas flowmeter design 79—32721
reading, viscosity change influence compensation *(Russian)* 77—65823
reference, development for irrigation water mains 80—96325
reference installations, development prospects for meas. computer complexes 80—96320
reference standard US flowmeter error component estimation 77—80248
reliability, overview 78—30382
repeatability, test procedure 78—30379
reproducibility conditions analysis and obs. 77—80240
resistors, pad and quad type, use in flowmeter inside pipe 77—65818
respiratory, hot-wire, evaluation for clinical appls. 80—72346
respiratory flowmeter switching device incorporating delay for synchronisation with mass spectrometer 80—17160
respirometer, flowmeter-polarographic electrode sensor, for respiratory function telemetering 78—80995
review of available devices 77—39367
rheometer, orthogonal, inertial effects in rheometrical flow systems, theory 77—51016
rolling bottle device, for measuring flow of liqs. and powders 80—6174
rotary flowmeter for hot water 77—47120
rotary gas flowmeter error anal. *(Russian)* 78—71407
segmental orifice flowmeters, discharge coeffs. meas. 79—68867
selection, performance-application compromise 80—87822
selection guidelines for fluid flow meas. 78—71404
sharp-lip capillary nozzle production and meas. precision 77—80246
slit type, linear slit profile anal., gas-saturated liquid flow meas. appl. 78—5835
small gas consumption meas., construction principles *(Russian)* 77—72393
solid-state water current meter for wave direction sensing 79—21070
stabilizing liquid flows for flowmeter appls. 80—103084
static plate type, automatically controlled, for flow meas. in pulsating flow 79—68870
supersonic flowmeter using laser beam and Fabry-Perot interferometer 79—7420
tachometer flowmeter for exact measurement and reproduction of high gas flow rates 79—77309
tachometric, testing with volumetric dynamic flowmeter installation 80—96324
tagging flowmeter, signal processing 80—10328
tank water, digital IC pneumatic bubbler probe system appl. 77—41569
temperature-difference based, for slow motion meas. *(French)* 79—86536
test equipment 77—72384
test system based on anal. of synthetic model 80—103082
testing, by comparison with standard instruments 77—76007
testing, design principles for comparative testers 80—96319
testing in working conditions, use of model EM flowmeter 77—76008
thermal measurement systems for flow rate and flow composition *(Russian)* 80—69953
thin orifice plate, turbulent flow numerical modelling 78—34229
throttle, standardisation in Soviet Union 77—76003
throughflow recording and measuring equipment, survey *(German)* 80—1707
time constant determining, using hydromechanical oscillatory system 77—76009
time differential clamp on ultrasonic flowmeter, performance and appls. 78—30390
total flow meas. using auxiliary pipe line *(Japanese)* 78—79395
transducer calibration, using computerised system 80—79416
transfer function, determination using hydropulsator 80—103083
transfer standard flowmeters, critical appraisal 77—84370
transfer-standard, calibration in water test rigs for comparison of laboratories 79—23389
trip-wire vel. probe, sphere with preceding trip-wire for turbulence 78—34239
true mass flowmeter for two-phase mass flow rate meas. in fission reactors 80—778
tubeless siphon apparatus, elongational flow meas. in dil. polymer soln. 77—7486
tubes with ball seatings, basic groups, appl. in flowmeters *(Russian)* 78—67287
turbine, calibration for solar collector testing facility 77—39387
turbine, historical development 78—51262
turbine and vortex, comparison 78—55699
turbine and vortex meter comparison, theory of operation 77—84350

flowmeters continued
turbine flowmeter, flow straightening effect on accuracy 79−32716
turbine flowmeter, for gaseous hydrocarbon, construction and performance, review 78−34244
turbine flowmeter, linear and nonlinear specific gravity digital compensation 78−34242
turbine flowmeter, universal viscosity curve, errors 78−34243
turbine flowmeter for high press. 79−55431
turbine meter uncertainty, uncertainty pattern statistical anal. 78−30381
turbine meters, appl. to gas flow under high press. 79−68884
turbine meters, appl. to present day flowmetering requirements 77−84362
turbine transmitter with radial rotor, low liq. flow meas., geometrical props. effects 79−68849
turbine-type, effect of measured gas parameters on steady-state characts. 77−72383
turbine-type, made in Bulgaria, survey *(Bulgarian)* 80−6173
turbulent air flowmeter for long-term monitoring in patient-ventilator ccts. 77−64149
turbulent flow measurement by laser Doppler anemometry, concentration and size of tracer particles, theoretical limits 78−59514
two phase flow in pipe lines, on-line holdup or quality meter 80−106858
types and usage 78−55698
U-bend open channel meter *(Japanese)* 78−22440
ultrasonic, applications and development 79−68893
ultrasonic, distorted profile effects 79−68860
ultrasonic, for pure and high polluted fluids *(German)* 79−77319
ultrasonic, frequency difference method 79−68851
ultrasonic, non-intrusive, theoretical and expt. uncertainty determ. 78−30391
ultrasonic, wide beam 80−106856
ultrasonic cross correl. flowmeter 78−30393
ultrasonic flowmeter *(Japanese)* 79−98837
ultrasonic flowmeter for natural gas industry 78−30392
ultrasonic flowmeters 79−50832
ultrasonic open channel flowmeter with microprocessor 79−68877
urinary flow rate meas. device 77−48906
US, appl. to meas. of discharge from partly filled pipes 79−68857
US, computer interface development 78−38426
US, correlation and spectral props. of flow modulated US signals 77−42948
US, Danfoss, using electronic unit and piezoelectric transducers 80−6172
US, for flow meas. of fluids in pipe *(French)* 79−1274
US, for measuring rapidly changing gas flows, freq. range, excitation and signal processing *(German)* 78−83502
US, for Na cooled FBR coolant flow meas. *(Japanese)* 78−78455
US, metrological properties *(Polish)* 78−51265
US, microcomputer-controlled 80−24111
US, multichannel time-freq. type, operating principle 77−72387
US, optimisation for two-phase prepolymer flow meas. 77−31410
US, performance anal. 79−14500
US, PLL cct. *(Japanese)* 80−79414
US, propagation time of acoustic signal 80−6175
US, recalc. of characts. and calibration 80−103086
US blood flow velocimeter, MTI filter, with inherent A/D 79−16263
US blood flowmeter, noninvasive Doppler device 77−44733
US blood flowmeter *(Japanese)* 78−31875
US blood flowmeters, early history 77−77946
US compensation-type flowmeters *(Russian)* 80−83866
US cross-correlation, performance evaluation, HWR appl. 78−25283
US directional Doppler blood flowmeter, transducer design 77−25535
US Doppler, bandwidth depend. on beam geometry rel. to flow parameter estimation 80−53894
US Doppler, new modulation method, blood flow meas. 80−45989
US Doppler blood flowmeter, geometrical spectrum broadening anal. 77−86567
US Doppler blood flowmeter modulation *(Japanese)* 79−2115
US Doppler blood flowmeters, induced soft tissue temp. increases, thermographic meas. 79−62294
US Doppler device in detect. of fat particles in blood, digital signal processing 77−25525
US Doppler flowmeter average frequency processor 79−83873
US Doppler flowmeter employing continuous wave modulation *(Japanese)* 79−37429
US Doppler flowmeter spectra for asymm. transducers 78−31880
US Doppler shift signal processing, maximum frequency follower 79−62320
US Doppler spectra, transit time and geometrical broadening 78−44576
US Doppler type, transcutaneous arterial elasticity assessment 77−77948
US flowmeter, 240 Clampitron, applicability study 80−24108
US flowmeter, multichannel 80−103089
US flowmeter cell unconventional designs 78−59528
US flowmeter data processing, transfer function modelling of arteries 78−61225
US flowmeter for LMFBR Na flow meas. 80−32412
US flowmeter output characteristic linearity 78−42685
US flowmeters, petroleum and similar fluids 80−43804
US flowmeters, thermal boundary layers, diffraction effects on sound transit time 80−14858
US FM blood vol. flowmeter processing technique 78−31878
US for measurement of pulsating temp. and vel. in internal combustion engine 80−1704
US for small time-interval meas., methods *(Russian)* 77−65824
US implantable CW Doppler blood flowmeter, optimal system design 78−53460
US implantable IC CW Doppler flowmeter 78−31877
US mean frequency Doppler modulator performance, blood flow meas. appl. 80−45991
US phase flowmeter, pulsating flow rate meas. error evaluation 77−72388
US pulse Doppler, arterial flow in man 80−104805
US pulsed Doppler flowmeter, vel. accuracy and range resolution 77−77945
US volume flowmeter, in vivo validation 79−83872
USSR testing aggregate as basis for single metrological testing system 79−94752
V-delta-P digital flowmeter 77−84363
V-notch weir, approach channel and sedimentation effects 78−30386
VA meters, calibration at low flow rates 79−68847
for vacuum system, gas throughput meas. 77−67451

flowmeters continued
variable area, physical function calc. by programmable pocket calculators *(German)* 78−30377
variable area flowmeter calibration, gas flow modelling 78−14115
variable area flowmeter calibration, gas flow modelling 79−90353
variable area flowmeter standardisation *(German)* 79−50834
variable press. drop method, accuracy and design analysis *(Russian)* 79−7427
variable pressure drop flowmeters, drainage coefficient reliability 77−58824
variable pressure-drop flowmeter parameter optimisation 77−58826
velocity probes for non-uniform gas flow in large ducts 80−48829
venturi, stabilizing the conversion function 79−68832
vibrating wire flowmeters, performance 77−84375
vortex, development and appl. trends 80−75017
vortex, turbine or orifice, which one to choose? 77−84359
vortex, vibrating wire type 78−30371
vortex flowmeter, calibration and appl. 77−84374
vortex flowmeter calibration data and appl. 78−34231
vortex flowmeter design, theoretical and practical aspects *(Polish)* 80−103092
vortex flowmeter for student laboratory use 79−7424
vortex shedding, characts. improvement in low Reynolds number *(Japanese)* 78−79396
vortex shedding flowmeter, stabilisation in low Reynolds number range 80−83865
vortex shedding flowmeter principles and potential 78−22432
vortex shedding principle applic. 77−42934
well-type flowmeter with radiation detector 77−68724
Na flowmeter principles *(Japanese)* 80−28585
Pb-Bi eutectic alloy flow rate meas. apparatus 77−79412
Si strip mass flowmeter 79−77302

fluctuations
see also Brownian motion; critical fluctuations; current fluctuations; noise; random processes
1/f noise, phys. models 77−71272
1/f noise mechanisms, linearity 78−45568
acetone, transient pressure-drop fluctuations in electroviscous effect 80−15286
acoustic Love waves and light scattering in photoelastic films *(Russian)* 77−28543
acoustic signal coherence limits in random ocean environment 80−46193
adsorbed phases, coverage fluctuations 78−14573
albumin, bovine serum, solutions, fluctuation transport theory 78−70057
amorphous ferromagnetic alloys, micromagnetic eqns. for case of dipolar and magnetocryst. fluctuations 80−11171
amorphous ferromagnets, dispersion rels. and spin-wave spectroscopy, spatial fluctuations of magnetisation modulus *(Russian)* 79−7983
amorphous semiconductors, fluctuations and non-randomness in continuous network models 80−49112
amorphous solid, phonon scatt. by density fluctuations and thermal cond. 80−10626
angular correls. random perturbations, asymptotic attenuation coeffs. 77−30507
anisotropic dielectric crystal, EM fluctuations 79−19857
W.Antarctic ice sheet, fluctuations in Antarctic Peninsula area 80−94549
antiferromagnet, crit. fluctuation of staggered magnetisation, AC susceptibility meas. 80−60219
applications of fluctuation and random event theory *(Hungarian)* 77−49679
arc plasma, thermal density fluctuations, light scatt. using CW CO_2 laser and heterodyne detection 78−59677
arcs parameters determ., natural fluctuations of voltage and emitted light correlation *(French)* 80−19654
aridity in Andhra Pradesh, fluctuations 77−56661
aromatic compounds, oxidative bromination, chem. oscills. 80−3335
arrival position fluctuations, geometric optics analysis limitations 78−46530
astronomical radio sources, ionospheric phase fluctuations meas. by radio-link interferometer 77−5452
atmosphere, liq. water content and temp. fluctuations in laser beam cloud clearance zone *(Russian)* 78−44999
atmosphere, synoptic object localisation, long-period tidal fluctuations *(Russian)* 78−81321
atmosphere electric field over oceans, short-period fluctuations 79−39816
atmosphere humidity fluctuations meas., correction for different wet and dry bulb response in thermocouple psychrometry 80−98472
atmosphere scintillation, theory for millimetre and submillimetre wavebands 80−61884
atmosphere submillimetre emission and absorpt., freq. spectrum of fluctuations 77−41308
atmosphere surface layer temperature, fluctuations investigation via acoustic method 80−67434
atmosphere temperature fluctuations, heat flux and struct. functions meas. with acoustic Doppler sodar 80−105023
atmosphere total O_3 content, natural fluctuations 79−29819
atmospheric optical intensity fluctuations, frozen turbulence hypothesis expt. *(Russian)* 78−61557
atmospheric precip., daily precip. fluctuations modelling with Markov-I chain 80−101401
atmospheric pressure fluctuations, influence on Earth surface tidal tilts *(Russian)* 78−88790
atmospheric turbulence effects on IR and near-millimetric-wave propagation 80−61902
atmospheric variables, spectra deduced from ground-based radiometry 79−92567
atomic engines, efficiency of coherent amplification 78−33717
atomic motion in resont fluctuating laser radiation 80−43310
atomic transition in stochastic field, saturation and Stark splitting 80−9546
auroral zone current system, fluctuations rel. to geomag. pulsations 77−87188
autocatalytic reaction system, sustained oscills., deterministic and stochastic theories 78−95922
Baltic Sea currents, Eulerian fluctuations rel. to Lagrangian meas. of horizontal mixing 80−17290
BBGKY hierarchy, scaling method of kinetic eqn. derivation 78−54286
Belousov-Zhabotinski reaction, chem. oscill. mechanisms 80−3304
Belousov-Zhabotinski reaction, oscill., thermal props. 80−7762

fluctuations continued
Benard instability, critical fluctuation, slowing, optical and acoustic study 79—77075
Benard system, convective instability, hydrodynamic fluctuations 77—35143
Bernard convection, and linear fluctuation theory, Markovian processes and irreversibility 80—87766
bimolecular reaction kinetics, role of density fluctuations 78—44351
binary gas mixture thermal fluctuations in renormalised kinetic theory 77—22492
biological membranes, single-file diffusion, for teaching 78—54127
biomembrane conductance fluctuations and ionic pores, review 77—90752
bispectrum and nonlinear wave coupling for three-wave coupling 80—52038
black hole, quantum gravitational fluctuations, energy dissipation mechanism 78—57572
black hole fluctuations, thermodynamics and time asymmetry 77—2451
black hole formation, effect of zero point fluctuations 78—12286
black hole formation by collapsing cloud of quantal particles 79—2552
boiling, pool saturated, subcooled, in narrow spaces, interferometry obs. 78—94527
boiling, two-phase boundary layer, temp. fluctuations 78—51222
boiling two-phase flow in two parallel horizontal tubes in solar collector receiver tubes *(Japanese)* 79—79377
Boltzmann eqn. for fluctuations in μ-space 77—17929
Boltzmann equation, stochastic, hydrodynamic fluctuations 80—68158
Boltzmann gas, stochastic theory of hydrodynamic systems 79—75476
book 80—73104
Bose fluid, structure factor determ. 78—34667
bound state spectra in ϕ^4 theory and Gross-Neveu model, temp. depend. 78—4770
boundary layer flow, fluctuations in external vel. 77—51043
Boussinesq fluids in turbulent convection, power spectra of temp. and vel. fluctuations 80—98543
Brownian interacting particle system, light scatt. theory diffusion coeff., lineshape 77—27254
Brownian motion, fluctuating hydrodynamics, slip coeff. fluctuation-dissipation theorem 78—8348
Brownian motion, generalised Einstein theory for nonequilibrium fluctuations 80—31672
Brownian motion, kinetic theory, fluctuation effects 80—150
Brownian motion, renormalisation theory 79—54060
Brownian motion, stochastic calculus, derivation from path integral expansion of conditional probability density 79—67227
Brownian motion due to fluid stress tensor fluctuations 78—16738
Brownian motion in external field, quantum description 77—49687
Brownian particles, k-dependence of long-time diffusion 80—5645
Brownian sphere, long time fluctuations 79—85077
Brusselator, two-box model, multiple stable steady states, chem. hysteresis 79—100428
bubble formation during gas injection into liq. through orifice, interfacial area, press. *(German)* 79—18937
BWR boiling noise, local and global component obs. and calc. 78—94066
BWR core flow fluctuation and neutron noise obs. 78—94060
BWR dynamics, multivariable autoregressive identification 78—94107
calcium alginate gels, Raleigh scatt., spectral broadening, density fluctuations 79—1776
cascade showers generated by muons in ionisation calorimeter, fluctuations anal. 79—84618
Caspian Sea, small-scale temp. inhomogeneities assoc. with thermocline, sonar obs. *(Russian)* 77—13132
CDW structure, incommensurate, phase fluctuations, Coulomb effects and long-range order 77—43524
cell population auto-activation, math. model 78—77017
chaos, onset and characteristics 80—82723
chemical instabilities, fluctuations in multiple steady state systems 79—11813
chemical instabilities, renormalisation group approach 78—15657
chemical instabilities, stochastic approach, anomalous fluctuation and transient behaviour 80—89465
chemical reaction, conc. fluctuations, use of master and Langevin eqns., diffusion effect 78—3313
chemical reactions, fluctuations, irreversible thermodynamics 77—52616
chemical reactions, macroscopic equivalence of fluctuation descriptions 77—77734
chemical reactions, oscill. thermal props. 80—7762
chemical system, equilibrium fluctuations, deviations from Poisson behaviour, molecular dynamics 80—86211
chemical systems, non-equilib., mol. dynamics studies of long range and short range fluctuations 80—21318
chemically oscillatory systems, critical fluctuation universality, soluble master eqn. 79—75454
chemisorption, spin-fluctuation description 77—76666
cholesteric liquid crystal, thermal fluctuations, spatial correl. function *(Russian)* 78—2005
cholesteryl oleyl carbonate, isotropic phase, polarisation of scattered light 79—78691
classical fluid near critical point, nonequilib. steady state fluctuations with laminar shear flow 79—81844
classical plasma dynamics 80—83888
classical system with long-range forces, eqn. props., BBGKY eqn., neutrality, screening, sum rules 80—62569
climate, temp. and precip. temporal fluctuations averaged for Europe and N.America 78—92958
climate fluctuations, relation of moistening to thermal regime 78—92937
cluster approximation, wavevector depend. of fluctuations, appl. to one-dimens. Ising model 80—12999
collective plasma density fluctuations, far IR scatt. apparatus obs. 79—32818
collimated laser beam propag. in turbulent atm., phase fluctuations spectrum 78—78914
colloidal systems, dynamical props., correlation and response functions 80—22286
colloids, interfacial electric polarisability, and interactions 80—108751
compressible supersonic turbulent boundary layers, compressible press. gradient effects 79—60001
conducting medium, inhomogeneous, anisotropic, thermal fluctuations of current density, EM fields, and charge density 78—23067
conference on nonlinear nonequilibrium statistical mechanics, Kyoto, Japan, (Jul. 78) 79—75441
contracted description of fluctuating systems 80—90781

fluctuations continued
cosmic inhomogeneities physical origin, conjecture 80—56986
cosmic microwave background, pregalactic fluctuations visibility and upper limit on q_0 80—8717
cosmic microwave background small-scale fluctuations *(Russian)* 80—109576
cosmic ray intensity fluctuations, two-particle distrib. function eqn. 78—28457
cosmic ray neutrons, hysteresis, fluctuations and barometric and ionospheric effects 79—84604
cosmic X-ray background spatial fluctuations, search for correl. with light of galaxies 80—56977
cosmological fluctuations, spontaneous prod. 80—94902
cosmology, primaeval fluctuation spectrum rel. to covariance function 9 Mpc break 78—65688
CP^{n-1} model, quantum fluctuations in the one-instanton sector 79—85209
critical dynamics, classical systems, Fokker-Planck description 78—21057
critical mixtures, shear and critical fluctuations, instantaneous mapping of velocity gradients 80—79420
critical scattering theory, book 79—25913
cyano-biphenyl, nematic liq. crysts., director fluctuation quenching by mag. field *(French)* 78—87613
cylinder, circ., oscillating in turbulent water flow, press. fluctuations 79—59995
deep ocean, low freq. press. fluctuations prod. by surface waves 78—81184
dense gas, of dipolar mols., electron localisation, density fluctuation, mol. orient. 78—38446
density fluctuations in classical and quantum liquids, general theory 79—35628
destructive thermal fluctuations under transient conditions 79—72861
deterministic systems with multiple steady states, small fluctuations effects 79—80526
diagnostic method based on distorted signal 77—41540
dielectric, time-correlation functions of permanent dipole moments and induced polarisation 80—11316
dielectrics, fluctuation theorem 79—47381
dielectrics with periodic boundary conditions, fluctuation theorems 80—80735
differential pressure flowmeters, errors due to pressure fluctuations 79—68862
diffusion in bistable potential, systematic WKB treatment 80—46975
digitised signals from PWR ex-core ion-chamber, transform and filtration methods of anal. 77—54312
dilute gas, Boltzmann-Langevin eqn., light scatt. and density correlation function 77—11307
disordered and amorphous mag. materials, position entropy solids, exchange and anisotropy noise 79—11295
disordered materials, fluctuation-induced tunnelling cond. 80—65516
disordered multicomponent solid solutions conc. fluctuation waves, microscopic theory 80—44327
disordered solids, light scatt. from configurational fluctuations 79—11428
disordered system, residual resistivity 78—87954
displacive ferroelectrics, model, fluctuation effects 79—33063
dissipation theorem for excess noise 78—70059
dissipative dynamical system, iterative transitions between periodic and turbulent 78—62159
dissipative dynamical systems, erratic solns. 78—16737
dissipative spin system, oscills. and fluctuations 80—27224
dissipative structures, fluctuation effects, appearance of optically active states 79—83442
dissipative structures, fluctuation effects on chem. oscill. systems 79—83441
dissipative structures, origins and perspectives *(French)* 80—151
dissipative system instabilities; nonlinear fluctuations 77—87696
distributed temperature sensor of optical path fluctuations, calibration 77—2688
distributive processes in discrete systems 79—80504
DNA in soln., mol. wt. determ. by fluctuation spectroscopy 77—10800
Duffing oscillator, damped, fluctuations, systematic expansion theory 77—13716
dust ball, nonsingular collapse in quantum conformal geometry 79—97284
dynamic theory of fluctuations, Liouville operator and eqn. anal. *(Russian)* 79—6051
dynamical fluctuation theory basic eqn. physical anal. 80—36946
dynamical fluctuations in simple fluids, kinetic theory 77—7652
dynamical theory, nonequilib. statistical operator method *(Russian)* 77—67378
dynamics of fluctuations in systems far from thermal equilibrium 79—40472
Dyson eqn., exact soln. for mean value of Green's function 78—4559
early universe, adiabatic density perturbations evolution 79—25769
early universe density-temp. fluctuations, present observability 80—82554
early Universe initial density fluctuations implications of origin of baryons in Universe 79—62938
Earth annual polar motion, many-year var. rel. to atmospheric circulation many-year fluctuation *(Chinese)* 80—104848
Earth atmosphere, lower, temp. skewness budget, turbulence modelling implications 80—21816
Earth crust resistivity near Palmdale, California, fluctuations after rainy period 79—16373
Earth rotation, amplitudes of components of ΔTs, depend. on observatory geographic position *(French)* 77—86741
Earth rotation, harmonic fluctuations correl. with secular geomag. field vars. 78—73302
EBBA, isotropic phase, order fluctuations, self-diffusion, and rot. motion, proton spin relax. meas. 79—87328
electric power conversion in circuits, power from energy fluctuations 79—100536
electrical circuit, power conversion of energy fluctuations, rel. to 2nd law of thermodynamics 80—17911
electrical noise in equilibrium conditions 79—56274
electrolyte solutions, fluctuations rel. to acoustic relaxation and light scatt. 77—15497
electron microscopes high-voltage supplies, capacitive meas. of slow fluctuations 77—13826
electron plasma with nonparabolic energy dispersion relation, EM fluctuations 80—2413

fluctuations continued
electronic transport coeff., soln. between Mori-Green-Kubo formulae and Boltzmann approx. 78—79971
EM field of infinite medium with spherical inhomogeneity, finite temp. Green's functions 78—1126
EM fluctuations in dielec. slab resonator 79—3672
energy density fluctuation, at fixed wavevector, max. below T_c 79—69225
enzyme dynamics, statistical phys. 80—21439
equation of motion for fluctuations in nonequilib. state 77—41538
ethane-propane, binary mixture near crit. point, conc. fluctuation decay rate, spectrosc. obs. 77—81108
ethanol, aq. soln., conc. fluctuations, shear and longit. relax., Brillouin scatt. and pulse techniques 78—71792
European Grosswetterlagen, temporal vars. and possible causes 79—58081
expanding universe, density fluctuations rel. to struct. development 78—93489
expanding universe, density perturbations three-point correl. function and higher order functions prediction 78—65730
extragalactic radio sources low-freq. variability, ripple radiation effect 79—21450
eye, accommodation microfluctuations in humans 80—12124
eye, induced optical anisotropy fluctuation in lens 78—35838
F_2-layer vertical sounding, radio signal Doppler spectrum and arrival angle meas. *(Russian)* 78—61651
F-region electron density, power spectra rel. to travelling ionospheric disturbances and assoc. gravity waves 78—28394
ferroelectric transitions, diffuse, existence of fluctuations 79—33628
ferromagnetic fine particles, thermal fluctuations, Brownian motion theory 80—11226
ferromagnetic spin system, Lee-Yang theory and normal fluctuations 79—69681
field fluctuations of two-photon coherent states 79—13937
field intensity moments, in randomly inhomogeneous medium, region of fluctuation saturation *(Russian)* 79—3630
field intensity relaxation, in medium with quasi-static fluctuations *(Russian)* 79—2715
finite fluctuations, Monte Carlo simulation 77—87693
fire gas velocity measurement by cross correlation of random thermal fluctuations 77—58812
first-order phase transitions, influence of quenched impurities 79—73289
fission, isobaric widths, frozen quantal fluctuations, charge equilibration 80—37365
fixed-point interactions with wave vector depend. struct. 77—65000
FKG inequalities and fluctuations, probabilistic approach 80—77712
flames, turbulent, calc. in one-dimensional approach 80—30236
flames, turbulent, contrib. of flow vel. fluctuations to noise 77—51127
Florida Current, fluctuations in transport at periods between tidal and two weeks 80—72551
flow, combined visualisation-anemometry technique, appl. to turbulent boundary layer 78—91044
flow, in pipe, struct. similarity in radial correlations and spectra of longitudinal vel. fluctuations 79—32482
flow, round heated jet, heat and momentum transport, intermittency, entrainment 79—32608
flow, transversely sheared, unsteady motion scatt. and distortion 79—59997
flow, turbulent, in pipe, vel. components during ejections and sweeps *(French)* 79—1166
flow boundary layer, stochastic model of fluctuations 78—90818
flow in open channel, turbulent intensity modelling 79—1172
flow measurement, hot-wire calib., for vel. and temp. meas., low-freq. effects 79—50825
flow of viscous cond. fluid on porous plate in rot. medium with transverse mag. field 79—90340
flow over plate with suction, heat transfer, skin friction 78—87389
fluctuating plasma, Trivelpiece-Gould mode parametric decay 78—75321
fluctuation-dissipation theorem for classical systems 78—49764
fluid, dense, depolarised light scatt. due to orientational fluctuations 77—47318
fluid, dense, depolarised light scatt. due to orientational fluctuations 77—47319
fluid, dense, statistical mech. of stationary state fluctuations 79—54035
fluid, internal energy calcs. 77—28025
fluid, ion mobility, long wavelength fluctuations effect 79—77786
fluid, one phase, bulk distribution functions and fluctuation theorems for one phase fluid 78—8346
fluid, rough sphere, kinetic theory, density fluctuations 78—131
fluid dynamics, Rayleigh-Benard convection, randomly forced 80—79314
fluid fluctuations about hydrodynamic nonequilibrium steady states, Langevin method calcs. 80—53761
fluid-like viscoelastic liquid, coupling of orientational and translational motions, LF depolarised (VH) scatt. 77—7642
fluidised bed, free-space and external heat transfer fluctuations 77—84319
fluids, corrections to linear hydrodynamics eqns., low-freq. sound dispersion *(Russian)* 79—3990
fluids, simple, thermally induced surface fluctuations 80—88403
fluids with nonuniform velocity fields, light scatt., and pair correl. functions 79—61389
Fokker Planck equation, non-linear, asymptotic representation of master equation 77—74325
Fokker-Planck dynamics, in stationary state, fluctuation-dissipation theorem 78—45567
Fokker-Planck model, transport equation renormalisation 80—82732
four-point field coherence function, strong fluctuations of wave intensity 80—63927
fracture phenomena due to random thermal fluctuations 77—15489
free convection, fluctuating boundary layer flow 77—11183
gamma-Lorentzian intensity fluctuations, integrated, statistics 80—102685
gas, dilute, kinetic-hydrodynamic transition obs., Brillouin scatt. 77—7508
gas, thermal fluctuations of optical absorpt., noise *(Russian)* 77—31423
gas, thermal fluctuations of optical absorpt. *(Russian)* 77—31422
gas with fast disturbance, slowing down, nonlinear Boltzmann eqn. 79—98196
gas-laser beam intensity fluctuations, spatial distrib. 79—18458
gas-lasers, single-mode, fluctuations of laser beam diameter, lens effect 80—64090

fluctuations continued
gaseous mixtures, conc. fluctuation meas. using catalytic wire 77—26291
gases, chem. reacting, kinetic fluctuations *(Russian)* 78—59552
gaussian fluctuations of mol. field 80—70918
Gaussian stochastic processes, unified treatment of fluctuation theories 78—32761
generalised Langevin eqn. with Gaussian fluctuations 78—32760
generation of fluctuations whigh arbitrary power spectrum, algorithm 78—73927
geomagnetic field fluctuations at synchronous orbit, power spectra 78—96358
Gibbs equation, generalised, heat fluctuations 79—76940
Ginzburg-Landau model system, quenched, fluctuations growth 78—41260
gravitational interactions in Brownian motion theory of quantum mechanics 79—12699
gravitational wave interferometer, quantum mechanical radiation press. fluctuations 80—90770
H-space fluctuations, Boltzmann eqn., master eqn. for drift motion 79—146
Hafke-Gilles reaction, oscill., thermal props. 80—7762
hard sphere fluid mixture, density fluctuations 77—19657
harmonic lattice, impurity motion, generalised hydrodynamics and microscopic theory of long time tail *(Korean)* 77—49683
harmonic oscillator, general time depend., quantal fluctuations and invariant operators 80—36898
heat fluctuations near crit. point 80—47005
heat flux fluctuations, Fokker Planck eqn. in extended irreversible thermodynamics 80—86205
heated horizontal pipe flow, temp. and vel. fluctuations obs. 77—75894
Heisenberg chain, classical, energy fluctuations 80—80472
Heisenberg chain, one dimensional classical energy fluctuations 80—70924
heterophase fluctuations in two component systems, distrib. function 79—80563
hydrodynamic fluctuation theories 78—87327
hydrodynamic fluctuations as Mori variables in generalised Langevin scheme 77—72279
hydrodynamic singularities and the renormalization group 79—54063
hydrodynamical fluctuation theory far from equilibrium 80—98856
incommensurate epitaxies at finite temps., substrate pot. effect 80—88451
incommensurate systems, discrete lattice effects 80—107402
incompressible homogeneous decaying turbulence, press. and vel. fluctuations calcs. 79—32475
information measures and thermodynamic criteria of motion 80—8947
information theoretical aspects of gravit. field, space-time fluctuations 77—57266
instabilities and fluctuations in systems far from thermodynamic equilibrium 79—21671
instanton quantum fluctuations, in 2-D nonlinear theories *(Russian)* 80—4868
intensity fluctuation linewidth, Jakeman-Pike approx., black-body and laser models 78—58960
intensity fluctuations, statistical props. of sum of partially correlated complex variables 77—79754
intensity fluctuations and fourth-order coherence function in random media 80—78774
intensity fluctuations at two wavelengths in turbulent medium 80—87318
interference pattern fluctuation statistics in turbulent atmospheric layer 78—53727
International Atomic Time fluctuations, autoregressive integrated moving average model 77—57297
interparticle percolation, statistical mech. anal. 79—96281
interplanetary magnetic field fluctuations, simulated, cosmic ray scatt. 80—51626
interplanetary magnetic fields, probability distrib. functions of microscale fluctuations during quiet conditions 78—4053
interstellar dust grains, temp. fluctuations 80—26938
interstellar magnetic field, irregular fluctuations rel. to interstellar polarisation 80—26926
ionic conductor, charge fluctuations, collective dynamics 78—67841
ionic fluids binary mixtures, critical conc. fluctuations 78—34596
ionosphere, electron temp. and density fluctuations meas. by Aeros-B, global distrib. 79—58160
ionosphere, total electron content fluctuations rel. to scintillation of VHF and GHz waves 80—109302
ionosphere, turbulent fluctuations, rel. to strong turbulence in partially ionised plasmas 80—79499
ionosphere electric field, ULF fluctuations obs. in dayside auroral oval 80—98505
ionosphere F-layer, large-scale artificial inhomogeneity spectrum 80—98515
Ising dilute magnetic alloys, local mag. fields and fluctuations 77—40061
Ising ferromagnet, gaussian fluctuations of mol. field, magnetisation and free energy 80—70918
jet, 3-dimens., at wall, two-point statistical props. 79—1223
jet, axisymmetric, turbulent bulge struct. 78—90955
jet, circ., controlled perturbation, smoke visualisation 78—90956
jet, free, turbulent flow, large scale struct., discrete values meas. 78—90840
Josephson junction parametric inductance fluctuations, upconvertor 80—25052
kinetic equation for a linear dynamic system with Poisson parameter fluctuations 80—31675
kinetic equation for a weakly-coupled test-particle 79—54039
kinetic fluctuations of Brownian motion 79—25984
kinetic systems, noise power spectrum matrix 78—48617
kinetic theory of gases, stochastic approach and functional models 79—60091
Landau-Ginsburg model, droplets free energy, Jost function 79—40469
Landau-Ginzberg ferromagnet, static and dynamic correl. functions near magnetization curve 79—15318
Landau-Lifshitz hydrodynamic fluctuations in nonequilib. systems, Boltzmann eqn. reduction 78—81929
Langevin equation, equivalence to master equation 77—71273
Langevin-equation approach, generalised phase space method 78—54303
laser, two-mode, with coupled transitions, quantum theory 80—43319
laser beam, intensity fluctuations in snowfall *(Russian)* 80—94602
laser beam amplitude fluctuation statistics in turbulent atmosphere 80—106458

fluctuations continued
laser beam in liquid waveguide, random fluctuations rel. to sound generation 78—1539
laser beam intensity fluctuations in turbulent atm. over water surface *(Russian)* 78—69449
laser beam propagation in atmosphere, detection effects on statistics of intensity fluctuations 79—16672
laser propagation in turbulent atm., detector nonlinearity effects on statistics of fluctuating signal 78—55301
laser scattered light intensity, recurrence rate correl. 78—66760
lattice constant fluctuations, influence on thermal props. of cryst. 79—77715
lattice constant fluctuations, rel. to theory of eqn. of state for crystals 78—30732
lens, intensity fluctuations in turbulent atmosphere, with (without) central screening 79—7080
LF, dissipation and relaxation props., universality 80—84687
light flux fluctuations, limiting factors in photoelectric meas. 80—13136
light intensity, higher-order correls. and photoelectron time-interval distrib. 77—61932
light intensity fluctuations behind lens, receiving aperture shape effect 80—95980
light intensity in turbulent medium, two-freq. fluctuations correl. 79—98280
light intensity strong fluctuations, spatial correlation functions, numerical calculation 80—18995
light scattering in solids, general theory 79—61324
light strong intensity fluctuations in turbulent medium, space struct. 79—98278
light wave propagation in randomly inhomogeneous media, moments of field calc. 79—72497
Ligurian Sea continental shelf, currents low-freq. fluctuations rel. to wind fluctuations 80—85675
limit cycle entrainment by periodic external excitation 77—61020
linear Boltzmann system, stochastic model of spatially heterogeneous fluctuations *(Russian)* 77—22497
linear Boltzmann system, theory of fluctuations, Tolubinskii's method *(Russian)* 77—22495
linear dynamic system with many fluctuating parameters, single group approx. *(Russian)* 78—62154
linear response theory, many-body van Hove limit 78—62156
liquid, classical, density fluctuations, SCF method, coherent scatt. function 78—18527
liquid, ionic, binary mode coupling theory of charge fluctuation spectrum 80—92451
liquid crystal, ferroelec., helicoidal, smectic-C, dynamics 79—1396
liquid interface, mol. light scatt., heat fluctuations *(Russian)* 78—23477
liquid metal, bulk modulus, calc. using press. fluctuation in microcanonical ensemble 80—2106
liquid metals, turbulent temp. fluctuations, in heated pipe flow, theory 77—84246
liquid with spectral resolution of 10^{14}, registration of central peak *(Russian)* 79—4812
liquid-vapour interface struct. and thermodynamics, density fluctuations, grand ensemble formulation 78—22932
Lithuanian river groundwater discharge long-term fluctuations *(Russian)* 79—92554
LMFBR subassembly local boiling detection by outlet temp. fluctuation analysis 79—13390
local fluctuations in chemical reactions, nonlinear master eqn., dimensionality expansions, augmented mean field theory 78—73019
local temperature fluctuations, determ. of reactor coolant state *(Russian)* 79—67845
long range force $1/R^{d+\sigma}$ problems with $d=\sigma$ 77—13701
Lorentz model, statistical dynamics 77—26231
Lorenz model, transient behaviour in periodic regions 79—17346
Lorenz model, turbulence in dissipative dynamical systems 80—90784
lossless energy-storing system, thermodynamic limits to nonlinearity 79—54090
Lotka-Volterra chemical reaction model, effect of fluctuations far from equilibrium 77—28983
macromolecules, interacting, spherical, light scatt., conc. fluctuations, transport eqn. 79—1775
macromolecules, internal coordinates fluctuations, effect on dimensions 80—74266
macroscopic open systems, hard mode stationary states generated by fluctuations 79—12721
macroscopic system, reduction description method of nonequilib. states and fluctuations *(Russian)* 78—21089
macroscopic system, unstable state decay, deterministic description 79—17347
magnetic fluctuations in magnetosheath and magnetosphere, anal. rel. to Pc pulsations reson. theory 79—80092
magnetic fluid, thermoconvective instability, with mag. field perturbations 78—94847
magnetic recorder, output characteristics rel. to carrier velocity fluctuations 77—26279
magnetisation thermal fluctuations, diamagnetic contrib. 78—23240
magnetosheath, microscale mag. fluctuations during quiet conditions, probability distrib. functions 78—4053
many particle spectra, statistical props., two point correlations and fluctuations 78—86216
Markov process generated by Langevin equations, WKB-type expansion 80—86212
mathematical formulation, review, book contrib. 80—73267
matrix theory of small oscillations, for teachers 78—61986
MBBA, isotropic phase, order fluctuations, self-diffusion, and rot. motion, proton spin relax. meas. 79—87328
MBBA, nematic liq. crysts., AC excited, dynamic light scatt., orient. fluctuations 79—1769
MBBA, order fluctuations, self-diffusion, rot. motion, proton spin T_1 relax. 77—32285
MBBA-d_{13}, nematic phase, mol. order and director fluctuations, ^{2}D NMR meas. 79—90529
membrane, rel. to 2-D phase transformation 77—1980
membranes, excitable, statistical theory, nonlinear force-flux reln. and fluctuation 77—9179
mesosphere winds at equatorial latits., random fluctuations 78—36229
metal cluster, electronic spectrum fluctuations, appl. to Ni and Ti 79—19501

fluctuations continued
metallic one component systems, normal cryst. growth fluctuations theory 80—15025
metals, resistance fluctuation spectroscopy, power spectrum of density fluctuations 79—65428
metastability, rigorous molecular theory, review, book contrib. 80—73271
metastable state, quantum kinetics of phase transitions *(Russian)* 79—51235
metastable state relaxation, critical point region nucleation in thermodynamic systems *(Russian)* 80—13026
metastable states, relax. and fluctuation theory 78—49769
meteor trails, causes of fluctuations in effective linear electron density 78—73687
methane, gas density fluctuations, orthopositronium annihilation rate depend. 78—37773
methane jet, turbulent conc. field meas. by Raman spectrum, data interpretation 79—32609
MHD equilibria, stochastic stability 79—77414
microscopic free energy zero fluctuation 77—5740
miscible fluids, concentration fluctuations, statistical theory 77—42810
mode coupled fluctuations and 1/f noise 77—79035
molecular, rotation vibration emission in turbulent flowfield spectral absorpt. coeff., temp. depend. 80—52987
molecular dynamics studies of the role of diffusion in chemical models with absorbing boundary states 79—8424
molecular fluid, optical scatt. dielec. screening and susceptibility fluctuations 77—90162
molecular low dimensional system, spontaneous symm. distortion 80—96456
molecular reorientation, dielec. friction theory 78—87599
molecular spectra, effect on emission spectra 77—58055
molecules, linear, forced rot. diffusion, nonlinear aspects 79—90503
molecules, nonrigid, orientational correlation times, tensor correlations 79—4220
molten salt, binary, charge and mass fluctuations in hydrodynamic limit *(French)* 77—31573
molten salt, hydrodynamic correlation functions 77—31577
Mossbauer spectrum line intensity fluctuations accompanying coherent US modulation *(Russian)* 78—10815
mountain ridge snow cover effect on ultrashort wave diffraction field 77—64395
multiplicative stochastic processes in statistical physics, appls. 80—22289
multiplicative stochastic processes in statistical physics 79—25980
multistable system, dissipative steady state, stability 79—9187
muscle fibre tension fluctuation meas. during contraction 78—20153
music, amplitude fluctuations rel. to musical consonance, psychoacoustic foundations *(German)* 77—5007
musical sounds, freq. fluctuations *(German)* 77—828
N complex random variables, sum, statistical anal., atm. laser beam propag. appl. *(Italian)* 77—45796
narrow sound bundle reflected from irregular surface, amplitude and phase var. 77—46825
nematic liq. cryst., nonlinearities and fluctuations at hydrodynamic instability threshold 78—87614
nematic liquid cryst., orientational fluctuations effect on evanescent modes of transmitted EM wave 80—64889
nematic liquid crystal, pretransitional effects, mol. statistical calc. 77—27990
nematic liquid crystals, hydrodynamic correlation functions, propagating modes 78—94988
neurosecretory structure particle motion, effect of increased K^+ concs. 78—77046
night sky brightness at Sacramento Peak Observatory, fluctuations 80—12545
non-equilibrium systems, statistical mechanics of steady states 79—54038
non-gaussian field, clipped time autocorrelation function of intensity fluctuations 80—106472
non-Markovian equilibrium dynamics and fluctuation-dissipation theorem 78—62157
non-uniform system, crit. behaviour 78—12660
nondegenerate electron gas, classical fluctuation theory, existence of an infinity 80—31666
nonequilbrium steady states, irreversible processes, Lyapunov functions 80—95049
nonequilibrium critical phenomena, probability density functions, fluctuations 78—54327
nonequilibrium electron gas, fluctuation theory, reviews 79—54043
nonequilibrium fluctuations, by Kubo and Callen-Welton formulae *(Russian)* 79—17351
nonequilibrium fluctuations in driven systems 80—86210
nonequilibrium open systems, phase transitions, expt. studies, review 79—75483
nonequilibrium phase transition, dynamical features *(Chinese)* 78—83030
nonequilibrium processes in open systems, fluctuation dissipation relations, p-n junction appl. *(Russian)* 79—58668
nonequilibrium state, eqns. of motion, variance eqn. 77—5762
nonequilibrium state, Langevin type eqns. applic. to linear response theory, scatt. cross section 78—16726
nonequilibrium states, Langevin type eqns. from projection operator method 79—97293
nonequilibrium states subject to Fokker-Planck eqns., thermodynamic props. 77—67396
nonequilibrium statistical mechanics, scaling for space-time coarse graining 79—40521
nonequilibrium statistical thermodynamics, covariant formulation 77—41542
nonequilibrium steady states, irreversible processes, Liapunov criterion 80—13023
nonequilibrium steady states of open systems, 2nd order type transitions and fluctuations 77—49680
nonequilibrium steady-states in chemical systems, fluctuations 77—28988
nonequilibrium thermodynamics, steady state fluctuations 79—49187
nonequilibrium transitions induced by external noise 80—152
nonisotropic medium near critical point, space-time correlation functions of hydrodynamic fluctuations 77—30123
nonlinear hydrodynamics, fluctuation theories 79—77055
nonlinear irreversible process fluctuations 79—67229
nonlinear irreversible processes and fluctuations 80—82724
nonlinear Markov systems, Langevin eqn. approach 77—33946
nonlinear Markovian system, fluctuations 79—75460

fluctuations continued
nonlinear master equation, asymptotic expansion 77−49682
nonlinear media containing chaotic inhomogeneities, equation closure for average field 79−81601
nonlinear oscillator with fluctuating parameters, dynamics, thermal noise 80−101729
nonlinear rate processes with multiple stationary states, stochastic theory, metastable state relax. time 79−2725
nonlinear relaxation and fluctuation 79−30373
nonlinear system, active, self-consistent soln. method for calc. of power spectrum of fluctuations 78−16735
nonlinear system, thermal fluctuations, general theory *(Russian)* 77−22484
nonlinear transport and dynamics of fluctuations 79−44884
nonlinear wave in turbulent medium, with random inhomogeneities *(Russian)* 79−27134
nonpolar fluid, excessive electrons near crit. points 80−92836
nonstationarity near cylinder in air cross-flow *(Russian)* 79−7382
nonuniform nonequilibrium systems, approx. scheme for fluctuations study 79−58637
Norwegian Current, evidence for baroclinic instability 77−60385
nuclear density fluctuations, scatt. theory 79−517
nuclear reaction cross sections, direct reaction contrib. 77−50102
nuclear reactor noise analysis, irreversible circulation parameter 78−94069
nuclear reactor noise theory, fluctuation coarse-graining and normality preservation 78−94068
nuclear reactors, coupled-core, irreversible circulation of fluctuation 80−27700
nuclear reactors, process monitoring and parameter estimation, multivariate signal analysis algorithms 80−47585
nucleation in early stage, stochastic process 79−80521
Nyquist relation, generalised, validity 77−45797
O(3) nonlinear σ model, quantum fluctuations of instantons 79−71610
ocean, vel. fluctuations in barotropic motion over continental shelf, bottom friction effect 79−48509
ocean, vel. fluctuations scaling in surface mixed layer 77−45009
ocean upper layer, small-scale temp. fluctuations statistical regularities *(Russian)* 80−94528
one-dimensional chain, thermal fluctuation induced rupture, computer simulation 78−91378
one-dimensional chains, diffusion of labelled particles, density fluctuations 79−4426
one-dimensional conductors, disordered, resistance fluctuations 80−80256
one-dimensional magnetic models, fluctuations in energy-energy correlation function 79−73726
one-dimensional system, fluctuations and localisation 77−35883
open binary mixtures, fluctuation theory, entropy prod. and energy dissipation *(German)* 78−64879
open dynamic subsystem, nonlinear eqn. with fluctuating parameters derivation 80−94991
open dynamical system, equations with fluctuating parameters 80−62584
optical, bistability, cooperative effects and fluctuations 78−17885
optical beams in randomly inhomogeneous media, strong fluctuations of fields 80−99634
optical bistability, nonlinear polarisability model 80−37976
optical bistability, scatt. light spectrum atomic fluctuations 78−94383
optical bistability and spectrum of fluctuations, quantum anal. 78−71067
optical bistable systems, fluctuations when driven by coherent external light field 79−18387
optical cavity, one-dimens., with output coupling, thermal radiation, fluctuation-dissipation theorem 79−978
optical goniometer accuracy effect of atm. turbulence 78−55461
optical image processing, noise fluctuations and coherence 78−66771
optical phase fluctuations, interferometric anal. of deep random-phase screens 80−101834
optical phase fluctuations in turbulent medium 78−33668
optical plane wave intensity fluctuations in turbulent medium *(Russian)* 78−1156
ordered continuously degenerate systems, props. 79−93040
Ornstein-Uhlenbeck process, devrivation from fluctuation quanta model, boson fields 80−12988
oscillator systems, nonlinear stochastic models 79−80525
N Pacific Ocean, wind stress fluctuations rel. to water temp. anomalies vertical struct. 78−73394
pair configuration space diffusion eqn., thermal fluctuations, kinetic theory 79−17362
parametric instability, space-time random fluctuations 78−30431
partially coherent beam intensity fluctuation calc. in turbulent atmosphere 80−78775
particle diffusion in nonuniform medium, thermal fluctuations 77−87709
particle motion in stochastic force fields 78−73928
particle motion through matter, fluctuations in cascade processes 80−5456
particle transport theory, fluctuation problem, probability balance eqn. 77−37829
particle transport theory, fluctuation problem 78−8363
percolation theory, fluctuations of infinite network 80−73278
permanent one-dimens. flow, small unsteady perturbations *(French)* 77−51024
perturbed flow, moisture form. kinetics 80−79387
phase fluctuations, in incoherent response method for space plasmas study 78−45184
phase transitions, nonequilibrium transient behaviour 80−93732
photochromic flow visualisation, effect of turbulence on precision of vel. and vel. fluctuation data 77−68714
photoelectron statistics, joint moment method, phase radiation 80−23647
photon bunching in thermal radiation, temp. depend., photodetector thermal fluctuation 78−24748
photon counting and fluctuation of molecular movement 79−29686
photon counting with dead time, inversion problem 80−99682
photon synchronisation effect on intensity interference *(Russian)* 80−48200
photosphere brightness fluctuations, two-dimensional spectral anal. of disc centre granulation 77−53520
physical theory, fluctuations and noise 77−87
plasma, density and current fluctuations, mode-coupling theory 79−23398
plasma, density fluctuations, laser heterodyne meas. 77−15246
plasma, electron density fluctuations, collective spectrum 77−47148

fluctuations continued
plasma, fluctuation-dissipative relation in nonlinear electrodynamics *(Russian)* 78−79410
plasma, ion-acoustic fluctuation absorption of laser light 77−51209
plasma, kinetic fluctuations *(Russian)* 78−59552
plasma, magnetised and nonuniform 79−41831
plasma, nonequilib., nonlinear wave interaction and stationary fluctuation spectrum *(Russian)* 78−14153
plasma, nonequilibrium, nonlinear EM fluctuation field correlation functions *(Russian)* 78−9756
plasma, one-component, dilute, kinetic eqns. and fluctuations in μ space 77−89230
plasma, with power distrib. of particles, time variation *(Ukrainian)* 77−72408
plasma Alfvenic fluctuations in inner solar system, mag. fields obs. 79−58212
plasma density fluctuation evaluation by microwave interferometry 78−67437
plasma ion temp. meas. by 10.6 μ scatt. from thermal fluctuations 78−67431
plasma MHD, two dimens. turbulence, stationary states in non-dissipative limit 80−24169
polarization fluctuations in regions bounded by equi-potentials 79−82917
polyacetylene, doped, fluctuation-induced tunnelling cond. in metallic regime 80−65516
polycarbonate, glassy state, enthalpy relax., thermal density fluctuations 80−59678
polyethylene, uniaxially stretched, density fluctuations 78−75587
polymer, glass transition, fluctuation theory and thermodynamics *(German)* 79−51242
polymer blends, fluctuation dynamics, spinodal decomp. 80−79943
polymer in solution, Brownian motion, fluctuation-dissipation theorem 80−46980
polymer solutions, random coil, intramol. fluctuations by photon correl. spectroscopy 77−48184
Potts model, Monte Carlo simulation in three dimens. 80−163
power reactor, neutron density fluctuations, stochastic nonlinear model, Fokker-Planck eqn. 78−58316
power-law fluid, fluctuating flow past porous flat plate 77−68639
precipitation, seasonal, in Jerusalem, temporal fluctuations 80−72618
pressure fluctuations in heat transfer channels with surface boiling *(Russian)* 78−14088
pressure fluctuations in homogeneous turbulence associated with shear and gravity effects, correlations *(French)* 79−50708
pressurised water reactor, fluctuation anal. of apparent malfunction, frequency and time domains 77−54313
primordial background radiation, temp. fluctuations due to gravit. waves 78−65728
probability derivation in statistical mechanics, distribution function coarsening evolution 80−36937
Proca's eqn. stochastic derivation, Weyssenhoff top fluid considerations, velocity of light random fluctuations 79−97247
propane-air mixture, turbulent combustion zone, initial temp. fluctuations influence on reaction evolution *(French)* 79−15998
proportional counter, energy loss of relativistc electrons and its fluctuation 78−94171
pseudo-first-order phase transitions in one dimension 80−22270
pulsed laser radiation intensity fluctuations, thermal selfinteraction in turbulent medium 80−102781
pulsed light rangefinder, amplitude error in presence of signal fluctuations 80−28332
PVC-C composite, fluctuation-induced tunnelling cond. 80−65516
pyroelectric thin film detector, temp. fluctuation noise 80−77861
QCD vacuum, quantum liq. model, gauge and rotational invariances of colour fields 80−13283
quantum diffusion, particle in fluctuating medium, memory effects 79−49180
quantum fluctuations and particle struct. in field theory model 79−30659
quantum fluctuations in atomic bound states 80−42918
quantum fluctuations near the classical space-time singularity 80−8893
quantum fluctuations of instantons 78−54530
quasiharmonic signals periods, determ. via time-interval analyser with visual display 77−37850
quasistatic, average field weakening calc. 79−71367
quenched critical fluid, time evolution of fluctuation spectrum 78−65893
quenched time-depend. Ginzberg-Landau model 79−40470
radar signal reflection from sea surface, spatial intensity fluctuations 80−109170
radiation, intensity fluctuation spectrum, theory of registration *(Russian)* 78−1199
radiation counting rate meter output at threshold, fluctuation and arrival shift by computer simulation 80−106240
radiation detector fluctuations, computer simulation 77−3218
radiation field, mean specific emission intensity, fluctuation effects *(Italian)* 79−18346
radiation fluctuations from light source 80−95857
radio emission of cloudy atmosphere, expt. characts. of fluctuation 80−67399
radioactive atoms in critical reactor, fluctuation in numbers, anal. 77−3076
radioactive concrete calibration sources for radiometric field instruments, gamma-ray output fluctuations 79−5633
radiowave phase fluctuations in anisotropic turbulent atmosphere when emitted by moving source 80−17352
rainfall short-period fluctuations for New Zealand 77−25746
Raleigh model, nonlinear fluctuations 79−7433
random, moment behaviour of soln. processes for nonlinear stochastic differential eqns. *(Japanese)* 80−95039
random impurity system, density of states tails, fluctuations and mobility edges 78−67983
random medium with finite inhomogeneity correl. range, EM wave fluctuations *(Russian)* 78−78870
random process, stationary behaviour testing, comparison of actual and predicted fluctuations 77−37817
random surface fluctuations on shallow water, effect on normal mode sound field *(Chinese)* 77−34982
randomly inhomogeneous layer, statistical moments of wave field, strong fluctuations of wave intensity 80−57107
randomly inhomogeneous medium, fluctuations in phase arrival angle and freq. correl. of spherical waves 80−106456

fluctuations continued
randomly perturbed one dimens. wave eqn., multiple-scales space-time anal. 78—8247
rangefinder with fluctuating phase shift, systematic averaging error elimination 77—67469
rarefied supersonic CO_2 flow, fluctuations in intensity of radiation excited by electron beam in jet core 77—55104
ray paths in a fluctuating environment 79—9129
Rayleigh scattering, reson. enhancement in absorbing media, fluctuation theory 78—72533
reactor noise anal., system size expansion method 77—26830
relaxation rate between widely spaced levels, due to gas (liq.) fluctuations, temp. depend. 79—30366
resin slab, stress response, fluctuating external moisture (temp.) effects 78—55620
resistor, fluctuations in resistance and enthalpy, response to current changes 78—34871
RF SQUIDs, quantum transitions phase fluctuations rel. to noise theory 77—87685
tRNA, conformation and intensity fluctuation spectroscopy, melting curves 78—35798
scaling, nonequilibrium systems near instability point, anomalous fluctuation theorems in extensive region 77—2612
scaling theory of instability, nonlinear fluctuation and formation of microscopic structure 80—4653
scaling theory of transient phenomena near instability point 77—33945
scattered radiation spatial structure statistical characts., optical thickness, particle conc. depend. 80—5694
Schrodinger eqn., model of stochastic origins 80—81
Schrodinger equation, randomly fluctuating interaction term, uncertainty in nature 80—62499
sea level, off S.Sicily coast, power spectra of 'Marrubbio' phenomenon 77—53062
sea level fluctuations along west coast of N.America, alongshore correl vars. 78—73381
sea upper layer, wind waves components of temp. fluctuations spectrum *(Russian)* 78—53655
second law of thermodynamics, time, struct. and fluctuations *(Czech)* 80—13016
second order phase transitions, with fluctuations, symmetry changes 77—63220
second-order radiometry, fluctuating sources 78—50879
secondary ion images observation, using channel plate *(French)* 79—58840
seismic P-waves, millisecond travel time vars. systematic monitoring near Palmdale, California 79—57863
selection game, fluctuation theory 77—26241
self turbulence in free particle motion 78—86177
self-oscillating reaction system under periodic external force, thermal fluctuations 79—66338
self-oscillating system close to harmonic, width of spectrum *(Russian)* 77—82462
semiconductor, current fluctuations in quantizing elec. field *(Russian)* 77—28175
semiconductor, optical thermal breakdown, fluctuations and wave processes 80—20587
semiconductor, temperature waves in nonequilib. conditions 77—43397
semiconductor laser with dielec. transverse mode confinement, light intensity fluctuations 80—48258
semiconductors, kinetic fluctuations, global estimation 78—43376
semiconductors, mobility-fluctuation description of 1/f noise 80—84496
semiconductors, nondegenerate, flicker noise, mobility fluctuation possibility 79—91108
shock tube driver gas flow with fluctuations 80—96282
short-lived large energy fluctuations, semiphenomenological collective treatment, Arrhenius approx. 78—43168
signal detection characteristics, evolution of influence of destabilising factors 80—9825
signal statistics, effects of nonlinear detectors 78—24735
silicate glasses, vol. of fluctuation microcavities calc. 79—65000
simple fluids, fluctuation expressions for nonequilib. distrib. functions in adiabatic flows 80—92441
simplified hydrodynamic theory of nonlocal stationary state fluctuations 80—98857
single-impurity Kondo system, fluctuation conductivity 78—76064
smoke-particle aggregates, long-range correlations 79—46369
Smoluchowski process, number fluctuation anal. of random locomotion 78—54318
solar constant fluctuations, prod. by convection zone struct. adjustments 80—82321
solar continuum brightness, fluctuations rel. to trapped gravity waves in solar atmosphere 80—72898
solar corona radio emission, fluctuations 78—45311
solar non-isothermal atmosphere, hydrodynamics/radiative transfer coupling rel. to temp. and rel. fluctuations 78—20794
solar photosphere, granular brightness fluctuations centre to limb var. 79—66971
solar radio noise storm, drifting pulsations obs. 80—62105
solar wind, multispacecraft obs. of microscale fluctuations 77—87224
solar wind, stream-assoc. fluctuations rel. to radial var. of average wind parameters 77—45278
solar wind plasma, density fluctuations from three-satellite radio wave propag. meas. 80—101518
solid laser, fluctuations in laser theories 80—83587
solid-liquid pipe flow, cross correlation method anal. 79—32638
solidification and crystal nucleation 78—83761
solids, large thermal fluctuations, kinetic eqns. for many-body treatment 79—54037
solutions, fluctuation transport theory 78—70057
space-time, wave propagation in one-dimensional medium, spectral correlation field characts. 79—71260
spatially periodic convective flow, stability and fluctuations 80—19394
spectral props. of physical processes of Markov-correlated events, quantum systems, carrier trapping fluctuations 79—21665
spectral temperature measurement, line-reversal method, turbulent fluctuation effects 77—30147
spin glasses, fluctuation theory, mag. susceptibility and sp. ht. 79—24176
spin glasses, Ising type random bond, scaling, eqn. of state and instability 79—73753
spin glasses, phase transition, fluctuations of local spins, mean-field theory 80—34661

fluctuations continued
spin systems, far-from-equilib. states, metastability and anomalous fluctuations 79—80561
squid joint axon membrane potential fluctuations, cross-correlations 78—92616
starlight interstellar polarisation, fluctuation theory 80—82442
stationary Markov systems, generalised fluctuation theorems 78—62153
statistical mechanical theory of the kinetics of phase transitions, review, book contrib. 80—73270
statistical mechanics, stationary states far from equilib., regression of fluctuations 80—42138
statistical mechanics of nonequilib. steady states, microscopic theory 79—58623
statistical theories, nonlinear, fluctuation effects, truncation schemes of cumulant hierarchies 80—68133
statistical thermodynamics, foundation of theory based on thermodynamic theory of measurement 79—85075
steady-state process, probability characts. error calcs. 80—42145
stellar Balmer-index photometry, bandpass fluctuations as noise source 78—96404
stellar mass fluxes, fluctuation theory 79—53804
stellar mass loss from O and Of stars, fluctuation theory involving stochastic accel. 80—90413
stochastic gravitational fluctuations in a self-consistent mean field theory, review 80—90734
stochastic one-variable system, growth of fluctuations from marginal eqn. 80—86213
Stratonovich calculus, superiority over Ito for stochastic processes with non-additive fluctuations 79—85078
Stratonovich calculus, superiority over Ito for stochastic processes with non-additive fluctuations 79—85079
streamwise velocity fluctuations spectrum, following channel wall roughness step 78—90861
strong VLF waves in ionosphere, pulse amplitude vars. 79—48613
structural phase transitions, Landau theory 80—92639
structural stability in physics (conference, Tubingen, Germany, May and Dec. 1978) 80—8739
structurally incommensurate systems, fluctuation spectrum, incommensurate phases 78—91419
superfluorescence, macroscopic quantum fluctuations 79—76651
superfluorescence, oscill., quantum statistics 79—917
superfluorescence, phase-wave fluctuations 80—23652
superfluorescence delay times, intrinsic quantum fluctuations 80—58492
superfluorescent pulse fluctuation 80—58490
superradiance, relaxation from complete inversion, fluctuations, scaling theory 77—38840
symmetry breaking in the decay of unstable states 80—57188
synergetics, chemical processes far from equilib., conf. Bordeaux, France (Sept. 78) 80—3334
synergetics, nonequilibrium phase transitions and laser instability hierarchy 80—1180
synergetics approach 78—16717
temperature, downstream of heat source in turbulent boundary layer *(French)* 77—911
temperature, HF fluctuations, in stream of vortical plasmatron, holographic interferometry obs. 77—43068
temperature, in turbulent round buoyant jets, flow 79—55403
temperature fluctuations in turbulent flow, ramp model 77—3819
temperature measurement, line-reversal method, effect of fluctuations and nonuniformities 78—8404
thermal equilibrium statistics, by fluctuation in thermodynamic theory of meas. 79—85074
thermal fluctuation of self oscillating reaction system under periodic external force 80—50828
thermal fluctuations, driven nonlinear resistive system 79—25981
thermocouple temperature transfer functions, theoretical and expt. determ. *(German)* 78—49827
thermodynamic density fluctuations effect on low of mass action and kinetics *(Russian)* 78—60990
thermodynamic nonlinear fluctuation-dissipation theory 80—36963
thermodynamic variable, nonlinear fluctuations, Onsager-Machlup function 78—36957
thermodynamics, irreversible, extended, hydrodynamical fluctuations 80—86235
thermodynamics, Riemannian geometric model, appl. to pure fluid 80—17910
thermodynamics at nonequilib. steady states 79—6068
thermopile, harmonic temp. variations generation, analytic method 78—79193
thermosphere, equatorial, density perturbations during geomag. storm *(French)* 79—96846
thin films, substrate supported, temp. fluctuation noise 80—92949
time averaged magnitude fluctuations during measuring process *(Russian)* 78—73923
TMMC, field-suppression of spin fluctuations, NMR obs. 78—91971
Tolubinskij's stochastic theory of nonequil. processes and rel. to kinetic eqns. *(Russian)* 78—21053
traffic current fluctuation on expressway, observance of Burgers eqn. 78—49765
transient nonlinear fluctuations, scaling theory, macroscopic order formation 79—80520
transient nonlinear interactions of opposed waves, fluctuations 77—62011
tribromomethane-propyl alcohol conc. fluctuation kinetics, holographic study *(Russian)* 78—19508
turbojet engine noise interaction of entropy fluctuations with turbine blade rows 77—80149
turbulence, fully developed, origin of intermittency 77—58658
turbulence, homogeneous, diffusion of passive scalar, statistical approach 80—38391
turbulence, intermittency model in three-dimensions 78—59376
turbulence, Kolmogoroff's theory, high Reynold's no. model, laser beam atmospheric propag. 79—7368
turbulence, onset, effect of nonequilib. fluctuations 78—18272
turbulence in systems with small parameters 80—105571
turbulence in the motion of a free particle and de Broglie waves 80—57189
turbulence universality and scaling, review 79—58548
turbulent advection, scalar spectrum model 79—32474
turbulent boundary layer, large-scale modes obs. 78—90859
turbulent boundary layer, pressure-fluctuation spectra, reasons for roughness 77—58665

fluctuations continued
turbulent boundary layer, temp. and vel. fluctuations, spectral analogy 77—7376
turbulent flow, negative prod. of temp. fluctuations, spectral anal. *(French)* 77—19592
turbulent flow, press. fluctuation spectrum, elastic boundary compliance effect 78—63422
turbulent flow, temp. and conc. fluctuations *(German)* 78—59372
turbulent fluctuations, amplitude scale characteristic 78—18273
turbulent shear flow with streamline curvature, algebraic stress-heat flux model 79—27625
turbulent wake, fluctuations in boundary 79—27646
two component Boltzmann gas, fluctuating kinetic eqn. 80—171
two-level atomic system, superfluoresc. fluctuations 80—23651
two-level system, in nonstationary field, fluctuation and relax. props. 78—33715
two-level system, Rabi oscillations in partially coherent field 80—102688
underwater illumination fluctuations, nonstatistical model *(Russian)* 77—2173
underwater light field fluctuations under rough sea surface, numerical modelling *(Russian)* 77—33090
underwater light-field fluctuations, experimental studies of spatial struct. *(Russian)* 78—53656
underwater sound, acoustically relevant statistics for stochastic internal-wave models 77—46854
underwater sound, amplitude and phase fluctuation periods for long-range propag. 77—50808
underwater sound, amplitude fluctuation spectra of tone-burst signals refl. from ocean surface 77—3695
underwater sound, cancellation of turbulent boundary-layer press. fluctuations 77—88978
underwater sound, estimation and interpretation of acoustic CW phase fluctuation spectra 77—46850
underwater sound, low-freq. fluctuations, rel. to internal gravity waves in ocean 77—50809
underwater sound, ocean temporal fluctuations rel. to general source extraction problem 77—84043
underwater sound field, fluctuations using parabolic vel. profile 77—31159
underwater sunlight fluctuations in sea spatial and temporal correlation 80—94533
uniaxial ferroelectric-crystal, with one-dimensional inhomogeneity, fluctuations of order parameter 80—15995
universe, Friedmann model, with decoupled radiation field, density perturbations growth 80—109567
Universe, tenacious myths about cosmological perturbations larger than horizon size 80—105408
Universe density perturbations, consequences for evolution nonlinear stage of neutrino rest mass *(Russian)* 80—105414
Universe density perturbations spectrum, consequences of neutrino rest mass *(Russian)* 80—109576
unstable states, relax. and fluctuation theory 78—49769
unstable systems, anomalous fluctuation and relax., multimacrovariables 77—79033
unstable systems, evolution eqns. of long wavelength fluctuation spectra 77—87695
unstable systems, fluctuation dynamics in Ginzburg-Landau models 77—49685
van der Waals force in cond. media, fluctuating electrodynamics 78—30876
VHF signals, ionospheric radio fluctuation obs. from geostationary satellite 79—21091
viscoelasticity, stress/strain relationships, fluctuations 80—17802
Vlasov dynamics and fluctuations in 1/N limit of interacting classical particles 78—130
wave intensity fluctuations, use of physical concept in multiple scatter problems 79—21561
wave propagation in one-dimensional medium with space-time inhomogeneities, spectral-correlation characts. evolution *(Russian)* 79—2634
wave scattering, second order approx. in planar linear sheet 80—17812
wave-number spectrum moments, correlation method for estimation 78—16732
weather, severe convective event numerical simulation and prediction, Navier-Stokes eqns. initialisation 80—31111
Wiener-Khinchin theorem 78—57851
wind, long-term fluctuations rel. to ocean nonlinear coastal and equatorial jets 80—51427
wind field variability, relationship with ocean internal waves 80—31052
wind velocity gust factors, analytical approach 78—88897
winds in lower stratosphere over Jicamarca, fluctuations from full day radar meas. 79—25308
Yang-Mills multi-instantons, quantum fluctuations, Seeley coeffs. 80—77934
Al film, lattice and bulk heat capacity meas. for normal and supercond. states 80—92684
Al, liquid, bulk modulus, calc. using press. fluctuation in microcanonical ensemble 80—2106
Ar gas, thermally excited density fluctuations, neutron scatt. 79—23392
Ar, liq., numerical anal. of density fluctuations 78—21051
CO_2 film, adsorbed on KBr, density fluctuations 79—42391
CO_2, turbulent flow field, mol. vibr.-rot. bands, spectral absorpt. coeff., temp. depend. 80—52987
CS_2, in CCl_4, orientational fluctuations, depolarised Rayleigh relax. time obs., temp. and conc. depends. 79—4809
CdS, intensity fluctuations of nonlinearly amplified phonons, Brillouin scatt. meas. 77—90163
$CsNiF_3$, ^{19}F NMR, spin fluctuation suppression 78—91970
Fe_3O_4, magnetite, coercive force spectrum at high temps., thermal fluctuation analysis 77—91111
GaAs, heavily doped, fluctuation-induced tunnelling cond. 80—65516
H II regions density fluctuatons, statistical approach 80—77468
He gas, temp. fluctuations 79—19414
He I liquid, temp. fluctuations 79—19414
He-Ne laser with anisotropic cavity, fluctuations of field polaris. 79—27242
He-Ne lasers, discharge reson. props. effect on radiation fluctuations, expt. 78—74883
He-Ne single mode lasers, meas. of intensity of sources of inherent fluctuations 80—32958

fluctuations continued
^3He, liquid, surface fluctuation influence on free energy, surface tension *(Russian)* 80—92746
^3He, superfluid A-phase, composite soliton in narrow circ. cylinder, satellite freq., thermal fluctuations 80—34266
^4He, liq., dynamic scaling, possible breakdown at lambda point 78—91498
^4He, superfluid, fluctuations in turbulent counterflow, vortex line density fluctuation power spectra 80—84335
^4He, superfluid, superflow dissipation near lambda point 79—55947
^4He superfluid, temp. fluctuations 79—19414
^4He, superfluid, vel. fluctuation spectrum 80—34262
$Hg_{3-\delta}AsF_6$, one-dimens. liq., fluctuations and freezing in order-disorder transitions 79—82301
n-InSb, semicond. plasma, Raman scatt. of waves of fluctuations *(Russian)* 79—94299
n-InSb, US absorption in alternating elec. field *(Russian)* 78—30959
$KTa_{1-x}Nb_xO_3$, paraelectric phase, defect induced fluctuations, Raman meas. 79—15423
N_2, liq., computer-simulated ang. correlations and rot. motion 77—11461
Na-Cs alloy, liq., conc. fluctuations, X-ray transmission meas. 77—47329
NaO_2-B_2O_3 glass melts 79—94865
Nd:YAG laser, influence of birefraction and cooling on output characteristics *(Italian)* 79—50299
Ni-Fe, thermal fluctuation aftereffect meas. by pulse field method 80—88837
$O_2(^1\Sigma)$ airglow, fluctuations appl. to gravity waves study 79—29918
Pb_{1-c}-Li_c (As)(Ag)(In)(Sn)(Sb)(Te)(Au)(Tl)(Bi), liquid alloys, local fluctuations and quadrupolar relaxation 80—66060
$^{32}S(d,\alpha)^{30}P$, statistical fluctuations at 135°, 2.0-2.5 MeV 78—89882
$^{32}S(d,p)^{33}S$, statistical fluctuations, at 135°, 2.0-2.5 MeV 78—89882
Tl_2Te-Tl liquid system, conc. fluctuation, time-of-flight quasielastic neutron scatt. obs. 80—88324
W (100) surface, fluctuation, thermal impurity depinning and commensurate-incommensurate transition of CDWs 79—42611
ZnO, intensity fluctuations of nonlinearly amplified phonons, Brillouin scatt. meas. 77—90163

fluctuations in superconductors
used only for thermal (thermodynamic) fluctuations around the order parameter near the critical point
A15 type compound, props. and one-dimensionality 80—2530
alkali tungsten bronzes, dynamic fluctuations between local struct. states in supercond. TI phase 78—26981
charged superconductors, collective excitations and longitudinal US spectrum 79—56389
composites, magnetic instabilities 77—80889
correlation functions, two-particle, below transition temp. 77—24640
crossover near fluctuation induced phase transitions, appl. to nematic-smectic A liq. cryst. transition 78—80098
dirty, type II superconductors, fluctuation induced elec. cond. 79—38251
dirty layer superconductors, fluctuation sound attenuation, depend. on critical temp. *(Russian)* 80—34553
dirty superconductor, fluctuation diamagnetism *(Russian)* 79—51721
dirty superconductors, anisotropic, fluctuation magnetoconductivity 79—56393
dynamic instabilities in high T_c materials 78—10607
dynamical electrical conductivity below transition temp. 78—2623
effective dimensionality crossover for supercond. surfaces in parallel mag. fields 77—40000
electron gas propagation, normal phase, in long superconductors of small cross-section 79—78274
ferromagnetic superconductor, critical behaviour, coexistence near supercond.-ferromag. multicritical point 79—47197
ferromagnetic superconductor, paramagnetic fluctuations, influence on superconductivity 80—70900
ferromagnetic superconductor, spin correls., effect on nonlocality 79—82708
film, resistive transition 80—7049
film, ultrathin, two-layer model 78—14849
finite fibre, fluctuation magnetocond. 80—24956
flux-flow noise voltages, oscillations in V-I curves 80—15671
granular microbridges, fluctuations and crit. current determ. 80—84562
granular microcylinder, flux quantisation phenomena above T_c *(Russian)* 80—70899
granular superconductors, effect of charging energy on transition temp. 79—91181
hard superconductor, critical state stability and oscillations 80—107959
incommensurate 1-D Peierls system, flucutation conductivity 78—91817
insulator to superconductor in DC electric field 78—6481
intercalated dirty layered superconductor, fluctuation cond. 80—49994
intermediate state, thermal conductivity giant fluctuations *(Russian)* 78—34922
Josephson effect, radiation line width, eddy fluctuation influence *(Russian)* 78—19186
Josephson junctions, collective excitations in superconductors below T_c, tunnel current fluctuations 79—33403
Josephson tunnelling junctions, supercond. fluctuations, below trasntiion temp. 78—84354
layered superconductor in parallel mag. field *(Russian)* 79—78262
LF current fluctuations in stationary states, statistical mechanics *(Japanese)* 80—15658
local electronic spin susceptibility, effect of superconducting fluctuations 77—72943
longitudinal electric field in superconductors and oscillations 80—15664
magnetoconductivity induced by supercond. fluctuations in anisotropic bulk and fibrous samples 79—95545
metal, granular superconductivity, instability 80—103796
metal inhomogeneous granular, superconductivity 80—103795
metallic ultrathin filaments, dielectric and superconducting fluctuations, Peierls transition *(Russian)* 80—65742
nearly two-dimensional superconductor, crit. exponent 78—14884
nonequilibrium state stability with respect to finite fluctuations 80—103782
nonequilibrium superconductivity, oscill. of order parameter caused by quasiparticle injection 79—42697
nonequilibrium superconductor, optical pumping, transition point *(Russian)* 77—12064
nonequilibrium superconductors, ferromag. ordering of quasi-particles and rise of domains 80—107958

fluctuations in superconductors continued
nuclear spin relaxation rate fluctuation growth, mag. field effect 78—10606
one-dimensional electron system, generalised susceptibilities in mag. field, fluctuations *(Russian)* 77—80750
order parameter fluctuations, pair tunnelling, review 79—1642
order parameter reson. fluctuations rel. to tunnel current *(Russian)* 78—31019
paraconductivity, mag. impurities effect *(Japanese)* 77—43785
paraconductivity in supercond. containing mag. impurities, effect of perpendicular mag. field 77—85389
paramagnetic metals, nonphonon mechanism of supercond. and static screening *(Russian)* 79—78258
paramagnetically limited superconductor, supercooling curve meas. 78—14885
rare earth cpds., $RMo_6S_8(Se_8)$ and RRh_4B_4, coexistence of supercond. and mag. ordering *(Russian)* 80—84542
rare earth superconductors, upper crit. fields in the dirty limit, depend. on intra- and interaction exchange interactions 79—56461
relaxation of effective nuclear moment of Van Vleck ions, effect of superconducting fluctuations 79—7936
selfconsistent treatment of fluctuations in superconductors 80—100549
stability, against localised disturbances of limited magnitude 78—39264
stability of superconducting states out of thermal equilib. 80—2526
technical superconductors, preparation velocity of normal-conducting zone 79—24096
three-dimensional organic chain conductors, one-dimensionalisation by impurities 78—91681
$(TTT)_2I_{3+\delta}$, 1 dimens. conducting chains, supercond. fluctuations 78—39099
two-dimensional fluctuation-induced cond. above crit. temp. 78—10608
type I, defects in nucleation of superconducting phase *(Russian)* 77—36025
type II, collective modes and relax. effects 77—76996
type II, perturbation series for crit. behaviour near H_{c2} 77—8233
type II superconductor, fluctuations in crit. region near upper crit. field 80—25048
type II superconductors, fluctuation induced diamagnetism above H_{c2} 78—80097
type II superconductors, flux jumps and oscills. *(Russian)* 80—7052
ultra-thin films, transition temp., interface and fluctuation phenomena 80—84527
Al, bulk superconducting fluctuations in elec. resist 80—49995
Al film, granular, crit. field anisotropy and fluctuation cond. 78—26994
Al film, supercooling mag. field and thermal fluctuations 78—34925
Al, film in presence of Formvar, excess elec. cond. above T_c 78—60250
Al particles, small supercond. nuclear spin-lattice relax. meas.. 80—88681
Al particles, Zeeman crit. field, NMR spin echo meas. 79—56453
Al, resistivity well above T_c, supercond. effect up to $2T_c$ 80—6810
Al, small particles, Josephson-coupled, local fluctuation effects 78—72308
Al strips, supercond., order-parameter relaxation meas. 79—47207
Al, supercond., order-parameter relax. time calc. 79—4618
Al, superconducting particles, nucl. relax. and supercond. fluctuations 78—60251
Al-Ag, type-II superconductor, torque oscillations in mag. field *(Russian)* 80—103800
Al-Al_2O_3-Pb Josephson junction, nonuniform, paracond., fluctuation effects 77—59359
Al-formvar-Sn junction, supercond. order parameter fluctuations below T_c 77—66227
Bi, amorphous film, resist. transition 78—10609
Bi, amorphous films, supercond. fluctuation effects in perpendicular mag. fields 79—60980
$ErRh_4B_4$, supercond. transition temp., upper critical field, local spin fluctuations 79—38250
Ga ultrathin metallic filaments, appearance of dielec. instability, coexistence with supercond. 80—103784
Hg filament, ultrathin, influence of fluctuations on supercond. transition 77—8234
Hg ultrathin metallic filaments, appearance of dielec. instability, coexistence with supercond. 80—103784
$Ho_{1.2}Mo_6S_8$, supercond. transition temp., upper critical field, local spin fluctuations 79—38250
In film, current-induced resistive state, fluctuations in flux nucleation process 79—38252
In ultrathin metallic filaments, appearance of dielec. instability, coexistence with supercond. 80—103784
In—Gd film, dil., fluctuation induced cond. above supercond. transition temp. 79—47196
$La_{18}Au_{22}$, amorphous, evidence for short wavelength cutoff in fluctuation spectrum 78—68113
$La_{78}Au_{22}$, amorphous supercond., T_c and fluctuation cond. under high press. 79—7935
$La_{1-n}Ce_n$, supercond. mag. alloy, effect of interconfigurational fluctuations 78—19175
$(La_{1-n}Ce_n)_3Al$, mag. impurity effects in normal and supercond. state, NMR 78—2622
$(La_{1-n}Gd_n)_3Al$, mag. impurity effects in normal and supercond. state, NMR 78—2622
$La_{1-x}Gd_xMo_6Se_8$, supercond. transition temp., upper critical field, local spin fluctuations 79—38250
$(La_{1-x}Th_x)_{1-n}Ce_n$, supercond. mag. alloy, effect of interconfigurational fluctuations 78—19175
Na_xWO_3, dynamic fluctuations between local struct. states in supercond. TI phase 78—26981
Nb and alloys, dynamic destruction of supercond. 77—69461
Nb, bulk granular supercond., thermal fluctuations compared to Josephson weak link array 78—43520
Nb, clean supercond., fluctuations and sound attenuation near $T_{c2}(B)$ 77—15996
Nb, fluctuation contrib. to sound attenuation near H_{c2} 79—33397
Nb, superconducting, deformed, oscillation in current-voltage characts. near H_{c2} 79—28491
Nb-NbO_x-Pb tunnel junctions with high normal resists.,, crit. currents 79—56399
Nb_3Al, quasi-one-dimensional supercond., giant enhancement of nucl. relax. rate near T_c 78—56257
NbN granular films, supercond., crit. props. 80—88661
$NbS_{1.6}Se_{0.4}$, layered supercond., fluctuation induced diamag. and dimensionality 77—77006

fluctuations in superconductors continued
$NbSe_2$, layered supercond., fluctuation induced diamag. and dimensionality 77—77006
Nb_3Sn, quasi-one-dimensional supercond., giant enhancement of nucl. relax. rate near T_c 78—56257
Pb film, near supercond. transition temp., Hall effect 79—42698
$Pb_{55}Bi_{45}$ film, amorphous; supercond. energy gap and transition temp. 78—14866
$(SN)_x$, supercond., fluctuation cond., crit. mag. fields 80—39712
$(SN)_x$, supercond. props., review 78—6474
$(SN)_x$, superconducting fluctuation induced magnetoconductivity in anisotropic bulk and fibrous samples 79—95545
$(SN)_x$, thermopower from 0.15 to 4.2K 80—34427
Sn, diamag. moment meas., dislocation supercond. above crit. temp. *(Russian)* 79—4619
Sn, film, superconducting fluctuations, transition temp. *(Russian)* 80—65740
Sn, film at supercond. transition temp. thermal noise fluctuations 78—47907
Sn, homogeneous supercond., phase stratification in microwave field *(Russian)* 79—82711
Sn, small particles, Josephson-coupled, local fluctuation effects 78—72308
Sn superconducting films, Ge-covered, effect on excess elec. cond. 80—65741
Sn, superconducting fine particles, specific heat exam., fluctuations in zero mag. field 77—28295
Sn superconducting thin-film bridge, IV curves oscill. instability and quasi-particle recomb. *(Russian)* 80—44769
Sn ultrathin metallic filaments, appearance of dielec. instability, coexistence with supercond. 80—103784
$Sn_{1.2(1-x)}Eu_xMo_{6.35}S_8$, supercond. transition temp., upper critical field, local spin fluctuations 79—38250
$TaS_2(pyridine)_{1/2}$ intercalated layered supercond., fluctuation induced diamag. and dimensionality 77—77006
V film, resist. supercond. transition 80—25033
V film, scaling behaviour of resistive supercond. transitions 79—56363
V, fluctuation contrib. to US attenuation in mag. field near H_{c2} 77—47936
V, fluctuation contrib. to sound attenuation near H_{c2} 79—33397
V-C sandwiches, energy gap fluctuations *(Russian)* 78—34930
V-Ti superconducting film, electron spin effects 79—28488
$Zr_{75}Rh_{25}$, amorphous, evidence for short wavelength cutoff in fluctuation spectrum 78—68113

fluctuations of cross sections *see statistical theory of nuclear reactions and scattering*

fluerics *see fluidics*

fluid composition control *see chemical variables control*

fluid composition measurement *see chemical variables measurement*

fluid dynamics
see also aerodynamics; biological fluid dynamics; drag reduction; electrohydrodynamics; flow; hydrodynamics; Navier-Stokes equations; rarefied fluid dynamics; relativistic fluid dynamics; surface waves (fluid); turbulence; wakes
$\varepsilon grad^2 u=\delta u/\delta y$, $0<\varepsilon\ll 1$, over rectangle, asymptotic soln., MHD appl. 77—9863
advection, pseudo-upstream finite difference scheme 80—106773
anisotropic micropolar fluid theory 80—31515
applied mechanics computing, conference, New York (1976) 77—67285
astrophysical media, relativistic and nonrelativistic gas flows, low press. limit 77—9655
astrophysics, higher order fluid eqns. for multicomponent nonequilib. stellar atmospheres and star clusters 80—105156
asymmetric weighted residual method 77—79421
asymptotic results for model eqn. for low Reynolds no. flow 79—14371
axial pressure variations of two communicating parallel flows 77—42040
axially symmetric form of biharmonic eqn., elec. analogue technique for approx. soln. 77—27502
axisymmetric accretion in astronomy, energy considerations 77—33335
backflow of quasiparticles, dynamics of classical systems 79—27614
barotropic Stokes fluid, Lagrangian finite element method 77—68562
Bernoulli's theorem, misinterpretation 77—87614
Boltzmann eqn., nonlinear, soln. of Cauchy problem 79—40497
Boltzmann linear time depend. operator as semi-group generator 77—87651
bond graph fluid line models for inclusion with dynamic systems simulations 80—27136
book, annual review 80—17722
boundary deform., Galkerkin finite element technique for multidimensional flow 80—86089
boundary element methods versus finite elements 78—73860
Burger's equation, coupled stream function-vorticity eqns., Method of Lines compared to finite difference scheme 78—79291
Burgers' nonlinear eqn. soln., finite element method 78—36835
calculation of force of resistance of a medium to motion of particles of various shapes at Reynolds numbers exceeding unity 80—106775
California Institute of Technology hydrodynamics research facilities, 1976 77—51147
channel design using global variational method 78—38408
chaotic flows of autonomous dissipative systems 80—73176
circular cylinder carrying flow, unsteady fluid dynamic forces rel. to stability anal. 78—13936
circular cylinders in confined fluid, hydrodynamic mass anal. 77—80099
classical fluids, linear irreversible thermodynamics, derivation 79—2740
classical unidimensional model of fluid motion, Burgers eqn., absence of turbulence 78—87328
coarse mesh methods appl. *(German)* 77—88197
compact stars, axisymmetric accretion theory 77—33334
compressible fluids, Fokker-Planck description 79—80498
compressible viscous fluid flow in domain, eqns. soln. 77—51078
computer drawn fields for diverse configurations, program 77—22401
computer simulation of fluid structure and dynamical props. using Monte Carlo and mol. dynamic methods *(German)* 80—69757
conference, computation fluid dynamics, Rhode-Saint-Genese, Belgium (March 1977) 77—80134
conference, Olsztyn-Kortowo, Poland (Sept. 1977) 79—46277
conference on advanced problems and methods, Poland (Sept. 1975) 77—51018
conservation laws, convex extensions and Cauchy problem 77—17933
conservation laws hyperbolic systems, soln. decay 77—49599

fluid dynamics continued
convection approx., upstream differences critical evaluation 77—900
convection in numerical fluid dynamics, tensor viscosity method 79—72888
Cosserat continuum, kinetic energy, linear and angular momentum densities, invariance 80—74829
Cosserat eqn., couple stress-tensor, associated with friction 79—7366
counterflow processes, nonlinear modelling using weighted residual methods 80—69754
coupled finite element-finite difference anal. of hydrodynamic and elastoplastic problems 77—71200
creeping flow in closed cylindrical cavity, numerical calculation 80—16976
critical fluctuations analogy in turbulence, intermittency exponents, book contrib. 77—84214
decomposed partial peeling and limit bundler 77—60919
dilute soln., spheroid-cylindrical mols., dynamics 80—44090
directional integration method for 2-D fluid transients 78—683
disc galaxies, effects of dissipation on gas response to oval distortions 78—12355
disc-halo galaxies gaseous components, boundary layer circulation 78—57627
discontinuities, subgrid resolution in tracking methods 80—105506
discrete equations of fluid flow and elasticity 78—65781
droplets, saturated, impinging on heated vertical surface, heat transfer characteristics and dynamic behaviour 80—14688
drops, liquid, charged, dynamics, symmetric and asymmetric stabilities 80—79366
duct flow eigenvalue problem, FEM soln. with Hermitian elements 80—74983
Earth fluid core with inward growing boundaries, dynamics 80—76934
EBR-II, whole core thermal-hydraulic phenomena, experimental study 77—88206
eigenvalue problem for Lagrangian systems 77—49601
elastic half space, torsional oscillations due to rigid annular disc 78—28958
electrodynamics, evaluation of electrofluidic pumps and generators, appls. *(German)* 79—94724
elliptic systems and numerical transforms. 78—65780
energy-momentum tensor, effect of motions, meson field and perfect fluid 78—73903
Euler equations, group analysis in presence of rot. symmetry and exact solns. 80—8799
Euler equations, solid-body boundary conditions, numerical implementation 78—90814
evolution equations in fluid dynamics, soln. by second order backward difference method 79—92950
Falkner Skan eqn., exact soln. 79—98680
FEBIE—a combined finite element-boundary integral equation method 79—2633
FFT pseudo-spectral technique for non-periodic problems 78—59359
finite element mesh, optimum design 80—36867
finite element method 79—9119
finite element method appls. 77—26158
finite element method for partial differential eqns. 77—80135
finite element methods, nonconventional, book contrib. 79—30257
finite element methods 77—80138
finite element techniques, book 77—903
finite elements in fluids, book 79—32441
finite-difference schemes, comparative criteria 78—5720
first-order Cosserat fluid kinetic energy decay with heat and mass transfer 78—94524
fission reactor fluid dynamic transient analysis using ASWR method with staggered meshes *(German)* 80—83176
fission reactors, thermodynamics and fluid dynamics, photographic techniques *(Spanish)* 77—71635
flow acoustics, characteristic phenomena 77—75903
flow field of a point force in an infinite fluid 79—59961
flow field round body at small Reynolds no. *(Russian)* 78—42584
flow in curved tube, finite difference anal. method 80—106846
flow in irregular geometries, numerical method calcs. 78—94522
flows with large density gradients, Eulerian finite difference technique 77—79424
fluid bifurcation phenomena numerical anal. *(French)* 80—19319
fluid dynamics, macroscopic relativistic approach to numerical simulation 79—9122
fluid flow, finite difference methods 79—9117
fluid interaction with obstacles, method of deformable coords. *(Ukrainian)* 78—65776
fluid motion in open basin, free boundary problem *(Italian)* 79—18868
fluid-solid dynamic interactions and wave forces, numerical treatment 79—3944
forced convection in annuli, experimental study *(Italian)* 79—37322
forced motion within an ellipsoid *(Russian)* 78—5719
free boundary flow, surface tension effects, finite element fluid flow simulators 80—82647
free surface problems, resolution methods, review 77—54954
fundamental principles *(Japanese)* 80—28484
fundamental problems in general fluid dynamics and hydromag. dynamo theory, book contrib. 77—84213
fundamentals *(Japanese)* 79—97210
fundamentals *(Japanese)* 80—10225
fundamentals *(Japanese)* 80—23982
Galerkin method, fluid flow appl. 79—9118
gas flow, isotropic ideal, dimensionless characts., rel. to determ. methods 77—23930
gas motion, nonstationary, invariant solns. of eqns. 79—41652
gasdynamic expansion of a cylindrical cloud 79—81837
gasdynamic modeling and computational accuracy 79—72872
gasdynamics, nonequilib., sonic discontinuities growth and decay 78—34209
geophysical fluid dynamics, specialist symposium, (Munich, 6 to 9 September 1977) 79—57951
geophysical fluid dynamics, use of similarity theory in Soviet work *(Russian)* 78—16174
geophysical fluid dynamics theory, book 80—105443
geophysical systems, conf., Aug. 1978, Strasbourg, France 80—36764
glass micropipette, mechanics of pulling 80—56295
glycerine-water drops, collision dynamics, ang. of incidence influence *(Russian)* 78—83461
gravity current, front motion down incline 80—106819

fluid dynamics continued
gravity current slumping 80—103052
groundwater flow, finite element eqns., Newton iteration and modified conjugate gradient method 80—77622
Hamilton's principle in fluid mechanics 77—68559
harmonic waves propag. in viscous fluid contained in cylindrical shell *(Russian)* 77—23969
helical axisymmetrical motion, of perfect fluid through diffuser, function series soln. 78—49669
higher order, possessing dissipative dynamical system props., Onsager symm. 77—65728
homogeneous ellipsoidal figures evolution 77—33333
Hopf equation in random force field with arbitrary distrib. *(Russian)* 77—30012
Howard's formula applicability 78—55622
HTPBR, gas injector to reduce pyrocarbon deposits *(German)* 78—29633
hybrid finite element methods 79—9120
hyperbolic systems, high-order methods, dynamic problems 80—68033
ideal fluid within three-dimens. toroidal geom., stagnation pts. existence 77—51020
ideal fluids, fundamental matrix for motion eqns. 80—1509
image processing applications at IBM Madrid Scientific Center 80—102657
immersed body with active flexible skin in perfect incompressible fluid *(French)* 78—59362
incompressible flow fields, finite element dual variational anal. 79—40375
incompressible flow including heat and mass transfer, vel.-press. coupling treatment 80—69832
incompressible flows, numerical solns., conservation of momentum and total pressure test 80—36862
incompressible fluid flow, one dimensional, calc. 80—79402
incompressible liquid, viscous and conductive, fluid mechanics eqns. invariant solns. 79—90272
inertial motion of continuum, shock waves form. 79—18861
inhomogeneous diffusion equations, analytic solutions, and diffusion coeffs. 78—34267
initial boundary-value problems for partial differential equations 79—30256
interfaces, pure, thermodynamics and dynamics rel. to Spacelab 79—28910
interrupted wall channels heat transfer and flow anal., appl. to heat exchangers 79—81883
inviscid fluid conservation law eqns., coeff. matrices for implicit finite difference soln. 78—42580
irrotational flow problems with free surface, inverse variable domain finite element anal. 77—68563
Jupiter atmosphere, equatorial light and dark spots obs. rel. to fluid dynamics 78—57493
Kepler problem, non-compact Anosov flows and hyperbolic motion *(Russian)* 77—7360
laminar coaxial annular jets in a circular cylinder and influence of temperature on them 80—14770
Lax-Wendroff difference scheme, appl. in fluid dynamics 78—65758
linear hyperbolic initial boundary value problems, hydraulic system appl. *(German)* 79—9115
linear viscoelastic fluids, Stokes' problems 78—51142
liquid, ideal incompressible flow, topological measuring of canonical Clebsch variables 80—69758
liquid penetrant testing, continuum fluid mechanics aspects 80—43818
liquid phase jet optimal profiling, Lagrange multiplier method appl. 77—72394
liquids, momentum transfer, cooperative effects 80—68160
liquids in vessels, undirectional vibration displacement *(Russian)* 79—32726
LMFBR, radial blanket assembly, flow split meas. 78—13209
LMFBR, squeeze flow between two adjacent subassemblies, discrete model 78—86634
local Green's function method for heat conduction and fluid flow problems 77—79420
Magnus method appl. to nonlinear eqns. near stability boundaries *(Russian)* 78—87331
mantle plume, fluid-dynamic model of ascending flow 80—12370
marker and cell technique 79—9121
Mars rampart craters, impact in viscous-liq. targets rel. to fluidised material ejecta deposits 78—65530
mathematical model, for hydraulic calc. of steam boilers 79—68816
mean residence times in steady-flow and non-flow systems 78—83357
measuring bell jar pressure and flow rate constancy under rapid shift 77—58825
method of generalised coords. 77—75877
microgravity environments 80—1720
micropolar fluid eqns., soln. exist. and uniqueness 77—19583
micropolar fluid theory, regularization theorem 79—9114
micropolar liquid flow between two infinitely slowly rotating discs 77—35150
micropolar unidirectional plane flow, spin-vorticity relation 77—19584
micropolar viscoelastic fluid motions, universal stability 77—11165
mid-oceanic ridge axes, topography and tectonics from fluid dynamic models 80—41433
mixture, unified theory of dynamics and thermodynamics *(Japanese)* 78—8244
mixtures with dynamic interaction, basic eqns. 79—50692
model eqn. of Lagerstrom 79—12612
modified Benjamin-Ono eqn., N-periodic wave and N-soliton solns. 80—28518
molecular dynamics method in statistical physics, dense media, review 80—18895
molten salt, possibility of plasmon mode obs., struct. dynamics 80—10477
momentum theory, generalised formulation for transient phenomena 80—62474
moving grids construction methods for problems with strong deforms. 77—54961
multidimensional flux-corrected transport algorithms 79—68672
multiparameter splitting schemes for solution of spatially three-dimensional nonstationary problems 80—68047
multisoliton solutions in two-layer finite depth fluid 78—55621
Newtonian fluid, incompressible, between parallel plates, effect of wall slip on drag flow and pressure flow *(German)* 80—87810

fluid dynamics continued

- non-homogeneous flows with vanishing initial density *(French)* 79−53983
- nonhomogeneous fluid, compact manifold boundary, Euler equations 80−62476
- nonordinary Poisson flows, moment dynamics 80−22280
- nonrelativistic fluids, Lagrangian perturbation theory 78−49305
- nonstationary motion in one-dimens. continuous medium, partial analytic solns. *(Russian)* 78−73859
- nonuniform fluid kinetics, statistical approach 79−10541
- nuclear engineering transient fluid and structural dynamics problems, flow singularity methods 78−86633
- nuclear reactor, fluid-structure system dynamics, reactor safety anal., computational algorithms 77−71669
- nuclear reactor fuel rod bundles, square array, shear stress distribution, axial flow 80−47679
- nuclear reactor subcompartment anal., inclusion of momentum flux 77−50224
- nuclear reactor thermal-hydraulic conservation eqns., analytic integration 77−83012
- numerical anal. in applied engineering science (conf. May 1977) 77−67249
- numerical methods, book 77−57201
- numerical methods, conf., Enschede, Netherlands (July 1976) 77−54953
- numerical methods, conference, Tbilisi, USSR (June 1978) 80−17717
- numerical methods based on polynomial spline interpolation 77−58636
- numerical methods comparison 79−9123
- numerical simulation 80−17805
- numerical simulation of fluid motion, conf., Melbourne, Australia (1976) 79−9116
- oil-bearing layer with input parameter correction, discrete dynamic model 80−83778
- Petrov-Galerkin finite element method, boundary layer behaviour 78−69989
- pipe containing flowing fluid, forced oscillations *(Russian)* 80−38304
- pipe containing water, pressure pulse propagation 80−33475
- pipeline hydrodynamical resistance reduction by dynamical effects *(Ukrainian)* 79−32670
- pipelines with liquid, stability and oscillations 80−14612
- pipes carrying fluid flow, oscillation stability *(German)* 78−87298
- piping systems, pipe rupture and steam/water, hammer design loads for dynamic anal. 78−41868
- piston problem, one-dimensional, in non-ideal gas, time-dependent soln. 80−82185
- planetary fluids, displacement and rectification 77−45002
- plate tectonics, fluid dynamical model rel. to subduction angle 78−11865
- Poisson equation, non-uniform grid, finite-difference, matrix decomp. technique 80−69756
- Poisson equation solver for potential and press. fields on staggered grid with obstacles 77−54959
- polyatomic fluids, nonsymmetric pressure tensor 79−75350
- potential flow, 3-D, about arbitrarily shaped bodies, direct matrix embedding technique 80−64511
- potential flow, elliptic PDE with discontinuous coeff., finite difference soln. 78−89347
- potential flow, finite difference stencils from isoparametric elements 78−4472
- potential flow, surface source and vorticity panel method 79−46278
- potential flow problems, partition technique integral eqn. method 78−49652
- principles of advanced mathematical phys., book 79−63090
- prismatic plate structs. submerged in liquid, natural freq. and vibr. modes 78−79256
- pulsating incompressible fluid in elastic tube, pressure wave propagation through tube 80−96228
- quasilinear hyperbolic systems, smooth solns., inviscid compressible fluids *(Italian)* 77−68553
- random choice soln. of nonlinear hyperbolic systems of conservation laws 77−7362
- rapidly occurring processes in perturbed gas, shearing interferometer obs. 77−7489
- reactor containment response to HCDA anal. with MICE code 77−42029
- reduced model theory, hydrodynamical approach for vel. autocorrelation functions 80−27135
- relaxation methods for time depend. conservation eqns. 77−80137
- renormalisation group anal. 80−17838
- reservoir with inclined bottom, gas motion under press. penetration *(Russian)* 77−81952
- reverse pseudo-unsteady aerodynamic calculation methods *(French)* 80−69759
- review of progress in last thirty years 78−89290
- Reynolds equation, asymptotic soln. 79−14369
- Ritz-Galerkin approximations use 77−54955
- Rossby wave, critical layer evolution 78−79329
- Runge-Kutta method appl. to nonlinear partial differential eqns. solution 77−42796
- Saint Venants eqns., three point weighted scheme for numerical soln. 78−30356
- self-similar power driven expansion into vacuum 79−64622
- selfgravitating liquid ring with inner flow *(Russian)* 78−65783
- semiconvection in stars, semitheory 78−69787
- sethlets, generalised singular points 79−46
- shallow water theory, exact solns. to eqns., appls. 80−58998
- shell, aerohydroelastic opening of shell in nonstationary flow *(Ukrainian)* 79−32258
- shock formation and decay for conservation law in several dimens. 77−53788
- slightly dissipative systems, stochastic behaviour 80−22290
- solar wind, models 79−25428
- solar wind, plasma fluid aspects 80−90313
- stationary motion of finite mass of fluid 79−23331
- statistical concepts, for teaching 79−35501
- steady viscous flows, finite element formulations 80−36859
- stochastic-dynamic system asymptotic behaviour 80−12474
- Stokes law, Reynolds no., erythrocyte sedimentation rate, for teaching 78−49610
- Stokes problem, for infinite vertical plate with const. heat flux 80−79108
- Stokes problem, second-order difference scheme 80−90678

fluid dynamics continued

- Stokes problem in multiple connected domain, soln. by stream function method *(French)* 77−68555
- Stokes problem with conforming Lagrangian finite elements, soln. error estimates *(French)* 78−62085
- stratosphere, Lagrangian motion of air parcels 80−109215
- structure-fluid interaction between vibrating wall and channel flow 77−38325
- submersion of a body into a fluid *(Ukrainian)* 80−33610
- summer school at Les Houches 1973, book 77−84210
- suspensions, fluid dynamical aspects of operating conditions of suspension stirrers *(German)* 80−26058
- theoretical gas dynamics, numerical aids, book contrib. 80−1513
- thermodynamics, pressure-volume work exercises illustrating the first and second laws, for teaching 80−22173
- thermodynamics of polarisable and magnetisable fluids in electromag. fields 77−57291
- thin body with ventilated cavity, inclined entry into ideal imponderable liquid 80−99984
- thin profile near interface of two heavy fluids, steady motion 77−58633
- three dimensional layer theory, using shell geometrical concepts 78−90815
- three-dimens. low Reynolds no. flows with free surface 77−49600
- torus, added-mass coefficients 78−32683
- transformation group techniques appl. to nonlinear fluid and plasma eqns. *(French)* 80−77623
- transient 3-D potential flow problems, fluid and structural dynamics 80−48668
- transient 3-D potential flow problems and dynamic response of surrounding structures, singularity method 80−48667
- transient flow, split band Cholesky eqn., strategy for finite element anal. 78−46923
- truncation error estimation due to upstream differencing, consistency check 79−23294
- tube bank efficiency in cross-flow, graphoanalytic method *(Russian)* 79−7365
- two dimensional fluid transient analysis, nearcharacteristics method 78−89349
- two-dimensional nonstationary Euler eqn. solution in time-dependent bounded domain *(Italian)* 78−69986
- two-stream mixing, variational soln. 78−38266
- unconfirmed aquifer flow, anal. by asymptotic ray method 80−36863
- universality class of asymmetric fluid critical points 80−57098
- unsteady flow, two-dimens., method of characteristics soln. 80−53740
- variable property flow, in curvilinear orthogonal coords., numerical calc. 79−44746
- viscosity, effect on energy eqn., book contrib. *(German)* 80−1516
- viscous flow around periodically positioned particles, asymptotic solns. *(Russian)* 78−41158
- viscous flow in channel, existence theorem of eigenvalue problem 77−33871
- viscous fluid, incompressible, motion in curved pipe of elliptical cross-section 80−74989
- viscous fluid, shear processes, local order theory 80−59687
- viscous fluid flow in pipeline, wave mechanism for control *(Ukrainian)* 78−1675
- viscous incompressible flow, finite element models 77−68561
- viscous liquid emerging from slot, nonlinear differential equation, Runge-Kutta numerical integration 80−52030
- Von Karman eqns., generic bifurcation theory, symmetry props. 79−44748
- water critical flow states through pipe, modified Bernoulli theory 78−30345
- water sprinkler, rotating, range calcs. 77−13528
- water-wave transmission through barriers with small gaps 77−15046
- weakly coupled linear systems, block iterative LU solution technique 77−60941
- weather forecasting as a problem in fluid dynamics 79−84359
- weighted residual classification of approximate methods 79−10540
- weightless liquid systems, acoustic manipulation in space 77−49716
- weirs, classical studies on the discharge over a broad-crested weir *(Italian)* 80−6016
- CO_2 supercritical boilers, forced flow, frictional pressure drop 80−14689
- H-He fluid planets, dynamics and He distrib. 78−28555
- He transfer lines for cooldown or warmup of superconducting magnets 79−63234
- ^{4}He, superfluid, properties in zero gravity, appl. as cryogen on spacecraft 77 31822
- Na, liquid, heat transfer characteristics of flow field *(Japanese)* 78−54815

fluid flow *see flow*

fluid instability *see flow instability*

fluid mechanics

- *see also capillarity; cavitation; compressibility of gases; compressibility of liquids; fluid dynamics; hydrostatics; Mach number*
- acoustic motion and transport eqns. for moving fluids 80−53523
- annual review of fluid dynamic, book 80−94927
- applied mathematics, conf., Delft, Netherlands, Jan. 1978 79−2617
- asymptotic methods, review, book contrib. *(French)* 77−87653
- Bernouilli and Lagrange-Cauchy integrals, p/γ term 78−65779
- book, annual review 77−46981
- book, annual review (1978) 78−59357
- book, for undergraduates 78−59358
- CAI source for final year B.Sc. students 77−60877
- coherent structures in fluids, appl. to plasma physics, review 79−10621
- compressible micropolar fluids, decay of kinetic and thermal energy 79−12611
- computational aspects, book contrib. 78−59366
- computer simulation of fluid structure and dynamical props. using Monte Carlo and mol. dynamic methods *(German)* 80−69757
- conference, Davis, Calif., USA, Jun 1976 77−39295
- coupled Burgers equation, numerical solution for turbulent fluid motion 79−40378
- Dirichlet problem for semilinear eqn. $\Delta^k u = f$ on a disc, approx. techniques 79−40377
- Dirichlet problem for semilinear eqn. $\Delta^k u = f$ on a disc, series soln. 79−40376
- dispersed and heterogeneous systems, mechanics, spatial averaging, cellular scheme 80−48788

fluid mechanics continued
dissipative dynamical systems of macroscopic phys., common formal struct. of kinetic theory, fluid mechs., nonequilibrium thermodynamics 79—140
edgetone generation, flow geometries 78—13835
education, conservative discrete models, difference eqn. formulation, nonlinear solid, fluid phenomena, computer calc. 77—78924
extensible string motion in nonviscous fluid *(Russian)* 78—77718
falling horizontal cylinder, low Reynolds number, horizontal plane boundary effect 80—87757
falling plate onto another in fluid, final stages 77—31411
finite element methods, book contrib. 77—45702
finite element methods, book contrib. 79—32446
finite-differential element nets, topological props. 77—67247
flotation of solid body on liquid surface, equilib. state *(Russian)* 78—67029
fundamental laws and constitutive equations, in space of any dimension *(Japanese)* 78—41160
helical curve motion and soliton eqns., scaling invariance 78—49667
history of fluid mechanics at Cambridge, book contrib. 78—57726
incompressible viscous fluid, slow motion of small sphere outside cylinder 80—96239
laws of motion of solid body for Reynolds number 0.6 to 800, anal. *(German)* 77—31270
liquid-liquid mixing analysis, lamellar model 80—15246
long wave-short wave resonance equations, complete soln. for fluid mechanics and plasmas 79—37334
microcontinuum, singular solns. 77—60940
microstretch fluid motion, stability 79—35566
migmatite rise, numerical expts. based on continuum dynamics 80—51381
miscible fluid mixtures, mechanics and thermodynamics, variational approach 79—93084
mixtures, Ornstein-Zernike relation transformation 79—98855
multiplanes, design theory 79—37284
nematic liquid crystals, nonlinear stability of motion *(French)* 77—84623
non-Newtonian fluid mechanics, scope, critical examination 77—3849
nonlinear dissipative system, successive bifurcation leading to stochastic behaviour 77—14975
nonlinear interaction of deformable body with liquid pressure wave *(Ukrainian)* 78—65777
numerical methods and associated problems, book contrib. 77—89087
optimal blowing problem using low Reynolds number theory 79—32440
optimal coordinate theory, appl. to physical problems 77—71211
photon correlation techniques in fluid mech., conf., Cambridge, England (March 1979) 80—56998
relation to statistical physics, book contrib. 80—94959
space environment, fluid behaviour, review 79—46410
Stokes fluids, in space of any dimension, continuum mechanics *(Japanese)* 78—41165
structured fluid theory, appl. to substruct. redistrib. kinetics 78—13983
unsteady flow soln. by spline functions *(Chinese)* 79—72873
viscometric flows of general fluids *(Japanese)* 78—87425
viscous fluid cosmological model in general relativity 78—61944
wave and force measurement system 79—41780
fluid theory, dense *see liquid theory*
fluid valves *see valves*
fluidic amplifiers
see also hydraulic amplifiers
bistable wall attachment fluid amplifier, flow field anal. *(Japanese)* 80—53743
chemical laser flameout using fluidic switching 78—29943
flow meas., linearisation of output press. with nonlinear detector 77—65818
flow measurement, using laser Doppler anemometer *(German)* 77—961
free jet dynamic response investigation 77—37842
pneumatic amplifier pump, for supercritical fluid chromatography, control and programming 78—88665
fluidic devices
attached jet characteristics, aspect ratio effect *(Japanese)* 80—87791
convertors, electrohydrodynamic and electropneumatic, flow regime alteration by corona discharge *(Russian)* 77—11269
curved wall power fluidics characts. 80—103053
flowmeter, state of art and semiconductor tensometric membrane based design *(Czech)* 78—26213
intra-aortic balloon heart assist device fluidic drive system 78—53566
oscillator channels, heat transfer 77—58677
resistors, pad and quad, flow meas. appl. 78—42688
sensors and meas. systems *(German)* 77—53886
strain gauge load cell 80—37024
temperature sensor, capillary 78—24793
vortex rate gyro, dynamic response characteristics, ang. rate meas. 78—21125
wall reattachment device, loading effects on switching *(Japanese)* 79—10548
fluidic logic
heart assist energy convertors control, thermal and electrical 79—53286
liquid oscillations in cavity in solid body, effect on solid body control device motion *(Russian)* 78—14031
nonstationary flow meas. by laser Doppler velocimeter with frequency tracker *(Japanese)* 78—55707
fluidics
mixing nozzle reattachment of two-dimensional turbulent jet 79—23347
turbulent structure determ. using thermoprobe unit *(Bulgarian)* 80—28584
fluidised beds
100 MW fluidised bed combustion district heating plant burning high S content residual oils 80—108777
200 MW atmospheric fluidised-bed combustion steam generator, comparison of three designs 80—108776
adsorbent fixed bed, temp. profiles 79—23359
air fluidised sand bed, large diameter, local bubble characts. obs. 77—58781
atmospheric fluidised-bed combustion boiler development facility, first year of operation 80—108775
axial dispersion, in liq. fluidised systems, correlating parameters 79—46381
axial flow through moving bed, press. drop *(German)* 79—68797
axial heat transport and solid phase displacement 79—14473
bed to surface heat transfer, fluidised bed of large particles 78—63269
fluidised beds continued
binary finely dispersed bed, local struct., random pseudoturbulent motion 77—75977
biomass growth, fluidised bed expansion 80—14803
bodies in fluidised beds, resistance to motion 78—47030
bodies in granular bed, heat and mass transfer 78—9701
body immersed in fluidised bed, max. drag forces 80—14808
boiling layer, axial mixing of solid phase *(Russian)* 78—47035
boiling layer, laser radiation probe of bed space 77—15115
boiling liquid in granular bed, heat transfer enhancement 78—9533
bubble average vel. in bed with packing material 78—22416
bubble characteristics in three phase fluidised beds 78—9680
bubble distribution, eruption diam. in fluidised bed with horizontal tube bundle 80—14781
bubble growth due to coalescence, theory 78—26191
bubble growth in fluidised bed with nonlinear interphase interaction 79—68798
bubble induced heat transfer 77—7435
bubble observation using probes and X-rays 80—79379
bubble populations simulation in gas fluidised bed 78—22415
bubble raise rate in nonuniform fluidised bed 78—67263
bubble size, correction for wall effect in point probe meas. 78—9681
bubble size, rise velocity in screen-packed fluidised beds 77—31372
bubble size prediction, math. models exam. 80—6135
bubble sizes in fluidised bed at 20 to 300°C 77—943
bubbles in fluidised bed, interphase mass transfer 79—7405
bubbles in fluidised beds, light probe detector 78—30376
bubbles of gas, rise velocities 80—64610
bubbling, conc. profile for mass transfer, appl. Kunii-Levenspiel model 77—11256
bubbling electrofluidised bed, heat transfer rates 78—87242
bubbling fluidised beds, theoretical bounding relations, for bubble void fraction 80—96296
catalytic, effect of granulometry and nature of catalyser on heat transfer *(French)* 77—68689
catalytic fluidised bed reactors, simulation by transient axial dispersion model 79—77289
coal, fluidised bed firing, technological state and economic chances *(German)* 79—92050
coal, pressurised fluidised bed combustion, alkali emission and fixation 80—30352
coal combustion, operation of a centrifugal fluidized bed with continuous feed and removal of bed material 80—30349
coal gasification, low-BTU gas production, ash agglomeration process appl. 79—48065
coal gasification system, Westinghouse, low-Btu fuel gas production 79—48058
combustion, energy conversion, Conf., San Diego, CA, USA (Aug 1978) 79—48038
combustion, future energy concepts, Conf. London, England (Jan.-Feb. 1979) 79—43709
combustion facility, radiation heat transfer, particle size and flow parameter effects 80—69641
continuous gas-solid, min. carrying vel. of particles prediction 80—33670
creeping flow mass transfer in size distrib. cloud drops, high Schmidt number 80—14783
critical height reduction anal. of particle ejection 80—106842
cylinder array, convective mass transfer with surface reaction 78—79369
dehydration of solutions and suspensions, rel. to granulation 80—81373
dispersion model, residence time distrib. calc. approx., Peclet no. depend. *(German)* 78—22421
dispersion profiles, non-destructive meas. method using dye 78—26214
drag force generated at high Reynolds numbers, effect of particle proximity 80—96306
drag of blocked fluidised bed 79—64758
drying, heat transfer between plate and fluidised bed 77—11243
effective density calc. 78—34195
electrical conduction theory 80—18988
electrochemical electrode, particulate-bed, H_2-evolving, mass transfer rate obs. 79—57243
electrode system, extractive metallurgy appl. 79—57249
electrodes, appl. in electrodeposition of Cu at high current density 79—100063
electrodes, appl. in electrodeposition of metals, math. model 79—100062
electrodes, kinetic behaviour for quinone electrochem. reduction 79—57235
electrostatic paint and powder spray coating developments 79—83363
electrostatic separation of vibrated bed electrostatic separation using vibrated bed 80—16641
electrowinning, using fluidised bed cathodes, const. current density operation 79—24456
electrowinning, using fluidised bed cathodes 79—24455
expansion characteristics of gas-fluidised beds, void fractions 77—68686
expansion of air fluidised sand and silica gel beds, high porosity packings *(Russian)* 78—59480
expansion of an inhomogeneous fluidised bed 78—63492
external heat transfer rate 78—9707
fission reactors, fluidised bed concept, diffusion theory 80—68729
fixed to spouted bed transition, theory 77—39338
flow in packed beds, effective heat transfer parameters, theoretical prediction 80—14802
fluid-solid flow, holdup, expt. 78—79361
fluidisation, initial problem 78—42661
fluidisation uniformity, disturbance criterion with uniform coding medium flow distrib. 80—43772
fluidised bed, particle motion 80—24090
free convective heat transfer in liq. saturated porous bed at high Rayleigh number *(German)* 80—33605
fuel particle coating, gas distrib. system optimisation in fluidised bed *(German)* 80—23104
fusion reactors, divergent impulsive crossflow over packed columnar arrays 80—47702
gas, bubble formation 77—39339
gas backmixing, solids movement, bubble activities, large scale bed 78—30349
gas blowing from orifice to fluidised bed 80—1678
gas bubble growth, inhomogeneous bed, expt. and model 78—1739
gas bubbles, low Reynolds number anal. in fluidised beds 77—11255
gas distribution in a deep granular bed injected by flat jets 80—19501
gas flow, anal. 79—94703

fluidised beds continued
gas flow division between bubble and interstitial phases in beds of fine powders 78—26189
gas flow in reactor 78—83468
gas fluidised bed, heat transfer assisted by alternating electric field 78—9697
gas jet discharge into stationary bed of granular material 77—42905
gas motion, statistical characts., expt. determ. method 77—65790
gas stream distrib. near plane jet in granular layer 79—14471
gas-bubble motion in nonuniform bed, governing laws 79—72941
gas-fluidised, flow distrib. between phases analysis 80—14804
gas-liquid cocurrent downflow in fixed bed in pulsed regime, mass transfer fluctuations 80—19485
gas-liquid countercurrent packed column, with intermittent voids, residence time distrib. studies 80—19483
gas-liquid flow in granular layer, hydrodynamic modes 78—9712
gas-liquid fluidised beds, axial and radial dispersion in dispersed plug flow model 80—10290
gas-liquid fluidised beds, axial liq. dispersion in plug flow model 80—10289
gas-particle heat transfer in shallow fluidised beds 77—35227
gas-solid, particle temp. meas. 78—83464
gas-solid, radioactive tracer for solids mixing investig. 77—35269
gas-solid, solid circulation 78—79359
gas-solid fluidisation, solid pot. flow around rising bubbles 79—86501
gas-solid layer, mech. agitated, fully- (partly-) fluidised, thermal evolution *(French)* 78—34193
gas-solid packed column, gas and solid phase axial dispersion at trickel flow 80—14807
gas-solid suspension flow through packed beds, convective heat transfer 79—4075
gas-solid systems at high Archimedes numbers, hydrodynamics, variational formulation 77—11257
gaseous hydrocarbons pyrolysis, quantitative model conceptions *(German)* 77—73448
geological materials, acoustic fluidisation prod. by strong transient wave field, theory and appls. 80—85653
granular bed, aerosol filtration efficiency, triboelec. effects 80—38487
granular bed, fluidisation, theory 77—35229
granular bed fluidised by gas flow, instability 78—5795
granular bed fluidised by gas stream, stability 79—18946
granular bed in conical system, fluidisation 79—90327
granular layer, bubble coalescence for jet injection under constrained flow conditions 77—89197
granular solids bed, shock wave attenuation 77—51110
graphite fuel element and C combustion for HTGR U recovery 78—13314
grid design using orifice eqn. 78—91006
grid effect on bed inhomogeneity 78—79367
heat and mass transfer, flow anal., separated flow model 78—9700
heat and mass transfer, jet channelling theory 78—9702
heat and mass transfer for low Peclet numbers 78—94799
heat and mass transfer in bed with vibro-rotational motion 78—9709
heat and mass transfer in oscill. mode 78—22417
heat exchange intensification using bubble motion control 79—86508
heat exchange rate control, using magnetic field *(Russian)* 77—55083
heat exchange with surface within bed, physical model 77—42918
heat exchanger, scale control and corrosion tests, geothermal power plant appl. 79—48090
heat exchanger for geothermal plant appl., flow distribution models 79—52879
heat transfer, from immersed bank of smooth tubes 79—77241
heat transfer, modified packet theory 77—35230
heat transfer, steady-state 78—9704
heat transfer, to horizontal tube surface, adaptability for air cooled heat exchanger *(Japanese)* 77—58785
heat transfer 78—9703
heat transfer and drag on moving bodies 78—9706
heat transfer between a dispersed system and a vertical heating or cooling surface 79—1069
heat transfer between a freely-rising slug and a fluidised bed 80—96307
heat transfer between air fluidised beds and horizontal Cu tubes 80—79317
heat transfer bibliography, Japanese works 79—23317
heat transfer coeff. between bed and vertically inserted tube wall 80—74971
heat transfer coeffs. from tube bundles to vibrated bed 78—9711
heat transfer fluctuations, free-space and external 77—84319
heat transfer from hot surface in vibrated beds 78—9710
heat transfer from immersed heater 78—71391
heat transfer from particle to fluid, stochastic model 78—51234
heat transfer from surface of fixed body 78—79368
heat transfer in fixed glass hallotini-packed beds, at low/intermediate Reynolds nos. 79—1244
heat transfer in fluidised bed with immersed horizontal tubes *(Russian)* 80—74880
heat transfer in horizontal direction, thermal conduction coefficients determ. 79—60058
heat transfer in packed bed heat recuperators, precision anal. 77—75974
heat transfer in two-level coolers 78—9705
heat transfer intensification, surface-to-bed, at controlled gas distrib. 79—1246
heat transfer of liquid fluidised bed, enhanced by turbulent jet 79—72940
heat transfer parameters, in packed beds, estimation from radial temp. profiles 78—83467
heat transfer to horizontal tube *(German)* 78—59387
heat transfer to staggered tube bundle 78--9708
heat treatment appl., development *(German)* 77—41596
heat treatment of tool steels 79—20087
heated fluidised beds, stability operation, depend. on temp. investig. 80—19502
heterogeneous fluidised system, aerodynamic aspects of transfer processes, crit. state 80—79394
high-S coal, continuous sorbent regeneration in pressurized fluid bed combustion 80—30351
high-temperature, radiant, conductive-convective components of external heat exchange 80—43709
horizontal immersed tubes in fluidised bed, heat transfer, surface roughness effects 80—6044
horizontal tubes in fluidised beds, local heat transfer coeffs. 80—74875

fluidised beds continued
HTGR fuel reprocessing pilot plant development 79—45397
HTR fuel elements, bed criticality *(German)* 77—18656
hydrodynamic structure effects of DC mag. field. *(Russian)* 77—65801
incipient fluidisation, particle to gas heat transfer, axial gas thermal dispersion coeffs. 80—10238
instability waves and bubble origin, two-fluid eqns. 80—92205
interparticle electrical forces, meas. 78—63491
ion exchange resins, liquid fluidised beds, mass transfer at low Reynolds number 77—68684
jet, vertical steady discharge, into fluidised bed 77—65789
jet and bubble formation 77—84318
jet discharge, bubble form. and growth 77—47084
jet entering fluidised bed, aerodynamics and mass transfer 80—14809
jet penetration depth of multiple vertical grid jets 80—38486
jet pseudoturbulent mixing efficiency in fluidised bed 77—39342
jets issuing into bed, quasisteady axisymmetric jet 78—83470
kinetic energy of particles in fluidised bed rel. to bubbling phenomena, theoretical anal. *(Russian)* 80—74965
kinetic eqns. soln. *(Russian)* 79—10610
Knudsen flow, through periodically constricted pores *(Japanese)* 79—72911
large particle fluidised beds, gas convection model of heat transfer 80—14801
light force effect on stability of uniform fluidisation 77—11259
liquid, axial dispersion obs. 80—59106
liquid, expansion props., void fraction effect *(French)* 77—68685
liquid, mass transfer at low Reynolds number 78—9698
liquid, particle mixing and classification 79—90330
liquid elimination from porous body by fluidised porous particles system, kinetics 79—86510
liquid fluidisation, mass transfer models *(French)* 79—37390
liquid fluidisation, study of mass transfer between a liquid and a mobile object in a bed *(French)* 78—83465
liquid fluidised bed, mass transfer time fluctuations 80—79380
liquid fuel fluidised bed combustion, heat transfer to horizontal steam generator surfaces 80—48549
liquid radial spread in random beds 79—4078
liquid-like behaviour, book contrib. 77—47089
liquid-liquid, drop coalescence 79—50783
liquid-solid evaporator, wall to liq. heat transfer, distillation plant 79—1245
liquid-solid fluidised beds, particle segregation, transition regions 79—46379
liquid-solid semi-fluidisation characts. for heterogeneous mixtures 77—36792
liquid-solid semifluidised, prediction of pressure drop 79—41746
loose material forced displacement processes in pipes, gas flow filtration effect 77—58783
magnetic stabilization of the state of uniform fluidization 80—19484
mass transfer, high Peclet number, to sphere in fixed or fluidised bed 77—35226
mass transfer, Karman-Pohlhausen method and concentric spheres free surface model 80—79378
mass transfer correlations for flow between fluidised spheres and liquid 80—14805
mass transfer factors for gas flow in packed beds 77—39340
mass transfer to power law fluids in fluidised beds 80—100032
minimum fluidisation vel. of spherical particles by liq. *(French)* 78—75196
minimum fluidisation velocities in beds of mixed solids 78—91005
moisture evaporation in fluidised bed of inert particles 77—15113
momentum transfer from body in fluidised bed 79—81961
moving bed solid flow in inclined pipe leading to fluidised bed., gas leakage 80—64619
moving bed solids flow in inclined pipe leading to fluidised bed 80—64620
multifuel fluidised bed combustion packaged boiler to supply 10000 lb/h saturated steam at 100 psig 80—108779
multistage countercurrent fluidized-bed heat exchanger, optimal heating surface 77—89200
multistage fluidised coal combustor 80—30345
non-Newtonian flow through porous media, fluidised beds, solid-fluid interaction *(Portuguese)* 80—38454
nonisothermal fixed bed adsorpt. column with nonlinear equilib., heat and mass transfer 77—80209
nonuniform, force on fixed sphere, rising gas bubble force field 78—59476
nonuniform fluidised bed, external heat exchange mechanism 77—47085
object immersed in shallow fluidised bed 78—91004
open channel flow of fluidised solids 80—14826
otpical probe for fluidised bed meas. 79—82000
packed bed, appl. of limiting current method to mass transfer at very low Reynolds number 77—39337
packed bed, flow conditions, examination by local meas. 80—14806
packed bed, interphase mass transfer at very low Reynolds no. 77—80208
packed bed, mass transfer coeff. at low Peclet no. 79—4077
packed bed, mass transfer time domain evaluation from chromatograph peaks 80—19496
packed bed, optimal control of heat and mass transfer *(Ukrainian)* 79—32655
packed bed, particle to fluid mass transfer, dispersion coeffs. 79—18940
packed bed, temperature profile for concurrent air-water downflow, latent ht. effect 79—50789
packed bed heat recuperator, film coefficient for dry sorbent solids 78—5742
packed bed of spheres, heat transfer coeff. determ. by quasistationary cyclic method 77—15116
packed bed reactor, creeping flow, mass transfer 77—80227
packed bed thermal storage systems, single- and two-phase models 78—91009
packed bed with horizontal flow, lateral thermal diffusivities 79—50788
packed beds, gas-liquid concurrent, wall heat transfer 79—50790
packed beds, heat transfer, length effect 78—9695
packed beds with gas-liquid concurrent upflow mass transport phenomena and hydrodynamics 79—50784
packed column, liquid distrib. and redistrib., expt. 79—18939
packed column, liquid distrib. and redistrib., theory 79—18938
packed-bed particle-to-fluid heat transfer coefficient, determination from radial heat transfer measurements 78—9699

fluidised beds continued
- particle chaotic motion, statistical characteristics determ. 77−51140
- particle size distributions, calc. for discrete cuts in fluidised bed reactor 80−14812
- particle-fluid heat transfer in fixed and fluidized beds 79−68552
- particle-to-fluid transfer coeff., fluid diffusivities in packed beds 77−31378
- plasma jet cooling mechanism 78−79371
- pneumatic transport of granular material 79−72927
- polydisperse filter bed, immobile, heat and mass transfer eqns. soln. 77−7446
- polydisperse particle entrainment in gas flow, low Reynolds no. 77−65791
- polydisperse particles in spouted bed, particle cycle times, size depend. 79−46365
- porosity measurement device, exam. 78−60911
- porous bed with permeable boundary, natural convection 79−77238
- porous particle bed, liq. removal from porous particles 79−72942
- powder, Knudsen diffusion, gas diffusion relationship of Knudsen flow permeametry 77−55087
- powder, Knudsen diffusion, pore size distrib. effect on surface areas obtained by diffusion meas. and Hg porosimetry 77−55088
- powder fluid bed forming in vacuum under vibratory action model 78−11147
- powders, air fluidisation, bubbling behaviour rel. to particle size 77−31362
- power law fluids, laminar flow through granular beds 80−38488
- pressed powder bed, bottom pressure distrib., meas. by scattered light photoelasticity *(Japanese)* 79−75543
- pressure drop through fixed beds of spherical particles 78−83466
- pressure field determ. during pumping and injection of water 79−77237
- pressurized fluidized bed combustor/steam generator design evaluation for combustion of high-S coals 80−30346
- probing using optical fibres 80−19533
- pseudofluidised layer, hydrodynamical eqns. *(Russian)* 77−35233
- PVC/coal blends, fluidized bed combustion of plastic waste with coal, removal of HCl 80−30347
- pyrocarbon, deposition from fluidised bed, quantitative aspects 77−50239
- pyrocarbon coating deposition by gaseous hydrocarbon pyrolysis, theoretical anal. 77−40459
- pyrocarbon coatings preparation in fluidised bed 77−46381
- pyrocarbon deposition in fluidised bed, qualitative model, investigation with Stromungsrohr 78−56595
- pyrocarbons, coating, of nuclear fuel particles, production *(German)* 80−18585
- radial gas content profiles of rising swarm of bubbles in vertical pipe *(German)* 77−47062
- radial heat conduction in liq. fluidised bed 77−42916
- radiative contribution to total heat transfer 80−19384
- radiative heat flux absorbed in radiative heating 77−39362
- radioactive low-level waste, vol. reduction, fluidised bed dryer/incinerator 80−9378
- random bed, area porosity profiles, stratified model 80−19495
- random bed, porosity estimation based on Lichtenstein Liapunov expansion functional 78−14078
- random packed beds, local voidage meas., fluoresc. method 78−9729
- random pulsations in a coarsely disperse fluidized bed 80−24089
- reaction near grid in fluidised beds, two-phase model 78−67280
- reactor, solid-circulation model, steady-state multiplicity 79−86524
- reactor, steady states multiplicity 79−4086
- reactors, mathematical modelling *(German)* 79−41767
- regimes of fluidization for large particles 78−83463
- relaxation autooscillations, gas quasifluidised bed, math. model 77−75975
- relaxation autooscillations of granular bed 78−59472
- review of current fluidisation research 77−24022
- Richardson-Zaki eqn. for spherical particle in bed 78−59465
- Richardson-Zaki equation, effective gravity force calc. 77−31382
- rotating bubbling beds, heat and mass transfer 78−30351
- sectionalised equipment for solution granulation 79−14472
- semifluidised bed, mass transfer rate 80−59105
- semifluidised liquid beds, residence time expts. 78−94814
- shallow fluidised bed heat transfer investigation 79−7404
- slug in fluidised bed, mass transfer, wall effect 79−4079
- solid aerosol collection in spouted bed, electric field effect 78−91019
- solid particle bed fluidisation characts. from hydrodynamic instability 80−6140
- solid-liquid bed, particle distrib., particle dynamics 78−59464
- solids circulation in column with spouting bed *(Ukrainian)* 79−32656
- solids wettability effect on liq. fluidisation 79−32654
- solids-gas countercurrent vertical flow 80−10288
- space above inhomogeneous fluidised bed, heat transfer 77−55085
- sphere immersed in a fluidised bed, mass transfer *(French)* 80−92214
- sphere-packed beds, limiting Sherwood and Nusselt nos. 78−18339
- spouted bed, fountain region height and struct. 79−46380
- spouted bed, temp. distrib. meas., heat transfer characts. for appl. to PyC use *(Japanese)* 77−50275
- spouted bed, theory for predicting maximum spoutable height 78−14077
- spouted beds of spherical particles, spout termination, parameters 80−64621
- steam generating system to supply 100000 lb/h of saturated steam burning high S coal 80−108778
- structured, particle mixing, diffusion model for longitudinal particle transport 77−47087
- surface boiling heat transfer from transverse streamlined cylinder 80−43708
- surface temperature measurement using infrared photoresistors *(Russian)* 80−82763
- temperature profiles in fluid bed boilers 79−32663
- temperature pulsations of immersed body, heat transfer problem 77−47086
- three-phase, bubble wake solids content 78−42660
- three-phase, containing fine/light solids, contraction or expansion 80−28557
- three-phase, electrocond. technique for meas. of axial var. of holdups 78−67286
- three-phase, heat transfer 79−60056
- transitional mass-transfer behavior from packed-bed conditions to onset of fluidization 79−86505
- with tube bundles, large particle mixing, effective axial diffusion coeff. *(Russian)* 78−47034

fluidised beds continued
- turbulent fluidised beds, solids circulation and heat transfer to immersed tube banks 80−6141
- two-dimensional, with transverse gas supply, fluid dynamics obs. *(German)* 78−34192
- two-dimensional gas fluidised, mixing characts. of large particles 79−86503
- two-phase gas-liquid mass transfer in packed beds, review 77−31381
- two-phase model, moment method 79−37391
- uniform and nonuniform smoothly varying water stream, erosional capacity, rel. to particle size of granular bed material 77−84316
- vertical forces acting on horizontal discs in fluidised bed 77−7448
- vertical gas jet in fluidized bed, temp. field and dynamics 77−11258
- vertical pneumatic transport by retarded compact layer, energy efficiency 79−14474
- vibrational fluidisation of shallow granular bed, model 79−72939
- vibrofluidised, shallow, vibr. grid gas flow influence on hydrodynamics 79−86509
- viscosity, of water-fluidised bed, by oscills. damping meas. 78−59475
- voidage variation at wall of packed bed of spheres 77−31379
- vortex flow, 2D unsteady diffusion eqn., numerical soln. 77−84320
- wall to bed heat transfer 77−31380
- wall to liquid mass transfer 78−1736
- wall-to-liquid mass transfer, local particle influence 79−94713
- water-water vapour flow through packed bed 80−38484
- wood gasification using fluidized bed wood gasifier 80−30348
- C-graphite materials, fluidised bed, carburising of metals, diffusion saturation 79−20276
- CaO-Cu concentrate pellet, fluidised bed roasting 77−4934
- Cu particles, electrical conductivity of electrodes, expt. meas. 77−48652
- H_2, isotope separation in Ti-fluidised bed 80−18676
- KCl crystal growth in fluidised bed, comparison to dissoln. *(French)* 80−16167
- MoO_3, fluidised bed roasting, operating variables effect 77−4933
- Ni, fluid bed electrolysis, deposition 80−55672
- SiC coatings, CVD on microspheres in fluidised bed, parametric investig. 77−40457
- UF_6 conversion to UO_2 by fluid bed 79−97879
- ZnS, oxidation in fluidised bed 77−4929

fluidised powders *see powders*

fluidity *see viscosity*

fluids
- *see also bubbles; classical theories of fluid structure; disperse systems; fluid mechanics; fluidised beds; gases; gravity waves; liquids; non-Newtonian fluids; quantum fluids; quantum theories of fluid structure*
- Coulomb systems, statistical mechanics, review 80−52119
- micropolar incompressible fluids, kinetic and thermal energy decay 78−5648
- thermoelastic, stability of motion anal. 80−10221

fluorescence
- *see also atomic fluorescence; fluorescent lamps; fluorescent screens; molecular fluorescence; nonradiative transitions; X-ray fluorescence analysis*
- 5-acetyl-5H-benzo[b]carbazole-5H-benzp[b]carbazole, singlet-singlet energy transfer *(German)* 80−93402
- acridene-toluene-phenol, luminescence of complexes with hydrogen bonding at 4.2-77K 79−87486
- acridine orange in ethanol, soln., excited single state lifetimes, aggregates, visible luminesc. spectra, conc. depend. 80−55172
- activated condensed medium, trapping of radiation 79−69890
- 2-adamantanone, absorption and fluoresc., high-press. 77−52113
- adenine film, polycryst., energy conversion processes, quantum yields, 4 to 10 eV 80−88589
- aerodynamic isotope separation technique based on vel. slip in freejet expansions 80−19441
- aerosol size distribution by means of laser-induced fluoresc. 77−40576
- air pollution detection, optical methods *(Czech)* 78−69444
- albumin-unsaturated fatty acid binding kinetics, fluoresc. anal., rel. to struct. lability of biomembranes 78−15755
- alcohol solutions, fluoresc. damping curves in reson. quenching by one-photon counting method 78−10978
- algae, Chlorella pyrenoidosa, delayed emission, temp. effects 77−29118
- aliphatic tertiary amines, laser action feasibility, emission spectra, two photon excitation 80−23683
- alkali halide, activated, luminesc. and stored light sum 78−6738
- alkali halide, chalcogen^{2-} vacancy centres, absorpt. and fluoresc. spectra 78−48204
- alkali halide phosphors, $Pb^{2+}(Sm^{2+})$ doped, luminesc. props., press. effects to 140 kbar 77−40278
- alkali-alumino-phosphate:U, rontgenoluminesc. and fluoresc., radiative transitions obs. 80−103977
- alkaline aqueous soln., fluorescence detection limit 79−30575
- alkaline earth halides:Eu^{2+}, fluorescence lifetime and quantum efficiency for 5d→4f transitions 80−100681
- alkane:toluene, radiolysis at 77K, luminesc., excited singlet toluene form., energy transfer mechanism 77−16846
- 6-amino-7-hydroxy-4-methylcoumarin solutions, additions effect on fluoresc. 80−2833
- 3,4-amino-N-methylphthalimide, intermolecular orientational relax. ‘upwards’, fluorescence spectra displacement *(Russian)* 79−78748
- 9-aminoacridine fluorescence quenching method of chloroplast membrane proton gradient and osmotic vol. determ. 78−28143
- amorphous solids, electron-phonon interactions, fluoresc. line broadening and spectral diffusion 78−84655
- angiographs, of vascularised cornea, using camera slit lamp 78−48855
- angiography, colour and black and white, use of interference filters 78−48856
- anisotropy decay determ. by single photoelectron counting 78−84635
- anomatic hydrocarbon high density excitation effects on fluoresc. 79−1782
- anthracene:2-hydroxyanthracene, site-selective photochem., fluoresc. spectra at 3K 78−80756
- anthracene: tetracene, singlet exciton trapping mechanism, fluoresc. mag. field modulation obs. 77−77267
- anthracene:acridine(carbazole), fluoresc., structural traps for singlet excitons 78−19542
- anthracene:rhodamine, triplet exciton density, isotope substitution effect, in weak mag. field 77−90184
- anthracene:tetracene, crysts., triplet kinetics model *(German)* 79−4518
- anthracene:tetracene, delayed fluorescence excitation spectra 78−39594

fluorescence continued
anthracene:tetracene, fluorescence decay with X-irrad., energy transfer by excitons 77—20915
anthracene:tetracene, nonlinear quenching of fluoresc. 79—65924
anthracene:tetracene, singlet exciton fission, fluoresc. in mag. field 79—69877
anthracene:tetracene, upper excited vibronic states optically pumped energy transfer matrix fluoresc. 78—76512
anthracene:tetracene (pentacene), effect of elec. field on fluoresc. *(Russian)* 78—56521
anthracene, and related derivatives, fluoresc. and photoreactivity 77—48668
anthracene, cryst., exciton aggregate possible form. under intense optical pumping, fluoresc. spectra 80—84772
anthracene, cryst., fluoresc. spectra, press. tuning 77—28612
anthracene, cryst., heat pulse propag., exciton condensation, time-resolved fluoresc. spectra 80—84771
anthracene, excitation spectra of exciton fission in organic crystals 78—92116
anthracene, exciton sounding of α-particle induced radiation defects 77—12423
anthracene, fluoresc. from (001) surface and sub-surface excitons 79—33763
anthracene, fluoresc. spectra and decay curves, 4-300K, reabsorpt. in cryst. *(German)* 78—68561
anthracene, high exciton conc., low temp. fluoresc. *(Russian)* 77—28623
anthracene, in stretched polymer film, mol. distrib. determ. 78—27298
anthracene, isotopically mixed cryst., exciton dynamics 80—29329
anthracene, light polarisation depend. on energy transfer from excited to emitting mols. *(German)* 78—37677
anthracene, liq. chromatography, sublimation, zone refining, exciton fluoresc., mobility meas., melt grown crystal 79—38736
anthracene, noncryst. solid, excimers, time resolved fluoresc. obs. 79—52006
anthracene, nonlinear fluorescence quenching 78—52562
anthracene, photo-oxidised, current oscills. due to recomb. instability in high field domain 77—4353
anthracene, pure and doped, singlet exciton diffusion lengths, fluoresc. quenching by dye 78—43923
anthracene, reflectivity and fluoresc. of (001) surfaces, sub-surface exciton states 79—15508
anthracene, single cryst., fluoresc. decay, Monte-Carlo simulation *(German)* 79—61440
anthracene, single cryst., X-ray radiation damage, delayed fluoresc. meas. *(Japanese)* 79—37736
anthracene, single cryst. with photoinduced local centres, luminesc. 79—61433
anthracene, singlet and triplet excitons as probes for photochem. reactivity 79—74406
anthracene, singlet exciton fission, fluoresc. in mag. field 79—69877
anthracene, singlet exciton fission, prompt and delayed fluoresc. mag. field depend., temp. effects 78—52540
anthracene, temperature independent intersystem crossing 78—39030
anthracene, thick crystals, excitation spectrum of fluorescence 80—76068
anthracene, thin surface layer, delayed fluoresc. obs., surface trap influence 77—77291
anthracene, triplet energy migration in polystyrene matrix, rate meas. 78—35185
anthracene, triplet excitons, phosphoresc. and delayed fluoresc. excitation spectra 78—63986
anthracene, UV irrad. effects on fluoresc. emission at room temp. 79—83019
anthracene crystal, singlet-triplet exciton annihilation 78—31240
anthracene crystals, basal dislocations, fluoresc. spectra and etching obs. 77—84755
anthracene crysts., nonlinear fluorescence quenching, recomb. of free excitons 80—7397
anthracene crysts., structural imperfections and delayed fluorescence 78—68551
anthracene in 2 methyl-THF glass, low temp. fluoresc. bandshape, excess energy effects 78—76509
anthracene-2-methyltetrahydrofuran, glassy solution, site-selective impurity phonon coupling 77—81142
anthracene-dimethylpyromellite-imide, CT complex, reaction yield detect. double reson., delayed fluoresc. quenching *(Russian)* 78—88230
anthracene-phenanthrene-tetracyanobenzene, CT-cryst., mini-excitons and lattice dynamics, ESR, optical and Raman spectra 80—60406
anthracene-PMDA, charge transfer cryst., 2K, zero-phonon lines, singlet spectra 78—23484
anthracene-TCNB charge transfer cryst., phosphoresc. and delayed fluoresc. detected mag. reson. 79—33565
anthracene-tetracene amorphous films, host-guest energy transfer 78—60505
anthracene-tetracenebenzene, triplet excitons annihilation, mag. reson. sign reversal 79—65769
anthracene/TCNB, charge-transfer cryst., fluoresc., 1.2-300K, mobile triplet excitons 78—43913
anthracenes, long-lived luminesc. in solid state *(German)* 78—23528
apomyoglobin-arylaminonapththalenesulfonate system, fluorescent behaviour 79—39359
aqueous solution fluorescence spectra, refr. correction 78—93766
aromatic hydrocarbons-amine, π-axciplexes, intermolecular interactions 80—43134
aromatic media, electron excitation, delayed fluoresc. 79—52024
atomic spontaneous emission, fluctuation spectroscopy 77—434
automatic fluorescence microscope photometry data processing and display *(German)* 80—86369
azomethines, photochromic, intramol. proton phototransfer sensitisation, organic cation energy transfer 78—53230
backward Raman amplifier for excimer laser pulse compression, parasitic superfluoresc. suppression 80—69453
bacteria, effect of mag. field on recomb. fluoresc. 80—35856
bacterial picosecond fluorimetry obs. 79—92178
benzene, cryst., vibronic spectra using 2-photon fluoresc. excitation 79—47493
benzene, isotropically mixed crysts., singlet and triplet exciton percolation theory 78—26818
benzene, solid, fluoresc. decay times and quantum yields, rel. to vap. phase 80—55154
benzene, soln., fluoresc., quenching in pulsed proton and alpha particle irrad., radiation quality effects 80—66259

fluorescence continued
benzene cryst., electron irrad., phenylcyclohexadienyl radical form., absorpt. and fluoresc. spectra study 80—89035
benzene in dilute cyclohexane solution, fluoresc. quenching on pulsed proton irrad., temp. depend. 80—21307
benzophenone: diphenylmethylene, mixed cryst., emission and absorpt. spectra, 2-30K, excitation-phonon coupling 79—99900
Bethe random lattice, spectral diffusion, total conductance distribution probability 80—8928
bilirubin, soln. luminesc. 79—31572
bimolecular exciton recombination kinetics, limited by anisotropic diffusion 77—4295
biological sample, cell and tissue, appl. of nanosecond fluorometric system 77—17010
biological technique, use of fluoresc. marker conc. dynamics as probe of mobility 77—9303
biomembrane, distance meas. by radiationless energy transfer, transition probabilities 78—24187
bis(p-toluene sulphonate) diacetylene, partially polymerised, defect-induced absorpt. and fluoresc. 77—44030
borate glass: $UO_2^{2+} \rightarrow Ho^{3+}$, energy transfer processes 78—10969
bronchoscopy for localisation of small lung tumours, fibre optic system 77—86580
calcite, luminescence spectral anal. of polycyclic aromatic hydrocarbon impurities 80—71483
calorimetric techniques for excited states detection 78—32847
carbocyanine dyes, fluoresc. probes, effect on Ca-depend. K efflux 77—12896
cell analysis in flow systems, geometry for orienting flat cells 78—77161
cell membrane translational dynamics, fluorescence redistrib. after photobleaching obs. 80—21491
cell nuclei structural change in the physiological pH interval 79—79492
cellular fluorescein excitation and emission polarisation spectra obs., involvement of mitochondria 80—30683
cellular fluorescence polarisation measurements in flow systems, epi-illumination optical design 80—89908
cetyltrimethylammonium bromide and chloride aqueous micelle, fluoresc. showing coexistence of rod-like and globular struct. 79—61910
charge transfer complex high density excitation effects on fluoresc. 79—1782
charge-transfer crystals, long lived emission 79—33752
chlorella, delayed fluoresc., ns laser pulse excited, fast phase kinetic anal. 79—24951
chlorella cells and pea chloroplasts orientated in a mag. field, fluoresc. polarisation 80—51055
chlorophyll, a and b, lowest singlet-singlet transition, solvent effects 79—24952
chlorophyll, photosystem 2, activation energy and lifetime of fluoresc. 80—35842
chlorophyll a in photosynthetic material, luminesc. 79—34498
chlorophyll-a, crystalline film, energy levels and carrier generation by photocond. and fluoresc. 77—16909
chloroplast in intact cell of green alga Haematococcus pluvialis 78—24037
chloroplasts, bean, chromatic transitions 77—25389
chlorotetracycline self-fluorescence probe in transport by bacillus megaterium 79—24971
chronospectroscopic method of investigation, improvement in resolution using phase spectra 79—54199
circular dichroism detection, direction dependent opt. activity by photoselection 77—36279
colour reproduction of halftone prints, effects of fluorescent brightening agents *(Japanese)* 77—26417
combustion diagnostics, laser Raman and fluoresc. techniques 78—88635
combustion products, Raman scatt., fluoresc. interference 78—15728
condensed phase, reson. Raman and reson. fluoresc. spectra, density matrix approach 78—80323
condensed phase fluoresc., double reson. excitation spectroscopy 80—86438
Condon approximation, shape of absorpt. and fluorescence bands, effect of electron-phonon coupling *(Russian)* 77—48212
continuous oil-in-water meas. by towed fluorometer 80—45846
contour plotter, automated, 3-dimens., for fluoresc. meas. 78—58046
cooperative resonance fluorescence, multiple sidebands, semiclassical calcs. 80—99685
cooperative resonance fluorescence, photon statistics and absorption spectrum 78—42311
copper (I)-butyrate, dimorphism, X-ray diffr. and fluoresc. *(German)* 79—51090
correlation, clip-correlator *(Russian)* 80—42270
correlation spectroscopy, effect of clipping 78—55198
coumarin, aq. soln., response to high LET radiation from $^{10}B(n,\alpha)^7Li$ reaction 78—24149
coumarin 6-diethylamine, soln. fluoresc. induced by laser, vibr. relax. 79—26984
crystalline solid of two-level atoms, resonance fluorescence 79—56844
cyanine dye monolayer/p-chloranil crystal, charge carrier injection rate const. determ., energy transfer vs. charge transfer method 79—83031
9-cyanoanthracene:perylene, exciplex emission 78—60513
9-cyanoanthracene, cryst., excimer emission, spectra, photochem. and multiphonon processes 78—10914
9-cyanoanthracene, quenching of solid state photodimerisation reaction by cryst. doping 78—68547
cytochrome-c, coherent reson. Raman scatt. and incoherently broadened reson. fluoresc., condensed phase 78—60429
cytofluorometer, imaging system for correlating fluoresc. cell meas. in flow 78—61240
cytofluorometric measurements by fluorescence extinction through a diaphragmed objective 80—67319
cytometry, hydrodynamic orientation of sperm heads in flow systems 78—77162
decay, nonrandom errors, moment index displacement calcs. 77—6835
decay time, phase-shift and modulation techniques, pulsed light sources high harmonic content 80—69179
decay time meas., photomultiplier wavelength depend. errors, correction method 79—30558
detection, of weak fluoresc. by drift free integration 77—40581
detection system for HPLC 78—48735
3,5-di-tert-butyl-4-hydroxybenzylidenemalononitrile, excited-state proton transfer, cryst. and mol. struct. 78—84630

fluorescence continued
dianthronylidene ethane, luminescent excimer geometries, intermol. shift 78—27294
dibenzofuran:anthracene, cryst., prompt fluoresc., temp. depend., trap effects *(German)* 80—93400
1,4-dibromonaphthalene, triplet-triplet exciton annihilation in quasi-1-dimens. cryst. 78—27297
dicarbonitrile-anthracene solutions, absorpt. and emission spectra, solvent influence 80—43083
9,10-dichloroanthracene, cryst., singlet-triplet absorpt. spectra, delayed fluoresc. 77—8619
9,10-dichloroanthracene, mag. field effect on exciton processes and photodetrapping 77—4668
dilute systems, donor fluorescence at high trap concentration 80—71479
dimesitylboranes, phenyl substituted, absorption and emission 78—27311
dimethylsulphoxide, $Eu^{3+} \rightarrow Pr^{3+}$ and $Eu^{3+} \rightarrow Er^{3+}$ non-radiative energy transfer 79—47510
1,6diphenyl 1,3,5, hexatriene cholesteryl chlorided cholesteryl laurate mixture, nematic, polarisation fluoresc. meas. 79—78723
1,3-diphenyl-5-(p-chlorophenyl)-2-pyrazoline, singlet excitation energy migration in cryst. and glassy states 79—95831
9,10-diphenylanthracene, luminesc. quantum yield, fluoresc. spectra polarisation effect, solvent viscosity depend. 78—27303
diquinolyl cyanomethane, fluoresc. quantum yields, viscosity effects 80—60646
disordered molecular system, exciton percolation, book contrib. 77—36297
disordered system, pair decay model of time depend. spectral transfer 79—43015
disordered system, spectral and spatial diffusion, Monte Carlo calc. 79—4848
disordered systems, fluoresc. energy transfer, conc. depend. 80—50413
disordered systems, optical excitation spectral transfer, generalised models 79—43027
disordered systems, random walk of energy to traps 80—55155
disordered systems spectral transfer, time development models 78—84643
ditetraethylammonium manganese bromide $^4T_1$ excited state, absorpt., MCD, Jahn-Teller model 78—43907
DNA, luminescence, excitation wavelength depend. in UV/VUV region 78—31768
DNA bases, thymine type, polarised fluoresc. in neutral aq. soln. 80—21445
donor fluorescence, t-matrix analysis 80—100679
double-beam fluorescence spectrophotometry 77—21435
dye, photon counting using clip-correlator *(Russian)* 80—42271
dye adsorption by cells, permeab. polarity and control by phytochrome 78—77025
dye liquid layers, fluorescence angular distribution, evanescent wave excitation 79—51996
dye medium, short laser pulse superposition, numerical anal. 79—31891
dye molecules adsorbed on Ag, Au and Cu films, absorpt. and luminesc. study 80—103981
dye solutions, mixed, fluoresc. conc. quenching, sensibilisation 79—24347
dyes in rigid matrices, solvent reorientation relax. effect on luminesc. 79—43009
EBBA, nematic, ordering parameter temp. depend. 79—23517
EBBA-dimethylaminonitrostilbene mixture, nematic, polarisation fluoresc. meas. 79—78723
Ehrlich ascites carcinoma cell fluoresc. after X-irrad. 78—69143
Ehrlich ascites vital cell UV primary fluoresc. rel. to ^{60}Co γ-ray dose 78—69142
elastic scintillation, fluoresc. meas. 78—86747
electrocrystallisation, recent progress in electrochem. and physical methods *(French)* 80—7510
electron beam fluorescence technique for hypersonic turbulent flow 77—35282
electron optical picosecond chronoscopy, 140 MHz repetition rate, fluoresc. lifetime meas. 78—78019
electron-vibrational transitions in presence of several minima of adiabatic potentials 77—81150
emission spectra, absorpt. method regularization 79—98250
epoxy resins, strain anal. by fluoresc. meas. *(French)* 79—47846
erbium ethylsulphate, cryst. laser-excited fluoresc. intensity 79—33751
erythrocyte membrane, X-ray induced structural changes, fluorescent probe obs. 79—88129
erythrosin, aq. soln., polarisation of fluoresc. spectra, aggregation of mols. 78—31227
ethylbenzocarbazole, soln., luminesc., effect of electronic excitation energy vibr. 80—55174
europium B-diketone chelate solns., fluoresc. quenching by appl. voltage, display devices appl. 79—87497
excimers and exciplexes, decreased stabilisation energy in polymer matrices 80—25431
eye lens fluorescence due to UV stimulation, appl. to pupillary response meas. 78—64977
fast fluorescence decay meas., appl. of curved microchannel plate photomultipliers 78—12743
film, method for refr. index and thickness determ. 80—40175
films on substrates, electron probe anal., charact. fluoresc. effects calc. 80—81408
fluorene:benz(f)indan(anthracene), single cryst., γ-irrad. rel. to luminesc. decay 77—12417
fluorene:dibenzofuran, mixed cryst., dipole-forbidden guest-host energy transfer 79—38585
fluorene:pyrene-d_{10}, exciton-guest, triplet-triplet annihilation, impurity traps effects 80—25433
fluorene:pyrene-d_{10}, single cryst., host-guest triplet pairs, mag. field effect 80—60649
fluorene, exciton band struct., two-photon fluoresc. excitation 78—64402
fluorene, lowest singlet state, exciton band struct. calc. 78—63983
fluorene, near 6K, two-photon excitation spectrum, g-exciton states location 78—64393
fluorescein angiography of the ocular fundus 80—67185
fluorescein in mammalian cells, appl. of fluoresc. polarisation meas. by flow cytometry 77—52942
fluorescence detected circular dichroism, theory 77—30914
fluorescent materials, reflective radiance factor meas. by two-monochromator method *(Japanese)* 80—68237
fluorimeter/spectrophotometer for university biochem. course 77—33807
fluorometric techniques and instrumentation 80—45845
fluorophotometer, slit lamp type, for tear measurements 77—2064

fluorescence continued
fluorophotometric measurement, supplementary unit for hand ophthalmoscope 78—48907
frozen gas matrix, refr. index determ. by emission spectrosc. 80—90884
frozen solution spectra, inhomogeneous broadening and phonon effects 79—33725
gated constant-fraction discriminator for use with fast-focused photomultiplier tubes 78—58063
germanate glass:Bi^{3+}, time-resolved spectra, radiative and nonradiative processes 79—47501
germanate glass:Bi^{3+},Eu^{3+}, time resolved spectra for Bi-Eu energy transfer 79—33748
germanate glass:Nd^{3+}, spectral behaviour under narrow-line excitation 79—33747
glass:Eu^{3+}, spectroscopic props. of excited states of ions, laser induced fluorescence line narrowing meas. 79—38641
glass:Nd^{3+}, ED-2 glass, spectral behaviour under narrow-line excitation 79—33747
glass:Nd^{3+}, ED-2 laser glass, transition probabilities and quantum efficiency 77—58330
glass:Nd^{3+}, line narrowed fluorescence spectra and site dependent transition probabilities 79—38640
glass:Nd^{3+}, spectral props. *(Chinese)* 80—60645
glass:Nd, fluoresc. decay data from minicomputer-operated spectroscopy equipment 77—74526
glass, coloured, for short wavelength cutoff filters, fluoresc. data 79—61411
glass, fluoresc. linewidth 80—34978
glass, fluorescence linewidth, anomalous of impurity ions, theory 80—50404
glass, structural analysis, using fluorescence excitation *(German)* 80—38923
glass-plumbite-treated cotton, form. of coating at interface 79—15058
glasses for fluorescence standards in radiophotoluminesc. detector reading device 77—67944
glycerine solutions, fluoresc. damping curves in reson. quenching by one-photon counting method 78—10978
greening bean leaf low-temp. fluorescence induction obs. 79—39354
halophosphate phosphors, radiation stability, recomb. processes effect *(Russian)* 80—7424
Hercules X-1, fluorescent origin of Fe K-line emission during X-ray low state 80—105393
2,4-hexadyne-1,6-diol-bis-p-toluene sulphonate, fluoresc. of localized states in single crystal 78—6756
high temperature metallic species, absorpt. and fluoresc., high temp. fast flow reactor technique 80—42231
human carcinoma cells, binding and internalization of epidermal growth factor 79—92189
hydrocarbon carcinogenesis, fluoresc. meas. in cells 79—39343
8-hydroxy, 1,3,6-pyrene trisulphonate, picosec. proton ejection, ultrafast pH jump 79—83475
II-IV-V_2 semiconductor, electronic struct. determ. 77—76751
II-VI luminophore, broad fluoresc. bands, spectral distrib. of emission probability 77—8653
III-V semiconductor, electronic struct. determ. 77—76751
immunofluorescence, laser appls. as biomedical research probe 77—9298
impurity atom in solid, reson. fluoresc., transient spectrum, intensity, and intensity correl. 80—84777
impurity atoms in solids, photon antibunching in reson. fluorescence 79—43025
impurity centres, electron-phonon coupling from structured optical spectra, review 80—89038
impurity luminescence, effects of reson. laser radiation on O-O line 78—6728
incoherent resonance decay and coherent optical ringing from coherently prepared electronic states 77—10698
indigo derivatives, fluorescence decay times, meas. by synchroscan streak camera 80—84759
indocyanine green fluoresc. spectrum in blood and other solvents, rel. to angiography 78—28057
indole, in PMMA matrix, high press. luminesc. 78—84629
indole soln. containing histidine, fluoresc. rel. to soln. pH 80—2826
inert gas crystal, benzene-doped, luminescence excitation investig. 77—77276
inhomogeneous solid, determ. of homogeneous impurity spectra 79—73982
inner filter effects in front face and total refl. fluoresc. 78—88357
intensity analysis, absorption and self-absorption quenching effects 77—37693
internal combustion engine, conc. fluctuation meas. 80—71973
internal field reson. struct., implications for optical absorpt. and scatt. by microscopic particles 79—10259
interstellar dust fluoresc., as source of emission lines in nebulae visible spectra 79—53874
ion trap sensitivity for spectroscopic applications, $^{137}Ba^+$ ground state hyperfine splitting 80—22447
ion-molecule reactions (thermal), emission spectra obs. using pulsed ICR cell 77—19108
ions in solids, time resolved fluoresc. line narrowing 79—38611
IR laser induced fluorescence cell for multiple photon processes 78—54475
4-isocyanate-trans-stilbenes, donor substituted, anisotropic fluoresc. in low viscosity solvents *(German)* 80—93401
2-isopropoxyphenyl-N-methyl carbamate, fluoresc. and phospheresc. in solns. 79—61426
lanthanide ion fluorescent probes, spectroscopic obs. system 78—11573
lanthanides in molten $LiNO_3$-KNO_3, transition probabilities in absorpt. and fluoresc. spectra 79—50085
laser, pulse width, meas. by two-photon absorpt. fluoresc., contrast ratio variation 79—76737
laser dyes, fluoresc. efficiency and standards 78—35205
laser fluorescence appl. in time-of-flight vel. selection system 77—49804
laser fusion fuel configurations, cryogenic, survival in fluorescence energy 77—50288
laser induced fluorescence spectroscopy, saturation effects 77—44526
laser induced fluorescence system for OH and trace gas meas. 80—36425
laser pulse asymm. detect. by three-photon fluoresc. meas. 78—1289
laser pump fluctuations, influence on resonance fluoresc. radiation intensity correlation 80—37981
laser spectroscopy, high-resolution, using fast ion beams 78—86975
laser spectroscopy, resonance fluoresc. in strong field 79—35846

fluorescence continued
laser-based methods for transient chem. events meas. 80—40801
level crossing detection through photon counting distrib. second factorial moment meas. 80—99485
life time decay curve meas. and anal. 78—54465
lifetime measurement, ratio correction for photomultiplier time response variation with wavelength 77—18065
lifetime measuring system with picosecond resolution using CW laser and AM radio 78—41357
light microscopy, simple preparation technique *(German)* 79—97429
line narrowing, line-shape deconvolution 80—89039
line narrowing, time depend. effects, appl. to $Pr_{0.2}La_{0.8}F_3$ 78—31244
linear laser spectroscopy, fluorescence spectroscopy, review of technique 78—29170
liposome structural lability, fluoresc. anal. 78—24033
liquid crystal display, fluorescent utilising elec. field induced cholesteric-nematic transition 78—16781
liquid crystals, static and dynamic props., time depend. fluoresc. depolarisation obs. 80—29786
localised centres in strong EM fields, multiquantum transitions 78—10936
lubricant film, thin, thickness meas. using laser based fluorescence technique 79—49201
lucensomycin interaction with cholesterol in membranes, spectral parameters 77—9177
lung cancer localisation using laser fibre optic bronchoscope 78—48921
lymphocytes, mouse thymus, X-irradiation effects on UV fluorescence 79—66491
Mars surface materials, chemistry, anal. of Viking X-ray fluoresc. spectrometer data *(German)* 78—85884
MBBA, nematic, ordering parameter temp. depend. 79—23517
MBBA, uniaxial, orientational order, polarised fluoresc. meas. 79—55655
membrane fluorescence test, rapid modification base on Microtiter system 78—20334
membrane surfaces, antibody association kinetics with spin-label haptens 80—66787
membranes, structural order of lipids and proteins, fluoresc. anisotropy data eval. 80—97873
metallic film, phonon fluorescence stimulated by laser radn. 79—87504
metaphosphate glasses, $n(M_2O.P_2O_5).(1-x)Y_2O_3.xTb_2O_3.3P_2O_5$, M=Li, Na, K, excitation and emission spectra 80—40150
methylene phenanthrene cryst., delayed fluoresc., mag. field effect, sense depend. 77—73160
5-methylindole, in PMMA matrix, high press. luminesc. 78—84629
3-methylpentane, γ-irradiated, isothermal luminescence in presence of aromatic solutes at 77K 78—76519
micelle forming detergent solutions, fluoresc. quenching by O_2, dynamic parameters and solubility characts. 79—83513
microscopical technique in diagnostic microbiology 78—20339
microscopy, incident light, specimen prep. method 80—82755
microscopy, water pollution abatement, self-cleaning capacity of epipelic biocenoses 79—79702
microscopy of living cells, low level, appls. of image intensification 80—94432
microspectrofluorometry, low temp., design of cold chamber 78—57144
minerals, physical theories for origin of colour 78—69323
molecular crystal, delayed fluoresc., anisotropic spin relax. effects 79—61416
molecular crystal, sensitised fluoresc., energy transfer rate 79—38586
molecular crystals, diffusion mediated exciton processes, mag. field depend. of fission and fusion 79—37998
molecular crystals, electronic energy transfer, review, book contrib. 77—39789
molecular pair, fluoresc. depolarisation, using stochastic Liouville eqn. with radiative terms 80—16074
molecular solid, disordered, exciton migration, dynamical approach 79—65916
molecular solid, intermolecular interactions, laser induced phonon probe 80—79891
molecular solids, Raman, fluoresc. and nonlinear props. 79—33702
molecules embedded in small particles, Raman and fluoresc. scatt., coherent results 79—41338
molecules embedded in small particles, Raman and fluoresc. scatt., incoherent results 79—41337
monodispersed spheres, dye impregnated, fluorescence angular distribution, evanescent wave excitation 79—51996
3-monomethylamino-N-methylphthalimide solns., fluoresc. and excitation spectra 79—61425
multicomponent fluorescent mixtures, quantitative anal. of data 78—27833
multicomponent sample, anal. method 77—70350
multicomponent systems, video fluorometer anal., rank annihilation method appls. 78—92546
muscle, cross bridge rotation during contraction, fluctuations in polarised fluoresc. 80—97856
muscle, tryptophan fluorescence polarisation 80—97877
nanosecond emission spectroscopy, developments 77—34037
nanosecond pulse stretcher, appl. to laser-excited time-resolved fluorescence spectrometer 79—67390
naphthalene:β-chloronaphthalene, reaction rate constants of triplet excitons 78—80407
naphthalene:anthmacene, singlet exciton energy transfer dynamics, time resolved spectra 79—83032
naphthalene:anthracene, pure and doped, delayed fluoresc. *(French)* 80—80846
naphthalene:anthracene, two-photon picosec. excitation, sensitised fluoresc. kinetics 79—47516
naphthalene:azulene, reson. fluoresc., Raman spectra, single vibronic level relax. 79—38588
naphthalene, 2-methylnaphthalene and anthracene doped, single cryst., sensitised fluoresc. 78—68548
naphthalene, $^1B_{2u}$ supertransfer, exciton percolation, fluoresc. spectra obs. 77—55482
naphthalene, and deutero derivatives, fluoresc., absorpt. spectra under Shpolskii conditions 80—2825
naphthalene, cryst., fluoresc. spectra, press. tuning 77—28612
naphthalene, cryst., singlet exciton interactions, prompt fluoresc. decay 78—60500
naphthalene, cryst., singlet exciton interactions fluoresc. decay 79—47027
naphthalene, crystalline, singlet exciton diffusion coeff. meas., fluorescence quenching anal. 78—67945

fluorescence continued
naphthalene, doped, fluoresc., impurity centre struct. depend. *(Russian)* 77—48231
naphthalene, fluorescence decay induced by electron pulse, exciton interactions 77—16403
naphthalene, in stretched polymer film, mol. distrib. determ. 78—27298
naphthalene, mag. effects on delayed fluoresc. at high and low triplet exciton density 77—8634
naphthalene, multiphoton excitation 79—61414
naphthalene, nonlinear fluorescence quenching 78—52562
naphthalene, triplet exciton annihilation at high triplet densities 79—37996
naphthalene, triplet excitons, phosphoresc. and delayed fluoresc. excitation spectra 78—63986
naphthalene β-chloronaphthalene, optically induced detrapping of triplet excitons 79—28828
naphthalene cryst., anthracene doped, fluoresc., two-photon excited 78—68560
naphthalene crysts., nonlinear fluorescence quenching, recomb. of free excitons 80—7397
naphthalene-d_8:naphthalene, betamethylnaphthalene, $^1B_{2u}$ naphthalene exciton percolation kinetics, exciton coherency 79—33750
2-naphthol-3,6-disulphonate, picosec. proton ejection, ultrafast pH jump 79—83475
2-naphthol-toluene-phenol, luminescence of complexes with hydrogen bonding at 4.2-77K 79—87486
nematic liq. cryst. with luminesc. impurity, luminesc. and absorpt., order parameter determ. 79—4240
nonexponential resonance decay, role of exciting light source 77—42348
obsidian, Lipari and Teotihuacan origin, Mossbauer, magnetisation, X-ray diffr. and fluoresc. study 80—46173
n-octane-3,4,6,7-dibenzpyrene impurity, fluorescence impurity spectra, phonon free line broadening *(Russian)* 80—108279
ODMR, spin-lattice relax. and triplet-triplet. absorpt. effects 79—19807
oil, fluoresc. props., appl. to oil films thickness meas. on polluted water 79—79437
opaque samples, proposed indices of degree of fluoresc. 78—54425
optical couplers, switch operation, exam. by fluorescence method 78—38049
organic compounds, inductive-resonance energy transfer, heterogeneous electron level broadening *(Russian)* 78—23530
organic crystals, kinetic model of triplet exciton dynamics 78—67948
organic matter dissolved in seawater, fluoresc. spectra *(Russian)* 77—13083
organic mixed crystals, energy transfer 78—76515
organic molecular crystals, intermolecular interactions, spectroscopic studies, review 80—103958
organic photoconductor, electric field-induced fluoresc. quenching 80—34967
organic solid, motion of localised excitations 77—31961
organic solids, decay time and emission spectra obs. *(Spanish)* 77—69873
oxide glasses:Sm^{3+}, optical transitions 79—61430
[2.2]paracyclophane, delayed luminesc. in cryst. and rigid glass solns. 79—15510
particles with embedded molecules, Raman and fluoresc. scatt. 79—64177
pentacene in naphthalene (p-terphenyl), mol. mixed crysts., optical dephasing and vibronic relax. 80—95957
pentacene in p-terphenyl, intermolecular interactions, laser induced phonon probe 80—79891
percolation model, one-dimens., spectral diffusion 78—80411
perfluorocarbons, γ-irrad. solns., mag. field effect on fluoresc. 80—55677
perylene, cryst., fluoresc. at low temp. 78—27299
perylene, cryst., fluoresc. spectra, time-resolved, excimer and excitons 79—78724
perylene, excitation spectra of exciton fission in organic crystals 78—92116
perylene, exciton fission in excimer forming cryst., fluoresc. 79—15511
perylene, fluoresc., exciton fission in excimer forming cryst. dynamics 79—61423
perylene, intermolecular interactions, laser induced phonon probe 80—79891
perylene, organic soln., picosec. fluoresc. for rot. diffusion 79—56839
phase fluorometer for measurement of picosecond processes 78—66691
phenanthrene:anthracene, cryst., triplet-triplet annihilation, shallow traps effect, 77-293K 79—11446
phenanthrene:anthracene, delayed fluores. of cryst. in mag. field 79—52023
phenanthrene, two-photon excitation spectra, exciton-phonon and intramol. vibronic coupling 80—84774
pheophytin containing monolayers, phase separation and domain interaction, surface press. and fluoresc. meas. 79—100580
pheophytin reduction obs. in higher plant photosystem II 79—43817
phosphate glass: UO_2^+, Sm^{3+}, energy transfer from UO_2^+ to Sm^{3+} 79—78732
phosphate glass:Nd^{3+}, spectral behaviour under narrow-line excitation 79—33747
phosphate glass:Sb^{3+},Dy^{3+}, fluorescence and energy transfer obs. 78—6778
phosphate glass:Tm^{3+}, eigenstates and radiative transition probabilities calcs. 77—77265
photobleaching recovery, investigation using grid-gated photomultiplier photometer with subnanosecond time response 80—37071
photobleaching recovery experiments, criticality of beam alignment 80—56296
photobleaching recovery method, bleaching light effect on membrane diffusion meas. 80—94434
photoelectrochemical cells, metal, electrodes in contact with fluoresent dye solns., photovoltage generation, comprehensive model 80—40871
photomacrography, bone growth and remodelling exam. 78—31982
photon catalysis, analytical, meas. of gas phase concs. to $10^4/cm^3$ 77—52685
photoreceptor fluorescence rel. to UV sensitivity, fly 79—92219
photosynthesis, chloroplast fluorescence, investigated using laser spectrofluorimetry 80—81558
photosynthesis, fluoresc. induction modelling by elec. diagram 79—57589
photosynthesis, fluorescence picosec. kinetics in chromatophores and reaction centres from R.sphaeroides, 295 to 80K 80—35857
photosynthesis of higher plants, energy migration and electron transport 78—20150

fluorescence continued
- photosynthetic apparatus repression b 2-deoxy-D-glucose, low-temp. fluoresc. spectra of intact Chlorella cells 80−81559
- photosynthetic organisms, reson. energy transfer, fluoresc. decay times 77−81479
- phthalocyanine, metal-free, solid, fluoresc., lifetimes temp. depend., polymorphic modification 78−80388
- phthalocyanine, X-metal-free in polyvinylacetate, elec. field induced fluoresc. quenching, carrier photogeneration 78−48207
- phthalocynanine, doped photovoltaic cell, photoconductivity, elec. field induced flouresc. quenching, charge carrier photogeneration 80−84485
- picosecond fluorescence spectroscopy, competing events 78−58051
- picosecond pulse techniques in spectroscopy, fluoresc. and other research areas 79−17504
- pigment reversible changes due to illumination of leaves 79−43818
- planar collector-concentrator, for solar energy conversion 80−45745
- planet surface, environmental remote sensing, molecular absorpt. methods 80−72651
- plastic scintillator, degree of fluorescence light polarisation, energy depend. *(German)* 78−37677
- plastic scintillator detectors, fluorescent response to heavy ions, $Z<36$, $E<170$ MeV 77−3228
- plastic scintillator props. meas., streak camera technique 78−66450
- PMMA crosslinked by dimethacryloxymethylanthracene, radiothermoluminesc. *(Russian)* 78−73068
- polarisation apparatus, for simultaneous meas. of orientation and mobility in uniaxial media 78−86320
- polarisation measurements, correction for finite apertures 78−21224
- polarisation microscope for cell membrane fluidity screening 77−44855
- poly(N-vinylcarbazole) film, fluoresc. and phosphoresc., energy transfer mechanism 80−16112
- poly-1-vinylnaphthalene solution, time-resolved fluoresc. spectroscopy, excimer form. and dissoc. 79−38637
- poly-2,6-dimethylphenyleneoxide, fluoresc. correction in light scatt. meas. 79−1771
- poly-N-vinylbenzocarbazole, soln., luminesc., effect of electronic excitation energy vibr. 80−55174
- poly-N-vinylcarbazole:2,4,7-trinitrofluorenone, fluoresc. kinetics, stroboscopic meas. 79−11443
- polyacenaphthalene, glassy soln., fluoresc. yield, polarisation and decay., temp. depend. 80−89043
- polyacenaphthalene-methylmethacrylate copolymer 80−89043
- polyacrylamide-fluorescein conjugates, fluoresc. polarisation, high press. obs. 80−20683
- polyaspartamides, soluble, fluorescent labelling 80−58426
- polybutylene terephthalate film, photoluminesc. exam. 78−48213
- polyethylene terephthalate film, photoluminesc. exam. 78−48213
- polyethylene-2,6-naphthalate fluorescence, transparency decay, possible appl. as polymer scintillators *(Chinese)* 79−93870
- polymer, uniaxial, fluoresc. polarisation, orientation and mol. dynamics effects 78−76516
- polymer orientation measurement, in solid, by spectroscopic techniques, mech. anisotropy 78−75558
- polymer solution, rigid, exciton transport 79−69431
- polymer solution, surface fluorescence, determ. using SPEKOL spectrocolorimeter 79−79301
- polymethinium dye, excitonic fluoresc., absorpt. trapping spectra 78−27302
- polymonochloroparaxylylene film, photoluminesc. exam. 78−48213
- polynitramines, solid cyclic, luminesc. meas. 77−32424
- polyparaxylylene film, photoluminesc. exam. 78−48213
- polyphenyls, fluoresc. and sensitization props. 79−38599
- polyribonucleotides, dye tagged, aqueous solns., elec. induced fluoresc. changes 80−85346
- polystyrene, end group modified, chain dynamics studied by fluorescence depolarization 80−19724
- polystyrene photophysical behaviour, solvent effect obs. *(Spanish)* 79−57267
- polystyrene solution, time-resolved fluoresc. spectroscopy, excimer form. and dissoc. 79−38637
- polyvinylbenzocarbazole, weak solution, intramolecular energy transfer by singlet and triplet excitons 80−34971
- polyvinylcarbazole, weak solutions, intramolecular energy transfer by singlet and triplet excitons 80−34971
- pressure calibration system improvement using ruby R_1 fluorescence 80−98928
- proteins, inductive resonance energy transfer, struct. and conform. changes 79−27120
- proteins, UV irradiated, luminesc. quenching, EPR and absorpt. spectra 78−15768
- pseudo-Kossel lines in high press. X-ray diffr. pattern using diamond anvil cell 80−79623
- pulsed laser spectroscopy, review 79−26140
- PVC, film, uniaxially stretched, effect of mol. orientation on anisotropy of Young's modulus 77−86076
- PVC film, uniaxially stretched, mol. orientation, polarised fluoresc. investig., deform. mechanism 77−52440
- pyrene, excimer form. process, ps laser fluoresc. obs. 79−11448
- pyrene, triplet state, excitonic energy transfer, phosphoresc. and delayed fluoresc., 2 to 300K 80−84776
- pyrene cryst., delayed fluoresc., mag. field effect, sense depend. 77−73160
- pyrene crystals, anomalous emission excited near absorption edge 80−100682
- pyrene-3-sodium sulphonate solubilised in didodecyldimethylammonium bromide-benzene inverted micelles 80−3417
- pyronin dye, use as fluorescent indicator of energetic state of mitochondria 77−66790
- quadratic electron-phonon interaction and impurity-ion band shape in impurity absorption and fluorescence spectra 78−6731
- quantum efficiesncie and lifetimes, environmental effects, semiclassical approach 80−7393
- quantum yield measurements, real, observed and mol. parameters, ref. soln. standards 78−32898
- quinine bisulphate, aq. soln., abs. fluoresc. quantum efficiency, optoacoustic determ. 78−16849
- quinoline, in binary solvents, luminesc. props. 80−7409
- radiation convertors, thin film waveshifter coatings 80−32574
- radiation problems, semiclassical theory 78−74684
- Raman spectra, time-resolved, fluoresc. suppression via mode-locked Ar^+ laser 77−53984

fluorescence continued
- Raman spectroscopy, fluoresc. interference, theory 77−71382
- random packed beds, local voidage meas., fluoresc. method 78−9729
- rare earth activated phosphors, for low press. fluoresc. lamps, luminesc. characts. 78−10960
- rare earth cobalticyanides, $R(Co(CN)_6)n.H_2O$, ($R=La$ to Lu), optical spectra 78−39566
- rare earth compound, crystal field and Slater parameters and coordination 78−6771
- rare earth ions in soln., absorpt. and fluoresc. spectra, book contrib. 80−45112
- rare earth orthovanadates:Eu^{3+}, ligand field parameters 78−2453
- rare earth oxyhalides: Eu^{3+}, fluorescence spectra obs. *(French)* 80−89042
- rare earth oxysulphides, R_2O_2S:$(Eu^{3+})(Tb^{3+})(Pr^{3+})$, branching ratios for fluoresc. 79−33807
- rare earth pentaphosphates:Ce^{3+},Tb^{3+}, energy transfer between dopants, excitation spectra, laser appls. 78−10961
- reflected-light fluorescence microscope, LABOVAL 2a.fl, for routine and research 80−56300
- resonance fluorescence, detailed balance, Lyapunov stability and entropy 79−13941
- resonance fluorescence, Doppler-free obs., fluorescence-line-narrowing method and improvement 79−13840
- resonance fluorescence, optical bistability and cooperative effects 79−3668
- resonance fluorescence, time and spectral resolution 77−58305
- resonance fluorescence in Markovian stochastic fields 80−83573
- resonance fluorescence of thin crystal films, superradiance 78−68573
- resonant, air pollution detection appl. *(Czech)* 78−81359
- resonant transitions in strong chaotic fields, saturation and Stark splitting 79−72542
- retinal autofluorescence in land snails 79−53103
- rhodamine 101, quenching of emission in methanol and latex particle suspensions 80−3374
- rhodamine 6G, in Triton X-100 water soln., energy migration and laser performance 77−71982
- rhodamine 6G, solns., delayed fluoresc. of simple associates 79−56847
- rhodamine B adsorbed on anthracene, electron-hole pair in external elec. field 79−73558
- riboflavin in various solvents, absorpt. spectra, relative quantum yields, electronic transitions 77−52149
- ruby:Cr, lifetimes of laser-induced population density gratings, comparison with fluoresc. lifetimes 79−64276
- ruby, energy diffusion distance, upper limit within fluoresc. lifetime 80−29789
- ruby, fluoresc. R-lines appl. to press. calibration, ambient and low temps. meas. 77−18106
- ruby, fluoresc. spectrum, appl. to glass transit fluid press. determs. 77−26321
- ruby, fluorescence line narrowing, energy transfer studies 78−84642
- ruby, heat-pulse induced energy transfer, time-resolved optical spectroscopy 77−24456
- ruby, nonradiative spectral and spatial energy transfer 77−44037
- ruby, optical energy storage and retrieval 77−73165
- ruby, optical hole burning, Stark and pump-probe studies 80−48356
- ruby, optically excited, diffusion of bottlenecked 29 cm^{-1} phonons 80−6472
- ruby, optically induced two-phonon processes connecting ^2E states 80−25443
- ruby, phonon bottleneck effect, 29 cm^{-1} phonons 78−68562
- ruby, phonon spectrum of high energy heat pulses generated in thin metal films 77−20140
- ruby, piezo-spectroscopy of exchange coupled Cr^{3+} pairs 79−33783
- ruby, quantum efficiency, photoacoustic meas. 80−73472
- ruby, radiative spectral transfer, time resolved fluoresc. 78−2900
- ruby, spatial diffusion of weakly bottlenecked 29 cm^{-1} phonons, quasi-stationary techniques 79−73996
- ruby, spin dependency of optical feeding into $\bar{E}(^2E)$ metastable doublet 79−28812
- ruby fluorescence line shift, condensed gas phase transitions obs. in diamond-anvil cell 80−73381
- ruby R_1 zero phonon line, resonance fluoresc. meas. 80−89055
- sapphire, F-centre, fluorescence decay below 75K 80−60664
- sapphire, neutron bombard., F-centre fluorescence, photoluminescence 80−100676
- sapphire, optical detection of acoustic phonons at THz freqs. 80−75320
- scanning fluorescence spectroscopy, new rapid technique and instrument 77−90650
- selective excitation of probe in luminesc. technique development for chem. analysis 80−40797
- SEM cathodoluminescence detection system for transmission optical fluorescence analysis 78−23999
- SEM cathodoluminescence microscopy, mirror detector system 78−24000
- semiconductor, impurity study by visible and far-infrared laser spectroscopy 77−74524
- semiconductor, phonon fluorescence stimulated by laser radn. 79−87504
- semiconductor-liquid junction solar cells, use of fluorescent windows in cell design 80−101114
- semiconductors, recombination processes, review 79−38088
- short fluorescence lifetime meas. by single photon counting 77−5883
- single-photon counting fluorescnece decay-time spectrometer 77−82620
- Smoluchowski equation, with Coulomb pot., appl. to fluoresc. quenching 78−73051
- sodium dodecyl sulphate micelles, diarylalkane intramolecular excimer formation, microfluidity and fluoresc. meas. 78−80791
- sodium fluorescein dil. soln., luminesc. absolute quantum yields, thermal blooming method 78−72582
- sodium fluorescein-rhodamine B, energy transfer in luminescent mixed solutions 80−103976
- sodium salicylate, UV convertor layer, fluoresc. props. *(French)* 77−4676
- sodium salicylate, vac. UV scintillators, characteristic props. at 253.7 nm 79−71525
- sodium tetraphenylborate solns., electrolyte, steady state electrochemiluminesc. or fluoresc. spectra 79−57250
- sodium uranyl acetate, fluoresc., circ. dichroism 79−38598
- solar energy conversion, fluorescent collectors, principles and feasibility *(German)* 79−70462
- solar EUV spectrum, CO fluoresc. obs. 78−93184

fluorescence continued
solar EUV spectrum, H_2 fluoresc. from H Lyman α excitation 79—16908
solar transition region, Bowen fluoresc. rel. to electron density determ. 78—93179
solid, impurity atom fluoresc. radiation, intensity correlation, low temp. limit 80—80847
solid, photoacoustic measurement of absolute quantum efficiencies 79—19924
solid and liquid samples, composition determ. using Neva spectrofluorometer 79—30576
solid laser dynamics, Auger recombination effects 80—69398
solid solutions, inhomogeneity and site selective impurity-phonon coupling effects 78—84625
solid surface fluorescence analysis, calibration curves 78—31719
solution, fluorescence energy transfer in the rapid-diffusion limit 79—92151
solution, multicomponent, excitation energy transfer 78—84621
solutions, containing quenching agents, emission spectra, temp. effects *(Russian)* 78—15227
solutions, quantum yields, optoacoustic determ. 77—12415
solutions and suspensions, polarised fluoresc. in elec. field, mol. props. deriv. 80—84785
specific volume meas., for ruby R_1 fluoresc. press. gauge calibration, 0.06-1 Mbar 78—70150
spectral files, for chem. characterisation, data compression by Fourier transformation 78—35744
spectrofluorimetric system, multifunctional, for luminesc. meas. 78—80811
spectrometer system for investigating light polaris. dynamics in nanosecond band 79—2834
spectrometry, anal. appls., historical review 78—93507
spectrometry, beam splitter and cell window errors 80—31897
spectrophotometric detection system for HPLC 78—48737
spectroscopy, advantages at low quantum efficiency 77—52684
spectroscopy using pulsed lasers, time-resolved 80—57393
sputtered particle light emission, review 80—35036
stilbene:rhodamine-6Zh, luminesc. of adsorbed mols., excitonic energy transfer to surface 78—31255
trans-stilbene, cryst., triplet excitons, $S_0 \rightarrow T_1$ transition 78—76518
styrene-phenylacetylene copolymer, fluoresc. emission, energy redistrib. 78—39580
subnanosecond decays, meas. by sampled single-photon detect. 78—21219
subnanosecond fluorescence lifetime meas., photon counting system 77—2699
superconductor, nonequilibrium excitation of quasiparticles and phonons 77—43783
superfluorescent systems, fluctuations, semiclassical theory 77—58301
superradiance in solid state physics, review 79—51988
surface, meas. by SPEKOL spectrocolorimeter 79—80664
synchrotron radiation, appls. 78—74825
synchrotron radiation with single photon counting or phase shift techniques, for fluoresc. lifetime meas. 79—13841
tellurate perovskites, $M_2^{2+}Y^{2+}TeO_6$, M=Ba,Sr,Ca,Cd, Y=Ba,Sr,Ca,Cd,Zn,Mg, luminesc. on activation by Eu^{3+}, Tb^{3+}, Dy^{3+}, Er^{3+} 79—4838
tellurite glass:Nd^{3+}, spectral behaviour under narrow-line excitation 79—33747
tellurite glass:Tm^{3+}, eigenstates and radiative transition probabilities calcs. 77—77265
terbium chelate solns., fluoresc. quenching by voltage appl. 79—87498
ternary solutions, spectral relax. of fluoresc. 79—65920
p-terphenyl, cryst., highly excited states decay, mag. field effects 78—10962
p-terphenyl, fluoresc. quenching by 4-aminobenzophenone in different dielec. const. solvents *(German)* 79—83030
p-terphenyl, single cryst., delayed fluoresc., mag. field depend., 130-300K 79—69879
p-terphenyl, substituted, dye laser and spectral characts., output power, conversion efficiency 80—23681
p-terphenyl, vac. UV scintillators, characteristic props. at 253.7 nm 79—71525
p- terphenyl cryst., low lying single state 80—97320
tetrabenzo[a, cd, j, lm]perylene evaporated film, crystn., time depend. as function of purity 80—88449
tetrabutylammonium europium yttrium isothiocyanate, conc.-depend. electron-phonon coupling, and self-quenching 80—60657
tetracene:pentacene, exciton migration, picosec. meas. 78—15207
tetracene:pentacene, pressure-induced phase transition, mag. field effect on guest fluoresc. 79—33083
tetracene:pentacene, thermally activated heterofission, fluoresc. 77—85787
tetracene, cryst., fluoresc. decay time, synchrotron radiation excitation 77—4675
tetracene, cryst., prompt fluoresc., mag. field depend. 77—85788
tetracene, cryst., solid-state transitions, Raman spectra, prompt fluoresc. in mag. field 79—99865
tetracene, cryst., triplet exciton pair kinematics, diffusion model, prompt fluoresc. decay 78—79931
tetracene, disordered, vapour deposited on glass substrate, fluoresc. and energy transfer 80—84761
tetracene, fluoresc. time decay, exciton interaction depend. 77—8618
tetracene, fluorescence, effect of weak external electric field *(Russian)* 78—80416
tetracene, press.-induced phase transition, fluoresc. mag. field depend. 77—1728
tetracene, single cryst., exciton interactions, ps laser pulse intensity depend. 77—63448
tetracene, singlet exciton fission, kinematic theory 78—87913
tetracene, singlet exciton fission and fluorescence, mag. field depend. 78—39026
tetracene, triplet exciton diffusion and double photon absorpt., delayed fluoresc. obs. 77—36287
tetracene, unrelaxed fluoresc., direct picosecond obs. 80—89046
tetracene in alcoholic glasses, laser-induced hole burning mechanisms, zero-phonon fluoresc. 78—43912
tetracene surface states, electric field effects, exciton-charge carrier interactions *(Russian)* 80—24989
1,2,4,5-tetracyanobenzene, CT complex in micellar soln., fluoresc. and photolysis study 79—61911

fluorescence continued
tetramethylammonium manganese chloride, energy migration rel. to impurity trap behaviour 77—55811
N,N,N′,N′-tetramethylparaphenylenediamine, recomb. fluoresc., elec. field quenching 78—92107
thin layer chromatography, luminesc. meas. methods 78—53305
three two-level atoms system, continuously incoherently-pumped, radiation rate, spectrum 80—5716
thymine film, polycryst., energy conversion processes, quantum yields, 4 to 10 eV 80—88589
Time dependence of long-range energy transfer 78—27281
time development of fluorescence in presence of traps, general theory 80—11478
time-dependent fluorescence, anal. by method of modulating functions 78—48715
time-resolved spectroscopy using pulsed laser excitation source 80—9051
toluene-1-hexene(1-pentene), radiolysis at 77K, fluoresc., energy transfer processes 78—20037
tryptophan soln. containing histidine, fluoresc. rel. to soln. pH 80—2826
two-photon absorption in liquids, optical system 79—17500
tyrosine fluorescence at 345 nm in proteins lacking tryptophan 79—39360
ultratrace inorganic ion determination by laser excited fluoresc. 79—34372
underwater chlorophyll *a* fluorescence sensing, sunlight penetration depth estimation 79—79874
uniaxial liq. crystal polarised fluoresc. emission 80—80838
uranyl salts, cryst., multiphonon relax. 80—15208
ureilite meteorites, fluorescent accessory phases in carbonaceous matrix 79—40143
UV laser 2-photon excited fluorescence detector, for high pressure liq. chromatography 78—7266
UV laser possible pumping by synchrotron radiation, NaCl:I(Br) luminesc. 78—66835
UV photography and fluoresc. photography techniques 80—18033
Venus upper atmosphere, solar Lyman α fluoresc. scatt. rel to dayglow spectrum 1250 to 1430 Å 80—77311
very weak, photon correlator for meas. transient waveforms 80—87250
video fluorometer, computer-controlled, multichannel, features 79—20495
N-vinylcarbazole-1-vinylnaphthalene copolymer, triplet-triplet annihilation carrier photocurrent, delay fluoresc. 78—2513
virus size measurement using optical microscope, Virometer design 78—61296
viscous solution, conc. depolarisation of fluoresc. *(Russian)* 77—85799
water, fluorometric dye meas. background variation expts. 80—45844
water pollutants, airborne monitoring by fluorescence spectroscopy 79—2397
zero-phonon impurity lines in absorption and fluorescence spectra, temp. broadening and shift 77—8643
zinc porphin, in n-alkane crystals. at 4.2K, Zeeman spectra for Jahn-Teller instability 78—27256
zinc porphin in n-octane, population hole-burning using triplet reservoir 79—87491
$AgUO_2(NO_3)_3$, fluoresc. decay rates, temp. depend. 80—25429
Al_2O_3 anodised film, surface impregnated by organic phosphors, fluoresc. spectrum *(Japanese)* 80—55170
Al_2O_3, sintered, residual stress meas., piezospectroscopic technique 78—52704
η-Al_2O_3, surface, laser Raman fluoresc. background, OH^- excitation 78—10875
Al_2O_3:Cr^{3+}, ruby, reson. scatt. and trapping of 29 cm^{-1} acoustic phonons 80—93403
Al_2O_3-La_2O_3:Eu^{3+} system, optical and struct. exam. 77—4674
β-Al_2O_3-Na_2O:Cr, absorpt. and emission spectra, mag. susceptibility 79—15495
Al_2O_3-P_2O_5:Nd^{3+} glass, high Nd conc., spectroscopy and lasing obs. 78—46609
Al_2O_3-SiO_2 glass ceramic, surface streaks and blisters, UV fluoresc. study 80—84347
$3Al_2S_3.La_2S_3$:Ho^{3+}, radiative and multiphonon relax. 79—33794
^{75}As, nucl. reson. fluoresc. meas., spins and level widths determ. 77—61379
BCl_3, visible fluoresc., IR laser induced, acousto-optical effects *(Chinese)* 79—78733
$BaBr_2$:Sm^{2+}, radiationless coupling, $4f^55d$ band effects, spectra 77—8627
$BaBr_2$:Sm^{2+}, spectra, ^5D states, Lauer-Fong formula and SCC model 79—15513
$Ba_{15}Ca_{27-x}Nd_xAl_{31}Be_{27}F_{231+x}$, $0 \leq x < 8$, optical props. and vitreous domain 79—65820
$BaCl_2$:Sm^{2+}, radiationless coupling, $4f^55d$ band effects, spectra 77—8627
$BaCl_2$:Sm^{2+}, spectra, ^5D states, Lauer-Fong formula and SCC model 79—15513
BaClF:Sm^{2+}, energy levels, optical props. 78—84631
BaClF:Sm^{2+}, radiative and radiationless transition rate meas. using tunable pulsed dye laser 77—24891
BaF_2:Er^{3+}, fluoresc., importance of defect clustering 79—33827
BaF_2:Er^{3+}, fluoresc. spectra of charge compensated cryst., multiphonon and energy transfer relax. 79—87496
BaF_2:Er^{3+}, single-site multiphonon and energy transfer relax. 78—52547
BaO-B_2O_3 glass, $Mn^{2+} \rightarrow Nd^{3+}$ energy transfer, fluoresc. obs. 77—8621
BaO-B_2O_3: UO_2^{2+}, Eu^{3+} glass, nonradiative energy transfer 77—59602
BaO-B_2O_3:UO_2^{2+}, Nd^{3+} glass, radiative and nonradiative energy transfer 78—60508
BaO-B_2O_3:$UO_2^{2+} \rightarrow Er^{3+}$ glass, energy transfer 78—2895
BaS:Cu, thermoluminesc. and decay 78—80426
BaS-CaS:Cu phosphors, X-ray diffr. and fluoresc. spectra 80—40148
Ba*+Ba*, radiative collisional fluoresc. at sum freq. 79—18261
BeF_2:Eu^{3+} glass, struct., Monte Carlo simulations 80—96448
BeF_2:Pr^+, glass, optical homogeneous linewidths 80—7395
BeF_2-KF-CaF_2-AlF_3:Nd^{3+} (Er^{3+}) glass, multiphonon relax., fluoresc. obs. 78—15219
BeF_2-KF-CaF_2-AlF_3-EuF_3 fluoroberyllate glass, Eu^{3+} fluoresc. linewidth 80—66285
$Bi_2Al(Ga)_4O_9$, fluoresc. and X-ray data 78—80403
$Bi_4Ge_3O_{12}$, temp. depend. luminesc. meas. 77—20910
$Bi_4Ge_3O_{12}$:Er^{3+}, host-sensitised energy transfer, laser time resolved spectroscopy 79—83013
$(CH_4)NMnCl_3$, nearly-one-dimensional cpd., energy migration rel. to impurity trap behaviour 77—55811
$(CH_3)_4NUO_2(NO_3)_4$, fluoresc. decay rates, temp. depend. 80—25429
$CaCO_3$, Iceland spar natural crystals, optical characts. 77—10988

fluorescence continued

- CaF_2, optical detection of acoustic phonons at THz freqs. 80−75320
- $CaF_2:Dy^{3+}$, fluoresc. spectra, A-centres and B-centres, Stark levels 80−25428
- $CaF_2:Dy^{3+}$, high temp. fluorescence using Ar^+ and N_2 lasers 78−56514
- $CaF_2:Er^{3+}$, fluoresc. spectra of charge compensated cryst., multiphonon and energy transfer relax. 79−87496
- $CaF_2:Er^{3+}$ laser fluoresc. of Er^{3+} sites, defect equilibria 78−6748
- $CaF_2:Eu^{2+}$, tunable optical detection and generation of THz phonons 79−65149
- $CaF_2:Ho^{3+}$, fluoresc., relative intensities, lifetimes 78−27296
- $CaF_2:Ho^{3+}$, site-selective spectroscopy 80−29791
- $CaF_2:Pr^{3+}$, multisite system, laser selective excitation and energy transfer 78−84634
- $CaF_2:Sm^{2+}$, phonon spectrum of thermal pulses by fluorescence 79−95860
- $CaF_2:Yb^{2+}$, luminesc. polarisation, elastic uniaxial compression effect, radiative state model 78−6739
- $CaF_2:Yb^{3+}$, Er^{3+}, and CdF_2-$CaF_2:Yb^{3+}$, Er^{3+}, IR to visible upconverting system 77−44035
- $CaF_3:Ho^{3+}$, laser excited fluoresc. rise and decay meas., expt. 80−22448
- CaO F-centre luminesc. and PMDR 79−95832
- CaO, photoionisation of F-centre, luminesc. and photocond. meas. 80−66270
- CaO-Li_2O-Al_2O_3-$SiO_2:Nd^{3+}$, CaO enriched, laser-type glasses, spectroscopic behaviour 78−60497
- CaO-Li_2O-B_2O_3, calibo glass, Dy^{3+} alone and in presence of Ho^{3+}, nonradiative energy transfer 79−65925
- CaO-Li_2O-B_2O_3 calibo glass, diffusion limited energy transfer from $Tb^{3+} \rightarrow Ho^{3+}$ 78−31235
- CaO-Li_2O-$B_2O_3:Dy^{3+}$ glass, optical excitation energy transfer from $Dy^{3+} \rightarrow Nd^{3+}$ 79−15515
- CaO-Li_2O-B_2O_3:Er, Tb, calibo glass, nonradiative energy transfer 78−19541
- $Ca(PO_3)_2:Eu^{3+}$, amorphous, phonon-assisted site-to-site electronic energy transfer, fluoresc. line narrowing obs. 77−81140
- $Ca_5(PO_4)_3F:Nd^{3+}$, optical fluorescence intensity and cryst. field parameters 78−52570
- $Ca_5(PO_4)_3F:Nd^{3+}$ site symmetries, EPR and spectral obs. 78−6571
- CaS:Ce, Na, photon sidebands in emission and excitation spectra, pseudolocalised vibrs. 79−28800
- CaS:Mn,Ce, phosphor, fluoresc. spectrum, fine struct., $^4T_{1g}(^4G) \rightarrow {}^6A_1(^6S)$ transition 80−45130
- CaS:Tb,Eu phosphors, fluoresc. spectra under X-ray excitation 80−16083
- CaS-Pb,Mn, phosphors, thermoluminesc. and fluoresc. spectra 78−64396
- $CaSO_4$ phosphors:Ce(Eu)(Dy)(Tm), gamma-irradiated valency conversions in rare-earth ions 80−55198
- $CaSO_4$:Ce(Eu) phosphors, fluorescence spectra, thermolum. glow curve 80−2879
- $CaSO_4$:Dy, thermolum. origin, test of model on $CaSO_4$:Eu 77−85813
- $CaSO_4$:Sm phosphors, X-ray induced fluorescence and phosphorescence 80−55179
- $CaWO_4:Nd^{3+}$, thermal behaviour of shape and width of 9145 Å laser line 78−6755
- $CaY_2Ge_3O_{12}$:Nd, energy levels and laser action, fluoresc. meas. 79−81438
- $CaY_2Mg_2Ge_3O_{12}:Nd^{3+}$, optical absorpt. and fluoresc. intensities 80−29793
- Cd complex, Cd (II) halide with 8-aminoquinoline, cryst. 77−52152
- $CdF_2:Er^{3+}$, selective monochromatic excitation of $^4S_{1/2}$-$^4I_{15/2}$ transition *(French)* 77−85765
- $CdF_2:Er^{3+}$, Tm^{3+}, evidence for $Er^{3+} \rightleftharpoons Tm^{3+}$ energy transfers, fluoresc. expts. 80−60655
- $CdF_2:Eu^{3+}$, luminesc. spectra conc. and annealing depend. 79−65917
- $CdF_2:R^{3+}$, cooperative luminescence influenced by symmetry of centres 78−6791
- CdS, biexciton fluoresc. line shape 77−44059
- CdS:Cl, heavily doped, fluoresc. spectrum upper threshold calculated 78−52568
- $Cl^{q+}+Cu$, K X-ray production and radiative electron capture, fluoresc. yield determ. 80−99553
- Cr complex, organic mol. singlet excited state energy transfer to complex quartet levels 77−25291
- CsBr:Th, absorpt., excitation, fluorescence spectra 79−43032
- CsF, EPR of self trapped exciton and MCd meas. 77−48091
- $CsMnF_3$, exciton-magnon interactions in optical transition, absorpt. and emission spectra meas. 80−70981
- $Cs_2NaBiCl_6$, optical props. 78−68549
- $Cs_2NaEuCl_6$, mag. dipole transitions $^5D_3 \rightarrow {}^7F_4$, interpretation 79−42505
- Cs_2NaYCl_6:Re,Tm, fluorescence, two-step blue up-convertors 78−95603
- $Cs_2UO_2Cl_4$, fluoresc. decay rate of pure and impure cryst. 79−47487
- $Cs_2UO_2Cl_4$, low-lying excited electronic levels, fluoresc. decay meas. 79−47491
- $CsUO_2(NO_3)_3$, fluoresc. decay rates, temp. depend. 80−25429
- $CuAl_5S_8$, cryst. growth, struct., and fluoresc. 77−48328
- $CuInS_2$, optical and elec. phenomena 78−39605
- Cu_2S-Ga_2S_3 alloys, cryst. growth, struct. and fluoresc. 77−48328
- 1,6-di-(N-carbazolyl)-2,4 hexadiin, cryst. struct., luminesc., γ-ray polymerisation 78−18629
- ErAlG:Ho, Tm, Et$\rightleftharpoons$Ho and Er$\rightleftharpoons$Tm energy transfer, fluorescence meas. 78−27305
- ErP_5O_{14}, single cryst., radiative and non-radiative transitions 79−19920
- Eu complex, benzoyltrifluoro-acetone-chelate, refr. index determ. of fluoresc. films 80−40175
- Eu complex, europium benzoyltrifluoroacetane chelate layers, fluorescence lifetime changes induced by variable optical environments 80−93386
- Eu complex Eu dibenzoylmethane chelate with piperidine, vibronic and IR spectra 79−82981
- Eu^{3+} fluoresc. lineshape in glass, temp., time and conc. depend., two-phonon Raman scatt. 78−64406
- EuP_5O_{14}, 4f-level press. depend., fluorescence exam. 77−72841
- $F+H_2(D_2)$, absolute rate coeffs. at 295-265K 80−81303
- $F_2+SiH_4(SiD_4)(Si)$, chemilum., at. absorption, and laser-induced fluoresc. obs. 80−3315
- $Fe_3[Co(CN)_6]_2.12H_2O$ struct. dehydration fluorescence and IR studies 80−28976
- GaAs, polariton fluoresc., spatial and spectral features 79−33760
- GaAs, reson. polariton fluoresc. obs. 77−85785
- GaP:N, excited states of excitons bound to NN_i pairs, fluoresc. obs. 77−44039

fluorescence continued

- $(GaP)_x(ZnS)_{1-x}$ solid solutions, X-ray fluorescence spectra, photoluminescence *(Russian)* 79−74003
- $3Ga_2S_3.La_2S_3:Ho^{3+}$, radiative and multiphonon relax. 79−33794
- $GdAlO_3:Cr^{3+}$, mag. field effects on fluoresc. 80−2850
- $GdBr_3$, frozen aq. soln., fluoresc. and absorpt. spectra 79−43022
- $GdCl_3$, frozen aq. soln., fluoresc. and absorpt. spectra 79−43022
- $Gd(ClO_4)_3$, frozen aq. soln., fluoresc. and absorpt. spectra 79−43022
- $Gd_3Ga_5O_{12}:Nd^{3+}$, optical absorpt. and fluoresc. intensities 80−29793
- $GdVO_4:Eu^{3+}$, absorption and fluoresc. spectra, SU(2) chain *(French)* 78−28912
- $GeO_2:Pr^+$, glass, optical homogeneous linewidths 80−7395
- H_2, plasma, resonance fluorescence diagnostics 80−48971
- $Hg_{3-x}AsF_6$, supercond., absence of surface Hg 80−20350
- HgI_2, cooperative fluoresc. by excitonic reson. pumping 79−33732
- $KAlSi_3O_8$:rare earth ion, glass, nonradiative energy transfer and fluoresc. quenching 77−20905
- $KBr:Ga^+$, luminescence decay times, fluorescence kinetics, 1.6-300K 79−33825
- $KBr:I^-$, OH^-, luminesc. of interstitial atomic H 80−89062
- KBr:In, type A long-wave luminesc., polarisation obs. 78−10944
- KCl, with colour centres, laser stimulated luminesc. 78−6749
- $KCl:Au^-$, fluorescence, stress and mag. field depend., Jahn-Teller effect and relax. processes 77−48220
- $KCl:Eu^{2+}$, radiationless processes 78−80391
- $KCl:Eu^{2+}$, zero phonon lines, time-resolved fluoresc. spectra 77−77269
- $KCl:Eu^{2+}$ crystals, photostimulated afterglow investigation at room temp. 80−108259
- $KCl:I^-$, H, fluorescence of interstitial H-centres 79−73987
- $KCl:Sm^{2+}$, spectra, ^5D states, Lauer-Fong formula and SCC model 79−15513
- KCl:Tl, 375 nm emission band 79−95834
- $K_5Eu(MoO_4)_4$, electric dipole transition cross section and effective site symmetry of Eu^{3+} 78−52556
- KI:In(Tl), type A long-wave luminesc., polarisation obs. 78−10944
- $KMgF_3$:Ni, Ni-Ni pair optical spectra 80−45042
- $KMgF_3:Yb^{3+}$, cryst. field parameters, optical, EPR spectra, spin-lattice relax. time 77−51950
- $KMnF_3$, exciton dynamics by time resolved emission spectroscopy 80−54615
- K_2MnF_4-Ni^{2+}, and undoped, magnon spectra, Raman, far IR and fluorescence meas. 77−20573
- $KNdP_4O_{12}$, determ. of fluoresc. quantum efficiency and laser emission cross sections 80−48264
- $KNdP_4O_{12}$, laser emission cross sections, fluorescence spectra, radiative lifetimes, quantum efficiency 80−23694
- K_2O-BaO-$SiO_2:Nd^{3+}$ glasses, absorption and fluoresc. spectra, density 80−25417
- $K_2UO_2Cl_4$, fluoresc. decay rate of pure and impure cryst. 79−47487
- $KUO_2(NO_3)_3$, fluoresc. decay rates, temp. depend. 80−25429
- $K_2UO_2(NO_3)_4$, fluoresc. decay rates, temp. depend. 80−25429
- $KY_3F_{10}:Eu^{3+}$, fluoresc. intensity, 77 to 4K, cryst. field parameters of Eu^{3+} 78−72580
- $KZnF_3:Ni^{2+}$, mechanism of conc. quenching of fluoresc. from T_{2g} of Ni^{2+} 77−59605
- $KZnF_3:Yb^{3+}$, cryst. field parameters, optical, EPR spectra, spin-lattice relax. time 77−51950
- $((La,Lu)O)_2S:(Eu^{3+})$, spectra 79−64957
- $La_2Be_2O_5:Nd^{3+}$, optical absorpt. and fluoresc. intensities 80−29793
- $LaBr_3:Np^{3+}$, energy level anal., polarised absorpt. and fluoresc. spectra 80−76056
- $LaBr_3$:Pr, continuous wave and pulsed laser pumped Pr IR quantum counters 79−93219
- $LaBr_3:Pr^{3+}$, laser-induced fluoresc. line-narrowing, hyperfine struct. and Zeeman effect 77−85789
- $LaBr_3:U^{3+}$, luminesc., fluoresc. lifetimes 79−33768
- $LaCl_3:Np^{3+}$, energy level anal., polarised absorpt. and fluoresc. spectra 80−76056
- $LaCl_3:Np^{3+}$, phonon-induced relax. in excited optical states, linewidth temp. depend. meas. 80−100688
- $LaCl_3$:Pr, continuous wave and pulsed laser pumped Pr IR quantum counters 79−93219
- $LaCl_3:Pr^{3+}$, hyperfine Zeeman effects, fluorescence line-narrowing technique 77−62881
- $LaCl_3:Pr^{3+}$, second order Zeeman hyperfine effect *(French)* 77−52162
- $LaCl_3:Pr^{3+}$, Zeeman second-order effects, fluoresc. line narrowing technique 80−16103
- $LaCl_3:U^{3+}$, cryst., spectrum anal., cryst. field parameters 80−76057
- $LaF_3:Ce^{3+}$, UV fluoresc. potential tunable laser 2760 to 3220 Å 78−15206
- $LaF_3:Dy^{3+}$, $^4F_{9/2}$ and $^4I_{15/2}$ levels, radiative decay rates 79−61415
- $LaF_3:Dy^{3+}$, high temp. fluoresc., Dy^{3+} G-level emission 78−27295
- $LaF_3:Dy^{3+}$, laser excited fluoresc., lifetimes meas. 79−24353
- $LaF_3:Er^{3+}$, optically excited, direct-process spin-lattice relaxation 80−93378
- $LaF_3:Eu^{3+}$, absorpt and laser fluoresc. spectra 77−52159
- $LaF_3:Ho^{3+}$, laser excited fluorescence absorption spectra, symmetry groups 78−60514
- $LaF_3:Ho^{3+}$ single crysts., multiphonon relax., fluoresc. obs. 79−47495
- $LaF_3:Ho^{3+}(Dy^{3+})$, laser excited fluoresc. rise and decay meas., expt. 80−22448
- $LaF_3:Nd^{3+}$, laser-excited fluoresc., self-adsorpt. 78−15210
- $LaF_3:Nd^{3+}$, luminesc. decay times 80−2811
- $LaF_3:Nd^{3+}(Er^{3+})(Tm^{3+})$, VUV fluorescence and tunable coherent sources from 1650 to 2600 Å 77−688
- $LaF_3:Pr^{3+}$, fluoresc., time resolved excitation technique 79−95820
- $LaF_3:Pr^{3+}$, laser-induced fluoresc. line narrowing 77−40280
- $LaF_3:Pr^{3+}$, Nd^{3+}, fluorescence linewidth and energy transfer 77−8635
- $LaNbO_4$, Raman scatt. and fluoresc. spectra 80−20625
- $LaPO_4$:Bi, fluoresc. props., blue emission mechanism 79−52002
- $La_{1-x}Pr_xP_5O_{14}:Pr^{3+}$, fluorescence spectrum 79−83014
- $La_2S.3GaS_3:Ho^{3+}$, fluoresc., visible and IR spectra assignments 77−52150
- $La_2S_3.3Ga_2S_3:Er^{3+}$ glass 78−23514
- $LiAl_5O_8:Cr^{3+}$, fluoresc. and excitation spectra, zero phonon lines 79−33785
- LiCl:Ag, fluoresc. and UV absorpt. spectra 80−80844
- $LiF:U^{3+}$, absorption and laser-excited fluoresc. 79−99927
- $LiGa_5O_8:Cr^{3+}$, fluoresc. and excitation spectra, zero phonon lines 79−33785
- $LiNbO_3$, exciton migration, laser time-resolved spectra obs. 79−69861

fluorescence continued
- $LiNbO_3$, luminesc. props., Li/Nb ratio effect 80—97323
- $LiNd(PO_3)_4$ laser with external and Fabry-Perot resonators, 1.05, 1.32 μm CW oscill. 80—23693
- $LiNdP_4O_{12}$ laser, fluoresc. and oscill. characts. at 1.317 μm 78—5473
- $LiNdP_4O_{12}$, laser emission cross sections, fluorescence spectra, radiative lifetimes, quantum efficiency 80—23694
- Li_2O-B_2O_3:Eu^{3+} glass, laser induced fluoresc. line narrowing, struct. 79—38613
- $LiY_{1-x}Eu_xP_4O_{12}$ phosphor, prep. and fluoresc. 77—48219
- $LiYF_4$:Ce^{3+}, laser transition at 325 nm, large fluoresc. linewidth 79—72574
- $LiYF_4$:$Nd^{3+}(Er^{3+})(Tm^{3+})$, VUV fluorescence and tunable coherent sources from 1650 to 2600 Å 77—688
- $LiYF_4$:Pr^{3+}, mag.-dipole transitions obs. in fluoresc. 80—11451
- $LiYF_4$:Pr^{3+}, polarized absorpt. and fluoresc. spectra, 10 to 300K, energy levels and live intensities 79—95836
- $LiYF_4$:Pr^{3+}, spectroscopic determ. of ground config. energy levels 80—34969
- $LiY_{1-x}Tb_xP_4O_{12}$ phosphor, prep. and fluoresc. 77—48219
- $Li_{14}ZnTa_4O_{18}$:Eu, fluorescence and cryst. symm. 77—24886
- LuF_3:Ce^{3+}, UV fluoresc. potential tunable laser 2760 to 3220 Å 78—15206
- LuF_3:$Nd^{3+}(Er^{3+})(Tm^{3+})$, VUV fluorescence and tunable coherent sources from 1650 to 2600 Å 77—688
- $Lu_{2-x}Si_2O_7$:Eu_x, synthesis and spectroscopic study 80—84846
- $LuVO_4$:Eu^{3+}, absorption and fluoresc. spectra, SU(2) chain *(French)* 78—28912
- MgO, surface, laser Raman fluoresc. background, OH^- excitation 78—10875
- MgO:Cr^{3+}, axial centres, EPR and fluoresc. meas. 78—2731
- Mn complexes, verification of laws of luminesc. of solids 78—60506
- MnF_2, biexciton decay, time resolved laser spectra 78—75999
- MnF_2, fluorescence props. 79—73994
- MnF_2:$Eu^{3+}(Er^{3+})$, fluorescence props. 79—73994
- MnF_2:Ni^{2+}, IR fluoresc., field depend., exchange energy 78—68543
- MnF_2:Zn, shift and broadening of optical transitions 79—38579
- NH_4Br:Tl, absorption, excitation and fluorescence spectra 79—33824
- $NH_4UO_2(NO_3)_3$, fluoresc. decay rates, temp. depend. 80—25429
- Na vapour, saturation of transient reson. nonlinear processes 77—68243
- Na-He model pot. calcs., fluoresc. line profile 79—36723
- NaBr(I), optically activated F→F′ centre conversion in mag. field 80—108253
- NaF, with colour centres, laser stimulated luminesc. 78—6749
- $Na_3La_{1-x-y}Ce_xTb_y(PO_4)_2$, optical props. *(French)* 80—103991
- $NaNO_2$, cryst., delayed fluoresc., triplet excitons, dopant effects 78—10963
- $NaNdP_4O_{12}$, laser emission cross sections, fluorescence spectra, radiative lifetimes, quantum efficiency 80—23694
- $Na_2Nd_2Pb_6(PO_4)_6Cl_2$, high-Nd conc. laser material, oscillator strengths and laser effect 79—55140
- Na_2O-Al_2O_3-P_2O_5:Eu glasses, fluorescence line narrowing meas. *(French)* 80—34975
- Na_2O-B_2O_3 glass, $Eu^{3+}\rightarrow Nd^{3+}$ diffusion-limited energy transfer, quantum efficiency 78—31238
- Na_2O-BaO-SiO_2:Nd^{3+} glasses, absorption and fluoresc. spectra, density 80—25417
- Na_2O-CaO-SiO_2:UO_2, energy spectrum of UO_2 ions, fluoresc. and absorption spectra 77—66531
- Nd crystals, determ. of fluoresc. quantum efficiency and laser emission cross sections 80—48264
- Nd^{3+} in glass and cryst. hosts, fluoresc. branching ratios 78—29956
- Nd:glass laser, mode-locked, ultrashort pulse duration meas., two-photon fluoresc. 79—27302
- Nd^{3+}:glass, fluoresc. line narrowing, hole burning and ion-ion energy transfer 79—89912
- Nd^{3+}:glass, laser induced fluoresc. line narrowing, site depend. 79—33819
- Nd^{3+}:$LaCl_3$, laser-induced fluoresc., hyperfine structs. 80—100677
- Nd^{3+}:$LaCl_3$, laser-induced fluoresc. energy transfer effects 80—100678
- $NdAl_3(BO_3)_4$, LPE for thin film miniature lasers 79—74101
- $Nd(Ga,Cr)_3(BO_3)_4$, cryst. growth by LPE, Nd^{3+} fluorescence, lattice constants 80—29883
- Nd_2O_3-Y_2O_3-As_2O_5 glass, spectroscopic props., rel. to possible appl. in lasers 78—84624
- NdP_5O_{14}, fluoresc. decay times meas. 79—8187
- NdP_5O_{14}, fluoresc. lifetime meas., IR and photoacoustic spectroscopy 80—60652
- NdP_5O_{14} laser, flashlamp excited, emission cross section at 1.32 μm 79—59701
- NdP_5O_{14}, laser site-selection time-resolved spectroscopy 78—76524
- NdP_5O_{14} single crystals, fluoresc. decay times, excitation density effect 80—7390
- NdP_5O_{14}, spectral line intensity anal. 78—43888
- $NdTa_7O_{19}$:$Nd^{3+}(^4F_{3/2})$, fluorescence intensity and lifetime rel. to mini laser prod. *(French)* 77—71988
- $Nd_xY_{1-x}P_5O_{14}$, conc. quenching 79—61435
- $Nd_xY_{1-x}P_5O_{14}$, fluorescence quenching 77—69903
- $Nd_xY_{1-x}P_5O_{14}$, fluoresc. conc. quenching, decay rate consts. 78—64404
- $Nd_xY_{1-x}P_5O_{14}$, fluoresc. energy transfer and radiationless relax. 79—38625
- P_2O_5-glass, diffusion of Cu^+, fluoresc. meas. 78—59980
- P_2O_5-K_2O-CdO-Na_2O glass:Nd^{3+}, highly doped, spectroscopic props. and CW laser action *(French)* 79—41385
- P_2O_5-R_2O_3-$M_2O(M'O)$, (M=alkali metal, M′=alkaline earth, R=Y or rare earth), metaphosphate glass phosphors, fluoresc. props., activation conc. effect 80—89058
- $POCl_3$:Pr^{3+}, fluoresc. and lifetimes of excited states 80—71466
- $POCl_3$:$ZrCl_4$:$Nd^{3+}(Er^{3+})$, radiative transition probabilities within 4f configs. 77—8617
- $POCl_3$-$SnCl_4$, Sm^{3+} fluoresc. quenching temp. depend., near reson. interaction 79—65915
- $POCl_3$-$SnCl_4$: Tb^{3+}, Sm^{3+}, lifetime and quantum yield of fluoresc. emission 77—20909
- $POCl_3$-$ZrCl_4$:Yb^{3+}, Er^{3+}, energy transfer from Yb^{3+} to Er^{3+}, agglomeration formation 78—64405
- PbI_2, cooperative fluoresc. by excitonic reson. pumping 79—33732
- PbI_2 laminar semicond., phase transition of first kind by exciton spectroscopy *(Russian)* 79—82334
- $PbMoO_4$, colour study from absorption, fluorescence and thermoluminesc. exam. 78—31245

fluorescence continued
- $PbMoO_4$, near-edge absorpt. band, fluoresc. and photocond. 77—44017
- Pm^{3+}:$POCl_3$-D_2O soln., visible and IR spectra, fluoresc. assignments *(French)* 77—66514
- Pr based, IR quantum counter imaging system, resolution, sensitivity 79—81541
- Pr^{3+}-based IR quantum counters, photon avalanche 79—97431
- $PrCl_3$, spectral energy transfer 78—19550
- PrF_3, spectral energy transfer 78—19550
- $Pr_{0.2}La_{0.8}F_3$, fluorescent line narrowing, time depend. effects 78—31244
- $Pr_xLa_{1-x}P_5O_{14}$, laser emissions, fluoresc. 79—72572
- PrP_5O_{14}, laser emissions, fluoresc. 79—72572
- $PrVO_4$, energy levels, opt. and NMR measurements 78—80226
- $Pr_xY_{1-x}P_5O_{14}$, laser emissions, fluoresc. 79—72572
- RbBr:I^-, OH^-, luminesc. of interstitial atomic H 80—89062
- RbCl:I, H, fluorescence of interstitial H-centres 79—73987
- RbCl:Tl, origin of 3.55 eV emission band 80—7401
- $RbMg_xMn_{1-x}F_3$, impurity induced fluorescence, thermal depend. 77—85776
- $RbMnF_3$:Ni, antiferromag., exchange splitting of $^3T_{2g}E$ state, fluorescence meas. 77—12419
- $Rb_2UO_2Cl_4$, fluoresc. decay rate of pure and impure cryst. 79—47487
- $RbUO_2(NO_3)_3$, fluoresc. decay rates, temp. depend. 80—25429
- ^{187}Re in W, WSe_2 and Nb, nuclear resonance fluorescence obs. of emission line shape 77—4136
- Ru complex, $Ru(2,2'\text{-bipyridine})_3Cl_2$-$6H_2O$, photocond., optical absorpt. and fluoresc. 77—80807
- S_2 mol. $B^3\Sigma_u^- \rightarrow X^3\Sigma_g^-$ fluorescence induced by N_2 laser *(Japanese)* 80—14175
- SRF_2:Er^{3+}, laser excitation of single ion and clustered ion sites 77—69879
- Si:Li X-ray detector, escape peaks and internal fluoresc., general geometry case 77—18150
- α-SiC (6H) laser excited thermostimulated luminescence light sum dose depend. *(Russian)* 80—16111
- SiF electronic transition laser non-feasibility, from $F_2+SiH_4(SiD_4)(Si)$ spectra obs. 80—3315
- SrF_2, optical detection of acoustic phonons at THz freqs. 80—75320
- SrF_2:Er^{3+}, fluoresc. spectra of charge compensated cryst., multiphonon and energy transfer relax. 79—87496
- SrF_2:Eu^{2+}, tunable optical detection and generation of THz phonons 79—65149
- SrF_2:Sm^{2+}, spectra, ^5D states, Lauer-Fong formula and SCC model 79—15513
- SrO, neutron- or proton-irrad., F^+ centre fluoresc. yield and lifetime, 5 to 140K 80—55181
- SrO, proton, neutron irradiated, fluorescence from anion vacancies, F^+ centre model 78—48221
- SrS:Hf, phosphor fluoresc. spectra, host lattice defect 77—12416
- SrS:Zr(Zr,Mn), yellow and red fluoresc. mechanism 77—32419
- Tb, phonon spectrum, obs. of one phonon transitions by nucl. reson. fluoresc. 79—38416
- $Tb^{3+}\rightarrow Nd^{3+}(Ho^{3+})$, diffusion limited energy transfer in DMSO soln., fluoresc. obs. 79—61428
- $Tb_xY_{1-x}PO_4$, H_2 VUV laser excitation, fluoresc. decay characts. 78—60510
- TeO_2-Li_2O glass:Nd^{3+}, highly doped, spectroscopic props. and CW laser action *(French)* 79—41385
- $ThBr_4$:U^{4+}, single cryst., absorpt. and emission spectra 77—90174
- $TlR(MoO_4)_2$, (R=Eu, Dy, Er), fluoresc. spectra at 77, 300K 79—56848
- $TlR(WO_4)_2$, (R=Eu, Dy, Er), fluoresc. spectra at 77, 300K 79—56848
- Tm^{3+}, in oxide glasses, multiphonon relax. rates and fluoresc. lifetimes 77—77266
- U, laser spectroscopy, using induction heated oven 78—21230
- U, sputtered atoms, laser fluorescence spectroscopy 80—66359
- UO_2^{2+} glass, Nd^{3+} or Ho^{3+} doped, fluoresc. appl. in improved planar solar convertor 80—40904
- UO_2^{2+}, in $HClO_4$ soln., photoluminesc. intensity, conc. depends. of uranyl and H^+ 77—68069
- Xe, cryst., X-ray and photoluminesc. 79—87480
- XeF discharge laser, gain and fluorescence meas. at high energy loading 77—79844
- Y, X-ray fluorescence of L_α spectrum *(Russian)* 77—63491
- YAG:Ce^{3+}, excited-state absorpt. meas., tunable laser model system 79—42994
- YAG:Eu^{3+}, reson. fluoresc. spectra, showing multiple Eu^{3+} sites 80—2812
- YAG:Ge^{3+}, excited state absorpt. loss, 5d→4f rare earth lasers 78—90417
- YAG:Mn, impurity-induced O^- colour centres, absorpt. and fluoresc. spectra 77—1709
- YAG:Nd, with improved fluoresc. lifetime of $^4F_{3/2}$ state 77—687
- YAG:Nd^{3+}, energy transfer between Nd^{3+} ions, laser-excited time-resolved site-selection spectroscopy 79—95839
- $Y_3(Al_{1-x}Ga_x)_5O_{12}$:Nd, fluoresc. energy transfer and radiationless relax. 79—38625
- $Y_3(Al_{1-x}Ga_x)_5O_{12}$:$Nd^{3+}$, time-resolved site-selection spectroscopy, energy transfer 80—2814
- $YAlO_3$:Cr^{3+}, fluorescence R-lines anisotropy, effective Hamiltonian parameters 77—16368
- $Y_{1-x}Eu_xP_3O_9$ phosphor, prep. and fluoresc. 77—48219
- YF_3:$Nd^{3+}(Er^{3+})(Tm^{3+})$, VUV fluorescence and tunable coherent sources from 1650 to 2600 Å 77—688
- $Y_3Ga_5O_{12}$:Nd^{3+}, energy transfer between Nd^{3+} ions, laser-excited time-resolved site-selection spectroscopy 79—95839
- $Y_3Ga_5O_{12}$:Tb^{3+}, fluoresc. and absorption spectra 77—32422
- Y_2O_3:Eu, fluoresc., cathodoluminesc. and thermal quenching 79—47488
- Y_2O_3:Eu^{3+}, absorpt. spectra, fluoresc., electron beam excitation 78—92093
- Y_2O_3:Eu^{3+}, cubic, laser-induced polarised fluoresc., Stark levels and cryst. field parameters 79—95838
- Y_2O_2S:Eu, phosphor, temp. meas. by line shift method 77—13750
- $Y_{1-x}Tb_xP_3O_9$ phosphor, prep. and fluoresc. 77—48219
- YVO_4, pure and Bi^{3+} doped, absorpt. and emission props., excitons 79—38592
- YVO_4:Eu, fluoresc., cathodoluminesc. and thermal quenching 79—47488
- YVO_4:Eu^{3+}, absorption and fluoresc. spectra, SU(2) chain *(French)* 78—28912
- YVO_4:Eu^{3+}, absorpt. spectra, fluoresc., electron beam excitation 78—92093
- YVO_4:Eu^{3+}, laser site-selection spectroscopy investigation 78—68556

fluorescence continued
$YVO_4{:}Eu^{3+}(Er^{3+})$, energy transfer, laser time-resolved spectroscopy 78−27306
$YVO_4{:}Nd^{3+}$, absorption and fluoresc. spectra of laser states 77−38900
$YVO_4{:}Nd^{3+}$, energy transfer processes, laser-excited time-resolved spectroscopy 80−84765
$YVO_4{:}Nd^{3+}$, fluoresc. lifetime of $^4F_{3/2}$ state 79−87494
Y_2WO_6, new structural type, unit cell, space group, fluorescence spectra 79−1420
$Y_2WO_6{:}Eu^{3+}$, luminesc., rel. to crystallographic data 79−33793
$Y_6WO_{12}{:}Eu^{3+}$, crystal struct., fluorescence spectra, exam. 78−52558
$(Y_{0.80}Yb_{0.19}Er_{0.01})F_3$ phosphors, IR to visible conversion 78−48210
$(Y_{0.80}Yb_{0.19}Ho_{0.01})F_3$, IR to visible conversion 78−48210
$Zn_4B_6O_{13}{:}Tb^{3+}$, fluoresc. and thermophosphoresc. spectra *(Spanish)* 77−90188
ZnO phosphor fired with Zn, luminesc. in green and red region 80−66265
ZnO, red, electronic and opt. props., electrographic props. 77−57419
$ZnO\text{-}TeO_2$ glass, Ho^{3+} or Er^{3+} doped, visible green emission 79−15523
ZnS type lattices, luminescence, constants, temperature dependence, activation energies 79−99923
$ZnS{:}Cr^+$, Fe^{3+}, luminesc., cond. and paramag. centre conc. parameters 78−6724
$ZnS{:}Eu^{3+}$, origin of red fluoresc., occurrence of rare earth oxysulphide inclusions *(French)* 77−69875
$ZnS{:}Mn^{2+}$, $^4T_1$ excited state, absorpt., MCD, Jahn-Teller model 78−43907
$ZnS{:}Mn^{2+}$, Jahn-Teller effect in fluorescent level 78−52566
$ZnS{:}Tm^{3+}$, charge compensation and polytypism influences on fluorescence 80−89051
$ZnSe{:}Cr^+$, Fe^{3+}, luminesc. cond. and paramag. centre conc. parameters 78−6724
$ZnSe{:}Mn^{3+}$, Jahn-Teller effect in fluorescent level 78−52566
ZnTe doped with group I impurities, spectra meas. 78−10949
$ZrF_4\text{-}BaF_2\text{-}NdF_3$ glass, vitreous domain, prep. and optical props. 78−27304
^{91}Zr, nuclear reson. fluoresc., γ-ray spectra 78−588

fluorescence of atoms *see atomic fluorescence*

fluorescence of molecules *see molecular fluorescence*

fluorescent lamps
biological effects, intermittent exposure effect on lifespan of human diploid fibroblasts in culture 77−77936
chromatic adaptation effects and colour appearance at various illum. levels *(Japanese)* 78−92628
colour photographic fluorescent lamp suitability evaluation by image psychophysical and subjective estimations 79−71555
colour-reference-standard fluorescent lamp with colour rendering index of 99 80−78925
high colour rendering, visual clarity investigation 78−48809
method of indirect comparison of luminous fluxes *(Polish)* 79−93200
phosphors, characts. of emission and absorption *(Japanese)* 80−89067
phosphors with aluminate host lattices, behaviour 79−11453
rare earth activated phosphors, for low press. fluoresc. lamps, luminesc. characts. 78−10960
total luminous energy transfer, scatt. medium effect 77−65577
vacuum UV fluorescence lifetime meas. instrument 77−49785
white light source for colour photography, evaluation of suitability *(Japanese)* 77−26415
$MgO\text{-}NH_4F\text{-}GeO_2{:}Mn$ phosphor, luminance. spectra due to UV irrad., 26-294°C 79−83005

fluorescent screens
see also electroluminescence
cathodoluminescence yield, calorimetric method determ. *(Russian)* 77−20938
cathodoluminescent screens, luminous emittance, photometric characts. *(Russian)* 77−1739
CRT, luminescent-cathodochromic sodalite powders, prep. and props. 77−20925
electroluminescent memory screens, evaluation of X-ray defectoscopic parameters 78−72992
electron beam pumped semiconductor laser as TV tube screen 78−29969
electron-optical convertor screen luminance, effect on observer's eye pupil diameter 80−35890
extra-fast shutter, for soft X-ray photography *(French)* 78−41397
glass, uranyl-doped, appl. in planar solar energy convertor and concentrator 78−71213
insulating material monitoring by electroluminescent screens, defect imaging 78−53083
IR laser and defectograph, semicond. flow detection 78−3299
IR laser radiation visualiser 77−38974
mammographic X-ray screen sensitivity and resolution 78−7449
medical X-ray and fluorographic film sensitometry 77−48858
metal-backed, appl. to high temp. RHEED obs. 80−75126
phosphorescent detectors and X-ray convertors, Symposium, Riga, USSR (Oct. 1966) 79−6243
phosphors, cathodoluminesc. investig., appl. to cathode ray tube screening 80−108282
radiographic screen characteristic X-ray reabsorption calc. 79−74753
radiography applic., X-ray and γ-ray *(German)* 77−180
rare-earth X-ray intensifying screens, calibration in 15-70 keV energy range 77−26446
resolution of luminescent screens with thermal quenching 78−21131
sensitivity threshold determ. under continuous IR radiation 80−31873
sodium salicylate, UV convertor layer, fluoresc. props. *(French)* 77−4676
texture anal. of phosphor screens using optical Fourier transform 77−23751
thermophotography, exposure conditions var. 77−171
X-ray image intensifier output screens 78−4755
X-ray intensification, new approach to line spread function meas. 79−20665
X-ray intensifying screen, efficiency determ., standard method 80−37140
X-ray intensifying screen, role of reflective layer 80−62816
X-ray phosphors, use in mammography, speed and resolution 77−90883
X-ray phosphors and screens based on compounds activated with rare-earth elements 79−8169
X-ray screens consisting of scintillating crystal fibers, for nondestructive testing 79−6244
X-ray topographic images, direct display systems, review 77−68899
BaFCl:Eu X-ray intensifying screen 78−11735

fluorescent screens continued
$CaWO_4$ and rare-earth X-ray intensifying screen sensitivity to scattered radiation 78−7450
CdS:Ag, Ni thermographic phosphor luminesc. screen, for IR laser pulse recording 79−64342
CsI based powdered phosphors and screens possible appl. in X-ray radiography and fluorography 79−6245
CsI:Na phosphor screen, absolute efficiency under fluoroscopy conditions 78−82084
CsI:Tl powdered phosphor screen for X-ray image intensifier 79−6246
CsI:Tl single crystal gamma-optical converting screens, factors influencing relative afterglow intensity 79−8173
Gd neutron radiographic amplifying screen sensitivity 78−7448
LaOBr:Tb phosphor X-ray mottle reduction by multilayer screen construction 78−4756
LaOBr:Tm X-ray emission spectra and screen-film system design 78−11024
$Y_2O_2S{:}Eu$, phosphor, temp. meas. by line shift method 77−13750
$Y_2O_2S{:}Tb$, cathodoluminesc. efficiency at low electron energy 78−6790
ZnCdS:Ag, phosphor screen, electron beam excited, light ang. distrib., modulation transfer function 80−45150
ZnCdS:Ag screen, electron beam excited, light emission spectra 80−25466
ZnS:Ag, Ni thermographic phosphor luminesc. screen, for IR laser pulse recording 79−64342
ZnS:Cu,Co, phosphor luminesc. screen, spectral characts. determ. of IR pulsed lasers 79−10341
ZnS-CdS phosphor coating for large-screen IR visualiser 78−18070
ZnS-CdS:Ag, Ni luminophor, temperature-sensitive, biological effect of microwaves determ. 80−36186

fluorimetry *see spectrochemical analysis*

fluorine
see also nuclei with ......
abundance meas. in meteorites 77−87342
air pollution, stack sampling apparatus for the collection of gaseous and particulate pollutants *(French)* 80−7986
alkali metal chloride: $F^-(Br^-)(I^-)$, anion impurities substitution, energies of soln., association and migration 78−83831
atom, ab initio effective valence shell Hamiltonian for neutral and ionic valence states 80−74117
atom, and 1st row ats., Compton profiles, momentum distribs., correlation effects 77−88429
atom, and isoelectronic series, Z=10-100, L-shell energy struct. and level classification 78−55129
atom, beam-foil populations, charge state distribs., independent electron model 77−19035
atom, binding energy of 1s electrons, rel. to adsorption of fluorobenzene *(French)* 79−69346
atom, electron affinity, modified variational approx. 78−66679
atom, electron affinity, variation-perturbation approach 77−54513
atom, electron scatt., d-wave resonances, close coupling calcs. 78−33610
atom, electron scatt., low energy d-wave resonances 78−33609
atom, energy levels of $1s^22s^22p^N3d$, (N=2,3,4) configurations 77−46509
atom, ground state energy, HF calc., second-order correction 78−86784
atom, ground state static polarisability and hyperpolarisability, numerical SCF method 79−36567
atom, He (I) PES 78−37609
atom, kinetic spectroscopy in far vacuum UV, oscillator strengths of transitions 78−13457
atom, many electron autoionisation states, perturbation theory Z-expansion, numerical results 80−52863
atom, min. basis of Slater-transform-Preuss functions 79−59343
atom, model pots., STO calcs. 77−408
atom, photoionisation cross sections and ang. distribs., outer p subshell 80−9572
atom, pionic X-ray transitions, strong interaction line widths and shifts 77−23586
atom, Raffenetti-type atomic basis set calcs. 79−97974
atom, Raman scatt. cross section for transitions between ground fine-struct. electronic states 80−23349
atom, s-shell spin polarisation calcs. 77−75318
atom, SCF electron-gas local-spin-density model including correlation 80−9488
atom, spectral lines, neutral, in shock tube plasma, Stark widths and shifts 78−9117
atom, spin-orbit splitting and $^2P_{1/2}$ radiative lifetime, absorpt. spectrosc. meas. 80−87063
atom+H_2, reactive collision, semiclassical dynamics on multiple electronic surfaces, 3-dimens. calcs. 78−27746
atom conc. meas. via HCl titration 77−36830
atom recombination, homogeneous, room temp. rate consts. 77−32766
atom source using thermal decomposition of KrF_2 in duralumin reaction vessel 79−24724
atoms, recombination const. meas. 77−36749
bare nucleus+He, electron capture to excited states, X-ray cross-sections 77−71814
basalts of Iceland and Reykjanes Ridge, F contents and outgassing 79−57900
Black Sea water, F content 78−32118
bone, F content measurement by neutron activation anal. 77−86592
catalytic effect on phase separation and crystn., $SiO_2\text{-}Al_2O_3\text{-}CaO\text{-}K_2O$ system glasses 79−60280
chemical laser, combustion driven nozzle, F_2 absorption meas. 78−79011
chemisorbed on Si (111), electronic energy struct. calcs. 79−78144
combustion studies, 2-compartment bomb calorimeter 80−57300
concentration profiles determ. in Mg alloy scales using $^{19}F(p,\alpha\gamma)$ 78−88678
content in natural water supply, hot springs in Kohu City, Japan, appl. *(Japanese)* 79−70821
depth profiling by $^{19}F(p, \alpha)$ and $^{19}F(p, \alpha\ \gamma)$ 80−45607
desorption from polycryst. W ribbon, electron stimulated 77−11793
determination, by instrumental neutron activation anal. 78−7262
determination, in atm. samples by $^{19}F(p,\alpha)^{16}O$ react. using low energy accelerator 78−85239
determination in steel making slag. by 14 MeV neutron activation anal. *(Japanese)* 79−20484
determination of fluorine in food samples, by $^{19}F(p,p'\gamma)$ 79−5218
discharge, stationary vol., reduced power meas. 80−75115
elastic scattering amplitudes, for high energy electron scattering, by ionised atoms, numerical calcs. 80−49057

fluorine continued
- ethylene+F, dynamics, stochastic reduction for reactions with complex form. 78—3315
- EXAFS amplitudes, wave function relaxation and chemical effects 78—46365
- F+dichloromethane, reaction products, modulated mol. beam mass spectrosc. obs. 80—97742
- flowing afterglow, thermal electron dissoc. attachment rate consts. 77—10773
- fluorination of Fe-Ni alloys, chem. nature of fluoride film 80—101035
- formaldehyde+F reactions, rate consts. by EPR 80—93736
- gas, eqn. of state, second virial coeffs., intermol. pot. at low temp. 79—46416
- glow discharge, positive column elec. props. 79—50916
- hot spring water content *(Japanese)* 79—8648
- hot spring water content measurement, Japan *(Japanese)* 80—31074
- human enamel, F density distrib. meas. with $^{19}F(p,\alpha\gamma)$ 77—56292
- inert gas-F_2 mixtures, excimer emission bands *(Russian)* 77—71885
- ion, in Fe(Ni)(Co), transient mag. field discontinuity 80—24515
- ion+solid target collisions, K-shell ionisation, X-ray emission cross sections 77—19069
- ion addition to β-Al_2O_3, effect on structural state 78—76620
- ion-foil interaction, K-shell vacancies and residual excitation 77—50519
- isoelectronic sequence, X-ray spectra 80—87071
- isoelectronic series, Fe XVIII, Zn XXII, Ge XXIV, Se XXVI, spectral line identification 79—72230
- K_α X-ray satellite struct. and KLL Auger electron spectra, solid-state effects 80—89089
- laser, atomic, hollow-cathode discharge, using He-$NF_3(SF_6)$ mixtures 80—48289
- laser, atomic, produced by He-NF_3 fast pulsed discharge, pumping mechanism 79—81410
- laser, discharge pumped, 1578 Å emission 79—31877
- laser, discharge pumped multiwavelength *(Chinese)* 80—102703
- laser, doublet and quartet transitions, spectral press. depend. 77—58318
- laser, simple high-power TEA, operating in visible and near IR 79—94251
- laser UV transitions of ion, performance and spectroscopy 78—22111
- lasing in atomic lines obs. in excimer XeF laser 77—83858
- liquid, hard sphere model with attractive interactions 80—96434
- liquid, mol. dynamics of '2-Lennard-Jones centres' pair pot. liq. 79—73082
- liquid, principle of corresponding states for viscosity 77—84959
- liquid, thermodynamic and struct. props., pair pots. calcs. 77—58939
- liquid, viscosity, density depend., theory 77—20105
- magnetic hyperfine field in ferromag. Fe, Ni, Gd, temp. depend. 80—20141
- MAGNOX fuel canning material, corroded, F conc. profiles determ. using $^{19}F(p,\alpha\gamma)^{16}O$ reaction 79—92035
- microanalysis in microcracked Cr plate by $^{19}F(p,\alpha\gamma)^{16}O$ 79—79351
- molecular charge density contours for cryst. struct. 78—38645
- molecular laser, high power, electron beam excited 79—932
- molecule, ^{19}F chem. shielding, temp. and internuclear distance depend. 77—75068
- molecule, bond order and Raman intensity, delta function eqn. 77—61693
- molecule, bonding, spin density functional theory 78—17558
- molecule, charge distrib. anal. rel. to Berlin's binding and antibonding regions 79—6875
- molecule, Compton scatt. profile, SCF MO theory calcs. 78—58577
- molecule, continuous UV absorpt. spectrum, temp. depend. 77—23506
- molecule, dissoc. attachment by 0-8 eV electrons 78—74776
- molecule, dissoc. electron attachment, negative ion prod. rates 80—18938
- molecule, dissociation, weak bias and anharmonicity effects 78—82661
- molecule, dissociation by electron beam or electron-beam-sustained discharge 77—68126
- molecule, dissociative attachment of electrons, current density meas., in controlled discharge 77—23566
- molecule, effective core potentials, all-electron calcs. 78—62704
- molecule, electron dissociative attachment rate consts. at 300 and 500K, in discharge plasma 80—43849
- molecule, electron impact dissoc., influence on KrF* laser props. 78—50756
- molecule, electron impact excitation, dissoc. of lowest electronic state 80—63839
- molecule, eqns. of motion method, transition energies, oscill. strengths, electron impact Born cross section 77—18983
- molecule, ground and ionised states, Koopman's theorem and Mo relax. in ab initio calcs. 78—1035
- molecule, ground state, determination and use of molecular α values in MSXα calcs., MTX$\bar{\alpha}_R$ meth. 79—10032
- molecule, ground state, multiconfig. function, perturbation theory calcs. 79—13644
- molecule, ground state pot. energy curve, improved ab initio effective core pot. calc. 80—32625
- molecule, He(II) photoelectron spectra 80—91601
- molecule, LCAO-GTO $X\alpha$ calc., rel. to other LCAO calcs. 80—52871
- molecule, mag. shielding and susceptibility, finite perturbation mol. orbitals calcs. 77—46513
- molecule, MSXα calc., partial wave expansion, binding energy and orbital energy 80—37738
- molecule, pot. curves, binding and ionisation energies and config. variational cellular method 80—32597
- molecule, pot. curves and electronic phototransitions 79—63935
- molecule, pseudopot. calcs. 80—91446
- molecule, pseudopotential calcs., dissoc. energy, bond length, force const. 77—26964
- molecule, relativistic Dirac-Fock multiconfig. SCF calcs. 80—99456
- molecule, rot. relax., in free jet expansion, rot. temp. meas. 77—88538
- molecule, statistical correlation energies 78—78637
- molecule, threshold photoelectron spectra, photoionis. threshold, resonant autoionis. 77—499
- molecule, UV laser system 80—83597
- molecule, vertical valence ionis. pot., many-body Green's functions 78—22051
- molecules PE curve, spectroscopic consts., perturbation theory appl. 80—23341
- muonic free atom, obs. from Larmor freq. meas. 77—23585
- muonic K-shell X-ray transitions, nuclear charge radius 78—66195
- neutron activation analysis using small deuteron accelerator 79—100475

fluorine continued
- NMR chemical shift in AMF_6 cryst. and MF_2+AF melts, (A=alkali metal, M=transition metal) 79—56619
- plasma, electron beam excited plasma UV absorpt. by diatoms 79—68907
- proton activation analysis for determ. in human dental enamel 79—70608
- proton activation analysis for determ. of F_2 pollution from brick kiln 78—20504
- seawater, potentiometric determ. 78—3820
- silicate optical glass chemical stability, F effect 79—76777
- solubility and diffusivity in solid Cu, electrochem. meas. 79—46808
- spin-spin coupling constants, review 77—23511
- viscosity coeffs., modified hard-sphere calcs. 77—11295
- VUV high-power laser, laser-induced fusion 78—58996
- X-ray spectra from light ion bombard. studies 80—71518
- X-ray transitions for F and O ions moving in Ne, Ar, Kr gases and C foils and slabs 77—69020
- $^{18,19}F$ ion diffusion in dental enamel at pH 7, obs. 79—29553
- Ar-F_2, mixtures, low-press. excimer form. and quenching by e-beam excitation 79—50071
- Ar-F_2 excimer laser, kinetics of excimer formation 80—14328
- Ar-Kr-F_2, nucl. pumped laser, high energy beam deposition 80—63999
- Ar-Kr-F_2 discharge, inelastic electron collisions, energy distrib. and rate consts. 80—87980
- Ar-Kr-F_2 excimer laser, kinetics of excimer formation 80—14328
- Ar-Kr-F_2 mixture, electron beam pumped, spectroscopy and kinetics of 248, 414 nm bands 78—63081
- Ar-Kr-F_2 mixture, nucl. induced excimer fluoresc. for I laser excitation 80—78846
- Ar-$N_2(Cl_2)(F_2)(H_2O)$ laser, energy pathways by proton excitation 78—5459
- Ar+Xe(F_2), proton excited mixtures, energy transfer processes 78—66647
- Br+F_2, reaction kinetics, mass spectroscopic obs. 77—77743
- CO_2-F_2-Ar mixture, vibr. relax. in shock wave, 4.3 μm radn. 78—1062
- CO_2-T_2-F_2 chemical laser using energy transfer from TF to CO_2 77—58322
- CaO:F, phosphon, luminesc., electron-hole recombination processes 79—65919
- CaO:F, X-ray and UV luminesc., electron-hole recombination processes *(Russian)* 78—76528
- CdS:F, shallow donors electronic Raman scatt., reson. enhancement 80—45068
- Cs+F_2, electronic excited states, chemiluminesc. in flame, spectra 77—52643
- CsBr:F, luminescence investig. of F_H-centre lifetime. 77—20917
- Cu+F_2, chemiluminesc. reactions, mol. beam study 80—97702
- Cu+X^{n+}, X=F, Al, Si, S, K X-ray production, target thickness depend. 77—75280
- F $(^2P_{1/2})+H_2$, quenching, classical path calcs. 79—22800
- F I, absorpt. spectrum, 730-620 Å 79—26923
- F I, reson. transitions, radiative lifetimes, astrophys. appls. 78—62767
- F I isoelectronic sequence, forbidden transition probabilities for ground terms 77—2376
- F II, $2p^3nl$ terms, beam-foil lifetime meas. 79—81173
- F II, Stark broadening of isolated lines by plasma 78—9116
- F II lines, Stark broadening 77—27024
- F II to VIII, mean lives, beam-foil spectrum in far UV 79—59389
- F III, IV, beam-foil spectra, mean lives, 2150-3200 angstrom 78—55224
- F IV, m-representation approach to atomic structure 79—45645
- F IX, and isoelectronic series, in laser-produced plasma, Balmer fine struct. (broadening) 80—48860
- F ions recoiling in gases, hyperfine interactions 78—74735
- F ions+Ne(Ar)(Kr) and C foil and slab, K shell X-ray spectra 78—17599
- F isoelectronic series, transitions between $1s^22s^2p^5$-$1s^22s^22p^43d$ and $1s^22s^22p^5$-$1s^22s^22p^43s$ configs. 79—26925
- F Kα, 676 eV X-ray source for ESCA 78—53301
- F Kα X-ray line, from KF, for excitation of electron spectra 78—29865
- F V, F VI, transition probabilities calcs. 79—54792
- F VI, 2s3p $^3P_1$-$2s^2\ ^1S_0$ intercombination line transition probabilities 80—18823
- F VI, intercombination lines, transition probabilities determ. 79—89645
- F VIII, 1s2p $^3P_0$ and $^3P_2$ levels, lifetimes, hyperfine quenching effects, UV beam foil spectra 80—47931
- F^-, electron impact detachment cross sections, test of classical scaling theory 79—31693
- F^-, excitation of Limulus ventral photoreceptors 80—8065
- F^-, free-ion polarisability, empirical values 77—20792
- F^- hydration, ab initio MO calcs., fractional charge model 77—34547
- F^-, in He, ion reduced zero field mobilities and free diffusion coeffs. 77—47139
- F^- ion, PAC meas., octahedral $(MeF_6)^4$ complex Sternheimer antishielding 78—10818
- F^- ion influence on Si anodic oxidation and Si-SiO_2 interface 79—15842
- F^-, ion mobility in Ar, flow drift tube meas. 77—72405
- F^- ions in Kr and Xe; mobilities and diffusion coeffs. determ. 80—100048
- F^-, mobility in He, flow-drift tube meas. 80—43831
- F^-, near threshold electron detachment cross section, effect of resons. 77—42403
- F^-, photodetachment cross section, Stieltjes imaging method 78—55149
- F^- positron complex, ground and excited states theoretical studies 80—42934
- F^-, second order correl. energy, Z depend. of irreducible-pair energies 80—91417
- F^-, static electric dipole polarisability 79—76332
- F^-, Thomas-Fermi-Amaldi eqn., approx. variational soln. 80—52870
- F^-, Xα method predicting unstable state 78—82640
- F^{6+}, 1s3s3p $^4p^0$ state, Hartree-Fock function, third-order energy 78—37569
- F^{7+}, 1s2p $^3P_1$ collisional quenching, perturbation theoretic calc. 77—54602
- F^{7+}, resonant coherent excitation in transmission through Au and Ag 78—43058
- F^{7+}, resonant coherent excitation of channeled ions 79—51178
- F^{8+}, resonant coherent excitation of channeled ions 79—51178
- F^{n+}, lifetimes and fluoresc. yields calcs. 79—45668
- F^--$(H_2O)_n$, complex struct., coord. numbers 79—7049
- F+Al, molecular K X-ray transitions, mol. radiative electron capture effect 78—58802

fluorine continued
F+Ar(Xe), coupled channel study, rel. to elastic approx. 79—81255
$F+C^{2+}(N^{2+})(O^{2+})$, K Auger electron spectra 79—89758
$F+CH_3I(CF_3I)$, IF product internal rot.-vibr. distribs., fluoresc. obs. 80—48078
$F+CH_3I(CF_3I)(ICl)$ reactions, product state analysis using laser-induced fluoresc. 80—11915
F+CO in Ar matrix, vibr. and electronic spectra, valence force potential determ., mol. photodissoc. obs. 80—85170
F+carbonyl compounds, HF IR chemiluminesc., vibr. and rot. energy disposal 77—86318
F+chlorobenzene→fluorobenzene+Cl, statistical theory, phase space theory 79—74369
F+Co(Fe) recoil, transient mag. field 78—29838
$F+D_2$, electronic-to-rot. energy transfer cross sections 78—86935
$F+D_2$, reaction rate constants, modified collision theory expression, comparison with exact expression 79—74370
F+DX, (X=I, Br, Cl), H abstraction, absolute reaction rate, H/D isotope effect 78—80721
F+ethylene, intermediate complex reaction, vibr., translational distrib., pot. hypersurface calc. 77—52612
F+ethylene (benzene) derivatives, deuterated, IR chemiluminesc. 80—102506
F+formic acid (formaldehyde), microscopic reaction dynamics, branching ratio, IR chemiluminesc. 78—73021
$F+H_2$, 3-dimens. electronic nonadiabatic reactive collision theory, electronuclear basis 78—3321
$F+H_2$, atom transfer reactions, reaction rate computing, trajectory calcs. 79—74371
$F+H_2$, collinear quasiclassical trajectory study 78—80718
$F+H_2$, collinear trajectories, reaction dynamics calcs. 79—70311
$F+H_2$, collinear trajectories, statistical behaviour and detailed dynamics 80—16664
$F+H_2$, collinear trajectories, pattern recognition 80—45481
$F+H_2$, collision in intense laser field, formalism for mag. dipole interaction 79—98190
$F+H_2$, electronic-rot. energy transfer, for $F(^2P)$ 79—36740
$F+H_2$, electronic-rot. energy transfer, partial cross-section interweaving 79—59538
$F+H_2$, electronic-to-rotational energy transfer 77—3431
$F+H_2$, Franck-Condon factors in reactive collision dynamics 77—36741
$F+H_2$, Franck-Condon factors in reactive collisions dynamics, vibr.-rot. distribs. 77—36742
$F+H_2$, hot-atom reactions, Boltzmann eqn. for hot-atom relax. 79—100423
$F+H_2$, in pulsed HF chem. laser, kinetic modelling, rot. nonequilib. 79—36888
$F+H_2$, in pulsed HF chem. laser evolution, irreversible thermodynamic anal. 79—31887
$F+H_2$, quenching, rot. energy transfer, quantum mech. calcs. 77—50499
$F+H_2$, reaction probabilities, information theoretic anal. 77—16799
$F+H_2$, reaction products ang. distribs., Franck-Condon theory 79—87835
$F+H_2$, reaction quantum dynamics, reson. model, transition state props. 79—11781
$F+H_2$, reaction rate constants, Monte Carlo quasi-classical trajectory calculations 79—74366
$F+H_2$, reaction rate constants, modified collision theory expression, comparison with exact expression 79—74370
$F+H_2$, reactivity, multiple electronic surface effects 77—21363
$F+H_2$, reactivity-selectivity, bounds derivation 80—66763
$F+H_2$, rotated Morse curve-spline pot. function 78—80729
$F+H_2$, transition states, trapped trajectories and classical bound states in continuum 78—88630
$F+H_2$, two electronic pot. energy surfaces, collinear quantum calcs. 80—16646
$F+H_2$ chemical laser, vib. populations in V→V, V→R,T energy transfer corrections 77—32794
$F+H_2$ chemical laser threshold times, reaction product rot. distribs., relax. rates 80—28222
$F+H_2$ dynamics, Franck-Condon factors rel. to information theory for vib.-rot distribs. and isotopic branching ratios 77—60041
$F+H_2$ nonadiabatic effects, scatt. theory, coupled-channel calcs. 78—22010
$F+H_2+\hbar\omega$, reactive scatt. and inelastic collision in laser field, semiclassical calc. 79—47948
$F+H_2(Cl_2)(HCl)$(methane), delay and decay times of stimulated emission 78—3317
$F+H_2(D_2)$, absolute rate coeffs. at 295-265K 80—81303
$F+H_2(D_2)$, absolute reaction rate coeffs., time resolved IR emission meas. 79—68258
$F+H_2(D_2)$, rate consts., temp. depend. 80—81302
$F+H_2\rightarrow FH+H$, collinear probability, quantum calc. using pot. energy surface 78—64829
$F+H_2\rightarrow FH+H$, vibr.-rot. energy distrib. of HF, DWBA calc. 78—80722
$F+H_2\rightarrow HF+H$, 3-dimens. vibrot. reaction probabilities from collinear results, information theoretic synthesis 79—74354
$F+H_2\rightarrow HF+H$, DWBA transition amplitude kernel 80—81310
$F+H_2\rightarrow HF+H$, reson. struct., quantum scatt. calc. 79—61847
$F+H_2\rightarrow HF+H$ energy profile, minimal basis ab initio VB calcs. 78—50477
$F+HBr(HI)\rightarrow HF+Br(I)$, electronic and vibr. energy transfer 77—63899
$F+HCl(DCl)\rightarrow HF(DF)+Cl$, dynamical props., pot. energy hypersurface computer anal. 77—77735
F+HCl(HBr)(DBr)(HI), H abstraction reactions, temp. depend., laser photolysis IR fluoresc. obs. 80—93744
$F+HCl\rightarrow HF+Cl$, time resolved vibr. chemiluminesc. and rate consts. 80—61069
$F+HD\rightarrow HF+D(DF+H)$, branching ratios, information theory test by classical trajectory calcs. 78—64822
F+HI, $^2P_{1/2}$-state excited I form. 78—23923
$F+HN_3$, production of $NF^*(a^1\Delta$ and $b^1\Sigma^+)$ 79—11770
$F+HN_3$, strong interactions in gas-phase reactions, arrested relax. IR chemilum. obs. 80—7773
F+HX, (X=I, Br, Cl), H abstraction, absolute reaction rate, H/D isotope effect 78—80721
F+He+Ar, VUV spark emission spectra 79—3457
F+hydrocarbon (substituted methane)(inorganic hydride), HF IR chemiluminesc., H abstraction rel. rate consts. 77—86319

fluorine continued
$F+I_2\rightarrow IF+I$, energy partitioning, vibr. populations and rot. temp., population inversion 80—50832
F+iodobistrifluoromethylphosphine, reaction mechanism and kinetics, ESR 77—86294
F+methane, reaction in Ar matrix, IR spectra obs. 79—96293
F+methyl radical, IR chemiluminescence obs. 80—61080
F+muonium (H)(D)(T), exothermic triatomic exchange reactions, dynamics, anal. theory 78—3322
$F+N^{4+}$, bonding effect on Kα satellite struct. 79—59392
F+Na(K)(Cs), quasiclassical charge transfer cross section, rel. vel. depend. 77—19073
F+Ne(Ar)(Kr), thermal energy interaction pots., crossed beam study 79—68288
$F+O_2$, quantum reactive scatt. theory, 3-dimens. 80—55637
$F+O_2+M\rightarrow FO_2+M$, flash photolysis IR chemiluminesc., rate const. 78—3311
$F+O_3$ reaction, $FO(X^2\Pi_i)$ radical VUV photoelectron spectra 80—104455
$F+SiO_2$, heterogeneous reaction, discharge-flow tube meas. 80—21274
$F+T_2\rightarrow TF+T$, rate meas. using TF-molecule chemical laser 77—86291
F+Xe, collision in laser field, ang. momentum anal., quantum mech. theory 78—74733
F+Xe, differential scatt. cross sections, crossed beam study, interaction pot. 79—3517
F+Xe, enhanced quenching in intense KrF laser light, computer modelling 78—55232
$F^-+Ar^+(Ar_2^+)(Kr^+)(Kr_2^+)$, in Ar, high press. ion-ion recomb. rate calcs. 78—31621
F^-+atom (Z=10-57), K-shell ionisation, X-ray prod. in transition region, collision symmetry effects 80—43163
F^-+fluoromethane, S_N2 reaction, ab initio LCAO SCF calcs. 77—81402
F^-+H_2F, proton transfer reaction, polarisation model 79—39131
F^-+H_2O, interaction energy calc. using minimal basis sets 80—9678
$F^-+H_2(He)(CO_2)(Ar)(Li)(Na)(Mg)$, negative ion stripping, at. beam form. 77—6926
F^-+HF, proton transfer reaction, polarisation model 79—39131
F^-+He, electron gas model, polarisation inclusion 78—37699
F^-+Kr^++Ar, three body ion-ion recombination probability, Monte Carlo simulation 80—85160
F^-+methane, MINDO/3-FORCES study, reactant energy, products and paths 78—95926
F^-+Na(K), differential cross-section, small angle scatt. 79—98186
F^-+O_2, 0.2-100 eV, collision cross section meas. 77—63902
$F^-+SF_6\rightarrow SF_5+F+F$, electron affinity of SF_5 radical 80—45495
F^-+Si(S)(Ar)(Kr), inner-shell ionisation, X-ray cross sections 80—58369
$F^-+X_2^+\rightarrow[X_2F]^*$, 300K, 50 atm., recombination rates 78—46576
$F^-+X^++X\rightarrow XF^*+X$, (X=inert gas), ionic recomb. 78—46574
F^-+Xe, elastic differential cross-section, 250-500 eV, well depth of XeF^- 79—86027
F^++H_2, empirical and ab initio correlation diagrams, pot. energy surfaces 78—40041
$F^++H_2\rightarrow FH^++H$, rot. effects 78—27744
F^{6+}+He, 10 to 40 MeV, F^{6+} K-vacancy production, role of excitation 80—37859
$F^{7+,8+}+H_2(He)$, 20-56 MeV, F K X-ray cross sections, inner shell Coulomb excitation 77—19025
F^{8+}+He, X-ray prod. cross sections resulting from electron capture and electron excitation of F^{8+} ions 79—3557
F^{9+}+Ne, double K-shell electron capture, theory 79—68315
F+ethylene, transition state, ab initio calc. 78—48640
F^{n+}+Ag foil, 10-40 MeV, Ag L-shell X-ray production 77—71856
F^{n+}+Al, X-ray prod. and electron transfer cross-section 79—45790
$F^{n+}+SiH_4$, X-ray emission from gaseous target, q=4-9, 1 and 2 MeV/amu 79—83060
F^{q+}+He, (q=1-9), X-ray prod. by electron excitation, ionisation and capture 79—76379
F^{q+}+Ne, MO X-ray prod. obs. 79—45663
F^{q+}+Ne, radiative electron capture X-ray profiles from fast collisions, calcs. 79—49975
F^{q+}+Ti(V)(Cr)(Fe)(Co), target and projectile cross-sections, X-ray prod. yields 79—81269
F^{x+}+He, electron capture, K X-ray emission ang. distrib. 77—57919
F_2 absorption diagnostic, sensitive technique, for chem. laser flow 78—74896
F_2, canonical exchange energy modulation parameters, MTXα calc. 79—97997
F_2, chemical shielding temp. depend. 78—5250
F_2, correlated wavefunctions, ionisation pot. 77—67986
F_2, electron energy loss spectra, 0-17 eV, 5-140°, repulsive valence states excitation 80—32844
F_2, electron impact, low energy, vibr. excitation and dissociative attachment 78—46453
F_2 gas chromatography 77—63982
F_2, multipole expansion of diatomic overlap, MEDO calcs. 78—46264
F_2, nucl. spin-spin coupling, scanning MO HF LCAO calc. 79—50045
F_2, photoexcitation and ionisation cross sections, Stieltjes -Chebyshev static exchange calc. 80—53060
F_2, total Xα energy, LCAO calc., rel. to local density models 80—32607
F_2, valence electronic states, $^1\Pi_u\leftarrow X^1\Sigma_g^+$ absorption spectrum 79—63920
F_2, vertical ionis. pots. calc., CNDO approx. in Green's function method 80—18799
F_2^-, absorption coeffs., shape resonance in e-F_2 scatt. 78—17792
F_2^- in alkali metal halides, mag. reson. absorpt. spectrum 77—73079
F_2^-, mag. dipole terms evaluation, internucl. distance depend. 78—82864
F_2-Ar mixtures, electron attachment rate to F_2, elec. cond. meas. 79—7019
F_2-H_2 mixture, parameters influence on flame propag. velocity, rej to HF chem. laser 80—50855
F_2-He, high-press. mixture, neutral atomic F laser lines 79—86167
F_2-inert gas mixtures, transport and attachment processes 78—59542
F_2-Ne(He) mixtures VUV emissions, mol. F_2 laser at 1575 Å 77—75487
F_2+Cu, photon yields, chemi- and photo-luminesc. 79—5157
F_2+D, DF initial vibr. energy distrib., IR chemiluminesc. obs. 80—45497
F_2+H_2 chain reaction, rotational nonequilibrium mech. vibr.-rotational energy exchange effect 80—48230
F_2+H(D), exothermic triatomic exchange reactions, prod. energy distrib., statistical dynamic model 78—92455

fluorine continued
F_2+H(D)(T)(Mu), impulsive triatomic reaction, vibr. state distrib., impulsive energy release model 78−92456
$F_2+H \rightarrow HF+F$, 3-dimens. vibrot. reaction probabilities from collinear results, information theoretic synthesis 79−74354
$F_2+H \rightarrow HF+F$, vibr. adiabatic and static distorted wave Born approx. calcs. 80−7768
F_2+He(Ar), vibr. relax. times, 3D semiclassical theory 78−25667
$F_2+K_2(Cs_2)$, ionisation reactions, absolute cross sections 80−99565
$F_2+Kr(^3P_2)$, KrF* bound-free oscill. emission spectra calc. 80−7799
F_2+Kr(Xe), XeF, KrF form., relax. and quenching 80−81314
F_2+Li, electron transfer reactions, semiempirical pot. energy surfaces calcs. 78−73022
F_2+Mg(Ca)(Sr)(Ba), crossed beam chemilum., kinetics and mechanisms 80−21264
F_2+Mu, isotope effects and collision theory 79−57273
F_2+Mu (H)(D)(T), exchange reaction, quasiclassical dynamics calcs. 79−91942
F_2+Ne*, quenching rate const. for metastable $Ne(^3P_2)$, flowing afterglow 78−46295
$F_2+Si(SiO_2)(Si_3N_4)$, plasma etching, electron or ion bombardment, Ar^+ enhancement 79−82073
$F_2+TeH_2(TeD_2)$, TeF radical form., chemiluminescence obs. 80−43058
F_2+UO_2, reaction kinetics, molecular beam study 78−46157
$F_2+X \rightarrow XF+F$ (X=Mu, H, D, T), exoergic reaction, calcs. 79−61851
$F_2+X \rightarrow XF+F$ (X=Mu,H,D,T), isotope effects, quantum mech. and information theoretic calcs. 78−44360
F_2+XeF*, quenching rates for XeF in (B) state 78−58730
F_2+XeF*+Xe, temp. dependent quenching rate constants 80−63701
$(F_2)_2$, mol. beam. elec. deflection obs. 80−53080
F_3^+, heat of formation, from OF_2 core electron binding energies 77−3417
$FO(X^2\Pi_i)$ radical from $F+O_3$ reaction, VUV photoelectron spectra 80−104455
$F(^2P)$ isoelectronic series, Sternheimer valence shielding and antishielding factors 80−18807
$F(^2P_{1/2})+H_2(j=0)$ quenching, quantum mech. study, ortho-para mixing role 79−76485
$F(^2P_{1/2})+H^+(Xe)$, nonadiabatic collision processes, electronic degrees of freedom, classical model 79−64062
F_2S_2, electronic struct. and stability of isomers, gaussian SCF MO calc. 79−93921
^{18}F, bone imaging radiopharmaceutical local accumulation model 78−24127
^{18}F labelled compounds, rat prostrate imaging expts. 80−51215
^{18}F penetration in Ge single crysts., charged particle activation anal. 80−93828
^{18}F, prep. with an electron linear accelerator, medical and biological appls. 80−98136
^{18}F, production from ^{18}Ne, carrier free $H^{18}F$ acid 79−29626
^{18}F, radioactivity meas. using Cherenkov liquid scintillator counter 79−26817
^{18}F recoil ranges in Au by irradiation of O, with ^3He and ^4He particles 80−71931
^{18}F recovery during transport from reactor 78−78821
^{18}F-F_3COF-^{18}F radiopharmaceutical synthesis procedure 79−29619
^{18}F-5-fluorouracil studies in humans and animals 80−109000
^{18}F-labelled acetic acid, carrier-free, production via a recoil labelling method 80−104756
$^{18}F+H_2$, hot atom reaction, nonequilib. time-depend. theory 80−61126
$^{18}F+H_2$, hot-atom reaction, nonequilib. vel. distrib. and reaction rate calcs. 77−63942
$^{18}F+H_2$, nuclear recoil reaction, steady state hot atom kinetic theory calc., rate coeffs. 78−35712
^{18}F+hexafluoropropylene nonequilibrium effects in moderated nuclear recoil experiments 80−89509
^{18}F+methane, nonequilibrium effects in moderated nuclear recoil experiments 80−89509
^{19}F, chem. shielding in isolated haloalkanes, temp. depend. 78−86888
^{19}F IX, high n states, laser induced resonances 77−83548
^{19}F NMR in one-dimensional ferromagnet $CsNiF_3$ 78−91970
^{19}F, pionic 2p-1s X-ray transitions 79−18319
^{19}F, spin-rot. tensors in trichlorofluoromethane and ClO_3F, appl. to liq.-phase rot. diffusion 80−43068
$^{19}F^-$, in lyotropic liquid crystals, chemical shift anisotropy obs. 80−20478
$^{19}F+^{60}Nd(^{67}Hd)(^{79}Au)$, target Lα X-ray prod., projectile charge state depend. 79−47549
^{19}F+Z, Z=22 to 57, 2 to 28 MeV, prod. of target atom K-shell X-rays 79−18285
F^*+H_2, quenching of excited state, semiclassical studies, comparison between reactive and nonreactive processes 80−106375
$F^*(^2P_{1/2})+H_2$, appl. of classical model for electronic degrees of freedom 79−98192
$(F^-;e^+)$ complex, ab initio LCAO SCF calc., positron affinity and excitation energy 79−49945
$F^-.e^+$, positron energy levels, rel. to Rydberg levels of Na, NO 79−86089
Fe:F, lattice location of implanted F rel. to mag. hyperfine fields 77−59041
Fe^{3+}-F^-, overlap and covalency contrib. to zero field splitting, LCAO-MO calc. 80−24850
FeOOH:F, quadrupole interaction, Mossbauer spectra 80−15895
Fl^+, reson. line regularities in plasma Stark widths and shifts 80−43881
$F_2(\nu=0)+Mu \rightarrow MuF(\nu' \leq 3)+F$, (Mu=muonium), quantum mech. calcs. 77−21366
$H+F_2$, vibr. prod. distrib., Einstein coeffs. 78−92448
$H+F_2(Cl_2)$, reaction probability, information theoretic anal. 77−16799
H_2/F_2 laser, initiation using surface spark discharge UV light source 80−78923
H_2-F_2 pulsed laser, flame out 77−27284
H_2-F_2-He chemical CW laser, flows *(Russian)* 78−74895
H_2-F_2-O_2, chem. laser mixture, multiatm., spontaneous explosions 78−73044
H_2+F_2, branched chain reaction, role of thermally nonequilibrium atoms and molecules 80−76507
H_2+F_2 reaction, coherent emission efficiency 78−17928
H_2+F(H), collinear reactive scattering, coupled eqns., soln., R-matrix calcs. 77−16812
H_2+H(F), minimum energy reaction path, reference coord. approach 78−40025

fluorine continued
H_2+H(F)(Cl), collision induced IR laser absorpt., rate enhancement, theory 79−66275
$HF(\nu=1)+F \rightarrow HF(\nu=0)+F$, vibr. relax. rate const., 100-3000K 77−3434
He-F, doublet series laser lines near 700 μm, hyperfine splitting and broadening meas. 78−63070
He-F gas mixture, electron drift velocities, laser modelling 78−63061
He-F laser, press. depend. of atomic F laser transition intensities 77−659
He-F mixture, RF discharge, mass spectroscopy, floating double probe meas. 80−84016
He-F_2, dissociative electron attachment, rate coeffs., appl. to lasers 78−46575
He-Xe-F_2 mixture, pulsed avalanche discharge at high gas press., homogeneous form. conditions 80−49027
$He^*(2^3S)+F$, Penning ionisation and excitation transfer, unified treatment 78−25672
InSb:F, acceptor props. and diffusion coeff. of F 80−70643
K:F^-, ground states and core hole states, self-consistent soln. using density functional formalism 79−69467
KCl:F^-, modes of vibr. due to U-centre and additive anion impurities 80−44280
Kr-F_2 mixture, preionised electric discharge stability 79−64865
Kr-Xe-F_2 excimer laser, kinetics of excimer formation 80−14328
Kr^++F^- and $Kr_2^++F^-$, ionic recomb. rates in buffer rare gases 79−8425
$Li+F_2(Cl_2)(NO_2)$, $4^2S_{1/2}$ excited atom crossed beam collisional ionisation 79−64087
MgO:F, hole processes in photostimulated luminesc., electron emission, X-ray irrad., ESR relaxation 79−69889
MgO:F, impurity-induced UV luminesc. 79−83037
MgO:F^-, shortwave luminesc., V-centre electron recomb., impurity effects *(Russian)* 77−20921
Mn^{2+}-F^-, overlap and covalency contrib. to zero field splitting, LCAO-MO calc. 80−24850
$Mu+F_2 \rightarrow MuF+F$, 300 to 400K in N_2 moderator, reaction rate determ., tunnelling 78−48682
N_2-F_2 mixture, fast Blumlein discharge excited, intense 3371 Å laser emission 79−41365
N_2H_4-F_2 flame, chemiluminesc., HNF A-X emission spectrum 79−50033
Na:F^-, ground states and core hole states, self-consistent soln. using density functional formalism 79−69467
NaCl:F^-, energy of migration of F^- 77−43380
NaCl:F^-, lattice relaxation around tetragonal and rhombic defects 79−95110
NaI:F, electron-lattice coupling of F-centres, optical props. 80−60641
Ne-Xe-$F_2(NF_3)$, excited states quenching 79−18406
Ni:F, ion-implanted, mag. hyperfine field, anomalous temp. depend., PAC meas. 79−4754
Ni:F, lattice location of implanted F rel. to mag. hyperfine fields 77−59041
$Pb+F_2$, chemiluminesc. spectrum of PbF 79−24742
Si:F, amorphous, heat resistant, prep., elec. cond., IR absorpt., annealing 80−65719
Si:F, amorphous, implantation effects on elec. props. 80−49716
Si:F, amorphous, thermal stability, comparison with Si:D 80−49542
Si:F, amorphous, vibr. excitations at defect sites, IR and Raman spectra calc. 80−49329
Si:F, amorphous alloys, RF sputtering prep. in SiF_4-Ar gas mixture, spectra 80−80772
Si:F, amorphous film, effect of F on elec. cond. 80−34444
Si:F,H, amorphous, elec. and optical props. 80−60031
Si:F,H, amorphous, glow discharge deposited elec. props. and device aspects 80−44744
Si:F,H, amorphous efficient carrier generation for solar photovoltaic energy conversion 80−92906
Si:F(,H), amorphous, electronic struct., orthogonalised LCAO calc. 80−44486
Si:H,F, amorphous, photocond., dark cond. and photoluminesc. 80−49802
Si:H,F, amorphous, Schottky barrier profiles, depletion region width 80−49871
Si:H,F,O amorphous, plasma deposited, comp. and optical props. 80−50441
Si-F-H:P, film, dark cond., struct., Raman scatt. 80−88588
Si-SiO_2 interface, ^{19}F implantation effects on charge density 79−10865
$Si+F_2$, fast flow reactor, second order rate coeff. determ. 78−80723
$Si+F^{q+}$, q=3-9, Si K-shell ionis., electron transfer cross sections, solid targets 79−10192
$SiO+F_2$, matrix reaction, $OSiF_2$ prod., IR spectra and force consts. calcs. *(German)* 80−97718
SiO_2:F, ion implanted, F influence on oxidation-induced stacking faults 80−65011
SiO_2:F, silica fibres, numerical aperture and attenuation, drawing from preforms 78−1449
SiO_2:F fibre preform plasma chemical deposition *(German)* 78−33926
SiO_2:F fibre preparation by plasma-activated CVD *(German)* 78−33927
SiO_2:F layers, deposition from $SiCl_4$-SiF_4-O_2 gas mixture by plasma CVD method 78−95699
SiO_2:F-ion implanted, mobile-ion drift compensation 79−19664
$Sm+F_2(N_2O)$, chemiluminesc., absolute photon yields determ. 77−86317
SnO_2:F films, elec. and optical props., solar energy conversion appl. 79−65945
SnO_x:Sb,F film CVD for bistable storage CRT 77−77410
$Ta+F_2$, reaction, 690-930K modulated mol. beam mass spectrometry expts. 77−70341
$Ta+F_2$ reaction, modulated molecular beam mass spectrometry 78−15678
U+F surface reactions, UF_6^- form. 77−73465
$UF_4+F_2 \rightarrow UF_5$, UF_6, IR matrix isolation spectra 77−12787
$V^{2+}F^-$, $V^{2+}F^-V^{2+}$ π-electron systems, transferred hyperfine interaction, HF calc. 80−24859
W-O-F system, gas phase, comp. and chem. transport reactions in discharge lamp *(German)* 77−32826
Xe-F two module discharge laser, gain and temporal characts. 80−87385
$Xe+F_2$, collision induced photoabsorpt. indicating $Xe+F_2+H\nu \rightarrow XeF^*+F$ 78−27786
XeF*(B), nuclear pumped laser, buffer effects 80−37617

fluorine continued
ZnSe:B(F), ion implantation, photocond. and cathodoluminesc. meas. 78−26586
ZnSe:F, signal enhancement by field modulation, ODMR expts. 78−56406

fluorine compounds
alkaline earth fluorides, cryst. growth in reactive atmosphere 80−80962
diatomic fluorides, exact force field calcs. using at. force consts. 78−62739
ESCA shifts and effective charges 80−78648
fluoride crystals, rutile-type, interionic pots., cohesive energy, bulk modulus, calc. 80−79741
fluoride mixtures, molten, for Ge powder electrodeposition 80−60797
fluoride solid electrolytes 80−70464
fluoride systems, fundamental condition for glass formation 80−44135
fluoride-oxide slags, elec. cond., Al and Si addition agents influence *(Russian)* 80−39572
fluorides, chem. formulae, advances in preparative chem. 79−47915
fluorides, electric field gradient, time-differential-angular-distrib. method 80−60463
fluorides, gaseous and solid, meas. in atmosphere *(Dutch)* 80−3567
fluorides, molten, significance of variable oxygen electronegativity in binary oxides 78−5157
fluorides, polyatomic with He and Ar, VUV spark emission spectra 79−3457
fluorides, XPS *(Japanese)* 80−16154
fluorites, natural colour centres and associated rare earth ions 79−61408
fluoroborates in non-aq. solns., ^{19}F-^{11}B spin-spin coupling 77−23512
fluorocarbon ozone problem, evaluation of current knowledge *(German)* 79−96826
fluxing material, effect on oxidation of graphite crucibles *(Japanese)* 78−84755
Freon-12, modelling two-phase hydrodynamic phenomena during nuclear reactor LOCA 80−5267
gaseous and particulate F compounds accumulation by forage vegetation and limed filter paper samplers 77−78407
ground states, mol. parameters, MINDO calcs. 78−41955
hexafluorides, electron affinities, MS Xα calc. 77−30778
materials review *(Japanese)* 79−96282
molecular effects in F K-shell ionisation by 0.5 to 1.5 MeV protons 77−50515
$Ba_2M_{II}M_{III}'F_9$, (M_{II}=Fe, Co, Ni, Zn; M_{III}'=V, Cr, Fe), solid state synthesis and cryst. chem. study *(French)* 79−41988
CC UF_6 conversion to UO_2, reactor fuels, review 80−23099
F donor reagent+inert gas, quenching, excimer form. 79−63953
F-bearing gases, K X-ray yields induced by proton bombardment 79−45736
F+H_2, gas phase H-atom transfer reactions, struct.-reactivity correl., pot. energy surfaces 80−104433
$(F\text{-}H\text{-}F)^-$, strong H-bond, using recent difinition 79−98240
FBO, electronic struct. calcs. 77−30772
FBr^- centre in alkali halides, analysis of spin-Hamiltonian parameters of heteronuclear XY^- defects 80−88509
$FBrO_3$, gas-phase electron diffr., mol. struct., force field, vib. amplitudes 77−547
FCN, ^{14}N quadrupole coupling consts., ab initio calcs. 80−58283
FCN, and isotopic forms, force field calc., freqs., rot. consts. 79−22691
FCN, CNF, isomer pairs, mol. orbitals calcs., using PLA and LEDO integral approx. methods 78−13418
FCN, CW for IR mol. laser, optical pumping with $^{16}CO_2$ and $^{18}CO_2$ lasers 80−74343
FCN, collisional transition obeying nondipolar selection rules between M-levels, laser-microwave double reson. 77−83627
FCN, general quartic force field, Machina-Overend parameters 78−50532
FCN, IR laser Stark spectra, C-F stretching mode, dipole moments, rot. consts. 78−1022
FCN, IR-microwave double reson. and double photon transitions, HF Stark effect 77−14464
FCN, in interstellar mol. clouds, search for J=2-1 transition 77−60808
FCN, laser-microwave two-photon spectroscopy, appl. of tunable source 79−30579
FCN, linear mol., Compton profile bond additivity, HF calc. 79−68268
FCN, photoelectron spectrum 77−30920
FCN+N_2, rot. spectra and geom. struct. of FCN 78−82725
FCO, radical, struct. and props. calcs. 80−74112
F_2CO, dipole moment derivatives, MINDO/3 semiempirical calcs. 77−75055
FCP, microwave spectrum, struct., dipole moment and vibr.-rot. props. obs. 80−91549
FCl^- centre in alkali halides, anlaysis of spin-Hamiltonian parameters of heteronuclear XY^- defects 80−88509
$FClO^+$, radical cation, struct. and electronic props., ab initio RHF SCF MO calc. 80−52883
FD+H(D), low barrier quantum model, vibr. deactivation 80−69216
FH, indirect nucl. spin-spin coupling const., Hartree-Fock and polarisation propag. calcs. 78−9170
FH, numerical coupled HF hyperpolarisabilities, basis set depend. 79−76357
FH, one-electron props., review of expt. and theoretical data, Hartree-Fock calcs. 77−67980
FH, quadratic vibr. force const., from X-ray scatt. factors 79−45864
FH, X-ray and high-energy elastic electron scatt., vibr. averages 79−81279
FH-OH_2(dimethyl ether), H-bonded complexes, cubic force consts. calcs. 80−47868
FH+Be→BeF+H, collinear, pot. energy surface study 79−11782
FH+H(D), low barrier quantum model, vibr. deactivation 80−69216
FH+H(D) low barrier quantum model, vibr. deactivation 80−69216
FH_2, pot. energy surface, valence states, VB diatomics-in-mols. method 79−85920
$FH_2{}^+$, reactive processes, ab initio MCSCF-CI and diatomics in mols. calc. 78−56881
$FH_3{}^+$, stability, ab initio calcs. 77−30775
$FHCl^-$, deuteron quadrupole coupling const., nuclear mag. shielding, geometry depend. 78−58586
FHF ion, H-bond excited electronic states, CI calc., dissoc. and autoionising states 80−5489
FHF^-, deuteron quadrupole coupling const., nuclear mag. shielding, geometry depend. 78−58586

fluorine compounds continued
FHF^-, H bonds, vibr. dynamics calcs. 80−23397
FHF'end, existence in alkali tetracyanoplatinate complexes, IR spectra 77−77184
$F^-(H_2O)_2$, 3-body pots., SCF energy partitioning calcs. 80−18953
$F^-(H_2O)n(n=1,2)$, FSGO-pair-pot. calcs. *(German)* 80−74278
FH($^1\Sigma^+$), diatomic molecular form factors, vibr. average, study of convolution approx. 79−50926
FHe^+, fragmentation and potential energy curves from FT β-decay 78−56910
FNNF, mol. struct., cis effect 80−91434
FNO, electronic transitions, limited GSMO and ESMO CI calcs., oscillator strengths, spectra 78−70750
FNO, excited states, SCF scheme 79−6885
FNO, four electron three centre bonding units, ab initio valence bond calcs. four electron three centre bonding units, ab initio valence bond calcs. 80−27949
FNO, ground and lowest excited states, SCF ab initio calcs. 78−37544
FNO_2, UV photoabsorption spectrum 79−10123
FO free radical, detection by CO_2 laser mag. reson. 80−45594
F_2O, absorpt. band freq. and intensities, electro-optical parameters, pot. energy, IR spectra 80−37812
F_2O, geometry, electron spectrum, vert. ionis. pot. ab initio calc. 80−58187
F_2O, inertia defects and dipole moments by kinetic consts. method 80−928
F_2O_2, geometry, SCF CI calcs. 78−55126
FOCl, ab initio vertical ionis. pot., corrections to Koopmans' theorem 78−25749
FOH, nucl. mag. shielding and susceptibility, SCF calcs. 77−14351
FOO radical, struct. and props. calcs. 80−74112
F_5S-F bond energy, upper and lower bounds, from chemiluminesc. data 79−86081
F_6S-Ar, compressibility 0 to 50°C, second virial coeffs. calcs. 77−15147
F_6S-Kr, compressibility 0 to 50°C, second virial coeffs. calcs. 77−15147
$F_4S_4N_4$, SCF-Xα-CNDO/BW calcs., comparison 78−25435
FSO (FOS), struct. and props., SCF calcs. 80−106260
FSO_4, electrolytic polishing of Ta and Ta alloys 78−85094
F_2SO, A′-force consts., 4th-order secular eqn., L-matrix approx. vs. HLFS methods 79−36556
FSO_2OF, wide-line NMR anal. of mol. struct., chem. shielding tensor 77−83622
FSS, struct. and props., SCF calcs. 80−106260
FSSF, SSF_2, and ^{34}S isotropic forms, matrix IR and Raman spectra *(German)* 79−89674
$F_3SiOSiF_3$, vibr. bands, normal coord. calcs. *(Russian)* 78−70814
$F_3SiOSiF_3$, vibr. anal., normal coordinates, siloxane bridge vibr. band struct. 79−50003
^{19}F, isotropic hyperfine coupling consts. in small radicals 80−52894
HF, variation-perturbation minimal Gaussian geminal basis sets correl. energy calc. 78−78629
HF-ClF complex, and isotopic forms., mol. beam elec. reson. spectra, config., bonding, spectroscopic consts. 77−30860
He-NF_3 laser, F* relax., generating 250 kW at 0.6-0.75 micron, for 2-3ns *(Russian)* 78−1219
N_2F_4, collisionless dissociation kinetics in highpower IR radiation field 80−66853
$(N_2H_6)_2F_2[TiF_6]$, X-ray cryst. struct. determ. 80−54182
Na^{18}F, transverse section imaging in acute myocardial infarct 80−46015
ONF_3, vibr. anal. using Green function 77−57962
SF_6 insulated switching installations and devices, gas chromatography appl. *(German)* 78−88668
SO_3F, dye laser excitation of vibr. levels of upper electronic state, mol. fluoresc. meas. 80−83402

flux (magnetic) *see magnetic flux*

flux (neutron) *see neutron flux*

flux creep
see also flux pinning
flux jump in magnetic field, at slow sweep rate, calc. and obs. 79−4632
hard superconductor influence of thermally activated flux creep on AC response 79−33416
hysteresis loops, minor, of type II supercond., direct obs. of flux creep 78−6487
magnetic flux structures in superconductors, book 79−91199
magnetic instability of superconducting wire in the changing magnetic field 80−34569
superconducting surface sheath, Brownian motion 79−19708
vortex array, pinning of flux lines by randomly-spaced pinning centres 78−52172
NbZr, thermally activated flux creep, effect on AC response 79−33416
$Pb_{83}In_{17}$, voltage current characts. 77−20508
V, creep effect in periodically swept minor hysteresis loops 79−60964

flux crystal growth *see crystal growth from solution*

flux flow
see also flux pinning
AC permeability of defect-free type II supercond. 77−8250
composite superconductor, flux jumps and training 80−70911
crystals of magnetic flux, review 79−99664
current induced superconducting to normal transition mechanism 79−56468
current-voltage characts., and their mag. field depend. 78−23217
cylinder, flux-density gradient and pinning force, flow stress effect *(German)* 77−24653
ferromagnetic superconductors, self-induced vortices, magnetisation, Gibbs free energy 80−70916
film, pin-free, vortex chain size effect and negative resist. 77−80888
foil, effects of current-induced mag. field on flux flow 77−77012
forces acting on vortices, microscopic theory *(Russian)* 77−12068
Ginzburg-Landau eqn. generalisation, nonlinear transient phenomena 77−32110
granular films as weak link in Josephson devices, vortex flow model 80−88685
hard superconductor flux jumps under time depend. external conditions 80−7038
induced flux-flow noise in type II superconductor 77−4476
irreversible, flux flow in transverse mag. field 79−7949
Josephson junction, flux flow characteristics 78−84351
Josephson junction, vortex motion induced by phonon injection 79−4622
Josephson vortex in inhomogeneous junction, EM radiation due to vortex motion 79−73642

flux flow continued
- layers, mixed state struct. rel. to Josephson effects 79−4628
- long Josephson junctions, microwave induced vortex motion 80−39715
- Lorentz transform law for EM field, fluxoid motion example 80−67954
- magnetic flux annihilation in a large Josephson junction 80−11139
- magnetic flux structures in superconductors, book 79−91199
- nearly pure superconductor, flux line motion, semiphenomenological theory 78−52171
- noise in rectangular sample, flux bundle effect 77−63043
- noise voltage, flux-flow, rel. to presence of oscills. in V-I curve 80−15671
- nonlinear effects during vortex motion, kinetic eqn. *(Russian)* 77−80890
- $Pb_{80}In_{20}$ foil, flux-flow crit. freq. and generalised bundle size depend. on fluxoid traversal distance and length 80−7054
- plastic deformation in flux-line lattice, flow stress *(German)* 77−24652
- plastic deformation of flux line lattice effect on flux transport 77−36035
- rare-earth, mag. supercond., appl. of boson theory to mixed state 80−7050
- reversible type II superconductor, AC flux penetration on force free config. 79−56464
- superconducting bridge, quantized vortex formation *(Russian)* 78−43521
- superconducting loop broken by damped Josephson junction, anomalous flux penetration 80−97033
- superconducting surface sheath, Brownian motion 79−19708
- superconductor, flux flow curves as function of temp. 78−84344
- superconductor flux-flow noise theory 79−24115
- surface, static electric potential structure 78−43535
- thin film superconductors, flux lattice melting, phase diagram 80−84571
- type II supercond., rot. in mag. field, flux density distrib. 78−43536
- type II superconducting wire, nonideal, flux penetration in transverse mag. field *(Japanese)* 80−60154
- type II superconductor, inductive response to trapezoidal magnetic field 78−39277
- type II superconductor, thermomag. effects and crit. state stability 80−20353
- type II superconductors, flux jumps and oscills. *(Russian)* 80−7052
- type II superconductors, longitudinal currents in a system of Abrikosov vortices, Ginzburg-Landau eqn. anal. 80−70914
- type II superconductors, metastable states, boundaries 80−54848
- type-I superconductor, current induced resistive state, noise in flux tube nucleation 79−24109
- voltage pulses, flux flow, in superconds. 79−56466
- Al granular film, vortex chain size effect and negative resist. 77−80888
- Al superconducting film, transition to zero vorticity, long-range topological order 80−93039
- Cu-Nb_3Sn multifilamentary tapes, in situ formed, crit. current density anisotropy 80−84576
- In film with dirty type II supercond. props., flux flow resistivity 77−51859
- In-Bi, mixed state, pinning centre distrib. statistics, I-V characts. *(Russian)* 80−100571
- Nb foil, cross correlation measurements on moving vortex arrays 79−24117
- Nb foil, flux flow noise cross-correl. functions 77−36034
- Nb foil, time behaviour of local flux flow noise 79−24116
- Nb microbridges, heating and flux flow, I-V curves and microwave mixing 79−28474
- Nb, neutron irradiation, low temp., 15 MeV, effect on superconducting props. 78−52179
- Nb-Hf (26 at.%), mixed state, ultrasonic velocity meas. 79−60974
- Nb-Ta type II supercond., defect-free, AC permeab. 77−8250
- Nb-Ti-Zr wire, longit. critical currents in AC mag. field, flux flow instability [-] type II superconductors 77−72958
- Nb-Zr, crit. current, flow-flow resist. depend., allowance for superheating *(Russian)* 80−93061
- Nb_3Ge, amorphous film, supercond., flux flow resist., vortex pair dissoc. 80−88701
- Nb_3Ge, amorphous nongranular thin superconducting film, thermodynamic and resistive transitions 80−34571
- NbN weak links, granular, Josephson behaviour 80−75681
- Nb_3Sn, multifilament superconductor, pulsed mag. field losses and critical current densities 80−54853
- NbTi, RF magnetoresistance, flux flow resistivity 79−61002
- NbTi, superconductor, acoustic emission during flux jump 80−39724
- $(Nb_{0.99}Zr_{0.01})_3Sn$, AC power losses in parallel AC and DC mag. fields 80−97041
- Pb film, current-induced flux motion, studied at 100 ns time resolution 79−47208
- Pb, supercond. strips, losses due to flux flow dissipation 79−56443
- Pb-2n, work hardening in mixed state *(Russian)* 79−42707
- Pb-Cd, oriented lamellar superconductor-normal composite, supercond. 79−1650
- Pb-Cd eutectic composite, mag. flux entry in proximity effect regime 79−33418
- Pb-In (40-60 at.%), type II superconducting Ettingshausen effect, transport entropy of vortices 78−56272
- Pb-In alloys, strong coupling effects in temp. depend. of flux-flow resist. near H_{c2} 77−36036
- Pb-PbO_x-Pb, long Josephson tunnel junction, current steps induced by vortex motion 79−47199
- Pb-Tl, low κ type II supercond., vortex motion anisotropy, intermediate-mixed state 78−47918
- PbIn cylinder, longitudinal geometry 78−14902
- $Pb_{0.8}In_{0.2}$, flux-flow noise 79−95556
- $Pb_{40}In_{60}$, mixed state supercond., Hall and Ettingshausen effects, vortex entropy transport 80−44780
- $Pb_{80}In_{20}$ foil, current-voltage characts., and their mag. field depend. 78−23217
- $Pb_{80}In_{20}$ foil, deformed, annealed, correlation between pinning strength and flux flow noise charges 77−43792
- $Pb_{0.871}Sn_{0.129}$, supercond., hysteresis in flux flow characts., normal metal precipitates 78−80107
- Sn-Sn_xO_y-Sn long Josephson tunnel junction, flux flow, crit. conditions 80−80452
- V foil, flux flow noise cross-correl. functions 77−36034
- V foil, time behaviour of local flux flow noise 79−24116
- V_3Ga, multifilament superconductor, pulsed mag. field losses and critical current densities 80−54853

flux-line lattice
- AC permeability of defect-free type II supercond. 77−8250
- antiferromagnetic superconductor, isolated vortex line 80−70912
- axial and azimuthal fluxes, contained in cylinder in force-free config. 79−82728
- continuum approach of physical line structs., appl. to flux line lattice of supercond. 78−81859
- correlation with cryst. lattice in type II superconductors 77−1526
- critical current angular dependence in supercond. with long narrow defects 77−69463
- critical current density, depend. on past history of mag. field and temp. 78−6491
- critical currents, in non-transverse mag. fields, theory 77−55646
- crystals of magnetic flux, review 79−99664
- current density distrib. in cylindrical sample 79−38270
- cylinder, helical force-free current and flux density distribs. 77−24654
- defect-flux line interaction potential, vol. pinning force 77−43790
- dielastic interaction with internal stresses of cryst. imperfections, change of elastic consts. 78−14906
- dielastic interaction with internal stresses of cryst. imperfections 78−56270
- distorted vortex lattice, generation of soln. to Ginzburg-Landau eqns. 79−56467
- distorted vortex lattice, order parameter and mag. field appl. to flux pinning 77−77013
- distorted vortex lattice, order parameter and mag. field appl. to flux pinning 77−77014
- elastic response, large, of fluxoid lattice, plausible arguments for 77−63040
- elastic vortex lattice, pinning by lattice defects 79−56465
- electron vortex microscopy and decoration for mag. flux quanta obs. 77−47945
- elementary interaction force between flux-line lattice and precipitates 78−10623
- Faraday effect direct obs. of flux-line gradients and vol. pinning forces 77−24651
- ferromagnetic superconductor, vortex structure 80−25055
- field lines of intersecting flux lines in type II supercond. 79−69641
- filamentary superconductor, upper and lower crit. fields 80−25053
- film, crit. region near H_{c2} rational approx. 79−91198
- film, inversion temp. in pinning of vortices by periodic struct. 78−56274
- film, pin-free, vortex chain size effect and negative resist. 77−80888
- films with periodic thickness modulation, pinning effects 80−88702
- flux pinning by point pinning centres 77−28321
- flux pinning force, derivation from a potential 78−68128
- flux-line cutting model 80−50017
- fluxoids, equilibrium misalignment with applied magnetic field, due to anisotropy effects, direct obs. 79−24112
- gauge choice in superconductors, vortex line free energy formulation 77−51838
- hexagonal lattice with planar pinning forces, elastic response 78−19195
- ideal vortex lattice strength *(Russian)* 77−80886
- imperfect vortex lattice, small angle neutron scatt. 79−42710
- Josephson contact, vortex pinning and energy *(Russian)* 78−68117
- Josephson junction, current-carrying, in strong mag. field *(Russian)* 79−33411
- Josephson junction composed of N series loops, kinetic momentum quantum effect 79−87199
- Josephson tunnel junction, nonresonant vortex motion 80−97037
- magnetic flux structures in superconductors, book 79−91199
- neutron diffraction, small angle, integral reflectivity calc. *(German)* 77−85398
- nonideal superconductor, magnetic behaviour under longitudinal mag. field, irreversible force free current 80−7053
- nonideal superconductor, reversible motion of fluxoids in pinning phenomena *(Japanese)* 80−2537
- periodic pinning structures, supercond. vortices 79−38269
- phase transition between triangular and square lattices 78−76202
- pinning, deformation of flux line lattice in type II superconductor 79−47213
- planar imperfections effect on stability 78−23218
- plastic deformation of flux line lattice effect on flux transport 77−36035
- rare-earth, mag. supercond., appl. of boson theory to mixed state 80−7050
- rotation and inversion symmetry props. 77−32128
- shear modulus of flux line lattice 77−1527
- shear modulus of flux-line lattice in case of low flux density 77−1528
- spiral-vortex expansion instability, helical perturbation growth 77−63041
- stress tensor theory of AC permeability 78−56271
- superconducting order parameter perturbation flux pinning 80−103801
- superconductor, type II, longit. current, continuous vortex cutting 80−88704
- superconductor Faraday effect obs. in polarising microscope 80−70892
- superconductors, tilted vortices, mixed state features in surface layers *(Russian)* 80−29512
- theory, rel. to plane elasticity of anisotropic media with antisymmetric stress tensor *(German)* 79−86338
- thin film superconductors, flux lattice melting, phase diagram 80−84571
- type II supercond., rot. in mag. field, flux density distrib. 78−43536
- type II superconductor, bounded, intermediate state struct. form. near crit. field, role of surface 80−80465
- type II superconductor, dilutely pinned, threshold criteria for pinning force 80−15668
- type II superconductor, neutron scatt. from imperfect flux-line lattice 79−56474
- type II superconductor, nonideal, with dense pinning centres, threshold criterion 80−88703
- type II superconductor vortex state, elastic energy calcs. on high inductions 77−36030
- type II superconductor vortex state, elastic energy calcs. on low inductions 77−36031
- type II superconductors, cubic, flux-line lattice anisotropy, boson method calc. 80−2536
- type II superconductors, flux-line cutting 80−7055
- type II superconductors, flux-line-cutting threshold 80−88705
- type II superconductors, longitudinal currents in a system of Abrikosov vortices, Ginzburg-Landau eqn. anal. 80−70914
- type II superconductors, order parameter change near H_{c2}, influence of transport current 80−75690
- volume pinning force for combined attractive-repulsive flux-line defect interaction pots. 77−59363

flux-line lattice continued
- volume pinning force for periodical interaction forces between defects and flux line lattice 79—95553
- vortex chain interaction with periodic pinning pot., crit. currents 79—56469
- vortices, local mag. flux density and elec. current density 80—84572
- vortices in supercond., solns. of Gorkov and Ginzburg-Landau theories 79—65624
- X-ray and neutron small-angle scattering, review 79—10752
- Al granular film, vortex chain size effect and negative resist. 77—80888
- Al granular films, vortex noise at supercond. transition 80—84530
- Al, supercond. cylinder, order parameter enhancement by microwave irrad. 80—70896
- $ErRh_4B_4$, ferromag. superconductor, vortex phase 80—80441
- In, film, flux nucleation meas. in current induced resistive state 78—27002
- In, superconducting bridge, Josephson effect, flux tube nucleation 77—36028
- Nb, bicrystal, parelastic interaction between grain boundary dislocations and flux line lattice 79—24114
- Nb, cylindrical specimen, flux-line gradients and pinning forces, Faraday obs. 77—24651
- Nb, flux pinning by proton irradiation damage 77—47947
- Nb, fluxoid lattice, eqn. props., small-angle neutron diffraction measurements 80—34573
- Nb, fluxoid lattice, eqn. props., magnetisation measurements 80—39725
- Nb, intermediate mixed state investig. by small-angle neutron scatt. 77—63042
- Nb, plastic deform., Shubnikov phase penetration, Faraday effect obs. 79—82731
- Nb, plastically deformed, flux density gradients and pinning forces, Faraday effect obs. 79—61010
- Nb pure single crystal, low-κ type II superconductors, determ. of low field critical parameters 79—11278
- Nb pure single crystals, anisotropy in flux-line lattice symmetry of low-κ type II superconductor, neutron diffr. study 79—11279
- Nb, supercond., field history effect of flux gradient 78—91828
- Nb, supercond. fluxoid line lattice neutron scatt. study 79—42712
- Nb, type II superconductor, equilibrium misalignment, fluxoids and appl. mag. field, anisotropy interaction 79—24112
- Nb, with Nb_2N precipitates, flux pinning, magnetization, bulk flux density gradient, and neutron scatt. meas. 79—56472
- Nb:N, H_{c2} anisotropy, impurity and temp. dependence 78—43533
- Nb-Hf (38 at.%) superconductor, peak effect, summation problem, mag. history flux pinning force 80—20362
- Nb-Ta (13 wt.%) alloy, flux line bending by transport currents, neutron diffr. 77—8247
- Nb-Ta type II supercond., defect-free, AC permeab. 77—8250
- Nb-Ti, pinning mechanism at high mag. fields 79—95555
- NbCn, superconducting film, high field critical current densities and resistive transition 79—73648
- Pb-In (50 wt.%), supercond., pinning effect 80—15669
- Pb-In cylinder, vortex-surface interaction, vortex field *(Russian)* 78—27003
- Pb-Tl, small κ type II supercond., flux line lattice, triangular/square transition 78—31025
- Pb-Tl alloys, pinning parameters 78—52173
- $Pb_{80}In_{20}$, flux pinning and flux flow noise 79—56473
- $Pb_{0.871}Sn_{0.129}$, supercond., hysteresis in flux flow characts., normal metal precipitates 78—80107
- V (-Ti), supercond., rotating discs, hysteresis losses and mag. phenomena 80—75695
- V_3Si superconducting bridge junctions, vortex model appl. *(Russian)* 79—60986

flux line motion *see flux flow*

flux pinning
- *see also flux creep; flux flow*
- chain of superconducting rings with trapped mag. flux, elastic length change *(Russian)* 77—63039
- chaotic states of anharmonic systems in periodic fields 80—22288
- Clarke solder-blob junctions, hysteresis studies 79—28478
- critical current, fluxon pinning in supercond. with regularly spaced defects 78—39276
- critical current density, depend. on past history of mag. field and temp. 78—6491
- critical currents, in non-transverse mag. fields, theory 77—55646
- current induced superconducting to normal transition mechanism 79—56468
- cylinder, flux-density gradient and pinning force, flow stress effect *(German)* 77—24653
- DC flux flow voltage and flux flow noise power spectrum local primary interactions 77—72953
- defect-flux line interaction potential, vol. pinning force 77—43790
- deformation of flux line lattice in type II superconductor 79—47213
- dilutely pinned superconductors, nonlinear I-V characts. 79—56479
- distorted vortex lattice, order parameter and mag. field appl. to flux pinning 77—77013
- distorted vortex lattice, order parameter and mag. field appl. to flux pinning 77—77014
- elastic response, large, of fluxoid lattice, plausible arguments for 77—63040
- elastic vortex lattice, pinning by lattice defects 79—56465
- Faraday effect direct obs. of flux-line gradients and vol. pinning forces 77—24651
- film, vortices, static and dynamic interaction with periodic pinning potential 78—52170
- films with periodic thickness modulation, pinning effects 80—88702
- flux pinning force, derivation from a potential 78—68128
- fluxoid-void interaction in type-II superconductors 79—7950
- fluxon dynamics, perturbation anal. 79—11280
- foil, effects of current-induced mag. field on flux flow 77—77012
- foil, rel. to DC voltage induced by superposition of AC mag. field 77—85395
- geometrical peak effect in superconds. with Frank networks, pinning force *(German)* 77—43791
- hard superconductor, flux trapping, penetration depth determ. 80—100572
- hard superconductor influence of thermally activated flux creep on AC response 79—33416
- hard superconductors, mag. instabilities 77—89908

flux pinning continued
- hexagonal lattice with planar pinning forces, elastic response 78—19195
- imperfect vortex lattice, small angle neutron scatt. 79—42710
- inhomogeneous superconductors, nonlocal pinning, inversion temp., and crit. current 79—56475
- Josephson contact, vortex pinning and energy *(Russian)* 78—68117
- Josephson interferometer flux detrapping by ground plane thickness modulation 80—2523
- loss-free current, max. possible, of type-II supercond. with flux pinning 80—84579
- magnetic field dependence of critical current, peak effect in second order supercond. *(Russian)* 78—47924
- magnetic field response, intensity, and direction-varying, nonrot. vortices 80—2535
- magnetic flux structures in superconductors, book 79—91199
- magnetisation, critical state model in nonideal type II supercond. 79—47212
- nonideal superconductor, reversible motion of fluxoids in pinning phenomena *(Japanese)* 80—2537
- nonideal type II superconductor, pin distrib. rel. to V-I characts. *(Japanese)* 79—33421
- one-dimensional analogue model, for pinning study in type II supercond. 78—88086
- one-dimensional system, flux line pinning *(Japanese)* 80—39726
- $Pb_{80}In_{20}$ foil, flux-flow crit. freq. and generalised bundle size depend. on fluxoid traversal distance and length 80—7054
- peak effect, static and dynamic crit. currents obs. *(Russian)* 77—85399
- periodic pinning structures, supercond. vortices 79—38269
- pinning strength, rel. to cooling of sample 80—11141
- by planar imperfections, Ginzburg-Landau theory 78—23218
- plastic deformation of flux line lattice effect on flux transport 77—36035
- point pinning centre flux pinning 77—28321
- randomly pinned type II superconductors, I-V characts. 79—56478
- rotating disc, flux expulsion and trapping 78—6488
- scaling relations in mag., mechanical and superconducting pinning theory 77—76403
- summation curves from TEM data 78—52165
- superconducting foil, pin distribution effect on DC voltage-current characts. 79—99666
- superconducting order parameter perturbation flux pinning 80—103801
- superconductors, tilted vortices, mixed state features in surface layers *(Russian)* 80—29512
- superconductors, type II, determination of surface and bulk props. 79—61011
- superconductors, type II, vortex pinning at edge dislocations, electrostatic mechanism 80—103802
- surface barrier interaction, effect of modulated conc. of impurities 77—55645
- surface sheath, dynamic pinning model of elec. dissipation 77—28320
- technical superconductor radiation damage obs. 79—33422
- trapped flux removal by thermal gradient technique 80—75694
- type II annular superconductor, field replication and flux shielding 77—28286
- type II supercond., rot. in mag. field, flux density distrib. 78—43536
- type II superconductor, cylindrical, rotating in mag. field, dissipation determ. 77—28309
- type II superconductor, dilutely pinned, threshold criteria for pinning force 80—15668
- type II superconductor, hysteretic, flux cutting 79—73647
- type II superconductor, inductive response to trapezoidal magnetic field 78—39277
- type II superconductor, neutron scatt. from imperfect flux-line lattice 79—56474
- type II superconductor, nonideal, with dense pinning centres, threshold criterion 80—88703
- type II superconductor influence of structure defects on resistive and Hall effects *(Russian)* 79—33419
- type II superconductors, magnetic hysteresis and flux profiles, review 79—1651
- type II superconductors, pinning centres influence on voltage-current characts. 79—56470
- type II superconductors, scaling law 79—99663
- type II superconductors, vortex line pinning and I-V characts. *(Russian)* 79—65623
- type II superconductors with current, effect on mag. field distrib. 79—65622
- type superconductor with field-dependent surface barrier, AC losses 79—87216
- volume pinning force for combined attractive-repulsive flux-line defect interaction pots. 77—59363
- volume pinning force for periodical interaction forces between defects and flux line lattice 79—95553
- vortex array, pinning of flux lines by randomly-spaced pinning centres 78—52172
- vortex chain interaction with periodic pinning pot., crit. currents 79—56469
- vortices in supercond., solns. of Gorkov and Ginzburg-Landau theories 79—65624
- Al film perforated with triangular lattice of 1 μm holes, critical currents due to flux pinning 77—28332
- Al superconducting film, edge pinning in perpendicular mag. fields 79—4633
- Al:O, perforated supercond. film, RF resist. in mag. field, pinning force const. 79—56471
- Al:O supercond. film, RF complex impedance meas., dynamic pinning 80—84573
- Al-Ag, torque oscillations in mag. field *(Russian)* 80—103800
- Al-Ag(10 at.%), torque meas., decomp. effect 77—1525
- Al-Na alloy, supercond. flux pinning by precipitates 77—47948
- Cu-Nb_2Sr, multifilamentary supercond. composites, in situ formed, critical currents 79—65625
- Cu-Nb_3Sn superconducting composite, crit. props., AC hysteretic losses 80—50014
- $Cu_{2.5}Mo_6S_8$, evaporated two-phase, crit. current and scaling laws 78—91831
- $Cu_xMo_6S_8$, inhomogeneous superconductor, scaling laws for pinning forces 79—47214
- $Cu_xMo_6S_8$, sputtered, supercond. crit. currents and scaling laws 78—47923
- $Hf_{0.65}Nb_{0.35}$, superconducting alloy, transition temp. and flux line pinning 77—43772

flux pinning continued
- In-Bi, mixed state, pinning centre distrib. statistics, I-V characts. *(Russian)* 80—100571
- In-Pb-In thin film bridge, instability current enhancement in perpendicular mag. field 77—85396
- $LaMo_6S_8$ thin films, crit. currents and pinning forces 80—34575
- $(Mo_{0.6}Ru_{0.4})_{80}Si_{10}B_{10}$, amorphous supercond. matrix, flux pinning by MoRu precips. 80—65756
- Nb and Nb alloys, superconductor, flux pinning under heavy ion irradiation 78—52167
- Nb, bicrystal, flux pinning by grain boundaries 79—24114
- Nb, critical current density, deviation from critical state model 80—84578
- Nb, cylindrical and ellipsoidal, rotational magnetisation and torque meas. in mag. field 78—43515
- Nb, cylindrical specimen, flux-line gradients and pinning forces, Faraday obs. 77—24651
- Nb film, struct. and electrophys. props. at 4.2K 80—80436
- Nb, flux pinning by proton irradiation damage 77—47947
- Nb, flux pinning by voids during neutron irrad. 77—40008
- Nb, high crit. flux density gradient near surface 79—87221
- Nb, irradiated superconductor, fluxoid defect interactions 78—52166
- Nb, neutron irradiation, low temp., 15 MeV, effect on superconducting props. 78—52179
- Nb, nonequilib. mixed state, with pinning centres, mag. flux interactions *(Russian)* 78—39275
- Nb, peak effect due to vortex pinning in subsurface layer *(Russian)* 80—93060
- Nb, plastically deformed, flux density gradients and pinning forces, Faraday effect obs. 79—61010
- Nb, proton irrad., dislocation loops and mag. flux pinning 79—56463
- Nb, single crysts., fluxoid pinning by small nitride precips. 80—70913
- Nb, supercond., dielastic interaction of flux line lattice with internal stresses of cryst. imperfections 78—56270
- Nb, superconducting, hysteresis in time depend. fields up to 3 kOe 77—24637
- Nb, torque anisotropy due to defects, flux line pinning 77—20509
- Nb, type II superconductor, Faraday effect, flux density gradient determ. 79—24113
- Nb, with Nb_2N precipitates, flux pinning, magnetization, bulk flux density gradient, and neutron scatt. meas. 79—56472
- Nb:O, type II supercond., radiation-induced flux pinning 78—80106
- Nb-Ge film, CVD and sputter deposited, critical current density and stability 77—28327
- Nb-H single crysts., critical current and flux pinning *(Russian)* 77—47946
- Nb-Hf (38 at.%) superconductor, peak effect, summation problem, mag. history flux pinning force 80—20362
- Nb-Ta, supercond., transport current distrib., neutron small angle scatt. study 79—42711
- Nb-Ta (54 at.%) cylinder, superconducting mag. and resistive behaviour 77—8252
- Nb-Ti, optimised pinning struct., crit. data 1.8-4.2K 77—89913
- Nb-Ti, pinning curves, high field J_c and scaling behaviour 80—93064
- Nb-Ti, pinning mechanism at high mag. fields 79—95555
- Nb-Ti, sheet, flux trapping, appl. to mag. shielding and levitation 80—31806
- Nb-Ti, superconductivity after heavy ion irradiation at low temps. and high fluence 77—69437
- Nb-Ti alloys, crit. current density, scaling law 78—31027
- Nb-Ti/Cu composite disc, crit. state model for crit. current determ. 79—99665
- Nb-Ti/Cu sheet composite, flux trapping and shielding capabilities in transverse fields 80—15667
- Nb-Ti-Ta, pinning curves, high field J_c and scaling behaviour 80—93064
- Nb-Ti-Zr, superconducting, critical current density and microstruct. correlation *(Japanese)* 79—61748
- Nb-Ti(Mo), AC loss minimum, pinning, flux distribution 80—84574
- Nb-Zr, deformed strip, pinning force, widely varied j_c, temp. and mag. field variations *(Russian)* 79—7948
- Nb-Zr, type II supercond., radiation-induced flux pinning 78—80106
- Nb_3Al multifilamentary cable fabrication and props. 79—33438
- Nb_3Ga, critical data, under hydrostatic pressure to 15 kbar 79—47217
- $Nb_3(Ge, X)$, X=Si, Ga, CVD tapes, supercond. props. at high mag. fields 79—38279
- Nb_3Ge, CVD, hysteretic losses, precipitates and deposition temp. effects 77—28319
- Nb_3Ge, CVD, impurity doping effect on supercond. crit. props. 78—52174
- Nb_3Ge CVD tapes, supercond. props. at high mag. fields 79—38279
- Nb_3Ge, CVD-prepared, high field props. and scaling 79—56455
- Nb_3Ge film, critical current density and flux pinning 77—20510
- Nb_3Ge film, prepared by cosputtering, supercond. props. 79—4634
- Nb_3Ge films, correl. between crit. current density and microstruct. 79—38277
- Nb_3Ge, inhomogeneous superconductor, scaling laws for pinning forces 79—47214
- Nb_3Ge, projected critical current, comparison with $PbMo_6S_8$ 79—69642
- Nb_3Ge, supercond., projected upper limits to crit. current density 77—36037
- Nb_3Ge, supercond. film, prep. by chem. transport reaction, critical props. 79—47635
- $Nb_2Ge_{1-x}Ga_x(Sn_x)$ CVD films, supercond. props., 4.2 to 19K 79—42713
- $Nb_3Ge_{1-x}M_x$ (M=Ga,Sn), pseudo-binary, scaling laws for supercond. crit. currents 79—24118
- NbN, critical data, under hydrostatic pressure to 15 kbar 79—47217
- NbN diffusion wires, crit. currents and supercond. crit. field under high press. 79—38287
- $NbSe_2$:Mn, supercond., anomalous flux flow and matching 77—12069
- Nb_2Sn, filamentary segments, flux pinning, proximity effects, percolation thresholds 78—56269
- Nb_3Sn, AC losses, low field behaviour, morphology depend. 77—24655
- Nb_3Sn bronze process, flux pinning scaling law depend. on strain 80—75696
- Nb_3Sn composites, crit. currents and microstruct. 79—38280
- Nb_3Sn, crit. current ang. depend., prep. conditions effect 77—47949
- Nb_3Sn, crit. current density, low dose fast neutron irrad. effect 78—14910
- Nb_3Sn, critical current density 78—52176
- Nb_3Sn, critical current enhancement by low temp. fast neutron induced flux pinning centres 78—52177

flux pinning continued
- Nb_3Sn, critical data, under hydrostatic pressure to 15 kbar 79—47217
- Nb_3Sn, dependence of max. trappable field on supercond. cylinder wall thickness 77—72952
- Nb_3Sn, filamentary superconducting composite, TEM 77—80887
- Nb_3Sn, flux density gradient determ. by Faraday effect 80—107969
- Nb_3Sn, flux trapping and shielding capabilities in transverse fields 80—15667
- Nb_3Sn multifilament conductors, strain effect on crit. props. 78—80108
- Nb_3Sn, multifilament superconductor, pulsed mag. field losses and critical current densities 80—54853
- Nb_3Sn multifilamentary composite superconductor, effect of heat treatment on supercond. props. 79—33376
- Nb_3Sn multifilamentary composites, crit. currents, flux pinning, and crit. field 79—78280
- Nb_3Sn multilayered supercond. power line conductors, elec. props. and growth morphology 77—28325
- Nb_3Sn, neutron irrad., crit. current change rel. to temp. and metallurgy 78—80109
- Nb_3Sn, neutron irradiation at 8K, supercond. crit. current and crit. temp. meas. 77—28334
- Nb_3Sn, radiation damage effect on superconducting props. 78—52127
- Nb_3Sn, supercond., effect of trapped mag. flux on AC losses 79—33420
- Nb_3Sn, supercond., production of high current carrying strip *(Russian)* 79—33435
- Nb_3Sn, supercond., projected upper limits to crit. current density 77—36037
- Nb_3Sn, supercond. diffusion layer, Zr content and Nb cold working effects 77—16015
- Nb_3Sn, superconducting, formed from Cu-Sn alloy, props. 79—42709
- Nb_3Sn superconducting multifilamentary wire, stress effects 79—33431
- Nb_3Sn, superconducting props., effect of radiation induced atomic disorder 78—52133
- Nb_3Sn superconductor, low temp. deuteron irradiation 78—52182
- Nb_3Sn, vap. deposited supercond. film, effect of N_2 and tape heating 78—34939
- $Nb_3(SnGa)$, wire, neutron effect on T_c, I_c and flux pinning 79—38216
- $Nb_3(Sn_{1-x}Ga_x)$, bronze processed wires, critical current densities in fields up to 23.5 T 78—47922
- $Nb_{73}Ta_{27}$, supercond., flux density distrib. meas. 77—32129
- $Nb_{73}Ta_{27}$, supercond., flux pinning by precipitates 77—47948
- NbTi multifilamentary wires, 30 GeV proton irradiated, effect on crit. currents 77—89911
- NbTi, superconducting, orientation effects on magnetisation 77—28287
- NbZr, thermally activated flux creep, effect on AC response 79—33416
- Pb foil, crit. current density, pinning force density, shadow electron microscopy obs. 80—88696
- Pb-Bi (12 at.%), Sn fibre reinforced type II superconductor, flux pinning *(German)* 77—85397
- Pb-Cd, oriented lamellar superconductor-normal composite, supercond. 79—1650
- Pb-In, containing Ag particles, flux pinning in superconducting matrix 80—2534
- Pb-In (5%), supercond. mobile dislocation density, instantaneous flux change meas. 80—15670
- Pb-In (50 wt.%), supercond., pinning effect 80—15669
- Pb-In alloys, flux pinning at grain boundaries 80—34572
- Pb-In alloys, vortex pinning on grain boundaries *(Russian)* 77—89910
- Pb-In film, supercond. surface sheath, dynamic pinning model of elec. dissipation 77—28320
- Pb-In-Ag, transport current distribution in longitudinal mag. field 80—25057
- Pb-Na, peak-effect supercond., flux pinning 78—95403
- Pb-Na (8.4 at.%), supercond., surface flux pinning, crit. state model 80—97044
- Pb-Na alloy, with Pb_3Na precips., flux pinning, crit. currents obs. *(German)* 78—14907
- Pb-Sn, proximity and pinning effect up to 7K *(French)* 77—51858
- Pb-Tl alloys, pinning parameters 78—52173
- $Pb_{0.8}In_{0.2}$, flux-flow noise 79—95556
- $Pb_{80}In_{20}$, flux pinning and flux flow noise 79—56473
- $Pb_{80}In_{20}$ foil, deformed, annealed, correlation between pinning strength and flux flow noise charges 77—43792
- $PbMo_6S_8$, inhomogeneous superconductor, scaling laws for pinning forces 79—47214
- $PbMo_6S_8$, projected critical current, comparison with Nb_3Ge 79—69642
- $PbMo_6S_8$, sputtered film, critical current density meas. 78—84369
- PbNa, type-II superconductor, regularly ordered precipitates, peak effect, crit. current meas. *(German)* 78—19196
- $Pb_{0.871}Sn_{0.129}$, supercond., hysteresis in flux flow characts., normal metal precipitates 78—80107
- PnBa, supercond., flux density distrib. meas. differential magnetisation loop method 77—32129
- $(SN)_x$, supercond., obs. of Meissner effect 78—6478
- V, superconducting, fluxoid pinning by VC_x precipitates 78—52169
- V, superconducting props., effect of voids 78—52168
- V-H single crysts., critical current and flux pinning *(Russian)* 77—47946
- V_3Ga, high current density multifilament wire, neutron effects on equilibrium and transport props. 78—52126
- V_3Ga, multifilament superconductor, pulsed mag. field losses and critical current densities 80—54853
- V_3Ga multifilamentary wires, effect of low temp. neutron irrad. 77—32132
- V_3Ga, pinning characteristics *(Japanese)* 78—91829
- V_3Ga, supercond., projected upper limits to crit. current density 77—36037
- V_3Si, H_{c2} anisotropy in high field, grain boundary flux pinning 78—43532
- V_3Si, neutron irrad., volume pinning force, summation and saturation behaviour 79—95554
- V_3Si, supercond. mixed state, low temp. tetragonal-domain-reorientation phenomena, US expts. and thermal props. 80—60141
- Zr-Nb (20%), low-j_c supercond. vortex pinning *(Russian)* 77—80885

flux vortex flow *see flux flow*

flux vortex lattice *see flux-line lattice*

fluxmeters
- *see also magnetic field measurement; magnetic flux*
- development review, 1980 status *(French)* 80—95114
- electronic, construction, appls. *(German)* 77—74467

fluxmeters continued
- gaussmeter, Hall-probe adapter cct. for use with digital multimeter, leakage detect. 80—37014
- Hall-effect magnetic field detection, for fields down to 10^{-3} T 80—244
- magnetic saturation measuring coil and fluxmeter system 78—93738
- measurement range extension 78—57993
- micro, MHD motion in water 78—79384
- MIS-3M magnetic measuring system (USSR), testing small permanent magnets 80—62699
- radially resolving diamagnetic loop, appl. to flux conservation test 78—12734
- superconducting, quantum, with 15 to 20 kHz passband 80—57345
- testing, using semiautomatic potentiometric apparatus 77—74464

fluxoid array *see flux-line lattice*

foams
- *see also bubbles*
- black foam films stability, review 80—104463
- breakdown, syneresis, drainage rate rel. to time 80—11954
- bubble size distribution, changes due to interbubble gas diffusion 78—85204
- colloidal crystal latex, nonlinear electro-optical props. 79—61337
- detergent foams, UHF radiation scatt. *(Russian)* 77—6978
- education, bubble cohesion in foam, binding energy calc. 78—61978
- electrical conductivity, rel. to degree of aeration 79—57299
- emulsive foams, UHF radiation scatt. *(Russian)* 77—6978
- ethylene-propylene-diene terpolymer, sulphonated, ionically cross-linked, foam elastomer, thermo-mech. props. 78—48362
- explosive charge detonation, shock wave parameters 77—15062
- fibre reinforced polyurethane foam, with chopped fibres, morphology and fracture 77—36447
- gas-liquid emulsions and foams, electrical conductivity 80—11961
- glass fibre reinforced polyurethane foam fracture toughness, modulus increase 78—44196
- graphite foam, thermal props. 77—48689
- interbubble gas diffusion, effect of initial bubble size distribution 79—79304
- latex particles, kinetics of flocculation under effect of protein 80—11958
- liquid-saturated open cell foam in circular tube acoustic wave propag. 79—41470
- LMFBR postulated core meltdown, onset of foam flow regime in volume heated boiling pool 79—31015
- metal, solidification in space environment, fluid flow effects 79—47674
- methane-O_2 aquamechanical foam, propag. characts. of detonation waves 78—31713
- nozzle, convergent-divergent, choked foam flow 79—64750
- nozzle, convergent-divergent, choked foam flow 80—74940
- ocean surface simulation, spectral characts. of microwave thermal emission from foams *(Russian)* 78—69353
- oil-water system, vibrational mixing and periodic struct. formation in artificial weightlessness *(Russian)* 77—59118
- optical glass, K8, foam form. and suppression methods during polishing 80—28364
- physical chemistry of surfaces, book 77—25310
- plastic, shock absorbing capacity determ. *(German)* 80—19877
- plastic foam layer beneath sheets, NDT *(German)* 77—1896
- plastic modular solar energy collector with reticulated foam 80—16833
- polyethylene, electron beam crosslinking process for high voltage power cable 80—66846
- polyethylene, foam growth, thermomech. anal. 80—3416
- polyethylene, low density foam, two-step heating process *(Japanese)* 77—52369
- polyethylene, low density foam production, viscosity meas., comparison with polystyrene *(Japanese)* 77—52276
- polyhedral foams, limiting cond. at low density, theory 78—44410
- polyisocyanurate foams, strength, cellular struct. effect 80—40518
- polymer, foamed, rigidity 78—95769
- polymeric foams, cell cracking 79—11701
- polystyrene foam, X-band microwave dielectric spectra 79—87376
- polystyrene hollow microspheres form., kinetic regularities *(Russian)* 79—57307
- polyurethane, foam, for organic material sampling in ambient air 78—20080
- polyurethane, foaming parameters determ. from US wave vel. 80—71885
- polyurethane, insulation for cylindrical cryogenic container, estimation of steady state heat link 79—35750
- polyurethane, press. wave propag. and refl. characts. 77—35634
- polyurethane, rigid, thermal expansion behaviour, mech. differential dilatometer method *(German)* 79—37859
- polyurethane foam, fast-neutron gauging for void detection 78—7157
- polyurethane foam, processing machines and systems, motor car components appl. *(German)* 80—71955
- polyurethane foam, rigid, gaseous thermal decomposition products, IR anal. *(German)* 79—29348
- polyurethane foam, SiO_2 particulate filled, mechanical props. 79—11666
- polyurethane foam, X-ray exam. *(German)* 78—75596
- polyurethane foam layers, open-cell, refl. characts. for ultrasound in air 78—83139
- polyurethane foam plastics, sorbents for marine oil pollution 79—53011
- polyurethane foam plate, response to acoustic noise impulse *(French)* 79—1033
- polyurethane foam solar concentrator, thermal and thermohydrolytic ageing 78—92281
- polyurethane foams, strength, cellular struct. effect 80—40518
- polyurethane rigid foam, fracture props. over range of densities 79—79106
- polyurethane solid foams, creep laws *(German)* 80—65139
- pool boiling with foam form., anal., fission reactor safety appl. 77—31341
- porous medium, foaming, liquid and gas relative permeabilities 80—33669
- propane-O_2 aquamechanical foam, propag. characts. of detonation waves 78—31713
- PVC, density rel. to rheological, surface props. of PVC pastes *(Polish)* 78—85212
- PVC, plasticised, foam growth, thermomech. anal. 80—3416
- shock wave dispersion 79—46359
- soap foam, arrangement of cells in a net rel. to grain sections of polycryst. 80—70225
- solar-energy concentrator, foam-film parabolic-cylindrical, surface fabrication 80—21372

foams continued
- sound-absorbing foam materials, effects of outdoor exposure 77—88985
- stabilisation by polymer solns. *(French)* 80—21323
- stability, interfacial phenomena interpretation using schematic density profiles 78—60012
- stability relation to structure, criteria derivation w.r.t. drainage stage 80—69904
- syneresis in Plateau-Gibbs channels of foams with high press. gradients, capillary press. 80—74948
- thermal radio emission from foam structures 79—29497
- thermoplastic structural foams, charact. by equidensitometry and radiography 77—44417
- thin films with nondeformable surfaces, generalized equations of hydrodynamics 80—10224
- thin liquid film, instability and rupture 80—34279
- urea-formaldehyde resins, book 80—73114
- urethane foams for noise abatement, physical and acoustical props. 79—18592
- US characts. of open-cell polyurethane foam layers for airborne appls. 80—96597
- C, glassy, props. 77—24976
- C-C composite material, syntactic-foam type properties 78—44169
- H_2O foams, shock wave propagation 79—64737

focused collision sequences *see sputtering*

focusing
- *see also self-focusing*
- 3-electrode axisymmetric lens, cardinal elements 77—30221
- Abbe's theory of imaging, lecture-room demonstration 78—41120
- aberration-free lens, near focus intensity distribs. for Gaussian and const. intensity beams 77—615
- acoustic beam, computer-controlled, with variable frequency array transducers 80—38191
- acoustic beam, self-focussing by thermal self-action 77—3692
- acoustic focusing device, with interdigital transducer 78—9520
- acoustic focusing systems, nonlinear effects 79—32126
- adaptive focusing of light in inhomogeneous nonlinear medium, interf. criteria 80—99633
- adaptive optical components, seminar, Washington (1978) 79—59792
- annular aperture lenses for scanning otpical microscopy, depth of focus 77—65054
- annular beam profile changing by aperturing diffr. pattern 80—18991
- astronomical telescope focusing mechanism, semi-kinematical design 79—96918
- atmospherically degraded beam, intensity fluctuations at focus of large lens 77—64425
- atomic beam, focused with laser beam, Na beam and dipole forces 79—7066
- atomic beam focusing by reson. radiation press., quantum fluctuations influence 80—58217
- attenuated total reflection with focused light, appl. to guided waves on grating 78—74992
- autofocus camera, mechanisms *(Japanese)* 79—75640
- automatic camera lens focusing, using optolinear chip 78—54480
- automatic focusing of cameras using self-contained IC 78—82069
- automatic focusing system, Visitronic, description for photo- and film cameras *(German)* 79—6200
- background limited system, defocused slit aperture, partial coherence 77—618
- beam line magnet misalignment effects 77—30688
- beam propagation in focusing media with random-axis misalignments: Second- and higher-order moments 79—17236
- bent glass optics 78—45767
- Busch method for determ. of specific charge on electron, errors in textbook treatment *(Russian)* 78—9311
- camera, Polaroid Sonar One-Step, US automatic focusing 78—78011
- camera, resolving power type, sinusoidal targets design and construction 77—53999
- camera, SX-70, automatic focusing by US echo ranging 79—93239
- camera automatic focusing mechanism principles and designs 79—30595
- camera lenses, automatic focusing systems 80—18028
- caustics, crit. exponents from catastrophes, focusing and twinkling 78—22084
- centrifugal electrostatic shaping of high intensity electron beams 80—13183
- CERN Proton Synchrotron focus control, pole face winding design and field correction 79—31299
- channel for high-current beam transportation, design parameters 79—59291
- charged particle beam focusing, using aberrational quadrupole lens system 79—26180
- charged particle beam focussing by cryst. film for colliding beam expt. *(Russian)* 79—67426
- charged particle motion in alternating elec. fields, scaling conditions 80—63903
- charged particle motion in mag. field, acceleration and focusing 78—1142
- charged-particle beam, axisymmetric, focusing in hyperbolic electrostatic field 78—50688
- Cherenkov counter, ellipsoidal mirrors, fabrication and use 80—47818
- Cherenkov counter, multiplexed focusing, optical system 80—47819
- Cherenkov radiation focusing, electric piston effect, appls. 79—55041
- chromaticity corrections, second order effects in sextupole-corrected SPS lattice 79—76196
- clinical microwave focusing thermography 80—3771
- close focusing, new optical solns., macro mirror lenses 79—93240
- close focusing, new optical solns., spherical aberrations 79—97453
- coherent anti-Stokes Raman spectroscopy, with focused laser beam, power generation 78—4701
- cold neutron beam polarising supercond. hexapole magnet 79—31300
- collimated light beam, focus and alignment sensing 78—59065
- collimator critical focusing, auto-collimation technique modification 78—42424
- combined focusing and deflection systems, electron trajectory aberration formulae 78—45756
- contact microscope for medical laboratory use 80—85540
- continuous zoom forward-looking IR optical system design and implementation 79—23046
- CW laser beam stablisation by spatially dependent absorption 79—76740
- cyclotron, AVF, central region, changes of puller shape, axial focusing 80—74050

focusing continued
- cyclotrons, alternate gradient focusing 80−27841
- cylindrical capacitor with oblique ends, ion optical coefficients determ., first-order focusing 80−63912
- cylindrical condenser, electrostatic prism appls. 77−6992
- cylindrical fibre with symmetric index distrib., matrix analysis 77−84001
- cylindrical parabolic focusing collector for distributed-collector solar power system 79−62108
- cylindrical particle analyser, fringing field 78−94165
- defocus spread and illumination aperture effect, in brightfield electron microscopy 79−231
- defocused optical system under partially coherent illumination, apodised aperture performance 77−10847
- deformation measurement, out-of-plane, using holographic interferometry and speckle photography, comparative accuracy 80−78804
- differential spectroscopy of charged particle beams, cylindrical mirror 77−50600
- diffused channel waveguides, direct index meas. 80−87562
- dissociation of SF_6, focussed beam approach 78−42369
- distorted image convolution deblurring by Fourier-Bessel transform holograms *(Russian)* 79−22897
- double focusing bending magnet, meas. of optical props. with thin alpha source 78−55073
- double focusing mass spectrometer, second order, aberrations, stigmatism 78−21256
- double-focusing electron spectrometer, new effective transmission determ. from focalization props. 78−17463
- dye laser fast light deflection, ultrahigh resolution 78−63178
- dynamic-focusing mirror system, umbrella-type 79−36971
- dynamically focused array imaging systems, induced Doppler distortions 79−46117
- dynamically focused electronic sector scanner based on CCDs 80−98042
- dynamically focused US diagnostic phased array 78−61232
- earthquake, stick slip, rupture propag. and energy focusing in foam rubber model 80−3947
- electric-magnetic focusing deflection system, relativistic aberrations formulae 78−13653
- electro-optical image sensors, performance evaluation of focal planes for aerial reconnaissance 79−31833
- electron beam, high-current, focusing in vac. chamber with dielec. walls *(Russian)* 77−83801
- electron beam, relativistic, focusing limitations in low-press. gas 79−41322
- electron beam, small perturbation anal. 77−50602
- electron beam distrib. function in focusing mag. field *(Russian)* 78−82898
- electron beam focal spot size, input phase characteristic nonlinearity effect 80−5678
- electron beam focusing theory, nonlinear differential eqns. *(Chinese)* 79−31783
- electron beams, intense, ion focusing and mag. self-focusing 78−331
- electron beams, point focusing through different vacuum lines 79−45499
- electron beams, shaped practical focus-deflection system 79−76572
- electron gun, triode, keV anode-controlled telefocus, focusing props. 78−342
- electron image, focusing with strong magnetic field in image convertor 78−5556
- electron lens, unipotential, focal and aberration props. calc. 77−68162
- electron lens system for optimum deflection sensitivity 80−23615
- electron micrograph, 500 kV, atomic resolution, computer image processing 80−100149
- electron micrograph optical and digital spatial freq. filtering 78−70231
- electron microscope defocusing depend. of lattice plane image contrast *(German)* 78−38594
- electron microscope image interpretation, instrumental, environmental conditions *(Polish)* 79−30623
- electron microscope objective lens focus and spherical aberration meas. 77−54024
- electron microscope resolution improvement for crystal structure imaging and atomic movement dynamic obs. 80−70090
- electron microscopy, imaging of thin phase objects, tilted and extended 80−99617
- electron optical devices, static multipole fields, numerical calc. 77−588
- electron probe, compensation of aberrations, dynamical focusing with stigmator 80−87291
- electron resonant motion in polarised EM plane wave, spontaneous phase focusing 79−68357
- electron spectrometer with double focusing, adjustment with nonuniform mag. field 77−6606
- electron-beam focusing optimisation with specified image parameters 78−86385
- electron-ion wedge-shaped beam, focusing electrodes shape calc. 80−53202
- electron-lens systems used in low-energy electron or ion scattering, geometries and focal props. 79−50202
- electrons, transverse focusing at large emitter currents *(Russian)* 80−87280
- electrostatic analyser, spherical, focusing using supplementary electrodes 77−9155
- electrostatic analyser with oblique cut plates, focusing props. 77−54667
- electrostatic crossed lens, for electron microscopic devices 80−87289
- electrostatic double cylinder lenses, spherical aberration coeffs. and focal props. 79−86124
- electrostatic energy filter, telescopic, with cylindrical mirror analysers 80−87296
- electrostatic lenses, focusing of GeV particle beams 80−74061
- electrostatic mirror, approx. cylindrical field, focal line correction 77−50599
- electrostatic mirror, ion beam focusing for low energy heavy ion accelerator 77−14654
- electrostatic mirror, second order focusing space charge effects 77−50598
- electrostatic mirrors for heavy-ion manipulation and focusing 77−10520
- electrostatic transaxial lens, curved charged particle beam focusing, image coords. and aberrations 78−46503
- ellipsoidal particles, by electrostatic fields, theory 78−5411
- elliptical Gaussian beam, propagation and focusing anal. 79−50873
- EM field, in focal region of wide-angular annular lens and mirror systems 78−90485
- EM wave propagation in inhomogeneous uniaxial anisotropic medium 80−32890

focusing continued
- energy distribution of converging spherical wave for small Fresnel nos. 79−3626
- energy-focused atom probe design and performance 78−85276
- exact transport eqn. for randomly perturbed focusing medium 79−81344
- Fabry-Perot focusing properties in multiple-beam holography system 79−13927
- Fabry-Perot interference rings, focusing props. 77−58454
- Fabry-Perot type interferometers focusing and beam shifting props. 79−6168
- Faraday double transmitting cup, ion optical control device 78−82556
- Fermilab, 100 GeV beam storage, improved chromaticity control 79−76187
- Fermilab neutrino focusing horn, pulse stretching in high current power supplies 77−83367
- fibre, gradient-index light-focusing, image enhancement 80−69501
- fibre preforms, index profile determ. using focusing technique 79−50464
- fibre-optic integral data source/receiver package 78−63179
- fibre-optic light source for curved platen illumination 78−63163
- field generation, geometric and analytic solns. *(Russian)* 79−64164
- flat-field spectrograph design, holographic grating appl. 80−68264
- focal plane design and optimal processing for scattered optical fields 78−78935
- focometer, F-1, for lens focal length meas. 80−64138
- four-channel laser system with four-ellipsoidal-mirror set-up for focusing laser beams 79−94276
- four-point field coherence function meas. in laser random focusing region *(Russian)* 78−58910
- Fresnel images, depth of focus 80−1145
- gas, harmonic generation by divergent radiation *(Russian)* 78−22170
- gas, resonance four-photon shift, optimal focusing of high-power pumping 80−95574
- Gaussian beam, focused truncated, spot size evaluation 79−59737
- Gaussian beam propagation, Fresnel-Kirchhoff integral anal. 79−45984
- Gaussian laser beam focus, intensity distrib. determ. 79−14002
- glint tracking by adaptive optical techniques 77−19458
- gradient-index imaging, theory 80−69331
- grainless focusing screen for cameras and microscopes, light scatter reduction appl. 80−101836
- grating acoustic scanner for material defects 79−47878
- grating coupler, chirped and curved, for focusing beam 80−78979
- gravitational lens effect, focusing by slowly rotating relativistic spherical mass 80−105155
- grazing incidence spectrograph-monochromator with focusing toroidal mirror 79−75617
- gross surgical specimen photography, centimetre rule/elevator rod technique 78−61287
- heavy ion, alternating phase focusing in linac 77−38476
- heavy ion beam focusing, accelerated, decelerated beam, electrostatic lenses 78−89588
- heavy-ion intense beam, periodic focusing, mag. channels 78−55079
- heavy-ion simulated neutron damage facility at ORNL 77−75011
- heavy-ion superconducting linac, alternating phase focusing 77−3194
- heptafluoroiodopropane light amplifier, wave-front distortion due to photolysis-gas dynamic effects 79−18412
- high-current electrostatic scanner-deflector 77−13820
- high-perveance electron beams with Brillouin focusing 77−83802
- holographic optical element, mathematical equivalence with ultra-high index lens 79−59653
- holographic plane gratings, self-focusing, aberrations 77−58450
- holography, long-wavelength hologram focusing parameters, estimation method using focused pattern 80−14304
- horn design for focused SAW radiation into waveguide 78−1542
- hyperopic eye functional visual acuity at intermediate range 78−48791
- image contrast theory of electronic focus 79−13914
- image formation with ultracold-neutron waves 80−78752
- image sharpness adjustment, teleobjective types characteristics *(Hungarian)* 78−12780
- imaging plastic focusing fibre with parabolic refractive index distribution 77−19437
- infrared telescope, 6032 image conversion tube 80−42020
- injection laser, for scanning applic. 77−19324
- instrument focusing to take account of eye accommodation 80−101811
- intense ion beam, production and focusing from self-pinched relativistic electron beam 77−24206
- intense relativistic electron beam focusing with large aspect ratio diodes 77−23610
- interstellar charged dust grains, EM focusing to solar mag. equator 80−4300
- ion beam, in dense plasma with 100 A to 10 kA current *(Russian)* 77−7561
- ion beam, intense, adiabatic wall focusing for thermonuclear microexplosion ignition 77−61611
- ion beam, intense, neutralised, ballistic focusing in pinched electron beam diode 78−9859
- ion beam, propag. and defocusing in plasma background 77−11359
- ion beam, quasineutral, intense, focused, max. current density, Coulomb interaction 77−54666
- ion beam focusing and neutralised transport 78−50323
- ion beam focusing by means of mag. insulated diodes 78−50324
- ion beam focusing designs for sputter deposition 79−78880
- ion beam focusing from quadrupole mass filter using electrostatic lens 79−229
- ion beam focusing in intense mag. insulated ion diode, particle diagnostics 78−9858
- ion beam production in spherical magnetically insulated diode 79−85200
- ion beams, prod. and focusing for fusion 78−50322
- ion beams for pellet fusion, focusing and prod. 77−83353
- ion imaging for ion implantation and micromachining *(French)* 80−34027
- ion linacs, permanent magnet quadrupoles, development 77−38494
- ion linear accelerator, synchronous phase focusing, standing wave continuous interaction *(Russian)* 77−38444
- ion optical focusing in cylindrical mirror analyser, space charge effects 78−25791
- ion optics, sector mag. analyser, fringing fields and focusing 79−41328
- ion-beam optimal focusing, compensated beams in plasma *(Russian)* 77−76109
- ion-optical system, planar, axisymmetric mag. focusing, foci outside field 80−5680

focusing continued
ions, trajectory in const. mag. field plus orthogonal sinusoidal elec. field 78—50687
IR laser system alignment using Smartt interferometer 80—33072
ISOCELE high-current on line separator development 77—26922
JOSEF gas filled separator, focusing and dispersive props. 77—26426
kidney stone contactless destruction by US shock waves 79—48300
large F-number optical system, focal spot shift 78—1175
large-spot laser damage meas., multibeam apparatus 77—19286
laser, multiple-beam pellet irradiance, diffraction analysis 78—50845
laser beam, far-field profile, focal plane technique 78—87087
laser beam, focused, scattering by moving particles 80—48149
laser beam, Gaussian, apertured, focal length and target range estimation 77—19299
laser beam, high power, focusing props., influence of nonlinear refractive index medium *(French)* 78—46696
laser beam, low power, in inhomogeneous plasma 79—73014
laser beam, monochromatic, multielement objectives synthesis, optical storage system design appl. *(German)* 77—68231
laser beam deflected by prismatic polygon mirror, focus path 77—19267
laser beam defocusing reduction, by circ. scanning *(Russian)* 77—83917
laser beam diffraction focusing by sequence of irises 79—50332
laser beam distrib. in focal region, transmission monitoring through pinhole 78—90441
laser beam divergence meas., focus errors 78—46692
laser beam focused in plane target, jet form., investigation using wavefront method 80—75103
laser beam focusing, geometrical optics model, focusing system design 77—7109
laser beam focusing, wave front convolution effect *(Russian)* 79—45990
laser beam focusing by reflection kinoform 77—79780
laser beam metal-coated apodising apertures 77—19439
laser beam optimal focusing conditions for freq. doubling 79—14036
laser beam with retractable focus, ionis. path form. in gases 79—18992
laser beam-exploded aerosol, light focusing and defocusing 80—8426
laser collimation and focusing at given distance *(Russian)* 78—29959
laser diffraction-limited system, resolution, intensity, and power distribution 77—58425
laser focus movement, nonlinear optical technique 80—74446
laser focusing lens design for hot spot elimination 79—72658
laser focusing lens design for nucl. fusion 77—18706
laser focusing objectives, flare image danger reduction 79—22997
laser focusing onto spherical plasma target, max. absorpt. optimisation 77—3967
laser focusing optics for fusion appl., lens and mirror design 77—3641
laser focusing optimisation in spherical plasma *(Russian)* 78—1863
laser fusion reactors, optical design, focusing optics 78—82518
laser light, effect on melting of steel *(Russian)* 77—59823
laser linear, annular and radial focusing with axicons, laser maching machining appl. 78—66856
laser material processing, workpiece focal point window tolerances 80—5776
laser microphotometry with laminar hydrodynamic focusing 77—37965
laser radiation, prism raster focusing device 77—19272
laser radiation distrib. characteristic determ. in vicinity of focus 79—50871
laser radiation focusing device 78—13742
laser recording with truncated Gaussian beams and focusing lens 79—81474
laser resonator, compensation of coma and astigmatism 77—34898
laser resonator-focusing system, power density improvements, anal. 79—50335
laser speckle for focus-position sensing 79—59785
laser spherical target irradiation symm. calcs. 80—23140
laser system, high energy, thermally induced optical distortion 80—38051
laser velocimeter optical scanning system 77—58481
lattice image formation, many-beam theory, TEM 80—38879
Lau effect, explanation based on coherence theory 80—23619
lens, gradient-index rod, evaluation by imaging 80—69485
lens, intensity fluctuations in turbulent atmosphere, with (without) central screening 79—7080
lens, three-electrode , crossed, electron focusing, spherical aberration 78—33659
lens aperture, rel. to depth of focus 78—12489
lens centring monitors design, using variable parameter system *(Russian)* 78—50883
lens system design with extended depth of focus, Version 14 optimisation program 78—90489
lens-array photographic system, depth of sharp focusing, resolution 80—62763
lens-axicon doublet illuminated by Gaussian beam, ring focal pattern 78—55421
light, in Kerr metric, appls. of geometrical optics, analytical results 77—29637
light beam, in moving nonlinear media, using gradient method 80—106578
light beam streaking by electro-optically induced travelling lens 79—46045
light concentration using inversion of wave front technique *(Russian)* 78—63154
linac, superconducting heavy-ion, hybrid solenoid as focusing element 77—38460
linac bunch shape meas. and double drift harmonic buncher 77—38471
linac Buncher, high efficiency for injection 77—38472
linear accelerator, hollow-beam, with phase focusing, limiting current 79—18065
linear accelerator incompatibility theorem, stability and focusing 77—3195
linear accelerator with solenoid focusing, stable particle motion 79—72000
linear accelerators, postacceleration and bunching of 150 MeV ^{58}Ni ions 77—34484
linear accelerators with space uniform quadrupole focusing 79—71998
linear high current ion accelerators utilising electron neutralisation 79—72016
linear proton accelerator, parameter errors, theory 77—30678
linear proton accelerators, possible use of quadrupoles with permanent magnets 77—23320
liquid surface deform. due to laser radiation thermal action, lens effect 80—33048

focusing continued
low-aberration focusing fibre, optimum diffusion exchange and heat treatment 78—1378
luminescence spectroscopy using Weierstrass sphere geometry 77—49777
magnetic focus generation for NMR biological meas. *(Japanese)* 79—12041
magnetic focusing of electrons in Cu 79—65540
magnetic lens, wide-angle focusing device for low energy π collection 78—70664
magnetic prism, design, for TEM energy filter 80—86523
magnetic spectrometer, corrected second-order aberrations 80—87013
magnetic vector man analyser, stigmatic focusing condition 78—70215
magnetoplasma, coaxial Gaussian EM beams cross focusing, plasma wave generation 79—32779
mask linewidth meas. effects of optical microscope operating parameters 77—37977
mass spectrometer electrostatic analyser attachment 78—86377
mass spectrum, second order image aberration correction by electrostatic hexapole lens 78—70216
mass-separator beam, quadrupolar focusing lens system 80—47801
matching focons, optical props. 79—27168
matrix multiplying optical system resolution calc. *(Russian)* 79—98456
mega-ampere ion beam production and focusing using self-pinched electron flow 77—24205
metal target, gas breakdown near surface, pulsed CO_2 laser focusing effect 79—52051
microdensitometer precision focus control 79—58769
microinterferometer limiting sensitivity and accuracy characteristics 77—79142
microscope, computerised focusing technique 77—22596
microscope, focusing technique for digital image anal. system 80—68250
microscope focusing screw mechanism improvement 77—30201
microscope objective, piezoelec. and electrodynamic automatic focusing servo mechanisms 80—73445
microwave ultrasound, using ZnO concave transducer 77—7276
miniature slow proton source for focusing efficiency obs. 78—78538
mirror, electrostatic, transaxial, for large-incidence ang. ion beams 78—37798
mirror, off-axis parabolic, for laser fusion expt., fabrication process 79—23103
mirror focusing in grazing-incidence region spectroscopy 80—14250
moire technique for image alignment, focus and scaling 77—27362
molecular beam, electrostatic space focusing 80—28118
molecular beam, state selection and focusing, appl. to NH_3 hyperfine spectrum 80—28119
monochromator, constant-deviation, defocusing compensation with concave diffr. grating 78—46792
moving objective lens and Fraunhofer condition for predeflection 79—41316
multi-lens focusing systems for energy Nd:glass lasers 78—50848
multibeam microwave therapy with computer control 80—3766
multichannel focusing collimator, computation of efficiency distrib. functions 77—10519
multidithered segmented COAT mirror, surface wave control 78—46752
multimode focusing fibre with random bends, optical power loss 79—7214
multimode irregular fibre, with fluctuation focusing ray calcs. of power loss 80—33195
Multiple Mirror Telescope guide alignment system 79—75107
multiple-pass Raman gain cell 80—48334
multiply reflected Gaussian beams in circular cross section 79—18343
multistage cylindrical analyzer for simultaneous detection of several beams with different energies 79—22891
neutral beam dynamics, paraxial approximation, single particle motion across magnetic fields 78—29890
neutral beam injectors, multi-aperture extraction systems 80—42301
neutrinos, beam focusing system, Protvino Inst. 78—37477
neutron guide tube, axial peaking of ultra cold neutrons 77—14295
neutron spin echo, matrix anal. 78—86715
neutrons, imaging and focusing by zone plate 80—106433
neutrons, ultracold, zone mirrors for high resolution image form. 78—87003
NMR J cross-polarisation in liquids, refocusing method 80—22406
nonlinear crystals, focused beam SHG, temp., wavelength and angle bandwidths 79—50343
ocean wave energy conversion techniques and subsystems 80—45627
off-axis gaussian beam focusing props. optical system primary spherical aberration depend. 79—76735
optical fibre, single mode, refractive index profile meas., focusing method 80—33144
optical fibre index profiles, focusing method, nondestructive meas. 79—27375
optical fibre preform, refractive index profile and cross-sectional geometry meas. method 80—91893
optical fibre preform index profiling, automatic nondestructive focusing method 79—50448
optical imaging with defocusing, partial coherence effect *(German)* 77—75430
optical memory beam positioning and focusing system combination *(Russian)* 79—7194
optical microscope, accommodation focusing control 80—82814
optical parametric oscillator, singly resonant, optimal focusing of pump radiation 79—7176
optical storage focus error detection, skew beam and Foucault knife-edge techniques 80—102649
optical systems with parabolic filters, point spread function, effects of defocusing 78—13776
optical waveguides, deflection and focusing of radiation by stepwise inhomogeneities 78—83093
optimum focusing, for direct higher harmonics generation *(German)* 79—10349
optimum focusing conditions for twelfth optical harmonic generation *(German)* 80—64098
pancratic objectives, aberration stabilisation during focusing 80—102799
particle accelerator, laser focusing, phase-adjusted 80—63434
particle beam, relativistic, focusing by nonuniform plane EM waves *(Russian)* 77—6988
particle beams, superconducting magnets appl. 80—68990
permanent-magnet focusing systems, complex shaped pole pieces, induction distrib. anal. *(Russian)* 77—83786
phase anomaly in focused light beams, intuitive explanation 80—99622

focusing continued
phase fluctuation effect on deform. of caustic surfaces 79—94152
phase gratings, coherently illuminated, defocused diffr. images 78—46523
phonon imaging, ballistic, in solids, low-temp. 80—10605
photodetector, position-sensitive, for focusing on variable luminous mark 79—75598
photographic wide-angle lens, Flektogon F/2/8-20 mm 79—35869
photomicrography, low-power, use of auxiliary telescope 80—13165
pinched beam diode, geometrical focusing of intense ion beams 78—58898
plano-cylindrical Fresnel plastic lens, design and performance analysis as solar collector 80—53403
plasma, collisionless, enhanced Raman backscatt. of Gaussian laser beam from plasma wave 79—86566
plasma, Gaussian ripple on uniform EM beam, growth in magnetoplasma 79—19041
plasma accelerator, stationary erosion elec. arc type, with mag. cathode spot confinement, flow *(Russian)* 79—98996
plasma lower-hybrid waves, focusing and channelling during HF-breakdown of gas *(Russian)* 80—106890
plasma-optical focusing of Hall-current accelerator beam 77—7605
plastic focusing fibre for imaging appls., fabrication and characts. 77—62040
plastic light focusing fibre, heat drawing process prep. 77—14815
plastic rods, light focusing, prep. by two step copolymerisation of diallyl phthalate with methyl methacrylate *(Japanese)* 79—37064
prism-scanning panoramic camera for reconnaissance aircraft 77—79181
proton beam, 20 GW, geom. focusing using magnetically insulated diode 77—67533
proton beam, using unipotential plasma lens 79—41326
proton beam 70 GeV, for Protvino Inst. neutrino expts., characts. 78—37475
proton beam focusing to micrometer dimensions 77—46444
proton beams, parametric focusing 77—57421
proton dynamics in linear accelerator with variable phase focusing, space charge effect, simulation 79—13561
proton synchrotrons, non-linearities 78—78897
Proton-Electron Tandem Ring Accelerator magnet field meas. 79—31271
PVF$_2$ film composite resonator for concave focusing US transducer 79—46155
quadrupole lenses with sector magnets, nonzero emittance beam focusing conditions 80—23612
quasi-fixed adjustable-focus reflector array solar collectors 79—62106
racetrack three cavity variable energy microtron with intra-sector beam focusing 77—65369
radiative damping effect for ultrarelativistic channelled particles 78—67758
radio waves in lower ionosphere, nonlinear thermal focusing 77—60511
radiography, convergent wide-angle beam, for polycrystals 80—40634
radiography, RMS focal spot, validity considerations 80—81691
radiowave gravitational focusing in interstellar medium, model *(Russian)* 78—81905
radiowaves, ionospheric focusing at boundary of zone of silence 77—13158
radiowaves in ionosphere, focusing rel. to statistical characts. of refl. signals 78—45092
random phase screen, geometrical focusing, speckle effects 77—79755
Rayleigh-Debye scattering with focused laser beams 78—71030
reflecting telescopes with zero expansion material mirrors, temp. defocusing *(Russian)* 79—96912
reflector geometry for acoustic microscopy and NDT 79—47874
reflex cameras, lens-array focusing system tests 80—86479
refractive index, profile determ. of light focusing rod, Interphako interf. microscopy method 80—101832
refractive index determ., focusing method 79—27374
relativistic charged-particle beam, collimation by coherent radiation *(Russian)* 77—61156
relativistic electron beam, diode compression 77—24197
relativistic electron beam, focusing and energy transfer on to target 77—42186
relativistic electron beam in plasma, coherently radiating, radiation press. at surface 78—9314
relativistic electron beams, mag. focusing, equilib. surface ripples 79—3618
retrofocus lens system designs for film cameras *(German)* 77—54768
RILAC, variable freq. heavy ion linac 77—38454
ring-type state selector and space focuser for mols. with positive induced dipole moment, appl. to mol. beam maser 78—54503
rod, tapered gradient-index, geometrical optics 80—69322
rotationally symmetric periodic electrostatic focusing system field distrib. 79—76574
ruby laser, focusing effects during emission in relaxed state *(French)* 77—34896
scanning focus by interferometry, beam shear change 80—52301
scanning microscope, increased depth of focus using slit aperture, MTF degradation 78—45689
scattered wave focusing in periodically inhomogeneous layers *(Russian)* 78—1158
Seemann-Bohlin focusing method, using modified Chirana cylindrical cameras *(Czech)* 79—26192
seismic body waves, focusing at epicentre antipode 79—16399
self-imaging multiplexer and branching couplers 80—106629
Selfoc lens, aberration improvement by glass composition and ion exchange process parameter choice 80—69486
SEM, automatic focusing and stigmating system 79—12893
SEM, focusing and stigmating system using minicomputer 78—37113
SEM fiducial grid prep. by electron resist. technique 77—25230
sharpness index autofocus system, depth of convergence 77—79913
SHIVA laser optical component manufacture and testing 79—22980
Shiva optical system 78—59039
shock wave focusing at an arete 79—37352
single-polepiece magnetic lens axial field distrib. 80—69317
single-polepiece objective and projector lenses for electron microscope 80—68326
solar concentrator, fixed mirror type, concentrated flux characts., expt. 77—23733
solar concentrator, plano-cylindrical Fresnel lens, anal., expt. 77—23732
solar cylindrical parabolic collector geometry 79—62109
solar energy concentrator designs for underdeveloped countries 79—62125

focusing continued
solar focusing collectors, cylindro-parabolic mirrors *(Rumanian)* 80—50934
solar thermal collector, line-focus Fresnel lens and secondary concentrator 79—62112
Solar Thermal Test Facility, 5 MW, heliostat focus and alignment system 78—50894
sonic booms focusing conditions 77—50804
sound beam, defocusing and absorpt. coeff. enhancement 78—9471
sound waves, mutual focusing in nonlinear elastic medium *(Russian)* 78—26001
space charge lens for high current ion beams 78—55075
speckle, white light, contrast at defocused image plane 80—23621
spherical particles beam, focusing by axisymmetric mag. fields 80—78755
spherical X-ray wave, diffraction focusing effect *(Russian)* 79—23500
STEM, defocus and astigmatism, automatic correction method 80—68298
STEM, non-optimal apertures 80—62801
STEM using shadow image processing, a posteriori focusing 79—80726
step-stare spaceborne optical system smear compensation by focal plane manipulation 80—82172
stimulated Brillouin scatt., three dimensional, for focused Gaussian beam 80—69456
straubel apodisation filter systems, effects of defocusing on point spread function 78—25804
stress wave focusing in paraboloids of revolution, internal fractures 80—83762
strong radio waves in ionosphere, self-focusing instability near caustic 78—45107
subwavelength focused light beam, knife edge scanning meas. 77—75641
superconducting quadrupole magnet design for ion beam fusion linac 79—36433
symmetry properties of focused fields 80—83550
synchrotron radiation, separated function focusing monochromator system 78—62278
synchrotron radiation, X-ray optics and monochromators 77—54027
synchrotron radiation from electron storage ring, focusing condition 77—42584
synchrotron radiation from electron storage ring, focusing on single point 77—10991
synthetic focus digital acoustic imaging for nondestructive evaluation 79—52611
Tandem Wadsworth spectrographs, horizontal foci calcs. 79—49298
telecentric imaging system focus detector 80—53397
telescope, AZT-24, design formulas for construction elements 79—35133
TEM, contrast of fold domain boundaries and microsectors in polyethylene single crystals 80—107065
tenuous particle scattering of focused laser beams 79—36836
tester for focusing adjuster, optimal parameters anal. 78—83070
thermal lens in laser cavity, focal length 77—61977
thermo-gasdynamic control in laser beam guidance, review of developments 78—74942
thin-film lenslike light guide focusing properties 77—54786
tokamak, beam focusing, by aperture displacement, in two-stage acceleration system 79—46496
tomograph information characteristics 77—25541
toroidal mirror as focusing element for stigmatic grazing incidence spectrometer 79—71539
tower-top focus solar receiver designs 79—62114
transition radiation emitted by ultrarelativistic particle 77—19153
two-beam laser fusion target illumination system design 77—19292
ultrasound, convergent sources using flexurally vibrating circular diaphragms 77—50845
uncharged spherical particle stream, longitudinal focusing by elec. fields in vac. 79—64165
underwater sound, bottom-reflected field defocusing in inhomogeneous antichannel 78—1484
underwater sound, focusing by spherical compliant-tube Luneburg lens, theory 77—46842
upconversion, three-freq. parametric, beam focusing effects 80—48340
US and hypersonic waves, stationary self-focusing in nonlinear media 77—813
US annular array with dynamic focusing 77—32947
US beam, dynamic, for nondestructive testing and medical diagnosis appl., use of analogue-switch phase shifters 77—52856
US bulk wave electromagnetoacoustic excitation 79—57195
US field focusing upon transmission using annular transducer 78—44574
US flaw detection, focusing probes 80—104383
US focusing device with IDT on thin piezoelectric plate 80—1398
US generator, general purpose broad-band, for biological object handling 79—48381
US imaging, digital focusing in near field of sampled acoustic aperture 77—60232
US reflectors in kidney stone destruction by shock waves 77—32946
US tracking focusing annular array transducer *(French)* 80—26301
UV photography and fluoresc. photography techniques 80—18033
variable magnification three component system, fabrication errors 77—88895
variable-focus US membrane transducer, medical imaging appls. 77—39185
VICKSI beam line instrumentation and control system 77—83401
Viking Lander camera performance and data reduction 77—41286
vision, psychophys. and electrophysiological effects of defocus 77—90768
water, aerated, laser beam focusing by vertical temp. gradient 78—33661
whistler-mode waves focusing and interference in spatially varying mag. field 78—65465
X-ray and visible streak camera for subpicosecond laser fusion diagnostics 77—18122
X-ray crystal spectrometer with conical focusing, astronomical appls. 77—5443
X-ray diffraction focusing, with (n,m)-positioning of crystals 80—87989
X-ray focal spot, MTF, modified meas. method 80—37149
X-ray spectrometer, Cauchois focusing with oblique-cut quartz analyser cryst. 79—52815
X-ray tube, microfocus, electron source with single pole mag. lens and novel focusing system 78—32964
zoom lens focusing system *(Japanese)* 80—31922
Ar$^+$ ion beam designs for sputter deposition 79—89841
As$_2$S$_3$ focusing diffraction grating with const. spacing 79—23096

focusing continued
- CO_2 laser beam focal zone rel. to luminesc. duration of NaCl particle 80−34983
- CO_2 laser fusion system alignment by IR Smartt interferometer 80−74425
- CO_2 laser Gemini fusion system optical performance 80−74392
- CO_2 laser Helios fusion target positioning with orthogonal telescopes 80−74421
- CO_2 TEA laser oscillator, transverse mode locking by short pulse injection 80−38045
- Fe lenses for muon beam transport 77−30685
- Ge, autofocusing of X-rays and γ-rays 79−12916
- H^- beam, intense, from Penning surface-plasma source, ion-optical characts. 79−13892
- H^+ beam, 0.5 TW pulses, production with spherically focusing mag. insulated diode 79−31288
- H^+ beam, pure, production by four-lens Hall accelerator, focusing 78−66441
- I laser, high-power, beam quality, gain saturation effect, for fusion ignition 78−63149
- ICl, mol. beam focusing in rot. states 79−18317
- Li cylindrical lens for high energy particle focusing, aberrations 77−14649
- $LiNbO_3$ acousto-optical SAW interaction multicolour image scanner 77−58483
- MgO-ZrO_2 ceramic sublimation at optical furnace focal spot *(Russian)* 79−95983
- N_2-He plasma, laser produced, high press. amplified stimulated emission 80−78843
- Na atomic beam focusing and defocusing using reson. radiation press. 80−47143
- Na neutral atom beam, focusing and defocusing forces, radiation press. from CW dye laser 80−52944
- Tl vapur, ruby laser third harmonic generation, flowing degree influence 80−48348

focusing, particle *see focusing; particle optics*

fog
- acoustic sounding of radiation fog 78−69419
- actual light scattering coefficient as meas. in haze and fog 79−80013
- advection fog formation from aerosol particles 80−21808
- advection fogs at sea, droplet spectra formation, numerical model 79−34916
- advection-radiation fog near Lake Michigan, visibility meas. 77−81996
- advective fog formation, theory *(Russian)* 78−36228
- aerosol size distribution by inverting spectral turbidity data 80−95796
- air-water fogs, audible sound propag. 78−1473
- aqueous, formation in shock tube 80−19531
- artificial, optical thickness change due to CO_2 laser pulses 77−75591
- artificial, size distrib. meas. by light, extinction-sedimentation inversion technique 78−37042
- artificial condensation nuclei effects on radiation fogs, numerical model 77−70788
- artificial mist, laser radiation propag., intensity fluctuations *(Russian)* 78−37806
- atmosphere, aerosol optical attenuation statistics, spring and autumn 79−84484
- atmosphere boundary layer, IR radiation rel. to dynamics and fog development 79−39815
- Belgium, freq. of occurrence *(French, Flemish)* 78−11978
- brightening of disperse media, role of laser fluctuations 79−41405
- California coast, marine fog form and fog-stratus systems development 80−77060
- California coastal fog and stratus microstruct. 78−61505
- Cheddar Gorge, England, oblique false-colour photograph 78−57290
- clearance, by laser-beam induced heat and mass transfer 78−93635
- clearance of persistent fog 80−41523
- clearing by laser beam, thermal self-defocusing effect 77−64432
- cloud condensation nuclei from paper mill effluents, induced fog *(French)* 78−96270
- dangerous weather phenomena prediction, research prospects 79−34932
- definition *(French)* 77−81978
- density monitoring in pollution chamber 78−45059
- diffusion coefficients deduced from closing times of helicopter-produced clearings in fog 79−39810
- DMSP visible imagery, fog as cause of anomalous grey shades 80−77111
- droplet spectra in fogs, new meas. instrument 77−53219
- droplets, size distrib. models, and visible and IR volume extinction coeffs. 77−25750
- EM pulse propagation in atmosphere with scatterers, diffusion theory 79−66775
- EM pulsed beam wave propag. 78−12000
- evaporation fog, growth and disappearance during cold air mass transformation 80−56585
- evaporation fogs formation theory and prediction 78−61522
- extinction coefficients, spectral correls., theory 79−96812
- forecasting using point discharge current 77−70748
- formation conditions in frontal zone, theory 80−41532
- frequency of fog, smoke concentrations in Midlands, England 79−84458
- glory formation, diffr. model 80−82053
- haze and fog vertical struct., effects on visible and IR extinction 79−58086
- heterogeneous photocondensation process initiation by laser radiation 80−67410
- hole boring with pulsed high-energy lasers 79−16662
- holography through fog, coherence requirements for light source 78−58949
- holography through fog, new version 79−912
- homogeneous fogs, lidar returns, doubly scattered radiation effects 79−53516
- ice crystals, holographic meas. of shapes, sizes and concs. 79−25364
- ice nucleation on AgI aerosols at different supercooled fog temps. *(Russian)* 77−27983
- ice nuclei in fog water off Nova Scotia coast during 1975 Summer 78−16104
- ice-crystal, aerodynamic and opt. props. 77−90648
- incinerator smog reduction by US vibration induced water mist 77−32845
- inhomogeneities in water props. 77−49135
- IR broadband transmission rel. to meteorological events 80−85744

fog continued
- IR extinction and absorption, linear relation to water content 80−56603
- IR extinction spectra of liquid droplet smokes and fogs 77−78416
- IR radiation extinction coeffs. for haze and fog droplet polydispersions 77−9496
- IR radiative transfer in cloudy sky, theoretical scheme 80−51540
- IR wavelengths extinction by aerosols in coastal fog 78−81400
- Irkutsk airport, fog prediction model 80−85736
- large transparent sphere effective extinction efficiencies using weakly collimated light 79−72487
- laser beacon visibility in fog, range extension technique 80−101434
- laser beam, multiple scatt. by radiational and advective fogs 79−100950
- laser beam attenuation at mountain altitudes by fog and clouds *(Russian)* 79−48566
- laser beam broadening and depolarization in dense water-droplet fogs 78−92981
- laser beam nonlinear propag. through fog, thermal blooming 77−91268
- laser beam off-axis propag. in low visibility weather conditions, non-small-angle scatt. 80−102621
- laser beam transmission, heating, ion emission 78−59063
- laser blue-green pulsed propagation through fog 79−39846
- laser light nonlinear transmission 80−1256
- laser radiation intensity fluctuation in fine-droplet water aerosol at 630 nm 80−4109
- laser radiation transmission meas. at 10.6 μm 78−92977
- lidar probing of fogs and clouds, double scatt. approx. 78−73512
- Lidar return from fogs, effect of non-uniform extinction coeff. on double scatt. contrib. 79−100952
- lidar returns from fog, doubly scatt. radiation contrib. 78−77326
- lidar scattering, four-component polarisation meas. 78−44996
- Lidar visibility measurements, using Raman/aerosol ratio method 79−100953
- light extinction, absorption effects 78−33667
- light scattering by haze of arbitrary shape nonuniform particles 77−7003
- liquid water content, organic aerosol effects 78−73465
- liquid water content rel. to atm. visibility 78−81404
- marine, characts. of air mass histories, Nova Scotia, 1975 August 79−70847
- marine advection fog, water distrib. rel. to droplet size, salt particle nuclei 79−5570
- maritime boundary layer model for fog prediction 77−78293
- measurement on motorways 79−16608
- microphysics in fog models 80−41517
- mist and wind-driven fog exchange between vegetation and atmosphere 78−44909
- multiple scattering, radiative transfer iterative calcs. 79−98276
- New South Wales, Australia, fog devil, photographic obs. 77−81985
- Ona, Norway, synoptic and climatological characteristics 77−17176
- optical probing, homogeneous particle model 79−66790
- organic material impact on fog and cloud processes 78−73467
- particle size distribution, Rocky Mountain air in winter 79−100887
- pH of hydrometeors, detailed struct. 79−92111
- photochemical smog, effect of latit. on form. pot. 77−2227
- photochemical smog, transferred contaminant air pollution model *(Japanese)* 78−32217
- photochemical smog dynamics and control strategies *(Japanese)* 78−32220
- precipitation onto surfaces, quantitative meas. gauge 80−56654
- radiation fog, relationship to dew 78−73446
- radiative fog and stratus cloud, form. and evolution in atmosphere boundary layer *(Russian)* 77−49104
- radiative transfer through fog, 2D numerical soln. algorithm 78−71032
- real-time holographic viewing in moving fog 80−102676
- remote measurement of water density and size distribs., using laser radar 77−91299
- solar radiation attenuation in visible and near IR 77−45153
- sound attenuation obs. 77−34981
- spectral transmission data, IR propag. and performance modelling 80−90218
- steam fog in Fenlands, obs. after heavy rain, (1979 May 1) 80−98431
- streamflow generation rel. to fog drip 77−64405
- supercooled, crystn. by means of powdered synthetic zeolite 77−37296
- supercooled, dispersal using compressed air 77−49185
- supercooled fog, −20°C, influence of aersol particle size on AgI ice-forming activity 79−53465
- temperature profiles in fog, meas. via shipboard use of low-level atmospheric thermograph 80−105073
- thermal emissivity 80−95795
- turbulent and radiative transport interaction in development of fog and low-level stratus 78−81313
- vapour-gas mixture containing fog, mass transfer in vapour condensation 77−58772
- visibility range of objects in horizontal direction, atm. haze effect 78−16161
- visibility temporal vars. beside motorway, England 79−39852
- visual range and radiation-fog microphysics 80−109195
- warm fog, modern thermo-kinetic dispersal system for commercial airports 80−51576
- warm fog and steam clouds, emission spectra variations, evidence for clusters in vapour phase 79−39849
- warm fog dispersed with electrostatically charged bubbles 78−20546
- warm fog dissipation by electrically enhanced coalescence, charged drop seeding 78−7714
- warm fogs, haze droplets effects on visibility in natural and treated fogs 79−100951
- water droplets in mists, clouds, size, density distrib. meas., laser remote sensing technique *(Japanese)* 78−49175
- water droplets size distrib. in mist, vol. extinction coeff. at visible and IR wavelengths 77−37287
- water evaporative cooling, convection and mass transfer, fog formation in boundary layers 80−79293
- water evaporative cooling, heat and mass transfer coeffs., fog formation effects 80−79294
- wave patterns in marine fog revealed by Apollo-Soyuz photographs 79−88395
- CO_2 laser radiation influence on liquid drop cloud medium, dissipation 79−39858
- ^{222}Rn meas. during marine fog off Nova Scotia 78−40624

foils
alloy, solute redistrib. during in situ irrad. in HVEM 80—107324
alloy, X-ray fluorescence correction in thin foil analysis 80—85256
alloy, X-ray microanal., thin foils, data correction for absorpt. effects 80—85255
anode foil changing system for heavy-current field-emission electron accelerator 78—9005
bimetal, magnetic-transforms., Mossbauer spectroscopy *(Russian)* 78—6607
β-brass, spinodally decomposed, morphology and characts. 80—60863
cellulose nitrate thin foil manufacture for α particle track detector *(Spanish)* 80—74091
chemical analysis, by electron microscopy *(French)* 80—50899
chemical mapping with high spatial resolution by electron energy loss spectroscopy 79—61934
dislocation elements, finite co-planar, interaction in finite medium 77—51375
dislocation loop growth during HV electron microscope irrad., thin foil point defect profile 80—2018
electrolytic foils, porosity meas. by electrochemical reaction 78—3265
electron backscattering, eikonal approx. 77—48289
electron micrograph, theoretical, of dislocation, foil surface stress relax. effect 77—31665
electron microscopy on etched thin foils, comparative SEM, STEM and TEM analysis 80—100144
electron probe analysis, orientation effects in quantitative X-ray microanal. 80—85259
electron scattering, appl. of Monte Carlo type calc. *(French)* 77—7636
electron scattering, most probable transmitted scatt. angle calc. *(French)* 77—68901
electron transmission, normalisation of ang. distrib. curves *(French)* 77—4026
electroplated, appl. of thermoelectric props. to measurement of neat flux 80—37026
electropolishing technique for transmission electron microscope specimen preparation 78—57919
electrothinning, laser-monitored, for preparing ultrathin metal foils 78—53074
emissivity, low temp., calorimetric meas. technique 80—17941
energy dispersive X-ray microanal. 77—60153
fluorocarbon foil, Ftoroplast, homogeneity study *(Polish)* 80—35278
flux-distortion factor for a foil in a exponentially varying flux 78—89930
glass, heat treated, thin foil prep. for TEM obs. 78—7154
Grafoil, ^{4}He crit. superflow, two-dimens. random bond model 80—15319
Incoloy 901, foil prep. for TEM exam. 80—88001
laser, electron beam controlled, electron beam parameter optimization and choice of foil 80—48269
laser pulse heating enhancement with pulsed air jet *(Russian)* 78—22533
lattice defects, dynamical image contrast in electron microscopy 77—15422
low atomic number target, anomalous energy dissipation of tightly pinched relativistic electron beam 80—29833
magnetic foils, thin, field distrib. mapping by holographic processing 79—89868
mechanical testing methods, review 80—40637
membrane waves excit. 78—90578
metal, crack propag. electron microscope obs. 77—63792
metal, ductility tester 77—63864
metal, foil, surface temp. meas. during laser irradiation heating *(Russian)* 79—74030
metal, for X-ray filters, electrolytic production method 79—95947
metal, He depth profile meas. 77—12858
metal, thermal diffusivity and emissivity, expt. transient technique and theory for foils 78—43353
metal, thickness, X-ray fluoresc. meas. method, appls. *(Russian)* 78—56582
metal foil bulge-test samples, shape meas. by optical contouring 77—63843
metal foil photoetching profile, quantitative obs. 78—39943
metal foil with thin film coating, failure by laser pulse *(Russian)* 78—23561
metal foils, electron irrad., loss of pt. defects 79—73215
metal foils, low energy heavy ion multiple scatt. in finite range potential 80—70283
metal foils, $Z=6$ to 79, energy loss of light 300 keV ions, using magnetic analyser 79—4350
metal foils for pulsed laser appls. 78—5480
metal powder, method for TEM study 80—84038
metal ultrathin foils, laser monitored electrothinner *(German)* 79—34219
metallic foil, continuous electrochemical perforation *(Russian)* 78—20020
mounting technique, wrinkle-free 80—77767
multilayer heterostructures, prep. and ion etching of thin foils for electron microscopy 79—12779
naturally passivated metal foils, ESCA, sputter etching 77—70218
plastic, foil prod. by extrusion blowing *(German)* 80—20786
polyester foil, static polarisation depend. on heat ageing 78—60688
polyethylene foils, deuterated, prep. technique 77—88313
polyethylene ultrathin foil prep. by film casting 78—48340
polymer, electron irradiated, charge dynamics, computer simulation 79—82915
preparation apparatus, for X-ray diffr. study of lattice defects 79—37585
quantitative microanalysis, by energy loss spectroscopy *(French)* 80—50900
recrystallisation during heating in column of electron microscope *(Russian)* 78—48421
reference fission foils preparation by fluoride deposition, characterisation 80—23218
steel, C, cementation process testing, foil samples method 79—70238
steel, microanalysis by energy dispersive X-ray spectrometry *(French)* 80—85250
steel, stainless, depth distrib. of swelling, TEM exam. 80—15165
steel, stainless, TEM foils, white band contrast 80—75134
steel, stainless 316, stress-strain behaviour of micron thickness foils 79—52327
strain gauges, small high-elongation foil, as fatigue damage indicators 79—32417
superconducting, type II, effects of current-induced mag. field on flux flow 77—77012

foils continued
superconductivity in metal foils, sensitive detection by change in penetration depth of electromag. fields 79—56372
superconductor, type II, DC voltage induced by superposition of AC mag. field 77—85395
surface density meas. method using X-rays or backscattered γ-rays *(Czech)* 77—50323
surface guided modes, excitation by electrons 77—59310
surface scattering, precision table 79—60907
target, thickness measurement using ^{14}C β-ray thickness gauge 79—26030
Teflon foils, cryst. struct. and texture changes due to polarisation process *(Polish)* 80—35209
TEM, plasma etching use for foil thinning *(Slovak)* 80—45405
TEM obs., preservation technique *(German, English)* 79—96263
tensile strength, thickness depend. *(Russian)* 77—59852
thermally induced structural changes, specimen surface influence 80—103559
thickness measurement method, X-ray microanal. technique 80—85256
thin crystal, large angle electron scattering by dependent Bloch wave model 79—99257
thin foils, electron scatt., Monte Carlo study 79—67745
thin metal films, for electron microscopy, production by jet polishing apparatus 78—86247
thin metallic foil prep. for TEM obs. *(German, English)* 79—91885
transition metal foil-electrolyte interface, optical and elec. expts. 78—88644
vacuum deposited resistive, powder alloy manufacturing technique *(Polish)* 80—35124
vacuum deposited resistive foils, manufacture and props. of multicomponent alloys *(Polish)* 80—35131
X-ray microanalysis in electron microscope *(French)* 80—61191
Ag, conduction electron spin disorientation at surface 80—75855
Ag, electron scatt., appl. of Monte Carlo type calc. *(French)* 77—7636
Ag foil, interface with liq., oxide props., refl. and scatt. light spectroscopy 80—60702
Ag foil-electrolyte boundary reactively formed oxide layers, differential reflectance 79—69856
Ag foils, trapezoidal splitting of partial dislocations 77—51376
Ag, proton energy straggling determ., at 0.35, 1, and 1.75 MeV, γ-emission reactions 79—4354
Ag, surface plasma-wave reflectance and roughness-induced scatt. 80—66228
Ag, surface-plasmon resonance, roughness-induced wavelength corrections 80—108288
Al, 150-400 keV electron transmission coeffs., Monte Carlo calc. continuous deceleration model 77—50604
Al, activated, determination of fast neutron contamination in X-ray beams 79—6724
Al alloys, use of electrospark cutting for preparing thin foils for electron microscope exam. 77—52590
Al, anodic oxidation, characterisation by nucl. methods *(French)* 77—73378
Al, anodising, behaviour of emulsion particles during electrodeposition 80—104357
Al, α-particle irrad. under fusion reactor conditions, He bubble alignment during deform. 80—107345
Al, burn-through by laser-driven ablation 80—33794
Al, electron-irrad., interstitial trapping on impurities 79—99242
Al, fluxural oscillations in longitudinal mag. field, sound attenuation, magnetoelasticity *(Russian)* 80—54844
Al foil, electrical conduction, electron mean free path, surface scatt. 80—88535
Al foil, electron diffr. effects and images from inclined grain boundaries 79—82241
Al foil, internal friction changes during low temp. plastic deform. *(Russian)* 80—100304
Al foil, laser irrad., fracture props. *(Russian)* 80—108523
Al, foil, secondary electron emission due to α-particle irrad. *(Russian)* 80—66344
Al foil, sputtering with ^{252}Cf fission products, desorbed secondary ions 78—68596
Al foil, straggling of relativistic electrons, 0-4000 eV 78—14393
Al foil electrolytic perforation, surface film phase composition obs. *(Russian)* 80—61004
Al, high strength, vapour deposited on curved surfaces, quantitative characterisation 80—80144
Al, in chemically enhanced opening switch for generating high-voltage pulses 77—49744
Al, influence of O_2-pressure on oxidation rate, TEM study 80—104355
Al powder thin foil, prep. for TEM study 80—42310
Al, quenched, vacancy-Fe interactions 78—47412
Al thickness uniformity determ. from proton backscatt. yield 77—10510
Al, thin foil, adhesion and friction, rel. to observed dislocation density 78—64706
Al, thin foil, Monte Carlo calcs. of electron transmission 77—80555
Al thin foil, thin foil, electron irrad., observation of triangular loops at twin boundaries 80—34005
Al, with Au overlay, impedance-match expts. using laser-driven shock waves 80—29119
Al, X-ray induced electron emission, secondary electron energy distrib. 77—59669
Al-Be, two-layer foils, mech. props. *(Russian)* 78—51858
Al-Cd hypomonotectic alloy, rapid solidification and decomposition 80—50638
Al-Mg, oxidation in O_2 atm., TEM study 80—104356
Al-Mg-Si-Mn foil, planar defect spacing meas. by TEM 78—2135
Al-Ni, vapour deposited, multiply twinned particles, electron microscopy 77—28083
Al-Zn-Mg-Cu foil, STEM-microanal., specimen thickness effect on X-ray count rates 77—70374
Au, electron scatt., appl. of Monte Carlo type calc. *(French)* 77—7636
Au, electron secondaries from α-particle and fission products 77—24918
Au, film with micron-size pinhole, low energy electron scatt. 79—81351
Au foil, radiation damage, in situ study by HV electron microscopy 78—6101
Au, grain boundary structure, high resolution HVEM 80—103360
Au, growth of stacking fault tetrahedra 80—19815
Au, ion imaging of thin specimen 79—99035
Au, proton energy straggling determ., at 0.35, 1, and 1.75 MeV, γ-emission reactions 79—4354

foils continued
- Au, spatial resolution of X-ray microanalysis 80—101065
- Au, sputtering in a high voltage electron microscope 77—36328
- Au, stopping cross sections of protons, 350 to 650 keV, backscatt. technique 79—4352
- Au, thin film bicrystal, diffraction effects from inclined grain boundaries 80—103362
- Au, thin foil, enhanced electron energy deposition heated, soft X-ray vacuum UV spectra 80—80901
- Au, X-ray induced electron emission, secondary electron energy distrib. 77—59669
- Au-Ni, composition-modulated, elastic modulus enhancement 77—52382
- Bi foil, splat quenched, preferred orientation 80—40381
- C, 40-100 keV He ions, electronic energy straggling 77—15471
- C, amorphous foil, electronic energy straggling of light ions, at. number depend. 77—11612
- C, electron secondaries from α-particle and fission products 77—24918
- C, energy loss of Ne ions (40-120 keV), and Ar ions (40-240 keV), as function of emergence ang. 79—4357
- C evaporated film, yield tensile strength 80—23214
- C foil, electron impact knock-on damage at 4K, electron microscope obs. 79—55786
- C foil, extreme UV induced forward photoemission 80—76137
- C foil, H_2^+ transmission yield 80—100732
- C foil, He^+ and HeH^+ impact, quantum beat pattern depend. on foil thickness 80—58343
- C foil, ion irrad., crystallographic transform. 79—55794
- C foil, ion irradiation, correlation of energy loss and crystallographic transform. 80—23215
- C foil, transmitted H^+ energy loss, ang. distrib. and charge fractions 80—2102
- C foil+$H_2^+(H^+)$, 0.5-2.5 MeV, forward electron vel. distrib., peak shape 78—78794
- C foils, forward photoemission and transmittance meas. 80—25516
- C, iron irrad., graphitisation rel. to lifetime, relevance to beam-foil spectroscopy 80—15166
- C, irradiation with 1.2 MeV Ar^+, electron diffraction study 80—103397
- C, Kr^+ incident, equilib. charge state distribs. and multiple scatt. angles 80—59532
- C, passage of ^{14}N and ^{20}Ne ions, energy-angle distribs. 79—10889
- C, plasma production by laser, mol. ions studied by mass spectrosc. 79—90429
- C stripper foils for heavy ions, preparation method 79—22516
- C, thin, for charging effects elimination in proton induced X-ray emission spectrometry 79—92024
- Cd foil, splat quenched, preferred orientation 80—40381
- Cd, monocrystalline, anisotropy of size effect 79—38048
- Cfoil, HeH^+ impact, dissoc. emitted light polarisation meas. 80—58361
- Co-P, amorphous, complex permeability and eddy currents, annealing induced short-range order 77—8360
- Cr foil, laser irradiated, low-angle X-ray scatt., angular block misalignment and hardness *(Russian)* 80—103413
- Cr isotope target foil preparation by electrolysis 78—21110
- Cu, Ar^+ ion irradiated, defects study by electron microscopy *(German)* 80—2087
- Cu, Ar^+ ion irradiated, small defect clusters, electron microscopy contrast *(German)* 79—99253
- Cu, conduction electron spin disorientation at surface 80—75855
- Cu, electron irradiated at low temps., annealing, form. of clusters of atomic defects 77—15416
- Cu, electron scatt., appl. of Monte Carlo type calc. *(French)* 77—7636
- Cu, electron-irrad., interstitial trapping on impurities 79—99242
- Cu foil, determ. of oxides on surface 77—90682
- Cu foil, laser irradiated, low-angle X-ray scatt., angular block misalignment and hardness *(Russian)* 80—103413
- Cu foil, sputtering with ^{252}Cf fission products, desorbed secondary ions 78—68596
- Cu, foil recrystallisation during annealing in high voltage electron microscope, grain growth *(Russian)* 79—100159
- Cu foils, cyclotron beam intensity monitors 77—38578
- Cu, interstitial impurity interaction investigation by stage II isochronal recovery expts. 78—47423
- Cu, ion irrad., Frank loops, electron microscope image contrast 80—6326
- Cu, pulsed action of laser radiation, dimens. effect *(Russian)* 77—16437
- Cu, role of grain-boundary porosity in superplasticity *(Russian)* 78—56690
- Cu, total emissivity meas. by calorimetric technique 80—17941
- Cu-Al(10 at.%) foils, trapezoidal splitting of partial dislocations 77—51376
- Cu-Bi foil, electron diffr. effects and images from inclined grain boundaries 79—82241
- Cu-Pd, composition-modulated, elastic modulus enhancement 77—52382
- Cu-polymer composite foils, fracture surface exam. by XPS *(German)* 78—84992
- CuO surface, contaminated, cleaning treatments, ion scatt. anal. 78—53307
- Cu_2O foils, electron microscope exam., Cu precipitates and CuO form. 79—1462
- Cu_2O polycrystalline and single cryst. mech. behaviour 78—95777
- Fe, electrodeposited, microstruct., internal stress and mech. props. 80—20807
- Fe foil, electrodeposited, phys. and mag. props. 79—91275
- Fe, foil, fatigue crack, low growth rate, microstruct. round top 77—16674
- Fe foil, Lamb-Mossbauer factor at 4.2K 80—20561
- Fe:^{133}Xe, heavy ion implantation, recovery, Mossbauer effect meas. 78—52393
- Fe:N, ion implanted foil, Mossbauer effect study, nitride form. 78—27149
- Fe-Cr-Ni, in situ oxidation in HVEM 80—104354
- Fe-Ni-(C), thin foil martensite, TEM obs. 77—51378
- $Fe_{75}P_{15}C_{10}$ foils, amorphous, ferromag. domain orientation, Mossbauer study 78—15000
- Ge, [110] oriented, seven-beam lattice images of defects 80—107209
- Ge, epitaxial growth of very thin electron microscopy specimens 80—100793
- Ge foil, thinning for electron microscopy 79—49217
- Ge-Si alloy foils, prep. by improved jet thinning 78—88589
- Hf-V foil, rapidly quenched and heat treated, supercond. props. 80—54852
- $La_{1-x}Ga_x$, amorphous foil, Hall coeff. meas. 80—20153

foils continued
- Mo, device for electrolytic thinning from wire, for electron microscopy 80—85105
- Mo, electron energy loss spectra 80—7452
- Mo foil electrolytic perforation, surface film phase composition obs. *(Russian)* 80—61004
- Mo, ion irrad., dislocation loops and stacking fault tetrahedra, electron microscope image contrast 80—6326
- N_2^+ + first row transition metal surface reactions 79—96363
- Na_2O-CaO-SiO_2 glass foils, HVEM in-situ straining expts. 80—104216
- Nb, coated with thin H-permeable Pd film, AES and SIMS 79—52467
- Nb, electron energy loss spectra 80—7452
- Nb, electron energy losses due to H, obs. by scanning TEM 80—79850
- Nb foils, polycryst., proton irrad., diffusion of nuclear react. products *(German)* 77—35756
- Nb, oxidised, electron irradiation damage, AES study 79—28015
- Nb, plastically deformed single crystal, foil, damage free prep. for TEM and X-ray topography *(German, English)* 80—30200
- Nb-Sn, supercond. foils, phase anal. by Mossbauer spectra 78—64305
- Nb_3Ge film, supercond., TEM obs. of microstruct. foil prep. method 77—55642
- Ni 78—7099
- Ni foil, critical exponent β determ. by microwave transmission 77—69575
- Ni foil, hydrogenated, thermoelectric and Hall effects 79—65559
- Ni, foil, polycryst., channelling micrographs using accelerators, defects investig. 77—11445
- Ni foil, sputtering with ^{252}Cf fission products, desorbed secondary ions 78—68596
- Ni foil electrolytic perforation, surface film phase composition obs. *(Russian)* 80—61004
- Ni, foil substrate with Ag island film, elec. props. 77—43745
- Ni foils, cyclotron beam intensity monitors 77—38578
- Ni, Frank loops, growth kinetics and 'preference factor' during electron irradiation 78—22723
- Ni, hydrogenated, thermoelec. and Hall effect 78—43364
- Ni, microwave transmission, parallel RF and mag. fields 77—59462
- Ni, phonon generation and attenuation at FMR 80—39875
- Ni single crystal foil, H_2 induced deform. during thinning, electron-optical obs. 79—57059
- Ni superalloy, STEM microanal. of precipitates and their nuclei 80—81067
- Ni, surface IR wave propag. distance 77—28641
- Ni thin foil, single cryst., cyclically deformed, HVEM in-situ deform. study 80—103339
- Ni-Al (6.35 wt.%), radiation-induced precipitate redistrib. 78—30681
- Ni-Al(Si), ion irrad., surface effects on precip. morphology 80—104168
- Ni-Co-Cr TEM foils, white band contrast 80—75134
- Ni-In, ion-implanted, impurity defect interaction and diffusion, Rutherford backscatter and TDPAC expts. 80—34039
- Ni_3Ga, stacking fault form. in situ obs. by stretching thin foils in electron microscope 77—62547
- Pb, fluxural oscillations in longitudinal mag. field, sound attenuation, magnetoelasticity *(Russian)* 80—54844
- Pb, splat-cooled and vapour-deposited, metastable structs. 79—87018
- Pb, type I supercond., crit. current density, pinning force density, shadow electron microscopy obs. 80—88696
- $Pb_{80}In_{20}$, flux-flow crit. freq. and generalised bundle size depend. on fluxoid traversal distance and length 80—7054
- $Pb_{80}In_{20}$ foil, deformed, annealed, correlation between pinning strength and flux flow noise charges 77—43792
- PbSb foil production for TEM by electrolytic and ion beam thinning *(German, English)* 77—49812
- Pd, surface IR wave propag. distance 77—28641
- Pd-Cu-Si, laser melting and splat quenching to form foils for TEM obs. 80—29986
- Pd_3Fe foil, $L1_2$ superstructure, antiphase boundary orientation and energy 80—39112
- PdH_x, supercond. props. 77—32114
- Pt, quenched, 1.2 MeV electron irrad., subthreshold irrad. effects 78—51585
- Pt, surface IR wave propag. distance 77—28641
- Pt:^{181}Hf, interaction of implanted impurity with radiation induced lattice defects, TDPAC meas. 80—24494
- Pt-Fe alloy foils prep. by electrodeposition of Fe 80—35113
- Rh foil, work function determ. rel. to heat treatment temp., extrinsic photoeffect meas. 77—39918
- Sb, splat-cooled and vapour-deposited, metastable structs. 79—87018
- Si, amorphous foil, electronic energy straggling of light ions, at. number depend. 77—11612
- Si, computer simulation of high resolution images of defects 80—107208
- Si, foil, thinning for electron microscopy 79—49217
- Sn, electron inelsatic MFP from photoionisation cross sections and ang. var. studies 77—66572
- Sn foils, 1-3.5 GeV electron impact, transition X-ray emission, comparison with theory *(Russian)* 80—60704
- Sn, irradiated by laser beam, psec optical shutter 78—1350
- Sn, thin layers, EM field penetration, depend. on temp. in mixed and intermediate states 79—65598
- ^{119}Sn, thin foil, 19.6 keV conversion e^- energy, ang. contrib., Monte Carlo calc. 79—11360
- Ta, coated with thin H-permeable Pd film, AES and SIMS 79—52467
- Ta, crack growth resistance straining stage in SEM 77—25124
- Ta, electron energy loss spectra 80—7452
- Ta, periodic chemical var. effect on mech. props. 79—91590
- Ti foil, 150-400 keV electron transmission coeffs., Monte-Carlo calc., continuous deceleration model 77—50604
- Ti foil electrolytic perforation, surface film phase composition obs. *(Russian)* 80—61004
- Ti Nb-Ge, β phase decomposition, electron microscopy struct. investigation *(Russian)* 79—83172
- Ti-Ni, laser melting and splat quenching to form foils for TEM obs. 80—29986
- U_3O_8, supported fission foils for laser excitation, preparation method 77—68218
- ^{235}U foil, sputtered, energy spectrum, fission track technique 78—68593
- V, coated with thin H-permeable Pd film, AES and SIMS 79—52467
- V, electron energy loss spectra 80—7452
- V, electron energy losses due to H, obs. by scanning TEM 80—79850
- W, adsorption and condensation of Fe, meas. by thermal desorption in time-of-flight mass spectra 79—15023

foils continued
W foil, electron diffr. effects and images from inclined grain boundaries 79—82241
W foil, integral heating by msec laser pulses *(Russian)* 77—59824
W foils, adsorption of Sm, kinetics meas. by flux modulation method 79—69363
W, surface IR wave propag. distance 77—28641
Zn foil, splat quenched, preferred orientation 80—40381
Zr, convergent beam thickness determ. 79—4215
Zr, foil bending by in situ ion irrad., neutron damage simulation, room temp. oxide growth 80—107342
Zr-V foil, rapidly quenched and heat treated, supercond. props. 80—54852
ZrO_2 foils, production for TEM 79—74087

Fokker-Planck equation
ϕ^4 system, metastable state, decay rate calc. 80—22301
absorptive optical bistability, transmitted light spectrum and dynamic response function 80—99789
absorptive optical bistability transient, local relax., quantum statistical treatment 80—91838
aerosol particle settling and diffusion from stationary gas in tube or duct 77—52678
aerosol particles diffusion and gravitational settling in tube 78—90976
alpha-particle heating in an open-field-line plasma 80—48908
approximate solutions *(Japanese)* 77—13682
atom+vibrator, stochastic theory, master or Fokker-Planck eqn. numerical solns. 77—30965
atomic resonant interaction with light wave 77—18854
atomic system, two-level, collective behaviour in external field, thermodynamics 80—86236
atoms, reson. radiation force, quantum mech. fluctuations, influence on at. motion 80—58233
bistable potential model, renormalised transport eqns. 80—36957
bistable potentials, diffusion, Schrodinger and Fokker-Planck equations 80—62528
boundary-value problem, two-point, statistical variant using Einstein-Fokker-Planck eqn. *(Russian)* 78—81924
Brownian motion, Fokker-Planck eqn. deriv. from generalised kinetic eqns. 78—36936
Brownian motion, generalised Einstein theory for nonequilibrium fluctuations 80—31672
Brownian motion, new method of setting up eqn. 77—26202
Brownian motion, nonlinear response to external field, in low-friction limit 80—4652
Brownian motion, quantum mech. treatment 79—9186
Brownian motion, Smoluchowski equation in presence of hydrodynamic interactions, Chapman-Enskog method 80—46979
Brownian motion in periodic potential, correlation functions, Fokker-Planck eqn. method 79—165
Brownian motion in periodic potential, in presence of temp. and elec. potential gradients 80—4650
Brownian motion of revolving particles, solution *(Russian)* 78—77802
Brownian motion of rotating spherical particles *(Russian)* 77—41539
Brownian oscillators, non markovian diffusion and Fokker Planck eqn. 77—57285
Brownian particle, Fokker-Planck equation, systematic soln. for high-friction case 78—49767
Brownian quasiparticle model 80—46976
Brownian rotation in external fields, relaxation times 78—62160
Brusselator, dynamic correl. functions, Mori-Zwanzig formalism 80—25988
butane, flexible chain molecules, momentum space diffusion eqns. 80—75142
catastrophe time scales and conventions 80—42173
channelling of relativistic particles 79—60413
channelling of relativistic protons in bent crysts., theory 80—96581
Chapman-Enskog procedure, complete 78—65860
linear Chapman-Enskog procedure, evolution equations of hydrodynamic variables 80—49075
charged particles transport in fluctuating mag. fields, interplanetary appl. 79—27752
Chebyshev polynomial approx., numerical soln., first passage time probability density functions 77—37744
chemical master eqns., Poisson representation 78—35638
chemical reaction system, nonequilibrium thermodynamics, stochastic approach 79—52749
chemical systems, single variable, master eqn. approximation by Fokker-Planck type eqns. 80—77702
chemical transition rates, Brownian motion theory 77—36731
classical damped motion, role played by trajectory in Fokker-Planck solns. *(French)* 79—30347
classical nonlinear stochastic dynamics 77—45740
collision operators as generators of Markov processes and their spectra 79—63150
colloidal solution, flow alignment, transition from isotopic to nematic phase 80—84060
colloidal systems, dynamical props., correlation and response functions 80—22286
complex molecular systems, collision phenomena by stochastic model, observables distribs. and information entropy 78—25640
compressible fluids, Fokker-Planck description 79—80498
constrained systems, Hamiltonian construction and diffusion eqns. derivation 80—73258
continuous-time linear system, varying environment, state estimation methods 79—12581
correlation and response functions, Fokker-Planck dynamics 78—45566
corrosion under random exposure conditions 80—40579
coupled random walk process, spatial structure, regression to steady states 79—25986
coupled random walk process theory, Fokker-Planck eqn. calcs. 80—77710
covariance, Riemann differential geometry 80—42137
critical behaviour of first order transition, mean-field theory, master eqn. and nonlinear Fokker-Planck eqn. 78—8375
critical dynamics, classical systems, Fokker-Planck description 78—21057
critical dynamics in Fokker-Planck formalism 77—22514
current generation by RF travelling waves in tokamaks, numerical anal. 80—1800
damped harmonic oscillator, eqns. of motion in quantum statistical theory *(French)* 78—89399

Fokker-Planck equation continued
dechannelling theory, axial and planar conditions, anal. methods for dechannelled fraction calc. 79—4359
dense fluids, rot. and translational motion, Fokker-Planck eqn. calcs. 77—5736
dense fluids, translational motion, modified Fokker-Planck eqn. 78—75517
derivation, for teaching 79—71188
diffusion, formal soln. using operator approach 79—35647
diffusion in bistable potential, systematic WKB treatment 80—46975
diffusion process modelling, equivalence of different methods 78—57818
diffusion process with critical point, eigenvalues discretisation technique 80—172
diffusion processes, stochastic description 78—41253
diffusive motion in periodic potentials, low friction nonlinear mobility 79—35645
DITE Tokamak, beam driven current meas. 80—106940
eigenfunction expansion soln. extension, first order system 80—31668
eigenvalues of Fokker-Planck operators 80—98863
electron distribution function, steady state response to applied electric field, e^-e^- collisions 80—83883
electron oscillations in fully ionized plasma 79—41814
electron-hole drop nucleation, Fokker Planck treatment 80—6732
electrostatic wave, electron Landau damping and electron collisions, Fokker-Planck model 78—47111
energy deposition of fast ions in plasma, Green's function calc. methods 79—14559
exact time dependent soln. 79—63125
extrema, asymptotic analytic theory for Fokker-Planck processes 80—12992
fast charged particle, dechannelling from planar channel, stochastic theory 80—96579
fast ion Fokker-Planck code FIFPC 78—34342
ferrofluids, dissipative process in non-homogeneous mag. field 80—59119
Feynman path integrals, white noise approx., inertialess Brownian system 78—57859
first order phase transition in laser with saturable absorber 79—18394
fission reactor neutron gas, nonequilibrium thermodynamics *(Japanese)* 78—62595
fluctuations and nonlinear irreversible processes. II 80—82724
fluid, low-density limit, ang. and orientational correlation times 77—84380
fluid structure, orientational correl. time 79—23512
Fokker-Planck-Coulomb systems, collective modes, 1-dimens. case 77—45809
Fokker-Planck-Vlasov eqn., weak solns., uniqueness and stability 79—92951
four-photon parametric oscillator theory 79—86216
free energy role in systems governed by Fokker-Planck eqn. *(French)* 77—26254
functional integral definition 80—65
gas kinetics, integro-differential eqn. approx. by Fokker-Planck type 78—91049
gases, weakly ionised, electron motion, stochastic theory of homogeneous systems, review 80—77735
generalised equation, derivation for non-Markovian system with time reversal asymmetry 79—30369
gross variables, microdynamics and nonlinear stochastic processes 80—101754
heat flux fluctuations, Fokker Planck eqn. in extended irreversible thermodynamics 80—86205
heavy ion collisions, ang. momentum dissipation of fragments 79—36260
heavy ion collisions, dynamics of statistical fluctuations, collective approach 77—14092
heavy-ion collisions, mass exchange and ang. distrib., dynamical treatment 77—61454
Heisenberg model, validity of Fokker-Planck equation 77—89920
hot electron quantum energy distribution function in crossed elec. and mag. fields 77—32019
hydrodynamic equations derivation by multiple time scale method 79—44861
information theoretic derivation, drift and diffusion characterised relax. 77—49699
inhomogeneous, eigentheory 78—29068
integration method, plasma appl. 78—91067
interacting particle diffusion in periodic pots., two particle model, random motion 79—46828
Ising model, magnetisation probabilities and metastability 80—29516
itinerant oscillator model, anal. for dielectric relax. and incoherent neutron scatt. 79—90509
Josephson junctions, Fokker-Planck solution for thermal noise 77—89906
kinetic effects due to detailed equilibrium violation, elastic scatt. *(Russian)* 80—31687
Kramers equation, eigenvalues calc., Fokker-Planck eqn. for Brownian motion in a potential 80—86215
Kramers theory of friction and vel. in chemical kinetics 80—50826
Lagrangian for non dimensional non constant diffusion processes 80—31688
laminar medium, Fokker-Planck equation solution *(Russian)* 78—45584
Landau-Fokker-Planck eqn., for arbitrary statistics, relativistic and nonrelativistic case 80—36935
Landau-Zener problem, random nature of motion role in intersecting terms problem 80—8937
Langevin equations, Fokker Planck Dynamics approach 80—57194
Langevin equations, stochastic integrals, removal of ambiguity, invariance postulate 78—70061
laser, approx. analytic solution 77—54689
laser, containing saturable absorber, bistability, semiclassical and quantum theories 78—82943
laser, continuum mode, with spatially inhomogeneous dissipation and excitation 77—54687
laser, continuum mode, with spatially inhomogeneous dissipation and excitation, stationary soln. 77—54688
laser, single-mode, photon statistics, cooperative atomic interactions 80—43318
laser, two-mode, with coupled transitions, quantum theory 80—43319
laser fields, stochastically fluctuating, saturation and Stark splitting of resonant transitions 80—53245
laser Fokker-Planck equation solutions, polynomial expansion method 80—91771

Fokker-Planck equation continued
laser plasmas, hot electron energy relaxation and transport *(Japanese)* 80—96347
laser with saturable absorber, near threshold, correlation functions, renormalised Fokker-Planck eqn. 80—48208
laser with saturable absorber, stationary state, nondiffusive approx., comparison with renormalised Fokker-Planck eqn. 80—19076
lasing systems exhibiting first order like phase transition threshold behaviour, correl. functions 77—71969
limit cycle fluctutions near bifurcation point, Fokker Planck, Langevin eqn. calcs. 80—77709
linear response approach to heavy ion deep inelastic collisions, dissipation, quantal fluctuations 78—46043
Liouville problem, quasi-particle dynamics from a given kinetic eqn., inverse 80—101749
liquid, non-Markovian system, Fokker-Planck eqn. 77—47313
LMFBR materials, interstitial loop nucleation and growth during irradiation, Fokker-Planck equation, numerical soln. 80—57857
LMFBR materials, interstitial loop nucleation and growth during irradiation, Fokker-Planck equation, numerical soln. 80—68796
Lorentz Fokker-Planck, kinetic theory 79—46413
macromolecular solutions, light scatt., ionic charge effects calc. 77—79714
magnetisation vector of superparamag. particles 79—56494
manifolds of equivalent path integral solns. 80—4687
many-particle system, generalised diffusion processes 78—73942
Markov process, Fokker-Planck-Kolmogorov type equations *(Russian)* 80—145
Markov processes, transition probability densities calc. using Fokker-Planck eqn. 80—42047
master eqn., derivation and expansion 77—5785
master equation, path integral solns., stationary Markov process 78—86233
master equation, two expansions in terms of jump size 77—82472
mobility, system in periodic pot., 1-D, elec. field perturbed, mobility 78—32776
molecular rotation and translation interaction 80—69262
molecules, Fokker-Planck eqns., stochastic modeling 80—43128
moment and Fokker-Planck eqns. for growth and decay of small objects 80—82709
multidimensional bistable potential, diffusion, WKB calc. 80—101770
multigroup formalism to solve the Fokker-Planck equation characterizing charged particle transport 80—68159
multiplicative stochastic processes in statistical physics, appls. 80—22289
multiplicative stochastic processes in statistical physics 79—25980
multistationary behaviour systems, stochastic approaches 80—98854
Navier-Stokes fluid, Fokker-Planck description 78—94632
neutron density fluctuations in on-off controlled reactor, exact stochastic anal. 79—36308
non-linear, with nonconstant diffusion, non-Gaussian time dependent 80—31686
nonequilibrium effects, Fokker-Planck eqn., rel. to path sums, Feynman proof 77—2629
nonequilibrium phase transitions in presence of external non-white noise 80—42182
nonequilibrium states, variational approach to Fokker-Planck eqn. 77—87717
nonequilibrium states subject to Fokker-Planck eqns., thermodynamic props. 77—67396
nonequilibrium statistical mechanics, kinetic eqns. derived 77—57269
nonequilibrium statistical thermodynamics, covariant formulation 77—41542
nonlinear, asymptotic representation of master equation 77—74325
nonlinear, path integral representation proof using Fourier series 78—45580
nonlinear Brownian motion with control parameter fluctuations 79—75456
nonlinear diffusion process, path integral evaluation, by Fourier series 78—70075
nonlinear Fokker-Planck eqns., master eqns. 79—40503
nonlinear irreversible process fluctuations 79—67229
nonlinear irreversible processes, Fokker-Planck eqn. asymptotic solns., generalised Onsager-Machlup theory 78—36955
nonlinear rate processes with multiple stationary states, stochastic theory, metastable state relax. time 79—2725
nonlinear second order system, eigenfunction expansion solutions of Fokker Planck eqn. 80—73172
nonlinear stochastic model, statistical mechanics 79—2724
nonlinear stochastic processes, space-time structure 79—67226
nonMarkovian Langevin n-dimensional eqn. approx. 80—57191
nonrelativistic Markoff field, stochastic quantisation 79—67181
nonspherical body, rot. Brownian motion, ang. vel. 77—33860
nonspherical molecules, rot. and translational motion, modified Fokker-Planck equation 78—75518
nonstationary generalised Langevin eqns., methods of multiplicative stochastic processes 77—57270
nonvolatile liquid, boiling, nucleation eqn. in phase space 79—27495
nuclear reactor, point reactor without delayed neutrons, moments of probability distrib. calc. 77—57705
nuclear reactor model, statistical anal. of neutron density fluctuations 77—26818
one-dimensional diffusion, soluble model potentials 79—35649
one-mass vibroshock system, forced random oscills., treatment by Markov process methods 79—14335
optical bistability, Fokker-Planck eqn. from master eqn. 79—13935
optical bistability, nonlinear polarisability model 80—37976
optical bistability dynamic behaviour, time depend. Fokker-Planck eqn. soln. 80—37980
optical bistability in bad cavity limit, Fokker Planck eqn. approach 80—64116
optical communication, channel displacement and diffusion coefficient determ. *(Russian)* 79—98303
optical fibres, randomly bent, ray theory 78—66921
optical harmonic generation, second harmonic and subharmonic, master eqn. approach 78—33773
optical parametric processes, generalised eqn. 79—3663
optical parametric processes, photocounting statistics 79—3664
optical stability, absorptive, two-level atom system, photon antibunching 80—58486
particle in velocity-dependent random force 77—22493
particle motion in stochastic force fields 78—73928

Fokker-Planck equation continued
particle number conservation in charged particles diffusive transport 78—75266
path integral method of soln. 77—2628
path integral soln. for eqn. with spatial coordinate-dependent moments 80—77688
path integrals for inertial classical particles, rapid stochastic processes 78—57858
path-integral methods in nonequilibrium thermodynamics and statistics 79—26018
perturbation expansion for Fokker-Planck dynamics 79—88879
phase-space density from Liouville equation, as a soln. of system of N one-dimens. free particles 79—97305
picosecond intramolecular dynamics in solution, Fokker Planck eqn. 80—28891
plasm drift-cyclotron instability, collisional effects 77—55144
plasma, electron beam injection, collisional relax., Fokker Planck computational treatment 80—64738
plasma, electron three-body recomb., Fokker-Planck theory extension 77—62332
plasma, hot, energetic charged particle transport, moment method 78—22458
plasma, ion beam-induced currents, kinetic theory 79—32746
plasma, Langmuir waves, collisional damping in collisionless limit 78—34295
plasma, laser fusion, long MFP electrons 78—22462
plasma, magnetised, unstable, turbulent, stochastic photon diffusion 79—48662
plasma, mirror trap, end-stoppered, ion losses, linearised Fokker-Planck eqn. 78—34357
plasma, Monte Carlo Lorentz collision operator 77—76028
plasma, multicomponent, runaway electron motion in momentum space 79—37449
plasma, nonlinear wave, statistical description of trapped particles, relax. time 77—31465
plasma, trapped electron regime, elec. resistivity, collisional theory 77—84412
plasma, two-dimens. guiding centre, kinetic eqn. derivation 78—26241
plasma current, fluctuations, diffusion and beam-induced currents in Culham Superconducting Levitron 80—28616
plasma heating, ion-cyclotron, Tokamaks and mirrors, quasilinear model 78—59626
plasma in const. elec. field, electron distrib. function 79—4106
plasma transport theory, Fokker-Planck linearized collision operator appls. 77—3923
plasma-relativistic electron beam interaction, transverse mag.-field induced enhanced energy deposition 77—62377
polydisperse system, turbulent coagulation in force field 79—57297
polymer solution dynamics, generalised Fokker-Planck eqn. appl. 79—1386
power and temp. fluctuations for reactor with temp. feedback, exact statistical anal. 79—36309
power reactor, neutron density fluctuations, stochastic nonlinear model, Fokker-Planck eqn. 78—58316
projection operator construction, nonequilibrium states, Fokker-Planck eqn. 79—21670
QED of strong field, nonrelativistic treatment *(Russian)* 77—6064
quantised dissipative systems, noise operator approach 77—30099
quantum dynamical semigroups, neutron diffusion eqn. 77—61034
quasiadiabatic solutions, time-dependent drift, fluctuation coefficients 80—90785
quasideterministic Fokker-Planck dynamics 78—93627
quasistationary distribution functions for kinetic eqns. 78—9755
quenched-in vacancies, clustering, stochastic theory, solvable model 79—65074
radiating molecules, in upper atm., rot. relax., IR emission and vibr.-rot. transitions calcs. 77—65462
random walk process, memory effects 80—27232
reactive and translational dynamics coupling 78—60988
relativistic free particle, in thermal radiation within classical electrodynamics, equilib. distrib. 80—8935
relaxation process as contraction of Markovian type multidimensional one 80—31671
resonance transfer rate of electron excitation, model of convergent terms, effect of diffusional motion of particles 80—8936
resonant medium with small degree of ionisation, radiation transfer mechanism, description by Fokker-Planck eqn. *(Russian)* 79—37453
ring laser, coherence theory, counter-rotating laser modes 78—55387
rotational Brownian motion of a symmetrical top 79—54061
scaling, nonequilibrium systems near instability point, anomalous fluctuation theorems in extensive region 77—2612
scaling theory of transient phenomena near instability point 77—33945
semiconductor, hot electrons, photoexcited in quantizing mag. field, energy distrib. calcs. 79—42586
short time propagators in Riemann geometries 79—63129
Smoluchowski equation derivation with corrections for Fokker-Planck and BGK collision models 79—80499
solid state self-diffusion 80—39340
Sonine polynomial soln. 77—17794
sonine polynomial soln. *(Japanese)* 77—45681
spherical stellar system, distrib. of stars around massive central black hole 78—65660
star escape from isolated clusters, Fokker-Planck eqn. generalization *(Polish)* 78—36645
stationary state, response and correlation in Fokker-Planck dynamics 78—45567
steady states of weakly dissipative systems 78—81918
steepest descent approx. 79—80516
stellar dynamics, in fixed inhomogeneous gravit. background, numerical integration method 78—32526
stochastic diffusion in a periodic potential 80—12994
stochastic one-variable system, growth of fluctuations from marginal eqn. 80—86213
stochastic quantisation, path integral formulation of Fokker-Planck equation 78—86228
stochastic quantisation processes, review, Markov processes, Martingales, quantum dynamics 80—94969
stochastic quantization and detailed balance in Fokker-Planck dynamics 80—4645
stochastic systems, relay-type scalar, fundamental response properties *(Japanese)* 77—2519

Fokker-Planck equation continued
  Stratonovich calculus, superiority over Ito for stochastic processes with non-additive fluctuations 79—85078
  Stratonovich calculus, superiority over Ito for stochastic processes with non-additive fluctuations 79—85079
  string, nonlinear stretched, randomly excited, anal. 78—83312
  structural vibrations under random excitation, energy anal. 79—27568
  superionic conductors, theoretical models, review 80—107465
  symmetric top molecule dense fluid orientational relax. 78—5996
  symmetry breaking in the decay of unstable states 80—57188
  system interacting weakly with heat bath, Fokker-Planck eqn. derivation 80—17900
  Tokamak plasma, beam driven currents, trapped electrons effect 80—70011
  toroidal plasmas, beam driven currents, trapped electrons effect 80—70011
  transition operator for Markov and non-Markov processes, interpolation model 80—8910
  transport equation renormalisation 80—82732
  transport properties of electrons with narrowly defined bands at low temp. *(Russian)* 80—103656
  trapped ion, laser cooling, theory 80—58414
  triatomic molecules, C_{2v} symm., vector statistical distrib., mol. dynamics computer simulation 80—63734
  truncated generalized equation, appl. to Poisson process 80—8938
  turbulence, observable motions, Navier-Stokes eqns. 80—10230
  turbulence kinetic theory, fundamental soln. 80—27137
  two-level atom, relax. and reson. fluoresc. in phase-modulated laser light, calcs. 77—54535
  two-level atom in coherent monochromatic field, transmitted and fluorescent light spectra 79—49981
  unstable state decay, trajectory time spread, laser photon statistics 80—83585
  variational method for soln. 77—33928
  variational techniques application 78—89415
  vibration systems simultaneous continuous and discrete stochastic processes, compact eqn. *(German)* 79—55337
  void nucleation, continuum description 78—87707
  weak diffusion master eqn. expansion, critical points 80—57228
  Wick's theorem, relation between canonical and Fokker-Planck dynamics 79—17329
  Wick's theorem and Fokker-Planck dynamics 79—40504
  Wicks theorem and Fokker Planck dynamics 77—87715
  X-rays transfer through optically thick shell 78—65488
  D-T fusion reactor core plasma, α-particle heating, dynamic characts. 77—74985
  DT reactor, alpha-particle heated, steady-state and dynamic characts. 78—5016
  He, film, Brownian motion, boundary layers and quantised vortex prod. 80—6579
  ^{4}He, superfluid film, dynamics of vortex pairs using Fokker-Planck equation 79—69313
  Mg atoms, cooling to broad band reson. light press. 80—48835
  Rb, Fokker-Planck eqn. for non-Markovian system 77—47313
  ^{120}Sn+^{132}Xe, deeply inelastic, relative motion mass transport and dynamics 79—13320
  ^{236}U fission as multi-dimensional Brownian motion, Fokker-Planck soln. *(Chinese)* 80—99197
  ^{238}U+^{238}U, deeply inelastic, relative motion mass transport and dynamics 79—13320

food processing industry
  baking, EHD augmented, corona wind impingement effects 78—87235
  cryogenic equipment for freezing and in-transit temp. control 79—58714
  freeze-drying of food models, heat and mass transfer 79—1098
  freeze-drying systems, information systems models 79—58727
  irradiated beef and ham, failure to induce genetic alterations in Drosophila 80—17009
  isotopic meas. of liquids, density, based on gamma radiation absorption 79—44903
  measuring transducers for automation in the sugar industry *(Polish)* 80—42212
  microwave appl., w.r.t. economics and safety 80—3754
  noise control, conflict with sanitation requirements 79—18593
  noise reduction materials 78—38132
  photometric determination and control of solution components, automatic method 79—79350
  physical strength of foodstuffs, materials testing machines made by Instron Ltd. 80—35452
  radiation and isotopes appl., development trends 78—55041
  spectrophotometer, high-energy, 0.25-2.4 μm, for rapid food constituent anal. 79—17508
  sugar mills, noise reduction of cane locomotives, shredders, and steam systems 79—18586
  sugar-cane extractors, windmills appl. in rural India 79—70419
  thermal energy storage, appl. to waste heat recovery in food processing industry 80—30585
  ultrasonic inspection, welded joints in sugar extraction diffusion apparatus 80—93703
  UV irradiation unit appl., Brown, Boveri, for surface sterilisation, foodstuffs and pharmaceutical industries appl. 79—62302
  vegetable washers, effluents meas. via plexiglass HS flumes 77—62321
  yeast survival rate obs., millimetre-waves influence *(Russian)* 79—2100
  N_2, liquid, use as cooling agent 79—58709

forbidden gap *see energy gap*

Forbush decreases *see cosmic ray variations*

force
  see also atomic forces; coercive force; Coriolis force; force control; force measurement; molecular force constants; nuclear forces
  biomechanics using a crane boom 78—81759
  centrifugal, simulation, on overhead projector, teaching appl. 77—41438
  classical mech. and field theories, force concept 77—49
  education, momentum flow as force, alternative conceptualisation for teaching mechanics 80—67993
  education, simplified relativistic force transformation equation 79—25791
  Faraday and the concept of force 80—57048
  Galaxy, gravit. force field normal to galactic plane 80—46669
  Galaxy disc, local K_z-force field rel. to interstellar matter z-distrib. 80—62271
  methane, intensity pertubations due to ν_3/ν_4 coriolis interaction 79—98087

force continued
  standards for industry 80—42198
  transmission through incompressible viscous fluid-isotropic elastic solid interface 78—43252
  two finite bodies problem, development of force function *(French)* 77—13218

force constants *see lattice dynamics; molecular force constants*

force control
  controllable force supply for human muscle voluntary reactions meas., design features 79—100801
  electron microscope, UHV, const.-load tensile device and appls. to materials science 78—11462
  mechanical prestressing, compensation of isolated muscle specimens *(German)* 80—36201
  optimum vibration isolation forces for system with random excitations 77—39240

force measurement
  see also dynamometers
  1 MN combination load/bending moment transducer *(German)* 77—79080
  1 MN meas. rig, with direct force introduction *(German)* 78—41301
  250 kN ONERA force standard machine, precision improvements 79—35728
  acceleration compensation of force transducers and weighing systems *(German)* 79—35733
  adhesion, intracorneal, human skin, piezoelectric transducer, skin disease diagnosis appl. 77—48819
  aircraft rudder-bar, strain-gauge dynamometer appl. *(French)* 78—49825
  artificial muscle, load meas. in animals 77—44852
  axial load meas. of leg prostheses, electronic storage system *(German)* 79—84006
  biomechanical force measuring platform *(Polish)* 80—36212
  bone mechanical properties characterisation by dynamic response 80—76782
  cable tension meas. using transverse vibration technique 79—37269
  cellular elastomer selection for use in biomechanical capacitive force transducers, measuring device *(German)* 80—85545
  centripetal force apparatus, modifications 77—71171
  conference, Braunschweig, W.Germany (Sept. 1978) 79—35725
  contact-resistance transducers using electrically conductive paper 77—13747
  deadweight standard machines, 100 kN, investigation of parasitic effects 79—35731
  digital force transducer, design, features 78—21116
  digital impulse meter, 5 to 500 N range 78—191
  distribution under human foot, online meas. system 78—96110
  dynamic damping effect in small force measurement *(Russian)* 78—12687
  dynamic errors in spring-mass-damping system *(German)* 79—12794
  dynamic force meas., method for processing results *(Hungarian)* 77—117
  dynamic force meas. device comparison *(German)* 77—79089
  dynamometer calibration, for exact meas. up to 10 N *(German)* 77—53897
  dynamometers, multicomponent, practical experimental designs for calibration 79—35729
  dynamometers, performance evaluation by compensation curves *(German)* 78—192
  dynamometers, time ageing determination using bonded resistance foil strain gauges 79—35726
  dynamometric transducers based on granular conducting material contact resistances 79—35706
  elastic devices, booklet 77—57322
  electro-mechanical sensors, mechanical compensation methods influence on error characts. *(German)* 78—16786
  electromechanical force meas. devices, long-term stability tests *(German)* 77—79088
  elongation measurement for polyethylene single crysts. 79—87700
  fibre optical interferometers for length, temp., pressure and force meas. 80—98971
  fluidic strain gauge load cell 80—37024
  foot function assessment system, normal and pathological feet, computerised system 79—100760
  foot vertical force during walking, continuous meas. device *(Japanese)* 78—73273
  force sensor, inductively coupled, high bandwidth 79—6118
  force transducer transformation analysis *(German)* 77—74380
  force-frequency measuring gauge based on oscillating quartz crystal 80—31727
  forearm crutch with built-in load indicator, walking retraining after fractures *(German)* 79—8563
  friction apparatus for meas. normal displacement of sliding body 80—99977
  gait analysis, for daily orthopaedic practice, 2-D cinephotography, 6 component force measurement 77—48908
  gait instrumentation for foot/ground interaction meas. and display 79—96696
  gravitational force on freely falling electrons, meas. apparatus 77—30080
  hand function, normal finger functional strength meas. 79—92276
  hip dynamic contact force distribution meas. 79—39624
  horse's hoof movement/load relationship camera and multicomponent force meas. panel *(German)* 79—16352
  impact force vs. displacement curves, expt. determ. 78—83344
  inductive transducer calibration characts., calc. and expt. *(Russian)* 77—10005
  insect lift and drag using two-component dynamic wind-tunnel balance 80—22350
  interaction energy, procedure for precision meas. of condensed bodies under various physicochem. conditions 79—21736
  isometric muscle contraction meas., fibre-optic force transducer 79—79715
  knee, human, ligament primary and coupled load transmission meas. 79—92271
  knee joint, gait anal. system 77—44774
  knee-joint forces, routine clinical assessment method 79—83831
  large forces, metrological provisions in COMECON member countries 79—75523
  leg loading determination using instrumented shoe, portable device 77—29217

force measurement continued
  limb muscle dynamic force meas. by surface EMG 79−34689
  load cell design and development for materials testing 80−105628
  load cell transducers, shear force, mathematical modelling and design 79−35722
  load cells, automatically controlled, method for digitizing measured values *(German)* 79−35721
  load cells and force transducers 80−86276
  load transducers, sensitivity to temp. gradients and transient environments 79−35716
  loading machines, comparison with German PTB force scale *(German)* 79−35734
  magneto-anisotropic transducer appl. *(Russian)* 77−65021
  magnetoelastic load cell and performance of force transducers *(German)* 79−35714
  magnetoelastic transducer, Fe-cored, choke-type, operation and characts. *(Polish)* 78−12684
  magnetostriction force transducer 79−2757
  mass standards for calibration of force standard machines *(German)* 79−35735
  mica surfaces in aq. poly(ethylene oxide) soln., forces meas. 79−23833
  molecular attraction forces between crossed fibres, meas. technique, appl. to Pt and quartz 77−27216
  moment of forces on truncated rotor, edge effect *(Russian)* 80−28135
  motor vehicle in impact test, force meas. *(German)* 79−34271
  myopotential controlled elec. operated hand with sensory feedback 79−57815
  occlusal force by human teeth, using small piezoelec. triaxial cell *(German)* 78−20303
  optoelectronic meas. methods appl., with twin diodes *(German)* 80−13064
  optoelectronic strain gauge, force and strain measurements giving high accuracy and resolution *(German)* 79−98673
  oral force monitoring, piezoelectric transducer 77−48888
  orthodontic appliance mechanical behaviour determ., computer-controlled device 78−44727
  oviduct contractile activity, extraluminal meas. using Si force transducer 77−40805
  pathological gait assessment, foot force meas. device 79−20701
  photoelastic substrate technique for dynamic measurements of forces exerted by moving organisms 79−39621
  piezoelectric dynamometer for dynamic force meas. *(Hungarian)* 78−65918
  piezoresistive strain gauge transducers for millinewton force meas. with millisecond response time 79−12793
  pneumatic force transducer, features 78−45611
  pneumatic force transducer 78−21128
  ponderomatic meas. for fluid detection in chem. anal. 78−68953
  pressure-force transducer using 32.768 kHz X-Y flexure watch crystal 78−57934
  resistive transducers, normalisation *(Rumanian)* 80−4699
  rolling mill strain meas. system, using semiconductor strain gauge based extensometer 78−41296
  semiconductor force transducer suitable for use with small muscles 80−72395
  sensitivity limitations on force and weight meas. in vac. 78−65908
  shear force instrument, force-balance 78−51263
  shearing forces on the sole of the foot, meas. system 80−72342
  shock absorbers, telescopic, dynamical force measurement *(German)* 79−35732
  silastic strain gauge as in vivo muscle force transducer 79−29680
  slot-effect transducer, appl. of energy principle for calc. force upon electret *(German)* 77−3706
  standard force measuring machine, calculation method of finding errors when certifying direct loading equipment 80−17934
  standard machines of national institutes for metrology, technical specifications 79−26022
  standards and force measuring apparatus, Hungarian *(German)* 79−35730
  standards for compression force measurement, 0.5 to 30 MN 79−35727
  state of the art and development prospects in the USSR 80−62621
  strain gauge, load cells, characterisation of creep response 79−35718
  strain gauge dynamometer system, body of rotation form, non axially symm. load 80−73350
  strain gauge load cells, small dead weight machines with compensator and computerized data processing 79−37266
  strain gauge load cells, stabilisation and compensation of temp. dependent errors *(German)* 79−35717
  strain gauge load cells, testing for suitability in electromechanical weighing machines *(German)* 79−35682
  strain gauge transducers in testing machine and as force standards 80−42215
  strain gauge with screw tenso-resistor, linearity anal. *(Russian)* 78−89475
  strain-dependent resistors, in force meas., noise limitations 78−16771
  strain-gauge force meas. rod bending moment compensation by parallel resistors *(German)* 77−79078
  surgical wound preoperative force meas., transducer device 78−36041
  tensile force measurement instruments developed as first order reference standards *(German)* 80−105635
  tensile testing machine with automatic null-balancing load meas. instrument, dynamic behaviour and optimal adjustment *(German)* 77−60005
  tensile testing machine with automatic null-balancing load meas. instrument, dynamic behaviour investig. and control *(German)* 77−60006
  tension of threads using instrum. based on inductive transducers 79−17414
  tenso-resistive strain gauge output error anal. *(Russian)* 78−89474
  tensometer, semicond., with parallel channel, operation principle *(Russian)* 80−73352
  tensometer with one-piece sensitive element, electric circuit analysis *(Russian)* 78−49824
  thick target projectile penetration model based on pressure bar force meas. 78−30174
  transducer for small muscle meas. 80−41281
  transducer using amorphous ribbon core 78−93669
  transducers, force, calibration using theoretical calcs. 79−35719
  transducers, force, designs and appls. 79−35720
  uniplanar force meas. system for orthodontic appliances 78−31970
  units and standards, relationship with mass and weight 80−27273
  walking, synchronisation of optical press. distrib. and 3-dimens. force meas. under sole human foot *(German)* 78−35975

force measurement continued
  wave and force measurement system 79−41780
  wind-tunnel balance, 6-component, using load cell techniques *(German)* 79−37268

force meters *see force measurement*

forecasting, technological *see technological forecasting*

forecasting theory
  autoregressive-moving average models for Wolf sunspot data, new models 79−12442
  pollution episodes in Venetian region, real-time forecasting via Kalman predictor 80−82046
  River Nile, Kalman forecasting model 80−31081
  streamflow, model, identification of seasonal water supply forecasting models using Akaik's information criterion 80−67386
  time series, conference, Nottingham, England (Mar. 1977) 80−82580

forging
  alkali halides, finished optical components, forging 77−46824
  billet shape during stamping *(Russian)* 79−98630
  borsic fibre reinforced Al, hot pressed forged, plasma sputtered *(Russian)* 78−35330
  circular blank, stress-strain state *(Russian)* 79−52231
  deformation of metal determ., in closed dies, theory and expt. comparison *(German)* 80−25745
  die filling and densification in hot extrusion forging of porous preforms 78−23645
  disk and strip forging for the determination of friction and flow strength values 78−85004
  fibre reinforced composites densification in free forging, exam. of specific work and kinetics 80−16218
  metal, sinter-forging process, powder charact. effects 77−59714
  metals, cold forging, upset tests anal., stress-strain law determ. appl. *(French)* 79−20064
  powder forging, review 79−43166
  rotor, crack detection, US holography method 77−66730
  steel, 18H2N4WA, hot-worked, kinetics of austenite grain growth, rel. to deformation degree *(Polish)* 80−45322
  steel, alloy, nonsteady temp. fields during cooling, calc. 80−16346
  steel, alloy, type 25Gs, increasing fatigue resistance by surface plastic deformation 78−88530
  steel, alloy hot forging for differential pinion gear 78−15337
  steel, CC Cr-Ni, soaking at forging temp., effect on struct. and mech. props. *(Czech)* 78−64628
  steel, Cr modified, heat resist. rel. to thermomech. treatment 79−20084
  steel, Cr-Mn, powder forged, fracture processes and fracture toughness 78−72870
  steel, Cr-Mo, cast and forged, difference in mech. props. 77−48465
  steel, Cr-Mo, martensite to ferrite transform. by fatigue deform. *(French)* 79−66056
  steel, Cu-Mn-Zn, Zn addition effects in powder forgings produced by liquid solid alloying 78−11157
  steel, eutectoid, U8, cold hydraulic press. forging effect on transform. and heat treatment *(Russian)* 79−52235
  steel, friction and wear during hot forging 80−89358
  steel, high speed R8F8K7M6, cast, forged, sintered, struct. and props. 77−77516
  steel, low alloy, microsegregation testing using electron microprobes *(Croatian)* 77−36516
  steel, low alloy, quenched and tempered, formation of stony fracture during forging 79−79059
  steel, Nb, high and medium C, austenite grain growth 78−11249
  steel, Ni-Mo, powder forged, as-forged props., effect of process variables 77−59715
  steel, Ni-Mo, powder forged, fracture processes and fracture toughness 78−72870
  steel, powder, rotary forging, porosity and deform. 78−23646
  steel, powder forged, fatigue, surface treatment effect 80−85048
  steel, powder forged for carburizing appl., core props., mech. props. 78−15339
  steel, powder-forged, fracture toughness 79−66155
  steel, stainless, fibre reinforced Al alloy, exam. of deformation, fracture and forging behaviour 80−11681
  steel forgings, expt.-calc. model of quenching, temp. meas. across cross section 80−16345
  steels, spring, 60S2A and 50KhFA, heat treatment and mech. working effect on mech. props. *(Russian)* 80−20962
  unidirectionally reinforced composite, plane strain deform. processing limits 77−55918
  upset forgings, grain flow structure 79−38872
  Al alloy, cast, forging and heat treatment effects on diamond planishing treatment 79−43237
  Al alloys, 6061, A356, forging of liquid and partially solid alloys 78−80569
  Al alloys 2024, thixoforging into net-shapes 80−16339
  Al bronze, creep forging 77−59848
  Al-Cu alloy, press-forming under coexisting state of liquid and solid, mech. props. 77−81240
  Al-Zn-Mg-Cu alloy, type 7050 and AZ 74.61, engineering props. 79−70219
  B fibre reinforced Al, X-ray investigation of internal stresses *(Russian)* 77−73290
  B fibre reinforced H, hot pressed forged, plasma sputtered *(Russian)* 78−35330
  $Bi_4Ti_3O_{12}$ ceramics, ferroelectric, hot-forged, grain orientation and dielectric props. 80−40076
  CaF_2, fine-grained, forging and bulk optical props. 80−33103
  CaF_2, hot forged, laser window material, fabrication, props. 77−46773
  CaF_2, laser windows, intermediate temp. forging 77−46775
  CaF_2, press forged, mech. and optical props. 80−38079
  Cu, hot forged powder compact 77−24981
  Cu, sintered preform, porous, ductile fracture criterion, rel. to forging process 77−56105
  Fe and Fe-C, (0.8 wt.%), sintered, hot forging ahd chemicothermal treatment, effect on wear resistance 80−25606
  Fe, powder-forged, elastic consts., density depend. 80−84987
  Fe-C (graphite, 0.3 wt.%), powder-forged, elastic consts., density depend. 80−84987
  KCl surface texture and optical props. after forging between polished dies 80−33102
  KCl:RbCl, $SrCl_2$, laser window material, prep., grain boundary stability 77−46774

forging continued
LiF mech. and optical props. rel. to forging conditions 80—33101
LiF, press forged, mech. and optical props. 80—38079
$MgAl_2O_4$, spinel materials press forged, mech. props., IR appl. 78—39722
Mo-Ti-Zr alloys TZM and TZC, superior powder metallurgy die alloys for isothermal forging mech. props. 79—74201
NaCl Czochralski crystal growth for large CO_2 laser windows 80—74525
Sn-Pb (15 wt.%), forging of liquid and partially solid alloys 78—80569
Ti alloy, microstruct. and mech. props., room and elevated temps. 77—36554
$\alpha+\beta$Ti alloy VT3-1, drop forgings, grain orientation and props., combined mech. working, hardening and high-temp. heat treatment influence *(Russian)* 80—20973
Ti-Al-Sn, alloy 6242, dynamic effects of flow and fracture during isothermal forging 80—76343
Ti-Al-V (6, 4 wt.%), deform. charact. under isothermal forging conditions 77—36600
U/(Zr-Cu-Mo alloy) welded joints, mech. characts. determ. 20 to 750°C 79—29113
U/Ti welded joints, mech. characts. determ. 20 to 750°C 79—29113
U-Mo (1.5 wt.%) metallurgical study of forging *(French)* 78—21737
W fibre reinforced Ni, high temp. stability 77—48372
Zn-Al, high strength superplastic alloy, exam. of precise forging method 79—4929

form factors, atomic *see atomic structure*

form factors (elementary particles)
see also form factors (nuclear)
0^- meson, EM form factor in straton model *(Chinese)* 80—22616
(1+1) dimensional field theoretic models with soliton behaviour, exact S-matrices and form factors 79—26240
(1/N) expanded nonrenormalisable interactions, nonlocality investigation 79—30652
σ model, $SU_2 \times SU_2$, modified Goldberger-Treiman relation, pseudoscalar form factor 80—27421
$(\phi^3)_6$ theory, composite particle form factor, asymptotic behaviour 80—86595
ϕ^4 model, Pade approximants, EM form factor, pseudoscalar particles 78—74122
Abelian gauge theories, charge screening and mass spectrum, form factor anal. 79—75686
Abelian Higgs model, classical vortex soln. 77—2752
an asymptotic connection between processes of deep inelastic scattering and inclusive annihilation 79—22105
analytic representation and radii determ. of hadrons and light nuclei 77—30386
axial vector form factor from current algebra, π PCAC and covariant threshold electroprod. amps. 80—414
axial vector matrix elements, chiral limit, renormalisation effects 79—17190
bag model, quark-quark interaction anal. 78—33029
baryon decay, algebraic formulation, vector and axial vector operators, SU(3), form factors 77—71512
baryon decay, semi-leptonic weak interactions, book contrib. 78—78162
baryon form factor predictions and Melosh transformations 77—54105
baryon octets, semileptonic decays, SU_3 theorems 80—32030
baryon resonances, EM transitions, multipole moments in single quark transition model 80—62985
baryonic state even wave harmonic oscillator theory, structure functions versus form factor 79—393
bi-local field in external source, scatt. amplitude 78—74182
bi-local field interaction with external field 78—66030
Bjorken asymptotic behavior of deep inelastic scattering form factors and the general principles of field theory 79—21958
bound state, relation to binding potential using nonrelativistic Schrodinger eqn. 78—58187
bounds on scatt. amplitudes and form factors 77—13878
causality props. of form-factors of one particle matrix elements of current commutator 77—30385
charge asymmetry and charge dependence of two nucleon scattering 78—4899
charged current induced weak one pion prod., form factors from PCAC 80—18129
charmed meson prod. in e^+e^- annihilation, quark model 78—8680
charmed meson semileptonic decay, effective chiral Lagrangian method 78—74254
composite particle EM form factors, asymptotic behaviour 80—62927
composite particles, form factors in terms of inelastic Jost functions 77—2831
compound system, form factor behaviour on approach to asymptotically high transferred momenta *(Russian)* 77—67655
Compton scatt. polarisability, use of Ward identity on off-shell form factors 78—66120
Compton scattering, γ-rays off bound electrons, nonrelativistic form factors, Fortran program 77—10252
conformal invariance breaking and quark counting rule for form factors 77—30381
conformal spin-1/2 systems 77—38085
conserved axial second class current, sum rule, commutation relations and axial formfactor 80—18090
consistent S-matrix with nonlocal Yukawa interaction and relativistic form factor 79—93300
continuum shell model, recoil corrections for nucleon-nucleus scattering 78—8751
core polarisation effects on Coulomb form factor 77—30474
covariant quantisation of solitons in gauge theories 78—16916
deformed nuclei, single nucleon form factor for knockout and pick-up reactions, (p,2p) calcs. 78—93999
deuteron, EM form factor, data anal. and asymptotic behaviour 79—89155
deuteron, EM form factors relation to wave functions 78—37210
deuteron, EM quadrupole form factor peak value, determination of percentage D-state 78—93950
deuteron, meson exchange currents in ed scatt. 77—18290
deuteron, six-quark state and EM struct., two nucleon bound state model *(Russian)* 79—13031
deuteron electromagnetic form factors, D-wave admixture in the dispersion approach *(Russian)* 79—30737
dilepton energy bounds, form factors anal. 78—41549

form factors continued
double-logarithmic quark and form factors and the evolution of parton jets 80—68421
E_7 exceptional group, calc. of 6_j symbols 78—57800
$e^+e^- \to \pi^+\pi^-(\pi^0\omega)$, $\rho'(1250)$ description, EM form factors, bound states, N/D method *(Russian)* 80—42465
elastic EM form factor analytic struct., complex coupling const. plane, Pade approximants 78—29335
elastic form factors, asymptotic behaviour, Callan-Symanzik eqns. *(Portuguese)* 80—18137
elastic form factors at large momentum transfer, dimens. counting model 77—18235
electromagnetic multipoles and form factors 77—67701
electron, in two-dimens. QED *(Russian)* 77—46003
electron+nucleus scattering, three body correlations, influence on charge form factor of closed shell nuclei 79—6571
electron scatt. form factors, effects of proton size folding 78—29372
EM form factor and Zweig rule, anal. props. *(Russian)* 79—9374
EM form factors, vector dominance model 77—74645
EM form factors in Bjorken limit and their Fourier transforms on light cone 79—26246
exact from factors in field theoretic models with soliton behaviour 78—82211
exclusive processes in QCD, baryon form factors at large momentum transfer 79—89153
fermion inelastic form factor, gauge theory, quark scatt. *(Russian)* 78—45883
fibre bundles almost complex manifold approach, curvature form 78—12915
g_A/g_V ratio in $\Sigma^- \to ne^-\bar{\nu}_e$ 77—26522
geometrodynamics for quarks and hadrons, form factors and currents 78—45809
hadron, form in dual parton model 77—67619
hadron electromag. and weak form factors, SU(6) scheme of relativistic quark model 78—41500
hadron electroprod., $\Delta(3,3)$ region, low hadronic mass, Δ, τ, and nucleon axial vector form factors 78—74259
hadron form factors in quantum chromodynamics, asymptotic form *(Russian)* 78—17021
hadron interactions, inclusive, large momentum transfer, quark counting, EM form factors 80—68498
hadronic, asymptotic behaviour in quark model *(Russian)* 77—61289
hadronic form factor asymptotics in QCD *(Russian)* 80—62983
hadronic structure functions and form factors in low-order QCD with Migdal regularization 79—30720
hadronic wave functions at short distances and the operator product expansion, QCD tests 80—57564
hadrons, axiomatic local constraints *(Russian)* 78—58190
hadrons, e.m. form factors in quark model 78—21429
hadrons, from parton model *(Russian)* 79—93381
hadrons, parton distribs. calc. 78—421
Hardy spaces, role in form factor bounds 79—30735
heavy ion inelastic scatt., folding model, macroscopic formalism, form factors 78—25227
heavy ion inelastic scattering, form factors 79—26458
heavy ion one- and two-nucleon transfer reactions 77—46188
heavy-ion transfer reactions, DWBA form factors 79—13322
inclusive, new scale variable *(Russian)* 79—36079
inelastic final state interactions, unitarity, coupled-channel approach 77—2835
inelastic nucleon form factors, spectral representation *(Russian)* 78—37212
IR singularities in gauge theories, renormalisation group method, coupled massless field theories 78—54538
isoscalar E1/broad resonances (T=0) 79—13250
K_l form factors and (8,8) model of chiral breaking, unitarisation 77—18286
large $|t|$ proton-proton scattering and quark-quark scattering 79—13161
lattice Schwinger model, form factors of dipole states 78—66029
light nuclei correlation struct. from elastic electron scatt. 77—18532
loosely bound composite particles, elastic scatt., disintegration 77—301
matrix equations for two-fermion systems with magnetic interactions 79—21904
meson, and integral representation of wave function in straton model *(Chinese)* 77—34124
meson, relativistic covariant quark model *(Russian)* 80—9140
meson form factor in dual model with spontaneous vacuum transitions *(Russian)* 77—49967
meson states in model with extended meson fields as alternative to quark confinement 77—22642
mesons, bound state wave function, probability interpretation, form factors, Bethe-Salpeter eqn. *(Chinese)* 80—101930
multichannel problem, coupled, soln. of form factor 78—29277
muon bremsstrahlung in collisions with nonpointlike nuclei 78—8803
muon capture, induced pseudoscalar form factor upper bound 77—82872
N-body scatt. theory, form factor approach 79—79
neutrino form factors in 2-D approx. of QED 80—9132
neutron charge form factor, new data anal. 79—67549
neutron charge structure, Clemental-Villi model 77—2830
neutron-proton mass difference, classical electrodynamic model 77—6123
non local theory, canonical quantization, with form factor in interaction Lagrangian 79—75691
non-Abelian gauge theory, colour-singlet quark form factor anal. 77—65084
nonlocal, field theory, form factor props. 77—87903
nuclear bag states containing quarks, detection 78—70465
nuclear charge, pion exchange currents effects 77—18379
nuclear charge form factors, multiquantum excitation calc. 77—41885
nuclear currents, microscopic anal. of elementary particle description 78—82304
nuclear EM, asymptotic behaviour, colour quark statistics 77—10301
nuclear one particle momentum distrib. 77—6206
nucleon, at t=9.58 GeV^2 from $\psi \to p\bar{p}$ data 77—6118
nucleon, dispersion theory, review 77—34155
nucleon, EM radii calcs. *(Russian)* 77—74687
nucleon, inelastic, form factors, spectral representation *(Russian)* 78—93881
nucleon axially-symmetric form factor, π electroproduction at threshold *(Russian)* 77—10267
nucleon charge form factor, quark model 78—62352
nucleon EM form factors and radii 77—2837

form factors continued
nucleon EM structure, $\psi(3.1)$ in VDM of nucleon form factors 78—50034
nucleon form factors, asymptotic relations from quark-gluon model, scaling violation 80—42463
nucleon form factors, Lorentz invariance and nuclear photoabsorpt. 77—88110
nucleon form factors and light front dynamics *(Russian)* 77—38172
nucleon in time domain, EM form factor *(Russian)* 78—78183
nucleon isovector, via $\pi^- p \to e^+ e^- n$ 275 MeV *(Russian)* 77—82764
nucleon structure functions from quark distrib. functions anal. of μp and μd interactions 78—50035
nucleon transfer reactions, centre-of-mass corrections to overlap factors 77—308
nucleon-nucleon potential, nuclear form factor behaviour at high transferred momenta 79—9485
nucleonic form factor, pion exchange, model 80—22608
nucleons, quark-diquark model 77—87937
nucleus$+\gamma$, electron pair production, screening corrections for intermediate, high energies, using relativistic form factors 78—93986
one-pion exchange current, conservation and form factors 77—38098
OPE formfactor and pd backward elastic scatt. in Δ-reson. region *(Russian)* 79—54353
P-wave isovector $\pi\pi$ phase shift, pion form factor left hand cut contrib. 80—27504
Pauli principle effect in nuclear matter, exchange of interacting two pions 78—12983
photon form factor, asymptotic behaviour in QED 80—18096
photon nonlocal form factors, extended extremal approach 77—61227
photoproduction of relativistic parapositronium, and muonium perturbation expansion *(Chinese)* 79—49432
pion, determ. from pion electroprod. cross-section *(Russian)* 77—10267
pion EM form factor zeros 77—6126
pion EM formfactor, upper bounds on derivatives 77—6125
pion EM props., dressed quark model *(Russian)* 80—52508
pion form factor, ω and ϕ effects G-parity violation 79—35963
pion form factor and its asymptotic behaviour 79—30734
pion form factors from $e^+e^- \to \pi^+\pi^-$ at 400 MeV *(Russian)* 79—3034
pion-quark scattering model for lepton pair production from $q\bar{q}$ annihilation 79—13056
polarisation, lepton and photon nuclear interactions, bremsstrahlung, pair production *(Russian)* 77—88104
pomeron current model for diffraction dissociation 78—4843
progenitor sum rules, nuclear theory appl., meson$+$nucleon interaction, inelastic form factors 78—54690
proton, harmonic anal. with Lorentz group *(Russian)* 77—46051
proton charge form factors, K_{min} approx. in ^{16}O, and ^{40}Ca 79—9456
proton electroproduction struct. function, elastic form factor, scaling function, causal representation 79—13138
proton form factor extrapolation using Pade type approximants 79—6341
proton proton form factor, influence on Coulomb-nuclear interference 79—49534
proton-hadron elastic scatt., Chou Yang droplet model anal., form factors 78—21464
proton-neutron mass difference, higher intermediate hadronic states 78—45920
pseudoscalar Dalitz decays, form factor slopes, VDM with subtracted dispersion relation 78—58181
QCD, 2-dimens., confinement effects on analyticity meson inelastic form factor, scatt. amplitude 79—333
QCD, 2-dimens., IR structure, EM form factors and inelastic struct. functions *(Chinese)* 79—58935
QCD, asymptotic precictions for exclusive processes, form factors, struct. functions, and low-mass jets 79—71701
QCD, infrared behaviour, colour-singlet quark form factor 78—24948
QCD exclusive processes, π, K, ρ form factors, hadronic wavefunction evolution eqns. 80—18135
QCD jet calculus, inclusive p_T distrib. with exclusive form factors consistency 80—391
quantum chromodynamics, two dimens., confinement form factors, deep inelastic scatt. 77—30322
quark, gauge-group singlet, infrared structure 77—45964
quark bag model, large transverse momentum processes of hadrons, EM form factors *(Russian)* 79—26308
quark double logarithmic form factor derivation, QCD, hard semi-inclusive processes 78—93862
quark exclusive form factor, leading IR behaviour in QCD 77—54074
quark form factor, asymptotic behaviour 78—89660
quark form factor, non leading contribs. to asymptotic behaviour 78—8586
quark form factors in quantum chromodynamics, renormalisation method *(Russian)* 78—45882
quark magnetic form factor, significance of instantons 78—70339
quark model of resonances, $SU_6 \times O_3$, form factors, review 77—67624
quark model relativistic generalisation minimal boosting of SU(6) scheme, meson, baryon props. 77—41814
quark models, axial vector mesons decoupling from local currents 77—87938
quarks, EM form factors in instanton fields 80—99102
quarks and quark systems, structures in hadrons, form factors 77—41810
quasi-relativistic quark model with confining pot., hadron form factors 77—46020
radiative corrections, fourth order, book contrib. 78—82213
Regge trajectories relation to form factors of composite states 77—82742
relativistic, clusters with nonrelativistic wave functions 77—30382
relativistic harmonic oscillator quark model, N and $\Delta(1236)$ form factors 78—93852
relativistic many-body bound systems, electron scatt. form factors 77—74765
relativistic oscillator formalism for hadron struct. and props. 80—9144
scaling, deep inelastic scattering, form factors, Tauberian theorems in quantum field theory 80—68375
semileptonic decay of charmed particles, formalism using helicity amplitudes 78—4852
sine-Gordon soliton form factors, massive Thirring model S-matrix 77—45952
singlet quark form factor exponentiation in leading logarithm approx. 80—91091
soliton conservation laws, construction of form factors and correl. functions *(German)* 79—9274
spectral function zeros for EM form factors 79—13125

form factors continued
spectral representation for nucleon form factors in electroprod. process 78—12914
stable analytic continuation with rational functions 80—37266
stripping form factors anal. 78—21538
Sturm-Liouville expansion method, one- and two-particle transfer form *(Russian)* 78—89844
SU(2) nonlinear σ model, kink solns., form factor interpretation 78—24964
$SU(3)_E$-invariant form factor for pseudoscalar mesons 77—61288
superpositronium, form factor corrections, short-dist. mag. moment behaviour of electron 77—83772
three nucleon, finite range microscopic form factors, zero range DWBA calcs. 79—6525
three particle system, dispersion relations, one channel N/D method, form factors *(Russian)* 79—40689
three quark operators, anomalous dimensions, baryon form factors and quantum numbers 80—22568
three-particle nucleus, virtual decay, vertex form factors *(Russian)* 77—26607
transition, quark mass differences inducing symmetry breaking 79—93400
trinucleon bound state using Paris pot., binding energy and form factors 78—89803
trinucleon props. with one-boson exchange potls. 77—18421
two fermion eqn. with form factors and EM high mass resonances 79—93322
two pion exchange charge density in static approx. ^{3}He, ^{3}H form factors 78—66222
two-fermion relativistic eqns with form factors, anomaloys mag. moment interactions 78—372
vector meson-nucleon interaction, SU(3) symm., coupling consts., form factors 77—13886
vertex form factor radiative corrections in 2 dimensional QED approx. *(Russian)* 80—418
vertex function expansion an arbitrary reference frame *(French)* 77—49614
vertex function expansion parameter, two-dimens. approx. QED *(Russian)* 79—6301
weak charmed-baryon resonance prod., neutrino inclusive interactions, scaling behaviour 78—8645
weak neutral couplings to hadrons in neutrino inclusive, semi-inclusive and elastic reactions 79—36064
weak nucleon formfactors in modified vector dominance model *(Russian)* 80—68437
Wigner-Weisskopf model form factor construction from eigenfunctions 77—78995
Yukawa pot., superposition, off-shell Jost function 78—29415
β decays of ^{6}He, ^{19}Ne, ^{35}Ar, recoil ion energy spectra anal. 78—21525
d, 6 quark system, wave function, elastic form factor, NN forces, spectroscopy *(Russian)* 78—50015
d, charge form factor falloff at large q^2 in dispersion approach *(Russian)* 79—3027
d, EM form factor, relativistic description 79—54340
d, EM form factor determ., relativistic impulse approx. 77—65158
d, EM form factor determ. 77—61287
d, EM inelastic form factors, exchange current effects in electrodisintegration 79—93418
d, elastic form factor calcs. with Bethe-Salpeter eqn. 79—67554
d, form factors relation to wave functions 78—70462
d, six-quark model, form factors and struct. functions 78—45871
D and D* prod. from e^+e^- annihilation, form factors and free quark model 78—37222
d charge, π-contrib., unity of relativistic corrections and meson exchange currents 79—67553
d charge form factor accompanying high imparted momentums *(Russian)* 78—58189
d EM form factors at large transferred momentum, six-quark state *(Russian)* 78—89715
d inelastic screening, form factor at $t \neq 0$ 80—91070
$D \to K\pi l\nu$, charm-changing weak hadronic current, models 80—57585
$D \to K\pi l\nu$, current algebra calcs., form factors and decay distribs. 80—42447
D mesons, e.m. props. 78—8668
d wave function with $\Delta\Delta$ reson., effect on EM form factors 77—18486
D^+-D^0 mass difference, form factors, SU(4) coupling, vector meson dominance model 79—391
D^{*+}-d^{*0} mass difference using form factors and vector meson interactions 78—21427
dN relativistic scattering, elastic and inelastic form factors 79—30752
dnp vertex form factor, ed elastic scatt. at high momentum transfer 80—82977
e scattering by boson of arbitrary spin, differential section *(Russian)* 78—25049
ed, elastic and deep inelastic scatt. at large momentum transfer, quark model *(Russian)* 78—86529
ed, nucleon structure from electron scatt., EM form factors 80—42468
ed$\to$ed, nucleon forces, meson exchange current effects, impulse approx., review 80—57603
ed elastic scatt., d form factors and struct. functions, charge and struct. radius *(Russian)* 79—40841
ed elastic scatt., EM form factors, relativistic harmonic oscillator model 79—54327
ed elastic scatt. at high momentum transfer, form factors at γNN and dnp vertices 80—82977
ed inelastic scatt., electrodisintegration at high energy and momentum transfer, exchange currents 79—6342
ed quasi-elastic scatt., en coincidence, n electric form factor 79—67563
ed tensor polarisation and d wave function short range behaviour 79—67564
$e^+e^- \to$ hadrons, scaling and quark struct. 80—425
$e^+e^- \to$ heavy spin-1/2 particles, form factors and decay parameters meas. 77—26536
$e^+e^- \to$ jets, on-shell QCD quark form factor from two particle correlations 80—86740
e^+e^- annihilation into boson resonance pair, multipole form factors, parametrisation of EM vertex *(Russian)* 77—74701
$e^+e^- \to p^-X$, charmed baryon pair prod. cross section, pole-dominated form factor 78—12922
$e^+e^- \to p\bar{p}$, 1925-2180 MeV total energy, form factors and cross sections 80—427

form factors continued
$e^+e^-\to\pi^+\pi^-$, 0.78 to 1.34 GeV, π form factor meas. 78—33076
$e^+e^-\to\pi^+\pi^-$, near threshold, π form factor *(Russian)* 80—4996
$e^+e^-\to\pi^+\pi^-$, vector meson dominance anal. for π form factor 78—70370
$e^+e^-\to\pi^+\pi^-(K^+K^-)$, $\sqrt{s}=1.5$ GeV, EM timelike form factors for π and K 80—91089
$e^+e^-\to\rho\varepsilon$, transition form factors, dispersion theory 79—63495
eN→eX, form factors and structure functions, review, book contrib. 80—47294
eN elastic scatt., pol. e, nucleon form factors, P violating symmetry, Weinberg-Salam calcs. 80—68461
$eN\to e\pi\Delta$, low energy, ΔN axial form factors soft-pion theory 78—70380
$eN\to e\pi N$, π form factor determ. 78—66128
eN inelasticcatt., low energy pion electroprod. and hadron form factors, book 79—85306
ep, nucleon structure from electron scatt., EM form factors 80—42468
ep deep inelastic scatt., EM form factors asymptotic behaviour, Fourier transform singularities 79—40789
ep elastic scatt., absolute differential cross sections, form factors and charge radius 80—27509
ep elastic scattering, longitudinally polarised, 6.5 GeV, cross section asymm., p form factors 77—6131
$ep\to ep\pi^0$ or $en\pi^+$, threshold cross section slope, form factors, π axial mass and radius 78—62411
$e\bar{p}\to e\pi^{-+}n$, longitudinal and transverse contribs., π^+ EM form factor 78—66126
ep scatt., deep inelastic, Lorentz invariant generalized functions, rel. to EM form factors 78—8544
$e^-p\to e^-p$, elastic scatt., polarisation of final lepton *(Russian)* 77—26529
$e\pi$ inelastic scattering, asymptotic bounds on π form factor 78—12917
$\eta\to\mu^+\mu^-\gamma$, branching ratio and η EM form factor 80—105899
$\eta'\to\mu^+\mu^-\gamma$, in π^-p interactions at 25 and 33 GeV/c, form factors *(Russian)* 80—4984
$F^+\to\pi^+e^+e^-$, enhancement due to π^+ EM form factor, generalised PCAC applicability 78—82164
$\gamma\to\pi\omega$, transition and π form factors, p'(1200) resonance *(Russian)* 79—22098
γ radiative decays, unified mechanism, form factors *(Chinese)* 77—57540
$\gamma^*n\Delta_{1236}$ transitional form factors, review *(Russian)* 78—54636
$\gamma^*p\Delta_{1236}$ transitional form factors, review *(Russian)* 78—54636
$\gamma d\to nn\pi^+$, threshold form factors 79—85453
$\gamma N\Delta_{33}$ form factors in πN collisions 79—63515
γNN vertex form factor, ed elastic scatt. at high momentum transfer 80—82977
$\gamma p\to V^0p$, one-pion exchange contrib., vertex corrections 78—50039
$\gamma^+p\Delta^+(1231)$ vertex transition form factor from $ep\to eN\pi$ *(Russian)* 80—37269
K, bound state relativistic effective range approx., EM form factors and charge radii 80—95270
K, extended vector meson dominance model 78—25046
K, form factor extraction from high energy scatt., Chou-Yang model 77—6127
K, momentum anal. of K pairs in $e^+e^-\to K^+K^-$ 77—46064
k, quark-antiquark systems combined by Coulomb type attractive force 78—89677
K decay, semi-leptonic weak interactions, book contrib. 78—78162
K electromag. form factor, Veneziano-type scatt. amplitudes *(Japanese)* 78—17019
K form factor and charge radii, isovector part using dispersion relations 79—22096
$K\to\pi^+\pi^-e^+\nu$ decay form factors, relativistic quark model 77—38160
$K\to\pi^+\pi^-\mu\nu$ decay rate 77—6113
$K\to\pi e(\mu)\nu$, form factors, SU(3) σ-model one loop calc., chiral symmetry breaking 80—52506
K^- EM form factor direct meas. from elastic scatt. cross section 80—86716
$K^0{}_{e3}$ and $K^0{}_{\mu3}$ decays, form factor parameters anal., SU(3) symm. violation *(Russian)* 78—450
$K^+\to\pi^0\mu^+\nu$, $K^+{}_{\mu3}$ decay spectrum and form factors 80—57587
$K^+\to\pi^+\pi^-e^+\nu$, $\pi\pi$ energy, phase shift difference, hadronic current form factors, scatt. length 77—41840
$K^\pm\to\pi^0l^\pm\nu_l(\bar{\nu}_l)$, decay form factors in relativistic symmetry $SO(4,2)\otimes SU(3)\otimes SU(3)$ 79—36068
$K_{e3}{}^0$ decays, vector form factor slope parameter *(Russian)* 79—67547
$K_L{}^0\to\pi^-\mu^+\nu_\mu$, transverse polarisation of μ, violation of time-reversal invariance 80—68448
$K_L{}^0\to\pi^\pm e^\mp\nu$, vector form factor meas. in large H bubble chamber 78—93875
$K_L{}^0\to\pi^\pm\mu^\pm\nu$, form factors 4-momentum depend., μe universality *(Russian)* 80—68449
$K_L{}^0\to\pi e\nu$, Dalitz plot anal., form factors 78—37204
$K_L{}^0\to\pi\mu^+\nu_\mu$, form factor from μ polarisation meas. 77—38161
$K_L{}^0\to\pi\mu\nu$, Dalitz plot anal., vector and scalar form factors 79—71744
K_{l3} decay, form factor and propagator bounds *(German)* 80—37265
K_{l3} form factors, parameter-free hard-meson prediction 77—49954
K_{l3} scalar form factor, chiral symmetry breaking model 77—71506
K_{l4} decay in relativistic quark model, axial vector form factors and decay rate 78—66109
K_{l4} decay vector form factor *(Russian)* 80—105900
$K_{l4}\to\pi\pi\gamma$, form factors in chiral quantum field theory *(Russian)* 79—67550
μ magnetic moment, pionic contrib., using exact soln. of Meiman problem concerning form factors 78—78182
μ magnetic moment form factor 80—18138
$\mu^-p\to\mu^-p$, elastic scatt., polarisation of final lepton *(Russian)* 77—26529
(N,N′) microscopic description of direct processes, effective interaction 78—12979
N, axial vector form-factor determ. from $\nu d\to\bar{\mu}pp_s$ 78—33055
n, charge form factor zeros 80—413
N, dispersion theory anal. of $\pi^-p\to e^+e^-n$ cross sections *(Russian)* 77—10253
N, EM form factors, dipole fit and scaling law, electroproduction in Δ_{33} energy region 80—22625
n, EM form factors from MIT bag model 79—93419
n, elec. form factor from ed quasi-elastic scatt. 78—82210
n, electric form factor determ. in $^2H(e,e'p)n$ 79—3138
N, Mandelstam representation, double dispersion relation 78—74256

form factors continued
n, studied by $^{12}C(d,p)^{13}C^*$ reactions leading to unbound states 77—26775
N, Thomas-Fermi type picture of EM structure 80—9170
N, vector and axial form factors, care model asymptotic behaviour, polarised struct. functions 77—6086
n charge distrib., $N\Delta$ mass difference, quark model anal. 77—67653
n charge struct., form factor in quark-parton model 77—54106
$N\to\Delta(1232)$ electromagnetic transition form factor and pion-nucleon dynamics at moderate energies 80—57598
N EM form factors, EM effects in precision anal. of low-energy np interaction data 78—93896
N elastic form factor, exclusive and almost exclusive process asymptotic behaviour, renormalisation group 80—42464
n electric polarisability, from photoabsorption cross-section 80—57597
N form factor, isovector, meson field theory, pseudoscalar πN interaction 80—62986
N form factors, parton separation determ. 78—33026
N form factors, weak, asymptotic behaviour within QCD dipole and triplepole formulae 80—62987
N isovector form factors, dispersion theory calc. of inelastic contrib. 77—13950
N renormalisation const., bounds on form factors and propagators 77—34092
N-N* EM transition form factors 77—22735
n-p system, EM form factors in multipole parametrisation formalism 78—17022
N* EM transition form factors 80—102049
$NN\to NN\pi$, effect of π-baryon from factors on ang. depend. of cross sections 79—85318
NN nonrelativistic 1-boson exchange potentials based on generalised meson field theory 78—70459
np→np, polarisation phenomena in close-to-forward scatt., intermediate energy region 80—78086
ν, EM form factors and mag. moments, Weinberg-Salam model and extensions *(German)* 80—62904
ν, EM properties, weak neutral current and form factor *(Russian)* 77—61270
νN, deep inelastic scatt., structure functions, form factors, negative scaling violation 78—74241
(p,p′) and (e,e′) scattering, core polarisation, microscopic models, transitions, cross sections, form factors 78—604
P, EM form factors from MIT bag model 79—93419
p, form factor extraction from high energy scatt., Chou-Yang model 77—6127
p, hadron distributions in quark jets 79—54317
p charge form factors, linear pot. model with gluon exchange 78—45873
p Dirac form factor and QCD 78—45864
p EM form factor, VDM of ep elastic scatt. *(Russian)* 78—17026
p EM form factors calc. 77—67654
p electric polarisability, from photoabsorption cross-section 80—57597
$p+e\to\pi+N$, form factor determ. *(Russian)* 79—9382
$\bar{p}d\to e^+e^-+n_s$, proton EM form factors, $p\bar{p}$ annihilation *(Russian)* 80—68457
$p\bar{p}\to e^+e^-$, magnetic nucleon form factor, p-meson type contribs. 80—57596
pp→pp, polarisation phenomena in close-to-forward scatt., intermediate energy region 80—78086
(π,π) elastic scatt. on light nuclei, optical pot. and scatt. amplitude model *(Russian)* 78—89918
π, analytic and unitary representation at all Q^2 accommodating higher vector meson states 78—58188
π, and Bloom-Gilman duality 79—9352
π, determ. from $e^+e^-\to\pi^+\pi^-$ obs. *(Russian)* 78—45915
π, dispersion theory anal. of $\pi^-p\to e^+e^-n$ cross sections *(Russian)* 77—10253
π, EM form factor and P-wave isovector $\pi\pi$ phase-shift data consistency 79—3025
π, expt. behaviour, influence of left-hand cut on second Riemann sheet 80—13304
π, form factor, resonant space and time like, radiative correction, ρ resonance interference 79—54341
π, form factor extraction from high energy scatt., Chou-Yang model 77—6127
π, hadron distributions in quark jets 79—54317
π, in QCD, light cone Bethe-Salpeter eqn. soln. 79—80827
π, inelastic effect of $\omega\pi^0$ channel calc. 77—46062
π, modified quark loop model, form factors, struct. functions, radiative decay 80—91088
π, momentum anal. of π pairs in $e^+e^-\to\pi^+\pi^-$ at 1.6 GeV 77—46064
π, Roy's eqn., inelastic effects 78—8669
π, Thomas-Fermi type picture of EM structure 80—9170
π decays and π electromag. form factor, σ-model with quarks 79—22100
π EM form factor, asymptotic behaviour in scale-invariant quark model 78—37211
π EM form factor, dispersion theoretic study, mass, charge radius 77—67652
π EM form factor, large-Q^2 behaviour 77—6002
π EM form factor asymptotics in QCD perturbation theory, partonic interpretation *(Russian)* 80—62984
π EM form factor factorisation and asymptotic behaviour in QCD 80—91090
π EM form factor via $e+p\to e'+n+\pi^+$ σ_L, σ_U separation 77—79269
$\pi\to e\nu\gamma$, branching ratio, axial vector form factor determ. 78—74247
$\pi\to e\nu\gamma$, isospin violation in form factor, induced by current quark mass 80—32069
$\pi\to e\nu\gamma$, vector form factor, quark masses and isospin breaking 79—13111
$\pi\to e\nu\gamma$ and $SU(3)\times SU(3)$ σ-model 80—78054
Π field in nuclei, μ absorpt. and doubly radiative Π absorpt. as probes 77—88063
π form factor and charge radius data anal., inconsistency, indistinguishable models 77—38170
π form factor around ϕ peak, unitary and gluonic corrections 80—22615
π form factor at $s<(m_\omega+m_\pi)^2$, influence of $\pi\omega$ inelastic channel 77—2838
π form factor via $\pi^-p\to e^+e^-n$ 275 MeV *(Russian)* 77—82764
π form factors, axial-vector and structure dependent, vector meson dominance model 80—62989
π form factors, Omnes-Muskhelishvili eqns. with inelastic unitarity 79—9371

form factors continued
π in parton model and Bethe-Salpeter wave function 77—41820
π phenomenological form factor for radius and EM mass difference 77—65156
π phenomenological form factor, EM mass difference, appl. to pionic ats. *(Korean)* 79—9372
π^- EM form factor meas. 78—17020
$\pi^0 \to e^+e^-$, form factor slope meas. 78—41537
$\pi^0 \to \gamma\gamma$, u-d quark mass difference effects, form factors 79—89159
π^+, electroproduction at threshold, weak form factor 79—22107
$\pi^+ \to e^+\nu_e\gamma$, decay rate calc. in SU(2)×SU(2) sigma model 78—8659
$\pi^+ \to e^+\nu\gamma$, u-d quark mass difference effects, form factors 79—89159
$\pi^-d \to nn$, mechanism, cross-sections, EM form factors 79—89181
$\pi^+d \to pp$, calc. including form factor at absorption and scatt. vertex 77—6155
$\pi^+d \to pp'$, effect of form factors on disintegration 77—6156
$\pi\Delta\Delta$, appl. to off-shell continuation of pion-baryon vertices 79—67552
$\pi\Delta N$, appl. to off-shell continuation of pion-baryon vertices 79—67552
πe elastic scatt. at 50 GeV/c, π EM size 78—4862
πN coupling, induced pseudoscalar nucleon form factor *(Russian)* 79—9375
πN form factor determ. in modified Chew-Low model 77—6152
πN form factor in Chew-Low theory 78—41574
πN off shell scatt. near Δ resonance, parameter free form factor 80—9168
πN S-matrix, inelastic effects in sidewise dispersion relations for nucleon EM form factors 78—82212
πN scatt., separable potl. model 77—6153
πNN, appl. to off-shell continuation of pion-baryon vertices 79—67552
πNN, Veneziano-type, test by fitting to $np \to pn$ and $\bar{p}p \to \bar{n}n$ $d\sigma/dt$ data 79—17725
πNN form factor, $\Delta(1236)$ contrib., calc. 80—22609
πNN form factor; relativistic calc. of $\Delta(1232)$ contribution to imaginary part *(Korean)* 80—47292
πNN form factors, influence on two nucleon data, one particle exchange 78—70369
πNN form factors for one off-shell nucleon, dispersion relation calc. 79—9373
πp elastic scatt., Chou-Yang model and π form factor 78—45960
$\pi^- p \to e^+e^-n$, induced pseudoscalar nucleon form factor, current algebra appl. *(Russian)* 78—78212
$\pi^- p \to e^+e^-n$, induced pseudoscalar nucleon form factor, current algebra framework 79—22131
$\pi\pi$, form factor and propagator bounds *(German)* 80—37265
$\psi \to f\gamma$, form factor depend. in relativistic harmonic oscill. model 79—89156
ρ form factors ratio, high momentum transfer behaviour in QCD 78—70340
ρ-meson, EM form factor, elec. quadrupole and mag. dipole moments 78—12913
$\tau \to \nu\pi\omega$, decay width and form factor calc. using vector dominance hypothesis *(Russian)* 80—47271
$V \to p\mu^+\mu^-$, vector meson decay EM form factors in bag model *(Russian)* 80—62982
$^{12}C+\nu$, neutral current processes in nuclei, elementary particle approach 79—93606
^3He charge form factors at high momentum transfer, relativistic interactions, N form factors 80—32205
$^ALi+\nu$, (A=6,7), neutral current processes in nuclei, elementary particle approach 79—93606

form factors (nuclear)
$0f_{7/2}$ and $0g_{9/2}$ nuclei, mag. form factors, core polarisation and exchange current effects 80—13409
A=12, recoil polarisation in muon capture, arbitrary nuclear spin, form factors 79—75978
A=16 system, 0^+-0^- transitions, nuclear structure effects on weak nuclear form factors 80—18246
A=3 system, Panofsky ratio, auxial vector form factor 79—574
A=3 system, struct. and form factor models 79—45274
A=3 systems, charge form factor and bound nucleon polarisation 80—22708
A=4n, densities, form factors, transitions, multipole moments in s-d shell, HFC 80—37321
A-odd deformed axially symmetric nuclei, EM form factors 79—9458
centre-of-mass effects in high-energy scattering by light nuclei 77—26642
charge density waves in finite nuclei 77—54144
collective props. of nuclei deduced from electron scatt., deformed nuclei, review 78—50064
conference on few body systems and nuclear forces, Graz, Austria (Aug. 1978) 79—80880
conference on heavy ion reaction dynamical props., Johannesburg, S.Africa (Aug. 78) 80—17715
Coulomb, core polarisation effects 77—30474
Coulomb problem and the separation of electromagnetic effects in few-nucleon systems 77—23014
deeply inelastic nucleon transfer form factors, shell model calc. 79—89265
deuteron form factors and spectroscopic factors in heavy spherical nuclei, shell model *(Russian)* 80—63078
dispersion relation approach, pole and quark-counting model 77—26568
doubly closed shell nuclei 77—6274
(e,e), elastic and inelastic A=12-40, 22 79—63571
effective form factor pot. due to unbound core after direct process, asymptotic behaviour 80—27560
electronuclear sum rules, linear energy weighted, nuclear struct. determ. method 79—75897
elementary particle method for nuclei in weak and EM processes, book contrib. 79—97663
EM form factors at infinite four-momentum transfer, limiting values 80—27503
EM isovector form factors of bound nucleons 80—78134
exact finite range calculations of light-ion induced two-neutron transfer reactions 79—63639
exact finite range DWBA form factor for heavy-ion induced nuclear reactions, calc. program adaption 80—9271
few nucleon correlations from high energy scatt., review *(Russian)* 80—68549
first order SU(3) theorem for weak and EM form factors, possible expt. verification 80—415
folding model description of heavy ion inealstic scattering 78—25227

form factors continued
heavy ion fusion, sensitivity to friction form factor, dissipative and conservative properties 79—67807
heavy-ion deeply inelastic collisions, form factors determ. within statistical model 78—50205
heavy-ion induced two-proton transfer reactions, sequential amplitudes 79—9608
HF calcs., translationally invariant self-consistent field theories 77—74788
imaginary inelastic transition form factor, microscopic theory 78—50175
imaginary part of the nuclear optical potential and inelastic form factor 79—93581
impulse approx. with nuclear current conservation, off-shell form factors 80—52632
inelastic nuclear factors, properties from inversion formula for energy weighted sum rules 78—37319
isovector M6 excitations, open shell RPA calcs., appl. to electron scatt. form factors 78—50112
light nuclei, inelastic form factors for abnormal parity states, K-harmonic method *(Russian)* 78—25113
light nuclei, pole and quark counting model 77—26568
light nuclei inelastic form factors in the K-harmonics method 78—25113
M1 magnetic form factor and spin oscillations 79—67652
many-body exchange currents and the tri- and four-nucleon charge form factors 78—33169
meson exchange currents, effect in electron inelastic scatt., book contrib. 80—480
microscopic theory of the imaginary inelastic transition form factor 78—50175
momentum and mass distribs., form factors, short range correlation effects 80—105959
mono-energy pair conversion of nuclear multipoles, form factors, Hartree-Fock-Slater wave functions *(Russian)* 79—93555
multipole moments, form factors, energy weighted sum rules, cnetre-of-mass bounds 80—27590
muon capture progress, weak interaction form factors 80—42643
nuclear charge form factors, effect of N* (1688) resonance 79—93501
nuclear currents, elementary particle description, microscopic anal., book contrib. 79—97664
nuclear density fluctuations and electron scattering at high-energy *(Russian)* 78—86529
nuclear muon capture, weak form factors 78—62508
odd-A deformed nuclei, EM and electron scatt. form factors, selection rules 79—9458
off shell form factor model, NN scatt. appl. 80—86800
one-hole states, in double magic nuclei, form factors, spectroscopic factors, centroid energies 78—17090
one-hole states in double magic nuclei 78—17090
one-nucleon transfer reactions on spherical nuclei, Pauli principle *(Russian)* 77—6393
particle-vibration coupling form factor from simple model 80—57663
pion exchange currents and nuclear charge form factors 77—18379
radial wave functions of valence nucleons 80—73788
relativistic harmonic oscillator model, hadron EM interactions and props. 80—37225
rotational nuclei, A=159-181, transverse form factors from projected HF approach 80—105965
semi-leptonic weak and electromagnetic interactions with nuclei' isoelastic processes 77—18528
shell model, elastic and dynamic form factors, with correction for motion of centre of mass *(Russian)* 78—8753
single-nucleon form factor for knock-out and pick-up reactions in deformed nuclei 78—93999
spherical nuclei, dipole states, transition densities and electroexcitation, GDR form factors *(Russian)* 80—52611
spherical nuclei, one nucleon transfer reacts. 77—6393
surface deformation effect *(Russian)* 77—46108
three nucleon bound states, Δ (1236) effects, on binding energy and form factors 79—75858
three-nucleon system, bound state calc. program PERFECT 80—13390
trinucleon charge form factor 77—34238
trinucleon properties with one-boson-exchange potentials 77—18421
two-nucleon stripping process with Skyrme-type potentials 78—58287
vertex, in peripheral model, (p,d) (d,p) cross-sections *(Russian)* 77—82889
vertex factor of virtual decay of three particle nucleus 77—26607
vibrationla nuclei, electron scatt. 77—6356
weak decays, EM effects and form factor renormalisation 79—54411
(α,α), antisymmetrisation effects, form factor, spt, model anal. 78—82366
$(\alpha,\acute{\alpha})$, form factors in Coulomb-nuclear interference region 78—66288
(d,t), DWBA anal., form factors and d-t overlap integral S- and D-state components 80—18320
d, polarisation meas. in ed scatt. and d percentage D state 80—420
(e,e), A=2, 3, 4, scaling laws in relativistic impulse approx. model, spin effects 80—52662
(e,e), form factors, magnetisation density, mag. moments and valence nucleon orbits 80—22690
(e,e), text of effective interactions in 1s-od shell 77—61400
(e,e) elastic scatt., spectroscopic information and form factors 80—9260
(e,e'), cross section near quasielastic maximum, shell and optical models *(Russian)* 80—91179
n, polarisation meas. in ed scatt. and d percentage D state 80—420
NNN bound state problems, hyperspherical harmonic expansion, review 80—91136
(p,α) microscopic form factors, DWBA cluster form factor replacement 80—47478
(p,π), DWIA calcs. 77—82932
p, polarisation meas. in ed scatt. and d percentage D state 80—420
(π,π), 1 GeV, nucl. struct. studies 77—14197
π decay constant, EM form factor, quark EM self-energy in QCD 80—37242
π^3He^3He coupling on basic of PCAC 80—32196
πNN vertex, virtual nucleon propagator, and pionic vertex, form factor enhancement 80—22700
t+nucleus, form factors for two-nucleon stripping process wth Skyrme potentials, DWBA 78—58287
^{24}Mg, K-band struct. electroexcitation form factors 79—17811
^{150}Nd, K^{π}-O* octupole band form factors 79—9447
^{207}(e,e'), transverse scatt. amplitude suppression, form factors, neutron hole states 80—91129

form factors continued
^{27}Al, inelastic electron scatt., charge distrib., Coriolis band mixing calc., C2 form factors 79−529
^{27}Al(e,e′) 77−34288
^{27}Al(e,e′), 62 to 112 MeV, form factors, ^{27}Al energy spectrum, transition probabilities 77−34288
^{27}Al(e,e′), 70-340 MeV, odd parity state electroexcitation, form factors, transition probabs. 80−78208
A(π^+,2p)B*, effect of nuclear form factors *(Russian)* 78−25248
^{10}B(e,e′), 67-194 MeV, form factors, transitions and ground state radiative width 79−75898
^{11}B (e,e′) 120-250 MeV, excited state form factors, shell and diagram model anal. *(Russian)* 79−40852
^{11}B(e,é), 121 to 250 MeV, levels, form factors *(Russian)* 79−40852
^{12}B average polarisation, form factors and partial capture rate from ^{12}C(μ^-,ν), polarised π^- 79−22263
^{12}B, beta decay weak form factors 78−37312
^{12}B→β^-+^{12}C, alignment correlation meas. by Zeeman technique, vector currents and form factors 78−37312
B(e,e), A=10, 11, form factors, Hartree Fock calcs. 78−58263
B(e,e) form factors 78−58263
^{9}Be, decay widths and charge form factors 78−46015
^{9}Be, molecular model, n and α-particle decay widths, charge form factors 78−46015
^{9}Be, struct., size, quadrupole moment, generator coord. method calc. 79−71788
^{9}Be(e,X), transverse and longit. form factors for electrodisintegration, small momentum transfer *(Russian)* 79−80927
^{9}Be(e,e), longitudinal form factor for 1/2$^+$ resonance 80−22682
^{A}C, A=12, 13, nuclear critical opalescence, M1 form factor, pion field and condensation 80−73809
^{12}C 1$^+$(T=1, 15.1 MeV) state excitational pionic modes, M1 form factor for (p,p′), (e,e′) 80−78195
^{12}C 2$^+$ level, transverse EM form factor, convection current contrib. 80−63076
^{12}C, 4-α model elastic and inelastic form factors 79−30798
^{12}C, α-cluster model, binding energy, RMS radii, and form factors 79−75825
^{12}C, charge transition density, sum rules, oscillation form factors *(Russian)* 79−22186
^{12}C, EM transition form factors 78−41662
^{12}C, E2 transitions, correction currents, spin magnetisation 79−13244
^{12}C, electron elastic and inelastic scatt., form factor calc. 78−50108
^{12}C, excitation cross sections, form factors for 2$^+$ and 3$^-$ levels *(Russian)* 78−41684
^{12}C, excited state struct., α-particle model 80−47385
^{12}C M1 (15.11 MeV) form factor, evidence for nuclear pion field critical opalescence 80−32232
^{12}C M1 form factor, pion field critical opalescence, ρ role, polarisation phenomena 80−68552
^{12}C, M1 form factor, pion field, rho meson role 80−105970
^{12}C, M1 form factor, threshold pion prod. 78−62519
^{12}C mag. transition form factors, core polarisation and exchange current effects 79−75899
^{12}C, oscillation form factors, sum rules *(Russian)* 79−22186
^{12}C struct., determ. of Brink's model parameters, calc. of binding energy, 2$^+$ level lifetime 79−85358
^{12}C, weak hadronic form factor and recoil polarisation in muon capture 78−62508
^{12}C+^{13}C, identical core neutron transfer, coupled channel anal., form factors 79−13319
^{12}C+^{13}C, nucleon transfer form factors 79−13319
^{12}C+ν, neutral current processes in nuclei, elementary particle approach 79−93606
^{12}C(K$^+$,K$^+$′), form factors, cross sections, interior probing capability 80−73866
^{12}C(d,p)^{13}C*, neutron form factors 77−26775
^{12}C(e,e′), allowed weak and EM transitions, improved impulse approx. treatment 78−41662
^{12}C(e,e′), E2 transitions, convection currents and spin magnetisation 79−13244
^{12}C(e,e') 57-215 MeV, 2$^+$ (4.43 MeV) state, transition DWA anal., electron scatt. form factors 79−67704
^{12}C(e,e), 180° scatt., transverse inelastic form factors and spectra, collective 2$^+$ state 80−9261
^{12}C(e,e) , 12.71 and 15.11 MeV level struct. and isospin mixing from form factors 80−32186
^{12}C(γ, π^-)^{12}N$_{gs}$, threshold prod., 15.11 MeV M1 form factor 78−62519
^{12}C(γ,π^+)^{12}B, nuclear critical opalescence study 80−105988
^{12}C(μ,γ), exclusive radiative capture, axial currents and induced pseudoscalar form factors 79−97699
^{12}C(μ^-,ν)B, polarised form factors 79−22263
^{12}C(μ^- ν_μ)^{12}B, induced tensor and pseudotensor form factors 77−38253
^{12}C($\mu^\pm$,$\nu\mu$)^{12}B, induced tenson and pseudotenson form factors 77−38253
^{12}C(p,α), 45.2 MeV, cross sections, finite range DWBA anal., cluster form factors 80−68666
^{12}C(p,p′), (e,e′), shell model 77−46164
^{12}C(p,p′), Glauber model, shell model wave functions, EM form factor, spin effects 77−46164
^{12}C(p,p′) proton polarisation and natural parity level excitations *(Russian)* 80−5144
^{13}C, giant resonance, isospin splitting, form factors 78−577
^{13}C(p,α)^{10}B$_{g.s.}$, 65 MeV, pol. p, DWBA form factor 80−52559
^{40}Ca, 1$^-$, T=0 state at 6.95 MeV, isospin forbidden electroexcitation 78−25177
^{40}Ca, 1$^-$T=O state isospin forbidden electroexcitation 78−25177
^{40}Ca, proton charge form factor 79−9456
^{40}Ca, two-parameter nucleon density distrib., form factors calc. 77−65193
^{40}Ca(^{13}C,^{14}N)^{39}K, sensitivity to ^{39}K+p form factor, DWBA anal. 77−34345
^{40}Ca(n,n′)^{40}Ca, imaginary inelastic transition form factor, microscopic theory 78−50175
^{40}Ca(t,p)^{42}Ca, form factors from effective interactions 78−610
^{40}Ca(t,p)^{42}Ca, form factors for two-nucleon stripping process wth Skyrme potentials, DWBA 78−58287
^{40}Ca(t,p)^{42}Ca, two-nucleon stripping process with effective interactions 78−610
^{42}Ca(p,d) form factors, Pauli principle *(Russian)* 77−6393
^{42}Ca(p,t) form factor, hole and continuum contribs. for pick-up reactions 80−78256

form factors continued
^{48}Ca(^{18}O,^{16}O) 50 MeV, cross sections, DWBA multipole expansion calcs., form factors 79−13325
^{48}Ca(^{18}O,^{16}O)^{56}Ca, microscopic tow nucleon transfer form factors 79−13325
^{140}Ce, E1 form factors, giant monopole state 79−3125
^{140}Ce(e,e′), giant dipole resonance, E1 form factor and breathing mode existence 79−3125
^{55}Co, spectroscopic study in ^{54}Fe (ζ,d) and ^{54}Fe(ζ,dp) 77−88029
^{57}Co, (3/2$^+$ state), anomalous analyzing power, DWBA calc. from ^{60}Ni(p,α) 80−86894
^{A}Cr(e,é), (A=53,54), 1.43 MeV level form factors *(Russian)* 78−54746
^{52}Cr(α,α), 15-19 MeV, inelastic scatt. form factors, Coulomb-nuclear interference region 78−66288
^{52}Cr(e,e′), 90-226 MeV, excitation of low-lying states *(Russian)* 78−54746
^{53}Cr(e,e′), 90-226 MeV, excitation of low-lying states *(Russian)* 78−54746
^{A}Dy(^{3}He,d), 46.5 MeV, A=162,164, form factor effects 77−14138
^{158}Dy(p,t), react. anal. 77−74747
^{18}F (e,e′), polarised e, parity mixing and form factors from elementary particle theory anal. 79−89233
^{20}F β-decay, calc. of recoil order matrix elements 77−79337
^{56}Fe(α,α), 15-19 MeV, inelastic scatt. form factors, Coulomb-nuclear interference region 78−66288
^{56}Fe(e,e′), Coulomb form factor for O$^+$→4$^+$ transition, collective 4$^+$ states, shell model 80−57664
^{1}H(γ,π^+), 3.4-18 GeV, πNN form factor and differential cross sections, one pion exchange 80−68526
^{2}H breakup spectra, 8.5 MeV, comparison with Faddeev calcs. 77−18548
^{2}H charge operator, retardation, quasipot. eqns. and rel. corrections 80−99122
^{2}H EM form factor 77−61287
^{2}H, EM props. in relativistic one boson exchange model 79−67678
^{2}H, EM quadrupole form factor 77−71571
^{2}H, EM quadrupole form factor 78−93950
^{2}H form factor, relativistic effects 77−18519
^{2}H pionic disintegration 77−88177
^{2}H, quadrupole form factor and D-state probability 77−71571
^{2}H, quadrupole form factors 78−70462
^{2}H, retardation currents 77−34234
^{2}H, weak and EM lepton reactions, exchange currents, isobaric excitations and form factors *(German)* 79−93523
^{2}H(N,N), off-shell effects, calcs. with phase equiv. separable pots. of rank two 77−18553
^{2}H(e, np), EM inelastic form factors, exchange current effects in electrodisintegration 79−93418
^{2}H(e,e′), 56.4 MeV, cross sections, form factors, meson exchange current contrib. 80−68649
^{2}H(e,e), EM form factors, relativistic formulae, moment corrections 80−63075
^{2}H(e,e), form factors, tensor pol., and two-nucleon force calcs. 80−106045
^{2}H(γ,nnπ^+), threshold form factors 79−85453
^{2}H(n,n), off-shell effects 77−18553
^{2}H(p,p) large angle elastic scatt., d form factor at large q^2 80−102189
^{2}H(p,π^0)^{3}He, (p,π^+)^{3}H, 250-800 MeV, distorted-wave impulse-approx. calc. 77−82932
^{2}H(π,p)^{1}H, threshold to 3,3 resonance region, disintegration model containing absorption 77−88177
^{2}H(π,π), 142, 256 MeV, form factor−backward scatt. correlation, tensor polarisation 80−99189
^{2}H(π^-, n)n, mechanism, cross-sections, EM form factors 79−89181
^{3}H charge form factor calc. with pair and recoil exchange currents 77−34238
^{3}H charge form factor from nd reaction 77−18439
^{3}H, EM form factors, 3-nucleon wave function calc. 80−95302
^{3}H, meson exchange currents, effect on charge form factors 80−105990
^{3}H, partly non-local pots. model 77−54157
^{3}H, partly nonlocal pots. 77−54157
^{3}H, rms radius, binding energy, form factor 78−54693
^{3}H, three nucleon observables with meson theoretical interactions, binding energy, form factors 79−67676
^{3}H(π^+,γ)^{3}He, elastic scatt., charge exchange and symmetries, and ^{3}H, ^{3}He form factors meas. 79−80959
He, A=3,4, form factors determ. by pole and quark-counting model 77−26568
He isotopes, EM struct. 77−54208
^{3}He change form factor, relativistic corrections for three nucleon observables 79−85383
^{3}He charge form factor, 3N bound state with separable interactions, Faddeev theory corrections 80−13388
^{3}He, charge form factor, n+d collision anal. 77−18439
^{3}He, charge form factor calc. using centre-of-mass effects 77−26642
^{3}He charge form factor calc. with pair and recoil exchange currents 77−34238
^{3}He, charge form factor one-boson exchange pot. 78−41652
^{3}He, charge form factor with Reid soft core pot. 80−13389
^{3}He, charge form factors, recent developments in lepton scattering 79−80929
^{3}He charge form factors at high momentum transfer, relativistic interactions, N form factors 80−32205
^{3}He, EM form factors, 3-nucleon wave function calc. 80−95302
^{3}He form factor from ^{3}H wave function anal. form 80−47410
^{3}He, meson exchange currents, effect on charge form factors 80−105990
^{3}He, nuclear charge form factor, two-boson exchange charge density π, ρ, ω exchanges 80−63073
^{3}He, one-body charge form factor computer code listing 80−57673
^{3}He, rigorous bounds for charge densities from form factor data 80−5055
^{3}He, trinucleon bound state problem, binding energy, form factors and mag. moment 80−22710
^{3}He(e, e), charge formfactors, second Born approx. and pole model 80−18155
^{3}He(e,e), charge density distrib., charge form factor, of ^{3}He 78−29453
^{3}He(e,e), charge form factor 78−29453
^{3}He(e,e), charge formfactors, second Born approx. and pole model 80−78133
^{3}He(e,e), form factors and dimensional scaling quark model 78−93991
^{3}He(e,e), relationship to ^{3}He(π^-,π^-) 80−78323

form factors continued
^{3}He(e,e) 170 to 750 MeV, EM structure, form factors and distribs. 77−54208
^{3}He(γ,π^{+})^{3}H, threshold π prod., and axial vector form factor 79−574
^{3}He(γ,π^{+})^{3}H, threshold form factors 79−85453
^{3}He(π,π), 145, 180, 195 MeV, differential cross section, mesonic exchange effects, form factors, optical pot. 79−85376
^{3}He(π^{-},γ)^{3}H, Panofsky ratio and axial vector form factor 79−574
^{3}He(π^{-},π^{-}), 145, 180 and 195 MeV, relationship to ^{3}He(e,e) 80−78323
^{3}He(π^{-},π^{0}), form factor sensitivity in Glauber multiple scatt. formalism 80−105964
^{3}He(π^{-},π^{0})^{3}H, Panofsky ratio and axial vector form factor 79−574
^{4}He (π^{-}, π^{-}p), 5GeV/c, quasielastic scatt., cross section, form factor, final state interactions 80−99190
^{4}He, binding energy, charge form factors 78−54678
^{4}He, binding energy, radius, charge form factors *(Russian)* 78−25123
^{4}He, binding energy and form factor calcs., Reid interaction 78−54678
^{4}He, charge form factors of doubly closed shell nuclei 77−6274
^{4}He, nucl. binding energy, radius and charge form factor, Brueckner calcs. 79−71787
^{4}He nuclear charge density determ. using form factor analyticity 80−63077
^{4}He, recent developments in lepton scattering 79−80929
^{4}He, short range correlation and nuclear charge form factor 78−8746
^{4}He, soft-core radial wave function, photo-disintegration calculation 80−18209
^{4}He, struct. effects on α-decay of superheavy nuclei 78−17158
^{4}He, structure in the translation-invariant oscillator basis *(Russian)* 78−25123
^{4}He+^{3}H, form factors from generator coordinate method 78−13122
^{4}He(e,e), cross section anal., nuclear charge form factor, short range correl. 78−8746
^{4}He(e,e), form factor, influence on superheavy nuclei half lives 78−17158
^{4}He(e,e), form factors and dimensional scaling quark model 78−93991
^{4}He(e,e) 170 to 750 MeV, EM structure, form factors and distribs. 77−54208
^{6}He$\rightarrow^{6}$Li+e+$\bar{\nu}$, tensor form factor 78−21525
^{A}He, (A=Z,4), form factors and dimens.-scaling quark model 78−93991
^{A}He, A=3,4, EM form factors and structure at large momentum transfer 79−67710
He(e,e), A=3,4, many-body exchange effects, charge form factors calc. 78−33169
He(e,e), A=3 and 4, high momentum transfer, elastic struct. functions 78−62521
Ho, A=163,165, collective state form factor effects in Dy(^{3}He,d) at 46.5 MeV 77−14138
^{A}K, A=37,39, levels, excitation and microscopic form factors, DWBA calcs. from Ca(p,α) 80−32185
^{6}Li, 5.36 MeV level electroexcitation form factor via ^{6}Li(e,e′)^{6}Li at 40.5 and 50.5 MeV 77−54177
^{6}Li, (αnp) 3 body model using hyperspherical harmonics, bound states 78−70469
^{6}Li (μ^{-},^{3}H)^{3}H, muon capture form factors 79−40907
^{6}Li, charge form factor, short range Jastrow correls. in harmonic oscillator shell model 78−70467
^{6}Li, charge form factors Jastrow correlations 78−70467
^{6}Li, EM form factors and spectroscopic factors in phenomenological cluster models 80−496
^{6}Li, EM form factors and vertex consts. 78−12958
^{6}Li, electroexcitation of 5.36 MeV transition 77−54177
^{6}Li, form factors determ. by pole and quark-counting model 77−26568
^{6}Li, form factors in K-harmonics model 78−70469
^{6}Li, self-consistent desorption using four and two body substructures 79−63611
^{6}Li, three body model, hyperspherical harmonics 78−29411
^{6}Li, three-body model using hyperspherical harmonics 78−29411
^{6}Li+^{4}He, form factors from generator coordinate method 78−13122
^{6}Li(H,ν)^{3}H^{3}H, muon capture in ditriton channel by elementary particle model 79−40907
^{6}Li(e, e), charge formfactors, second Born approx. and pole model 80−18155
^{6}Li(e,e′), 102, 123 MeV, excitation form factor, ^{3}H-^{3}He cluster model 80−78190
^{6}Li(e,e′), 140-330 MeV, 3.65 MeV 0^{+} state form factor at high momentum transfer 80−495
^{6}Li(e,e′), 76-141 MeV, form factors, appl. to (π^{-},γ), phenomenological model 80−83068
^{6}Li(e,e), charge formfactors, second Born approx. and pole model 80−78133
^{6}Li(e,e), elastic and inelastic charge form factors from shell model wave functions 80−68523
^{6}Li(γ,η)^{6}Li*(3.56 MeV), partial photoproduction reactions, large momentum transfer anal., form factor choice 80−22808
^{6}Li(γ,π°)^{6}Li*(3.56 MeV), partial photoproduction reactions, large momentum transfer anal., form factor choice 80−22808
^{7}Li charge form factor with resonating group wave function, quad. moment, charge radius 80−102110
^{A}Li+ν, (A=6,7), neutral current processes in nuclei, elementary particle approach 79−93606
^{24}Mg, 6 MeV 4^{+} state, configurational anal. 78−25115
^{24}Mg(e,e′), 6^{-}T=1 resonance 77−41940
^{24}Mg(e,e), 4$_{1}{}^{+}$4.12 MeV and 2$_{2}{}^{+}$4.24 MeV level resolution, E2 and E4 form factor meas. 79−17811
^{24}Mg(e,e) form factor calc., test of 1s-0d shell effective interactions 77−61400
^{25}Mg(e,e), 40-260 MeV, cross sections, Coulomb multipole moments and magnetic form factor 78−25178
^{25}Mg(e,e), multipole moment distrib., form factors 78−25178
^{25}Mg(e,e) M1,3,5, form factors 79−40844
^{14}N(e,e) in storage ring, elastic form factor 80−22819
^{15}N, 9.7 to 14.7 MeV levels electroexciation, form factors 78−25175
^{15}N(e,e′), excitation of energy levels 9.7 to 14.7 MeV, 60-194 MeV, EM form factor meas. 78−25175
^{15}N(e,e′), form factors meas., obs. of low-lying states 78−12976
^{18}N(e,é), low lying states, form factors 78−12976
^{20}Na, β-decay, calc. of recoil order matrix elements 77−79337
^{93}Nb(e,e), M1,3,5, form factors 79−40844
^{150}Nd(e,e′), possible K$^{\pi}$=0^{-} octupole band, e scatt. form factors 79−9447

form factors continued
^{18}Ne analogue and nonanalogue states, π double charge exchange form factors from ^{18}O(π^{+},π^{-}) 80−13405
^{20}Ne, from ^{16}O(α,γ), 10.27 MeV, first T=1,2^{+} state radiative width meas. rel. to analogue β-decays 78−549
^{20}Ne quadrupole transitions, electron scatt. form factors, shell model calcs. 78−62523
^{20}Ne, T=1,2^{+} state, radiative widths 78−549
^{22}Ne(e,e'), 60 to 110 MeV, spin, parity, form factor, reduced transition prob. determ. 79−63661
Ni(^{16}O,^{18}O), surface transparent pots., and CCBA anal. of diffractive behaviour 78−50206
^{58}Ni, isovector M8 strength fragmentation, inelastic electron scatt. meas. 78−37305
^{58}Ni, M8 isovector strength fragmentation, form factors 78−37305
^{58}Ni(d,d), 10 MeV, multishell form factors 79−93636
^{58}Ni(e,e′), 120-264 MeV, J$^{\pi}$=6^{+}, 5.125 MeV state isoscalar character, form factors, transition strengths 80−9262
^{58}Ni(e,e′) 5.125 MeV J$^{\pi}$=6^{+} state excitation, isoscalar character 79−22227
^{58}Ni(p,d) form factors, Pauli principle *(Russian)* 77−6393
^{59}Ni, K-electron radiative capture 77−61384
^{60}Ni(α,α), 15-19 MeV, inelastic scatt. form factors, Coulomb-nuclear interference region 78−66288
^{16}O, 0^{+} states, appl. of K-harmonics method 78−54685
^{16}O, 3 α forces, ground state energy and form factor 80−86817
^{16}O form factor effects, zero range DWBA calcs. from ^{18}O(p,t) 80−491
^{16}O, inelastic form factors for abnormal parity states, K-harmonic method *(Russian)* 78−25113
^{16}O, O^{+}state, form factors, K-harmonics calcs. 78−54685
^{16}O, proton charge form factor 79−9456
^{16}O, two-parameter nucleon density distrib., form factors calc. 77−65193
^{16}O, weak hadronic form factor and recoil polarisation in muon capture 78−62508
^{16}O(e,e), T=1 level form factors, Helm model, pion photoprod. and muon capture appls. 80−52553
^{16}O(γ, p)^{15}N and ^{16}O(γ, n)^{15}O, 60-300 MeV, absorpt. mech., residual nucleus form factor 78−70511
^{16}O(γ,n)^{15}O, 60 to 300 MeV, residual nucleus form factor 78−70511
^{16}O(γ,p)^{15}N, 60 to 300 MeV, residual nucleus form factor 78−70511
^{16}O(μ,γ), exclusive radiative capture, axial currents and induced pseudoscalar form factors 79−97699
^{16}O(p,p′), proton polarisation and natural parity level excitations *(Russian)* 80−5144
^{17}O, charge distrib. differences between A=16, 17, and 18 isotopes 79−63583
^{17}O, core polarisation, mag. form factor exchange current effects 78−46003
^{17}O, giant reson., form factors 78−4930
^{17}O, giant resonance, isospin splitting, form factors 78−577
^{17}O, mag. form factor, core polarisation and exchange current effects 78−46003
^{17}O(e,e), mag scatt., form factors, HF calcs., core polarisation effects 80−42579
^{17}O(e,e), transverse form factor, ground state mag. distrib. 79−63658
^{17}O(n,n′)^{17}O, imaginary inelastic transition form factor, microscopic theory 78−50175
^{18}O(e,e′), 80-165.7 MeV, giant dipole and quadrupole resonances, form factors 80−102168
^{29}P populated in (^{3}He,d) 77−82934
^{207}Pb+e, high resolution inelastic scatt. cross sections, induced charge of neutron, form factors 78−78366
^{207}Pb(e,e), cross sections, form factors, induced charge of neutron 78−78366
^{207}Pb(e,e), magnetisation distrib. from elastic mag. form factors, core polarisation, exchange currents 80−47372
^{208}Pb (e,e′), 2^{-} giant resonance twist mode excitation, B(M2) values, form factors 80−78246
^{208}Pb, electroexcitation of high spin states 77−14116
^{208}Pb, high-spin states, form factors for electroexcitation 77−14116
^{208}Pb region, mag. transition strength, core polarisation effects, form factor shape 80−86850
^{208}Pb+^{40}Ar, deeply inelastic collisions, form factors determ. within statistical model 78−50205
^{208}Pb(^{40}Ar,X), deeply inelastic collisions, form factors, microscopic calcs. 80−18339
^{208}Pb(e,e), scatt. from levels up to 6.2 MeV and J=10 77−310
^{108}Pd, vibr. states study, elastic and inelastic electron scatt., anharmonic vibrator model 78−62520
^{108}Pd(e,e), form factors for vibrational states 78−62520
^{32}S(e,e) form factor calc., test of 1s-0d shell effective interactions 77−61400
^{127}Sb states, collective neutron excitation role, spectroscopic factors and form factors from ^{30}Te(p,α) 79−67622
^{45}Sc(α,p)^{48}Ti, 26 MeV, form factors, energy levels 79−45202
Si isotopes ground state distrib. 77−54142
^{A}Si, A=28,30, charge distrib. of excited states 77−54142
^{A}Si(e,e'), 126-293 MeV, A=28,29, levels and form factors, particle-phonon coupling anal. 80−105977
^{28}Si, transition densities, form factors and transient radii 79−6481
^{28}Si(e,e′), 6^{-} T=1 resonance form factor, mag. strength quenching, meson exchange currents 80−86882
^{28}Si(μ^{-}, $\gamma\nu$), $\gamma-\nu$ ang. correlation, pseudoscalar and tensor form factors, particle-hole model 79−13256
^{28}Si(μ^{-},ν)^{28}Al*, moon capture form factors 79−13256
Si(p,ṕ), blocking and form factors 78−82336
^{120}Sn+^{40}Ar, deeply inelastic collisions, form factors determ. within statistical model 78−50205
^{120}Sn(^{40}Ar,X), deeply inelastic collisions, form factors, microscopic calcs. 80−18339
^{124}Sn, giant multipole reson. E1$\rightarrow$E7 transition form factors *(Russian)* 78−78349
^{181}Ta, ground state rotational band, electroexcitation 78−33168
^{181}Ta(e,é), rotational band form factors 78−33168
^{232}Th(d,t)^{231}Th, influence of form factors and multistep effects 77−79388
Ti(p,d),A=46,48,50, DWBA calcs., rms radius, form factors, spectroscopic factors 79−541
Ti(p,d), rms. radius, form factors, spectroscopic factors 79−541
^{238}U(e,e′), scatt. from octupole band, vibrational form factors 78−37333
^{238}U(e,é), octupole band form factors 78−37333

form factors continued
^{51}V(e,e′), shell model calcs. and effective charges 77-26674
^{51}V(e,e′), shell model calcs., effective charges 77-26674
^{64}Zn(α,α), 15-19 MeV, inelastic scatt. form factors, Coulomb-nuclear interference region 78-66288
Zr-region, two nucleon transfer reactions, spectroscopic amplitudes, form factors, ang. distrib. 80-22779
^{90}Zr(^{16}O,^{14}C), 80 MeV, coupled channel Born approx. anal., form factors, sequential amplitudes 79-9608
^{90}Zr(α,α), E=26.2-166 MeV, antisymmetrisation effects, α pot., form factor, optical model anal. 78-82366
^{90}Zr(α,α), form factor, coupling between real and imaginary optical potential 80-68680
^{90}Zr(e,e′), 2^- giant resonance twist mode excitation, B(M2) values, form factors 80-78246
^{92}Zr($\vec{p}$,α)^{89}Y, 35 MeV, analysing power study *(French)* 79-75981
Zr(α,α), 40 to 120 MeV, Woods-Saxon form factors 78-13123

formal languages
contrastive linguistics, P-struct. C-struct. grammar 78-69959

formal logic
see also threshold logic
axiomatisation of set of formulae of intuitionistic logic 78-57730
causal struct. of space-time, covariant representation of Galilean logic 77-5619
combustion process hazard modelling and logic theory 79-91953
education, logical abilities and success in physics courses, correl. 80-17731
foundational studies, A. Mostowski, book 80-57015
Herbrand theorem for ω^+-valued logic 78-57731
history of mathematics, causal and formal logic unification 78-77639
nuclear reactor design appl. 78-33247
permutation matrices using graphical methods of spin algebras, Serber coupling 79-6833
Polish logic and philosophy of science after Second World War 78-12529
quantum logic interpretation of orthocomplemented quasi modular lattice 80-12950
quantum mechanics, operational logics, state-generated effects measures 79-75401
quantum theory, logical structures and hidden models 78-41190

formation, heat of *see heat of formation*

forming processes
see also casting; electroforming
butadiene rubber, polymer melt, extrusion at constant deformation rate 78-68744
composite discs, fibre-reinforced, rotating strength, stress distrib., failure criterion rel. to mould process 78-76701
ethylene-propylene-diene terpolymer, sulphonated, ionically cross-linked, foam elastomer, thermo-mech. props. 78-48362
explosive forming, computer numerical simulation 80-59560
extrusion and forming of solids, plastic deform., nonNewtonian flow, numerical solns. 78-19824
fibre bundle cables termination, using portable tools 77-79977
fibre lightguide form., from tubular blank, optimisation 77-75719
fusion reactor, TFTR outer poloidal field coil insulation and mould design 80-91261
glass forming processes, review 78-3090
glass industry forming machines, review 78-3091
glass-ceramic, aligned, hot extrusion method for prep. 77-32552
high strain rate processes, review 80-84864
hot metal, dynamic yield characts. during multistage deform., plastometer design 80-85135
hydrostatic forming, novel industrial appls. 77-44191
ingot formed in EM crystalliser, control of metal melt circulation *(Russian)* 78-84790
ingot forming from melt, liq. containment by EM field 80-35120
injection molding, flow anal. of non-isothermal 2-D filling process 79-77038
injection-moulded article mech. props. rel. to process parameters 79-78929
limit curve for bending processes 80-7627
metal extrusion process, stress and deform. distribs., elastic-plastic anal. 77-48364
metal forming, limit anal. appl., book contrib. 78-11140
metal forming process, forming conditions and material characts. 80-30032
metal sheets, theories of necking and limit strain calc. 79-29115
metallic glass, moulding process 78-80536
microelectrode puller with high temp. heating element 77-61059
multistage continuous extrusion process by viscous drag 77-55912
nylon, steady-state deform. and its effect on struct. and morphology 78-15459
opical element polishing simulation calc. and results *(German)* 80-87566
optical component blank pressure shaping, semiautomatic apparatus 79-72731
optical fibre connectors, hot forming versus epoxy bonding of bundles, single fibre techniques 78-42482
polyethylene, high density, plastic deform. during hydrostatic extrusion 77-63722
polyethylene, high-density, effect of fillers and moulding process parameters on strength *(Russian)* 78-60640
polyethylene, steady-state deform. and its effect on struct. and morphology 78-15459
polyethylene, ultraoriented, prep. comments 77-85983
polyethylene film-resin melts, die swell, prep. method depend. 78-34099
polyisobutylene, polymer melt, extrusion at constant deformation rate 78-68744
polymer, filled, thermosetting, anisotropic structure on injection moulding *(German)* 78-76625
polymer melting, during extrusion, integral energy-balance model 77-46899
polymer sheet, stretching, with suction and blowing, heat and mass transfer 78-34033
polymers, hydrostatic extrusion effects on subsequent mechanical behaviour 77-90392
polystyrene-polybutadiene block copolymer, oriented microlattice obs. 78-2025
porous moist body, contact heating moulding, temp. distrib. heat/mass transfer 77-75784

forming processes continued
PVC, oriented mouldings, struct. order 80-60896
sheet metal, punch stretching, friction coeff. determ. method 78-27647
sheet metal forming, material behaviour 78-95787
sheet metal forming, strain hardening and strain rate sensitivity 78-7000
sheet metals, strain-induced changes in mech. props. and press formabilities 78-19781
shell, fracture behaviour, forming severity and metal flow in deep drawing 79-38975
shells, plastic, explosive forming, computer numerical simulation 80-59560
solar concentrator facet quality evaluation for deformational forming 78-90483
spinning, filament velocity measurement, streak photography 78-41367
steel, C and alloy, cold formability *(French)* 78-60681
steel, creep-resistant influence of temp., holding time, cooling rate on formability *(German)* 78-84901
steel, creep-resistant pipe steel, influence of chemical comp. on formability *(German)* 78-84900
steel, high-speed tool, properties, powder metallurgy prep. method *(Czech)* 80-60800
steel, inclusion effect on cold formability 80-29975
steel, laser erosion value depend. on metallic props. anisotropy during plastic deform. *(Russian)* 78-31452
steel, low C, forming limit diagram, eval. of applicability of theoretical anal. 78-60682
steel, low C, quenched, hardening during explosive forming 79-87650
steel, Si-Mn, 27SG, heat treated sheets, underwater explosive forming *(Polish)* 79-34052
steel, stainless, clad Al, sandwich sheet material, forming limits 80-3131
steel, stainless, ferritic, 430 Zr, oxidation, forming and mech. props. 80-11680
steel U8, struct. and mech. props., effect of hydrostatic extrusion *(Russian)* 77-56022
steels, hot forming property and struct. *(German)* 80-25730
superplasticity, deformation mechanisms, review 80-50691
thin shell forming processes, geom. props. *(Russian)* 78-51061
Al, circular tube, forming limit of free bulge-forming *(Japanese)* 80-55477
Al, extrusion, pick-up form. on surface 78-39882
Al membranes, circular, plastic deform. under impulsive loading by underwater wire explosion 79-100208
Al-Ca-Zn (5,5 wt.%) superplastic sheet alloy, mechanical properties, superplastic forming behaviour 80-60920
Al-Cu alloy, press-forming under coexisting state of liquid and solid, mech. props. 77-81240
Al-Cu-Mg alloy, extruded, press forming in liquid/solid coexisting state, mech. props., Mg effects 78-11151
Al-Mg-Si, type 6010, microstruct. characts. influence on formability. heat treatment 80-81090
C mixes, extruded, preoxidation treatment effect on transverse breaking strength 77-63767
C mixes, rheological props. at very low shear rates using capillary rheometer 77-65691
C mixes, rheological props. using capillary rheometer, binder content depend. 77-65692
Fe, Armco, struct. and mech. props., effect of hydrostatic extrusion *(Russian)* 77-56022
Fe, isochronous annealing recovery, in cold rolled and explosively formed samples 79-100166
Li$_2$O-SiO$_2$ glass ceramic, aligned, prep. by hot extrusion and microstruct. 77-32552
Na$_2$O-CaO-SiO$_2$ glass, vol. relaxation and thermal history during forming process 80-70130
Nb-Ti (46%) composite superconductor, fabrication 77-24989
PbMo$_6$S$_8$, supercond. wires prod. and characteris. 77-69462
^{238}Pu fuel form facility at Savannah River Plant 79-9846

FORTRAN
complete computer program in FORTRAN, for analysis of variance and means 80-98792
least-squares approximation program, lateral absorbed dose distrib. for 25 MeV electrons appl. *(Japanese)* 78-74505
PWR dynamical behaviour modelling in FORTRAN 80-91217

Foucault currents *see eddy currents*

fountain effect *see superfluid helium-4*

Fourier analysis
see also Fourier transforms; harmonic analysis; waveform analysis
2A 0311-227 optical counterpart, binary star, light curve Fourier anal. 80-82549
acoustic propag. in absorbant fluid, Fourier propag. theory *(French)* 80-33288
acoustic spectra, appl. of cepstral techniques to ground refl. effects 77-31165
acoustics, near field parametric emission study *(French)* 80-33291
adsorption, selective, correlation of intensity features with at.-surface pot. Fourier components 79-15013
alloy, Fermi surface and phase stability 77-77459
almost periodic functions with values in Banach spaces, convergence of Fourier series 77-82367
angle between two Fourier subspaces 77-64922
anharmonic temperature factors, site symmetrised Fourier invariant treatment 79-33040
arterial curvature sites anal. of unsteady component of pulsatile flow 77-56408
astronomical images, bidimensional Fourier filtering *(Italian)* 79-58269
astronomical spectral line profiles anal. 77-22105
astronomy, integral evaluation for Fourier analysis of eclipsing binary light curves 78-45236
atmosphere temp. in Madrid in 1871-1975 period, Fourier series *(Spanish)* 77-9486
atmospheric pressure field, Fourier expansion rel. to intensity of atmosphere meridional motions *(Russian)* 77-53154
atom-surface scattering potential, hard corrugated wall model, Fourier components 79-61485
atomic profile determ., Fourier analysis, deconvolution of Fabry-Perot interferograms *(French)* 80-48972
atoms, Compton profile, Fourier anal. 79-89588
SX Aurigae, eclipsing binary, light curves anal. by automated Fourier techniques 79-92798

Fourier analysis continued
- automated technique for stellar light curve analysis 79—17020
- beat Cepheids, Fourier anal. 78—69811
- biomechanical data, mathematical function fitting 79—48278
- biomedical signals, development of common struct. for filters, correlators and Fourier analysers *(German)* 78—88748
- blood pressure waves, physiological interpretation of spectra, heart rate, respiration waves 79—29540
- boson system, 1-D, with δ-function interactions, time-depend. Hartree approx. 79—9184
- boundary-value problems of unrestrained rod 77—39258
- β Canis Majoris, β Cephei star, Fourier anal. of radial vel. changes 80—105246
- l Carinae, Cepheid variable, Fourier anal. of light var. 80—90442
- Cepheid variable stars, double-mode, freq. anal. 80—31308
- chemical reactions, Fourier sensitivity analysis, improved freq. sets 78—31628
- Cherenkov effect in spatially dispersive media 80—105516
- circular cylinder with variable thickness free flexural vibrations 79—68620
- clay layer, non-homogeneous, consolidation estimation via pore water press. Fourier anal. 79—58110
- Comet Bradfield (1974 III), nuclear brightness meas. using deconvolution technique 79—84745
- computer representation of geometrical configuration of vocal tract *(Russian)* 80—46111
- computerised tomography principles, X-ray, axial, medical diagnosis appl. *(Spanish)* 79—20698
- concrete, aggregate, shape and texture anal. by modified Fourier method, orientation effects 77—77691
- cooling tower supporting columns and reinforcing rings, displacement analyses 78—38187
- cosmic ray intensity diurnal variation, Fourier series method 79—29953
- cosmic rays, annnual and semiannual vars. 80—26704
- crystallography, determinantal inequalities, invariant joint probability distrib., heuristic derivation 79—32927
- crystallography, tangent-formula development, and refinement and Fourier synthesis, theoretical weighting scheme 79—99027
- cuboid surrounded by infinite elastic space, stress field due to initial strains 78—55565
- CVD, interface morphology on profiled substrates, calc. of development 78—60040
- daily precipitation stochastic models, estimation of Fourier coeffs. to describe parameters seasonal vars. 79—53481
- data with closely spaced frequencies, erroneous results 78—89298
- deconvolution, Fourier analysis of methods, pitfalls 78—24638
- deconvolution of exptl. curves. Fourier series 77—54493
- difference schemes for Laplace eqn. in rot. symm. system, Fourier anal. 78—77677
- diffraction of plane EM wave by grating at interface 79—27139
- diffraction-profile Fourier analysis, determ. of microstruct. parameters 80—49042
- diffusion equation, Fourier expression, appl. *(Japanese)* 80—49400
- diffusion process, nonlinear, path integral evaluation by Fourier series 78—70075
- diffusion-convection equation, stability of finite difference approximations 80—82730
- discrete Fourier transform filter in spectrum analyser 79—1032
- early-type stars photospheric expansion, meas. via. Fourier anal. technique 78—93224
- Earth surface temperature, determ. of diurnal var. in mountainous terrain 80—82011
- Earth surface topography, polynomial and Fourier trend surfaces computation 78—32245
- earthquake magnitude determ. from seismograms by Fourier anal. 77—73655
- earthquakes strong ground accel., empirical model for scaling Fourier amplitude spectra 77—9361
- echocardiogram of anterior mitral leaflet 78—28028
- eclipsing binary star light curve anal. in freq. domain by automatized Fourier technique 80—22039
- eclipsing binary star light curve analysis technique 79—58261
- eclipsing binary star light loss analysis techniques 79—58262
- eclipsing binary stars, Fourier anal. of light curves, geometric elements soln. 79—25634
- eclipsing binary stars, Fourier anal. of light curves, reduction of integrals 78—20856
- eclipsing binary stars, Fourier anal. of light curves 77—87474
- eclipsing binary stars, Fourier anal. of light curves 78—24525
- eclipsing binary stars, Fourier anal. of light curves 78—69830
- eclipsing binary stars, Fourier anal. of light curves for transit eclipses 78—96506
- eclipsing binary stars, light curve analysis by Fourier techniques 80—72993
- eclipsing binary stars, light curve analysis by Fourier techniques 80—72994
- eclipsing binary stars, light curves Fourier anal. 77—9769
- eclipsing variable stars, Fourier anal. of light curves, photometric perturbs. for partial eclipses 79—25635
- eclipsing variable stars, Fourier anal. of light curves 77—49428
- eclipsing variable stars, Fourier anal. of light curves 78—20854
- eclipsing variable stars, Fourier anal. of light curves 78—93311
- eclipsing variable stars, Fourier anal. of light curves 79—25632
- eclipsing variable stars, Fourier anal. of light curves 79—25633
- eclipsing variable stars, Fourier anal. of light curves 79—30088
- eclipsing variable stars, Fourier analysis of light curves, error anal. in freq. domain 80—31214
- eclipsing variable stars, light curves Fourier analysis, appls. to eccentric orbits 79—25630
- eclipsing variable stars Fourier anal., $B_{n,m}{}^q$ integrals explicit expression 79—35298
- eclipsing variable stars light curves, photometric perturbations for total and transit eclipses 78—12291
- eclipsing variable stars with extended atmospheres, Fourier anal. of light curves 80—46604
- eclipsing variables, Fourier anal. of light curves, photometric perturbs. 78—96507
- eclipsing variables, Fourier analysis of light curves 79—8945
- eclipsing variables, Fourier analysis of light curves 79—8946
- eigenfunction expansions assoc. with vector-matrix differential eqn., convergence 78—69965

Fourier analysis continued
- Einzel-type electrostatic field with rot. symmetry, Fourier-Bessel soln. 78—82878
- elastic plug in elastic region contact problem, numerical quadrature method 77—53747
- elastic radiation from spherical wave sources, seismic model 79—8612
- electrolytes, aq. solns., X-ray, neutron diffr. data, termination errors, Fourier anal. 77—47299
- electron diffraction data of Al_2O_3 amorphous films 80—20046
- electron micrograph, 500 kV, atomic resolution, computer image processing 80—100149
- electron microscopy, conically tilted projections, 3-D reconstruction 80—99618
- electroplasticity, skin effect 80—21046
- elementary neutron slowing down equation, infinite series soln. 79—17951
- EM and acoustic fields around bodies of complex form *(Russian)* 78—46486
- ν Eridani, β Cephei star, Fourier anal. of radial vel. changes 80—105246
- evoked potential optimal filtering in sequential range *(German)* 78—85401
- exponential densities on SD(3) for rotational processes, function representation and optimal estimation 77—17782
- Fermi fluids, nonlinear response of strongly coupled fluids, appl. to polarisation diags. 77—7931
- Fermi surface parameter determ. from Fourier anal. of Compton profiles 77—4285
- field problems in multilayer composites, produced by line charge 78—29875
- fluid and isotropic solid acoustic harmonic generation 77—27417
- forces exerted in walking and running 80—94266
- FORTRAN program for Fourier analysis with splines 79—12582
- FORTRAN program for Fourier coeffs. of assoc. generalised Legendre polynomials of generalised spherical harmonics in texture analysis *(French)* 77—15279
- Fourier series, recursive evaluation, for teachers 79—35477
- frequency analysis of low-amplitude δ Scuti stars 79—35276
- frequency analysis of low-amplitude δ Scuti stars 79—35275
- gamma ray spectra anal., fast Fourier transform *(Chinese)* 80—77762
- gammagraphy, 3-dimens. image processing appl. to coded aperture imaging *(French)* 78—57067
- geophysical anomaly source models, statistical parameters rel. to pot. fields obtained by superposition *(German)* 79—34783
- geophysical data acquisition *(Italian)* 80—109254
- geophysical fields, shortened Fourier expansions *(Russian)* 79—62624
- grain size and strain determ. by Fourier anal. of X-ray diffr. profiles 78—88588
- gravimetric and magnetometric anomalies, interpretation *(Rumanian)* 79—58123
- harmonic anal. on Lorentz group as dynamical relativistic Fourier anal. 77—82406
- harmonic waveforms, Fourier analysis using SR56 calculator 78—36986
- harmonic waves, introduced through Fourier synthesis, for teaching 80—27080
- heart beat rate signals, fast Fourier transforms, beatquency domain 77—81595
- heat conduction, nonlinear Fourier eqn. soln., minorant-majorant aprox. 80—79105
- heat diffusion in solid sphere, Fourier theory 80—31456
- Hirshfeld type deformation functions, and elec. field gradients calcs. by Fourier series 79—73479
- horizontal ground acceleration, Fourier amplitude spectra estimation 79—16389
- human vision, Fourier anal. and texture discrimination 78—96051
- hyperfunctions, appl. to quantum field theory 77—38084
- impact response of layered composite containing a crack, Fourier and Laplace transforms 77—50991
- infinite plate reinforced by finite beam set and driven by point force, sound radiation anal. 78—1496
- inhomogeneous medium, effective cond., iteration series and variational estimates, Herring method 80—70663
- insect visual system elementary movement detectors 77—2001
- integral determ. from derivative of given function *(German)* 78—49644
- ionograms, Fourier anal. rel. to pulse spreading and unresolved spread-F 77—78557
- ionosphere sounding, pulse synthesis technique for improving ionosonde resolution 78—28411
- ionospheric travelling disturbances, medium-scale, diurnal and seasonal var. modelling 79—58181
- Korteweg-de Vries, eqn., recurrence of initial state, numerical soln. using Fourier expansion 79—92924
- Korteweg-de Vries equation, numerical solution, comparison of computation methods 80—46814
- lamellar structures, deconvolution method for evaluating small angle X-ray scattering 79—10756
- laser, high-intensity, multimode, dynamics theory 79—41363
- light curve analysis for eclipsing binary stars 79—21349
- light curves, Fourier analysis for partial phases of eclipsing variable stars 79—21350
- liquid phase band contours, data processing, band shape corrections 78—27215
- Lorentz group in function space outside light cone, Fourier expansion 79—71246
- magnetic field calc., Fourier anal. within finite elements 77—71903
- magnetic induction, in cylindrical geometry, rel. to plasma probes 77—65907
- membrane profiles, asymmetric, struct. determ., iterative Fourier method 79—43810
- meteorological fields, objective analysis method *(Russian)* 78—81272
- metrological reliability, indication errors and Hilbert space *(Rumanian)* 79—40523
- modal analysis techniques applied to acoustic problems, review 79—18651
- molecules, Compton profile, Fourier anal. 79—89588
- 1 Monocerotis, δ Scuti star, photometry and Fourier anal. 78—32495
- multicomponent exponential functions, differential technique 77—78955
- multidielectric stack control using chromatic maximeter, Fourier series anal. of signal *(French)* 78—83111
- multidimensional contour resolution into components 79—84941
- multipurpose Fourier spectral analysis program for analytical chemistry 78—64896

Fourier analysis continued
- muscle, skeletal, deriving viscoelastic modulus from transient pulse propag. 78—77077
- musical acoustics, Fourier anal., phase determ. *(French)* 79—90100
- nerve spike train analysis 80—12070
- neural response evaluation and statistical judgement to sinusoidal stimulation with superimposed drift and noise 79—88068
- neutron diffusion equation, Fourier expansion for xyz-geometry 80—9326
- neutron transport eqn., factorised kernels and DKPL soln. 79—80968
- neutrons, thermal, diffusion eqn. in medium with cylindrical hole, soln. 80—51548
- noise, Fourier transform as perturbation criterion, appl. to NMR intensity 78—65948
- non-equilibrium quantum statistics validity of Fourier expansion method 77—53829
- nonlinear interaction of acoustic beams in absorbing fluid, parametric emission, Fourier anal. *(French)* 79—94388
- nonlinear wave envelope equations for plasma physics, Fourier's method convergence 79—55463
- nuclear medicine, fourier reconstruction with a distortion function 80—8174
- numerical-valued Fourier transform in two-sided operational calculus 77—67219
- ocean waves, comparison between synthetic aperture radar imageries and surface truth 79—5497
- optical phase tracking, Fourier series and estimation appl. 78—25812
- Ornstein-Zernike eqn. with Yukawa closure for a mixture of spherical molecules 79—27893
- parallel optical Fourier transform techniques for Fourier spectroscopy 80—95161
- parametric decay spectrum of heating near LH frequency in Petula 80—28761
- particle profile charact. rel. to profile Fourier coeff. 78—11142
- particle shape *(Japanese)* 79—88506
- pendulum, simple, large-amplitude, Fourier anal., for teaching 80—17767
- phase meter system expt. error evaluation algorithm *(Russian)* 77—41636
- physical optics farfield inverse scatt., mathematical inversion technique for nondestructive eval. 80—69580
- pinhole and continuous projections, limited angle 3-D reconstruction 80—61667
- planar positron cameras, 3-D reconstruction using Fourier deconvolution of generalised tomograms 78—40295
- plane wave diffraction by periodic surface *(French)* 80—37939
- plasma drifting, cold or hot, radiation potential of immersed point antenna, DRFT computation 80—14906
- Poisson's eqn. in 3-d, direct solns. using algorithms 78—20954
- polycrystal Debye-Scherrer line profile analysis moment methods using Fourier representation *(German)* 77—55202
- polymer, vibrational spectra of chain, Green's function anal., Fourier method for perfect infinite chain 78—18725
- polymer chains, Coulombic contributions, LCAO-SCF-CO method, Fourier representations 80—32862
- polymers, Fourier anal. of X-ray diffr. patterns 80—15016
- polymers, thermal diffusivity, Fourier theory 80—31456
- polyoxymethylene, electron density calc. in cylindrical coordinates, Fourier method 79—13852
- positron camera proportional chamber, Fourier deconvolution technique 78—40297
- potential field transformation from relief to single reference plane, Fourier anal. appl. *(Russian)* 78—53759
- power reactor resonance determ. by rod-drop method, Fourier anal. 79—22407
- protein crystallography, min.-variance Fourier coeffs. from isomorphous replacement method by least squares anal. 77—52938
- protein structures, Fourier refinement 80—51037
- pseudo-differential eqns., Fourier integral distribs. and Denjoy-Carleman classes *(French)* 77—67198
- psychophysical response to transients, human visual perception appl. 77—25441
- pulse-excited systems for nondestructive materials testing, using eddy current method *(Czech)* 79—39071
- radiography, straight-line tomography, linearising mechanisms 78—35934
- random data, effects of detrending and smoothing 78—40685
- reactor containment expts., Fourier transform anal. of transient condensation heat transfer coeff. 79—22410
- real-time Fourier spectrum analysis, using acousto-optic devices 77—58285
- reflectance data analysis, Fourier series algorithm 77—85679
- regular growth, entire and meromorphic functions, Fourier series method *(Russian)* 79—12565
- resonant antenna system, anomalous radiation and electrodynamic characts. 80—69302
- resonator, transient process, excited by beam 79—81347
- respiratory system, freq. characts. determ. 77—5093
- Riesz summability of Fourier series and its conjugate 78—54155
- rigid body impact on elastic half-space, Fourier synthesis of steady state vibr. 77—80101
- rocks single layer folds, arc lengths, comparison between theory and obs. 79—53345
- sandwich panels, discrete field mechanics 77—62151
- SAW chirp filters based Fourier transformation processors 79—7270
- SAW in periodic structures, noniterative technique using Languerre functions and Fourier series 79—81596
- scattering, inverse problem, determ. of shape of cylindrical obstacle 80—83543
- scattering density variance minimisation criteria for Fourier synthesis 78—55774
- scintiallation camera collimators, point spread function study 79—35910
- σ Scorpii, β Cephei star, Fourier anal. of radial vel. changes 80—105246
- segmental cylindrical shells vibrations 80—58958
- seismic oscills., Fourier and response spectra 77—56597
- seismic SH-waves at epicentral distances greater than 90°, Fourier anal. 77—81811
- seismic waveforms extrapolation 79—34978
- seismology, rapid convolution and correl. *(Russian)* 79—39959
- seismometers, automated high-precision amplitude and phase calibration 77—9519
- shape and surface texture anal. of planar sections of particles 77—77690
- shape differences comparison, between two-dimensional irregular forms, computer program 77—87639
- shortening operators used in gravity interp. data processing techniques 77—64179
- signal processing system for vibrs., shock and noise 77—68335
- signature analysis systems with Fourier analyzer 78—87195
- solar heating of buildings calc., transient thermal flux model 79—62144
- solar line profiles, broadening by finite sized eddies, Fourier anal. appl. 77—17500
- solar quiescent prominences, Ca II K spectra and vertical struct. of line of sight and vel. field 77—53522
- solitary wave, diffraction by circular island in ocean, shallow-water theory *(French)* 80—83803
- space-like surfaces, mass ≠0, definition of transformations 77—29995
- space-like surfaces, zero mass case 77—45680
- Spar Buoy Oceanographic Telemetry System software engineering 80—46308
- speech signals, time-domain algorithms for harmonic bandwidth compression 79—46125
- star light changes in eclipsing binaries 79—75247
- star light curves in eclipsing binaries, series expansions 79—75248
- stars, eclipsing variables, light curve Fourier analysis, eclipse parameters, geometrical determinacy 78—96503
- statistical equality connecting zero Fourier harmonics with average quantities 80—133
- steady state evoked potentials, recording and appls. review 78—35823
- stellar atmosphere motion field, macro- and microturbulent filter functions for weak lines 79—53803
- stellar light curves, eclipsing variable element determ. 77—45484
- stellar rotational vel. determ. from stellar spectrum by Fourier method *(Russian)* 79—80240
- stellar speckle interferometry for stars cold satellites searches, Fourier spectra *(Russian)* 80—12672
- stellar spectral line profiles, Fourier deconvolution for mag. fields detect. 80—72949
- stellar spectral lines, Fourier anal. rel. to lower main-sequence stars rot. vel. determ. 80—51767
- stellar systems dynamics, purely discontinuous random processes in field of irregular forces *(Polish)* 78—16465
- stress analysis of plastic zone during rolling under plane strain conditioner, Fourier calcs. *(Russian)* 78—80555
- stress intensity factors for semi-infinite crack under 3-D loading 77—80115
- strong (J, p_n) summability 79—58525
- surface profile waviness and roughness separation technique *(German)* 77—74352
- time series, rest frame spectra deduction from spectra computed in moving frame 77—25795
- Toeplitz determinants calc. produced by substantially limited functions *(German)* 80—26
- tomography, computed, 3-D image reconstruction, Fourier deconvolution method 80—61669
- truncated autocorrelation functions, numerical inversion 80—57097
- turbulence problems, functional smoothing method 79—86407
- two-dimensional higher-order Hermite-Gaussian beam scatt. by offset cylinder 79—55056
- two-phase fluid velocity meas. by radiation intensity correlation 77—75996
- 4U 1700-37 (HD 153919), uncertainty of 97 min. periodicity 79—40295
- ultrasonic transducers, study of nonlinear parametric radiation using Fourier anal. *(French)* 79—41485
- unsteady viscous flow in curved elastic tube 79—92281
- US Doppler-shift arterial flow signals 77—29187
- US frequency analysis, Fourier model 77—40504
- US image feature enhancement via digital processing 78—73183
- vector function expansions, appl. to vibr. of shells of revolution *(Russian)* 77—54921
- vector groups, multiplier representation, translation-invariant traces, Fourier anal. 79—6023
- vibration of circular plate on eccentric annular elastic support 80—14601
- visual environment, spatial frequency analysis, anisotropy and carpentered environment hypothesis 79—53137
- visual illusion, cortical simple receptive field neurons, spatial freq. response approximating Fourier analyser 79—53089
- visual physiology and psychophysics polar coordinate data 78—56988
- waves in magnetised plasma, kinetic eqn., velocity Fourier transform solution of a model collision operator 79—94785
- X-ray diffr. line profile analysis, on-line computer routine 78—79498
- X-ray diffraction profile, appl. to N content determ. of sputtered Ta films 77—76693
- X-ray line profile analysis, direct determ. of Fourier coeffs. by least squares method *(French)* 77—27775
- X-ray line-shape anal., simplifications using Fourier series, appl. to Mo film on Si 79—82123
- CO_2, atmospheric, conc. vars., cycles and trends 79—84381
- Cs+Xe, Cs spectral line profile and absorpt. transitions 80—47944
- Cu, bulk and (001) film, extended tight-binding calcs. 80—70592
- LiH, cryst., Compton profile, position space anal. 79—47536
- Ni powder, neutron diffr. study of Debye-Waller factor using reverse Fourier time-of-flight method 80—49050

Fourier series *see series (mathematics)*

Fourier transform optics
- *see also Fourier transform spectroscopy*
- 2-D acoustic Fourier transform of optical images 80—74308
- aberrated diffraction pattern obs. with computer-generated holograms 80—102681
- acoustic hologram correction for nonuniform relative motion 79—46119
- acoustic image scanning, optical processing, photon integration technique *(French)* 79—32147
- acousto-optic real-time radar and sonar signal processing 79—72515
- acousto-optic spectrum analysis, wideband high-resolution, hybrid technique 79—76597
- acousto-optical devices for real- and near-real-time signal processing 80—10024
- acoustoelectric SAW image scanner applications 79—45912
- acoustooptic snapshot PROM, real-time optical, signal spectrum analyser 78—90494
- adaptive Fourier transformation by acousto-optic convolver 79—55079
- aerial photograph statistical spatial filtering 79—13908
- ambiguity function display, improved coherent processor 77—42492
- ambiguity processing by joint Fourier transform holography 80—58468

Fourier transform optics continued
- analogue data processing systems, polarised modulation of light *(Russian)* 80−91884
- analogue image processing, Japanese achievements 77−50634
- analytic, information encoding by complex zeros 80−23628
- annular lenses in microscopes, imaging props., calcs. 80−22426
- apodisation, optimal, Fourier spectrometry 80−99641
- applied inverse problems, book 79−49017
- astigmatic coherent processor analysis 78−78927
- astronomical telescope, diffraction figure calc. by Fourier transform. *(French)* 79−48672
- axial patterns diffracted from optical pupils, Fourier analysis of Fabry-Perot spectrograms 79−27188
- binary computer-generated holograms 80−19004
- biological cell diffr. pattern, Fourier optical extraction of morphological parameters 78−92749
- biological cell size meas. by static light scatt. Fourier transform 80−81793
- biological cells in flow system, paraxial anal. of light scatt. 79−11907
- blood cell smear pathology differentiation by optical transform method 78−69248
- cellulose nitrate film, ion track density, quantitative assessment using Fourier transform techniques 79−86610
- cervical cancer detection, comparison of coherent optical transform processing systems 78−48922
- channel waveguide array in fan-out pattern for high resolution optical imaging 80−38129
- chest radiograph optoelectronic processing for pulmonary venous hypertension detect. 79−74754
- chirped grating lenses anal. 80−87563
- chromatic Fourier hologram as matched filter, for spatially coherent white light correlator 79−3642
- chromosome metaphase spread, automatic finding, prep. and eval. of object spectra 80−98168
- circularly symmetric positive filter function realisation by transparent rings 80−87343
- coded image obtained with nonredundant pinhole array, digital deconvolution 77−61919
- coded-aperture images, pre-folded Fourier filter reconstruction 80−53222
- coding of spatial and chromatic information by Fourier holography 77−3555
- coherence properties modification of light beam, optical processing appls. 80−78769
- coherent information processing by a pair of lenses in spherical wave illumination 80−95816
- coherent light valve optical processor for GHz bandwidth signals 78−78937
- coherent optical data processing fundamentals 78−78923
- coherent optical feedback analogue computer for partial differential eqns. with inhomogeneous terms 79−76870
- coherent optical Fourier transform operator numerical accuracy improvement 79−76628
- coherent optical implementation of generalized two-dimensional transforms 79−94174
- coherent optical implementation of generalized two-dimensional transforms 80−95835
- coherent optical information processing systems, operations achievable 77−10861
- coherent optical iterative extrapolation of 2-D band-limited signals 80−78780
- coherent optical processing, cervical cytological samples 78−36007
- coherent optical processing equipment, cervical cytological samples screening 78−36006
- coherent optical processing of biological cells, exam. of Fourier spectrum analyzer with optical transducer 78−36008
- coherent optical processor, input object vibr. effects on spatial freq. spectrum 77−46686
- coherent optics fundamentals 78−78910
- colour image archival storage using Fourier multicolour holograms 80−102674
- colour image evaluation from tristimulus values transfer functions measurements 80−87333
- compact real-time matched-filter optical processor 78−74869
- computer controlled optical system for quantitative diagnosis of early pulmonary oedema 77−77981
- computer generated holograms, x-y plotter display 79−55088
- computer-generated double-phase holograms, Fourier transform subcells and phase coding 79−27200
- computer-generated hologram spectrum shaping and image reconstruction, iterative method 80−106475
- computerised tomography, Fourier transform image reconstruction, polar sampling theorems 79−92373
- computing, conference, London (1978) 79−72511
- confocal scanning microscope, image form. 80−68249
- conjugate Fourier series approach to optical data analysis 78−90378
- contemporary optics, book 79−81353
- correlation function of single-mode radiation in a quasi-classical approximation 80−95815
- Correlation image formation with an axicon 80−48162
- correlator, wavefront propagation error effects 79−50232
- cross-correlation matrix processing 79−13910
- cylindrical surface two-wavelength speckle pattern intensity distrib. at optical transform plane 80−106487
- deconvolution of electronographic images 79−75112
- deflection contour generation, Fourier filtering of white light speckle patterns 80−98881
- defocused grainy photographs, digital restoration by noise cheating and Fourier techniques 77−50626
- diatom photography characterisation by Fourier transform differences 79−79697
- differentiation by spatial filtering 78−1171
- diffraction and causality principle 78−55295
- diffraction pattern and AM sideband parallelism *(German)* 79−89854
- diffraction point spread function second moment as image quality criterion 80−9818
- diffuser for Fourier transform hologram recording 80−43285
- directional filtering two-dimensional patterns, hybrid character recognition system *(German)* 77−83819
- disordered crysts., optical transforms 80−78783
- distorted image convolution deblurring by Fourier-Bessel transform holograms *(Russian)* 79−22897

Fourier transform optics continued
- dither signals for binary display of images, computer-aided design 79−94161
- double beam system, data storage and processing appl. *(Russian)* 80−28165
- driven equilibrium Fourier transform sensor operating at 100 MHz 80−74612
- dynamic laser speckle interferometry, appl. to transient flexure 78−32861
- edge enhancement of optical images, by Fourier transform optical system 78−33680
- edge image analysis, Walsh functions used in Fourier transforms 79−72507
- education, geometrical optics, lens Fourier transform properties 80−57024
- electro-optical spatial light modulator resolution, stored point charge effects 80−106616
- electron diffraction patterns, and optical transforms of atomic aggregates, symmetry aspects using computer simulation 79−7525
- electron microscope, image formation in partially coherent illumination including inelastic scatt. 78−32956
- electron microscopy, optical Fourier transformation of two-dimens. image signals *(German)* 78−32932
- electron microscopy of biomacromolecules, image analysis *(Czech)* 78−31983
- electron optical systems, optimisation using orthogonal functions 80−63908
- equalizing and coherence measure correlators 79−13911
- ERG, human corneal, frequency domain anal. 80−45888
- evaluation techniques, user-oriented, for optical design 79−86131
- exact spatial frequency plane of Fourier transforming lens 78−63012
- fast image recognition by generalised harmonic analysis *(Russian)* 80−63930
- fibre refractive index profile nondestructive determ., fast Fourier transform method 79−64307
- fibre sizing using Fraunhofer diffraction 79−171
- fibre waveguide mode properties, computation by propagating beam method 80−69502
- fibres, graded-index, multimode, differential mode delay and attenuation meas., optimal excitation calc. 80−99842
- fibres with arbitrary index profile, pulse propag. and dispersion 80−78984
- filter function, circularly symm. positive, realisation by transparent rings 78−94448
- filter plane resolution requirements for coherent optical correlators 77−34828
- fluid section flow pattern speckle photography 80−103096
- folded spectrum processor, signal demodulation and radar processing appls. 78−5429
- four-component system design for optical data processing 78−42282
- Fraunhofer diffraction, dispersion relations 79−81356
- Fraunhofer diffraction of apertures, analogy with SSB modulation 80−48138
- Fraunhofer diffraction pattern processing for real-time meas. 79−76621
- fraunhofer diffraction patterns from apertures illuminated with nonparallel light, for teaching 79−35465
- Fraunhofer diffraction symmetry, series expansion of Fourier transform 79−50212
- Fresnel diffr. patterns and in-line holograms, FT analysis 77−88637
- Fresnel diffraction pattern, spatial freqs., spectral analysis *(French)* 77−58269
- Fresnel hologram recording, quasi-Fourier transform reconstruction of object 79−59652
- Fresnel images, form. of 2-D transparencies with extended periodic struct., theory 78−82920
- generalised holographic form. of lensless Fourier transform, different geometries 80−19003
- geodesic lens design for integrated optics signal processing 80−33247
- geomagnetic surveying, optical filtering of airborne and ground data 77−25797
- geophysical mapping and remote sensing by optical filtering 80−101458
- graded-index multimode fibres, dispersion calc. by propag. beam method 79−98465
- graded-index optical fibres, mode eigenfunction computation propagating beam method 80−95988
- graphological elements meas. using optical Fourier transform *(Italian)* 78−50707
- gratings optical imaging, embedded, for meas. by moire fringes *(German)* 80−23805
- Gulf of Alaska SeaSat Experiment synthetic aperture radar wave imagery 80−46199
- handwriting, linear prediction of optical parameters *(French)* 79−3640
- Hankel transforms, quasi fast, algorithm for evaluation 77−83826
- helical motion of rigid body, meas. by double exposure speckle method 78−16775
- high-contrast point-image holography in turbulent atmosphere *(Russian)* 80−63943
- hologram, resolving power characts. *(Korean)* 77−50638
- hologram, sampled, interpretation, simplification technique 78−1181
- hologram generation, synthetic, variable magnification imaging system 79−3655
- hologram memory using one dimensional Fourier transform image hologram 78−87032
- hologram optimisation, computational method 77−50639
- hologram optimisation 77−19209
- hologram recording and reconstruction, using materials with low resolving power *(Czech)* 78−90399
- hologram recording in optical system with synthetic aperture 80−95852
- holograms, binary Fourier, wavefront coding by Lee method 77−75441
- holograms, computer-generated, three-dimensional, image reconstruction using line printer 77−42506
- holograms, long-wavelength, recording and reconstructing schemes 78−87029
- holograms, stacked Fourier, reconstruction 80−87348
- holographic disc with high data transfer rate, audio response memory appl. 80−58477
- holographic filters and character identification *(German)* 77−88668
- holographic Fourier transform lenses for matched-filter optical processor 79−45913
- holographic image scanning by SAW on monolithic MIS structure 77−23771

Fourier transform optics continued
- holographic interference correlators, theory 78—78969
- holographic lensless Fourier transform, spherical wave illum. 80—74312
- holographic lensless Fourier transform, wavelength difference between recording and reconstructing wavefronts 80—58471
- holographic matched filter, increasing information capacity 78—25815
- holographic memory, lens aberrations effect on storage capacity 77—19202
- holographic memory readin system parameter optimisation *(Russian)* 78—13670
- holographic nondestructive testing at Fourier plane 78—46536
- holographic pattern recognition of the Korean alphabet using matched spatial filters *(Korean)* 79—22920
- holographic recording medium, optimal linear transfer function determ. 80—23635
- holography, computer-generated, review 80—9827
- holography, Fourier transform computer-generated, generalisation *(Japanese)* 77—34847
- holography, lensless, expt. and digital simulation results *(Japanese)* 78—30133
- holography, maximum recordable number of particles 78—58946
- holography, reference and illuminating sources size effect 79—72531
- holography, super resolution technique in Fresnel transform holography 80—9840
- holography method, fast Fourier transform 78—71064
- hybrid image processing trends and prospects 80—32927
- hybrid optical-digital image processing, appl. to handwriting and aerial photos 77—68178
- image correlation, real-time high-resolvance, by Bragg diffr. in saturable absorbers 80—48159
- image display, Fourier domain aliasing and quantization 79—81372
- image formation by inversion of scatt. field data, expts. and computer simulation 79—89852
- image formation in scanning microscopes with partially coherent source and detector 78—58923
- image forming systems, fundamentals for electronics engineer 78—22089
- image Fourier transform correlator using US light modulator *(Russian)* 77—58264
- image irradiance moments optical calc., wave optical accuracy limitations 80—74302
- image multiplication using duplex spatial sampling filtering 79—7090
- image processing by spatial freq. spectrum phase modulation *(Korean)* 78—22090
- image reconstruction, iterative computer method 80—102634
- image reconstruction and partially coherent objects from mutual intensity samples 78—9333
- image reconstruction by modified back projection methods, reconstruction error determ. 78—33682
- image reconstruction from kinoforms and distorted holograms *(Russian)* 78—13664
- image reconstruction from partial Fourier transform 78—33691
- image reconstruction using polar sampling theorems 79—81366
- image reconstruction with limited angle projection data 79—66508
- image rotation and magnification, optical system 80—48376
- image subtraction via processing simultaneously recorded holographic images 77—46700
- imaging, significance of Fourier transform *(German)* 78—50709
- imaging system using intensity triple correlator 78—74846
- imaging systems in water, point and beam spread functions 78—5426
- implicit sampling for noncoherent optical data processing 80—99652
- in-plane vibration measurement, real-time speckle interferometry with aid of liq. cryst. light valve 80—53734
- incoherent image two-dimensional Fourier transform by optoacoustic transducer 79—50243
- incoherent method, fully parallel, high-speed, for performing discrete Fourier transforms 78—33684
- incoherent optical discrete Fourier transform processing system 80—74303
- information encoding and propagation in scattered fields by complex zeros 79—50238
- information encoding by complex zeros, analytic Fourier optics, comment 80—87326
- inhomogeneously amplifying medium, light beam deflection 77—88689
- integrated optical circuit for Fourier transform 77—39111
- integrated optical multimode waveguides, Fourier domain propagation calc. 80—64219
- interferogram analysis, point spread function and OTF determ. for optical system testing 79—76616
- interferometric determination of complex Fourier spectra 80—87327
- interferometric imaging through scatt. media with achromatic interferometer 79—58778
- interferometric two-dimens. imaging of rotating objects 78—1176
- inverse radon transform by optical convolution 78—66777
- inverse sampling spatial filtering for image multiplication 77—23627
- joint Fourier transform processing with thermoplastic device 79—72512
- joint-Fourier-transform correlator, dual-axis, hologram recording 79—59649
- Kanji character generation by holographic memory system 78—37854
- Kirchhoff diffraction integral validity *(German)* 78—9339
- Kirchhoff integral, cosine factor, rel. to Fourier optics *(German)* 80—18997
- Kirchhoff integral, Fourier optics as approximation *(German)* 79—18357
- Kirchhoff integral approximation *(German)* 79—27186
- Kirchhoff integral approximation *(German)* 79—31814
- laser beam profile measurement using spatial sampling, Fourier optics and holography 79—86201
- laser line art optical processor, optimal enhancement filter 79—59648
- laser pulse autocorrelation by optical processing of Fabry-Perot spectrograms 80—58465
- laser pulse shaping by passive optical Fourier techniques 77—10934
- laser speckle photography, double-exposure, magnification change effect 79—40607
- lateral shearing interferometry for stochastic inputs, data reduction 77—26386
- lens, Fourier transform, design and structural characts. *(Chinese)* 79—45911
- lens, spatial invariance test 80—69492
- lens array, Fourier transform, for shortening optical correlator length 79—59646

Fourier transform optics continued
- lens design, least squares fitting of Zernike's polynomials to wave aberration function 80—83660
- lens film system resolution computation from numerical MTF data 79—44960
- lenses, simple, as Fourier transform elements, performance meas. techniques 78—94374
- LF signal optical processing procedure 78—9343
- light pencil and interferometer for amplitude and phase profiles 80—102680
- line spread function, notation 77—620
- linear inverse problems in Fourier optics, regularisation 79—50240
- linear multiplane coherent optical processors, iterative Fourier transform description 79—94164
- linear systems, Fourier transforms and optics, book 79—41350
- liquid crystal image transducer, spatial frequency spectrum temporal meas. 79—76810
- Lohmann hologram, detour phase error 79—41351
- long-wave imaging with super-resolution by wavelength diversity 80—102675
- magnetic thin films, substructural defect anal. by coherent methods *(Russian)* 79—61190
- matched filter visibility effects on the correlation function 80—96031
- matched filtering improvements for coherent optical pattern recognition 80—78786
- matched filtering using binary digital hologram, Fourier domain quantization 77—3544
- matched spatial filter optimisation for diatom recognition 80—48180
- medical tomography, image reconstruction of non-scalar parameters 79—66510
- memory systems, using Fourier transform hologram, alignment and design conditions 78—29901
- metal vapour pulsed lasers, quantum amplifiers, image distortion 79—18433
- metaxial optics, centred refracting systems, undiaphragmed and without aberration *(French)* 78—94369
- methods for optical system analysis 78—13665
- microprocessor-based optical/digital processor 78—63027
- microscope, scanning and conventional, Fourier imaging of phase information 80—73444
- microscope, with optical spatial filtering 78—58028
- microwave holography 77—54676
- mirror segment, parabolic, general Fourier transforming configuration 77—46687
- modular chirp Z transform equivalent to two-lens optical Fourier transform 78—78943
- moire-holographic fringes, differentiation by wavefront reconstruction with white light sources 79—86145
- Mueller matrix photopolarimetric meas., Fourier analysis of single detected signal 78—74048
- Mueller-Stokes matrix determ. using Fourier anal. 77—42496
- multichannel long integration time techniques 80—91751
- multidielectric spectral filters, synthesis and realisation *(French)* 78—74998
- multilayer synthesis program, Fourier transform model 79—7196
- multimode optical fibre bandwidth computation from refractive index profiles 79—76815
- multiple image form. by addition of optical signals 78—66776
- multiple imaging by lensless Fourier transform holography 79—81389
- multispectral size-averaged incoherent spatial filtering 80—33146
- n-dimensional FFT tomography applied to electromagnetic inverse scattering theory 80—9784
- Newton's formula validily in Fourier transform. config. 78—42281
- noncoherent methods 79—76624
- nonradiating partially coherent sources, scalar theory 79—64189
- numerical holography application 78—33692
- object reconstruction from Fourier transform modulus 78—74852
- object restoration and image extrapolation 79—50236
- object restoration beyond Rayleigh limit in presence of noise 80—102661
- object-plane Fourier processing with volume-hologram filters 79—94172
- one-dimensional Fourier hologram line data recording scheme *(Russian)* 79—22912
- one-dimensional linear coherent processing by single optical element 79—94165
- operator algebra description 80—48163
- optical computing, appls., review 77—10852
- optical data processing, appls., book 78—90388
- optical diffraction analysis, in microscopy 80—32926
- optical fibre diameter measurement using fast Fourier transform 80—91894
- optical imaging, systems theory appl. *(German)* 78—74851
- optical surface statistical properties and scattering angular dependence relations 79—50219
- optical transform masks, manufacture, model drawing programs 79—40334
- optics for electronic engineers *(Japanese)* 80—43272
- optimisation of inversion of convolution products 79—76601
- parallel optical Fourier transform techniques for Fourier spectroscopy 80—95161
- paraxial approx. of scalar diffraction theory without using Kirchhoff integral 80—95838
- partially coherent imaging, edge ringing, performance function 77—46699
- partially coherent object, coherence props. in image 77—34833
- particle motion detection in transparent liquids, Fourier transform acoustooptical system performance 80—87680
- pattern recognition, deformation invariant, space variant, book contrib. 79—76619
- pattern recognition, Fourier-Mellin transforms 77—10854
- pattern recognition, hybrid method, suboptimal statistical transform *(French)* 77—46703
- pattern recognition, Mellin transform method 78—63021
- pattern recognition by thermoplastic complex filter 80—99656
- pattern recognition of coal-workers' pneumoconiosis, optical-digital system 78—40389
- perceptual coding in the cosing transform domain 80—102635
- phase accuracy of Fourier processor, coherence effects 78—90377
- phase computation from intensity meas. 78—66768
- phase error model for simple Fourier transform lenses 78—71037
- phase measurement in real time using photodetector array, Fourier transform computation 80—9013

Fourier transform optics continued
- phase plate consisting of bleached holographic lens, for noise-free coherent imaging systems 79−31817
- phase problem in astronomy, sky brightness distrib. 80−46258
- phase problems, image recovery from Fourier transform modulus 78−82918
- phase recovery from single intensity distrib., using spatial filter 77−83825
- phase retrieval and polarisation identity 78−71042
- phase retrieval from intensity meas., uniqueness question 79−13915
- phase retrieval using zero information 79−76612
- phase shifter in hologram recording, deterministic phase code synthesis 78−37835
- phase values reconstruction from phase differences, matrix formulation 79−59642
- phase-frequency signal intensity characteristics *(Russian)* 79−94176
- photodichroic spatial light modulator for joint Fourier transform correlation 80−106617
- Photoelectric recording of optical fields by correlation processing 78−71048
- photoelectric registration of Fourier transform of optical field distrib. 78−82925
- photopolarimeter with rot. polariser and analyser for meas. Jones and Mueller matrices 78−54435
- plano-plano interferometer modes, FFT computation, Fresnel numbers 80−86392
- pockels readout optical modulator, for optical/digital processing systems 78−79125
- Pockels readout optical modulator, image and signal processing appls. 78−79123
- post-detection compensation for atm. distortion of faint scene images 77−45322
- power spectrum determination of random pattern, comparison between numerical and analogic processing methods *(French)* 78−58922
- profile digitised diffractographic data processing 77−58276
- projector having a thermoplastic target and operator's eye, characts. 80−96023
- pseudocolour encoding, of holographic imaging, new technique 78−78963
- pulmonary venous pressure estimation from routine chest radiographs using hybrid optical-electronic system 78−44657
- pulse shaping and compression using electrooptic deflector with Fourier optical elements 80−53421
- qualitative and semiquantitative Fourier transformation using a noncoherent system 80−5698
- quartz, far IR ordinary-ray optical constants 80−45025
- quasi-monochromatic incoherent optical image processing 79−76626
- radar, synthetic aperture system, coherent optical simulation 77−27260
- radar ambiguity function, optical processing techniques 78−78938
- radar ambiguity function display and one-dimensional correlation/convolution by coherent optical processors 78−78950
- radiative transfer problem soln., limitations of approx. Fourier techniques 80−37952
- radio-holograms, complex one-dimens. Fourier, recording and processing *(Russian)* 77−19207
- radioastronomical aperture synthesis imagery data optical reconstruction 78−69702
- radiographic 3D imaging with a restricted view angle 80−17066
- radiographs, signal and graininess relationship 80−95808
- radionuclide tomographic image reconstruction, optical processing 77−73572
- real 1D signal convolution and correlation by freq. plane filtering 80−32919
- real-time incoherent subtraction of irradiance 80−74301
- real-time optical Fourier spectrum analysis using acousto-optic diffr. 78−5430
- real-time recognition of microscopic phase objects 79−7085
- reconstruction, three-dimensional, from planar projections 80−99639
- reconstruction from projections via deconvolution 79−55070
- regularization in Fourier-synthesis 2-D image reconstruction 79−74748
- regularized object restoration, resolution beyond the diffr. limit 80−87324
- repetitive image visibility, two-dimensional Fourier spectrum description 77−58282
- resonators, unstable, Fourier transform spline soln. to deal with sharply cut off fields at mirror edges 79−94263
- restoration, of optical objects using regularisation 78−78929
- rotating wedge spatial filter, pattern recognition of biological speciemens (algae) 78−33837
- rough surface power spectrum measurement 80−36989
- sampling theorems in polar coordinates 80−28169
- satellite derived cloud imagery, optical Fourier transform anal. 78−85749
- SAW and optical signal processing techniques compared 80−48173
- SAW delay line acousto-optic signal processing devices 79−94328
- Sayce test patterns, structure and spatial freq. spectrum 80−1136
- scanning microscopes, partially coherent and confocal, imaging of periodic structs. 80−5700
- scatterplate interferometer, energy distrib., Fourier optics approach 80−31850
- scatterplate interferometer, scalar diffraction theory 80−73432
- scatterplate interferometer principles, limitations and tolerances 80−73436
- schlieren system, phase object projection, imaging characts., recording conditions 78−25977
- self-image techniques, optical computing 80−18998
- self-imaging, light-optical experiments *(German)* 80−63938
- self-imaging of plane periodic objects, Fourier image theory 79−81379
- self-imaging process, partially coherent light effects *(French)* 77−23621
- sharpness criterion, rel. to redundant spacing interferometry 78−5427
- signal detection, optical vs digital Fourier transform computers 79−27181
- signal detection methods, optical/digital components evaluation in hybrid processor 78−63026
- signal processing in integrated optical format 78−50950
- sine condition derivation via Fourier optics 79−98297
- skeletal muscle disease, Fourier optical evaluation of histopathologic findings 77−37091
- sky image coherent-optical processor for moving object location 78−78944
- space variant optical transfer with Fourier filter in extrapupilar position 77−10846

Fourier transform optics continued
- space variant processors using coordinate transforms 77−88649
- space-variant linear processing of 1D signals 77−42490
- space-variant processing of 1D signals, direct output and output spectrum displays 77−42491
- spatial coherence analysis using reversing front interferometer 78−277
- spatial convolution and correlation of optical fields via degenerate four-wave mixing 78−71044
- spatial filtering, real time operations on spectral and temporal envelopes 78−22093
- spatial filtering for obtaining first and second order derivatives 77−27259
- spatial filtering of Fourier transform of half-tone picture using photographic replica 79−27184
- spatial filters, square root type phase image differential linear intensity output digital simulation 78−33839
- spatial filtration in coherent optics system *(Russian)* 80−28164
- spatial frequency analysis of Fourier and Fresnel images *(German)* 77−79764
- spatial frequency sampling by phase modulation, multiple image generation 77−79759
- spatial power spectra estimation in speckle interferometry S/N ratio calc. 79−76608
- speckle applications to correlation and information processing 77−19189
- speckle axial structure, Fourier description 79−72494
- speckle imaging phase estimation, FFT-based algorithm 79−76605
- speckle interference fringes, lens aberration effects 80−105700
- speckle interferometry, lens aberration effects, optical system pupil complex amplitude changes *(French)* 79−50237
- speckle patterns, photographic recordings, fringes generated in Fresnel plane 78−66763
- speckle shearing interferometer for studying aberration of optical system *(French)* 77−65616
- speckle technique, for meas. of out of plane tilts 77−13735
- spectral intensity filtering for image recognition 78−46529
- spectral interpolation by zero fill or convolution 78−25803
- spectral-temporal effects, white-light interferometry and phase-locked pulse anal. 77−88656
- spectrum analyser, energy spectrum smoothing using multimode laser radiation 78−55311
- spectrum analyser for radar signal processing 78−78942
- spherical-cylindrical lens combination, combined 1-D image-orthogonal Fourier transform processing 80−58658
- spherically symmetric objects, reconstruction from slit-imaged emission, appl. to spatially resolved spectroscopy 78−78930
- stack of dielectric layers, Fourier description of analysis and synthesis operations 78−94449
- statistical reversal methods of linear transforms. *(Russian)* 78−1179
- stellar interferometer, imaging using aperture synthesis 79−58244
- stochastic image restoration procedure 77−10858
- surface acousto-optic lens, Fourier and Mellin transform props. 78−78926
- surface layer, reflection related to density profile Fourier transform *(Russian)* 78−31269
- surface roughness measurements by means of polychromatic speckle patterns 80−31708
- surface roughness measurements using optical Fourier spectrum analyzer 79−49195
- surface scattering rel. to microroughness, surface transfer function 78−58917
- surface-wave acousto-optic signal processors 80−102640
- synthetic aperture radar image coherent-optical simulation 77−50632
- synthetic ternary-complex Fourier holograms *(German)* 77−58293
- systems analysis using two-dimensional FFT algorithm 80−78986
- teaching, diffr. and spatial filtering 77−57120
- thermoplastic-photoconductor films for optical data processing 78−50875
- thin film rib waveguide, numerical anal. by mode-matching method 80−48421
- threaded article parameter measurement by spatial spectra analysis 79−30409
- three-dimensional image reconstruction, direct Fourier transform techniques 77−12986
- three-dimensional imaging by coded aperture and shadow casting techniques 79−74757
- tomography, transaxial scanners for reconstructing objects from their X-ray projections, review 80−102632
- transaxial topography, optical method, optical fibre, refr. index meas. *(French)* 78−66778
- tuning fork for clock, vibr. anal. using speckle method 79−21737
- turbid medium, infinite plane wave, mutual coherence function propag. 78−1163
- two dimensional unitary transforms for image processing 78−58928
- two-dimension Fourier holograms recorded and decoded in polychromatic light 80−37970
- two-dimensional, props., image sampling/scanning appl. 78−58929
- two-dimensional acoustic processor 79−72514
- two-dimensional Gauss-Markov field, pinned Karhunen-Loeve transform 77−83827
- two-dimensional photoacoustic image processing with longitudinal waves 79−50244
- two-dimensional program, for image processing system *(Japanese)* 78−9330
- two-dimensional structure in-plane vibr., stress analysis by laser speckle method 80−103006
- undersampled images, bounds on errors in reconstruction 79−89858
- underwater US video system *(German)* 78−94471
- uneven interface of media with different refractive indices, statistical characts. of images 80−87331
- US blood flow spectral anal. using coherent optics 78−53459
- US image processing device status and prospects 80−48446
- US lateral and range resolution improvement by optical computer 79−53203
- Vander Lugt filter, effect of recording errors 77−23624
- variable-scale single-lens optical transform systems 80−58656
- virtual Fourier transform as analytical tool, appl. to single lens processing system 78−71036
- vision model using optical engineering theory concepts 79−96555
- visual perception, spatial Fourier transform model 79−11940
- visual prosthetic device, bioengineering and biomedical aspects of focal surface model 78−48942
- Walsh functions in polar co-ords., appls. 77−23626

Fourier transform optics continued

- wave field three-dimensional energy distrib. 78−71009
- white light speckle method of experimental strain analysis 79−37255
- Wiener image filtering, object fast restoration after PSF degradation 78−90379
- Wigner distrib. function and Hamilton's characts. 80−1143
- Wigner distribution function and its application to first-order optics 80−37958
- Wigner distribution function applied to optical signals and systems 78−50713
- Wigner distribution function display using coherent optical processor 80−48160
- X-ray systems for 3-D imaging, MTF 77−40851
- xerographic image, measurability of structure fluctuations 77−18119
- Zernike's three-slit interferometer, Fourier optical synthesis 78−65960
- CO_2 laser Antares fusion system optical diffraction computation 80−74424
- CO_2 laser fusion system optical design and analysis 80−74391
- CdS film SAW two-dimensional image processor 77−39164
- CdS-$LiNbO_3$ monolithic two-dimensional Fourier transformer 79−72516
- CsD_2AsO_4 Fourier transform plane superposition multiplier, for optical processing 79−7084
- $LiNbO_3$ acousto-optical SAW interaction multicolour image scanner 77−58483
- $LiNbO_3$:Fe electro-optic crystal holographic storage data error probability 80−43304
- Nd:glass laser, with metallic grating in cavity, Fourier spectrum and periodic mode fields distrib. *(Russian)* 79−31915

Fourier transform spectroscopy

- absolute IR intensities, Fourier transforms spectrosc. obs. 79−93993
- absorption cell for heated gas IR spectroscopy 80−98987
- absorption meas. method 79−49300
- air pollutant gas detection by dye laser and Fourier transform method 79−57558
- air pollutant measurement by absorption spectrum Fourier transform 80−81514
- air pollution measurement 78−61564
- airborne IR astronomical obs. 78−61747
- alcohols, OH-stretching vibr. band in overtone region, IR-Fourier spectral investig. *(German)* 80−976
- aliasing distortion in power spectra, digital processing of interferograms 77−45904
- alkali halide, ReO_4^- doped, saturable absorber at 10.6 μm 80−53384
- analytical chemistry, IR spectroscopy appls. 78−61092
- aperture distortion correction methods *(Russian)* 77−82615
- apodisation, optimal, Fourier spectrometry 80−99641
- aromatic hydrocarbons, in airborne particulates, gas chromatography/mass spectrometric, NMR analyses 77−13116
- astronomy, Doppler broadening parameters and Doppler shifts meas. without spectrograph 78−20646
- atmospheric emission obs. by Fourier transform IR spectrometer *(Japanese)* 80−12541
- atmospheric IR laser beam transmission 77−70873
- atmospheric pollutant detection, spectral interfernece correlation method 79−8727
- atmospheric pollution, SO_2 detect., interferential spectrum correl. *(French)* 79−21059
- atmospheric reactions, IR Fourier transform spectroscopic obs. 79−66785
- atmospheric spectroscopy, transmittance calc. 80−12555
- atmospheric submillimetre spectrum meas. 77−87133
- atmospheric submillimetric-wave interferometric spectrometry 79−34979
- atmospheric transmission meas. using IR lasers and Fourier spectroscopy 77−70885
- atomic spectrochemical measurements using Michelson interferometer Fourier transform spectrometer 78−3399
- background spectral radiance and contrast in the 1.5 to 13 micrometer region 79−8694
- benzyl alcohol, C-C spin coupling, two-dimens. Fourier transformation 78−90194
- Brownian motion and NMR spin relax., book 78−15054
- capillary column gas chromatography at nanogram resolution using dual beam Fourier transform IR spectroscopy 80−89554
- cervical smear screening with coherent optical processing 77−21653
- cholesterol, proton-coupled ^{13}C NMR spectrum, double Fourier transform 78−78725
- coal, cleaved surface, photoacoustic IR spectra 80−87104
- coal and mineral content characterisation by Fourier transform IR spectroscopy 80−104474
- complex biological systems, Fourier transform. IR obs. 78−68945
- complex systems, pyrolysis and combustion charact., Fourier transform IR spectroscopy 80−86462
- composite transparent film layer thickness meas. 77−10093
- computer coupled, high data rate spectrometer system *(German)* 79−49212
- computerised vibrational spectroscopy, using piezoelectric polymer transducers 78−29105
- concentration fluctuations, chem. species in unsteady flow, Raman spectrosc. obs. 79−66379
- conference, Columbia, USA (June 1977) 78−58067
- convolution Fourier transform ion cyclotron resonance spectroscopy 79−75648
- COOB, solid state dimorphism and cryst.-smectic transition, Raman study 80−45063
- correcting errors in optical path difference, computational method 78−70192
- coupled spin systems, multiple quantum transitions, excitation, detection, Fourier transform multiple quantum NMR 80−31819
- cyclopropane, adsorption on Pt, NMR and PMR obs., chem. shift 77−51591
- cytidine, pulse Fourier transform proton mag. resonance, equivalent to CW INDOR 77−32293
- data handling, minicomputer appls., errors 78−92543
- deconvolution of spectral lines, improved method 79−97439
- delay compensation, sampling error reduction 79−30566
- demonstration for students 78−57722
- dichlorodifluoromethane, study of ν_6 fundamental 79−31526
- dichroism, linear and circular, Fourier transform spectroscopy-differential interferometery meas. 79−71514

Fourier transform spectroscopy continued

- dielectric spectrometer, in vivo, for tissue dielec. loss and permittivity meas. 79−57743
- differential absorption at high modulation frequencies using a Fourier transform infrared spectrometer 80−95160
- diffuse reflectance, FT IR spectrometric meas. 79−35858
- diffuse reflectance Fourier transform IR spectroscopy using diamond anvil cell 80−101855
- digitisation noise in Fourier transform IR spectroscopy and gain ranging 79−97448
- dimethylamino radical$+O_2(NO)(NO_2)$, reaction rate constants, FTIR obs. 80−16652
- dispersive, appl. to gases, liquids and solids, bibliography 79−58806
- dispersive, measurements using liquid He cryostat 79−54135
- dispersive, millimetre and submillimetre wavelengths, low-loss materials dielec. meas. 77−37916
- dispersive, mode of operation of polarising interferometer 78−78003
- dispersive, phase errors 77−45902
- dispersive, submillimetre wave, with variable thickness variable temp. liquid cells 77−37915
- dispersive, with liquid cells of varying thickness and temp. 77−38039
- dispersive Fourier transform spectroscopy, lossy liq., far IR 77−2700
- dispersive Fourier transform spectroscopy, phase spectra determ., role of origin of computation 79−30567
- dispersive measurement of opaque solid at 6K 79−2841
- dispersive refl. Fourier interferometer, sample holders for use at 4.2K and 300K 79−30587
- dispersive reflection spectroscopy using commercial Michelson interferometer 77−45903
- dispersive reflectivity meas. on highly absorbing solids, using modular interferometer 78−89568
- dispersive-reflection spectroscopy at liq. He temps. using Michelson interferometer 80−31910
- DNMR, multiple-quantum, tickling 80−23446
- Doppler spectroscopy, appl. to reactive collisions 79−80692
- double beam weighting 78−29169
- double resonance NMR, two- and three-spin systems 78−80249
- double-beam, with interferometric background compensation 77−38038
- double-beam spectrometer, for weak IR absorpt. meas. 80−105725
- double-pass rapid-scanning spectrometer, for plasma diagnostics 80−103190
- education, Fourier transform interferometry, visible reflectivity spectra 77−33765
- electron spectroscopy, deconvolution methods, review 79−26188
- electron spin echo envelope modulation, 2-dimens. Fourier transform 80−63680
- encoding figure of merit, Hadamard transform comparison 77−5922
- energy dispersive X-ray spectra, anal., computer techniques 79−43690
- errors, due to mirror oscills. in spectrometer, mathematical corrections *(Russian)* 77−87849
- ESR spectra, simulation by FFT 79−19763
- far IR, appls. in laboratory, industry and environment 78−58069
- far IR, meas. techniques and data reduction methods 78−62240
- far IR, spectrum distortion by multiple reflections using Michelson interferometer 80−82837
- far IR absorbent solid dispersive reflection meas., using Fourier spectrometer and cryostat 79−30580
- far IR and near MM wave power energy meter calibration 80−57373
- far IR atmospheric emission and absorption spectrum calc. program 79−35020
- far IR dispersive Fourier transform spectroscopy, complex refr. index determ. of solids 78−92042
- far IR Fourier spectrometer automation *(Russian)* 79−6192
- far IR Fourier spectroscopy, attainment of high resolution 78−86361
- far IR Fourier transform spectrometry improvements 79−30582
- far IR interferometer for obtaining Fourier sine transform of spectrum 79−97422
- far IR interferometry, (1950-76) 78−4456
- far IR modular Fourier interferometer construction, very high resolution 80−57401
- far IR transparent solid dispersive transmission meas., using Fourier spectrometer 79−30581
- far IR-submillimetre range, Fourier and laser spectroscopy comparison, meas. in V_3Si film 79−93237
- fast-scanning Fourier spectrometer automatic adjustment method 79−80705
- fast-scanning Fourier spectrometer with electrodynamic drive 79−75630
- field meas. Fourier transform spectrometer 80−86470
- finite zero filling, error estimates 80−37061
- fixed groove depth lamellar grating Fourier transform spectrometer 80−77885
- fluid, three-body correlation determ., heterodyne coincidence spectroscopy 77−10118
- fluoromethane, gas, optical rotary saturation 79−27338
- formic acid, vibr. states, rot. and Coriolis parameters IR Fourier transform spectra 80−32709
- formyl radical, atmospheric oxidation, IR Fourier transform spectroscopic obs. 79−66785
- Fourier transform ion cyclotron double resonance, complicated ion-molecule reactions 78−80808
- Fourier transform NMR spectroscopy, review 80−104486
- Fourier transform spectroscopy, Doppler-limited high-accuracy, 10^6 samples 78−58068
- FT NMR, digitisation and data processing 80−95115
- FTNMR, effect of inhomogeneous mag. field on line shape and resolution enhancement 79−63289
- full photon counting Rayleigh spectrometer, minicomputer system using autocorrelation or FFT 78−41351
- gamma-ray spectral anal. using FFT *(Japanese)* 78−90047
- gas cell, multiple-path, for Fourier spectrometer, small f-number optics 79−58805
- gas chromatographic effluents, FT IR spectrometric identification 78−73091
- gas dispersive Fourier transform spectrometry, using modular interferometer 78−89567
- gas phase IR absorpt. spectrometry, 714-1667 μm 77−83765
- gaseous pollutants, remote meas. using mobile Fourier transform interferometer 80−12043
- gases, high resolution vibr. spectra by Fourier transform far IR spectroscopy 80−86461
- ghostline intensity in far IR 80−73480

Fourier transform spectroscopy continued
glass fibre reinforced plastics, coupling agent/matrix interface investigation by Fourier transform IR spectroscopy 80—20884
haloalkyl peroxy radical+NO_2, haloalkyl peroxynitrate form., FT IR obs. 79—34283
heavy water optical constants, 70 to 450 cm^{-1}, reflection dispersive Fourier transform spectrometric obs. 77—40203
high resolution spectrometer, 0.005 cm^{-1}, for 0.6 to 100 μm spectral range 78—70204
high-resolution NMR by double Fourier transform, chem. shift and spin echoes 77—57375
hologram spectrograph, parameters 78—37858
INDOR, pseudo, heteronuclear selective decoupling, automatic, using Fourier transform NMR spectrometer appl. 79—93185
industrial IR analysis using Fourier transform spectrometer 78—61091
interference spectrometric detection of atmospheric pollutants 80—35813
interference spectroscopy, Fourier decomposition technique appl. 77—49784
interferograms, dispersive two-beam, computation 79—97424
interferograms, effect of random errors in sampling interval on spread function of Fourier spectrum 80—18020
interferograms, undispersive two-beam, computation 79—97423
interferometer, two beam, comparison of refl. and refr. optics in condensing element 78—77968
interferometer drive nonlinearities effect 77—61127
interferometric data from GC Fourier transform IR spectroscopy, functional group anal. 80—89548
interferometric IR spectrometer, performance evaluation 78—29181
interferometric microwave spectroscopy, modern aspects, book contrib. 80—52330
interferometry, imperfect blackbody sources effects 77—38032
interferometry, multimode fibre optic, applications 80—86387
iodomethane, liq. (liq. mixtures), vibr. relax. and reorientation, symmetric C-H bending mode 1st overtone 78—62884
ion + molecule, elastic collision frequency, determ. by Fourier transform ICR spectroscopy 79—50105
ion cyclotron reson. mass spectroscopy, freq. sweep excitation 80—101810
ion cyclotron resonance spectroscopy 79—2877
ion resonance spectroscopy of ions undergoing collisions with mols. 80—35598
IR, absorbance compensation technique, anal. appls. 78—74083
IR, chem. and environmental anal. appls. 78—20100
IR, choice of radiation source 80—27362
IR, dual beam Fourier transform spectrometer, sensitivity improvement by using Digilab 496 interferometer 80—90910
IR, dynamic range improvement 78—89565
IR, emission optimisation for nearly transparent gases 77—5931
IR, factor anal. appls. 79—96378
IR, focal shift photometric errors 78—86358
IR, for space appl., thermal behaviour *(German)* 79—35091
IR, immersion microsampling technique 78—12777
IR, Jacquinot (throughput) advantage, limitations 77—82626
IR, least squares curve fitting, appls. to polymer systems 78—15726
IR, matrix isolation appls. 78—45740
IR, pharmaceutical anal. quality control 79—97449
IR, real-time, for liq. chromatography detect. system 78—86357
IR, scatter eliminated spectrometry 78—89564
IR, signal to noise ratio meas. 77—49790
IR, variable field of view techniques 77—40586
IR absorption technique for airborne atm. comp. meas. 78—61604
IR astronomy applic. 78—16309
IR complex refr. index spectra, FT interferometry, errors in liquid-cell expts. 77—87814
IR detector with gas chromatograph collects, stores spectral data, monitors functional groups 78—92560
IR diffuse reflectance, Fourier transform spectrophotometer 77—5929
IR diffuse reflectance spectrometry, spectrochemical anal. appl. 79—34387
IR Fourier spectrometers, grid polarisers 80—105724
IR microspectrophotometer for surface anal., lubrication problem appls. 80—13162
IR molecular investigations using UFS-01 high-resolution Fourier spectrometer 79—35862
IR spectra, interference fringe elimination, computer method 79—12872
IR spectra differentiation using Fourier transforms 79—67397
IR spectra of magnetic materials, apparatus for absorption meas. by Fourier transform 77—177
IR spectrometer, dual beam 78—70201
IR spectrometer, for satellite, optical design problems *(German)* 78—86360
IR spectrometer, radiation source stability *(Russian)* 79—26150
IR spectrometer, sensitivity 78—74082
IR spectrometer for balloon-borne telescope, lamellar grating type 78—16294
IR spectrometer software package for phase correction 80—95162
IR spectrometers, dispersion and FT interferometric types, comparison 77—82624
IR spectrometers, spectral compensation, instrument line shape and resolution effects 79—40631
IR spectrometers history, current status and commercial future 78—58072
IR spectrometry, absorbance subtract, wedging errors diagnosis and correction 80—11967
IR spectrophotometer, underlying principles 80—36812
IR spectrophotometer *(Japanese)* 79—75627
IR spectrophotometers, grating and FT types, rel. advantages of interferometers and monochromators 78—16861
IR spectroscopy, microscopic technique for sub-ng level anal. 78—32901
IR spectroscopy, multiple order spectra 77—74527
IR spectroscopy, use in atm. chem. 80—55743
IR spectroscopy, use in polymer research as vibr. spectroscopy tool 80—55744
IR system, km pathlength, for trace pollutants detect. and meas. 79—5624
IR technique, for in situ identification of TLC spots 78—15727
IR transmission spectroscopy, appl. to natural and model membrane study 80—17218
IR vibrational circular dichroism 79—99845
Ku-band microwave Fourier transform spectrometer, construction, appls. 80—68265

Fourier transform spectroscopy continued
lamellar grating Fourier spectrometer for sub-mm and mm spectroscopy *(Japanese)* 77—67504
lamellar-grating spectrometer, high resolution, for submm. region 78—70203
laser time resolved spectroscopy 78—303
laser wavelength calibration using optogalvanic effect, atlas 80—62727
Lau effect, diffr. expt. with incoherent illum., appl. to Talbot interferometer, Fourier spectrometer 79—41333
light divider phase distortion compensation improvement 78—58073
light pipe gas cell, Au coated internally, for gas chromatography/Fourier transform IR spectroscopy 80—89555
line deconvolution by Fourier analysis 79—12861
line narrowing, selective population transfer induced 80—31827
linear motion gas bearing for Fourier spectrometers 80—31893
linuron, herbicide, interaction with soil, Fourier transform IR spectra 77—9142
liquid chromatography, high performance, direct-coupling to FT-NMR 79—34412
liquid chromatography effluents on line anal., micro liq. chromatograph-interfaced Fourier transform IR spectrophotometer 80—73483
liquid crystal, thermotropic mesophase, DMR chain segments assignment 80—24356
liquid crystals, protonated multiple quantum transitions, excitation detection, Fourier transform multiple quantum NMR 80—31819
liquid dielec. permittivity meas., sub-mm wave, using laser- and Fourier transform-spectrometry 78—95568
lyo-mesophases, induced chem. shift, NMR obs. 79—33548
lysozyme, spin echo and spin lock ^{13}C Fourier transform NMR 79—43824
Martin-Puplett interferometer, use as Fourier spectrometer and for OTF meas. 78—70179
matched filtering, real time spectral recognition 78—37822
MBBA, ^{13}C spin-lattice relax., Fourier-transform NMR, NOE 78—48064
methane, $\nu_1+\nu_4$ vibration-rotation spectrum, spectroscopic constants *(French)* 79—13709
methanol, vap., rot. spectrum, 8-50 cm^{-1}, 293K 79—72305
methyl alcohol submillimetric high-resolution Fourier transform spectra 79—31509
methyl chloride submillimetric high-resolution Fourier transform spectra 79—31509
methyl cyanide submillimetric high-resolution Fourier transform spectra 79—31509
Michelson Fourier spectrometer modified for far IR spectroscopy 78—45741
Michelson Fourier transform stellar spectrometer 80—98552
Michelson interferometer, all-refl., for far IR Fourier spectroscopy 78—70205
Michelson interferometer, tilt-compensated, for Fourier transform spectroscopy 79—9239
Michelson interferometer for Fourier transform IR spectroscopy 78—49914
Michelson interferometer misalignment nonlinear phase errors 79—30535
Michelson type Fourier interferometer and gaseous molecular spectra 80—68275
Michelson-Fourier transform spectrometer for night airglow visible spectra 80—36424
microreactor assembly to study heterogeneous catalyst system, IR emission spectra anal. 80—98988
mixture chemical analysis, direct interferogram comparison of chromatography/Fourier transform IR spectra data 79—100458
modular interferometer for FT spectroscopy in far IR 77—82629
modular Michelson interferometer for Fourier transform spectrochemical meas. 78—29177
molecular crystal, Stark modulation of Lorentzian line shapes, Fourier anal. 77—1691
molecule, large, ^{1}H spin-spin coupling consts., accurate meas. method 79—31555
molecules, 3-dimens. scatt., vel.-angle distribs., Fourier transform Doppler spectroscopy 77—49776
molybdates, ^{95}Mo and ^{97}Mo Fourier transform NMR, chem. shifts and Larmor freqs. *(German)* 77—59473
multichannel long integration time techniques 80—91751
multiplex advantage, conventions and values 78—32882
multiplex advantage, Hadamard transform comparison 78—32883
multiplex and high throughput spectroscopy 80—95145
narrowband optical signal, spectral width estimation 80—102627
natural rubber latex ^{13}C NMR spectra 80—15816
nematic liquid cryst., one-deuteron system, multiple quantum spin-echo spectroscopy 80—31832
neopentane adsorbed on graphite, quasi two-dimens. fluid, NMR 80—102525
neutron Fourier TOF spectroscopy, influence of higher harmonics in chopper modulation function 77—6609
neutron spin-echo integral transform spectroscopy 80—4748
new developments—passive heterodyne spectrosc. and diode laser absorpt. spectrosc. 80—95148
NMR, clipped free induction decay signal anal. 77—63976
NMR, commercial spectrometer modification for rot. frame spin-lattice relax. meas. 80—22407
NMR, computer appl. *(Czech)* 80—17984
NMR, computer programmable digital pulse generator 80—98959
NMR, digital quadrature detect. 78—24833
NMR, double quantum, operator formalism 78—2750
NMR, fully automatic soft ware correction 77—43891
NMR, line-broadening mechanisms, dispersion-absorption plots 78—89512
NMR, pulse system, commercial waveform analyser use 80—17977
NMR, pulsed field gradient system 80—57353
NMR, resolution enhancement, digital filtering by sinusoidal window 79—93195
NMR, resolution enhancement by digital filtering with sinusoidal window function 77—18060
NMR, resolution enhancement using double exponential function 79—35804
NMR, rot. frame, ^{13}C spin-lattice relax. using proton decoupled Fourier transform spectra, errors origin 80—18945
NMR, rot. frame spin-lattice relax. in presence of off-reson. RF field 79—93193

Fourier transform spectroscopy continued
- NMR, S/N ratio optimisation, influence of receiver circuit and digital processing *(Czech)* 79—17461
- NMR, selective excitation, theory and appls. 78—77953
- NMR, selective excitation with single-freq. off-reson. decoupling 80—17981
- NMR, small signals meas. in presence of intense peaks 79—93196
- NMR, standard spectrometers use for multicomponent self-diffusion meas. by spin echo 80—22401
- NMR, two-dimens., sensitivity, comparison with one-dimens. FT NMR 78—78724
- NMR, two-dimens. spin-echo spectra, anomalous spinning sidebands 80—17976
- NMR, water-eliminated, WEFT, modified pulse sequence technique 77—26373
- NMR chemical shift between two sites in rapid exhange limit, Fourier transform method 79—24743
- NMR Fourier transform spectroscopy, free induction decay, resolution enhancement function 79—80656
- NMR meas. of spin-lattice relax. time by variable nutation angle method 77—49757
- NMR multiple-quantum transition orders separation, using pulsed field gradients 80—50222
- NMR of ^{13}C, modified DEFT pulse sequence use 79—93191
- NMR recording, of low gyromag. ratio nuclei, by mag. coherent transfer technique 77—90068
- NMR sensitivity improvement for spectrometer using double-tuned receiver coil 80—31824
- NMR spectra, flip angle depend., pulse cascade description 80—28036
- NMR spectral phase and intensity anomalies reduction for Varian XL-100 spectrometer 77—45873
- NMR spectral segments, Fourier transform interpolation 77—26374
- NMR spectrometer, magic-angle rot. 80—105688
- NMR spectrometer, TESLA BS 497 adaption *(Czech)* 79—6157
- NMR spectrometers, time-sharing control by minicomputer 79—93192
- NMR spectroscopy, high-field, of biological systems 79—39457
- NMR spin echo, rotating solid sample, Fourier transform anal. 79—65759
- NMR spin echo two-dimensional J spectroscopy, suppression of spurious signals 78—15057
- NMR thermometer, for multinuclear Fourier transform NMR 80—57292
- noise compensation, using improved InSb photodiode preamplifier circuit 80—73474
- noise levels in broad band absorpt. spectrometry 77—45901
- noise reduction by averaging over optical path 77—18080
- nonlinear processing of interferogram 78—89553
- nonuniform samples, Fourier transform IR spectroscopic meas. 78—15730
- NQR, electronics appls. 80—63668
- nuclear spin-lattice relax. time meas. using single-scan Fourier transform method 77—20741
- nuclear spin-lattice relaxation meas., variable nutation WEFT, biochemical appl. 80—20482
- O-B stars, Fourier transform spectroscopy in 4800-10200 Å range 79—16993
- optical pulse Fourier transform spectroscopy, coherent transients 78—86974
- optical pulse Fourier transform technique 77—26405
- organosilane coupling agent interphase of glass-fibre reinforeced plastics, molecular organisation 80—44195
- Orion Nebula, near IR Fourier spectroscopy 77—57071
- oxide crysts., Fourier transform Ir spectroscopy of vibr. states at high temp. 80—97256
- parallel optical Fourier transform techniques for Fourier spectroscopy 80—95161
- PBLG solns., dielec. meas., using pseudorandom noise dielectric spectrometer 78—15084
- pentachlorotoluenes, positional isomers, ^{13}C Fourier transform NMR spectrometry, struct. and compositional anal. 80—91576
- photoacoustic FT IR spectroscopy of liquid and solid samples 80—90911
- photoacoustic rapid-scan Fourier spectroscopy and methyl alcohol interferograms 79—30585
- photoelectron spectra, lineshape transformations for Fourier transform resolution enhancement 77—90250
- photon and detector noise quantitative limit, definition *(German)* 80—9049
- planetary atmosphere, remote sensor, high resolution Fourier transform spectropolarimetry 78—57469
- plasma device, JIPP T-II, electron cyclotron emission meas. using double-pass optical spectrometer 80—54035
- plasma proteins adsorbed on polymer surface, Fourier transform IR spectrometry 80—16899
- PMMA, atactic, FT IR spectrum, ^{18}O substitution effects 80—23581
- polarising submillimetric Fourier interferometer with achromatic internal modulation 78—65959
- poly(ϵ-caprolactone)-PVC system, Fourier transform infrared spectroscopic exam. 80—25361
- poly(tetramethylene tetraphthalate), IR studies of α crystal phase 77—62486
- polyacrylonitrile, thermal degradation, Fourier transform IR obs. 78—92474
- polybutadiene, C black filled, struct., Fourier transform IR obs. 77—50571
- polycrystalline material, crystallite size distrib., X-ray diffr. determ. 77—27777
- polyethylene, brominated, single cryst., IR analysis 80—25362
- polyethylene, linear, glass transition temp. upper limit, ^{13}C Fourier transform NMR 79—14918
- polyethylene single cryst., FT IR spectra, CH_2 rocking mode 78—2843
- polyethylene single cryst., FT IR spectra, CH_2 wagging mode 78—2842
- polyethylene single crystal in suspension, Fourier transform IR study 78—10877
- polymer film, formation, time-lapse IR spectroscopic obs. 79—74458
- polymer system, Fourier transform IR spectroscopy appl. 78—58870
- polymethylacrylate, tacticity from peak-eliminated Fourier transform NMR 77—563
- polypropylene, Fourier transform IR study of ordered and amorphous phases 78—27225
- polystyrene, atactic, stereoregularity study using Fourier transform IR spectroscopy 79—59612

Fourier transform spectroscopy continued
- polystyrene, atactic, uniaxially oriented, Fourier transform IR spectroscopic exam. 80—25360
- polystyrene, isotactic gel film, Fourier transform IR spectrum 80—104465
- polystyrene, stress cracking, pressure-induced, mechanism 80—35361
- polystyrene amorphous film, cyclically fatigued, molecular behaviour 80—35310
- polystyrene film, Fourier-transformed IR photoacoustic spectra 80—34993
- potassium palmitate-d_{31}, spin-lattice relax., chain position and temp. depends. 78—68405
- power transmission spectrometry, use of approx. expressions 80—98982
- propylene ozonide formation mechanism, Fourier IR spectra 77—33132
- pseudocolour density encoding, white-light, using contrast reversal 80—83560
- PTFE, γ-ray effects on 19 and 30°C phase transitions, Fourier transform IR spectroscopy 80—103387
- pulse Fourier transform NMR, vomplex spin system nonequilib. state, Liouville space description 78—48057
- pulse Fourier transform NMR, weakly coupled complex spin system 78—48058
- pulsed Fourier transform NMR spectroscopy resolution enhancement, multiple pulse technique 79—40595
- pulsed NMR methods, analogue Fourier transform calculations 80—47085
- pulsed NQR, automation for Zeeman studies of single crystals 80—66066
- purple membrane, polarized IR spectroscopic struct. study 79—43809
- PVC, thermally induced conformational changes, Fourier transform. IR spectroscopy 78—9287
- quantitative IR spectrometry, matrix isolation microsampling procedure 79—100460
- Raman, signal modulation within elec. bandpass 78—82041
- rapid scan, use of opto-acoustic effect 78—78004
- rapid scanning, very high resolution, data processing aspects 80—95150
- rapid scanning Fourier transform time resolved spectroscopy, practical aspects 80—86464
- real Fourier spectrometer, spread function determ. 80—31892
- reflection dispersive Fourier interferometer window eliminating backlash error 80—57402
- remote identification of solids in solar system, Fourier transform spectroscopy appls. 77—87273
- resolution limits 77—2701
- resolution of 0.010 cm^{-1} by Fourier spectrometer, 20 to 1200 cm^{-1} 79—75603
- resolution of Fourier spectrometer, determ. using solid-state Fabry-Perot etalon 78—89569
- $tRNA_{yeast}^{phe}$, Fourier transform PMR in aq. soln., ^{1}H exchange and relax. rates meas. method 78—15049
- S/N ratio 78—32885
- satellite methods and problems *(German)* 80—36477
- satellite problems, mechanical disturbance effects on optical elements *(German)* 80—36478
- scanning interferometer designs 79—75612
- secondary interferograms, effect on reconstituted spectra *(French)* 78—82043
- selective modulation interferometric spectrometer, theory, design 78—58054
- silane, coupling agent on E-glass fibre, structure, Fourier transform infrared spectroscopy 78—60643
- silane, coupling agent on porous silica, Fourier transform infrared spectroscopy 78—60642
- single-channel quadrature detection, improvement of technique 77—45875
- sinusoidal interference modulation and path difference control *(Russian)* 78—29176
- SNR enhancement by elec. filter compensation of slide velocity errors 80—95151
- solar spectra, Fourier transform spectroscopy at South Pole 80—98448
- solid dielectric complex and power reflectivity determ., 100 GHz to 3 THz 80—15999
- solid mixture charact. discrete fourier transform, spectroscopy, computer simulation 78—63859
- solid/gas interfaces, in situ Fourier transform IR spectroscopy 80—37100
- solids, IR photoacoustic Fourier transformed spectroscopy 80—86465
- specimen holder for transmission dispersive far IR Fourier transform spectrometry 80—86468
- spectral smoothing under white and background-noise-limited expts. 79—35861
- spectral subtraction in Fourier transform IR spectroscopy 79—83525
- spectrometer, balloon-borne, using focal plane detector array 80—95147
- spectrometer, high resolution ruggedized 80—95152
- spectrometer, problems in optical measurements 79—85187
- spectrometer for recording holograms 79—68369
- spectrometer performance, instrumentation for assessment 80—95165
- spin echo, rot., in solids, anisotropic interaction recovery 78—68410
- spin-echo Fourier transform NMR spectroscopy, multiple pulse technique 80—37063
- spread function variation anal. *(Russian)* 77—18104
- stellar projected rotational vel. determ. method 77—29655
- stellar spectral energy distributions, results from Fourier transform spectrometry 77—82215
- stratosphere trace molecule Fourier transform spectrometer optical design 80—82099
- student laboratory experiment using inexpensive interferometers 78—49609
- submillimetre-wave precision measurement of gases at NPL 77—18111
- subsurface layers, attenuated total refl. Fourier transform spectra 77—71379
- subtractive dispersion monochromator for Fourier transform spectroscopy *(French)* 78—83079
- surface analysis using FT-IR spectroscopy 78—76943
- tetrachloromethane, fluid, collision induced light scatt. intensity 80—103955
- tetrahedral mol. fluids, collision induced light scatt. intensity 80—103955
- thiirene and deuteroderivatives, Fourier transform IR spectra using Ar matrix isolation, vibr. band assignments 80—14142
- time domain dielectric spectroscopy, discrete Fourier transform appl. errors *(French)* 80—13105
- time resolved, improvements 78—58070

Fourier transform spectroscopy continued
time resolved Fourier infrared spectroscopy of transient samples 77−75339
time-resolved, time-freqn. error product 77−173
tissue macrostructure determ. by swept-frequency US scatt. 77−64120
Tokamak, PLT, electron cyclotron radiation Fourier transform diagnostics 80−59292
Tokamak diagnostic Fourier transform spectrometer calibration by liquid N_2 cooled microwave absorber 80−59304
Tokamak far IR Fourier transform spectroscopic Michelson interferometer 80−59294
Tokamak far IR Fourier transform spectroscopy resolution limits 80−59298
transient system, IR spectroscopic techniques 78−58071
2,3,4,- tri-O-acetyl-1,6,-anhydro-β-D-mannopyranose, pulse Fourier transform proton mag. resonance equivalent to CW INDOR 77−32293
trifluoromethyl systems, in smectic liq. cryst. soln., Fourier transform ^{19}F NMR 77−79631
trimethyl phosphate, ^{31}P normal Fourier transform spectra, line narrowing, selective population transfer induced 80−31827
tryptophan, Fourier transform PMR in aq. soln., ^{1}H exchange and relax. rates meas. method 78−15049
Twyman-Green spectrometer alignment, for high temp. reflectivity meas. 79−17498
uridine, pulse Fourier transform proton mag. resonance, equivalent to CW INDOR 77−32293
US spectral tissue identification by colour-coded B-scan display 77−64112
UV, vacuum, investigation of feasibility of extending spectral range down to 170 nm 79−54198
variable-thickness cell for liquid MM-wave Fourier transform and laser spectroscopy 80−57403
vinyl acetate, pulse Fourier transform proton mag. resonance, equivalent to CW INDOR 77−32293
visible and UV range 78−58060
water optical constant submillimetric wave meas. 79−33656
water optical constants, 70 to 450 cm^{-1}, reflection dispersive Fourier transform spectrometric obs. 77−40203
weak IR emission studies of overlayers on meter surfaces 79−67399
wedge fringes in Fourier spectrograph, method using spectrum recorded in parts *(German)* 77−41698
zeugmatography, rotating frame 79−93186
ArHBr, ArHCl, and isotopic forms, rot. spectra, mol. struct., mol. consts. 80−58246
AsD_3, IR spectra, vibr. relax., rot. reorientation in solid phase 78−19463
AsH_3, IR spectra, vibr. relax., rot. reorientation in solid phase 78−19463
CN, Fourier spectrometry of $A^2\Pi \rightarrow X^2\Sigma$ transition 77−57995.
CO, and isotopic forms, fundamental bands, absolute wavenumbers, mol. consts. 79−59458
CO submillimetric high-resolution Fourier transform spectra 79−31509
CO-myoglobin, mol. tunnelling, isotope effect, time resolved IR Fourier transform obs. 80−72126
$CO+CO_2$, vibr. level depend. quenching of CO(ν=1-16) 80−32808
CO_2, $30^01_{II} \leftarrow 00^00$ band, meas. at different temps. of absolute intensities, line half-widths and broadening by Ar and N_2 78−86865
CO_2, $30^01_{I} \leftarrow 00^00$ and $30^01_{IV} \leftarrow 00^00$ bands, absolute intensity meas. at different temps. 78−86864
CO_2, and isotopic forms, bending fund. region, IR spectra, rot. consts. 80−47988
CO_2 and isotopic species, high-resolution Fourier spectra near 4.3 micron 80−47982
CO_2, ν_2 fundamental, absolute IR intensities, Fourier transform spectrosc. obs. 79−93993
^{13}C Fourier transform NMR, method for tailored detection of signals 79−40597
^{13}C NMR with off-reson. proton spin decoupling, proton chem. shift calc. methods 78−27101
^{13}C pulsed NMR, simultaneous T_1 and T_2 meas., Fourier transform. visualization 78−24838
^{13}CH fragment, selective population transfer expts., density matrix formalism appl. to NMR spectroscopy 78−15059
Cs_2ZnCl_4:Cu^{2+} electron spin echo envelope, Fourier transform ^{133}Cs modulation 80−58291
Cu complexes, Cu(I)-P tetrahedral, ^{63}Cu FT-NMR 80−53021
$CuGaS_2$, lattice vibr. modes, Fourier transform spectroscopy 79−33701
^{63}Cu,^{65}Cu, Fourier transform NMR studies 78−94262
DF* prod. from D+PTFE, Fourier transform IR spectroscopy 80−87105
$D_2{}^{16}O$, IR spectra, ν_2 band, rot. struct. 78−982
$FePO_4$ coating on Armco Fe, Fourier transform IR absorpt.-reflection spectra 80−71500
$Ga+H_3PO_4$, interaction in aq. soln., ^{71}Ga and ^{31}P NMR obs. 79−22729
GaAs:Ge,Se transmutation shallow donor transition obs. 80−59925
$H+NO_2 \rightarrow OH+NO$, vel. and angular distrib., Fourier transform Doppler spectrosc. obs. 79−80692
$H^+ + He(Ar)$, H(n=4) s-d coherence, zero-field quantum beats obs. 80−32676
H_2O, $4\nu_2$ band, hot vap., Fourier transform spectrum, rot. consts. 80−32712
H_2O gas submillimetric high-resolution Fourier transform spectra 79−31509
H_2O vapour, refr. index calc. and dispersive Fourier transform spectrometry 79−32736
$H_2{}^{16}O$, $H_2{}^{18}O$, determ. of line intensities from Fourier absorpt. spectra *(French)* 79−18186
$H_2{}^{18}O$, line positions and intensities, $\nu_1+\nu_2$ and $\nu_2+\nu_3$ bands 78−74656
$H_2O+Cl_2O=HOCl$, equilib. const., Fourier transform IR determ. 80−7765
HOCl, photolysis product of Cl_2-O_3-H_2 dil. mixtures, absolute integrated IR band intensities 80−26033
HO_2NO, unimol. dissoc., rate consts., temp. depend., atmospheric implications 78−7175
$HOONO_2$, FT IR spectral obs. of $HOO+NO_2 \rightarrow HOONO_2$ 77−28993
^{1}H spin systems, NMR, two-dimensional Fourier transform. of spin echoes 79−3463
Hg, IR arc spectrum, fine struct., HFS and isotope shifts 77−79559
I_2, 5350 Å band rot. anal., Fourier transform spectroscopy 77−27081
I_2, absolute absorption spectrum measured by Fourier transform spectroscopy 79−75622
I_2 absorpt. spectrum, wavenumber meas. in visible region *(French)* 77−57407

Fourier transform spectroscopy continued
I_2 visible spectrum, Fourier transform spectroscopy, B-X system 79−94007
I2 fluoresc., Ar^+ laser excited, high resolution and sub-Doppler Fourier transform spectroscopy 80−43089
$In_{1-x}Ga_xAs_yP_{1-y}$ far IR reflection spectrum 80−60612
KBr pellet, appl. to IR spectroscopy of inorganic species 80−22455
KCl far IR complex permittivity meas. by dispersive Fourier transform spectroscopy, 7 to 300K 80−15940
KH_2PO_4, soft mode behaviour, dispersive Fourier transform spectroscopy 77−7823
K_2OsCl_6, Cl NQR spectra by Fourier transform methods 80−75879
$KTaO_3$, dielec. response temp. depend. meas., dispersive Fourier transform spectroscopy 79−15449
KrHBr, KrCHl, and isotopic forms, rot. spectra, mol. struct., mol. consts. 80−58246
$^{138,139}La$, Fourier transform NMR 80−57354
$LiTaO_3$ high-temp. ferroelec. transition, soft mode IR reflectivity spectroscopy 79−33692
MnII-ATP system, exchange mechanism, FT NMR and EPR obs. 79−22733
$^{14,15}N_2$, Fourier spectrometry and IR emission spectra 80−83368
NH, atmospheric, IR emission studied using Fourier spectroscopy 80−95628
NO, and isotopic forms, $X^2\Pi$ state, IR obs., mol. consts. 78−42045
NO, and isotopic forms, ν=0 electronic states, spin-rot. doubling 80−5540
NO, Fourier transform spectra, intensity and self-broadening coeff. meas. 80−102503
NO, IR emission Fourier transform spectroscopy, mol. rot.-vibr., RKR potential curve calc. 80−95618
$NO_2+ROO \rightarrow ROONO_2$, ($R=C_nH_{2n+1}$), Fourier transform IR spectroscopic meas. 78−53194
N_2O submillimetric high-resolution Fourier transform spectra 79−31509
^{14}N NMR, single cryst., separation of dipolar and quadrupolar splittings, new technique 80−25217
^{15}N NMR chem. shift references evaluation 78−24835
^{15}N NMR heteronuclear spectroscopy, two dimensional Fourier transform technique 80−31818
^{15}N-$^{1}H^+$ NMR, coupling consts., double reson., difference proton Fourier transform spectroscopy 79−3467
Nd:glass, Fourier-transform photoacoustic spectroscopy 79−9246
Ni/SiO_2, adsorption of CO, scavenging effect of H_2, in situ Fourier transform IR spectra obs. 80−39410
OCS, ν_3 band absolute wavenumbers *(French)* 79−98099
P I, IR spectra and HFS 80−91478
P I, spectra and term anal. 80−91481
P_2, $b^3\Pi_g$-$w^3\Delta_u$ and $A^1\Pi_g$-$W^1\Delta_u$ systems, IR emission spectrum 78−94244
$Pb_{1-x}Ge_xTe$ epitaxial layers, phase transition obs. by far IR reflectivity spectroscopy 79−33691
$Pb_{1-x}Ge_xTe$ magnetoplasma reflectivity and transmission spectra 80−71428
SO_2, conc. determ. for coal-burning power plant stack, Fourier spectrometry appl. 77−49196
SeF_6, in Kr matrix, temp. reversible IR spectral changes, site struct. dynamics 80−102505
Si compensated monocrystal, IR absorption spectra 80−60644
Si complex reflectivity determ., absolute method 79−30584
Si:O(C) wafers, impurity meas. by Fourier transform IR spectra 80−89030
Si:O(C) wafers, impurity meas. by Fourier transform IR spectra at low temp. 80−89031
^{119}Sn NMR by pulse Fourier transform, T_1, T_2 and chem. shifts 77−55715
Te_2, laser excited fluoresc. Fourier transform spectrosc. obs., isotope effects 79−59504
U emission spectrum, wavenumber meas. in visible region *(French)* 77−57407
YO, $A^2\Pi-X^2\Sigma^+$ and $B^2\Sigma^+-X^2\Sigma^+$ systems, Fourier transform spectroscopy anal. 79−22718

Fourier transforms
see also fast Fourier transforms; Fourier analysis; Fourier transform optics
acoustic holography, numerical image reconstruct., applicability conditions for Fourier transform *(Japanese)* 78−59208
acoustic radiation coupling of disc to plane and back or to disc, exact soln. 77−46828
acoustic signal processing, Fourier efficiency using analytic translation and Hilbert samples 80−48519
acoustic system identification, from multiple input/output data, comment and reply 78−83179
acoustic system matrix parameter determ., transient test principles 79−68527
acoustooptic effect calc., integrated 80−91944
action functional in distrib. spaces 78−54207
alloy, quenched, binary, time evolution, computer simulation of three-dimensional model system 78−31433
analysis code for automated reduction of gamma ray data 78−23978
analytic signal model, physical justification 79−909
annular and circular fan duct noise, radial and circumferential mode meas. 79−68529
APS, extended fine struct. above appearance pot. thresholds, use of Fourier transforms 79−83058
APS, extended fine struct. anal., use of Fourier transforms 79−43066
arterial system impulse response determ. 79−79594
astronomical observations, transforms of data sampled at unequal intervals 78−69697
atomic scatt. factors and momentum densities, asymptotic form 80−74105
audio recording and playback system, hypothetical cct. and characts. 79−3879
band-pass filter synthesis, acoustic surface waves, transfer characts. *(Russian)* 77−58510
binary alloy, determ. of distortion field 80−44536
binary star orbital elements calc. using Fourier transform of eqns. 77−56832
binary star orbits solution, Fourier transform method 80−26899
biomembranes, radial autocorrelation function, significance in X-ray diffr. patterns 80−51048
boomeron equation, asymptotic behaviour (in t) of solutions 79−9082

Fourier transforms continued
- canonical Fourier transform of quantum-mechanical pair 79—44781
- catalase, electron microscope exam. of new cryst. form, Fourier transform. method 77—11447
- Cauchy problem, linear eqns. with const. coeffs., absolute instability, 3-dimens. 79—12622
- cell external elec. fields, Fourier transform anal. 79—62223
- cepstrum performance, improvement through windowing of log spectrum 78—89303
- chirp transform processors using US strip dispersive delay lines, implementation 80—53577
- cloud motion estimation, Fourier phase difference technique 79—21046
- coagulating dispersions, light scatt. data, Fourier inversion anal. 78—76932
- complex contour resolution into components, Fourier method 77—31561
- Compton profiles, one dimens. 77—73187
- computer aided tomography, reconstruct. by exact interpolation 80—21538
- computer constructed optical-rose diagrams 77—9505
- contrast profile method of vector mag. field meas., Fourier transforms appl., for solar meas. 78—53839
- cosmic ray spectra, leakage error 78—89023
- crystal, Fourier transforms of Compton profiles, LCAO calc. 79—83050
- crystal structure least squares refinement technique based on fast Fourier transform algorithm 78—91197
- crystallography, electron distributions, aspherical-at. least squares refinements combined with Fourier methods 78—71633
- crystallography, elimination of finite-range effect on block-size distrib. from Fourier transform 77—31547
- cylinder, composite circular, transient thermal stresses 78—79217
- cylindrical viscoelastic waves, diffraction by circular obstacle, calc. *(Russian)* 77—54895
- data compression, spline approximation of input signal 79—35533
- data sampled in unequally spaced segments, astron. appl. 79—35140
- diamond-structure semiconductor, Compton profile interpretation 80—29820
- dielectric properties time domain meas., multicomponent exponential decay curves, analysis method *(French)* 77—52007
- diffraction-profile Fourier analysis, determ. of microstruct. parameters 80—49042
- diffuse wave scatt. by short range order, improved mean spherical approx. 79—9127
- diffusion equation, from space-time transport eqn., for anisotropic random media 80—62595
- diffusion equation, with non-linear terms, Fourier transform 80—103514
- directional light beams, necessity for spatial coherence, equivalence theorem 78—42398
- Dirichlet problem, Fourier transform technique for boundary condition of infinitely long strip 77—45679
- discrete, passive sonar appl., using directional transducer arrays *(Spanish)* 80—69586
- discrete Fourier transforms, fundamental concepts and use 79—47
- discrete Hilbert transform, 2-dimensional, computational complexity aspects 79—84937
- discrete-time windows, optimum low-order 77—5631
- dispersive wave equation, spatial discretisation effect on steady state and transient solns. 77—30014
- distributions theory and EM radiation fields application 77—6974
- domain restoration from scattering data *(Russian)* 77—5630
- drag on sphere accelerating rectilinearly in elastico-viscous fluid, Fourier transform technique 78—51145
- dykes magnetic anomalies interpretation using Fourier transforms 79—58106
- Earth gravity field, Fourier transform anal. and relation to geoid anomalies 80—3897
- earthquake true ground motion reconstruction using Fourier transforms 77—86787
- eclipsing variable stars, Fourier transforms of light curves 77—49428
- edge dislocation, displacement field, in elastic strip, Fourier transform technique 79—46658
- EEG analysis, Fourier-Haar transform 77—44823
- EEG data processing, discrete Fourier transformation 80—26385
- elastic consts. and internal friction meas. in small specimens 79—14357
- elasticity, micropolar continua, static problems, nonhomogeneous eqn. of equilibrium, Green's functions and Fourier transforms 80—58905
- elastostatic problems, three-dimens., mode I loading, soln. method 80—92086
- electrodynamic suspension system, current coil interaction with semiinfinite superconducting sheet *(Russian)* 80—83539
- electrodynamics, null infinity, full canonical formalism, Maxwell field theory 78—12581
- electron distribution, Hylleraas-type wavefunction transform. to momentum space 79—54757
- electron image formation, partial coherence and inelastic scatt. 78—58897
- electron micrographs of deformed filaments, image processing 77—57428
- electron microscopy support film, phase contrast, Fourier spectrum analysis 80—95199
- electron optical devices, static multipole fields, numerical calc. 77—588
- electron wave function pair Fourier transforms, at., mol. and solids, by $(\gamma,2e)$ and $(e,3e)$ *(Russian)* 77—71878
- electron-molecule scattering, Schrodinger eqn. Fourier transform 79—64105
- elliptical galaxies, ang. size determ., 2-D Fourier transform technique 79—35373
- EM field theory, unification of various representations *(Czech)* 80—37931
- EM form factors in Bjorken limit and their Fourier transforms on light cone 79—26246
- EM plane waves, diffr. by staggered parallel plates, spectral diffr. coeff. in Fourier transform domain 78—22071
- EM radiation scattering by dielectric spheroids and ellipsoids, integral eqn. soln. 78—85622
- EM scattering problem solns. 80—23605
- EM wave Gaussian beam at normal incidence on dielectric sandwich slab, reflection and transmission 79—7062
- EM wave propagation appl. 77—58235
- EM wideband freq. response conversion to transient response using segmented transform. 78—77349
- Euler-Lagrange eqns., generalised solns. 78—54206
- EXAFS measurements, appl. to local struct. anal. *(Japanese)* 79—38691

Fourier transforms continued
- experimental data components isolation, Fourier transforms appl. 78—36434
- Fermi surface mapping from one-dimens. Fourier transform of Compton profile 77—39764
- film, HF formalism for calc. of total energies and charge densities 80—49850
- filter functions, Savitzky-Golay, freq. response plots 77—53741
- finite length theoretical gravity anomaly interp. 78—61299
- fluid, Wigner representation, Fourier transform., replacement by series *(French)* 79—9181
- fluorescence spectral files for chem. characterisation, data compression by Fourier transformation 78—35744
- Fokker-Planck equation, manifolds of equivalent path integral solns. 80—4687
- Fourier deconvolution technique for TEM computerised three-dimensional image reconstruction from projections under limited view angle 80—9078
- Fourier-Laplace transform asymptotic behaviour, wave eqns. with memory, oscillatory integrals *(Russian)* 79—92990
- Fraunhofer diffraction symmetry, series expansion of Fourier transform 79—50212
- galaxies optical redshifts determ., Fourier transform filtering and cross correl. techniques 80—56936
- gamma emitting organs, 2 and 3-dimens. digital Fourier reconstruction 80—101705
- generalised Fourier transforms 78—54205
- generalised X-ray scattering factors, two-centre case with Slater type orbitals 78—79491
- generalized Fourier transform diffraction theory for parabolically anisotropic media 78—38107
- geodesy, altitude obs. Fourier transform. *(German)* 78—61312
- geomagnetic anomalies, interpretation with end-corrected Fourier transforms 78—65418
- granular solids, cracks, stress concentrations and shapes, Fourier transform methods 80—83761
- gravity anomalies, second derivative method formulae evaluation by Fourier transform 79—100987
- gravity anomalies due to faults, general expression for Fourier transform 78—61300
- gravity anomalies due to finite inclined dykes, interpretation using Fourier transform. 77—53223
- gravity anomalies of two idealised bodies, theoretical transforms 79—5441
- gravity effect of two-dim. triangular prism interp. 78—3703
- Griffith crack, cross shaped, surface stress distrib. 78—30240
- Griffith crack at rigid-elastic media interface, transform soln. method 77—897
- Hamiltonians, effective, appl. to atomic pot. transferability in hydrocarbons 80—42933
- Hankel transforms, numerical evaluation via Gaussian-Laguerre polynomial expansions 79—84938
- heat diffusion in cylinder, with radiation boundary conditions 78—45577
- heated finite electric coil, temp. distrib. calc. using integral cosine Fourier transform *(Polish)* 77—54865
- heteronuclear double-resonance spectra, modulations 78—86897
- HF scatt. from multiple-edge diffraction at shadow boundaries 77—38781
- hologram binary coding mask, computer appl. *(Russian)* 78—37831
- Hubbard and similar models, functional Fourier transform 80—84416
- image reconstruction, Fourier techniques evaluation in relation to number of X-ray sums 78—77112
- image reconstruction by projection, review *(Italian)* 79—53207
- inductor-screen-ingot systems, EM fields calcs. *(Russian)* 77—46671
- infinite harmonic crystal, dynamics and ergodicity 80—10598
- infinite strip, with elliptical hole, definition of stress *(Russian)* 78—55562
- instant Fourier transform based on harmonic anal., real-time appls. 77—22402
- integral eqn. soln. for 3-D wave propagation in cracked elastic solid 79—46251
- interdigital transducer transverse electrostatic end effects 77—27453
- interfacial tension, electrochem. data numerical differentiation by Fourier transformation 78—41139
- inversion methods for integral transforms of class L_2 functions *(Russian)* 78—20940
- ionisation, electron wavefns. for at. and mol. $(\gamma,2e)$ and $(e,3e)$ processes, high energy, double Fourier transform 78—17628
- Korteweg-de Vries equation, numerical methods of solution, difference and transform schemes, accuracy 80—46833
- Kramers-Kronig transforms, Fourier method numerical soln. by computer 78—2825
- Lame eqns., fundamental soln. to displacement and strains 79—35559
- LEED, Fourier transform deconvolution procedure, multiple scatt. effects 79—32862
- LEED analysis, Fourier transform deconvolution procedure, multiple scatt. effects 80—6322
- LEED data anal., Fourier transform-deconvolution procedure, multiple scatt. effects 79—41914
- LEED data analysis, Fourier transform-deconvolution procedures, multiple scatt. effects 79—41913
- Lie groups, nilpotent, smooth functions Fourier transforms 80—99067
- linear transport operator with periodic boundary conditions, spectral decompositions 77—33961
- liquid structure factor, pair correlation function errors, dilute hard sphere approx. 78—79514
- local modes in disordered crysts., two-time Green's functions 80—6480
- Lorentz group functionals, Fourier expansion in light cones 79—21604
- α Lyrae (Vega) rot. rate determ. from line profile photoelec. obs., Fourier transforms 80—77408
- macromolecule, star type, characteristic function of distrib. of square radius of gyration 77—79717
- matrix relationship with Walsh spectra, physiological data processing appl. *(Russian)* 78—26
- maximum likelihood spatial filtering examples 78—63038
- Maxwell fluid, unsteady flow past flat plate, transform technique 78—59428
- mechanical impulse testing techniques, computer evaluation, high-speed film recording 78—44343
- metal, surface relax. from LEED, Fourier transform-convolution method 79—4459

Fourier transforms continued
meteorological temp. data Fourier transform anal., cyclic behaviour 77—33179
microprocessor in real-time Fourier analysis *(German)* 79—67266
microwave holography by rotational scanning of object 78—42302
minicomputerized automatic radiocardiogram analysis *(Japanese)* 79—29614
mixed Fourier Walsh transforms, appl. to seismic array processing 77—81819
molecular dynamics, semiclassical study of bound states 80—9693
molecular dynamics data, space-time Fourier transform 77—7647
molecular structure, forces acting upon nuclei, Fourier transform calcs. 78—86774
multicomponent systems, higher-order partial struct. factors 77—31572
multidimensional neutron transport equation, spherical harmonics soln. by finite Fourier transform. 78—17269
multiple input/output data, system identification 77—37750
musical scale, 12-tone, tempered Fourier transform 80—87671
Navier, and Beltrami-Michell eqns., fundamental solns. in deform. of elastic space, dynamical case 80—12908
Navier's eqn. soln. in cylindrical coords. 79—44744
nerve field, isolated sciatic nerve in volume conductor 77—21505
neutron slowing down eqn., resonance interaction effects 77—14207
neutron slowing-down kernel moments, MAGGIE code 78—29540
NMR, high resolution in inhomogeneous field, free decay and side bands in Fourier transforms *(French)* 77—51965
NMR, Voigt profile analysis, Fourier transform approach and least-squares curve fitting 77—20729
nonlinear, evolution equations soln. using spectral transform method 78—57745
nonlinear evolution equation with linearly x-depend. coeffs., spectral transform, single soliton soln. 78—57746
nonlinear oscillators, Brownian motion, projection operator method, double well potential oscillator appl. 79—2723
nonlinear wave propagation, spectral and pseudospectral methods, turbulent sound wave appl. 77—5672
nuclear relaxation, low temp. stimulated by paramagnetic impurity 79—33563
numerical, singularity expansions and product integration 78—89316
numerical evaluation method 79—17194
numerical Fourier and Bessel transforms in logarithmic variables 79—9089
numerical-valued Fourier transform in two-sided operational calculus 77—67219
ocean continental shelf waves, generation by alongshore vars. in bottom topography 80—51424
ocean directional wave spectrum, new meas. method, description 79—16706
Oldroyd liquid, unsteady flow between two porous walls 78—63452
optical fibre impulse response measurement system, time to freq. domain transform. by minicomputer 77—19406
optical image processing, two-dimensional high-speed acoustic Fourier transform 79—36844
optical imaging, Fourier transform, using SAW memory-correlator 78—83090
optical systems, correlation coeffs. of planar sources and their far fields 78—66750
optical systems, electronic analogy, systems concepts from communications theory *(German)* 77—3542
orthorhombic base centred lattices, Fourier transform of dipole-dipole interaction 78—76404
orthorhombic lattices, Fourier transform. of dipole-dipole interaction 78—64334
particle dimension determination, by direct Fourier cosine transformation, of expt. SAXS data 80—79624
partitioned signal detection by discrete cross-spectrum analysis 80—91966
phase coding with high quality computer holograms 77—628
piano notes, anal. Fourier transform methods 78—26009
plane sound sources, radiation pattern *(German)* 77—42639
plate, containing infinite row of holes, effect of couple-stresses on stress concentration 78—41159
Poincare Bertrand formula, proof by Fourier transform of distribution 77—82366
point process sampling for spectral analysis 79—68498
Poisson's formula for two dimens. wave eqn., direct soln. by Fourier transform 77—37727
polar molecule, dielec. friction effect on reorientation in liq. 80—40048
polymers, long-range Coulombic interaction, Fourier transform technique calcs. 79—31748
polystyrene, sol, light scatt. data, Fourier inversion anal. 78—76932
positron focused tomogram object reconstruction 78—40314
potential fields due to vertical circular cylinder and dike, Fourier transforms anal. 79—34972
potentials, two-body, configuration of systems of interacting particles with minimum potential energy per particle 80—23491
pseudocontinuum theory, correspondence between representations 79—35553
pulsars, axisymmetric magnetosphere models, Fourier transform method 79—92794
quantum harmonic oscillators, multidimensional, soln. with time depend. frequencies 80—8822
quantum mechanical appl. of fractional order Fourier transform 80—82665
radiation intensity in finite slab, integral Fourier transform technique 77—67389
radiative heat transfer, rigorous constructive solns., integral Fourier transform technique 78—9553
radiative transfer in slab with boundary refl., Fourier transform soln. 79—90119
radio astronomy, direct transform hardware processing of rot. synthesis data 78—85856
radio astronomy, direct transform hardware processing of rot. synthesis data 78—85857
radiographic imaging, 3-dimens. 80—85486
radiography, computerised tomography, MTF meas. method appl. to EMI head scanner 77—48864
radionuclide angiography technique for assessment of regional wall motion abnormalities 80—85488
radiotelescope, surface meas. with two feeds 79—12403
radiotelescope reflector surface errors, rapid meas. method 77—41301

Fourier transforms continued
real-time Fourier transform. via acousto-optics 79—46112
reconstruction accuracy of 2D emissive intensity contours from ID projection limited no. 79—77422
retinal photoreceptors, small angle X-ray data processing 80—81536
review, role of Fourier transforms in struct. determ. 77—27772
sarcoplasmic reticulum membranes, small angle X-ray data processing 80—81536
SAW EM transducer model and flexible design for NDT 77—23844
scalar diffraction theory, near-field, Fourier transform appls. 80—31455
scalar wave diffraction by two parallel slits in plane 78—49671
scalar wave diffraction problem for slit, soln. using Fourier orthogonal functions transform. 77—13599
scattering experiments, deconvolution of thermal averaging using integral transform methods 78—92442
Schrodinger equation, one dimensional *(French)* 77—37766
scintillation detector MTF calc. on programmable pocket calculator 77—66844
seismic data migration by Fourier transform 78—77341
semiconductors, Fourier transformed X-ray Compton profiles 80—35004
SH waves due to shearing-stress discontinuity in viscoelastic half-space, displacement 80—56405
shallow water wave propagation, Pekeris operator resolvant 78—90575
signal detection, optical vs digital Fourier transform computers 79—27181
SL(2,R), universal covering group, Plancherel formula 80—68393
Slater 1s orbital four centre mol. integrals, Fourier transforms 80—74104
Slater-type orbitals, Z centre case, generalised X-ray scattering factors and Fourier transforms 79—99020
soil consolidation under distributed shear loads, complex Fourier and Laplace transform. technique 79—57936
solar coronal mag. field determ., fixed mesh soln. to Laplace's eqn. 77—2392
solar magnetic fields, meas. from saturated and blended lines via Fourier transform techniques 77—22165
sound absorption mechanism of porous material 80—38170
spectroscopic binary stars, massive, Fourier transform anal. rel. to low eccentricity orbits detect. 79—67060
speech processing, preservation of phase 79—59875
spherical Fourier transform, summation formula *(French)* 79—9078
spherical wave diffraction by absorbing plane, bidimensional spatial Fourier transform 77—46830
spherical wave reflection at fluid plane interface with porous medium 78—42484
spinless particle scatt., plane waves on the impact parameter group *(Russian)* 79—2668
standard sieves, Fourier transform method for verification of wire screens 77—53874
stationary point processes, estimation procedures 77—2517
STEM and conventional TEM, bright-field image contrast and resolution 80—95200
stress concentration, in plate containing infinite row of holes, effect of couple-stresses 78—38192
stress intensity factor for a flat elliptical crack in an elastic solid under uniform tension 79—27525
strings, stretched, vibr. control by an external distributed force 78—83308
TEM, wave aberration sign 77—22623
tetrahedrally coordinated semiconductors, electronic struct. and Fourier transformed Compton profiles 79—38689
texture anal. of phosphor screens using optical Fourier transform 77—23751
three dimensional mixed dynamic problem theory, new method 79—84958
three-dimensional contour, resolution into components 79—84939
time dependent, time dependent spectrum density *(Korean)* 77—22384
tissue characterisation by US backscattering 79—70595
turbulence dynamics, Fourier transform ambiguity 77—5300
turbulence problem, physical and spectral space methods *(French)* 80—28493
turbulent homogeneous fields, spectral modelling *(French)* 77—75890
two-centre charge distrib., Fourier transform, STO general expression derivation 80—58119
two-dimensional neutron diffusion eqn. for triangular region 78—78432
uncorrelated jet model, evaluation of phase-space vols. and inclusive spectra 77—26496
underwater sound, source location in random dispersive media using generalised reduction methods 80—43509
upper atmosphere neutral gas expansion differential eqns. soln. 79—12325
US field calibration from acousto-optic data using Fourier techniques 77—84054
US holography, electronic reference generation of spherical wave by microcomputer 79—81646
US image reconstruction processing limitations 78—73184
US pulse echo digital processing 77—32948
vector potential pf parallel conductors between metallic half-spaces, Fourier integral transform appl. *(Polish)* 77—54645
vision, receptive fields in area 17 of cat visual cortex, linear and nonlinear properties 80—104583
visual cortex local spectral anal., image description model 78—40143
visual perception, colour aftereffects, spatial frequency contingent range 79—2071
visual processing models, adaptation to spatial impulse 77—9191
visual system spatial and temporal information separation model 78—40167
volume-conductor fields of isolated axon, linear filtering problem 78—3463
wave function determ. by position and momentum distributions 78—93548
wave-broadened spectral line profiles, anal. of Fourier transforms 79—80229
weldable butt joints, calc. of temp. field for nonideal thermal contact *(Russian)* 80—10121
X-ray crystallography, Fourier transforms of Gaussian orbital products 78—38573
X-ray diffraction line broadening, of crysts. containing small angle boundaries, Warren-Averbach anal. 79—37578
X-ray reconstruction by finite field transforms 77—67549

Fourier transforms continued
- X-ray small angle scattering, radial electron density distrib. calcs. indirect Fourier transform method 77—76246
- X-ray small-angle scattering, rel. to elec. resist. 79—19125
- 2-zinc insulin, rhombohedral, cryst. struct. refinement, experience with fast Fourier least squares 78—92595
- ep deep inelastic scatt., EM form factors asymptotic behaviour, Fourier transform singularities 79—40789
- β'Cu-Al martensite, stacking order, disorder anal. by continuous Fourier transformation of diffracted intensities 80—39115
- GaAs n^+2n^+ epitaxial multilayers, carrier conc. from Fourier transform anal. of magnetoresist. signal 79—38205
- LiF, expressions for Fourier transformed anharmonic force consts. 79—55843
- NaCl, expressions for Fourier-transformed anharmonic force consts. 79—55843
- NiO (001), diffr. of He atoms, wall corrugation parameters from Fourier transform of diffracted intensities 79—61487
- $RbCaF_3$, cubic to tetragonal phase transition, ^{87}NMR meas. 80—7187

fractional-horsepower motors
- DC micromotor controls feed rates in syringe pumps 78—48923
- deep slip motor starting characteristics, industrial cinefilm winder motor appl. *(Russian)* 78—29199
- $CeCo_5$ hard magnets, appl. *(German)* 77—80966

fractionation *see distillation*

fracture
- *see also brittle fracture; crack-edge stress field analysis; cracks; creep fracture; ductile-brittle transition; ductile fracture; embrittlement; fatigue; fracture toughness; stress corrosion cracking*
- ABS polymer, fracture behaviour, rubber content effects 77—32676
- acoustic emission, phenomenological model, calc. of intensity 78—85110
- acoustic emission signal simultaneous recording with fracture monitoring 80—55599
- acrylic surgical bone cement fracture behaviour 80—56277
- activation of fracture mechanisms 78—63380
- adhesion of solids, review of physical mechanisms *(French)* 78—6231
- adhesional bonds, stressed state and strength during breaking *(Russian)* 80—76478
- adhesive fracture mechanics, review 78—60773
- adhesive fracture specimen, DCB, crack tip stress field anal. 78—55602
- adsorption-sensitive fracture processes, control and appl. 77—52468
- β-Al_2O_3-Na_2O, geometrical aspects of breakdown, TEM study 79—79096
- alite paste, mature, microstructure study by SEM, TG and X-ray diffr., corrosion 78—92381
- alkali halide, electron-irrad., Monte Carlo modelling 77—69038
- alkali halide crystals, exciton mechanism of complex active centre formation at fracture 79—33033
- alloy hard, binary carbide with Ni-Mo binder, physicomech. props. 77—90461
- alloys, austenitic, neutron irradiation effect on tensile, creep-rupture, deform., fracture props. 79—65120
- alloys, electron irradiated, temp. depend. spall threshold 78—48504
- alloys ferrous and nonferrous H_2 related failure studies, overview 78—11322
- alumina, diametral compression test, parametric study 78—44282
- amber, natural, optical strength and laser induced rupturing 78—7039
- ammonium tartrate, triboluminescence and cryst. fracture dynamics 80—50437
- amylose, micromech. fracture anal. 78—68784
- analysis, use of microfractography 77—32750
- analysis using SEM 79—61834
- angled elliptic notch problem under biaxial loading, strain failure criterion 80—79235
- anharmonic atomic chain breakup, molecular dynamics calcs., deformation dynamics 80—29117
- annular crack at spherical voids, stress intensity factor estimates 80—106757
- Araldite D cured with triethylenetetramine, fracture stability 80—30070
- arbitrary criterion, weakest link theory reformulated 78—90786
- arteriograft opening characts. as fracture phenomena 78—92746
- atomic chain, loaded, phonon model of breaking 80—70301
- atomistic model for crack propagation 77—72193
- beam, cracked, transverse loading by stamp, stress and fracture anal. 80—10187
- beam bending, internal damage induced instability 77—7341
- beams in pure bending, distributed damage theory, cracks, fracture 80—64474
- bearings, plain, fracture 80—81170
- bench scale prebaked anode fracture, coke and formulation variables effect during Al smelting 79—52371
- biaxial load effects, review 79—43433
- biaxial stress field, stress ratio effect on fatigue crack growth 77—58617
- biaxially fibre reinforced composites, two dimens. mixture theory, dynamic crack appl. 78—87301
- biological material freeze-fracture preparation for SEM 78—61290
- biological membranes and proteins, plastic deformation during freeze-cleavage, review 78—14400
- biological specimen prep. freeze-fracturing with a new specimen table 79—5425
- biological specimens, cryosectioning for X-ray microanal. 79—39626
- biological specimens, new freeze-etch unit 79—5423
- bisphenol-A-diglycidyl ether epoxies, struct., fracture and mech. response, cure and crystallisation conditions effects 79—15779
- blister test specimen, effect of adhesive layer elasticity 77—16778
- blood cells, red, human, frozen section prep. for electron probe anal., fracturing or cutting 79—39625
- bonded plate or membrane strips, exam. of adhesive fracture 78—59342
- bone, compact, fracture mechs., effects of density and specimen thickness 78—3534
- bone, compact, human, microscopic struct. rel. to fractures 80—56106
- bone, crack velocity depend. of longitudinal fracture, bovine tibia 80—97965
- bone, human tibia, ultrasonic assessment, surgical manipulations effect 80—3745
- bone, US propag. 78—24105
- bone morphology and fracture, exam. 78—57036
- bone regeneration, morphology, effect of US 80—41111
- bone tissue, human, subjected to longit. extension, acoustic emission 77—25495

fracture continued
- boundary-integral equation method, stress anal. fracture mechs., computer calcs. 77—80111
- branching criterion, invalidity of proof based on energy balance arguments 80—33536
- α/β brass, bicrystal, dynamic obs. of fracture phenomena 79—5040
- α-brass, bicrystal, grain boundary fracture at intermediate temp. *(Japanese)* 79—15774
- brass, circular plate perforation and deformation by square section punch 79—34100
- brass, failure obs. with optical microscope 78—11472
- brass, hot ductility and torsional deform. *(Japanese)* 79—57069
- α-brass, stress corrosion cracking in 15N ammonia solns., fractographic aspects 80—16547
- brass, textured thin specimens, fracture 78—60816
- brass, two phase α/β bicrystal, transgranular slip and fracture across an interface 80—81150
- α-β brass, two phase bicrystal, deform. and fracture at 450K 80—16409
- α-β-brass, two phase bicrysts., deform. and fracture at 150K 80—16388
- $\beta'+\gamma$- brass, two-phase, acoustic emission from β' plastic flow and γ cracking 80—16452
- α-β brass, two-phase bicrystals, plastic deform. and fracture mechanism 78—84898
- brass (37%Zn), workhardened thin specimens, fracture, anisotropy coeff. role *(French)* 80—104276
- brittle fibre reinforced composite, brittle reaction zones at interfaces, tensile strength 79—52306
- brittle material, surface energy determ. from AE, automatic system 79—91899
- brittle solid, atomically sharp cracks, TEM study 80—71729
- brittle solids, microfracture resulting from anisotropic shape changes 80—88254
- bulk cold working processes, fracture criterion 78—56775
- butt welded joint dynamic strength, partial penetration and slag inclusion effects 79—83288
- BWR fuel rod relocation, gap conductance anal. 80—83192
- cantilever beam method to investigate J_{1c} and J_{1scc} *(Chinese)* 78—15488
- carbon fibre reinforced plastic, fracture energy improvement by delamination promoters 77—8909
- carbonate rock, interrelation of flow or fracture and phase transition during deform. 80—51389
- case hardened components, exam. of fracture surface by TEM. *(Japanese)* 78—52949
- cavity growth, creep mechanisms, independent and sequential 80—55480
- cellulose fibre hydrolysability increase on gamma-irrad. *(Russian)* 80—61121
- cellulose hydrate, nondestructive control of mech. props. anisotropy, appl. of capacitance method 77—86277
- cement, hardened paste, fracture meas. 77—4837
- cementite, in white pig Fe, deform. and fracture 77—4827
- ceramic, fracture stress, rel. to flaw and fracture mirror sizes 78—11309
- ceramic, spherical cavity effect on fracture 79—66145
- ceramic bars, fired, high Al_2O_3, modulus of rupture, relative humidity depend. 80—40473
- ceramic building materials, breakdown kinetics by X-ray diffr. 80—108526
- ceramic compact, morphological investigations significance 79—33988
- ceramic composite, mech. props. *(Polish)* 78—31481
- ceramic material fracture mechanics, n review 80—45373
- ceramic materials, subject to elastic/plastic indentation, crack initiation threshold 79—70157
- ceramics, cracking characterisation by double torsion test *(French)* 80—104369
- ceramics, fracture mech., probability, micromech. models of crack growth 80—108571
- ceramics, fracture mech. appl. 79—43426
- ceramics, fracture mechanism maps for materials which cleave 79—91774
- ceramics, high temp. failure mechanisms, statistical model 80—39210
- ceramics, microstructure dependence of mechanical behaviour, fracture energy and path 78—88533
- ceramics, polycrystn., porosity, twinning and grain-size depend. on spontaneous cracking 80—44253
- ceramics, polycrystn., strength-grain size relations 79—79081
- chemically-assisted fracture, atomic modelling at crack tips 80—106754
- chemisorption modification of strength of solids 79—51423
- citric acid monohydrate, triboluminescence and cryst. fracture dynamics 80—50437
- combined bend mode specimens, calc. of stress intensity factors 78—79284
- combined loads effects, maximum energy release rate criterion 79—32384
- combined mode cracks, energy fracture criteria, complex variable method 79—27596
- combined mode cracks, fracture criteria 78—79285
- compact specimen, J-integral evaluation 80—5986
- compact tensile test pieces with starting notches, photoelasticity obs. *(German)* 77—58619
- compact tension specimen, J-integral eval. *(Japanese)* 78—9607
- composite, biaxial analogs of triaxial stresses 79—55345
- composite, brittle particulate, fracture, theoretical aspects 79—70156
- composite, separation failure 78—9610
- composite beam, multilayered, anisotropic, exam. of shear stress distrib. under transverse loading 79—18731
- composite beams, shearing stresses distrib. under three point flexure, fracture due to surface peeling 78—44183
- composite discs, fibre-reinforced, rotating strength, stress distrib., failure criterion rel. to mould process 78—76701
- composite elastic media, crack retardation at boundary *(Russian)* 79—23275
- composite fracture with bonding strength defects between components, computer simulation 80—11771
- composite laminate in combined stress state, fracture models 80—10211
- composite material, fracture and fatigue, review 78—68781
- composite material, heat exchange during rupture *(Russian)* 77—48517
- composite material strength criteria 80—10208
- composite materials, crack growth, conc. criterion 80—65146
- composite materials, failure predictions 80—10200
- composite materials, fracture kinetics 80—11770
- composite materials, fracture mechanics 80—10202
- composite materials, lecture *(Japanese)* 77—8928

fracture continued
composite materials, physical nature of fracture 78—80653
composite materials, stochastic fracture models, and strength test results statistical anal. 80—64470
composite materials, unidirectional, three-dimens. fracture 80—64471
composite materials damageability, NDT methods 80—11867
composite piezoelectric medium, integral parameters at longit. shear *(Russian)* 78—30232
composite structures, fracture initiation prediction 80—11870
composites, appl. of exptl. methods to fracture 80—11869
composites, micro- and macro cracks 80—11767
composites with stress gradients, failure anal. 80—10199
compression failure anal., glassy materials investigation 78—55608
concrete, crack growth, computer simulation using Monte Carlo method 78—76764
concrete, crack propagation, uniaxial compressive stress *(Japanese)* 78—11330
concrete, deformation under complex loading, mathematic description 80—25783
concrete, microcrack phenomena, geometric probability calcs. 79—57091
concrete, plain, deform. and fracture 79—70167
concrete, reinforced slabs, nonlinear statical props. anal. 80—25809
concrete, role of aggregate in fracture 79—79076
concrete plates, cracked, and beams existence of critical strain energy release rate 78—76765
conic-section simulation finite element anal. 77—3773
continuum mechanics, non-local, at atomic scale 78—12563
copolyimide glass based on benzophenone tetracarboxylic acid dianhydride 77—63720
Cr, strain hardened metal and microalloys, low temp. brittleness 79—96140
crack, stress intensity factor, near doubly riveted stiffeners 78—67152
crack extension process and nonlinear fracture criterion, finite element anal. 80—53702
crack fracture parameter estimation bv long wavelength scatt. 79—24709
crack growth, 3-D geometric effects, implications for composite material structures 80—10204
crack growth, quasistatic, nonlocal model, thermodynamics of irreversible processes basis 78—83324
crack growth determination, in mixed mode loading system 78—67105
crack growth law derivation, linear viscoelastic solids, fracture process zone concept 80—92088
crack growth thermodynamics for elastic, almost elastic and viscous bodies *(Russian)* 80—1481
crack initiation in elastic/plastic indentation fields, model 78—5668
crack propagation, fracture viscosity and plastic flow calc. *(German)* 77—54934
crack propagation, subjected to mode I and II loading, rupture criteria *(French)* 80—14616
crack propagation theory, Lamb's problem for a point source 80—56375
crack resistance, characteristics correlation of material α_p and γ 80—21075
crack stress intensity factor determ., using numerical method *(Italian)* 80—14625
crack tip singularity models, assessments for use with isoparametric elements 79—50652
crack tips, near boundaries or other geometrical discontinuities, stress intensity factors 80—1484
crack trajectory, unstable crack extension, stress field anal. 80—64462
cracked holes and rings, loaded with polynomial crack face pressure distrib., stress intensity factor solution 78—83335
cracked lug, test and analysis 78—67153
cracked thick walled cylinder, elastic plastic fracture anal. under displacement controlled loading 78—67119
cracks, planar, growth under hydraulic fracture 80—28469
criteria, integral eqn. 78—79279
cropping and blanking, plastic flow, fracture, crack propagation 80—74761
cross-plied factors controlling transverse cracking 77—77566
crystal cleavage due to dislocation tilt wall splitting 78—91377
crystal plasticity, surface effects, review 77—47505
crystalline bodies, plastic strain and microcrack propag. 80—81199
crystalline materials, fracture, stress relaxation effect 80—88256
cutting tools, diffusive wear, mag. field effect 80—60985
cylinder, rupture under wave conditions, stress-strain state for explosive loading *(Russian)* 80—79220
cylinder elastic orthotropic brittle, under axisymmetric thermal and press. loading failure probability anal. 78—34078
Czochralski-grown crystals, cracking 78—31323
damage model, crack growth and instability 79—41614
damage parameter in continual fracture mechanics review *(Polish)* 79—32382
damage tolerant fibre reinforced sheet metal composites, crack growth 77—81319
DCB specimen, fast fracture simulation using Kanninen's model 78—19866
debond dynamics for elastic strip, Timoshenko beam props. and steady motion 78—55604
defect dimension determination by acoustic emission 80—104381
defective material, with strength, anisotropy induced by pretreatment, limiting state probability calc. 77—86123
defects, influence on solid-state props., review 77—7709
deformable solids, fracture and hardening kinetics 80—35210
deformation criterion for local fracture *(Russian)* 78—9604
delamination failure mode of composite bars in compression 80—11772
delaminations in thin sheets, elongated, interaction with Lamb waves, book contrib. 79—98574
destructive thermal fluctuations under transient conditions 79—72861
diamond, high press. appl. by spherical diamond indentor, plastic deform. obs. method 78—35619
dielectric, thermal mechanism of plastic deformation and fracture by laser beam 77—11553
dielectric materials, electromagnetic radiation in crack formation process, exam. 78—76771
differential geometry of fracture 79—27581
diffusion controlled stress rupture in polycrystalline materials 79—14878
diffusion controlled stress rupture in polycrystalline materials 79—14879
diffusive cavitation of grain interfaces, non-equilib. models 79—46668
disc specimens, photoelastic study of fracture process under superimposed static and dynamic loading *(German)* 79—34267

fracture continued
dislocation distrib., fracture relation, plastic flow at crack tip, slip line theory 80—64482
dislocation structures, and fracture surfaces in fatigue *(Japanese)* 80—65144
dispersed fracture of unidirectional composites 80—11768
DNA-cetavlate crystal growth and morphology 77—66583
dolomite, impact and static compression studies rel. to strain rate depend. and failure mode 77—44977
double cantilever beam adhesive joint, cohesive fract., stress anal. 77—65721
double cantilever beam model, for K_{Ic} determ. *(Chinese)* 80—54306
dry hot rock hydraulic fracture characterisation acoustic instrumentation 77—33221
ductile-fibre composites, strengthening effects of brittle zones 77—8946
dynamic crack propag., two dimensional anal. validation 79—50662
Earth crust, fluid-filled fracture mechanical interaction with Earth surface 79—79779
Earth upper mantle, micromechanisms of flow and fracture 78—69331
earthquake faulting process and prediction using fracture mechanics *(Chinese)* 77—91012
earthquakes stress relaxation models, finite difference calc. 77—73682
edge problem of fracture mechanics, plasticity theory inadequacy 79—3978
education, chimney breaking while falling 77—33768
effect of simulated fission products on mech. props. 80—73922
elastic, linear and non-linear solids, rupture mechanics using contour integrals *(French)* 80—14615
elastic adhesion problems, rel. to linear fracture mechanics *(French)* 80—14617
elastic body with plane cracks of normal fracture, 3D problems *(Russian)* 80—79219
elastic crack problem, soln. by superposition of finite elements and singular fields 78—38249
elastic crack tip enclave model, fracture stress 80—71730
elastic fracture analysis, 2D linear, finite element anal. vs. the edge function method 80—99963
elastic fracture mechanics, boundary integral eqn. anal. 80—14622
elastic fracture mechanics problem, two-dimensional, Green's function method 79—23272
elastic fracture of solids containing arrays of cracks 80—1473
elastic half-plane, wave propagation for non-uniform motion of displacement discontinuities 80—1478
elastic media, longit. shear fracture, dynamical problem for region with curvilinear cuts 78—81842
elastic solid with doubly periodic array of cracks, fracture mechs. 78—34085
elastic-perfectly plastic material, theory of stable crack growth 78—79272
elastic-plastic, finite element method appl. 80—1489
elastic-plastic, hardness and fracture 78—34090
elastic-plastic crack tip characterisation, relation to R-curves 78—56767
elastic-plastic fracture mechanics for structure design 77—14961
elastic-plastic materials, finite deformation anal. of crack-tip opening 78—51126
elastic-plastic solids, crack tip deformation and fracture 79—27591
elasticity and damage, interrelation *(French)* 79—90182
elasto-diffusive solids, singularity movement, appl. to fracture propag. 78—30235
elasto-plastic material, crack tip stress and strain fields and fracture behaviour, work hardening 78—22304
elastodynamic fracture analysis of plane crack extension 78—5693
elastomeric block copolymer properties obs. 78—27560
elastomers, tackiness, fracture mechanics theory *(French)* 80—38344
elastomers, vulcanised, tensile failure and network fracture mechanism, particle reinforcement 80—41928
elastoplastic bodies fracture, estimation of load required to start a crack *(Russian)* 79—14346
elastoplastic fission reactor materials, fracture zone analysis *(Spanish)* 79—66139
elastoplastic fracture mechanics, finite element analysis *(German)* 77—54935
elastoplastic fracturing structures, boundary value rate problem, extremum theorems 80—48596
elastoplastic solid, fracture and yield conditions 79—14344
electrotechnical porcelain, bend tests, fracture stress distrib. at various loading rates 78—15529
elongation, dynamic, of material, stress/strain curve up to scabbing, meas. method 79—7348
EM sensor window materials, particulate erosion 80—38080
energy rel. to inelastic behaviour 79—60429
energy release rate expression, Leibnitz's rule appl. J-integrals 79—18831
Epikote 828 cured with tetraethylenepentamine, fracture stability 80—30070
epoxide resin, low temp. crack propag. 80—85020
epoxy laminate, glass-fibre reinforced, with circular holes, tensile fracture 80—25789
epoxy materials, crack blunting mechanisms 80—66624
epoxy resin, destruction by diffused water 78—48511
epoxy resin, fracture energy under plane strain conditions 78—80624
epoxy resin, plastic deform. effect on crack propag. 80—97563
epoxy resin DGEBA, cured with TETA, crack propag. and fractography 79—70154
epoxy resin-Al alloy 5086, scarf joint test specimen, mixed mode adhesive fracture, bond angle effect 78—68768
epoxy resins, adhesion to metals fracture mech. study 77—4888
epoxy resins, expt. exam. of fracture by peeling method *(Russian)* 80—71761
epoxy resins, struct. changes under mag. field action 80—40516
epoxy system, rubber-modified and unmodified, sub-T_g annealing expts. 79—11643
epoxy-metal joints, environmental fracture and effects of shrinkage stresses 80—16635
equivalent energy method in fracture mechs. anal., critical evaluation 77—80113
expansion process, associated differential geometry 79—67159
explicit finite difference method, anal. of dynamic crack and fracture 77—75860
explosive fracture, time criteria, kinetic theory appl. 79—14347
failure mechanisms and metallography, review 79—61833

fracture continued
  failure micromechanisms, classification according to failure type *(Russian)* 80—108557
  fast fracture and crack arrest, finite difference anal., appl. to steel, epoxy resin 78—1607
  fatigue cracks, Dugdale crack closure analysis, under const. amplitude loading 79—50650
  faulting, far-field body waves generated by elliptically expanding rupture 77—81804
  femoral bone, bovine, slow fracture propagation obs. 79—79592
  femur, bovine, crack vel. and fracture mech. 79—57690
  ferrous material fractured surface exam., oxide scale removal 78—95886
  fibre cross-reinforced layered composites, moment effects in plane problem 80—64393
  fibre reinforced composite, deform. diagram construction method, based on statistical distrib. of strength of fibres 77—52437
  fibre reinforced composite, energy release rate for cracks 77—66690
  fibre reinforced composite, fibre geometry and filler vol. influence on fracture stresses 80—45397
  fibre reinforced composite, new, physical props. 77—8797
  fibre reinforced composite, oriented, statistical theory of fracture and scale factor effect in reliability 77—70171
  fibre reinforced composite failure analysis by acoustic emission 78—80691
  fibre reinforced composite laminate, fracture mode determ. by AE 79—57187
  fibre reinforced composites, brittle zone on fibre surface, deform. and fracture 77—56104
  fibre reinforced composites, conf. Moscow, USSR (Nov. 1978) 80—8733
  fibre reinforced composites, crack growth 80—10212
  fibre reinforced composites, failure, probability bounds 79—87716
  fibre reinforced composites, fracture mechanics, review 79—27597
  fibre reinforced composites, fracture mechanics appl. to failure 77—52453
  fibre reinforced composites, fracture processes modelling, digital computer appl. 80—65147
  fibre reinforced composites, intralaminar-shear charact., 10 deg off axis test 78—35422
  fibre reinforced composites, materials properties, unsolved problems, review 77—4843
  fibre reinforced composites, micro- and macrocracks 80—65148
  fibre reinforced composites, strain rate effect on AE 78—44193
  fibre reinforced composites, stress redistribution dynamics during fibre rupture 80—64394
  fibre reinforced composites, theory 80—89351
  fibre reinforced composites, transverse strength rel. to fracture mech., stress interactions 80—16421
  fibre reinforced composites, unidirectional, mixed mode fracture 80—100302
  fibre reinforced composites with high work of fracture 80—81029
  fibre reinforced epoxy, laminate, static and impact props. 77—63725
  fibre reinforced epoxy laminates, interlaminar failure 80—81207
  fibre reinforced laminated hybrid, tensile first cracking strain and strength 80—81175
  fibre reinforced nonlinearly elastic matrix, unidirectionally reinforced, deform., strength, and failure 80—3134
  fibre reinforced plastic, fracture mechanism study, cumulative failure model 78—92315
  fibre reinforced plastic, props., implications for structural design 80—81174
  fibre reinforced plastics, bent thin-wall constructions, rupture 80—64472
  fibre reinforced plastics, exam. of strength criteria 78—75105
  fibre reinforced polymer, pressurised wound tube, failure from longitudinal defects 77—16660
  fibre reinforced polyurethane foam, with chopped fibres, morphology and fracture 77—36447
  fibre reinforced resin matrix composite deform. and fracture in combined stress states 77—70106
  fibreboard, made from Asplund pulp-PMMA composite, props. *(Japanese)* 80—7664
  fibrous composite, thermal crack propagation anal. 80—10205
  fibrous composite materials, brittle interlayers influence on tensile strength and rupture stress *(Russian)* 80—21006
  fibrous laminated composite, tensile failure, quantitative fault tree anal. 77—59891
  fibrous material failure kinetics, internal stresses, computer simulation *(Russian)* 80—40479
  filament-wound pipe, microscopy of failure mechanisms 79—24604
  film, stability and rupture using perturbation analysis 78—79911
  film adhesion testing, use of fracture mechanics concepts 80—50802
  finite element anal. of problems with non-removable singularities 77—72250
  finite element analysis, symmetry and nonlinearity 77—3791
  finite element dynamic anal. appl. to fracture mechanics 77—3790
  finite element mesh optimisation for fracture problems soln. 78—34070
  finite element model of crack movement with fracture propagation *(Russian)* 79—77017
  fission reactor coated fuel particles, failure statistics 77—74945
  fission reactor materials, clad failure prediction during FBR overpower transiency, JANE code 80—78363
  fission reactor pipework integrity assessment 79—22431
  fission reactor pressure vessel, failure risk due to manufacturing defect 79—22432
  flaws, 2D, irregularly shaped, fracture mechanics transfer function 80—99970
  flow of solute atoms near crack tip, time dependent, exam. 78—75722
  fluoropolymer adhesive joints, fracture and surface anal. by SEM and ESCA 77—55434
  fractography, applications *(Japanese)* 80—16446
  fracture mechanics, conformal mappings to delete singularities, finite element anal. 77—72251
  fracture mechanism in various temperature and stress intervals *(Russian)* 79—24600
  fracture mechanism maps, usefulness 80—84245
  fragile materials, mech. props. and fracture mech. *(French)* 80—104274
  fully yielded components, stable and unstable cleavage fracture, moving cracks 79—64586
  fusion reactor blanket structures, linear elastic fracture mech. anal. 80—86979
  fusion reactor ceramics, Weibull probabilistic design approach 79—93822

fracture continued
  generalised fracture mechanics, predictions of fracture energies in highly extensible solids 77—62208
  generalised three dimensional work of fracture specimen, stability considerations 78—67140
  geological faults, fracture, creep and strain 78—69345
  geological structures, structural fracture and stress fields, review *(Chinese)* 79—53343
  GFRP, shrinkage stress calc. 78—19869
  GFRP, unidirectional, compressive fracture mode 77—21251
  glass, dense, mirror-to-flaw size ratio, comparison with polycrysts. 80—25841
  glass, industrial cylindrical tubular elements under internal and external press., deform. and failure resistance 78—35460
  glass, surface flaw density, statistical determ. 78—11310
  glass bead, impact fracture *(Japanese)* 78—92338
  glass bonded Pt-Au thick film conductor, adherence fracture energy, Al_2O_3 substrate effects 77—56075
  glass ceramic, fracture stress rel. to flaw and fracture mirror sizes 79—11689
  glass fabric reinforced organic-matrix, interlaminar fracture studies 80—55495
  glass fibre reinforced cement, durability in wet and dry conditions, fibre length and content effect 80—71726
  glass fibre reinforced composite, failure anal. by fault tree technique 79—29193
  glass fibre reinforced composites, energy absorption during axial collapse 79—96112
  glass fibre reinforced concrete, flexural strength 78—11288
  glass fibre reinforced epoxy, short aligned fibres, mech. charact., SEM and optical obs. 78—72761
  glass fibre reinforced epoxy cross ply laminates, transverse cracking and long. splitting, strain effects 79—61723
  glass fibre reinforced epoxy laminate, failure, fractographic study 79—96111
  glass fibre reinforced epoxy laminate, mech. strength meas., comparison with theory, tensor polynomial failure criterion 78—39886
  glass fibre reinforced epoxy resin, destruction by diffused water 78—48511
  glass fibre reinforced epoxy resin, destruction by freezing or boiling of phase separated water 78—48512
  glass fibre reinforced plastic, fracture dynamics 80—100906
  glass fibre reinforced plastic, punching shear tests under static and impact loadings *(Japanese)* 80—55512
  glass fibre reinforced plastic, ring, exposed to press., transverse prop. effect on bearing capacity 77—86177
  glass fibre reinforced plastic laminates, failure models, reinforcement struct. effect 80—66641
  glass fibre reinforced plastics, cylindrical shells, compressive and flexural strength *(Japanese)* 80—81115
  glass fibre reinforced plastics, damage summation in nonstationary cyclic loading 80—60969
  glass fibre reinforced plastics, microstructure rel. to mech. props. 80—11685
  glass fibre reinforced polyester, 90° cross-ply laminates, multiple transverse fracture 77—8913
  glass fibre reinforced polyester, filament wound pipe, winding angle effect on failure 79—43379
  glass fibre-reinforced polyester cross-ply laminates, effect of resin failure strain on tensile props. 78—3212
  glass fibres, flaw generation by indentation fracture technique 80—81156
  glass plates, biaxially stressed, anal. of localised impact damage 78—68772
  glass plates, thermally tempered, strength degradation 78—48505
  glass reinforced laminates, damage accumulation during tensile loading 79—83262
  glass rods, compressively clad, residual stresses, comparison of optical and fractographic meas. 80—108539
  glass textolite, failure charact., effect of test conditions 78—27635
  glass-epoxy laminate post failure behaviour, stress concentration 77—48521
  glass-metal seal, finite element anal. of stresses, photoelastic meas. 79—29197
  glass/C reinforced epoxy resin, hybrid effects, conditions for positive or negative effects vs. rule of mixtures, mech. props. 78—68769
  glass/polymer/glass plate in temp. field, failure 80—43674
  glasses and fragile materials, fracture energy, direct meas. *(French)* 80—104376
  glassy organic polymers, total fracture surface energy, theory 79—43406
  grain boundaries decohesion energy, solute adsorption influence 80—65009
  granite, exam. of fracture mech. under dynamic loading 79—29218
  granite, failure expts., pore press. stabilisation 80—90079
  granite, hydraulically induced fractures for geothermal energy extraction 79—34424
  granite, shear and tension hydraulic fracture 77—91119
  granite, slow crack growth anal., appl. to rad waste disposal 79—89452
  graphite, deform. and fracture mech., high temp. effects 77—63763
  graphite, failure in lab. tests, fracture mech. approach, finite element stress anal. 77—4149
  graphite, fracture, stress gradient effect 78—92321
  graphite, fracture criterion 77—48552
  graphite, fusion reactor applications, mechanical constitutive laws for irradiation behaviour 80—32448
  graphite, isotropic, nonlinear stress/strain relationship effect on band strength 79—20119
  graphite, silicized, fracture analysis, deform. 78—15530
  graphite fabric reinforced organic-matrix, interlaminar fracture studies 80—55495
  graphite fibre filled polyimide composite laminates, space environment, phys. and mech. response 80—81140
  graphite fibre reinforced composites, energy absorption during axial collapse 79—96112
  graphite fibre reinforced epoxy laminate, fracture, comparison of anal. and expt. 79—61713
  graphite materials, isotropic, resist. to deformation and fracture under complex stress conditions 80—16479
  graphite reinforced epoxy laminate, fracture behaviour 79—83294
  graphite reinforced epoxy laminate, fracture by three point bend 79—83297

fracture continued
- graphite reinforced epoxy laminate, mech. strength meas., comparison with theory, tensor polynomial failure criterion 78—39886
- graphite reinforced epoxy laminates, cracked, deformation and failure in biaxial stress fields 79—47763
- graphite reinforced epoxy laminates, imminent fracture detection using acoustic emission 79—20302
- graphite ring, eccentric, under radial thermal load, stress state 80—76351
- PAN graphite-Al composites, fracture characteristics and props. 80—11779
- graphite-epoxy resin, hydrothermal ageing 77—52367
- graphite/epoxy composite laminates, splitting process charact. 80—25843
- graphite/epoxy laminate with third phase reinforcement, static and impact behaviour 77—40447
- Griffith type, analysis for large scale yield conditions 77—3771
- grinding, fracture and deform. mech., SEM obs. *(Japanese)* 79—15620
- guillotining materials, mechanics, fracture and burr formation 80—14619
- hardening of materials, plastic and viscous, steady and cyclic loading 77—4793
- Hastelloy X, creep props. and appl. to structural design *(Japanese)* 77—59862
- helical, in cylinders 77—56063
- heterogeneous structured materials, fracture theory using kinetic statistical approach, with discrete model, review 80—7678
- high alumina cement pastes, accelerated conversion, acoustic emission 77—36726
- high strain rate processes, review 80—84864
- hip replacements, total, causes of failure 77—81662
- Homalite, specimen geometry effect on crack propag. and arrest 79—34148
- Homalite-100 plates, modified compact-tension specimens, dynamic anal. 80—97561
- hot dry rock geothermal reservoir fracture mapping techniques 80—81419
- HTGR coated particles, failure rate prediction during neutron irradiation 77—79466
- hydraulic fracturing for stress meas. in hard and soft earthen material 77—9577
- hydraulic fracturing operations, material and structural simulations 78—31540
- hydrogen embrittlement, role of plastic fracture processes, exam. 78—60810
- hypoelastic materials with internal variable, work-hardening, hysteresis, fracture law 77—62177
- ice shelves, floating, tidal flexure cracks, fracture mechanics 78—69368
- ideal fibre reinforced composites, finite plane deformation and energy dissipation 78—79274
- impacted pretensioned plate, dynamic finite element and photoelastic analyses 78—67111
- Incoloy 903, microstruct. and effect of H_2 charging 77—86143
- Inconel 600 safe-end cracking failure at Duane Arnold reactor 80—104295
- indentation fracture mechanics, residual stress effects 79—83300
- Indiana limestone fracture toughness, confining pressure effect 78—57197
- influence function method, fracture mechs. and residual fatigue life anal. of power station cracked components 77—80109
- initiation, crack opening displacement and crack tip plastic strain energy 79—18819
- initiation location in disc under biaxial tension, statistical distrib. 77—58607
- initiation site prediction, idealized polycrystalline materials, stress and strain fields 78—34092
- initiation under metal working conditions 78—64662
- integral I and elastic-plastic fracture criteria *(Chinese)* 78—75100
- integral J_1, calculation by finite element analysis 78—67129
- intensity factor, single edge V-notched plates in tension 78—90782
- interface crack, singularity anal. 80—10201
- interfacial cohesion, adsorption-induced losses 80—65010
- intergranular, at elevated temps. 77—48545
- intergranular, at elevated temps. 78—19897
- intergranular, low temp. mechanism 78—60795
- internal elliptic cracks in thick plate, fatigue growth calcs. 77—80112
- internal heat source action in material 78—67025
- ionic crystal, ion-electron mechanoemission mechanism 78—3002
- ionic crystals, in mag. field 78—59855
- isotropic material, criterion of rupture and plasticity *(Russian)* 78—13973
- J_c data, indirect elec. determ., specimen config. effects 78—7011
- J-integral appl., review *(Japanese)* 79—81817
- J-integral as thin section fracture criterion 77—56067
- J-integral evaluation for CT specimen 78—67131
- jets produced by shaped explosive charges, particle size distribution in breakup 80—23957
- Kapron fibre reinforced phenolic resin, fracture kinetics, interface props. 80—66640
- karate, exertion of physical force using bare hand 79—88792
- Kevlar 49, fibre, mech. props., environmental effects incl. sunlight, ionising rad. 77—36560
- kevlar fibre reinforced composites, energy absorption during axial collapse 79—96112
- kinetics, static, dynamic loading, comparison 78—87738
- laminate, post-failure behaviour, no stress conc. 77—28895
- laminated composites, effective length of reinforcing component 80—25797
- laminates, combined fracture and delamination, simple idealised example 77—68529
- laminates, failure mechanics, damage development 79—43427
- laminates, multiple fracture 80—10206
- laminates, plane strain state with transverse crack 80—38338
- laminates, symmetric, new results on edge effects 77—46971
- Larson-Miller parameter, rel. to stress rupture and creep 77—72192
- lattice instability theory 80—84244
- lattice-statics approach, review 80—39212
- lattices, two-dimensional, detonation, shock propagation, computer simulation 79—64554
- layered structures, intercalation, crack propag. theory 80—97559
- layered thin composites, optimum design and strength 80—10210
- lecture on fracture toughness *(Japanese)* 80—90595
- lens, Schott S-1005, static fracture resist. rel. to thickness 78—81063

fracture continued
- limit torsion problems, finite element method, failure torque 79—72820
- limiter materials, for Doublet III fusion research machine, selection 78—55026
- limiting load assessment for cracked body from deform. resist. criteria *(Russian)* 78—9606
- linear 3-D fracture mechanics, displacement hybrid finite element model 77—3792
- linear elastic and post yield fracture mechs., thermal and residual stresses 77—89066
- linear elastic fracture mechanics, stress singularities interfaces 78—34079
- linear fracture mechanics parameters, in fatigue life estimation, sensitivity study *(Japanese)* 80—64468
- linear theory of elasticity, in fracture mechanics 80—64458
- longitudinal-shear crack refraction, Wiener-Hopf method calcs. 80—87743
- LWR pressure vessel, unstable fracture *(Japanese)* 79—9767
- macrofracture of solids, mechanism and kinetics 80—92600
- macroscopic examination procedures for failure analysis 79—66254
- magnesite-dolomite refractories, tar bound, fracture and wear 80—104287
- matched asymptotic expansions, in nonlinear fracture mechanisms 78—51127
- material divagation, appl. to fracture 78—67109
- material minimum lifetimes, failure probability after proof testing, exam. using Monte Carlo method 78—79273
- material strength, stability in fracture mechanics 79—57117
- material with initial defects 80—38339
- of materials, conf., Waterloo, Canada (June 1977) 78—56763
- materials under complex stress, with local dynamic loading, strength 79—91768
- maximum stress criterion on the equal strain energy density line *(Chinese)* 79—32371
- mechanics, conf., Washington, USA (Sept.78) 79—43422
- mechanics, fundamental aspects and new developments *(Italian)* 78—34086
- mechanics, linear elastic, appl. to crack stability in brittle struct., elastic-plastic conditions 78—90800
- mechanics, techniques, review 79—41635
- mechanics, variational bounds, qualitative method 78—67134
- mechanics, variational bounds and qualitative methods 78—79283
- mechanics appl. to wear 80—11792
- mechanics of cracking, computing, based on three-dimensional models and finite element analysis *(German)* 80—58976
- mechanics stress intensity calibration in four-point bending, expt. determ. 77—77558
- mechanism maps, exam. of development 78—56764
- metal, BCC, intracrystalline fracture *(Russian)* 79—5031
- metal, current pulse effects on structure at crack tip *(Russian)* 77—44332
- metal, inhomogeneous strain effects on surface props., rel. to fracture model development 77—72907
- metal, interbubble fracture mech. of blister form., He irrad. 78—6109
- metal, lattice decohesion due to H_2 78—15533
- metal, plasticity under hydrostatic pressure *(Russian)* 78—68726
- metal, sinter-forging process, powder charact. effects 77—59714
- metal, spalling produced by elastoplastic waves 77—80574
- metal, stress-induced EM effect, phys. model 78—55909
- metal, tensile fracture, transient elec. and mag. field form. 77—4148
- metal, thin sheet, crack growth, effect of strain rate 77—1869
- metal arc welds, chevron cracking, initiation and propagation 79—38981
- metal cutting, separation process tool tip, fracture detection, acoustic emission method *(Japanese)* 80—1388
- metal failure, due to hydrostatic pressure, exam. of kinetics 78—52944
- metal foil with thin film coating, failure by laser pulse *(Russian)* 78—23561
- metal matrix-fibre composites, brittle interface layers and tensile strength 79—79039
- metal rods, stress state and fracture in pulsed mag. field 80—81201
- metal-glass material, relation between struct. and props., prod. by hot densification 78—11145
- metal-metalloid amorphous systems, thermal instability, crystn. characts. 77—4044
- metallised coating on polyethylene terephthalate film, fracture under laser irrad. *(Russian)* 80—76333
- metallography, failure analysis appl., conf., Houston, USA (July 1977) 79—61832
- metallurgical coke, mech. behaviour charact. *(French)* 80—104371
- metallurgically bonded plates, structural integrity determ. by high energy impulse 79—39111
- metals, deformation resistance, rel. between uniaxial stress state and breaking stresses in shear 80—3147
- metals, effect of hydrostatic pressure and stress on plasticity 78—52907
- metals, FCC, BCC and HCP, fracture mechanism maps for materials which cleave 79—91774
- metals, fracture due to laser irrad. and shock compressed plasma *(Russian)* 80—55500
- metals, fracture during laser working, depend. on physico-chem. props., heat cond. *(Russian)* 80—55432
- metals, H effect on mech. props., review 80—50718
- metals, mechanical props., testing and modelling 80—25811
- metals, physicomechanical characts., review 79—52368
- metals and alloys, FCC, fracture mechanism maps and construction 79—61693
- meteoroids atmospheric breakup, effects on crater field form. 80—94760
- meteors thermal fracture, detached particles mean dia. 80—62081
- methodological questions in determ. of failure criteria in complex stressed states and complex loading *(Russian)* 78—67089
- microanalysis of fracture surfaces by energy dispersive X-ray spectrometry with Si(Li) diodes *(French)* 80—89571
- microcrack enlargement in heterogeneous materials, conc. criterion 80—11769
- microfractographic characts., in determ. of failure stages in repeated loading 77—40490
- microfractography *(Japanese)* 80—71841
- micromechanical models in risk anal. 80—108572
- mild steel, circular plate perforation and deformation by square section punch 79—34100
- mineral-fibre composites, treatment for increased fracture and cracking resistance 77—8798

fracture continued
mode II fracture test specimen, boundary-collocation anal. and photoelastic expt. 77—50982
mode III cracks, steady propag. followed by nonuniform growth, stress intensity factor 77—65716
monocarbide, cubic, calc. of surface energy, rupture energy, and theoretical strength 77—11775
moving interfacial cracks, dynamic stresses, finite difference approx., iterative process 77—46966
Mylar film/adhesive/Al foil laminate, mech. interactions 80—81112
Ni-base wrought superalloy, creep and stress rupture behaviour in air and vacuum 80—60918
Nimonic 105, creep and stress rupture props., trace elements influence 80—66602
Nimonic 80A, struct., fracture characts. 80—3071
Nomex, fibre, mech. props., environmental effects, incl. sunlight and ionising rad. effs. 77—36560
non-linear theories for onset of stable and unstable crack growth 77—72248
nonlinear elastic systems, incremental approach to the solution of snapping and buckling problems 79—76975
nonlinear fracture mechanics, exam. of J-integral criterion for crack growth initiation 78—60775
nonlinear fracture mechanics, matched asymptotic expansions method, longit. shear of elastic-perfectly-plastic specimen 77—35087
nonlinear fracture mechanics, matched asymptotic expansions method, longit. shear of elastic work hardening plastic specimens 77—35088
nonlinear materials, Mode I fracture behaviour, finite element anal. 80—84237
nonlinear mechanics 78—79261
notched fibre reinforced composites, tensile fracture 78—52991
notched rectangular bars, stresses at plastic deflection *(German)* 78—34025
nozzle, primary coolant inlet of PWR vessel, fracture mech. exam of integrity *(German)* 78—17327
nuclear fuel pellet-cladding interaction phenomenon investig. 77—46299
nuclear reactor materials, crack propag., fracture, and ductile-brittle transition *(Spanish)* 79—36316
nuclear reactor materials, crack-front tunnelling, investigated by single specimen compliance technique 80—70300
nuclear reactor Pilgrim I nozzle-to-press. vessel weld discontinuities, fracture mechs. anal. 77—80110
nuclear reactor piping system, crack initiation and propagation, fracture mechanics 80—83193
nuclear reactor pressure vessel ZR-6M rupture test using scaled simulation *(Hungarian)* 78—89964
nuclear reactor pressure vessels, radiation embrittlement, allowable crack size, unstable fracture 77—10465
nuclear reactor technology, fracture problems 78—78472
nuclear reactor valve bellows, effect of service parameters on fatigue life and fracture 78—58348
nuclear reactor vessel cracks and elastic fracture mechanics 77—67843
nuclear reactors, seismically qualified piping, failure probability, ASME code limits 80—78365
numerical anal. of fracture initiation 77—75861
numerical solutions of three dimensional dynamic crack problems and simulation of dynamic fracture phenomena by a 'non-standard' finite difference method 79—41613
numerical treatment of boundary integral eqns., three-dimens. elastostatic anal., fracture mechs. appls. 77—46909
nylon 6, notched sheet, deform. mech., fracture, X-ray obs. *(Japanese)* 77—59863
Nylon 6, unidirectionally reinforced, mech. props. and fracture 77—21252
nylon 6 fibres, chain rupture during tensile deform. 79—15740
oil shale, dynamic fracture strength, expt. determ. method 79—48584
oil shale, shear and tension hydraulic fracture 77—91119
olivine, fracture surface energy 79—16462
one-dimensional crystal, deform. and fracture simulation 78—47470
one-dimensional crystal subjected to deform., static and dynamic equilib. 79—28037
opening mode crack problems, Westergaard method, critical re-examination 80—38337
optical fibre, long length for communications cable, proof testing 77—54818
optical fibre, spark-induced fracture for low-loss joints prep. 78—1441
optical fibre, statistical data, graphical and analytic statistical model depiction 77—83975
optical fibres, breaking strain estimation for long lengths of fibres 78—30060
optical fibres, fractographic analysis 79—59828
optical waveguide long-term stress failure probability estimation 80—58745
organic fibre composites, lifetime prediction, expt. verification of accelerated test 77—50993
organic fibre reinforced plastics, failure 80—11774
organoplastics, fracture characts., effect on strength 80—66642
orthorhombic crystals, triboluminescence and piezoelectric behaviour 79—95861
osteons with crossed lamellae, micromech. study 77—25493
p-convergent finite element approx. in fracture mechanics 78—38252
pacemaker, lead wire fracture 78—57134
paper sheets and single fibres, SEM investigation 79—34149
paraboloids of revolution, internal fractures due to stress wave focusing 80—83762
particles, abrasive, mech. strength determ. 79—87781
PBI fibre, mech. props., environmental effects, incl. sunlight and ionising rad. effs. 77—36560
pearlite, SEM obs. of tensile deform. and fracture 78—84897
perforated plate, global stress strain behaviour 80—10169
perspex spheres, internal fractures due to stress wave focusing 78—18239
Perspex spheres, times to fracture due to point explosive loading 77—50989
PET, IR, spectra of prefractured state 77—69032
PET, rigid, unoriented, prefracture state study, forced high-elastic deform. 77—59931
PET film, relation between deform. and rotational isomerism 77—52438
Phobos, impact fracturing rel. to grooves distrib., morphology and possible origin 80—72837
Phosphate conversion coatings on steel 78—3251
photoelastic determination, of mode I stress intensity factors 78—90781

fracture continued
photoelastic determination of stress intensity factors *(Chinese)* 79—32395
piezoceramic, compression tests, fracture stress distrib. at various loading rates 78—15529
piezoelectric materials, fracture mechanics, deform. anal., crack development 77—24349
pin loaded single edge notched tension specimens, K-COD relationship 78—67133
pipeline, pressurized, steady-state crack propagation 77—58614
along planar slip bands 80—107262
plane strain conditions, crack propag., fracture energy criteria, displacement discontinuity method 80—48648
plane strain fracture mode criterion based on plastic zone size-thickness correlation 80—43670
plant fibres, fracture mechanism 80—35931
plant material, cryofracturing and low temp. SEM 78—24207
plastic deformation, appl. of continuum theory of dislocations fracture mechanics 78—67767
and plastic deformation 78—88497
plastic fracturing materials, work inequalities and stress-strain relations 80—103000
plastic materials, crack resistance *(Russian)* 78—63377
plastic solids, rupture mechanics using contour integrals *(French)* 80—14615
plasticised cellulose acetate sheet, post-yield fracture 80—25859
plasticity, couple-stress theory and plane boundary problem *(Russian)* 79—86358
plasticity and fracture mechanics, finite element anal., review 79—41612
plasticity model, dislocation based, geometrically consistent 78—30242
plates and tubes, thick-walled growth characts. of part-through cracks 77—58613
plates under uniaxial load, optimum hole shapes, cracks and fracture appl. 80—64479
plexiglass composite, long term strength and durability 80—75294
PMMA, crack growth rate effect, fracture surface structure 80—16466
PMMA, crack velocity depend. on critical stress in fracture, static and dynamic loading 77—63768
PMMA, critical stress-intensity factor, determ. under mixed mode loading conditions by shadow optics 78—68868
PMMA, defect build up in service, effect on notch sensitivity 77—66694
PMMA, destruction of microsec. time scale, tensile stresses 79—70172
PMMA, fracture morphology in notched tension, mol. wt. effects 77—52487
PMMA, fracture surface parabola markings, temp. 78—52969
PMMA, notched, sheet, deform. mech., fracture, X-ray obs. *(Japanese)* 77—59863
PMMA, pulsed dielectric breakdown, mech. stress photoelasticity obs. *(Russian)* 78—2800
PMMA, solid, stress-strain behaviour, strain rate and temp. effects, cryogenic temps. *(Japanese)* 78—11315
PMMA, struct.-prop. relationship between mol. wt. and fracture surface energy 78—80633
PMMA, time independent fracture criterion 79—83298
PMMA, uniaxial tension, fractographic anal. of crack growth kinetics 80—40519
PMMA bar, notched and perforated, fracture produced by longitudinal impact 79—43388
PMMA biaxially stressed plate, fracture trajectories 77—70152
PMMA notched beam, fracture due to central impact 80—16426
PMMA plate with angled elliptic notch in tension, exptl. investig. 78—38257
PMMA-mortar composite, thermocatalytically polymerised, fracture morphology and mech. props. 78—27595
point defect model for materials failure 77—16669
point-loaded centre cracked plates 78—19884
political and social decision making rel. to fracture, failure, risk anal. and safe design 78—77661
poly(butadiene-co-styrene), rubber, radiation cured, dynamic phys. props. 77—69003
polyarylate, rupture mechanism 79—52372
polyaxial stress states, fracture statistics 79—41625
polybutadiene, elastic fracture, polymer chain entanglement criterion 78—79290
polycapromide, fracture, interatomic bonds deform. 79—57107
polycarbonate, notched sheet, deform. mech., fracture, X-ray obs. *(Japanese)* 77—59863
polycarbonate, notched specimens deform. and fracture 78—11293
polycarbonate, particles, critical stress 77—28869
polycarbonate, plane strain fracture energy instability and mixed mode crack propag. 78—68775
polycarbonate, theoretical prediction of temp. rise at tip of running crack 80—2114
polycarbonate notched beam, fracture due to central impact 80—16426
polycarbonate of bisphenol bar, notched and perforated, fracture produced by longitudinal impact 79—43388
polycarbonate plates, modified compact-tension specimens, dynamic anal. 80—97561
polycrystalline materials, diffusion controlled stress rupture 77—32681
polycrystalline materials, diffusion-controlled stress rupture 80—3186
polyethylene, effects of mol. rot. and crosslink on specific draw ratios *(Japanese)* 79—96099
polyethylene, extended chain crystal, fine structure and nucleation mechanism 78—14287
polyethylene, fracture energy determ. 77—62208
polyethylene, high density, effects of draw rate and temp. on necking stress *(Japanese)* 79—91757
polyethylene, high density, necking stress *(Japanese)* 77—56036
polyethylene, high-density, tensile necking, specimen size and loading conditions effects 79—61672
polyethylene, high-density unorientated, damage buildup kinetics under creep conditions, during prolonged loading 80—60932
polyethylene, nonoriented partially cryst., kinetic damage accumulation cure 80—71753
polyethylene, notched sheet, deform. mech., fracture, X-ray obs. *(Japanese)* 77—59863
polyethylene, stress rel. to draw ratio during ultra draw *(Japanese)* 79—91759
polyethylene, uniaxially oriented, relation between deform. and rotational isomerism 77—52438
polyethylene films, lifetime under small loads 79—95301

fracture continued
polyethylene reinforced with graft polymers, molecular failure mechanism, IR spectra 77—16682
polyethylene stabilized with home-made antioxidants, thermal resistance *(Polish)* 79—52328
polyethylene terephthalate, exposed to aq. medium and γ-radiation, lifetime levels and fracture 80—40520
polyethylene terephthalate, fracture, interatomic bonds deform. 79—57107
polyisocyanurate foams, strength, cellular struct. effect 80—40518
polymer, activation energies of fracture and deform., comparison *(Russian)* 78—11303
polymer, crosslinked, amorphous probabilistic theory of time to fracture 77—90448
polymer, deform. polarisation effect on interaction with liquid environment, fracture *(Russian)* 77—25166
polymer, deformation, ultimate regimes for flexible chains 78—19844
polymer, drawing properties, role of interfibrillar tie mols. 78—76706
polymer, failure, book 78—92361
polymer, filled, tensile strength calc., rel. to fracture *(German)* 80—25795
polymer, fracture time variability, endochronic prediction 78—76734
polymer, glossy, generality of plastic fracture process 80—35321
polymer, rubbery state, correl. between strength and relaxation props. 77—28848
polymer, solid, impact compression crushing at low temps. *(Japanese)* 78—7032
polymer, time depend. fracture, mol. motions effect 79—15780
polymer coated metal spheres, flow, degradation mechanism 77—9036
polymer crystals, deform. and fracture, submicrocrack nucleation and supermod. struct. 78—52918
polymer reinforcement, fracture mechanics 80—10207
polymer rod, fluid-permeable, longit. stability during creep 79—57066
polymer-metal laminate, bone fixation plate fabrication, fracture stabilisation 79—79685
polymeric materials, thin-wall tubes, rupture time determ. 80—64473
polymers, mech. props., at 4.2K depend. on chemical struct. and physical struct. form. 77—28847
polymers, plastic deformation during freeze-cleavage, review 78—14400
polymers, solid-liquid state transitions, state before breakdown 78—63842
polymers, specific fracture surface energy, meas., review *(French)* 80—104275
polypropylene, (Moplen) influence of temp. and mol. wt. on high speed fracture mechanics 80—76341
polypropylene, fracture exam. using microscopic obs. *(German, English)* 79—20186
polypropylene, interatomic bonds deform. 79—57107
polypropylene, notched sheet, deform. mech., fracture, X-ray obs. *(Japanese)* 77—59863
polypropylene, oriented, microcracks diagnostics by paramag. probe method 80—66736
polypropylene, stability under radiation sterilisation 77—60245
polypropylene fibre reinforced polyoxyethylene, fracture kinetics, interface props. 80—66640
polypropylene fibrillated film reinforced cement, loading capacity, cracking 78—72759
polypropylene fibrillated film reinforced cement matrix for low cost sheeting 80—80996
polypropylene reinforced with graft polymers, molecular failure mechanism, IR spectra 77—16682
polypyromelliteimide, fracture, interatomic bonds deform. 79—57107
polystyrene, amorphous, failure in methanol and ambient air 80—3165
polystyrene, coarse shear bands and fracture, SEM study, craze fracture surfaces 79—29191
polystyrene, elastic fracture, polymer chain entanglement criterion 78—79290
polystyrene, particles, critical stress 77—28869
polystyrene, rubber-modified, crazing and fracture, Dugdale model 77—8907
polystyrene, rupture mechanism 79—52372
polystyrene film, craze growth and fracture 79—83319
polystyrene film, temp.-stress depend. of rupture life under hydrostatic pressure 80—16467
polystyrene-polyethylene(ethylene-propylene) blends, copolymer modified, mech. props., morphology 79—57088
polystyrene-polymethylmethacrylate system, phase relationships and fracture surface morphology 79—61571
polystyrenes, monodisperse, static and dynamic props., mol. wt. effect 78—84938
polyurethane, tensile fracture stress eval. for prosthetic heart valve 77—56533
polyurethane foam/glass reinforced plastic/Al, sandwich construction, nonsymmetric, flexural fracture 79—74233
polyurethane foams, strength, cellular struct. effect 80—40518
polyvinyl alcohol fibre reinforced epoxy resin, fracture kinetics 78—3222
polyvinylbutyrals, rupture activation energy and structurally sensitive coeff. *(Russian)* 77—21282
polyvinylidene fluoride, γ-ray irradiation effect on mech. props., in presence of triallyl trimellitate *(Japanese)* 77—86091
porous materials, fracture behaviour estimation using simulation model and finite element method 77—42777
portland cement paste, microstructure study by SEM, TG and X-ray diffr., corrosion 78—92381
post yield solutions for fracture mechanics analyses of cracks emanating from elliptic holes 79—68643
powder, tensile strength data and failure loci from Jenike shear cell tests 78—31476
Prandtl-Reuss plastic material with scalar and tensor internal variables 79—68589
precipitative processes and intercrystallic failure, quantitative methods *(Czech)* 78—60672
prediction on basis of acoustic emission 80—104382
prefracture zone, similarity conditions in vicinity of contour of microcrack *(Russian)* 78—30233
preservation and cleaning, for fractography 80—71866
pressure diecast automatic components, processing condition effect on performance 78—88623
pressure tube explosive rupture anal. using scaled-down model of CIRENE reactor 80—18449
pressure vessel components reliability, conf. Vienna, Austria, 1977 79—17986

fracture continued
pressure vessels, thin-walled, containing surface flaws, fracture mechanics and acoustic emission exam. of failure 78—84981
pressure vessels, warm prestressing effects, fracture mechanics during severe thermal shock 79—22411
pressurized containers, crack propagation and arrest 77—58611
probabilistic fracture mechanics anal., nuclear power station structural components 77—81317
profilometric anal. 78—88600
propagating rectangular fracture in semi-infinite elastic medium 78—57168
propagation, Stefan problem approach 77—14964
propagation rate meas. by fracture sensors 80—50796
propergol, rheological props. during polymerisation *(French)* 78—23762
PVC, plasticised, fracture energy determ. 77—62208
PVC, rigid, viscoelastic props. rel. to thermal, mech. history 79—5016
PVC, rubber-modified, stress whitening and yield mechanism 79—8324
PVC, solid, stress-strain behaviour, strain rate and temp. effects, cryogenic temps. *(Japanese)* 78—11315
PWR pressure vessel failure probability from pressure transients, OCTAVIA computer code 79—18011
Pyrex, stress intensity factors of surface cracks and fracture stress, acoustic meas. 79—47845
Pyrex glass, near-surface H embrittlement, effect on deform. and fracture props. 79—29180
pyrex glass, statistical analysis of Hertzian fracture using Weibull distribution function 80—66623
Pyroceram, enhanced failure by combined pulse and CW laser 79—29182
quantitative fractography review 79—39072
quantum solid, lifetime-under-load, temp., depend. 77—15487
quartz, thin layer, interaction with gas-discharge plasma *(Russian)* 78—14178
quasi static crack growth, in sheet materials 78—67106
reactor containment liner seismic reliability under statistical uncertainty, cracking 78—89948
reactor fracture safe design, appl. to elastic-plastic fracture mechanics params. 78—30241
reactor fuel pin rupture detection system, using meas. of time differential of acoustic emissions 80—102282
reactor press. vessel nozzle under internal press. safety against bursting *(German)* 78—17326
reactor primary system under operating and accident conditions 78—66342
reactor technology, conference, Berlin, Germany (Aug. 1979) 80—77539
Rebinder effect in breakdown of dielectrics 77—44328
recognition from stereo photographs 78—54140
reference theta pinch reactor, first wall thermal-mechanical anal. 77—57750
refractories, hot compressive strength 77—12677
refractory, rheological behaviour at high temp. *(French)* 77—56016
refractory, thermal stresses produced by temp. gradient, finite element anal. *(Japanese)* 80—33538
refractory composites, fibre reinforced, directionally solidified tensile tests, in HVEM, deform. and fracture *(French)* 78—68785
refractory oxide, thermal shock resist. mechanisms 80—25860
reinforced concrete containment model behaviour under thermal gradients and internal pressure 80—42837
reinforced masonry shear wall, elastoplasticity and crack-growth anal. *(Chinese)* 79—94506
reinforced plastics, failure of thin walled flexural structures 80—10209
reinforced polymer, strength, statistical struct. parameter effects *(German)* 77—56095
reinforced shell of revolution, failure in bending 79—90185
resin, highly crosslinked, fracture, review 77—4846
resin beams with glass fibres, crack propag. expt. 78—15521
resin matrices and their contribution to composite properties 80—81028
Rochelle salt, depend. on mechanoluminescence on charge prod. during fracture 78—88370
rock, computer modelling in uniaxial compression *(Japanese)* 80—12379
rock, failure process under compression, fracture mechanics *(Japanese)* 79—57915
rock, fracture mechanics approach to in situ stress field determ. via hydrofracturing 78—81435
rock, laminar, stress distrib. during sliding failure 79—2225
rock, symmetrically extending plane crack, self-similar pressure profiles 78—69340
rock fracture, assoc. microacoustic signals anal. 78—32070
rock half-space, impact of steel cylinder and effects 80—85649
rock jointing, Griffith crack concept appl. 77—53048
rock volume changes during fracture and frictional sliding 79—16450
rockburst fault gouge microscopic features, SEM obs. 79—74891
rocks, dilatancy and fracture induced vel. changes rel. to frictional sliding 79—16458
rocks, edge-fracture anal. method 77—21765
rocks, electrical resistivity changes during frictional sliding and fracture 79—16457
rocks, faulting and flow during deform. expt. in transmitted light 77—86860
rocks, fracture intensity, expressed as fracture surface area per vol. 80—8301
rocks, fracture propagation by transient cooling 79—84236
rocks, fracture regularities with internal friction and dilatancy 78—85537
rocks, fracture under uniaxial compression *(Chinese)* 77—37183
rocks, fractures effect on compressibility, anal. using new model 80—8300
rocks, hydrofracturing stress meas. techniques, American field results 77—9576
rocks, hydrofracturing stress measuring method and recent field results 79—29885
rocks, microfracture *(Japanese)* 78—7020
rocks, rings, discs, under diametral compression, tensile strength calcs. *(French)* 77—70638
rocks, shatter cones geometry and description procedure 80—51398
rocks laboratory hydraulic fracturing 77—73723
rollers, steel casting installation, effect of thermal stresses on fracture characts. 78—64650
rubber, cutting resistance measurement in absence of friction 79—5035
rubber, ethylene-propylene, fracture energy determ. 77—62208
rubber, fracture in viscoelastic systems under cyclic loading 80—81195

fracture continued
rubber, natural, tensile fracture strength eval. for prosthetic heart valve 77—56533
rubber, rupture life calc. 77—59933
rubber, vulcanized, longevity computation, fracture 79—96131
rubber balloon bursting under biaxial strain, tear behaviour 80—19287
rubber filled epoxy polymers, dense-woven, fracture characts. 80—11757
ruby, structural defects due to laser irrad. *(Russian)* 80—100303
running crack, cohesive fracture zone, thermodynamic laws 80—43676
rupture processes and fracture mechanics *(French)* 80—5989
rupture time, entropy criterion estimate 80—55535
sandstone, fluid injection effects on fracture 78—7622
SAP 895 (Al-Al$_2$O$_3$) alloy containing ^{4}He and ^{3}H, tensile props. 80—34129
sapphire, fracture anisotropy of ⟨1$\bar{2}$10⟩ zone 79—61726
SBR, fracture energy determ. 77—62208
sea ice, failure by compression *(Japanese)* 78—88841
seismic faulting, rupture propag. in presence of friction and inhomogeneous initial stress 77—86835
seismic vel. changes during fracture and frictional sliding 79—16408
self-adaptive finite elements 77—72249
SEM fractograph quantitative analysis, develop. and exptl. verification 77—60023
SEM obs. *(Chinese)* 80—11849
SEM/acoustic emission in situ techniques *(German)* 79—96240
semibrittle, damage process preceding fracture, plastic strain depend. 77—32692
separation energy rate for crack advance 78—56765
shallow shell, pressurized, cracked, fracture mech. anal. 77—72240
sharp-pointed stress concentrators with various types of angular recovery points *(Russian)* 78—9605
sheet metal forming, material behaviour 78—95787
shell, by periodic shock waves 77—89068
shell, fracture behaviour, forming severity and metal flow in deep drawing 79—38975
Sialon, reaction sintered, mech. props., effect of composition and X-phase 77—56013
Sih fracture criterion formal extension, elastic stress field near crack *(German)* 79—1139
silica paricle filled epoxy resin, mech. props., fracture by slow crack growth 77—40443
silicone rubber, tensile fracture stress eval. for prosthetic heart valve 77—56533
simulation of inelastic material behaviour in struct. anal. 78—34041
single phase system, microfracture from thermal expansion anisotropy 79—19314
singular crack borders, constitutive preps. 78—67108
skew crack propagation, induced dynamic stresses, numerical soln. 79—1137
skin, mech. and struct. response to X-irradiation 80—35994
slitlike crack arrays, plastic and strain hardened materials, fracture characts. 78—90798
snow, acoustic emission response 79—87801
snow, shear fracture precipitated by strain softening rel. to dry slab avalanche release 80—8338
snow, uniaxial tension, strain rate and fracture *(Japanese)* 78—88855
solid composite propellants, fracture criterion, fracture time computation 78—75106
solid popellant, delayed fracture and crack propagation *(French)* 80—108521
solidifying ingot, temp., strain and stress distrib. *(Russian)* 77—25041
specimen configuration effects, tensile and precracked data 80—16413
spheres at high pressure, contact stresses and spreading resistance 78—71296
split birefringent coating on birefringent material, determ. of dynamic stress intensity factors 79—50684
stability conditions in fracture mechanics 78—13974
stable crack extension and nonlinear fracture criteria, finite element anal. *(Chinese)* 80—10184
stable crack-growth, fracture criteria, numerical approach 78—67104
stable progressively fracturing solids 77—7347
statistical approach to fracture, fatigue crack growth of defects 80—1487
statistical methods for creep, fatigue and fracture data analysis 80—58936
statistical treatment, maintenance procedures 79—43538
statistics, relation between volume and surface distributed cracks 79—50664
statistics for polyaxial tension, approx. treatment 77—58602
steel, austenitic, alloy and stainless, fuel-element cans, deform., failure, rigid loading scheme 79—91765
steel, austenitic, hot isostatically pressed superalloy A286, fracture path 78—23824
steel, austenitic, Kh17N13M3T, activation characts. of rupture, 630-730°C, Sb and Nb microalloying effects *(Russian)* 79—5033
steel, austenitic, types 304 and 316, fracture-mechanisms, tensile specimens 80—85039
steel, austenitic heat resistant, zig-zag grain boundaries, strength 77—73308
steel, austenitic heat-resisting, deformation and fracture rel. to grain-boundary reaction nodules 78—80591
steel, austenitic stainless, ageing at high temp., effect on creep props. SEM 80—97516
steel, austenitic stainless, Cr-Ni (16, 16 wt.%), in-pile rupture strength, cold work and soln. annealing effects 77—63687
steel, austenitic stainless, DIN 1.4970, influence of He on high temp. mech. props. 79—7636
steel, austenitic stainless, grain boundary segregation studies, intergranular fracturing technique for stress corrosion cracking investigation 79—39057
steel, austenitic stainless, He implanted 1.4970, high temp. fracture 77—86186
steel, austenitic stainless, liquation cracking during welding, comp. influence 80—66645
steel, austenitic stainless, tensile fracture, phase transform. effect, comparison of stable and metastable phases 78—60798
steel, austenitic stainless type 316, σ phase precipitation during long term high temp. creep, fracture 79—74157
steel, austenitic stainless type-316, fracture mechanics study of stress corrosion cracking 80—16580
steel, bonded with epoxy resin, effect of adhesive bond thickness on mech. resist. *(French)* 77—63882

fracture continued
steel, C, cold rolled sheet, spot welded joints, static fracture appearance 80—55538
steel, C, effect of pre-straining on torsional fracture strain *(Japanese)* 80—3183
steel, C, explosively fractured, struct. of white etching band 79—61722
steel, C, fracture, effect of cementite *(Russian)* 78—7037
steel, C-Mn, types SA-516-70, SA-105-B, fracture energy criterion determ. by static and dynamic testing 80—40651
steel, carburised, microstruct. and fracture 79—24658
steel, cast, fractographic features of coarse grained intercrystalline fractures *(Czechoslovakian)* 77—36627
steel, cast, heat-resist., subcrit. crack growth 80—97581
steel, cast 18OSKhNM, fractographic investigation 77—21266
steel, cast automatic couplings, yield strength, crack propag. resistance and ductile-brittle transition temp. 80—104281
steel, cast structural, heat treatment and mech. working influence on mech. props. *(Russian)* 80—40392
steel, Charpy type bars of AISI 4340, varying notch root radii, fracture initiation and propag. at notch root 80—85050
steel, Ck 45, alternating bending, fracture surface appearance *(German)* 78—52995
steel, correlation links between mech. props. controlled rolling effect 80—35234
steel, Cr-C, segregation of P, C, and Cr to γ-boundary and carbide/γ-interface *(Japanese)* 79—61593
steel, Cr-Mo:P (2.25, 1 wt.%), stress relief cracking, effect of P segregation 80—89324
steel, Cr-Mo, cast and forged, difference in mech. props. 77—48465
steel, Cr-Mo (2.25, 1.0 wt.%), fracture-mechanisms, tensile specimens 80—85039
steel, Cr-Mo (2.25, 1 wt.%), temper embrittlement trace elements, Mo, intercritical heat treatment effects 77—36634
steel, Cr-Mo weld metal, reheat cracking, residual elements and microstruct. influence 80—66553
steel, Cr-Mo-V, press. vessel, fracture, effect of tempering 78—60799
steel, Cr-Mo-V low-alloy, mech. props. and stress relief cracking, effects of impurities and deoxidation practice 80—66599
steel, Cr-Mo-V low-alloy, stress relief cracking, impurity and alloy content effects 80—66654
steel, Cr-Mo-V low-alloy with high residual element content, cavitation control 80—66663
steel, Cr-Mo-V pressure vessel, microstruct. parameters and yielding rel. to plastic deform. 80—89318
steel, Cr-Ni-Mn, adiabatic shear band determ. by surface obs. 80—97579
steel, Cr-Ni-Mo, 'spots' *(Chinese)* 80—104248
steel, Cr-Ni-Ti-B, grain size effect on mech. and struct. props. *(French)* 80—45361
steel, crack resistance, −196 to 500°C 80—71750
steel, crack tip opening displacement and J-integral fracture criteria 77—3777
steel, cratered overheating facets 77—52482
steel, CrMoNi, cantilever beam method to determ. J_{Icc} and J_{Iscc} *(Chinese)* 78—15488
steel, delayed fracture, hydrogen and impurities 78—84988
steel, elastic plastic material, critical stress intensity factor determ., fracture mech. method *(German)* 79—11694
steel, elastic-plastic fracture, plastic zone correction application 79—70147
steel, fission reactor pressure vessel, reliability 79—22430
steel, flaw detection in macrostruct. of large specimens 79—87777
steel, forged axle spindle, fractographic anal. of shear fracture 78—68821
steel, fracture obs., shell-shaped fracture 77—25153
steel, free cutting, with MnS inclusions, tensile flow and fracture 78—11290
steel, heat resistant 15Kh1M1FL, cast, crack development at various stages of fracture, prolonged load 77—63802
steel, high C, tensile strength, working and heat treatment effects *(Japanese)* 80—104209
steel, high Mn, mech. props., strain induced martensitic transform., effect of austenite predeformation 77—16649
steel, high speed, matt-facet fractures *(Chinese)* 78—95793
steel, high strength, dislocation sweeping model for hydrogen assisted subcritical crack growth 80—97577
steel, high strength, low alloy, critical stress for delamination fracture 79—1907
steel, high strength, low alloy, splitting of tensile and impact specimens 77—63777
steel, high strength, subcritical crack growth, role of time delayed H_2 assisted plastic zone growth 80—97576
steel, high strength sheets, finite element anal. of crack propag. expts. 80—40498
steel, high-speed, shiny nonfusion rings in friction welding, origin 78—23872
steel, inclusion behaviour investigations using SEM 78—23916
steel, intergranular failure, role of grain boundary composition 79—20155
steel, intergranular fracture, impurity effects 77—8842
steel, laminar, high hardness, ballistically damaged, fracture mech. approach to residual strength 77—56050
steel, low alloy, A533B, fatigue crack prop. 78—35517
steel, low alloy, fibrous component zones size, depend. in fracture on impact test temp. and notch radius 80—21076
steel, low alloy, fracture strength investigation under various types of loading 78—7042
steel, low alloy, quenched, tempered martensite embrittlement, role of retained austenite and cementite 79—74251
steel, low alloy, quenched and tempered, formation of stony fracture during forging 79—79059
steel, low alloy 30KhGSA, sheet, regression anal. of critical stages of fracture process 79—15786
steel, low alloy Mn-Sb(2, 0.12 wt.%), reversibility of temper embrittlement, studied by XPS and AES 77—32667
steel, low C, plastic props., fracture, effect of strain rate in static tensile tests *(Czech)* 77—59866
steel, low C, rephosphorised static strain ageing 77—70079
steel, low C, transition behaviour, bending speed effect *(Japanese)* 78—11222
steel, low C, type 08Yu, influence of nonmetallic inclusions on microfailures, during strain *(Russian)* 79—34128

fracture continued

steel, low pearlite, Nb microalloyed, ageing at 600°C, mech. props. *(German)* 77—36542
steel, low S, overheating 77—21185
steel, low-alloy, hardened deoxidised, delayed failure, influence of internal adsorpt. of impurities 80—60974
steel, maraging, N12K6M5TYu, fracture, influence of high-temp. thermomechanical treatment on characts. *(Russian)* 78—27591
steel, maraging, Ni, H_2 assisted crack growth 77—73346
steel, maraging 350, produced by powder metallurgy, mech. props. 78—15334
steel, maraging influence of H content on γ-α transform. during welding *(Russian)* 79—78962
steel, martensitic-aged, plastic deformation influence in type N17K12M5T steel on mech. props. *(Russian)* 80—76305
steel, medium C, deformed, H_2 enhanced load relaxation 79—61635
steel, medium C, Ni-Cr-Mo, overheated, fractographic study *(Chinese)* 80—66616
steel, medium C, shell-shaped fracture due to B embrittlement *(Chinese)* 80—55493
steel, mild, X-ray meas. of conc. stress at crack tip *(Japanese)* 77—77570
steel, mild plate, explosive hardening of one end 77—36531
steel, Mn-C-Si-Cu (0.95, 0.85, 0.25, 0.16 wt.%), fibrous-banded fracture mechanism 80—104280
steel, Mn-Nb-Al-C, crack progag. and hot ductility during straightening concast strand 80—66646
steel, Ni and Cr-Mn for liquefied natural gas appl., material and weld props. 79—61735
steel, Ni-Co-Mo-Ti, microfractographical features, embrittlement and grain size influence on fracture behaviour *(German)* 80—30053
steel, Ni-Cr temper embrittlement by P 77—40448
steel, Ni-Cr-Mo, type 4340, equivalence of K_{Ic} and J_{Ic} fracture toughness meas. for range of yield stress 79—38934
steel, Ni-Cr-Mo and Ni-Cr, impact strength, effect of modified ausforming *(Japanese)* 79—11692
steel, normalised, C-Mn-P, P effect on mech. props. 77—63745
steel, notched bar, plastic zone determ. near rupture *(French)* 78—88515
steel, pearlitic, deform. microstruct. and cementite fracture, −196 to 700°C 78—27576
steel, pearlitic, heat-resist., secondary phase precipitation, deform., and fracture during creep *(Russian)* 80—50669
steel, pearlitic, temp. relationship of failure charact. 78—3158
steel, perlitic, ferritoperlitic and bainitic, stress state influence on fracture *(French)* 79—79093
steel, quenched, adsorption of P on austenite grain boundaries rel. to tendency to delayed fracture of type 18Kh2N4VA *(Russian)* 80—45378
steel, quenched 40Kh2N5SM and 18KhNVA, nature of delayed fracture 77—90456
steel, shelf energy rel. to fracture surface dimensions *(Czech)* 77—59917
steel, sintered, fracture of residual pores 80—76352
steel, spalling prod. by sheet charge explosion and collision of plate 78—44198
steel, spheroidised, H_2 embrittlement, fracture characts., electron probe anal. of inclusions 79—57109
steel, stainless, 316, nuclear fuel cladding, crack nucleation 78—72864
steel, stainless, creep limit, cyclic load component effect at high temps. 80—104231
steel, stainless, duplex, hot ductility and fracture mechanism 78—60731
steel, stainless, fast reactor cladding tubes subjected to thermal transients, rupture behaviour 80—37465
steel, stainless, FBR fuel pin cladding, in-reactor endurance and rupture life 80—13599
steel, stainless, FBR fuel rod cladding damage correl. for rod perform. predictions 80—18424
steel, stainless, fibre reinforced Al alloy, exam. of deformation, fracture and forging behaviour 80—11681
steel, stainless, fracture micromechanism when kept isothermally in sulphur pulp 80—76355
steel, stainless, in-reactor deformation and fracture behaviour of EBR-II driver fuel cladding 80—42769
steel, stainless, type 304, elastoplastic fracture mechanics for reactor piping 78—68777
steel, stainless, type 304, piping cracks, metallurgical exam., failure anal. 79—67849
steel, stainless 304, recrystallisation, effect of dislocation structure 77—32595
steel, stainless brittle zone Al 3 component composites deform. and fracture 77—56104
steel, stainless type 304, rupture of tubes, appl. of fracture mechanics 77—3794
steel, stainless type 321, role of crack blunting in sustained load crack growth 80—21098
steel, stainless wire reinforced Al-Zn-Mg system, resistance to crack propagation 79—43409
steel, stretch-bend test strain distribution obs. 77—70243
steel, structural, classification according to ductile-brittle transition temp. 78—11298
steel, structural, impurity effect on crack initiation, dynamical loading *(Czech)* 80—60955
steel, structural, influence of deform. heat on the mech. props. *(German)* 78—84904
steel, structural, lithoidal fracture surfaces *(Russian)* 77—8905
steel, structural, macroscopic and microscopic features of fracture 80—81179
steel, structural, sharp notched bending specimens, fracture stress, temp. depend. anal. 77—56062
steel, structural, St37-2, large plastic deform., fracture behaviour, COD concept validity *(German)* 79—47764
steel, temper embrittled, grain boundary failure model for intergranular fracture modes 80—25825
steel, temper embrittlement, fracture mech. of grain boundary segregated phases 78—48531
steel, tool, blanking punch, chipping behaviour *(Japanese)* 79—100250
steel, type 12Kh1Mf and 15Kh1M1F, damage accumulation during prolonged high-temp. creep fractography study 79—57026
steel, type 12KhN4MDA, deformation and fracture props. on extension and twisting *(Russian)* 80—55504

fracture continued

steel, type 304, faceted fracture surfaces, selected area channelling patterns 77—77565
steel, type 4052Kh, thermomechanical working influence on mech. props. *(Russian)* 80—93578
steel, type 4340 and 1018 dynamic fracture initiation 80—35333
steel, type 4Kh5MFS, 5KhNM, 5KhNMFS, stress conc. effect on low-cycle fracture results 79—87697
steel, type AISI 4340, quenched and tempered, U-notched bend specimens, effect of H_2 on fracture 79—61716
steel, ultra-high strength, H induced delayed plasticity and cracking 80—21100
steel, use of impressions for fracture study under optical microscope 77—56185
steel, W, high C, amorphous, rapidly quenched from melt, mech. and thermal props. 79—38874
steel, white layers forming at high rates of friction, struct. props. *(Russian)* 79—15800
steel, wooden fracture pattern obs. *(Chinese)* 79—43376
steel 15Kh1M1F, microstruct. changes rel. to creep and fracture *(Russian)* 79—24572
steel 30L, critical size of nometallic inclusions in fracture 79—83322
steel 81B45, chevron fracture in tube reduction by spinning 78—64664
steel case hardened and structural, fracture obs. by SEM *(German)* 77—60032
steel core/sheath tube system, non-fracturing core, stress transfer mechanism 77—52454
steel fibre reinforced epoxy composite, static tensile behaviour *(Japanese)* 78—15482
steel fibre reinforced Pb, fabrication, mech. props. *(Korean)* 77—12579
steel for nuclear pressure vessels, transient finite element crack propag. model 77—3106
steel fracture mode, determ. from shear lip width 80—60968
steel rod reinforced concrete, laterized columns, random axial loading, compressive strength to failure 78—27614
steel sheet, hot and cold rolled, cold formability, notched tensile test and stretch bend test *(German)* 80—61031
steel shot, cast, impact fracture *(Japanese)* 78—92338
steel St3kp, deformability at 600 to 950°C 77—70117
steel welding, development and results of an instrumented restrained cracking (IRC) test *(German)* 78—85060
steel wire, high C, fatigue and fracture 80—55531
steel-Cu M3 bimetal, eutectic alloy, crack development, failure energy capacity *(Russian)* 80—40480
steels, austenitic and type 316, neutron irradiation effect on tensile, creep-rupture, deform., fracture props. 79—65120
steels, free-machining, fractography and X-ray photoelectron spectroscopy 80—7673
steels, high strength, optical crack profile meas. and correlation with mech. props. *(German)* 80—21108
steels, solute segregation and intergranular fracture 80—60957
steels 20Kh and 38Kh2N2VA, tensile testing, deform. rate effect 79—70115
stochastic models, appl. to composites and polymers 80—10198
strain and failure relationship of stressed solids 78—9574
strain cumulative fracture, plane, criterion 79—60432
strength calculations for parts with an unsafe volume in a probability formulation 80—33537
stress intensity factor, of simplified geometries of structural parts, experimental determ. 78—68866
stress intensity factor criterion for combined loading *(Chinese)* 79—32372
stress intensity factor determ. along crack path., numerical method 80—74808
stress intensity factors, UNCLE finite element system calcs., appls. in fracture mechanics 78—67098
stress intensity factors by enriched finite elements 78—90774
stress intensity factors calc. using special 3-D elements 79—94556
stress intensity factors for internal multiple cracks in thick-walled cylinders stressed by internal pressure using load relief factors 79—46261
structural analysis, inelastic response, constitutive modelling 77—3093
structural element design calc. under creep conditions 80—48598
structural materials in complex stress state, criterion for strength at low temp. 78—71292
sugar, mechanical relax. time, determ. from tribolum. 77—1173
sugar, triboluminescence and cryst. fracture dynamics 80—50437
sugar, triboluminescent intensity, fracture in air and liq. anhydrous diethylether 78—19582
sugar crystals under stress, fracture-initiation time from triboluminesc. 77—59065
superconducting magnet epoxy fracture after low-temp. irradiation 79—34147
superplasticity, region I characteristics 80—107357
surface anal. by SEM microtopography 80—68312
surface gas washing, by explosive detonation products 77—77611
surface temperature meas. via secondary ions, intensity correction by total ion monitoring 78—12796
sustained load, ambient temperature 79—43424
symposium, USA-USSR, 1978, on composite materials fracture 80—11766
tartaric acid, triboluminescence and cryst. fracture dynamics 80—50437
tartaric acid, troboluminescent intensity, fracture in air and liq. anhydrous diethylether 78—19582
teaching, description of Open University course 'Materials under Stress' 78—57720
teaching in universities 78—77645
tectonic fracture system, statistical anal. *(Chinese)* 80—41417
tensile fracture device for Auger electron spectroscopy 80—73530
tensile fracture stress pulse emission in glass rods 77—15486
tensile to shear fracture mode transition, in fatigue crack propogation 79—79101
tetrafluoroethylene-vinylidene fluoride copolymer, exporide-diphenylolpropane resin filled, viscoelastic and strength parameters 79—91730
tetraglycidyl 4,4′ diaminodiphenyl methane, diaminodiphenyl sulphone cured, failure and tensile mech. props., moisture effect 80—50735
theory, future trends and appl. 78—90799
thermal fluctuation fracture phenomena 77—15489
thermally activated crack propagation 78—18247
thermoplastic pipes, apparatus for time-to-failure determ. *(Polish)* 79—74328

fracture continued
- thermoplastics, homogeneous, fracture under plane strain and plane stress conditions 78—52941
- thermoplastics, internal stresses revealed by artefacts produced in SEM 78—35634
- thick walled tube, shape of fracture and state of stress *(German)* 77—48551
- Ti, IMI-125, strain rate effect on mech. behaviour 80—3153
- α-Ti alloy, deformation and failure, microstructural, mechanism in biaxial stress state 79—66132
- Ti alloys, gas-saturated layer effect on cracking after welding 77—44359
- Ti-Pd (0.15 wt.%), IMI-260, strain rate effect on mech. behaviour 80—3153
- timber, determ. of critical Rice integral *(French)* 80—16412
- toluene sulphonate diacetylene polymer, vibr. modes, strain depend. using Raman spectra 80—20626
- topography-microstruct. correlations in SEM 77—32687
- torsional deformation testing for plastic deformation, fracture *(Hungarian)* 80—97659
- toughness tests, holographic interferometry 77—9034
- triangular quarter point element as elastic and perfectly-plastic crack tip elements 77—14956
- triboluminescence kinetics in crysts. 77—77306
- unidirectional composites, appl. of linear elastic fracture mech. to longitudinal fracture 79—91784
- US inspection of fracture surface by replicas, determ. of reflector size by scanning 78—27689
- use in engineering, industry and crafts, review 80—50702
- vessels and piping, two-parameter fracture criterion 77—58618
- viscoelastic bodies, adhesion and fracture mechanics, review 78—83336
- viscoelastic mass, detachment of glass sphere, crack tip *(French)* 78—42536
- viscoelastic materials, thermodynamics and fracture, integral expansions 77—3736
- viscoelastic solid, crack growth law using energy and COD fracture criteria 79—32378
- viscoelastic solid, cracked linear, dynamic anal. by finite element method 80—53706
- viscous solids, rupture mechanics using contour integrals *(French)* 80—14615
- void growth, coalescence, ahead of moving crack tip, finite element anal. 78—1609
- Weber sandstone, hydrofracture at high confining pressure and differential stress 77—64272
- wedge stress singularities, inversion theorem for conical regions, elasticity and fracture appls. 79—68578
- Weibull parameter estimation, for fracture characterisation 80—79224
- Weibull statistical theory 78—51132
- Winkler layer, axisymmetric deform. by internally loaded elastic half-spaces 78—26044
- wound healing, var. of mech. props. in different areas 78—27984
- X-ray study *(Japanese)* 79—66117
- Zircaloy clad fuel rod burst behaviour in simulated PWR LOCA 79—36337
- zircaloy cladding tubes of irrad. fuel, flattening test *(Japanese)* 77—42054
- Zircaloy-2, effects of simulated fission products on mechanical props. 80—52740
- Zircaloy-2 cladding tubes, heat treatment influence on texture and mech. anisotropy 79—91694
- zircaloy-2 cladding tubes, post neutron irrad. ring-tensile props. prehydriding effect 77—42053
- Zircaloy-4, failure strain prediction under non-stationary loading conditions 80—93640
- Zircaloy-4, fuel cladding, burst criteria under LOCA conditions 80—73931
- Zircaloy-4, strain rate dependent mech. response 77—21254
- Ag-MgO, laws of plasticity of dispersion strengthened materials 78—84832
- Ag-Ni (10 wt.%) wire, plastically deformed, fracture struct. *(German)* 80—71744
- Al 6061 alloy, B fibre reinforced, fracture 80—11773
- Al alloy, 2618 A, crack closure effect *(French)* 79—20172
- Al alloy, 5083-0, pressure vessel material, delay effects 78—35515
- Al alloy, creep crack growth 80—60976
- Al alloy, fracture of large second phase particles 78—7010
- Al alloy, laminates, fracture of bonded 2024-T3/7075-T6 78—56722
- Al alloy 7075, fracture props., effect of thermomechanical treatment 78—60793
- Al alloy 7075-T6, acoustic emission response 79—87801
- Al alloy AK4-1, crack growth rate prediction under creep conditions 80—85107
- Al alloy AZ5G, age hardening heat treatment effect on mech. props. microstruct. *(French)* 77—52370
- Al alloy OT4-1u, with varying H_2 content, rel. to loading condition *(Russian)* 77—70148
- Al alloys, 7075-T6, H_2 effects and Cd segregation to grain boundaries 78—84764
- Al alloys, cryogenic, AMg5 and AMg6, mech. props. at −196°C 77—63748
- Al alloys, deformation processes in sheet materials, application of failure maps 78—56718
- Al alloys, fracture relief formed in fatigue crack growth, rel. to failure mechanism 80—76347
- Al, alloys, limiting plastic props. *(Russian)* 78—88504
- Al alloys 7178 and M580, chevron fracture in tube reduction by spinning 78—64664
- Al anodic films, acoustic and electron-emission during deform. 80—80143
- Al, anodised, photostimulated exoelectron emission, effect of oxide thickness 78—80461
- Al, circular plate perforation and deformation by square section punch 79—34100
- Al foil, laser irrad., fracture props. *(Russian)* 80—108523
- Al, fracture due to shock waves leaving surface, shear stresses 78—51128
- Al, fracture mechanism, plastic strain role 79—38977
- Al, fracture mechanism 80—100903
- Al fracture speed during phase explosion due to electron beam irrad. *(Russian)* 80—76336
- Al, plane stress calc. with two dimensional elastic-plastic computer program 78—35465

fracture continued
- Al plastic deformation depend. on mag. field at 4.2K *(Russian)* 79—91754
- Al, plate, explosive hardening of one end 77—36531
- Al polycrystalline, exoelectron emission under tensile deform. and fracture *(Japanese)* 77—55870
- Al sheet alloy D16AT, regression anal. of critical stages of fracture process 79—15786
- Al smelting cathodes, comp. and props. 77—28740
- Al, workhardened thin specimens, fracture, anisotropy coeff. role *(French)* 80—104276
- Al-Al_2 eutectic, abrasive fragmentation *(Czech)* 78—64715
- Al-Al_2O_3 composite, brittle zone on fibre surface deform. and fracture 77—56104
- Al-Al_6Fe, fibre reinforced eutectic, deformation behaviour by rolling, TEM and SEM study 79—29129
- Al-B fibre-D16 alloy welded composites, structure, strength and fracture props. *(Russian)* 80—108524
- Al-Cu, precipitation hardened, hysteretic plastic work as failure criterion in Coffin-Manson type relation 77—32657
- Al-Cu, type 2219-T851, fracture mechanics and surface chemistry of fatigue crack growth 80—81168
- Al-Cu (4 wt.%), supersaturated and aged conditions, high strain deform. 80—60907
- Al-Cu (4 wt.%) fractography *(German)* 78—19982
- Al-Cu (4.6 wt.%), cold work and ageing influence on ductility and fracture behaviour *(Japanese)* 80—89295
- Al-Cu-Mg-Li alloy extrusions, microstruct., embrittlement and fracture props. 80—60965
- Al-Cu-Mg-Mn (4.5, 1.5, 0.6 wt.%), alloy 2024-T3, exam. of residual strength of plate containing crack, fracture anal. 78—90792
- Al-$CuAl_2$, directionally solidified eutectic, structural changes during strength tests *(Russian)* 80—7543
- Al-$CuAl_2$ aligned, fracture, effect of growth speed, orientation, environment 77—28907
- Al-Cu(Ag), tensile ductility, effect of ageing and impact velocity *(Japanese)* 78—15465
- Al-Cu(Mg), age-hardenable, US cavitation erosion mechanisms, effects of comp. and heat treatment 78—53002
- Al-Cu(Mg), liquid impact erosion 80—108598
- Al-Li-Mn (2.8, 0.3 wt.%), recrystallised sheet, fracture behaviour, SEM and TEM study 80—97566
- Al-Mg (2 wt.%), hardening and fracture characts., β-phase dissolution role 80—81178
- Al-Mg alloys, for liquefied natural gas appl., material and weld props. 79—61735
- Al-Mg alloys, overheating effects on microstruct. and props. 77—63698
- Al-Mg-Si, type 6010, microstruct. characts. influence on formability, heat treatment 80—81090
- Al-Mg-Si alloys, effects of dispersoids upon micromechanism of crack propagation 79—83286
- Al-Si eutectic, secondary creep and fracture time *(Czech)* 80—35267
- Al-Si-Cu-Mg-Ni, piston, secondary creep and fracture time *(Czech)* 80—35267
- Al-Si-Cu-Mg-Ni cast alloy, fractography *(German, English)* 79—87809
- Al-Zn-Mg, cavitation during superplastic deform. *(Japanese)* 78—15464
- Al-Zn-Mg, weldable, microstruct. and intercrystalline fracture 77—48550
- Al-Zn-Mg (6, 2.5 wt.%) alloy, intergranular fracture mechanism due to ledge formation 79—57089
- Al-Zn-Mg alloy 7075, unstable shear failure 77—48516
- Al-Zn-Mg-Cu alloy 7075-T651, adiabatic shear localisation and erosion 79—96157
- Al_2O_3 (96 wt.%), fractographic criteria for subcritical crack growth boundaries 80—81155
- Al_2O_3, atomically sharp cracks, TEM study 80—71729
- Al_2O_3, ceramic, delayed fracture 77—44342
- Al_2O_3, dense, surface segregation of Ca under exposure to steam and steam-CO 78—85013
- Al_2O_3, high-purity, modulus of rupture, expt. test of Weibull scaling theory 77—21258
- Al_2O_3, hot pressed, fracture stress-reflecting spot relations 80—71731
- β''-Al_2O_3, Li_2O stabilised, hot-pressed and sintered, fracture props. 77—36626
- Al_2O_3, spray dried agglomerates, compaction response, fracture, deform. 79—43172
- Al_2O_3 strength-size relation 77—21255
- α-Al_2O_3/graphite mixtures, high corrosion resistance refractory materials, fracture anal. *(French)* 79—70137
- Al_2O_3/Nb laminates, metal to ceramic joints, adherence props. 80—45386
- Al_2O_3-BaO, fracture *(German)* 77—28882
- Al_2O_3-TiC, composite, fracture behaviour in three-point bending 80—60951
- Au, metallised coating on polyethylene terephthalate film, fracture under laser irrad. *(Russian)* 80—76333
- B fibre reinforced Al alloy, influence of band strength on failure *(Russian)* 79—43387
- B fibre reinforced Al laminate with discontinuities, fracture 78—19877
- B fibres, quality evaluation from morphological and fractographic characteristics *(Russian)* 79—70150
- B, filament, light emission during fracture 77—28896
- B-fibre reinforced Al, with imperfect separation boundary, material stability *(Russian)* 80—54307
- B_4C absorber pin in-reactor rupture test 79—93701
- B_4C, TEM investigation using C replicas 80—61034
- BN, TEM investigation using C replicas 80—61034
- $BaTiO_3$, ferroic materials, fracture processes 80—79869
- $BaTiO_3$, powder compacts, sintered, physical and chem. inhomogeneities 79—87594
- Be, fracture and strength properties, dynamic ageing effects 80—81202
- Be, grain size effect on mech. props. *(Russian)* 79—47749
- Be, strain hardened metal and microalloys, low temp. brittleness 79—96140
- C fibre, morphological charact. rel. to fracture, SEM obs. 77—63791
- C fibre, structural and mech. characts. 77—28737
- C fibre and glass fibre hybrid reinforced plastics, review of physical properties 80—55496
- C fibre reinforced Al, factors affecting struct. formation and some props. 78—15346
- C fibre reinforced C, processing, room temp. mech. props., and low temp. expansion 80—25820

fracture continued
C fibre reinforced composites, kinking as structural degradation mode 78—52893
C fibre reinforced Cu, mech. props. *(Japanese)* 77—63723
C fibre reinforced epoxy, activated C, storage life effect on shear strength *(Russian)* 78—35483
C fibre reinforced epoxy cross ply laminates, transverse cracking and long. splitting, strain effects 79—61723
C fibre reinforced plastic, stress analysis of butt strap joint 79—43300
C fibre reinforced plastic, deform. and failure using AE method *(Russian)* 80—40630
C fibre reinforced plastic, fractography of fracture surface under three-point bending *(Japanese)* 80—55506
C fibre reinforced polymers, strategic reinforcement of hybrid, impact props. 78—15502
C fibre-polymer composite, C fibre surface effect on fracture 80—11777
C fibres, from mesophase pitch, tensile strength, fracture surface SEM study 79—79031
C stripper foils, lifetime enhancement, heavy ion bombardment 78—94156
C-C composite, oxidised, SEM study 77—52522
C-fibre reinforced cement, review 77—21082
CaF$_2$, hot forged, laser window material, fabrication, props. 77—46773
CaF$_2$, laser windows, intermediate temp. forging 77—46775
CaF$_2$, strength-controlling fracture energy depend. on flaw-size to grain-size ratio 80—81152
β-CaSiO$_3$ fibre, continuous unidirectional crystallisation from melt 78—95739
Ca$_3$SiO$_5$, fracture surfaces, quantitative anal. using energy dispersive X-ray spectrometry *(French)* 80—89571
Ci-Bi (0.0115 wt.%), fracture paths, TEM study 79—27998
(Co,Ni)-Cr$_{23}$C$_6$ eutectic, microstruct. effect on fracture energy 80—7662
Co-base superalloy, machine thixocast, mech. prop. deficiencies 79—74244
Co-CoAl, two phase, interaction between deform., fracture initiation and propag. 80—85006
Co-Cr-C-Al (39, 2.2, 2 wt.%), directionally solidified eutectic alloy, Larson Miller C const. 79—70162
Co-Cr-W-C, hardfaced coating for high temp. liquid Na service, deposition and wear 77—32724
Cr, deposited by high rate sputtering, mech. props. 77—36630
Cr-Mo pressure vessel steel, improvement through electroslag remelting 77—42104
Cu, circular plate perforation and deformation by square section punch 79—34100
Cu, fracture due to shock waves leaving surface, shear stresses 78—51128
Cu fracture speed during phase explosion due to electron beam irrad. *(Russian)* 80—76336
Cu, hot ductility and torsional deform. *(Japanese)* 79—57069
Cu, metallic adhesion, use of fracture mechanics and contact resistance meas. 77—70271
Cu, metallised coating on polyethylene terephthalate film, fracture under laser irrad. *(Russian)* 80—76333
Cu, powder, sprayed, effect of start props. in struct, and porosity of sintered products *(Czech)* 77—85960
Cu, spallation, temp. effect on breaking strength 78—31536
Cu, tough pitch wire, cupping fracture surface, SEM study *(Japanese)* 79—79087
Cu wire, tough-pitch, cupping fracture, Cu$_2$O particle size effect 80—66668
Cu-Al (9.3 wt.%), in torsion, deformation temp. depend., superplasticity due to grain size, dislocation density *(Russian)* 79—74200
Cu-Bi, grain boundary struct. intergranular fracture, segregation role 80—66648
Cu-Ni diffusion couple, diffusion bonding process, fracture surface exam. *(German)* 77—35762
Cu-polymer composite foils, fracture surface exam. by XPS *(German)* 78—84992
Cu-Zn-Al, polycrystn., β-phase, fatigue life, intergranular cracking 79—38974
α-Cu-Zn(Al), solid soln., intermediate temp. embrittlement *(Japanese)* 79—20158
α-Cu-Zn(Al) fracture behaviour, effect of deform. temp. and alloying content *(Japanese)* 79—20159
α-Fe, 0.14 wt.% P addition effect on creep 77—90420
Fe, [110] and [410] single crysts., push-pull fatigue 79—74257
Fe based amorphous alloys, delayed fracture in atmosphere, effect of alloying additions *(Japanese)* 79—96212
Fe, cast, grey, fracture surface after dynamic fracture, Mg conc. effect 80—100909
Fe, cast, heated in CO atm., obs. cracks around graphite flakes *(Japanese)* 78—84974
Fe, cast, Mg micro distrib., microprobe anal., electron fractography 77—70373
Fe, cast, notch strength, non-uniform stress distrib. effect *(Japanese)* 79—79090
Fe, cast ferritic, spheroidal, graphite nodule size and distrib. effect of fracture *(French)* 79—20176
Fe, commercial, deformability at 600 to 950°C 77—70117
Fe, fatigue fracture strength and failure, at 77K after cyclic loading at room temp. 78—84996
Fe, fracture mechanism in various temperature and stress intervals *(Russian)* 79—24600
α-Fe, grain boundary segregation of C, N$_2$ and C Auger spectroscopy 78—72778
Fe, grey cast, deform. and fracture regions in microzones *(Russian)* 78—80585
Fe, grey cast, tensile testing of mechanical props., from room temp. to liquidus *(Japanese)* 80—7728
Fe, metallic adhesion, use of fracture mechanics and contact resistance meas. 77—70271
Fe, plastic deform. and fracture, H$_2$ effect, studied by electron microscopy and Auger spectrography *(French)* 77—77545
Fe, powder, consolidated, exam. of mech. and electrical props. 78—56599
Fe, pure, fracture-mechanisms, tensile specimens 80—85039
Fe, pure, neutron irrad. and H$_2$ absorption effects on mech. props. 78—34546
Fe, sintered, fracture behaviour, microscopic obs. 79—47771
Fe, sintered, fracture mechanics *(German)* 77—8948

fracture continued
Fe static loading over wide deform. and temp. range, acoustic emission, plastic flow, fracture 77—90424
Fe, whisker, H$_2$ effect on deform. 78—68755
Fe-CaF (6 and 9 wt.%), sintered, elevated temp. mech. props. 77—28878
Fe-Cr-Al-Ti-Y$_2$O$_3$ (20, 4.5, 0.5, 0.5) type MA956, strain rate effect on fracture behaviour at 1366K 80—16458
Fe-Cr-Co, ductile magnet alloys, mech. props. 80—85001
Fe-Cr-Co-V-(Ti) hard magnets, V and V-Ti effects on mag. and mech. props. 79—91810
Fe-Cr-Mo(Ni)(Mo-NI), AES using peak-to-peak value *(Japanese)* 79—20485
Fe-Cr-Ni, two-phase ($\alpha+\gamma$), and metastable austenitic, uniform elongation peak 77—77547
Fe-Cr-Ti-Mo ferritic alloy, annealed, cold rolled, fast reactor material, mech. props. 78—21646
Fe-Cu-Ti, improvement of irradiation-enhanced Cu embrittlement by Ti addition 79—43393
Fe-Mo-CaF (15, 9 and 6 wt.%), sintered, elevated temp. mech. props. 77—28878
Fe-Ni-Al-Co-Cu alloy, sintered single-crystal mag. prod., props. 77—66709
Fe-Ni-Al-Co-Cu-Ti YuNDK type, S effect on mech. props. 80—60927
Fe-Ni-Al(2.5, 7.5 at.%), fracture surface morphology, ageing temp. effects 77—16600
Fe-Ni-C, martensitic, mech. charact., effect of ageing and tempering *(Slovak)* 78—19791
Fe-Ni-C, martensitic, mech. and fracture charact., effect of starting austenite heterogeneity *(Slovak)* 78—19792
Fe-Ni-C (31, 0.1 wt.%), metastable austenite, fractography 77—59919
Fe-Ni-Cr (35, 15 wt.%) superalloy, stress rupture and tensile props., C and B additions effect *(Chinese)* 80—104244
Fe-Ni-Cr based alloy, KhN35VTYu, temp. depend. of energy of fracture, influence of γ' phase *(Russian)* 80—81147
Fe-Ni-Cr-Ti-Al, Ti and Al effect on microstruct. and mech. props. *(Chinese)* 79—74130
Fe-P, P equilib. grain boundary segregation 79—38835
α-Fe-P, static strain ageing 77—70079
Fe-Si, rapid cracks self-arrest potential, −196-0°C 80—100911
Fe-Si (2.6 wt.%) single cryst., crack propag., controlled plastic crack tip opening rate 80—60943
Fe-Si (3 at.%), acoustic emission response 79—87801
Fe-Ti alloys, kinetic trapping model for H$_2$-induced grain boundary cracking 79—29164
Fe$_2$O$_3$-FeO, sinter, heating and reduction effect of phase transform. and fracture *(Russian)* 78—15375
GaP/Si heterostruct., differential thermal contraction, plastic deform., fracture 80—108494
Ge, atomically sharp cracks, TEM study 80—71729
Ge, high press. appl. by spherical diamond indentor, plastic deform. obs. method 78—35619
H$_2$ embrittlement cracking and impurity atom migration *(Chinese)* 80—104247
Ir, fracture mechanisms, and cleavage criteria 79—74253
Ir-W (0.3 wt.%), P segregation to grain boundaries, effect on high temp. ductility 78—95754
Ir-W (0.3%), grain boundary comp., trace element additions effect 80—66661
LiF bicrystals, intergranular fracture due to single slip 78—34520
LiF, crystal fracture induced surface charge, elec. signal meas., double elec. layer approx. 80—44254
LiF, pulsed dielectric breakdown, mech. stress photoelasticity obs. *(Russian)* 78—2800
(Li$_{0.5}$Fe$_{2.5}$O$_4$)$_{0.8}$(CuFe$_2$O$_4$)$_{0.2}$, struct., magnetic props., rectangular hysteresis loop 77—20645
Li$_2$O-Al$_2$O$_3$-SiO$_2$ glass-ceramic, near-zero thermal-expansion heat treatment effect in fracture behaviour 80—66537
Li$_2$SO$_4$, triboluminescence and cryst. fracture dynamics 80—50437
MgAl$_2$O$_4$, strength-controlling fracture energy depend. on flaw-size to grain-size ratio 80—81152
MgO, crack propagation during in-situ deform., plastic zone formation 80—16468
MgO single crystals, crack formation process, micro-deformation and fracture *(Japanese)* 80—24530
MnZn ferrite, O$_2$ stoichiometry effect on fracture 80—25826
MnZn ferrite, spray dried agglomerates, compaction response, fracture, deform. 79—43172
Mo alloy TsMb, mech. props., effect of gaseous H$_2$ *(Russian)* 78—31508
Mo, C doped sheet, electron beam welded, low temp. ductility 79—87685
Mo, dislocation structure, temp. depend., at crack tip, of fractured single cryst. 79—29210
Mo, exam. of H$_2$ embrittlement mechanisms, effect on mech. props. 78—39891
Mo fibre reinforced Al and Al alloys, SEM study *(Slovenian)* 78—84923
Mo, fracture and crack propag. tested in tension along [001] axis *(Russian)* 80—50697
Mo, fracture and crack tip plastic zones, in situ obs. 80—108686
Mo, microcrack formation, structural singularities, TEM obs. *(Russian)* 79—1905
Mo, proton irradiated, annealed and rolled, void form. 78—22774
Mo sheet, conc. of interstitial elements on lamination surface 77—86038
Mo, sintered, grain boundary segregation of S and N 79—56982
Mo, strain hardened metal and microalloys, low temp. brittleness 79—96140
Mo/Nb welded joints in sheet metal, detect. and exam. of cracks, initiation, development 77—73385
Mo-B, Mo-B-Fe(Ni), microalloying influence on mechanical props., cold rolling, plasticity *(Russian)* 80—40502
Mo-B-Al-C system, fractography of static and fatigue fracture 79—87729
Mo-C (0.07 wt.%), two-phase alloy, fracture and deform. characts., struct. depend. *(Russian)* 77—32635
Mo-Mn alloy, plasticity, fracture, strength depend. on C content *(Russian)* 80—35257
Mo-Nb-TiN, dispersion hardened with strong interface, fracture mechanism 79—5058
Mo-O system, grain boundary segregation and intergranular fracture 80—55516

fracture continued
Mo-O-C system, grain boundary segregation and intergranular fracture 80−55516
Mo-Re alloy, type MR47VP, fractographic of static and fatigue fracture 79−87729
Mo-Re alloy wire, high-strength, fracture mechanism *(Russian)* 77−25126
Mo-W (30 wt.%), wrought, fracture, characteristic features 80−104278
Mo-Zr (0.15 wt.%), wrought, fracture, characteristic features 80−104278
Mo_2 single crysts., surface orientation effect as high temp. creep and fracture type 80−16403
NaCl, damage process preceding semibrittle fracture, plastic strain depend. 77−32692
NaCl, pulsed dielectric breakdown, mech. stress photoelasticity obs. *(Russian)* 78−2800
Na_2O-CaO, enhanced failure by combined pulse and CW laser 79−29182
Na_2O-CaO glass, (K_I,V) diagram determ. *(French)* 80−108558
Na_2O-CaO glass, abrasion-resistant, high strength 80−76369
Na_2O-CaO-SiO_2, dynamic hardness testing, pendulum attenuation, yield stress obs. 79−24699
Na_2O-CaO-SiO_2, expt. errors in estimating time to failure 77−16666
Na_2O-CaO-SiO_2, glass, transition from slow to fast crack propag., effect of different liquids 78−23828
Na_2O-SiO_2 glass, microcracking about NiS inclusions, fracture mech. description 80−89333
Na_2O-SiO_2 glass, OH^- content effect on mech. and other props. 80−89337
Na_2O-SiO_2 glass, scoring, deform. and fracture mech. approach 80−89332
Nb, dislocation-free single crystal, deformed at 180K, X-ray topographic obs. 79−24587
Nb-Cr(Mn)(Mo)(Zr), internal impurity adsorption effect on bond type of intercrystallite zones 77−16684
Nb-Zr-C (0.1, 0.01 wt.%) plastic deform. influence on electronic state of Nb atoms 80−40463
Nb-ZrN alloy, high temp. hardness and short duration tensile strength *(Russian)* 77−44266
Nb_3Sn composite wires, supercond., degradation mech. under tensile strain at 4.2K 79−38284
Nb_3Sn filamentary superconducting composites, mechanical property variations between composites 79−57054
Nb_3Sn microfilamentary superconducting composite, critical currents, fracture props. 80−107970
Ni alloy ZhS6KP, heat-resist., superplastic deformation, effect on struct. 79−96090
Ni alloys, liquation cracking during welding, comp. influence 80−66645
Ni base alloy IN792, carbide morphology 77−36508
Ni, cavitation-erosive wear in surface-active media, dislocation struct. and fracture study by FMR *(Russian)* 79−52384
Ni, ductility and fracture, nonmetallic inclusions effect 80−104221
Ni films, adhesion on graphite 80−80141
Ni, low-temp. fracture, electron fractography obs. *(Russian)* 77−90437
Ni, metallised coating on polyethylene terephthalate film, fracture under laser irrad. *(Russian)* 80−76333
Ni, pure, fatigue crack propagation, quantitative stereoscopic fractography study 79−74238
Ni/Ni_3Al-Ni_3Nb, directionally solidified lamellar eutectic alloy, deform. anisotropy and fracture 77−36604
Ni-Al-Cr, precipitation-strengthened, mechanical props. 78−84968
Ni-B, hydrogen embrittlement, effect of B additions *(Japanese)* 78−84973
Ni-Cr-Al sintered alloy, hot vac. pressure, fracture and mech. characts. 80−66667
Ni-Cr-Co-Mo-Al-Ti (10, 15, 3, 5.5, 4.5 wt.%), superalloy, exam. of creep and fracture behaviour 78−48464
Ni-Cr-Co-Mo-Ti-Al, powders, HCl surface treatment to prevent TiC precipitation, fracture props. 79−8397
Ni-Cr-Ti (19.51, 4.2 wt.%), quench-ageing and fracture *(German)* 77−70088
Ni-Cr-ZrO_2, dispersion hardened, sintered, rupture 77−21272
Ni_3Al, ductility, tensile and compressive tests *(Japanese)* 77−52414
Ni_3Al-B, $L1_2$ type intermetallic cpd. room temp. ductility improvement by B addition *(Japanese)* 80−35263
Ni_3Al-Ni_3Nb, eutectic alloy, crack development, failure energy capacity *(Russian)* 80−40480
$Ni_3(Al.Ti)$, single crysts., flow and fracture behaviour tested in tension 79−79075
$Ni_{36}Fe_{32}Cr_{14}P_{12}B_6$ metallic glass, mech. props. and thermal stability 80−76362
$Ni_{49}Fe_{29}P_{14}B_6Si_2$ glass, flow and failure 80−40438
NiTa C-13, advanced fibre reinforced eutectic superalloy, creep and rupture 77−63744
Pb-Sn, with brass insert, tensile flow and fracture 78−11290
$Pb_xSn_{1-x}Te$ surfaces, fractured and etched, Raman scatt. spectra of monolayer oxide and Te films 77−48211
$Pb(Zr,Ti)O_3$, ferroic materials, fracture processes 80−79869
$Pb(Zr,Ti)O_3$, fracture and deform. 80−79870
$Pb(Zr,Ti)O_3$ polycrystalline ceramic, fracture and strength, surface treatment effects 80−11704
$Pd_{77.5}Cu_6Si_{16.5}$, cold drawn wires, surface markings, fracture stresses 79−56997
$Pd_{80}Si_{20}$, glass, deform. localisation, plastic instabilities and fracture 80−89320
Pt-Au glass-bonded printed thick-film conductor, adherence fracture energy 77−9037
239PuO_2, stoichiometric, high-temp. deformation 80−81111
S-based composite, engineering props. 77−86093
Si, atomically sharp cracks, TEM study 80−71729
Si, elastically bent, strain canc. determ. by microfluorescent densitometry of X-ray topography 80−79245
Si, high press. appl. by spherical diamond indentor, plastic deform. obs. method 78−35619
Si, near (111), fracture by painted indenter, SEM study 80−71734
Si, single crystal, fracture under several liq. environments 80−81157
Si wafers, scribing and subsequent fracture 80−11743
Si-Al C fibre composite technological coatings, liquid phase method preparation *(Russian)* 80−108375
Si-SiC composite, high temp. time depend. strength 77−56083
SiC, atomically sharp cracks, TEM study 80−71729

fracture continued
SiC, electron microscopical fractography *(Russian)* 77−25146
SiC fibre reinforced Al-Si alloy, liq. phase process prep. effect on mech. props. 79−70020
SiC, hot pressed, bending strength *(German)* 79−24571
SiC, hot pressed, K_{Ic} and delayed fracture meas. 79−61701
SiC, identation plasticity and microfracture 79−70158
SiC, pressureless-sintered, high temp. strength *(Japanese)* 80−104299
SiC, reaction densified, controlled surface flaw initiated fracture 77−8919
SiC single crystals, friction, deform., and fracture, crystal orientation effect 79−96150
SiC, spray dried agglomerates, compaction response, fracture, deform. 79−43172
SiC, TEM investigation using C replicas 80−61034
SiN film, on Si substrate, thermal stresses and cracking resist. 78−63958
Si_3N_4, cracking characterisation by double torsion test *(French)* 80−104369
Si_3N_4, evidence for cavitation crack growth, SEM study 79−79086
Si_3N_4 film, on Si substrate, thermal stresses and cracking resist. 78−63958
Si_3N_4 first pressed, mixed mode fracture from controlled surface flaws 78−27603
Si_3N_4, hot pressed, fracture phenomenology, fracture surface energy, crack propagation 79−57090
Si_3N_4, hot-pressed, fracture in bending *(Japanese)* 79−79113
Si_3N_4, pyrolytic, amorphous and crystalline, chemical vapour deposited fracture surfaces rel. to struct. features 79−5038
Si_3N_4, reaction bonded, fracture mech. pararucters, microstmet. amd temp. effect 79−24598
Si_3N_4, reaction-sintered, elastic moduli, fracture mechanics parameters, and strength 77−28889
Si_3N_4, reaction-sintered, SEM fractographs 79−86933
Si_3N_4, sintering under high press., modulus of rupture tests 77−44202
Si_3N_4 with Y_2O_3 and Al_2O_3 additions, hot pressed, exam. of mech. props., grain boundary crystallization 79−20009
Si_3N_4/Zr laminates, metal to ceramic joints, adherence props. 80−45386
Si_3N_4-$Y_2O_3(CeO_2)$, hot pressed, sintered, microstruct., flexural strength and fractographic anal. 80−40293
Si_3Ni_4, hot pressed, subcritical crack growth boundaries at internal fracture origins 80−11748
SiO_2 film, on Si substrate, thermal stresses and cracking resist. 78−63958
SiO_2, fused, single particle impact damage 80−40508
SiO_2-Al_2O_3 refractories, thermal shock props., fracture mech. appl. *(French)* 79−96109
SiO_2-Na_2O-$CaCO_3$ sheet glass, rupture upon local contact loading 80−50725
SiO_2-TiO_2 antireflection coating, 1.064 μm laser damage, barrier 80−33059
$SmCo_5$, sintered, anisotropic thermal expansion and fracture of radially oriented toroids *(Chinese)* 80−10686
Sn, molten drops, gas evolution on quenching 78−39818
Sn-Pb (38 wt.%), graphite fibre reinforced, effect of interface on fracture characts. 78−76723
Ti alloy, fracture surface and metallographic features exam. by precision sectioning 77−36638
α-β-Ti alloy, stress, H segregation, fracture 77−40450
Ti alloy, VT23, ht. treatment effects on fracture *(Russian)* 78−80623
$\alpha+\beta$ Ti alloys, fracture, influence of phase comp. in VT16 and VT9, quenching effects *(Russian)* 78−56665
α-βTi alloys, high strength, heat-treated weldments, intergranular fracture 80−21097
α-Ti, electron fractography 77−63778
Ti, fracture mechanism at different temps. 77−63785
Ti-Al, age-hardened, deform., order effects in Ti_3Al and temp. effects 77−25111
Ti-Al-Mo alloy VT14, fracture anisotropy, with varying H_2 content, rel. to loading condition *(Russian)* 77−70148
Ti-Al-Sn, alloy 6242, dynamic effects of flow and fracture during isothermal forging 80−76343
Ti-Al-Sn-Zr-Mo (6,2,4,6 wt.%), α-β type 6246, fusion zone fracture behaviour in weldments 80−30093
Ti-Al-Sn-Zr-Mo (6,2,45 wt.%), surface cracking under unidirectional loading 78−56753
Ti-Al-V (6, 4 wt.%), hot isostatically pressed casting, fatigue crack initiation 79−79078
Ti-Al-V (6, 4 wt.%), solution treatment temp. effect on fracture morphology 79−61620
Ti-Al-V (6,4 wt.%), effect of air exposure on fracture characts. 80−100890
Ti-Al-V (6,4 wt.%), metallographically prepared, fracture surface, phase anal. by energy dispersive X-ray microanal. *(German, English)* 77−48606
Ti-Al-V (6,4 wt.%), surface cracking under unidirectional loading 78−56753
Ti-Al-V-Sn (6, 6, 2 wt.%) weldments, heat treated, transangular fracture 80−40524
Ti-Al-V-Sn (6,6,2 wt.%), α-β type 662, fusion zone fracture behaviour in weldments 80−30093
Ti-Al-V(Sn) alloys, plastic deformation and fracture characts. at low temps. *(Russian)* 80−7624
Ti-Hastelloy-N, homogenization 79−61606
Ti-Mo, fracture behaviour and tensile props. at elev. temp. 78−60822
Ti-V-Si (30, 1 at%), quenched and aged, hardness, tensile behaviour and phase transform. 79−11646
TiC-Ni-Mo sintered hard alloy TN-20, fracture surfaces 80−7684
(U,Pu)C, fracture and crack healing, SEM study 79−79080
U, one dimensional spall 77−80579
α-U, strain rate effect on flow and fracture 80−100887
α-U, strain rate effect on tensile flow and fracture 80−84992
U-Mo (1.5 wt.%) metallurgical study of forging *(French)* 78−21737
UO_2, unrestructured fuel, intergranular fracture during film boiling 80−3169
UO_2, Zircaloy sheathed, CEA expt. on transient behaviour *(French)* 80−18417
V-Mo, effect of ion plated Mo on corrosion in liquid Na, mech. props. 78−53020
VC-Ni, fracture mode determination, using Auger electron spectroscopy 80−7680

fracture continued

- W, (100) oriented cryst., plastic relax. effect on semi-brittle fracture 77−69036
- W bicrysts., crack propag. across grain boundaries, crack speed meas. technique appl. 80−108575
- W, drawn wire, microstruct. effect on fracture 80−3177
- W, fibre reinforced Cu composite, temp.-load depend. of time-to-rupture *(Russian)* 78−11299
- W, LEED and electron microscopic investigs., review *(Hungarian)* 77−47654
- W, plasma coating, thick, struct. and mech. props. 77−28716
- W, with different microstructs., temp. depend. of yield strength 80−16404
- W, with impurities, grain boundaries, effect on high temp. plasticity *(Russian)* 79−79057
- W-Mo, vapour deposited, long-term strength and thermocyclic creep 80−16405
- W-Ni-Fe(Co)(Cr), structural characterisation *(French)* 77−56074
- WC-Co, elastic and plastic charact. 80−35280
- WC-Co, fracture mode determination, using Auger electron spectroscopy 80−7680
- WC-Co, rupture of bending specimens, use of quantitative metallography and stereology *(French)* 77−28899
- WC-Co, various combinations, fracture characts. in bending, compression, and toughness tests 78−60808
- WC-Co (10 wt.%), elevated temp. bend deform. and fracture, effect of C 77−59877
- WC-Co (6 to 20 wt.%), bend deform. and fracture up to 1000°C 77−48510
- WC-Co alloys fracture, spatially constrained crack tip opening displacement 77−77580
- WC-Co carbide, crack paths, SEM study *(Japanese)* 80−50710
- WC-Co cemented carbide, bending strength, surface roughness effects *(German)* 77−8947
- WC-Co cemented carbide, carbide grain size effect on strength rel. to structural defects 77−32689
- WC-Co cemented carbide, relation between transverse rupture and tensile rupture *(Japanese)* 77−52473
- WC-Co cemented carbide, indentation fracture, operative fracture mode survey 77−70183
- WC-Co hard alloy composite, calc. of weakest link in struct. 80−11730
- WC-Co hardmetal, defect initiated fracture and bond strength 78−11319
- YH_x, mech. props. 77−44333
- Y_2O_3 ceramics, strength under mech. and thermal actions 80−97554
- Y_2O_3, grain size depend. of fracture energy, SEM study 79−34130
- Y_2O_3, strength-controlling fracture energy depend. on flaw-size to grain-size ratio 80−81152
- Zn-Al (22 at.%), heat treatment and straining effect on fracture and corrosion 79−87672
- Zn-Al (22 wt.%), superplastic eutectoid cavitation evidence 77−63741
- Zn-Al(Cu), mech. and technological props. *(Polish)* 80−89286
- ZnSe, CVD, delayed failure 79−99462
- Zr alloys, acoustic emission during tensile testing 77−90433
- Zr-Al (4.6 wt.%), microstruct. effect on mech. props. 79−20080
- Zr-CR (1.9 wt.%), β-quenched and tempered, tensile props. rel. to tempered conditions, SEM study 79−66109
- Zr-Nb, fracture resistance, atomic reactor material *(Russian)* 77−25140
- Zr-Nb (2.5 wt.%), cold worked, press. tubes, secondary cracking obs. 78−80630
- Zr-Nb (2.5 wt.%), heat treatment effects on slow crack growth, cold working effects 77−28836
- Zr-Nb (2.5 wt.%) pipe, fracture resistance, hydrogenation effect 80−104279
- ZrC based cermets, strength and gas-abrasive wear resistance 77−25163
- ZrC, fracture by laser beams, macrocrack propag. 79−15789
- ZrH_x, mech. props. 77−44333
- ZrO_2, metastable, tetragonal, erosive damage depth, martensitic transform. effect 79−61738
- ZrO_2, partially stabilized, precipitation hardening effect on fracture mode 77−90353
- ZrO_2, partially stabilized, precipitation effects on fracture mode 77−90354
- ZrO_2, partially stabilized, processing defects 80−97558
- ZrO_2, porous, sintered stabilised microspheres, strength and fracture studies 80−85019
- ZrO_2, spray dried agglomerates, compaction response, fracture, deform. 79−43172
- ZrO_2, stabilised, coating for turbine components, degradation due to internal stresses 79−24671
- ZrO_2-Ta and ZrO_2-Y_2O_3-Ta aligned eutectic composites, solidification and fracture behaviour 77−48387
- $ZrSiO_4$, plasma dissociated, improved thermal shock resistant refractories 79−52350

fracture strength *see fracture toughness*

fracture strength testing *see fracture toughness testing*

fracture toughness

see also notch brittleness; notch ductility; notch strength

- ABS resin, craze growth and fracture 80−50705
- ABS samples with 25 and 30% rubber, fracture toughness 80−16438
- ABS-rubber modified, two-phase struct. influence on fracture toughness *(German)* 80−66666
- acoustic emission, amplitude distrib. anal. 80−66713
- acrylic bone cement containing second phase dispersions, strength 77−81663
- acrylic plastic, stretched, fracture toughness 79−15778
- acrylonitrile-butadiene-styrene copolymers, micromechanism of deform. and rupture *(German)* 80−35276
- alloy, high temperature, mechanical, thermal and corrosion props. 78−95763
- alloy, precipitation hardened, containing narrow soft zones at grain boundaries, fracture toughness 77−77553
- alloy B95T1 with surface cracks, fracture toughness determ. *(Russian)* 77−25141
- alloys, fracture toughness and impact strength, correl. breakdown 80−55523
- alloys, fracture toughness rel. to microstruct. characts., alloy design 79−43423
- alumina, diametral compression test, parametric study 78−44282

fracture toughness continued

- alumina, grain size and fracture toughness, effect of fracture toughness test methods 78−72883
- alumina, multiaxial fracture, general approach to statistical anal. 78−90785
- amorphous metals, mech. characts., review *(Japanese)* 77−86109
- amylose, micromech. fracture anal. 78−68784
- Araldite B, crack arrest toughness determination 78−72867
- Araldite B specimens, dynamic fracture toughness, influence on dynamic crack propag. 80−99966
- aramid fibre reinforced acrylic bone cement, tensile strength and fracture toughness, SEM study 79−29667
- asbestos fibre reinforced cement, strength and fracture props. 80−108533
- asbestos fibre reinforced cement mortar, strength and fracture properties 79−100241
- asbestos fibre reinforced Portland cement analytical fracture resistance curve expression 78−76756
- austenitic steel neutron-irradiated weld toughness rel. to ferrite content 79−83327
- Barre granite, crack growth and development during creep 79−84237
- Barre granite, static and dynamic fracture strength 77−44976
- bone tissue, compact 80−12178
- bone-prosthetic material composites 77−37108
- boride coatings, high temp. resist. and struct. 79−39008
- borsic fibre reinforced Ti, unidirectional, K-calibration and compliance curves 78−88518
- brass, crack opening displacement, rel. to flow stress 78−68810
- brittle circular disc under impact loading, fracture mech. 78−88514
- brittle cracks, stability, propagation, fracture mech. *(Czech)* 78−79257
- brittle fracture, statistical theory, dislocation mechanism, crack propagation *(Chinese)* 80−106755
- brittle fracture, structure design, method of calculation 78−72869
- brittle fracture in ductile material, model and applic. to H embrittlement 78−23814
- brittle materials, crack propagation under compression, finite element anal. *(Japanese)* 78−42567
- brittle materials, influence of structural parameters on fracture toughness 79−96133
- brittle materials, splitting of fracture toughness into two terms, elastic deform. and plastic deform. *(German)* 78−35468
- brittle materials, under multiaxial loading, fracture toughness characterisation 80−33530
- brittle materials, water drop impacted, damage thresholds 80−81149
- brittle rotating disk, probability theory appl. to rupture strength 80−43662
- carboxyl terminated butadiene nitride-diglycidyl ether of bisphenol A epoxy resin, struct. and mech. props. 78−52901
- cast iron, white, high Cr-Mo, fracture toughness 80−50726
- cellulose fibres, from jute, crystallinity percentage, estimation by X-ray methods 79−7553
- cemented carbides, hardmetal, bending strength and fracture toughness 79−20181
- cemented carbides, indentation fracture, surface fracture toughness nature 78−60849
- ceramic, critical stress intensity factor and fracture energy concepts applic. *(French)* 77−32672
- ceramic composite, toughening by oriented nucleation of microcracks 77−8921
- ceramic material fracture mechanics, n review 80−45373
- ceramic multilayer capacitors, fracture mechanics approach to structural reliability assessment 80−89328
- ceramics, coarse-grained, dimensional anal. of grain size depend. of fracture strength 80−70299
- ceramics, crack extension micromechanisms, review 80−108567
- ceramics, fracture toughness, exam. of methods of enhancing, merits and limitations 78−60771
- ceramics, high temp. props., conf., Baden-Baden (Feb. 1978) *(German)* 79−70135
- ceramics, mechanical behaviour, book 79−38983
- ceramics, transformation toughening, martensitic transforms. in crack-tip stress fields 80−104154
- ceramics and brittle solids, abrasive wear, role of plastic deform. and fracture 80−108594
- ceramics containing metastable tetragonal ZrO_2, grinding induced tempering 80−89260
- chevron notched short bar specimens, compliance and stress intensity coefficients 80−96232
- chrysotile asbestos fibres, texture rel. to mech. props. 77−81300
- cleavage fracture toughness models 80−40515
- coated fibre-reinforced composites of strain-rate sensitivity 77−16664
- coke, breakage behaviour rel. to struct. 80−85026
- coke, metallurgical, industrial strength meas. methods, critique 80−85117
- Columbia Resin, CR-39, fracture mirrors, static and impact tests 78−27601
- composite, crack extension micromechanism 80−108566
- composite materials, fibre-reinforced, impact responses perpendicular to fibres *(Japanese)* 79−43377
- composite materials, fracture, elastic mismatch and interfacial bonding influence 80−40506
- composite materials, rational bonding of structures, fracture resistance 80−5990
- composites, single fibre-brittle zone model, fracture behaviour 80−97570
- concrete, cracking along anchored deformed reinforcing bars 79−96122
- concrete, glass or steel fibre reinforced 79−87706
- concrete, prestressed hollow beams in combined torsion and bending 79−96087
- concrete, stress distribs. under splitting loads *(Japanese)* 78−35495
- concrete cylinders, fracture, fluid pressure testing using H_2O and N_2 gas 78−60750
- concrete slab, explosive shock resist., tensile fracture 80−85065
- constitutive equations of continuum creep damage mechanics 78−67054
- constructional materials, use of J-integral method for assessing fracture toughness *(Russian)* 79−24602
- continuous bodies under gravity load, centrifugal force, optimum strength shape 79−98665
- crack, plain strain arrest charact. 77−44367
- crack development resistance anal., stereoscopic fractography anal. 79−90189

fracture toughness continued
- crack extension criterion of maximum shear or principal stress 78—79278
- crack growth, at rubber springs bonds, energy calc. and meas. 79—83316
- crack length dependence 78—67120
- crack tip, plastic deform., metallographic anal. by recrystn. 80—85029
- crack tip plastic zone, thermal props. calcs. 80—7659
- crack tip strain distribution measurement by recrystn. *(German, English)* 77—56203
- cryogenic alloys, and structural strength 77—59927
- curve fitting, to toughness data 80—40511
- cyclotrimethylene trinitramine, high explosive, fracture surface energy determ. 77—44337
- cylinder, transversely isotropic brittle elastic, stress and failure probability analysis for internal press. and thermal loading 77—50990
- cylindrical specimen with external crack reaching surface of annular stress concentrator, tension and bending 79—14349
- dental amalgam, exam. of fracture toughness and critical strain energy release rate 78—48933
- dental restorative materials, empirical eqn. including fracture toughness for friction 78—61283
- determination from fatigue test results in circular bending 78—15526
- disk test study of combined mode fracture criterion *(Japanese)* 79—66153
- double cantilever beam, fracture behaviour, quasistatic energy anal. 79—18817
- double cantilever beam, fracture studies 80—53708
- ductile fracture, computer model based on plastic strain, fracture toughness prediction, comparison with steel data 79—32383
- ductile materials, tearing, fracture strength determ. 79—43385
- ductile notched fracture toughness specimens, instability prediction, approx. flow stress model 78—34082
- Duralumin, effect of alloy purity and ageing on fracture mechanism, and resultant toughness 79—5049
- dynamic, conf., London, England, (July 1976) 77—36714
- dynamic analysis with Lagrangian finite difference method 77—35095
- dynamic fracture toughness, influence on dynamic crack propag. 80—99966
- elastic-plastic materials, K_{Ic}-value determination, fracture mechanics method 80—45376
- elastic-plastic solid containing holes in vicinity of crack tip, finite element anal. 78—67147
- elasto-plastic fracture mechanics, critical assessment 79—38943
- elastomers, viscous flow, strength characteristics, activation energy, fracture behaviour *(German)* 79—57105
- engineering structures, welded exam. of fracture processes, review 78—60777
- epoxy, elastomer-modified, loading rate depend. fracture prop. 80—76342
- epoxy, thermomech. props., rel. to hardener type and conc. 79—1913
- epoxy, three-component modified, development for dynamic photoelastic obs. of fracture 78—35474
- epoxy resin, low temp. irradiation effects on mechanical props., use in superconducting magnets 78—60737
- epoxy resin systems, synthesis review, phys. and mech. props. at low temps. 80—25650
- epoxy resin-cemented glass joint, temp. relationship of fracture toughness 80—3196
- epoxy resins, fracture props. study at cryogenic temps. 80—25869
- epoxy-polyglycol elastomers, fracture strength under compression 79—38929
- epoxy-rubber particulate composite, toughness and fracture mech. 80—71727
- ethylene-base ionomers, impact tensile props. *(Japanese)* 79—96120
- ethylene-vinyl acetate-vinyl chloride graft copolymers, rel. between morphology and toughness *(German)* 80—66665
- evaluation method, review *(Japanese)* 79—8342
- evaluation method *(Japanese)* 78—92330
- failure criterion considering stress state at crack apex 79—57113
- fatigue fracture toughness use in fracture toughness determ. 79—46747
- femora, bovine, critical crack length, plastic zone size 79—43948
- femoral subtrochanteric fracture stress anal. 79—79591
- fibre composites impetus of composite mechanics on test methods 80—11868
- fibre reinforced cement, mech. and rheological props. *(German)* 79—20129
- fibre reinforced ceramic, strength and fracture 79—87723
- fibre reinforced composites, cracking and fracture, review 78—60772
- fibre reinforced composites, fracture toughness, fibre bunching effects 79—61699
- fibre reinforced composites, Monte Carlo study of strength 80—25844
- fibre reinforced composites, unidirectional, mixed mode fracture 80—100302
- fibre reinforced concrete beam, load-deflection curves in flexure 78—35437
- fibre reinforced plastic laminate with circular holes, stress conc. and breaking strength *(Japanese)* 78—23816
- fibrous composite, short steel wire reinforced (polymer impregnated) concretes, cracking and toughening 78—80626
- finite centre crack specimen, biaxial and nonlinear effects on energy release rate, J-integral 78—18232
- fission reactor pressure vessel supports, fracture-safe design in neutron environment 79—93700
- fission reactor welded pressure components, effect of material property changes on operating conditions 79—20197
- float glass, toughening by ion exchange, selection of technology parameters 78—84757
- fracture mechanics, recent theoretical and experimental developments, review 78—60776
- fracture mechanics of yielding materials, review 78—31521
- fracture mechanism maps, usefulness 80—84245
- fracture mechanisms review 80—35296
- fusion reactor materials, fracture resistance 78—82515
- gelatin in nuclear photoemulsion, effect of pulsed elec. field on physical and mech. props. *(Russian)* 78—869
- GFRP cross-ply laminate, constrained cracking 78—19870
- glass, annealed and tempered, impact damage, strength 80—85025
- glass, electrical energy losses and causes, atm. humidity effect 80—55498
- glass, silicate, ultimate strength, and max. breaking rate 80—25863
- glass, strength degradation from impact with spheres 78—27663
- glass bead, impact fracture *(Japanese)* 78—92338
- glass bead epoxy resin, direct obs. of debonding at crack tips 80—3167

fracture toughness continued
- glass ceramic rods, strengthened, residual stress determ. 78—23830
- glass fibre, reinforced polycarbonate, dynamic fracture toughness, absorbed energy and crack propagation velocity *(Japanese)* 80—16447
- glass fibre reinforced epoxy, fatigue, time and temp. depend. 80—21095
- glass fibre reinforced epoxy, fracture mechanics 80—35294
- glass fibre reinforced epoxy-aniline, laminate, work required to rupture along interfaces 79—43413
- glass fibre reinforced laminate, failure process 78—31529
- glass fibre reinforced plastic, centrifuged laminate, fracture characts. determ. *(German)* 79—38967
- glass fibre reinforced plastic, impact tensile fracture energy *(Japanese)* 78—39888
- glass fibre reinforced plastic, time depend. probabilistic failure model 80—40477
- glass fibre reinforced plastic, unwinding resistance of hardening layers, fibre tension effect 77—32691
- glass fibre reinforced plastic laminate, crack resistance under prolonged loading 77—21276
- glass fibre reinforced plastic laminate, mixture law of tensile and fracture strength and variation *(Japanese)* 79—43337
- glass fibre reinforced plastics, stress conc. effect on spread of strength and fatigue life *(Japanese)* 79—96117
- glass fibre reinforced polyamide thermoplastic, stiffness and strength 78—27600
- glass fibre reinforced polycarbonate, fatigue crack propag., mean stress effect *(Japanese)* 79—66151
- glass fibre reinforced polyurethane foam fracture toughness, modulus increase 78—44196
- glass laminate 27-63S, shear fracture toughness charact., strain rate effects 77—8950
- glass panel, dynamic stresses and failure under inertial loading 77—56073
- glass reinforced plastics, static and fatigue failure, fracture mechanics 78—19898
- glass systems, binary and tenary, structure toughness-composition relationship 80—104257
- glass-ceramic composite, internal stress effects on mech. props. 77—21250
- glass-filled ABS, deform. and fracture behaviour, 293-353K 77—56077
- glass/C fibre reinforced plastic, hybrid effects between interlaminar and translaminar config., mech. props. 79—52351
- glasses, mech. strength fracture dynamics, behaviour forecasting *(French)* 77—73344
- grain boundary decohesion, exchange type soft solute segregation in hard hosts 80—54258
- graphite, coarse grained, fracture toughness *(German)* 80—76358
- graphite, failure criterion, J-integral critical value 78—84999
- graphite, failure energy of polycrystalline sample considered as heterogeneous medium, porosity effect 79—96138
- graphite, fracture mode criterion, combined, disk test study *(Japanese)* 79—66153
- graphite, fusion reactor first wall appl., radiation damage 79—86822
- graphite, neutron irradiation effects on thermal shock resist. and fracture toughness *(Japanese)* 80—66622
- graphite, pyrolytic, structural factor effect on strength 79—66135
- graphite, thermal shock resistance and fracture toughness during graphitising heat treatment *(Japanese)* 80—71843
- graphite epoxy laminate, mixed mode fracture, fracture strength 77—70156
- graphite fibre reinforced Al, mech. props., comparison with B-Al composite 77—52470
- graphite fibre reinforced epoxy, fracture mechanics 80—35294
- graphite fibre reinforced panels, low energy impact testing 78—72845
- graphite fibre/epoxy laminates, free edge induced failure 80—11775
- graphite reinforced epoxy resin, average stress failure criterion appl. 78—88519
- graphite-epoxy laminates, AS/3501-5, compressive fracture strength 79—43396
- graphites, reactor, strength and deformation under conditions of cyclic variation in load and temp. 79—43355
- graphitic materials deformation, crack and fracture behaviour, SEM exam 80—11706
- gypsum plaster, plain and glass reinforced, fracture energy 77—36621
- hard alloy bar, slide rule for calc. transverse rupture strength 80—40530
- Hastelloy C-4, loaded at high temp., useful life 80—40523
- Hastelloy X, heat resistant superalloys, for nuclear plants in He, creep props. *(Japanese)* 79—83263
- heat-resisting alloy, EP199, creep-rupture strength in NH_3 and decomp. products *(Russian)* 77—52534
- high strength, crack propagation behaviour, stress, temp. and fracture toughness effects *(German)* 78—31494
- high strength ductile materials, condition for crack growth 80—10190
- high strength materials, exam. of flow localisation and fracture toughness 78—60764
- high strength structural mats., microstruct. influences on fatigue and fracture resist. 78—56728
- high-C steel, strength characts. with controlled hardenability after bulk-surface hardening 77—56156
- Homalite 100, dynamic fracture toughness 78—60740
- Homalite-100 plates, modified compact-tension specimens, dynamic anal. 80—97561
- hydrostatic pressure effects on fracture, exam. 78—60779
- hydroxylapatite, dense, fatique and fracture strength from diametral tests, after various treatments 80—60953
- impact damage in elastic response regime 78—71785
- impact test, finite element analysis 78—68806
- Incoloy, 800 and 807, heat resistant superalloys, for nuclear plants in He, creep props. *(Japanese)* 79—83263
- Incoloy 800, and 800H, proposed specification changes 79—43298
- Incoloy 800, mech. props. above 600°C 79—43370
- Incoloy 800 and 802, influence of carburisation on mech. props. 79—20254
- Incoloy 800 for HTR appls., correlation of carburization behavior, mechanical property degradation, and exposure conditions 80—5244
- Inconel, 617 and 625, heat resistant superalloys, for nuclear plants in He, creep props. *(Japanese)* 79—83263
- Inconel 600 and 601, influence of carburisation on mech. props. 79—20254
- Inconel alloy 718, exam. of struct., properties and continuum synthesis of ductile fracture 78—76736

fracture toughness continued
indentation analysis, relation of hardness, toughness and brittleness 79—100249
index, K_{ic}, accuracy of values, assessment *(Russian)* 78—11300
intergranular fracture energy, effects of segregated impurities 79—38928
J_{Ic}-integral value determination steel, low strength, through compact tests 80—45451
J-integral rel. to crack tip opening displacement *(Japanese)* 78—42569
J-integral/strain energy correlation, expt. study *(Chinese)* 79—100236
jade, fracture parameters and crack propag. resist., rel. to fibrous microstruct. 77—8908
Kevlar fibres, effect of crystallinity and orientation on mech. props. *(Japanese)* 79—38952
Kevler fibre, mech. props. in aq. H_2SO_4 soln. *(Japanese)* 79—47753
kinetics, analytical description 77—11139
lecture on fracture toughness *(Japanese)* 80—90595
limestone, fracture toughness meas., influence of microstruct. and environment *(French)* 77—81874
LMFBR, effect of cracks in fast neutron embrittled hexagonal subassembly ducts 78—74446
long-term strength of materials under load and accumulation of damage *(Russian)* 77—59892
low-alloy cast steel, high-strength, fracture toughness 77—56109
membranes, two-layer protective, with circular slits, strength 79—87730
metacarpi, equine, fracture toughness 80—3694
metal, fracture and tensile props., effect of strain rate and temp. 77—36662
metal, fracture toughness and temp.-rate sensitivity of plastic flow stress 78—35501
metal, notched sheet, thickness effect on deform. and fracture under tension 79—70113
metal, overload effect on fatigue crack growth, fracture toughness prediction *(Polish)* 79—34134
metal, stress to rupture strength charact. at high temps. 77—81321
metallic alloys, fracture toughness and fatigue crack growth data, compendium of sources 78—84963
metallic glasses, mats. props. review 77—4043
metallic glasses, strength and stiffness 77—8899
metallic material, fatigue cracking, cyclic fracture toughness determ., critical state *(Russian)* 79—29173
metallic materials, crack propag. mech. and fracture toughness, microstruct. effects 78—19859
metals, crack resistance, high temp., during creep due to stress relaxation *(Russian)* 79—52348
metals, fracture toughness charact. in fatigue 79—15790
metals and alloys, fracture toughness determ. in conditions of similarity to local fracture *(Russian)* 78—31505
metals and alloys, micromechanical modelling *(Russian)* 78—31504
microcrystalline alloys, metastable, rapidly quenched particulates, props. appl. and production 80—84887
mineral-fibre composites that resist fracture and cracking 77—8798
modified glassy polymers, thermal stresses 77—77567
multiaxial, general approach to statistical anal. 78—90785
NASICON solid electrolyte, processing and phys. props. 80—60820
Navy vessel fracture mechanics and flow separation, instability phenomena 80—99971
Nimonic EhI437B, heat resistant, true breaking stress in rapid air stream 79—66163
nitrided layer, fracture toughness determ. from hardness impressions *(German, English)* 80—97575
notch analysis for fracture toughness and fatigue crack propagation threshold 77—35086
notch creep rupture strength under longit. shear and torsion 78—5689
notch-tip geometry, influence on stress and strain distrib. 80—33535
notched beam, fatigue crack emanates from notch root, fracture strength 78—72866
notched specimen, brittle fracture characts. under impact bending 78—23810
nuclear fuel pin failure, pressure in duct due to gas discharge 78—675
nuclear piping, impact loading *(Japanese)* 79—43373
nuclear reactor materials, crack-front tunnelling, investigated by single specimen compliance technique 80—70300
nylon, partially crystn., temp. effects on fracture 77—63771
Nylon 6, injection moulded, yield stress and fracture toughness 80—38951
ophthalmic lenses, thin, chemtempered, static load strength testing 80—5812
optical fibre, fast fracture and time depend. strength meas. 77—46818
optical fibre, fracture surface anal. 80—58754
optical fibre, influence of surface defects *(Japanese)* 78—37987
optical fibre, mechanical strength, fractographical analysis, review *(Japanese)* 80—35319
optical fibre, rupture stress rel. to ageing *(German)* 78—38009
optical fibre, statistical data, graphical and analytic statistical model depiction 77—83975
optical fibre fracture strength and degradation factors 78—1383
optical fibre moisture effect on fracture strength 79—37019
optical waveguide fibre, screen tested, fatigue strength meas. 80—19098
oxides on Al alloys, mech. props. and influence on substrate fatigue 77—44408
parameters J and G^{Δ}, effect of load biaxiality 78—67128
pentaerythritol tetranitrate, high explosive, fracture surface energy determ. 77—44337
PFFE, impact fracture toughness, rate effect 78—56741
phosphate bonded refractory plastics, hot modulus of rupture, 1500 to 2500°F 78—19855
phosphate glass-Al alloy seals, elec. and mech. props., glass transition 80—81018
photopolymer, biaxial stress-strain test 80—40417
phthalocyanine polymer, dynamic mech. props. and fracture energy 80—100866
plane strain fracture mode criterion based on plastic zone size-thickness correlation 80—43670
plant fibre, fracture energy 79—52355
plaster, fracture mode criterion, combined, disk test study *(Japanese)* 79—66153
plastic material, material scale length as meas. of fracture toughness in fracture mechanics 78—68763
plate, thin, fracture toughness from plastic deform. induced thickness contraction 78—75109
PMMA, crack velocity meas. using US fractography 79—15772

fracture toughness continued
PMMA, cracking kinetics, effect of small vibrs. 79—57108
PMMA, craze shape, fracture toughness, −30 to 45°C 77—48542
PMMA, craze shape and fracture, temp. depend. 77—52486
PMMA, durability over extensive time temp. range 77—90460
PMMA, effect of mol. orientation on fracture toughness 78—52992
PMMA, effects of notch shapes on Charpy impact values, tensile props., fracture surfaces *(Japanese)* 79—38951
PMMA, fracture stress 78—3216
PMMA, fracture toughness for moving crack 77—44365
PMMA, fracture toughness under biaxial stress 78—76760
PMMA, instantaneous crack resist. during stable crack propag. 80—85058
PMMA based composite (acrylic bone cement), effect of $BaSO_4$ and glass particle dispersions, on fracture behaviour 78—76753
PMMA-filled with SiO_2, degrading effect of filler on polymer fracture energy 78—52939
point-loaded centre cracked plates, fracture studies 78—19884
polycarbonate, crack instability under impulse loads, dynamic fracture toughness 77—48518
polycarbonate, deform. and failure modes, surface craze characts. 79—91753
polycarbonate, dielec. relax. and ductile brittle transition 78—52438
polycarbonate, effect of mol. weight on craze shape and fracture toughness 80—25858
polycarbonate, notched specimens, impact fracture behaviour 77—28888
polycarbonate craze shape temp. depend. 78—48529
polycarbonate plates, modified compact-tension specimens, dynamic anal. 80—97561
polycarbonate structure foams, fracture toughness 78—15500
polyester resin, cross-linked unsaturated, synthesis and fracture toughness 80—93634
polyester resin, reinforced with glass chopped strand mat and woven roving fabric, fracture toughness and crack-growth meas. 79—83299
polyethylene: (Dy_20_3), mech. props. and transfer to steel surfaces 80—16496
polyethylene, filled, linear, struct., strength 79—29149
polyethylene, filled with SiO_2, degrading effect of filler on polymer fracture energy 78—52939
polyethylene, high-density, longevity prediction, effect of surface active media 77—12729
polyethylene, high-density, submicroscopic cracks form. and residual strength, hydrostatic press. influence 79—20185
polyethylene, impact fracture toughness, rate effect 78—56741
polyethylene total joint replacement, props. improvement by C fibre reinforcement, SEM obs. 78—24183
polyethylene-propylene copolymers, branching effect on struct. and mech. props. *(Russian)* 79—52333
polyimide fibre reinforced polyamide-12 80—11754
polymer, fracture kinetics, book 79—29222
polymer, glassy, strength and safe stress calcs. for brittle state *(Russian)* 77—59898
polymer concrete, fracture toughness meas. 79—70168
polymer endoprosthetic joint, fatigue life 80—40521
polymer fibre, lifetime under load, in presence of UV radiation stress depend. 78—48534
polymer fibre, lifetime under load, in presence of UV radiation, stress depend. 78—48535
polymer film, semicrystalline, tear resist. 77—52488
polymer strength, kinetic nature 78—15524
polymers, low mol. wt., mol. theory of fracture toughness 79—66140
polymers, mol. struct. rel. to bulk props. 77—32553
polyphenylene sulphide, high mol. wt. soluble resin, prep., mech. props. 80—60828
polypropylene, crystalline, morphological aspects of crack growth 78—76761
polypropylene, fracture toughness eval. with surface crack specimens 79—15777
polypropylene, homopolymer, effect of mol. orientation on fracture toughness 78—52992
polypropylene partially crystn., temp. effects on fracture 77—63771
polypropylene/peanut-hull flour composite, strength 79—8365
polystyrene, fracture toughness eval. with surface crack specimens 79—15777
polystyrene, rubber modified, two-phase struct. influence on fracture toughness *(German)* 80—66666
polystyrene, rubber-modified, fracture, temp.-effect −120-20°C 77—4838
polystyrene, rubber-modified, fracture mechanics anal. of effect of rubber content, craze formation 79—29190
polystyrene, rubber-modified, temp.-effect −120-20°C 77—4838
polyurethane rigid foam, fracture props. over range of densities 79—79106
polyvinylethylal, durability over extensive time temp. range 77—90460
porcelain, crack propag. data applicability to failure prediction 80—81154
porous materials, pore geometry effects on tensile strength 80—30048
pressure vessel, strength analysis, by thermal shock 78—68819
pressure vessels, elastoplastic fracture modelling, acoustic emission 80—35303
PVC, biological media effect on. physiomech. props. 79—96168
PVC, kinetic nature of strength 78—15524
PVC, rigid, craze and yield zones in fracture 80—50701
PVC, rigid plate, notching method effect on Charpy impact values, fractographic considerations *(Japanese)* 80—108541
PVC, slightly plasticised, fracture toughness tests, impact tests 79—5037
PVC extruded films, mech. props. *(Polish)* 79—70037
PVC-Cu composites with chemically deposited ultrafine copper particles 80—93534
α-quartz seed plate fracture strength, etching and annealing effects 77—36661
quasi-cleavage fracture, characteristic length parameter, correlation with fracture toughness *(Chinese)* 80—104246
reactor graphite, thermal shock fracture toughness eval. by arc discharge heating 78—72835
reactor graphite, up to 2600°C 78—68760
reference curve development 80—97588
refractories, fracture toughness role in spalling resistance *(German)* 77—73316
refractories, role of fracture toughness in thermal shock resistance *(French)* 78—80618

fracture toughness continued
  refractory, fracture under thermal shock, AE study 80—25865
  refractory fibre, effect on high-temp. strength of refractory coatings *(Russian)* 77—52536
  reinforced axisymmetric shells stratified by shear, bearing capacity 79—3979
  reliability of fracture sensitive structures, materials related aspects 78—42570
  residual stress effect in quasi-static cracking of materials 77—84193
  rock, deformation and fracture under general triaxial stress states, anisotropic dilatancy *(Japanese)* 78—56750
  rocks, dynamic fracture strength 79—62486
  round bars, endurance limit under combined tension and torsion 79—32387
  rubber-like polymer, molecular relaxation process effect on strength *(German)* 78—31440
  S glass-Ni sphere composite, exam. of crack shape and fracture toughness 78—72886
  safety guide for material treatment and working *(German)* 78—15534
  sapphire, white, brittle fracture, microstruct. depend. 80—16469
  sapphire fibre reinforced, Mo, strength at rupture 80—104286
  silica optical fibres, surface flaws obs., fracture strength 77—14793
  silicate glass 79—57190
  silk, spider, tensile, fracture strength, elongation and ageing effects 80—41072
  sital, structural glass component, strength in complex stress state 79—91763
  small crystals, fracture strength and triboluminesc. 78—64420
  β-spodumene-mica glass ceramic, thermal expansion thermal shock and moduli of rupture and elasticity 78—60736
  stainless cast high-strength steel, fracture toughness 77—56109
  stainless steel type 316, ductile crack initiation, detection and toughness characterisation 77—16662
  steel, 12 MKh, creep-respective strength and fracture mode in H_2 *(Russian)* 77—52461
  steel, 15G2AFDps and boiler steel, fracture toughness determ. from fatigue test results in circular bending 78—15526
  steel, 24Kh2NMFA, crack resistance, yield strength, ductile-brittle transition temp., optimum tempering of 24Kh2NMFA 77—63787
  steel, 30CrMnSiNi2A, fracture toughness parameter K_{ISCC} 80—21099
  steel, 30KhGSA, fracture toughness, tempering effects 77—90463
  steel, 30N9K4, effects of Mo, V, and N on grain growth, tempering, hardenability, strength and toughness 78—44202
  steel, 35, fracture characteristics, notch sharpness effect in impact tests 79—52536
  steel, 35Kh3MFS, strengthening involving austenite fine grain processing *(Russian)* 77—52358
  steel, (0.36 wt.% C) Ni-Cr-Mo, electroslag refined, fracture toughness and fatigue behaviour 80—81171
  steel, AISI 4140, cyclic crack opening displacement behaviour during high-amplitude block loading 80—45375
  steel, AISI 4340, austenitised at low and high temps., toughness evaluation 77—16621
  steel, AISI 4340 toughness evaluation austenitized at high and low temps. 77—86155
  steel, Al-Ti-(Mo), Al-Ti-V-(Mo), Al-Ti-Nb-(Mo) and Al-V-(Mo) low-alloy, toughness improvement through Ti additions 80—66525
  steel, alloy, 300M, fracture toughness and strength, effect of heat treatment on microstruct. 78—15436
  steel, alloy, C-Cr-Mo-V, exam. of fracture toughness and critical flow anal. 78—72848
  steel, alloy, crack arrest toughness determination 78—72867
  steel, alloy, cyclic strength after strain hardening and tempering, precip. hardened 40FT and 40 78—52988
  steel, alloy, Fe-Cr-Mo-Si-V, various steels, short rod stress intensity factor tests up to 700K, exam. 78—60815
  steel, alloy, Fe-Cr-Ni-Mo-Al, (13, 8, 2, 1, wt.%), H_2 effects on fracture, exam. 78—60809
  steel, alloy, maraging, 18% Ni, effect of solution and ageing treatments, on microstruct., tensile props., fracture toughness 78—80648
  steel, alloy, maraging, 250-grade, ductility and toughness of hot isostatically pressed powder 78—52925
  steel, alloy, mechanical properties, morphology, transform. kinetics and composition interrelations 77—86146
  steel, alloy, medium and low C, quenched and tempered, fracture resist., nonmartensitic transformation products effect 79—96054
  steel, alloy, Mn-Si-C, exam. of fracture toughness for sheets, using linear elastic fracture mechanics 78—56762
  steel, alloy, Ni (5.5 wt.%), fatigue fracture toughness, crack propag., at low temp. 78—68823
  steel, alloy, nonmartensitic decomposition of austenite, fracture strength of high tempered products *(Russian)* 78—11304
  steel, alloy, sheet, crack-propag. resist. in heat-affected zone in presence of H, rolling direction and preliminary plastic tensile strain effects 80—60971
  steel, alloy, toughness evaluation inconsistency of AISI 4340 austenitised at increasing temp. 78—52982
  steel, alloy, type 4340, fracture toughness, effect of partially dissociated N_2 78—80642
  steel, alloy 4340, fracture and high temp. props., 533K to 1255K 78—60821
  steel, alloy cast, optimal alloying, carburising effect 80—50771
  steel, austenite decomposition, controlled rolling rel. to substruct., props. 79—29014
  steel, austenitic, 30KhGSA, heat treatment, preliminary, cold deform., elec. heating rel. to mech. props. 79—24554
  steel, austenitic, AISI 4340, effect of step quenching on microstruct. and fracture toughness 78—84834
  steel, austenitic, ASTM A533B and A542, H_2 embrittlement behavior of unirrad. steels for nuclear reactor press. vessels 79—8340
  steel, austenitic, fracture toughness effects on friction force in abrasive wear *(German)* 77—4860
  steel, austenitic, fracture toughness meas. by Charpy impact testing, welding, heat treatment, neutron irrad. effects 79—5062
  steel, austenitic, fracture toughness props. of A533B, prior austenite grain size effect 78—60780
  steel, austenitic, high-temp. crack resist., B and Mo influence *(Russian)* 80—16435
  steel, austenitic, low-C, transform. kinetics rel. to temp., deform., struct., mech. props. 79—24519

fracture toughness continued
  steel, austenitic, martensitic transform. effect on hardening kinetics and fracture resist. of friction surface of 45Kh12G8 and 110G13 *(Russian)* 80—50727
  steel, austenitic, Mn-base, as LNG storage and transportation system material 79—70133
  steel, austenitic, overheated, ESR, low alloy, fatigue crack growth rate 79—34141
  steel, austenitic, reliability of stress intensity factor values 80—55530
  steel, austenitic, strength, ductility and fracture toughness, N and Cr effects 80—100878
  steel, austenitic stainless, 12Kh18N10T, deformed, phase comp. and props. after prolonged heating 80—30040
  steel, austenitic stainless, biphase, ferritic, ageing and thermomech. treatment effects on struct. and props. 80—35226
  steel, austenitic stainless, Cr-Mn, austenite stability during deform. 77—70050
  steel, austenitic stainless, cylindrical specimens with crack. fracture characts. in inelastic strain, test methodology 80—25839
  steel, austenitic stainless, fracture toughness and transition temp., T_{50}, effect of cooling rate and supercooling temp. 78—84987
  steel, austenitic stainless, mech. props. correl. methodology development for fusion environments 80—29068
  steel, austenitic stainless, reliability of stress intensity factor values 80—55530
  steel, austenitic stainless, supercond. magnets, mech. and phys. props. at 4K 80—86976
  steel, austenitic stainless in liq. Na, mechanical props., review 79—20150
  steel, brittle fracture resistance, welding and heat treatment effects 80—50723
  steel, C, brittle fracture resistance, C effect 80—3163
  steel, C, composite layered specimen influence of contact strengthening by intermediate layer, on fracture toughness *(Russian)* 79—15768
  steel, C, corrosion carcking by sulphide, effect on props. 80—55587
  steel, C, crack opening displacement, rel. to flow stress 78—68810
  steel, C, crack resistance, preliminary loading condition effects in crack appl. 78—56739
  steel, C, cyclic loading and fracture toughness 80—35298
  steel, C, cylindrical specimens with crack. fracture characts. in inelastic strain, test methodology 80—25839
  steel, C, fracture criterion determination, using 3-point bending 79—29216
  steel, C, heterogeneous structure, fracture characts. 79—38961
  steel, C, inclusions, influence on toughness and fatigue props. 80—40533
  steel, C, microduplex, ferritic-martensitic, struct. effect on tensile fracture *(Japanese)* 79—96113
  steel, C, plates, residual elements effect on through-thickness props. 80—66660
  steel, C, pressure vessel and piping, factors affecting notch toughness 79—61730
  steel, C, residual elements, effect on props. 80—66643
  steel, C, spheroidal, fracture toughness, cementite particles, effect., obs. 77—70165
  steel, C, spheroidised, fracture toughness, cementite particle effects, optic and electron obs. 78—60785
  steel, C, structural strength, increase by high temp. mech. treatment with austenite isothermal decomp. 79—24555
  steel, C, tempered martensite embrittlement, and retained austenite, exam. 78—56754
  steel, C, type 35, low temp., non-metallic inclusions influence *(Russian)* 79—52346
  steel, C, weldable, ferrite-pearlite, Widmanstatten structs., resist. to fracture 79—29203
  steel, C and alloy, notched beam, fatigue crack emanates from notch root, fracture strength 78—72866
  steel, C and low alloy, structural, ductile and brittle fracture resist. in stable crack growth stage 79—52369
  steel, C content influence on brittle and tough fracture, heat treatment *(Russian)* 80—40500
  steel, C type 45, martensitic needle size, effect on mech. props. after induction hardening 80—11672
  steel, C-Mn-Cr-Mo (0.4, 0.8, 1.1, 0.25 wt.%) C, Ni, Mo, Cr addition effects on toughness of bainite 78—11327
  steel, C-Mn-Nb, structural for seamless line pipe tube, brittle fracture resistance *(Czech)* 77—70161
  steel, C-Mn-V and Cr-Mo-V, power station component, fracture toughness and fatigue characts. 79—20192
  steel, C-Mo-P, intergranular fracture and grain boundary segregation, P, H, Mo effects *(Japanese)* 79—15775
  steel, cantilever bend specimen, side grooving effect on compliance relationships 78—35472
  steel, carburised, fracture resistance 79—24612
  steel, cast, effect of non-uniform struct. on props. 78—84850
  steel, cast, high tensile strength, heat treatment 80—16358
  steel, cast, low alloy, fracture toughness 77—4835
  steel, cast C and C-Mn steels, fracture toughness 77—4836
  steel, Charpy V-notch toughness test, computer simulation 79—70138
  steel, Ck35N and 37MnSi5, fatigue strength estimation, separation method suitability *(German)* 78—27644
  steel, Co-Cr-Mo type HY-180M, mech. props. and SCC, overageing effect 80—108634
  steel, comp. and processing effects on microstruct. and props. rel. to low temp. applic. 77—52365
  steel, compliance correction for determining load-line energies for compact fracture toughness specimens 79—57186
  steel, constructional, fracture toughness in cyclic loading 78—72860
  steel, Cr, cast, fracture toughness and fatigue crack propagation, structural components of hydro-turbines, in water and air 78—68822
  steel, Cr, tempering resist., mech. props., Cu addition effect 79—79012
  steel, Cr (12wt.%), mech. props, carbide phase struct. 79—15702
  steel, Cr (13 wt.%), fatigue, effect of toughness *(Japanese)* 78—7025
  steel, Cr (40 wt.%), Sn and P segregation effects on impact toughness *(Chinese)* 77—73313
  steel, Cr-Mn, powder forged, fracture processes and fracture toughness 78—72870
  steel, Cr-Mo, effect of Mo on high-temp. props. 80—85005
  steel, Cr-Mo, Mn-V, V, fracture toughness, pressure vessel appl. *(Czech)* 79—79094
  steel, Cr-Mo, toughness of heat treated steels of equal tensile strength *(German)* 80—25727

fracture toughness continued
steel, Cr-Mo (10-14, 2-6 wt.%), heat-resist., creep-rupture strengths 80−104271
steel, Cr-Mo (1.25, 0.5 wt.%), creep, fracture, Ti and Ti+B effects 77−36603
steel, Cr-Mo-(Ni), fracture resistance, H_2S in H_2 effect *(French)* 80−16461
steel, Cr-Mo-V, hydrogen embrittlement resist. evaluation *(Czech)* 80−35308
steel, Cr-Mo-V, medium strength, correlation between crack initiation, propag. and microstruct. 78−60787
steel, Cr-Mo-V, stress rupture strength at high temps. *(German)* 80−40474
steel, Cr-Ni, effect of tempering under load on mech. props. 80−16354
steel, Cr-Ni, hydrogen effect on strength, ductile and fracture characts. 79−38960
steel, Cr-Ni, soaking at forging temp., effect on struct. and mech. props. *(Czech)* 78−64628
steel, Cr-Ni (14, 5 wt.%), tempering resist., mech. props., Cu addition effect 79−79012
steel, Cr-Ni-Sr (18.15, 17.64, 2.4 wt.%), rare-earth additions effect on impact fracture *(Chinese)* 80−66617
steel, Cr-Si-Mn-Ni-Mo-C, resist. to deform. and fracture, C effect 80−71757
steel, Cr-W-V-Mo (3.9 to 4.5, 1.5 to 2, 0.9 to 1.2, 3.9 to 4.4 wt.%), heat resistant, type 8Kh4M4V2F1-Sh, mech. props. 80−16464
steel, crack opening displacement appl. to fracture toughness eval. *(Italian)* 79−52378
steel, crack opening displacement in deeply notched specimens 78−27617
steel, crack resist. reduction in surface-active media *(Russian)* 79−52441
steel, cracking resistance of high-strength 40Kh and 35KhGSA, tempering temp. influence *(Russian)* 79−52252
steel, CrMoV, compact tension specimen, thickness effect 78−68764
steel, CrMoV, failure in post yield regime using single edge notched tension specimens 78−68765
steel, cryogenic, and structural strength 77−59927
steel, decarburised layer effects on fracture toughness of 60S2 77−59930
steel, deoxidised, AlN and V carbonitrides precip. effect on mech. props. *(French)* 80−45311
steel, die, with high heat resist. and toughness 78−84989
steel, ductile structural, crack resistance and cohesive strength 80−50722
steel, duplex ferrite-martensite, microstructure resistance optimisation 80−40482
steel, electroslag welded sheet, impact strength and toughness, welding effect *(German)* 77−86139
steel, embrittled N18K8M3TYu, toughness enhancement by double quenching 77−59922
steel, fast fracture toughness 77−44362
steel, fatigue damaged, fracture toughness 80−89353
steel, fatigue life, structural parameters and chem. comp. effects, rel. to test parameters 77−59928
steel, fatigue strength, low-cycle, under severe loading, friction-strengthening treatment effect *(Russian)* 79−52435
steel, Fe-Cr-C, austenitizing temp. effect on microstruct. and mech. props. 80−16341
steel, Fe-Mn, improvement of cryogenic mech. props. through thermal/mech. treatments 79−79098
steel, ferritic, cleavage fracture toughness, temp. and strain rate depend. 80−85028
steel, ferritic, low to intermediate strength, fracture toughness, upper shelf temp. depend. 77−73330
steel, ferritic-bainitic welded by electron beam, morphology and struct. of heated zone *(French)* 77−73292
steel, ferritic-martensitic, fatigue crack tip plastic zone *(Japanese)* 80−71738
steel, fibre reinforced Al composite, role of brittle layers at elevated temps. 79−96135
steel, fibrous crack extension, micromechanisms 80−108563
steel, fission reactor pressure component, fracture charact., implications for reliability 79−20199
steel, for pressure tanks, yield point influence on brittle fracture, tensile strength *(German)* 80−40539
steel, fracture micromechanisms, fracture toughness, exam. 78−56766
steel, fracture toughness, temp. and loading rate effect 77−36663
steel, fracture toughness and dynamic strength, surface active agent effects *(Russian)* 78−56812
steel, fracture toughness and impact strength, correl. breakdown 80−55523
steel, fracture toughness charact. in fatigue 79−15790
steel, fracture toughness determ., rel. to mech. props. 77−21277
steel, fracture toughness determination, from crack propagation measurements *(German)* 79−43421
steel, fracture toughness eval. by equivalent energy method *(Slovak)* 79−43402
steel, fracture toughness of nuclear pressure vessels 80−81172
steel, fracture toughness testing, obs. of crack initiation and stable growth processes *(Japanese)* 78−52954
steel, gas pipe, H_2 press. tests appl. to H_2 transmission 79−74550
steel, hard, high speed and tool, linear elastic fracture mech. appl. 78−48518
steel, heat-treatment furnace trays, in service embrittlement, microstruct. and props. changes 77−63784
steel, heavy section, pressure vessel rupture tests 78−44212
steel, high C, resist. to crack propag. and abrasive wear, role of retained austenite 79−83330
steel, high Mn-Cr, austenitic struct. stability and low-temp. toughness *(Japanese)* 80−76356
steel, high speed, AISI M2 and M7, fracture toughness 77−86141
steel, high speed, M2, fracture behaviour and fracture toughness 79−24609
steel, high speed, props. after electroslag remelting 80−104139
steel, high speed, sintered, and wrought, type T6 strength and toughness 80−30102
steel, high speed type M-50 and 18-4-1, fracture and fatigue 80−16457
steel, high speed YXM62, heat treatment, mech. props., wear, fracture toughness for cutting tool 78−19864
steel, high strength, 300-M, slow fatigue crack growth, threshold behaviour, temper embrittlement, impurity segregation effects 77−86152
steel, high strength, alloy, initiation of cracks at delayed fracture, AE study 78−72868

fracture toughness continued
steel, high strength, heat resistant, fracture resistance at low temps. 80−104284
steel, high strength, hypereutectoid, low alloy, microcrack frequency and fracture toughness rel. to martensitic struct. *(Czech)* 77−70163
steel, high strength, increasing resistance to cracking, use of overheating before quenching *(Russian)* 77−25135
steel, high strength, low alloy, mech. props. 78−60739
steel, high strength, low alloy, rare earth treated, ductile fracture mech. 78−64658
steel, high strength, Nb(C, N) precipitation in austenite, effect on mech. props. *(Japanese)* 77−21186
steel, high strength, produced bh extrusion of Ni-coated steel powder, enhanced fracture resist. 80−81169
steel, high strength weld metal, fractography, microstructure and reheated zone toughness effects *(Japanese)* 80−108543
steel, high-alloy die, electrothermal treatment 80−29996
steel, high-speed, 30Kh2N2SMKt, deform. effects on physicomech. props. 78−23741
steel, high-speed, cast, mech. props. at high temps. 79−20135
steel, high-speed, fracture toughness, carbides influence *(French)* 80−108559
steel, high-speed, fracture toughness of powder metallurgy vs. conventionally produced steels 78−64647
steel, high-speed, N effects on struct. and props. 77−59799
steel, high-strength, criteria for determining struct. strength and reliability 77−60021
steel, high-strength, gun barrel, fracture mechanics 77−77569
steel, high-strength, specific energy of fracture, adsorption lowering by H_2, H_2S, HCl and CH_4 gases *(Russian)* 79−52440
steel, high-strength and mild, fatigue of V-bent specimens 77−16681
steel, high-strength maraging, N18K9M5T, improvement in mech. props. under applied stress influence during ageing 80−20985
steel, high-strength maraging, N18K9M5T, nitriding effect on fracture resist. 80−21092
steel, high-strength reinforcing, 20GS2, local microstresses on creep strength in hydrogenating media *(Russian)* 77−52462
steel, high-strength structural type StE47, specimen geometry and plastic deform. effect on fracture mechanics *(German)* 80−66613
steel, high-strength tool steel D7KhFN, remelting effect on mech. props. 80−76284
steel, high-tempered bainite and mass martensite, shock toughness, −196°C *(Russian)* 77−16663
steel, hollow cylinder, thick walled, effect of thermomech. treatment 80−11674
steel, hot forging die type, fractography *(Japanese)* 80−108547
steel, hot rolled, M1 tool type, microparticle distributions and mech. response 77−44279
steel, hydrogen embrittlement, experimental test of Petch-Stables theory 78−60738
steel, hypereutectoid, type FS-01, HF-1, brittle fracture, fragmentation due to blast loading 80−50699
steel, hypereutectoid type HF-1, microstruct. effects on fracture toughness, ductility, strength 79−74255
steel, hypoeutectoid, fracture toughness, effect of Widmanstatten ferrite 80−35315
steel, inclusion effect on cold formability 80−29975
steel, Kh17N2, endurance limit, effect of residual stresses caused by Cr plating and cyaniding 77−86184
steel, large forging, mech. props. 77−4797
steel, linepipe, S content influence on H_2 induced fracture 80−30088
steel, low alloy, bainite transform. behaviour, struct., toughness 78−27513
steel, low alloy, blunt-notched, fracture mechanism and failure assessment 80−16450
steel, low alloy, brittle fracture, quenched and tempered 80−11677
steel, low alloy, directional fracture toughness and sulphide modification 78−27618
steel, low alloy, exam. of fatigue crack growth, and Paris Law parameter relationship 78−92343
steel, low alloy, high strength, correlation between fracture toughness, tensile props., fracture morphology 78−60789
steel, low alloy, metallurgical factors and toughness in structural steel welds *(Japanese)* 79−52377
steel, low alloy, microstruct. effects on fatigue at intermediate and high crack growth rates 79−74247
steel, low alloy, naval, stretch zone width meas., COD for ductile crack initiation 78−68813
steel, low alloy, press. vessel, fracture toughness in post yield regime 77−16671
steel, low alloy, pressure vessel and piping, factors affecting notch toughness 79−61730
steel, low alloy, radiation embrittlement, heat treatment effects 78−19893
steel, low alloy, St 52-3, structural, fracture toughness, fatigue precracking and grain size effect 78−60782
steel, low alloy, strength, Cr and N effects 80−104277
steel, low alloy, tempered martensite embrittlement and crack initiation *(Japanese)* 79−66149
steel, low alloy, tempered martensite embrittlement mechanisms 79−8351
steel, low alloy, thermally fatigued, fracture toughness 78−72872
steel, low alloy, toughness, effect of packet size and lath width 77−16677
steel, low alloy, type SNCM 8, rotor disc, exam. of fracture, using a J integral approach 78−92352
steel, low alloy effect of grain size, and amount of pearlite on fracture resistance 79−100255
steel, low alloy press. vessel, fracture toughness determ. from invalid compact tension specimens 77−4848
steel, low alloy structural, type 30KhGSA, effect of thermomech. treatment on strength, fracture toughness and fatigue props. 80−11676
steel, low C, and hardened and tempered, impact specimen fractures, stress concentrator sharpness effect on size of tough component 78−7015
steel, low C, brittle fracture of notched specimens, ferrite grain size and notch geometry effects 78−19860
steel, low C, effect of heat treatment on resistance to fatigue crack propag. 80−11675
steel, low C, endurance limit, effect of coatings *(Russian)* 77−25145

fracture toughness continued
- steel, low C, martensitic, fracture toughness variations during tempering 78—60812
- steel, low C, microalloyed, heat treatment, mech. props. 79—24551
- steel, low C, Nb-V microalloyed, Nb, V effect on impact and toughness props. 78—15515
- steel, low C, notched specimens, brittle fracture stress, effect of ferrite grain size, notch acuity and notch length 79—20187
- steel, low C, structural, AE rel. to crack tip plasticity *(Japanese)* 79—66150
- steel, low C structural, fracture toughness and X-ray diffr. obs. of surface *(Japanese)* 80—66634
- steel, low S, ESR, overheating effect on toughness 78—52860
- steel, low Si, martensite struct. and mech. props. *(Korean)* 80—93614
- steel, low strength, blunting effects on fracture toughness 78—68814
- steel, low-alloy, fracture resist. assessment from stable crack length *(Russian)* 79—15765
- steel, low-alloy, fracture toughness and brittle fracture, S and rare earth additions effect 79—87720
- steel, low-alloy, residual elements, effect on props. 80—66643
- steel, low-alloy, V effect on mech. props. 80—35312
- steel, low-alloy samples with fatigue crack, work of crack propag. and fracture toughness 79—38959
- steel, low-alloy sheet, welded hydraulic turbine volute chamber, strength and toughness 78—68820
- steel, low-C, Cr, ferritic, optimal heat treatment development 79—38869
- steel, low-C, fracture toughness, electroslag remelting effect 77—63788
- steel, low-C, kinetics of void development in fracturing A533B tensile bars 80—76357
- steel, low-C, with Nb-B addition, transform. characts. and mech. props. *(French)* 79—43253
- steel, low-C and low-alloy types, Nb effect on cold resist. 79—38954
- steel, low-C martensitic, Ni addition influence on toughness and ductile-brittle transition 80—30099
- steel, maraging, (18 wt.% Ni), solution annealed, exam. of cryogenic tensile, fatigue, and fracture props. 78—92311
- steel, maraging, crack resistance, effect of external stress during ageing *(Russian)* 77—59902
- steel, maraging, effect of deformation on props. 80—21032
- steel, maraging, fracture toughness data, comparison with equivalent energy and energy per unit area data 78—52965
- steel, maraging, fracture toughness of thin sections 78—27616
- steel, maraging, inert gas atomised, hot isostatic pressing temp. effect 79—24460
- steel, maraging, Ni (18 wt.%), grain boundary precipitation, scanning Auger electron obs. 78—3132
- steel, maraging, Ni (18 wt.%), with aged struct. at low temp., delayed failure crack and fracture toughness 78—7047
- steel, maraging, pressure vessel, with defects, failure anal. 77—44361
- steel, maraging, prior austenite grain size effect on tensile ductility and fracture toughness 79—100226
- steel, maraging N18K9M5T, crack propag. resistance under stress corrosion 77—70224
- steel, maraging stainless, phase transformation and mech. props. rel. to heat treatment *(Chinese)* 80—66501
- steel, martensite, brittle fracture resistance, struct. after quenching effects, tempering effects 79—57104
- steel, martensite-ferrite combined microstructure, two-phase, tensile fracture strength 78—60783
- steel, martensitic, as LNG storage and transportation system material 79—70133
- steel, martensitic, Cr (12 wt.%), temper embrittlement 79—87722
- steel, martensitic, Cr-Co-Ni-Mo, notch toughness, rel. to sensitivity to stress conc. 78—31532
- steel, martensitic, delayed fractures suppression, by neutron irradiation *(Czech)* 78—67743
- steel, martensitic, impact bending failure resistance, initial crack length and tempering effects 78—31530
- steel, martensitic, quenched, strength variation rel. to H behaviour 77—59924
- steel, martensitic ferritic struct., fracture toughness *(Russian)* 77—77560
- steel, martensitic-bainitic, lath morphology effect on yield stress, martensitic and ductile-brittle transition temps. 79—100215
- steel, material scale length as a measure of fracture toughness in fracture mechanics of plastic materials 78—68763
- steel, medium alloy, constructional, strength-toughness relationship 77—70137
- steel, medium and low-alloy with ferritic pearlitic struct., fracture toughness rel. to pearlite conc. 79—15787
- steel, medium C, Cr-Mn-Mo, austenising temp. effect on microstruct. and fracture toughness *(Chinese)* 80—66542
- steel, medium C 80—11752
- steel, medium strength, fracture toughness eval. by J-integral and equivalent energy method *(French)* 77—77578
- steel, medium strength, fracture toughness eval. of small specimens 78—60762
- steel, medium strength plate, quenched and tempered, fracture toughness in ductile-brittle range 78—7036
- steel, metastable austenitic, resistance to failure 77—4852
- steel, mild, cold-rolled, rate-sensitive, fracture initiation, loading rate and temp. effects 80—40532
- steel, mild, fracture toughness meas. with reinforced-double-cantilever-beam specimen 77—4842
- steel, mild, grain size depend. of cleavage fracture toughness 79—8359
- steel, mild, plate, effect of striking velocity on perforation energy 78—68818
- steel, mild, tempered and quenched, dynamic fracture toughess 77—36665
- steel, mild, yield strength and fracture toughness, microstruct. effect, heat treatment 78—27615
- steel, Mn, as rolled bainitic, tensile, impact and machinability props., transport appl. 78—88503
- steel, Mn, hydrogen embrittlement resist. evaluation *(Czech)* 80—35308
- steel, Mn (1.10 to 1.55 wt.%), reactor vessel material, assessment of weld heat affected zone mech. props. 79—29217
- steel, Mn-C-Si-Cu (0.95, 0.85, 0.25, 0.16 wt.%), fibrous-banded fracture mechanism 80—104280
- steel, Mn-Cr-V, crack propag. resist. at hardness indentation, and fracture toughness *(German)* 79—29220

fracture toughness continued
- steel, Mn-Cr-V, tool, quenched and tempered, fracture toughness *(German)* 80—25726
- steel, Mn-Mo, castings, mech. props., Cu and Sn trace elements effect 80—66596
- steel, Mn-Ni-Mo, hydrogen embrittlement resist. evaluation *(Czech)* 80—35308
- steel, Mn-Ni-Mo low alloy steels for nuclear appl., toughness and heat treatment 80—5239
- steel, Mn-Si, St 52-3, cleavage fracture toughness, temperature and notch sharpness influence *(German)* 80—35291
- steel, Mn-Si, St 52-3, fracture toughness determ. from yield strength and cleavage fracture strength *(German)* 80—35292
- steel, Mn-Te, structural, brittle fracture resistance, Ti addition effect *(Czech)* 80—45392
- steel, Mo-Nb microalloyed sheet, fracture toughness evaluation *(Slovak)* 79—38948
- steel, Mo-V, creep rupture strength, heat treatment effects *(German)* 78—72834
- steel, natural gas environment effects on strength *(Russian)* 78—11401
- steel, Ni, cross girder connections, fatigue strength, design stress 78—64700
- steel, Ni, cryogenic fracture toughness enhancement through grain refinement 77—36651
- steel, Ni, welded joints on LNG carriers mech. props. and fracture toughness 80—85017
- steel, Ni (23 wt.%), crack propag. in the presence of H_2 *(French)* 78—15517
- steel, Ni (9 and 5 wt.%), for liquefied natural gas appls., material and weld props. 79—61736
- steel, Ni (9 wt.%), effect of repeated tempering on notch strength *(Japanese)* 79—43280
- steel, Ni (9 wt.%) static and dynamic fracture toughness 77—36664
- steel, Ni-Co-Cr, high-strength medium C, Cr effect on props. 80—76339
- steel, Ni-Co-Mo-Ti, hot formed, recrystallization and grain boundary precipitation effect on mech. props. *(German)* 79—66073
- steel, Ni-Cr-Mo, cleavage fracture toughness, temperature and notch sharpness influence *(German)* 80—35291
- steel, Ni-Cr-Mo, fracture toughness determ. from yield strength and cleavage fracture strength *(German)* 80—35292
- steel, Ni-Cr-Mo, Ni effect on fracture toughness, heat treatment effect *(Korean)* 79—91781
- steel, Ni-Cr-Mo, type 4340, equivalence of K_{1c} and J_{1c} fracture toughness meas. for range of yield stress 79—38934
- steel, Ni-Cr-Mo SNCM8, delayed fracture, specimen thickness and threshold stress intensity effect *(Japanese)* 80—104268
- steel, Ni-Cr-Mo-U, ferritic, B segregation and high temp. embrittlement 78—7040
- steel, Ni-Cr-Mo-V, stress corrosion cracking 77—52542
- steel, Ni-Cr-Mo-V, temper embrittled, crack initiation strength *(Japanese)* 77—52474
- steel, Ni-Cr-Mo-V, turbine rotor shaft, fracture toughness, validity criterion for K_{IC} 78—72861
- steel, Ni-maraging weld metal, increasing fracture toughness by heat treatment 78—72871
- steel, Ni-Mo, powder forged, fracture processes and fracture toughness 78—72870
- steel, Ni-Mo-Cr, critical value of J-integral determ. *(German)* 80—25827
- steel, Ni-Ti, high-alloy, precipitation hardening, fatigue strength 79—79103
- steel, nil ductility transition temp., and Charpy V-notch fracture appear transition temp. relationship between them, determ. *(Czech)* 79—91783
- steel, notched 1018, air fatigue in endurance limit range 77—36631
- steel, nuclear pressure vessel, SA533B-1 and SA302B, fracture toughness prediction using crit. fracture stress and strain models 80—25855
- steel, nuclear pressure vessel, type A533B-1, three point bending, yield stress, exam., Charpy V-notch and precracked specimens 78—92310
- steel, nuclear pressure vessel time A533 grade B class 1, thermal shock fracture toughness at elev. temp. *(Japanese)* 79—83304
- steel, pearlitic, heat treatment effect on fracture resistance, microstruct. and mech. props. 80—104191
- steel, pearlitic, strength, fracture, microstructure effect 77—40449
- steel, pearlitic eutectoid, crack initiation and effective grain size for cleavage fracture 80—30085
- steel, powder-forged, fracture toughness 79—66155
- steel, precipitation hardening, strength and struct. *(German)* 79—47701
- steel, prestrained pressure vessel, correl. between dynamical toughness characteristics 78—68816
- steel, prestrained pressure vessel, dynamic toughness characts., expt. correlations 79—15783
- steel, quenched, reheating, to improve plasticity and notch toughness 77—63701
- steel, quenched and tempered, microstructure effect on cleavage fracture toughness 79—74252
- steel, rail, toughness, effect of Sn, SEM exam. 80—97569
- steel, rare earth additions, effect on physicomechanical props. 77—12639
- steel, reactor vessel, neutron irrad. effect on brittle fracture characts. *(Slovak)* 78—50254
- steel, RPV type, toughness values compilation, temp.-range validity 77—48611
- steel, SA540, fracture toughness props. for nuclear bolting appl. 78—35514
- steel, SAE 4340, depend. of fracture roughness on crack velocity 79—47772
- steel, SHE 4340, tempered martensite embrittlement 80—30084
- steel, Si-Mn-C (1.6-2.0, 0.4-0.6, 1.1-1.4 wt.%), cast graphitised, heat treatment effects on mech. props. and wear resist. 79—96050
- steel, Si-Mn-Cr-C (1.1, 0.9, 1.0, 0.29 wt.%) 30KhGSA, heat treatment effect on strength and toughness 78—15437
- steel, silchrome, thermomech. hardening 78—23736
- steel, sintered, mech. props., effect of small cold reduction 79—39048
- steel, St 37-3 and St 52-3, fracture mech. specimen, effect of fatigue precracking condition *(German)* 77—21240
- steel, stainless, 10Kh18N9TL, S, Se, Te and Bi additions effect on mech. props. 79—83312
- steel, stainless, 321, internal pressure creep rupture strength of boiler tubes, anisotropy effect 78—23825
- steel, stainless, austenitic, CC Ni-Al, γ-phase, fracture mechanical aspects of abrasive friction, wear, chip formation 78—72865

fracture toughness continued

- steel, stainless, deformation temp. determ. for high yield strength 78—44177
- steel, stainless, FBR fuel pin cladding, burst strength eval. 79—89378
- steel, stainless, ferritic, Cr-Mo-Ni (29,4,2 wt.%) 77—44276
- steel, stainless, ferritic, subjected to 475°C embrittlement, exam. of fracture toughness 78—84982
- steel, stainless, fibre reinforced wustite, strength and toughness 78—27602
- steel, stainless, fracture toughness, −20 to +22°C, of type UNS-S 15500 79—70145
- steel, stainless, fracture toughness improvement by applying Pb-Sn-Cd coating to crack tip 79—43416
- steel, stainless, maraging, high strength, notch toughness, effect of ageing *(Japanese)* 78—11311
- steel, stainless, martensitic, crack resistance of type VNS-2, heat treatment effects 79—100196
- steel, stainless, strength down to 4.2K; influence of stress raisers 80—71754
- steel, stainless and low alloy, PWR primary circuit constituent materials, design features verification *(French)* 79—17976
- steel, stainless FBR fuel pin cladding, failure stress and strain 811 to 1644K 79—89377
- steel, steam pipes, 12Cr1MoV, selection of allowable stresses based on minimum possible strength data 80—104237
- steel, structural, CrN-modified, tempering and quenching effects on struct. and props. 77—59835
- steel, structural, effect of rare earth metals on cold temper brittleness 79—29202
- steel, structural, effect of structural factors 77—59923
- steel, structural, rel. between static and dynamic fracture toughness 78—68815
- steel, structural, second phase particle effects on impact strength 80—108581
- steel, structural, type St 37, microstruct. rel. to fracture toughness and fracture load of bending specimens *(German)* 80—89352
- steel, structural 78—68808
- steel, structural 15Kh2NMFA, use of linear and nonlinear fracture mech. for crack propagation resist. determ. 79—5056
- steel, tempered, high strength, internal stresses and mech. props. 80—3200
- steel, tempered or quenched, exam. of fracture toughness tests, for C shaped specimens 79—29215
- steel, thermal shock cracking, fracture mechanics and fractographic exam. *(Japanese)* 78—52964
- steel, Ti (0.1 to 0.55 wt.%), strengthening by carbide precipitation 77—25062
- steel, tool, abrasive wear rate rel. to fracture toughness and microstructure *(German)* 79—29232
- steel, tool, type KhBG, carburising and quenching, effect on fracture toughness 80—29997
- steel, tool, W-Mo, heat treatment effect on props. 80—50656
- steel, toughness, review of joint tests *(German)* 80—65142
- steel, TRIP, strength and plasticity rel. to thermomech. treatments 77—44281
- steel, type 28Kh3SNMVFA, strain hardened martensite, resist. to tempering, exam. 80—16348
- steel, type 52100, heat treatment effect on microstruct. and mech. props. 80—29993
- steel, type A533B-1, fracture toughness meas. using small specimen strength ratio 79—70143
- steel, ultrahigh C, heat treated, mechanical properties and microstructure 79—57012
- steel, V and V-N , high strength, mech. props. and strain ageing, processing variables effects 77—59819
- steel, V-Nb and Cr-Mo-V-Nb, supercooled austenite isothermal decomp., struct., strength and fracture characts. 80—60966
- steel, V-Nb microalloyed sheet, fracture toughness evaluation *(Slovak)* 79—38948
- steel, W-Mo, sintered high-speed, naphthalenelike grain form., quenching effect on fracture toughness 80—30103
- steel, welded joints, durability in repeated impact loading, low temp. effects 77—63800
- steel, yielded pipeline, fracture resistance changes, impact tests 77—16667
- steel 35KhGSA, resist. to fracture after low temp. temperating, P content and grain size effects *(Russian)* 78—48490
- steel 40Kh, surface working effects on crack resist. *(Russian)* 78—56734
- steel A533A, review of data in reln. to fracture toughness at upper shelf temp. 79—15797
- steel AF1410, wear against stainless steel, repetitive impact, microstruct. effect 79—74263
- steel bimetal, low-alloy austenitic ferritic stainless steel, fracture toughness *(Russian)* 78—35482
- steel boiler tubes, Cr-Ni-Mo austenisation conditions effect obs. 80—3151
- steel Cr-Mn (13, 19 wt.%), for liquefied natural gas appls., material and weld props. 79—61736
- steel fibre reinforced porous mat. prod., mat. props. 77—59723
- steel for nuclear reactor press. vessels, criteria for brittle fracture, neutron effects *(German)* 77—34389
- steel plates, C and alloy steels, comparison of dynamic tear and Charpy V notch impact props. 78—92357
- steel pressure vessel, nuclear, fracture toughness at elevated temps. 79—20193
- steel shot, cast, impact fracture *(Japanese)* 78—92338
- steel susceptibility to H_2 embrittlement, fracture toughness *(Czech)* 77—59915
- steel/steel bimetal, creep-rupture strength in corrosive environment *(Russian)* 77—52533
- steels, 08kp and 03Kh13AG19, cyclic and static fracture toughness, low temp. effect *(Russian)* 79—52344
- steels, die, mech. props. high temp. thermomech. treatment 79—20086
- steels, irradiated pressure vessel, reference fracture toughness curves 80—100921
- steels, secondary hardened, microstruct. rel. to mech. props. 80—25851
- steels, structural St 37-2, cleavage fracture, report 80—25868
- steels, tool, cold hydrostatic extrusion rel. to struct., props. 79—20068
- steels, wide plate and V-notch bending tests evaluation on basis of materials mechanics *(German)* 80—66571

fracture toughness continued

- steels, with yield pt. of about 260 to 800 N/mm^2, specimen thickness influence of fracture mechanics parameters *(German)* 80—66614
- steels, with yield pt. of about 420 to 720 N/mm^2, correlation between yield pt./tensile strength ratio and toughness *(German)* 80—66615
- strength of structures and fracture mechanics role 78—34073
- stress intensity coefficient, determ. at crack start 79—87711
- stress intensity factor calc., infinite similar element method 78—79277
- stress intensity factors for circumferential crack from notch in round tensile bar 79—41618
- stretch zone width and striation spacing. The comparison of theories and experiments 80—85051
- stretched zone anal. by means of stereo matching method *(Japanese)* 80—108544
- structural alloys, fracture at temps. approaching absolute zero 78—72877
- structural components subjected to proportional cyclic loading, rupture life estimates 77—35089
- structural steel cracking, plastic deform. and fracture toughness obs. *(German)* 77—59936
- structural steels and alloys, conf., Kiev, USSR (Sep. 1976) 77—59921
- sugar crystals under stress, fracture-initiation time from triboluminesc. 77—59065
- superalloy, microstructure resulting from alloying and heat treatment, effect on creep, fatigue, fracture strength 78—11246
- Tennessee sandstone, Carrara marble, fracture toughness, double torsion testing method 79—84239
- test-piece dimensions influence on delayed fracture resist. *(Russian)* 79—52478
- thermoplastics, effect of mol. orientation on fracture toughness 78—52992
- thin sheet impact strength study *(Czech)* 80—59571
- thin skin structures, residual strength prediction, using crack resistance curves 78—90795
- β-III Ti alloy, powder compacted by hot swaging, tensile and toughness prop. 79—38764
- α+β Ti alloys, prior β grains and α platelet morpholgoy, exam. 78—76679
- β-Ti-Mo (15wt.%) metastable alloy, strength enhancement 77—66650
- tooth, artificial-denture base joint, adhesion, fracture mech. 79—16350
- toughness-porosity phenomena 78—72874
- wear resistance rel. to specific fracture energy for various materials *(Russian)* 78—85005
- weld defects, toughness, crack growth anal. 79—43429
- weld metal, submerged arc irradiated, reference fracture toughness curves 80—100921
- wood, Douglas fir, crack front width effect on fracture toughness 77—56060
- wood, fracture toughness variations with specimen size, statistical approach 80—100889
- wood fibre reinforced cement, coupling agent effect on strength 80—35295
- wood fibre reinforced Portland cement composite, strength 80—100822
- wood-epoxy bond system, cleavage fracture toughness *(Japanese)* 77—77574
- yield zone form., fracture resistance, influence of specimen configuration 78—68817
- Zircaloy, irradiated spent fuel cladding, annealing effects 79—89382
- Ag vacuum deposited coating on glass, strength 80—55505
- Al, 6061-T651, fracture toughness 80—35301
- Al alloy, 2124-T851, rel. to acoustic emission 78—7109
- Al alloy, 5083-0, fatigue crack growth and fracture resistance meas., at 295, 111, 76 and 4K 78—35509
- Al alloy, adhesive-bonded-laminated, fatigue props. 80—50695
- Al alloy, D16, Fe and Si impurity effects on K_{Ic} 78—84990
- Al alloy, effect of specimen thickness 77—70151
- Al alloy, forge-rolled AK4-1T1 alloy slabs, fracture toughness scatter assoc. with plane deform. 78—7014
- Al alloy, fracture of large second phase particles 78—7010
- Al alloy, fracture toughness determ., rel. to mech. props. 77—21277
- Al alloy, fracture toughness and struct. *(Russian)* 77—25134
- Al alloy, fracture toughness anisotropy and struct. *(Russian)* 77—25139
- Al alloy, low-cycle fatigue strength, isothermal hardening effect 79—38863
- Al alloy 01205, mech. props. at cryogenic temps. 79—29206
- Al alloy 2024-T4, compact shear specimen, finite element anal. rel. to fracture 80—16423
- Al alloy 7075, fracture toughness, hydrostatic press. depend., tensile ductility 78—3209
- Al alloy 7075, precipitation hardening, toughness and microstruct. *(Japanese)* 78—15509
- Al alloy AK4-1 with surface cracks, fracture toughness determ. *(Russian)* 77—25141
- Al alloy AK4-1T1, endurance at elev. temp. of strip with loaded hole 77—86181
- Al alloy A356-T61, creep rupture props. 78—27612
- Al alloy D16, cyclic and static fracture toughness, low temp. effect *(Russian)* 79—52344
- Al alloy V93, high strength, notch sensitivity in static and repeated loading 78—27639
- Al alloys, 1201 and 01381, cryogenic, and structural strength 77—59927
- Al alloys, (5083, 6061, 2219), supercond. magnets, mech. and phys. props. at 4K 80—86976
- Al alloys, cyclic fracture toughness *(Russian)* 79—52343
- Al alloys, D16At and V95A, fatigue crack growth *(Russian)* 77—52463
- Al alloys, extrusion, purity effect on fracture props. 79—100248
- Al alloys, fracture micromechanisms, fracture toughness, exam. 78—56766
- Al alloys, fracture toughness under plane stress 78—92316
- Al alloys, microstruct. effects on strength, fracture toughness, fatigue cracks 79—43434
- Al alloys, quenching rate rel. to mech. props., residual stresses, optimum quench coolings *(French)* 78—64562
- Al alloys AMg6M, AMg6, 5083, weld at cryogenic temps., mech. props. 79—66136
- Al alloys D1 and AK6, cylindrical specimens with crack. fracture characts. in inelastic strain, test methodology 80—25839
- Al vacuum deposited coating on glass, strength 80—55505
- Al/Cu laminates, vapour deposited, strength enhancement 79—24576
- Al/Mg soldered samples, UTS and fracture surface comp., 20 to 500°C 79—38941

fracture toughness continued
- Al-Al_2Cu, eutectic composite, abrasive fragmentation *(Czech)* 80−30110
- Al-Al_3Ni, eutectic composite, abrasive fragmentation *(Czech)* 80−30110
- Al-alloy, type D20, cryogenic welded vessels, structural strength 80−16477
- Al-Cu, effect of alloy purity and ageing on fracture mechanism, and resultant toughness 79−5049
- Al-Cu alloy 1201, thermomech. treatment effect on strength characts. and fracture toughness *(Russian)* 80−40391
- Al-Cu-Mg, type D16 alloy, stress intensity coeff. determ. 79−87711
- Al-Cu-Mg-Mn (4.5, 1.5, 0.6 wt.%), thin sheet, exam. of fracture toughness, and fatigue crack growth 78−92353
- Al-epoxy adhesive systems, opening and edge-sliding fracture toughness 78−95805
- Al-Fe (0.5 wt.%)-Ti-Cr, Ti, Cr addition effects on toughness/microstruct. relationship *(Japanese)* 77−48525
- Al-$Fe_{78}Mo_2B_{20}$ wire composite, mech. props. 80−40441
- Al-Mg, fracture resistance at low temps. 80−104284
- Al-Mg, type AMg6, cryogenic welded vessels, structural strength 80−16477
- Al-Mg (4.4 and 6 wt.%), for liquefied natural gas appls., material and weld props. 79−61736
- Al-Mg (7 wt.%), β-phase soln. behaviour and mech. props. *(Korean)* 78−11277
- Al-Mg alloy AMg6, mech. props. of welded joints, impurity effects 78−95789
- Al-Mg-Li alloy, subboundary brittleness due to horophilic Na *(Russian)* 77−21244
- Al-Mg-Si-Mn, Mn addition effects on fracture 78−60791
- Al-Si-Cu, fracture resistance at low temps. 80−104284
- Al-Zn-Mg, atmosphere effect on fatigue crack propag. *(Japanese)* 80−81161
- Al-Zn-Mg, effect of microstruct. on localised shear failure 78−52996
- Al-Zn-Mg, type 7075-T651 plate, thickness direction inhomogeneity of mech. props. and fracture toughness 80−100892
- Al-Zn-Mg (6, 2.5 wt.%), fracture toughness-transgranular fracture relation 77−52447
- Al-Zn-Mg (6.0, 2.5 wt.%), aged, grain, size depend. of fracture toughness 78−48495
- Al-Zn-Mg alloy V95, two-stage ageing kinetics, mech. props. effects 79−83238
- Al-Zn-Mg-Cu, alloy 7075, effect of purity level, dispersoid type, heat treatment, on fracture toughness 78−80636
- Al-Zn-Mg-Cu, fracture toughness 78−7044
- Al-Zn-Mg-Cu alloy, laminated, adhesively bonded alloy 7075-T6, exam. of fracture resistance 78−76754
- AlN-Al_2O_3 composites, hot-pressed 77−52275
- Al_2O_3, anodic film on Al, strain to failure, failure characts. 77−12734
- β''-Al_2O_3, conductive, Li_2O stabilised, sintering and annealing 77−59724
- Al_2O_3, dense, effects of oxide sintering additions on strength *(German)* 77−1866
- Al_2O_3, fracture toughness specimen, appl. of wedge indentation technique for precracking 78−85087
- Al_2O_3, fracture toughness meas. using Knoop indentation method *(German)* 80−25830
- Al_2O_3, fracture toughness determ. using four-point-bend specimens 80−108536
- Al_2O_3, hot-pressed, crack-growth boundaries, subcritical, fractographic criterion 79−100243
- Al_2O_3, polycrystalline, fracture probability under static bending and tensile loading at 800°C *(German)* 78−23806
- Al_2O_3, polycrystalline, fracture toughness and acoustic emission rel. to microstructure, temp. depend. 80−11745
- Al_2O_3, polycrystn., high-temp. fatigue and strength 80−60954
- Al_2O_3 refractories, fracture, J-integral meas. 80−108537
- Al_2O_3 substrates, tape-casted, fracture strength analysis 80−60948
- Al_2O_3, vitreous-bonded, mech. behaviour under various stress-time schedules 79−38968
- β-Al_2O_3:MgO, strength and delayed fracture behaviour 80−35290
- Al_2O_3/Al soldered samples, UTS and fracture surface comp., 20 to 500°C 79−38941
- Al_2O_3/Nb, fracture mech. parameter determ. at high temps. *(German)* 79−70136
- Al_2O_3-B_2O_3-SiO_2 sheet glass, solar energy appl., optical and mech. props. 80−87447
- Al_2O_3-Ca (0.6 to 1.6 at.%), fracture behaviour, Ca segregation effect 80−40504
- β-Al_2O_3-Na_2O, fracture stress, effect of microstruct. defects 77−44338
- β-Al_2O_3-Na_2O, hot pressing and phys. props. 79−4940
- β''-Al_2O_3-Na_2O solid electrolyte, processing and phys. props. 80−60820
- β''-Al_2O_3-Na_2O solid electrolyte, strength degradation under electrolytic conditions 80−61329
- Al_2O_3-Nb composites, influence of gas impurities on solid-state bonding on annealing 80−11739
- Al_2O_3-SiO_2 glass, annealed and tempered, fracture strength studies under dynamic conditions 79−96132
- Al_2O_3-W cermet, sintered pressed compact, compressive and transverse rupture strength 78−19850
- Al_2O_3-ZrO_2, dispersion hardened, fracture toughness improvement by induced microcracking *(German)* 78−31501
- Al_2O_3-ZrO_2 composite, fracture toughness increase by microcracking in energy dissipative zone near crack tip 79−20156
- Al_2O_3-ZrO_2 dispersed system, fracture toughness, inclusion induced microcracking effect 78−11296
- $3Al_2O_3.2SiO_2$-ZrO_2 composites, sintered, in situ-reacted, fracture props. 80−81158
- $Al_2O_3.3P_2O_5.5H_2O$-SiO_2 composite, binding and struct. 79−66030
- Au vacuum deposited coating on glass, strength 80−55505
- B fibre, Griffith criterion appl., tensile test 77−12684
- B fibre, prep. by closed CVD system, mech. props. and surface defects 79−52311
- B fibre reinforced Al, crack tip damage and fracture toughness 79−57093
- B fibre reinforced Al, fracture toughness 77−70157
- B fibre reinforced Al, fracture propag. 78−23823
- B fibre reinforced Al, fracture mechanical study, unidirectional composites 78−88520
- B fibre reinforced Al, unidirectional, K-calibration and compliance curves 78−88518

fracture toughness continued
- B fibre reinforced Al laminate, effect of ply by-up sequence on fracture toughness 78−35492
- B fibre reinforced epoxy, fracture mechanical study, unidirectional composites 78−88520
- B fibre reinforced epoxy, fracture mechanics 80−35294
- B fibre reinforced epoxy composites, notched, tensile strength and failure modes 80−81205
- B fibres, surface morphologies rel. to mech. props. 80−11749
- B reinforced Al laminates, applic. of linear elastic fracture mechanics 77−28893
- BN, toughening by stress-induced phase transforms. 78−80635
- Ba hexaferrites, mech. and mag. props. 79−70151
- $BaTiO_3$, effect of phase transformation on fracture behaviour 78−48507
- Be fibre reinforced Ti-Al-V (6.4 wt.%), synthesis and mech. props. 77−32544
- Be, high-strength, fracture toughness determ. 77−73336
- β-epoxy composite, intermittently bonded, water and ice effects 77−12685
- C adsorbent, granules and artifacts, strength, mech. characts. 78−23771
- C fibre reinforced C, appl. as refractories, toughness props. 79−38782
- C fibre reinforced plastics with mixed fibres, exam. of fracture toughness and shear strength 79−20151
- C fibre reinforced polyamide thermoplastic, stiffness and strength 78−27600
- C fibres with large breaking strain, prep., mech. props., struct., appl. 78−44077
- C mixes, extruded, preoxidation treatment effect on transverse breaking strength 77−63767
- CaF_2, press forged, mech. and optical props. 80−38079
- CaF_2, whiskers and crysts., flux growth and charact. by morphology and fracture strength 79−19987
- Co-$(Cr,Co)_7C_3$ eutectic, oxidation effect on toughness and strength 80−89404
- Co-Cr-Ni-W-TaC (15.7, 9.5, 3, 12.77 wt.%) alloy Co50B3W, temperature cycling effect on rupture strength 78−39898
- Co-Zr, amorphous phase form. in Zr-poor region, hardness and fracture strength *(Japanese)* 80−84914
- Cr vacuum deposited coating on glass, strength 80−55505
- Cr-$(Cr,Co)_7C_3$ eutectic, oxidation effect on toughness and strength 80−89404
- Cr-Ni steel, strengthening by elastic deform. at −196°C 77−55987
- Cr-Ni VKh-4 alloy, deformation and fracture mechanism investigation *(Russian)* 80−11738
- Cr-V-B-Y system, fatigue strength and fatigue fracture at 20 and 1100°C, SEM study 80−3194
- Cu clad steel, bond strength through intermediate Zn layer *(Korean)* 79−66213
- Cu, diffusion welding, tensile fracture strength *(Japanese)* 80−7663
- Cu-Al (10 wt.%), annealed, tensile fatigue strength at high temp. in vacuum *(Japanese)* 78−35493
- Cu-Al (5 wt.%), subjected to tension-compression fatigue, deform. and fracture strength *(Japanese)* 80−93644
- Cu-Al-Fe, mech. props. rel. to heat treatment 80−50682
- Cu-Al-Ni-Fe-Mn, cast Ni-Al bronze, fracture metallography 78−27597
- Cu-$Fe_{78}Mo_2B_{20}$ wire composite, mech. props. 80−40441
- Cu-Zr amorphous alloys, mech. props. *(Japanese)* 77−86179
- $Cu_{46}Zr_{54}$, devitrification effect on mech. props. 80−30082
- $Cu_{56}Zr_{44}$ metallic glass, devitrification and its effect on mech. props. 80−33893
- Fe alloy, fracture toughness of cryogenic temp. 78−72878
- Fe alloys, cast, fracture toughness prediction 79−5045
- Fe, Armco, cyclic loading and fracture toughness 80−35298
- Fe, Armco, fracture stress, effect of Pb melts *(Russian)* 77−21246
- Fe, Armco, fracture toughness characts. under cyclic loading 79−11703
- Fe, cast, ferritic SG ductile fracture initiation and propagation 78−64661
- Fe, cast, fracture mech. and fractography *(Japanese)* 78−7031
- Fe, cast, grey, abrasive wear rate rel. to fracture toughness and microstructure *(German)* 79−29232
- Fe, cast, grey pipe, resist. to fracture under hydraulic pressure 79−96124
- Fe, cast, rare-earth-Mg nodular, fracture toughness and fatigue *(Chinese)* 78−95791
- Fe, cast, Si, ferrite heterogenisation, phase separation and embrittlement, Si effects 79−96125
- Fe, cast, thermal treatment influence on mechanical props. *(German)* 80−29980
- Fe, cast alloyed, struct., props., heat treatment 77−16623
- Fe, cast flake and nodular, rupture strength, circumferential notch *(Japanese)* 80−93649
- Fe, ductile, influence of crack tip sharpness and morphology of graphite on K_{1c} *(Chinese)* 80−81144
- Fe, porous, density, elec. cond., Young's modulus, toughness 78−64645
- Fe, porous, volume strained, correlation between strength and acoustic props. 77−16770
- Fe, sintered PZh1M, fracture resistance subject to thermomechanical treatment 77−77517
- Fe-B_4C sintered material, mech. props. and struct. characts. 79−100084
- Fe-BeO, dispersion hardened alloy, struct.-props. relationships 77−66652
- Fe-Co-Cr-Mo (20, 15, 5 wt.%), maraging, stainless alloy fracture toughness 77−73326
- Fe-Cr (26 wt.%) effect of Ni content and austenite phase, on low temp. toughness and embrittlement 78−60754
- Fe-Cr-Mo, (30,2 wt.%) Bridgman-type, unexpected embrittlement phenomena, hydrostatic tensile test *(Japanese)* 80−55517
- Fe-Cr-Mo, white cast, optimising fracture toughness and abrasion resist. 80−85042
- Fe-Cr-Mo alloy castings, thick-section, factors affecting 80−108374
- Fe-Cr-Ni-Si, sintered, carbide coated, crack propag. energy in impact bending 79−66162
- Fe-Mn (up to 8 wt.%), microstructure, mech. props. and fracture *(Japanese)* 80−35304
- Fe-Mn-B, B effect on intergranular embrittlement 80−108555
- Fe-Mn-Ni, fracture toughness, thermomechanical treatment effects 78−60794
- Fe-Mo-Ta, ternary Laves phase strengthening 80−108466
- Fe-Ni, fracture toughness at cryogenic temp. 78−72878
- Fe-Ni, reactive metal alloy, effects of thermomechanical processing on strength and toughness 79−70112

fracture toughness continued
Fe-Ni-Al (18.2 wt.%) aged, fracture toughness and mode, grain size depend. 77—12700
Fe-Ni-Al-(Cu) (12, 0.5, 0.5 to 3 wt.%), Cu addition strengthening at 77K, mech. props. 80—60875
Fe-Ni-Al(Ti)(V)(Nb), cryogenic toughness, strength, rel. to reactive metal addition 78—39885
Fe-Ni-C (9, 0.1 wt.%), effect of intercritical tempering on impact energy, exam. of mech. props. 78—52861
Fe-Ni-Co-C, substruct. effect in mech. props. 80—30086
Fe-Ni-Cr-Mo superalloy, mech. props., η-phase form. effect *(Chinese)* 80—20925
Fe-Ni-Cr-Si, superalloy, Cr and Si effect on mech. props. and microstruct. *(Chinese)* 79—100207
Fe-Ni-Cr-Ti-Mn-Mo, (25.8, 14.04, 2.17, 1.27, 1.30 wt.%), superalloy A-286, precipitation hardening, exam. of fracture toughness and mech. props. 78—92355
Fe-Ni-Mo alloy, high-strength ferritic, for cryogenic service, mech. characteris. 77—70143
Fe-Ni-Mo(13,3wt%), welded alloy, fracture and strength for cryogenic service 79—38930
Fe-Ni-P-B, metallic glasses, fracture toughness, shear rupture failures, critical thickness 79—52365
Fe-Ni-Ti-(Cu) (12, 0.25, 2 wt.%), Cu addition strengthening at 77K, mech. props. 80—60875
Fe-Ni-V-(Cu) (12, 2, 2 wt.%), Cu addition strengthening at 77K, mech. props. 80—60875
Fe-Ni-(Cu) (12, 0.5 to 3 wt.%), Cu addition strengthening at 77K, mech. props. 80—60875
Fe-Si (3.12 wt.%), brittle fracture, work hardening effect at notch tip 78—44220
Fe-Zr, amorphous phase form. in Zr-poor region, hardness and fracture strength *(Japanese)* 80—84914
$Fe_{80}B_{20}$, amorphous, deform. and annealing effects on mag. and mech. props. 77—12717
$Fe_{40}Ni_{40}P_{14}B_6$, amorphous, deform. and annealing effects on mag. and mech. props. 77—12717
$Fe_{29}Ni_{49}P_{14}B_6Si_{12}$, Metglas fibre reinforced mortar, fracture props. 79—70159
K_2O-Al_2O_3-SiO_2 system, crystallisation of glasses in primary phase field of leucite 78—67658
LiF mech. and optical props. rel. to forging conditions 80—33101
LiF, press forged, mech. and optical props. 80—38079
Mg-Zn-Zr rare earth alloy, mech. props., effect of microshrinkage during solidifaction 79—43234
$MgAl_2O_4$ spinel, single cryst., fracture behaviour, temp. depend. 80—40503
MgO-ZrO_2, dispersion hardened, fracture strength and texture, rel. to temp. *(German)* 79—43378
Mo, fibre, brittle to tough transition, impact strength meas. 80—40527
Mo, stress-to-rupture strength at high temps., struct. effect 77—70175
Mo-TiC lamellar eutectic composite, deformation and strength, room temp. to 2073K *(Japanese)* 80—71702
Mo-Ti(B)-Zr(Al)-C, stress cycling at room temp. *(Russian)* 77—25148
Na_2O-B_2O_3-SiO_2 glass fibre, plastic coating influence on strength 80—58697
Na_2O-B_2O_3-SiO_2 glass-Ni compact, indented, strength and fracture toughness 80—93636
Na_2O-B_2O_3-SiO_2 glass, fracture toughness, effect of microheterogeneous struct. 80—104256
Na_2O-B_20_3-SiO_2, mechanical strength and swelling in liq. 80—85024
Na_2O-CaO-SiO_2 glass, annealed and tempered, fracture strength studies under dynamic conditions 79—96132
Na_2O-CaO-SiO_2 sheet glass, pristine and scratched, fracture behaviour during bending 78—23829
Na_2O-NaF-CaO_xZnO_{1-x}-Al_2O_3-SiO_2, opal glasses, strength, surface composition 80—30066
Na_2O-SiO_2 glass, coated with SnO coeff. of friction and fracture toughness 78—80657
Na_2O_3-B_2O_3-SiO_2, glass, effect of composition on mech. props. 78—48435
Na_2O_3(CaO)-Al_2O_3-SiO_2, effect of composition on mechanical props. 78—48435
Nb fibre glass composites, new technique for producing fine metal fibres 80—108384
Nb-Fe(Co)(Ni)(Os), alloying element influence on strength, ductility, surface and grain boundary energies *(Russian)* 79—74234
Nb-low alloys, strength and ductility at high temp. and different strain rates 80—16401
Nb-Mo-Ti-Zr, influence of C content on creep charact. and creep-rupture strength *(Russian)* 77—48483
$Nb_{40}Fe_{40}P_{14}B_6$, metallic glass, explosive compaction, mech. props. 80—89176
Ni alloys, heat resistant EI437B and EI929, surface condition, air stream effect 80—76409
Ni alloys, plasticity, heat treatment effect 80—76277
Ni base alloy, directionally solidified, fatigue crack propag. 77—36639
Ni base superalloy, directionally solidified, struct. and props. *(Chinese)* 80—20918
Ni spheres in glass matrix, brittle composites, fracture 79—66141
Ni wire reinforced epoxy resin, crack propagation 79—29188
Ni-Al bronze, fracture resistance of tubes 78—19867
Ni-Al bronze 77—81312
Ni-Al_2O_3 cermet, fabrication and mech. characts. 79—38781
Ni-Cr-Co base superalloy APK1, hot isostatically pressed, heat treatment, fracture props. 77—73251
Ni-Cr-Co superalloy, σ-phase effect on mech. props. *(Chinese)* 79—74229
Ni-Cr-Co superalloy IN-792, crack growth resistance, metallurgical effects 77—36655
Ni-Cr-Mn alloy solidification, effects of Si, Mo and Co alloying 79—83193
Ni-Cr-W (20, 10 to 40 wt.%), phase composition, struct. and props. 80—21034
Ni-Cr(Mo), solid soln., US effect on mech. props. *(Russian)* 78—23819
Ni-Fe solid soln., precip. hardened, paramag.-ferromag. transition on ageing 78—52255
Ni-Fe-Cr (18, 18 wt.%) superalloy, mech. props., 4-295K 77—44327
Ni-Fe-Cr base superalloy, addition effect on mech. props. *(Chinese)* 80—20998

fracture toughness continued
Ni-Fe-Cr superalloy 718, heat treatment effect on room temp. and elevated temp. fracture toughness response 80—100922
Ni-Zr, amorphous phase form. in Zr-poor region, hardness and fracture strength *(Japanese)* 80—84914
Ni(Cr)-Mo-V, fracture toughness data, comparison with equivalent energy and energy per unit area data 78—52965
PbO-B_2O_3 phase-separated glass, fracture toughness, Vickers indentation method 80—85023
Pd-Si-Sb, mostly crystalline, rapidly quenched, mech. props. 79—61610
α-Pu and δ-stabilised Pu-Ga alloy, strain rate effect on tensile props. 77—21284
α-Pu, plane strain fracture toughness 77—25161
Si/SiC ceramic composite, room temp. props., effect of SiC content and orientation 78—27599
Si-Al-O-N, high-temp. fracture and diffusional deform. mechanisms 80—40509
Si-Al-O-N sintered ceramic, microstruct., phase composition and transformation mech., mech. props. 80—40309
SiAlON, pressureless sintered with low amounts of sintering aid, rupture modulus 79—66029
α-SiC, effect of cryst. shape and size on plastic deform. to rupture and strength 77—56043
SiC, fracture toughness specimen, appl. of wedge indentation technique for precracking 78—85087
SiC, fracture toughness and high-temp. slow crack growth 80—81153
SiC, fusion reactor first wall appl., radiation damage 79—86822
SiC, low blow Charpy impact 79—34122
SiC single crystal, fracture toughness 78—7019
SiC, strength assessment by Young's modulus meas. up to 1400°C *(German)* 78—11253
β-SiC whisker, failure and defects 79—96145
SiC-fibre reinforced glass, fabrication, thermal expansion, flexural and fracture toughness 80—40319
Si_3N_4, effect of oxide impurities on physicomechanical props. 80—16396
Si_3N_4, fracture toughness meas. using Knoop indentation method *(German)* 80—25830
Si_3N_4, grain-boundary-crystallized, thermal shock resistance 78—11308
Si_3N_4, HS-130, dynamic mode I fracture toughness and flexural strength 77—21248
Si_3N_4, hot pressed with different grain struct., mech. props. 79—61700
Si_3N_4, hot-pressed, fracture toughness determ. using specimens with chevron and straight through notches 80—108538
Si_3N_4, hot-pressed, strength anisotropy origins 80—89330
Si_3N_4, optimization of props. as tool material, for high fracture toughness and hot pressing prod. 79—95987
Si_3N_4, pyrolytically-deposited, engng. significance 79—38746
Si_3N_4, reaction bonded, pore size and distrib. effect on strength 79—29165
Si_3N_4, reaction-bonded, biaxial fracture strength 79—38969
Si_3N_4-based refractories, strength and microstruct. rel. to sintering 77—63610
Si_3N_4-MgO, (5 wt.%), hot pressed, fracture toughness as function of initial α-phase content, SEM 80—3174
α-Si_3N_4-MgO (5 wt.%), hot-pressed, mech. strength development 78—44195
Si_3N_4-Y_2O_3 (8.0 wt.%), hot pressed, mech. props. 79—70134
Si_3N_4-ZrO_2, sintered and hot pressed, exam. of mech. props. 78—48509
SiO_2, fused optical fibre, strength, appl. of Weibull type analysis 77—19418
SiO_2-B_2O_3-Na_2O-K_2O glass, strengthening by partial leaching 80—60993
Sn-Pb (38 wt.%), graphite fibre reinforced, effect of interface on fracture characts. 78—76723
steel, Cr-Mo-V, charact. investigation 78—72857
strengthened by lattice transformations, mech. props. study *(Japanese)* 79—43332
Ta foil, electron beam deposited, periodic chemical var. effect on mech. props. 79—91590
Ta_2O_5, anodic film on Al, strain to failure, failure characts. 77—12734
ThO_2, sintered, fracture props. studied by Hertzian indentation technique 80—50703
α-β Ti alloy, fracture toughness rel. to microstruct. 77—16673
Ti alloy, fracture toughness determ., rel. to mech. props. 77—21277
Ti alloy, microstruct. and mech. props., room and elevated temps. 77—36554
Ti alloy, microstructure resulting from heat treatment, alloying, effect on creep, fatigue, fracture strength 78—11246
Ti alloy, VTS-1kt, cryogenic, and structural strength 77—59927
Ti alloy, VT23, ht. treatment effects on fracture *(Russian)* 78—80623
Ti alloy TA6V, toughness and rate of fatigue, cracking, structural morphology effects *(French)* 77—77579
Ti alloy VT20, endurance in cyclic bending 77—63798
Ti alloy VT3-1, fracture toughness improvement by applying Pb-Sn-Cd coating to crack tip 79—43416
Ti alloy VT3-1, fracture toughness, rel. to struct. 79—79105
Ti alloys, data handbook of low temp. mech. and phys. props. 80—22153
Ti alloys, toughness and behaviour under dynamic loads *(French)* 80—45383
Ti alloys fracture toughness-mech. props. interrelations 77—86154
Ti, high purity, data handbook of low temp. mech. and phys. props. 80—22153
Ti, plastic deform. dynamics, mech. characts. and phys. props., effect of O_2 *(French)* 80—45353
Ti-Al-Cr-Fe-Si alloy AT6, and weldments, mech. and corrosion props. 77—90409
Ti-Al-Mo alloy VT-14, spherical pressure vessel, correlation between fracture stresses and mech. laboratory characts. 80—25838
Ti-Al-Mo-Cr (4.5, 5, 1.5 wt.%), CORONA-5, effect of microstructure and heat treatment on fracture 78—60805
Ti-Al-Mo-Sn-Si (4,4,2,0.5 wt.%), fracture toughness and crack propagation 78—39892
Ti-Al-Mo-V (8, 1, 1 wt.%), Widmanstatten colonies, fracture toughness 80—85031
Ti-Al-Sn (5, 2.5 wt.%), fracture mechanism at cryogenic temps. 78—64642
Ti-Al-Sn (5, 2.5 wt.%) alloy, fatigue under combined alternating bending and torsional stresses 77—8923
Ti-Al-V, (6.7, 4.3 wt.%), fatigue crack growth and fracture resistance enhancement, due to annealing 78—35510
Ti-Al-V (6, 4, wt.%), texture influence on fracture toughness and deformation 79—91801

fracture toughness continued
- Ti-Al-V (6, 4 wt.%), friction characts. improvement by O_2 dissolution and controlled surface hardening *(French)* 80−45401
- Ti-Al-V (6, 4 wt.%), textured, anisotropy of fracture toughness over various specimen orientations 79−8353
- Ti-Al-V (6, 4 wt.%) slow crack growth in air and fracture toughness, H content effect *(French)* 80−45385
- Ti-Al-V (6,4 wt.%), improved toughness from prior β-grains 78−15522
- Ti-Al-V (6,4 wt.%), strongly textured, influence of cryst. orientation on fracture toughness 78−84951
- Ti-Al-V (6,4 wt.%), to H effect on fracture props. and microstruct. 80−40512
- Ti-Al-V-Sn (5.5, 5.3, 2.3 wt.%) fatigue crack growth and fracture resistance enhancement, due to annealing 78−35510
- Ti-Al-V-Sn(Mo-Fe), heavy section extrusion, fabrication and mech. props. 78−6985
- Ti-Al-Zr-Mo-Si (6,5,0.5,0.25 wt.%) fracture toughness and crack propag. 78−39892
- Ti-alloys, methods of studying effect of H on service behaviour 80−16478
- αTi-Fe, plastically deformed, $\alpha \rightarrow \omega$ transform. 78−3095
- β-Ti-Mo-Cr-Al (8, 4.5, 2.5 wt.%), metastable, tensile ductility, α-phase morphology and distrib. effect 77−86098
- Ti-Mo-Fe-Cr-Al, alloy VT3-1, influence of constitution on fracture toughness *(Russian)* 77−77559
- Ti-V-Cr-Mo, fracture resistance at low temps. 80−104284
- Ti-V-Fe-Al (10, 2, 3 wt.%), fracture toughness and stress corrosion resistance 80−100904
- Ti-Zr-Mo alloy, effect of O_2 on elec. resistivity, microhardness, mech. props. 77−56092
- TiC coated WC-Co cemented carbides, fracture toughness 80−85046
- TiC coating on C fibre, by CVD TiC coated C fibre compatibility with Al *(Japanese)* 79−78898
- TiC, tool carbide, thermal shock resistance and fracture strength 77−21257
- TiC-Mo_2C-TiN-Co, fracture toughness, effect of microstructural defects *(Japanese)* 77−56087
- TiC-steel alloy, struct. form. during sintering, strength, rel. to heat treatments 77−59717
- (U,Pu)C, fracture and crack healing, SEM study 79−79080
- U-Mo(2 wt.%), mech. props., effect of ageing 77−8914
- U-Ti(0.75 wt.%), mech. props., effect of ageing 77−8914
- UAl_2-Al dispersion fuel, effect of reactions on Young's modulus and rupture strength *(German)* 78−62596
- UO_2 fracture strength meas. of sintered specimens by diametral compression testing, effect of temp. and deformation rate 79−79074
- V-low alloys, strength and ductility at high temp. and different strain rates 80−16401
- V-Nb-Ti-N alloy, dispersion hardened, fracture characts. 79−15794
- VC, exam. of brittle fracture props., using Hertzian indentation 79−11686
- W alloy, nonlinear compliance curves, caused by crack closure and fracture tests 77−56064
- W, fibre, brittle to tough transition, impact strength meas. 80−40527
- W-Cu fibre reinforced composites, interface shear strength, critical aspect ratio 77−4826
- W-Ni-Fe (5(2), 5(2) wt.%) pore formation, effect on mech. props. 80−45396
- W-Ni-Fe(Cu), liquid phase sintered, interfacial embrittlement 79−57101
- W-ZrC(-Re) eutectic alloy, Re effect on breaking stress, lattice parameters, electron struct. *(Russian)* 79−1845
- WC, tool carbide, thermal shock resistance, fracture strength 77−21257
- WC-Co, comparison of indentation crack resistance, and fracture toughness 78−76739
- WC-Co, rupture stress, microstructure and other effects 77−73343
- WC-Co, various combinations, fracture characts. in bending, compression, and toughness tests 78−60808
- WC-Co (10 to 30 wt.%) transverse rupture strength, residual stresses due to surface grinding effects 77−63789
- WC-Co (10 wt.%), high temp. transverse rupture strength 77−63790
- WC-Co alloy, short-time creep rupture strength, C content effect 400° to 900°C *(Japanese)* 78−48487
- WC-Co alloy, transverse rupture strength rel. to grain size and strain rate, 400° to 900°C *(Japanese)* 78−48486
- WC-Co alloys, fracture toughness model 80−84243
- WC-Co alloys, single edge notched beams, exam. of fracture toughness 78−52975
- WC-Co cemented carbide, fracture toughness meas., model for variation with microstruct. 78−60806
- WC-Co cemented carbides, high temp. transverse rupture strength, effect of domain size of binder phase *(Japanese)* 78−92329
- WC-Co cemented carbides, rel. between Palmqvist indentation toughness and fracture toughness 79−70155
- WC-Co cemented carbides, transverse-rupture strength obs., w.r.t. domain size of binder phase *(Japanese)* 80−11741
- WC-Co hard alloy-steel welds, effect of intermediate layer composition on structural changes and mechanical properties 78−60616
- WC-Co hard alloys, hot pressed, mech. props. 79−100260
- WC-Co particle-matrix composite, fracture and cleavage strength 77−73342
- WC-Ni (10 wt.%), room temp. transverse rupture strength *(Japanese)* 77−63774
- WC-TaC-Co, cemented carbide, strength improvement by hot isostatic pressing 78−84969
- WC-TiC-TaC-Co cemented carbides, at 600 to 1000°C *(Japanese)* 79−43374
- Y-Si-Al-O-N glass, prep. and props. 80−25647
- Zn, brittle fracture, temp.-time depend. of strength in embrittlement region *(Russian)* 77−25125
- Zr TA6V6E2, tensile and toughness props. after isothermal quenching and continuous cooling *(French)* 77−59833
- Zr-Al (8.0 wt.%), tensile props. and fracture toughness after fast neutron irradiation 80−3198
- Zr-Al (8.6 wt.%), fast neutron irradiated, tensile props. and fracture toughness 80−84994
- Zr-Nb, (2.5 wt.%), cold-worked pressure tubing for CANDU reactors, slit burst testing 79−26532
- Zr-Nb (2.5 wt.%), crack resistance, influence of ZrH_x fracture toughness 80−16444
- Zr-Nb (2.5 wt.%), nuclear fuel channels, neutron effects on ultimate fracture strength, 293 to 573K 80−85054

fracture toughness continued
- Zr-Nb (2.5 wt.%) pipe, fracture resistance, hydrogenation effect 80−104279
- ZrC, high-temp. strength, affecting factors 77−63794
- ZrH_x, fracture toughness, influence on crack resistance of Zr alloys 80−16444
- ZrO_2, containing metastable tetragonal phase, stress induced phase transform. effect on props. 78−68683
- ZrO_2, MgO partially stabilized, microstruct. development during ageing 79−91710
- ZrO_2, partially stabilised, toughening mechanism 77−56084
- ZrO_2, partially stabilised ceramics, strengthening, post-sintering heat treatment 80−97518
- ZrO_2, partially stabilized, precipitation effects on fracture mode 77−90354
- ZrO_2, partially stabilized, transform. toughened, fracture toughness 79−91775
- ZrO_2 stabilised with Nd_2O_3, refractories prod. and long-term high-temp. behaviour 77−59725
- ZrO_2, tetragonal polycryst., sintering and props. 79−29008
- ZrO_2, transformation toughened, localised impact damage 80−7665
- ZrO_2-Zr cermet composite, hot pressed, fracture toughness 78−27604

fracture toughness testing
- *see also notch testing*
- acoustic emission, inspection technique 78−68860
- adhesive joints, fracture toughness meas., CDCB specimens 77−4874
- alloys, influence of test piece geometry 78−84951
- alumina, grain size and fracture toughness, effect of fracture toughness test methods 78−72883
- amplifier to record heat pulse during material fracture 78−60921
- annular fatigue crack prod. in cylindrical specimens *(Russian)* 77−52559
- austenitic steel, Cr-Ni alloyed, Ti stabilised, nuclear reactor pipeline appl. *(Hungarian)* 77−18658
- automatic crack growth recording using PSR-1-19 potentiometer 78−39971
- automation of method of forming and measuring circular crack depth in cylinders 79−43531
- bar-to-block based testing method for materials characteris. in high-vel. tension 80−85133
- biaxial strength tests, finite element anal. 80−89431
- boiler steel fatigue crack propagation test results *(Hungarian)* 79−83293
- bone, long, bending strength prediction, from bending stiffness and bone mineral content meas. 78−11787
- brass, crack initiation at high strain rates, uniaxial and biaxial tests 80−85141
- brittle, notch angle effects obs. *(Japanese)* 80−6459
- brittle materials, diametral compressive stress considering Hertzian contact, fracture and tensile strength meas. *(Japanese)* 78−72946
- brittle materials, strength measurement using hydraulic bursting technique 80−35443
- brittle materials, ultimate tensile strength determ. by radial compression testing 78−7132
- brittle nommetallic material 79−57190
- C-shape compact specimen 78−7108
- C-shaped fracture-toughness test specimens, stress, strain and deflection meas. 78−19963
- castings, fracture toughness characteristics, using double torsion method 78−68863
- cemented carbide, simple evaluation method 77−32748
- ceramic material fracture mechanics, n review 80−45373
- ceramics, wedge indentation technique for precracking, appl. to Al_2O_3 and SiO_2 78−85087
- ceramics diametral compression test, parametric study 78−44282
- Charpy tests, instrumented, evaluation of reliability 77−25243
- chevron notched short bar specimens, compliance and stress intensity coefficients 80−96232
- compact specimen, for plane strain crack arrest toughness testing 80−76433
- compliance correction for determining load-line energies for compact fracture toughness specimens 79−57186
- concrete, US testing of strength under load and of reinforced concrete structs. 77−36707
- concrete slab perforation by missiles, nuclear plant appl. 77−38352
- concrete slab perforation by missiles, nuclear plant appl. 77−38353
- concrete slab perforation by missiles, nuclear plant appl. 77−38354
- concrete splitting test, nonlinear numerical analysis 77−7339
- constructional material, K_{1c} determ. from mech. props. and struct. parameters *(Russian)* 77−60010
- constructional materials, brittle failure resistance, calc. characts., expt. methods 77−77662
- crack growth gauge for assessing flaw growth potential in structural components 78−68859
- crack propag. toughness testing 77−44449
- crack propagation initiation, meas. by elec. resist. meth. *(Chinese)* 77−9005
- crack propagation speed, calc. for testing with energy accumulator 80−3262
- crack resistance in materials under long term static loading, evaluation methods 80−45461
- cracking-resistance evaluation, apparatus for rapid determ. of K_{Iscc} 77−77671
- cracks, critical opening determ. *(Russian)* 79−52479
- critical stress intensity coeff. under plane deform., expt. determ. standards 77−77663
- critical stress intensity factor determ. from crack development vel. and test temp. 78−7130
- cyclic toughness determ. in low-cycle fatigue testing of plane specimens in simple bending *(Russian)* 77−52560
- cylindrical notched specimen, four-point bending, crack resist. tests 80−53735
- cylindrical specimen with segmental crack *(Russian)* 78−11301
- cylindrical specimens, fatigue and crack generating and meas. device 79−52508
- deformation strength props., simultaneous meas. of several samples, polymer films appl. 79−15896
- diametral compress test using circular anvils *(Japanese)* 78−72947
- diamond surface soldered to metal film, contact strength determ. device 78−60910

fracture toughness testing continued
disc test measurement of combined mode fracture toughness stress analysis 78—92432
double torsion fracture toughness test, 3-dimens. finite element anal. 80—30203
ductile, procedure for determ. using J-integral technique 79—52542
ductile material, dynamic toughness determ. 77—44452
dynamic, by instrumented impact tests 78—68861
dynamic, conf., London, England, (July 1976) 77—36714
dynamic analysis of test results 77—36715
dynamic impact test method, new *(German)* 79—11740
dynamic meas., test specifications 77—36721
dynamic method using compact tension tests 79—34218
dynamic stress/strain measurements under superimposed high press., torsion bomb machine 80—85130
eddy current sensor, for detecting induced fatigue cracks in Al, Ti alloys 80—45459
elastic-plastic material behaviour, K_{Ic} values determ., specimen size effects 80—45376
elastoplastic range, computer simulation 80—21217
electrical potential method, unusual potential drop 77—16761
energy measurement and significance in acoustic emission testing 78—31594
exoemission defectoscopy in initial stages of fatigue fracture 78—53126
fastening materials, specimen for testing 80—61050
fibre, failure charact. determ. by electrical simulation, feasibility study 77—52597
film, diamond indentation and draw tester for meas. of ultra-adherence 78—72944
fractographic study on evaluation of fracture toughness 78—68865
fracture ductility determ. from fracture diagram, method 79—43511
fracture evaluation at high loading rate by extrapolation method 77—36723
fracture mechanics anal. and NDT/destructive test correlations 77—90526
fracture sensitive structures, materials related aspects 78—42570
glass, fracture mechanics studies, specimen *(French)* 77—73401
glass, stress intensity factors by double torsion method, crack growth *(French)* 77—73345
glass components, life testing under flexing load *(French)* 80—89432
glass fibre reinforced plastic, bending tests, specimen size and shape selection 77—52575
glass fibre reinforced plastic, woven-roving type, high-speed punching, failure mechanisms 80—85143
graphite, constructional, fracture toughness testing methods 78—7129
graphite, diametral compressive testing method 80—35495
graphite, effective specific work of fracture, evaluation method 79—57170
graphite, fracture toughness measurement, by disc test comparison with stress analysis of disc test 78—92432
graphite, structural, impact toughness, reln. to compressive strength 78—88605
graphite materials, mech. characts. under stress using acoustic emission analysis *(German)* 79—15881
graphite thermal shock resistance and fracture toughness meas. *(Japanese)* 79—91868
Griffith fracture tests, for plastic deform. *(Hungarian)* 80—97666
hard metal, tensile strength meas., bend test-piece geometry effect 80—30184
heat resistance testing, massive sample for mech. prop. changes obs. 78—7124
Hertz indentation test and Auerbach's law, computer simulation 78—19967
Homalite, stress intensity factor measurement, dynamic fracture toughness determination from isopachics of a running crack [holographic interferometry] 79—34257
Homalite 100, dynamic fracture specimens, dynamic photoelastic analysis 77—44364
Homalite-100 plate, dynamic finite element and photoelastic analyses 77—7340
impact bending, specimen parameter effect on crack propag. 77—86242
impact machines, pendulum, energy meas. using optical system 80—69746
impact penetration damage, probability based fracture mechs., appl. to Al panels 78—1606
impact testing equipment for small specimens 77—52578
impact three point bend testing for notched and precracked specimens, testing and data analysis procedures 78—53053
impact toughness testing at cryogenic temps., temp. determ., using thermocouples 80—25942
impact-fatigue method *(Chinese)* 80—3258
Inconel, compact ductile fracture toughness specimens, load line displacement measurement method at elev. temps. 78—27700
inertial peak under impact loading, possibility of diminishment *(German)* 77—66726
installation for in-reactor study of creep and stress-to-rupture, plane stress mode 78—39996
instrumented impact testing, critical review 77—36725
irradiated reactor component testing facility 79—79201
J_{Ic}-integral value determination by compact tests 80—45451
J_{Ic}-testing, statistical eval. of different techniques, applic. to A-533 B steel 78—56828
J integral, work for failure and work for plastic deform. 80—61061
J integral and its components, determ. method 80—45458
J integral estimation procedure, summary and comparison 78—85088
K_{Ic} determ. for reduced size specimens *(Russian)* 78—56830
Kassem method 78—92412
laboratory tests automation, using 500 kN and 2.5 MN ATE *(Czech)* 80—66710
layer, double torsion method of crack propag. study 79—83412
limestone tubes, dynamic torsional failure obs. 80—85648
low temperature testing, design of cooling installation 80—21216
marble, diametral compressive testing method 80—35495
marble, fracture toughness measurement, by disc test comparison with stress analysis of disc test 78—92432
metal, US propag. factor rel. to fracture toughness props. 78—80698
metal in atomized NaCl solutions, fatigue strength testing unit 77—77677
metallurgically bonded plates, structural integrity determ. by high energy impulse 79—39111

fracture toughness testing continued
metals, crack resistance determination, cyclic loading, methodological instructions 80—108660
metals, ductile-brittle transition temperature evaluation, as function of thickness 80—3261
metals, test method applicability and interpretation 79—15950
method of unloading in experimental fracture mechanics *(Russian)* 78—56829
miniature test-pieces, multipurpose apparatus *(Russian)* 77—52558
NDT, role in fracture mechanics evaluation 78—68862
notch production with small root radius on test samples *(German)* 78—64795
nuclear components, struct. integrity assessment mat. prop. variations 78—89953
ophthalmic lenses, basic principles of fracture testing 79—96233
optical fibre fracture stress and mirror size obs. 79—37020
optical fibres, breaking strain estimation for long lengths of fibres 78—30060
oscillograph determ. of charact. in impact bending 79—66231
photoelastic, isochromatic fringes, comparison of stress intensity factor determ. methods 77—84197
plane strain, simple meas. method 77—73381
plane strain, testing with C-shaped specimens 78—92414
plaster, fracture toughness measurement, by disc test comparison with stress analysis of disc test 78—92432
plastic film tear test, fracture mechanical analysis *(Japanese)* 77—81351
plastic material, impact-torsion test machine *(German)* 77—52595
plastic zone, direct meas. in side grooved fracture toughness specimens 78—68864
plastic zone obs., holography 77—9034
PMMA, plane strain, simple meas. method 77—73381
PMMA dental biomaterials, fracture toughness testing 80—50800
PMMA fracture toughness, flame-retardant additive effect obs. 80—16470
PMMA plates with flawed fastner holes, static fracture testing 80—97651
polyethylene, high-density, impact fracture behaviour, adiabatic heating at crack tip 80—85142
polyethylene pipes, lifetime determ., crack growth in thermoplastics under various conditions 78—39981
polymer, fracture energy spectrometer 79—57181
polymer glass, method *(Russian)* 78—11457
polystyrene, impact-torsion testing *(German)* 77—52595
post yield fracture mechanics analysis of 3-pt bonding specimens rel. to toughness testing 77—56168
precompression cracking method appl. *(Japanese)* 78—15612
pressure vessels, brittle fracture probability using reactor surveillance capsule data 78—80641
quartz, fused, plane strain, simple meas. method 77—73381
radial expansion technique for fracture strain meas. at high strain rates 80—85134
refractories, strength and thermal properties, automated test system 80—100986
refractory concrete fracture strength, test apparatus simulating usage conditions 80—71824
refractory products, toughness measurement, expt. problems *(French)* 80—104368
repeat impact testing machine 77—52604
ring segments, radially cracked, displacement coeffs. from boundary collocation anal. 78—71298
rocks, under downhole stress conditions, expt. technique for meas. fracture toughness 79—43543
rope with transverse load, tensile testing to rupture, device 80—25962
round compact specimen, mode I stress intensity factor testing, boundary collocation method 78—27702
rupture strength testing under cycic loading, AIMA-5 machine modification 79—52506
sample design improvements for brittle failure characts. determ. 78—39970
sandstone, fracture toughness and acoustic emission characts. *(Japanese)* 79—34810
sharp notch tension testing, screening procedures 77—56169
sheet materials, testing method 78—3277
siltstone rock, plane strain, simple meas. method 77—73381
specific potential energy method *(German)* 80—21239
specimen fracturing device for ion microprobe analyser, and appl. to grain boundary segregation 77—21341
specimen loading method *(Russian)* 77—28941
split Hopkinson pressure bar application 80—85140
static and dynamic loads, correlation 77—60022
static bend testing of cracked samples until failure, −60 to 20°C 78—23893
statistical processing of results, cold brittleness crit. temps. determ. 80—100980
steam turbines, structural stresses, experimental anal. 80—93727
steel, A533B, dynamic fracture toughness testing 77—77650
steel, acoustic-emission analysis of fracture-toughness tests 80—55596
steel, alloy, single specimen determ. for J_{Ic} 80—100989
steel, alloy A533B1, neutron irrad., flow growth characts. by acoustic monitoring 80—100918
steel, at low temps. *(Russian)* 77—25206
steel, austenitic, approx. method for high-temp. cracking resistance estimation 78—23914
steel, brittle fracture, J-integral fracture criterion *(Japanese)* 77—48597
steel, C(1 wt.%) fracture, dynamic, testing apparatus 77—44450
steel, cast, cold resistance determination, quick method 80—100997
steel, construction, fracture toughness determ. under developed plastic deform. conditions 77—77664
steel, dynamic fracture toughness meas. by instrumented impact bend and compact K testing 77—36718
steel, effect of side-grooving on K_{IC} meas. by bending *(Japanese)* 78—35614
steel, ferritic, Charpy impact testing criteria 79—47855
steel, ferritic, criteria for Charpy impact testing 80—7752
steel, ferritic nuclear pressure vessel, methodology for fracture props. variability evaluation 78—33257
steel, fracture ductility, determ. in bending tests and US emission 78—23899
steel, fracture initiation moment, I-integrals critical value determ., ultrasonic method 80—61049

fracture toughness testing continued

- steel, fracture toughness dynamic, interlaboratory data, statistical analysis 77—36717
- steel, heat-treated, toughness factor statistics *(Russian)* 77—44418
- steel, low strength, impact tests with oscillography, exam. of fracture toughness using new method 80—21215
- steel, low-alloy, fracture toughness characts., loading rate effect 80—100897
- steel, low-alloy, testing cracked specimens for impact bending, expt. planning method appl. 80—71831
- steel, maraging thin sheet, fracture toughness testing *(German)* 77—66728
- steel, mild, dynamic flat fracture resistance, shear lip effects 77—44451
- steel, mild, welded struct., dynamic initiation of brittle fracture, testing 77—36716
- steel, notched bar impact bending test, Robertson test and drop-weight test relationship 77—81364
- steel, precompression cracking method, fracture toughness testing *(Japanese)* 78—15612
- steel, RPV type, toughness values compilation, temp.-range validity 77—48611
- steel, Sn (1.5 wt.%) and Mn-Mo (3, 0.4 wt.%), specimen fracturing device for ion microprobe analyser, to grain boundary segregation 77—21341
- steel, stainless, 316, ductile, prestrained, method of J_Q and δ_i determ. 77—36724
- steel, stainless, thin sheet, fracture resist., critical opening of crack criterion 80—61048
- steel, structural, susceptibility to brittle fracture criteria, comparison of notch impact and fracture toughness testing *(German)* 77—70237
- steel, structural, wide plate tensile testing eval. *(German)* 80—100969
- steel, tensile test pieces, comparison of micro and standardised size *(German)* 79—83414
- steel, types A533B and KAS, fracture toughness meas. using elect. potential method *(Japanese)* 80—93722
- steel, using oscillograms, optimum heat treatment 79—57169
- steel 45G2, fracture resistance, from impact bending tests and oscillograms 80—61047
- steel , welded specimen AE testing by external static loading of cold cracking susceptibility 78—40013
- steel components, safety anal. for loading conditions 78—39979
- steel transition temp. determ. from fibrous structure in fracture, exam. of method 78—85080
- steels, brittle transition temp. determs. from impact ductility tests, comparative evaluation 79—15888
- steels, test for determining reheat cracking susceptibilities of heat affected zones *(French)* 80—16633
- strain gauging techique for monitoring fracture mech. specimens during environmental testing 78—31606
- strained samples, K_I determ. *(Chinese)* 77—75856
- strength testing, long-term of specimens with fatigue crack 78—7131
- stress intensity factor, reliability of values 80—55530
- stress intensity factor measurement, dynamic fracture toughness determination from isopachics of a running crack [holographic interferometry] 79—34257
- stress rupture test using photoelectronic monitoring of tube deform. 78—78470
- structural grade steel, dymamic meas. 77—56167
- structural materials, crack resist. determ. 80—81258
- Stycast-1266, mechanical props. at low temps. 80—57286
- surface crack shape change in bending fatigue, resonant fatiguing apparatus 78—72950
- thermal shock fracture toughness eval. by arc discharge heating 78—72835
- thickness criterion, modified 78—7107
- thin sheet, fracture toughness testing *(German)* 77—66728
- thin-sheet failure, fracture toughness, resistance curve and stable crack extension 77—44416
- transverse rupture of hard alloys by mag. loss on polarity reversal 77—59879
- triaxial loading test, plastic flow and fracture 78—27701
- tubular specimens, tensile testing with delayed necking 77—90522
- US, crack extension monitoring 77—16758
- welded joints in dissimilar Al alloys, fishbone test piece axis of symmetry, residual stresses, cracking coefficient effects 80—7725
- Al alloy, 2124-T851, acoustic emission 78—7109
- Al alloy, crack arrest toughness, used to estimate plane strain for toughness 77—63863
- Al alloy, crack initiation at high strain rates, uniaxial and biaxial tests 80—85141
- Al alloy, crack propag. toughness testing 77—44449
- Al alloy, creep rupture testing, metallographic studies of fracture test specimen 77—63862
- Al alloy, fracture toughness determ., dynamic mode II 77—36720
- Al alloy, fracture toughness testing, acoustic emission, inspection technique 78—68860
- Al alloy, plane strain, simple meas. method 77—73381
- Al alloy, semifinished materials, fracture toughness determ. after tempering 78—7128
- Al alloys, wide range specimen thicknesses, new rig design 77—60011
- Al-Cu, type 2024, fractography of fatigue 80—40488
- Al-epoxy adhesive joints, cohesive-interfacial mixed-mode fracture 79—39110
- Al_2O_3 brittle ceramic fracture toughness meas. notch requirements *(German)* 77—59937
- Al_2O_3, fracture toughness testing by AE *(German)* 79—70234
- B fibre reinforced epoxy, tensile anal. of edge notch 77—70159
- C materials, mech. characts. under stress using acoustic emission analysis *(German)* 79—15881
- Cr-Mo-V steel, creep rupture tests on notched cylindrical specimens at 600°C 77—32670
- Fe base superalloy, type A-286, elevated temp. fracture toughness testing of thin section irrad. materials 80—61063
- Fe cast, dynamic tear charact. 77—44448
- Fe, cast, instrumental dynamic tear tests 77—44447
- Fe, cast, white, fracture toughness testing by double torsion bend test 78—27705
- Fe, pig, white, mech. props. meas. *(French)* 80—104370
- Fe, sintered, porosity estimation by screen image of brittle fracture 77—52585
- Si solar cells, production process effect on fracture strength 80—93656
- SiC, instrumented Charpy impact testing 77—36719

fracture toughness testing continued

- Si_3N_4, hot-pressed, fracture mech. parameters, indentation-precracking and double-torsion methods 80—104364
- UO_2 fracture strength meas. of sintered specimens by diametral compression testing, effect of temp. and deformation rate 79—79074
- WC/Co cemented carbides, fracture toughness testing 80—104410
- WC-Co, fracture toughness testing by double torsion bend test 78—27705

francium

- *see also nuclei with ......*
- atom, evidence for optical transition *(French)* 78—86829
- atom, radioisotopes, hyperfine spectroscopy, nucl. props. 80—57677
- electrical resistivity, data tables, 1-2000K 79—78072
- emission spectra measurements *(French)* 79—26918
- properties from melting point to 7500K, prediction *(Russian)* 80—44296
- Fr I, wavelength estimate of first and second resonance lines 78—58617
- Fr I isoelectronic series, transition probabilities, oscill. strengths, lifetimes, branching ratios 78—33470
- ^{212}Fr, low energy ions systematic range meas. in Ar and N_2 gases 79—1472

francium compounds

- No entries

Franck-Condon factors

- acetones, fluorinated, absorpt., fluoresc. spectra, quantum yields, decay times meas., mechanism 77—3410
- acetylene, core ionised, core-excited and shake-up states, ab initio MRD-CI methods 80—42950
- alkali halide, Tl^+-type centres, struct. of Jahn-Teller induced B absorption band 77—12410
- aromatic hydrocarbon derivatives, low-temp. singlet-triplet conversion probability rel. to optical parameters 79—54898
- bent triatomic mol., photodissoc. rot. distrib. 80—95694
- benzaldehyde in methylcyclohexane, $n^3\pi^*$ spectra 80—63627
- benzene, $^1A_{1g}\rightarrow{}^1B_{2u}$ absorption band, Franck-Condon factors calc. 79—36701
- benzene, deuterated mixed crysts., phonon assisted trap-trap triplet energy migration, 0K limit, phosphoresc. obs. 77—48218
- benzene, intramol. nonradiative transitions, Franck-Condon principle at high energies 77—14478
- benzene, reson. Raman cross sections, forbidden electronic transitions, depolaris. ratios 78—42075
- benzene, SVL fluoresc. band intensities, Franck-Condon factors, Fermi reson. 77—10700
- benzophenones, triplet state fine struct. parameters and phosphoresc. spectra 79—50065
- bound continuum vibr. transitions, Franck Condon matrix elements calcs. 80—69191
- bound-free transitions, harmonic and flat pots., exact wavefunctions 78—969
- C_{3v}-type mols., doubly degenerate electronic states, Jahn-Teller interaction 78—50536
- camphorquinone, vapour, nonradiative electronic relax. rate, excess energy depend. 77—38687
- chemical laser systems, ion-molecule reactions, thermal energy, book contrib. 77—50668
- chemical reaction dynamics, Franck-Condon factors rel. to information theory for vib.-rot. distribs. and isotopic branching ratios 77—60041
- in chemical reactions 77—28990
- Comet Kohoutek (1973 XII), spectrum interpretation by means of Franck-Condon factors, Rydberg-Klein-Rees method calc. *(French)* 77—17428
- computer program for calcs. 77—50341
- conjugated molecules, resonance Raman spectra calc. 78—984
- cytochrome C, vibronic theory of reson. Raman scatt. 79—94004
- diatomic astrophysical molecules, review of spectroscopic information in visible and UV regions 77—88459
- diatomic hydrides of first and second row elements, PNO-CI and CEPA calc. 79—768
- diatomic molecule, calc. by factorisation method 77—6855
- diatomic molecule, electronic states calc. using five-parameter pot. function *(Russian)* 77—3270
- diatomic molecule, Franck Condon factors, vibr. rot. interaction effect 80—74198
- diatomic molecule, reson. Raman scatt. amplitudes estimate based on Airy approx. for Franck-Condon amplitude 79—36649
- diatomic molecule, rot. perturbed Morse oscillator, eigenfunctions and Franck-Condon factors 77—42309
- diatomic molecule, vibr.-rot. interaction effect on Franck-Condon factors 77—23485
- diatomic molecule, vibr.-rot. states, high accuracy wave functions and energies 80—74159
- diatomic molecule, vibrational transitions, Franck-Condon matrix elements 80—9645
- diatomic molecules, Franck-Condon factors, isotope effects calcs. 78—1031
- diatomic molecules, Franck-Condon factors for high J, Morse oscill. calcs. 78—37548
- diatomic molecules, Franck-Condon factors for Morse pots. 79—72365
- discrete-continuum electronic states coupling, appl. to He+Ar 79—10193
- electrochemical redox reactions, Franck-Condon approx. 77—1929
- electron and exciton transfer rates, effect of nucl. degrees of freedom 78—60057
- electronic transitions, band shape in multimode weak coupling limit, multidimens. subspace theory 80—87178
- emission spectra and phonon relax. 77—77279
- energy transfer, unified model, arbitrary Franck-Condon offset and temp. 79—1781
- $ethane^+$, stability and struct., CI-SCF ab initio calc., Franck Condon anal. 77—54575
- ethylene, core ionised, core-excited and shake-up states, ab initio MRD-CI methods 80—42950
- ethynylradical, photodetachment, parturbation theory calcs., ICR spectroscopy obs 79—98166
- Faulkner Richardson method, generalisation 80—1027
- Faulkner Richardson method, generalisation and test 80—5583
- ferricenium complex, Franck-Condon light scatt. transitions 77—57999
- fluoromethanes+$Ne^{+\cdot}$($He^{+\cdot}$)($Ar^{+\cdot}$)($Kr^{+\cdot}$)($Xe^{+\cdot}$)($N_2^{+\cdot}$)($CO^{+\cdot}$)($CO_2^{+\cdot}$)($N_2O^{+\cdot}$), thermal energy charge transfer reactions mechanism 77—63889
- Franck-Condon overlap, coherent state representation 79—10153
- interference structure in Franck-Condon overlap functions 78—94287

Franck-Condon factors continued

- intermediately coupled localised electron-phonon system, transient reson. Raman scatt. Franck-Condon-like excitation 79—8141
- intramolecular radiationless transitions, Franck-Condon factors of polyatomic mols. 77—14478
- large molecule, novel ultrafast two-pulse excitation spectroscopy 78—94331
- linear triatomic molecule, photodissoc. dynamics, moment anal. 78—13557
- local mode mols., normal mode spectra 80—95687
- methyl radical, HeI photoelectron spectrum, Franck-Condon factors 77—34692
- molecular $\pi\pi^*$ and $n\pi^*$ states, rel. positions, single-triplet conversion probability, low temp. 79—816
- molecular electronic spectra, vibrational struct., determ. by Franck-Condon method, book contrib. 78—21911
- molecular vibrational wave functions, semiclassical Gaussian basis set method 80—9583
- molecule, diatomic, Franck-Condon factors calc. using Rydberg-Klein-Rees pot. 78—70878
- molecule core 1s and 1b, photoelectron bands, vibr. excitations, ab initio calc. 80—63543
- molecule dissociation, transition amplitudes, semiclassical evaluations 78—62860
- naphthalene, vibronic fluorescence spectrum, intensity distribution 79—3477
- near reson. Raman lines, relative intensities, A-term method 79—81205
- nonadiabatic collisions, Franck-Condon approach for electronic state quenching 78—66640
- nonradiative decays, complex Franck-Condon overlap integral 79—50066
- nonradiative quenching of hot luminesc. in F centres 80—11467
- photochemistry two-photon, photo-fragment distrib., isotope separation appl. 80—81344
- photoelectron angular distribs., oriented or rot. resolved unoriented mols., dynamic and struct. data 78—37682
- photoionisation, vibrationally-excited ions form. in Franck-Condon gaps, threshold photoelectron spectra obs. 79—68262
- photosynthetically relevant mols., electronic structural props. 80—16902
- photovoltaic effect mechanism, expt. obs. of thermal and spectral variations in the photovoltaic current in ferroelectrics 78—91719
- polyacenes, electronic transition bands, Franck-Condon factors, PPP SCF MO/CI calc. 78—33430
- polyatomic molecule, dissoc., natural collision coords. 78—44373
- polyatomic molecule, Franck-Condon principle and sum rules for vibronic transitions 77—30927
- polyatomic molecule, nuclear γ-transitions, Franck-Condon principle *(Russian)* 79—59522
- polyatomic molecule, selected fragment vibr. energy distrib. in dissoc. processes 78—1036
- polyatomic molecule, vibronic transitions, dynamical symm., Franck-Condon theory 77—34575
- polyatomic molecules, Franck-Condon factors calcs. 78—17723
- polyatomic molecules, Franck-Condon integrals calcs. *(Russian)* 78—33555
- polyenes, photoiosomerisation, triplet pot. energy surfaces and normal mode anal. 80—108700
- polymer formation, interstellar molecules and prebiological evolution 79—92842
- r-centroid approximation accuracy 79—89661
- Raman excitation profiles and mol. spectra synthesis, vibronic and exciton-in-mol. theory 78—42076
- reactive collision dynamics, general theory applic. 77—36741
- reactive collision dynamics, vibr.-rot. distribs. in atom-diatom reactions 77—36742
- resonance Raman scattering from small molecule, vibronic theory 79—94004
- semiempirical three-parameter pot. functions 77—18986
- thiophosgene, second excited singlet state emission spectroscopy 80—69157
- transition metal complexes, excited states geometrical parameters, Franck-Condon anal. 77—27047
- triatomic exchange reactions, exothermic, semiclassical dynamics calcs. 80—25999
- triatomic mols., close coupling methods, bound-free bidimensional nonseparable FC factors 77—71834
- vibration frequency change influence 80—106312
- water solar photodecomposition, redox reaction thermodynamics 80—35697
- Wigner distrib. function 80—99520
- $Ag_2SO_4:CrO_4^{2-}$, polarised electron spectrum assignments, red colour explained 77—85753
- Al, continuous UV emission under inert gas ion bombard. 78—84664
- AlI, electronic spectrum, Franck-Condon factors, r-centroids 78—62817
- AlO, A-X transition, Franck-Condon factors computation, iterative method compared with Langer's method 78—86762
- AlO, $D^2\Sigma$-$X^2\Sigma$, Franck-Condon factors and V-centroids *(Russian)* 78—74642
- AlO, Franck-Condon factors and r-centroids for $D^2\Sigma$-$X^2\Sigma$ transition 79—94037
- AlO, rot. quantum number effect 79—31613
- AlO, spectra, vibr. consts., pot. curves, Franck-Condon factors and r-centroids 78—42243
- BH, rot. quantum number effect 79—31613
- BO, rot. quantum number effect 79—31613
- Br_2, $B^2\Pi(O_u^+)$ predissoc. rates, analytical interpretation 80—91617
- BrF, laser excitation spectrum, 4850 to 5200 Å, rot. anal. 77—6840
- C_2, Phillips system, rot. depend. of Franck-Condon factors 77—27058
- C_2, reson. fluoresc. statistical equilib. calc., appl. to comets 78—1016
- C_2, rot. quantum number effect 79—31613
- C_2, Swan, Phillips, Deslandres-d'Azhambuja and Fox-Herzberg systems, rotational dependence 78—74701
- C_2, Swan bands, variation of electronic transition moment with internuclear separation 79—826
- C_3, $\bar{A}^1\Pi_u$ state, orbital angular momentum 80—78514
- CH A-X, B-X and C-X systems, rotational dependence 78—74701
- $(C_2H_5)_2Fe^+$ complexes, vibrational electronic (Franck-Condon) Raman transitions 78—42070
- CN $(A^2\Pi$-$X^2\Sigma^+)$ transition, by Langer's approx. method 78—37685
- CN, RKR Franck-Condon factors and r-centroids for $B^2\Sigma$-$A^2\pi$ transition 79—81195
- CN, red and violet band systems, rotational dependence 78—74701

Franck-Condon factors continued

- CN^-, spectrosc. consts. for ground and excited states, ab initio, CI calcs. 80—78551
- CO, (CO^+), Franck-Condon factors, isotope effects calcs. 78—1031
- CO A-X system, rotational dependence 78—74701
- CO, $A^1\pi$-$X^1\Sigma$ system, Franck-Condon factors, r-centroids calc. program 77—27121
- CO, ejected electron spectroscopy of autoionising states using electron-electron coincidence technique 79—3587
- CO, fourth positive system in 1115-4759 Å range 77—49291
- CO, Franck-Condon factors appl., rot. depend. 79—10154
- CO, high resolution lifetime meas., perturbation and collisional transfer correl. 78—78699
- CO, inner-shell ionisation, vibr. struct., sudden approx. calcs. 79—50002
- CO, rot. quantum number effect 79—31613
- CO, valence X-ray photoelectron spectrum, satellite struct. 77—61800
- CO, vibr. struct., core and valence ESCA spectra, Frank-Condon and HF anal. 80—32602
- CO, $X^2\Sigma^+$, vibr. levels, UPS electron attachment obs. 80—95683
- CO_2, Franck-Condon transition amplitudes for mol. dissoc., semiclassical evaluations 78—62860
- $CO(d^3\Delta_i$-$X^1\Sigma^+)$ fluoresc. from CO_2 photodissoc. 77—6836
- CS, CS^+, emission band systems after $He(2^3S)+CS_2$ reaction 77—14473
- Ca_2, $A^1\Sigma_u^+$-$X\Sigma_g^+$ system, laser induced fluoresc., pot. energy curve and mol. consts. 80—58307
- Ca_2, rot. perturbed Morse oscillator eigenfunctions and Franck-Condon factors 77—42309
- Ca_2, vibr.-rot. states, high accuracy wave functions and energies 80—74159
- CaH, rot. quantum number effect 79—31613
- CaS, $A^1\Sigma^+$-$X^1\Sigma^+$, Franck-Condon factors and r-centroids 79—36700
- $Cu+N_2$, Cu*, preferential energy transfer from N_2 to specific Cu energy levels 80—43152
- CuH, vibr.-rot. interaction influence on band intensity parameters 79—49999
- $^{63}Cu_2$, $B^1\Sigma_u^+$-$X^1\Sigma_g^+$ transition, Franck-Condon factors, r-centroids and pot. curves 80—43114
- $^{63}Cu_2$ $A^1\Pi_u$-$X^1\Sigma_g^+$ transition, Franck-Condon factors and r-centroids 80—95690
- D_2, Lyman bands, Morse Franck-Condon factors and R-centroids 77—58088
- DCN, electronic spectra, vibr. struct., ab initio calc. 78—9166
- $F+H_2$, Franck-Condon factors in reactive collision dynamics 77—36741
- $F+H_2$, Franck-Condon factors in reactive collisions dynamics, vibr.-rot. distribs. 77—36742
- $F+H_2$ dynamics, Franck-Condon factors rel. to information theory for vib.-rot distribs. and isotopic branching ratios 77—60041
- GaAs:O, deep level, Franck-Condon shift, photocond. and Hall effect study 80—70642
- GaAs:O, high-resist., extrinsic photocond. meas., Franck-Condon shift determ. 77—85255
- GaO, B-X band system, electronic spectrum, struct. and anal. 79—45732
- GeO, Franck-Condon factors and r-centroids of A-X band system 77—65513
- GeO, RKRV Franck-Condon factors and r-centroids, $(A^1\Pi$-$X^1\Sigma^+)$ transition, pot. energy curves 78—29817
- GeS, band system vibr. anal. 80—48009
- H, Lyman α-line wings, Stark effect 79—22648
- H, Stark broadened line shape, unified Franck-Condon-JWKB method 77—10635
- H-bond complex formation, enthalpy change due to electronic excitation, spectroscopic determ. 78—92496
- $H+Cl_2$, Franck-Condon factors for reactive collision processes 77—36741
- $H+Cl_2$, Franck-Condon factors in reactive collision dynamics, vib.-rot. distribs. 77—36742
- $H+Cl_2$, stochastic-collision complex model theory 80—108696
- $H+Cl_2$ dynamics, Franck-Condon factors rel. to information theory for vib.-rot. distribs. and isotopic branching ratios 77—60041
- $H+H_2$, Franck-Condon factors in reactive collision dynamics, vibr.-rot. distribs. 77—36742
- $H+H_2$ dynamics, Franck-Condon factors rel. to information theory for vib.-rot. distribs. and isotopic branching ratios 77—60041
- H+LiF, laser-induced nonadiabatic collision process, classical model 80—97701
- H_2, electron energy loss spectra, $B^2H_u^+$ state cross sections, Franck-Condon factors 78—13616
- H_2, electron energy-loss spectra in afterglow, ground state vibr. conc. 77—31012
- H_2, Lyman bands, Morse Frank-Condon factors and R-centroids 77—58088
- H_2, photoelectron ang. distrib., 304 Å line, vibr. state depend. 79—45764
- H_2, predissoc., interference effects, lineshape obs. 80—83432
- HCN $(A^1A''\rightarrow X^1\Sigma^+)$, fluoresc. spectrum, using ArF laser excitation 79—36675
- HCN, electronic spectra, vibr. struct., ab initio calc. 78—9166
- HCN, Franck-Condon transition amplitudes for mol. dissoc., semiclassical evaluations 78—62860
- HCN predissoc. Frank-Condon amplitudes 80—95694
- HCN(DCN), photodissoc. dynamics, rot. (vibr.) energy disposal 78—48672
- HD, ionisation, Franck-Condon factors calcs. 77—58102
- HD, Lyman bands, Morse Franck-Condon factors and R-centroids 77—58088
- HD, predissoc., interference effects, lineshape obs. 80—83432
- $H(D)CN(C^1A')\rightarrow H(D)+CN(B^2\Sigma^+)$, photofragment excitation spectra measurement 79—45777
- $HI+D\rightarrow H+DI$, Franck-Condon theory 78—60984
- H_2O, $(D_2O)(HDO)$, photoelectron spectrum, Franck-Condon, factor calc., geometry and vibrs. *(French)* 77—83652
- H_2O, ESCA and soft X-ray emission, vibr. excitation 80—23433
- H_2O threshold PES, OH^+ fragment obs. 80—78647
- HOCl, photodissoc. rot. distrib. 80—95694
- H_2S^+, $^2B_1$, $^2A_1$ and $^2B_2$ electronic states, pot. energy curves, CI calcs. 80—87048
- He+OCS, emission spectra in He afterglow 80—87139
- He^++CS_2, dissoc. charge-transfer, $CS^+(B^2\Sigma^+$-$A^2\Pi_i)$ emission prod., Morse pot. Franck-Condon factors calc., vibr. anal. 80—99539
- He^++OCS, dissoc. charge-transfer, $CS^+(B^2\Sigma^+$-$A^2\Pi_i)$ emission prod., Morse pot. Franck-Condon factors calc., vibr. anal. 80—99539

- **Franck-Condon factors** continued
  - HgCl, HgBr, HgI, $B^2\Sigma$-$X^2\Sigma$ systems, Franck-Condon factors and r-centroids 79−64051
  - I_2, B-X band system, intensity factors 78−25551
  - I_2, B-X fluoresc. band system, intensity and relative band strengths meas. 80−102540
  - I_2 lines, Franck-Condon factors, Ar^+, Kr^+ and He-Ne laser excitation 80−58320
  - IBr, $B^3\Pi(0^+)$ states, Franck-Condon factors, RKR turning pts. 77−34681
  - ICN, Franck-Condon transition amplitudes for mol. dissoc., semiclassical evaluations 78−62860
  - ICN, photodissoc. dynamics, moment anal. 78−13557
  - ICl, $A^3\pi(1)$-$X^1\Sigma^+$ emission spectrum, near-IR, rotational analysis 80−47991
  - ICl, $B^3\Pi(0^+)$ states, Franck-Condon factors, RKR turning pts. 77−34681
  - IF, $B^3\Pi(0^+)$ states, Franck-Condon factors, RKR turning pts. 77−34681
  - $^{127}I_2$, $^{129}I_2$, $B^3\Pi 0_u{}^+$-$X^1\Sigma_g{}^+$ systems, fluoresc., mol. consts., Franck-Condon factors 77−34680
  - $I(5^2P_{1/2})$+benzene-d_0(-d_6), fluoresc. quenching, spin-orbit interaction, isotope effect obs. 78−62763
  - LaF, Franck-Condon factors and R-centroids, rot.-vibr. effects 78−50596
  - LaO, Franck-Condon factors rot. depend. 80−58319
  - LaO, spectral intensity of $B^2\Sigma$-$X^2\Sigma$ bands, Rydberg-Klein-Rees pot. 79−31611
  - Li_2, A-X band intensity distrib. Franck-Condon calcs. validity 77−65511
  - $^7Li_2$, $B^1\Pi_u$-$X^1\Sigma_g{}^+$ band system, absorpt. and laser fluoresc. spectra 79−68256
  - $^7Li_2$ $A^1\Sigma_u{}^+$-$X^1\Sigma_g{}^+$ band system anal. 77−83565
  - Mg_2, $A^1\Sigma_u{}^+$-$X^1\Sigma_g{}^+$ system Franck-Condon factors, J-depend., fluoresc. pot. and predissoc. 77−58067
  - Mg_2 $A^1\Sigma_u{}^+$-$X^1\Sigma_g{}^+$ system, discrete and continuous Franck Condon factors, J-depend. 78−66811
  - MgD, emission spectra, 600 to 850 nm, rot. anal., dissoc. energies 78−62815
  - MgH, and MgD, $B'^2\Sigma^+$-$X^2\Sigma^+$ band system, ab initio CI calcs. 79−93970
  - MgH, emission spectra, 600 to 850 nm, rot. anal., dissoc. energies 78−62815
  - MgO, Franck-Condon factors rot. depend. 80−58319
  - MgO, red and near UV bands calc., rel. to sunspot spectra 80−12736
  - N_2, -semiempirical three-parameter pot. functions 77−18986
  - N_2, ($N_2{}^+$), Franck-Condon factors, isotope effects calcs. 78−1031
  - N_2, rot. perturbed Morse oscillator, eigenfunctions and Franck-Condon factors 77−42309
  - N_2, rot. quantum number effect 79−31613
  - N_2, vibr. struct., core and valence ESCA spectra, Franck-Condon and HF anal. 80−32602
  - $N_2{}^+$, rot. quantum number effect 79−31613
  - $^{14,15}N_2$, Fourier spectrometry and IR emission spectra 80−83368
  - N_2+He($2^{1,3}S$,$2^{1,3}P$), Penning ionis., $N_2{}^+$, $B^2\Sigma_u{}^+$ state effective cross sections 77−79688
  - $N_2{}^+$+He collisions, vibronic excitation, curve-crossing trajectories 80−23520
  - ND c $^1\Pi$-a $^1\Delta$ system, improved Franck-Condon factors 80−9612
  - NH c $^1\Pi$-a $^1\Delta$ system, improved Franck-Condon factors 80−9612
  - NH_3, ESCA and soft X-ray emission, vibr. excitation 80−23433
  - NH_3, Franck-Condon factors calcs. 78−17723
  - NH_3, vibr. excitation in soft X-ray emission and core ESCA spectra 80−69163
  - NO, ang. distrib. valance photoelectron spectra, vibr. depend., autoionisation and Franck-Condon factors 79−72356
  - NO, ionic ground state, photoelectron spectra vibr. intensity 77−79650
  - NO, UV photoelectron spectrum, autoionisation from Rydberg state, vibr. progressions, Franck-Condon factors 78−50583
  - NO^+, $A^1\Pi$-$X^1\Sigma$ system, Franck-Condon factors, r-centroids calc., program 77−27121
  - NO^+, R_e-function of A-X system, rel. to astrophysical meas. 78−13554
  - NO+Kr^+, charge-transfer reaction rel. to vibr. state of NO^+ 77−1916
  - NO_2, 8920 Å band temp. depend., location of 000-000 band of A^2B_2-X^2A_1 transition 78−70826
  - NO_2, electronic struct., $A^2B_2 \leftarrow X^2A_2$ and $B^2B_1 \leftarrow X^2A_1$ absorpt. bands 77−3257
  - N_2*, metastable, collisional form., C-B emission spectrum 77−19019
  - Na_2, A-X band intensity distrib., fluoresc. spectrum Franck-Condon calcs. validity 77−65511
  - Na_2, Franck-Condon factors direct meas. 78−25618
  - Na_2, rot. perturbed Morse oscillator eigenfunctions and Franck-Condon factors 77−42309
  - Na_2, two-photon transition, velocity tuned, polarisation depend. and Franck-Condon factors 78−90250
  - NaOH:$CrO_4{}^{2-}$($NO_2{}^-$), electron tunnelling, pulse radiolysis 80−108722
  - NaOH:$Fe(Cn)_6{}^{3-}$, electron tunnelling, pulse radiolysis 80−108722
  - O_2, rot. quantum number effect 79−31613
  - O_2, Schumann-Runge band system in sunspots UV spectrum 80−12735
  - O_2, semiempirical three-parameter pot. functions 77−18986
  - $O_2{}^+$, Franck-Condon factors calc. using Rydberg-Klein-Rees pot. 78−70878
  - $O_2{}^+$, $X^2\Pi_g$ photoelectron spectra, vibr. intensity, Franck-Condon factors 77−42352
  - O_2*, vibrationally excited, study by variable temp. photoelectron spectroscopy 78−21972
  - PO, $C^2\Sigma^-$-$X^2\pi_r$ state, Franck-Condon factors and r-centroids 77−65512
  - ^{18}PO, spectral intensity of $E^2\Sigma$-$X^2\Pi$ transition 79−50084
  - Pd(100) surface, of O, obs. of O^- and O^+ during electron bombardment 79−95883
  - PtH(D), pot. energy curves, r-centroids, Franck Condon factors, rot. depend. 80−28082
  - Rb_2, B-X system vibr. consts. from mag. rot. spectra 79−76530
  - S_2 B-X system, Franck-Condon factors 79−94035
  - SIO, Franck-Condon factors rot. depend. 80−58319
  - SO_2, 193 nm photodissoc., photofragment translational energy distrib. 79−74402
  - SO_2, single vibronic level fluoresc. spectra 80−91597
  - SO_3($SO_3{}^+$), Jahn-Teller interaction, Franck-Condon factors and vibronic energy level calc. 78−50536
  - Sb atom, Franck-Condon factors and r-centroids for $^1\pi$−$X^1\Sigma$ of p^{121} Sb and p^{123} Sb 80−42992
  - ScF, Franck-Condon factors and R-centroids, rot.-vibr. effects 78−50596
- **Franck-Condon factors** continued
  - ScO molecule, $B^2\Sigma$-$X^4\Sigma$ system, Franck-Condon factors and r-centroids 80−1025
  - ScO, r-centroids and Franck-Condon factors for $A^2\Pi$-$X^2\Sigma$ and $B^2\Sigma$-$X^2\Sigma$ systems 77−61809
  - SeO, IR bands of 10296 and 10491 Å, rot. struct. 78−5224
  - SiH, A state new predissociations, improved dissoc. energy value from rot. level lifetimes 79−3496
  - SiO, valence-excited bound states, spectroscopic consts., radiative lifetimes 77−6752
  - SiO, vibr. wavefunctions, Franck-Condon factors, at low quantum numbers 78−55203
  - SiS, chemiluminescent flame spectra, electronic states and rot. struct. obs., vibr. assignments, Franck-Condon factors determ. 80−85179
  - SiS, Franck-Condon factors and r-centroids for ($D^1\Pi$-$X^1\Sigma^+$) transition using R-K-R-V 78−5293
  - SnO, D $^1\Pi$-$X^1\Sigma$ transition 79−41179
  - SnO, $D^1\Pi$-$X^1\sigma$ transition Franck-Condon factors and r-centroids, calc. using RKB pot. 79−41197
  - SrF, $B^2\Sigma^+$-$X^2\Sigma^+$ system, rot. anal. using a cw tunable dye laser 78−9165
  - TiO β system, electronic transition moment and effective vibr. temp. 77−68078
  - TiO, Franck-Condon factors rot. depend. 80−58319
  - TiO, γ'-system, Franck-Condon factors, r-centroids and Einstein coefficients calcs. 80−74163
  - TiS, $C^3\Sigma_2$-$X^3\Sigma_2$, Franck-Condon factors and r-centroids 79−36700
  - XeF, 3500 Angstrom band, vibr. anal. 78−70843
  - XeF, X, B, and D-states, spectra, vibr. and rot. consts. 78−70844
  - YF, Franck-Condon factors and R-centroids, rot.-vibr. effects 78−50596
  - YH, YD, 3800-9000 Å negative glow spectra, triplet and singlet systems 77−79608
  - YO, spectra, 4500-6900 Å, mol. consts. 78−50551
  - ZrO, $C^3\Delta$-$X^3\Delta$ system, electronic transition moment depend. on internuclear dist. 77−68079
  - ZrO, Franck-Condon factors rot. depend. 80−58319
  - ZrO, vibr.-rot. interaction influence on band intensity parameters 79−49999
  - ZrS_3, excitonic transition, reson. Raman spectra, Franck-Condon factors 80−97252
- **Frank-Read sources**
  - dislocation ensembles, local heating at low temps., parallel glide planes, temp. distribution *(Russian)* 80−29020
  - dislocation pile-up formation, by Frank-Read source, emission of sound 79−37705
  - electric field depinning of charge density waves 79−73454
  - grain boundary dislocations, Burgers vectors, grain boundary dislocations 78−87680
  - kinetics, quasistatic nucleation and expansion of dislocation loops 80−33999
  - metals, time dependent plastic deformation, thermodynamic model 80−76309
  - personal recollections of F.C. Frank 80−62442
  - plasticity, rate-independent, axiomatic model 80−87717
  - screw dislocation control of plastic deformation in crystals 78−51605
  - steel, stainless, Frank-Read dislocation source obs. in grain boundary 77−84756
  - Al, acoustic emission from moving dislocations during tensile tests 77−19964
  - Cu-Al (10 at.%) alloy, TEM obs. 77−19958
  - Si, zone melting, swirl defects A-type as source of dislocation generation on macroscopic scale 80−25554
  - Si:B, ion implanted, structure defects formation and behaviour under annealing in various ambients 80−65033
  - Si:B(Ga)(Sb), plastic deform. and formation of dislocation loops, effect of Au atoms 79−69184
  - Zn, line energy of basal screw dislocation, exptl. determ. 80−88154
- **Fraunhofer lines** *see solar spectra*
- **free-electron approximation**
  - alkali metals, cohesive energy, teaching 80−90630
  - amorphous metals, electron-phonon coupling const. and Eliashberg function 80−39567
  - amorphous metals, electron-phonon interaction effect on thermopower 80−29393
  - Bloch generalised density matrix approx. solns., free and lattice electrons 77−31923
  - brass, α and β phases, Hume-Rothery rules for phase stability 79−99292
  - cyanine dyes, substituted symmetric, optical nonlinearities, free-electron like model 79−41407
  - degenerate free electron metal, cyclotron wave propag., finite $\omega\tau$ effect 77−20228
  - diamond-like structure, interatomic matrix elements between s- and p-like states, LCAO calc. 80−10857
  - diamond-structure semiconductor, Compton profile interpretation 80−29820
  - dislocation elec. resistivity 78−6371
  - education, deep one-dimens. periodic pot., zero energy gaps, Kronig-Penney model 80−62426
  - electron state density calcs. by linearly analytical tetrahedron method *(Russian)* 79−82507
  - ground-state energy of free-electron gas, transcorrelated method 80−34373
  - HF wave dispersion for complex wave numbers, ordinary waves 80−70740
  - iterative method, for band theory wave function detn. 78−22996
  - itinerant magnets and superconductors, structural instabilities, phase diagrams 78−14922
  - liuqid simple metal, mag. susceptibility rel. to theories of electronic structure 77−1536
  - metal, electron density behaviour near impurity charge 80−75518
  - metal, hypothetical, electron momentum distrib., reconstruction from point-geometry positron-annihilation data 79−56883
  - metal, proton energy losses, Bohr equipartition rule 77−15467
  - metal, struct. induced surface plasmon polariton modes using ATR, theory 79−60890
  - metal, surface region, absorption of EM radiation 78−43456
  - metal fibre, micron sized, light scatt. 77−65571
  - metal surface, influence of submonolayer films on props., free electron model calc. *(Russian)* 80−2273
  - metallic thin film, conductivity, Kubo formalism 79−7909

free-electron approximation continued
metallic thin films, optical props., theory including electron surface scatt. 80—29817
metals, electron theory, internal press. 80—92802
metals, free electron approx. and symm. Hermitian pseudopot. *(Russian)* 79—28263
metals, free-electron, model-independent constraints on many-electron XPS asymmetries 77—52219
metals, interface energy and charge oscills. 77—62984
metals, monovalent, magnetic susceptibility, impurities effect, free electron gas model 79—91206
noble metal, thermal resistivity temp. depend., free electron approx., phonon spectrum 77—66152
one-dimensional conductivity, with arbitrary bandfilling, Peierls instability 80—59968
one-dimensional systems, exchange effects in plasmon dispersion 79—60741
paramagnet, free electron, muonic and hydrogenic Knight shifts 78—43759
phase comparisons for Sondheimer size effect oscills. 78—34823
photoemission, angle-resolved, from bulk bands of solids 79—4895
review of metal theory *(Japanese)* 77—47710
SCF calcs., electron exchange and correlation phenomena, effect of local electron speed 79—95356
solid-liquid transition, optical reflectance spectra 80—24569
d-transition metal hydride, mag. suscept. and quasirigid model *(Russian)* 78—26805
transition metals and their alloys, amorphous, elec. resist. 78—60103
XPS lineshape asymmetries, free-electron-like metals 78—14681
Ag (111), angle-resolved photoemission, free-electron final state model 79—4896
Au, films, optical props. meas. rel. to electron surface scatt. theory 80—29818
Au, thermal radiative props. at cryogenic temps., comparison with model predictions 77—15604
BiIn$_2$, dHvA effect, Fermi surface determ., free-electron model 77—15744
Cs, elec. and thermal resist. calc. using modified noncentral force model 79—91016
Cu-Sn, amorphous, electron-phonon interaction effect on thermopower 80—29393
Fe, interband optical conductivity, self energy correction 80—2792
Fe$_3$O$_4$, magnetite, charge carriers, optical props. 80—34874
Ga-M, liq. alloys, mag. susceptibility *(Russian)* 77—24671
K, ideal thermal resist. calc., anisotropic continuum dispersive model 77—51724
K, intermediate-wavelength cyclotron waves and Fermi-liq. effects 79—77986
Li, elec. and thermal resist. calc. using modified noncentral force model 79—91016
Li, ideal thermal resist. calc., anisotropic continuum dispersive model 77—51724
Mn ferrites, Fe-excess, charge carriers, optical props. 80—34874
Na, X-ray edge shape, band struct. role 77—16425
Ni, interband optical conductivity, self energy correction 80—2792
Rb, ideal thermal resist. calc., anisotropic continuum dispersive model 77—51724
Sc, dielectric screening and lattice dynamics 77—35646
n-Si:Ar(P), single cryst., positron annihilation parameters, energy-band struct. on surface in free-electron approx. 79—15555
SmS, metallic, rel. to thermal modulation of reflectivity, 1.2-3.8 eV 79—99909
Sn, liq., optical props., 0.62-3.7 eV 80—75996
SnO$_2$ doped films for spectral-selective surfaces, refl. and elec. props. meas. 79—74013
Y, dielectric screening and lattice dynamics 77—35646

free electron lasers
amplifier, multimegajoule free-electron, nonlinear forces utilisation 80—9847
amplifier storage ring appl. 80—871
basic characteristics and possible developments of free electron laser-electron storage ring system 79—68019
basic mechanisms, stimulated Raman and Compton backscattering 79—7106
beat radiation of electron waves 80—43314
beats of coherent electron beams 79—55106
boundary deformation and Robinson-Liouville theorem 80—48202
bremsstrahlung, resonator consideration *(Japanese)* 80—5721
characterisation and optimisation of gain and efficiency 79—68400
characteristics and limitations of mag. bremsstrahlung, Compton and Cherenkov lasers *(Chinese)* 79—31851
Cherenkov and Smith-Purcell effect based, and TW amplifiers, operation regimes 79—919
Cherenkov-Smith-Purcell, collective and single electron interactions, book contrib. 79—27234
classical multimode theory of the free electron laser 79—27228
classical theory, in moving frame 79—76655
classical theory, saturation, perturbation calcs. 80—83580
coherent dynamics, conservation law, small signal theory and gain-spread relation 80—83582
coherent dynamics with arbitrary magnet geometry 80—83581
coherent quasi-classical states 80—53251
coherent radiation novel sources, book 79—27231
coherent states in single mode and multimode cases 80—102689
coherent transients, laser lethargy and coherence brightening 79—94204
coherent X-ray generation from CO$_2$ laser backscattered relativistic electron beam 80—53252
collective and single-electron interactions of electron beams with EM waves and free-electron lasers 78—55330
common properties 79—98331
Compton laser, scatt. stimulation by decelerated EM waves, semiclassical theory 78—29926
construction, operation, future developments *(French)* 80—32951
efficiency improvement by rippled mag. field strength increase 79—72548
electron energy sensitivity of free electron laser, reduction 79—94246
energy transfer, computer simulation 80—83578
equations of motion, approx. technique for integration 79—64193
feasibility of design without external inducing source *(Russian)* 78—50746

free electron lasers continued
free charged particle interacting with intense laser pulse, energy momentum gain 80—101963
free electron laser, enhanced gain 78—63050
frequency determination, energy-momentum conservation calc. method 78—37866
gain, exact classical electron dynamic approach 79—41362
gain, small-signal, space charge effect 79—920
gain mechanism for short wavelength 78—46557
gain-spread generalised expressions 80—53249
intense-beam free electron laser, beam quality expts. 80—58619
IR and millimetric waves and applications, conf., Miami Beach, USA (Dec. 1979) 80—57009
kinetic theory, appl. of radiative processes in relativistic plasmas 78—42316
laser description, population inversion existence 79—59665
laser fusion appl. 79—31919
laser fusion applications 78—58974
lasers and accelerators 79—72015
LEDA-F storage ring dedicated to free electron laser operation, preliminary design 79—68030
longitudinal relativistic, amplification in spatially periodic optical waveguide 78—37865
low gain, analytic soln. of quasi-Bloch eqns. 80—87363
low-energy electron beam excited high-power CW efficient tunable UV-visible-IR laser system 79—64194
magnetic free-electron laser, output power 80—32947
microwave to X-ray up-conversion under kinematical conditions 77—62006
momentum distribution function, classical single particle theory 78—58973
multiphoton analysis 80—78826
multiphoton stimulated Compton scattering of relativistic electrons 80—48198
nonlinear force of laser-electron interaction, system working without cyclotron radiation *(German)* 80—9845
nonlinear formation and efficiency enhancement 80—32948
nonlinear free electron laser dynamics with space charge and wiggler effects 80—58500
nonlinear phase equation, numerical solns. 78—87035
nonlinear saturation, thermal effects using EM pump 80—87364
nonlinear theory, efficiency enhancement 80—43317
nonlinear theory, gain, saturation, recoil and velocity spread, book contrib. 79—27148
nonlinear wave equation for free electron lasers driven by single-particle currents 80—69355
O-type relativistic electron devices, linear theory 80—43242
one-body analysis, book contrib. 79—27233
one-body dynamics, electron beam form. 78—17893
operation 77—46734
optical frequency electron wave beat-driven free electron laser 80—43315
orotron, Smith-Purcell effect 80—5720
oscillation characts. of free electron laser based on stimulated Raman scatt. by relativistic electron beam 80—99688
output increase using dielectric effects 79—27229
physical processes and construction problems 80—102691
plasma laser, new free electron laser 79—98329
pulse amplification through energy exchange with electron beam via nonlinear radiation press. effects 80—95776
pulse propagation equations 80—53250
pulse radiator, miniature, based on semicond. quantum generators with electronic excitation 79—3707
pulsed laser dynamics, coherent picosecond pulse propag. calcs. 80—95860
quantum and multimode theory, Bloch-like model 80—48203
quantum description 79—98330
quantum mechanical and classical theories 80—83579
quantum theory 80—23656
quantum theory for strong fields 80—83583
quasicircular undulator system 79—55102
radiated energy, mean and mean squared, rel. to spontaneous power spectrum 79—50277
reaction kinetics measurement and control using laser technology, free electron laser appl. 80—81349
recirculating, electron heating elimination using isochronous storage ring 80—48204
relativistic, rippled static mag. field, simulation, waves and instability 77—54686
relativistic Compton laser, power potentiality *(Russian)* 78—90405
relativistic electron beam, in periodic transverse mag. field, stimulated emission 78—42318
relativistic electron beam amplification in spatially periodic mag. field 80—19014
relativistic electron beam Raman laser 78—74877
research status 78—82940
review 78—90406
review 80—9794
saturation, classical theory 80—23655
saturation behaviour from barrier reflection 80—9846
saturation effects, classical theory 80—95864
simulations using relativistic EM plasma simulation codes 79—68376
single particle classical model, stimulated Thomson scatt. 78—42317
small signal gain of free electron lasers with nonuniform wigglers 80—58499
small signal theory for gain in strong axial mag. field 80—78825
Smith-Purcell effect laser, theory 79—50276
static guide magnetic field laser, computer simulation and theoretical study 79—68377
stimulated backscattering from relativistic unmagnetized electron beams, book contrib. 79—27334
stimulated Cherenkov radiation, relativistic electron beams in dielec. resonators, book contrib. 79—27150
stimulated emission and absorption in classical systems 78—63047
stimulated processes in strong fields, quantum theory *(Russian)* 79—86155
stimulated Raman backscattering regime, megawatt sub m.m. range 79—7107
stimulated undulator radiation from relativistic electrons, physical processes 79—45921
storage ring laser, Boltzmann simulation 79—72547
storage rings, free electron laser amplifier operation 79—68399

free electron lasers continued
storage-ring laser, synchrotron motion 79—55103
strong wave amplification by electron scatt. in spatially periodic mag. field 79—76654
theory, 1979 strate of art and development *(Japanese)* 80—37658
theory, relativistic steady-state formulation 80—43316
theory 78—37867
theory 80—48205
travelling microwave radiation stimulated, theory 79—18392
travelling wave amplifier analysis, book contrib. 79—27232
two-element, efficiency improvement 80—43313
inuniform magnetic field 79—94203
velocity narrowing using electron echo techniques 79—55105

free energy
A15 compounds, elec. struct., 3-D k.p model 78—2405
A^4-phonon theory, free energy and phase transition 78—41257
acetonitrile-water mixture, electrolyte transfer, thermodynamic props. 80—3395
adamantane crystals, variation of free energy with tetragonal distortion at room temp. 79—73119
adsorbed layers, clustering, bulk vapour pressure behaviour 79—4473
adsorption, direct eval. of free energy change from single isotherm 77—35807
adsorption thermodynamics, symmetrical, case of noninert adsorbent 80—80059
ageing media, thermodynamic pots. in creep theory *(Russian)* 78—63318
alcohol-aliphatic hydrocarbon mixture, critical soln. temp. 79—37844
alcohol-inert soln., assoc. soln. thermodynamics, enthalpy, Gibbs free energy 78—31670
alcohol-solvent, associated, excess free energy and enthalpy of mixing 78—31680
Alfven wave system, eqn. of state, thermodynamic props., Bose-Einstein statistics 78—87397
aliphatic acids, thermodynamics of adsorption at air/aqueous soln. interface 80—10752
aliphatic alcohol, thermodynamics of adsorption at air/aqueous soln. interface 80—10752
alkali halide, electric-dipole ordering of tunnelling impurity centres 80—2215
alkali halide, migration enthalpy and entropy for cation vacancy motion 77—35750
alkali halides, free energy of formation of vacancy determ. 77—76597
alkali halides, premelting elec. cond., heat capacity 78—91445
alkali metal halides, solid phase free energies, Debye-Huckel theory 80—15263
alkali metals, anharmonic effects in thermodynamics *(Russian)* 78—43145
alkali metals, condensed phase, free energy, Debye-Huckel theory calcs. 80—79958
alkali metals and alloys, liq., internal energy, chem. pot., critical consts. 78—34422
n-alkane binary mixtures, melting and solid-state transition 77—72685
alloy, binary, atomic misfit effect on coexistence and spinodal transform. boundary 78—60644
alloy, binary, with arbitrary mole fraction, order disorder transition in case of FCC lattice 80—88295
alloy, free energy calc. for any conc. of implanted atoms, diffusion current in chem. pot. gradient *(Russian)* 78—34657
alloy, multicomponent, thermodynamic partial molar quantities, calc. from known quantity of one component 77—72703
alloy, role of phase boundaries in phase transformations 78—72772
alloy, thermodynamic and structural changes in deform. twinning 78—2139
alloy surface, free energy of segregation 80—29256
alloys, determ. by X-ray and neutron scatt. expts. 78—83974
amorphous insulator, phase diagram and statistical mechanics 78—52268
amorphous magnet, random anisotropy axis model in the infinite-range limit 80—88761
amorphous magnetic metals and alloys, high temp. 77—16078
amorphous systems, mag. pros. effect of random anisotropy 79—4686
anharmonic crystal, statistical theory, quasi-classical expansion *(Russian)* 78—38803
anharmonic crystal, thermal expansion contribution to free energy and heat capacity to order λ^4 78—6138
anharmonic crystals, unsymmetrised SCF approx. 78—63830
anilines, substituted, in benzene, dielectric relax. and mutual viscosity, obs., molar free energy 79—38449
anilines, substituted, in nonpolar solvent, dielec. relax. obs. 80—55022
anisotropic antiferromagnet, phase transition, with external mag. field 79—11316
anthracene, chemical thermodynamic props. 80—21312
anthracene-acridine, order parameters and lattice energy, mean field approx. 78—22688
antiferroelectric transition, phenomenological theory Kittel's free energy for sublattice polarisation 79—4771
antiferromagnet, linear-chain, sine-Gordon solitons 80—80543
antiferromagnet, second-order phase transition, weakening of effect of fluctuation in order parameter near crit. point 79—15316
antiferromagnetic chain, random, quantum spin-1/2 Heisenberg soln. 80—11148
antiferromagnetic Ising model on triangular lattice, phase diagram, free energy 78—23283
antiphase boundary motion, microscopic diffusional theory, appl. to domain boundary coarsening 79—61563
aqueous multicomponent multiphase equilibria, free energy minimisation method, comput. algorithm 80—40724
atomic cluster, crystalline, microscopic capillarity approx. 80—5654
atomic clusters, Becker-Doring and Lothe-Pound theory 78—22063
benzene-cyclohexane system, vap. press., excess free energies, isotope effects 78—59939
benzene-p-xylene, excess vol., enthalpies, Gibbs free energies 80—44335
2,3-benzo-1,6-methano(10)-annulene, mol. geom. and gas phase thermodynamic props., minimisation scheme 78—78829
benzylidene aniline series, nematic liq. crysts., depolarised scatt. strength, free-energy, coherence length anisotropy 77—62470
binary alloy, ordered BCC to disordered FCC transition 77—43327
binary alloy, quenched, time evolution of struct. function free energy 78—55937
binary alloy with BCC type lattice, order-disorder transition 79—78957

free energy continued
binary liq. mixture, chain assoc., excess Gibbs free energy 77—16860
binary liquid mixture, surface tension, free energy density expansion 78—91509
binary molten salt mixture, excess free energy of mixing, conformal ionic soln. theory 77—1230
biological intracellular energy transform., phys. aspects 77—86462
black lipid membranes and bilayer vesicles in solution, thermodynamic stable states anal. 80—45856
bond free energies, table for chem. student use 80—22171
boson gas, interacting, approx. equilib. states 80—46962
boundary free energy for phase interface, scalar-prod. expression, Ising model and cluster approx. 78—34591
bounds, upper and lower, renormalisation group methods 80—68162
brass, α and β phases, Hume-Rothery rules for phase stability 79—99292
β-brass, cryst. struct., elastic consts., central force model 78—51637
brass, liquid, thermodynamic props. *(German)* 80—66482
brittle fracture energy condition for uniform extension *(Russian)* 80—33534
α,βbromonaphthalenes, thermodynamic functions calcs. 298-1500K 77—31418
t-butyl alcohol, self-assoc., linear and nonlinear dielec. effects obs. 80—60484
n-butylamine-n-propanol, isothermal vapour-liquid equilib. 80—59639
canonical ensembles, Monte Carlo estimation of free energy differences 77—2632
capillary condensation and adsorption, adsorptive pot. boundary layer approx. 78—2366
capillary condensation and adsorption, Gibbs free energy, unitary approach 77—76643
carbonyl frequency correlation of aromatic derivatives with nonaromatic analogues 79—22709
dl-carvoxim, order parameters and lattice energy, mean field approx. 78—22688
CDW ordered state in coupled chains of BGD model, props. 80—6756
CDW phase transition, 1-D electron-phonon system, thermodynamic props. 78—14682
charge-density waves, lock-in transition, effect of thermal fluctuations on harmonics 79—19338
charged hard sphere system, restricted primitive model 79—27890
charged particles in continuous dielectric medium, free energy, hard core pot. effects 79—37600
chemical equilibrium, displacement by elec. field *(French)* 77—25299
chemical equilibrium teaching, computer method using minimisation of free energy 79—30168
chemical potential, algebraic theory for usual gauge group 80—31661
chemical reaction kinetics, mixing entropy for activation barrier 78—19993
chemiluminescence reactions, electron exchange initiated, kinetics correl. with free energy changes 80—50856
chloroform+acetone, isotropic light scattering, excess Gibbs function 79—8150
chloroform-methanol mixtures, thermodynamic props. 79—87865
chloroform-tetrahydrofuran system, excess free energies and vols. 79—82357
β-chloronaphthalene, thermodynamic functions calcs. 298-1500K 77—31418
o-chlorotoluene(-benzene), liq. and dilute soln., microwave absorption and relax. processes 79—82920
cholesteric liquid crystal, large-scale continuous theory *(Russian)* 79—46568
cholesterylpelargonate, cholesteric-smectic A transition, metal-supercond. analogue 79—23712
classical spins, linear chain, with random Dzyaloshinski-Moriya interactions, exactly soluble model 79—61118
colloidal plates, parallel, polymer adsorption, excluded volume effects, polymer-solvent interactions 80—45568
colloids, rel. to thermodynamic stabilisation 80—81369
commensurability in one dimension at nonzero T 79—35655
commensurate phases, spatially modulated, in simple Ising model 80—79909
condensation of pure vapour, use of chem. pots. 79—86880
condensed media, low-temp. particle transport theory, impurity electron transfer 80—19974
configurational free energy of chains Monte Carlo approach 78—16742
continuous quantum systems, variational principle for pressure, entropy, free energy, convexity consequences 79—40453
continuous spin model, exactly soluble, for mag. and distortive systems 77—85470
continuous spin systems, thermodynamic limit of free energy and correl. functions 77—9962
convex-envelope formulation for separable interactions 79—71355
Coulomb gas, classical, two-dimens., screening props. from sine-Gordon eqn. 79—4524
creep and long-term strength 77—11139
cresols, ideal gas thermodynamic props. 78—75250
critical isotherm free energy, analyticity violation, thermodynamical scaling hypothesis 77—74341
critical opalescence, nonuniform fluid struct. factor calc., thermodynamical treatment 77—40198
critical phenomena, renormalisation group theory, numerical method for calc. of free energy and correl. length of generalised Ising model 80—4664
critical point of infinite type, exact sol. in one dimens. 79—9199
crystal, energy of step on rough face 77—43421
crystal, statistical thermodynamics with collective vibrations 78—54289
crystal growth from soln., thermodynamic formalism for adsorbed layers 77—76336
crystal hydrates, thermodynamic functions, Karapetyants-Rozenfeld equation *(Russian)* 79—66332
crystal with many particle interactions, variational quasiharmonic approx. *(Russian)* 77—11642
crystal-liquid phase boundary, pair distrib. functions and free energy functionals 80—24734
crystallisation of phase A from A+B melt, Helmholtz free energy 80—79911
cubic crystal, self-diffusion and melting 77—31803
cubic crystals, temp. series in statistical theory, Vlasov eqn. 80—17895
cubic lattices, fully frustrated, phase transitions, Gaussian and spherical model, free energy calcs. 80—60281

free energy continued
  cubic margules solution model, miscibility gap and crit. point behaviour 78−59925
  cubic Margules solution model, miscibility gap and critical point 79−65199
  cyclic ethers-HF H-bonded complexes, calorimetry, IR spectra and MO calcs. 79−52738
  cytochrome c_3 film, anhydrous, elec. cond. 79−66439
  de Haas-van Alphen effect, quasiparticle approach 80−10897
  defect energy of formation, Gibbs free energy 78−91332
  deformation kinetics, Gibbs eqn. and nonequilibrium thermodynamic models *(Ukrainian)* 78−90720
  degenerate semiconductors, heterogeneous state, first-order phase transition, Ginzberg-Landau method analogue 80−70372
  diamond-structure crystals, lattice anharmonicity 77−89549
  dicalcium lead propionate, improper ferroelectric, dielectric props., IR radiation pyroelectric detection 80−80711
  o-dichlorobenzene(-benzene), liq. and dilute soln., microwave absorption and relax. processes 79−82920
  Dicke-like model structural stability of 2nd order phase transitions 77−26259
  dielectric medium, continuous, free energy due to Coulomb and hard-core pots., activity coeffs. 80−45537
  diffusion with wave fronts, definition *(French)* 77−67386
  dilute metal solutions in molten salts, optical absorption, F-centre model for bound state 80−89023
  dilute systems of dipoles and dipolar charged particles, Mayer resummation method 78−83710
  dimerised Ising chain, free energy, mag. moment, static susceptibility 77−55651
  dipole relaxation in electric field, teaching 80−90625
  dislocation-creep, minimisation of free energy due to viscoelastic strain and dislocations 77−24348
  disordered spin systems, nonrandom free energy in macroscopic limit 79−40477
  disordered systems, simple inequality 77−47593
  dispersed two-phase single-component system, modification of charact. functions by interphase boundary and surface tension 77−90647
  distribution functions, high order, truncation procedure, compatibility problem 80−47004
  double Ising chain, model in external field *(Russian)* 79−82735
  double Ising chain, model in zero external field *(Russian)* 78−84430
  Earth mantle elements compounds and modifications, high press. and temp. thermodynamics 80−81874
  elastic body, non-negativity of specific heat, rel. to dynamic stability 77−42723
  elastic media, dissipative, relativistic electrodynamics 80−73219
  elasto-plastic metal-dislocation system, stress-activated dislocation motion, thermodynamic theory *(Chinese)* 78−83868
  electrets, free energy and Gibbs energy determ. 77−28513
  electrochemical electron transfer at electrodes in soln., review, in book, for teaching 78−8203
  electrode systems, nonequilib. polaris. states props. overvoltage theory, in book, for teachers 78−8205
  electrode-electrolyte systems, absolute half-cell EMFs and single ion free energy of solvation 77−73449
  electrolytes, Blum's theory, derived conclusions involving Helmholtz free energy, correlation functions 77−48651
  electrolytes, due to Coulombian and hard core pots. 79−23748
  electrolytes, in soln., free energy due to Coulomb and hard-core pots., activity coeffs. 80−45537
  electrolytes, strong, specific adsorption, electrical double layer, interface excess activity coeff. 80−49523
  electron gas, two dimensional, classical, hypernetted chain solns. 78−67963
  electron gas in metal, free energy virial expansions *(Russian)* 78−10380
  electron transfer reactions, free energy, anharmonic intramol. quantum mode depend. 77−12781
  electronic system with two-fold degenerate band, free energy change due to electron-phonon coupling 79−42500
  entropy production in stochastic model of open system 78−4574
  enzyme catalysis, electron pairing as source of cyclic instabilities 78−95953
  enzyme dynamics, statistical phys. 80−21439
  equilibrium and nonequilib. thermodynamics organised and unorganised systems, philosophy 79−40344
  ethylene oxide-d_0, -d_4, centrifugal distortion const., thermodynamic functions 79−41149
  ethylene sulphide, centrifugal distortion const., thermodynamic functions 79−41149
  Euclidean $\phi_3{}^4$ theory, phase space cell expansion, Borel summability 78−8501
  exactly solvable statistical mechanical models with nonpolynomial interactions, free energy density calcs. 79−63124
  excess Gibbs free energy, general calc. method from isothermal vapour-liq. equilibria 77−89552
  extended defects of arbitrary shape and size near solid surfaces, dilatation energy 78−34508
  FCC lattice, phase transitions of fully frustrated models 80−29517
  FCC metals and alloys, grain boundary energy and self-diffusion, effect of solute segregation 78−15412
  α-Fe alloy, ferromagnetic, thermodynamic analysis of solubility and miscibility gap 79−60508
  fermion 1-D systems, free energy independence 79−40448
  ferroelastic crystal, nonideal, domains struct. 78−2191
  ferroelastic transitions, order parameter symm., free energy expansions 80−49164
  ferroelectric, acoustic activity near ferroelectric transition 77−90114
  ferroelectric, eight-site order-disorder model, influence of tunnelling 80−2709
  ferroelectric, incommensurate-commensurate transitions 78−60404
  ferroelectric, uniaxial, crit. behaviour, electrostrictive coupling role 80−71329
  ferroelectric crystal classification by transition mechanisms *(Russian)* 78−60401
  ferroelectric semiconductor, phase transition temp., rel. to free carrier conc. 78−10860
  ferroelectric semiconductor, spin susceptibility near ferroelec. transition 80−2710
  ferroelectric semiconductor, vibronic model, fluctuation effects 77−90113

free energy continued
  ferroelectric substances, electron microscopy investigations, review *(Japanese)* 80−71366
  ferroelectric transition, displacive, effect of strong cubic anisotropy of lattice anharmonicity, mol. field theory 77−52026
  ferroelectrics, vibronic model, fluctuations of order parameter and anharmonic interaction 77−52022
  ferroics, nonmagnetic secondary and higher-order, order-parameter symmetries for the phase transitions 77−85668
  ferromagnet, uniaxial one-dimens., role of Bloch walls in statistical mechanics 77−40079
  ferromagnet, with mag. axial symmetry, magnetisation 77−85487
  ferromagnet containing void, Gibbs free energy, numerical calc. 80−29597
  ferromagnetic binary alloys, strictly regular, quasi chemical model 78−39316
  ferromagnetic classical vector model, extension of high temp. free energy series 80−7062
  ferromagnetic film, ϕ^4 domain walls, magnetisation, occurrence of crit. point 78−95500
  ferromagnetic Ising model, spin-one three dimensional, single-ion anisotropy, crit. behaviour 80−80540
  ferromagnetic nondegenerate semiconductor, magnetoresistance 80−11019
  ferromagnetic polycrystals, cubic, domain structure under torsion *(Spanish)* 79−91246
  ferromagnetic single crystal with cubic symmetry, mag. and magnetoelastic props. 79−15332
  ferromagnetic superconductors, self-induced vortices, magnetisation, Gibbs free energy 80−70916
  ferromagnetic systems, inhomogeneous, Ginzburg-Landau theory, free energy and Curie temp. 79−51789
  finite disordered Hubbard cluster, thermodynamic and mag. props. 77−85409
  first order phase transitions, droplet models, renormalisation, singularities 80−95050
  first-order phase transitions, influence of quenched impurities 79−73289
  first-order transition induced by cubic anisotropy 79−4688
  fluid, classical, density functional theory, direct correlation function-free energy relation 77−76285
  fluid, dense, with square-well+hard core pot., equilib. props., quantum corrections 79−27891
  fluid, hard dumbbell mols., reference pot., perturbation theories, spherical reference systems 80−28898
  fluid, hard-spheres, eqn. of state, quantum corrections 78−34592
  fluid, inhomogeneous, free-energy theory 80−10751
  fluid, multiphase system, vapour bubble collapse, charact. functions 78−18156
  fluid, randomly-stirred, vel. correlations, variational principle for path-integral functionals 78−81846
  fluid, simple, thermodynamic props. in hard-sphere reference system 77−76575
  fluid interfacial stress and struct., gradient theories 79−19428
  fluid membrane multilayer system, free energy of interaction 78−44463
  fluid polar, complex modified free-energy averaged pot. 80−48833
  fluid with triangular-well potential, eqn. of state, quantum corrections 79−69222
  fluid-solid type phase transition, one dimens. model 78−63838
  fluids, polarisable and magnetisable, thermodynamic theory in electromag. EM fields 77−57291
  fluorobenzene(-benzene), liq. and dilute soln., microwave absorption and relax. processes 79−82920
  Fokker-Planck eqn. governed systems, role of free energy *(French)* 77−26254
  freezing, molecular theory, eqn. of state, free energy, from 1st BBGKY eqn. 78−67804
  gas, thermodynamic props. review 80−31694
  gaseous diffusion in stressed thermoelastic solid, thermodynamic struct. 78−51065
  gases, self-trapped electron effective mass, appl. to He 79−60090
  generalised Gibbs function for equilib. and non-equilib. processes *(Russian)* 77−41555
  Gibbs, misconceptions in school thermodynamics 77−60865
  Gibbs eqn., generalised, second-order fluids 80−24331
  Gibbs equilibrium thermodynamic pot. second derivatives, discontinuity surfaces rel. to phase boundaries of q-component systems 79−82304
  Gibbs phase rule, history and development *(German)* 77−78943
  glassy state, thermodynamics, multiple order parameter 78−14283
  granulated superconductors, phase transitions, Josephson energy *(Russian)* 80−84540
  graphite+O_2 reaction, standard Gibbs free energy change, electrochemical determ. 77−29041
  graphite-diamond equilibrium, thermodynamic stability 79−65184
  Griffiths singularity, and upper bounds on cluster distrib. functions 79−7958
  group IIIa dihydrides, structs. and stabilities 80−107146
  haemoglobin, mol. system, with N associating particles, free energy virial expansion 77−55336
  1-haloalkanes, microwave spectra, conformation 78−21913
  hard core fluid with Yukawa tail, eqn. of state 80−24330
  hard quadrupolar diatomics, free energy, perturbation theory and Monte Carlo calc. 79−90361
  hard sphere fluid, thermodynamic props., quantum corrections 79−4219
  hard-core square lattice gas, 3-parameter isotropic atom distrib. 78−24740
  hard-sphere dense fluid, equilib. props., semiclassical limit 77−76281
  harmonic crystals, Helmholtz free energy, vacancy defects interactions calc. by cell cluster method 80−107443
  harmonic crystals, thermodynamic props., effects of vacancy defects determ. by cell cluster method 80−79959
  harmonic solids, free energy, vacancy defect effects calcs. 77−1198
  Heisenberg antiferromagnet, uniaxial, props. by Green's function method 77−85406
  Heisenberg ferromagnet, classical one-dimensional, transfer integral and collective coordinate results for free energy 80−93067
  Heisenberg ferromagnet, classical spin field model in mag. field, statistical mechanics in one dimens. 78−43544
  Heisenberg ferromagnet in critical region, Bloch renormalised spin wave approx. 79−82784
  Heisenberg linear chain magnets with unlike spins, exactly soluble model 77−16030

free energy continued
Heisenberg metamagnet, collinear, mag. phase diagram 80—71035
Heisenberg model, classical spin, with three or four spin interactions, linear chain 80—70923
Heisenberg model, long-range interaction, free energy 78—56282
Heisenberg model, operator formulation of renormalisation transformation 77—59376
Heisenberg model, phase transition, free energy and susceptibility 78—43595
Heisenberg model, random, thermodynamics, cluster approx. 77—16032
Heisenberg n-component classical model, low temp. renormalisation group and symm. breaking perturbation, closed form expression for correlation function and free energy 79—15315
Helmholtz free energy, approx. expressions 77—16024
Helmholtz free energy in Falicov-Kimball model, upper and lower bounds, conditions for phase transitions 79—86906
heteroazeotropic system, thermodynamics in Gibbs pot. metrics *(Russian)* 79—96355
heterogeneous nucleation, appl. of thermodynamic pots. 77—7948
heterogeneous nucleation systems, crit. conditions characterising formation 78—56023
heteropolymer in random mag. field, Ising chains, statistical mechanics, free energy, numerical calcs. 78—77803
highly degenerate multicomponent plasma thermodynamic props. 80—33739
highly dispersed systems, phase size effect 80—6488
Hubbard Hamiltonian, coupled spin and charge fields 77—32147
Hubbard model, extended, phase transitions 78—6531
Hubbard model, ferromag. phase transition 77—77062
Husimi-Temperley model under a random field 79—97313
ideal type II superconductor, thermodynamics of inhomogeneous mixed phase 78—84365
incommensurate phase transitions under existence of Lifshitz invariant 78—22822
Inconel 617, mass spectrometric study, high temp. reactor system appl. 79—43663
induced moment systems, effect of spin fluctuations 80—2585
inhomogeneous charged fluids, density functional theory, rel. to molten salts surfaces 80—79660
interaction site cluster series for Helmholtz free energy 77—36780
intercalation compound electrodes, thermodynamic and transport props. 80—66963
interface, noncritical, near a crit. end pt., struct. and tension 77—84885
interface free energy and transition temp. 77—73041
interface tension, density-gradient term in free energy near crit. temp. 77—89617
interfacial tension var. with supersaturation, one-layer adsorpt. model 80—103563
intermediate state, superconducting-spot and normal-spot models 79—11275
interstitial solutions, impurity subsystem free energy, impurity distrib., temp. depend. 80—44232
interstitial-FCC soln., thermodynamics based on kinetic considerations 77—62651
ion+polar molecule collision freq., thermodynamic model 80—43145
ion $(H_2O)_n+H_2O \rightleftarrows$ ion$(H_2O)_{n+1}$, standard free energies of reaction 79—34348
ion solvation, in polar media, continuous charge distrib. model, quantum mech. calcs. 78—68913
ionic clusters, struct., thermodynamic functions, energy surfaces and SIMS 80—63881
ionic crystal, sublattice disorder, phenomenological models 77—35663
ionic crystals, vibrational surface modes, vibrational contributions to surface thermodynamic functions 77—47659
ionic crysts., thermodynamic ion-vacancy complexes *(Spanish)* 80—75222
ionic molecules, vapours, thermodynamic properties, classical partition function, dimens. anal. 80—43829
ionic solvation, electrostatic free energy, multilayered continuum model 79—57282
ionic solvation energy, statistical calc., gas approx. 80—40731
irradiation induced crystalline to amorphous transition, Gibbs energy 80—70371
Ising antiferromagnet, triangular, improved mol. field approach 79—73745
Ising chain, disordered, equivalent formulations for thermodynamics 77—28346
Ising chain, disordered, linear renormalisation transformations, appl. to dil. soln. model 78—34941
Ising chain, random bond, low temp. behaviour 80—57211
Ising chain, two-component random, in zero field, free energy and derivatives 77—59371
Ising chain of alternating spins of 1/2, and general S, appl. of transfer matrix method 80—80529
Ising chains, random bond, thermodynamics and correl. functions 79—15270
Ising disordered spin system on Cayley tree 79—51783
Ising double chain, compressible, mag. susceptibility and thermodynamic props. 79—15320
Ising ferromagnet, 2-D, with quenched bond disorder, critical temp. 78—56328
Ising ferromagnet, gaussian fluctuations of mol. field, magnetisation and free energy 80—70918
Ising ferromagnet of spin 1/2, Lee-Yang theorem 78—45572
Ising ferromagnetic half-plane, surface, pinned domain wall, free energy and magnetisation profile 80—60361
Ising fourth-neighbour models on FCC lattice, coexistence curves 79—80543
Ising free energy, direct high-temp. star graph expansion 80—46985
Ising magnet coupled to isotropic elastic medium, first order transition, renormalisation method 80—68151
Ising model, 2-D, metastability 79—58648
Ising model, 3D, long range pot., phase transform. 77—66379
Ising model, BCC, spin phase boundaries, struct. and excess free energy 77—59097
Ising model, boundary free energy, natural iteration and cluster variation methods, critical points 77—17913
Ising model, continuous, first and second order phase transitions 77—9965
Ising model, disordered, thermodynamic pot., ferro-and antiferromagnetic bonds, mag. moment and entropy *(Russian)* 79—19714

free energy continued
Ising model, exact renormalisation group equations 79—73749
Ising model, free energy, recursion method calcs. 78—52186
Ising model, free energy, variational calc. for 3 dimens. system 80—42167
Ising model, free energy and susceptibility inequalities, phase transition 78—43541
Ising model, generalised compressible, one-dimens., exact thermodynamics, renormalisation group method 77—20525
Ising model, high-temperature low field expansions extension 79—93045
Ising model, interface free energy and crit. line, nearest and next nearest neighbour interactions 78—39352
Ising model, low temp. expansions for 4-D simple hypercubic lattice 79—61025
Ising model, modulated phase with solitons, phasons and devil's staircase 80—95044
Ising model, one-dimensional, long range, metastability 80—42166
Ising model, one-dimensional, with mag. field, renormalisation group soln. 77—24664
Ising model, spin 1/2, susceptibility and fourth field derivative for $T>T_c$ and $d=4$ 79—61024
Ising model, spin glass in Bethe-Peierls-Weiss and other mean-field approximations 79—65682
Ising model, spin-one, high temp. series expansion, arbitrary biquadratic exchange, field and anisotropy 77—20526
Ising model, three dimensional, free energy, lower bound approx. 78—10707
Ising model, two-dimens., interface free energy 78—60261
Ising model eigenvalue analytic continuation and free energy 77—26236
Ising model free energy upper bound by renormalisation group methods 77—61026
Ising model strip, spin $^1/_2$, critical wall perturbations and a local free energy functional 80—80533
Ising model with nearest and next-nearest neighbour interactions, nonuniversality 79—44870
Ising model with transverse field, method of two-time Green's functions 80—2543
Ising spin glass, spherical approx. 77—28392
Ising spin glass, three-dimensional mag. correlations 80—103849
Ising spin glass free energy for $m\to\infty$ m-component spins 79—11320
Ising spin systems with random bonds, thermodynamic props. at low temp. 79—28532
Ising system with quenched impurities, high temp. expansion methods 79—78422
Ising systems, finite thickness, renormalization-group transformation, real-space 80—15749
Ising triangular model, in mag. field, Markov process anal. 77—13708
Ising two-dimens. random bond model, evidence against spin-glass order 80—15747
isotropic spin system, momentum-shell recursion relations in $2+\varepsilon$ dimensions 78—6498
itinerant ferromagnet, thermodynamics 79—4645
itinerant ferromagnetism, statistical mechanics of spin waves 79—82746
Josephson effect higher harmonics, flux tunnelling, thermodynamic free energy 80—60147
Kac-Baker model of partially finite spin systems 77—20621
kaolinite rare-earth complexes, relax., molar free energy of activation for dipole relax. 80—88919
Landau crit. point, mean-field theory, scaling theory and crit. exponents to second order in ε^2 79—4395
Landau model, anisotropic one dimens., correl. length complex order parameter amplitude fluctuation effect 80—46995
Landau theory of phase transitions 77—30120
Landau-Ginsburg model, droplets free energy, Jost function 79—40469
lattice free energy, anharmonic contrib. 77—20088
lattice gas model, three phase eqns. of state 78—22818
lattice model, analyticity and cluster props. of unbounded spin systems 78—45571
lattice spin models, high-density limit 78—29056
lattice systems with long range random Hamiltonians, existence of free energy 79—88886
lattice systems with many ground states, low temperature expansion 79—88887
layered crystal, electron gas statistical and thermodynamic props. *(Russian)* 79—87051
Lennard Jones system, nonphysical sampling distribs., Monte Carlo free energy estimation, umbrella sampling 77—26229
Lennard-Jones liq., press. and temp. consistent, approx. theory, Helmholtz free energy 78—63647
limit relations for model system in case of degenerate state of statistical equilib. 78—8337
linear viscoelastic media with concealed parameters, free energy concept *(French)* 77—42754
liquid, simple, free energy and radial distrib. function expansion rel. to fundamental system 78—26402
liquid, undercooled, Gibbs free energy change for crystallisation 80—25676
liquid, Zwanzig perturbation expansion convergence, free energy 77—76274
liquid alloy, Gibbs energy interaction parameters with O_2 and N_2 79—56961
liquid crystal, ferroelec., helicoidal, smectic-C, dynamics 79—1396
liquid crystal, nematic, molecular theory, orientation-average pair correlations 79—60272
liquid crystal with slowly varying orientational order parameters *(Russian)* 78—75533
liquid crystals, stability of mol. orientational distrib. 79—94880
liquid crystals, unified Landau theory, for nematic, smectic-A and smectic-C phases 77—55238
liquid crystals *(Chinese)* 80—79696
liquid metal, electronic theory of thermodynamics and struct., summer school lecture series 80—6353
liquid metal structure determ. by hard sphere model of repulsive interatomic pot. 79—55650
liquid mixture, excess Gibbs free energy, quasilattice local composition model, phase equilib. 78—31681
liquid mixture, modified Heil-Prausnitz eqn. for excess Gibbs energy 77—62652
liquid mixture, nonideality, prediction and meas. of thermodynamic excess functions 78—27818
liquid mixtures, local mole fractions consistency 78—83702

free energy continued
  liquid phases, non-uniqueness in phase, chem. react. equilib. computations 79—43612
  liquid surface tension, statistical mechanical theory 79—82414
  liquid systems, pure component Gibbs energy using structural group contribution method 79—90797
  liquid-gas critical point in 3.3 dimensions 79—7684
  liquid-gas system near critical point, sound attenuation and dispersion, renormalisation group calcs. 79—42149
  liquid-vapour equilibrium, systems with components of very different volatility, total press. static method meas. 79—14922
  liquid-vapour interface and stability rel. to spinodal decomposition, Cahn-Hilliard theory departure 79—77752
  liquid-vapour interface struct. and thermodynamics, density fluctuations, grand ensemble formulation 78—22932
  liquids, diatomic, hard and soft core, free energy difference, Monte Carlo calcs. 80—92436
  liquids, polar, thermodynamics, electrostatic approximations using Onsager model 80—55693
  liquids, simple, surface tension and density profile from expression for excess free energy 77—80681
  lithium ammonium tartrate, piezoelec., proper ferroelastic transition 78—2812
  local equilibrium hypothesis extension 80—27249
  localised soft mode theory for martensitic transforms. 78—10159
  macromolecules, crystallisation thermodynamics, various degrees of coiling 78—51445
  magnetic alloy, disordered Heisenberg binary, with mixed exchange interaction, compensation point *(Russian)* 77—51898
  magnetic contributions to phase stability calc. 78—6141
  magnetic objects, current loops, thermodynamics, teaching 80—90633
  magnetic system, random 78—2634
  magnetic systems with random interactions, upper bounds to be quenched free energy 80—103845
  magnetisation theory, of slab of finite thickness, role of positive surface energy 80—15724
  many-particle separable short range interaction system, trial Hamiltonian 77—26238
  many-particle systems, distrib. functions and thermodynamic functions 77—57273
  martensite energy due to order inherited from austenite 77—28813
  massive transformations, free energy, microstruct., growth and nucleation 77—4776
  melting curve maximum phenomenon, computer simulation using two species soft core model 78—6146
  melting/diffusion, linear correlation 77—20108
  metabolism, energy conservation 77—81459
  metal, crystal melt interfacial free energy calc. from exptl. radial distrib. function data 79—10926
  metal, electrochemical reaction on surface in aq. soln. 79—83387
  metal, entropy/free energy relation 78—15368
  metal, eqn. of state from statistical electronic free energy 79—99495
  metal, HCP, regular soln. model for interstitial soln. 77—15591
  metal, localised atomic states, resist. and free energy calc. 77—8069
  metal, mag. susceptibility, effects of impurities and temp. *(Russian)* 78—84429
  metal, monovalent, low temp. eqn. of state 78—22820
  metal, surface free energy of solid, at MP, estimated from liq. surface tension data 77—31866
  metal, thermodynamic props. of grain and phase boundaries, review *(German)* 79—34012
  metal, vacancies and change of surface free energy at melting point 79—42219
  metal surface free energy for BCC, FCC and HCP structs. etch pit depend. 80—29258
  metal to ceramic reaction welding, interfacial free energy rel. to noble metal corrosion 78—53035
  metal-H system, elastic interaction and phase transition, book contrib. 79—83178
  metallic soln., association 78—15373
  metals, adsorption of S, thermodynamics of two-dimen. and three-dimen. sulphides 80—20036
  metals, dislocation cell diameter rel. to free energy during creep 79—91756
  metals, eqns. of state based on free energy expressions, isothermal compression moduli *(Russian)* 79—90753
  metals, melting theory for small particles, Helmholtz free energy 80—59629
  metamagnetic model in field of arbitrary direction 79—95593
  metastability, spinodal fixed point, renormalisation group anal. 79—40509
  methane, liq., surface tension and density profile from expression for excess free energy 77—80681
  methane, liq., thermodynamic perturbation theory, equilib. props. 79—64976
  methane-ethane liq. mixture, phase equilib., heat of mixing, vol. change, data evaluation 80—15233
  1,6-methano(10)-annulene, mol. geom. and gas phase thermodynamic props., minimisation scheme 78—78829
  micellar systems, aqueous, thermochemistry 80—61133
  microcluster formation, free energy, curvature-depend. surface tension effect 80—100056
  microemulsion, border between lyophobic and lyophilic colloids, thermodynamic stability 80—40747
  microemulsions, thermodynamic stability, theory 78—85203
  micropolar fluids, thermodynamical aspects, non-linear approach 80—105598
  microscopic free energy zero fluctuation 77—5740
  Migdal-Kadanoff renormalisation scheme, surprising effectiveness 79—35652
  mixture, derivation and extension of UNIQUAC eqn. 79—14933
  mixtures, binary and ternary, activity coeffs. rel. to excess Gibbs free energies 80—96665
  mixtures of heavy and light gases, kinetics and thermodynamics *(Russian)* 77—76015
  mobile pinning points on dislocations, equilibrium distrib. 80—79792
  model phospholipid membrane, structural changes, aggregation 79—66451
  molar free energy functions at high temp., semi-empirical eqn. 79—47956

free energy continued
  molecular electron-donor-acceptor complexes, solvent effect on charge transfer absorpt., thermodynamic props. 77—83615
  molecular fluid perturbation theory, Pople expansion third order term, anisotropic pot. 78—79510
  molecular liquid, thermodynamic functions, interaction site model calc. 78—71661
  molecular solvation, in polar media, continuous charge distrib. model, quantum mech. calcs. 78—68913
  molecular system, with N associating particles, free energy, virial expansion 77—55336
  molecular vap., conformational changes, microwave spectroscopic intensities 77—75227
  molecular volume effects in the excess functions of binary mixtures *(Spanish)* 80—15261
  molecule desorption and surface diffusion from critical deposition rate 80—92786
  molten salt mixtures, binary, excess thermodynamic props. and US vel. *(French)* 77—27943
  monodisperse polymer solution, thermodynamic fluctuations, light scattering 77—52107
  2(4)-monooxopyrimidines, gaseous, matrix, soln., tautomeric equilib., IR and UV absorpt. spectra 80—58256
  Mott transition in Hubbard long range model, isostructural instability, thermodynamic props. *(Russian)* 80—65454
  multicomponent fluid mixtures, renormalised one-chain approx. 77—11452
  multicomponent systems, phase diagrams and thermodynamic data, electrochem. determ. 80—71922
  multicomponent systems, use of polynominal representation of excess free energy, in phase diagram calc. 79—10914
  multiple layer adsorption, on foreign substrate, surface roughness and surface free energy variation 77—24497
  n-component spin system, energy-energy correl. function calc. 80—31697
  1- and 2-naphthol, ideal gas thermodynamic props., vibr. fundamentals, rot. isomerism 79—24813
  narrow band electron systems, unified theory of magnetism 80—70928
  nematic liquid crystal, cluster variational const.-coupling theory, thermodynamic props., nematic-isotropic transition 77—24265
  nematic liquid crystal, intermol. forces, in anisotropic mean field, hard spherocylinder model 77—35468
  nematic liquid crystal, pure splay, geometric approach to problem of stable configurations 79—27914
  nematic liquid crystal, validity of Landau approx. 77—27989
  nematic liquid crystals, Frank elastic consts., statistical mech. theory 80—29104
  nerve axon, squid giant, transient polarisation currents 77—86477
  neutron star matter, superfluid phase transition 79—59025
  Newton black soap film, interaction forces, contact angles 79—77870
  Nimonic PE 13, mass spectrometric study, high temp. reactor system appl. 79—43663
  NLC, effective ion mass and mobility calcs. *(Russian)* 80—79694
  non-stationary thermodynamics of polarisable and magnetisable dissipative fluid media 80—47002
  nonequilibrium superconductivity, oscill. of order parameter caused by quasiparticle injection 79—42697
  nontranslationally invariant spherical model, exact soln., phase transition 77—37833
  nonuniform one dimensional classical fluids, Lennard-Jones pot. interactions, Percus Yevick approx. and density functional calcs. 80—64864
  nuclear free energy, variational description 79—45199
  nucleation, heterogeneous theory, appl. to precipitate nucleation at Guinier-Preston zones 77—36509
  nucleation, theory for high and low supersaturations, review 80—49142
  nucleation free energy of nucleus formation, influence of elec. field 77—35702
  nucleation kinetics for non-spherical nuclei, and high pressure effects 80—19730
  nucleation theory, atomistic models of microclusters, exact free energy barrier 77—62612
  nucleation theory, role of replacement free energy, review 77—62611
  octafluorocyclobutane+n-butane mixtures, 233K, surface tension meas., excess Gibbs function 79—19371
  octamethylcyclotetrasiloxane-cyclohexane liq. mixtures, u.p. and excess Gibbs free energy determ. 77—30225
  one dimensional continuous quantum systems, limit Gibbs state 78—93599
  one-dimensional classical spin chain with random interactions, exact calcs. 79—4687
  one-dimensional diatomic chain, order-disorder transition, simple model 79—4394
  one-dimensional fluid, triangular well pot., perturbation theory 77—35455
  optimal truncation procedures in renormalization-group calculations 79—63075
  order-disorder transitions, cluster approach 79—94943
  order-parameter expansion of free energy, appl. to some phase transition models 78—43099
  organic binary mixtures, with weak charge transfer interactions, thermodynamic props. 80—54360
  organo tin dichlorides, tetrahedral, dilute soln., dielec. and thermodynamic behaviour, microwave region 77—36170
  orientationally ordered liquids, Helmoholtz free energy, generalised van der Waals theory 80—44119
  paraelectric-ferroelectric-antiferroelectric phase transitions, electrostrictive effects 80—97209
  n-paraffin, rotator phase transformation, lattice dynamics Helmholtz free energy 78—34585
  paramagnetic semiconductor, heavily doped, linear response functions and magnetoresist. 77—51770
  partition function of the hydrogen system in the metallic state 79—73458
  percolation model, singularity of the analogue of free energy 78—36943
  PET, crystallization, lamellar growth kinetics and thickness 80—103266
  phase boundaries in first-order phase transitions, dynamics stability 80—107403
  phase boundary, impurity conc., free energy and equilib. eqns. 80—34038
  phase diagrams optimisation by least squares method using simultaneously different types of data 78—6143
  phase transitions with several order parameters, catastrophe and renormalisation theories 78—32782
  phenanthrene, chemical thermodynamic props. 80—21312

free energy continued
phenol, ideal gas thermodynamic props. 78—75250
planar micelles, structural changes, aggregation 79—66451
Planck function, replacement for free energy function 80—62603
plasma, free energy, exchange quantum correction 78—47091
plasma, MHD equilibria in mag. quadrupole field, secular instability 80—10427
plasticized triblock copolymers, thermodynamic theory 78—15377
polar fluid, translationally invariant correlation function, thermodynamic and dielectric props. 77—35457
polar fluids, intermol. and thermodynamic potentials, angle-depend. pot. 78—22618
polar fluids, intermol. and thermodynamic potentials, preaveraged pot. 78—22617
polar lattices, Monte Carlo results 77—4594
polar liquids, solns., mol. rot., kinetics 77—51984
polar mol.+ion, statistical and thermodynamic theory 80—99562
polarisable hard sphere fluid, thermodynamic props. 79—42277
poly(vinylidene fluoride) phase II, field induced phase transitions 80—96640
poly-arylate-dimethyl siloxane, polyblock copolymers, struct., thermodynamic stability *(Russian)* 80—64931
polyamide-12 plasticized with sulphonamides, relaxation props. *(Russian)* 80—55031
polyethylene, high density, effects of draw rate and temp. on necking stress *(Japanese)* 79—91757
polyethylene, high density, necking stress *(Japanese)* 77—56036
polyethylene, orthorhombic and triclinic lattices, eqns. of state 79—28069
polyethylene, oxidation rel. to spherulitic crystn. *(Russian)* 78—71689
polyethylene, uncrosslinked amorphous matrix embedded cryst. orientation distrib., strain energy and hydrodynamic pot. effects 78—9968
polyethylene (orthorhombic), intermol. pot. functions, force consts., vibr. assignments, thermodynamic props. 77—39639
polymer, isotropically swollen networks, vol. depend. of elastic eqn. of state 78—67832
polymer, stressed, config. free energy change due to partial crystn. of chains, distrib. of cryst. orientations 79—94923
polymer chain, elasticity for different vibr. modes, algorithm 78—66696
polymer chains in cubic lattice solvent, thermodynamic props., Monte Carlo method, computer simulation *(Russian)* 77—31787
polymer crystal and melt, stat. thermodynamics using Midha-Nanda cryst. state theory 79—41979
polymer crystallisation, thermodynamic analysis of nucleation *(Russian)* 77—19881
polymer flexible lattice chain in limited vol., behaviour *(Russian)* 78—70992
polymer melting, theoretical aspects 80—59633
polymer network in solution, free energy of deform. 80—38900
polymer protonated and deuterated mixtures, partial miscibility 80—107037
polymer solutions, free energy of mixing, modelling, critical exponents 80—44106
polymers, heterophase mixtures, excess energy 78—53264
polyolefins, triboelectric charging, linear free energy relationships 78—6431
polyoxymethylene, kinetics of epitaxy and over-growth on needle-like single crystals 78—14291
polystyrene, glassy, thermally activated deform. 79—20126
polystyrene-methylcyclohexane, coexistence curve, comparison obs. and free energy calc. 80—88323
polyurethanes, vapour press. of solvent above swollen crosslinked networks rel. to rubber elasticity theory 80—45536
polyvinylidene fluoride, cryst., struct. phase transition theory, free energy, uniaxial stress 80—64924
polyvinylidene fluoride, thermodynamical model, applications *(French)* 80—39315
porous solid with below-freezing pt. adsorbate, isothermal adsorption and dimensional changes obs. 78—75925
position-space renormalization approach 79—30404
Potts model, four state, series studies 79—85088
Potts s-state model on Cayley tree Bethe-Peierls critical coupling 80—103844
protein-water system dynamic model 77—21470
pseudocritical phenomena near the spinodal point 78—65894
quantal spin systems, classical representation and scaling props. of spin Hamiltonians 78—14919
quantum compressible Ising model, critical behaviour 80—108016
quantum crystal, ground-state lattice vacancies and Bose-Einstein condensation 77—7943
quartz, stressed, Dauphine twinning growth, thermodynamic theory 79—23619
quasi-one-dimensional systems, free energy of Ginzburg-Landau field, equiv. Hamiltonian 78—6293
quasi-one-dimensional systems, statistical mech., thermodynamic props., mag. transition 77—26246
quenched random system, dual relations 80—34664
random Ising chain, Bethe approx. for free energy 79—78287
random Ising model, variational principle for distrib. function in the Bethe approx. 80—15674
random ordered phase, effective field approx. 79—1676
random system, density of states, essential singularities, sp. ht., free energy 78—18729
rare earth (III) complexes, cysteinates, thermodynamics of form. 80—89515
rare earth compounds, mag. moment and valence fluctuations 78—23244
reacting polymer system, convergence to equilibrium, free energy 79—52624
reaction rates, magnitude and variation, with energy, structural modifications of reactants 79—74349
real gas, nonpolar, ideal eqn. of state curve features 78—1776
renormalisation theory, variational principles 78—73951
Rochelle salt, phase transitions, free energy in symm. group representation of parent phase 79—69790
Rochelle salt family, rectilinear system of transition parameters 78—48126
rocks, rings, discs, under diametral compression, tensile strength calcs. *(French)* 77—70638
rods, with anisotropic surface free energy, stability 80—20013
roughening models, step free energies, and correlation functions in X-Y models 78—67675

free energy continued
Schottky defect, possibility of enthalpy decreasing with increasing temp. 80—2012
semiconductor, binary, estimation of heats of formation from melting temp. 78—27810
semiconductor, n-type, thermodynamic pot. for anodic dissolution, rel. to photoelectrochem. cell efficiency 78—26948
semiconductor p-n junction, conversion of chem. energy into elec. power thermodynamic props. 79—11219
separable many-particle interactions, free energy per particle, convex-envelope formulation 78—32781
silicate, polymerised binary melts, activities and free energy of mixing 77—47596
simple liqs. with repulsive forces, thermodynamically selfconsistent theory 80—75139
simple metals, monovacancy formation parameters, temp. depend. 78—75658
small polaron theory, translational symm. breaking transform. 80—92838
smectic A to smectic A phase transition 79—69229
smectic liquid crystal, piezoelectric domains, free energy minimisation and Euler eqns. calc. 77—51319
soap film, Newton black, contact angle meas. 78—47640
sodium ammonium tartrate, ferroelec., thermodynamic theory of phase transitions 77—90112
soft mode catastrophe indices rel. to thermodynamic pot. function isotropy 78—14431
solid solution, free energy extrema characterised by two long-range order parameters *(Russian)* 77—76576
solid solution, ordering, characterisation by long range order parameters *(Russian)* 79—1489
solid solutions, congruent transformation pt., regular soln. theory 79—60477
solid-liquid interface free energy anisotropy clustering influence 80—80054
solid-liquid phase equilib., binary and ternary systems, excess Gibbs free energy 78—30736
solid-liquid transition, thermodynamic potential calc. 77—20049
solid-on-solid model, screw dislocations, rel. to correl. in X-Y model 78—63691
solids, polarisable and magnetisable, theory of in electromag. fields 77—57291
soliton free energies calcs., WKB approx. failure 80—42073
solute hydrophobic interaction, mol. aggregation, free energy, entropy and enthalpy, scaled particle theory 77—84609
solution, aq., hydrophobic apolar spheres interaction, Monte Carlo simulation 80—6335
solution, aq., hydrophobic hydration around apolar species pair, Monte Carlo simulation 80—6336
solution, Gibb's excess energy, thermodynamic restrictions on analytic expression 78—27817
solutions, dilute, Monte Carlo free energy calcs. in isothermal-isobaric ensemble 78—92498
solvent effects on chemical reactions, semiempirical model 80—25986
solvent-rod mixture, two phase, interfacial free energies, quartic van der Waals theory 80—59377
spin $^1/_2$ Ising model in four-dimens., hyperscaling test 80—46986
spin glass, infinite range model, stability and susceptibility in Parisi's soln. 80—88762
spin glass, mean field theory and ε-expansion 78—10705
spin glass, principle of minimum free energy 80—88773
spin glass, random molecular fields, Edwards-Anderson theory 78—80164
spin glass, Sherrington-Kirkpatrick model, thermodynamic props. 79—51797
spin glass free energy, phase transition dynamical instability 79—33493
spin glass in d dimensions, Ashkin Teller model 79—65691
spin glass model, stability of Sherrington-Kirkpatrick soln. 78—56319
spin glass transition, cumulant expansion of free energy of disordered systems 80—71067
spin glass transition in system with competing ferromag. and antiferromag. interaction 77—20616
spin glasses, free energy, order parameter expansion, random bond model 80—84609
spin glasses, Ising type random bond, scaling, eqn. of state and instability 79—73753
spin glasses, metastable states, crit. free energy 80—88764
spin glasses, RKKY free energy, pair approx. 79—56557
spin glasses, second virial coeff., magnetic field depend. 79—65690
spin systems, one-dimensional, free energy series expansion, renormalisation group series 78—31081
spin-flip process, non-increasing free-energy 77—73031
spin-glass model, stability of Sherrington Kirkpatrick soln. 78—80152
spin-glasses, order parameter expansion of free energy, random site model 80—88772
spin-S XY-model, susceptibility series expansions 79—28540
spin-systems, double-time Green functions method, thermodynamics 79—15313
spinels, entropy of cation transitions 79—11812
spinodal decomposition, light scattering, depend. on method of quench 78—18782
spinodal decomposition, near interface, continuum mechanics *(German)* 80—45272
spinodals and swallowtails, rel. to phase diagrams 77—7844
square lattice finite thickness slabs, long self-avoiding walks, steric stabilisation model 78—54309
stability of critical behaviour, critical-exponent renormalization and first-order transitions 79—44895
statistical approach, calculation of inductive, mesomeric contributions 79—49957
statistical mechanics, stability, equilib., and metastability 80—31659
steam, crit. region, universality, revisions and corrections to scaling 78—38810
steam critical behaviour of thermodynamic potential 80—42175
steel, alloy with additions of Mn, Si, Ni, Cr, Mo, Cu, thermodynamic prediction of Ae_3 temp. 78—64524
steel, aluminising, thermodynamic anal. of phase transforms. 80—76413
steel, hydrogenation in HCl, influence of conc. depend. of anilines additives on time to fracture, principle of linearity of free energy *(Russian)* 79—15854
steel, medium and high C, deformation ageing, entropy, free energy, dislocations *(Russian)* 80—66581
steelmaking, thermodynamics of rare earths 77—4782

free energy continued
  stored energy determ., analytical method *(Russian)* 77−25096
  stress corrosion weakening, subcritical crack velocity, free energy considerations 79−8374
  strong-coupling superconductors, meas. of small changes in free energy 77−33988
  structural and mag. phase transforms., integral rational basis of invariants *(Russian)* 80−62602
  structurally complex crystals, continuous phase transitions, Landau theory, subgroup approach 78−14441
  sublattice metamagnet, temp. dependent anisotropy, magnetisation curves, mag. transitions, classical approx. 80−39795
  substitutional solid solutions, new phase nucleation mechanism 80−61135
  superconducting films, inhomogeneous crit. dynamics 77−8230
  superconducting order parameter perturbation flux pinning 80−103801
  superconducting surface sheath, dynamic pinning model of elec. dissipation 77−28320
  superconducting-magnetic sandwich, Landau free energy 77−47924
  superconductor, high T_c, dynamic instabilities 78−10607
  superconductor, inhomogeneous, equilibrium order parameter 78−2616
  superconductor, type-II, magnetisation, rel. to anisotropy of upper crit. field 80−54832
  superconductor type II, perturbation series for crit. behaviour near H_{c2} 77−8233
  superconductor with crystalline-field-split mag. impurities, free energy and thermodynamical crit. field 77−32127
  superconductors, magnetic impurity low temp. behaviour, transition temp., specific heat, free energy 80−88691
  superfluid density in two-dimens., XY model 79−95242
  superionic crystals, phase transitions 78−75826
  superlattice, electron gas statistical and thermodynamic props. *(Russian)* 79−87051
  supersaturated vapour, critical clusters, theory and Monte Carlo simulation, review 80−82734
  surface, anisotropic, method for absolute meas. 77−85062
  surface tension, review of theory 79−77866
  symmetry principles and 1/f noise 80−68136
  1T-TaS_2, nearly commensurate phase, harmonics effect on phase transitions 78−14462
  TCNQ anion radical salts, phase transitions, solid solns., thermodynamic props. 77−47571
  temperature induced antiferromagnetic-ferromagnetic phase transition, s-f two-band Hubbard model 80−60253
  ternary dil. soln., free energy of transfer determ. by vapour press. method 78−64871
  ternary system isothermal Gibbs-Duhem eqn., direct numerical soln. 79−1511
  tetramethylsilane, thermodynamic props. of polymorphic phases 77−84943
  thermodynamic study of form. 78−48685
  thermodynamics of solids, corrections from electron-phonon interactions 80−49387
  thermoosmotic concentration difference meas. for gaseous mixtures across membranes 79−83508
  thermorheological behaviour and coupling problem of struct. materials 77−3718
  thermorigid dielectrics, nonlinear thermodynamic theory 80−10149
  Toda lattice, statistical mechanics and solitons 79−49176
  transition metal carbides, thermochemistry 79−43617
  transition metal dichalcogenides, trigonal-prismatically coordinated layers, phenomenological theory of CDW state 80−80200
  transition metal sulphides, liq. and solid thermochemistry 78−23962
  transition metals and alloys, group IV, electronic basis for ω-phase stability 79−91616
  triangular lattice, thermodynamic props., effect of vacancy defects determ. by cell cluster method 80−79959
  triangular lattice, two-dimens., vacancy pair free energy 79−14799
  triangular well fluid, Helmholtz free energy, Barker-Henderson perturbation theory 79−4218
  triangular-potential fluid, Zwanzig's perturbation theory, appl. to thermodynamic props. 79−41920
  triplet superconductivity, incomplete Meissner effect 79−15255
  TTF-TCNQ, Landau free energy function, CDW-libron interaction, sp. ht. near phase transitions 80−19963
  TTF-TCNQ, Landau theory of phase transitions 80−92666
  two dimensional real matter, low density free energy in canonical thermodynamics plasmas 80−87852
  two order parameter systems, Landau-Ginzburg-Devonshire theory 78−10164
  two-centre Lennard-Jones liquids, free energy, perturbation theory 80−79656
  two-dimensional electron system in strong mag. field, crystallisation 78−30966
  type II magnetism in mixed magnets and spin glasses 78−23281
  type II superconductor, bounded, intermediate state struct. form. near crit. field, role of surface 80−80465
  type II superconductor, ideal, wire, macroscopic current in longitudinal field 78−84366
  type-II superconductors, anisotropic, lower crit. field 80−60153
  ultradisperse particles, spinodal decomposition singularities, conc. profiles *(Russian)* 79−82340
  unbounded n-component spin systems on lattice, statistical mech. 77−4477
  uncorrelated-pairs approximation for anharmonic free energy, tests 78−59920
  uncorrelated-pairs approximation for the free energy of a crystal 79−42200
  uniaxial magnet, free energy of system with weak exchange interactions and high mag. anisotropy *(Russian)* 78−68213
  univalent gaseous ions, free energy of solvation, 1-layer continuum model 78−95944
  unstable compounds, free energy of formation calcs., FORTRAN program for ternary phase equilibria. 80−10683
  vacancy, 2-dimensional triangular lattice, classical high temp. limit free energy 77−65974
  van der Waal's crystal P-V-T diagram, Holmholtz free energy, mean-field model, for teaching 77−33784
  vaporisation of liquid, free energy change, classroom example for teaching thermodynamics 80−42010
  vapour-liquid equilibria data reduction, vapour phase composition effect, excess Gibb's function 77−59091

free energy continued
  vibronic ferroelectric semiconductor, mag. susceptibility calc. 80−2711
  vibronic ferroelectric semiconductor, tunnel effect 78−10853
  viscoelastic materials, glass-transition temp., thermodynamic criterion 77−59783
  volatile liquid, statistical thermodynamics of new phase form. *(Russian)* 78−18739
  wall and boundary free energies, ferromagnetic scalar spin systems 78−155
  wall and boundary free energies, general domains and complete boundaries 79−49182
  water, uniform and two-phase states, thermodynamic model interpolation 80−24565
  water vapour, dissociated, thermodynamic props. *(Japanese)* 77−80263
  weak superconductor with current in external mag. field, free energy 80−25046
  X-Y($s=1/2$) model, renormalisation group method, triangular lattice 77−26247
  X-Y model, quantum, phase transition, free energy and susceptibility 78−43595
  X-Y model, spin 1/2, thermodynamic props., high temp. series expsn. 78−47929
  X-Y model classical one-dimensional, free energy in mag. field 77−4484
  (Ag, Tl, Ca)NO_3, aqueous solutions, vapour press. meas. 80−6504
  Ag film, on mica, microstruct. changes 78−72013
  Ag halide grains, surface free energy, effect of adenine adsorption *(German)* 79−39175
  Ag-Bi-Tl, system calculated from optimised binary boundary systems *(German)* 77−16545
  Ag-Cu (8 wt.%), deformed, free energy changes in process of discontinuous precipitation 80−3054
  Ag-Sn system intermetallic formation rate, H_2 adsorption effect 79−90819
  Ag-Zn, liquid, thermodynamic props. *(German)* 79−87615
  Ag-Zn, molten, EMF meas. of activities using ZrO_2 solid electrolytes *(Japanese)* 80−88339
  AgBr, photographic emulsion, adsorpt. of Br^-, cyanine, thermodynamics 78−32908
  AgCl:Cd^{2+}, heavily doped, free energy and point defect distrib., integral eqn. method 80−107219
  AgCl:$CdCl_2$, point defect model, free energy and radial distrib. functions 80−44201
  $AgNO_3$-$TlNO_3$-$Cd(NO_3)_2$-H_2O mixtures, Henry's law, excess free energy 78−68908
  $AgNa(NO_2)_2$, Landau behaviour of sp. ht. close to nearly tricritical ferroelec. phase transition 78−10861
  Ag_2S, α-β transform., heterogeneous solid state reactions, role of phase boundaries, dynamic equilib. at interfaces 78−71848
  Ag_2S, α-β transform., role of phase boundaries in heterogeneous solid state reactions 78−71849
  $Ag_2S(Se)(Te)$, thermodynamic props., growth of single cryst. by chem. transport reaction 77−36380
  Al, elastic grain boundary responses, thermodynamic props., computer calc. 77−39593
  Al, monovacancy thermodynamic parameter calcs., temp. dependence 78−2114
  Al, surface energy and adhesion props. 80−10774
  Al-Ag, discontinuous decomposition *(Polish)* 78−52808
  Al-Ag (40 wt.%), deformed, free energy changes in process of discontinuous precipitation 80−3054
  Al-B, enthalpies and free energies, effusion and mass spectra, phase diagram 78−23665
  Al-Ga-In, liq. alloys, excess Gibbs functions 633 to 1173K 78−60655
  Al-Ga-In system, thermodynamic anal. 79−60512
  Al-Ga(In) systems, thermodynamic anal. 79−60512
  Al-Mg-Si liquid alloy, exam. of thermodynamic props at 780-820°C *(Czech)* 79−91626
  Al-Zn, discontinuous decomposition *(Polish)* 78−52808
  Al-Zn (40(50)(65) wt.%), deformed, free energy changes in process of discontinuous precipitation 80−3054
  Al-Zn-Hg alloy, cathodic protection characts., surface free energy, lattice struct. 79−29281
  Al_4C_3, stability at 1873K, Gibbs energy of formation determ. 78−39745
  $Al_{20}Cu_{25}Zr_{55}$ metallic glass, inelastic deform., free energy spectra 80−71699
  Ar adsorbed monolayers, on graphite, equilib. config. and lattice consts. 80−54524
  Ar adsorbed on graphite, nonregistered-registered phase transition 80−39414
  Ar, effect of high mag. fields on vapour pressure 78−38825
  Ar, liq., surface properties of classical Lennard-Jones liquid *(Russian)* 79−77869
  Ar, liq., surface tension and density profile from expression for excess free energy 77−80681
  Ar small crystallite,s self consistent phonon calc. of struct. and thermodynamic props. 77−62596
  Ar, solid, equilib. props., uncorrel. pairs approx. 80−84303
  Ar, solid, FCC and HCP, free energy difference, from Ar-O_2 vapour press. meas. 77−11700
  Ar-Kr, liq. mixture, excess thermodynamic props. 78−75836
  Au-Ag, surface segregation 79−77873
  Au-Fe, liq., thermodynamic mixing effects, mass spectrometric meas. eval. *(German)* 77−59123
  Au-M, liq. alloys, M=Ga,In,Sn,Sb,Te, ΔG^E of mixing, exptl. determ. 77−4920
  Au-Ni, liquid alloy system, determ. of thermodynamic props. using Knudson effusion method, phase diagram calc. *(German)* 78−51707
  Au-Ni-Cu phase diagrams, thermodynamic calc. *(Korean)* 78−68672
  Au-Si, liq. alloy, thermodynamic activity meas. by Knudsen-cell mass spectrometry *(French)* 80−10684
  Au-Zn, molten, EMF meas. of activities using ZrO_2 solid electrolytes *(Japanese)* 80−88339
  AuCu-Al thin film bilayer system, phase formation, backscattering spectra 80−96728
  p-azotoluene-azulene, order parameters and lattice energy, mean field approx. 78−22688
  B, CVD from BCl_3-H_2 and BBr_3-H_2 gas mixtures onto inert substrate, thermodynamic approach *(French)* 78−44020
  B, CVD from BCl_3-H_2 mixture, on metallic substrate, thermodynamic exam. *(French)* 78−27412

free energy continued
B, CVD on inert and metal substrates, Gibbs free energy minimisation 80—16201
BN, high temp. compatibility with insulating oxides 77—24995
Ba, silicates, solid state reactions, thermodynamics and kinetics *(German)* 80—76236
$BaFe_2O_4$, free energy of form. 77—4924
$BaMnF_4$, pure and Co doped, ferroelec. antiferromag., dielec. anomalies 80—71288
$BaPO_3F$, prep. from $BaCO_3$, H_3PO_4 and NH_4HF_2, props. 79—52147
$BaTiO_3$, thermodynamic props. 77—39680
$BaTiO_3$-type ferroelectrics, existence of noncommensurate phases due to gradient term in free energy 79—69792
Ba_2TiO_4, $Ba_6Ti_{17}O_{40}$, standard Gibbs free energy of formation, EMF meas. at 673K 80—85207
Ba_3WO_6, Ba_2WO_5, and $BaWO_4$, chem. thermodynamics, galvanic cell study 80—21315
Bas and B_6As, standard values of thermodynamic functions 77—24414
Bi-S liquid soln., S activities meas. by EMF method *(Japanese)* 80—70425
Bi_2O_3, energies of formation, solid-state electrochemical techniques 80—6527
C-C interaction energy, thermodynamics of steels 80—93793
C_3, linear, high temp., rot.-vibr., anharmonicity, thermodynamic function calcs. 80—43830
CO, liq., thermodynamic perturbation theory, equilib. props. 79—64976
CO_2, linear, high temp., rot.-vibr., anharmonicity, thermodynamic function calcs. 80—43830
CO_2, liq., thermodynamic perturbation theory, equilib. props. 79—64976
CO_2(g), standard enthalpies of solution and formation, standard Gibbs energies of formation and standard entropy 79—57285
Ca-Ag(In), liquid alloy, thermodynamic exam 78—75848
Ca-Zn liquid alloys, thermodynamics 79—52173
CaBr(Cl)(I), Gruneisen γ and other thermodynamic props. at zero and elevated press. 78—43142
CaCl, aq., mean activity and osmotic coeffs., free energy, 298.15K, review 77—81411
$CaGa_2O_4$ and $CaGa_4O_7$, cryst., thermodynamic parameters of reactions of form., thermodynamic stability 80—108726
CaO-ZrO_2 solid soln., thermodynamic investig., by EMF method 77—36485
$Ca(O_2)_2$, standard heat, entropy and free energy of form. 79—87869
$CaWO_4$, cryst. growth from solns. in melts, kinetics parameters and thermodynamic props. 80—59424
Cd-In-Sb, liq. alloy, Cd thermodynamic activities, Gibbs free mixing enthalpy *(German)* 80—45279
Cd-Zn-Hg alloys, liq., comp. and temp. depend. of Hg VP, activity, free energy and enthalpy *(Russian)* 77—20087
CdP_4, thermodynamic functions, 55-300K 80—34203
CdSb, thermodynamic functions, heat of formation 79—77768
CdX_2-RbX-H_2O, X=Cl,Br,I, Gibbs free energy, H_2O activity, 25°C *(Russian)* 78—31678
Ce-S-O equilibrium in molten Fe *(Chinese)* 80—104423
Ce_2O_2S, free energy of formation and nonstoichiometry of CeO_2 79—83498
^{249}Cf, vapour pressure, thermodynamic functions 80—6509
Cl^- hydration complexes, gas phase, electrostatic calcs. 80—100055
Co bi-univalent cpds., soln., activity coeffs., osmotic coeffs., water activity, Gibbs energy, molality depend. 80—51963
Co, liquid, N activity coeff. 77—72699
Co-Fe(Ni)(Cr), liquid, N activity coefficient 77—72699
Co-W-C system at 1150°C, phase equilibria, isothermal reactions and thermodynamic study 78—31385
Co_2GeO_4-Mg_2GeO_4, solid solubility and cation distrib., free energy 77—35700
$Co(NH_3)_5\ Br^{2+}$, aquation, polyelectrolyte catalysis, high pressure effect 80—55656
Cr, liquid, N activity coeff. 77—72699
Cr, spin density wave state, phenomenological free energy density description 80—75720
Cr-Ge, thermophysical props., at elevated temp. 80—103493
Cr-N system, thermodynamic anal. 77—77461
Cr-Ni-O, computer-assisted anal. and calcs. of phase diagrams 80—25667
Cr-Ni(Co)(Fe), liquid, N activity coeff. 77—72699
CrF_2, thermodynamic props. meas., electrochem. method 77—7874
$Cr_{11}Ge_8$, Cr_3Ge, thermodynamic functions 77—84948
$Cr_{12}Ge_{19}$, CrGe, thermodynamic props. 77—36779
CrO_2F_2, determ. of thermodynamic props. from vibrational freqs. and moments of inertia 77—31415
Cs-CsCl, liq. mixture, enthalpy of fusion, Gibbs energy of mixing and excess entropy 80—19947
Cs-SiO_2-Al_2O_3 system interactions, getter development for radiocaesium 80—83208
$CsNiF_3$, one dimensional planar model with symm. breaking fields, thermodynamics, static props. 80—97111
$CsPO_3$ formation, from dihydroorthophosphate dehydration, reaction thermodynamics 79—52643
$CsPbBr_3$, cubic-to-tetragonal phase transition, critical anomalies, phenomenological eqns. 80—39275
$CsPbCl_3$, cubic-to-tetragonal phase transition, critical anomalies, phenomenological eqns. 80—39275
$CsPbCl_3$, O_h^1-D_{4h}^5 transition, US and thermodynamic props. 78—67826
Cu bi-univalent cpds., soln., activity and osmotic coeffs., H_2O activity, Gibbs energy, molality depend. 80—51964
Cu, elastic grain boundary responses, thermodynamic props., computer calc. 77—39593
Cu, grain growth during isothermal annealing *(Russian)* 79—52259
Cu-Ag (8 wt.%), deformed, free energy changes in process of discontinuous precipitation 80—3054
Cu-Al, heat capacity of phases, 233 to 800K, heat of transform. and entropy 77—47589
Cu-Al (In), eutectic systems, phase boundary Gibbs free energy *(German)* 79—29016
Cu-Al-Ni, stress induced martensite 77—36500
Cu-Ge, liq. alloy, thermodynamic activity meas. by Knudsen-cell mass spectrometry *(French)* 80—10684
Cu-Ge-O, phase diagram and thermodynamics, electrochem. study 80—50617
Cu-In liquid alloy, thermodynamic props., potentiometric exam. *(French)* 77—59126

free energy continued
Cu-Ni-Zn system, free energy surfaces 80—24404
Cu-O system, liq., thermodynamic study *(Japanese)* 78—64529
Cu-Sn liquid alloys, thermodynamic meas. 78—52765
Cu-Sn system intermetallic formation rate, H_2 adsorption effect 79—90819
$CuGaO_2$, Gibbs free energy of formation, 680-1000°C 77—36489
$CuGa_2O_4$, Gibbs free energy of formation, 680-1000°C 77—36489
CuI, γ and β phases, phonon contribs. to Gibbs free energy and entropy 77—80633
CuO-Cu_2O-TiO_2, phase equilibria, thermodynamics of Cu_3TiO_4 phase 80—55374
Cu_2O, meas. of standard molar free energy of form. by EMF method at high temp. *(Japanese)* 78—11546
Cu_2O, standard free energy of formation, by EMF method with solid oxide electrolyte at low temps. *(Japanese)* 80—88338
Cu_xS-CdS solar cells, Cu_xS transform. behaviour rel. to topotaxial growth, cell efficiency 77—11814
$CuSe_2$, CuSe, Cu_3Se_2 and Cu_2Se, thermodynamic props., 298 to 420K *(Russian)* 77—69098
$Cu_{40}Z4_{60}$, $Cu_{56}Zr_{44}$, and $Cu_{60}Zr_{40}$ metallic glass, inelastic deform., free energy spectra 80—71699
$Cu_xZn_{1-x}SiF_6.6H_2O$, heat capacities and thermodynamic props., 14 to 300K, cooperative Jahn-Teller transition 80—21314
p-D_2, order-disorder phase transition 78—79726
D_2O, liq., ionisation const., thermodynamic props. determ., 298-523K 77—32821
DyF_3, thermodynamic props., galvanic cell meas. 80—21316
$DyMnO_3$, thermogravimetric study of phase stability 79—100121
ErF_3, standard enthalpy of formation 79—91990
ErF_3, thermodynamic props., galvanic cell meas. 80—21316
$ErMnO_3$, thermogravimetric study of phase stability 79—100121
$ErRh_4B_4$, ferromag. superconductor, vortex phase 80—80441
$EuFeO_3$, thermodynamic study of form. 78—48685
$Eu_3Fe_5O_{12}$, thermodyn. props. 77—84947
Fe alloys, magnetic sp. ht., Curie temp., alloying effects model 79—61116
Fe, α and γ phases, electronic free energy, HF calc. 79—11611
Fe, α-, γ-, liq., thermodynamic data *(German)* 80—40328
Fe base melt, thermodynamic props. *(Russian)* 77—55363
Fe, Gibbs energy in BCC and liquid states rel. to FCC, Fe-C and Fe-N phase diagrams 80—60846
Fe, liquid, N activity coeff. 77—72699
Fe, phase transition thermodynamics 78—18769
Fe rich binary alloys, effect of transition impurities on structural stabilisation 77—76552
Fe-Al, antiphase boundary motion, microscopic diffusional theory, appl. to domain boundary coarsening 79—61563
Fe-Al, equilibria of Fe, Al ordered phase *(Japanese)* 79—70042
α-Fe-Be(P)(Mo)(W)-Co, effect of Co on solubility anomaly due to mag. transition, free energy and phase diagrams *(Japanese)* 79—42257
α-Fe-Be(Ti)(Mo)(P)(Sb), effect of mag. transition on solubility of alloying elements, phase diagrams and free energy curves *(Japanese)* 79—42256
Fe-C phase diagram, thermodynamic anal. 80—60846
Fe-Co(Ni)(Cr), liquid, N activity coefficient 77—72699
Fe-Cr-C system, isothermal sections, 873 to 1373K, computer plotting 78—6894
Fe-Cr-Ni system, austenitic, energetic particle bombardment, thermodynamic and dimensional stability 77—27904
Fe-Cr-O, computer-assisted anal. and calcs. of phase diagrams 80—25667
Fe-Cr-O-C, stability diagrams, characteristics and calc. 79—10917
Fe-Cr-W-C, carbide/austenite equilibria, expt. and thermodynamic study 77—36459
Fe-Cu, generation of self-consistent Gibbs energy functions 79—11565
Fe-Ge, liquid alloy, thermodynamic mixing function determ. by mass spectrometric meas. 79—29025
Fe-lanthanid-O systems, thermodynamic props., composition and lattice constants 78—31390
Fe-Mn, thermodynamic props. *(Czech)* 77—85990
Fe-Mn-C, thermodynamic analysis 77—32563
Fe-Mn-C system, Gibbs energy, high temp. phase relations 78—80779
Fe-Mn-C system, isothermal sections, 873 to 1373K, computer plotting 78—6893
Fe-Mo-C system, isothermal sections, 973 to 1273K, thermodynamic analysis 78—6895
Fe-N phase diagram, thermodynamic anal. 80—60846
Fe-Ni, FCC and BCC lattices, X-ray characteristic temp. *(Russian)* 78—67797
Fe-Ni-Cr system, absolute partial pressures and chem. activities of component metals 80—50600
Fe-Ni-O, computer-assisted anal. and calcs. of phase diagrams 80—25667
Fe-Ni(Cu)(Al)(Si) liquid alloys, thermodynamic characts. calc. *(Russian)* 80—15264
Fe-O, exam. of thermodynamic data, using a computer aided strategy 79—11592
Fe-P-C, amorphous alloy, crystallisation 79—100112
Fe-Zn, homogeneous phases, Gibbs free energies of form., Knudsen effusion method 80—66481
$FeBO_3$, magnetisation near crit. temp., up to 3 kbar hydrostatic press., scaling theory 77—8316
Fe_3BO_6, weak ferromagnetism and spin reorientation, antiferromag. reson. spectra 78—6580
$Fe_3B_7O_{13}I$, improper ferroelectric, dielectric props., IR radiation pyroelectric detection 80—80711
$FeCl_2$, soln., activity coeffs., osmotic coeffs., water activity, Gibbs energy, molality depend. 80—51963
Fe_2Mo, standard Gibbs energies, enthalpies, entropies of formation 78—61042
Fe_3Mo_2, standard Gibbs energies, enthalpies, entropies of formation 78—61042
$FeMoO_3$, standard Gibbs energies, enthalpies, entropies of formation 78—61042
$Fe_{1-x}O$, wustite, vaporisation, mass spectrometric analysis of gaseous phase 78—48652
Fe_3O_4, electron energy band theory, thermodynamic functions *(Korean)* 79—7785
Fe_3O_4, magnetite, vaporisation, mass spectrometric analysis of gaseous phase 78—48652

free energy continued
  Fe_3O_4, standard free energy of formation, by EMF method with solid oxide electrolyte at low temps. *(Japanese)* 80—88338
  Fe_xO, standard free energy of formation, by EMF method with solid oxide electrolyte at low temps. *(Japanese)* 80—88338
  $2FeO.SiO_2.2MnO.SiO_2$ melt, free energy of mixing 79—61572
  $2.33FeO.TiO_2.2.33MnO\text{-}TiO_2$ melt, free energy of mixing 79—61572
  FeS_2, marcasite and pyrite phases sp. ht., thermodynamics of transform. 77—28016
  FeV_2O_4, free energies of form., 1400-1750K, electrochem. method determ. 79—43613
  Ga liquid, solubility and activity of O_2 77—59122
  Ga-Cu liquid alloy, solubility and activity of O_2 77—59122
  Ga-Ge-Zn ternary alloys, thermodynamic props., EMF meas. 80—81033
  Ga-In(Al) systems, thermodynamic anal. 79—60512
  GaAs(Sb), high-temp. thermodynamic data and quantitative fits to liquidus line 77—63637
  GaN film, heteroepitaxial deposition, growth kinetics and catalytic effects 79—4487
  $GdCrO_3$, magnetisation, appl. of molecular field theory 79—4637
  GdF_3, standard enthalpies of formation 79—24810
  Gd_6WO_{12}, thermodynamic and X-ray investig. at 1200-1400K 77—36778
  Ge, liquid, solubility and activity of O_2, 1233 to 1397K 78—44109
  Ge, thermodynamic functions and normalised moments 79—51279
  Ge-Cu, liquid, solubility of O_2 at 1373K, in equilibrium with GeO_2 78—44109
  Ge-Si, phase diagrams near melting point, Helmholtz free energy, heat of solution 80—70379
  Ge-Sn, liq. alloys, thermodyn. props. 77—51518
  GeO_2, free energy of form., EMF meas. 80—35566
  GeP, thermodynamic characts. 10-300K, interatomic bond elasticity 80—59677
  H_2 embrittlement adsorption or decohesion, mechanism 80—97643
  H_2, liquid, perturbation theory and quantum effects, thermodynamic props. and quantum stat. corrections *(Russian)* 78—22867
  H_2, metallic, solubility of He, Gibbs energy, fluid state model, He conc. in giant planets 79—60602
  o-H_2, order-disorder phase transition 78—79726
  HBr-HCl, thermodynamics of binary liquid mixtures 78—64876
  HBr-Xe, thermodynamics of binary liquid mixtures 78—64876
  HCO_3^-(aq), standard enthalpies of solution and formation, standard Gibbs energies of formation and standard entropy 79—57285
  HF oligomers, Gibbs free energies, gas. equilib., ab initio calc. 79—20456
  H_2O, free energy of liq. water, ab initio Monte Carlo calc. 78—83975
  H_2O, liquid, free energy calcs. by random network model 80—92688
  $(H_2O)_n$, n=8, 64, cluster thermodynamics calcs. using Monte Carlo method 77—58219
  HOCO and HOCO*, thermochem. props., 100-300K 78—27805
  HSO, thermochem. props. 79—5173
  ^{3}He, BCC, four-spin interaction effects on ordering processes 77—39721
  ^{3}He, liquid, surface fluctuation influence on free energy, surface tension *(Russian)* 80—92746
  ^{3}He, quasiparticle interactions, transport coeffs. and superfluid free energy 79—95234
  ^{3}He, superfluid, A-phase, slowly rotating, textures and free energy 79—60587
  ^{3}He, superfluid, Bogoliubov transform for spatially varying gap, gradient free energy 78—38901
  ^{3}He, superfluid, free energy, strong coupling corrections, spin-fluctuation theory 78—38899
  ^{3}He, superfluid, frequency sums for free energy 79—33148
  ^{3}He, superfluid, Ginzburg-Landau free energy 77—28063
  ^{3}He, superfluid, phase transitions not controlled by stable fixed points 77—47640
  ^{3}He, superfluid, point and line singularities 78—47625
  ^{3}He, superfluid, strong-coupling effects 77—11758
  ^{3}He, superfluid A phase, planar textures 78—79837
  ^{3}He, superfluid A phase, slowly rotating, textures 79—95236
  ^{3}He, superfluid A-phase, composite solitons, mag. reson. 78—51779
  ^{3}He, superfluid A-phase, rotational textures 79—11002
  ^{3}He, superfluid A-phase, topological struct., nucleation and screening effect 79—1537
  ^{4}He film, Bose-Einstein condensation, thermodynamic functions 79—82399
  ^{4}He, liq., lambda transition free energy in Feynman's model *(French)* 78—71895
  ^{4}He, quantum cryst., ground-state lattice vacancies and Bose-Einstein condensation 77—7943
  ^{4}He, rotating superfluid, vortex patterns and energies 80—6578
  ^{4}He superfluid, acoustic vibration field density of states in piecewise const. parameter media 80—6483
  ^{4}He, superfluid, stress tensor form 77—51558
  ^{4}He, superfluid, vortex ring energy and momentum for large core radius 77—4231
  Hf, liquid, viscosity at melting point, free energy *(Russian)* 80—92699
  $HfB_{2.036}$, $HfC_{0.968}$, ht. capacity, thermodyn. props., 5-350K 77—47590
  Hg-U system, thermodynamic props., vap. press. and EMF expts. 79—91625
  Hg_2Br_2, ferroelastic, Brillouin and Raman scatt. spectra 79—95770
  Hg_2Br_2, nonintrinsic ferroelastic, thermal expansion and thermodynamic potential 80—88344
  $HgCl_2$, second order phase transition, elastic consts. meas., Brillouin scatt. 78—10908
  Ho, thermophysical properties at high temps., exam. *(Russian)* 79—28105
  HoF_3, enthalpy of formation by calorimetry 80—7843
  HoF_3, thermodynamic props., galvanic cell meas. 80—21316
  I^- hydration complexes, gas phase, electrostatic calcs. 80—100055
  I_2 solid charge-transfer complexes, determ. of thermodynamic form. values 80—45540
  In-Cd alloy crystal, phenomenological study of FCC$\rightleftharpoons$FCT transform. *(Japanese)* 79—100140
  In-Sb, metallic soln., association 78—15373
  In-Te, molten thermodynamic props. determ. by EMF method 77—51504
  In-Tl liquid alloy, thermodynamic props. and struct. *(German)* 77—48400
  InAs(Sb), high temp. thermodynamic data, quantitative fits to liquidus line 77—63637
  InSb-Sn(Pb)(Bi), metallic soln., quasibinary alloy, association 78—15373
  IrS_2, thermodynamic props. by effusion technique 77—40570

free energy continued
  K, self-diffusion, high temp. bulk modulus determ. 80—79976
  K, thermodynamic props. at high press. *(Russian)* 78—47536
  KCl:Sr, Ca, simultaneous diffusion, coefficients meas. 78—79813
  KCl-NaCl mixed crystals, contact angles and free energies at solid/melt interface 80—64937
  KDP-type crystals, polarisation, dielec. const. thermodyn. props. 77—59527
  KH_2PO_4, Landau-Devonshire coeffs. 78—15116
  KH_2PO_4, press. and deuteration effects on static ferroelec. props., four-particle cluster approx. 80—34861
  KH_2PO_4, variational treatment of proton-photon system 78—88261
  $KMnF_3$, cubic-to-tetragonal phase transition, critical anomalies, phenomenological eqns. 80—39275
  $K_2Pt(CN)_4Br_{0.3}3H_2O$ incommensurate linear conductors correlation length in 77—80745
  K_2SeO_4, unpolarised-noncommensurate-polarised phase transition, phenomenological theory, based on free energy function 79—15422
  Kr adsorbed on graphite, nonregistered-registered phase transition 80—39414
  Kr-NO, thermodynamics, monomer-dimer assoc. of NO, vap. press. meas. 79—90798
  $LaMnO_3$, stoichiometric manganite form. reaction, thermodynamic characts. 80—108727
  $LaNbO_4$, Raman scatt. and fluoresc. spectra 80—20625
  La_2NiO_4, free energy of formation 77—1240
  $(LaPr)Sn_3$, supercond., free energy and thermodynamical crit. field 77—32127
  Li, thermodynamic props. at high press. *(Russian)* 78—47536
  $Li/TiS_2(TiSe_2)(Ti_{1.1}S_2)$, electrochem. obs. of Li intercalation 80—61216
  Li-Pb, quasi-ionic, thermodynamic props. using EMF meas. 78—51705
  Li-Sb(Bi), thermodynamic props., 355-600°C 78—34634
  Li-Te alloys, liq., electrochem. investig. of thermodynamic props. 77—1244
  LiAl, β phase thermodynamic props., chem. diffusion coeff., electrochem. meas. 80—39308
  $LiAlCl_4$, fast ionic conductor, thermodynamic and phase props. 80—89211
  $LiAlCl_4$, solid and molten electrolyte, thermodynamic stability 80—107447
  $Li_{0.5}Al_{2.5}O_4$, spinel struct. magnetodielectrics, free energy of form. 79—83493
  $LiBF_4$, thermal decomposition, equilib. decomposition press. and enthalpy of form. 79—91983
  $Li_{0.5}Fe_{2.5}O_4$, spinel struct. magnetodielectrics, free energy of form. 79—83493
  $Li_{0.5}Ga_{2.5}O_4$, spinel struct. magnetodielectrics, free energy of form. 79—83493
  Li_xMO_2 (M=transition metal), thermodynamic investigations 80—89210
  Li_2MoO_4, Li_2MoO_7, $Li_2Mo_3O_{10}$ and $Li_2Mo_4O_{13}$, thermodynamic props. 77—12822
  Li_3N, heat capacity 5 to 350K, thermochem. props. to 1086K 78—92500
  Li_3N, vaporisation, studied by Knudsen effusion method 80—92662
  $LiNO_3\text{-}NaNO_3\text{-}AgNO_3$, molten salt mixture, excess thermodynamic props. and US vel. *(French)* 77—31720
  $LiPO_3$ formation, from dihydroorthophosphate dehydration, reaction thermodynamics 79—52643
  $LiRbSO_4$, order-disorder phase transitions with many-minimum potential, thermodynamic props. 80—96623
  $Li_2Si_2O_5$ glass, steady state crystal nucleation rate 79—90564
  $Li_2Si_2O_5$ glass, steady state crystal nucleation rate 79—90565
  $\beta\text{-}Li_xV_2O_{5-y}$ bronzes, thermodynamic props. by coulometric titration 80—34209
  Lu, thermophysical properties at high temps., exam. *(Russian)* 79—28105
  Mg, phonon spectrum and thermodynamic functions, inelastic coherent cold neutron scatt. *(Russian)* 78—55917
  Mg-Cd, thermodynamic props., order-disorder transitions based on Helmholtz free energy 79—37853
  $MgIn_2O_4$ free energy, entropy of form. 78—91433
  Mg_2SnO_4, Gibbs' free energy of form., electrochem. determ. 78—11548
  $Mg_yU_{1-y}O_{2+x}$, thermodynamics from EMF meas., high Mg conc. 78—43143
  Mn bi-univalent cpds., soln., activity and osmotic coeffs., H_2O activity, Gibbs energy, molality depend. 80—51964
  Mn-Ge, thermophysical props., at elevated temp. 80—103493
  $Mn(CO)_5Cl(Br)(I)$, thermodynamic props. tabulation 79—24808
  MnSe, and $MnSe_2$, thermodynamic props. 80—19958
  Mo_2C, free energy of form. and thermodynamic props. of C in solid Mo 80—15266
  MoF_5, vapour, thermodynamic props. calc. 78—38826
  MoO_2, Gibbs energies of form., form. enthalpies and standard entropies 79—52742
  Mo_4O_{11}, Gibbs energies of form., form. enthalpies and standard entropies 79—52742
  N_2, effect of high mag. fields on vapour pressure 78—38825
  N_2, liq., surface tension and density profile from expression for excess free energy 77—80681
  N_2, liq., thermodynamic perturbation theory, equilib. props. 79—64976
  NH_3, ND_3, crystals, rotation mol. motion *(Russian)* 78—87762
  NH_4Br, $\beta\text{-}\gamma$ phase transition, critical anomalies, phenomenological eqns. 80—39275
  $NH_4H_2PO_4$, improper antiferroelec. phase transition, elastic props., free energy, thermodynamic theory 78—80299
  NH_4HSeO_4, ferroelec. phase transition, pyroelec. props. 80—60513
  $(NH_4)_2SO_4(BeF_4)$, order-disorder phase transitions with many-minimum potential, thermodynamic props. 80—96623
  NH_4X, (X=Cl, Br, I), tricritical points, free energy, phenomenological expansion 79—7695
  Na, monovacancy thermodynamic parameter calcs., temp. dependence 78—2114
  Na, thermodynamic props. at high press. *(Russian)* 78—47536
  Na-Cs, liq., struct. factor, free energy of mixing, and electrochem. pot., thermodynamic calc. 80—96436
  Na-Ga liquid alloy, thermodynamic props. 79—37854
  Na-K liquid alloy, electron theory of chemical potential and activity *(Japanese)* 77—72702
  Na-Te system, liq., electrochem. determ. of thermodynamic props. rel. to temp. 77—1245
  Na_2CO_3(s), $NaHCO_3$(s), standard enthalpies of solution and formation, standard Gibbs energies of formation and standard entropy 79—57285

free energy continued
NaCl, Gruneisen γ and other thermodynamic props., vol. depend. 77—76577
NaCl-KCl, aq. solns., isopiestic studies, 383 to 474K 80—21320
$NaCrO_2$, thermodynamic props. 77—69099
Na_xMS_2 (M=Ta,Ti), Na chem. pot. and free energy of intercalation, electrochemical meas. 79—100396
Na_2NiO_2, thermodynamic props. 77—69099
Na_2O-B_2O_3-GeO_2 system glass-forming melts, mass spectrometry obs. of thermodynamic props. 80—97468
Na_2O-Fe_xO_y, (where x=1,2,3, y=1,3,4), thermodynamic props. 77—69099
Na_2SO_4, liq., standard free energy of formation from 1160 to 1220K 78—56911
Na_2SiO_3-K_2SiO_3, molten, thermodynamics of mixing at 1100°C, CaO addition effects 77—47581
$NaUO_3$, ht. capacity and thermodyn. props., 5-350K 77—43343
Nb-H, modulated ordering, elastic free energy theory 79—94945
Nb-K melts, thermodynamic characts., elec. resistivity, single parameter rigid sphere calcs. *(Russian)* 80—34410
Nb-Re(Ru)-N, α-solid soln., thermodynamics *(German)* 77—12600
Nb_3Al, prep. by reduction of Nb_2O_5 and Al_2O_3 by CaH_2, thermodynamic calc. 80—100809
$NbSe_2$, thermal dissociation 78—44370
$NdCo_5$, ferromag., thermomag. charact. in mag. field *(Russian)* 78—23273
Ni alloy, GAB 286, austenitic energetic particle bombardment, thermodynamic and dimensional stability 77—27904
Ni alloys, aluminising, thermodynamic anal. of phase transforms. 80—76413
Ni base melt, thermodynamic props. *(Russian)* 77—55363
Ni bi-univalent cpds., soln., activity coeffs., osmotic coeffs., water activity, Gibbs energy, molality depend. 80—51963
Ni, liquid, N activity coeff. 77—72699
Ni-Cr(Co)(Fe), liquid, N activity coeff. 77—72699
Ni-Cr(Fe)(Cu) alloy, matrix effect in SIMS anal. using O_2^+ primary beam 80—76576
Ni-Ge, liq. alloy, thermodynamic activity, mass spectrometric determ. *(German)* 78—20052
Ni-Nb (5 to 45 at.%) alloys, free energy and thermodynamic props. investigation using EMF method *(Russian)* 79—52160
Ni-S system, Knudsen effusion and thermodynamics 78—79759
Ni-Sn system intermetallic formation rate, H_2 adsorption effect 79—90819
$NiCl_2$-tetra-n-butylammonium iodide melts, densities and kinematic viscosities 79—77793
NiO, meas. of standard molar free energy of form. by EMF method of high temps. *(Japanese)* 78—11546
NiO-$NiAl_2O_4$-Al_2O_3, heterogeneous solid state reactions, role of phase boundaries, dynamic equilib. at interfaces 78—71848
NiS_2, model for weak ferromag. 79—65632
$NiWO_4$, Gibbs' free energy of formation 77—73262
O_2, effect of high mag. fields on vapour pressure 78—38825
O_2, liq., thermodynamic perturbation theory, equilib. props. 79—64976
OH, UV light absorpt. at 3080 Å, for Gibbs free energy of mol. 79—100425
P, crystalline to amorphous transition, thermodynamic functions 80—54354
Pb bi-univalent cpds., soln., activity and osmotic coeffs., H_2O activity, Gibbs energy, molality depend. 80—51964
Pb, impurity diffusion and self-diffusion activation volumes 80—2209
Pb liquid, O_2 activity from electrochem. meas. 80—55695
Pb-Ag, liquid alloy, exam. of thermodynamic props. using solid oxide galvanic cell 78—75851
Pb-Bi, thermodynamic props. 77—59743
Pb-In films, atom redistrib., ion-ion emission obs. *(Russian)* 78—18926
Pb-Sn, lamellar eutectic alloy, proximity effect, entropies, free energies and transition temps. 77—51849
$Pb(Fe_{2/3}W_{1/3})O_3$-$Pb(M_{3/2}W_{1/2})O_3$, (M-Mn, Co, Ni), ferroelec. phenomenological theory 79—99831
$Pb_{1-x}Ge_xTe$, Raman scatt. from soft TO-phonon modes 79—95773
$Pb_{1-x}Ge_xTe$, TO phonon interaction with acoustic phonons near phase transition temp. 79—90776
PbO, standard free energy of formation, by EMF method with solid oxide electrolyte at low temps. *(Japanese)* 80—88338
PbO-Bi_2O_3, thermodynamic props. 77—59743
PbO-$PbSO_4$ melts, thermodynamics, determination of free energies of mixing at 1253K 78—83976
PbO-$PbSO_4$ system, discussion of thermodynamics of oxide-sulphate melts 79—82358
PbO-$PbSO_4$ system, thermodynamics 79—82359
PbO-TiO_2, solid phase reactions, thermodynamic anal. 77—12603
PbSe, enthalpy, heat capacity, 300 to 1480K 79—60523
$PbSiO_3$ and Pb_2SiO_4, vitreous, free energy of form. at elevated temps. 79—43195
PbTe, thermodynamic props. 77—28023
Pd-Pt alloys, soln. of H_3, partial thermodynamic parameters determ. 77—66027
Pd-Rh alloys, soln. of H_2, partial thermodynamic parameters determ. 77—66027
$Pd_{0.9}Ag_{0.1}$:H(D), free energy, enthalpies of soln. 78—15692
PdO, free energy of form. using impedance dispersion analysis 80—108728
$Pd_{80}Si_{20}$ metallic glass, inelastic deform., free energy spectra 80—71699
$PrFeO_3$, thermodynamic study of form. 78—48685
Pt-Al(In)(Sn) alloys, Fermi energy influence on thermodynamic props. *(German)* 80—24619
Pt-Zr(Hf), high temp. thermodynamic props. 77—63633
$PuO_{(2)}$, spectroscopic data rel. to thermodynamic functions 80—34208
Rb-Cs liquid alloy, electron theory of chemical potential and activity *(Japanese)* 77—72702
$RbH_3(SeO_3)_2$, ferroelec., thermodynamic theory of phase transitions 77—90112
$RbPO_3$ formation, from dihydroorthophosphate dehydration, reaction thermodynamics 79—52643
RbX-CdX_2-H_2O, X=Cl,Br,I, Gibbs free energy, H_2O activity, 25°C *(Russian)* 78—31678
Ru complex, $(2,2'\text{-bipyridyl})_3\text{ruthenium}^{2+}$, excited-state redox processes, electron transfer theory 79—39126
α-S, under hydrostatic press., deformable mol. lattice statics 80—49175
Sb, liquid, diffusion of O_2, activity coeff. 80—65267

free energy continued
Sb liquid, O_2 activity from electrochem. meas. 80—55695
Sb, liquid, solubility and activity of O_2 *(German)* 79—90793
Sb-Bi, melting kinetics of solid soln. during high heating rates, superheating *(Russian)* 78—15358
Sb_2O_3, energies of formation, solid-state electrochemical techniques 80—6527
Sb_2O_3, standard free energy of formation, by EMF method with solid oxide electrolyte at low temps. *(Japanese)* 80—88338
SbSI, free energy function, temp. depend. and anisotropy of dielec. const., ferro- and paraelec. phases 78—64330
α-Se, monoclinic, heat capacities and thermodynamic properties, 3-300K 78—95162
Se, monoclinic to trigonal conversion, thermodynamic stability and associated investigs. 80—24592
$1/2S_2(g) \rightleftarrows S(l)$ equil. reaction, improved ΔG^0 values calc. 77—32822
Si:Se, impurity states, A- and B-centres, electron, hole thermionic emission rates 80—96813
β-SiC, thermodynamic props., temp. depend., 5 to 300K 80—96666
Si_3N_4-Al_2O_3-AlN, isothermal sections, free energy of formation 80—55363
SiO_2, reduction by C using a plasma, thermodynamic computer anal. 77—40530
SiO_2-Al_2O_3, calculated thermodynamic data and metastable immiscibility 78—27495
SiO_2-Al_2O_3-Si_3N_4, isothermal sections, free energy of formation 80—55363
SiP, thermodynamic characts. 10-300K, interatomic bond elasticity 80—59677
$SmMnO_3$, thermogravimetric study of phase stability 79—100121
$Sn_xGe_{1-x}Te$, ferroelec. semicond. structural phase transition, X-ray study 79—37836
SnO_2, electrochem. determ. of free energy 79—82360
SnO_2, electrochemical determination of free energy of formation 79—11797
SnTe, standard free energy of form. 79—57287
Sr Nb_2O_6, crystallography, polymorphism and isomerism, X-ray diffr. and DTA study 80—100216
$SrTiO_3$ ceramic, sp. ht and electrocaloric effects at low temps. 77—59518
$SrTiO_3$, thermodynamic props. 77—39680
$SrWO_4$ cryst. growth, from Na_2WO_4 melts, thermodynamic props. 80—107084
Ta BCC lattice, strain ordering in interstitial solutions 80—107420
Ta-D system, thermodynamic stability of Ta_2D, rel. to long-range order parameters *(Japanese)* 78—15376
Ta_2D_{1+x}, phase relations in terms of long-range order 79—38808
$Tb_2(MoO_4)_3$, improper ferroelectric, dielectric props., IR radiation pyroelectric detection 80—80711
$Tc(CO)_5Cl(Br)(I)$, thermodynamic props. tabulation 79—24808
TcF_6, heat capacity, entropy Gibbs energy, 2.23-350K 78—38852
Te-$TeBr_4$ system, Gibbs free energy of reaction, electrochem. e.m.f. expts. 79—91991
Te-$TeCl_4$ system, Gibbs free energy of reaction, electrochem. e.m.f. expts. 79—91991
Te-TeI_4 system, Gibbs free energy of reaction, electrochem. e.m.f. expts. 79—91991
$(Th,U)O_2$, burnup simulated, high O_2 pot., chem. state 80—91220
Th-Os(Ir) system, phase diagram and thermodynamic props. *(German)* 79—47958
$ThCl_4$, in LiCl-KCl and Na-K eutectic solns., thermodynamic props. 77—86345
$ThO_{(2)}$, spectroscopic data rel. to thermodynamic functions 80—34208
Ti, liquid, viscosity at melting point, free energy *(Russian)* 80—92699
Ti, surface and grain boundary free energy, zero-creep determ. 79—4313
Ti-Al-V (6,4 wt.%), surface and grain boundary free energy, zero-creep determ. 79—4313
Ti-Co alloys, absorpt. of H_2, thermodynamic parameters calc. 80—2268
Ti-Cu system, appl. of metal-hydrogen equilibration determ. thermodynamic props. 79—77772
Ti-Ir alloys, Ti-rich, thermodynamic study at high temp. using Knudsen cell mass spectrometry 80—45539
Ti-Ir system, high temp. thermodynamic investig. of Ir-rich portion by Knudsen cell mass spectrometry 77—12595
Ti-Ni alloys, absorpt. of H_2, thermodynamic parameters calc. 80—2268
$TiCl_3$, layer compound, theoretical study of phase transition, energy bonds calc. 79—10945
TiO_2, rutile, reduction by C, thermodynamic and struct. study, 1400 to 1600K 79—52650
TiO_{2-x}, nonstoichiometric and Nb_2O_5 doped rutile, defect struct. and thermodynamic props. 79—86790
Ti_nO_{2n-1}, long-range strain and localised relax. energies of crystallographic shear structs. 79—94948
Tl-Pb-Hg system, thermodynamic props. *(Russian)* 77—25018
Tl_xTe_{1-x}, thermodynamic evidence against large scale fluctuations in composition in heterogeneous transport models 77—28172
TmF_3, thermodynamic props., galvanic cell meas. 80—21316
U bi-univalent cpds., soln., activity and osmotic coeffs., H_2O activity, Gibbs energy, molality depend. 80—51964
$UAs_2(Sb_2)$, heat capacities, antiferromag.-paramag. transitions 78—76253
UH_3, UD_3, dissoc., isotope effect 80—26174
$UO_{(2)(3)}$, spectroscopic data rel. to thermodynamic functions 80—34208
U_3Si, heat capacity and thermodynamic props., 1 to 1203K 77—72697
V, liquid, viscosity at melting point, free energy *(Russian)* 80—92699
V-Ge, thermophysical props., at elevated temp. 80—103493
V-S system, order-disorder transition of metal vacancies, statistical thermodynamics 78—43012
VO_2, metal-insulator transition, electron correls. and spin dimerization, thermodynamical study 80—70615
VO_x, diffuse scatt., relation to curvature of free energy surface 79—99025
V_3S_4-V_5S_8 system, exam. of thermodynamic props. at temp. from 650 to 800°C 78—52784
VSb_2, free-energy, heat and entropy of formation, 430-600°C *(Ukrainian)* 80—7837
VSi_2, thermodynamic props. determ. using ternary phase equilibria 78—91449
V_3Si, mixed state, ultrasonic anomaly 77—55644
V_3Si, mixed state A15 struct., Gibbs free energy and lower crit. field temp. depend. 77—55643

free energy continued
- V_3Si, thermodynamic props. determ. using ternary phase equilibria 78−91449
- V_5Si_3, thermodynamic props. determ. using ternary phase equilibria 78−91449
- W, self-diffusion, high temp. bulk modulus determ. 80−79976
- W-Re, neutron irrad. effects on phase stability free energy changes 79−11566
- WO_3, force field, normal coord. anal., kinetic consts. method, thermodynamic props. 78−25504
- Xe adsorbed monolayers, thermodynamic props. and lattice const., quasi-harmonic theory 79−42380
- Y, thermophysical properties at high temps., exam. *(Russian)* 79−28105
- Y-Fe-O, phase equilib. and thermodynamics, solid state high temp. electrochem. obs. 79−56967
- $YFeO_3$, dissociation press. and Gibbs energy of form. 79−11816
- $YFeO_3$, thermodynamic study of form. 78−48685
- $YMnO_3$, thermogravimetric study of phase stability 79−100121
- YbF_3, standard enthalpies of formation 79−24810
- $YbMnO_3$, thermogravimetric study of phase stability 79−100121
- Zn-Al, near eutectoid alloy, deformation kinetics analysis 79−29161
- Zn-bearing binary substitutional solutions, thermodynamics 80−44337
- $Zn_3(OH)_4(NO_3)_2$, sp. ht., 5-300K, thermodynamic props. 79−55900
- $Zn(OH)(NO)_3.H_2O$, sp. ht., 5-300K, thermodynamic props. 79−55900
- $Zn_5(OH)_8(NO_3)_2.2H_2O$, sp. ht., 5-300K, thermodynamic props. 79−55900
- $Zn(g)+H_2O(g)=ZnO(s)+H_2(g)$, standard Gibbs free energy of reaction 79−11815
- Zr, liquid, viscosity at melting point, free energy *(Russian)* 80−92699
- Zr-Nb, phase transformation sequences, prediction using free energy composition diagrams 79−4951
- Zr-Nb (20 wt.%) ω-phase transform., structural model, intensity distrib. in neutron diffr. 77−77472
- Zr-Ta (5 wt.%) martensite, β_1 precipitation, thermodynamics 79−74164
- ZrI_4, high-temp. enthalpy, X-ray powder diffr. data 80−107446
- $ZrN-Al_2O_3$ sintering reaction thermodynamics 80−2989
- ZrN-Mo, cermet, sintering reaction thermodynamics 80−2989
- ZrO_2, doped, ionic cond., theoretical model 80−107552
- ZrO_2, substoichiometric, thermodynamic props. at lower phase boundary 80−29185

free field rooms *see anechoic chambers*

free induction decay (optical) *see optical coherent transients*

free radical reactions
- abstraction-addition step, free radical-bonded pair reactions, Yamaguchi theory 77−52624
- acetyl radical decomposition and recombination, in acetone photochem. and photophysics expts. 78−17706
- N-acetylglucosamide, substrate-inhibitor of lysozyme, localisation of unpaired electrons 78−68992
- acetylperoxy radicals, absorpt. spectrum and reaction kinetics 80−91571
- adamantane, radiation chem. alkylation 77−48663
- addition, rate consts. calc. 78−40023
- adrenaline, acid aq. solns., pulse radiolysis, H., OH. react. kinetics, UV spectra 77−16841
- air-acetylene flame, atom form., theory 78−7208
- albumin, Reanal serum, mag. field effect on photoinduced reactions 79−92154
- aliphatic nitroxyl radicals, quenching of triplet state aromatic hydrocarbons, energy transfer 78−35651
- alkali metal salt solution, Ar saturated, sonoluminesc. as acoustic cavitation probe 79−60437
- allyl chain free radical, decay kinetics in γ-irrad. polyethylene state depend. 78−76855
- allyl free radical decay, in irrad. polyethylene, const. diffusion controlled rate const. 78−15651
- D-amino acid oxidase, crit. residues, pulse radiolysis and inactivation study 78−27897
- amino acids, aq. solns. EPR of spin-trapped radicals, hydrated electron reactions 78−27796
- anthracene anion+dimethylaniline cation, recombination reaction in soln., time-resolved mag. field effect 80−3308
- anthracene anion radicals, enthalpy of disproportionation, calorimetric determ. technique 79−96296
- aromatic radical ion recomb., mag. field modulation, Liouville eqn. soln. 77−28995
- aromatic substitution mechanisms 77−9056
- ascorbic acid, action with perhydroxyl radicals, radiolytic study 80−35523
- bacterioviridin, photochem. oxidation mechanism 77−25370
- benzophenone ketyl radical, in micelle, decay rate in mag. field, photolysis meas. 80−85154
- bilirubin, aq. soln., pulse radiolysis 78−48761
- bromomethyne radical+paraffins (olefins)(O_2)(NO), absolute reaction rate parameters 77−1909
- bromotrifluoromethane, IR multiphoton selective dissoc., effect of acceptor radicals 80−66854
- butyl radical$+O_2$, reaction rate consts. meas. 80−45490
- carbohydrate solutions, irradiated, lyoluminesc. and carbohydrate peroxy radical reactions 77−48665
- carbohydrates, reactions with hydrated electrons and hydroxyl radicals, rate constants obs. 80−50825
- cationic polymerisation promotion by free radicals 79−34301
- cellulose, nitrated, strength, deform. and disintegration, influence of stable free nitroxyl radicals 80−11717
- chemically induced dynamic polarisation in strong mag. field, radical rotation influence 80−76509
- chlorophyll photo-oxidation mechanism, effect of spectral composition of light 77−25369
- CIDEP, examples of $S-T_{\pm 1}$ polarisation 78−86891
- compartmentalised free radical polymerisation reactions 79−24748
- copolymerisation, reactivity ratios, press. directional effect 79−100362
- copolymerisation kinetics, monomer reactivity ratios under high press. conditions, meas. methods 79−91950
- correlated radical pairs recomb., const. and oscill. mag. fields effects 77−86311
- cycloalkane radical ion charge transfer reaction 79−45774
- cytosine monohydrate single cryst., X-irrad., OH addition radical and decay product 77−86447

free radical reactions continued
- diazonium, amplifying material, kinetic and sensitometric props. *(German)* 79−43607
- dichlorodifluoromethane+OH reaction, rate const. and tropospheric lifetime 77−64366
- difluoromethane, IR laser-induced reactions 77−77792
- dimethylamino radical$+O_2(NO)(NO_2)$, reaction rate constants, FTIR obs. 80−16652
- diradical+singlet reaction, SCF calc. involving orbital symm. forbidden reaction pathway 79−98004
- DNA, single-stranded, alkali-labile sites and post-irrad. effects induced by H radicals 78−68994
- doublet and quartet states, abstraction reactions, pot. energy surfaces calcs. 78−31627
- doublet with singlet ground state electronic system, long range interaction energy, CNDO approx. 80−53089
- electron pairs, destiny in chem. reactions 79−52652
- emulsion polymerisation, ideal, first-stage kinetics calcs. *(Russian)* 79−66295
- ethane, X-irradiated, 4.2K, pairwise radical trapping mechanism, EPR obs. 79−100412
- ethyl radical decomposition, mol. dynamics, trajectory studies 80−7780
- ethylene polymerisation and dissociation in high-freq. discharge 77−70299
- ethylperoxy radical$+NO_2$, reaction rate const. meas. 80−21262
- ethylperoxy radicals+NO reaction, flash photolysis and kinetic spectroscopy obs. of rate consts. 79−83470
- fast reaction kinetics meas. by ESR of free radicals 80−21286
- ferricytochrome, photoreduction in presence and absence of electron donor 78−53337
- fluoroethyl radical, unimol. dissoc., pot. energy characts. and energy partitioning calcs. 80−45488
- fluoromethylene$+NO \rightarrow HF+CNO$, vibr. energy distrib., lasing action in dichlorofluoromethane-O_2 78−48644
- fluoromethylene$+O_2 \rightarrow HF+CO_2$, vibr. energy distrib., lasing action in dichlorofluoromethane-O_2 78−48644
- furil, photochem. reduction by pentachlorophenol, zero-field CIDNP study 77−90625
- haloalkyl peroxy radical$+NO_2$, haloalkyl peroxynitrate form., FT IR obs. 79−34283
- Heisenberg models, local spin symmetry conservations of biradical species 77−32778
- hexafluoroethane, RF discharge chemistry, added H_2 effect 80−33832
- hydrated electrons, photochem. generated in solns., decay kinetics 77−52656
- imidazoles, reaction with photochemically generated α-hydroxyalkyl radicals, EPR study 80−35558
- imidazoline nitroxide radical, H-bonding with H donors, NMR, DNP and spin lattice meas. 79−15971
- indole, aq. solns., flash photolysis, transient absorpts., 600 to 800 nm 78−53228
- indoles, laser flash spectroscopy in presence of nitroxide radicals, protein-membrane interaction probing 79−87855
- interstellar dense clouds, molecular composition 77−29892
- intratrajectory reacts. in radiolysis of aq. solns. by recoil particles from $^{10}B(n,\alpha)^7Li$ *(French)* 77−12812
- invertase, S-containing glycoprotein, gamma-irrad., secondary radical reactions, EPR 77−9175
- iodoheptafluoropropane, photolysis, reaction rate consts. meas., photodissociation I laser characts. 79−52671
- iodotrifluoromethane, IR multiphoton selective dissoc., effect of acceptor radicals 80−66854
- iodotrifluoromethane, photolysis, reaction rate consts. meas., photodissociation I laser characts. 79−52671
- ion pair geminate recomb., polar solvents, mag. field modulated, stochastic Liouville eqn. 77−86302
- isobutane$+HO \rightarrow H_2O+$iso(or t-)C_4H_9, 700 and 100 torr, 25°C, FT-IR anal. 77−25247
- jasmone and intermediate compound synthesis *(Japanese)* 79−8436
- ketone chemiluminescence during disproportionation, nonradiative transition processes 79−87846
- lactate dehydrogenase+free radicals, reactions, pulse radiolysis 78−7214
- laser studies of relaxation and reaction of species in defined quantum states 80−11918
- Liouville generalised eqn. solns., density matrices 78−27739
- lipid free radical oxidation, UV effect on lipid-protein complexes and membranes 77−36874
- lipid free radical oxidation kinetics rel. to lipid composition, photoreceptor membrane 78−80872
- liquid crystal alignment by O_2 RF plasma exposed solid surfaces 77−76307
- liquid phase, cage model, solvent effects 77−16811
- mechanisms, mathematical theory 78−48647
- methane, X-irradiated, 4.2K, pairwise radical trapping mechanism, EPR obs. 79−100412
- methanethiol+OH radical, reaction rate const., 299-426K 77−40525
- methanol glass, H atom abstraction by methyl radicals, 15-100K, limiting rate const. rel. to tunnelling 77−60037
- methyl(-d) radical recombination rate const. calcs. in low press. limit 77−4891
- methyl radical+ethylene(acetylene)(propene)(allene), reaction pot. surfaces, MINDO/3 calcs. 79−22601
- methyl radical$+O_2$ (NO), mass spectra, absence of reaction in combustion system 78−53195
- methyl radical+O(F), infrared chemiluminescence obs. 80−61080
- methyl radical decay in methanol glass, accumulation and dark decay kinetics 79−74352
- methylamine+OH radical, reaction rate const. 299-426K 77−40525
- 6-methylmercaptopurine riboside, 4 MeV electron irrad., 77K radicals form., EPR obs. 78−39405
- MO calculation of radical and unsaturated polymer interactions 77−44481
- muon spin rotation in free radical chemistry 79−57209
- naphthalene anion radical$+H_2O$, react., H_2 prod. 78−92460
- naphthalene radical anion+TCNQ, electron transfer reactions, theory 78−15661
- nitroaromatic compound+anion radical, photo-CIDNP, acid-base equilib. effects 77−75185
- nitrosodisulphonate ion salt dimerisation, ESR of dimers in triplet state *(French)* 77−12791

free radical reactions continued
nitroxyl radical reduction kinetics, modelling non-enzymatic influence of membranes 78-64945
Norrish type II reaction biradicals+O_2, diffusion controlled rate const. 77-90617
paramagnetic centre unpaired electron density rel. to reactivity 77-52633
pentafluoroacetone, IR laser induced decomp., free radical mechanism 80-71924
peptide aqueous solution, EPR of spin-trapped radicals, OH radical reactions 78-68993
peroxymethyl radical+NO, reaction rate const. 79-61848
peroxymethyl radical+peroxymethyl radical, reaction kinetics, H_2O vap. depend 79-61844
phenol derivatives, neutral aq. solns., flash photolysis, N_2O and alcohol effects 78-40065
phenoxy radical dimer, reversible diffusion controlled dissoc., detailed equilib. principle 80-7770
photo-initiated, CIDNP 78-13526
photoinduced radical pair recombination in high mag. field, Monte Carlo method 79-87861
photoinduced recombination of atoms and radicals 79-5170
photolytically initiated, high temp. kinetics meas. technique 80-61085
photoreceptor membrane viscosity and component dynamics, recombination kinetics method 79-39366
polyethylene, low-density, γ-irrad., spin trapping reaction 80-39873
polymer, charged particle detect., graft-and-dye method 78-17520
polymerisation chemistry, mol. wt., chain-unit struct. control, review 77-40544
polymers, multiphoton photodestruction, free radical formation 79-39177
polynucleotides, single-stranded, reaction of O_2 with radiation-induced free radicals 78-48759
polynucleotides poly(A+U), double-stranded, radiolysis in presence of O_2 78-48760
polyvinyl cyclohexane, head-to-head, prep., characterisation 79-70036
protein-lipid model systems, chemiluminesc. on exposure to formalin 77-56329
pyrene+N,N-dimethylaniline (deuterate)(3,5 dimethoxy-N,N-dimethylaniline), geminate recomb., solvent, isotope, mag. field effects 78-56888
radiation-induced chemical carcinogenesis, redox model 80-26298
radical+radical, mag. field effects on rates, theory, projection rule 77-86312
radical+radical reactions, reaction path calc. using perturbation expansion *(German)* 79-34300
recombination, rate consts. meas., student expt. 79-48996
recombination kinetics of radical pairs, solid matrix, 1, 2 and 3 dimens. theory 78-27793
recombination probability in liqs., HF mag. field, reson. effect 80-93737
recombination reaction kinetics in atm. chem. 79-53410
recombination reactions, mag. field modulation, time depend. soln. 78-15662
recombination reactions, short time behaviour, spin multiplicity of radical pair 77-81393
retina of developing frog eye, free radical reactions rel. to mitosis, daily vars. 77-56376
rhodamine 6G in soln., photochem. stability 78-37878
secondar free radicals, primary reacting with substrated, CIDEP relax. time, theory 78-25573
selection rules 78-7181
spin-dependent reaction probabilities theory 78-20002
spin-selective reactions, density matrix description 77-12790
stiff boundary valued problems in kinetics and diffusion, numerical methods 79-86525
stilbene, radiolysis, electron transfer and protonation, vis. spectra, isomer effects 77-60085
styrene divinylbenzene, viscosity meas. during radical copolymerisation 80-3344
submitochondrial particle succinic dehydrogenase, interaction of ubisemiquinone with Fe-S centre, EPR 78-69016
symmetry selection rules for ro-vibronic states 77-81385
tetracene anion radicals, enthalpy of disproportionation, calorimetric determ. technique 79-96296
tetrafluoroethylene radical ion+tetrafluoroethylene, cycloaddition 78-13533
tetrafluoromethane, RF discharge chemistry, added H_2 effect 80-33832
thiamine (vitamin B_{12}), aq. soln., radiation induced reactions 80-93779
toluene, H at. abstraction by free radical, transition state charge development 79-83438
transient radicals, generation for EPR spectrosc. 80-11271
2,4,6-tri-tert-butylnitrosobenzene, reactions in γ-irrad. tetrahydro-2-methylfuran glass 78-10776
trifluoromethane, RF discharge chemistry, added H_2 effect 80-33832
trifluoromethyl radical reactions, prod. and meas. by IR multiphoton dissoc. of iodotrifluoromethane 80-26036
tryptophyl peptides, pulse radiolysis, hydrated electron reaction 78-48679
unsaturated fatty acids, free radical oxidation, mag. field effects 79-15992
AgBr crystal produced by action of free radicals, developability 80-66838
$Ar^{+\cdot}$+fluoromethanes, thermal energy charge transfer reactions mechanism 77-63889
BrO+ClO, reaction rate consts., mass spectrometry meas. 78-3316
C, activated+H_2, react., EPR spectra, paramag. props. alteration 77-63957
$C_3+NO(O_2)$, reaction kinetics, laser induced fluoresc. obs. of allene photolysis 80-66820
CCl+alkynes, absolute reaction rate consts. 78-27728
$CCl_3O_2+NO+NO_3$, photolysis, $CCl_3O_2NO_2$ thermal decomposition in stratosphere 79-57256
$CF_3+CH_4(H_2)(HCL)$, H abstraction, energies of activation calc. 78-31632
$CH_2+H_2 \rightarrow CH_4$, MINDO/3-FORCES calc., acativation energy and enthalpy of reaction 78-66472
$CH_2+H_2 \rightarrow$methyl radical, SCF calc. involving orbital symm. forbidden reaction pathway 79-98004
$CH_3+CH_4(H_2)(HCl)$, H abstraction, energies of activation calc. 78-31632
$CH_3+O_2 \rightarrow OH+H_2CO$, 368K, rate const. upper limit 80-7771

free radical reactions continued
$CH_3^{\cdot}$+ethylene, transition state, ab initio calc. 78-48640
$C_2H_2+OH^- \rightleftharpoons C_2H^- +H_2O$, equilib. consts., ab initio SCF and CEPA calcs. 78-3361
CHO short-lived radical recombination, intracavity laser spectroscopy obs. 79-61858
CH_3O_2, radical, form. and decay rates, UV absorpt. spectra 77-48631
CH_3O_2+NO, rate const., flash photolysis and kinetic spectroscopy 79-70305
$(CH_3)_3SnH$, radical initiated dissoc., Sn isotope separation *(Russian)* 79-59604
$CH(X^2\Pi)$ radical, prod., detect. and reactions 79-61842
CN+NO, reaction rate constants 79-1935
$CN+O \rightarrow CO+N$, flash photolysis, absorption spectrosc. obs. 79-66289
CO+OH(+isobutane), reaction rate consts., press. depend. 78-35654
$CO^{+\cdot}$+fluoromethanes, thermal energy charge transfer reactions mechanism 77-63889
$CO_2^{+\cdot}$+fluoromethanes, thermal energy charge transfer reactions mechanism 77-63889
$C_2(a^3\Pi_u)$+methane(acetylene)(ethylene)(ethane)(O_2), reaction rate consts. and quenching, multiphoton UV photolysis, fluoresc. obs. 79-74355
$C_2(a^3\Pi_u)$+NO(vinyl cyanide)(ethylene), laser-generated radical kinetics 79-100352
Cl+methane-methane-d_2, free radical chain reaction, D isotope photochem. enrichment 79-36790
$Cl+OH^* \rightarrow HCl^*+O$, reaction dynamics, vibr. excited reagent and product 77-81392
ClO+formaldehyde, expt. showing no reactivity, stratospheric implications 80-90119
$ClO+HO_2$, reaction rate consts. and products at 298K, discharge flow mass spectra 80-67391
$ClO+NO_2+M \rightarrow ClONO_2+M$, react. in stratosphere, $ClONO_2$ form., photolysis 77-33154
$ClO+O \rightarrow Cl+O_2$, reaction kinetics, 220 to 426K, at. fluoresc. obs. 77-21380
$ClONO_2+O(^3P)$, photolytic gas phase kinetics at 245K 79-52719
ClOO+NO, reaction in stratosphere 79-34889
$Cl.+XHC{=}CH_2$, free radical reaction theory, ab initio calc. 77-52624
DO_2+NO, reaction kinetics, near IR chemiluminesc. determ. 80-21261
$F+SiO_2$, heterogeneous reaction, discharge-flow tube meas. 80-21274
$F^{\cdot}$+ethylene, transition state, ab initio calc. 78-48640
$H^{\cdot}$, S-$T_{\pm 1}$ polarisation, CIDEP in pulse radiolysis 77-48656
H+C, surface chemical reaction of thermal at. H 78-20071
$H+CH_4 \rightarrow H_2+CH_3$, transition state, UHF method in INDO approx, 79-43578
$H+NH_2 \rightarrow NH_3$ react., force, density anal. 78-60997
HCO, prod. by formaldehyde photolysis, vibr. relax., chem. kinetics and spectra 79-11808
$HCO+NO(O_2)$, reaction rate consts. 78-31617
$HO+CO \rightarrow H+CO_2$, 700 and 100 torr, 25°C, FT-IR anal. 77-25247
HO_2 radical, atmospheric reactions studied by laser mag. reson. spectroscopy 80-12511
$HO_2+CO(HO_2)$, in H_2-O_2-CO, 500°C, rate consts. 78-35646
HO_2+Cl react. rate const. determ. at 298K *(French)* 78-64817
$HO_2+ClO \rightarrow HOCl+O_2$, reaction rate consts. 79-5140
$HO_2+H_2O_2$, Haber-Weiss reaction kinetics, chain mechanism 79-83444
HO_2+HO_2, gas phase reaction mechanism, FT IR spectrosc. obs. 80-85163
HO_2+HO_2, reaction rate, press. depend. 80-7766
$HO_2+HO \rightarrow H_2O+O_2$, rate coeff. meas. by laser mag. reson., atm. chem. appl. 77-52614
HO_2+NO, reaction kinetics, near IR chemiluminesc. determ. 80-21261
HO_2+NO_2, UV irradiated, kinetics and mechanism, peroxynitric acid form., smog 77-63885
$HO_2+NO \rightarrow OH+NO_2$, kinetics temp. depend. 80-3313
$HPO_4^-(H_2PO_4)$ radicals + organic compounds, reaction rate consts. 78-15669
$He^{+\cdot}$+fluoromethanes, thermal energy charge transfer reactions mechanism 77-63889
I radical recombination in dense liquids, stochastic trajectory simulation 80-45487
$Kr^{+\cdot}$+fluoromethanes, thermal energy charge transfer reactions mechanism 77-63889
$LiH+H \rightarrow Li+H_2$, $Li+H_2 \rightarrow LiH+H$, LiHH pot. function calcs. 77-6699
$N_2^{+\cdot}$+fluoromethanes, thermal energy charge transfer reactions mechanism 77-63889
N_3+NCl, reaction rate consts. calc. 79-74342
N_3+O, NO chemilum. obs. in NaN_3 thermal decomp. N_3 form. 79-100351
$NCNO \rightleftharpoons NC+NO$, ground state pot. energy surface, ab initio calcs. 77-90593
$ND^*+DN_3 \rightarrow ND_2^*+N_3$, chemiluminesc. reaction of electronically excited species, rate const. 78-80771
NF+H(NF), electronically-excited free radical reactions 80-97707
NF_2+H(O)(N), electronically-excited free radical reactions 80-97707
NH, ND, $(b^1\Sigma^+)$ states quenching by deuterated cpds., kinetic isotope effects 77-63891
NH, photofragment, energy distrib., chemiluminesc. reaction rates 77-90618
NH reactions obs. using photolysis of HN_3 in C_2H_6 or C_3H_8 soln. 79-83471
NH_2 free radical recombination meas. using intraresonator laser spectroscopy 77-86292
NH_2+HO_2, rate const., in NH_3+O_2 flash photolysis 79-47943
NH_2+NO_2, reaction rate const. meas. 80-7772
NH_2+O_3, reaction mechanism, flash photolysis obs. 80-104425
NH_3+radical ion, thermal energy charge transfer, reaction mechanism 77-16796
$NH_3^{\cdot +}+H_2O \rightarrow NH_4^+ +OH^{\cdot}$, statistical phase space theoretical anal., vibr. depend. cross section 78-15660
$NH_3^{\cdot +}+NH_3 \rightarrow NH_4^+ +NH_2^{\cdot}$, statistical phase space theoretical anal., vibr. depend. cross section 78-15660
$NH(X^3\Delta^-)$ radical, form., detect. and reactions 79-64036
NO dimerisation, equilib. const. anal., trans-/cis-$(NO)_2$ zero pt. correlation energy difference 78-11509
NO+formaldehyde(-d_2), laser beam-induced free radical reactions, quenching 78-44387
NO+OH radical-molecule reactions, relax. and rate consts. 80-11918
$NO_2+ROO \rightarrow ROONO_2$, $(R=C_nH_{2n+1})$, Fourier transform IR spectroscopic meas. 78-53194

free radical reactions continued
- $Ne^{+\cdot}$+fluoromethanes; thermal energy charge transfer reactions mechanism 77—63889
- O in methane-air flame, reactions, radical overshoot 79—34308
- O+biradical, from γ-methyl valerophenone photolysis, lifetime and quantum yield meas. 77—60086
- O+$ClONO_2$, in stratosphere, rate constants 77—33134
- O+methane→OH+methyl reaction, photolytically initiated, high temp. kinetics meas. technique 80—61085
- O_2^-+H_2O_2, Haber-Weiss reaction kinetics, chain mechanism 79—83444
- $O_2^+AsF_6^-$, thermal decomposition, Raman spectra study, free radical mechanism 80—55652
- $O(^1D)$+chlorofluoromethane, stratospheric chem. reactions 79—53499
- $O_2F.+Cl+O_2$, $ClF^*(B^3\pi_0+)$ prod., B-X emission spectrum 79—57216
- OH, radical, atmospheric reactivity with organic compounds 79—61860
- OH radical, reactions with ester vapours, reaction rate consts. determ. at 292k 78—27729
- OH radical participation in terminal muon spur for muonium prod. 79—57271
- OH+2-methyl-2-butene, reaction rate consts. meas. 78—61001
- OH+acetylene (CO), reaction rate consts. meas. 78—35663
- OH+alkanes (alkenes), photooxidation, 305K, absolute and rel. rate consts. 77—16782
- OH+alkene, absolute rate consts., 297K 79—100353
- OH+allene (1,3-butadiene)(3-methyl-1-butene), absolute rate consts. 78—23927
- OH+benzene-(toluene)(1,3,5-trimethylbenzene), cross mol. expt., product anal., 300K 78—44353
- OH+CO, HOCO and HOCO* form., thermochem. props. 78—27805
- OH+CO, reaction mechanism, HOCO radical stability 77—73436
- OH+CO, reaction rate consts. at 296K, press. effect 77—73435
- OH+$COS(CS_2)$(dimethyl thioether), reaction rate consts., 299-430K 78—35653
- OH+$ClONO_2$, in stratosphere, rate constants 77—33134
- OH+$ClO(Cl_2)(Cl_2O)$, rate const. at 298K, rel. to stratospheric O_3 depletion 79—87831
- OH+dimethyl ether (vinyl methyl ether) reaction rate consts., 299-427K 77—86301
- OH+dimethyl sulphide, flash photolysis reson. fluoresc. rate consts. determ., pollution aspects 78—95913
- OH+dimethylamine, rate const., 298-426K, Arrhenius expressions and activation energy 78—48619
- OH+ethylamine, rate const., 298-426K, Arrhenius expressions and activation energy 78—48619
- OH+ethylene, reaction rate consts., 229-425K 77—40535
- OH+formaldehyde (acetaldehyde), rate consts., 299-426K, UV flash photolysis, reson. fluoresc. obs. 78—68873
- OH+gaseous S compounds, lower atmos. chem. 80—61870
- OH+H_2O_2, reaction rate const., 298K, flash photolysis-reson. fluoresc. obs. 79—57215
- $OH+H_2O_2 \rightarrow HO_2+H_2O$, reaction rate consts., laser induced fluoresc. 80—101017
- OH+H_2SO_4, collisional reaction probabilities atmospheric chem. 80—90168
- OH+H_2(CO), in H_2-O_2-CO, 500°C, rate consts. 78—35646
- $OH+HBr \rightarrow H_2O+Br$ absolute rate const., 249-416K 79—70303
- OH+HCN, reaction rate, press. depend. 78—85135
- OH+HCl, reaction rate const. temp. depend., stratospheric implications 78—31616
- $OH+HO_2 \rightarrow H_2O+O_2$, rate const. meas. *(German)* 79—52629
- OH+halocarbons rate consts., appl. to tropospheric degradation 79—52622
- OH+methane+M, absolute rate consts., 296K, flash-photolysis reson. absorpt. technique 77—86290
- OH+n-propyl acetate (sec-butyl acetate) (tetrahydrofuran) (peroxyacetyl nitrate), raction rate consts., in irrad. NO_x mixture 78—7171
- $OH+O_3 \rightarrow HO_2+O_2$, reaction rate const., 238-357K 79—47902
- OH+$OCS(CS_2)$, flash photolysis reson. fluoresc. rate consts. determ., global S cycle 78—95914
- OH+$OCS(CS_2)$, lower atmosphere chem. 80—61870
- $OH+OH \rightarrow H_2O+O$, rate meas. by UV absorpt., 1200 to 1800K 78—35642
- $OH+RH \rightarrow H_2O+R$, radical substitution reaction 80—81321
- OH+SO_2, role for stratospheric HSO_3 layer, reaction rate consts. 78—32202
- OH+trans-2-butene, reaction products, O_2 and NO_2 effects obs. 80—85156
- OH+trichloroethane, 1,1,1- and 1,1,2-isomers, reaction kinetics, 298-460K, lower atmos. chem. 80—16657
- OH+trichloroethane→$H_2O+CH_2CCl_3$, rate const. and tropospheric chem. 80—16658
- OH+trimethylamine, rate const., 298-426K, Arrhenius expressions and activation energy 78—48619
- OH+vinyl halides, reaction rate consts., 299-426K 77—81389
- $OH^\cdot+CH_3SH$, $OH^\cdot+CH_3NH_2$, reaction rate consts., 299-426K 77—40525
- $OH^\cdot$+$CO(N_2O)$, rate consts. 77—16781
- $OH^\cdot$+O, $OH^\cdot$+CO, reaction rates, mechanism, flow discharge chemilum. obs. 77—52610
- $^{18}OH+CO_2(CO)$, evidence for at. exchange 79—47910
- OH.+N_2O reaction, rate const. meas., N_2O atmospheric residence time appl. 77—21352
- ON+azomethane, rate const. meas. 80—7771
- $O(^3P)+CHF \rightarrow HF+CO$, product vibr. energy distrib. 79—61853
- PH_3+radical ion, thermal energy charge transfer, reaction mechanism 77—16796
- PO_4^{2-} anion radicals + organic compounds, reaction rate consts. 78—15669
- $(SN)_n^*$ radicals polymerisation to $(SN)_x$ in thin films, optical spectra 80—16656
- $SO_2+H_2O+O_2(N_2)(Ar)$, condensation nuclei form., ion polarity and age depend. 79—39220
- U_2O_8, radioiodine release in O_2 and inert gas atm., chem. identities 77—57712
- $Xe^{+\cdot}$+fluoromethanes, thermal energy charge transfer reactions mechanism 77—63889

free radicals
- *see also free radical reactions; paramagnetic resonance of free radicals*
- σ^*, ESR of radical in N-bromosuccinimide, X-irrad. 80—66037
- acetaldehyde photolysis, HCO product microwave spectra 79—5163

free radicals continued
- acetaldehyde radical cation, fragmentation, MO calc. 79—18109
- acetate ion radicals, solns., pulse radiolysis, CIDEP, viscosity depend. 77—75189
- acetate radical CIDEP, appl. of ns time-resolved EPR in pulse radiolysis 80—43075
- acetophenone enolate anion radicals, substituted, electron photodetachment cross sections, reson. states 80—1030
- acetyl radical, absorpt. spectrum obtained by flash photolysis and kinetic spectroscopy 79—13731
- acetyl radical, photofragment spectroscopy, collision dynamics 78—25636
- N-acetyle DL-methionine, γ-irradiated, radical cation EPR, ^{33}S hyperfine coupling 77—40559
- N-acetylglycine, X-irrad., stable radical electronic and mol. struct., ENDOR and ESR 80—80637
- acetylperoxy radicals, absorpt. spectrum and reaction kinetics 80—91571
- acid amide+H_2O_2, aq. solns., photolysis, EPR study of spin-trapped radicals formed during photolysis 78—68996
- acyloxy radical ion, in irrad. Rochelle salt, decarboxylation, pulse radiolysis and EPR obs. 78—70854
- adamantane, γ-irrad., free radicals EPR and ENDOR 80—69170
- L-α-alanine, cryst., cationic radicals, EPR 78—11537
- albumin, human serum, kinetics of eosin-sensitised photochemilum. of solns. 78—68991
- albumin, pulsed laser study of adsorbed aromatic mol. excited states 77—86448
- alcohol dehydrogenases, yeast and horse-liver, radiation chem. evidence for differences in amino acid composition 78—40116
- alkali ion pairs, intramolecular cation migration, freezing out by crown ether addition 77—58047
- alkanes, electron localisation and solvation, radical ion theory 78—87936
- n-alkanes, single cryst., γ-irrad., ESR, energy deposition rel. to alkyl radical form. 77—16844
- alkoxy, proton hyperfine coupling in X-irrad. hydroxy cpds., ENDOR obs. 80—50863
- alkoxy free radicals, produced by X-irrad. of hydroxy containing cpds., characterisation by ESR and ENDOR 78—95938
- alkoxy primary radical, prod. by X-irrad. of α-methyl-D-glucopyranoside, ESR and ENDOR study 80—45526
- alkoxy radical, trapped in nucleosides or nucleotides, EPR, INDO calcs. 77—90623
- N-alkyl free radicals, ESR study, conformational anal. of N-alkyl group 78—62831
- alkyl halide and σ^* anion radicals, stability 80—89468
- alkyl substituted diacetylene radical cations, optical emission and photoelectron spectra, fragmentation decay 80—53004
- allyl cation and radical, ab initio non-paired spatial orbital wavefunctions 77—26968
- allyl radical, ab initio SCF solns., doublet stability 78—33423
- allyl radical, doublet state, open shell RPA unitary group formulation, Hartree Fock stability eqns. 80—52860
- allyl radical, ionisation potential, ab initio valence bond calcs. 79—31407
- allyl radical, restricted ab initio SCF LCAO solns., doublet stability 77—79539
- allyl radical, restricted SCF and MC SCF calc. of C_{2v} and C_s structs. 80—83289
- allyl radicals, in irrad. polyethylene, distrib., trapping regions 78—91957
- amino acid, in polycryst., γ-irrad. induced radical pair form., 77K, EPR obs. 78—85292
- amino acids, technique for study of radiation in induced free radicals using lyoluminesc. 77—29230
- α-aminoisobutyric acid, cryst., γ-irrad., cation radicals, ESR obs., SCF-MO-INDO calcs. 78—11537
- p-aminophenol, oxidation in aq. soln., chem. equilib. of free radicals, review 79—43573
- anthracene, α-induced radical production beyond Bragg peak 79—24773
- anthracene, cryst., radiation induced radicals, optical absorpt. bands, SCF-CI MO calc. 79—91463
- anthracene, radical cation, EPR, acidic surface anisotropic rot. diffusion 78—27095
- anthronyl radicals, ESR, temp. depend. phenyl twist angles 79—18210
- atmospheric, meas. by matrix isolation EPR 78—46374
- atmospheric meas. by matrix isolation and EPR 78—73535
- bacteriochlorophyll radicals, role in primary charge separation of Rhodopseudomonas viridis 80—63688
- bacteriochlorophyll-800, implication in picosec. electron transfer to bacteriopheophytin in R.rubrum reaction centres 80—35844
- bacteriophage T7, radiation inactivation 78—65083
- bacteriopheophytin b radicals, role in primary charge separation of Rhodopseudomonas viridis 80—63688
- benzene, cation radical, charge exchánge reagent appls. 78—70929
- benzene, plasma polymerisation in glow discharge, thin film IR and free radical EPR obs. 80—2964
- benzene, substituted cations, spectroscopy, substituent effects 78—58709
- benzene radical anion, ab initio MO calcs., struct. 79—18113
- benzene radical cation in solid Ar, fluorescence spectra obs. 80—83382
- 1,3,5-benzene triyltris (1,5-diphenyl-3-verdazyl), rot. diffusion in nematic phase, EPR spectra 77—36135
- benzophenone, aqueous system, LET depend. of transient yields in deuteron and alpha pulse radiolysis 77—63940
- benzophenone betyl radical, photochem. yield mag. field effect on spin rephasing, double-pulse technique 77—90615
- benzophenone in isopropanol, submicrosecond time resolved EPR, lser photolysis, CIDEP polarisation mech. 78—80764
- benzophenone ketyl radical, in micelle, decay rate in mag. field, photolysis meas. 80—85154
- 1,4-benzosemiquinone, monoprotonated radical, spin distrib., INDO calcs. 77—14357
- p-benzosemiquinone monoprotonated radical, submicrosecond time resolved EPR, lser photolysis, CIDEP polarisation mech. 78—80764
- N-benzoylaminomethyl radical, from X-irrad. hippuric acid, ^{14}N and ^1H ENDOR study 80—71240
- 3,4-benzphenanthrene cation radical, in boric acid glass, spectrum 200-1400 nm, MO calcs., assignments 77—75174
- benzyl, $1^2B_2 \rightarrow 2^2B_2$ electronic excitation, natural orbital occupation numbers calcs. 79—45638
- benzyl bromide, photolysis, free radical form., investig. 80—102523
- benzyl chloride, photolysis, free radical form., investig. 80—102523
- benzyl radical, 1^2B_2-3^2B_2 transition in absorpt. spectrum, extinction coeffs. 80—102523
- benzyl radical, IR absorpt. spectra, matrix isolated at 77K 79—22706

free radicals continued
benzyl radical, MINDO/3-FORCES, geom. of heat of formation 78—66472
benzyl radical trapped in X-irrad. potassium hydrogen bisphenylacetate, ENDOR 77—10695
benzyl radical-halide ions, form. by dissoc. electron attachment in matrix, charge transfer band 77—16854
benzyl radicals, monomtheyl- and dimethyl-substituted, electronic spectra and electron affinity 80—63618
benzyne, struct. and IR spectrum, MNDO calc. 79—31403
binaphthyl anion radicals, photoisomerisation, local heating effects 78—85179
binary complex, quinone-phenol radical pair EPR, geometry calc. 78—90101
biphenyl single crysts., γ-ray induced radicals, EPR and optical absorpt. studies 80—44921
biradical, triplet state, S-T$_0$ CIDNP, biradical scavenging rate const. from mag. field depend. CIDNP 79—3461
biradical magnetic field dependent ^{13}C and ^{1}H CIDNP, hyperfine coupling 79—3460
biradical metal chelates, rot. motion in polar solvents, rel. to ESR lineshape 80—27994
1,3-bisdiphenylene-2-(p-chlorophenyl)-allyl, antiferromag. resonance, antiferromag. phase transition 78—6579
bromanil and radical anion, Raman and IR freq. shifts 78—33516
1-bromoadamantane, orientationally disordered, γ-irrad. free radical defects, positron probe obs. 79—23647
bromobenzene -d$_0$(-d$_5$) radical cation, electron impact dissoc., secondary isotope effect 80—63836
bromodifluoromethyl radical, IR matrix isolation spectrum, stretching fundamentals 78—27788
α-bromofluoro alkyl pi-radical, signs of hyperfine and quadrupole couplings, ESR determ. 80—97141
bromofluoromethylene radical, laser-induced fluoresc., $^1A''$-$^1A'$ transition 80—91589
bromomethyne radical+paraffins (olefins)(O$_2$)(NO), absolute reaction rate parameters 77—1909
butadiynyl radical, interstellar, detect. towards (IRC+10216) 78—93374
t-butanol, aqueous system, LET depend. of transient yields in deuteron and alpha pulse radiolysis 77—63940
cis-butene, ozonolysis, radical form., matrix ESR spectrosc. 80—16653
n-butoxy radicals, intramol. isomerisation, following n-butyl nitrite pyrolysis 79—20355
n-butyl radical, matrix isolation IR spectrum 78—33510
t-butyl radical, VUV photoelectron spectrum, geometry, vibr. struct. and ionisation pots. 78—50577
butyl radical+O$_2$, reaction rate consts. meas. 80—45490
t-butyl radicals, ab initio geometry calc., ^{13}C hyperfine coupling 77—10580
calcium tartrate tetrahydrate, X-ray irrad. single cryst., free radical EPR 77—63936
carbazole cation radical, optical absorpt. spectra 77—40564
carbenes, triplet state g-tensors and hyperfine coupling tensors 80—52895
carbonyl oxide, config. interaction calc., using DODS natural orbit approach 78—66476
carboxylic esters, γ-irrad. glass, trapped radical photolysis, ESR 78—85178
carbyne and interstellar grains 78—69859
carotenoid pigments, radical ions, radiolysis generation, absorpt. spectra, MO calcs. 77—65488
chloranil and radical anion, Raman and IR freq. shifts 78—33516
α-chloro radical in X-irradiated 5-chlorodeoxyuridine single crysts., ESR, ENDOR 77—4916
chloroethane diradical, MINDO/3 for optimised geometry and heat of form. 78—78830
chlorofluorocarbene, ($^1A''$) state, radiative lifetime, quenching rate, press. depend., laser-induced fluoresc. obs. 78—5259
chlorofluoromethanes, laser photolysis, product vibr. relax. rates and diffusion coeffs. 80—55680
chlorofluoromethylene, radical, laser-induced fluoresc. excitation spectra 79—98131
chlorofluoromethylene radical, gas phase laser-induced floresc. spectroscopy 80—14173
chloromethylene radical, MINDO/3 for optimised geometry and heat of form. 78—78830
chlorophyll a, cation radical formation by pulse radiolysis, oxidation and demetalation rate consts. 80—61505
chlorophyll a, photo-oxidation by p-benzoquinone, nature of electron-excited state 78—76991
chlorophyll radical cations, NMR, hyperfine coupling 79—8482
chlorophyll-a radical cation lifetime in water-acetonitrile soln. 80—72136
chlorophyll-a radical cations, in disordered systems, electron spin echo envelope modulation, isotope effects 78—61141
chlorotrifluoroethylene, multiphoton dissoc., fragment energy partitioning 80—55681
chlorotrifluoroethylene radical anions, EPR spectra and struct. 79—31558
cholesteric products, gamma irradiation, effect of presence of organic solvents 79—24777
chondromucoprotein, effects of ^{60}Co γ-irrad. 78—7400
chromosome aberration form. by gamma irrad. in lymphocytes, protection by free radical scavenging 78—20216
CIDEP, examples of S-T$_{\pm1}$ polarisation 78—86891
CIDEP of radicals prod. by flash photolysis 78—13535
CIDEP of radiolytically produced radicals 78—13534
citric acid, single cryst., X-irrad., EPR and ENDOR, 4.2K radical identification 79—65764
ClF$_6$, EPR of matrix, isolated radical 79—85977
collision-induced state-changes, intermol. pot. well depth role 79—81257
comets neutral atmospheres, average random walk model for mol. phot. dissociation 80—77351
concanavalin A-carbohydrate interactions, implication of protein aromatic amino acids, radiolysis 78—40110
condensed media, electron localisation and solvation, radical ion theory 78—87936
coronene trimer radical cation, spin densities in CH$_3$Cl$_2$-CH$_3$NO$_2$ solvent mixture, −100°C 80—5565
coumarin, aqueous solution, fast neutron irrad., dosimetry appl. 78—44613
crystal, electron-irradiated, free radical stabilisation, filler content effects *(Russian)* 77—56241

free radicals continued
cyanoacetylene, photoelectron spectra, electronic states of radical cations 79—22756
cyanomethyl radical, electronic struct. and props. 79—49938
cyclopentadienyl radical, pot. surface and vibronic states, ab initio CI calcs. 80—47897
cyclopentadienyl radical, vibronic valence isomerisation, Jahn-Teller effect, D$_{5h}$ symmetry 79—97986
cyclopropenyl radical and anion, planar, E state pot. surfaces, CI and SCF calcs. 78—5155
L-cysteine HCl, free radical formation by two photon absorpt. at 3371 Å 77—32815
cytidine-5′-monophosphate, γ-irrad. aq. soln., spin-trapped radicals, liq. chromatography and EPR spectroscopy 78—53340
di-(2,2,6,6-tetramethyl-4-piperidinyl-1-oxyl)-suberate, spin densities, polarised neutron diffr. meas. 80—50037
di-t-butyl nitroxide, in benzene, solvent-solute interactions, ESR, DNP 78—17698
di-t-butyl nitroxide radical, in soln., proton relax., meas. of H-bonding 78—27103
di-t-butylnitroxide radical, solid, nucl. and electron spin relax. times meas. 78—60350
diacetylene, single cryst., photopolymerisation, intermediate states, struct. changes 80—30235
diacetylene radical cation, and deuterated forms, electronic spectrum in solid inert gases 79—94026
N,N′-dialkyl dipyridinium cation radicals, struct., INDO calcs., EPR obs. 77—71821
diatomic radicals, wavefunctions, populations and orbital energies, Roothaan calcs. 78—86773
1,3- and 1,4-dichlorobenzene radical cation, emission and photoelectron spectra, lifetimes meas. 78—86905
dichlorocarbene, $^1B_1$ state, radiative lifetime, quenching rate, press. depend., laser-induced fluoresc. obs. 78—5259
dichlorocarbene, electronic spectrum, ab initio CI calcs. 79—85948
dichlorodifluoromethane, UV photolysis, free radical emission 80—30263
dichloromethylene, radical, emission and excitation spectra, in Ar matrix 77—34657
dichloromethylene, radical, laser-induced fluoresc. excitation spectra 79—98131
dichloromethylene radical, MINDO/3 for optimised geometry and heat of form. 78—78830
dicyanoacetylene radical cation, $\tilde{A}^2\Sigma_g^+ \rightarrow \tilde{X}^2\Pi_u$ emission band system 79—22721
dicyanodiacetylene radical cation, photoelectron and emission spectra 80—5558
1,3- difluorobenzene radical cation, and deuterated forms, laser-induced fluoresc. matrix. study 79—98138
difluorocarbene, $\tilde{A}^1B_1$-$\tilde{X}^1A_1$ system spectrosc. and photophysics 80—5577
difluorodiacetylene radical cation, $\tilde{A}$-$\tilde{X}$ band emission spectra, $\tilde{A}$ state lifetime 79—72327
difluoroethene, cis- and trans-, photoelectron-photoion coincidence study, fluoresc. obs. 80—95678
difluoromethane, triplet state emission spectra, phosphoresc. and energy transfer 78—53196
dihalodiacetylene radical cations, $A^2\Pi_u$-$X^2\Pi_y$ system, emission spectra and state lifetime 79—10121
dihalogenated benzene derivatives, 77K, gamma radialysis radical pair formation, EPR 79—29334
dihalogenoacetylene radical cations, C$_2$X$_2^+$, emission spectra, $A^2\Pi \rightarrow X^2\Pi$ band systems 78—17679
α-diketone radical anions, spin-lattice relax. in soln. 79—22735
dimethyl-diacetylene, radical cation, fluoresc. spectra, matrix isolated 79—45752
dimethylamino radical+O$_2$(NO)(NO$_2$), reaction rate constants, FTIR obs. 80—16652
dimethylseleniumchloride, formed by X-irrad. of Ph$_3$SeCl cryst., ESR study 79—39167
9,10-diphenylanthracene, electrogenerated chemiluminescence, T$_2$ state emission 78—60524
diphenylketyl radical, fluoresc. lifetime and quantum yield, organic matrix, 77-130K 78—42110
dispiro compound I, pyrolysis, CIDNP, S-T mixing, nuclear Overhauser effect 77—6803
DNA, transforming, X-ray sensitivity rel. to presence of free radicals 78—68995
DNA lesion production, role of radicals, E. coli X-ray endonuclease specificity 77—52745
doublet states, positive ion potential anal. in CNDO/BW calc. 80—91452
DPPH, mag. susceptibility of solvent-free and DPPH-benzene complex 78—70963
DPPH-benzene, organic radical, pressure induced mag. ordering *(Russian)* 78—88120
DSO, radical, electronic spectrum and struct. 77—75147
duro-semiquinone monoprotonated radical, submicrosecond time resolved EPR, lser photolysis, CIDEP polarisation mech. 78—80764
duryal radical in durene matrix, optical coherent transient spectra 79—76764
n-eicosane, single cryst., electron irrad., free radical pair form., ESR 77—4913
electron spin echo theory, in nonviscous soln. 77—3386
ENDOR spin-echo lineshape, density matrix, free radicals in soln. 78—35064
ESR studies of transient free radicals in irradiated food components 79—52699
ethane, X-irradiated, 4.2K, pairwise radical trapping mechanism, EPR obs. 79—100412
ethenoxy, config. interaction calc., using DODS natural orbit approach 78—66476
ethyl radical, $^{13}C_\alpha$ and H$^+$ hyperfine interactions, EPR spectra, vibr. anal. 80—23443
ethyl radical, C-C bond barrier rot., IR spectra 80—76536
ethyl radical, geom. struct., Hartree-Fock calcs. 78—62722
ethyl radical, photochemical studies 80—3373
ethyl radical, photoelectron spectra, first ionis. pot. 77—58078
ethyl radical proton exchange reaction with ethylene matrix, indirect ESR obs. 80—16700
ethylene, ozonolysis, radical form., matrix ESR spectrosc. 80—16653
ethylene radical cation, electronic states assignments, ab initio SCF CI calcs. 77—10584

free radicals continued
ethylperoxy radical+NO_2, reaction rate const. meas. 80−21262
ethynyl radical, emission spectra and pot. energy surface, ab initio MRD CI calc. 79−41099
ethynyl radical, interstellar abundance and distrib. 78−65664
ethynyl radical, vertical electronic spectrum, CI calcs. 77−34656
ethynylradical, photodetachment, parturbation theory calcs., ICR spectroscopy obs 79−98166
fibrinogen solution, effect of scavengers on radiation-susceptible sites 78−11701
flames, diagnostic techniques, ion-molecule thermochemistry 80−55664
fluorene: acridene, radical pair form. from excited states, optical nucl. polarisation obs. 80−14155
fluorobenzene radical anion, ab initio MO calcs., struct. 79−18113
fluorobenzene radical cations, in gas phase, laser-induced fluoresc. 79−27022
fluorobenzene radical cations, matrix laser fluoresc. spectra 80−1009
fluorobenzene radical cations in solid Ne, laser-induced fluoresc. spectra, vibr. struct. of excited and ground states 80−95671
fluorobenzenes, radical cations, $B(\pi^{-1})$ excited states, radiative relax. 78−13546
fluorobromomethanes, matrix photoionisation and radiolysis, IR spectra of free radicals 79−24765
fluoroethyl radical, unimol. dissoc., pot. energy characts. and energy partitioning calcs. 80−45488
formaldehyde anion radical, hyperfine coupling consts., vibr. depend,, ab initio calcs. 80−87150
formyl radical, -d_0, (-d_1), first ionis. pot., photoelectron spectrosc. determ. 80−48039
formyl radical, atmospheric oxidation, IR Fourier transform spectroscopic obs. 79−66785
formyl radical, electronic struct., dissoc. energy and pot. energy surface many body perturbation theory and couple cluster doubles calc. 80−23296
formyl radical, form., vibr. relax., spectrosc. 79−36746
formyl radical, laser mag. reson. spectrum at 5.3 micron 80−47981
formyl radical, lower electronic states, ab initio calc. of pot. energy surface, hydrocarbon flame band 79−68287
formyl radical-d_0,-d_1, microwave spectroscopy, high field Zeeman effect 78−37631
galvinoxyl, radical in a smectic liq. cryst., ENDOR study 79−78567
galvinoxyl radical in phenol matrix, ESR spectra 80−54950
geminate species, recomb. in presence of a scavenger, probability calcs. 79−31644
germyl radicals, benzil adducts, organometallic group dynamic migration, EPR 77−58049
glyceraldehyde-3-phosphate dehydrogenase radiolysis, active-site and SH loss 78−77000
glycine, cryst., cationic radicals, EPR 78−11537
glycyl anion radical, in α-glycine cryst., struct., ESR obs. 78−33530
glyoxal-photoreduction-product-radicals, kinetics and intramol. dynamics 77−32808
halide dioxide radical form., H_2O_2 decomposition of halide-coated surface, EPR obs. 80−7851
haloacetylenes, photoelectron spectra, electronic states of radical cations 79−22756
halogenoacetylene radical cations, C_2HX^+, emission spectra, $A^2\Pi \rightarrow X^2\Pi$ band systems 78−17678
halogermane radical anions, ESR spectra and struct. 80−87153
5-halouracils, solid, radiation damage, free radicals in 5-fluorouracil single crysts. 80−71926
heat capacities, molar, correlation coeffs., data collection 78−85188
hexafluoride radicals, prep. and EPR spectra comparison, hyperfine splitting 78−68381
hexafluorobenzene+bisdiphenylenephenylallyl radical, solvent effects on collisions, dynamic nucl. polaris., spin-lattice relax. 77−63303
hexafluorobenzene anion-radicals in squalane, ESR spectrum optical detection 80−95655
hexafluorobenzene radical anion, ^{13}C hyperfine interaction, EPR obs. 80−83392
1, 3, 5-hexatriene, radical cations, emission spectra of cis and trans isomers 77−6793
1,3,5-hexatriene radical cation, in Ne matrix, laser induced fluoresc. and emission spectra 80−87163
high resolution spectroscopy *(Japanese)* 79−79355
high-temperature molecules, matrix isolation spectra, review 78−46340
hydrocarbon radicals, ab initio calc. of spin densities 79−93938
hydrocarbon radicals, planar and nonplanar, g-factors, π-σ delocalisation 78−58580
1-hydronaphthyl radical, 4.2K absorpt. spectrum *(French)* 80−80809
1-hydronaphthyl radical, in naphthalene single cryst., anisotropic oscill. strength 78−50591
hydronaphthyl radicals embedded in naphthalene cryst., optical transition energies and ionisation energies 80−78595
hydroxycarbene, intermediate formaldehyde photochem., ab initio calc. methods 79−61880
hydroxymethyl radical+solvated electron, reaction in methanol, dose and base effects 78−20043
hydroxymethyl radicals, adsorption on A-type zeolites, electron spin echo obs. 78−21947
hydroxymethylene intermediacy in low-temp. matrix photolysis of formaldehyde, IR obs. 78−76877
hydroxymethylene radical cation stability, $CH_2O^{+\cdot}$ isomers, ab initio MO study 80−42965
hyperfine struct., EPR cepstra method determ. 80−102531
iminoxyl radical, addition to MBBA liq. cryst., domain struct. parameter depend. *(Russian)* 77−58948
iminoxyl radicals, influence on elec. cond. of MBBA, EBBA liq. crysts. *(Russian)* 78−67641
in flame, with low press. counterflow, spectrosc. and probe obs. *(Russian)* 77−36755
interstellar molecules, matrix isolation spectra, review 78−46340
iodomethyl radical, vibr. excited, photofragmentation IR emission obs. 80−87162
β-iodophenylacetylene radical, PhC_2I^-, from γ-irrad. morpholine β-iodophenylacetylene complex, EPR obs. 77−52652
isocyanoethynyl radical, theoretical study and rot. const. 78−33633
isocyanomethyl radical, electronic struct. and props. 79−49938
isopropyl radical, Ar matrix isolated, IR spectra and UV photolysis 80−66827

free radicals continued
ketyl radical+benzophenone, triplet-doublet energy transfer, viscosity and mag. field effects 77−71850
laser fluoresc. detection with high time resolution 80−9632
lipids of membranes, free radical formation on UV irrad. 80−81647
liquid crystal:aromatic free radical, D quadrupole splittings, ENDOR and TRIPLE reson. obs. 77−51989
lithium acetate dihydrate, γ-irradiated single crystal, $CH_3...CO_2$ pairs, e.s.r. 77−9100
magnetic field modulation of geminate recombination of radical ions in polar solvent 77−4912
matrix isolation spectra, radicals formed by collision with AR 79−50008
matrix isolation spectroscopy 79−80688
metalloporphyrin, cation radical formation by pulse radiolysis, oxidation and demetalation rate consts. 80−61505
β-methallyl radical, formed in photolysis, extinction coeffs. 77−1938
methane, X-irradiated, 4.2K, pairwise radical trapping mechanism, EPR obs. 79−100412
methanol multiphoton photolysis-produced radicals luminesc. 78−3358
methoxy, Jahn-Teller induced rovibronic effect, nuclear spin-electron spin hyperfine Hamiltonian 80−83298
methoxy detection by submillimetric laser spectrometer 77−40623
methoxy free radical, laser mag. reson. submillimetre spectrum, linear Zeeman effect 77−46579
methoxy radical, LMR spectra anal. 80−63677
methoxy radical and deuterate, vibronic level fluoresc. spectrum 80−58305
methoxy radical fluoresc. spectra induced by laser, UV region 79−59498
methoxy radical prod. from 266 nm photolysis of methyl nitrite 80−76534
methoxy radical UV emission spectra from methanol+Ar(Kr) reactions 80−91572
methyl isocyanide photodissoc., cyanide radical energy partitioning chemical laser determ. 78−73063
methyl radical, ab initio projected unrestricted Hartree-Fock calcs. 78−58582
methyl radical, HeI photoelectron spectrum, Franck-Condon factors 77−34692
methyl radical, hyperfine coupling, in ground and excited states, Green's function calcs. 77−6692
methyl radical, hyperfine coupling consts., vibr. depend., ab initio calcs. 80−87150
methyl radical, in γ-irrad. lithium acetate dihydrate, ENDOR, line-shape model appl. 79−73853
methyl radical, vibr. excited, photofragmentation IR emission obs. 80−87162
methyl radical+ethylene(acetylene)(propene)(allene), reaction pot. surfaces, MINDO/3 calcs. 79−22601
methyl radical and anion, electron affinity determ., ab initio SCF and CI calcs. 78−5149
methyl radical in glassy organic matrices, electron spin-lattice relax. 78−76312
methyl radicals, reactions behind shock waves, UV absorpt. obs. 78−46362
2-methyl tetrahydrofuran radical formation on liq. phase γ-radiolysis. 77−60080
methyl thiyl radical, emission spectrum, collisional quenching 78−13543
γ-methyl valerophenone, photolysis, biradical form., lifetime, interaction with O 77−60086
4-methyl-2,6-t-butylphenol, γ-irrad., electron-methyl group spin-spin interaction 77−85572
methylbenzene cations, photodissoc. spectra, substituent effects 78−58710
methylchloride, $CH_3Cl^{\cdot +}$, photofragmentation at 366 nm 78−58752
methylene, $^1B_1$-$^1A_1$ separation, ab initio 80−106251
methylene, classical stretching dynamics 80−23400
methylene, triplet state g-tensors and hyperfine coupling tensors 80−52895
methylene, zero-field splitting, absolute sign, EPR determ. 77−10692
methylene+$HD(D_2)(H_2)$, isotopic exchange, interstellar implications 80−61087
methylene diiodide, in 3-methyl pentane, γ-radiolysis 79−24776
methylene isolectronic radical, separation of two lowest states, comparison with NH_2^+ 80−53047
methylene peroxide, struct., energy levels, ab. initio UHF and MRUHF NO CI calcs. 80−83287
methylene radical, vibronic bands obs. in pulsed supersonic jet 80−28024
methylene radical anion and dimer, semiempirical CNDO/2 and nonempirical SCF calcs. 77−79535
methylene radicals, rotational transitions, laser mag. resonance spectra 80−5538
3- methylhexane, glass, γ-irradiated, trapped electron-radical mag. energy transfer, ELDOR, cross relax. 77−16209
6-methylmercaptopurine riboside, S-substituted nucleoside, ESR and ENDOR obs. 77−36766
2-methyltetrahydrofuran, glass, γ-irradiated, trapped electron-radical mag. energy transfer, ELDOR, cross relax. 77−16209
methyoxy radical, electronic absorpt. spectra, visible, vibr. freqs., vibronic intensities and oscill. strengths 80−28025
microwave spectroscopy of short-lived molecules, review 79−50010
MINDO/3 unrestricted open-shell calcs. of geometries and electronic struct. 77−23429
molecular cryst., triplet exciton annihilation and triplet exciton quenching by free radicals, analytical form of mag. field depend. of rate consts. 79−15094
monoalkylbenzenides, anion radicals, EPR, temp. depend., vibronic interaction, proton HFS 77−34666
muonic radicals, μSR precession freqs. 79−55004
muonic radicals, μSR spectra obs. 80−69279
muonic radicals, muon spin resonance frequency spectra, theory 80−1088
muonic radicals formation 79−57277
muonium-substituted transient radicals observed by muon spin rotation 78−74678
N-acetyl-L-leucine, single crysts., X-ray induced free radicals 80−45525
N-alkylated phenazine type radicals, mag. props. 79−73671
naphthalene:1-hydrodynaphthyl, cryst., charge transfer optical transitions 77−44027
naphthalene, $C_{10}H_8$ and $C_{10}D_8$, optical absorpt. spectra of hydronaphthyl radicals, isotope effects 78−60487

free radicals continued
naphthalene, cryst., radiation induced radicals, optical absorpt. bands, SCF-CI MO calc. 79—91463
(naphthalene)$^-$(naphthalene)$^+$ radical pairs, ESR absorption, optical detection 80—7166
naphthalene radical anion, ethereal soln., far IR spectra 78—62796
naphthalene radical anion+TCNQ, electron transfer reactions, theory 78—15661
naphthalene radical cation, in organic glass, 77K, reson. Raman spectra 78—78704
naphthalenes, methyl substituted radical cations, UHF spin densities, additivity model calcs. 80—58139
neutral free radicals, in Ar matrix, IR spectrosc. evidence 78—66546
neutral radical proton interactions, applic. of anisotropic HFS tensors for double zeta functions 77—35903
nitrobenzene, adsorbed radicals, oxide surface chem., ESR 77—21417
nitrone, config. interaction calc., using DODS natural orbit approach 78—66476
nitroxide free radicals, neutral, EPR spectra, localised solvent-radical adducts 79—96290
nitroxide free radicals in liquids, electron spin-echo obs. 80—63685
nitroxide radical ELDOR obs. for discriminating rot. and transl. correl. times in liqs. 77—1619
nitroxide spin probes, solubilised, ESR obs. in cetyltrimethylammonium bromide micelles 78—21950
nitroxyl radical, aromatic hydrocarbon singlet state quenching, triplet form. 77—88487
nitroxyl radical rotation in liquids, ESR, dielec. relax. 77—28447
nitroxyl radicals, cyclic, conform. flexibility, EPR obs. 80—91581
2-norbornyl radical, photolysis prod. and EPR, hyperfine splitting 77—56237
Norrish type II reaction biradicals, spectra, extinction coeffs., solvent effect on lifetime 77—90617
Norrish type II reaction photogenerated biradical lifetimes, solvent effects 79—11804
octane radical cations in γ-irrad. pentane matrices, ESR 77—36765
organic, solid, selective pulse NMR expts. 80—60452
organic Π-radicals, open shell systems, spin density calc., program for semiempirical calc. *(Rumanian)* 79—72241
organic doublet radicals in nematic and smectic liq. crysts., ENDOR obs. 80—91585
organic radicals, HFS coupling const. calcs., RHF+CI method in INDO approx. 79—770
oxiphenol, radical transform. in aqueous solns., chem. equilib. *(Russian)* 79—39138
perfluorohexadiyne radical cation, $\tilde{A}$-$\tilde{X}$ band emission spectra, $\tilde{A}$ state lifetime 79—72327
perfluoropentadiyne radical cation, $\tilde{A}$-$\tilde{X}$ band emission spectra, $\tilde{A}$ state lifetime 79—72327
peroxy chain radicals, reactivity and struct., EPR spectra, trapped in PTFE 80—66783
peroxy radicals, in polluted tropospheric air 79—62560
peroxymethyl radical+NO, reaction rate const. 79—61848
peroxymethyl radical+peroxymethyl radical, reaction kinetics, H_2O vap. depend 79—61844
perylene, anthracene, radical cation, EPR, acidic surface anisotropic rot. diffusion 78—27095
phenol biradical prod. from O+benzene(-d), crossed mol. beam investig. 80—71902
phenoxy radicals, electronically excited states, photochem., flash photolysis obs. 77—77797
phenoxyl type radical, ^{1}H and ^{13}C ENDOR studies in soln. 78—94266
phenyl radical intermediate, spin trapping in γ-radiolysis of benzene, EPR 78—7218
4-phenyl-3-thiosemicarbazide, single cryst., X-irrad., EPR, ENDOR, radical identification 79—31560
9-phenylanthronyl radical, ESR, temp. depend. phenyl twist angle 79—18210
phenylcyclohexadienyl radical form in electron irrad. benzene cryst., absorpt. and fluoresc. spectra study 80—89035
pheophytin-a, photochem. generation of cation-radical, spectral-kinetic characts. 78—96008
phosphonatomethylene radical, EPR spectra and rot. barrier height, comparison CNDO calcs. 79—74409
phosphoranyl radicals, Ph_3PBr, trapped in X-irradiated triphenyliminophosphonium bromide, ESR study 79—56611
photoionisation, expt. techniques, processes, theory, review 77—14402
photolysis, excimer laser UV obs. 80—16711
piperdinyloxy 2,2,6,6-tetramethyl radical, recrystallised samples, EPR study 80—100615
planar cyclic radicals, C-H proton isotropic hyperfine consts., C hybridisation 80—95646
polyatomic radical cations, excited states, decay processes 80—28055
polyethylene, elec. trees free radical ESR study 78—60393
polyethylene matrix, trapped free radicals, decay in single crystal and diffusion 77—52657
polymer, photoradiative processes in free radical form. *(Russian)* 79—57269
polymer particle change with time in emulsion polymerisation 79—47923
polymerisation, from emulsion, homogeneous nucleation 79—29354
polymethylene flexible biradicals CIDNP and chain dynamics, field depend. 77—88473
polypropylene, electron bombarded, radical formation, piezoelectric and pyroelectric effects, ESR study 80—7169
polystyre, irrad, thermoluminesc. 78—2931
polystyrene film, in MIM struct., elec. conduction and free radicals 80—20340
prop-1, 2-dienyl radical, ab initio SCF HF MO calc., electronic struct. and one electron props. 77—42231
propyl compounds, photolysis, photofragment free radicals, mass spectra *(Japanese)* 78—7220
propyl halides, photoionisation mass spectrometry 80—40779
n-propyl radical, and propane, struct., ab initio calc. 79—98006
n-propyl radical, matrix isolation IR spectrum 78—33510
PTFE, peroxy radical labelled, temp. dependent rots., EPR obs. 80—28125
pyrene solutions, radical ion pairs, pulse radiolysis, time resolved EPR spectra meas. by ODMR of fluoresc. 80—83395
pyrene-DMA-methanol solution, photoinduced radical ion pair geminate recombination, triplet yield 78—76879

free radicals continued
pyrene-naphthalene complex radical cation, in γ-irrad. glass, visible spectrum obs. 78—44385
pyridine, near Ag electrode, intense Raman spectra, free radical form. 80—55076
pyridinyl radicals, hyperfine splitting consts., vibronic effects 77—57890
pyridyl imidazoline-1-oxyl radical, trifluoroacetic acid solns., ^{1}H scalar dynamic polaris. 78—23371
pyrimidine H-addition radicals in single crystals, long range proton hyperfine coupling, EPR and INDO 77—54568
pyrometallic dianhydride radical anion, MTHF glass, 77K, reson. Raman spectra 78—78704
pyrrole, free radicals produced by X-irrad. and decay of tritium atom, EPR study 78—48676
radical cation EPR spectra, ion-pair effects 79—13742
radical ion pair formation, ESR spectroscopic obs. 78—73038
radical pair generation, diffusion, spin motion, recombination in soln. nanosecond scale 77—77798
radical pairs, electron spin motion, diamag.-paramag. exchange, mag. field effect 79—98123
radical radiation formation in solid organic compounds 80—85201
RHF CI INDO spin density calc. 80—919
Rochelle salt, X-irrad., radical II struct. and location, ENDOR 77—51991
RX$^-$, radical anion stability conditions, pot. energy diagrams 80—85161
sec-butyl radicals, intermol. potential well depth estimation method 79—86034
secondar free radicals, primary reacting with substrated, CIDEP relax. time, theory 78—25573
semiquinones in protic solvents, saturation behaviour, ESR 77—6808
silyl radical, conform., hyperfine struct., nonempirical calcs., vibr., effects 79—97998
silyl radicals, benzil adducts, organometallic group dynamic migration, EPR 77—58049
singlet biradical species, correl. effects, spin density wave calcs. 77—18796
small radical, isotropic hyperfine coupling consts. MINDO/3 calcs. 80—52894
solution, relaxation process effect on coefficient of dynamic polarisation *(French)* 78—39446
solvent effect in π(PPP-like) and CNDO calcs. on radical ions and mols. 77—38622
solvent effect in π-approx. calcs. of electronic transitions and spin densities 77—38623
solvent effect in CNDO and INDO calcs. of electronic spectra by Longuet-Higgins-Pople and Roothaan methods 77—38624
spectroscopic determ., on polymer surface *(German)* 80—7892
spectroscopy, review, book contrib. 77—38653
spin exchange, anisotropic spin-density distrib. 80—102526
spin relaxation, Heisenberg exchange interaction between unlike free radicals 78—84490
spin-dependent magneto-optical rotation for free radicals and for singlet-triplet transitions 79—10129
spores exposed to pulsed electron irrad., decay of potentially lethal O_2-depend. damage 78—20217
stilbene anion radicals, photoinduced isomerisation, 77K 80—66818
cis-stilbene radical anion, ESR, proton coupling const. 78—21948
stilbene radical anion, form. in tetraphenylcyclobutane pulse radiolysis 79—16019
styrene, plasma polymerisation in glow discharge, thin film IR and free radical EPR obs. 80—2964
TANOL, spin flopping transition, temp. depend., mag. anisotropy energy 80—54890
TCNQ$^{-\cdot}$, ESR probe for phospholipid membrane polar head motion study *(French)* 80—45865
TCNQ salts, spin density distribs., estimation from EPR fine struct. and cryst. data 79—11347
p-terphenyl anion radicals, photoisomerisation, local heating effects 78—85179
1,4,5,8-tetraazanaphthalene radical ion pairs, EPR spectra 79—50051
tetracene, radical cation, EPR, acidic surface anisotropic rot. diffusion 78—27095
tetrafluoroethylene anion, EPR spectra in organic matrix 79—76453
tetrafluoroethylene radical anion, isotropic and anisotropic EPR spectra, conform. 78—13532
tetrahydro-2-methylfuran glass, γ-irrad., spin trapping of radicals by BNB, EPR obs. 78—10776
2,2,6,6tetramethyl piperid-4-one N-oxide, aq. soln., ESR spin probe for H_2O struct. alteration 77—59460
2,2,6,6-tetramethyl-4-oxopiperidine-1-oxyl, aq. soln., nucl. spin-lattice relax. times, cross-correl. method 79—95679
TGS, X-irrad., glycine radicals, geom. struct. by ENDOR and INDO calc. 79—24230
thiomethoxyl anion, and deuterate, electron photodetachment, affinities, vibr. freq. and spin-orbit splitting 80—53063
thionine triplet+haloanilines, electron transfer reaction, radical yield meas. 80—3330
l-thioproline single cryst., X-irrad., ESR and ENDOR study of radicals 80—45528
three-spin systems in nematic liq. cryst., EPR 77—14463
thymidine, frozen aq. solns., final products of gamma radiolysis 78—77001
thymidine-5-monophosphate, γ-irrad. aq. soln., spin-trapped radicals, liq. chromatography and EPR spectroscopy 78—53340
thymine+muonium, radical form. in aq. soln., spin reson. obs. 78—74679
transient radicals, EPR time profiles, CIDEP, electron spin-echo method 79—6953
1,3,5-trichloro,2,4,6-trifluorobenzene radical cation, $B^2A_2' \rightarrow X^2E''$ laser-induced fluoresc. spectra 80—14172
1,3,5-trichlorobenzene radical cation, emission and photoelectron spectra, lifetimes meas. 78—86905
trichlorobenzene radical cation, gas and matrix isolated vibr. resolved electronic spectrum 79—68252
trichlorobenzene radical cation, symm. substituted, fluoresc. and emission spectra in Ne matrix 79—89702
trichlorofluoromethane+OH reaction, rate const. and tropospheric lifetime 77—64366
trichloronitromethane, visible and near UV spectra, 295K, photoabsorpt. cross-section 79—22720
trichloronitrosomethane, visible and near UV spectra, 295K, photoabsorpt. cross-section 79—22720

free radicals continued
- triethylenediamine cation radical, ESR 77–24745
- trifluoroacetamide, single cryst., X-irrad., transient radical form., INDO and ESR calcs. 77–12814
- 1,3,5-trifluorobenzene radical cation, laser induced fluoresc. spectra, vibronic anal., Jahn-Teller distortion 79–3470
- trifluorobenzene radical cation, symm. substituted, fluoresc. and emission spectra in Ne matrix 79–89702
- β,β,β-trifluoroethyl radical in Ar matrix, EPR, F and H^+ hyperfine interaction and motional effects 77–14460
- trifluoromethyl, from iodotrifluoromethane IR multiphoton dissoc., meas. of reaction rate consts. 80–26036
- trifluoromethylperoxy radical, in $Ar:O_2$ matrix, IR spectra 80–50845
- trifluoronitrosomethane, visible and near UV spectra, 295K, photoabsorpt. cross-section 79–22720
- 2,2,5-trimethyl-1,3-dioxane-4,6-dione, cryst., X-irradiated, methyl group hindered rot. tunnelling, EPR, ENDOR, and ELDOR 79–68328
- trimethylene biradical, rot. barrier of mol., INDO calc. 79–68192
- trimethylene diradical, generalised Hartree-Fock natural orbital config. interaction approach 77–75062
- trimethylene diradical, geometry optimisation by generalised Hartree-Fock 78–25427
- trimethylene diradicals, geometry optimisation ab initio SCF CI calcs., energy gradient 79–85903
- triphenylamine cation radical, condensed and vapour phase geometry, photoelectron spectra 79–31597
- triphenylmethyl, in triphenylamine, photon-echo decay, in lowest doublet-doublet electronic transition 77–79903
- triphenylmethyl-^{13}C phosphonium chloride, Ph_3P^+-$^{13}CH_2$· EPR, reorientation and hyperfine coupling tensor 78–6574
- triphenylstannyl radical, EPR in single cryst. matrix, ^{119}Sn hyperfine coupling tensors 78–23346
- trishydrazyl radical in s-butylbenzene, slowly slowly tumbling triradicals EPR 80–32748
- L-tryptophan-HCl radical form. after X-irrad. 78–64940
- vanadyl octaethylporphyrin, radical cation EPR linewidth inversion, relax. theory 77–10693
- vanadyl porphyrins, anion radicals and dianions, reson. Raman spectra 77–471
- vinyl radical, MINDO/3-FORCES, geom. of heat of formation 78–66472
- 1-vinyl-o-carborane, orientationally disordered, γ-irrad. free radical defects, positron probe obs. 79–23647
- vinylidene chloride copolymer, stretched free radical form., meas. using indirect scavenger method 79–61923
- Yang's biradical, EPR, g- and D-tensors, electronic struct., deuteration and conformation effects 77–42343
- yeast cell suspensions, vac. UV irrad., 163 nm, lethal and genetic damage 77–21573
- Zeeman terms, mag. field splitting of hyperfine components 78–25610
- zinc etioporphyrin I anion radical, photoreduction obs. *(Russian)* 78–23958
- zinc porphyrins, anion radicals and dianions, reson. Raman spectra 77–471
- AlBr, UV emission spectrum, vibr. consts., isotope displacement and dissoc. energies 77–3381
- AlF, radical, form. in arc plasma, spectra 77–28989
- AlH^+ radical cation, EPR matrix isolation obs., hyperfine components calcs. 80–14158
- AlH_3, AlH_3^-, ground electronic states and geometries, ab initio calcs. 77–57863
- AlO radical, ground state dissoc. energy 80–53159
- AsF_5^-, form. from AsF_6^- by radiolysis, ESR spectrum 77–16845
- AsO_3H^-, localised near impurity in irrad. ferroelec. KH_2AsO_4, ENDOR 77–24762
- AuCa radicals, rotational analysis for near IR bands *(French)* 77–61741
- AuSi radicals, rotational analysis for near IR bands *(French)* 77–61741
- BF_2 radical, thermomechanical studies by mass spectrometry, enthalpy of form. and ionisation pot. determ., chem. bonds 80–81382
- BH^+, spin-extended Hartree-Fock ab initio calculations for small radicals 78–70746
- BH_3F^-, B-F bond, interference density and kinetic energy 78–74566
- BO_2, fluoresc. excitation spectra, vibronic level fluoresc., Fermi reson., force field 77–79643
- BO_2, gas, optically detected mag. reson. spectrum, $X^2\Pi$ rovibronic sublevels 78–82756
- BO_2, intermodulated fluoresc. spectra using stabilised dye laser 79–27020
- BO_2, laser saturation spatial spectroscopy of diffusion coeff., interaction pot. 77–75341
- BO_2, Π vibronic states, laser induced fluoresc. obs. 80–58301
- BeH radical, hyperfine splitting const., electronic energy, UHF-type, CCI calcs. 80–52909
- BeH, spin-extended Hartree-Fock ab initio calculations for small radicals 78–70746
- BeOH, struct. and electronic props., ab initio calcs. 80–74113
- BrF_6, EPR of matrix, isolated radical 79–85977
- BrO, free radical, Ar matrix absorpt. spectra, mol. vibronic states obs., spectroscopic const. determ. 80–83387
- BrO, Ir spectra in Ar matrix at 10K 79–89669
- $BrO(X^2\Pi_i)$ radical, ionisation potential, photoelectron spectroscopic determ. 78–25612
- C-$^+NH_3$ radical, exchangeable H^+ hyperfine coupling, ENDOR obs. 79–36669
- C_2, $(a^3\Pi_u)$, prod. from IR multiphoton dissoc. of acrylonitrile 80–63723
- C_2, band system transition moment ab initio SCF and CI calcs. 79–13770
- C_2, emission in halogenated compound flames *(German)* 79–52668
- C_2, laser fluoresc. detection with high time resolution 80–9632
- C_2, low lying $a^3\Pi_u$ state produced in intense IR field, fluoresc. and quenching obs. 80–11931
- C_2, luminesc. assignments in excimer laser photolysis of CBr_4 and CF_2Br_2 79–39184
- C_2, multiple photon dissoc. of C_2H_3CN, photofragment spectroscopy by laser-induced fluoresc. 80–11937
- C_2, primary radicals, from ethylene photolysis, dye laser obs. 77–16851
- C_2, Swan band system, vibr.-rot. interaction on pot. energy curves 80–27965
- C_2^-, matrix isolated, vibr. energy transfer, fluoresc. 78–46382
- C_2+NO, laser-induced chemilum. reaction 80–61101

free radicals continued
- C_2+O_2, $C_2(X^1\Sigma_g^+)$ and $C_2(a^3\Pi_u)$ intersystem crossing and free radical kinetics 80–95668
- $C_2+O_2(NO)$, IR laser photolysis of polyat. mols. photochem. appls. 80–66835
- C_3, $(^1\Pi_u)$ radical excited state radiative lifetimes and the collisional deactivation 79–27018
- C_3, electron spectrum, ab initio MRD CI calcs. 78–90089
- C_3 production by IR multiphoton allene photolysis, vibr. relax., chem. kinetics 80–66820
- CCN radical in solid Ar, emission and excitation spectra 78–70868
- CCO radical, heat of form. calc., geometries excitation energies and vibr. freq. calc. using POL-CI wave functions 80–89512
- CCl, reaction rate const. determ. using laser-induced fluoresc. technique 80–97682
- CCl_2, reaction rate const. determ. using laser-induced fluoresc. technique 80–97682
- CClF, reaction rate const. determ. using laser-induced fluoresc. technique 80–97682
- $CCl_2FO_2+NO(NO_2)$, reaction, photolysis obs. 79–74931
- $CCl(\tilde{X}^2\Pi)$+methylhalosilanes, reaction rate const. determ. by kinetic absorpt. spectroscopy 80–97683
- CF_2, absolute IR intensity of fundamental vibrs. 78–58743
- CF_2, fluoresc. and radiative lifetime obs. in dibromodifluoromethane UV laser photolysis 80–16703
- CF_2, in Ar matrix, conc. determ. by intensity calcs. 78–68941
- CF_2, luminesc. assignments in excimer laser photolysis of CBr_4 and CF_2Br_2 79–39184
- CF_2 radical, UV emission in microwave discharge, assignments 77–50461
- CF_2, time-resolved optical absorption obs. in IR multiphoton dissoc. of CF_2HCl 80–16702
- CF_2, $X\ ^1A_1$ radical, form. in chlorofluoromethane collision-free multiphoton dissoc., translational energy meas. 78–92491
- CF_2+H, IR matrix isolation spectra 80–97706
- $CF_2+He(Ne)(N_2)(SF_6)$, vibr. deactivation of CF_2 first excited single state 79–94061
- CF_3, absolute IR intensity of fundamental vibrs. 78–58743
- CF_3, CF_3^-, and CF_3^+, optimised struct. and bonding, ab initio SCF MO calc. 80–23334
- CF_3, in Ar matrix, conc. determ. by intensity calcs. 78–68941
- CF_3 radical, dipole moment from beam mass spectrometric anal. 79–59596
- $CF_2(^3B_1)$ triplet-triplet annihilation, CF_2, $CF_2(^1B_1)$ energy distrib. 80–50861
- CF_2Cl^+, and parent cations, IR spectra in matrix radiolysis and photoionis. of Freons 78–80767
- CH, $A^2\Delta$ state, radiative lifetime 77–34698
- CH, $B^2\Sigma^-$ state predissoc., calcs. and time resolved spectrosc. 80–23576
- CH, CD, interstellar, Λ-doublet population inversion by collisions 80–22065
- CH, CH^+, interstellar molecules, book contrib. 77–33625
- CH, chemiluminesc. in flowing afterglow of Ar+methane 78–64839
- CH, emission in halogenated compound flames *(German)* 79–52668
- CH, far IR laser mag. reson. spectrum 79–3466
- CH, force constants, local mode approx. 77–71791
- CH, formed by laser photolysis of methylamine fluoresc. obs. 80–97710
- CH, interstellar, ground state inversion, collisional excitation 78–28503
- CH, interstellar, rot. levels struct., excitation mechanisms 78–21908
- CH, photoionis. and photodissoc. near ionis. threshold, SCF MO CI and Steltjes imaging 78–58749
- CH, radiative lifetimes, electron-photon delayed coincidence meas. 78–50594
- CH radical, SCF theory, multiconfig., direct orbital optimisation 80–87049
- CH radical, sputtered, rotational and vibrational excitation 80–69224
- CH radical, sputtered from acetone chemisorption layer on Si, rot. and vibr. population distrib. 78–64436
- CH^+, ‘π ‘Σ band systems, vibr.-rot. interaction on pot. energy curves 80–27965
- CH^+, CD^+, $A^1\Pi$-$X\ ^1\Sigma^+$ band system, spectroscopic consts. and radiative lifetimes 78–5237
- CH^+, continuum electron wavefunction, electron capture width 78–78805
- CH^+, excitation energies and transition moments in a second order polarization propagator approach 79–10051
- CH^+, excitation energy and transition moment anal. of electronic transitions 78–25620
- CH^+, expt. oscillator strength 77–34693
- CH^+, photodissoc., $A^1\Pi$ state shape resonances 79–54924
- $CH+H_2$, doublet and quartet states, abstraction reactions, pot. energy surfaces calcs. 78–31627
- $CH+p\text{-}H_2(He)$, collisional pumping of Λ-doublet transitions, pot. energy surface 80–23516
- CH_2 and CH_2^+, valence states, ab initio calcs. 79–6859
- CH_2, line search in photographic IR spectrum of C stars 77–78786
- CH_2, photoprod. from ketene, singlet-triplet energy separation and rovibronic level obs. 80–11936
- CH_2 radical, fluoresc. induced by laser 588.9-595.6 nm, $(a^1A_1-X^3B_1)$ energy separation 78–42121
- $CH_2+H_2\rightarrow$methyl radical, SCF calc. involving orbital symm. forbidden reaction pathway 79–98004
- CH_3 average internal excitation formed in $F+CH_3I(CF_3I)$, fluoresc. obs. 80–48078
- CH_3, experimental determ. of the geometry and electron affinity 78–82860
- $CH_3\text{-}d_n$, matrix isolation IR spectra, rot. and vibr. struct. 77–83589
- C_4H_3, in flash photolysis of thiophene, transient absorption spectrum 78–46354
- C_6H_4 radical, force constants, local mode approx. 77–71791
- C_6H_5 radical, force constants, local mode approx. 77–71791
- $C_6H_6^+$, gas, laser-induced-fluoresc., rel. to photodissoc. and Jahn-Teller X and A states distortion 79–72345
- $CH(A^2\Delta)$ radicals, electronically excited, lifetimes and quenching rate constants meas. 80–69188
- CH_2CCH radical, electronic struct., geometry, INDO calcs. 77–14358
- $CH_3(CH_3^+)(CH_3^-)$, HF, GVB and CI calcs. 77–75063
- CH_3CO', low lying states, struct., energetics, ab initio STO calcs. 77–61682
- CHF radical, $\tilde{A}^1A''$-$\tilde{X}^1A'$ transition, laser induced fluoresc. 80–95660
- $CHF+O(^3P)\rightarrow HF+CO$, product vibr. energy distrib. 79–61853

free radicals continued
CH_2F, far IR laser mag. reson. spectrum 78−9174
C_3H_5NH radical, valence shell ionis. pot. determ. 77−31014
$C_5H_6NNHCSNH_2$ radical, prod. in X-irrad. 1-phenyl-3-thiosemicarbazide, ESR, ENDOR 77−36770
CH_3NN', low-lying states, struct., energetics, ab initio STO calcs. 77−61682
CH_3O_2, radical, form. and decay rates, UV absorpt. spectra 77−48631
$CH(X^2\Pi)$ radical, prod., detect. and reactions 79−61842
$CH_2(a^1A_1\text{-}X^3B_1)$ energy separation 79−8443
$CH_2(b^1B_1)$, radiative lifetime from $b^1B_1 \rightarrow a^1A_1$ emission in electron irrad. methane 77−3476
CN, $(A^2Pi_i \rightarrow X^2\Sigma^+)$ and $(B^2\Sigma^+ \rightarrow X^2\Sigma^+)$ yields from HCN photodissoc. 80−87141
CN $(A^2\Pi)$, chem. prod., CN number densities for gain, emission and absorpt. meas. 78−63112
CN, $(X^2\Sigma^+)$, prod. from IR multiphoton dissoc. of acrylonitrile 80−63723
CN (0,0) vibr. band in Comet Mrkos (1957 V) 78−20734
CN, A- and B-state lifetimes, collisional transfers and perturbations 78−78756
CN, abundance in comets from radiance of violet CN spectra bands 78−16348
CN, $B^2\Sigma^+ \leftarrow A^2\Pi$ 0-0 and 1-0 bands, laser excitation spectra 80−91588
CN, CN^-, HF electron affinity, SCF calcs. 77−67979
CN, fluoresc. spectra, time resolved, radiative decay and radiationless deactivation in Ar 79−98142
CN, form. by photodissoc. of parent mols., possible detect. in comets 78−61798
CN formed by laser photolysis of methylamine, fluoresc. obs. 80−97710
CN free radical, $A^2\Pi\text{-}X^2\Sigma^+$ Red system, perturbation analysis 80−87247
CN, free radical, anticrossing spectra for fine struct. consts. 79−68270
CN, free radical, electron affinity 77−47375
CN, from ICN photodissoc., internal state distrib., laser-induced fluoresc. 77−36773
CN, from IR photolysis of cyanomethane, photoluminesc. spectroscopy 77−73452
CN, internal energy distrib. following vinyl cyanide photodissoc., temp. depend. 80−78638
CN photodissociation laser, IR stimulated emission due to BrCN photolysis 79−31888
CN, prod. by RCN photodissoc., fluoresc. obs. 79−52725
CN, radical, $(A^2\pi\text{-}X^2\Sigma)$ fluoresc. predissoc. in HCN photodissoc. 77−38691
CN, radical, $A^2\pi$ state, collisional deactivation, fluoresc. quenching obs. 77−83642
CN, radical, adiabatic electron affinity, CI calcs. 79−68197
CN, radical, electronic, vibr. and rot. energy partitioning obs. following ICN photolysis 77−16853
CN, radical, nonradiative transition rates, matrix isolated molecule 78−78740
CN radical, photofragment spectroscopy of A-X transition 79−52726
CN, radical, $X^2\Sigma^+$ ground state, microwave absorpt. spectrum 78−17657
CN, radical fluoresc. excitation spectrum and laser emission from ICN photolysis 78−76892
CN radicals, electronic transition laser, using C_3F_7CN and $(CN)_2C_4F_8$ photodissociation 78−50769
CN, solar lines in 7100-7600 Å range, table 78−77495
CN, spectral absorpt. coeffs. for fundamental and first overtone vibr.-rot. bands 77−14405
CN, time behaviour in laser-initiated thermal isomerisation of CH_3NC 80−11887
CN, time resolved chemilum., in C_2+NO(vinyl cyanide)(ethylene), laser-generated radical kinetics 79−100352
CN^-, enthalpy of formation and electron affinity 77−35506
$CN+O \rightarrow CO+N$, flash photolysis, absorption spectrosc. obs. 79−66289
$CN(B^2\Sigma)$, from electron impact dissoc., of HCN, near-threshold emission 79−54975
CNC radical vibr. and electronic spectra, in VUV photolysis of matrix-isolated cyanomethane 78−85180
CNN, matrix isolation spectrum, 2600-1900 Å 78−86880
CNN, matrix-isolated, $^3\Pi\text{-}^3\Sigma^-$ system, laser-induced temporal and wavelength resolved spectra 77−83637
CNN radical, matrix isolation spectra, $23.5\text{-}25.6 \times 10^3$ cm^{-1}, vibr. relax. and Renner splitting 77−83612
CN(X), free radicals, state distribs. rel. to prod. by photolysis of dicyanoacetylene 77−9107
$CN(X^2\Sigma^+)$, IR laser photofragmentation of cyanomethane, energy partitioning, rovibronic distrib. 77−61813
$CN(X^2\Sigma^+)$, translational-electronic-vibr.-rot. energy partitioning in photolysis of C_2N_2 77−48667
CN^*, $B^2\Sigma^+$ state, fluoresc. decay dynamics, collisional quenching and radiative lifetimes 80−58306
CO^+, $A^2\Pi\text{-}X^2\Sigma^+$ system, (2,0) band, rot. anal., $^2\Pi$ state Λ-doubling *(French)* 77−10681
$CO_2\text{-}O_2^-$ radical, on MgO surface, ESR spectrum, mobility effects 80−43076
CS, heat of formation from electron impact dissoc. of CS_2 and OCS 78−73074
CS, nonexponential decay of $a^3\Pi\text{-}X^1\Sigma^+$ luminesc., Π sublevel radiative lifetimes, matrix isolated spin-orbit 79−89699
CS+He, Penning ionisation, $CS^+(B^2\Sigma^+ \rightarrow A^2\Pi_i)$ fluoresc., flowing afterglow 80−14197
CS_2, electron impact dissoc., CS heat of form. determ. 78−73074
$CS(a^3\Pi)$ production, CS_2 photodissoc. below 1600 Å, quantum yield, rate const. 77−48658
CSiH, matrix Hartree-Fock calcs. 79−5874
CX_n radical, $(X=H,D;\ n=1,2,3)$, thermodynamic function in ideal gas state 80−14871
^{13}C, CIDNP, obs. in reactions of organic and inorganic radicals during pulse radiolysis 80−63660
^{13}C-labelled organic radicals, ^{13}C- and proton-ENDOR in soln. 78−55190
^{13}CH, predicted Λ-doubling spectrum 77−30857
CaCl, free radical, $A^2\Pi\text{-}X^2\Sigma^+$ system obs. by saturation spectroscopy 78−46353
$Ca^{35}Cl$, radical, rot. spectrum, $X^2\Sigma^+$ state, laser MODR 78−5257
CdF, mol., ESR spectra in inert gas matrix 79−76455

free radicals continued
2-chlorothiophene, σ^* anion radical, prod., ESR spectrum assignment 78−11539
Cl_2^-, near Ag electrode, intense Raman spectra, free radical form. 80−55076
ClCF, radical in Ar matrix, vibr. relax., multiphonon processes, fluoresc. 77−65430
ClCF radical in solid Ar, emission and excitation spectra, vibr. anal. 78−9164
ClCO radical, struct. and props. calcs. 80−74112
ClF_4, geom., ab initio MO calcs. 79−89610
ClO, $A^2\Pi\text{-}X^2\Pi$, UV absorpt. spectrum 78−74673
ClO, bandstrength determ. of fundamental vibr.-rot. spectrum 78−70872
ClO, free radical, Ar matrix absorpt. spectra, mol. vibronic states obs., spectroscopic const. determ. 80−83387
ClO, laser excited fluoresc. 79−50077
ClO, laser spectroscopy relevant to stratospheric photochemistry 78−88951
ClO radical, 2-0 vibrational overtone band, laser magnetic resonance spectroscopy study 80−48021
ClO radical, IR vibr.-rot. spectra, background data for atm. meas. 78−58679
ClO radical in stratosphere, in situ obs., rel. to O_3 depletion 78−36241
ClO, remote meas. in stratosphere 79−58005
ClO, UV absorpt., lab. spectra rel. to atmos. identifications 77−34653
$ClO+H_2 \rightarrow HOCl+O_2$, reaction rate consts. 79−5140
ClO_2, laser mag. reson. spectra tuned by Zeeman level crossing avoidance, perp. spectra 79−68229
ClO_2, laser mag. reson. spectra tuned by Zeeman level crossing avoidance, high-field spectra 79−76424
ClO_2, laser-microwave double reson. of ν_1 band 80−48022
ClO_2 radical, laser mag. reson., ν_1 band 78−94263
ClO_3 radical, in $KClO_4$ EPR obs., X-irrad. creation 78−76311
$ClONO_2$, photolysis products, very-low press. meas. 79−29376
ClOO radical, struct. and props. calcs. 80−74112
$ClO(X^2\Pi_i)$ radical, first ionis. pot., photoelectron spectrosc., vibr. struct., bond length 77−14495
$ClO(X^2\Pi_i)$, radical, He(I) photoelectron spectrum, ΔSCF calcs. 79−72359
Cn free radical, $B^2\Sigma^+$ state lifetime, photon-photon cascade meas. 78−5273
CrO_3^- radical in K_2CrO_4 and $KCrO_3Cl$, g-factor anisotropy 78−67994
DO_2, IR spectra, config. of $^2A'$ and $^2A''$ states 79−36636
DO_2, ν_2 fundamental band, 9.8 micron, laser mag. reson. spectroscopy 79−85961
DO_2+NO, reaction kinetics, near IR chemiluminesc. determ. 80−21261
F compounds, ground states, mol. parameters, MINDO calcs. 78−41955
FCO, radical, struct. and props. calcs. 80−74112
FHF, struct. and stability, ab initio SCF and CI calcs. 77−71887
FO free radical, detection by CO_2 laser mag. reson. 80−45594
FOO radical, struct. and props. calcs. 80−74112
$FO(X^2\Pi_i)$ radical from $F+O_3$ reaction, VUV photoelectron spectra 80−104455
$Fe(NO)_3CO$ radical, form. by $Fe(CO)_5$ photolysis in NO soln., EPR spectrum 80−53024
GeX_n radical, $(X=H,D;\ n=1,2,3)$, thermodynamic function in ideal gas state 80−14871
H, stored in solid H_2, equilib. conc., upper bound 77−46510
H_3, interrelationships between effective hamiltonians 77−30767
HC_2, ground state energy surface, ab initio SCF calc. 78−33446
HC_2 radical, electron affinity, ab initio SCF and CI calcs. 78−50468
$HCC \rightarrow H+C=C$ dissoc., trajectory calcs., random vibr. excitation 80−45491
HCCN, free radical, matrix isolation spectra and ab initio calcs. 78−46329
HCCN, matrix isolation IR and UV spectra, vibr. anal., struct. 77−65457
HCN^-, SCF ab initio ground state pot. energy surface, geometry, rel. to HCN 78−78646
HCNH radical, valence shell ionis. pot. determ. 77−31014
H_2CNH_2 radical, valence shell ionis. pot. determ. 77−31014
H_3CNH_3 radical, valence shell ionis. pot. determ. 77−31014
HCO, formation in acetaldehyde photodissoc., wavelength depend. 79−83490
HCO, IR spectra of ν_2 fundamental, laser elec. reson. 78−5226
HCO, microwave spectra, hyperfine struct. 77−75139
HCO, ν_2 fundamental band, laser mag. reson. spectra 78−5256
HCO, UV matrix isolation spectra, 14K, 210-260 nm, C-X transition 78−62819
HCO, vibr.-rot. transitions, IR laser mag. resonance 77−27098
HCO', low lying states, struct., energetics, ab initio STO calcs. 77−61682
HF_2, neutral free radicals, in Ar matrix, IR spectrosc. evidence 78−66546
HFF, struct. and stability, ab initio SCF and CI calcs. 77−71887
HF^*+NH^*, microscopic vibrotational-electronic energy transfer, IR chemiluminesc. obs. 79−31662
$HGeCl^*$, chemiluminescence obs., vibr. levels 77−81406
HNC^+, radical cation, charge exchange mass spectrometry, HNC^+ ion recombination and ionisation pot. 78−76838
HNN', low-lying states, struct., energetics, ab initio STO calcs. 77−61682
$HNO(A^1A'')$, state-selected fluoresc. lifetimes, collisional quenching rates 79−36674
HNOO, singlet and triplet diradicals, unrestricted 79−97975
HO fluorescence detection, interference suppression by sampling method 80−8431
HO radical form. from H_2+N_2O reaction on Pt surface, laser-induced fluoresc. obs. 80−108738
HO_2 free radical, dipole moments and Stark effects from microwave spectra 80−63623
HO_2, IR spectra, 1.43-1.51 μm emission bands 79−36635
HO_2, in polluted tropospheric air 79−62560
HO_2 prod. from $H+O_2+Ar$, rate const. calc. 80−101026
HO_2 radical, EPR spectrum, ground state parameters 78−90193
HO_2 radical, microwave spectrum 77−57983
HO_2 radical, near IR emission bands, vibr. and vibronic transitions 78−37633
HO_2 radical, ν_3 fundamental band, laser mag. reson. 78−66566
HO_2, vertical electronic spectrum, MRD-CI calcs. 78−37646
$HO_2+ClO \rightarrow HOCl+O_2$, reaction rate consts. 79−5140

free radicals continued
HO_2+HO_2, gas phase reaction mechanism, FT IR spectrosc. obs. 80−85163
HO_2+HO_2, reaction rate, press. depend. 80−7766
HO_2+NO, reaction kinetics, near IR chemiluminesc. determ. 80−21261
HO_2+O_3, reaction kinetics, laser mag. reson. obs. 80−102528
H_2O^-, trapped in γ-irrad., Y-type zeolites, ESR obs. 77−9099
H_3O radical, stability, ab initio UHF-CI calcs. 78−5137
HOCO and HOCO* formed by OH+CO, thermochem. props., ideal gas state 78−27805
HOCO, prod. in OH+CO reaction, stability 77−73436
HOO radical, lowest doublet electronic states, rel. to photodissoc. 79−93914
HPO, vibrational freqs., by rot. anal. of spectra 79−54831
$HPO_4^{\cdot -}$, in γ-irrad. $K(H_{1-x}D_x)_2PO_4$, 77K, optical and EPR obs., form. mechanism 78−68379
$H_2PO_4^{\cdot}$, in γ-irrad. $K(H_{1-x}D_x)_2PO_4$, 77K, optical and EPR obs., form mechanism 78−68379
$HPO_4^-(H_2PO_4)$ radicals + organic compounds, reaction rate consts. 78−15669
HS_2, ground and first excited states, geometry, ab initio SCF calcs. 78−50657
HS_2 radical, ab initio calcs. of geometry and spectra 77−34552
HSO, ground and first excited states, geometry, ab initio SCF calcs. 78−50657
HSO radical, Doppler-limited dye laser excitation spectroscopy, rot., distortion and spin-rot. interaction const. determ. 80−83383
HSO, radical, electronic spectrum and struct. 77−75147
HSO radical, ground and excited first states, ab initio SCF and CI calcs. 77−30776
HSO, thermochem. props. 79−5173
HgBr radical, laser action by $HgBr_2$ photodissociation, ArF excimer laser pumping 78−13695
HgPh, photoionisation effectiveness curves 78−25633
IO, free radical, Ar matrix absorpt. and emission spectra, mol. vibronic states obs., spectroscopic const. determ. 80−83387
KN_3, ab initio calcs. of elec. props. of N_4^- 79−95363
KPF_6, γ-irrad., trapped free radicals EPR obs. 80−63683
$^{83}Kr_2F$ radical, in UV-irrad. Kr/CF_3OF, 10K, ^{83}Kr hyperfine EPR spectrum, struct. 78−42101
LiH^+, spin-extended Hartree-Fock ab initio calculations for small radicals 78−70746
LiHH, pot. function by trial function method 77−6699
MgOH, struct. and electronic props., ab initio calcs. 80−74113
N_3 generation in NaN_3 thermal decomp. 79−100351
ND, $b^1\Sigma^+$ state, radiative lifetime, Einstein coeff. 78−90217
ND $c\ ^1\Pi$-$a\ ^1\Delta$ system, new bands, spectroscopic consts. 80−9612
ND, dissoc. energy, calc. from $c^1\ \Pi$ state predissoc. *(German)* 78−90237
ND radical, metastable $b^1\Sigma^+$ state, tunable laser fluoresc. obs. 79−22744
ND radicals, metastable, production in discharge, spectra, rot., vibr. consts. determ. *(German)* 77−34642
ND, singlet-triplet transitions, high resolution spectrosc. with new emission source *(French)* 80−57383
$ND_2(NH_2)$, ν_2 band, laser mag. reson., 9-10 micron 80−9601
$ND(b^1\Sigma^+)$, quenching rate consts. *(German)* 79−41189
NF, $b^1\Sigma^+$ state, enhancement by I laser pumping, lasing potential 78−79012
NF, chem. pumped electronic transition laser system, chem. and scale-up 78−63103
NF, excited, lasing potential, prod. by $N+O_2F$ reaction 78−63106
NF produced by $H+NF_2$ in subsonic CW laser device $a^1\Delta$ state scale up 77−79815
NF+H(NF), electronically-excited free radical reactions 80−97707
NF_2, IR spectra, ν_1 and ν_2 bands, vibr. excitation and spin-rot. interaction, doublet splitting 80−28011
$NF_2+H(O)(N)$, electronically-excited free radical reactions 80−97707
NF_3, NF_3^-, and NF_3^+, optimised struct. and bonding, ab initio SCF MO calc. 80−23334
NF*+HF*, microscopic vibrotational-electronic energy transfer, IR chemiluminesc. obs. 79−31662
$NF(a^1\Delta)+I(^2P_{1/2})$ system, electronic angular momentum transfer, chem. kinetic model 78−63104
$NF(b^1\Sigma^+)$ enhancement by I laser pumping 78−63105
NH, 3Π states, MC wavefunctions, rot.-vibr. anal. 79−13652
NH, $b^1\Sigma^+$ state, radiative lifetime, Einstein coeff. 78−90217
NH, $c^1\Pi$ state anomalous populations following NH_3 photodissoc. 79−10133
NH, dissoc. energy, calc. from $c^1\ \Pi$ state predissoc. *(German)* 78−90237
NH, laser-excited A-X system fluoresc. 79−50060
NH, lower valence states, predissociations, Franck-Condon anal. 80−5590
NH, ND, $(b^1\Sigma^+)$ states quenching by deuterated cpds., kinetic isotope effects 77−63891
NH, ND, $X^3\sigma^-$ state vibr. relax. Ar matrix, energy gap law breakdown 77−30963
NH, radiative lifetimes, electron-photon delayed coincidence meas. 78−50594
NH radicals, metastable, production in discharge, spectra, rot., vibr. consts. determ. *(German)* 77−34642
NH, singlet-triplet transitions, high resolution spectrosc. with new emission source *(French)* 80−57383
NH^+, interstellar, Λ-doublet population inversion by collisions 80−22065
NH_2 fragments, multiple photon dissoc. of CH_3NH_2 and NH_3, laser-excited fluoresc. obs. 80−11938
NH_2, ground state mol. consts., absorption spectra 80−28030
NH_2, hyperfine level crossing spectroscopy of (0, 9, 0) and (0, 10, 0) vibr. states 78−17728
NH_2, hyperfine struct. of u-state, microwave optical double reson. 79−68246
NH_2, isotope effect on spectroscopic parameters *(Russian)* 77−54577
NH_2, microwave modulated saturation spectroscopy, hyperfine energy levels 79−68245
NH_2, radical, laser mag. reson. spectra in 9 μm region, ν_2 band 79−45724
NH_2 radical, mag. hyperfine interactions, zero-point vibrs. effects 80−58167
NH_2, vibr.-rot. transitions, IR laser mag. resonance 77−27098
NH_2, vibronic levels, excited by blue CW dye laser 78−86907

free radicals continued
NH_2, X^2B_1, A^2A_1 and B^2B_2 states, ab initio SCF CI calcs. 78−29746
NH_2^-, mol. geom., diffuse functions in SCF calcs. 79−10226
$NH_2^{\cdot}$ radical, heat of form., a diabatic electron affinity, from proton affinity meas. 79−91987
NH_2+H rot. energy transfer in vibronic levels, absolute transfer rates 80−9701
NH_2+O_3, reaction mechanism, flash photolysis obs. 80−104425
NH_2+propylene, reaction kinetics, laser reson. absorpt. obs. 77−9096
NH_3^+, in γ-irrad. NH_4ClO_4 single cryst., EPR obs., g-tensor, hyperfine splitting 78−2739
NH_3^+ radical, EPR in X-irrad. K_2SO_4:$(NH_4)SO_4$ 80−11272
NH_3^+ radical, mag. hyperfine interactions, zero-point vibrs. effects 80−58167
$N_2H_4^+$ radical, mag. hyperfine interactions, zero-point vibrs. effects 80−58167
N_3H_3 radical, lowest two electronic states 80−925
$NH(A^3\Pi, c^1\Pi)$ radicals, electron impact of NH_3, H_2NNH_2 and organic mols., emission spectra 77−83752
NH_2CO', low-lying states, struct., energetics, ab initio STO calcs. 77−61682
NHD, electronic absorption spectrum, 5750-6450 Å, rot. assignments 79−64013
NH(D) radical, and isotopic species, laser mag. reson., hyperfine parameters 77−10694
NHD radical, dipole moment determ., optical Stark spectroscopy 80−23455
$NH_2(F_2)(Cl_2)$, SCF-MO-HF calc., struct. and one-electron props., population anal. indices 79−76338
$NH(NH_2)$ obs. in laser photolysis of methylamine, fluoresc. obs. 80−97710
NH_2O_2, long-lived radical prod. by photolysis of ammoniacal KO_3 soln. 77−16838
$NH_2(X^2B_1)$, laser mag. reson. spectra, Zeeman and hyperfine effects, rot. consts. 77−30892
$NH_2(X^2B_1)$, MODR, hyperfine coupling consts., spin rot. consts. 78−1010
$NH_2(X^2B_1)$ radical, and ND_2, ionisation pot., vibr. anal., ab initio calcs. and vacuum UPS obs. 80−53047
$NH(X^3\Delta^-)$ radical, form., detect. and reactions 79−64036
$NH(b^1\Sigma^+)$, quenching rate consts. *(German)* 79−41189
NO $(\upsilon=1)$, vibr. fluoresc. detection of trifluoroformamide photodissoc. 78−74712
NO, diffusion in plastic solids, ELDOR 77−1618
NO, fluoresc. spectra, $3s\sigma(A^2\Sigma^+)$ Rydberg state, vibr. relax. 79−13759
NO, hyperfine splitting const., H-bond contrib. 78−74799
NO, radical spin labels, appl. to solvent-solute interactions 78−17698
$NO^{\cdot}$ radical-paramagnetic transition metal interactions, EPR spectra rel. to dipolar interactions 79−95647
$NO^{\cdot}$ radicals, saturation transfer EPR effects anal. using hole-burning concept 79−94022
NO_3, detect. in polluted troposphere by differential optical absorpt. 80−77036
NO_x biradicals, conform., spin probe appls. 78−86895
NOH polycryst. radicals, low temp. PMR 80−25220
NS radical chemiluminescence produced by active $N+S(S_2Cl_2)$, kinetics study 79−39151
NaOH, aqueous system, LET depend. of transient yields in deuteron and alpha pulse radiolysis 77−63940
O+biradical, from γ-methyl valerophenone photolysis, lifetime and quantum yield meas. 77−60086
O_2^- superoxide ion as cause of O_2 effect, X-ray induced cell lethality 77−25513
$O_2^{\cdot -}$, superoxide radical role in lipid photoperoxidation in isolated chloroplasts 78−77016
OBrO, Ir spectra in Ar matrix at 10K 79−89669
OD, $^2\Pi_{3/2}$ state EPR spectra 78−21949
OD radical, in $NiSiF_6.6D_2O$, optical absorption spectrum, 300 and 80K 79−73966
OD, spectra, A-X system Einstein coeffs. 79−36703
$O_2F+N \rightarrow N_2(NF)$, lasing potential of excited fluorides 78−63106
$O_2F(Cl)(Br)$ radicals, matrix IR spectra, bonding 78−90160
OH, 13.4 GHz absorpt. line width *(French)* 77−61801
OH $(A\ ^2\Sigma^+)$ radical, predissoc. investig., shock-radiational recombination method 77−1924
OH, $(A^2\Sigma^+ \rightarrow X^2\pi)$ fluoresc. prod. by H_2O photodissoc., cross sections 78−25604
OH, $(A^2\Sigma^+)$, abnormal rot. following H_2O photodissoc., semiclassical calcs. 78−40069
OH $(A^2\Sigma^+)+H_2(N_2)(Ar)$, collisionally induced population change rates, laser-induced fluoresc. obs. 78−5326
OH, $A^2\Sigma$ state, predissoc. rates, high freq. deflection meas. 78−62864
OH, $A^2\Sigma^+$ state, predissociation and tunnelling 78−29823
OH, $A^2\Sigma^+$ state, predissociation, tunnelling 78−29824
OH, $A^2\Sigma^+{}_{1/2}$ state, g-factor meas. by quantum beat obs. 79−18176
OH, $A^2\Sigma^+$-$X^2\Pi_i$ system, vibrational and rotational levels, transition probability determ. 80−43034
OH column densities in stratosphere from far IR rotational lines 80−36367
OH conc. in troposphere, rel. to halocarbons, SF_6 and N_2O concs. 77−45069
OH, conc. meas. in atm. boundary layer by monitoring CO oxidation 79−58012
OH concentration profile in methane-air flames 80−35534
OH, continuum opacity oscillator strength rel. to solar atmosphere model 79−40162
OH, determ. in flames, spectrosc. method 77−32853
OH, Dunham pot. energy coeffs. 78−41979
OH, exact hyperfine struct. and Einstein A-coefficients, astrophys. appl. 77−83762
OH, excitation in interstellar clouds 78−65669
OH, excited free radicals, form. by ion-mol. reactions 78−56890
OH, fluoresc. lidar instrument for stratospheric temp. and press. determ. 79−80033
OH, free radical, vibr.-rot. level population determ., including unresolved doublet struct. *(Russian)* 77−68033
OH, fundamental vibr. band, mag. rot. spectrosc. obs. 80−86446
OH in flames, laser excitation dynamics 80−74201
OH, in inert gas matrix, H-bonding and charge transfer, fluoresc. 78−25602
OH, in lower atm., vibr. energy distrib. 77−25735

free radicals continued
OH, in polluted tropospheric air 79−62560
OH inactivated papain, optical density, amino acid composition and fluoresc. 78−53344
OH, J=9/2 Λ-doublet line detect. in W3(OH) 78−65670
OH lifetime in comets at 1 AU 80−46488
OH Meinel bands intensity distrib. in airglow, OH* quenching mechanisms 78−65447
OH, microwave spectral line breadth in NH_3, H_2O, NO_2, SO_2, O_2, H_2, He, N_2, chloromethane 79−45806
OH, mol. beam electric reson., hyperfine Λ-doubling transitions 79−36628
OH, multipredissoc. of $A^2\Sigma^+$ state, multichannel scatt. theory 79−94046
OH, OD, interstellar, Λ-doublet population inversion by collisions 80−22065
OH, optimum mol. consts. and term values, $X^2\Pi$ and $A^2\Sigma^+$ states, vibr.-rot. and microwave freqs. 80−95577
OH, product state distrib. in $O+H_2$ reaction, laser photolysis-laser induced fluoresc. meas. 79−83446
OH, Pt catalytic oxidation of H_2 and D_2, matrix isolation and laser fluoresc. obs. of prods. 80−66865
OH, radiative lifetimes of $A^2\Sigma$ state and A-X Einstein coeffs. 79−36703
OH, radical, atmospheric reactivity with organic compounds 79−61860
OH, radical, far IR laser mag. reson. spectra, fine struct. transition 79−76454
OH radical, gas phase EPR, rot. states electronic struct. and Zeeman parameters 78−86896
OH radical, in Earth's atmosphere, pure rot. lines 79−92593
OH radical, matrix-isolated, from H_2 oxidation on Pt, laser diagnostics 80−5572
OH radical concentration in methane-O_2-N_2 flames, hook method meas. 77−77762
OH radical concentration in troposphere, determ. via atmospheric ^{14}CO meas. *(German)* 80−8419
OH radical in premixed laminar methane-air flame, fluoresc. meas. of rot. temp. 79−80622
OH radical in upper atmosphere, meas. using lidar from Space Shuttle 80−51590
OH, radical $\nu=1^2\Pi_{3/2}$ state, microwave spectrum 79−26972
OH radicals, microwave spectra data tables 78−50542
OH radicals in glow discharge, rot. levels distrib., temp. meas. 78−47169
OH radicals vibrationally excited in stratosphere, instantaneous rate model 77−5273
OH, rot. transitions broadened by press., laser mag. reson. study 79−94020
OH spectroscopy using freq.-doubled dye laser radiation *(Dutch)* 79−50039
OH, spin-extended Hartree-Fock ab initio calculations for small radicals 78−70746
OH, spontaneous vibr.-rot. Raman scatt. from $X^2\Pi$ state 79−36646
OH, UV light absorpt. at 3080 Å, for Gibbs free energy of mol. 79−100425
OH, vibr. ground-state, MFS, rot. spectra and electronic band anal. 78−5206
OH, vibrationally excited, high-resolution hyperfine Λ-doubling spectrum 78−90153
OH^- adsorbed on defect site of TiO_2 surface, electronic struct. 79−47150
OH^-, proton affinity, integral Hellmann-Feynman theorem 78−70767
OH+2-methyl-2-butene, reaction rate consts. meas. 78−61001
OH+acetylene (CO), reaction rate consts. meas. 78−35663
OH+CO(trichloroethane), reaction rate consts. and quenching kinetics, reson. fluoresc. obs. 79−72349
OH+dimethyl ether (vinyl methyl ether) reaction rate consts., 299-427K 77−86301
OH+ethylene, reaction rate consts., 229-425K 77−40535
OH+ethylene (and halogenated derivatives), reaction rate consts. 77−21356
OH+gaseous S compounds, lower atmos. chem. 80−61870
$OH+H_2O_2$, reaction rate const., 298K, flash photolysis-reson. fluoresc. obs. 79−57215
$OH+H_2O_2\rightarrow HO_2+H_2O$, reaction rate consts., laser induced fluoresc. 80−101017
$OH+H_2O(NO_2)(CH_3Cl)(N_2)(H_2)(He)$, mean collision cross sections from microwave spectroscopy 80−1046
OH+haloalkanes (haloalkenes), reaction kinetics in microwave discharge, reson. fluoresc. obs. 77−77744
OH+halomethane(haloethane), reaction rate consts., reson. fluoresc. meas. in discharge-flow system 79−72350
OH+He, O_2, N_2, H_2, NO_2, H_2O, NH_3, SO_2, chloromethane, rot. inelastic collision, microwave spectra 79−45806
$OH+OCS(CS_2)$, lower atmosphere chem. 80−61870
OH+organic compounds photooxidation reactions in atmosphere, rates, reactivity and mechanism 80−72104
OH+p-H_2(He), collisional pumping of Λ-doublet transitions, pot. energy surface 80−23516
$OH+RH\rightarrow H_2O+R$, radical substitution reaction 80−81321
OH+trans-2-butene, reaction products, O_2 and NO_2 effects obs. 80−85156
OH+trichloroethane, 1,1,1- and 1,1,2-isomers, reaction kinetics, 298-460K, lower atmos. chem. 80−16657
OH+trichloroethane$\rightarrow H_2O+CH_2CCl_3$, rate const. and tropospheric chem. 80−16658
$OH(A^2\Sigma^+)$ form. during H_2O photodissoc., luminesc. spectrum 79−57270
$OH(A^2\Sigma^+)$, form. from $H_2O+Kr(^3P_1)$, internal energy distrib. 79−10183
$OH(A^2\Sigma^+)+N_2(O_2)(H_2O)$(air), quenching rates and fluoresc. efficiency, rel. to atmosphere 80−14199
$OH(A^2\Sigma_{1/2}{}^P)$, and OD, hyperfine struct. determ. by freq.-doubled dye laser radiation 79−72333
$OH(C^2\Sigma^+)$, prod. by water radiolysis, time-resolved emission, quenching rate consts. 79−10138
OH(OD), $A^2\Sigma^+$ state, vibrational energy transfer in collisions, rot. resolved fluoresc. 78−74742
OH(OD) radical, photoelectron spectra 77−27113
$OH(^2\Pi)$, rot and translational temps. in gas discharge 78−5243
$OHX^2\Pi$ radical, ground and vibr.-excited ($\nu\leq6$) levels, microwave spectrum 79−63985
$O(^3P)+CHF\rightarrow HF+CO$, product vibr. energy distrib. 79−61853
OPCl radical, absorpt. spectra, PO (β and B′-X) systems, vibr, numbering 77−75173
P_2, perturbations in $b^3\Pi_g$ state, existence of $^5\Sigma_g{}^+$ state, visible and IR systems *(French)* 77−68035
P_2 radical, $A^1\Pi_g$-$X^1\Sigma_g{}^+$ transition, vibr. consts. *(French)* 77−75176
P_2 radical, $b^3\Pi_g$-$a^3\Sigma_u{}^+$ transition, perturbed by $1^5\Sigma_g{}^+$ state *(French)* 80−18855
PF_4, MS $X\alpha$ calcs., pot. energy surface, electronic struct. 77−57877
PH, $(b^1\Sigma^+)$ state, radiative lifetime, time resolved spectra 78−78750
PH, far IR laser mag. reson. of $X^3\Sigma^1$ and at $^1\Delta$ states 79−54869
PH_2, laser mag. reson. spectra. 9-9.6 μm, ν_2 band 79−89694
PH_2 radial, pot. energy curves. config., ab initio SCF-MO calcs. 77−50419
PH_2 radical, laser-induced fluoresc. 78−94277
$PH_2(F_2)(Cl_2)$, SCF-MO-HF calc., struct. and one-electron props., population anal. indices 79−76338
$PH(PH_2)$, excited state dynamics, laser photolysis of PH_3 79−16023
PO, $SiCl_2$ band system reassignment to PO and P_2 radicals 77−23505
$PO_4{}^{2-}$ anion radicals + organic compounds, reaction rate consts. 78−15669
PS, electronic transition $B^2\Pi$-$X^2\Pi$, vibr. and rot. anal. *(French)* 78−78716
l-proline monohydrate single cryst., X-irrad., ESR and ENDOR study of radicals 80−45528
$S_3{}^-$, stabilized on MgO surface, CNDO calcs. of g-tensors and hyperfine coupling consts. 77−83625
$(SCN)_2{}^-$, and $(SCN)_2$, vibr. anal., bond strengths 80−9582
$(SCN)_2{}^-$, reson. Raman spectrum, vibr. freqs. 79−18189
S_2Cl, blue absorpt. in Ar matrix 79−5149
SCl(Br), unstable radicals, matrix-isolated, IR spectra force const. *(German)* 80−43053
SF_5, IR spectrum, form. by VUV photolyses in Ar matrices 78−981
SF_6, equilib. electron-transfer reactions in gas phase involving long-lived neg. ion radicals 78−58807
SF_3BF_4;SF_3, cryst., γ-irrad., radical form., EPR 78−91955
SH, $(X^2\Pi_i)$ radical, UPS in VUV region showing vibr. struct. 79−98153
SN, electronic states, ab initio, SCF, and CI calcs. 77−75053
$(SN)_n{}^*$ radicals polymerisation to $(SN)_x$ in thin films, optical spectra 80−16656
SO, and isotopic forms, $X^3\Sigma^-$ state, CO_2 laser mag. reson. spectroscopy 80−9602
SO_3F, dye laser excitation of vibr. levels of upper electronic state, mol. fluoresc. meas. 80−83402
SO_3F, laser fluoresc. spectrum 80−28047
SO_3F, visible spectrum, heating and laser excitation of $S_2O_6F_2$ dimer 78−35647
SOH, ground and first excited states, geometry, ab initio SCF calcs. 78−50657
SOH radical, ab initio SCF and CI calcs., electronic states and transitions 77−46488
ScF_2, ESR spectra of radical in Ar matrix, 12K, hyperfine splitting 79−98122
$SeH(X^2\pi_{3/2})$, far IR LMR spectrum 78−66564
SeO_2, free radicals, pulse radiolysis obs. 78−20040
o-semiquinone, radicals, intra- and intermolecular H^+ transfer, ESR 77−16840
Si biradical, six-coordinate, mol. mobility two-spin probe investig. 80−102529
SiCH, matrix Hartree-Fock calcs. 79−5874
$SiCl_2$, band system reassignment to PO and P_2 radicals 77−23505
$SiCl_4{}^-$, ESR of radical in adamantane matrix, γ-irrad. of $SiCl_4$ in adamantane matrix 79−27011
SiF, $A^2\Sigma(\nu'=0)$ state, radiative lifetime meas. 77−27110
SiF_3, low-lying electronic states, ab initio HF calcs. 77−54512
SiF_3Cl^-, radical anion struct. and ESR spectrum 78−25571
SiH, emission spectroscopy, in H_2-SiH_4 glow discharge 80−69984
SiH, rot. transition freqs. calc., rel. to search in interstellar space 78−93100
SiH^+, rot. transition freqs. calc., rel. to search in interstellar space 78−93100
SiH_3 radical, hyperfine coupling consts., vibr. depend., ab initio calcs. 80−87150
SiH_3X^-, X=Cl, Br, I, and isotopic forms, EPR spectra, mol. struct. 79−94023
SiX_n radical, (X=H,D; n=1,2,3), thermodynamic function in ideal gas state 80−14871
$SnX_3{}^{\odot}(SnX_2{}^{\odot})$(X=Br,Cl,I), structs., electron affinities, formed by electron impact 77−61865
^{119}Sn free radicals, dynamic nucl. polarisation in solution 77−88475
SrF, $B^2\Sigma^+$-$X^2\Sigma^+$ system, rot. anal. using a cw tunable dye laser 78−9165
SrF radical, rot. spectrum of $X^2\Sigma^+$ state, MODR 78−9176
T in solid H_2, equilib. stability 77−81396
TeF, chemiluminesc. from oxidation in $F_2+H_2Te(D_2Te)$ emission spectrum obs. 80−43058
XeF*, $B^2\Sigma^+$ and $C^2\Pi_{3/2}$ states, fluoresc. decay dynamics, collisional quenching and radiative lifetimes 80−58306
ZnF, mol., ESR spectra in inert gas matrix 79−76455

freezing
see also refrigeration
adhesive hard sphere fluids, clustering phenomena, theory of freezing 79−7533
aerosol large particles ingestion by cloud, ice nucleation by freezing 77−37308
alkali halides, binary liq. mixtures, freezing pt. depression 77−43312
annular region, perturbation soln. for melting/freezing interface 78−59286
aqueous solution, effect of surface condition on crystallisation in capillaries 79−56037
atmosphere freezing nuclei sources, large aerosol particle conc. 80−41512
baceteriophages, freeze drying method for electron microscopy 80−104826
BBOA, polymorphism, radiothermoluminescence and differential scanning calorimetric study 80−24570
beach sediments, lower St. Lawrence Estuary, Quebec, frost effects 78−7609
bifurcation of crystalline solutions and freezing 78−67814
binary alloy, non-equilibrium thermodynamic processes 80−34167

- **freezing** continued
  - binary alloy, numerical calc. and simulation of nonsteady mass transfer by moving phase boundaries *(German)* 77−8811
  - biological cells, mechanism of dehydration on thawing 77−81478
  - biological material, prep. for X-ray microanal. of diffusible elements, methods of drying ultrathin cryosections 78−77166
  - biological material cryofixation, fast freezing device 78−28138
  - biological material freeze-fracture preparation for SEM 78−61290
  - biological material freezing, multi-purpose cryostat 78−15940
  - biological material prep. for X-ray microanal. of diffusible elements, rapid freezing and ultrathin section prep. 78−77165
  - biological materials, freeze-drying technique using modified freeze-etching device 77−70572
  - biological materials, multipurpose cryostat 78−40437
  - biological materials, thermal history of cells 79−62419
  - biological membrane, egg yolk, freezing injuries, membrane destabilisation *(French)* 79−48221
  - biological sample microtoming, freezing technique for long specimens of small width/depth 78−3695
  - biological specimen freeze drying technique for SEM 80−104828
  - biological specimen freeze-drying process obs. by SEM 78−28142
  - biological specimen prep. freeze-fracturing with a new specimen table 79−5425
  - biological specimen rapid freezing under controlled and reproducible conditions 78−57139
  - biological specimen replication at −150°C with improved freeze-fracture apparatus 80−85560
  - biological specimens, new freeze-etch unit 79−5423
  - biological tissue around cryosurgical probe, Stefan-like problem analysis 77−17005
  - biological tissue prep. without chem. fixation, freeze-drying for electron microscopy 78−65164
  - bone, fresh and preserved by freezing, bending strength 77−25488
  - bone, marrow and leucocyte preservative freezing apparatus 79−39617
  - bricks, extensometer for meas. of linear expansion due to freezing 78−53062
  - British Isles, freezing level during rainfall 77−29391
  - carbon tetrachloride, freezing and melting of stable and metastable phases 77−27984
  - cell drying, critical point drying alternatives for specimen prep. 78−24210
  - cell freeze conservation control unit *(German)* 79−5410
  - cell organelle lipid anti-radical activity change due to freezing at −78 and −196°C 77−70426
  - cell structure and function, freezing patterns and post-thaw survival 78−64960
  - cell water permeability during freezing and thawing, cryomicroscope multiple nonlinear regression analysis 79−92197
  - cells, mouse embryo, innocuous freezing during warming 80−94175
  - cells, volumetric changes during freezing and thawing, thermodynamic model 80−108863
  - ceramic compounds, lyophilisation parameters, freeze-drying synthesis 80−97453
  - charged fluids near freezing point, static dielectric behaviour 78−56417
  - ciliated surface preservation for scanning electron microscopy 79−74805
  - classical hard sphere system, statistical theory of freezing 80−33868
  - colligative properties of simple solns. 77−21466
  - computer simulation, using array processor 80−54353
  - concrete, flowing, expt. studies *(Japanese)* 80−89298
  - corrosive materials, freeze-drying 77−41580
  - cryobiology, freezing and cryofixation 78−28136
  - cryobiology, H_2O-NaCl-sucrose phase diagram 78−15777
  - cryobiology, struct. and functional aspects of freezing techniques 78−28137
  - cryogenic equipment for food and medical industrial appls. 79−58714
  - cryogenic fluids cooling and freezing by vapour space evacuation 77−57331
  - cryogens, porous solids, gradientless heat transfer, cryogenic liq. crystn. 79−59903
  - cryosurgery, math. and biophys. foundation 77−40920
  - cuboid, heat-balance integral calcs. 77−27981
  - Darcy flow, chilled pipe freezing zone, finite difference method 78−94734
  - decane: pyrene (coronene), quasiline spectra, multiplet struct., freezing conditions and solvent effects 79−1786
  - dendritic ice form. in pipe, cooling rate effect 78−90690
  - dendritic ice formation in flowing water pipes, blocking mechanism 77−47092
  - determination using ruby fluoresc. spectra shift in high press. cell 77−26321
  - diffusion cloud chamber, freezing and sublimation expts. with ice forming nuclei *(Spanish)* 77−87046
  - dioxan-$H_2{}^{16}O(H_2{}^{18}O)(D_2{}^{16}O)$, solns., FP determ., equilib. method 77−20048
  - dispersed medium freezing, origin of water aspiration 77−60130
  - EBBA, polymorphism, radiothermoluminescence and differential scanning calorimetric study 80−24570
  - n-eicosane, freezing, control by natural convection 80−39262
  - electron microscopy, cold-stage system for fast-frozen liquids 79−71573
  - erythrocyte survival after slow freezing in glycerol, temp. depend., human cells 78−77019
  - erythrocytes, human, effect of hydration on water content 77−16921
  - erythrocytes, slowly frozen human cells, phys.-chem. basis of protection by glycerol 78−77020
  - ethanol-water system, metastable states, hydrates existence and props., low temp. 78−71835
  - fast reactor ceramic fuel-steel system, freezing of flowing liquid in melting tube, simulation expt. 79−30981
  - fibre coating, freeze and viscous coating technique 78−48350
  - finite domains not initially at fusion temp., singular perturbation theory 77−66014
  - finite medium freezing (melting), variational anal., radiation and convection effects 80−38244
  - first principles order-parameter theory 79−77718
  - foodstuffs and biological materials, information systems models relevant to developed freeze-drying systems 79−58727
  - freeze drying microscope stages 78−45681
  - freeze-drying of food models, heat and mass transfer 79−1098
  - freeze-drying techniques; mass transfer, appl. of calorimetric instrumentation 77−25628
  - freeze-etching improvement using evaporated film 80−85558

- **freezing** continued
  - freeze-fracture electron microscopy freezing method evaluation by low temp. X-ray diff. 78−57145
  - freeze-fracture specimen temp. changes during rapid quenching in liq. coolants 78−57140
  - freeze-fracturing preparation technique, methods and results, review 78−24776
  - frost depth in soils of Urals and W.Siberia 79−57986
  - frost formation, struct. model of frost layer growth 78−79200
  - frost properties, rel. to frost formation types 77−80614
  - geological conductors, water-bearing, effect of freezing on elec. props. *(German)* 79−5472
  - glass fibre reinforced epoxy resin, destruction by freezing or boiling of phase separated water 78−48512
  - haeme protein solns., resonance Raman spectra at low temp. 77−23588
  - half-space, plane Stefan problem soln., degenerate hypergeometric transformations method 79−86332
  - heat balance integral method, refinement 79−14229
  - heat conduction, at freezing/melting boundary, model for approx. calcs. 78−5630
  - Heisenberg spin-glass, crit. dynamics 78−60295
  - hexane:pyrene (coronene), quasiline spectra, multiplet struct., freezing conditions and solvent effects 79−1786
  - hydrated tissue section prep. for X-ray microanalysis using satellite vacuum coating and transfer system 78−24200
  - ice, bacteria as biogenic sources of freezing nuclei 79−20948
  - ice, detection using surface acoustic waves 78−18129
  - ice, nucleation threshold on Cu_2S, Ag_2S, Mo_2S and CdS photosensitive surfaces 77−55343
  - ice, on CuS aerosol prepared by burning pyrotechnic mixture, freezing temps. 78−96279
  - ice crystal size from droplet accretion growth 79−79933
  - ice growth in laminar flow through a channel with two parallel flat walls 79−3908
  - ice layer formation of given thickness by accumulation on cooled-cylindrical surface 77−7850
  - ice nucleation on AgI, exptl. verification of ice-forming activity theory 80−101406
  - ice on Great Lakes, formation, freeze-up, breakup predictions 77−45038
  - ice phase formation in natural and seeded storms 78−61509
  - ice-maker heat pumps, two plate-type, Remcor and 'no-penalty' harvest schemes comparison 79−48165
  - ice-water interface, dynamic light scatt. during freezing 79−33074
  - ice-water interface struct., fluctuations during solidification 78−59935
  - ice-water phase boundary, conc. depend. solute redistrib., spontaneous convection, chloride solns. 78−26665
  - inert gas fluid, nucleation of freezing by positive ions 77−84893
  - kidney, tissue water freezing study, ^{1}H NMR obs. 80−8027
  - Lake Shlavantas, deep autumnal cooling and freezing *(Russian)* 78−36213
  - latent heat storage materials, high temp. corrosion resistance and thermodynamic stability 80−30582
  - latex, monodisperse, reflectivity obs. of phase separation into ordered and disordered phases 77−70345
  - liquid flow blockage in circular tube below freezing point, theory and expt. 78−94830
  - liquid flow in tube with frozen layer, crust profile method 78−30359
  - living cell volumetric changes in freezing and thawing, thermodynamic model and expt. 79−92192
  - LMFBR accident anal., noncondensible void fraction effect on freezing of flowing fluids 79−31013
  - LMFBR in HCDA transition phase analysis, material relocation and freezing 77−46329
  - LMFBR transient over power accident, plateout and thermal loading of ejected fuel 79−30982
  - lyophilisation, effect on free radical states of animal cells 77−25391
  - Matanuska Glacier, Alaska, meltwater subglacial freezing, evidence from O isotope investigation 79−79884
  - material systems containing aqua solns., heat cond. with freezing 79−50565
  - metal, freezing at mean heat exchange intensity in irregular mode stage *(Russian)* 79−52193
  - metal fixed points, limitations caused by trace impurities 80−105644
  - metastable liquid, instability and freezing, theory 78−18746
  - metastable liquid, nonlinear diffusion eqn., multi-mode one dimens. anal. 78−87771
  - molecular dynamics simulation, Gaussian core model 78−67811
  - molecular theory, bifurcation, density depend. 77−1213
  - molecular theory, eqn. of state, free energy, from 1st BBGKY eqn. 78−67804
  - monolayers, Lennard-Jones system, melting in external field, freezing, temp. determ. 80−65362
  - multidimensional problems in arbitrary domains, numerical method 78−90693
  - nematic liquid crystal, Merck 389, polymorphism, radiothermoluminescence and differential scanning calorimetric study 80−24570
  - noble gas fluids, press. induced transition in neighbourhood of alkaline earth impurity 78−51770
  - numerical calculations, for third kind boundary conditions 77−84891
  - octane: pyrene(coronene), quasiline spectra, multiplet struct., freezing conditions and solvent effects 79−1786
  - oscillatory ice states in water internally heated and cooled from above 77−73759
  - permafrost, freezing rel. to N.Canadian hummocky microrelief dynamics 77−64285
  - pharmaceuticals, freeze drying 77−70010
  - phase change derivation, phys. chem. textbook assumption removal 80−17772
  - physiological sample, fusion progression during rapid freezing for electron microscopy 80−3884
  - plant and animal tissue, freeze-substitution, for localisation of water-soluble cpds. by electron probe microanalysis 77−37115
  - plant material, cryofracturing and low temp. SEM 78−24207
  - plant root transport studies using ion localisation, freeze substitution method 80−85569
  - plant tissue preparation for ion localisation studies, freeze substitution method 77−9309
  - polymorphous material, Stefan problem, melting or freezing, interfacial boundaries 80−64350
  - polyvinylidenefluoride, melting and freezing, effect of structural factors *(German)* 78−15389

freezing continued
porous ceramics, frost action under one dimens. heat flow *(Japanese)* 79—79140
porous solid with below-freezing pt. adsorbate, isothermal adsorption and dimensional changes obs. 78—75925
puddle water, nighttime disappearance with ice needles growth and daytime reappearance 77—29334
pyroelectric polymer film for electron microscope sample preparation, rapid cooling effects *(German)* 80—13185
red blood cell freezing, cryopreservation and refrigeration 80—67262
reference standards for radiation pyrometry, silver and copper freezing points 78—57888
resin-embedded unicellular organism preparation for ultrathin sectioning 79—70724
Ross Ice Shelf (Antarctica), basal freezing, confirmed by core drilling 80—101393
salt solutions, freezing in cells, heat and mass transfer with phase change 80—6493
saltwater drop falling in organic phase, ice growth 80—15218
saturated liquid, freezing-controlled penetration into cold tube 77—80219
saturated porous media, effect of seepage flow on freezing 79—1241
sea water freezing, induced haline convection expts. *(Japanese)* 78—88843
seawater freezing point depend. on salinity 78—3803
secretory granule membrane, particle clustering induced by centrifugation, freeze-fracture anal. 80—85559
SEM cold stage microscopy, thin frozen hydrated specimens, temp. rise and sublimation of water 78—24198
SEM sample preparation apparatus for freeze drying and vacuum evaporation 78—335
semiinfinite slab, with const. heat flux boundary, transient interface position and temp. field 79—94481
skin freezing temperature, human finger 77—21486
sodium oleate, frozen soln., NMR study of phase transitions 79—56617
soil, freezing, effect of moisture exchange and heaving 77—25702
soil, freezing, migrational flow of moisture 77—25704
soil, freezing processes, finite element simulation 79—16527
soil, frost heave in Tomakomai, Hokkaido, 1976 to 1977 *(Japanese)* 78—92860
soil, moisture change-of-state front advancement in freezing and thawing 77—91163
soil, prediction using weather records 79—88379
soil, seasonal freezing or thawing depth calc., eqns. eval. 77—78243
soil, struct. changes during freezing and thawing 77—25707
soil creep induced by freeze-thaw cycles, rate meas., lab. expt. 77—81868
soil freezing, water migration obs. *(Japanese)* 78—88862
soil freezing velocity meas., recording device design *(Japanese)* 77—82033
solidifying sphere, thermal contraction and density change effects upon freezing 79—64517
spherical particles, force exerted by freezing interface 80—107083
spray-freezing unit for prep. of specimens for freeze-etching 77—41581
stability of solid freezing front 78—63844
statistical mechanical theory, appl. to Lennard-Jones fluid 78—47499
statistical mechanical theory of freezing transition 77—7846
steam condensation heat transfer on below-freezing pt. surface 78—75042
steel, killed ingots, freezing process, liq. core movement *(Russian)* 80—20921
Stefan-like problems, soln. improvements 79—23181
supercooled aqueous solution, freezing, generalised analytical soln. 80—92142
teaching demonstration of freezing by boiling, using low capacity pump without acid 78—8192
TEM specimen freeze drier, all-glass design 80—82854
temperature meas., theoretical aspects, thermometric reference materials 77—67436
thermal problems, one-dimens., with phase change, efficient numerical technique 78—59270
tissue, normal and diseased, rel. to cryosurgery 78—44685
tissue molecular dynamics and freezing phase transition studied by proton spin relax. 78—68983
transient freezing of liquids in turbulent flow inside tubes 80—6494
tube flow, heat transfer problem of flowing liquid solidification onto a melting wall 78—94585
turbulent flow between parallel plates, steady-state soln. 77—58680
turbulent liquid flow in tube, freezing, steady state 78—33998
two-phase Stefan problem, numerical anal. by variational inequalities 79—82315
ultrathin cryo-section stabilization by freeze-drying 78—54349
universality of melting and freezing indicators, additivity of melting curves 77—1214
Van der Waalsian theory, 3D Ornstein-Zernike equation 78—91424
Van der Waalsian theory 78—22821
water:Cu(II) adsorbed on silica surface, EPR spectrum, freezing props. of water 77—4555
water, adsorbed on cellulose, NMR relaxation times 79—78552
water, cylindrical and two-dimens. freezing with varying wall temp. 77—1217
water, forced laminar convection in horizontal pipe, density inversion effects, numerical anal. 78—90900
water, particle engulfment, theoretical model 80—54351
water, supercooled, probability of ice nuclei form. 78—3909
water, transient natural convection in horizontal pipe with const. cooling rate through 4°C 77—42828
water, viscosity of nonfreezing thin interlayer between ice column and quartz capillary 80—54475
water at interfaces, mol. struct. and dynamics 77—31873
water droplet freezing process under supercooled conditions 80—65192
water drops, ice envelope splitting during freezing *(Russian)* 77—27982
water drops, ice splinter production during riming 78—85662
water drops, kinetic parameters of AgI-type crystallising reagents *(Russian)* 77—81963
water in capillary, freezing and melting behaviour, dilatometry, elec. cond. meas. 78—75908
water supercooled, dispersed within emulsions, freezing, differential scanning calorimetry meas. 77—15552
water supercooled droplets, on ice substrate after low speed collision, freezing behaviour, cryst. struct. 80—29152
water-ice transition, production of stimulated coherent radiation 78—83920

freezing continued
yeast cell suspension in salt soln., dynamic effects of freezing 79—70533
Al-Cu alloy, nonstationary mass transfer in front of moving phase boundaries in mormal freezing *(German)* 77—44238
$3Al_2O_3.2SiO_2$, mullite, synthesis by freeze drying 80—16252
Ar, two-dimensional freezing, on differently graphitised carbon 79—77896
C-O white dwarf freezing, C-O eutectic model 80—77405
Cu, freezing point, precise determ. 78—30740
$Cu(NO_3)_2$, frozen aq. soln., phase transitions, struct., ESR 77—16154
Fe, cast, white, freezing rate and Si content effect on graphitisation *(Japanese)* 77—56009
H_2, on inner surface of spherical polymer shell, cryogenic targets for laser-driven fusion 78—86688
$HN(SO_2Cl)_2$, physical props. meas. 79—51293
^4He, density, 0.1 to 0.82K, and entropy of solid 77—7925
^4He, Lennard-Jones model at 0K, props. using Monte Carlo method 79—82401
^4He, liq., nucleation of freezing by positive ions 77—84893
LiCl, frozen soln., NMR study of phase transitions 79—56617
N_2, two-dimensional freezing, on differently graphitised carbon 79—77896
NaCl, frozen soln., NMR study of phase transitions 79—56617
O_2, phase equilibria near 298K, Raman spectral study of solid and fluid 80—19937
PbO mixtures with various oxides, solvents for garnet growth, cryoscopic study 80—24393
Pt, freezing point determ. 77—26288
Pt ribbon, melting temp. determ. from continual melting and freezing 77—51476
SF_6 partial press. meas. in mixtures with N, using separation by freezing 79—71478
^{99m}Tc-diethylentriaminepentaacetic acid freeze-dried kit prep. 79—88189
UO_2, molten fuel freezing in shield plug following LMFBR HCDA 78—8941
UO_2, simultaneous freezing and melting in finite media 80—620
Y_2O_3, digital pyrometry in solar furnace *(Japanese)* 78—32821
Zn-Al, impure and pure, as cast, endogenous-exogenous freezing 78—19736
ZrO_2, digital pyrometry in solar furnace, freezing point *(Japanese)* 78—32821

Frenkel defects
acceptor-donor-acceptor complex, Frenkel excitons and ionic excited states 80—92824
alkali halide, Frenkel defect pairs formation mechanism *(Russian)* 80—10542
alkali halide, shock recomb. mechanism of defect generation in cation sublattice *(Russian)* 77—31656
alkali halides, irradiated at room temperature, stored energy 80—79839
alkali perchlorates, elec. transport during struct. transforms. 78—59971
alkaline earth halide crystals, thermal transport of charged point defects 80—15293
diffusion-controlled defect annealing, theory 80—92520
discrete lattice model, Frenkel pair annihilation 77—59009
doped semiconductor, radiation defect, form. mechanism associated with electron transitions 79—69155
electron interaction for Frenkel pair form. in solids, computer simulation *(Russian)* 80—6402
electron irrad. effect on electrolum., defects form. and quenching obs. 80—55194
FCC metal, Frenkel pair annihilation, discrete lattice model *(Russian)* 78—10042
graphite, point defects and self diffusion 78—63758
HCP lattice, Frenkel pair stability 79—60353
inert gas:H, quasifree electron energy, inference from ESR studies 79—69459
ionic crystal, influence of defect interaction upon their recomb. 80—84207
ionic crystal, intrinsic electronic excitations and defects, review *(Russian)* 80—10881
ionic crystal, sublattice disorder, phenomenological models 77—35663
ionic crystals, efficiency of radiation-induced F-centre accumulation *(Russian)* 79—69102
ionic crystals, radiation defect accumulation temp. depend. 80—19803
ionic crystals, spatial separation of components of primary radiation defect pairs 78—14376
linear crystal, donor-acceptor complex, Frenkel excitons and ionic excited state mixing 79—99485
long-lived point defect formation from unstable vacancy-interstitial pairs 77—59008
low-energy radiation damage, temp. depend. 78—6099
metal, BCC, neutron irradiated, spontaneous recombination volumes of Frenkel defects, rel. to compressibility 78—71765
metal, HCP, long-range interstitial migration rel. to c/a ratio 79—28125
metal, irrad., containing self-interstitials and vacancies, electronic transport props. 78—60105
metal, irradiated, determ. of time threshold energy for Frenkel pair creation 77—47444
metals, thermal instabilities due to recomb. of radiation-induced Frenkel pairs 79—23597
Mossbauer spectroscopy exam. of radiation defects in solids 78—31139
quartz, comparison of different radiation effects 78—26596
radiation-induced processes, unstable Frenkel pair mechanism 80—34050
rare earth metals, HCP, point defect production during electron irrad. at low temp. 80—49273
semiconductor, collective magnetoexciton transition under action of light *(Russian)* 78—79939
semiconductor, Frenkel pair defect formation threshold energy during particle irrad. 79—90647
semiconductor, Frenkel pair formation threshold energy during particle irrad. 79—90646
semiconductor, threshold energy for displacement of atoms 78—47428
semiconductors, asymmetry in displacement energy for Frenkel-pair prod. 78—2116
semiconductors, fast particle irrad., Frenkel defect formation threshold energy 80—6404
semiconductors, glassy, diamag., photostructural changes, mechanism 80—92557
steel, austenitic stainless, Cr-Ni, resist. damage rate during neutron irrad. at 23K 80—96571

Frenkel defects continued
superionic conductor, with fluorite struct., activation vol. 80—107557
superionic conductors, cooperative phenomena within generalized lattice gas models 79—46827
unstable, form. and collapse, defect migration, electron irrad. effects, computer simulation 80—92523
Ag film, electronic stopping power on irrad. by He, Li, C ions, damage-rate measurements 79—77654
Ag film, Frenkel pair prod. by light energetic ions, elec. cond., changes 77—59050
Ag, Frenkel defect production associated with He and light ion implantation, exam. 78—47443
Ag, ion-irradiation studies of damage function 79—37746
Ag, proton irrad., radiation-annealing effects in energetic displacement cascades, film resist. meas. 78—26603
Ag-halide microcryst., space charge characts. 78—15097
AgBr, Br^- diffusion plot, anomalous curvature 79—60548
AgBr, electron simulation, luminescence and hidden image formation *(Russian)* 79—47515
AgBr, Frenkel defects, interstitials, neutron scatt. study 79—42059
AgBr, high-temp. transport anomaly from Na tracer obs., mechanism 77—62669
AgBr, self-diffusion of ^{82}Br by both single vacancies and vacancy pairs 78—55978
AgBr, thin epitaxial layer, surface ionic cond., lattice disorder, space charge region 77—11730
AgBr thin film interstitials, Frenkel and space-charge contributions 79—18494
AgBr:Pb^{2+}, cubic microcryst., ion influence on ionic cond. and space charge characts. 79—55928
AgBr-AgCl, mixed crystals, pure and I doped, lattice defect parameters, Frenkel defect form. energy, ionic cond. 80—44359
AgBr(:Pb^{2+}), ionic conductivity, Frenkel defects 77—51542
AgBr(Cl), formation vol. of Frenkel defect 78—79606
AgBr(Cl), ionic transport, defect form. and migration energies, quasiharmonic model 80—107538
AgCl, electron simulation, luminescence and hidden image formation *(Russian)* 79—47515
AgCl, Frenkel defects, interstitials, neutron scatt. study 79—42059
AgCl, ionic mobility, diffusion coeffs., defect mobility energies 80—65284
AgCl:Na^+, Frenkel defect formation energy, impurity diffusion and migration 79—99179
AgCl(Br), enhanced defect form., mean field theory 80—107220
AgI, B1 phase, high press. elastic props., thermally activated rel. anomaly 80—44261
β-AgI, ionic cond. and Frenkel pair form., dielec. loss meas. 79—33112
β-Ag_2S, electrogalvanic and elec. props., and range of existence *(French)* 78—43175
α-Ag_2S, electronic and electrogalvanic props., completely ionised Frenkel defects *(French)* 78—84237
Ag_2Se, electronic and electrogalvanic props. in α-phase region *(French)* 80—107820
Al, Al-Ag(Mg) dil. alloys, electron irrad., stage I_E recovery, interstitial trapping 77—15405
Al, electron irradiated, di-interstitial formation within small defect clusters 78—26566
Al, irradiation defects, intrinsic thermal expansion meas. 79—95186
Al, low temp. thermopower of Frenkel defects 78—19024
Al, low-field galvanomag. props., Fermi surface and defect struct. effects 77—4323
Al, neutron irradiated, phonon dispersion curves, neutron scatt. meas. 77—43290
Al, with dilute pt. defects, thermopower, Hall effect and magnetoresist. 79—65458
AlN, asymmetry in displacement energy for Frenkel-pair prod., n-type to p-type conversion 78—2116
β-Al_2O_3, stoichiometric, Raman and IR spectra, Frenkel defects, order-disorder transition and cation cond. 80—55086
β-Al_2O_3-M_2O, M=Ag, K, Rb, Na, Eu, X-ray diffuse scatt. 78—71725
Au, electron irradiated, low temp., Frenkel defects, diffuse X-ray scatt. study *(German)* 79—23601
Au, proton irrad., radiation-annealing effects in energetic displacement cascades, film resist. meas. 78—26603
$BaCl_2(F_2)$, sp. ht. meas., Schottky-type diffuse phase transitions, defect form. energies and entropies 80—107441
BaF_2, influence of O_2 on elec. cond., 450-1150°C, anion Frenkel disorder model *(French)* 77—47619
BaF_2, ionic cond., activation vols., freq. depend. cond., press. effects 80—100354
BaF_2, NMR relax., ionic cond. and self-diffusion 78—23362
BeF_2, vitreous, ionic transport and defect struct. 80—107472
Bi, electron irrad., displacement threshold energy *(French)* 79—23649
β-AgI, ionic cond. and dielec. meas., Frenkel defect formation energy 78—87814
CaF_2, entropy of form., Green function calc. 80—19898
CaF_2, ionic cond., activation vols., freq. depend. cond., press. effects 80—100354
CaF_2, mol. dynamics studies of superionic conductors 80—107547
CaF_2:Y, absorpt. spectra, radiation defect formation energy, F to M centre conversion kinetics 79—65079
CdF_2, ionic cond., activation vols., freq. depend. cond., press. effects 80—100354
CdS laser irrad. native defect formation, influence on photoelectric props., IR luminescence *(Russian)* 80—11039
CdS, neutron irradiated, photoelectric props. 77—35962
CdTe, electron induced defect creation rates 78—41892
CdTe-HgTe, semicond. solid solns., effect of reactor irrad. on electrophys. props. 77—51744
Co, electron irradiated, mag. after-effect spectrum, 20-350K 77—1570
$Co_{1-y}O$, self-diffusion and defect struct. 78—22889
Cr, atomic displacements in electron irrad. cryst. 79—46705
CsBr, X-irradiated, release of stored energy 78—38753
Cu, defect-phonon perturbations after neutron irrad., neutron scatt. study 80—44278
Cu, elastoresistivity of Frenkel pairs, defect migration *(French)* 80—2073
Cu, electron irrad. at 4.7K, recovery of Frenkel defects, defect-agglomerate effects *(German)* 77—84797
Cu, electron irradiated, dia- and paraelastic effects 77—76482
Cu, electron radiated, formation of Frenkel pairs 79—23598

Frenkel defects continued
Cu, film, Frenkel pair prod. by light energetic ions, elec. cond. changes 77—59050
Cu foil, electron irradiated at low temps., annealing, form. of clusters of atomic defects 77—15416
Cu, Frenkel defect production associated with He and light ion implantation, exam. 78—47443
Cu, Frenkel defects, diffuse X-ray scatt. obs. *(German)* 79—23600
Cu, Frenkel pair production threshold energy, temp. depend., exam. 78—51530
Cu, ion-irradiation studies of damage function 79—37746
Cu, proton irrad., radiation-annealing effects in energetic displacement cascades, film resist. meas. 78—26603
Cu, pure and dil. alloys, Frenkel pair recombination radius, temp. depend. 77—89427
Cu, thermal vibr. and zero-point motion effects on low-energy collision cascades 78—87705
Cu-Au(Be)(Sb), dil., electron high dosage source for residual resistance specimens and irradiation expts. *(German)* 78—21274
Cu-Cr, dil. alloys, Frenkel defects, effects on anomalous resistivity and thermopower 77—8084
CuCl, pure and Cu_2S doped, rel. to ionic cond., 60-370°C 77—47617
Cu_2O:Mn, photomemory mobility components, charged centre conc. 80—103725
Fe, BCC, neutron-irradiated, Frenkel defect spontaneous recomb. volumes 79—60355
α-Fe, defect creation anisotropy in electron irradiated samples 77—31994
Fe, electron irrad. damage, elec. resist., 20K *(French)* 78—2160
α-Fe, Frenkel defect recombination zone, effect of uniaxial compression 78—6987
Fe, irradiated with electrons then annealed, magnetoresistance at 20K *(French)* 80—103677
GaAs, low temp. gamma irrad., donor-acceptor pair formation 79—69158
GaAs, point defect equilib., non-stoichiometry 79—90644
GaAs, primary radiation defect separation by elec. field 80—92522
Ge, electron or γ-irrad., metastable close Frenkel pair form. 77—80501
Ge, gamma irrad. above threshold, defect formation impurity ionisation mechanism 80—6433
Ge, gamma-irradiated, number of Frenkel defects 78—14377
Ge, ion bombarded, radiation defect formation, atom-atom collision cascades modelling 80—10582
Ge, lattice defects formed on γ-irrad., effect on elec. props. 80—19839
Ge:Sb, electron-hole drop lifetime, quenching temp. influence 80—59889
He, solid, ion current modulation by thermal waves 78—91506
^{3}He, solid, low temp. mag. and thermal props. due to bound state Frenkel vacancies 79—56019
$Hg_{1-x}Cd_xTe$, grown from melt, Kirkendall and Frenkel effects 80—100365
HgTe, self diffusion of Hg and defect struct. 79—23775
InSb, energy spectra of impurity atoms under 4.2K gamma irradiation 77—89471
n-InSb, influence of electron irradiation intensity on defect formation 79—73216
KBr, cation defects creation mechanism 80—75224
KBr, defect accumulation under electron irrad. at 4K 80—107233
KBr, defect recombination, 4.2 to 77K 78—72606
KBr, electron irrad., F-centre formation kinetics, interstitial stabilisation mechanism 79—69103
KBr, electron irradiated, defect accumulation kinetics of low temps. 80—10577
KBr, radiation-induced F-centre accumulation efficiency *(Russian)* 79—69102
KBr, recomb. in ionic crysts., defect interactions 80—84207
KBr, stored energy after X-irrad. at low temp., 10-50K 77—76459
KBr, thermolum. and reactions of freed interstitial and trapped hole centres 78—23538
KBr, with Frenkel cation defects, EPR and thermolum. of V_F, V_2-centres 78—10769
KCl, defect recombination, 4.2 to 77K 78—72606
KCl, ionic cond., defect parameters, diffusion coeffs. 80—79978
KCl, temp. depend. of F-colouring efficiency 80—44204
KCl, with Frenkel cation defects, EPR and thermolum. of V_F, V_2-centres 78—10769
KCl, X-irradiated, formation of cation defects 78—91359
KCl, X-irradiated, release of stored energy 78—38753
KCl:$Sr^{2+}(SO_4{}^{2-})$, ionic cond., defect parameters, diffusion coeffs. 80—79978
KCl:$Sr^{2+}(SO_4{}^{2-})$, defect parameters, self-consistent set, ionic cond. meas. 80—107487
$KClO_4$, AC electrical conductivity meas., mechanism involving Shottky and Frenkel defects 79—99367
β-K_2O-Al O_3, cation distrib. 77—80487
$K_2[SnCl_6]$, defects determ., dipole relax. in phase transform. *(German)* 78—22711
LiH, defect form. at low temp., EPR, thermolum. and TSC study 80—107222
Lu, effect of low-temp. electron irradiation 77—43249
Lu-H, effect of low-temp. electron irradiation 77—43249
MgO, electron irradiation damage, cryst. defects 80—107320
MgO:Fe^{3+}, Mn^{2+}, X-irrad. induced anion Frenkel defects, stabilisation by Fe^{3+}, optical and ESR obs. 77—68969
Mo, BCC, neutron-irradiated, Frenkel defect spontaneous recomb. volumes 79—60355
Mo, gamma-ray irrad. positron annihilation during radiation defect annealing *(Russian)* 79—99970
$Na_8Al_6Si_6O_{24}Cl_2$, radiolytic radiation damage, Frenkel pair formation on Cl sublattice 79—7628
$Na_6Al_6Si_6O_{24}(NaX)_{2n}$, X=Cl, Br or I, sodalites, thermal destruction of colour centres *(Russian)* 80—84169
NaBr Frenkel pairs, interactions forming enrichment centres 80—96518
NaBr-U-centre containing cryst., X-ray radiation induced cation vacancy generation 80—39078
NaBr(:I), exciton ionisation and decay, photoluminesc. in elec. field 77—44046
NaCl, formation during fast electron beam irrad. *(Russian)* 77—7716
NaCl(Br), X-ray or UV irradiated, cation defects creation mechanism 80—75224
Ne:Xe(Ar), electronic relax. cascades in Wannier and Frenkel type exciton states 79—33759
Pb, O ion irradiated, damage rate decrease 78—26604

Frenkel defects continued
- Pb superconducting junction, neutron irradiated, tunnel spectroscopy 78—10618
- $PbBr_2(Cl_2)(I_2)$, ionic cond. and activation volumes, high press. effects 80—100353
- PbF_2, cubic and orthorhombic, press. and temp. depends. of ionic cond. 79—95207
- β-PbF_2, solid electrolyte, mobile species mobility and conc., temp. depend. 77—20113
- PbF_2, sp. ht. meas., Schottky-type diffuse phase transitions, defect form. energies and entropies 80—107441
- PbTe, epitaxial film on fluorphlogopite, effects of annealing in Te vapour 77—80709
- Pt, deuteron irrad., energy release and resist. recovery, self-interstitial-atom interaction energies 79—95002
- Pt, electron and deuteron irrad., close Frenkel pair recomb. during annealing 78—87716
- Pt, Frenkel defect migration and reactions, by subthreshold recoil events, exam. 78—47364
- PuO_{2-x}, O_2 chem. diff., dilatometry and thermogravimetry study *(French)* 79—73339
- RbCl(Br), cation defects creation mechanism 80—75224
- n-Si, defect charge states, complex form., gamma-ray effects 80—96564
- p-Si, electron irrad., influence of acceptor impurity conc. and irrad. temp. on defect formation 79—19281
- Si, gamma-irradiated, number of Frenkel defects 78—14377
- Si, ion bombarded, radiation defect formation, atom-atom collision cascades modelling 80—10582
- Si, ion-implanted, secondary defects development, three-stage model 78—87725
- Si, local electron irrad., Frankel pair separation, influence on photo EMF 80—44203
- Si material processing, point defect thermodynamics 78—6054
- p-Si, X-irrad., subthreshold defect prod., Hall meas. of carrier conc. and photocond. spectra 77—89470
- Si:As, 1.5 MeV H^+ and He^+ irradiations of As diffused layers 78—47447
- Si:O,C, electron irradiated, indirect vacancy-interstitial recomb., IR absorpt. meas. 77—43209
- Sn, tetragonal β-phase, neutron-irradiated, Frenkel defect spontaneous recomb. volumes 79—60355
- $SnSe_yTe_{1-y}$, semicond. chalcogen interdiffusion coeffs., antifrenkel defects, interstitials *(German)* 77—43375
- $SrCl_2$, anion diffusion mechanism 80—2201
- $SrCl_2$, pure and doped, disorder and defect props. 80—107217
- $SrCl_2$, sp. ht. meas., Schottky-type diffuse phase transitions, defect form. energies and entropies 80—107441
- SrF_2, ionic cond., activation vols., freq. depend. cond., press. effects 80—100354
- Ta, BCC, neutron-irradiated, Frenkel defect spontaneous recomb. volumes 79—60355
- Ta, near-threshold displacements in single crysts., electron-irrad. induced defects, resistivity meas. 79—60356
- ThO_2, ^{18}O self-diffusion, isotope exchange meas. 77—11725
- TiC, low-temp. reactor irrad., calorimetric investig. 77—80547
- β-Tl_2O-Al_2O_3, cation distrib. 77—80487
- UO_2, point defects and electronic props., theoretical survey 77—31657
- UO_{2+x}, configurational entropy of defect complexes, Mayer cluster theory calcs. 79—77591
- $UO_{2\pm x}$, model of response of fission gas bubbles to dynamic behaviour of point defects 79—37735
- W, BCC, neutron-irradiated, Frenkel defect spontaneous recomb. volumes 79—60355
- W, Frenkel pair creation and stage I recovery of electron irrad. cryst. near threshold 79—1463
- Zn, α-irradiation damage and stage I recovery 78—38759
- Zn, electron irradiated, diffuse X-ray scatt. exam. of self interstitials 79—73213
- Zn, electron irradiated, diffuse X-ray scatt. exam. of interstitial clustering during thermal annealing 79—73214
- ZnO, defect struct. calc., doping effects 80—107218
- ZnO single crysts. with stoichiometry deviations, intrinsic defects, thermodynamic analysis 79—42485
- ZnTe, irradiation induced radiative centers obs. 80—66290
- Zr, HCP, neutron-irradiated, Frenkel defect spontaneous recomb. volumes 79—60355
- ZrC, low-temp. reactor irrad., calorimetric investig. 77—80547

frequency agility
- *see also information theory*
- SAW frequency synthesizers for fast frequency hopping 77—39176

frequency allocation
- counter sophistication 77—71307
- EM spectrum, overcrowding and use by radio astronomy 80—85874
- IEEE International EMC Symposium, Atlanta (1978) 78—82876
- radiocommunication services, propagation factors relating to freq. allocation 80—12613
- space appl. and research, WARC 1979 impact 80—105147

frequency changers *see frequency convertors*

frequency control
- *see also automatic frequency control*
- 30th Annual Frequency Control Symposium, Atlantic City (1976) 77—37852
- 31st Annual Frequency Control Symposium, Atlantic City (1977) 78—57905
- 32nd Annual Symposium, Atlantic City (1978) 79—54100
- automatic frequency trimming, in double-frequency gas laser *(Russian)* 80—1217
- clocks, non-autonomous (secondary) *(Czech)* 79—40540
- clocks and watches, crystal controlled, accuracy setting and control *(Czech)* 79—40541
- crystal ovens using temp. gradient-free change of state for quartz cryst. standard *(Polish)* 79—30481
- digital clocks, 1 min. interval signal from standard freq. transmitter *(German)* 78—57902
- electron linear accelerators, freq. control methods *(Chinese)* 79—54619
- field-frequency lock, for a superconducting spectrometer 78—86312
- laser continuous broadband dynmaic freq. adjustment using selective resonator *(Russian)* 78—1239
- laser frequency stabilizer using single-photon detection, D/A lock-in circuit 79—50334

frequency control continued
- mass spectrometer, spectrum sweep using HF pickup control 77—13812
- modular control system for coupled-cavity structures in high duty factor accelerator 79—67992
- multichannel wide-range oceanographic sonar 80—46295
- NQR spectrometer, fast pocket computer frequency-controlled 79—80655
- quartz clock, accuracy, radio signal control *(French)* 80—95079
- RF accelerating structures, improved reference cavity design for freq. tracking 77—83176
- SAW filters, fine frequency adjustment by modifying propagating direction 78—18125
- selective digital voltmeter, electronic control of tuning frequency 77—10052
- solid-state oscillator with superconducting sapphire resonator, freq. stabilisation 79—12823
- synchronous machine phase shift control cct. 78—22054
- telescope drive, controlled 300 Hz freq. supply 78—61746

frequency convertors
- *see also frequency dividers; frequency multipliers; mixers (circuits); optical frequency conversion*
- for amateur radiotelescope 79—21189
- amplitude-digital convertor IC, for meas. of polarisation of short light pulses 79—17465
- analogue meas. of frequency, using NC 170 convertor *(Czech)* 80—13043
- cardiac sound frequency shifting stethoscope 79—29647
- cyclotron-resonance maser amplifier with freq. conversion 78—55329
- deaf speech and hearing aids, vocoders, frequency lowering and lipreading cues 80—12309
- differential frequency convertor cct. *(Russian)* 78—77872
- digital frequency-to-temp. convertor for use in radio telemetry systems 80—8119
- digital voltmeter with intermediate freq.-pulse conversion *(Russian)* 77—71347
- FM, bioelec. process mag. recording appl. 78—7469
- high resolution IR mol. spectroscopy with difference frequency generation, refinements 78—90321
- improved effectiveness of differential circuits used to suppress low-frequency noise 79—52608
- intermittent sinusoidal voltage phase difference meas. device 78—77941
- Josephson junction, pumped, noise down-conversion 79—56432
- Josephson junctions in self-pumping mode of operation, anomalies of freq. conversion 80—54839
- materials testing using frequency convertors with mechanical resonators 77—73400
- microwave devices and their use for generation and freq. conversion of microwave oscillations 80—15534
- optical glass melting in Pt crucibles, power supply freq. convertors 79—72728
- point contact and Schottky diodes, submm. mixing for heterodyne detect. 77—5910
- polarization convertors for 2-freq. optical interferometers 80—18005
- radiotelescope receiver, Croce del Nord, new front-end receiver with 30 to 408 MHz amplifier-convertor *(Italian)* 79—2478
- sideband upconversion in injection lasers 78—79047
- specialised freq. meter combination *(Russian)* 77—71346
- superconducting point contacts, sub mm band mixer 77—49774
- thyristor power supply for optical glass melting 77—50780
- tunable IR solid-state laser characteristics and principles 80—87406
- AlAs-GaAs three-layer heterostruct. spectrum convertor, in Nd:YAG laser pumping system 79—27272
- CdTe linear electro-optic translation of IR laser wavelengths 80—78878
- Nb bridges, variable thickness, microwave mixing 77—85390
- TiO_2:Fe^{3+}, microwave second harmonic generation and freq. conversion 80—50166

frequency dividers
- digital frequency-offset lock system designed for use with stabilised lasers 78—29960
- digital temp. meter appl. *(German)* 78—29110
- laser-to-microwave frequency division using synchrotron radiation 79—76562
- multifunctional programming unit for self-contained oceanographic instruments 79—2391

frequency division multiplexing
- contradirectional frequency-selective couplers for guided-wave optics 80—102803
- ECG transmission, 3-lead, over Post Office telephone network, central computer analysis appl. 77—86698
- EEG analogue multiplexer for FM tape recording 79—34691
- frequency-domain nonvolatile optical storage scheme 80—43282
- holocinematography, high speed, acousto-optic beam deflection for spatial freq. multiplexing 78—74860
- incoherent optical correlation operations 80—99650
- integrated optical mixer in waveguide based on phase diffr. gratings, for multichannel optical communication lines 79—18554
- interval modulation semiconductor laser communication system 78—9331
- light source with monolithically integrated DFB lasers 77—34958
- multimode digital system wavelength multiplexing constraints in 850 nm region 80—63942
- optical communication, conference, Amsterdam, Netherlands (Sep. 1979) 80—46733
- optical demultiplexer, using coupling between nonidentical waveguides 79—10380
- optical demultiplexer, using diffraction grating, for FDM fibre transmission system 80—5845
- optical fibre, multimode, wavelength multiplexing 77—79926
- optical fibre links, transparent GdAs LED for optical wavelength multiplex transmission system appl. 78—30063
- optical fibre transmission system filtering prism *(Japanese)* 78—9441
- optical fibre waveguide link, colour multiplexing 78—42444
- optical multiplexers/demultiplexers for single-fibre WDM transmission 80—43475
- optical techniques for wide-band FM system 79—64308
- optical wavelength-division multiplexing transmission via single fibre, multiplexer design 80—33222
- pulse interval modulation optical fibre communication system field expt. 78—1424
- SAW digital FM compression system *(Russian)* 78—55541
- tape recorder single-track multiplex FM conversion unit 77—45828

frequency division multiplexing continued
- telephony development in Australia, optical fibre systems advances 77—65630
- wavelength multiplexing for information transmission 79—22906

frequency-domain analysis
- *see also frequency-domain synthesis*
- 200 to 500 MHz A-scan defect characterisation 79—47873
- acoustic system matrix parameter determ., transient test principles 79—68527
- atomic reference frequency stability transfer to quartz crystal oscillator 79—54108
- biological nonlinear system Wiener kernel estimation 77—1973
- dominant noise process slope intersections, time/frequency-domain conversion 79—54107
- ECG frequency-domain analysis 80—85521
- EEG frequency-domain numerical analysis 77—9292
- EEG signal processing, frequency-domain instrumentation 79—83743
- EEG slope descriptor computation, time and frequency domain comparison 78—57115
- evoked frequency stabilisation in cat brain electrical activity 79—34533
- Gaussian filter for nuclear pulse amplifiers, direct synthesis, freq. domain anal. 77—3239
- glass fibre drawing process, characterization and control 80—58826
- graded-index optical fibre intermodal dispersion, frequency-domain meas. 80—58729
- AK Herculis, eclipsing system, anal. of light changes in freq. domain 77—53635
- lateral geniculate nucleus of cat, oscillatory neural activity entrainment 79—92216
- multicomponent noise signal decomposition 79—3210
- multimode optical fibre dispersion rel. to wavelength, frequency-domain meas. 78—1401
- ophthalmic tissue signature characterisation by US frequency-domain analysis 77—40857
- optical fibre frequency response meas., combined time/frequency domain technique 79—76809
- photosensor array aliasing and MTF effects 77—39086
- pressurised water reactor, fluctuation anal. of apparent malfunction, frequency and time domains 77—54313
- raylography, acoustic medium characterisation and imaging, non-biological model expt. 77—25528
- raylography, freq. domain deconvolution technique for pulse echo ultrasonography 77—25527
- real-time and frequency-domain processor simulation 79—81643
- remote sensing of stratified media, pulse-spectrum technique, permittivity determ. 79—8722
- seismic data processing, Fourier transform wave filter appl. *(Chinese)* 79—96838
- seismology, multichannel subtracting filters synthesis *(Russian)* 78—49156
- speech adaptive noise cancellation by short-time Fourier transform 80—91976
- speech enhancement by frequency-domain spectral weighting 79—94416
- speech signals, time-domain algorithms for harmonic bandwidth compression 79—46125
- US transducer evaluation in exptl. and theoretical domains 79—46153
- Volterra integral equations 77—9854

frequency-domain synthesis
- *see also frequency-domain analysis*
- disc impedance meas. and US transducer CAD program 79—46157
- He speech unscrambling by nonlinear power spectrum conversion 79—46134

frequency doublers *see frequency multipliers*

frequency measurement
- *see also atomic clocks*
- 2D linear prediction for freq. and bearing estimation 79—64409
- 10^{-2}-10^{-4} Hz freq. signal analyser operational principles *(Russian)* 78—45598
- absolute wavelength measurement, ^{127}I stabilised He-Ne laser, pressure scanning Fabry-Perot interferometer appl. 78—73971
- acoustic signal mean frequency meas. *(Russian)* 78—81441
- analogue, using NC 170 frequency convertor *(Czech)* 80—13043
- analogue cct. for fast-response measurement, used for foetal heart rate 79—21708
- analyzer for room quality meas. for HiFi *(German)* 79—46140
- analyzing equipment, device for scientific education in oscillatory phenomena 78—41126
- atomic freq. standards, transfer of freq. stability to quartz-crystal resonator 80—17927
- atomic time and frequency standards development at Shanghai observatory, China 80—105617
- auditory frequency measurement based on neural timing 77—5011
- automatic frequency meters, construction and performance *(French)* 80—62658
- baseband frequency response meas. system, for fibre transmission system components 78—42404
- beat frequency meter, using LED bar-graph display 79—63191
- capacitor discharge frequency meter for 10-500 Hz range *(Russian)* 77—53864
- clock error with a Wiener predictor and by numerical calculation 80—82748
- CMOS ICM 7216B multifunction counter used for time, frequency or period measurement *(German)* 80—74092
- cochlea model, for signal anal. 77—26281
- comparator based on delay line, generator spectral line width measurement appl. 79—6144
- Compton electron wavelength, determ. by cryogenic metrological technique 78—37165
- counter, high quality using wideband preamp and LSI pair 77—87782
- counter selection, principles 79—12775
- counter sophistication 77—71307
- counter-timer, Phillips PM 6610 and 6620 series, features *(Italian)* 77—26340
- counting and timing circuits, optimum solution with Philips instruments 77—112
- crystal ovens using temp. gradient-free change of state for quartz cryst. standard *(Polish)* 79—30481
- DCF 77 standard time and frequency receiver, display ccts. *(German)* 77—13737

frequency measurement continued
- design principles and characteristics of freq. and time standards, radiation effects 77—22533
- differential frequency convertor cct. *(Russian)* 78—77872
- digital counter and timer instruments, accurate meas. techniques 78—45605
- digital filter appl. *(Russian)* 80—57264
- digital freq. counter in probe, 0 to 750 kHz, using CMOS ICs 79—49209
- digital freq. meter for operation with freq. convertor *(Russian)* 77—71346
- digital frequency meter impulse noise effect on accuracy *(Russian)* 77—41575
- digital universal counter, TTL, amateur constr. *(German)* 78—12727
- Doppler signal centre freq. estimation using quadrature zero-crossing counter, US blood flowmeters 78—31879
- dye laser multimode beam, spectral distrib. meas. using speckle patterns 77—14730
- elastic element characteristic vibrational-frequency meas. errors 77—74391
- electromagnetic meas., precision, conf., Braunschweig, Germany (Jun. 1980) 80—98903
- electronic counting instruments, review 78—21164
- equipment calibration using standard frequency broadcasts 79—67258
- error probability anal. *(Russian)* 80—90823
- far IR, Josephson device high-harmonic mixing props. for freq. meas. 79—26120
- far IR laser, optically pumped, for freq. metrology 77—54725
- far IR laser line frequency meas. by klystron harmonic comparison 77—7113
- ferromagnetic-resonance linewidth meas. method and apparatus 80—22411
- flip-flop used to indicate frequency differences in CRO 79—88919
- fluctuation characts. evaluation apparatus 80—22333
- frequency counters, phase-locked transfer oscillator automatic computing system 77—5862
- frequency meter, UHF pulse carrier freq. meas. appl. 77—37917
- fundamental problems, time measurement, simple mathematical approach *(French)* 77—53865
- gas lasers, frequency stabilised by saturated absorpt., synthesis and measurement of optical frequencies, review *(French)* 79—31966
- gastrointestinal electrical rhythm frequency estimation by autoregressive modelling 78—56948
- hearing aid measurement system comparison 78—65151
- induction motors, piezoelectric pick-up appl. *(Russian)* 78—65911
- instantaneous frequency measurement of micro-wave range by two different point detected signals *(Japanese)* 80—73327
- insulator parameters meas., freq. and mode variation in cavity 80—13102
- International time and freq. comparison using Loran-C radio waves *(Japanese)* 78—81951
- ionosphere HF radiowave propag., freq. standard utilisation 78—93027
- ionospheric EM wave propagation in HF and MF bands, Doppler meas. accuracy 78—77417
- laser, far IR optically pumped, monitoring by piezoelec. transducers 80—102729
- laser, interference methods, accuracy 78—17997
- laser, precision of interferometric meas. based on Doppler shift 77—165
- laser as wavelength reference standard, He-Ne, with Ne or iodine cell 77—7124
- laser beam interferometric wavelength measurements through post-detection signal processing 80—42254
- laser freq. meas., review and extension to 197 THz 78—81952
- laser frequency meas. using diode laser, appl. to CO_2 weak transitions 77—88693
- laser frequency measurement of I ion line, by harmonic mixing 77—83919
- laser frequency measurement using supercond. point contacts 80—90824
- laser frequency synthesis 78—12675
- laser spectroscopy conf., Jackson Lake Lodge, WY, USA, 1977 July 78—82666
- laser wavelength measurement using digital interferometer 80—37079
- laser wavelength measurements, why? how? and how accurate? 78—89446
- laser-Doppler-velocimeter, digital, signal processor accuracy testing *(German)* 78—86242
- lasers, precise meas. in submm. and IR regions 80—99698
- LF direct meas. cct. for heart beat disturbances anal. *(German)* 79—96671
- LF meas. technique 79—21717
- LF measurement using counters and monostables 77—113
- linear displacement transducer using vibrating string *(German)* 79—71441
- LORAN-C type standard freq. signal, time and freq. calibration standard comparison *(Rumanian)* 79—40542
- maser standard, H_2, stability improvements and cavity tuning 78—21099
- methanol optically pumped laser, frequency instability meas. at 70.5 and 118 μm 80—1254
- methyl alcohol laser, freq. meas. at 4.25 THz using Josephson harmonic mixer and phase lock techniques 80—95078
- metrological Cs frequency standard MTs-1, description 77—79063
- microwave and IR, appl. of Na Rydberg state two-photon spectroscopy 80—43018
- microwave time and frequency standards 80—47026
- microwave to visible frequency synthesis 80—48319
- microwaves, meas. with 10 MHz resolution in upper microwave bands 77—5868
- multimeter, automatic storage *(German)* 77—10044
- national time and frequency standards of Finland 80—47031
- NBS, development up to NBS-6 77—45825
- NQR spectrometer, super-regenerative, continuous freq. monitoring 79—63190
- optical, by an heterodyne technique *(French)* 79—40602
- optical fibre bandwidth measurements employing use of mode scrambler 79—50438
- optical frequency measurement and synthesis, near IR and visible ranges 79—35808
- optical frequency standard, Doppler-free stimulated-emission technique 78—93765
- oscilloscope appl. *(German)* 77—13766
- photodetector frequency response meas. using laser mode beating 78—8442

frequency measurement continued
precise time dissemination via OMA-50 kHz 80—47032
quantum frequency store and Cs atomic transition frequency comparison system 77—79064
quantum oscillator, phase automatic freq. control parameters, optimal values *(Russian)* 80—77814
quantum standards, output signal sidebands/resonator detuning effects on accuracy 77—87743
quartz crystal, new method of freq. spectrum determ. and appls. 78—23402
quartz crystal oscillator checking against standard frequencies in LF/VLF ranges 77—74372
radiointerferometric frequency and coordinate meas. accuracy, tropospheric fluctuation constraints 79—8848
Raman laser freq. meas. with MIM diode, spectroscopy in 5.3 μm region 77—10935
Raman laser IR freq. synthesis with MIM diode 77—19277
Ramsey separated oscillatory field method, two-freq. excitation, appl. to freq. standards 78—36974
reference standard derived from 22.3 KHz signal 77—61049
refractory, resonant frequency meas. apparatus, elastic props. investigations 77—19576
reinforced concrete structural integrity assessment, NDT method 78—56847
remote, using VHF/UHF receivers *(German)* 78—4631
RF frequency standard transmission, phase instability due to effect of ionosphere 78—41279
secondary frequency standard, using colour TV burst signal 78—24826
secondary standard, source for BBC 200 KHz signal 78—24766
short duration low frequencies, digital measurement equipment description *(German)* 77—87735
small frequency shifts meas. using two open resonators at mm wavelengths 78—81949
spectral analyser appl., accuracy improvement *(French)* 77—65023
spectrum analyser using FFT *(Spanish)* 80—90825
SQUID RF measurement system, future of superconducting instruments in metrology 79—26020
standard, atomic, Cs beam, Millman effect origin and expt. determination 77—5810
standard, establishing common scale for COMECON member countries 80—42200
standard, passive quantum, static AFC system parameter optimisation 77—9989
standard, precision oscillator freq. stability meas. *(Japanese)* 78—4596
standard frequencies in SW and VLW ranges, dynamics of seasonal variations obs. 77—79061
standard frequency receiver XKE 2, 10 to 200 kHz, for regulating crystal and atomic freq. references 79—67259
standard signals and applications *(German)* 77—71301
standards, electrically tuned far infrared lasers appl. 78—174
standards, time, freq. and physical measurement, unified standard 79—26038
standards comparison, improved accuracy 80—95062
standards using divergent beams, stability limits 79—26037
submillimetric and IR laser absolute frequency meas. 77—79882
Swedish measurements establishment for time and freq. standards *(Swedish)* 79—75503
techniques, book 79—176
three-phase frequency meas. transducers with saturating transformers 78—77893
time and frequency, conf., Helsinki, Finland (Aug. 1978) 80—46728
timebase for frequency counter, precision 77—74432
unplated piezoceramic plate frequency response meas. 78—248
users' manual on time and freq. meas. 80—94934
USSR State Standard of time and frequency 77—79062
USSR state time and frequency standards *(Russian)* 78—161
USSR State Time and Frequency System data collection and processing automation 77—79074
USSR time and freq. state service 79—93103
USSR Time and Frequency Service collaboration with international organisations 78—41280
very low frequency counters, use digital time interval conversion with microprocessor control 77—74430
vibration freq. meter, for vibr. etching of rolled wire technical parameters meas. 79—14356
visible lasers with 80-GHz freq. offset, beat freq. generation 80—1253
visible light, direct freq. meas. method 80—47041
visible region, absolute freq. meas. using ^{20}Ne laser 79—93104
VLBI, improvement of freq. stability of local oscillators *(Japanese)* 80—17504
VLF, cct. for heart beat rate monitoring in animals, range 0.01 to 10 Hz *(German)* 79—34709
VNG-derived frequency reference, adapting for astronomy 79—35139
voice, using fast freq. meter *(German)* 78—3518
voltmeter with offset zero used for freq. meas. *(French)* 80—22331
X-band frequency standard, high Q cavity resonator *(Polish)* 77—26342
x-t chart recorder, frequency marking 77—53947
Ag beam mag. resonance apparatus as freq. standard, features 78—89458
CO_2 isotope laser transitions, abs. freq. calibration, heterodyne technique 77—19230
CO_2 laser, accurate frequency meas. *(Japanese)* 80—9850
CO_2 laser, stabilized, meas. of freq. 80—99699
CO_2 laser freq. and wavelength meas., speed of light determ. 77—49708
CO_2 laser transition absolute freqs. by multiplication of difference-freqs. 78—90445
CO_2 laser transition absolute freqs. by multiplication of difference freqs. 80—37992
CO_2 laser transitions, absolute freq. meas. by multiplication of CO_2 difference freq. 80—105618
CO_2 laser wavelength standards 77—17945
CO_2/$^{192}OsO_4$ laser, absolute light oscill. freq., universal const. variation meas. possibilities *(Russian)* 80—5723
Cs atomic time standard data combination 77—5814
Cs beam atomic freq. standards, Millman effect on freq. shift 78—32797
Cs beam deflection system for time and freq. primary standard 78—89453
Cs beam freq. standards, freq. offset due to spectral impurities 78—89455
Cs beam frequency standard, frequency stability *(Japanese)* 77—108
Cs clocks made by Oscilloquartz Company, investigation of metrological characts. 80—101787
Cs frequency standard, construction of improved system (NRLM-II) 78—45599
Cs maser freq. standard, stability determ. method 77—83842
Cs primary frequency standard, recent progress of PTB 77—17942
Cs primary standard, TAI freq. estimation 77—17952
Cs standard frequency line, for receiver-controlled references 79—6099
D_2O laser phase locking to freq. standard, CO_2-OsO_4 laser freq. meas. 80—95080
H maser frequency, nonuniform magnetic field effect 80—99687
H masers, with automatically tuned resonators 80—95859
H oscillator with flexible walls, wall induced freq. shift meas. 79—2749
H time and frequency standards with redundancy 77—79065
He-Ne, 1.15 μm laser line, 260 THz freq. synthesis using $CdGeAs_2$, Ag_3AsS_3 crysts. 79—64263
He-Ne laser, laser system for 3.39 μm freq. synthesis 78—18001
He-Ne laser, methane-stabilized at 88 THz 80—73304
He-Ne laser, methane-stabilized, meas. of freq. at 88 THz accurate to ±3 parts in 10″ 80—99700
He-Ne laser, stabilized, meas. of freq. 80—99699
He-Ne laser reference IR frequency meas. installation 77—79068
He-Ne lasers, iodine- and methane-stabilised, reproducibility comparison 77—7135
I_2, line near 520 THz, HFS, direct freq. meas. 80—53266
NH_3 81.5 μm subMM laser, freq. meas. by CO_2 laser difference freq. comparison 80—74415
$^{15}NH_3$ frequency standard, 22.79 GHz, feasibility study 79—71418
Ne laser line, 260 THz, direct freq. meas. 80—53266
Rb atomic frequency standard, optical pumping phenomenon and techniques, review 77—65022
Rb freq. standard, Measurement Standards Laboratory, capability improvement 78—54332
Rb frequency standard, Rb lamp stability and reliability factors, expt. 77—17955
Rb frequency standard XSRM 78—41281
^{85}Rb unperturbed hyperfine transition frequency determ. 77—7047
^{85}Rb, unperturbed hyperfine transition freq. meas. 77—17954
^{87}Rb atomic frequency standard, resonant frequency change, due to spectral profile of pumping light 78—45590
^{87}Rb pumping light passed through ^{85}Rb filter cell, freq. displacement meas. 77—41702
W-Ni(Co) point-contact diodes as harmonic generators and mixers, DC bias dependence 80—75653

frequency meters
see also wavemeters
5 MHz digital frequency meter *(German)* 78—62206
10^{-2}-10^{-4} Hz freq. signal analyser operational principles *(Russian)* 78—45598
100 MHz counter, microprocessor controlled, Hewlett Packard (5315A) *(French)* 79—88938
automatic, construction and performance *(French)* 80—62658
automatic, electronic, for stationary and ergodic random processes obs. *(Bulgarian)* 80—27283
capacitor discharge type for 10-500 Hz range *(Russian)* 77—53864
capacitor discharge- and differential voltage-types, appl. *(German)* 77—41584
constant-display frequency meter 79—21718
counter, high quality using wideband preamp and LSI pair 77—87782
counter design, 1 GHz, use of custom LSI 80—8973
counter design technology 80—8974
counter modification, for pulse duration below 1 μsec meas., use of time interval shaping circuit 77—10060
counter sophistication 77—71307
counter-timer-frequency meter for teaching, evaluation 78—28901
counter/timers, avoiding compromise in accuracy 80—8970
counters and timers, var. in counting cct. techniques 80—8971
counting and timing circuits, optimum solution with Philips instruments 77—112
difference and ratio meters using thyristors 78—4649
digital, accuracy and noise rejection increase, weighting method *(Russian)* 80—27281
digital, for LF meas., using TTL ICs 78—86296
digital, for LF with short duration meas. *(German)* 77—87735
digital, for use with freq. convertor *(Russian)* 77—71346
digital, impulse noise effect on accuracy *(Russian)* 77—41575
digital, manufacture in Rumania *(Rumanian)* 77—74452
digital, up to 50 MHz, with seven-digit display *(Czech)* 80—8979
digital, using variable measuring times and automatic scale conversion *(Spanish)* 78—49862
digital, with high noise immunity 78—8412
digital CMOS seven digit 200 MHz range 77—74427
digital freq. counter in probe, 0 to 750 kHz, using CMOS ICs 79—49209
digital freq. counters and counter-timers, new range using MSI 80—27318
digital frequency meter, for burst-like laser Doppler-signals 77—72376
discrete-time Doppler frequency meter for blood flow imaging 79—57704
F571, in digital integrator for pulsed NMR spectrometer 77—26372
Heathkit IM-4100 multi-function, circuit diagrams and performance data *(French)* 80—73348
high precision laser freq. meas., sigmameter, motionless two-channel Michelson interferometer 78—89449
inductance meas. circuit, resonance, using self-excited oscillator 77—5867
LF and infra-LF, with digital positive feedback, improvements with aid of computer simulation *(Russian)* 78—4656
LF meter used for measuring period between pulses 79—85128
LF meter with instantaneous response 79—40539
low-frequency, cardiac rate meter appl. *(Czech)* 77—37084
LSI counting circuit *(Japanese)* 77—18003
microwave counters, modern techniques 78—32831
NMR magnetometer display using freq. to magnetic field convertor 79—71490
precision, eight digit 250 MHz device counting and reading, portable 77—71339
series TF 2430, digital display, LSI 77—53936
technology trends *(German)* 79—71437
UHF pulse carrier freq. meas. appl., 2.1-4.1 GHz range 77—37917
universal timer-counter, design aspects 80—8972

frequency meters continued
US pulse velocity meas. by time selector and frequency counter *(German)* 78—13876
Watford Electronics 0-050 MHz digital frequency meter measures frequency and time intervals 80—68191
ZnSe-Si n-n heterojunction photovoltaic effect, freq. meter in visible wavelength *(Korean)* 79—60915

frequency modulation
see also frequency shift keying; pulse frequency modulation
acoustooptic FM and freq. shifted heterodyne CO_2 laser system 78—5568
AF PLL lock indicator and event alarm for multiplexed seismograph telemtry 79—62597
afferent elec. nerve stimulation with ref. to prosthesis sensory feedback 77—90962
analogue multiplexer for FM tape recording 79—34691
auditory system, evidence for direction-specific channels in processing of FM 79—96573
bandpass filters, technique, construction, appl. *(German)* 79—50544
blind children's CW FM sonar 79—70708
brain unit and slow-wave field activity, telemetry with FM pulse subcarrier 77—25625
cardiac valve motion obs. CW FM sonar 78—61230
coupled laser oscillators, injection modulation 80—99773
CW FM sonar with aural displays, improvements 78—87221
dye laser, optogalvanic effect to freq. lock to discharge transition freqs. 77—19309
dye laser jet stream, thickness meas. in real time, by optical technique 78—82975
electro-optical modulator with rot. elec. field, appl. to laser Doppler velocimeters 77—42620
electron beam, optical frequency modulation depth, Pendellosung effect 80—33859
electrooptic polarization modulated injection laser 80—58591
Fabry-Perot resonator, laser mode sweeping dynamics, optical length effects 78—83001
far IR lasers, optically pumped, frequency modulated noise measurements 78—55392
flaw-detection apparatus, noise immunity, sounding signal freq. modulation 80—89441
fluoromethane far IR laser FM and stabilisation by Stark effect 78—59056
FM-CW acoustic sounder resolution rel. to modulation noise *(Japanese)* 78—30137
frequency to voltage convertor using SAW linear FM chirp filter 80—19182
hearing, theory of detection for low modulation freqs. 80—61586
integral pulse freq. modulator, spectral props., heart-rate variability meas. 77—90951
ionosphere, heating by powerful radio emission with random modulation of carrier freq. 80—109310
Josephson effect appl., review 79—82724
laser, double heterostruct. junction type, US wave freq. modulation anal. 78—83009
laser gas analysers, freq. modulation appls. 80—85246
laser interferometers, AM and FM operation and applications *(German)* 80—86389
laser radiation, frequency shifting via rotating half-wave retardation plate rel. to ang. Doppler effect 80—9800
laser radiation internal modulation, freq. limitation 79—72607
LF real-time spectral analyser design and operation *(French)* 78—20538
liquid level-to-frequency converter 79—6080
low-distortion FM demodulator using SAW delay device 78—51014
low-frequency acoustic parametric radiator 77—39128
microwave backscatter modulation by shoaling ocean waves 78—57212
microwave spectrometer baseline suppression using FM and harmonic detection 78—82866
mm-wave Fabry-Perot tuning and freq. modulation by electrically variable external reactance 79—68409
multimode optical fibre incoherent chirp pulse transmission 78—1374
multiterminal ECG processing system experiences 79—39573
muscle contraction strength control during elec. stimulation, using PWM and FM 77—40929
non-redundant scanning, high efficiency freq. modulation, of light beam in half space 78—78907
NQR spectrometer, digital freq. modulation 78—21189
optical communications, FM, using electrooptically tuned semicond. lasers 80—14351
optical fibre analogue signal transmission system *(German)* 80—58679
optical slip-ring for transmission of transducer signals 78—13814
optical techniques for wide-band FM system 79—64308
optical video disc, acoustooptic travelling wave transcription signal recording 79—36986
optical waveguide with moving boundaries, p-i-n structure modulator 80—19099
optical zone plate, frequency-modulated, for coherent noise reduction 79—86134
photoelectronic phase and frequency modulation 78—79131
piezoelectric powder, electroacoustic echo form. by FM mechanism 78—19421
radio signal diffraction in homogeneous dispersive medium, space time geometric theory 79—4149
ring laser gyroscopes, multioscillator approach to locking problem 78—79042
SAW digital FM compression system *(Russian)* 78—55541
shot noise limited stimulated Raman gain laser system for monolayer vibr. spectroscopy 80—62744
sonar ranging systems, pulse compression techniques 80—33350
superconducting FM resonators, analysis and appls. 77—26893
surface roughness estimation using linear FM signal *(Russian)* 78—77353
tape recorder single-track multiplex FM conversion unit 77—45828
tape recording, low freq. FM, of nerve action potentials 79—57832
telemetry, low power PAM/FM system for ventricular press. and cardiac dimension meas. 78—44747
underwater acoustic transducers, reciprocity calibration by FM signal correl. methods 77—68298
underwater sound measurement, FM signal correl. Methods 77—62086
US blood vol. flowmeter processing technique 78—31878
CO_2 laser, detuning effects of FM mode-locking 80—69434

frequency modulation continued
CO_2 laser intracavity freq. modulation, transient behaviour 80—14374
CO_2, single mode laser, internal freq. modulation up to 350 MHz 77—19308
Cs beam frequency standards, quadrupole and hexapole magnet combination 77—5813
$Ga_{1-x}Al_xAs$ DH injection laser, FM at microwave freq. rates 80—58610
H_2 generator, resonator tuning methods 77—88294
He-Ne 3.39 μm laser, FM eliminated CH_4 locked freq. stabilisation in dual feedback control 80—99772
He-Ne laser, beat freq., high displacement sensitivity meas. 80—95926
He-Ne ring laser beat frequency deviation rel. to dispersion and modulation 79—68410
$Nd_{0.5}La_{0.5}P_5O_{14}$ laser, FM mode-locked 79—86184

frequency multipliers
angle meas., photodetector freq. doubler nonlinear distortions effect on meas. errors 78—36968
broadband frequency multiplier for type KM-2 quantum magnetometer using optical pumping 77—37951
Josephson absorption effect current steps, inflexion point structure anal. 77—20496
LF measurement using counters and monostables 77—113 •
superconducting weak links for freq. multiplication 79—11273
superhigh frequencies, high multiplication factor 78—4636
wide-band transistor frequency doubler 78—4635

frequency regulation *see frequency control*

frequency response
AC voltmeter noise response, equivalent noise bandwidth approximation 78—4662
acoustic noise sources, time delay bias errors in estimating frequency response and coherence functions 79—18614
acoustic piezoceramic transducer, in liquid, bandwidth and freq. response 77—14871
adsorption calorimeter, freq. response rel. to dynamic characts. 78—24796
aerosol layer depth remote meas. by microwave-modulated laser *(Russian)* 78—57338
ambulatory blood pressure recording in man, transducer and perfusion system 79—53271
anemometer, constant-temperature hot-wire, freq. response and electronic testing 77—58820
anemometers, hot wire, used for turbulence meas. in marine environment, freq. response 77—33214
arterial O_2 tension, generation of variable amplitude sinusoidal changes for freq. response anal. 77—56563
back diode amplifier, use at low temp. 80—57324
blood pump pressure servovalve control, moving coil system *(German)* 78—24182
cold-wire thermometers used for atmospheric turbulence meas. in marine environment 80—56650
compensation, instrum. for joint operation with broadband amplifier 77—45862
complex dynamic systems, elements of statistical energy anal. 77—75740
complex lumped parameter linear systems 78—5610
composite strip piezoceramic US receiving array 78—42511
concatenated fibre-optic cable, cumulative baseband frequency response models 80—78983
condenser microphones with flat freq., response up to 500 kHz 78—33968
deformable metal mirror characterisation techniques 79—59798
digital bandpass filters instrumental realisation, operator parameters selection rel. to freq. response *(Russian)* 79—74984
dynamic measurements of a nuclear reactor using low-peak-factor excitation signals 79—36349
ear, external, and artificial ear model *(Chinese)* 80—56063
Earth strain-tides, spectroscopy 78—73301
EEG evoked frequency response polygons, computer anal. technique 77—40961
electromanometric system frequency response visualisation device 77—48890
EM fields created by currents in confined conductors, freq. and transient responses 79—29702
energy losses in magnetically soft materials, determ. *(Russian)* 79—8014
far IR laser hybrid output couplers, metal mesh dielectric mirror design and fabrication 80—58554
ferroelectric cylinders, radially polarised, electroacoustic response calc. by normal-mode methods 77—62131
filter functions, Savitzky-Golay, freq. response plots 77—53741
flexural-mode mechanical filter resonances 77—27435
gapped pot core and Permalloy foil pressure transducer 79—75520
hand-arm vibration, analytical model of hand vibr. response characts. 77—64074
hearing aid measurement system comparison 78—65151
heat receivers with moving heat carrier, freq. characts. 80—4733
imaging system, maximum likelihood spatial filtering examples 78—63038
insect mechanoreceptor sensory transduction nonlinear anal. 77—64061
internally lossless transducer conjugate matching, power transfer and backing impedance 79—46158
invertors, anal. *(Russian)* 77—53761
IR charge transfer device imaging arrays 78—77990
Josephson tunnel junction in arbitrary cct., response 78—39265
LED, GaAs-(Ga,Al)As DH, as function of design parameters 77—79941
Limb Infrared Monitor of Stratosphere, radiometer spatial frequency response 79—101048
linear structures' greatest maximum response analysis 78—38241
loud speaker, echo chamber meas. *(German)* 77—75762
loudspeaker system amplitude and phase response rel. to driver alignment on baffle 80—92010
modulated backscatter from reed switch loaded dipole 77—75386
MOS inversion layers, freq. response of charge transfer 80—88638
multidelay system coherence function meas. 79—68530
multielement acoustic array characterisation by acousto-optic diffraction 80—99911
multimode optical fibre transmission, perturbation soln. 78—1380
multimode SAW resonators, optimum design 77—23823
multiple input systems, effect of input cross spectra on freq. response estimation 79—55261
multiplier unit for acoustic and electronic wattmeters 77—79118

frequency response continued
nuclear research reactor ZED-2, two-phase control absorber development 79—85697
optical fibre, graded index, baseband freq. response meas. 79—41439
optical fibre, multimode, wavelength depend. 77—27341
optical fibre, multimode step-index, baseband freq. response meas. using mode scrambler 77—19402
optical fibre, multimode W-type, baseband signal frequency response 77—83969
optical fibre, transfer function meas., baseband frequency response *(French)* 77—79919
optical fibre frequency response meas., combined time/frequency domain technique 79—76809
optical fibres, baseband freq. meas., interpretation 78—46777
optical fibres, baseband freq. response meas. by modulated InGaAsP laser beam, dispersion characts. 80—1308
PCM optical fibre communication system numerical aperture optimisation *(German)* 78—38017
photodetector, meas. using laser mode heating 78—8442
physiological system anal. using swept sine wave 78—28133
piezoceramic transducer for laser freq. stabilisation *(Russian)* 79—10315
piezoelectric modulation transducers for alternating pressures 78—77891
piezoelectric receivers, amplitude-freq. response determ. for acoustic emission 80—87699
plasma, automatic control investigation 79—10649
pointer instrument, determ. using stroboscopic methods *(Polish)* 78—29102
pulse preamplifier for fast photocond. decays meas. 80—57326
PVF$_2$ bulk wave transducers for nondestructive evaluation 79—57199
quartz crystal gravitational radiation antenna, Q factor 78—16715
relaxational frequency spectra, simultaneous meas. by digital signal processing 80—15959
Renshaw cells dynamic properties, freq. response characts. 78—3462
reverberation chamber LF sound power injection analysis and response averaging 78—42496
SAW devices, automatic response measurements for large time-bandwidth SAW devices 80—74677
SAW filter using waveguide between input and output transducers, freq. response 77—39162
SAW inverse filter for NDT 77—28970
SAW transmitting hydrophone development and performance 79—53586
seismic receivers, cable and amplifier system, freq. characts. *(Russian)* 79—84529
seismic recording channel, phase-freq. response and input cct. parameters matching *(Russian)* 79—39920
seismic sensors, mechanical, influencing factors *(Japanese)* 78—85722
seismic wide-band recorders specification 79—39908
sound level meter meas. accuracy 78—59211
space applications of LF supercond. sensors inc. SQUID devices 80—56691
spatial light modulator with CCD address 80—48445
step index multimode fibre, baseband frequency measurement, mode scrambler technique *(Japanese)* 78—37983
thickness mode piezoelec. US probe design factors 79—68540
transmission system design, influence of optical component baseband frequency response 78—1415
underwater sound backscattering from fluid sphere, response from marine organisms 77—46846
unplated piezoceramic plate frequency response meas. 78—248
veins, simulation of collapse 78—44535
vibrating structure, modelling by freq. response data curve fitting 77—54922
vibrator, flexural piezoelectric, split-electrode, suppression of spurious responses *(Japanese)* 78—83204
VLF signal phase velocity calc., curvature correction/frequency relationship 77—60543
GaAs CW DH laser, inherent oscillations and subharmonic resonances obs. in light output 78—74910
GaAs LED absorption effect on freq. characteristic 79—8189
GaAs-Al$_x$Ga$_{1-x}$As buried-heterostructure laser, wideband optical sources *(German)* 78—37904
GaAs-AlGaAs DH lasers, multipeak freq. response obs. 78—17940
Ge, amorphous film 79—56334
He cooled reactor turbine control experiences Fort St. Vrain HTGR *(German)* 80—57927
LiIO$_3$, cryst. transducer in US pulse-phase interferometer, 0.2 to 100 MHz 77—14868
Se photocell optical vibration transducer 80—77768
Si accelerometer, batch fabricated 80—73328

frequency shift keying
MFSK freq. acquisition and tracking, Jupiter probe-to-relay communication 77—64613
optical communication receiver, direct detection, performance for intensity subcarrier FSK 77—39033
telemetry data buoy for coastal operation 78—36320

frequency stability
see also frequency control; laser frequency stability
1.2 GHz temperature stable SAW oscillator 78—59226
1/f fluctuations *(Japanese)* 78—43448
400 MHz SAW timing filter for optical fibre transmission 79—50415
440 Hz standard A tone generator 78—46863
atomic clock long-term frequency variations, heuristic model 77—37854
atomic frequency standard prediction error analysis 78—57906
atomic reference frequency stability transfer to quartz crystal oscillator 79—54108
digital monitor for rotational-speed instability 79—97363
electron cyclotron maser, fundamental mode, linear theory 80—58496
field-frequency lock, for a superconducting spectrometer 78—86312
high-performance quartz crystal oscillators, systems approach 79—54109
horseshoe bat echolocator signal, freq. stabilisation model 78—20195
hydrophone quartz transducer stability analysis 77—11102
IMPATT source, frequency-stabilised, 115 GHz 80—67573
Josephson junction, frequency-agile, biasing for precise freq., analogue computer study 79—28455
laser, rel. to interferometry 77—694
laser cooled ion storage frequency standard possibilities 79—54102
laser scanning system design, stable fixed freq. 77—58478
microwave interferometer, freq. stabilized, laser prod. plasma density decay meas. 77—84524

frequency stability continued
NTS-2 satellite Cs frequency standard stability estimates 79—54110
oscillator quartz cuts for improved temp. stability 79—55292
phase and frequency instabilities in precision frequency sources, characterisation and mathematical models 79—2750
Pioneer Venus Programme stable quartz oscillator 77—41288
plasma etched SAW resonator ageing effects 77—39148
Polish voiced consonant fundamental frequency variations 79—68501
quartz, electroded doubly-rotated thickness-mode resonators, temp.-induced frequency 79—55298
quartz resonators, freq. instability rel. to time scales *(Italian)* 79—17400
quartz SAW resonator deep etching 78—59248
α-quartz SAW temp. depend. 78—51813
quartz temperature-stable shallow bulk acoustic wave devices 79—55293
quartz-LZT wide-range instrument transducer, practical feasibility 78—51035
radio time signal coding and clocks for private and industrial use *(German)* 78—89445
resonator ageing mechanisms 79—46161
sapphire single-crystal clocks and frequency standards 78—57915
SAW deeply-etched resonators, long-term aging improvement 79—55290
SAW narrow pass band filter *(Japanese)* 78—90603
SAW oscillator frequency stability developments 78—59253
solid-state oscillator with superconducting sapphire resonator, freq. stabilisation 79—12823
stable frequency standards comparison by TV carrier beat note transmission 78—57909
standard, precision oscillator freq. stability meas. *(Japanese)* 78—4596
standards using divergent beams, stability limits 79—26037
string transducer auto-oscillator cct., using ICs *(Russian)* 77—13741
superconducting resonators, high stability oscillators, appl. to fundamental physics, metrology, freq. stability 79—26034
time and frequency, conf., Helsinki, Finland (Aug. 1978) 80—46728
time and frequency stability, characterisation and meas. 80—47025
voltage-controlled SAW resonator oscillators 77—27450
Cs atomic beam frequency standard performance and environmental effects 77—37858
Cs atomic beam tube velocity distributions 77—37856
Cs atomic frequency standard, optically pumped, buffer gas mixture optimisation 77—37859
Cs beam freq. standard research at PTB, beam optics, Majorana transitions 79—21709
Cs beam frequency standard, frequency stability *(Japanese)* 77—108
Cs beam frequency standard errors due to excitation asymmetries 77—5816
Cs beam frequency standard design for satellites 78—57911
Cs beam frequency standard drift and noise performance rel. to velocity distributions 78—57912
Cs dual atomic beam tube performance 77—37857
Cs frequency standard, NRLM-I, improvement of freq. stability 78—62184
Cs maser freq. standard, meas. method 77—83842
Cs optically pumped frequency standard stability limitations 79—54104
Cs primary standard operation limitations 77—5812
H atomic passive frequency standard 77—37860
H frequency standard undisturbed transition evaluation 77—79066
H generator, freq. shift due to atomic collisions with storage flask walls 78—77870
H maser, atomic resonance effects on long-term freq. stability 77—75465
H maser design for NAVSTAR Global Positioning System satellite clock 78—58969
H maser failure mode identification 77—37862
H maser improvements at Smithsonian Astrophysical Observatory 78—58971
H passive maser frequency standard 79—55100
H VLG-11 maser, performance evaluation 79—55098
H$_2$ maser, time-dependent freq. shifts obs. 79—21713
He-Ne laser, I$_2$ stabilised, wavelength intercomparison 77—19305
He-Ne laser, methane stabilised, intercomparisons 77—19304
^{3}He gas thermometer secondary standard for 0.5 to 40K 80—82762
^{199}Hg$^+$ trapped ion frequency standard 78—57914
LiNbO$_3$ 400 MHz saw filters 79—23158
LiTaO$_3$ temperature-stable shallow bulk acoustic wave devices 79—55293
NH$_3$ special-purpose frequency standard and clock 78—57913
Rb frequency standard, Rb lamp stability and reliability factors, expt. 77—17955
Rb maser oscillator, freq. domain meas. 80—83574
^{87}Rb maser and related oscillators, time- and frequency-domain stability 78—58968
^{87}Rb passive frequency standards, line inhomogeneity effects 79—54106
Si single-crystal clocks and frequency standards 78—57915

frequency synthesizers
see also frequency convertors
digital, 10-29.999 MHz freq. range 77—45860
digital synthesis of low-freq. signals, performance data for LEA GSN 20 and GSN 80 series *(French)* 80—73393
Doppler sonar controller 80—43575
music, sample and hold facility 78—46865
NMR spectrometer, programming device for control of frequency synthesizers 80—22400
octave synthesizer, teaching appl. 79—44680
quantum frequency store and Cs atomic transition frequency comparison system 77—79064
SAW frequency synthesizers for fast frequency hopping 77—39176

frequency synthetizers *see frequency synthesizers*

frequency triplers *see frequency multipliers*

friction
see also internal friction; lubrication
abraded surfaces, topography rel. to contact area and abrasion mechanism 80—58986
acrylic gel, US observation of critical behaviour *(French)* 79—29414
acrylic resin wear and cutting surface against brass *(Japanese)* 78—56779
adhesive wear and friction, state of the art 77—8955
aerodynamic base pressure correlation technique, turbulent supersonic flow, conical bodies 77—89146
aerodynamic drag on heated spheres and cylinders, effective Reynolds no. 77—89090

friction continued
- aerodynamic wave drag, nonplanar singularity distribs., Hayes' algorithm extension 77—84271
- aerosol, solid phase motion, large Reynolds no., carrying agent drag 78—79363
- aerosol, spherical particle phoresis in multicomponent gas mixtures 78—22446
- air flow, urban area effect on frictional convergence and convective precip. 78—81338
- air turbulent flow in heated channel, effect of gravitational field 80—64533
- air-water annular flows, interfacial drag and wall layer height 77—39324
- alloy, friction and wear, effect of oxides 79—20203
- alloy testing for use in heat treatment furnace, disc tribometer with high temp. pin 78—95900
- alloys, ion implantation in tribology and corrosion science, overview 79—14830
- Alpine fault, New Zealand, frictional metamorphism, Ar depletion and tectonic stress 80—41440
- alumina, wear, effect of liquid environment, use of pendulum scratching sclerometer *(Russian)* 77—16693
- angle detector for meas. *(French)* 78—92434
- asbestos-reinforced friction materials, wear and thermal processes 80—40559
- asperity deformation models, slip-line field anal., wear and friction regimes 79—87739
- aspherical clusters of galaxies, dynamical friction effects 78—16547
- asymmetrical friction in piston-cylinder device and effect on melting curves of In, Bi 80—86292
- N.Atlantic Ocean, bottom friction rel. to wind-induced sea level changes on Scotian shelf 80—72531
- atmosphere, cumulus friction and moisture budget in tropical wave-CISK 79—16580
- atmosphere, friction with Earth surface rel. to Earth rot. multiyear vars. excitation 79—96734
- atmosphere, role of horizontal friction forces in tropical circulation *(Russian)* 78—65360
- atmosphere boundary layer, coeffs. of mechanical resist. law over tropical ocean 77—45066
- atmosphere tides in joint presence of friction and rot., f-plane approximation 79—66847
- atom near metal surface, friction coeff. calc. 77—59312
- atomised-Fe powder, friction of compaction process *(Japanese)* 77—59716
- avalanches and landslides, mechanism based on law of dry friction 80—8314
- average flow model, appl. to lubrication between rough sliding surfaces 80—16497
- Babbitt grade Bk-2Sh, improvement in antifriction layer props. by impulse discharge *(Russian)* 79—1917
- bar, stability against self-excited frictional oscillations *(German)* 77—54916
- biharmonic equation, analogue technique, cylinders falling between parallel walls 78—55628
- bimaterial full-plane with crack at any angle to interface 77—14965
- bimetal rolling, calc. of strains by variational method *(Polish)* 80—45323
- bluff body, turbulence scale rel. to mean drag 77—27518
- bluff body, two-dimens., drag and wake *(Japanese)* 78—55647
- bodies in fluidised beds, resistance to motion 78—47030
- bone, anelastic deform. and friction stress 78—19871
- boundary friction effects on elastic wave propag. 79—46242
- boundary friction study by ultramicrosclerometry, dislocation generation 80—34131
- boundary layer, intermittent laminar/turbulent transition, local skin friction 78—30260
- boundary layer, laminar, skin friction, determ. with small Pitot probe 78—18269
- boundary layer, laminar, small temp. factor, high Mach no. 78—34156
- boundary layer turbulence, burst cycle and drag reduction 77—15003
- boundary layers influence on friction, effects of adding MoS_2 80—21125
- brass, α-β phase transformation caused by friction 80—76378
- brass, cold rolling, inhomogeneous texture 80—89251
- brass, frictional wear, effect of alloying and metal oxide compounds *(Russian)* 78—31541
- brass, repeated friction contact, form. of thick hardened surface layer 79—39056
- brass rings, sliding against mild steel, prow formation processes *(Japanese)* 80—35336
- in brittle fracture, transition from plastic to brittle contact *(Russian)* 78—53000
- bronze, Al, wear on 13% Cr steel in presence of aviation fuel 80—11781
- bronze, Al and Ti, sintered frictional material, wear resistance, effect of matrix struct. 77—28911
- bronze, P type, experimental analysis of junction growth with a junction model 79—47783
- Brownian motion, bistability effects in periodic potentials 80—68139
- Brownian motion, nonlinear response to external field, in low-friction limit 80—4652
- Brownian particle, freq.-depend. friction coeff. in fluid near crit. pt. 78—73929
- Brownian particle in a gas, coeff. of friction, Kirkwood-Kubo method 78—4558
- bubble of gas rising in fluid filled tube, wall effects *(French)* 79—7399
- camera lens shutters, friction coefficient nonreproducibility evaluation 80—62765
- car tyre, friction and traction, for teachers 78—81751
- carbonaceous hard insulating film, phys. props. 77—39752
- ceramic artificial hip joint, wear and friction tests *(German)* 79—8568
- channel, axisymmetric, with axial press. gradient injection, turbulent boundary layer characts. 79—37304
- channel flow with longitudinal press. gradient, friction meas. 77—58792
- channel flow with rough walls, drag 79—86512
- chip formation, frictional interactions between chip and rake face 79—52387
- circular cylinder, local heat transfer by turbulence of free-stream flow of viscous liquid, theoretical determ. of influence *(Russian)* 80—96252
- close binary stars, tidal friction theory 77—57013
- closed crack tip terminating at interface, asymptotic anal., friction effects 79—64595
- coatings for wear and lubrication 79—19494

friction continued
- coefficient, effect of surface curvature 78—87310
- Colmonoy, friction behavior in high temp. Na environment *(Japanese)* 80—40546
- Colmonoy hardfacing materials, friction characts. in high temp. Na *(Japanese)* 80—89356
- composite friction and bearing materials, development, friction and wear theory, review 80—60979
- composite materials, water lubrication, wear studies 80—60984
- compressible laminar boundary layer, development and separation with adverse press. gradient 78—26144
- compressible turbulent boundary layer, improved Van Driest skin-friction formula 77—58712
- condensation in channel, local (total) heat transfer coeffs., friction factors 78—51045
- conducting fluid, uniform current, flow past conducting porous sphere 78—34204
- conducting medium, high temp. plane flow turbulence, mag. field effect *(Russian)* 77—65811
- cone/plate system in fluid, friction heating and convection 78—87238
- conference, drag reduction and turbulence struct., Washington, USA (June 1976) 78—22329
- contact, frictionally heated, thermoelastic deform. 80—83764
- contact compression of circular cylinders with rough surfaces *(Ukrainian)* 79—50671
- contact fatigue life, traction and microgeometry effects 79—20205
- contact friction problems, associated and non-associated sliding rules 79—14351
- contact friction stress problems, soln. using superposition principle 79—32394
- contact of two plane bodies, loading distrib. intensity, slope and curvature discontinuities 79—86386
- contact planform effect, roughness, friction and wear 80—64497
- contactless gyroscope, influence of nonconservative moments on precession *(Russian)* 79—80421
- convection, forced, turbulent, in square cavity, shear effect 79—1180
- convection, laminar mixed forced/free, about sphere, buoyancy effects 77—75907
- convection, natural, over uniform heat flux vertical surface, higher-order approx. 78—59388
- Couette flow, striated boundary effect on viscous drag 78—59367
- Coulomb friction, elast. solid with one-sided contact *(French)* 80—64485
- Coulomb friction, elastic theory 80—33539
- Coulomb friction forces during rotation *(Polish)* 79—64597
- Coulomb friction in mechanical systems, simulation 80—53723
- crack anal., frictional contact 80—1475
- creep, high temp., friction stress 78—11289
- crossblow, by cone over thread, numerical solution *(Russian)* 78—55612
- cutting alloy detonation coating, struct. and friction *(Russian)* 78—15537
- cutting mechanism model during grinding 79—79124
- cylinder, permeable, in viscous fluid, friction coeff. 79—46385
- cylinder contact with visocelastic lubricant, friction 78—7056
- cylinder in cross flow, skin friction and vortex shedding freqs. 78—94758
- cylinder in near-critical flow, influence of acoustic surface vibrs. on drag 78—5729
- cylinders, aerodynamic noise vs. drag relationships 79—32550
- cylinders, circ., various arrangements, flow interference, review 78—46985
- delamination wear, macroscopic effects 80—35343
- delamination wear, mechanics of crack propag. 78—3231
- dental restorative materials, empirical eqn. including fracture toughness for friction 78—61283
- device for kinetic coeff. of friction meas. between surface and granular mass 78—31603
- diamond, friction in contact with W, temp. depend. *(Russian)* 77—73350
- diamond, frictional anisotropy, cathodoluminesc. study 80—35340
- diamond stylus, sliding on rubber, orientation effects, expt. test of theory 77—86188
- disk and strip forging for the determination of friction and flow strength values 78—85004
- dislocation behaviour during fatigue, friction stress and back stress from hysteresis loop anal. 79—42076
- dispersion hardened alloy, friction stress for high-temp. creep 78—11289
- drag, on circular cylinder low Reynolds number 77—84218
- drag force on sphere moving in medium with variable viscosity 78—67173
- drag minimised bodies, given length and base, Newtonian theory calcs. 77—84267
- drag on a sphere moving axially in a long rotating container 79—50734
- drag on bodies of revolution, effect of distributed boundary layer suction 77—46998
- drag prediction, of bodies of revolution, importance of near wake 77—23962
- drag reducing flow, mean vel. and turbulent energy closures 78—22331
- drag reducing fluid, turbulent fluctuations in viscous wall region 78—26160
- drag reducing pipe flow, boundary turbulence 77—68578
- drag reduction, dilute polymer soln., wall roughness effective slip depend., turbulence model 78—26162
- drag reduction, PEO 301 dilute soln., pipe flow turbulence struct. drag reduction 78—26196
- drag reduction, Polyox coagulant effects on turbulent boundary layer 78—26165
- drag reduction and burst cycle mechanism, dil. polymer soln. 78—26164
- drag reduction by compliant wall, numerical simulation of turbulent boundary layer 78—26114
- drag reduction enhancement by mol. aggregates in polymer soln. 78—26161
- drag reduction in turbulent boundary layer with compliant wall 78—26193
- drag reduction polymer additive in helicoidal flow, screw pump press. head 78—26166
- drag reduction with compliant coatings, review 78—26115
- drag reduction with surfactants at elevated temp. 77—68579
- drag-reducing flows, calc. of velocity profiles 77—35185
- dry friction problems, graphical soln. for teaching 78—12511
- dry sliding wear, role of dynamic recrystallisation 80—108599
- dry-friction periodic relay system analysis *(Russian)* 79—10455
- duct, noncircular, with sharp corners, friction factors 79—81968

friction continued
- duct, turbulent air flow, small streamline curvature effects 79—60064
- in ducts of non-circular cross section 78—18342
- dynamic rigid indentation induced by sliding frictionless contact 78—75107
- Earth asthenosphere, frictionally heated shear flows stability 79—44164
- earthquake mechanics based on nonuniform friction 79—20766
- earthquake slip, frictional heating on fault zone with finite thickness 78—36124
- education, circular motion with friction, numerical and analytical solns. 80—57029
- education, knots, topology friction and strength 77—33769
- education, speed and displacement relations for tire skids, program for PET 80—57038
- education, work and kinetic energy, automobile min. stopping distance 77—78929
- EHD, lubricating layer *(Russian)* 78—47061
- elastic contact and friction mechanisms, for rough surfaces 78—87309
- elastic contact problem with friction, solution using nodal parameters *(French)* 78—63401
- elastic contact problems, in fracture mech., friction effects 78—67142
- elastic contact problems with friction, nodal parameter soln. *(French)* 79—10475
- elastic layer on substrate, frictional slip caused by normal load 80—33541
- elastomers, surface roughness, friction and adhesion 80—66674
- elastometric materials, friction testing using reciprocating friction and wear tester 80—76451
- elastoplastically deformed strengthened material, stress deformed state during rolling *(Russian)* 80—54299
- elbor, friction in contact with W, temp. depend. *(Russian)* 77—73350
- electromagnetic clutch material, sintered, friction, hardness, wear props. 78—11339
- elementary theory 78—15543
- emulsion, relative drop-drop and drop-wall motions, slow 79—32641
- entrainment process in stratified fluid, role of side-wall friction in laboratory expts. 80—51405
- epoxy resin wear and cutting surface against brass *(Japanese)* 78—56779
- epoxy-steel system, friction and wear 78—44229
- experimental device for measuring friction between ski and snow 78—92410
- external friction reduction by forced piezoelec. oscillation 80—92096
- extrusion, benefit of vibrations 78—51135
- failure, temp. gradient model 79—42142
- Fe, cast, mechanism of boundary lubrication with zinc dithiophosphate 79—79120
- ferroelectric narrow walls, steady-state motion 80—11356
- fibre passing over moving curved surface, apparent friction paradox 77—31263
- fibre suspension, rheology, rel. to turbulent drag reduction 78—22315
- film rupture in laminar and turbulent lubrication, inertia forces effect 80—74813
- finite difference numerical solns 78—9661
- floors, friction coeff. meas. method 79—52540
- floors, small mobile apparatus for meas. coeff. of friction 80—69747
- flow, creeping, about sphere, general soln. of linear Navier-Stokes eqn. 78—71307
- flow, downward, entrained, of gas-liq. mixture in vert. channel 79—94704
- flow, fully-developed, in non-circ. passages, prediction method 79—1254
- flow, laminar, incompressible, about bluff body, separation, reattachment, eddies, drag 79—59964
- flow, of anisotropic spatially inhomogeneous viscosity fluid, variational principle 79—37367
- flow, Reynolds analogy extension for fully rough surface 78—51159
- flow, rot., between rot. and static discs, with radial flow, numerical method 78—59403
- flow, rough surface boundary layer calculation methods 80—1595
- flow, rough-wall incompressible boundary layer, calc. model 79—1165
- flow, separated, internal, computation using coupled boundary layer-inviscid core, elliptic representation 80—1549
- flow, steady, in porous region between rot. spheres 79—46382
- flow, Stokes law, Reynolds no., for teaching, erythrocyte sedimentation rate 78—49610
- flow, stratified, stress-driven entrainment expts. scaling 79—50768
- flow, swirled, in pipe, friction law and form parameters 79—37329
- flow, transonic wedge, parabolic series method, drag coeff., press. distrib. 77—89142
- flow, wall jet, 3-dimens., surface layer props. computation 80—1667
- flow behaviour and transport phenomena in agitated vessels, correlation eqns. *(Japanese)* 78—38300
- flow between coaxial rotating cones, frictional moment coeff. determ. *(Japanese)* 77—39299
- flow between porous walls, 2-dimens, laminar 79—14477
- flow between rot. disc and fixed wall, friction coeffs. 78—63439
- flow between rotating spheres, frictional moment 78—79301
- flow in annular channel with vortex generators, crit. heat flux, hydraulic resistance *(Russian)* 78—83397
- flow in narrow annular channel, heat exchange, hydraulic resistance *(Russian)* 77—72299
- flow in pipe, laminar friction factor and heat transfer, finite-element technique 80—10247
- flow in pipe, swirled, integral calc. method 79—37402
- flow instability, two-phase, in parallel channels 78—94810
- flow normal to perforated plates, heat transfer and friction loss 78—94733
- flow over 79—46308
- flow over plate with simultaneous injection and suction, turbulent layer friction and vel. profile 78—83469
- flow past cavitating bluff bodies, constrained, drag and vortex shedding 78—47006
- flow through porous media, friction factor 78—91008
- fluid drag on group of cylinders 77—58703
- fluid spheres in viscoelastic fluid, drag coeff., low Reynolds number *(Japanese)* 78—9694
- fluid-solid interface, sliding friction coeff., calc. method 77—14987
- fluidised bed, nonuniform, force on fixed sphere, rising gas bubble force field 78—59476
- fluoro epoxy resins, surface props., appls., wear resistance and friction 78—64713

friction continued
- fluorocarbon polymer film, prep. by RF sputtering and plasma polymerisation, props. 77—55890
- fluorocarbon polymer thin films for lubrication of Au contact surfaces 80—89157
- foam PS-4-40, microslip, effect of friction 77—77588
- fretting fatigue crack, initiation and propag. 77—73353
- friction, lubrication and wear, review of papers published 1974 to 1976 79—15806
- friction, stochastic quantisation, nonlinear Schrodinger equation 80—27164
- friction machine, residual stresses meas., appl. to wear resist., surface wear 78—60906
- frictional torque nonstationary brake flow in liquid filled cylinder *(German)* 77—72304
- galactic disc, dynamical friction theory 79—35367
- galaxies, colliding, dynamical friction effects 79—44600
- galaxies binary systems, luminosity/separation correl. as dynamical friction effect 80—36700
- gas, reson. oscills. in channel, local heat transfer coeffs. 78—1659
- gas, with variable physical props., pipe flow, turbulent momentum and heat transfer calc. 78—90869
- gas flow through cracks, surface roughness influence 80—69929
- gas friction, detector using active permanent magnet suspensions 78—24829
- gas lubricated bearings, test equipment to examine friction and wear, exam. of design 79—52522
- gas subsonic flow in tubes, friction factor determ. method *(Russian)* 77—19635
- gas-liquid annular two-phase flow, wave and interfacial friction characts. 78—67249
- gas-liquid flow, hydraulic resistance 80—24077
- gas-liquid mixture, bubble mode of flow in vertical pipe 80—24081
- gas-liquid mixture, flow struct. and distrib. effects in pipe 79—27682
- GCFR fuel rod roughness elements, pressure drop meas. 80—581
- glacier, sliding friction on plane strewn with hemispherical obstacles *(French)* 79—8640
- glacier friction law, shadowing function of Gaussian probability curve *(French)* 79—8641
- glass, viscoplastic, gas-vapour interlayer problem 80—49490
- glass ball rolling on adhesive viscoelastic material, contact area 79—52394
- glass fibre reinforced PTFE and polyacetal, friction and wear against glass and steel 78—56783
- glass on rubber rolling friction, humidity effect 79—79118
- glass/MoS_2 reinforced PTFE, fibre orientation effect on friction and wear 79—79125
- graphite, fibre reinforced epoxy, fibre orientation effect on friction and wear 79—79125
- graphite, time to formation of adsorbed molecular monolayers at contact spots during friction 77—43425
- graphite fibre reinforced, Cu-Sn exam. of high speed tribological props. in friction expts. against steel 79—15809
- graphite fibre reinforced metal, fibre orientation effect on wear 79—87744
- graphite fibre reinforced metals, tribological behaviour, fibre origin effects 79—96158
- graphite fibre reinforced polyimide composites 79—52381
- graphite filled PTFE, carbon aspect ratio effect on friction and wear characts. 77—59945
- graphite reinforced Al, wear volume/sliding time relationship 79—61743
- ground effect wings, minimum induced drag 77—7367
- gyroscope, unsteady oscillations reduction using inner gimbal-base elastic damping coupling *(Ukrainian)* 77—30143
- haemodynamic friction, effect on parietal microenvironment 80—16973
- haemodynamic parietal friction meas. by pulse type Doppler velocimeter 80—17206
- hard ellipsoid sliding on rubber, orientation effects, theory 77—86188
- heat and mass transfer and friction under complex thermogasdynamic conditions 79—1209
- heat exchanger, with lamellar surfaces and smooth ribs, gas flow resistance, heat exchange *(Russian)* 78—83218
- heat pipe, high temp., subsonic vapour flux, heat exchange and friction 77—75779
- heat pipe, with header and single or two-phase artery systems 78—90981
- heat transfer and drag on moving bodies 78—9706
- heat transfer and friction factors for laminar flow through finned tube 78—94730
- high contact speed, sliding friction coeff. determ. 78—87308
- high speed rubbing, thermomechanical interactions 80—83769
- hip prostheses, expt. study of friction and lubrication 80—17189
- hydraulic machines, liquid and dry power losses calc. method 78—85009
- hydrodynamic, sticking and slipping boundary conditions, friction of rot. bumpy cylinder 78—63410
- hydrodynamic boundary conditions and radii, appl. to rot. rough sphere friction with chloroform 78—9926
- hydrodynamic resistance reduction by surfactant, rel. to micelle form. 77—7438
- hydrodynamic thermal breakdown in viscous fluid, Couette flow between cylinders 78—83391
- hydroplaning of a rotating cylinder on water 78—63522
- hydroplaning plate, lift, drag 78—63523
- hypersonic flow around blunt bodies, surface friction, physiochemical processes in shock layer 78—46997
- hysteretic, in small velocity approx., linear viscoelasticity eqns. 79—37252
- ice single crystal, friction of steel ball load, velocity and temp. depend. *(Japanese)* 78—88537
- ice single crystal, friction of WC ball, anisotropy *(Japanese)* 78—88539
- ice single crystal, friction of WC ball, slider size effect *(Japanese)* 78—88538
- impact interaction of microroughnesses of rubbing surfaces *(Russian)* 79—100265
- imprinigement flow, skin friction and heat transfer meas., hot and cold-film sensors 77—27629
- Inconel hardfacing materials, friction characts. in high temp. Na *(Japanese)* 80—89356
- inequality conditions, consequences in crack and friction contact problems 79—37242
- inert gases, viscosity rel. to ionis., skin friction of wetted oscill. disc 78—34252

friction continued
- interface flaw extension with friction, basic mathematical anal. 79−18810
- interface of two solids, sliding mechanism without slipping 78−51136
- ion, near metal surface, friction parameter and Brownian motion 80−15584
- ionic lattice/moving dielec. medium, molecular friction force *(Russian)* 78−13975
- jet, subsonic, flow and heat near blunt body stagnation point 77−65774
- jet impact system with unilateral outlet, air flow, heat exchange *(Russian)* 78−83449
- junction growth mechanism during friction *(Japanese)* 79−32391
- Kevlar fibre reinforced epoxy, fibre orientation effect on friction and wear 79−79125
- kinematic examination of constraint systems realised on pairs of surfaces in contact *(German)* 77−31262
- Lagneborg particle by-passing model, creep rate stress exponents and friction stress 80−55481
- laminar boundary layer, with press. fluctuations heat transfer, friction *(Russian)* 77−89114
- laminar boundary layer with press. fluctuations, friction and heat transfer 79−64652
- laminar film condensation from moving vapour, with suction 78−59459
- laminar flow, of fluid with free surface, in triangular-shaped open channel *(Russian)* 77−51028
- linear elastic half space, frictional unloading problem 80−33542
- linear elastic half-space, frictional unloading problem, variational soln. for stress analysis 78−59350
- linear models of frequency-independent internal friction *(Russian)* 79−18834
- liquid film, in vertical tube with turbulent gas flow, friction coeff., press. losses 77−89189
- liquid film turbulent flow, heat transfer, friction factor 77−42819
- liquid flow around cylinder, thermophys. characts. rel. to friction and heat transfer *(Russian)* 78−38328
- liquid motion in channels with permeable walls, hydraulic resistance 78−5797
- liquid pipe flow, heat exchange and resistance calc. 78−94819
- liquid system, turbulent flow, drag reduction, neutral stability 77−7380
- liquid-friction bearing tester, description and improvements over existing designs 80−64503
- low velocity friction pair, friction microgeometry influence on $\mu(a_s)/\mu(a_k)$, slip-stick amplitude 78−26091
- lubricant at friction boundary *(German)* 77−86190
- lubricant evaluation, using four ball friction machine 80−25951
- lubricated elastomers in contact with regularly spaced sliders, frictional dynamics 79−20213
- lubrication film temp. and traction, rel. to solidification and glass transition temp. 79−28041
- lubrication of cylindrical surfaces with Rivlin-Ericksen fluid *(French)* 77−80126
- machine, type SMTs-2, exam. of electronic loading cycle counter 79−52527
- machine SMTs-2, self adjusting fixture for block specimens 80−25944
- macromolecular liquids, flow alignment, non-Newtonian viscosity and normal press. 77−35183
- macroscopic van der Waals interaction contrib. to friction forces *(Russian)* 77−16867
- macroscopic Van der Waals interactions, contrib. to frictional force 78−55613
- material, current state of prod. and development trends review 78−19902
- materials and lubrication media, for frictional pairs, choice by energy criteria *(Russian)* 78−31541
- materials under melting, intensity calc. 80−103416
- measurement methods at lubricated sliding surfaces, machine bearings *(German)* 79−81826
- measuring instrument for single fibres in various media 77−27498
- mechanical treatment in aq. salt soln., material transport rel. to wear 80−16506
- membrane, weak ion exchange, nonequilib. props., steady flow in const. elec. field 78−23966
- metal, abrasive wear resistance rel. to physicomechanical props. 79−91804
- metal, friction and slip during cold rolling 78−64707
- metal, friction during working stresses and rheological charact. at high temps. *(Russian)* 77−66702
- metal, friction equation 77−16699
- metal, friction heating during cutting 79−39055
- metal, friction pair, seizure centres on contacting surface *(Russian)* 77−70185
- metal, frictional forces during polishing in vacuum 80−28365
- metal, internal stresses during rolling friction and their evaluation 77−28912
- metal, kinetic friction re-examination using modified pin and disc machine 80−55547
- metal, load-bearing surfaces, secondary structures obs. by electron microscopy, specimen thinning method 79−52484
- metal, pack rolling, bonding, deform. struct., small reduction before seizing 77−90503
- metal, plastic deform. and sliding friction 79−87743
- metal, polymer coated, wear and friction 77−21328
- metal, pure, friction stress for high temp. creep 78−11289
- metal, surface layer transform. and failure, kinetic charact., under dry friction 77−52506
- metal cutting, direct SEM obs. of adhesion and frictional sliding 80−104412
- metal mechanical property effects on frictional behaviour 80−55548
- metal surface, AES anal. in adhesion, friction and wear 78−53179
- metal surface, spectroanalytical investig. of friction processes and subst. transfer products *(Russian)* 79−34418
- metal surface $H_2 \rightleftharpoons H+H$ reaction rel. to catalysis, friction coeff. calc. 77−77807
- metal transfer in frictional contact of rough hard surface 78−64739
- metal wear energy balance under abrasive and boundary friction, expt. 78−85006
- metal-insulator pairs, frictional heating at cryogenic temps., rel. to supercond. magnet technology 80−66671
- metal-metal interface, effect on adhesion and friction 77−24488
- metal-polymer contacts, methods of decreasing wear 79−20209
- metal-polymer friction pairs, triboelec. effects 80−11784

friction continued
- metal-sapphire interface, effect on shear strength of adsorbed species 80−49485
- metalforming processes, finite element anal., introduction of friction, appl. to ring compression 79−81818
- metallic glasses, friction coeff. determ. using sliding friction rig 80−89355
- metallic ion plated soft film, friction and wear 78−15549
- metallic powder materials, deform., boundary conditions on sliding surfaces 80−60978
- metallic sliding contact, resistance at single point, friction force *(Japanese)* 78−11343
- metals, abrasive wear testing under conditions of rolling friction 79−15894
- metals, FCC, texture changes in running surface as result of frictional stress 79−91699
- metals, friction and wear rel. to comp., struct. and props., review 80−25872
- metals, ion-implanted, friction and wear, review 80−40555
- metals, rheological interpretation of planar deformed state in extremal friction regime *(Russian)* 80−64385
- metals, scoring resistance under dry friction *(Russian)* 79−99267
- metalworking, role of friction, and energy saving in deep drawing 80−76271
- methyl α-n-alkylacrylate methyl methacrylate copolymer, friction and wear 77−63809
- MHD convective viscous flow past porous plate with suction, mass transfer effects 78−87398
- MHD flow between parallel plates, temp. field, vel. field, skin friction, heat transfer 77−68700
- MHD free convection about semi-infinite plate in strong cross field, skin friction, heat transfer 77−15134
- MHD slip flow regime over porous plate, skin friction and heat transfer 77−31392
- MHD turbulent boundary layers in rot. circ. vessel, drag 80−33697
- MHD turbulent heat and momentum transfer in 2-dimens. channel with transverse mag. field 78−94848
- microslip, effect of friction 77−77588
- mineral oil lubricants, behaviour in line contact and oscillatory movement *(Spanish)* 79−98671
- miniature drag force anemometer 78−14117
- molecule, moving in compressible viscous fluid, hydrodynamic drag 79−27732
- monolayer formation on solid surface as friction protection 78−47663
- Mossbauer spectroscopy appl. to friction, lubrication and wear studies 80−40547
- mountain streams, channel roughness coeffs., Chezy-Manning relation 78−49045
- moving rigid punch on unlubricated viscoelastic half plane 79−64598
- multiple contact points, theoretical representation of coeff. of friction 79−61742
- multiply variable struct. systems, periodic regime anal. method *(Ukrainian)* 80−10134
- n-octadecyl methacrylate methyl methacrylate copolymer 77−63809
- nematic thin slab fluid, friction coeff. *(French)* 77−27829
- Ni, friction props. of surface films in air and high vacuum 78−60850
- Nichrome-silicate glass-CaF_2 multicomponent self-lubricating coating, prep. by plasma spraying, and props. 80−40604
- Nimonic 90, creep rate stress exponents and friction stress, comparison with Lagneborg particle by-passing model 80−55481
- Nimonic 90, dispersion hardened, friction stress rel. to initial and secondary creep 80−11711
- non-Newtonian flow along thin needle, vel. profile, skin friction 78−67229
- non-Newtonian lubricant, frictional behaviour 79−87736
- noncircular prismatic block between parallel frictional platens, press. distrib. and bulging profiles during compression 78−18207
- noncoherent powder, pressure exerted on vertical screen *(French)* 78−42572
- nonlinear friction element output with stochastic input 79−50674
- nonlinear vibrating systems, fourth order parametric resonance, influence of frictions 77−58620
- nonslender body, minimal drag determ. 77−39306
- nonspherical particle, friction coeffs. in incompressible fluid with spin 78−87350
- nonsteady flow of dropping compressible liquid in pipes, effect of friction laws 77−55091
- nozzle of rocket, compressible turbulent boundary layers, heat transfer and skin-friction 79−14451
- nuclear reactor components, lubrication, friction system in liquid Na and Ar 79−59176
- numerical integration of eqn. system for nonadiabatic compressible gas flow in tube *(Russian)* 78−83427
- nylons, exam. of frictional behaviour *(Japanese)* 78−64714
- ocean, bottom friction effect on barotropic motion over continental shelf 79−48509
- optomechanical device frictional elements, solid lubricant tests 79−52388
- oscillator with dry friction, forced vibrs., response random process treatment *(Russian)* 80−36841
- parallel plate porous slider, magnetohydrodynamic, optimum profile 79−47781
- periodic solutions of systems with friction *(German)* 79−90199
- permeable cylinder in sheet of viscous fluid, translational frictional coeff. 80−19500
- permeable plate gas screen region, heat transfer and friction laws 79−1250
- permeable spheres in incompressible fluid, hydrodynamic interaction, mobility tensors 78−71395
- permeable spheres in incompressible fluid, hydrodynamic interaction vel. fluid, friction consts. 78−75202
- physicochemical processes during frictional contact leading to H_2 generation *(Russian)* 77−52496
- pipe, heated, vertical, gas buoyancy effect on downward flow and heat transfer 78−74427
- pipe, porous, uniform air outflow, turbulent momentum flow and friction coeffs. formula 78−1737
- pipe entrance region boundary layer, turbulent temp. and vel. fluctuations *(Japanese)* 78−38301
- pipe flow, triggered laminar to turbulent transition, random coiling macromolecular soln. 78−26195

friction continued
pipe flow, turbulent, temp.-depend. viscosity effect on convective heat transfer 78—90884
pipe resistance with ball packing, calc. 77—72356
plane punch on viscoelastic half-plane, hysteretic friction 77—68450
planet-satellite systems of solar system, tidal friction secular effects 79—8860
plasma, MHD flow in channel, wall friction 78—14092
plastic, antifriction, self-lubricating, behaviour at elevated temps. in friction process 77—86192
plastic, load-bearing surfaces, secondary structures obs. by electron microscopy, specimen thinning method 79—52484
plastic flow round crack under friction and combined stress 78—79280
plate tectonics, roles of boundary friction, basal shear stress and deep mantle convection 78—57188
plume, turbulent, thermal, along vert. wall, struct. and heat transfer 78—90880
PMMA, molecular interaction in frictional-contact zone, absorpt. spectra 79—78688
PMMA-steel pair, temp. calc. under severe friction 80—40550
polyacrylamide solution, tube flow, friction and convective heat transfer, rheological changes effect 79—1220
polyamide resin wear and cutting surface against brass *(Japanese)* 78—56779
polyamide-Cu system, antifrictional props., struct. 80—40552
polycaproamide, molecular interaction in frictional-contact zone, absorpt. spectra 79—78688
polycarbonate resin-steel pair, temp. calc. under severe friction 80—40550
polyethylene, branched, frictional props., normal force/shear for relationship 79—47785
polyethylene, branched, frictional props., true area of contact 78—64735
polyethylene, friction and wear with lubrication by thermooxidative destruction products 77—52504
polyethylene, high density, friction and transfer 77—52512
polyethylene, molecular interaction in frictional-contact zone, absorpt. spectra 79—78688
polyethylene, ultra high molecular weight, wear limit, γ-irradiated and unirradiated *(Japanese)* 78—27649
polyethylene oxide soln., drag reduction of highest mol. wt. fractions 77—68636
polyethylene pellets, falling in air in pipe, equilib. region press. drop, friction factor 78—63479
polyethylene terephthalate, molecular interaction in frictional-contact zone, absorpt. spectra 79—78688
polyethylene terephthalate monofilaments, friction and adhesion 79—52386
polyethylene-glass pair, contact interaction under elastic strain, friction and γ-ray effects 80—40549
polyethylene-steel pair, temp. calc. under severe friction 80—40550
polyethylenoxide additive mixing, turbulent drag reduction, schlieren obs. 78—26163
polyimide, carbonized layer form., friction, wear *(Japanese)* 77—52502
polyimide films, effect of atm. and temp. on wear, friction and transfer 78—85003
polyimide films, mol. relaxations, mol. orientation and friction characts. 77—59939
polyisobutylenes, dilute solns., turbulent drag reduction, influence of mol. wt. and mol. conformation 77—80189
polymer, calc. of coeff. for isotropic surface contact 78—64716
polymer, changes in material performance 77—52509
polymer, composition coatings for rubbing mechanisms 78—29198
polymer, friction coefficient calc. for contact surfaces with nonspherical asperities 79—20200
polymer 77—4859
polymer additives in pseudo-turbulent flow, nonlinear dumbbell model 78—51206
polymer elastic deform. meas., occurring under reversible slippage, friction method 77—52598
polymer film, dynamic loading influence on sliding friction 79—50675
polymer films, between contacting surfaces, effect of contact pressure and temp. 78—60842
polymer films, stick-slip motion and surface deformation 79—37253
polymer in dilute solution, friction tensor, microscopic treatment 78—22314
polymer reaction with metal formates in frictional contact zone 78—7057
polymer soln., translational friction coeff. conc. depend., multiple scatt. formulation 77—20102
polymer soln. pipe flow, fluid friction 78—5769
polymer soln. turbulent flow over plate, drag reduction 78—5768
polymer solution, channel flow, drag reduction, viscous sublayer struct. 78—22385
polymer solution, drag reduction, elec. field effects 77—72334
polymer solution, drag reduction in pipe flow, flow time scales 78—22386
polymer solution, drag reduction in turbulent flow 78—26159
polymer solution, logarithmic equations fo resistance of turbulent friction 77—51042
polymer solution, rheology, rel. to turbulent drag reduction 78—22315
polymer solution, semidilute, hydrodynamic interaction of two permeable spheres, method of reflections 78—71394
polymer solution, turbulence structure, drag reduction 78—22381
polymer solution, turbulent boundary layer, drag reduction 78—22414
polymer solution, turbulent mass transfer to pipe flow 78—1695
polymer solution elongational flow through porous bed, drag increase 78—22419
polymer solution pipe flow, drag reduction 78—42631
polymer solutions, dilute, internal viscosities, frictional coeffs. calcs. 78—6171
polymer solutions, turbulent, mass transfer rate, frictional force *(French)* 79—37357
polymer solutions, viscosity, intrinsic, friction coeff., porous sphere model 78—71301
polymer-metal pair adhesive interaction during friction 78—3227
polymer-polymer pair, adhesive interaction 78—3227
polymeric composites, sliding wear mechanisms at metal surfaces, microscope obs. 79—87742
polymers, abrasive wear resistance rel. to physicomechanical props. 79—91804
polymers, entanglement, topological theory, chain centre friction coeffs. 80—91709

friction continued
polymers, friction and wear, role of mech. props. 78—52998
polymers, frictional props., crystn. effect 80—40551
polymers, shear strength and friction 78—39913
polyorganosiloxane fluids, temp. determ. in friction zone accompanying breakdown, using TV *(Russian)* 80—7688
polyox solution, turbulent flow in tube with large surface roughness 78—1651
Polyox-701 aq. soln., turbulent press. suppression, spectral effects in pipe flow 78—5771
polyphenylquinoxalines, graphite filled, behaviour during friction 80—40553
polypropylene, molecular interaction in frictional-contact zone, absorpt. spectra 79—78688
polypropylene, thermoplastic, supramolecular struct. and frictional props. of surface layers 77—70188
polystyrene, conc. soln., friction const., Rayleigh scatt. 77—35737
polystyrene, conc. solns., diffusion and sedimentation, frictional coeff., crit. soln. temp. 79—95195
polystyrene in cyclohexane, dil. theta soln., translational diffusion coeffs., conc. depend., Rayleigh scatt. meas. 79—90812
polystyrene solution, drag reduction, mean vel. profile 78—22384
polyurethane, stress plate in contact zone with solid indentor 78—1624
pore size determ. of powder and wire gauge filter materials 77—12776
porous composite slider bearing, hydrodynamic lubrication 78—39915
porous materials, contact stresses in hot rolling 77—77515
porous plate boundary layer, vel. and friction stress distribs. 77—84243
porous plate skin friction, injection or removal from boundary layer due to turbulent wall jet 78—47029
press forming of sheet metal, frictional surface damage 78—76768
protective coatings, role in mechanical failure prevention, conf., Caithersburg, USA (Oct. 1975) 77—21327
pseudoplastic fluid flow in pipes, press. loss 79—98765
PTFE, friction and transfer 77—52512
PTFE, sliding charact., friction and wear *(Japanese)* 78—56778
PTFE, wear, sliding speed, contact press. and rubbing surface temp. 80—76372
PTFE impregnated porous bronze, coeff. of friction, temp. effect 78—64737
PTFE-steel pair, temp. calc. under severe friction 80—40550
pulsating laminar-boundary layer, heat transfer and skin friction 78—94711
PVC, rheology, viscoelasticity 79—3982
pyrex, plates, exam. of friction, wear and elastic constant mechanisms 78—87309
quadratic friction quantisation, point object in viscous field 80—68076
radial ply motor tyres, deformation on road surface, anal. *(German)* 79—90201
rarefied gas, thermal transpiration, thermal and friction forces 77—35171
rebound of elastic bodies in oblique impact 77—50873
reciprocating magnetic refrigerator for 2-4K operation 80—2577
rectangular vibrating plates separated by liquid filled gaps, viscosity friction calc. *(German)* 80—105504
reinforced composite pull-out forces, effect of matrix stresses 77—21334
resin impregnated glass tape, friction and rheological props. 77—63806
Reynolds equation, numerical soln. with slip boundary conditions and large bearing number 79—90197
rib-roughened surface, friction factor and heat transfer correlations with rib characts. 78—87233
rigid circular cylinder in confined flow, fluctuating lift and drag forces 77—15118
rigid cylinder rolling on a rigid perfectly plastic half space 79—41629
rigid indentor and elastic halfspace, dynamic contact with perfect adhesion and frictional slip 80—58980
rigid slider, deformational contact and friction on viscoelastic substrates 79—50677
road vehicle stopping distance, weight transfer effect, for teaching 79—25800
rock and rock joints, empirical laws of friction and fracture 77—21762
rock friction and earthquake prediction, conf. (Stanford, 28-30 April 1977) 79—16448
rock friction effect of confining pressure, temp. and pore pressure 79—16455
rock friction modelling, expt. results and constitutive eqns. 79—84240
rock friction modelling, preseismic slip simulation 79—84241
rock samples with saw cut, fracture and frictional sliding, earthquake prediction appl. *(Chinese)* 79—100825
rock volume changes during fracture and frictional sliding 79—16450
rocks, dilatancy and fracture induced vel. changes rel. to frictional sliding 79—16458
rocks, electrical resistivity changes during frictional sliding and fracture 79—16457
rocks, frictional sliding, asperity-surface interaction and surface damage 79—16456
rocks, frictional sliding, displacement rate effects in Tennessee sandstone 79—16461
rocks, rupture and particle velocity during frictional sliding 79—20820
rocks, slip propag. along frictional surfaces 79—25236
rocks, time-depend. friction and stick-slip mechanics 79—16459
rocks 79—16451
rolling, ball on rough plane 79—95076
rolling contact with dry friction, Duvorol computer code 79—90194
rolling discs, coeff. of friction 79—14360
rolling object, frictional force, student lab. expt. 80—17764
rough materials, stressed state on contact 80—38352
rough surfaces in contact, stochastic approach to deform. mode 77—59950
roughness persistence between surfaces in static contact 77—11632
rubber, C black filled, friction behaviour sliding against Al, applied voltage effects 79—74266
rubber, cutting resistance measurement in absence of friction 79—5035
rubber, friction against paper and polymer film surfaces, microroughness effect 80—71763
rubber, role of adhesion, friction coefficient determ. *(French)* 77—52495
rubber, Schallamach waves, rel. to friction of elastomers 79—29225
rubber, surface texture effect on hysteretic friction 79—61741
rubber containing $CuSO_4$ paired with steel, selective transfer mechanism 80—55544
ruled three layer shell, large coefficient of friction between layers, stresses-strained state calc. 79—14354

friction continued
- sandpaper, standardised, for Taber abraser, influence of relative humidity an abrasive quality *(Japanese)* 79—8369
- Schrodinger equation, nonlinear time-depend., one dimens. wave packet soln., Fortran prog. 77—9897
- sealing materials, friction and wear tests *(German)* 79—38987
- secondary flow prediction , three-dimens. turbulent boundary layers, skin-friction 78—22341
- seismic faulting, rupture propag. in presence of friction and inhomogeneous initial stress 77—86835
- seismic vel. changes during fracture and frictional sliding 79—16408
- self-excited vibrations in lubricated friction 80—58984
- self-lubricating, struct. and props. 79—100267
- SEM specimen chamber use for dynamic expts., state-of-the-art review 78—23918
- semiinfinite elastic solid, frictional shear effect on dynamic stresses 79—10537
- SH-waves refl. and refr. in presence of slip and friction 79—46243
- shallow water basin, wind-driven current, eddy viscosity, bottom friction 78—65319
- shear loaded interface crack, friction effects, contact zones, stress fields 80—79225
- shear-thinned fluid, laminar heat transfer and drag 79—68764
- sheet metal, punch stretching, friction coeff. determ. method 78—27647
- shock-wave boundary-layer interaction, wall shear stress meas. 79—1212
- shuttlecock, terminal vel. in vertical fall 80—90627
- signature response, for friction and wear 80—40541
- simulative testing, systems analysis data sheet for friction and wear tests 77—28967
- simulative wear study critically reviewed 77—28968
- sintered frictional material, environmental effects on props. 78—11338
- sintered parts for frictional units 78—11342
- Sitall, microcrystalline glass, exam. of frictional props. under end-end rubbing 80—16488
- sitall base composites, antifriction props. 77—77591
- skin friction, meas. by viscosity balance method, appls. to three dimensional flow 77—19645
- skin friction, Reynolds number depend. of bulk flow varibles in duct flow 78—94827
- skin friction coefficient, correl. with momentum thickness Reynolds number and free stream press. gradient 78—94640
- skin friction in turbulent boundary layers, meas. techniques 78—1770
- skin friction measurement, comparison of viscosity balance and Preston tube methods 77—55109
- skin friction meter using viscosity balance principle for metal surfaces 77—35266
- skin friction variation with Reynolds number, viscosity balance meas. compared with Preston tubes 77—72377
- slab, surface displacements for high speed rubs 80—83767
- slender cones, in hypersonic flow drag meas. using mag. suspension and balance 79—4039
- sliding bodies, friction apparatus for meas. normal displacement 80—99977
- sliding contact, friction, wear, temp. anal. 80—93659
- sliding contact problems, heat conduction, temp. and heat source distribs. 79—98588
- sliding fit, stick-slip phenomena 80—5996
- sliding friction coefficient, between liquid and solid, method for experimental det. 78—22307
- sliding in metallic solids, anti-scuffing rating 80—14629
- slip flow, MHD, over porous plate, with variable suction, heat transfer 78—79337
- slip friction characteristics in nonstationary motion *(Russian)* 80—43652
- slip of friction-controlled mass excited by earthquake motions *(Japanese)* 79—70753
- slip progressing into contact zone of crack 80—16417
- slurry flow, pressure loss reduction by addition of surfactants 77—84297
- soft metal used as solid lubricant, compatibility effects 77—21291
- soft metallic films, role in reducing friction between metal surfaces 80—55592
- soil, sliding masses, residual strength and frictional resist. *(Japanese)* 78—11919
- solid body, reduced by mechanical vibrations, piezoelectric drive *(German)* 77—35101
- solid friction damping of mech. vibrs., math. model approach 77—42764
- solid systems, non-linear vibration properties *(French)* 77—54937
- solids, pneumatic transport, flow, friction effects *(German)* 78—34181
- solids, surface energy and theory of friction 77—51609
- sphere drag coeff. correlation method, continuum and rarefied flows 77—84349
- sphere in unsteady motion in liq., drag. calc. 78—67170
- spherical bearings with stone pillow blocks, friction and wear *(French)* 79—18832
- spherical cap, free translation and rot. in linear shear flow, Stokes resistance 78—26095
- spherical indentation mechanics, appl. to reversible and irreversible contact between rough surfaces 78—13976
- spinning top, on surface with friction, behaviour 79—58467
- spiral vibration of rotating shaft rubbing against interference element *(German)* 78—87252
- square cylinders, smooth/turbulent lift, drag, vortex shedding 77—89109
- stagnation point boundary layer on subliming surface with roughness elements 78—94635
- steady flow in collapsible tubes 78—57033
- steady state sliding, elementary results of dimensional analysis 77—12711
- steam-generating tube, bubble/plug flow boiling regimes, elevated press., drift vel. and void fraction determs. 78—87379
- steam-water, flow characts. at high press. 78—94805
- steel, 12KhN3A, case-hardened, friction austenite, electron diffr. obs. *(Russian)* 77—21286
- steel, 40Kh, heat-treated, wear during friction under extreme conditions 78—85007
- steel, alloy, friction surface and lubricant nature, effect on adsorption and temp. stability of lubricant layers 78—15544
- steel, alloy, friction with cast Fe, boundary and oil-abrasive, adsorption effect 80—55546
- steel, austenitic, fracture toughness effects on friction force in abrasive wear *(German)* 77—4860
- steel, austenitic, friction in vacuum of type U8 steel under microshock loading *(Russian)* 80—108583

friction continued
- steel, austenitic, martensitic transform. effect on hardening kinetics and fracture resist. of friction surface of 45Kh12G8 and 110G13 *(Russian)* 80—50727
- steel, austenitic, precipitation hardenable, friction and wear under abrasive conditions *(German)* 77—59951
- steel, austenitic stainless, friction in vac. at elevated temps. 80—55542
- steel, austenitic stainless, unlubricated, friction, wear and microstruct. of types 304, 316 and Nitronic 60 80—108589
- steel, C, 45, surface wearing ability, surface finishing method and running-in effects 80—11794
- steel, C, annealed, rolling wear under dry contact conditions 79—52391
- steel, C, friction faces, S, O content, secondary ion-ion emission obs. 80—55545
- steel, C, rubbed surface, continuous hard layer *(Japanese)* 77—52501
- steel, C, struct. changes in centres of galling 79—38985
- steel, C, wear charact. of worn surface layer under lubrication *(Japanese)* 78—35526
- steel, C and Cr, surface damage during friction, struct. effect 80—35339
- steel, C-Cr (0.6, 13 wt.%), friction during working stresses and rheological charact. at high temps. *(Russian)* 77—66702
- steel, case hardening and carbonitriding treatment, mech. props. testing *(French)* 77—59991
- steel, case-hardened cast, contact endurance rel. to austenizing *(Russian)* 78—56805
- steel, Ck 45, cylindrical bodies rolling over one another, plastic deformations caused by frictional forces 80—11735
- steel, Cr-Ni-Nb, LKh16N4B, high temp. frictional characts. 80—21118
- steel, eutectoid, wear due to impulsive friction, device for exam. 80—25957
- steel, fatigue, impact loading, friction, wear in surface active media *(Russian)* 79—29268
- steel, fatigue strength, low-cycle, under severe loading, friction-strengthening treatment effect *(Russian)* 79—52435
- steel, fatigue strength of 30 KhGSNA, 12 KhN3A, effect of friction in abrasive medium after hardening 78—35507
- steel, friction and wear during hot forging 80—89358
- steel, friction measuring test for use under conditions of high normal interfacial force 80—76454
- steel, hypoeutectic, texture development from frictional stress *(German)* 78—53003
- steel, low C, surface layer struct. under sliding friction 79—52393
- steel, mechanism of boundary lubrication with zinc dithiophosphate 79—79120
- steel, medium C (0.42 wt.%), wear charact. in unidirectional and reciprocating friction *(Japanese)* 79—100266
- steel, mild, conical rider on Cu surface plastic deform. and wear at friction junction, SEM exam. 78—88542
- steel, mild, experimental analysis of junction growth with a junction model 79—47783
- steel, Mn (13.5 wt.%) hardening mechanism during friction 79—96152
- steel, roller-bearing, high-temp. wear resistant coating treatment *(German)* 79—24629
- steel, sheet galling, development of quantitative test 78—92433
- steel, sheet structural changes during rolling influence of lubricants on friction and wear 78—95815
- steel, sintered bearing material, standardisation, wear and friction props. 78—19901
- steel, stainless, austenitic, Ni-Al, γ-phase, fracture mechanical aspects of abrasive friction, wear, chip formation 78—72865
- steel, stainless, Cr-Ni-Mo-Mn (16.55, 10.23, 2.28, 1.34 wt.%), hardfacing materials, friction characts. in high temp. Na *(Japanese)* 80—89356
- steel, stainless, sintered Kh18N10T, friction and corrosion props. for frictional units of nuclear plants 78—60845
- steel, stainless AISI 304, wear at high sliding speed 78—3237
- steel, stainless/Al laminate, sandwich sheet material, plane strain compression and rolling 79—57062
- steel, type 1Kh17N2, alloying element redistrib. during friction *(Russian)* 77—81326
- steel, type 1Kh17N2, white zone formation and props. during friction in vac. *(Russian)* 80—40542
- steel, wear resist., effect of rolling friction strengthening, oil abrasive environment *(Russian)* 79—15799
- steel, white layers forming at high rates of friction, struct. props. *(Russian)* 79—15800
- steel 45, fractional fatigue, microcrack formation in surface layers 77—86193
- steel 45-antifrictional alloys friction pairs, electrochem.-mech. investigation *(Russian)* 80—76367
- steel 9Kh18, wear resistance during friction, effect of retained austenite 77—21288
- steel AISI 1020, wear at high sliding speed 78—3237
- steel core/sheath tube system, non-fracturing core, stress transfer mechanism 77—52454
- steel matrix-bronze surface, water lubricated bearing material, manufacture, friction, corrosion and erosion 78—11341
- steel ShKh15, high C, wear tests in fuel oil, O_2 conc. effect in oil *(Russian)* 77—16694
- steel wire reinforced Portland cement mortar, wire pull out, inelastic behaviour 78—56681
- steel-polymer pair, temp. calc. under severe friction 80—40550
- steels, 110G13 and 40Kh10G10, hardening and structural transformations during friction *(Russian)* 77—52527
- steels, C, friction in liq. Sn, Rebinder effect *(Russian)* 79—29269
- steels, contact resist. in working media in static, dynamic loading, testing unit 79—15900
- steels, self lubricating composite, frictional props., Ag-Cu-Zn-Cd lubricant 78—11340
- Stellite, friction behavior in high temp. Na environment *(Japanese)* 80—40546
- stellite hardfacing materials, friction characts. in high temp. Na *(Japanese)* 80—89356
- stick-slip phenomena, mathematical model 80—16504
- stochastic quantisation, nonlinear wave eqn. 80—98825
- Stokes flow ellipsoid of min. drag, limited by cylindrical front *(French)* 79—53982
- Stokes problem for infinite vert. plate, hydromagnetic free convection effects 80—10318
- straining experiments, in situ, strong frictional force, quantitative anal. 80—100244
- strongly anisotropic rough surfaces, statistics 79—91805

friction continued
structures with convex strain energy density, friction problem, variational approach 79—27601
superlow friction effect 77—12705
supersonic flow over cones with near-critical and supercritical vertex angles 79—81918
supersonic intense gas blowing through wedge wall, dividing static press. determ. 77—84273
supersonic wave drag of planar singularity distributions 78—83430
surface analysis, appl. to lubrication problems, review *(French)* 80—45616
surface coatings, materials conservation and optimum tribological performance 80—34130
surface contacts, tribological props. 79—19469
surface friction meas. *(German)* 79—68668
surface roughness effect on abrasive wear 77—28915
surface strength, structural and energy conditions *(Russian)* 77—56111
surfaces, wear meas. using profilograph mould producing material quality factors 78—7116
surfaces meas., lubricated *(German)* 80—14643
surfactant solns., rheological props., hydraulic loss reduction in tube flow 77—65768
suspension, Brownian rotational-translational particles, at finite conc., dynamics and hydrodynamics 79—7401
suspension, hydrodynamic screening and viscous drag at finite conc. 78—35725
suspension of asbestos fibres, heat transfer and friction coeffs. for tubular flow 78—22405
teflon, microslip, effect of friction 77—77588
Teflon-4, gamma irrad., wear resistance and antifriction props. 80—7691
temperatures reached during sliding 80—16505
terrestrial gyrocompass dry friction anal. *(Russian)* 78—77899
test friction machine, exam. of design 79—52526
test machine, SMTs-2, broadening of test capabilities by modification 78—60919
test machine SMTs-2, automatic loading device 79—70257
test simulation in lubricated condition *(French)* 79—57189
tester, variable speed 80—100990
testing equipment for use at high temp. in air 78—56839
testing in various media, device 79—29319
theory, wear, new charact. of asperity interactions 77—16697
thermal desorption with large variable friction constant 78—71974
thermal pipes, sonic restriction on power at high temp. 80—103023
thermomechanical approach *(Ukrainian)* 77—68537
tidal propagation in shallow rivers, frictional forces rel. to diffusive model 79—2303
tobacco shreds, determ. of filling capacity, friction effects *(Japanese)* 78—7167
top rising by friction, exact mathematical soln. 78—83343
torque suppression in mech. stirred liqs. and multiphase systems, additives 77—3864
transient sliding motion under idealized dry friction, earthquake faulting appl. 78—34093
transients during passage from one steady state to another, role in failures 77—35096
translational friction, for arbitrary shaped objects, modified Oseen tensor calcs. 78—71311
transonic flow, two- and three-dimens., perturbation soln. method 79—1208
transonic turbulent boundary layer, Mach 0.8, skin friction reduction by slot injection 77—39309
transonic vel. profiles, local skin friction coeff. 78—67214
Tribaloy 700, hard surfacing in Na, friction, wear and corrosion 79—24628
tribology, review of current understanding 77—59066
tribology study reactor fuel element, PEC type, in Na at high temps. *(Italian)* 78—58362
tribometry development, friction reduction and meas. 80—23973
troposphere circulation in equatorial latits., role of horizontal friction 79—29821
tube, horizontal, laminar combined convection, circumferentially nonuniform heating effect 78—71331
tube banks, heat transfer, viscous flow, numerical anal. 79—55375
tube flow, drag reducing additives and sudden enlargement of diam. 79—37397
tube flow, with spiral blades, heat transfer, drag resistance 78—1672
tube wall heating during steady state tube drawing *(German)* 78—84899
turbulence, free-stream, effect on heat transfer and skin friction 78—30276
turbulence flow struct., in tube, suspended particles influence 77—75969
turbulent air flow in round tube, high-temp., friction resistance, cooling *(Russian)* 78—75135
turbulent axisymmetric boundary layer, skin friction, weak and strong disturbances effect 78—90857
turbulent boundary layer, axisymmetric body, surface roughness 78—9630
turbulent boundary layer, compressible, extended mixing length appls. 78—94655
turbulent boundary layer, drag reduction, compliant wall motion 78—22336
turbulent boundary layer, drag reduction 78—26107
turbulent boundary layer, fully rough, accelerated stability conditions 77—84240
turbulent boundary layer, large eddy destruction effect on skin friction 78—90860
turbulent boundary layer, separation region, oscillatory flow effects 78—75127
turbulent boundary layer, skin friction coeff. determ. 77—84242
turbulent boundary layer, supersonic, wall temp. effect 78—94765
turbulent boundary layer, surface friction meas. using plane Pitot tube 80—79284
turbulent boundary layer analysis for air and combustion products *(Russian)* 78—5732
turbulent boundary layer flow, drag reducing additives, 2-D channels and circular pipes 78—26167
turbulent boundary layer on rough surface with blowing, heat transfer behaviour 78—71334
turbulent boundary layer with surface roughness and injection 78—94654
turbulent compressible boundary layer on permeable rough surface with heat transfer 79—1176
turbulent drag reduction by polymer additive, mech. mixing 77—68637

friction continued
turbulent flow, drag reduction scale-up criteria 78—22330
turbulent pipe flow, fully developed, friction factors calcs. 79—98812
turbulent pulsating tube flow, friction resistance and energy losses *(Russian)* 77—51039
turbulent wall flows, struct. 78—18281
turbulent water film, with different initial flow conditions and high temp. gradients, heat transfer 78—90862
two solids in friction, thermal contact resistance, relative slipping speed effects *(French)* 79—94469
two spinning bars with Coulomb friction bearing, differential equation of motion 79—64601
two-phase channel flow with friction 78—59458
two-phase flow, compressibility effect on hydrodynamics, resistance coeff. 78—55684
two-phase flow, frictional energy dissipation, appl. to nuclear fuel assemblies *(Japanese)* 77—55074
two-phase flow, turbulent boundary layer, drag reduction 78—22414
two-phase flow, unstratified, in permeable tube, hydraulic resistance 77—35205
unilateral interface, elastic wave interactions, frictional slip effects 79—94542
unsteady pipe friction coefficients *(Japanese)* 78—14086
US inspection of friction materials 78—60931
US reflection from interface experiencing state versus dynamic friction 77—27494
variable resistance boundary layers, frictional resist. effects on motion of bodies 80—96243
variational method of investigating contact problems with slip and cohesion 78—63398
vibrating string, acceleration discontinuity propagation due to solid friction *(French)* 80—22196
viscoelastic and inelastic fluid flow past sphere, creeping and boundary layer flows, drag coeff. 77—51090
viscoelastic flow in tube, eddy diffusion reduction for heat and momentum transfer 78—22382
viscoelastic fluid, reduction of turbulent friction, rheological model 79—86408
viscoelastic fluid, turbulent flow, frictional drag reduction 78—1696
viscoelastic liquid steady flow about porous rotating disc 79—32586
viscoplastic liquid film on vertical vibr. wall, with slip, shaking loose 78—59371
viscous liquid, logarithmic equations for resistance of turbulent friction 77—51042
viscous liquid flow through annular clearance over rotating inner cylinder 80—64626
vortex chamber, friction losses on end walls, Kantorovich method 77—47021
water bodies, contained, surface friction vel. rel. to wind-induced drift 79—48512
water surface, free, roughness determ., from air flow struct. anal. 78—63441
water-entrained gas flow, force on moving body 78—63480
wave propagation in rocks, frictional attenuation, amplitude depend. 80—31034
wear and friction, material aspects in manufacturing processes 80—81210
wear frictional heating and oxidational theory 80—44255
wear mechanism review 78—72891
wear of specimens on friction machine, device for continuous recording 80—55604
wear resistance, surface treatments, selection procedure, review 78—72892
wear tests with plastic lubricants, friction machine attachment 78—3273
Westerly granite, high temp. frictional sliding mechanisms 78—73357
wheel temperature in railroad service, effect of brake shoes 80—93660
wind tunnel, low-Reynolds-number turbulent boundary layers 80—1556
wing, rectangular, with tip clearance in channel, aerodynamic characts. 78—59415
wing, swept, 3-dimens. turbulent boundary layer, numerical anal. 80—1621
wood cutting, stress distrib. and frictional coeff. at tool-chip interface, specific gravity effect *(Japanese)* 80—1492
wood-metal interface 77—1167
wool fibre, directional friction obs. by capstan method 78—19899
zinc dialkyldithiophosphate surface film, prep. and nature 80—104300
Ag alloy, wear resistance, internal oxide effect *(French)* 77—52503
Ag, cold rolling, inhomogeneous texture 80—89251
Ag, electrical contact material with liquid lubricant, prod. and appl. 78—10559
Ag, sliding charact., friction and wear *(Japanese)* 78—56778
Al alloy matrix, reinforced with fibrous and particulate nonmetals, wear, friction 77—4758
Al, cold rolling, inhomogeneous texture 80—89251
Al, experimental analysis of junction growth with a junction model 79—47783
Al FCC single crystal, crystal rotation accompanying scratch deform. *(Japanese)* 79—15733
Al, surface subjected to friction, wear, exoelectron emission, rel. to O_2, H_2O, gaseous adsorpt. 79—1816
Al, thin foil, adhesion and friction, rel. to observed dislocation density 78—64706
Al, tribological investigation using two-cylinder tribometer *(German)* 77—25164
Al, wear volume/sliding time relationship 79—61743
Al-graphite particulate composite, exam. of friction, wear and tensile props. 78—72890
Al-Mg (2.2 at.%), high temp. creep mech. determ. by stress-relaxation 77—12670
Al-Si-Cu-Ni alloy casting, thermal props. 78—95814
Al_2O_3(-TiO_2) coatings, detonation deposited on steel, prep., wear resist., antifriction props. 78—60877
Au film, ion plated, defect growth structs., SEM obs., and effect on mech. props. 80—24768
Au, friction props. of surface films in air and high vacuum 78—60850
Au, sliding charact., friction and wear *(Japanese)* 78—56778
B coating on steel 45, effect of abrasive particle size on wear 78—44225
B-Cu(Al) coating on steel 45, effect of abrasive particle size on wear 78—44225
BC, sintered and hot pressed, friction and wear, 20 to 1500°C 78—60844

friction continued
- BN, pyrolytic, in contact with various metals, friction and transfer behaviour 78−88535
- BO_2, laser saturation spatial spectroscopy of diffusion coeff., interaction pot. 77−75341
- C diamondlike layers, RF plasma deposited, frictional props. 80−71762
- C fibre, expt. and ahesion theory 77−1877
- C fibre reinforced PTFE and polyacetal, friction and wear against glass and steel 78−56783
- C fibre reinforced polyethylene matrix, ultra high molecular weight, wear limit, γ-irradiated and unirradiated *(Japanese)* 78−27649
- C fibre rubbing on rotating cylinder, friction and wear 77−52498
- C, ion-plated, on metal, deposition method, graphitic struct., and tribological props. 78−11440
- C materials, graphitised and ungraphitised, in P_2O_5 vapour, 300-600°C 79−79116
- $(CF_x)_n$ rubbed films applied to different finished surfaces, obs. 79−83332
- CO_2, viscosity rel. to ionis., skin friction of wetted oscill. disc 78−34252
- Cd film, dry lubrication on C steel, tribological behaviour 80−89364
- Co base alloys, unlubricated, adhesive wear study 80−108593
- Cr, sliding charact., friction and wear *(Japanese)* 78−56778
- Cr_3C_2, $Cr_{23}C_6$, plasma sprayed coatings for gas-cooled reactor appl. 79−24676
- Cr_3C_2-Ni, friction and wear, 20-1000°C 80−30112
- Cu, FCC single crystal, crystal rotation accompanying scratch deform. *(Japanese)* 79−15733
- Cu film, ion plated, defect growth structs., SEM obs., and effect on mech. props. 80−24768
- Cu, friction and prow form. in scratch process by diamond cone 78−11349
- Cu, friction mechanism, HV TEM expts. 80−35341
- Cu, friction props. of surface films in air and high vacuum 78−60850
- Cu, friction surface structural investigation, O_2 surface diffusion *(Russian)* 80−96726
- Cu, friction under electrolyte immersion condition 78−64738
- Cu, mechanical twinning in (110)[$\bar{1}$12] single crystal under plane strain compression *(German)* 77−36616
- Cu pin against steel ring, dry sliding wear, role of dynamic recrystallisation 80−108599
- Cu pin-on-disc friction and wear under boundary lubrication, dissolved O_2 effect 80−76365
- Cu, single crystal, fatigue and fretting initiated fatigue, crystallographic orientation effect 77−70182
- Cu single crystals, influence of friction and geometry of deformation, on texture inhomogeneities during rolling 78−72792
- Cu, sintered strip, external friction of rolling 77−1845
- Cu, sliding charact., friction and wear *(Japanese)* 78−56778
- Cu solid soln., wear 78−3233
- Cu surface, interacting mechanisms with organic sulphides rel. to friction and lubrication behaviour 80−45546
- Cu surface subjected to friction, wear, exoelectron emission, rel. to O_2, H_2O, gaseous adsorpt. 79−1816
- Cu, tribological investigation using two-cylinder tribometer *(German)* 77−25164
- Cu, wear volume/sliding time relationship 79−61743
- Cu-Al(Sn), effect of Al and Sn on friction and wear 78−11348
- Cu-C bushings, powder metallurgically prepared, exam. of friction and wear charact. 79−15813
- Cu-Cu pair, He environment 4.2-80K 78−48543
- Cu-ferrous alloy, hard inclusion composite exam. of wear resistance props. 79−34153
- Cu-graphite brushes, friction and wear under severe sliding conditions against steel 79−38991
- Cu-graphite starter brushes, effect of high velocities, current densities on wear, friction 78−88544
- Cu-M alloys (M=Zn,Al,Sn,Mn,Pb), diffusive redistrib. during friction *(Russian)* 78−52999
- Cu-Sn industrial bronzes, Sn diffusion in deform. zone influence on wear resistance, friction *(Russian)* 80−108582
- Cu-Sn-P (5, 1-5 wt.%), effect of P on friction and wear characts. 80−16494
- Cu-Sn-Pb-Fe-graphite, bronze-based, sintered alloy, silica additions effect 77−63807
- Cu-steel and Cu-brass system, realisation of selective transport mode with friction, effects of normal stresses 79−87735
- Cu-TiC precipitation hardened composite, struct. effect on friction 78−11337
- Fe alloy granule reinforced Cu M2 wear resistance in rubbing with lubrication 80−16490
- Fe alloy granule reinforced Cu, friction in vacuum 80−25880
- Fe alloy granules in Cu binder, exam. of wear characteristics without lubrication 79−96154
- Fe and Fe-Cr alloys, friction behaviour in oxygen, development of wear-protective oxides and influence on sliding friction 80−30111
- Fe, Armco, friction in vac. at elevated temps. 80−55542
- Fe, cast, sintered, friction and wear 79−91806
- Fe, cast, wear mechanism of friction couples 79−83329
- Fe, cast, wear resist., effect of rolling friction strengthening, oil abrasive environment *(Russian)* 79−15799
- Fe, friction at elevated temps. 78−15548
- Fe, friction in liq. Sn, Rebinder effect *(Russian)* 79−29269
- Fe, friction props. of surface films in air and high vacuum 78−60850
- Fe, grey cast, friction and wear, phosphating effect 77−70190
- Fe powder compact, apparent density, mixing, and friction, zinc stearate lubricant effect 80−45403
- Fe, sintered, friction and wear 77−59946
- Fe surface, interacting mechanisms with organic sulphides rel. to friction and lubrication behaviour 80−45546
- Fe, surface subjected to friction, wear, exoelectron emission, rel. to O_2, H_2O, gaseous adsorpt. 79−1816
- Fe, wear of surface due to friction, surface hardening 78−44227
- Fe-(Mo)-CaF_2, sintered, friction and corrosion props. for frictional units of nuclear plants 78−60845
- Fe-based materials, wear resistance, surface hardening processes, review 78−72894
- Fe-based sintered friction material, wear rate, depend. of phase struct. 79−15801
- Fe-C-Pb, sintered, antifriction props., Pb introduction effect 79−96155
- Fe-Cr, friction and wear in controlled environment, effect of sliding mode and specimen geometry 78−15542

friction continued
- Fe-Cr, friction at elevated temps. 78−15548
- Fe-Cr (5 wt.%), friction and wear in controlled environments, oxide film effect 78−15546
- Fe-Cr-Mo-C, X-ray investigation after friction and oxidation 78−52997
- Fe-Cu-Ni-Cr_3C_2-C based sintered friction material, wear, surface geometry and struct. effects 80−25875
- Fe-glass porous material, wear resist. under dry friction 80−25876
- Fe-MoS_2, exam. of props., using differential thermal analysis, and metallography *(Russian)* 79−15653
- Fe-P, sintered frictional material, friction and wear rubbing pair under moderate load 77−21208
- Fe-P base frictional material, sintered, friction and wear under moderate load 77−12704
- Fe-P(S) sintered materials, antifriction props. 79−24626
- FeO compacted powder, effect of wall groove orientation and wall lubricants, on WC wall friction 78−23831
- Fe_2O_3, plasma sputtered coatings, oxide dissociation, coating props., struct. and composition *(Russian)* 80−54577
- Fe_2O_3, powder, compression in moulds, meas. apparatus *(Dutch)* 77−44205
- Ge, supecond, friction layer formed during friction between Ge and Pb *(Russian)* 78−52143
- Ge-Ge (Sn) friction pairs, elec. cond. of Ge tribolayers at He temp. 79−87140
- He, flow, of liq.-vap. mixture, frictional press. drop, adiabatic and heated conditions 78−90983
- He, near-critical, friction factors for flow in curved tubes 78−83367
- HfC-HfB_2 alloys, wear in vacuum, role of boride phase 80−21113
- HfC-$HfBr_2$, preparation and high temp. antifriction props. 79−1918
- I_2, laser saturation spatial spectroscopy of diffusion coeff., interaction pot. 77−75341
- In film, friction and fear in ultrahigh vacuum, effects of speed, film thickness and substrate surface roughness 79−20202
- LiF, mech. excitation, luminesc. electron emission, friction, static electrification, meas. method *(German)* 77−24904
- MgO single crystal, wear and friction on sintered Al_2O_3 in vacuum 77−12710
- Mn cast Fe, W effect on transform. in thin surface layers during dry sliding friction 77−21289
- Mo sintered composite, MoS_2 containing, friction and wear props. 80−11786
- Mo-Mo pair, He environment 4.2-80K 78−48543
- MoS_2, friction coeff. temp. depend., 300 to 80K 77−35631
- MoS_2, lubricating properties in CO_2 medium 77−86194
- MoS_2, RF sputtered layers with variable stoichiometry, lubrication props. 80−40557
- MoS_2, self-propag. high-temp. synthesis, wear props. 80−2975
- MoS_2, sliding charact., friction and wear *(Japanese)* 78−56778
- MoS_2 solid lubricant, antifriction and elec. props. depend. on oxidation temp., dopant influence 80−108584
- $MoS_2(Se_2)(Te_2)$ coatings, growth kinetics and friction coeffs. 77−16731
- N_2, viscosity rel. to ionis., skin friction of wetted oscill. disc 78−34252
- N_2O_4, dissoc. flow in tube, heat transfer and drag 78−71402
- N_2O_4, dissociating, turbulent pipe flow, heat transfer, resistance 78−91026
- Na, liq., in vert. pipe, hydraulic resistance under boiling conditions 78−90968
- Na_2O-SiO_2 glass, coated with SnO coeff. of friction and fracture toughness 78−80657
- Nb-Nb pair, He environment 4.2-80K 78−48543
- $NbSe_2$ solid lubricant, antifriction and elec. props. depend. on oxidation temp., dopant influence 80−108584
- Ni base alloys, unlubricated, adhesive wear study 80−108593
- Ni, sliding charact., friction and wear *(Japanese)* 78−56778
- Ni, surface subjected to friction, wear, exoelectron emission, rel. to O_2, H_2O, gaseous adsorpt. 79−1816
- Ni-base superalloy, ⟨111⟩ monocrystals under compression, inhomogeneous deformation 77−63736
- Ni-Cr (20 wt.%), high temp. frictional characts. 80−21118
- Ni-Cr (20 wt.%) alloy LNKh, room-temp. friction characts. 80−25874
- Ni-SiC(WC), dispersion hardened coating, chemically deposited using electroless baths, exam. of protection props. 79−34208
- Ni-Zn ferrites, hot-pressed, key props. 78−15348
- NiCr-AlY sintered fibre metal struct. abradable seal material, friction and wear 78−56785
- O_2, viscosity rel. to ionis., skin friction of wetted oscill. disc 78−34252
- Pb film, friction and fear in ultrahigh vacuum, effects of speed, film thickness and substrate surface roughness 79−20202
- Pb, friction, wear in supercond., normal states *(Russian)* 78−39914
- Pb, pure, friction stress for high temp. creep 78−11289
- Pb-Pb pair, He environment 4.2-80K 78−48543
- Pb-Sb, improvement in antifriction layer props. by impulse discharge, impulse discharge treatment *(Russian)* 79−1917
- Se, amorphous, friction and wear under lightly loaded contact 78−64740
- SiC abrasive papers, frictional force amplitude effect on degradation 79−74264
- SiC, single cryst., friction and wear behaviour in sliding contact with various metals 80−21112
- SiC single crystal, friction and fracture in contact with itself and Ti 80−11780
- SiC single crystals, friction, deform., and fracture, crystal orientation effect 79−96150
- Sn, sputtered film, exam. of frictional props. 79−15814
- TaC-TaB_2, exam. of high temp. friction and wear, and deformation behaviour 79−34152
- Ti alloy, VT3-1, vacuum-chromized, fretting-corrosion in couple with unprotected BT3-1 and steel 40KhNMA *(Russian)* 78−56804
- Ti alloy VT1-0, wear resistant coated, metallic and intermetallic, electrospark applied *(Russian)* 79−1916
- Ti alloys, lubrication by chloroparaffins, friction and wear *(Russian)* 80−93657
- Ti, antifriction props. 77−90467
- Ti base composite sintered bearing materials, metallic solid lubricant infiltrated, antifriction props. 80−60981
- Ti, friction surface structural investigation, O_2 surface diffusion *(Russian)* 80−96726
- Ti, tribological investigation using two-cylinder tribometer *(German)* 77−25164
- Ti, wear and corrosion resistance, effect of surface alloying with Nb and Si *(Russian)* 77−25191

friction continued
- Ti, wear at high sliding speed 78−3237
- Ti-Al-V (6, 4 wt.%), friction characts. improvement by O_2 dissolution and controlled surface hardening *(French)* 80−45401
- Ti-Al-V alloy, friction coeff. reduction on injection with TiC particles 80−85086
- Ti-bronze, friction with diamond, characts. 78−48541
- Ti-Cr, sintered, friction and wear, structural factors 78−60843
- Ti-Cr-TiC, sintered, friction and wear, structural factors 78−60843
- Ti-Mg-ZrC(HfC)(TiC)(TiB_2) sintered, friction and wear props. 79−70019
- Ti-TiC system, sintered, friction and wear, structural factors 78−60843
- Ti-Zr-Nb-Si, Nb and Si surface alloying effects on wear and corrosion resistance *(Russian)* 77−25191
- TiC coatings, RF sputtered, on 440-C steel, adherence, friction, and wear props. 79−47823
- TiC, frictional characts. and contact-zone deform. in homogeneity range 80−66673
- TiC reactively sputtered coatings on Ni-Cr-Mo-Ti (19,11,3 wt.%), adherence, XPES and wear study 80−25565
- TiC-Ni-Mo hard alloy, wear resistance under end face friction cond. 78−60846
- TiC-TiB_2, friction characts., comp. depend., 20-1000°C 80−3203
- TiC-TiB_2, preparation and high temp. antifriction props. 79−1918
- TiC-TiB_2, strength and antifriction props. over wider range of concs. 80−50673
- TiC-TiB_2 alloys, wear in vacuum, role of boride phase 80−21113
- UO_2 powder compaction, friction between particles and die walls 80−71620
- WC cutting tools, TiN, TiC coated, frictional characts. 79−20218
- WC-Co (15 wt.%), alloy VK15 coating on Ti-Al, detonation sprayed, antifriction props. 80−21188
- WC-Co hard alloys, hot-pressed, wear resist. under abrasive friction, heat treatment effect 80−66555
- WC-Co sputter deposited film, friction and wear 78−72918
- WS_2, self-propag. high-temp. synthesis, wear props. 80−2975
- WS_2 solid lubricant, antifriction and elec. props. depend. on oxidation temp., dopant influence 80−108584
- WS_2-NbS_2 system, compds., elec., antifriction props. 79−38066
- WSe_2, lubricant, prep. by self-propagating high-temp. synthesis, technological characts. 78−35338
- Zn-glass, friction, loading time effect *(Japanese)* 78−34095
- ZrC-ZrB_2, friction characts., comp. depend., 20-1400°C 80−3203
- ZrC-ZrB_2, preparation and high temp. antifriction props. 79−1918
- ZrC-ZrB_2, strength and antifriction props. over wider range of concs. 80−50673
- ZrC-ZrB_2 alloys, wear in vacuum, role of boride phase 80−21113

friction, internal *see internal friction*

frictional electricity *see triboelectricity*

FSK *see frequency shift keying*

fuel
- *see also coal; fission reactor fuel; pulverised fuels*
- 100 MW fluidised bed combustion district heating plant burning high S content residual oils 80−108777
- alcohol, diesel engines auxiliary fuels 80−61230
- alcohol, ethanol and methanol, fuel for vehicles, gas turbines, and boilers, Brazil 80−61229
- alcohol fermentation, octane booster for inferior regular unleaded gasoline 80−55783
- alcohol fuel production, practical aspects of a fractional distillation column 80−55774
- alcohol fuel production from biomass 80−55773
- alcohol fuel production from wood, Brazil, ethanol and methanol 80−30328
- atactic polypropylene waste, pyrolytic conversion to fuel oil 80−35627
- biochemistry and biotechnology, conf., Helsinki, Finland, 27-31 Aug. 1979 80−57001
- biomass, an alternative to fossil hydrocarbons 79−87985
- biomass, H_2 production from water using biomass feedstock and bromination process 80−61459
- biomass and peat, utility fuel cells development 79−52930
- biomass energy R and D 80−66922
- biomass options for the Big Island of Hawaii 80−66921
- black locust biomass, surface mine reclamation 80−7894
- boiler, sawdust waste of timber mills *(German)* 80−40805
- Boston, air quality during fuel shortage 77−64424
- chrysler's electronic lean burn system 80−16868
- coal, fluidised bed gasification, power generation fuel gas manufacture for combined cycle gas turbines 80−26104
- coal gasification, potential fuel source 80−93842
- coke, metallurgical, microstruct., using refl. light microscopy and image anal. 80−66732
- combustion, flame propagation through stratified charge combustion channel, model 79−64795
- combustion, NO_x and SO_2 form., oxidizing agent excess depend., thermodynamic anal. 78−15677
- condensed, combustion and extinction in stagnation pt. boundary layer 79−29356
- conservation, concept of available work, utilisation factor 80−35629
- droplet evaporation at elevated press. and temp., math. model investig. 77−52675
- droplet on hot surface, evap. and ignition 79−96310
- droplet on hot surface, evap. and ignition 79−96311
- droplets, mathematical models of transient heat flow 79−18673
- drops, liquid, blast wave initiated detonation waves 79−64691
- electricity/fuel substitution coefficients, energy units and balance sheets *(French, English)* 79−92053
- energy-political questions nationally and internationally for West Germany *(German)* 80−101072
- ethanol, as petrol substitute, increased use in USA *(Dutch)* 80−72004
- ethanol fuel production from municipal cellulosic wastes using enzymatic hydrolysis 80−55779
- fluidised bed combustor, control and instrumentation 80−30350
- fossil, appl. of cross-polarisation ^{13}C NMR with magic angle spinning 80−77819
- fossil, combustion in atm., effect of CO_2 on climate 79−2359
- fossil fuel fired power plants, standardisation, feasibility, advantages, limitations 80−16775
- fossil fuel in situ extraction, US DOE R and D program 80−40814

fuel continued
- fossil fuel use consequences, atmospheric CO_2 concentration increase 80−12041
- fossil fuel utilisation, reliability, maintainability and availability engineering 80−61234
- fossil fuel vs. wood as source of atm. CO_2 excess 77−53162
- fossil fuels, global distribution *(French)* 80−16770
- fossil fuels for use in MHD power stations 80−72074
- French energy research projects *(French)* 79−74497
- furnace combustion chamber and radiative transfer, fuel substitution effects, review 79−3903
- fusion reactors for synthetic fuels 80−13793
- future reserves, projections to 2050 *(Dutch)* 80−61221
- gas field performance anal., effect of formation compressibility and edge water encroachment 80−30355
- gas research with a view to energy savings in France *(French)* 79−39272
- gasdynamics of explosions, reactive systems, conf., Stockholm, Sweden (Aug. 1977) 79−64690
- gasohol, appl. to improving octane rating of unleaded petrol 80−30329
- gasoline consumption, structural/econometric model 79−79366
- H production, theoretical design of solar engine 80−30598
- health hazards from alternative electricity generation fuel cycles 78−11791
- household fuel uses, ORNL model 79−79387
- hydrocarbon fuels combustion prod. plasma with alkali impurity, elec. cond. 79−55466
- hydrogen fuels, safety aspects of a future hydrogen technology 79−74551
- kerosene, combustion in air rel. to press. 3-15 $kgf.cm^{-2}$ 79−66297
- liquid, blend of recycled alcohols, mineral spirits, solvents and other combustible liquids 80−55782
- liquid, coal derived, direct appl. to power generation 79−48056
- liquid and gaseous, from waste, technology and economics, critical analysis 80−7893
- liquid fuel supplies and synthetic fuel prod. 80−97753
- liquid fuels from biomass, biotechnology appls. 80−61225
- liquid H_2 fuel for commercial aircraft, production and liquefaction facilities 80−45818
- methane, production process in context of Nuclear Long Distance Energy System *(German)* 80−3483
- methane as fuel, solid state storage device study using physisorption data *(German)* 79−96414
- methane production from cellulose by sewage bacteria 80−72005
- methanol derivation from lignite, fuel appl. 80−61223
- MHD generator combustion products plasma with mixed alkali impurities, elec. cond. calc. 79−86621
- motor fuel prod. from plants, technical and economic feasibility *(French)* 80−3479
- natural gas demand forecasting in California 79−79367
- natural gas tunnel burner, heat transfer, computer model predictions test 78−59504
- oil, multi-dimens. simulation of flow nonuniformities in fissured porous media 80−28559
- oil, shale, in-situ oil recovery projects 79−87953
- oil, shale, Michigan Antrim, simulated in situ retorting 79−87954
- oil, shale, true in situ fracturing 79−87955
- oil, shale research outlook 79−87952
- oil demand projections to 1985, review 80−3482
- oil recovery from Utah tar sand deposit, by in situ combustion 79−48046
- oil resources in US, estimation of undiscovered sites 80−21361
- oil shale, in situ retorts, computer simulation of ignition with hot inert gas 80−30356
- oil shale, in situ technological developments, review 80−30354
- oil shale retort dispersion, effect of particle size distrib. and flow nonuniformities 80−28560
- oil shale retort flow nonuniformities c.f. numerical predictions 80−28492
- oil-shale, resource, Colorado's Green River Formation, vertical modified in-situ processes 79−48049
- oils, shale, from five different sources, comparison w.r.t. boiling-point composition, elemental content and physical properties 79−48050
- organic fuel prep. by CO_2 reduction using photoelectrochem. solar cells 80−55880
- peat, resources in United States 80−40806
- peat gasification process for synthetic fuel prod. 80−30340
- petrol, prod. via $ZnCl_2$ hydrocracking of solvent refined coal 80−30333
- petrol utilisation for transportation in USA, econometric anal. 80−3477
- petroleum, world oil markets and the business cycle 80−21359
- petroleum fractions from USSR fields, isobaric integral heats of condensation *(Russian)* 79−65181
- petroleum samples, extinction coeff., refractive index meas., 0.25-25 microns 79−65818
- petroleum spills on water, control using gellants 80−61496
- petroleum-acetylene-O_2 combustion products, seeded, elec. cond., for MHD power plant 78−34256
- polymer interrelations, raw material 80−63876
- PVC/coal blends, fluidized bed combustion of plastic waste with coal, removal of HCl 80−30347
- quiescent fuel mists, ignition and flame quenching 79−8437
- refuse derived, conversion to elect. energy at St. Louis refuse fuel demonstration project 80−93846
- resources and future prospects, 1970s trends 79−57347
- rocket propellants, thermodynamic evolution, extension of Huff's method 78−75054
- smoke plumes SO_2 conversion *(Dutch)* 77−70825
- solid propellant stress transducer evaluation 80−81245
- solid waste utilization in integrated community energy systems 79−100359
- steam-gas system, joint use of nucl. and organic fuels 80−40807
- substitute fuel prospects *(French)* 79−92055
- supply, implications for national defence, social, economic and political well-being 80−3500
- synthetic and fissile fuel prod. by Cat-D fueled SAFFIRE reactors 80−99280
- synthetic fuel, alternative programmes, decision anal. 79−83548
- synthetic fuel development in New Zealand 80−21357
- synthetic fuel manufacture using peat 80−97754
- synthetic fuel prod. by direct radiolysis using fusion radiation sources 80−61227
- synthetic fuel production, environmental effects 80−21417

fuel continued
- synthetic fuel production, falling-bed high temp. fusion blanket design 80−13814
- synthetic fuel production from fusion, economic prod. pot. 77−34467
- synthetic fuel production in a particle-beam driven fusion reactor 80−55780
- synthetic fuels from peat gasification 80−30340
- synthetic fuels from wood, gasification of biomass in developing countries 80−61231
- synthetic fuels R&D and electric power 80−35624
- synthetic liquid fuel production using high temp. gas cooled fission reactor 80−55781
- transportation effects, public, future outlook 80−35621
- tree form energy plantations, woodchip transport and handling 80−30327
- UK policy suggestions for future, coal to oil and gas conversion, nuclear power 80−61224
- undersea resources and related topics, world-wide survey 80−35622
- USSR and Eastern Europe resources, production, consumption and imports and exports forecasts 80−26100
- waste heat utilisation, opportunities and potential 80−35628
- waste materials as fuels, refuse derived fuels, pyrolysis, hydrolysis, fluidised beds 80−66920
- wood, hybrid poplar, direct hydrogenation to liq. and gaseous fuels 79−87945
- wood, model for gasification process 79−61937
- wood energy in W.Virginia 80−72006
- wood energy program; industrial, New England 80−61233
- wood fuel resource, coordinated energy sources for production of heat, steam, electricity 80−61232
- wood gasification using fluidized bed wood gasifier 80−30348
- wood sawdust, flash pyrolysis, cyclone, solar gas-solid chemical reactor *(French)* 80−61296
- wood waste gasification using flash pyrolysis and concentrated solar energy *(French)* 80−61226
- wood waste processing, gasifier design and construction 80−7895
- wood-burning in heating plants, calorific values *(German)* 80−40815
- wood-waste fired power plants, economic feasibility anal. 80−66923
- worldwide energy prospects, synthesis of studies published in 1976 and 1977 *(French)* 79−29443
- C-based fuel production by CO_2 thermochem. reduction using solar energy 80−76610
- H, electrolytic prod. by ocean thermal energy conversion 80−30546
- H fuel, health benefits derived from a planned hydrogen community 80−55947
- H fuel storage and distrib. for automotive vehicles, techno-economic feasibility study 80−45820
- H, produced by photolysis of H_2O *(French)* 80−55776
- H production by H_2O dissociation using solar energy 80−30597
- H production by H_2O electrolytic dissociation, review 80−30429
- H production by H_2O photocatalysis on TiO_2 using solid C 80−26150
- H production by seawater electrolysis utilisation of ocean hydropower systems 80−30374
- H production from radioactive waste heat and utilisation in gas turbines 80−30326
- H production using nuclear process heat from HTRs 80−30595
- H storage, transmission and distribution, review 80−30596
- H storage in metal hydrides 80−61445
- H, survey of liquid hydrogen container technology for highway vehicle fuel system applications 80−30607
- H-rich synthetic fuel prod. and transportation for solar energy utilisation 80−51015
- H_2 as an energy source 80−108816
- H_2 automotive fuel, technico-economic feasibility of storage, transportation, distrib. 80−16766
- H_2, electronic fuel injection techniques for H_2-powered internal combustion engines 80−45622
- H_2 for single cylinder diesel engines 80−61228
- H_2 fuel, safety anal. 79−74552
- H_2 fuelled aircraft, kinetic model anal. of pollution 80−40816
- H_2 fuelled vehicles, design and engine modifications with Fe-Ti hydride storage 80−40925
- H_2 generation for automotive appls. utilising gas permeation and steam-on-iron processes 80−55778
- H_2 internal combustion engines, electronic fuel injection techniques 80−72094
- H_2, liquid automobile fuel, cryogenic storage, and semiautomatic refueling station 80−40926
- H_2 photocatalytic production by carbohydrate conversion using $RuO_2/TiO_2/Pt$ photocatalyst powder 80−94120
- H_2 production, electrolysis of steam, high temperature, in fusion reactors, synfuel production 80−72099
- H_2 production, high temperature fusion blanket design for synthetic fuel plant 80−99275
- H_2 production by water electrolysis, economics and technology *(French)* 79−100543
- H_2 production from coal by centrifugal separation from gasification products 80−76643
- H_2, storage as metal hydrides, props. and appls. 80−76661
- H_2, storage in form of metal hydrides 80−72096
- H_2, synthetic fuel production, Tokamak high-temp. blanket 78−74479
- H_2/hydrocarbon fuel prod. via biomass conversion wastes by solar H_2O photoelectrolysis 80−89653
- H_2+O_2 fuel, equilib. compositions, 1000 to 6000K *(Ukrainian)* 79−50571

fuel batteries *see fuel cells*

fuel cells
- 1 kW battery using methanol and methane, development and thermodynamic layout *(German)* 80−3510
- anode, electrochemical oxidation of H_2 and CO in fused alkali metal carbonates 80−72040
- battery voltage stabilisation on basis of electrolyte, stabilisation methods *(Russian)* 79−70467
- biofuel cell, pacemaker power supply, dog implants 77−52935
- biogalvanic and biofuel cells, animal expts. 77−81657
- biogalvanic implanted pacemaker performance 77−81732
- cathodes, voltage losses 80−104503
- ceramic materials appl., fireproof *(Czech)* 79−70455
- development status and prospects *(French)* 79−79389
- development trends and appls. 80−35672

fuel cells continued
- developments in electrochemical energy sources *(German)* 80−97770
- electric power generation, H_3PO_4 and molten carbonate fuel cell developments 80−66966
- electric vehicle power sources, fuel cell/secondary battery hybrid appls. *(Dutch)* 80−72037
- electrocatalytic O_2 reduction mechanism with metal chelate coating 78−23951
- Electrochemical Society Meeting, Boston, USA, (May, 1979) 79−91959
- electrochemistry, power sources and energy science 80−101023
- electrode performance with H_2SO_4 electrolyte, WC and iron phthalocyanine 80−21293
- formamide oxidation at Pt alloy catalytic electrodes 79−57245
- harnessing tomorrow's energy sources, prospects 79−100484
- high-temperature meas. using pellet sample holder 79−88928
- history of development 79−70448
- honeycomb-type structures for high power batteries and fuel cells, possible use 80−72027
- hydrazine, long life, with high reliability and easy maintenance *(Japanese)* 79−83590
- implantable, effect of O_2 on Pt black anode 77−60309
- materials needs, in energy conservation and storage 80−66958
- methanol-air, 50 W, with hydrophobic air electrodes 80−89609
- methanol-air fuel cells, methanol oxidation mechanisms at Pt electrodes in acid electrolytes 80−45661
- molten carbonate, development of S-tolerant compounds 80−72039
- molten carbonate, effect of temp. and press. on fuel gas comp. and cell perform. 80−30474
- molten carbonate, scaled-up, performance and current distrib. model 80−55837
- molten carbonate, thermal stability of $LiAlO_2$ matrix support material 80−50952
- molten carbonate fuel cell, electrolyte comp. effect on electrode kinetics 80−101092
- molten carbonate fuel cell based, coal fired power plants for electric power generation 80−30471
- molten carbonate fuel cell gas seal, corrosion protection using $LiAlO_2$ coating on stainless steel 79−39293
- molten carbonate fuel cell performance, H_2S effect, mixed pot. anal. 80−81431
- molten carbonate fuel cell performance model for cycle studies 80−30473
- molten carbonate fuel cell power plant, eng. development 80−66969
- molten carbonate fuel cell systems development program 80−30469
- nonequilibrium thermodynamics, heat release mechanisms and voltage 80−45660
- operating principles and uses, catalyst choice 80−35671
- output voltage stabilisation theory *(Russian)* 80−3511
- oxygen electrodes, galvanostatic switching curve shapes 80−66965
- power plant, economics 79−57424
- power plant development and commercialisation program 80−16797
- power plants for utility appls. 80−66967
- power station, 4.8 MW DC 80−89608
- reactor-condenser systems, thermal operating regimes selection 79−87987
- rechargeable fuel cell battery output power stabilisation theory 80−35674
- refractory oxide layer growth by high-temp. electrochemical vapour deposition 78−23627
- semiconductor p-n junction, conversion of chem. energy into elec. power thermodynamic props. 79−11219
- solid electrolyte fuel cell for electric utility power generation 80−30470
- space power systems, 1979 state of art and development trends 79−100506
- space power systems appls. 80−30465
- trifluoromethanesulphonic acid monohydrate, electrochemical props. and use as fuel cell 79−61969
- types and construction principles *(Dutch)* 80−72038
- utility, for biomass fuel, Swedish development 79−52930
- vehicle propulsion appls. technical and economic eval. 80−30475
- vehicular use, Fiat research, Italy 80−35673
- C gas-diffusion O_2 electrode in acid, electrochem. performance 78−31652
- H-Cl electrochemically regenerative fuel cell, electrode kinetics and cell perform. 80−89610
- H-O, with self-control of external humidity exchange, operation analysis 79−34429
- H_2-air alkaline fuel cell system, applications and prospects 80−40854
- H_2-air fuel cell with proton conducting solid electrolytes, performance meas. 80−16796
- H_2-air-H_3PO_4 fuel cell performance, effect of NH_3 80−108795
- H_3PO_4, assessment of alternative fuel cell designs for residential and commercial cogeneration 80−66970
- H_3PO_4, fuel cell efficiency 80−30472
- H_3PO_4 fuel cell power plant with high temp. steam reforming and autothermal reforming 80−30466
- H_3PO_4 fuel cell scale-up for prod. of low-cost stacks 80−30467
- H_3PO_4 fuel cells, commercial prototype plant for dispersed electric power generation 80−66968
- H_3PO_4 fuel cells, technology development for commercial systems, review 80−30464
- H_3PO_4, heat transfer 79−48121
- H_3PO_4, technology advances w.r.t. cost reduction 79−48122
- H_3PO_4, with WC anodes and C/Pt cathodes 80−30468
- $HUO_2PO_4.4H_2O$, rapid H^+ cond. 77−76602
- $LaAlO_3$ perovskite electrolytes for high-temp. fuel cells 79−29467
- $LiAlO_2$, fine particle size, heat treatment synthesis, molten carbonate fuel cell appl. 80−21395
- $LiAlO_2$, fuel cell electrolyte matrix, prep. and struct. characts. 78−80488
- molten carbonate fuel cell efficiency 80−30472
- NH_3 high temperature solid electrolyte, overpot. and product selectivity characts. 80−104504
- Ni catalysts, thermoanalytic investigation *(German)* 79−74420
- Ni powder, sintered, use of extruded porous materials as fuel cell electrodes 80−40853
- Ni-H_2 sealed storage battery, characts., charging, transient, stationary regimes 77−63930
- O_2 electrodes, galvanostatic transients, curve shape, 0 to 5 msec. 80−93868

fuel cells continued
- Pt and Pt/Ru electrocatalysts for methanol oxidisation in acid electrolyte with improved steady state activity for fuel cell appls. 80—76629
- Pt electrode O_2 reduction kinetics in conc. H_3PO_4, H_2SO_4 and $HClO_4$ 78—23952
- Pt, on C electrode, surface area loss in H_3PO_4 80—101091
- S-tolerant components development for molten carbonate cell 80—89611

fugacity
- *see also kinetic theory of gases*
- adsorbed monolayer, effective two particle potential 79—11012
- Angra dos Reis meteorite, O fugacities as function of temp. 77—82187
- gas mixtures containing common polar and nonpolar components 77—31417
- hard-core lattice gas with tricrit. point, phase transition behaviour 80—8926
- hydrocarbon-simple fluid gas streams, second virial coeffs. calcs. 78—1777
- infinite dilution activity coeffs. determ. from total press. VLE data, eqn. of state influence 80—40727
- Lennard-Jones gas, Ising model, critical parameters from cluster integrals 77—11297
- point particle gas, grand partition function, zero distrib., logarithmic interaction 77—11296
- vapour-liquid equilib., component fugacity coeffs. 79—23716
- vapour-liquid equilibria, generalised method for calc. and prediction at high press. 78—87780
- vapour-liquid equilibrium, supercritical components, standard state fugacities 80—15230
- weakly ionised gas non-ideal behaviour, virial eqn. of state and fugacity coeffs. 80—79424
- CO_2, fugacity at high temps. and press. from exptl. decarbonation reactions 79—16439
- $(Fe_{0.5}Mg_{0.5})Ti_2O_5$, armalcolite, stability as function of press. and O_2 fugacity 77—64275
- Ne, molar volumes and thermodynamic props., 25 to 150C, up to 7 kbar 77—42957
- O_2 electrochem. fugacity meas. rel. to geothermometry 77—2256
- O_2 fugacity of basaltic magmas, role of gas forming elements 78—77218
- O_2, measurement with aid of solid electrolytes *(Czech)* 77—77779

full wave rectification *see rectification*

full wave rectifiers *see rectifiers*

function approximation
- *see also Chebyshev approximation; interpolation*
- anisotropic multigroup transport cross sections, low order approx. 77—34364
- automatic piecewise linear approximation of yield function in ideal plasticity 77—46929
- beam mode function series approximating beam field *(Japanese)* 77—22427
- bivariational bounds on soln. of two-point boundary-value problems 77—5646
- bordering functions based interpolation method 78—81816
- bordering functions based numerical method 78—81815
- boundary value problem for linear partial differential eqns., approx. soln. *(Russian)* 77—57170
- capacitive sensor characts. linearisation, in vicinity of working point *(Slovak)* 79—40547
- chemical composition centre waves, periodic chaotic, Pade approximant scheme 78—80716
- compressible flow, subsonic, finite element method *(French)* 77—47037
- constructive methods based on analytic characterizations and their application to nonlinear elliptic and parabolic differential equations 79—71225
- Coulomb excitation functions, numerical calc. of limiting props. 79—9604
- Debye lattice, thermal props., WINIMAX approx. appl. 80—49333
- elastic EM form factor analytic struct., complex coupling const. plane, Pade approximants 78—29335
- elastic shells, two-dimensional eqn. system *(Ukrainian)* 78—89342
- elliptic variational equality, of Bingham type *(French)* 77—47048
- error summation using piecewise-polynomial distribution functions 77—67246
- first derivatives, construction of approximations of high order of accuracy *(Russian)* 77—9873
- flow density function, compressible, subsonic *(Hungarian)* 79—14421
- furnaces, walking-beam, numerical soln. of two-dimens. temp. field, boundary condition modification *(Polish)* 80—87706
- Gammel-Baker generalised Pade approximations construction for function with given singularity 77—45687
- Green's function mean value, Dyson eqn. approx. anal. *(Russian)* 77—74201
- heat equation, semilinear, blowing up of finite difference soln. 77—54854
- high-temp. dissociated water vapour thermodynamic functions *(Japanese)* 77—80263
- inverse problems with piecewise continuous solns., approx. soln. 78—20943
- Legendre Pade approx., Yukawa scatt. and impact parameter amplitudes 80—22227
- Legendre Pade approximants to scatt. amplitudes, convergent sequences 79—85014
- matrix Pade approximants, Fortran IV calc. subroutine 77—9877
- microhardness of Fe electrodeposited coatings, Ha_5 design appl. 79—39069
- minimum norm, numerical methods convergence 78—54166
- multidimensional integrals, numerical calc. 78—89323
- multivariate approximants with branch points, off diagonal approximants 78—54160
- multivariate approximants with branch points, practical evaluation 78—54161
- mutual diffusion coeffs., calc. by computer for Fe-Mn diffusion pair 79—69299
- neutron density in slab geometry, transport soln. props., piecewise polynomial variational approx. 77—54269
- neutron diffusion and transport theory, discontinuous variational approx. 78—46129
- noncompact operators, numerical approx. of spectra *(French)* 77—67242
- nonlinear theory of simple dipolar elastic solid, successive approx. method 77—39221
- one-dimensional oscillator, matrix elements of position coord., upper and lower bounds 79—35578
- orthogonal polynomials expansions, summation procedure 78—81805

function approximation continued
- Pade approx. and low-energy Lagrangian field theory 77—61220
- Pade approximants, variational approach to NN dynamics 78—62427
- Pade approximants via continued fraction approach 78—61972
- parabolic nonlinear eqns., control to meet finitely many terminal conditions 77—5647
- partial differential approximants for multicritical singularities 77—85466
- phase-frequency signal intensity characteristics *(Russian)* 79—94176
- plasma dispersion function, multipole approx., modified asymptotic Pade method 80—48853
- polynomials, smoothing, averaging method 80—31
- power series, class of algorithms for obtaining rational approximants 78—54169
- quantal particle, inverted Morse pot. barrier, transmission, reflection coeffs., phase-integral approx. 77—53801
- Rayleigh-Schrodinger, appl. of Pade approximants 78—65806
- scattering amplitude, punctual Pade approx. as regularisation procedure for partial wave expansions 79—17639
- Schrodinger eqn. eigenvalue and eigenfunction computation by stepwise potential function approximation 77—17853
- smooth interpolation and approximation of data by anal. curve method 77—26159
- special functions for phase integral approx. 79—75321
- stochastic approx. procedures in continuous time 78—69969
- time dependent Hamiltonian, scale gauge transforms., adiabatic approx. principle, suitability for teaching 78—45506
- transport equation, Galerkin type methods for approx. soln. 77—87706
- variational methods for solution of electrodynamic and electrostatic problems 80—1105
- Voigt profile, fast calculational algorithm, line-by-line transmittance 78—7767
- Volterra nonlinear integral eqns., soln. using two-point rational approximants 79—40351
- Weierstrass elliptic function rational approx. 77—17793
- weighted residual classification of approximate methods 79—10540

function evaluation
- arbitrary square matrix with multiple eigenvalues 77—74188
- asymptotic series coefficient, generalised calculus using steepest descent method *(Rumanian)* 78—89304
- atomic struct., numerical HF radial function during SCF iteration, convergence 78—58574
- D-optimal design for quadratic regression on a hypercube 79—92921
- Earth gravity field spherical functions, numerical development *(German)* 78—61311
- fibre-optic digital transmission, shot noise probability distribution function 78—50717
- fluid dynamics, pseudo-spectral FFT technique, non-periodic problems 78—59359
- FORTRAN function writer, FURI, polynomial expansion 78—16631
- hand calculator, appls. 78—12483
- heat eqn. Cauchy problem, numerical procedure 77—5644
- image correlation of geometric distortion, optimal window functions 79—45907
- Meijer's G-function, sums of series 78—24639
- regression experimental design, unbiased, practical appls. 79—97184
- $U(t,t_o)$ operator, approximate sequence *(Chinese)* 79—92925
- Ursell functions, group functions and derivatives 78—70049

function generators
- *see also pulse generators; signal generators; square-wave generators; time bases*
- analogue-digital function generator, for pulsed AAS *(Russian)* 78—70199
- digital based triangular wave generator for Mossbauer spectroscopy 78—55113
- digitally controlled, and storage instrum., electronic modelling appls. 78—77937
- ECG simulation, adjustment of electronic machine *(French)* 79—83968
- Echosimulator, function generator for meas. of US diagnostic equipment characts. *(German)* 80—104685
- electronic sweep of magnet field in microwave spectrometer 78—12717
- LF function generator/controller using X-Y recorder 78—21108
- microcomputer-based speech synthesis system 79—94421
- Mossbauer effect work, function generator using IC 80—68334
- Mossbauer systems, synchronous digital triangle generator and servo loop pre-amp 77—88351
- optical wideband ambiguity function generator with Doppler compensation 78—78936
- proton synchrotron, CERN, online function generation optimisation 78—834
- scan-forming unit for controlling coupled beams from an electron-beam probing device 80—52366
- sinewave, simultaneous supply of fifty strain transducers, ship vibration testing 80—62652
- square wave, CRO calibrator, Y amplifier, cct., constr., amateur radio appl. 77—30183
- sweep, x-y recorder, sweep speed dependent on four terminal network transfer charact. 80—62649
- tape and chart recorder timing waveform generator 79—17415
- technology trends *(German)* 79—71437
- Thornton's electronics modules for physics courses, evaluation 77—57133
- triangular voltage, IC, for electrochemical meas. *(German)* 77—52724

functional analysis
- *see also harmonic analysis*
- ϕ^3 interaction, four-dimensional Green's function model *(Russian)* 78—77775
- abstract averaging theorem 77—2510
- Airy functions, asymptotic behaviour of derivatives 80—17830
- Airy functions, stress problem solns., teaching appl. 78—86063
- algebra of pseudodifferential operators and the asymptotics of quantum mechanics 78—93547
- analysis, manifolds, calculus and other fundamental maths. book 78—28918
- analytic continuation of the Fourier Series on connected compact Lie groups 78—93511
- analytic function determ. from conjugate harmonic 79—71227
- analytic function theory, plane/parallel fields and boundary problems in piecewise inhomogeneous anisotropic media *(Russian)* 79—62996
- applied inverse problems, book 79—49017
- applied inverse problems, introduction 79—49018

functional analysis continued
  arbitrary scalar functions, divergence relns. and multipole expansions 79—6434
  asymptotic functions, general assumptions and definitions 79—40350
  atomic and mols., ionisation and excitation energies, ΔE SCF, transition functional method 77—88404
  atomic Banach lattices, operator props. *(French)* 77—49558
  bar, rectangular, torsion crack problem, harmonic function continuation technique soln. 80—99969
  Bessel polynomials 77—22385
  bifurcation into invariant tori at points of reson., use of Poincare maps 79—44707
  Bose system, Jastrow wavefunction, hypernetted chain method 80—17866
  branching continued fractions for double power series *(Russian)* 79—12567
  broken linear transformations, baker's transformation 77—71186
  canonical ensemble partition function, hidden connections and functional integral representation 79—30361
  catastrophe theory as tool for physical scientists 78—41136
  Cauchy problem, general case, class of nonlinear Schrodinger equations 79—84994
  Cauchy problems average boundary conditions 77—2561
  Chandreskhar's operator valued H-function, analytic continuation, appl. to neutron transport 78—37388
  classical functions, expansion problems 77—22390
  classical impact theory, Carnot functional *(Russian)* 79—25856
  composite multidimensional function decomposition into its components 80—79625
  continuum mechanics applications *(French)* 77—67292
  Dalembertian functions of celestial mechanics, props. *(Russian)* 78—24454
  dielectric plate, determ. of index profile from scatt. data 79—49067
  diffraction integral transform 77—5635
  diffraction waves on arbitrary surface, Gaussian functional integral method 79—76902
  dimensional base selection in expt. design and planning 78—49636
  dimensional regulation, SU_2 gauge theory, instantons 80—18066
  discrete operator spectra *(Russian)* 78—28916
  distribution functions, high order reduced, truncation procedure 78—36958
  domain restoration from scattering data *(Russian)* 77—5630
  doubly orthogonal function construction 80—32888
  dusty gas, unsteady flow in cylinders, numerical soln. 78—51231
  dynamical systems, homoclinic and heteroclinic points in Hemon mapping, analyticity 80—82634
  elastostatics, nonlinear, boundary value problem of space and traction, error energy, and error norm 80—53631
  elctromagnetic inverse scattering, linear delay integral equations 79—55033
  elementary particle scattering, phenomenological approach to the inverse problem 79—49498
  EM prospecting, inverse problem 79—53583
  endomorphism bifurcation, universal metric props. 79—25827
  equivalent linearization, existance and uniqueness of solns. 79—9080
  Euler's infinite sine product 77—67210
  extrapolation towards interior points from a cut, analytic continuation of functions of physical interest 80—12952
  extremal problems, theory, book 79—63001
  Fermi system, Jastrow wavefunction, hypernetted chain method 80—17866
  field quantisation, number operators for distinguishing Bose, Fermi and parastatistics 78—93562
  finite range potentials, inverse problem 79—49097
  fission reactor, functional anal. of multigroup neutron diffusion problem 78—58317
  flat galaxies, bi-orthogonalization of Toomre's surface-density functions 79—80356
  form convex functions and the WYDL and other inequalities 79—30200
  fracture analysis, 2D linear, elastic, finite element anal. vs. the edge function method 80—99963
  fracture mechanics, appl. of method of pots. 78—51121
  functional restoration from functional derivatives 80—31485
  gauge field theory, double counting, collective coordinate resolution of identity of unity 80—68359
  gauge theories, quantisation, without fixing gauge, functional technique 80—57471
  Gaussian generalised stochastic fields, Markov property 80—22287
  Gegenbauer functions, expansion formulas and addition theorems 77—5634
  GM and GL type spaces, basic props., future appls. to physical axiomatics 78—45458
  gravitational field eqn. solution by functional method 80—17847
  Green's functions in space and time 79—58474
  H-functions of radiative transfer problems, representation for multiplying media 78—53808
  Helmholtz equation, 1-D three-body problem, Sommerfeld Maluzhinetz transformation 80—62524
  hydrogeological parameter determ. method, semipervious stratified aqu. layers *(Russian)* 78—32236
  hypergeometric functions asymptotic series calcs. 78—45468
  hypergeometric partial solutions in the problem of two Coulomb centers 80—4582
  induced potential problem in 3-D, functional analytic approach 78—58880
  integral method appl. to classical and quantum spin models 80—15676
  internal scalar pressure determ. in atom or molecule, density functional theory 80—47857
  invariant props. of n-point functions and functionals due to translationally invariant formal measure 78—45500
  inverse gravity/mag. problem, appl. of linear programming, basic numerical techniques 79—53581
  inverse methods applied to continuation problems in geophysics 79—53579
  inverse problems, analytic extrapolations in high energy physics 79—49499
  inverse problems of reconstructing functions with discontinuous derivatives 79—2600
  inverse scattering method for solving nonlinear evolution equations 79—49096
  inversion-like integral equations, construction and appl. 79—49095

functional analysis continued
  Ising model, critical temperature, modulated Pade approximant 80—84605
  Josephson effect, appl. of elliptic sine equations in two space dimens. 77—55640
  Jost function treated by the F-matrix phase integral method 79—25884
  Kampe de Feriet function expansion in terms of generalised prolate spheroidal wave function 79—17259
  Kolosov-Muskhelishvili functions in generalized symmetrical problems of elasticity theory *(Ukrainian)* 79—75340
  Laguerre polynomials 77—22385
  laminar boundary on surface of circular cylinder moving in fluid, flow pattern and heat transfer 80—28487
  laminar stationary 2D viscous duct flow, generalised Prandtl eqns., soln. methods 78—5726
  Lauricella function, analytic continuations 79—17645
  linear functionals in nonlinear problems, general estimates 78—49643
  linear inverse problems in Fourier optics, regularisation 79—50240
  linear inverse theory with a priori data, geophysics appl. 79—53580
  local seismic foci, soln. of inverse problem 79—53582
  magnetic alloys, dilute, static suscept., Anderson model, functional integral approach 80—50050
  Markov process, continuous, using Onsager-Machlup Lagrangian 79—80522
  Markov process generated by Langevin equations, WKB-type expansion 80—86212
  material with internal variables, condition equivalent to existence of non-equilibrium entropy and temp. 79—44890
  Mayer function, delta-function expansion, virial coeffs. appls. 79—4221
  mechanical systems, follower load type, time invariant functionals 80—77609
  membrane and plate vibrations, functionals method for lateral vibr. freqs. determ. *(Japanese)* 80—12918
  MHD two-dimens. problems, function averaging *(Russian)* 78—26209
  Minkowski spaces, estimates for constants of local unconditional struct. 78—89299
  mixed continuous mechanics problems, orthogonal functions *(Russian)* 78—49659
  multidimensional interpolation by polynomial roots 80—18778
  multiplication of distribs. by non-standard anal. 79—30292
  neural transformations of random signals, Wiener and of functionals of Markov chain 80—76727
  neutron transport Boltzmann equation in parallelepiped functional methods use 77—57701
  neutron transport equation, perturbation method to estimate functionals 80—27698
  neutron transport multigroup theory 80—13525
  Newtonian mechanics inverse problem, transition between second order and first order systems 79—53968
  noise distorted function resolution into sum of exponentials, characteristic eqn. coeffs. 80—77707
  non-convex functional, minimum, appl. to nonlinear integro-differential eqn. soln. *(French)* 79—53963
  non-gradient algorithm of functionals minimization *(Russian)* 79—12566
  nonlinear eigenvalue problems, approx. method of first eigenvalue 77—64921
  nonlinear monotonic functions with selectable intervals, constitutive eqns. appl. 79—46230
  nonlinear operators and differential eqns. in Banach space, book 77—2516
  nonlinear oscillator, stroboscopic phase portrait and strange attractors 78—54177
  nuclear reactor suboptimal control method 77—71636
  oceanic induction and spectrum shifting method 78—20353
  off-shell continuation of scattering amplitude in quantum mech., inverse method 79—49423
  one dimensional function, resolution into sum of exponentials, roots of polynomial 80—77603
  optical system with annular pupil, orthogonal polynomials, appl. to Fraunhofer diffr. 78—50714
  optimal control of 1-D linear distributed parameter systems with cost functionals 78—59257
  Orr-Sommerfeld eqn. eigenvalues, series representation 78—38280
  Pade approximant, modulated, applied to Ising model critical temperature 80—84605
  plane eikonal eqns., class of complete integrals 77—49562
  potential flow about bodies of revolution, general analytic method 78—1629
  principles of advanced mathematical phys., book 79—63090
  pump, centrifugal, impeller flow, quasi two-dimens. method of singularities 78—46986
  quantum field theory, conformally invariant, functional representations 77—5708
  quantum field theory, Euclidean approach in curved spacetime, functional anal. 80—27181
  quantum field theory, lattice-limit definition of functional integrals 80—27396
  quantum field theory, nonperturbative generating functionals for Green's functions 80—73588
  quantum field theory *(French)* 79—54016
  quantum mechanics, Feynman path integrals with Gaussian measure, Laplace transform method 80—62522
  quantum pendulum representation of canonical relns. 80—42084
  radiative transfer, two-dimens. expansions, for isotropic scatt. semiinfinite medium 78—42522
  ray theoretical inverse methods in geophysics 79—53578
  real-time transfer function analysis, instrum., for rapid meas. of system kinetics 77—41578
  Regge amplitude construction through soln. of S-matrix equations 79—49413
  relativistic QFT, inverse scatt. problem and 5th Painleve transcendent 79—54260
  relaxation distribution function, approx. methods and num. inversion of Laplace transform. 80—84720
  scalar wave diffraction problem for slit, soln. using Fourier orthogonal functions transform. 77—13599
  scattering theory, general case, class of nonlinear Schrodinger equations 79—84995
  Schrodinger eqn., radial, general pot. props. for soln. by hypergeometric functions 80—4581

functional analysis continued
Schrodinger operator, minimal, self-adjointness 80—17836
Schrodinger operator, scatt. and local absorpt. 78—93546
self inverse Sheffer sequences 77—22392
self-adjoint operator, eigenvalue bounds, variational approach *(German)* 79—25886
shells of revolution, thin-walled, heated, temp. field, thermostatic control 78—67003
singular potentials, Gel'fand-Levitan theory of the inverse problem 79—49098
singularity methods in math. phys., boundary value problems appl. 77—74198
spectral transform method for solving nonlinear evolution equations 79—49019
spherical delta functions, multipole expansions for fields, using Cartesian Taylor series 78—86118
spherical harmonic gradient formula, generalisation 79—17271
spheroids, harmonically oscillating, unsteady airload prediction, analytical soln. 78—51184
spin systems, functional method *(Chinese)* 79—63064
stable analytic continuation with rational functions 80—37266
Stieltjes functions and approximate solutions of an inverse problem 79—49094
stochastic fields, functional integral methods 79—25973
stochastic inverse problem in the radiation of noise 79—49168
stochastic linear systems with nonwhite parameter fluctuations, differential anal. 79—85082
stochastic methods and techniques for quantum mechanics, book 80—4584
Stratonovich-Hubbard scheme for grand canonical partition function determ., linearization by functional integral 79—63141
Sturm Liouville inverse discrete problem, different spectral data *(French)* 79—53964
Sturm-Liouville discrete inverse problem, algorithms *(French)* 79—49022
symmetrical free vibrations of a thin elastic plate with initial condition as a generalized function 79—59939
tensor functions, irreducible representations *(French)* 77—74190
thermal conductivity, nonlinear, variational formulation, counter functional, exactness of soln. *(Russian)* 80—90800
Toeplitz determinants calc. produced by substantially limited functions *(German)* 80—26
transport eqn. 77—14209
turbulence homogeneous, incompressible conducting fluid 78—18355
turbulence theory, expectation of an exponential function of an integral 78—32686
turbulent boundary layer on a moving surface, integral and numerical methods 78—63421
turbulent shear flows, coherent motions, critical points 80—33571
Ursell functions and cluster estimates, representations 80—8900
vacuum polarisation function 79—21578
viscoelasticity, Il'yushin kernels, analytical representation 78—67055
Voigt function and its derivatives, complex probability function 79—45675
wave and Dirac operators, conformal group representations 77—33895
wave equation, reduced, fixed incident field, inverse problem 80—62484
He, Schrodinger eqn. solns., existence criterion, for teachers 78—41117

functional equations
alkali metals, vacancy formation energy calcs., electron density functional method 80—19801
approximation functionals, simplification in elastoplasticity theory *(Russian)* 78—63328
bifurcation of stable stationary solns. from symmetric modes 78—57752
Boltzmann eqn., stability anal. by Lyapunov functionals 78—29069
boson system, many particle, radial distribution function, functional derivative 78—137
closed time path Green's functions, transform. props. *(Chinese)* 80—105491
composite multidimensional function decomposition into its components 80—79625
confluent hypergeometric functions, high order nonlinear eqns., sum rules, zeros 79—92923
confluent hypergeometric functions, nonlinear eqn. infinite system, zeros 79—92922
continuum mechanics, macroscopic determinancy principle corollaries *(Russian)* 78—77714
crystal-liquid phase boundary, pair distrib. functions and free energy functionals 80—24734
cubic array of identical spheres, dielec. const. calc. 80—25271
diffraction waves on arbitrary surface, Gaussian functional integral method 79—76902
directed cell locomotion model, turning-angle and run-length distributions 77—21502
dual strings, functional integrals for partition functions 77—67628
dynamic contact problem, for thermoelastic half-space 77—62215
elastic eqns. of uniform systems, general integral solns., appl. *(Russian)* 79—14272
electron spin density functional gradient expansion, local approx. calcs. 80—44792
Euclidean QFT, appl. of virial expansion derivation 78—37131
exponential function, growth and compound interest 77—5637
extended hadrons, functional eqns. soln. by stochastic methods 78—21376
Fermi-Pasta-Ulam lattice with cubic nonlinearity, novel first integrals 77—65003
finned-pipe solar energy collector, optimal material distribution 79—83631
fission reactor, functional anal. of multigroup neutron diffusion problem 78—58317
fluid computations using infinitesimal functionals, variational approach 79—14365
Fokker-Planck equation, functional integral definition 80—65
functional methods, introduction to use in quantum field theory 77—57458
geophysical inverse log.-potential problems, integral and functional eqn. analysis 77—40968
Gibbs random fields described by generating functional method 80—31698
Guderley's transonic small disturbance equation, exact solns. 80—19315
heterogeneous, continuous functional differentiation, appl. to Feynman path integral 78—4504

functional equations continued
Hilbert space, quantum mechanics and integration, functional integrals 79—97246
hydrodynamics, random velocity field perturbations, 3-dimens. characteristic functional eqns. 80—12909
linear stochastic diffusion equations, two-dimens. system, asymptotic behaviour of functional for distribs. from argument of soln. *(Russian)* 78—21083
many-body systems with weak coupling between remote particles, novel first integrals 77—65003
Markovian causal nonrandom vectorial functionals of random processes with independent increments *(French)* 77—26144
membrane and plate vibrations, functionals method for lateral vibr. freqs. determ. *(Japanese)* 80—12918
metals, cohesive energy using Kohn-Sham density functional formalism 79—60749
metals, ground state of solids, spin density functional method, binding energy, compressibility 80—65477
microhardness of Fe electrodeposited coatings, Ha_5 design appl. 79—39069
multiplicative functionals on diffusion processes 80—73286
neutron stochastic transport, functional theory 80—37413
nonlinear differential equation, compactness of bounded trajectories of dynamical systems 80—82636
nonlinear functional equations, group representation theory and branch points 77—67195
nonlinear transformations, universal metric props. 80—52000
nonlocal QFT within Bogolyubov axiomatic approach, mapping abstract classes *(Russian)* 80—22530
optimal control, differential eqn., canonical, functional relation expressed by Volterra series *(French)* 80—73159
orthogonal decomposition of 2-D periodic discrete vector fields 77—67196
partial inversion of oparator for summator functional equation with kernel of the form of periodic Mathieu functions 79—21562
perturbation theory, variational methods, evaluation of second-order matrix elements 80—12936
phase space functional integrals of quantum mechs., Hamiltonian quantization 78—41194
plasma in uniform mag. field, complementary variational principles on elec. conductivieies 79—46430
QCD_2, fermionic Green function and functional determinant, closed representation 80—13269
quasiclassical asymptotic behaviour of functional integrals, scatt. amplitude 78—62325
random functional equations, stochastic approx. in Banach space *(Japanese)* 80—95038
random heat conduction in solids, functional eqns. 78—83210
Saint-Venant torsion problem, classical, integral and functional eqns. 78—57780
Schwinger functionals, positive extensions, moment problems, representations 78—8505
simple metal, Knight shift, single-ion approach 80—44935
simplex volume in constant-curvature spaces, integral representation *(German)* 77—57163
soliton lattice melting, functional integral method 80—17883
state depend. delay difference eqns., jump discontinuities 77—41456
statistical thermodynamics of quasi relativistic electron gas, pathway integral application *(Russian)* 80—22277
stereology, estimation of linear functionals of size distributions 77—61056
strong Markov process time change *(French)* 78—62151
super-multiplicative functions, generalisation to fundamental theorem 79—93047
superposition of numerical graphs, functional changes *(Ukrainian)* 78—89293
transport theory, discontinuous trial functions, classical functionals 77—53842
two or three electrons, interacting with localised mag. moment, wave function determ., Sommerfeld's method, soln. of linear functional eqn. *(French)* 79—12636
viscoelasticity, nonlinear functional relations and superposition principles 80—42065
viscosity of water, multiparameter viscosity-temp. eqns. analysis 80—15283
Volterra expansion, detect. memoryless nonlinear functional of random process in white noise 79—86296

functionals *see functional equations*

functions
see also Bessel functions; Boolean functions; describing functions; Green's function methods; random functions; recursive functions; transfer functions; vertex functions; Walsh functions
Γ-integral, invariance props. *(Russian)* 77—71187
ζ-function regularisation, symmetric spaces of rank 1, physical instabilities 80—57519
amplitude distributions, appl. in practical data assessment problems 80—27107
angular covariance functions for galaxies, correl. anals. of deep samples 79—67104
Appell function F_1, generating functions 77—17777
biharmonic function difference eqn., improved, appl. for elasticity 77—68411
book, Brownian motion, Hardy spaces and bounded mean oscillation 77—67180
book, mathematical methods for physics 77—45670
Boussinesq-Papkovich displacement functions, generalisation to anisotropic medium 78—12570
characteristic functions, monotone decrease 77—33843
conjugate functions theory, appl. to long-range prediction of averaged meteorological fields 78—3905
continuous descent functions for polynomial eqns. 77—13581
covariance function, of galaxy clustering N-point simulations 80—31373
D-optimal design for quadratic regression on a hypercube 79—92921
diffusion, non-stationary one-dimensional, psi-functions 78—54322
Dirac-Coulomb, radial integrals with finite energy loss 77—23000
distribution function transformation, second-degree regression effects *(German)* 79—80417
distribution function $y=ax^b \exp[-c(\ln x)^2]$, props. *(German)* 78—77686
dual strings, functional integrals for partition functions 77—67628

functions continued
- empirical orthogonal functions, stability 77—67224
- expansion theorem for $(r')^{m-1}\exp(-\alpha r')$ for $m=-1$ case 79—12569
- exponential, single-step numerical method anal., approx. of exponential function 80—94950
- exponential function, appl. to problems of steady inflation 77—13576
- Gaussian distribution, unconventional calc. of moments 78—49647
- generalised integrals involving elliptic functions, appl. to stellar structure 77—71107
- generating functions, increasing entropy-like, for shocks in hyperbolic systems *(French)* 77—13573
- geophysical prospecting, fundamental functions for horizontally stratified Earth 77—21918
- geophysics, analytic continuation of function for Earth surface *(Russian)* 79—35008
- Gortler functions, uniqueness, laminar boundary layer flow *(German)* 80—52034
- gravity disturbance covariance functions, upward continuation integrals 78—85468
- H-function for anisotropic scattering, in radiative transfer 80—36491
- H-function of radiative transfer integral eqn. spectrum, calc. for semi-infinite medium 80—67540
- H-function of two variables applic. in heat cond. 79—94450
- Hamiltonian, quantification of geodesic flow of sphere S^n *(French)* 78—54151
- heat conduction, stationary, in piecewise homogeneous bodies, generalised functions theory methods *(Ukrainian)* 80—23861
- kernel functions in EM closed region problems, singularity extraction 78—66728
- Laguerre functions, appl. to nuclear medicine washout curves 80—81521
- Laguerre polynomials generating functions, Lie group viewpoint *(French)* 77—71181
- laminar boundary layer flow, Gortler functions, uniqueness *(German)* 80—52034
- Laplace expansion of Earth potential, generalisation to Earth's surface 77—60337
- Legendre function for impulsive wave propag. in spherically symmetric model, analytic inverse transform. 79—74849
- log-concave functions and convex interaction terms for quantised fields 77—57232
- Mathieu, Lame and parabolic, in representations of M(2), SO(3) and O(2,1) groups 77—45675
- Mathieu's elliptical functions, appl. to elastic waves propag. in elliptical cylinders *(German)* 77—62186
- Mathieu modified functions, second kind, integer order for small values of parameter, limiting form *(French)* 78—86113
- mechanical systems with non-holonomic constraints, existence of potential function *(French)* 78—86128
- Meijer's G-function, differential props. 80—86072
- mixtures, multicomponent, anal., by method of additions 80—61187
- natural nonorthogonal functions, appls. to geomag. S_q-field seasonal and latit. vars. 78—36359
- natural orthogonal functions, appl. to forecasting of data of breakup of Amur basin rivers *(Russian)* 77—53088
- Neumann's operator in potential theory, contractivity 78—69966
- nonstationary one-dimensional diffusion under forced convection, Omega functions as auxiliary functions 78—93631
- normalized distrib. functions, comparative behaviour *(German)* 79—25826
- ocean remote sounding instruments, quasi-optimum operating functions *(Russian)* 78—77362
- parabolic cylinder functions, asymptotic approximations 78—89301
- parabolic cylinder functions, asymptotic expansions, comment on previous letter 78—89302
- Payne-Rayner isoperimetric inequality, extension to N dimensions *(French)* 78—54323
- perturbed Hamiltonian systems, soln. via accelerated elimination technique 77—60585
- potential theory inverse problem, soln. uniqueness *(Ukrainian)* 77—71183
- radiative transfer, exit function for unified treatment of reflected and transmitted intensities 78—85838
- radiative transfer H-function, expression using Laplace transform and Wiener-Hopf technique 79—35111
- random function of universal time, determ. 80—46120
- regression experimental design, unbiased, practical appls. 79—97184
- renewal equations system, extension of Feller's renewal theorem 77—33841
- Riemann function derivation for Klein-Gordon eqn. with nonconstant coeff. 77—57153
- Riemann functions of mixed problems for wave eqn. in plane stratified media, singularities 77—30017
- Riemann functions of mixed problems for wave eqn. in plane stratified media, singularities 77—30018
- Rosin statistical function, appl. to meteorite chondrules mass distrib. 79—35201
- sesquiholomorphic functions, symbolic calculus and second quantisation *(French)* 77—53804
- shadowing function of Gaussian probability curve rel. to glacier friction law *(French)* 79—8641
- Sheffer, one variable, main diagonal necessary and sufficient conditions 78—54152
- skewness distribution of functions, rel. to flood sequences apparent regional skew 77—64355
- solid harmonics, props. determ. 77—71185
- stellar spectra macro- and microturbulent filter functions for weak line profiles 79—53803
- stellar spectral line shapes, convolution function for combined expansion and rot. effects 78—53920
- stochastic linear system moment and cumulant functions *(Russian)* 78—32759
- Voigt functions, partial derivatives 78—89052
- Weibull distrib. function, applicability to atmospheric radioactivity data 77—2230
- Weibull statistical function, appl. to meteorite chondrules mass distrib. 79—35201
- Weierstrass-Mandelbrot fractal function 80—52063
- Wightman fields, algebra of test functions 77—18186
- window functions, in geodesy, influence on prediction *(German)* 77—86749
- zeta function of quartic oscillator 80—62532

fundamental constants *see constants*

fundamental law tests
- Aspect experiment, objective reality, causality in QED 80—99076
- Eotvos expts. and weak interactions, anal. 78—78129
- equivalence principle tests in Earth orbit 78—45551
- general relativity, astronomical tests 80—36934
- general relativity, light bending by eclipsed Sun, star field obs. *(French)* 78—20634
- general relativity, potential blue shift, Cs beam clock meas. 79—12704
- general relativity, radio signal retardation by solar gravity, Viking expt. results 80—36933
- general relativity, Viking radio signals time of flight test 78—16716
- gravitation, inverse square law test in laboratory 80—31657
- probability of laws being zero 77—33820
- relativistic synchronization procedures, geophysical tests in rotating frame 78—24662
- scientific laws neither deterministic nor probabilistic 77—33819
- special relativity, time dilation meas. for relativistic muons 77—71210
- strong principle of equivalence, test using redshift of X- and γ-ray lines of neutron stars 78—40814
- variable rest masses, relativistic theories, tests and consequences 80—31396

fundamental particles *see elementary particles*

fundamental physics concepts *see physics fundamentals*

fundamentals of physics *see physics fundamentals*

furnaces
- *see also electric furnaces; refractories*
- annealing furnace O_2 gettering by NiSi or Pd_2Si 79—100160
- atomic absorption graphite furnace analysis, matrix interferences reduction with L'vov Platform, Pb analysis 79—92020
- blast furnace, simulated, interaction between gas and liq. flow 80—10300
- blast furnace blocks, carbon-containing, apparatus for thermal conductance determ. 77—57329
- burner with diffusive control, intermixing of gas streams with transverse swirled air flow 78—87418
- carbon furnace for IR source, practical consideration 78—81976
- combustion chamber and radiative transfer, fuel substitution effects, review 79—3903
- combustion modelling, for large gas-fired furnaces 79—32710
- control, Nicrosil-Nisil alloy thermocouple appl. 78—49831
- DC glow discharge, for high-rate carburizing of automotive components 79—83370
- diffusion furnace temp. profile meas. systematic errors, theoretical model *(German)* 80—8989
- diffusion furnaces, temp. profile meas., systematic errors *(German)* 80—37030
- fast reactor fuel fabrication using high temp., low-power furnace 79—49823
- flue gas anal. using RF mass spectrometric method 77—71403
- furnace tube HK40 alloy remaining creep life testing *(Japanese)* 77—28950
- gas fired, radiative heat transfer 78—1557
- gas temp. meas. by multiple-thermocouple method 77—49728
- glass melting, gas consumption through ports, monitoring and control system 79—58692
- glass melting furnaces, development and prospectives, review 78—3088
- glass tank furnace, physical models, selection criteria for liquids to simulate melted glass 79—8263
- gradient and mirror furnaces for Swedish materials science expt. in Texus 1 and 2 sounding rockets 80—104362
- graphite, used for pulling optical fibres, effect of drawing conditions on tensile strength 79—50469
- graphite furnace, between-sample cleaning 79—87889
- graphite furnace, HGA-2200, operating parameters 79—34384
- graphite furnace atomic absorpt. spectrometry heated by capacitive discharge, determ. of elements 80—66892
- graphite furnace atomic absorption spectrometry, electrothermal atomisation 79—24852
- graphite furnace-flame atomic absorption technique, for thermoanalytical investigs. 79—100477
- heat transfer and pollution *(French)* 79—16001
- high temp. furnace control methods in creep testing 80—30187
- high-temperature furnace, for small-angle neutron scatt. expts. 77—84591
- horizontal epitaxial reactor having multiple elongated-inclined susceptors 78—80475
- imaging furnace, appl. to thermal cond. and emissivity meas. of Ta 80—103667
- industrial, heat recovery from exhaust gases *(German)* 80—38224
- industrial plants, heat exchanger installations, heater min. furnace diameter determ. *(German)* 80—38234
- insulation, C materials *(French)* 78—44345
- lehr, position of radiation burners *(Polish)* 77—65036
- LPE, multi-layer, furnace design and fabrication *(Japanese)* 80—108366
- luminous radiation, vision problems, Swedish report *(Swedish)* 77—77896
- Martin bath, blowing with oxygen, smelting dust phase comp. determ. 77—52705
- melting furnace of high efficiency using hot plate and spherical mirror 80—68202
- metal sample preparation facility, multipurpose 79—180
- metallic thin films, vacuum deposition, ultra-high vac. technique 80—100791
- metallurgical, interior temperature meas., by means of radio transmission *(Czech)* 77—2659
- mirror furnace at Czochralski growth 80—60766
- molybdenite ore treatment using 2 kW solar furnace 80—3107
- Mossbauer furnace, high-precision for use up to 1100K 78—66021
- Mossbauer furnace for amorphous alloy investigations 80—98916
- multimirror radiation furnace, optical-energy characts. investigation 80—17945
- multiple hearth, biomass gasification process, Garrett Energy Research 79—48040
- municipal incinerators, fly ash and trace organic compounds anal. 80—45584
- neutron scattering chamber with high temp. resolution, 370 to 770K, furnace design 77—55212
- NMR probe heating furnace for high mag. field use 80—247
- optical component blank pressure shaping, semiautomatic apparatus 79—72731

- **furnaces** continued
  - optical vacuum furnace for Raman and Brillouin spectroscopy 78—58062
  - Oxford spectroscopic furnace, temp. meas. by photoelectric pyrometer for Fe I oscillator strengths 79—36584
  - photographic pyrometry technique and external calibration 79—93144
  - plasma furnaces, mineralogy and extractive metallurgy appls. *(French)* 80—28849
  - plasma melting, for steel industry, development in GDR *(German)* 78—22522
  - plasma smelting furnace, burning arcs 78—1944
  - plasma torch furnace, modified, doped MgO single cryst. growth *(Japanese)* 79—95923
  - precession camera furnace with indirect heating 77—10028
  - production, Nicrosil-Nisil thermocouples appl., 538°C to 1177°C 80—68198
  - pyrolysis tube, materials evaluation with creep damage model 77—52445
  - pyrometer, temp. meas. of bodies heated in solar furnaces 80—86312
  - quenching-tempering apparatus with recirculation tempering furnace, thermal charact. 77—67438
  - radiant heat exchange calc. by generalised zonal method 77—14885
  - radiation flux model 78—93689
  - radiative transfer in internally fired furnace 78—5643
  - RF, floating-zone melting with viscous torque control 80—89140
  - single-crystal diffraction measurements, microfurnace 78—32817
  - sintering furnace for remote nucl. fuel fabrication 79—89479
  - solar, appl. to La_2O_3 reduction by Si *(French)* 80—16784
  - solar, high temp. refractory study *(French)* 79—70268
  - solar, Pd membrane diffusion-cell for separation H_2 containing mixtures 80—92245
  - solar, temp. meas. using digital pyrometry system 77—37896
  - solar, thin films production appl. 80—89148
  - solar furnace, focal spot thermal analysis 80—21383
  - solar furnace, high temperature *(Japanese)* 78—45631
  - solar furnace, materials melting process dynamics rel. to automatic control 79—39317
  - solar furnaces, two mirror, high power, optical characts., calc. for design 80—40824
  - space solar furnaces, for materials-science expts. 80—108786
  - spectroscopic techniques, achievement of high-temp. and material selection *(Japanese)* 78—45726
  - technology, IR applications 80—86431
  - temperature distrib. measurement using thermocouples and wire bridge cct. 80—31758
  - temperature meas., dipping depth effect of thermometer elements on accuracy *(Polish)* 77—53910
  - temperature meas. using two-colour pyrometer 79—6129
  - temperature measurement with pyrometer and thermocouple, accuracy 77—5845
  - temperature-rise controller up to 1000°C 77—17980
  - tensile test specimens, furnace for up to 1400°C 80—3265
  - tensile testing, prolonged high temp. testing method with subseqeunt microscopic exam. 77—52581
  - thermogravimetric method for recording mass transport of materials under action of radiant fluxes 80—17944
  - thermostat system, automatic, for high temps. 79—6112
  - thyristor temp. regulation circuits, for creep testing devices 80—25956
  - tunnel furnace, natural gas fired, heat transfer, 3-dimens. computer model predictions test 78—59504
  - ultra-high extraction furnace for inert gas analysis 78—77918
  - vacuum, high-temp. processing and testing 77—49730
  - vacuum furnace, inexpensive design 77—2657
  - vacuum melting furnaces and casting techniques 78—84727
  - vehicle emission control, nitrogen oxides reduction on industrial furnace 79—52995
  - walking-beam, numerical soln. of two-dimens. temp. field, boundary condition modification *(Polish)* 80—87706
  - water thermolysis, solar furnace, thermodynamic analysis 79—83625
  - Woodriff furnace, for SO_4^{2-} determ. in natural water by at. absorpt. spectroscopy 77—40595
  - X-ray diffraction furnace, using thermal image technique, for high temp. molten salt diffr. studies 77—15280
  - X-ray diffractometer, temp. calibration using eutectic transitions of alloys *(Japanese)* 79—6128
  - C fibres, thermal expansion coeff. meas. using TEM fitted with furnace 80—102966
  - C furnace, for at. emission spectrometry, atomisation temp. effects 77—40583
  - C vapour molecular source for flowing systems 77—14616
  - H_2, combustion, heat transfer calc. *(French)* 80—19218
  - Ta foil lining of graphite furnace, at. spectrosc. 78—74078
  - WC vacuum sintering furnace systems 78—84737
  - Xe-lamp imaging furnace, crystal growth of refractory materials *(Japanese)* 80—50547
- **Furry theorem** *see quantum electrodynamics*
- **fuses, electric** *see electric fuses*
- **fusion** *see melting*
- **fusion, nuclear** *see nuclear fusion*
- **fusion-fission reactors** *see hybrid reactors*
- **fusion reactor ignition**
  - *see also fusion reactor materials; plasma heating; plasma production*
  - 2XIIB magnetic mirror device, neutral beam injection 80—28782
  - 100 kJ CO_2 laser, Antares, status report 80—64075
  - 100 mA low emittance ion source for ion beam fusion 79—68069
  - A-FLINT advanced-fuel pellet design, inertial confinement fusion 80—23125
  - ablation driven thermonuclear implosion targets, high efficiency 77—88272
  - ablative acceleration of laser-irradiated thin-foil targets 79—71952
  - ablative laser fusion implosion, scaling laws and spatial struct. 80—87915
  - accelerated Mach wave in nonhomogeneous cumulation cone 79—68925
  - accelerator grid assemblies, 120 keV, fabrication and brazing 78—66379
  - active burn control of nearly ignited plasmas 80—48909
  - advanced fuel reactor, plasma ignition condition 77—83098
  - advanced fuels for inertial confinement fusion 77—83102
  - advanced lasers for fusion, modelling and anal. 78—50819
  - alpha particle heating of fast-solenoid fusion reactor plasma, self-consistent anal. 79—31187
  - ANTARES and advanced CO_2 laser-fusion systems 80—32502
  - Antares CO_2 laser power amplifier, design 80—69423
  - ANTARES device, target-induced parasitic oscills. 78—59072
- **fusion reactor ignition** continued
  - Antares laser fusion project, 300 kJ, 200 kA Marx energy storage module 80—68954
  - Argus two beam system, 5 TW performance 78—46656
  - ASDEX fusion experiment, toroidal field coil construction features *(German)* 78—54877
  - Asterix III and German laser fusion programme 78—63136
  - auto-resonant ion acceleration concept, computer simulation 77—24208
  - automatic target alignment of Helios CO_2 laser system 80—74416
  - ballistic focusing of intense neutralised beam in pinched electron beam diode 78—9859
  - Baseball II-T experiment, microcomputer-based pellet trajectory guidance system 78—62623
  - beam direct conversion 78—13329
  - beam direct conversion for fusion injection at energies above 100 keV 78—13330
  - beam injection, ripple-assisted, magnetics design for ISX-B and TFTR Tokamaks 78—62643
  - beam stop calorimeter for high intensity neutral beam 80—13885
  - beam-pellet fusion, electron and ion beams 77—67892
  - beams, neutral, high-power, high-energy, for reference mirror reactor 79—49836
  - beat heating, system, using double-barrelled laser 78—67386
  - Berkeley multifilament ion source, plasma characts. 79—94807
  - Berkeley type ion source, long life cathode 78—66375
  - biconical profiled explosion-induced compression of matter 79—67938
  - black body radiation imploding in small cavity as inertial confinement fusion driver 80—86984
  - break-even in a bi-conical explosion system 79—71944
  - Brillouin backscatter saturation, underdense plasma target 80—14886
  - catalysed D fusion reactor start-up characts. *(Japanese)* 80—86983
  - cavitons in laser irradiated fusion plasmas, EM wave propag., supersonic density humps 80—24178
  - cavity gas response to particle beam target explosions 80—37602
  - chain reactions, kinetics, high electron temps., interactions with D-T plasma 80—68945
  - characterization techniques for high quality ICF targets 80—86986
  - Chinese research 80—78447
  - CLEO stellarator, heating, confinement and fluctuations 80—24225
  - coil design, cost anal., for neutral beam magnets 78—55005
  - collective ion acceleration by controlled motion of virtual cathode in relativistic electron beam 77—24210
  - collective ion acceleration by relativistic electron beam localised pinch model, simulation 78—9826
  - collective ion acceleration following relativistic electron beam injection into low press. gas 77—24209
  - compact ignition experiments, designs, numerical computation 80—13853
  - compact ignition test reactor, engineering design using Bitter type magnet 80—102310
  - compressible fast liner, adiabatic plasma heating and fusion energy production 79—31182
  - compression, laser-induced, expt. and theoretical obs. 77—43003
  - concentric compression of plasma, possibility of generating singular densities 77—68840
  - concentric hyperdetonation shock wave 79—7464
  - concentric shock wave, const. speed, in nonhomogeneous medium, thermonuclear microfusion 78—83281
  - conference, controlled fusion and plasma physics, Oxford, England (Sept. 1979) 80—77545
  - conference, fusion technology, Padova, Italy (Sep. 1978) 80—8741
  - conference, inertial confinement fusion, San Diego, USA, (Feb. 1978) 78—46171
  - conference, inertial confinement fusion technical digest, San Diego, CA, USA (Feb. 1980) 80—57012
  - conference on fusion reactor materials [Miami Beach, Florida, Jan. 1979] 80—31407
  - control, laser appls. *(Spanish)* 79—26748
  - critical surface, enhanced stimulated Brillouin scatt. due to light refl. 80—1750
  - cryogenic laser fusion target quality assessment by wavefront shearing interferometer 79—97417
  - cryogenic laser fusion targets, fabrication 78—58485
  - cryogenic laser fusion targets, irrad. systems 78—58486
  - cryogenic spherical shell target implosion by laser 77—74977
  - cryopumps for high power neutral injectors, design and performance 78—74494
  - cryopumps for PLT neutral beam injectors 78—58439
  - CTR neutral beam source, SCR series switch and impulse crowbar 78—66395
  - CTR neutral-beam injection system, plasma source design 77—24105
  - CTR potential 78—37442
  - cumulated shock waves, coming to free surface, optimal conditions 79—45414
  - cylindrical ion implosion fusion using radially convergent beams 80—23137
  - D-D neutron and X-ray yields from high-power deuterium beam injectors 79—67942
  - dense matter, laser driven fusion, laboratory expts. 80—75077
  - deuterium-tritium thermonuclear ignition, high current density approach, expt. 78—54874
  - deuteron linear for fusion reactor ignition 79—71991
  - diode design review, intense mag. insulated ion diodes 78—9857
  - direct energy conversion optimisation with charged particle parabolic trajectories 80—37585
  - DITE Tokamak neutral injection system 80—13886
  - double shell targets, low aspect ratio, for high density and high gain 78—58479
  - double-sided electron beam generator for KrF laser excitation, fusion appl. 80—68956
  - Doublet III, neutral beam injection system, overview and status 80—13868
  - Doublet III, neutral beam injection system, parametric study 80—13869
  - Doublet III noncircular Tokamak, neutral beam injection system 78—54970
  - duopigatron ion source, modified, ion composition 78—54914
  - duopigatron ion source for PLT injectors 78—54913
  - E-beam sustained large amplitude CO_2 laser discharge, for fusion appls. 78—55382
  - eight-beam CO_2 laser system, high-voltage engineering 78—58492
  - eight-beam CO_2 laser system, minicomputer-CAMAC control system 78—58493

fusion reactor ignition continued

- electron accelerator for inertial confinement fusion, Angara 5 features and design principles 80—63384
- electron accelerators, pulsed power technology for fusion expts. 78—50321
- electron and ion beam generation at high power, review 80—13988
- electron beam, energy coupling to expanding thick-shelled target 80—96365
- electron beam, relativistic, high-current, self-focused, energy dissipation at focus 80—5674
- electron beam (relativistic)-plasma interaction, transverse mag.-field induced enhanced energy deposition 77—62377
- electron beam accel., ignition of thermonuclear microexplosions 77—27686
- electron beam focusing and target irrad. in Angara-I accelerator 78—54911
- electron beam fusion, appl. of coaxial Marx generator 79—76177
- electron beam fusion, pellet and pellet-blanket neutronics and photonics 80—74006
- electron beam fusion, pulsed power requirements for breakeven 77—23278
- electron beam fusion accelerators, data acquisition and processing 78—37469
- electron beam fusion compression targets, fuel preconditioning studies 79—81076
- electron beam fusion of D-T pellets, neutronics and photonics 80—52781
- electron beam heated linear solenoids as fusion sources 78—5043
- electron beam impact on hemispherical target, implosion dynamics 77—47228
- electron beam induced fusion, power requirements for target implosion expt. 77—23277
- electron beam inertial confinement thermonuclear fusion 80—27803
- electron beam irradiated pellet, holographic interferometry of plasma blowoff vel. and density 77—23279
- electron beam pinching from discrete cathodes 78—50318
- electron beam propagation in plasma channels for ICF reactors 80—1812
- electron beam targets, thick-shell shock-focusing 78—30454
- electron beam transport, beyond diode, Z-pinch plasma 77—87874
- electron beam transport for inertial fusion, high current density generation 77—67870
- electron beam use in controlled nuclear fusion *(Japanese)* 77—61608
- electron cyclotron heating, high power MM wave source—gyrotron *(Japanese)* 80—23654
- electron gun, large-area cold-cathode grid-controlled, for Antares CO_2 laser amplifier 80—68955
- electron-beam fusion coupled pellet-blanket neutronics 80—47717
- electron-beam fusion research, appl. of electron-photon cascade model 77—68157
- energetic neutral beams, development to MW power level of controlled thermonuclear research 79—45508
- energy multiplication factor and ignition parameter 78—21763
- Engineering Test Facility/International Tokamak Reactor, plasma physics characts. 80—95420
- excimer laser Raman pulse compression for appl. to laser fusion 79—59756
- excimer laser Raman pulse compressor systems for laser fusion 79—59757
- exploding liner gas confinement, liner velocity effects 80—79541
- exploding pusher laser fusion 79—54596
- exploding pusher target, performance of fixed laser power theory 78—58481
- exploding pusher targets, expts. of Lawrence Livermore Lab 78—58482
- exploding-pusher-tamper areal density, neutron activation meas. 80—91237
- explosion compression of plasma up to critical values of thermonuclear microfusion 77—67872
- explosion compression of plasma up to critical values of thermonuclear microfusion 77—67873
- explosion induced compression, neutron yield optimisation in crucial systems 80—5328
- explosion induced conical system, internal break even possibilities 79—94811
- explosion-induced longitudinal-cylindrical compression of plasma 79—89496
- explosive implosion of polyethylene shell in D_2-filled cone, fusion neutron prod. 78—82510
- explosive implosion of variable density shell, neutron generation in a plane system 79—18035
- explosive implosion of variable density shell into conical region, neutron output determ. 79—22454
- explosive-pusher-type laser compression experiments with neon-filled microballoons 80—23132
- Fabry-Perot interferometer transients, for ultrashort laser pulse generation 78—58019
- fast charged particle beam density effect on stopping in matter 78—14180
- fast ion beam, in Tokamak plasma, quasilinear relax. *(Russian)* 78—87457
- fast ions in laser-produced plasma, nonlinear plasma-wave interaction 80—24183
- fast-liner reactor, fusion power from fast imploding liners 79—76119
- feedback controlled particle suspension system for laser initiated target expt. mag. mirror fusion facility 78—1864
- feedback laser fusion using direct nucl. pumped laser 78—58445
- field-reversing E- and P-layers, generation and stability 77—74988
- fissionable highly-compressed pellets, neutron kinetics 77—38315
- focus, current sheath struct. diagnostics, fast particle beams, deuterated polyethylene fusion 77—76206
- focus, low-energy, neutron yield props., filling press. depend. 77—74992
- focused beam ray tracing for laser fusion 80—83218
- four-channel laser system with four-ellipsoidal-mirror set-up for focusing laser beams 79—94276
- free electron laser, fusion appls. 78—58974
- FT Tokamak, RF additional heating system 80—13879
- fuel pellet implosion, laser compression efficiency, wavelength depend. calcs. 77—35369
- fuelling profile sensitivities of trapped particle mode transport for TNS 78—58421
- fusion reactor neutral beam transport system 78—54968
- gas filled microballoon targets, laser produced implosion dynamics 80—24198

fusion reactor ignition continued

- gas-filled microballoons, radiation effects MEDUSA code calcs. 80—83220
- Gekko IV, four beam phosphate glass laser system for fusion expts. 78—46650
- glass laser high power system for thermonuclear fusion *(Japanese)* 78—8970
- glass microballoon imploded by laser, X-ray transmission analysis *(French)* 80—54011
- glass microballoons, laser driven compression, calc. results *(Chinese)* 79—63807
- glass microbubbles, permeation eccentricities of He, Ne and D-T 78—47598
- glass microshell, high-power glass laser interaction 78—9804
- glass microspheres, separation by diameters and wall thicknesses to obtain correct. laser-target shells 78—8969
- glass sphere laser fusion targets, fabrication, liquid-droplet and dried-gel systems 80—32440
- glass-CO_2-hybrid laser system for plasma prod. and heating in mag. traps 80—24196
- Group IV photolytic laser expts., for fusion research 78—63101
- Group VIA photolytic laser systems, for fusion research 78—59002
- gyrating charged particle beam compression, modeling with finite circuit element code 80—14930
- gyrotrons and gyrokylstrons, small signal theory, fusion reactor appl. 78—70633
- gyrotrons for high power millimeter wave generation 78—62611
- heavy current electron beams prod., survey 78—33337
- heavy ion 1.5 megavolt preaccelerator, high intensity, ion beam fusion appl. 79—67970
- heavy ion acceleration, time-depend. study, fusion ignition appl. 80—86997
- heavy ion beam inertial confinement fusion, US programme 80—23136
- heavy ion beam linac, 12.5 MHz, for ion beam fusion 79—76158
- heavy ion fusion, linear accelerator facilities at Argonne 78—50327
- heavy-ion fusion preaccelerator, 1.5 MeV, fibre-optic remote control system 80—73993
- Helios CO_2 fusion laser alignment accuracy 80—33071
- Helios CO_2 fusion laser alignment system 80—33070
- Helios gas laser system, ICF expt. program as LASL 80—32501
- hemispherical laser fusion target fabrication using Si-based technology 79—89495
- high current switch, fast closing, for fast discharge expt. 78—74483
- high current switch, fast-closing, for Doublet III poloidal field circuit 78—74484
- high density plasma, thermonuclear reaction wave, propag. stages, computer simulation 78—742
- high field ignition test reactor using adiabatic compression 79—89500
- high n flux fusion heating, $^{6}Li(n,t)^{4}He$ use 78—89975
- high power laser, review *(German)* 77—54361
- high power laser appl. *(French)* 80—13785
- high power lasers for thermonuclear synthesis *(Russian)* 77—26879
- high power neutral injectors, review 80—18656
- high-power pulsed laser requirements and performances 78—83592
- hollow-cathode multipole boundary ion source, IBIS, plasma prod. and containment system 78—74521
- homopolar generator, radially stacked drum type, for Tokamak Ohmic heating coils 78—13337
- homopolar machine, fast discharging, 10 MJ model, for fusion device 78—13335
- homopolar motor-generator energy storage system 78—5044
- hot-ion-mode ignition in a Tokamak reactor 80—73999
- hyperdetonation eccentric shock wave, approx. soln. 78—67070
- hyperdetonation shock wave passage through jump like nonhomogeneity 78—67069
- ICF, production and energy flux concentration of REB accelerator 80—74026
- ICF targets, laser driven, materials problems 80—32438
- ICF targets, material response and implosion dynamics obs. 78—58477
- ICF targets, semiconductor process technology for mass production 80—32439
- ICTR walls, thermal response and stress problems 78—813
- Ignition Test Reactor remote maintenance system requirements 79—9885
- ignition test reactor with high field operation 79—71965
- ignition Tokamak, neutral beam system 78—54973
- imploding liner fusion, USA expt. and theoretical studies 80—23129
- imploding liner reactors, stabilised, optimisation 80—13859
- imploding liquid metal liner dynamic stabilisation 79—89494
- implosion heating coil, radially fed, design, fabrication 78—55006
- implosion velocity, minimum non-spherical for inertial confinement fusion 79—67937
- induction linac for heavy ions, pellet-fusion appl., design/cost study 79—67982
- inductor for high power impulse production, Joint European Torus appl. *(German)* 78—50293
- inert gas hydride laser, use two-step nucl. fusion dissipative confinement of doubly isotopic boron hydrides 78—82506
- inertial confinement, by laser and electron beams, conf. summary 77—76174
- inertial confinement, HF laser conceptual design 79—86192
- inertial confinement, ion-beam fusion 78—756
- inertial confinement, reaction gains, reheat calcs., collective model 78—59664
- inertial confinement, temporally shaped laser pulse generation 78—50831
- inertial confinement fusion, appl. of advanced lasers, review 79—18435
- inertial confinement fusion, electric power generation 78—50314
- inertial confinement fusion, electron beam-target interaction 78—755
- inertial confinement fusion, high yield Li injection fusion energy convertor 79—85772
- inertial confinement fusion, LASNEX code simulation 78—58478
- inertial confinement fusion, light ion and electron beams appl. 80—5323
- inertial confinement fusion, pulsed power aspects, overview 80—63382
- inertial confinement fusion, requirements for commercialization 78—50330
- inertial confinement fusion at NRL, laser and ion drivers 80—23131
- inertial confinement fusion at Osaka, laser energy drivers, REB fusion research 80—23135
- inertial confinement fusion by high energy heavy ions 78—5040
- inertial confinement fusion by high-energy heavy ions 79—18047
- inertial confinement fusion gains using collective model for electrodynamic laser compressions 80—23138

fusion reactor ignition continued
- inertial confinement fusion model targets, shock focusing in implosions 79—49832
- inertial confinement fusion pellets, neutron moderation, effects on damage and radioactive inventory 80—47704
- inertial confinement fusion power system, nuclear pumped laser coupling 79—85775
- inertial confinement fusion reactors, appl. of intense charged particle beams overlap 80—91242
- inertial confinement fusion reactors, use of black-body radiation as fusion driver 80—91241
- inertial confinement fusion research at Los Alamos, recent progress 80—23133
- inertial confinement fusion research system of high power lasers *(Japanese)* 80—5324
- inertial confinement fusion targets 78—50299
- inertial confinement pellet fusion, perturbation theory for sensitivity and uncertainty anal. 80—68946
- inertial confinement targets, hollow H_2 droplet prod. by acoustic excitation of superheated liq. H_2 jet 79—85766
- inertial fusion by oscillating relativistic electron beams in magnetic mirror *(French)* 79—54595
- inertial fusion reactors, feedback-controlled laser-guided pellets 80—73997
- inertial fusion results from Shiva 80—92358
- inertial-confinement ion-beam wet-wood-burner fusion neutron source 80—32489
- inertially confined fusion, high density effects 80—86981
- inertially confined fusion with heavy ion beams 78—50313
- Ingra injector, control and data acquisition system 80—13913
- insulated power transport expts. using MITE accelerator 79—90471
- intense ion beam, production and focusing from self-pinched relativistic electron beam 77—24206
- intense ion beam propag. in z-discharge plasma channels, straight and tapered 80—83948
- intense particle beams, production and handling 79—76117
- intertial confinement fusion, implosion of black body radiation 80—73990
- inverse bremsstrahlung absorption intensity depend., in inhomogeneous standing wave, laser fusion appls. 78—67382
- inverse-bremsstrahlung absorption rate in an intense laser field 80—24201
- ion+electron, energy transfer term in rate eqn., fusion targets 80—5331
- ion accelerators and their use for controlled thermonuclear reactions, review *(German)* 79—67933
- ion accelerators for fusion ignition, neutron resistant ceramic insulator development 80—37639
- ion beam, intense, adiabatic wall focusing for thermonuclear microexplosion ignition 77—61611
- ion beam, intense, supercompression in collapsing pinch 77—80379
- ion beam, low ang. momentum, for pellet fusion 78—50326
- ion beam accelerator, multimegawatt, high-voltage power system, design philosophy 78—62613
- ion beam accelerators, high voltage protection, using floating deck modulators 78—66392
- ion beam direct conversion 78—54920
- ion beam dump, design and development 77—83441
- ion beam focusing and neutralised transport 78—50323
- ion beam focusing by means of mag. insulated diodes 78—50324
- ion beam focusing in intense mag. insulated ion diode, particle diagnostics 78—9858
- ion beam periodic transport system, K-V distrib. stability 78—50329
- ion beam prod. in spherical mag. insulated diode, fusion ignition appl. 79—85200
- ion beam-spherical target, deflagration wave 80—28694
- ion beams, intense, space charge field 79—41325
- ion beams, prod. and focusing for fusion 78—50322
- ion beams, space charge neutralisation 79—45507
- ion beams, transport, space charge effects, computer simulation 78—50328
- ion beams from pulsed linear accelerator for inertial fusion 78—50325
- ion cyclotron heating, Tokamaks and mirrors, quasilinear model 78—59626
- ion cyclotron instability induced by perpendicular beam injection into a plasma 79—14565
- ion diode, dual current feed magnetically insulated for internal confinement fusion studies 79—93851
- ion extractor electrode CAD *(Japanese)* 78—86680
- ion extractor for large area plasma source 77—84466
- ion multifilament source at Berkeley, model 78—13332
- ion source, insulator coated grid with precel voltage, effect on ion optics 78—9014
- ion source, Periplasmatron, for neutral beam injection systems 78—54915
- ion source for JT-60 neutral beam injector 78—54912
- ion-ring igniter for inertial fusion 78—78497
- IRIS implosion experiment experience using four-beam system *(French)* 78—14187
- ISX-B neutral beam injector expt. on prototype beam line 80—74039
- JAERI experimental fusion reactor, neutral injection system 78—54972
- JIPP T-II, simultaneous neutral beam injection and lower hybrid heating 80—79516
- Kal'mar-1 pulsed electron accelerator, relativistic electron beam for fusion 80—32543
- KMSF laser implosion fusion programme, neutron yield and peak fuel density 80—23130
- laminated coatings, for fuel confinement, strength optimisation 78—60883
- large aperture contact ionized Cs^{+1} ion source for an induction linac for fusion 79—76229
- laser, alignment system for large high-power pulsed CO_2 laser fusion system 78—59075
- laser, fusion experiment alignment accuracy meas. 78—55731
- laser, multiple-beam pellet irradiance, diffraction analysis 78—50845
- laser ablated microballoon, 10^6 W cm^{-2}, density modification obs. by optical technique 78—14206
- laser acceleration of reactor-fuel pellets 78—86687
- laser alignment accuracy on target, Hartmann test, direct meas. 79—23004
- laser appl., 'Argus' system *(Czech)* 79—67943
- laser applications *(French)* 79—41037
- laser automated alignment, CO_2 10 kJ laser for fusion research 79—76703

fusion reactor ignition continued
- laser beam alignment, accuracy, Snout test 78—59073
- laser beam appls., future prospects in electrotechnology *(French)* 78—37446
- laser beam Faraday optical shutter, highly uniform mag. field production 78—13719
- laser beam focused on $Z>5$ targets, ion diagnostics of produced plasma 77—68868
- laser beam steering, investig. using hole grating attenuator 78—59071
- laser compressed D-T spheres, fusion neutron heating, Monte-Carlo anal. 77—6553
- laser compression of advanced H-^{11}B fuel, reaction feasibility 77—83084
- laser compression of advanced H-^{11}B fuel, reaction feasibility 77—83085
- laser compression of D_2 filled SiO_2, observations *(Russian)* 78—8968
- laser compression of inertially confined plasmas, future energy developments 80—23120
- laser compression of sphere rel. to controlled fusion *(French)* 77—15216
- laser design for inertially confined fusion reactor 78—58423
- laser driven, non-classical aspects, Zhabotinsky effect and communications theory 77—38404
- laser driven compressions, uniformly redundant array imaging 79—60189
- laser driven fusion, teaching approach 80—42012
- laser driven implosion, anomalous interaction 78—8986
- laser driven implosion, expts. using the Shiva target irrad. facility 78—58483
- laser driven implosion of gas-filled microballoons 78—50317
- laser driven inertial confinement fusion, pulse power technology 80—63385
- laser driven microshell implosion, α-particle and proton meas. 77—10486
- laser driven plasma, vacuum insulation against suprathermal electrons 80—18598
- laser energy absorpt. in practical target illumination schemes 79—23434
- laser energy deposition in planar target, expansion and X-ray emission obs. 78—9810
- laser engineering and appls., conf., Washington, USA (May-June 1979) 80—1216
- laser facility, Shiva Nova, diagnostics of high-yield thermonuclear events 79—41034
- laser focus movement, nonlinear optical technique 80—74446
- laser fusion, 1 TW high power system, Asterix III 77—88765
- laser fusion, 4 TW system 78—74471
- laser fusion, appl. of inert gas halogen pumped I laser 77—34883
- laser fusion, beam transport optics 78—83017
- laser fusion, CO_2 eight-beam Helios laser, evaluation of diamond-turned Cu mirrors 79—23044
- laser fusion, CO_2 single beam irrad., diagnostics 78—51329
- laser fusion, electric power generation 78—50315
- laser fusion, electron thermal cond., plasma hydrodynamic calcs. 77—68750
- laser fusion, energy flux limitation by ion acoustic turbulence, anomalous transport coeffs. 77—43009
- laser fusion, energy transport, implosion, pellet design study by GEKKO II glass laser *(Japanese)* 79—14585
- laser fusion, fast optical shutters for Nova 78—66854
- laser fusion, free electron lasers appl. 79—31919
- laser fusion, interaction and transport processes, continuous pulse shaping 80—28766
- laser fusion, laser heated solenoid reactors, nuclear pumped laser concepts 78—5041
- laser fusion, Nd:glass laser systems 77—88764
- laser fusion, Nd:YAG laser, actively modelocked and Q-switched 79—45980
- laser fusion, operation of short pulse high energy CO_2 laser 77—88758
- laser fusion, plasma confinement, laser compression, Li activation *(German)* 80—52783
- laser fusion, prepulse damage to targets and alignment verification 79—54593
- laser fusion, present state of research *(French)* 78—29645
- laser fusion, progress at Lawrence Livermore Lab., USA 80—57945
- laser fusion, pulse generation using Nd:YAG 77—88809
- laser fusion, scattered energy focusing 77—84467
- laser fusion, self-adjusting laser-target system 79—14024
- laser fusion, status of large Nd:glass JANUS, CYCLOPS, ARGUS and SHIVA systems 77—38929
- laser fusion, suprathermal electron transport, dual treatment 80—18599
- laser fusion, target support fibre, heated by return current 79—45416
- laser fusion, truncated Maxwellian electron vel. distrib., ion expsn. 78—51326
- laser fusion, wavelength scaling 78—51328
- laser fusion cryogenic target characterisation by wavefront shearing interferometer 80—74008
- laser fusion diagnostics, techniques and appl. 80—49009
- laser fusion diagnostics with axisymmetric grazing incidence X-ray microscope 78—75422
- laser fusion DT target, conical, for implosion studies with CO_2 laser 79—41849
- laser fusion experiment, off-axis parabolic mirror fabrication 79—23103
- laser fusion experiments, Nd:glass Argus laser system performance 77—88759
- laser fusion experiments, performance of Argus Nd:glass laser system 78—55361
- laser fusion experiments appl. of eight beam Nd:glass laser 80—33035
- laser fusion experiments at KMSF 80—92355
- laser fusion exploding pusher targets, theoretical performance model 79—82081
- laser fusion expt., damage history of Argus 4 TW Nd system 79—18463
- laser fusion expts., tamper temp. and compression, simultaneous proton and α-particle meas. 78—83607
- laser fusion expts. at Osaka, pellet compression 78—50300
- laser fusion implications of resonance absorption and associated electrostatic field pressure 80—24176
- laser fusion implosion, subns, fast Fourier transform streak photography diagnostics 79—71945
- laser fusion implosion, X-ray diagnostics 78—51362
- laser fusion implosion and target interaction physics 77—88276
- laser fusion ion temp. meas., neutron time of flight techniques 78—17413
- laser fusion microballoon wall-thickness meas. 77—50289
- laser fusion microsphere production, low pressure gas filling 80—32441
- laser fusion Optical Evaluation Laboratory, Antares CO_2 laser system 80—14346
- laser fusion physical processes, investigation 80—74024

fusion reactor ignition continued
laser fusion plasma, HF EM wave swelling effect near crit. density 77—84443
laser fusion power plants, design and operating characts. of optical system 79—76136
laser fusion programme diagnostics, plasma physics on micron and picosecond scale 79—23452
laser fusion reactor concepts 78—58422
laser fusion reactor engineering design aspects of SOLASE 78—58425
laser fusion reactor materials, fusion microexplosion emission, resulting problems 77—30663
laser fusion reactor study, SOLASE, laser, optics and pellet design 78—58426
laser fusion reactor study, SOLASE 78—58424
laser fusion reactor targets, energy partition and neutron spectra 78—58451
laser fusion reactors, conceptual, first wall response to energy deposition 77—34429
laser fusion reactors, optical design, focusing optics 78—82518
laser fusion research, advanced components and systems for beam lines 79—18466
laser fusion research, glass laser feasibility 79—13979
laser fusion research, prep. of solid H_2, D_2 targets using cryostat 78—17417
laser fusion research, present (1977) status *(Japanese)* 78—37439
laser fusion research, progress in Europe 80—74025
laser fusion simulation, hydrodynamical behaviour *(Chinese)* 80—1823
laser fusion system, CO_2 eight beam, SF_6 saturate absorber effects on optical performance 80—106577
laser fusion system beam quality, Laser Optical Train Simulation code 80—78886
laser fusion systems, electrooptic prepulse suppression using Pockels cells 80—102743
laser fusion target, energy transport 78—47143
laser fusion target, fast ions 78—51327
laser fusion target, loading and kinematic positioning 78—58487
laser fusion target, solid-fuel-layer technology 79—49834
laser fusion target chamber, stimulated Raman scatt. 79—9873
laser fusion target interactions at 10.6 μm 77—88274
laser fusion target materials, cryogenic processing 80—32443
laser fusion target microradiographs, wall thickness meas., 2D modelling 79—63804
laser fusion target pellets, mass spectrometer determ. of AR contents 80—32442
laser fusion target uniformity, interferometric meas. 78—47158
laser fusion targets, automated prod. system 78—62608
laser fusion targets, cryogenic technology 80—68939
laser fusion targets, interferometric meas. of microsphere wall thickness variations 79—17470
laser fusion targets, spatially resolved α-emission 77—68811
laser fusion targets, X-ray meas. using least squares fitting 80—32425
laser fusion technology 78—754
laser fusion the Japanese way *(German)* 78—66838
laser fusion theory, computer simulation, expt. 77—34440
laser fusion with 1000 times compression, and kiloJoule laser energy *(German)* 78—41858
laser high energy systems, conference, Reston, VA, USA (Apr. 1977) 78—50783
laser high power system, performance characts. of BETA 77—88761
laser high power system, spatial filter imaging relays 77—88760
laser imploded glass microspheres, numerical modelling 77—24115
laser imploded targets, compressed core density and radius, X-ray spectroscopy meas. calcs. 78—59685
laser implosion, of structured pellet, model 79—10684
laser induced, 1979 development trends and supercompression *(Czech)* 80—23122
laser induced fusion, high-efficiency high-power lasers development *(Japanese)* 78—5486
laser induced thermonuclear fusion, turbulent mixing effect on shell target compression *(Russian)* 80—5332
laser inertial confinement fusion research, 100 kJ CO_2 laser optical design 78—82990
laser inertial containment, principles and problems *(French)* 80—78437
laser interaction and implosion at Centre d'Etudes de Limeil 80—24197
laser irradiated freely falling glass microballoon, hemispherical shock wave 79—63809
laser irradiated target, mag. field transport, nonlocal cond. effects, simulation 78—59637
laser irradiation facility, OMEGA fusion system 78—50811
laser pellet implosion dynamics, high compression, hinged ramp pulse 78—41859
laser plasma compression, computer simulation of implosion struct. *(Japanese)* 79—14587
laser plasma density profile modification by ponderomotive force 78—59634
laser plasma simulation code, PHD-IV 78—59640
laser plasmas, wave absorpt. and superreflectivity due to EM struct. resonances 80—24177
laser processes, Lagrangian vs. Eulerian framework 77—50284
laser produced plasma, flux-limited thermal conduction 78—5899
laser pulse shaping 77—88806
laser pulse shaping for inertial confinement fusion expts. 77—83905
laser pulse synchronisation system 77—88807
laser research, highly repetitive picosecond YAG and glass laser systems 77—88762
laser saturable absorber cells for CO_2 fusion, parasitic oscills. suppression 78—87066
laser short pulses generation in Nd:YAG, laser fusion appl. 78—9404
laser solenoid appl. 77—47250
laser spatial intensity distrib. effect on ablated polystyrene target plasma characts. 78—9811
laser spherical target irradiation symm. calcs. 80—23140
laser start-up system for mag. mirror fusion 77—62383
laser startup system for magnetic fusion 77—18704
laser system, Asterix III, nuclear fusion D, T appl. *(German)* 78—13744
laser system, high energy Ng:glass, multi-lens focusing systems 78—50848
laser system, intense sub ns pulse attenuation and reshaping 77—88870
laser system, multibeam, OMEGA-10, automatic alignment system 78—50847
light beam laser system, multiline energy extraction meas. 77—88275

fusion reactor ignition continued
laser system, p-Ge as saturable absorber 77—88869
laser system, performance of SAIL-1 at. I laser 77—88766
laser system, Shiva Nd:glass, for fusion expts. 78—50812
laser systems, Ge:Ga and SF_6 as saturable absorbers 77—88868
laser systems, photolytic atomic I and rare gas oxide lasers 77—46403
laser systems, solid state lasers 77—88763
laser target behaviour, anal. in CASTOR 2 code 79—86594
laser target compaction, turbulent mixing effects *(Russian)* 79—31191
laser target insertion system 78—46172
laser target irradiation in high mag. fields 78—8989
laser targets, H isotopes condensation 77—42190
laser targets, preparation and parameters, book contrib. 80—23148
laser thermonuclear fusion, large laser control system, evolution from Shiva to Nova 80—9894
laser thermonuclear fusion, shell target parameters meas. using X-ray schlieren method 80—14942
laser thermonuclear fusion problems and progress 78—74500
laser-driven fusion, state-of-the-art review *(Japanese)* 78—21768
laser-driven implosion, Rayleigh-Taylor instability, nonlinear development, calcs. 78—58475
laser-driven implosion experiments 78—58490
laser-driven isentropic hollow-shell implosion, ignition problem 79—31183
laser-driven shock wave inside D_2-filled glass microballoon target 78—41856
laser-driven stable implosion scheme 79—4161
laser-fusion, KMSF group results 77—54358
laser-fusion hydrodynamics calcs. 77—79477
laser-fusion pellet injection accuracies, accelerations and deflections 79—85774
laser-fusion plasma confinement, α-emission recoil force effect 80—6275
laser-fusion reactor producing neutrons for direct nuclear pumped laser 78—9364
laser-fusion system, multibeam, illumination and energy deposition 79—98429
laser-imploded pellets, spatially resolved X-ray diagnostics, book contrib. 77—51242
laser-induced implosion, expt. and theoretical investig. 77—43002
laser-irradiated solid target, nonlinear dynamics 80—28767
laser-produced plasma, high-energy charged particle diagnostics, rel. to nucl. fusion products 77—24190
laser-produced plasma, microsphere implosion, symm. and stability of thermally generated mag. field 77—24118
laser-produced plasma, suprathermal electron effects, sheath generation effects on implosion dynamics 77—24191
laser-produced plasma expts., optical absorpt. 80—14931
laser-produced thermonuclear alpha particle pinhole imaging 77—67934
laser-target illumination reduction, enhanced stimulated Raman plasmon scatt. 77—84470
lasers for fusion appls., energy storage and nonstoring laser media 78—79027
Lawson criterion, impurity losses, numerical soln.of energy balance eq. *(Korean)* 78—17414
layered shell explosive implosion into D-plasma region of compression 79—22455
linear accelerators, recent progress and plans for heavy ion fusion 79—71992
linear high current ion accelerators utilising electron neutralisation 79—72016
liner implosion, energy focusing method 79—31185
load coil, 1.5 MA, 10 MJ, for pulsed homopolar machine 78—13336
lower hybrid heating, nonuniform density, particle simulation model 78—14185
LWHR, source driven, Li-free neutron sources, feasibility and comparisons 79—13383
Mach wave generation, two stage process 79—68924
Mach wave parameters in cumulation cone 79—18034
macroparticle accel. by laser induced ablation pressure, wavelength scaling 77—76156
macroparticle acceleration, megagauss fields 80—47789
magnetic cusp, relativistic electron beam driven inertial fusion, transport calcs. 78—75268
magnetic field generation by Rayleigh-Taylor instability 78—58476
magnetic linac as driver for impact fusion, design 79—67983
magnetic-gun igniter for controlled thermonuclear fusion, travelling wave linac. 80—91238
magnetically insulated vacuum power transmission lines, pulse propag. 79—85765
magnetically stored energy, fast switching into external load, for pellet fusion 78—13339
magnetogasdynamic energy storage in controlled thermonuclear fusion 80—57951
mega-ampere ion beam production and focusing using self-pinched electron flow 77—24205
megavolt and megampere diagnostic techniques for pulsed power particle beam fusion drivers 80—49010
metal hydride target for relativistic electron beams 78—8980
MeV cluster ion beam diagnostics by calorimetry and time of flight spectra 80—13882
micro-explosions, electron beams initiated, progress and future applicability *(French)* 78—746
microdiscs, energy transport to rear surface under high laser irrad. 80—33797
microexplosion ignition by hypervelocity supercond. projectiles 79—89493
microexplosion of pellet, debris energy deposition in wall 78—54890
micropellet implosion in toroidal mag. field with new lens system 77—67535
microshell compression by fast ions generated by laser radiation 78—22526
microwave power, review 80—23151
microwave start-up of Tokamak plasmas near electron cyclotron and upper hybrid resonances 78—94137
MIGMA, colliding beam fusion power source, review 79—18031
minimum beta at ignition, analytic calcs. for transport scaling laws 79—71947
Mirror Fusion Test Facility, neutral beam injection, optimisation by computer graphics 78—66376
mirror machine, 2XIIB, neutral-beam-injected, field reversal expts. 79—86589
mirror-damage thresholds for laser-fusion pulse shapes 78—74467

fusion reactor ignition continued
- multichannel configuration, relativistic electron beam driven inertial fusion, transport calcs. 78—75268
- multiple shell ICF capsules, stability 78—58474
- muon catalysed fusion in cold H, new development *(German)* 79—67805
- MW impulse generator system, for ion cyclotron heating 78—70635
- Naval Research Laboratory, USA, inertial confinement fusion programme 78—59042
- Ne, in glass microbubble, laser-imploded, compression, X-ray emission 78—18454
- negative ion beam, generation, transport and accel. 78—66378
- negative ion beam, intense 150 kV test stand electronics system 78—54934
- negative ion beam acceleration to energies up to 120 keV 78—54918
- negative ion source and beam development at BNL 79—45411
- negative ions from accelerated hydrogen clusters, fusion ignition appl. 80—13883
- neutral atomic beam source, power supply system 78—66393
- neutral beam, 120 keV, calorimetric and optical diagnostics 78—54933
- neutral beam, charged particle separation by space target blowup 78—9018
- neutral beam, pulsed, arc (arc filament) power supplies 78—70637
- neutral beam accelerator electrodes, spark discharge protection 78—62609
- neutral beam filament supply, 15 V 10^3 A, programmable, regulated 78—70630
- neutral beam generation, negative ion revolving multiple beam instabilities *(French)* 80—47798
- neutral beam high-voltage test stand 78—70632
- neutral beam injection, charge exchange and ionis. rate coeffs., analytical approx. 79—86590
- neutral beam injection, control by high voltage switch tubes 80—13875
- neutral beam injection, energy and power requirements for Tokamak reactors 80—91243
- neutral beam injection, fuelling profiles effect on plasma transport props. 80—19596
- neutral beam injection, impurity contaminated Tokamak 80—9403
- neutral beam injection drift ducts for Tokamaks 80—13870
- neutral beam injection efficiency using ion sources with 3 and 4 grids extraction systems 80—13872
- neutral beam injection scenarios for TNS 78—58464
- neutral beam injection system power supply, 80 to 150 kV, development program 78—13367
- neutral beam injection systems based on negative ions, review 80—42852
- neutral beam injection USA research 80—27808
- neutral beam injection vac. components 78—74493
- neutral beam injector, 150 kV, 80 A solid state power supply 80—13888
- neutral beam injector, beam line studies 78—54969
- neutral beam injector, decel voltage effect 78—9015
- neutral beam injector, high voltage series protection by cross field interrupter 80—13884
- neutral beam injector, monoenergetic, power flow and gas flow models 78—66398
- neutral beam injector, simulation of neutral particle transport 80—37600
- neutral beam injector, test device for discharge interrupter 79—85771
- neutral beam injector system, for 2XIIB expt., automated control 78—62620
- neutral beam injectors, continuously operated, grid convective He cooling 79—81083
- neutral beam injectors, electrostatic energy recovery system 78—66400
- neutral beam injectors, fast, for TFR 77—76140
- neutral beam injectors for mirror reactors, arc snubbers 78—13333
- neutral beam injectors for the mag. fusion energy program, development and appl. 79—45404
- neutral beam line improvements from gas flow reduction 79—22511
- neutral beam line pipe, He cryotrapping capability 80—18638
- neutral beam line upgrade for laser initiated target expt. 78—13334
- neutral beam module, 80 keV 78—54917
- neutral beam power supply, series switch/regulator system, 40 kV, 80 A, 10 ms 78—66366
- neutral beam power system, for Princeton TFTR fusion reactor 78—70639
- neutral beam source 8 MW voltage series regulator 78—70631
- neutral beam system, 120 keV 78—66377
- neutral beam system for Princeton Large Torus 78—9019
- neutral beam system for TFTR Tokamak 78—13331
- neutral beam systems, computerised, development and operation 79—93849
- neutral beam test facility, 150 keV 78—62660
- neutral beam test facility, D-D neutron meas. 80—37710
- neutral beam test stand, 120 keV, computer based diagnostic and control system 78—66389
- neutral beams, continuously operating, mech. design criteria 78—66380
- neutral beams for fusion research, review 79—45406
- neutral injection, RIG 10, on RF ion source capability 80—13876
- neutral injection beam line, parameter studies, computer programme 78—66390
- neutral injection beam line, Ti getter pump, corrugated surface and pumping speed 78—74491
- neutral injection fast protection and control circuit 80—13874
- neutral injection heam power monitor system 78—54944
- neutral injection power supply system, for Princeton large torus fusion reactor 78—70638
- neutral injection system, cold gas flow pattern evaluation 78—66397
- neutral injector system, operation above 50 KV 80—13873
- neutral-beam divergence due to imperfect magnetic shielding 78—78489
- neutron generation by implosion of D_2 gas target 78—54869
- non K-V beams, space charge limited transport and bunching in heavy ion fusion 79—76227
- non-linear theory of collective processes in laser-pellet interaction and soliton generation 80—24199
- non-self-sustaining thermonuclear reaction in Tokamak 78—94138
- nonlinear inverse bremsstrahlung and heated-electron distributions 80—48927
- Nova: the laser fusion scientific feasibility experiment 78—59040
- Nova, mechanical design, overview 80—91279
- NOVA laser facility and future programs 80—37590
- Nova laser system design for fusion 78—46652
- nuclear pumped laser fusion blanket optimisation in space and time 80—37616

fusion reactor ignition continued
- nuclear pumped lasers, 'next step' expt., inertial confinement fusion appls. 78—58997
- NUMAK reactor design, fast wave heating via mode conversion and ICRF scaling 80—28815
- Oak Ridge TNS reference design, 1978—plasma engineering considerations 80—13795
- ohmic heating energy storage for power reactor, costing 78—58495
- ohmic heating system for TFTR Tokamak 78—55017
- ohmic heating to ignite fusion in stellarator 78—8978
- OMEGA laser system, design parameters, performance 78—46655
- OMEGA laser system for fusion expts. 78—46649
- Omega laser system for fusion studies, Rochester Univ. 78—59041
- optical system for laser induced plasma compression 80—14382
- optics in adverse environments, conf., San Diego, USA (Aug. 1977) 78—82976
- particle accelerators, power flow studies 78—50320
- particle beam fusion, laser beam with retractable focus, ionis. path form. in gases 79—18992
- particle beam interactions with plasma, inertial fusion appls. 80—59250
- particle beam target, for inertial confinement fusion, mag. field prod. and heating in fuel 78—58480
- particle-beam fusion experiments for fusion ignition, pellet compression and long solenoid approaches, breakeven experiments 80—47720
- particle-beam-induced fusion, inertial confinement 77—42184
- parylene disc, high-power glass laser interaction 78—9804
- pellet ablation in hot plasmas, magnetic nozzle model 80—839
- pellet ablation layer, Rayleigh-Taylor stability 78—58473
- pellet collision fusion, compact exptl. determ. of efficacy 80—18594
- pellet dynamics for heavy ion or laser induced fusion *(German)* 79—49853
- pellet fusion by relativistic pinched electron beams, beam propag. expt. 77—68163
- pellet fusion reactors, heavy ion accelerators and storage rings 79—678
- pellet fusion targets, fast protons energy deposition 78—58404
- pellet heated by multi-GeV heavy ions, filamentation instability 78—89976
- pellet implosion, scheme for stable implosio n, asymptotic theory derived 78—29649
- pellet implosion reactor engineering, use of advanced fuels 78—58444
- pellet targets, laser beam interaction obs. 77—43007
- perturbations accompanying compression of shell target by laser radiation *(Russian)* 78—13321
- phosphate glass 4TW laser system for fusion ignition *(Japanese)* 79—81457
- planar streak tube, for X-ray and optical cameras, laser fusion appls. 78—59686
- planar targets, laser beam interaction obs. 77—43007
- plane hyperdetonation wave generation, optimum conditions 78—67068
- plasma, subignited, α-particle heating 80—92340
- plasma and the controlled thermonuclear reaction, review of practical problems of energy prod. 79—93826
- plasma compression for microfusion, bilinear systems, thermodynamic optimisation 79—67939
- plasma confinement, compact devices, D-T fusion ractions *(Italian)* 80—52778
- plasma focus, recent developments to increase neutron yield 79—14567
- plasma heating by modulated relativistic electron beam-plasma interactions, instability 79—98929
- plasma implosions, mag. field generation due to Nernst refrigeration 79—27811
- plasma instability, in ambipolar traps, appl. to fusion reactors *(Russian)* 79—55535
- plasma ion emission, cylinder and transverse slot ion optics, theory 80—43250
- plasma polymerised films on glass, as laser fusion targets, deposition method 78—60860
- plasma prod. by electrically exploded liquid threads, MHD instability 77—15220
- plasma production by CO_2 laser *(Japanese)* 79—14586
- plasma science, conference, Monterey, CA, USA (May 1978) 79—37442
- plasma sheath driven targets, simulation, fusion yields 80—48898
- plasma source for Tokamak fusion test reactor beam lines 78—54916
- plasma source of high current low energy beams 77—5962
- plasma triode ion beam production, anode design for reflex operation without impedance collapse 78—9862
- plasma-wall heat transfer, fusion appls. 77—11367
- plating discrete microparticles for laser-fusion targets 79—15841
- PLT, ECR fundamental ordinary mode absorption and emission 80—43943
- PLT, neutral beam injectors, component design 78—54966
- PLT, neutral beam lines, development and testing 78—54967
- PLT, neutral beam test stand, data acquisition system 78—62622
- PLT, start-up phase, vol.-second consumption 80—18603
- PLT neutral beam injection, impurity studies expt. ORMAK 78—58438
- PLT neutral beam injection system cryopump, liq. He-cooled 78—74495
- PLT neutral particle injectors 78—58437
- polarized light interferometer for laser fusion studies 80—31855
- polyethylene microspheres, deuterated, variable density, laser fusion targets, prep. 78—74468
- polyethylene pellets, heating using CO_2 laser 79—1331
- polymer shells in laser fusion 78—8987
- polymer-coated laser fusion targets, compression to 10×liq. DT density 80—83964
- polymeric laser fusion targets, cryogenic fuel config. 78—8988
- polytropic plastic gas, nonstationary shock wave propag., closed form soln., thermonuclear microfusion 80—28534
- profiled cylindrical explosion-laser compression of plasma up to hyperhigh densities 77—68837
- profiled shock wave disintegration at cumulation point 79—7463
- proton beam, intense, space charge neutral, trapping in mag. mirror, simulation 78—9825
- proton beam, radially convergent, production by cylindrical double diode 78—9856
- proton collective acceleration in intense relativistic electron beams 78—9864
- pulse shaping effects on interaction processes in laser prod. plasmas 80—43946
- pulse-power particle beam sources as fusion drivers, review 79—18066
- pulsed energy storage in high-β systems 77—74984
- pulsed laser, electronic instrumentation systems 78—78498

fusion reactor ignition continued
pulsed linear accelerators for inertial fusion driver appls. 80—13842
pulsed power acceleration for fusion reactor ignition 80—63383
pulsed power conversion with inductive storage, for particle accel. in fusion device 78—13340
pulsed thermonuclear reactor, ignition of D-T target using electron beams 79—71955
quasi-stationary, Tokamak type, HF plasma heating methods 77—34445
radiation absorption in magnetoplasma, rel. to laser fusion 80—92273
radiation diffraction in high power low system, theory and expt. 79—90431
rare earth halide vapour, discharge, potential fusion laser systems 78—63074
Rayleigh-Taylor instability for impulsively accelerated shells in pellet fusion 77—62384
Rayleigh-Taylor instability generation of mag. fields, effects on laser fusion 79—19025
reflectionless shock-waves used to homogenise a jump-inhomogeneous medium 78—83568
reflex triode system for generation of intense magavolt proton beam 77—24203
relativistic electron beam, anomalous interaction with solid target 80—28709
relativistic electron beam, energy deposition in high temp. targets 79—4157
relativistic electron beam, energy deposition in plane solid low Z target 78—5894
relativistic electron beam, focusing and energy transfer on to target 77—42186
relativistic electron beam acceleration accompanied by beam focusing, for pulsed fusion 77—34054
relativistic electron beam diode, annular cathode, pinching rot. and reflexing in axial mag. field 78—9860
relativistic electron beam diode, intense slow space charge generation appl. to collective ion acceleration 78—9863
relativistic electron beam induced fusion *(Japanese)* 78—1859
relativistic electron beam pinching and combination for inertial confinement fusion 78—50319
relativistic electron beam target design, jacket material and design, Monte Carlo method 78—17416
relativistic electron beam-solid target interaction, fusion induction 77—42187
relativistic electron beams, transport in laser prod. plasma channel 78—71568
research, plasma temp. increase 80—18607
review of potential, thermal insulation and plasma conditions 77—75000
RF phased waveguide heating, thermal eddies form., probe obs. 80—24193
RF plasma heating, effect of wall corrugations on lower hybrid wave spectrum 80—33787
rotationally stabilized liquid liner implosion for fusion plasma production 77—23274
Sandia Labs. particle beam fusion programme 80—23134
Sandia particle beam fusion accelerator facilities 80—37592
saturable absorber gases, for CO_2 laser gain isolation 78—59095
scaling laws for plasma production and pellet acceleration by laser 79—55527
second-harmonic generation of upper-hybrid radiation in a plasma 80—79506
self-excited cumulative flow, compression dynamics and heating *(Russian)* 78—22469
shell, laser compression, two-dimens. effects *(Russian)* 77—4124
shell, thin-walled spherical, for laser-fusion reactor, Taylor instability evolution *(Russian)* 77—46400
shell target monitoring by X-ray Schlieren method 80—86263
SHIVA, 30 TW Nd glass laser system for inertial confinement fusion 79—22978
Shiva, laser-target and laser isolation 78—59035
Shiva alignment systems 78—59033
Shiva fusion laser, development of components and subsystems 78—5491
Shiva high-radiance nd-doped disc laser amplifiers 78—59036
Shiva laser, 25 MJ energy storage and delivery system 78—55015
Shiva laser, 25 MJ energy storage and delivery system 78—59038
Shiva laser beam diagnostics 78—59037
Shiva laser computer control system 78—59034
Shiva laser fusion facility construction, optical engineering problems 78—82989
SHIVA laser optical component manufacture and testing 79—22980
Shiva laser performance, nominal interstage beam energy, power 78—59032
Shiva laser system for laser fusion 78—50820
Shiva mechanical systems 78—63135
Shiva optical system 78—59039
Shiva pulse power conditioning, isolation and control system 78—54935
shock wave induced fusion, multiple refraction problems in layered medium 80—5330
shock wave thermal ionisation production method 80—13902
small-aspect-ratio torus for demonstrating thermonuclear ignition 79—71966
Solase laser fusion reactor, wall protection scheme 78—58491
SOLASE laser fusion reactor design and its technological implications 79—71974
solid pellet acceleration using plasma gun 79—90470
solid target-intense CO_2 laser beam nonlinear interaction, radiation obs. 78—22562
space charge ion optical systems, expt., theory 78—9020
space time implosion characts. of fusion targets, X-ray obs. 77—27725
spherical implosion, of coalesced weak shocks, approx. anal. soln. 77—55161
spherical implosions, instability growth and saturation simulation 77—79480
spherical laser fusion target, uniform illumination 78—13317
spherical laser target hydrodynamic compression stability *(Russian)* 80—106159
spherical shell targets, laser-driven compression and neutron generation obs. 77—42188
spherical target in multichannel laser system, irrad. symm. calc. 78—13323
stellarator, possibility of medium energy neutral beam injection 77—31489

fusion reactor ignition continued
superpinch implosion, isentropic compression of thermonuclear plasma 78—5032
symmetrical implosion system, charged reaction products, electrostatic field effects 80—32499
synchrotron high energy accelerator system for intense heavy ion beam, inertial fusion igniter 79—72040
target fabrication of CVD of Mo_2C 78—60861
target production, for inertial confinement fusion power plants, costs. 78—58488
targets, six-beam irrad. and implosion, laser focus depend. 80—14919
targets for energetic ion beams, design 79—54218
targets for laser and electron beam fusion, design space 79—18037
TEA-CO_2 laser pulse interaction with dense H plasma 80—38683
telescoping beams for heavy ion fusion 79—76228
TFR 604, circular periplasmatron ion sources for injection system 80—13871
TFTR, neutral beam injection system 78—54971
TFTR neutral beam injector, calorimeter and beam dump design 78—66382
TFTR neutral beam injectors, neutronics calcs. 79—59253
TFTR neutral beam source, power supply system 78—66394
TFTR prototype neutral beam injector, test facility 78—62659
TFTR Tokamak, 120 kV neutral beam injector, development status 80—13887
TFTR type neutral beam system, ion accelerator design and fabrication 78—66381
thermonuclear combustion in plasma with electron thermal cond. *(Russian)* 78—13319
thermonuclear energy prod. by imploding pre-heated plasma 77—10489
thermonuclear explosion microfusion, internal break-even neutron number eval. 79—71943
thermonuclear fusion by laser, Soviet progress report *(Russian)* 77—26878
thermonuclear fusion expts. 78—41857
thermonuclear fusion plasma, laser coupling and implosion 77—43006
thermonuclear fusion plasmas, elem. processses and role of atomic, ionic and mol. data 80—14916
thermonuclear microexplosion reactor, heavy ion beam ignition and inertial confinement 79—59252
thermonuclear microexplosions ignition by acceleration of magnetically insulated foils to ultrahigh vels. 78—46163
thermonuclear neutron production of action of laser on conical target *(Russian)* 78—13320
thermonuclear neutron pulse, electron beam generated, scintillator-photomultiplier response 78—51357
thermonuclear plasma, nonspherical implosion geometry 78—21762
thermonuclear reaction wave in high density plasma 77—10487
thermonuclear reactions, laser compressed, thermalising and electrodynamic coupling 77—11374
thermonuclear reactions in laser fusion, emitted particle spectra, Monte Carlo calcs. *(Russian)* 80—52780
thermonuclear target, electron beam heating and compression 77—42185
theta-pinch, linear, solid end plugs and mag. mirrors, fusion reactor 77—89294
theta-pinch description form classical electrodynamics 79—90436
theta-pinch plasma column, design of Marshall implosion coil for shock heating 77—23267
three-phase pellets for inertial confinement systems burning waste U from fission reactors 77—61600
TMX injector system, mech. design 78—66403
TMX neutral beam power supply, 40 kV, 25 ms 78—62610
$n\tau$ criterion for fusion plasmas, fusion-fission analogy 78—74469
TNS, ignition test reactor, decision modelling 78—50362
TNS Tokamak plasma, small radius start-up, moving limiter effects 78—50360
Tokamak, advanced fuel, start-up, T enrichment effects 77—88278
Tokamak, catalysed-D, startup investig. 77—34470
Tokamak, characts. of low temp. ignition 77—18699
Tokamak, characts. of low temp. ignition 77—18700
Tokamak, cycled, energy optimisation of burn phase 77—38406
tokamak, decision model for near term (TNS) ignition reactor 78—58415
Tokamak, driven, plasma parametric studies and appl. 80—42865
Tokamak, dynamic model for energy optimisation of cycled reactor 78—13318
Tokamak, effect of fuel pellet injection velocity on energy parameters 80—32490
Tokamak, experimental power reactor, plasma studies 78—66418
Tokamak, heating by accelerated neutralised change carriers *(German)* 78—67377
Tokamak, high field compact, plasma cahracts., start up scenario 78—8975
Tokamak, ignition demonstration reactor development 79—18045
Tokamak, lower hybrid heating to ignition 80—18605
Tokamak, lower-hybrid-freq. heating, parametric instabilities 79—90426
Tokamak, multimegawatt neutral beams, review 79—76234
Tokamak, neutral beam injection, low density ignition scenarios 80—48937
Tokamak, pellet fuelling, effects of transport on injection 79—89501
Tokamak, Petula, vac. vessel and RF coils for compressional transit time mag. pumping heating 78—70634
Tokamak, reactor size, diffusive losses and scaling law 78—87478
Tokamak, start-up phase, plasma impurities effects 77—14265
Tokamak, startup anal. 79—49843
Tokamak fusion ignition, lower hybrid heating system 78—70636
Tokamak fusion reactor, ignited operation regimes 80—10423
Tokamak He-cooled solid breeder system, UWMAK-II, conceptual design 77—3160
Tokamak heating by plasma column mixing, electrotech. method 79—32789
Tokamak high field ignition test reactor using Bitter magnets 78—58417
Tokamak ignition equilibria and thermal stability 80—74005
Tokamak ignition test reactor, TNS, consideration of bundle divertors 78—58440
Tokamak magnetic confinement, recent progress in Tokamak expts. for fusion energy prod., review 79—71948
Tokamak plasma, fueling profiles and radial transport 78—66421
Tokamak plasma, RF power coupling antennae for ion cyclotron heating 80—13878

fusion reactor ignition continued
Tokamak plasma overheated underdense, two-zone model and 1-D transport code 80—63376
Tokamak plasma power coupling by 500 KW RF amplifier 80—13877
Tokamak plasma startup system 78—62612
Tokamak plasmas, advanced-fuel, ignition and thermal stability 80—86970
Tokamak power reactor, electron-cyclotron-reson.-heated, characts. 79—31188
Tokamak power reactors, initiation pulse prod. methods in ohmic heating circuits 78—55730
Tokamak reactor, fuel injection, dynamic burn control 1-D transport code 80—68948
Tokamak reactor, short-pulse D-T, burn phase control 79—86604
Tokamak reactor, toroidal magnetic field ripple, burn control 80—63375
Tokamak reactor, UWMAK-III, using closed cycle He gas turbines 77—6555
Tokamak reactor with injection of deuterium and tritium ions, calc. of characts. 78—37447
Tokamak superconducting toroidal field coil concept 79—31200
Tokamak TNS studies 80—27810
Tokamak with poloidal divertor, discharge startup 80—48942
toroidal fusion reactor design based on reversed field pinch 79—71977
toroidal plasma, D-T to catalysed-D operation, trapped ion scaling law 78—66419
toroidal plasma compression by imploding plasma liner 80—33811
tritium filling and monitoring apparatus for particle beam inertial confinement fusion targets 80—57949
TTT, current penetration and resistivity, probe diagnostics 79—32821
Twin Beam Mirror, effect of hot beam injection angle 80—48939
twin beam mirrors, effect of hot beam injection angle 78—58466
two component plasma vortex approach to fusion 79—85770
two electrode ion beam formation system 78—9016
two-component torus, reactivitity calcs. 77—23299
two-stage 150 keV accelerator, ion beam optics 78—9017
two-stage cumulation method 79—68923
ultraintense heavy ion beam generation, by radiation cooling in long drift tube 78—58489
vacuum arc fusion switch development 78—13341
vacuum beam diodes, repetitively pulsed for inertial confinement fusion 80—63386
Wendelstein VII A, injector design 78—54965
wire explosion to create controlled supercritical fission for pulsed D-Li reactor 77—15221
X-ray emission in laser imploded targets, three-dimens. reconstruction 80—79563
X-ray microradiographs of laser fusion targets, improved image analysis techniques 80—79562
X-ray pinhole photography of the target pellet in laser fusion *(Chinese)* 79—97458
X-ray stream camera, ultrafast X-ray diagnostics for laser fusion experiments 77—79185
Z-pinch for CO_2 laser pellet simulation expts. 78—55742
Z-pinch plasma, focused ion beam microinstability, pellet fusion appl. 79—32785
Z-pinch thermonucl. imploding liner, model calcs. 77—74995
α-particle generator pellet for commercial power production 77—50285
D plasma, explosion fusion, optimisation of Ar admixture 79—41031
D-T pellet, ideal gas treatment, implosion and shock waves 78—55735
DD reaction for neutron generation in thermonuclear reaction initiation *(Russian)* 80—42848
Al coated glass microballoon targets for laser implosion expt., search for shell disintegration 80—33792
Al microdisc targets for single beam laser expts., prod. method 78—1865
$Ar^{16,17+}$ filled glass shell, symmetric laser compression 80—64759
Au pellet fusion target-particle beam system, radiative opacity 80—10365
^{11}B-p, microexplosion ignition schemes 79—18030
$^{11}B(p,\alpha)2\alpha$, fuel for advanced fusion plant 77—83100
CF_3I, I laser medium, UV absorption profile modification by vibr. excitation, for fusion ignition 78—58717
CO-O_2-SF_6, efficient CO_2 laser radiation 3rd harmonic generation, for fusion ignition 78—59087
CO_2 dual beam laser system for fusion ignition *(Japanese)* 79—81456
CO_2 laser, Antares system, 100 kJ, for fusion expts. 78—46665
CO_2 laser, nsec pulse amplification at efficiencies greater than 20% 78—50818
CO_2 laser, optical isolation by flowing gaseous saturable absorbers 78—59096
CO_2 laser amplifier, short pulse amplification calcs. 78—58979
CO_2 laser Antares fusion system power amplifier optics 80—74394
CO_2 laser Antares fusion system beam alignment 80—74422
CO_2 laser Antares fusion system, mirror quality specifications 80—74423
CO_2 laser Antares fusion system optical diffraction computation 80—74424
CO_2 laser Antares system, power amplifier module 78—46666
CO_2 laser Antares system, optical design and anal. 78—46667
CO_2 laser Antares system, energy extraction, pulse shaping 78—46668
CO_2 laser beam-diagnostics techniques, laser beam parameter monitoring 80—64089
CO_2 laser fusion effort at Los Alamos Scientific Lab. 78—33290
CO_2 laser fusion systems, optical design approach for design and assembly 79—86193
CO_2 laser fusion system optical design and analysis 80—74391
CO_2 laser fusion system alignment by IR Smartt interferometer 80—74425
CO_2 laser fusion system wavefront correction, deformable mirror design 80—74427
CO_2 laser fusion system phase conjugation 80—74429
CO_2 laser fusion system, optical design considerations 80—78868
CO_2 laser fusion target alignment 78—46706
CO_2 laser Gemini fusion system optical performance 80—74392
CO_2 laser Gemini fusion system, wavefront error correction by deformable mirror 80—74426
CO_2 laser Helios fusion system, multicomponent gaseous saturable absorber optimisation 80—74393
CO_2 laser Helios fusion system, beam simultaneity system 80—74419
CO_2 laser Helios fusion system alignment 80—74420
CO_2 laser Helios fusion target positioning with orthogonal telescopes 80—74421
CO_2 laser Helios fusion system beam diagnostics 80—78882
CO_2 laser system, pulsed, for fusion research 80—58556

fusion reactor ignition continued
CO_2 laser systems for laser fusion appls. 78—50817
CO_2 laser-plasma interaction, stimulated Brillouin backscatter saturation 80—24175
CO_2 long-pulse 2 GW single longit. mode source for laser-matter expts. 80—78860
CO_2-laser radiation filamentation in underdense H_2 plasma, X-ray diagnostics 80—14941
D catalysed plasmas, critical impurity conc. 78—37445
D fuel pellets, laser acceleration for injection into thermonuclear reactor *(Russian)* 80—52779
D pellet, ionisation by Nd laser irrad. 80—43949
D plasma, amplification of laser implosion velocity 79—68938
D plasma, density optimisation in conical system for explosion fusion 79—41032
D plasma neutron generation by CO_2 laser implosion of polyethylene shell into conical region 78—87468
D, shell target compression on laser heating *(Russian)* 80—47718
D source, magnetically insulated, pulsed, peak beam parameters 80—32548
D^- ions. equil. charge state fractions of 3.3-39 keV D atoms and ions in Mg vapour 77—57788
D^-, neutral beam production for plasma injection heating research 77—76118
D^-, prod. of 100 keV beam, transport, accel. and diagnostics 77—83440
D^- source using surface ionis., continuous beam prod. 78—9021
D^+ beam production in relativistic electron beam oscill. diode 78—9861
D-Ar mixture, effect of Ar admixture on plasma temp. 79—37446
D-D plasma interaction with relativistic electron beam, thermonucl. reaction, neutron and proton prod. 80—37575
D-fusion, shock wave induced, Ar admixture optimisation 80—5329
D-T ball, compressive plasma fusion using CO_2 lasers 78—82507
D-T ball, laser driven compression with profiled explosion induced precompression 77—68838
D-T burning test facility for JT-60 79—71963
D-T charges, explosion-induced compression for thermonuclear microfusion, power station parameters 78—82508
D-T compression, explosion-induced, cylindrical system with heavy inertial layer, neutron yield 80—68944
D-T concentric plasma compression, optimum output of fusion neutrons 79—41030
D-T explosion induced compression, neutron yield 79—67940
D-T explosion induced compression, neutron yield, thermal conduction effects 79—67941
D-T filled glass microshell, laser-irrad., plasma electron energy profile steepening, polarimetry obs. 78—34349
D-T filled glass shells, plasma polymerisation coating method 78—60859
D-T filled laser fusion microballoon targets, fuel content characterisation and press. retention meas. 79—54594
D-T fuel temperature in laser fusion targets, neutron energy spectra obs. 77—89317
D-T gaseous core fusion, crit. parameters, dense medium profiled explosion 79—45413
D-T laser fusion target, fabrication using cold-gas jets 79—49833
D-T plasma, density optimisation in conical system for explosion fusion 79—41032
D-T plasma, kinetics of compression induced fusion chain reaction 78—50297
D-T plasma, thermonuclear reaction product kinetics effect on parameters 80—5327
D-T plasma ball, critical continuously shaped concentric explosive compression, approx. estimate 78—87473
D-T plasma compression by profiled explosion, neutron output 80—13782
D-T plasmas, ignition toroidal expt., equilibrium configs. and heating 80—28704
D-T target, laser pulse compression, thermonucl. reaction initiation *(Russian)* 77—23249
D-T Tokamak, high-density, ohmically-heated, transport calcs. 80—24142
D-T tokamak plasma effect of particle confinement and recycling on thermally stable regions 79—97900
$D+T \rightarrow He^4+n+17.6$ MeV, possibility of using U^+ accelerated ions *(Norwegian)* 79—30871
D_2 filled glass microspheres for multibeam laser-target expts. 78—82509
D_2 plasma, compression by microfusion explosion, expt. biconical system 80—13783
D_2-^3He, filled microspheres, implosion expts. 78—59672
DD advanced fuel, fusion dynamics reactivity coeffs. 77—23296
DD laser produced plasma in shell target, diagnostic methods 77—62408
DD, microexplosion ignition schemes 79—18030
DT gas-filled shell, cryogenic, laser fusion 78—8985
DT glass microballoon, Ne seeded, compression by CO_2 laser 79—22466
DT laser compression, computer simulation, shock and thermal waves *(Chinese)* 79—90428
DT linear mag. fusion reactor, thermal cond. and alpha-particle restraints 79—9870
DT near critical explosion compression, neutron output 77—67867
DT plasma, amplification of laser implosion velocity 79—68938
DT plasma in biconical system, neutron generation by shell implosion 79—37524
DT plasma in glass shell, laser-induced fusion, spectrum and absolute yield of α-particles 77—79482
DT reaction rate in laser fusion pellets, effect of high energy ion loss 80—32495
DT sphere compression, neutron yield, self-similar hydrodynamic model 77—18703
DT thermonuclear miniexplosion produced by explosion compression, energy output minimisation 77—67896
DT-Pu plasma, neutron induced fission, fission fragment slowing down 79—26749
DT-Pu plasma, neutron induced fission, enhancement of neutron prod. and fusion rate 79—26750
DT-Pu plasma, neutron induced fission, plasma heating effect 80—27800
F_2, VUV high-power laser, laser-induced fusion 78—58996
H ion source, hollow cathode device 78—54921
H isotopes, transition radiation from neutral beams, beam foil ionization 79—18299
H^- cluster ion beam high power injector 80—13889
H^-, production by Hall accelerator in Cs vapour, space-charge effects 78—67375
H^- sources for neutral beam injection 78—54919
H^+ beam production and 0.5 TW pulse driven implosion 79—31288

fusion reactor ignition continued
H^+, intense beam generation, appl. to controlled fusion 77−76119
H_2 plasma, neutral H ats. penetration, kinetic theory 79−32782
H_n^+ multispecies beam, particle species evolution in neutral-beam injection lines 79−85846
HF, high-energy laser, energy extraction, beam quality, for fusion ignition 78−63102
HF laser possible use as laser-fusion drivers 79−22979
H_2O, dielectric insulation for electron accelerators and impulse current generators *(Russian)* 78−75430
$H(1s)+O^{8+}(He^{2+})(H^+)$, charge transfer, 0.025-200 keV/amu 79−22823
HgCl discharge laser, electron beam sustained, operation, appls. 78−59043
I laser, high-power, beam quality, gain saturation effect, for fusion ignition 78−63149
I laser possible use as laser-fusion drivers 79−22979
KrF laser beam, Raman pulse compression, for fusion expts. 78−59086
Li+doubly charged ions, electron capture excitation, theoretical predictions in fusion plasma 80−63810
^6LiD advanced fuel, fusion dynamics, reactivity coeffs. 77−23296
$^6Li(n,\alpha)T$, mechanism for driving ^6LiD pellet to fusion temp. 79−93823
$^6Li(p,\alpha)^3He$, fuel for advanced fusion plant 77−83100
Na vapour, electron and ion beam transportation channel form., reson. saturation based laser ionis. 79−77410
Nd:BeF_2 glass lasers for fusion expts. 78−46661
Nd:glass, fluorophosphate glass for fusion lasers 78−46660
Nd:glass laser irradiated fusion targets, time and space resolved harmonic emission 79−82095
Nd:glass laser system, multichannel, for fusion experiments, model 80−58557
Nd:glass laser system, pulse shaping 78−46658
Nd:glass lasers, optimisation for 1-10 ns pulses operation 78−46651
Nd:YAG short-pulse oscillator, for Shiva 78−63134
$NdCl_3$-$AlCl_3$ vapour complex, optical gain at 1.06 μm, rel. to appl. in fusion laser amplifier 78−33742
Ne microballoon, laser compression, X-ray emission diagnostics of explosive pusher mode 79−54598
Ne plasma, compression, spectra, temp. and density calc. model 78−59663
Ne spectral line broadening as diagnostic for compressed laser fusion targets 79−98979
OCS laser, two-quantum excitation, photolysis, energy transfer, for fusion expts. 78−59003
Pb, mass ejection from shocked surface during fusion 78−47186
Pd alloy membrane pump, for thermonuclear fusion devices 78−89980
Se photolytic fluorescence pumped gas laser system 78−62606
SiO_2, laser-fusion microballoon, expansion density profile, 10.6 μm irrad. 78−86686
T breeding and burning within laser compressed pellets 77−83103
T low inventory for inertially confined fusion, high thermonuclear gains 78−50339
Tb-Al-Cl vapour complex, fusion laser gain medium 78−63073
$TbCl_3$-$AlCl_3$, vap., high-energy laser medium props., for fusion ignition 78−63075
$TbCl_3$-$AlCl_3$ vap. complex, kinetics and laser fusion pot. 79−98343
U, profiled explosion-induced compression 78−50296
UF_6, plasma expts. related to plasma core reactors 78−8977
UF_6-He mixture, ballistic piston fissioning plasma 78−5038
XeF(B) nuclear pumping, candidate laser fusion driver 79−86171
XeF*-UF_6, nuclear pumped excimer fusion lasers, kinetic model 79−18410
XeF*(B), nuclear pumped laser, buffer effects 80−37617

fusion reactor materials
see also fission reactor materials; radioactive waste
A15 superconductors, radiation induced Tc, gap anisotropy effects 78−52125
advanced fuels, reactivities for two-component calcs. 77−23299
advanced nuclear energy systems, emerging concepts, conf., Graz, Austria (March 1978) 79−13381
alkali metal, liq., reactions with refractory metals and oxides, relevance to reactor technology 80−85173
alloy damage effects, simulation of likely neutron environment 78−8972
alternative advanced fuels, cat-D, D-T and D-^{3}He comparison 80−99310
ANS annual meeting, 1977 78−663
ATJ graphite, ultrahigh vac. compatibility, outgassing characts. 79−81080
atom displacement and He prod. using fusion reactor first wall neutron spectrum 78−46168
austenitic stainless steel 316, trapping up to 7 eV D, depth profiles 78−71751
barium aluminosilicate glass coating on NbZr, d and He ion irrad., blistering 77−35605
blanket designs, near term, thermal-hydraulic and mechanical anal. 78−58452
blanket designs for catalysed D-D and D-^{3}He Tokamak reactors 78−74480
blanket first wall time-depend. thermal stress model 78−787
blanket material impurity hazardous activity and dose rates, biological hazard pot. 80−102315
blanket models, calc. of T breeding per source neutron 79−67934
blanket neutronic performance in CTR, influence of design variations, variational interpolation techniques 77−34437
blankets for fusion augmented steam turbine 79−22475
brittle materials, swelling, blistering by 140 keV p, d and He ion irrads. 77−35603
bubble nucleation, He-assisted, computer simulation 78−86625
C and graphite cloths and fibres, neutron irradiation effects 78−78496
catalysed D fusion reactor blanket, gas-suspended, B_4C cooled, nuclear characts. 78−58400
cavity gas response to particle beam target explosions 80−37602
ceramic insulation joints for Frascati Torus 80−18653
ceramic ring assemblies, brazing techniques for TFTR injector and pumping ports 80−32476
ceramics, applications in fusion systems, neutron effects 80−32473
ceramics, design criteria for blanket and first wall regions 80−32474
ceramics, design methodology and anal. 80−32475
ceramics, erosion in high temp. steam and H atmosphere 80−35334
ceramics, TEM study of radiation damage, review 79−86816
ceramics, Weibull probabilistic design approach 79−93822

fusion reactor materials continued
ceramics utilization in nuclear industry, current status and future trends, review 79−45349
charged particle prod. cross sections for 14 MeV neutrons, Ti, V, Cr, Mn 80−42648
Chinese research 80−78447
coated heat sink materials, evaluation studies 80−32453
coated heat sink materials for fusion appl., thermal shock testing 80−18651
coating materials for inner vac. liner of ORMAK 77−30669
coatings for fusion reactor environment 80−18618
cold gas blankets for RINGBOOG II reactor *(Dutch)* 80−32498
cold turbulent plasma blanket, anomalous heat transport 80−18604
compact Tokamak fusion reactor, materials comp. and weight of blanket and shield 79−71970
composite liners, thermal fatigue tests 80−32460
composition changes in neutron-irradiated materials, calculation methods 77−62565
compound superconductors, radiation effects on critical currents 78−52175
concrete shields, neutron activation props. 80−13787
conduction cooled min. activity blanket for TNS and EPR fusion reactors 78−781
conference on fusion reactor materials [Miami Beach, Florida, Jan. 1979] 80−31407
constitution changes due to radiation effects 80−34048
coolant compatibility with structural materials 80−32462
cryogenic inertial confinement fusion target fabrication system operable inside room-temp. chamber 80−106152
cryogenic targets for laser-driven fusion, H_2 freezing on inner surface of spherical polymer shells 78−86688
CTR, engineering and technology considerations *(Spanish)* 79−36399
CTR, model blanket expt., neutron spectra sensitivity analysis 78−29648
CTR blanket design *(Japanese)* 78−46164
CTR blanket model with graphite reflector, tritium prod. anal. 77−61609
CTR first wall, high power ion-irrad. test 80−78443
CTR first wall materials, irradiation effects 77−6561
CTR first walls, high power ion-irrad. test 80−68941
CTR first-wall irradiation environment, appl. of dual-ion accelerator 78−13325
D_2 target fabrication for laser fusion *(Japanese)* 78−8971
damage energy functions for compounds and alloys 78−86692
deuterium distillation at desalination plants 77−67894
development of fusion mats. 80−33804
development studies, irradiation sources 80−32478
development trends 77−46401
dielectric target fabrication for electron beam fusion 78−50302
discrete ordinates method, sputtering calc. 78−86689
divertor target material choice 79−665
Doublet III, limiters, materials selection 78−55026
Doublet III, toroidal field coils, Cu alloy plate defect size restrictions 80−91257
DT self-propelling pellets for fusion-reactor refueling 79−677
electrical contacts, for homopolar generators, tests at high surface vels. and current densities 78−54964
electrical insulators, radiation effects on organic polymers and ceramics 78−95082
electron beam fusion, pellet and pellet-blanket neutronics and photonics 80−74006
electron beam fusion compression targets, fuel preconditioning studies 79−81076
environmental aspects of the fusion materials resource cycle 80−18616
epoxy glass based poloidal coil insulation system, for JET, mechanical tests 80−18669
exotic fuels charged particle cross section meas. 77−23293
fast neutron spectra, activation technique determ., fusion reactor blanket model appl., unfolding program 77−79500
FINTOR-DEMO fusion reactor, fibre-reinforced epoxy resins for cryogenic support 80−32434
first wall, enhanced diffusion simulation by fission fragment irrad. of α-brass 79−63810
first wall, fusion product. bombard., prompt and non-prompt contrib. 80−106156
first wall, materials science 79−97899
first wall, metal surfaces, scatt. of H ions 77−36337
first wall, prod. of H, D and He by 15 MeV neutrons 79−93831
first wall, radiation damage simulation using fission reactor test facilities 80−57950
first wall, sputtering coeff. calcs., 1 keV H^+, D^+, T^+ and He^+ *(Russian)* 77−8697
first wall, surface resist. 80−42853
first wall and divertor plate material selection 78−94129
first wall design, safety study of primary coolants 79−9871
first wall erosion, blister-induced, alpha incident velocity and poloidal angle distribs. 80−37583
first wall material, mobile He inclusion in void swelling rate theory model 80−34069
first wall materials, compatibility with impure He 80−32469
first wall materials, depth profile of near surface C contaminant 77−34433
first wall materials, H release 80−37579
first wall materials, H trapping characts. 79−45407
first wall materials, light ion sputtering studies 80−18647
first wall materials, mechanical, corrosion and irrad. behaviour requirements 77−67875
first wall materials, sputtering by H^+, D^+, T^+ ions 77−36343
first wall materials, thermal stress and creep fatigue limitations 79−76132
first wall materials development evaluations, fatigue crack growth testing optimisation 80−35444
first wall model, mechanical anal. using state variable approach 80−32452
first wall neutron spectra prod. around 14 MeV point source, feasibility study 79−54597
first wall of thermonuclear reactor, diffusive action of radiation *(Russian)* 78−29639
first wall radiation damage, H and He gas prod. from stainless steel 78−82512
first wall structural materials, prediction of life limiting props. 78−62605

fusion reactor materials continued
first walls, hydrogen profiles 80—37578
first-wall alloy program, appl. ORR fission reactor for simulation of neutron environment 78—8973
first-wall material, computer model, design lifetimes determ. 78—82513
first-wall materials, ionisation-assisted damage processes 77—34432
first-wall materials, sputtering model 78—82514
first-wall structural mats., stress and lifetime limitations 80—32447
first-wall/blanket and associated structural mats., performance, safety and economics 80—32432
fission cross sections meas. In YAYOI reactor, fast neutron spectrum 77—42013
fissioning matter in blanket, parameters of Tokamak type hybrid reactor 77—34446
FMIT accelerating struct. design 79—76160
FMIT damage parameters spatial variations, implications 80—34065
FMIT neutron source, energy spectra and yields, fusion reactor mat. development appl. 80—32552
fracture resistance determ. 78—82515
fuel, fussion-triggered fusion pellets design, review 79—13519
fuel cycles, reactor types, future role of nuclear energy *(German)* 78—29579
fuel pellets, coupled nuclear-thermohydrodynamic anal. of laser-fission-fusion systems 79—13520
fuels for inertial confinement systems 77—10491
fusion and fast breeder reactors, a comparison, book 78—78430
fusion devices, controlled, surface effects, conf., San Francisco, USA (Feb. 1976) 77—30659
Fusion Materials Irradiation Test Facility, high flux neutron source for material development 80—32551
fusion reactor first walls, temp. and displacement transients 78—58427
fusion reactor first-wall performance under ion bombardment and cyclic stresses, in-reactor materials testing 80—104407
fusion-fission hybrid reactor, mirror confinement, fuel design consideration 79—22472
fusion-fission hybrid reactor fuel cycle considerations 79—22474
fusion-fission hybrids, mag. mirror blankets and drivers 79—13517
fusion-fission symbionts, nuclear fuel trajectories, fissile and fusile fuel characterisations 80—68947
gaseous impurity origin, meas. by mass spectroscopy in JFT-2 Tokamak 79—1339
glass, blister formation by 150 keV He$^+$ irrad., effects of gas diffusivity 77—35604
glass and polymer shells fabrication for inertial confinement fusion 78—50316
glass fibre reinforced epoxy, as electrical insulation for Tokamak toroidal field coils, mech. props. 78—64610
glass fibre reinforced epoxy prepreg, PDX TF coil insulation 78—62656
glass fibre reinforced epoxy resin, mech. props. 78—64582
glass fibre reinforced polymer matrix laminates, compressive strength 78—64609
glass microbubbles, method for polishing bubbles into hemispheres 78—95869
glass microsphere laser targets, He and H_2 permeation 77—83078
glass microsphere laser targets, He and H_2 permeation 77—83079
glass shells fabrication 78—50301
glass sphere laser fusion targets, fabrication, liquid-droplet and dried-gel systems 80—32440
graphite, chemical sputtering by H$^+$ ions 77—36341
graphite, cloth erosion by 20 keV H_2^+ and He$^+$ ions 79—46725
graphite, conditioning of surface by atomic H 80—93665
graphite, CTR material, the ion injection effect 78—34557
graphite, D$^+$ bombardment, surface damage, sputtering, SEM study 80—32459
graphite, degassing rate measurement 80—102306
graphite, energetic deuteron irradiated surface struct. quantitative meas. 78—95210
graphite, energetic ion sputtering, appl. of AES-SIMS (IMA)-FDS combined systems to physical and chemical processes 78—95636
graphite, energy deposition from pellet microexplosion 78—54890
graphite, fusion reactor first wall appl., radiation damage 79—86822
graphite, ion bombarded, light gases, structural study using TEM 80—92570
graphite, irradiated with MeV He ions, exptl. study of effects 79—4341
graphite, mechanical constitutive laws for irradiation behaviour 80—32448
graphite, neutron damage at 1200°C, fusion reactor first-wall appl. 79—93829
graphite, permeable, 0.6, 3.5 MeV He$^+$ irrad., surface erosion, porosity effects 77—35602
graphite, pyrolytic, behaviour of implanted D and He 78—95071
graphite, pyrolytic, sputtering yield meas. on first wall materials of thermonuclear fusion devices *(Japanese)* 77—85865
graphite, radiational size stability, effect of technological factors 79—26527
graphite, sputtering, physical and chemical, by H_2 and He, 600 to 7500 eV 77—36340
graphite, sputtering yield, use as first wall material 78—95629
graphite, surface erosion by 100 keV ^{4}He$^+$ and 200 keV H_2^+ 78—23569
graphite, surface erosion by ion bombardment crystal anisotropy effect 78—23845
graphite, surface morphology changes after irrad. with energetic He ions 78—21767
graphite, Tokamak mag. limiter plate, electron irrad. and thermal shock 78—66416
graphite, tritium effects, first wall controlled thermonuclear reactor conditions, simulation 79—647
graphite, unipolar arc damage in hot, dense D plasma 79—3235
graphite, wall and limiter material for Tokamaks, induced desorption diffusion and gas production by 100 eV electrons and ions 79—675
graphite blanket concept for Tokamak reactor 78—780
graphite blanket design concepts at BNL, appl. to Tokamak 77—3164
graphite damage function in neutron irrad. up to 15 MeV 80—34059
graphite limiters for ISX-A expt. 80—32457
graphite liner, thermal response 80—32456
graphite liners, thermal fatigue tests 80—32460
graphite sputtering by low energy H and D 78—95630
graphite structure Li$_2$O cooled blanket, thermal, mech. and neutronic design 78—62652
graphite-Th assemblies for fusion blankets, neutronic calcs. using 14 MeV source 79—59262

fusion reactor materials continued
gross blanket breeding ratio determ., neutronic cell calc. by Monte Carlo methods 79—18033
handling system for ^{3}H, materials considerations 80—32463
Hastelloy N, air contamination effect on compatibility with liquid Li in stainless steel vessels at 600°C 78—25285
Hastelloy X, H permeability using permeation method *(Japanese)* 78—51740
Hasteloy B, equilibrium surface bombarded with high dose He$^+$ ions 78—95091
Haynes alloy 188, H_2 permeability 77—46399
heavy ion irradiation swelling theory 80—34090
high temperature materials problems, review 77—65329
high-temperature materials, technological requirements, R and D, report 80—45222
hybrid, ^{3}H and Pu reproduction problems 77—38403
hybrid blanket data and development, review, simulation test facilities 80—106170
hybrid reactors, materials implications for reactor design 80—32430
hydrogen permeation characts. 79—67948
ICF reactor, first wall protection schemes 80—32437
ICF reactor fuel pellet fabrication techniques and quality factors, optical systems 80—32436
ICF reactor mats., particle-beam-driven, critical environmental considerations 80—32444
ICF reactors, material implications of design and system studies 80—32431
ICF targets, laser driven, materials problems 80—32438
ICF targets, semiconductor process technology for mass production 80—32439
ICFR, first walls, void growth, analytical model 80—63377
ICFR, interstitial loop formation, point defect clustering 80—63378
ICTR walls, thermal response and stress problems 78—813
impurity effects in Tokamak expts., numerical modeling 79—659
impurity flux in scrape off layer of Tokamaks TFR 400 and 600 79—652
in-situ analysis of ion irradiation and implantation effects 79—45408
Inconel, sputtering and blistering from H$^+$ and He$^+$ bombardment 78—79649
Inconel 600, equilibrium surface bombarded with high dose He$^+$ ions 78—95091
Inconel 600, fusion reactor vac. vessel, air, N, adsorpt., thermal desorpt., heat treatment effects 78—54880
Inconel 600, Neutron irradiation using HFIR for evaluation as fusion reactor material 78—13324
Inconel 600, surface composition depend. on H atom influx, AES 79—5192
Inconel 600, thermal outgassing after various surface preparations 79—67952
Inconel 617, mass spectrometric study, high temp. reactor system appl. 79—43663
Inconel 625, electron yields under ion bombardment for clean and oxidised surfaces 80—66368
Inconel 675, wall and limiter material for Tokamaks, induced desorption diffusion and gas production by 100 eV electrons and ions 79—675
Inconel 718, H plasma effects on fusion device vacuum vessel 80—21111
Inconel 718, heat capacity 313 to 1053K 79—10964
Inconel 718 gas-cooled blanket, mech. and thermal design 78—66387
Inconel-625, hydrogen permeation characts. 79—69295
inertial confinement fusion pellet centre burnup of fission reactor actinide waste 79—31181
inertial confinement fusion target, formation of uniform solid fuel layers 80—95432
insulation for supercond. magnets, gamma irrad. effects 80—34051
insulation system for fusion magnets and coils *(German)* 80—27817
insulators, radiation damage calcs. using MORSE code 80—34061
ion bombarded, swelling induced stresses, crystalline orientation effects 80—34093
ion implantation for radiation damage studies 77—80530
ion-beam fusion reactor, first wall costs 78—811
irradiated, defect cluster nucleation, He injection effect 80—34091
irradiation creep by the climb-controlled glide mechanism in Tokamaks 80—102304
irradiation creep facility, materials testing for fast and fusion reactors 79—57192
irradiation effects, Fusion Materials Irradiation Test facility initial target design 80—95410
irradiation test facility, higher energy neutrons, shielding calcs. 80—13786
K-ramic^R, ultrahigh vac. compatibility, outgassing characts. 79—81080
laser driven fusion reactors, assessment of engineering problems 79—36413
laser fusion, energy transport, implosion, pellet design study by GEKKO II glass laser *(Japanese)* 79—14585
laser fusion fuel configurations, cryogenic, survival in fluorescence energy 77—50288
laser fusion microballoon wall-thickness meas. 77—50289
laser fusion microsphere production, low pressure gas filling 80—32441
laser fusion reactor materials, fusion microexplosion emission, resulting problems 77—30663
laser fusion reactors, calculated neutron and gamma irradiation response of metallic mirrors 80—23121
laser fusion target, 4π interferometric meas. of defects 78—50307
laser fusion target, gas content anal. 78—50306
laser fusion target, microradiographic meas. of microspheres 78—50308
laser fusion target, microradiography using monochromatic X-rays 78—50310
laser fusion target, semiautomated anal. of radiographs 78—50309
laser fusion target materials, cryogenic processing 80—32443
laser targets, preparation and parameters, book contrib. 80—23148
laser-fusion reactor SOLASE-1, first wall and blanket design 78—812
limiter materials response for long duration plasma burns 80—32455
limiters; thermal and stress environment effects 80—32461
liquid metal two phase flow, gaseous phase redistrib. in strong mag. field 79—37410
low and intermediate energy radiation physics 80—19845
low energy ion erosion expts., Kaufman source appl. 80—68942
low Z coating development program 80—106182
macrotor, metal influx 79—650
magnetic confinement system, surface problems caused by dissolved H_2 80—57946

fusion reactor materials continued
magnetothermal conductivity measurement for selected metals, 4 to 20K 79−67317
material requirements exam., review 78−50257
material requirements for fusion reactors, exam. 78−50255
metal, clean surface, H release rate 78−95187
metal, interbubble fracture mech. of blister form., He irrad. 78−6109
metal, reactive, trapping of energetic H^+ ions 78−10096
metal atoms sputtered by light and heavy particles, velocity distrib. meas. by fluorescence spectroscopy 78−95626
metal hydride target for relativistic electron beams 78−8980
metal impurities, DITE Tokamak plasma, N-ion backscatt. anal. 79−4182
metal impurity origin in DIVA, ion sputtering, evaporation and arcing 79−656
metal surface, 14.8 MeV neutrons, radionuclide product ejection range 78−15257
metallic surfaces in contact with flowing electrolyte, mag. field effects on electrochemical reactions 77−73369
metals, He embrittlement, grain boundary cavity model 80−34075
metals, point defect and microstruct. behaviour during irrad., appl. to fusion reactors 79−23638
metals and alloys, microvoid form., gaseous impurity atom effects, positron annihilation study 80−49275
MFTF, intense neutron environment, test cell side wall design, shielding materials 80−102318
microballoons, batch processing technique 78−50312
microparticle array preparation device 78−94139
microspheres, computer modelling, image analysis of X-ray radiographs 78−50311
microstructure evolution under irradiation 80−34041
microstructures development in simulated irradiations 80−34072
MIGMA, colliding beam fusion power source, review 79−18031
mirror fusion test facility, beams and supercond. magnets 79−49849
multifilamentary and cabled superconductors, cryogenic stability anal. 79−59260
neutron 14 MeV irradiation, Fusion Materials Irradiation Test Facility 80−91361
neutron activation cross section meas. on wall and blanket materials 77−26881
neutron and heavy ion damage correlation, predicted temp. shift on swelling with radiation dose rate change 79−7630
neutron induced nuclear recoil emission probabilities 78−15256
neutron irrad., low temp., materials research *(Japanese)* 77−72637
neutron irradiation effects on organic insulators at 5K for superconducting magnets 80−107336
neutron multipliers for D-T solid breeder fusion reactors to improve T breeding ratio 80−102296
neutron multipliers for fusion blankets, comparative anal. 79−18049
neutron primary damage, energy depend. 80−34064
neutron production D, laser fusion, neutron production from conical target 79−22467
neutronics analysis using ENDF/B-V cross-section covariance data 80−47710
Nimomic PE-16, equilibrium surface bombarded with high dose He^+ ions 78−95091
Nimonic PE16, He injected, bubble-void transitions in Ni ion bombard. 80−34095
Nimonic PE-16, damage in high energy fluence D plasma 77−34427
NOEL (no external leak) blanket concept 79−18048
nuclear, social aspects *(Dutch)* 80−106153
nuclear energy synergetics, characts. of integrated systems 79−13382
nuclear fusion reactor R and D, technical problems review *(Japanese)* 80−5325
nuclear response functions library, MACKLIB-IV 79−67950
organic materials, adhesives and bulk materials, mechanical characterisation at low temps. 78−64611
ORMAK, contamination buildup on Tokamak liner anal., laser refl. technique 77−34436
ORMAK, first wall, surface impurities and cleaning techniques 77−34435
pellet fusion reactor, thermomech. dynamic behaviour of solid wall 80−95396
pellet implosion reactor engineering, use of advanced fuels 78−58444
physical sputtering model for fusion reactor first-wall materials 78−80445
plasma cooling by metal snow, expt. evidence 78−71495
plasma cooling by metal snow, origin of effect and elimination 78−71494
plasma impurity deposition, in ISX-Tokamak, time resolved measurements 80−38694
plasma impurity flux and differential wall changes, in Alcator-A Tokamak, surface probes 80−38664
plasma spraying utilisation in research work 79−83117
plasma-wall interactions in controlled fusion devices conf., Abingdon, England (April 1978) 78−94917
PLT, vacuum vessel wall surface conditions, long term changes 79−653
point defect production in irradiation, swelling, cascade diffusion theory 80−34044
polyethylene, deuterated, microspheres for laser fusion targets 78−46173
polyethylene microspheres, deuterated, variable density, laser fusion targets, prep. 78−74468
polystyrene, spherical pellets, ablation rates in Q-pinch plasma 77−89265
post-irradiation examination, hot cell complex test facilities in Japan *(Japanese)* 80−63255
proton irradition, 10 to 16 MeV, resistivity changes 80−2082
pulsed radiation effect on void growth and swelling 80−34043
pulsed system first wall, point defect kinetics 79−93827
pure elements, potential reactor materials, He generation by 14.8 MeV neutron 79−67944
pyrocarbon, deposition from gaseous hydrocarbons, kinetic model *(German)* 78−23851
pyrocarbon, methane formation during p and d irrads. and thermal release of K 77−36788
quartz, forming machine for helical or toroidal tubes 78−54886
quartz TFTR diagnostic windows, radiation damage 80−34063
radiation blistering, material distortion *(Russian)* 77−76160
radiation damage, appl. of dynamic computer models to high energy cascades 80−34046

fusion reactor materials continued
radiation damage, range calculations using multigroup transport methods 80−34070
radiation damage, review *(Japanese)* 79−81011
radiation damage problem, systematic approach 78−4984
radiation damage simulation using triple ion beams 79−45410
radiation effects, appl. of simulation expts. 78−46167
radiation effects in superconductors conf., Argonne, Il., USA (June 77) 78−52120
radiation induced exchange reaction kinetics of H_2, D_2 and T_2, review 78−61005
radiation-induced embrittlement and swelling due to void form, ASTM research 78−13231
radioactivity minimization by elemental substitution and isotopic tailoring 79−22463
rate equations, transport theory formulation for fusion reactor materials 79−95050
refractories, neutron irrad., microstruct., voids, nucleation TEM study 80−29065
refractory metals and oxides, reactions of liq. alkali metals, relevance to reactor technology 80−85173
refractory oxide development for fusion reactor first walls, chem. environment effects 80−83221
refuelling pellet penetration depth and fuel deposition 80−78446
research at Lawrence Livermore Lab. 77−57742
review of props. *(Dutch)* 80−68938
RFPR, direct-cycle steam generating blanket design 80−37615
rotating target neutron souces, appl. to high energy neutron induced effects on fusion reactor materials 79−45493
SAP 895 (Al-Al_2O_3) alloy containing ^{4}He and ^{3}H, tensile props. 80−34129
SAP thermosyphon breeding blanket, neutronics and thermal-hydraulic anal. 78−785
sapphire TFTR diagnostic windows, radiation damage 80−34063
scrape-off layer of poloidal limiter, transport code calcs. rel. to plasma parameters 79−669
seawater distillation, heavy water concentration, numerical model calc. 79−26514
secondary ion emission due to H ion bombardment 79−8216
shield integral expts. at ORNL 80−47709
shielding, radiation attenuation meas., sensitivity response of liquid scintillator detector 79−67951
SOLASE, tritium pathways and handling problems in a laser fusion reactor 79−36411
solenoid, partially disintegrated superhigh field, for fusion reactor *(Russian)* 77−7584
solid breeding blanket for commercial Tokamak reactors, materials and design 80−95441
solid H_2 pellet ablation, in Tokamak plasma 77−89264
solid H pellet interaction with magnetised plasma 80−78451
sputtering erosion in inertial confinement fusion reactors 79−22462
sputtering yield meas. on first wall materials of thermonuclear fusion devices *(Japanese)* 77−85865
sputtering yield meas. using torsion var. microbalance *(Japanese)* 78−19622
stainles steel, type 316, irrad. in simulated environment, tensile props. 80−34076
stainless steel, 316, long term radioactivity minimisation 78−772
stainless steel, compared to V alloys, performance and economics 80−32433
stainless steel, effect of pulsed radiation on swelling 79−31190
stainless steel, energy deposition from pellet microexplosion 78−54890
stainless steel, ferritic SUS 410 type, coated with organometallic complexes and Ti alkoxides 80−34078
stainless steel, first wall lifetime considerations 78−17419
stainless steel, neutron dose determ., from isotope abundance ratio, mass spectra obs. 80−61220
stainless steel, T exposure, methane growth 77−50296
stainless steel, type 316, first wall structural materials, prediction of life limiting props. 78−62605
stainless steel, type 316, neutron induced charged particle spectra 78−5024
stainless steel first wall, swelling and irradiation creep, FWLTB computer code 80−32446
stainless steel He cooled blanket design for Tokamak 80−37613
stainless steel panel with graphite liner, first wall thermal response during cyclic operation 78−62651
stainless steel surface erosion under ion impact, temp. depend. 77−36350
stainless steel Tokamak blanket design concept 80−13815
steam generator alloys effects of T permeation 80−34250
steel, austenite, blistering after 40 keV He ion bombard. 80−39175
steel, austenitic, annealed, Ni ion bombardment, swelling temp. depend. effect of He implantation 80−29080
steel, austenitic, gas implantation effects, fusion reactor first wall damage simulation 80−29079
steel, austenitic, in liquid Na, corrosion resistance and degradation of mechanical props., influence of N 80−16567
steel, austenitic, thermonuclear reactor walls, ferromagnetic layer form. magneto-optical testing method 80−35465
steel, austenitic and ferritic, corrosion effects of Li 80−35398
steel, austenitic stainless, corrosion by Li and Li:LiH at 873K 80−35397
steel, austenitic stainless, first wall material, radiation damage by simultaneous accelerator microscope irrad. 79−45402
steel, austenitic stainless, fusion reactor blanket struct. material, low cycle fatigue behaviour 80−30073
steel, austenitic stainless, fusion reactor first-wall and blanket material, mech. props. 80−34074
steel, austenitic stainless, H plasma effects on fusion device vacuum vessel 80−21111
steel, austenitic stainless, H trapping studies in fusion first wall materials 79−45407
steel, austenitic stainless, He role in neutron induced microstruct. evolution 80−29064
steel, austenitic stainless, mech. props. correl. methodology development for fusion environments 80−29068
steel, austenitic stainless, microarcing studies in low temp. RF-plasma 80−96407
steel, austenitic stainless, neutron irrad., mag. props. 80−29067
steel, austenitic stainless, neutron irrad. effects on fatigue crack propag. 80−29069
steel, austenitic stainless, stressed state blistering 78−95085

fusion reactor materials continued
steel, austenitic stainless, type 316, D-T fusion neutron and Ni^{2+} ion damage 78—14388
steel, austenitic stainless, types 304, 316, tensile props., effect of exposure to Li and LiH 80—35219
steel, austenitic type 316, continuous gas generation effects in neutron and simulation environments 80—34068
steel, Cr (13 wt.%), sintered, organometallic complex addition effects on mech. props. 80—25595
steel, He ion irrad., 20 keV, 700-800K, surface blister bursting 77—36349
steel, martensitic, first wall/blanket material 80—32451
steel, stainless, 0Kh16N15M3B, blistering under high He^{+} irradiation 80—29095
steel, stainless, 304, D trapping in fusion reactor materials, temp. dependence 80—37577
steel, stainless, 304L, T grainboundary diffusion and trapping, autoradiographic exam. 78—51738
steel, stainless, 305, surface composition changes with plasma discharges 77—34434
steel, stainless, 316, neutron irradiation embrittlement, pre-irradiation treatment and composition modification 80—3171
steel, stainless, 316 and 304, equilibrium surface bombarded with high dose He^{+} ions 78—95091
steel, stainless, 321 and 304, D implanted, thermal desorption and bombardment induced release 78—95072
steel, stainless, absorption of O ions 79—1547
steel, stainless, blistering owing to He^{+} bombard., 2 MeV 80—49279
steel, stainless, constitution changes due to radiation effects 80—34048
steel, stainless, CTR, first wall material, Li compatibility, H$_2$ influence 80—23149
steel, stainless, D depth distrib. determ. using D(^{3}He,p)^{4}He 79—4326
steel, stainless, D transport through membranes at low driving press. and 15 keV D bombardment 78—34552
steel, stainless, design calculations for A 14-MeV neutron collimator 79—59257
steel, stainless, design of materials irradiation experiments utilizing spectral tailoring 80—102305
steel, stainless, electron-bombardment surface prep. for Princeton Large Torus 77—59957
steel, stainless, embrittlement by low energy ionic and atomic H particles 78—95809
steel, stainless, first wall/blanket system, thermal-hydraulics and fatigue life modelling 78—58453
steel, stainless, fusion blanket structures, NAA 80—23145
steel, stainless, fusion reactor He embrittlement simulation, splat cooling in development of B doping 80—30072
steel, stainless, H recycle from Tokamak walls using plasma-wall interaction simulator 78—94131
steel, stainless, He effects on microstruct. in ion-irrad. 80—29078
steel, stainless, He induced blistering, during simultaneous sputtering 79—1808
steel, stainless, He ion bombard., in situ electron microscope examination 80—34094
steel, stainless, He ion irrad., fracture behaviour, in-situ HV electron microscopy 80—29089
steel, stainless, ion bombardment, primary recoil energy spectra characts. 78—10103
steel, stainless, ion induced release of trapped D 78—95095
steel, stainless, irradiation-induced creep anal., proton simulation of first wall environment 79—24707
steel, stainless, laser fusion reactor first wall, void growth charact. 80—34042
steel, stainless, Li compatibility, H$_2$ influence 78—68844
steel, stainless, liner for TFR 400, D, O, and limiter material spatial and depth implantation distrib. 80—18648
steel, stainless, low energy D implanted, microstruct. 78—95073
steel, stainless, low energy H^{+} sputtering 80—40198
steel, stainless, N toughened, electron beam welding, fusion reactor component fabrication 80—32472
steel, stainless, neutron activation of struct. components 78—74476
steel, stainless, oxidised, sputtering yield meas. by atomic fluoresc. spectroscopy 80—80922
steel, stainless, permeation by ^{2}H(^{3}H) in fusion reactor, oxide film inlfuence 80—34241
steel, stainless, reduction of oxide layer by H atoms 80—40738
steel, stainless, reflection of H ions 77—36336
steel, stainless, spatial distribution of limiter material and impurities on the first wall of TFR 400 79—651
steel, stainless, sputtering and chem. attack by H ions of 100 eV energy 78—95635
steel, stainless, sputtering by low energy H and D 78—95630
steel, stainless, sputtering yield meas. using AES 80—18654
steel, stainless, sputtering yields of 1 to 20 keV light ions 77—36339
steel, stainless, surface, roughness factor measurement, energetic D^{+}, He^{+}, Ar^{+} irradiation 80—39172
steel, stainless, surface damage under high dose ^{4}He^{+} ion irradiation 78—95092
steel, stainless, surface treatment of plane and hollow components in glow discharges 79—1923
steel, stainless, swelling, effect of free surface 78—10097
steel, stainless, Tokamak first wall, angular effects in sputtering by H ions 79—46458
steel, stainless, Tokamak fusion reactor first walls, hydrogen profiles 80—37578
steel, stainless, trapping and replacement of 1 to 14 keV H and D 78—95070
steel, stainless, type 304, electron stimulated desorption rel. to CTR first wall appl. 78—51818
steel, stainless, type 316, cold worked, precipitation response to neutron irrad. 80—34073
steel, stainless, type 316, corrosion in flowing Li 80—35399
steel, stainless, type 316, corrosion rates in molten Li salts 80—35400
steel, stainless, type 316, fusion reactor blanket materials for Argonne Experimental Power Reactor 80—32450
steel, stainless, type 316, neutron irrad., Ni ion bombard. effects of injected interstitials on void volume 80—34092
steel, stainless, Type 316, neutron irrad. effects on tensile props. and microstruct. 80—65059
steel, stainless, type 316, plasma chamber material for power generating Tokamak, suitability tests 80—32449

fusion reactor materials continued
steel, stainless, type 316, struct. life anal. for fusion reactor first-wall appl. 78—13326
steel, stainless, type 316L, thermal outgassing properties 80—18649
steel, stainless, type AISI 321, surface damage and mech. changes after H atom irrad. 80—39182
steel, stainless, unipolar arc damage in hot, dense D plasma 79—3235
steel, stainless, vacuum transfer technique for Tokamak in situ surface anal. 79—2778
steel, stainless, wall and limiter material for Tokamaks, induced desorption diffusion and gas production by 100 eV electrons and ions 79—675
steel, stainless, with Pd coating, interdiffusion at reactor wall temps., Rutherford backscatt. obs. 80—39361
steel, stainless, X-ray induced desorption of gases from surface 77—35813
steel, stainless 316, blanket struct. for JAERI fusion reactor 78—62654
steel, stainless 316, fatigue behaviour of materials containing significant amounts of irrad.-induced He 80—100917
steel, stainless 316, first wall, thermal stress and creep fatigue limitations 79—76132
steel, stainless 316, ion sputtered, surface anal. by Auguer effect and SEM 78—95632
steel, stainless 316, irradiated, D trapping 78—95069
steel, stainless type 304, ion bombarded, He effects 80—29076
steel, stainless type 316, first wall material, compatibility with impure He 80—32469
steel, stainless types 361 and 304, He and He prod. cross sections for 15 MeV neutrons 77—50291
steel, type 316 stainless, Neutron irradiation using HFIR for evaluation as fusion reactor material 78—13324
steels, austenitic 316-SS, 321-SS, hydrogen permeation characts. 79—69295
structural, fast neutron induced H and He producing reaction 80—13841
structural alloys, constituent segregation during irradiation 79—55791
structural materials, accident-related dose rate calc. 80—95411
structural materials for inertial confinement fusion reactors, scaling laws for structural loads and stresses 79—76137
structural metals, non-metals, radiation environment, materials technology since 1974, review 79—76134
superconducting compounds, neutron effects 78—52121
superconducting fusion magnets, radiation effects 78—50294
superconducting magnet, large system, structure, insulators, conductors 80—32471
superconducting magnet materials, irradiation damage *(Japanese)* 78—54873
superconducting magnets, magnetic confinement of plasmas in fusion reactors 79—23441
surface analysis in Princeton Large Torus 77—57743
surface erosion, review 77—57741
surface erosion, sputtering, unipolar arcs, heat pulses in plasma solid interaction 80—38665
surface impurities during start up and early operation of ISX-A, surface anal. with sample transfer 79—654
symbiotic energy system, U fuelled, economic anal. using SYMECON code 80—106172
symbiotic system, managing fusion burn, economic analysis 80—106173
synthetic chemical fuel, non-electric fusion energy applications 80—42866
T$_2$ release, air detritiation operation, computer model and scale expt. 78—66413
tandem mirror hybrid reactor, gas cooled blanket 80—37608
tandem mirror hybrid reactor, nucl. performance sensitivity of Be/molten salt blanket 80—37606
target, arc-resist., for divertor of fusion reactor 80—13784
target fabrication for electron beam initiated fusion 78—46174
TETR Tokamak hybrid blanket design, breeding and power capabilities 78—62615
TEXTOR, technical materials for first wall 77—34430
tFTR blanket module experiments 80—37609
TFTR breeding modules, neutronics 80—37611
TFTR coil materials, neutron irrad. effects 80—34060
TFTR diagnostic windows, radiation damage 80—34063
TFTR exptl. blanket modules, mechanical design 80—37610
thermal shock resistance of limiter and first wall materials for fusion reactor 79—3239
Thor Tokamak, wall conditioning by cleaning H discharges 80—78440
Tokamak, blanket and shield of high-field compact reactor 78—74475
Tokamak, DITE, time resolved metal impurity conc. using RBS anal. 79—1329
Tokamak, mag. limiter plate, electron irrad. and thermal shock, Mo, SiC and graphite 78—66416
Tokamak, UWMAK II, thermal hydraulic and mechanical design of blanket 77—6556
Tokamak blanket, Li-cooled, parametric anal. of design parameters 79—22464
Tokamak blankets, neutronic materials with different coolants and structural arrangements 79—81087
Tokamak devices, blistering and flaking by He atoms 78—86690
Tokamak first wall low-Z materials, impurity radiation from medium density plasmas 79—55472
Tokamak first-wall characterisation by in situ Auger electron spectroscopy 78—5022
Tokamak fusion reactor, blanket structural material selection and development *(Japanese)* 79—97901
Tokamak fusion-fission breeder, blanket fuel selection 79—22468
Tokamak He-cooled solid breeder system, UWMAK-II, conceptual design 77—3160
Tokamak ISX-A, impurity expts. 79—1328
Tokamak noncircular experimental power reactor, blanket and shield design 77—3161
Tokamak plants, neutron wall loading and structural lifetime goals 78—58408
Tokamak plasma exhaust, packed distillation column for isotopic enrichment 80—838
Tokamak plasma fusion products, deposition and thermalisation 80—83895
Tokamak plasmas, advanced-fuel, ignition and thermal stability 80—86970
Tokamak reactor, material and design options for superconducting TF magnets 79—85801
Tokamak reactor, resistive requirements of vacuum wall 78—66410

fusion reactor materials continued
Tokamak reactor, UWMAK-III, using closed cycle He gas turbines 77—6555
Tokamak reactor first wall, coating materials and techniques 78—8974
Tokamak reactors and structural materials, plasma-wall interactions 80—32428
Tokamak-driven hybrid breeder reactor, liquid metal coolant, MHD effects 79—17974
Tokamaks, lifetime of reactor components 80—32445
toroidal fusion magnet systems, radiation damage effect on max. attainable magnetic field 78—50295
transition metals, implantation of He$^+$, range profiles and thermal release 80—39138
transmutation and activation of fusion reactor wall and structural materials 80—32509
vacuum deposited film, as first wall material, sputtering yield mea. *(Japanese)* 80—25513
void, and interstitial loop evolution in pulsed fusion reactors 80—84217
void nucleation, continuum description 78—87707
wall released impurity transport in limiter scrape off layer of Tokamak 79—670
water, decomposition by fusion energy, H_2 prod., synthetic fuel 78—50335
water cooled and moderated reactors in Soviet Union nuclear power generation 79—642
water splitting thermochemical cycle for synthetic fuel prod. 78—58458
Ag, energy reflection coefficient for 5 to 10 keV He ions 78—95639
Ag film, light energetic ion damage rel. to fusion reactor wall appl. 77—59050
Ag, Frenkel defect production associated with He and light ion implantation, exam. 78—47443
Ag, light ion (H, D, He, Li) irrad., defect prod. and electronic stopping power 80—34088
Ag, sputtered, angular distrib. during He$^+$ and Ar$^+$ ion bombardment 78—95624
Al, 20 keV He$^+$ implantation, gas re-emission, critical dose, temp. effects 77—35596
Al, Al ion irradiated, void swelling and annealing of voids, electron microscopy study 80—88216
Al alloy 6061 79—675
Al and Al-Cu (1.5 at.%), vacancy charact. study by electrical resistance derivative method, rel. to temp. 78—47361
Al and SaP 930, 300 keV He irrad., blistering, flaking, gas re-emission 77—35601
Al, annealed and neutron irrad., exam. of positron lifetimes in voids and other defects 78—47426
Al blanket/shield design, high field ignition test reactor 78—54899
Al blanket/shield designs, minimum-activity, for D-T and D-^{3}He fusion blankets 79—85796
Al conduction cooled blanket, thermal analysis 78—62653
Al, damage production rates of 5 MeV Al ions 78—47444
Al, electron backscatter fractions, exptl. determ. 80—18617
Al, expt. and statistical model determ. of α-prod. by 14.8 MeV neutrons 80—95397
Al foil, α-particle irrad. under fusion reactor conditions, He bubble alignment during deform. 80—107345
Al, He bubble behaviour during high plastic deform. 80—29087
Al, impurity-vacancy binding energy, clustering effects calc. 78—47411
Al, laser fusion target simulation, press. ionisation 80—63374
Al low activity blanket for Tokamaks 77—6560
Al min. activity blanket design for TFTR upgrade 78—58460
Al sintered powder, 100 keV He ion irrad., surface erosion due to blistering 77—35600
Al sintered powder coatings, form. and behaviour under particle bombard. 80—35029
Al, sputtering and chem. attack by H ions of 100 eV energy 78—95635
Al, struct. metal, effective damage levels in neutron radiation environment 79—36236
Al, surface exfoliation and blistering induced by He ion bombard. in energy range 10-80 keV 80—39173
Al, vacancy-solute interaction 78—47413
Al-Cr(Ti), electron irradiated, interstitial trapping and detrapping at undersized impurity atoms 78—47424
Al-Li cold worked neutron irrad. alloys, the bubble behaviour, microstruct. changes 77—54359
Al-Si, effect of irrad. on the nucleation of incoherent precipitates 79—8303
Al-Si coatings, form. and behaviour under particle bombard. 80—35029
Al_2O_3 coatings, form. and behaviour under particle bombard. 80—35029
Al_2O_3, D plasma interaction, surface structure, chemistry and resistivity changes 78—53010
Al_2O_3, displacement functions calc. 80—34047
Al_2O_3, limiter and liner, results in Tokamak Petula 79—655
α-Al_2O_3, neutron damage, fusion/fission ratio 80—34066
Al_2O_3, permeability and solubility of H_2, 1200-1450°C 80—39351
α-Al_2O_3, rapid firing, XPS study of cryst. struct. 78—68663
Al_2O_3, refractory, chemical reduction by atomic hydrogen 79—93830
Al_2O_3, thermally stressed insulator surfaces, behaviour under vacuum 80—18652
Al_2O_3, void formation by fast neutron irradiation, TEM exam. 78—51591
Al_2O_3, X-ray induced desorption of gases from surface 77—35813
Al_2O_3-BaO-SiO_2 glass coatings in fission and fusion reactors, permeation, elec. cond. and dielectric breakdown 80—18439
Ar contents in laser fusion target pellets, mass spectrometer determination 80—32442
Ar, response to spherical blast waves, effect on first wall protection 80—91245
Au, energy reflection coefficient for 5 to 10 keV He ions 78—95639
Au, low energy H$^+$ sputtering 80—40198
Au, neutron damage, defect clusters 80—34067
Au, polycrystalline, low energy H$^+$ scatt., computer study 77—36338
Au, sputtered with 15 or 30 keV H$^+$, He$^+$ and Ar$^+$ ions, energy and angular distrib. 78—95625
Au, sputtering and chem. attack by H ions of 100 eV energy 78—95635
Au, X-ray induced desorption of gases from surface 77—35813
B and B-rich borides, protective coatings, in situ prep. for controlled nuclear fusion devices 79—3238
B coatings on graphite, fusion reactor appl. 80—23147
B, protective coatings for first wall, prep. by means of low press. plasma CVD 80—35103

fusion reactor materials continued
BC, ion bombarded, chemical effects on secondary photon and ion emission 78—95637
BC_4 gas-suspended, cooling of D-D fusion blanket, neutronics calc. 80—834
B_4C, chem. erosion by H-plasma, first wall of fusion reactor 77—36676
B_4C coating, erosion rates under H$^+$ ion bombard., fusion reactor appls. 80—39179
B_4C, first-wall coating for Tokamak, H retention and release 80—18620
B_4C, low energy ion erosion expts., Kaufman source appl. 80—68942
B_4C reflector-shield concept for fusion reactor designs 80—102293
B_4C, sputtering yield, use as first wall material 78—95629
B_xCy, protective coatings for first wall, prep. by means of low press. plasma CVD 80—35103
BN, low-Z material, outgassing expts. 79—209
^{11}B-p advanced fuel development and confinement 79—13516
Be, amorphous, reflection of D and T, Monte Carlo study 80—40197
Be blanket material, neutron multiplication meas. 79—59255
Be, blistering model, correlation between blister diameter and skin thickness 78—95067
Be, CTR blanket materials, neutron multiplication factor studies 80—18628
Be coated limiters, first wall protection 80—32483
Be coating, erosion rates under H$^+$ ion bombard., fusion reactor appls. 80—39179
Be, double differential neutron cross sections at 5.9, 10.1, and 14.2 MeV 77—67743
Be, implanted D and He, interaction and radiation enhanced oxidation 80—39120
Be, ion bombarded, chemical effects on secondary photon and ion emission 78—95637
Be, low energy ion erosion expts., Kaufman source appl. 80—68942
Be, plasma-sprayed, response to He$^+$ bombardment determ. 78—86691
Be, plasma-sprayed coatings on Cu and stainless steel, fusion reactor appl. 80—18619
Be range profiles of Li$^+$, appl. of (n,p) and (n,α) reactions 80—61200
Be sintered powder, 100 keV He ion irrad., surface erosion due to blistering 77—35600
Be, sputtering by H$^+$, D$^+$, He$^+$, weight loss measurements 80—35028
Be, surface morphology, effect on low energy H ion erosion yield 79—42121
Be-Li-V, phase diagram, metallurgical aspects for fusion blanket use 80—32467
BeF_2, molten, symm. stretching freq. calc. using mol. dynamics method 77—71790
BeO film, 5 keV D implantation 80—100268
BeO, low-Z material, outgassing expts. 79—209
BeO, radiation induced detrapping of implanted D by ^{3}He and proton irradiation 80—32482
BeO, sputtering by H$^+$, D$^+$, He$^+$, weight loss measurements 80—35028
BeO, sputtering by low energy H and D 78—95630
Bi, breeding zone in molten-salt blanket, effect on ^{232}Th and ^{235}U fission rates 80—99272
C CVD coating, surface damage and erosion under energetic D$^+$ and ^{4}He$^+$ irrad. 80—39174
C coating on Pt temp. depend. of H_2^+ sputtering 78—95634
C coatings for fusion applications 80—23146
C, D implanted, trapping of D, calibration for particle energy meas. in plasma boundary of Tokamaks 79—98983
C, glassy, surface erosion by ion bombardment crystal anisotropy effect 78—23845
C, interaction with D$^+$ ions, 5-30 keV, temp. depend. of methane formation 78—79645
C, ion bombarded, chemical effects on secondary photon and ion emission 78—95637
C limiter for JFT-2 Tokamak 79—85768
C, low energy ion erosion expts., Kaufman source appl. 80—68942
C, neutron differential elast. and inelast. scatt. from 9-15 MeV, cross-section meas. 77—2984
C pyroceramic, sputtering and blistering from H$^+$ and He$^+$ bombardment 78—79649
C, pyrolytic, 0.6 to 3.5 MeV He$^+$ irrad., surface erosion, porosity effects 77—35602
C, pyrolytic, energy depend. of methane prod. during deuteron bombardment 78—95939
C, reflection of H, D and He ions 78—95640
C reinforced composites, first wall, limiter, beam dump appl. 80—32458
C surface, pyrolytic, roughness factor measurement, energetic D$^+$, He$^+$, Ar$^+$ irradiation 80—39172
C, trapping of 6 to 15 keV D, temp. depend. and depth profile 77—30664
C-graphite materials for HTR and fusion reactors 80—73928
CaO, displacement functions calc. 80—34047
Ce binary alloys, absorpt. of D, T-getters for CTR evaluation 78—51683
Co, (n,2n) 14 MeV cross sections 80—91181
^{59}Co+n, calc. using pre-equil. statistical model code GNASH 78—4946
Cr, (n,2n) 14 MeV cross sections 80—91181
Cr-Ni, blistering after 40 keV He ion bombard. 80—39175
Cr-Ni, Inconel, first wall material thermal response 80—32456
Cr-Ni, Inconel 718, fusion reactor blanket materials for Argonne Experimental Power Reactor 80—32450
Cr-Ni alloy, 01Kh18N40M5, blistering under high He$^+$ irradiation 80—29095
Cr-Ni first wall material, compatibility with impure He 80—32469
Cr-Ni-Fe, Inconel 625, plasma chamber material for power generating Tokamak, suitability tests 80—32449
CrB, crystallographic relationship with αMoB, UBC, ThBC 79—42025
Cr_3C_2, $Cr_{23}C_6$, plasma sprayed coatings for gas-cooled reactor appl. 79—24676
Cr_2O_3-stainless steel system under fusion reactor first wall condition, oxide dispersoid stability 80—40374
Cu, blistering by He atoms, (10-20 keV), exam. of skin structure, thickness, He distribution and swelling 79—60412
Cu, doubly peaked He depth profile and blistering 78—10078
Cu, electron backscatter fractions, exptl. determ. 80—18617
Cu, energy reflection coefficient for 5 to 10 keV He ions 78—95639
Cu, expt. and statistical model determ. of α-prod. by 14.8 MeV neutrons 80—95397
Cu film, light energetic ion damage rel. to fusion reactor wall appl. 77—59050

fusion reactor materials continued
Cu, Frenkel defect production associated with He and light ion implantation, exam. 78−47443
Cu, Frenkel pair production threshold energy, temp. depend., exam. 78−51530
Cu, He conc. profile meas. rel. to blistering 78−95089
Cu, He defect complexes and depth distribution, production theory 77−31686
Cu, inertial confinement fusion reactor, surface damage and thermal effects from transient thermonuclear radiation 79−648
Cu, inertial confinement reactor first wall response to thermonuclear radiation 79−76133
Cu, ion radiation damage 78−22773
Cu, isochronal recovery of high energy d-Be neutron damage 78−51592
Cu, light ion (H, D, He, Li) irrad., defect prod. and electronic stopping power 80−34088
Cu, low energy ion erosion expts., Kaufman source appl. 80−68942
Cu, low temp. D$^+$ irradiated, radiation blistering onset 80−2081
Cu, neutron damage, defect clusters 80−34067
Cu, neutron damage and gas prod. spatial variation in Li(d,n) radiation damage facility 77−42207
Cu neutron production of free interstitials 80−34071
Cu, neutron spectra meas. and calcs. 80−23142
Cu, polycrystalline, low energy H$^+$ scatt., computer study 77−36338
Cu, proton irradiation, 10 to 16 MeV, isochronal annealing meas. 80−2083
Cu, proton irradiation, 10-16 MeV, neutron damage simulation 80−34089
Cu, proton irradition, 10 to 16 MeV, resistivity changes 80−2082
Cu, sputtered with 15 or 30 keV H$^+$, He$^+$ and Ar$^+$ ions, energy and angular distrib. 78−95625
Cu, stabiliser for fusion reactor supercond. mag., neutron irrad. effects on magnetoresistance 80−34062
Cu, volume change due to point defects and He bubbles, isotropic elasticity theory 78−47445
Cu, X-ray studies of fusion energy neutron damage 78−51593
Cu$_3$Au, radiation disorder model of phase stability 80−16297
D trapping in fusion reactor materials, temp. dependence 80−37577
D-^{3}He, advanced fuel development and confinement 79−13516
D-^{3}He, driven Tokamak fusion reactor, plasma parametric studies and appl. 80−42865
D-^{3}He satellite fusion power plants 79−76143
D-D advanced fuel development and confinement 79−13516
D-D fusion reactor blankets and shields, effect of neutron source ratio on nuclear characts. 79−41033
D-T, laser pellet, structured, implosion model 79−10684
D-T fusion fuel, liquid-vapour equilib., Raoult's law 79−67947
D-T fusion reaction, $D+T \rightarrow n+{}^4He$, chain carriers 80−86969
D-T fusion reactor, tritium recovery using Zr, Y *(Japanese)* 78−29646
D-T fusion sources, light water hybrid breeding reactors, source driven 79−13518
D-T reactor first wall, feasibility of in situ regeneration by vapour deposition processes 77−18701
D+T, guiding centre distrib. spatial separation, reaction rate enhancement 80−33737
D_2^+ molecular ions, dissociation in migmacells II and III, advanced fusion fuel expts. 77−83088
D_2-DT-T_2, three-phase region, temp.-press.-composition correlations 77−84889
D_2-DT-T_2 mixture, solid and liq., props. for fusion reactor applications 78−66415
D_2-T_2-H_2, fusion reactor fuel, isotopic exchanges, equilib. consts., 4.2-300K 77−70331
DD advanced fuel, fusion dynamics, reactivity coeffs. 77−23296
DD fusion reactor blanket, thermal blanket and blanket shield designs, comparative study 79−22457
D(^{6}Li)-T, inertially-confined, high thermonucl. gain with low T inventory 78−58403
DT fast neutrons in blankets and shields, neutrons, associated particle method 77−71690
DT fill system for laser fusion targets 78−50303
DT filled microballoon, gaseous content anal. 78−50305
DT filled microballoons, fuel content characterisation 78−50304
DT pellets, auto-irradiation effects, thermal and electric stresses 79−41036
DT, solid and liq., fusion reactor applications 78−66415
DT-loaded glass microbubbles, interference fringes, forbidden zone 77−18702
(Fe,Ni,Co)$_3$V, long-range ordered alloy for fusion reactor appl. 80−32481
Fe, (n,2n) 14 MeV cross sections 80−91181
Fe alloy containers for liquid Li, corrosion resistance properties 79−47815
Fe, amorphous, radiation damage simulation 80−34045
Fe, amorphous, reflection of D and T, Monte Carlo study 80−40197
Fe and Fe alloys, fast neutron irradiated at high temps., mech. props. 79−51157
Fe, Armco, corrosion and mechanical behaviour in liquid Li 78−53036
Fe, BCC, void nucleation following electron irrad. 80−29054
Fe, impurity atoms in hot plasma, radiation energy loss 78−18441
Fe, neutron experiments for data testing 78−5023
Fe, permeation by H in fusion reactor 80−34242
Fe, proton irrad., 10-16 MeV, neutron damage simulation 80−34089
Fe, proton irradiation, 10 to 16 MeV, isochronal annealing meas. 80−2083
Fe slab *(Japanese)* 80−18595
Fe struct. metal, effective damage levels in neutron radiation of environment 79−36236
Fe-Ni-Co-V alloys, effects on fusion reactor neutronics performance 80−47705
Fe-Ni-Cr, compatibility with Li_2O pellets, mass spectrometric study of Li_5FeO_4 evaporation 79−8385
Fe-Ni-Cr, pulsed HVEM irrad., effect on microstruct. evolution 80−34053
Fe-Ni-Cr (20, 15 wt.%), dual-ion irrad. effects on microstruct. and mech. props. 79−45403
Fe-Ni-Cr (20, 15 wt.%), single and dual ion irrad., microstruct. studies 80−29077
^{56}Fe, gamma-rays from 14 MeV neutron scatt. in extended samples 77−57739
H atom, reaction with ethylene chemisorbed on W 77−36789

fusion reactor materials continued
H isotope, removal from flowing Ar, U and Ce as hydriding materials 78−17438
H isotope trapping, materials exposed to high power discharges in PLT 80−37576
H isotopes, techniques for uniform charged particle generation, fusion reactor fuel 78−86682
H, solid pellet ablation, lifetime anal., rel. to reactor refuelling 77−23272
H-related materials problems, in situ anal. using Li nuclear microprobe method 78−7299
H-T fusion fuel, liquid-vapour equilib., Raoult's law 79−67947
H_2, isotope separation in Ti-fluidised bed 80−18676
H_2 uniform solid spheres, prod. apparatus 77−74409
$H_2(D_2)(T_2)$, ortho-para transition, catalytic-, radiation-, and self-induced conversion, review 77−90633
^{2}H-^{2}H molten-salt-cooled fusion reactor blankets, nuclear heating and radiation leakage 78−78490
^{3}H, behaviour in graphite, gettering in Ti, permeation in oxide covered metals 80−18633
^{3}H, losses in primary and steam circuits in FINTOR-D, control system 80−18634
He accumulation fluence dosimetry for fusion materials neutron irrad. testing 80−32479
He cooled molten salt hybrid blanket for TCT-hybrid reactor 78−62614
He, hydraulic resistance to forced two-phase flow in narrow channels 78−87383
He, liq. and vap., dielectric breakdown across epoxy insulation 78−62658
He prod. in materials, integral meas. comparison with ENDF/B calcs. 77−23214
He production, Hauser-Feshbach calcs. of (n,α), (α,n) rates for Fe group elements 77−23100
He unit requirements, for superconductive energy appl. in USA 78−89999
He$^+$ implanted stainless steel, microstructure anal. 78−82516
^{4}He transport models for solid breeders 78−17424
I, radioactive, adsorption on charcoal filter, safety evaluation *(Japanese)* 78−33267
In, amorphization by ion implantation 78−52135
In, film, embedded with He particles, superconductor ion implantation study of inhomogeneities 78−52181
La binary alloys, use as tritium extractors from breeder blankets 79−67946
Li and hybrid blanket assemblies, absolute fission rate distribs. 77−67871
Li, blanket, for Tokamak thermonuclear reactor, MHD flow modelling *(Russian)* 78−47146
Li, blanket, isotopic exchange equilib. for H and D 79−49845
Li blanket, thermoelectric MHD 79−50806
Li, blanket coolant for Tokamak reactor, flow resist., MHD effects 78−66423
Li blankets, experimental model studies 77−71694
Li boiler, a high-temp. fusion reactor T breeding blanket 80−13818
Li cooled first wall/blanket system, thermal-hydraulics and fatigue life modelling 78−58453
Li, energy deposition from pellet microexplosion 78−54890
Li, estimates of economically recoverable resources for nuclear fusion appls. 80−52788
Li fall fusion reactor, dynamic loading of structural wall 79−93821
Li, isotope separation by plasma centrifuge, static characts. anal. *(Japanese)* 80−5326
Li, liq., ^{7}Be impurity control, fusion reactor appl. 80−32466
Li liq., deuteron activated, shielding 80−99286
Li, liq., first wall/blanket concepts, thermal hydraulic anal. 78−62650
Li, liq., impurity monitoring and control system for fusion reactor 80−32465
Li liq. blanket, T removal by Y 80−95434
Li, liquid, coolant and T fuel source, safety anal. and support facilities 80−63380
Li, liquid, fusion reactor blankets, chemical processing 80−32512
Li, liquid, solubility of LiD 78−2259
Li, liquid, solubility of Li_2O, determ. by fast neutron activation 79−42252
Li, liquid, trapping efficiency for 20 keV tritium ions 77−50290
Li metal sphere, T prod. meas. using new methods of neutron source strnegth determ. 78−74470
Li, molten, estimate of diffusion coeff. of Pb 79−93828
Li, neutron experiments for data testing 78−5023
Li, reactions with dissolved salts in fusion reactor regime 80−32464
Li requirements for fusion power plants, survey 79−45401
Li resources, energy reserves of D-T fusion, recovery costs 78−46162
Li solid compounds, removal of bred T 80−32513
Li, space depend. T formation rate 77−26881
Li, T breeding performance eval., multigroup neutron and photon transport calc. 80−13831
Li thin films on inclined surface, flow stability 79−22458
Li Tokamak breeding blankets, T breeding perform. comparative eval. 80−95398
Li-Al alloys, T recovery 78−58455
Li-Bi(Al), sorption of tritium, for appl. in thermonuclear reactor 77−1301
Li-D equation of state under extreme conditions, solid state to plasma region 80−69976
Li-LiH system, liquid Li, dilute solns., equilib. H press., solubility, heat of soln., CTR materials 77−14266
Li-LiH(D)(T), decomposition in $(\alpha+\beta)$ field 79−15652
Li-Pb eutectic alloys for fusion reactor solid breeder blankets, reactions with water 80−102297
Li-Pb-cooled blanket for tandem mirror fusion reactor, neutronic anal. 80−99273
Li-SAP alloys, T recovery 78−58455
Li+d, 40 MeV, target system neutron spectra 79−9595
$LiAlO_2$ solid breeding banket, low temp. T cyclic purging 79−59256
β-Li_5AlO_4, microcryst., neutron irrad., ^{3}H diffusion studies, fusion blanket appl. 80−18627
Li_2BeF_4-Na(K)BF_4, phase diagram 77−21119
Li_2C_2 solubility in Li 80−13840
Li(D,T), prep. via exchange reaction 77−9109
LiF, gamma-rays from 14 MeV neutron scatt. in extended samples 77−57739

- **fusion reactor materials** continued
  - LiF, ns. slowing down time, expt. obs. 78−58319
  - LiF-LiCl-LiBr, molten, H electrochemical extraction, appl. to fusion reactor blanket processing 78−53217
  - LiF-NaF-KF molten mixture, diffusivity and solubility of H_2 78−34640
  - Li_3N, vaporisation, studied by Knudsen effusion method 80−92662
  - LiO_2, Monte Carlo anal. of asymmetric effects 78−74464
  - LiO_2 pellets, T release due to recoil process 79−85767
  - LiO_2, reactions with Mo in fusion blanket feasibility tests 80−26055
  - LiO_2 sintered pellets, neutron irradiated, T release 78−5014
  - LiO_2 sintered pellets, reaction with 316 stainless steel, Incoloy 800, Hastelloy X-R, Inconel 600 and pure Ni 79−39137
  - LiO_2, T breeding performance eval., multigroup neutron and photon transport calc. 80−13831
  - Li_2O, 2.7 MeV triton recoil range from $^6Li(n,\alpha)^3H$ 80−63372
  - Li_2O, Ar^+ implantation, depth distrib. by proton backscatt. 78−51577
  - Li_2O blanket breeding material, single crystal synthesis using vacuum fusion technique 80−71585
  - Li_2O gas carried fusion reactor blanket, neutronics and photonics 77−67880
  - Li_2O, heat capacity 306 to 1073K 79−10965
  - Li_2O, lattice energy calc. 78−79556
  - Li_2O, Li^+ ion self-diffusion coeff., sectioning technique 80−15296
  - Li_2O, microspheres for gravity flow bed fusion reactor, fabrication research 80−32468
  - Li_2O, neutron irrad. effects, optical absorpt. spectra 80−75271
  - Li_2O packed bed blanket, T transport 80−37612
  - Li_2O pellets, neutron irrad., microstruct. and Vickers mircohardness meas. 79−8339
  - Li_2O pellets, neutron irradiated, temp. distrib. 80−86968
  - Li_2O pellets, sintered, neutron irradiated, ESR study 80−92566
  - Li_2O pellets, thermal neutron flux distrib. inside and outside 80−47700
  - Li_2O, porosity, dependence on thermal diffusivity and thermal conductivity, 200-900°C 80−92726
  - Li_2O, single crysts., growth by floating zone method 79−43139
  - Li_2O solid state breeding blanket for controlled thermonuclear reactors *(Japanese)* 79−9869
  - Li_2O Tokamak breeding blankets, T breeding perform. comparative eval. 80−95398
  - Li_2O_1 fund. optical absorpt. edge, number of displaced atoms from $^6Li(n,\alpha)^3H$ reaction 78−51594
  - Li_2O_2, thermal decomposition and heat capacity 301 to 566K, enthalpy 80−3322
  - Li_xO_y, gaseous, mass-spectrometric study of thermochemistry 79−10940
  - LiOH(D)(T), thermal decomposition rates 530-690K, activation energy and enthalpy meas. 80−3321
  - Li_7Pb_2, fusion reactor breeding material, reaction with H_2O 80−13830
  - Li_7Pb_2, T breeding fusion blanket with boiling water coolant 80−99274
  - Li_7Pb_2, T breeding performance eval., multigroup neutron and photon transport calc. 80−13831
  - Li_7Pb_2 Tokamak breeding blankets, T breeding perform. comparative eval. 80−95398
  - LiT, retention and distrib. of ^3He NMR studies 79−69153
  - ^6LiD advanced fuel, fusion dynamics, reactivity coeffs. 77−23296
  - ^6LiD pellet, fusion prod. by $^6Li(n,\alpha)$ T 79−93823
  - ^6LiD sphere, T prod. under 14 MeV neutron irradiation 79−59254
  - ^6Li+d, thermonuclear reaction rate parameters calc. 77−61436
  - $^6Li(n,\alpha)^3H$, 3-800 keV, cross section meas. 78−89865
  - MgO, displacement functions calc. 80−34047
  - MgO, ion irrad. induced vol. changes, optical absorpt. expts. 77−59053
  - Mn, (n,2n) 14 MeV cross sections 80−91181
  - Mo, (n,2n) 14 MeV cross sections 80−91181
  - Mo, activation anal., charged particle prod. cross sections by 14 MeV neutrons 80−93829
  - Mo, air contamination effect on compatibility with liquid Li in stainless steel vessels at 600°C 78−25285
  - Mo alloy, TZM, long term radioactivity minimisation 78−772
  - Mo alloy:Re, effect of Re on mechanical props. 80−35196
  - Mo alloys, fusion reactor first wall and blanket material, props. for struct. appl. 80−30071
  - Mo alloys, fusion reactor first-wall and blanket material, mech. props. 80−34074
  - Mo alloys (MChVP and TsM10VD), erosion, effect of ion bombardment dose and previous surface treatment 80−89419
  - Mo, amorphous, reflection of D and T. Monte Carlo study 80−40197
  - Mo, BCC, void nucleation following electron irrad. 80−29054
  - Mo, blister erosion reduction by multi-groove surface microstruct. 78−95211
  - Mo, blistering and surface roughening, room temp. ageing effects Ar^+ ion bombardment 78−34550
  - Mo, candidate refractory for Tokamak, thermal fatigue failure testing 80−32454
  - Mo, D^+ impact, surface blistering, SEM study 78−71774
  - Mo, damage profile resulting from Ni^{2+} and He^+ ion bombardment 78−10100
  - Mo, dual beam ion bombardment 79−7634
  - Mo, energetic deuteron irradiated surface struct. quantitative meas. 78−95210
  - Mo, energy deposition from pellet microexplosion 78−54890
  - Mo, fusion reactor appl., quick heating thermal fatigue test, ultra-high vac. environment *(Japanese)* 80−93716
  - Mo, H and D trapping, enhancement due to He ion damage 77−31698
  - Mo impurity flux, time resolved, in DITE Tokamak 80−63373
  - Mo, in-situ coating, vacuum deposition on Hastelloy-X substrate 79−3237
  - Mo, inertial confinement reactor first wall response to thermonuclear radiation 79−76133
  - Mo, ion bombardment, N interaction with vacancies 79−82261
  - Mo, ion bombardment by Ni^{2+}, TEM study of damage depth distrib. 78−10101
  - Mo, irrad. between 425 and 1000°C, ductility in bending 80−39164
  - Mo, irradiated by H^+ and $H_2{}^+$ ion beams, grain ejection from surface 78−6819
  - Mo limiter for JFT-2 Tokamak 79−85768
  - Mo, low energy ion erosion expts., Kaufman source appl. 80−68942
  - Mo, microstruct., swelling induced by ion bombard., He injection effects 80−29083
  - Mo, neutron irradiated, radiation softening and hardening 80−34083
  - Mo, neutron irradiated, void swelling and shrinkage, TEM study 80−34079
  - Mo, ordered void obs. 79−86786
- **fusion reactor materials** continued
  - Mo, particles sputtered with low energy Ne^+ ions, surface microstructure effect on angular distrib. 79−100004
  - Mo, proton irradiated, annealed and rolled, void form. 78−22774
  - Mo, reflection of H, D and He ions 78−95640
  - Mo, SiC coating, CVD and stability under thermal cycle conditions 80−7500
  - Mo single crystal 78−52136
  - Mo, sintered, fusion reactor blanket struct. material, low cycle fatigue behaviour 80−30073
  - Mo, sintered, thermally induced surface composition variations 79−5078
  - Mo, sputtered, angular distrib. during He^+ and Ar^+ ion bombardment 78−95624
  - Mo surface, low energy ion scattering of absorbed layers 79−1807
  - Mo surface, rolled, $H_2{}^+$ ion bombard, large blister form. 80−75274
  - Mo, surface erosion due to $H_2{}^+$ and He^+ bombardment 79−85769
  - Mo, surface impurities, depend. on prep. method, ion scatt. spectroscopy 80−40200
  - Mo, TFTR protective plate, sputtering and surface damage by D^+ irrad. 80−18645
  - Mo Tokamak limiter, surface observation, infrared techniques 80−38693
  - Mo, Tokamak mag. limiter plate, electron irrad. and thermal shock 78−66416
  - Mo, unipolar arc damage in hot, dense D plasma 79−3235
  - Mo-Ti, irrad. between 425 and 1000°C, ductility in bending 80−39164
  - Mo-Ti-Zr, D trapping in fusion reactor materials, temp. dependence 80−37577
  - Mo-Ti-Zr, first wall materials, compatibility with impure He 80−32469
  - Mo-Ti-Zr (0.5, 0.1 wt.%), neutron irradiated, void swelling and shrinkage, TEM study 80−34079
  - Mo-Zr, heavy ion irradiated, void swelling, phase instability 80−29084
  - α-MoB, crystallographic relationship with CrB, UBC, ThBC 79−42025
  - Na, incipient boiling in the presence of a mag. field 79−37411
  - $NaBF_4$-$LiBF_4$(KF)(LiF), phase diagram 77−21119
  - NaCl Polytran laser windows, for CO_2 lasers, fusion appls. 78−59067
  - NaI-LiI, phase diagram 77−21119
  - NaK, liquid metal, blanket coolant, natural convection under transverse magnetic field 80−69827
  - Nb, (n,2n) 14 MeV cross sections 80−91181
  - Nb, activation anal., charged particle prod. cross sections by 14 MeV neutrons 80−93829
  - Nb, air contamination effect on compatibility with liquid Li in stainless steel vessels at 600°C 78−25285
  - Nb alloy, He ion irrad., 20 keV, 700-800K, surface blister bursting 77−36349
  - Nb alloys, fusion reactor first wall and blanket material, props. for struct. appl. 80−30071
  - Nb alloys, fusion reactor first-wall and blanket material, mech. props. 80−34074
  - Nb and Nb alloys, superconductor, flux pinning under heavy ion irradiation 78−52167
  - Nb and Nb-Zr (1 wt.%), fusion reactor blanket struct. material, low cycle fatigue behaviour 80−30073
  - Nb and Nb-Zr (1 wt.%), ion irradiated, void ordering 78−22770
  - Nb, Ar ion surface erosion 77−36342
  - Nb, BCC, void nucleation following electron irrad. 80−29054
  - Nb based alloys, He and simultaneous damage production simulation 80−32480
  - Nb, blister form. on single crystal under Ne^+ ion bombardment 78−71772
  - Nb blistering by 5-15 keV He ions, dose rate and temp. effects 77−35595
  - Nb, blistering by He atoms, (10-20 keV), exam. of skin structure, thickness, He distribution and swelling 79−60412
  - Nb, blistering by He^+ bombardment at thermonuclear reactor energies 80−34104
  - Nb, depth distrib. meas. of He 77−30665
  - Nb, depth profiling of Li ions using $^7Li(p,n)$ reaction 77−80534
  - Nb, effect of O ion irradiation on supercond. 78−52131
  - Nb, energy deposition from pellet microexplosion 78−54890
  - Nb, fast neutron sputtering 78−15255
  - Nb, fusion neutron damage effects on mech. props., simulation by 16 MeV protons 78−71768
  - Nb, fusion reactor first wall material, cyclic deform. tests 80−30074
  - Nb, H_2 isotope release 80−37580
  - Nb, He ion irrad., 20 keV, 700-800K, surface blister bursting 77−36349
  - Nb, He^+ bombardment, high dose 800 to 1400°C 77−36344
  - Nb, irradiated superconductor, fluxoid defect interactions 78−52166
  - Nb, isochronal recovery of high energy d-Be neutron damage 78−51592
  - Nb, neutron damage and gas prod. spatial variation in Li(d,n) radiation damage facility 77−42207
  - Nb, neutron damage and sputter yields 77−57742
  - Nb, neutron irrad. effects on mech. props. 78−91361
  - Nb, neutron irradiation, low temp., 15 MeV, effect on superconducting props. 78−52179
  - Nb, neutron spectra meas. and calcs. 80−23142
  - Nb, polycrystalline, 10 to 1500 keV $^4He^+$ irrad., blister skin thickness, meas.-calcs. correl. 77−35597
  - Nb, polycrystalline, low energy H^+ scatt., computer study 77−36338
  - Nb, radiation blistering by $^4He^+$ ions implanted sequentially at different energies, 3 to 500 keV 77−35594
  - Nb, radiation damage in fusion reactors, computer expts. 80−13839
  - Nb, radiation hardening and yield strength correlations for 16 MeV H^+ and (D,T) neutron effects 78−14389
  - Nb, reactive, trapping of energetic 18 keV deuterons 78−10096
  - Nb, recovery and recrystallisation, fast neutron irradiation effects 77−70069
  - Nb, reflection of H ions 77−36336
  - Nb, resistivity studies of interstitial He mobility 79−14800
  - Nb simulation of 14 MeV neutrons by higher energy protons 79−1469
  - Nb, sputtering by energetic neutrons and protons, round robin expt. 78−11052
  - Nb, stress distrib. from He ion irrad., vol. expansion, calcs. 77−35599
  - Nb, superconductor, neutron irradiation, low temp., effect on critical current 78−52180
  - Nb, surface behaviour under ion irrad., in fusion reactor 77−57740
  - Nb, surface carburisation with propane 79−8382
  - Nb, surface damage caused by He^+ ion bombard. 80−39177
  - Nb, trapped He, temp. depend. 77−31685
  - Nb, unipolar arc damage in hot, dense D plasma 79−3235
  - Nb:He, mech. props. and microstruct. 80−85003

fusion reactor materials continued
Nb-Mo-Zr, erosion coeff., temp. depend. reactor wall swelling due to He ion bombardment 78—17418
Nb-Rh, radiation disorder model of phase stability 80—16297
Nb-Sn(Ge), A-15 compound formation by ion implantation 78—51572
Nb-Ti, radiation effects on critical currents 78—52175
Nb-Ti, superconductivity after heavy ion irradiation at low temps. and high fluence 77—69437
Nb-Ti, void volume fraction reduction, Ni^+ ion irradiation 79—51162
Nb-Zr, deformed, α-peak, internal friction meas. between 90 and 300K 79—100205
Nb-Zr, first wall material, compatibility with impure He 80—32469
Nb-Zr (1 wt.%), D_2 diffusion coeffs., 923-1148K 77—84991
Nb-Zr (1 wt.%), He bubble growth, α-particle effects 78—67749
Nb-Zr (1%), He bubbles and voids with ringed images SEM and TEM exam. 78—51529
Nb-Zr-C, erosion coeff., temp. depend. reactor wall swelling due to He ion bombardment 78—17418
Nb_3Al, multifilamentary wires, supercond. props. 78—64175
Nb_3Ge, neutron irradiated, A15 compound, recovery of T_c by annealing 78—52132
$Nb_3Ge(Sn)$, electron irradiation at cryogenic temps., effect on T_c and transport props. 78—52122
Nb_3Sn, critical current density 78—52176
Nb_3Sn, critical current enhancement by low temp. fast neutron induced flux pinning centres 78—52177
Nb_3Sn, degradation mechanism of superconducting transition temp. under high energy neutron irradiation 78—52124
Nb_3Sn, effect of O ion irradiation on supercond. 78—52131
Nb_3Sn, filamentary, fatigue tests on small coils 78—64652
Nb_3Sn, irradiated, critical current density 79—38293
Nb_3Sn, low temp. neutron irrad. expts., $E_n=14$ MeV 79—33424
Nb_3Sn, multifilament conductors, strain-crit. current meas. 78—64174
Nb_3Sn, neutron irrad. effect on supercond. fusion magnet props. 78—52128
Nb_3Sn, radiation damage effect on superconducting props. 78—52127
Nb_3Sn, superconducting props., effect of radiation induced atomic disorder 78—52133
Nb_3Sn superconductor, low temp. deuteron irradiation 78—52182
Nb_3Sn, X-ray study of fission fragment induced structural damage 78—51589
$Nb_3Sn(Al)$, neutron irradiated, A15 compound, recovery of T_c by annealing 78—52132
$Nb_3Sn(Ge)$, resistivity and T_c measurement after low temp. neutron irradiation 78—52123
NbTi, neutron irrad. effect on supercond. fusion magnet props. 78—52128
^{93}Nb, in RTPR blanket, Bondarenko formalism to account for resonance self-shielding effects 77—23300
Ne spectral line broadening as diagnostic for compressed laser fusion targets 79—98979
Ni, (n,2n) 14 MeV cross sections 80—91181
Ni, air contamination effect on compatibility with liquid Li in stainless steel vessels at 600°C 78—25285
Ni alloys, constitution changes due to radiation effects 80—34048
Ni, blistering, He^+ ion energy and irradiation temp. effects 80—34103
Ni, blistering due to 20 keV He ion irradiation, temp. depend. 79—73228
Ni, blistering model, correlation between blister diameter and skin thickness 78—95067
Ni, cavity evolution in 500 keV $^4He^+$ irrad. 80—29082
Ni, deuteron irrad. induced creep/mechanisms 80—39171
Ni, fusion neutron damage effects on mech. props., simulation by 16 MeV protons 78—71768
Ni, H permeability using permeation method *(Japanese)* 78—51740
Ni, irradiated, numerical simulation of void nucleation 79—73208
Ni, irradiated, with He^+ bubble depth distrib. meas. by TEM and blister form. mech. 78—95088
Ni, irradiated with Cu and Ni ions, depth depend. damage profile 79—14857
Ni light ion (H, D, He, Li) irrad., defect prod. and electronic stopping power 80—34088
Ni low energy H^+ sputtering 80—40198
Ni, permeability and diffusivity of hydrogen *(Japanese)* 78—66345
Ni, point defect-dislocation loop interaction, effect on dislocation loop growth kinetics 78—47415
Ni, porosity depth distrib. of annealed samples following bombardment by 1 MeV Ar^+ ions 80—5333
Ni, radiation hardening and yield strength correlations for 16 MeV H^+ and (D,T) neutron effects 78—14389
Ni, reflection of H, D and He ions 78—95640
Ni, self-ion irradiated, He effect on void form. 78—6112
Ni, sputtering of adsorbed layers 77—36335
Ni, stress distrib. from He ion irrad., vol. expansion, calcs. 77—35599
Ni surface, adsorbed CO and H_2 layers, laser induced desorption expt. 79—1548
Ni, surface erosion by He blistering during operation 79—69166
Ni, thermal neutron cross sections for He prod. 77—23079
Ni, transient irrad.-induced creep under D bombardment, mechanism 78—80597
Ni, unipolar arc damage in hot, dense D plasma 79—3235
Ni, void swelling rates in self-ion irrad. sample 80—29081
Ni:^{235}U (0.1 at.%), exam. of saturation defect conc. and elec. resistivity meas., for neutron irrad. at 7K 78—47435
Ni-base alloys, Nimonic PE-16, type 718 and type 625, neutron irrad. effects on fatigue crack propag. 80—29069
Ni-base binary alloys, solute segregation and precip. under heavy-ion bombard. 79—11623
Ni-Cr-Co-W (47.5, 25, 12, 8.75 wt.%), vaporization of IN-643, high-temp. mass spectrometry 79—7685
Ni-Cr-Fe Alloy 600, acid intergranular corrosion rel. to caustic stress corrosion cracking stress relieving effect 77—66712
Ni-Cu, sputtering rate, radiation-induced segregation and preferential sputtering effects, kinetic model 80—40199
Ni-Mo, sputtering rate, radiation-induced segregation and preferential sputtering effects, kinetic model 80—40199
Ni-Si, proton irrad., γ' precipitation, early stages 80—34096
Ni-ThO_2, irradiated with 5 MeV Ni^{++}, ThO_2 redistrib. 78—71771
Ni_3Si coatings, form. and stability during high temp. irrad. 80—35088
Pb, breeding zone in molten-salt blanket, effect on ^{232}Th and ^{235}U fission rates 80—99272

fusion reactor materials continued
Pb, effect of O ion irradiation on supercond. 78—52131
Pb-Li alloys, ^3H breeding blanket for fusion reactor, ^2H solubility 80—18626
Pb-Li liq. alloy internal spectral shifter and energy converter for laser fusion reactor 79—49841
Pd, reactive trapping of energetic 18 keV deuterons 78—10096
Pt, isochronal recovery of high energy d-Be neutron damage 78—51592
Si, D implanted, trapping of D, calibration for particle energy meas. in plasma boundary of Tokamaks 79—98983
Si, impurity atoms in hot plasma, radiation energy loss 78—18441
SiC, 0.6, 3.5 MeV He^+ irrad., surface erosion, porosity effects 77—35602
SiC, 10 keV H^+ irrad., C deposition, surface swelling, surface morphology changes 77—35608
SiC, chem. erosion by H-plasma, first wall of fusion reactor 77—36676
SiC, energetic deuteron irradiated surface struct. quantitative meas. 78—95210
SiC, energetic ion sputtering, appl. of AES-SIMS (IMA)-FDS combined systems to physical and chemical processes 78—95636
SiC, exam. of T_2 diffusion coeffs. and D_2 solubility 78—79816
SiC, fusion reactor first wall appl., radiation damage 79—86822
SiC limiter for JFT-2 Tokamak 79—85768
SiC on graphite substrate, Tokamak mag. limiter plate, electron irrad. and thermal shock 78—66416
SiC, pellet, rise in temp. involving reaction sintering 77—12555
SiC, permeability and solubility of H_2, 1200-1450°C 80—39351
β-SiC powder compact, microstruct. changes and β to α transform., Si vapour influence 78—19738
SiC, pyrolytic particles for high temp. reactor fuel, X-ray and SEM study *(French)* 78—22734
B SiC, sintered, effect of Al trace amounts on specimen props. 79—83289
SiC, sputtering, physical and chemical, by H_2 and He, 600 to 7500 eV 77—36340
SiC, sputtering processes by energetic ions, combined SIMS-AES study 80—40201
SiC, sputtering yield, use as first wall material 78—95629
SiC surface, H^+, D^+ and Ar^+ bombardment, 5 to 15 keV, meas. of erosion yield 78—79647
SiC surface, roughness factor measurement, energetic D^+, He^+, Ar^+ irradiation 80—39172
SiC, surface characterisation by combined AES-IMA system, for first wall material of fusion devices *(Japanese)* 79—74039
SiC-C, sputtering and blistering from H^+ and He^+ bombardment 78—79649
SiL, neutron damage at 1200°C, fusion reactor first-wall appl. 79—93829
Si_3N_4, low-Z material, outgassing expts. 79—209
SiO_2, laser-fusion microballoon, expansion density profile, 10.6 μm irrad. 78—86686
Sn, effect of O ion irradiation on supercond. 78—52131
steel, stainless, He cavitation, rel. to TiC precipitation 80—45399
T and fissile fuel exchange between hybrids, fission power reactor and T prod. reactors 80—47703
T breeding costs in critical fission reactor 78—58456
T breeding in fusion-fission Tokamak, optimisation with geom. program 78—74477
T breeding in TFTR, tritium breeding test blanket module design 80—99304
T control by glove box containment 78—46169
T, environmental control of use and release at TFTR 80—13829
T facility at Lawrence Livermore Laboratory, quality assurance of systems 77—50297
T fuel handling, safety and control systems for TFTR 78—50364
T, fuel handling systems, for TNS Tokamak 78—50363
T gas, container prep. effect on growth of protium and methane impurities 80—78436
T gas exposed to stainless steel, methane growth 77—50296
T handling, breeding and containment in Tokamak designs UWMAK II and III 77—6557
T handling systems, Monsanto-Mound Laboratory eng. development 77—50295
T health effects during normal and off normal release in CTR's 78—774
T permeation, scoping studies 78—769
T permeation in steam generators and T content in CTR coolants 77—50293
T permeation through steam generator alloys 80—34250
T prep. from liquid Li by molten salt extraction, kinetic studies of tank mixing characteristics 80—13824
T processing systems for inertial confinement fusion facilities 78—50338
T prod. meas. in Li metal sphere using new methods of neutron source strength determ. 78—74470
T, recovery from molten Li by Y getters 80—32470
T recovery from solid Li-Al and sintered Al product blanket materials 78—58455
T release control and environmental monitoring *(Japanese)* 79—81078
T removal from air streams of reactors by catalytic oxidation and water adsorption 77—50292
T removal from inert gases, feasibility of chemical getter beds 78—41861
T, removal from liq, K and Li by sorption onto Y 78—66411
T removal from solid Li compounds in blanket 80—32513
T self sufficient 1600K process heat fusion reactor blanket concept 80—37614
T separation from Li at low conc. using Y 80—83219
T system design for near-term Tokamak, effect of plasma perform. parameters 79—76131
T systems test assembly, containment and cleanup technology 78—767
T systems test assembly at LASL 78—17421
T transport in fusion reactors, limitations 78—70628
T_2, cryocondensation pumping, smooth surface at 4.2K, fusion reactor application 78—74492
T_2, transport models for solid breeders 78—17424
T_2 valve, pulsed gas feed into Tokamak reactor 78—66412
TZM, D^+ impact, surface blistering, SEM study 78—71774
TZM, irrad. between 425 and 1000°C ductility in bending 80—39164
Ta, unipolar arc damage in hot, dense D plasma 79—3235
TaC-C fibre composite, neutral beam target appls. 78—66399
TaO, displacement functions calc. 80—34047
Th blanket in hybrid system, reaction rate calc., central DT neutron source, ENDF/B-IV cross sections 80—13792

fusion reactor materials continued
^{232}Th, mirror hybrid reactors 80−42860
^{232}Th, neutron spectra meas. and calcs. 80−23142
Ti, 300 keV He^+ irrad., exfoliation, flaking, blistering, in-situ SEM obs. 77−35598
Ti, (n,2n) 14 MeV cross sections 80−91181
Ti alloy, radioactive structures, recycle time 78−58457
Ti alloys, first wall and blanket structure, impact of H_2, phase stability and solubility 80−32435
Ti alloys, fusion reactor first-wall and blanket material, mech. props. 80−34074
Ti based alloys, He and simultaneous damage production simulation 80−32480
Ti, blister form. by He and H ion bombardment, target struct. effect 78−95087
Ti coated Nb, reduction of void number density and size by ion irradiation 78−51600
Ti, D bombarded surface, ion fraction and energy anal. of sputtered particles 77−36345
Ti, D profiles after D_3^+ implantation 80−37581
Ti, film, CO surface contamination effect on deuteriding 77−35814
Ti, first wall material, thermal response 80−32456
Ti fusion reactor structural alloys, dual-ion irrad. effects 79−45403
Ti, getter pump, corrugated surface and pumping speed, fusion reactor application 78−74491
Ti, H_2 isotope release 80−37580
Ti impurity flux, time resolved, in DITE Tokamak 80−63373
Ti, overlaid thin films, D pumping speed 78−33286
Ti, permeation of H plasma reduced by layer of interstitially built ϵ-Ti_2N 80−16566
Ti, plasma chamber material for power generating Tokamak, suitability tests 80−32449
Ti, reactive, trapping of energetic 18 keV deuterons 78−10096
Ti, reflection of H, D and He ions 78−95640
Ti spongy metallic protective gettered coating for thermonuclear reactor walls *(Russian)* 80−106154
Ti, sputter-erosion and impurity emission under low energy ion bombardment 78−95628
Ti, Tokamak fusion reactor first walls, hydrogen profiles 80−37578
Ti, trapping coeff. of energetic H at high doses 77−31699
Ti:D, ion implanted, depth profiles, temp. depend. 80−100270
Ti-70A superalloy, fusion reactor blanket structures, radiation resistance 80−63379
Ti-Al (6 wt.%), D profiles after D_3^+ implantation 80−37581
Ti-Al-V, (6,4 wt.%), single and dual ion irrad., microstruct. studies 80−29077
Ti-Al-V, fusion reactor blanket structures, radiation resistance 80−63379
Ti-Al-V (6,4 wt.%), D profiles after D_3^+ implantation 80−37581
Ti-Al-V (6,4 wt.%), D trapping in fusion reactor materials, temp. dependence 80−37577
Ti-Al-V (6,4 wt.%), heavy ion irrad. effect on microstructure 79−10884
Ti-Al-V (6,4 wt.%), ion irradiated, microstruct. study using TEM 80−96572
Ti-Co, radiation disorder model of phase stability 80−16297
Ti-Fe-C-N, ion irradiated, microstruct. study using TEM 80−96572
Ti-Ru, radiation disorder model of phase stability 80−16297
TiB_2 CVD coating, surface damage and erosion under energetic D^+ and $^4He^+$ irrad. 80−39174
TiB_2 coated limiters, first wall protection 80−32483
TiB_2 coating, erosion rates under H^+ ion bombard., fusion reactor appls. 80−39179
TiB_2 coatings for Tokamaks, H trapping and re-emission, annealing effects 80−37582
TiB_2, first wall material, activation energies and populations of H traps 79−45409
TiB_2, first-wall coating for Tokamak, H retention and release 80−18620
TiB_2, ion microanalysis and implantation applied to fusion surface research 79−45405
TiB_2, plasma sprayed, low energy ion erosion expts., Kaufman source appl. 80−68942
TiB_2, plasma-sprayed coatings on Cu and stainless steel, fusion reactor appl. 80−18619
TiC coated limiters, first wall protection 80−32483
TiC coating, erosion rates under H^+ ion bombard., fusion reactor appls. 80−39179
TiC, plasma-sprayed coatings on Cu and stainless steel, fusion reactor appl. 80−18619
TiC, sputtering yield, use as first wall material 78−95629
TiD_2, nucleation and growth in D_3^+ implanted Ti, TEM study 80−97717
UO_2, refractory, chemical reduction by atomic hydrogen 79−93830
^{238}U, mirror hybrid reactors 80−42860
^{238}U, neutron spectra meas. and calcs. 80−23142
V, 80 keV ^{4}He irrad., depth profiles, migration, release, surface effects, blistering 77−35606
V alloys, compared to stainless steel, performance and economics 80−32433
V alloys, first wall thermal stress and creep fatigue limitations 79−76132
V alloys, first wall/blanket system, thermal-hydraulics and fatigue life modelling 78−58453
V alloys, fusion reactor first wall and blanket material, props. for struct. appl. 80−30071
V alloys, fusion reactor first-wall and blanket material, mech. props. 80−34074
V, and V-H, fusion reactor first wall material, cyclic deform. tests 80−30074
V, annealing after irradiation with 210 keV He at 625°C at high fluences 78−67751
V based alloys, He and simultaneous damage production simulation 80−32480
V, blister behaviour during 200, 2000 keV He irrad, temp. depend. 77−35607
V, blister form and stress build-up, under the bombardment, surface prep. effects 78−95094
V, blister form. by He and H ion bombardment, target struct. effect 78−95087
V, blistering after Ar^+ ion bombard., irrad. mode effect 80−39176
V, D bombarded surface, sputtered particles, ion fraction and energy anal. 77−36345
V, effect of O ion irradiation on supercond. 78−52131
V, evap. layer, ion bombardment effect on superconducting transition temp. 78−52136
V, first wall material, irrad. with 40 keV ^{4}He ions, blistering 78−55897
V, H_2 permeability, surface impurity layer effect 77−24440
V, interstitial impurity and substitutional solute interaction, internal friction meas. 78−10082
V, ion implanted with 2 MeV He under pulsed conditions, microstructure obs. 80−29088
V, irradiation with 2 MeV He ions, low cycle at elev. temp. 78−95086
V, neutron irradiated, saturable trap anal., of solute segregation applied to O_2 trapping 79−77645
V, proton bombard. induced blistering 77−7770
V, sputter-erosion and impurity emission under low energy ion bombardment 78−95628
V, superconducting props., effect of voids 78−52168
V, superconductor, neutron irradiation, low temp., effect on critical current 78−52180
V, void formation from 200 to 700°C following heavy-ion irradiation 78−10104
V:N, ion bombard., void form. 80−34097
V:O, neutron irrad., void form., 673-1073K 80−29066
V-Cr (15 wt.%), dual-ion irrad. effects on microstruct. and mech. props. 79−45403
V-Cr (15 wt.%), radiation-induced solute segregation 80−29086
V-Cr (wt.%), 3.5 MeV $^{51}V^+$ irrad. induced void swelling and solute segregation 79−7637
V-Cr-Ti, fusion reactor first wall structural materials, prediction of life limiting props. 78−62605
V-Mo, effect of ion plated Mo on corrosion in liquid Na, mech. props. 78−53020
V-Nb, mech. props., −196-1000°C, comp. depend. 78−39847
V-Ni, ion bombard., void form. 80−34097
V-O alloy, temp., dose and conc. depend. of void form. following V^+ ion beam irradiation 78−10105
V-Ti, and V-Ti-Be(Zr), 4 MeV Ni^{++} irrad., He gas bubble form. 80−29085
V-Zr-C, erosion coeff., temp. depend. reactor wall swelling due to He ion bombardment 78−17418
VBe_{12}, coated limiters, first wall protection 80−32483
VBe_{12} coating, erosion rates under H^+ ion bombard., fusion reactor appls. 80−39179
VBe_{12}, low energy ion erosion expts., Kaufman source appl. 80−68942
VBe_{12}, plasma-sprayed coatings on Cu and stainless steel, fusion reactor appl. 80−18619
V_3Ga, high current density multifilament wire, neutron effects on equilibrium and transport props. 78−52126
V_3Ga, neutron irradiation and annealing 78−52130
V_2HfZr, C-15 cryst. struct. supercond. props. 78−64173
V_3Si, neutron irradiated, A15 compound, recovery of T_c by annealing 78−52132
V_3Si single crystal, radiation damage and superconductivity 78−52129
VTi alloys, blister behaviour during 200, 2000 keV He irrad. temp. depend. 77−35607
W, amorphous, reflection of D and T, Monte Carlo study 80−40197
W, candidate refractory for Tokamak, thermal fatigue failure testing 80−32454
W, FIM study of lattice damage caused by low-energy He ion bombardment 78−95090
W, reflection of H, D and He ions 78−95640
W, unipolar arc damage in hot, dense D plasma 79−3235
W-ThO_2, candidate refractory for Tokamak, thermal fatigue failure testing 80−32454
Y, D bombarded surface, ion fraction and energy anal. of sputtered particles 77−36345
Y, solubility of T, 250-400°C, rel. to possible appl. for T recovery from molten Li blanket in fusion reactor 79−90784
Zr, 10 keV deuteron irradiated, retention and precipitation 80−34099
Zr alloys, creep and growth, irradiation induced, microstruct. depend. 80−93602
Zr, deuteron implanted, temp. depend. depth profiles of deuterons 78−95076
Zr foil, determ. of T diffusion coeff. 80−15306
Zr, proton irradiation, 10 to 16 MeV, isochronal annealing meas. 80−2083
Zr, proton irradition, 10 to 16 MeV, resistivity changes 80−2082
Zr, reactive, trapping of energetic 18 keV deuterons 78−10096
Zr-Al getter modules, transient getter scheme for Tokamak fusion test reactor 80−79584
Zr-H system, δ and ε phases, neutron irrad., radiation swelling investigation 78−18685
Zr_3Al, ordered, exam. of Young's modulus and thermal expansion coeff. 78−72805
Zu, reflection of H, D and He ions 78−95640

fusion reactors
see also fusion reactor ignition; fusion reactor materials; hybrid reactors; plasma heating
1-MJ plasma focus expt., neutron yield, current distrib., scaling law 77−74991
2XIIB, liq. N_2 cooled liners 78−50406
2XIIB magnetic mirror device, neutral beam injection 80−28782
2XIIB plasma, evidence for neutral-beam-injected O impurities 79−37547
34MW 120MJ pulsed DC supply for Divertor & Injection Tokamak Expt. 79−31214
475 MVA pulsed motor generators for TFTR 78−58498
600 MW pulsed energy convertors for toroidal field coil, design philosophy 78−58496
θ-pinch plasma with antiparallel trapped mag. field axial behaviour 79−41857
A-FLINT advanced-fuel pellet design, inertial confinement fusion 80−23125
ablation of hydrogen pellet in fusion plasma, scaling law 77−35354
adiabatic compression heating 77−68821
advance fuel fusion power reactors, nuclear analysis 80−13821
advanced designs, Conf., Chicago, IL, USA, Nov. (1978) 80−23123
advanced fuel bumpy tori studies 78−58430
advanced fuel bumpy torus reactor 77−83105
advanced fuel cycle fusion reactors utilising octopole plasma confinement 79−76144

fusion reactors continued
advanced fuel development and confinement 79−13516
advanced fuel fusion impact on electric power transmissions 77−83087
advanced fuel fusion reactor, SURMAC, employing axisymmetric surface mag. confinement 78−58431
advanced fuel fusion reactor wall loading limitations and stability index beta 80−99311
advanced fuel fusion reactors, high efficiency, minimum activity blanket design 80−13822
advanced fuel Tokamak, ILB systems, bundle divertor designs and appls. 78−62618
advanced fuels for inertial confinement systems 77−10491
advanced nuclear energy systems, emerging concepts, conf., Graz, Austria (March 1978) 79−13381
advanced Tokamak integration with closed Brayton cycle gas turbine, design study 77−38395
air cool transformers for fusion reactors, computer aided design 80−18662
air detritiation operations, computer modelling and bench-scale testing 79−85784
Alcator A Tokamak, disruptive MHD activity during plasma current rise 80−32487
Alcator A Tokamak, spatial profiles of light impurity ions 80−48948
Alcator Tokamak, radiative and particle power losses, bolometric meas. 80−73996
Alcator-A Tokamak, D_2 thermal desorption meas. 80−79588
Alcator-C, mag. coil systems 78−50355
Alfven and magnetoacoustic wave heating for fusion plasmas 80−24188
alpha particle transport in thermonuclear Tokamak plasma 78−94895
alpha particles, fusion-generated, producing plasma transport 78−83533
alpha particles interaction with mag. plasma fluctuations in D-T reactor 80−24204
alpha-particle heating, compact expts. proposals 77−62379
alpha-particle heating in an open-field-line plasma 80−48908
alpha-particles anomalous diffusion in nonlinear trapped-ion regime 77−11319
alpha-particles energy spectrum resulting from turbulent diffusion 77−11318
alternative magnetic confinement systems 78−58428
American Nucl. Soc. winter meeting 1977 78−58315
American Nucl. Soc. Winter Meeting 1977 78−82408
American Nuclear Society 25th Annual Meeting (Atlanta, GA, USA (June 1979)) 80−12847
American Nuclear Society proceedings (conf. Las Vegas, NV, June 1980) 80−94920
analogue safety data link, for Princeton Large Torus control room 78−54938
anisotropic B_T-coil two-dimens. finite element anal. of laminate sliding 78−50382
anisotropic neutron transport calc. using scatt. kernel without polynomial expansion 79−67936
ANS annual meeting, 1977 78−663
arc, high-press. gas blast, local thermal recovery, current zero model calcs. 78−9892
arc quenching system for transient and statistical flashover 78−75455
Argonne experimental power reactor, equilib. field coil system design 78−50367
Argonne National Laboratory energy storage and transfer program 78−55031
Argonne National Laboratory Experimental Power Reactor, superconducting magnet system 78−50372
Argonne/GA TNS Tokamak reactor supercond. ohmic heating coil design 79−31197
ASDEX, 30 kA ohmic heating system, tests and performance 80−13848
ASDEX, assembly and commissioning, review 80−102334
ASDEX, extraction grid for high power ion source 80−102372
ASDEX, feedback system and plasma position determination 80−18667
ASDEX, neutral beam injection, beam line design 80−99395
ASDEX, neutral beam injectors, HV power supply system, thyristor control 80−99332
ASDEX, vacuum vessel, voltages and currents induced by plasma disruptions 80−18665
ASDEX circuit breaker system, design, calcs. and tests 78−55032
ASDEX divertor Tokamak, status and design principles 80−13847
ASDEX divertor Tokamak, toroidal and poloidal mag. field coils 78−50352
ASDEX vacuum vessel stress anal. 80−18655
ATC machine, lower hybrid heating using pulsed UHF TV klystron 78−66404
Augean, fission prod. toxicity reduction 80−106175
axial shock heating applied to compact toroid plasma formation 80−95402
B_T-coil stress anal., constraint finite element anal. for contact problem 78−55004
bakeable seals development for large noncircular ports on Tokamak fusion test reactor 80−82777
ballooning limit of non-circular small aspect ratio Tokamak 80−28801
ballooning mode stability in gas insulated plasma boundary layer 80−10415
beam and plasma direct converters 80−42861
beam dump, design and development 77−83356
bellows valve, large rectangular for mirror fusion reactors 78−50404
Belt Pinch IIa, transport phenomena, density profiles 80−24219
Belt Pinch Screw Reactor, neutronics characteristics 80−18624
belt shaped screw pinch, reactor design study 80−13857
bending free toroidal shell shapes for Tokamak fusion reactors 79−64503
Beta II, field reversed expt., device description 80−91274
beta limits for Tokamak experiments 80−83937
Beta-II, magnetised coaxial plasma gun mechanical design and construction 80−91271
bi-conical system of concentric explosive compression of D-T 79−50880
bi-liner method for implosive compression of plasma 79−50881
blanket, analysis of a water-cooled blanket for a commercial Tokamak reactor 80−13819
blanket, gas-cooled, mech. and thermal design 78−66387
blanket, graphite struct., Li_2O cooled, thermal, mech. and neutronic design 78−62652
blanket, high-temp. design for synthetic fuel plant 80−99275
blanket, NOEL (No External Leak), thermal anal. and tests 80−95459
blanket, response matrix formulation for particle transport 77−34458

fusion reactors continued
blanket, thermal stresses and cyclic creep-fatigue 78−62655
blanket boundary layer, high-density gas, localised drift mode stability 80−43956
blanket concept, 1500 to 2000K Li boiler for process heat/electric power generation 80−37633
blanket design, for catalyzed D-D and D-^{3}He fusion reactors 77−88279
blanket design, impact of module size on the tritium breeding and energy conversion experiments in an ETF/INTOR reactor 80−102295
blanket design for a small field-reversed mirror reactor 80−13816
blanket design for toroidal fusion reactor 78−62649
blanket designs, near term, thermal-hydraulic and mechanical anal. 78−58452
blanket first wall time-depend. thermal stress model 78−787
blanket integral neutronics expts. 80−13820
blanket model *(Russian)* 77−47103
blanket neutronic performance in CTR, influence of design variations, variational interpolation techniques 77−34437
blanket neutronics, acceleration of Monte Carlo simulation 77−23280
blanket region, neutron-gamma energy absorpt. chem. appls. 78−5021
blanket structure design for JAERI experimental fusion reactor 78−62654
blanket structures, linear elastic fracture mech. anal. 80−86979
blanket temp. variation with slab geometry 78−78495
blanket thickness, improvements to cellular design 80−18630
blanket thickness, minimization calcs., implication of cellular struct. 80−18629
blanket with synthetic fuel prod., neutronics and heating analyses 80−13812
blankets, conduction cooled, thermal analysis 78−62653
blankets, experimental model studies 77−71694
blankets, plasma physics, conf., Varenna, Italy (Sept. 1977) 79−98869
blankets, redundant coolant capability 78−58454
blankets, structure mechanics at elevated temps. and high fluences 80−86978
blankets for synthetic fuel production, two dimensional heating anal. 80−18631
breakeven condition on hot-ion mode 80−78439
breeding blanket design, parameter matching 78−784
breeding characteristics, comparison of hybrid fission-fusion plant and fast breeder 77−88269
bremsstrahlung cross-sections, 1- and 2-photon, Debye shielding corrections 80−106157
Bumpy Torus plasma, NASA Lewis, optimisation and scaling of ion heating 77−24110
bumpy torus plasma, weak vertical mag. field effect on fluctuation induced transport 80−48946
bumpy torus reactor, beam driven 80−42859
bundle divertor design 79−664
burn period plasma current maintenance, rectifying first wall, cct. anal. 80−102307
capacitor banks, optimum design rules, neutral beam power supply 78−74487
capacitor energy storage, propylene film-paper-phthalate ester capacitors 78−74486
capacitor fed fusion expts., computer based control system 80−13912
capacitors, 10 kV foil-and-paper, low-cost energy storage 78−74485
catalysed D-D noncircular Tokamak, graphite blanket design 78−74480
catalysed-D Tokamak reactors, direct energy converter attachment 77−88277
cavity design for compact electron beam or light ion beam reactor using nonspherical blast waves 80−9405
cavity wall loads and stresses, scaling 78−58446
chaotic motion theories with appl. to controlled fusion research, review 78−93605
charge exchange meas. in Tokamak plasma, active beam method 80−48991
charged particle cloud, nonadiabatic compression by mag. field, energy density 77−61610
charged particle confinement in superposed cylindrical cusp field and biconical cusp field 78−18435
chemonuclear, gamma-neutron, chem. reaction parameters 77−34466
Chinese research 80−78447
circuit breaker, liquid metal plasma valve, tokamak and stellarator heating circuit 78−74488
clean fusion concepts, survey 77−83082
CLEO stellarator, heating, confinement and fluctuations 80−24225
cluster test facility, design 80−90835
coil, multilayer structs., laminated beam theory anal. 78−55011
coil design codes 78−66367
coil insulation and winding techniques 79−31210
cold blanket shielding of wall from hot plasma core 77−61603
cold-ended dense liner-fusion plasma, equilib. profiles calc. 77−19745
combined heat and power, appls. *(German)* 79−67935
commercial Tokamak fusion power reactor remote systems requirements 79−13525
commercial Tokamak reactor, 1000 MWe energy storage and transfer systems 79−76127
commercial use, future prospects, United States 77−10488
commercialisation of fusion, generalised requirements and R&D 77−34462
commercialisation of fusion energy, research review 79−76146
commerical fusion energy, utility requirements and economics 79−76145
commited site evaluation 80−37628
committed site development, technical and economic aspects 80−95437
compact ignition test reactor, engineering design using Bitter type magnet 80−102310
compact reverse-field pinch for small demonstration fusion reactor 80−95413
compact Tokamak fusion reactor, conceptual design of commercial reactor 79−71970
compact Tokamak fusion reactor, nucleonic design for blanket and shield 79−81086
compact toroidal ignition experiment, support struct. anal. by numerical code 80−106167
comparability study of fission and fusion reactors w.r.t. safety, costs and development time 79−59114
component development, mag. systems and plasma engineering, programs status review 80−99299
composite superconductor continuous resistive transition self-field instability depend. 78−50369

fusion reactors continued
composite superconductors for fusion magnets, current distrib. and losses 77−28331
computer models of magnetically confined plasmas, review 77−11388
computerised control and data acquisition 80−13890
conceptual design, review, confinement systems 77−57749
conduction cooled min. activity blanket for TNS and EPR fusion reactors 78−781
conference, accel. engineering and technology, Chicago (March, 1977) 77−83184
conference, controlled fusion and plasma physics, Oxford, England (Sept. 1979) 80−77545
conference, fusion technology, Padova, Italy (Sep. 1978) 80−8741
conference, inertial confinement fusion technical digest, San Diego, CA, USA (Feb. 1980) 80−57012
conference, nuclear cross sections and technology, Washington, USA (March 1975) 77−22826
conference, plasma science, New York, USA (May 1977) 77−84396
conference, San Diego, Calif., USA (June 1978) 79−17972
conference, San Diego, Calif., USA (June 1978) 79−49650
conference, San Francisco, USA (Nov. 1979) 80−91248
conference, world nuclear energy, Washington, D.C., USA (Nov. 1976) 77−34361
conference on ionised gas physics, Dubrovnik, Yugoslavia (Aug.-Sept. 1978) 80−36779
conference on nuclear engineering remote systems technology, San Francisco, USA (Nov.-Dec. 1977) 79−45438
conference summary 77−74997
confinement, alternative approaches, literature survey 78−87477
confinement, pulsed high-density linear systems 77−74983
confinement of fusion plasma by cold gas blanket 77−61602
confinement scalings determ. 78−17431
control valve, low-noise, rolling closure 78−54888
Controlled Fusion Atomic Data Center 78−17432
controlled fusion research *(Japanese)* 77−83094
controlled nuclear fusion, progress and problems review 79−36415
controlled nuclear fusion development, confinement and laser ignition 79−31176
controlled thermonuclear fusion, contemporary state of research 79−680
controlled thermonuclear fusion reactor problems and prospects 79−81075
controlled thermonuclear fusion with submillimetric plasma diagnostics 77−38416
cooling system operational principles *(Slovenian)* 77−67858
coupled explosion current plasma compression, numerical anal. 79−50884
coupled explosion-current compression of plasma, self-similar approximation 79−50883
critical comparison to fast breeders *(German)* 79−93832
cross section requirements, for CTR design program 77−23294
cryo-pumps, nucl. heat deposition, Monte-Carlo method 78−66414
cryocondensation pumping, for fusion research 77−57746
cryogenic laser fusion targets, fabrication and characterisation 78−58484
cryogenic pumping of D_2 and H_2, large-capacity, for nucl. fusion 78−21151
cryogenic pumps *(Russian)* 79−36417
cryogenic refrigerators for fusion research 79−679
cryogenic refrigerators role 79−49840
cryogenic technology and superconductivity in controlled thermonuclear reaction programs 79−54600
cryopump neutral beam compatibility test 78−17423
cryopumps, neutron irrad. effects on pumping characts. 79−44915
cryopumps, radiation-induced degassing 79−85780
cryopumps and cryogenic ancillary equipment for JET machine 77−30670
cryopumps for Tokamak reactors 77−30672
cryosorption pumping, D_2-He (5 at.%), on mol. sieve, 5A, 4.2K 78−74499
cryosorption pumping of D at 6 to 20K, fusion reactor appl. 78−70626
cryosorption pumping of He by charcoal, cryopump design for fusion reactor 80−105654
cryosorption vac. pumping of D, H and He at 4.2K 77−50298
CTR, engineering and technology considerations *(Spanish)* 79−36399
CTR, for power generation, design 77−3157
CTR, nuclear energy strategy, Japan, possibility of FFHR 80−42868
CTR, plasma physics *(German)* 77−14264
CTR, review of present state and future possibilities 77−65326
CTR blanket, neutron heating sensitivity to cross section variations 78−29642
CTR blanket design *(Japanese)* 78−46164
CTR blanket design and associated problems *(Japanese)* 77−50286
CTR central power station waste management 78−773
CTR devices, surface effects related to voltage breakdown 77−35356
CTR first wall design, surface phenomena importance 77−34431
CTR technology 78−37444
Culham conceptual Tokamak, remotely operated shield door 80−74009
Culham Conceptual Tokamak Reactor Mk II, reactor costs and maintenance 77−74978
Culham fusion expts., distributed control systems using microcomputers 80−13909
Culham fusion expts., integrated data network for microcomputer based diagnostics 80−13910
Culham fusion studies, appl. of microcomputer to data acquisition and control 80−13908
cusp field with RF plugging, appl. thermonucl. plasma 77−76169
cycles involving charged particles only, cross sections for p, d and ^{3}He induced reactions on ^{6}Li 77−23297
cyclotron radiation transport in plasmas by neutron transport techniques 80−38660
D-^{3}He-fueled bumpy torus reactors, design study 79−18044
D-D cross sections for thermonuclear synthesis 80−18608
D-D fusion reactor blankets, nuclear characteristics 79−45415
data adjustment experience and trends 79−9881
DC superconducting magnets, pot. damage due to HF EM wave propag. 78−50371
DEALS, demountable superconducting magnet system, for fusion reactors 80−52777
Demonstration Power Tokamak Reactor, vacuum outer containment and metal seals feasibility study 80−95458
dense H_2 plasma generator for research appl. 77−34448
with dense plasma confined by crimped mag. field 77−34442

fusion reactors continued
dense plasma focus, capacitor bank system design and safety 78−54889
dense plasma focus, thermonucl. erosion of wall materials 77−23273
dense plasma focus Julich I, neutronics, fusion plasma investigation 77−35396
design, afterheat and radioactivity probs., ^{94}Nb(n,γ)^{95}Nb, ^{95m}Nb reaction 77−23060
design, considerations on the minimum size of a tritium burning, preferably self-sustaining Tokamak with a breeding blanket 79−76139
design, engineering and technology developments since 1974, review 79−71958
design, nuclear data requirements 77−23291
design and economics, confinement physics effects 78−50358
design and performance requirements, cost and systems anal. 78−50357
design computations, quantitative cross-section data assessment 78−9047
design concepts, [conf. Madison, WI, USA, Oct. 1977] 79−71957
design schemes based on multi-jet mixing chamber *(Russian)* 80−840
design sensitivity anal., reference theta-pinch reactor example 77−67879
designs and alternative fusion concepts, systems studies 80−27805
deuteron linac as neutron generator for materials irradiation and fusion reactor investigation 77−34486
development, review of expt. accomplishments, program strategies and system test facilities 80−57958
development and advantages of Doublet III type 77−34472
development and appl. 77−38417
development in Europe and USA *(German)* 78−29647
development of fusion power, pure and hybrid reactor options, review 80−63389
development programs, outlook 77−34450
development research at Debrecen, Hungary *(Hungarian)* 80−91240
development status, review, energy balance, confinement, designs *(German, English)* 77−67874
diagnostics, mech. techniques in fluctuating mag. fields 78−54946
diagnostics, visible spectrum monochromator, scanning drive 78−54940
dielectric joints, effect on struct. behaviour of Tokamak 78−62657
diffusion time scale Tokamak code, G2M, two dimens. 78−42795
direct current accelerator for 14 MeV neutron prod., thermal-mech. design 78−66383
direct energy conversion from fusion plasma exhaust of divertor 78−54898
disc laser amplifier design 77−19340
discrete cross-section expansion for discrete ordinate codes 79−69162
DITE, behaviour review including injection and bundle divertor 80−74021
DITE MkII divertor, coil and struct. system design 80−13924
DITE Phase II ion source, characteristics 80−83223
DITE Tokamak, arcing investigation 79−658
DITE Tokamak, divertor expts. 79−663
DITE Tokamak, impurity density, soft X-ray meas. 80−19616
DITE Tokamak bundle divertor, Mk.II design 80−91268
DITE-II, neutral beam ion source particle beam identification 80−99397
DIVA, D^+ plasma with H^+ minority component, ICRF heating 80−18601
DIVA, divertor expt. for impurity control 79−662
DIVA, X-ray emission from Au impurities in H_2 plasma 79−32820
DIVA Tokamak, confinement and MHD characts. of very low q discharges 80−64765
divertor collector plate, pot. drop across electrostatic plasma sheath 80−13833
divertorless Tokamaks, limiter pumping system 80−95463
Doublet fusion programme, Tokamak designed 77−23250
Doublet III, computer control system 80−99321
Doublet III, limiter performance, design and material selection 80−106162
Doublet III, neutral beam injection system, overview and status 80−13868
Doublet III, neutral beam injection system, parametric study 80−13869
Doublet III, neutral beam injection system, two-gap magnet design and performance 80−92379
Doublet III, neutral beam injector system, instrumentation and control 80−99322
Doublet III, neutral beam interlock system using IR detector 80−106228
Doublet III, neutral beam test tank design 80−99301
Doublet III, noncircular toroidal plasma confinement expt. 79−49846
Doublet III, noncircular toroidal Tokamak, design and construction 79−49847
Doublet III, ohmic heating E-coil vacuum breaker system, function and operation 80−102323
Doublet III, plasma density, shaping and characteristics 80−74018
Doublet III, plasma shape control, 1.5 Megawatt DC chopper power supply 80−102333
Doublet III, possible Dee configs. 80−91269
Doublet III, toroidal field coils, Cu alloy plate defect size restrictions 80−91257
Doublet III, vacuum vessel neutral beam armour 80−95462
Doublet III beamline, review, component relation and config., design constraints 80−99382
Doublet III beamline calorimeter, three dimens. heat transfer anal. 80−99381
Doublet III device design and construction 79−49854
Doublet III fusion research device, United States, construction 77−46404
Doublet III fusion testing 79−85763
Doublet III indented vac. vessel, mech. design 78−74490
Doublet III neutral beam injector system, outgassing rate meas. and residual gas anal., coating props. 80−95457
doublet reactor, neutron wall loading, two-dimens. calc. 78−66407
Doublet Tokamak devices, TNS to demo, review 79−71968
Doublet-III, frequency generator-rectifier system performance 80−102326
drift loss cone instability in inhomogeneous mag. field 80−48934
drift wave stability and transport theory in fusion systems 80−28653
driven magnetic fusion reactors, conf., Erice-Trapani, Italy (Sept. 1978) 80−41948
DT, in magnetoplasma, effect on diffusion and thermal cond. 77−76031
DTHR, advanced bundle divertor design 80−99281
EBT, neoclassical transport 80−32488
EBT, radial transport in collisionless electron regimes 80−32491
EBT expts., simple annulus power balance 80−48947
EBT heating, electron-cyclotron absorption and microwave propagation 80−64749

fusion reactors continued
EBT reactor, new design arising from plasma research 80—27806
EBTR, parametric anal. of thermonuclear burn dynamics and energy balance 80—37597
economic anal. 78—788
economic and environmental consequences of fusion power 78—33285
economic feasibility *(German)* 77—38400
economics, standard costing methods 78—790
eddy currents in vacuum vessel when plasma current is disrupted, calc. *(German)* 80—68937
electric power generation by light nuclei fusion of charged particles 79—18032
electrical output power profiles, utility interface 78—54906
electromagnetic insulation systems, features 78—89506
electron and ion rings, strong, truncated exponential-rigid-rotor model, fusion confinement 79—41860
electron beam driven Tokamaks, review 80—99317
electron beam heated solenoid reactors for fusion power and fissile fuel breeding 78—8992
electron beams, insulator flashover in HV vacuum transmission line, mag. effects 77—24236
electron cyclotron absorption of the ordinary wave at normal incidence 80—19570
electron cyclotron heating in toroidal systems 77—76141
electron diodes, relativistic, low impedance, behaviour in converging mag. gradient 77—370
electron emission, secondary, effect on energy transport to limiter of Tokamak 79—3236
electrostatic end plugging, open-ended mag. confinement system 78—55743
electrostatic levitation, control and transport in high rate, low cost production of inertial confinement fusion targets 80—47723
electrotechnical component practicalities, operational safety and economics *(German)* 78—94140
elementary reactions in thermonuclear fusion plasmas 79—85762
ELMO, bumpy torus, self-consistent operating point calcs. 79—85779
ELMO Bumpy Taurus, trapped-particle instabilities 79—31184
ELMO Bumpy Torus, electron cyclotron heating, density and temp. 80—28780
Elmo bumpy torus, electron cyclotron heating program, review 80—28750
ELMO bumpy torus, macroscopic MHD stability and beta limit 79—31186
ELMO Bumpy Torus, microwave coupling 80—99328
Elmo bumpy torus, physics and engineering aspects 78—54981
ELMO Bumpy Torus, ring power balance optimisation 80—99316
ELMO Bumpy Torus, scaling studies 80—78444
ELMO bumpy torus design 78—58429
ELMO Bumpy Torus Proof-of-Principle, proposed mag. system 80—99296
ELMO Bumpy Torus reactor, design and operation 79—76120
ELMO bumpy torus reactor, design characts. 78—5039
Elmo bumpy torus reactor, economics 78—54994
Elmo Bumpy torus reactor evaluation 77—38405
ELMO bumpy torus reactor reference design 78—803
ELMO Bumpy Torus Reactor toroidal magnet system design 79—31196
EM implosion of large diameter liners 77—26876
energy option, recent developments 79—36416
energy policy, prospective role 80—13843
energy research, superconducting magnet *(Japanese)* 79—18039
energy storage, 10 MJ homopolar machine, superconducting magnet design 78—54927
energy storage, inductive, appl. of homopolar generator 78—54948
energy storage for Tokamak reactor cycles 78—62661
engineering aspects of fusion expts. 80—9402
engineering developments review 79—3240
engineering problems, conf., Knoxville, USA, (1977) 78—50342
engineering problems, TFTR experience 78—54974
Engineering Test Facility: progress and plans 80—95418
Engineering Test facility, R and D program 80—95419
Engineering Test Facility work on magnetic confinement 80—52787
environmental and safety aspects 78—766
EPR-1, status of HF and iodine lasers as laser-fusion drivers 79—22979
EPRI single-cell field reversed mirror reactor, neutral beam design for plasma heating 80—13836
ETA-BETA fusion expt., data acquisition and anal. programs 80—13914
ETA-BETA II, reverse field pinch, expt. tests and performance 80—102312
Eta-Beta II, reverse field pinch toroidal machine, design parameters 80—13851
ETA-BETA II RFP, diffuse pinch, temp. and confinement results 80—74028
ETA-BETA II RFP, vacuum system design and operation 80—95450
ETF, design considerations 80—95438
ETF, design considerations for remote maintenance 80—68950
ETF, engineering challenges, review 80—95422
Euratom Data Acquisition Co-ordinating Committee activities 80—13904
EURATOM test coil, conceptual design 80—13921
European energy strategy, fusion research programme 80—45652
European engineered fusion experiment, objectives and design 77—34438
European fusion program, technology base review 80—13867
European thermonuclear fusion programme, role of technology 80—86982
exhaust to divertor target by collisionless processes 79—63808
exotic fuels charged particle cross section meas. 77—23293
experimental devices, neutron source strength, comparison of neutron yields 79—85795
experimental power reactor, energy storage and transfer system 78—54955
experimental Tokamak device, pulsed homopolar power supply 77—23286
falling bed high temp. blanket design 80—13813
falling-bed high temperature fusion blanket design for a synthetic fuel production 80—13814
Faraday MHD generator with thermonuclear reactor, efficiency 78—75432
fast circuit-breaker driven by magnetic pressure 80—13899
fast liner reactor conceptual design, nucleonics 80—13790
fast neutron induced nonelastic reaction cross section data, $E_n \geq 14$ MeV 77—23058
FAST power cycle, high efficiency 79—49861

fusion reactors continued
fast-magnetosonic-wave heating of the conceptual NUWMAK Tokamak reactor 80—6264
fast-wave heating, two freq. regimes consideration 77—67884
Ferromak, helical mag. configuration produced by ferromagnetic materials 80—48936
few-nucleon data needs 77—18657
FFHR, tailoring the breeding-fission ratio by neutron moderation with iron 78—21677
fibre optic signalling in experiment control 80—13919
fibre optic telemetering for high voltage test stand, Lawrence Livermore lab. 78—54939
fibre optics, use in controlled fusion expt. shielding and earth loop elimination 80—74007
field coils, fabrication effects on structural behaviour 80—9406
field reversed mirror, self sustained, fueling requirements 79—49844
field reversed mirror neutral beam startup, hybrid plasma code simulation 80—99313
field reversed mirror reactor, 2nd generation design calcs. 78—58465
field reversed mirror reactor, parametric anal. and preliminary conceptual design 79—71973
field reversed mirrors, fusion product energy distribs. 80—37595
field reversed mirrors 80—43961
field reversed theta pinch, model for angular rotation 80—37596
field reversing electron and proton layers, recent results 80—28789
field reversing ion rings, precessional mode stabilisation by multipole fields 77—89298
field-reversed mirror, reactor parameters 78—8983
field-reversed mirror fusion reactor pilot plant 80—13794
field-reversed mirror reactor 80—42857
field-reversed mirrors, stability of low-frequency modes 79—86606
field-reversed mirrors as fusion power reactors 78—8979
Filippov dense focus, time and space resolved neutron emission meas. 77—58896
Filippov plasma focus apparatus fundamental characteristics *(Japanese)* 77—51244
finite element anal., high-energy water-cooled heat sink and 25 MW power tube 79—49838
FINTOR Tokamak, force calc. on D-shaped coils in normal and fault conditions 80—13927
FINTOR-D, demonstration reactor, preliminary design for superconducting toroidal magnet system 79—67953
FINTOR-D, T breeding blanket, Monte Carlo calcs. 80—99283
first wall, hydrodynamic response of Xe protective buffer gas after absorbing target debris 79—85777
first wall, life extension by periodic annealing 80—102344
first wall, lifetime calc. in FWLTB program 80—18646
first wall, thermal response to X-rays, effect of inert gases 79—85776
first wall blanket, cylindrical module, reference design 80—106181
first wall design, reduction of effective sputtering yield by honeycomb structures 79—23440
first wall design, safety study of primary coolants 79—9871
first wall of He cooled blanket, design of segment struct. and coolant ducts 79—13528
first wall problems, ^{6}Li(^{3}He,d)^{7}Be and ^{7}Li(^{3}He,t)^{7}Be cross section meas. 80—13791
first wall-blanket-shield system for commercial Tokamak reactor, molten-salt-cooled design 80—13817
first wall/blanket concepts using liq. Li, thermal hydraulic anal. 78—62650
first-wall alloy program, appl. ORR fission reactor for simulation of neutron environment 78—8973
first-wall structures, fatigue life criteria 80—86980
first-wall/blanket modules maintenance, impact and design approach 80—18612
Fiscatron fusion reactor principle, Z-pinch device using ^{6}LiD 78—78492
fluid-wall inertial confinement fusion reactor concept, tritium breeding control 79—85773
fluorphosphate glass developments, SHIVA laser appl. 78—37440
fly-through particle recovery unit for external-injection injectors, parameter eval. 79—71956
flywheel energy storage system for JT-60 toroidal field coil 78—62662
focus, neutron and X-ray sources space-time struct., scintillator diagnostics 77—74993
focus device dynamics, 120 and 20 kV, neutron and X-ray emission diagnostics 77—74990
Fokker-Planck equatn. numerical solutn. 80—18622
force cooled superconductor cryostability expt. 78—50378
force-cooled superconductor design for large fusion magnets 79—31216
Frascati high field Tokamak, technological aspects 78—50351
Frascati Tokamak, 1MJ plasma focus dynamics, neutron production scaling 80—24220
FT Tokamak, liquid nitrogen system design, construction and operating experience 80—13923
FT Tokamak, non-thermal electron distrib. function 80—83891
FT Tokamaks, expt. results 80—74014
FT-1 Tokamak, electron cyclotron heating expt. 80—75071
FT-1 Tokamak, lower hybrid heating, energy balance 80—79523
FT-1 Tokamak neutral density profile, absolute meas. by H_α line reson. fluorescence 80—24250
FTR, equilib. field coils, electrical supply system, optimisation and computer aided performance anal. 80—91288
fuel feed and removal systems, plasma heating and vacuum technology problems *(German)* 78—50298
fuel handling system for TNS, and cost model 78—58441
fueling and thermonuclear instability, cold plasma layer surface fueling source 80—59196
fuelling by plasma gun 78—760
fundamentals and perspectives *(German)* 78—41862
fusion and fast breeder reactors, a comparison, book 78—78430
fusion as a future power source, plasma confinement and technological problems 79—26752
fusion burner concept 77—10490
fusion design team, undergraduate education 78—58469
fusion devices, controlled, surface effects, conf., San Francisco, USA (Feb. 1976) 77—30659
fusion plant design costs 78—791
fusion plasma, MHD behaviour computation *(Japanese)* 79—31178
fusion possibilities and plasma confinement and interactions in mag. config. Tokamak, review *(French)* 80—54017
fusion power commercialisation 78—58405

fusion reactors continued

- fusion products, thermalisation orbits, wall-loadings and microinstabilities 77–88284
- fusion reaction rate increase in plasma strongly perturbed by longitudinal wave 80–27815
- fusion reactor, beam-profile fast scan monitor 78–54941
- fusion reactor, diagnostics of radial plasma transport rate, data acquisition and handling system 78–54937
- fusion reactor design, dynamic analysis of electromagnetomechanical field by finite element method *(Japanese)* 78–8967
- fusion research at the Inst. of Plasma Physics, Nagoya Univ., present status *(Japanese)* 80–47699
- fusion technology progress 78–62607
- fusion-fission hybrid reactors, fissile fuel breeding potential 77–50287
- fusion-fission reactors, performance parameters, design and fuel cycle anal. 79–17973
- fusion-fission system, basic characts., breeding ratio, thermal power ratio 77–50283
- fusion-MHD power plant, exhaust plasma pulsed accel. 78–62644
- fusion-Synfuel blankets, thermal, hydraulics 79–85800
- fusion/fission reactors, inertial confinement systems, review 79–13519
- future nuclear power technology, impact of nuclear research in India 80–95345
- future prospects, technical, economic and political review *(Spanish)* 79–59116
- GAMMA 6, tandem mirror confinement expt. 80–28786
- Garching Belt Pinch, very fast power crowbar system 80–13901
- gas-fueled plasma core reactors, fission-fueled 78–5036
- General Atomic PGFR concept, 10 tesla toroidal field magnet system 79–49835
- getter pump, nonevaporable, appl. in fusion reactor 77–57745
- getter pump, Zr-Al, for fusion reactor 77–57748
- graphite blanket concept for Tokamak reactor 78–780
- graphite reflected Li assembly, cross section sensitivity anal. of U(n,f) rates 78–46166
- gross blanket breeding ratio determ., neutronic cell calc. by Monte Carlo methods 79–18033
- HBTX1A experimental reversed field pinch machine, parameters and layout 80–13850
- heating, neutral beam injection systems 77–67886
- heating, neutral injection in thermonuclear reactor 77–67888
- heating, neutral injection systems at Princeton plasma lab. 77–68826
- heating and refuelling by injection in ASDEX divertor Tokamak 77–67889
- heating by relativistic electron beam injection 77–76130
- heating injection systems at Princeton plasma lab. 77–68825
- heating systems for Argonne expt. power reactor 77–67891
- heavy ion accel. for inertial fusion 77–83189
- heavy ion-pellet fusion, liquid wall boiler and moderator 78–810
- heavy-ion beam inertial-confinement fusion, commercial power generation 79–6762
- heavy-ion-beam fusion reactor conceptual design 80–95414
- HEGLF, Antares power amplifier 78–54958
- Heliotron D, RF heating, equilibrium and stability 80–28777
- Heliotron E, helical coil design, mag. field perturbations 80–99300
- Heliotron E, neutral beam injector ion source power supply 80–99333
- Heliotron E, vacuum chamber construction using electron beam welding 80–106180
- Heliotron E project, design concepts 80–13855
- Heliotron E project for fusion reactor plasma confinement *(Japanese)* 79–81077
- Helitron E, power supply and control systems 80–13897
- HFCTR, demonstration reactor conceptual design, high force density magnets and modularisation 80–95439
- HFITR, preliminary DEALS magnet system design 80–13925
- high beta MHD theory, stellarator equilibrium and stability, mirror traps and reverse field machines 80–28778
- high beta stellarator, l=2,3 helical fields, stabilisation effects 80–28779
- high current diffuse vac. arc, stable mode with ring array rod electrodes 78–9894
- high density reactors, new concepts 78–5042
- high energy gas laser facility, energy storage system design 78–55030
- high field compact Tokamak reactor, conceptual design for operation at high power density 79–71971
- high field ignition test reactor, Al blanket/shield design 78–54899
- high temp. plasma diagnostics and control *(Japanese)* 78–46165
- high temperature efficient energy conversion 80–86985
- high temperature fusion reactor design for high temp. process heat and electricity prod. 80–32514
- high-power pulsed laser systems 77–19338
- high-Z spectral shifter 78–782
- homopolar generator, fast discharge machine, design, fabrication, testing 78–54952
- homopolar generator design for fusion reactor energy storage 80–68953
- homopolar machine, 10 MJ, fast-discharging 78–54950
- homopolar machine power supply, calc. of steady state mag. fields 77–23288
- homopolar pulse power machine, current collection system 78–54949
- HVDC interrupter test facility, dual 30 kA systems 78–55035
- hybrid blanket assemblies absolute fission rate distribs. 77–61607
- hybrid fusion-fission energy systems prospects 79–49831
- hybrid reactors, laser induced photonuclear and fusion-fission reactions 77–61599
- hybrid tandem mirror reactors, design, fissile fuel production 80–27811
- HYLIFE converter concept, remote systems requirements 80–18614
- hypercompression of matter by thermonuclear miniexplosion 79–50882
- HYPERFUSE: a novel inertial confinement system utilizing hypervelocity projectiles for fusion energy production and fusion waste transmutation 80–102300
- ICF, pellet and laser beam space-time interaction system study 80–13802
- ICF, pool type reactor driven by heavy ion beam 80–37601
- ICF magnetically protected cavities, modelling 80–37603
- ICF reactor design considerations 78–50331
- ICF reactors, MHD decelerators for removal of fuel pellet microexplosion energy 80–13801
- ICFR, divergent impulsive crossflow over packed columnar arrays 80–47702
- ignition test reactor, design features 78–54978
- ignition test reactor, remote maintenance system requirements 79–45420
- Ignition Test Reactor remote maintenance system requirements 79–9885

fusion reactors continued

- ignition TNS Tokamak reactor, engineering parameters 78–50359
- ignitrons, high current, for plasma physics expt. equipment *(German)* 78–75435
- imploding liner fusion system 78–54979
- imploding liners for LINUS-O, high press. gas generator 78–54904
- implosion of dense liner at medium vel., fast fusion reactor, energy regime 77–74996
- impurity and gas throughput control 78–54907
- impurity radiation loss, for corona equilib. 78–91074
- Impurity Study Experiment, mag. field calcs. using GFUN-3D programme 78–66368
- induction coil, superconducting, for a doublet Tokamak reactor 77–30657
- inductive and rotating machinery energy storage and transfer 79–85782
- inductive storage technology, new applications, review 78–55019
- inertial and inductive energy storage programs at LASL 77–23284
- inertial confinement, advanced engineering requirements, review 80–95421
- inertial confinement, advanced fuel D pellets, opaque tamper shell requirements 80–102303
- inertial confinement, ion-beam wet-wood-burners using limited mass targets 80–102301
- inertial confinement, liquid Li waterfall concept 78–808
- inertial confinement, liquid metal protection schemes for first wall 79–76118
- inertial confinement, parametric studies 80–32507
- inertial confinement, preliminary assessment of heavy ion fusion 80–102299
- inertial confinement, T self-sufficient A-FLINT pellet, optimised design 80–102302
- inertial confinement, USA research 80–78448
- Inertial Confinement and Tokamak systems survey *(German)* 79–41038
- inertial confinement economics, parametric study 80–32506
- inertial confinement from reactors, remote system needs 79–45421
- inertial confinement fusion, appl. of advanced lasers 79–18435
- inertial confinement fusion, commercialisation anal. 78–58410
- inertial confinement fusion, review 77–88273
- inertial confinement fusion generating remote systems, laser driver sources 79–9886
- inertial confinement fusion mag. wall reactor cavity concept, new plasma model 79–86602
- inertial confinement fusion programme 78–752
- inertial confinement fusion reactor, appl. PWR fuel rod reenriching 80–106174
- inertial confinement fusion reactor, surface damage and thermal effects from transient thermonuclear radiation 79–648
- inertial confinement fusion reactor and generating station concepts 78–753
- inertial confinement fusion reactor system integration 80–102298
- inertial confinement fusion reactors, scoping studies 78–807
- inertial confinement fusion technology in USA, status *(German)* 80–68952
- inertial confinement pellets, neutronics modelling 80–37593
- inertial confinement plasmas, energetic charged fusion product slowing 80–37594
- inertial-confinememt fusion targets, Rayleigh-Taylor instability 77–51174
- inertial-confinement, design constraints due to microexplosions 79–49858
- inertially confined DT plasma, nucl. fusion yield due to reheat 78–82517
- inertially confined plasma, charged particle energy deposition 77–83081
- inertially-confined, pellet neutron moderation on blanket neutronics 80–836
- inhomogeneous plasma, relativistic electron beam propagation effects 78–9797
- integrated composite conductor for LCS program 78–62631
- interferometric phase detection system, using high speed digital techniques 78–62629
- international cooperation on fusion research *(Japanese)* 80–63371
- international fusion technology program, review 80–95423
- International Tokamak Reactor (INTOR) Workshop, R and D status report 80–95417
- ion+atom, projectile charge dependence *(Dutch)* 79–50121
- ion accelerators pulsed power, for inertially confined fusion *(Russian)* 77–67915
- ion beam, energetic, propag. through fusion target chamber, stability 78–26303
- ion beam-pellet, power balance and systems anal. 78–809
- ion cyclotron EM wave instability, oblique, due to monoenergetic fusion alphas 79–37491
- ion energy analysis on a plasma focus device, rel. to fusion plasmas 79–90465
- ion ring, field-reversed, anomalous decay of induced electron current 80–24206
- ion-beam fusion reactor, first wall costs 78–811
- ion-cyclotron and first harmonic heating of large Tokamak 77–51204
- ISX, coil design and fabrication 78–50353
- ISX, Tokamak, assembly details 78–54883
- ISX Tokamak program, status review 80–37586
- ISX-A Tokamak, H pellet fuelling expts. 79–22465
- ISX-B, differentially pumped bellows 78–55025
- ISX-B, electron cyclotron microwave heating 80–99329
- ISX-B, high power neutral beam injection studies 80–79545
- ISX-B, neutral beam power system 80–91283
- ISX-B, neutral beam system 80–99388
- ISX-B, with bundle divertor, structural anal. 80–91254
- ISX-B impurity study program, in situ Tokamak expts. 80–37589
- ISX-B noncircular Tokamak for expts. on the physics of high-β toroidally confined plasmas 80–37588
- ISX-B tokamak, design of bundle divertor expt. 80–102341
- ISX-B Tokamak, expt. program, review 80–78435
- ISX-B Tokamak for impurity study expts., program objectives 80–37587
- ISX-B toroidal field coil finger joints, fatigue life, structural evaluation 80–91253
- ITR vacuum vessel, free standing, structural design 78–54900
- JAERI experiment fusion reactor neutral gas fuelling problems 79–76128
- JAERI experimental fusion reactor, design problems 79–76126
- JAERI large Tokamak, fast acting movable rail limiters, R and D programme *(Japanese)* 79–13524

fusion reactors continued
JAERI large Tokamak JT-60, vacuum vessel R and D programme *(Japanese)* 79—13523
Japanese Tokamak research, impurity control, low-q discharge, scaling law, RF heating 80—74015
JET, 1978 annual report 80—42850
JET, combined DC power supply 80—13892
JET, control and data acquisition system, CODAS 78—62619
JET, control and data acquisition system 80—13905
JET, control system, communications, diagnostics, data storage and anal., NORD computers 80—68943
JET, cryopumps 78—50399
JET, design, construction, physics 80—74023
JET, development of relevant technologies of vacuum vessel, toroidal field coils, and remote handling 79—71961
JET, experimental system for studying cryopumping under operating conditions 79—58753
JET, extraction element design for long pulse multi-megawatt neutral beam 80—102373
JET, high voltage network to load AC/DC pulse power conversion 78—58497
JET, inner poloidal field coil mechanical design 78—50387
JET, large flywheel-generator-diode convertor, modelling and simulation 80—13894
JET, laser driven pellet refuelling 80—9408
JET, neutral injector overvoltage injection system 80—99398
JET, periplasmatron ion source for intense neutral beam 80—99380
JET, state of development *(Dutch)* 77—61604
JET, synchronous generator, bridge convertor and ohmic heating systems, digital simulation 78—54960
JET, synchronous-generator/bridge-convertor/ohmic heating circuit anal. 80—13893
JET, toroidal field coil design and manufacture 78—50349
JET, transport calcs. for approach to ignition 80—92263
JET, vacuum vessel, development and construction 80—18639
JET, vacuum vessel construction 78—55024
JET additional heating power supply and protection 78—66391
JET fusion exp., remote handling 77—50299
JET poloidal coil insulation system, mechanical tests 80—18669
JET project, design proposals report 79—3241
JET project, EEC five-year plan, development *(Italian)* 77—14267
JET project, fusion as power source, evaluation study 80—32484
JET project, project description and proposed expt. programme 78—89977
JET project, scientific and technical developments 1976 79—3242
JET project, status, 1978 80—18670
JET project, technical developments, administrative and managerial aspects 78—54986
JET project description 78—58399
JET pulse power supply system 78—25327
jet target intense neutron source 78—66384
JET Tokamak inner poloidal field coil design 79—31209
JET Tokamak toroidal field coil design 79—31205
JET Tokamak toroidal field coil manufacture 79—31206
JFT-2 Tokamak, impurity ion sputtering 80—79554
JFT-2 Tokamak, radiation loss meas. using thin-film thermometer 80—47698
JIPP T-II, neutral beam injection system, design and expt. test 80—106226
JIPP T-II Tokamak, current density profile control 80—32493
JIPP-T-II Tokamak plasma, time resolved spatial profiles of impurities 80—48950
Joint European Torus, fusion and energy sufficiency 79—81090
JT60 critical plasma testing device, status report 80—27801
JT-60, alternating mag. field, three dimens. finite element anal. 80—18663
JT-60, control system 80—13906
JT-60, fault current anal. in grounding system 80—99307
JT-60, grounding system design 80—102313
JT-60, grounding system pot. rise during lightning strike, anal. 80—102314
JT-60, high current DC circuit breaker 80—13898
JT-60, poloidal field coil internal voltage oscills. 78—50386
JT-60, poloidal field DC power supply developments 80—102325
JT-60, poloidal field power supply system, AC voltage behaviour, simulation 80—91287
JT-60, prototype neutral beam injector unit 80—106225
JT-60, seismic anal., design changes 80—95425
JT-60, status report 1978 80—18672
JT-60, vacuum vessel, construction and parameters 80—18641
JT-60 large Tokamak device, position and cross-section control 78—50366
JT-60 Tokamak vacuum vessel, stress anal. 78—66371
JT-60 toroidal field coil, brazed connection, nondestructive test methods 80—13930
Jupiter, based on plasma confinement by elec. and mag. fields 77—34444
JXFR, neutral beam injection system, gas-beam interaction secondary particles 80—106227
JXFR, superconducting mag. system conceptual design 80—99295
L-2 stellarator, current equilibrium and effective ion charge 80—24228
L-2 stellarator, solid H_2 pellet injection parameters and effects 80—28775
large coil excitation at const. current and voltage by flywheel generator converter 80—13895
Large Coil Program, coil winding development support 80—106190
Large Coil Program, cryostabilised conductor cooling system 78—50393
Large Coil Program, General Dynamics Convair conceptual design test coil 78—50389
Large Coil Program, General Dynamics Convair/IGC manufacturing engineering 80—106169
Large Coil Program, General Electric test coil conceptual design 78—50390
Large Coil Program, He liquefier-refrigerator and distrib. system 78—50398
Large Coil Program, insulation system cryogenic elec. test 80—91263
Large Coil Program, low temp. stability, joints, design method 80—106195
Large Coil Program, Nb_3Sn forced flow superconducting test coil, Westinghouse design 80—99337
Large Coil Program, Nb_3Sn forced flow superconductor design considerations 78—50394

fusion reactors continued
Large Coil Program, NbTi, superconducting test coil, General Dynamics Convair Division, Intermagnetics General Corp. design 80—99338
Large Coil Program, NbTi superconducting test coil, General Electric design and manufacture program 80—102319
Large Coil Program, pool boiling mag. quench press. calc. 80—106199
Large Coil Program, pulse coil concepts 78—50397
Large Coil Program, research and development activity 80—99336
Large Coil Program, struct. response of toroidal field coils, finite element anal. 78—50396
Large Coil Program, superconducting mag. coil struct. design status 80—106189
Large Coil Program, superconducting toroidal field coils for Tokamaks 78—50388
Large Coil Program, support struct. conceptual design 78—50395
Large Coil Program, test heater conceptual designs 80—91251
large Coil Program, Westinghouse coil cooldown and warmup 80—106193
Large Coil Program. Westinghouse coil stability testing, pulsed induction heating 80—106194
Large Coil Program, Westinghouse Electric conceptual design for test coil 78—50392
Large Coil Program, Westinghouse superconducting mag. elec. design 80—91250
Large Coil Segment test, struct. anal., mag. force loadings 78—50373
Large Coil Task, CC NbTi, pool cooling superconducting test coil, Japanese design 80—99340
Large Coil Task, CC NbTi forced flow superconducting test coil, Swiss design 80—99341
Large Coil Task, NbTi, forced flow superconducting test coil, EURATOM design 80—99339
Large Coil Test Facility, instrumentation system design 80—95446
Large Coil Test Facility, liq. He cooling system 80—102321
Large Coil Test Facility test stand design description 80—102320
large toroidal fusion expts., power supply situation 80—18635
LARTS, extended burn operation, physics, engineering and economics 80—95440
lase fusion, wavelength scaling, benefits of lasers with wavelength less than one micron 80—75073
laser, Nd:glass 20-beam fusion laser focusing lens design 77—18706
laser, Nd:YAG two-beam irradiation facility 77—18705
laser beam appl., semiconductors *(Italian)* 77—26868
laser beam metal-coated apodising apertures 77—19439
laser beams appl. 77—26867
laser commercial plants, systems for protective Li falls 79—85785
laser controlled 77—6563
laser controlled fusion reactor, safety considerations 79—89497
laser driven, fast electrons, X-rays and ions, motion evaluation 80—19557
laser driven, Monte Carlo study of asymmetric effects of LiO_2 blanket 78—74464
laser driven fusion reactors, assessment of engineering problems 79—36413
laser dual beam CO_2 module for nuclear fusion expts. 77—19336
laser flash method, error evaluation in heating disc 77—6552
laser fusion, CO_2 laser prepulse elimination by SF_6 saturable absorber 77—19337
laser fusion, CO_2 laser subnanosecond pulse generation by Pockels cell modulator 77—19357
laser fusion, comparative review of high-power lasers 77—7062
laser fusion, critical surface bubbles and corrugations 77—11376
laser fusion, HYLIFE reactor chamber response to fusion microexplosion 79—89499
laser fusion, National Program of USA 77—34473
laser fusion, thermonuclear power station development, Yugoslavia *(Croatian)* 80—833
laser fusion, transparent microtargets, nondestructive inspection 77—9012
laser fusion 78—59635
laser fusion apodised apertures, Faraday rotators, and spatial filters 77—19290
laser fusion blanket, neutronics and photonics 78—5025
laser fusion concept, high yield injection fusion energy chamber design 79—49862
laser fusion deployment scenario 78—58411
laser fusion generating stations, safety, environmental effects 78—50337
laser fusion in power engineering, future prospects 77—38401
laser fusion power plant, capital cost data base 80—32504
laser fusion power plant, conceptual design 79—71975
laser fusion power plants, final optics 78—50334
laser fusion power stations, potential accidents 78—776
laser fusion process heat systems, criteria for industrial applications 80—57953
laser fusion process heat systems, reliability and maintainability anal. 79—18042
laser fusion reactor, environment and safety features 78—50333
laser fusion reactor, Pb-Li liq. alloy internal spectral shifter and energy converter 79—49841
laser fusion reactor, wetted-first-wall, falling liq. film 78—66408
laser fusion reactor design, pellet X-ray spectra calc. 79—36410
laser fusion reactor design 78—50332
laser fusion research, safety aspects, control measures and protective eye-wear 77—40711
laser fusion system studies model, TROFAN 80—32505
laser fusion system using Shiva 78—54990
laser fusion systems, optical developments 77—19289
laser fusion targets, plating methods 78—60862
laser fusion targets, vapour deposited coatings, surface finish obs. 78—60863
laser fusion with conical target, neutron production 79—22467
laser heated fusion reactor, design of 20 tesla pulsed solenoid 77—23270
laser induced magnetically enhanced reactor, LIME 78—58434
laser plasma prod., penetration length of alpha particles 77—15214
laser produced nuclear fusion, review 80—63381
laser produced plasma in cusp field, RF plugging 80—28783
laser pulse stackers, comparative flexibility and efficiency 77—19291
laser reactor Li_2O blanket, Monte Carlo and discrete ordinate scoping models 78—62603
laser rod amplifier of 4 cm diam., design and performance 77—19339
laser solenoid concept, fusion reactor development 78—54980
laser solenoid fusion concept 78—58435
laser solenoid radiation test facility 77—83430

fusion reactors continued
laser specification 77—18696
laser systems development, CO_2 79—49859
laser systems using CO_2 77—19335
laser target, cylindrical shell, thermal vibrs., general soln. 80—95433
laser technique using H-B reaction, research in Australia 79—3234
laser thermonuclear fusion, review 77—34449
laser thermonuclear synthesis for future energy production *(Russian)* 78—89978
laser-controlled thermonuclear fusion, expt. studies *(Russian)* 77—24114
laser-fission-fusion systems, coupled nuclear-thermohydrodynamic anal. 79—13520
laser-fusion program, LLL, X-ray diagnostic instrumentation 77—76213
laser-fusion reactor, surface heating of 1st wall by pulsed photon and ion irrad. 78—89979
laser-fusion reactor SOLASE-1, first wall and blanket design 78—812
laser-induced, attenuation of 10.6 μm retropulse by elec. initiated laser-driven plasma 77—34424
laser-induced acceleration of macroparticles 80—27813
laser-induced fusion reaction *(German)* 77—65328
lasers for fusion, conference, Reston, Va., USA (Mar. 1976) 77—34895
LASL toroidal reversed-field pinch programme, energy loss meas. 80—23127
Levitron experiment, Culham, plasma fluctuation and by microcomputer system 80—13911
light ion sputtering in fusion reactors, discrete ordinates method calcs., ANISN code 78—92158
linear, heating of cold plasma blanket 79—59258
linear induction accelerator for heavy ions as power source 77—38483
linear laser solenoid, 20 tesla pulsed solenoid design 77—35373
linear magnetic liner, liquid metal, performance calc. 79—50885
linear magnetic solenoid reactor plasmas, dynamic behaviour 80—64751
linear reactor, impurity seeded multiple-mirror end plug 78—63580
linear reactor system with impurity-seeded multiple-mirror end plug 78—78493
linear spheromak, conceptual design 80—95412
liner implosion, anomalous transport processes in radially compressed reversed-field configurations, numerical simulation 80—64689
LINUS, imploding liq. liner system, engineering anal. 80—99315
LINUS approach, using controlled imploding liners 79—49860
LINUS conceptual reactor 78—58432
LINUS program 77—26875
LINUS-O prototype liner implosion system 78—54902
liquid He cryopump, for fusion machines, degassing 78—54382
liquid liners with annular piston drive, hydrodynamic model expts. 78—54903
liquid metal imploding liner fusion system, rot. electron beam stabilisation 77—74994
liquid metal linear implosion systems with blade lattice for rotational stabilisation 80—73994
liquid metals in metallic containers, thermoelectric MHD 79—64787
LMFBR, inherent safety features 80—106145
LMFBR DNB oscillatory temp. and thermal stress anal. by finite element method 79—6767
LMFBRs, national development programmes, status assessment 80—106104
LOCA accidents in Li cooled fusion blankets 78—777
long pulse extraction from modified duoPIGatron for neutral beam fusion reactor system 80—91355
long pulse high current ion source electrode cooling 80—91360
long solenoid reactors, charged particle beam heating 77—67893
long-term nuclear energy strategies, role of fission and fusion 80—78354
low frequency heating wave, parametric instabilities induction in mag. confined plasma 80—24187
low power Tokamak experimental fusion power plant, scoping studies with empirical scaling, SISYFUS code 80—102309
low-activity first-wall and blanket designs, thermal-hydraulic analysis 77—34463
lower hybrid resonance heating theory of Tokamak plasmas 80—28745
LPTT, engineering design 80—102308
LWHR, energy multiplication and T breeding 78—5031
LWHR, source driven, Li-free neutron sources, feasibility and comparisons 79—13383
magnet, high current density superconducting coils, cryostability 80—106201
magnet coil, 125 kG, 1 m, design, fabrication 78—55008
magnet design module for system design studies 77—23261
magnet stability, press. induced flow cooling, highly stable superconducting mag. systems 80—106192
magnet systems for commercial power reactors, structural design 80—86975
magnet systems safety 78—770
magnet technology, conference, Bratislava (1977) 79—30499
magnetic, 1978 status, expt. results survey 79—49864
magnetic, current status 77—23290
magnetic, Tokamak and tandem mirror reactors, neutral beam injection and superconducting magnets 80—63391
magnetic coil systems, EM field, force and inductance calc. by EFFI code 78—62648
magnetic confinement, structural anal., combined interactive/batch computer environment 80—91255
magnetic confinement near term designs, overview 78—58413
magnetic confinement of plasmas 78—94928
magnetic confinement research developments 80—13844
magnetic confinements, international collaboration 80—63390
magnetic diverters for experimental Tokamaks and fusion reactors 80—18621
magnetic fields, biological implications 78—768
magnetic fusion energy program, mirror approach 80—42855
magnetic fusion program in US, recent exptl. results 79—85781
magnetic mirror, transverse confinement of high press. plasma in corrugated mag. field 80—48944
magnetic mirror 2XIIB, first wall surface conditions control 77—31501
magnetic mirror configurations, program at LLL 80—37620
magnetic mirror fusion experiments 78—50343
magnetic mirror research, compact fusion power plants 78—744
magnetic surface with free boundary, eqn. soln. based on one-dimens. model *(Chinese)* 77—76159
magnetic system power source, capacitive energy stores, ultrapowerful, improved service life development problems 79—81089

fusion reactors continued
magnetically confined plasma, numerical computation of MHD flow in Scyllac 77—80282
magneto-electrostatic reactor, power gain factor 80—48933
magnetron, with split electrodes, radial ion (electron) cluster rot., fusion appl. 78—17415
magnets, constitutive model for struct. anal. of elastic-plastic and slip deformation 80—86977
magnets, W.European development 79—31194
main field coil, D-shape, for ASDEX fusion expt., W.Germany 77—61601
maintenance, cassette blanket and vacuum building concepts 78—66386
maintenance considerations 79—45417
Marshall coil, epoxy-insulated, fabrication 78—66388
mathematical simulation of equilibrium plasma configurations and power supply operating conditions in Tokamak-type devices 79—76125
Maxwellian reactivities, convenient computational forms 77—74999
metal vapour columnar arc instability, mag. fields effect, up to 67 kA 78—9893
MFTF, BBC CQK 200-4 modulator tube for sustaining neutral beam power supply 80—99290
MFTF, cryogenic system 80—106163
MFTF, electrical systems, overview 80—91278
MFTF, end loss region high energy plasma gettering 80—102343
MFTF, exception handling control system 80—99325
MFTF, ion and neutral beams dumps, design 80—102317
MFTF, mag. cryostability 80—106198
MFTF, Mirror Fusion Test Facility design and construction 80—37618
MFTF, neutral beam accel power supply protection 80—102380
MFTF, neutral beam module component design and development 80—91270
MFTF, neutral beam source development 80—102368
MFTF, plasma buildup, contaminant control 80—95461
MFTF, plasma diagnostics system 80—95444
MFTF, plasma streaming system, description 80—91280
MFTF, power supply system, digital simulation using EMTP code 80—91286
MFTF, start up neutral beam power supply system 80—91281
MFTF, superconducting mag. quench vent rate 80—106197
MFTF, supervisory control and diagnostics system, database management system 80—99326
MFTF, supervisory control and diagnostics system, database management system, data structs. 80—99327
MFTF, supervisory control and diagnostics system software 80—99324
MFTF, sustaining neutral beam power supply, cct. anal. using ASTAP and EMTP codes 80—91284
MFTF, sustaining neutral beam power supply, shunt preconditioner, IBM-ASTAP anal. 80—102332
MFTF, sustaining neutral beam power supply system, modelling with ASTAP code 80—91285
MFTF physics experiments 80—37623
mFTF plasma diagnostics Data Acquisition System 80—99319
MFTF superconducting mag. design and construction 80—101008
MFTF-B, full tandem extension, description 80—99294
MFTF-B, upgrade of MFTF 80—37619
MHD coolant flows in fusion reactor blankets, 3-D model 80—23119
MHD duct flow studies 78—29651
MHD equilibrium and stability in three dimens. configurations 80—28776
mHD gas turbine energy conversion for mirror fusion reactors 79—41885
microexplosion containment vessel, structural design 78—50341
microexplosion reactor neutronics, adjoint transport eqn. technique 80—47713
microparticle dispenser for laser fusion target fuel cones 78—46170
microprocessor applications in data acquisition and control 80—13918
MIGMA, colliding beam fusion power source, review 79—18031
migma advanced fuel fusion reactor, design 77—83076
migma electron velocity space distrib. function strapping 77—83091
migma fusion reactor, single particle orbits 77—83077
migma ion distrib. in phase space, shaping 77—83090
MIGMA IV, stability study of plasma density buildup 79—13522
migma programme of controlled fusion, 1976 status 77—83086
Migma-type solutions of the Vlasov equation in cylindrical coordinates 79—81082
Migmacell, diamag. limitations to fusion rate 78—42791
Migmacell, low gain driven fusion power amplifier as interim energy source 78—54875
migmacell advanced fuel fusion appl. to manned space propulsion 77—87236
migmacell II, Si detector for fusion products 77—83089
Migmacell III, Tnτ values 77—83104
migmacells II and III advanced fuel expts., orbit diagnostics and lifetime meas. 77—83088
miniexplosion, critical masses in fission-fusion hybrid systems 77—3158
minor reactor, high beta, simple binary collision theory 79—86603
mirror, standard, tandem and field-reversed types, conceptual designs 79—49857
mirror fusion central power station, 1 GW, tritium containment and blanket design problems 77—38414
mirror fusion device, plasma buildup, model 78—8981
mirror fusion reactor design, first-wall and blanket designs, superconducting magnets, neutral beam injectors, direct energy convertors 80—32429
mirror fusion reactors, remote servicing features 78—58448
mirror fusion test facility, beams and supercond. magnets 79—49849
mirror fusion test facility, design and construction 79—49850
mirror fusion test facility, procurement, schedules and status 79—49851
mirror fusion test facility, project scope and objectives 79—49848
mirror fusion test facility, supercond. coils for plasma confinement field 79—36402
mirror fusion test facility, supercond. magnet prod. system 79—36408
Mirror Fusion Test Facility, superconductor core manufacturing and quality 80—93521
mirror fusion test facility 79—49856
mirror fusion test facility 80—43962
Mirror Fusion Test Facility supercond. coil development 79—31202
mirror fusion-fission reactor, safety 79—22461
mirror fussion test facility, supercond. Yin-Yang coil fabrication 79—36403
mirror machine, fusion reactors, survey 80—47721
mirror machine confinement, theoretical status, review 77—38398

fusion reactors continued
mirror machines, 2XIIB neutral-beam-heated, extreme UV spectroscopy 80—74002
mirror machines, field reversal studies 80—27802
mirror machines, nonaxisymm., quadrupole field and orbital reson. 79—59250
mirror machines, superconducting magnets 80—42862
mirror plasma, electron heating using external power 78—87482
mirror reactor, convective loss-cone instability is absolute 79—64900
mirror reactor, direct energy conversion 78—5018
mirror reactor, flute mode axial feedback stabilisation 77—80344
mirror reactor dynamics, parametric anal. 78—17430
mirror reactor studies 77—74980
mirror reactors, economic significance of Q 80—47722
mirror reactors, finite orbit treatment of plasma building 80—37631
mirror reactors, small size field reversed D-^{3}He fuelled 78—799
missile ejection from confining magnets, kinetic energy release 78—779
modern atomic and nuclear physics (book) 80—11
molecular beams, intense condensed, for injector for heating and fuelling of toroidal plasma expt. 77—24179
molten-salt blanket, effect of Pb and Bi neutron multiplication zones on the fission rates of ^{232}Th and ^{235}U 80—99272
motor generator set, for inductive energy storage systems, voltage protection scheme 78—55037
moving plasmoid heater fusion reactor concept, operating parameters 80—13800
moving plasmoid reactors using advanced fuel, modularisation 80—99312
multi-baseball magnetic trap system, plasma confinement 79—23443
multimegawatt gyrotron design for controlled thermonuclear reactor heating 80—59256
multiple mirror, coil design and economic optimisation 80—99284
multiple mirror reactor with depressed ion temp., power balance 78—67393
multiple-laser-beam expts., Compton-induced refl. 77—993
multipole fusion confinement with 2 MA levitated superconducting coil 80—106191
muon catalysis of d-t fusion 80—78438
muon catalysis of hot fusion 78—743
Nagoya Bumpy Torus, confinement studies 80—78445
near-future Tokamak power reactor remote servicing considerations 79—9887
Netherlands fusion expts., data acquisition and anal. systems 80—13915
neutral atom distribution near wall, temp. grad. effect 80—19555
neutral beam diagnostics of ion temp., Princeton large torus 78—54942
neutral beam injection, 120 keV, ion source 80—91357
neutral beam injection, 24 MW 400 keV H beam 80—91356
neutral beam injection, comparison of series and shunt regulation for power supply 77—23271
neutral beam injection, trace identification of Cs and Na 80—95401
neutral beam injection reionisation power losses in duct, model 80—99385
neutral beam injecto cryogenic pumping panel chevron baffles, black coating materials, selection 80—95456
neutral beam injector, continuous operation, water cooled U-tube extraction grid 80—99392
neutral beam injector for tandem mirror fusion reactor, delivering 1.2 MeV D atoms 79—22509
neutral beam injector mag. cusp plasma source, design and fabrication 80—99377
neutral beam injector vacuum system transient simulation anal. 80—95453
neutral beam source, 40 kV for TMX, engineering design 80—91358
neutral beam targets, water-cooled swirl tubes, heat transfer calcs. 78—67018
neutral beam-injected mirror-confined plasma transport 78—22461
neutral injection heating of large Tokamaks and reactors 77—68828
neutral-beam requirements for compression-boosted ignited Tokamak plasmas 78—78494
neutron cross section requirements of CTR program model calcs. 77—23292
Neutron diagnostics for pulsed high-density thermonuclear plasmas 79—90462
neutron energy spectra from beam-driven toroidal plasmas 78—5034
neutron flux, high intensity, modelled by deuteron linac 77—38464
neutron induced activity and biological dose rates in and around JAERI reactor 78—54872
neutron intense high-energy sources for fusion reactors and radiotherapy 77—83419
neutron irradiation damage in fusion reactors *(Japanese)* 79—31180
neutron multipliers for fusion blankets, comparative anal. 79—18049
neutron plasma source, PROMETHEUS, potential mirror concepts for materials testing 77—83431
neutron production in dense focus 77—74989
neutron source, 3 ns pulsed beam-target, thermonuclear neutron burst simulation 80—87008
neutron source, high intensity, high energy for fusion reactor developments *(Japanese)* 79—31179
neutron sources, pulsed power appl. 77—83432
neutron streaming along fusion reactor ducts, perturbation and variational corrections 80—23143
neutron time depend. transport, discrete transfer cross section expansion 79—80969
neutron yield depend. on interelectrode insulating system shape 80—74027
neutronics, fundamental problems *(Japanese)* 80—57944
neutronics, higher-order variational functional derivation 79—9880
neutronics analysis using generalised variational principles 80—57947
neutronics rel. to energy problem 77—26827
neutronics simulation using low energy neutron source 78—5030
NOEL (no external leak) blanket concept 79—18048
non-circular Tokamak field shaping coils, current optimisation 80—95426
non-electric fusion energy applications 80—42866
non-superconducting magnet structures for near-term, large fusion experimental devices, magnet and structural design 80—86973
nonelectrical appl., US DOE perspective 80—42849
nonelectrical applications, review 80—57952
nonmagnetic dense thermonucl. plasma confinement, electron beam heating 77—76171
NOVA, high speed rot. mech. shutter design for pre-pulse protection 80—96032

fusion reactors continued
NOVA, pulsed power control system, fibre-optic multi-tapped computer bus 80—95443
nuclear, social aspects *(Dutch)* 80—106153
nuclear energy, appl. and processes *(Portuguese)* 77—3189
nuclear energy options, for future, fusion-fission concepts, accelerator breeding 80—13838
nuclear energy synergetics, characts. of integrated systems 79—13382
nuclear fusion reactor R and D, technical problems review *(Japanese)* 80—5325
nuclear power, role of fusion in future, European point of view 79—26751
NUWMAK, blanket and power conversion system design 80—18625
NUWMAK, toroidal field magnet system 79—36406
Oak Ridge National Laboratory superconducting coil fabrication development 78—50370
Oak Ridge TNS program (1976/1977) 78—54975
Oak Ridge TNS reference design, 1978—engineering considerations 80—13796
Oak Ridge TNS reference design, 1978—plasma engineering considerations 80—13795
Ogra-3 mirror device, loss mechanism due to cyclotron instabilities 80—28788
ohmic heating, electron power balance, TFR device 77—67885
ohmic heating coil, fast ramp superconductor 78—62638
ohmic heating pulsed superconducting coil 78—62640
ohmic heating superconducting solenoid, Tokamak TNS appl. 78—54928
ohmic heating system, superconducting 78—62634
Ohmic pumping by means of externally driven tearing modes 80—28706
oil shale extraction in situ retort utilising fusion reactor 80—108780
open system, AC direct energy convertor 79—4197
open trap with ambipolar mirrors, thermonuclear plasma behaviour 77—76167
open traps, axially symmetric, transverse particle losses 80—28784
ORMAK, impurity and surface studies 77—31517
ORMAK, plasma equilib. feedback control 77—3976
ORMAK, poloidal magnetic field fluctuations 80—18597
ORMAK Tokamak, solid H pellet injection as refuelling test 78—5020
ORNL fusion power demonstration study, review 79—71969
ORNL Tokamak, hybrid equilib. field coils, power supply 78—54895
ORNL/TNS and ETF, tokamak reactor poloidal field system study 80—95436
ORPUS-3, pulsed superconducting solenoid for poloidal field coils 78—62641
parametric anal. of utility operations 78—58409
particle diagnosis of fusion plasma 77—35397
particle-beam fusion reactors, first wall protection by inert cavity gases 80—91245
passive notch circuit for pulsed-off fusion power compression fields 77—23266
PCX facility, intense laser radiation effects on mag. confined plasma 78—66405
PDX, 6 MW Neutral Beam Project, overview 80—106223
PDX, assembly, description 80—99308
PDX, data acquisition systems, networking and distrib. processing improvements 80—99318
PDX, flexible work platform and balcony design 80—106161
PDX, initial operation 80—79555
PDX, large Tokamak, design and future use 80—79534
PDX, mech. design and assembly 78—50350
PDX, neutral beam elec. power system, ion source supply upgrade 80—102330
PDX, ORNL prototype neutral beam injection system, ion source development 80—99391
PDX, shaping field-equilib. field power supply rectifier upgrade study 80—91290
PDX, toroidal field coil and frame struct., anal., finite element anal. 80—106165
PDX canned poloidal coils, design, fabrication and mag. alignment 78—50385
PDX device, overview and status report 78—54985
PDX machine, poloidal field power supplies, performance 78—54956
PDX magnetic islands anal. 78—62646
PDX neutral beam injector, ion accel. structural anal. 80—102375
PDX neutral beam injector, multi-aperture ion accel. electrodes thermal anal. 80—102371
PDX neutral beam injector development 80—99375
PDX poloidal field coil power tests 78—50384
PDX power test results, struct. finite element anal. 80—91265
PDX Tokamak, finite element anal. using computer graphics 80—95424
PDX Tokamak, neutron skyshine Monte Carlo calcs. 80—47711
PDX Tokamak, struct. anal. by finite element method 80—106166
PDX Tokamak, surface analysis station 80—79586
PDX Tokamak, Ti density meas. using Ti XVII forbidden line 80—32496
PDX Tokamak program, status review 80—37586
PDX toroidal field coil joint fatigue testing 80—91252
PDX toroidal field coil mag. force distrib. anal. 78—50380
pebble bed inertial confinement blankets, prod. of high temp. industrial process heat 80—13807
pellet re-fuelling feasibility, review 80—91246
pellet refuelling of a divertor Tokamak 80—91247
perturbation theory developments for anal. and design, review 77—14227
PETULA Tokamak, lower hybrid heating expts. 80—83958
Petula Tokamak, transit time magnetic pumping 80—24186
PGFR seismic risk anal. 80—99298
PHIBEX, poloidal field power supply for ignition, computer based cct. anal. 80—102329
photonuclear processes, obs. in TFR Tokamak 77—34441
pinch experiment, high energy Cu foil fuse for implosion in multimegajoule region 77—24218
pinch-tormac, device using theta pinches and tormac-like end sections 80—24213
pinched electron beam diode, proton current density meas. using biased charge collecting probe 77—55166
plasma, RF heating limitations, Alfven's critical ionisation velocity phenomena 80—28717
plasma boiler moving in ambient plasma, fusion reaction rate enhancement 79—18038
plasma column, confinement by ablation front from cold gas plug 80—28793

fusion reactors continued
plasma confinement, alternative mag. configurations for commercial fusion reactor development 79—71949
plasma confinement, quasisteady, scaling laws rel. to fusion reactor operation 79—27812
plasma confinement and heating, basic problems rel. to extraterrestrial plasmas 78—69672
plasma contamination, sputtered particles, energy and mass distribs. 80—84822
plasma diagnostics for controlled thermonuclear fusion experiments *(Spanish)* 79—63805
plasma diffusion in low-beta devices, finite element analysis 77—80277
plasma divertor experiment, management techniques and procedure 78—54891
plasma flow driven by fusion-generated alpha particles 79—14592
plasma focus as high intensity neutron source 77—83433
plasma focus as large fluence neutron source 77—88315
plasma fuelling, collisional drift modes, anomalous skin effect, enhanced particle penetration nonlinear theory 80—64703
plasma heating, conference, Varenna, Italy, (Sept. 1976) 77—65885
plasma heating and confinement, review 80—63388
plasma heating by collisional slowing of fast ions in noncircular Tokamaks 80—95403
plasma impurities, effects, diffusion, wall erosion 77—67877
plasma impurity control using neutral gas blankets 80—13835
plasma impurity diversion through ambient boundary layer flow 80—19603
plasma in mag. confinement, review of required diagnostic techniques 79—71951
plasma models for standard mirror reactors 80—6273
plasma neutron diagnostic techniques with good spatial and energy resolution 79—46478
plasma physics, and controlled nuclear fusion, conf., Berchtesgaden (1976) 77—43020
and plasma physics magnets, USA development 79—31193
plasma reaction rates, velocity-space methods 77—79475
plasma recycling at surfaces using self-consistent model 77—35355
plasma rotation induced by 3.5 MeV alpha-particle losses 78—18384
plasma science, conference, Monterey, CA, USA (May 1978) 79—37442
plasma transport, unified slowing down theory 78—18383
plasma transport processes in toroidal stellarators and torsatrons, viability as fusion reactors 79—90381
plasma valve design with liq. metal cathodes, high-power conversion/switching appls. 78—9865
plasma vortex struct. compression 79—9888
plasma wall interaction in ATC during high power neutral beam injection 77—31502
plasma-wall interaction, boundary layer 77—47216
plasma-wall interaction, permissible degree criterion 78—89981
plasma-wall interaction in ASDEX divertor expt. 77—31504
plasma-wall interactions in controlled fusion devices conf., Abingdon, England (April 1978) 78—94917
PLT, coil stress and deflection analysis, ANSYS computer code appls. 78—50356
PLT, D_2 flux and energy incident on probe, power balance, impurity generation 80—79553
PLT, data acquisition systems, networking and distrib. processing improvements 80—99318
PLT, fusion neutron yield during D neutral beam injection 80—79522
PLT, fusion-produced T confinement 79—98955
PLT, ICRF heating for two-ion regime 80—83959
PLT, neutral beam duct reionisation losses, obs. and power loss model 80—99383
PLT, neutral beam injection, power input and plasma temp. reconciliation 80—106224
PLT, neutral beam injection and ICRF heating, charge exchange meas. 80—83892
PLT, ohmic heating system operation 78—66401
PLT machine, multi-channel TV-Thomson scatt., apparatus, mech. aspects 78—54932
PLT toroidal field coils, operational deflection meas. 78—62627
pollution hazards assessment *(Czech)* 78—86681
poloidal coil air-core system for experimental power reactor 77—26873
poloidal field coil design and development of JT-60 Tokamak 79—31204
power conversion system, (PULSAR), with inductive storage 78—55029
power development program plan 77—34461
power generation by thermonuclear reactions 77—65330
power plant simulation model 80—13865
power plants, engineering limitations 78—74473
power supply, three-phase system, computer aided cct. design 78—54959
power supply using air powered fibre optic coupled pulser 78—13342
pressurized spark gap switch with high repetition rates in multimegawatt average power range 77—23275
primary wall swelling due to ion bombardment 78—17418
Princeton Large Tokamak, D electrodisintegration neutron spectrum 77—84521
Princeton large Tokamak, obs. of electrodisintegration neutron prod. 78—5029
Princeton Large Torus, engineering tests on toroidal and internal poloidal field coils 77—23264
Princeton large torus 3-coil test 78—54945
process heat source for secondary energies 80—13863
progress review *(Spanish)* 77—67869
projected inertial confinement fusion reactor target evaluation by buoyancy analysis 80—78442
prospects and the future of nuclear fusion, discussion *(French)* 80—18609
protium beam injection into protium-deuterium plasmas, fusion neutron production 79—23430
PULSATOR I Tokamak, wall analysis, impurities 77—31515
pulse power supplies development 78—8990
pulsed, based on θ-pinch with a liner 77—34443
pulsed, plasma MHD generator for modelling energy conversion 77—3165
pulsed fusion experiments, computer-based control systems 78—62624
pulsed high-β devices, CTR radiation test facilities appls. 77—23256
pulsed homopolar power supply, misalignment and eccentricity anal. 77—23287
pulsed power supply using fast discharging homopolar demonstration model 77—23283
pulsed superconducting coils, high voltage test 80—13929

fusion reactors continued
pulsed Tokamak, load-levelling considerations 79—85799
pulsed Tokamak reactor, poloidal mag. field design 80—13858
pulser system, air-driven fibre-optic coupled for Los Alamos ZT-40 expt. 78—54943
pumping and vacuum requirements 77—57744
Q-enhanced mirror fusion system, plasma-surface interaction 78—94130
quasisteady fusion reactor, gas blanket confinement, drift mode instabilities 78—18403
R-OM stellarator, MHD resonant HF heating 80—79518
radioactive waste management 78—21766
radioactivity calc. code and decay chain data library, DKR 78—786
radioactivity considerations in reactor operation 79—63811
radiological hazards, reliability requirements 78—58447
radiological protection aspects of fusion power, review 80—9411
re-entrant boundary conditions for toroidal transport and diffusion 80—18592
reactant distribution functions in fusion reactors, fast computing method using Legendre polynomials expansion 78—78491
recirculating power, unit costs, thermal pollution 78—29643
rectangular plasma generator, advanced ion source for ion injectors 80—99376
reference theta pinch reactor, first wall thermal-mechanical anal. 77—57750
refuelling by pellets, ablation rate, injection vel. effects 80—13881
relativistic electron beam fusion reactor, parametric anal. 78—50340
relativistic electron beams as plasma heating mechanism for solenoid systems 80—24190
remote leak detection for Tokamak Fusion Test Reactor 78—50403
remotely operable large vacuum seals for fusion reactors 78—50405
research, appl. as future energy resource, review 79—49839
research and development in Japan 80—47701
research and development in thermonuclear fusion *(Japanese)* 77—83095
research philosophy 80—42854
research program strategy 79—59251
reversal field mirror, alpha-particle effects 78—58468
reversed field experiment, performance predictions comparison to ZETA 78—30466
reversed field mirror reactors, startup using coaxial plasma guns, scaling laws 80—99279
reversed field pinch, burn stability 78—58467
reversed field pinch, expt. and comp. studies 80—23128
reversed field pinch, reactor burning calcs. 77—23253
reversed field pinch, RFX constructional details 80—91277
Reversed Field Pinch, thin walled toroidal vacuum chamber design 80—18642
reversed field pinch experiment, ignitron switching problems 80—13900
reversed field pinch experiments, vacuum design and discharge cleaning 80—18650
reversed field pinch machines, plasma stability anal. 80—24214
reversed field pinch reactor, 600 MWe, plasma physics and reactor parameters 79—71976
reversed field pinch reactor, choice of parameters for 600 MW net electrical output 78—58471
reversed field pinch reactor, physical principles, design, operation and plasma stability 78—58470
reversed field pinch reactor, preliminary engineering design 78—58472
reversed field pinch reactor 78—58433
reversed magnetic fields induced by a rotating e-beam 80—28790
reversed-current ion ring reactor, image current interaction 79—85778
reversed-field pinch, formation, relaxation and heating studies 80—24215
reversed-field pinch burn dynamics, global computer code 78—63579
reversed-field pinch reactor 80—37626
reversed-field-pinch reactor, superconducting windings 80—27804
review 77—42182
review of international fusion research 77—46402
RF driven current generation by lower hybrid waves in Tokamak 80—103116
RF driven currents in steady state Tokamak reactors 80—28687
RF plasma heating, effect of wall corrugations on lower hybrid wave spectrum 80—33787
RFC-XX, coil system, design, fabrication, testing 78—55007
RFC-XX, cusp end plugging MW quasi-steady wide band RF system 80—13880
RFP, plasma stabilizing passive shell and active feedback windings 80—18666
RFPR, direct-cycle steam generating blanket design 80—37615
RFPR, T transport in packed bed Li_2O fusion blanket 80—37612
RFX field system design 78—54884
RINGBOOG II, cold gas blanket design *(Dutch)* 80—32498
RINGBOOG II, design and construction 80—13849
RINGBOOG II, poloidal field configuration 80—18664
RINGBOOG II, toroidal discharges with cold blankets 80—83901
rotating plasma reactors, longitudinal confinement, stability equilibrium and heating problems 80—74001
rotationally stabilised liquid-liner fusion system, finite liner compressibility effects 79—18036
RST, RF driven steady state toroidal expt., design 80—91276
RST, support struct. 80—102342
RTPR, Bondarenko formalism to account for resonance self-shielding effects 77—23300
safety, consequences to the first wall during a major plasma disruption 80—13823
safety, environmental control of use and release of T at TFTR 80—13829
safety, radiation exposure and maintainability 80—13828
safety, reliability criteria determ. by consideration of radiological hazards 80—13826
safety and environment contamination factors *(German)* 79—13527
safety and environmental aspects 77—34454
safety and environmental impact 77—67876
safety and environmental pollution *(German)* 80—63370
safety of superconducting fusion magnets: twelve problem areas 80—102348
SAFFIRE, Cat-D fueled, synthetic and fissile fuel prod. 80—99280
Sandia particle beam fusion program, objectives and current status 80—37591
screw pinch, force free current induction by boundary displacements 79—32796
screw pinch, reactor design parameters 77—23254

fusion reactors continued
screw-pinch high-β Tokamak, field generation using transverse rotating mag. field 80—19606
Scylla IV-P, computer-based control and data acquisition system for CTR 78—62621
Scylla IV-P linear theta-pinch, material end plugging 78—55744
Scyllac fusion test reactor design 77—23252
Scyllac reactor, feedback stabilisation system 78—54887
Scyllac sector feedback stabilisation expt., engng. aspects of on-line operation 77—23268
second generation designs, safety anal. 78—771
segmented compact Tokamak reactor, poloidal field coil system 80—13866
self-sustained advanced-fuel field reversed mirror reactor, preliminary design 79—85786
shielding, multigroup libraries from radiation shielding information centre 78—13399
shielding, sensitivity-based cross-section data assessment 78—9048
shielding and maintainability in an experimental Tokamak 80—99287
shielding experiment, cross-section sensitivity calcs., one- and two-dimensional models 80—27799
shiva and Argus target diagnostics vacuum systems 79—81079
Shiva Faraday rot. coils, circuit and mag. anal. 78—54951
Shiva laser fibre-optic digital links 79—85804
Shiva project, control and alignment systems, development trends 79—85764
single-cell field reversed mirror fusion reactor, mechanical struct. 80—13825
SIT with neutral injection heating, transport calculations 80—9409
SLPX, supercond. long pulse expt., design features 80—13854
SLPX, Superconducting Long-Pulse Experiment, scoping study 80—91275
SLPX TF coil, stress anal. using COSMIC-NASTRAN 80—106168
small-aspect-ratio torus for demonstrating thermonuclear ignition 79—71966
SOLASE laser fusion reactor, Monte Carlo shielding calc. for mirror-laser beam duct system 80—23174
SOLASE laser fusion reactor design and its technological implications 79—71974
solenoid, orthotropic, finite element stress anal. 78—55010
solenoidal, instability-driven anomalous transport, review 78—22460
solid breeder blankets for D-T reactors, operating temp. limits for T release and recovery 80—102294
solid breeding blanket for commercial Tokamak reactors, materials and design 80—95441
SORB-AC wafer getter pumps, fusion reactor appl. 80—18637
Sorb-ac wafer pumps, behaviour in plasma machines, review 78—70627
spark gap overpressure, 0.2 MA, design and appl. 78—75456
special engineering problems 79—6766
spent fuel streams, impurity removal and recovery processes 79—85783
spherical multipole electromagnet development 79—31208
spheromak, toroidal reactor low aspect ratio limit 80—23139
Spheromak fusion reactors, MHD equilib. and stability, numerical anal. 80—74000
sputtering, rel. to fusion research 78—764
sputtering by neutrons from Nb, Mo, V, 316 SS meas. 77—36321
sputtering erosion in inertial confinement fusion reactors 79—22462
sputtering erosion of cavity walls, comput. procedure 77—38410
stability and dynamic properties transfer function anal. for fusion system 79—93825
staged heating using laser irrad. and mag. compression 77—19736
Starfire, commercial Tokamak power plant, conceptual design 80—57957
Starfire Commercial Tokamak design, utility evaluation criteria 80—37624
STARFIRE project, an overview 80—106183
STARFIRE project, design parameters 80—106184
STARFIRE project, first wall and blanket design 80—106188
STARFIRE project, impurity control system 80—102345
STARFIRE project, maintenance considerations 80—102346
STARFIRE project, superconducting poloidal coils design study 80—106185
STARFIRE project, T handling and vacuum requirements 80—106187
STARFIRE project, toroidal field coil system preliminary assessment 80—106186
stationary ion source construction 80—91359
stationary turbulence as confinement layer 77—68844
status and prospects of fusion power 77—67878
status report on fusion, April 1977 IFRC report 79—6760
steady-state Tokamak reactors with RF driven currents 80—27818
steam turbine, fusion augmented, high efficiency, power cycles 79—22475
stellarator, ohmic plasma heating 77—65333
stellarator, plasma losses, quasi-neoclassical law 80—79544
stellarator, with 3 mag. axes, Doublestar, numerical study 78—91140
stellarator reactor studies, review 78—30467
stellarators, controlled thermonuclear fusion expts. at Kharkov Inst., Ukrainian SSR *(Russian)* 79—13526
stellarators, equilibrium and stability calcs. 80—83982
stellarators, magnetic hill effects on equilibrium 80—79558
stellarators, research status 80—74013
stochastic ion heating by electrostatic wave in sheared mag. field 80—28705
streaming ray technique for particle transport calculations 80—47716
structure neutron activation, experimental power reactor 78—74476
superconducting 7.5 Tesla segment test facility 78—54929
superconducting cables for PF and TF coils, losses and transient field effect 78—62635
superconducting coil, multifilamentary composite losses 78—62637
superconducting composite, eddy current losses 78—62636
superconducting energy storage coil 78—54924
superconducting energy storage coils, conductor design 78—62639
superconducting fusion magnetic systems, struct. anal. methods and standards 80—86972
superconducting fusion magnets for mirror systems 79—36401
superconducting magnet cooling system design 77—23289
superconducting magnet development 77—26869
superconducting magnet failure experience rel. to fusion reactors 77—26870
superconducting magnet for fusion research, Nb_3Sn multifilamentary cond. development 77—28760

fusion reactors continued
superconducting magnet for magnetic flux compression, compression generator, PULSAR, design optimisation 80—68957
superconducting magnet for mirror fusion test facility, conductor fabrication 78—62642
superconducting magnet joints, resistance welding 80—91259
superconducting magnet magentoelastic energy calcs., finite element anal. 78—55002
superconducting magnet system, appl. to Tokamak 78—54925
superconducting magnet systems, USSR designs 79—31192
superconducting magnet systems 77—19759
superconducting magnet systems for Tokamak design 77—71691
superconducting magnet testing instrumentation and methods 77—26882
superconducting magnets, composite superconductors, stability anal. by thermal analyser digital computer program 78—54995
superconducting magnets, cooling system using liquid He 78—54998
superconducting magnets, force-cooled conductors design 78—54999
superconducting magnets, high field test facility, and initial performance 79—30447
superconducting magnets, hollow conductors, cooled by supercritical He 78—54997
superconducting magnets, pulsed, stability studies, fusion reactor appls. *(Japanese)* 80—106158
superconducting magnets, recovery, laboratory obs. and computer calc. 79—30494
superconducting magnets, structural alloys, props. at 4K 80—86976
superconducting magnets, structural design 80—86974
superconducting magnets, toroidal field coil thermal design and anal. 78—50368
superconducting magnets cryostabilisation using superfluid He 78—54996
superconducting magnets safety and structural aspects 77—26874
superconducting material and device requirements for thermonucl. fusion *(French)* 78—13322
superconducting ohmic-heating coils for Tokamak fusion reactors, simulation expts. 79—36404
superconducting pulsed solenoid ORPUS-1, for Tokamak reactor 77—26352
superconducting quadrupole magnet design for ion beam fusion linac 79—36433
superconducting ring, buckling in toroidal mag. field 79—64550
superconducting Tokamak TF coil system, protective control features 78—62625
superconducting Tokamak toroidal magnet system development, cluster test facility 79—30495
superconducting toroidal coil, TESPE, for Tokamak fusion plasma containment 79—54223
superconducting torus, magnetoelastic buckling experiments 79—64549
superconducting Ying-Yang magnet system for mirror fusion test facility 78—54922
superconductor coils appl., based on Nb-Ti *(French)* 80—95399
superconductor optimisation for 12 Tesla toroidal field coils from Nb-Ti and Nb-Ti-Ta alloys 80—91272
superconductor strain and mag. system design parameters, closed-form anal. 78—50377
superconductors, built-up, current transfer 78—62633
superheating-diffusion instability, thermonuclear burn 80—32500
suprathermal alpha particle effects, phase space grouping techniques 77—79479
surface effects in controlled thermonuclear fusion 77—26866
surface effects of neutral beam injectors and beam direct convertors 80—47719
surface erosion phenomena in CTR appl. 77—71695
surface magnetic confinement devices for advanced fuel fusion 77—83101
surface problems in controlled fusion *(Chinese)* 79—97904
switch, 100 kA, explosively actuated, 70 μs opening time 78—8984
switch for mag. cct. supply *(German)* 78—37441
switches, supercond., high specific breaking power 78—55020
switching and regulating elements, high-power tetrodes appl. 79—54592
synfuel blanket design for mirror or Tokamak reactors 80—95407
synfuel blanket module in neutron beam, 2-D heating anal. by computer simulation 80—95406
synthetic fuel prod. using fusion reactors 80—13793
synthetic fuel production appl. 80—13864
synthetic fuel production from fusion, economic prod. pot. 77—34467
synthetic fuel production in a particle-beam driven fusion reactor 80—55780
synthetic-fuel producing blanket, nucleonic anal. 79—85802
T-10 M tokamak toroidal field coil shape struct. anal. 78—50374
T-10 Tokamak, electron temp. meas. from cyclotron emission 80—19617
T-10 Tokamak, plasma thermal-loss process and behaviour of impurities 79—27805
T-10M Tokamak, normal and supercond. inductive energy storage and switching 78—55018
tandem minor reactor maintainability study 80—18615
tandem mirror confinement studies 80—28785
tandem mirror device, operation, Q-factor calcs. *(Russian)* 78—74466
tandem mirror end plugs, ICRF fuelling 79—19070
tandem mirror experiment, mag. field requirements 78—54988
tandem mirror experiment, system design 78—54987
Tandem Mirror Experiment, vacuum system 78—55023
tandem mirror experiment 78—54885
tandem mirror fusion reactor, mechanical design 78—800
tandem mirror fusion reactor, parametric design 78—794
tandem mirror fusion reactor with barrier pot. between plug and solenoid 80—9407
tandem mirror fusion reactors, axisymmetric sloshing-ion plugs 80—73998
tandem mirror physics, fusion plasma confinement 80—43960
tandem mirror plasmas, alpha particle dynamics 80—83986
Tandem Mirror Reactor, end plug mag. system design 80—102347
tandem mirror reactor, new central cell design 80—37625
tandem mirror reactor, new plasma confinement scheme with high system Q 77—42183
tandem mirror reactor parametric anal. and preliminary conceptual design 79—71972
Tandem Mirror Reactor power plant, maintenance and handling economics 80—102311
Tandem Mirror Reactor startup and shutdown, simulation and control 80—99277
Tandem Mirror Reactor steady state, simulation and control 80—99278

fusion reactors continued
Tandem mirror reactors, anomalous and classical transport effect 80—13862
tandem mirror reactors, DT and DD operation 78—8982
tandem mirror reactors 80—42856
technology transfer, adoption in developing countries 77—57751
temperature distribs. in first wall systems 78—58450
TESPE coil, finite element method calc., winding package modelling 78—50376
TESPE coils, design constraints 80—13922
Texas experimental Tokama, homopolar generator, eddy currents, EM forces (torques), due to misalignment 78—54953
Texas fusion plasma research Tokamak, power supply system 77—23258
Texas turbulent heating experiment, fast crowbar switching system 77—23260
TEXT, assembly plan 80—99305
TEXT, motor-generator power supply system 80—99292
TEXT, poloidal coil systems power supplies 78—54957
TEXT, poloidal field power systems, design and anal. 80—102328
TEXT, pulsed homopolar generator power supply, engineering and design 78—55016
TEXT, regulating resistors and interrupters 78—55038
TEXT, Tokamak structural system 78—54882
TEXT, toroidal and poloidal field coil design 78—50354
TEXT, toroidal field coil fabrication 80—91267
TEXT, toroidal field coil power supply, thyristor controlled 80—91289
TEXT data acquisition, multichannel AD subsystem 78—54936
TEXT fusion plasma research facility 78—54984
TEXT iron core Tokamak, design formalism for OH and VF coil system 77—23259
TEXT overview and status report 80—91273
TEXT poloidal field coils 78—62645
TEXT toroidal field coil stress anal. 78—50381
TEXTOR, computerised control system design 80—13907
TEXTOR, mag. diagnostics and monitoring systems data acquisition 80—99320
TEXTOR, plasma position feedback control 80—18659
TEXTOR, plasma wall interaction experimental studies, design features 80—13845
TEXTOR, plasma-wall interaction study reactor, mechanical struct. design 80—13846
TEXTOR, poloidal coil system power distrib. system 80—102327
TEXTOR, poloidal field problems, num. anal. 80—18661
TEXTOR, poloidal field system, transient behaviour 80—18660
TEXTOR, poloidal field system splittable coil, design and testing 80—18658
TEXTOR, toroidal field magnet design 78—50348
TEXTOR, toroidal field magnet design 80—13920
TEXTOR, vacuum vessel and pumping system 80—18636
TEXTOR, vertical plasma position control by fast response unit 80—13896
TEXTOR program at KFA, Julich 77—31505
TF superconducting magnet, demountable, for catalysed D-D and D-^{3}He fusion reactors 77—88280
TFR, electron cyclotron frequency emission and transmission meas. 80—79575
TFR, electron cyclotron heating, computer simulation 80—79517
TFR, extraction grid for high power ion source 80—102372
TFR, high power neutral beam injection and ion power balance, anomalous heat conduction 78—82511
TFR, ICRF heating at ion-ion hybrid reson. 80—74020
TFR, ICRF heating obs. by all metal antenna 80—18606
TFR, ion energy balance, heating by fast neutral injection 77—43023
TFR, neutral injection heating, ion power balance 77—67887
TFR 600, ^{2}H ion flux, temp., and density meas. 80—48940
TFR 600, plasma equilibrium and stability, iron core influence 80—23150
TFR 600 Tokamak, electron heat transport anomaly 80—79449
TFR 600 Tokamak, soft X-ray meas., mag. topology near $q=1$ surface 80—79580
TFR 604, circular periplasmatron ion sources for injection system 80—13871
TFR discharge, energy balance obs. 77—43021
TFR machine, impurity behaviour, radiation losses and wall effects 77—31516
TFR Tokamak, microcomputer data acquisition system 80—13916
TFTR, AC distrib. system for pulsed loads 78—54963
TFTR, assembly 80—102335
TFTR, blanket module expts., engineering test station design 80—102338
TFTR, ceramic insulator rings 78—55022
TFTR, diagnostic interface systems, problems 78—62626
TFTR, eddy current theory for structural materials 80—95427
TFTR, electrical power blanket module, conceptual design 80—102339
TFTR, energy conversion and storage systems, fault detection and protection 80—95431
TFTR, engineering design problems 78—751
TFTR, field coils cooling water system 80—106160
TFTR, gas injection assembly 80—99342
TFTR, general arrangement of diagnostics 80—95445
TFTR, heating, compression clamping, controlled thermal runaway 77—67890
TFTR, high energy heat sink, ion beam dump and calorimeter 80—99394
TFTR, high power direct energy convertors for beams and plasma 80—99334
TFTR, High Voltage Switch Tube, for Neutral Beam Power System 80—99291
TFTR, hollow cathode mag. multipole ion source 80—102369
TFTR, HV switch tube development 78—66385
TFTR, interrupter and hybrid-switch testing 80—99289
TFTR, isodose contour map construction using DOT 3.5 computer code 79—67949
TFTR, large noncircular ports, development of bakeable seals 80—95454
TFTR, large section water cooled Cu conductor, brazing joints 80—91260
TFTR, neutral beam injector prototype, construction and performance 80—99390
TFTR, neutral beam injector test facility construction 80—102336
TFTR, neutral beam line cryopanels, cryogenic supply systems 78—55027
TFTR, neutral beam line final design 80—99309
TFTR, neutral beam line injectors, cryopumping system 78—55028
TFTR, neutral beam power system 80—91282
TFTR, neutral beam source, arc current modulator design 80—102379
TFTR, neutral beam sources overcurrent protection during spark down 80—102331
TFTR, neutral beam-torus connecting duct 80—99302
TFTR, neutron spectrometer mech. design 80—95498
TFTR, neutronics anal. of neutral beam injectors 79—59261
TFTR, physics/engineering interface 78—750
TFTR, plasma generation and confinement 80—42864
TFTR, plasma physics research tool 78—749
TFTR, plasma position control, linear feedback optimal method 78—50365
TFTR, power line, variable freq. AC harmonic content 80—99293
TFTR, preoperational test plan, manpower loading and scheduling 80—102340
TFTR, remote segmentation approach 80—68949
TFTR, role in development of Tokamak physics 78—748
TFTR, T fuel handling, safety and control systems 78—50364
TFTR, T gas injection system transient response 80—102337
TFTR, three-dimens. solid finite element anal. for simulating composite windings 78—55003
TFTR, transient getter scheme 80—79584
TFTR, tritium breeding test blanket module design 80—99304
TFTR, vacuum chamber for neutral beam injection system 78—55021
TFTR, vacuum pumping system 80—95447
TFTR, vacuum system design, performance curves 78—70625
TFTR, vacuum vessel bellows, strength and fatigue anal. 80—95455
TFTR auxiliaries, power distrib. system 78—54962
TFTR device, neutral beam injection and adiabatic compression heating 77—65332
TFTR energy conversion system simulation 80—99303
TFTR engineering developments in remote handling and maintenance vacuum vessel design 79—76129
TFTR engineering features 78—747
TFTR exptl. blanket modules, mechanical design 80—37610
TFTR Flexibility Modification, in-torus surface pumping, Ti and Zr/Al gettering 80—95451
TFTR mag. field coil electrical insulation system and test results 80—95429
TFTR neutral beam injectors, concrete shielding calcs. 80—47734
TFTR neutral beam support system 80—102376
TFTR neutral-beam injectors, shielding calcs. 80—23172
TFTR outer poloidal field coil insulation and mould design 80—91261
TFTR poloidal coils power system 80—13891
TFTR poloidal field coil system, characts. 80—95430
TFTR poloidal field coils, tooling and manufacture 80—91262
TFTR poloidal field coils design details 78—50383
TFTR pulsed loads, AC electrical distribution system protective relaying 80—63387
TFTR status report, 1978 80—18671
TFTR technology and Tokamak engineering 78—50344
TFTR test cell, calc. dose rates from induced activity, Monte Carlo methods 80—57967
TFTR thermal response of first wall limiters 80—79585
TFTR toroidal field coil case design 78—50347
TFTR toroidal field coil design 78—50346
TFTR toroidal field coil support restraint struct. 80—95428
TFTR vacuum pump system, radiation exposures during maintenance 80—13788
TFTR vacuum system, description, operation, safety 78—74497
TFTR vacuum system transient simulator 78—74496
TFTR vacuum vessel, T permeation and wall loading 79—45412
TFTR-II, high density Tokamak design studies 79—71962
thermal hydraulics anal., reln. to magnetic fusion blanket design 80—27816
thermalisation of energetic charged particles in fusion plasma, QED effects 77—65834
thermionic topping cycles appl., preliminary assessment 79—48161
thermonuclear Alfven instability stabilisation in high press. tokamak, mag. surface distortion *(Russian)* 79—27758
thermonuclear energy from ball lightning, design concept 80—32516
thermonuclear fusion and the Tokamak, review *(Italian)* 79—31177
thermonuclear fusion devices, atomic and mol. data 77—68741
thermonuclear fusion research, economic factors 80—73991
thermonuclear fusion research, user-engineered command language 80—27819
thermonuclear instabilities, Tokamak reactor fuelling, α-particle interactions 77—88281
thermonuclear plants, international collaboration 77—79481
thermonuclear plasma, radn. losses at impurities, $n_e\tau$ parameter *(Russian)* 79—68908
thermonuclear plasma surrounded by cold blanket, density profiles, thermo-elec. forces effect 79—31189
thermonuclear power station based on microexplosion-induced D-T initiation 78—82508
thermonuclear power station based on theta-pinch reactor with cumulating liner, engineering level and economic charact. *(Russian)* 80—68951
thermonuclear react. rates, computation with STEEP code 78—18375
thermonuclear reactor development *(German)* 77—34425
thermonuclear research in the Soviet Union *(Hungarian)* 80—91239
thermosyphon energy removal system design 77—34465
theta pinch, field reversed, ion beam injection, fusion appl. 79—22476
theta pinch, hot linear, end plugging effect on stability and parameters 80—24223
theta pinch, linear, end losses, stoppering, instabilities and heating 80—24224
theta pinch, linear, with strong and fast rising mag. field 80—24222
theta pinch fusion reactor, switching technology for supercond. mag. energy storage system 77—23285
theta-pinch, high β, plasma evolution and thermonuclear yield 77—89287
theta-pinch, high density linear system, fusion power appls. 77—23255
theta-pinch, linear, solid end plugs and mag. mirrors, fusion reactor 77—89294
theta-pinch, reverse field expts., equilibrium, confinement, stability 80—28787
theta-pinch, Scylla I-C, laser beam-plasma interaction 77—24090
theta-pinch device for modelling fusion reactor operation 78—89972
theta-pinch fusion system with liner exploded by thermonuclear neutrons 80—79547

fusion reactors continued
theta-pinch reactor, fast feedback stabilisation 77—23269
time depend. diffusion eqn. for neutronic calcs., use of exterior differential forms 78—54871
time-dependent tandem mirror confinement, start-up and alpha particle build-up 80—10419
TMX, config., liq. N_2 supply and operation of vacuum system 80—95448
TMX, injector system mech. design and installation 80—99393
TMX, installation and operation of cryoliners in vacuum system 80—95449
TMX, mag. control system 80—95442
TMX, magnet construction and alignment 80—91266
TMX, magnets, mech. design 78—58494
TMX, neutral beam control systems 80—99323
TMX, neutral beam system startup 80—99306
TMX design and construction 80—37622
TMX tandem mirror experiments 80—37621
TNS, air core and Fe core ohmic heating systems 78—66402
TNS, compact poloidal divertor reference design 79—71960
TNS, design related RD&D assessment 78—54976
TNS, electrical design costing 78—55014
TNS, electron cyclotron heating startup system, design 80—99330
TNS, negative-ion neutral-beam system design for plasma heating 80—13837
TNS, review of plasma engineering, design and program planning for future developments 79—71959
TNS, T handling system design 78—62616
TNS conceptual design, parametric anal. 78—54991
TNS Tokamak, T fuel handling system design 78—50363
TNS Tokamak first wall, thermal consequences due to plasma disruption 80—37598
TNS Tokamaks, costing and sizing, computer code 78—50361
TNS Tokamaks, trade study anal. 78—54992
Tokamak, 2-D neutronics model for major penetrations 78—5027
Tokamak, 'drift' thermonuclear instabilities *(Russian)* 78—25326
Tokamak, advanced fuel 77—83099
Tokamak, advanced fuel type, bundle divertor design 77—38413
Tokamak, Al low activity blanket 77—6560
Tokamak, alpha transport and blistering of first wall 79—19069
Tokamak, anomalous diffusion of α-particles due to trapped ion mode 80—48951
Tokamak, arbitrary cross-section, self consistent two dimens. transport eqns. 79—49842
Tokamak, ATC, free expansion expt. 78—30469
Tokamak, axially symmetric, α-particle escape in nucl. fusion, azimuthal distrib. *(Russian)* 77—18694
Tokamak, axisymm. MHD instability, feedback stabilisation 78—87484
Tokamak, beam heated, critical impurity conc. for power multiplication 78—29641
Tokamak, beam-driven, nucl. reactions among energetic ions 77—34469
Tokamak, blanket and first wall design concept, thermal and hydraulic anal. 80—95460
Tokamak, blanket and shield of high-field compact reactor 78—74475
Tokamak, bounce effects on cyclotron instability caused by trapped alpha particles 77—76060
Tokamak, catalysed D operation, plasma and reactor parameters 78—33287
Tokamak, cold layer formation, wall protection 78—30470
Tokamak, compact high-density, system of field coils 77—34464
Tokamak, comparative anal. with hybrid reactors 79—18043
Tokamak, computational method for neutron transport problems 78—22538
Tokamak, conceptual designs 77—34453
Tokamak, construction, objectives and performance of future devices 77—34452
Tokamak, counterstreaming-ion, plasma refuelling and heating 77—71693
Tokamak, D-T steady-state fusion *(Russian)* 77—18693
Tokamak, demonstration and commercial prototype 79—49855
Tokamak, design consideration for maintenance access 77—3163
Tokamak, diffusion of runaway electrons across mag. field 78—87480
Tokamak, DITE, recycling in gettered and diverted discharges 78—94132
Tokamak, DITE expt., plasma surface interaction program 77—31503
Tokamak, DITE H conc. meas. in walls and limiters 78—94136
Tokamak, DIVA, impurity shielding and sweeping out, axisymm. divertor 78—86685
Tokamak, DIVA, radiation loss and power balance, pyroelectric detection 78—86684
Tokamak, divertor expts. for controlling plasma-wall interactions 78—94125
Tokamak, doublet reactor, parallel connected ohmic heating coil 78—54930
Tokamak, eddy current analysis, finite element circuit method 78—66373
Tokamak, eddy currents, 3-dimens., perturbation-polynomial expansion calcs. 78—66372
Tokamak, effects of blanket-shield penetration on performance, Monte Carlo anal. 78—21765
Tokamak, efficient particle removal using liq. Li getter 77—38411
Tokamak, electrostatic drift waves, numerical anal. of instability and transport 80—48871
Tokamak, energetic ion slowing and transport coeff. by Makokot code 80—83899
Tokamak, energy balance, computing method 78—54982
Tokamak, experimental fusion reactor preliminary design 77—74981
Tokamak, experimental power reactor, plasma studies 78—66418
Tokamak, expt. power reactor, first wall/blanket/shield system, mech. design 78—74482
Tokamak, expt. power reactor, neutronic and photonic calcs., blanket and shield design 78—29644
Tokamak, fast ion injection, energy amplification 77—71692
Tokamak, fast wave heating in ion cyclotron freq. range 77—65890
Tokamak, finite element anal. of structural response of superconducting magnet 77—3166
Tokamak, flux conserving reactor 78—8976
Tokamak, flux-conserving, high power density, performance characts. 80—23124
Tokamak, fuel-pellet relax. time effects 77—38407
Tokamak, fusion power plant economics, effect of major design parameters 79—76141
Tokamak, fusion power reactor design 77—74982

fusion reactors continued
Tokamak, fusion reactor, axisymmetric, slowing-down alpha particle loss, Monte-Carlo calc. 78—59653
Tokamak, fusion-product bombardment of first wall 77—38409
Tokamak, heat transfer in wall region *(Russian)* 78—87501
Tokamak, heating by pulsed elec. fields, hot ion prod. 80—24192
Tokamak, helical, alpha particle absolute confinement condition 78—42782
Tokamak, high beta, theory 78—25324
Tokamak, high energy α-particle flux at walls due to mag. field rippling *(Russian)* 77—68841
Tokamak, high field compact, plasma cahracts., start up scenario 78—8975
Tokamak, high-beta, with force-free currents, MHD stability 78—87481
Tokamak, high-temp. blanket, generating efficiency and H_2 synthetic fuel prod. 78—74479
Tokamak, HP flux-conserving equilibria 77—35379
Tokamak, ignited plasma, temp. control by toroidal field ripple 78—5033
Tokamak, ignition demonstration reactor development 79—18045
Tokamak, ignition form, theory 80—74010
Tokamak, impacts of plasma perform. parameters on vacuum and T system design 79—76131
Tokamak, impurity beam trapping instability 77—34428
Tokamak, impurity control and plasma transport in plasma-edge region 80—13832
Tokamak, impurity control by neutral-beam injection 80—32494
Tokamak, influence of ergodic magnetic limiter on impurity content 79—661
Tokamak, interaction and protection of superconducting poloidal field coils 77—42189
Tokamak, ISX-B, design improvements for neutral particle heating 78—54881
Tokamak, JFT-2, plasma parameter improvement by Ti gettering 79—671
Tokamak, large aspect ratio, two-dimens. drift-wave stability 80—79479
Tokamak, lower hybrid-driven steady-state reactors, power requirements 80—95415
Tokamak, LT-3, disruptive instability, spectroscopic observations 78—87483
Tokamak, Macrotor, metallic impurity suppression by electron injection 79—32781
Tokamak, magnet coil radius optimisation 77—42191
Tokamak, magnet conceptual design 78—54983
Tokamak, magnetic field system 78—21761
Tokamak, neutral beam injector penetrations, limiting neutron streaming, neutron flux calc. 80—95400
Tokamak, neutron emission and yield *(Russian)* 78—13328
Tokamak, neutron source and toroidal geometry neutronics effects 77—34457
Tokamak, non circular, small-aspect-ratio, high mode number ballooning instabilities, max. β-value 80—73995
Tokamak, nonaxisymmetric, reduced fusion neutron production 78—63577
Tokamak, noncircular section construction with axisymmetric divertor JFT-2a, Japan 77—61605
Tokamak, octopole, obs. of RF driven plasma current 80—48910
Tokamak, ohmic heating coil, nonuniform current density distrib. 78—17427
Tokamak, ohmic heating coil arrangement 78—54896
Tokamak, ohmic heating solenoids, engineering design solns. 78—54893
Tokamak, optimum conceptual scaling 78—54908
Tokamak, perturbed mag. field phase slip 80—48982
Tokamak, physics of burn control 80—37599
Tokamak, plasma diffusion in divertor scrape-off layer 79—667
Tokamak, plasma diffusion in divertor scrape-off layer 79—668
Tokamak, plasma limiter design 78—54910
Tokamak, plasma simulation using nonuniform spatial mesh technique 77—79478
Tokamak, plasma-wall interactions, review 78—94123
tokamak, plasma-wall-divertor model 78—58462
Tokamak, PLT, disruptive instabilities, X-ray study 78—89974
Tokamak, PLT, photo-neutron prod. 77—30668
Tokamak, poloidal divertor, mag. configuration 80—48938
Tokamak, power supply requirements 80—837
Tokamak, radiofrequency divertor 79—666
Tokamak, ray tracing in axisymmetric toroidal coords. 77—84476
Tokamak, recycling processes 78—94126
Tokamak, RF and neutral beam plasma heating 77—65331
Tokamak, RIGGATRON, neutronic anal. of two-dimensional models 80—13789
Tokamak, runaway electron bombardment of limiter during startup 77—30666
Tokamak, self-sustained, power balance model 78—5017
Tokamak, space-depend. thermal stability of reacting plasma 79—19068
Tokamak, stable equilibria using supplemental heating 80—91244
Tokamak, stainless steel He cooled blanket design 80—37613
Tokamak, startup anal. 79—49843
Tokamak, steady state resistive toroidal field coils 80—91264
Tokamak, structural anal. 77—3162
Tokamak, superconducting heating coils and toroidal field coils design 77—6559
tokamak, superconducting toroidal system, force anal. for all fault conditions 80—91258
Tokamak, superconductor design considerations for poloidal field coils 79—63236
Tokamak, superthermal alpha transport and wall bombardment 79—649
Tokamak, surface effects and impurity production 78—94127
Tokamak, surface interactions and conditioning techniques 78—94124
Tokamak, surface processes in plasma-wall interactions 78—94121
Tokamak, T-10, plasma parameters 77—43071
Tokamak, T-20 installation, demonstration, characts. 77—38402
Tokamak, temp. fluctuations and heat transfer 80—74003
Tokamak, TFR, internal disruptions and current breakdown, X-ray diagnostics 77—43027
Tokamak, TFR, variable-radius Mo and graphite limiters 78—63600
Tokamak, TFR-600, surface conditioning and mass spectroscopy 79—672
Tokamak, thermal and dynamic flow props. of liq. Li falls 77—38412
Tokamak, thermal stabilisation by controlled ejection of fusion α-particles 77—38408
Tokamak, thermonuclear Alfven instabilities, toroidal effects direct mag. field approx. *(Russian)* 77—51166

fusion reactors continued
Tokamak, TNS, equilib. field coils and free boundary equilib. considerations 78—58420
Tokamak, toroidal field ripple effect on particle and energy transport 77—11315
Tokamak, use and performance of graphite and metal ISSECS 78—41860
Tokamak, UWMAK II, thermal hydraulic and mechanical design of blanket 77—6556
Tokamak, UWMAK II and III, T handling breeding and containment 77—6557
Tokamak, wall protection from hard disruptions 77—31508
Tokamak advanced fuel power plant, capital cost anal. 79—18046
Tokamak and CTR reactors, mobile diaphragm operation mode *(Russian)* 80—83966
Tokamak and JET, development trends *(German)* 77—6551
TOKAMAK and other fusion reactor realisation, plasma beam control, Boltzmann eqn. 79—97903
Tokamak and stellarator, progress in experiments 78—94122
Tokamak blanket, Li-cooled, parametric anal. of design parameters 79—22464
Tokamak blanket, liq. Li module stresses due to changing poloidal mag. field 80—95435
Tokamak blankets, neutronic materials with different coolants and structural arrangements 79—81087
Tokamak central station fusion power reactors, potential safety 77—6562
Tokamak collisional plasmas, poloidal asymmetry of impurity spectral line emission 80—32485
tokamak confinement, next step beyond TFTR 78—58414
Tokamak constant tension D-shaped coils, lateral support struct. 78—55013
Tokamak construction criteria *(Norwegian)* 78—74474
Tokamak contamination, comparison of different refuelling methods 78—94133
Tokamak CTR research 77—67882
Tokamak D-^{3}He fuelled reactors 78—806
Tokamak D-D fuelled reactors, conceptual design 77—83083
Tokamak demonstration power reactors, engineering problems rel. to system components 80—32511
Tokamak designs, impact of key plasma parameters 78—17429
Tokamak device, control coil optimum design, nonlinear optimisation 77—27744
Tokamak devices, aspects 77—79473
Tokamak discharge, anomalous drift-wave transport anal. 79—32745
Tokamak divertor, toroidal field mag., vacuum system 78—54909
Tokamak divertor mag. piston action, elec. AC power direct generation 80—102324
Tokamak divertor slot design to enhance mag. shielding 78—5028
Tokamak doublet geometry, shape control of doublets 80—48943
Tokamak energy storage superconducting solenoids 78—66369
Tokamak experiment for a positive energy balance fusion reactor *(Spanish)* 80—32427
Tokamak experimental power reactor, burn cycle dynamics, confinement scaling laws and heating 77—23263
Tokamak experimental power reactor, first-wall/limiter design 79—85797
Tokamak experimental power reactor, plasma position control and sensor requirements 78—62628
Tokamak experimental power reactor, remote maintenance considerations 79—45418
Tokamak experimental power reactor, shielding of major penetrations 77—34455
Tokamak experimental power reactor 79—71967
Tokamak Experimental Power Reactor remote maintenance considerations 79—9883
Tokamak Fe cores, design advantages 78—54897
tokamak first wall, 3.5 MeV alpha bombardment 78—58463
Tokamak first wall, fusion product bombardment 78—5019
Tokamak for surface and impurities studies 77—31531
Tokamak fusion devices, likelihood of success 80—52784
Tokamak fusion power generation 78—74472
Tokamak fusion power plant, cost sensitivity anal. 78—17412
tokamak fusion power plants, major cost drivers 78—58443
Tokamak fusion power reactors 78—21764
Tokamak fusion power stations, economic evaluation 79—76147
Tokamak fusion reactor, electron emission effect at divertor target 79—660
tokamak fusion reactor, generic PSAR for TF coil system 78—58407
Tokamak fusion reactor, RF injection for refuelling and impurity control 80—87921
Tokamak fusion reactor, steady-state, lower hybrid wave-driven, design constraints 80—10424
Tokamak fusion reactor, wall bombarding high energy α-particle characts., drift *(Russian)* 77—47214
Tokamak fusion reactor geometry, optimum plasma parameters rel. to reactor parameters 79—76140
Tokamak fusion reactor maintainability considerations 79—9882
Tokamak fusion reactor plasma, trapped α-particle cyclotron instability 79—73024
Tokamak fusion reactor prefabricated toroidal supercond. field magnet system 79—31211
Tokamak fusion reactor supercond. toroidal coil bending moment computation 79—41867
Tokamak fusion reactors, commercial feasibility 78—58406
Tokamak fusion reactors, doublet research, plasma shape control, MHD stability 80—28837
Tokamak fusion reactors, MAXAMAK and MULTIMAK approaches 78—804
Tokamak fusion reactors, model of impurity control techniques 78—17428
Tokamak fusion reactors, neutral beam driven, physical basis and engineering parameters, review 77—54360
Tokamak fusion reactors, plasma modelling and first wall interaction phenomena 77—30660
Tokamak fusion reactors, pulsed electrical power systems, computer design and simulation 80—13827
Tokamak fusion reactors, refuelling pellets, self-propulsion force exerted by anisotropic ablation 80—106969
Tokamak Fusion Test Reactor, conceptual digital computer control systems 77—23281
Tokamak fusion test reactor, cross section sensitivity, uncertainty anal., design parameters 77—6554

fusion reactors continued
Tokamak fusion test reactor, dose rates from induced activity in test cell 80—23144
Tokamak Fusion Test Reactor, elec. resistance bellows for vacuum vessel 78—50407
Tokamak fusion test reactor, engineering design 77—23265
Tokamak Fusion Test Reactor diagnostic penetrations, neutron streaming calc. 79—9877
Tokamak Fusion Test Reactor neutron collimator design 79—9876
Tokamak Fusion Test Reactor remote handling and maintenance 79—9884
Tokamak fusion test reactor remote maintenance 79—45419
Tokamak graphite blanket design concepts at BNL 77—3164
Tokamak He-cooled solid breeder system, UWMAK-II, conceptual design 77—3160
Tokamak heating by fast magnetosonic wave excitation 80—24189
Tokamak high field compact reactor 78—805
Tokamak ignition test reactor, scoping studies 78—793
tokamak induction heating coils, 50 kA prototype superconducting cable, critical current 80—106196
Tokamak IT-60, first wall design and related expts. 79—673
Tokamak machine with iron cct., flux mapping and current distrib. 79—41866
Tokamak machines, eddy currents, numerical and exptl. anal. 78—66374
Tokamak magnetic fusion R+D, ISX and PDX programs 80—37586
Tokamak magnets, EM forces, TORMAC computer program 78—62647
Tokamak maximum toroidal mag. field value by core constraint 80—102349
tokamak medium field ignition test reactor, plasma engineering 78—58419
Tokamak Mk. II reactor, remote separation and rejoining of coolant pipes 78—29650
Tokamak neutral beam injectors, HV power supplies 79—22456
tokamak neutral beam ion source, core snubber network design, fabrication and testing 80—102378
Tokamak next generation reactors, remote servicing considerations 79—45422
tokamak next step designs, system size and cost trends 78—58416
Tokamak noncircular experimental power reactor, blanket and shield design 77—3161
Tokamak ohmic heating pulsed power supply digital simulation 78—8991
Tokamak plant, superconducting toroidal field magnet model 78—17425
Tokamak plants, neutron wall loading and structural lifetime goals 78—58408
Tokamak plasma, ISX, plasma position dynamics 78—66420
Tokamak plasma, neutral atom transport by multigroup methods, time reduction techniques 78—18385
Tokamak plasma, quasi-mode parametric excitations in lower-hybrid heating 80—64748
Tokamak plasma, real and simulated, impurity behaviour 78—94128
Tokamak plasma, RF driven electron currents for confining poloidal field 78—91145
Tokamak plasma, runaway electrons and current dirve 80—74004
Tokamak plasma, superthermal fusion products, α-particle transport theory 78—66417
Tokamak plasmas containing momentum sources, impurity transport 80—48935
Tokamak poloidal divertor, compact, reference design 78—54894
Tokamak power plants, impact of major design params. on economics 78—792
Tokamak power plants, impact of technology and maintainability on economic aspects 80—27807
tokamak power reactor, electron cyclotron reson. heating by gyrotrons 80—99331
Tokamak power reactor, fuelling by high speed pellet injection 78—758
Tokamak power reactor, position control and sensor requirements 78—5035
Tokamak power reactor, steady state, lower hybrid wave driven 80—48945
Tokamak power reactor supercond. coil design, experimental 79—31198
Tokamak power reactor supercond. poloidal magnet system design, experimental 79—31207
Tokamak power reactor toroidal field coil design and manufacture 79—31201
tokamak power reactors, design approaches for engineering feasibility 78—58442
Tokamak power reactors, remote system requirements 79—45423
Tokamak power systems, economics 78—54993
Tokamak power systems technology 78—50345
Tokamak reactor, commercial, plasma driving system requirements 78—54954
Tokamak reactor, driven, two-component and hot ion, modes of operation 80—42863
Tokamak reactor, first wall stress anal. 77—83093
Tokamak reactor, fuelling requirements 78—757
tokamak reactor, impurity effects on α-particle loss 78—58461
Tokamak reactor, neoclassical regime, stationary temp. profile 77—74987
Tokamak reactor, overhaul procedure 78—54905
pulsed Tokamak reactor, parameters and parameter sensitivity, comparison with reversed field pinch reactor 80—9410
Tokamak reactor, radiation shielding 78—25323
Tokamak reactor, resistive requirements of vacuum wall 78—66410
Tokamak reactor, supercond. toroidal field magnets, large coil program 79—36400
Tokamak reactor, thermal thermonucl. instability 77—74986
Tokamak reactor, turbulent plasma blanket generation *(Russian)* 79—55566
Tokamak reactor, two-component, efficiency, fast ion quasilinear relax. 79—37509
Tokamak reactor, UWMAK-III, using closed cycle He gas turbines 77—6555
Tokamak reactor blanket and shield, nucleonic design 79—85803
Tokamak reactor blankets, effects of neutral beam injection tubes, shielding calcs. 80—23173
Tokamak reactor design, influence of physics parameters 79—36414
Tokamak reactor feasibility 80—18610
Tokamak reactor first walls, thermal response during cyclic operation 78—62651
Tokamak reactor modelling, time-depend. computer codes 77—34468
Tokamak reactor refuelling, magnetic field distortion near an ablating H_2 pellet 80—64734

fusion reactors continued
Tokamak reactor shielding requirements, penetration size effects 79—9875
tokamak reactor superconducting toroidal field magnet computational model, technical and economic 78—50375
Tokamak reactor toroidal magnet system, technology-constrained scaling 79—76138
Tokamak reactor with high-temperature blanket 80—27809
Tokamak reactor with turbulent transport coeff., energy balance 79—71953
Tokamak reactors, fuelling by ripple assisted injection of energetic neutral beams 78—759
Tokamak reactors, prod. of noncircular discharge, ohmic heating expts. (Doublet III) 80—52785
tokamak reactors, radiation shielding of major penetrations, theory 79—36412
Tokamak reactors, role of α-particles review 80—86971
tokamak reactors, status and prospects 80—102292
Tokamak reactors, supercond. toroidal magnets, mag. and thermal loading 79—36407
Tokamak reactors, supercond. toroidal magnets, max. mag. fields, mech. stress calcs. 79—36405
Tokamak reactors, toroidal magnetic field strength requirements, physical parameters, cost 77—19777
Tokamak reactors and structural materials, plasma-wall interactions 80—32428
Tokamak reactors with elongated plasmas, parametric and economic anal. 78—795
Tokamak research, current state of art 80—13903
Tokamak structural and mechanical design guidelines 79—6764
Tokamak studies in the USSR 80—74022
Tokamak superconducting coils, active energy transfer rate control using inductor-convertor bridges 78—13338
Tokamak superconducting toroidal field coils, pulsed field losses, expt. simulation 77—26871
Tokamak systems, fusion power station development, Yugoslavia *(Croatian)* 80—832
Tokamak test reactor, in-vessel maintenance remote manipulator system 80—18611
Tokamak test reactor, neutron activation code REBATE 79—49852
Tokamak test reactor vacuum vessel, flow-related heating/cooling problems 79—85798
Tokamak TFR, electron temperature profile meas. by Thomson scatt. with single laser shot *(French)* 78—9840
Tokamak thermonuclear reactor, MHD modes drift phenomena, kinetic method *(Russian)* 80—1827
Tokamak TNS reactor, plasma engineering innovations 78—66422
Tokamak TNS studies 80—27810
Tokamak toroidal field coil shielding calc. 79—31212
Tokamak toroidal field coil system for homopolar generator power source 77—23257
Tokamak toroidal field coils, reduction of bending moments 80—47697
Tokamak toroidal field coils, superconducting 78—62632
Tokamak toroidal field magnet 77—31496
Tokamak toroidal magnet supercond. cluster test design 79—31199
Tokamak transport simulation models 77—79474
Tokamak two stroke reactor 80—48941
Tokamak type, boundary conditions for cryopumping 77—30671
Tokamak type, neutron flux and released energy in blanket, calc. 77—34447
Tokamak type, uncertainties in heating and radiation damage in toroidal field coil from cross section errors 77—67881
Tokamak wall, model of unipolar arc 79—657
Tokamak XFR, toroidal magnet design 79—76135
Tokamak zero moment toroidal field coils, compatibility calcs. 79—93824
Tokamak-7, circulating superconducting magnet system, design and operational tests 79—89498
Tokamak-fusion reactors, He exahust 80—75084
tokamak-like equilibria at beta close to unity 80—19604
Tokamak-type experimental power reactor, interaction and protection of supercond. and pulsed coils 77—23262
Tokamak-type reactors, conceptual design studies 79—71964
Tokamak-UWMAK systems, magnet design of toroidal field coils 77—6558
Tokamaks, current disruption effects 80—74012
Tokamaks, density upper limit from thermal stability data 80—18600
Tokamaks, design modifications to simplify remote maintenance 80—18613
Tokamaks, elongated, axisymm. MHD stability 78—86683
Tokamaks, gas breakers for ohmic heating circuits 78—66396
Tokamaks, high-β, expt. and comp. studies 80—23128
Tokamaks, high-beta, heating, confinement, dynamics studies 80—24218
Tokamaks, ideal MHD mode stabilisation and optimisation 80—79480
Tokamaks, impurity models 78—765
Tokamaks, low Z_{eff} operation 78—762
Tokamaks, lower hybrid resonance cones 80—28791
Tokamaks, magnetic divertors for impurity control 78—763
Tokamaks, maintenance design requirements and economics 80—99285
Tokamaks, meas. of impurity conc. 78—761
Tokamaks, MHD stability and reactor requirements 79—98911
Tokamaks, neutral beam heated, radial transport/Fokker-Planck model 77—15224
Tokamaks, secondary ion emission, appl. to impurity control 80—37584
Tokamaks, small-scale, review 78—42831
Tokamaks and reactors, applic. of bundle divertors, collisionless exhaust flow 80—27814
Tokamaks of arbitrary cross section, wall stabilized high β equilibria 77—84477
Tokamaks with iron core transformer, self-consistent MHD equilibria 80—19608
Tokamaks with shear, scaling law for trapped ion anomalous diffusion 80—32492
Tokapole II, poloidal divertor, plasma production and confinement studies 80—18602
Tokomak, impurity control, divertor and gas blanket model 79—90445
Tormac, confinement system, magnetoacoustic heating studies 80—24217
Tormac DT fusion reactor, power gain and net output 78—58402
TORMAC fusion reactor design points 80—37627
toroidal, hot ion mode, exotic fuel cycles 79—97905
toroidal axisymmetric plasma, ideal and resistive ballooning modes 80—83936

fusion reactors continued
toroidal beam-driven, fusion reactivities, power multiplication factors 77—18697
toroidal coil system, D-section 79—6761
toroidal coil system, Oak Ridge Experimental Power Reactor 77—26872
toroidal device with nonplanar mag. axis, magnet and coil engineering 78—55009
toroidal discharge, dynamic stabilisation in weak longit. mag. field *(Russian)* 78—87476
toroidal field coil, 10 Tesla 77—27692
toroidal field coil design and development for JT-60 Tokamak 79—31203
toroidal field coil finite element stress anal. 80—91256
toroidal field coil in-plane bending stress, struct. support design 80—106164
toroidal field coil stress anal., cost effective procedures for TFTR 78—50379
toroidal field coils, bending-free, for Tokamak reactor 78—55012
toroidal field coils, EM parameters calcs. of current paths in homogeneous media *(Japanese)* 80—106155
toroidal field coils, stress anal. by finite element method 80—13926
toroidal field coils for JET, manufacture and testing 80—5334
toroidal field magnet system utilizing normal metal trimming coils 78—54931
toroidal field magnets conceptual design for expt. fusion reactor 78—50391
toroidal field ripple effects, computer simulation 78—54892
toroidal field superconducting coil cryogenic stability and field anal., design parameter 80—106200
toroidal field windings design for fusion-driven actinide burner 77—27693
toroidal fusion reactor, common problems in control system software design 77—23282
toroidal fusion reactor design based on reversed field pinch 79—71977
toroidal geometry, Monte Carlo calcs. 77—34456
toroidal geometry effects in neutron transport eqn., discrete ordinate S_N method 78—13327
toroidal high-β plasma, liner compression 77—26877
toroidal mag. confinement, physics and technology 80—78450
toroidal magnet coil design and testing 79—31195
toroidal magnet for FINTOR 1 77—27694
toroidal magnetic confinement, progress, rel. to fusion reactor requirements 80—59261
toroidal plasma, 2-D neutral H transport 78—59661
toroidal plasma, Monte Carlo treatment for neutral particle transport 80—33750
toroidal reactors, α heating 80—13861
toroidal reactors, confinement scaling, effect on economy and unit size 80—13860
toroidal reversed field pinch reactor, engineering desing 80—13856
toroidal system, MHD plasma control by feedback and HF fields 80—28781
toroidal systems, engineering and technological problems 80—78449
toroidal theta pinch fusion reactor for investigating plasma instability problems, expt. 77—23251
toroidal Z-pinch, ZT-40 78—54989
toroidally linked mirror reactors, Q calcs. 77—34439
toroidally-linked mirrors 80—42858
torsatron, superconducting mag. engineering design 80—99297
Torsatron T-1, demountable resistive joint for high current superconductors 80—106202
torsatrons, neutral beam injection calcs. 80—48949
TORTUR I, heating by current driven turbulence 80—24191
TORTUR II Tokamak, liner currents and forces calcs. 80—18644
torus 2, vacuum chamber module 80—18640
Torus II, poloidal field system 80—18657
TORUS II SUPRA, superconducting Tokamak, conceptual design 80—13852
TORUS II Tokamak, toroidal field coil, fatigue test results 80—13928
torus with superconducting toridal coils, TESPE 78—54926
torus with three coil arrangements, simulation 78—18434
TOSCA, β optimisation studies 80—83990
transient data recorder for fusion expts. 80—13917
transient gas feed in Tokamak discharges, numerical investigation of buildup phase of neutral H layer near wall 78—94135
transient neutral gas interactions with plasmas and walls 78—94134
transmutation of fission product waste using DT neutrons 80—32383
transmutation waste management program effectiveness, ^{90}Sr disposal case 77—34460
transmutation waste management system, chemical separation efficiency 80—37482
trends 79—6763
TTR, Thomson scattering system based on two-detector spectrometers 80—32426
tubular flow reactor, ion density and Z_{eff} profiles, neutral beam attenuation technique 80—6282
turbomolecular pump in pulsed mag. field, operational effects 78—50402
turbomolecular pump with mag. bearings, fusion expt. device appl. 78—50400
turbomolecular pumping systems for nuclear fusion devices in JAERI *(Japanese)* 79—49837
turbulent plasma blanket, anomalous heat transport 80—83224
turbulent plasma blanket 79—59259
two-beam laser fusion target illumination system design 77—19292
two-dimensional mag. flux shell model for MHD simulations of cylindrically symmetric plasmas 80—1838
two-stage opening switch technique, for high inductive voltage generation 78—55034
ultra high vacuum technology developments *(Japanese)* 78—49845
United States fusion power, overview 80—95395
unstable continuous spectrum and ballooning modes 80—19569
upgradable ignition test reactor, engineering features 78—54977
US magnetic fusion program, survey 80—91249
USA, mirror machine research progress 80—74016
USA fusion energy development program 80—74011
USA Tokamak fusion research 80—74017
USA-Japanese cooperation in science and technology 79—58518
UWMAK II, conceptual demountable TG magnet design 78—17426
UWMAK-III, non-circular, Tokamak, power reactor design 77—74979
vacuum arc plasma, fault current limiter mode, temp. distrib. diagnostics 78—9851
vacuum engineering for fusion reactors *(Japanese)* 78—58401

fusion reactors continued
vacuum gap following high-current arcing, dielec. recovery strength 78−9891
vacuum interrupter, for for high voltage DC current 78−74489
vacuum outer containment, safety, T control and monitoring 78−74498
vacuum pumping systems for fusion expts. 77−57747
vacuum pumping using compound cryopumps, performance 80−95452
vacuum technology development, wall contamination avoidance *(German)* 78−21769
vacuum vessel, large, ultra high vacuum, design and manufacturing problems 80−99276
vacuum vessel, magnetic stress induced by plasma motion, 3-dimens. anal. 78−66370
vacuum vessel, of General Atomic TNS, toroidal resist. and low Z armour/limiter 78−54901
vacuum vessel, performance of silver-coated metal seals, 20 to 450C *(German)* 78−81996
vacuum vessel welds, ultrasonic scanner 80−99288
W VII-A stellarator, m=2 mode at q=2 80−24227
W VII-A stellarator, Ohmic heating, energy and particle confinement 80−24226
W VII-A stellarator, particle and energy transport 80−83222
wall confined shock heated fusion reactor, design 80−99314
wall interaction, impurity introduction mechanism, review 77−42990
wall problem, reactor modular set up *(German)* 78−54879
wall-plasma interaction, impurity prod. *(Russian)* 78−25325
water-water reactor parameters optimisation 77−74912
waveguide array for lower hybrid wave excitation 80−48911
WEGA stellarator, lower hybrid heating 80−79515
WEGA torus, plasma position control by MVA amplifier 80−18668
Wendelstein VII, neutral beam injectors, HV power supply system, thyristor control 80−99332
Wendelstein VII-A, neutral beam injectors, performance 80−99389
working reactor progress at Culham, descriptive survey 77−83073
X-rays to electricity conversion scheme for advanced fusion reactors 78−70641
z-pinch, high plasma density, conceptual fusion reactor 78−5015
Z-pinches of intense energy density driven by high-voltage storage lines 80−24216
Zephyr experiment, toroidal chamber, ASDEX project *(German)* 80−73992
ZT-40, power crowbar system design 78−55033
ZT-40, reverse field pinch engineering prototype 80−102316
ZT-40, switching components development 78−55036
ZT-40, toroidal pinch, power supply crowbar transformer, low leakage and high current 80−102322
ZT-40, toroidal Z-pinch, circuit design and plasma simulation 78−54961
ZT-40 torus, ceramic torus fabrication 80−32477
α-particle, generation and loss problems 79−97906
p-^{11}B fuel, potentiality for controlled thermonuclear fusion 77−30667
Ar magnetic helical arc electrode, for MHD generator, visible, RF and probe diagnostics 78−9867
B-H, possibility of thermonuclear fuel in relativistic plasma *(Russian)* 80−37573
^{11}B-p, microexplosion ignition schemes 79−18030
$^{11}B+p \rightarrow {}^{4}He+{}^{8}Be \rightarrow 3({}^{4}He)$ fusion power feasibility 77−38310
$^{11}B+p \rightarrow 3\ {}^{4}He+6.8$ MeV, feasibility calc. 77−83092
^{11}B(p,3α), 35.4-1500 keV, resonance cross sections, astrophysical S-factor, fusion fuel 79−36213
CO_2 laser driven fusion plant layout 80−32503
D beam formation via negative ions 77−46636
D plasma, compression and heating by shell, thermonuclear neutron output *(Russian)* 77−371
D^- ion source for high voltage neutral beams for fusion reactors 80−99379
D-^{3}He, clean fusion reactor feasibility study 78−33288
D-^{3}He, confined by levitating supercond. ring, neutron effects 80−47715
D-^{3}He catalysed fusion blanket design 78−783
D-^{3}He field-reversed mirror concept appl. to small, flexible fusion plant 80−23126
D-^{3}He fuelled bumpy torus, blanket/shield designs, minimum-activity 79−85796
D-^{3}He satellite fusion power plants 79−76143
D-^{3}He satellite fusion reactor, field-reversed mirror confinement 78−70643
D-^{3}He Tokamak, blanket design, Al layers with organic coolant 78−74480
D-D, neutronics aspects of a porous blanket 80−83217
D-D catalysed fusion blanket design 78−783
D-D catalytic fusion-fission breeder, synergetics 79−22460
D-D fusion blanket cooling by gas-suspended B_4, neutronics calc. 80−834
D-D fusion reactor, heliotron *(Japanese)* 78−54878
D-D fusion reactor blankets, nuclear characteristics calc. 77−61606
D-D fusion reactor blanket, nucl. characts., summary 78−89973
D-D fusion reactor blankets and shields, effect of neutron source ratio on nuclear characts. 79−41033
D-D fusion reactor blanket, radioactivity and afterheat 80−9404
D-D fusion reactor plasmas, pure and catalysed, thermal stability 80−24207
D-D nonideal system, generalised feasibility criterion 77−46398
D-D nonideal systems, generalised feasibility criterion 77−30658
D-T, muon catalysed fusion for pellet ignition 77−3063
D-T blankets, two-phase flow cooling, nuclear performance, effect of coolant volume fraction 80−68940
D-T fuelled HFITR, blanket/shield designs, minimum-activity 79−85796
D-T fusion, energy deposition, damage and neutronics data 77−26880
D-T fusion reactor, T window study for laminar flow *(Japanese)* 78−17433
D-T fusion reactor core plasma, α-particle heating, dynamic characts. 77−74985
D-T linear mag. fusion device, particle end loss reduction 78−33289
D-T magnetoplasma, fusion effects on diffusion and thermal cond. 77−67883
D-T plant 78−37443
D-T plasma, Monte Carlo anal. of particle spectra 79−72992
D-T plasma, reaction rate with suprathermal ions, ^{6}Li seeded 79−676
D-T reactor, neoclassical transport props., model 77−68756
D-T reactor first wall, feasibility of in situ regeneration by vapour deposition processes 77−18701
D-T steady state Tokamak, neoclassical diffusion 77−3159

fusion reactors continued
D-T Tokamak reactor, costing and sizing using COAST code 79−76142
D-T toroidal plasma, steady state, thermally self-sustained by thermonuclear fusion reaction 77−83080
D_2 fusion reactors, catalysed, power balance calc., plasma confinement 80−42847
D_2, high-density Alcator Tokamak discharge, neutron yield 78−18438
D_2-DT-T_2 fuel, cryogenic data rel. to mag. fusion energy 80−8746
DD fusion reactor blanket, thermal blanket and blanket shield designs, comparative study 79−22457
DD, microexplosion ignition schemes 79−18030
DT fuelled reactor concepts for high-temp. process heat sources 80−52786
DT fusion reactors, environmental aspects, review *(German)* 79−54599
DT laser-driven plasma, thermonuclear burn wave with electron- and α-conductivities 77−18698
DT multiple mirror reactor, power balance, impurities 77−74998
DT plasma, free expansion hydrodynamics 78−70629
DT reactor, alpha-particle heated, steady-state and dynamic characts. 78−5016
H atoms, Rayleigh scatt. from n=2 states, fusion plasma diagnostics appls. 80−43002
H cryogenic isotope distillation for fusion power reactors 79−93833
H flux to walls, ang. and time resolved meas. techniques 79−674
H flux to walls, novel meas. technique 78−29640
H ion beam, intense and small emittance, formation by BPD source 77−6593
H, pellet ablation in thermonuclear plasma, reactor refuelling 77−88282
H, pellet ablation in thermonuclear plasma, electron space charge and refuelling 77−88283
H prod. appl. of fusion heat 80−51012
H production by thermochemical cycles using fusion energy source 80−51010
H production from fusion reactors coupled with high temp. electrolysis 80−45771
H production using fusion reactor heat and gas dynamic compression heating 80−35793
H radiative recombination in quasistationary thermonuclear plasma *(Russian)* 77−39465
H synfuel prod. by high temp. electrolysis using fusion energy 80−35792
H synfuel prod. from fusion power using hybrid thermochem. $Bi_2O_3.SO_3$ cycle 80−40931
H_2 fuel pellet ablation in thermonucl. plasma, atomic processes effects 80−18596
H_2, neutral, behaviour calc. in wall region of high temp. plasma, wall interaction 77−35377
H_2 plasma reactor design, heat transfer and flow 80−38697
H_2 production, electrolysis of steam, high temperature, in fusion reactors, synfuel production 80−72099
H_2 production by fusion reactor-high temperature electrolysis system 79−18041
H_2 production in fusion-synfuel blanket, thermal hydraulics 80−106176
H_2 production technologies, high temperature electrolysis of steam 79−52915
H_2 production using fusion reactor heat, from $2CO_2 \rightarrow 2CO+O_2$, CO+-steam$\rightarrow CO_2+H_2$ 80−67014
H_2, synthetic fuel production, Tokamak high-temp. blanket 78−74479
H(D) recycling model in Tokamak, influence on discharge behaviour 80−10393
^{2}H-^{3}H fuel pellet electrostatic injection *(Japanese)* 80−78434
$^{2}H^{3}H\mu \rightarrow {}^{4}He+n+\mu^{-}+17.6$ MeV, muonic catalysis in synthesis reactions *(Russian)* 80−52706
^{3}H breeding ratio maximisation by geometric programming 79−9879
^{3}H(d,n)^{4}He, neutron fluence and energy transfer standard 80−102194
He cryosorption pumping at 4.2K by type 5A molecular sieve 78−17422
He distrib. system for Large Coil Test Facility 78−55001
He, liq., narrow channel flow and heat transfer characts., void fraction in steady and transient states 78−55000
He requirements for superconducting power network 79−50897
$^{3}He+{}^{3}He \rightarrow 2p+{}^{4}He$, fusion power feasibility 77−38310
laser fusion, Nd glass gain coefficient determ. for fusion laser amplifiers 77−19261
Li blanket assemblies, absolute fission rate distribs. 77−61607
Li blanket models, Monte-Carlo and discrete ordinates calcs. *(German)* 77−83096
Li cooling system, corrosion inhibition by Al addition 80−108646
Li, liq. cooled pulsed fusion reactor blanket heat transfer, numerical calc. 78−94141
Li sphere, neutron spectra and T prod. meas. 78−62604
Li_2O gas carried blanket, neutronics and photonics 77−67880
$^{6}Li+{}^{6}Li$ reactions, effect on reaction rates for ^{6}Li(p,α)^{3}He cycle reactors 79−22459
^{6}Li+d reactions, low-energy, CTR appl. 77−83097
^{6}Li+p propagating fusion fuel cycle 80−37629
N_2 fixation using fusion energy heat source 80−32510
N_2 high intensity arc anode region, temp., current density, flow field, numerical anal. 78−9827
Nb-Ti 10 kA conductor development for Tokamak toroidal coil 79−31217
Nb-Ti superconductor, for fusion facility, cold-pressure-welded joints 78−62630
Nb_3Sn multifilament conductor critical current rel. to mech. strain 79−31215
Nb_3Sn multifilamentary conductor production and testing 79−32809
Nb_3Sn multifilamentary conductor for fusion research 79−35797
NbTi cabled and soldered superconds. with low losses, for fusion research magnets, development 79−35796
NbTi superconducting magnet, 0.8 m free bore toroidal magnet module 78−54923
Ni-Cr foil strain gauge, for cryogenic anal. of supercond. structs. in high mag. fields 78−54947
^{90}Si transmutation in fusion reactors 79−26559
T breeding fusion blanket with boiling water coolant 80−99274
T chemistry in nuclear fusion research, review *(Japanese)* 79−63806
T high-pressure equipment 77−50294
T inventory associated with metal-getter recovery systems 77−38415
T production, cross section sensitivity calc. using SENSETWO code 80−835
T release control and environmental monitoring *(Japanese)* 79−81078
T self sufficient 1600K process heat fusion reactor blanket concept 80−37614

fusion reactors continued
T systems test assembly, containment and cleanup technology 78—767
T systems test assembly at LASL 78—17421
T_2 valve, pulsed gas feed into Tokamak reactor 78—66412
U plasma core reactor expts. 78—5037
^{A}U, A=235, 238, fission and activation by fusion plasma neutrons 79—13521
Z-pinch, noncylindrical, dynamics and particle accel. mechanism 77—76170

g-factor
see also gyromagnetic ratio; Zeeman effect
A≥208, accurate g-factor measurement using heavy-ion induced reactions 77—26572
N-acetyle DL-methionine, γ-irradiated, radical cation EPR, ^{33}S hyperfine coupling 77—40559
acetylene, sign of rot. g-factor, mol. beam expt. 79—59600
alkali halides, spin lattice relax. and g-shift 80—15799
alkali metal halide crystals, g-tensor anal. of S— and Se^- centres, ESR 80—84650
alkali metal halides, analysis of spin-Hamiltonian parameters of heteronuclear XY^- defects 80—88509
alkali metal-hexamethylphosphoramide, low temp. glass, EPR of solvated K, Cs and Rb 78—91927
alkaline earth molybdates, luminesc. centres, EPR meas. *(Russian)* 77—28442
alkaline earth tungstates, luminesc. centres, EPR meas. *(Russian)* 77—28442
alkoxy free radicals, produced by X-irrad. of hydroxy containing cpds., characterisation by ESR and ENDOR 78—95938
alkoxy radical, trapped in nucleosides or nucleotides, EPR, INDO calcs. 77—90623
α-aminoisobutyric acid, cryst., γ-irrad., cation radicals, ESR obs., SCF-MO-INDO calcs. 78—11537
antiferromagnet, substitutionally disordered, Raman scatt. by mag. excitations 77—55775
antiferromagnetic semiconductor, magnon-spin flip excitations in Raman scatt., g-factors 77—66494
arbitrary spin particles in EM field, mag. dipole g-factor 78—93829
atomic wave functions, weighting factors determ. from g-factors 79—98237
band crossing in interacting boson model, E2 transition probabilities and g-factors 80—102101
benzophenone, high resolution ODMR and optically detected ENDOR 79—19811
n- $(Bi_{1-x}Sb_x)_2Te_3$, magnetoresist. in quantising mag. field 80—24953
biological systems, containing Fe, electronic and mag. struct., semiempirical MO cluster calcs. 78—62733
bis(diethylammonium) copper tetrachloride, mag. susceptibility, EPR spectra 78—68193
bis(p-toluene sulphonate) diacetylene polymer, spin conc., g-values of single cryst. from EPR study 78—48037
1,2-bis(p-tolysulphonyloxymethylen)-l-buten-3-inylen, ESR of X-irrad. cryst., 77K 79—11806
5-bromodeoxyuridine, single cryst., X-irrad. at 77K, $C_{5'}$-centred deoxyribose radical 78—20032
bromomethane, microwave spectrum obs., B rot. and centrifugal distortion consts. 77—75135
carbenes, triplet state g-tensors and hyperfine coupling tensors 80—52895
carbonyl chlorofluoride, rot. Zeeman effect, g-factors and mag. suscept. anisotropies, microwave meas. *(German)* 77—57993
CESR line-width and g-shift anisotropy, singularities, appl. to Ag 77—20705
chloroacetamide, X-irrad., ESR of $CH_2ClCO^{\cdot}$ radical 78—76882
5-chlorodeoxyuridine, single cryst., X-irrad. at 77K, $C_{5'}$-centred deoxyribose radical 78—20032
chromocene, mag. suscept., zero-field splitting, ligand field, 1-303K 77—89924
compressed D_{4h} cluster, g_{zz}-g_0 value 77—80756
copper (II) complex, bis(dithiocarbamate), HF-Slater-LCAO calcs., mag. coupling parameters and optical spectrum 80—99447
copper di-isopropyldiselenophosphate, soln. anisotropic g and hyperfine tensors, ESR linewidth meas. 79—85978
copper dipyridine dichloride, dynamic shift of the ESR field 80—2630
copper porphine, Xα multiple scatt. calcs., EPR and electronic spectra 78—13426
cross conjugate nuclei, correl. between g-factors of cross-conjugate pairs of states 79—460
trans-crotonaldehyde, rot. Zeeman effect, microwave spectra, mol. parameters 79—3491
cytochrome P-450_{cam}, Fe^{3+} zero-field splitting, Orbach relax. rates 77—21483
cytochrome P-450, anomalous T^7 temp. depend. of Raman spin-lattice relax. 77—21482
degenerate semiconductor, electron g-factor determ., Shubnikov-de Haas type oscills. 80—20070
$DEM(TCNQ)_2$, ESR study 80—97127
diamond, magnetic field and stress splitting of GR1 line 78—60095
diatomic $^1\Delta$ states, corrections to effective orbital g-factor 79—7036
diatomic molecule, rel. to theory of high-precision Zeeman effect 77—14486
diatomic radical, vib. quantum no. depend., ESR 77—18949
1,3difluorobenzene, rot. Zeeman effect, g-tensor, mag. susceptibility 77—497
dimethyl ammonium copper manganese tetrachloride, EPR study *(German)* 80—54941
diphenylhaloselenium radical trapped in single crysts., FSR, struct. 80—44919
ditetraethylammonium manganese bromide $^4T_1$ excited state, absorpt., MCD, Jahn-Teller model 78—43907
effective mass and exchange current effects in finite nuclei 80—78171
electron, g-2 technique, evolution and future prospects 77—34154
electron g-factor, sixth order contributions, anal. evaluation of graphs 77—6066
electron in sixth order, g-factor analytic contributions 80—22612
elementary particle properties from atomic phys. expts., parity, time-reversal, g-2 of electron 77—34578
EPR determination, using Picein 80 cement as standard 79—80658
EPR parameters for orbital singlet of d^1 ion in cryst. 78—10751
$f_{7/2}$ shell nuclei, shell model study in pure $f_{7/2}{}^n$ config. 79—36162

g-factor continued
F- and F_A-centres, EPR and spatial extn. of relaxed excited state 79—73812
F-centre, vibronic scheme of relaxed excited state 79—90989
Fermi liquid, multicomponent ferromag., g-factor 77—80724
ferric haeme protein, anal. of low-spin ESR spectra 77—60185
ferromagnetic alloys, hyperfine field rel. to paramag. reson. of shift 77—24537
ferromagnetic semiconductor, Raman scatt. due to magnon-spin flip of cond. electrons 77—20839
finite perturbed chains, g-factor, use of exact one electron solution *(French)* 80—59858
fluctuating hyperfine field I-depend. 77—22880
fluorite type crystal; $Tm^{2+}(Yb^{3+})$, axial g-values of $4f^{13}$ ions with trigonal symmetry *(Korean)* 79—24135
fluoroacetylene, and -d_1, vibr. Zeeman effect, g-factors 78—46391
formaldehyde, triplet state g-tensors and hyperfine coupling tensors 80—52895
g-2 technique, evolution and future prospects 77—34154
garnet:Fe^{3+}, spin Hamiltonian parameters, g-factors, temp. depend. EPR obs. 77—48038
garnet:Mn^{2+}, spin Hamiltonian parameters, g-factors, temp. depend. EPR obs. 77—48038
garnets, mag. props. of V^{4+} ion, effect of covalency 78—64010
gas, photon echo in a magnetic field at small areas of the exciting pulses 80—95961
glass:Fe^{3+}, EPR line shape, H to g transforms. 77—12193
glass:Fe, thermally detected EPR meas. 77—63273
glass:Mn^{2+}, EPR, low-field hyperfine struct. 78—95513
glycine-$AgNO_3$, single cryst., X-irrad., oxidation product form. 77—48660
graphite, polycryst., EPR meas. rel. to temp., crystallite orientation, paramag. suscept. 78—35023
graphite intercalation compounds with acceptor molecules, CESR 78—48042
haemoglobin, human, EPR spectrum, g-value during oxygenation-deoxygenation reaction 78—53333
haemoglobin g-value change obs., EPR *(Japanese)* 77—90724
heavy atoms, g-factor anomalies and strongly forbidden M1 transitions 78—78825
heavy atoms, strongly forbidden M_1 transitions, g-factor anomalies *(Russian)* 78—78648
Heisenberg magnet, pseudo-one-dimens., EPR freq. temp. depend. 77—32241
high spin d^5 system, isotropic g-tensor 78—10757
hydrocarbon radicals, planar and nonplanar, g-factors, π-σ delocalisation 78—58580
3-hydroxyxanthine, monocrystals, UV-induced nitroxide radical and pair species 79—24775
hyperfine fields on fast ions in ferromagnetic media, review 78—37283
II-VI compounds, g-factor exam. 78—39393
II-VI semiconductor:Mn^{2+}, superhyperfine struct. tensor and g-shift 78—39056
interdoublet EPR spectrum ang. depend. for ions with arbitrary electron and nuclear spins in strong axial cryst. field 80—93164
ions in $^6S_{5/2}$ ground state, ESR line with 3.33 isotropic g-factor 80—15787
ions with S=3/2 and S=5/2, effective g values from EPR 79—42825
iron porphin in triphenylene, ESR 78—60329
Ising antiferromagnet, induced staggered mag. fields, g-factor mechanism 77—55676
isomeric A=48-50 nuclei, mag. moments and core polarisation 78—37274
Jahn-Teller centre optical band polarisation dichroism, forbidden transitions 80—55062
Jahn-Teller impurity centres, piezo-optics and magneto-optics 78—39579
liquid solution, relaxation studies in magnetic resonance spectroscopy 79—73841
liver tissue, mouse, appearance of free radical centres on low temp. oxidation 78—69013
magnetic susceptibility of s=1/2 crystallographic two sublattice system 78—14914
measurement technique for standard EPR samples 77—26370
meson presence in nuclei, nuclear g-factor exchange current controls., EM interaction role 80—22706
metal, CESR and inhomogeneous broadening due to local moments 79—99769
metal, paramagnetic, CESR spin-orbit perturbation, spin-phonon scatt. 77—63285
metallic slab, theory of Larmor waves, Fermi-liquid interactions, Fermi-surface and g-tensor anisotropy 79—69397
metals, magnetic impurity-conduction electron interaction, g factor renormalisation 79—69652
metals, non-S-state impurities, coupled ESR 79—47326
methyl vinyl ether, rot. Zeeman effect, g-values, mag. susceptibility, quadrupole moments 77—490
methylammonium chromium alum, single cryst., Cr^{3+} EPR, g-factor, hyperfine splitting 78—2729
3-methylfurane, rot. Zeeman effect, g-tensor, mag. susceptibility 77—497
6-methylmercaptopurine riboside, 4 MeV electron irrad., 77K radicals form., EPR obs. 78—39405
molecular complex, g-tensor components, semi-empirical LCAO calc. 77—18794
molecular polycrystals, effect of high hydrostatic press., EPR meas. 78—19307
molecule, diatomic, Zeeman effect, relativistic corrections 77—83646
molecules, electronic transitions, g-factor determ. by polarisation plane mag. reson. rot. *(Russian)* 78—70954
muon, g-2 technique, evolution and future prospects 77—34154
muon anomalous mag. mom., review of theoretical contribs. 77—30384
N=50 isotones populated in heavy-ion beam reactions, mag. moments, proton core polarisation 78—21598
nitrobenzene, anion radical, in benzoate crysts., EPR and X-ray diffr. obs. 77—1597
nitroxide free radicals, neutral, EPR spectra, localised solvent-radical adducts 79—96290
nitroxide radicals, q- and A-tensor components, rot. mobility 2 mm EPR spectrosc. determ. 80—102530
NMR recording, of low gyromag. ratio nuclei, by mag. coherent transfer technique 77—90068
nohle metal, g-factor on the Fermi surface 78—18949

g-factor continued
- nonlinear absorption method in magnetic field for spectral line width and shift meas. 80—37066
- nonlinear spectroscopic determ. of g-factor difference between atomic transition levels 80—23346
- nonrelativistic quantum mechanics and anomalous part of g-factor 77—74238
- nuclear, corrections due to Skyrme's interaction 77—65196
- nuclear compound deformed state g-factors and moments of inertia *(Russian)* 77—74757
- nuclear exchange mag. moments, meson exchange currents, field theoretical approach 80—52574
- nuclear giant magnetic resonances and effective Mλg-factors, RPA anal. 77—2897
- nucleotide sugar-phosphate region, γ-irradiated, deoxycytidine 5′-phosphate alkoxy radical EPR 79—5249
- odd-odd deformed nuclei, mag. props. 77—82822
- optical absorption spectra, correl. with g-shifts 78—23485
- organic charge-transfer salts, comparison of ESR spectra 80—50164
- palladium porphin, triplet state, optically detected EPR and Zeeman meas. 79—19809
- palladiumporphin in n-octane cryst., lowest triplet state, ESR-optical detect. 77—58050
- phenanthrene-pyromellitic acid dianhydride, single cryst., EPR, delocalised and localised charge transfer excitons 77—85545
- phosphate-tungstate semicond. glass, W (V) complex, EPR and electronic spectra interpretation 77—69682
- photoabsorption and beta decay, exchange current effects on orbital g-factor 77—41950
- piperdinyloxy 2,2,6,6-tetramethyl radical, recrystallised samples, EPR study 80—100615
- polydextran, γ-irrad. frozen gel, electron trapping, EPR and optical obs. 78—20030
- porphyrexide solutions, EPR meas., isotropic hyperfine coupling constants and g-factor determ. 77—81009
- positron, g-2 technique, evolution and future prospects 77—34154
- pure metal, derivation and validity of Elliott relation 79—19780
- pyrocarbon:B, g-factor anisotropy *(Russian)* 79—47001
- quanidinium aluminium sulphate hexahydrate:Fe^{3+}, EPR, zero-field splitting 77—8395
- quasi-one dimensional organic systems, ESR 78—52358
- rare earth alloy, dil., anisotropic exchange Hamiltonian, rel. to ESR spectrum 77—20696
- rare earth ethyl sulphate nonahydrates:Gd^{3+}, $g_\parallel$, EPR obs. 78—35031
- rare earth orthocobaltites, $R_{1-x}Sr_xCoO_3$, ferromag. reson., Lande g-factor 80—25215
- rare earth salts, phonon field contrib. to g-shift, symm. restrictions 77—55500
- relativistic average of config. wavefunctions, applicability to at. and ionic intermediate coupling props. 78—17574
- renormalisation of g_s factors in conversion transitions, spin-force consts. 77—61347
- ruby, E, 2A levels, laser excitation, Zeeman spectra 78—43908
- ruby, ENDOR of Cr^{3+} ions, elec. field effect *(Russian)* 79—8071
- ruby, Zeeman effect of R-absorpt. lines 79—47416
- semicond. alloy, spin splitting and effective g-factor of T-holes *(Russian)* 77—51643
- semiconductor, p-type, determ., g-values, spin temp., from Raman spectra 78—43856
- shape isomers, spontaneous fission, static and decay props. and excitations, review, book contrib. 78—82402
- shell-model, mag. dipole moments 78—82280
- Shubnikov-de Haas quasi-periodic oscill. curves, harmonic analysis, computer method *(Russian)* 78—39132
- Skyrme interaction, mag. moments, polarisability, gyromag. factors 78—21501
- sodium oxalate:Cu^{2+}, anhydrous spin Hamiltonian and bonding parameters and orbital-reduction factors 80—60408
- spectral simulation via finite elements, variational method and stochastic-Liouville eqn. 79—85157
- spin Hamiltonian consts., computation from EPR single cryst. data 77—90013
- spin-phonon interaction shift of EPR line 79—65712
- strongly deformed nuclei, shortlived states, g-factor meas. method 80—52577
- superconductors with paramag. impurities, NMR theory in singlet state 79—28445
- superposition model of g-shift of S-state ions 77—72838
- systems with anisotropic g-tensor, EPR spectra, extra absorpt. peaks 79—51839
- tC $FeCr_2S_{4-x}Se_x$ chalcospinels, ESR spectrum and paramag. susceptibility 80—15789
- (TCNQ)$(TTF)_{1-x}$-$(TSeF)_x$, quasi 1-D metal, mag. susceptibility, temp. depend. 77—8267
- TCNQ salt, TMTTF-TCNQ, mag. gaps, EPR meas. 77—8390
- tetrafluoromethane, sign of rot. g-factor, mol. beam expt. 79—59600
- tetrathiotetracene, charge transfer state parameters, evaluation by mag. field effect *(Russian)* 80—10924
- thioformic acid, g-values, mag. susceptibility, quadrupole moments, rot. Zeeman effect, isomer effects 78—25520
- TMNB, ferromag. chains with easy-plane anisotropy, exchange const., anisotropy const. and g-value 77—80927
- TMNC, ferromag. chains with easy-plane anisotropy, exchange const., anisotropy const. and g-value 77—80927
- $(TMTSF)_2PF_6$, ESR g-factor, linewidth, spin susceptibility, metal-insulator transition 80—103887
- transient ESR line profiles, $S=I={}^1/_2$ system, calcs. 78—88170
- transition metal 3d, spin-orbital interaction effect on NMR, g-factor anisotropy *(Russian)* 77—24752
- transition metal-rare earth alloys, amorphous, mag. props., mean field anal. 79—4701
- triatomic molecule, rot. vibr. electronic Hamiltonian, Born-Oppenheimer approx., breakdown 80—87097
- triatomic molecules, microwave spectra, mol. parameters 79—31513
- β,β,β-trifluoroethyl radical in Ar matrix, EPR, F and H$^+$ hyperfine interaction and motional effects 77—14460
- triphenylantimony, single crystal, irrad. by UV, diphenylantimony radical prod., ESR 78—31662
- TTF-TCNQ type salt, trimethylene-TTF-TCNQ, unsymmetric cation, phys. props. 78—76059

g-factor continued
- vanadyl octaethylporphyrin, radical cation EPR linewidth inversion, relax. theory 77—10693
- vinyl formate, rot. Zeeman study, g-factors, mag. susceptibility, quadrupole moments 78—50572
- violanthrone, free radical, EPR meas. 78—27094
- W-dichalcogenide, valence band nature, elec. and mag. props 78—39014
- Yang's biradical, EPR, g- and D-tensors, electronic struct., deuteration and conformation effects 77—42343
- Zeeman interaction, relativistic corrections and very small g-shifts, contrib. to EPR 78—72393
- zinc blende structure semiconductors, cyclotron reson. *(German)* 78—10337
- zinc formate dihydrate, Co^{2+}-doped, EPR spectrum, g-factor anisotropy for A- and B-sites 77—77089
- e, meas. at low energy and 110 keV 78—57777
- e gyromagnetic ratio in Coulomb field 80—82870
- e$^-$ anomalous mag. moment calc. 78—37254
- μ, (g−2) value, second order weak correction in arbitrary gauge models 78—62301
- μ, anomalous mag. moment meas. 77—46094
- μ g-factor, (g−2) expts., review, book contrib. 80—68403
- ^{4}He(3^3P), fine struct., level crossing obs. 78—82686
- Ag, conduction electron spin props., g-factor, de Haas-van Alphen oscill. amplitudes 77—35858
- Ag, obs. of CESR using reflection technique 77—20702
- Ag:Er(Dy), orbit-lattice coupling, nonuniform strain effects 78—88182
- Ag-Er film, stress-induced g-anisotropy, EPR of Er 77—85566
- AgBr, optical absorpt. of indirect exciton in high mag. field 78—60486
- AgBr:Pd, EPR of Pd$^+$ ions 78—27087
- $AgBr_{1-x}Cl_x$, ESR of self-trapped holes, Jahn-Teller and reorientation effects 78—27092
- $AgBr_{1-x}Cl_x$:Cu^{2+}, EPR of $(AgBr_6)^{4-}$, Jahn-Teller effect 79—91294
- AgCl, optical absorpt. of indirect exciton in high mag. field 78—60486
- AgCl:Cd^{2+}, Pb^{2+},Br$^-$, EPR anal., mechanism for photoinduced decomposition 78—80219
- AgCl(:AgBr), intrinsic ODMR spectrum mechanism, doping effect 78—43682
- $AgClO_3$, ClO_2 spin Hamiltonian 78—60326
- ^{105}Ag high spin states and bands, g-factor and isomeric state from ^{103}Rh(α, 2nγ) 79—36125
- ^{108}Ag, populated in ^{108}Pd(p,nγ), level struct., spin and parity, isomeric state lifetimes and g-factors 77—18392
- ^{110}Ag, populated in ^{110}Pd(p,nγ), level struct., spin and parity, isomeric state lifetimes and g-factors 77—18392
- ^{110}Ag^m, oriented, T-reversal test and struct. study 78—86505
- Al, CESR lineshape and A/B and g-values 77—63284
- Al, with plastic surface coating, g-factor and spin relax. time of cond. electrons 77—32258
- Al, with plastic surface coating, CESR obs. at 60 GHz in refl. spectrometer 77—32259
- Al:Er(Dy), orbit-lattice coupling, nonuniform strain effects 78—88182
- Al:Fe(Cu), CESR, effect of ion implantation 77—20701
- AlH$^+$ radical cation, EPR matrix isolation obs., hyperfine components calcs. 80—14158
- Al_2O_3:V^{3+}, $g_\perp/g_\parallel$ determ. by freq. crossing spectroscopy using thermal phonons 78—23055
- β-$Al_2O_3.Na_2O$:Cu, EPR, localisation of Cu^{2+} and linewidth effect 78—39395
- Al_2SiO_5, EPR of Fe^{3+} at V-band and the pair spectra 78—80204
- Ar, implantation in Fe, perturbed ang. distrib. 78—12969
- ^{40}Ar:^{41}K, matrix isolation model system 78—45722
- As_2S_3, amorphous, optical detection of ESR 79—38408
- ^{69}As 1306 keV state mag. moment, g-factor, rot. aligned band 80—86807
- ^{72}As, new 87 ns isomer, g-factor via ^{59}Co(^{16}O,2pn) 53-56 MeV 77—54149
- ^{207}At, g-factor of $25/2^+$ isomeric state, evidence for neutron excitation 78—70447
- ^{212}At high spin states, decay, g factor, J^π assignments, level energies from ^{208}Pb(^{7}Li,3n) 80—5042
- Au, conduction electron g-factor meas. 77—35859
- Au, conduction electron spin props., g-factor, de Haas-van Alphen oscill. amplitudes 77—35858
- Au, de Haas van Alphen meas. of g-factor 77—11847
- Au-Er, dil., cold-worked, EPR expts. 80—39864
- Au-Er film, stress-induced g-shift, ESR meas. on Er 77—51951
- BO_2, gas, optically detected mag. reson. spectrum, $X^2\Pi$ rovibronic sublevels 78—82756
- Ba II, $6p^2P$ fine struct. g-values, laser excitation of fast ion beam 77—10645
- $Ba_2Cu(OH)_6$, EPR, g-values 79—19770
- BaF_2: rare earth, far IR electronic transitions 77—4657
- BaF_2:Cd^2 X-irrad., ESR of Cd$^+$ centres 77—59459
- BaF_2:Ce^{3+}, EPR of low-symmetry sites 79—47332
- BaF_2:Tm^{2+}, EPR meas. of Tm^{2+} ion pair interactions 79—95641
- $Ba_2Mg_2Fe_{12}O_{22}$, hexagonal ferrite, with anisotropic g-factor, ferromag. reson. 77—69700
- BaO-B_2O_3-SiO_2:Ti^{3+}, Ti^{4+}, glass EPR spectra, variation of g-factor with temp. 79—99757
- $BaSO_4$, X-ray irrad., electron and holes traps, g-factors, ESR obs. 80—50183
- $BaTbO_3$:Tb^{4+}, perowskite struct., EPR, cryst. field parameters determ. *(Italian)* 78—52350
- ^{136}Ba, mag. moment of 2140.2 keV 5^- state 79—59009
- ^{138}Ba, 6^+ state, nucl. g-factor and nucl. spin relax. in Xe 77—22884
- Be_2SiO_4:P, EPR and ENDOR 78—76295
- $(Bi_{1-x}Sb_x)_2Te_3$, highest valence band struct., Shubnikov-de Haas effect 78—14661
- C powder magnetisation thermometry for very low temps. 79—63219
- CO, elec. and mag. props., mol. beam elec. reson. spectroscopy 77—61791
- ^{15}C 0.74 MeV $5/2^+$ state g-factor, shell model interpretation from ^{3}H(^{13}C,p) 80—32176
- Ca, hyperfine field of highly stripped atom, recoil distance method 78—37760
- CaF_2, low symmetry U^{5+} centres 78—76307
- CaF_2: Ni crystals, X-irradiated, EPR study of Ni$^+$ and Ni^{3+} 80—75849
- CaF_2:Cd^{2+}, X-irrad., ESR of Cd$^+$ centres 77—59459
- CaF_2:Ce, Stark struct., phototransitions, g-factors 78—67995
- CaF_2:Ce^{3+}, Na$^+$, ^{23}Na ENDOR meas. 77—69730

g-factor continued
CaF_2:Er, hydrogenated and deuterated, optical and EPR specra 79—61209
$CaF_2:PrF_3$, EPR of cubic Pr^{3+} 79—28607
$CaF_2:Tm^{2+}$, EPR meas. of Tm^{2+} ion pair interactions 79—95641
$CaF_2:U^{3+}$, cubic site substituent, EPR spectra obs. 78—72392
$CaF_2:U^{5+}$, single cryst., EPR 78—19325
$CaMoO_4:Er^{3+}$, phase relax. time rel. to g-factor anisotropy, electron spin echo obs. 80—29615
$CaMoO_4:Mo^{5+}$, g-factor, ground state, line broadening, EPR obs. 80—39863
$CaO:Cr^{2+}$, APR spectra 79—87313
$CaO:Mg^+$, EPR exam., hyperfine const. determ. 77—8388
$CaO:Mg^+$, g-shift anal. 80—29313
$Ca(OH)_2:Ni^{2+}$ single cryst., X-irrad., Ni^+ EPR, g-factors and point-charge model 80—2626
$CaSO_4$, γ-irradiated, ESR and bleaching studies of radical ion centres 80—2637
$CaV_2O_6:W^{6+},Mo^{5+}$, g-factors and hyperfine coupling parameters of V^{4+}, ESR 77—12196
$CaWO_4:Yb^{3+}(Nd^{3+})$, phase relax. time rel. to g-factor anisotropy, electron spin echo obs. 80—29615
^{107}Ca $21/2^+$ 2679 keV three quasiparticle state, nuclear struct. of isomeric states using g-factor 77—88039
Cd, Breit-Margenau correction, relativistic calcs. 77—3281
Cd II $(4d^95s^2\ ^2D_{5/2})$, high order mode-crossing signals, g-factors 79—796
Cd_3As_2, anisotropy of electronic g*-factor 80—44483
Cd_3As_2, band struct. and g-factor, Shubnikov-de Haas oscills. meas. 80—49598
Cd_3As_2, depend. of g-factor on electron conc. at low temps. 77—69218
Cd_3As_2, electronic g-factor, effective mass and density of states 79—60691
$CdBr_2:Ag^{2+}$, strong Jahn-Teller coupling, EPR 79—28605
$CdBr_2$:Co, spectroscopic studies of interactions 80—29769
$CdBr_2:Co^{2+}$, ground state g-value, EPR meas. 77—16159
$CdCl_2:Ag^{2+}$, strong Jahn-Teller coupling, EPR 79—28605
$CdCl_2$:Co, spectroscopic studies of interactions 80—29769
$CdCl_2:Co^{2+}$, ground state g-value, EPR meas. 77—16159
$CdCr_2Se_4$, deviation from Kittel's mag. resonance formula near T_c 79—87322
$CdCr_2Se_4$:Cu(Ag), ferromag. reson. and ESR line widths 80—60413
CdF_2:Cu, paramagnetic centre coordination, g-tensor orientation by anisotropy of ^{19}F ENDOR 80—54993
n-$Cd_{0.245}Hg_{0.755}Te$, magnetophonon reson. and quantum oscillations 77—39902
$CdInGaS_4:Er^{3+}$, cryst. field parameters, thermal and mag. props. calc. 77—20540
$CdIn_2S_4:Er^{3+}$, cryst. field parameters, thermal and mag. props. calc. 77—20540
Cd_3P_2, g-factor of conduction electrons at low temp. 79—56118
CdS electronic two- and one-photon Raman scatt. via biexcitons, stimulated config. obs. mag. field shift 80—103963
CdS, magnetoreflectance and magnetoluminesc. of A exciton 78—39597
$CdS:Mn^+$, cryst., X-band ESR 78—2730
CdSe, magnetoreflectance and magnetoluminesc. of A exciton 78—39597
CdTe and CdTe:Cl, grown by travelling heater method, EPR defect charact. 77—40125
p-CdTe, ESR optical detect., Overhauser shift, g-factor 78—80252
CdTe, optical detection of ESR 79—65770
^{107}Cd, g-factor of 845.6 keV state, differential PAC 77—6225
Ce, F states, radiative lifetime and g-factor determ. 79—41138
Ce^{3+}, in Van Vleck paramagnets, EPR meas. 77—12199
$CeRu_2$, type II supercond., ESR of Nd^{3+} meas. 79—28444
^{252}Cf fission products, g-factors of isomeric states 77—22890
Cl_2^-, in ion pairs with metals, ESR, in AR matrix, V-centre theory 77—16172
ClCN, ground and first excited bending, vibr. state, props., mol. beam elec. reson. 80—37823
ClO_2, gas-phase electron g-tensor, magic doublet rot. Zeeman spectra 78—90212
Co complex, cobalt pyridine chloride, EPR, effective g-values 79—42825
Co complexes, 1,2-bis(diphenylphosphino)-ethane in-plane ligand ^{31}P hyperfine interaction, ESR obs. 77—77087
Co Schiff base complex, N,N′-ethylene-bis (salicylideniminato)-Co II pyridine doped in Znsalenpy crystal, ENDOR, EPR studies 80—34819
Co-P, amorphous, ferromag. antireson. 24 GHz microwave transmission, mag. props. 80—34778
$Co_{1-x}B_x$, polycrystalline and amorphous sputtered films, Brillouin spectra 80—2775
$CoCl_26H_2O$, g-tensor and exchange parameters, mag. reson. studies 79—87324
$CoCl_2.6H_2O$, antiferromag., spin flop and paramag. resons. at very low temp. 77—66426
$Co_{75-x}Fe_xSi_{15}B_{10}$, quenched ferromag. ribbon, Brillouin spectra 80—2776
Cr complex, dimer di-μ-diphenylphosphinatoacetylacetonatochromium(III), EPR of exchange coupled Cr^{3+} pairs 78—88172
Cr complex, influence of anisotropy of spin-Hamiltonian parameters on EPR spectra *(Russian)* 77—28432
Cr I to XXIV, energy levels, ionis. pots., g-factors, from spectral data review 77—79556
$CrBr_3(Cl_3)$, two-dimensional mag. insulator, cryst. field splitting, spectroscopic g-factors 79—47059
$Cr(^{16}O,^{16}O'\gamma)$, 36 MeV, g-factors of first 2^+ states in $^{50,54}Cr$ 78—13138
CrO_3^- radical in K_2CrO_4 and $KCrO_3Cl$, g-factor anisotropy 78—67994
Cs^+ dipole and quadrupole polarisability fine struct. intervals and g-factor interval 80—91477
$^{133}Cs^+/Cs$ g-factor ratio, NMR and zeeman transition freqs. 78—17817
$CsAsF_6$, γ-irrad., EPR spectra, hyperfine interactions and g-value determ. 77—81416
CsBr, F-centres, EPR in relaxed excited state, detection via saturated optical pumping 78—6606
CsBr, gamma irrad., EPR of Br_2^- ions 79—51838
CsBr, second relaxed excited state of F-centre, optically detected EPR 79—87335
$CsCdCl_3:Co^{2+}$, ground-state g-value, EPR meas. 77—16159
CsCl, F-centres, EPR in relaxed excited state, detection via saturated optical pumping 78—6606
$Cs_2HfCl_6:Mn^{2+}$, ESR of mol. jumps, zero-field splitting tensor 77—51944
$Cs_2NaRCl_6:Er^{3+}(Gd^{3+})$, R=lanthanide, EPR parameters and interpret. 77—59456

g-factor continued
$CsSbF_6$, γ-irrad., EPR spectra, hyperfine interactions and g-value determ. 77—81416
$CsUF_6$, D_{3d} distortion on octahedral UF_6^- complex 77—47779
$Cs_2ZrCl_6:Mn^{2+}$, ESR of mol. jumps, zero-field splitting tensor 77—51944
$Cs_2ZrCl_6:Np^{4+}{}_6$, EPR of np^{4+} ground state 80—44903
^{129}Cs $11/2^-$ isomer, g-factor and lifetime in CsI cubic environment from $^{127}I(\alpha,2n)$ 79—6394
Cu, CESR linewidth and *g*-value, freq. and temp. influence, 4.2-50K 79—87318
Cu, CESR meas., 4.2K, selective transmission method 78—39401
Cu complex, bis(1,1-diisobutyl-3-benzoyl-selenoureato)Cu(II), single cryst. ESR, ^{77}Se hyperfine struct., bonding 77—77086
Cu complex, diaquobis(2,3-dihydroxy-2-methyl propanato) copper(II), cryst., EPR, room-temp. 79—82861
Cu complex, glycylglycinatocopper trihydrate, mol. g values, EPR meas. *(French)* 77—43874
Cu complex, with acetylene, Ar matrix-isolated EPR obs., bonding 78—50564
Cu complexes, spin coupled ion pair, singlet-triplet splitting 77—85552
Cu complexes of amino acids and α-hydroxy acids, bonding effect on spin-orbit coupling 77—1399
Cu complexes with glycine, in aqueous soln., EPR meas. 77—36115
Cu, conduction electron g-factor, Fermi surface 78—23011
Cu, conduction electron spin props., g-factor, de Haas-van Alphen oscill. amplitudes 77—35858
Cu^{2+} complexes, ground state wave functions, g-factor anisotropy, lattice structs. 77—24536
Cu^{2+}, dopant, ground state wavefunctions and Δg 78—64012
Cu^{2+}, g-anisotropy and ground state wave functions in crysts. *(German)* 78—23065
$Cu:Du^{3+}$, EPR, g-factor, hyperfine struct. 77—48046
Cu-Fe, dil., transmission ESR meas. 2 to 40K 78—68364
Cu-Mn, dil., Kondo deviations of Mn electron spin relax. and g-factor, NMR meas. 79—51747
$CuCl_2.2H_2O$, submillimetre ESR meas. using pulsed high mag. field 80—44905
$CuCl_2.2H_2O$, X-band ESR magneto-microwave effects 77—28434
$CuCl_4.2NH_3$, g-tensor components, LCAO calcs. 77—18794
$CuCr_2Se_4$, mag. reson. and valence state of Cu and Cr ions 80—60413
$CuF_2.2H_2O$ powder, EPR and Cotton-Mouton Voigt effect in Q-band *(French)* 79—8045
$CuF_2.2H_2O$, X-band ESR powder spectrum and related magneto-microwave effects 79—24214
$Cu(NH_3)_n(ClO_4)_2$, (n=4 or 5), EPR parameters and dilatometry 80—39850
$Cu(NH_3)_4SO_4.H_2O$, submillimetre ESR meas. using pulsed high mag. field 80—44905
$Cu(NH_4SO_4)_2.6H_2O$, X-band ESR magneto-microwave effects 77—28434
Cu_2O, optical absorpt. due to paraexciton, exchange energy and g-factors 77—28596
^{62}Cu 390 keV state populated in $^{60}Ni(\alpha,pn\gamma)$, ferromag. effect, spin assignment 77—2903
$D_2^+(HD^+)$, g-factors and related mag. props., calc. theory 79—41124
Dy^+ spectra, exam. of $4f^{10}6s$ and $4f^{10}5d$ configs. *(French)* 77—50385
Dy^{3+}, in Van Vleck paramagnets, EPR meas. 77—12199
^{152}Dy high spin isomeric states, g-factors from $^{140}Ce(^{16}O, 4n)$ 80—13377
$Er(C_2O_4)(C_2O_4H).3H_2O$, single cryst., mag. susceptibility, 1.5-20K, g-factors 77—77094
ErH_3, Mossbauer spectra of Er^{3+}, gyromagnetic ratios and cryst. field parameters determ. 78—19388
$Er(OH)_3$, g-values and hyperfine interaction parameters, calc. for Er^{3+} 79—15123
^AEr, A=159,160, energy levels, deexcitation γ-rays, g-factors and hyperfine interaction from $^{28}Si(^{136}Xe, xn)$ 80—102114
^{168}Er, 80 and 1094 keV states, g-factors from ang. correlation methods 80—83035
Eu absorption spectrum, 2100-7200 Å, wavelengths, intensities, J- and g_J-values determ. 77—14383
Eu, metal, g-shift, EPR 77—48045
$EuCl_3$, solns., $^7F_0 \rightarrow {}^5D_1$ and $^7F_1 \rightarrow {}^5D_0$ transitions, MCD 79—31566
$EuCl_3.6H_2O:Gd^{3+}$, EPR spectrum, g-tensor and zero-field splitting 77—55706
$Eu_2Mg_3(NO_3)_{12}.24H_2O$, Zeeman effect in ahsorpt. spectrum 77—63402
EuO nonstoichiometric film, ESR spectra and exchange interaction 80—93176
^AEu, A=145, 147, 149, mag. moments of $11/2^-$ states 79—40846
Fe, A=54,58, mag. moments of 2^+ first excited states, g-factors 77—88041
Fe complexes, electronic and mag. struct., semiempiricial MO cluster calcs. 78—62733
Fe complexes, rhombic, g-values and zero-field splitting 79—78061
α-Fe particles, in fused SiO_2, g-values and anisotropy consts., FMR study 79—82876
Fe, polycryst., g-factor meas. 77—24748
Fe, transient magnetic field velocity and Z depend. 80—39904
Fe:^{95}Nb NMR 77—59482
Fe:Xe, gyromagnetic ratios of first 2^+ states in Xe, implantation PAC 78—12966
$Fe_{1-x}B_x$, polycrystalline and amorphous sputtered films, Brillouin spectra 80—2775
$Fe_{100-x}B_x$, quenched ferromag. ribbon, Brillouin spectra 80—2776
$Fe_{80}B_{20}$, ferromagnetic metallic glasses, Brillouin scattering 78—92085
$FeCO_3:Mn^{2+}$, far IR host and impurity excitations, antiferromag. and paramag. temp. ranges 77—52140
$FeF_2:Co^{2+}$, impurity-induced magnon, influence of localisation 80—11182
Fe_xGd_{1-x}, $0.5>x>0.65$, amorphous film, FMR, spin wave spectra 77—16181
Fe(III) Laeme complex, EPR g-value anal. 80—30657
$Fe_{76}Mo_4B_{20}$, quenched ferromag. ribbon, Brillouin spectra 80—2776
$FeNb_2O_6$, magnetisation, 1.4-80K, antiferromag. ordering 78—10666
$Fe_xNi_{80-x}B_{20}$, quenched ferromag. ribbon, Brillouin spectra 80—2776
$Fe_{32}Ni_{36}Cr_{14}P_{12}B_6$, Metglas 2826 A, ferromag. reson. for g-values and relax. parameters, 77 to 430K 77—63289
$Fe_{40}Ni_{40}P_{14}B_6$, ferromagnetic metallic glasses, Brillouin scattering 78—92085
$Fe_{40}Ni_{40}P_{14}B_6$, Metglas 2826, ferromag. reson. for g-values and relax. parameters, 77 to 430K 77—63289

g-factor continued
$Fe_{40}Ni_{40}P_{14}B_6$, Metglas 2826, ferromag. antireson. transmission at 24 GHz, 26 to 270°C 77−69696
$Fe_{29}Ni_{49}P_{14}B_6Si_2$, Metglas 2826 B, paramag. reson. for g-values and relax. parameters, 77 to 430K 77−63289
Fe_2O_3-NiO-Na_2O-Li_2O-B_2O_3-SiO_2 glass, EPR meas. of exchange interactions 77−32243
Fe_3O_4, magnetite, ferrimag. reson. at 9.3 GHz near Verwey temp., g-factors *(French)* 78−91959
$^{54}Fe^{m}$, static moments, perturbed ang. distribs. with combined dipole and quadrupole interactions 78−62482
$^{54}Fe(^{16}O,^{16}O'\gamma)$, 36 MeV, g-factors of first 2^+ states in ^{54}Fe 78−13138
$(Fe^{3+})d^5$ config. in C_{4v} and C_{2v} symmetries, appl. to ferrihaemoglobins 78−39071
Ga, A=66, 68 isomeric state from $^{56}Fe+^{13}C$ and $^{56}Fe+^{15}N$ reactions, lifetimes, g-factors 78−33147
GaAs epilayers, high-quality, sharp-line transitions due to donor-acceptor recomb. 78−6768
GaAs, optical detection of CESR 77−36155
GaAs:Co^{2+}, EPR expts., y-factor determ. 78−76301
GaP, MCD of phonon-assisted exciton transitions, g-value of hole forming free exciton 78−92053
GaP:N, spin dependent exciton recombination at N_2 isoelectronic traps 77−69734
GaP:Ni, optical and EPR study of two-electron-trap state 79−73806
GaP:S(Se)(Te), pot.-depend. g-values and quenched diamag., props. of donor states 77−62861
GaP:S(Se)(Te), pot.-depend. g-values and quenched diamag., pseudoacceptors D^0, X 77−62862
GaS, optical detection of triplet excitons 80−29650
p-GaSb, interband optical pumping, optical detection of EPR 77−28483
n-GaSb, Shubnikov-de Haas effect, effective mass, Dingle temp., and g-factor 79−51602
GaSe, optical detection of triplet exciton reson. 79−33567
Gd, metal, g-shift, EPR 77−48045
Gd^{3+} impurity ions, EPR spectra, linewidth narrowing due to spin-lattice relax. of lanthanide Kramers host ions 80−108061
Gd^{3+}, in Van Vleck paramagnets, EPR meas. 77−12199
Gd-Al, amorphous film, microwave mag. reson. 78−91948
$GdAl_2$-$GdCo_2$ system, EPR and mag. props. 79−33478
GdAs(Sb)(Bi), antiferomag., EPR meas., Neel temp. determ. 77−32242
$Gd(Co_xIr_{1-x})_2$, C15 Laves phase struct., g shift, linewidth EPR meas., Fermi level movement interpretation 79−61210
$Gd_{1-x}Dy_xAl_2$, EPR bottleneck, Dy substitution effect 77−63281
$Gd_{0.5}Dy_yY_{0.5-y}Ir_2$, effect of dil. Dy substitution on Gd ESR 79−82868
$GdFe_2$ films, electron beam deposited, amorphous and cryst., mag. and struct. props. 79−4710
$Gd(Fe_xAl_{1-x})_2$, magnetic behavior 80−108079
$Gd_xLa_{1-x}Pd_3$, EPR of Gd, g-factor and thermal broadening, temp. and comp. depend. 77−48048
$Gd_xLa_{1-x}Pd_3$, ESR linewidths, g-shifts, effective electron interaction, spin-lattice relax., spin-flip scatt. 78−68372
$GdNi_x$, (x=3, 3.5, 8.5), ferrimag., mag. reson. above and below Curie temp. 80−97148
$Gd_2Ni_{17-x}Al_x$, EPR of Gd^{3+} ions 80−97139
$Gd(Rh_{1-x}Fe_x)_2$, $x\leq0.15$, magnetisation and EPR studies 80−34767
GdS(Se), antiferromag., EPR meas., Neel temp. determ. 77−32242
$Gd_xY_{1-x}Fe_2$, effective g-values, ferromag. reson. meas. 77−20720
^{A}Gd A=144,146,147,148, high spin isomer g-factors yrast traps from $(^{28}Si,^{28}Si')$, (α,α') 80−78146
^{A}Gd, A=146, 147, g-factors of yrast states 79−17800
^{A}Gd, A=146-7, high spin yrast traps, g-factors 79−63578
Ge, amorphous, EPR 78−88167
Ge, luminescence circular polarisation in mag. field, Landau levels paramag. splitting 77−32435
Ge:Al, excitation spectra of shallow acceptors, Zeeman effect, expt. 80−7381
Ge-Al film, amorphous, EPR meas. 78−80212
Ge-Cu film, amorphous, EPR meas. 78−80212
GeF_4, sign of rot. g-factor, mol. beam expt. 79−59600
$^{72}Ge^{32}S$, $^{74}Ge^{80}Se$, $^{74}Ge^{130}Te$, rot. g_J-factor meas., $^1\Sigma$ ground state *(German)* 77−30865
$Ge_{42}S_{58}$ glass, Cu(Ag)(I) impurity effect on e.p.r., dangling bonds 77−4553
$^{70}Ge(^{16}O,^{16}O'\gamma)$, 36 MeV, g-factors of first 2^+ states in ^{70}Ge 78−13138
H $(1^2S_{1/2})$ to ^4He (2^3S_1) electronic g-factor ratio from Zeeman resonance meas. 78−13467
H, bound electron to free electron g-factor ratio, $g_J(^1H,1^2S_{1/2})/g_s(e)$, optical pumping 77−79587
H_2, 3d-triplet complex, Zeeman effect, eigenvectors and g-factors, rovibronic states 79−72353
H_2, Zeeman effect in 3d singlet states, g-values 78−50571
$H_2^+(HD^+)$, g-factors and related mag. props., calc. theory 79−41124
HO_2 radical, EPR spectrum, ground state parameters 78−90193
H_2O^-, trapped in γ-irrad., Y-type zeolites, ESR obs. 77−9099
He, Lande g-factor determ. from free radn. beats 77−18880
He-Ne laser, double reson., RF mag. field strength and g-value depend. *(Japanese)* 78−9359
^4He (2^3S_1) to H $(1^2S_{1/2})$ electronic g-factor ratio from Zeeman resonance meas. 78−13467
^4He, electronic g_J-value of 2^3S_1 state, by atomic beam mag. reson. method 77−23446
$^4He^+$, g_J-factor determ., optical pumping method 80−87085
$He(2^3S_1)$, isotopic g_J-factor ratio 77−10608
HfI, at spectrum, g-values, Zeeman effect, LS-coupling, ionisation pot. 77−3292
^{178}Hf, g-factor for K=6, $J^\pi=6^+$ isomer, perturbed ang. distrib. meas. 78−37277
Hg, 8^3S_1 level, Lande factor *(French)* 77−430
Hg, Breit-Margenau correction, relativistic calcs. 77−3281
Hg, odd isotopes, Lande factor of 6^3P_0 metastable level *(French)* 78−5162
$Hg_{1-x}Cd_xGe$, quantum oscillations of magnetoresistivity *(Russian)* 80−11007
$Hg_{1-x}Cd_xTe$, CESR *(Russian)* 78−23344
$Hg_{1-x}Mn_xSe$, band struct. from anomalous Shubnikov-de Haas effect 80−20080
$Hg_{1-x}Mn_xTe$, semimetallic, giant spin splitting induced by exchange interactions 77−28150
$Hg_{1-x}Mn_xTe$, Shubnikov de Haas effect and quantum oscills. of thermoelec. power 80−49781

g-factor continued
HgSe, Shubnikov-de Haas oscills., electron conc., g-factor and Dingle temp. 77−69354
HgSe, Shubnikov-de Haas determ. of electron g factors 80−6704
HgSe:Mn^{2+}, temp. depend. of EPR of ^6S state ions 80−80593
HgTe, Γ_8 symm. acceptor centre hole mag. props. *(Russian)* 80−88733
^{190}Hg, 21 ns isomer $(\nu i_{13/2})^2$ interpretation from g-factor meas. 80−105945
$(Ho_{0.58}Tb_{0.2}Dy_{0.22})Fe_2$, microwave mag. props. 80−65860
Hz, 3d complex, radiative lifetimes, hyperfine constants 78−70873
I_2, anomalous visible band effects near B state dissoc. limit 77−6816
^{127}I atoms in Xe matrices, ESR spectrum 80−1005
n-InAs, Shubnikov-de Haas effect, effective mass, Dingle temp., and g-factor 79−51602
$In_{1-x}Ga_xP_{1-z}As_z$, lattice matched to InP, electroreflectance obs. 80−93416
n-InSb, doping and strain depend. of quantum props. 79−60690
n-InSb, effective g-value of electrons determ. by spin flip Raman scatt. and electric-dipole-excited ESR 78−52494
n-InSb, effective mass and Lande factor, stress depend. calcs. *(German)* 79−95313
n-InSb, Shubnikov-de Haas effect 80−11015
InSb, spin flip Raman scattering, gain, linewidth, effective g-value 78−22167
InSb:Te, anomalous anisotropy of magnetoresist. and g-factor 77−47831
^{A}In, A=109,110, nucl. g-factor NMR-ON meas. on Fe-In alloys 78−37275
^{111}In $21/2^+$ isomeric state g-factor and relaxation time from $^{109}Ag(\alpha,2n\gamma)$ 80−73794
^{112}In, half-lives and mag. moments of two high spin states, γ-ray spectra 77−22940
Ir, A=191, 193, hyperfine struct. of low lying fine struct. levels, hyperfine anomaly, electronic g-factor 78−66214
^{191}Ir, excited nuclei mean precession time depend. on γ-spectral width, g-factors *(Russian)* 80−78211
^{192}Ir ground state spectroscopic quadrupole moment, g-factor, hyperfine quadrupole splitting 79−89235
(K,Na) $(AlSi_3O_8)$, feldspar, N^{2-} ESR spectrum parameters *(Ukrainian)* 79−38366
K I to K XIX, energy levels, tabulated data 80−51966
K, implantation in Fe, perturbed ang. distrib. 78−12969
KBr:Li(Na), F_A centres, optical detection of ESR 79−99793
KBr:Na, U-centres, HFS and g-factor, EPR spectra 80−39869
KBr:Tl^{2+}, relation between bonding and g-shift 80−39492
KBr(F), orbital g-factor and spin-orbit splitting of F-centre excited state, magnetoabsorpt. and MCD 78−2886
K_4CdCl_6:Co^{2+}, ground-state g-value, EPR meas. 77−16159
KCl, MCD, magneto-optical parameters of R-centre in H_3-mol. model 77−77253
KCl, mag. circular dichroism of R-center, point-ion lattice model 79−69814
KCl:Ag, Br, EPR spectra of $Ag^0(Br_1)$ paramag. centres *(French)* 79−11346
KCl:Au, EPR and optical absorpt. 78−39397
KCl:Au^-, absorption bands and MCD, electron-lattice interaction 77−55808
KCl:Ga(In), ESR of impurity centres, impurity optical absorpt. bands 80−29618
KCl:Na, F_B centres, optical detection of ESR 79−99793
KCl:$SnCl_2$, X-ray irrad., polarised luminesc. and EPR study of Sn^{3+} centres 80−39868
KCl:Tl^+ cryst., A band, mag. field effect 80−34897
KCl:Tl^{2+}, relation between bonding and g-shift 80−39492
KCl(Br), second relaxed excited state of F-centre, optically detected EPR 79−87335
KCl.Pb^{3+}, relation between bonding and g-shift 80−39492
$K_2Cr_5F_{17}$, monocrystal, cryst. field and mag. props., EPR and optical absorpt. spectra 79−19773
KF:U^{5+} EPR of U^{5+} centre meas. 77−20684
KF(Cl)(Br), mag. props. of relaxed excited state of F-centre, vibronic theory 78−60502
$K_3Fe(CN)_6$, electronic struct., electron density, elec. field gradient, mag. susceptibility and g-tensor 79−91006
$KFeS_2$, magnetic reson. meas. 78−95524
KH_2AsO_4:Cr^{5+}, ferroelec. phase transition, EPR intensity and linewidth meas. 79−4721
KH_2PO_4:KH_2AsO_4, X-irrad., EPR 77−32257
KH_2PO_4:VO^{2+}, EPR spectra, Hamiltonian parameters, ferroelec. transition 78−39387
KI:In^+, luminesc. decay, excited state symm. and g-value 79−99922
KI:Sn^{2+} luminesc. decay, excited state symm. and g-value 79−99922
$KMgF_3$, F-centre, superhyperfine interaction, g-factor, symmetry, ENDOR obs. 80−39893
$KMgF_3$:Fe^{2+}, super hyperfine struct., Zeeman splitting and dynamic Jahn-Teller effect 77−85555
$KMgF_3$:Fe^{2+}, transferred hyperfine interactions, EPR exam. 78−31105
$KMgF_3$:Ni^{2+}, EPR meas., g-factor, spin-orbit coupling const. and mag. moment determ. 77−80999
K_2MnF_4, EPR g-shift and anisotropic mag. susceptibility 77−85546
KN_3, X-irradiated, N defect, EPR obs. 79−82870
K_2O-TeO_2 glass, radiational EPR centres, struct. model *(Russian)* 77−28426
$K_2Pt(CN)_4Br_{0.3}.xH_2O$, one-dimensional cond., effects of dehydration on mag. props. 77−85549
KUO_3, EPR and mag. susceptibility, temp. depend. 79−33451
^{39}K, ground-state g-factor, rel. to ^{87}Rb, spin-exchange optical pumping meas. 77−34596
^{43}K 738 keV state g-factor, PAC technique 77−6227
^{43}K, $(7/2)^-$ 738 keV state g-factor and lifetime 77−10367
Kr, g-factors meas. by optical pumping and mag. reson. 80−14246
^{84}Kr, 1.84 μs isomeric state, g-factor meas. 78−17101
$^{138}La/^{139}La$ nuclear electric quadrupole moment ratio, laser RF double reson. obs. 80−23447
La-Sm-Lu iron garnet film grown as NdGaG substrates, mag. props. 80−44888
LaF_3:Ce, cryst. field parameters, optical transitions and g-factor determ. 78−2456
LaF_3:R^{3+}, R=rare earths, crystal field anal., intensity calcs. 80−100670
LaM_2-Gd, M=transition metal, correl. between g-shift and stability, EPR study 80−88874
$LaRu_2$, type II supercond., ESR of Nd^{3+} meas. 79−28444

g-factor continued
$(LaTmCa)_3(Fe_{5-x}Ge_x)O_{12}$ film, high g, for mag. bubble applics. 77—85529
^{125}La $27/2^+$ 2737 keV three quasiparticle state, nuclear struct. of isomeric states using g-factor 77—88039
Li, atomic beam mag. reson., Ramsey patterns of field depend. transitions 77—71767
$Li_3AsO_4:CrO_4{}^{3-}$, EPR, 4.2K, cryst. field parameters 79—28586
$LiCrO_2$, EPR of Cr^{3+} ion, g-factor and effective mag. moment 77—73073
$LiErF_4$, EPR studies, lowest levels of rare-earth ions, submillimetre freq. 80—39865
LiF, F-centre, excited state, optical absorption 77—20267
LiF:OH, neutron irrad., interstitial H-centres, ESR obs. 80—93175
LiF:U, Mn, EPR of Mn^{4+} centre, g-values and hyperfine struct. 77—12192
$LiH_3(SeO_3)_2:VO^{2+}$, ferroelectric, 298K, EPR 79—51846
$LiHoF_4$, EPR studies, lowest levels of rare-earth ions, submillimetre freq. 80—39865
Li_2O-TeO_2 glass, radiational EPR centres, struct. model *(Russian)* 77—28426
$Li_3PO_4:CrO_4{}^{3-}$, EPR, 4.2K, cryst. field parameters 79—28586
$LiRF_4$ (R=Tb,Ho,Er), cryst. field parameters, mag. susceptibility meas., 0.3 to 100K 80—60214
$LiTbF_4$, EPR studies, lowest levels of rare-earth ions, submillimetre freq. 80—39865
$LiUO_3$, EPR and mag. susceptibility, temp. depend. 79—33451
$Li_3VO_4:CrO_4{}^{3-}$, EPR, 4.2K, cryst. field parameters 79—28586
$LiYF_4:Dy^{3+}$, spectrum, Stark struct. 77—85756
$LuIr_2$-Nd^{3+}, dil., ESR, hyperfine crysts. of $^{143,145}Nd$, g-factor, crystalline field splitting 78—52349
$LuRh_2$-Nd^{3+}, dil., ESR, hyperfine crysts. of $^{143,145}Nd$, g-factor, crystalline field splitting 78—52349
$MgCl_2:Co$, spectroscopic studies of interactions 80—29769
$MgCl_2:Co^{2+}$, ground-state g-value, EPR meas. 77—16159
$Mg_xFe_{3-x}O_{4-y}$ precipitates, g-factor, ferrimag. reson. meas. 78—60337
MgO:Cr, high resolution far IR spectroscopy of lower energy levels of Cr^{2+} 80—80822
$MgO:Cr^{2+}$, APR spectra 79—87313
$MgO:Cr^{2+}$, APR under applied stress 80—88865
$MgO:Cr^{3+}$, ODMR study, Cr^{3+} ions in tetragonal symm. sites 80—88892
$MgO:Cr^{3+}$, strain modulated ESR 78—88175
MgO-Ti^{3+}, orthorhombic distortion, Jahn-Teller effect 77—66140
$MgSiF_6.6H_2O:Ni^{2+}$, EPR meas., low temp. phases 77—63269
$MgTe:Cr^+$, cryst. growth and EPR 78—39393
$MgTiF_6.6H_2O:Ni^{2+}$, EPR meas., low temp. phases 77—63269
Mn^{2+}-Cu^{2+} coupled pair, ESR spectrum, strong isotropic exchange model 80—29606
MnF, MnF_2, EPR, in inert gas matrices, high spin mag. parameters, level diagrams 78—66565
MnF_2, antiferromag., magnetocryst. anisotropy, susceptibility, static torque meas. 77—69545
MnSi, itinerant ferromag. spin dynamics field depend. 79—38315
Mo complex, influence of anisotropy of spin-Hamiltonian parameters on EPR spectra *(Russian)* 77—28432
Mo-dichalcogenide, valence band nature, elec. and mag. props. 78—39014
$MoO_3:Re$, ESR and optical absorption obs. 77—36127
$(Mo_xV_{1-x})_2O_5$, mag. and spectroscopic investigation 80—25206
^{92}Mo, mag. moments of 8^+ and 11^- states anomalous orbital magnetism 79—6391
^{95}Mo, first excited $3/2^+$ state, g-factor determ. 77—26574
^{99}Mo first excited state g factor from $^{96}Zr(\alpha,n)$ and $^{98}Mo(d,p)$ 79—17801
^{93m}Mo, nucl. g-factor NMR-ON meas. on Fe-Mo alloys 78—37275
N, HFS and g_J factor, precision meas. ground state 77—88412
N_2, $B^3\Pi_g$ state, Hanle effect on rot. level 77—58090
$(NH_4)_2Cd_5Fe_3Al(SO_4)_{12}.18H_2O$, EPR above ferrimag. transition 78—10762
NH_4ClO_4, γ-irrad. single cryst., $NH_3{}^+$ EPR obs., g-tensor hyperfine splitting 78—2739
$(NH_4)_2Co(SO_4)_2.6H_2O$, submillimetre ESR meas. using pulsed high mag. field 80—44905
$(NH_4)_2CuCl_4.2H_2O$, submillimetre ESR meas. using pulsed high mag. field 80—44905
$NH_4H_2AsO_4:Cr^{5+}$, antiferroelec. phase transition, EPR intensity and linewidth meas. 79—4721
$(NH_4)_2InCl_5:Fe^{3+}$ EPR, site g-tensor, spin Hamiltonian factors 77—63270
$(NH_4)_xTl_{1-x}Al(SO_4)_2.12H_2O:Cr^{3+}$, zero field splitting, g-values, EPR spectra obs. 80—50169
NO, Zeeman modulation spectroscopy, line shape analysis 80—74197
NO_2, EPR, mag. dipole transitions, Zeeman parameters 78—17697
NO_2, g-factors of electronic transitions determ., use of resonance optical rot. 79—54876
NO_2, optical RF double reson. for $^2B_2$ state g values 79—64022
$NO_3{}^{2-}$, ENDOR and ESR obs., ^{14}N hyperfine coupling and g-tensors 77—50455
$^{14}N_2{}^{16}O$, elec. and mag. props., hyperfine struct., mol. beam elec. reson. obs. 78—62792
^{14}N, g-factor, lifetime meas. of 5.106 MeV 2^- state of ^{14}N 78—93965
^{14}N, meas. of nucl. g-factor of 5.11 MeV 2^- state by recoil distance technique 78—37268
Na small particle, model calc. of size depend. of CESR g-shift 79—61220
Na_4 $Fe(CN)_6.10H_2O$, single cryst., X-irradiated product ESR, 4.2K 77—48659
NaCl, second relaxed excited state of F-centre, optically detected EPR 79—87335
NaCl:Au, EPR and optical absorpt. 78—39397
NaCl:Ga(In), ESR of impurity centres, impurity optical absorpt. bands 80—29618
NaCl:Li, U-centres, HFS consts., g-factor, EPR spectra 80—39869
NaCl(Br), orbital g-factor and spin-orbit splitting of F-centre excited state, magnetoabsorpt. and MCD 78—2886
$NaCrX_2$, X=S, Se, EPR meas., g-factors, effective mag. moments, and dipolar shifts 79—8043
$NaF:K^+$, γ-irradiated, $H_A(K)$ centres, EPR obs. 77—69689
$NaLa(MoO_4)_2$, luminesc. centres, EPR meas. *(Russian)* 77—28442
NaN_3, X-irrad., EPR of $N_2{}^-$ 77—66421

g-factor continued
Na_2O-$B_2O_3:Se$, EPR, γ-ray effects *(Russian)* 78—31109
Na_2O-TeO_2 glass, radiational EPR centres, struct. model *(Russian)* 77—28426
^{23}Na, ground state g_J factor, meas. from weak-field Zeeman spectra 78—33469
$NbSe_3$, oscillatory magnetotransport, Fermi surface anisotropy, Hall effect, g-factor, Dingle temp. 78—51975
$NbSe_3$, Shubnikov-de Haas oscills. 78—2502
^ANb, nucl. g-factor, A=90, 92 m, NMR-ON meas. on Fe-Nb alloys 78—37275
^{91}Nb, $17^-/2$ state, g-factor meas. 80—32179
^{91}Nb $21/2^+$ state, lifetime, g-factor meas. 77—30487
^{91}Nb, 3.8 μs isomeric state, mag. moment, TDPAD meas. 78—41634
NdF_3, Zeeman splitting in mag. fields up to 100 kG 78—52483
$^ANd(^{32}S,^{33}S^1)$, 56 MeV, A=144,146,148, first excited 2^+ state mag. moment meas. 79—17798
Ne, $2p^53p$ config., Lande factors, double reson. meas. *(French)* 78—9113
Ne, $2p^53s^3P_0$ state, optical pumping, g-factor, metastability exchange cross section 80—947
Ne, g-factors meas. by quantum beat spectroscopy 79—93955
Ne I, wave functions, weighting factors determ. from g-factors 79—98237
Ne, optical-optical double reson., $2p_4$ and $2s_2$ level g_J-values by mode crossing 77—50411
^{20}Ne with backbending, first excited 4^+ state g-factor 80—78144
^{21}Ne, recoil into vacuum g-factor meas. of $5/2^+$ state, 0.350 MeV 78—37272
^{21}Ne, TDPAC obs. on ions recoiling in vacuum 77—22942
$^{21}Ne^*$, produced in $^2H(^{20}Ne,p)^{21}Ne^*$, 351 keV $^5/_2{}^+$ state lifetime and mag. moment 78—41631
^{22}Ne, first excited 2^+ state, mag. moment determ. 77—18388
$^{22}Ne(2^+)$, g-factor and τm via $^4He(^{19}F,p\gamma)$ 38.5 MeV 77—34224
Ni complex, $Ni(5\text{-methylpyrazole})_4X_2$, (X=Cl, Br, I), mag. props., EPR, ligand field calcs. 77—62880
Ni complexes, with CO, O_2 and NO ligands, in NiCa-Y zeolite, EPR, UV obs. 77—63949
Ni, ferromagnetic antiresonance transmission at 24 GHz, temp. depend., g-factor and magnetisation 77—51959
Ni isotopes, even determ. of g-factor of $2_1{}^+$ states 78—43697
Ni-Fe, split bands rel. to sp. ht., g-factor and magnetostriction data 77—72977
Ni-V, ferromag. reson. meas., anisotropy consts. determ. 78—39410
$Ni(BrO_3)_2.6H_2O$, low temp. EPR meas. 77—81001
$Ni(ClO_4)_2.6H_2O$, EPR and IR spectra, 98-298K, phase transition at 224K 78—84477
$Ni_{2-x}Co_xBaFe_{16}O_{27}$, ferromagnetic reson., anisotropy and g-factor, spin-orbit interactions 77—24749
$NiNb_2O_6$, antiferromag., principle mag. susceptibility and field induced magnetisation meas. 77—20589
NiO, with spinel-type defect struct., ferromagnetic reson. meas. 78—43647
$NiSiF_6.6H_2O$, single cryst., EPR, 77-300K, Debye temp. 77—85551
NiTi alloy single cryts., ferromag. reson., g-value and linewidth 80—71186
O_2, Zeeman effect, g_s values 79—3492
O_3, mol. beam electric resonance, electric and mag. props. determ. 77—27055
OD, $^2\Pi_{3/2}$ state EPR spectra 78—21949
OH, $A^2\Sigma^+{}_{1/2}$ state, g-factor meas. by quantum beat obs. 79—18176
OH radical, gas phase EPR, rot. states electronic struct. and Zeeman parameters 78—86896
ONF, J transitions, rot. Zeeman effect 80—63707
$O(^5S_2)$ metastable state g_J factor, TOF at. beam mag. reson. obs., rel. to $He(^3S)$ 79—3593
^{15}O, nucl. g-factor and lifetime of 5.24 MeV $5/2^+$ level 78—37269
^{16}O, transient fields in magnetised Fe, g-factor meas. 77—22887
^{18}O, 2^+ 1.98 MeV level lifetime and g-factor determ. from high velocity recoil in vacuum 77—18474
^{20}O first excited state, g-factor and lifetime from $^3H(^{18}O, p\gamma)$ 80—102115
^{183}Os $9/2^+$ [624] ground state g-factor from NMR 80—83037
Pb, 1^+ state and effective g-factor anal. 77—74764
Pb, phase smearing and mag. interaction, de Haas van Alphen effect 79—37961
PbI_2 (2H), layer cpd., band parameter determ. 79—95332
$PbMoO_4:Fe^{3+}$, ESR, effective g-factors, Fe^{3+} sites 77—51947
$^{208}Pb^{32}S$, $^{203}Pb^{80}Se$, rot. g_J-factor meas., $^1\Sigma$ ground state *(German)* 77—30865
PbSe. electron gas magnetisation, energy band parameters determ., use of Faraday effect 80—45047
$Pb_{1-x}Sn_xSe$, energy band parameter determ. from Shubnikov-de Haas effect 77—69227
$Pb_{1-x}Sn_xSe$ solid solns., photoluminesc. spectra, energy band parameter determ. 80—71484
$Pb_{1-x}Sn_xTe$, energy band parameters from IR Faraday rotation 78—48154
$Pb_{1-x}Sn_xTe$, epitaxial layers, photolum. in mag. field 79—83033
$Pb_{1-x}Sn_xTe$, lattice and electronic props. and g-value 80—80161
$Pb_{1-x}Sn_xTe:In$, carrier spectroscopic g-factors, magnetoresistance, temp. depend. 80—6705
PbTe, far IR spin flip reson. 79—82979
p-PbTe, Fermi surface parameters depend. on carrier density, Shubnikov-de Haas oscills. 79—42435
PbTe, phase convection for effective g-factors and role of g-factors in Knight shifts 79—51473
^{202}Pb, $4_1{}^+$ state g-factor 77—30491
Pd, CESR obs., g-factor and susceptibility enhancement factor 79—65734
Pd, g tensor of d holes near X point in Brillouin zone 79—23890
Pd, Lande g-tensor for d-holes 79—61221
Pd-Fe alloys, hydrogenated and unhydrogenated, EPR and demagnetisation field 77—32250
Pd-Mn, dil. alloy, very temp. magnetisation 80—34692
Pd-Mn, ESR meas., evidences of bottlenecked relax. for Mn^{2+} ion 78—72401
^{143}Pm high spin states, J^π, transitions, isomer g-factors from (d,2N), (α,2N) 80—32154
^{151}Pm 255.676 keV level 77—54173
^{209}Po, $31/2^-$ isomeric state, g-factor meas. 77—10317

g-factor continued
PrX:Dy^{3+}, (X=P,As,Sb), singlet-ground-state paramagnets, EPR meas. 77−20695
^{139}Pr isomeric 11/2^{-} state, half-life, g-factor, and nuclear orientation relaxation from ^{140}Ce(p,2nγ) 79−75837
Rb, lowest metastable autoionising level identification by RF spectroscopy 77−426
RbCl:Au, EPR and optical absorpt. 78−39397
RbCl:Na, U-centres, HFS consts., g-factors, EPR spectra 80−39869
RbUO$_3$, EPR and mag. susceptibility, temp. depend. 79−33451
^{87}Rb, ground state g-factor, rel. to ^{39}K, spin-exchange optical pumping meas. 77−34596
^{85,87}RbCl isotope enriched cryst., optical registration of EPR F-centres *(Russian)* 80−103886
^{187}Re, 206 keV state, g-factor, time differential PAC meas. 78−505
^{212}Rn, Knight shift and absolute mag. moment meas. 78−37278
^{212}Rn, shell model states, semiempirical calcs. half lives, mag. moments, excitation functions 80−63083
^{99}Ru ground state g-factor, relaxation time 80−83036
S containing small paramag. ions on MgO g-tensors and spin densities 78−46270
S$_3^{-}$, stabilized on MgO surface, CNDO calcs. of g-tensors and hyperfine coupling consts. 77−83625
SF$_6$, mol. beam mag. resonance, rot. mag. moment spectrum 77−34661
SF$_6$, sign of rot. g-factor, mol. beam expt. 79−59600
SO, and isotopic forms, X$^3\Sigma^-$ state, CO$_2$ laser mag. reson. spectroscopy 80−9602
SO, Zeeman effect, g$_s$ values 79−3492
^{A}S(α,$\alpha'\gamma$), 8-9 MeV, A=32, 34, 2$_1^+$ state transient field g-factor meas. 79−36151
^{32}S, transient field g-factor meas. on 2$_1^+$ states 78−37273
^{34}S, transient field g-factor meas. on 2$_1^+$ states 78−37273
Sb, A=115, 117, 11/2^{-} isomeric states, half-life, and g-factor 78−33122
Sb, nucl. spin-lattice relax., 4.2K 78−91984
Sb, spin splitting meas. from de Haas-van Alphen effect, g-factors 78−51881
^{A}Sb, A=113,115,117,119, high spin states, J$^\pi$ assignments, decay schemes and lifetimes from Cd(^{6}Li,3n) 79−54381
^{114}Sb, 8^{-}, 210 μs state, mag. moment, PAC of liq. Sn:^{114}Sb 77−26609
^{115}Sb g-factor of 19/2^{-} and 11/2^{-} isomers from ^{115}In(α,4n) 79−40845
^{115}Sb, g-factor of 19/2^{-} isomeric state, time differential perturbed ang. distrib. method 79−22192
^{122}Sb, 5^{+} isomeric state, mag. moment determ. from ^{122}Sn(d,2n)^{122}Sb 78−21493
^{122}Sb, 5^{+} state, mag. moment, g-factor meas. 77−71567
^{43}Sc, g-factor of 3/2^{+} hole state meas. in (α,p) react. 78−21492
^{44}Sc, 68 keV state, g-factor, time differential PAC meas. 78−505
Se$_2$, Lande factor meas. by Zeeman quantum beats *(French)* 79−45761
^{80}Se$_2$, Lande factors measurement in B $^3\Sigma_u^-$ state 77−34648
^{80}Se$_2$, B $^3\Sigma_u^-$ state, Lande factor meas., mol. perturbations 79−45756
Si, amorphous, EPR expts. 78−88167
Si, amorphous, undoped and B doped, ESR-linewidth temp. depend. meas. 80−20459
Si amorphous film, saturation meas. on ESR signals 79−33535
Si, diamagnetism of excitons and biexcitons, recomb. spectra *(Russian)* 80−7412
Si, heavily irrad., ESR study of annealing characts. 78−10771
n-Si inversion layer, resist. minima in surface quantum oscills. 78−60215
n-Si inversion layers, electronic g-factor, spin-split Landau levels 80−80346
n-Si, inverted MOSFET surface, evidence for Lande factor g=2, finite valley splitting 80−6989
Si:Al, bound exciton and bound multiexciton complexes, electronic structure, luminesc. obs. 79−56139
Si:B(P), recombination spectra of bound multiexciton complexes, Zeeman splitting *(Russian)* 79−38526
Si:K, bound exciton luminescence in mag. field *(Russian)* 80−108278
Si:O, EPR spectra of heat treatment centres 78−48039
Si:O, evaporated amorphous film, effect of O$_2$ on props., ESR spectra 80−11265
n-Si:P, heavily depend., spin-lattice relax. at high temp. 78−39403
Si:P, heavily doped, 100 GHz ESR of impurity band 79−95631
Si:P, ion-implanted layers, CESR meas., impurity distrib. inhomogeneity 78−2738
Si:P, neutron transmutation doped, EPR obs. of annealing behaviour 79−1453
Si:P^{-}, Zeeman energy transfer at surface layer 80−11247
Si-SiO$_2$ interface, anisotropic photoinduced ESR 78−23345
Si-SiO$_2$ interface, electrically active paramag. centres detect., photocond. reson. obs. 80−50185
SiC:Al, g-values, spin temp., determ. from Raman spectra 78−43856
SiF$_4$, sign of rot. g-factor, mol. beam expt. 79−59600
Si$_{1-x}$Ge$_x$, amorphous, ESR centres, effect of annealing 77−55701
SiO amorphous thin film capacitor, EPR, elec. cond. 78−68358
SiO$_2$, g-tensor and ^{29}Si hyperfine tensors of E$_1$'-centre for model of O^{-} vacancy 79−19777
SiO$_2$, g-tensor of interstitial O and broken Si-O bond, MO model calc. 79−78520
^{28}Si, high vel. recoil in polarised Fe, transient mag. fields 77−43910
SmB$_6$:Gd^{3+}(Eu^{2+}), mixed valence compound, ESR g-shifts and linewidths 78−48035
SmS:Eu, excited-state exchange interactions, EPR meas. 78−68374
Sm$_3$S$_4$:Eu, excited-state exchange interactions, EPR meas. 78−68374
SmSe:Eu, excited-state exchange interactions, EPR meas. 78−68374
SnO$_2$:W^{5+}, EPR parameters, g hyperfine and superhyperfine tensors 77−85560
^{120}Sn^{32}S, ^{120}Sn^{80}Se, ^{120}Sn^{130}Te, rot. g$_J$-factor meas., $^1\Sigma$ ground state *(German)* 77−30865
^{A}Sn(^{35}Cl,^{35}Cl'), 108 MeV, A=112-124 even isotopes, 2$_1^+$ mag. moments and shell model struct. 80−86805
^{112}Sn 6^{+} isomeric state g-factor and relaxation time from Cd(α,2nγ) 80−73794
Sn^{+}(5s5p^2)^{4}P$_{1/2}$ level, lifetime and Lande g-factor *(French)* 80−52938
Sr, Zeeman effect of J=2 states, interacting Rydberg states 78−17609
SrCl$_2$:Fe^{2+}(Co^{2+}) electronic absorption spectra in far and middle infrared 78−68537
Sr$_2$Cu(OH)$_6$, EPR, g-values 79−19770
SrF$_2$:Cd^{2+}, X-irrad., ESR of Cd^{+} centres 77−59459
SrF$_2$:Ce^{3+}, EPR of low-symmetry sites 79−47332
SrF$_2$:Tm^{2+}, EPR meas. of Tm^{2+} ion pair interactions 79−95641

g-factor continued
SrF$_2$:Yb^{3+}, trigonal centres, superhyperfine interaction, model 78−88114
Sr$_5$(PO$_4$)$_3$Cl:CrO$_4^{3-}$, EPR, cryst. field parameters 79−87309
SrTiO$_3$:Cr^{5+}, nonlinear Jahn-Teller coupling, local dynamics, near struct. transition 80−2625
^{86}Sr, 8^{+} state, nucl. g-factor and nucl. spin relax. in Kr 77−22884
Ta, Mossbauer states at 6.2 keV, freq. modulation 80−7212
TaSe$_3$, oscillatory magnetotransport, Fermi surface anisotropy, Hall effect, g-factor, Dingle temp. 78−51975
^{181}Ta, 136 keV level, g-factor meas. 79−6387
^{181}Ta NMR, obs. of Knight shifts in W and Ta 79−11369
Tb II, Zeeman patterns, g-factors 79−22651
Tb(OH)$_3$:Er^{3+}, g-values and hyperfine interaction parameters, calc. for Er^{3+} 79−15123
TbPO$_4$, zircon struct., cryst. field analysis 80−80232
^{A}Tc, A=93-95, nucl. g-factor NMR-ON meas. on Fe-Tc alloys 78−37275
^{134}Te, levels, J$^\pi$, 6^{+} isomer level mag. moment 77−82824
ThOS:Gd^{3+}, EPR study, g-factor and cryst. field parameters 80−25204
ThRu$_2$, type II supercond., ESR of Nd^{3+} meas. 79−28444
^{232}Th, thermal Westcott g-factor meas. 78−37287
TiF$_2$(TiF$_3$), ESR spectra in rare-gas matrices at 4K 77−88474
TiO$_2$:Mn^{2+}(Mn^{4+}), anatase single cryst., ESR spectra at 77K, 300K 78−10764
TiO$_2$:Mo^{5+}, interstitial EPR, g-tensor and hyperfine tensor 80−84647
^{45}Ti, 40 keV level spin and g-factor via ^{42}Ca(α,n) 77−74761
^{45}Ti, 5/2^{-} 40 keV level, g-factor meas. 77−57599
^{45}Ti, integral rot., hyperfine field and g-factor of 3/2^{+} state 77−50052
^{47}Ti, integral rot., hyperfine-field and g-factor of 7/2^{-} state 77−50052
^{A}Tl, A=203, 205, excited state g-factor from Tl(^{40}Ca, ^{40}Ca'γ) 79−22191
Tm$_3$Al$_5$O$_{12}$:Yb^{3+}, g-shift meas., EPR 78−56376
TmX:Dy^{3+}, (X=P,As), singlet-ground-state paramagnetics, EPR meas. 77−20695
^{169}Tm, 316 keV state, g-factor 79−63586
^{171}Tm, g factor of 635.4 keV level meas. 77−10316
U I, gf-values, level mean lifetimes, electronic excitation and delayed coincidence meas. 78−21878
UCl$_5$, ESR, g-factor 77−43864
UCl$_5$, mag. susceptibility, ESR and g-value, crystal field model anal. 79−91292
V^{4+}, doped in single crysts. bonding character and g-factor interpretation 77−55704
V$_2$O$_5$, reduction in butyllithium, ESR study 80−100611
V$_2$O$_5$-P$_2$O$_5$ glass, EPR investig., samples with varying V^{4+} content and cond. 77−8389
mV$_2$O$_5$.(100-m)P$_2$O$_5$, (m=100-2), V(IV) complexes conc., absorpt. and ESR spectra 78−64266
W, conduction electron g-factor, US vel. quantum oscills. 77−28100
WO$_3$, single cryst. and amorphous film, ESR of defects 78−10770
Xe, excited levels Lande factors *(French)* 79−68326
Xe, g-factors meas. by optical pumping and mag. reson. 80−14246
^{126}Xe, first 2^{+} excited state g-factor 77−18389
(Y,Ca)$_3$(Fe)$_2$(FeGe)$_3$O$_{12}$ film, exchange const., ferromag. reson. meas. 79−8023
(YErCa)$_3$(Fe$_{5-x}$Ge$_x$)O$_{12}$ film, high g, for mag. bubble applics. 77−85529
YFe$_{2x}$Mn$_{2-2x}$, mag. props. and FMR 79−95581
Y$_{1.3}$GdYb$_{0.7}$GaO$_{12}$, epitaxial film, ferromagnetic reson. exam. 77−85579
YH$_3$:Er, Mossbauer spectra of Er^{3+}, gyromagnetic ratios and cryst. field parameters determ. 78−19388
YIG:Si(Ge), Fe^{2+} spectroscopic props., nontrigonal cryst. field effects 80−44553
YM$_2$-Gd, M=transition metal, correl. between g-shift and stability, EPR study 80−88874
Y(OH)$_3$:Er^{3+}, g-values and hyperfine interaction parameters, calc. for Er^{3+} 79−15123
YVO$_4$:Nd^{3+}, zircon struct., cryst. field analysis 80−80232
^{88}Y 14 ms 8^{+} isomeric state, g-factor from ^{87}Rb(α,3n) 80−63080
YbF($^2\Sigma^+$), matrix isolated ESR spectra 78−86890
YbH(YbD), and isotopic forms, optical and EPR matrix isolated spectra, HFS, bonding 77−83613
^{A}Yb(^{40}Ca,^{40}Ca'), A=170,172,174, 168 MeV, rotational g-factor meas. using transient field interactions 80−18193
Zn$_x$Cu$_{0.1}$Fe$_{2.9-x}$ O$_4$, ferromag. reson., g-factors, Jahn-Teller ion effects 80−66043
Zn$_x$Fe$_{3-x}$O$_4$, ferromag. reson., g-factors, Jahn-Teller ion effects 80−66043
Zn$_x$Hg$_{1-x}$Se, galvanomagnetic effects, Shubnikov-de Haas oscill. determ. of band struct. 80−6884
ZnIn$_2$S$_4$:Er^{3+}, cryst. field parameters, thermal and mag. props. calc. 77−20540
ZnO:Co^{2+}, polarised optical absorpt. spectrum, crystal field transitions 77−48206
ZnS, Fe^{3+}-Cu^{+} complexes and A-centres, g-factor anisotropy *(Russian)* 77−20271
ZnS:Mn^{2+}, ^{4}T$_1$ excited state, absorpt., MCD, Jahn-Teller model 78−43907
ZnSe, cubic, magnetoreflectance of Γ_6-Γ_8 exciton ground state 78−23495
ZnSe, cubic, valence band parameters, magnetoreflectance of Γ_6-Γ_8 exciton 78−60056
ZnSe, magnetoreflectance of exciton-polaritons, semiclassical treatment 79−99857
ZnSe, optically detected mag. reson., donor g-factor 77−69732
ZnSe, valence-band parameters and g-factors from free-exciton magnets reflectance 79−73905
ZnSe:Ti^{2+}, EPR meas. 80−80594
ZnSe(Te):Cr^{2+}, spin Hamiltonian parameters and wave function coeffs., LCAO theory 77−39804
ZnSiF$_6$.6H$_2$O:Co, influence of hydrostatic press. on Co^{2+} EPR spectrum 78−27084
ZnTe, magnetoreflectance meas. on Γ_6-Γ_8 exciton 78−6656
ZnTe, spin flip scatt. of laser light 77−43976
ZnTe, spin flip scatt. of laser light 77−43977
ZnTe:As(P), spin flip acceptor scatt. 78−92072
ZnTe:P(As), g-values, spin temp., determ. from Raman spectra 78−43856
^{A}Zn, A=64, 66, 68, 70, transient mag. field g-factor meas. 79−67653

g-factor continued
  ^{A}Zr(^{35}Cl,^{35}Cl′), 90 MeV, A=92, 94, 2_1^+ levels mag. moments 80—105968
  ^{94}Zr, 2^+ state, recoiling in Fe, enhanced transient fields 78—37284

gadolinium
  see also nuclei with ......
  AC susceptibility, temp. modulation studies, domain property thermal relaxation 79—61072
  adsorption and absorption of $H_2(D_2)$ 77—4257
  adsorption on W in field ion microscope *(Russian)* 77—47662
  AES, by computer *(French)* 80—7890
  alkaline earth fluoride:Gd^{3+}, ligand ENDOR, spin Hamiltonian and hyperfine parameters 77—43903
  alkaline earth fluoride:Gd^{3+}, model of ligand hyperfine interaction 80—6792
  amorphous, exhibiting Mossbauer spectra, mean mag. props. *(French)* 80—80489
  atom, electronic spectra of 4s level, many-config. approx. 80—32615
  atom, highly selective multistep ionisation by laser radiation 79—59408
  atom, ion induced K-shell ionisation cross-sections determ. by comparison with nuclear Coulomb excitation 79—76500
  atom, isotope shifts and deform. obs. 77—65433
  atom, laser isotope separation by two step photoionisation 77—61720
  atom, long-lived autoionisation state *(Russian)* 78—94216
  atomic polarisability, effective potential approximation method 77—88587
  atoms, populations of metastable levels during electron beam evap. 77—57926
  band structure, relativistic spin polarised calc. 77—85128
  band structure and Fermi surface using KKR formalism 79—77993
  band structure calcs. 80—15441
  BCC, β-phase, self-diffusion coeff. meas. *(French)* 77—15616
  clusters in faujasite type zeolites, mag. suscept. temp. depend. 78—14925
  coil noise due to permeability fluctuations at phase transition temp. 80—84598
  cover, effective energy cut-off determ., rel. to neutron flux meas. in high-temp. reactor 78—86573
  criticality control of U/Pu reprocessing systems 79—85729
  crystal hyperfine fields at positive muons 79—56662
  crystal structure, P-T phase diagram 78—84776
  cubic metal:Gd, influence of cryst. field on EPR 78—52346
  de Haas-van Alphen effect, Fermi surface 80—15435
  de Haas-van Alphen effect, Fermi surface determ. 78—84138
  dilute impurity hyperfine fields, comparison with model 78—14954
  dipole field anisotropy, at interstitial sites, lattice-deformation effects 79—33584
  displacive phase transition, S ion spin Hamiltonian parameter dependence on order parameter 80—70356
  domain effects near order-disorder and order-order ferromagnetic transitions 80—65886
  electrical resistivity meas., 4.2-600K 78—14706
  electron energy loss spectrum and surface electron states 77—85860
  electron irradiated, defect annealing, recovery spectra 79—23648
  electron irradiated, relation of defect densities to Rayleigh parameters 77—62517
  EPR, g-shift determ. 77—48045
  EPR in polycrystalline cubic metallic cpds., cryst. field effects 77—77096
  EPR linewidth and spin-spin relax. near T_c 78—68369
  EPR near Curie temp. 78—19321
  Fermi surface and de Haas-van Alphen effect frequencies meas. 77—69217
  ferromagnet, static and dynamic magnetoelastic coupling 77—20665
  ferromagnetic, activation energies using transient enhancement of AC permeability 77—59431
  ferromagnetic, crit. sp. ht. and thermal expansion 80—60343
  ferromagnetic, Fermi surface and band struct., press. effects, dHvA expts. 78—14656
  ferromagnetic, hyperfine fields at positive muons 78—43758
  ferromagnetic, isotopically enriched single crystals short-range order 79—4653
  ferromagnetic, local mag. field at positive muon 77—85637
  ferromagnetic, magneto-optical reson., optical consts. determ. 78—6657
  ferromagnetic, positive muons as light isotopes of H, book contrib. 79—82907
  ferromagnetic, RKKY oscills. in surface spin density 77—20512
  ferromagnetic, self-consistent relativistic band struct. calc. 78—91609
  ferromagnetic, spin polarised electron gas model 77—8034
  ferromagnetic, temp. depend. of μ^+ hyperfine field 78—43761
  ferromagnetic, temp. depend. of hyperfine field at interstitial positive muon 79—15300
  ferromagnetic, temp. depend. of hyperfine fields for F 80—20141
  ferromagnetic, transient enhancement of AC susceptibility, domain wall pinning 77—20633
  ferromagnetic, transport props., crit. behaviour 80—65522
  ferromagnetic, vel.- and Z-depend. of transient mag. fields 78—43698
  ferromagnetic domain struct., small-angle neutron scatt. 77—66382
  ferromagnetic reson. line width *(Russian)* 78—39406
  film, Auger emission from excited atoms 77—20967
  film, deposited by cylindrical magnetron sputtering, internal stresses 80—24773
  film, elec. resist. results 78—84326
  film, energy loss and straggling of $^4He^+$ ions 80—88231
  film, hydride form. under water vap. 79—91997
  film, magnetoelastic excitations, phonon spectroscopy and forbidden transitions 79—82853
  film, O_2 and H_2 contamination effect on elec. resist. 77—80856
  film, thermoreflectance dispersion curves at 315K and 97K 80—7332
  film, vacuum deposited and VPE, deposition parameters effects on struct. 79—90912
  film, vacuum deposition, using liq. He cooled cryopumping panel 78—56581
  films, electrical props. correlation with microstructure 80—97009
  foil, domain and domain wall structure 77—69603
  fused salt electrorefining, evaluation of electrolytes 78—92215
  galvanomagnetic effect, longit., in single crystals *(Russian)* 78—56132
  gamma ray TDPAC using ^{161}Dy, hard core correl. 78—10809
  gettering effect 79—63241
  HCP, ferromag. band struct. and Fermi surface, KKR band calcs. 77—62815
  hyperfine field at positive muon 80—40029

gadolinium continued
  hyperfine interaction of ^{188}Os, PAC expts. 78—48102
  hyperfine interaction of ^{197}Au, Mossbauer obs. 77—20773
  impurities in s-p metals, isomer shifts 80—15839
  impurity hyperfine fields 79—99518
  indirect magnetic interactions, NMR anal. 80—71193
  internal fields, positive muon investigation 78—68438
  interstitial site determ., μSR technique 80—71287
  isotope separation, laser two-step photoionisation 78—46461
  lanthanum ethyl sulphate.$9D_2O$:$^{160}Gd^{3+}$, EPR transition energies at low mag. fields 77—12198
  lanthanum ethyl sulphate:Gd^{3+}, EPR lineshape distortion in weak fields with zero-field splitting 77—48034
  lanthanum ethyl sulphate:Gd^{3+}, spin Hamiltonian, higher-order spin terms 77—48044
  lanthanum ethyl sulphate:Gd^{3+}, X-band EPR, near room temp., spin Hamiltonian parameters 77—63275
  lanthanum ethylsulphate:Gd^{3+}, zero-field splitting, contributory mechanism 80—80231
  liquid, electrical resistivity calc., spin disorder contrib. 80—6803
  liquid, mag. susceptibility, elec. resistivity 80—20377
  liquid, resist. and thermoelec. power, t-matrix calc. 78—26840
  liquid, trivalent, electrical resist. 79—42514
  local magnetic fields probed by μ^+ 78—48103
  magnetic crystalline anisotropy, Fermi level, electronic density of states 80—84596
  magnetic domain struct., 230-293K 80—88783
  magnetic domain struct., 77K 78—84447
  magnetic domain structure obs. 78—6542
  magnetic domains, Lorentz microscopy obs. 78—84448
  magnetic hysteresis, departure from Rayleigh law in low mag. fields 77—40086
  magnetic short range order, 80 to 425K 79—42784
  magnetic susceptibility and temp. modulation near Curie point 77—4515
  magnetic transient hyperfine fields, IMPAC obs. 77—8464
  magnetisation, easy axis, as function of press. and temp. 77—63231
  magnetisation, easy direction, meas. with aid of phase theory 80—65963
  magnetised, nature of dynamic mag. fields acting on ^{82}Se, gamma-ray spectra meas. 78—43697
  magneto-optical Kerr effect spectra in UV region using synchrotron radiation 77—52127
  magnetocaloric effects and magnetisation *(Russian)* 78—34985
  magnetocrystalline anisotropy, high quality single cryst. 78—84413
  magnetocrystalline anisotropy, temp. and press. depend. 77—20586
  magnetoelastic anomaly at 240K, spin reorientation region 77—40105
  magnetoelastic excitations and ferromagnetic resonance 79—82879
  magnetoresistance, 4.2-220K, temp. depend., anisotropy 77—62903
  magnetoresistance anisotropy, Fermi surface model 79—91025
  metallic monopnictides:Gd, coupling between 4f electrons and conduction electrons, EPR linewidth 78—52347
  metastable high-pressure phase, conversion into stable phase 77—55357
  microcontact magnon spectra, electron-magnon interaction *(Russian)* 80—54768
  muon spin rotation; freqs., and relax. rates 80—55006
  neutron detector using (n,γ) on ^{157}Gd, ^{177}Hf foils, proportional chamber detection of conversion electrons 78—37517
  neutron radiographic amplifying screen sensitivity 78—7448
  neutron radiography uses 77—66722
  nonmagnetic inclusions, effect on easy direction 77—77052
  Oklo natural fission reactors, migration in core sample, appl. to dating of reactions *(French)* 80—21760
  optical conductivity, direct interband transitions 80—15488
  optical conductivity meas., 0.5-3.1 eV *(Russian)* 80—45100
  optical constants, reflectance meas. *(French)* 78—2869
  optical consts., polarimetric meas., mag. ordering effects 78—15184
  optical properties, 0.5-3.1 eV *(Russian)* 79—11432
  oxidised surface, comparative sputtered neutral mass spectrometry and SIMS studies 79—90856
  $Pb_5Ge_3O_{11}$:Gd^{3+}, ESR spectra, electric-field effect and reversible permittivity 80—29614
  photoabsorption spectra, band struct., at. ionisation mechanisms, electron energy loss spectra 77—24909
  pinned domain wall motion, magnetic damping studies 80—65956
  point defect production during electron irrad. at low temp. 80—49273
  purification by electrorefining, exam. 78—52721
  PWR, safety aspects of using Gd as burnable poison 80—13662
  rare earth ethyl sulphate:Gd^{3+}, host lattice effects on EPR spectra 77—69684
  rare earth ethyl sulphate nonahydrate:Gd^{3+}, high-precision EPR of cryst. 79—69717
  rare earth garnet: $^{154}Gd^{3+}$, hyperfine interactions, PAC 77—43909
  rare earth sulphate:Gd^{3+}, hydrated, EPR spectra, host lattice effects 78—95516
  rare earth trichloride hexahydrate:Gd^{3+}, EPR meas. 78—15017
  rare earth trinitrate hexahydrate:Gd^{3+}, EPR, spectral parameters 79—4720
  resonance recomb. lines in AES and photoelectron spectra 80—97390
  RKKY interactions, anisotropic effects from spin-split bands 80—15712
  small ion-getter pump 78—89487
  small-core approx. and structural phase stability 79—99498
  sound attenuation anomaly near mag. transition temp. 78—15004
  specific heat, mag. contrib. 79—28538
  specific heat near T_c, scaling behaviour 77—66333
  spin reorientation transition, crit. behaviour of elec. resist. 79—51787
  spin wave exam. 78—56306
  spin wave temp. depend., exchange coupling role 78—68199
  spin-reorientation transition, spontaneous 77—36073
  sputtered vapour, neutral ground state population, laser obs., appl. to isotope separation *(Russian)* 78—29759
  surface, O_2 layer thickness, reson. α-scatt. from ^{16}O 78—64778
  surface ionisation on W (110) 79—87142
  texture formation during cold rolling *(Russian)* 78—92275
  thermal conductivity critical behaviour near Curie point 80—75540
  thermal diffusivity, conductivity and elec. cond. 110 to 2100K 79—42516
  thermal diffusivity and electrical resist., T>1100K 77—24548
  thermal expansion, near ferromag. transition 78—31084
  thermoelectric power, absolute, temp. variation 77—11900
  thermoelectric power anisotropy at high temp. 79—23952
  thermoreflectance meas. 79—69816
  thin layer chromatography 78—20105

gadolinium continued
- transient magnetic fields at stopping nuclei in ferromag. phase, stopping power 78−34555
- transition metal intermetallics, ESR of Gd^{3+} 79−87315
- transport props., anisotropy, high temp. obs. 78−26843
- UV absorption exam. of 4f-shell optical excitations 77−1698
- water assemblies, poisoned, thermal neutron diffusion calc., absorption discontinuity effect 78−13191
- working medium in mag. Stirling cycle wheel, refrigerator and heat engine modes of operation 78−57964
- X-ray absorpt. edge, plasmon excitation 80−7437
- X-ray diffraction obs. of magnetostriction and phase transitions 77−73068
- X-ray L_3 absorpt. discontinuity 77−85840
- X-ray L_{III} absorption discontinuity, bidirectional orbital interpretation 77−16423
- X-ray photoabsorption near 3d edges 77−38645
- XPS valence band spectra meas. 77−48306
- β-$Al_2O_3:Gd^{3+}$, EPR, ion site occupancy 77−81003
- $BaCl_2:Gd^{3+}$, EPR, electrostatic versus superposition model 78−23337
- $BaF_2:Gd^{3+}$, dielectric relax. and EPR line broadening 79−56608
- $BaF_2:Gd^{3+}$, high-order EPR transitions of Gd^{3+} centre 78−23335
- $BaF_2:Gd^{3+}$, phonon reson. and IR absorpt. 80−84752
- $BaF_2:Gd^{3+}$, spin-lattice coeffs., EPR study 80−66032
- $BaF_2:Gd^{3+}$ film, Gd^{3+} luminesc. spectrum and kinetics 78−6763
- $BaF_2:Gd^{3+}$-m^+ complex, cryst. field parameters, EPR 78−10768
- $BaF_2:Y^{3+},Gd^{3+}$ production and mech. props. 79−72638
- $Ba_2NaNb_5O_{15}$, Gd substitution, effect on linear thermal expansion, possible BSN replacement 78−43153
- $BaTiO_3$:Gd, positron lifetime spectra meas. 78−43956
- Be intermetallics, Gd-doped, exchange parameters, ESR obs. 77−4557
- $CaAl_4O_7:Gd^{3+}$, ESR, symm. effects 77−36130
- CaF:Gd, dimer reorientation activation volume 80−107285
- CaF_2:Eu,Gd, single crystal predisintegration phenomena, SEM cathodolum. obs. 80−59502
- CaF_2:Gd, triply ionised, lowest energy 4f-5d transition 79−24345
- $CaF_2:Gd^{3+}$, cubic, strain effects on EPR by UMER method 77−1592
- $CaF_2:Gd^{3+}$, ENDOR of ^{19}F ligands, under uniaxial stress 77−16207
- $CaF_2:Gd^{3+}$, effect of strain on cryst. field, EPR longitudinal and shear strain parameters 77−90027
- $CaF_2:Gd^{3+}$, Eu^{2+}, natural, EPR study of impurity centres 78−19318
- $CaF_2:Gd^{3+}$, ITC spectra of impurity aggregate 78−71883
- $CaF_2:Gd^{3+}$, $Li^+(K^+)$, elec. field gradient at nuclei on orthorhombic sites, vs. elec. zero-field splitting 79−87070
- $CaF_2:Gd^{3+}$, ligand ENDOR cubic centres, elec. field effect *(Russian)* 78−60357
- $CaF_2:Gd^{3+}$, Mn^{2+}, photo- and radioluminesc. investig. of intracentric energy transfer 77−16378
- $CaF_2:Gd^{3+}$, S-state splitting, investigation by ESR and ENDOR at high pressure 78−52345
- $CaF_2:Gd^{3+}$ evaporated film, struct. of impurity centres, substrate temp. effects 79−99943
- $CaF_2:Gd^{3+}$ film, Gd^{3+} luminesc. spectrum and kinetics 78−6763
- $CaF_2:Gd^{3+}$-M^+, (M=Li, Na, K, Rb, Cs, Ag), electric field effect expts., EPR line breadths, lattice distortions 78−80210
- $CaF_2:Gd^{3+}$-m^+, complex, cryst. field parameters, EPR 78−10768
- CaF_2-SrF_2-$BaF_2:Gd^{3+}$, luminescence spectrum of Gd^{3+} ion and solid solution region obs. 78−84638
- CaO:Ce,Gd phosphors, trap distrib., phosphoresc. decay characts. obs. 80−29773
- $CaO:Ce^{3+}$, Gd^{3+}, sensitization of Ce^{3+} luminesc. by Gd^{3+} 80−97326
- $CaO:Gd^{3+}$, crystal growth from molten solvent LiF-20 mole % CaF_2 77−77358
- $CaO:Gd^{3+}$, quadrupole hyperfine interaction, ENDOR 78−23370
- CaS:Zr, Gd phosphors, thermoluminesc., trap distrib., activator effects 78−2929
- $CaWO_4$:Gd, site occupation 79−28608
- $CaWO_4$:Gd, thermally stimulated depolarisation current, 100 to 300K 80−7280
- $CdCr_2S_4$:Gd, ferromag. reson. and electrical cond. 79−28626
- $CdCr_2S_4$:Gd magnetic semiconductor growth, structural defects, physical properties 80−60759
- CdF_2:Gd, semicond., symmetry of optical centres, optical and elec. props. 77−59592
- $CdF_2:Gd^{3+}$, hydrostatic press. and temp. effects on EPR spectrum 78−76304
- $CdF_2:Gd^{3+}$, investigation of superhyperfine struct. in EPR spectra 79−51851
- $CdF_2:Ge^{3+}$, Ce^{3+}, in semicond. state, elec. cond. and Hall meas. 78−10443
- $3CdSO_4.8H_2O:Gd^{3+}$, EPR, spin Hamiltonian 79−42833
- $CeP_5O_{14}:Gd^{3+}$, EPR and emission spectra *(French)* 77−69686
- $Ce_2(SO_4)_3.8H_2O:Gd^{3+}$, single cryst., EPR study, spin Hamiltonians 80−80606
- $CsCdBr_3:Gd^{3+}$, EPR of coupled pairs of Gd^{3+} ions 78−19322
- $CsCdBr_3:Gd^{3+}$, EPR spectra of mag. coupled Gd^{3+} ions 78−35032
- $CsMgCl_3(Br_3):Gd^{3+}$, EPR spectra of mag. coupled Gd^{3+} ions 78−35032
- $Cs_2NaRCl_6:Gd^{3+}$, R=lanthanide, EPR parameters and interpret. 77−59456
- $CsSrCl_3:Gd^{3+}$, structural transitions, EPR meas. 78−34619
- $EuAsO_4$:Gd, dynamical interactions, EPR meas. 80−7162
- $EuCl_3.6H_2O:Gd^{3+}$, EPR spectrum, g-tensor and zero-field splitting 77−55706
- EuO:Gd, 4f-photoelectron spin polarization, temp. depend. 79−78842
- EuO:Gd, critical specific heat depend. on doping, microwave cond. 79−95602
- EuO:Gd, elec., mag., and optical props. rel. to electronic conc. 80−96880
- EuO:Gd, elec. cond. under hydrostatic press., Curie temp. 80−96881
- EuO:Gd, electron mobility below Curie temp. 78−91696
- EuO:Gd, ferromag. semicond., electron spin polarisation and conduction band struct. 80−65449
- EuO:Gd, mag. props. and instability phenomena 79−1666
- EuO:Gd, photoelectron spin polarisation, temp. depend. 77−69966
- EuO:Gd, photothreshold changes below mag. ordering temp. 80−97406
- EuO:Gd, surface depolarisation of photoelectrons 78−15286
- EuO:Gd, surface mag. props. 80−71566
- Eu_2O_3:Gd, neutron activation anal. of Gd impurity 77−16874
- EuO(S):Gd, indirect exchange 78−23264
- EuS:Gd, electronic struct., mag. exchange and elec. transport props. 78−87974

gadolinium continued
- EuSe:Gd, mag. props. explained by band struct. 78−43324
- $EuVO_4$:Gd, dynamical interactions, EPR meas. 80−7162
- GaP:Gd, magnetic susceptibility, impurity states 79−61044
- GaSb:Gd(Yb), elec. props., dopant effects 79−87115
- Gd I and II spectra, 3930 to 4140 Å, isotope shift meas. 77−61713
- Gd^{3+} crystal field, spin correlation effect calc. 78−23058
- Gd^{3+}, ESR in cubic intermetallic compounds, AB_2, (A=Y, La, Ce, Lu; B=Ir, Rh) 77−85564
- Gd^{3+}, ground state, fourth-order spin-Hamiltonian parameters 77−69278
- Gd^{3+}, hyperfine interactions, relativistic CI using many-body calcs. 78−78638
- Gd^{3+} impurities in metals, value of interconfigurational energy for S-state ion 79−19563
- Gd^{3+}, impurity ion in frozen aq. solns., effect on Fe^{3+} spin-spin relax., Mossbauer obs. 79−33573
- Gd^{3+} impurity ions, EPR spectra, linewidth narrowing due to spin-lattice relax. of lanthanide Kramers host ions 80−108061
- Gd^{3+} in host lattices, energy transfer from sensitizer to activator 79−38628
- Gd^{3+} in lanthanide ethyl sulphate nonahydrates, $g_{\parallel}$, EPR obs. 78−35031
- Gd^{3+} in $Pb_5Ge_3O_{11}$, SrF_2, β-PbF_2 and BaF_2, spectral diffusion in coherent effects in ESR 79−51852
- Gd^{3+} in $R_2(SO_4)_3.8H_2O$, (R=Pr, Nd, Sm, Eu, Yb and Y), EPR 80−20458
- Gd^{3+} in rare earth trichloride hexahydrate hosts, EPR meas. and linear point charge model predictions 80−25200
- Gd^{3+} in rare-earth trichloride hexahydrates, Tb to Yb, spin Hamiltonian parameters, EPR 77−36128
- Gd^{3+}, in Van Vleck paramagnets, EPR meas. 77−12199
- Gd^{3+}, Zeeman interaction, relativistic corrections and very small g-shifts, contrib. to EPR 78−72393
- $Gd:^{160}Tb$, hyperfine interaction for ^{160}Tb *(Russian)* 77−63347
- $Gd:^{177}Hf$, polycryst. ferromag., impurity hyperfine field polarisation, IPAC 77−73106
- $Gd:^{75}As$, mag. hyperfine field determ. by PAC 77−8459
- Gd:Ra, hyperfine field determ. 77−85622
- Gd^{3+}-doped crystals, mag. susceptibility, cryst. field calc. 78−76035
- $Gd+H^+$, K-shell ionisation, 7-15 MeV, relativistic effects 78−82830
- ^{155}Gd $L_{2,3}$ subshell X-ray fluorescence and Coster-Kronig yields from ^{155}Eu decay 80−69102
- $^{156}Gd/^{155}Gd$ isotopic ratio, eval. of neutron temp. in Oklo natural reactors *(French)* 80−21766
- ^{157}Gd quadrupole electric moment determ. 79−31723
- ^{157}Gd, splitting factor determ. by computer fit in Gd II spectrum 79−31723
- H, and He, stopping powers meas. 80−42904
- $HoVO_4$:Gd, indirect superhyperfine interaction, EPR line width meas. 80−2633
- $KCdF_3:Gd^{3+}$, EPR, spin Hamiltonian parameters 79−65725
- $K_2M(SO_4)_2.6H_2O:Gd^{3+}$, M=Co, Ni, EPR, low-symmetry effects 77−48043
- $KSc(MoO_4)_2:Gd^{3+}$, hyperfine struct. of ESR spectrum 77−8399
- $KTaO_3$:Gd semicond., temp. depend. of thermal diffusivity and Seebeck coeff. 78−10481
- $KTaO_3:Gd^+$, influence of external elec. field on EPR 78−15020
- $KZnF_3:Gd^{3+}$, EPR, spin Hamiltonian parameters 79−65725
- $LaAl_2:Gd^{3+}(Eu^{2+})$, cryst. field parameters, relax. rates 78−84482
- $LaAl_2$:Gd(Ce), supercond., electronic thermal cond. 77−12063
- $LaBe_{13}$:Gd, ESR, crystalline field single ion effects 78−84481
- $LaCl_3:Gd^{3+}$, ^{139}La ENDOR, hyperfine and elec. quadrupole interactions 77−20749
- $LaCl_3:Gd^{3+}$, EPR spectra, linear-electric-field effect 79−73808
- LaF_3:Gd, cryst. field anal. of triply ionised ion spectra 80−2796
- $LaNi_5$:Gd, ESR, exchange induced g-shift, H_2 uptake effect 77−4556
- $La_2(SO_4)_3.9H_2O:Gd^{3+}$, single cryst., EPR study, spin Hamiltonians 80−80606
- $La_{3-x}V_xS_4:Gd^{3+}$, EPR study of interaction between localised mag. moment and conduction electrons *(Dutch)* 77−63277
- $La_{3-x}V_xS_4:Gd^{3+}$ localised moment-conduction electron interact., ESR obs. 78−88183
- $La_{3-x}\square_xS_4:Gd^{3+}$, localised moment-cond. electron interactions, EPR data interpretation 77−63280
- $LuBe_{13}$:Gd, ESR, crystalline field single ion effects 78−84481
- $LuPO_4:Gd^{3+}$, zircon struct. EPR investig., rel. to radiation resistance 80−97138
- $LuPO_4$:Sc, Gd^{3+} EPR spectrum, satellite resonances 78−2734
- $Na_2S:Gd^{3+}$, EPR and ENDOR meas., spin-stress Hamiltonian 77−63278
- $Na_2S:Gd^{3+}$, $PbFCl:Gd^{3+}$, crystal field splitting, parametrisation of temperature dependence 78−91652
- Nb film, supercond. props., Gd ion implantation effects 77−39986
- $NdCl_3.6H_2O:Gd^{3+}$, EPR spectra, angular var. calc. 80−54940
- $Nd_3Mg_3(NO_3)_{12}.24H_2O:Gd^{3+}$, EPR spectra, spin Hamiltonian anal. 79−33527
- $Nd_2(SO_4)_3.8H_2O:Gd^{3+}$, EPR, zero field splittings, spin-Hamiltonian parameters 78−91949
- $Nd_2Zn_3(NO_3)_{12}.24H_2O$, EPR of Mn^{2+}, Gd^{3+} doped single crystal 79−24212
- $PbF_2:Gd^{3+}$, EPR and ENDOR of Gd^{3+} at cubic sites 80−7161
- $Pb_5Gd_3O_{11}$, trigonal Gd^{3+} centre structure 79−69720
- $Pb_5Ge_3O_{11}:Gd^{3+}$, discrete saturation of ESR, due to superhyperfine interaction 77−28440
- $Pb_5Ge_3O_{11}:Gd^{3+}$, EPR hyperfine struct. 79−82867
- $Pb_5Ge_3O_{11}:Gd^{3+}$, ferroelec. transition, temp. depend., EPR study 80−66127
- $PbMo_6S_8$:Gd, EPR meas. *(French)* 80−54947
- $PbMo_6S_8:Gd^{3+}$, powder EPR spectra, cryst. field, supercond. energy gap 80−34769
- $Pb_3(PO_4)_2:Gd^{3+}$, EPR near ferroelastic transition point 79−15350
- $Pb_3(PO_4)_2:Gd^{3+}(Eu^{2+})$, EPR spectra of α- and β-phases 80−11261
- PdH_x-Gd, EPR of Gd^{3+} in temp. range 1.6 to 30K 77−43882
- PrAs(Bi)(P)(Sb):Gd, EPR relax. of impurity in Van Vleck paramag., host ion fluctuation spectra 77−48049
- $PrIn_3$:Gd, EPR relax. of impurity in Van Vleck paramag., host ion fluctuation spectra 77−48049
- $PrIn_3$:Gd, indirect nuclear exchange interactions, ESR-linewidth meas., sp. ht. determ. 80−103825
- $Pr_2Mg_3(NO_3)_{12}.24H_2O:Gd^{3+}$, EPR X-band, fine struct., low field lines 79−15351

gadolinium continued
- Pr_2O_3:Gd^{3+}, EPR, zero-field splitting 79—51850
- PrSb (Bi):Gd, Gd ESR, Gd-Pr exchange, conduction electron effects 79—69719
- PrSb:Gd, ESR study, relaxation narrowing 79—99765
- $Pr_2Zn_3(NO_3)_{12}.24H_2O$:Gd^{3+}, EPR 78—64270
- $RbCaF_3$:Gd, shift of first order transition under hydrostatic press. EPR of Gd^{3+} meas. 80—59649
- $RbCaF_3$:Gd^{3+}, $O_h{}^1$-$D_{4h}{}^{18}$ struct. transition, ESR obs. 80—50178
- $RbCaF_3$:Gd^{3+}, struct. phase transition, EPR study 80—71171
- $RbCaF_3$:Gd^{3+}, uniaxially stressed, transcrit. behaviour, EPR obs. 79—33086
- $RbCdF_3$:Gd^{3+}, EPR 79—91289
- $RbCdF_3$:Gd^{3+}, $O_h{}^1$-$D_{4h}{}^1$ struct. transition, ESR obs. 80—50178
- $RbCdF_3$:Gd^{3+}, struct. phase transition, EPR study 80—71171
- $RbIn(MoO_4)_2$:Gd^{3+}, hyperfine struct. of ESR spectrum 77—8399
- $RbIn(WO_4)$:Gd^{3+} hyperfine struct. in ESR spectrum 77—8399
- $RbSc(MoO_4)_2$:Gd^{3+}, hyperfine struct. in ESR spectrum 77—8399
- $RbSc(WO_4)_2$:Gd^{3+}, hyperfine struct. of ESR spectrum 77—8399
- $ScH_{1.9}$:Pt, Gd, effect of Pt on Gd^{3+} ESR lineshape 78—68371
- $ScPO_4$:Gd^{3+}, zircon struct. EPR investig., rel. to radiation resistance 80—97138
- n-Si:Gd, depth of energy levels of As and P from impurity photocond. 79—90996
- Si:Gd, impurities behaviour 79—78568
- p-Si:Gd, irradiated, elec. props. 79—51613
- Si:Gd, magnetic props. and interaction of impurities 79—11286
- Si:Gd, photoconductivity anomalies due to mag. impurities *(Russian)* 80—103722
- Si:Gd, radiation defect form., effect of Gd impurities, elec. and optical meas. 78—71764
- Si:Gd, radiation defects effect on elec. props. 77—28184
- Si:P, Gd, optical orientation of ^{29}Si nucleus, effect of donor level implantation depth *(Russian)* 77—8452
- SmB_6:Gd^{3+}, mixed balence compound, ESR g-shifts and linewidths 78—48035
- $SmCl_3.6H_2O$:Gd^{3+}, X-ray band EPR lines, exact anal. using intensity operator 80—20448
- $Sm_2(SO_4)_3.8H_2O$:Gd^{3+}, cryst., EPR 77—59455
- $Sm_2(SO_4)_3.8H_2O$:Gd^{3+}, EPR, zero field splittings, spin-Hamiltonian parameters 78—91949
- $Sm_2Zn_3(NO_3)_{12}.24H_2O$:Gd^{3+}, EPR X-band, fine struct., low field lines 79—15351
- $SnMo_6S_8$:Gd, EPR meas. *(French)* 80—54947
- $SnMo_6S_8$:Gd^{3+}, powder EPR spectra, cryst. field, supercond. energy gap 80—34769
- $SrCl_2$:Gd^{3+}, hyperfine interaction, X-band ENDOR 80—60457
- $SrCl_2$:Gd^{3+}, Na$^+$, elec. field gradient at nuclei on orthorhombic sites, vs. elec. zero-field splitting 79—87070
- $SrCl_2$:Gd^{3+}, small dielec. particles, cryst. field size effects 80—44913
- $SrCl_2$:Gd^{3+}-m$^+$ complex, cryst. field parameters 78—10768
- $SrCl_2.6H_2O$:Gd^{3+}, evaporation technique prep. of $SrCl_2$:Gd^{3+}, H_2O content, EPR powder spectrum obs. 80—60416
- SrF_2:Gd, cryst. field parameters calc. and model of tetragonal Gd^{3+} centres 79—28328
- SrF_2:Gd, dipolar complex exam. 79—38435
- SrF_2:Gd, hydrogenated IR and EPR spectra 77—69865
- SrF_2:Gd^{3+}, cryst. field parameters calc. 77—8048
- SrF_2:Gd^{3+}, dielectric relax. and EPR line broadening 79—56608
- SrF_2:Gd^{3+}, dipole relax. and equilib., ionic thermocurrent obs. 77—48121
- SrF_2:Gd^{3+}, dipole strengths and conc. effects influenced by dipole-dipole interactions 79—69718
- SrF_2:Gd^{3+}, high-order EPR transitions of Gd^{3+} centre 78—23335
- SrF_2:Gd^{3+}, Na$^+$(Kr$^+$)(Rb$^+$)(Ag$^+$), EPR of orthorhombic Gd^{3+}-univalent metal ion complexes 80—11262
- SrF_2:Gd^{3+}, orientation kinetics of Gd^{3+}-F$^-$ dipole complexes 77—51952
- SrF_2:Gd^{3+}, spin-lattice relax. of Gd^{3+}, EPR line shifts meas. 78—72404
- SrF_2:Gd^{3+} film, Gd^{3+} luminesc. spectrum and kinetics 78—6763
- $ThBe_{13}$:Gd, ESR, crystalline field single ion effects 78—84481
- ThO_2:Gd^{3+}, ENDOR, nuclear mag. moment and HFS, stress-induced splitting 77—51990
- ThOS:Gd^{3+}, EPR study, g-factor and cryst. field parameters 80—25204
- $TmAsO_4$:Gd, cooperative Jahn-Teller system, dipolar and random strain effects 77—40124
- $TmPO_4$:Gd^{3+}, EPR spectrum and Jahn-Teller induced nonuniform dynamic strains 77—85565
- TmS(Se)(Te):Gd^{3+}, EPR studies of valence states of Tm 77—77095
- TmSb:Gd, Gd ESR, Gd-Pr exchange, conduction electron effects 79—69719
- $TmVO_4$:Gd^{3+}, EPR linewidth temp. var., random strains due to Jahn-Teller effect 77—12200
- YAG:Gd^{3+}, cathodolum. intensity, temp. depend., comparative study with other YAG:R^{3+} crysts. 79—99953
- YAG:Gd^{3+}, cathodolum. efficiency rel. to activator conc. 80—11479
- YAG:Gd^{3+}, EPR absorpt. spectrum 78—76305
- YAG:Gd^{3+}, ESR absorption spectra, line broadening 78—91940
- YIG:Gd, Ga, optical probing of magnetoelastic Rayleigh waves 79—78495
- YIG:Gd^{3+}, mag. relax., hyperfine field interactions, PAC expts. 78—27128
- YPO_4:Gd^{3+}, zircon struct. EPR investig., rel. to radiation resistance 80—97138
- $YbCl_3.6H_2O$:Gd^{3+}, EPR, temp. depend., spin-lattice relax. time 80—93173
- ZnO:Gd, electrolum. brightness, field strength and freq. depend. 80—100696
- ZnO:Gd, phosphor, photoluminesc. and electroluminesc. spectra 79—11457

gadolinium alloys
- amorphous, mag. props. and ferromag. reson. 80—54952
- Curie temperature and saturated mag. moment, nonmag. solute effects. 78—39301
- dilute, in CsCl type alloys, exchange between localised 4f and cond. electrons 77—63279
- ferromagnetic, hyperfine fields of 4d and 5d impurities 78—31133
- ferromagnetic, nuclear spins as probe for mag. coupling and crystallographic order 78—10799
- GdCo amorphous film, magnetic compensation walls 77—8375

gadolinium alloys continued
- $La_{1-x}Gd_xRu_2$, mag. ordered superconductor, re-entrant superconductivity 78—88059
- magnetically concentrated cubic Laves phase cpds., ESR 80—71174
- noble metal-Gd, dil., hyperfine fields of rare earth impurity, calc. 80—15486
- pseudobinary Laves phases, mag. reson. 79—87323
- transition metal alloys, amorphous film, galvanomag. effects, Hall detector 77—89882
- Ag(Au)-Gd, dilute, thermoelec. power, crystal field and interaction effects 77—66158
- AlGd alloys, μ^+ depolaris. rate 79—56695
- Au-Gd, dil., conduction electron-local moment interactions using dHvA waveshape anal. 79—77981
- Au-Gd, dil., conduction electron-local moment exchange interaction meas. 80—60191
- Au-Gd, dil., crystal-field splitting of localised Gd^{3+} moments, ESR obs. 79—82869
- Au-Gd, dil., fine struct. splitting, magnetisation meas. 79—56498
- Bi-Gd system, heats of form. 80—89517
- Cd-Co(-Mo), amorphous films, thermal stability of mag. props. *(Japanese)* 79—47307
- α-Ce-Gd, dil., ESR study of mag. prop 78—39398
- $Ce_{1-x}Gd_xRu_2$, superconductivity and ferromagnetism coexistence, 60 mK-4.2K, spin echo NMR 78—84349
- $Ce_{1-x}Gd_xRu_2Zr_2Co$, spin-pairing state investig. via Josephson effect 77—47942
- $CePd_3$-Gd, dil., EPR 80—25201
- $CePd_3$-Gd, EPR of Gd^{3+} impurities in host with interconfig. fluctuations 78—56377
- $CePd_3$-Gd, ultralow interaction temp. and cryst. field effects for Gd impurities 79—61100
- Co-Ga, spin glass materials, mag. field dependence of susceptibility peak 80—103840
- Co-Gd, dilute, magnetic annealing effect, induced anisotropy 77—73054
- Co-Gd amorphous film, struct., mag. anisotropy consts., saturation magnetisation *(Russian)* 79—99735
- Co-Gd film, amorphous, prep. conditions influence on supernetwork struct. 77—76709
- Co-Gd film, amorphous, stripe domains and mag. anisotropy by Lorentz microscopy 77—63243
- Co-Gd film, magneto-optic coeff. and refr. index, ellipsometric determ. 80—71501
- Co-Gd-B, rules of cmpd. form. in related systems 79—34010
- Co-Gd-Mo, amorphous film, mag. props., temp. depend. 78—10734
- Co-Gd-Mo amorphous films, resist. and extraordinary Hall effect, thermal annealing effect 80—70852
- Co-Gd-Mo films, sputtered, O effects on mag. props. during annealing 80—89374
- Co-Gd-Mo-Ar film, amorphous, mag. props. 78—80182
- Co-Gd-Mo(Au) film, amorphous Hall effect 77—85347
- Co-Gd-Sm magnet, prep. and characterisation 77—8351
- $Co_2Ga_{2-x}Cu_x$, mag. and struct. phases from magnetisation, neutron, X-ray diffr. techniques 78—52253
- $Co_2Ga_{2-x}Ni_x$, mag. and struct. phases from magnetisation, neutron, X-ray diffr. techniques 78—52253
- CoGd, H_2 and N_2 contaminated amorphous films, mag. props. 79—1690
- Dy_xGd_{1-x}, mag. anisotropy energy, composition depend. 77—16071
- $Dy_{1-x}Gd_xAl_2$, ferromag, easy axis rot., ^{163}Dy NMR obs. 79—78562
- $Dy_{1-x}Gd_xAl_2$, ordered alloys, ^{163}Dy NMR, hyperfine field 78—10801
- $Dy_{1-x}Gd_xAl_2$, ordered alloys, hyperfine field, anomalous con. depend. NMR 80—75868
- $Er_{1-x}Gd_xAl_2$, effective mol. field at ^{167}Er, NMR meas. 80—71197
- $Er_{1-x}Gd_xAl_2$, nuclear hyperfine field, quadrupolar splitting, NMR study 80—39888
- Fe-Gd amorphous film, struct. and mag. props. 80—20439
- Fe-Gd amorphous films with comp. gradient, volume and surface hysteresis *(Russian)* 78—88148
- Fe-Gd film, amorphous, mag. props., mean field analysis 78—64236
- Fe-Gd film, amorphous, O_2 contamination effects on mag. props. 78—64231
- Fe-Gd film, magneto-optic coeff. and refr. index, ellipsometric determ. 80—71501
- Fe-Gd films, crystallisation, electron microscope obs. 79—15034
- Fe_3, effect of adsorbed H on mag. props. 77—63129
- FeGd, H_2 and N_2 contaminated amorphous films, mag. props. 79—1690
- Fe_xGd_{1-x}, $0.5>x>0.65$, amorphous film, FMR, spin wave spectra 77—16181
- $GDCo_2$, forced vol. magnetostriction and induced moment 77—36106
- $(Gd,Dy)Al_2$, spin adjustment, NMR spin echo obs. 78—15058
- Gd-Ag, vap. quenched alloys, struct. and mag. props. 78—84461
- Gd-Ag (0-16 at.%), vapour-quenched, struct. and mag. props. 78—38980
- Gd-Ag(Cu) alloy film, amorphous, struct. and mag. props. 78—52318
- Gd-Al, amorphous alloy films, mag. phase diagram, spin glass and ferromag. regions 78—68234
- Gd-Al, amorphous film, microwave mag. reson. 78—91948
- Gd-Al, XPS valence band spectra meas. 77—48306
- Gd-Al sputtered amorphous films, spin glass state 77—66393
- Gd-Al_2, cubic Laves phase compounds, exchange striction determ. 80—44895
- Gd-Al-Co, H sorption props. for H storage, influence of Al 80—45794
- Gd-Al(C)(Cu)(Ga)(Ni)(Pd)(Rh), amorphous, mag. and elec. props. 80—80499
- Gd-Al(Cu)(Ga)(Rh)(Pd), amorphous alloys, mag. coupling of rare earth moments 78—88108
- Gd-Au, dil., Mossbauer exam. of mag. hyperfine field at ^{197}Au impurity 78—88244
- Gd-Cd, dil., elec. field gradient, at ^{111}Cd impurities, temp. depend. 79—28642
- Gd-Ce(Eu)(Yb), magnetocrystalline anisotropy, magnetisation and torque curve meas. 80—65859
- Gd-Co, amorphous, RF sputtered, prep. and props. 79—1693
- Gd-Co, amorphous, sputtered very thin film struct. 77—15707
- Gd-Co, amorphous film, anisotropy due to resputtering effect 77—89989
- Gd-Co, amorphous film, RF sputtering, DC bias role 77—16494
- Gd-Co, amorphous film, with cylindrical mag. domains, sputtering prep. *(Russian)* 77—12176
- Gd-Co, amorphous films, mag. props. ferromag. reson. meas., 20-520°C *(Russian)* 80—97144
- Gd-Co, and Gd-Co-Mo films, amorphous, mag. props., annealing effects 78—64235

gadolinium alloys continued
Gd-Co, and Gd-Co-X (X = Mo, Cu, Au), sputter deposited amorphous alloy, substrate bias, magnetic anisotropy, annealing 78—48006
Gd-Co, CPA calcs., moments and transition temps. 78—52252
Gd-Co, disordered, saturation mag. moment calc., CPA 77—20515
Gd-Co, evap. amorphous film, mag. props. 77—24720
Gd-Co, evap. amorphous films, anisotropy, magnetisation and FMR meas. 77—66392
Gd-Co, evaporated amorphous film, perpendicular anisotropy by controlled O_2 contamination 77—89990
Gd-Co, LV multitarget sputtered film, substrate bias effect on anisotropy 77—16125
Gd-Co, sputtered film, growth induced anisotropy 77—16123
Gd-Co, thermally evap. amorphous film, mag. anisotropy 77—16122
Gd-Co alloy, mag. anisotropy origin 79—38319
Gd-Co alloy, sputtered film, mag. props. determ. *(Chinese)* 78—2714
Gd-Co alloy amorphous thin films, anisotropic mag. and microstruct. props. 78—95487
Gd-Co alloy film, sputter yield ratio, combined ion deposition and etching 80—71594
Gd-Co amorphous film, DC or RF sputtered, mag. props., He^+-backscatt. investig. 77—20650
Gd-Co amorphous film, mag. anisotropy 77—20649
Gd-Co amorphous film, magnetisation processes near compensation point 77—69644
Gd-Co amorphous film, sputtered perpendicular mag. anisotropy 79—56576
Gd-Co amorphous film, sputtered, perpendicular anisotropy exam. 79—73707
Gd-Co amorphous film, sputtered, FMR spectra 79—73822
Gd-Co amorphous film 80—34725
Gd-Co amorphous films, annealed, short-range order and perpendicular mag. anisotropy 80—15765
Gd-Co amorphous films, correlation between struct. and mag. props. *(Chinese)* 80—54532
Gd-Co amorphous films, mag. anisotropy, static and ferromag. reson. expts. 79—33477
Gd-Co amorphous films, mag. struct., mag. bubbles, electron diffr. study *(Chinese)* 80—71126
Gd-Co amorphous films, model calculations for anisotropy formation induced by resputtering processes 78—64242
Gd-Co amorphous films, O_2 adsorption, effect on perpendicular anisotropy 80—34713
Gd-Co amorphous films, RF sputtered, magnetisation ripple effects 80—11232
Gd-Co amorphous films, struct. and mag. anisotropy 80—20438
Gd-Co amorphous films, uniaxial perp. anisotropy induced by resputtering effect, expt. *(Japanese)* 77—55885
Gd-Co amorphous films of rare earth transition metal system, preparation by co-sputtering 79—56928
Gd-Co amorphous ribbons, mag. props. and Invar effects 80—2574
Gd-Co amorphous sputtered films, magnetoelastic contrib. to perpendicular anisotropy, internal stress meas. 78—95490
Gd-Co amorphous sputtered film, magnetostriction and anisotropy 80—39821
Gd-Co amorphous thin film, mag. and optical props., conc. depend 79—19748
Gd-Co amorphous thin films, crystn. process and domain struct. *(Chinese)* 80—54533
Gd-Co based amorphous sputtered films, microstruct. variability and mag. anisotropy, implanted ion effects 80—88459
Gd-Co film, amorphous, Ar sputtered, struct. 78—63946
Gd-Co film, amorphous, ferrimagnet, mag. anisotropy, effect of ion bombard. during prep. 79—1692
Gd-Co film, amorphous, for bubble device appl., prep. and perpendicular anisotropy 77—69641
Gd-Co film, amorphous, inverted and biased loops 77—89996
Gd-Co film, amorphous, magnetisation and anisotropy meas. 77—8370
Gd-Co film, amorphous, magnetisation processes near compensation point 77—40101
Gd-Co film, amorphous, microstruct. and magnetism 78—64230
Gd-Co film, amorphous, perpendicular uniaxial anisotropy, dominant contrib. of preferential resputtering effect 77—36103
Gd-Co film, amorphous, phase separation as source of perpendicular anisotropy 78—64244
Gd-Co film, amorphous, preferential resputtering effect induced anisotropic distrib. of atomic pairs 78—63950
Gd-Co film, amorphous, selective resputtering-induced anisotropy 78—72376
Gd-Co film, amorphous, stability of small bits to temp. and mag. field changes 78—68314
Gd-Co film, amorphous ferrimagnet, anisotropic short range order effects on mag. props. 79—1691
Gd-Co film, bias-sputtered, dipolar mechanisms for mag. anisotropy 78—64233
Gd-Co film, evaporated and sputtered, struct. and mag. anistoropy, electron microscopy 79—56578
Gd-Co film, homogeneity of films prepared by bias sputtering 78—72379
Gd-Co film, sputtered, inert gas incorporation effect on uniaxial anisotropy 78—64232
Gd-Co film, sputtered from segment target, composition and mag. props. 78—27062
Gd-Co film, temp. depend. of mag. aftereffect *(Russian)* 79—8021
Gd-Co film, vapour quenched, amorphous, struct., electron diffr. meas. 77—28086
Gd-Co film, with layer struct., mag. torque and anisotropy 77—63246
Gd-Co films, amorphous, mag. anisotropy from torque meas. 77—47987
Gd-Co films, anomalous magneto-optical hysteresis loops obs. 77—12174
Gd-Co influence of gaseous phase on mag. props. *(Polish)* 80—39820
Gd-Co intermetallic compounds, magnetocrystalline anisotropy obs. *(Japanese)* 77—80926
Gd-Co sputtered amorphous films, resistivity anomalies, 42 to 300K *(Chinese)* 80—7001
Gd-Co sputtered films, preparation process, props. 77—59688
Gd-Co thin films sputtered from mosaic target, thickness and composition distrib. 80—6676
Gd-Co-Au amorphous magnetic films, domain wall obs. by Lorentz electron microscopy 77—80979
Gd-Co-B system, phase composition, struct., phase equilibria 78—35355
Gd-Co-Cu film, amorphous, influence of biased magnetron deposition parameters on props. 77—43856

gadolinium alloys continued
Gd-Co-Fe film, amorphous, bias-sputtered, uniaxial perpendicular anisotropy 78—64234
Gd-Co-Mo, amorphous, sputtered very thin film struct. 77—15707
Gd-Co-Mo amorphous film, MCD, oxide surface layer effect 77—90132
Gd-Co-Mo film, amorphous, bubble and stripe domain wall vel. meas. 77—40094
Gd-Co-Mo film, amorphous, mag. props., ion implantation damage effects 77—89991
Gd-Co-Mo film, amorphous, mag. bubble dynamics 77—89997
Gd-Co-Mo film, amorphous, Ar sputtered, struct. 78—63946
Gd-Co-Mo film, amorphous, in-plane susceptibility near compensation point 78—64238
Gd-Co-Ni series intermetallics, induced moments, magnetisation meas. 77—63138
Gd-Co(-Au) amorphous film, domain wall dynamics near compensation point 79—1696
Gd-Co(-Au) film, ferrimag. amorphous, coated with Permalloy films, mag. props. 79—1695
Gd-Co(-Mo) films, amorphous, inhomogeneities of mangetization and anisotropy 79—65698
Gd-Co(Fe) amorphous films, microstruct. and mag. anisotropy 79—82838
Gd-Co(Fe)(Ni), amorphous film, Kerr and Hall effect meas. 77—24722
Gd-Co(Ni)(Cu)(Rh)(Ru)(Pd)(Ga), amorphous, mag. props. and ferromag. reson. 80—75862
Gd-Cu, amorphous alloy films, mag. phase diagram, spin glass and ferromag. regions 78—68234
Gd-Cu amorphous alloy film, mag. props. 77—16121
Gd-Cu sputtered amorphous films, ferromag. props. 77—66393
Gd-Cu(Fe) splat-cooled, internal friction exam. 77—20012
Gd-Dy, dil., impurity component of elec. resist. meas. 1.5 to 390K 77—39831
Gd-Dy, galvanomag. effect, longit., in single crysts. *(Russian)* 78—56132
Gd-Dy, mag. anisotropy, magnetisation meas. 77—12115
Gd-Dy, magnetic and electric hyperfine fields at Gd, NMR spin echo 77—77123
Gd-Dy, magnetostriction contrib. to thermal expansion *(Russian)* 77—12184
Gd-Dy alloy, magnon contribution to electrical resist. *(Russian)* 78—39087
Gd-Er, mag. anisotropy, magnetisation meas. 77—12115
Gd-Er, magnetic and electric hyperfine fields at Gd, NMR spin echo 77—77123
Gd-Fe, amorphous film, Kerr readout characts. 79—15439
Gd-Fe, amorphous film, stress induced anisotropy 77—89989
Gd-Fe, amorphous film, thermomagnetic writing 78—84428
Gd-Fe, amorphous sputtered film, magnetostriction 79—47320
Gd-Fe, CPA calcs., moments and transition temps. 78—52252
Gd-Fe, co-evap. amorphous film, anomalous hysteresis loop, domains obs. 77—89995
Gd-Fe, DC bias RF sputtered film, mag. props. 77—16124
Gd-Fe, disordered, saturation mag. moment calc., CPA 77—20515
Gd-Fe, LV multitarget sputtered film, substrate bias effect on anisotropy 77—16125
Gd-Fe, mag. moment of Fe, multiplet splitting in photoemission 79—78846
Gd-Fe, sputter deposited amorphous alloy, substrate bias, magnetic anisotropy, annealing 78—48006
Gd-Fe alloy, amorphous thin films, anisotropic mag. and microstruct. props. 78—95487
Gd-Fe amorphous alloys, mag. props. and crystn. 79—90557
Gd-Fe amorphous film, atomic diffusion of deposited Co 79—73346
Gd-Fe amorphous film, prep. by dual-source evaporation, mag. props. 77—89988
Gd-Fe amorphous films, anisotropy dispersion, FMR meas. 79—73824
Gd-Fe amorphous films, O_2 adsorption, effect on perpendicular anisotropy 80—34713
Gd-Fe amorphous films, stress contrib. to perpendicular anisotropy 80—75819
Gd-Fe amorphous films with CeO_2 coatings, Kerr magneto-optical effect enhancement 79—19866
Gd-Fe amorphous sputtered films, magnetoelastic contrib. to perpendicular anisotropy, internal stress meas. 78—95490
Gd-Fe film, amorphous, contact printing 77—73061
Gd-Fe film, amorphous, in-situ ion beam sputtered, microstruct. and Lorentz mag. struct. 78—63947
Gd-Fe film, amorphous, mag. props., annealing effects 78—64235
Gd-Fe film, amorphous, microstruct. and magnetism 78—64230
Gd-Fe film, amorphous, preferential resputtering effect induced anisotropic distrib. of atomic pairs 78—63950
Gd-Fe influence of gaseous phase on mag. props. *(Polish)* 80—39820
Gd-Fe-B ternary systems, phase equilibria and cryst. struct. *(Ukrainian)* 80—11626
Gd-Fe-O system, O-stabilised intermetallic $Gd_{12}Fe_{32}O_2$, prep. and characterisation 77—8956
Gd-Fe-Si, phase diagram 79—52158
Gd-Fe-Y, amorphous film, thermomagnetic writing 78—84428
Gd-Fe(Co), mag. interactions, exchange fields, mol. field model 77—4498
Gd-Fe(Co), thin amorphous system, resistance and hardness, chemical comp. and temp. effect 80—15625
Gd-Hg, dil., mag. hyperfine field, TDPAC meas. 78—52414
Gd-Ho, mag. anisotropy, magnetisation meas. 77—12115
Gd-Ho dil. alloy, nucl. spin-lattice relax. of ^{165}Ho 78—48069
Gd-Ir, dil., hyperfine interaction of ^{193}Ir, Mossbauer effect meas. 78—52413
Gd-La, magneto-optic reson. *(Russian)* 79—47426
Gd-La alloy, optical freq. cond. in 0.5-3.1 eV range, paramag.-ferromag. transition 80—29761
Gd-Mg, X-ray determ. of Debye temp., mean amplitude of vibr. 78—38802
Gd-Mn alloy, mag. props. and effect of H_2 absorpt. 78—19250
Gd-Mn(-Co), amorphous, ferrimag. props. and Hall effect 79—73692
Gd-Mo-Mo amorphous film, domain drag effect obs. 78—91911
Gd-Ni, amorphous, Mossbauer spectra 80—25262
Gd-Ni, CPA calcs., moments and transition temps. 78—52252
Gd-Ni, ferromag., elec. resist. temp. depend. 80—96843
Gd-Ni-Al, (Gd < 33.3 at.%), isothermal section, 800°C, X-ray and microscopic anal. *(Russian)* 79—27950

gadolinium alloys continued
Gd-rare earth metal, dil. resist. anisotropy due to impurities 77—62902
Gd-Sc, dil. alloy, ferromag. hyperfine field determ. 77—43919
Gd-Sm(Eu), mag. props. at low temp. in high mag. fields 79—56570
Gd-Ta, dil., elec. field gradient at ^{181}Ta, temp. depend., TDPAC meas. 79—95689
Gd-Ta, dil., mag. hyperfine field and elec. field gradient at ^{181}Ta impurities, TDPAC meas. 79—47361
Gd-Tb, elasticity modulus, ΔE-effect, internal friction, magnetic transformations *(Russian)* 79—91723
Gd-Tb, magnetic and electric hyperfine fields at Gd, NMR spin echo 77—77123
Gd-Tb (10 wt.%) film, nuclear echo signals, crystal anisotropy consts. *(Russian)* 79—99790
Gd-Ti(V)(Cr)(Mg)(Nb)(Ge)(Si)(Au) amorphous films, spontaneous Hall effect and elec. resist. 80—80251
Gd-Tm, mag. anisotropy, from magnetisation meas. at 4.2K 78—68216
Gd-Tm, magnetic and electric hyperfine fields at Gd, NMR spin echo 77—77123
Gd-Y, Kaufman approach to calc. of intra-rare earth phase diagrams 80—25657
Gd-y, magnetic-field variations of velocity of sound 79—90101
Gd-Y (40 wt.%) single crystal, elastic, magnetic props. 78—14957
Gd-Y alloy, anomalous thermal expansion, interferometric meas. 78—52333
Gd-Y alloy, metal sphere prod. by spark erosion technique 78—81956
Gd-Y alloys, mag. crit. temp. gap 80—60260
Gd-Yb(Ir), dil., ferromag., mag. hyperfine fields of ^{170}Yb and ^{193}Ir, Mossbauer effect meas. 79—24242
Gd-Zn, X-ray determ. of Debye temp., mean amplitude of vibr. 78—38802
GdAg, amorphous, bulk mag. props., field, time and temp. depends. 77—89932
Gd$_{56}$Ag$_{46}$, amorphous, susceptibility and magnetisation, 6-300K *(French)* 77—36060
GdAg$_{1-x}$In$_x$, elec. and Hall resist. 80—96844
GdAg$_{1-x}$In$_x$, magnetic transition temp., effect of hydrostatic press. 78—76244
GdAl$_2$, amorphous, mag. heat capacity 77—89969
GdAl$_2$, anisotropic magnetostriction, temp. depend. 80—39841
GdAl$_2$, anisotropy and magnetostriction 78—10741
GdAl$_2$, anomalous change of Curie temp. 78—47976
GdAl$_2$, ferromag., spin reorientation 78—39334
GdAl$_2$, ferromagnetic, extraordinary Hall effect 80—39560
GdAl$_2$, hyperfine fields, ferromagnetic coupling between rare earth spins, NMR study 80—39880
GdAl$_2$, orbital and spin polarisations of cond. electrons 80—65791
GdAl$_2$, spin reorientation, NMR features rel. to preferred magnetisation direction change 77—63213
GdAl$_2$, spin reorientation 78—39335
GdAl$_2$, thermal expansion and heat capacity Curie temp. determ. 77—1559
GdAl$_2$-GdCo$_2$ system, EPR and mag. props. 79—33478
GdAl$_3$ thin films, polytypism 79—99446
GdAl$_4$, mag. props., mag. exchange strength 77—85440
Gd$_{0.37}$Al$_{0.63}$, amorphous film, anomalous resonance field shift 79—73821
Gd$_{0.37}$Al$_{0.63}$ film, amorphous, spin-glass order parameter meas. 77—28396
Gd$_{0.37}$Al$_{0.63}$ sputtered film, amorphous, conc. spin glass, microwave reson. spectrum obs. 78—15018
Gd$_2$Al, magnetic properties, 4.2 to 400K, metamagnetism 77—32193
Gd$_{37}$Al$_{63}$ amorphous film, spin glass, microwave mag. resonance, freq. dependence 80—39798
Gd(Al$_{1-x}$Cu$_x$)$_2$, C15 struct., elec. resist., comp. depend. 78—14705
Gd(Al$_{1-x}$Cu$_x$)$_2$, thermoelec. power, exchange interactions 80—24881
Gd(Al$_x$Fe$_{1-x}$)$_2$, intermetallic compounds, pseudobinary, Mossbauer studies 80—75887
Gd(Al$_{1-x}$Mn$_x$)$_2$, alloys soft X-ray emission spectra investigation 79—91537
Gd(Al$_{1-x}$Mn$_x$)$_2$, ordering on crystallographic sites, X-ray diffr. 78—38662
GdAu$_3$, mag. props. *(German)* 79—51761
GdAu$_{3.6}$, ordering temps. and effective moments 78—60283
Gd$_2$Au, mag. props., 4.2-300K 79—7972
Gd$_{80}$Au$_{20}$, amorphous ferromag., critical phenomena and mag. props. 77—85469
Gd$_{80}$Au$_{20}$, amorphous ferromag., mag. and transport meas. 77—89930
GdAuNi$_4$, mag. props. 77—20595
GdAuSn, mag. props. 77—85439
GdBi, LCAO calc., electronic struct. *(Russian)* 77—39777
GdCO$_2$, lattice parameter determ. 79—14737
Gd(CO$_x$Ni$_{1-x}$)$_2$, mag. interactions, effects on moments *(Rumanian)* 79—15296
Gd$_{1-x}$Ca$_x$Al$_2$, mag. props. and phase relations 80—107991
Gd$_x$Ce$_y$La$_{1-x-y}$Be$_{13}$, high electron lattice relax., Gd EPR meas. 78—2736
Gd$_x$Ce$_{1-x}$Ru$_2$, magnetic ordering by ^{155}Gd Mossbauer spectroscopy 78—27139
Gd$_x$Ce$_{1-x}$Ru$_z$, coexistence of supercond. and spin glass mag. freezing 77—28283
GdCo, amorphous film, MCD *(Japanese)* 78—39530
GdCo amorphous film, O$_2$ contaminated, TEM obs. of source of perpendicular anisotropy 78—14993
GdCo amorphous sputtered film mag. props. from Mossbauer effect obs. *(Japanese)* 80—15933
GdCo, amorphous thin film, for thermomagnetic recording *(Japanese)* 80—11562
GdCo film, amorphous, sputtered, in-plane anisotropy induced by rare gas annealing 78—84458
a-GdCo film, magneto-optical Kerr effect spectra 77—12458
GdCo film, sputtered amorphous, incorporation of Ne, Ar and Kr 77—44163
GdCo film structure, dependent on substrate type *(Russian)* 80—24747
GdCo sputtered amorphous film, third elements effect on mag. anisotropy 79—91260
GdCo$_2$, ^{59}Co hyperfine field, temp. depend. splitting 77—8447
GdCo$_2$, adsorption of H$_2$, effect on mag. props. 77—20185
GdCo$_2$, dilute ferromagnets, press. effect on Curie temp. 80—65873
GdCo$_2$, magnetovolume effects in itinerant electron ferromagnets 79—8038

gadolinium alloys continued
GdCo$_2$, spontaneous vol. magnetostriction and thermal expansion meas. 77—12183
GdCo$_3$, effect of absorbed H$_2$ on mag. behaviour 79—33483
GdCo$_3$, X-ray absorpt. edge shifts 80—25483
GdCo$_5$, domain wall grooving due to mech. polishing 79—70232
GdCo$_5$, Gd$_2$Co$_{17}$, Mossbauer effect 77—85635
GdCo$_5$, large Barkhausen discontinuities, effect of dynamic elastic stresses *(Russian)* 78—39364
GdCo$_5$, spin polarised energy band struct., APW calc. 78—10342
GdCo$_x$, mag. interactions, effects on moments *(Rumanian)* 79—15296
Gd$_{1-x}$Co$_x$, amorphous alloys, thermal stability, elec. cond. enthalpy 80—100172
Gd$_{1-x}$Co$_x$ amorphous thin film, magnetostriction 79—91281
Gd$_{1-x}$Co$_x$, CPA calcs., mean mag. moments 77—72997
Gd$_{1-x}$Co$_x$ film, amorphous, Curie and compensation temps., effect of O or Ar impurity 77—40093
Gd$_{1-x}$Co$_x$, film, resistivity, Hall effect, domain wall density 78—76169
Gd$_{1-x}$Co$_x$, temp. depend. of magnetisation 77—77043
Gd$_2$Co, amorphous ferromag. obtained by splat cooling, local and bulk mag. props. 79—1685
Gd$_{2+x}$Co$_{17-x}$, magnetocryst. anisotropy, stoichiometry and temp. effects 77—8296
Gd$_2$Co$_{17}$, NMR spin echo meas., dipolar field anisotropy 80—71236
Gd$_{25}$Co$_{75}$, amorphous film, low-field magnetoresistance and domain drag. 78—68014
Gd$_{65}$Co$_{35}$, amorphous, amg. ordering, susceptibility, magnetisation and hysteresis meas. 78—68190
Gd$_{67}$Co$_{33}$, amorphous, elec. resist. and magnetoresist. 80—49693
Gd$_{67}$Co$_{33}$, amorphous ferromag., mag. and transport meas. 77—89930
Gd$_x$Co$_{1-x}$ annealing amorphous film, ferromag. reson. 77—85580
GdCoAl, mag. props. 78—2659
Gd$_2$Co$_6$Al$_{11}$, NMR and mag. susceptibility 79—15367
(Gd$_x$Co$_{1-x}$)$_{1-y}$Ar$_y$ amorphous films, effective anisotropy field, ferromag. reson. obs. 80—71123
GdCoAu amorphous film, bias field depend. of domain drag propagated bubble domains 79—78471
a-GdCoAu(Mo) films, perpendicular anisotropy temp. depend., Lorentz microscopy 77—28419
GdCo$_3$B$_2$, ferromag. ordering and saturation moments 77—24711
Gd$_{0.12}$Co$_{0.59}$Cu$_{0.29}$, sputtered film prep. for bubble device 77—16493
GdCo$_2$(Fe$_2$), amorphous alloys, atomic order, mag. behaviour 78—19221
Gd(Co$_x$Fe$_{1-x}$)$_2$, mag. props., composition and temp. depend. 79—15289
Gd$_3$Co$_3$Ga, crystal struct., X-ray determ. *(Russian)* 79—27951
Gd(Co$_x$Ir$_{1-x}$)$_2$, C15 Laves phase struct., g shift, linewidth EPR meas., Fermi level movement interpretation 79—61210
Gd(Co$_x$Ir$_{1-x}$)$_2$, struct. and mag. moments, comp. depend. 79—86743
GdCoMo amorphous alloy films, mag. cobalt alloys susceptibility, uniaxial anisotropy field 80—54930
GdCoMo film, amorphous, sputtered, ferrimag., in-plane susceptibility near compensation point 78—64240
GdCoMo film, sputtered amorphous, incorporation of Ne, Ar and Kr 77—44163
Gd$_{6.9}$Co$_{74.0}$Mo$_{12.8}$Ar$_{6.3}$, amorphous film, spin wave reson. 79—73823
Gd(Co$_{1-x}$Ni$_x$)$_2$ compounds, NMR and thermal expansion 80—66070
Gd(Co$_{1-x}$Ni$_x$)$_5$, mag. props. and mag. reversal phenomena *(Russian)* 77—51924
GdCo$_{5c}$Ni$_{5-5c}$, intrinsic coercivity, anisotropy, exchange and cryst. field interactions 80—75806
Gd(Co$_x$Ni$_{1-x}$)$_2$, EPR exam. 79—28600
Gd(Co$_x$Ni$_{1-x}$)$_2$, Gd(Fe$_x$T$_{1-x}$)$_2$, Mossbauer spectra, mag. props. 80—20563
Gd(Co$_x$Ni$_{1-x}$)$_2$, mag. props., composition and temp. depend. 79—15289
GdCu, electrical resistivity and length changes with temp., hysteretic behaviour 80—97600
Gd$_x$Cu$_{1-x}$, amorphous film, magnetisation meas., fully aligned moment 78—68309
GdCu$_4$Ag, mag. props. and cryst. struct. 77—20562
Gd$_2$Cu$_6$Al$_{11}$, NMR and mag. susceptibility 79—15367
Gd(Cu$_{1-x}$Gd$_x$), pseudobinary alloy, mag. susceptibility and elec. resist. at low temp. 80—34602
GdCuGe, Gd$_6$Cu$_8$Ge$_8$ and GdCu$_2$Ge$_2$, magnetic props. 77—32180
GdCu$_2$Si$_2$/Mo, point contact spectroscopy of magnons 79—38312
GdCuSn, mag. props. 77—85439
GdCu$_{1-x}$Zn$_x$, mag. struct. determ. 79—87238
Gd$_{1-x}$Dy$_x$Al$_2$, EPR bottleneck, Dy substitution effect 77—63281
Gd$_{0.5}$Dy$_y$Y$_{0.5-y}$Ir$_2$, effect of dil. Dy substitution on Gd ESR 79—82868
Gd$_x$Er$_{1-x}$Rh$_4$B$_4$, effects of Gd ion on supercond. transition temp., mag. transition temp. and upper crit. field 79—56392
Gd$_x$Er$_{1-x}$Rh$_4$B$_4$, ferromag. and structural transitions, low temp. calorimetric meas. 79—55888
Gd$_2$(Fe,Co)$_{17}$, mag. anisotropy fields by singular pt. detection 79—24156
Gd$_2$(Fe,Co)$_{17}$, magnetic anisotropy meas. by singular point detection method 77—63170
GdFe amorphous film, Mossbauer and mag. meas. 80—15844
GdFe, amorphous films, thermal stability of mag. props. *(Japanese)* 79—47307
GdFe film structure, dependent on substrate type *(Russian)* 80—24747
GdFe homogeneous amorphous films, compensation point switching, magneto-optical Kerr signal anal. 80—15726
GdFe$_2$, amorphous, small angle neutron scatt. study of mag. order and mag. microstruct. 79—15283
GdFe$_2$, easy direction of magnetisation 80—20535
GdFe$_2$, electronic heat capacity coeffs. 80—39787
GdFe$_2$ films, electron beam deposited, amorphous and cryst., mag. and struct. props. 79—4710
GdFe$_2$, Mossbauer sample, X-ray diffr. obs. 78—22737
Gd$_{1-x}$Fe$_x$, amorphous film, cosputtered, struct. and mag. props. 78—60323
Gd$_{1-x}$Fe$_x$, CPA calcs., mean mag. moments 77—72997
Gd$_{1-x}$Fe$_x$, temp. depend. of magnetisation 77—77043
Gd$_2$Fe$_{17}$, Mossbauer effect 77—85635
Gd$_x$Fe$_{1-x}$ amorphous film, crystn., TEM obs. 79—87019
Gd$_x$Fe$_{1-x}$ amorphous foil, EELS as analytical tool, data handling and processing 80—81407
Gd$_x$Fe$_{1-x}$ film, mm-wave ferrimag. reson. using optically pumped waveguide laser source 77—55710
GdFeAl, scatter order cpd., mag. props. 77—51891
Gd(Fe$_{1-x}$Al$_x$)$_2$, magnetisation, Curie temps., and mean mag. moments 79—51817
GdFe$_4$Al$_8$, mag. props. 78—52250

gadolinium alloys continued
$Gd(Fe_xAl_{1-x})_2$, magnetic behavior 80—108079
$(Gd_{65}Fe_{35})_{100-x}B_x$ glasses, mag. props. 79—73693
$(Gd_{65}Fe_{35})_{90}B_{10}$, amorphous, mag. props., Mossbauer study 80—93093
GdFeBi, amorphous ferrimag. films, magneto-optical props., optical spectra 80—76008
$(Gd_{1-x}Fe_x)_{1-y}Bi_y$ amorphous films, saturation magnetisation, Kerr and Faraday rotation 80—40093
GdFe(Co), amorphous film, XPS meas. 79—87295
$Gd(Fe_xCo_{1-x})_2$, ferromag. reson. of pseudobinary cubic compounds 78—91961
$Gd(Fe_xCo_{1-x})_2$, Mossbauer effect at 78 and 300K, ^{57}Fe hyperfine fields 80—2677
$Gd(Fe_xCo_{1-x})_2$, paramag. behaviour, itineracy 78—39289
$Gd_2(Fe_{1-x}Co_x)_{17}$, hyperfine interactions, Mossbauer spectra 78—2780
$Gd_x(Fe_{1-y}Co_y)_{1-x}$, evap. amorphous film, mag. anisotropy due to pair ordering 77—32219
$GdFe_2Ge_2$, magnetisation, 4.2-273K, and Neel temp. 77—8310
$Gd(Fe_{1-x}Mn_x)_2$, phase struct., mag. and Mossbauer meas. 77—20563
$Gd_{18}Fe_{82-x}Ni_x$, amorphous film, mag. and galvanomag. props. 77—24715
$Gd_2(Fe_{1-x}Ni_x)_{17}$, Mossbauer spectra, hyperfine field interactions 78—6614
$Gd(Fe_xRh_{1-x})_2$, mag. props., Mossbauer spectra 80—25108
$GdGa_2$, mag susceptibility, 1.5-300K and Neel temp. 78—68184
$Gd_{11}Hg_{45}$, cryst. struct. determ. 79—77555
$Gd_{0.99}Ho_{0.01}(Rh_{1-x}Fe_x)_2$, spin echo meas. on ^{165}Ho, quenching effect of Fe substitution 78—48079
$GdIn_3$, magnetisation 80—25106
Gd_2In, mag. props., 4.2 to 270K 79—56512
Gd_2In, mag. props. 80—108009
Gd_3In, mag. props. 80—108009
Gd_5Ir_2, cryst. struct. 80—96473
$Gd_{0.9}La_{0.1}Al_2$, ferromag., NMR of ^{139}La 78—52377
$Gd_xLa_{1-x}Al_2$ ($x<0.05$), Hall effect measurements 80—44569
$Gd_xLa_{1-x}Al_2$, cryst. fields and exchange parameters, ESR meas. 80—71175
$Gd_xLa_{1-x}Be_{13}$, $0.001 \lesssim x \lesssim 1$, EPR, indirect exchange, bottleneck effect 77—16171
$Gd_xLa_{1-x}Be_{13}$, high electron lattice relax., Gd EPR meas. 78—2736
$Gd_{0.9}La_{0.1}Ni_2$, Ni contrib. to ordering, ^{139}La NMR spin echo 77—63317
$Gd_{0.1}La_{0.9}Ni_5H_x$, $Gd_{0.1}La_{0.9}Co_5H_x$, ^{155}Gd Mossbauer spectra 77—63340
$Gd_xLa_{1-x}Pd_3$, EPR of Gd, g-factor and thermal broadening, temp. and comp. depend. 77—48048
$Gd_{1-x}La_xRh_2$, NMR, contribution of Gd neighbours to Gd hyperfine field 77—8423
$Gd_xLa_{1-x}Zn$, magnetisation and paramag. suscept. 78—88101
GdM_2, (M=Mn, Fe, Co, Ni, Rh, Ru, Ir, Al), H_2 sorption props. 79—86980
GdM_x, M=3d transition metal, hyperfine interactions 78—19401
GdMg, canted mag. struct. in S-ion compound, neutron diffr. obs. 78—34962
GdMg, noncollinear mag. struct., nonlinear band behaviour 80—75706
GdMg, sp. ht., magnetisation and stability of canted struct. 79—78412
$GdMg_3$, mag. props., Mg conc. depend. 78—84392
$GdMg_3$, mag. props. 78—72346
$GdMn_{12}$, mag. interactions, mag. meas. and neutron diffr. 77—63103
$GdMn_2$-$GdAl_2$ intermetallics, mag. props., 80-650K 78—60282
$GdMn_2$-$GdAl_2$ system, mag. and structural studies 80—108006
Gd_6Mn_{23}, magnetic moments, magnetisation 80—25094
Gd_6Mn_{23}, noncollinear mag. struct., magnetization meas. 79—78322
$(GdMn_2)_x(GdAl_2)_{1-x}$, mag. and struct. investigations of intermetallic systems 78—95440
$(Gd_{1-y}Nd_y)_{1-x}Fe_x$ amorphous bubble films with good temp. characts. 79—95616
$Gd_xNd_{1-x}Zn$, ferromag., mag. susceptibility and magnetisation, temp. depend. 80—70975
$Gd(Ni,Cu)_2$, spin disorder resist. evaluation, influence of antiferromagnetic order 77—73035
GdNi, single cryst., magnetocrystn. anisotropy 80—88746
GdNi-DyNi, FeB-CrB type stacking variations, cryst. struct. 80—64952
GdNi-YNi FeB-CrB type stacking variations, cryst. struct. 80—64952
$GdNi_5$, anomalous behaviour near Curie point 78—91880
$GdNi_5$, Gd_2Ni_{17}, Mossbauer effect 77—85635
$GdNi_x$, ($x=3, 3.5, 8.5$), ferrimag., mag. reson. above and below Curie temp. 80—97148
$Gd_{1-x}Ni_x$, CPA calcs., mean mag. moments 77—72997
$Gd_{1-x}Ni_x$, temp. depend. of magnetisation 77—77043
$Gd_{68}Ni_{32}$, amorphous ferromag., mag. and transport meas. 77—89930
$Gd_{69}Ni_{31}$, amorphous, Curie temp., mag. susceptibility and coercive force, 4.2 to 300K 80—93092
Gd_xNi_{1-x} sputtered amorphous films, mag. props. and Hall meas. 78—95488
$Gd_2Ni_{17-x}Al_x$, cryst. struct., X-ray obs. 79—65034
$Gd_2Ni_{17-x}Al_x$, EPR of Gd^{3+} ions 80—97139
$Gd_2Ni_{17-x}Al_x$, mag. behaviour in paramagnetic region 79—73675
$GdNi_2H_4$, effect of absorbed H_2 on struct. and mag. behaviour 78—2682
$GdNi_2H_4$, effect of H_2 absorption on struct. and mag. behaviour 78—10685
$GdNiSi_3$, mag. susceptibility, 80-1200K *(Russian)* 77—66281
$GdNi_2$; Mossbauer effect of ^{57}Fe 77—69743
Gd_3Os, cryst. struct. 80—96474
$Gd_xPd_{82-x}Si_{18}$ amorphous alloys, mag. susceptibility, 4.2-300K 77—66248
$GdPt_5$, low temp. mag. susceptibility 80—93075
$GdPt_x$, $Gd_{1-x}A_xPt_2$ (A=Sc, La), Laves phase alloy, NMR, nonstoichiometry 77—63298
Gd_2Pt, mag. susceptibility meas., mag. transitions obs. 80—60222
Gd_3Pt_4, mag. props., 4.2 to 160K 79—78343
$(Gd_{1-x}R_x)(Co_{1-y}M_u)_5$, R=rare earth, M=Cu, Ni, Pt, origin of hyperfine fields acting on Gd, Mossbauer study 80—44967
$Gd(Rh_{1-x}Fe_x)_2$, $x \leq 0.15$, magnetisation and EPR studies 80—34767
$GdRh_2H_x$, struct. and mag. props., Mossbauer and magnetisation meas. 80—71271
$GdRu_2H_x$, struct. and mag. props., Mossbauer and magnetisation meas. 80—71271
$Gd_{1-x}Sc_x$, Mossbauer spectra, hyperfine interactions 80—15923
$Gd_{1-x}Sm_xCo_2Ni_3$, giant intrinsic magnetic hardness 78—56347
$GdSn_3$, Neel temp., hydrostatic press. depend. 80—29549
GdTb alloy, transport props., anisotropy, high temp. obs. 78—26843
GdTb, elec. resist. and thermal diffusivity anisotropy *(Russian)* 77—85192

gadolinium alloys continued
GdTb, ferromag., magnetisation and microwave absorpt. 80—65816
$Gd_{70}Tb_{30}$, magnetisation, AC susceptibility and microwave absorption meas. 80—60221
$Gd_xTh_{1-x}Ru_z$, coexistence of supercond. and spin glass mag. freezing 77—28283
$Gd_{1-x}Y_x$, Mossbauer spectra, hyperfine interactions 80—15923
$Gd_xY_{1-x}Al_2$ ($x<0.05$), Hall effect measurements 80—44569
$(Gd_xY_{1-x})Al_2$, ferromag. and spin glass like behaviour, magnetisation meas. 80—75734
$(Gd_xY_{1-x})Co_2$, mag. interactions, effects on moments *(Rumanian)* 79—15296
$Gd_xY_{1-x}Co_2$, transferred hyperfine interactions, ^{155}Gd Mossbauer effect and ^{165}Ho NMR expts. 77—63339
$(Gd_xY_{1-x})_4Co_3$, Curie temp. and resist.-temp. curves, comp. depend. 80—71020
$Gd_xY_{1-x}Fe_2$, effective g-values, ferromag. reson. meas. 77—20720
$(Gd_xY_{1-x})Fe_2$, Fe mag. behaviour, FMR measurements, mag. props., Vangsness relation anal. 79—78336
$(Gd_xY_{1-x})Fe_2$, high temp. mag. behaviour 77—1538
$Gd_xY_{1-x}Fe_2$, s-d exchange interaction integral, change due to hydrostatic compression 78—88199
$Gd_xY_{1-x}Fe_3$, saturation magnetisation, magnetostriction, Curie temp., ferrimag. ordering, exchange field *(Russian)* 78—68343
$Gd_xY_{1-x}Ir_2$, ESR meas., bottleneck and relax. rates 79—38369
$(Gd_{0.5}Y_{0.5})Ni$, FeB struct., cryst. field effects on mag. struct. 78—52226
$Gd_xY_{1-x}Zn$, ferromag., mag. susceptibility and magnetisation, temp. depend. 80—70975
GdZn, magnetoelastic consts. 78—15005
$GdZrFe_2$, hyperfine field at Gd, TDPAC meas. 80—93214
$Gd[Co_xFe_{1-x}]$, NMR, hyperfine fields, conc. depend. 77—43902
Ge-Fe amorphous film, sputtered, stress induced anisotropy 79—73706
$Ho_{0.01}Gd_{1-x}Y_xNi_2$, spin echo meas. on ^{165}Ho, limited quenching of Ho moment by cryst. field 79—73851
In—Gd film, dil., fluctuation induced cond. above supercond. transition temp. 79—47196
$(La,Gd)Al_2$, dil. alloy, magnetoresistivity determ. 79—73495
$(La,Gd)Al_2$, mag. props. 78—52299
$(La,Gd)Al_2$, magnetic impurity effect on thermal cond., normal and supercond. states 77—63027
$(La,Gd)Al_2$, normal and supercond. state, US attenuation, freq. depend. and mechanisms 80—49992
$(La,Gd)Al_2$, reverse Kondo alloy, transport props. at finite mag. field 80—6812
$(La,Gd)Al_2$, spin glass, cluster glass and magnetisation characts. for different comps. 77—69585
$(La, Gd)Al_2$ spin glass, suscept. and sp. ht., mag. field depend. 79—61173
$(La,Gd)Al_2$, spin glass materials, mag. field dependence of susceptibility peak 80—103840
$(La,Gd)Al_2$ spin glasses, reversible and irreversible mag. susceptibility 80—15738
$(La,Gd)Al_2$ spin glasses, time depend. mag. props. 80—65909
$(La,Gd)Al_2$, very dil., resist. 79—23958
$(La,Gd)B_6$, dil. alloy, spin glass behaviour, 4.2 to 200K AC mag. susceptibility, RKKY calcs. 78—47994
La-Gd, dil., DHCP, impurity effects on supercond. T_c, electron pair breaking 77—36013
La-Gd, EPR investig. of local moment, correl. with supercond. props. 77—63282
La-Gd, exchange-coupled localised moments, Korringa relaxation rate 80—75851
La-Gd (8 at.%), FCC, under hydrostatic pressure, resistivity meas., comparison with positive-J spin glasses 80—59958
La-Gd/AlO_x/Al tunnel junctions, cond. meas., cryst. field effects 80—88694
La-Gd-An, amorphous, high Gd content, bulk mag. props. 77—59426
La-Gd-Au, amorphous, mag. field depend. of resist. minima 77—59275
La-Gd-Au, amorphous spin glasses, mag.-cluster description 79—42776
$La_{1-x}Gd_xAg$, ^{139}La NMR 78—15038
$La_{1-x}Gd_xAg$, antiferromagnet, spin echo NMR anal. 80—15821
$(La_{1-n}Gd_n)_3Al$, mag. impurity effects in normal and supercond. state, NMR 78—2622
$(La_{1-x}Gd_x)Al_2$, dil., reverse resistance anomaly 78—76054
$La_{1-x}Gd_xAl_2$, Gd^{3+}, ESR meas. 78—68370
$(La_{1-x}Gd_x)Al_2$, spin glass, susceptibility maximum freq. depend. 79—61172
$La_{1-x}Gd_xAl_2$, spin glass, thermoremanent and isothermal remanent magnetisation 79—87276
$La_{1-x}Gd_xAl_2$, supercond., nucl. relax. and impurity magnetism 77—20495
$La_{80-x}Gd_xAu_{20}$, amorphous dil. alloy, RKKY interaction, magnetisation meas. 77—32207
$La_{80-x}Gd_xAu_{20}$, amorphous, supercond. and spin-glass regime, magnetisation and resist. meas. 77—36011
$La_{3-x}Gd_xIn$, mag. impurity ordering and superconductivity, EPR exam. *(Russian)* 77—8400
$La_{1-x}Gd_xZn$, ^{139}La NMR 78—15038
$(La_{.993}Lu_{.007})_{1-x}Gd_xRu_2$, exchange enhanced supercond., compensation effect on H_{c2} 77—4474
LaM_2-Gd, M=transition metal, correl. between g-shift and stability, EPR study 80—88874
$LaNi_5$-Gd, dil., ESR spectra, fine struct. and random stresses 80—25203
Lu-Gd, dil., positive exchange Kondo system, magnetisation and resist. 78—68158
Lu-Gd, positive exchange const. Kondo system, resistivity meas. 78—47775
Mg-Gd, dil., magnetoresist., anomalous Hall effect 80—15502
Pd-Gd, dil., EPR, 35 and 9 GHz, very dil. limit 78—15019
Pd-Gd (1 at.%), lattice distortion around impurities determ. by polarised neutron method 79—1372
Pd-H-Gd, dil., ESR exam. of low temp. region of phase diagram, and electronic props. 80—29930
Pd-H-Gd, dil., Pd-H phase diagram determ. using Gd^{3+} EPR 79—87608
$Pd_{0.98}Fe_{0.01}$ $Gd_{0.01}$, Pd-Gd exchange const., neutron diffuse scatt. meas. 80—71002
$Pd_{0.98}Fe_{0.01}Gd_{0.01}$, ferromag., Pd-Gd exchange const. and Pd polarisation, neutron scatt. meas. 80—25122
$Pd_{0.95}Gd_{0.05}$, mag. transition temp. determ., magnetisation data 77—12123

gadolinium alloys continued
PrGd, magnetic interactions, Mossbauer spectra quadrupole splitting, crystal field parameters 80−39907
$PrNi_5$-Gd, dil., single crystal, ESR study 80−75850
$PrNi_{5-x}Gd_x$, nucl. cooling agent, relax. and exchange, EPR and NMR study 80−25237
Sc-Gd, dil., reverse resist. anomaly and negative magnetoresist. 80−84459
Sc-Gd, spin glasses, low temp. sp. ht. and magnetisation 80−65913
Sc-Gd, spin glasses, low-field susceptibility, role of single-ion anisotropy 77−48000
Sc-Gd spin glass, sp. ht., 0.3-10K 80−25145
$ScAl_2$-Gd, dil., EPR, comparison with YAl_2, La Al_2, $LuAl_2$ 77−63276
$Sm_{1-x}Gd_xAl_2$, hyperfine fields, ferromagnetic coupling between rare earth spins, NMR study 80−39880
$Sm_xGd_{1-x}Co_5$, permanent mag. materials with low reversible temp. coeffs. 79−82822
$Sm_{2-x}Gd_xCo_{17-y}Mn_y$, saturation magnetisation and anisotropy field temp. depend., suitability for microwave/millimetre wave TWT 79−82824
$Sm_{0.6}R_{0.4-x}M_xCo_5$ (R=Gd, Dy, M=Pr, Nd), temp. coeff. of magnetisation 80−34688
Tb-Gd, elec. resistivity and thermopower critical behaviour 80−15499
Tb-Gd, ferromag. monocrystalline, crit. behaviour of elec. resist. 77−62886
Tb-Gd, mag. anisotropy, contrib. from single-ion cryst. anisotropy and anisotropic exchange *(Russian)* 80−29546
Tb-Gd, mag. ordering temp. and indirect exchange integrals *(Russian)* 79−95590
Tb-Gd, spontaneous striction and phonon contributions to thermal expansion *(Russian)* 79−90800
Tb-Gd alloy, spin orientation transition obs. 79−99714
Tb-Gd single cryst., mag., magnetoelastic and elec. props. *(Russian)* 78−2677
Tb_xGd_{1-x}, orientation phase transitions near Curie pt., magnetization and magnetocaloric effect meas. *(Russian)* 79−87261
$Tb_{1-x}Gd_xAl_2$, effective mol. field at ^{159}Tb, NMR meas. 80−71197
$Tb_xGd_{1-x}Al_2$, magnetic anisotropy, magnetostriction 78−56364
$(Tb_{1-x}Gd_x)_3Co$, intermetallic cpd. mag. props., phase transform, and mag. hystersis *(Russian)* 80−93113
$TbMg_3$, mag. props. 78−72346
Th-Gd (1 at.%), Heisenberg exchange, residual resist. meas. 80−75558
Th-Gd spin glass, low temp. sp. ht. 79−51795
Ti(Zr,Hf)-Gd-B system, phase equilib. 80−11629
Y-Gd, de Haas-van Alphen effect, Fermi surface 80−15435
Y-Gd, dil., reverse resist. anomaly and negative magnetoresist. 80−84459
Y-Gd, mag. susceptibility, 4.2 to 300K, Neel temps. 79−19735
Y-Gd, spin glasses, low temp. sp. ht. and magnetisation 80−65913
Y-Gd spin glass, sp. ht., 0.3-10K 80−25145
$Y_{1-x}GdCo_5$, exchange interactions and magnetocrystalline anisotropy 80−34618
$Y_{1-x}Gd_xCo_2$, NMR meas. of ^{59}Co 77−85585
$Y_{1-x}Gd_xCo_2$, NMR of ^{59}Co 78−52376
$(Y_{1-x}Gd_x)Co_2$, spin echo NMR of mag. states 80−7190
$(Y_{1-x}Gd_x)_2Co_{17}$, ^{59}Co NMR, hyperfine fields and contrib. of 4f electrons 77−20727
$Y_{1-x}Gd_xCo_5$, ferrimag., magnetisation, exchange interactions, mag. anisotropy 80−80565
YM_2-Gd, M=transition metal, correl. between g-shift and stability, EPR study 80−88874
YPd_3-Gd, ultralow interaction temp. and cryst. field effects for Gd impurities 79−61100
$YbAl_2Gd$, dil., EPR and mag. susceptibility 80−15797
$Yb_{0.99}Gd_{0.01}CuAl$, intermediate Yb valence states, mag. props. 79−51743
$Zr_{40}Cu_{60-x}Gd_x$, amorphous, mag. ordering and local random anisotropy 78−68273
$Zr_{40}Cu_{60-x}Gd_x$, amorphous alloy, mag. interactions 78−95432
$Zr_{40}Cu_{60-x}Gd_x$, magnetically dil. glass, 4f moments, mag. susceptibility and magnetisation meas. 79−95575

gadolinium compounds
see also gadolinium alloys
acetate, L_3 X-ray absorpt. discontinuity 77−85840
alkali metal-gadolinium oxides, $MGdO_2$ synthesis and physicochem. props. 77−48216
and UO_2-Gd_2O_3 solid soln., high temp. thermal expansion, 298-1700K 78−83979
crystal field and Slater parameters and coordination 78−6771
exchange striction in NaCl type compounds 78−84409
ferrite aluminates, prep. 77−85970
formate, IR spectra and phase transitions, under pressure 78−31179
gadolinia-based fuel pins, efficient diffusion theory parameterization 79−67840
GdH_3, mag.-ordering at 1.8K 80−50062
ionic, elec. field gradients 79−91004
ionic, magnetic interaction potential 78−10682
oxalate, L_3 X-ray absorpt. discontinuity 77−85840
phthalocyanine solutions, bleaching by ruby laser beam 78−30030
pnictides, band struct., semicond.-metal trend 77−28111
Al_2O_3-Gd_2O_3, phase diagrams at high temps., exam. 78−44114
Al_2O_3-Gd_2O_3 system, phase diagram at high temp. *(Japanese)* 80−45290
$(Ba,Gd)TiO_3$, flux growth and chem. characts. 78−23595
$BaGd_4X_5O_{17}$ (X=Si,Ge), cell consts., luminesc. of various rare-earth activators 80−93376
$Ca_{0.5}Gd_{0.5}H_n$, H_2 dissociation press., phase behaviour and struct. 78−2260
$Ca_xGd_{2-x}Sn_{2-x}Sb_xO_7$, pyrochlorate struct. form. 80−92504
CdF_2:CdF_3 films, electroluminesc. meas. *(French)* 79−11471
$Cd_3Ga_5O_{12}$ melt, simulation of fluid flow 78−31321
Cu-Gd_2O_3, high sp. ht. metal for supercond. composite 77−40404
$(Er,Tb,Gd_3)Fe_5O_{12}$ plate, pseudouniaxial, domain struct., magneto-optical obs. 80−11221
$Er_{1-x}Gd_xRh_4B_4$, supercond. and mag. transitions at press. up to 19 kbar 79−38236
$Er_{1-x}Gd_xRh_4B_4$, supercond., phase diagrams and upper crit. fields 80−2531
$Er_{1-x}Gd_xRh_4B_4$, ternary superconductor, mag. interactions 79−73613
$Eu_{1-x}Gd_xO$, mag. props., transport meas. 80−97117
$Eu_{1-x}Gd_xO$, mag. semicond., specific heat and magnetocaloric effect 79−69688

gadolinium compounds continued
$Eu_{1-x}Gd_xO_{1-x}N_x$, ferromag. semicond., prep., ferromag. props. *(French)* 77−69550
$Eu_{1-x}{}^{2+}Gd_x{}^{3+}O_{1-x}N_x$, lattice parameters, mag. and elec. props. 80−100578
$EuGd_2S_4$, nonstoichiometric, elec. transport props., semicond. and metallic cond. 80−107786
$Eu_{1-x}Gd_xS$, concentrated system with ferromag. and antiferromag. interactions, spin-glass props. 80−34639
$Eu_{1-x}Gd_xS$ films, mag. and elec. props. 80−15766
$Eu_{1-x}Gd_xS$, spin glass, transition temp., freq. depend. 80−97113
Eu_2O_3-Gd_2O_3-Ta_2O_5 system at 25, 50 and 75 mole.% Ta_2O_5, cross section investig. 77−12607
Eu_2O_3-R_2O_3-Ta_2O_5, R=La, Gd, Y, quasibinary cross sections 77−90333
$Eu_{1-y}X_yS$ (X=Sr,Gd), spin-disorder-induced Raman scatt. from phonons, expt. investigation 80−20635
$Eu_{1-y}X_yS$ (X=Sr,Gd), spin-disorder-induced Raman scatt. from phonons, theory 80−20636
$(Gd, Bi)_2$ $(Fe, Ga)_5O_{12}$ magneto-optic LPE garnet films, high-energy heavy ion irrad., props. 80−71390
$(Gd,Bi)_3,(Fe,Al,Ga)_50_{12}$ LPE film, 180° Bloch wall pinning at etched nucl. tracks 78−39376
$(Gd,Bi)_3(Fe,Ga)_5O_{12}$ magneto-optic film, ion irrad. effect on storage props. 78−52324
$(Gd,Bi)_3(Fe,Ga)_5O_{12}$, LPE film, coercivity, influence of nuclear tracks 79−51829
$(Gd,Bi)_3(Fe,Ga)_5O_{12}$ epitaxial garnet film, nucl. tracks effect on mag. props. 80−11234
$(Gd,Lu)_3(Fe,Mn,Al)_5O_{12}$ epilayer with orthorhombic anisotropy, domain wall vel. 78−52322
$(Gd,Tm,Y)_3(Fe,Ga)_5O_{12}$ film, magnetocrystalline anisotropy 79−78450
$(Gd,Tm,Y)_3(Fe,Ga)_5O_{12}$ LPE garnet thin films, magnetocrystalline anisotropy 80−93147
$(Gd,Tm,Y)_3(Ga,Fe)_5O_{12}$, bubble domain gradient propag., elliptical distortion and bias compensation 78−19292
Gd complex, benzoylacetonate, energy transfer at high pressures 78−52541
Gd Ni_2Si_2, mag. props., 4.2-200K 80−84602
Gd^{3+} in solution, absorpt. spectrum intensity *(Russian)* 78−35169
Gd-C-N system, isothermal section at 1200°C, X-ray investigation *(German)* 80−93543
Gd-Ga garnet growth, effect of buoyancy parameter of Czochralski bulk flow 79−61512
Gd_3, chem. binding, 4d X-ray spectra obs. 79−69910
GdAG, electrostatic model of cryst. field 80−59945
GdAG:$^{154}Gd^{3+}$, hyperfine interactions, PAC 77−43909
Gd_2ASe_5, A=Ge, Sn, diffuse refl. spectra and band gaps 79−51963
$GdAlO_3$, ^{155}Gd excited states, determ. of nuclear parameters using Mossbauer effect 79−28646
$GdAlO_3$, antiferromag. reson. relax., multimagnon processes 77−4564
$GdAlO_3$, bicrit. and tetracrit. behaviour, susceptibility obs. 77−47992
$GdAlO_3$, canted antiferromagnetic, Mossbauer meas. 80−97171
$GdAlO_3$, crossover effects near spin-flop multicritical point 78−68245
$GdAlO_3$, magnetoelec. susceptibility, mag. struct., mag. phase diagram and crit. coeffs. 77−66303
$GdAlO_3$, magnetoelectric susceptibility, crit. behaviour 78−10743
$GdAlO_3$, spin-flop bicritical line obs. 77−66306
$GdAlO_3$:Co, Ti, effects of Co and Ti ions on cryst. growth 77−28711
$GdAlO_3$:Cr^{3+}, mag. field effects on fluoresc. 80−2850
$GdAlO_3$:Er^{3+}, $^4S_{3/2}$ to $^4I_{9/2}$ transition laser action, optical and luminescence spectra 80−16082
$GdAlO_3$:La, antiferromag., random-field crit. and multicritical behaviour 80−65939
$GdAlO_3$:La, random antiferromagnets, crit. and multicritical props. 80−60332
$Gd_3Al_5O_{12}$ phase obtained by crystallisation of amorphous $Gd_2O_3.5/3Al_2O_3$ by quenching 78−92224
$GdAl_3[BO_3]_4$, thermal stability, X-ray struct. anal., refractive indices 79−4297
$GdAsO_4$, ferroelectricity, dielec. meas. 80−60515
GdAs(Sb)(Bi), antiferomag., EPR meas., Neel temp. determ. 77−32242
GdB_2, high press. synthesis 78−18608
GdB_4, antiferromag. props. *(French)* 77−20566
GdB_4, mag. and elec. props., metallic character 80−20386
GdB_6, crystal preparation, elec. resistance, phase transitions 80−97427
GdB_6, L_3 X-ray absorpt. discontinuity 77−85840
GdB_6 single crystals, mag. behaviour and structure change at low temp. 80−71018
GdB_6, thermophys. props., 700 to 1200K 79−37850
$GdBO_3$:$Eu^{3+}(Tb^{3+})$ and $GdBO_3$:Bi^{3+},Eu^{3+}, vacuum UV excitation spectra and quantum efficiencies 79−28811
GdB_3O_6:Bi^{3+} , Tb^{3+}, energy transfer from sensitiser to activator, intermediate role of Gd^{3+} 80−50389
GdBi, thermal expansion, thermal cond., 300-900K 78−91453
$GdBr_3$, chem. binding, 4d X-ray spectra obs. 79−69910
$GdBr_3$, frozen aq. soln., fluoresc. and absorpt. spectra 79−43022
GdC_2, mag. susceptibility, temp. depend. 79−87239
GdCa garnets, solid soln., mag. and cryst. chem. props. 77−16057
$GdCl_3$, crystn. field parameter of Gd^{3+} 80−10930
$GdCl_3$, frozen aq. soln., fluoresc. and absorpt. spectra 79−43022
$GdCl_3$, heat capacity, 5 to 350K entropy 77−47588
$GdCl_3$, interaction parameters, high freq. meas. of adiabatic differential susceptibility 78−68211
$GdCl_3$, uniaxial ferromag., nonuniversal props. in dipolar crit. region 77−24703
$GdCl_3$, vapour press. and sublimation thermodynamics, mass loss effusion meas. 80−88313
$Gd(ClO_4)_3$, frozen aq. soln., fluoresc. and absorpt. spectra 79−43022
$Gd(ClO_4)_3$, osmotic coeffs. 80−45556
$GdCl_3.6H_2O$, cryst. field parameters computation using Ewald method lattice sums 79−91003
$GdCl_3.6H_2O$, thermal decomp., X-ray emission luminesc. *(Japanese)* 80−55763
$GdCl_3(s)+1.5L_2Cl_6(g)=GdL_3Cl_{12}(g)$, (L=Al,Fe), entrainment, quenching, and chem. transport, rel. to appl. for GdIG CVD 80−24750
$(Gd_{1-x}Co_x)_{1-y}Ar_y$ amorphous mag. film, elec. and mag. prop. depend. on Ar 80−80410
$GdCo_2Ge_2$, magnetism and hyperfine interactions 78−76228
$Gd_{0.27}Co_{0.64}Kr_{0.09}$, amorphous film, thermal release of Kr and H, meas. using UHV mass spectrometric technique 80−3439

gadolinium compounds continued
$GdCoO_3$, spin state of Co^{3+} ion, X-ray photoemission line broadening 79—82751
$GdCo_2Si_2$, mag. props. 80—107988
$GdCrO_3$, EPR linewidth, Neel point to 700K 80—39849
$GdCrO_3$, Faraday rot. and linear birefr. meas., 0.8 to 2 μm 77—77180
$GdCrO_3$, magnetisation, appl. of molecular field theory 79—4637
$GdCrO_3$-$GdAlO_3$ solid solutions 80—20887
$GdCu_2Ge_2$, magnetism and hyperfine interactions 78—76228
Gd_2CuO_4, catalytic props., mag. and elec. props. 79—66350
$Gd_xDy_{1-x}C_2$, solid soln., mag. susceptibility, temp. depend. 79—87239
$Gd_xEr_{1-x}Rh_4B_4$, mag. and supercond. transitions 78—68127
$Gd_xEr_{1-x}Rh_4B_4$, mag. ordering near supercond. region 79—73696
$Gd_xEu_{1-x}B_6$, solid solns., mag. susceptibility, 80 to 1000K *(Russian)* 80—88713
GdF_3, bomb calorimetric determ. of enthalpy of formation 80—50879
GdF_3, chemically reacted film on ferroelectric-ferroelastic $Gd_2(MoO_4)_3$, characterisation 79—15057
GdF_3, crystal growth by Bridgman-Stockbarger method 78—52660
GdF_3, mol. force, compliance and Coriolis consts. 79—31726
GdF_3, standard enthalpies of formation 79—24810
GdF_3:H films, H, F profiles meas. by sputter-induced optical emission 78—47407
$GdF_3:Tb^{3+}$, cryst. fields, luminesc. spectra 78—19563
GdF_3-BaF_2-ZrF_4 glass fibres, IR transmission, losses, fabrication 80—87516
GdF_3-RF_3, R=Tb, Ho, Er, Yb, stabilisation of rhombic β-YF_3 type struct. 78—67700
$GdF_3(Cu_3)(Br_3)$, L_3 X-ray absorpt. discontinuity 77—85840
$Gd(FOD)_3$.n-hexylamine, flexible chain dynamics, NMR, steric effects calcs. 77—6800
GdFe garnet, thermomagnetic recording on magnetised single cryst. plate 79—47285
$GdFe_2$, cubic Laves-phase cpd., spark machining 77—90501
$GdFeB_4$, mag. susceptibility meas., paramag. Curie-Weiss behaviour 79—61041
$GdFe_2B_2$, compounds with $CeAl_2Ga_2$ structure type *(Ukrainian)* 79—32970
$GdFe_3(BO_3)_4$, solubility in Bi_2O_3-B_2O_3 melt and crystallisation 80—19736
$GdFe_2Ge_2$, magnetism and hyperfine interactions 78—76228
$GdFeO_3$ orthoferrite, rare earth-Fe interactions 79—56525
$Gd_3Fe_3O_{12}$, electron irrad., primary-ion charge compensation using SIMS 79—57322
$Gd_3Fe_5O_{12}$, formation mechanism from metallic oxides 77—48376
$Gd_3Fe_5O_{12}$, nucl. gamma reson., anomalous behaviour of intensity 77—12289
GdGa garnet, appl. as X-ray monochromator for high-angle double-cryst. diffr. 77—43111
GdGa garnet, Czochralski grown, substrate material dislocation propagation 78—59771
GdGa garnet, microwave losses 77—4531
GdGa garnet single cryst. substrate surface quality *(Russian)* 77—44371
$Gd_3Ga_{5-x-y}Mg_xZr_yO_{12}$, cryst. growth, coupled substitution of Ga by Mg and Zr 78—31325
$Gd_2Ga_5O_{12}$, cryst. growth by Czochralski technique, dissociation products calcs. 79—47615
$Gd_3Ga_5O_{12}$, brilliance, sparkliness and fire of diamond simulants 78—90363
$Gd_3Ga_5O_{12}$, Ca, Zr and Mg substituted artificial garnets, track registration props. 78—62679
$Gd_3Ga_5O_{12}$, chem. binding, 4d X-ray spectra obs. 79—69910
$Gd_3Ga_5O_{12}$ crystal growth from melt, X-ray topography meas. *(Hungarian)* 80—11556
$Gd_3Ga_5O_{12}$, Czochralski grown, effect of melt flow phenomena on perfection 78—88419
$Gd_3Ga_5O_{12}$, decorated dislocations, large interstitial climb loops round precip. particles 77—19960
$Gd_3Ga_5O_{12}$, dielectric constant, effect of degree of purity and perfection 77—48117
$Gd_3Ga_5O_{12}$ dislocation anal. at inclusions by repeated etching technique 80—29024
$Gd_3Ga_5O_{12}$, elec. cond. meas. 79—23961
$Gd_3Ga_5O_{12}$, flux growth and nucleation temp. determ. *(Chinese)* 80—60761
$Gd_3Ga_5O_{12}$, garnet substrate, surface polishing, damage, abrasion, brittle fracture model *(German)* 77—73357
$Gd_3Ga_5O_{12}$, garnet substrate surfaces, working damage, electron microscope investig. 77—77605
$Gd_3Ga_5O_{12}$, garnet-perovskite transform 80—15239
$Gd_3Ga_5O_{12}$, grown by automatic diameter control, growth striae 77—69979
$Gd_3Ga_5O_{12}$, growth of 3″ diameter crystals 78—68616
$Gd_3Ga_5O_{12}$, high energy heavy ion irrad., lattice strain 80—49278
$Gd_3Ga_5O_{12}$, IR refl., ATR, Voigt and Faraday expts. 80—66180
$Gd_3Ga_5O_{12}$, interface processes with $(YSm)_3(FeGa)_5O_{12}$ film, LPE, horizontal dipping obs. 80—49552
$Gd_3Ga_5O_{12}$, mag. phase diagram, AC susceptibility meas. 80—60265
$Gd_3Ga_5O_{12}$, magnetic interactions and short range order 79—78401
$Gd_3Ga_5O_{12}$ monocrystal optical homogeneity requirement for light beam control 79—82952
$Gd_3Ga_5O_{12}$, opt. dispersion 78—64343
$Gd_3Ga_5O_{12}$, optical birefringence images of edge dislocations 77—1129
$Gd_3Ga_5O_{12}$, planar defects, X-ray topography obs. *(French)* 80—2008
$Gd_3Ga_5O_{12}$, precipitates assoc. with dislocation climb trails *(German)* 77—35567
$Gd_3Ga_5O_{12}$, single cryst., helical dislocation obs. by etching 77—11558
$Gd_3Ga_5O_{12}$ single crystal polishing characteristics, comparison chemical, mechanical methods, magnetic bubble device appl. *(Japanese)* 79—5067
$Gd_3Ga_5O_{12}$, single cryst. growth for mag. appls., book contrib., review 79—69968
$Gd_3Ga_5O_{12}$, substrate, electron examination of microstruct. and microsegregation 78—67919
$Gd_3Ga_5O_{12}$, synthetic, cryst. growth, review *(German)* 79—33926
$Gd_3Ga_5O_{12}$, X-ray topography and double-crystal diffraction 80—92534
$Gd_3Ga_5O_{12}:Er^{3+}$, laser active media, nonradiative losses due to $^4I_{11/2}$-$^4I_{13/2}$ transition 79—31911
$Gd_3Ga_5O_{12}:Ho^{3+}$, stimulated emission at low temps. 80—106526

gadolinium compounds continued
$Gd_3Ga_5O_{12}:Ho^{3+}(Er^{3+})$, stimulated emission and Ho^{3+} cascade laser action 79—91466
$Gd_3Ga_5O_{12}:Nd^{3+}$, cryst. field anal. 78—64013
$Gd_3Ga_5O_{12}:Nd^{3+}$, growth, stimulated emission, spectral props. 78—95593
$Gd_3Ga_5O_{12}:Nd^{3+}$, optical absorpt. and fluoresc. intensities 80—29793
$Gd_3Ga_5O_{12}:Nd^{3+}$ pulse-pumped laser action at 1.054 μm 80—64030
$Gd_2Ge_2O_7$, polymorphism under pressure *(French)* 78—95150
$Gd_2Ge_3O_7(OH)_2$, cryst. struct. 78—71714
Gd_2GeSe_5, elec. props., 300 to 1100K 79—51585
$Gd_2Gi_2O_7:Nd^{3+}$, spectroscopic props. 77—69866
GdH_2, lattice thermal expansion and point defect form. energy 77—51524
$GdH_{2.92}$, electrical resistance anomalies at high pressures 80—29381
GdH_3, magnetisation and mag. suscept. 77—43821
GdIG, amorphous, Mossbauer specfra, mag. props. 80—15849
GdIG, crystal and static mag. props. 79—99166
GdIG, empirical formula for lattice const. calc. 79—27968
GdIG, expts. on chem. equilib. for possible appl. in CVD 80—24750
GdIG, IR refl., ATR, Voigt and Faraday expts. 80—66180
GdIG, local mag. anisotropy in stress field of single dislocation 80—88744
GdIG, mag. props. meas. in high mag. fields, review *(Japanese)* 78—52303
GdIG, one-magnon light scatt. with and without compensation temps. 78—31062
GdIG single crystal plates for magnetooptical information storage 79—7997
GdIG, spin struct. obs. by Faraday rotation expts. in fields up to 200 T 77—69809
GdIG, spin wave intrinsic relaxation, magnon damping at low temps. 80—29543
GdIG, spin-orientation phase transitions, magneto-optic and visual exam. 77—24675
GdIG, thermal effect on re-entrant hysteresis loop and coercive force 78—2702
GdIG, thermoelec. power, elec. cond., 500-1200K, ferrimag. Curie temp. 79—99543
$GdIG:^{154}Gd^{3+}$, hyperfine interactions, PAC 77—43909
$Gd(IO_3)_3$, cryst. struct., X-ray diffr. obs. 77—84718
Gd_3InO_6, high press. synthesis, cryst. struct. 77—68955
$Gd_xLa_{1-x}B_6$, solid solns., mag. susceptibility, 80 to 1000K *(Russian)* 80—88713
$Gd_{0.67}La_{0.33}P_5O_{14}$, photoemission spectra, 4f, 5p and 5s giant reson. enhancement 78—95660
$Gd_xLa_{1-x}Pd_3$, ESR linewidths, g-shifts, effective electron interaction, spin-lattice relax., spin-flip scatt. 78—68372
$GdMn_2Ge_2$, magnetism and hyperfine interactions 78—76228
$Gd_2(MoO_4)$, ferroelec., Raman scatt. from soft modes 77—85706
$Gd_2(MoO_4)_3$, and isotypes exam. of crystal growth, and defect generation 78—68617
β-$Gd_2(MoO_4)_3$, antiferromag., polarised ferroelec., ferroelastic, magnetothermodynamics 79—7996
$Gd_2(MoO_4)_3$, cryst. field parameters for Gd^{3+} 77—66142
$Gd_2(MoO_4)_3$, crysts., elastic props. during domain switching under mech. loading 79—55809
$Gd_2(MoO_4)_3$, domain structure obs. by GdF_3 decoration 78—84544
$Gd_2(MoO_4)_3$, domain wall motion dynamics 80—108030
$Gd_2(MoO_4)_3$, EM wave diffr. by domain walls 79—69799
$Gd_2(MoO_4)_3$, effect of ferroelec. ordering on refractive index 79—33653
$Gd_2(MoO_4)_3$, electro-optical properties 78—88281
$Gd_2(MoO_4)_3$ electroacoustic interaction obs. 77—11966
$Gd_2(MoO_4)_3$, electron microscope exam. of ferroelec. and ferroelastic props., domain walls and cryst. defects 77—69786
$Gd_2(MoO_4)_3$, electron microscopy investigs. of ferroelec. substances, review *(Japanese)* 80—71366
$Gd_2(MoO_4)_3$, ferroelastic, laser-induced twinning 77—76422
$Gd_2(MoO_4)_3$, ferroelec., anomalous damping of phonons, Raman spectra, stress and temp. effects 79—38503
$Gd_2(MoO_4)_3$, ferroelec., amorphous Si:H coating, domain wall motion, image scanning 80—83663
$Gd_2(MoO_4)_3$, ferroelec. and ferroelastic, electron microscopic study 77—85675
$Gd_2(MoO_4)_3$, ferroelec. ferroelastic, domain wall motion, crit. field var. 77—81075
$Gd_2(MoO_4)_3$, ferroelec. ferroelastic, electron microscope exam., antiphase boundary, image analysis 78—15134
$Gd_2(MoO_4)_3$, ferroelec. temp. depend. of spontaneous biref. and electrooptic reponse 79—33662
$Gd_2(MoO_4)_3$, ferroelec.-ferroelastic, photolum. and photocond. meas. 80—84768
$Gd_2(MoO_4)_3$, ferroelectric domain decoration 78—10862
$Gd_2(MoO_4)_3$, ferroelectric, polarisation reversal, electric field induced phase transform. 80—103925
$Gd_2(MoO_4)_3$, improper ferroelectric, electro-opt. props. 78--76426
$Gd_2(MoO_4)_3$, low temp. optical absorpt., external mag. field influence 78—43896
$Gd_2(MoO_4)_3$, matrix-addressed analogue ferroelec. memory 80—103926
$Gd_2(MoO_4)_3$, nonlinear piezoelec. coeffs. near phase transition 79—95710
$Gd_2(MoO_4)_3$, one-dimensional ferroelectric image sensor with polymer photoconductor 80—80729
$Gd_2(MoO_4)_3$, optical activity, gyration tensor determ. near Curie point 79—33660
$Gd_2(MoO_4)_3$, optical activity *(Japanese)* 79—65832
$Gd_2(MoO_4)_3$, passivation of c surface against attack by HF by inert ion beam irradiation 78—35545
$Gd_2(MoO_4)_3$, photoelastic tensor components 77—48146
$Gd_2(MoO_4)_3$, piezoelectric and electrostriction coeffs. near ferroelastic transition *(French)* 77—40182
$Gd_2(MoO_4)_3$, prismatic domain exam. 78—56441
$Gd_2(MoO_4)_3$, spontaneous birefringence, pulsed field switching, compression effect, domain movement 78—27187
$Gd_2(MoO_4)_3$, spontaneous electrooptic effect, role of induced birefringence 78—68480
$Gd_2(MoO_4)_3$, spontaneous rot. of plane of polarisation of light in external field 80—93282
$Gd_2(MoO_4)_3$, surface study using AES and ion scatt. spectroscopy 80—65339
$Gd_2(MoO_4)_3$, uniaxial stress effect on ferroelec. transition, Raman scatt. 78—80360

gadolinium compounds continued
$Gd_2(MoO_4)_3$, variable frequency SAW resonator on ferroelectric-ferroelastics 78−33977
$Gd_2(MoO_4)_3$:Nd^{3+}, optical spectrum, free ion wavefunctions, radiative transition probabilities 79−24339
Gd_2MoO_5, cryst. struct., IR spectra, elec. and mag. props. 80−33954
$GdMo_6S_8$, Chevrel phase, RE mag. isolation and supercond. 80−44470
$GdMo_6S_8$, coexistence of antiferromagnetism and superconductivity, neutron diffraction study 79−99685
$GdMo_6S_8$, long range mag. order in supercond. state 79−65653
$Gd_{1.2}Mo_6S_8$, low temp. heat capacity anomaly rel. to antiferromag. transition in supercond. state 80−25044
$Gd_{1.2}Mo_6S_8$, low temp. magnetisation meas., and supercond. props. 79−8018
$Gd_xMo_6S_8$, Chevrel phase, lattice instabilities, X-ray diffr. meas. 78−34491
$Gd_{0.1}Mo_6Se_8$, mag. supercond., low temp. sp. ht. meas. 79−56380
$Gd_{1.2}Mo_6Se_8$, coexistence of supercond. and long range antiferromag. order 80−84534
$Gd_xMo_6Se_8$, Gd^{3+} ESR meas., 1.4-290K 78−88184
$Gd_xMo_6Se_8$, supercond., mag. props., 0.7 to 295K 77−32113
GdN, and $GdN_{1-x}O_x$, mag. interactions 80−60218
GdN, m.p. N_2 press. depend., Pirani-Alterthum meas. 78−43103
GdN, mag. interaction and carrier conc. 80−71005
GdN, miscibility with UC *(German)* 80−96654
GdN-EuO soln., ^{151}Eu Mossbauer spectroscopy 78−6610
GdN-RN systems, (R=La,Ce,Nd), mutual solubilities *(German)* 79−19374
$Gd(NO_3)_3$, L_3 X-ray absorpt. discontinuity 77−85840
$Gd(NO_3)_3$, osmotic coeffs. 80−45556
$Gd(NO_3)_3$, use in fuel dissolution criticality control 79−85728
$GdN_{1-x}O_x$, magnetic interaction and carrier conc. 80−71005
$GdNbO_4$-$CaWO_4$, phase transitions of fergusonite-scheelite *(French)* 80−19942
$GdNbTiO_6$:Eu^{3+} emission under UV excitation 78−6770
$Gd_2Ni_{12}As_7$, crystal. struct., X-ray diffr. obs. 79−1411
$GdNi_2Ge_2$, magnetism and hyperfine interactions 78−76228
GdO film, new reduced variant due to annealing 77−89660
GdO, high resolution visible emission spectrum 77−18932
Gd_2O, Gd_2O_2, GdO_2, atomisation energies and stand. ht. of formation 77−54622
Gd_2O_3, ^{161}Dy TDPAC, hard core correl. 78−10809
Gd_2O_3, 'monoxide' film reidentified as sesquioxide formed by oxidation by hydride 79−19474
Gd_2O_3 additive, neutron radiography contrast enhancement obs., ordnance appl. 80−30177
Gd_2O_3, B-type monoclinic, DC(AC) elec. cond., thermoelectric power, dielectric const., temp. depends. 80−59980
Gd_2O_3 bearing BWR fuel rods, spatial depletion meas. 79−67844
Gd_2O_3, C-phase, specific heat, 1.4 to 18K, antiferromag. ordering 79−38351
Gd_2O_3, chem. binding, 4d X-ray spectra obs. 79−69910
Gd_2O_3 coatings, neutron collimators, comparison with enriched ^{10}B coatings 78−82564
Gd_2O_3 densely sintered and granular ceramics prep. physicomechanical props. 77−32548
Gd_2O_3, elec. cond., thermoelec. power, dielectric const. 79−69763
c-Gd_2O_3, electrical cond., dielectric const. mag. susceptibility, polymorphic transition 77−59505
Gd_2O_3 film on CaF_2 substrate, computational algorithm for optical consts. determ. 78−72617
Gd_2O_3, isotopically enriched target preparation using electron gun 80−23226
Gd_2O_3, L_3 X-ray absorpt. discontinuity 77−85840
Gd_2O_3, microhardness anisotropy of single cryst. *(French)* 77−52489
B-Gd_2O_3, monoclinic single cryst., Raman spectrum 80−103953
Gd_2O_3 photoabsorpt. spectra, band struct., at ionisation mechanisms, electron energy loss spectra 77−24909
Gd_2O_3, polycryst. monoclinic, Gd self-diffusion 80−24655
Gd_2O_3, reaction with liq. Li and liq. Li-N 79−66276
Gd_2O_3:Eu^{3+}, luminesc., rel. to crystallographic data 79−33793
Gd_2O_3-Al_2O_3 glasses, crystallization 79−50998
Gd_2O_3-Fe_2O_3-PbO-B_2O_3, primary crystallisation regions 77−12604
Gd_2O_3-Ga_2O_3 system, phase diagram relationships of garnet-perovskite transform. 80−97460
Gd_2O_3-GeO_2 system cpds. physicochem. characteris. 80−97469
Gd_2O_3-UO_2, behaviour as control rod in commercial reactor 78−8918
Gd_xO_y film, struct., electron microscope and diffr. obs. 79−11028
$Gd(OH)_3$, dynamical effects of interaction between 4f electrons and optical phonons 80−108196
$Gd(OH)_3$, heat capacity from near 5 to 350K, lattice and Schottky contribs. 80−49374
$Gd(OH)_3$, mol., XPES, satellite phenomena 79−27035
$GdOHCO_3$, $Gd_2O_2CO_3$, synthesis of rare earth carbonates under hydrothermal conditions 78−72714
Gd_2O_2S, compact specimen prep. 77−85951
Gd_2O_2S scintillation convertor screen characterisation, portable neutron radiographic system 77−40510
Gd_2O_2S scintillator screen, neutron radiographic film imaging systems, MTFs and resolution capabilities 80−66758
Gd_2O_2S:Eu^{3+}, luminesc. props., charge transfer effects 78−15214
Gd_2O_2S:Eu^{3+}, luminesc., excitation spectra, cooperative phonon sidebands 79−33771
Gd_2O_2S:Tb, recomb. processes and emission spectra *(Russian)* 78−6797
Gd_2O_2S:Yb^{3+},Ho^{3+}, anti-Stokes emission band assignments, energy transfer mechanism 77−40277
$Gd_2O_2SO_4$, antiferromag., specific heat, 0.6 to 30K 79−33487
$Gd_2O_2SO_4$, antiferromag., mag. props. 1.6 to 40K 79−33464
GdP, electronic struct., mag. exchange and elec. transport props. 78−87974
GdP, vapour comp. and dissoc. pressure 77−84916
GdP-GdS systems, mag. exchange interactions, free carrier conc. 78−60278
$Gd(PO_3)_3$, mag. susceptibility, 2-27K, appl. as mag. thermometer 79−63224
$GdPO_4$, rotating Carnot-cycle magnetic refrigerators for use near 2K 78−57965
$GdPO_4$:Dy^{3+}, $Bi^{3+}(Sb^{3+})$, energy transfer from sensitiser to activator, intermediate role of Gd^{3+} 80−50389
$GdPO_4$:Eu^{3+}, vac. UV luminesc.-excitation spectra 77−85774

gadolinium compounds continued
Gd_3PO_7 and $(Gd,Nd)_3PO_7$, IR and Raman spectra, vibr. assignments, cryst. struct. characts. 80−97258
GdPS, PbFCl-type struct. deriv. 77−80489
$Gd_xPb_{1\pm x}Mo_{6+y}S_8$, sputtered supercond. props. 80−50019
$(GdPrBi)_3(FeGaIn)_5O_{12}$, pure and In^{3+} doped, near IR absorpt. and Faraday rot. 78−95580
$Gd(ReO_4)_3.4H_2O$, $(ReO_4)^-$ ion vibrs. rel. to static field, Raman investig. *(Russian)* 78−76470
$Gd(ReO_4)_3.4H_2O$, Raman spectra, $(ReO_4)^-$ ion normal vibrs. rel. to static field 79−65858
$GdRh_4B_4$, cryst. struct., X-ray diffr. 77−89423
$GdRh_4B_4$, ferromag. Curie temp. 77−89893
$GdRh_4B_4$, magnetic and electrostatic props., NMR study 80−93195
$GdRh_4B_4$, NMR and sp. ht. in supercond. and mag. ordered phases 80−7037
GdS, Debye-Waller factor, X-ray diffr. meas. 77−11659
GdS, electronic struct., mag. exchange and elec. transport props. 78−87974
GdS, FCC metallic phase, Raman scatt., phonon density of states 78−19480
GdS, L_3 X-ray absorpt. discontinuity 77−85840
GdS, low temp. phase transitions, mag. moment orientation, spin flip 79−99700
GdS, meas. of opto-magnetic interactions at low mag. fields 80−2735
GdS, metallic FCC antiferromag., phonon Raman scatt. 78−60458
GdS, vaporisation thermodynamics and dissoc. energy obs. 78−67822
Gd_2S_3, antiferromag. to ferromag. and semiconductor to metal transitions *(Russian)* 79−33485
Gd_2S_3, resonance excitation of Nd^{3+}, luminescence, absorption spectra *(Russian)* 80−50381
Gd_2S_3, semimetallic, elec. and thermal transport meas. 78−10442
Gd_2S_3 with excess Gd, magnetoresist. meas. 80−49777
α-Gd_2S_3:Nd^{3+}, spectroscopic props. from absorpt., photoluminesc. and excitation spectra 80−34968
Gd_2S_3-1.8 Ga_2S_3 glass, vibr. spectra, electronic transitions, short range order 77−69820
$Gd_{3-x}S_4$, ferromag., elec. props. near Curie temp. 80−107788
$Gd_{3-x}S_4$, mag. ordering and elec. cond. 78−10681
Gd_xS_y, nonuniform ferro-antiferromag. ordering, 1.6 to 300K range obs. *(Russian)* 77−69504
$Gd_2(SO_4)_3$, L_3 X-ray absorpt. discontinuity 77−85840
$Gd_2(SO_4)_3.8H_2O$, pressed powder and single crystal, low temp. thermal cond., mag. field depend. 79−23789
$Gd_2(SO_4)_3.8H_2O$, rotating Carnot-cycle magnetic refrigerators for use near 2K 78−57965
GdS(Se), antiferromag., EPR meas., Neel temp. determ. 77−32242
GdS(Se)(Te), metallic, phonon density of states, Raman scatt. expt. 78−23451
$Gd_3Sc_2Al_3O_{12}$:$Er3^+$, laser active media, nonradiative losses due to $^4I_{11/2}$-$^4I_{13/2}$ transition 79−31911
GdScFe garnets, mag. props. 77−47979
GdSe, low temp. phase transitions, mag. moment orientation, spin flip 79−99700
Gd_2Se_3, mag. susceptibility 77−40032
Gd_2Se_3/PbTe, N type selenide segmented element fabrication, thermoelectric props. 80−107835
Gd_2SiO_5, atomic positions, high resolution electron microscopy 80−100220
$Gd_xSm_{1-x}S$ K X-rays chem. shifts, electronic phase transition, semicond.-metal transition 77−28116
$Gd_ySn_xMo_6S_8$, supercond. props. 80−97023
$Gd_{0.85}Sr_{0.15}(Ca_{0.15})CrO_3$ self formed Gd coating, vaporisation protection 79−5069
$Gd_{1-x}Sr_xCoO_3$, electronic and mag. props., itinerant ferromagnetism obs. 78−10660
$Gd_{1-x}Sr_xVO_{3-0.1x}$, elec. cond. and mag. susceptibility, temp. depend. 77-300K 77−47816
$GdTaO_4$, heat of form. 79−83494
$(Gd_{1-x}Tb_x)_2O_2S$ phosphor, concentration quenching of Tb^{3+} luminesc. 80−29785
GdTe, low temp. phase transitions, mag. moment orientation, spin flip 79−99700
$GdTiO_3$, bulk mag. and struct. props., ferrimag. order 80−107993
$Gd_2Ti_2O_7$, ferroelec., layer type struct., cryst. growth 80−108348
$Gd_2Ti_2O_7$, ferroelec., temp. depend. of SHG intensity 79−24267
GdTmGa garnet bubble film, ion implanted, pot. wells under charged wells 80−34717
$GdV_{1-x}M_xO_3$ (where M=Cr or Fe), solid solns., elec. and mag. props 79−23967
$GdVO_3$, flux growth and chem. characts. 78−23595
$GdVO_4$, ^{155}Gd excited states, determ. of nuclear parameters using Mossbauer effect 79−28646
$GdVO_4$, antiferromag., US attenuation at 9 GHz 77−24728
$GdVO_4$, electron energy loss spectra, primary excitation processes in cathodoluminescence 79−11490
$GdVO_4$, hyperfine field and exchange interactions, Mossbauer meas. 79−47370
$GdVO_4$:Eu^{3+}, absorption and fluoresc. spectra, SU(2) chain *(French)* 78−28912
$GdVO_4$:Eu^{3+}, ligand field parameters, computed from fluoresc. and absorption data 78−2453
$GdVO_4$:Ho^{3+}, optically excited doublet splitting in magnetically ordered state 78−19238
$GdVO_4$:R^{3+}, R=Nd, No, Tm, Sm, Dy, Er, Eu, Tb, electronic struct. and spectra of VO_4, RO_8 clusters 78−10953
$GdVo_3$, phase transitions and Jahn-Teller distortions 79−28548
$Gd_2(WO_4)_3$, mag. susceptibility, paramag. Curie temp., 300-900K 79−82753
$Gd_2(WO_4)_3$, molar mag. susceptibility, DC elec. cond., thermopower meas. 79−15172
Gd_2WO_6, growth from soln. in melt 77−1806
Gd_6WO_{12}, thermodynamic and X-ray investig. at 1200-1400K 77−36778
$Gd_{1.8}Y_{1.2}Fe_5O_{12}$, nucl. gamma reson., anomalous behaviour of intensity 77−12289
$Gd_xY_{1-x}Rh_4B_4$, mag. and supercond. transitions 78−68127
$Gd_{0.9}YTm_{1.1}1Ga_{0.44}Fe_{4.56}O_{12}$, ion implanted, ferromag. reson. meas. 78−68385
$Gd_xZr_{1-x}O_{2-x/2}$, elec. cond. of ceramic solid solutions 80−107554
$Gd_xZr_{1-x}O_{2-x/2}$, fluorite and pyrochlore solid solutions, electrical conductivity meas. 80−65287

gadolinium compounds continued
- $Gd_xZr_{1-x}O_{2-x/2}{:}Tb^{3+}(Eu^{3+})$, energy transfer, luminesc. 79−51999
- Gd_2ZrS_5, mag. and sp. ht. meas. on polycrystalline samples 78−23253
- $Gd_{3-x}\square_xS_4$, transport and mag. props., mag. Wigner localisation 80−97069
- $GeFeO_3$, field induced spin reorientation temp. depend. 77−63200
- HfO_2-Gd_2O_3, phase relations 78−72769
- $KGd(WO_4)_2{:}Ho^{3+}$, stimulated emission at low temps. 80−106526
- $KTaO_3{:}Gd_2O_3$, semiconducting, elec. props. 79−78097
- $(La,Gd)B_6$, mag. susceptibility, zero field, 0.04 to 10K 78−10696
- $(La_{1-x}Gd_x)_{1.0}Mo_6Se_8$, Gd-rich, supercond. state, phase transition, lambda-type sp. ht. anomaly obs. 78−6480
- $La_{1-x}Gd_xMo_6Se_8$, supercond. transition temp., upper critical field, local spin fluctuations 79−38250
- $La_{1-x-y}Pr_xGd_yCl_3$, satellite lines in optical absorpt. spectra, Zeeman effect 79−65912
- $LiGd(MoO_4)_2$, defect struct. and phase transitions 79−28697
- $Li_2Gd_4(MoO_4)_7$, Czochralski growth, struct. and optical props. 78−27397
- $MnGd_2S_4$, mag., struct. and Mossbauer effect study 78−51507
- $Na_5GdSi_4O_{12}$, ionic conductivity and struct. 78−18826
- Nd-Gd-Te alloys of R_2Te_3-T_3Te_4 region, physicochem. props. 78−52017
- $NdGa_3(BO_3)_4$ crystal structure by X-ray spectral microanalysis 79−46621
- PdGdH, diagram of state elec. props., indirect exchange interaction, EPR study *(Russian)* 80−50179
- $RbCaF_3{:}Gd_2O_3$, Gd^{3+}-O^{2-} pair, EPR study of displacive transform. *(French)* 78−27088
- $Sc_{0.995}Gd_{0.005}H_{1.9}$, low temp. anomaly, Gd^{3+} EPR linewidth and X-ray meas. 77−69687
- Si_3N_4-SiC-Gd_2O_3, reactively sintered, microstruct. and strength 80−25631
- $Sm_{0.8}Gd_{0.2}S$, low temp. phase transition, X-ray diffr. expts., 110-293K 77−59115
- $Sm_{0.8}Gd_{0.2}S$, single cryst., fracture stresses meas. 77−31718
- $Sm_{0.8}Gd_{0.2}S$, valence transition, positron annihilation study 80−15454
- $Sm_{0.85}Gd_{0.15}S$, metal-semicond. transition, X-ray diffr. obs. 90-473K 79−95333
- $Sm_{1-x}Gd_xS$ ($x=0.15$ to 0.18), magnetic susceptibility meas., phase transition 77−63071
- $Sm_{1-x}Gd_xS$, calorimetric exam. of metal-semiconductor transition 78−18967
- $Sm_{1-x}Gd_xS$, electron mechanism of high temp. phase transform., X-ray K-line shift obs. *(Russian)* 77−89704
- $Sm_{1-x}Gd_xS$, metal-insulator transition, induced by temp. and press. *(Japanese)* 79−51488
- $Sm_{1-x}Gd_xS$, metal-semicond. isomorphous transition curve, low temp. crit. point, lattice parameter changes 79−95334
- $Sm_{1-x}Gd_xS$, phase transition temp. depression by mag. field, hybridisation 77−62828
- $Sm_{1-x}Gd_xS$, press. induced electronic transitions 78−68058
- $Sm_{1-x}Gd_xS$, resistivity investig. of metal-semicond. transition, press. effects 77−62829
- $Sm_{1-x}Gd_xS$ system, equilib. of isomorphous phases and crit. point 78−34772
- $Sm_{1-x}Gd_xS$ system, semicond. to metallic isomorphous phase transition mechanism 80−2338
- $Sm_{1-x}Gd_xS$, XPS, electronic struct. excitonic effects, insulator to metal transition 78−43988
- $(Sm_{1-x}Gd_x)_3S_4$, mixed valence compound, elec. cond. transition 80−70777
- SmS-CdS system, T-p-X diagram, semicond.-metal transition 79−69421
- SmS-GdS system, crit. effects and phase equilibria 79−7692
- $SrCl_2$-$GdCl_3$, prep. and purification 78−88420
- $SrF_2{:}GdF_3$, absorpt. spectra of γ-irrad. cryst., 77K, 200-700 nm 78−84615
- $SrGdFeO_4$, Neel temp. and spin reorientation, Mossbauer study 80−39934
- $SrO.Gd_{1-x}Sr_xVO_{3-0.1x}$, solid solns., elec. and mag. props. 77−89819
- $Tb_{0.7}Er_{1.3}Gd_{1.0}Al_{0.2}Fe_{4.8}O_{12}$, garnet plate, domain struct. 80−2602
- $Tb_cGd_{1-c}VO_4$, cooperative Jahn-Teller effect, linear birefringence 77−76550
- $Tb_xLa(Y,Gd)_{1-x}.DAM.Sal_3$, DAM=diantipyrylmethane, luminesc. *(Russian)* 77−55830
- $(U,Gd)O_2$ sintered pellets, homogeneity determ. by ceramographical method *(German)* 79−49804
- UO_2-Gd_2O_3, determ. of H_2O, Hz content by hot extraction methods *(German)* 79−49808
- UO_2-Gd_2O_3, interfacial energy meas. 77−59763
- $(Y,Gd,Tm)(Fe,Ga)_5O_{12}$, cylindrical mag. domain behaviour in external mag. field *(Russian)* 78−6553
- $(Y,Gd,Yb,Bi)_3(Fe,Al,Ga)_5O_{12}$ films, magnetic bubble domains, domain wall motion examined 78−19294
- $(Y,Gd,Yb,Bi)_3(Fe,Al)_5O_{12}$ film, nonreciprocal effects in domain boundary motion in inhomogeneous field 77−24726
- $(Y, Gd, Yb, Bi)_3(Fe, Al)_5O_{12}$ epitaxial film, domain wall motion and oscill. 80−2616
- $(Y,Gd,Yb,Bi)_3(Ga,Al,Fe)_5O_{12}$, bubble conversion to anomalous behaviour 78−23309
- $(Y,Gd,Yb)_{3-x}Bi_x(Fe,Al)_5O_{12}$, garnet single cryst. film, possible bubble appl. 78−6552
- $(Y,Gd,Yb)_{3-x}Bi_x(Fe,Al)_5O_{12}$, LPE, for magneto-optical appls. 78−48341
- $(Y,Gd,Yb)_3(Fe,Ga)_5O_{12}$ film, magnetisation processes and domain struct. near compensation temp. 78−14996
- $(Y,Gd)BO_3{:}Eu^{3+}$, phosphor, vac. UV excitation spectra, appl. to gas discharge display 80−2816
- $(Y,Gd)_3(Fe,Ga)_5O_{12}$, thin film lightguide, noninteracting mode conversion *(Russian)* 78−1347
- $(Y,Gd,Yb)_{3-x}Bi_x(Fe,Al)_5O_{12}$ film growth on $Gd_3Ga_5O_{12}$ substrates 79−78623
- $Y_{1-4}BiFe_{3.8}Ga_{1.2}O_{12}$ garnet films, bistable bubble domain 79−15331
- $Y_3Fe_5O_{12}$ LPE growth on $Gd_3Ga_5O_{12}$ substrates, substrate orientation effect 80−66438
- $(Y_{0.8}Gd_{0.2})AlO_3{:}Er^{3+}$, spectroscopic props. 77−85791
- $Y_{1-x}Gd_xAl(Sc)O_3{:}Ho^{3+}$, stimulated emission of Ho^{3+} ions 77−81126
- $(YGdBi)_3(FeAl)_5O_{12}$ films, Faraday effect in transverse mag. field, orientation depend. 80−88971
- $Y_{1.4}Gd_{0.6}BiFe_{3.8}Ga_{1.2}O_{12}$ film, bistable bubble domains, static, dynamic and optical props. 79−28574
- $Y_{3-3x-2z}Gd_{3x}Ca_{2z}Fe_{5-z-u}V_zSi_uCo_uO_{12}$, mag. props., effect of V substitution 77−20582
- $Y_{1-x-y}Gd_xEr_yAlO_3$, $Y_{1-x-y}Gd_xEr_yScO_3$, stimulated emission of Er^{3+} ions 78−6705
- $Y_{2.3}Gd_{0.6}Fe_{4.7}Al_{0.4}O_{12}$ garnet, effect of Gd on magnetite exsolution in a garnet matrix 79−11624
- $Y_{3-x}Gd_xFe_{5-y}Al_yO_{12}$, solid solns., IR absorpt. spectra, physical props. 80−55082
- $Y_{2.01}Gd_{0.99}Fe_{4.925-x}Mn_xO_{12}$, comp. depend. of mag. props., and stress sensitivity control 78−27057
- $Y_{3-x}Gd_xFe_5O_{12}$, effect of electron bombardment on mag. and elec. props. 79−42103
- $Y_{3-x}Gd_xFe_5O_{12}$, FMR, influence of Gd^{3+} substitution on linewidth 77−8416
- $Y_{3-x}Gd_xFe_5O_{12}$, field depend. of susceptibility *(Russian)* 78−68176
- $Y_{3-x}Gd_xFe_5O_{12}$, mag. phase diagrams, mag. transitions, exchange interaction *(Russian)* 80−54896
- $Y_{3-x}Gd_xFe_5O_{12}$, solid solns., IR absorpt. spectra, physical props. 80−55082
- $(YGd)(GaFe)_5O_{12}$ epitaxial film, nonlinear magnetoelastic effects *(French)* 80−34745
- $Y_{2.55}Gd_{0.45}GaFe_4O_{12}$, garnet thin films, magnetisation orientation, temp. depend. 80−71125
- YGdIG, with various domain wall orientations, natural spin reson. 80−66040
- $Y_{1-x-c}Gd_xNd_cScO_3$, crystal, absorption, luminescence, stimulated emission spectra 78−15220
- $Y_{1-x}Gd_xRh_4B_4$, mag. supercond., anomalous temp. depend. of upper crit. fields 80−29510
- $Y_{1-x}Gd_xRh_4B_4$, supercond., phase diagrams and upper crit. fields 80−2531
- $YGdTmFe_{4.3}Ga_{0.7}O_{12}$ epitaxial films, bubble-domain lattices with specified parameters 80−60386
- $(YGdTm)_3(FeGa)_5O_{12}$ epitaxial film, formation of lattice of cylindrical mag. domains from stripe domains *(Russian)* 80−80579
- $(YGdYbBi)_3$ $(FeAl)_5O_{12}$ epitaxial film, diffuse domain wall, bubble domain expansion 80−25170
- $Y_{0.9}Gd_{1.1}Yb_{0.7}Bi_{0.3}Al_{0.9}Ga_{0.2}Fe_{3.9}O_{12}$ films, cylindrical mag. domain form. *(Russian)* 77−40098
- $(YGdYbBi)_3(FeAlGa)_5O_{12}$ film, motion of mag. bubble domains in inhomogeneous pulsed mag. field 78−27064
- $(YGdYbBi)_3(FeAl)_5O_{12}$, epitaxial garnet film, with mag. compensation point, behaviour of 'compromise' phase boundary 78−60321
- $(YGdYbBi)_3(FeAl)_5O_{12}$, garnet, epitaxial film, interior domains 79−91268
- $(YGdYbBi)_3(FeAl)_5O_{12}$, epitaxial film, 360° domain walls with periodically distrib. Bloch lines 80−7127
- $(YGdYbBi)_3(FeAl)_5O_{12}$ ferrite-garnet films, effect of in-plane field on dynamics of domain walls 80−65979
- $(YGdYbBi)_3(FeAl)_5O_{12}$ epitaxial garnet film, uniaxial ferromagnet domain struct., phase transition *(Russian)* 80−108044
- $(YGdYbBi)_3.(FeAl)_5O_{12}$ films, substrate orientation influence on max. vel. of domain boundaries 79−15330
- $Y_{1.3}GdYb_{0.7}GaO_{12}$, epitaxial film, ferromagnetic reson. exam. 77−85579
- Y_2O_3-Gd_2O_3-Nd_2O_3 solution phase diagrams and thermal conductivity *(Russian)* 78−88448
- ZrO_2-Gd_2O_3, solid solution with fluorite and pyrochlore structure; exam. of elec. conductivity *(German)* 79−23766
- ZrO_2-$GdO_{1.5}$ (80 mol.%), X-ray diffr. exam. of continuous transition 78−68684
- ZrO_2-Y_2O_3-Gd_2O_3, spectral determ. of crystal stabilisation 78−27203

gain (amplification) *see amplification*

gain control
- *see also automatic gain control*
- channel plate electron multiplier, gain, detection dynamics *(French)* 78−46229
- photomultiplier gain stabilisation with high counting rate, feedback resistor series effect appl. 80−106232
- single-fibre EMG oscilloscope trace selective gain control 77−44864

gain measurement
- automated gain measurement system for high-energy chemical lasers 79−36914
- bipolar junction transistor, common-emitter current gain β, measurement of low values 79−63268
- communications satellite system measurements 78−61712
- dye laser, flashlamp-pumped, relative-gain curve determ. 78−25878
- intracavity dye laser spectroscopy, gain probing technique 77−7092
- laser gain measurements using amplified spontaneous emission 80−37986
- mass spectroscopy, electron multiplier gains determ. for various ions by pulse counting method 80−57418
- solid state laser, refraction effects and gain meas. 79−31905
- underwater transducers, gain characts. meas. by FM signal modulated by smoothed random telegraph signal 78−18130
- CO_2 amplifier, pulsed, large-vol., small-signal gain meas. 80−91772
- Nd:glass lasers, gain coeffs. meas. and modelling 77−88726

gain regulation *see gain control*

galactic cosmic rays
- 11 year cosmic-ray cycle, galactic and sdlar protons anal. 77−53360
- 11-year cycle, modulation coeff. energy depend. 78−28460
- 11-year solar modulation cycle obs., review 77−13196
- 27 day modulation by solar wind *(Russian)* 78−16257
- 27-day cycle, amplitude, quasistationary treatment 77−53369
- 27-day cycle and anisotropy rel. to solar activity epoch 77−53370
- γ-ray emission from inverse Compton scatt. 77−73911
- acceleration, by galactic mass infall 77−78583
- acceleration, by interstellar shock waves 78−49241
- acceleration by EM radiation 78−7840
- acceleration by supernova shock waves 80−82154
- acceleration by supernova shocks in interstellar medium 80−31179
- acceleration in shock fronts 78−32302
- acceleration in shock waves, energy loss effect *(Russian)* 80−17449
- acceleration mechanism and transport, model 79−35077
- acceleration mechanisms, cosmic-ray source composition probe 80−31178
- acceleration models, inconsistencies 80−82155
- age, derivation from ^{10}Be abundance 78−12060
- age distribs. in galactic convective halo 80−51625
- age distribution of interacting, decaying and secondary particles 77−5401
- angular distribution at heliosphere boundary, results from muon intensity vars. 79−80116
- anisotropic diffusion in interplanetary space, 11-year var. 77−25891

galactic cosmic rays continued
- anisotropic diffusion in interplanetary space, radial and transverse gradients 77–49248
- anisotropic diffusion in interplanetary space, rel. to annual vars. 77–60550
- anisotropy, 10^{11} to 10^{20} eV 79–66892
- anisotropy, implications for cosmic ray origin and local anisotropy 79–44313
- anisotropy at extremely high energies, from EAS data, rel. to origin 79–80115
- anisotropy in directional distribution of 6×10^{13} eV radiation *(Hungarian)* 77–53343
- anisotropy measurement by spinning charged particle detectors, COS approx., computer simulation 77–5457
- anisotropy of 1-100 TeV particles, pitch angle scatt. 80–17451
- annual and semiannual variations, phase reversals. rel. to Sun polar mag. fields reversals 78–40780
- anomalous intensity during 20th solar cycle rel. to solar total mag. field 79–80132
- antimatter model for galactic nuclei and quasars *(Chinese)* 78–73771
- antiparticles in primary cosmic radiation and collisions in interstellar medium 80–77241
- antiprotons and antihelium, relative abundance in primary cosmic radiation 78–73594
- antiprotons balloon-borne superconducting-mag. spectrometer obs. 80–17457
- arrival directions, galactic halo magnetic field effects *(Russian)* 80–67872
- Biostack experiments, radiobiology of cosmic galactic radiation heavy nuclei 78–20236
- charge state of anomalous He component, expt. test 78–7847
- charged particles acceleration on shock front, temporal characts. 79–80121
- composition determ. from tracks in lunar and meteoritic feldspars 78–20603
- conference, non-solar gamma-rays (Bangalore, India, May-June 1979) 80–77548
- confinement, rel. to interstellar gas hydrostatic equilib. and galactic radio emission 77–29919
- confinement in dynamical halo, age, matter traversal distrib. and anisotropy for nuclei 78–4043
- confinement in dynamical halo, electrons energy spectrum and spatial distrib. 78–4044
- correlation with interplanetary cosmic ray protons 80–77243
- cosmic ray halo, size constraints from galactic gamma-ray data 78–12353
- cosmic rays propagation and distribution in Galaxy 78–69621
- density and current inside interplanetary mag. sector 79–80120
- differential spectra, model description, solar modulation theory 79–80130
- diffusion, mean and local coeffs., connection 79–21110
- diffusion and turbulent galactic mag. field 79–48627
- diffusion equation solution, isotropic diffusion for random energy depend. 77–9632
- diffusion in large-scale turbulent magnetic field 79–58203
- diffusion in low-latitude solar wind 77–53344
- diffusion model for galactic cosmic ray propag. 80–56684
- discrete gamma-ray sources rel. to galactic cosmic ray distrib. *(Russian)* 78–65719
- discrete sources, statistical theory of propag. 79–44312
- distribution in galaxy, results from gamma ray obs. 77–26083
- distribution of cosmic rays and mag. field, from synchrotron radio and gamma-ray obs. 80–4207
- dynamical halo model and cosmic ray path length var. with energy 79–53675
- dynamics and γ-ray production rel. to galactic matter distrib. 78–4349
- Earth atmosphere, effects of energetic particle precip. on middle atmosphere chemical comp. 80–109213
- electron component, diffusion model of cosmic ray propag. 79–53679
- electron spectrum below 1000 MeV 79–5718
- electrons, contrib. to diffuse X-ray flux in 2 to 7 keV range 80–98745
- electrons, diffusion models for galactic halo low-freq. radio emission 78–12433
- electrons, discrete galactic sources 79–35078
- electrons, distrib. rel. to spiral struct. and continuum radiation 77–13465
- electrons, energy spectrum and fundamental props. *(Chinese)* 80–105138
- electrons, energy spectrum meas. by transition-radiation detector and shower detector combination 77–57844
- electrons, evidence for large-scale gradients in Galaxy 77–33299
- electrons, in galactic radio halo 77–9631
- electrons, propag. rel. to galactic radio background distrib. 77–5602
- electrons, radio emission and cosmic ray confinement 77–73910
- electrons, source spectrum rel. to diffusion model of propag. 79–53677
- electrons, spatial distrib. perpendicular to galactic plane 77–53338
- electrons, spectrum determ. from radio emission rel. to Galaxy gamma-rays prod. 80–62257
- electrons and positrons, fluxes in closed galaxy model 77–13189
- energy dependent diffusion in dynamic halo model 80–82156
- energy loss and modulation in solar system 78–32308
- energy loss and modulation in solar system 78–49245
- energy loss in expanding areas of Galaxy *(Russian)* 78–93055
- energy spectra, obs. between 1-9 AU 78–4046
- energy spectra, of nuclei with $4\leq Z\leq 26$ and $0.3\leq E\leq 2$ GeV amu^{-1} 77–56800
- energy spectra from pulsars 80–31319
- energy spectrum, determ. from stratospheric cosmic rays eleven-year cycle 80–4212
- energy spectrum and arrival direction of >10 EeV cosmic rays 80–67480
- energy variation in interplanetary space 80–101505
- equatorial modulation and north-south asymm. due to interplanetary mag. field 78–16253
- equilibrium configurations stability, hydromagnetic energy principle 80–82448
- flux rel. to solar wind vel. and interplanetary magnetic field, Mars 2-7 meas. 78–16252
- Forbush decreases, struct. 77–91385
- Forbush decreases and interplanetary mag. field disturbances 77–60551

galactic cosmic rays continued
- Forbush decreases in August 1972, summary of solar/interplanetary events 77–25991
- Forbush effect, galactic cosmic ray currents obs., interplanetary mag. field inhomogeneity 79–80124
- galactic γ-ray lines, balloon investigation using Ge(Li) spectrometer 80–8677
- galactic γ-rays from low energy cosmic ray interactions with interstellar medium 80–8678
- galactic centre, cosmic ray flux, predicted from high energy γ ray observations 80–72731
- galactic centre, gas, dust, high energy particles and star form. 80–36713
- gamma radiation, possible origin, data from COS-B and SAS-2 satellites *(French)* 78–85776
- gamma radiation in 0.03-4.1 MeV range Kosmos 461 meas. 77–67144
- gamma ray bursts, sise spectrum, idealised galactic distrib. of sources 78–65716
- gamma ray observations interpretation *(Polish)* 79–58451
- gamma rays, discrete source component 79–35436
- gamma rays, medium energy, from galactic centre region, obs. 79–9030
- gamma rays, origin 77–87213
- gamma rays, prod. by relativistic electrons inverse Compton interactions 80–17448
- gamma rays from annihilation of positrons produced by pulsars, 511 keV line 80–46590
- gamma rays from galactic disc, obs. between $-45° < l^{II} < 45°$ in 80 keV to 8 MeV energy range 80–82540
- gamma-ray 511 keV positron annihilation line, galactic component in atmospheric meas. 80–41582
- gamma-ray astronomy and cosmic ray origin 79–29951
- gamma-ray background and protogalaxy formation model 80–62325
- gamma-ray bursts, galactic origin 78–32303
- gamma-ray bursts, intensity distrib., galactic origin *(Russian)* 79–16772
- gamma-ray bursts and cosmic fireballs 78–54087
- gamma-ray burts, distance limit for non-relativistic source models 78–32612
- gamma-ray diffuse background from inverse Compton scatt. in halo 77–53711
- gamma-ray diffuse component from galactic centre and anticentre 79–62901
- gamma-ray flux, 60 keV to 5 MeV range, from ensemble of point sources 79–53933
- gamma-ray flux from galactic plane, cosmic ray diffusion influence 77–64854
- gamma-rays, 0.511 MeV energy, meas. with balloon-borne Ge(Li) spectrometer 77–53373
- gamma-rays, diffuse component origin in elementary interactions 80–17450
- gamma-rays, galactic disc bremsstrahlung emissivity and local interstellar electron spectrum 79–25417
- gamma-rays, galactic struct. determ. 78–16538
- gamma-rays, non-thermal electron bremsstrahlung prod. in galactic disc. 78–24414
- gamma-rays, spectra rel. to cosmic ray electrons flux and cosmic ray gradients 78–40784
- gamma-rays, ultrahigh energy, detect. by obs. of Cherenkov flashes of EAS 79–80368
- gamma-rays and origin 77–78584
- gamma-rays from disk and inverse Compton effect of electrons on starlight 80–26702
- gamma-rays from galactic plane 79–71105
- gradient in 1971-4 period derived from Gorlovka meteorite 78–61695
- halo, relativistic electrons spectrum from radio obs. 78–96544
- halo around Galaxy obs. and anal. 77–53687
- hard gamma-rays from galactic centre and diffuse background, Kosmos 561 obs. 79–84597
- hard X-ray background, pregalactic black hole origin 80–56978
- Helios 1 measurements, 1974 Dec.-1975 Sept., quiet time spectra, radial gradients 78–20592
- highest energy nuclei and EAS records 78–57413
- injection into dense supernova shells by pulsars 78–65638
- intensity and modulation out to 18 AU, Pioneer 10 and 11 obs. 80–90297
- intensity modulation in interplanetary space taking into account royal zones in solar activity distrib. 79–80138
- intensity pulses, north-south anisotropy of Earth based obs. 80–56687
- intercloud cosmic ray ionisation rate 78–85989
- interplaetary propagation, drift as essential energy loss process 80–8498
- interplanetary anisotropies, quiet time obs. from Pioneer 10 and 11 78–77442
- interplanetary density distrib. 77–17305
- interplanetary diffusion and solar cycle var., effect of directional medium-scale interplanetary vars. 77–29605
- interplanetary diffusion in presence of Alfven waves, Fokker-Planck theory 77–29606
- interplanetary flux, Mars spacecraft meas. (1971-74) 78–96365
- interplanetary gradient meas. 78–49243
- interplanetary modulation allowing for generalised anisotropic diffusion tensor 80–101504
- interplanetary propagation, cosmic ray flow lines and energy changes 80–82158
- interplanetary propagation, modulation, analytic solns. 78–7844
- interplanetary transport, particle drift effects and analytical soln. to modulation problem 78–28456
- interstellar arks, cosmic-ray shielding 77–49264
- interstellar electron spectrum in local interstellar medium, determ. from bremsstrahlung gamma radiation 79–25417
- interstellar grains, destruction by sputtering 78–45382
- interstellar local electron spectrum determ. from galactic radio background 78–93056
- interstellar matter interaction, exclusion from dense mol. clouds 77–13190
- interstellar medium, cosmic ray ionisation coupling to acoustic instability 79–97044
- interstellar medium interaction, gamma-ray flux from Cygnus X region rel. to CG 78+1 nature 79–92895
- interstellar molecular clouds, cosmic ray penetration 79–8979
- interstellar molecular clouds rel. to cosmic rays and spiral struct. in Galaxy 77–87544

galactic cosmic rays continued
- interstellar propagation, compound diffusion in inhomogeneous mag. field 77−67127
- ionization of ionospheres of Saturn, Uranus and Neptune 78−4142
- isotopes composition rel. to origin and containment time 78−53781
- isotopic composition, meas. with isotope spectrometer on International Sun-Earth Explorer C spacecraft 78−85797
- isotopic composition of Fe-group elements, balloon meas. 78−89024
- K-captured isotopes content calc. in galactic cosmic rays 79−80114
- latitude variations determ. from chondrite cosmogenic isotope radioactivity 80−101507
- light isotopes abundances in galactic cosmic rays, rel. to interstellar gas density 80−17456
- long term composition changes from lunar fossil tracks 77−60552
- low energy cosmic rays diffusion, existence of strong spatial inhomogeneities 77−5402
- low-energy interplanetary background, evidence for galactic origin from Venera 9 and 10 meas. 78−4049
- low-rigidity cosmic rays, weak turbulence diffusion theory rel. to mean free paths 80−98524
- lunar ancient regolith, record of solar and galactic radiations 77−60695
- Mariner-Jupiter-Saturn low energy charged particle expt. 77−70971
- metagalactic nuclei, ultrahigh-energy, spectrum calc. 77−53342
- MeV protons, effects on IR spectra of interstellar Mg silicates 77−45534
- modulation, 27 day period 77−17307
- modulation by solar total mag. field 79−80131
- modulation depth in interplanetary space, pitch-angle depend. 79−80139
- modulation rel. to solar wind high speed streams 80−41673
- Monte Carlo propagation model 78−20591
- Musala station, obs. of anisotropy 78−49253
- neutrinos, emission by binary pulsars 79−2550
- north-south gradient rel. to solar polar coronal holes 78−89019
- nuclear component, diffusion model of cosmic ray propag. 79−53678
- nuclei abundance, time averaged for $Z\geq 50$, tracks in meteorite minerals 80−101513
- nuclei from 3000 MeV to 50 GeV per nucleon, charge comp. and energy spectra 78−93059
- origin, appl. of galactic models with halo to proton nucleon component 80−61971
- origin, flare stars as source, hypothesis 80−46559
- origin, homogeneous galactic model and halo model 79−44314
- origin, source model rel. to electron-proton abundance ratio 77−49252
- origin and accel. at interstellar medium interaction with stellar wind 80−77512
- Parker instability with curved magnetic field lines 79−5889
- particle radiation satellite obs. *(Danish)* 78−69631
- path-length distribution, concept extension to nonrelativistic energies 79−88558
- positrons, annihilation and gamma radiation spectrum 79−44309
- positrons, primary source, prod. rate, and escape probability 80−109319
- primary cosmic ray N and O, isotopic comp. with consequences for source models 79−84609
- primary cosmic-ray electrons, 30-1000 GeV, emulsion chamber obs. 80−85827
- propagation, in spherically symmetric solar wind 79−53681
- propagation, leaky-box model 78−57409
- propagation, two-zone model, radioactive cosmic ray isotope appl. 79−66891
- propagation in dynamical halo, retrodictive probability approach 78−65467
- propagation in finite solar cavity, theoretical model 78−69623
- propagation in Galaxy, convective model 77−25890
- propagation in Sun's heliosphere, longit. intensity modulation, models 80−90298
- proton/electron ratio 78−69633
- protons, as extraterrestrial source of atmospheric water vapour 78−69416
- protons, spectrum vars. meas. by Venera 9 and Venera 10 probes 77−91388
- radial gradient effect on solar wind vel. 80−101506
- radiation doses meas. by Molniya 1 satellite 79−8774
- radio background, linear polarisation between 408 and 1411 MHz, reductions 77−2500
- relativistic particles, anisotropies assoc. with solar rotation 80−67481
- review, cosmic gamma radiation, sources and detection 78−12059
- screening effect on interstellar cloud stability 79−67077
- secondary electrons, in dense interstellar clouds 77−33593
- secondary electrons and positrons rel. to nonthermal galactic radio background 78−49527
- secondary $\bar{p}$, confinement models 78−12061
- semiannual variation, solar mag. cycle depend., origin 79−16777
- short pathlengths, evidence for deficiency and no-near-sources model 79−84596
- short-term intensity variations, 1964-67 period 77−64550
- sidereal variation of 10^{11} eV particles and interplanetary mag. fields 80−17452
- soft X-rays, astrophysics rel. to 0.1-2.0 keV X-rays diffuse background 78−16581
- solar activity effect on cosmic rays 77−53340
- solar equator vicinity, daily cosmic ray flows during solar cycle 78−69622
- solar modulation, isotropic and anisotropic diffusion, asymm. conditions 78−40777
- solar modulation, latit. depend. 77−2314
- solar modulation, nucleonic flux and solar indices correl. 77−22026
- solar modulation, numerical models of particle drift effect on cosmic ray transport 80−31180
- solar modulation, particle drift effects 77−37488
- solar modulation absence during glacial period 79−80129
- solar system access at polar heliographic latits. 77−25893
- source isotopic abundances, secondary tracer approach 79−96864
- sources, coronal-type ionisation model and flare star contributions 78−49240
- St. Severin meteorite, flux of low energy particles in solar system 77−82096
- stellar daily variation, semiannual modulation 78−69626
- streaming cosmic rays, generation of anisotropic MHD interstellar turbulence 77−45532
- streaming or mirror instability effects on pulsar scintillations 80−51845
- subcosmic rays rel. to active solar processes 78−61693

galactic cosmic rays continued
- super-high energy cosmic rays, anisotropy in galactic disc direction *(Russian)* 78−57410
- supernova γ- and X-rays, recorded by Antarctic ice NO_3^- content 80−31314
- supernova remnants, cosmic rays escape and adiabatic energy losses 79−16771
- tracks in olivine from Marjalahti meteorite, abundance of VVH nuclei 78−36414
- transient cosmic ray intensity vars., solar flare origin 78−89021
- transient cosmic ray intensity vars., solar source 78−89022
- transient variation origin, rel. to flares with type IV radioemission 79−40043
- transport coeffs. in supernova remnants 79−101033
- ultra high energy cosmic rays, discussion *(French)* 80−21879
- ultraheavy $(Z>52)$ nuclei abundances, long-term averages from pallasites 77−9641
- ultrahigh energy cosmic ray origin and propagation 78−49242
- ultrahigh-energy cosmic rays, possible source in galactic centre 80−46351
- variation with solar cycle and coronal mag. field 78−7974
- vector and tensor anisotropy rel. to Musala expt. 77−17302
- velocity diffusion, turbulent mag. field, Monte Carlo calc. 78−53777
- Voyager cosmic ray detector system, energetic particle studies in outer heliosphere 78−24434
- Voyager low energy charged particle experiment 78−20618
- μ, long-period variation in galactic cosmic-ray distrib. 77−53382
- p, inside magnetosphere, local energy spectra calc. *(Russian)* 78−16258
- $\bar{p}$ flux, upper limit for secondary production 78−12062
- ^{7}Be, cosmic ray accel. probe 78−81512
- ^{10}Be abundance rel. to age, balloon meas. technique 77−29602
- ^{40}Ca source abundance meas. 80−8502
- Fe nuclei in galactic cosmic rays, isotopic comp. 80−72729
- H and He fluxes, modulation in 1974-1975 near solar minimum 77−33304
- Ne, Mg and Si isotope abundances, high resolution meas. 80−51631
- ^{22}Ne/^{20}Ne ratio, meas. 79−101036

galactic radio waves *see radiofrequency cosmic radiation*

galaxies
- *see also BL Lacertae-type objects; clusters of galaxies; H I regions; H II regions; intergalactic matter; nebulae; The Galaxy*
- 1mm continuum emission galaxies, obs. 78−36720
- 145-IG-03, interacting galaxies, apparent luminous bridge 77−17681
- 0816+526, cD galaxy, classical double radiosource, 4885 MHz obs. 80−109545
- 0915+320, wide-angle-tail radio source in group of galaxies, 4.9 GHz map 78−93441
- 0934.5+01, compact galaxy, optical variability 77−26051
- 0957+561A, B, double quasar, intervening galaxy IR obs. and holometric luminosity 80−73065
- 1008−3814, southern ring galaxy in Vela, struct. and spectrum 79−58413
- 1401−33, radio structure and spectrum 77−29942
- A0035, large southern ring galaxy, obs. 77−45559
- A non 0945−30, X-ray detect. and intermediate luminosity X-ray galaxies contrib. to background 79−2578
- Abell 193 cluster, BV photometry of galaxies *(Russian)* 77−22319
- Abell 2256, X-ray cluster of galaxies, head-tail radio galaxies obs. 80−36726
- Abell and Shane-Wirtanen catalogues, cross-correl. anal. 78−4118
- abnormal galaxies dynamics, discrete states of redshift 77−22307
- absolute luminosities of galaxies containing giant H II regions 79−8973
- absolute mag.-redshift var. in magnitude-limited samples 79−101189
- absorption features radial gradients rel. to metallicity 79−40254
- accretion disk models 80−36659
- accretion disks in quasars and active galactic nuclei, theoretical review *(Polish)* 80−26739
- accretion on massive black holes in galactic nuclei 79−80335
- accretion wake model of galactic and quasar jets in clusters 79−71135
- accretion wake model of radio jets *(Japanese)* 79−84857
- active centre, relativistic astrophys. *(Russian)* 77−13233
- active galactic nuclei, conference, Cambridge, (England 1977) 79−75281
- active galactic nuclei, emission line spectra rel. to ionised gas and dust 79−88730
- active galactic nuclei, extreme nonthermal radiation 80−90531
- active galactic nuclei, H emission-line spectra 78−96557
- active galactic nuclei, irradiated stars evolution 80−56949
- active galactic nuclei spectra, Monte Carlo simulation of relativistic Comptonisation 80−90566
- active galactic nuclei X-ray sources, hard X-ray emission mechanism 79−97080
- active galaxies, black holes possible existence in nuclei 79−48842
- active galaxies, forbidden lines theory 78−93408
- active galaxies, gravit. focusing by slowly rotating relativistic spherical mass 80−105155
- active galaxies, rel. to faint radio source counts at 5 GHz 78−32588
- active galaxies narrow line region physical conditions 80−31364
- active nuclei, black hole gravity power model 78−57667
- active nuclei, brightness var. rel. to supermassive stars *(Russian)* 79−25764
- active nuclei, continuous optical spectra 78−57644
- active nuclei, cosmic ray driving of gas 77−29915
- active nuclei, dense clouds form. and confinement 79−30117
- active nuclei, emission-line, radiatively accelerated clouds, structure, shape and evolution 80−17685
- active nuclei, energy mechanism, Penrose photoproduction processes 80−31365
- active nuclei, energy source, supermassive black holes 79−40213
- active nuclei, energy sources, review 77−87539
- active nuclei, envelope parameters and mass 79−35392
- active nuclei, high energy neutron beams 78−69881
- active nuclei, IR obs., future prospects 78−57651
- active nuclei, line transfer calcs. 79−48902
- active nuclei, local space density 78−57676
- active nuclei, masses of central bodies *(Russian)* 77−45566
- active nuclei, massive black hole binaries model 80−109546
- active nuclei, models of supercritical accretion discs around black holes 80−105272
- active nuclei, models of unsaturated Compton accretion discs around supermassive black holes 80−22033

galaxies continued
- active nuclei, non-thermal X-ray sources syntheses of X-ray background 80—27021
- active nuclei, optical and UV spectra 79—97094
- active nuclei, Penrose pair prod. in massive extreme Kerr black holes 79—21322
- active nuclei, physical props. from emission-line spectra 78—57650
- active nuclei, probing via high-energy neutrino astronomy 80—4432
- active nuclei, radiation from relativistic blast waves 77—74156
- active nuclei, radio obs., future prospects 78—57652
- active nuclei, role of UV obs. *(Italian)* 78—32577
- active nuclei, spectroscopic and photometric obs. 77—37650
- active nuclei, strong gravity effect on light curve 79—16812
- active nuclei, theories and X-ray production 79—58421
- active nuclei, thick accretion discs models rel. to supercritical luminosities 80—101614
- active nuclei, X-rays from inverse Compton refl. 79—48920
- active nuclei and quasar broad line regions, luminosity and radio emission 80—105340
- active nuclei contrib. to diffuse X-ray background 78—36733
- active nuclei energy sources, choice between, magnetoid, black hole and compact star cluster *(Russian)* 77—78885
- active nuclei galaxies, distance determ. method *(Russian)* 80—51880
- active nuclei in spiral and Seyfert galaxies 78—57653
- active nuclei physical conditions, role of inelastic collisions 77—45599
- active radio galaxies, dust lane origin, explosion model 79—62910
- active southern objects, JHKL obs. 79—40270
- activity, scheme for quasars, radio galaxies, N galaxies and Seyferts 77—45541
- ages, determ. from N/O ratio 79—25728
- alignment in linear clusters, visible obs. 80—90516
- AM-2, possible Local Group low-mass dwarf galaxy, description 79—25651
- angular correlation functions from South Galactic Pole wide angle surveys 80—90536
- angular diameter counts, determ. of selection criteria for deep Schmidt plates 77—91623
- angular momenta, distrib. 78—20886
- angular momentum in Local Group 78—93400
- angular momentum redistrib. by spiral waves, computer models 79—53909
- angular momentum transport and gas distrib. secular change near corot. reson. by bar 79—48933
- Anon 0050+72.8, peculiar emission line galaxy 77—91627
- anonymous galaxy in Canes Venatici, discovery obs. of SN 80—67759
- anonymous galaxy in Cygnus 79—5846
- anonymous galaxy near k Centauri, supernovae discovery and magnitudes 80—85962
- anticorrelation rel. to dark intergalactic matter in galactic haloes 79—2567
- apparent distribution, intragalactic factor due to interstellar clouds 78—96552
- apparent flattening 77—78873
- apparent luminosity function to 21st magnitude 80—31350
- apparent magnitudes estimation rel. to zodiacal light brightness *(Russian)* 78—93389
- Arakelian, emission line spectra 77—74138
- Arakelian 120, optical and IR photometry of class 1 Seyfert 79—58423
- Arakelian 120, Seyfert 1 galaxy, optical variability 79—40259
- Arakelian 120, Seyfert 1 type, UBV photometry, brightness and colour vars., models 80—26983
- Arakelyan 120, Seyfert, spectrophotometry 79—62913
- Arakelyan 120, Seyfert galaxy nuclei, optical variability, UBV obs. 80—73049
- Arakelyan 120, X-ray obs. of Seyfert 1 galaxy 80—105344
- Ariel 5 active galaxy survey, X-ray obs. 78—24554
- Arp QSO-galaxy associations, nature 80—90564
- associations with QSOs, spectroscopic search 80—105355
- associations with quasars, statistical analysis 79—9024
- astrophysics, symbiosis with solar and stellar astrophysics 77—9736
- Australian Astronomical Society, conf. Melbourne, Australia (May-June '77) 78—69655
- axisymmetric nucleus stellar system, stellar motion anal. 77—17687
- axisymmetric scalar-tensor gravit. field, galaxies, oblate bodies 77—33917
- axisymmetrical stellar systems, periodic orbits of stars 80—17619
- B0844+31, relaxed double galaxy with radio jet, 5 GHz obs. 77—29945
- B2 1502+28, head-tail galaxy in Abell 2022, Westerbork obs. of spectral index and polarisation distrib. 80—36727
- B2 1506+34, peculiar radiogalaxy, H I absorption detection 78—54048
- B2 radiogalaxies of low luminosity, polarization at 1.4 GHz 79—71141
- B 0844+31, extended radio galaxy, multifreq. obs. 80—56963
- bar, lens and ring components, morphological survey, secular evolution in struct. 79—30119
- bar length rel. to bulge size in barred galaxies 80—98713
- bar-driven spiral density waves in disk galaxy 80—8684
- barred galaxies, star formation and active nuclei 80—105341
- barred spiral dynamics using gas as tracer 80—51869
- barred spiral galaxies gas dynamics, gaseous density waves and galactic shocks 80—12819
- barred spirals, large-scale shock wave formation 77—2470
- barred spirals, occurrence freq. 80—73037
- barred spirals, ring-like structures, mass accretion 79—75271
- barred spirals, self-gravitating gas flow 80—90521
- barred spirals in Virgo cluster, surface photometry 77—13453
- bars, extent 80—46666
- basic properties, rel. to anthropic principle of cosmology and physical world struct. 79—48973
- bidimensional stellar systems in uniform rot., stability for nonaxisymm. modes 78—85980
- binary galaxies, anal. of Turner's (1976) sample 80—67849
- binary galaxies, angular measures, rotation and morphological type 79—53914
- binary galaxies, dynamics 78—4354
- binary galaxies, dynamics and masses from 21 cm obs. 80—105332
- binary galaxies, excess of early type galaxies, mass overestimation 80—73037
- binary galaxies, late type, mass-to-light ratios from luminosity-weighted averages 78—8113
- binary galaxies, mass-luminosity ratios 79—84863
- binary galaxies, radial vels. and masses of 44 pairs 80—26990

galaxies continued
- binary galaxies and massive halos 77—33644
- binary galaxies peculiarities, luminosity function and colours 80—41900
- binary galaxy systems, luminosity/separation correl. as dynamical friction effect 80—36700
- binary galaxy systems formation by tidal encounters 77—41410
- binary stellar systems, tidal disruption and coalescence 78—93330
- black hole halos, form. in tepid early universe 78—20919
- black hole in galactic nucleus, sustenance 78—57632
- blue compact emission-line galaxies, H I content 77—87542
- blue compact galaxies, chemical comp. and evolution 80—36711
- blue compact Zwicky galaxies, spectroscopic survey 79—58417
- blue dwarf galaxies, morphology of 15 objects on red Asiago plates 79—101200
- blue galaxies, star form. 78—12356
- blue galaxies in distant cluster, photometry and red shift 78—12377
- blue radio quiet objects, spectrographic obs. of optical counterparts 79—101212
- branched spiral struct., density wave theory 77—26067
- bridges and jets, hydromagnetic break-up into aligned objects 77—49475
- bright galaxies, 1415 MHz continuum survey 80—94869
- bright galaxies, Arecibo 2380 MHz, survey 78—57470
- bright galaxies, comparison with positions of Tololo quasar candidates 80—77506
- bright galaxies, distrib. of ang. distances from optically variable quasars 79—58438
- bright galaxies, UBVRI photoelectric photometry 78—32578
- bright galaxies and compact galaxies apparent associations 78—41040
- bright galaxies associated with nearby Abell clusters, position and magnitude 80—67880
- bright galaxies vicinity, background radio sources distrib. and density 80—56964
- bright galaxies with low red shift, red shift-magnitude relation 80—101639
- bright galaxies with nearby QSOs, non-cosmological redshifts 80—105386
- bright galaxy nuclei, optical and radio survey, sample selection and obs. 80—73039
- bright galaxy nuclei activity, emission line sources and radio sources 80—98709
- bright nuclei, survey of 448 galaxies 78—32569
- bright objects, integrated magnitude and colours in UBV system, catalogue 79—12509
- bright phase in evolution, intergalactic gas ionization 77—26065
- bright southern galaxies, H I obs. 77—57084
- bright southern galaxies, photoelectric photometry 79—21436
- brightness distrib., decomposition of profiles into spheroid and disc components 78—8115
- broad emission line galaxies in southern sky 78—20891
- 3C111, new very large radioenergy source in core of radio galaxy *(German)* 78—16558
- 3C273, spectroscopic obs. and redshift of associated galaxy 78—77606
- 5C2 survey revised distances of optical objects from radiosources 78—57472
- 5C3 sources, optical idents., spectroscopic results 80—46689
- 3C 105 optical counterpart, identification and source struct. 79—35413
- 3C 111, 3C 236, radio galaxies, 150 GHz obs. 80—41908
- 3C 111, radio galaxy, obs. at 1.38 cm wavelength with resolutions up to 8″ *(Russian)* 80—109558
- 3C 111, spectrum and redshift of luminous N-type galaxy 77—33666
- 3C 120, emission-line nebulosity morphology 79—80363
- 3 C 120, galaxy and nucleus, UBV photoelectric obs. 79—44601
- 3C 120, IR variability, 2 μm obs. 79—30118
- 3C 120, radio galaxy, linear polarisation and flux density vars. 77—9805
- 3C 120, radio galaxy, vars. in optical spectrum *(Russian)* 80—90540
- 3C 120, Seyfert galaxy, IUE and visual spectrophotometry 79—92856
- 3C 120, Seyfert galaxy, spectrophotometric obs. of assoc. nebulosity 80—67890
- 3C 120, Seyfert galaxy, X-ray emission detect. 77—78890
- 3C 120, Seyfert galaxy nuclei, optical variability, UBV obs. 80—73049
- 3C 123, brightness and polarisation distrib. at 3.7 and 6 cm wavelength 78—4340
- 3C 123, radio struct. at 2.7 and 15 GHz 78—54050
- 3C 129, head-tail galaxy with radio jet, 5 GHz obs. 77—29945
- 3C 129, orbital dynamics of head-tail radio galaxy around nearby supergiant galaxy 78—49518
- 4C 13.17A, B, in X-ray cluster of galaxies Abell 401, radio emission distrib. 80—98731
- 3C 132, 3C 192, radio galaxies, study of bridges metre and centimetre wavelengths 77—91658
- 3C 219, double radio galaxy, high-resolution 80—77500
- 3C 227 and 382 radiogalaxies, spectral-flux distrib. in 0.36-3.5 μ range 78—36710
- 3C 236, high resolution VLBI obs. of compact central component 79—92878
- 3C 236, radio galaxy, 6-49 cm obs. of double source 80—82528
- 3C 236, VLA obs. of extended radio core of giant radiogalaxy 79—75288
- 3C 264 (NGC 3862), radio galaxy, high resolution radio maps 77—5582
- 3C 273, search for hard X-ray emission 77—29939
- 3C 285, 3C 265, 3C 390.3, optical emission in radio lobes 78—57630
- 3C 285, double radio galaxy, discovery of optical emission in radio lobes 77—64866
- 3C 286, quasar, intervening galaxy model for optical absorpt. lines 80—4454
- 3C 288, complex extragalactic radio source, radio brightness distrib. model 80—90558
- 3C 293, radio galaxy, radio and optical obs. 78—93418
- 3C 303, double radiosource, radio struct. and optical field 78—16519
- 3C 303b, N-galaxy, gravit. lens effect on 3C 303a 77—78878
- 3C 310, 326, relaxed double radio sources, implications of fine scale struct. 80—51891
- 3C 310, extended radio galaxy, multifreq. obs. 80—51890
- 3C 310, relaxed double galaxy with radio jet, 5 GHz obs. 77—29945
- 3C 315, radio galaxy, high resolution radio maps 77—5582
- 3C 319, radio struct. and optical identification with elliptical galaxy 80—31377
- 3C 31, linear polarization obs. of radio galaxy at 1.4 and 2.7 GHz 79—48925
- 3C 31, multifreq. radio obs. of galaxy with jets and peculiar spectra 78—16533

galaxies continued
3C 31, radio emission obs. at 2.7, 4.8, and 10.7 GHz 79−35375
3C 31, radio galaxy, mag. field struct. in radio jets 80−82526
3 C 31, radio jet brightness and shape rel. to beam and slingshot models 79−25741
3C 31 (NGC 383), dynamical interpretation of radio jet, galaxy interactions 79−9020
3C 326, very large radio galaxy, multifreq. obs. 78−28810
3C 33, 98, 184.1 and 218, rotation axes 80−26997
3C 33, optical emission detect. in SW radio lobe 78−57665
3C 33, radio galaxy, optical line emission rel. to physical conditions in compact head 80−51892
3C 33, rot. axis. of assoc. optical galaxy 78−4355
3C 33 and 327, double radiogalaxies, spectrophotometry 78−54066
3C 343.1, distant radio galaxy, spectroscopy and photometry, redshift 78−8123
3C 371, polarisation at 2.2 μm, nonthermal emission 79−2566
3C 382, 3C 386, radio galaxies, two-freq. high resolution obs. 78−86031
3C 382 (B2 1833+32), variability of optical counterpart 78−41053
3C 388, galaxy in Abell 643, classical double radiosource, 4885 MHz obs. 80−109545
3C 390.3, 3C 111, 3C 129, radio galaxies, search for hard X-ray emission 77−29939
3C 390.3, obs. of radio galaxy with International UV Explorer 79−67101
4C 39.04, powerful giant radio galaxy, multifreq. obs. 80−17682
4C 39.11, N galaxy, radio and optical obs. 78−16553
3C 427.1, brightness and polarisation distrib. at 3.7 and 6 cm wavelength 78−4340
3C 449, radio jet structure at 1465 and 4885 MHz 80−12823
3C 452, spectral index variation 77−82309
3C 465, extended radio galaxy, multifrequency UHF and SHF obs. 80−105338
4C 47.51, complex radiogalaxy, aperture synthesis obs. 80−94883
3C 48, 3C 295, radio galaxies, scintillation at 25 MHz rel. to ang. struct. 78−65711
3C 48, quasar, galactic disc model of assoc. nebulosity 77−13487
4C 53.37 (1638+538), tailed radiogalaxy, dual curved jets 80−62265
3C 61.1, 3C 33, 1.4 GHz aperture synthesis obs. of circular polarisation 77−29656
3C 6.1, 265 and 352, spectrophotometry of high-redshift radio galaxies 79−92876
3C 84 (NGC 1275), study of emission variability in millimeter wave range *(Russian)* 80−90559
3C 98, 3C 178, 3C 192, 3C 327, narrow-line radio galaxies, optical spectra 77−33664
5C areas, optical identifications 77−37665
4C radio galaxies, structs. and optical identifications 79−71137
4C radiosources, brightness and polarisation distrib. 77−26076
4C radiosources, optical identifications 77−26077
3C radiosources, systematic optical identification 78−36709
4C radiosources clustering, statistical analysis 79−5761
Calar Alto IR objects, search for continuum radio emission 77−41418
Canes Venatici I galaxy group, neutral H obs. of NGC 4136, 4144, 4190, IC 4182 and (DDO 133) 79−84853
Carafe galaxy, peculiar ringed Seyfert, spectroscopic and photographic obs. 79−35387
catalogue of galaxies and clusters of galaxies in SMC direction 78−96410
catalogue of galaxies near galactic plane between l=245° and 255° 77−2346
catalogue of galaxies within 10 Mpc 80−51670
Catalogue of Southern Peculiar Galaxies and Associations, preliminary results 77−82129
cD and related galaxies in poor clusters, pencil beam obs. of radio emission at 6 cm 80−62293
cD and related objects in poor clusters, 1400 MHz pencil beam obs. 80−62263
cD galaxies, ellipticity 80−22076
cD galaxies, form. by dynamical friction in aspherical clusters 78−16547
cD galaxies, in poor clusters 77−22111
cD galaxies in poor clusters, photometry, spectra and redshifts 79−48907
cD galaxies in poor clusters, radial vel. meas. 79−8994
cD galaxies in X-ray clusters observed by HEAO 1, positions rel. to X-ray source locations 79−97090
cD galaxy in Abell 2029, dynamics and struct. 79−92850
cD galaxy in Abell 401, spectral obs. of halo 78−32584
cD galaxy in cluster Abell 2029, radio and SAS 3 X-ray obs. 80−82519
Centaurus A, giant quasiperiodic mm wavelength bursts in nucleus 79−48928
Centaurus A, nuclear γ-rays detect. 77−13482
Centaurus A, nuclear gamma-ray lines, origin in relativistic plasma 80−41890
Centaurus A, X-ray struct., radio-lobe energy source evidence 80−26978
Centaurus A, X-ray variability, OSO-8 obs. 78−41082
Centaurus A (NGC 5128), detect. of X-ray emission from giant radio lobes 78−41055
Centaurus A (NGC 5128), X-ray and gamma-ray lines prod. by nonthermal ions 78−36725
central explosions, rel. to very large H II regions form. 80−56951
central surface brightnesses, extrapolated, upper limits 79−25705
Cepheid variables in different galaxies, progression in period-amplitude diagrams characts. 78−53956
chains of galaxies, stabilisation by continuous background *(Russian)* 78−73765
chemical evolution, anal. of effect of heavy element abundance on stellar evolution 80−105231
chemical evolution, O and N abundance in H II region 80−46680
chemical evolution, review 77−26068
chemical evolution of two-component galaxies, numerical calcs. 79−25715
chronometric cosmology, tests using galaxy and quasar samples 80−86022
chumpy irregular galaxies 79−97072
Circinus, discovery of large new galaxy 77−41409
Circinus galaxy, H I 21 cm line obs. 77−33652
Circinus Sb galaxy, Mt. Stromlo Schmidt red plates *(Swedish)* 78−69877
circular rotation from simple two component model 77−45550
classical field component of galaxies, test 77−33658

galaxies continued
classification, structure and origin, review 78−49541
classification of galactic collisions 77−45544
classification of N-galaxies and Seyferts 79−97071
close pairs, excess radio emission 78−57658
cluster galaxies, gas ejection rel. to intracluster Fe-enriched gas origin 78−93390
cluster galaxies, interaction with intracluster hot gas 78−12374
cluster galaxies, luminosity function 78−54058
cluster galaxies, luminosity function rel. to clusters Bautz-Morgan classes 78−54057
cluster galaxies, luminosity functions and morphology 78−12383
cluster galaxies, morphological characts. and correl. with cluster parameters 79−17109
cluster galaxies, number densities and radial cumulative distribs. 79−40278
cluster galaxies, number density rel. to cluster Bautz-Morgan type 78−28804
cluster galaxies, redshift determ. using Image Dissector Scanner, visible spectra 80−90544
cluster galaxies distribution determination, maximum likelihood method 80−56954
cluster galaxies evolution, ISIT photometry of Cl 0024+1654 and 3C 295 78−24557
cluster galaxies evolution, nearby clusters galaxy content 79−17108
cluster galaxies orientations, Monte-Carlo simulation 80−90528
clustering, N-body simulations covariance function 80−31373
clustering, scaling law determ. 80−82522
clustering about extragalactic radio sources, cross-correl. anal. 80−22103
clustering models, discrimination of statistical measures 79−35404
clustering spectrum, low mass portion anal. 78−81695
clustering spectrum, rel. to cosmic luminosity 78−81696
in clusters, number density, radial number density and radial cumulative galaxy distrib. 80−73050
in clusters, review of props. 77−64862
clusters first brightest galaxy, multiplicity rel. to cluster Bautz-Morgan type 79−92873
collapse times from N-body simulations of clustering 79−44620
colliding galaxies, dynamical friction effects 79−44600
colliding galaxies, mechanism of encounter 80−73047
colliding-cloud system, struct. and spectrum and relationship to QSOs 78−28836
collinear configs. of point masses, three body problem 77−71139
collisionless disc systems anisotropic instability and galactic plane bending *(Russian)* 77−60827
collisionless gravitating systems, gravitational pot. nonlinear eqns. determ., astrophysical appl. 80−67560
collisions, classification for galaxies of unequal dimensions 79−84850
collisions, deformation caused by tides, computer simulation *(French)* 80−56952
collisions, effect on dynamics and evolution of groups and clusters 79−75282
collisions between compact galaxies and large spirals *(Norwegian)* 78−4361
collisions between model spherical galaxies 80−51864
collisions in dense groups, effects on galaxies size and struct. 77−45573
colour-absolute magnitude relation for elliptical and S0 galaxies 78−8108
colour-magnitude relation for cD, E and S0 galaxies 80−31351
Coma cluster, galaxies rel. to intergalactic optical surface brightness 77−87550
Coma cluster galaxies, luminosity function and distrib. 77−45574
Coma Cluster galaxies, photometry 78−12381
Coma cluster radio galaxies, rel. to electrons in halo radio source 77−26073
Coma I cloud galaxies, redshifts, morphology and luminosity function 77−45575
GQ Comae Berenicis, QS0 or N galaxy, spectrophotometry obs. 80−77488
X Comae Berenicis, Seyfert, optical variability 77−74139
compact, distrib. in compact groups of galaxies *(Russian)* 78−61926
compact, in Morphological Catalog of Galaxies, discovery, apparent distrib. and props. 78−28792
compact, mean surface brightness and integral brightness relation 78−93412
compact, optically variable, calibration of photoelec. comparison sequences 77−87537
compact, spectroscopic and photometric obs. 78−77603
compact and interacting southern galaxies with emission line spectra 78−41048
compact central components in 17 extended radiosources, VLBI detect. 77−17703
compact double radio sources, relativistic blast-wave model for superlight motion 78−28807
compact extragalactic source model, stellar collisions near Kerr black hole 79−12490
compact galaxies, equidensitometric determ. of angular diameters 78−16308
compact galaxies diameters and magnitudes, study of galaxy catalogues *(Russian)* 78−49514
compact galaxies in compact cluster Shakhbazian 1, photometry *(Russian)* 78−93428
compact galaxies in compact groups, tenth list 80−26991
compact galaxies in fields near M3 and M92, selection, statistics and photometry with two telescopes 80−77485
compact galaxies in neighbourhood of Abell 193, list of 140 objects 79−88736
compact galaxies in systems of galaxies, redshifts 77−71143
compact galaxy, review 80−17668
compact galaxy detect. method *(Russian)* 77−49302
compact groups of compact galaxies, seventh list *(Russian)* 77−22110
compact groups of galaxies, survey 77−22320
compact nuclei, scattered X-ray flux 78−4363
compact nuclei, stellar collisions, binary star components periodic collisions 78−8061
compact objects in 27 compact groups, morphology *(Russian)* 79−9008
compact objects on UK Schmidt plates 78−81687
compact radio galaxies, particle accel. and flux vars. 77−13479
compact radio sources, struct. and time vars. 78−57669
compact radio sources in bright galaxies, very long baseline interferometry 79−48943

galaxies continued
compact radiosources, flux density and linear polarisation at 3.7 and 11.1 cm wavelength 77—49490
compact radiosources in and near bright galaxies 78—49548
compact structure in double radio sources 79—17113
compact X-ray source galaxies, observational consequences of synchrotron self-Compton models 77—29961
compact Zwicky galaxy assoc. with giant radio source 4C 73.08, multifreq. obs. 79—25745
composite object 0246+18, bright galaxy with superposed variable star, UBV colours 79—71130
conference on high redshift objects, IAU Symposium 92, Los Angeles (August 1979) 80—101669
conformally invariant gravit. theory, astrophysical appl. 77—82428
Contopoulos potential, field of directions of motion *(Russian)* 80—62205
cool stellar discs, equilib. 78—54037
cool stellar discs, radial modes of oscill. 78—57628
coronae, ionisation struct. and absorpt. line spectra 77—13448
coronae, production by supernovae rel. to intracluster medium origin and quasar absorpt. lines 80—31355
correctionless observational cosmology 79—53946
correlation function, computer simulation of catalogue *(Russian)* 80—36729
correlation function evolution, N-body Monte Carlo model 80—62292
correlation function for density perturbations in expanding universe, linear theory 78—4417
correlation functions, BBGKY eqns. integration for development of nonlinear clustering in expanding universe 78—8175
correlation functions, for density perturbations in expanding universe 78—65730
correlation functions and relative peculiar vels., rel. to cosmic virial theorem 77—17726
correlation functions for galaxy counts, interstellar medium effects *(Russian)* 79—25740
correlations, gravit. instability evidence in dense universe 77—33712
corrugation waves in differentially rotating gas layer, theory 77—5571
cosmogony based on spatial distrib. of matter 77—37652
cosmological distance determination, new method, appl. to weighing of Universe 79—9003
cosmological objects in nonradial motion, redshifts, special and general relativistic anal. 79—80212
couble galaxies, H I 21 cm. line obs. 80—51886
counter-rotating relativistic disks 79—16822
counts, up to 25th apparent magnitude *(Russian)* 80—51879
counts and colours of faint galaxies 80—105351
counts and galactic reddening determ. 79—5875
counts in $21<B<25$ apparent mag. range 80—105352
covariance function, explanation for 9 Mpc break 78—65688
covariance function, extension to small scales 79—101197
covariance function, technique for shape determ. at small scales 80—82506
3CR, radio galaxies, spectrophotometry spectral energy distrib. 79—21413
3CR radio galaxies, optical spectra 79—71124
3CR radio galaxies, redshifts, strong emission line spectra 77—33666
3 Cr radio sources, spectral index breaks 79—67108
3CR radio sources counterparts, optical field investigations to faint limiting magnitudes 78—54067
3CR radiosources, optical identification 80—90555
Curtis-Schmidt thin prism survey for extragalactic emission line objects, Univ. of Michigan list I 77—71012
Cygnus, obs. of two obscured galaxies 77—29922
Cygnus A, giant cD radio galaxy, extended X-ray source 79—67109
Cygnus A, models for central compact radiosource 79—17073
Cygnus A, optical struct. 77—9802
Cygnus A, polarization maps at 23 GHz 79—71109
Cygnus A, radio galaxy, 150 GHz obs. 80—41908
Cygnus A, radio obs., digital hologram reconstruction 77—64653
Cygnus A, radiogalaxy structure at 150 MHz 80—101646
Cygnus A, rot. axis of assoc. optical galaxy 78—4355
Cygnus A (3C 405), radio galaxy, obs. at 1.38 cm wavelength with resolutions up to 8″ *(Russian)* 80—109558
Cygnus A model, radio source powered by M87 type knots 78—57661
Cygnus A region, X-ray obs. of 3U 1957+40 with ANS 77—53700
D and cD galaxies in poor clusters struct. and classification 78—32580
DA 240, radio galaxy, high-vel. gas in jet 78—28773
David Dunlap Observatory (DDO) galaxy distrib. 79—12520
de Vaucouleurs' groups of galaxies, type-redshift relation 77—17693
deep galaxy samples, correct anals. 79—67104
deep samples and meas. of faint images 80—62285
dense nuclei, black hole ang. momentum reduction by star capture 77—29874
dense nuclei, disruptive stellar collisions 78—65621
dense nucleus, stellar tidal disruption by black hole, QSO model 77—33674
dense stellar system, high-density gaseous disc formation and evolution 77—5549
density oscillations in uniformly rotating disc galaxy 78—57635
density wave, co-rotational singularity *(Chinese)* 79—97084
density wave evolution at unstable stage *(Chinese)* 78—28787
density wave induced star formation rel. to surface brightness 80—17649
density wave propag. through disc 78—20894
density wave theory, book 78—36700
density wave theory, non-linear effect on gravit. instability for adiabatically deformed case 78—20864
density wave theory for normal spirals, review 80—67873
density wave theory for spiral galaxies, finite spiral arm inclination regime in stellar dynamics 78—49534
density wave-star interaction in spiral galaxies 77—45545
density waves, excitation at Lindblad and corotation resons. by external potential 80—22072
density waves, maintenance and phase shifts between stellar and gaseous arms 79—44618
density waves, maintenance of spiral struct. and discrete spiral modes 77—33638
density waves, nonlinear growth *(Chinese)* 79—97085
density waves, nonlinear instability in the region of corotational circle *(Chinese)* 80—4438
density waves, nonlinear stationary finite-amplitude waves in thin layer of stars 79—88739

galaxies continued
density waves, tightly wound, nonlinear self consistent theory and mechanism for shock wave formation 79—101206
density waves excitation and evolution 78—65684
density waves in self-gravitating disc, accretion-induced overstability 78—73752
development in expanding Universe *(Danish)* 78—86019
diameter luminosity relation, Hubble constant determ. *(French)* 79—30128
diameter-luminosity relation, magnitude system 77—45551
differentially rotating spiral system, density wave-star interaction 78—69871
diffuse gamma-ray emission from active galaxies 80—12806
diffuse [O I] emission and Hα lines, warm interstellar gas 78—4312
dimensions and masses, relationship to fundamental constants *(French)* 80—22081
disc $\alpha\omega$ dynamo theory for mag. field generation 80—46663
disc galaxies, co-rotation singularity effect on density wave *(Chinese)* 77—87554
disc galaxies, density waves excitation by wave energy transfer 77—7532
disc galaxies, effects of dissipation on gas response to oval distortions 78—12355
disc galaxies, evolution from spiral galaxy 79—92867
disc galaxies, masses and mass-luminosity ratios 77—78871
disc galaxies, nonlinear stability theory for rotating gravitating disc 80—17488
disc galaxies, stability anal. of finite uniformly rotating disc 79—88732
disc galaxies dynamical props. and two-dimens. classification 77—33654
disc galaxies nuclei, superdense gaseous cores form. 80—90526
disc galaxies of finite thickness, distrib. of matter *(Chinese)* 79—80349
disc galaxy, axisymmetric disturbances growth rates 79—21410
disc shaped, global dispersion reln. for density waves 79—62916
disc shaped galaxy, local gravit. instability of double gas disk 80—8691
disc systems in Virgo and Hercules clusters, cluster, disc galaxies sizes 79—75269
disc-halo galaxies, boundary layer circulation 78—57627
disc-shaped, enhanced growth rate of unstable spiral modes 77—41414
disclike galaxies, stability, numerical expts. 78—89251
disclike galaxies in massive halos, stability, models 78—93403
discrete spiral modes, spiral waves and local dispersion relationship 79—17080
discrimination from stars on astronomical plates, Bayesian approach to optimal classification 80—21920
discs, chemical evolution and formation 78—49525
disk equilib. and stability, effect of galactic halos 80—62275
disk galaxies, relation between S0 and spiral galaxies 80—82483
disk galaxy, hydrodynamical model *(Chinese)* 80—85996
dispersion of local disturbances and spiral waves in disk-halo galaxies 80—56934
distance determ. using UBV data and light curve models for Type II supernovae 79—62856
distance from photometric props. of type II supernovae 79—44511
distance indicators, tertiary, appl. to extragalactic distance scale 79—25708
distance indicators, test of four techniques 77—91641
distance scale, spiral galaxies distances from tertiary indicators 79—30120
distance scale from IR magnitude/H I vel.-width relation 80—82480
distance scale using H II region fluxes and parent galaxy diameters 79—44576
distance scale using H II region isophotal diameters 79—44575
distances, determ. from H I line profiles 77—29920
distances determination, appl. of H II regions rel. dispersions 80—31360
distant objects, problems 79—97068
distant satellites of Galaxy, spectra of giant stars 78—40926
distribution, angular covariance function estimation 79—62920
distribution, correl. functions, inversion of Limber's formula 77—33646
distribution, statistical anal. of galaxy catalogues 80—26987
distribution correl., appl. to Universe structure and evolution theory, review 79—62912
distribution evolution 80—62287
distribution via correl. anal. of deep samples, techniques and appl. to two-colour sample 78—41056
Doppler shift distributions in Universe, extragalactic peculiar motions 78—4416
double galaxies, data anal. and galaxian mass (M/L) determ. 80—4428
double galaxies, mass discrepancy 77—37657
double galaxies, redshift intervals periodicity 80—56923
double gaseous discs model, local gravit. instability criteria *(Chinese)* 79—17099
double radio galaxies, symmetry rel. to dressed slingshot effect 78—12359
double radio sources, evolutionary characts. *(Chinese)* 80—86007
double radio sources, struct. and evolution, plasma and twin exhaust models *(Chinese)* 79—40284
double radiosources, relativistic and nonrelativistic gas flows, low press. limit 77—9655
double radiosources, statistical props. 79—92877
double radiosources, steady-state configs., Cygnus A models 78—45416
double radiosources, twin beam models, dynamical calcs. 78—49547
double spiral galaxies, UBV photometry, magnitudes and colour indices 79—62914
Draco dwarf galaxy, giant stars effective temp. from photometry and spectral obs. 80—72941
Draco dwarf galaxy, masses of anomalous Cepheids 77—2434
Draco dwarf galaxy, metal abundance determ. from red giant obs. 79—17078
Draco dwarf spheroidal galaxy, anomalous Cepheids instability strip 78—28695
Draco dwarf spheroidal galaxy, red giants metal abundance 80—73030
Draco dwarf spheroidal galaxy, stellar colour magnitude diagram and proper motion 80—73029
Draco dwarf spheroidal galaxy, stellar metal abundances 77—91638
dwarf galaxies, discovery of three new members of Local Group 79—5907
dwarf galaxies, H I redshifts rel. to absolute solar motion and discrete redshift 78—49530
dwarf galaxies, nearby, 6 cm continuum emission limits from compact components 79—30126
dwarf galaxies NGC 5128 group 79—25738

galaxies continued
dwarf irregular galaxies near Local Group and M81 group, photographic obs. 79—35363
dwarf irregular galaxy identified in Phoenix 77—26057
dwarf nearby galaxies, search for intergalactic H I clouds 79—71126
dwarf ring galaxy, discovery, luminosity, diameter and distance 77—49482
dwarf spheroidal, anomalous Cepheids binary system model 77—45451
dwarf spheroidal galaxies, evolution 80—22088
dwarf spheroidal galaxies, H I content upper limits 78—57633
dwarf spheroidal galaxy in Draco, BV photometry 79—97076
dwarf spheroidal galaxy in Draco, foreground interstellar reddening 79—97077
dwarf spheroidal galaxy in Ursa Minor, possible membership of eclipsing binary with RRc primary 80—109505
dwarfs in Nilson's Uppsala General Catalogue, H I 21 cm line survey 79—92846
dynamical effects in formation and evolution 78—41051
dynamical evolution, effects of time-varying gravity 78—24459
dynamical evolution of stellar systems, anal. rel. to hidden masses *(Russian)* 77—91583
dynamics, appl. of problem of four fixed centres 78—28493
dynamics, stability of one-dimensional self-gravitating isothermal systems 80—73008
dynamics, trapping of particles in time-depend. Hamiltonian 77—13217
dynamics of colliding bodies systems in gravit. field, transversal viscosity effects 77—67026
dynamics rel. to cosmological turbulence theory, observationsl tests 80—98747
E and S0 galaxies, CO and JHK photometric obs. 78—36684
E and S0 galaxies, luminosity functions 79—97057
E and S0 galaxies, new colours, magnitudes and types 78—89246
E and S0 galaxies, UBVR and JHK photometric obs. 79—58412
E galaxies in Abell clusters, UR surface photometry 79—12525
E/S0 radio galaxies, ionized gas obs. 79—17105
early type disks, H I distrib. and vel. structure, 21 cm line obs. 79—35357
early-type, energy distribs. from OAO UV photometry of severn objects 79—35360
early-type, in Virgo cluster, H I survey 79—30123
early-type, metallicity effects on integrated colours, calibration 78—89227
early-type bright spiral galaxies, multiaperture UBV photometric props. 80—98706
early-type galaxies, H I obs. 78—45401
early-type galaxies, photometric determ. of twists in three objects 79—25703
early-type galaxies, relative distance moduli 80—22080
early-type galaxies, relative luminosities and distances 80—31363
early-type galaxies, rot. curves meas. 78—54034
early-type galaxies, sequences and populations 79—58415
early-type galaxies accretion phenomena, role of gas-rich dwarfs 80—31349
early-type galaxies in NGC 7331 field, distances 80—4435
early-type spiral galaxies, H I obs. 77—64838
edge-on spirals, H I 21 cm line obs. of 14 objects 79—97075
element abundance determ. from metal rich H II regions 80—82461
element evolution 80—22084
ellipsoidal stellar system, hot model with complex vel. distrib. function 77—45570
elliptical, ang. size determ., 2-D Fourier transform technique 79—35373
elliptical, anisotropic vel. distribs. generation 80—36715
elliptical, apparent flattening rel. to absolute magnitude 79—9004
elliptical, formation model, stellar population explosions 79—35388
elliptical, H I detect., upper limits 77—53685
elliptical, H I emission search, gas content determ. 80—46657
elliptical, in Abell 426 and 1367 clusters, surface brightness and colour distribs. 78—81681
elliptical, in Coma cluster, surface brightness and colour distribs. 78—41063
elliptical, internal dynamics 79—53902
elliptical, IR obs. of late-type stars 77—91639
elliptical, massive central objects rel. to halo formation 78—4366
elliptical, search for H I emission 78—65681
elliptical, ultralow dispersion spectroscopy 79—53733
elliptical and dwarf spheroidal galaxies, mass-energy-density rel. 80—22049
elliptical and IO galaxies, HI content, 21 cm obs. 79—97066
elliptical and lenticular, gas content 78—16544
elliptical and S0 field and cluster galaxies, photometry, colour distribs. 79—17071
elliptical and S0 galaxies, absorpt.-line strengths 80—4430
elliptical and S0 galaxies, H I obs. 77—64838
elliptical and spiral, tidal interaction theory, ang. momentum calc. 78—8106
elliptical galaxies, average ellipticity compared with galaxy groups ellipticity 80—12820
elliptical galaxies, central luminosity spike and dynamics of dense stellar kernel *(Russian)* 80—67871
elliptical galaxies, chemical evolution 80—67843
elliptical galaxies, correl. between isophotal twisting and flattening 80—41896
elliptical galaxies, equilib. systems models rel. to rot. vels. and vel. dispersion 80—94865
elliptical galaxies, form. by tidal interactions 77—78865
elliptical galaxies, hot gas interstellar medium rel. to head-tail radio sources form. 80—36703
elliptical galaxies, isophotes struct. 78—41058
elliptical galaxies, mass and radius, star formation by contraction 80—67868
elliptical galaxies, mass to light ratios 80—98707
elliptical galaxies, normal, giant ellipsoidal shells discovery 80—86000
elliptical galaxies, relation between dynamics and flattening 77—71140
elliptical galaxies, rot. meas. rel. to oblate models 78—16529
elliptical galaxies, star form. theory 77—33636
elliptical galaxies, surface photometry 78—57625
elliptical galaxies, three-dimensional figures anal. 80—36704
elliptical galaxies, vel. dispersion radius depend. 80—51876
elliptical galaxies cores light distrib., effects of seeing 80—12814
elliptical galaxies formation, refutation of spiral galaxies merging hypothesis 80—98723

galaxies continued
elliptical galaxies in Virgo and Coma clusters, ellipticity profiles 78—28785
elliptical galaxies stellar population, evolutionary synthesis for late M giants, comp. effects 78—57626
elliptical galaxy dwarf companions, Palomar plate search 77—33653
elliptical galaxy near Cygnus A, photometry and foreground reddening 77—9802
elliptical galaxy rotation curve determ. 80—46675
elliptical protogalaxies, dynamical evolution 78—32571
elliptical radio galaxies, large radio sources preferred orientation rel. to parent galaxy 79—92880
ellipticals, colour rel. to flattening, possible correlation 79—71122
ellipticals, ellipticity var. with radius 79—101202
ellipticals, extended radio sources, optical positions 80—105331
ellipticals, extended radio sources, partial synthesis maps at 2.7 and 8.1 GHz 80—105330
ellipticals, formation, analytical model 78—69868
ellipticals, intrinsic shape *(Russian)* 79—40272
ellipticals, intrinsic shapes 80—56942
ellipticals, lack of spiral arms and lifebearing planets 77—64845
ellipticals, oblate or prolate spheriods 79—71121
ellipticals, optical posns. for identified radiogalaxies 79—97074
ellipticals, photometric data on twists 80—56932
ellipticals, polarisation by interstellar matter 78—93399
ellipticals, rotation 78—54052
ellipticals, scale free axisymmetric models with little ang. momentum 80—82493
ellipticals, surface photometry, numerical mapping by interactive procedure *(Italian)* 80—98572
ellipticals, three-dimens. shapes 80—51868
ellipticals 79—84851
ellipticals assoc. with B2 radiosources, orientation 80—77501
ellipticals in cD clusters Abell 401 and 2670, surface brightness distrib. 79—97073
ellipticities of galaxies in Abell 193 and 2255 clusters *(Russian)* 79—8986
emission line galaxies, review 77—64855
emission line galaxies, spatial distrib. rel. to clusters, visible spectra obs. 80—73046
emission line objects, classification system and list of 116 objects 77—22308
emission line objects from Curtis Schmidt thin prism survey, second list 78—28537
emission-line, galaxies and active radio-emitting nuclei, red and IR spectral obs. *(French)* 79—48815
emission-line, UBV obs., light vars. 79—30134
emission-line galaxies, high-excitation, HEAO 1 X-ray obs. 79—62907
emission-line galaxies, phys. conditions in nuclei *(Russian)* 79—80359
emission-line galaxies in dense clusters 78—65703
emission-line galaxies with IR excesses, 8000-11000 Å spectra 77—67124
emission-line objects, Univ. of Michigan List IV 78—77494
emission-line objects in Curtis Schmidt thin prism survey, third list 78—28538
energy sources in quasars and nuclei of galaxies 77—60849
ES type galaxies, UBV photometry obs. 80—73053
ESO 012-G21, Seyfert 1 galaxy, spectrum, redshift, UBV photometry and X-ray identification 80—8695
ESO 012-G21, type I Seyfert galaxy, Ariel V X-ray spectra 80—90539
ESO 103-G35, Seyfert galaxy and possible X-ray source 79—88741
ESO 103-G35, type I Seyfert, optical counterpart of H 1834—653 X-ray source 78—96547
ESO 113-IG45, galaxy and/or quasar, spectrum, photometry and struct. 78—28782
ESO 113-IG 45, interacting galaxy, Type 1 Seyfert spiral with bright central quasar 78—8126
ESO 113-IG 45 (=Fairall 9), Seyfert galaxy, spectroscopic and multiaperture photometric obs. 80—31362
ESO 140-G43 (Fairall-51), new southern Seyfert 1 galaxy discovery 78—54044
ESO 153-G27, supernova discovery and magnitudes (1979 August 19 to October 15) 80—26892
ESO 290-G50, spectral obs. of type I supernova 78—96496
ESO/Uppsala galaxies, second catalogue 78—77497
ESO/Uppsala galaxies, spectroscopic obs., first catalogue 77—22113
ESO/Uppsala survey of ESO(B) Atlas of southern sky, fifth list containing 2395 objects 78—20653
ESO/Uppsala survey of ESO(b) Atlas of southern sky, fourth list, 2920 objects 77—26059
ESO/Uppsala survey of ESO (B) Atlas of S. sky, pt.VII 80—56722
ESO/Uppsala survey of ESO (B) Atlas of southern sky, sixth list containing 3162 objects 79—8850
evolution, automated faint object counts to J=24 mag. 79—71120
evolution, effects of intergalactic matter 80—109543
evolution, state of fundamental knowledge inferred from study of globular clusters 80—90488
evolution, three-dimens. computer simulation 78—81551
evolution and automated faint galaxy counts 80—105350
evolution and classification 77—91637
evolution and cosmology, investigation via galaxy counts and colour-redshift relations 77—33627
evolution and QSOs 79—97095
evolution and spiral structure of a spiral galaxy 80—17667
evolution and stellar populations, Yale conference (May 1977), report 78—69879
evolution in groups and clusters, model 80—85992
evolution of galaxies in clusters 79—71132
evolution of stars and gas, review 80—77486
evolution rel. to quasar evolution 78—57693
evolution rel. to star formation mechanisms 80—12811
evolution rel. to stochastic self-propagating star formation 80—12810
evolutionary processes 77—67125
expanding universe, galaxy correls. time evolution, gravit. instability, model 79—17145
exploding galaxies and supermassive black holes, review 79—80355
explosions, source and nature in galactic nuclei 78—96546
extended radio galaxies, multiple ejection theory 77—45592
extended radio galaxies, multiple explosion model 80—41894
extended radio galaxies (>1 arcsecond), large-scale struct. 78—57668
extended radio sources, relativistic Kelvin-Helmholtz instabilities 78—45419

galaxies continued
extended radiogalaxies, instability rel. to cool regions in relativistic plasma 80−17486
extended radiosources, models, review 77−26079
extended radiosources and elliptical galaxies, search for radio cores using Very Large Array 78−81700
extended radiosources and elliptical galaxies, small-diameter components in extended structs. 78−81699
extinction in IR-emitting nuclei 79−44599
extragalactic astronomy meeting (Paris, 11-13 December 1978) 79−97121
extragalactic distance scale, rel. to Hyades Cluster distance 78−8121
extragalactic distance scale, review of distance indicators 78−93396
extragalactic distance scale 77−91640
extragalactic objects clustering in Universe *(Polish)* 78−96580
extragalactic research, conf., Potsdam, Germany 1975, Oct. 77−37644
extreme compact object in Hydra I cluster 80−41898
faint blue objects, nature and distrib. 80−82476
faint blue objects in field of open cluster M67, spectroscopic obs. 77−22329
faint galaxies, number magnitude counts 80−26976
faint galaxies, spectroscopy and photometry rel. to evolution 80−105353
faint galaxies apparent distrib. 79−21444
faint galaxies near quasi-stellar objects with low-redshift absorpt. systems, search 79−17121
faint galaxies radial vel. meas. from objective prism plates 77−45562
faint galaxy counts, rel. to Friedmann cosmological model *(Russian)* 77−87584
faint objects in two fields near SGP 79−25739
Fairall 160, 182, UBV photometry 80−82349
Fairall 9=ESO 113-IG45, companion galaxy to Seyfert 79−44616
Fairall 9, X-ray emitting Seyfert galaxy 78−28790
Fairall 9 and Fairall 51, spectrophotometry, Seyfert 1 class galaxies 79−17076
Fairall-9 (ESO 113-IG 45), extreme Seyfert galaxy, IR and visible photometry 79−25720
far IR (30-300 μm) emission 80−51861
far IR background contrib. at high galactic latitudes 77−53712
far UV spectrophotometry using Faint Object Telescope 79−25481
Faraday rotation in galaxies and quasar absorption lines *(Russian)* 79−40273
field galaxies, luminosity function 78−16526
field galaxies, luminosity function and space distrib. 79−88731
field galaxies and nearest groups, distances from secondary indicators 79−8987
field galaxies space distrib., redshifts and photometry of complete sample 79−21418
fields of galaxies, stochastic simulation 80−90530
fission of self gravitating rotating elongated gaseous disc 77−87546
flare stars, large-scale winds driven by mass loss, effects on interstellar matter 78−32464
flat; pot.-density relations 80−109548
flat disc galaxies, retrograde stars effect on global bar-forming mode 79−21411
flat discs, negative mass instability 78−45393
flat galaxies, bi-orthogonalization of Toomre's surface-density functions 79−80356
flat galaxies dynamical struct., statistical characts. 80−62269
flat galaxies dynamics, integral eqn. for normal modes in matrix form 77−33637
flat galaxies puffing up by rapid stripping and S0 galaxies form. 79−62908
flat galaxies with double-peaked rot. curves, spiral struct. generation 80−46679
flat spectrum radio galaxies in 5 GHz S4 survey, Westerbork obs. 79−58435
flat spirals, scattering of trapped star orbits, bananas 78−16464
flat systems, stellar kinetics, relaxation times 77−13405
formal third integral of motion for resonance *(Russian)* 77−57062
formation, adiabatic cosmological perturbations propag. through matter-radiation decoupling era 80−62337
formation, adiabatic theory rel. to high-vel. H I clouds parameters 80−46677
formation, anisotropic gravit. collapse 78−4344
formation, appl. of pair prod. in intense mag. fields 77−13505
formation, cylindrical relativistic shock waves propag. in presence of mag. field 79−53708
formation, density perturbations development after recomb. 78−49569
formation, dissipative processes 78−4343
formation, dynamical development and struct. of six collapsing models 79−25710
formation, early evolutionary stages of universe spatially inhomogeneous models *(Russian)* 80−4467
formation, fragmentation of cosmic gas clouds 77−33628
formation, free collapse of stars rotating sphere 78−93325
formation, implications of origin of baryons in Universe 79−62938
formation, in chaotic cosmology 77−57112
formation, origin of rotation *(Russian)* 77−82334
formation, pregalactic evolution model 79−92863
formation, relativistic cylindrical shock propagation through a magnetic field 79−94796
formation, role of primordial black hole form. in universe 78−32507
formation, role of shock damping and entropy prod. in relativistic simple waves 77−17725
formation, role of shock formation and shock structure in the cosmological radiative era 80−4463
formation, stable shapes for axisymm. gravitating incompressible fluid body 77−53414
formation, tenacious myths about cosmological perturbations larger than horizon size 80−105408
formation, violet gas dynamics 78−86018
formation, vortex generation in protogalactic medium 80−62360
formation adiabatic theory, H recomb. kinetics in presence of primordial black holes *(Russian)* 79−17152
formation and assoc. microwave background fluctuations 78−28865
formation and clustering rel. to core condensation in heavy haloes 78−54051
formation and entropy prod. from nonlinear adiabatic fluctuations 78−8172
formation and evolution, review 79−17100
formation and gravit. clustering, efficiency 79−48903

galaxies continued
formation and superclusters 80−36728
formation as gravitational field stochastic fluctuations 79−44837
formation by dissipationless collapse, limiting ellipticity 80−26973
formation by gravit. instability, role of ang. momentum 80−98722
formation epoch in hot big bang model 77−29968
formation era, metagalactic shock waves thermal processes 80−46678
formation from perturbations in Friedmannian universe 80−101656
formation from primordial material and dissipative processes 78−57654
formation from rotating gas clouds, gravit. axisymm. adiabatic collapse 78−7875
formation in cold early universe, influence of black holes 78−16585
formation in Eddington Lemaitre universe 79−62909
formation rel. to cosmic turbulence decay 78−49568
formation theories, microwave background angular distrib., constraints 80−62329
formation theories rel. to enriched gas in clusters and dynamics 78−77596
formation theory, statistical approach 79−97086
Fornax A, obs. of central region of double radiosource at 4.9 GHz 79−5912
Fornax cluster bright galaxies, surface photometry 78−96548
Fornax dwarf elliptical galaxy, giant branch colour-magnitude diagram 80−4431
Fornax dwarf galaxy, detection and props. of identified planetary nebula near centre 78−41005
Fornax dwarf galaxy, integrated colours of globular clusters 78−16469
Fornax galaxy, very red giant stars discovery 80−51768
Fornax system density rel. to open or closed Universe 80−90587
Fourcade-Figueroa galaxy near NGC 5128, resolution, redshift and distance 78−73758
fragmentation and interaction, rel. to evolution *(Russian)* 77−82312
Freeman's elliptical stellar cylinder model, stability 78−28731
G 307.1+1.2, G 309.7+1.7, low-latit. radio galaxies, optical and radio obs. 79−12535
G-varying cosmology, galaxy and QSO magnitude/red shift relations 80−56980
galaxies distance scale, determ. from IR magnitude/H I vel. width rel. to expansion rate outside Local Supercluster 80−105325
gamma-ray emission, observational and physical review 79−80373
gamma-ray emission, radio galaxies as source of 1-10 MeV background 77−87213
gas motion in rotating disc-shaped galaxies 79−21424
gas poor disc galaxies, radio and optical props. 77−22310
gas replenishment rates, stripping of spirals to form S0 galaxies 79−40253
gas/dust ratio in disc galaxies 79−53903
gaseous halos rel. to evolution 80−17675
gaseous protoclusters spatial struct. and galaxy form. 78−93415
gaseous sphere, gravitational contraction vel., virial based soln. 79−48665
gaseous warps persistance, test particle calc. for NGC 5907 79−71112
giant E and cD galaxies, optical extent 77−45557
giant elliptical galaxies and quasars, rel. to quasars clustering 78−16564
giant ellipticals, luminosity evolution from 2.2 μm studies 80−105358
giant ellipticals, V−K colours and IR Hubble diagram 80−105359
giant galaxies in clusters, radioactive accretion flow 78−93433
giant radio galaxies, 26-100 MHz obs. of four objects 80−56961
global gravitational instability of disc galaxies 79−48931
global gravitational instability of gaseous discs 79−48932
gravitating ellipsoid with halo, rotationally symmetric oscills. 79−5905
gravitating spiral system, dispersion relation 77−87538
gravitational encounters in rich clusters of galaxies 79−17110
gravitational instability in collisionless stellar disc, quasilinear saturation *(Russian)* 79−16824
gravitational instability role in galaxy and star form. theories *(Czech)* 80−41718
gravitational lens action of intervening galaxy on double QSO 0957+561 AB, IR spectrum 80−77510
gravitational potential, three dimens., generalised model 80−109551
gravitational radiation 77−9825
gravitationally bound systems, primordial gravitational wave effects 79−58599
gravothermal catastrophe enhancement in two-component isothermal spheres 78−4297
gravothermal catastrophe of finite amplitude 79−2476
Great Debate of galactic astronomy, actual proceedings 77−29979
group membership, probability density function appl. 80−86002
haloes, tidal effects on mass profile 80−86001
halos of spiral galaxies: photometry and mass-to-light ratios 79−5892
Haro 15, spectrophotometry and morphology of galaxy with UV excess *(Russian)* 78−93387
HB13, radio galaxy with jets, 151 MHz obs. 79−48926
head-tail radio galaxies, galaxy counts in surrounding region rel. to tail orientation 78−54060
head-tail radio galaxies, intrinsic parameters distrib. 80−17653
head-tail radio galaxies, VLA obs. 79−48945
head-tail radio galaxies in clusters, radial vels. 79−9014
head-tail radio galaxies in poor clusters, radio and optical obs. 78−96530
head-tail radio galaxies velocities with respect to intracluster medium 78−49516
heavy halos, resulting twisted and warped discs 78−65694
Hercules supercluster, basic redshift data 80−36725
high energy neutrinos of extraterrestrial origin, possible detection with DUMAND 79−80179
high surface brightness, spectra, redshifts absolute magnitudes *(Russian)* 77−49467
high surface brightness, spectral obs. *(Russian)* 77−49466
high-luminosity spirals, rotation curves for Sa→Sc types 79−17092
high-order clusters, existence 78−12386
Holmberg II, irregular galaxy, aperture synthesis obs. 77−2475
hot accretion disks in galactic nuclei, pair production and gamma-ray luminosities 80−56930
Hubble's law, galaxies recession and quasar redshifts *(Swedish)* 77−71144
Hubble classification system, 50th anniversary 77−33657
Hubble const. distance depend. caused by ScI galaxy luminosity distrib. *(German)* 77−45620
Hubble constant and extragalactic distance indicators *(German)* 78−45442

galaxies continued
Hubble diagram, deceleration parameter rederivation 77−13457
Hubble diagram for E and S0 galaxies in the local region 79−35359
Hubble diagram for type I and II objects supernovae 78−53967
Hubble diagram statistics, q_0 determ. and luminosity evolution rel. to quasars 79−71102
Hubble morphological classification, elliptical disc galaxy discontinuity 78−41043
Hubble parameter determination, homogeneity of galaxies sample 77−13506
Hubble ratio, local value, and extragalactic distance scale *(French)* 77−60826
Hubble sequence, ang. momenta and time scales of galaxies early evolution 79−8997
Hubble sequence, dynamical interp. using Brosche theory 77−82303
Hubble sequence, influence of galactic winds 79−8989
Hubble sequence rel. to mag. fields, new theory of galaxies 77−71142
Hubble Sequence rel. to massive star evolution 77−91651
hydrodynamic expansion of relativistic gas, Euler eqns. 77−33331
hydrodynamics of collisionless spherical stellar systems in a steady state 79−5865
IAU 13S6A, strong southern radiosource, optical identification 77−64865
IC239, H I distrib. determ. 79−53910
IC 10, H I emission obs., unusual kinematics 79−67098
IC 10, irregular galaxy, giant H I envelope obs. 79−67094
IC 1613, colour-magnitude diagram and luminosity function for brightest stars 77−5561
IC 1613, dwarf irregular, luminous stars, visible spectra and photometry 80−82345
IC 1613, structure and content of Local Group dwarf galaxy 78−86006
IC 310, outer structure from electronographic obs. 78−16521
IC 342, CO emission from late-type galaxy 78−89250
IC 342, detection of extragalactic ammonia 79−48886
IC 342, H_2O maser emission detect. 78−45417
IC 342, Scd galaxy, central regions IR emission and star form. 80−62256
IC 342, Scd galaxy, discovery of companion 80−36712
IC 342, Scd galaxy, H I large-scale struct. obs. 80−67857
IC 342, Scd galaxy, struct. from H I obs. 80−73045
IC 342, spiral galaxy radio continuum obs. 77−74132
IC 3576, peculiar galaxy possibly 4U 1232+07, HEAO 1 obs. 80−12832
IC 4296, double-double radio galaxy 1415 MHz obs. 77−41412
IC 4329 A, X-ray obs. of extreme type 1 Seyfert 79−12515
IC 4329A, Seyfert galaxy, photographic photometry and optical spectrum 80−36706
IC 4329A, spectrophotometry of extreme Seyfert, possible quasar 79−101190
IC 5152, low-luminosity barred galaxy, struct., rot. curve and redshift 80−56950
IC 5201, supernova discovery report 79−44514
IC 708, Papillon radio galaxy, morphology, polarization 79−92855
IC 708 and 711, head-tail radiogalaxies in Abell 1314, 1.4 GHz obs. 77−60833
identification and spectroscopy of distant radiosources 77−17705
II Zw 70/II Zw 71, compact galaxies, H I maps, tidal interactions 78−96531
inhomogeneous spherical gravitating systems dynamics, simplest hydrodynamic models 80−17620
inner Lindblad resonance, nonlinear theory including bars 78−20863
inner Lindblad resonance nonlinear theory, response density 79−35366
instabilities, variational principles for complex eigenvalues 79−21527
integrated Brandt masses 78−93398
interacting and peculiar galaxies, radial vels. determ. *(Russian)* 79−80358
interacting components in VV 644, compact 'nest' of galaxies *(Russian)* 80−94879
interacting galaxies, atlas of 1500 objects, galaxy fragmentation theory 77−41320
interacting galaxies, causing background quasars absorpt. lines 77−17714
interacting galaxies, luminosities and diameters 80−17677
interacting galaxies, numerical models appl. *(Russian)* 78−93421
interacting galaxies, physical characts. *(Russian)* 77−57097
interacting galaxies with compact components, UBV photometry 78−20888
interacting glaxies, radial vels. and luminosities 77−78874
interacting nonequilibrium systems near bright galaxies 78−36682
interaction and fragmentation *(Russian)* 77−26062
interaction with central objects, active nuclei 79−58428
intercloud medium and spiral galaxy struct. 77−17664
intergalactic hot gas formation by ejection from galaxy in early explosive era 78−45408
interstellar abundances 78−16542
interstellar gas chem. comp. differences within and among galaxies 78−4369
interstellar gas flow stability in disk-halo galaxies 80−56933
interstellar gas self-gravity effects on galactic shock waves 78−73761
interstellar H I clouds in distant galaxies, colour pictures of Doppler shifts 77−17383
interstellar medium, differentially rotating kinetic theory questions *(Russian)* 77−91617
interstellar reddening freq. distrib., selection effects in SMC *(German)* 77−74113
intervening galaxies, rel. to quasar image doubling assoc. with absorpt. systems 80−22112
intervening galaxy hypothesis rel. to absorption spectra of QSOs and BL Lacertae objects 79−5894
intervening galaxy in front of BL Lacertae object PKS 0735+178, multiple absorpt. components obs. 79−25707
intrinsic flattening, anal. using iterative method 80−36701
IR astronomy development progress *(German)* 77−67138
IR emission, rel. to Byurakan classification *(Russian)* 77−22305
IR luminosity/H I vel. width relation and distance scale 79−44596
IR-bright nuclei, photometry at 10 μm 78−41045
irregular and late-type southern galaxies, survey, classification 77−91618
irregular galaxies, chemical comp. and evolution 80−36711
Irregular II galaxies origin 78−77601
irregular objects, star-forming activity 79−9001
isolated galaxies, continuum survey at 5 GHz 80−105333

galaxies continued
isolated galaxies, search of Turner-Gott field galaxies 78−4352
isolated pairs, radio continuum survey 78−57657
isophotes of elliptical galaxies, ellipticity study and classification 79−101194
IUE obs. 80−105357
BL Lacertae, spectrum and magnitude of associated galaxy 78−24552
large galaxies, H I mapping survey, 21 cm obs. 80−94870
Large Magellanic Cloud, giant filamentary shell N51D, nature and dynamics 80−105343
large-scale distribution and motion, in adiabatic theory of form. 78−54056
large-scale structure in universe, formation and development 79−12526
Las Campanas survey of bright southern galaxies, new classification for 153 systems 79−71113
late-type galaxies, integral props. derived from H I obs. 78−86015
late-type spirals, luminosity class correl. with obs. parameters 77−33655
lenticular, H I 21 cm line obs. 79−67090
lenticular, photographic obs., morphology and H I content *(French)* 79−2570
lenticular galaxy origin 80−51872
Leo A, H I 21 cm. line survey of dwarf irregular galaxy 78−81688
Leo I dwarf galaxy, 23 new variables discovered 78−53953
LGS 3 in Local Group, 21 cm line obs. of new dwarf galaxy 79−101195
AP Librae, extended source obs. by photoelectric photometry 78−4348
Lick catalogue of galaxies, new reduction 77−71013
Lick galaxy counts, correl. with QSOs from extragalactic objects catalogues statistical anal. 79−25700
Lick reduced galaxy counts, smoothing method 80−41897
light emission, search for correl. with cosmic X-ray background 80−56977
light neutral leptons, dynamical role in cosmology 79−35407
LMC, 30 Doradus chemical comp. and struct. obs. 80−62226
LMC, Apollo 16 for UV spectra 77−33634
LMC, Apollo 17 far UV spectra 77−13461
LMC, Balmer line photometry of 30 Doradus nebula 79−62888
LMC, blue to red supergiant star ratio across face, rel. to star form. 80−26984
LMC, bright stars luminosity function and comparison with galactic luminosity function 80−82499
LMC, BVI obs. of Cepheids, period-luminosity-colour relation 79−71055
LMC, BVI photometry of supergiants 77−33490
LMC, C stars possibly assoc. with open clusters 78−49428
LMC, C stars VRI photometry, optical spectroscopy and evolutionary implications 79−71019
LMC, candidate symbiotic stars optical spectroscopy and IR photometry 80−62139
LMC, catalogue of 302 C stars 78−20654
LMC, catalogue of radical vels. 79−101089
LMC, catalogue of UV obs. in 30 Doradus region 77−64844
LMC, Cepheid variables intrinsic colours 79−84797
LMC, Cepheids in Dunsink II region, BV photographic photometry 78−45340
LMC, colour magnitude diagram and metal abundances of Hodge 11 cluster 78−69850
LMC, discovery of nova near HV 12080 (1977, February 26) 77−37605
LMC, distance from OB stars spectroscopic obs. 79−71111
LMC, dynamics of giant filamentary shell (N70) 80−90511
LMC, dynamics of giant interstellar shells from line profiles 80−46674
LMC, electronographic photometry and colour-magnitude diagram of cluster (Hodge 11) 79−40230
LMC, electronographic photometry and colour-magnitude diagram of star cluster (NGC 2231) 79−92813
LMC, emission line objects *(French)* 78−69875
LMC, emission nebulae with strong S II forbidden lines 77−29891
LMC, faint clusters, colour magnitude diagrams, BV photometry 80−94841
LMC, far IR obs. of H II regions 78−81671
LMC, far UV extinction anomaly in 30 Doradus region 78−45386
LMC, four super-giant H II shells obs. 78−86012
LMC, giant H II ring obs. rel. to energetic stellar winds 78−77593
LMC, gravit. warping of plane of Milky Way 77−45540
LMC, H 0544-665 X-ray source, obs. of optical candidate 80−36737
LMC, H I+molecular/H II shells from 1 to 2000 pc dia. obs. 79−25678
LMC, H I distrib. from absorpt. in 30 Doradus direction 78−24541
LMC, hot supergiant stars with stellar winds, luminosity and extinction values, UV obs. 80−77477
LMC, instrumental colour-magnitude diagrams for 24 stellar clusters 77−22279
LMC, integrated photometric props. 78−54054
LMC, internal motions in bubble-like nebula N51D 80−105295
LMC, interstellar 4428 Å feature 79−35335
LMC, interstellar and nebular lines obs. towards 30 Doradus central object (HD 38268) 80−51839
LMC, interstellar Ca II and Na I obs. in 30 Doradus nebula 80−46643
LMC, interstellar extinction and stellar population in 30 Doradus region 78−96517
LMC, interstellar extinction meas., UV sky-survey telescope obs. 79−35384
LMC, IR obs. with HJKL filters of second nova 77−33518
LMC, IR survey of 30 Doradus, 2 μm sources in central region 78−32544
LMC, IUE and ground based obs. of S Doradus 80−101595
LMC, IUE obs. and 2200 Å feature detection towards reddened supergiants 79−16959
LMC, IUE obs. of UV spectra and flux distribs. of supergiants 80−101593
LMC, kinematics and dynamics compared to galaxies of Magellanic type *(German)* 80−105348
LMC, long time baseline VBLUW photometry of most luminous supergiants HD 33579, 35343, HDE 286757, (269006) 80−22007
LMC, longtime baseline VBLUW photometry of most luminous supergiants (HD 33579, HD 35343, HDE 268757 and HDE 269006) 80−36630
LMC, luminous composite stars 79−58375
LMC, M-type supergiants spectral types and luminosities 79−62820
LMC, main sequence luminosity function 78−8111
LMC, massive stars, evolution 79−101191
LMC, metal abundance of cluster (NGC 2209) 78−8122

galaxies continued
LMC, metal-poor intermediate-age cluster NGC 1868, BV photometry 80—51814
LMC, N 59 nebular complex filter photography 79—17052
LMC, nebulous filaments around 30 Doradus nebula 79—67076
LMC, new Wolf-Rayet stars discoveries 79—67018
LMC, Nova 1977b, photometry, light curves, distance modulus 78—8019
LMC, nova discovery confirmation, magnitude, photometric obs., premax. spectra 78—49456
LMC, obs. of A0538-66 recurrent X-ray transient source 78—54085
LMC, obs. of luminous extended X-ray source 78—16570
LMC, obs. of three luminous C stars 78—28670
LMC, optical candidate star for A 0538—66 X-ray burster 80—73076
LMC, optical obs. of bright core of 30 Doradus nebula 80—67827
LMC, photometric obs. of nova 77—60769
LMC, planetary nebula obs. in red globular cluster NGC 1852 77—17668
LMC, probable nova discovered 1978 March, position and magnitude 78—45341
LMC, probable nova discovery and spectrum 79—8931
LMC, radio model of 30 Doradus region 78—96523
LMC, radiosources at 3.4 cm, catalogue and spectral indices 78—65695
LMC, red stars survey in 30 Doradus region, list of 298 stars 79—48794
LMC, ring-shaped nebulae diameter rel. to number of embedded stars 80—77457
LMC, RR Lyrae stars, list of 76 objects 77—91549
LMC, sinusoidal Cepheids, first overtone pulsations, photometry obs. 80—77422
LMC, SNR N49, Pioneer Venus Orbiter obs. of 1979 March 5 gamma-ray transient 80—77518
LMC, SNRs identification from Einstein Obs. X-ray meas. 80—26980
LMC, space orientation and translational motion *(German)* 77—53684
LMC, spectra of bright A-type supergiant stars, line intensities 77—22215
LMC, spectral analysis of HD 34664 (S 22) peculiar emission-line supergiant 80—77416
LMC, spectral types and magnitudes of supergiant stars, catalogue of 1882 objects 78—32361
LMC, spectrophotometric study of Henize S22, emission line star 78—69803
LMC, spectroscopy and IR photometry of emission line stars 77—13348
LMC, spectrum and semi-accurate position of LMC X-1 optical candidate 80—67908
LMC, spiral struct. 77—29924
LMC, star density distribution of red and blue globular clusters 79—92811
LMC, stellar photoelectric UBV photometry *(German)* 80—21932
LMC, supergiant stars, long-term light vars. 78—45326
LMC, supernova remnant line intensity ratio evolution 77—17656
LMC, supernova remnant N132 D, rapidly moving material, visible and UV obs. 80—82449
LMC, supernova remnant N49 as source of fast intense unusual gamma-ray transient 80—73073
LMC, supernova remnant N49 as source of gamma-ray transient event of 1979 March 5 80—73074
LMC, supernova remnant N49 origin of 1979 March γ-ray burst 80—105270
LMC, supernova remnant N49 possible assoc. with gamma ray burst (1979, March 5) 79—58441
LMC, supernova remnants, SHF obs. 80—67864
LMC, supernova remnants obs. in O III and S II forbidden lines 77—91607
LMC, tilt determ. from Cepheid obs. 79—53912
LMC, unique interstellar Ca II K-line profile in 30 Doradus direction 80—51850
LMC, UV absorpt. by interstellar gas near 30 Doradus 80—85978
LMC, UV reddening law in 30 Doradus complex 78—96516
LMC, UV surface brightness meas., TD-1 sky survey 79—71125
LMC, uvby photometry of O-type stars 77—60756
LMC, uvbyR surface photometry of 30 Doradus region 77—91600
LMC, Wolf-Rayet stars discovery in 30 Doradus nebula 79—16980
LMC, X-ray obs. of gamma-burst field near N49 SNR 80—27019
LMC, X-ray survey using HEAO 1 scanning modulation collimator 80—17648
LMC, yellow star search from low-proper-motion stars 77—5576
LMC, yellow stars UBV photometry and LMC members number 78—93417
LMC bar, soft X-ray source identification 80—82491
LMC disc population structure, obs. of central regions underlying stellar component 77—33633
LMC H II regions, ANS UV obs. of exciting stars 79—71017
LMC interstellar extinction, visible and UV obs. 80—51877
LMC nova, UBV photometric meas. (1977, March-April) 77—53608
LMC OB and supergiant stars, deep objective prism survey catalogue 79—40090
LMC stellar population structure, count-brightness ratios for central regions 78—89245
LMC supergiant stars, comments on catalogue of Stock et al. *(French)* 78—53941
LMC supergiants spectra, diffuse interstellar 4430 Å feature 80—73033
LMC X-1, X-2 and X-3, positions from HEAO 1 modulation collimator 79—5923
LMC X-1 region (MC76 and 77), 2 cm obs. 80—51875
LMC X-4, Ariel 5 obs. of eclipses and identification confirmation 77—74161
LMC X-4, closeness of A0538—66 bursting source, Ariel 5 obs. 77—82321
LMC X-4, identification with eclipsing binary system, review *(German)* 78—81713
LMC X-4, possible optical counterpart OB star 77—29959
LMC X-ray source light curves, Ariel V obs. 77—74164
LMK, faint star clusters detection, size distrib., visible obs. 80—73011
local cluster, satellite galaxies and globular clusters, radial vels. and galactic mass 78—49522
Local Group, distances for six nearest galaxies 78—89247
Local Group, initial mass function rel. to massive star formation 79—30053
Local Group, Local Cloud and intergalactic gas clouds 77—91642
Local Group, new dwarf galaxy member discovery near (NGC 6822) 79—84852
Local Group galaxies, Cepheid variables freq.-period distribs. 78—28694

galaxies continued
Local Group galaxies, interstellar gas 77—91644
Local Group galaxies, kinematics and solar motion rel. to centroid 78—12376
Local Group galaxies, number of globular clusters correl. with spheroidal system luminosity 77—91594
Local Group galaxies, possible new members from solar motion solns. 77—22321
Local Group galaxies gravitational encounters, numerical expts. 77—57098
Local Group gas concs. and Magellanic Stream 77—91646
Local Group motion rel. to Sc I galaxy vel. anisotropy 77—91643
local peculiar vels. 80—62284
local radio luminosity function of elliptical galaxies 77—57086
low surface brightness galaxies, luminosity function, props. 78—96532
low surface brightness galaxies in clusters and groups, comparisons *(Russian)* 79—80357
luminosity classifications, systematic and accidental errors 79—12510
luminosity criteria for E-S0 objects 79—97065
luminosity function, anomalous, of galaxies in compact groups 80—82520
luminosity function, of galaxies in small groups 78—12385
luminosity function models, observational test 78—77605
luminosity function of galaxy systems, from single galaxies and small groups to rich clusters 80—12808
luminosity functions for complete samples, observational magnitude cutoff bias elimination 80—56940
luminous obscured galaxy assoc. with G127.11+0.54, optical spectroscopy and photometry 80—31371
M100 (NGC 4321), discovery of possible type II supernova before max. 79—48835
M100 (NGC 4321), precise position of SN 1979C 80—85962
M100 (NGC 4321), SN 1979c detect. as radio source 80—82402
M100 (NGC 4321), spectrophotometry of SN 1979c and distance estimate 80—62166
M101, chemical comp. of H II regions 78—93359
M101, distance from 21 cm line widths and optical methods, H_0 global value determ. 77—9827
M101, extended H I envelope obs. 79—62904
M101, gas and stellar mass determ. in NGC 5471 H II region *(Russian)* 78—93426
M101, giant spiral galaxy, companion galaxies integral props. from H I meas. 78—49532
M101, H I distrib. and motions in giant spiral 79—44613
M101, Mars model from gas kinematics 79—35371
M101, spectra of H II regions, comp. gradient across spiral galaxy 78—65683
M101, spectra of type II supernova 1970g 78—8030
inner M101 galaxy group, H I obs. 80—67885
M104, galactic-scale magnetic field from optical polarisation obs. 77—22313
M104, number of globular clusters correl. with spheroidal system luminosity 77—91594
M104 (Sombrero), radial distrib. and total number of globular clusters 77—74140
M104 (Sombrero galaxy), mass spectrum of star form. 77—17675
M15, possible second planetary nebula detect. in Hα 77—17655
M31, anomalous nova-like object obs. 79—80316
M31, aperture synthesis obs. complemented by short spacing data fron single dish obs. 79—66928
M31, central region, near IR surface photometry 78—28791
M31, classical novae minimum number of outbursts determ. 78—28692
M31, CO and H I distrib. comparison 78—36694
M31, CO partial radial distrib. meas. 78—8117
M31, dark nebulae catalogue 80—72787
M31, disc colour gradient photoelec. surface photometry obs. 80—73032
M31, formaldehyde detect. 79—48929
M31, former globular clusters considered as H II regions *(Russian)* 80—31347
M31, gas-to-dust ratio determ. 78—8120
M31, globular cluster distribs. 79—12513
M31, globular cluster populations uniformity 77—53654
M31, globular clusters colour indices, rel. to interstellar absorpt. law 78—28796
M31, Hα survey, catalogue of 981 H II regions 78—40840
M31, H I emission in NE.region, 21 cm obs. 80—90537
M31, H I emission in SW region 80—51873
M31, H I in outer regions 78—16532
M31, H I sheets ejected by M32, multiple disk radial vels. computer simulation 78—16523
M31, high-resolution H I obs., spectra and major axis rel. plots 78—41057
M31, identification of H II regions and distant galaxies previously considered as globular clusters *(Russian)* 78—12370
M31, inertial frames of reference determ. from rot. vels. 79—21433
M31, inner nuclear regions, spectral features and dwarf content 78—86005
M31, integrated colours of globular clusters 78—16469
M31, interstellar polarization, wavelength depend. 79—92835
M31, line intensity distrib., contour maps, vel. profiles, 21 cm HI line survey 80—73038
M31, luminosity distrib. of globular clusters 80—36708
M31, M32 nuclei, luminosity-sensitive spectral features obs. 78—49431
M31, M33, IR detect. of luminous blue variable stars 78—49437
M31, M33, obs. of luminous variable stars 78—28686
M31, M51, M81, spiral galaxies, polarisation detect. at radio wavelengths 77—5575
M31, M51, nuclei, isophotometry 79—71114
M31, near IR polarization of nucleus 78—24556
M31, near IR vel. dispersion for nuclear bulge 78—49521
M31, near-IR energy distribs. 79—12512
M31, nearby blue objects and 5C3 radiosources optical counterparts obs. 77—91526
M31, new Bonn 21-cm survey, first results 77—91645
M31, novae identified as Population II stars 79—30074
M31, open star clusters obs. rel. to spiral struct. 79—75270
M31, photometric obs. of blue star-like objects 77—9744
M31, polarised radio emission detect. 78—86017
M31, polarised radio emission distrib. rel. to large-scale mag. field 80—41899
M31, population synthesis models, nonuniqueness 80—82489
M31, position angle of major axis of nuclear region 77—53682

galaxies continued
M31, possibility of black hole existence at centre 77—26025
M31, radio continuum survey at 2695 MHg comparison with optical data 77—57085
M31, radio emission obs. at 102.5 MHz *(Russian)* 78—49512
M31, reddening of 22 H II regions 79—71082
M31, rocket far UV imagery 79—5897
M31, rotation of nuclear region 78—45395
M31, search for globular clusters in disc and minor axis fields 78—32568
M31, semistellar nucleus, possible M-dwarf enrichment 80—51862
M31, spiral arm S4 struct. from Cepheids investigation *(Russian)* 80—82515
M31, stellar absolute proper motion meas. *(Russian)* 77—71106
M31, studies of luminous stars in Baade's Field IV 80—36622
M31, suspected OB star obs. 77—37601
M31, triaxial models of bulge 77—45539
M31, UBV photoelectric photometry of star clusters *(Russian)* 80—36680
M31, UBV photometry of star clusters *(Russian)* 79—17034
M31, UBV photometry of star clusters 79—62879
M31, UV image 80—98716
M31, vel. dispersions and dynamical model of nuclear bulge 79—35370
M31, vel. dispersions in nucleus and bulge 77—26049
M31, X-ray sources, obs. 80—26979
M31 (Andromeda galaxy), Cepheids associated with interstellar gas and star complexes *(Russian)* 80—90455
M31 (Andromeda galaxy), planetary nebulae astrometric catalogue 79—40087
M31 (Andromeda galaxy), planetary nebulae obs. 78—28737
M31 (Andromeda Galaxy) and companions, planetary nebulae props. 80—109520
M31 (Andromeda nebula), space motion derivation from solar motion 77—91518
M31 and M32, IUE spectra of nuclei 79—71117
M31 and M81 nuclei, UV continua, spectrophotometry obs. from ANS satellite 80—77478
M31 central bulge, energy distrib. from OAO UV photometry 79—35360
M31 nuclear bulge, rotational vels. meas. 80—41888
M31 spiral arm pattern, M32 gravit. effects 79—21408
M32, ejection of runaway planetary nebula 80—46626
M32, orbital decay and accretion by M31 galaxy 79—92845
M32, photoelectric scanning of elliptical *(Italian)* 79—21435
M32, spectrophotometry and filter photometry of planetary nebula, (M32-1) 79—25664
M32, stellar population spectral synthesis and galaxy age 80—67842
M32 is in front of M31, evidence from planetary nebula (M32-1) 78—93394
M33, clumping factor in H II regions 78—20870
M33, density wave motion obs. evidence from star form. and evolution 77—45552
M33, detect. of H_2O maser emission 77—29926
M33, detection of SNRs, by strong S II forbidden line emission 78—36665
M33, emission regions catalogue 80—46416
M33, far IR obs. of H II regions 78—61923
M33, H I distrib. obs. and spiral struct. 80—56948
M33, H I large-scale struct. 78—96539
M33, identification of star clusters, list of 58 candidates 79—9002
M33, ionisation of interarm medium 77—67131
M33, IUE UV spectra of giant H II region (NGC 604) 80—77467
M33, M101, vel. dispersion meas. in giant H II regions 79—44606
M33, N/S abundance gradient, SNR evidence 80—56929
M33, new variable star discovery 78—73717
M33, radio and optical obs. of supernova remnants *(Italian)* 79—53890
M33, radiocontinuum emission obs. at 14850 MHz 78—28783
M33, spectral obs. and identification of Wolf-Rayet stars 77—64779
M33, spectral obs. of supernova remnants 79—35354
M33, supergiants distrib. rel. to spiral struct. and star form. 79—21437
M33, supernova remnants catalogue 80—41734
M33, supernova remnants optical identification 79—62894
M33, UV integrated magnitudes of spiral galaxy 80—31368
M33, warped optical plane obs. 80—56944
M33 central region, optical supernova remnant candidates 79—21402
M33 direction, H I 21 cm emission/absorpt. obs. 80—62262
M33 H I tail, obs. rel. to adjacent high-vel. H I cloud 80—12815
M49, globular clusters space distrib. 78—93393
M51, high resolution obs. at 21 and 49 cm 77—29921
M51, ionized gas velocities 79—75268
M51, orientation model 79—71115
M51, radio continuum obs. 77—74135
M51, radio spectral index distrib. 78—8119
M51, spiral, mag. fields config. from Faraday rot. data 79—48934
M51, spiral arm struct. and star form. 78—73762
M51 and 81, stellar arm-gas arm phase shift, calc. 80—8690
M51 system, extended H I obs. 78—89253
M51 system, photometric study 79—30125
M81, enigmatic dark lines identified as galactic high latit. nebulosity 80—56947
M81, kinematics of gas in nuclear disc 77—9795
M81, M51, spiral galaxies, phase shifts between gaseous arm and stellar arm *(Chinese)* 79—17098
M81, near IR vel. dispersion for nuclear bulge 78—49521
M81, spiral, dynamics, axisymmetric models and stellar density wave 80—105335
M81, spiral, gas dynamics and HI regions 80—105336
M81 (NGC 3031), two component mass model construction 80—98710
M81 and 82 interacting galaxies, H I 21 cm obs. 77—45561
M81 nucleus, small radiosource obs. 77—13484
M81-82 system, 2.7 GHz continuum survey of intergalactic gas stream 78—36691
M82, 2 to 8 μm spectrophotometry 78—12363
M82, 87.2 GHz continuum obs., Ne abundance 78—41042
M82, bright ridge detected in 2.2 μ emission 79—40269
M82, compact radio source 41.9+58 in nucleus 78—93442
M82, dust model for light scatt. in halo, constraints on nature of intergalactic dust 77—87543
M82, exploding, galaxy hypothesis questioned 79—75279
M82, H125α recomb. line, SHF obs. 80—82486
M82, H 102α radio recomb. line detect. 77—49476
M82, interstellar HCN and CS search 77—53661

galaxies continued
M82, Irr II galaxy, high angular resolution H I study 77—33626
M82, irregular, aperture synthesis obs. of H I emission 79—17077
M82, irregular galaxy, colour distrib. 77—37653
M82, M104, VLBI obs. of galactic nuclei at 18 centimetres 80—22078
M82, model with galaxy drifting through dust 77—33632
M82, nature of radio recomb. lines in extragalactic sources 78—45418
M82, Ne II 12.8 micron emission obs. and galactic dynamics 79—17082
M82, nuclear source nature from IR obs. 80—82485
M82, OH absorption and emission obs. 77—5565
M82, optical polarisation wavelength depend. 80—67861
M82, polarimetry of irregular galaxy 77—17692
M82, radial vel. field from TAURUS imaging device 80—82205
M82, radio recomb. line emission detect. 77—57093
M82, radio structure at 23 GHz 79—71119
M82, stimulated recomb. line emission obs. 77—41408
M82, surface photometry and gross struct. of irregular galaxy 80—31367
M82, UBV colours and surface brightness distrib. 79—9006
M82, [O III] 88.35 microns and [O I] 63.2 microns fine struct. lines search 80—12794
M82 as exploding radiogalaxy, image tube spectrogram evidence 78—69880
M82 central regions, kinematics 78—45394
M82 nucleus, λ6 cm formaldehyde absorpt. detect. 79—17088
M82 nucleus, Brackett-line obs. 79—25704
M82 nucleus, obs. of compact radio source 77—78869
M83, H II regions spectral characts. and chemical abundances 80—56927
M83, star formation rate, rotational dynamics and interstellar gas density 80—51870
M83, UBVR surface photometry 79—44598
M83 and centaurus group, distance 80—4434
M84, M86, positional coincidence with extended X-ray emission 78—54090
M86, elliptical galaxy, X-ray evidence for hot gas retention 80—90535
M87, 2 and 6 cm VLA obs. of jet 80—105345
M87, anisotropic vel. distribs. model rel. to necessity of supermassive black hole 80—82500
M87, central giant galaxy in Virgo cluster, excess X-ray emission 80—41907
M87, central luminosity spike and dynamics of dense stellar kernel *(Russian)* 80—67871
M87, central regions luminosity distrib., isothermal core, point source or black hole models 79—71110
M87, dynamical evidence for central mass concentration 78—49529
M87, elliptical galaxy, enormous mass rel. to extended X-ray source model 78—28775
M87, emission-line filaments and active accreting nucleus 80—56931
M87, evidence for supermassive object in galaxy nucleus from SIT and CCD area photometry 78—49528
M87, Faraday rot. in radio/X-ray halo 80—67844
M87, giant elliptical galaxy, appl. of black hole theory *(French)* 79—92866
M87, giant elliptical galaxy, model for compact X-ray source in nucleus 78—28847
M87, globular cluster populations uniformity 77—53654
M87, halo globular clusters metallicity 78—89244
M87, high-resolution X-ray spectroscopy, O VIII emission line detect. 80—26977
M87, luminosity profile and outer corona 78—41035
M87, millisecond radio bursts discovery 80—73034
M87, model for optical knots in jet 79—30127
M87, nature of jet 78—54055
M87, number of globular clusters correl. with spheroidal system luminosity 77—91594
M87, photographic surface BV photometry of giant elliptical 78—69867
M87, photometric structure of jet 79—92848
M87, planetary nebulae, possible origin of extended emitting regions *(Russian)* 80—77492
M87, relativistic plasmon ejection *(Russian)* 80—67870
M87, search for hard X-ray emission 77—29939
M87, spectroscopic evidence for large central mass 80—94873
M87, spectroscopic obs. of nucleus 79—92858
M87, UV spectrum, IUE obs. 80—82502
M87, very high resolution radio obs. of nucleus 77—33663
M87 (NGC 4486), vel. dispersion from a population model 80—77490
M87 and Virgo cluster, X-ray emission, Ariel V SSI obs. 79—12528
M87 galaxy, jet, nonlinear Poynting flux for radio emission 80—26736
M87 halo, Fe XVII-XXIV X-ray line complex obs. 79—21425
M87 jet, imaging polarimetry 78—41076
M87 jet, internal shocks in plasma beam 78—93416
M87 jet, optical photograph deconvolution by maximum entropy 80—62032
M87 jet, radiation from knots rel. to model *(Russian)* 80—36719
M87 jet, synchrotron optical and radio emission origin *(Russian)* 80—8694
M87 jet knots, polarisation, spectroscopic and radio props. 80—12817
M87/Virgo cluster X-ray source spectrum, 1.1 keV Fe line emission discovery 79—25758
M89, elliptical galaxy, associated optical jet discovery 79—25731
M 101, giant spiral galaxy, distance 80—67852
M 101, IUE UV spectra of giant H II region (NGC 5471) 80—77467
M 31 spiral structure, morphological approach 78—65690
M 33, core-halo struct. of H II region (NGC 604) 80—85984
M 33, H_2O maser emission detect. 78—45417
M 81, CO emission upper limits 78—36693
M 81, spiral galaxy, aperture synthesis obs. at 1415 and 610 MHz 77—33639
M 87, radio continuum halo at 2.7, 4.8 and 10.7 GHz 79—48915
Maclaurin spheroids discs in halos, second-harmonic oscills. 79—8993
Maffei 2, CO emission obs. 78—16530
Magellanic Cloud clusters, spectral types of red supergiants 79—40190
Magellanic Cloud supernova remnants, high-resolution mapping in coronal [Fe XIV] emission 79—97051
Magellanic Cloud supernova remnants, optical emission from shocks 79—92831
Magellanic Clouds, C and M-type giant stars distrib. 78—32460
Magellanic Clouds, C stars in red globular clusters 79—101143
Magellanic Clouds, chem. comp. of H II regions, photoelec. spectrophotometry 78—77607
Magellanic Clouds, chemical comp. of planetary nebulae 77—37632

galaxies continued
Magellanic Clouds, chemical composition, model nebulae anal. 80—22085
Magellanic Clouds, colour luminosity-amplitude relations for Cepheids 77—91554
Magellanic Clouds, comparison of intrinsic colours of luminous stars *(German)* 77—17560
Magellanic Clouds, direct photography of SNRs 77—91612
Magellanic Clouds, evolution struct., and intensity, review *(French)* 79—71131
Magellanic Clouds, extrinsic model of anomalies in Cepheid variables 80—4361
Magellanic Clouds, F-type supergiants Ca abundances 80—98655
Magellanic Clouds, gaseous corona, evidence from stellar spectra 80—82490
Magellanic Clouds, general description 80—73048
Magellanic Clouds, giant and supergiant interstellar shells obs. 80—94858
Magellanic Clouds, H II regions chem. comps. 78—93381
Magellanic Clouds, He, N, O abundances of planetary nebulae 78—4338
Magellanic Clouds, high luminosity stars UBV intrinsic colours 80—26855
Magellanic Clouds, IR photometry of late-type supergiant stars 79—35254
Magellanic Clouds, lists of planetary nebulae 79—58405
Magellanic Clouds, masses determ. for globular clusters 79—5867
Magellanic Clouds, monochromatic photographs of giant H II regions 77—45516
Magellanic Clouds, orbit rel. to Magellanic Stream simulation and Milky Way mass 77—91622
Magellanic Clouds, planetary nebulae, identification, luminosity function and numbers 80—67815
Magellanic Clouds, planetary nebulae excitation classes 77—91611
Magellanic Clouds, planetary nebulae space distrib., excitation classes and comps. 80—109519
Magellanic Clouds, ratio of total-to-selective absorpt. from Cepheid obs. 77—29927
Magellanic Clouds, shell nebulae survey in S II, N II and O III forbidden lines and Hα 79—67085
Magellanic Clouds, SNR populations *(Italian)* 79—53887
Magellanic Clouds, SNR spectroscopic study 77—91613
Magellanic Clouds, spectral classification of O and B0 supergiants 77—78777
Magellanic Clouds, spectrophotometry of nebulae suitable as standards 78—12350
Magellanic Clouds, stellar winds from O and B supergiants 80—51863
Magellanic Clouds, supergiant stars birthrate and mass function 80—67699
Magellanic Clouds, supernova remnants optical obs. review 79—75259
Magellanic Clouds, tabulated light curves for 108 eclipsing variables 78—16536
Magellanic Clouds, turbulent wake in galactic halo forming Magellanic Stream 78—8125
Magellanic Clouds, UV brightness maps and UV spectra 80—85994
Magellanic Clouds, very-low-excitation compact nebulae obs. 78—32556
Magellanic Clouds, Wesenheit function, reddening correction for Cepheids 77—91553
Magellanic Clouds, Wolf Rayet binaries, spectroscpic orbits 80—109479
Magellanic Clouds 77—26060
Magellanic Clouds in binary state, galactic disc bending and Magellanic Stream 77—91620
Magellanic Clouds stars, five-channel photometric obs. 78—16398
Magellanic dwarf irregular galaxies/ gas distrib., motions and dynamics 78—36690
Magellanic Plane 77—91649
Magellanic Stream, origin and dynamics 79—44594
Magellanic Stream, turbuelnt wake of Magellanic Clouds in galactic halo 78—69884
Magellanic Stream H I regions, fine struct., 21 cm obs. 80—90523
Magellanic type galaxies, review *(German)* 80—105348
magnetic fields from light polarisation obs. 78—69872
magnetised accretion disc model, for quasars and active galactic nuclei 79—35425
Markarian, 3.2 mm and IR continuum obs. 77—22317
Markarian, with broad emission lines, spectroscopic obs. *(Russian)* 77—45567
Markarian 132, spectrum and redshift systems 78—89248
Markarian 185, 186, UBV surface photometry *(Russian)* 77—91614
Markarian 205, Seyfert galaxy, distance 79—97058
Markarian 205, weak radio emission 79—48912
Markarian 231, IR emission obs. 77—5570
Markarian 231, IR polarisation obs. 78—4360
Markarian 231, Seyfert 1 galaxy, optical variability 79—40259
Markarian 231, Seyfert galaxy, spectra, photometry and electronograph 77—45558
Markarian 231, Seyfert galaxy, substructure with UV excess, UV and visible obs. 80—82512
Markarian 290, multicolour photometry of Seyfert galaxy *(Russian)* 77—64848
Markarian 295, 296, 297, spectroscopic and 21 cm line investigations 79—44608
Markarian 296, clumpy irregular galaxy, spectroscopic and 21 cm line investigations 79—44608
Markarian 298 (=IC 1182-4), multicolour photometry *(Russian)* 78—57641
Markarian 325, irregular galaxy, emission clumps observational props. 80—67869
Markarian 335, Seyfert galaxy, spectroscopic investigation *(Russian)* 79—101204
Markarian 348, Seyfert, H I halo rel. to nucl. activity 80—82505
Markarian 348, Seyfert galaxy, spectrophotometry 79—88735
Markarian 359, peculiar emission line spectrum 79—17075
Markarian 374, Seyfert galaxy, spectra of double nucleus components 78—69882
Markarian 3, 231, Seyfert galaxies, optical polarisation obs. 80—90533
Markarian 3, class 2 Seyfert, visible spectra obs. 80—85999
Markarian 3, Seyfert, radio maps, 5HF obs. 80—82501
Markarian 421, optical and radio obs., identification with 2A 1102+384 X-ray source 79—5899
Markarian 421 (B2 1101+38=2A 1102+384), soft X-ray flux discovery 79—25721

galaxies continued
Markarian 464, 766 and 841, Seyferts, historical light curves 79—58425
Markarian 464, type I Seyfert galaxy, Ariel V X-ray spectra 80—90539
Markarian 501, BL Lacertae object, identification with 4U 1651+39, by HEAO 1 modulation collimator 79—5918
Markarian 501, optical variability 77—78867
Markarian 501, optical variability meas. 77—78886
Markarian 501, UV and X-ray obs. of BL Lacertae-type object 80—36717
Markarian 509, brightness variability meas. *(Russian)* 77—17671
Markarian 541, massive X-ray halo evidence 79—35369
Markarian 668, Seyfert galaxy, radio emission in 2.3-14.4 GHz range 79—88740
Markarian 668 (=OQ 208), Seyfert, H83α and H99α radio recomb. lines detect. 80—94864
Markarian 668 (OQ 208), radio spectrum 79—12531
Markarian 79, analysis of spectra of type 1 Seyfert 79—71103
Markarian 79, Seyfert galaxy, IUE and visual spectrophotometry 79—92856
Markarian galaxies, emission line intensities depend. on colour index *(Russian)* 77—17672
Markarian galaxies, Hubble modulus 78—49538
Markarian galaxies, morphological and colorimetrical obs. 77—37646
Markarian galaxies, nature from photometry and classification 78—28781
Markarian galaxies, obs. with RATAN-600 radiotelescope 79—88737
Markarian galaxies, radio continuum obs. at 1410, 2380 and 5000 MHz 80—46668
Markarian galaxies, radio continuum obs. at 1410 MHz and 2700 MHz 77—87548
Markarian galaxies, radio spectra 77—37647
Markarian galaxies, spectroscopic obs. *(Russian)* 77—49465
Markarian galaxies 508 to 700, optical positions 79—21417
Markarian galaxies frequency on objective prism photographs at Tautenburg Observatory 77—67128
Markarian galaxies in poor cluster ZwCl 1122.3+6317, radial vels. 80—26989
Markarian galaxies of Tautenburg objective prism survey, high-resolution spectra and redshifts 80—4436
Markarian galaxies origin of radio and optical radiation 77—17682
Markarian II, spectra of stellar population 78—54047
Markaryan 372, Hβ profile of Seyfert galaxy 80—26972
Markovian 297, IUE UV spectra of clumpy irregular galaxy 80—26981
Markovian 348, Seyfert, H I envelope, 21 cm obs. 80—82504
mass and ang. momentum, statistical relations 80—8689
mass density, Burbidge-Prendergast integral eqn., exact soln. 80—17652
mass distrib. models, regularization method *(Russian)* 79—12507
mass structure, rel. to N-body simulations of galaxy clustering 80—67879
mass to luminosity ratio of spiral and irregular galaxies 77—17684
masses, determ. from H I total profile widths 80—56937
masses and angular momenta, anal. and rel. to morphological types *(Chinese)* 79—17097
masses and spiral formation 79—12522
masses rel. to quasars greatest redshifts 77—49480
massive black hole ejection from galaxies, quasar-galaxy association 77—22263
massive galactic haloes rel. to rapid global bar formation 79—88745
massive gas clouds, cooling, dynamics and fragmentation rel. to masses and radii of galaxies and clusters 77—60857
massive haloes, form. and evolution 78—28777
massive halos, contrib. of heavy stable neutral leptons 78—93091
massive objects ejection from centre of stellar disc, theory for ejections in plane of disc 80—82495
massive objects ejection from centre of stellar disc, theory for ejections out of disc plane 80—82496
master list of non-stellar objects 77—78668
MC2 and MC3, optical identifications, 11^h28^m to 17^h00^m right ascensions 78—20900
MCG—6-30-15, type 1 Seyfert galaxy, X-ray and optical obs. 80—82479
MCG 10-16-117, supernova classification and spectrum 78—69818
MCG 10-16-117, supernova discovery 78—69817
MCG 43223, spectrum of Type V supernova 78—93288
MCG 5-23-16, X-ray emission detect. 78—41052
MCG 8-11-11, Seyfert, hard X-ray emission detect. 80—46660
MCG 8-11-11, Seyfert galaxy inside error box of 2A0551+466, optical spectra 77—74130
MCG 8-11-11, X-ray obs. of Seyfert 1 galaxy 80—105344
MCG 8-11-11, X-ray Seyfert galaxy, recent optical activity in nucleus 79—25701
MCG 8-11-11 (2Ariel 0551+466), Seyfert galaxy, brightening of nucleus 78—41053
MCG —3-34-61, discovery of 17 mag. supernova 80—72989
MCG —3-34-61, Type I supernova, 1980 June spectrum analysis 80—82401
MCG -5-23-16, spectroscopic obs. of possible X-ray source 78—45404
MCG -6-30-15, X-ray emission in 2-10 keV range 78—45405
MCG-4-32-23, possible supernova discovery 78—53968
MCG-5-9-22, supernova discovery 78—81643
MCG-5-9-22, supernova obs. and red shift 78—81644
McLauren cool discs, equil. and stability w.r.t. perturbations, gravitating mass effect *(Russian)* 79—92860
mergers, rel. to slowly rotating elliptical galaxies origin 79—48919
mergers, stellar populations mixing processes 80—67860
merging, cosmological N-body simulations 80—56922
merging galaxies, numerical simulations 80—36716
merging of galaxy pairs, N-body simulation 78—77600
microwave background radiation fluctuations, in adiabatic and entropic theories of galaxy form. 79—62942
Milky Way companion galaxy, synthesis obs. at 0.610 GHz rel. to identification 77—29941
Milky Way companions, kinematics rel. to Hypergalaxy mass 77—5573
millimetre temps. of planets, galactic and extragalactic sources 78—28556
missing mass, role of brown dwarfs and black holes 78—61879
missing mass problem, implication of neutrino rest mass *(Russian)* 80—105414
mm emission from extragalactic objects, luminosities, spectra, microwave background contrib. 77—17677
models, comparison of algorithms for numerical orbit computation 80—67797

galaxies continued
models, numerical orbit computation algorithms comparison 79—12497
models with variable spiral structure, computer simulations 78—32574
Morphological Catalogue, galaxy distrib. homogeneity *(Russian)* 79—8849
morphological evolution and galactic cannibalism 78—93404
morphological types, occurrence freqs. in Morphological Catalogue of Galaxies 80—17662
morphological types in rich clusters, catalogue 80—85872
morphology in clusters rel. to spiral galaxy evolution 80—90543
morphology in rich clusters, implications for galaxies form. and evolution 80—62255
morphology of bright galaxies in UVK colour plane 78—49539
N-galaxies as new class of X-ray sources 79—2572
N-type, colours as indicators of spiral and elliptical components 77—74137
N-type, morphology, electronographic obs. *(French)* 79—88759
N-type, optical spectra 79—40258
narrow-line emission galaxies, near IR broad-band photometric obs. 80—46659
nearby bright galaxies, optical obs. 79—97062
nearby extragalactic systems, interstellar reddening law and dust content *(German)* 80—67850
nearby galaxies, quantitative probabilities of group membership 79—62919
nearby galaxies nuclei, CO survey 80—62276
nearby galaxy in Orion, H I 21 cm obs. 79—30131
nearby normal galaxies, X-ray luminosity limit 80—4443
neutrinos, high energy, emission from point sources and detect. techniques 79—2484
new Sculptor-type dwarf elliptical in Carina, discovery 77—82311
new type of galaxy with prolate structure 79—21427
NGC1023, H I distrib. determ. 79—53910
NGC, 4151, Seyfert, periodicity of optical variations 78—41047
NGC 1023, SB0 galaxy, H I obs. rel. to rot. and mass/luminosity ratio 80—67886
NGC 1023, SB0 galaxy, surface photometry, brightness distrib. 77—22316
NGC 1052, 4278, VLBI obs. of galactic nuclei at 18 centimetres 80—22078
NGC 1052, active elliptical, radio and optical study 78—65693
NGC 1052, elliptical, electron density and N II/Hα line intensity ratio in nucleus 77—33642
NGC 1052, elliptical galaxy, field, H I emission mapping and line profiles 80—98719
NGC 1052, elliptical galaxy, H I obs. 78—69873
NGC 1052, H I detect. in elliptical galaxy 78—41041
NGC 1055, 681, 4594, rot. curves and mass distribs. *(Russian)* 80—90541
NGC 1068, 87.2 GHz continuum obs., Ne abundance 78—41042
NGC 1068, light polarisation in Seyfert galaxy 78—54046
NGC 1068, Seyfert, 2-2.5 μm spectrum, H_2 detect. 78—57636
NGC 1068, Seyfert, UBV photometry 77—67132
NGC 1068, Seyfert galaxy, forbidden O III lines high-resolution profile 80—46665
NGC 1068, Seyfert galaxy, IR photometry and polarimetry 78—54035
NGC 1068, Seyfert galaxy, nucleus, H_2 existence and form. 80—12816
NGC 1068, Seyfert galaxy, radiative transfer in dust rel. to spectral flux distrib. 77—29914
NGC 1068, type 2 Seyfert, recombination spectrum and reddening 80—90519
NGC 1073, quasars in spiral arms 79—53904
NGC 1073 obs. of three QSOs lying in spiral arms 80—22110
NGC 1084, NGC 7331, spiral galaxies, surface photometry and mass distrib. 79—40265
NGC 1087 and 1090, surface B photometry and mass distribs. in spirals 80—46676
NGC 1097, jets on image-processed plates of galaxy 78—61922
NGC 1167, S0 galaxy, extended core radio source 14.8 GHz mapping 79—25727
NGC 1199, possible mag. 17 SN, 1979 Sept. obs. 80—41846
NGC 1199 and silhouetted compact high-redshift object 78—41031
NGC 1265, 1275, in Perseus cluster, low-resolution aperture synthesis map at 408 MHz 80—56958
NGC 1265, outer structure from electronographic obs. 78—16521
NGC 1265, twin jet model for radio trails 79—75290
NGC 1265, VLA obs. at 4886 MHz 79—21428
NGC 1275, central giant galaxy in Perseus cluster, excess X-ray emission 80—41907
NGC 1275, compact X-ray source, synchrotron self-Compton model 77—29961
NGC 1275, double nucleus, radio and emission line obs. *(Russian)* 79—21439
NGC 1275, explosive phenomena in nuclei 80—26970
NGC 1275, form. of optical filaments in surrounding cooling gas 80—67862
NGC 1275, ionization and excitation mechanisms in surrounding filaments 79—71107
NGC 1275, IR variability, 2 μm obs. 79—30118
NGC 1275, multicolour photometry of Seyfert galaxy *(Russian)* 77—64848
NGC 1275, nucleus, daily vars. in optical continuum flux 79—71118
NGC 1275, Perseus A, refutation of colliding elliptical and spiral galaxies theory 78—57639
NGC 1275, photometric and spectrum vars. 80—22075
NGC 1275, possibly BL Lacertae object 78—45406
NGC 1275, Seyfert, optical outbursts *(Russian)* 77—82301
NGC 1275, Seyfert, radio and optical variability of nucleus 78—28793
NGC 1275, Seyfert, search for regular optical brightness vars. of nucleus *(Russian)* 77—60828
NGC 1275, Seyfert galaxy, emission line variability and nucleus conditions 77—37649
NGC 1275, Seyfert galaxy, IR polarisation obs. 78—4360
NGC 1275, Seyfert galaxy, nucleus, ralation between gas and radio source structs. *(Russian)* 79—48936
NGC 1275, Seyfert galaxy, nucleus model 77—41411
NGC 1275, Seyfert galaxy, nucleus struct. *(Russian)* 80—62288
NGC 1275, Seyfert galaxy, spectrograms 77—22314
NGC 1275, Seyfert galaxy, spectroscopic obs. *(Russian)* 77—17670
NGC 1275, Seyfert galaxy, vars. of emission line spectrum and conditions in nucleus envelope 77—17688

galaxies continued
NGC 1275, spectroscopic and photometric obs. 77—33630
NGC 1275, stellar populations, visible UV obs. 77—91628
NGC 1275, vel. field mapping 78—81680
NGC 1275, X-ray emission rel. to Perseus cluster soft X-ray struct. 79—9009
NGC 1275 (3C 84, Perseus A), Seyfert galaxy, 5′ halo SHF obs. 80—105372
NGC 1275 (3C 84), Seyfert galaxy, optical and 3 mm radio vars. similar struct. 79—67102
NGC 1275 (3C 84), Seyfert galaxy, search for variability at 408 MHz *(Russian)* 77—17710
NGC 1275 as pair of interacting galaxies, spectra and structure 80—26969
NGC 1275 nucleus, structural changes at 2.8 cm wavelength 80—31359
NGC 128, S0 galaxy, rot. curve 77—33631
NGC 1291 and 1326, kinematics of lenticular galaxies 79—53908
NGC 1313, 5236 and 7552, barred spirals, emission regions, visible obs. 80—82510
NGC 1313, barred spiral, interferometric study 77—49474
NGC 1313 barred spiral galaxy, asymmetric rot. *(French)* 79—97082
NGC 1316 (Fornax A), optical study of giant radiogalaxy 80—77479
NGC 1365 and 1386, IR and optical props. of emission-line galaxies 80—51867
NGC 1411, discovery of SN in elliptical galaxy 77—67104
NGC 147, Local Group galaxy, identifications and radial vels. of planetary nebulae 77—33596
NGC 1510, tidal interaction with NGC 1512 companion galaxy 78—81682
NGC 1510, young elliptical galaxy 77—87541
NGC 1512 and 1510, interacting galaxies, optical and H I study 79—80348
NGC 1566, Sbc galaxy, spectrophotometry of nucleus and nine H II regions 80—51824
NGC 1569, dwarf irregular galaxy, H I obs. 80—90538
NGC 1569, irregular galaxy, optical linear polarization obs. from Durham 77—74126
NGC 157, spiral galaxy, surface photometry and mass distrib. 79—40264
NGC 1672 and 2997, nuclei morphology, Hα obs. 80—67867
NGC 1809 rel. to PKS 0502-696, no connection 79—30129
NGC 185, Local Group galaxy, identifications and radial vels. of planetary nebulae 77—33596
NGC 1961, rotation curve for massive spiral 79—62898
NGC 205, UV image 80—98716
NGC 2110, Seyfert 2 X-ray galaxy, optical studies 80—22071
NGC 2110, X-ray/radiogalaxy, elliptical morphology questioned 79—21426
NGC 2146, peculiar spiral galaxy, extensive H I obs. 77—17676
NGC 2366 H II region visible and radio obs. 80—77475
NGC 2377, H I absorption within radiogalaxy 79—5910
NGC 2403, distance 77—2471
NGC 2403, distance from 21 cm line widths and optical methods, H_0 global value determ. 77—9827
NGC 2403, Sc III type, surface photometry 78—32581
NGC 253, 87.2 GHz continuum obs., Ne abundance 78—41042
NGC 253, barred spiral galaxy, detailed surface photometric study 80—105327
NGC 253, detection of extragalactic ammonia 79—48886
NGC 253, H_2O emission detection at 22.235 GHz 78—16534
NGC 253, interstellar HCN and CS search 77—53661
NGC 253, Ne II 12.8 μm emission and galactic dynamics 79—92844
NGC 253, nuclear source nature from IR obs. 80—82485
NGC 253, radio continuum obs. at 8.7 GHz 79—92853
NGC 253, radio recombination line obs. 80—56941
NGC 253, Sc galaxy, aperture synthesis obs. of H I distrib. 77—74131
NGC 253, Sc-type galaxy, two-micron spectrophotometry 80—4442
NGC 253, spiral, H102 alpha recomb. line detect. 77—87540
NGC 253, spiral galaxy, gas outflow from nucleus rel. to nucleus stellar population 78—28776
NGC 2623, interacting galaxy, H I absorpt. and emission obs. 79—17087
NGC 2639 companion galaxy, nearby UV excess objects discoveries and redshifts 80—56965
NGC 2685, geometry of flattened system 79—12511
NGC 2685, H I 21 cm line survey 80—56943
NGC 2685, polarization of peculiar galaxy *(Russian)* 79—35390
NGC 2685, possible explosion in peculiar galaxy *(Russian)* 79—30135
NGC 2715, 5033, 5055, rot. curves and orientation parameters 79—12517
NGC 2742, spiral galaxy, rot. and mass. *(French)* 78—89255
NGC 2768, optical and IR photometric study 78—36683
NGC 2776, rotation and mass from image-tube spectra *(French)* 79—101199
NGC 2782, peculiar hot-spot nucleus galaxy, vel. field 78—4357
NGC 2823, obs. of nearby double radiosource 78—24562
NGC 2903, 5005 and 5055, spirals, masses, mass-luminosity ratios and classifications 77—78871
NGC 2903, photometric obs. of bright patches in spiral arms *(Russian)* 77—64847
NGC 2903, spiral galaxy, nucleus identification and visual energy distrib. 80—62273
NGC 2915, southern galaxy, optical and H I obs. 77—67126
NGC 2974, 4105, 5846, elliptical galaxies, H I contents 79—62906
NGC 2997, late-type galaxy, rot. and mass 79—21409
NGC 2997, morphology and hot spots around nucleus, obs. 80—62282
NGC 2997 and 5128, morphology from ESO 3.6 m telescope obs. 79—97063
NGC 300, nearby intergalactic dust obs. 77—45553
NGC 300, NGC 1365, southern galaxies, H II regions comp. 80—4441
NGC 300, spiral, aperture synthesis obs. of H I, outer plane warping 79—53905
NGC 3067, galactic Ca II absorpt. lines in spectrum of quasar (3C 232) 78—36719
NGC 3079, peculiar edge-on spiral galaxy, 2.7 and 8.1 GHz obs. 78—36692
NGC 3079, rotation and mass from image tube spectra *(French)* 77—29931
NGC 3115, lenticular galaxy, photometry and struct. 80—36707
NGC 3115, optical and IR photometric study 78—36683
NGC 3115, s0 galaxy, photometric obs. 77—29917

galaxies continued
- NGC 3115, S0 galaxy, rotation and mass of inner 5 kiloparsecs 80−105326
- NGC 315, giant radio galaxy, jet structure and polarization 79−35379
- NGC 315, NGC 6251, very large radio galaxies, 11.1 cm obs. 78−86014
- NGC 315, radio galaxy, mag. field struct. in radio jets 80−82526
- NGC 3226, elliptical galaxy, supernova discovery 77−33537
- NGC 3227, 3516, Seyfert galaxies, optical polarisation obs. 80−90533
- NGC 3227, Seyfert galaxy, photoelectric and spectroscopic study and comparison with galaxy chain (VV 150) 80−98724
- NGC 3256, peculiar galaxy, kinematics 78−96537
- NGC 326 (B2 0055+26), radio galaxy with precessing beam model 79−17118
- NGC 3309, in Hydra I cluster, photometric obs. 77−33659
- NGC 3310, peculiar spiral galaxy, 2.7 and 8.1 GHz obs. 77−29929
- NGC 3310, peculiar spiral galaxy, near nuclear H II regions exploratory investigation 80−62235
- NGC 3311, in Hydra I cluster, photometric obs. 77−33659
- NGC 3312 in Hydra I cluster, ram-pressure sweeping of interstellar medium 78−93429
- NGC 3379, elliptical galaxy, spectroscopic obs. rel. to rot. and vel. dispersion 78−49529
- NGC 3379, elliptical galaxy as luminosity distrib. standard 80−22073
- NGC 3379, luminosity profile of elliptical rel. to formation model 78−69868
- NGC 3379, surface photometry, computerised analysis 78−12101
- NGC 337 and 6745, galaxy chain interpretation *(Russian)* 80−17658
- NGC 3384, quasars aligned across galaxy 79−53927
- NGC 3448, optical and H I 21 cm line obs., peculiar nucleus 78−36696
- NGC 3516, SBO type Seyfert, extended nebulosity, UV and visible obs. 80−82487
- NGC 3516, Seyfert, search for regular optical brightness vars. of nucleus *(Russian)* 77−60828
- NGC 3516, Seyfert galaxy, charge transfer reactions rel. to low excitation forbidden line 80−56701
- NGC 3516 Seyfert galaxy, optical spectrum 77−26052
- NGC 3556, edge-on galaxy, multi-freq. radio continuum study 79−44607
- NGC 3620, southern emission-line galaxy at low galactic latitude 78−86022
- NGC 3627, obs. of type II supernova 1973r 77−49407
- NGC 3628, detection of emerging H I plume at 21 cm wavelength 78−54038
- NGC 3631, H II regions and spiral struct. 77−45538
- NGC 3665, elliptical galaxy with dust lane, radio obs. 79−58414
- NGC 3672, high luminosity spiral galaxy, extended rotation curves 78−8124
- NGC 3686 galaxy quartet, surface photometry, mass distribs. and group stability 80−62297
- NGC 3718, peculiar early-type galaxy, H I survey, interaction with NGC 3729 79−35383
- NGC 3733, discovery of mag. 15 supernova (1980 March 17) 80−51793
- NGC 3733, supernova spectrophotometry (1980 March 22) 80−62164
- NGC 3780, probable supernova 79−5848
- NGC 3783, possible X-ray emitting Seyfert galaxy 77−13467
- NGC 3898 and 4036, B photographic photometry 78−54045
- NGC 3904, elliptical galaxy, H I content from 21 cm line 77−87545
- NGC 3913, B magnitude and spectrophotometry of supernova 79−44513
- NGC 3913, supernova discovery report 79−44512
- NGC 3913, type I supernova and likely max. magnitude (1979 March) 79−48834
- NGC 3928 C (Markarian 190), identification as miniature spiral galaxy 80−105347
- NGC 3962, elliptical, large scale H I distrib. 79−80347
- NGC 4038-9, giant H II regions in interacting galaxies 79−97053
- NGC 4038/39, interacting galaxy pair, H I kinematics and distrib. 79−35365
- NGC 4088, rotation curve and mass of spiral galaxy *(French)* 78−36698
- NGC 4151, compact X-ray source, synchrotron self-Compton model 77−29961
- NGC 4151, Compton emission model for Seyfert galaxy using gamma-ray data 80−67902
- NGC 4151, gamma-ray emission from Penrose powered black hole 80−56925
- NGC 4151, optical polarization of Type 1 Seyfert 79−53906
- NGC 4151, OSO 8 X-ray obs. of flare in Seyfert galaxy 79−17093
- NGC 4151, outer structure from electronographic obs. 78−16521
- NGC 4151, search for 1-20 MeV gamma rays, balloon-borne obs. of Seyfert galaxy 80−67912
- NGC 4151, Seyfert, gamma-ray emission, Compton scatt. model 80−98711
- NGC 4151, Seyfert, gamma-ray energy spectrum *(Russian)* 79−88748
- NGC 4151, Seyfert, hard X-ray emission detect. 80−46660
- NGC 4151, Seyfert, nuclear region far UV spectrum 78−32573
- NGC 4151, Seyfert, optical and X-ray variability correl. *(Russian)* 79−21440
- NGC 4151, Seyfert, optical polarimetry, circumnuclear dust envelope 78−61916
- NGC 4151, Seyfert, X-ray absorpt. increase 78−12367
- NGC 4151, Seyfert galaxy, 21 cm line obs. 77−57087
- NGC 4151, Seyfert galaxy, companion galaxy and spiral arm obs. 78−16522
- NGC 4151, Seyfert galaxy, for UV line profiles 80−22083
- NGC 4151, Seyfert galaxy, IR polarisation obs. 78−4360
- NGC 4151, Seyfert galaxy, low energy gamma-ray obs. 78−12368
- NGC 4151, Seyfert galaxy, low-energy γ-ray spectrum 80−31370
- NGC 4151, Seyfert galaxy, optical variations of nucleus 77−82305
- NGC 4151, Seyfert galaxy, repeated X-ray flaring obs. 80−90534
- NGC 4151, Seyfert galaxy, UV spectrum 77−13468
- NGC 4151, UV photometry and extended spectrum of Seyfert galaxy 78−89249
- NGC 4151, X-ray emission, two-component model 78−45399
- NGC 4151, X-ray emission monitoring by Ariel V, evidence for flare 77−2491
- NGC 4151, X-ray emitting Seyfert galaxy, Uhuru obs. 78−12411
- NGC 4151, X-ray flares in Seyfert, thermal model and central black hole 78−93407
- NGC 4151 (3U 1207+39), Seyfert galaxy, high-energy X-ray obs. with balloon-borne telescope 77−45610

galaxies continued
- NGC 4151 (3U 1207+39), weak X-ray source, ANS meas. 80−46701
- NGC 4151 (4U 1206+39), hard X-ray variability of Seyfert galaxy 80−17647
- NGC 4151 (4U 1206+39), Seyfert galaxy, hard X-ray spectrum 78−49537
- NGC 4214, barred Im galaxy in Canes Venatici I group, H I obs. 79−92862
- NGC 4235, Seyfert galaxy, spectrum and radial. vel. 78−49536
- NGC 4248, H I obs. 78−4358
- NGC 4258, aperture synthesis obs. complemented by short spacing data fron single dish obs. 79−66928
- NGC 4258, gas flow in disk, two-dimens. model 79−48913
- NGC 4258, high resolution 21 cm line obs. 80−56946
- NGC 4278, elliptical, H I detect. 78−4342
- NGC 4278, elliptical galaxy, H I content meas. 77−22312
- NGC 4278, possible supernova near nucleus 77−53616
- NGC 4278, possible visual obs. of supernova 77−29865
- NGC 4314, barred spiral galaxy, UBV surface photometry of central region 80−77482
- NGC 4319, weak radio emission 79−48912
- NGC 4321, JHKL mags. of SN, 1980 Jan. obs. 80−41847
- NGC 4321, spectrograms of supernova (1979 April) 79−48836
- NGC 4321, spectrophotometry of type II supernova 79−67044
- NGC 4321, spectrum, lightcurve and magnitudes of type II supernova 79−71061
- NGC 4321, supernova, visual magnitude estimates, 1979 May-Jun. 79−75229
- NGC 4321, supernova UBV photometry, light curve and type 79−67045
- NGC 4321, supernova UBV photometry 79−53835
- NGC 4321, type II supernova characts. and 1979 April UBV and visual obs. 79−58364
- NGC 4321, UBVRI photometry and visual mag. estimates of supernova (1979 April-June) 79−80330
- NGC 4321 (M100), interstellar Na I and Ca II absorption 80−51847
- NGC 4321 (M100), supernova UBVR photometry 80−77428
- NGC 4378, anaemic Sa galaxy, extended rot. curve 79−8990
- NGC 4410a/b, interacting pair, possible HEAO 1 obs. 80−12832
- NGC 4449, emission nebulae content 79−84848
- NGC 4449, irregular, optical obs. of possible SNR with broad emission lines 79−17057
- NGC 4449, irregular, radio emission detect. from possible SNR 79−17056
- NGC 4449, irregular galaxy, extraordinary supernova remnant spectrophotometry 80−56895
- NGC 4472, very weak radio galaxy, struct. and radio power 78−65708
- NGC 4472 and 5846, luminous giant ellipticals, B−V colour profiles 80−51865
- NGC 4473, flattened elliptical, spectroscopic obs., dynamics 78−57631
- NGC 4485/90 interacting system, radio continuum and H I obs. 80−62274
- NGC 4490/4485, interacting galaxy pair, 2.7 and 8.1 GHz obs. 78−36692
- NGC 4565, dark halo population model 79−62905
- NGC 4565, edge-on spiral galaxy, grid photography of halo 80−62261
- NGC 4565, spiral galaxy, minor axis brightness profile rel. to massive halos problem 78−93409
- NGC 4565, spiral galaxy, optical halo detect. 78−12364
- NGC 4565, warped Sb galaxy, H I distrib. 21 cm obs. 80−109542
- NGC 4593, Seyfert galaxy, spectrophotometry 80−51878
- NGC 4593, var. X-ray emission from bright type 1 Seyfert 79−84856
- NGC 4594, search for O I 6300 Å forbidden line from warm neutral interstellar medium 79−71129
- NGC 4594, Sombrero galaxy, H I content, stellar rotation curve, mass-to-light ratio 77−53680
- NGC 4631, edge-on spiral galaxy, high freq. radiocontinuum obs. 77−74129
- NGC 4631, edge-on spiral galaxy, radio continuum halo obs. 77−26054
- NGC 4631, spiral galaxy nucleus, IR photometry 78−45412
- NGC 4631 group, tidal interactions model 78−54059
- NGC 4631/NGC 4656, neutral H aperture synthesis obs. 78−54043
- NGC 4636, elliptical, H I emission detect. 78−32570
- NGC 4636, elliptical galaxy, H I content from 21 cm line 77−87545
- NGC 4636, elliptical galaxy, H I large-scale distrib. 78−45400
- NGC 4647, supernova classification and time since maximum 79−25620
- NGC 4647, supernova discovery 79−25619
- NGC 4697, elliptical, axisymmetric galaxy, three dimens. mass model 80−109549
- NGC 4725/47 interacting pair, 21 cm line obs. of H I distrib. 80−46662
- NGC 4736, spiral, ring-like structs. as Lindblad resonance tracers 77−2469
- NGC 4736, spiral galaxy, H I study 77−57090
- NGC 4736, spiral galaxy, multifrequency radio continuum study 77−17683
- NGC 4762, S0 galaxy, rot. curve and dynamics 78−28774
- NGC 4861, SBm galaxy, obs. of supergiant H II region (Markarian 59) 80−98705
- NGC 4889, cD galaxy, assoc. with line of peculiar galaxies in Coma cluster 77−64860
- NGC 488, NGC 977, supernovae photometry 79−62857
- NGC 488, Sb galaxy, rotation curve from emission line spectra 80−62266
- NGC 4902, supernova discovery and magnitude (1979 August) 79−88693
- NGC 4944, obs. of supernova 1973f 79−21318
- NGC 4945, late-type spiral galaxy, excited gas kinematics, obs. 80−109547
- NGC 4945, spiral, H I absorpt. obs. 77−33651
- NGC 4945, strong H_2O maser emission detected 79−40271
- NGC 4945, water vapour emission obs. 78−93427
- NGC 5012, B and R imagery of S0 galaxy 79−92847
- NGC 5102, lenticular galaxy, dust and young stars obs. 79−44609
- NGC 5102, peculiar SO galaxy, obs. 77−13452
- NGC 5128, Centaurus A, stellar population and dust lane 78−20890
- NGC 5128, H I, OH and formaldehyde absorpt. line obs. 77−33649
- NGC 5128, inner structure of optical jet 79−12516
- NGC 5128, NE halo, compact emission regions and BSOs 79−17095
- NGC 5128, southern radio galaxy, OAO UV photometry, energy distrib. 79−40255

galaxies continued
NGC 5128, struct. and evolution from multicolour photography 79—53913
NGC 5128 (Centaurus A), dark lane, extended 10 μ emission 79—21429
NGC 5128 (Centaurus A), fast ray of nucleus at 13.5 mm wavelength 77—87564
NGC 5128 (Centaurus A), formaldehyde absorpt. obs. at 14 GHz 80—17657
NGC 5128 (Centaurus A), gamma-ray emission from Penrose powered black hole 80—56925
NGC 5128 (Centaurus A), gamma-ray line emission 79—44641
NGC 5128 (Centaurus A), globular clusters deficiency 80—26986
NGC 5128 (Centaurus A), high-resolution spectroscopy and tubelike model of dust band 80—56945
NGC 5128 (Centaurus A), narrow band photography 79—92854
NGC 5128 (Centaurus A), nucleus, radio and X-ray variability model 80—90522
NGC 5128 (Centaurus A), radio and X-ray var. of nucleus 78—36711
NGC 5128 (Centaurus A), radio galaxy, obs. at 1.38 cm wavelength with resolutions up to 8″ *(Russian)* 80—109558
NGC 5128 (Centaurus A), slowly varying flux component, 22 GHz confirmation 80—56939
NGC 5128 (Centaurus A), struct. and evolution from photographic and spectroscopic obs. 80—4429
NGC 5128 (Centaurus A), X-ray structure 78—24569
NGC 5128 (Centaurus A), X-ray variability, Ariel V Sky Survey obs. 78—16574
NGC 5128 (Centaurus A) optical struct., picture processing anal. 79—53907
NGC 5128 (lentaurus A), image tube spectrograms 80—41892
NGC 5195, companion of M51, rot. and relative mass 77—22306
NGC 5195 (M51 comparison), struct. obs. using negatives superposition method *(Russian)* 77—13251
NGC 520, Irr II galaxy, new photographic and spectroscopic obs. 80—41889
NGC 520, tidal interaction in peculiar galaxy 79—48916
NGC 5236, radial vars. of emission line ratios 80—82497
NGC 5236, spiral galaxy peculiar nucleus continuum and reddening 80—73031
NGC 5236 (M83), Sc galaxy, CO obs. 78—65689
NGC 5253, SN 1972e spectrum 80—41844
NGC 5253, surrounding star clusters, fossil evidence for star form. burst, visible obs. 80—77489
NGC 5291, massive gas-rich peculiar lenticular galaxy in IC 4329 cluster 79—71127
NGC 5296 (NGC 5297 companion), obs. of nearby quasar 77—13489
NGC 5296/7 and nearby quasar, radio obs. 78—93419
NGC 5363, radiosource and compact core 77—49468
NGC 5383, barred spiral, kinematic study *(French)* 77—71141
NGC 5383, barred spiral, radio continuum emission obs. at 1415 MHz 78—73753
NGC 5383, barred spiral galaxy, optical surface photometry 79—9000
NGC 5383, barred spiral galaxy, vel. field 78—24549
NGC 5383, gas flow in barred spiral 79—17091
NGC 5383, H I 21 cm line obs. of barred spiral 80—8687
NGC 5406, 1977, March 28 photovisual magnitude of Lovas' supernova 77—57002
NGC 5406, discovery of 14th magnitude supernova 77—33535
NGC 5474, peculiar Scd galaxy, H I distrib. and kinematics 80—8683
NGC 5506, IR obs. of X-ray Seyfert-like galaxy 78—65696
NGC 5506, Seyfert 2 galaxy, detect. of flare in X-ray emission 80—17656
NGC 5506, X-ray Seyfert, spectra 78—93411
NGC 5506 (3U 1410—03), probable X-ray galaxy, optical spectrum and morphology 77—13466
NGC 55, photoelec. sequence for stars surrounding galaxy edge 80—73007
NGC 5728, barred spiral, vels. and mass distrib., visible spectra obs. 80—94863
NGC 5854, discovery of mag. 15 Type I supernova (1980 March 20) 80—51793
NGC 5866, edge-on galaxy, luminosity obs., BV photometry 80—82511
NGC 5907, rotation and mass of edge-on galaxy from spectra *(French)* 78—77595
NGC 5920, cD galaxy in poor cluster MKW 3s, extended X-ray emission obs. 80—51884
NGC 6034 radio tail galaxy in Hercules cluster, Westerbork obs. at 0.6, 1.4 and 5 GHz 78—36706
NGC 6051, cD galaxy in poor cluster AWM 4, extended X-ray emission obs. 80—51884
NGC 6052, possible collision of two late type spiral galaxies, observational evidence 80—8681
NGC 612, rotation of lenticular radio galaxy 80—51874
NGC 612 (PKS 0131—36), radio galaxy with disc, struct. 79—2568
NGC 6166, cD galaxy, B—V profiles 80—51865
NGC 6217, spectra of nucleus *(Russian)* 79—92869
NGC 6221 and NGC 7213, optical spectrophotometry of X-ray galaxies 79—35377
NGC 6240, unusual radio galaxy, radio and optical, obs. 80—4440
NGC 6240 (=VV 617+MCG 0-43-4), interacting Seyfert with reddening *(Russian)* 79—58426
NGC 6251, elliptical galaxy, nuclear jet radio obs. 78—41059
NGC 6251, extended radio galaxy, polarisation at 610 MHz 78—61918
NGC 6251, radio galaxy, CCD photometry rel. to central supermassive object 80—26966
NGC 6251, radio galaxy, radio jets misalignment, VLBI obs. 80—27001
NGC 6251, radio jet brightness and shape rel. to beam and slingshot models 79—25741
NGC 6251, very large radio galaxy with exceptional jet 78—12394
NGC 628, evidence against discrete states of redshift 77—60820
NGC 628, Sc I galaxy, extensive H I envelope, 21 cm obs. 80—90520
NGC 6306, active galaxy, spectrophotometry and morphology *(Russian)* 78—28768
NGC 660, barred spiral, photometry and spectroscopy 77—5566
NGC 672 and IC 1727, interacting galaxies, H I obs. and computer modeling 2 km line obs. 80—67853
NGC 6745, peculiar ring-like galaxy, struct. *(Russian)* 79—25732
NGC 6822, CO emission upper limits 78—36693
NGC 6822, dwarf irregular, luminous stars, visible spectra and photometry 80—82345

galaxies continued
NGC 6822, irregular galaxy, interferometer study of H I assoc. with optical core 78—20889
NGC 6822, irregular galaxy, planetary nebula spectrophotometry and comp. 80—41867
NGC 6822, new compact H II regions discovery 80—51854
NGC 6822, struct. and content of irregular galaxy 77—41405
NGC 6822, UBV photometry of dwarf irregular 79—62903
NGC 6872, remarkably large barred spiral galaxy 80—31358
NGC 6902, H I rich southern supergiant spiral galaxy, opticals studies 80—8680
NGC 6946, CO emission from late-type galaxy 78—89250
NGC 6946, radio continuum emission from H II complexes and nonthermal disc 77—41407
NGC 6946, search for radio emission from four young SNRs 80—77473
NGC 6946, spiral, N overabundance in nucleus *(French)* 78—89257
NGC 7213, IR photometry of lenticular Seyfert X-ray galaxy 78—89262
NGC 7213, S0 galaxy with Seyfert nucleus, spectra and direct obs. 78—86024
NGC 7217, spiral, extended rot. curve, mass distrib. 79—21414
NGC 7331, search for radio emission bridge to Stephan's Quintet 77—57099
NGC 7331/Stephan's Quintet area, obs. at 1421 MHz 78—12392
NGC 7385, optical-radio knot obs. in elliptical galaxy 79—35362
NGC 741, 1316, 7626, radio galaxies, dynamics 80—94871
NGC 7469, Seyfert galaxy, spectrum 77—57089
NGC 7479, barred spiral, surface photometry, struct. 78—81690
NGC 7541, rotation curve and mass distrib. in spiral *(Russian)* 80—94874
NGC 7582, narrow emission line X-ray emitting nucleus, UV spectra 80—101640
NGC 7603, Seyfert galaxy, spectrum variations 77—13463
NGC 7714—7715, peculiar interacting pair, discovery of two nearby quasars 78—28835
NGC 7723, dynamics of barred spiral 79—5893
NGC 772, false companions identified as refl. nebulosities *(Russian)* 80—36723
NGC 7743, barred spiral, surface photometry, struct. 78—81690
NGC 7793, Hα interferometry 77—53683
NGC 7793, late-type galaxy, ionized gas phys. conditions and mass-luminosity distrib. 80—26967
NGC 891, edge-on disc galaxy, radio continuum obs. 78—28786
NGC 891, HI 21 cm. obs. of edge-on Sb galaxy 79—48914
NGC 891, radio continuum obs. at 8.7 GHz 79—92853
NGC 891, radio halo, Westerbork obs., electron propag. and magnetic fields 78—61920
NGC 925, barred spiral galaxy, high-resolution H I obs. 80—105329
NGC 931, interacting Seyfert galaxy, struct. and spectra 79—25716
NGC 935-IC 1801, close pair of spiral galaxies, rot. curves and mass distribs. 77—45556
NHC 4594 (Sombrero Galaxy), H II regions and ionised interarm gas detect. 78—36685
night sky model for artificial satellite search systems 77—73923
Nilson dwarf galaxies, H I survey statistical props. 79—92851
ninth catalogue of galaxies with UV continuum *(Russian)* 77—49464
non-linear high-frequency waves in relativistic cosmology 79—48968
nonflat components (halo), mass limits 80—62291
nonlinear interaction between monochromatic wave and particles in gravitating system *(Russian)* 77—82285
nonlinear nonradial oscillation of two-dimens. models 77—87480
nonlinear periodic waves in self-gravitating fluid rel. to galaxy formation 79—70946
nonlinear phenomena in gas subsystems of flat galaxies *(Russian)* 77—74143
normal galaxies, contrib. to diffuse X-ray background 79—17141
North Galactic Pole region, galaxy distrib. in 36 sqaure degree field 79—40261
northern galactic plane galaxies on POSS E prints 80—62280
nuclear black holes, destruction in isothermal sphere rel. to black tide model of QSOs 77—78884
nuclei, accel. of supermassive compact objects by emission of asymmetric radiation 77—45481
nuclei, accretion and radiation spectrum of gas debris from star disrupted by black hole 80—90467
nuclei, dense stellar systems fates 79—25652
nuclei, distrib. and consumption rate of stars around massive collapsed object 77—45497
nuclei, fate of stellar mass loss material 80—67858
nuclei, IR astronomy 77—53433
nuclei, massive black holes existence 79—25713
nuclei, regular optical variability 77—45598
nuclei, rotating supermassive magnetized disc model 79—84849
nuclei, stellar population synthesis 78—36688
nuclei, superfine radiostructure determ. using interstellar scintillations *(Russian)* 80—77297
nuclei and radiogalaxy matter and energy ejection *(Italian)* 77—87552
nuclei bright line emission, contrib. of H II regions and shock waves 80—109552
nuclei energy source, rel. to supernovae relativistic particles total energy upper limit in early explosion stages 79—71059
nuclei of bright galaxies, stellar populations and H II regions, spectral anal. 80—98708
nuclei of massive galaxies, recurrent activity 78—89261
nuclei of nearby galaxies, stellar population models 77—2467
nuclei of nearby galaxies, vel. dispersions 77—57083
null radiation gravitation deflection by relativistic spherical masses 79—58600
number density profiles in clusters 78—12382
objective-prism spectra meas., computer control of Joyce-Loebl microdensitometer 80—105173
Ohio radio sources, optical identification using radio and optical positions meas. by Texas interferometers 78—28808
optical and radio props. rel. to identifications of 3CR sources 78—28830
optical counterparts of 5C radiosources and blue objects, spectrographic obs. 79—101212
optical identifications for 2A X-ray sources 78—89273
optical identifications of extragalactic radio sources 80—105373
optical nebulosities associated with active nuclei 79—97069
optical redshifts, of 719 bright galaxies 78—89252
optically bright galaxies, 3 cm obs. of 141 objects 80—73040

galaxies continued

- optically bright galaxies, radio survey at 1400 MHz, 248 radiosources detect. 77−60627
- OQ 208, red shift difference between broad and narrow emission lines 79−67100
- orbit segregation in nonhomologously changing nonlinear gravitational field 78−4351
- orbits, near particle resonance of galaxy, numerical study 79−88746
- origin, spontaneous prod. of cosmological fluctuations 80−94902
- origin, structure and evolution, review *(Chinese)* 77−87551
- origin and early evolution, review 80−17669
- origin and evolution, developments 80−36718
- origin and evolution, discussion (London, England, 14-15 Feb. 1979) 80−36770
- origin of galaxies in expanding Universe, plasma cond. and instabilities, MHD soln. 80−62283
- origins, galactic angular momenta and magnetic fields 78−93405
- oscillating spherical stellar system, growth of density correl. 77−57095
- OX+029, nearby extended variable object 79−67096
- pairs, axis ratios and posn. angles 78−93430
- pairs containing one Markarian and one normal galaxy, morphology 78−96535
- pairs with Markarian components, spectroscopy *(Russian)* 77−37648
- paradoxical redshifts compatibility with gravitation theory 78−73757
- parallaxes, meas. via radiointerferometric techniques 78−53796
- Parkes 2700 MHz survey, optical identifications 77−49489
- particle acceleration in collisionless shocks, regulated injection and high efficiency 79−44311
- particle dynamics in spheroidal mass distribs., third integral of motion 77−74101
- particle reacceleration in radio galaxies 79−71104
- particle resonance, nearby stellar orbits theoretical study 80−26914
- peculiar and interacting galaxies in southern sky, emission line obs. of 37 objects *(Russian)* 78−49511
- peculiar compact galaxy and quasar near companion galaxy NGC 5296, redshifts 77−13489
- peculiar extragalactic sources, multiaperture UBV photometry 78−28772
- peculiar galaxies in Coma cluster, calc. and obs. 77−64859
- peculiar galaxies radio emission detect. 77−17674
- peculiar giant galaxies with fragmentation *(Russian)* 77−26063
- peculiar hot-spots nuclei 79−30130
- peculiar motion, kinetic energy density 77−37651
- peculiar nuclei, relation to galaxy type 78−73759
- peculiar velocities, influence of interaction with long-wave primordial gravit. radiation 80−17661
- periodicity investigation at 21 cm 80−82529
- PHL 1070, spectrum of halo surrounding quasar 78−28771
- photographic observations, image processing techniques 77−9664
- photographic photometry of bright galaxies, Numerical Mapping Technique *(Italian)* 77−91443
- photography, image picture processing system for colour 77−49303
- photometry, B system magnitudes, luminosity curves and photometric parameters 77−49469
- photometry, background subtraction problem *(Italian)* 80−98570
- photometry, magnitudes and colours from multiaperture UBV photoelectric photometry 77−49470
- photometry, reduction of Shapley-Ames magnitudes to B_T system 77−49472
- photometry, reduction to B_T system of Ames, Reiz and Zwicky catalogues of Virgo cluster area 79−58411
- photometry, reduction to B_T system of southern galaxy magnitudes 77−49473
- photometry, revised standard total magnitudes and colours of multiply observed galaxies 78−8116
- photometry, standard total magnitudes of 139 bright galaxies in Virgo cluster area 78−65685
- photometry, total magnitudes and colours in BV from Holmberg photographic photometry 77−49471
- photometry of galaxies in Virgo area, reduction of magnitudes to standard B_T system 79−92852
- photon helicity detection for matter/antimatter star discrimination 78−12092
- Pictor A, powerful radio galaxy, photographic and spectrophotometric obs. 77−49481
- PKS 0211−47 and 0634−20, giant radiogalaxies, optical and radio obs. 78−81702
- PKS 0528−250, neutral stellar object with no emission and rich absorption 78−49551
- PKS 1345+12, radio galaxy, optical spectrum 78−4341
- PKS 1402+044, dissector scanner obs. of red object with 3.20 redshift 78−65710
- PKS 1718−649, radio and optical study 77−45564
- PKS 1934−63, spectrophotometry of radiogalaxy 78−54066
- PKS 2201+04, compact galaxy, optical variability 77−26051
- PKS 2322-12, narrow-line radio galaxy, optical spectrum 77−33664
- plane galactic orbits, epicyclic approx. 80−36674
- Poissons equation for finite thickness disks, effect of thickness on density waves 80−17666
- polytropic gaseous disc galaxies with Toomre density distrib., global instability 80−98725
- pregalactic gas cloud, thermal instability, fragmentation 78−4421
- prestellar gas, element separation by gravitational diffusion 79−21386
- primaeval galaxies, model emission spectra 80−46655
- primaeval giant elliptical galaxies, observable props. 78−89260
- primeval, appearance in X- and γ-ray regions, contrib. to background rad. 80−8692
- primeval, investigation of red shift 80−31372
- primordial heavy leptons halos, annihilation contrib. to cosmic gamma-ray background 78−93479
- prolate stellar systems, instability 80−101642
- proper motion programmes, importance of coords. determ. *(Russian)* 78−12079
- protogalaxies, disc accretion in soft potential well 80−8532
- protogalaxies, numerical simulation of systems of colliding bodies in gravit. field 77−29634
- protogalaxies, rot. and star form. rate 79−35374
- protogalaxies formation in zero press. Friedmann-Lemaitre universe 77−49512
- protogalaxy formation age and γ-ray background 80−62325
- protogalaxy interactions in newly formed clusters rel. to luminosities, colours and intergalactic gas 78−41060

galaxies continued

- protogalaxy-hadrons dipole magnetic fields *(Russian)* 79−8985
- Q 0957+561, double quasar, intervening galaxy obs. rel. to gravit. lens hypothesis 80−27005
- QSO candidates, spectroscopic obs., indentifications 80−31385
- QSO redshifts and field galaxies 78−89271
- QSO-galaxy and QSO-QSO pairs, discrepant red shift assocs. statistical anal. 79−8999
- QSO-galaxy pair, redshift meas. 77−26075
- QSO/galaxy associations, redshifts and distances 80−31369
- twin QSOs 0957+561 A and B direction, possible detect. of galaxies between QSOs 80−17686
- QSOs discretions, intervening galaxies rel. to absorpt. line regions physics 78−57680
- quasar absorption lines, intervening galaxies hypothesis and $z=1.95$ peak in redshifts 78−57685
- quasar luminosity model, galactic nucleus evolution with stellar coalescence and supernovae 77−87568
- quasar-galaxy associations, ang. separations 77−60846
- quasar-galaxy associations, search using Jodrell Bank 966 Hz survey 78−24566
- quasar-galaxy pairs and surface density of quasars 78−12404
- quasar-like objects, black hole model for IR and optical emission 78−20905
- quasars, continuous and emission-line spectra and relationship with Seyfert galaxies 79−2571
- quasars, gravit. and Doppler redshifts, interpreted as massive black holes ejected from galaxies 80−46695
- quasars, low-redshift, optical struct. rel. to underlying galaxies 78−32596
- quasars absorption lines, survey in QSOs of small and intermediate emission redshift 80−31218
- quasars and galaxies active nuclei, conference, Copenhagen, Denmark, (1977 June 27 to July 2) 78−57675
- quasars intervening galaxies, search for 21 cm absorpt. 80−4453
- quasistellar objects possible assoc. with radio galaxies and rich clusters of galaxies 78−8142
- radial vel. meas. in clusters of galaxies 77−64856
- radial velocities for 39 objects 78−45410
- radial velocities measurements, distortion by night sky spectrum 77−41406
- radial vels. for 42 southern objects 80−41902
- radiation belts, trapped electrons as radiowave source 80−26982
- radiation pressure in spectral lines in gaseous systems with axisymm. motions, kinematics 79−88579
- radiation-driven outflow models of nonthermal energy source 78−57687
- radio and cD galaxies, optical props. 78−93413
- radio and Seyfert galaxies, optical spectra 77−17686
- radio continuum emission, obs. at 11 cm 80−94872
- radio continuum obs. of nearby galaxies, review *(German)* 80−109544
- radio emission, correl. with mean surface brightness *(Russian)* 77−91615
- radio emission, flux densities at 1.35 cm wavelength *(Russian)* 77−64868
- radio emission, rel. to galactic dynamo numerical models 79−40262
- radio emission of active and normal nuclei, review 78−57646
- radio galaxies, ang. size-redshift test for double sources 77−57100
- radio galaxies, anisotropic explosion of rotating, self-gravitating uniform spheroids 79−8822
- radio galaxies, bivariate size-luminosity function determ. 78−65687
- radio galaxies, book 78−24564
- radio galaxies, broad-line Mg II 2798 Å and Hβ emission, line profiles 80−12807
- radio galaxies, double, statistical props., asymmetry and components flux ratio 80−67892
- radio galaxies, double source structs. form. and superluminal expansion 78−8141
- radio galaxies, elliptical, minor axes orientations rel. to radio sources orientations 80−82527
- radio galaxies, energy source, supermassive black holes 79−40213
- radio galaxies, energy supply and press. balance 77−41417
- radio galaxies, evidence on origin of rot. measures 77−5584
- radio galaxies, flux densities and spectra meas. at centimetre wavelengths 77−37664
- radio galaxies, flux densities and variability at 2.7 GHz 77−53694
- radio galaxies, form. of knots in relativistic flows rel. to compact synchrotron sources variability 80−105369
- radio galaxies, internal dynamics and brightness distribs. of extended source models 77−22323
- radio galaxies, interpretation and theory of extended and compact components 78−57670
- radio galaxies, log N-log S relation rel. to Dirac cosmology 77−22334
- radio galaxies, low luminosity, radio struct. and fluxes, Westerbork obs. 77−82306
- radio galaxies, model for superlight vels. 77−29944
- radio galaxies, models, rel. to solar flare physical mechanisms 77−17499
- radio galaxies, narrow-lined, spectrophotometry 78−93391
- radio galaxies, new complete sample, struct., redshifts 79−17096
- radio galaxies, obs. with Cambridge 5 km telescope at 5 GHz 78−12391
- radio galaxies, optical catalogue 80−21931
- radio galaxies, optical emission in radio lobes 78−57630
- radio galaxies, optical emission-line spectra 78−57643
- radio galaxies, optical identifications using accurate radio and optical positions 77−37660
- radio galaxies, optical positions 77−78881
- radio galaxies, optical spectra, morphological classification rel. to spectroscopic classification 78−41038
- radio galaxies, orientations 79−53911
- radio galaxies, origin of aligned inner and outer double struct. 77−45582
- radio galaxies, radio brightness distrib. obs. with RATAN-600 telescope 78−65698
- radio galaxies, radio emission from intense EM beam-plasma system 79−84663
- radio galaxies, red shift dependence of proper densities and colours 80−62286
- radio galaxies, relativistic electrons in situ accel. by shock waves 78−49241
- radio galaxies, relativistic fluids flow through channels, self-similar solns. and stability 80−62006
- radio galaxies, relativistic jets and beams 78−96541
- radio galaxies, search for H I clouds 78−12316

galaxies continued

- radio galaxies, southern, of large ang. extent, emission spectrum vars. 80—17683
- radio galaxies, statistical props. of compact features as function of flux density 78—41071
- radio galaxies, variable, 18 cm obs. 77—37662
- radio galaxies, variable, obs. at 0.95 and 1.65 cm wavelength 78—16552
- radio galaxies, variable, ten-year study at centimetre wavelengths 78—89267
- radio galaxies, variable radio emission temporal characts. *(Russian)* 80—62307
- radio galaxies, vars. at 7.9 GHz 77—37661
- radio galaxies, with strong millimetre-wave emission, 90 GHz obs. 78—16548
- radio galaxies and quasars, redshift-apparent dia. relation 77—87559
- radio galaxies and quasars, VLBI hybrid mapping of nuclei 80—105356
- radio galaxies components, fly away velocities upper limits *(Russian)* 80—62306
- radio galaxies in Abell 1367 cluster, Westerbork obs. rel. to interaction with intracluster medium 79—2574
- radio galaxies in Abell clusters, Westerbork aperture synthesis obs. 78—12360
- radio galaxies in Abell clusters fields, Westerbork obs. 78—96549
- radio galaxies in clusters interferometer obs. 77—53693
- radio galaxies in Coma cluster, optical obs. 78—12358
- radio galaxies nuclei, gamma-ray source model 79—25747
- radio galaxies search for variability at 18 cm wavelength, complete sample obs. 78—89268
- radio galaxies south of declination −75°, optical identification 77—64863
- radio galaxies suspected of decimetric flux density vars., 610 MHz VLBI obs. 77—78879
- radio galaxies with dust lanes 79—44604
- radio galaxies with radio jets, optical spectra of nuclei 79—84859
- radio galaxies with short wave radio emission excess, flux densities and variability at 1.35 cm *(Russian)* 78—57666
- radio galaxies with tail-bridge struct., spectral index, radio polarisation, mag. field 79—58416
- radio galaxies with tails, review *(French)* 78—41054
- radio galaxy 1159+583, wide-angle tailed, radio obs. and models 80—31352
- radio galaxy with superluminal vels. review 77—78882
- radio jets, Hα and 450 nm obs. 80—51889
- radio jets in radio galaxies, particle acceleration 80—31379
- radio luminosity and source size rel. to cluster membership 79—25729
- radio luminosity v volume emissivity diag. of galaxies in Virgo cluster 77—17696
- radio observations of lunar occultations of bright galaxies, spectra and struct. 79—9005
- radio recombination line obs. 79—101193
- radio recombination line studies of nearby galaxies 78—93397
- radio recombination lines, stimulated emission 78—86030
- radio sources, ang. size-redshift diagram interpretation 80—22101
- radio sources, compact, relativistic jets model 80—4448
- radio sources, compact, ripple radiation rel. to low-freq. variability 79—21450
- radio sources, compact, strong mag. dipole model 79—17115
- radio sources, complex, in Abell clusters, 2.7 GHz obs. 79—92881
- radio sources, double, collimation 80—22098
- radio sources, double, gas dynamical calcs. 79—67107
- radio sources, double, separation depend. on redshift 80—22096
- radio sources, extended, MHD instabilities and electron accel. 80—27000
- radio sources, extended, relation between radio luminosity and spectrum 80—51894
- radio sources, extended, statistical evidence on dynamical evolution 79—88757
- radio sources, jets brightness and shape rel. to beam and slingshot models 79—25741
- radio sources, jets configuration and propag. 80—31374
- radio sources, position coincidence optical identifications using Texas Interferometer radio positions 79—88753
- radio sources, rapidly varying, relativistic plasmoids dynamics 78—93438
- radio sources, superluminal, mag. dipole model 80—56959
- radio sources from B2 catalogue, optical identifications and 5 GHz flux meas. 79—40283
- radio sources from NRAO-Bonn 5 GHz survey, optical identifications 77—78880
- radio sources from NRAO-MPIfR 6 cm surveys, 21 cm flux density meas. 79—88754
- radio sources in clusters of galaxies, props. 78—12398
- radio sources in clusters of galaxies, review of obs. 78—12397
- radio sources in directions of Zwicky clusters of galaxies, statistical investigation 78—4378
- radio sources in south polar cap, optical identifications 79—75284
- radio sources in Zwicky galaxy clusters, detailed interferometer obs. and anal. 80—22099
- radio sources of Parkes 2700 MHz survey, new optical identifications 79—75289
- radio sources with speeds exceeding speed of light, geometric models *(Danish)* 78—36715
- radio tail galaxy in Abell 2634 cluster, spectrum and radial vel. 77—64857
- radio-galaxies with $13.0 \leq m_{corr} \leq 15.5$, peculiar radial rel. distrib. 77—9798
- radioastronomical obs. by amateurs *(Italian)* 78—7887
- radioastronomical obs. of galactic struct. *(Spanish)* 79—40275
- radiogalaxies, 1.4 GHz aperture synthesis obs. of circular polarisation 77—29656
- radiogalaxies, colour and space density, redshift dependence 79—75278
- radiogalaxies, cosmic ray accel. 80—82192
- radiogalaxies, extended, VLBI obs. of compact components 80—17680
- radiogalaxies, faint southern objects, identification and spectrophotometry 80—56935
- radiogalaxies, hot spots in outer lobes 78—69899
- radiogalaxies, linear polarisation meas. at 99 GHz 78—93439
- radiogalaxies, optical and radio props. 78—28829
- radiogalaxies, optical spectroscopy and redshifts for 18 objects 80—56966
- radiogalaxies, polarisation props. 79—53920
- radiogalaxies, polarized brightness distrib. at 2695 and 8085 MHz 79—35410

galaxies continued

- radiogalaxies, redshift-magnitude relation and cosmological test 78—28798
- radiogalaxies and quasars, models of extended and double sources 78—16557
- radiogalaxies and quasars, spectrophotometric survey 78—28828
- radiogalaxies and supermassive black holes 78—61882
- radiogalaxy, particle acceleration and plasma heating by turbulent Alfven waves 77—13227
- radiogalaxy interaction with intergalactic medium *(Italian)* 77—87562
- radiogalaxy luminosity function and past population evolution 79—44597
- radiogalaxy models, relativistic channel flow, soliton soln. stability 80—56962
- radiosources, linear polarisation meas., SHF obs. 80—73058
- radiosources, method for distance determ. 80—109559
- radiosources, optical identifications, spectrophotometric obs. 79—92879
- radiosources, spectroscopic identification of three southern PKS sources 79—25744
- radiosources from 13th part of Parkes 2700 MHz survey, optical identifications 78—20901
- radiosources optical identifications, statistical anal., data selection 78—61928
- RC1 galaxies, nuclei, lenses, rings diameters for 532 galaxies 80—90525
- red compact galaxies, surface photometry 77—53679
- red shift anisotropy and local supercluster *(Russian)* 79—92875
- red shifts, cosmological implications of composite Hubble diagram 77—22333
- red shifts, evolution free test for non-zero cosmological const. 80—4465
- red shifts angular anisotropy, additional evidence and interpretation 77—2472
- red shifts of galaxies in Abell 2255 cluster 79—40276
- reddening determ. method 78—54039
- redshift discrete states, systems of galaxies 77—37643
- redshift distrib. and luminosity function *(Chinese)* 80—4437
- redshift distribution, implications for evolution of galaxies 80—90527
- redshift errors, Simkin effect and Hg I 4047 Å night sky contamination 78—41032
- redshift-distance relation, evidence for linearly expanding Universe 80—31354
- redshift-distance square law 79—67095
- redshift-distance square law statistical scrutiny 78—81683
- redshift-magnitude bands, internal struct. and galaxies morphological evolution 80—22070
- redshift-magnitude bands and galactic evolution, obs. of Perseus and A1367 clusters 78—54033
- redshift-magnitude bands and galaxies evolution, data anal. 78—57629
- redshifts, discrepant, in quasar-galaxy associations and galaxy groups, examples 79—25722
- redshifts, Doppler shifts distrib. for relativistic gas 78—65492
- redshifts, evidence for large-scale uniformity of physical laws 80—73079
- redshifts, Kirshner, Oemler, Schechter sample rel. to universe mean mass density 79—75298
- redshifts, optical, of 59 galaxies 80—56936
- redshifts, vel. dispersions and line strengths meas. 77—29916
- redshifts and superluminal expansion vels., kinematic model 77—26050
- redshifts for 196 bright galaxies and two QSOs 80—46661
- redshifts for supernova parent galaxies 79—44612
- redshifts for three radiogalaxies 79—97060
- redshifts of cluster galaxies, interpretation 80—4427
- redshifts of radio tail galaxies in clusters 78—69889
- redshifts rel. to photon damping in discrete space-time *(Chinese)* 77—67145
- redshifts survey, data reduction techniques 80—22074
- relative velocities, missing mass problem 77—13478
- relaxation from aspherical initial conditions 78—96538
- resonances of discrete symmetric dynamical systems, appl. to axisymmetric galaxies 79—67066
- review of outstanding problems and future instrumental prospects 77—91626
- rich cluster at 00^h47^m, $-29°46'$, galaxies static props. using COSMOS meas. 79—40279
- ring galaxies, diversity and origin *(Russian)* 77—26064
- ring galaxies, form. and evolution 77—33635
- ring galaxies, H I survey 79—5901
- ring galaxies, radio continuum emission 80—67846
- ring galaxies, relative abundance and probability of ring structs., collisional form. 79—92868
- ring galaxies, review 80—62281
- ring galaxies near rich clusters, catalogue 77—33629
- ring galaxy, physical characts. *(Russian)* 77—57097
- ring galaxy A0035 (Cartwheel), H I 27 cm line obs. 77—64852
- ring galaxy discovery in Bootes on Palomar Sky Survey prints, radio flux meas. 80—26985
- ring structure, original rel. to instability of gravitating rot. viscous gaseous systems 77—17690
- ring structures form. by collisions with intergalactic gas clouds *(Russian)* 78—93425
- ring-like structures rel. to galactic nuclei activity *(Russian)* 80—36720
- RMB 56 (1216+141), compact blueshifted galaxy, photometry and spectrum 78—16527
- rotating galactic bar, isolating integrals of motion for stellar orbits 80—4404
- rotating gaseous disc with gravitation, shock waves, spiral galaxy model *(Russian)* 79—88749
- rotating gravitating disc of stars, Jeans' instability self-suppression *(Russian)* 78—93422
- rotating gravitating gas disc, explosive instability *(Russian)* 77—87260
- rotating stellar bar, gas response 79—48930
- rotating stellar systems, collapse and relaxation 79—62902
- rotating stellar systems, two-dimensional, nonlinear nonradial oscills. stability 78—53992
- rotation, ang. moments mass depend. rel. to self-similarity 80—36490
- rotation, contrib. from galaxy merging 80—4439
- rotation, tidal torque theory, N-body simulation 80—17670
- rotation, tidal torque theory, numerical simulations 79—25730
- rotation curve determ. review 77—33643
- rotation curves, rel. to nearby galaxy presence *(Russian)* 80—77496
- rotation in turbulent layers with proto-galactic eddies 78—54040
- rotational momenta, rel. to gravidynamic theory for large cosmical masses *(Russian)* 77—17351
- rotational properties, role of dissipation and galaxies merging 80—4444

galaxies continued
S0 and E galaxies, luminosity functions 79—97057
S0 and elliptical galaxies, absorpt.-line strengths 80—4430
S0 galaxies, disc struct., ring distrib. 77—13418
S0 galaxies, H I obs. 77—2466
S0 galaxies, radio continuum and H I obs. 77—87549
S0 galaxies, struct. and origin disc-to-bulge ratios 80—46656
S0 galaxies, surface photometry, luminosity struct. 80—62258
S0 galaxies relation to other types, evidence from assoc. in pairs 79—53901
S0 galaxies structure and origin, luminosity distrib. perpendicular to plane of discs 80—36705
Sa spiral galaxies, H I study 80—98714
Sa type spiral galaxies, redshifted 21 cm line profiles, radio obs. 80—73041
Sagittarius dwarf irregular galaxy, discovery on ESO Schmidt plates 78—20887
Sb-type galaxies, luminosity classification rel. to Hubble const. local value 80—62339
Sc galaxies, rot. props. from major axis visible spectra obs. 80—90517
SC galaxies, space distrib., large-scale struct. 79—71106
Sc I and II types, integrated B and V photometry 77—5559
Sc I galaxies, vel. anisotropy rel. to motion of Galaxy and Local Group, data 77—5560
Sc I galaxy vel. anisotropy rel. to motion of Galaxy and Local Group 77—91643
Sc I types, vel. anisotropy rel. to motion of Galaxy and Local Group 77—9796
Sc-type, colours of nuclei *(Russian)* 77—13471
Sc-type, nuclear regions stellar content 77—9793
Sc-type galaxies of Rubin et al. sample, study of Milky Way interstellar absorpt. 78—49533
Sculptor dwarf, dynamics rel. to extratidal variables 79—67088
Sculptor dwarf galaxy, photoelectric sequence and preliminary colour-magnitude diagram 77—53429
Sculptor dwarf irregular galaxy, 21 cm obs. 77—64843
Sculptor dwarf irregular galaxy, discovery by ESO 3.6 m telescope 77—22311
Sculptor dwarf spheroidal galaxy, abundance vars. on giant branch rel. to ω Centauri anomaly 79—5904
Sculptor dwarf spheroidal galaxy, catalogue of 602 variable stars 79—58431
searches for primaeval galaxies 80—105354
secondary distance indicators 78—93402
self-gravitating disk, resonant interaction of three density waves 77—67130
self-gravitating star system dynamics, time depend. soln. 80—4405
self-similar gravitational clustering, theory 80—4447
self-similar relativistic disks in rotation 79—16823
Seyfert, charge exchange model for broad emission line prod. 77—53681
Seyfert, class 1, theoretical and obs. anal. of He I triplet lines in spectra 78—49519
Seyfert, classification, jets and spirals existence *(Chinese)* 78—69878
Seyfert, contrib. to low-energy γ-ray background 78—86007
Seyfert, cosmic ray driving of gas in active nuclei 77—29915
Seyfert, energy source and time variation accreting massive black holes 79—40214
Seyfert, Fe II emission profiles interpretation 77—9791
Seyfert, Fe XI 7892 Å forbidden line emission 78—49520
Seyfert, gaseous envelopes *(Russian)* 77—87535
Seyfert, IR emission by dust grains near variable primary sources 79—44358
Seyfert, linear polarisation obs. at 7.2 cm wavelength 77—64870
Seyfert, list of 33 objects 78—77602
Seyfert, Mg II 2798 Å and $H\beta$ emission, line profiles 80—12807
Seyfert, morphology, electronographic obs. *(French)* 79—88759
Seyfert, near IR broad-band photometric obs. 80—46659
Seyfert, nuclear structure *(Russian)* 77—64846
Seyfert, source of diffuse cosmic γ-ray background 78—57700
Seyfert, survey of 80 objects based on large-scale image-tube plates 77—45323
Seyfert, type 1, nuclei props., UV emission, colour index *(French)* 79—48923
Seyfert, UBV obs., light vars. 79—30134
Seyfert, X-ray sources, review *(Polish)* 79—101223
Seyfert 1, disk struct. and nucl. activity 80—82503
Seyfert 1, Fe II permitted emission, excitation mechanism 79—21412
Seyfert 1, O I 8446 Å emission excitation mechanism, visible and IR obs. 80—85991
Seyfert 1, theory of asymm. broad H I emission lines 79—71108
Seyfert 1 and 2 nuclei, observational differences 79—97070
Seyfert 1 galaxies, emission line intensities rel. to colour index 80—26971
Seyfert 1 galaxies, forbidden line emission suppression 79—35358
Seyfert 1 galaxies, permitted Fe II emission, obs. 79—35361
Seyfert 1 galaxies, spectrophotometry 78—4346
Seyfert 1 galaxy 1224+04, discovery from spectrophotometry obs. 80—77488
Seyfert 1 galaxy nuclei, luminosity function and implications for X-ray background 80—8682
Seyfert 1 nuclei, synchrotron radiation model for IR emission 80—31387
Seyfert 1 objects, HEAO 1 scanning modulation collimator X-ray obs. 80—51859
Seyfert 1 X-ray emitting objects, HEAO 1 spectra 80—51860
Seyfert 2 galaxies, spectrophotometry 78—93391
Seyfert 2 X-ray galaxies, nucleus spectra and photometry obs. 80—98712
Seyfert and radio-galaxy nuclei, optical spectra of ionis. gas region, model 78—93420
Seyfert and related galaxies, 1415 MHz survey 77—9800
Seyfert emission line asymmetry 79—101214
Seyfert emission lines, hard X-ray effects 80—26974
Seyfert galaxies, accretion discs thermal continuum as optical emission source 78—54075
Seyfert galaxies, accurate optical positions 78—89254
Seyfert galaxies, broad H lines prod. by suprathermal protons passing through neutral gas *(Russian)* 78—57642
Seyfert galaxies, continuous and emission-line spectra and relationship with quasars 79—2571
Seyfert galaxies, depend. of emission line intensity on colour index *(Russian)* 78—28769
Seyfert galaxies, exploratory obs. of gas near nuclei 79—48906

galaxies continued
Seyfert galaxies, gas cloud containment by particle flux 79—8820
Seyfert galaxies, H I survey 79—8988
Seyfert galaxies, IR emission obs. 79—17083
Seyfert galaxies, IR energy distribs. obs. 78—57645
Seyfert galaxies, IR spectra rel. to metagalactic IR flux 77—29964
Seyfert galaxies, nearby, photographic study of morphology 80—82478
Seyfert galaxies, optical emission-line spectra 78—57643
Seyfert galaxies, powered by pregalactic black holes? 80—56978
Seyfert galaxies, profiles and redshifts of broad lines 78—16566
Seyfert galaxies, radio props. 78—49535
Seyfert galaxies, rate coeff. for He I $2^3S \rightarrow 2^3P$ transition electron impact excitation 79—48664
Seyfert galaxies, spectral line profiles interpretation *(Russian)* 79—101203
Seyfert galaxies, submillimetre photometry 78—4353
Seyfert galaxies, thermal IR emission vars. 80—67865
Seyfert galaxies, type 1, dust as source of IR luminosity 78—12357
Seyfert galaxies, Type 1, obs. with HEAO-1 scanning modulation collimator 79—92864
Seyfert galaxies, type 1, permitted Fe II lines form. and low excitation region parameters 80—62278
Seyfert galaxies, X-ray spectra and variability 78—32611
Seyfert galaxies and quasars, Fe II emission obs., spectrophotometry 78—4347
Seyfert galaxies from lists of Markarian galaxies, spectroscopic obs. *(Russian)* 79—80360
Seyfert galaxies nuclei, optical variability from U, B, V and $H\alpha$ photometry 78—96543
Seyfert galaxies nuclei, stellar debris clouds model 78—32597
Seyfert galaxies spectra, Mg II and Fe II lines excitation 80—67896
Seyfert galaxies spectra, theory of H line emission from dense plasmas 80—51900
Seyfert galaxies with large z, electronographic survey 77—91624
Seyfert galaxies X-ray emission, Uhuru obs. 78—93392
Seyfert galaxies X-ray emission detectability in deep X-ray surveys 78—96567
Seyfert nuclei, absolute spectrophotometry 79—12508
Seyfert nuclei, black flash model 78—57673
Seyfert nuclei, emissive regions, self-consistent models 78—57686
Seyfert nuclei, fast spectral line variability interpretation *(Russian)* 80—77286
Seyfert nuclei, spectroscopic obs. 77—9792
Seyfert nuclei as successive supernovae 77—91652
Seyfert recognition, inclination effects 80—62264
Seyfert type 1 objects, supercritical disc accretion, on to black hole, model 80—41850
Seyfert type 1 spectra, permitted Fe II lines 79—44602
Seyfert type I, optical counterpart of 3C 111, position 79—48948
Seyfert-like galaxies, medium-redshift, redshift-magnitude-ang. dia. data statistical anal. 78—86016
Seyferts, obs. at 1.3 and 2.8 cm wavelength, spectra 78—69866
Seyferts, possible origin for background isotropic radiation excess at 1 MeV 80—77522
Seyferts, quasars and red shift controversy 77—2476
Seyferts and QSOs, He I lines in spectra 78—36717
Seyferts and quasars, broad line emission from black hole accretion disc 77—60819
Seyferts and radiogalaxies, Penrose pair production as power source 79—44352
Seyferts detected as X-ray sources by Ariel V satellite 78—49540
Seyferts in 12th list of galaxies with UV continuum *(Russian)* 80—17659
Shahbazian 1 group of galaxies, internal vel. dispersions and group dynamics 80—67878
Shane-Wirtanen galaxies, two- and three-point correl. functions 78—8132
Shapley-Ames southern galaxies, Las Campanas survey and classifications 78—45409
shock wave props., density wave theory *(Chinese)* 77—71145
shock waves generated in intergalactic medium at large redshifts 79—21442
single galaxies abundance and cosmological significance 77—53688
small galaxies, accurate 21 cm H I spectra 79—35382
SMC, 30 Doradus, central object R 136, struct., colour, mass, photometry obs. *(German)* 80—67825
SMC, abundances in 10 H II regions 78—4320
SMC, atlas of variable stars, clusters, emission regions and supergiant stars, book 79—44619
SMC, C stars in NGC 419 globular cluster 78—53962
SMC, deep X-ray survey 79—25702
SMC, discovery of dusty star 77—45461
SMC, eclipsing W-R binary HD 5980, photoelectric curve 78—45366
SMC, faint planetary nebulae identification 79—17081
SMC, five colour photometry of Cepheids rel. to interstellar dust content 77—29923
SMC, globular cluster NGC 419, cluster membership of nearby C- and M-type stars 80—26921
SMC, identification of globular cluster Kron 3 with X-ray source (4U 0.026—73) 79—5919
SMC, lack of absorption of 1 keV diffuse X-rays 79—35381
SMC, obs. of new faint outlying open clusters, (AM-3) 79—25651
SMC, photoelec. UBV and RI sequences 77—82307
SMC, photometric study of wing and eastern halo 78—86011
SMC, radial vels. of individual stars in young cluster (NGC 330) 80—67803
SMC, radial vels. of supergiant stars 78—93237
SMC, ratio between total and selective interstellar absorpt. *(German)* 80—67851
SMC, red variable in NGC 371 OB association 78—53961
SMC, search for Wolf-Rayet stars 79—67014
SMC, spectral classification of 26 supergiants 77—29936
SMC, star cluster colour magnitude diagrams and stellar identification charts photometry obs. 80—73014
SMC, star formation regions and star clusters 79—62900
SMC, stellar content of NE outer arm and halo 78—86013
SMC, stellar populations, distrib. and evolution 80—94868
SMC, struct. and kinematic behaviour *(French)* 78—89258
SMC, structure and kinematics from supergiants 79—101192
SMC, structure from supergiant distrib. 77—45549
SMC, supergiant MK classifications 77—87390

galaxies continued

- SMC, surface brightness meas. with UV Sky Survey Telescope 78—93414
- SMC, UBV photoelectric photometry *(German)* 78—77594
- SMC, UBV photometry of open, intermediate and globular clusters 79—17033
- SMC, very early O-type star discovery 79—5820
- SMC, Wolf-Rayet stars spectral classification 78—73716
- SMC globular clusters, gas content upper limits 80—22047
- SMC M-type supergiants rel. to low metallicities 79—96995
- SMC probable members and foreground stars, additional tests 79—40091
- SMC Shapley wing, UV obs. from S2/68 sky-survey telescope 79—25717
- SMC star clusters catalogues, identifications and coordinates 78—89086
- SMC stars, Herschel catalogue rel. to CPD 79—44337
- SMC supergiant stars, radial vel. determ. by spectrographic and photometric data study 79—101147
- SMC wing, photoelectric UBV sequence 78—69874
- SMC X-2, SMC X-3, discovery, hard spectra, high luminosity rel. to galactic X-ray sources 78—49559
- SMC X-2, SMC X-3 optical counterparts, spectra 78—93469
- SMC X-2 and X-3, SAS 3 discovery of new sources 77—91667
- SN in anonymous galaxy in Centaurus, discovery, posn. and magnitude 80—85961
- SNR candidates in nearby galaxies, catalogue 80—62037
- SO -alaxies, radio and IR photometry 78—16531
- southern, strong emission line spectra, characts. 79—21432
- southern bright elliptical and S0 galaxies, 5 GHz survey 77—49479
- southern compact and bright nucleus galaxies 77—74136
- southern compact and bright-nucleus galaxies, spectroscopic survey 79—84683
- southern compact and bright-nucleus galaxies, spectroscopic survey 80—94725
- southern galaxies, UBV photometry of 262 objects 79—35364
- southern galaxies with strong emission lines spectroscopic obs. 77—17679
- southern hemisphere galaxies, search for H_2 2.1 μ emission 80—22059
- southern interacting galaxies with emission lines 77—91653
- southern late type and irregular galaxies, visible survey 80—105334
- southern late-type and irregular galaxies, survey, morphology, luminosity 79—21420
- southern Molonglo radio galaxies, optical spectra 78—96555
- southern Parkes radiosources, redshift obs. 78—20899
- southern peculiar galaxies and pairs, morphologies, spectra and redshifts 78—32579
- southern peculiar galaxies and pairs, spectra and radial vels. 78—45411
- southern peculiar objects, UK Schmidt plates, analysis 78—20896
- southern radio galaxies, obs. with Fleurs synthesis telescope 78—4385
- southern radiosource identifications 77—45591
- space distribtuion of distant galaxies, evolution effects 79—40260
- space distribution determination, statistical anal. of galaxy catalogues 80—46417
- spatial distrib., spatial pair-correl. function 78—4350
- spatial distrib. in southern galactic hemisphere 79—12518
- spatial distribution of different types of galaxies 79—84862
- spectral study, of galaxies with UV excess and double and multiple nuclei 80—67848
- spectral var. in brightest cluster galaxies 78—41030
- spectrophotometric gradients *(Russian)* 79—92861
- spherical, gravit. stability of rotating embedded gas discs *(Russian)* 78—61915
- spherical compact galaxy pairs, UBV obs. 77—37645
- spherical galaxies acting as gravitational lenses, multiple images 80—90532
- spherical galaxy obeying $r^{1/4}$ law, tables of physical functions 77—13454
- spherical protogalaxy collapse and violent relaxation 80—31366
- spherical stellar systems, dynamical relaxation, tidal perturbations by external systems 77—49443
- spherical stellar systems, marginal mode to second order *(French)* 78—32527
- spherical stellar systems, potential *(Russian)* 78—93386
- spherical systems of gravitating bodies with ellipsoidal vel. distrib. *(Russian)* 79—40274
- spherically symmetric accretion with self-gravitation, criteria for enhanced accretion 79—71098
- spheroidal component struct. parameters of brightness profiles in compact and normal galaxies 78—16524
- spheroidal galaxies, interstellar medium equilib. forms *(Russian)* 77—91616
- spinar model for active nuclei 79—17090
- spiral, central holes in stellar discs, rel. to evolution 80—62268
- spiral, CNO isotopes as probes of chem. evolution 77—91636
- spiral, composition gradients rel. to density wave theory 77—2468
- spiral, density wave amplitude and long-term maintenance 77—45571
- spiral, density wave evolution *(Chinese)* 78—86020
- spiral, density wave evolution at unstable stage *(Chinese)* 77—60831
- spiral, early-type, absolute magnitude-colour relation 77—74133
- spiral, gamma-ray luminosity, contrib. to diffuse background above 100 MeV 78—93481
- spiral, in Coma cluster, nuclear radio emission upper limits 78—8107
- spiral, in Virgo cluster, H I deficiency *(Russian)* 79—21438
- spiral, interpretation of line intensity gradients across discs 77—13459
- spiral, interstellar matter distrib., density wave theory 78—16540
- spiral, irregular struct. rel. to star formation 77—13450
- spiral, light absorpt. by interstellar dust 79—35393
- spiral, magnetogasdynamic mechanism of rotation *(Russian)* 77—87536
- spiral, nearly edge-on illusionary warps in H I discs 78—65682
- spiral, radial vels. from H I 21 cm line obs. 79—21419
- spiral, radio continuum flux from discs, theory 77—13460
- spiral, ring structs., nonlinear density wave theory *(Russian)* 78—93423
- spiral, ring-like structs., H II regions and OB associations distrib. *(Russian)* 78—93424
- spiral, rot. curves, mass distrib. and total masses 77—49477
- spiral, search for nearby radiosource pairs 77—26074
- spiral, star formation and mechanism for maintenance of galactic density wave *(Chinese)* 77—60830
- spiral, star orbits in region of inner Lindblad resonance, numerical studies 78—45396
- spiral, UBVR surface photometry and mass distrib. 79—71123
- spiral, with large redshifts, optical obs. 77—29933
- spiral, with unusual radio morphology, radio continuum obs. 77—60822
- spiral and elliptical, optical surface brightness, dust effects 80—90518

galaxies continued

- spiral and elliptical galaxies in Virgo cluster, redshift differences 77—17694
- spiral and irregular galaxies, brightest superassociations as distance indicators 80—62260
- spiral arm development, sufficiency conditions 80—77483
- spiral arm instability origin 77—13456
- spiral arms, CO emission detect. 77—33641
- spiral arms form. by central explosions 79—8996
- spiral density wave caused by orbiting retrograde companion, props. 78—96533
- spiral density waves, driving mechanisms, observational constraints 80—17650
- spiral density waves, illustrated by periodic stellar orbits superposition 79—84828
- spiral density waves, local density-pot. relation 79—84860
- spiral density waves, loosely wound, hydrodynamic model 79—101207
- spiral density waves, non-linear theory 78—32576
- spiral density waves, response near corotation radius to central bar 77—17689
- spiral density waves, tidal disturbances of material arms and star clusters *(German)* 79—17086
- spiral density waves as solitons in gaseous and stellar discs *(Russian)* 77—45569
- spiral density waves in embedded discs 79—88734
- spiral density waves in plane galaxies *(Russian)* 77—87553
- spiral density waves individual stellar orbits, response 79—44570
- spiral disturbances in flat galaxies caused by Kelvin-Helmholtz instability *(Russian)* 77—74142
- spiral galactic potential, planar stellar orbits 78—69845
- spiral galaxies, BV magnitudes and dias. rel. to galactic extinction coeff. amplitude 80—17664
- spiral galaxies, central density min. in stellar disc 80—17663
- spiral galaxies, density wave theory *(Swedish)* 79—92859
- spiral galaxies, extended H I regions as probe for galactic struct. and intergalactic medium 78—12354
- spiral galaxies, formation *(French)* 80—4446
- spiral galaxies, interstellar gas hydrodynamic flows in regions of Lindblad resons. 78—96527
- spiral galaxies, local mass-to-light ratio radial var. 80—31361
- spiral galaxies, non-linear corrugation waves numerical computations 80—67859
- spiral galaxies, normal, post-explosion gas depletion in central regions 80—62272
- spiral galaxies, number of companion rel. to morphology and luminosity 80—77481
- spiral galaxies, periodic orbits near particle reson. 78—49484
- spiral galaxies, props. from stochastic star form. model 80—12818
- spiral galaxies, rot. direction determ. by means of edge-on systems *(Russian)* 80—36722
- spiral galaxies bulges, vel. dispersions meas. 80—26965
- spiral galaxies corotation circle, angular motion of trapped stars *(French)* 79—88705
- spiral galaxies formation, model 80—90529
- spiral galaxies from Uppsala Catalogue, position angle distrib. *(Russian)* 78—41049
- spiral galaxies nuclei, stellar population 80—56926
- spiral galaxies pair at low galactic latit., discovery 78—96536
- spiral galaxies stellar vel. dispersion determ. *(Chinese)* 80—85995
- spiral galaxies studied at Westerbork, optical surface photometry 80—17655
- spiral galaxy, density wave theory 79—48939
- spiral galaxy orientation anisotropy in Abastumani Catalogue of Bright Galaxies 77—17678
- spiral modes in disc galaxies, density wave theory 78—54053
- spiral modes in gaseous cylindrical systems 79—66914
- spiral of limited thickness, model for pattern and rotation *(Chinese)* 80—8688
- spiral perturbation near corotation resonance, density response of disk stellar population 79—71077
- spiral structure, accretion theory *(Russian)* 77—45568
- spiral structure, bar driven 80—105337
- spiral structure, density wave theory, review *(German)* 79—17103
- spiral structure, density wave theory 77—71146
- spiral structure, density wave theory and very hot interstellar gas 80—31356
- spiral structure, gaseous theory of origin 80—82517
- spiral structure, obs. foundations for density wave models 79—62915
- spiral structure, rel. to stochastic star formation 78—93395
- spiral structure, variability in numerical models 79—25725
- spiral structure and dust lane gravitational collapse 79—92849
- spiral structure formation, plasma density wave analogy *(Russian)* 77—13470
- spiral structure formation, role of Population II stars 77—13469
- spiral structure of galaxies, density wave theory 79—75280
- spiral structure persistence and stellar orbits 78—41046
- spiral structure theory, density waves energy and lifetime and spiral galaxies classification 80—98715
- spiral structure theory, developments 79—97061
- spiral structures, geophysical and astrophysical 80—77287
- spiral structures, origin 79—25714
- spiral systems, Lin's density-wave theory, observational possibilities *(German)* 78—73756
- spiral systems, redshifted 21 cm absorption line clouds 80—62310
- spiral waves in disc galaxies, barlike perturbations 78—49523
- spiral waves in galaxies discs, nonlinear interaction with stars near corotation radius *(Russian)* 80—62289
- spirals, 408 MHz obs. 80—98720
- spirals, dust complexes optical anal. method, visible obs. 80—101638
- spirals, extended optical-rotation curves 79—97083
- spirals, H II regions and dust presence 80—82484
- spirals, influence of star vel. ellipsoidal distrib. *(Chinese)* 80—77484
- spirals, primordial star generation rel. to heavy haloes 78—61946
- spirals, radio continuum morphology, review 77—26071
- spirals, radio haloes 78—89263
- spirals, resonant stellar orbits, disc equilib. for Lindblad resonances 78—49524
- spirals, search for extended H I envelopes, 21 cm obs. 80—90520
- spirals, types Sab to Scd, luminosity, freq. distrib. 80—82482
- spirals, wind from disc, hydrodynamic model 78—45397
- spirals in double systems, radio continuum emission 80—105342

galaxies continued
stability of rotating spheroidal stellar systems 80−62203
stable heavy neutrinos, dynamical interactions and astrophys. effects 79−5743
stable method heavy leptons, astrophysical mass constraint, condensation in stars and galaxies *(Russian)* 80−72768
star complexes rel. to gas complexes *(Russian)* 79−35391
star formation, suppression rel. to delayed star form. problem 80−105349
star formation in non-elliptical galaxies, two colour diagram 80−67875
star formation rate and extragalactic background light 78−36687
star formation rate in external galaxies, numerical simulation 77−45555
star formation rates, in normal and peculiar galaxies 78−24550
star formation rates and IR radiation 78−49526
stars and star systems, conference, Uppsala, Sweden (1978 August 7 to 12) 80−51959
statistical mechanics of gravitating systems 79−35311
statistical virial theorem appl. 79−5926
steep spectrum radiosources, spectral index dependent props. 80−36730
stellar bar, dynamics, computer model 79−30093
stellar dynamics, global particular solution to initial value problem 79−35314
stellar dynamics, gravitational instability of loosely wound spiral density wave 80−85998
stellar dynamics in thin disk galaxies, hydrodynamic eqns. 79−92809
stellar H-R diagrams, appl. to studies of galaxies 78−81619
stellar motion in gravitational field of uniformly rotating galaxy *(Russian)* 80−94838
stellar orbits, 2/1 reson. 80−67796
stellar orbits, applicability of approximate third integral of motion 80−67798
stellar orbits, nonlinear behaviour near corotation in spiral systems 80−98694
stellar orbits in growing spiral field in galaxy near corotation resonance 78−61891
stellar planar orbits, in spiral galaxy with extensive inner Lindblad reson. 79−88704
stellar population synthesis, spectral inversion technique 80−90339
stellar populations, Wing-Ford 9910 Å molecular band as mass function constraint 77−17673
stellar populations in central regions 79−97064
stellar space density derivation methods, systematic comparison 78−61917
stellar systems dynamics, collision integral determ. *(Polish)* 80−67799
stellar systems dynamics, limiting radii of direct and retrograde satellite orbits 79−88572
stellar systems nonradial-oscillations, homogeneous models *(Russian)* 77−57063
stellar velocity distribution maximum anisotropy *(Russian)* 77−82313
stochastic simulation of fields of galaxies 77−45546
stochastic simulation of fields of galaxies 80−62295
strong lined ellipticals, overabundances of Na and Mg heavy isotopes 77−13464
structural features, origin rel. to galaxy form. *(Russian)* 77−17691
structure, collisions with intergalactic neutral clouds rel. to interstellar super 80−98717
structure of the universe, book 78−32628
structure parameters from star counting 80−82507
structuring mechanism 79−48924
super massive star in dense stellar system, evolution 79−12465
supergiant elliptical galaxies nuclei, CCD photometry rel. to supermassive object in (NGC 6251) 80−26966
supernova discovery in anon. galaxy in Grus, position 78−93289
supernova in anonymous galaxy, discovery report 79−2549
supernova in anonymous galaxy in Cygnus, photometric and spectrophotometric obs. 79−5847
supernova in anonymous galaxy in Grus, discovery and magnitudes (1980 May 23 to July 12) 80−94820
supernova radial distrib. in galaxies, correction for galactic diameters 77−2465
supernova rate in Sc galaxies, max. likelihood estimate 78−45402
supernova remnants, identification in nearby galaxies *(Italian)* 79−53884
supernova remnants, interaction rel. to evolution and galaxy gas ejection 80−4423
supernova statistics 77−87460
supernovae, external galaxy investigations of nature 77−49408
supernovae, theoretical review *(Norwegian)* 79−80329
supernovae, Type I, number depend. on galaxy class rel. to origin from short-lived stars 79−88692
supernovae, types I and II, radial distribs. in spiral and elliptical galaxies 80−62163
supernovae and SNR radial distrib., exponential law 77−45473
supernovae in anonymous galaxies, three new discoveries 80−46589
surface brightness distributions in elliptical galaxies 79−40268
surface brightness parameters, tests of galactic evolution 77−13462
surface brightness rel. to evolution, cosmological appls. 77−9801
surface brightnesses distrib. in Coma cluster *(Russian)* 78−49543
surface photometry, computerised analysis method 78−12100
Syeferts from Zwicky lists, spectrophotometry 79−75274
symmetric struct. in slingshot theory of radiogalaxies 77−45542
Sz 80, southern emission-line galaxy at low galactic latitude 78−86022
tailed radio galaxies, Westerbork synthesis obs. of Abell clusters 80−56957
thermal evaporation of gas within galaxies by hot intergalactic medium 77−41413
thin disc galaxies, stellar dynamics, hydrodynamic and orbit theories 78−8059
thin disc galaxies, stellar hydrodynamics 79−25706
tidal deformation by primordial gravitational waves, numerical simul. 79−92865
tidal disruption by a massive black hole and collisions in galactic nuclei 78−77597
tidal hypothesis for ang. momentum origin 79−48927
tidal interaction in clusters 79−35395
tidal interactions, rel. to massive halo hypothesis 77−91625
tidal interactions in expanding Universe, prolate systems form. 79−71164
tidally interacting galaxies, evolution of mass and tidal radius 78−65699
Tololo emission line galaxies, size, morphology and spectroscopy, visible obs. 80−73044

galaxies continued
Tololo emission-line galaxies, nature from photometric and spectroscopic obs. 78−49531
Tololo list of emission line galaxies, spectroscopic and radio survey 77−64851
Ton 1542, electronographic photometry *(French)* 77−45547
Ton 1542, Seyfert galaxy nucleus, optical polarisation *(French)* 77−26053
trapped orbits in time-dependent potential 80−8664
triaxial galaxy model, nonexistence of three-dimensional tube orbits around intermediate axis 80−22046
triaxial stellar system in dynamical equilib., numerical model 80−4433
turbulent accretion onto massive black holes 79−62865
twisted accretion discs, time-dependent eqns. 79−12395
two component Emden sphere model, theory 80−22045
two-component galaxies chemical evolution, analytical approach 79−25711
two-component galaxy, polytropic model 79−25712
two-point correlation function, integral constraint on evolution 77−5578
4U 0241+62, identification with QSO or Seyfert nuclei-like object 78−16572
UBV photoelectric photometry and photometric parameters, meas. for forty galaxies 80−67855
UBV photoelectric photometry of 16 galaxies in Hydra I (Abell 1060) 80−51887
UBV photometry of southern galaxies 79−101198
UGC 5196 revealed as plate flaw 80−4445
UKS 1927−177 and 2323−326, 21 cm. obs. of new dwarf irregulars 78−65697
ultrahigh-energy neutrinos production, fluxes and detect. techniques 78−49264
unidentified high latitude radiosources 78−57672
universal structural evolution 80−17700
Universe and general field clumpy structure 78−45443
universe model, computer simulation of galaxy distrib . in Lick catalogue 78−81718
unseen galaxies, H I obs. rel. to limits on space density 77−29925
Ursa Minor dwarf spheroidal galaxy, abundance vars. on giant branch rel. to ω Centauri anomaly 79−5904
UV continuum galaxies, eighth list *(Russian)* 77−22109
UV continuum galaxies, eleventh list *(Russian)* 78−28767
UV continuum galaxies, tenth list *(Russian)* 77−91445
UV continuum galaxies, twelfth list 80−67585
UV continuum galaxies with broad emission lines, rel. to QSOs 77−64840
UV continuum objects, photoelectric UBVR photometry *(Russian)* 80−36721
UV excess galaxies, second list 80−67584
UV excess objects, list of 136 new galaxies 80−26968
UV galaxies, double nuclei, visible spectra obs. *(Russian)* 80−77495
UV galaxies with double and multiple nuclei *(Russian)* 78−61914
UV obs., implications 80−105390
UV radiation, contrib. to diffuse cosmic UV background spectrum 80−17696
UV spectra, International Ultraviolet Explorer (IUE) obs. 78−96540
UV surface brightness and morphology rel. to activity *(Russian)* 78−49513
variable compact object discovery in Perseus, bright blue N-galaxy, photometry and spectrum 79−12524
variable galactic nuclei, props. and observing techniques 78−81691
variable radio emission, nature of cm radiation quasisteady component 79−21456
velocity dispersions, Doppler broadening parameters meas. technique without spectrograph 78−20646
velocity dispersions in rich clusters 80−56956
velocity distrib. of galaxies in clusters 77−53690
velocity field multiplicity, ergodicity of motion *(Russian)* 77−37623
velocity field of bright nearby galaxies, Local Group peculiar motion rel. to Virgo cluster 80−36699
velocity-distance relation, history 80−12880
velocity-distance relations and Local Supercluster Hubble ratio 80−17698
Virgo A, core object, comparison of 5 and 23 GHz maps 80−82488
Virgo A (M87), 1.3 cm obs. 78−49550
Virgo A (M87), Westerbork map at 610 MHz 80−62302
Virgo cluster galaxies, 1.4 GHz continuum survey 80−98721
Virgo cluster galaxies, masses rel. to globular clusters luminosity distrib. 78−12308
Virgo cluster galaxies, photographic surface photometry 77−78870
Virgo cluster spiral galaxies, H I deficiency from 21 cm obs. 80−62277
Virgo galaxies globular clusters, luminosity function and Hubble const. new determ. 79−92902
virial mass discrepancy, in groups and clusters of galaxies 78−28803
visual magnitude-radial vel. rel. for normal galaxies *(Russian)* 78−28789
VV 126, multicomponent interacting galaxies, visible spectroscopy obs. *(Russian)* 80−77494
VV 150, galaxy chain, photoelectric and spectroscopic study 80−98724
VV 243, edge-on spiral and minichain or galaxy pair *(Russian)* 80−17658
VV 493 (UGC 07910), unusual extragalactic object, morphology and spectrum rel. to probable nature 80−98718
VV 5-26-14=Zw 155-16=Anon. 1045+26, supernova discovery and position 77−22257
VV 5-32-63/64 in Abell 1775, supermassive double galaxy theory questioned 80−8693
VV 5-42-11(=Zw 171-20), probable supernova in interacting galaxy 77−53615
VV 617 (NGC 6240), obs. of nucleus in type II Seyfert *(Russian)* 79−67103
VV 794 H II regions, photographic and spectral obs. *(Russian)* 80−77493
VV 8, rotation mass and surface brightness obs. *(Russian)* 79−48937
VV interacting galaxies search for clumpy irregular galaxies 79−101201
14W12, radio galaxy in X-ray cluster of galaxies Abell 401, radio emission distrib. 80−98731
warp precession due to invisible galactic halo 80−82508
warped H I discs, obs. 77−5567
warping of galactic plane and ellipticity changes 78−69847
warps in disks, excitation mechanism 80−105339

galaxies continued
weak radio galaxies, relationship between radio power and enhanced emission regions separation 79—25726
weak radio nuclei in galaxies and quasars 77—17680
white dwarfs formation rate 78—28674
WLM galaxy (A2359), BV photometry 77—82302
X-ray clusters, galactic content correl. with X-ray luminosity 78—32585
X-ray clusters, galaxies classification rel. to gas stripping from spirals 78—32586
X-ray coronae, hot gas dynamics simulation 80—82481
X-ray emitting galactic nuclei, luminosity function and variability time scale 78—57701
X-ray galaxies, review of compact sources and Seyferts 79—58422
X-ray galaxies, spectral lines profile evolution due to Comptonisation, Monte Carlo computations 79—66916
X-ray sources correl. with radiosources from 26.3 MHz survey 78—65707
X-ray spectrum and variability of active galaxies 79—58420
Yerkes poor cluster members, redshifts 80—51858
young galaxies, contribution to X-ray background 80—82550
young galaxies, form., evolution and relation to quasars 78—32582
young galaxies, rel. to galaxy form. theory 77—33645
young galaxies in catalogues of quasars and radiosources 78—28799
young massive halos, spectral energy distribs. at large redshifts 77—78866
III Zw, radio outburst, 14.5 GHz flux density increase 78—12373
II Zw 136, Seyfert galaxy nuclei, optical variability, UBV obs. 80—73049
Zw 1400+0949 cluster (NGC 5416 group), 21 cm obs. 80—22090
I Zw 18, dwarf blue compact galaxy, blue star emission spectra 77—37593
I Zw 1, analysis of spectra of type 1 Seyfert 79—71103
III Zw 2, compact galaxy, radio outburst obs. 79—75277
III Zw 2, IR variability, 2 μm obs. 79—30118
III Zw 2, quasar, spectrophotometry of assoc. galaxies and nebulosity, redshifts 79—21460
III Zw 2, type I Seyfert, X-ray emission detect. 78—20895
III Zw 2, X-ray and radio emission from compact galaxy 78—65691
III Zw 2, X-ray emitting Seyfert galaxy, VLBI obs. 79—5903
Zw 310-31 = VV 11-10-52 faint galaxy, discovery of mag. 16 supernova 78—4259
II Zw 40, 70, 71, CO emission upper limits 78—36693
II Zw 40, dwarf blue compact galaxy, blue star emission spectra 77—37593
II Zw 40, dwarf galaxy, radio obs. 79—8992
VII Zw 421 and II Zw 67, spectrophotometry of S0 galaxies 80—51866
VII Zw 466, ring galaxy, UBVR photometry 79—8991
II Zw 70, optical and radio obs., evidence for star form. 79—16935
I Zw 92, III Zw 77, compact galaxies with broad emission lines, spectra 78—73760
Zwicky's compact galaxies, properties 78—49542
Zwicky catalogue magnitude scale, comparison with Holmberg and de Vaucouleurs galactic magnitudes 77—22309
Zwicky compact galaxies, spectroscopic survey 79—17074
Zwicky galaxies, luminosity function slope 80—36709
3C 348, 3C 111, multiple radio galaxies, intermediate latit. H I absorpt. obs. 79—12503
CH, detect. in NGC 4945, NGC 5128 and LMC 80—46673
CO emission obs. at 2.6 mm 77—45543
^{13}CO in external galaxies, ^{12}CO/^{13}CO intensity ratios 80—4416
Cygnus A, intensity and polarisation at 9 mm wavelength 80—36732
Fe/H abundances of extreme Population II stars in globular and dwarf galaxies 78—40939
H I 21 cm line widths correl. with absolute magnitude and type 79—5900
H I deficient spiral galaxies in Abell 1367 and coma cluster 79—17072
H I extent from centre, 21 cm line study 79—97067
H I gas, pervasiveness of intercloud medium 80—51825
H I large-scale distrib. in early type galaxies 80—8685
H I layers large-scale warping 78—16543
H I observations of active and interacting galaxies 79—67091
H I profile shapes rel. to Hubble type 77—64841
H I profile width distances for disc galaxies rel. to Hubble constant 78—41050
H I profiles classification system for dwarf galaxies, discrete redshift and asymm. 78—49517
H I profiles of nearby galaxies, obs. 80—41895
H I surface density distrib. at periphery of galaxies, effects of ionising background radiation 78—65729
H I survey of 500 southern galaxies 77—33650
H II region diameters, applicability to Hubble constant determ. 80—41887
H II region vel. dispersions rel. to linear diameters 77—33595
H II regions, line intensity data compilation 79—88721
H II regions, spectra anal. and models 80—73024
H II regions as distance indicators, obs., struct. considerations 79—40231
H_2O absorption and coolest stellar component of E and S0 galaxies at 2 μ 78—41034
Mg index in old galaxy populations 78—41033
N/O abundance ratio 80—8686
O I 7990 Å and 11287 Å branching ratios, astron. appl. 79—41134

gallium
see also nuclei with ......
1/f noise, meas. in solid and liq. phases 78—64073
3d and $L_3M_{4,5}M_{4,5}$ binding energy, Ga, GaAs and Ga_2O_3, ESCA absolute energy calibr. 78—92171
3d subshell photoionisation partial cross-section, energy depend. meas. 80—29850
abundance in ordinary chondritic meteorites 80—8595
acoustic effect in crystallisation and melting *(Russian)* 79—51238
acoustic wave drag, acousto-elec.-mag. effects *(Russian)* 79—19638
adsorbed on W and Mo (001), struct., FIM obs. 80—103576
adsorption on W, field emission, FIM 77—16470
alkali halide:Ga^+, cryst. field effect on spectral characts. 77—24880
alkali halides:Ga^+, Jahn-Teller effect, EPR study 78—43690
alkali halides:Ga^+, optically detected EPR in relaxed excited states of Ga^+ 78—72437
amorphous film, elec. field gradient 80—25264
amorphous film, X-ray diffr. 79—51451
amorphous metal films, crystallisation with and without mag. field 80—70570
anomalous US penetration at low temp., effect of trajectorial electron transfer *(Russian)* 77—43670
atom, and isoelectronic ions, excited-state energy level k-ordering, l-patterns 77—88406
atom, electron impact excitation cross sections 79—54972
atom, ground-state hyperfine struct., differential Stark effect 80—42990
atom, HF oscillator strength calculations, relativistic, $np^2P_{1/2,3/2} \rightarrow (n+1)^2S_{1/2}$ and $np^2P_{1/2,3/2} \rightarrow nd^2D_{3/2,5/2}$ transitions 79—89609
atom, isotope shift and HFS, isotope effects, UV spectra obs. 80—42973
atom, L_{23}-$M_{4\ 5}M_{4\ 5}$ principal and satellite Auger spectra 78—42030
atom, L-shell soft X-ray emission spectra, oscillator strengths 80—32651
atom, lowest S-state lifetime meas. 77—65436
atom, reson. states lifetimes, electron-at. crossed beams expt. 77—68013
atom, reson. X-ray Raman scattering, IR divergence of Compton effect 78—21873
atomic and ionic spectra 79—59388
atomic electron impact excitation cross sections calc. *(Russian)* 78—55240
atomic gas, Raman transitions, active reson. spectroscopy 77—27003
atomic oscillator strengths and radiative lifetimes 79—54811
atomic weight from GaAs stoichiometry meas. 78—42234
atomic weight from solid-source mass spectra 77—541
atomic-transition lasers based on two-photon dissociation of metal-triiodide vapors 80—23679
atoms and ions, regularities within Stark widths of reson. lines 78—78662
Auger LMM spectra, transition probabilities, term splittings and effective Coulomb interaction 77—44126
Auger spectra, LMM, rel. to L_{23} photoelectron spectra 77—77348
Auger spectrum, effect of $L_1L_{2,3}M$ Coster-Kronig processes 78—72681
chemisorption on Si (111) surface, Ga-induced surface states 79—19644
chemisorption site geometry and interface electronic struct. on GaAs (110), photoelectron spectra 80—49843
complexation by amino acids, with basic or heterocyclic groups *(French)* 78—53318
concentration determ. in atm. and rainwater in Vizcaya, Spain *(Spanish)* 78—57264
concentration measurement in Si_3N_4 thin film by CAMECA probe *(French)* 77—86411
conference, Marseille, France (Nov. 1976) 78—14243
contact angle meas. between melt and crystal during Czochralski growth 78—64461
controlled diffusion in Si, open-tube system 80—19822
creep near MP, influence of cryst. orientation *(Russian)* 77—8878
crystal growth, rate equations for dislocation-free and dislocation-assisted growth 79—4262
crystal growth by pulling, thermal parameters governing purity *(French)* 78—2046
crystal growth from melt, effect of small Cu additives 77—32515
crystal growth from melt dissolution, morphology *(German)* 77—24283
crystal structures, high press., X-ray diffr. obs. 78—42952
Czochralski growth, heat transfer during drawing *(French)* 78—48309
de Haas-van Alphen effect, expt. and interpretation 78—84132
deep planar diffusion in Si 79—69290
desorption, from W oxidised polycryst. surface, kinetics 78—75939
determination, in flux-grown magnetic garnets, by AAS 78—92585
determination in bauxite, X-ray fluoresc. method 77—36849
diffusion coefficient of As at 720°C during LPE growth 80—54419
diffusion in Ge along dislocations 79—82385
diffusion in Ge single cryst., effects of ultrasound 77—69119
diffusion in In-P melt, coeff. determ. 77—85927
diffusion into Si through SiO_2 layer, junction depth 78—51574
dislocation structure on melting of nearly perfect crysts., Borrmann topography 77—31663
elastic moduli, temp. depend., anharmonic effects *(Russian)* 77—31708
electric field gradient at nucleus calc. 78—39079
electrical props. of metastable β-phase in normal and supercond. states *(Russian)* 80—65520
electrode, crystallite interfacial impurities, electrochem. effects, microprobe anal. 77—44569
electronic struct. under pressure, Fermi surface meas. using magnetoacoustic technique *(Russian)* 77—47716
entropy of fusion, vibr. contrib. 77—47601
epitaxial layer, crystal defects influence on luminesc. obs. 79—87511
EXAFS, anisotropy of white line in K-absorption spectrum 80—89086
EXAFS, orientation depend. at 5K 79—52043
FCC hypothetical struct., stability calcs. 78—18766
field ion microscopy using mag.-sector atom probe, ionisation characts. 79—43106
film, freshly deposited, 77K, refl., annealing effect, thickness depend. 77—16413
film, monoclinic, elec. cond., classical size effect 77—89881
film, on GaAs or Si, anodic oxidation, Ga_2O_3 film prep. 77—81338
film, polymorphism, electron diffr. obs. *(French)* 78—18922
film, quench-condensed, disorder effect on optical cond. and band struct. 77—1746
film, vapour deposited on polymer, ageing, adhesion, elec. cond., electrochem. pot. *(Russian)* 79—33362
film optical props., 2-15 eV 77—77308
films, distorted, crit. mag. fields *(Russian)* 78—39273
gaseous reduction and extraction from mica 78—92216
Gaussian basis sets, Ga, Ge, As, Se, Br, and Kr, HF calcs. 77—38611
heat pipe meas. of corrosion and vapour press. 80—23878
horizontally dipped LPE film, inhomogeneities, spin wave reson. meas. 79—91298
ion implantation in Al, defect structures obs. 80—59494
ion source, high intensity, emission characts., atom-probe FIM obs. 80—80950
ion source, liquid, emission characts. obs. 80—62810
ion source, possible applications of a high brightness Ga source to ion microprobes 79—2896
ionisation mechanism on W field emitter 80—76156
ionisationj ionisation at field emitter, optical emission 80—93461
J_1J_2 transition from LS, revised assignments for $d^9s^2p^2$, $d^9s^2p^3$ 79—45630
laser from GaI_3 photodissoc., stimulated emission obs. on 417.2 nm line 79—89897
liquid, Brillouin scatt. obs. 77—24858

gallium continued

- liquid, Brillouin scattering from reflections of surface ripples 78—48188
- liquid, contact angle with Nb and Zr substrates 79—77864
- liquid, effective pair pot. and thermodynamical props. 77—47600
- liquid, effective pair potential and entropy *(French)* 78—14267
- liquid, EHD ion source for microprobe, design 77—21444
- liquid, elec. resist. calc., 19 and 35°C, using calc. and expt. struct. factors *(Russian)* 78—56124
- liquid, electrode metal-solvent interaction rel. to elec. double layer struct., adsorpt. 78—61023
- liquid, electrodiffusion conc. of impurities 80—54414
- liquid, electron transfer of rare earth metal impurities *(Russian)* 77—59132
- liquid, electron work function meas., dynamic capacitor method 77—39919
- liquid, embrittlement of Al 78—64653
- liquid, field ion source emission characts. 80—74059
- liquid, field ionisation, surface temp. and elec. field depend. 79—78849
- liquid, heating of glass substrate, surface temp. of substrate 79—97390
- liquid, interference function temp. depend. from X-ray diffr., elec. resist. calc. 77—47332
- liquid, Knight shift of ^{69}Ge 77—12271
- liquid, mol. motions from NQR, viscosity and sound damping 77—1615
- liquid, neutron diffr. room temp. to 1303K, struct. model 78—51405
- liquid, nucl. acoustic reson. Knight shift, rel. to spin-lattice relax. 78—19351
- liquid, nucl. quadrupole relaxation, Sternheimer antishielding and fluctuating elec. field gradients 77—55726
- liquid, nuclear quadrupole relax. rate for ^{69}Ga, 20-150°C, calc. 77—36151
- liquid, optical density of states, low-energy photoemission meas. 77—77341
- liquid, self-diffusion coeffs. by radioactive tracer technique 80—49392
- liquid, solubility and activity of O_2 77—59122
- liquid, spreading kinetics on Cu surface 80—10742
- liquid, struct., X-ray diffr. obs. 77—84619
- liquid, structure factor shoulders and interatomic pot. rel. to electron theory 77—7658
- liquid, supercooled, double hard sphere model 77—43128
- liquid, supercooled, dynamics 79—27902
- liquid, surface tension, low-temp. H_2 plasma influence, elec. double layer form. 79—33160
- liquid, thermal props. at high temp. 80—75536
- liquid, tracer diffusion studies using metallic ^{67}Ga 80—24629
- liquid, viscosity, 370-1800K 77—1254
- liquid, X-ray diffr., 323 and 203K *(French)* 77—84575
- liquid, X-ray diffr. exam. of struct. at 203 and 323K *(French)* 78—14268
- liquid and solid, photoemission, conduction electrons 79—87566
- liquid metal field emission ion source, characts. 80—108326
- liquid metal ion source, energy distrib. meas. 80—95493
- liquid particles-He(N_2)(CO_2)(air), nonequilib. Laval nozzle flow calib., numerical soln. 77—75967
- liquid point anodes, field-ion emission 80—2928
- liquid spreading over Ag thin film, kinetic eqn. *(Russian)* 80—59376
- liquid struct. factor, short range repulsive forces 78—75520
- liquid-Ag interface, γ-phase interlayer growth, two-dimens. electron diffr. 79—19487
- liquid-metal, high-intensity scanning ion probe with submicroscopic spot size 79—54225
- liquid-solid phase transition, photoacoustic detection 78—75810
- liquid-solid transition, collective mode dynamics, quantum corrections 77—15554
- magnetic susceptibility near melting point 80—60186
- magnetoresistance, oscillatory, freq. spectrum meas., Fermi surface model 77—62898
- medical use of Ga radionuclides, history 79—53955
- melt, adhesive props. on Ti and graphite, 300 to 1200K *(Russian)* 77—15663
- melting point, thermometric standard 77—82516
- melting point as temp. calibration standard 77—41611
- melting-point apparatus for thermometer calibration, enzymologic appl. 78—85460
- melting-point standard, near 30°C, clinical chemistry appl. 78—80997
- metal and alloy high-temp. couplants for acoustic transducers 79—14195
- metal-GaAs contacts, use of Ga to eliminate large As loss peaks 80—80370
- metastable phases, melting curve under atm. and high press. by microcalorimetry *(French)* 77—43314
- metastable states, supercooling and polymorphism *(French)* 78—14325
- molten, thermomigration in Si and GaAs 77—69118
- monolayers on W field ion image qualities and work function 78—35272
- nonlinear sound wave interactions, sound attenuation in weak superconducting state *(Russian)* 80—75310
- NQR, press. depend. of elec. field gradient and Knight shift tensors 78—19366
- optical properties in 0.3 to 5 eV range 78—31196
- optical properties in 0.5-60 eV range, dielectric const. and loss functions *(French)* 77—12353
- orthorhombic asymmetry temp. depend. 77—51339
- overlayers on GaAs (110), interfacial electron states, UPS and LEED obs. 80—80377
- p-type, electrode, flatband pot. determ. from differential stress meas. 80—75638
- photoacoustic effect at solid-liq. phase transition 80—70320
- photoemission, reson. shake-up and Auger processes at 3p photothreshold 80—100748
- photoemission, transition from ordered solid to disordered liquid 80—45217
- plastic deform. and fracture obs. by acoustic emission of Zn single crysts. in metal melt *(Russian)* 78—56737
- polymorphism at high press. *(French)* 78—47279
- positron annihilation lineshape factors, effect of thermal expansion 77—44084
- positron lifetime meas., comparison with theory 77—63483
- quadrupole interaction in orthorhombic metal of $9^+/2$ states of ^{71}As and ^{73}As 77—8467
- quench-condensed films, superconducting transition temp., elastic stress and strain effects 80—70883
- reaction with InSb 78—23682
- residual resistivity, bulk, in ultra-pure single crystals 80—10950

gallium continued

- rutile: Ga, Mg, intersecting defect structures, TEM study 79—51123
- solid and liquid, positron annihilation temp. depend. 80—108296
- solid-liquid transition, optical reflectance spectra 80—24569
- solubility in CdSe in presence of Cu 78—22856
- spectrophotometric determination, in aq. organic medium using eriochrome cyanine R 77—36829
- spiral cyclotron waves excited by US in open Fermi surface metals *(Russian)* 79—99771
- spreading kinetics on thin Ag films, influence of melt-support interaction *(Russian)* 79—37903
- superconducting film, crit. transverse mag. fields and transition temp. *(Russian)* 80—7048
- superconducting film, T_c and residual resist., variation with coating thickness 78—47900
- superconducting high pressure phase, sp. ht. 80—70894
- superconducting modifications in bulk samples *(Russian)* 79—65574
- superconducting thin film, tunnelling meas. in high mag. field 78—68120
- superconductor, US anomalous penetration along electron trajectories in mag. field *(Russian)* 79—87191
- surface, He^+ ion neutralisation 78—35237
- surface (3×3) superstructure on W(011) and Mo(011), FIM obs. 79—99425
- surface coating on W field emitter, stability 77—12500
- surface props. rel. to adsorbed O_2, H_2O vapour, work function determ. 78—60187
- thermal contact agent for low temperatures 77—49731
- thermopower quantum oscillations 80—15505
- thermoreflectance, in near IR, down to 0.3 eV 77—85722
- triple point temp. determ. 80—42223
- ultrasonic absorpt., intermediate state 77—72942
- ultrathin metallic filaments, appearance of dielec. instability, coexistence with supercond. 80—103784
- vacancy equilibrium configuration, pseudopot. estimation 77—39582
- vacuum deposited film characterisation *(French)* 79—51447
- whisker growth from GaN/Ga layered films 80—92800
- work function, electrochem. determ., rel. to In-Ga alloys 77—44489
- X-ray emission spectra, L_l and L_η 78—39631
- X-ray K absorpt. edge, effective ionic charge and bonding schemes 80—29827
- Ag-Ga thin film couple, room temp. interactions 80—2220
- Al single crystals, liq. metal embrittlement by Ga 80—7675
- Al:Ga, impurity low-field galvanomag. coeffs., 4 OPW calcs. 77—69304
- Al:Ga, pulsed electron-beam annealing, lattice site location improvement 80—107303
- $Al_xGa_{1-x}As$:N, photoluminesc. and optical absorpt. spectra of N impurity bound-excitons 79—47496
- As_2S_3:Ga system chalcogenide glasses, thermophysical and struct. props. 80—15007
- a-As_2Se_3:Ga, doped film, photoluminescence intensity and lineshape study 80—50448
- $BaTiO_3$:Ga, annealed in H_2 and O_2, valence change in phase stability 80—20600
- $Bi_{12}GeO_{20}$:Ga,Ca, photocond. suppression by simultaneous Ga and Ca doping, and appl. to electro-optic light valve 79—78134
- $C(NH_2)_3Al(SO_4)_2.6H_2O$:Ga, temp. depend. quadrupole coupling const. for $^{27}Al^{3+}$ and $^{71}Ga^{3+}$ 78—19368
- $CdCr_2S_4$:Ga, resist. and magnetoresist. meas., effect of donor impurities 79—19608
- $CdCr_2S_4$:Ga magnetic semiconductor growth, structural defects, physical properties 80—60759
- $CdCr_2Se_3$:Ga, synthesis and photoferromag. effect 77—51936
- $CdCr_2Se_4$:Ca, temp. driven metal-semiconductor transition, temp. and mag. field depend. *(Russian)* 78—88003
- $CdCr_2Se_4$:Ga, effect of doping on exchange interaction 78—43579
- $CdCr_2Se_4$:Ga, elec. props., vac. heat treatment effect 80—15518
- $CdCr_2Se_4$:Ga, elec. resist. and magnetoresist., 2 to 200K 80—96876
- $CdCr_2Se_4$:Ga, magnetic microregions caused by s-d exchange 77—77050
- $CdCr_2Se_4$:Ga, photoconductivity, photomagnetoresistance near Curie point *(Russian)* 80—100485
- $CdCr_2Se_4$:Ga, sp. elec. resist., temp. and mag. field depends. *(Russian)* 78—26893
- $CdCr_2Se_4$:Ga(Ag), and pure, photocond. and photomagnetoresist. spectra 77—80809
- $CdCr_2Si_4$:Ga, negative magnetoresist. effects near Curie temp. 79—11152
- CdS:Cu, In, Ga, spray deposited film, struct., X-ray obs. 78—71713
- CdS:Ga, cathodolum. on diffusion front 77—32447
- CdS:Ga crystal cathodoluminescence, SEM analysis 80—97349
- CdSb:Ga, p-n junction formation by laser radiation 80—96983
- CdTe:P,Ga, IR absorpt. investig. of localised vibr. modes of impurity centres 77—52136
- Co:Ga, temp. anomalies of hyperfine fields 78—23265
- $(Eu,Lu)_3Fe_5O_{12}$:Ga(Al)(Ca,Ge), bubble material, dynamic characterisation, comparison between transport and FMR methods 80—39833
- EuIG:Ga, mag. anisotropy, magnetisation meas. 80—60240
- in Fe meteorites, concs. rel. to chemical classification and nebular condensation 80—36594
- α-Fe_2O_3:Ga^{3+}, substitution effect on Morin transition, neutron diffr. study 80—44827
- Ga, amorphous thin films, supercond. surface resist. 77—72961
- Ga I, absorption spectrum 320-1000 Å, intersubshell correls., simultaneous ejection of two photoelectrons 77—50391
- Ga I, radiative lifetimes, calcs. and beam-foil spectra 77—75223
- Ga I, relativistic and cancellation effects in line strength ratios 78—82689
- Ga I, Rydberg series, disctete levels and continua of finite bandwidth 78—74603
- Ga II, $4s4d\,^1D$ and $4p^2\,^1D$ energies and lifetimes 79—59391
- Ga XXIII, 2p-4d and 2p-4s transition arrays, wavelengths and oscillator strengths 80—47933
- Ga^-, photodetachment cross-sections, crossed beam meas. *(German)* 77—42298
- Ga^+, photon coherent scatt., cross sections 77—50410
- Ga^{29+}, ^1P and ^3P energy levels, relativistic RPA calc. 80—47913
- Ga/Al ratio vars. along Reykjanes Ridge and Iceland 79—8617
- Ga-Ag tunnel junction, evidence for existence of anisotropy of supercond. energy gap 80—20357
- Ga-Al and Ge-Si fractionation in Hawaiian volcanic rocks 79—12112
- Ga-GaAs, surface reactions and interdiffusion, photoemission study 80—49532
- Ga-GaAs (110), Schottky barrier form., defect mechanism 80—49902

gallium continued
- Ga-GaAs interface immersed in electrolytic solns., elec. props. 78−95368
- Ga-GaAs melt, mutual diffusion from soln. kinetics, self-diffusion coeffs. 77−47608
- Ga-GaAs(110) structure, interface states, photoemission study 78−95359
- Ga-$GaCl_2$, finely disperse system, supercond. props. 77−85376
- Ga-insulator compound, obtained by impact compression method, superconducting properties *(Russian)* 79−7919
- Ga-NaX zeolite system, press. depend. of metal-insulator transition 78−88005
- Ga-Xe film, metal-nonmetal transition, optical and resist. meas. 77−89818
- Ga+As reaction temp. determ. for GaAs synthesis 77−24978
- $Ga+H_3PO_4$, interaction in aq. soln., ^{71}Ga and ^{31}P NMR obs. 79−22729
- $Ga+H^+$, 4 MeV beam-foil X-ray production cross-section 79−7003
- Ga+inert gas atom, diffuse series head lines, hyperfine components, broadening calcs. 80−32632
- $GaAs:C^+,Ga^+$, dual implantation of C^+ and Ga^+, sheet resist. and Hall effect meas. 78−67728
- GaAs:O(Cr), relax. semicond., Dember effects meas. 79−28372
- GaAs:Se, Ga, dual species ion implantation, elec. characts. 80−103377
- GaAs-Ga, (110) interface electron states, photoemission study, chemical shift, surface charge redistrib. 78−72259
- GaAs-In_2O_3 heterojunction solar cells, photovoltaic and rectifying props. 79−1618
- GaN/Ga layered films, Ga whisker growth 80−92800
- ^{31}Ga, L-shell X-ray prod. by H(He) ion bombardment 79−47548
- ^{31}Ga, origin of high and low freq. K-satellites in X-ray emission spectra 80−50466
- ^{67}Ga and other Al analogues, possible parathyroid imaging 80−101252
- ^{67}Ga, comparison of Anger tomographic scanner with 15 in scintillation camera for medical imaging 79−34658
- ^{67}Ga, Crohn's disease, value of ^{67}Ga-citrate scanning 79−100719
- ^{67}Ga imaging in abdominal disease 79−57772
- ^{67}Ga imaging in Hodgkin's disease and other malignant lymphomas 79−57769
- ^{67}Ga imaging of peritoneum and retroperitoneum, anatomic correls. 80−17097
- ^{67}Ga localisation in normally functioning allografted kidney 79−100717
- ^{67}Ga, mechanism of localisation in tumours 79−57768
- ^{67}Ga, metallic, prep. and appl. to tracer diffusion studies in liq. Ga 80−24629
- ^{67}Ga, role in inflammatory disease 79−57770
- ^{67}Ga, role in neoplastic disease imaging in children 79−100718
- ^{67}Ga, status in tumour detection 80−98074
- ^{67}Ga substraction scanning in Hodgkin's disease and lymphomas 79−74738
- ^{67}Ga, uptake in human melanoma cells 79−62217
- ^{67}Ga, use in diagnosis of pulmonary disorders 79−57771
- $^{67}Ga/^{99m}Tc$, computerised double-tracer subtraction scanning for inflammatory diseases 79−70612
- ^{67}Ga-scintigraphy, ultrasonography and computerised tomography, role in abdominal abscesses detect. 80−17096
- ^{68}Ga, ionic, pot. column chromatography generators 80−46050
- ^{68}Ga labeling of albumin and albumin microspheres 80−17137
- ^{68}Ga, new generator, medical appls. 80−76834
- ^{68}Ga-labelled human serum albumin microspheres, prep. 80−17131
- ^{73}Ga, β-decay rate for estimation of ultra-high pressure 78−77927
- Ge:Ga, amorphous, doping effects on Fermi level, electrical meas. 79−42546
- Ge:Ga, appl. of heat pipe to Czochralski growth, segregational behavior 79−61511
- p-Ge:Ga, carrier heating by weak elec. field, hole-hole collision influence 78−72161
- p-Ge:Ga, cryst. defects due to γ-irrad., annealing 79−55779
- Ge:Ga, cryst. defects due to neutron irrad., elec. cond. and annealing 79−55789
- p-Ge:Ga, dislocation density effect on carrier lifetime and deep recomb. centres 79−51598
- Ge:Ga, effects of destabilising vertical thermal gradients on cryst. growth and segregation 78−52659
- p-Ge:Ga, fast electron radiation defects, 0.52 eV absorpt. band, impurity photocond. and Hall effect meas. 78−27273
- Ge:Ga, fast-neutron irradiated, shallow radiation defect levels, electronic props. 78−23049
- p-Ge:Ga, heavily doped, elec. resist., 40 mK to 300K 79−38071
- Ge:Ga, heavily doped, structure defect evolution during heating *(Russian)* 78−43026
- p-Ge:Ga, lattice defects induced by γ-irrad. 80−29051
- Ge:Ga, magnetoacoustic resonance attenuation, Zeeman splitting of acceptor ground state 77−47869
- Ge:Ga, photoconductivity oscillation with respect to applied mag. field *(Russian)* 78−80026
- p-Ge:Ga, photoemission into electrolyte soln., energy diagram, Volta pots., voltage drop 77−62990
- Ge:Ga, polycrystalline film, electron transport props. 79−99642
- Ge:Ga, resonant phonon interaction with localised acceptor levels 80−6784
- Ge:Ga, resonant scattering of phonons by bound holes in temp. range 1 to 5K 80−75393
- p-Ge:Ga, saturation behaviour at CO_2 laser wavelengths 78−1307
- Ge:Ga, shallow acceptor ground state, thermal cond. meas. 77−43540
- Ge:Ga, shallow acceptor spectral line intensities 80−88517
- Ge:Ga, simultaneous multiline saturation at 10.6 μm 77−88868
- Ge:Ga, transmutation-doped, impurity cond., 1.5-4.2K 77−89758
- n-Ge:Ga, uniaxial compression, 0.6-2.9 mm radn. absorpt. 79−82629
- Ge:Ga, uniaxially stressed, far IR photocond. meas. 78−10496
- Ge:Ga,Sb, compensated, low temp. props. rel. to appl. in bolometry 80−31867
- Ge:Ga photoconductor detector performance in low optical background 77−37999
- Ge:Ga photoconductors in low IR backgrounds 79−63305
- Ge:Ga surface, antireflection coated, laser pulse damage resistance obs. 79−14020
- n-Ge:P,Ga, compensated, uniaxially compressed, anisotropy of mm. and submm. wave absorpt. 78−19074
- Ge-Se-Ga thin film, elec. cond., switching phenomena *(Polish)* 80−11120
- GeO_2:Al, Ga, EPR, transferred hyperfine interactions of impurity-related trapped hole centres 77−85568

gallium continued
- $Ge_{1-x}Si_x$:Ga,As, interimpurity radiative recombination, composition depend. 79−11465
- Gra II isoelectronic series, $4s4p^1P$ lifetimes meas. 80−42998
- $KBr:Ga^+$, Jahn-Teller effect in orbital triplet, optically detected EPR meas. 77−66441
- $KBr:Ga^+$, luminescence decay times, fluorescence kinetics, 1.6-300K 79−33825
- $KBr:Ga^+$, mag. circular dichroism meas. 79−42988
- KCl:Ga, ESR of impurity centres, impurity optical absorpt. bands 80−29618
- KCl:Ga, X-irradiated, EPR spectra 79−28613
- $KCl(Br)(I):Ga^+$, polarisation of Ga^+ centre A_T emission, temp. depend. 80−80842
- $KCl(Br)(I):Ga^+$ phosphor, press. effects on triplet relaxed excited states, quadratic Jahn-Teller interaction 78−23510
- $KI:Ga^+$, mag. circular dichroism meas. 79−42988
- $KI:Ga^+$, magnetic circular dichroism of A- and B-absorption band region 77−12412
- MgO:Ga, γ-irradiated, EPR and optical studies 79−73809
- NaCl:Ga, ESR of impurity centres, impurity optical absorpt. bands 80−29618
- NaCl:Ga, X-irradiated, EPR spectra 79−28613
- $NaCl:Ga^+$, polarisation of Ga^+ centre A_T emission, temp. depend. 80−80842
- Nb-Ga-Ir system, phase equilib. at 1000°C and supercond., Nb-rich portion 77−36480
- $Pb_{1-x}Ge_xTe$:Ga, Fermi level stabilization, transport props. meas., 77-400K 78−56065
- $Pb_{1-x}Ge_xTe$:Ga, influence of hydrostatic compression on elec. props. 79−73516
- $Pb_{1-x}Sn_xTe$:Ga, elec. props., dopant influence 79−51599
- $Pb_{1-x}Sn_xTe$:Ge, anomalous behaviour of impurity centres under press. *(Russian)* 80−65491
- PbTe:Ga, location, behaviour of Ga, electrophysical props. meas. 79−38016
- Si, diffusion of Ga in closed capsule, surface damage elimination 78−87691
- Si:Ga, As, sequential diffusion, radiotracer obs. 78−10073
- Si:Ga, binding energy, excited state spectra, photolum., semi-empirical short range pot. 80−44534
- Si:Ga, bound exciton lifetimes for acceptors 77−80738
- Si:Ga, bound-exciton absorption 78−56507
- Si:Ga, CC Si:Al(Ga), O_2 diffusion, conc. profile meas. 80−79990
- Si:Ga, diffusion of impurity into cryst., doping profile 79−77621
- Si:Ga, dopant solubility limit, laser irrad. effects 80−84295
- Si:Ga, edge luminesc. spectra of acceptors, multiexciton complexes 78−56517
- Si:Ga, electron excited, recomb. radiation, high resolution investigation 78−15233
- Si:Ga, electron irrad.-induced defects, DLTS meas. 80−24499
- Si:Ga, even-parity acceptor excited states, bound exciton two hole transitions 77−85793
- Si:Ga, extrinsic detector material props. 77−89797
- Si:Ga, gettering of Au and Cu during Ga diffusion 78−91350
- Si:Ga, heavily damaged, channelling investigation of diffusion behaviour 79−37877
- Si:Ga, heavily doped, form of occurrence of acceptor impurities 77−11581
- Si:Ga, IR absorption of dopant centres, spectral depend. on doping, impurity conc. and temp. 80−76053
- Si:Ga, IR spectra of acceptor levels 80−34953
- Si:Ga, impurity states, localised orbital approach 80−92851
- Si:Ga, ion implantation and pulsed laser annealing, supersat. alloy form. 80−54267
- Si:Ga, LPE growth on Si substrate, melt-back approach 78−80481
- Si:Ga, LPE on Si, technique and characterisation 79−38751
- Si:Ga, laser assisted doping for surface layers 80−19824
- Si:Ga, laser-doped, impurity distrib., Rutherford backscatt. and channelling anal. 80−59507
- Si:Ga, luminescence fine struct. from bound exciton and multiexciton complexes 77−32430
- Si:Ga, MBE, growth, struct. and elec. props. 77−89458
- Si:Ga, mean square dynamic displacement of atoms, effect of electron-phonon interactions *(Russian)* 78−10145
- Si:Ga, neutron irrad., Hall effect meas. of shallow donor levels 80−20124
- p-Si:Ga, neutron transmutation counterdoped, shallow defect levels, Hall effect and photocond. obs. 79−87055
- Si:Ga, plastic deform. and formation of dislocation loops, effect of Au atoms 79−69184
- Si:Ga, possibility of use in fabrication of fast response photodetectors 79−15184
- Si:Ga, spreading resist. calibration using Si:B 80−103690
- Si:Ga,P(As), sequential diffusions, comparison of interactions 77−80655
- Si:Ga epitaxial film, doping efficiency *(Japanese)* 79−73201
- n-Si:Ga laser doped, segregation, Rutherford backscattering 80−103483
- Si:Ga material for space solar cell 80−94007
- $Si:Ga^+$, impurity distrib. profiles using SIMS and Hall effect method 79−69152
- Si:Se,Ga, diffusion of Se, solubility and ionization levels, Hall effect and photocond. meas. 79−42486
- Si-Ga interface, electron energy loss spectra of Schottky barrier 77−48290
- $Si+Ga^+$ ion implantation at high current density, lattice disorder, proton backscattering 80−34085
- SiC:Ga, 4H-, 6H- and 3C-polytypes, melt growth and photoluminesc. 77−24885
- β-SiC:Ga, donor-acceptor pair emission 77−4682
- α-SiC:Ga, piezoresist. rel. to acceptor levels 78−60129
- SiC:Ga (6H), photoluminesc., site-depend. donor and acceptor levels 79−61421
- SiC:Ga (6H) LEDs, fabrication by rotation dipping technique, electrolum. mechanisms 80−50426
- 4H-SiC:Ga(Al), photoluminesc. spectra 77−66530
- SiO_2:Ga film, impurity distrib. after annealing, neutron activation anal. 80−24484
- Si;Ga, ground state of impurities 79−28313
- Ta-Ga phase relationships, X-ray anal. of struct. 77−36453
- $TiO_2:Ga^{3+}$, EPR spectra of trapped hole centre 78−80214
- VO_2:Ga, Mo, conductivity transitions 78−76121

gallium continued
VO_2:Ga, phase transforms., influence of nonstoichiometry 77−85274
YAG:Er^{3+}, Ga^{3+}, LPE and luminesc. 78−64408
YIG, epitaxial, temp. stabilisation of ferrimag. reson. field by Ga, La substitution 77−77104
YIG, pure and Ga-substituted diffuse refl. and thermorefl. spectra near Curie point 80−40131
YIG:Ga, crystal growth from high temp. soln., induced striation method 77−1802
YIG:Ga, diamagnetically substituted, annealing effects on cation distrib. 79−1455
YIG:Ga, magneto-optical Kerr effect, reflectivity spectra 80−66157
YIG:Gd, Ga, optical probing of magnetoelastic Rayleigh waves 79−78495
YIG:La,Ga, film, LPE-grown, Ga incorporation, depend. of magnetisation on growth rate 80−84627
YIG:La,Ga film, uniaxial anisotropy, variation along growth direction 77−28416
Zn-Ga, metal/liquid metal, exam. of crack propag. in liquid metal environment 78−60766
ZnO:Ga sputtered films, props. rel. to deposition conditions 80−107935
ZnP_2:Ga, optical absorpt. spectra in range 0.5 to 2.2 eV 80−66250
ZnS:Ga, deep traps, impurity electroabsorpt. and photocond. meas. 78−6707
ZnS:Ga, self-activated emission, A-centre ODMR 79−95685
ZnS:Ga^{3+}, $Cu^{+}(Ag^{+})$, interimpurity luminesc. at high press. 78−19532
ZnSe:Ga, 1.91 eV red emission, optically detected mag. reson. study 79−69750
ZnSe:Ga, defect struct., Hall effect and resist. meas. 79−1428
ZnSe:Ga, effect of thermal treatment and doping on elec. props. 77−85223
ZnSe:Ga, P, optically detected mag. reson. of P_{Se}-centre 79−33566
ZnSe:Ga, single cryst., diffused, blue luminesc. 78−39584
ZnSe:Ga,As, characts. of simultaneous incorporation, by Mn^{2+} ESR and X-ray fluoresc. anal. 80−34017
ZnSe:Ga(As), edge luminesc. 80−20699
ZnSe:Li(Na)(Ga) doped and pure cryst., donor-acceptor bands 80−11465
$ZnSiP_2$:Ga, effect of doping conc. on elec. cond. and Hall coeff. 78−76077
n-$ZnSiP_2$:Ga, elec. cond. and Hall meas., 77 to 1000K, scatt. mechanisms 79−11153

gallium alloys
see also gallium compounds
alloy high-temp. couplants 79−14195
rare earth intermetallics, RGa_2, AlB_2-type struct., electron transfer, bonding, heat of form. theory 78−92499
rare earth intermetallics, RGa_2, mag susceptibility, 1.5-300K and Neel temp. 78−68184
rare earth intermetallics, RGa_2, ordering and exchange interactions 80−39779
rare earth intermetallics, RGa, mag. props., 4.2 to 350K 77−63230
rare earth-Ga_2 intermetallics, mag. structs. 78−84394
rare earth-Ga alloys, phase diagrams 79−78932
refractory metal dichalcogenides and Ga alloys, mixing powders using US treatment 79−24454
thermodynamic properties 78−14480
Ag-Ga, α-phase, lattice sp. ht. calcs. 80−65246
Ag-Ga, α-phase alloy, thermopower at low temps. 78−84196
Ag-Ga, electric field gradient temp. depend., nearest neighbour impurity mass effect, TDPAC meas. 78−6612
Ag-Ga, Ga spreading kinetics, influence of melt-support interaction *(Russian)* 79−37903
Ag-Ga, thermopower at low temp., Fe impurities 79−65440
Ag-Ga (0.42 to 2.09 at.%), internal oxidation *(Japanese)* 77−63908
Ag-Ga (27 at.%), cooling rate depend. of thermal arrest, transform. temp. 79−29053
Ag-Ga based contacts to GaAs alloyed in As_2 beam 79−95495
Ag-Ga solid soln., internally oxidised, hardness *(Japanese)* 78−60744
Ag-Nb-Ga, phase relations, A15 phase diffusion layer formation 78−52764
Al-Ga, ab initio calcs. of partial enthalpy and result for enthalpy of mixing 79−43197
Al-Ga, band model of high temp. magnetism 78−26809
Al-Ga, dil., deviation from Matthiessen's rule, 4-OPW approx. calc. 79−19574
Al-Ga, dil., Dingle temp. calc. 78−39005
Al-Ga, dil., electronic transport coeffs. for point defect scatt., 4-OPW calc. 79−42531
Al-Ga, dil., Hall coeff. by OPW Fermi surface model 80−6816
Al-Ga, dil., low-temp. electron-diffusion magnetothermopower meas. 77−15833
Al-Ga, dil., neutron irrad., 4.2K, defect prod., recovery 77−1155
Al-Ga, electrical resist. and magnetoresist., 2 to 40K, Matthiessen rule deviations *(Russian)* 77−31996
Al-Ga, enthalpy of mixing, 'const. vol. alloy' formulation 79−28111
Al-Ga, face centred cubic struct. stability, melt equilib., α-Ga effects 78−18766
Al-Ga, internal friction and shear modulus, temperature and concentration dependence 77−86077
Al-Ga (10 wt.%), exam. of ^{27}Al diffusion by NMR technique 78−87813
Al-Ga dil. alloys, Hall coeff., residual resist., and relax. times 79−11107
Al-Ga-Ge, liq., enthalpy of form., direct reaction calorimetry, 713-1230K *(French)* 79−66336
Al-Ga-Ge, thermodynamic props. of mixing of binary systems, phase diagram 80−45275
Al-Ga-In, liq. alloys, excess Gibbs functions 633 to 1173K 78−60655
Al-Ga-In system, thermodynamic anal. 79−60512
Al-Ga(-Ge), and Al-Ge, Al activity, EMF study, phase diagrams 79−83175
Al-Ga(In)(Sn), interpretation of metallic phase diagrams, entropy of mixing 79−42274
$Al_{10.4}Ga_{0.08}V$, low temp. thermal expansion 78−95167
Au-Cu-Ga, solid soln., phase systems, valence electron density effects *(French)* 78−19724
Au-Ga, dil. alloys, dHuA meas. and phase shift analysis of electronic scatt. anisotropy 77−35932
Au-Ga, elec. resist. in liquid and solid state *(Russian)* 79−51549
Au-Ga, liq. alloys, Ga activities, ht. of mixing 77−4921

gallium alloys continued
Au-Ga, resist. and supercond. meas., electron-phonon interaction and Coulomb pseudopot. determ. 78−43358
Au-Ga, UPS exam. of valence bands 79−19511
Au-Ga based contacts to GaAs alloyed in As_2 beam 79−95495
Au-Ga dil. alloys, electronic struct. 79−37974
Au-Ga liq. alloys, ΔG^E of mixing from ht. of melting and sp. ht. of cpds. 77−4920
Au-Ga-In solid soln., elastic strain energy depend. of supercond. T_c 79−38229
AuGa, and $AuGa_2$, supercond. transition temp. and crit. field 79−38232
$AuGa_2$, core-level binding energy shifts and charge transfer 80−25268
$AuGa_2$ film, supercond., mag. susceptibility and Knight shift press. depend. 77−43777
$AuGa_2$ type supercond., mag. impurity and press. effect on crit. temp. *(Russian)* 78−23189
$AuGa_3$, supercond., press. depend. of thermodynamic props., theor. *(Russian)* 77−51843
$Au_2(MnGa)_2$ Heusler alloy, magnetic order and coupling 79−38303
$(Au_{1-x}Pd_x)Ga_2$, supercond. transition temp. and crit. field 79−38232
$Ba_{10}Ga$, cryst. struct. *(French)* 80−79749
Ce-Ga, liquid, solubility and thermodynamic props. *(Russian)* 78−19717
Ce-Ga, phase diagram *(Russian)* 78−27478
Ce-Ga system, phase equilib. and cryst. struct. of phases 80−35159
Co-Ga, binary alloy, small-angle neutron scatt. from superparamag. behaviour 78−19217
Co-Ga, β' phases, evidence of non-cubic lattice distortions around vacant sites 78−42956
Co-Ga, ferromag., local configuration studies, neutron scatt. and spin echo NMR 77−63114
Co-Ga, phase diagrams and cryst. struct., DTA, X-ray diffr. and microprobe anal. *(French)* 79−47660
Co-Ga alloys, transition metal partially substituted, elec. resist. anomalies 79−38044
Co-Ga binary system, lattice consts., phase transform *(Chinese)* 80−88108
Co-Ga β' quenched single crystals, annealing-out of point defects 80−55426
Co-Ga liquid and solid alloys, elec. resistivity at high temps., partial struct. factors 80−6806
Co-Ga system, exam. of thermodynamics of α and β' phases 78−71870
Co-Ga-B, phase diagram, metallographic, X-ray and electron probe anal. 78−92241
Co-Ga-Mn, small-angle mag. neutron scatt., states of mag. order study rel. to Mn and Fe substitution 79−11292
Co_2FeGa, alloy, site preference of Co and Fe, Mossbauer and neutron study 79−78577
β-CoGa, Cu addition effects on defect struct. *(German)* 77−11546
CoGa, defect struct. model 79−46648
CoGa, diffusion coeffs. of ^{60}Co, 800-1050°C 77−84966
CoGa, onset of ferromag., diffuse mag. neutron scatt. meas. 77−63113
CoGa, ordered electronic cpd., self-diffusion of ^{60}Co and ^{72}Ga 79−65238
$Co_{0.54}Ga_{0.46}$, frequency depend. magnetisation, superparamagnetic behaviour 80−84624
β-$Co_{52}Ga_{48}$, negative TCR obs. 80−75543
$Co_{54}Ga_{46}$, superparamag. response to low DC fields 80−44860
$Co_{56}Ga_{44}$, thermal release of injected He 77−31881
Co_xGa_{1-x} alloys, cluster spin glass, host and impurity NMR and AC susceptibility 80−71194
Co_xGa_{1-x}, β-phase, spin glass behaviour 80−44837
Co_xGa_{1-x}, cluster spin glass, AC susceptibility in DC mag. fields, 77 to 500K 80−34670
Co_xGa_{1-x}, NMR expts. interpretation 80−75870
Co_xGa_{100-x}, electrical resistivity anomaly, spin cluster model 79−99531
$Co_2Ga_{2-x}Cr_x$, ferromag., local configurational studies, neutron scatt. and spin echo NMR 77−63114
$Co_2Ga_{2-x}Cr_x$, ferromag., site selecting and moment distrib. 77−77031
$Co_2Ga_{1.95}Fe_{0.05}$, mag. behaviour, Mossbauer effect and DC magnetisation meas. 80−50244
$Co_2Ga_{2-x}Fe_x$, elec. resist., temp. and mag. field depend., mag. contrib. 80−96846
$Co_2Ga_{2-x}Fe_x$, mag. field depend. of resist., 5.80K 80−70676
$Co_2Ga_{2-x}M_x$ (M=V, Cr, Mn, Fe), mag. props. and order 77−12093
Co(GaTiV) alloys, ferromag. onset, electron conc. depend. 80−60203
$Co_2Ga_{2-x}V_x$, ferromag., local configuration studies, neutron scatt. and spin echo NMR 77−63114
$Co_2Ga_{2-x}V_x$, ferromag., site selectivity and moment distrib. 77−77031
CoGe, vacancy conc. in B2 phase exhibiting triple defects 79−42058
$Co_2Mn_xFe_{1-x}Ga$, hyperfine fields of Fe impurities, Mossbauer effect meas. 78−31130
$Co_{50}Mn_xGa_{50-x}$, cryst. struct. transform. of B2 type *(German)* 79−91642
$Co_{50}Mn_xGa_{50-x}$, ordering and disordering phenomena, mag. study 80−70154
Co_2VGa, ferromag., hyperfine fields meas. by NMR 77−63315
Co_2VGa, ferromag. Heusler alloy, spin echo NMR meas. 77−63319
Cr-Co(Ni)-Ga, phase equilibria diagrams at 800 and 600°C *(Ukrainian)* 78−92236
Cr-Fe-Ga system, phase obs. at 800 and 820°C *(Russian)* 78−23662
Cr-Ga, dil., Neel temp., elec. resist. and thermal expansion meas. 79−51778
Cu-Ga, binary alloy constituent EDS anal., secondary fluorescence, SEM study *(Chinese)* 80−85231
Cu-Ga, dil., impurity electron struct., self-consistent KKR Green's function calc. 79−78040
Cu-Ga, dil., magnetic susceptibility, impurities effect, free electron gas model 79−91206
Cu-Ga, dil., magnetic susceptibility, impurities effect, Fermi surface effects 79−91207
Cu-Ga, dil., Matthiessen's rule deviations above room temp. 79−91023
Cu-Ga, dil., optical props. and electronic struct. 78−35164
Cu-Ga, dil. alloy, thermopower and resistivities, validity of Nordheim-Gorter relation 78−91671
Cu-Ga, disordered, phonon dispersion curves, inelastic neutron scatt. study 79−51223
Cu-Ga, effect of ion bombardment on surface composition using differential reflectometry and AES 77−59189
Cu-Ga, high dislocation density alloys and oxide precipitated struct., NMR, spin echo 80−39892

gallium alloys continued

- Cu-Ga, ion bomard. effect on surface comp., reflectometry AES 77−81190
- Cu-Ga, lattice dynamical meas. and anal. *(Russian)* 77−62599
- Cu-Ga, liq., elec. cond., temp. and conc. depend., model interpret. and alloy struct. *(Russian)* 80−88528
- Cu-Ga, liq., mag. susceptibility, diamag. 78−72326
- Cu-Ga, magnetic susceptibility, comp. and temp. depend., melting effects 78−52202
- Cu-Ga, microconductors, cast, struct. and physical props. exam 78−44232
- Cu-Ga, plastic flow enhancement during massive transformations 78−48468
- Cu-Ga (17 wt.%), elec. resist. and TEM studies 80−108604
- α-Cu-Ga (3.4-15 at.%) cold-worked, lattice imperfections, X-ray obs. 77−55291
- Cu-Ga (4 at.%), anneal hardening mechanism 80−60879
- Cu-Ga alloys, α-phase, lattice sp. ht. calcs. 80−65246
- Cu-Ga alloys, massive phase ζ tempering, kinetics, order-disorder transform. *(French)* 78−44118
- Cu-Ga bulk and thin-film forms, reflecting surface absorpt. coeffs. at 10.6 μm 80−95984
- Cu-Ga periodic antiphases obs. *(French)* 77−4772
- Cu-Ga porous solid formed by shock compression 80−29905
- Cu-Ga-Fe, Mossbauer effect of Fe impurities 78−31131
- Cu-Ti-Ga, wetting of Al_2O_3, alloying effects 80−107617
- Cu-V-Ga dil. alloys with V_3Ga particles, supercond. props. and microstruct. 78−39278
- Cu-Zn-Ga martensite, thermally produced large single crystals 77−12615
- Cu-Zn-Ga martensites, internally faulted, shape memory mechanism 80−30010
- Cu-Zn-Gu, configs. of martensite variants, shape deform. matrices 77−12620
- CuGa alloys with Mn impurities, liq., elec. resistivity 79−51545
- $Cu_{0.83}Ga_{0.17}$, α-phase, photoelectron meas., impurity level 78−35247
- $Cu_{1-x}Ga_x$ liquid alloys, elec. resistivity 79−47073
- Cu_3Ga, interpretation of diffuse contours in electron diffr. *(French)* 79−19377
- Cu_3Ga, transition state between long range order and short range order, model, computer simulation *(French)* 80−49371
- $Er_6Ga_{1.5}Ni_{2.5}$, struct. determ. by X-ray powder method *(Ukrainian)* 80−39001
- Eu-Ga alloys, phase diagrams, struct. and comp. *(Russian)* 79−52163
- Fe-Ga, constitution between 10 and 50 at.% Ga, heat treatment depend., BCC phases *(German)* 77−90325
- Fe-Ga, dil., mag. hyperfine fields, Curie temp. and Mossbauer meas. 77−63190
- Fe-Ga, dil., short range order, NMR study 80−71237
- Fe-Ga, dil., XPS meas. 77−63538
- Fe-Ga, Mossbauer effect for phase transitions, 20-720°C, 25.7-28.3 at.% Ga *(German)* 78−68437
- Fe-Ga, phase constitution depend. on heat treatment, phase diagram *(German)* 78−39748
- Fe-Ga, solid soln., order-disorder transform. *(French)* 78−3121
- Fe-Ga, volume change during solid state transformation *(German)* 78−84802
- Fe-Ga (25 at.%), precipitation *(French)* 77−70057
- Fe-Ga (up to 50 at.%), liq., elec. resist., 1200-1800°C *(Russian)* 78−6341
- Fe-Ga-C melts, thermodynamics and C solubility *(Russian)* 80−39292
- Fe-Ge (10 to 50 at.%), phase diagram rel. to heat treatment, supercooling diagram *(German)* 78−92240
- Fe_2CoGa, alloy, site preference of Co and Fe, Mossbauer and neutron study 79−78577
- FeGa, dil., short-range order, neutron diffuse scatt. and spin echo NMR 80−50106
- Fe_3Ga, Ll_2 ordered alloy, positive temp. depend. on strength, phase destabilization 80−81203
- Ga/rare earth systems, direct calorimetric exam. 78−84775
- Ga-Al, effect of Al on solidification kinetics, and morphology of Ga 78−56628
- Ga-Al alloys, solubility of GaAs, in multilayer LPE of $Ga_xAl_{1-x}As$ 78−52690
- Ga-Bi liquid binary mixtures, phase separation under press. 80−34183
- Ga-Cu, fast quenching of A15-phases *(German)* 77−36014
- Ga-Cu liquid alloy, solubility and activity of O_2 77−59122
- Ga-Cu-Sn solders, exam. of structural transformations due to hardening, heat treatment *(Russian)* 80−7578
- Ga-Cu(Tl)(In), liq., mag. susceptibility *(Russian)* 78−6513
- Ga-Fe dilute alloy, Mossbauer spectrum 77−90080
- Ga-Ge, liq., enthalpy of form., direct reaction calorimetry, 713-1230K *(French)* 79−66336
- Ga-Ge-Sn, thermodynamic props. of mixing of binary systems, phase diagram 80−45275
- Ga-Ge-Zn ternary alloys, thermodynamic props., EMF meas. 80−81033
- Ga-In, dil., elec. resist., temp. and impurity depend., deviation from Matthiessen's b-axis crystals 78−51970
- Ga-In, liq., O diffusion coeff., thermodynamic activity and solubility 78−38860
- β′-Ga-In, metastable binary phase, X-ray diffr. determ. of cryst. struct. 80−1967
- Ga-In (2 and 4 wt.%), binary, kinetic conditions for two phase zone form. *(Russian)* 77−66633
- Ga-In eutectic system, diffusion coeff. depend. on composition *(Russian)* 80−59695
- Ga-In liq. alloy, repetitive pulses electron emission 79−24416
- Ga-In-Sn, thermal analysis, determination of liquidus and reactions 78−88446
- Ga-In-WSe_2 eutectic alloy, self-lubricating, struct. and props. 79−100267
- Ga-In(Al) systems, thermodynamic anal. 79−60512
- Ga-La, energy band struct. and atomic radius 79−73434
- Ga-Ni-R, (R=Dy, Ho, Er, Tm, Lu), struct. determ. by X-ray powder method *(Ukrainian)* 80−39001
- Ga-Pb, liquid alloy, thermodynamic activity determ. using Knudsen method *(German)* 79−34008
- Ga-rare earth alloys, phase diagram determ. 78−15366
- Ga-Sn, dil., elec. resist., temp. and impurity depend., deviation from Matthiessen's b-axis crystals 78−51970
- Ga-Sn alloys, compressibility, US velocity meas. *(Russian)* 77−59060

gallium alloys continued

- Ga-T alloys, relationship between struct. and thermodynamic props. *(German)* 78−91307
- Ga-Te, alloys, liq., thermodynamic functions, struct. 78−40075
- Ga-Te, liq., compressibility and US velocity meas. 77−51426
- Ga-Te, liq., mag. susceptibility 77−51881
- Ga-Te, solid and liq., thermodynamic props. 80−35567
- Ga-transition metal, phase diagrams and cryst. struct. *(French)* 79−47659
- Ga-Zn, dil., elec. resist., temp. and impurity depend., deviation from Matthiessen's b-axis crystals 78−51970
- Ga-Zn, eutectic system, diffusion coeff. depend. on composition *(Russian)* 80−59695
- Ga-Zn(In)(Ta)(Sn)(Bi)(Pb), liquid binary alloys, magnetic susceptibility *(Russian)* 77−24671
- GaAlAsSb avalanche photodiode for LW optical communication systems 80−10043
- GaAlSb avalanche photodiode for LW optical communication systems 80−10043
- $Ga_{1-x}Co_x$, cluster spin glass system, host and impurity NMR studies 79−65745
- GaIn, liq. alloys quad. relax. rates, 3-particle correls., ^{71}Ga and ^{115}Sn 77−12272
- GaP-M, M=Cd, Sn, Pb, polythermal cross sections 77−52300
- Gd-Ga, amorphous, mag. and elec. props. 80−80499
- Gd-Ga, amorphous, mag. props. and ferromag. reson. 80−75862
- Gd-Ga, amorphous alloy, mag. coupling 78−88108
- Gd_3Co_3Ga, crystal struct., X-ray determ. *(Russian)* 79−27951
- $Gd(Cu_{1-x}Gd_x)$, pseudobinary alloy, mag. susceptibility and elec. resist. at low temp. 80−34602
- Ge-Ga, segregation of Ga due to barometric mol. diffusion in gravitational, centrifugal fields 78−14472
- Ge-Ga (1.13 wt.%), US wave vel. meas. for anal. of solid soln. breakup 78−23887
- Ge-Ga alloys, amorphous, far IR absorption 78−88306
- Ge-Ga amorphous alloy, co-evaporated elec. and optical props. 80−70860
- Ge-Ga film, codeposited, amorphous and polycryst., struct. and elec. props. 80−24766
- Ge-Ga film, polycryst., struct. props. determ. 79−4494
- Ge-Ga liq. alloys, thermodyn. props. 78−26695
- Ge_2FeGa, and Fe_2CoGa, site preference and local environment effects, Mossbauer and NMR expts. 78−43710
- GaNi-rare earth intermetallics, struct. by X-ray powder method *(Ukrainian)* 80−10529
- Hf-Co-Ga system, crystal atomic struct. and phase equilibria *(Ukrainian)* 78−84772
- Hf-Cr-Ga, X-ray microanalysis of phase equilibria *(Ukrainian)* 78−6898
- Hf-Ge-Ga, X-ray microanalysis of phase equilibria *(Ukrainian)* 78−6898
- Hf-Nb-Ga, phase equilibria X-ray study at 800°C *(Ukrainian)* 79−95998
- Hf-Ni(Cu)-Ge, alloys, phase diagrams and cryst. struct. *(Russian)* 80−25658
- Hf-Zr-Ga, phase equilibria X-ray study at 800°C *(Ukrainian)* 79−95998
- Ho-Ga-Ni (60, 30 wt.%) cryst. struct., isostructural compound structural study 80−33930
- HoAlGa, mag. props. and struct. 78−39302
- $HoAl_xGa_{2-x}$, mag. props. and phase transitions 80−25133
- In-Ga, eutectic alloy, zero point determ. from uncharged surface pot. 77−90611
- In-Ga, work function, electrochem. determ. rel. to Ga 77−44489
- In-Ga alloy, electrode metal-solvent interaction rel. to elec. double layer struct., adsorpt. 78−61023
- In-Ga liquid alloy, low-resistance ohmic contacts in ZnSe, LED fabrication appl. 80−70823
- InGa-GaSe interface, microplasma electrolum. at 300K 79−11469
- InGaAsP avalanche photodiode for LW optical communication systems 80−10043
- K_3Ga_{13}, X-ray cryst. struct. determ. 80−92479
- $La_{0.8}Ga_{0.2}$, amorphous, Hall effect at 4.2, 78K and room temps. 79−60797
- $La_{1-x}Ga_x$, amorphous foil, Hall coeff. meas. 80−20153
- $La_{1-x}Ga_x$ foils, amorphous, splat cooled, calorimetric and resistive meas. 79−33417
- $La_{75}Ga_{25}$, amorphous, local symmetry around glass-former sites, elec. quadrupole effects, NMR 80−80618
- Mg-Ga, form. enthalpies and excess entropies, differential scanning calorimetry *(German)* 79−51278
- Mg-Ga, metastable cryst. and glassy phases, X-ray struct. anal. and electron microscopy *(German)* 79−46601
- Mg-Ga, X-ray spectra, electronic struct. *(Russian)* 77−48279
- Mg-Ga (6 wt.%), precipitation, lattice const., ageing effects *(Chinese)* 79−43279
- Mg-Ga system, thermodynamic props. of metastable and glassy phases *(German)* 79−52743
- Mg-Ga-In(Tl), phase diagrams and electrochem. props. *(Russian)* 80−40330
- Mg-Li-Ga, phase diagram, isothermal cross section *(Russian)* 80−20900
- Mn-GA system, cryst. struct. and degree of order *(Chinese)* 79−51048
- Mn-Ga, DO_{22} type alloys, magnetic props., crystal struct. *(Japanese)* 78−59784
- Mn-Ga, Elinvar charact. *(Japanese)* 79−61638
- Mn-Ga, mag. and cryst. struct. in conc. region of gamma phase, temp. depend. *(Russian)* 79−65649
- Mn-Ga (19 to 30 at.%), phase equilib. diagrams, X-ray diffr., thermal expansion, and mag. meas. *(Japanese)* 78−39743
- Mn-Ga (19.0 to 31.2 at.%), exam. of phase diagram, using X-ray diffr., thermal expansion and mag. meas. 78−76634
- Mn-Ga (24.1 wt.%), reversible memory of form, X-ray diffr. expts. *(Russian)* 79−5006
- Mn-Ga system, X-ray struct. investigation, solubility *(Chinese)* 80−88084
- Mn_3Ga, formation of DO_{22} superstruct. and para-antiferromag. transition 79−19737
- Mn_3GaC, mag. symmetry of ordered phases 78−71698
- MnGaGe film, mag. domains and amorphous to cryst. phase transition, electron microscopy obs. 80−71129

gallium alloys continued

- Mn_3GaN, sp. ht., 6 to 350K, mag. and crystallographic phase transitions 80—71060
- Na-Ga, solid and liq., mag. susceptibility and elec. cond. *(Russian)* 80—29522
- Na-Ga liquid alloy, thermodynamic props. 79—37854
- Na-Ga liquid alloy, thermodynamic props. of mixing derivation method 80—54385
- Nb-Ga, A15 type, melt produces specimens, supecond., homogeneity, transition temp. *(German)* 78—2608
- Nb-Ga, fast quenching of A15-phases *(German)* 77—36014
- Nb-Ga, phase system form. and stability of A15 phase 77—90347
- Nb-Ga, supercond., high press.-high temp. treatment, phase props. 77—28746
- Nb-Ga, superconductor, phase diagram determ. using various methods up to temp. of 2200°C 79—8414
- Nb-Ga (16 to 28 at.%), transition temp., upper critical field and magnetisation curves 77—80866
- Nb-Ga-C, phase equilib. and supercond. 80—50593
- Nb-Ga-Cu, fast quenching of A15-phases *(German)* 77—36014
- Nb-Ga-Cu, phase diagram, metallographic and X-ray study, annealed and as-cast supercond. crit. temp. *(Russian)* 78—56617
- Nb-Ga-Fe ternary system, phase equilib. at 1000°C, supercond. transition temp. 80—35158
- Nb-Ga-Ir, phase equilib. at 1000°C, cryst. data for intermediate phases 78—52763
- Nb-Ga-Sc, superconducting transition temp., X-ray, microscopic and microprobe anal. *(Ukrainian)* 80—75667
- Nb-Ga-Y system, X-ray and microprobe anal., isothermal section and supercond. transition temp. *(Ukrainian)* 79—38793
- Nb-Ge-Fe, effect of Fe on supercond. and mag. props. 79—56351
- Nb_3Al-Nb_3Ge-Nb_3Ga system, supercond. crit. temps. 77—8218
- $Nb_{0.75}Ga_{0.25}$, A 15 phase high transition temp., sp. ht. determ. 80—60140
- Nb_3Ga, comp. and LRO effects on supercond. T_c 77—39992
- Nb_3Ga, composition effects on T_c 77—76993
- Nb_3Ga, critical data, under hydrostatic pressure to 15 kbar 79—47217
- Nb_3Ga, Debye temp., determ. from elec. resist. meas. *(French)* 77—4322
- Nb_3Ga, electronic struct. calcs. 79—47005
- Nb_3Ga, electronic struct., electron-phonon interactions, and low temp. anomalies 79—60701
- Nb_3Ga film, quasiamorphous, supercond. phase formation by heat pulse 77—63017
- Nb_3Ga film, RF sputtered, supercond. and struct. props. 77—28274
- Nb_3Ga Josephson junctions, excess current anal. 79—28465
- Nb_3Ga, NQR freq. temp. depend., supercond. transition temp. 80—93207
- Nb_3Ga, supercond. crit. temp. and struct., heat treatment and stoichiometry effects 77—43769
- Nb_3Ga, supercond. transition temp., rel. to A15 phase stability 78—52137
- Nb_3Ga, temp-depend. of elec. resist. 80—103675
- Nb_3Ga, thermodynamic and expt. study of CVD 79—24441
- Nb_3Ga with structure A15, apparatus for rapid hardening from liquid state 80—76275
- Nb_3Ga, X-ray $M_{IV,V}$ emission bands *(Russian)* 80—45170
- Nb_3Ga:^{93}Nb, NQR spectra, NQR signal disappearance in supercond. state 78—19369
- Nb_3Ga-Nb_3Pt, supercond. crit. temp., comp. depend. *(Russian)* 77—59347
- Nb_4Ga_5, cryst. struct. and homogeneity range 78—42957
- $Nb_{78}Ga_{22-x}Mn_x$, supercond. props., influence of Mn mag. impurities 80—54825
- $Nb_{80}Ga_{20-x}Mn_x$, supercond. props., influence of Mn mag. impurities 80—54825
- Nb_3(Ge, Ga) CVD tapes, supercond. props. at high mag. fields 79—38279
- $Nb_3Ge_{1-x}Ga_x$, applicability of scaling law for supercond. crit. currents 79—24118
- $Nb_3Ge_{1-x}Ga_x$ CVD films, supercond. transition temp. depend. on lattice parameter 79—38219
- $Nb_3Ge_{1-x}Ga_x$ CVD films, supercond. props., 4.2 to 19K 79—42713
- $Nb_{78}Gn_{22-x}Fe_x$, $Nb_{80}Ga_{20-x}Fe_x$, A15 phase supercond. 79—87181
- Nb_3(SnGa), wire, neutron effect on T_c, I_c and flux pinning 79—38216
- $Nb_3(Sn_{1-x}Ga_x)$, bronze processed wires, critical current densities in fields up to 23.5 T 78—47922
- Nd-Ga, heat of form. and soln., calorimetric meas. *(Russian)* 78—27806
- Nd-Ga, phase diagram *(Russian)* 78—27478
- Nd-Ga alloy, phase diagram, DTA, X-ray and metallographic obs. 79—24494
- Nd_3Co_3Ga, crystal struct., X-ray determ. *(Russian)* 79—27951
- $(Ni,Fe)_3Ga$, magnetovolume effects near crit. conc. for ferromag. 79—56591
- Ni Ga, defect struct. 78—30608
- Ni-Ga, band model of high temp. magnetism 78—26809
- Ni-Ga, dil., ferromagnetic, hyperfine field and relax. time obs. of impurity heavy nuclei 80—75533
- Ni-Ga, phase diagrams and cryst. struct., DTA, X-ray diffr. and microprobe anal. *(French)* 79—47660
- Ni_3GA single crystals, anomalous temp. depend. of strength, dislocation struct., optical and TEM 79—74228
- NiGa, defect struct. model 79—46648
- NiGa, point defects, lattice parameter determ. 78—38695
- NiGa, vacancy conc. in B2 phase exhibiting triple defects 79—42058
- Ni_3Ga, form. mech. of superlattice intrinsic stacking faults 77—27897
- Ni_3Ga, off-stoichiometric alloy, inverse mag. susceptibility rel. to defect conc. 80—60216
- Ni_3Ga, stacking fault form. in situ obs. by stretching thin foils in electron microscope 77—62547
- Ni_3Ga, strongly enhanced itinerant paramag., theory of anomalies in field depend. of magnetisation 77—69488
- Ni_3Ga, temp. depend. of mech. props. *(Russian)* 79—38895
- Ni_3Ga, with $L1_2$ struct., dissociated struct. of superlattice dislocations 79—37706
- Pb-Ga amorphous films, supercond. transition temp. and residual elec. resist. *(Russian)* 79—19680
- Pd-Cu-Ga, cold work and annealing-induced hardening, X-ray diffr. anal. and metallographic exam. *(Russian)* 79—38844
- $Pd_{55}Ga_{45}$, ordered BCC phases at high temp. 79—32948

gallium alloys continued

- Pr-Ga (0 to 50 at.%), phase diagram and cryst. structs. of intermetallic cryst. 80—3002
- Pr_3Co_3Ga, crystal struct., X-ray determ. *(Russian)* 79—27951
- Pt_3Ga, Ll_2 ordered alloy, positive temp. depend. on strength, phase destabilization 80—81203
- Pu-Al-Ga system, phase diagram 77—21108
- Pu-Ga, $\delta \rightarrow \alpha$ transform. kinetics 77—25047
- Pu-Ga (1 wt.%), alloy powder, hydriding kinetics 80—76503
- Pu-Ga (1 wt.%), single cryst. elastic consts. US wave vel. meas. 77—20005
- Pu-Ga (1 wt.%) delta-stabilised, heat transport props., room temp. to 500°C 77—20294
- Pu-Ga (1-8.56 at.%) alloys, enthalpy sp. ht. determ. at elevated temp. 78—78458
- Pu-Ga (3.3 at.%), oxidation in air, 250-400°C 77—44401
- Pu-Ga (3.4 at.%), δ-stabilised, strain rate effect on tensile props. 77—21284
- Rh_2MnGa, mag. and cryst. props. 77—20568
- Sc-[Co,Ni,Cu]-Ga, phase equilibria, diagrams of state, X-ray, microstructural study *(Russian)* 80—55356
- Sc-Ga system, phase diagram from 20-75 at.% Ga, intermetallic compound identification *(Russian)* 77—55944
- ScGa and Sc_5Ga_3, exam. of X-ray K spectra of pure Sc, Ga in alloys *(Russian)* 79—15562
- $ScGa_2$ atomic structure determ. using single crystal method *(Ukrainian)* 80—70165
- Sm-Ga, phase diagram *(Russian)* 78—27478
- Sm_3Co_3Ga, crystal struct., X-ray determ. *(Russian)* 79—27951
- Sn-Ga, temp. regime of crystn. on rapid cooling *(Russian)* 80—66495
- Sn-Mn(Fe)-Ga, isothermal sections of phase diagram *(Ukrainian)* 78—92235
- $SrGa_2$, layered, dispersion of acoustic phonons, inelastic neutron scatt. 78—47484
- Ta-Ga, crystal struct. at high press., polymorphism 80—88112
- TbAlGa, mag. props. and struct. 78—39302
- $TbAl_xGa_{2-x}$, mag. props. and phase transitions 80—25133
- Tb_3Co_3Ga, crystal struct., X-ray determ. *(Russian)* 79—27951
- $TbGa_2$, mag. props. and struct., neutron diffr. patterns at 4.2, 300K 77—63109
- $TbGa_2$, noncollinear magnetic order and spin wave spectrum in presence of competing exchange interactions 80—65834
- Ti-Co-Ga, Th_6Mn_{23} type struct., mag. susceptibility *(Russian)* 79—42736
- Ti-Fe-Ga, Th_6Mn_{23} type struct., mag. susceptibility *(Russian)* 79—42736
- Ti-Ni-Ga, Th_6Mn_{23} type struct., mag. susceptibility *(Russian)* 79—42736
- TiGa, $TiGa_2$, Ti_5Ga_3, X-ray K- and L-bands, electronic struct. *(Russian)* 79—1797
- Ti_3Ga, lattice period and crystallographic struct., temp. depend. *(Russian)* 78—55835
- Tm-Ga, exam. of phase diagram, using differential thermal and X-ray phase anal. *(Russian)* 79—11555
- U-Ga system cpds., elec. resist., paramag. susceptibility magnetis., temp. depend., mag. struct. 77—20559
- UGa_2, cryst. struct., mag. and magnetoelastic props. *(Russian)* 79—38364
- UGa_2, mag. and magnetoelastic props. 80—15775
- UGa_3, thermoelectric power, 5-300K 79—65444
- $(V,Fe)_3Ga$, solid soln. form. and supercond. T_c *(Russian)* 78—80512
- $(V,Nb)_3Ga$ solid solns., supercond. T_c, absolute thermal EMF, microhardness 77—36006
- $V_3Ga_{1-x}Sn_x$, lattice props. supercond., ^{119}Sn Mossbauer shift meas., 5-300K 77—1627
- V/Cu-Ga, composite superconductor, V_3Ga phase form., TEM obs. *(Russian)* 80—84933
- V-Ga, fast quenching of A15-phases *(German)* 77—36014
- V-Ga-C, phase equilib. and supercond. 80—50593
- V-Ga-Cu, phase diagram *(Russian)* 77—25014
- V-Ga-Sc, phase diagram, metallographic and X-ray meas., solubility boundaries *(Russian)* 78—56618
- V_3 Ga, high T_c supercond., electron-phonon coupling, effect of electronic density of states sharp struct. 78—14877
- $V_{75-x}Fe_xGa_{25}$, Mossbauer exam. 77—90078
- $V_{0.75-x}Ga_{0.25+x}$ ^{51}V, nucl. spin-lattice relax. time, annealing and neutron effects 79—82710
- $V_{1-x}Ga_x$, A-15 cpds., nucl. mag. relax. in normal and supercond. state 80—49993
- $V_{1-x}Ga_x$, nuclear spin-lattice relax. and supercond. 79—56387
- V_2Ga, phonon density of states, temp. depend. 79—42183
- V_3Ga, A15 compound, exam. of deformation processing, review 78—39864
- V_3Ga, A15 cpd., hydrogenation effects on supercond. transition temp., lattice parameters 80—103772
- V_3Ga, band theory, semiself-consistent band calcs. 78—2406
- V_3Ga, cast, effect of hydrostatic extrusion on supercond. props. *(Russian)* 77—21215
- V_3Ga, coherence parameter, nonlinear high temp. supercond. elements with A-15 lattice *(Russian)* 80—60127
- V_3Ga, composite-processed, with improved current carrying capacities in high mag. fields 79—38272
- V_3Ga, diffusion-processed layer, texture meas. 79—82726
- V_3Ga, electronic struct., electron-phonon interactions, and low temp. anomalies 79—60701
- V_3Ga, electronic struct. calcs. 79—47005
- V_3Ga, filamentary conductors, type-II, low temp. 30 GeV proton effects on critical props. 78—52178
- V_3Ga, grain size in A-15 reaction layers 78—14911
- V_3Ga, high current density multifilament wire, neutron effects on equilibrium and transport props. 78—52126
- V_3Ga, high-current A-15 microcomposite material 80—44781
- V_3Ga layer on bronze, diffusion of Ga *(Russian)* 80—65297
- V_3Ga, long-range order parameter variations determ. and correls. with supercond. T_c 77—11504
- V_3Ga multifilament superconductors, AC losses 79—60979
- V_3Ga, multifilament superconductor, pulsed mag. field losses and critical current densities 80—54853
- V_3Ga multifilament wire, crit. current props. above 4.2K 77—32135
- V_3Ga multifilamentary stranded compd. supercond., design, processing, mech., supercond. props. 77—76999

gallium alloys continued
V_3Ga, multifilamentary supercond., prod. by ECN powder metallurgy method, and props. 77−28762
V_3Ga multifilamentary supercond. wire, fabrication and props., crit. review 79−38271
V_3Ga, multifilamentary wire, stress effect on critical currents 77−80891
V_3Ga, multifilamentary wire, crit. current props. with third element additions 79−61013
V_3Ga, NMR and mag. suscept. *(Russian)* 78−39420
V_3Ga, neutron irrad. effect on upper crit. field and crit. current 77−72954
V_3Ga, neutron irrad. effects on transition temp. *(Japanese)* 79−82707
V_3Ga, neutron irradiation and annealing 78−52130
V_3Ga, nuclear magnetic relaxation, near T_c *(Russian)* 79−42852
V_3Ga, phonon densities of states and Debye temp. calcs. 79−51212
V_3Ga, self-consistent APW band struct. calc. 78−47697
V_3Ga, single crystal prep. by iodine transport, supercond. T_c meas. 78−48294
V_3Ga, structure effects on supercond. props. and electron spectrum *(Russian)* 77−80862
V_3Ga, supercond., μ^+ probe study *(Russian)* 79−7946
V_3Ga, supercond., neutron-induced disorder revealed by isochronal annealing 77−72938
V_3Ga, supercond., pinning characteristics *(Japanese)* 78−91829
V_3Ga, supercond., prep. from V-Al and Cu-Ga, crit. temp. and field 78−43506
V_3Ga, supercond., projected upper limits to crit. current density 77−36037
V_3Ga, supercond. A15 phase, prep. by controlled precip. 80−81000
V_3Ga, supercond. and high mag. fields 79−87215
V_3Ga, supercond. μSR meas. 79−56667
V_3Ga superconducting composite, bronze process, metallurgy 80−3004
V_3Ga superconducting multifilamentary wires, effect of low temp. neutron irrad. 77−32132
V_3Ga superconducting multifilamentary wires, critical current densities 79−69645
V_3Ga superconducting tape, diffusion-processed, cryst. textures, X-ray pole figures 79−11266
V_3Ga superconducting tape, stress effect on critical current *(Japanese)* 80−50020
V_3Ga, superconducting transition temp. and electron density of states 77−32105
V_3Ga, superconducting transition temp., metallurgical processing, struct. 77−63019
V_3Ga, superconductive fixed points for temperatures above 0.5K 79−63221
V_3Ga-Cu, high-current A-15 microcomposite material 80−44781
V_3Ga-Cu, supercond. in situ composites, stress effects on crit. props. 80−65757
V_3Ga-Cu composites, supercond. props. 79−95557
V_3Ga-Nb_3Sn concentric solenoid magnet system, 17.5 T operation 77−26353
V_3Ga-NbN point-contact Josephson junction, fabrication and characts. 78−19189
V_3Ga-V_3Pt, supercond. crit. temp., comp. depend. *(Russian)* 77−59347
$V_{3-x}M_xGa$, M=Ti, Cr, Mn, Fe, Co, Ni, cryst. struct. and microhardness meas. 79−86740
$V_{75-x}M_xGa_{25}$, M=Ti, Cr, Mn, Fe, Co, Ni, supercond. transition temp. and electron-phonon coupling parameter 79−60952
V(Nb)-Ga-Cu, rapidly quenched, comp. and phase equilib. 80−76235
V_3Si-Ga solid soln., supercond. T_c and paramag. susceptibility *(Russian)* 77−59348
Ve-Fe-Ga system, phase obs. at 800 and 820°C *(Russian)* 78−23662
Y_3Co_3Ga, crystal struct., X-ray determ. *(Russian)* 79−27951
Yb-Ga, phase diagram, differential thermal and X-ray analysis *(Russian)* 78−56615
Yb-Ga system, phase diagram, cryst. structs. of phases 79−52169
$YbGa_2$, intermediate valency cpd., paramag. susceptibility, 1.4 to 1060K 77−63079
Zn-Ga, temp. regime of crystn. on rapid cooling *(Russian)* 80−66495
Zn-Ga liquid soln., thermodynamic props. determ., invariant method appl. 77−59742
Zr-Co-Ga, mag. susceptibility in phases of structural type Th_6Mn_{23} *(Russian)* 79−24130
Zr-Cu-Ga, mag. susceptibility in phases of structural type Th_6Mn_{23} *(Russian)* 79−24130
Zr-Nb-Ga, phase equilibria 800°C *(Ukrainian)* 80−35157
Zr-Sc-Ga, phase equilibria 800°C *(Ukrainian)* 80−35157
Zr_2CoGa_3, crystal struct. determ. by single crystal method *(Ukrainian)* 79−51049

gallium arsenide
(110) surface structure, rotational relaxation, cluster model *(Chinese)* 80−107621
400 MHz TW laser modulator 80−87541
absorption coefficients, method of meas. 78−83048
acceptor bound exciton Auger and radiative transition rates, radiative recomb. 80−6733
acceptor ground state calc. 77−28113
acoustic phonon disturbances, effect on conductivity 78−91697
acoustic plasmons in MOS inversion layers 78−18983
adsorbed mol. lifetimes and desorption activation energy meas. 78−20072
adsorbed O_2^- EPR spectrum, HFS 77−40118
adsorbed O, (110), surface electronic struct., synchrotron irradiated photoemission 78−43453
adsorption and field-desorption of O_2 and Au, FEM studies 80−34304
adsorption enhancement by electron beam excitation of gas mols. 78−43238
adsorption of Cs on (110) surface, work function meas., adsorption site model 79−23839
adsorption of Cs on (110) surface 77−72794
adsorption of In, N, P, and As, UPS and EELS study, tight-binding calcs. 80−49496
adsorption of O_2, adsorption states and Ga depletion, UPS, AES, and thermal desorption meas. 79−46952
adsorption of O_2, H_2, H_2O and H_2S on (110), surface photovolt. spectroscopy 80−49499
adsorption of O_2 on (110) ordered and disordered surfaces, XPS meas. 80−49498

gallium arsenide continued
adsorption of O_2 on (110) surface, oxide form., XPS/UPS study 80−49497
adsorption of O_2 on Cs-covered (110) surface, initial oxidation, soft XPS obs. 80−10793
adsorption of Sb_2, surface state exam. by energy loss spectra 77−15935
adsorption of water and methanol on GaAs(110) surface, UPS study 80−6632
adsorption-desorption of Zn, thermal desorpt., at. beam adsorpt., AES, SEM, RHEED 78−14591
aircraft IR window appl., development 77−72038
n-$Al_xGa_{1-x}As$, large-lattice relax. model for persistent impurity photocond. 77−85261
$Al_xGa_{1-x}As/Al_yGa_{1-y}As$ heterostructure lasers, prep. characts., and CW reliability 80−58586
alloying with Au and Au alloy ohmic contact metallisations, SEM and optical study 80−70820
amorphous, EXAFS, evidence for inequivalent environments of Ga and As 79−15558
amorphous, localised gap states, hopping cond. and chem. bonding 78−23052
amorphous, localised gap states, variable range hopping, susceptibility and EPR 77−72866
amorphous, mobility gap temp. derivative calc., polar contrib. 78−26861
amorphous, optical absorpt. edge shape, band edge fluctuations 77−20880
amorphous, switching obs. 79−11190
amorphous film, composition, study by nondispersive X-ray anal. *(French)* 79−8457
amorphous film, effective medium theory and freq. depend of conductivity 79−24090
amorphous film, EXAFS, optical and elec. props. 80−49547
amorphous film/GaAs crystal junction, optical and elec. props. 79−99611
amorphous layer formation, ion implantation, IR spectra 78−95063
amorphous layers, ion-implanted, low-temp. epitaxial regrowth 80−92790
amorphous sputtered films, hydrogenated, photoinduced optical absorpt. 80−50362
amorphous state, thermal stability, elec. cond. obs. 80−33888
Anderson-Gruneisen parameter, bulk modulus temp. depend. 78−10154
annealed, surface cond. change, n-p double layer 78−64095
annealing, growth of noncrystalline Si_3N_4 layers by CVD for encapsulation 79−19994
annealing rel. to stoichiometry deviation, Hall effect, electron microscope meas. 77−24410
anodic films, XPS study 80−71562
anodic MOS structs., interface-state band model 80−11093
anodic native oxides for MOS devices, quality assessment 79−61767
anodic oxidation, under dark and illuminated conditions, behaviour of cell voltage 77−16826
anodic oxidation 77−16710
anodic oxidation and MOS devices 77−80845
anodic oxidation in O plasma 79−66188
anodic oxidation mechanism, temp. and electrolyte comp. effects 80−3220
anodic oxidation using O plasma, and oxide layer evaluation 78−85015
anodic oxide, analysis using low-energy ion scattering spectrometry *(French)* 79−52845
anodic oxide, electrical props. 79−38170
anodic oxide, quantitative chem. depth profiles 77−72799
anodic oxide, refl. and transmission, 0.01-6 eV 78−95613
anodic oxide, refr. index meas., Sellmeier eqn. 77−12454
anodic oxide, states, electrochemical meas. 80−80176
anodic oxide chem. depth profiles, neutron activation analysis and Auger spectroscopy 77−77619
anodic oxide film, optical props. 78−72626
anodic oxide film, self drifting of ionic charges, detection by surface potential decay method 78−72295
anodic oxide film comp. profile anal., radioactive tracer technique 77−59956
anodic oxide film growth, in situ differential refl. obs. 77−73354
anodic oxide film on surface, direct current-voltage characts. 78−23186
anodic oxide film prep. by plasma anodisation of O-sputtered surfaces, MOS device characts. 79−66176
anodic oxide films, composition meas. by ion scatt. spectrometry, influence of current density 80−11802
anodic oxide films, optical studies using rot. light-pipe reflectometer 80−76096
anodic oxide for device application, crystallisation dynamics 79−66190
anodic oxide formation, galvanostatic obs. 77−77620
anodic oxide growth rate in mixed electrolyte 77−44382
anodic oxide layers, chem. depth profiles, XPS determ. 80−3222
anodic oxide system, multiple angle incidence ellipsometry, meas. at λ=632.8 nm 79−63294
anodic oxides, MOS struct. leakage currents 79−38169
anodically oxidised, etch pits, defect characterisation 77−56122
anodisation, ellipsometric study *(Japanese)* 80−97610
anodisation, for MAOS diode with stable charge storage 77−15960
anodisation, initial film form. in tartaric acid-water-propylene glycol 77−21301
anodisation, O incorporation at oxide-electrolyte interface, ion microprobe mass anal. 77−25273
anodisation at low substrate temp. by low pressure O_2 plasma 80−104314
anodisation ellipsometric and IR spectroscopic studies of oxide film 80−11493
anodisation in HF O_2 plasma, oxide film form. mechanism and kinetics *(Japanese)* 80−93667
anodisation obs. by in situ differential refl. 80−50732
anodised, interfacial reactions, Raman scatt. obs. 80−49544
anodised MOS, electrorefl. spectra 79−99901
anomalous avalanche breakdown 80−80284
anomalous diffusion of Sn from doped oxides due to dopant depletion effects 77−89461
anomalous scattering factors determ. near absorpt. edges, by one-intensity-ratio method 80−1888
antireflecting MOS solar cells, epitaxial and polycryst. using OM-CVD techniques 80−94072
Auger de-excitation of metastable state 79−65410
Auger recombination, luminesc. meas. 77−85850
Auger recombination, phonon assisted, scatt. mechanisms 77−85804

gallium arsenide continued
- Auger recombination cross sections associated with deep centres 78—47810
- autoepitaxial film growth, surface struct. and stoichiometry during molecular beam epitaxy, RHEED anal. 79—4921
- autoepitaxial layer, local impurity inhomogeneities *(Russian)* 79—23854
- autoepitaxial structure on heavily Te-doped GaAs substrate *(Russian)* 80—49556
- avalanche breakdown field, approx. formula 80—11025
- avalanche breakdown voltage for p-n junction, calc. 78—88020
- avalanche photodiode, reach-through, temp. depend. characts. 79—95482
- avalanche photodiode design, high speed 78—8446
- avalanche photodiodes, planar ion-implanted, fabrication and characterisation 80—22431
- back etching and growth by liq. phase epitaxy, surface morphology obs. 80—29287
- ballistic and near ballistic transport 80—96867
- ballistic electron motion at room temperature 80—80360
- band structure, modulation spectroscopy, two-ray methods *(Russian)* 78—54469
- band structure under high stress, nonperturbative calc. 78—10344
- biexciton stability, appl. of theory for polar crysts. 78—76002
- binary alloy constituent EDS anal., secondary fluorescence, SEM study *(Chinese)* 80—85231
- birefringence, photoelastic consts. dispersion 80—11361
- birefringence in presence of electroabsorpt. 77—32351
- blazed gratings in (110) oriented GaAs, preferential chemical etching 79—37067
- blocking effect, backscatt. method *(Chinese)* 79—90708
- boat-grown, deep levels *(Japanese)* 79—47043
- boundary scattering and phonon conductivity, 2-10K 78—63888
- bridges of Nb and Sn on GaAs substrates, variable thickness, props. 79—28464
- Brillouin scattering from surface ripples 79—15472
- Brillouin scattering from surface waves, appl. of surface Green's function mapping method 80—40125
- Brillouin scattering of refl. light, surface ripple mechanism 77—73149
- Brillouin spectra, light scatt. cross section for surface ripples 80—71434
- bulk acoustic phonons, light scatt. from phonon-induced surface ripples 78—75924
- bulk and epitaxial, meas. method for compensation and spatial fluctuation of impurities 78—6404
- bulk hot-electron properties, review 79—99553
- bulk purification by chemical vapour transport 79—24437
- carrier concentration and compensation microprofiles 80—80820
- carrier concentration determ. using electroreflectance 78—23483
- carrier concentration variations using electrolyte electroreflectance, topographical features 79—99562
- carrier Debye screening length, temp. depend. 80—88504
- carrier diffusion in transient response regime 80—103688
- carrier lifetime, radiation induced changes, edge luminesc. spectra 77—8664
- carrier lifetime profile, depth depend. 78—68036
- carrier mobility profiles meas. at room temp. by Corbino effect 78—60128
- carrier removal, after H_1^+, H_2^+, and H_3^+ implantation 77—8115
- cascade capture of carriers by attractive impurity centres, cross section 78—56157
- CESR, optical detect. by spin orientation techniques, anal. 78—80251
- CESR, optically detected, g-factor determ. 77—36155
- charge accumulation and transmission, physical modelling *(Bulgarian)* 80—6947
- charge carrier UHF heating using lumped-capacitance resonators 80—20203
- chemical bond, modulation X-ray diffr. obs. 80—96464
- chemical etching processes, review 78—95832
- chemical transport by water vapour, growth kinetics of epitaxial layers 77—16500
- chemical transport equilib., with I_2, in gaseous phase *(French)* 77—55876
- chemical transport equilib. with I_2 in gaseous phase *(French)* 77—55877
- chemically etched surface, Auger characterisation 77—25169
- chemisorption, of O_2 79—95466
- chemisorption and oxidation states of (110) surfaces 79—24049
- chemisorption and thin oxide layer form., synchrotron radiation meas., review 79—60637
- chemisorption geometry, of Cl on cleaved (110) surface 80—6659
- chemisorption of Al, surface barrier formation, localised orbital theory 79—51671
- chemisorption of Al on (110) surface, electronic struct., tight binding calc. 80—49842
- chemisorption of Cl on (110) surface, photoemission spectra and tight-binding calcs. 80—6629
- chemisorption of Cs, isobars, LEED and loss spectroscopy meas. 77—4262
- chemisorption of O_2, effect of surface index and atomic disorder AES, LEED and optical ellipsometry 79—60638
- chemisorption of O_2 on (110) surface, bonding sites 78—38938
- chemisorption of O and Al on (110) surface, ab initio theory 80—75612
- chemisorption of O on (110), surface EXAFS meas. 80—50460
- chemisorption on semiconductor surfaces, book contrib. 80—107648
- chemisorption site geometry and interface electronic struct. of Al and Ga on (110) surface, photoelectron spectra 80—49843
- circuit effects in time-of-flight diffusivity meas., Monte Carlo method 80—88563
- cleaved (110) face, interaction with O_2, influence of cleavage defects 80—66684
- coeff. and surface conc. 80—39122
- colar cell arrays, for earth orbital and orbit transfer missions 80—94044
- compensated, electron mobility temp. depend. 80—96868
- compensated, influence of electron gas heating on negative magnetoresist. 77—89778
- compensated, magnetoresist. and Hall effect 77—66176
- compensated, magnetoresist. and magnetothermoelec. power meas. 77—43627
- compensated, photoabsorption, expt. 78—19521
- compensated, Shubnikov-de Haas oscills. 77—11941
- compensated VPE thin film, electron Hall mobilities 80—107932
- complex luminesc. centres at 1.20 and 1.30 eV 77—16386
- conduction band, three-level struct., from high-stress and high-field obs. 77—15764

gallium arsenide continued
- conduction band effective mass, influence of high uniaxial stress 80—80162
- conduction band mapping by angle-resolved photoemission 79—83105
- conduction band minima, ordering and props. 77—28114
- conduction band nonparabolicity and coupled plasmon-phonon modes, IR refl. spectra 80—55110
- conduction band ordering, velocity field characts., Monte Carlo calcs. 78—18957
- conduction band structure 78—6271
- conductivity of complementary error function n-type diffused layers 77—35944
- conference, Edinburgh, Scotland (Sep 1976) 78—3039
- conference, St. Louis, MO, USA (Sept. 1978) 80—8737
- controlled doping during VPE growth using trimethylgallium and arsine 78—6855
- core exciton binding energies 80—80188
- core level spectra, electronic polarisation effects 80—6765
- creep and dislocation velocities 78—95783
- crystal defect obs. by TEM *(Japanese)* 77—84752
- crystal growth, effect of thermal and elastic consts., eval. 80—92586
- crystal growth, LEC, using pyrolytic BN crucibles 78—6841
- crystal growth by MBE 78—39707
- crystal pulling, liquid encapsulated compounding and Czochralski growth of semi-insulating GaAs 79—43136
- crystal structure stability, P-T diagrams 78—51886
- cubic, noncentrosymmetric, electrooptic effect 79—69812
- cubic semiconductor, Zeeman split acceptor levels, calc. method 79—28322
- current instabilities in semiconductors, theory and expts. *(Hungarian)* 77—39857
- CVD, S doping behaviour during growth, electron conc. 78—26784
- CVD for solar cell applications 77—77412
- CVD in Ga-$AsCl_3$-H_2 system with different input supersaturations *(Russian)* 78—68098
- CVD mechanism, product catalysed reaction of Me_3Ga with AsH_3 77—48345
- CVD of SiO_2 on GaAs, using tetraethoxysilane oxidation 78—60582
- CVD on W coated graphite, characterisation, and Schottky barrier solar cell characts. 79—28930
- CVD using Ga-As-H-Cl system, theoretical anal. of equilib. adsorption layers 79—23858
- Czochralski grown, pure and doped, elec. props. 80—10989
- Czochralski growth kinetics, total emittance determ. 80—75193
- DC— and microwave-biased extrinsic GaAs photoconductors 80—70750
- DC biased, filamentation of laser radiation 80—74428
- Debye temperature, atomic mean square displacement 78—87757
- deep bound states, temp. depend. of ionisation energies 77—31975
- deep centre free energy level determ. by transient capacitance technique 80—103641
- deep centres, collective thermal emission of electrons 80—10918
- deep centres, electron and hole capture cross sections 79—99510
- deep centres, electron struct., transition element impurities 78—39060
- deep centres, many-electron effects 79—15117
- deep centres, wave functions and optical cross sections 78—34801
- deep centres due to transition metals, model 79—78045
- deep impurity levels, activation energy 80—107742
- deep level, strongly anisotropic field ionisation 79—28317
- deep level defects, review 80—24841
- deep level impurities *(Japanese)* 77—89723
- deep level photoionisation, absorpt. by derivative surface photovoltage spectroscopy 79—99575
- deep level profile anal., double correlation technique 77—80830
- deep level trap emission identification by indirect conduction minima technique 78—84163
- deep level traps, transient and thermally stimulated capacitance meas. *(Chinese)* 79—91072
- deep levels, optical and thermal spectroscopy, lattice relaxation *(French)* 80—66248
- deep levels, photocapacitance meas. under hydrostatic press. 77—85259
- deep levels, photoionisation of impurities 80—65484
- deep radiation centres from heat treatment, γ-irrad., deform., probability of nonradiative electronic transitions 80—50408
- deep trap characts. by photocapacitance spectroscopy 78—6398
- deep trap study by free exciton refl. spectra 79—60761
- deep traps exam. by capacitive method 77—11869
- defect cluster annealing, pot. barrier height determ. 80—84209
- defect clusters induced by γ-rays and neutrons, effect on elec. props. 80—29408
- defect processes, electronic stimulation 80—24665
- defect state identification associated with Ga vacancy 77—69269
- defects from proton irradiation, thermal transients and optical capacity *(French)* 80—59534
- deformation, acoustic emission rel. to cracks, dislocations 80—35441
- degenerate, impurity band struct. for dense donors and acceptors 80—29348
- degenerate, nonequilib. electron distrib. functions 77—63394
- density of states, spontaneous emission rate calcs., 120, 160, 200K 77—4292
- desorption properties of Sb on (100), AES obs. 80—80074
- destruction mechanisms by intense IR laser radiation *(Russian)* 78—39633
- device compatible anodic oxidation technique 78—44236
- device isolation with deuteron bombardment 80—75248
- DH injection laser, modulation behaviour, appl. in high bit-rate fibre optical communications 78—1281
- DH injection lasers, ambipolar transport 80—64025
- DH laser, alloying of ohmic contacts, Nd:YAG laser irrad. 80—43357
- DH laser, life test at room temp. 78—17937
- DH laser, planar stripe geometry and channelled substrate, lateral current confinement 78—66823
- DH laser/fibre transmission system modulation and injection 77—50764
- diffraction gratings, photoresist and GaAs, exposure and etching time optimalisation 80—23816
- diffraction gratings prod. by interference photoetching 77—46805
- diffusion and power spectral density and correl. function of vel. fluctuation for electrons 80—65576
- diffusion in Au-refractory thin film systems obs., by combination of scattering techniques 80—65308
- diffusion of Cr and Ag, radiotracer profiles 80—24680
- diffusion of ion implanted Be, SIMS and electrical profiling 78—47605

gallium arsenide continued
diffusion of Se 77−51547
diffusion of Sn, surface stability, effect of As vapour press. 80−2208
diffusion of Zn, low-temp.-selective process using anodic oxides [illegible]
diffusion-type stripe-geometry injection laser using V-groove, structure, fabrication process and props. 79−27277
diode, high temp. and freq. characts., made by gas-transport method 79−19654
diode, quantum efficiency and nonequilibrium carrier lifetime 77−12442
diode, reverse-biased, current-controlled negative resist., switching investg. 77−69410
diode, with Schottky barrier, photoluminesc. *(Russian)* 79−28410
diode laser, behaviour in optical feedback mode *(Dutch)* 79−76689
diode laser in communication system using PPM methods *(Rumanian)* [illegible]
diode lasers coupled to short external resonators, reson. amplifier model [illegible]
diode temperature sensors, characts. obs. at 4.2 to 393K 80−47054
direct energy gap, press. depend. up to 180 kbar 77−8020
direct gap semiconductor, gain spectrum of electron-hole liq. 80−66279
direct-gap epitaxial layers, optical compensation profiling 77−76450
directional-coupler switch with stepped $\Delta\beta$ reversal 77−79968
directional-coupler switch with stepped $\Delta\beta$ reversal 77−88962
dislocation density, ⟨100⟩ cryst., quantitative light microscopy 77−31661
dislocation density effect on polarisation and intensity of reflected $CuK_{\alpha 1}$ radiation 77−1131
dislocation dissociation, electron microscopy 79−46665
dislocation etching of {100} and {111} planes of As 77−43215
dislocation free, phonon-defect interaction 77−69061
dislocation half-loops, nucleation and generation 79−95009
dislocation loops, rel. to dark defects in LEDs 77−80509
dislocation states 79−60762
dislocation structure 79−82206
dislocation velocities for α- and β-dislocations in n- and p-type cryst., double-etch method 77−51382
dislocations, associated electron states 79−82544
dislocations, elec. effects 79−82586
disorder distribution extraction, semiempirical method of applying dechannelling correction 78−22781
disordered, ion implanted, elec. props. 78−84212
dissociated dislocations, statistics of kink formation 79−82207
dissociation during alloying with Au contact films 79−79357
domain dissolution for wide range of doping Gunn device, planar [illegible]
domain electrical instability in two-valley semiconds. 77−76842
donor and acceptor concs. determ. by optical method 78−19525
donor energy spectrum, mag. field effect, submm. photocond. meas. *(Russian)* 77−43666
donor van der Waals interactions, spectral lineshapes 80−11450
donor-acceptor type complex, mag. field splitting of photolum. line [illegible]
donor-acceptor-type complex 80−80837
dopant atom charge effect on lattice parameter 77−31631
dopant profiles for Zn diffusion, modification by proton irrad. 78−43043
doped, photoemission, calc. of escape probability of electrons *(Russian)* 79−24408
doped, radiative lifetimes, quantum mechanical model 80−55151
doping structures production and appl. *(German)* 78−95064
double hetero stripe-geometry laser, two-dim. anal. 78−1231
double-cavity laser with branching output waveguides 78−63128
dual implantation of C^+ and Ga^+, sheet resist. and Hall effect meas. [illegible]
dual species ion implantation, elec. characts. 80−103377
dynamic cathode contacts., pinned cathode and cond. current density calc. 77−20427
dynamical response of electron distrib. to high elec. field fluctuations [illegible]
effective mass, Raman spectrum determ. 80−24797
EHT calcs. of energy bands and pressure dependences *(Japanese)* 78−34747
electrical and optical props. at low temps. 80−39636
electrical conductivity, effect of As vapour press. at 200-1000°C 77−15846
electrical conductivity and thermoelectric power charge due to melting 80−100496
electrical properties of dislocations, review *(Japanese)* 78−6325
electrical properties of unintentionally doped layer grown by MBE [illegible]
electro-optic rib waveguide directional-coupler switch with stepped $\Delta\beta$ Schottky electrodes 79−98507
electroabsorption avalanche photodiode waveguide detector, freq. demultiplexing [illegible]
electroabsorption avalanche photodiode waveguide detector 78−65965
electroabsorption characteristics, valence band splitting 77−44018
electroabsorption signal, depend. on elec. field 80−103942
electrochemical sectioning and surface finishing 80−108611
electrode, electon injection in liq. NH_3 80−6977
electrode, interpretation of selective etching, electrochem. props 80−7703
electrode, photoemission into electrolyte solns. 77−24616
electrode liq. junction solar cells, photocurrent spectra, carrier recombination 78−76142
electrodeposition from molten soln. 78−64486
electrodes, n- and p-type, freq. depend. of impedance 77−12001
electrodes, photo-induced electrogenerated chemilum. and up-conversion 79−91510
electrodes in acetonitrile solns., liq. junction photovolt. cell 79−99617
electrodes in acetonitrile solutions, characterisation and photochemical behaviour 79−70341
electrodes in aqueous electrolytes, localised avalanche breakdown 79−4599
electroluminescent study of irrad. induced struct. damage, athermal annealing 80−108280
electrolytic decomposition and photodecomposition at GaAs-electrolyte contacts 78−95357
electromodulated reabsorption of luminesc. in MOS and Schottky systems 79−15524
electron and hole impact ionisation coeffs. 78−6389
electron and neutron irrad., defect clusters 80−2077
electron beam induced current, minority carrier generation distrib. 80−96906

gallium arsenide continued
electron beam induced defect annealing 77−80790
electron bombardment, absorption of energy 79−14847
electron capture by multiphenon emission at B centre 80−24830
electron distrib. function in alternating fields, single particle Monte Carlo method 77−89791
electron dynamic properties in strong electric field, anal. *(German)* 78−43404
electron effective mass, temp. depend. for various degrees of doping and compensation *(Russian)* 78−79923
electron heating under hydrostatic pressure, Monte Carlo calcs. 77−69334
electron irrad. induced defect levels, hydrostatic press. effect 80−92858
electron irradiated deep-level defect anal. using 2γ positron annihilation and IR absorption spectra 80−16120
electron mobility illumination, compensation, space charge regions, carrier scatt. 80−70691
electron mobility temp. depend. 79−91084
electron momentum distribution, anisotropy, positron annihilation *(Russian)* 78−84676
electron relaxation times, distribution functions 77−55541
electron scattering interaction with coupled plasmon-polar-phonon modes 79−42536
electron source, high intensity polarised, illum. of GaAs with polarised light 77−38520
electron source, spin-polarized 80−69000
electron speed, technique for doubling 79−38076
electron transient vel. characts., Γ-L-X cond. band ordering 78−79997
electron transport analytical model 79−91039
electron trap at E_c-0.75 eV, direct evidence for nonassignment to O 79−90988
electron traps in bulk and epitaxial crysts. 77−39865
electron-beam excited, efficient generation of electron-hole plasma 80−76051
electron-exciton collision influence on luminescence line profile due to bound excitons 80−29800
electron-hole drop transition to metallic condensed state, Hartree-Fock theory 79−56136
electron-hole interaction of d core levels 77−11880
electron-hole liquid, final state interactions in gain and absorpt. spectra 78−43305
electron-hole liquid form., luminesc. 79−33804
electron-hole liquid theory, generalised RPA 78−87914
electron-hole liquids in polar semiconds., phase diagram 77−89706
electron-hole plasma, Coulomb effects on gain and absorption spectra 80−50371
electron-hole plasma, ground state energy 78−84244
electron-hole plasma, thermalisation 79−95439
electron-hole plasma phase transition 80−24803
electron-spin relaxation and recomb. kinetics, time-resolved luminesc. study 80−108074
electronic density, multiple scatt. method, muffin-tin approx. 80−27924
electronic elementary excitations in far UV and X-ray region 79−95346
electronic Raman scatt. of polarised light on donor levels 80−93309
electronic states associated with 60° dislocations, tight-binding calc. 79−15114
electronic states of neutral vacancies 77−11875
electronic structure, mol. cluster model, SCF multiple scatt. method 79−42446
electronic structure, self consistent local description 80−20067
electronic structure, self-consistent localised description 79−42445
electronic surface structure, Cs(Rb)(Na) adsorpt. processes, AES, LEED, EELS, study 78−68068
electrooptic effect, birefr. harmonics, permittivity dispersion 77−52044
electrooptic switches and directional couplers, wavelength depend. 78−79143
electroplated Au-SnNi-Au ohmic contacts 78−35319
electroreflectance spectroscopy using synchrotron rad. 78−10912
ellipsometry of dielectric films on 79−69894
empty surface states and surface order effects on sorption 77−85281
encapsulants for high temp. annealing, photolum. and AES evaluation of SiO_2 and Si_3N_4 78−27657
encapsulation of preliminary heated specimens by sputtered deposits of Si_3N_4 and AlN *(French)* 77−32714
energy bands and wavefunctions, localised orbital description 78−18942
epilayer structures, patterned, MBE writing 78−56590
epilayers, high-quality, sharp-line transitions due to donor-acceptor recomb. 78−6768
epitaixal unintentionally doped layer growth using MBE 78−72741
epitaxial, deep level profile anal. by double deep level transient spectroscopy 77−20378
epitaxial, impurity gradients caused by surface states and substrate doping 77−84784
epitaxial, polycryst., monocryst. layers and whiskers growth by CVD, SEM obs. electron diffr. study *(French)* 79−43150
epitaxial, residual donor identification by far IR photocond. 80−60047
epitaxial, residual donor identification by far IR photoconductivity meas. 80−103717
epitaxial, Si and Ge doping 80−24470
epitaxial, trapping levels obs. using deep level transient spectroscopy, laser irrad. effects 79−99499
epitaxial and bulk n-type, IR reflectance meas. 77−32364
epitaxial deposition, growth kinetics *(French)* 80−2961
epitaxial deposition from organometallic cpds. 77−47689
epitaxial film, amorphous and polycrystalline, vol. plasmon energy and linewidth, electron scatt. obs. 80−50482
epitaxial film, chem. transport by water vapour, thermodynamic calcs. 77−12539
epitaxial film, deep centre reson. charging, photocapacitance meas. on Schottky barrier 78−26908
epitaxial film, donor characterisation by far IR photoconductive techniques 78−43501
epitaxial film, enhanced electrodiffusion purification in mag. field 80−66409
epitaxial film, field effect struct., elec. breakdown, negative resist. 77−12030
epitaxial film, magnetoresist. at low temp., geometric effect 80−93015
epitaxial film, photo-EMF echo at 4.2K 80−60038
epitaxial film, positron annihilation, impurity centre study 79−15554
epitaxial film, pure and Cr doped, heavy electron trapping, Gunn oscills. 80−6857

gallium arsenide continued
epitaxial film, radiative recomb. under influence of mech. stresses 80—66291
epitaxial film, surface trap exam. by surface doping and field effect 77—76896
epitaxial film on GaAs substrate, IR characterisation 78—23544
epitaxial film on GaAs substrate, two-interface surface polariton modes 78—60180
epitaxial film recombination props. *(Russian)* 80—49812
epitaxial films, deep levels, impurity photocond. 80—20247
epitaxial films on strongly doped substrate, basic parameter meas. utilising magnetoresist. and SEM techniques under cathodoluminesc. conditions 80—65728
epitaxial growth, CVD-organometallics method, reactional efficiency in solar cell elaboration 80—93498
epitaxial growth, gas-phase composition during growth by chloride method 77—12537
epitaxial growth, molecular beam, uncontrolled doping obs. *(Russian)* 80—2276
epitaxial growth, selective, using MBE and self-masking method 77—52256
epitaxial growth and etching rate meas. method 77—35829
epitaxial growth for microwave devices *(French)* 77—48360
epitaxial growth in $Ga(CH_3)_3$-AsH_3-H_2 system 78—35312
epitaxial growth in Ga-$AsCl_3$-He_2 system, expt.-statistical analysis *(Bulgarian)* 78—60580
epitaxial growth of undoped layers from nonstoichiometric solns., O_2 contamination sources 80—108362
epitaxial growth on Ge/Mo substrates 79—69988
epitaxial growth under different intake supersaturations in GaAs-$AsCl_3$-H_2 gas transport system *(Russian)* 78—26776
epitaxial layer, 1.06 μm two-photon absorption coeff., guided wave meas. 78—46707
epitaxial layer, AuGe ohmic contact production by laser alloying 78—88026
epitaxial layer, Be, O, Si, S, Zn and Sn impurity concentrations 80—49260
epitaxial layer, comparison of compensation ratios determ. by photolum. and elec. methods 79—28818
epitaxial layer, controlled electrochemical and selective etching, integrated optics appl. 77—14814
epitaxial layer, effective doping density, comparison of Hall and magnetoresistance meas. 77—11938
epitaxial layer, fast electron irrad., impurity distrib. profile obs. 77—76969
epitaxial layer, free-carrier density determ. by Hall meas., surface and interface depletion corrections 79—91170
epitaxial layer, laser mag. photoelec. spectra 79—82635
epitaxial layer, magneto-plasma-reflectivity effects, difference method meas., IR region *(German)* 77—12363
epitaxial layer, micron and submicron vap. phase growth, for FET 80—11577
epitaxial layer, nondislocation etch pits 80—92535
epitaxial layer, nonequilibrium carrier relax., recombination radn. 80—7416
epitaxial layer, photo- and cathodolum., doping distribs. *(Russian)* 77—48215
epitaxial layer, photoluminesc. defect complex 80—29804
epitaxial layer, polariton wave packet propag. in exciton reson. 80—2345
epitaxial layer, role of Cl in VPE, LEED, RHEED, and AES obs. 77—1327
epitaxial layer, surface morphology 79—90852
epitaxial layer, VPE, high purity, residual donors, photocond. effects 77—85174
epitaxial layer and Sn-doped bulk characterisation 79—82596
epitaxial layer growth, by pyrolysis, producing power GaAs MESFETs 78—23623
epitaxial layer growth, vapour-phase, transfer mechanism of Si 77—51616
epitaxial layer growth by chloride process, μ and subμ thickness 78—23624
epitaxial layer partition coefficients of impurities 77—15443
epitaxial layer resistivity meas. using Hg—n-GaAs barrier contact 79—60945
epitaxial layers, characterisation Hall effect and Schottky diode profile meas. 78—91791
epitaxial layers, doping profile degradation due to ion implantation 80—84194
epitaxial layers, electroepitaxy and thermal LPE growth, defect struct. and electronic characts. 80—2290
epitaxial layers, electron irrad. deep level trap energy depend. 80—80205
epitaxial layers, electronic surface props., photoluminescence exam. 77—20901
epitaxial layers, from mixed Ga solns., C solubility 80—15392
epitaxial layers, grain boundaries, deep level transient spectroscopy study 80—49234
epitaxial layers, growth below 700°C, electrophysical props. 79—1827
epitaxial layers, high density electron-hole plasma luminesc. 78—19537
epitaxial layers, inclusion obs., Raman microprobe-microscope appl. 80—62737
epitaxial layers, low freq. current noise between 4.4 and 300K 78—95388
epitaxial layers, MBE grown, Hall mobilities, substrate temps. 80—20335
epitaxial layers, meas. of doping profiles *(Hungarian)* 80—70545
epitaxial layers, multiexciton complex bound to neutral acceptors, photoluminesc. obs. 79—87503
epitaxial layers, non-doped, from Ga-$AsCl_3$-H_2 system, TEM and RHEED study of micromorphology and defects 79—65340
epitaxial layers, photocond., high field effects on carrier capture and recomb. 77—43646
epitaxial layers, quantitative anal. of oxygen by SIMS 79—5233
epitaxial layers, structural defect and conc. inhomogeneities influence on barrier diode I-V characts. 80—15602
epitaxial layers, substrate prep. effect on surface morphology 78—26780
epitaxial layers, surface impurity gradients, Schottky barrier capacitance. meas. 80—70782
epitaxial layers, transient processes during doping for large conc. jumps. 80—39134
epitaxial layers, undoped, recomb. of non-equilib. carriers, steady-state photocond. 77—85357
epitaxial layers and bulk, diffusion and elec. activity of Co 79—56333
epitaxial layers on conductive substrate, elec. characterisation 78—91790

gallium arsenide continued
epitaxial layers on polycryst. GaAs substrates, LPE growth characts. 80—75471
epitaxial multilayer, electron irrad. defect study by transient capacitance 79—99241
epitaxial multilayer photocathode structures, TEM obs. of dislocations generated 80—100241
epitaxial n^+n^{2+} multilayers, carrier conc. from Fourier transform anal. of magnetoresist. signal 79—38205
epitaxial n-n^+ structure, for CW microwave electroacoustic amplifier 78—59235
epitaxial pseudobinary compounds, lattice deform. determ. by X-ray diffraction 78—6242
epitaxial structures, impurity profile 77—39610
epitaxial thin film, nonuniform electroconductivity *(Russian)* 80—70753
epitaxial thin film prep. by low temp. CVD 80—60789
epitaxial thin films with neg. electron affinity, photoelectron energy distrib. 80—100755
epitaxial tunnel diode pressure sensors 78—57975
epitaxially grown (001), (111) and $(\bar{1}\bar{1}\bar{1})$ surfaces, LEED, AES, photoemission 78—38924
epitaxy, ultrathin film growth by cracking of organometallic compounds at 40 to 100 torr *(French)* 78—44023
epitaxy by metallorganic and chloride depositions, defect characterisation at growth interface 80—59817
epitaxy on GaAs and Ge, mechanism, effect of substrate surface struct. 77—51614
epitaxy using TMG and AsH_3, chloride etching effect 78—76606
ESCA absolute energy calibr., Ga 3d and $L_3M_{4,5}M_{4,5}$ and As 3d binding energies 78—92171
etch pit pattern made by light irradiated electrolytic etching 79—95012
etch solutions containing H_2O_2, correl. between etch and surface film characts. 80—71770
etchant, universal, multipurpose 78—53008
etched, saucer-pit defect identification 78—43021
etching and polishing with $AsCl_3$ 78—3243
etching soln. system H_3PO_4-H_2O_2-H_2O for MESFET fabrication 78—11379
EXAFS amplitudes, many-body effects 80—97379
exchange interaction, analytical and nonanalytical parts, from polariton spectra in mag. fields 80—50367
excited, LO phonon effective temp., Raman meas. 80—20639
excited luminescence, influence of IR illumination 80—76072
exciton effects in photocond., photoluminesc. 80—96797
exciton ground state and oscillatory absorption spectra in mag. fields, variational calc. 79—11071
exciton luminescence, excitation intensity depend. 78—52554
exciton motion under external electric field 79—56135
exciton parameters near absorption edge 79—73448
exciton quenching, obs. at room temp. using electrolyte electroreflectance 80—60546
exciton to neutral acceptor binding energy, calcs. using atomic-like variable wave function 78—79937
excitonic polariton reson. interaction with LA phonons 78—60481
excitonic spectra broadening, influence of phonons and impurities 77—1711
excitons, diamond like semiconductor, variational calculation of binding energies 78—79938
excitons, exciton-phonon interactions, review, book contrib. 80—49624
excitons, interaction with charged impurities 78—43906
excitons detect., precision method 79—19906
excitons in arbitrary mag. fields 80—96798
extended Huckel theory appl. 80—59916
extrinsic photoconductor detectors, DC and microwave bias comparison 77—37998
far IR photoconductivity 77—15893
far IR transmission spectrum 77—38041
far IR transmission spectrum 78—4713
Faraday effect meas. using IR magneto-optic polarimeter 77—34014
FET, continuous growth of LPE double layers 78—64487
FET, Cr influence on mobility of electrons 80—92910
FET amplifier, varactor-tuned, for UHF SQUID magnetometer 80—31814
FET double layer production by LPE growth procedure, sliding boat method of investigation *(Japanese)* 79—66014
FET structure, sharp line photolum. spectra 78—72248
FET with buffer, bias effects due to deep centres in struct. *(French)* 80—107917
field evaporation, atom probe field ion microscopy 78—80460
field ion microscopy 78—19644
field ionisation speed of shallow impurity levels, quantum-mechanical estimates 80—97412
field penetration in FIM, band bending 79—87567
film, differential mobility anisotropy effect on wave propag. 78—88050
film, electron scatt. cathodolum., loss spectra 80—104023
film, electroreflectance effects 79—43055
film, epitaxial deposition from gas phase, transient processes, elec. cond. 77—16501
film, epitaxial growth from noncondensed phases, kinetic anal. 80—54565
film, epitaxy on semiinsulating GaAs, elec. props. of transitional layers rel. to growth conditions 77—15977
film, growth kinetics for step-cooling LPE technique 77—40395
film, MBE grown, in situ surface characterisation by RHEED, SIMS and AES 77—43410
film, monocrystalline, lateral definition, prep. by MBE 80—108357
film, optical components, prep. by MBE using Si shadow masking technique 80—28358
film, photovoltage anomaly investig., p-n-p microjunction model 77—4398
film, plasma oxidation and oxide props. 78—95825
film, polycryst. for terrestrial photovoltaic energy conversion 79—15242
film, prep. by ionised-cluster beam deposition *(Japanese)* 80—25576
film, radiative relax. time, nonequilibrium carriers 78—84657
film, RF sputtered, ESCA, surface chemistry suitability for photovolt. appl. 80—7476
film, sample preparation for TEM studies 78—14258
film, selective anodisation, grain boundary edge passivation 79—11711
film, solar cell on large grains 79—100528
film, vapour-grown, effect of gas-phase stoichiometry on deep levels 78—10393
film and solar cell on graphite, struct. and elec. props. 80—2286

gallium arsenide continued
- film on recrystallised Ge film, solar cell appl. 78−19671
- film plasma oxidation process 77−77614
- film solar cell fabrication, substrate requirements 78−11125
- films for solar cells appl., deposition and characterisation 80−84853
- fine struct. in energy derivative reflectance spectra 79−78705
- fine structure of lowest exciton state *(Russian)* 80−96801
- fluorescence, reson. polariton, obs. 77−85785
- foils preparation, transparent, for TEM, ion sputtering technique appl. *(Czech)* 80−16619
- forbidden Raman scatt. by LO phonons 78−64367
- forward-biased diode structures, numerical anal. based on direct gap semicond. 79−65542
- Franz-Keldysh effect modulator parameters for integrated optics systems 80−106624
- fundamental absorption band, influence of phonons on long-wavelength wing 79−69857
- $Ga_{1-x}Al_xAs$ LPE growth: composition control and growth rate analysis 79−95946
- $Ga_xAl_{1-x}As$, optically oriented electron, nuclei spin instability *(Russian)* 80−70660
- gaAlAs diode sources for laser-doppler anemometry 79−14499
- n-GaAs:Cr(Si), deep-level extrinsic photocond. response, decay at 4.2K 80−2420
- GaAs:Fe, superparamagnetism, spontaneous magnetization 79−11285
- GaAs:O, growth, O_2 solubility determ. rel. to temp. 78−34624
- n-GaAs:Te, interaction of positrons with dislocations 79−99974
- p-GaAs:Zn, diffusional doping, photoluminesc. in mag. field 77−16384
- GaAs, back-wall Schottky barrier solar cell with interfacial layer 77−62993
- GaAs-$Al_xGa_{1-x}As$ DH laser for optical communication 77−50684
- GaAs-$Al_xGa_{1-x}As$ strip buried heterostructure laser densely packed monolithic linear array 79−45956
- GaAs-$Ga_{1-x}Al_xAs$ DH crystals, <110> oriented dark line defects 77−80510
- n-GaAs-Ge laser alloying to from ohmic contacts 80−58546
- gamma and electron irrad. defect formation depend. on interface, luminescence study 80−34057
- gamma irradiation, form. of defects, contrib. of inelastic nucl. reactions *(Russian)* 77−27905
- GaP/$In_xGa_{1-x}P$/GaAs:(Cs-O) high sensitivity transmission photocathodes, photosensitivity, electron diffusion length 79−78832
- gas-phase epitaxy, step stopping centre form. kinetics 80−65407
- gas-solid interface, EPR centres induced by microwave gas plasma 78−80215
- grain boundaries, extended Read model 80−96543
- grain boundaries investigation using DLTS techniques, photovoltaic material appls. 80−92539
- ground state of electron subsystem, quasimolecular model 79−69055
- grown-in dislocation density, impurity effect 78−51543
- growth, dual-bubbler CVD system, characts., for MESFET applics. 78−6856
- growth and heat treatment of single crystal *(Chinese)* 77−73222
- growth in strip and rod form, Stepanov method 78−3017
- Gunn diode, peak electron vel. and threshold field temp. depend. 77−32075
- Gunn diode, static domain form. 77−8111
- Gunn diode, velocity-field characts. at 35 GHz, impurity conc. var. 77−85306
- Gunn diodes, microwave oscill. generation at two freqs. 80−65614
- Gunn diodes, population inversion condition 77−77251
- Gunn domain appearance and movement, SEM obs. 77−80785
- Gunn effect, carrier generation-recomb. processes 79−38080
- Gunn effect, equal-areas rule 80−107798
- Gunn effect, influence of strong transverse mag. field 80−6854
- Gunn oscillations, IR field induced 78−30956
- Gunn oscillator, magnetoresist. meas. of mobility and noise 77−62948
- Hall effect sensor for mag. fields up to 23 T 77−10066
- Hall mobility, automatic electrochemical profiling 79−99615
- heavily doped, electron effective mass, Kane equation calcs. 79−77989
- heavily doped, fluctuation-induced tunnelling cond. 80−65516
- heavily doped, n-type, non-linear extrinsic luminesc., role of Auger recombination 79−52010
- heavily doped, self energy of phonons 80−44277
- heavily doped, strongly compensated, hopping cond. 79−47180
- heavily doped electron mobility due to scatt. by pot. fluctuations 80−2387
- heavily doped semiconductor, carrier Debye screening length, temp. depend. 80−88504
- heavily oxidised, photoemission, escape depth for electrons, energy depend. 77−69969
- heavily-doped, band gap, magnetoabsorpt. oscills. obs. 78−18960
- heavy metal migration, ESCA study *(French)* 78−75885
- heteroepitaxial layers, on Si and Ge from multiple component solns. *(Russian)* 78−15319
- heteroepitaxial layers, on Si substrates by LPE 79−1832
- heterojunction laser, origin of dislocation climb during laser operation 77−51380
- heterojunction lasers, degraded, TEM obs. of dark defects 78−14355
- heterolaser active layer, photoluminesc., temp. depend. *(Russian)* 79−10310
- heterostructures for integrated optics 77−39112
- high power Gunn diode developement and fabrication 80−16199
- high pressure electron transport props., three band model 80−15516
- high speed photoconductive integrated optical receiver 80−58816
- highly deformed samples, absence of dislocation-induced luminescence 79−4835
- highly doped, behaviour of buried O_2 implanted layers 80−59499
- hole effective mass, press. depend., theory and tunnelling expts. 78−75986
- hole traps characterisation in bulk and epitaxial crysts. 78−6392
- holes optical orientation, luminesc. 80−25452
- holographic grating transduction from bulk to surface acoustic waves 77−31199
- homoepitaxial interface, thermal degradation 77−11988
- homogeneity region calcs. 80−92681
- homojunction laser diodes, in transient state conditions, analysis of junction temp. rise 77−38889
- homojunction lasers active layer in steady state, thermal problems *(Polish)* 77−14717
- homojunction LED, mechanical stress induced degradation 80−2860

gallium arsenide continued
- homojunction LED signal source for fibre-optic communication 78−1413
- homojunction rib waveguide directional coupler switch 80−69554
- homojunction solar cell, temp. depend. of photovolt. solar energy conversion 79−43768
- homojunction solar cells, efficient large grained 80−94070
- hot carrier distribution, optically excited, picosec. time resolved reflectivity obs. 78−76495
- hot carrier impact ionisation, band struct. depend. 78−30934
- hot carrier noise, in epilayer for FET 79−24035
- hot electron distrib. function, inter-carrier scatt. effect 80−2395
- hot electron distrib. function with LO phonon kink, photoluminesc. 79−19925
- hot electron distrib. meas. and calc. 78−27318
- hot electrons, diffusion coeff. 79−15156
- hot electrons, mobility in mag. field 77−4368
- hot electrons and exciton-electron collision under external elec. field 78−43928
- hot electrons drift rate/field strength characteristic in microwave fields *(German)* 78−43430
- hot excitons, collisions with hot electrons 80−7415
- hot photoluminescence, polarisation anisotropy *(Russian)* 77−90195
- hot photoluminescence depolarisation in mag. field, 0.4 eV energy state electron lifetime *(Russian)* 80−16086
- hot photoluminescence spectrum on pumping across the L-valley *(Russian)* 80−103984
- HV diode, I-V characts. 79−24068
- hydrothermal oxidation kinetics, exam. 80−40566
- impact ionisation, electron band struct. effects obs. by temp. tuning 77−85232
- impact ionisation initiated by acoustoelectric effect 78−52038
- impact ionisation of excitons 79−38079
- impact ionisation of free carriers, orientation depend. rel. to cond. band 77−76836
- impact ionisation rates, temp. depend. 79−38077
- impact ionisation rates for electrons and holes, photocarrier multiplication obs. 78−87995
- impact ionisation rates for electrons and holes meas., elec. field orientation depend. 78−10453
- IMPATT diode, maximum efficiency single- and double drift region, 3 to 18 GHz range 79−24058
- implantation of Si, Al, Hf, Ta into InP and GaAs, form. of protective oxide 78−79622
- implantation of Si ions, annealing, damage recovery, surface carrier profile 77−4119
- implanted, IR refl. meas. of free carrier parameters 77−36244
- implanted amorphous layer reordering 77−76435
- implanted ion lateral spread *(Japanese)* 79−4322
- implanted p-n junction form. using laser pulse annealing 77−15946
- impurities, conc. of C, O, Si 78−59832
- impurity anal. by photoelectric spectroscopy, review 77−24584
- impurity analysis by photoluminescence *(Japanese)* 77−24888
- impurity band Hall mobility 80−70730
- impurity centres ionis. by Auger electrons, carrier relax. *(Russian)* 79−51594
- impurity density of states, effect of doping and injections, models and calc. method 79−73466
- impurity distribs. by chemical methods 77−43237
- impurity effect on grown-in dislocation density *(Japanese)* 78−6063
- impurity gettering by ion implantation damage 77−11579
- impurity scattering of current carriers in quantizing mag. field 78−51954
- impurity states and core excitons, binding energies, perturb. theory 80−49659
- impurity-point defect complexes 78−6097
- indirect band edge, determ. by quantum-well bandfilling 78−92120
- induced birefringence, temp. coeff. 80−93277
- inertia of intervalley redistribution of electrons, meas. of V(E) relationships by microwave method 79−82621
- inhomogeneities in single crystal doped with group IV elements 77−11556
- inhomogeneous, cylindrical and spherical localised inhomogeneities in magnetic field, anomalous elec. props. calcs. 80−44621
- injection laser, active region effect on single-freq. stimulated emission conditions 80−9884
- injection laser, electronic stabilisation of radiated power 80−23702
- injection laser, intensified luminesc. *(Russian)* 78−90416
- injection laser, output instabilities related to optical gain and lasing conditions 80−1203
- injection laser integration with Gunn oscillator on semi-insulating GaAs 78−71232
- injection laser with localisation of injection current, design and characts. 80−106543
- injection lasers, longitudinal mode spectrum, effect of carrier diffusion 78−71099
- injection lasers, spectral output, influence of diffusion and spontaneous emission 79−13965
- injection lasers with filament, junction current and carrier-conc. profiles *(Chinese)* 79−50292
- injection photodiode IR radiometer 79−75597
- InP-InGaAsP-InP, low threshold laser, threshold density temp. depend., LPE method *(Russian)* 78−22133
- insulating, generation of far IR radiation by freq. mixing 79−50347
- insulating, optically pumped electron-hole plasma, Raman scatt. 77−40236
- integrated LED/sphere-lens source for optical fibres, coupling efficiency calcs. 80−43433
- integrated multijunction photodetector with high output voltage 79−6178
- integrated optical coupler using p-n-i-n^+ semi-insulating struct. 80−64212
- integrated optics devices, recent advances 77−75712
- integrated optics technology, book contrib. 79−64362
- interband Faraday rotation, Roth theory calcs. 77−52046
- interband tunnel current, influence of press. 77−76910
- interface, energetic barrier height hypothesis 79−19657
- interface with anodic and thermal oxides, comparison of AES and ESCA 78−95980
- interface with oxide, photoemission obs. of energy levels induced by adsorpt. 80−93000
- interference grating blazed by ion-beam erosion 80−1302

gallium arsenide continued
interimpurity interaction effect on distrib. profiles of impurities diffusing simultaneously 77—76451
intervalley electron transfer, drift velocity and diffusion coefficient 80—39594
intervalley electron-electron scattering effect on optical transitions 80—108267
intervalley gap from Schottky diode meas., generalisation of thermionic emission theory 79—73586
intracavity modulation of polarization direction of CO_2 laser radiation, 80—102744
inverted hot electron states and negative cond. *(Russian)* 77—43612
ion beam induced annealing effects 80—59530
ion bombarded, defect distrib., photolum. meas. 77—20920
ion bombarded, H ions, carrier removal effects 80—92542
ion bombardment, composition changes, AES 78—72662
ion bombardment by alkali metal sputter ion source *(Japanese)* 79—54734
ion channelling meas. for lattice location of S and Mn implanted in single crystals 79—4332
ion damage, TEM study of laser annealing 80—88215
ion electron emission spectra, on 2-4 keV Ar^+ ion excitation 80—11529
ion etching, effects on optical props. and lattice disorder 78—83122
ion implantation, 1978 state of art review 79—42089
ion implantation, disordered layer physical props. 79—77624
ion implantation, effects on deep-level conc., transient spectroscopy techniques 80—2046
ion implantation, laser annealing 80—107296
ion implantation, range distrib. calc. 79—55760
ion implantation, review 78—6080
ion implantation, survey 77—76448
ion implantation, trends 80—39132
ion implantation damage, characterisation and appl. 80—92551
ion implantation damage, TEM exam. of variation with ion species and stoichiometry 78—59827
ion implantation disorder, flux and fluence depend., electrorefl. expts. 78—83833
ion implantation doping, developments 77—59028
ion implantation of high energy Se^{++} to produce active layers for device appls. 77—39605
ion implantation of S and Se 78—55884
ion implantation of semiinsulating materials, role of substrate in elec. props. 80—59488
ion implantation parameter determ. by microwave contactless mobility meas. 78—10527
ion implantation review 80—88184
ion implantation with proximity cap annealing 80—24475
ion implanted, capless annealed and dielectrically annealed, comparison of doping profiles 80—100278
ion implanted, diffusion of Zn and Ag, profiles 80—24681
ion implanted, effect of channelling on elec. props. 77—8114
ion implanted, encapsulation surface effects, RHEED 77—1883
ion implanted, laser annealing 79—69124
ion implanted, laser induced damage and recrystallisation by freq.-doubled Nd:YAG laser 79—73197
ion implanted, laser induced recrystn. and damage, ion backscatt. and Raman scatt. obs. 80—49248
ion implanted, laser pulse annealing 80—19825
ion implanted, layer thickness and refr. indices meas. 77—24837
ion implanted, mode-locked Nd:YAG laser annealing, recrystn. 80—19817
ion implanted, ruby laser pulse effects 79—69125
ion implanted films, optical and luminesc. props. 80—60699
ion irradiated, Auger electron spectra struct., possible surface diagnostic methods 79—69946
ion irradiation damage, strain effect contrib., channelling meas. 78—67752
ion-bombarded, energy band struct., electrorefl. obs. 79—19517
ion-implantation induced damage profile, ellipsometric study, annealing 80—103400
ion-implanted, capless anneal, effect of As partial press. 80—29038
ion-implanted, laser pulse annealing, TEM and channelling study 80—100264
ion-implanted, laser pulse annealing of amorphous surface layer, TEM 80—55436
ion-implanted layers, close contact capless annealing, elec. props. 80—84192
ion-implanted semiconductor, annealing, crystallisation, laser pulse energy depend. 78—34528
i.r. 10.6 μm absorption meas. using thermal emission 77—1649
IR absorption of isolated impurities 77—12407
IR thermometry, semiconductor material temperature measurement *(Spanish)* 80—47062
IR transparent materials, forward and backward scatt. data 78—59099
IR vibrational absorption, effect of fast neutron irrad. 78—75776
junction field effect structures, 2-D subbanding 78—64125
junction laser, spectral hole burning 79—50291
junction laser, spontaneous emission reduction at lasing with long delays 79—64226
k-linear coupling, E_1' transitions 78—91583
large dislocation-free single crystal growth 80—25550
laser, broadening mechanism, limitations to single mode power emission 79—961
laser, buried heterostructures, discrete or DFB 78—5499
laser, continuous-injection, with distributed Bragg mirrors, construction and operation *(Russian)* 78—29972
laser, DH, inherent oscillations and subharmonic resonances obs. in light output 78—74910
laser, directly modulated injection, HF noise enhancement effect 80—83608
laser, distrib. Bragg reflector, room temp., highly collimated broadside emission 78—13721
laser, double cavity, with branching output waveguides 78—37918
laser, electron beam pumped, far-field radiation pattern, optical confinement effects 79—86181
laser, electron-beam-pumped, transient waveguide effects and lasing time delays 78—37882
laser, epitaxial waveguide type with distrib. second-order feedback, electron beam pumped *(Russian)* 78—29973
laser, freq. retuning using electron beam excitation *(Russian)* 77—716

gallium arsenide continued
laser, high speed direct modulation, multimode operation effects 78—13738
laser, image emission, for optical information processing 77—58268
laser, injection, single heterostruct., mode competition effects, tuning characts. 80—48255
laser, one-sided heterostructure injection stability of output pulse power 77—83876
laser, operation characteristics *(Rumanian)* 78—87053
laser, optically pumped, DFB, with two dimens. Bragg reflectors 78—1252
laser, oxide-insulated stripe-geometry DH, low degradation rate at room temp. 77—23674
laser, permittivity at laser transitions freq., excess carriers effect 77—14719
laser, photopumping of quantum well heterostruct. $Al_xGa_{1-x}As$-GaAs-$Al_xGa_{1-x}As$ 79—22956
laser, pnpn-heterostructure barrier controlled low threshold 77—61966
laser, radn. coupling to thin-film and fibre waveguides 77—19426
laser, refractive-index profile and resonant modes 79—86179
laser, self-induced modulation, noise, instability 80—48250
laser, $Si_{1-x}C_x$ protective coating 80—5753
laser, single heterostruct., transient effects 79—98366
laser, single-channel injection, polarisation characts. 80—48256
laser, single-channel injection, radiative characts., single longit. mode 79—10309
laser, single-freq. injection, coherence of emitted radiation 79—31904
laser, single-freq. injection, CW operation 78—46606
laser, sinusoidal modulation 9 MHz to 1.1 GHz, appl. for fibre meas. 77—10966
laser, spectral depend. of gain calc. 77—23677
laser, stripe-geometry, interaction and spectral distrib. of lateral modes *(Russian)* 78—22134
laser, striped DH, anomalous behaviour at low temp. *(Chinese)* 80—87390
laser, surface temp. distrib. *(Russian)* 78—74909
laser, transverse modes, mirror reflectivity dependence 79—68404
laser, two dimensional, DFB, with distributed Bragg and acousto-optic reflectors 77—10946
laser, uncooled electron-pumped, degradation rel. to dislocation density 80—14344
laser, wavelength depend. of gain saturation 78—1229
laser action in photopumped ribbon whiskers 80—91801
laser alloying of Au-Ge ohmic contacts 79—73583
laser annealed, Ga precipitation, Rutherford backscattering and TEM study 79—79127
laser annealing, optical refl. meas. of melted layer 79—78796
laser annealing after ion implantation, temp. distrib. 80—54265
laser annealing of ion bombardment damage 80—25502
laser array, integrated, Si substrate package fabrication 79—18555
laser array source package 77—84007
laser array to channel groove waveguide coupling prism 78—38067
laser arrays, Si substrate packaged, thermal performance and limitations 78—46613
laser convex micromirror mode control 79—36920
laser crystallisation, for production of large grained sheets for solar cells 80—93570
laser damage, 10.6 μm CW CO_2 beam 77—63497
laser damage statistics rel. to structural defect statistics 80—91829
laser diode, CW injection, specification for integrated optical circuits 80—33034
laser diode, fabrication and characts. *(Korean)* 79—7144
laser diode, GaAs based 77—7088
laser diode, SEM electron beam induced current study, contamination effect 79—43773
laser diode, spontaneous emission reduction 80—95904
laser diodes, absorption edge effects on temp. depend. of threshold currents 77—58328
laser diodes, coupling light efficiency into parabolic-index fibres 78—94435
laser diodes, digital modulation for optical communication systems *(German)* 78—37919
laser diodes, junction temp. meas. method 79—36895
laser diodes for optical communication transmission *(German)* 80—28252
laser diodes stabilised using self-apertures facet coatings 80—58609
laser facsimile printer 80—30207
laser heating of lightly damaged material, carrier diffusion effect 80—84809
laser heterojunction diode as light source for fibre optical communication 80—58653
laser induced damage 79—56890
laser irradiated, origin of periodic surface struct. 78—91513
laser irradiation effects, capacitance spectra 79—99987
laser long time delays, internal Q-switching 77—79822
laser material, secondary dislocation climb during optical excitation 78—75672
laser reordering of implanted amorphous layers 78—43042
laser residual lattice absorpt., freq. and temp. depend 78—25910
laser source package for multichannel optical links 78—1266
laser structures, double and narrow stripe 80—64062
laser window material, surface and bulk absorpt., photoacoustic meas. 78—25912
laser with integrated interferometric reflectors 77—65642
laser-annealed ohmic contacts for microwave devices 79—73584
laser-annealing behaviour, Si_3N_4 encapsulation effect forming n-type layers 79—79131
laser-induced bulk breakdown and free carrier generation, photocond. meas. 80—35018
laser-induced recrystallisation and damage of ion-implanted amorphous samples 79—47557
lasers, at room temp., modulation at X-band frequencies 78—87079
lasers, comments on host dispersion in ultra-short pulse generation 80—64024
lasers, current research, fibre optic appl. 80—83613
lasers, degraded, climb asymmetry, TEM obs. 80—79802
lattice dynamics, overlap shell model, bond charge model 79—42156
lattice dynamics, phonon freq., bond bending force model calcs. 80—70335
lattice thermal cond. at high temp. 79—90838
lattice thermal cond. from three phonon scatt. relax. rate 78—51755

gallium arsenide continued
- lattice thermal conductivity, point defect scatt. relax. rate role 80—70478
- lattice vibration, thermal expansion and pressure effect 80—39233
- layer growth by electroepitaxy, thickness profiles 79—4486
- layer structures revealed by decoration method and electron microscopy 77—27902
- layers, grown by electroepitaxy and LPE, surface morphology 79—19478
- layers, LPE growth, graphite boat construction 78—31348
- layers and p-n junctions grown by current-controlled LPE, elec. characts. 78—6436
- LED, absolute internal quantum efficiencies of photoluminescence 77—63461
- LED, minority carrier lifetime determ. 79—42560
- LED, optimum p-n junction depth, photoluminesc. method 79—4598
- LED absorption effect on freq. characteristic 79—8189
- LED modulation bandwidth, influence of inhomogeneous current density distrib. 80—9993
- LEED, (110) clean surface, internal pot., interplanar spacing 77—89627
- light scattering spectra, interference effects 79—82977
- lightly doped, movement of dissociated dislocations in diamond cubic struct. 78—59806
- lightly doped, p-n structure, parameters of nonequilib. carriers, transient photoeffect method 79—11143
- liquid, semicond.-metal transition at high temp. and press. 77—51784
- liquid encapsulated Czochralski technique of single crystal growth using B_2O_3 80—11554
- liquid interaction parameters determ., 580-670°C 80—65197
- liquid-phase electroepitaxial growth kinetics, Peltier effect and solute electromigration 79—42401
- liquid-solid equilibrium of Ga-As system, Krupkowski model *(German)* 78—95132
- liquidus line, quantitative fits and high-temp. thermodynamic data 77—63637
- LMTO self consistent band struct. calc. 80—20078
- local mode sideband IR absorption and second harmonic intensity calc. for isolated impurities 77—85707
- localised defects, one-electron pseudopot. 77—24533
- longitudinal magnetophonon reson. and Fourier anal. 79—4569
- low temp. gamma irrad., donor-acceptor pair formation 79—69158
- low-current-threshold strip-buried-heterostructure lasers with self-aligned current injection stripes 79—72581
- low-field study of p^+nn^+ or p^+pn^+ structs. on forward direction 80—60072
- LPE, charge carrier conc. distrib. *(Russian)* 78—52694
- LPE, current controlled, for LAS diodes, optimum doping profiles 78—35318
- LPE, deep levels rel. to growth conditions 79—28314
- LPE, dislocations obs. by etching 79—95284
- LPE, gaseous impurity source and effect on purity 79—28959
- LPE, growth mechanism and kinetics 78—34726
- LPE, residual impurities and deep levels, FET fabrication 79—28964
- LPE, smooth, thin layers on nominally oriented substrate 78—44030
- LPE, temperature instability effect, report 80—66446
- LPE, transient-mode, on InP 78—72746
- LPE (001) layer, etching by molten KOH 78—34515
- LPE buffer layers for MESFET appls. 80—29887
- LPE edge-growth reduction method 78—30848
- LPE film, thickness comparison with $Ga_{1-x}Al_xAs$, for layers grown by linear cooling 78—87892
- LPE from Au-Ge-Ni melts, elec. props. of Ni/Au-Ge/GaAs contacts obs. 77—77437
- LPE from Ga soln., carrier conc., growth condition depend. 80—71584
- LPE growth, electric current controlled, on n^+ and semi-insulating substrates 77—73240
- LPE growth, for MM-wave and sub MM-wave receiver elements 80—11558
- LPE growth, high purity, using sliding boat method for FET buffers *(Japanese)* 79—28955
- LPE growth, wave morphologies on surface 77—40396
- LPE growth 78—18924
- LPE growth from supercooled soln., thickness uniformity 80—54547
- LPE growth of high purity layers by sliding boat method 78—76610
- LPE growth on O-implanted GaAs substrate elec. props. 78—2592
- LPE growth on O-implanted GaAs substrates, surface morphology 77—28732
- LPE growth rate calc., from GaP and GaAs LPE data 79—19485
- LPE growth surface, singular instabilities 77—24969
- LPE in graphite boat, total ionised impurity density 77—12550
- LPE in situ etchback calibration 79—83114
- LPE layer, deep levels, photocapacitance obs. 77—15790
- LPE layers, ambient O_2 effect on defects and elec. props. 77—76683
- LPE layers, baking effect on mobility and doping conc. 79—99641
- LPE layers, dopant tracing of terrace growth 78—75948
- LPE layers, voids and depressions in facet and terrace growth 78—38974
- LPE layers, X-ray topographic exam. of defects 78—30844
- LPE layers, X-ray topographic studies of defects 77—62772
- LPE on polycrystalline Mo 79—43157
- LPE with $AsCl_3$-saturated Ga/As solns. 78—63953
- luminescence, electron-hole plasma 79—47500
- luminescence by laser excitation, photocarrier thermalisation and polariton kinetics 77—66533
- luminescence due to deep centres, annealing effect on quantum efficiency 77—55825
- luminescence during streamer discharge *(Russian)* 77—55835
- luminescence emitted as a result of carrier heating 77—52185
- luminescence emitted by deep centres, illumination-induced change in internal quantum efficiency 79—91495
- luminescence emitted by travelling acoustoelec. domains 78—27329
- luminescence emitted from deep centres, γ-irrad. induced changes in internal quantum efficiency 80—20701
- luminescence emitted from deep centres, plastic deform. effect on internal quantum efficiency 80—60672
- magnetic circular dichroism at E_1 edges 78—92051
- magnetic freezeout in ultraquantum limit 78—76017
- magnetic susceptibility and absorption spectra, exam. 79—1778
- magnetoelectric susceptibility, nonlinear, three-dimens. model 80—39845
- maximum electric field in high-field domain in Gunn devices 78—79996
- MBE, growth and doping kinetics 77—76682
- MBE, growth temp. depend. and characts. 79—28946
- MBE, process anal. and appl. *(French)* 79—56937
- MBE, SnTe source of donor impurities 79—95035

gallium arsenide continued
- MBE, surface reaction steps 79—77941
- MBE, technology and epitaxial layers props. 79—33945
- MBE, undoped, growth and characterisation 80—10836
- MBE, with ionised dopant 77—40338
- MBE (001) layers, work function meas. 80—49870
- MBE developments in device fabrication 79—78902
- MBE epilayers, photoluminesc. and elec. characterisation 80—11500
- MBE growth, deep levels effect on electron and hole trap densities 80—49652
- MBE layer, Al_2O_3, film growth 78—39706
- MBE layer, directional coupler switch 79—76878
- MBE layers, H_2 effect on residual impurities, photolum. obs. and elec. characts. 79—47636
- MBE of autoepitaxial films, temp. range for growth, RHEED monitoring 78—44025
- MBE of doped cryst., thermodynamics and kinetics interplay 80—70144
- MBE of thin layers, growth conditions and phys. props. *(German)* 80—55307
- MBE physical characteristics and applications *(German)* 79—7618
- MBE prep., device props. 77—77417
- MBE process for thin film growth, military microwave, optoelectronic devices appl. 79—52129
- melt grown, improved elec. and luminesc. props. after short time heat treatment 77—63452
- melted zone displacement by current *(Russian)* 78—26727
- MESFET, deep trapping effects at GaAs-GaAs:Cr interface 78—72245
- MESFET layers, low-temp. halide epitaxial growth 77—77403
- MESFET struct., high-resolution deep level meas., photo-FET method 80—44531
- MESFET structure, buffered, LPE growth 80—40271
- metal contacts, use of Ga to eliminate large As loss peaks 80—80370
- metal interface, intervalley scattering electron transport mech., model obs. 77—89845
- metal-GaAs junctions, thermal stability improvement, with and without near noble metals 79—7143
- metal-gelatin-n-GaAs struct., C-V characts. and gelatin-semiconductor interaction rel. to photographic process *(Russian)* 80—49944
- metal-induced chem. reactions and surface states at Ga As-metal interface 80—20311
- metal-insulator transition in impurity band induced by mag. field and loss of dimens. 78—52042
- metal-semiconductor contact, surface doping effect *(Russian)* 77—47896
- metal-semiconductor thermoelectric coolers, effects of contact resist. and dopant conc. 80—81481
- metal/GaAs contacts, recent developments in investigations of preparation and props. *(French)* 80—107909
- metallisation, anodic oxidation anal. 78—80673
- microcharacterisation for device appls. 80—10922
- microhardness and charact. hardness 79—52376
- microscopic etching, laser induced 80—76379
- microwave biased n-type, fast rise-time modulation of 337 μm radiation 77—54794
- microwave devices and their use for generation and freq. conversion of microwave oscillations 80—15534
- microwave diode chips, elec. characterisation 78—91791
- migration of liquid inclusions, effect of DC current and temp. 77—7910
- minority carrier diffusion length, photon absorption reemission 79—87109
- minority carrier diffusion length, Schottky barriers, electron bombard. investigation 78—68037
- minority carrier diffusion length reabsorbed radiation effect 77—28191
- minority carrier diffusion lengths, contact metal effects 78—72260
- minority carrier diffusion lengths in semicond. SEM meas. interpretation 78—80002
- minority carrier lifetime at high temp., solar cell performance appl. 80—24947
- minority deep level investig. by new optical method 78—6331
- MIS capacitor, transient capacitance and C-V characts. 78—95374
- MIS devices, diffusion, chemical reactions, contamination, AES and SIMS 80—72066
- MIS devices, multidielectrics using composition-graded $Al_xGa_{1-x}As$ and oxidised AlAs 79—65333
- MIS diodes, interface states determ., by deep-level transient spectroscopy *(Japanese)* 80—49917
- MIS dynamic optically controlled transparencies 78—90523
- MIS Schottky barrier diodes, radiation effects 79—24078
- MIS solar cell, field shaping and barrier height 77—20454
- MIS solar cells, effects of thin oxide layers on characts. 80—89624
- MIS struct., with natural anodic oxide elec. props. 79—99634
- MIS structure, elec. props., effect of interface As domains 78—88032
- MIS structure, fabrication by reactive sputtering, and props. 78—39686
- MIS structure, GaAs based, as possible optical memory elements 79—65556
- MIS structure, interface with insulator, processes of electron emission from traps 79—73598
- MIS structure using LaF_3 insulator 79—78182
- MIS structures, C-U curves, surface state densities 77—85335
- MIS structures, photoelectric conversion *(Czech)* 79—83595
- MIS structures, review 78—95372
- MIS structures and metal-semicond. structures, effects of ultrathin oxides 79—1626
- MIS structures on GaAs, dielec. and interfacial characts. appl. to microwave MISFETs 79—60933
- mixed cryst. form. by ion beam synthesis, vibr. anal. 80—103376
- MM wave guiding and control by surface plasmons 80—103713
- model relating elec. props. to impurity concs. 77—51697
- molecular beam epitaxy for superlattices control 80—2283
- molecular clusters, eliminating α exchange parameter in multiple scatt. method 80—103652
- MOS capacitor characts. and anodic oxidation in nonaqueous electrolyte 79—38183
- MOS capacitor fabrication and transient response for minority carrier lifetime meas. 79—47103
- MOS capacitors, anodized, C-V characts., surface pot. 79—11227
- MOS capacitors, scanning photovoltage investigation 80—80396
- MOS device, new method of fabrication 78—47872
- MOS diodes, interface states, deep-level transient spectroscopy 80—44727
- MOS solar cells by anodisation in active region 80—101107
- MOS structure, props. of surface carriers 77—20453

gallium arsenide continued
  MOS structure, small signal admittance study 80—2478
  MOS structure, white light emission obs. 78—76148
  MOS structure with Al_2O_3 grown by molecular beam reaction under UV excitation 79—60927
  MOS structures, leakage current for anodic oxide layers, space charge trapping effects 80—60091
  MOS structures, native oxide growth by wet anodisation 80—70832
  MOS structures, props. of capacitance transient 80—25013
  MOS system, elec. meas. interpretation 78—43484
  MOS system, surface and interface exam. by derivative surface spectroscopy 79—82674
  MOSFETs, native oxides, annealing effects and inversion-layer mobility 78—6452
  multilayer liquid phase epitaxy, transition to faceting 80—96750
  multilayer with abrupt carrier conc. profile, vapour growth technique 78—11123
  multiphonon absorpt., IR spectra meas., phonon density of states interpretation 77—69833
  multiphonon IR absorpt. expt. 78—60461
  multiphonon IR absorption in highly transparent semicond. crysts. 78—10885
  multiphonon nonradiative transition rate for electrons in semicond. and insulators 78—60503
  multiple insulating layers on GaAs, Auger exam. 79—83345
  multiple layer epitaxial growth, VPE method 77—12545
  multiple layer LPE growth by controlled supercooling of Ga soln. 77—77429
  n^+-p^--n^+ ballistic structure 80—80359
  n^+-type, multiple energy proton bombard. effects on elec. characts. 77—39853
  n-i-n junction, photoelec. props. investig., 77 to 300K 77—28248
  n-i-n junctions, simulation of long-term relax. of nonequilib. conductivity 79—38156
  n-i-n three layer struct., transmitted phonon effect in strong mag. fields 77—20341
  n-tupe, LPE, impurity compensation, photolum. and free carrier conc. meas. 77—62558
  n-type, anodic oxide film, exam. using SIMS and ellipsometry 79—61770
  n-type, Auger transitions, nonlinear extrinsic luminesc. study sublinear emission 79—95833
  n-type, carrier compensation by O ion implantation C-V meas. 77—7747
  n-type, compensated, LF current instabilities 79—7859
  n-type, computer study of conditions for absolute negative resistance 77—4358
  n-type, conductivity relax. times in warm electron range, intervalley transitions 77—55537
  n-type, conversion to p-type after 1 MeV electron irrad. 79—77636
  n-type, coupled plasmon-LO phonon modes, Raman scatt. meas. 78—60472
  n-type, coupled plasmon-LO phonon modes and Lindhard-Mermin dielec. function 79—82540
  n-type, current-voltage characts., dislocation etch pits and perfect cryst. 80—70695
  n-type, deep electron traps, determ. by time-resolved capacitance meas. 77—39797
  n-type, deep trapping centre characterisation by Hall and photo-Hall meas. 80—88578
  n-type, deform. produced deep levels, DLTS meas. 80—54634
  n-type, density of states tail in heavily doped closely compensated semicond. 78—47689
  n-type, diffusion coeff., Monte Carlo calc., rel. to trapped domain behaviour 78—56152
  n-type, donor-acceptor pair recomb., isolated-pair model revisited 79—28825
  n-type, dopant conc. determ. using laser IR microscopy 79—86811
  n-type, doping by neutron transmutation 80—96553
  n-type, electrical instability, negative differential cond., electron heating by static and alternating elec. fields 79—11165
  n-type, electron and gamma ray irradiated, introduction and annealing of defects 78—67736
  n-type, electron drift rel. meas. at high elec. fields 77—39861
  n-type, electron irrad. defects, carrier removal rate, annealing effects 80—75269
  n-type, electron irradiated, defect energy levels, influence of irrad. temp., photocond. meas. 78—2446
  n-type, electron mobility, free-carrier absorpt., and compensation ratio 79—56218
  n-type, electronic transition scheme via radiative centres 77—69905
  n-type, epilayer, on semi-insulating substrate, elec. field distrib. *(French)* 80—20333
  n-type, epitaxial, electron mobility obs. 77—69435
  n-type, epitaxial, high temp. carrier transport 80—65725
  n-type, epitaxial, ionised donor pair spectrum 77—63477
  n-type, epitaxial film, defect clusters, charge-carrier mobility temp. depend. anal. 80—54701
  n-type, epitaxial film, surface mode phonon amplification, numerical analysis 78—34691
  n-type, epitaxial films, residual cond. meas., struct. perfection rel. to photomemory 80—7010
  n-type, epitaxial layers electrical parameter determ. by graphical method *(Russian)* 77—15975
  n-type, far IR propag. of surface EM waves 79—42615
  n-type, film, carrier wave amplification, external medium stratification effects *(Russian)* 78—34905
  n-type, freq. depend. of effective temp. of hot carriers 79—11135
  n-type, H-like impurities photocond., mag. field effect 79—82634
  n-type, heat treated, origin of 1.41 eV emission band, photolum. expt. 78—72579
  n-type, heat treatment effect on electron traps 78—6396
  n-type, heavily doped, impurity-band cond., DC cond., Hall mobility, and magnetoresist. meas. 80—49733
  n-type, heavily doped, test of cond. band edge random fluctuations by MCD 77—63438
  n-type, heavily-doped, with Gaussian band tails, modification of Einstein relation 80—80270
  n-type, high temp. mobility anal. in three-valley (Γ_6^c-L_6^c-X_6^c) model 79—99544
  n-type, hot carrier thermoelec. power, temp. depend. in mm wavelength range 79—23996
  n-type, hot electron magnetophonon resonance, Fourier anal. 80—54718

gallium arsenide continued
  n-type, hybrid-hybrid mode interaction in crossed elec. and mag. fields 78—51997
  n-type, impurity interaction and donor-acceptor recombination 80—16094
  n-type, in DMF solns., electrochem., photoelectrochem., redox. pot. determ. 79—96322
  n-type, influence of uniaxial stress on low field resist. 78—87976
  n-type, interband transition times, luminesc. depolarisation obs. *(Russian)* 79—33831
  n-type, interface with anodic oxide, C-V and I-V characts. 77—89863
  n-type, intrinsic avalanche response time, orientation depend. 79—51587
  n-type, intrinsic emission intensity, role of local centres in determ. of conc. depend. 78—39599
  n-type, intrinsic luminescence intensity, effect of 0.94, 1.0, 1.2 and 1.3 eV radiative centres 78—23517
  n-type, ion implanted, compensation 78—75680
  n-type, IR luminescence from acoustoelectric domains 77—55822
  n-type, IR luminescence of acoustoelectric domains 78—31258
  n-type, IR transmission, cond. variations effects 79—15158
  n-type, Landau level lifetimes for electrons 79—87112
  n-type, laser beam self-focusing in mag. field, carrier mechanism 78—33788
  n-type, lattice scatt. identified as cause of 1/f noise 78—64074
  n-type, limiting freq. of Gunn effect in polyharmonic LSA mode 80—6856
  n-type, low energy photolum., 77K, deep centre obs. 77—69877
  n-type, low temp. field generation of carriers, liberation from surface states 80—92959
  n-type, magnetised semiconductor, coupled LO phonon-plasmon modes, inelastic neutron scatt. 79—73459
  n-type, magneto-impurity effect, review 79—91081
  n-type, magnetophonon resonance, Fourier anal. 79—91080
  n-type, MBE, correl. between electron traps and growth processes 80—65387
  n-type, mechanical polishing damage effect on IR refl. and ATR spectra 77—20848
  n-type, mechanism of cyclotron reson. induced cond. 78—43396
  n-type, melt-grown, stoichiometry, photolum. obs. 78—72583
  n-type, metal-insulator transition in impurity band induced by loss of dimension 77—47732
  n-type, MIS struct., native oxide, effect on interface props. and removal by sputter etching 79—11228
  n-type, model describing removal and scattering of charge carriers by defect clusters 78—76069
  n-type, MOS capacitor struct., elec. props., annealing effects 80—34519
  n-type, nature of low temp. field generation of carriers, liberation from surface states 80—92960
  n-type, neutron irrad. and thermally induced defects, annealing stages 77—51409
  n-type, non-equilibrium acoustic phonon generation by hot electrons 80—6477
  n-type, non-Maxwellian electron distribution function, from electric field-depend. photolum. spectrum 79—11450
  n-type, ohmic contacts study 80—60083
  n-type, parametric interaction of HF waves, anal. 80—15554
  n-type, persistent photocurrents, Hall effect anal. 79—87130
  n-type, photo-Hall effect meas. of ionised impurity scatt. 78—56182
  n-type, photoemission and work function of (111A) and (111B) surfaces, energy states 77—20980
  n-type, photolum., rel. to n-Inp 77—40272
  n-type, piezo-absorpt. meas. 79—87455
  n-type, piezoelec. semicond., nonlinear interaction of acoustic waves with microwave elec. fields 79—42593
  n-type, preferential photoelectrochemical dissolution in Fe(III) based etches 78—7066
  n-type, proton irrad., $E_p=30$ MeV, defect form., orientation depend. 78—55898
  n-type, Raman scatt. by coupled phonon-plasmon mode, nonlocal theory 77—36222
  n-type, Raman scattering by wavevector dependent coupled plasmon-LO phonons 77—40232
  n-type, Raman spectra of coupled LO phonon-plasmon mode, de Haas-Shubnikov like quantum oscills. 78—43863
  n-type, real epitaxial surface, photoelec. spectroscopy mechanisms 78—34858
  n-type, recombination scheme for $h\nu_m \approx 1.0$, 1.2 and 1.3 eV luminesc. bands 77—69906
  n-type, Schottky barrier junction, SEM meas. of hole diffusion length, surface effects 79—87110
  n-type, semicond. electrode, electrolum. due to hole injection from electrolytes 77—20926
  n-type, semidegenerate, acoustoelec., gain and lattice attenuation, X-ray Brillouin scatt. and elec. meas. 79—15193
  n-type, shallow donors, elec. cond. and Hall coeff. meas. 77—11942
  n-type, smooth and continuous ohmic contacts using epitaxial Ge films alloyed with Ni 78—68086
  n-type, spectra, light induced, electrolyte and Schottky barrier techniques of meas. 80—76046
  n-type, stabilisation against photodecomposition, surface damage influence 80—76390
  n-type, strain sensitivity of specimens obtained from pressed powders 77—36177
  n-type, subject to crossed static elec. and mag. fields, microwave amplification 77—1440
  n-type, submillimetre cond. and carrier heating, two-electron-temp. model 77—20349
  n-type, surface states, photoemission yield obs. 77—16459
  n-type, switching time in low-temp. impurity breakdown 77—15923
  n-type, temp. depend. density of states, activation energy, screening, chem. pot. calcs. 79—56109
  n-type, thermoelec. power 79—60857
  n-type, three valley band struct., high temp. Hall mobility 80—29318
  n-type, transferred electron effects under hydrostatic pressure 77—32018
  n-type, transferred electron effects under hydrostatic press. 78—26871
  n-type, tunable far IR Landau emission with subnanosecond rise time 79—32015
  n-type, two stream instability 78—2509
  n-type, two-valley semicond., helicon wave instability 77—47842
  n-type, two-valley semiconductor, domain instability *(Russian)* 77—62934

gallium arsenide continued
  n-type, two-valleyed semicond., hot electron diffusion coeff., random walk calc. 78—68033
  n-type, ultra low resistance ohmic contacts 80—20307
  n-type, uncompensated, mech. of energy relax. at low temps. 77—62921
  n-type, undoped, proton radiation defect detect. by transient capacitance spectroscopy 79—11089
  n-type, Verdet const., free carrier density depend. 78—56462
  n-type, VPE, hi-lo, carrier conc. profiling by electrochem. methods 80—49958
  n-type, VPE layers, Hall mobility, effect of Cu contamination, photolum. expts. 80—54810
  n-type, X-band impact ionisation for 337 μm radiation modulation 77—39069
  n-type and p-type electrodes in acetonitrile solns., photoelectrochem. behaviour 79—4600
  n-type epitaxial, film, potential barrier height, temp. depend. *(Russian)* 78—68070
  n-type epitaxial film, undoped, correl. incorporation of donors, photocond. meas. at 4.2K 80—6898
  n-type epitaxial layer, planar diode, intervalley carrier transfer, dynamics of capture processes 78—47864
  n-type epitaxial layers, alloyed in As_2 beam, metal-Ga contacts 79—95495
  n-type epitaxial wafers, IR reflectance and elec. characts. 79—56293
  n-type far IR cyclotron emission 79—61226
  n-type film, cond. mechanism in strong elec. field determ. 77—1430
  n-type interface with insulator, elec. props. 78—95370
  n-type layer, VPE, influence of growth conditions on incorporation of deep levels 77—4310
  n-type layer, with SiO_2 overlayer, ohmic props. of Au-Ge contacts 80—2467
  n-type layers, heavily doped, formation by multiple ion implantation 80—59491
  n-type layers, heavily doped, formation by multiple ion implantation 80—88187
  n-type minority carrier trap meas. in Schottky barriers 78—26951
  n-type photoanodes for water photoelectrolysis 77—77789
  n-type surface recomb. vel. meas., diffr. from transient optical grating 79—1604
  n-type vapour phase epitaxial film electrophysical props. rel. to growth temp. *(Russian)* 80—49961
  n-type wafer, defect studies by ASLEEP, SEM and scanning AES 79—19256
  narrow-channel double-current-confinement CSP lasers, current distrib. effect on performance 80—58539
  native vacancies study using positron lifetime technique 79—83052
  negative differential mobility and geometrical magnetoresist. calc. 77—43624
  negative electron affinity cold cathode 79—87558
  negative resistance, current controlled, at low temps. 78—39133
  negative resistance and peak velocity in central (000) valley 79—73522
  neutron irradiated, effect on cryst. lattice period, X-ray diffr. meas. 79—37743
  neutron irradiated change in lattice period during annealing 77—55307
  neutron transmutation doping, shallow donors magneto-optical effects 80—20255
  nitridation, following oxidation, surface and contact props. of GaN produced 77—20436
  nitriding, GaN formation, preparation variables rel. to dielectric data 78—60591
  NMR under optical pumping conditions 80—25253
  noise calc. using Monte-Carlo method 80—75575
  nonalloyed ohmic contacts of TiPtAu by pulse-electron-beam annealed Se implants 80—2466
  nonequilibrium carrier conc. profile, photon transfer of excitation 77—69907
  nonlinear crystal, wavefront distortion compensation in thick inhomogeneous medium 80—102762
  nonlinear electro-optical susceptibility, coupled anharmonic oscill. model 80—2723
  nonlinear extrinsic luminescence 78—84645
  nonlinear light absorpt., photoluminesc. meas. 77—66528
  nonlinear light absorption, effect of deep impurity levels 77—77259
  nonlinear optical susceptibility and dispersion, electro-optic meas. 77—23707
  nonlinear refractive index dispersion at helium temp. 78—2820
  nonradiative capture, direct obs. of phonons 78—30976
  nonradiative capture and recomb. by multiphonon emission 77—43533
  nonradiative multiphnon carrier-capture cross sections of deep traps, intermediate-temp. depend. 78—43414
  nuclear spin levels, elec. induced shifts 80—34408
  ohmic contact fabrication using epitaxial Ge films 78—47871
  ohmic contact form. to n- and p-type samples by MBE, characts. 79—47159
  ohmic contacts, solid phase epitaxy formation, AES and channelling meas. 79—60658
  ohmic contacts fabrication, review 80—49901
  ohmic contacts to III-V cpds. *(Japanese)* 78—47869
  ohmic contacts using epitaxial Ge films 78—88027
  ohmic NiGeAu contact to GaAs, TEM obs. 80—75449
  one-photon absorption coeffs. calc. 77—20884
  one-sided abrupt junctions, distinction between avalanche and tunnelling breakdown 78—56211
  open tube diffusion of Zn 80—84326
  optical absorption near fundamental edge due to CO_2 laser pulses 78—39569
  optical absorption spectrum, effect of impurity wavefunction overlap 77—8613
  optical absorption spectrum dynamics using sub-ps. optical pulses 80—11431
  optical absorption spectrum in presence of optical pumping, low-temps. 78—15188
  optical cond. of free carriers 78—19436
  optical conductivity, constants, refractivity from IR absorption spectra 78—43873
  optical constants in 0.6 to 4.2 eV range 79—51928
  optical cross sections associated with deep levels, O centre obs. 80—6777
  optical inhomogeneity, physical basis 79—15430
  optical integrated circuits appl., properties and preparation 77—65644
  optical modulation by optical tuning of cavity 79—64314

gallium arsenide continued
  optical modulation spectra, proton damage effect 78—76487
  optical properties calc., dispersion relations approach, Velicky's method *(Spanish)* 77—90119
  optical transitions, effect of perturbed k-selection and gap shrinkage, thoery comparison with expt. 80—66257
  optical waveguide, periodic, phase-matched SHG obs. 77—19360
  optical waveguide, waisted-rib 80—74487
  optical waveguides, exam. of GaAs as cladding materials, for cutoff polariser 78—55474
  optical waveguides, oxide confined, formed by lateral epitaxial growth 80—58815
  optical waveguides, strain induced in epitaxial layers 79—27388
  optically pumped, absorption spectrum, band filling, hot electron effects 78—31199
  optically pumped laser, two-dimensional distributed Bragg reflectors, oscillation *(Japanese)* 78—42350
  optoelectronic devices, conf., Berlin, DDR 78—91755
  optoelectronic devices, thin-film optical waveguide periodic structures appls. *(Polish)* 78—50947
  optoelectronic switching in picosec. region 77—23742
  order-disorder interaction with O_2 on (110) surface, LEED anal. 80—75445
  organometallic VPE, with varying As/Ga ratios, deep states 80—65480
  orientation dependence of ballistic electron transport and impact ionisation 80—49758
  oscillatory electron drift rel. in non-ohmic regime at low temp. 79—33291
  oxidation, hardness and electromechanical polishing response 80—71776
  oxidation, initial process and oxide/semicond. interface formation 80—50739
  oxidation, of (110) surface, photoemission spectra obs. 77—16460
  oxidation, Raman scatt. obs. of GaAs-native oxide interface 77—85709
  oxidation, using low temp. plasma, and MIS struct. characts. 78—31546
  oxidation in multipole plasma, MOS elec. props. 80—44737
  oxidation of (110), 3d core level binding energy, multiple bonds 78—35543
  oxidation of (110) surface 77—32703
  oxidation of cleaved (110) surface, XPS exam. 78—31551
  oxidation saturation and MOS diode equivalent cct. 78—47875
  oxidation through Al film, AES and TEM 77—77621
  oxide, anodic, optical props., 1.5-6.0 eV 77—90209
  oxide, anodic heat treatment temp. effects, optical props. obs. 78—27658
  oxide, anodised native, influence of temp. on struct. and props. 77—81332
  oxide, grown in O plasma, physical and elec. props. 79—66189
  oxide, passivated layers, quantitative in-depth profile, AES-SIMS, thermal, anodic and plasma oxidations 78—84087
  oxide film, plasma-grown, analysis using Rutherford backscatt. and ion-induced X-rays 77—43438
  oxide film, thermal and anodic, in-depth profiles, XPS expts. 78—84086
  oxide film form., ion implantation effects 80—100266
  oxide film growth, thermal oxidation, optical obs., model 77—56120
  oxide film growth in As_2O_3 vapour, As incorporation 79—77928
  oxide film on surface, microscopy with an ellipsometric arrangement 80—17998
  oxide films, anodically and thermally grown, XPS study 80—16141
  oxide films grown by anodization in electrolytes, electron spectroscopy exam. *(German)* 79—15837
  oxide growth kinetics and physical props. 79—77937
  oxide layer, plasma grown, semiquantitative chemical depth profiles, Auger spectroscopy and neutron activation anal. 78—53284
  oxide layers prepared by anodic, thermal and plasma oxidation, in-depth profiles and annealing effects 79—61768
  oxides, appl. of selective chemical reaction concept for controlling props. 79—47790
  oxides, plasma-grown, in situ meas. and anal. with spectroscopic ellipsometry 80—76386
  oxidised surface, detection of excess crystalline As by Raman scatt. 78—19453
  p^+-ν-n diode, Cr-doped, nonlinear transport phenomena *(Japanese)* 80—6850
  p^+-n^0 junction photocurrent, hole diffusion length in lightly doped n-type region 77—28246
  p^+-n^0-n^+ structure, control of modulation of base resist. 79—91133
  p^+-n^- n^+ electro-optical directional-coupler switch 77—7217
  p^+-n diode, radiative hot carrier recomb., photoluminesc. and electroluminesc. meas. 79—38676
  p^+-n junction, deep level obs. 77—89834
  p^+-n-n^+ diode, ns modulation of 10.6 μm radiation by elec. injection 77—34937
  p-i-n avalanche photodiode, temp. depend. characts. 79—35835
  p-n homojunctions, elec. breakdown mechanism 79—87147
  p-n junction, as pressure/temp. transducers *(Polish)* 77—67424
  p-n junction, conductance oscillations in a two-dimensional impurity band 79—95477
  p-n junction, electroepitaxy and thermal LPE growth, elec. characts. 80—2290
  p-n junction, HV, current induced by electron probe in space charge region 79—24065
  p-n junction, piezotunnel current *(Russian)* 77—47890
  p-n junction, short-circuited, estimation of surface recomb. rates, electron-probe meas. 77—43713
  p-n junction, surface recomb. current reduction with $Al_{0.5}Ga_{0.5}As$:O surface layer 80—49878
  p-n junction, Zn^+ implanted, residual radiation defect influence on characts. *(Russian)* 78—84287
  p-n junction depth, and etch pit density, effect of As vapour press., for Cd diffused GaAs 78—26937
  p-n junction formation, laser assisted, TEM and elec. props. 79—69138
  p-n junction pressure transducer characteristics *(Polish)* 77—89832
  p-n junctions, direct biased, temp. depend. of low freq. voltage fluctuations 79—56298
  p-n junctions, planar, Be ion implantation, fabrication and characts. 78—88022
  p-type, carrier drag by photons 79—11185
  p-type, electron minority carrier diffusion lengths 80—29807
  p-type, electron-nuclear spin coupling, low field, under optical pumping conditions 77—77126
  p-type, electronic props. 78—68040
  p-type, field electron emission current-voltage characts. 80—45219

gallium arsenide continued
p-type, field emission, role of surface electron states 78—2993
p-type, hologram recording, photochem. etching control 80—28179
p-type, hot luminescence of semicond. with GaAs band struct. 78—39601
p-type, influence of light holes on transport props. 77—4367
p-type, intervalence-band transitions, saturation, theory 80—75997
p-type, IR plasma reflectivity spectra calc. 78—52511
p-type, linear polarisation of hot photoluminescence 79—38661
p-type, low-temp. resist. thermometers 78—223
p-type, MBE grown, As$_2$ and As$_4$ effects on photolum. 80—103974
p-type, minority carrier mobility calcs., including screening, scattering mechanisms 79—99545
p-type, photoemission into electrolyte soln., energy diagram, Volta pots., voltage drop 77—62990
p-type, photon drag optical rectification detectors, performance in 2 to 33 μm range 79—35834
p-type, piezoresistance, relax. time for heavy and light holes determ. 79—19599
p-type, Schottky barriers on polar (111) and $(\bar{1}\bar{1}\bar{1})$ surfaces 80—88631
p-type, spin relaxation of photoelectrons 77—85207
p-type circular polarisation of hot luminesc. 78—52572
p-type epitaxial layer, electron-hole plasma, quantum effects in magnetoluminesc. 78—72591
p-type epitaxial layer, thermalisation of electron-hole plasma, photolum. meas. 78—80408
p-type magnetoluminesc. of cond. band to acceptor transition 77—1716
p-type/heptyl viologen system, appl. in photoelectrochemical cells and photoelectrochromic displays 80—76640
particle detector, semi-insulating, VI characts., γ-ray sensitivity and performance 77—46467
passivated and unpassivated surfaces, heat treatment effects 79—73383
passivation, nitride-based, for reduced surface state density 80—16537
passivation by GaO$_x$N$_y$ films and multilayer systems 80—11809
Peltier induced growth kinetics of LPE 78—64485
Peltier LPE, absence of electromigration of As and Al 77—81230
periodic doping structure, nipi superlattices, HBE growth and characts. 79—95484
periodic surface corrugation generation by holography 78—55469
phonon assisted tunnel emission of electrons from deep levels 80—25532
phonon generation, anisotropic, in p-n junctions and GaAs epilayers 79—37784
phonon surface density, Brillouin elasto-optic cross section 78—72536
phonon viscosity tensor 78—34570
photo-field cathode, ageing and surface state effects *(Russian)* 77—28703
photoabsorption and magnetoabsorption effects 77—16332
photoacoustic measurements of ion-implantation and laser-annealing 80—47117
photoanode, using n/n$^+$ struct., power conversion efficiency 80—50990
photocapacitive MIS IR detector, spectral response, noise characts. 80—75644
photocarrier thermalisation by laser excitation spectroscopy 78—31250
photocathode, emitted electron transverse energy 77—12489
photocathode, high performance 77—48303
photocathode with Cs-O adlayer, negative electron affinity, core level photoemission of adlayer 79—19965
photocathodes, photoelectron emission, energy levels, influence of dimens. quantisation *(Russian)* 78—64447
photocathodes exhibiting negative electron affinity *(French)* 77—8724
photoconductive carrier lifetime meas. by optoelectronic gating technique 77—47857
photoconductivity, impurity induced, low energy edge spectral shift 80—65630
photoconductivity and photomagnetic effect spectra 79—11178
photoconductivity meas. of cyclotron resonance 79—82638
photoconductivity spectra with deep traps, interpretation 78—52030
photoconvertor, short-circuit current and load current depend. on angular sensitivity 79—83594
photodetector, determ. of theoretical threshold 78—37065
photodetectors, pin- and avalanche diodes, characts. *(Swedish)* 78—89545
photodiode, electroabsorpt. avalanche, as 1.06 μm waveguide detector 78—16842
photoelectric memory effect, effect of metallic island struct. on surface 77—55570
photoelectrons spin polarisation from (100) and (110) faces 80—11530
photoemission, angle-resolved, and valence band dispersions 80—7469
photoemission, from layers produced by pyrolytic synthesis 79—43100
photoemission characteristics, parameters of emitters with negative electron affinity 79—4898
photoemission modulation by IR illumination, saturation photocurrents 80—108318
photoemitter, negative electron affinity, face depend. of emission 77—32496
photoexcitation, high intensity, hot electrons and phonons 78—26905
photoexcitation phenomena, low density 78—27319
photoexcited, band edge absorpt. dynamics 79—19879
photoexcited, carrier relaxation determ. from time resolved transmission spectrum changes 79—99583
photoexcited carriers, relax. 78—19080
photoexcited hot electrons energy relaxation in near-surface region of semiconductors 80—92928
photoluminescence, ambient-enhanced, mol. adsorption and gas-flow effect 79—99925
photoluminescence, deep level trap emission capture 80—29805
photoluminescence, electron gas coding influence in ion-bombarded layers 80—108272
photoluminescence, electron-acceptor, from non-Maxwellian distrib. of photo-excited electrons 80—45138
photoluminescence and resonant Raman spectra, press. depend. 78—31251
photoluminescence at dislocations, band gap electronic levels 79—99926
photoluminescence at low temp., free exciton recomb. mechanisms *(Russian)* 77—32438
photoluminescence in polycrystalline samples at 5K, possible solar cell material 79—99929
photoluminescence intensity degradation caused by excitation-enhanced oxidation 78—15205
photoluminescence intensity of cleaved surface, ambient gas influence 78—88345

gallium arsenide continued
photoluminescence intensity rel. to heat treatment in S vapour *(Russian)* 78—48216
photoluminescence of defects, degraded layer form. by annealing 78—10968
photon drag effects 78—23134
photon transfer of excitation of nonequilibrium carriers, radiative recomb. 77—8639
photovoltage transients, expt. and model 77—89802
photovoltaic concentrator cells development project, developments, performances and future trends 80—45699
photovoltaic conversion characts. *(Czech)* 77—76903
photovoltaic solar system, appl. in electric utility system 80—55875
photovoltaic technology, conf., San Diego, CA, USA (Jan. 1980) 80—86041
picosecond absorption spectroscopy 79—47482
piezoelectric constant due to bond bending, electron redistribution effect 79—38457
piezoelectric coupling and dislocations 79—91377
piezoelectric film, surface phonon amplification 77—31864
piezoelectric oscillations, meas. by laser interferometry 77—118
piezoelectric phonon fields effect on absort. edge broadening 77—16302
piezoelectric powder, RF dynamic polarisation echo obs. 77—16254
piezoresistance and conduction band minima 78—51993
planar diffusion of Sn from doped SiO$_2$ films, for planar junction fabrication 79—69289
planar p-n junction fabrication by Be ion implantation 78—43470
plasma anodisation in DC discharge, AES and MIS diode expts. 78—95826
plasma region reflection effect of surface treatment methods *(Russian)* 79—69827
plasma-grown oxides, physical props., Auger and IR spectral anal. 79—91821
plasmon-phonon coupling, and IR refl. spectra of impure crysts. 79—56150
plastic deformation, produced by thermocompression bonding 77—76807
plastically deformed, elec. props. 77—28178
plastically deformed, photocond., spectral response and decay process 80—29435
point defect equilib., non-stoichiometry 79—90644
point defect generation by electron-hole recombination at dislocations 79—37699
point defects, laser annealing 80—107224
point defects, multiple scatt. Xα model 80—54636
polar modes, light scatt. intensities, wave vector depend. 77—77219
polariton scattering, free carrier effects 78—34783
polaritons, surface nonlinear interactions, Green's function theory 78—42379
polishing dislocation etch 78—6066
polycrystalline, carrier transport at grain boundaries 80—29411
polycrystalline, for solar cells 78—11124
polycrystalline, grain boundary resistance meas. effect on solar cell performance 80—93891
polycrystalline, wet and dry oxides, comparative study by AES, SIMS and XPS 80—80116
polycrystalline film growth for solar cells 79—33941
polycrystalline films, meas. of effective diffusion length by SEM 80—80424
polycrystalline solar cell diagnostics using IR electroluminesc. 80—93885
polycrystalline thin film solar cells 80—94066
polycrystalline thin film solar cells with grain boundary edge passivation, prep. and props. 80—81437
population inverted semicond., resonant Brillouin scatt., photoelastic consts. 80—89016
positron annihilation, deep acceptor level props. 79—11485
positron annihilation, mag. field effect, positronium states 77—16417
positron annihilation 78—72636
positron annihilation depend. on doping 80—60710
positron annihilation in disturbed surface layers 78—6809
positron annihilation rel.to surface treatment *(Russian)* 77—44081
positronium-like states, low temp., ang. correl. of annihilation photons 78—76549
powder, RF field depend. of memory echoes 79—8095
preferential etching, in $1NH_4OH.2H_2O_2$, facet formation *(Japanese)* 78—44242
primary radiation defect separation by elec. field 80—92522
proton irrad., effect on elec. props 80—65567
proton irradiated, low energy, deep level defects and hole diffusion length meas. 80—60000
proton isolation layer, lateral spread, elec. meas. 77—80520
proton range calcs. 77—76479
proton range data and deep proton-isolated lasers 79—36923
proton-bombarded, lattice strain, precision X-ray meas. 77—27922
pulled, dislocation generation, thermoelastic anal. 80—79787
pxidation of (110), 3d core level binding energy, single bonds 78—35544
radiation damage, influence on diffusion of implanted P and Kr atoms 78—6082
radiation damage in proton-bombarded material, observation using TEM 80—75276
radiation defects, Schottky diode characts. obs. 78—76024
radiation detector, characteristics 79—68139
radiative recombination, optical evaluation review 80—60647
radiative spectra from hot photocarriers 78—31249
radiative yield improvement by laser annealing 80—45128
radiometer, single-cell for artificial satellite measurement system 80—13147
Raman scattering, electron-phonon deformation potential coupling 78—52502
Raman scattering, two-phonon, room temp. meas. 77—81097
Raman scattering absolute cross section band struct. model calcs. 80—7349
Raman scattering from nonequilibrium LO phonons with picosecond resolution 80—80779
reactive ion etching of III-V compounds 80—58813
reactor irrad., opt. props. 77—90137
reactor-irradiated, anisotropy in diffuse small angle neutron scatt. 78—51598
recombination characteristics near surface, effect of γ- and electron irradiation 80—71478
recombination radiation, anomalous temp. depend. 80—2847

gallium arsenide continued
recombination velocity at III-V compound heterojunctions, $Al_xGa_{1-x}As$-$GaAs_{1-y}Sb_y$ solar cells 80—12010
reflection spectra, optical consts. *(Russian)* 79—38571
reflectivity, high resolution, down to 15K, Ga-3d-excitation 80—25415
refractive index and induced birefringence dispersion 80—2717
refractive index dispersion 79—24280
relaxed surface, (110), electronic states 79—51649
residual donors, ionisation energies determ. 78—6333
resonance enhancement of Raman scatt. by electron gas excitations 79—65878
resonance Raman scattering by 2 TO phonons and cond. band minima ordering 77—20854
resonant Brillouin scatt., book contrib. 79—42983
resonant Brillouin scatt. of excitonic polaritons 77—44010
resonant Brillouin scattering 79—78695
resonant Brillouin scattering and photoelastic consts. in population-inverted material 80—76042
resonant Brillouin scattering of exciton polaritons 80—11418
resonant Brillouin scattering of exciton polaritons 80—93357
resonant Raman scattering at indirect gap 79—73931
ribbons from Ga-$AsCl_3$-H_2 epitaxy 80—7498
S-shaped I/V characteristics based on laminated semicond. cryst. structures *(Russian)* 79—42628
SAW amplification 79—46907
SAW broadband generation by conversion from acoustoelectrically amplified bulk waves 77—54852
Schottky barrier, effect of oxide composition on elec. behaviour, AES meas. 79—87141
Schottky barrier, thermal emission from damage near interface, effect on TSC and transient current expts. 77—11982
Schottky barrier and semicond./insulator interface states formation 80—49906
Schottky barrier charge-accumulation detector, photosensitivity spectrum 77—55582
Schottky barrier diode, detection down to 70.5 μm 77—10103
Schottky barrier diode, under high neutron fluence, current transport 80—65679
Schottky barrier diodes, electron processes at metal-semicond. interface *(Russian)* 78—84301
Schottky barrier diodes, freq. and voltage depend. of impedance 78—64114
Schottky barrier diodes, strain sensitivity mechanism 79—38165
Schottky barrier electrorefl. under uniaxial stress, band struct. 77—48193
Schottky barrier ellipsometric electroreflectance spectra, energy band parameters 79—99853
Schottky barrier formation, Fermi-level pinning, defect mech. 78—95358
Schottky barrier height, semi-empirical tight-binding calc. 79—28408
Schottky barrier height rel. to chem. reactivity 80—25008
Schottky barrier solar cells, diffusion length meas. 79—61973
Schottky barrier solar cells with grain boundary edge passivation 79—83592
Schottky barrier with Au and Au-Ga contacts, high temp. annealing behaviour 77—43725
Schottky diode, impurity photolum. 80—29781
Schottky diode, trap levels, admittance spectroscopy 79—51672
Schottky diode, trap refilling, depth and capture cross section determ. 78—80052
Schottky diode, use in acoustic memory correlator 78—66989
Schottky gate FET struct., obs. of localisation in two-dimens. systems 78—60213
Schottky-barrier, linear and quadratic electroreflectance, minicomputer-controlled meas. 80—97241
Schottky-barrier diode submicron layer LPE reactor 77—77439
Schottky-contact, influence of surface states and hole traps *(Bulgarian)* 80—25006
screw dislocations in LPE layers, optical microscope obs. 77—35561
secondary ionisation coeffs., interband scatt. effects 78—43408
selective etching in nonaqueous bromine and iodine solns. 77—40453
selective plasma oxidation, interface props. 80—100933
self-compensation due to shallow and deep levels 80—24837
self-scattering in Monte Carlo calcs. of transient dynamic response 80—103687
semi-insulating, cond. mechanism, model explaining temp. depend. of elec. props. 79—51571
semi-insulating, conduction model 80—10986
semi-insulating, damage gettering of Cr during annealing of Cr and S implants 80—107304
semi-insulating, doping by neutron transmutation 80—96553
semi-insulating, effects of heat treatment characterised by SIMS 78—6091
semi-insulating, elec. characts., correl. with mass spectra anal. 78—39104
semi-insulating, LPE growth for FET buffer layers 79—66015
semi-insulating, magnetophotoconductivity as function of etching time 79—56265
semi-insulating, microwave permitt. meas. 80—60479
semi-insulating, optical and electron microscopy exam., line dislocation precipitates 80—70205
semi-insulating, surface layer thermal conversion mechanism, Hall effect meas. 80—49772
semi-insulating, thermal conversion, Hall effect and luminesc. meas. 78—6405
semi-insulating, undoped and Cr-doped, compensation mechanisms, Hall effect and optical absorpt. meas. 80—84477
semi-insulating substrate, characterisation and modification 77—81215
semi-insulating substrates, monolithic integration of optical and electronic devices 80—58543
semi-insulating substrates, whispering gallery lasers 80—69405
semiconductor-metal transition, press. calibration above 100 kbars fixed points 80—77808
shallow acceptor states exam. by far IR Fourier transform spectroscopy 78—31185
shallow core level spectra 80—104037
shallow donors, screening, energy spectrum of electrons and cond. mech. 79—7831
shallow impurity spectral linewidths, 4-10K 77—63443
shallow-homojunction solar cell by MBE, conversion efficiency 80—30476
shallow-homojunction solar cells, electron radiation effects 80—97798
Shubnikov-de Haas oscillations in semiconductor superlattice 77—62947
signal processing optical electronic devices 80—33242

gallium arsenide continued
single cryst., linear electro-optical props., temp. depend. 80—71376
single mode fibre cable, 4.15-km, interf. and polarisation characts. using AlGaAs laser 79—81535
site selective doping by ion implantation of radioactive nuclei 80—34023
solar cell, polycryst., grain boundary passivation by oxidation, AES, SIMS and XPS obs. 80—81467
solar cell, shallow homojunction, resist. to 1 MeV electron radiation 80—50953
solar cell, thin film, prep. by Peeled Film Technology 79—29472
solar cell film, large-grained, growth method 79—38737
solar cell polycrystalline conducting substrate, minority carrier diffusion length spatially-resolved meas. 80—94084
solar cell structs., photolum. props. 80—50958
solar cells, developments, appls., and economics of solar photovoltaic conversion *(German)* 80—26132
solar cells, developments and trends for automatic interplanetary stations, Venus-9 and Venus-10, and mooncar program 80—89613
solar cells, effect of grain size on efficiency 80—50968
solar cells, electron and proton radiation damage 80—94034
solar cells, electron-irrad., annealing kinetics 80—7937
solar cells, for satellite solar power systems, developments and future trends 80—45694
solar cells, ion-implanted and laser-annealed 79—79390
solar cells, low-high junction effect, theoretical anal. 80—89626
solar cells, multi-bandgap concentrator cells, Si and $Al_xGa_{1-x}As$ systems, operation with spectrum splitting filter 80—45698
solar cells, photoreactance of p-n junction diodes 80—81464
solar cells, polycrystalline and tandem, for high efficiencies, using compound semiconductors 80—72052
solar cells, shallow junction, damaged by electron irrad., recovery of short cct. current 79—29471
solar cells, shallow-homojunction, efficient, on single cryst. GaAs and Ge substrates 80—61364
solar cells, simultaneous radiation damage and annealing 80—94033
solar cells, thin film growth and grain size, effect on cell efficiency 80—81471
solar cells, thin film growth tech. and characterisation 80—89631
solar cells on Ge substrates, thin film shallow homojunction struct., quantum efficiencies 80—35677
solar cells with concentrators, prospects *(Italian)* 80—60025
solar cells with shallow homojunction on Ge substrates 80—26142
solid solubility of Se, SIMS 78—67830
solubility in Ga-Al alloys in multilayer LPE of $Ga_xAl_{1-x}As$ 78—52690
spin polarised electron source for LEED 78—83693
spin-dependent recomb., photoluminesc. obs. 80—60666
spontaneous luminesc. due to high density electron-hole plasma under nano- and picosecond pulse excitation 80—40157
spreading resistance, meas. for p- and n-type and Zn diffused samples 79—28343
sputtered film, structuring rel. to laser sputtering method *(Russian)* 77—59689
sputtered layers, EPMA of Kr content 80—3443
sputtered neutral mass spectrometry using post-ionisation in microwave plasma 78—92579
sputtered-etched surface, Schottky contact characterisation and its recovery by annealing 79—99603
sputtering at elevated temps. 80—7456
stepped surface exam., LEED vs. RHEED 77—72762
stimulated and spontaneous emission from degenerate electron-hole plasma at 300K 80—29762
stimulated emission and luminesc. obs., HV pulse excitation 79—59704
stimulated emission during N_2 laser pumping under appl. elec. field, gain anisotropy 77—61958
stoichiometry meas. by 15 MeV He^{2+} backscattering 79—99330
strain sensitivity of p-samples, piezoresistance *(Russian)* 79—82585
stripe-geometry laser, nonlinear temp. characteristics *(Chinese)* 80—43337
structural defects, detection by electrochemical etching 78—55872
structural defects in single cryst., first order distribs. eval. *(German)* 78—6049
substrate, (111), and homoepitaxial layers, characterisation by divergent X-ray beam diffr. 78—31352
substrate, Al MBE growth 80—24757
substrate, $CuInTe_2$ epitaxial layer growth and props. 80—108359
substrate, evidence for insulator film growth-induced damage from photolum. expts. 78—75953
substrate, MBE growth of insulating oxide films 79—77943
substrate, morphology and crystallography of CdS-CdTe double layers 80—34326
substrate, O implanted, LPE growth of GaAs film 78—2592
substrate, optical meas. of temp. *(French)* 79—35743
substrate, Pd/Ge film sintering, Auger spectra, Schottky barrier energy 79—69581
substrate, plasma polymerised polysiloxane film growth, dry etching process 80—25575
substrate, Ta film deposition and oxidation, form. of Ta_2O_5 79—61769
substrate, VPE growth of n-AlAs, for heterojunction devices 77—1814
substrate, ZnSe film on, transition layer form. kinetics 79—87007
substrate for Al_2O_3 film, ion beam etching defect detection 80—89155
substrate for AlAs epilayers, MBE growth, self-terminating thermal oxidation 78—92374
substrate for epitaxial growth, backscatt. anal. of surface prep. and anodic oxidation 77—25175
substrate for homoepitaxy, vicinal surfaces characterisation 77—20207
substrate for p-Ge film, cond., Hall effect and transverse magnetoresist., anisotropy 79—51697
substrate for sputtered GaSb film growth, Hall effect, impurity levels 80—20334
substrate surface, low loss electron and Auger images correl. 78—22944
substrates, out-diffusion of Cr 80—10708
subsurface atomic displacements, LEED exam. 78—71912
superconductor-semicond. device research, future prospects 79—28467
surface, {001} layer, dislocation etch pits revealed by molten KOH 78—63772
surface, {100}, interaction kinetics of As_2 and Ga 77—60115
surface, (001), clean or contaminated, Au film growth 78—26785
surface, (001), MBE and field emission deposition of Al and Au films, comparative study 79—87016
surface, (001), thermal treatment before MBE growth, RHEED-AES meas. 79—61754

gallium arsenide continued
surface, (100), pot., wave functions, spectrum and charge density calc. 77—20382
surface, (110), adsorption of one Cs atom, mol. orbital study *(French)* 78—38958
surface, (110), ang.-resolved photoelectron spectra 78—43984
surface, (110), atomic and electronic struct. 78—72223
surface, (110), atomic geometry from elastic LEED meas. 77—20170
surface, (110), bond angle and lengths of rearranged As and Ga atoms 78—71918
surface, (110), chemisorption of O_2, electronic struct. theory, oxidation, electron spectra interpretation 79—42376
surface, (110), electronic struct., pseudopot. calc., surface relax. model 80—29456
surface, (110), high resolution photoemission yield, surface states 77—69392
surface, (110), O_2 interaction, order-disorder effects, LEED, UPS anal. 80—6634
surface, (110), oxidation process, XPS study 79—15585
surface, (110), pseudocharge density calcs. 78—84275
surface, (110), relax. effects 77—24601
surface, (110), surface core-level binding-energy shifts 80—103737
surface, (110), surface states, angle-resolved photoemission meas. 77—20984
surface, (110), valence band Auger spectra 78—35230
surface, (111) epitaxial film, adsorption of Cs, Cs+O, ellipsometric study 80—29282
surface, AB etch reappraisal 78—6065
surface, Al-coated, surface phonon Brillouin spectra 79—78694
surface, Ar ion bombardment induced photon emission, rel. to target temp. 78—72612
surface, chem. prep., and AES and XPS characterisation 77—90477
surface, clean and O_2 covered, work function and photovoltage meas. 77—1446
surface, clean and oxidised, O_2 sticking coeff., ionicity effects, XPS expts. 77—85887
surface, cluster model approach for electronic struct. 78—56205
surface, $CO(O_2)$ interactions, surface electronic struct. (surface chem.) using synchrotron radiation 78—53254
surface, contact pot. difference meas. 77—20403
surface, distrib. of surface states 80—44692
surface, electron struct. and Fermi level pinning by O_2 and metals 80—11066
surface, electronic props., interaction with Au and O adsorbate layers 77—20385
surface, electronic struct. of clean and O_2 covered surface 77—43685
surface, electronic structure of (111) and $(\bar{1}\bar{1}\bar{1})$ surfaces 79—87137
surface, energy-minimisation approach to atomic geometry 78—95213
surface, growth of anodic Al_2O_3 and composite oxides 79—83344
surface, intrinsic gratings, low angle X-ray diffr. obs. 77—85035
surface, low temp. thermal nitridation 80—97607
surface, negative electron affinity, optically pumped, depolarization of emitted photoelectrons 79—8223
surface, O_2 sorption and excitonic effects, photoemission expts. 77—85055
surface, oxidation, water vapour and O_2 excitation effects, XPS obs. 79—100274
surface, oxide film influence on adsorption and electrophys. props. 79—42369
surface, pulsed electron beam processing, doping, annealing 80—75254
surface, thermally oxidised, in-depth comp. profile, Auger analysis 77—89621
surface, thermally oxidised, TEM obs. 78—72036
surface, vacancies, bound state energy level calcs., tight binding approx. 80—44694
surface (100), comp. and struct. of differently prepared surfaces, LEED and AES 78—91524
surface (100), electronic struct., scattering-theory formulation 79—42607
surface (100) etch pit density meas. using automatic struct. analyser EPI-QUANT *(German)* 77—72619
surface (110), absorpt.-desorpt. processes and phase transitions in alkali halide adsorbed layers 78—2361
surface (110), angle-resolved photoemission spectra 80—50516
surface (110), chemisorbed O_2, extrinsic surface states 78—91535
surface (110), clean, cleaved, surface states, work function meas. 80—49847
surface (110), clean and As covered, atomic struct., LEED study 80—49476
surface (110), comparison of LEED intensities for chemically polished and cleaved surfaces 78—18884
surface (110), correl. of short-range order and sputter dose, using vidicon-based LEED system 79—83082
surface (110), double-dangling-bond defects and band bending 79—69411
surface (110), electron states from transfer matrix method 78—56203
surface (110), electronic states and initial steps in oxidation 78—91534
surface (110), electronic struct., ang. resolved photoemission expts. and tight binding calcs. 78—91743
surface (110), energy distrib. of dangling-orbital surface states 80—80347
surface (110), exposed to O and O_2 photoemission spectra meas., Space Shuttle expt. 78—35246
surface (110), initial oxidation, XPS and AES study 80—11542
surface (110), kinematical LEED calcs. 77—85034
surface (110), LEED and AES study, comparison of MBE and ion bombard. surface prep. 80—54496
surface (110), LEED intensities, dynamical calc. 79—77462
surface (110), low O_2 exposure effects on electronic props. 79—47146
surface (110), reconstruction and oxidation initial stages, ab initio calc. 80—49473
surface (110), self-consistent pseudopotential calcs., electronic struct. and atomic co-ords. 80—49848
surface (110), semidynamical renormalised forward scatt. technique for LEED anal. 79—77877
surface (110), steps 80—49846
surface (110), struct., elec. props., effects of illumination, O_2 absorpt., electron bombard. *(French)* 78—34690
surface (110), struct. determ. by LEED, UPS, and EPR 80—49475
surface (110), subsurface atomic displacements, evidence from LEED/CMTA analysis 78—38920
surface (110), surface and interface states, effects of atomic and electronic rearrangements 77—85284

gallium arsenide continued
surface (110), surface and near-surface atomic struct., LEED 78—91515
surface (110), surface electronic struct. calcs. 80—80343
surface (110), surface states, photoemission spectroscopy and tight binding calcs. 77—85888
surface (110), surface states and matrix elements in angle-resolved photoemission 78—91741
surface (110), surface struct., EPR meas. and elastic energy minimisation calcs. 79—51405
surface (110), valence band Auger spectra, from Ga and As CCV transitions 78—92149
surface (110), wave functions and surface struct. 78—91519
surface (110), with Al or Ga overlayers, interfacial electron states, UPS and LEED obs. 80—80377
surface (110), with ultrathin Al and Cs overlayers, O_2 adsorption, comparative studies 80—50740
surface (110) atomic struct. 79—69331
surface (111), $(\bar{1}\bar{1}\bar{1})$, (110), XPS, photo-Auger ionisation cross section, electron mean free paths 78—56558
surface (111), O bonding, thermodesorption and ESCA meas. 77—86206
surface (111) and $(\bar{1}\bar{1}\bar{1})$, XPS study 79—83102
surface $(\bar{1}\bar{1}\bar{1})$, MBE prep., angular resolved UPS of surface states 79—47598
surface barrier diodes for nuclear radiation detection, deep trapping centres 80—92849
surface barrier particle detectors based on epitaxial GaAs 79—72203
surface carrier depletion layers, GaAs in MIS system 77—1469
surface characterisation by high resolution Rutherford backscatt. 80—25511
surface characterisation using SAW 80—11069
surface charge state change during thermodesorpt. 77—80825
surface chemisorption of Li, charge injection into space charge layers 80—100496
surface chemistry and electronic struct., adsorption of O_2, photoemission meas. 77—20985
surface composition vs. temp., low energy ion scatt. *(French)* 77—59663
surface condition, effect on ohmic contact barrier height 77—4435
surface crystal regularity by X-ray photoelectron diffr. 80—89112
surface electrical props. by SAW meas. 77—20387
surface electron states, (110), photoemission 80—25529
surface electron states, appl. of surface photovoltage spectroscopy 77—69391
surface electronic properties, contact potential difference and photoemission expts. 77—47884
surface exciton energy 80—92829
surface final-state effects on core electron transition energies 78—91745
surface grating relief pattern profile altering, oblique shadow deposition technique 79—68451
surface impurities, struct. and comp. of compounds using IR spectroscopy 78—63918
surface morphology during etching with H_2O vapour 80—39094
surface passivation using composite Al_2O_3 and native oxide, MIS characts. 80—93004
surface passivation using GaO_xN_y based multiple insulating layers 80—93006
surface passivation using Si_3N_4, interface characts. 80—93005
surface phonons, scatt. expts. 80—10772
surface photogalvanic effect, polarisation depend. photocurrents *(Russian)* 80—80322
surface photovoltage due to photo-thermo-ionization of surface states 78—14787
surface polaritons, of GaAs on degenerate n-Ge 80—6752
surface polaron in mag. field 79—23912
surface processing, residual film monitoring by ellipsometry 80—13124
surface protection, by KCl layer, LEED and Auger spectroscopy obs. 77—89628
surface recomb. vel., psec. optical techniques 80—70784
surface recombination rate reduction by Ru chemisorption 80—49866
surface recombination velocity, determ. from SEM expts. on p-n junctions 77—55601
surface recombination velocity, diffr. from picosecond transient free carrier gratings 79—47109
surface reconstruction, cryst. growth for screw dislocation free semiconductors 77—55251
surface relax. models, tight-binding calcs. 79—4594
surface segregation of implanted alkali metals, photoemitter prep. and props. *(French)* 78—60544
surface states, band struct. by discontinuous potential method 80—20276
surface states, contact pot. difference, photoemission, and low energy loss spectra expts. 77—85285
surface states, optical techniques 80—6939
surface states in bond orbital model 78—91749
surface states obs. by XPS 80—50515
surface states symmetry determ. using polarisation-depend. ang. resolved photoemission, for GaAs (110) 78—91742
surface states XPS 80—25528
surface structure and orbital symmetries of (110) surface state 78—72229
surface studies during MBE growth 79—90899
surface wetting with Hg, doping degree influence 80—92762
surface-barrier photodetectors, GaP and GaAs with Au film deposition 77—77423
surfaces, (100), reconstructed, ang. resolved photoemission from surface states, adsorption and annealing effects 80—16143
surfaces, electronic struct., tight-binding calc. 80—54755
surfaces (110) and (111)As, UPS and LEED 78—91514
switch, control of fast Pockel cell for active pulse shaping in ps domain 80—28257
switch, laser-activated, high-power switching with ps. precision 80—2416
switching conduction in ion-irradiated layers 78—34868
synthesis, Ga+As reaction temp. determ. 77—24978
synthesis in pyrolytic BN boat 78—6840
temperature rise induced by laser beam 78—11025
thermal conductivity, calc. using numerical soln. of Boltzmann eqn. 80—44373
thermal conductivity, design and fabrication of cryostatic system 80—52243
thermal equilibrium phonon populations, acoustic intensity meas. by Brillouin scatt. intensity obs. 80—45098
thermal oxidation, 450 to 760°C, Rutherford back scattering obs. 78—76780

gallium arsenide continued
thermal oxidation, film growth and characterisation 80—11808
thermal oxidation, vapour phase equilibria of As_2O_3 79—66181
thermal oxidation in As_2O_3 vapour 78—56792
thermal oxidation in wet and dry atm., 470-830°C 77—86204
thermal oxidation rate and activation energy obs., 470° to 830°C *(Japanese)* 77—52517
thermal oxides, electrical properties 78—2601
thermally stimulated relax. under internal field conditions 80—7279
thermodiodes and resistance thermometers thermometric characts. approx. 80—31746
thermometer, semiconducting resistance, for low-temp. measurement, 0.3 to 350K range 79—58687
thermomigration of molten Ga 77—69118
thick sample, atomic comp. determ., H^+ and He^+ induced X-ray anal. 79—5223
thin film, effect of O on thin film compositions obtained by secondary ion emission 80—26079
thin film external resonator for optimum SHG 79—18485
thin film polycrystalline Schottky barrier solar cells, grain boundary chemistry 80—94067
thin film polycrystalline solar cells, grain boundary edge passivated 80—94069
thin films, reactively sputtered, ESCA/XPS study 80—97430
thin Schottky barrier metallisations, thermal reactions 79—78176
three level cond. band struct., uniaxial stress effects, resist. and Gunn effect threshold meas. 77—85137
time of flight atom-probe mass spectra 78—92584
time resolved reflectivity of ps pulses 78—31217
time-resolved spectra, carrier relax. time, phonon lifetime 80—11433
trace element conc. meas. by Zeeman atomic absorpt. spectroscopy 80—29046
transferred electron devices, ohmic contacts 78—52082
transient dynamic response calculation by Monte Carlo techniques 80—107796
transmission spectrum under uniaxial compression 80—29714
transmutation doped, shallow donors, magneto-optical study, photocond. meas. 78—87996
transmutation doping by thermal neutrons 80—10581
transport phenomena, review 79—19587
travelling heater method growth, dislocation elimination 77—7684
tunable stimulated Raman scatt. in far IR, laser feasibility 79—50344
tunnel diode, electron beam bombard. induced defects, influence on excess current *(Russian)* 77—4424
tunnel diode, peak current press. sensitivity *(Russian)* 77—4423
tunnel MIS structures, surface states 77—85336
two dimensional impurity bands, Hall mobility 79—95509
two photon absorpt., hot electron-hole plasma, relax. time depend., picosecond spectra 79—51979
two photon absorption spectrum, band gap luminesc. 78—10888
two-hole species plasma, parametric instability 80—2410
two-phonon diffuse scatt. of X-rays 78—26374
two-photon 1.06 μm absorption coeff., absolute meas. 78—19527
two-photon absorption coefficient, 3-band model 79—78679
two-photon absorption of Nd:glass laser radiation 78—87107
two-photon electroabsorption by excitons 79—42944
two-photon interband transitions, carrier drag 79—7858
n-type, metal filmed photoelectrochemical cell, energy conversion characts. 80—101118
UPS, 5-450 eV, surface states, oxidation behaviour 77—66579
UV photoemission, polarisation-depend., angle-resolved spectroscopy 77—66573
vacancy, ideal, electronic struct., tight-binding calc. 79—4529
vacuum deposited Shottky barrier metallisation 79—78153
valence band fine struct. from light mod. with nonequilib. opt. phonons 78—39568
valence band struct. obtained by magnetophonon effect 77—76748
valence band structure, CPA, bond orbital calcs. 78—87909
valence band studies of clean and O_2 exposed surfaces 78—43298
valence-band dispersions, electron and hole lifetimes, angle-resolved photoemission 80—80947
vapor-phase etching, mechanisms and kinetics 80—100934
vaporisation during laser annealing 80—25495
vapour growth, element incorporation 78—30556
vapour phase CVD, surface anal. during growth using RHEED and Auger spectroscopy 80—66433
vapour phase epitaxial, appl. to hyperabrupt varactor fabrication 80—29288
vapour phase epitaxial growth, techniques and meas. of surface characterisation during growth *(French)* 77—1817
vapour phase epitaxy using computer control 79—38744
VPE, effects of growth conditions on incorporation of deep levels 80—20111
VPE, electron Hall mobility meas., attempted correlation with growth parameters 78—43417
VPE, growth method at low H_2 press. 79—28936
VPE, growth parameters effect 77—28726
VPE, hole diffusion lengths, effect of transition metal diffusional doping 80—15628
VPE, hole diffusion lengths, surface prep. and heat treatment effects, etchant evaluation 80—15627
VPE, influence of growth parameters, $AsCl_3$ transport method 80—29881
VPE, mass exchange during 79—78901
VPE, multi-wafer growth technique using $AsCl_3$-Ga-N_2 system with horizontal reactor 79—28934
VPE, partial press. diagrams use for thermodynamic represent. 79—33201
VPE, residual donor impurities 77—76679
VPE, review of growth techniques *(French)* 79—33935
VPE, selective in situ vapour etch of substrate and growth 80—2958
VPE, surface defects rel. to technological parameters 78—44015
VPE, thermodynamic analysis of Si contamination 79—28932
VPE, thermodynamic factor influencing growth rate and layer purity in Ga-$AsCl_3$-H_2 system 79—28933
VPE by CVD, vapour-solid interface, expt. anal. *(French)* 79—33940
VPE by Ga-$AsCl_3$-H_2 process, role of Si 77—40380
VPE by single temperature zone method, elec. props. 79—95526
VPE fast growth, at low temp. and high partial pressure 79—51446
VPE film growth in Ga-$AlCl_3$-H_2 system, O_2 injection effect 79—100057
VPE growth, by hydride technique, for FETs, and characterisation 78—27407

gallium arsenide continued
VPE growth, growth rate anal. 78—52680
VPE growth, in situ surface anal. 79—95937
VPE growth and characterisation, doping levels 80—10841
VPE growth of MESFET layers 77—90279
VPE growth of single flat temp. zone method, residual doping level 77—48352
VPE growth on {110} cryst. plane 80—10840
VPE in CVD systems, anisotropic phenomena 80—54563
VPE in Ga-$AsCl_3$-H_2 system at reduced temp. 79—11519
VPE in inert gas-H_2 mixed carrier system, thermodynamic analysis 78—11120
VPE layer growth with abrupt doping profile 80—24746
VPE layer on Ge, antiphase domain structures 77—69193
VPE layer props. control using boundary layer characts. 80—50561
VPE layers, back surface gettering, Cr out diffusion 80—10802
VPE layers, elec. props., semi-insulating substrates effect 80—11123
VPE layers, electron irrad., electron traps 80—25026
VPE layers, growth conditions effect on deep levels 79—95360
VPE layers, high resistivity, growth for microwave device appl. 79—100056
VPE layers, role of diffused Ga vacancy in degradation 78—95050
VPE layers for FET devices, impurity characterisation 80—29491
VPE on Ge substrate, and characterisation 78—72736
VPE thin layers, thickness uniformity, main factor anal. 80—76197
VPE using low press. organometallics 79—100054
VPE using organometallic method, deep trap levels 80—10923
VPE using organometallics and hydrides *(French)* 79—33936
VPE UV stimulated 78—35313
wafer, dissolution kinetics in undersaturated isothermal solns. in Ga-Al-As system 80—80106
wafer, double-etching technique for submicron channel fabrication, laser fabrication appl. 80—74387
wafer, H_3PO_4-H_2O_2-H_2O etching solution system and its kinetics 79—20229
wafer diagnostics, using computer automated scanning low-energy electron probe 79—4214
wafers, for semicond. lasers, cleaving process 78—37915
weakly excited, luminesc. from exciton polaritons, based on exciton-electron collisions 79—83020
whiskers grown on GaAs substrate by thermal decomp. method 77—55875
X-ray and Rutherford backscatt. yields from channelled $^4He^+$ ions 79—46730
X-ray anomalous scatt. factors and integrated intensities near K-absorpt. edges 77—19834
X-ray diffraction, integrated intensity meas. near absorption edge with synchrotron radiation 77—76253
X-ray K absorpt. edge, effective ionic charge and bonding schemes 80—29827
X-ray reflection intensity, near absorption edge, temp. depend 80—1889
X-ray structure factors and Debye-Waller factor, from Bragg case diffr. curves 77—62509
XPS, secondary illumination effects, band bending, level shifts 80—108324
zinc blende structure semiconductors, cyclotron reson. *(German)* 78—10337
(Al,Ga)As, CW long-life laser, use of half-wave Al_2O_3 facet coatings 77—23688
(Al,Ga)As, channelled substrate planar struct. injection lasers 77—71996
(Al,Ga)As DH diode laser, double-dovetail constricted, single mode CW operation 79—22949
(Al,Ga)As DH injection lasers, internal quantum efficiency, algorithm for meas. 78—66822
(Al,Ga)As DH injection lasers, sustained oscills. depend. on DC current bias 79—68392
(Al,Ga)As DH laser, effect of mounting on pulsed threshold 78—13711
(Al,Ga)As DH laser, pulsations produced by saturable absorber Q-switching, possible model 79—81426
(Al,Ga)As, DH laser, stripe geometry, threshold for amplitude-stabilised oscill. 77—7084
(Al,Ga)As DH laser degradation, facet oxide formation 79—86185
(Al,Ga)As DH lasers, temp. accelerated ageing and degradation characts. 78—22130
(Al, Ga)As DH lasers, water role in gradual degradation 80—74379
(Al,Ga)As DH lasers, superlinear emission characts., negative resist. obs. 80—95895
(Al,Ga)As, DH stripe-geometry CW laser, junction voltage saturation 77—23675
(Al,Ga)As DH wafer, Al distrib. meas. 77—7994
(Al,Ga)As double heterostructure laser, comparison of deep and shallow proton bombardment fabricated devices 80—99724
(Al,Ga)As double-heterostructure lasers degraded, deep-level changes during accelerated ageing at high temps. 80—74356
(Al,Ga)As injection lasers, pulsations and adsorbing defects 79—94234
(Al,Ga)As laser, ageing-induced self-pulsation stabilisation and initial degradation elimination by facet coatings 80—43347
(Al,Ga)As, laser, DH, light-current voltage characts. 77—3584
(Al,Ga)As, laser, DH, threshold current var., optical scatt. losses 77—3588
(Al,Ga)As long-lived DH injection lasers for fibre optic communication, degradation exam. 78—50778
(Al,Ga)As proton-bomard. stripe-geometry DH lasers, optical nonliniarities and optical spikes 79—55138
(Al,Ga)As:Zn planar stripe lasers with deep Zn diffusion, guiding mechanisms controlled by impurity concs. 80—78853
(Al,Ga)As/GaAs, LPE grown heterostructures, X-ray diffr. exam. of interfacial elastic strains 78—72019
(Al,Ga)As-GaAs laser, transverse junction stripe, high temp. single mode CW operation 78—74918
Al/GaAlAs, film, epitaxial growth on (100) GaAs by hot vac. deposition and characterisation 79—56085
Al-Al_2O_3-GaAs MOS struct., mol. beam reaction growth of Al_2O_3 film, C-V characts. 80—11095
Al-Al_2O_3-p-GaAs MOS diode, capacitance-voltage characts. 80—107914
Al-anodised Ta_2O_3/native oxide-n-GaAs MOS structure evaluation 80—84514
Al-Ga-As, light emitting heterojunction diode, $\eta_e \approx 40\%$ *(Russian)* 77—81157
Al-Ga-As heterostruct. with confined current flow, fabrication 78—68081
Al-Ga-As heterostructure formation by LPE 77—32517

gallium arsenide continued
- Al-Ga-As heterostructure photocell with a transition layer 79—19655
- Al-Ga-In-P(As)(Sb), III-V quaternary alloy, $A_xB_yC_zD$ or $AB_xC_yD_z$, energy band gap and lattice constant 79—4296
- Al-GaAs-Al sandwich-type sputtered film, elec. props. 78—91780
- Al-GaAs-$Al_xGa_{1-x}As$ Schottky barrier diodes, prep., characts. 80—6948
- Al-gelatin-GaAs, capacitance-voltage characts. after and before incorporation of $AgNO_3$ 79—51684
- Al-SiO_2-GaAs, oxide film sputter deposition and MIS struct. characts. 77—89864
- Al-Ta_2O_5-GaAs, oxide film sputter deposition and MIS struct. characts. 77—89864
- n-AlAs/p-GaAs, VPE growth for solar cells 77—77391
- AlAs-GaAs, binary heterostruct. LED, external quantum yield *(Russian)* 77—8661
- AlAs-GaAs, heterostructure electroluminesc. characts., active region electron density depend. 77—12446
- AlAs-GaAs, strip heterolaser, O^+ implantation optimisation, relative threshold current density *(Russian)* 78—1230
- AlAs-GaAs (001) interface and superlattice, electronic props., band struct. 79—95485
- AlAs-GaAs (100) superlattices, band struct. 78—30868
- AlAs-GaAs (110) interface, self-consistent calc. of interface states and electronic struct. 78—52066
- AlAs-GaAs double heterostructure, effective lifetime of nonequilibrium carriers 78—6435
- AlAs-GaAs film heterojunction, VPE growth and characts. 78—6439
- AlAs-GaAs heterojunctions, on graphite substrate, props., solar cell appls. 78—91760
- AlAs-GaAs heterostructure, fabrication by selective liq.-phase epitaxy 79—15618
- AlAs-GaAs LEDs, Ge or Zn-doped, mechanism of degradation 77—76911
- AlAs-GaAs monolayer crystal, two-photon absorpt. spectrum 78—52589
- AlAs-GaAs monolayered periodic cryst., optical props. 77—81079
- AlAs-GaAs multipass heterostructure, spectral and ang. charact. of luminesc. 77—20418
- AlAs-GaAs multipass heterostructures, external quantum efficiency of luminesc. 77—20419
- AlAs-GaAs solid solution, quantitative analysis, use of internal calibration technique developed by AES 77—36834
- AlAs-GaAs stripe heterojunction laser, O^+ implantation effect on threshold characts. 79—41383
- AlAs-GaAs:Ge double heterojunctions, efficiency of radiative recombination 77—77286
- AlGaAs buried heterostructure lasers, gain and absorpt. spectra meas. 80—91792
- AlGaAs CW heterolaser, hysteresis of output radiation power 79—64230
- AlGaAs CW injection heterostructure laser, with second order distributed Bragg reflectors, exam. 78—37907
- (AlGa)As, CW laser diodes, long-term lifetests at room temp. 79—22963
- (AlGa)As CW narrow stripe injection laser with induced waveguide, expt. props. 80—32988
- AlGaAs CW oxide defined stripe laser, optical feedback effects 78—79045
- (AlGa)As CW oxide-defined stripe laser, reliability statistical study 79—76687
- AlGaAs constricted DH diodes, stable single filament laser action obs. 78—55358
- AlGaAs constricted DH laser with large optical cavity, CW high-power single-mode operation 80—48276
- (AlGa)As DH, proton-striped, proton-induced defects, photoluminesc. study 80—48251
- AlGaAs DH, temp. depend. of intensities and times of radiative transitions 79—38660
- (AlGa)As DH CW laser diodes modulation characts. 77—38965
- AlGaAs DH diode laser, ps optical pulse generation with RF modulated 80—9882
- AlGaAs DH injection phase-locked laser, coherence 80—102726
- (AlGa)As, DH junction laser, stripe geometry second derivatives of elec. characts. obs. 77—10923
- (AlGa)As DH laser, insulating C film deposition to prevent facet deterioration 78—87049
- AlGaAs DH laser, self-pulsations due to proton bombarded region self-annealing during ageing 80—99728
- (AlGa)As, DH laser, threshold current temp. depend. 79—81431
- (AlGa)As DH laser degradation due to facet oxidation 78—42336
- AlGaAs DH laser epilayer struct. optimization for integrated optical circuits 80—99879
- AlGaAs DH laser mirror degradation mechanism and lasing characts. changes 80—9919
- AlGaAs DH laser with external grating oscillation properties 80—48247
- (AlGa)As DH lasers, catastrophic optical damage generation mechanism, TEM obs. of dark line defects 80—100239
- (AlGa)As DH lasers, comparison of 'normal' lasers and lasers exhibiting light jumps 80—106519
- (AlGa)As DH narrow stripe injection laser with rigid waveguide, expt. props. 80—32987
- AlGaAs DH short wavelength lasers, internal stress and degradation 79—68393
- AlGaAs DH stripe geometry lasers, spontaneous radiation, carrier conc., and threshold current, luminesc. meas. 79—36898
- AlGaAs DH stripe laser, spontaneous emission factor 77—75514
- AlGaAs DH stripe laser, side lobe suppression by Te facet coating 80—5744
- AlGaAs double heterostruct. laser, 'window-stripe', high power emission 79—72566
- AlGaAs electroluminescent heterostructures, LPE, appl. to LED fabrication 80—55308
- AlGaAs, heteroepitaxial waveguides for image transmission *(Russian)* 77—11037
- AlGaAs, heteroepitaxial waveguides, far radiation field characts. *(Russian)* 77—11038
- AlGaAs heterojunction laser, single transverse and longit. mode operation 78—37887
- AlGaAs heterojunction laser diodes for optical analogue link, evaluation 79—68395
- AlGaAs heterojunction diode as light source for fibre optical communication 80—58653
- AlGaAs heterojunction laser, lightwave sources and detectors 80—64068

gallium arsenide continued
- AlGaAs heterojunctions, nonradiative recomb. vel. estimate from edge luminesc. props. 80—65668
- AlGaAs heterojunction photocell with luminesc. wavelength converter 80—108800
- (AlGa)As heterostruct., proton irrad., photoluminesc. 80—29808
- AlGaAs heterostructures in integrated optics 77—75713
- AlGaAs high-power constricted DH diode laser, for optical recording 80—43351
- AlGaAs injection lasers, undoped, estimation of intra-band relax. time 80—43335
- AlGaAs injection laser, large optical cavity, with multiple active regions 80—106538
- AlGaAs integrated twin guide laser with distributed Bragg reflectors 77—88744
- AlGaAs junction laser, with optical waveguiding 77—42540
- AlGaAs, LPE layers, growth initiation and cathodoluminesc. irregularities 79—87010
- (AlGa)As laser, CW, accelerated ageing effect on optical props. 77—38898
- AlGaAs laser, monolithic integration with amplifier/detector by twin-guide struct. 78—42466
- AlGaAs laser array on Si heat sink, optical power detection 80—74383
- AlGaAs laser mode, fractional spontaneous emission coupling, power fraction, expt. evaluation 79—959
- (AlGa)As laser system, VPE growth and degradation mechanisms 80—99748
- AlGaAs lasers, CW high-power single-mode constricted DH lasers with large optical cavity 80—64076
- (AlGa)As lasers, facet protection using SiO_2 sputter deposition 79—81444
- AlGaAs lasers, relaxation oscillation rel. to carrier diffusion length, spontaneous emission 80—32986
- AlGaAs layer, epitaxial, grown from pre-heated Ga soln., photolum. study 78—39591
- AlGaAs leaky-mode buried heterostruct. injection lasers 77—68209
- AlGaAs mode-locked diode laser, optical pulse generation 80—95907
- AlGaAs multimode laser, longitudinal modes intensity fluctuations effect on high bit-rate optical transmission 79—68415
- (AlGa)As oxide-defined strip lasers, self-sustained oscillations, ageing effects 80—32991
- AlGaAs p-n diodes, I-V characts., tunnelling 80—100510
- AlGaAs pulse modulate DH laser, oscillatory longitudinal mode competition 79—81427
- AlGaAs resonant laser amplifier, gain and saturation power 80—53315
- AlGaAs rib waveguides, characts. 80—33177
- (AlGa)As self-pulsing junction laser, saturable absorpt. effects 79—72568
- AlGaAs semiconductor lasers, single-mode stabilisation by traps 80—95893
- AlGaAs, strip buried heterostruct. laser, linear light-current characts. 78—37908
- (AlGa)As strip buried heterostructure lasers, mode locking using external cavity 80—91791
- (AlGa)As, stripe geometry DH laser, emission nonlinearities 77—685
- (AlGa)As stripe geometry, proton-bombardment delineated DH laser, lifetime 80—106520
- AlGaAs stripe-geometry DH laser, filament displacement and refr. losses 80—58536
- AlGaAs transverse junction stripe lasers, single longit. and fund. transverse mode oscill. 78—22124
- (AlGa)As, transverse junction stripe single mode oscillating laser, gain spectra 78—55356
- AlGaAs transverse junction stripe laser with distributed Bragg reflector 80—106535
- AlGaAs tunnel diode, fabrication and appl. in cascade solar cell struct. 80—35682
- AlGaAs twin guide struct., monolithic integration of laser and laser amplifier or detector 78—38082
- (AlGa)As, visible CW heterojunction laser diodes, room temp. operation 77—38895
- AlGaAs, Zn diffused window structure laser, high optical power density emission 79—98394
- p- (AlGa)As:Zn, MBE grown, elec. props., shallow junction solar cell use 79—91175
- AlGaAs/GaAs monolithic series-connected solar cell arrays 80—97794
- (AlGa)As-GaAS DH lasers prep. by new LPE technique 77—40358
- AlGaAs-GaAs, DH laser material, singular instabilities of LPE growth surface 77—24969
- AlGaAs-GaAs, DH laser, with bent guide of planar struct. 78—1256
- AlGaAs-GaAs, DH semiconductor laser, influence of struct. parameters on lasing characteristics 79—45942
- (AlGa)As-GaAs, large area high efficiency solar cell fabrication, LPE process 77—36410
- AlGaAs-GaAs, TJS laser, single-mode oscill. with low threshold currents, optical communication appl. 80—14355
- AlGaAs-GaAs CW injection heterolaser, single freq., tunable by external dispersive resonator 80—28236
- AlGaAs-GaAs cascade solar-cell structure, fabrication and characteristics 79—43758
- AlGaAs-GaAs concentrator solar cells of high-efficiency characts. 79—48125
- AlGaAs-GaAs DH laser, bent-guide struct. 77—75544
- AlGaAs-GaAs DH lasers, accel. life test 77—79828
- AlGaAs-GaAs DH laser, impurity effects on relaxation oscillations 78—13710
- AlGaAs-GaAs DH laser, carrier leakage, physical mechanisms 78—66824
- AlGaAs-GaAs DH lasers, accelerated life test 78—66830
- AlGaAs-GaAs DH lasers, coupling efficiency between gain-induced guides 79—23094
- AlGaAs-GaAs double heterostructure laser lifetime, point defect generation model calcs. 80—32992
- AlGaAs-GaAs heteroepitaxial wafers, Mg doping, surface morphology and photoluminesc. props. laser applics. 77—3591
- AlGaAs-GaAs heterostructure, minority carrier lifetime, photon recycling effect *(Japanese)* 79—42556
- AlGaAs-GaAs heterostructures, luminescent characts., efficiency and radiative lifetime conc. depend. 80—55151
- AlGaAs-GaAs injection laser, spectral band homogeneous broadening and narrow band emission 79—98364

gallium arsenide continued
AlGaAs-GaAs lasers, defects and degradation *(Japanese)* 79—31899
AlGaAs-GaAs lasers for optical fibre transmission, defects and degradation 79—41382
AlGaAs-GaAs multimode laser, intensity fluctuations in each longit. mode 77—75512
AlGaAs-GaAs proton irradiated solar cells, deep-level defects, recombination mechanisms, performance characts. 80—81459
AlGaAs-GaAs proton irradiated solar cells, deep level defects and recombination parameters 80—94032
AlGaAs-GaAs remote junction heterostructure laser, recomb. enhanced annealing effect 79—98355
AlGaAs-GaAs ring laser, injection type, laser oscill. 77—75570
(AlGa)As-GaAs solar cells, theoretical perform. of multi-layer grid patterns 80—55846
AlGaAs-GaAs transverse mode stabilised plano-convex waveguide laser made by single step LPE 80—48274
AlGaAs-GaInAs cascade solar cells, AM 0-AM 5 spectra, anal. 79—79396
$Al_{0.25}Ga_{0.75}As$, optically oriented electron, nuclear spin systems, local anisotropy effects on states, resonances *(Russian)* 78—43679
n-$Al_{0.3}Ga_{0.7}As$, layer of (AlGa)As DH laser, deep levels 78—46605
$Al_{0.3}Ga_{0.7}As$:Te(SN), impurity effects on interface morphology of LPE films on corrugated GaAs substrates 78—88435
$Al_{0.3}Ga_{0.7}As$-GaAs DH mesa stripe laser, metalorganic VPE growth and characterisation 79—98391
$Al_{0.35}Ga_{0.65}As$-GaAs cascade solar cell structs., spectral response and junction characts. 80—93926
$Al_{0.35}Ga_{0.65}As$-GaAs N-p heterojunction diodes, current suppression by cond. band discontinuity 80—80362
$Al_{0.36}Ga_{0.64}As$, LPE films, Te-induced defects 78—43037
$Al_{0.4}Ga_{0.6}As$:Te, saturable optical absorpt. of deep Te-complex centre 79—99917
$(Al_{0.42}Ga_{0.58})As$, LPE grown layer, optical absorpt. coeff. meas. 78—6801
$Al_{0.42}Ga_{0.58}As$-GaAs-$Al_{0.42}Ga_{0.58}As$, etalon, optical bistability and modulation 80—58628
$Al_{0.5}Ga_{0.5}As$, first order phonon spectrum replicas 78—60467
$Al_{0.5}Ga_{0.5}As$:O surface layer, on GaAs p-n junction, surface recomb. current reduction 80—49878
$Al_{0.5}Ga_{0.5}As$-GaAs heterojunction phototransistors, growth by metalorganic vapour deposition 79—67380
$Al_{0.5}Ga_{0.5}As$-GaAs minimum heterojunction width determ. by sputter Auger techniques, interface broadening 79—69586
$Al_{0.7}Ga_{0.3}As$ layers, diffusion of Zn, comparison with GaAs 78—26589
$Al_{0.93}Ga_{0.07}As$-GaAs monolithic series-connected solar cell array 80—7939
$Al_{1-x}Ga_xAs$ laser, transverse junction stripe, with low threshold current and high efficiency 78—82985
$Al_{1-x}Ga_xAs$, transient-mode LPE on GaP 78—72746
$Al_xGa_{1-x}As$ CSP laser, analytical waveguide study 79—10302
$Al_xGa_{1-1}As$ heterojunction LED monolithic matrix fabrication 79—56301
$Al_xGa_{1-x}As$, analytic approx. for Fermi energy 78—63973
$Al_xGa_{1-x}As$ and GaAs planar local struct. synthesis by LPE 79—56097
n-$Al_xGa_{1-x}As$, Au-based ohmic contacts TEM obs. 80—34509
$Al_xGa_{1-x}As$ buried heterostruct. laser, fabrication, optical props. and reliability 80—53322
$Al_xGa_{1-x}As$ CW heterolaser, 10000 hr. lifetime tests, degradation of mirror surfaces 80—106542
$Al_xGa_{1-x}As$, CW low threshold, high efficiency injection laser props. 78—22126
$Al_xGa_{1-x}As$ CW multiwavelength TJS laser, MBE, single-longitudinal modes 80—64049
$Al_xGa_{1-x}As$, compensated, electron mobility temp. depend. 80—96868
$Al_xGa_{1-x}As$, cryst. growth by MBE 78—39707
$Al_xGa_{1-x}As$, DH, defect generation in active regions at high optical excitation rates 79—23845
$Al_xGa_{1-x}As$ DH, origin of $n\simeq2$ injection current, photolum. expts. 78—14799
$Al_xGa_{1-x}As$ DH laser, threshold current, stripe width influence 77—61952
$Al_xGa_{1-x}As$ DH laser, linear light output power depend. on effective gain width 77—75553
$Al_xGa_{1-x}As$ DH laser, accelerated ageing and uniform mode of degradation 77—83874
$Al_xGa_{1-x}As$ DH laser, with constricted active region, fabrication and characts. 78—37895
$Al_xGa_{1-x}As$ DH laser, rake-line form. in LPE growth, doping effects 80—2287
$Al_xGa_{1-x}As$ DH laser diodes, temp. rise under transient state conditions 77—68211
$Al_xGa_{1-x}As$ DH laser material, Ar laser induced catastrophic damage 79—86178
$Al_xGa_{1-x}As$ DH lasers, deep-level luminesc. 79—65913
$Al_xGa_{1-x}As$ DH lasers continuously operated, with 70°C lifetimes as long as two years 78—17952
$Al_xGa_{1-x}As$ DH p-n junction, surface recomb. effects on current, luminesc. expts. 78—72246
$Al_xGa_{1-x}As$ DH stripe-geometry lasers, degraded, capacitance spectroscopy 77—14715
$Al_xGa_{1-x}As$ DH superluminesc. diode, with unpumped region, time-delayed laser oscill. 77—54711
p-$Al_xGa_{1-x}As$, DH under optical orientation conditions, diffusion of spin labelled electrons 77—8189
$Al_xGa_{1-x}As$, DX photocond. centres, photocapacitance and DLTS meas. 80—11044
$Al_xGa_{1-x}As$, defect state identification associated with Ga vacancy 77—69269
$Al_xGa_{1-x}As$, dependence of energy spectrum of levels introduced by electron irrad. on composition 79—60766
$Al_xGa_{1-x}As$ double heterostructure laser, CW optical power 77—14716
$Al_xGa_{1-x}As$ double heterostruct. lasers, optical pulsations 79—98354
n-$Al_xGa_{1-x}As$, electrical props. 78—6381
$Al_xGa_{1-x}As$, electron mobility illumination, compensation, space charge regions, carrier scatt. 80—70691
$Al_xGa_{1-x}As$, energy band struct. calc. 78—23019
n-$Al_xGa_{1-x}As$, epitaxial, photolum. emission and excitation spectra 78—76526
$Al_xGa_{1-x}As$ epitaxial diode, neutron and γ-irrad. effects on cathodolum. in SEM 79—11473

gallium arsenide continued
$Al_xGa_{1-x}As$ epitaxial film, LPE growth and semi-insulating props. 77—44179
$Al_xGa_{1-x}As$ epitaxial films, microanal. in photoemissive electron microscope 79—16068
n-$Al_xGa_{1-x}As$ epitaxial films, elec. cond. press. depend. 79—56337
$Al_xGa_{1-x}As$ epitaxial film, microstruct., effect on elect. characts. of Schottky diode *(Russian)* 80—107671
$Al_xGa_{1-x}As$, epitaxial growth from limited vol. melt 79—70005
$Al_xGa_{1-x}As$, epitaxial layer struct., dislocation etching obs. 77—85095
$Al_xGa_{1-x}As$, epitaxial layer crystn. from soln. in melt, diffusion limited 78—35321
$Al_xGa_{1-x}As$, epitaxial layer, distribution of Te and Ge impurities 78—43046
$Al_xGa_{1-x}As$ epitaxial layers on GaAs, struct. study by scanning Auger electron microscopy 80—80110
$Al_xGa_{1-x}As$, fabrication of mesa-type waveguides by laser irrad. 80—5849
$Al_xGa_{1-x}As$ film, hot photoluminescence spectrum, polarisation depend. 78—31254
p-$Al_xGa_{1-x}As$ film, variable-gap photo-EMF 80—65626
$Al_xGa_{1-x}As$, graded band-gap heterostruct., photo-EMF 79—24072
$Al_xGa_{1-x}As$, graded-gap crystal, voltage-current characteristics 79—69613
$Al_xGa_{1-x}As$ grown by organometallic VPE, luminesc. efficiency 79—78892
$Al_xGa_{1-x}As$, growth of high-resistivity layers by liquid-phase epitaxy 79—70008
$Al_xGa_{1-x}As$, growth of uniform epitaxial layers 77—40393
$Al_xGa_{1-x}As$, Γ-X intervalley junctions 77—4433
$Al_xGa_{1-x}As$, Hall effect measurements to 40 kbar under hydrostatic pressure in piston-cylinder device, 150 to 300K 79—67337
$Al_xGa_{1-x}As$, Hall effect, press. temp. and composition depend. 80—49775
$Al_xGa_{1-x}As$, hetero junction light-emitting diode, construction and performance characts. *(Russian)* 77—85808
$Al_xGa_{1-x}As$ heterojunction laser diode, technology and spectral characts. 77—38885
$Al_xGa_{1-x}As$ heterojunction laser diode, accelerated step-temperature ageing 78—46599
$Al_xGa_{1-x}As$ heterojunction LED, fabrication by negative profiling of substrate and characts. 78—56523
$Al_xGa_{1-x}As$ heterojunction LED 79—28403
$Al_xGa_{1-x}As$ heterostructure laser, improved light-output linearity by antireflective coating 78—17953
$Al_xGa_{1-x}As$ heterostructures, photoelectric convertors of conc. solar radiation 80—12015
$Al_xGa_{1-x}As$, indirect, exciton-phonon coupling, photolum. meas. 79—47511
$Al_xGa_{1-x}As$, indirect-gap, laser oscill. involving N isoelectronic impurities 77—10919
$Al_xGa_{1-x}As$, injection laser, transmitter for fibre optical transmission lines 77—7134
n-$Al_xGa_{1-x}As$, ion implanted films, optical and luminesc. props. 80—60699
p-$Al_xGa_{1-x}As$, LED in red and IR region, multiple-pass heterostruct. 79—19653
$Al_xGa_{1-x}As$, LPE, cathodoluminesc. obs. 78—68565
$Al_xGa_{1-x}As$, LPE, effect of doping on interface morphology 77—81231
$Al_xGa_{1-x}As$, LPE, quantitative analysis by AES 77—89667
$Al_xGa_{1-x}As$, LPE layer, deep levels, photocapacitance obs. 77—15790
$Al_xGa_{1-x}As$, laser, spectral, threshold, power and time characts. 77—715
$Al_xGa_{1-x}As$ laser diode, reliability 80—53320
$Al_xGa_{1-x}As$ laser-alloyed stripe-geometry lasers 80—5745
$Al_xGa_{1-x}As$ layer, LPE, graded bond gap solar cell, composition profile, Rutherford backscatt. 78—76612
$Al_xGa_{1-x}As$ layers, graded band gap, growth and properties 79—60645
$Al_xGa_{1-x}As$, lower conduction band struct. 78—6270
$Al_xGa_{1-x}As$, MBE grown film, in situ surface characterisation by RHEED, SIMS and AES 77—43410
$Al_xGa_{1-x}As$ MBE layers, ionized beam doping, elec. and optical characts. 79—37721
$Al_xGa_{1-x}As$, metalorganic-CVD, photopumped laser operation meas. GaAs quantum well 79—10303
$Al_xGa_{1-x}As$, method for determ. of liquidus surfaces in Ga-Al-As phase diagram 77—28787
$Al_xGa_{1-x}As$, mode-stabilised injection laser, longitudinal-mode behaviour 79—962
$Al_xGa_{1-x}As$, modified-strip buried-heterostructure lasers, CW electro-optical properties 80—74359
$Al_xGa_{1-x}As$, monolithic optical integration for new devices 77—75714
$Al_xGa_{1-x}As$ native oxide, low leakage, MOS characterisation 78—91795
n-$Al_xGa_{1-x}As$, nonradiative donor related defect centre obs. 78—23497
$Al_xGa_{1-x}As$, optically magnetised, luminescence polarisation anisotropy, hysteresis effect symmetry props. 80—34982
$Al_xGa_{1-x}As$, organometallic VPE growth, and characterisation 79—78899
$Al_xGa_{1-x}As$ oxidised AlAs as multidielectric for GaAs MIS devices 79—65333
$Al_xGa_{1-x}As$, p-n homojunction, hot carrier recomb., overheating luminesc. 78—92122
$Al_xGa_{1-x}As$ p-n junction, photolum. and current, interface recomb. effects 78—95346
$Al_xGa_{1-x}As$, p-n junction solar cells, effect of interface recombination on photoluminescence and current 80—93893
$Al_xGa_{1-x}As$, point defects, recomb. enhanced interactions with dislocation networks 79—60398
$Al_xGa_{1-x}As$, press. coeff. of direct band gap from optical absorpt. meas. 80—11430
$Al_xGa_{1-x}As$ pulsating DH laser, spectral broadening 80—23686
$Al_xGa_{1-x}As$, pure and Ge doped, shallow acceptor photoluminescence 80—76064
$Al_xGa_{1-x}As$, Raman spectroscopy, characterisation of thin films and heterostructures 78—76439
$Al_xGa_{1-x}As$, resistor pressure sensors 79—2756
$Al_xGa_{1-x}As$ semitransparent photocathode, LPE, quantum efficiency spectrum 80—76153
$Al_xGa_{1-x}As$ solar cell, intermediate wavelength conversion for operation with concentrators 79—70451
$Al_xGa_{1-x}As$, solid soln., controlled electrochemical and selective etching, integrated optics appl. 77—14814

gallium arsenide continued
$Al_xGa_{1-x}As$ solid soln., epitaxial layer growth on GaAs by zone recrystallisation with temp. gradient 77—16510
$Al_xGa_{1-x}As$, solid soln., synthesis by ion implantation Al^+ ions 78—38741
$Al_xGa_{1-x}As$ stripe geometry DH lasers, proton bombarded, intensity pulsations 79—94235
$Al_xGa_{1-x}As$, temp. coeff. of resistance of pressure sensors 79—6108
$Al_xGa_{1-x}As$ thick epitaxial layer production, by zone recrystn. in temp. gradient 79—15619
$Al_xGa_{1-x}As$ thin graded band-gap layers, isothermal LPE growth 80—34325
$Al_xGa_{1-x}As$, transverse mode stabilized injection lasers 78—29964
$Al_xGa_{1-x}As$ triggerable semiconductor lasers made by deep proton bombardment 80—69408
$Al_xGa_{1-x}As$, VPE, recent advances, book contrib. 79—66011
$Al_xGa_{1-x}As$, VPE and LPE growth, electron mobility 79—91165
$Al_xGa_{1-x}As$, VPE growth and characterisation 78—35315
$Al_xGa_{1-x}As$, valence and core level photoemission spectra 79—19973
$Al_xGa_{1-x}As$ variable gap junction, photosensitivity 78—39204
$Al_xGa_{1-x}As$ variable gap thin structs., radiative recomb. photoluminesc. spectra 79—43036
n-$Al_xGa_{1-x}As$, variable-gap crystal, magnetoresistance 78—34850
n-$Al_xGa_{1-x}As$, variable-gap solid solns., diffusion length, photolum. meas. 79—38659
$Al_xGa_{1-x}As$, waveguide heterostruct. epitaxial growth with gradual composition change 79—42416
$Al_xGa_{1-x}As$: Sn(Te), persistent photocond., due to donor-related centres, symmetry 80—15558
p-$Al_xGa_{1-x}As$:Be layer, MBE growth, Be doping and diffusion 77—51397
$Al_xGa_{1-x}As$:Cr, deep level props. 79—69465
$Al_xGa_{1-x}As$:Cr, exptl. verification of Cr^{2+} models of photoluminescent transitions 78—27320
$Al_xGa_{1-x}As$:Cr, high resist. film, photolum. and photocond. meas. 78—72596
$Al_xGa_{1-x}As$:Cu, variable-gap semicond., impurity props., carrier recomb. 80—96907
$Al_xGa_{1-x}As$:Cu(Ag)(Au), LPE film, impurity levels, elec. and optical props. meas. 78—26862
p-$Al_xGa_{1-x}As$:Ge layer on GaAs substrate, Hall and elec. cond. meas., Hall mobility 80—2402
$Al_xGa_{1-x}As$:Ge(Te)(Zn), photo- and cathodolum., comp. depend. *(Russian)* 77—48215
$Al_xGa_{1-x}As$:Mg doping characteristics, elec. props., effective hole masses 79—78117
$Al_xGa_{1-x}As$:Mn epitaxial layers, Mn-O association, EPR meas. 77—69677
$Al_xGa_{1-x}As$:N, indirect band-gap, visible laser oscill. at 77K 77—79820
$Al_xGa_{1-x}As$:N, ion implantation, in situ annealing photoluminesc. obs. 80—10567
$Al_xGa_{1-x}As$:N, luminescent material, appl. in optically pumped lasers and electrolum. diodes *(Japanese)* 77—44069
$Al_xGa_{1-x}As$:N, photolum. excitation spectra 77—63451
$Al_xGa_{1-x}As:N^+$, (x=0.58), laser annealing of optically active impurities, photolum. charact. 80—20682
$Al_xGa_{1-x}As$:O, appl. as insulating layer in MIS struct. 78—64115
$Al_xGa_{1-x}As$:O-n-GaAs heterojunction for MIS device, capacitance voltage meas. 79—87157
$Al_xGa_{1-x}As$:Si, charge state of impurity atoms, positron annihilation meas. 78—39062
$Al_xGa_{1-x}As$:Sn(Te)(Ge), anneal-induced defects, photoluminesc. obs. 79—61422
$Al_xGa_{1-x}As$:Te, epitaxial film, elec. cond. and Hall coeff. rel. to donor levels 77—24630
$Al_xGa_{1-x}As$:Te, persistent photocond. trapping centre, donor complex model, photocapacitance meas. 79—65517
$Al_xGa_{1-x}As$:Zn DH laser, stripe geometry, horizontal transverse mode stabilisation, lasing characts. 77—19313
$Al_xGa_{1-x}As$:Zn epitaxial layers, composition and Zn carrier conc. 80—25585
$Al_xGa_{1-x}As/Al_yGa_{1-y}As$ DH lasers grown by metalorganic CVD, CW operation in wavelength range 760-780 nm 80—64053
$Al_xGa_{1-x}As$/GaAs heterojunction laser, appl. of stress distrib. calc. for multilayer heteroepitaxial struct. 77—72798
$Al_xGa_{1-x}As$-$Al_yGa_{1-y}As$ DH superluminesc. diode, for Nd:YAG laser pumping, room temp. CW operation 77—7122
$Al_xGa_{1-x}As$-Al_yGa_{1-y} DH laser, threshold current temp. depend., potential barrier height influence 80—53296
$Al_xGa_{1-x}As$-$Al_yGa_{1-y}As$ DH IR-visible (0.89-0.72 μm) MBE grown lasers 80—64058
$Al_xGa_{1-x}As$-Au interface, Auger depth profiling 77—89657
$Al_xGa_{1-x}As$-GaAs, CW 300k quantum-well heterojunction laser, optical and injection pumping operation 80—5735
$Al_xGa_{1-x}As$-GaAs, DH integrated optics development 80—33240
$Al_xGa_{1-x}As$-GaAs, diode pump system for YAG:Nd^{3+} laser 79—41396
$Al_xGa_{1-x}As$-GaAs, epitaxial heterostructure, influence of defects on diffusive distrib. of group I impurities 78—43045
$Al_xGa_{1-x}As$-GaAs, heterojunction, interface width, AES obs. 80—20290
$Al_xGa_{1-x}As$-GaAs, p-n heterojunction laser, low temp. operation 80—1204
$Al_xGa_{1-x}As$-GaAs, p-n heterostruct. laser, tunnel injection and phonon-assisted recomb. 80—5733
$Al_xGa_{1-x}As$-GaAs, quantum-well MO-CVD heterostructure lasers, band-filling props. 79—22954
$Al_xGa_{1-x}As$-GaAs, quantum-well heterostructure laser diode, temp. depend. of threshold current 80—87395
$Al_xGa_{1-x}As$-GaAs abrupt LPE heterojunction, Auger profiling 77—85101
$Al_xGa_{1-x}As$-GaAs DH injection laser, active region internal parameters determ., composite resonator use 80—106548
$Al_xGa_{1-x}As$-GaAs DH laser, short cavity, performance characts. 77—83889
$Al_xGa_{1-x}As$-GaAs DH lasers, metalorganic CVD growth and performance characts. 80—53312
$Al_xGa_{1-x}As$-GaAs DH laser diode, I-V characts., variation of ideality factor 80—64027
$Al_xGa_{1-x}As$-GaAs DH laser operation, phonon contrib. 80—102724
$Al_xGa_{1-x}As$-GaAs DH photodetector, optical power conversion at 8500 Å and I-V characts. 77—87833

gallium arsenide continued
$Al_xGa_{1-x}As$-GaAs heterostructure, effect of photon recycling on diffusion length and internal quantum efficiency 77—39929
$Al_xGa_{1-x}As$-GaAs heterostructure photoluminesc., origin of large dark spots 77—85763
$Al_xGa_{1-x}As$-GaAs heterostructure, nonradiative large dark spots rel. to minority carrier transport 78—9378
$Al_xGa_{1-x}As$-GaAs heterostructures, nonradiative large dark spots exam. 78—23149
$Al_xGa_{1-x}As$-GaAs heterojunction photodiodes, high-efficiency fast-response 78—52073
$Al_xGa_{1-x}As$-GaAs heterostructures, MO-CVD, phonon assisted recomb. and stimulated emission 80—1205
$Al_xGa_{1-x}As$-GaAs heterostruct. lasers, metallorganic CVD 80—23692
$Al_xGa_{1-x}As$-GaAs heterostructure, quantum-well, hot electrons and phonons 80—84505
$Al_xGa_{1-x}As$-GaAs heterostruct., varizonal, parameter determ. by photoluminescence method *(Russian)* 80—108291
$Al_xGa_{1-x}As$-GaAs interface, Auger depth profiling 77—89657
$Al_xGa_{1-x}As$-GaAs large-quantum-well heterostructures, induced phonon-sideband laser operation 80—95888
$Al_xGa_{1-x}As$-GaAs laser, made by organometallic CVD, continuous room temp. operation 80—1201
$Al_xGa_{1-x}As$-GaAs linear-gradient heterostruct., photoelec. props. 79—11205
$Al_xGa_{1-x}As$-GaAs long life laser, initial degradation, minority carrier lifetime reduction 77—71984
$Al_xGa_{1-x}As$-GaAs multilayer heterostructures, optical birefringence 78—64422
$Al_xGa_{1-x}As$-GaAs multilayers, LPE, using addition of GaCl vapour and new boat struct. 79—33950
$Al_xGa_{1-x}As$-GaAs multiple-quantum-well injection lasers grown by metalorganic CVD, room temp. continuous operation 80—1218
$Al_xGa_{1-x}As$-GaAs n-n heterojunction, LPE, Auger profiling and absence of rectification 78—95349
$Al_xGa_{1-x}As$-GaAs n-n heterojunction, interface width determ. 80—49887
$Al_xGa_{1-x}As$-GaAs phonon-sideband metalorganic-CVD quantum-well heterostructure laser 79—64244
$Al_xGa_{1-x}As$-GaAs photopumped quantum-well heterostructure lasers grown by metalorganic CVD 79—98390
$Al_xGa_{1-x}As$-GaAs quantum-well heterostructure laser, metalorganic CVD growth, CW operation 300 to 337K 79—10304
$Al_xGa_{1-x}As$-GaAs quantum-well heterostructure laser diode, threshold current temp. depend. 80—43331
$Al_xGa_{1-x}As$-GaAs quantum well heterostructure lasers, operation 80—53292
$Al_xGa_{1-x}As$-GaAs quantum-well heterostructures, phonon-assisted recomb. and stimulated emission 80—74358
$Al_xGa_{1-x}As$-GaAs quantum-well heterostruct., exciton in recomb. 80—103990
$Al_xGa_{1-x}As$-GaAs single-quantum-well heterostructure laser diodes grown by metalorganic CVD, continuous 300K operation 79—50309
$Al_xGa_{1-x}As$-$GaAs_{1-y}Sb_y$ solar cells, appl. of recomb. vel. at III-V cpd. heterojunctions *(Korean)* 80—54771
$Al_xGa_{1-x}As$-GaAs-$Al_xGa_{1-x}As$ photopumped quantum-well laser, room temp. CW operation 78—74908
$Al_xGa_{1-x}As$-GaAs-$Al_xGa_{1-x}As$ quantum well, carrier collection 79—15211
p-$Al_xGa_{1-x}As$-n-$Al_yGa_{1-y}As$ junction, electrolum. spectra at high press. 77—48246
p-$Al_xGa_{1-x}As$-p-GaAs-n-GaAs heterophotocells, optimal parameters for high solar-excitation level 80—93872
$Al_xGa_{(1-x)}As$-$Al_yGa_{(1-y)}As$ DH optically pumped laser, room temp. single pass gain 77—75511
$Al_yGa_{1-y}As$-$Al_xGa_{1-x}As$ laser struct., for integrated optics, MBE 78—13817
$Al_yGa_{1-y}As$-$Al_xGa_{1-x}As$, electrooptic rib waveguide modulators and switches 78—38046
AlGaAsP/GaAs heterojunction, X-ray characterisation of defects 78—95239
AlGaAsP(Sb), compositional grading by LPE 80—10844
AlGaAsSb LPE growth, lattice-matched to GaSb, characterisation 80—60794
AlGaAsSb, photodiode, lattice-matched to GaSb 79—71527
AlGaAsSb-GaSb heterojunction injection laser, radiative props. 1.4 to 1.8 μm range 80—91798
n-AlGaAsSb-GaSb-p-AlGaAsSb binary heterostructure injection laser, room temp. operation 78—9381
$Al_yGa_{1-y}As_{1-x}Sb_x$ heterostructure, electroluminesc., appl. to LED's 77—8663
$Al_yGa_{1-y}As_{1-x}Sb_x$ LPE phase diagram 78—11137
$Al_yGa_{1-y}As_{1-x}Sb_x$, LPE, strain effects near miscibility gap, importance 79—7759
$Al_yGa_{1-y}As_{1-x}Sb_x/GaAs_{1-x'}Sb_{x'}$, buried heterojunction electroabsorption modulator, report of operation 78—38044
$Al_yGa_{1-y}As_{1-x}Sb_x$-$Ga_{1-z}Sb_z$ buried heterojunction electroabsorption modulation 78—55439
$Al_xGa_{1-x}As$Zn-GaAs solar cells by LPE, open circuit voltage, fill factor 80—101108
$Al_xGa_{1-x-y}In_yAs$, LPE on InP, solid-liq. equilib. calcs. 78—84083
AlGaSbAs heterostructures and LED's luminesc. props. in 1-2 micron band 78—10988
As_2Te_3-GaAs, amorphous-monocrystalline heterojunctions, space charge limited conduction 78—64099
Au/oxide/n-GaAs struct., photocurrent relax. 80—92978
Au-$Al_{0.5}Ga_{0.5}As$ -GaAs heterojunction Schottky-barrier solar cells, barrier height enhancement 80—85284
Au-AlGaAs-GaAs heterojunction Schottky barrier solar cells, barrier height enhancement 80—94071
Au-Cr-GaAs Schottky-barrier diodes, effect of γ-radiation on current-voltage charact. *(Russian)* 80—2459
Au-GaAs, film-substrate interface alloying behaviour, electron microscopic study 79—60652
Au-GaAs, photosensitivity losses, field and spectral depend. 80—2452
Au-GaAs Schottky barrier, photocurrent, recomb. losses *(Russian)* 80—2470
Au-GaAs Schottky barrier diode, X-band applications 77—8192
Au-GaAs Schottky barrier solar cells, effect of interfacial oxide layer on cell characts. 80—61365
Au-GaAs solar cell, practical antireflection coatings 77—763

gallium arsenide continued

- Au-GaS, Schottky-barrier electroreflectance spectra under uniaxial stress 79—56767
- Au-n-Al_xGa_{1-x}As-n-GaAS Schottky barrier solar cells, prep. and props. 80—26140
- Au-n-AlGaAs-n-GaAs Schottky-barrier solar cells, band readjustment effect 80—81458
- Au-n-$Ga_{1-x}Al_x$As-n-GaP narrow-band variable-gap surface-barrier photoedetector 80—96944
- Au-n-GaAs Schottky diodes, interface state density model 77—39937
- Au-oxide-GaAs struct., steady-state and transient photocurrents 80—6994
- Au-oxide-n-GaAs MIS structures, reverse bias influence on photocurrent 80—107921
- Au-W-GaAs Schottky barrier, elec. and chem. props., AES 80—96973
- AuGe/n-GaAs, SIMS study Au behaviour during annealing 78—75947
- CC $Al_xGa_{1-x}As_ySb_{1-y}$, heterostructure composition profile by photoemission microanalysis 80—44717
- CdS-GaAs heterojunctions, current transmission mechanism *(Russian)* 77—39924
- CdS-GaAs solar cell heterojunctions, CVD fabrication, photovoltaic response 80—93878
- Cr-GaAs, metal-nn$^+$ Schottky diode, I-V characts., inverse branch, effect of dislocation defects *(Russian)* 79—15217
- Cr-GaAs, Schottky-barrier diode, surface electron states 79—73578
- epitaxial layer, C distribution, anal. by quasichem. reactions 77—11803
- etching by water vapour, rate 80—16519
- (Ga, Al, As) heterostructures and compounds, electronic props., empirical pseudopot. calc. 80—80366
- (Ga,Al)As CW diode laser, L(J) charact., external cavity induced nonlinearities 77—79824
- (Ga,Al)As DH lasers used for optical recording, hole machining in Te films 79—89954
- (Ga,Al)As injection laser parameters, homogeneous degradation calc. from initial rates 79—22951
- (Ga,Al)As, LPE growth of multilayered struct., explanation for meniscus lines on surfaces 77—76681
- (Ga,Al)As narrow double-current-confinement channelled-substrate planar laser fabrication, double etching technique 80—74371
- (Ga,Al)As transverse mode stabilised laser, direct obs. of saturation behaviour of spontaneous emission 78—46600
- (Ga,Al)As:Si, Ge, epitaxial layers, radiative recomb., compensation, cathodolum. study 80—66307
- (Ga,In)(As,P) DH lasers, 1.55 μm, low-threshold current densities 80—1221
- (Ga,In)As, growth of epitaxial layers 77—12542
- Ga-Al-As solid soln., liquidus surface in ternary phase diagram, simplex lattice method 77—7847
- Ga-As-O, equilib. phase diagram, GaAs oxidation 80—104130
- Ga-As-P, liquidus surface in ternary phase diagram, simplex lattice method 77—7847
- Ga-As-Sb system, two- and three-phase fields obs. 80—55373
- Ga-GaAs interface immersed in electrolytic solns., elec. props. 78—95368
- Ga-GaAs melt, mutual diffusion from soln. kinetics, self-diffusion coeffs. 77—47608
- Ga-In-As, liquidus surface in ternary phase diagram, simplex lattice mathod 77—7847
- Ga-In-As-Sb quaternary system, phase equilib. and heterojunctions 79—34016
- Ga-In-As-Sb system LPE layers, pseudoquaternary phase diagram 78—10293
- Ga_{1-x} Al_xAs, anodic oxide films, ellipsometric anal. 79—20234
- GaA-$Al_{0.27}Ga_{0.73}$As DH lasers grown by MBE, growth conditions influence on threshold current density 80—32984
- GaAS, semiinsulating, heat treatment effects 78—6382
- GaAS:Cr, mag. field depend. of single carrier parameters, mixed cond. anal. 79—91043
- GaAS-Al_xGa_{1-x}As, DH laser and modulation developments *(German)* 78—37903
- GaAS-AlGaAs LPE layers, defects formed by oxygen in ambient gas *(Japanese)* 77—70009
- GaAS-GaAlAs, DH laser, correlation between optical output characts. and time depend. behaviour 77—68210
- (GaAl) As/GaAs five layer heterostructure narrow beam laser, characts. 77—10920
- $Ga_{1-x}Al_x$ As, metal-gap channel waveguides, intensity modulation 78—66899
- GaAlAs actively mode-locked laser, bandwidth limited picosecond pulses 80—95905
- GaAlAs based heterojunctions, integrated optics appl., technology advancements *(Slovak)* 80—33226
- GaAlAs, buried-heterostructure injection lasers, threshold current reduction 77—10924
- (GaAl)As buried-heterostructure laser with buried optical guide, highly efficient operation 80—1219
- GaAlAs CW DH diode lasers, 1/f noise behaviour 78—1226
- (GaAl)As CW DH lasers with stripe geometry, LF intensity noise obs. 77—38887
- GaAlAs CW diode laser, external cavity control, 32 MHz single axial mode 78—1271
- GaAlAs DH, optically-pumped, degradation at elevated temps. 79—50295
- GaAlAs, DH CW diode laser, picosecond pulse generation 78—83002
- (GaAl)As DH diode laser, microscale degradation absorpt. centres 78—13704
- GaAlAs DH injection laser, half-ring, room temp. operation 80—58558
- (GaAl)As DH laser, gradual degradation accel. as exponent of driving current value 80—32990
- GaAlAs DH laser, In solder deterioration, Au diffusion in In 80—33019
- (GaAl)As, DH laser, LPE growth, meniscus lines as nucleation sites 77—15706
- (GaAl)As DH laser, low-current, proton-bombarded, design and characts. 78—87059
- GaAlAs DH laser, narrow stripe geometry, spontaneous carrier lifetime 80—87392
- GaAlAs DH laser, optimum p-n junction depth, photoluminesc. method 79—4598
- GaAlAs DH laser, stripe geometry, spatially resolved emission 79—27257
- (GaAl)As DH laser, threshold current density, growth terraces effect 80—99723

gallium arsenide continued

- GaAlAs DH laser diode, deep level associated with slow degradation 78—87050
- GaAlAs DH laser diodes, catastrophic degradation 79—50290
- GaAlAs DH laser diodes, long-lived high-power at 70°C, using Al_2O_3 film coating 79—50321
- GaAlAs DH laser diodes, small signal modulation, junction capacitance effect 80—83625
- GaAlAs DH laser diode, edge coupling to planar $LiNbO_3$:Ti waveguide 80—87559
- (GaAl)As DH laser wafer, photoluminesc. improvement with buffer layer 80—64014
- GaAlAs DH laser-diode-to-diffused-waveguide coupling calcs., Gaussian beam model 79—94372
- (GaAl)As, DH lasers, degradation mechanisms, temp. depend. 78—66825
- GaAlAs DH lasers, electron-hole recomb. effects 79—45944
- GaAlAs DH lasers, nonlinearity, second and third harmonic distortion 79—31898
- GaAlAs DH lasers, proton-bombard., nonradiative recomb., luminesc. time-response meas. 79—98371
- GaAlAs DH lasers, SiO_2 insulated, characts. and near field 80—64019
- GaAlAs DH lasers, self-sustained pulsation suppression, effect of SiO_2 facet coating films 80—95894
- GaAlAs DH p-n junction laser, construction and operating characts. 78—9377
- GaAlAs DH photovoltaic detectors, high efficiency 79—11198
- GaAlAs DH pump laser for photoluminescence lifetime meas. 78—74085
- (GaAl)As DH stripe contact injection lasers, local attached data fibre link appls. 80—19044
- GaAlAs DH stripe geometry lasers, degradation phenomena 80—53290
- GaAlAs, diode laser, CW radiation, intensity noise spectra of axial mode groups 77—34890
- GaAlAs embedded DH stripe laser with GaAsP strip-waveguide modulator 78—66957
- (GaAl)As heterojunction laser with distributed Bragg refl., mode switching 80—43336
- GaAlAs, heterostruct. formed by LPE, growth and dissolution kinetics 79—99439
- GaAlAs heterostructure lasers, fine-structure in spectra 80—19033
- (GaAl)As high performance diode laser, high-reflectivity cavity mirrors 78—82994
- GaAlAs injection DH laser and GaAs Schottky-gate FET, monolithic integration 80—58593
- (GaAl)As injection lasers, optimisation of power efficiency 77—42539
- (GaAl)As injection lasers, self-pulsations, Q-switching and mode-locking effects 78—66827
- GaAlAs injection lasers, AM characts. 79—50330
- GaAlAs injection laser, long wavelength radn. spatial distrib. 79—76686
- GaAlAs injection lasers, stability in single transverse mode operation 80—38027
- GaAlAs injection laser, monolithic integration with Schottky-gate FET 80—48275
- (GaAl)As injection lasers operating with optical fibre external resonator, characts. 80—58544
- (GaAl)As injection laser operating in external cavity, intensity self-pulsations 80—64013
- (GaAl)As injection lasers operating with optical fibre resonators 80—91812
- (GaAl)As, LPE, GaAs dissolution kinetic in undersaturated isothermal solns. in Ga-Al-As system 80—80106
- GaAlAs laser, coherent pulse generation by active modelocking 79—89941
- (GaAl)As laser, stripe struct. for horizontal transverse mode stabilisation 77—79859
- GaAlAs laser diode, CW, ps pulse generation 79—50329
- GaAlAs laser diode, for heterodyne communication systems, high frequency stability 80—99727
- GaAlAs laser nonlinearities, harmonic distortion 80—74357
- GaAlAs laser transmitter for optical fibre communication, features 78—90423
- GaAlAs laser transmitters using optical tap for feedback control, output power stability 79—64241
- (GaAl)As lasers, low threshold proton isolated, spectral and transient response 78—87052
- GaAlAs lasers, return-beam-induced noise generation model 80—48244
- GaAlAs lateral injection laser, low threshold, single mode operation 77—75545
- GaAlAs light intensity modulators using p-n junctions 80—99871
- (GaAl)As low threshold current proton isolated DH lasers 78—1258
- (GaAl)As low-beam-divergence CW DH laser, grown by low press. metallorganic CVD 80—74376
- GaAlAs, luminescence circular polarisation, electron optical orientation resonant variation *(Russian)* 80—84782
- GaAlAs mode stabilised separated multiclad layer stripe geometry DH laser, optical waveguide 80—64051
- GaAlAs mode-stabilised semiconductor lasers 78—46638
- GaAlAs, native defects, stoichiometry, doping effect 77—11541
- GaAlAs novel DH lasers fabrication 78—50803
- GaAlAs on GaAs thin film stacked multiple-bandgap solar cell structs., prep. using CVD techniques 80—94083
- (GaAl)As oxide-stripe geometry DH laser, cavity length effect on output 79—50323
- GaAlAs p-n heterostructures, current-flow mechanisms, luminesc. spectra 80—20298
- GaAlAs plasma grown oxide film, anal. by combined ion beam techniques 79—7760
- GaAlAs, SEM defect study, transmission cathodoluminescence 79—64964
- GaAlAs solar cells, appl. for navigational satellite power systems 80—35694
- GaAlAs stripe laser, longit. and transverse mode dynamics on junction plane 77—38890
- GaAlAs, surface vacancies, bound state energy levels calc. 80—80340
- (GaAl)As system, automated system for growth of multilayered structs. by LPE 79—38752
- GaAlAs terraced substrate laser, visible-light-emitting, characts. 80—106523
- GaAlAs visible diode laser for hologram recording of three-dimens. object 80—95839
- (GaAl)As, Zn diffused DH laser with twin transverse junctions, low threshold current 79—98393

gallium arsenide continued
(GaAl)As, Zn diffused proton bombarded stripe laser 79−98392
(GaAl)As:Be implanted DH stripe geometry laser 80−64044
n-GaAlAs:Sn LED DH donor-level analysis, DLTS obs. 79−47040
GaAlAs:Zn recombination radiation drift, charge carrier photon induced drift in varigap semicond. 80−50418
GaAlAs/GaAs, n-p-n heterojunction transistor, elec. props. 79−87149
GaAlAs/GaAs heterostructures, ellipsometric assessment of epitaxial layer during growth in organometallic VPE system 79−37933
GaAlAs/GaAs solar cells, efficiency optimisation at high and low current levels *(French)* 80−61348
GaAlAs/GaAs solar cells, Be and Zn behaviour 80−101111
(GaAl)As/GaAs-heterostructure lasers, degradation studies of sawn cavity lasers under pulsed operation 78−29953
(GaAl)As-GaAs, DH laser, degradation in water due to facet deterioration 79−22970
(GaAl)As-GaAs, double heterostructure laser, TEM study of dark line defect growth from dislocation clusters 79−33206
GaAlAs-GaAs, high efficiency heterostruct. solar cell grown by metalorganic CVD 78−11118
(GaAl)As-GaAs, long life lasers, initial degradation mode 77−14712
(GaAl)As-GaAs concentrator solar cells, series resistance effects 79−57427
(GaAl)As-GaAs DH laser, anomalous emission intensity, cavity competition 77−79823
GaAlAs-GaAs DH laser diodes, long-life diodes for optical fibre communication 80−48246
GaAlAs-GaAs DH lasers, degradation caused by growth of dislocation networks 80−53289
GaAlAs-GaAs double heterostructure, interfacial recomb. velocity, photolum. meas. 78−68075
GaAlAs-GaAs epitaxial heterostructures for integrated optics functional elements 78−50948
GaAlAs-GaAs heteroepitaxial devices, interstitial impurities and degradation, Auger obs. 80−99730
GaAlAs-GaAs heteroface solar cells, 1 MeV electron irrad., analytical and expt. study 79−70450
GaAlAs-GaAs heteroface solar cells, high open-cct. voltage, full-factor and efficiency 80−94081
GaAlAs-GaAs heterojunction prep., Zn conc. effect in epitaxial layer, high-power IR emission *(Spanish)* 77−39932
GaAlAs-GaAs heterojunction solar cells, high temp. props. 25 to 300°C 80−94035
GaAlAs-GaAs heterostruct. fabrication, using horizontal and vertical LPE furnaces 77−42538
(GaAl)As-GaAs heterostruct. lasers, factors affecting catastrophic degradation 77−75524
GaAlAs-GaAs heterostructures, electronic excitation effects on mobility of point defects and dislocations 78−2561
(GaAl)As-GaAs heterostructure lasers, factors affecting catastrophic degradation 78−17942
GaAlAs-GaAs heterostruct. solar cells, Al, P, Zn incorporation by LPE *(French)* 79−24899
GaAlAs-GaAs heterostruture, optical waveguide characteristics, mode spectrum, universal dispersion curves 79−72706
GaAlAs-GaAs heterostruc. lasers, interstitial impurities and degradation, Auger obs. 80−99730
(GaAl)As-GaAs laser, low temp. threshold behaviour 78−46604
GaAlAs-GaAs lasers, channelled substrate, prepared by combination of organometallic pyrolysis and LPE 80−99745
GaAlAs-GaAs n-n heterojunction, rectification 79−28402
(GaAl)As-GaAs narrow stripe laser, improved optical communication system performance 80−102733
GaAlAs-GaAs solar cell structs., photolum. props. 80−50958
(GaAl)As-GaAs twin-transverse-junction stripe laser with linear light/current characteristic and low threshold 79−36893
GaAlAs-GaAs-GaAlAs etalon, optical bistability 80−5781
(GaAl)As-heterostruct. stripe lasers, light/current characts. and near field shifts, waveguide self focusing effects 78−29952
$GaAl_xAs_{1-x}$, ion beam synthesis for photodetector fabrication 79−46688
$Ga_{0.1}Al_{0.9}As$ LPE layers containing low-cond. regions, charging effects in SIMS anal. 80−66348
$Ga_{0.5}Al_{0.5}As$-GaAs, DH, interfacial recomb., photolum. time decay meas. 78−95347
$Ga_{0.5}Al_{0.5}As$-GaAs(:Ge) DH structure, minority carrier lifetime and internal quantum efficiency of surface-free GaAs 79−43013
$Ga_{0.64}Al_{0.36}As$, plasma grown oxide, phys. and elec. props. 78−48550
$Ga_{0.65}Al_{0.35}As$ epitaxial layer on GaAs, two-dimensional lattice mismatch parallel to interfacial boundary 79−51439
$Ga_{0.65}Al_{0.35}As$, LPE growth, wave morphologies on surface 77−40396
$Ga_{0.7}Al_{0.3}As$-GaAs chemically etched mirror lasers, optical coupling effect 77−72000
$Ga_{0.9}Al_{0.1}As$, nucleation morphologies on $Ga_{0.65}Al_{0.35}As$ surfaces grown by LPE 78−15323
$Ga_{0.9}Al_{0.1}As$:Ge(Si) epitaxial layers, defect obs. by TEM 77−51618
$Ga_{1-x}Al_xAs$ DH injection laser diode, long-term-degraded, TEM obs. 78−71102
$Ga_{1-x}Al_xAs$-GaAs DH lasers, very low threshold, grown by metalorganic CVD 78−55365
$Ga_{1-x}AlAs$ (110) oxide-free Schottky barriers, surface comp. and characts., AES obs. 79−82661
$Ga_{1-x}AlAs$, LPE layers, electron mobility, scatt. processes 80−84519
$Ga_{1-x}AlAs$:Zn, acceptor energy level and elec. props. 80−65482
$Ga_{1-x}Al_xAs$, alternate monolayer crysts., MBE and props. exam. 78−10289
$Ga_{1-x}Al_xAs$, appl. of theory of electroepitaxy of multicomponent systems 80−65396
$Ga_{1-x}Al_xAs$, band struct. from I-V, C-V meas. on Schottky diodes 80−96989
$Ga_{1-x}Al_xAs$ based layer structures, optimum growth conditions, comp. and struct. perfection 80−104069
$Ga_{1-x}Al_xAs$ buried heterostruct. injection laser, degradation rate, optical flux density depend. 79−50313
$Ga_{1-x}Al_xAs$ buried heterostructure lasers for analogue communication 80−48297
$Ga_{1-x}Al_xAs$, channelled substrate, planar struct. and DFB lasers 78−79032
p-$Ga_{1-x}Al_xAs$ crystals, spectral characts. of photosensitivity, mechanism 80−44735
$Ga_{1-x}Al_xAs$ DH catastrophically degraded laser, TEM obs. of defects 80−32989

gallium arsenide continued
$Ga_{1-x}Al_xAs$ DH injection laser, FM at microwave freq. rates 80−58610
$Ga_{1-x}Al_xAs$ DH laser, LPE surface protective coating 78−35320
$Ga_{1-x}Al_xAs$ DH laser diode, long-lived, high-power, facet coated 80−58564
$Ga_{1-x}Al_xAs$ DH laser hybrid device, reliability 79−27281
$Ga_{1-x}Al_xAs$, DH stripe geometry laser, lasing-induced change in differential resistance 79−45943
$Ga_{1-x}Al_xAs$, deep level-dislocation interactions, DLTS meas. 80−29357
$Ga_{1-x}Al_xAs$, deep levels, pressure effects 80−49651
$Ga_{1-x}Al_xAs$, degraded DH LED, defect struct. by electrolum. topography and TEM obs. 79−60369
$Ga_{1-x}Al_xAs$ double heterostruct. lasers, aging characts. 79−72569
$Ga_{1-x}Al_xAs$ electrodes, interface capacitance meas., flatband pot., conduction and valence band boundaries *(French)* 79−33339
$Ga_{1-x}Al_xAs$, electrolum. study using high-gain image intensifier 80−55193
$Ga_{1-x}Al_xAs$, epitaxial, radiative deep states 80−76061
$Ga_{1-x}Al_xAs$, epitaxial layers on GaAs substrate, mismatch stress accommodated by tetrahedral distortion 77−55466
$Ga_{1-x}Al_xAs$, epitaxial layers, reflectivity meas. by wavelength modulation spectroscopy *(French)* 77−59632
$Ga_{1-x}Al_xAs$ epitaxial layers, spectroscopic technique for imaging spatial distrib. of nonradiative defects 78−23498
$Ga_{1-x}Al_xAs$, epitaxial layers, on GaAs substrates, X-ray double-cryst. diffractometry, state of strain 79−19480
$Ga_{1-x}Al_xAs$ epitaxial layer, absorpt. and transmission coeffs. *(French)* 80−2887
$Ga_{1-x}Al_xAs$ epitaxial layer, elec. cond., Hall effect, band struct. 80−49964
$Ga_{1-x}Al_xAs$ heterostructure, LPE prep., growth and dissolution kinetics, thermodynamic and kinetic models 80−75456
$Ga_{1-x}Al_xAs$, hot electron distrib. meas. and calc. 78−27318
$Ga_{1-x}Al_xAs$, IR refl. spectra and Raman spectra 80−20623
$Ga_{1-x}Al_xAs$ injection laser automatic bias control cct. 78−5498
$Ga_{1-x}Al_xAs$ integrated optical waveguide LPE 77−75703
$Ga_{1-x}Al_xAs$, intervalley energy gaps, temp. junction, exptl. determ. 80−80179
$Ga_{1-x}Al_xAs$ junction-up TJS laser electron injection efficiency improvement 80−48300
$(Ga_{1-x}Al_x)As$ LOC DBR laser integration with p-n junction detector 78−38066
$Ga_{1-x}Al_xAs$, LPE, growth mechanism and morphology on channelled substrates 79−28960
$Ga_{1-x}Al_xAs$ LPE crystals for DH laser, LEDs, TEM obs. of Ge, Si-doped epitaxial layers 79−1556
$Ga_{1-x}Al_xAs$ LPE film, with $x=0.23$ and 0.37, grown by linear cooling, thickness comparison with GaAs 78−87892
$Ga_{1-x}Al_xAs$, LPE growth and characterisation 80−50566
$Ga_{1-x}Al_xAs$ LPE layer photoluminescence obs. *(Polish)* 77−77268
$Ga_{1-x}Al_xAs$, LPE layer thickness depend. on soln. comp. 78−10295
$Ga_{1-x}Al_xAs$ LPE layer on GaAs, lattice mismatch using X-ray source 79−82470
$Ga_{1-x}Al_xAs$ LPE layers, comp. and refr. index, ellipsometry meas. 79−87011
$Ga_{1-x}Al_xAs$ laser, buried heterostruct., stable operation during accelerated ageing at 70°C 79−7125
$Ga_{1-x}Al_xAs$ laser, DH, enhanced localised degradation and anomalous emission spectra 77−680
$Ga_{1-x}Al_xAs$ laser, SHG with $KNbO_3$ 80−74431
$Ga_{1-x}Al_xAs$ laser, stripe-geometry DH, improved light output linearity 77−682
$Ga_{1-x}Al_xAs$, laser, temp. sensitive, enhanced degradation rates 77−79825
$Ga_{1-x}Al_xAs$ laser diode end facet protection by parylene coating 79−36921
$Ga_{1-x}Al_xAs$ lasers, processing stresses effect on residual degradation 79−72567
$Ga_{1-x}Al_xAs$ layer, surface conc. x determ. by rapid localised nondestructive optical method *(French)* 77−62725
$Ga_{1-x}Al_xAs$ layer form. on GaAs during dissolution in Ga-Al-As soln. 80−10799
$Ga_{1-x}Al_xAs$, liquid and solid comp. variations during LPE growth 79−99445
$Ga_{1-x}Al_xAs$ low threshold stripe geometry DH laser, Be implanted, on semi-insulating substrate 80−69409
$Ga_{1-x}Al_xAs$, MBE, state-of-the-art 79−24450
$Ga_{1-x}Al_xAs$ n-p_3-p_2-p_1-p_0 struct., degradation electrolum. 80−50428
$Ga_{1-x}Al_xAs$, NMR of optically oriented nuclei, quadrupole effects *(Russian)* 77−85592
$Ga_{1-x}Al_xAs$, non-shallow levels and cond. band struct. from Hall carrier conc. meas. 80−39607
$Ga_{1-x}Al_xAs$, ohmic contacts, metallisation systems 80−25010
$Ga_{1-x}Al_xAs$, optical detection of CESR 77−36155
$Ga_{1-x}Al_xAs$, p^+-n-n^+ heterostructure, distrib. of injected carriers, forward V-I characts. *(Russian)* 80−6973
$Ga_{1-x}Al_xAs$ p-i-n structure photoelectric props. 78−95353
$Ga_{1-x}Al_xAs$ p-n structure, charge-storage diode, variable-gap 80−11076
$Ga_{1-x}Al_xAs$, Peltier LPE, absence of electromigration of As and Al 77−81230
$Ga_{1-x}Al_xAs$, photoluminescence, deep level trap emission capture 80−29805
$Ga_{1-x}Al_xAs$, point defects and dislocation climb, interaction with deep level donor 79−82209
$Ga_{1-x}Al_xAs$, protection by reactively sputtered AlN *(French)* 78−23849
$Ga_{1-x}Al_xAs$, quantum magnetoresist. results, using pulsed fields up to 35 T 79−73528
$Ga_{1-x}Al_xAs$, rapidly degraded LED, defect struct. of ⟨100⟩ dark lines 78−10052
$Ga_{1-x}Al_xAs$, room-temperature CW laser structures and characteristics 77−19323
$Ga_{1-x}Al_xAs$, STEM techniques for simultaneous electronic anal. and obs. of defects 79−14812
$Ga_{1-x}Al_xAs$ Schottky barrier, oxide free, surface composition and fabrication 78−68084
$Ga_{1-x}Al_xAs$ Schottky directional coupler switch, construction and operation 78−25960
$Ga_{1-x}Al_xAs$, Se ion implantation *(French)* 77−68986
$Ga_{1-x}Al_xAs$, self-aligned three dimensional struct. MBE growth 77−59697

gallium arsenide continued
- $Ga_{1-x}Al_xAs$, semiconductor defects, spectroscopic study of electronic props. 80—84446
- $Ga_{1-x}Al_xAs$, Shubnikov-de Haas oscillation, in semiconductor superlattice 77—62947
- $Ga_{1-x}Al_xAs$, solar cells appl., technology advancements 79—43776
- $Ga_{1-x}Al_xAs$, solid solution, synthesized by ion implantation, Raman scattering 79—42972
- $Ga_{1-x}Al_xAs$ stripe laser with stable transverse mode structure 80—48298
- $Ga_{1-x}Al_xAs$ structures, STEM and scanning deep level transient spectroscopy in defect centre anal, cathodoluminesc. techniques 80—103642
- $Ga_{1-x}Al_xAs$ superlattices, multilayers, periodic and near-periodic, small-angle interferences of reflected X-rays 79—94846
- $Ga_{1-x}Al_xAs$, surface phonon polaritons, frustrated total internal refl. expts. 78—47656
- $Ga_{1-x}Al_xAs$ symmetrised epitaxial variable-gap waveguide, coherent radiation generation 80—38018
- $Ga_{1-x}Al_xAs$, topographical stoichiometry determ. using electroreflectance 78—23483
- $Ga_{1-x}Al_xAs$ transparent LED, optical wavelength multiplex transmission system appl. 78—30063
- $Ga_{1-x}Al_xAs$ transverse mode DH laser with inbuilt plano-convex waveguide 80—48296
- $Ga_{1-x}Al_xAs$, VPE, on-time comp. depend. 78—67915
- $Ga_{1-x}Al_xAs$ VPE layers, X-ray diffr. 80—29296
- n-$Ga_{1-x}Al_xAs$, variable gap photodetector, quantum efficiency 79—7903
- $Ga_{1-x}Al_xAs$, variation of optical transitions *(French)* 79—60708
- $Ga_{1-x}Al_xAs$, varizone layer photoelectron yield depth estimation 80—100745
- $Ga_{1-x}Al_xAs$, velocity saturation and cond. band struct. under press. 78—26863
- $Ga_{1-x}Al_xAs$ visible diode lasers, transverse-mode stabilised, nonstigmatic laser beams 79—76694
- $Ga_{1-x}Al_xAs$ visible diode lasers, degradation 80—43330
- $Ga_{1-x}Al_xAs$ visible diode lasers, degradation mechanisms 80—64026
- $Ga_{1-x}Al_xAs$ visible diode lasers, degradation due to macroscopic defects (<730 nm) and facet oxidation (>740 nm), life tests 80—99729
- $Ga_{1-x}Al_xAs$, Zn diffusion, depend. on Al content 78—59981
- $Ga_{1-x}Al_xAs$:Si, LPE, phase diagram, Hall effect meas., carrier conc., donor ionisation energies 77—72803
- $Ga_{1-x}Al_xAs$:Si, linear-gradient p-n junction, barrier capacitance 77—43705
- n-$Ga_{1-x}Al_xAs$:Si, room-temp. cond. and band struct. 80—96869
- $Ga_{1-x}Al_xAs$:Si, Si determ., spectrochem. method, photoluminesc. spectra, Hall effect meas. *(German)* 77—77851
- $Ga_{1-x}Al_xAs$:Si p-n junction, reemission effects 78—15230
- $Ga_{1-x}Al_xAs$:Si p-n junction, doping in LPE, elec. and luminesc. props. *(Czech)* 78—47851
- $Ga_{1-x}Al_xAs$:Si photoelectric convertors, broadband varizone creation 80—40856
- $Ga_{1-x}Al_xAs$:Sn, layer Schottky barrier, deep level spectroscopy 80—49666
- $Ga_{1-x}Al_xAs$:Te, plasmon-LO-phonon coupling, IR refl. obs. 80—50335
- $Ga_{1-x}Al_xAs$/GaAs heterostructure solar cell design for space usage 79—96450
- n-$Ga_{1-x}Al_xAs$-Au, Schottky barrier height as function of AlAs content 79—65535
- $Ga_{1-x}Al_xAs$-Au variable-gap surface-barrier struct., photoelec. effect 80—39634
- $Ga_{1-x}Al_xAs$-$Ga_{1-y}Al_yAs$ p-n heterojunction, minority carrier lifetime, elec. characts. and electrolum. meas. 78—2554
- $Ga_{1-x}Al_xAs$-$Ga_{1-y}Al_yAs$ DH laser, grown by organometallic CVD, room temp. operation 78—29950
- $Ga_{1-x}Al_xAs$-GaAs, abrupt quantum-well heterostruct. grown by metalorganic chemical vapour deposition 79—56933
- $Ga_{1-x}Al_xAs$-GaAs, CVD laser diodes, operation and growth processes 78—46598
- $Ga_{1-x}Al_xAs$-GaAs, grown by LPE, direct obs. of dislocations 79—65087
- $Ga_{1-x}Al_xAs$-GaAs, heteroepitaxial layers on GaAs(001), misfit dislocation asymmetry 77—47694
- $Ga_{1-x}Al_xAs$-GaAs, high efficiency solar cell, isothermal etchback-regrowth method 77—59701
- $Ga_{1-x}Al_xAs$-GaAs, injection lasers, defects, TEM anal. 79—23866
- $Ga_{1-x}Al_xAs$-GaAs, room temp. DH laser, CVD growth 78—37912
- $Ga_{1-x}Al_xAs$-GaAs channel guide laser grown by metalorganic CVD 79—10317
- $Ga_{1-x}Al_xAs$-GaAs DH injection lasers grown by metalorganic CVD, props. 80—99751
- $Ga_{1-x}Al_xAs$-GaAs DH lasers grown by metalorganic CVD, room temp. operation 78—1248
- $Ga_{1-x}Al_xAs$-GaAs heterostructure lasers grown by metalorganic CVD, prep. and props. 79—36918
- $Ga_{1-x}Al_xAs$-GaAs heterojunctions grown by metallorganic CVD 80—15599
- $Ga_{1-x}Al_xAs$-GaAs high-efficiency solar cell 79—29469
- $Ga_{1-x}Al_xAs$-GaAs injection laser, branching waveguide coupler fabrication by LPE 78—63202
- $Ga_{1-x}Al_xAs$-GaAs LPE multilayer heterostructure photovolt. solar cells, fabrication and performance 79—48128
- $Ga_{1-x}Al_xAs$-GaAs laser, degradation, appl. of dislocation climb model 77—1125
- $Ga_{1-x}Al_xAs$-GaAs laser, DH, grown by metalorganic CVD, room temp. operation 78—13702
- $Ga_{1-x}Al_xAs$-GaAs laser, distributed Bragg confinement, room temp. operation 78—74907
- $Ga_{1-x}Al_xAs$-GaAs low threshold room temp. DH lasers grown by metalorganic CVD 78—50804
- $Ga_{1-x}Al_xAs$-GaAs narrow stripe laser for improved communication performance 80—48299
- $Ga_{1-x}Al_xAs$-GaAs p-n and p-p-n heterojunction solar cells, high efficiency, prep., eval. and characters *(Japanese)* 80—61342
- $Ga_{1-x}Al_xAs$-GaAs p-n structures, variable-gap front layer, photoelec. props. 79—7884
- $Ga_{1-x}Al_xAs$-GaAs p-n solar cell, with thin variable gap layer, high efficiency 79—24064
- $Ga_{1-x}Al_xAs$-GaAs solar cell, deep level obs. 77—89834
- $Ga_{1-x}Al_xAs$-GaAs solar cells, photoluminesc. characterisation 80—3512
- $Ga_{1-x}Al_xAs$-GaAs solar cell, radiation resist., theoretical evaluation and optimisation 80—35681
- $Ga_{1-x}Al_xAs$-GaAs solar cells, computer anal. of cell characts. incl. band gap variation 80—55866

gallium arsenide continued
- $Ga_{1-x}Al_xAs$-GaAs:Si, momentum distrib. of valence electrons, positron annihilation meas. 79—51530
- $Ga_{1-x}Al_xAs$-GaAs-GaAs p-i-n heterojunction, photoelec. props. 78—26938
- $Ga_{1-x}Al_xAs$-GaAs-GaAs, p-p-n junctions, variable gap solar photocell with coordinate depend. band gap gradient 79—11213
- $Ga_{1-x}Al_xAs$-Ge, MBE of ultra thin film superlattices on GaAs substrates, TEM study 79—37932
- p-$Ga_{1-x}Al_xAs$-n-$Ga_{1-y}Al_yAs$, graded band gap, solar cells, theoretical efficiency *(French)* 77—62987
- $Ga_xAl_{1-x}As$ channelled-substrate planar struct. injection laser 77—88742
- $Ga_xAl_{1-x}As$ DH laser, suppression of output nonlinearities by use of misaligned mirrors 78—17954
- $Ga_xAl_{1-x}As$ diode laser, modulation characts. 77—83903
- $Ga_xAl_{1-x}As$ embedded stripe DH laser monolithically integrated with strip waveguide 78—59025
- $Ga_xAl_{1-x}As$ injection heterojunction distributed output laser, exptl. study 80—43369
- $Ga_xAl_{1-x}As$, LPE, charge carrier conc. distrib. *(Russian)* 78—52694
- $Ga_xAl_{1-x}As$, LPE, GaAs solubility in Ga-Al alloys investig. 78—52690
- $Ga_xAl_{1-x}As$ layer, optical guiding in Bragg configuration 78—1431
- $Ga_xAl_{1-x}As$, Schottky barrier, effect of oxide composition on elec. behaviour, AES meas. 79—87141
- $Ga_xAl_{1-x}As$ stripe-geometry laser, current carrier conc. distrib. and threshold props. 77—68212
- $Ga_xAl_{1-x}As$:Cu epitaxial layers, spatial distrib. of nonradiative defects, STEM imaging spectroscopic technique 77—89438
- $Ga_xAl_{1-x}As$-GaAs DH laser, degraded, nature of ⟨110⟩ dark-line defects, TEM 77—89439
- $Ga_xAl_{1-x}As$-GaAs DH laser, continuous room temp. operation 78—55363
- $Ga_xAl_{1-x}As$-GaAs double heterostructure laser diode, temp. depend. of photolum. 80—5734
- $Ga_xAl_{1-x}As$-GaAs heterostructure laser, suppression of internally circulating modes, effect on catastrophic degradation and efficiency 77—83896
- $Ga_xAl_{1-x}As$-GaAs heteroepitaxial layer distortion characterisation by X-ray multiple diffr. 80—96754
- $Ga_xAl_{1-x}As_x$ photodetector diode on GaAs substrate dark currents, tunnelling, energy gaps, effective masses 80—70805
- $Ga_xAl_{x-1}As$ laser, CW, 3-5 mW, optical communication appl. 77—3656
- GaAlAsP-GaAs T-Q DH laser, light induced misfit dislocation motion 77—75518
- $Ga_{1-x}Al_xAs_{1-y}P_y$ epitaxial film, nonradiative recomb. at dislocations 80—44213
- $Ga_{1-x}Al_xAs_{1-y}P_y$ epitaxial layer heterojunction, nonradiative recombination at misfit dislocations 80—96901
- $Ga_{1-x}Al_xAs_{1-y}P_y$ layer of uniform composition grown on GaAs by LPE, temp. diff. method appl. 79—23864
- $Ga_{1-x}Al_xAs_{1-y}P_y$-GaAs quaternary heterojunction strains and IR laser diode performance 78—9385
- $Ga_{1-x}Al_xAs_{1-y}P_y$-GaAs quaternary heterojunction, misfit dislocation charact. by synchrotron radiation white beam topography 78—63771
- $Ga_{1-x}Al_xAs_{1-y}P_y$-GaAs heterojunctions, light-induced misfit dislocation motion, photoluminesc. and X-ray diffr. meas. 79—11200
- GaAlAsSb/GaSb alloys, prep. and optoelectronic device appl. 80—25587
- GaAlAsSb-GaSb low bandgap solar subcell for high efficiency multibandgap convertors, LPE growth 80—93927
- GaAlAsSb-GaSb p-n heterojunction CCD, charge transfer, charge exchange 80—65658
- $Ga_{1-x}Al(In)_xAs$, $GaAs_{1-x}P_x$, substit. solid solns., comp. determ. from X-ray integral intensities 77—84584
- Ga(As,P):N, intermediate range model of N states 79—73467
- Ga(As,P):N, isoelectronic impurity states, long-range, short-range model 80—75524
- Ga(As,P):N, theory of bound states induced by disorder and isoelectronic pots. 77—35889
- Ga(As,P)/(In,Ga)P DH laser, red-emitting, optical and elec. characts. 78—66826
- GaAs (001)-Ag contact, surface stoichiometry and struct., and electronic surface states 78—95361
- GaAs (110)/Ge heterojunction, valence band discontinuity in XPS spectra, precise determ. 80—84834
- GaAs (110)-Al interface, XPS study of interface interaction, Al proximity effects and replacement reaction 79—100019
- GaAs (110)-Al(Ga) interface, interface states, photoemission study 78—95359
- GaAs (110)-Al(Ga)(In), Schottky barrier form., defect mechanism 80—49902
- GaAs (110)-Au Schottky barriers on ordered and disordered GaAs surfaces, props. 78—95360
- n-GaAs, absorption tails in surface depletion layer and bulk 78—64379
- n-GaAs, and Te doped, homogeneity, IR introscopy investig. 79—15446
- GaAs anodic MIS system, dynamic props. of interface state bands 80—49933
- GaAs, anodic oxide film, annealing effect on carrier density profile 78—88040
- GaAs base laminated epitaxial struct., surface plasmon phonon polaritons *(Russian)* 80—59905
- GaAs, chemical shift and effective atomic charges 78—88201
- GaAs, cryst. growth from large Ga:As solns., critical cooling rate 80—64938
- GaAs crysts., IR light scattering and absorpt. microscopy study of dislocations 80—107249
- GaAs DH stripe geometry laser, horizontal mode deform. and anomalous lasing props. 77—19253
- GaAs, deep levels investigation 77—76769
- GaAs distributed Bragg reflection lasers, large optical cavity, optimal design 80—38028
- GaAs, effective dielectric function calc., exchange interaction effects 79—99494
- GaAs electrooptically tuned external-cavity CW injection laser, FM optical communication appl. 80—14351
- GaAs epitaxial film, microstruct., effect on elect. characts. of Schottky diode *(Russian)* 80—107671
- GaAs epitaxial growth, in GaAs-$AsCl_3$-H_2 system, elec. field effect 80—2306
- GaAs, equation of state 79—82310
- GaAs, exciton-polariton reflectance spectra, exciton impact ionization and illum. intensity effects 79—42943
- GaAs, highly excited, LO phonon Raman lineshape 79—78683

gallium arsenide continued
GaAs, hot photoluminescence spectrum, polarisation depend. 78—31254
GaAs injection lasers, amplified luminesc. 80—2824
GaAs integrated optical circuits by wet chemical etching 79—32092
GaAs LPE layers, deep levels by photocapacitance and related techniques 78—6334
GaAs, LPE layers, outdiffusion of recomb. centres from substrate during growth 80—39466
GaAs laser reliability, protective facet coatings 79—81452
GaAs layers, from gas phase, impurity influence on growth micromechanism 80—45237
GaAs, lightly doped, p-n junctions, forward branches of current-voltage characts. 79—7890
GaAs, multilayer epitaxial growth with Sn doping 77—47690
GaAs n-p solar cells, theoretical perform. of multi-layer grid patterns 80—55846
GaAs on Ge thin film stacked multiple-bandgap solar cell structs., prep. using CVD techniques 80—94083
GaAs optical modulator for coupled-waveguides 78—71235
GaAs, optically pumped laser with acoustic distributed feedback 78—82977
GaAs, plasma-grown oxides, in situ anal. using spectroscopic ellipsometer 79—79138
GaAs, polariton fluoresc., spatial and spectral features 79—33760
GaAs, polycryst. Schottky barrier solar cells, effect of grain size on efficiency 80—50968
GaAs, polyethylene mixture, optical props., IR bandpass filter appls. *(Russian)* 78—90468
GaAs, Raman spectroscopy, characterisation of thin films and heterostructures 78—76439
GaAs rib-waveguide laser, propag. and radiation characts. 77—79933
GaAs, Schottky barrier electrorefl. meas. by sample rotating technique 80—60544
GaAs, shallow donors, excited state transitions 78—6710
GaAs, stripe geometry laser, optical losses of O^+ and B^+ implanted layers 77—79827
GaAs substrate, epitaxial growth of single crystal layers of $Cd_{1-x}Sn_xS$, close-spaced geometry 78—92198
GaAs, transient and steady-state electron transport props. 77—39812
GaAs, VPE growth, surface morphology study by optical microscopy 79—60651
GaAs, VPE growth rate variation with distance along substrate within const. temp. zone 78—2384
GaAs: Cr, annealing with Si_3N_4, Cr profiles meas. 79—90693
GaAs: Cr (O_2), impurity levels charact. using dark capacitance and photocapacitance transient techniques 80—59920
GaAs: Si(Te), radiative recomb. *(Russian)* 79—91499
GaAs:$^{119}Sn^m$, Mossbauer spectra 80—29667
GaAs:^{11}B, physicochem. and resistivity meas. 80—24933
GaAs:$^{56}Fe(^{57}Fe)$, paramag. centres, identification from ESR and ENDOR spectra 80—80600
GaAs:0, effect of displacement upon impurity levels, psuedopotential calc. 77—39803
GaAs:Ag, diffusion of Ag at 1000°C, profiles, Schottky barrier and Hall effect meas. 80—54435
GaAs:Al, optical detection of NQR 79—69752
GaAs:Ar^+-metal, capacitor, capacitance-voltage and current-voltage meas., assuming intermediate dielec. layer 79—56316
GaAs:Au, back surface gettering 80—10758
GaAs:B, deep levels, optically stimulated transient current method *(French)* 80—59919
GaAs:B, electron or neutron irradiated, low symmetry interstitial B centre 78—79605
GaAs:B, incorporation of B during growth 80—93471
GaAs:B(Ge)(Mg), impurity conc. profile by glow-discharge optical spectroscopy 80—49258
GaAs:Ba^+, Auger electron and charact. electron energy loss spectra 80—55235
GaAs:Be, annealing effect during MBE 78—79898
GaAs:Be, deep levels 80—29358
GaAs:Be, implantation and annealing, elec. props. 79—99540
GaAs:Be, implanted, determ. of Be concentration profiles by $^9Be(p,\alpha)$ reactions and SIMS anal. 79—4335
GaAs:Be, ion implanted, elec. profiling and optical activation expts. 77—89457
p-GaAs:Be, ion implanted, annealing characts., defect cond. profiling, electron diffr. obs. 79—4318
GaAs:Be, ion-implanted, photolum. spectra, effects of implantant depth distrib. 78—27293
GaAs:Be, ion-implanted, IR refl. and transmission meas. 80—34908
GaAs:Be,Se VPE layers, ion implanted, donor-acceptor pair radiative recomb. 79—91489
p-GaAs:Be layer, MBE growth, Be doping and diffusion 77—51397
GaAs:Be(C)(Ge)(Sn), MBE layers, photoluminesc. 80—29803
p-GaAs:C, ion implantation efficiency, elec. profile and compensation level meas. 77—27880
GaAs:C, Zeeman effect of effective mass acceptor, polarised luminesc. 79—4541
GaAs:C,O, impurity conc. determ. in LEC grown cryst. 77—39612
GaAs:C(Sn), diamagnetism quenching 80—6782
p-GaAs:Cd, (110) cleaved surface, defect-induced surface states 80—6925
GaAs:Cd, lattice defects caused by quenching, elec. cond. 79—56160
GaAs:Cd, time depend. of Cd diffusion from gaseous phase 79—46844
GaAs:Co, effect of complex formation on impurity diffusion 77—11736
GaAs:Co, neutral state of Co impurities, optical absorption and mag. susceptibility 78—39578
GaAs:Co VPE layers, bound-exciton luminesc., Zeeman anal. 79—95818
GaAs:Co^{2+}, EPR expts., y-factor determ. 78—76301
GaAs:Co^{2+}, piezoabsorption meas. tunnel splitting and Jahn-Teller effect in $^4T_1(P)$ state 79—15494
GaAs:$Co^{2+}(Ni^{3+})$, mag. and optical props. 78—10763
GaAs:Co(Ni), intra d-shell excitations of acceptors 80—84757
GaAs:Cr, 0.84 eV no-phonon luminesc., fine struct. and origin 80—103980
GaAs:Cr, acceptor levels, photocapacitance meas. 79—95443
GaAs:Cr, Be, ion-implanted, semi-insulating, carrier mobility and conc. temp. depend. 77—76808
GaAs:Cr, Be^+ implantation, atomic conc. and defect density profiles after annealing 80—39123

gallium arsenide continued
GaAs:Cr, bulk and epitaxial, ion implanted, Cr conc., depth distrib. and diffusion coeff. 80—49243
GaAs:Cr, carrier equilibrium effects, impurity states, elec. resistivity 80—65488
GaAs:Cr, carrier transport in p^+-ν junction based on relaxation semiconductors 79—65543
GaAs:Cr, Cr distrib. and heat-treatment migration studies by SIMS 80—107305
GaAs:Cr, Cr^+ and Cr^{2+} centres, thermal treatment effects, EPR 80—65492
GaAs:Cr, current voltage characterisation, deep levels and Fermi level determ. 79—7823
GaAs:Cr, deep acceptor level, DLTS and optical DLTS study 80—92852
GaAs:Cr, deep levels, wavelength-modulated photocapacitance spectroscopy 80—76055
GaAs:Cr, dislocation-free single crystals, point defects and rad. damage 80—88141
GaAs:Cr, EPR, annealing and IR excitation effect on Cr^+ signal, Cr content by colorimetry 77—69680
GaAs:Cr, effect of light on EPR centres 78—10767
GaAs:Cr, electroabsorption spectra obs. 80—50301
GaAs:Cr, epitaxial layers, MBE grown, Hall mobilities, substrate temps. 80—20335
GaAs:Cr, exptl. verification of Cr^{2+} models of photoluminescent transitions 78—27320
GaAs:Cr, far IR EPR spectroscopy, mag. field-modulation technique 80—15830
GaAs:Cr, fine structure in cathodoluminescence spectrum 78—56524
GaAs:Cr, gettering by back surface mech. damage 80—10759
GaAs:Cr, high resist., anomalously strong elec. field induced release of carriers from traps 78—6397
GaAs:Cr, high resistivity, specific resistance depend. determ. using impedance freq. depend. *(Czech)* 80—15536
GaAs:Cr, hole traps, ESR studies 80—75843
GaAs:Cr, hot electron relax. process and ionization of traps *(Russian)* 79—28354
GaAs:Cr, IR absorpt. determ., emissivity meas. 77—63421
GaAs:Cr, IR spectral detectivity 78—70184
GaAs:Cr, impurity conc. and segregation coeff., optical absorpt. meas. 79—56819
GaAs:Cr, impurity electron states by $X\alpha$ scattered wave cluster method, electron-electron interactions 80—6767
GaAs:Cr, intracenter radiative transition in Cr^{2+} ions 79—11463
GaAs:Cr, ion implanted, implantation damage profiles, laser annealing, ellipsometry study 80—79819
GaAs:Cr, local level near valence band, photocapacitance 79—11080
GaAs:Cr, local level parameters from thermally stimulated excitation curves, influence of variations of rate of heating 80—6769
GaAs:Cr, low dose n-type ion implantation obs. 77—39608
GaAs:Cr, low temp. gettering 80—96549
GaAs:Cr, luminesc. stress splitting, 4.2K 78—84627
GaAs:Cr, luminescence and absorption spectra, temp. depend. of fine structure 80—6779
GaAs:Cr, Mg, ion implanted, elec. meas. and optical activation studies 79—86806
GaAs:Cr, O, effect of O in photoluminesc. meas. 80—29799
GaAs:Cr, optical charging of paramag. centres, effect of potential relief 77—20694
GaAs:Cr, optical modulation study of proton bombardment 78—6720
GaAs:Cr, optical modulation spectra affected by 150 keV proton beam 78—10871
GaAs:Cr, optically excited, Hall effect meas. 77—20343
GaAs:Cr, optically induced transient EPR phenomena 80—50168
GaAs:Cr, origin of sharp near IR transitions 80—10913
GaAs:Cr, parameters determ. using cond., Hall-effect and magnetoresist. meas. *(Slovak)* 78—47802
GaAs:Cr, photoconductivity and photo Hall spectra 78—19091
GaAs:Cr, photoionisation transition $Cr^{3+} \rightarrow Cr^{2+}$, EPR studies 80—60638
GaAs:Cr, photoluminescence, YAG laser or krypton laser 80—60668
GaAs:Cr, photoluminescence in strong electric fields 80—108270
GaAs:Cr, plane-parallel plate subjected to laser illumination, photocond. meas., photodetector for far IR 79—93221
GaAs:Cr, redistrib. of Cr during laser annealing 80—88192
GaAs:Cr, Schottky barrier, effect of trapping processes on photocapacitance 77—76866
GaAs:Cr, Se implantation, carrier conc. and mobility profiles depend. on dose and annealing temp. 77—47479
GaAs:Cr, Se layers, ion implanted, ohmic contact form., contact resist. meas. 79—91158
GaAs:Cr, semi-insulating, i.r. induced modulation of cathodoluminescence, and specimen current 77—1737
GaAs:Cr, semi-insulating, TSC, carrier recomb. and trapping 77—32014
p-GaAs:Cr, semi-insulating, illumination effect on mobilities 77—32043
GaAs:Cr, semi-insulating elec. compensation, Hall and resist. meas. 77—62855
GaAs:Cr, semi-insulating, complex permittivity, 2.5-36 GHz, 300-400K 77—69763
p-GaAs:Cr, semi-insulating photoelectronic analysis 77—80804
GaAs:Cr, semi-insulating, deep impurity level anal. 78—6332
n-GaAs:Cr, semi-insulating, contact effects, trapping levels 78—10465
GaAs:Cr, semi-insulating impurity photomagnetoelectric effect 78—34861
GaAs:Cr, semi-insulating, characterisation by photoelectronic data 78—68051
GaAs:Cr, semi-insulating, I-V characts. and surface currents 79—56234
GaAs:Cr, semi-insulating, I-V characts. and photocond. spectra dependencies on Fermi level 79—99576
GaAs:Cr, semi-insulating, defect chemistry, EPR study 79—99754
GaAs:Cr, semi-insulating, Cr charge states conc., EPR determ. 80—20450
GaAs:Cr, semi-insulating, thermal conversion suppression by arsine-controlled capless-anneal, ion implantation 80—49245
p-GaAs:Cr, semi-insulating, mobilities and carrier concentrations, temp. depend. 80—70702
GaAs:Cr, semi-insulating, Cr redistrib. during thermal annealing as function of encapsulant and implant fluence 80—84199
GaAs:Cr, semi-insulating, Zeeman studies of 0.839 eV emission 80—103987
GaAs:Cr, semiinsulating, hole recomb. domains, Hall mobility and photocond. 77—15867

gallium arsenide continued
- GaAs:Cr, semiinsulating, LPE and elec. props. 77—44178
- GaAs:Cr, semiinsulating, I-V characts., photocond., Fermi level, and deep levels 78—39118
- GaAs:Cr, semiinsulating solid-state inductance, theory and expt. 78—56138
- GaAs:Cr, Si, deep centre photoluminescence spectra 78—95601
- GaAs:Cr, Si ion implantation and annealing, damage recovery, surface carrier profile 77—4119
- GaAs:Cr, single cryst., optical quenching spectrum, disappearance of stationary high-field domain 78—47830
- GaAs:Cr, site symmetry of Cr ions, ground-state splitting, ballistic phonon expts. 78—95273
- GaAs:Cr, strong quenching of thermally stimulated conductivity by elec. field *(Russian)* 77—1434
- GaAs:Cr, surface and bulk recombination parameter determ. from photoluminesc. spectra 77—55820
- GaAs:Cr, Te implantation, electron conc. and mobility profiles depend. on dose and annealing temp. 77—39607
- GaAs:Cr, thermally grown, DLTS study of Cr trap density 80—96815
- GaAs:Cr, VPE grown, exam. of doping GaAs using Cr(CO)$_6$ 78—72737
- GaAs:Cr, VPE growth, carrier conc. profiles 79—74099
- GaAs:Cr, zero-phonon struct. in Cr^{2+} (3d^4) optical absorption 80—60640
- GaAs:Cr, Zn(Se) shallow impurity implantation, elec. props. after annealing 80—24465
- GaAs:Cr,O, semi-insulating, photocond. anal. of levels 80—20243
- GaAs:Cr,O semi-insulating monocrystal development and four-level model 80—88191
- GaAs:Cr,Se, ion-implanted, semi-insulating effects of Cr redistrib. on elec. characts. 80—59982
- GaAs:Cr,Zn, implanted, doping profiles after laser annealing, elec. props. 80—2058
- GaAs:Cr (Cr-Te), and undoped, transverse-acoustoelec.-voltage spectroscopy 79—99586
- GaAs:Cr capless annealed, under As press., Cr redistrib., SIMS obs. 80—59503
- GaAs:Cr diffusion profile meas. 80—6554
- GaAs:Cr diode, high magnetosensitivity of negative resist. region 78—26946
- GaAs:Cr erosion by laser beams *(Russian)* 78—2950
- GaAs:Cr excess electron lifetime determ. by US method *(Czech)* 77—20336
- GaAs:Cr photoconductivity, large scale fluctuations of impurity electostatic potential 77—8145
- GaAs:Cr photoluminesc. meas. 78—6761
- GaAs:Cr plane-parallel photocond. plate, oscills. in current and light intensity in laser irradiation 80—49819
- GaAs:Cr plate, illuminated, oscills. in V-I charact. 80—11038
- GaAs:Cr pulsed electron beam induced recrystallisation and damage, amorphous layer formation 80—34052
- GaAs:Cr semi-insulating substrate, photoluminescence obs. of surface degradation during LPE growth 78—6865
- GaAs:Cr semi-insulating wafer, heat treatment technique for no thermal conversion 80—100857
- GaAs:Cr substrates and LPE layers, Au film deposition and annealing, Cr redistrib. 80—15312
- GaAs:Cr wafers, semi-insulating, surface degradation by heat treatment at 900°C 77—80820
- GaAs:Cr^{2+}, cluster calcs. of Cr^2 electronic states 79—87064
- GaAs:Cr^{2+}, dynamic Jahn-Teller effect, relaxation time for reorientation 80—6798
- GaAs:Cr^{2+}, effect of uniaxial stress and temp. variation on Cr^{2+} centre, EPR expts. 79—95636
- GaAs:Cr^{2+}, Jahn-Teller effect for ion impurities 80—107753
- GaAs:Cr^{2+}, US attenuation meas. of Jahn-Teller distorted Cr^{2+} centres 79—28048
- GaAs:Cr^{2+}(3d^4), Jahn-Teller distortion, photoinduced charge conversion, EPR 78—10758
- GaAs:Cr^{3+} (3d^3), EPR, 5K, evidence for strong Jahn-Teller effects 77—43875
- GaAs:Cr(O), deep impurity levels, AC photocond. meas. 78—19082
- GaAs:Cr(O), mechanism of thermal quenching of luminesc. and photocurrent stimulation 77—55821
- GaAs:Cr(O), photocapacitance of deep levels obs. 79—38021
- GaAs:Cr(Te)(Zn), dopant influence on hardness 77—84777
- GaAs:Cr(W), deep trapping centre exam. by thermally stimulated capacitor discharge method and luminesc. 77—55495
- GaAs:Cs, oxidation process, UPS obs. 80—50511
- n-GaAs:Cu, contaminated single cryst., deep level photoluminesc. model 78—68554
- GaAs:Cu, contamination equilibrium assessment 79—51134
- GaAs:Cu, diffused layers, photocond. spectra, hole conc. and mobility *(Russian)* 78—14758
- n-GaAs:Cu, electron-phonon interaction in optical transitions between deep impurity level and allowed bands 79—42591
- GaAs:Cu, epitaxial and bulk conductivities compared *(Russian)* 78—10585
- GaAs:Cu, Fe, Cr resistance thermometer expts., 0° to 200°C *(Russian)* 78—45627
- p-GaAs:Cu, impurity photocond. and absorpt. coeff., Hall meas. 80—6770
- GaAs:Cu, in MSM struct., phototrigger effect 78—56238
- GaAs:Cu, LPE, photoelec. meas. of electron density for different Cu introduction methods 78—43437
- GaAs:Cu, multiple scatt. Xalpha cluster model, impurity electronic states, dangling bond effect elimination 79—99504
- GaAs:Cu, photoionisation spectrum of deep impurities in presence of weak electron-phonon interactions 79—51529
- GaAs:Cu, sensitivity of impurity photocond., ordered surface irregularities 79—24018
- GaAs:Cu, supersaturated solid solns., decomp., surface impurity content 78—51681
- GaAs:Cu, Te, photoelec. props. 80—92936
- GaAs:Cu electrode photographic device, CO$_2$ pulsed laser output high-speed meas. 79—14008
- GaAs:Cu melt grown, 1.36 eV band luminescence studies, edge emission 79—87510
- GaAs:Cu(Cr) S-type diodes, thermal quenching of injection currents and current-voltage characts. 78—26942
- n—GaAs:Fe, diffusion doped compensated layers 80—15125
- p-GaAs:Fe, ESR line width, temp. depend., 4.2-330K 77—12195

gallium arsenide continued
- GaAs:Fe, exchange-coupled pairs, ESR 79—11343
- GaAs:Fe, for FET, VPE and characterisation 78—19672
- GaAs:Fe, impurity atom charge exchange, Mossbauer spectroscopy 79—47050
- GaAs:Fe, LPE, phase diagram 77—16509
- GaAs:Fe, ordering of Fe impurity, NMR anomalous line shift obs. 78—27102
- GaAs:Fe, p-π-ν-n struct., photoelec. props. 80—107862
- GaAs:Fe, photoionisation cross section meas. of deep levels 77—8042
- GaAs:Fe, profile of impurity optical absorption bands 78—56509
- GaAs:Fe, static magnetis. rel. to doping method and heat treatment conditions 77—36092
- GaAs:Fe epitaxial diode, photocapacitance meas. 77—43708
- GaAs:Fe LPE layers, negative resist. effects and deep acceptor model 77—72929
- GaAs:Fe p$^+$-n junction minority carrier trap meas. by photo-excited DLTS 80—96816
- GaAs:Fe reverse biased π-ν-n struct., switching effect 80—88628
- GaAs:Fe^{3+}, energy spectrum of deep centres, ESR spectrum 77—90023
- GaAs:Fe(Co)(Cu)(Ni), substitutional impurity elec. struct. 80—88513
- GaAs:Fe(Ni) O$_2$ effects on opt. props. 77—16350
- p-GaAs:Ge, (111) surface, LPE grown, cryst. struct., phys. and chem. props. by Auger obs. 79—73386
- GaAs:Ge, cryst. and epitaxial layers, ion-implanted, elec. props. 79—99542
- n-GaAs:Ge, film, substrate temp. depend. of Ge incorporation during MBE 80—76196
- GaAs:Ge, ion implanted, elec. props., comparison with Sn, Se and Te ion implanted samples 77—39879
- GaAs:Ge, ion-implanted, photoluminesc., deep emission centres 80—34965
- GaAs:Ge, LPE, on semi-insulating GaAs, film-substrate interface characterisation 78—72017
- GaAs:Ge, LPE growth, Ge incorporation 78—27423
- GaAs:Ge, MBE layers, complex free-carrier profile synthesis 80—54266
- GaAs:Ge, mol. beam epitaxy of n- and p-types 80—10839
- GaAs:Ge, solubility and point defect-dopant interactions 79—90689
- GaAs:Ge, stress depend. of donor-acceptor recomb. energy 79—15113
- GaAs:Ge, VPE, doping, electrophysical characts. meas. 78—43493
- GaAs:Ge, vap. grown, diatomic complex donor and acceptor model 78—80003
- GaAs:Ge,Se transmutation shallow donor transition obs. 80—59925
- n-GaAs:Ge epitaxial layer, ion-implantation doped, anomalous behaviour of impurities 78—18669
- GaAs:Ge film, MBE grown, heavily doped, elec. props. rel. to growth parameters 80—100537
- GaAs:Ge MBE power FETs with Sn surface impurities 80—80374
- GaAs:Ge p-n junctions by mol. beam epitaxy 79—56289
- GaAs:Ge(Sn), LPE layer growth, impurity effect on terrace form. 79—95288
- GaAs:H amorphous sputtered films, high field cond. props. 80—44607
- n-GaAs:H(D), ion implanted, carrier removal, capacitance-voltage profiling 80—84195
- GaAs:Li diffused, lattice imperfections, TEM 77—80521
- GaAs:Mg, photoluminesc. temp. depend., 4.2-293K 77—69878
- GaAs:Mg ion implanted, photoluminesc. and annealing characts. 77—16361
- GaAs:Mg(Be)(Cd)(Zn), implanted, low temp. photolum. spectra 78—39583
- GaAs:Mg(C)(Te)(Ge), ion implanted, laser annealing, ellipsometric and Hall meas. 79—73193
- GaAs:Mn, LPE layer, near band edge photoluminescence, 2K, low excitation intensities 78—48218
- GaAs:Mn, Mn-O association, EPR meas. 77—69677
- GaAs:Mn, p-type semiconductors, internal strain on bound hole-phonon interaction 78—91492
- GaAs:Mn, photoluminesc., emission props. and radiative mechanism 79—56842
- GaAs:Mn epitaxial layers, fabrication and electrical props. 77—80859
- GaAs:Mn(Ni), negative magnetoresist. meas. 77—51768
- GaAs:N, extended Huckel theory appl. 80—59916
- GaAs:n, ion implantation, hole conc. and mobility profile meas. 78—23082
- GaAs:N$^+$, ion implantation, disorder profiles meas. by Rutherford backscatt. and channelling 80—54270
- GaAs:Na, impurity solubility and diffusion 79—55930
- GaAs:Ni, behaviour of Ni impurity in 3d^8 state, optical absorption and photocond. meas. 78—47737
- n-GaAs:Ni, negative photocond. at low temps., impurity levels 80—6900
- n-GaAs:Ni(Zn), VPE, deep-level transient spectroscopy 80—34383
- GaAs:O, annealing effects, optical absorpt. and I-V characts. 80—29037
- GaAs:O, deep level, Franck-Condon shift, photocond. and Hall effect study 80—70642
- GaAs:O, deep traps, photocapacitance meas., complementary transition energy threshold determ. 79—19550
- GaAs:O, defect states, IR absorption spectra meas. 77—4666
- GaAs:O, electrolum., photolum., negative differential resist. rel. to recomb. processes 80—66304
- GaAs:O, electronic struct., multiple-scatt. Xα mol. cluster model 80—15445
- GaAs:O, evidence for metastable state of O centre, Schottky barrier photocapacitance meas. *(French)* 78—10556
- GaAs:O, Fe, temp. depend. of ionisation energies of O and Fe levels, electroabsorption meas. 78—47736
- GaAs:O, field depend. of radiative recomb. 80—20700
- GaAs:O, high-resist., extrinsic photocond. meas. 77—85255
- GaAs:O, impurity photocond. in high elec. field, 90K 78—19095
- GaAs:O, junction barrier depletion region, capture from free-carrier tails 80—70802
- GaAs:O, optical characterisation of deep O implants 77—55294
- GaAs:O, oxygen-compensated single GaAs cryst., photoelec. memory 79—11184
- GaAs:O, photocapacitance quenching effect 78—91727
- GaAs:O, photocond., electron traps, level-broadening, 90 to 150K 78—60158
- n-GaAs:O, photocond. associated with deep level at 0.4 eV 80—44640
- n-GaAs:O, press. depend. of deep level associated with O, transient capacitance meas. 78—64000
- GaAs:O, semi-insulating, excitation temp. effect on TSC 80—70717
- GaAs:O, slow domains, origin 78—60132

gallium arsenide continued
n-GaAs:O carrier removal profiles meas. 78—56154
GaAs:O epitaxial film, impurity states, photocapacitance spectra 80—65625
n-GaAs:O film, influence of O on elec. props. 79—11252
GaAs:O p-ν-n structs., injection current and negative photocond., saturation mechanism 80—92967
GaAs:P, form. of GaAs$_{1-\eta}$P$_{\eta}$ by diffusion 80—54389
GaAs:P films, epitaxial growth from melt with components introduced by ion bombardment 77—21044
GaAs:P^{+}, defect form. on P^{+} implantation at various temp., He^{+} backscatt. obs. 78—59828
GaAs:P^{+}, implantation profiles, backscatt. meas. 80—70238
GaAs:P^{+}, ion-implanted, refr. index, IR reflection and transmission meas. 77—1671
GaAs:p^{+}(N^{+}), struct. characts. of radiation damage produced by high energy ion implantation 79—4340
GaAs:S, depth profiling using Cs^{+} bombardment and negative SIMS in UH vac. 79—99232
GaAs:S, implantation depth profiles of S^{+} and S$_2{}^{+}$ using AES 79—55774
GaAs:S, ion implantation, expt. 77—11574
n-GaAs:S, Zn VPE film, LF current oscill., negative photocond. 77—80858
GaAs:S epitaxial layers, dopant conc. control method 77—1807
GaAs:S^{+} film, ion implanted carrier characterisation by cyclotron reson. 77—20472
GaAs:S(Se), ion-implanted, evaluation by contactless mobility meas. 79—1448
GaAs:S(Se), MBE grown, surface exchange doping using PbS(Se) captive sources 79—10864
GaAs:S(Si), ion-implanted, capless anneal in As controlled vapour 79—55767
GaAs:S(Te)(Zn), dislocation-free, TEM study of microdefects 79—82213
GaAs:Sb, resonance levels of isoelectronic impurities 80—107740
GaAs:Sb (100) surface, Sb-induced surface states 78—10529
GaAs:Se, fast diffusion of elevated temp. ion implantation, SIMS meas. 78—34527
GaAs:Se, implantation and laser annealing 80—24476
GaAs:Se, implanted, annealing with O-free CVD Si$_3$N$_4$ encapsulant 78—83834
GaAs:Se, implanted, depth profile, SIMS obs. 78—30655
GaAs:Se, implanted, multilayered encapsulation using SiO$_2$:As and Si$_3$N$_4$ 79—11715
GaAs:Se, ion implanted, surface state study from photoreflectance 79—91465
GaAs:Se, ion implanted, Cr redistrib. during annealing, SIMS anal. 80—10570
GaAs:Se, ion implanted, laser annealing 80—24482
GaAs:Se, LPE growth, Ga-As-Se phase diagram 79—1849
GaAs:Se, multiple scatt. Xalpha cluster model, impurity electronic states, dangling bond effect elimination 79—99504
GaAs:Se, pulsed electron beam annealing, doping profiles 80—6421
GaAs:Se cathodoluminescence decay obs. with SEM and streak camera, 90 to 300K 80—97348
GaAs:Se depth profiles, Cs^{+} SIMS anal. appl. 79—39265
GaAs:Se ion implanted samples, Q-switched ruby laser annealing, improvement in elec. props. 80—100460
GaAs:Se ohmic contacts, pulsed electron beam annealing donor density, mobility 80—65678
GaAs:Se^{+}, Cs^{+}-SIMS and negative ion spectrometry 79—12882
GaAs:Se^{+}, implanted semi-insulating, pulsed electron and laser beam annealing effects on elec. characts. 79—73196
GaAs:Se^{+}, TEM structural study, surface and interior damage 80—34025
GaAs:Se(Si), ion-implanted, capless annealing by melt-controlled ambient technique 80—75251
GaAs:Se(Sn), annealing kinetics of implanted donor ions 78—6079
GaAs:Se(Te), laser annealed, donor implanted, elec. props. 79—4556
GaAs:Se(Zn) polycrystalline film, Hall effect, resistivity meas. 80—96911
GaAs:Si, accelerated growth rate effect on MBE, Hall mobility and photolum. meas. 80—104067
GaAs:Si, activation by multiply scanned electron beams 80—75246
n-GaAs:Si, B, IR absorpt. spectra, reson. and localised modes 80—66172
GaAs:Si, charge state of impurity atoms, positron annihilation meas. 78—39062
GaAs:Si, Cr, carrier concs. from Hall effect, microscopy, localised vibrational modes absorption meas. 78—56104
GaAs:Si, current-controlled growth, segregation and amphoteric behaviour 78—31346
GaAs:Si, defect density before and after Zn diffusion, SEM and TEM obs. 80—96529
GaAs:Si, donor-acceptor pair defects absorpt. bands 80—16064
GaAs:Si, electrical activity of Si 79—15145
GaAs:Si, electron irradiated, LPE layers and Bridgman crysts., IR absorption and Hall meas. 77—16345
GaAs:Si, encapsulated by SiO$_2$ and Si$_3$N$_4$, ion-implanted As profiles 79—4319
GaAs:Si, epitaxial layers, photo- and cathodoluminesc. 77—77285
GaAs:Si, faulted and prismatic loops, TEM obs. 77—51386
GaAs:Si, film, conversion of type of conduction stimulated by ion bombardment 77—4457
GaAs:Si, hardening by solute-vacancy pairs 77—4794
GaAs:Si, heteroface solar cells, diffusion lengths 78—47849
GaAs:Si, IR absorpt. bands, localised modes, Si-related defects 80—76054
GaAs:Si, influence of stoichiometry on recomb. processes 80—93396
GaAs:Si, ion implantation, thermal annealing, Hall meas., SIMS atomic profile meas. 80—75243
GaAs:Si, ion implanted, effect on stoichiometry of annealing in ambient 77—51394
GaAs:Si, ion implanted, photoluminesc. 79—69887
n-GaAs:Si, ion implanted and/or annealed, As vacancy form., photolum. line 77—27875
GaAs:Si, ion-implanted, depth distrib. profiles of Si ions 77—43230
GaAs:Si, ion-implanted, elec. props. 79—46686
GaAs:Si, ion-implanted, annealing with Nd:glass laser 79—73194
GaAs:Si, LED, effect of struct., defects on quantum efficiency 79—11211
GaAs:Si, Li, IR absorpt., microstruct., charge compensation 80—107565

gallium arsenide continued
GaAs:Si, momentum distrib. of valence electrons, positron annihilation meas. 79—51530
GaAs:Si, neutron irrad., strain detection by local mode IR absorpt. meas. 77—69828
n-GaAs:Si, optically enhanced Hall mobility meas. 77—39884
GaAs:Si, positron lifetime temp. depend. 80—29826
GaAs:Si, pulsed laser annealing of implanted layers, defect structure and Hall effect meas. 79—69118
GaAs:Si, quantitative anal. with ion microanalyser *(Japanese)* 78—7292
GaAs:Si, single crysts., asymmetric deform. 79—23616
GaAs:Si, stacking fault prod. during heat treatment in As vapour 80—96547
n-GaAs:Si, thermally treated, photolum., acceptor levels obs. 79—38587
GaAs:Si, thick LPE layer growth and characterization 77—12511
GaAs:Si, transferred-electron devices by low-level ion implantation 80—92543
GaAs:Si,Cr, under layer of SiO$_2$, effect of annealing, on electron concentration and mobility, and impurity distrib. 79—4323
GaAs:Si encapsulated with AlN, Si$_3$N$_4$ layers, photolum., annealing effects 80—20681
GaAs:Si epitaxial films, elec. and photoelec. props., impurity distrib. 80—7006
n-GaAs:Si LEC crystal, carrier conc., B acceptor centres, Hall meas. and IR spectra 78—6717
GaAs:Si LED, with anti-Stokes phosphor 79—11204
GaAs:Si LED p-n structures, speed *(Russian)* 79—43044
GaAs:Si LEDs grown from restricted soln.-alloy bulk, props. *(Russian)* 79—43043
GaAs:Si LPE layers, surface morphology, substrate misorientation, initial supercooling effects 80—34329
GaAs:Si layers, MBE growth, elec. and optical props., doping characts. 80—10819
GaAs:Si p-n junction, electrolum. power, injection current and temp. depend. *(Russian)* 77—16401
GaAs:Si p-n junction LED, electroluminesc. efficiency 80—71491
GaAs:Si p-n light-emitting structs., soln. of general minority carrier transport eqn. 80—15597
GaAs:Si p-n structs., effect of growing conditions on distrib. of recomb. parameters 80—39668
GaAs:Si p-n structure, radiative recombination region 78—52071
GaAs:Si(Cr), LPE, spiral growth patterns, dopants role 77—72800
GaAs:Si(Ge) LPE layers, luminesc. props. rel. to substrate quality 78—52583
GaAs:Si(Mg), doped and undoped, sputtered epitaxial films, elec. props. 79—78234
GaAs:Si(Se), ion implanted, laser annealing, microwave device appl. 79—69139
GaAs:Si(Sn), ion implanted, laser annealed, high doping levels 80—88181
n-GaAs:Si(Te), radiative transitions induced by modest annealing, photoluminesc. spectra 80—55158
GaAs:Si(Te)(S), vapour phase epitaxial grown layers, photoluminesc. and emission spectra 80—29774
GaAs:Si(s), generation of high mobility n layers, SIMS 80—103375
GaAs:Sn, 1.39 eV luminescence, injection level depend., freq. response and thermal quenching 78—19529
GaAs:Sn, dopant segregation during liq. phase electroepitaxy 80—54384
GaAs:Sn, doping characts. during LPE 79—10866
n-GaAs:Sn, heavily doped, nonalloyed ohmic contact form. by MBE and metallisation 79—7895
GaAs:Sn, implantation, annealing, impurity-defect struct., Mossbauer study 80—54269
GaAs:Sn, influence of growth process in doping profile and mobility profile during LPE 79—70000
GaAs:Sn, LPE, growth rate and temp. depend. of impurity incorporation 78—3063
GaAs:Sn, LPE layers, electronic props., depend. on Sn incorporation 78—87883
GaAs:Sn, nature and conc. of point defects over conc. range 10^{17} to 6.10^{18} cm^{-3} 79—14802
n-GaAs:Sn, nonalloyed and in situ Ohmic contacts for FETs 79—56307
n-GaAs:Sn, photoluminesc. spectra 79—43031
GaAs:Sn, proton implantation and annealing behaviour *(Chinese)* 80—44224
GaAs:Sn, selective LPE, orientation dependent growth, luminesc. 77—12551
GaAs:Sn, solubility and point defect-dopant interactions 79—90688
GaAs:Sn, surface segregation of Sn during MBE, SIMS and AES 78—72031
n-GaAs:Sn, Te, compact IR laser source pumped by electron beam from field emission tube 79—59725
GaAs:Sn, Te, luminescence props. 79—52017
n-GaAs:Sn, VPE growth, reactor design 80—2956
GaAs:Sn diode, LPE grown, electron irrad. effect on characts. 80—39667
GaAs:Sn epitaxial layer, electronic props. and epilayer-substrate interface props. 77—89886
n-GaAs:Sn epitaxial layer, free carrier relax. time, transverse magnetoplasma refl. 77—90212
GaAs:Sn films, MBE 80—50563
GaAs:Sn films, MBE grown, doping profiles, carrier mobilities, RHEED and AES obs. 79—1447
GaAs:Sn layers for MESFET, MBE growth 77—15952
GaAs:Sn thermal diffusion from spin-on SnO$_2$/SiO$_2$ source 80—96691
GaAs:Sn^{+}, impurity-defect complex from ^{119}In implantation, Mossbauer study 80—59486
n-GaAs:Sn-p-GaAs:Ge-p-Al$_x$Ga$_{1-x}$As:Ge heterostructure solar cells, LPE growth techniques 80—66977
GaAs:Sn(Be) MBE films, elec. characterization 79—91168
GaAs:Sn(Te), epitaxial film, influence of impurities on stacking fault energy 80—103371
n-GaAs:Sn(Te), pure and doped, diffusion of Sn, radiotracer profiles 79—23782
n-GaAs:Te, 0.93-0.99 eV luminesc. band characts. 78—19560
GaAs:Te, amorphous, ion implanted layers, optical refl., 1.5-7.0 eV 79—8152
n-GaAs:Te, elec. cond. and Hall coeff. temp. depend. meas., three band model 79—33287
n-GaAs:Te, electron-irrad., absorpt. spectra *(Russian)* 78—15200
GaAs:Te, Ge, compensated, activated cond. 77—76968

gallium arsenide continued
n-GaAs:Te, heavily doped, interband luminesc. intensity, heat treatment effect 78—72593
GaAs:Te, heavily doped degenerate semicond., Kondo effect 79—61053
GaAs:Te, heavily-doped, annealing-induced prismatic dislocation loops and elec. changes 78—51546
GaAs:Te, implanted and laser annealed, surface crystallinity, refl. and channelling meas. 79—95036
GaAs:Te, impurity cond., microcathode-luminesc. investig. 77—8666
GaAs:Te, ion implanted, abrupt dopant profile 77—1143
GaAs:Te, ion implanted, laser annealing 79—73192
GaAs:Te, ion implanted, surface crystallinity and stoichiometry of laser annealed samples 79—73198
GaAs:Te, ion implanted, ohmic contacts produced by laser-annealing 79—73585
GaAs:Te, ion implanted optical transitions in modulated reflectivity spectrum 79—73972
GaAs:Te, LPE, Te induced defects, rel. to growth conditions 78—6067
GaAs:Te, laser annealing of implanted Te 78—35400
GaAs:Te, microcathodoluminesc. of effect of struct. defects on radiative recomb. 79—11475
GaAs:Te, phonon-dislocation interactions, nonstoichiometry effect *(French)* 77—43298
GaAs:Te, powder, quadrupole interactions in NMR spectra 79—51880
GaAs:Te, preferential precipitation on dislocation loops 79—7612
GaAs:Te, recombination barrier, dark cond., photocond., and Hall mobility meas. 80—15559
GaAs:Te, solubility and point defect-dopant interactions 79—90687
GaAs:Te, superdilation and defects, lattice parameter meas. and carrier mobility 80—10569
n-GaAs:Te, vibr. props. of 1.0, 1.2 and 1.3 eV luminesc. centres 77—55823
GaAs:Te diffused LED, electron irrad. effect on characts. 80—39667
GaAs:Te influence of fluctuations of impurity pot. on Burstein-Moss effect 78—48240
GaAs:Te Schottky barrier solar cells, diffusion length determ. using minority carrier SEM 80—61359
GaAs:Te$^+$(Se$^+$)(Sn$^+$)(Ge$^+$), ion implanted, laser annealing effect on elec. characts. 79—73195
GaAs:Te-implanted by laser-annealing, ohmic contacts 79—19658
GaAs:Te(Cd)(Mg)(B), ion implant depth distribs., AES and glow discharge optical spectroscopy meas. 80—65028
GaAs:V, ion implanted, luminesc., level splitting 80—97338
GaAs:W^{2+}, radiative transitions, photoluminesc. obs. 80—108271
GaAs:Zn, diffusion during LPE, impurity gradients and annealing effects 80—29882
GaAs:Zn, diffusion of Zn by two-temp. method, LED fabrication 80—49416
GaAs:Zn, distribution of radiative recombination efficiency 79—78725
GaAs:Zn, heavily doped, photolum. obs., above gap 80—29796
GaAs:Zn, high surface conc. Zn diffusion for good ohmic contact 77—11575
GaAs:Zn, implanted, furnace annealed, electrical, Rutherford backscattering and TEM meas. 80—100272
GaAs:Zn, implanted, hole conc. and mobility profiles meas. 78—23081
GaAs:Zn, implanted, laser annealing, elect., Rutherford backscattering and SEM meas. 80—100273
GaAs:Zn, ion implanted, TEM study after laser and furnace annealing 80—70234
GaAs:Zn, laser annealing of implanted layers 77—55296
p-GaAs:Zn, luminescent, ion doped MBE growth 80—44436
GaAs:Zn, MBE with ionized beam doping 77—77418
p-GaAs:Zn, Mn, degenerate, tunnel p-n junction and semicond.-metal struct., I-V characts. 78—72252
GaAs:Zn, pulsed laser annealing, expt. 78—34828
p-GaAs:Zn, Raman scatt. by LO phonon-plasmon coupled modes, wave vector non-conservation 80—16033
GaAs:Zn, Se, double doping during LPE, exam. of elec. cond. and Hall effect 79—4923
GaAs:Zn, sign inversion of the linear photogalvanic effect *(Russian)* 80—80321
GaAs:Zn, surface conc. control 79—55758
GaAs:Zn (110), spin polarised electron production by photoemission from Cs-O overlayer 79—95903
GaAs:Zn diffused, meas. of depth profiles, photoluminescence technique, LED applic. 78—72587
GaAs:Zn epitaxial layers, composition and Zn carrier conc. 80—25585
GaAs:Zn films, VPE growth and photoluminesc. props. 79—38642
GaAs:Zn ion implanted ionic alloy, electrophysical props., annealing 80—39133
GaAs:Zn MBE layers, ionized beam doping, elec. and optical characts. 79—37721
p-GaAs:Zn optical absorpt. spectra and photocond. after 2 MeV electron irrad. *(Russian)* 77—69859
GaAs:Zn optically pumped ribbon-whisker laser, picosecond pulses 80—99771
n-GaAs:Zn substrate, ion implantation as predeposition process 79—19268
GaAs:Zn waveguide, light coupling at fundamental absorption edge 79—23082
GaAs:Zn-$Al_{0.5}Ga_{0.5}As$ p-n junction, surface layer effect on surface recombination current 79—69585
GaAs:Zn(Cr), As precipitation at dislocations, TEM study 80—79820
GaAs:Zn(S), LPE, and doping characts. 79—33948
GaAs:Zn(Se), recrystn. of implanted amorphous layers, TEM and channelling obs. 77—89459
GaAs:Zn(Si)(Sn), etching rel. to dopant and carrier conc. 77—16704
GaAs/(Ga,Al)As, DH laser diode, electroluminescence near 1 eV 80—60682
GaAs/(GaAl)As channelled substrate narrow stripe lasers, with quarter-wavelength facet coatings 80—99746
GaAs/$Al_xGa_{1-x}As$ heterostruct., anomalous elec. and optical characts. 80—2865
GaAs/Al-Au interfaces, atomic interdiffusion, soft XPS studies 80—65302
GaAs/AlGaAs, DH laser, degradation under Ar laser irrad. 79—98375
GaAs/AlGaAs DH wafers and lasers, defect struct., X-ray topography 79—50312
GaAs/AlGaAs integrated twin guide injection lasers prepared by LPE, coupling coeff. and coupling length meas. 79—81458

gallium arsenide continued
GaAs/anodic oxide interface, characterisation of proposed model 80—103754
p-GaAs/Au-Be ohmic contact form. by ionised-cluster beam deposition 77—32528
GaAs/Au-Ge/Au structure, ohmic contact behaviour, alloying time effect 79—19659
GaAs/Au-Ge/Ni, Schottky barrier energy var. with interdiffusion 77—20435
GaAs/Au-Ge/Ni contact system, alloying behaviour, microprobe AES and X-ray diffr. 80—54548
n-GaAs/Au-Ti contacts, interdiffusion and Schottky barrier height variations 77—89849
n-GaAs/Au-W contacts, interdiffusion and Schottky barrier height variations 77—89849
n-GaAs/chalcogenide glass, elec. props. and band diagram 79—99609
GaAs/GaAlAs crowding effect lasers using whispering gallery mode on semi-insulating GaAs substrates 80—58589
GaAs/GaInP DH, MBE grown, optically pumped laser action at 77K 80—95890
GaAs/HBr system, heterogeneous reactions, modified entrainment method appls. 79—23551
n-GaAs/K_2Se-K_2Se_2-KOH/C solar cell, Ru (III) chemisorption on photoanode, effect on performance 80—3516
n-GaAs/K_2Se-K_2Se_2-KOH/C liq. junction cell, effect of Ru ion chemisorption on grain boundaries 80—55879
n-GaAs/N-GaAlAs heterojunctions, microwave detection 79—54186
GaAs/Ni film contact system, alloying reaction 80—96747
GaAs/Ni-Ge-Au cathode struct., with enhanced injection efficiency, contact resist. 77—20431
GaAs/oxide interface, interface states obs. by electrochem. method 79—99626
n-GaAs/Pt/Cr Schottky contact, barrier height change due to heat treatment 79—47165
p-GaAs/rare earth metal contacts, surface pot. barrier 80—60086
GaAs/SiO_2, substrate/film system, Ga content in SiO_2 after annealing at 730-940°C 78—43255
GaAs/SiON substrate/film system, interface formation during CVD, modelling 80—24764
n-GaAs/ZnSe:Mn/Au low threshold thin film DC electrolum. cell, pulse-excited characts. 80—76081
GaAs-(Ga,Al)As heterostructure transmission photocathodes, characts. and epitaxial growth *(French, English)* 78—52616
GaAs-(Ga,Al)As light modulators and distributed Bragg reflector laser, monolithic integration 78—50944
GaAs-(GaAl)As, DH laser, injection enhanced dislocation glide under uniaxial stress 77—27885
GaAs-(GaAl)As channelled substrate buried heterostruct. injection laser, fabrication 77—7087
GaAs-(GaAl)As DH injection laser with pillbox resonator, characts. and fabrication 80—58581
GaAs-(GaAl)As DH lasers, automated LPE growth, CW reliability tests 80—20804
GaAs-(GaAl)As DH stripe lasers, CW life tests 79—98383
GaAs-(GaAl)As epitaxial layers and DH lasers, deep centre 1.02 eV luminesc. 78—80387
GaAs-(GaAl)As injection lasers with circular resonator 80—74377
GaAs-(GaAl)As LOC-DBR laser, high differential quantum efficiency 78—79031
GaAs-(GaAl)As laser, SiO_2 stripe geometry, for wide band optical communication systems 78—42358
GaAs-(GaAl)As terraced-substrate injection lasers, fabrication and output characts. 79—50310
GaAs-(GaAl)As terraced substrate laser, fundamental transverse and longit. mode oscill. 79—98357
GaAs-$(SN)_X$, solar cell fabrication and efficiency 80—26143
GaAs-$(SN)_x$ semiconductor-polymer solar cell 79—15219
GaAs-Al (Ni-AuGe) contacts, elec. characts. 80—29476
GaAs-Al interdiffusion, 250-450°C, AES meas. 77—1263
GaAs-Al interface, ellipsometric anal. methods, correl. between optical props., thickness and surface roughness meas. *(German)* 80—55215
GaAs-Al interface, metal overlayer effect on semicond. (110) surface states 77—4441
p-GaAs-Al interface, produced by diffusion method using heavily doped GaAs, rectifying props. 79—28409
GaAs-Al interface, struct. study by X-ray total-external-refl.-Bragg diffr. 80—34321
GaAs-Al interface, thermal ageing of Al film, optical microscopy and SEM obs. 77—20203
GaAs-Al interfaces, chemically induced charge redistrib. 79—33342
GaAs-Al Schottky barrier diode, prep. by MBE on GaAs, and characts. 78—72257
n-GaAs-Al surface barrier diodes, influence of exciton effects on photo-EMF spectrum 78—10557
GaAs-$Al_{0.27}Ga_{0.7}$ 7_3As Dh lasers grown by MBE, influence of growth conditions on threshold current density 80—58587
GaAs-$Al_{0.2}Ga_{0.8}As$ periodic layered media, optical surface waves 78—43946
p-GaAs-$Al_{0.3}Ga_{0.7}As$, cladded dielec. waveguide, loss meas. using Raman scatt. 79—81539
GaAs-$Al_{0.3}Ga_{0.7}As$ n-N heterojunction, LPE grown, cond. band discontinuity, C-V profiling meas. 80—70801
GaAs-$Al_{0.3}Ga_{0.7}As$ laser diode, spontaneous radiation transfer 80—91796
GaAs-$Al_{0.4}Ga_{0.6}As$, p-n heterojunction, quantum confinement and compositional grading effects on band struct. 79—87151
GaAs-$Al_{0.5}Ga_{0.5}As$-Cr/Au MIS capacitors, characts. meas. 78—95371
GaAs-$Al_{1-x}Ga_xAs$ lar, PbO-SiO_2 glass optical coating 78—71113
GaAs-Al_2O_3 anodic oxide interface, elec. props., rel. to MESFET passivation 80—49934
GaAs-Al_2O_3 interface, fabricated by interactive oxidation, props. 80—49935
GaAs-Al_2O_3 MIS struct., interface props. and MISFET fabrication 79—65557
GaAs-Al_2O_3-Al backwall MIS Schottky barrier solar cell, anal. model 80—85289
GaAs-$Al_xGa_{1-x}As$ transverse junction lasers with low threshold current prep. by MBE on semi-insulating substrates 80—58588
GaAs-$Al_xGa_{1-x}As$, optically pumped multilayer struct. and DH, laser oscillations 77—3589
GaAs-$Al_xGa_{1-x}As$, integrated twin-guide laser with distrib. Bragg reflectors 77—19310

gallium arsenide continued
GaAs-Al$_x$Ga$_{1-x}$As, heterojunction photodiode, electric and photoelectric characts. 77—55604
GaAs-Al$_x$Ga$_{1-x}$As, DH laser, lateral current confinement by reverse biased junction 77—58339
GaAs-Al$_x$Ga$_{1-x}$As, single mode optical rib waveguides, MOS control of switches 78—1432
GaAs-Al$_x$Ga$_{1-x}$As, DH LED, self-aligned sphere lens array characteristics *(German)* 78—38014
GaAs-Al$_x$Ga$_{1-x}$As, single-mode rib waveguide switches electro-optical modulation 78—46839
GaAs-Al$_x$Ga$_{1-x}$As, optically pumped taper coupled laser, second order Bragg reflector 78—50788
GaAs-Al$_x$Ga$_{1-x}$As, DH laser, effect of bulk nonradiative recombination 78—82967
GaAs-Al$_x$Ga$_{1-x}$As, monolithic integrated optics, rib waveguide switches with MOS electrooptic control 78—87168
GaAs-Al$_x$Ga$_{1-x}$As, film waveguide, heterojunction lasers with Bragg mirrors, threshold characts. 79—23095
GaAs-Al$_x$Ga$_{1-x}$As, carrier transport across heterojunction interfaces 79—47158
GaAs-Al$_x$Ga$_{1-x}$As, negative differential resist., real-space electron transfer 80—6958
GaAs-Al$_x$Ga$_{1-x}$As, heterojunction and superlattice, magnetophonon reson., polaron mass 80—44715
GaAs-Al$_x$Ga$_{1-x}$As, current transverse junction lasers, low threshold, MBE prep. 80—83614
GaAs-Al$_x$Ga$_{1-x}$As buried-heterostructure laser, wideband optical sources *(German)* 78—37904
GaAs-Al$_x$Ga$_{1-x}$As buried-heterostructure lasers, current injection confinement, MBE/LPE hybrid technique 80—74374
GaAs-Al$_x$Ga$_{1-x}$As CW-diode laser, coupled to freq.-selective external cavity, self-pulsing 77—61982
GaAs-Al$_x$Ga$_{1-x}$As channelled-substrate-planar-struct. laser with lateral-evanescent-field distributed feedback 79—98398
GaAs-Al$_x$Ga$_{1-x}$As current injection multi-quantum-well heterostructure lasers, MBE grown 80—19042
GaAs-Al$_x$Ga$_{1-x}$As DH laser, high-temp. degradation *(German)* 78—37884
GaAs-Al$_x$Ga$_{1-x}$As DH laser, modulation with coherent light injection *(German)* 78—37922
GaAs-Al$_x$Ga$_{1-x}$As DH laser structures, high-resolution composition profiling with photolum. 78—71101
GaAs-Al$_x$Ga$_{1-x}$As DH laser, room temp. threshold current 78—79019
GaAs-Al$_x$Ga$_{1-x}$As double heterojunctions, dark-line defects and recomb. centres, scanning photocurrent microscopy 79—35822
GaAs-Al$_x$Ga$_{1-x}$As DH lasers, MBE grown, low current threshold, high lasing uniformity 79—64223
GaAs-Al$_x$Ga$_{1-x}$As DH broad contact pulse lasers, second-order coherence props. 80—23685
GaAs-Al$_x$Ga$_{1-x}$As DH lasers, very low current threshold, MBE grown 80—43353
GaAs-Al$_x$Ga$_{1-x}$As DH lasers, MBE grown, substrate temp. effect on current threshold 80—48243
GaAs-Al$_x$Ga$_{1-x}$As differentially doped heterojunction interface, two-dimens. electron gas obs. 80—49886
GaAs-Al$_x$Ga$_{1-x}$As DH laser, MBE grown, CW electro-optical props. 80—102725
GaAs-Al$_x$Ga$_{1-x}$As epitaxial layer heterointerface, toroidal defect obs. 79—77933
GaAs-Al$_x$Ga$_{1-x}$As electro-optic frequency- and polarisation-modulated injection laser 80—91810
GaAs-Al$_x$Ga$_{1-x}$As films for optical devices, masked MBE 78—38100
GaAs-Al$_x$Ga$_{1-x}$As heterostructure superlattice, construction of bound states in continuum 77—32076
GaAs-Al$_x$Ga$_{1-x}$As heterojunction, MBE, diffusion across interface, optical annealing expts. 78—2305
GaAs-Al$_x$Ga$_{1-x}$As heterojunction, avalanche phototransistors, detectivity and noise 78—2558
GaAs-Al$_x$Ga$_{1-x}$As heterojunctions, MBE grown, photocollection efficiency and interface charges 79—11199
GaAs-Al$_x$Ga$_{1-x}$As heterostruct., photon recycling, diffusion length and lifetime determ. 79—47499
GaAs-Al$_x$Ga$_{1-x}$As heterojunctions, inelastic light scatt. 79—65867
GaAs-Al$_x$Ga$_{1-x}$As heterojunctions, LPE grown, 2D electron gas obs. 79—99606
GaAs-Al$_x$Ga$_{1-x}$As heterojunction interface, two-dimensional hole gas obs., Shubnikov-de Haas meas. 80—80357
GaAs-Al$_x$Ga$_{1-x}$As heterostructures, real-space electron transfer by thermionic emission, analytical model 80—100512
GaAs-Al$_x$Ga$_{1-x}$As integrated optics structs., dry processing 77—27383
GaAs-Al$_x$Ga$_{1-x}$As integrated injection lasers and detectors with etched reflectors 77—62074
GaAs-Al$_x$Ga$_{1-x}$As integrated lasers and detectors fabricated by wet chemical etching 77—88961
GaAs-Al$_x$Ga$_{1-x}$As injection laser, direct modulation and spectral props. *(German)* 78—37921
GaAs-Al$_x$Ga$_{1-x}$As LPE heterojunction, interface states 78—19128
GaAs-Al$_x$Ga$_{1-x}$As multilayer struct., MBE, selective area growth using Si shadow masks 77—85946
GaAs-Al$_x$Ga$_{1-x}$As modulation-doped heterojunction superlattices, electron mobilities 79—7877
GaAs-Al$_x$Ga$_{1-x}$As multilayer, photoluminesc., electron spin orientation 80—25453
GaAs-Al$_x$Ga$_{1-x}$As MOS rib waveguide polarizers 80—64207
GaAs-Al$_x$Ga$_{1-x}$As MOS rib waveguide polariser, modulator and isolator 80—64217
GaAs-Al$_x$Ga$_{1-x}$As multilayers, two-dimens. transport at high mag. fields 80—65724
GaAs-Al$_x$Ga$_{1-x}$As optical modulator for coupled-waveguides 78—71235
GaAs-Al$_x$Ga$_{1-x}$As proton-isolated DH laser, threshold current optimisation *(German)* 78—37905
GaAs-Al$_x$Ga$_{1-x}$As single mode rib waveguide COBRA switches, MOS control 77—88970
GaAs-Al$_x$Ga$_{1-x}$As single heterostructure laser diode, pulse operating, anal. of temp. decrease in active region 78—13706
GaAs-Al$_x$Ga$_{1-x}$As stripe geometry DH laser, threshold current density, effect of optical mode losses 78—59008
GaAs-Al$_x$Ga$_{1-x}$As superlattice, mag. field induced dimensionality change 78—64381
GaAs-Al$_x$Ga$_{1-x}$As structures for DH lasers, LPE *(Polish)* 79—4922

gallium arsenide continued
GaAs-Al$_x$Ga$_{1-x}$As strip-buried heterostruct. laser with distributed feedback 79—76696
GaAs-Al$_x$Ga$_{1-x}$As strip buried heterostructure lasers 79—81425
GaAs-Al$_x$Ga$_{1-x}$As superlattice, electronic props. 80—11080
GaAs-Al$_x$Ga$_{1-x}$As strip buried heterostructure laser with passive DBR 80—14352
GaAs-Al$_x$Ga$_{1-x}$As transverse junction stripe laser, single-mode oscillation *(German)* 78—37885
GaAs-Al$_x$Ga$_{1-x}$As-GaP photocathodes, minority carrier diffusion length determ. by photoluminesc. 80—103992
GaAs-AlAs, alternate monolayer single cryst., optical waveguides 77—72065
GaAs-AlAs, epitaxial layer, partition coefficients of impurities 77—15443
GaAs-AlAs, epitaxial struct. with alternate layer comp. modulation, fabrication and characterisation 77—1322
GaAs-AlAs, heterolight diodes, mesoconstruction, output *(Russian)* 77—12441
GaAs-AlAs, heterostructure, effects of cation order on energy bands 80—11081
GaAs-AlAs, large area p-n heterojunctions, vapour phase epitaxially grown, elec. characterisation 77—11990
GaAs-AlAs, one-dimensional superlattice, X-ray diffr. 77—27860
GaAs-AlAs, pseudobinary alloy, phase diagram calc. 78—52786
GaAs-AlAs (100) interface, tight binding calc. of electronic struct. 78—95342
GaAs-AlAs abrupt (110) interface, electronic struct. 78—95339
GaAs-AlAs alternating epitaxial monolayers, Raman scatt. and zone-folding effects 77—90208
GaAs-AlAs alternating monolayers, zone folding effects on phonons 78—72510
GaAs-AlAs and related monolayer heterostructures, pseudopot. calc. 78—60198
GaAs-AlAs heterojunction, recombination currents 78—14806
GaAs-AlAs layered films, MBE prep., struct., rel. to optical props. 79—77950
GaAs-AlAs layered superlattices, deposited by MBE, exam. of crystal growth kinetics 78—72739
GaAs-AlAs mixed crystal, optical obs. of multiple-photon absorpt. NMR *(Russian)* 77—90073
GaAs-AlAs mixed crystals, valence charge distrib. and elec. field gradients 80—80239
GaAs-AlAs multilayer heterostructure laser, power and photoelectroluminescence characts. 80—53297
GaAs-AlAs superlattice, folded acoustic phonons obs., Raman scatt. 80—88996
GaAs-AlAs system, diffuse scatt. of X-rays by single crysts. *(German)* 78—30517
GaAs-AlGaAs CW laser coupled to external cavity, multimode operation, output intensity low freq. pulsations 79—68394
GaAs-AlGaAs DH, improved LPE growth, lasing characts. 77—81229
GaAs-AlGaAs DH injection laser, emission energy, wavelength depend. in strong mag. fields 80—48248
GaAs-AlGaAs DH injection laser with stripe contacts, radiation pulse stepped shape 80—91799
GaAs-AlGaAs DH laser, rapid degradation caused by process-induced defects 77—71985
GaAs-AlGaAs DH laser, improved lifetime by defects reduction during LPE 77—75547
GaAs-AlGaAs DH laser, impedance meas. 78—17939
GaAs-AlGaAs DH lasers, multipeak freq. response obs. 78—17940
GaAs-AlGaAs DH laser with buried facet 78—55373
GaAs-AlGaAs DH laser, degradation rate rel. to photocurrent 80—28233
GaAs-AlGaAs DH laser structure, defect assessment by differentiated cathodolum. topography 80—59819
GaAs-AlGaAs DH layers, tapered growth by wipingless LPE 77—66594
GaAs-AlGaAs distributed Bragg reflector integrated twin-guide laser, temp. characts. 78—87064
GaAs-AlGaAs double heterostructure, optically induced dislocation glide, cooperative phenomena 78—74911
GaAs-AlGaAs half-ring laser, fabrication by deep Zn diffusion 78—17960
GaAs-AlGaAs heterojunction superlattices, electron mobilities 80—29473
GaAs-AlGaAs heterojunction superlattices, obs. of intersubband excitations in multilayer two dimensional electron gas 80—29753
GaAs-AlGaAs heterojunction superlattices, inelastic light scatt. by two-dimens. electron gas 80—93360
GaAs-AlGaAs heterostructure thyristors, operation and elec. characts. 79—7891
GaAs-AlGaAs high-radiance LED for optical communication systems, power and modulation bandwidth 78—42416
GaAs-AlGaAs LPE growth, wipinglass method for DH laser *(Japanese)* 78—48304
GaAs-AlGaAs LPE layers, baking effect on surface morphology 78—14625
GaAs-AlGaAs laser array packaged with fibre lightguide array on Si substrate 78—46611
GaAs-AlGaAs multilayer stack, optical surface wave propag. 78—38090
GaAs-AlGaAs photoelectroluminescent diodes, characts., radiant power 80—6972
GaAs-AlGaAs solar cells *(Rumanian)* 80—93877
GaAs-AlGaAs solar cells with valley-transferred electrons for voltage and efficiency enhancement 80—93956
GaAs-AlGaAs superlattice, selective transmission of HF phonons 80—34154
GaAs-AlGaAs transverse junction stripe laser, single mode behaviour after 12000 hr ageing test 78—66831
GaAs-AlGaAs two-junction stacked solar cell, growth and characterisation 80—16811
GaAs-AlGaAs:Si heterojunction interface, two-dimens. electron gas, Hall effect and cyclotron reson. meas. 79—65530
GaAs-Al(Au) Schottky barrier diodes, Richardson consts. 77—20424
GaAs-Al(Ga)(Ge), surface reactions and interdiffusion, photoemission study 80—49532
GaAs-anodic oxide interfaces, struct. and chem. props., Raman scatt. obs. 79—47168
n-GaAs-anodic oxide MIS devices, inversion and accumulation layer form. at elevated temps. 79—60934
GaAs-anodic oxide MOS struct. oxide and interface props. 79—60929
GaAs-anodic oxide MOS struct., interface state band 79—60930

gallium arsenide continued
n-GaAs-anodic oxide-Al MOS struct., elec. instabilities and annealing effects 79—60928
GaAs-Au, quenching of exciton luminesc. by surface elec. field 80—29801
GaAs-Au, Schottky barrier energy var. with interdiffusion 77—20435
GaAs-Au interface, atomic modulation of interdiffusion, effect of reactive Al monolayers 80—49432
GaAs-Au polycrystalline Schottky barriers, transition with grain size from electrode-limit to bulk-limited cond. 80—65676
n-GaAs-Au Schottky barrier diode, thermally assisted tunnelling currents 77—20412
GaAs-Au Schottky barrier diodes, fabrication using LPE 77—40357
GaAs-Au Schottky barriers, PES and depth profiling obs. 79—42641
GaAs-Au Schottky diode, electroless plating of Au, fast characterisation of epitaxial layers 79—33347
n-GaAs-Au-Mo, RF sputtering, elec. props. of contacts, compensating damage centres form. 80—34507
GaAs-Au(Ag) Schottky barrier solar cells, interface problems, AES, SIMS and XPS study 80—89627
n-GaAs-Au(Al) Schottky diodes, interface state density model 77—80840
GaAs-Br$_2$(-Zn) system, filamentary cryst. prep. 78—52650
GaAs-C, ion implanted, obs. of localised vibrational mode absorption, effects of annealing temp. 80—16068
p-GaAs-Cd$_{1-x}$Zn$_x$S heterojunctions, elec. and photovolt. props. rel. to growth technique 80—29466
GaAs-CdS heterojunction, prep. by CdS CVD and etching 78—52062
GaAs-CdS n-n voltage-enhanced photoanode, solar cell efficiency 78—14810
n-GaAs-chalcogenide glass heterojunction, fabrication, characterization, switching 80—49892
GaAs-Cr Schottky barriers, interfacial structural defects effect on avalanche breakdown 79—42644
GaAs-Cs-O, negative electron affinity, secondary emission characts. 78—11031
GaAs-Cs-O, negative electron affinity, refl. of slow electrons, 0.4-3 eV 78—11038
GaAs-Cs-O film, polycryst., secondary emission props., activating coating effects 78—2957
GaAs-Cs-O photoemitter, negative electron affinity, fabrication and characts. 78—2979
GaAs-Cu:Tl, cathode luminescence spectra, Hall effect, cryst. defects 80—76087
GaAs-disperse metal film, photoluminesc. at interface 78—26953
n-GaAs-electrolyte interface, surface pretreatment rel. to photocurrent, spectral response 80—3204
GaAs-electrolyte interface, surface barrier electroreflection anisotropy *(Russian)* 80—34895
GaAs-element systems, solidus curves calc. for liq. phase epitaxy technology 77—8768
n-GaAs-ferrite layer struct., boundary spin wave amplification *(Russian)* 77—73016
GaAs-Ga, (110) interface electron states, photoemission study, chemical shift, surface charge redistrib. 78—72259
GaAs-Ga$_{0.7}$Al$_{0.3}$As channelled substrate buried heterostructure injection lasers 77—38932
GaAs-Ga$_{0.7}$Al$_{0.3}$As (001), (211), threading dislocation in single layer heteroepitaxial struct., bowing 79—65341
GaAs-Ga$_{0.7}$Al$_{0.3}$As n-n heterojunction, LPE, rectification 80—49888
GaAs-Ga$_{0.8}$Al$_{0.2}$As layered struct., LPE, optical surface waves 78—48244
GaAs-Ga$_{1-x}$Al$_x$Al superlattice, reson. Raman scatt., 2-D quantum states 77—8577
GaAs-Ga$_{1-x}$Al$_x$As, DH, dark line defects induced by mech. bending 77—683
GaAs-Ga$_{1-x}$Al$_x$As, monolithically integrated DFB diode laser, freq. multiplexing 77—702
GaAs-Ga$_{1-x}$Al$_x$As, DH, improved LPE growth method 77—4746
GaAs-Ga$_{1-x}$Al$_x$As, DH distributed Bragg reflector laser, room temp. operation 77—7085
GaAs-Ga$_{1-x}$Al$_x$As, optically pumped ring laser fabricated by LPE over chemically etched channels 77—10958
GaAs-Ga$_{1-x}$Al$_x$As, n$^+$-i-n heterojunction, radiative recombination under double injection *(Russian)* 77—77298
GaAs-Ga$_{1-x}$Al$_x$As, LPE growth for solar cells 77—77427
GaAs-Ga$_{1-x}$Al$_x$As, DH laser Al$_2$O$_3$ facet coating effect on degradation 78—13722
GaAs-Ga$_{1-x}$Al$_x$As, DH laser, characts. exam. for communication appl. 78—37891
GaAs-Ga$_{1-x}$Al$_x$As, superlattice umklapp processes in resonant Raman scattering 78—64362
GaAs-Ga$_{1-x}$Al$_x$As, ultrathin layer heterostruct., pseudopot. calcs. 78—95343
GaAs-Ga$_{1-x}$Al$_x$As, single-heterostructure laser diode with short current pulses, heat spreading analysis 79—76690
GaAs-Ga$_{1-x}$Al$_x$As, semiconductor superlattices by MBE 79—95939
n-GaAs-Ga$_{1-x}$Al$_x$As, superlattice, subband struct. and optical spectra, self-consistent calc. 80—15443
GaAs-Ga$_{1-x}$Al$_x$As, variable band gap, photo-EMF 80—20296
n-GaAs-Ga$_{1-x}$Al$_x$As, heavily doped superlattice, electronic props., perpendicular low temp. mobility 80—65660
GaAs-Ga$_{1-x}$Al$_x$As buried DH diode laser fabrication 77—75565
GaAs-Ga$_{1-x}$Al$_x$As DH lasers, X-ray topographic obs. of lattice defects rel. to degradation 77—15420
GaAs-Ga$_{1-x}$Al$_x$As DH lasers, long-term degradation due to facet erosion 77—50672
GaAs-Ga$_{1-x}$Al$_x$As DH strip CW laser for optical transmission *(German)* 77—68222
GaAs-Ga$_{1-x}$Al$_x$As double heterostructure LED and injection laser transmitters 77—68282
GaAs-Ga$_{1-x}$Al$_x$As DH injection laser, curved junction stabilized filament, struct. and characts. 78—33744
GaAs-Ga$_{1-x}$Al$_x$As DH laser, curved stripe, operation and appl. 78—42341
GaAs-Ga$_{1-x}$Al$_x$As DH lasers, electron beam induced current microscopy 80—95899
GaAs-Ga$_{1-x}$Al$_x$As half-ring laser, fabrication by LPE over chemically etched channels 77—684
GaAs-Ga$_{1-x}$Al$_x$As heterostruct. superlattice, props. in high mag. fields 79—73570
GaAs-Ga$_{1-x}$Al$_x$As heterostructures, quantum size effect in superlattices, electronic props. 80—29471

gallium arsenide continued
GaAs-Ga$_{1-x}$Al$_x$As laser, low threshold room temp. embedded DH, fabrication and characts. 77—681
GaAs-Ga$_{1-x}$Al$_x$As laser, optically pumped, longit. mode broadening due to transient heating 77—61953
GaAs-Ga$_{1-x}$Al$_x$As LPE wafer stress-free dislocation generation 77—75527
GaAs-Ga$_{1-x}$Al$_x$As multilayer struct., growth over preferentially etched channels, MBE 77—40388
GaAs-Ga$_{1-x}$Al$_x$As n$^+$-ν-n junction, avalanche carrier multiplication *(Russian)* 78—76140
GaAs-Ga$_{1-x}$Al$_x$As repeated monolayer heterostructure, electronic struct. 77—66197
GaAs-Ga$_{1-x}$Al$_x$As red LED, 4% quantum yield *(Russian)* 77—85809
GaAs-Ga$_{1-x}$Al$_x$As semicond. laser diodes, degradation, lattice defects *(Japanese)* 77—34889
GaAs-Ga$_{1-x}$Al$_x$As single heterostructure laser diode, anal. of temp. rise under transient-state conditions 77—61949
GaAs-Ga$_{1-x}$Al$_x$As superlattices, resonance enhanced Umklapp Raman process 78—39547
GaAs-Ga$_{1-x}$Al$_x$As superlattice, sub-band dimensionality 78—63981
GaAs-Ga$_{1-x}$Al$_x$As stripe geometry lasers 79—94245
GaAs-Ga$_{1-x}$Al$_x$As superlattice, Raman scatt., polar phonon anisotropy 80—45052
GaAs-Ga$_{1-x}$Al$_x$As thin film structs., LEDs, deep levels *(French)* 78—56218
GaAs-Ga$_{1-x}$Al$_x$As variable gap p-n junction, variable gap and photo EMFs 80—15596
GaAs-Ga$_{1-x}$Al$_x$As-Ga$_{1-y}$Al$_y$As n$^+$-i-n heterostructure, electroluminesc. characts., 80 to 330K *(Russian)* 79—28404
GaAs-Ga$_{1-x}$Al$_x$GaAs heterostructure, electron tunnelling theory 78—47861
GaAs-Ga$_{1-x}$In$_x$As heterojunction, thermally assisted tunnelling 78—19136
GaAs-Ga$_{2.2}$Al$_{0.8}$As:Be, LPE, diffusion of Be into GaAs substrate 80—103517
GaAs-Ga$_x$Al$_{1-x}$As, injection laser with external resonator, mirrors of Michelson interferometer 79—81455
GaAs-Ga$_x$Al$_{1-x}$As CW stripe geometry laser fabrication and performance 77—38933
GaAs-Ga$_x$Al$_{1-x}$As DH diode lasers, single longitudinal mode operation 78—1243
GaAs-Ga$_x$Al$_{1-x}$As double heterojunction laser structures, LPE growth with double source method 79—28962
GaAs-Ga$_x$Al$_{1-x}$As DH laser wafers, active layer inhomogeneities 79—74106
GaAs-Ga$_x$Al$_{1-x}$As DH lasers, dislocation effects 79—82221
GaAs-Ga$_x$Al$_{1-x}$As DH laser material crystal cathodoluminescence, SEM analysis 80—97349
GaAs-Ga$_x$Al$_{1-x}$As heterostructure, depend. of efficiency of radiative transitions on composition 78—2909
GaAs-Ga$_x$Al$_{1-x}$As injection laser, external resonator, radiative characts. 77—23703
GaAs-Ga$_x$Al$_{1-x}$As injection laser, large-optical-cavity, with low-loss distributed Bragg reflectors 78—1244
GaAs-Ga$_x$Al$_{1-x}$As laser, degradation, TEM obs. 77—51625
GaAs-Ga$_x$Al$_{1-x}$As superlattice, photoconductor with high sensitivity and reduced dark current appl. 79—7881
GaAs-Ga$_x$In$_{1-x}$P heterostruct., MBE layers, photolum. props., assessment as laser struct. 80—20705
GaAs-Ga$_x$In$_{1-x}$P heterostructure, elastic stresses and substrate/epitaxial film mismatch, X-ray diffr. method 80—92794
GaAs-Ga$_x$In$_{1-x}$P multilayer epitaxial films, MBE technology and epitaxial layers props. 79—33945
GaAs-GaAlAs, DH laser material, rapid optical degradation 77—7083
GaAs-GaAlAs, DH laser material, LPE grown, obs. of melt carryover 78—91553
GaAs-GaAlAs, double heterostruct. injection laser, curved junction stabilised filament, exam. 78—37911
GaAs-GaAlAs, heterostructure laser diode, lasing threshold calc. 80—28232
GaAs-GaAlAs, injection laser and MESFET monolithic integration on GaAs substrate 79—64242
GaAs-GaAlAs, inverted-ridge-waveguide DH injection laser with current and lateral optical confinement LPE growth 77—75540
GaAs-GaAlAs, stripe geometry laser, simplified fabrication process, characts. 79—76697
GaAs-GaAlAs, superlattice, subband related anisotropy in negative magnetoresistivity 80—11082
GaAs-GaAlAs, transverse Bragg-reflector injection lasers 78—74926
GaAs-GaAlAs 13 μm wide stripe CW DH lasers linear to more than 10 mW 78—42344
GaAs-GaAlAs (100) abrupt interface, carrier transmission and refl. coeffs. 79—69588
GaAs-GaAlAs (100) interfaces, carrier transport coeffs., tight binding calc. 80—49889
GaAs-GaAlAs bipolar transistor and heterostruct. laser, monolithic integration 80—102858
GaAs-GaAlAs CW diode laser, lateral mode stabilization using apertured facet reflectors 80—23708
GaAs-GaAlAs CW injection laser, stripe geometry DH, temporal coherence 80—38016
GaAs-GaAlAs channelled-substrate narrow-stripe lasers; low threshold currents 80—23706
GaAs-GaAlAs DFB and distributed Bragg reflector lasers, historical review 77—31102
GaAs-GaAlAs DFB diode lasers with separate carrier and optical confinement, room temp. operation 77—10926
GaAs-GaAlAs DH CW laser, growth by Peltier effect induced LPE 77—48357
GaAs-GaAlAs DH diode lasers with angled pumping stripes, operation 78—46602
GaAs-GaAlAs DH injection laser, integrated optics techniques 80—33033
GaAs-GaAlAs DH injection lasers, external cavity operated angled-stripe geometry, CW operation 80—64078
GaAs-GaAlAs DH internally striped planar laser with flat freq. response up to 2 GHz 78—66829
GaAs-GaAlAs DH LEDs, with thin active layer, Burrus type, internal interference in emission spectrum 78—27325
GaAs-GaAlAs DH LED, transient current trap spectroscopy 78—80049

gallium arsenide continued
GaAs-GaAlAs DH laser on semi-insulating substrate using carrier crowding 77—83886
GaAs-GaAlAs DH laser material, secondary dislocation climb in optical degradation 78—17935
GaAs-GaAlAs DH lasers, optical studies of defects and degradation 78—18654
GaAs-GaAlAs DH lasers, single longit. mode operation 78—22125
GaAs-GaAlAs DH laser, unsaturated optical gain spectra above threshold 78—29951
GaAs-GaAlAs DH laser diode, lateral modes 78—59009
GaAs-GaAlAs DH laser, beam scanning with twin-stripe injection lasers 79—10334
GaAs-GaAlAs DH laser with low threshold current, metalorganic CVD 79—50293
GaAs-GaAlAs DH lasers, strain-enhanced luminesc. degradation, photoluminesc. obs. 80—69392
GaAs-GaAlAs DH laser, O$^+$ isolation compared with SiO$_2$ isolation 80—74382
GaAs-GaAlAs DH material, dislocation glide and climb, electron diffr. 78—83824
GaAs-GaAlAs double heterostruct., self-absorpt. effects on radiative lifetime 77—39928
GaAs-GaAlAs double heterostructures for CW injection lasers, LPE growth 79—31931
GaAs-GaAlAs embedded stripe DH laser with polycryst. GaAsP, cleaved mirrors 77—75548
GaAs-GaAlAs embedded stripe DH laser with polycryst. GaAsP, etched mirrors 77—75549
GaAs-GaAlAs grating coupled lasers, output power efficiency 77—79858
GaAs-GaAlAs heterostructures, LPE growth, Peltier effect *(Polish)* 78—6861
GaAs-GaAlAs heterostructure, growth by metal-alkyl-hydride process 78—15313
GaAs-GaAlAs heterostructure injection lasers, room temp. operation with curved stripe waveguides 78—37909
GaAs-GaAlAs heterostructure, GaAs preferential etching, using O$_2$ and CCl$_2$F$_2$ 79—8373
GaAs-GaAlAs heterostructure lasers on semi-insulating substrates 79—13977
GaAs-GaAlAs heterostructures, saturation of free exciton absorption 79—61454
GaAs-GaAlAs injection lasers, on semi insulating substrates, using laterally diffused junctions 78—37910
GaAs-GaAlAs injection laser, branching waveguide directional coupler, fabrication and operation 78—38047
GaAs-GaAlAs injection laser sources, for fibre optic communications 78—46637
GaAs-GaAlAs injection lasers on semi-insulating substrates using laterally diffused junctions 78—55364
GaAs-GaAlAs injection laser sources for fibre optic communications, design 79—31923
GaAs-GaAlAs injection laser, radiation divergence reduction by non-waveguide mode excitation 80—91797
GaAs-GaAlAs injection lasers, narrow-stripe proton-implanted, high bit-rate modulation 80—91824
GaAs-GaAlAs LPE layers, laser material, shallow growth pits obs. 77—7985
GaAs-GaAlAs LPE layers, DH material, TEM obs. of crystal defects 78—6241
GaAs-GaAlAs large optical cavity injection layer with low loss DBRs 78—1430
GaAs-GaAlAs laser, degraded, characterisation by selective etching and photoetching 80—48252
GaAs-GaAlAs laser, high-spectral radiance source using integrated optics 79—36931
GaAs-GaAlAs laser, optical repeater using PFM at 1 GHz 79—98395
GaAs-GaAlAs laser with integral light intensity detector 79—89917
GaAs-GaAlAs monolithically integrated DFB lasers as freq. multiplexing source 77—34958
GaAs-GaAlAs multilayer struct., Hall mobility enhancement 80—100511
GaAs-GaAlAs multiple-stripe phase-locked laser array, behaviour 79—45955
GaAs-GaAlAs nonplanar large optical cavity laser, pulsed room temp. operation 80—28244
GaAs-GaAlAs optically pumped DFB laser, wavelength tuning effect 78—82979
GaAs-GaAlAs planar stripe DH laser, origin of dark line defects 77—75510
GaAs-GaAlAs room temp. DBR lasers, highly collimated broadside emission 78—1428
GaAs-GaAlAs stripe injection laser, CW double heterostruct., technology 79—31933
GaAs-GaAlAs stripe injection laser, high performance, design and characts. 79—31932
GaAs-GaAlAs superlattices, metalorganic VPE growth, in sites ellipsometry monitoring 80—70547
GaAs-GaAlAs superluminescent diodes for optical fibre links, modulation bandwidth 79—36993
GaAs-GaAlAs TJS lasers, high power density single mode operation, Si$_3$N$_4$ facet coating 79—86186
GaAs-GaAlAs wafers, defects and degradation, transmission cathodolum. evaluation 80—65395
GaAs-GaAlAs-GaAs rectifying semicond. struct., prep. by MBE and characts. 80—65657
GaAs-GaAs oxide interface layer characterisation by spectroscopic ellipsometry 80—50738
n-GaAs-GaAs:Cr, interface elec. props., substrate effects 78—6438
n-GaAs-GaAs:Cr. semiinsulating, low freq. current pulses 77—8176
GaAs-GaAs$_{0.5}$P$_{0.5}$ almost perfect epitaxial multilayers, TEM obs. 77—89668
GaAs-GaAs$_x$Sb$_{1-x}$, heteroepitaxial structs., mismatch dislocation nets 79—10855
GaAs-GaInAs structure, dislocation struct., TEM anal., appl. as IR LED 80—70206
GaAs-GaP, heterojunction, electronic processes *(Russian)* 79—56312
GaAs-GaP diffuse scatt. of X-rays by single crysts. *(German)* 78—30517
GaAs-GaP heterostructure, radiative recomb. under influence of mech. stresses 80—66291
GaAs-GaP(Sb), pseudobinary alloy, phase diagram calc. 78—52786

gallium arsenide continued
GaAs-GaSb, threshold energies for impact ionisation by electrons and holes 78—6390
GaAs-GaSe n-p heterojunction, elec. props., interface states 80—65670
GaAs-Ge, heterostructure, zincblende-on-diamond type systems, MBE growth, (110) orientation as preferred orientation 80—80099
GaAs-Ge, n-n isotype heterojunctions, fixed-interface-charge model 78—56215
GaAs-Ge (100) interface, electronic struct., scattering-theoretic approach 78—95340
GaAs-Ge (110), heterojunction chemistry, photoemission expts. 78—95244
GaAs-Ge abrupt (110) interface, electronic struct. 78—95339
GaAs-Ge abrupt interface, electronic struct., self-consistent wave mechanical calcs. 77—89837
GaAs-Ge abrupt interface, orientation depend. of interface dipole energies, XPS expts. 78—39196
GaAs-Ge heterojunction, band discontinuities, angle-resolved UPS obs. 79—7878
GaAs-Ge heterojunction, electronic structure 79—73572
GaAs-Ge heterojunction, interface geometry, model 80—49879
GaAs-Ge heterojunctions, electronic struct., tight-binding and pseudopot. models 79—42633
GaAs-Ge interface, abrupt, electronic struct., self-consistent calc. 77—24611
GaAs-Ge interface, electronic struct. of Ge overlayers on (100) GaAs 80—49880
GaAs-Ge interface, photoemission 80—25530
GaAs-Ge interface, surface and interface states of (111) surfaces 79—15206
GaAs-Ge interface, XPS obs. of electronic struct. 78—95341
GaAs-Ge interfaces, heteroepitaxial, misfit dislocations, TEM obs. 79—23610
GaAs-Ge n-p diode, microplasma breakdown 79—91140
GaAs-Ge structure, electronic struct., ang.-resolved photoemission obs. 80—49881
GaAs-Ge$_{1-x}$(GaAs)$_X$ n-p heterojunctions, hydrostatic press. effect on elect. and photoelectric props. 80—20304
GaAs-Ge$_3$N$_4$-Al structures and MISFETs based on them 79—60932
GaAs-HBr chemical vap. transport system, thermochem. data 78—6854
GaAs-In Schottky barrier interface, covalent bonding of metal atoms 77—20429
GaAs-In$_{1-y}$Ga$_y$P heterojunction, VPE, energy band gap and lattice parameter, lattice mismatch effects 78—95345
GaAs-In$_{2-x}$Sn$_x$O$_{3-y}$ SIS heterostructure solar cells, spray-deposited 80—101106
GaAs-In$_y$Ga$_{1-y}$P, CW room temp. DH lasers prep. by VPE 77—10942
GaAs-InAs, pseudobinary alloy, phase diagrams calc. 78—52786
GaAs-InP heterojunction laser output wavelength control 80—74384
GaAs-InSe, heterojunction, electronic processes *(Russian)* 79—56312
GaAs-InSe p-n junctions, 'optical' contacts, elec. props. 78—56222
n-GaAs-K$_2$Se-K$_2$Se$_2$-KOH/C thin film solar cell, 7.3% cell efficiency 80—93931
GaAs-metal contacts, excess capacitance, depend. on nonlinear dielectric susceptibility 78—43475
GaAs-metal diode, surface-barrier, excitons effect on photocurrent 79—82670
GaAs-metal interface form., chem. and electronic struct. 80—25009
GaAs-metal junction stabilisation by transition metal diffusion barrier 79—38161
GaAs-metal junction stabilisation by intermetallic diffusion barrier 79—38160
GaAs-metal Schottky barrier, surface states and barrier height, I-V (C-V) characts. meas. 77—85310
GaAs-metal Schottky barrier contacts, interface chemistry 79—74049
GaAs-metal Schottky barrier diodes, elec. props. under mech. stress 80—11087
n-GaAs-metal Schottky barrier, ultrathin native oxide, thickness determ. from C-V and photoresponse meas. 80—70821
GaAs-metal struct., photoresponse spectra, electron thermalisation *(Russian)* 79—15221
GaAs-n-Al$_x$Ga$_{1-x}$As heterojunctions, selectively doped, FET 80—80364
n-GaAs-n-Al$_x$Ga$_{1-x}$As rectifying heterojunction, cond. props. study 80—88626
n-GaAs-n-GaN, diffusion growth kinetics, morphology and electrical properties 80—20294
n-GaAs-n-GaP, in MIS structures, elec. controlled optical transparencies, optical processing use 77—85339
n-GaAs-n$^+$-Al$_x$Ga$_{1-x}$As heterostructure production, by MBE *(German)* 80—44711
p$^+$-GaAs-n-(Ga,In)As heterostructure, thermally assisted tunnelling currents 77—20412
GaAs-NaOH interface, inversion layer form. and surface states 80—2465
GaAs-native oxide interface, electronic props. 79—73590
GaAs-O$_2$ system, electron beam induced adsorption, ion beam effects 77—11778
GaAs-on-sapphire spatially distributed thermal light modulator 79—59839
GaAs-oxide, interface layer determ. by spectroscopic ellipsometry 79—95275
n-GaAs-oxide, plasma-grown, surface states, modified DLTS meas. 80—11094
GaAs-oxide interface, field effect 79—87160
GaAs-oxide interface, physical struct. 79—60644
GaAs-oxide interfaces, local atomic and electronic struct., high resolution XPS 80—49927
n-GaAs-oxide-Au structure, influence of reverse bias on photocurrent 80—20323
GaAs-Pb junctions, electron tunnelling under high press., transition temp., energy gap, phonon energies 79—15257
GaAs-Pd junction, contact reactions 79—56308
GaAs-plasma grown oxide interface, new resonant ellipsometric technique for characterisation 79—40606
GaAs-polyethylene mixture, optical transmission spectra, IR filter prep. using computer appl. 80—2763
GaAs-Pt interface states energy distrib. and relaxation time 79—33345
n-GaAs-Pt Schottky diode, microplasma breakdown 79—91140
GaAs-Pt-air system, far IR propag. distances of surface EM waves 79—42616
GaAs-S VPE layers, thickness and carrier conc. variations 79—100060

gallium arsenide continued
GaAs-Si eutectic alloy, effect of crystallisation rate on microhardness 79—96110
GaAs-Si heterojunction, IR quenching of photocapacitance 80—92968
GaAs-Si ion implanted, impurity profiles elec. props. 80—96550
GaAs-Si$_3$N$_4$ structure, photoluminesc. and collective effects 78—6727
GaAs-Si$_3$N$_4$ system, photoluminesc. edge line *(Russian)* 79—4852
n-GaAs-Si$_x$O$_y$N$_z$ interface, C-V and I-V characts. 77—89863
n-GaAs-SiO$_2$ interface, MOS capacitors, surface states from conductance and capacitance meas. 80—100533
GaAs-SiO$_2$ interface local props. *(Russian)* 78—10567
GaAs-SiO$_2$ MIS structures, fabrication and elec. props. 79—47166
GaAs-SiO$_x$-Al system, C-V characts. 79—65553
GaAs-Ta$_2$O$_5$ interface, fabricated by interactive oxidation, props. 80—49935
n-GaAs-W contact, Schottky barrier 78—39213
n-GaAs-YIG layered structure, magnetostatic surface wave amplification 78—88107
GaAs-ZnS p-n heterojunction, epitaxial, elec. props. *(Russian)* 78—88023
GaAs-ZnS p-n heterojunction, struct., multibeam electron microscopy obs. 79—11031
GaAs-ZnSe, solid solution crystals, grown by Bridgman method, exam. of resistivity and Hall effect 79—95919
GaAs-ZnSe, X-ray cond. 5.4 to 17.5 keV, spectral and dosimetric characts. *(Russian)* 77—35964
GaAs-ZnSe (110) interface, electronic struct., self-consistent calc. 79—95486
GaAs-ZnSe heterojunction, elec. and photoelec. props. *(Russian)* 77—32070
GaAs-ZnSe heterojunction, LF noise, I-V and C-V characts., illumination effects *(Russian)* 77—66200
GaAs-ZnSe system, heterovalent solid solns. of substitution, prep. and investig. 77—24553
GaAs-ZnSe system, phase diagram 77—28785
GaAs$_{1-x}$ P$_x$, hot photoluminescence spectrum, polarisation depend. 78—31254
(GaAs)$_n$-(AlAs)$_n$, multilayer heterostructure, cation order, effect on energy bands 79—1570
Ga$_{1-x}$As(Al,In)$_x$, heterojunction solar cells, optimum bandgap, computer anal. 79—43767
GaAs$_{0.84}$Al$_{0.16}$As, surface processing, residual film monitoring by ellipsometry 80—13124
(GaAs)$_n$(AlAs)$_m$ multilayers, MBE, interdiffusion, X-ray diffr. study 80—70474
GaAsGaAlAs coated heterostruct. etalon, optical bistability and ns modulation 80—64096
GaAsGa$_{1-x}$Al$_x$As DH laser material, rapid optical degradation obs. 77—75528
GaAs$_{1-x}$H$_x$, amorphous, vib. props., Raman and IR meas. 80—50322
GaAsP, composition dependence of phonon frequencies 78—75764
Ga(AsP), dislocation etching of (001) faces with H$_3$PO$_4$ etchant 80—15103
GaAsP epitaxial film, TEM obs. of misfit dislocation arrays, nucleation and multiplication 77—39742
GaAsP epitaxial films, planar waveguides for integrated optics appls. 79—10416
GaAsP epitaxial film, composition self modulation, defect struct. 80—34331
GaAsP epitaxial waveguide, electro-optic phase modulation of laser radiation 79—10417
GaAsP, negative-electron-affinity, photoemission transmission coeff. 78—56560
Ga(AsP) on GaAs, LPE, growth with Ge and Sn solvents, phase diags. 78—88434
GaAsP photocathode, negative electron affinity process obs. by laser beam scanning *(Japanese)* 80—55262
GaAsP strip-waveguide modulator with GaAlAs embedded DH stripe laser 78—66957
GaAsP, VPE, lattice forbidden band composition depend. *(Hungarian)* 80—6669
GaAs$_{0.1}$P$_{0.9}$:Zn, shallow Zn diffusion profile determ. using anodic oxidation and double radioactive tracer method 77—43239
GaAs$_{0.15}$P$_{0.85}$ ridged waveguide for electrooptic radiation modulator 80—91925
n-GaAs$_{0.6}$P$_{0.4}$, anodic oxide film, exam. using SIMS and ellipsometry 79—61770
GaAs$_{0.6}$P$_{0.4}$, anodic oxide, electronic props. 79—61771
GaAs$_{0.6}$P$_{0.4}$, CVD growth for LEDs 79—19998
GaAs$_{0.6}$P$_{0.4}$, deep level profile anal., double correlation technique 77—80830
GaAs$_{0.6}$P$_{0.4}$ LED, deep level radiative defects detection during degradation 77—76770
GaAs$_{0.6}$P$_{0.4}$ LED, luminesc. investig. of degradation, deep-level form. at dislocations 77—40287
GaAs$_{0.6}$P$_{0.4}$, low dark-current MOS photodiodes 77—32083
GaAs$_{0.6}$P$_{0.4}$ p-i-n diode, behaviour of turnover voltage under pulsed conditions 77—20408
n-GaAs$_{0.6}$P$_{0.4}$, reproducible ohmic contacts 79—73587
GaAs$_{0.6}$P$_{0.4}$ single cryst., defect distrib. near abraded surface 80—92533
GaAs$_{0.6}$P$_{0.4}$, surface processing, residual film monitoring by ellipsometry 80—13124
GaAs$_{0.6}$P$_{0.4}$, VPE, hole diffusion lengths, surface prep. and heat treatment effects, etchant evaluation 80—15627
GaAs$_{0.6}$P$_{0.4}$, VPE, hole diffusion lengths, effect of transition metal diffusional doping 80—15628
GaAs$_{0.6}$P$_{0.4}$:Be, implanted annealing studies, elec. resist., Hall effect meas. 78—84213
GaAs$_{0.6}$P$_{0.4}$:N, isoelectronic tape by ion implantation and CO$_2$ laser annealing 80—24464
GaAs$_{0.6}$P$_{0.4}$:Zn, control of Zn diffusivity by multiple implantation 78—38877
GaAs$_{0.6}$P$_{0.4}$:Zn$^+$(Ar$^+$), ion-implanted, thermal degradation of mechanical surface perfection and surface photolum. 77—77271
GaAs$_{0.62}$P$_{0.38}$, negative electron affinity, photoemission of spin polarised electrons 80—2916
n-GaAs$_{0.62}$P$_{0.38}$, optical absorpt. coeff. and minority-carrier diffusion length, differential photocurrent method of meas. 80—96896
GaAs$_{0.65}$P$_{0.35}$, gamma irradiated, deep level study using DLTS and photocapacitance methods *(Japanese)* 80—49665

gallium arsenide continued
GaAs$_{0.7}$P$_{0.3}$-In$_{0.34}$Ga$_{0.66}$P, CW heterojunction laser, visible, laser operation 77—38886
GaAs$_{1-x}$P$_x$, $0 \leq x \leq 1$, evidence for common nature of certain deep-level radiative centres 78—6767
GaAs$_{1-x}$P$_x$, anodic oxide films, ellipsometric anal. 79—20234
GaAs$_{1-x}$P$_x$ based structs., carrier conc., mobility calcs. from Hall effect meas. 78—60138
GaAs$_{1-x}$P$_x$, bending parameters calc. by pseudopot. method 78—26813
GaAs$_{1-x}$P$_x$, bound exciton, luminesc. reson. excitation 79—95840
GaAs$_{1-x}$P$_x$, chemical transport and crystal growth in closed tube *(Japanese)* 78—39673
GaAs$_{1-x}$P$_x$, continuously tunable electron beam pumped laser 78—50802
GaAs$_{1-x}$P$_x$, dependence of energy spectrum of levels introduced by electron irrad. on composition 79—60766
GaAs$_{1-x}$P$_x$, diffusion of implanted Zn ions, ion microbe analysis 78—95190
Ga(As$_{1-x}$P$_x$) electrode, equilib. establishment kinetics *(French)* 79—79259
GaAs$_{1-x}$P$_x$ electrodes, interface capacitance meas., flatband pot., conduction and valence band boundaries *(French)* 79—33339
GaAs$_{1-x}$P$_x$, electrolum. and related props., state-of-the-art, book contrib. 77—73173
GaAs$_{1-x}$P$_x$, electron irrad., radiation defects annealing 80—29059
GaAs$_{1-x}$P$_x$ epi-wafer, comp. profile of heterogeneous struct., anodisation-electrorefl. meas. 78—26782
GaAs$_{1-x}$P$_x$ epitaxial films, VPE grown, photolum. spectra 79—73997
GaAs$_{1-x}$P$_x$ epitaxial layer prep. for electroluminescent diodes *(Czech)* 77—21032
GaAs$_{1-x}$P$_x$, epitaxial layer, modulation of direct and indirect gaps, piezotransmission meas. 77—24819
GaAs$_{1-x}$P$_x$ epitaxial layers, charge carrier conc. determ. from low-field electrorefl. spectra 77—85320
GaAs$_{1-x}$P$_x$ epitaxial layers prep., photoluminesc. and electroluminesc. props. *(Czech)* 78—48233
GaAs$_{1-x}$P$_x$ films, use in recording phase relief holograms *(Russian)* 78—50741
GaAs$_{1-x}$P$_x$, heterogeneous struct. obs. by anodisation-electrorefl. technique 78—84088
GaAs$_{1-x}$P$_x$ heterostructure, LPE prep., growth and dissolution kinetics, thermodynamic and kinetic models 80—75456
GaAs$_{1-x}$P$_x$, high quantum efficiency photoemission 77—44115
GaAs$_{1-x}$P$_x$, indirect-gap, evidence for exciton localization by alloy fluctuations, photolum. 80—66276
GaAs$_{1-x}$P$_x$ LED, effect of band filling on emission spectra shape 78—48236
GaAs$_{1-x}$P$_x$ layer, growth by isothermal LPE 77—40398
GaAs$_{1-x}$P$_x$, localised exciton-phonon complex as intermediate state in light scatt. 78—39543
GaAs$_{1-x}$P$_x$, MBE growth on GaP, and crystallographic evaluation 77—8762
GaAs$_{1-x}$P$_x$, method for determ. of liquidus surfaces in Ga-As-P phase diagram 77—28787
GaAs$_{1-x}$P$_x$, mol. beam epitaxial growth, cryst. quality, composition investig. *(Japanese)* 77—55895
GaAs$_{1-x}$P$_x$, molecular beam epitaxial, effect of substrate temp. on composition ratio 77—1811
GaAs$_{1-x}$P$_x$, N doping using ionised beam in MBE 78—47400
GaAs$_{1-x}$P$_x$, N implantation, characterisation by photolum. and channelling 80—54262
GaAs$_{1-x}$P$_x$, N trap bound state, Hall effect determ. 78—19055
GaAs$_{1-x}$P$_x$, N$^+$ implantation photoluminesc. props. 77—68987
GaAs$_{1-x}$P$_x$, N$^+$ implantation, annealing props. 77—68988
GaAs$_{1-x}$P$_x$, piezomodulation spectra of indirect gap, zero-phonon and phonon-assisted transitions 77—48192
GaAs$_{1-x}$P$_x$, protection by reactively sputtered AlN *(French)* 78—23849
GaAs$_{1-x}$P$_x$, SIMS, energy distrib. of sputtered ions 79—38706
GaAs$_{1-x}$P$_x$, solid soln. comp. control during gas-phase heteroepitaxy 77—85091
GaAs$_{1-x}$P$_x$, solid soln., synthesis by ion implantation P$^+$ ions 78—38741
GaAs$_{1-x}$P$_x$, solid solution, synthesized by ion implantation, Raman scattering 79—42972
GaAs$_{1-x}$P$_x$, solid state diffused, conc. distrib. obs., electroreflectance and tracer sectioning obs. 80—54389
GaAs$_{1-x}$P$_x$, structural defects, optical props. effect 80—55208
GaAs$_{1-x}$P$_x$, thermal oxides, elemental composition and C-V characts. 79—61772
GaAs$_{1-x}$P$_x$, VPE, on-time comp. determ. 78—67915
GaAs$_{1-x}$P$_x$, VPE on Ge substrate, and LED characts. 78—72736
GaAs$_{1-x}$P$_x$:N, $0.6<x<1$, photoluminesc., comp. depend. 78—52546
GaAs$_{1-x}$P$_x$:N, film, optical absorpt. from photoluminesc. meas. 78—92134
GaAs$_{1-x}$P$_x$:N, Koster-Slater model and N-states 78—47732
GaAs$_{1-x}$P$_x$:N, LED, external quantum efficiency, press. effect 77—8655
GaAs$_{1-x}$P$_x$:N, N isoelectronic trap, model calc. of N$_\Gamma$ and N$_x$ electronic states 78—10398
GaAs$_{1-x}$P$_x$:N, photoluminesc. and optical absorpt. spectra of N impurity bound-excitons 79—47496
GaAs$_{1-x}$P$_x$:N, photolum. and electrolum. study of N isoelectronic traps 80—89061
GaAs$_{1-x}$P$_x$:N, upper branch of N isoelectronic trap., photo- and electrolum. expts. 77—63462
GaAs$_{1-x}$P$_x$:N epitaxial layers, absorption and photolum. spectra meas. 77—24894
GaAs$_{1-x}$P$_x$:N heterojunction, N$_x$ and N$_\Gamma$ bound states, high-press. effects on electroluminesc. meas. 77—11870
GaAs$_{1-x}$P$_x$:S, deep level, photoconductivity, carrier nonradiative recombination 80—20112
GaAs$_{1-x}$P$_x$:Te, thermoelectric figure of merit 79—69538
GaAs$_{1-x}$P$_x$:Zn, diffusion profile determ., ^{32}P/^{65}Zn double tracer technique 78—55888
GaAs$_{1-x}$P$_x$:Zn implanted, Zn diffusion 77—84993
GaAs$_{1-x}$P$_x$-Au, surface-barrier struct., photodetectors of visible and UV radiation 77—20437
GaAs$_{1-x}$P$_x$-GaP heterostructure, photomodulation spectroscopic exam. 77—40257
GaAs$_{1-x}$P$_x$-SiO$_2$:N,Zn ion-implanted multiple layers, ion range distribs., secondary ion microprobe meas. 79—42129
GaAs$_{1-y}$P$_y$-In$_{1-x}$Ga$_x$P$_{1-z}$As$_z$, DH laser, low threshold visible spectrum 78—5471

gallium arsenide continued
  $GaAs_xP_{1-x}$, surface phonon polaritons, total internal refl. *(Russian)* 79—38688
  $GaAs_xP_{1-x}$, band struct., CPA calc. based on linear combination of bond orbitals 79—87035
  $GaAs_xP_{1-x}$, elastic consts. and Debye temp. determ. 77—4142
  $GaAs_xP_{1-x}$, energy band struct., CPA based on LCBO *(Japanese)* 80—44495
  $GaAs_xP_{1-x}$, energy gap variation, CPA calcs. 78—43294
  $GaAs_xP_{1-x}$ epitaxial film nonlinear light absorpt., photoluminesc. meas. 77—66528
  $GaAs_xP_{1-x}$, liquid phase epitaxial growth on GaP, growth and properties 79—47641
  $GaAs_xP_{1-x}$ on GaP, heterojunctions, misfit dislocation banding, stress-induced birefr. 77—28542
  $GaAs_xP_{x-1}$, luminous intensity ang. distrib. and total light flux meas. device *(Chinese)* 78—82018
  $GaAs_yP_{1-y}$ alloy, composition effects in growth by MBE 80—59816
  $GaAs_{1-x}P_x(Te)$, bound exciton stress depend., piezoluminescence, photoluminescence 80—80206
  $GaAs_{1-x}Px$, heteroepitaxial solid soln., defects of struct 79—28223
  GaAsSb laser, optimum wavelength emission for fibre guides 77—7086
  GaAsSb/GaAlAsSb DH lasers, growth and props. 80—69412
  $GaAs_{1-x}Sb$, microprocessor controlled MBE growth 78—3058
  $GaAs_{1-x}Sb_x$, ($x \leq 0.05$), band gap, temp. depend., from edge photolum. meas. 80—71486
  $GaAs_{1-x}Sb_x$, cryst. growth by steady state LPE 78—44032
  $GaAs_{1-x}Sb_x$, DH, laser operation between 0.9 and 1.1 μm 77—10922
  $GaAs_{1-x}Sb_x$ electron intervalley transfer and drift velocity calc. 77—80778
  $GaAs_{1-x}Sb_x$ epitaxial n-n heterostructures, gap energies and interface pots., modulation electroabsorpt. meas. 79—11201
  $GaAs_{1-x}Sb_x$, LPE,phase diagram meas. 77—20047
  $GaAs_{1-x}Sb_x$ layer on GaAs, dislocation density reduction by improved LPE growth method 80—76202
  $GaAs_{1-x}Sb_x$, MBE grown, surface struct. exam. by MEED 78—87847
  $GaAs_{1-x}Sb_x$, narrow-gap film on wide-gap GaAs, energy gap grading, optical transmission meas. 77—20943
  $GaAs_{1-x}Sb_x$ on GaAs, LPE growth of GaAs 79—61519
  $GaAs_{1-x}Sb_x$ photodiode structures, current-voltage characts., photo-EMF spectra 80—29472
  $GaAs_{1-x}Sb_x$ photodiode, speed and sensitivity meas. 80—92937
  $GaAs_{1-x}Sb_x$ ternary phase diagram, LPE, band gap and elec. props. 77—55896
  $GaAs_{1-x}Sb_x$ undoped epitaxial layers, photoluminesc. meas. 80—20703
  $GaAs_{1-x}Sb_x$-$Al_yGa_{1-y}As_{1-z}Sb_z$, DH laser, threshold characts. and extended wavelength operation 78—9379
  $GaAs_{1-x}Sb_x$-$Ga_{1-x}In_xP_{1-y}As_y$ multilayer structure, continuously tunable electron beam pumped laser 78—50802
  $GaAs_{1-y}Sb_y$ organometallic VPE, use of trimethyl As and trimethyl Sb 80—45238
  $GaAs_{1-y}Sb_y$, organometallic VPE growth using trimethylantimony 80—60788
  $GaAs_xSb_{1-x}$, epitaxial layer, struct. defects rel. to luminesc. 78—72040
  $GaAs_xSb_{1-x}$, heterostructure composition profile by photoemission microanalysis 80—44717
  $GaAs_xSb_{1-x}$, lattice-matched LPE growth in InP substrates 79—42402
  $GaAs_xSb_{1-x}$ solid solution epitaxial layer, morphology and defect structure 77—1330
  $GaAs_xSb_{1-x}$-GaAs epitaxial films and multilayer heterostruct., SEM obs. under cathodolum. conditions 79—11023
  $GaAs_ySb_{1-y}$, miscibility gap, rel. to LPE 79—33090
  $GaAs_{1-x-z}Sb_xP_z$, LPE growth, constant compositional grading 78—6867
  $GaAs_{2-x-z}Sb_xP_z$, LPE growth, continuous comp. grading, use as secondary substrate 77—31913
  $GaAs_xSb_yP_{1-x-y}$, continuously graded comp. layers, LPE 77—24970
  $(GaAs)_{1-x}(ZnSe)_x$, LPE growth, resist., Hall effect and cathodoluminesc. meas. 77—28270
  $(GaAs)_x(ZnSe)_{1-x}$ single crystal, visible cathodoluminesc. spectra 80—20716
  p-$(GaAs)_x(ZnSe)_{1-x}$-nn$^+$.GaAs, avalanche heterojunctions, inverse branch of volt ampere characts. *(Russian)* 80—6974
  $GaAs(\bar{1}\bar{1}\bar{1})As$ surface, 3 states, comp., struct., surface states and O_2 sticking coeffs. 77—66080
  $Ga_yIn_{1-y}As_xP_{1-x}$-InP heterostructure, lattice matching and cryst. perfection 78—6437
  GaInAs, efficient photodiode for near IR detection 78—16848
  GaInAs, electron-pumped laser, far-field radiation pattern, optical confinement effects 79—86181
  GaInAs, photocathode with negative electron affinity, photoemission, influence of strong elec. field 79—8227
  GaInAs-InP, growth by low-pressure metalorganic CVD 80—71595
  GaInAs-InP injection lasers with longer wavelengths for optical fibre communications, review *(Japanese)* 78—25892
  $Ga_{0.47}In_{0.53}As$, electron and hole impact ionisation rates 80—49745
  $Ga_{0.47}In_{0.53}As$, HF carrier mobility, temp. depend., theory 80—75593
  $Ga_{0.47}In_{0.53}As$, homojunction avalanche photodiode, exam. of props. 78—37072
  $Ga_{0.47}In_{0.53}As$ homojunction photodiode, avalanche photodetector for 1.0-1.6 μm region 79—6179
  $Ga_{0.47}In_{0.53}As$, LPE growth and characterisation 80—10845
  $Ga_{0.47}In_{0.53}As$, MBE, $InP/Ga_{0.47}In_{0.53}As/InP$ DH laser fabrication and room temp. operation 78—74906
  $Ga_{0.47}In_{0.53}As$ p-n junctions, band-to-band tunnelling current 80—107895
  $Ga_{0.47}In_{0.53}As$, photodetector applications 80—95140
  $Ga_{0.47}In_{0.53}As/InP$ DH lasers double cladded with InP by LPE technique, 1.67 μm operation 79—50314
  $Ga_{0.7}In_{0.3}As$ photodiodes, fibre optic appls. 79—40613
  $Ga_{1-x}In_xAs$, and $Ga_{1-x}In_xAs_{1-y}P_y$, quantum magnetoresist. results, using pulsed fields up to 35 T 79—73528
  $Ga_{1-x}In_xAs$ epitaxial layer growth by organometallic pyrolysis, homojunction LED prep. 80—76194
  $Ga_{1-x}In_xAs$, IR reflectivity, cluster effect on optical phonons 80—97259
  $Ga_{1-x}In_xAs$, optical detection of CESR 77—36155
  $Ga_{1-x}In_xAs$ organometallic VPE, use of trimethyl As and trimethyl Sb 80—45238
  $Ga_{1-x}In_xAs$, organometallic VPE growth using trimethylarsenic 80—60788
  $Ga_{1-x}In_xAs$, photocathode, work function depend. of photoelectric emission 78—68071

gallium arsenide continued
  $Ga_{1-x}In_xAs$ photocathode, negative electron affinity, photoelectron scatt. in Cs-O film 79—28899
  $Ga_{1-x}In_xAs$ photodetectors for 1.3 micron PIN-FET receiver 80—13145
  $Ga_{1-x}In_xAs$ solid solns., electron scatt. by isoelectronic impurities in covalent crysts. 79—11129
  $Ga_{1-x}In_xAs$, VPE grown, refractive index, reflectance meas. 79—4780
  $Ga_{1-x}In_xAs$, VPE layers, main electron trap, transient capacitance spectroscopy obs. 78—34800
  $Ga_{1-x}In_xAs$:Mn grown by LPE, elect. props. 80—100541
  $Ga_{1-x}In_xAs$-GaAs epitaxial interface with small misfits, TEM image contrast 80—2275
  $Ga_{1-x}In_xAs$-GaAs low-misfit epitaxial interface, electron microscope contrast 79—73416
  $Ga_xIn_{1-x}As$, alloy film surface processes controlling growth by MBE RHEED and AES exam. 78—84084
  p-$Ga_xIn_{1-x}As$, Auger recomb., theory and luminesc. expts. 78—56518
  $Ga_xIn_{1-x}As$, cryst. growth on (100) InP by LPE 78—56591
  $Ga_xIn_{1-x}As$, energy gap variation, CPA calcs. 78—43294
  $Ga_xIn_{1-x}As$, far IR reflectivity spectrum, damped harmonic oscill. model 77—52070
  $Ga_xIn_{1-x}As$, method for determ. of liquidus surfaces in Ga-In-As phase diagram 77—28787
  $Ga_xIn_{1-x}As$, on ⟨111⟩B InP, LPE growth, characterisation of high purity lattice 80—104082
  $Ga_xIn_{1-x}As$ on InP, lattice matched LPE film growth and characts. 78—72033
  $Ga_xIn_{1-x}As$ p-n junction, growth and electrolum. spectra 77—20420
  $Ga_xIn_{1-x}As$, spontaneous and stimulated emission, electron beam excitation 77—58333
  $Ga_xIn_{1-x}As$, substrate orientation effect on liq.-solid distrib. coeffs., 600-700°C 80—2278
  $Ga_xIn_{1-x}As$, VPE growth, thermodynamic anal. 80—2933
  $Ga_xIn_{1-x}As$:Ge LED, by LPE, radiation emitted at 1.02 μm 78—48235
  $Ga_xIn_{1-x}As$-InP, lattice matched LPE film growth and characts. 78—15320
  $Ga_xIn_{1-x}As$-InP, MBE film growth, composition control obs. 80—84399
  $Ga_xIn_{1-x}As$-InP heterostructure, growth by MBE 79—8251
  GaInAsP alloys, materials and devices for long wavelength optical communication 80—99854
  GaInAsP DH laser diode CW modelocking 79—7126
  GaInAsP DH laser emitting at 1.55 μm, threshold currents 80—83609
  GaInAsP, diffusion-limited growth in LPE 80—10842
  GaInAsP diode lasers, self-sustained pulsations in light output 80—64012
  GaInAsP, electroabsorption 79—78652
  GaInAsP LEDs, 1.3-1.6 μm, appl. in long haul high data rate fibre optic communication systems 80—102854
  GaInAsP layers on InP substrate, conditions for lattice matching in LPE growth 78—6866
  GaInAsP on InP substrate, epitaxially grown, fabrication of avalanche photodiode 78—37071
  GaInAsP quaternary alloys, orientation effects in LPE growth 78—92203
  GaInAsP, rectifying and ohmic contacts 80—80376
  GaInAsP, VPE growth and props. 80—16194
  GaInAsP/InP, DH laser, low threshold current density, 1.3 μm emission 79—94249
  GaInAsP/InP 1.5-1.6 micron integrated twin-guide lasers with distributed Bragg reflectors 80—74380
  GaInAsP/InP buried heterostruct. laser, 1.6 μm, fabrication and room temp. CW operation 80—58568
  GaInAsP/InP DH lasers, with (100) substrate, 1.2-1.5 μm, LPE growth conditions 79—15617
  GaInAsP/InP DH lasers, direct modulation charact. meas. by sharp pulse method 80—1245
  GaInAsP/InP DH lasers, room temp. CW operation at 1.5 to 1.6 micron range, fabrication 80—58585
  GaInAsP/InP DH lasers emitting at 1.3 μm, growth and characts. 80—64057
  GaInAsP/InP DH stripe geometry lasers emitting at 1.3 μm, growth characterisation 80—69410
  GaInAsP/InP DH lasers, 1.3 μm wavelength, LPE growth and characterisation 80—69411
  (100)GaInAsP/InP DH lasers, 1.5-1.6 μm wavelength, two phase soln. LPE technique using anti-meltback layer 80—99750
  GaInAsP/InP integrated twin-guide lasers with first order distrib. Bragg reflector, room temp. operation at 1.3 μ 80—64077
  GaInAsP/InP integrated twin-guide lasers with distributed Bragg reflector, spectral behaviour 80—74381
  GaInAsP/InP lasers, 1.5 μm emitting, high temp. CW operation 80—95889
  GaInAsP/InP lasers, LPE grown, effect of p-doping on carrier lifetime and threshold current density 80—99726
  GaInAsP/InP narrow planar stripe lasers, lasing characts. 80—95897
  GaInAsP/InP system, chemical etching, fabricating laser diodes and integrated optical circuits 80—38030
  GaInAsP/InP terraced substrate DH lasers, fabrication and single transverse mode operation 80—58580
  GaInAsP-InP, broad-area and stripe-geom. DH laser, for fibre optic communication 78—42356
  GaInAsP-InP, lattice matched, emission spectrum half width rel. to peak wavelength 80—2820
  GaInAsP-InP avalanche photodiode, fabrication and characts. 78—54454
  GaInAsP-InP buried stripe DH laser, fabrication using meltback method and CW operation 79—3708
  GaInAsP-InP buried heterostructure lasers, 1.6 μm wavelength 80—64055
  GaInAsP-InP DH laser, 1.3 μm CW operation at room temp. 77—71986
  GaInAsP-InP DH laser grown by newly designed vertical LPE furnace 78—9380
  GaInAsP-InP DH laser, relaxation and delay in oscillations 78—13709
  GaInAsP-InP DH layers, lattice deform. and misfit dislocations 79—19473
  GaInAsP-InP DH lasers with low threshold, narrow-beam divergence 79—36892
  GaInAsP-InP DH laser, LPE and wet chem. etching techniques for integration 79—98388
  GaInAsP-InP DH laser, room temp. CW laser 80—28235
  GaInAsP-InP DH lasers made by melt-back method, operating characteristics 80—48287
  GaInAsP-InP DH lasers, LPE growth and operational characts. 80—53313

gallium arsenide continued
GaInAsP-InP DH injection lasers prep. by LPE, 1.11-1.67 μm operation 80—53321
GaInAsP-InP facet lasers with chemically etched end mirrors 80—1228
GaInAsP-InP integrated twin-guide lasers with first-order distributed Bragg reflectors, 1.3 μm 80—58567
GaInAsP-InP lasers and detectors, for fibre optic communications at 1.0-1.6 μm 79—3803
GaInAsP-InP mesa substrate buried heterostruct. injection laser, fabrication and lasing props. 80—53319
GaInAsP-InP planar stripe lasers, sputtered SiO_2 film as Zn-diffusion mask 80—48249
GaInAsP-InP stripe-geometry monolithic laser with etched mirror and monitoring detector 80—64054
GaInAsP-InP stripe laser, etched mirrors fabricated by wet chem. etch 80—99744
GaInAsP-InP surface emitting injection laser, fabrication and lasing props. 80—28234
GaInAsP-InP Zn diffused stripe geometry DH diode laser fabrication 79—98386
$Ga_{0.08}In_{0.92}As_{0.18}P_{0.82}$, band struct., optical studies 79—47013
$Ga_{1-x}In_xAs_{1-x}P_x$, VPE growth and characterisation 78—22970
$Ga_{1-x}In_xAs_{1-y}P_y$-InP DH laser, carrier lifetime meas. 77—61955
$Ga_{1-x}In_xAs_{1-y}P_y$-InP DH lasers, 1000-hour CW operation 78—1265
$Ga_xIn_{1-x}As_yP_{1-y}$, conduction band and phonons, Shubnikov-de Haas effect, magnetophonon resonance, Raman scattering 80—24795
$Ga_xIn_{1-x}As_{1-x}P_x$ film, energy band struct., photolum. meas. 79—7784
n-$Ga_xIn_{1-x}As_{1-y}P_y$, photoluminesc. of epitaxial films, isovalent substitution 80—16097
$Ga_xIn_{1-x}As_{1-y}P_y$, spontaneous and stimulated emission, electron beam excitation 77—58333
$Ga_xIn_{1-x}As_{1-y}P_y$:Ge(Sn)(Te), epitaxial film, elec. and optical props. 79—11251
$Ga_xIn_{1-x}As_{1-y}P_y$-InP, room temp. electron-beam-pumped laser with dielec. waveguide, output characts. 80—5761
$Ga_xIn_{1-x}As_xP_{1-x}$-InP buried-stripe DH diode laser, room temp. CW operation 77—50671
$Ga_xIn_{1-x}As_yP_{1-y}$, CVD by Ga-In-P-H-Cl system, 80—54159
$Ga_xIn_{1-x}As_yP_{1-x}$, epitaxial layers on InP, expt. determ. of effective masses 79—65370
$Ga_xIn_{1-x}As_yP_{1-x}$, thermal expansion coefficients, 25-400°C 79—46817
$Ga_xIn_{1-x}As_yP_{1-y}$, anodisation, effect of pH, current density and illumination 78—95823
$Ga_xIn_{1-x}As_yP_{1-y}$, electron effective mass, cyclotron reson. and magnetophonon effect meas. 80—103618
$Ga_xIn_{1-x}As_yP_{1-y}$, IR refl. spectra 80—60602
$Ga_xIn_{1-x}As_yP_{1-y}$ LPE layers matched to InP, comp. and lasing wavelengths 78—71103
n-$Ga_xIn_{1-x}As_yP_{1-y}$, transferred electron oscill., threshold field 77—85227
$Ga_xIn_{1-x}As_yP_{1-y}$/GaAs structure, LPE growth and lattice consts. matching conditions 80—59822
$Ga_xIn_{1-x}As_yP_{1-y}$-GaAs substrate, lattice matching 79—90901
$Ga_xIn_{1-x}As_yP_{1-y}$-InP, CW stripe-geometry lasers, fabrication and props. 77—10943
$Ga_xIn_{1-x}As_yP_{1-y}$-InP injection laser, partially loaded with distributed Bragg reflector 78—82986
$Ga_xIn_{1-x}As_yP_{1-y}$-InP, rib-waveguide injection lasers made by one-step LPE 79—59710
$Ga_xIn_{1-x}As_yP_{1-y}$-InP injection laser partially loaded with first-order distributed Bragg reflector 79—98387
$Ga_xIn_xAs_yP_{1-y}$-InP substrate, lattice matching 79—90901
$Ga_yIn_{1-y}As_xP_{1-x}$, LPE growth 80—66440
$Ga_xIn_{1-x}As_yP_{1-y}$InP laser, DH, 1500 h continuous CW operation 77—42537
$Ga_xIn_{1-x}As_yP_{1-y}$InP DH, LEDs and lasers, fabrication and operation in 1.5 μm region 78—37893
$Ga_{1-y}In_yAs_xSb_{1-x}$, LPE on GaSb, miscibility gap in liq. phase and lattice mismatch 80—15404
$Ga_xIn_{1-x}As_ySb_{1-y}$, epitaxial film and DH, luminesc. props. 77—686
$Ga_xIn_{1-x}As_ySb_{1-y}$ laser, efficient room temp. stimulated emission, 1.8 to 2.4 μm spectral range 79—10307
$Ga_xIn_{1-x}As_ySb_{1-y}$ tunable electron-beam-pumped laser parameters 80—106524
GaInPAs, CW strip heterolaser, characts. 78—9382
GaInPAs heterostructures and LED's, luminescent props. in 1-2 micron band 78—10988
GaInPAs laser using multicomponent solid soln., room temp. operation 77—75516
GaInPAs, narrow-band tunable injection laser, 1.06 μm 79—76713
GaInPAs/InP heterostructure DFB laser under optical pumping, lasing characts. 80—87396
GaInPAs-InP, high-efficiency LED 79—65545
GaInPAs-InP DH lasers, misplaced p-n junctions due to Zn contamination 78—87051
$Ga_{1-x}In_xP_{1-y}As_y$, carrier compensation and alloy scatt. 80—29490
$Ga_{1-x}In_xP_{1-y}As_y$, drift vel. elec. field characts., Monte Carlo simulation 77—39839
$Ga_{1-x}In_xP_{1-y}As_y$, electron transient drift vel., influence of effective mass and alloy scatt. 80—2384
$Ga_{1-x}In_xP_yAs_{1-y}$/InP DFB injection laser, one-step LPE 80—58575
$Ga_xIn_{1-x}P_yAs_{1-y}$, 111-A and 111-B faces, defect struct., etching and X-ray diffr. obs. 80—2026
$Ga_xIn_{1-x}P_yAs_{1-y}$, (0.5<y<0.9), LPE on InP, Ga, As distrib. coeffs., lattice matching 78—47673
$Ga_xIn_{1-x}P_yAs_{1-y}$-InP(GaAs), DH integrated optics development 80—33240
p-$Ga_xIn_{1-x}PyAs_{1-y}$/Au-Zn, specific contact resist. 80—84509
$Ga_xIn_{4-x}PyAs_{1-y}$, In rich bulk single crysts. growth from melt via gradient freeze method, and characterisation 78—68618
GaP, luminesc. emission band, electron-hole liquid 77—69245
GaP on GaAs, LPE, growth with Ge and Sn solvents, phase diags. 78—88434
GaP:H/GaAs, amorphous film/crystal junction, optical and elec. props. 79—99611
GaP:N, phonon satellite intensity distrib. in luminesc. spectrum 77—55832
GaP-GaAs, amorphous film/crystal junction, optical and elec. props. 79—99611
GaP-GaAsP planar heterostructure strip ridged waveguide under mech. load, polarisation modulation 80—96038

gallium arsenide continued
$GaP_{0.1}As_{0.9}$, gas-transport condensate with superlattice, structural and chemical inhomogeneity 77—85088
$GaP_{0.9}As_{0.1}$/GaP, heteroepitaxial structs., refined formulation of relative orientation criterias 80—44448
GaP_xAs_{1-x} $(0 \leq x \leq 0.32)$ epitaxial film, one-dimens. superlattice, X-ray spectrometer scanning, struct. variations 78—47681
GaP_xAs_{1-x}, exam. of magnetic susceptibility and absorption spectra 79—1778
GaP_xAs_{1-x}, ion beam synthesis for photodetector fabrication 79—46688
GaP_xAs_{1-x}, N doped, alloying induced shift between excitation and luminesc. of N bound exciton 79—52013
GaP_xAs_{1-x}, refractive index comp. depend., nonlinearity parameter *(German)* 77—32344
GaP_xAs_{1-x} solid soln., specularly smooth epitaxial layers, superlattice struct. 77—24959
GaP_xAs_{1-x} solid solns., edge absorpt. 77—16334
GaP_xAs_{1-x}, surface defects and comp. inhomogeneity during gas-phase heteroepitaxy 77—85090
GaP_xAs_{1-x}:N, impurity electron states, binding energies and wavefunctions 79—42488
GaP_xAs_{1-x}:N, luminesc. of N bound state excitons, local-environment effects 80—100691
GaP_xAs_{1-x}-GaAs one dimens. superlattice, possibility of X-ray and electron diffr. struct. determ. 80—54560
n-GaP_xAs_{1-x}-p-$Ga_{1-y}Al_yP_xAs_{1-x}$ single sided heterolaser, visible emission 78—46607
GaSb-GaAs-Ge system, props. and struct. 80—20232
$GaSb_{1-x}As_x$, disorder-enhanced Auger recomb. 79—43014
$GaSb_{1-x}As_x$, MBE RHEED meas. 78—18916
$GaSb_{1-x}As_x$-$In_{1-x}Ga_xAs$ heterojunction, prep. by MBE, transport props. 77—80827
$GaSb_{1-y}As_y$ alloy surface states obs., using electron energy loss spectra 79—15202
$GaSb_{1-y}As_y$, MBE-grown, substrate effect on lattice consts. 79—77942
$GaSb_xAs_{1-x}$ films, MBE growth and elec. props. 79—23863
Ge-GaAs, (100) interface, electronic struct. calc. 80—49861
Ge-GaAs, crystallisation at superhigh cooling rates 80—54349
Ge-GaAs, heteroepitaxial systems, misfit dislocations obs. using HV electron microscopy 80—100242
Ge-GaAs, p-n heterojunctions, surface electron states 79—73578
Ge-GaAs, p-nn$^+$ junction, I-V characts., inverse branch, effect of dislocation defects *(Russian)* 79—15217
Ge-GaAs (110) interface, relax., self-consistent pseudopotentials 78—30981
Ge-GaAs (110) interface, self-consistent calc. of interface states and electronic struct. 78—52066
Ge-GaAs (110) junction, interface states and electronic struct. 77—69408
Ge-GaAs heterodiode, interfacial structural defects effect on avalanche breakdown 79—42644
Ge-GaAs heteroepitaxial system, dislocation struct. in stress measurements 80—29030
Ge-GaAs heterojunction, electrostatic dipole shifts contrib. to valence band discontinuities 79—51657
Ge-GaAs heterojunction, elec. and recomb. props., interface defect effects 80—80365
Ge-GaAs heterojunctions, electronic struct. 78—19138
Ge-GaAs heterojunctions, effect of γ-radiation on current-voltage charact. *(Russian)* 80—2459
Ge-GaAs p-n heterojunction, current fluctuations 79—11209
Ge-GaAs p-n junction, microparameters determ. 79—11216
Ge-GaAs superlattice and interface, electronic struct. 78—52065
p$^+$-Ge-n-GaAs abrupt heterojunction, reverse currents *(Russian)* 78—10542
n-Ge-n-GaAs isotype heterojunctions, modelling, characts. 80—103747
$Ge_{0.8}(GaAs)_{0.2}$, metastable solid solns., decomp. kinetics 79—38789
$Ge_{1-x}(GaAs)_x$, metastable solid solution, fine struct. *(Russian)* 79—27960
IR spectra, manifestation of local vibrs. 78—88339
(In,GA)(As,P) binary, ternary and quaternary, hydride vapour phase epitaxy, cryst. growth and props. 80—66434
In-Ga-As system, heterophase equilibrium, phase diagram calc. 79—43212
In-Ga-As-P, phase diagram rel. to lattice matched LPE 78—39708
In-GaAs:Cu-In S-type diode, role of deep trapping levels in form. of current-volt. characts. 77—76948
p-$In_{0.77}$ $Ga_{0.23}As$/Ag photocathode, field assisted photoemission to 2.1 microns 80—76130
InGaAs detector, integrated optics appl. *(Czech)* 80—33227
(InGa)As film, growth kinetics for step-cooling LPE technique 77—40395
InGaAs, LED, 1.06 μm range, neutron and γ-irrad. effects 79—97433
InGaAs, LPE, diffusion-limited step-cooling technique, layer thickness and composition 80—84402
InGaAs, lattice-matched VPE on (100) InP, photodiode appl. 80—35102
InGaAs on (100) InP substrate, VPE 80—40267
InGaAs, transferred electron photoemission to 1.65μm 78—68600
(InGaAs)/(InGa)P, DH laser, threshold current temp. depend. 79—81431
InGaAs/InGaP struct. for transferred electron photocathodes, VPE growth and characterisation 80—76193
InGaAs-GaAs heterojunction with low misfit, misfit dislocation struct. 77—62783
InGaAs-GaSbAs periodic structures, with controlled emission 79—7880
InGaAs-$In_{1-x}Ga_xAs_yP_{1-y}$ DH laser, LPE fabrication, electroluminesc., lasing characts. 79—3709
InGaAs-InGaP vapour-grown ternary heterojunction laser struct., reliability 79—98385
InGaAs-InP heterojunction detector for 1.0-1.7 μm wavelength range 78—49895
InGaAs-InP p-p heterojunction, field-assisted minority carrier electron transport, in photocathode struct. 78—95651
InGaAs-InP punch-through type photodetector fabricated by VPE 80—68253
$In_{0.1}Ga_{0.9}As$, quantitative anal. with SIMS 80—101052
$In_{0.53}Ga_{0.47}As$, growth on (100)-oriented InP, from supercooled solution 79—70001
$In_{0.53}Ga_{0.47}As$, Hall mobility and Hall factor, temp. and donor conc. depend. 80—49773

gallium arsenide continued
$In_{0.53}Ga_{0.47}As$, incorporation of Ga during LPE growth on (111)B and (100)InP substrates 78—91557
$In_{0.53}Ga_{0.47}As$, interband magnetoabsorption study, quasi-Ge model application 80—50304
$In_{0.53}Ga_{0.47}As$, LPE growth on (100) InP, for field assisted photocathode appl. 78—15318
$In_{0.53}Ga_{0.47}As$, LPE layer on InP, electron mobility and energy gap 77—24627
$In_{0.53}Ga_{0.47}As$ p-i-n photodiodes, for long-wavelength fibre-optic systems 80—5826
$In_{0.53}Ga_{0.47}As$, phase diagram at 650°C and LPE growth of lattice-matched layer 79—96009
$In_{0.53}Ga_{0.47}As$ photodiodes with dark current limited by generation-recombination and tunneling 80—107893
p-$In_{0.53}Ga_{0.47}As$:Zn on InP, elec. and optical props. 80—75662
$In_{0.53}Ga_{0.47}As$/InP avalanche photodetector 80—4764
$In_{0.53}Ga_{0.47}As$-InP, 1.7 μm heterojunction lasers and photodiodes fabrication 78—25880
$In_{0.53}Ga_{0.47}As$-InP avalanche photodiode with guard-ring struct., characts. 80—96939
$In_{0.53}Ga_{0.47}As$-InP avalanche photodiode structure for 1 to 1.6 μm region 80—98978
$In_{0.53}Ga_{0.47}As$-InP heterostructure, LPE growth 80—11582
$In_{1-x}Ga_xAs$-$GaSb_{1-y}As_y$ superlattice, optical absorption 79—19887
$In_{1-x}Ga_xAs$, disorder carrier scatt., Green's function calc. 77—11906
$In_{1-x}Ga_xAs$, LPE, electron mobility and max. drift vel., microwave device appls. 77—77431
$In_{1-x}Ga_xAs$, LPE growth on InP, electron probe anal. of etched surface 79—23862
$In_{1-x}Ga_xAs$, LPE layer on InP substrate, phys., elec. and optical props. 78—39235
$In_{1-x}Ga_xAs$, LPE on InP substrate, comp. latching phenomenon and lattice mismatching effects 79—28961
$In_{1-x}Ga_xAs$ layer on InP, misfit dislocation free, LPE growth 80—108364
$In_{1-x}Ga_xAs$, MBE-grown, substrate effect on lattice consts. 79—77942
$(In_{1-x}Ga_x)As$, scattering of electrons by potential clusters 77—15842
$In_{1-x}Ga_xAs$-$GaSb_{1-y}As_y$, semiconductor superlattices by MBE 79—95939
$In_{1-x}Ga_xAs$-$GaSb_{1-y}As_y$, superlattice electronic subband struct. 77—72815
$In_{1-x}Ga_xAs$-$GaSb_{1-y}As_y$, new heterostruct. characts. 78—72247
$In_{1-x}Ga_xAs$-$GaSb_{1-y}As_y$ superfine heterostruct., MBE 78—95348
$In_{1-x}Ga_xAs$-$GaSb_{1-y}As_y$ superlattice, with nonlinear energy-wave and energy-momentum relationships 79—7871
$In_{1-x}Ga_xAs$-$GaSb_{1-y}As_y$ heterostructure devices 79—42624
$In_xGa_{1-x}As$ (x=0.03 and 0.05), grown as GaAs substrate, with InGaAsP buffer layer, exam. of dislocation density 80—44447
$In_xGa_{1-x}As$ avalanche diode, noise meas. 77—4431
$In_xGa_{1-x}As$, electron drift vel. in high elec. fields 78—30928
$In_xGa_{1-x}As$ epitaxial layer, waveguiding at 1.06 μm, losses 78—18052
$In_xGa_{1-x}As$, epitaxial solid soln. film, spectral depend. of transparency, absorpt. spectra calcs. 80—45161
n-$In_xGa_{1-x}As$ film, epitaxial growth on GaAs, using CVD system 77—1812
$In_xGa_{1-x}As$, heteroepitaxial, MBE grown, props. 78—84328
$In_xGa_{1-x}As$, heterostructure composition profile by photoemission microanalysis 80—44717
$In_xGa_{1-x}As$, LPE growth on GaAs 79—61519
$In_xGa_{1-x}As$ layers, on GaAs substrate, MBE fabrication and laser operation 80—10820
$In_xGa_{1-x}As$, MBE layers on InP substrates, elec. props., photoluminesc., X-ray and Auger obs. 79—51450
$In_xGa_{1-x}As$ MBE layers on InP substrate, lattice deformation, misorientation 79—90896
$In_xGa_{1-x}As$ multilayer struct., photoluminesc. and X-ray spectroscopic microprobe analysis 77—4687
$In_xGa_{1-x}As$ on GaAs, heterojunctions, misfit dislocation banding, stress-induced birefr. 77—28542
$In_xGa_{1-x}As$, planar photodiodes made by VPE 79—49286
$In_xGa_{1-x}As$, thick LPE growth, electrolum. obs. 78—60589
$In_xGa_{1-x}As$, VPE on (100), (111)A, and (111)B InP substrates 80—15382
$In_xGa_{1-x}As$:Si, p-n junction form. in LPE layers, In content effect on inversion temp. 77—4266
$In_xGa_{1-x}As$:Si p-n structs., electrolum. spectra, 77 to 300K 80—93408
$In_xGa_{1-x}As$:Zn, lattice matching to InP, LPE growth conditions 80—70541
$In_xGa_{1-x}As$-Au Schottky contacts, interfacial oxide layers used to increase effective barrier height 79—7896
$In_xGa_{1-x}As$-$In_yGa_{1-y}P$ DH laser, CW room temp. operation at 1.06 μm 77—19250
$In_xGa_{1-x}As$-$InAs_xP_{1-x}$ VPE mixed crystal composition rel. to vapour pressure *(Japanese)* 77—55893
InGaAsP, 1.3 μm LED, for high-bit-rate fibre data link 78—46825
InGaAsP, anodic oxidation, refractive indices 80—97601
InGaAsP avalanche photodiodes, leakage current, shot noise, quantum efficiency, gain saturation 79—67381
InGaAsP avalanche photodiode, 1.3 μm, noise performance, −190°C 80—57370
InGaAsP avalanche photodiodes, breakdown mechanism, donor conc. effect 80—70710
InGaAsP, bandgap energy by electroreflectance and photoluminesc. spectra 80—107700
InGaAsP buried stripe laser, modulation characts. 79—98418
InGaAsP DH, luminesc., quantum efficiency determ. 80—108273
InGaAsP DH laser characts., temp. depend. 80—1223
InGaAsP DH lasers with etched reflectors, fabrication, current density 80—64050
InGaAsP, dual-wavelength demultiplexing photodiode 79—63304
InGaAsP, epitaxial layer, defect evaluation by cathodoluminescence 80—2866
InGaAsP heterojunction cathode, transferred electron photoemission 78—48272
InGaAsP, high radiance CW LEDs emitting at 1.30 μm 78—22196
InGaAsP IR heterojunction photodiode detector 79—21813
InGaAsP InP DH lasers, optical power and wavelength stabilisation 80—38036
InGaAsP, injection heterojunction laser at 1.3-1.5 μm 79—89910
InGaAsP LED sources, for near-IR absorpt. meas. 80—77135

gallium arsenide continued
InGaAsP, LPE, diffusion-limited step-cooling technique, layer thickness and composition 80—84402
InGaAsP, LPE growth, orientation depend. of incorporation of Ga, As, and Zn 78—6869
InGaAsP, LPE growth on InP, influence of lattice mismatch on surface morphology 79—1553
InGaAsP, LPE growth techniques influence on composition 79—52130
InGaAsP, LPE growth, impurity depend. of distrib. coeff. 80—10843
InGaAsP, LPE grown, impurity effect on surface morphology 80—29291
InGaAsP LPE layers on InP substrate, material selective chemical etching 79—70188
InGaAsP laser, single-mode CW ridge waveguide, emitting at 1.55 micron for optical fibre links 80—9883
(InGa)(AsP) laser system, VPE growth using metal organic sources or halide transports 80—99748
InGaAsP, lattice matched, LPE growth on (100) InP, for 1.15-1.31 μm spectral region 78—64483
InGaAsP low-threshold 1.25-μm vapour grown CW lasers, emission characts. 79—50308
p-InGaAsP, on InP surface, diffusion coeff. and surface recombination velocity 80—39598
InGaAsP photocathodes for astronomical detectors, UV response 77—57387
InGaAsP quaternary alloy IR heterojunction detectors, props. 79—2823
InGaAsP, quaternary alloy, physical props. *(Japanese)* 80—15449
InGaAsP single-mode CW ridge-waveguide laser emitting at 1.55 micron 80—58584
InGaAsP strip-buried-heterostructure high-output power laser 80—58540
InGaAsP strip-buried heterostructure laser, high output power, operation 80—58559
InGaAsP, with and without InP cladding layers, low photolum. regions 79—33754
InGaAsP:Be, avalanche photodetectors annealing temp. effect on photolum. spectra 79—69872
InGaAsP:Be ion-implanted avalanche photodiode, struct. and characts. 79—17487
InGaAsP:Sn(Te)(Zn), LPE growth, influence of growth-solution dopants on distrib. coeffs. 79—47640
InGaAsP/InP, DH laser, 1.5 μm, with optical waveguide structure, fabrication 79—72587
(InGa)(AsP)/InP, DH laser, threshold current temp. depend. 79—81431
InGaAsP/InP, native oxide stripe laser 79—68405
InGaAsP/InP avalanche photodiode, ionisation coeff. 80—15590
InGaAsP/InP DFB injection lasers 80—5746
InGaAsP/InP DH, vapour phase growth by dual-growth-chamber method 80—50559
InGaAsP/InP DH lasers, Zn doping level 79—98373
InGaAsP/InP DH laser, self-aligned struct. 80—9893
InGaAsP/InP DH lasers, temp. depend. characts. 80—58541
InGaAsP/InP DH stabilised 1.3 μm laser diode-isolator module for hybrid optical integrated cct. 80—58583
InGaAsP/InP heterojunction, X-ray characterisation of defects 78—95239
InGaAsP/InP heterostruct. lasers as optical source, CW operation at room temp. 80—1220
InGaAsP/InP injection lasers for long wavelength (1.1 to 1.6 μm) optical communication 80—58582
InGaAsP/InP lasers and detectors for LW optical fibre communication 80—9885
InGaAsP/InP phototransistors, fabrication by LPE, photodetectors 80—95139
p-InGaAsP-Au, Schottky barrier height comp. depend., photoelec. meas. 77—20433
InGaAsP-InP, anomalous luminesc., near heterojunction interface 79—65932
InGaAsP-InP, double heterostructure laser, temp. sensitive threshold current 79—59700
InGaAsP-InP, double heterostructure laser lifetime, point defect generation model calcs. 80—32992
InGaAsP-InP, Zn diffused DH structures, oxide defined transverse junction stripe lasers 79—98389
InGaAsP-InP 1.27 μm CW DH injection lasers, 1.1 Gb/s pseudorandom PCM 78—55390
InGaAsP-InP bias assisted photocathodes, photoemission in 1-2 μm range 78—48289
InGaAsP-InP buried crescent injection laser emitting at 1.3 μm with low threshold current 80—87404
InGaAsP-InP buried heterostructure lasers emitting at 1.3 μm, accelerated ageing characts. 80—95898
InGaAsP-InP CW lasers, 1.5-1.7 μm, VPE 80—78861
InGaAsP-InP DH laser emitting at 1.27 μm, fast pulse behaviour, high speed direct modulation 77—23676
InGaAsP-InP DH lasers, direct modulation 78—42363
InGaAsP-InP DH lasers, carrier lifetimes meas. 78—66828
InGaAsP-InP DH laser, threshold depend. on active layer thickness 79—7127
InGaAsP-InP DH lasers, threshold characteristic 79—81430
InGaAsP-InP DH laser, optical gain meas., low-intensity luminesc. and absorpt. spectra 79—98356
InGaAsP-InP DH lasers, low temp. behaviour of threshold current and carrier lifetime 79—98374
InGaAsP-InP DH lasers, degradation by In solder 79—98402
InGaAsP-InP DH laser with self-aligned struct., oscillation characts. 80—38017
InGaAsP-InP DH laser, 1.55 μm, low temp. LPE growth for room-temp. CW operation 80—64045
InGaAsP-InP DH LED, high temp. aged, dark-spot defects, TEM obs. 80—66300
InGaAsP-InP DH lasers, interfacial recomb., influence on oscill. characts. 80—87393
InGaAsP-InP DH lasers, spatial hole burning, spontaneous emission saturation, direct obs. 80—95892
InGaAsP-InP DH lasers, temp. dependence of threshold and elect. characts. 80—99725
InGaAsP-InP DH lasers, perturbed InP growth, photoluminesc. study 80—106518
InGaAsP-InP DH laser, threshold current, temp. depend. 80—106521
InGaAsP-InP dual wavelength LED 80—15589
InGaAsP-InP embedded mesa strip lasers 80—14350

gallium arsenide continued
InGaAsP-InP heterojunction, LPE, lattice mismatch, Auger depth profile 79—87005
InGaAsP-InP high-gain heterojunction phototransistor 80—103745
InGaAsP-InP laser, LPE, 1.5 μm range, effects of double cladding struct. 80—48290
(InGa)(AsP)-InP laser system, 1 μm wavelength, lattice matching techniques 80—99748
InGaAsP-InP lattice-matched heterojunction, LPE growth and characterisation 77—21041
InGaAsP-InP lattice matched DH, growth by two-phase supercooled soln. technique 78—10296
InGaAsP-InP layers, grown by LPE techniques, lattice const., bandgap, thickness and surface morphology meas. 80—59818
InGaAsP-InP photodiodes, microplasma-limited avalanche multiplication at 1 to 1.3 μm 79—26128
InGaAsP-InP photodiodes antireflectively coated with InP native oxide 80—13137
InGaAsP-InP vapour-grown quaternary heterojunction laser struct., reliability 79—98385
InGaAsP-InP:Mg LEDS, for high-bit-rate optical communication systems 80—5823
$In_{0.79}Ga_{0.21}As_{0.54}P_{0.46}$, LPE layer, electroreflectance meas. 79—24290
$In_{0.8}Ga_{0.2}As_{0.5}P_{0.5}$, LPE growth 80—11557
$In_{0.84}Ga_{0.16}As_{0.46}P_{0.54}$, refractive index, at laser oscillating wavelength of 1.2 μm 79—64224
$In_{0.85}Ga_{0.15}As_{0.39}P_{0.61}$, deep impurity levels 79—87058
$In_{0.9}Ga_{0.1}As_{0.22}P_{0.78}$, effective mass meas. by Shubnikov-de Haas oscills. 78—34754
$In_{1-x}Ga_xAs_{1-y}P_y$ layers on InP substrate, LPE growth, quaternary phase diagram, and band gaps 79—42403
$In_{1-x}Ga_xAs_xP_{1-y}$, p-n junction diodes, fabrication by Be ion implantation 79—47156
n-$In_{1-x}Ga_xAs_yP_{1-y}$, cyclotron reson., cond. band nonparabolicity 80—29311
$In_{1-x}Ga_xAs_yP_{1-y}$, DH laser material, spatially resolved photolum. characterisation and optically induced degradation 79—47486
$In_{1-x}Ga_xAs_yP_{1-y}$ DH laser, low threshold current density, near equilibrium LPE growth 80—19040
$In_{1-x}Ga_xAs_yP_{1-y}$ DH lasers for 1.3 and 1.5 μm optical fibre communications 80—91817
$In_{1-x}Ga_xAs_yP_{1-y}$, electron effective mass from Shubnikov-de Haas meas. 80—80298
$In_{1-x}Ga_xAs_yP_{1-y}$ epitaxial layer, far IR refl. spectra, lattice vibrs. 80—97282
$In_{1-x}Ga_xAs_yP_{1-y}$, evidence for alloy scatt. from press. induced changes of electron mobility 80—88548
$In_{1-x}Ga_xAs_yP_{1-y}$ far IR reflection spectrum 80—60612
$In_{1-x}Ga_xAs_yP_{1-y}$, Hall mobility, comp. depend. 80—75587
$In_{1-x}Ga_xAs_yP_{1-y}$, hole mobility over temp. range 77 to 300K 80—60111
$In_{1-x}Ga_xAs_yP_{1-y}$, LPE growth on InP (100), lattice matched composition 78—87881
$In_{1-x}Ga_xAs_yP_{1-y}$ LPE layers, background carrier conc. and electron mobility. 79—95523
$In_{1-x}Ga_xAs_yP_{1-y}$, lattice vibrs., Raman study 78—91391
$In_{1-x}Ga_xAs_yP_{1-y}$, lattice matched to InP, band gap vs. comp., and Vegard's law demonstration 79—7782
$In_{1-x}Ga_xAs_yP_{1-y}$, oscillatory magneto-transmission, band parameters 79—60707
$In_{1-x}Ga_xAs_yP_{1-y}$ quaternaries VPE 0.75 to 1.35 eV band gap range 79—69987
$In_{1-x}Ga_xAs_yP_{1-y}$, vapour grown, alloy comp., thermodynamic calc. 79—99094
$In_{1-x}Ga_xAs_yP_{1-y}$:Be, ion implantation, hole conc. and mobility, junction depth 79—46685
$In_{1-x}Ga_xAs_yP_{1-y}$/InP 1.5 μm room-temp. CW laser fabrication and operation 80—64070
$In_{1-x}Ga_xAs_yP_{1-y}$-InP DH laser, fabricated on (100)-InP substrate, 500-hr CW operation 77—83890
$In_{1-x}Ga_xAs_yP_{1-y}$-InP DH lasers, fabrication and performance 78—5500
$In_{1-x}Ga_xAs_yP_{1-y}$-InP DH laser on InP (100) substrate 78—29965
$In_{1-x}Ga_xAs_yP_{1-y}$-InP DH laser, 10000 h continuous CW operation, dark-line and dark-spot defects 79—98384
$In_xGa_{1-x}As_{1-y}P_y$ epitaxial layers, characterisation and relation to lattice matching 80—100540
$In_xGa_{1-x}As_xP_{1-x}$-InP photodetectors, construction and performance 78—65966
$In_xGa_{1-x}As_yP_{1-y}$ layers on InP, LPE and opt. props. characteris. 79—28849
$In_xGa_{1-x}As_yP_{1-y}$ photodetector diode on InP substrate dark currents, tunnelling, energy gaps, effective masses 80—70805
$In_xGa_{1-x}As_yP_{1-y}$, surface and dielec.-semicond. interface props. 80—93001
$In_xGa_{1-x}As_yP_{1-y}$, valence band struct., CPA calc. 79—73435
$In_xGa_{1-x}As_yP_{1-y}$-InP n-p heterojunction photodiode, characts. 78—14800
InGaAsSb based injection heterolaser, 1.9 μm stimulated emission 79—18420
InGaAsSb, LPE growth, and appl. in GaSb/AlGaAsSb/InGaAsSb/AlGaAsSb/GaSb DH 80—16205
InGaAsSb-AlGaAsSb DH laser, room temp. operation at 1.8 μm wavelength 80—43358
$In_{1-x}Ga_xAs_{1-y}Sb_y$, LPE growth on (111)B-oriented InAs, growth conditions and lattice matching 77—24973
$In_xGa_{1-x}As_ySb_{1-y}$ laser, nonequilibrium carrier recombination, luminesc. study 80—50431
InGaP-GaAs junction, effect of elastic strain on energy band gap and lattice parameters 79—24057
InGaP-InGaAs solar cell, high internal collection efficiency, low bandgap 80—26134
$In_{0.5}Ga_{0.5}P$-GaAs heterojunction, interfacial recomb. vel. determ. 77—51809
$In_xGa_{1-x}P$-GaAs heterojunction, interface recomb. velocity determ. 77—89838
$In_xGa_{1-x}P$-GaAs lattice mismatched heterojunction, recomb. props. 78—13707
InGaPAs LPE layers, compositional inhomogeneity, photoluminesc. obs. 80—75451
InGaPAs-InP DH laser, threshold current temp. depend., potential barrier height influence 80—53296
$In_{1-x}Ga_xP_{1-y}As_y$ LPE films, hot electron and magnetotransport props. 78—26977

gallium arsenide continued
$In_{1-x}Ga_xP_{1-y}As_y$ lattice-matched epitaxial layers, LPE growth on GaAs(100), characterisation 80—75465
$In_{1-x}Ga_xP_{1-z}As_z$, DH, operated in external grating cavities, inhomogeneous and homogeneous line broadening 77—10921
$In_{1-x}Ga_xP_{1-z}As_z$, DH, diode and laser performance, limitations of direct-indirect transition 77—39927
$In_{1-x}Ga_xP_{1-z}As_z$ DH lasers, pulsed room temp. operation 77—10941
$In_{1-x}Ga_xP_{1-z}As_z$ DH laser, effective index of refr., wavelength depend. 77—61954
$In_{1-x}Ga_xP_{1-z}As_z$ DH lasers, multiple LPE, lattice matching 77—77421
$In_{1-x}Ga_xP_{1-z}As_z$ DH laser diode, defect and phonon assisted tunnelling 78—13708
$In_{1-x}Ga_xP_{1-z}As_z$ LPE DH laser with multiple thin layer active region 77—83887
$In_{1-x}Ga_xP_{1-z}As_z$, lattice matched to InP, electroreflectance obs. 80—93416
$In_{1-x}Ga_xP_{1-z}As_z$ near IR DH laser, constant temp. LPE, external grating cavity 77—75550
$In_{1-x}Ga_xP_{1-z}As_z$, room temp. visible heterojunction lasers 78—5501
$In_{1-x}Ga_xP_{1-z}As_z$ single thin active layer visible spectrum heterostruct. lasers 78—63120
$In_{1-x}Ga_xP_{1-z}As_z$, stimulated yellow-green emission under electron excitation, 80K 79—33846
$In_{1-x}Ga_xP_{1-z}As_z$ thin well in InP p-n junction, confined carrier luminesc. and laser modes 78—13703
$In_{1-x}Ga_xP_{1-z}As_z$, visible spectrum laser diode, continuous operation, 6280 Å, 77K 79—960
$In_{1-x}Ga_xP_{1-z}As_z$ well in InP, tunnel injection into confined particle states 78—19130
$In_{1-x}Ga_xP_{1-z}As_z$:Zn, x~0.12, z~0.26, LPE, DH lasers, tunnelling involving defects 77—65594
$In_{1-x}Ga_xP_{1-z}As_z$-$In_{1-X}Ga_XP_{1-Z}As_z$ visible spectrum multiple-quantum-well heterostruct. lasers 80—106537
$In_{1-x}Ga_xP_{1-z}As_z$-InP, single and multiple layer heterostruct., LEDs and lasers 78—46626
$In_{1-x}Ga_xP_{1-z}As_z$-InP, valence band discontinuity, quantum well luminesc. 79—91483
$In_{1-x}Ga_xP_{1-z}As_z$-InP coupled multiple quantum-well heterostructure laser diodes, threshold current temp. depend. 80—78855
$In_uGa_{1-u}P_vAs_{1-v}$-InP, LPE, lattice matching, phase 80—54350
InGaSbAs heterostructures and LED's luminesc. props. in 1-2 micron band 78—10988
In_{1-x}GaxAs, MBE, RHEED meas. 78—18916
In_2O_3-SnO_2/GaAs, solar cell, fabrication, characts. and interfacial chemistry 80—21401
InP/$In_{1-x}Ga_xAs_yP_{1-y}$ heterostruct., optically induced degradation 79—86791
InP/$In_xGa_{1-x}As_yP_{1-y}$ interfaces, sputter-profiled, depth resolution degradation by cone form. 80—80094
InP/InGaAs heterojunction phototransistor, high-sensitivity 80—100505
InP/InGaAsP avalanche photodiodes, with guard ring structure 80—100506
InP-$Ga_xIn_{1-x}As_{1-y}P_y$ heterojunctions, energy band diagram 77—16400
InP-$Ga_xIn_{1-x}As_gP_{1-y}$ systems, for optical devices in 1 to 1.6 μm region, LPE growth *(Japanese)* 79—28956
InP-Ga_xIn_{1-x}As-InP, DH fabrication, crack form. due to lattice mismatch 77—15704
InP-$Ga_xIn_{1-x}P_yAs_{1-y}$ heterostruct. lasers, growth and characterisation 80—23691
InP-GaInAsP buried heterostructure lasers of 1.5 μm region, fabrication and characts. 80—74388
InP-$In_{1-x}Ga_xAs_yP_{1-y}$-InP 1.55 μm DH room-temp. CW laser fabrication and operation 80—64071
InP-$In_{1-x}Ga_xAs_yP_{1-y}$-InP 1.53 μm single-mode CW ridge-waveguide laser 80—64072
InP-$In_{1-x}Ga_xP_{1-z}As_z$ quantum-well LPE heterostructure lasers, band filling and gain 79—22955
InP-$In_{1-x}Ga_xP_{1-z}As_z$ laser, phonon-assisted recombination 79—89906
InP-$In_{1-x}Ga_xP_{1-y}As_y$, LPE for optoelectronic devices *(German)* 79—95280
InP-$In_{1-x}Ga_xP_{1-z}As_z$ heterostructure laser, single and multiple quantum-well, liquid-phase epitaxial growth 80—38031
InP-In_xGa_{1-x}As alloy photocathodes, semiconductor photoemitters, field-assisted, 1-2 μm range 80—97396
InP-InGaAsP p-n junction avalanche photodiodes, surface passivation techniques 80—100508
InP-InGaAsP-InP DH diode lasers, room temp. CW operation 80—1222
InP-InGaPAs heterojunction lasers and LEDs, 1.0 to 1.2 μm 80—74362
InSb-GaAs, interface between two polar semiconds., optic-phonon-magnetoplasmons 78—23146
InSb-GaAs semiconductor plasmas, surface wave instabilities, temp. effects 79—78125
LED, luminous intensity ang. distrib. and total light flux meas. device *(Chinese)* 78—82018
n-type, hybrid mode instability 77—80800
O^+ implantation, effect on LPE growth and elec. props. 80—24477
O^+ implantation, energy levels, photoluminesc. 80—24838
optical constants of n- and p-type, 2.5-3.5 eV 79—15428
p-type, Fe-compensated, photocond. under strong excitation 77—15904
Pt-GaAs contacts, sintered, eval. of W, Ti, Mo and Hf barrier metals 77—8193
$(SNBr_{0.4})_x$-GaAs solar cells, single crystals and polycrystalline 80—16810
Si-GaAs heterojunction photothyristor, spectral characts. 78—10546
Si_xGe_{1-x}-GaAs, heterojunction, elec. and recomb. props., interface defect effects 80—80365
Si_xGe_{1-x}-GaAs, p-nn^+ junction, I-V characts., inverse branch, effect of dislocation defects *(Russian)* 79—15217
Si_xGe_{1-x}-GaAs heterodiode, interfacial structural defects effect on avalanche breakdown 79—42644
Si_3N_4-GaAs, layer struct., electron-hole liq. at interface 79—69434
SiO_2/GaAs, interface reaction during high-temp. heat-treatments 80—88439
SiO_x-GaAs, vacuum evaporated system, acoustoelec. signal, interface props. 80—75646
Sn, CVD onto GaAs surface, anal. of conditions 79—87584
in Sn, vap. press. of P and As 77—51485
SnO_2-GaAs heterojunctions, elec. and optical props., photovoltaic appls. 77—43714
surface, (110), electronic states near band gap 77—85290

gallium arsenide continued
$Zn_xCd_{1-x}S$/GaAs heterojunction solar cells, meas. of minority carrier diffusion length 80—26158
ZnSe solar spectrum convertor for GaAs solar cells 80—101117
ZnSe:Mn-n-GaAs, single cryst. substrate low threshold DC electrolum. 77—63465
ZnSe-GaAs epitaxial heterostructure, growth and struct. 78—43257
ZnSe-GaAs narrow junction lasers 80—43334
ZnSe-GaAs solid solns., chem. transport cryst. growth, struct. 78—43991
ZnSe-GaAs thin film DE electroluminescent cell with 20 V threshold voltage 78—76141
$(ZnSe)_{1-x}(GaAs)_x$ solid solns., photoluminescence spectra 80—40159
n-ZnSe—p-GaAs heterojunction high-detectivity threshold photodetectors 79—6181

gallium compounds
see also gallium alloys; gallium arsenide
carbon tetrachloride-$GaCl_3$-Nd^{3+} nontoxic liquid phosphor system, synthesis 80—55157
cathodoluminescence, bibliography of papers till 1977 79—21482
chalcogenate and chalcogenite double salts, form. laws and acid-base props. 80—101070
chalcogenide, layered materials, prep. and growth, book contrib. 78—19661
chalcogenides, cryst. struct. types 77—15392
chalcogenides, energy spectrum of local levels *(Russian)* 79—51517
chalcogenides, photoemission, book contrib. 77—44133
electron irrad. effect on electrolum., defects form. and quenching obs. 80—55194
$Ga_{1-x}In_xSb$, inverted diode, electron irradiation effect on props. *(Russian)* 78—14378
Ga_2S_3-Ga_2Te_3 phase diag. *(French)* 78—76635
Ga(AsP) on GaAs, LPE, growth with Ge and Sn solvents, phase diags. 78—88434
GaInAsP quaternary alloys, orientation effects in LPE growth 78—92203
n-GaP, quasidirect radiative recombination of free holes at neutral shallow donors 78—64410
GaP, reevaluation of bandgap and free exciton binding energy 78—60061
GaP/$In_xGa_{1-x}P$/GaAs:(Cs-O) high sensitivity transmission photocathodes, photosensitivity, electron diffusion length 79—78832
$GaSe_{1-x}Sx$, exciton spectrum nature and anisotropy of electron bands near absorption edge *(Russian)* 79—51483
p-GaSe, relaxational oscillations of photoconductivity and dark conductivity 77—69379
halides, (X=Cl,Br,I), charge transfer spectra 79—76441
halides, Wasastjerna pot. function, force consts., internuclear separations and binding energies 80—14187
hydroxygallium phthalocyanine, exciton electroabsorpt., optical density spectra 77—85746
InP-InGaAsP-InP, low threshold laser, threshold density temp. depend., LPE method *(Russian)* 78—22133
methylammonium alums, dielec. relax. near transition point 80—71301
methylammonium gallium selenate, lattice consts. and ferroelec. props. 79—33641
methylammonium-$Ga(SO_4)_2.12H_2O$, ferroelec. alum single crysts., dielec. dispersion and characts. 79—15408
methylammoniumgallium sulphate:Cr^{3+}, EPR and linewidth anomaly 77—12191
oxidation, water vapour and O_2 excitation effects, XPS obs. 79—100274
rare earth beryllogallates with melilite struct., synthesis 77—81236
rare earth gallium borates, high temperature crystallisation, composition, struct., props. 80—40253
rare earth gallium garnet, growth of crystals from $50PbO.40PbF_2.10B_2O_3$ flux 77—21014
selenites, binary, effect of nature of alkali metals on composition and props. of hydrothermal reaction products 77—24941
zeolites, and Ga analogues, IR spectroscopy to investigate structure 79—95744
$AgGaS_2$, up-conversion of 10.6 μm radiation into visible 78—33783
$AgGaS_2$, electroluminesc., mechanism *(Russian)* 77—69918
$AgGaS_2$, Raman spectrum, degenerate mods, temp. depend. 78—35150
$AgGaS_2$-$AgGaSe_2$ system, phase diagram, lattice consts., and IR spectra 80—60841
Ag_5GaS_4, form. in Ag-Ga-S system 79—87618
AgGaSe, exciton energy determ., electron beam excited luminesc. 79—38680
$AgGaSe_2$, and Ag_9GaSe_6, XPS, Auger and direct electron spectra 78—52620
$AgGaSe_2$, growth by Bridgman method, optical characts. 77—69980
$AgGaSe_2$, Schottky diodes with tunnel device characts. 78—39215
$AgGaSe_2$, ternary semiconductor crystals for nonlinear optical applics. 78—33782
$AgGaSe_2$ wavelength-modulated reflectance, optical electronic transitions, 1.5-5.5 eV 78—35170
$AgGa(Se_{1-x}S_x)_2$, crystal growth, phase studies, optical props. 78—48305
$AgGaSe_2(Te_2)$, phonons, far IR refl. obs. 78—60459
Ag_2S-Ga_2S system, phase diagram, DTA and X-ray diffr. meas. 77—15544
Ag_2Se-Ga_2Se_3, phase diagram in rich Ag_2Se region *(French)* 77—51472
Ag_2Se-Ga_2Se_3, pseudobinary phase diagram determ., DTA, X-ray diffr., cryst. growth investigs. 77—70036
Al-Ga-Sb, ternary phase diagram, appl. to LPE growth 77—59761
Al-Ga-Sb ternary phase diagram, calc., DTA and LPE expts. 80—29931
Al_xGa_{1-x}-GaP structure, LPE, double heterostruct. light modulator appl. 79—28963
$Al_xGa_{1-x}As$, epitaxial growth, orienting substrates effects 77—43444
AlGaAsP/GaAs heterojunction, X-ray characterisation of defects 78—95239
AlGaAsSb, photodiode, lattice-matched to GaSb 79—71527
AlGaAsSb-GaSb heterojunction injection laser, radiative props. 1.4 to 1.8 μm range 80—91798
n-AlGaAsSb-GaSb-p-AlGaAsSb binary heterostructure injection laser, room temp. operation 78—9381
$Al_xGa_{1-x}As_ySb_{1-y}$, heterostructure composition profile by photoemission microanalysis 80—44717
$Al_yGa_{1-y}As_{1-x}Sb_x$ heterostructure, electroluminesc., appl. to LED's 77—8663
$Al_yGa_{1-y}As_{1-x}Sb_x$, LPE, strain effects near miscibility gap, importance 79—7759
$Al_yGa_{1-y}As_{1-x}Sb_x$-$Ga_{1-z}Sb_z$ buried heterojunction electroabsorption modulation 78—55439

gallium compounds continued
$Al_xGa_{1-x}N$ epitaxial layers, growth and props. 79—11522
$Al_{2x}Ga_{2(1-x)}O_3$:Cr^{3+}, luminesc., lifetime, 77 and 4K, struct., energy transfer 79—28798
$Al_{2x}Ga_{2(1-x)}O_3$:Cr^{3+}, luminesc., lifetimes 79—33784
$Al_{1-x}Ga_xP$, IR phonons, lattice reflection spectra 78—51626
$Al_xGa_{1-x}P$, LPE, crystallographic obs. and electrolum. 80—88445
$Al_xGa_{1-x}P$, photoluminescence excitation spectra, bound excitons, Al conc. depend. 80—20687
$Al_xGa_{1-x}P$, proportional ingredient content determ. by X-ray fluoroscopy 80—97747
$Al_xGa_{1-x}P$, solid solutions, refr. index dispersion characts. *(Russian)* 77—81080
$Al_xGa_{1-x}P$, Zn diffusion behaviour, device appls. 77—11741
$Al_xGa_{1-x}P$(:Zn), solution-grown single crysts., photo- and electrolum. at 77K 79—52004
AlGaSb, growth and characts. for 1.0-1.8 μm heterojunction devices 78—6870
p-$Al_xGa_{1-x}Sb$ epitaxial layers, cathodoluminescence. investig. for varying x *(Russian)* 77—20931
$Al_xGa_{1-x}Sb$, LED, 1.54 μm efficient emission at 300K reproducible fabrication 79—42636
$Al_xGa_{1-x}Sb$, method for determ. of liquidus surfaces in Ga-Al-Sb phase diagram 77—28787
$Al_xGa_{1-x}Sb$ mixed crystal, two-phonon absorption meas., 15-48 μm 77—1682
$Al_xGa_{1-x}Sb$, photolum. intensity increase due to composition variation 79—15528
$Al_xGa_{1-x}Sb$, solid soln., epitaxial layer growth from liq. phase 77—85089
$Al_xGa_{1-x}Sb$, solid soln., depend. of forbidden-band width on composition 78—39602
$Al_xGa_{1-x}Sb$ solid solns., freq. dependences of form of luminesc. spectra 80—40160
$Al_xGa_{1-x}Sb$, soln.-grown, photolum. 80—71476
$Al_xGa_{1-x}Sb$, surface flatness depend. on LPE condition 79—15042
$Al_xGa_{1-x}Sb$, vibr. spectra, Raman light scatt. study 80—45080
$Al_xGa_{1-x}Sb$:Zn, impurity diffusion, p-n junction depth 80—24678
$Al_xGa_{1-x}Sb$:Zn(Si)(Ge)(Sn)(Pb), doping of solid solns. during LPE *(Russian)* 77—85087
$Al_xGa_{1-x}Sb$-Pd contacts, struct., preparation elec. props. 80—65684
$Al_xGa_{1-x}Sb$-Pd contacts, band gap depend. of barrier height 80—65685
AlGaSbAs heterostructures and LED's luminesc. props. in 1-2 micron band 78—10988
$Al_xGe_{1-x}Sb$, photolum. spectra 78—95602
$(AlSb)_x(GaSb)_{1-x}$, solid soln., LPE 77—40392
As-Te-Ga, glass, elec. cond., 190-300K *(Russian)* 80—54702
As-Te-Ga system, glass-forming region and props. 80—25674
Au-$Ga_{1-x}Al_xSb$ Schottky barriers, barrier height 80—96986
Au-n-$Ga_{1-x}Al_xAs$-n-GaP narrow-band variable-gap surface-barrier photoedetector 80—96944
$Ba_2Ga_2GeO_7$, gehlenite struct., synthesis and physicochem. props. 79—43181
$BaGeO_3$-$(0.25MgF_2.0.75YF_3)$-Ga_2O_3 glass, synthesis and props. 80—25648
BiTe-In(Gn,Sn)Te system, physicochemical anal., eutectic type phase diagram with solid soln. region 77—16556
CC GaP, improvements in synthesis, solute diffusion (SSD) growth 79—65992
$CH_3NH_3Ga(SeO_4)_2.12H_2O$, dielec. relax. near transition temp. 80—60493
$Ca_3Ga_2Ge_3O_{12}$, appl. as substrate for mag. bubbles 77—28418
$Ca_3Ga_2Ge_3O_{12}$, substrate, electron examination of microstruct. and microsegregation 78—67919
$Ca_{1+x}Ga_{1-x}N_y$, prep. *(French)* 77—44206
CaO-Ga_2O_3, vitrification, spectroscopic and petrographic anal. 77—15556
CaO-Ga_2O_3 phase diagram and Czochralski melt growth of $CaGa_2O_4$ 80—29934
CaO-Ga_2O_3-Bi_2O_3, vitrification regions 77—15557
$CdGa_2S_4$ double surface-barrier diodes, current-voltage characts. 80—92972
$CdGa_2S_4$, IR refl. spectra 80—60604
$CdGa_2S_4$, photoluminesc. and photocond. meas. 78—60159
$CdGa_2S_4$:Ag(In), photoluminesc. and photocond. meas. 78—60159
$CdGa_2(S_{1-x}Se_x)_4$ solid solns., band struct. behaviour w.r.t. comp. *(French)* 80—107699
$CdGa_2S_4(Se_4)$, band struct., pseudopot. method 80—92816
$CdGa_2Se_4$, IR refl. spectra, optical phonon dispersion 80—29746
$CdGa_2Se_4$, ordered vacancy compound, Raman scatt. 79—95749
$CdGa_2Se_4$ ordered vacancy compound, Raman scatt. 79—99870
$CdGa_2Te_4$ film, effect of thermal annealing on struct., optical absorpt. and photocond. 79—65342
$Cd_{1-x}Hg_xGa_2S_4$ solid solns., band struct. behaviour w.r.t. comp. *(French)* 80—107699
$CdInGaS_4$, far IR refl. and transmission spectra, lattice vibrs. 79—91439
$CdInGaS_4$, layered structure crystals, refractive index meas. method 80—98966
Cr_2O_3:Ga_2O_3 EPR, antiferromagnetic coupling energy temp. depend. *(German)* 78—10766
$CsGa_{1-x}Fe_xS_2$, tetrahedrally coordinated Fe atoms in low spin state, mag. props. and neutron diffr. study *(German)* 80—88714
$CuFe_2O_4$-$CuGa_2O_4$, physicochem. props. *(French)* 77—44233
$Cu_{0.5}Ga_{0.5}Cr_2S_4$, mag. struct. determ. 77—8272
$CuGa_xIn_{1-x}S_2$ solid soln., IR refl. spectra, comp. depend. 78—52498
$CuGa_{0.5}In_{0.5}Se_2$/$Zn_{0.29}Cd_{0.71}S$ heterojunction solar cell, preparation and props. 80—101110
$CuGa_xIn_{1-x}Se_2$, CVD, elec. and optical props., use as heterojunction solar cell absorber 79—52095
$CuGaS_2$, ESR assessment of S diffusion behaviour on annealing 78—35036
$CuGaS_2$, exciton energy determ., electron beam excited luminesc. 79—38680
$CuGaS_2$, photoelectronic props., 77 to 300K 78—34865
$CuGaS_2$, tetragonal distortion, crystal field splitting, temp. depend. 79—47060
$CuGaS_{2-2x}Se_{2x}$, mixed crysts., luminesc. spectra, lattice consts. and band gap energy 77—63454
$CuGa(S_xSe_{1-x})_2$, refl. spectra, comp. depend. 78—39570
CuGaSe, Schottky diodes with tunnel device characts. 78—39215
$CuGaSe_2$, film, spray pyrolysis prod. 79—95953

gallium compounds continued
CuGaSe$_2$ single crystals, elect. and optical props. for solar cell appl. 80−10981
CuGaSe$_2$, temp. depend. of fundamental absorpt. edge 78−92090
CuGaSe$_2$/Cu Schottky-barrier cells, photovoltaic effect 79−96440
CuGaTe$_2$, IR lattice vibr. spectra 79−28765
CuGeTe$_2$, electroreflectance data, direct gap obs., cryst. field splitting and hybridisation degree 78−39557
CuIn$_{1-y}$Ga$_y$Se$_{2(1-x)}$Te$_{2x}$ pentenary alloy compounds for photovoltaic solar energy conversion 80−93971
Cu$_2$S-Ga$_2$S$_3$ alloys, cryst. growth, struct. and fluoresc. 77−48328
EuGa$_3$(BO$_3$)$_4$, luminesc. spectra, local symmetry of rare earth ion determ. 80−16095
EuGaYIG film, bubble dynamics, anisotropy depend., ferromag. reson. expts. 77−63240
EuGaYIG:Cr, epitaxial garnet film, interaction pot. of domain walls with localised stress fields 80−44889
EuS-Ga$_2$S$_3$-GeS$_2$, chalcogenide glasses, conditions of form. of glassy prod. *(French)* 80−100325
Fe$_{1-x}$Ga$_x$BO$_3$, synthesis, cryst. chem. and mag. props. 78−31058
FeGa$_2$Se$_4$, elec. cond., mag. susceptibility 80−88301
FeS-Ga$_2$S$_3$ system, intermediate phases crystallographic study *(French)* 79−51061
GAP:N LED, acoustic emission study of defects 79−86799
(Ga, Al)As laser diode, operation and gain meas., importance of gap shrinkage effects 80−66257
(Ga,In)(As,P) DH lasers, 1.55 μm, low-threshold current densities 80−1221
Ga complex, photoluminesc. spectra, $\pi\rightarrow\pi^*$ and charge transfer L→M transitions, Stokes shift 78−64407
Ga complexes, ^{68}Ga-EDTMP and ^{68}Ga-DTPMP, skeletal imaging agents for position scintigraphy 77−9241
Ga-Al-In-P(As)(Sb), III-V quaternary alloy, $A_xB_yC_zD$ or $AB_xC_yD_z$, energy band gap and lattice constant 79−4296
Ga-Al-Sb, liq. phase epitaxy, phase diagram, X-ray microanal. 79−19491
Ga-Al-Sb, liquidus surface in ternary phase diagram, simplex lattice method 77−7847
Ga-AlSb-GaSb, phase diagram, LPE of (AlSb)$_x$(GaSb)$_{1-x}$ solid soln. 77−40392
Ga-As-Sb system, two- and three-phase fields obs. 80−55373
Ga-As-Se, exam. of phase diagram, rel. to LPE of GaAs:Se 79−1849
Ga-GaCl$_2$, finely disperse system, supercond. props. 77−85376
Ga-Ge-Se chalcogenide glasses, rare earth element doped, elec. props. 80−96885
Ga-Ge-Te system, GaGeTe formation, peritectic decomp. and struct. *(French)* 77−85995
Ga-In-As-Sb quaternary system, phase equilib. and heterojunctions 79−34016
Ga-In-Sb, solidus isotherms and isoconcentration lines 78−56624
Ga-In-Sb, ternary phase diagram, thermodynamic models of solidus and liquidus isotherms 79−24504
Ga-In-Sb system, phase diagram calcs. in Ga+In rich region 80−60842
Ga-In-Sb system, precipitation of solid phase from liq. phase, thermodynamical formulation *(French)* 77−28003
Ga-P-As-Sb, III-V quaternary alloy, $A_xB_yC_zD$ or $AB_xC_yD_z$, energy band gap and lattice constant 79−4296
Ga-Sb-Te, props. of ternary solid solution based on GaSb 79−7826
Ga-Se system, phase diagram and cryst. struct. of phases *(French)* 80−93544
Ga-Te, liq., reflectance, 0.65-3 eV, comp. depend. 78−72549
Ga-Te liquid alloys, mag. susceptibility 77−59383
Ga-Te system, phase diagram and cryst. structs. *(French)* 79−78946
Ga-Te system cpds., degree of dissoc. from curvature of liquidus line 78−22828
Ga-YIG, accelerated crucible rotation technique effect on cryst. growth by induced striation method 77−63553
Ga-Zn(Cd), excimer visible emission spectra in RF discharge, vibr. struct. 79−18201
Ga$_x$ In$_{1-x}$P, localised exciton-phonon complex as intermediate state in light scatt. 78−39543
Ga$_x$Al$_{1-x}$ melt, solubility of Si, ternary phase diagram *(French)* 77−51498
GaAlAs, LPE edge-growth reduction method 78−30848
GaAlAs, p-n and heterojunctions, superinjection coeffs., luminesc. obs. 80−50427
(GaAl)As:Be DH stripe geometry lasers with current confinement structure 80−58592
GaAlAs-GaAs heterostruct. solar cells, Al, P, Zn incorporation by LPE *(French)* 79−24899
GaAlAs-GaAs heterostruture, optical waveguide characteristics, mode spectrum, universal dispersion curves 79−72706
Ga$_{0.5}$Al$_{0.5}$As, heterostructure, cation order, effect on energy bands 79−1570
Ga$_{0.7}$Al$_{0.3}$As epitaxial film, inclusion-generated dislocation clusters 77−89445
Ga$_{1-x}$Al$_x$As DH laser, accelerated ageing test 79−76688
Ga$_{1-x}$Al$_x$As, LPE layers, grown under const. cooling rate conditions, cryst. composition 78−39710
Ga$_{1-x}$Al$_x$As, STEM techniques for simultaneous electronic anal. and obs. of defects 79−14812
Ga$_{1-x}$Al$_x$As-GaAs solar cells, computer anal. of cell characts. incl. band gap variation 80−55866
Ga$_{1-x}$Al$_x$As$_{1-y}$P$_y$ epitaxial film, nonradiative recomb. at dislocations 80−44213
Ga$_{1-x}$Al$_x$As$_{1-y}$P$_y$ layer of uniform composition grown on GaAs by LPE, temp. diff. method appl. 79−23864
GaAlAsSb/GaSb alloys, prep. and optoelectronic device appl. 80−25587
GaAlAsSb-GaSb p-n heterojunction CCD, charge transfer, charge exchange 80−65658
Ga$_{1-x}$Al$_x$N heteroepitaxial films, photoluminesc., cathodoluminesc. 80−66292
Ga$_{1-x}$Al$_x$N, VPE growth on sapphire, RHEED obs.of orientation rels. 77−20208
Ga$_x$Al$_{1-x}$N, epitaxial film, cathodoluminesc. 80−25469
Ga$_x$Al$_{1-x}$N film, growth and props. 78−39702
Ga$_{1-x}$Al$_x$P, bending parameters calc. by pseudopot. method 78−26813
Ga$_{1-x}$Al$_x$P, LPE grown, green electroluminescence 78−19571
Ga$_{1-x}$Al$_x$P, long-wavelength optic phonons, IR reflectance meas. 77−7804
Ga$_{1-x}$Al$_x$P, two-phonon optical absorpt. 78−88341

gallium compounds continued
Ga$_{1-x}$Al$_x$P varigap structs., crystallation 80−80993
Ga$_{1-x}$Al$_x$P:N epitaxial films, ion implanted, cathodoluminescence study 80−60684
Ga$_x$Al$_{1-x}$P high-temp. solar cell with 0.3 eV band gap 80−21400
Ga$_{0.5}$Al$_{0.5}$Sb, surface cleaning by sputter-etch technique 77−48560
Ga$_{0.72}$Al$_{0.28}$Sb avalanche photodiodes, ionization coeff. 79−17488
Ga$_{1-x}$Al$_x$Sb, dispersive energy and energy gap calcs. *(French)* 79−99478
Ga$_{1-x}$Al$_x$Sb, LPE growth and phase diagram *(French)* 77−24974
Ga$_{1-x}$Al$_x$Sb, melt growth and elec. props. 79−65999
Ga$_{1-x}$Al$_x$Sb p-n homojunction LPE and photovoltaic effect obs. *(French)* 78−64108
Ga$_{1-x}$Al$_x$Sb p-n structure, variable-gap, elec., photoelec. and electrolum. props. 77−11996
Ga$_{1-x}$Al$_x$Sb p-n structure, variable-gap, electroluminescence 78−52582
Ga$_{1-x}$Al$_x$Sb, second order Raman spectra, photon combinations *(French)* 80−34912
Ga$_{1-x}$Al$_x$Sb, small wave vector modes 78−75785
Ga$_{1-x}$Al$_x$Sb, surface oxidation, Raman spectra, residual Sb layers 80−71419
n-Ga$_{1-x}$Al$_x$Sb, transport phenomena in low and high mag. fields 78−80007
Ga$_{1-x}$Al$_x$Sb variable-gap p-n struct., selective photoelec. effect 77−76912
Ga$_{1-x}$Al$_x$Sb variable-gap p-n structures, wide-band photoelec. effect 79−42635
Ga$_{1-x}$Al$_x$Sb, variation of optical transitions *(French)* 79−60708
Ga$_x$Al$_{1-x}$Sb, VPE, closed tube transport technique 79−28935
Ga$_x$Al$_{1-x}$Sb, VPE with I$_2$ as transport agent 78−48325
Ga(As,P):N, intermediate range model of N states 79−73467
Ga(As,P):N, isoelectronic impurity states, long-range, short-range model 80−75524
Ga(As,P):N, theory of bound states induced by disorder and isoelectronic pots. 77−35889
Ga(As,P)/(In,Ga)P DH laser, red-emitting, optical and elec. characts. 78−66826
GaAs, (110) surface, trned in energy distribs. of Ga dangling orbital surface states 79−28397
GaAs, photomag. effect anomalies and state of surface layer 80−100482
GaAs, surface Brillouin scattering from acoustic phonons 80−55113
GaAs:Ni^{3+}(Co^{2+})(Fe^{+}), EPR assessment of 3d^7 transition metal impurity state 78−48031
GaAs/AlGaAs, DH laser, degradation under Ar laser irrad. 79−98375
GaAs/GaInP DH, MBE grown, optically pumped laser action at 77K 80−95890
p-GaAs-Al$_{0.3}$Ga$_{0.7}$As, cladded dielec. waveguide, loss meas. using Raman scatt. 79−81539
GaAs-Al$_x$Ga$_{1-x}$As DH lasers, MBE grown, low current threshold, high lasing uniformity 79−64223
GaAs-Ga$_{1-x}$Al$_x$As, LPE growth for solar cells 77−77427
n-GaAs-Ga$_{1-x}$Al$_x$As, superlattice, subband struct. and optical spectra, self-consistent calc. 80−15443
GaAs-Ga$_x$In$_{1-x}$P heterostructure, elastic stresses and substrate/epitaxial film mismatch, X-ray diffr. method 80−92794
GaAs-GaAs$_{0.5}$P$_{0.5}$ almost perfect epitaxial multilayers, TEM obs. 77−89668
GaAs-GaP diffuse scatt. of X-rays by single crysts. *(German)* 78−30517
GaAs-GaP heterostructure, radiative recomb. under influence of mech. stresses 80−66291
GaAs-GaP(Sb), pseudobinary alloy, phase diagram calc. 78−52786
GaAs-GaSb, threshold energies for impact ionisation by electrons and holes 78−6390
GaAs-GaSe n-p heterojunction, elec. props., interface states 80−65670
n-GaAs-n-GaN, diffusion growth kinetics, morphology and electrical properties 80−20294
GaAs-Sn-H$_2$-HCl, thermodynamic calcs., reduction of SnCl$_2$ by H$_2$ 79−86903
GaAs$_{1-x}$ P$_x$, hot photoluminescence spectrum, polarisation depend. 78−31254
GaAsO$_4$, XPS of cryst., inner shell binding energies of elements 79−43092
GaAsP, composition dependence of phonon frequencies 78−75764
Ga(AsP), dislocation etching of (001) faces with H$_3$PO$_4$ etchant 80−15103
GaAsP epitaxial film, composition self modulation, defect struct. 80−34331
GaAsP epitaxial waveguide, electro-optic phase modulation of laser radiation 79−10417
GaAsP, negative-electron-affinity, photoemission transmission coeff. 78−56560
GaAsP photocathode, negative electron affinity process obs. by laser beam scanning *(Japanese)* 80−55262
GaAsP, VPE, lattice forbidden band composition depend. *(Hungarian)* 80−6669
GaAs$_{0.1}$P$_{0.9}$:Zn, shallow Zn diffusion profile determ. using anodic oxidation and double radioactive tracer method 77−43239
GaAs$_{0.15}$P$_{0.85}$ ridged waveguide for electrooptic radiation modulator 80−91925
n-GaAs$_{0.6}$P$_{0.4}$, anodic oxide film, exam. using SIMS and ellipsometry 79−61770
GaAs$_{0.6}$P$_{0.4}$, anodic oxide, electronic props. 79−61771
GaAs$_{0.6}$P$_{0.4}$, CVD growth for LEDs 79−19998
GaAs$_{0.6}$P$_{0.4}$, deep level profile anal., double correlation technique 77−80830
GaAs$_{0.6}$P$_{0.4}$ LED, luminesc. investig. of degradation, deep-level form. at dislocations 77−40287
GaAs$_{0.6}$P$_{0.4}$, low dark-current MOS photodiodes 77−32083
GaAs$_{0.6}$P$_{0.4}$ p-i-n diode, behaviour of turnover voltage under pulsed conditions 77−20408
n-GaAs$_{0.6}$P$_{0.4}$, reproducible ohmic contacts 79−73587
GaAs$_{0.6}$P$_{0.4}$, surface processing, residual film monitoring by ellipsometry 80−13124
GaAs$_{0.6}$P$_{0.4}$, VPE, hole diffusion lengths, surface prep. and heat treatment effects, etchant evaluation 80−15627
GaAs$_{0.6}$P$_{0.4}$, VPE, hole diffusion lengths, effect of transition metal diffusional doping 80−15628
GaAs$_{0.6}$P$_{0.4}$:Be, implanted annealing studies, elec. resist., Hall effect meas. 78−84213

gallium compounds continued
$GaAs_{0.6}P_{0.4}$:N, isoelectronic tape by ion implantation and CO_2 laser annealing 80—24464
$GaAs_{0.6}P_{0.4}$:Zn, control of Zn diffusivity by multiple implantation 78—38877
$GaAs_{0.6}P_{0.4}:Zn^+(Ar^+)$, ion-implanted, thermal degradation of mechanical surface perfection and surface photolum. 77—77271
$GaAs_{0.62}P_{0.38}$, negative electron affinity, photoemission of spin polarised electrons 80—2916
n-$GaAs_{0.62}P_{0.38}$, optical absorpt. coeff. and minority-carrier diffusion length, differential photocurrent method of meas. 80—96896
$GaAs_{0.65}P_{0.35}$, gamma irradiated, deep level study using DLTS and photocapacitance methods *(Japanese)* 80—49665
$GaAs_{0.7}P_{0.3}$-$In_{0.34}Ga_{0.66}P$, CW heterojunction laser, visible, laser operation 77—38886
$GaAs_{1-x}P_x$ based structs., carrier conc., mobility calcs. from Hall effect meas. 78—60138
$GaAs_{1-x}P_x$, bending parameters calc. by pseudopot. method 78—26813
$GaAs_{1-x}P_x$, bound exciton, luminesc. reson. excitation 79—95840
$GaAs_{1-x}P_x$, chemical transport and crystal growth in closed tube *(Japanese)* 78—39673
$GaAs_{1-x}P_x$, continuously tunable electron beam pumped laser 78—50802
$GaAs_{1-x}P_x$, dependence of energy spectrum of levels introduced by electron irrad. on composition 79—60766
$GaAs_{1-x}P_x$, diffusion of implanted Zn ions, ion microbe analysis 78—95190
$Ga(As_{1-x}P_x)$ electrode, equilib. establishment kinetics *(French)* 79—79259
$GaAs_{1-x}P_x$ electrodes, interface capacitance meas., flatband pot., conduction and valence band boundaries *(French)* 79—33339
$GaAs_{1-x}P_x$, electrolum. and related props., state-of-the-art, book contrib. 77—73173
$GaAs_{1-x}P_x$, electron irrad., radiation defects annealing 80—29059
$GaAs_{1-x}P_x$ epi-wafer, comp. profile of heterogeneous struct., anodisation-electrorefl. meas. 78—26782
$GaAs_{1-x}P_x$ epitaxial films, VPE grown, photolum. spectra 79—73997
$GaAs_{1-x}P_x$, epitaxial layer, modulation of direct and indirect gaps, piezotransmission meas. 77—24819
$GaAs_{1-x}P_x$, heterogeneous struct. obs. by anodisation-electrorefl. technique 78—84088
$GaAs_{1-x}P_x$ heterostructure, LPE prep., growth and dissolution kinetics, thermodynamic and kinetic models 80—75456
$GaAs_{1-x}P_x$, high quantum efficiency photoemission 77—44115
$GaAs_{1-x}P_x$, indirect-gap, evidence for exciton localization by alloy fluctuations, photolum. 80—66276
$GaAs_{1-x}P_x$ LED, effect of band filling on emission spectra shape 78—48236
$GaAs_{1-x}P_x$ layer, growth by isothermal LPE 77—40398
$GaAs_{1-x}P_x$, localised exciton-phonon complex as intermediate state in light scatt. 78—39543
$GaAs_{1-x}P_x$, MBE growth on GaP, and crystallographic evaluation 77—8762
$GaAs_{1-x}P_x$, method for determ. of liquidus surfaces in Ga-As-P phase diagram 77—28787
$GaAs_{1-x}P_x$, mol. beam epitaxial growth, cryst. quality, composition investig. *(Japanese)* 77—55895
$GaAs_{1-x}P_x$, molecular beam epitaxial, effect of substrate temp. on composition ratio 77—1811
$GaAs_{1-x}P_x$, N doping using ionised beam in MBE 78—47400
$GaAs_{1-x}P_x$, N implantation, characterisation by photolum. and channelling 80—54262
$GaAs_{1-x}P_x$, N trap bound state, Hall effect determ. 78—19055
$GaAs_{1-x}P_x$, N^+ implantation photoluminesc. props. 77—68987
$GaAs_{1-x}P_x$, N^+ implantation, annealing props. 77—68988
$GaAs_{1-x}P_x$, piezomodulation spectra of indirect gap, zero-phonon and phonon-assisted transitions 77—48192
$GaAs_{1-x}P_x$, solid soln., synthesis by ion implantation P^+ ions 78—38741
$GaAs_{1-x}P_x$ solid solution, disorder scatt. Hall mobility meas. 77—69350
$GaAs_{1-x}P_x$, structural defects, optical props. effect 80—55208
$GaAs_{1-x}P_x$, synthesized by ion implantation, Raman scattering 79—42972
$GaAs_{1-x}P_x$, thermal oxides, elemental composition and C-V characts. 79—61772
$GaAs_{1-x}P_x$, VPE, on-time comp. determ. 78—67915
$GaAs_{1-x}P_x$, VPE on Ge substrate, and LED characts. 78—72736
$GaAs_{1-x}P_x$:N, $0.6<x<1$, photoluminesc., comp. depend. 78—52546
$GaAs_{1-x}P_x$:N, film, optical absorpt. from photoluminesc. meas. 78—92134
$GaAs_{1-x}P_x$:N, Koster-Slater model and N-states 78—47732
$GaAs_{1-x}P_x$:N, N isoelectronic trap, model calc. of N_Γ and N_x electronic states 78—10398
$GaAs_{1-x}P_x$:N, photoluminesc. and optical absorpt. spectra of N impurity bound-excitons 79—47496
$GaAs_{1-x}P_x$:N, photolum. and electrolum. study of N isoelectronic traps 80—89061
$GaAs_{1-x}P_x$:N, upper branch of N isoelectronic trap., photo- and electrolum. expts. 77—63462
$GaAs_{1-x}P_x$:N epitaxial layers, absorption and photolum. spectra meas. 77—24894
$GaAs_{1-x}P_x$:N heterojunction, N_x and N_Γ bound states, high-press. effects on electroluminesc. meas. 77—11870
$GaAs_{1-x}P_x$:S, deep level, photoconductivity, carrier nonradiative recombination 80—20112
$GaAs_{1-x}P_x$:Te, thermoelectric figure of merit 79—69538
$GaAs_{1-x}P_x$:Zn, diffusion profile determ., $^{32}P/^{65}Zn$ double tracer technique 78—55888
$GaAs_{1-x}P_x$:Zn implanted, Zn diffusion 77—84993
$GaAs_{1-x}P_x$-Au, surface-barrier struct., photodetectors of visible and UV radiation 77—20437
$GaAs_{1-x}P_x$-GaP heterostructure, photomodulation spectroscopic exam. 77—40257
$GaAs_{1-x}P_x$-SiO_2:N,Zn ion-implanted multiple layers, ion range distribs., secondary ion microprobe meas. 79—42129
$GaAs_{1-y}P_y$-$In_{1-x}Ga_xP_{1-z}As_z$, DH laser, low threshold visible spectrum 78—5471
$GaAs_xP_{1-x}$, surface phonon polaritons, total internal refl. *(Russian)* 79—38688
$GaAs_xP_{1-x}$, band struct., CPA calc. based on linear combination of bond orbitals 79—87035
$GaAs_xP_{1-x}$, elastic consts. and Debye temp. determ. 77—4142

gallium compounds continued
$GaAs_xP_{1-x}$, energy band struct., CPA based on LCBO *(Japanese)* 80—44495
$GaAs_xP_{1-x}$, energy gap variation, CPA calcs. 78—43294
$GaAs_xP_{1-x}$, liquid phase epitaxial growth on GaP, growth and properties 79—47641
$GaAs_yP_{1-y}$ alloy, composition effects in growth by MBE 80—59816
$GaAs_{1-x}Px$, heteroepitaxial solid soln., defects of struct 79—28223
GaAsSb/GaAlAsSb DH lasers, growth and props. 80—69412
$GaAs_{1-x}Sb$, microprocessor controlled MBE growth 78—3058
$GaAs_{1-x}Sb_x$, $(x\leq 0.05)$, band gap, temp. depend., from edge photolum. meas. 80—71486
$GaAs_{1-x}Sb_x$, cryst. growth by steady state LPE 78—44032
$GaAs_{1-x}Sb_x$ electron intervalley transfer and drift velocity calc. 77—80778
$GaAs_{1-x}Sb_x$ epitaxial n-n heterostructures, gap energies and interface pots., modulation electroabsorpt. meas. 79—11201
$GaAs_{1-x}Sb_x$, LPE phase diagram meas. 77—20047
$GaAs_{1-x}Sb_x$ layer on GaAs, dislocation density reduction by improved LPE growth method 80—76202
$GaAs_{1-x}Sb_x$, MBE grown, surface struct. exam. by MEED 78—87847
$GaAs_{1-x}Sb_x$ photodiode structures, current-voltage characts., photo-EMF spectra 80—29472
$GaAs_{1-x}Sb_x$ photodiode, speed and sensitivity meas. 80—92937
$GaAs_{1-x}Sb_x$ ternary phase diagram, LPE, band gap and elec. props. 77—55896
$GaAs_{1-x}Sb_x$ undoped epitaxial layers, photoluminesc. meas. 80—20703
$GaAs_{1-x}Sb_x$-$Al_yGa_{1-y}As_{1-z}Sb_z$, DH laser, threshold characts. and extended wavelength operation 78—9379
$GaAs_{1-x}Sb_x$-$Ga_{1-x}In_xP_{1-y}As_y$ multilayer structure, continuously tunable electron beam pumped laser 78—50802
$GaAs_{1-y}Sb_y$ organometallic VPE, use of trimethyl As and trimethyl Sb 80—45238
$GaAs_{1-y}Sb_y$, organometallic VPE growth using trimethylantimony 80—60788
$GaAs_xSb_{1-x}$, epitaxial layer, struct. defects rel. to luminesc. 78—72040
$GaAs_xSb_{1-x}$, heterostructure composition profile by photoemission microanalysis 80—44717
$GaAs_xSb_{1-x}$, lattice-matched LPE growth in InP substrates 79—42402
$GaAs_xSb_{1-x}$ solid solution epitaxial layer, morphology and defect structure 77—1330
$GaAs_xSb_{1-x}$-GaAs epitaxial films and multilayer heterostruct., SEM obs. under cathodolum. conditions 79—11023
$GaAs_ySb_{1-y}$, miscibility gap, rel. to LPE 79—33090
$GaAs_{1-x-z}Sb_xP_z$, LPE growth, constant compositional grading 78—6867
$GaAs_{2-x-z}Sb_xP_z$, LPE growth, continuous comp. grading, use as secondary substrate 77—31913
$Ga_2As_{49}Te_{49}$ glassy film, nonlinear current voltage characts., Poole-Frenkel effect 80—7007
ε-GaAse, optical consts. for ⊥ and ∥ light polarisation, reflectivity, interf. meas. 77—52077
$GaBO_3:Fe^{3+}$, ESR spectra, lattice parameters 80—93170
GaBi, possibility of existence with sphalerite struct. 80—33950
$GaBo_3$, coefficients of thermal expansions 80—39322
GaBr, rot. analysis of $^3\Pi_{0,1}$-$X^1\Sigma^+$ transition 80—69129
GaBr, rot. spectrum hyperfine struct. 79—13838
$GaBr_3$, D_{3h} point group, mol. consts., struct. effects 79—54992
$GaBr_3$, intramolecular force fields, compliance consts. and vibr. amplitudes 80—58234
$GaBr_3$, vibr. anal., pot. const. determ., mol., compliance and Coriolis coupling const. calc. 80—95579
$Ga_3Br_{10}^-$, vibr. spectrosc., in alkali metal compound crysts. *(French)* 78—6667
$GaBr_3.NH_3$, mol. struct., vap. phase electron diffr. obs. 77—65541
$GaCl_3$, cryst. struct., Zeeman split fine struct. lines, FT NQR obs. 80—54982
$GaCl_3$, D_{3h} point group, mol. consts., struct. effects 79—54992
$GaCl_3$, force and compliance consts., OVFF, UBFF and GVFF models 78—50663
$GaCl_3$, intramolecular force fields, compliance consts. and vibr. amplitudes 80—58234
$GaCl_3$, Raman spectral differences from liquid to glassy state, ionic equilib. interpretation 80—20619
$GaCl_3$, vibr. anal., pot. const. determ., mol., compliance and Coriolis coupling const. calc. 80—95579
$GaCl_3(I_3)$, gaseous, Raman spectra, struct., Fermi reson. and thermodynamic functions 77—18929
$Ga_{0.67}Cr_2S_4$, semiconducting thiospinelide, spin glass type mag. ordering *(Russian)* 80—50123
GaF+O matrix reaction, OGaF IR spectrum 79—11787
GaH_4^-, GaD_4^-, intramol. force fields, F_2 vibrs., isotope shifts 77—3336
$GaH_2P_3O_{10}$, crystn. from Ga_2O_3 in H_3PO_4 79—52641
$GaH(SO_4)_2.4H_2O$, cryst. parameters and X-ray powder diffr. data *(French)* 79—14765
GaI, $A0^+$-$X0^+$ and $B1$-$X0^+$ transitions, isotope shifts, UV and visible spectra obs. 80—53005
GaI, rot. spectrum, EHF spectra obs. 80—58245
GaI_3, intramolecular force fields, compliance consts. and vibr. amplitudes 80—58234
GaI_3, molten, electrical cond., press. effect, 0-1 kbar 78—55963
GaI_3, molten, isothermal compressibility obtained from adiabatic thermal press. coefficients 79—95065
GaI_3, vibr. anal., pot. const. determ., mol., compliance and Coriolis coupling const. calc. 80—95579
GaI_3-$SbCl_3$, total exchange of halogens, Raman spectra and phase equilibrium *(French)* 79—65874
$Ga_yIn_{1-y}As_xP_{1-x}$-InP heterostructure, lattice matching and cryst. perfection 78—6437
$Ga_{1-x}In_xAs$ organometallic VPE, use of trimethyl As and trimethyl Sb 80—45238
$Ga_xIn_{1-x}As$, prep. and props. 79—100047
GaInAsP DH laser emitting at 1.55 μm, threshold currents 80—83609
GaInAsP diode lasers, self-sustained pulsations in light output 80—64012
GaInAsP, electroabsorption 79—78652
GaInAsP layers on InP substrate, conditions for lattice matching in LPE growth 78—6866
GaInAsP, rectifying and ohmic contacts 80—80376
GaInAsP, VPE growth and props. 80—16194
GaInAsP/InP, DH laser, low threshold current density, 1.3 μm emission 79—94249

gallium compounds continued

- GaInAsP/InP buried heterostruct. laser, 1.6 μm, fabrication and room temp. CW operation 80−58568
- (GaIn)(AsP)/InP DH 1.27 micron lasers, nonradiative carrier loss and temperature sensitivity of threshold 80−43333
- GaInAsP/InP lasers, 1.5 μm emitting, high temp. CW operation 80−95889
- GaInAsP/InP lasers, LPE grown, effect of p-doping on carrier lifetime and threshold current density 80−99726
- GaInAsP/InP narrow planar stripe lasers, lasing characts. 80−95897
- GaInAsP/InP optical sources for 1.2 to 1.4 μm wavelength region, growth and props. 79−90023
- GaInAsP/InP system, chemical etching, fabricating laser diodes and integrated optical circuits 80−38030
- GaInAsP-InP avalanche photodiode, fabrication and characts. 78−54454
- GaInAsP-InP buried heterostructure laser with mesa substrate, linear light/current characts. 79−36894
- GaInAsP-InP DH laser grown by newly designed vertical LPE furnace 78−9380
- GaInAsP-InP DH laser, relaxation and delay in oscillations 78−13709
- GaInAsP-InP DH layers, lattice deform. and misfit dislocations 79−19473
- GaInAsP-InP DH lasers, for fibre optic communications 79−31924
- GaInAsP-InP DH lasers with low threshold, narrow-beam divergence 79−36892
- GaInAsP-InP DH laser, LPE and wet chem. etching techniques for integration 79−98388
- GaInAsP-InP DH lasers made by melt-back method, operating characteristics 80−48287
- GaInAsP-InP DH lasers, LPE growth and operational characts. 80−53313
- GaInAsP-InP DH injection lasers prep. by LPE, 1.11-1.67 μm operation 80−53321
- GaInAsP-InP double heterostructure laser, prep. by LPE growth and laser operation 77−3590
- GaInAsP-InP integrated twin-guide lasers with first-order distributed Bragg reflectors, 1.3 μm 80−58567
- GaInAsP-InP lasers and detectors, for fibre optic communications at 1.0-1.6 μm 79−3803
- GaInAsP-InP mesa substrate buried heterostruct. injection laser, fabrication and lasing props. 80−53319
- GaInAsP-InP Zn diffused stripe geometry DH diode laser fabrication 79−98386
- $Ga_{0.08}In_{0.92}As_{0.18}P_{0.82}$, band struct., optical studies 79−47013
- $Ga_{1-x}In_xAs_{1-x}P_x$, VPE growth and characterisation 78−22970
- $Ga_{1-x}In_xAs_{1-y}P_y$-InP DH laser, carrier lifetime meas. 77−61955
- $Ga_xIn_{1-x}As_yP_{1-y}$, conduction band and phonons, Shubnikov-de Haas effect, magnetophonon resonance, Raman scattering 80−24795
- n-$Ga_xIn_{1-x}As_{1-y}P_y$, photoluminesc. of epitaxial films, isovalent substitution 80−16097
- $Ga_xIn_{1-x}As_{1-y}P_y$:Ge(Sn)(Te), epitaxial film, elec. and optical props. 79−11251
- $Ga_xIn_{1-x}As_{1-y}P_y$-InP, room temp. electron-beam-pumped laser with dielec. waveguide, output characts. 80−5761
- $Ga_xIn_{1-x}As_xP_{1-x}$-InP buried-stripe DH diode laser, room temp. CW operation 77−50671
- $Ga_xIn_{1-x}As_yP_{1-x}$, epitaxial layers on InP, expt. determ. of effective masses 79−65370
- $Ga_xIn_{1-x}As_yP_{1-x}$, thermal expansion coefficients, 25-400°C 79−46817
- $Ga_xIn_{1-x}As_yP_{1-y}$, electron effective mass, cyclotron reson. and magnetophonon effect meas. 80−103618
- $Ga_xIn_{1-x}As_yP_{1-y}$, IR refl. spectra 80−60602
- $Ga_xIn_{1-x}As_yP_{1-y}$, LPE layers, growth and characterisation 78−38983
- $Ga_xIn_{1-x}As_yP_{1-y}$ LPE layers matched to InP, comp. and lasing wavelengths 78−71103
- $Ga_xIn_{1-x}As_yP_{1-y}$/GaAs structure, LPE growth and lattice consts. matching conditions 80−59822
- $Ga_xIn_{1-x}As_yP_{1-y}$-GaAs substrate, lattice matching 79−90901
- $Ga_xIn_{1-x}As_yP_{1-y}$-InP injection laser, partially loaded with distributed Bragg reflector 78−82986
- $Ga_xIn_{1-x}As_yP_{1-y}$-InP injection laser partially loaded with first-order distributed Bragg reflector 79−98387
- $Ga_xIn_xAs_yP_{1-y}$-InP substrate, lattice matching 79−90901
- $Ga_yIn_{1-y}As_xP_{1-x}$, LPE growth 80−66440
- $Ga_xIn_{1-x}As_yP_{1-y}$InP DH, LEDs and lasers, fabrication and operation in 1.5 μm region 78−37893
- GaInAsSb/GaSb DH lasers, 2 micron CW operation at 80K 80−53291
- $Ga_{1-y}In_yAs_xSb_{1-x}$, LPE on GaSb, miscibility gap in liq. phase and lattice mismatch 80−15404
- $Ga_xIn_{1-x}As_ySb_{1-y}$ tunable electron-beam-pumped laser parameters 80−106524
- GaInP, composition dependence of phonon frequencies 78−75764
- (GaIn)P, dislocation etching of (001) faces with H_3PO_4 etchant 80−15103
- $Ga_{1-x}In_xP$, mixed cryst., IR absorption by zone edge lattice vibrs. 78−19487
- $Ga_{1-x}In_xP$, zone edge phonons 78−76475
- $Ga_xIn_{1-x}P$ alloy films, surface processes controlling growth by MBE, RHEED and AES exam. 78−84084
- $Ga_xIn_{1-x}P$, band struct. enhancement of indirect transitions, piezoreflectance meas. 77−20823
- $Ga_xIn_{1-x}P$, Debye-Waller factors, X-ray diffr. determ. *(German)* 77−27959
- $Ga_xIn_{1-x}P$, diffuse X-ray scatt. investig. of cation distrib., segregation 77−24409
- $Ga_xIn_{1-x}P$ electrode, in aqueous electrolytes, impedance meas. *(French)* 79−87153
- $Ga_xIn_{1-x}P$, epitaxial film, diffusion of Cu(Au)(Zn), intrinsic impurity effects 78−87825
- $Ga_xIn_{1-x}P$, film, energy band struct., photolum. meas. 79−7784
- $Ga_xIn_{1-x}P$, flat band pot., impedance meas. and photoelectrochemistry *(French)* 80−49894
- $Ga_xIn_{1-x}P$, LPE producing coherent interface, model 77−59229
- $Ga_xIn_{1-x}P$ MBE layers, comp., Rutherford scatt. and X-ray diffr. meas. 80−75457
- n-$Ga_xIn_{1-x}P$, optical props. and energy spectrum of donors 78−72567
- n-$Ga_xIn_{1-x}P$ photoelectrochemical cells, bandgap energy, electronic transition mode, and diffusion length 80−72070
- $Ga_xIn_{1-x}P$, real struct. exam. by electron microscopy and channelling 78−2143

gallium compounds continued

- $Ga_xIn_{1-x}P$, refractive index comp. depend., nonlinearity parameter *(German)* 77−32344
- $Ga_xIn_{1-x}P$ solid soln. epitaxial layers, stabilisation of composition 78−18933
- $Ga_xIn_{1-x}P$ solid solns., isothermal liq. epitaxy 80−60793
- $Ga_xIn_{1-x}P$ solid solutions, single cryst prep. and props. 80−16162
- $Ga_xIn_{1-x}P$, undoped liquid epitaxial layers, effect of heat treatment on photoluminescence 78−60512
- $Ga_xIn_{1-x}P$, VPE, recent advances, book contrib. 79−66011
- $Ga_xIn_{1-x}P$, with indirect band struct., radiative recomb. of free excitons, cathodolum. meas. 77−90202
- $Ga_xIn_{1-x}P$:Mn, ESR of Mn 79−11341
- $Ga_xIn_{1-x}P$:N, Delta lattice parameter model, correl. with electronic props. 78−91560
- $Ga_xIn_{1-x}P$:N layers, LPE growth, luminesc. and direct exptl. obs. of band struct. effects 77−52157
- $Ga_xIn_{1-x}P$:Si, solid soln., splitting of ground state 79−51527
- $Ga_xIn_{1-x}P$-GaAs heterostructures, photolum. props., assessment as laser struct. 80−20705
- Ga_xIn_xP, LPE, with GaP saturation source wafer *(Polish)* 78−23633
- $Ga_zIn_{1-x}P$, piezomodulation spectra of cond. band struct. 77−48191
- GaInPAs, CW strip heterolaser, characts. 78−9382
- GaInPAs heterostructures and LED's, luminescent props. in 1-2 micron band 78−10988
- GaInPAs, narrow-band tunable injection laser, 1.06 μm 79−76713
- GaInPAs-InP DH lasers, misplaced p-n junctions due to Zn contamination 78−87051
- $Ga_{1-x}In_xP_{1-y}As_y$, carrier compensation and alloy scatt. 80−29490
- $Ga_{1-x}In_xP_{1-y}As_y$, drift vel. elec. field characts., Monte Carlo simulation 77−39839
- $Ga_{1-x}In_xP_{1-y}As_y$, electron transient drift vel., influence of effective mass and alloy scatt. 80−2384
- $Ga_xIn_{1-x}P_yAs_{1-y}$, 111-A and 111-B faces, defect struct., etching and X-ray diffr. obs. 80−2026
- $Ga_xIn_{1-x}P_yAs_{1-y}$, $(0.5<y<0.9)$, LPE on InP, Ga, As distrib. coeffs., lattice matching 78−47673
- $Ga_xIn_{1-x}P$(Sb), energy gap variation, CPA calcs. 78−43294
- p-$Ga_xIn_{1-x}PyAs_{1-y}$/Au-Zn, specific contact resist. 80−84509
- $Ga_xIn_{4-x}PyAs_{1-y}$, In rich bulk single crysts. growth from melt via gradient freeze method, and characterisation 78−68618
- GaInSb, Be ion implantation, device appl. 80−24478
- GaInSb, intervalley electron transfer, drift velocity and diffusion coefficient 80−39594
- $Ga_{0.3}In_{0.7}Sb$, negative differential mobility and geometrical magnetoresist. calc. 77−43624
- $Ga_{0.85}In_{0.15}Sb$, MIS struct., C-V characts., interface state densities and storage times meas. 77−89861
- $Ga_{1-x}In_xSb$, effective radiative recombination centre nature, photoluminescence spectra 79−90998
- $Ga_{1-x}In_xSb$, epitaxial, vapour-phase growth using open-tube flow system 79−33943
- $Ga_{1-x}In_xSb$, LPE on GaSb by stepwise grading, and characterisation 78−72745
- $Ga_{1-x}In_xSb$, press.-induced structural phase transition 78−30751
- $Ga_{1-x}In_xSb$, temp. gradient zone melting 80−50550
- $Ga_{1-x}In_xSb$, vapour phase epitaxial growth by open tube method 78−84109
- $Ga_{1-x}In_xSb$:Zn(Te), photolum. and stimulated emission obs. 78−72595
- $Ga_{1-x}In_xSb$-GaSb, lattice parameter meas. in epitaxic layers 79−11040
- $Ga_xIn_{1-x}Sb$, computer simulation of growth from In soln. 77−51332
- $Ga_xIn_{1-x}Sb$ diode, with Au metallisation, interdiffusion effect of heat treatment 78−14820
- $Ga_xIn_{1-x}Sb$, electron transport props. calc. by Monte Carlo method 77−76834
- $Ga_xIn_{1-x}Sb$, electron transport in RF field, Monte Carlo simulation 80−96932
- $Ga_xIn_{1-x}Sb$, electron vel. field characts., microwave heating method 79−91058
- $Ga_xIn_{1-x}Sb$, Ga-rich, prep. by Czochralski technique 80−60771
- $Ga_xIn_{1-x}Sb$, growth by LPE 78−27421
- n-$Ga_xIn_{1-x}Sb$ Gunn diode, high field domain characts. 80−59992
- $Ga_xIn_{1-x}Sb$ LO phonon obs. using Raman scatt. 78−35152
- $Ga_xIn_{1-x}Sb$, LPE, growth by vertical dipping method and elec. props. 77−85949
- $Ga_xIn_{1-x}Sb$ p-n junction photodiode fabrication, sensitivity as 1 to 2.5 μm detectors *(Japanese)* 80−52311
- $Ga_xIn_{1-x}Sb$, transferred-electron effect, and device performance estimation 78−19049
- $Ga_{1-x}In_xSe$, energy bands near absorpt. edge, transmission and photoluminesc. spectra 79−83022
- $Ga_{1-x}In_xSe$, energy spectrum and struct., X-ray diffr. and light absorption 79−11437
- $Ga_{1-x}In_xSe$, exciton spectrum nature and anisotropy of electron bands near absorption edge *(Russian)* 79−51483
- $Ga_{1-x}In_xSe$, layered, luminescence and photocond. obs., two-photon excitation 78−76521
- $Ga_{1-x}In_xSe$, magnetic susceptibility anisotropy, chemical bonds, electron density distribution *(Russian)* 80−50073
- $Ga_{1-x}In_xSe$, Raman scatt. spectra, optical phonon freq., cryst. vibr. freq. types 80−29744
- $Ga_{1-x}In_xSe$ solid solution, IR spectra of static reflectivity 79−69849
- $Ga_xIn_{1-x}Se$, fabrication, struct., elec. and optical props. 80−44180
- $(Ga_xIn_{1-x})_2Se_3$, $1\geq x\geq 0$, phases, lattice parameters and thermal expansion between room temp. and melting point 80−39031
- $GaKHP_3O_{10}$, crystn. from reaction of Ga_2O_3 with H_3PO_4 and K_2O 79−52642
- $GaK(PO_3)_4$, crystn. from reaction of Ga_2O_3 with H_3PO_4 and K_2O 79−52642
- GaKr, low-lying electronic states, PE curves, transition moments, emission coeffs. 79−6894
- $GaMn_3(C_{1-x}N_x)$, mag. struct., phase transition, rel. to valence instabilities in rare earth compounds *(French)* 80−34596
- $Ga_{1-x}Mn_xSb$ alloys, mag. phase transition obs. 78−52248
- $Ga_{1-x}Mn_xSb$, elec. cond., mag. susceptibility, Hall const., and thermo-EMF, 80 to 1000K *(Russian)* 80−88549
- $Ga(Mo_2Re_2)S_8$, synthesis and electrical props. of mixed tetrahedral cluster phases 80−2971
- $GaMo_5S_6$, mag. and struct. transition temps., press. effects, 0-6 kbar *(Russian)* 77−89956
- $Ga_xMo_6S_8$ Chevrel phase, synthesis, stability and characts. 80−71608

gallium compounds continued
  GaN and GaN:Zn epitaxial layers, doping effect on cathodoluminesc. 77—20935
  GaN CVD layer props. rel. to Ga-GaCl conversion efficiency and HN_3 decompositon 77—77404
  GaN, cryst. struct. refinement 77—84731
  GaN, deposition from plasma reactor, organo-metallic and donor-acceptor complex exchange in HF plasma 80—38839
  p-GaN, doping in nonequilibrium conditions 77—62556
  GaN, elastic constant calc., elastic wave propag. vel. 78—87734
  n-GaN elec. props., electron mobility calc. 78—30923
  GaN, electrolum. and related props., state-of-the-art, book contrib. 77—73173
  GaN, electron struct., ESCA study 80—89116
  GaN, epitaxial, cathodolum., 78-300K 78—19575
  GaN, epitaxial, refl. spectra, 5-12.5 eV 79—99967
  GaN epitaxial films, cathodoluminesc. spectra 80—71496
  GaN epitaxial films, planar waveguides for integrated optics appls. 79—10416
  GaN, epitaxial growth kinetics in Ga-HCl-NH_3 77—80710
  GaN, epitaxial growth on sapphire substrates, elec. props., X-ray diffr. anal., photoluminescence spectra 79—4919
  GaN, epitaxial layer, characts. from cathodoluminesc. 78—35208
  GaN, epitaxial layer, cryst. quality meas. by channelling 78—38986
  GaN epitaxial layer, magneto-plasma-reflectivity effects, difference method meas., IR region *(German)* 77—12363
  GaN, epitaxial layer prep. and elec. props. 77—85097
  GaN epitaxial layers, exciton cathodolum. *(Russian)* 78—76543
  GaN epitaxial layers, exciton cathode luminesc. 79—65933
  GaN epitaxial layers for LED, X-ray diffr. topography and cryst. characterisation 79—65336
  GaN epitaxy, sapphire substrate prep. 78—39929
  GaN film, deposition by pyrolysis of gallium trichloride and triiodide ammoniates 77—36402
  GaN film, heteroepitaxial deposition, growth kinetics and catalytic effects 79—4487
  GaN, film, secondary ion mass spectrometric qualitative anal. 78—7265
  GaN film, thermoelec. power and Hall coeff. meas. 77—55627
  GaN, formed from initial oxidation and nitridation of GaAs, surface and contact props. 77—20436
  GaN, growth and morphology of crystals *(Japanese)* 80—11548
  GaN, high-press. VPE and elec. characts. 78—14627
  GaN, indirect doping method *(Czech)* 80—24468
  GaN, initial growth, on Al_2O_3 and spinel *(German)* 80—107664
  GaN, interatomic interactions from XPS 80—49171
  GaN, ion implantation, indirect doping method 80—10568
  GaN, luminesc. centres 80—93405
  GaN, nonlinear susceptibility and coherence length, SHG meas. 78—25924
  GaN on Si, form. with GaCl-NH_3-H_2(He), ESCA and RHEED meas. 79—90909
  GaN, photoluminesc. characts. for 35 implanted elements 77—24884
  GaN, photoluminesc. spectra, energy distrib. 80—97339
  GaN, physical props. and appls. in integrated optics *(Czech)* 80—28355
  GaN, plasma deposition and elec. cond. 78—60585
  GaN, polarised electroluminescence emission, microstructure investigations 80—97344
  GaN preparation in sealed fused silica ampoules 80—80982
  GaN preparation technology, powder, thin film and volume crystals *(Czech)* 78—3037
  GaN, preparation variables rel. to dielectric data, GaAs conversion 78—60591
  GaN, pure and Zn-doped, epitaxial film lumins. 78—10955
  GaN, reactive sputtering, GaAs MIS struct. fabrication and props. 78—39686
  GaN single crystals, growth and morphology *(Japanese)* 79—43112
  GaN, stimulated emission under high one and two quantum excitation 78—35171
  GaN, thermal conductivity, 25-360K 77—35766
  GaN, thermodynamic anal. of prep. methods 80—55328
  GaN, VPE, on sapphire, crystallographic aspects 78—2387
  GaN, VPE, requirements and structural etching of Al_2O_3 substrates *(Polish)* 77—43440
  GaN VPE for blue LEDs *(French)* 79—28928
  GaN, VPE growth rate influence on elec. and luminesc. props. 80—100702
  GaN:Al, VPE grown, luminesc. and elec. props. depend. on doping conc., bound excitons 80—20688
  GaN:As(P), implanted single cryst. film, cathodolum. 78—60523
  GaN:Mg, and undoped, epitaxial growth from vapour, orientation, elec. props. 77—4740
  GaN:P, photoluminesc. 79—78730
  GaN:Zn, cathodolum. obs., recomb. model 79—11474
  GaN:Zn, cathodoluminesc., photocapacitance 79—38679
  GaN:Zn, epitaxial layer, effective electroluminesc., blue regime *(Russian)* 77—77302
  GaN:Zn, heavily doped, photocond. spectra 77—72887
  GaN:Zn, LED, blue, yellow and green emission, temp. depend. 77—8658
  GaN:Zn, low voltage LED, epitaxial layer, growth and electrolum. *(Russian)* 77—77297
  GaN:Zn, n-i struct., anomalous luminesc. 80—80865
  GaN:Zn, polarised electroluminescence, mag. field intensity depend. *(Russian)* 79—91502
  GaN:Zn, temp. and press. depends., electrolum. 78—19567
  GaN:Zn, VPE grown, optical cross sections, photoluminesc. and optical absorpt. meas. 80—55160
  GaN:Zn, VPE growth, photoluminesc. rel. to doping conditions 80—55159
  GaN:Zn, violet bipolar LED 79—38190
  GaN:Zn epilayers, growth parameters effect on props., device struct. 78—26975
  GaN:Zn epitaxial films, luminesc. spectra separation into individual bands by impurity absorpt. region excitation 79—74002
  GaN:Zn LED, electrolum. centres, rel. to growth morphology, Zn conc. and etch patterns 77—1733
  GaN:Zn LED, I-V characts., elec. cond. mechanism 77—55614
  GaN:Zn(Fe)(Ni)(Cr), lattice parameters, variation with stoichiometry and doping 79—73153
  GaN/Ga layered films, Ga whisker growth 80—92800
  GaN-AlN, solid solution, epitaxial growth and electrical props. 77—73236

gallium compounds continued
  $GaNbO_4$ decomp. due to electron beam heating in electron microscope 78—35711
  $GaNbO_4$, diffuse refl. and luminesc. spectra 78—56516
  $GaNbO_4$, electron beam induced decomp., high resolution lattice imaging obs. 78—6161
  $GaNbO_4$, polymorphic transition under high press. 80—100835
  $Ga_2Nb_2O_7$, and $Ga_2Nb_2O_{7.25}$, new phase of mixed oxide 78—59787
  GaO, B-X band system, electronic spectrum, struct. and anal. 79—45732
  Ga_2O, decomposition and desorption on Al_2O_3 $(10\bar{1}2)$ surface, effect of multiple binding states 78—44406
  Ga_2O, molecular beam, interaction with Al_2O_3 surface, mass spectroscopic anal. 77—40600
  β- and β''-Ga_2O_2-Na_2O, fast ion conductor, Na^+ self diffusion and Na-K exchange 79—28133
  Ga_2O_3, additive to plasma arc, influence in spectrochemical powder anal. *(German)* 79—54196
  Ga_2O_3, α to β monotropic transition heat determ. 80—54370
  β-Ga_2O_3, crystal structure, 2/m symm. deviation 77—35534
  β-Ga_2O_3, doped, photolum., emission centres struct. 78—52557
  Ga_2O_3, effect on thermal oxidation of Si 77—12722
  Ga_2O_3, entropy of beta→alpha transformation 77—36489
  Ga_2O_3 film, growth by reactive vapour deposition, optical and elec. props. 77—48347
  Ga_2O_3 film, on GaAs wafer, surface roughness by gas adsorption techniques 80—15398
  Ga_2O_3 film, prep. by anodic oxidation of Ga film on GaAs or Si 77—81338
  Ga_2O_3, Ga 3d and $L_3M_{4.5}M_{4.5}$ and O 1s binding energies, ESCA absolute energy calibr. 78—92171
  Ga_2O_3 in vitreous silica, effects on viscosity of impurity alkali oxide, OH, Al_2O_3 and Ga_2O_3 78—64580
  Ga_2O_3, L_l and L_η X-ray emission spectra 78—39631
  Ga_2O_3 on spinel and sapphire, VPE and orientation *(Japanese)* 77—51611
  β-Ga_2O_3, presence at oxide-GaAs interface 79—66190
  β-Ga_2O_3, pure and doped samples, UV luminesc. obs., 5 to 300K 78—80396
  Ga_2O_3 reaction with K_2O and H_3PO_4, $KGaHP_3O_{10}$, $KGa(PO_3)_4$ and $Ga(PO_3)_3$ crystn. 79—52642
  β-Ga_2O_3, rel. between rutile, hollandite, psilomelane, ramsdellite type structs. 79—37664
  Ga_2O_3 solubility in H_3PO_4, $GaH_2P_3O_{10}$ and $Ga(PO_3)_3$ crystn. 79—52641
  β-Ga_2O_3 spinel form. *(German)* 78—22894
  Ga_2O_3 thin films, reactively evaporated, props. *(Japanese)* 79—99648
  β-Ga_2O_3:Cr, temp. depend. of luminesc. characts. *(Russian)* 77—28621
  Ga_2O_3:Mg(Zr) single crystals, quenched, ionic and elec. props. 78—30922
  Ga_2O_3-As_2O_3, anodic ellipsometric and IR spectroscopic studies 80—11493
  Ga_2O_3-Fe_2O_3 system, anomalous Mossbauer lineshapes, incomplete annealing 77—51998
  Ga_2O_3-Fe_2O_3 system, anomalous Mossbauer line shapes, incomplete annealing 78—92006
  β-Ga_2O_3-K_2O/K ferrite, interfaces and solid soln., thermal expansion and lattice parameter variations 78—55959
  Ga_2O_3-Na_2O, β- and β''-phases, superionic conductors, Raman results 77—40234
  Ga_2O_3-Na_2O, β- and β''-phases, ionic cond., room temp. to 350°C 77—43368
  Ga_2O_3-Na_2O, β- and β''-phases, IR spectra 78—39552
  β''-Ga_2O_3-Na_2O, single cryst. growth by Na_2O evaporation from molten Na_2O-Ga_2O_3 77—44141
  Ga_2O_3-Na_2O, syntaxy between β and β'' structures, TEM 77—20075
  β''-Ga_2O_3-Na_2O-K_2O mixed crystals, cond. anomaly 79—46838
  Ga_2O_3-PbO, phase diag. 78—80524
  Ga_2O_3-R_2O_3:Nd^{3+} glass, prep., characts., X-ray diffr., absorpt. and thermal anal. obs. *(French)* 78—19704
  Ga_2O_3-SiO_2-X_2O (X-alkali metal) glass, acid resist. 80—21140
  Ga_2O_3-TeO_2, phas diag. 77—81252
  GaO_xN_y based multiple insulating layers for surface passivation of GaAs 80—93006
  GaO_xN_y films and multilayer systems, passivation of GaAs 80—11809
  α-GaOOD, powder neutron diffr. cryst. struct. exam. 78—2081
  $Ga_2O_3.6Bi_2O_3$, IR and Raman spectra, vibr. anal. 78—76464
  GaP, 1 MeV proton bombardment, lattice deformation investigation by Kossel effect 78—22775
  GaP, 3d core level spectra, electronic polarisation effects 80—6765
  GaP (III) B surface, negative-electron-affinity, photoemission transmission coeff., comparison with GaAsP 78—56560
  GaP, (001), adsorpt. of Cs, photoemission meas. 78—87874
  GaP (001), dislocation etch pits 78—14351
  GaP (100), prep. of negative electron affinity surface by Cs adsorption 80—10768
  GaP, (100) surface, thermal desorption props. of Cs and Cs-O adsorbed layers *(Japanese)* 80—15368
  GaP (100) thermal and vap. phase etching in H_2-HCl-PH_3, obs. 77—77612
  GaP (110), electronic surface states, initial steps of O_2 chemisorption 80—49844
  GaP (110), initial oxidation, XPS and AES study 80—11542
  GaP (110), surface bands in relaxed cleavage surface, tight binding model 78—91744
  GaP (110), surface struct., EPR meas. and elastic energy minimisation calcs. 79—51405
  GaP (110), wave functions and surface struct., EPR expts. 78—91519
  GaP (110) surface, oxidation process, XPS study 79—15585
  GaP, (110) surface, trned in energy distribs. of Ga dangling orbital surface states 79—28397
  n-GaP, acoustoelectric effect due to piezoelectrically active wave 80—80331
  GaP acoustooptic pulse modulator 78—46814
  GaP, adsorption and desorption of Cs, LEED, AES, and photoemission meas. 80—70532
  GaP, adsorption and field-desorption of O_2 and Au, FEM studies 80—34304
  GaP, amorphous, optical absorpt. edge shape, band edge fluctuations 77—20880
  GaP amorphous film, EXAFS, optical and elec. props. 80—49547
  n-GaP and p-GaP, photon drag-optical rectification detectors, performance in 2 to 33 μm range 79—35834

gallium compounds continued
GaP anodic MOS structs., interface-state band model 80—11093
GaP, anodic oxidation and MOS devices 77—80845
n-GaP, anodic oxide film, exam. using SIMS and ellipsometry 79—61770
GaP, anodic oxide film comp. profile anal., radioactive tracer technique 77—59956
GaP anodic oxide system, multiple angle incidence ellipsometry, meas. at λ=632.8 nm 79—63294
GaP, anodically grown insulating layers, prep. and props. *(German)* 78—64158
GaP, anomalous avalanche breakdown 80—80284
GaP, anomalous photoeffect on connected excitons *(Russian)* 80—92929
p-GaP, appl. as anode in stable photoelectrochemical cells for splitting of water 77—44484
GaP, atom probe field ion microscopy 78—80460
GaP, Au surface film deposition for constructing surface-barrier photodetectors 77—77423
n-GaP, Au-coated semicond. electrode, photoelectrochem. behaviour in water 77—21399
GaP, Be-Au and Si-Au ohmic contacts, metallurgical struct. 77—1485
GaP, birefringence, photoelastic consts. dispersion 80—11361
GaP, birefringence observations of strain and plastic deform. 80—50678
GaP, bound excitons in spherical model, low lying excited states 80—10883
n-GaP, CO$_2$ laser induced photon drag effect 79—42589
GaP, CVD epitaxy, book contrib. 77—12544
GaP, CVD mechanism, product catalysed reaction of Me$_3$Ga with PH$_3$ 77—48345
GaP, camel's back excitons, rel. to band structure 78—47707
GaP, camel's back induced stabilisation of electron-hole liquids 79—19524
p-GaP, cathode of photoelectrochemical cell 78—10552
GaP, cathodoluminesc. meas. of minority carrier lifetime 78—19572
GaP, chem. vapour growth in closed system 78—35283
GaP, chemical etching processes, review 78—95832
GaP, cleaved (110) surface, electron surface props. 80—11067
GaP, comparison of contact resistances of Au-Zn, Au-Zn-Sb, Au-Ge-Ni and Au-Ge-Ni-Sb alloyed contacts 80—70825
GaP, complex ^{119}Sn impurity-defect, Mossbauer study 80—75898
GaP complex band semicond. photogalvanic effect mechanism 80—11036
GaP, complex form of donor energy levels, optical spectra anal. 78—23045
GaP, containing matrix metal inclusions, internal friction study 79—42145
GaP, core exciton binding energies 80—80188
GaP, core levels, chem. shift and relaxation energy, temp. dependence 80—39520
GaP, core levels, temp. depend. of conduction band and core exciton energies 80—24828
GaP, cryst., characterisation by light scatt. *(Japanese)* 77—35498
n-GaP, cryst. growth, synthesis solute diffusion method, elec. characts. *(Korean)* 78—52653
GaP, cryst. growth for green luminesc. diode manuf. 77—40346
GaP, crystal, growth conditions rel. to dislocation struct. 80—88151
GaP crystal, structure defect formation due to annealing and stress, dendrites, slip, dislocations 80—29026
GaP crystals, radiation defects, TSC obs. 80—65588
GaP, Cs(Cs-O) activated, with negative electron affinity, thermalised electron emission 78—11073
GaP, Cs(Cs-O) activated, with negative electron affinity, near UV photoemission and secondary emission 78—11074
GaP, cubic cryst., lattice dynamics, overlap shell model and bond charge model 79—42156
GaP, current controlled LPE from finite volume melt 80—20805
GaP, d core levels, electron-hole interaction 77—11880
GaP, d-electron participation in chem. bonds 77—28682
GaP, Debye temperature, atomic mean square displacement 78—87757
GaP, deep centres, many-electron effects 79—15117
GaP, deep level defects, review 80—24841
GaP, deep level impurities *(Japanese)* 77—89723
GaP, deep level profiles at substrate-epitaxial interfaces, photoionisation meas. 79—38025
GaP, deep levels investigation 77—76769
GaP, deep O$^-$ state, model impurity calc. 80—6780
n-GaP, deep state controlled minority carrier lifetime 80—20211
GaP, defect processes, electronic stimulation 80—24665
GaP, deformation potentials of direct and indirect absorpt. edges 79—69854
GaP, density of states effective mass and cond. band energy minima 77—28101
GaP, diffusivity and solubility of Cu 78—51743
GaP diodes, TSCAP and admittance spectroscopy of gamma-ray induced defects 77—89472
GaP, dislocation etching of (001) faces with H$_3$PO$_4$ etchant 80—15103
GaP, dislocation loops and bipolar obs. by chemical etching 78—55873
GaP, dislocation obs., SEM EBIC vs SEM CL micrographs 77—80511
GaP, dislocation structure, optical microscopy obs. 80—24458
GaP, dislocations induced by diffusion of Zn with or without P 77—19955
GaP, disorder distrib. extraction, semiempirical method of applying dechannelling correction 78—22781
GaP, dispersion of refr. index and permittivity 77—55765
GaP, dispersion of vibrational excitations, Raman scatt. 78—84588
GaP, donor states theory, camel's back struct. influence 80—59921
GaP donor system, local mode, random force const. change 78—38800
GaP, donor-acceptor pair spectra, electron-phonon interactions 79—38631
GaP, donor-acceptor pair luminesc., excitation spectroscopy 80—25440
GaP, dopant dislocations, scanning electron micrographs, cathodoluminesc. 78—91340
GaP, double reson. in two-phonon Raman scatt. by longitudinal optical phonons 77—24852
GaP, EHT calcs. of energy bands and pressure dependences *(Japanese)* 78—34747
GaP, effective mass anisotropy at X$_{1c}$ and X$_{3c}$ minima of conduction band, optical absorpt. spectra 77—8021
GaP, effective partition coeffs. and elec. behaviour of group IV elements 77—7754
GaP, effects of hydrogen incorporation during deposition by sputtering 79—69981
GaP, elastic moduli, 80-700K, and elastic consts. 79—73245
GaP, elastic moduli and attenuation of elastic waves 77—51429

gallium compounds continued
GaP, electrical and optical props. at low temps. 80—39636
GaP, electrical recomb. behaviour at dislocations 79—82606
p-GaP electrode, for solar cell, differential capacitance meas. for flatband potential determ. 78—72256
n-GaP electrode, photoanodic dissolution rate, effect on surface electronic band energies 80—103748
n-GaP electrode, photoelectrochemical behaviour in acetonitrile solns. 78—31644
p-GaP electrode, photoelectrochemical effect 80—55673
p-GaP electrode, spectral response extension by metal adatoms 78—34895
p-GaP electrodes with metal adatoms, surface states form. due to impregnated H 80—54778
GaP, electrolum. and related props., state-of-the-art, book contrib. 77—73173
GaP, electrolum. efficiency degradation and deep level change in red LEDs 77—81155
GaP, electrolum. study using high-gain image intensifier 80—55193
GaP, electroluminescent diode, electron irradiated, negative resistance due to impact ionisation 77—15942
GaP electroluminescent diode struct. prep. by SSD and Czochralski methods, dynamic props. *(Czech)* 80—97425
GaP, electron hole droplet, motion damping, impurity and piezoelec. scatt. 78—67951
GaP, electron irrad., EPR of antisite-impurity defect 80—25211
GaP, electron irrad., radiation defects annealing 80—29059
n-GaP, electron mobility, 77 to 300K, intervalley scatt. of electrons *(Russian)* 79—95407
GaP, electron traps around dislocations in p-n junction and metal-semicond. structs. 80—34388
GaP, electron-hole drop, luminesc. 79—33812
GaP, electron-hole drops, self-consistent surface calculation 80—65464
GaP, electron-hole liq., cathodolum. spectra meas., 4.2-20K 77—63470
GaP, electron-hole liquid obs. by luminesc. spectra 77—51668
GaP, electron-hole liquid exam. 78—2430
GaP, electron-hole liquid, emission band from time-resolved spectra 78—43938
GaP, electron-hole liquid props., luminescence at high excitation intensity 79—69882
GaP, electron-hole plasma photolum. obs. 78—52559
GaP, electron-hole plasma luminesc. 79—38651
GaP, electronic elementary excitations in far UV and X-ray region 79—95346
GaP, electronic props. of paramag. antisite P(Ga) defect 78—43327
GaP, electronic states of neutral vacancies 77—11875
GaP, electronic structure of neutral phosphorus vacancy, empirical pseudopotential 79—78042
GaP, electroreflectance spectroscopy using synchrotron rad. 78—10912
GaP, epitaxial growth by GaPO$_4$-C system 79—99448
GaP, epitaxial growth from Sb and Bi melts 79—52131
GaP epitaxial growth from solution in melt, crystn. theory 80—16204
GaP, epitaxial layer, carrier recomb. at dislocations 77—20932
GaP, epitaxial layer, thickness and diffusion length, photocurrent meas. 77—32096
GaP, epitaxial layer prep. and elec. props. 77—85096
GaP, epitaxial layers, anisotropy of growth rate from soln. in melt 78—35322
GaP, epitaxial layers, dislocation recomb., SEM cathodoluminescence studies 79—42558
n-GaP, epitaxial layers, electrical parameter determ. by graphical method *(Russian)* 77—15975
GaP epitaxial layers, stable growth conditions, by molten salt electrodeposition on Si and GaP substrates 79—20000
n-GaP epitaxial layers, transverse magnetoresist. *(Russian)* 77—76964
GaP epitaxial layers for yellow-LEDs, prep. and props. *(Czech)* 78—48234
GaP epitaxial layers grown in Ga-PCl$_3$-H$_2$ system, surface defects 77—7993
p-GaP, epitaxial layers grown from liq., overcompensated, doping levels 78—91353
GaP, epitaxial struct., cathodolum. in SEM 78—10991
GaP, etching in aqua regia and bromine-methanol-water solns. 78—68833
GaP, exam. of magnetic susceptibility and absorption spectra 79—1778
GaP, excited 1s-level of S-bound excitons 79—82996
GaP, facets on pulling under concave interface conditions 78—23601
p-GaP, field electron emission current-voltage characts. 80—45219
GaP, field ion microscopy 78—19644
GaP film, deposited by RF sputtering, struct. and elec. props. obs. *(Czech)* 78—52667
GaP film, polycrystalline, with negative affinity, secondary emission *(Czech)* 78—52604
GaP films, RF sputtering on glass and Au film substrates, struct. and elec. props. 80—2311
n-GaP films, reduced work function, energy spectra of secondary electron emission 79—28867
GaP films on Si, epitaxial crystallisation by nanosecond laser pulses 80—107674
GaP, fine struct. in energy derivative reflectance spectra 79—78705
GaP, fine struct. of indirect exciton 78—19509
GaP, first order Mott transition of exciton gas 78—76535
GaP, freq. depend. of TO phonon decay parameter, and phonon-phonon interaction mechanisms 77—59084
GaP, frozen-in pt. defects annihilation 79—99949
GaP, GPE layers, nonradiative dark regions along surface ripples 77—59600
GaP, gain in stimulated Raman scatt. by coupled phonon-plasmon modes from spontaneous Raman spectra 79—68418
GaP, green cathodolum. from cryst. defects, SEM, TEM study 80—80870
GaP, green LED, degradation, appl. of dislocation climb model 77—1125
GaP, green luminesc. efficiency, review 77—28636
GaP, grown by SSD method, Zn diffusion for green LED fabrication 77—81208
GaP, growth, LPE method for green LED mass production 77—77422
GaP, growth and props. of LPE layers on Si substrates 78—6864
GaP, growth of dislocation free crysts. from stoichoometric melt. 77—81212
GaP, growth of epitaxial layers from limited of melt-soln. 78—19676
GaP, heteroepitaxial CVD on Si, dual process, film characts. 77—16503

gallium compounds continued
GaP, heteroepitaxial deposition on GaAs, Sn solvent inclusion, surface morphology *(German)* 79—28968
GaP, heteroepitaxial growth on Si, substrate misorientation effects 78—3055
GaP, heteroepitaxial growth on Si substrate by MBE 78—64481
GaP, high-energy ion-implanted, layer thickness and refr. indices meas. 77—24837
GaP, high-order Raman spectra, polariton scatt. 78—56483
GaP high-pressure reaction synthesis 77—77372
GaP, hole traps, rel. to two stage model for deep level capture 78—10396
GaP, hyperbolic singularity of dispersion law of excitons 79—42466
GaP, IR absorpt. spectra depend. on compensating defects and thermal treatment *(Russian)* 80—71465
GaP, impact ionisation theory, Auger processer 80—49752
GaP, impurity behaviour during crystallisation from melt 77—84772
GaP, impurity distribution ratios, correl. with covalent and ionic radii 80—54276
GaP, impurity interaction on excited acceptor states, luminesc. excitation spectra 79—15517
GaP, impurity-containing single crysts., refl. spectra 80—80823
n-GaP in DMF solns., electrochem., photoelectrochem., redox. pot. determ. 79—96322
GaP in Sn, vap. press. of P and As 77—51485
GaP, indirect exciton dispersion, 'camel's back' 79—73447
GaP, indirect exciton fine struct. in absorpt. spectrum, stress effects 79—42986
GaP, indirect exciton fine struct. and effect of uniaxial stress 79—95805
GaP, indirect free exciton, magneto-optical investigation of ground state 77—51670
GaP, influence of shear deform. on interband interaction 78—39116
n-GaP, interface-recomb.-controlled minority carrier lifetime obs. 77—12027
GaP, interimpurity interaction effect on distrib. profiles of impurities diffusing simultaneously 77—76451
GaP, internal friction calc. 80—2116
n-GaP, inversion layers, broken-symmetry ground states 77—47873
GaP, ion implantation, range distrib. calc. 79—55760
GaP, ion implanted, mode-locked Nd:YAG laser annealing, recrystn. 80—19817
n-GaP, ion implanted films, optical and luminesc. props. 80—60699
GaP, ion irrad. damage, strain effect contrib., channelling meas. 78—67752
GaP, ion-bombarded, energy band struct., electrorefl. obs. 79—19517
GaP, ion-implanted, form. and annealing of radiation damage 78—91363
GaP, ion-implanted, radiation damage, ellipsometry expts. 78—38735
GaP, ionised-cluster beam epitaxial growth on GaP and Si, characts. for LED 79—28951
p-GaP, irrad. by visible light, photoelectrolytic decomposition of water 77—77778
GaP, LEC, SSD and CVD samples, Zn tracer diffusion profiles in solids 78—95189
GaP, LEC crystal, cathodolum. and photolum. around dislocations 78—84663
GaP, LEC crystal, etch pit obs. 77—76387
GaP LEC crystal, imperfections obs. by light scatt. 78—6074
GaP, LEC growth of dislocation-free crysts., microdefects and striations 78—9974
GaP, LED, efficiency depend. on O_2 conc. 79—19613
GaP LED, N content by photovoltage meas. 77—11993
GaP LED, negative differential resistance and conductance associated with dielectric losses 77—63468
GaP LED, SEM study of charge collection and cathodoluminesc. 80—65661
GaP LED, surface treatment effect on surface recomb. vel. and leakage current 77—20410
GaP LED with S-shaped characteristic, negative resist. and red electroluminesc., expt. 78—48237
GaP LED's, current/voltage and light/voltage characts. 77—8662
GaP, LPE, cathodo- and electrolum., residual impurity and struct. defect effects 78—19570
GaP, LPE, LED fabrication and electroluminesc. characts. 77—28632
n-GaP, LPE, minority carrier bulk lifetime and diffusion coeff. meas. 77—11932
n-GaP, LPE, non-radiative recombination 78—19565
GaP, LPE at 650°C from In solvent, low Si contamination 78—80480
GaP, LPE edge growth reduction method 78—30848
GaP, LPE growth rate calc., model of LPE growth 79—19485
GaP, LPE layer for LED, photoluminesc. distrib. meas. *(Czech)* 78—48209
GaP, LPE layer perfection, effect of dislocation loops in GaP substrate 78—30843
GaP, LPE layers, comparison of growth rates with theoretical predictions 79—52134
p-GaP, LPE layers, Hall effect 78—91704
GaP LPE layers, low temp. growth from In solvent 79—56924
GaP LPE layers and LEC substrates, correlation between dislocation pits 78—38706
GaP, LPE layers high purity, invest. *(German)* 78—31353
GaP, LPE solvent choice, equilib. in In-Ga-P system 79—87589
GaP lamps, green emitting deep level photocapacitance spectra 77—69409
GaP, large cryst., optical birefr. images of dislocations 78—30627
GaP, laser damage, 10.6 μm CW CO_2 beam 77—63497
GaP, lattice dynamics, phonon freq. meas., valence-force-field overlap shell model 80—15205
GaP, lattice dynamics and phonon parameters bond bending force model 80—59595
GaP layers, heteroepitaxy, grown on Si and Ge from multiple component solns. *(Russian)* 78—15319
GaP layers, LPE growth, elec. props., residual impurities 79—38202
GaP, light emitting diode structure, effect of neutron irradiation on cathodoluminesc. 79—28843
GaP, light scatt. by LO phonons, high-resolution study 80—80798
GaP, light scatt. spectra of guided wave polaritons 79—15101
GaP, line shape and symmetry analysis of core-level electroreflectance spectra 77—8600
GaP, liquid interaction parameters determ., 580-670°C 80—65197
GaP, localised defects, one-electron pseudopot. 77—24533

gallium compounds continued
GaP, localised states in presence of P vacancy, pseudopot. calc. 78—18992
n-GaP low absorption monitors for HF laser 79—31964
GaP, low temp. selective Zn diffusion process using anodic oxides 78—47399
GaP, luminesc. from electron-hole drops, 2 to 77K 79—11454
GaP luminophor powders, SAW nonlinear acoustoelectro-luminescence 80—45143
GaP, MBE growth on GaP, and crystallographic evaluation 77—8762
GaP, MCD of phonon-assisted exciton transitions 78—92053
GaP, manifestation of local vibrs. of dislocations in IR spectra 78—88339
n-GaP, many-valley semiconductor, relative displacement of D_1 and D_2', bands under shear deform. influence 79—15080
n-GaP, many-valley semicond. anisotropic acoustoelectric effect, thermo-EMF anisotropy fluctuation depend. on ultrasound freq. 79—69562
GaP meas. of transition press. to conducting phase 79—54150
GaP, mech. props. and photomechanical effect 77—84833
GaP, metallic modification, supercond. transition temp. at high temp. *(Russian)* 77—80867
GaP, microscopic mechanism of film growth from non-condensed phases, kinetic anal. 80—54565
GaP, minority carrier lifetimes at dislocations, SEM meas. using photon counting 78—23109
GaP, minority carrier quasi-Fermi level meas. in illuminated photoelectrolysis cell 77—85308
GaP, minority carrier traps, detection using transient spectroscopy 79—65402
GaP, mol. beam epitaxial growth, cryst. quality composition investig. *(Japanese)* 77—55895
GaP, moments of phonon spectra from specific heats 80—15203
GaP, momentum distrib. of electrons, anisotropy, positron annihilation *(Russian)* 78—84676
GaP, Mott transition of exciton gas, cathodoluminesc. 79—33845
GaP, multiband and multivalley effective mass theory for impurities 79—65409
GaP, n-, p-type, electrode, impedance in alkaline medium *(French)* 79—43586
GaP, n-type, Zn diffusion, p-n junction depth 77—89841
GaP negative electron affinity cold cathodes, vidicon appls. 78—19133
GaP, non-radiative recombination and structural defects 78—19566
GaP, nonlinear optical susceptibility and dispersion, electro-optic meas. 77—23707
GaP, nonradiative capture and recomb. by multiphonon emission 77—43533
GaP, O_2 adsorpt. monitoring by Auger spectroscopy, electron beam effects 77—72777
GaP, O_2 adsorpt. monitoring by Auger spectroscopy, electron beam effects 78—6218
GaP, obs. of Γ-L indirect transition, phonon struct. 78—48194
GaP, obs. of Raman scatt. by Cu vapour laser 78—95586
GaP on GaAs, LPE, growth with Ge and Sn solvents, phase diags. 78—88434
GaP on GaAs substrate, heteroepitaxial layers, stuct. defects *(German)* 79—23865
GaP, one-sided abrupt junction, distinction between avalanche and tunnelling breakdown 78—56211
GaP, optical absorption and struct. of acceptor centres 78—48205
GaP, optical inhomogeneity, physical basis 79—15430
n-GaP, optical rectification due to free carriers, detector appl. 77—10967
n-GaP, optical rectification and photon drag 77—36224
GaP, optical transitions, effect of perturbed k-selection and gap shrinkage, theory comparison with expt. 80—66257
GaP, optoelectronic devices, conf., Berlin, DDR 78—91755
GaP, overlap integrals and Auger recomb. coeff. direct calc. 79—69524
GaP oxide, anodic, optical props., 1.5-6.0 eV 77—90209
GaP oxide films grown by anodization in electrolytes, electron spectroscopy exam. *(German)* 79—15837
GaP, p^+-n diode junction, admittance meas. and carrier traps 78—91757
GaP, p-i-n LED, I-V characts., electrolum., and photocond. meas. 77—20930
GaP p-n junction, capacitance-freq. dispersion and electroluminescence efficiency 78—64101
GaP p-n junctions, electron beam excited carrier avalanche multiplication 79—69587
p-GaP photocathode, charge transfer via surface states, water photoelectrolysis anal. 80—75636
GaP photoelectrode, role of Au overlayers 78—14812
GaP photoelectrode, stability 77—20422
GaP, photoelectron spectra at Schottky barrier *(Korean)* 79—11220
n-GaP, photoelement in UV radiation ratemeter 78—285
GaP, photoemission from (111) and $(\bar{1}\bar{1}\bar{1})$ surfaces 79—91562
GaP, photoexcited, Raman scatt. from plasmons 79—38541
GaP, photovoltage transients, intensity and chopping freq. depend. 77—47859
GaP, piezo-modulated spectroscopic investigation of N and N-N pairs, bound exciton 77—66474
GaP, piezobirefringence above direct gap 79—51929
GaP, plasma deposition and elec. cond. 78—60585
GaP, polar semicond., radiative recomb., electron-phonon interaction effects, calc. 80—49631
GaP, polar semiconductor, electron-hole liquid, electron-phonon interactions 80—6739
GaP, polariton dispersion, IR reflection spectroscopy 80—11415
GaP, polariton linewidth in k-space, anharmonicity and permittivity 77—85155
GaP, polished, technique for uniform etching 78—39928
GaP, polishing dislocation etch 78—6066
GaP polycrystals, subgrain boundaries, cathodolum. in SEM 79—1440
GaP, positron annihilation 78—72636
GaP, positron annihilation, deep acceptor level props. 79—11485
n-GaP, potential of Au overlayer, I-V curves 77—89848
GaP, powder, electroluminesc. excitation by SAW, nonlinear effects 80—16104
GaP, preferential etching of dislocations and stacking faults 77—39589
GaP, proton implanted, thermally stimulated current meas. 80—24943
GaP, pure and N doped, extended Huckel theory appl. 80—59916
GaP, radiation defect accumulation due to ion bombardment, optical absorpt. meas. 77—76438

gallium compounds continued
GaP, radiative and non-radiative recombination around dislocations 78—19576
GaP, radiative recombination, optical evaluation review 80—60647
p-GaP, Raman scatt. by coupled plasmon-phonon oscills. 78—6687
GaP, Raman scatt. from plasmon-phonon coupled modes 80—93337
GaP, Raman scatt. from surface polaritons, selection rules 77—52083
GaP, Raman scattering selection rules for surface polaritons 78—72091
GaP, Raman spectra, press. depend. optical phonon anharmonicity 77—8586
GaP, rare earth doped, photolum. and elec. props. *(Russian)* 78—52545
GaP, red LED degradation, diffusion model 77—8657
GaP, refr. index, 100 to 420K, permittivity calcs. *(Russian)* 77—90156
GaP, reson. Brillouin scatt., near indirect absorpt. edge 80—11423
GaP, reson. photoemission shake-up and Auger processes at 3p photothreshold 80—100748
GaP ribbon waveguide, vapour-grown, phase-matched SHG 80—48339
GaP, S-bound exciton stress depend. 80—29333
GaP, SEM, cathodoluminesc., impurity and defect detect. 78—83695
GaP, scatt. mech., mobility tensor 80—6826
GaP, Schottky barrier height, semiempirical tight-binding calc. 79—28408
n-GaP, Schottky barrier height data for several contact systems 80—60080
GaP Schottky barriers, voltage fluctuations, meas. 80—15604
p-GaP, Schottky barriers on polar (111) and $(\bar{1}\bar{1}\bar{1})$ surfaces 80—88631
GaP second order Raman spectrum, polarisation meas. 78—64368
GaP, semicond., ^{31}P nuclear mag. shielding 79—33549
n-GaP, semicond. electrode, electrolum, due to hole injection from electrolytes 77—20926
p-GaP semiconducting photoelectrode 80—101119
GaP semiconductor Raman laser 80—78864
p-GaP semiconductor-electrolyte solar cells for photochemical reduction of CO_2 to organic fuel 80—55880
GaP, semiconductor-metal transition, press. calibration above 100 kbars fixed points 80—77808
GaP, shallow impurity states, free exciton binding energy 78—79960
n-GaP, shallow trapping centres, electron lifetime from photocond. meas. 79—99563
GaP single cryst., defect distrib. near abraded surface 80—92533
GaP, single cryst., Raman scatt., effective cross-section rel. to nonlinear coeffs. *(Russian)* 78—71152
GaP single cryst., Raman scatt. cross section, nonlinear optical coeffs. 79—56784
GaP, single cryst. electrode, impedance, effect of freq., voltage and electrolyte comp. 78—19146
GaP single crystal, direct obs. of dislocations by birefringence 79—14810
GaP, single-crystal, anodically oxidised layers, AES measurements 78—91556
GaP, site selective doping by ion implantation of radioactive nuclei 80—34023
GaP, soln. growth of bulk crysts., luminesc. and elec. props. 78—92181
GaP, solubility in fused Sb, Bi, thermodynamics, rel. to epitaxial growth 78—34721
GaP, spectral depend. of O photoneutralisation cross-section near threshold, and band gap 79—1788
p-GaP, spin-flip Raman scattering, review 80—108209
GaP, stabilisation of electron-hole liquid by camel's back 80—6740
GaP, Stark effect at H-like impurity centres, forbidden electron transitions *(Russian)* 80—16009
GaP, stress-induced X_{1c}-X_{3c} conduction band mixing 79—19515
GaP, structural etching, characterizing $A^{III}B^{V}$ compounds, misfit dislocations 80—39099
GaP, substoichiometric native oxide layers, $^4He^+$ backscatt. obs. 77—77610
GaP substrate, transient-mode LPE of $Al_{1-x}Ga_xAs$ 78—72746
GaP surface, Ar^+ and e^- excited Ar Auger electron emission 79—47560
GaP, surface, chem. anal., low energy ISS compared with SIMS 78—64908
GaP, surface, contact pot. difference meas. 77—20403
GaP, surface, energy distrib. of photoemission *(Japanese)* 80—16145
GaP surface, quantitative XPS meas. 78—56559
GaP surface barrier structure, breakdown voltage exam., effect of proton irradiation 79—11225
GaP, surface characterisation using SAW 80—11069
GaP, surface cleaning by oxidation and heating, characterisation for electron emitter appl. 78—35548
GaP, surface energy evaluation, by a microindentation method 80—16473
GaP, surface layers produced by chemical treatment, comp. and struct. 79—96173
GaP, surface polariton linear photon and two photon absorpt. 80—49863
GaP, surface polaritons, freq. depend. of associated functions 79—78020
GaP, surface polaritons, light scattering studies, effect of surface roughness 80—6753
GaP, surface processing, residual film monitoring by ellipsometry 80—13124
GaP, surface protection, by KCl layer, LEED and Auger spectroscopy obs. 77—89628
GaP, surface sensitivity, low energy electron transmission optical modulation 78—76567
GaP, surface states, UPS meas. 78—14780
GaP, synthesis by gas chemical transport reactions, exam. of kinetics 79—95933
GaP, temp. coeff. of induced birefringence 80—93277
GaP, temp. depend. of Fermi Level, calc. 80—39491
GaP, temp. rise induced by laser beam 78—11025
GaP, thermal etch-pits, morphology 80—34002
GaP, thermal expansion below room temp. 80—79963
GaP, thermoelectric performance of Si-Ge alloy improvement 79—47115
GaP, Thomas-Fermi theory, dielectric functions, screening, dielectric constants 79—99497
GaP, transition metal deep centres, model 79—78045
GaP, transverse acoustoelec. voltage spectroscopy 80—49828
GaP, two photon absorption relative to Raman cross sections 78—87098
GaP, two-particle states and polariton spectrum 77—59261
GaP, two-photon absorpt., by surface polaritons 77—51676
GaP, two-photon absorption coefficient rel. to inverse Raman cross section 78—6678
GaP, two-stage vapour/liq. epitaxial growth on Si 78—3054
n-GaP, uniaxially deformed, piezoresist. exam. of donor levels 77—4346

gallium compounds continued
GaP, upper polariton branch obs. by ATR 78—68510
GaP, VPE, background deep level defects, transient capacitance obs. 77—62854
GaP, VPE cryst., electrolum. characts. 77—28631
GaP, VPE layer on Si or Ge, antiphase domain structures 77—69193
GaP, VPE layer structures for LED's, SEM, and TEM obs. of dislocation density reduction expt. 80—100425
GaP VPE layers, precision lattice parameter meas. by Umweganregung method 79—65047
GaP, vac. deposited film, structural, elec. and photoelectric props. 79—82698
GaP, valence band structure, CPA, bond orbital calcs. 78—87909
GaP, vapor-phase etching, mechanisms and kinetics 80—100934
GaP, vapour growth, element incorporation 78—30556
GaP, Zn diffusion into n-LPE layer, for high efficiency green LEDs 77—80519
GaP:^{56}Fe(^{57}Fe)(^{53}Cr), paramag. centres, identification from ESR and ENDOR spectra 80—80600
GaP:0 effect of displacement upon impurity levels, pseudopotential calc. 77—39803
GaP:As, form. of $GaAs_{1-\eta}P_\eta$ by diffusion 80—54389
GaP:Au, diffusion, solubility, and electrotransport of Au 78—91489
GaP:Bi,N, photoluminesc., electroluminesc., 4.2 to 300K, excitons and hole traps 80—108275
GaP:Bi(N), luminesc. decay kinetics 79—38646
GaP:C(Mg)(Zn), excited acceptor state investig. by photoluminesc. 77—8632
GaP:Ce(Dy)(Pr) epitaxial films, photoluminesc. spectra 80—66294
GaP:Co, deep levels, IR photoluminesc., stress effects 80—55163
GaP:Co, optical spectra and Zeeman anal. of Co 3d^7 state 80—66247
GaP:Co(Ni), photolum. excitation spectroscopy 80—80841
GaP:Cr, diffusion parameters and solubility and influence on elec. and optical props. 79—73343
GaP:Cr, ESR of doubly ionised Cr acceptor and IR luminesc. 78—56374
p-GaP:Cr, hole traps, ESR studies 80—75843
GaP:Cr, local level near valence band, photocapacitance 79—11080
GaP:Cr, origin of sharp near IR transitions 80—10913
GaP:Cr epitaxial layers, Cr conc. profile determ. 80—65029
GaP:Cr_2O_3, growth, dopant distribution, elec. resist. 78—34531
GaP:Cs-O simultaneous adsorption, oxidation interface chemical struct. 80—103584
GaP:Cu, deep levels, photoluminesc. and optical cross sections 79—38653
GaP:Cu, elec. and optical props., rel. to doping and heat treatment 80—16056
GaP:Cu, impurity absorpt. bands at 1.05, 0.75 eV 77—44032
GaP:Cu, LPE, photoconductive props. obs. 78—47836
GaP:Cu, Raman scatt. from acceptor state 80—11408
GaP:Cu, thermally and optical excited cond., deep level centres 78—72190
GaP:Cu p$^+$-n junction, deep level parameters, TSC meas., rel. to photocurrent techniques 78—72249
GaP:Cu-Ni, Schottky barrier, TSC meas., trap levels 78—91709
GaP:Dy, photolumines. spectra 79—52015
GaP:Fe, current-voltage characteristics p-i-n diodes, luminescence, absorpt. double injection methods 79—65407
GaP:Fe, diffusion, solubility, elec. activity and energy levels 77—55395
GaP:Fe, double electron trap state, ESR identification 77—36124
GaP:Fe, double Fe-thermal acceptor centre, energy states 80—96823
GaP:Fe, electron exchange via val. band between Fe acceptor centres, Mossbauer spectra 77—55741
GaP:Fe, heat treated, EPR spectra, struct. defects 80—7158
GaP:Fe, impurity atom charge exchange, Mossbauer spectroscopy 79—47050
GaP:Fe, optical absorption spectrum and Faraday effect 80—108245
GaP:Fe, photo-EPR study Fe(3d^6) centres and deep electron traps 80—44910
p-GaP:Fe, photoionisation spectrum of acceptor level 77—55810
GaP:Fe, profile of impurity optical absorption bands 78—56509
GaP:Fe n-i-n epitaxial struct., photoconductivity, recombination scheme *(Russian)* 80—15569
GaP:Fe^{2+}, absorpt. and luminesc. spectra 77—16388
GaP:Fe^{2+}(Co^{2+})(Ni^{2+}) d→d luminesc. spectra 80—7414
GaP:Fe^{3+}, deep impurity states investig. 77—15794
GaP:Fe^{3+} ESR spectrum, elec. field, uniaxial compression influence 80—103882
GaP:Fe(Cr), photo-ESR of annealed crysts. 80—15795
GaP:Ge, ENDOR study, superhyperfine interactions 80—93210
n-GaP:Ge, photomemory effect and thermal field impurity breakdown 77—20362
GaP:H/GaAs, amorphous film/crystal junction, optical and elec. props. 79—99611
n-GaP:In, LPE from In solvent, dislocation density reduction by doping 78—18919
GaP:M, M=substitutional impurities, lattice dynamics and local mode freqs. *(French)* 77—66011
GaP:Mg, ion implanted, elec. profiles 79—77628
GaP:Mn, ENDOR of cubic $^{55}Mn^{2+}$ 79—69749
GaP:N, appl. of temp. modulated photolum. induced by photoexcitation technique 78—95605
GaP:N, bound exciton absorpt. line asymmetry, electroabsorption spectra 80—71459
GaP:N, bound excitons, low temp. photoluminesc. thermal quenching 77—48228
GaP:N, Cd(Zn),(C), interimpurity recomb., acceptor binding energies 78—34796
GaP:N, electron binding by N pairs 79—90990
GaP:N, electron charge distrib. in vicinity of substitutional N 77—24531
GaP:N, electron-hole liq., luminesc. obs. 80—25438
GaP:N, electronic energy levels calc., optimisation 79—28315
GaP:N, epitaxial layer, determination of nitrogen concentration from cathodoluminescence spectra 78—38744
GaP:N, epitaxial layer doping 77—51396
GaP:N, epitaxial layers, N concentration determination by two independent methods 80—39142
GaP:N, excited states of excitons bound to NN_i pairs, fluoresc. obs. 77—44039
GaP:N, luminesc. from electron-hole drop 79—33813
GaP:N, N doping profiles in GaP grown by LPE, cathodoluminesc. data 79—23631

gallium compounds continued
GaP:N, photoluminesc., temp. depend., exciton recombination mechanism 78—88355
GaP:N, photoluminescence, temp. modulated 79—38623
GaP:N, quenching of luminesc. by charged defects 78—23531
GaP:N, radiative recomb. from electron-hole drops, impurity induced transition 78—19547
GaP:N, radiative recomb. of electron-hole liq. 79—73442
GaP:N, spin dependent exciton recombination at N_2 isoelectronic traps 77—69734
GaP:N, temp. modulated photoluminesc. 77—55818
GaP:N, temp.-modulated photoluminesc., phonon assisted tunnelling process 78—23511
n-GaP:N,O,S,C end, dielec. const. from S-C donor acceptor pair spectra 79—65788
GaP:N LED, acoustic emission, NDT of dislocation motion 78—91759
GaP:N LED, deep level studies, growth by time difference method at controlled vapour pressure 80—39522
GaP:N LED structures, local dopant conc. determ. using SEM cathodolum. spectra 80—101057
GaP:N p-n structure yellow light emitting source 77—69412
GaP:N VPE LED, deep level centres, DLTS studies 79—42493
GaP:N VPE layers, thermal emission energies, trapping, and carrier lifetimes, deep level capacitance spectroscopy 79—42487
GaP:N(N,O) epitaxial struct., luminesc. study of degradation during heat treatment 80—45139
GaP:N(Te), ion implanted at 40 keV, refl. spectra, 210-2000 nm, annealing *(Russian)* 78—80386
GaP:Ni, absorpt. and luminesc. spectra 79—42996
GaP:Ni, deep traps, near IR luminesc., polarised spectra meas. 80—16077
GaP:Ni, electron-hole recombination via deep state 79—99560
GaP:Ni, Hall effect and absorpt. spectrum investig. of acceptor level 77—44033
GaP:Ni, Ni contaminant, detection through IR photoluminescence 78—15212
GaP:Ni, optical and EPR study of two-electron-trap state 79—73806
GaP:Ni, whisker growth on surface 79—33212
GaP:Ni(Fe), multivalence impurities, EPR and optical absorpt. meas. 80—75844
GaP:O, EPR investig. of deep donor centre, delocalisation 77—28428
GaP:O, impurity concentration determ. by donor-acceptor luminescence 78—6090
GaP:O, multicharged state of O, TSC and photoinduced currents 79—7808
GaP:O, optical transitions via deep levels, phonon interaction 78—87939
GaP:O, optical transitions via deep levels, cross section temp. depend. 78—87940
GaP:O, photoionisation of deep impurity levels 80—34386
GaP:O, wave functions and optical cross sections associated with deep centres 78—34801
GaP:O^-, two electron state, electron capture 78—39054
GaP:O^-, two-electron O^- state evidence, ODMR, IR emission, phonon replicas 80—15828
GaP:rare earth, magnetic susceptibility, impurity states 79—61044
GaP:S, defect struct. and tetrahedral precipitates, TEM study 80—107246
GaP:S, ENDOR meas., symmetries, hyperfine parameters 78—72435
GaP:S, effects of uniaxial stress on luminesc. 79—78739
n-GaP:S, elastic moduli and mode gammas 79—73242
GaP:s, elec. props. following 1.7 MeV electron irradiation 78—80005
GaP:S, ground and excited states of bound exciton complex, stress effects 80—65463
GaP:S, Se, Te, Si, shallow donors, excitation spectra 77—81128
GaP:S, shallow donor states, Stark effect and inversion splitting, electroabsorption spectral obs. 80—50385
n-GaP:S electrical properties investigation, Hall effect and resistivity meas. *(Japanese)* 77—39840
GaP:S LEC grown crystals, HVEM investig. of defects 79—60376
GaP:S(Se), donor bound exciton excited states 80—66284
GaP:S(Se)(Te), pot.-depend. g-values and quenched diamag., props. of donor states 77—62861
GaP:S(Se)(Te), pot.-depend. g-values and quenched diamag., pseudoacceptors D^0, X 77—62862
GaP:S(Se)(Te)(Si)(C)(Zn), IR photocond. response spectra 79—56257
n-GaP:S(Te), IR absorpt. cross-section 79—38582
GaP:S(Te), photostimulation spectra, bound electron phonon interactions *(Russian)* 77—1712
GaP:Sb(Bi), gap vibrs. and impurity conc. determ. 79—69869
GaP:Si p-n struct., on n-$Ga_{1-x}Al_xP$ and n-GaP substrates, electrolum. spectra 79—24368
GaP:Si(s)(O)(Ta), donor centre struct. and conduction band nonparabolicity 78—14695
GaP:Sn, LPE growth from Sn soln., elec. resist. and Hall coeff. meas. 78—2593
GaP:Sn(Sb), lattice location of implanted atoms, ion backscatt. and ion-induced X-ray obs. 77—84785
GaP:Te, defects formed due to precipitation of Te, metallography and TEM exam. 77—84769
n-GaP:Te, doping parameters calc., by means of Hall data analysis 78—51925
GaP:Te, ENDOR meas., hyperfine interactions and elec. field gradient 79—42869
GaP:Te, Hall effect and elec. cond., 80-400K 78—91705
n-GaP:Te, LPE layers, Hall effect 78—91704
GaP:Te, photon drag, optical rectification response meas., anomalous polarisation depend. 78—33769
GaP:Te, struct. imperfections, prep. and doping effects 77—89451
GaP:Te, VPE grown layers, precision lattice parameter determination 80—24429
GaP:Te epitaxial layers, dopant distrib. obs. by amalgam polarography 77—39609
GaP:Te on GaAs, LPE growth fron Sn, exam. of impurity band conduction effects 79—11249
GaP:Te(S), nucl. relax. rel. to donor density 80—11284
GaP:Ti(Co)(Ni), positron annihilation meas. rel. to deep levels study 80—60712
GaP:V, ESR exam. 79—11344
GaP:Zn, diffusion profile determ., $^{32}P/^{65}Zn$ double tracer technique 78—55888
GaP:Zn, dopant diffusion profiles at 900°C, radiotracer meas. 77—59147

gallium compounds continued
GaP:Zn, doping from gas phase during LPE 80—55312
GaP:Zn, Hall effect and elec. cond., 80-400K 78—91705
p-GaP:Zn, Hall effect determ. of hole mobility temp. depend., scatt. mechanisms 77—4364
GaP:Zn, implanted, elec. profiling using anodic oxidation in N-methylacetamide 80—54690
GaP:Zn, isolated Ga vacancy due to electron irrad., EPR study 78—95519
GaP:Zn, light attenuation by impurity precipitates 79—11441
GaP:Zn, luminesc., acceptor-bound multiple excitons 80—11476
GaP:Zn, O, influence of impurity-absorbed illumination on luminesc. 80—93395
GaP:Zn, O LED, neutron irrad. effects on capacitance, I-V and electrolum. characts. 77—66543
GaP:Zn, Raman spectra of Zn acceptor 77—77187
GaP:Zn, shallow Zn diffusion profile determ. using anodic oxidation and double radioactive tracer method 77—43239
GaP:Zn, Sn doped epitaxial layers, Hall const., hole mobility and conc. 80—15143
GaP:Zn, Te, epitaxial layers, determ. of Zn conc. 79—77614
GaP:Zn, thermodynamics of Zn doping by liquid phase expitaxy 78—83832
GaP:Zn,O, Auger coeff. from luminesc. decay and Hall effect 77—48226
GaP:Zn,O, Auger coeff. from luminesc. efficiency and Hall effect 77—48227
GaP:Zn,O, bulk electrolum. degradation in LEDs 77—81156
GaP:Zn,O, degradation of bulk luminesc. induced by laser excitation 77—1715
GaP:Zn,O, epitaxial p-n junction, IR electroluminesc. exam. *(Russian)* 78—35207
GaP:Zn,O, kinetics of X-ray luminesc. 78—10984
GaP:Zn,O, photodiodes, high temp. emission spectra *(Russian)* 77—66545
GaP:Zn,O, red LED, deep-level changes associated with degradation 77—1472
GaP:Zn,O LED, 76K electrolum, spectrum, γ-irrad, and forward bias effects 79—78756
p-GaP:Zn,O-n-GaP:Te,N diode struct., radiative recomb. 80—7419
p-GaP:Zn,S, spin polarisation of donors and acceptors in mag. field, optical and microwave study 80—93393
plGaP:Zn-electrolyte interface, electrochemical LED, luminescence obs. 80—84507
GaP:ZnO, LED, degradation, temp. and current depend. 79—87144
GaP:Zn(Mg)(Cd), multiple bound excitons, photoluminesc. obs. 79—95837
p-GaP/Au-Be ohmic contact form. by ionised-cluster beam deposition 77—32528
GaP/Si heterostruct., differential thermal contraction, plastic deform. fracture 80—108494
GaP/Te(S), IR lattice band profile, electron spin reversion in mag. field, Nf-R curve 79—28771
n-GaP-(Ge-Au)/Ni, specific contact resistance calc. 78—43474
GaP-Ag(Au), Schottky barrier, stress effects on elec. props. 80—34512
GaP-$Al_xGa_{1-x}P$, DH electrooptical strip modulator *(Russian)* 78—1344
GaP-AlGaP, stripe-geometry electrooptical modulator 80—23798
GaP-anodic oxide devices, optoelectronic device, processing appl. 78—84304
GaP-anodic oxide MOS struct. oxide and interface props. 79—60929
p-GaP-aqueous CO_2 liq. junction solar cells, CO_2 photoelectrochemical reduction 78—88649
GaP-based III-V solid solns., bonding and energy gap, mag. meas. 78—18580
GaP-Cs-O, negative electron affinity, secondary emission characts. 78—11031
GaP-electrolyte contact, electrolytic decomposition and photodecomposition 78—95357
GaP-GaAlP, heterojunction cold cathode 79—69965
GaP-GaAlP-GaP, lattice-matched, LPE layer growth under P vapour pressure and reduced O_2 contamination 79—51445
GaP-GaAs, amorphous film/crystal junction, optical and elec. props. 79—99611
GaP-GaAsP planar heterostructure strip ridged waveguide under mech. load, polarisation modulation 80—96038
GaP-Hg, elec. props. using Schottky barrier capacitance techniques 78—47870
GaP-In LPE layers, carrier diffusion lengths and escape probabilities optical absorpt. and photoemission meas. 79—87559
GaP-InAs solid solns., energy band struct., edge absoprtion spectra 78—39018
GaP-InP, pseudobinary alloy, phase diagram calc. 78—52786
GaP-InP solid solution, quantitative analysis, use of internal calibration technique developed by AES 77—36834
GaP-liq. NH_3 soln. junctions, elec. characts. *(French)* 80—2460
GaP-M, M=Cd, Sn, Pb, polythermal cross sections 77—52300
GaP-metal Schottky barrier diodes, elec. props. under mech. stress 80—11087
GaP-metal Schottky barrier height rel. to chem. reactivity 80—25008
n-GaP-n-GaAs, in MIS structures, elec. controlled optical transparencies, optical processing use 77—85339
GaP-NH_3 electrolyte interface, photo-assisted electron injection 79—87152
GaP-$Ni^{3+}(Co^{2+})(Fe^{+})$, EPR assessment of $3d^7$ transition metal impurity state 78—48031
GaP-Pd contact system, low temp. alloyed contact formation 80—100519
GaP-Sb, Sb solubility in region of GaP primary crystn. 79—86891
GaP-Si, heteroepitaxial growth, electronic and optical props. 80—104075
GaP-Si, heterostructure, zincblende-on-diamond type systems, MBE growth, (110) orientation as preferred orientation 80—80099
GaP-ZnS, solid solns., microstruct. investig. 78—2128
GaP-ZnSe heterojunction, elec. and photoelec. props. *(Russian)* 77—32070
GaP-ZnSe solid solutions, spectral studies *(Russian)* 79—91498
$GaP_{0.1}As_{0.9}$, gas-transport condensate with superlattice, structural and chemical inhomogeneity 77—85088
$GaP_{0.9}As_{0.1}$/GaP, heteroepitaxial structs., refined formulation of relative orientation criterias 80—44448
GaP_xAs_{1-x} $(0 \leq x \leq 0.32)$ epitaxial film, one-dimens. superlattice, X-ray spectrometer scanning, struct. variations 78—47681
GaP_xAs_{1-x}, exam. of magnetic susceptibility and absorption spectra 79—1778

gallium compounds continued
GaP_xAs_{1-x}, ion beam synthesis for photodetector fabrication 79—46688
GaP_xAs_{1-x}, N doped, alloying induced shift between excitation and luminesc. of N bound exciton 79—52013
GaP_xAs_{1-x}, refractive index comp. depend., nonlinearity parameter *(German)* 77—32344
GaP_xAs_{1-x} solid soln., specularly smooth epitaxial layers, superlattice struct. 77—24959
GaP_xAs_{1-x} solid solns., edge absorpt. 77—16334
GaP_xAs_{1-x}, surface defects and comp. inhomogeneity during gas-phase heteroepitaxy 77—85090
GaP_xAs_{1-x}:N, impurity electron states, binding energies and wavefunctions 79—42488
GaP_xAs_{1-x}:N, luminesc. of N bound state excitons, local-environment effects 80—100691
GaP_xAs_{1-x}-GaAs one dimens. superlattice, possibility of X-ray and electron diffr. struct. determ. 80—54560
n-GaP_xAs_{1-x}-p-$Ga_{1-y}Al_yP_xAs_{1-x}$ single sided heterolaser, visible emission 78—46607
GaP(As)(Sb), modulation spectroscopy in far UV, electroreflectance and thermoreflectance 77—66516
$(GaP)_x(InAs)_{1-x}$ solid solution, IR reflection spectra 77—69830
$Ga(PO_3)_2$, vitreous, microhardness 80—25864
$Ga(PO_3)_3$, crystn. from Ga_2O_3 in H_3PO_4 79—52641
$Ga(PO_3)_3$, crystn. from reaction of Ga_2O_3 with H_3PO_4 and K_2O 79—52642
$GaPO_4$ film growth on GaP, XPS exam. 78—31552
$GaPO_4$, high-low cristobalite transitions, DTA meas. 79—82335
$GaPO_4$, XPS of cryst., inner shell binding energies of elements 79—43092
$GaPO_4.2H_2O$, orthorhombic, thermal dehydration 79—79234
GaP(Sb), avalanche breakdown voltage for p-n junction, calc. 78—88020
GaP(Sb), electronic surface props., contact potential difference and photoemission expts. 77—47884
GaP(Sb), refractive index dispersion 79—24280
GaP(Sb), surface (110), energy distrib. of dangling-orbital surface states 80—80347
GaP(Sb), surface states, contact pot. difference, photoemission and low energy loss spectra expts. 77—85285
$(GaP)_x(ZnS)_{1-x}$ solid solutions, X-ray fluorescence spectra, photoluminescence *(Russian)* 79—74003
$(GaP)_x(ZnSe)_{1-x}$, solid solution, reaction of Zn with Se during Czochralski growth and LPE 79—8238
$(GaP)_x(ZnSe)_{1-x}$, two-photon absorpt. at ruby laser freq., clarification *(Russian)* 79—15505
$(GaP)_x(ZnSe)_{1-x}$/GaP, epitaxial heterostructures, chem. microinhomogeneity 77—80831
GaS, absorpt. edge, exciton levels and Raman scatt., press. effects above 40 kbar 77—48187
GaS, angle resolved UPS, energy band dispersion curves determ. 79—100022
GaS, anisotropic phonon dispersion 77—84864
GaS, anti-Stokes photon replica emission under two photon excitation 77—52175
GaS, birefringent layer cryst., indices of refraction 77—20815
n-GaS, Bridgman crysts., hole traps, photocond. and thermal quenching study 80—75580
GaS, Brillouin scatt. by pure transverse phonons 79—78696
GaS, Davydov splitting of degenerate lattice modes 79—61382
GaS, direct and indirect two photon processes 77—40261
GaS, elastic prop. anisotropy, Debye temp. *(Russian)* 80—88244
GaS, electrolum. and electroabsorpt., 77K 77—48247
GaS, factor-group analysis of high-symmetry layer dynamics 79—42160
GaS, growth by I_2 vapour transport using temp. oscill. method 77—77355
n-GaS, hopping and impurity cond. anomalies 77—59287
GaS, indirect excitons *(Russian)* 77—89709
GaS, infrared optical props., polarisation depend., vibr. modes 80—100658
GaS, lattice dynamics parameters, X-ray diffr. study *(Russian)* 80—29146
GaS, layer compound, long-wavelength phonons and elastic consts. 80—65175
GaS, layer cpd., lattice dynamics 79—95105
GaS layer crystal, differential indirect exciton spectra 79—8159
GaS layer semiconductor, IR derivative absorpt. spectra 78—6666
GaS, layered, conduction band photoelectron spectroscopy 77—52217
GaS, luminescence excited by high-intensity two-photon pumping 77—44038
GaS, mag. susceptibility anisotropy, chem. bonding *(Russian)* 79—61045
GaS, optical absorption edge under hydrostatic press. 78—23487
GaS, optical and nonlinear optical props. *(Russian)* 79—51943
GaS, optical phonons, IR and Raman scatt. meas. 78—59903
GaS, optimisation of crystal growth conditions by I_2 vapour transport 78—68611
GaS, photoemission props. of III-VI layer compounds 79—65976
GaS, polarisation selection rules for photoemission spectra, test of band struct. calcs. 77—52216
GaS, reflectivity from 4 to 32 eV, Kramers-Kronig anal. 80—34943
GaS, refr. index in far IR, permitt. meas. 78—64360
GaS, refr. index meas. 78—10864
GaS, reson. Brillouin scatt. 80—89010
GaS, semiconductor layer cpds., band struct. calc. using tight-binding method 79—65376
GaS, shallow core level spectra 80—104037
GaS, sp. ht., vibr. spectra and Debye temp. 78—87796
GaS, sp.ht., 2-30K, expt. compared wih theory 78—18791
GaS, space group, determ. by convergent-beam electron diffr. 80—49154
GaS, sputtering conditions effect on film struct. and optical absorption *(Russian)* 77—12525
n-GaS, TSC, electron traps 80—11002
GaS two-photon absorpt., cond. and luminesc. meas. 77—52166
GaS, two-photon photoemission 79—28890
GaS, UPS, polarisation effects 77—12494
GaS, valence and conduction bands, synchrotron radiation photoemission spectra 77—63536
GaS, XPS and valence band density of states, tight binding approx. 78—63974
GaS:Bi_2S_3, photocond. and optical obsorpt. 79—51634
GaS-SmS system, phase diagram 79—78939
GaS-YbS system, phase diagram, reacts., thermal, mag. and elec. meas. 79—11578
Ga_2S, partial vapour press., above Ga_2S_3, anomalous temp. depend. 77—62634
Ga_2S_3, d-electron participation in chem. bonds 77—28682
α-Ga_2S_3, defect semicond., optical absorption meas. 78—15186
Ga_2S_3 glass *(French)* 80—71369
Ga_2S_3, IR refl. spectra, linear chain model for lattice vibrs. 78—27235
Ga_2S_3, partial vapour press. of Ga_2S, anomalous temp. depend. 77—62634
αGa_2S_3, single crystal, lattice phonon exam., Raman and IR spectra of polycrystalline samples *(French)* 78—27229
Ga_2S_3-L_2S_3 system, L=La, Ce, Dy, Er, Y, phase diag. *(French)* 78—3108
Ga_2S_3-La_2S_3-Nd_2S_3:Nd^{3+} chalcogenide glass, Nd^{3+} emission and absorption spectra, nonradiative relax. 77—40268
Ga_2S_3-PbS system, phase diagram and crystallographic study *(French)* 80—29937
Ga_2S_3-R_2S_2, R=rare earth, glasses *(French)* 77—19877
Ga_2S_3-rare earth sulphide glasses, vibr. spectra electronic transitions, short range order 77—69820
GaS_xGe_{1-x}, valence band states, composition depend., photoemission spectra study 80—100434
GaS(Se), polar optical phonon ang. behaviour, IR refl. meas. 80—20633
$GaS_{0.6}Se_{0.4}$, angle resolved UPS, energy band dispersion curves determ. 79—100022
GaS_xSe_{1-x}, grown by iodine vapour transport, X-ray struct. studies 79—4411
GaS_xSe_{1-x}, IR reflectivity and transmission spectra, stacking transform. 77—32371
GaS_xSe_{1-x}, indirect exciton spectrum and phase transition, luminesc. and absorption spectra 79—8160
GaS_xSe_{1-x} layered system, neutron diffr., IR and Raman scatt. 79—87443
GaS_xSe_{1-x}, multiphonon reson. Raman scatt., excitonic transition 77—59574
GaS_xSe_{1-x}, optical phonons, IR and Raman scatt. meas. 78—59903
GaS_xSe_{1-x}, recomb. radiation intensity, temp. depend. *(Russian)* 79—33830
GaS_xSe_{1-x} solid solutions, two-mode behaviour of optical phonons, IR reflect spectra 79—78680
GaS_xSe_{1-x}, two photon absorpt. 77—69841
GaS_xSe_{1-x}, wavefunction symm. and binding energies, synchrotron radiation photoemission spectroscopy 80—50532
$GaS_xSe_{(1-x)}$ solid solns., electrical props. meas. 78—84216
GaS(Se)(Te), electronic struct., tight-binding calcs. 80—15448
$GaS_{1-x}Te_x$, solid soln., single cryst., crystallography and optical props. 79—55711
Ga_2S_2Te, peritectic decomp., Ga_2S_3-Ga_2Te_3 phase diag. *(French)* 78—76635
Ga_2S_2Te, single cryst. X-ray data, struct. determ. *(French)* 79—60316
GaS(Te)(Se), elastic characteristics, Debye temp., ultrasonic study *(Russian)* 80—79872
GaSb, 3d core level spectra, electronic polarisation effects 80—6765
GaSb (100) surface, Sb-induced surface states 78—10529
GaSb (110), chemisorption of Cl, photoemission spectra and tight-binding calcs. 80—6629
GaSb (110), oxidation, initial stages, photoemission study 80—16529
GaSb (110), surface core-level binding-energy shifts 80—103737
GaSb, (110) surface, trned in energy distribs. of Ga dangling orbital surface states 79—28397
GaSb (110) surface and InAs-GaSb (110) interface, electronic states, Green's function technique, tight binding approx. 80—49855
GaSb (110)/Au interface, heat-treated, struct. and chem. state, angle-resolved XPS 80—97400
GaSb, accumulation layer localised carriers interaction with LO phonons, Raman interference lineshapes 80—93338
GaSb, acoustic wave attenuation, phonon viscosity and dislocation drag 80—70319
GaSb, adsorption and desorption of Cs, LEED, AES, and photoemission meas. 80—70532
GaSb, amorphous, optical absorpt. edge shape, band edge fluctuations 77—20880
GaSb, amorphous, two-circle SSD diffractometer appl. in angle dispersive mode 79—14641
GaSb amorphous film, elec. props. *(French)* 78—14843
GaSb and alloys, struct. defect, photoluminesc. 80—25459
GaSb, Anderson-Gruneisen parameter, bulk modulus temp. depend. 78—10154
GaSb, anharmonic force consts. from third order elastic consts. at 300K 77—59074
GaSb, Au overlayer adatom interactions, photoemission obs. 79—33898
GaSb, Auger coeffs. calc. 79—15160
GaSb, Auger recombination, luminesc. meas. 77—85850
GaSb based eutectics, thermal cond. and diffusivity, 300-700K, phonon mechanism 80—103526
GaSb, bound excitons at doubly ionisable acceptors 79—42459
GaSb, bulk and epitaxial, IR reflect. meas., carrier conc. and mobility determ. 80—80769
GaSb, CESR, optical detect. by spin orienation techniques, anal. 78—80251
p-GaSb, CESR, optically detected, giant Overhauser shift 79—4722
GaSb, CVD using organometallics, epitaxial growth 80—29879
GaSb, chemical shift and effective atomic charges 78—88201
GaSb, chemisorption and oxidation states of (110) surfaces 79—24049
GaSb, cond. band L-states, i.r. absorption, uniaxial stress 77—1674
p-GaSb, cond. mechanisms, uniaxial compression effects 77—20312
GaSb, core exciton binding energies 80—80188
n-GaSb, coupled LO-phonon-plasmon modes, Raman spectrum 80—11409
GaSb crystal, phonon dispersion curves, valence force field 78—95121
GaSb, crystal growth by travelling heater method 80—11553
GaSb crystals, uniaxial deform., effect on polarised luminesc. 78—10957
GaSb, cubic cryst., lattice dynamics, overlap shell model and bond charge model 79—42156
GaSb, Debye temperature, atomic mean square displacement 78—87757
GaSb, defect concentration determ. model, Hall effect 80—103385
GaSb, degenerate valence band, diamag. excitons and oscillatory magnetoabsorpt. 77—76754
GaSb, diffusion of In, 520 to 712°C 80—79995

gallium compounds continued

- GaSb, dislocation velocities, double etch technique exam. 78−30629
- GaSb, E_1 and $E_1+\Delta_1$ edges using electroreflectance, Franz-Keldysh oscills., high mag. fields 77−66518
- GaSb, effect of n-doping on Debye temp. 80−2175
- GaSb, elastic scatt. of He^+ ions by atomic chains, screening 80−2915
- p-GaSb, elec. cond., Hall effect, mobility and carrier concentration *(Russian)* 79−19603
- GaSb, electrochemical sectioning and surface finishing 80−108611
- GaSb, electroliquid epitaxial growth 80−89160
- p-GaSb, electron irrad., annealing 77−51407
- GaSb, electron-hole plasma, ground state energy 78−84244
- GaSb, electronic elementary excitations in far UV and X-ray region 79−95346
- GaSb, electrorefl. spectra from 0.6 to 26 eV 77−20825
- GaSb, electroreflectance spectroscopy using synchrotron rad. 78−10912
- GaSb film, gamma-irradiated, struct., TEM and SEM obs. 79−15033
- GaSb film, ion bombard. effects on elemental Sb incorporation probability during sputter deposition 79−83120
- GaSb film, polycrystalline, Hall mobility 80−97015
- GaSb films, amorphous and cryst. vac. evaporated, Elec. cond. thermoelec. power and optical absorpt. 80−2504
- GaSb films, elemental incorporation probability modification by ion bombard. during growth 80−80118
- GaSb films, MBE growth and elec. props. 79−23863
- GaSb, fine struct. in energy derivative reflectance spectra 79−78705
- n-GaSb, galvanomagnetic effects 78−72172
- p-GaSb, heavily doped, LO phonon-carrier interaction, Raman interf. lineshapes 80−93319
- p-GaSb, heavy and light holes scattering 78−91692
- GaSb high temp. thermodynamic data, quantitative fits to liquidus line 77−63637
- GaSb high-purity and doped layers grown by LPE and VPE methods 78−6863
- p-GaSb, hot exciton luminesc., LO phonon Raman scatt. 80−11474
- GaSb, interaction of exciton recombination with LO phonons 79−38647
- GaSb, interband masses of E_1 and $E_1+\Delta_1$ edges 77−32353
- p-GaSb, interband optical pumping, optical detection of EPR 77−28483
- GaSb interface with oxide, photoemission obs. of energy levels induced by adsorpt. 80−93000
- GaSb, inversion of Γ and L conduction bands under uniaxial stress, photoluminescence meas. 79−33229
- GaSb, inverted diode, electron irradiation effect on props. *(Russian)* 78−14378
- GaSb, LEC growth, Hall coeff. 80−89133
- GaSb LEC single crystal growth, novel encapsulant material 80−93475
- GaSb laser, electron beam excited, spectral and power characts. 77−50676
- GaSb, lattice dynamics, phonon freq., bond bending force model calcs. 80−70335
- GaSb, lattice vibration, thermal expansion and pressure effect 80−39233
- n-GaSb, local resist. near dislocations, eqns. 78−60123
- GaSb, MIS struct., C-V characts., interface state densities and storage times meas. 77−89861
- GaSb, manifestation of local vibrs. of dislocations in IR spectra 78−88339
- GaSb, many-valley semiconductor, space charge, contrib. of different charge carriers *(French)* 80−34458
- GaSb mesa photodetectors with very high quantum efficiency between 1.3 and 1.6 μm 80−47102
- GaSb, migration of liq. inclusions, effect of DC current and temp. 77−7910
- GaSb, molten, temp. depend. of vel. of sound and adiabatic compressibility 77−27944
- GaSb, oscillatory magnetoabsorption and excitons 77−55777
- GaSb oxide, anodic, optical props., 1.5-6.0 eV 77−90209
- GaSb oxide films grown by anodization in electrolytes, electron spectroscopy exam. *(German)* 79−15837
- GaSb oxidised surface, detection of excess crystalline Sb by Raman scatt. 78−19453
- GaSb p-n junction as presssure/temp. transducers *(Polish)* 77−67424
- GaSb p-n junction pressure transducer characteristics *(Polish)* 77−89832
- GaSb, p-type, effects of accumulation layer on photocond. *(French)* 77−24582
- GaSb, phonon density of states 79−90744
- GaSb, photoemission investig. of surface states, effects of O_2 and alkali metals 77−48312
- GaSb, photolum., electrolum. meas. in p-n junction, temp. influence 78−72594
- GaSb, photolum. spectra under hydrostatic press. 79−19930
- GaSb, piezoresistive vibrating circular membrane, reflectance light modulation 80−97232
- GaSb, proton range data and deep proton-isolated lasers 79−36923
- GaSb, pulled crystal, microfacet obs. near irregularly remelted surfaces 78−91278
- GaSb pulled crystal, wavy impurity patterns beside twin boundary 78−18674
- GaSb, real surface elec. props., light effects *(French)* 77−72906
- GaSb, relations pressure-volume under high pressure 80−39219
- GaSb, reson. two phonon Raman scatt. near E_1 and $E_1+\Delta_1$ gaps 78−60470
- p-GaSb, saturation characts. over CO_2 laser spectrum 80−83646
- GaSb, Schottky barrier and semicond./insulator interface states formation 80−49906
- GaSb Schottky barrier formation, Fermi-level pinning, defect mech. 78−95358
- GaSb, second order Raman scatt. meas., comparison with photon density of states calc. 77−8579
- GaSb, separate and combined solubilities of donors and acceptors 77−15434
- n-GaSb, Shubnikov-de Haas effect, effective mass, Dingle temp., and g-factor 79−51602
- GaSb, single crystal, stress-induced phase change 79−23720
- GaSb, single crysts., grown by vertical and horizontal travelling heater method, growth parameters and cryst. quality 79−24421
- GaSb, site selective doping by ion implantation of radioactive nuclei 80−34023
- GaSb, solid solns., impact ionisation, cond. and valence band effects 80−65583
- GaSb, sputtered films, on GaAs, growth, Hall effect, impurity levels 80−20334
- n-GaSb, stress-induced elec. props. of point defects, piezoresistance effect 79−56726
- GaSb substrate for Al_2O_3 film, ion beam etching defect detection 80−89155
- GaSb, surface, electron struct. and Fermi level pinning by O_2 and metals 80−11066
- GaSb surface, quantitative XPS meas. 78−56559
- GaSb surface, temp. depend of work function *(French)* 80−6949
- GaSb, surface chemistry and electronic struct., adsorption of O_2, photoemission meas. 77−20985
- n-GaSb, temp. distrib. around dislocations, due to Joule heating, calc. 78−71734
- GaSb, thin film prep. for TEM 77−9027
- GaSb thin layers, directed crystn. on sapphire, props. 80−35111
- GaSb, transport phenomena, review 79−19587
- GaSb, two-phonon diffuse scatt. of X-rays 78−26374
- GaSb, UPS, 5-450 eV, surface states, oxidation behaviour 77−66579
- GaSb, undoped, impurity band parameters calc. 79−51516
- GaSb, undoped, intrinsic acceptors, parameters determ. 79−51515
- GaSb, valence band structure, CPA, bond orbital calcs. 78−87909
- GaSb, vibr. spectra, lattice dynamics ang. force model 80−29127
- GaSb:Cd(Te)(Zn), carrier density dependence on impurity conc., rel. to solubility limit 77−8047
- GaSb:Cd(Zn)(Se)(Te), thermal sensitivity, −170 to +180°C, resist. meas. 77−39906
- GaSb:Fe, shallow acceptor level, electrical meas. 79−11087
- GaSb:Gd(Yb), elec. props., dopant effects 79−87115
- GaSb:Li, dopant behaviour 77−51696
- GaSb:Mn(Sm), struct., thermo EMF, galvanomag. props. rel. to dopants, eutectic $Mn_{0.6}Ga_{0.4}Sb$ form. 77−15869
- GaSb:S, cond. and Hall coeff. relax., impurity config. model 80−6786
- n-GaSb:S, inhomogeneous, temp. depend. of elec. resist. 78−2482
- n-GaSb:S, thermal quenching of residual cond. 78−56188
- n-GaSb:S-metal surface barrier struct., elec. and photoelec. props. 78−56229
- n-GaSb:Se, resonant and bound impurity states, Hall effect and resistivity press. depend. 77−28143
- GaSb:Sn, p-n junction, electroluminesc. and photoluminesc. 80−66306
- p-GaSb:Te, effective radiative recombination centre nature, photoluminescence spectra 79−90998
- n-GaSb:Te, elec. transport mechanism in cond. band from Hall mobility and transverse mangetoresist. meas. 79−73531
- n-GaSb:Te, Hall coeff., carrier conc. and mobility, elec. cond., 290 to 550K *(Russian)* 79−19604
- n-GaSb:Te, heavily doped, electron-hole recomb., photoluminesc. spectra 78−84644
- n-GaSb:Te, heavily doped, spontaneous radiative recomb. vel., photoluminesc. spectra 79−11458
- GaSb:Te, indirect gap photolum. 80−29797
- GaSb:Te,Zn(Te,Mn), prep. and electrophys. props. 79−87116
- n-GaSb:Te(Se), forbidden optical band gap, Moss-Burstein effect 78−88335
- p-GaSb:Zn, hole transport props. from 77 to 300K 79−73530
- p-GaSb:Zn film, epitaxial, lifetime of nonequilib. carriers, determ. from circular polarisation of luminesc. 77−24898
- GaSb/InSb superlattice thin films, sputtered, ion-bombardment-enhanced diffusion during growth 78−87882
- GaSb-Ag, phase diag. 77−90327
- GaSb-anodic oxide MOS struct. oxide and interface props. 79−60929
- GaSb-Au contacts, interface struct., technology rel. to elec. props. *(German)* 77−72915
- GaSb-Au Schottky barriers, PES and depth profiling obs. 79−42641
- GaSb-Au structure, metal-semicond. interaction, soft XPS meas. 78−60203
- GaSb-Bi system, molten, enthalpy change due to mixing *(German)* 79−86892
- GaSb-$Ga_{1-x}In_xSb$ p-n heterojunction, electrolum. spectra and elec. props. 77−12444
- GaSb-GaAs-Ge system, props. and struct. 80−20232
- GaSb-Ge eutectic alloy, effect of crystallisation rate on microhardness 79−96110
- GaSb-InAs (001) superlattice, electronic struct., tight binding calcs. 78−95350
- GaSb-InAs (001) superlattices, two-dimens. effects and effective masses 80−49883
- GaSb-InAs (100) superlattice, electronic struct., self-consistent pseudopot. method 80−49884
- GaSb-InAs heterojunction, photoelec. props. 77−28245
- GaSb-InAs heterostruct. superlattice, props. in high mag. fields 79−73570
- GaSb-InAs superlattices, two-dim. electronic structure 78−75995
- GaSb-InAs superlattice, semiconductor-semimetal transition obs. 80−44710
- GaSb-InAs superlattices, crystallography, Rutherford backscatt. and channelling obs. 80−49533
- GaSb-InAs superlattices, semicond.-semimetal transition obs. 80−49882
- GaSb-InAs system, (110) surface and interface electronic struct. 80−100494
- GaSb-InSb solid solns., heavily doped, electronic props. 77−80727
- GaSb-InSb(AlSb), liq., mixing enthalpies *(German)* 79−77755
- GaSb-Pb junction, Ar ion bombard. effect on tunnelling props. 80−54783
- GaSb-Zn(Cd)Te, quasibinary system, phase equilibrium, intermol. interaction 77−12601
- $GaSb_{1-x}As_x$, disorder-enhanced Auger recomb. 79−43014
- $GaSb_{1-x}As_x$, MBE RHEED meas. 78−18916
- $GaSb_{1-x}As_x$-$In_{1-x}Ga_xAs$ heterojunction, prep. by MBE, transport props. 77−80827
- $GaSb_{1-y}As_y$ alloy surface states obs., using electron energy loss spectra 79−15202
- $GaSb_{1-y}As_y$, MBE-grown, substrate effect on lattice consts. 79−77942
- $GaSb_xAs_{1-x}$ films, MBE growth and elec. props. 79−23863
- $(GaSb)_{1-x}Ge_x$ films, single-cryst. metastable semicond., growth and phase stability 80−80115
- p-GaSb−n-$Ga_{1-x}Al_xSb$, photodiode, LPE, spectral response, quantum efficiency 78−47850
- GaSe, ^{110}Ag diffusion, temp. depend. and solution *(Russian)* 80−70467

gallium compounds continued
GaSe, 4 to 12 μm tunable down-conversion from $LiNbO_3$ parametric oscillator 78−66865
GaSe, absorpt. and electroabsorpt. near indirect edge 77−20827
GaSe, absorpt. edge, exciton levels and Raman scatt., press. effects above 40 kbar 77−48187
GaSe, absorpt. spectra, electron-hole system at high densities 77−69854
GaSe, additional IR electrolum. band obs. at 77K 78−72607
GaSe, angle resolved UPS, energy band dispersion curves determ. 79−100022
GaSe, anisotropy effects on electroreflectance spectra at oblique incidence 77−52042
GaSe, anodic film form., in situ ellipsometric study 80−104318
GaSe, anodic oxide films, two-dimens. nucleation and growth 80−11807
p-GaSe, back wall Schottky barrier cells, diffusion length, RT spectral response meas. 80−107806
GaSe, band struct., tight-binding calc. 77−80729
GaSe, band struct. and electron density of states in two-dimens. approx. 79−37987
GaSe, band struct. from ang. resolved photoemission 77−59673
GaSe, band structure calc., semi-empirical tight-binding method 77−47726
GaSe, basal plane orientation determ. in vertical Bridgman grown single crysts. 78−19658
GaSe based layer crystals, three dimensional electron state nature near absorpt. edge 79−90960
GaSe, birefringent layer cryst., indices of refraction 77−20815
GaSe, Brillouin scatt. by pure transverse phonons 79−78696
GaSe, cascade resonant Raman processes 80−25385
GaSe, cathodolum., 115 and 285K 79−87512
GaSe, constant current anodisation, representation of layer periodicity 80−3218
GaSe, core level excitation effects, synchrotron radiation UPS study 80−40234
GaSe, core-level photoemission anisotropy 78−11076
GaSe, deep free and constrained excitons and biexcitons, collective interactions *(Russian)* 80−66282
GaSe, direct and indirect two photon processes 77−40261
GaSe, direct exciton excited state hot luminescence, band struct. props. 80−55183
GaSe, down-conversion of $LiNbO_3$ optical parametric oscillator output, 4 to 18 μm 79−86215
GaSe, electron beam excited free exciton luminesc. 79−19940
GaSe, electron spectroscopy, energy loss and photoemission 78−72682
GaSe, electron-phonon interaction and optical props. 80−34942
GaSe, excitation spectra and structural props., X-ray Laue diagrams and optical transmission *(French)* 80−50358
GaSe, exciton, excitation-induced absorption and luminesc. 78−60516
GaSe exciton absorpt., change under a pulsed dye laser 78−92088
GaSe, exciton absorpt. spectra, additional light wave 77−63445
GaSe, exciton absorption under intense excitation 77−77235
GaSe, exciton absorption spectrum, polariton effects 77−85747
GaSe, exciton luminesc. kinetics, intermediate electron-hole states 80−93389
GaSe, exciton magneto-optical spectra 80−25347
GaSe, exciton spectra at 4.2K rel. to layer struct. 77−16336
GaSe, exciton-phonon bound state, photocond. and visible absorpt. spectra obs. 80−50369
GaSe, exciton-phonon quasibound states, photocond. and luminesc. study 80−96800
GaSe excitonic spectra fine struct., reflection and transmission spectra *(Russian)* 80−55126
GaSe, factor-group analysis of high-symmetry layer dynamics 79−42160
GaSe, Faraday rot. near absorpt. edge, optical dispersion meas. 80−80757
GaSe film, amorphous, I-V characts. in strong elec. fields, 173-373K 78−56248
GaSe film, charge transport models *(Russian)* 78−60233
GaSe film, structure, influence of laser beam 79−7761
GaSe films, optical props. at lattice vibr. freqs., IR and Raman spectra 80−60696
ε-GaSe films, optical props. in IR region, metal substrate effect 80−71502
GaSe, fine struct. of exciton spectrum 78−39567
GaSe, group theoretical anal. of phonon assisted optical transition 78−39564
GaSe, growth by I_2 vapour transport using temp. oscill. method 77−77355
GaSe, growth of crysts. with natural facets at large angles to layers 78−15305
GaSe, Hall mobility anisotropy 78−68041
GaSe, high resistivity, electric field stimulated conduction 77−66172
GaSe, highly excited, polarisation of luminesc. spectra and electron-hole plasma radiation 77−52169
GaSe, highly excited photoluminesc. exciton-exciton and exciton-carrier scatt. 77−48244
n-GaSe, hopping and impurity cond. anomalies 77−59287
GaSe, impurity photocond., induced illumination corresponding to fundamental absorption region 80−92933
GaSe, interlayer interaction and exciton spectra study 77−52165
GaSe, isolated layer model, lattice dynamics and elastic props. 80−24547
GaSe, lamellar crystal, exciton translational mass from magneto-Stark effect *(Russian)* 78−48153
GaSe, lattice dynamics, in one-layer approach 79−14900
GaSe, lattice dynamics and elastic props., Born-von Karman model study 80−70337
GaSe, lattice dynamics parameters, X-ray diffr. study *(Russian)* 80−29146
GaSe, layer, upper valence bands using bond-orbital model 79−15078
GaSe, layer compound, long-wavelength phonons and elastic consts. 80−65175
GaSe, layer compounds, lattice instability, deformation dipole model 80−39249
GaSe, layer cryst., elastic props. rel. to zone-centre phonon freqs. 79−46736
GaSe layer semiconductor, IR derivative absorpt. spectra 78−6666
GaSe, layer struct., fine independent elastic const. using Brillouin scatt. 79−19896
GaSe, layered, conduction band, photoelectron spectroscopy 77−52217

gallium compounds continued
GaSe, layered, DC hopping cond. due to stacking disorder and electron localisation 77−47819
GaSe, layered, electronic band struct., direct evaluation by angle resolved photoemission 77−51652
GaSe, layered, photoelectromag. effect meas. of transport parameters 77−59301
GaSe layers, band struct. and state density calc. by empirical tight-binding method 79−42443
GaSe, long wavelength IR refl. spectra 80−11401
ε-GaSe, long-wavelength lattice vibr. 80−92631
GaSe, luminesc. emitted by electron-hole plasma 77−85795
GaSe, luminesc. from exciton-electron and exciton-exciton collisions 77−52168
GaSe, luminescence and absorpt. spectrum in region of high-energy resonance 77−44044
GaSe, luminescence excited by high-intensity two-photon pumping 77−44038
GaSe MSM struct., inelastic tunnelling investigation of lattice dynamics, electron-phonon interaction 80−20330
GaSe, mag. susceptibility anisotropy, chem. bonding *(Russian)* 79−61045
GaSe, magnetoluminesc. at 4.2K 79−61345
p-GaSe, monocrystal, temp. depend. of mechanical strength *(Russian)* 79−10892
GaSe, multiphonon reson. Raman scatt., excitonic transition 77−59574
GaSe, multiple-phonon reson. Raman scatt. processes 77−4634
p-GaSe, negative residual photoconductivity 79−51632
GaSe, nonlinear cryst., IR parametric image conversion from 10 μm to near-IR 79−89970
GaSe, nonlinear susceptibility, SHG 78−30019
GaSe, one-carrier SCl currents in solid with two sets of traps distributed in energy 78−72158
GaSe, optical and nonlinear optical props. *(Russian)* 79−51943
GaSe, optical consts. at fundamental absorpt. edge 77−66471
GaSe, optical detection of triplet exciton reson. 79−33567
GaSe, optical excitation, excitonic spectra, stimulated luminesc. 80−40132
GaSe, optical orientation and free exciton alignment on reson. excitation *(Russian)* 77−69812
GaSe, optical orientation and alignment of free excitons, on resonant excitation *(Russian)* 77−90196
GaSe, optical phonons, IR and Raman scatt. meas. 78−59903
GaSe, optimisation of crystal growth conditions by I_2 vapour transport 78−68611
GaSe, photocond., influence of stacking disorder 80−2422
GaSe, photocond. at high excitation rates 78−52036
n-GaSe, photoconductivity and TSC investig. of trapping centres 77−20359
GaSe, photoemission props. of III-VI layer compounds 79−65976
GaSe, photolum. decay 79−15518
GaSe, photolum. under strong optical excitation 79−24364
GaSe, photoluminescence between 4.2 and 40K 78−10974
n-GaSe, photomagnetoelec. and photocond. current spectral distrib. 79−42585
n-GaSe, photomagnetoelectric effect, photocond., in presence of traps 80−39631
GaSe, photosensitivity anisotropy in polarised light, pleochroism coeff., suitability as photoelec. analysers 79−60873
GaSe, photovoltaic spectra 80−20240
GaSe, photoyield reson. enhancement near Se 3d core threshold, photoelectron spectra obs. 80−45207
GaSe plate in elec. field, photostimulated ocills. 79−65799
GaSe, Pockels effect 79−51933
GaSe, polarisation selection rules for photoemission spectra, test of band struct. calcs. 77−52216
GaSe, polarized exciton luminesc. 78−6734
GaSe polytypes, electronic band struct. calcs. 77−51650
GaSe polytypes, tight binding study of electronic states 79−60705
GaSe, population dynamics and spin relax. of excitons 77−66122
GaSe, press. induced metallic and supercond. state 80−75666
GaSe, pressure-induced polytypic transforms. and edge absorpt., exciton lines 77−28595
GaSe, radiative decay of direct and indirect excitons 78−10975
GaSe, radiative transitions, cathodoluminescence 78−10997
ε-GaSe, Raman scatt., hydrostatic press. effect 80−84745
GaSe, reflectivity from 4 to 32 eV, Kramers-Kronig anal. 80−34943
GaSe, refr. index 0.45 to 330 μm, interf. and refl. meas. methods 77−63387
GaSe, refr. index meas., temp. variation 300 to 75K 80−25328
GaSe, refr. index meas. 78−10864
p-GaSe, resist. and Hall-mobility meas. at 77-850K 77−59295
p-GaSe, resistivity, anisotropy 77 to 750K 79−4559
GaSe, reson. Brillouin scatt. 80−89010
GaSe, SHG, absorpt. coeffs. and temp. variation of refr. index difference 80−14390
GaSe, semiconductor layer cpds., band struct. calc. using tight-binding method 79−65376
GaSe, semiconductor-metal contact, photovoltaic props. 77−59330
GaSe, shallow core level spectra 80−104037
GaSe, single cryst., dispersion of refr. indices and exciton absorption 79−73947
p-GaSe, single cryst., negative photocond. induced by elec. field 79−19623
GaSe, sp. ht., vibr. spectra and Debye temp. 78−87796
GaSe, space-charge-limited currents at different temps. 77−43607
GaSe, spatial symm. of valence band struct. by angularly resolved XPS 77−69961
GaSe, spontaneous and stimulated emissions due to exciton-electron and exciton-exciton collisions 77−32421
GaSe sputtered film microhardness, influence of gas discharge *(Russian)* 80−49560
GaSe, stacking disorder effect on Wannier excitons 77−62834
GaSe, stimulated eimission due to electron-hole plasma recomb. 80−50374
GaSe, thin film, photoelectrical props. at high electric field *(Russian)* 79−11247
GaSe thin films, electroabsorpt. spectra, exciton line splitting 80−107716
GaSe, thin layers, far IR refractive index 80−80799
GaSe, triplet excitons ODMR 80−25252

gallium compounds continued
GaSe, triplet indirect bound exciton, level anticrossing effect on magnetolum. 79—47513
GaSe, tunable medium IR source, difference freq. mixing of Nd^{3+}:YAG and dye lasers 79—55183
GaSe, two and three dimensionality of electron states, normal photoemission obs. 77—32503
GaSe, two-photon absorpt., cond. and luminesc. meas. 77—52166
GaSe, type II crysts., triplet exciton resonances 79—47359
GaSe, UPS, polarisation effects 77—12494
GaSe, valence and conduction bands, synchrotron radiation photoemission spectra 77—63536
GaSe, valence band struct., angle-resolved photoemission spectroscopy 77—1360
GaSe, wave function symmetries of valence band states revealed by polarisation effects in angle-integrated photoemission spectroscopy 79—67395
GaSe, zone-centre optical phonons, Raman scatt. meas. 78—10141
GaSe:Cu(Cd, Sb), photovoltaic spectra 80—20240
n-GaSe:I, SCL currents, expt. test of theory for insulator with two sets of traps distribution in energy 77—89768
GaSe:Mn, ESR spectra, influence of temp. and antiferromag. inclusions 79—99763
GaSe:Sn, ^{113}Sn diffusion, temp. depend. and Sn solubility *(Russian)* 80—70466
p-GaSe:Sn, majority carrier drift mobility meas. 80—92895
GaSe:Sn, single crystal, transient photoconductivity *(Russian)* 79—11171
GaSe:Sn, single crystal, space-charge-limited currents *(Russian)* 80—11001
GaSe-InSe, heterojunction, electronic processes *(Russian)* 79—56312
GaSe-InSe, heterostructure fabrication using laser radiation 79—73580
GaSe-SnO_2 heterojunction, elec. props. and electrolum. spectra 77—59328
GaSe-SnO_2 heterojunction photocell, fine struct. of photo-EMF spectra 80—6967
GaSe-SnO_2 heterojunctions, photoelec. props. 80—96945
GaSe-SnO_2 spray heterojunction, electro-optical props. 78—64102
GaSe-SnSe system, phase diagram and lattice consts. of solid solns. 79—34014
Ga_2Se_2, sublimation growth, closed tube, mass flow and press. meas. 77—63550
$\alpha(\beta)$-Ga_2Se_3, cryst. growth, optical, X-ray diffr. and SEM study 80—71587
β-Ga_2Se_3, cryst. struct. 77—27862
Ga_2Se_3, evaporation, thermodynamic props. 80—54365
Ga_2Se_3, film, electrical and optical props. 77—1505
Ga_2Se_3, IR refl. spectra, linear chain model for lattice vibrs. 78—27235
Ga_2Se_3, physical properties, application as lens or laser window materials 79—98450
Ga_2Se_3 semiconductor, basis of ionising radiation detectors 78—86743
Ga_2Se_3, single cryst., bistable cond. switching effect 77—51783
Ga_2Se_3, solid solution, elec. cond. 80—88301
Ga_2Se_3, vapour phase deposited films, struct. 78—2383
Ga_2Se_3-FeSe, phase diagram, elec. cond., mag. susceptibility 80—88301
Ga_2Se_3-Ga_2S_3 solid solutions, IR refl. spectra, linear chain model for lattice vibrs. 78—27235
Ga_2Se_3-In_2Se_3, semiconducting props. of four stable phases 77—55528
Ga_2Se_3-In_2Se_3 solid solution system, X-ray diffr. exam. 77—63639
Ga_2Se_3-MnSe system, crystallographic study, phase diagram, DTA and X-ray diffr. determ. *(French)* 79—24506
Ga_xSe_{1-x}-SnO_2 heterostruct., amorphous, photovoltaic effect 78—14803
GaSe(S), layer dynamics of high-symmetry crystals with atom-atom interactions 78—71799
$GaSe_{1-x}S_x$, magnetic susceptibility anisotropy, chemical bonds, electron density distribution *(Russian)* 80—50073
$GaSe_{1-x}S_x$, polytypes, exciton gap energies, luminesc. study 80—54611
$GaSe_{1-x}S_x$, stimulated photoluminesc. excitons role 77—48201
$GaSe_{1-x}S_x$, struct. transition, Raman scatt. obs. 79—99888
$GaSe_xS_{1-x}$, layered semicond., electroabsorpt. in fundamental absorpt. edge region 77—52043
$GaSe_xS_{1-x}$, X-ray diffr. investig. of stacking sequences 77—43198
GaSe(Te), optical spectra in 2 to 50 eV range 78—10915
$GaSe_{0.9}Te_{0.1}$, undulation spectra associated with acceptor complexes 78—80392
$GaSe_{1-x}Te_x$, energy bands near absorpt. edge, transmission and photoluminesc. spectra 79—83022
$GaSe_{1-x}Te_x$ layered crystal, photoluminesc. meas. 77—1725
$GaSe_{1-x}Te_x$, Raman scatt., optical phonons and phase transition 80—66202
$GaSe_{1-x}Te_x$, Raman spectra, phonon freq. 80—97286
$GaSe_{1-x}Te_x$, room temp. electroreflectance meas. 77—12361
$GaSe_{1-x}Te_x$, zone-centre optical phonons, Raman scatt. meas. 78—10141
$GaSe_xTe_{1-x}$ mixed crystals, near-band-edge optical props., absorption edge spectra 79—61401
$GaSe_xTe_{1-x}$, solid solns., exciton luminesc. 78—10992
Ga_6SnTe_{10}, cryst. struct. *(French)* 79—78946
GaTe, ^{110}Ag diffusion, temp. depend. and solution *(Russian)* 80—70467
GaTe, cryst. struct., TEM and X-ray diffr. study 80—79757
GaTe, cryst. struct. *(French)* 79—78946
GaTe, exciton polariton effect on absorpt. edge, absorpt. and refl. spectra, 4.2 to 300K 80—20664
GaTe, exciton polariton effect on absorpt. edge, thickness depend. of absorpt. 80—20665
GaTe, excitonic absorpt. edge, transmission and refl. meas. 80—40133
GaTe film, amorphous and polycryst., memory effects 77—20368
GaTe, Hall mobility, resistivity anisotropy 79—11150
GaTe, hexagonal, vacuum deposited, physical parameters and substruct. 78—2393
GaTe, laser modulated reflectance meas. 77—63424
GaTe, layer cryst., polarised IR refl. spectra 80—97279
GaTe layer semiconductor, UV-visible wavelength derivative and thermorefl. spectra 78—6666
GaTe, long wavelength phonons, Raman and far IR spectra obs. 79—69210
GaTe monocrystal, far IR polarised complex reflectivity obs. 80—60609
GaTe, reflectivity, 1-35 eV, electron props. determ. 77—20872
GaTe, resist. anisotropy in layer plane 79—51581
p-GaTe, scatt. by homopolar optical phonons, Hall effect meas. 77—28197
GaTe, Schottky barrier, photovoltaic props. 79—7854

gallium compounds continued
α-GaTe, single cryst., Raman scatt. 80—60599
GaTe, single cryst. prep. and electroabsorpt. spectra investig. 80—103968
α-GaTe single crystals, Raman spectra 79—99883
GaTe, sp. ht., vibr. spectra and Debye temp. 78—87796
GaTe, transport anisotropy 79—23975
GaTe, transport properties under hydrostatic pressure 80—75589
GaTe, vibr. spectrum 77—89513
GaTe, X-ray cryst. struct. determ., direct method *(French)* 80—28956
GaTe, zone-centre optical phonons, Raman scatt. meas. 78—10141
GaTe:Sn, electroabsorption spectra 79—19901
GaTe-SnO_2 heterojunctions, photoelec. props. 80—96945
GaTe-SnO_2 spray heterojunction, electro-optical props. 78—64102
GaTe-SnTe, melt, temp. and composition dependence of elec. cond. and thermo EMF 79—95430
GaTe-SnTe, phase equilib. 77—86006
$Ga_{0.25}Te_{0.75}$ amorphous film, time evolution of nanosecond switching 80—6921
$Ga_{0.25}Te_{0.75}$ amorphous film, nanosecond switching, resist. fluctuations in low-resist. state 80—44676
$Ga_{0.25}Te_{0.75}$, amorphous film, off-state recovery after nonosecond switching 80—44681
$Ga_{1-x}Te_x$ amorphous films, elec. cond., optical absorpt. and transparency, band gap energy 79—56335
$Ga_{20}Te_{80}$, amorphous, splat cooled, thermoelectric props. 78—43426
Ga_2Te_3, liq., elec. resistivity meas. up to 30 kbar 79—38070
Ga_2Te_3, nuclear gamma resonance of ^{57}Fe, isomer shift scale construction *(Russian)* 78—35070
Ga_2Te_3, physical properties, application as lens or laser window materials 79—98450
Ga_2Te_3 semiconductor, basis of ionising radiation detectors 78—86743
Ga_2Te_3, single cryst., elec. cond. meas.. 79—11124
Ga_2Te_3 single crystals, switching effect., carrier trapping 80—6919
Ga_2Te_3, vapour phase deposited films, struct. 78—2383
Ga_2Te_3:Sn, impurity atom electron shell compression by matrix *(Russian)* 77—28146
Ga_2Te_3-Cu system solid solns., elec. cond. 78—51988
Ga_2Te_5, cryst. struct. *(French)* 77—72589
Ga_2Te_5, cryst. struct. *(French)* 79—78946
$GaTe_{1-x}Se_x$, exciton spectrum nature and anisotropy of electron bands near absorption edge *(Russian)* 79—51483
p-$GaTe_xSe_{1-x}$, resistivity and Hall effect meas. 77—24556
$Ga_4Ti_{x-4}O_{2x-2}$ (where x=odd) type structures, rel. between rutile, β-gallia, hollandite psilomelane type structs. 79—37664
Ga_xVO_2, reduced, microstruct., crystallographic shear planes, electron microscope obs. 79—1443
$Ga_xV_{1-x}O_2$, resistivity, EPR, enthalpy and entropy meas., rel. to semicond.-metal transition 78—88004
$(Ga_xV_{1-x})_2O_3$, impurity doping effects, elec. props. obs. 80—75609
GaYIG, magnetoelastic surface wave attenuation 77—20667
^{67}Ga citrate, use in detect. and follow-up of extrapulmonary tuberculosis 80—46012
^{67}Ga-citrate images obtained with rectilinear scanner and large-field Anger camera 77—66841
Gal, Brillouin spectra, light scatt. cross section for surface ripples 80—71434
Gap-Ge, compensated, photosensitivity 79—19624
GdGa garnet, Czochralski grown, substrate material dislocation propagation 78—59771
GdGa garnet, microwave losses 77—4531
$Gd_3Ga_5O_{12}$, garnet substrate, surface polishing, damage, abrasion, brittle fracture model *(German)* 77—73357
$Gd_3Ga_5O_{12}$, garnet substrate surfaces, working damage, electron microscope investig. 77—77605
Gd_2O_3-Ga_2O_3 system, phase diagram relationships of garnet-perovskite transform. 80—97460
GdTmGa garnet bubble film, ion implanted, pot. wells under charged wells 80—34717
p-Ge in DMF solns., electrochem., photoelectrochem., redox. pot. determ. 79—96322
Ge-GaP system, phase analysis 78—23674
Ge-GaSb, metastable continuous solid solutions 79—8284
Ge-In-Ga system, microscopic and X-ray phase anal. 77—12606
Ge-S-Ga amorphous thin film, memory switching effects 80—88605
Ge-S-Ga system glasses, photoinduced changes 80—24365
Ge-Se-Ga system glasses, vitreous phase struct. 77—76320
n-$Ge_{1-x}Al_xAs$:Te, long-lifetime photocond. effect obs., Hall effect meas. 77—89795
$Ge_{1-x}(GaSb)_x$, metastable solid solution, fine struct. *(Russian)* 79—27960
$(Ge_{1-x}Ga_x)_{1-x}Te$, rhombohedral and cubic phases, transport effects 78—2481
GeS_2, single crystal, far IR transmission 80—80800
Ge_4Se_5Te, amorphous layers, charge carrier transport mechanism 80—54708
GeTe-Ga_2Te_3, electrophys. props. 77—48403
$HgCr_{2-x}Ga_xSe_4$, temp. depend. of ESR linewidth, 105-300K 80—71161
$HgGa_2S_4$, energy band struct. calc., empirical pseudopot. method 80—24793
$HgGa_2Se_4$, energy band struct. calc., empirical pseudopot. method 80—24793
HoGa garnet, mag. ordering induced by hyperfine interaction, neutron diffr. meas. 77—66265
(In, Ga)Sb, sputter deposited amorphous film, impulse stimulated explosive crystallisation 78—84098
In-Ga-As-P, phase diagram rel. to lattice matched LPE 78—39708
In-Ga-P ternary system, low temp. phase diagram rel. to epitaxial growth 80—84916
In-GaP, phase diag. cross section 77—48410
In-In-P-GaP, liquidus surface obs. 78—22829
InAs/GaSb (001) superlattices, electronic struct., two dimensional effects 80—11064
InAs-$Al_xGa_{1-x}Sb$ heterojunctions, elec. and photoelec. props. 79—11206
InAs-GaSb superlattice energy struct. and semiconductor-semimetal transition 79—23893
InAs-GaSb superlattice, cyclotron resonance, energy level quantisation 79—73430
InAs-GaSb superlattice, electronic struct., self-consistent pseudopot. calc. 80—29470
InAs-GaSb superlattices, mag. field induced semimetal-semicond. transition 80—65656

gallium compounds continued
InAsSb/GaSb broad-spectral-band IR detector, backside-illum. heterostructure approach 80−73450
InGa-GaSe interface, microplasma electrolum. at 300K 79−11469
InGaAs p-n junction, carrier multiplication and ionisation coefficients 77−8188
(InGaAs)/(InGa)P, DH laser, threshold current temp. depend. 79−81431
InGaAs-GaSbAs periodic structures, with controlled emission 79−7880
InGaAs-InGaP vapour-grown ternary heterojunction laser struct., reliability 79−98385
$In_{1-x}Ga_xAs$-$GaSb_{1-y}As_y$ superlattice, optical absorption 79−19887
$In_{1-x}Ga_xAs$ alloy surface states obs., using electron energy loss spectra 79−15202
$In_{1-x}Ga_xAs$-$GaSb_{1-y}As_y$ superlattice, with nonlinear energy-wave and energy-momentum relationships 79−7871
$In_xGa_{1-x}As$-$In_yGa_{1-y}P$ DH laser, CW room temp. operation at 1.06 μm 77−19250
InGaAsP avalanche photodiodes, leakage current, shot noise, quantum efficiency, gain saturation 79−67381
InGaAsP avalanche photodiode, 1.3 μm, noise performance, −190°C 80−57370
InGaAsP avalanche photodiodes, breakdown mechanism, donor conc. effect 80−70710
InGaAsP, bandgap energy by electroreflectance and photoluminesc. spectra 80−107700
InGaAsP DH, luminesc., quantum efficiency determ. 80−108273
InGaAsP, dual-wavelength demultiplexing photodiode 79−63304
InGaAsP heterojunction cathode, transferred electron photoemission 78−48272
InGaAsP IR heterojunction photodiode detector 79−21813
InGaAsP, LPE, diffusion-limited step-cooling technique, layer thickness and composition 80−84402
InGaAsP, LPE growth, orientation depend. of incorporation of Ga, As, and Zn 78−6869
InGaAsP, LPE growth on InP, influence of lattice mismatch on surface morphology 79−1553
InGaAsP, LPE growth techniques influence on composition 79−52130
InGaAsP LPE heterostructs., interface grading, Auger depth profile 80−103585
InGaAsP LPE layers on InP substrate, material selective chemical etching 79−70188
InGaAsP, lattice matched, LPE growth on (100) InP, for 1.15-1.31 μm spectral region 78−64483
InGaAsP low-threshold 1.25-μm vapour grown CW lasers, emission characts. 79−50308
p-InGaAsP, on InP surface, diffusion coeff. and surface recombination velocity 80−39598
InGaAsP, quaternary alloy, physical props. *(Japanese)* 80−15449
InGaAsP strip-buried heterostructure laser, high output power, operation 80−58559
InGaAsP, with and without InP cladding layers, low photolum. regions 79−33754
InGaAsP:Be, avalanche photodetectors annealing temp. effect on photolum. spectra 79−69872
InGaAsP:Be ion-implanted avalanche photodiode, struct. and characts. 79−17487
InGaAsP:Sn(Te)(Zn), LPE growth, influence of growth-solution dopants on distrib. coeffs. 79−47640
InGaAsP/InP, native oxide stripe laser 79−68405
InGaAsP/InP avalanche photodiode, ionisation coeff. 80−15590
InGaAsP/InP DH, vapour phase growth by dual-growth-chamber method 80−50559
InGaAsP/InP DH lasers, Zn doping level 79−98373
InGaAsP/InP DH laser, self-aligned struct. 80−9893
InGaAsP/InP heterojunction, X-ray characterisation of defects 78−95239
InGaAsP-InP, Zn diffused DH structures, oxide defined transverse junction stripe lasers 79−98389
InGaAsP-InP buried heterostructure lasers emitting at 1.3 μm, accelerated ageing characts. 80−95898
InGaAsP-InP DH laser, room temp. operation, 1.27 μm emission 77−88743
InGaAsP-InP DH laser, optical gain meas., low-intensity luminesc. and absorpt. spectra 79−98356
InGaAsP-InP DH lasers, low temp. behaviour of threshold current and carrier lifetime 79−98374
InGaAsP-InP DH laser with self-aligned struct., oscillation characts. 80−38017
InGaAsP-InP DH laser, 1.55 μm, low temp. LPE growth for room-temp. CW operation 80−64045
InGaAsP-InP DH LED, high temp. aged, dark-spot defects, TEM obs. 80−66300
InGaAsP-InP DH lasers, perturbed InP growth, photoluminesc. study 80−106518
InGaAsP-InP DH laser, threshold current, temp. depend. 80−106521
InGaAsP-InP heterojunction, LPE, lattice mismatch, Auger depth profile 79−87005
InGaAsP-InP high-gain heterojunction phototransistor 80−103745
InGaAsP-InP laser, LPE, 1.5 μm range, effects of double cladding struct. 80−48290
InGaAsP-InP lattice matched DH, growth by two-phase supercooled soln. technique 78−10296
InGaAsP-InP layers, grown by LPE techniques, lattice const., bandgap, thickness and surface morphology meas. 80−59818
InGaAsP-InP vapour-grown quaternary heterojunction laser struct., reliability 79−98385
$In_{0.79}Ga_{0.21}As_{0.54}P_{0.46}$, LPE layer, electroreflectance meas. 79−24290
$In_{0.85}Ga_{0.15}As_{0.39}P_{0.61}$, deep impurity levels 79−87058
$In_{1-x}Ga_xAs_xP_{1-y}$, p-n junction diodes, fabrication by Be ion implantation 79−47156
n-$In_{1-x}Ga_xAs_yP_{1-y}$, cyclotron reson., cond. band nonparabolicity 80−29311
$In_{1-x}Ga_xAs_yP_{1-y}$, DH laser material, spatially resolved photolum. characterisation and optically induced degradation 79−47486
$In_{1-x}Ga_xAs_yP_{1-y}$, electron effective mass from Shubnikov-de Haas meas. 80−80298
$In_{1-x}Ga_xAs_yP_{1-y}$ epitaxial layer, far IR refl. spectra, lattice vibrs. 80−97282
$In_{1-x}Ga_xAs_yP_{1-y}$, evidence for alloy scatt. from press. induced changes of electron mobility 80−88548

gallium compounds continued
$In_{1-x}Ga_xAs_yP_{1-y}$, Hall mobility, comp. depend. 80−75587
$In_{1-x}Ga_xAs_yP_{1-y}$, hole mobility over temp. range 77 to 300K 80−60111
$In_{1-x}Ga_xAs_yP_{1-y}$, LPE growth on InP (100), lattice matched composition 78−87881
$In_{1-x}Ga_xAs_yP_{1-y}$ LPE layers, background carrier conc. and electron mobility. 79−95523
$In_{1-x}Ga_xAs_yP_{1-y}$, lattice vibrs., Raman study 78−91391
$In_{1-x}Ga_xAs_yP_{1-y}$, lattice matched to InP, band gap vs. comp., and Vegard's law demonstration 79−7782
$In_{1-x}Ga_xAs_yP_{1-y}$, oscillatory magneto-transmission, band parameters 79−60707
$In_{1-x}Ga_xAs_yP_{1-y}$ quaternaries VPE 0.75 to 1.35 eV band gap range 79−69987
$In_{1-x}Ga_xAs_yP_{1-y}$, traps in device quality n- and p-type LPE material 80−10999
$In_{1-x}Ga_xAs_yP_{1-y}$, vapour grown, alloy comp., thermodynamic calc. 79−99094
$In_{1-x}Ga_xAs_yP_{1-y}$:Be, ion implantation, hole conc. and mobility, junction depth 79−46685
$In_{1-x}Ga_xAs_yP_{1-y}$-InP DH laser, fabricated on (100)-InP substrate, 500-hr CW operation 77−83890
$In_{1-x}Ga_xAs_yP_{1-y}$-InP photodetectors, high-efficiency with selective wavelength response, 0.9-1.7 μm 79−21810
$In_{1-x}Ga_xAs_yP_{1-y}$-InP DH laser, 10000 h continuous CW operation, dark-line and dark-spot defects 79−98384
$In_xGa_{1-x}As_xP_{1-x}$-InP photodetectors, construction and performance 78−65966
$In_xGa_{1-x}As_yP_{1-y}$ layers on InP, LPE and opt. props. characteris. 79−28849
$In_xGa_{1-x}As_yP_{1-y}$, surface and dielec.-semicond. interface props. 80−93001
$In_xGa_{1-x}As_yP_{1-y}$, valence band struct., CPA calc. 79−73435
$In_xGa_{1-x}As_yP_{1-y}$-InP n-p heterojunction photodiode, characts. 78−14800
InGaAsSb based injection heterolaser, 1.9 μm stimulated emission 79−18420
InGaAsSb, LPE growth, and appl. in GaSb/AlGaAsSb/InGaAsSb/AlGaAsSb/GaSb DH 80−16205
InGaAsSb-AlGaAsSb DH laser, room temp. operation at 1.8 μm wavelength 80−43358
$In_{1-x}Ga_xAs_{1-y}Sb_y$, LPE growth on (111)B-oriented InAs, growth conditions and lattice matching 77−24973
InGaP/InGaAs struct. for transferred electron photocathodes, VPE growth and characterisation 80−76193
InGaP-GaAs junction, effect of elastic strain on energy band gap and lattice parameters 79−24057
$In_{0.3}Ga_{0.7}P$, N free and implanted, photoluminescence study 80−97322
$In_{0.5}Ga_{0.5}P$-GaAs heterojunction, interfacial recomb. vel. determ. 77−51809
n-$In_{1-x}Ga_xP$, direct-gap semiconductor, cathodoluminesc., electron irrad. effects 80−108283
$In_{1-x}Ga_xP$, epitaxial film, cathodolum. obs., recomb. mechanisms 78−72613
$In_{1-x}Ga_xP$, epitaxial growth from melt, optimisation of growth conditions 79−52132
$In_{1-x}Ga_xP$, epitaxial layers, compositional inhomogeneity 80−88444
$In_{1-x}Ga_xP$, homogeneous bulk, growth from soln. with predetermined cryst. comp. 78−11097
$In_{1-x}Ga_xP$ LEDs and electron-beam-pumped lasers, LPE and VPE growth 80−2281
$In_{1-x}Ga_xP$, LPE, conditions, reacts. in In-Ga-P system 79−11525
$In_{1-x}Ga_xP$, LPE, on $GaAs_{1-y}P_y$, photo- and cathodolum. 78−19559
$In_{1-x}Ga_xP$, non-isodisplacement of P atoms in long-wavelength optical phonons 79−47444
$In_{1-x}Ga_xP$, phonon density of states, cluster Bethe lattice treatment 80−6475
$In_{1-x}Ga_xP$, quantitative characterisation of chemical disorder from wavelength-modulated no-phonon absorpt. 79−15482
$In_{1-x}Ga_xP$, solid soln., evaporation of P during LPE 79−95948
$In_{1-x}Ga_xP$, solid soln. film, photoluminesc. meas. 78−27321
n-$In_{1-x}Ga_xP$ solid solns., electron scatt. mechanisms *(Russian)* 79−4568
$In_{1-x}Ga_xP$, temp. depend. of forbidden band width, photoluminesc. meas. 78−19556
$In_{1-x}Ga_xP$, two-phonon IR absorpt. 78−52493
$In_{1-x}Ga_xP$:N_2, N-trap bound states, photoluminesc. and absorption data 77−1719
$In_{1-x}Ga_xP$:N(Te), composition depend. of bound state luminesc. transitions 78−39595
$In_{1-x}Ga_xP$:Te,Zn, photolum. and electrolum., direct transition region 77−8659
$In_{1-y}Ga_yP$-GaAs heterojunction, VPE, energy band gap and lattice parameter, lattice mismatch effects 78−95345
$In_xGa_{1-x}P$ on GaP, heterojunctions, misfit dislocation banding, stress-induced birefr. 77−28542
$In_xGa_{1-x}P$, proportional ingredient content determ. by X-ray fluoroscopy 80−97747
$In_xGa_{1-x}P$, solid solns., gas phase epitaxy from Ga-In-HCl-PH_3-H_2 systems 78−34722
$In_xGa_{1-x}P$, TEM foil preparation, using polishing set 'Elypovist' *(German)* 79−9264
$In_xGa_{1-x}P$-GaAs heterojunction, interface recomb. velocity determ. 77−89838
$In_xGa_{1-x}P$-GaAs lattice mismatched heterojunction, recomb. props. 78−13707
InGaPAs LPE layers, compositional inhomogeneity, photoluminesc. obs. 80−75451
InGaPAs LPE multilayered DH lasers exhibiting quantum size effects 78−1227
InGaPAs, LPE-grown on (001)-InP, lattice mismatch study using X-ray double-cryst. diffr. 79−99440
$In_{1-x}Ga_xP_{1-y}As_y$ LPE films, hot electron and magnetotransport props. 78−26977
$In_{1-x}Ga_xP_{1-y}As_y$ lattice-matched epitaxial layers, LPE growth on GaAs(100), characterisation 80−75465
$In_{1-x}Ga_xP_{1-z}As_z$ DH lasers, multiple LPE, lattice matching 77−77421
$In_{1-x}Ga_xP_{1-z}As_z$ DH laser diode, defect and phonon assisted tunnelling 78−13708
$In_{1-x}Ga_xP_{1-z}As_z$ LEDs and electron-beam-pumped lasers, LPE and VPE growth 80−2281
$In_{1-x}Ga_xP_{1-z}As_z$, lattice matched to InP, electroreflectance obs. 80−93416

gallium compounds continued
$In_{1-x}Ga_xP_{1-z}As_z$, room temp. visible heterojunction lasers 78—5501
$In_{1-x}Ga_xP_{1-z}As_z$ single thin active layer visible spectrum heterostruct. lasers 78—63120
$In_{1-x}Ga_xP_{1-z}As_z$ solid solution, radiative transitions 79—11476
$In_{1-x}Ga_xP_{1-z}As_z$, stimulated yellow-green emission under electron excitation, 80K 79—33846
$In_{1-x}Ga_xP_{1-z}As_z$ thin well in InP p-n junction, confined carrier luminesc. and laser modes 78—13703
$In_{1-x}Ga_xP_{1-z}As_z$, visible spectrum laser diode, continuous operation, 6280 Å, 77K 79—960
$In_{1-x}Ga_xP_{1-z}As_z$ well in InP, tunnel injection into confined particle states 78—19130
$In_{1-x}Ga_xP_{1-z}As_z$:Zn, x~0.12, z~0.26, LPE, DH lasers, tunnelling involving defects 77—65594
$In_{1-x}Ga_xP_{1-z}As_z$-$In_{1-X}Ga_XP_{1-Z}As_z$ visible spectrum multiple-quantum-well heterostruct. lasers 80—106537
$In_{1-x}Ga_xP_{1-z}As_z$-InP, LPE heterojunctions, lattice matching and dislocations 78—23150
$In_{1-x}Ga_xP_{1-z}As_z$-InP, single and multiple layer heterostruct., LEDs and lasers 78—46626
$In_{1-x}Ga_xP_{1-z}As_z$-InP, valence band discontinuity, quantum well luminesc. 79—91483
$In_{1-x}Ga_xP_{1-z}As_z$-InP coupled multiple quantum-well heterostructure laser diodes, threshold current temp. depend. 80—78855
$In_uGa_{1-u}P_vAs_{1-v}$-InP, LPE, lattice matching, phase 80—54350
$In_xGa_{1-x}P_yAs_{1-y}$, electron effective mass and Dingle temp., Shubnikov-de Haas oscills. 80—59859
InGaSb, LPE growth characteristics, substrate surface contamination dependence 80—39470
$In_{0.58}Ga_{0.42}Sb$, interband magneto-optical transitions, arbitrary field orientation 79—42948
$In_{1-x}Ga_xSb$ alloy system, interband magnetooptical study using Schottky barrier 79—8124
$In_{1-x}Ga_xSb$, band parameter variations 80—20084
$In_{1-x}Ga_xSb$, drift velocity of electrons 77—20327
$In_{1-x}Ga_xSb$, energy gap, temp. depend. and photovoltaic effect 80—70746
$In_{1-x}Ga_xSb$ film, epitaxial growth by multitarget RF sputtering 77—44157
$In_{1-x}Ga_xSb$ films, elec. props., preparation 80—100473
$In_{1-x}Ga_xSb$, multitarget sputtering using decoupled plasmas 77—12529
$In_{1-x}Ga_xSb$-Au, photovoltaic effect and Schottky barriers 80—49897
$In_xGa_{1-x}Sb$, influence of annealing on microstruct., exam. 78—56669
$In_xGa_{1-x}Sb$, molecular beam epitaxy 79—47638
$In_xGa_{1-x}Sb$, vertical Bridgman Stockbarger growth, magnetic field effect 78—60565
InGaSbAs heterostructures and LED's luminesc. props. in 1-2 micron band 78—10988
$In_xGa_{1-x}Se$ single crystals, exciton absorption spectra 80—20663
$In_2Ga_6Te_{10}$, X-ray cryst. struct. determ. *(French)* 79—23580
InP homojunction solar cell, antirefl. coated, high-efficiency 80—104505
InP/GaP system, two-layer structs., relaxation of internal stresses 80—34341
InP/$In_{1-x}Ga_xAs_yP_{1-y}$ heterostruct., optically induced degradation 79—86791
InP/$In_xGa_{1-x}As_yP_{1-y}$ interfaces, sputter-profiled, depth resolution degradation by cone form. 80—80094
InP-$Ga_xIn_{1-x}As_gP_{1-y}$ systems, for optical devices in 1 to 1.6 μm region, LPE growth *(Japanese)* 79—28956
InP-GaInAsP buried heterostructure lasers of 1.5 μm region, fabrication and characts. 80—74388
InP-GaP, solid soln. crystallization from stoichiometric melt, solidus construction 77—85927
InP-$In_{1-x}Ga_xP_{1-z}As_z$ heterostructure laser, single and multiple quantum-well, liquid-phase epitaxial growth 80—38031
InP-InGaPAs heterojunction lasers and LEDs, 1.0 to 1.2 μm 80—74362
InSb-GaSb, compositionally modulated sputtered superlattice, growth and interlayer diffusion 79—56930
InSb-GaSb, directionally solidified, determination of non-constant distrib. coeffs. 78—76641
InSb-GaSb alloys, directionally solidified, composition variations, electron probe anal. 79—24513
InSb-GaSb solid solution ingots, orientation, twinning and orientation depend. reflectance 79—28001
InSb-GaSb superlattice, interlayer diffusion 77—85086
$In_{2-x}Sn_xO_{3-y}$-$Ga_xIn_{1-x}P$(-InP_yAs_{1-y}) heterojunction solar cells, chemistry and prep. 80—94073
$K_2Ga_2P_8O_{24}$, cryst. struct., atomic coordinates, anisotropic temp. corrections 80—33974
K_2O-Ga_2O_3-P_2O_5-H_2O, reactions, 150-500°C 80—35514
$K_2O_{5-x}Ga_2O_3.xFe_2O_3$, K ion cond. 78—83998
$LaGaOS_2$, cryst. struct. determ. *(French)* 78—79575
La_2O_2S-AgS-Ga_2S_3, ionic conducting glasses *(French)* 78—79804
La_2O_2S-Ga_2S_3 system, phase diagram determ. by DTA and X-ray diffr. *(French)* 77—43309
La_2S_3-Ag_2S-Ga_2S_3 glass system, prep., thermal and elec. props. *(French)* 80—89192
$La_2S_3.3Ga_2S_3$:Er^{3+} glass, fluoresc., and possibility of lasing 78—23514
La_2Se_3-Ga_2Se_3-$GeSe_2$ ternary system, phase diags., glass formation *(French)* 78—3109
LiGa ferrite, substituted ferrospinel, spin configuration determ. *(Russian)* 77—32162
$Li_{0.5}Ga_{0.85}Cr_{1.625}O_2$ spinel, tetrahedral coordination of Cr^{3+} ion, electronic spectra, X-ray and neutron diffr. *(French)* 79—65031
$Li_{0.5}Ga_{0.095}Fe_{1.55}O_4$ ferrites, linear magnetostriction in weak field, 150 to 300K *(Russian)* 77—80983
$Li_{0.5}Ga_xFe_{2.5-x}O_4$, polycrystalline, ferromagnetic reson. theory applicability limits *(Russian)* 77—55709
Li_2O-Ga_2O_3, rapidly quenched glasses, Li ion cond., elec. cond. 80—100346
Li_2O-Ga_2O_3 quenched glasses, crystn. and ionic cond. 80—33899
Li_2O-GeO_2-Ga_2O_3, glass, electrode props., dissolution kinetics 80—89387
MgO-Ga_2O_3-SiO_2 system, subsolidus phase equilib. 78—44106
$Mn_{0.75}Ga_{2.17}S_4$, twinning and cryst. struct. determ. *(French)* 78—83798
$Mn_{0.6}Ga_{0.4}Sb$, eutectics, galvanomag. props., thermo EMF 77—15869
Na_2O-Ga_2O_3 system, new superionic conductor *(French)* 78—14504
Na_2O-Ga_2O_3 system β and β″ phases, fast ion cond., prep. and phase comp. 80—59716
Na_2O-SiO_2-Ga_2O_3-Al_2O_3-B_2O_3-SnO_2 glasses, ion exchange reactions with $NaNO_3$ and KNO_3 melts 80—16673

gallium compounds continued
Na_2O-SiO_2-Ga_2O_3-Al_2O_3 glasses in mixed $AgNO_3$-$NaNO_3$ melts, ion exchange 80—21282
β″-$Na_2O.Ga_2O_3$, reaction with water, particle size effect 77—21379
$NbGa_2O_x$, O stabilised cpd., struct. determ. 80—103301
Ni-n-GaP:Si(Ge) contacts, doping effect in elec. props. 80—6983
$NiGa_2O_4$ spinel form., effect of Ga^{3+} chemical diffusion in NiO *(German)* 78—22894
P_xAs_{1-x}, periodic structs. characts. determ. by means of satellite Bragg reflections 79—46510
PbTe-Ga_2Te_3, phase interaction, DTA, XPA and microstructural anal. 80—96625
$RbGa(SO_4)_2.12H_2O$, ENDOR of $^{57}Fe^{3+}$ in trigonally distorted octahedral sites 79—38405
$RbGa(SO_4)_2.12H_2O$, spin-Hamiltonian with trigonal S^3I terms for describing $^{57}Fe^{3+}$ ENDOR spectra 80—75885
Si-GaP, heterojunction, photosensitivity spectrum, characts. 79—24071
Si-GaSe n-p heterojunction, elec. characts., interface states 80—70812
SiTe-GaTe, solid solns., mag. suscept. meas., defects 78—43552
SiTe-GaTe, thermo-EMF, elec. cond. and solubility 77—20346
SmGa garnet film, scratch-modified mag. domain patterns 78—48007
Sm_2O_3-Ga_2O_3 system, garnet-perovskite transform., phase diagram relationships 80—97460
$Sn_{1-x}Ga_xMo_5S_6$, heat capacity meas., singularities at low temp. 80—49985
$SnGa_6Te_{10}$, X-ray cryst. struct. determ. *(French)* 79—23580
SrF_2-Ga_2O_3, carrier for impurity anal. of U-Pu oxides by emission spectrography 78—68944
SrO-Ga_2O_3, vitrification, spectroscopic and petrographic anal. 77—15556
SrO-Ga_2O_3-Bi_2O_3, vitrification regions 77—15557
TbGa garnet, mag. ordering induced by hyperfine interactions, neutron diffr. meas. 77—66265
TbGa garnet, Verdet const. meas. with pulsed mag. field 78—68486
$TbGa_3(BO_3)_4$, luminesc. spectra, local symmetry of rare earth ion determ. 80—16095
TiO_2:Ga_2O_3, impurity influence on polymorphic crystn. 79—78858
TiO_2-Ga_2O_3, crystallographic shear planes and defect pair splitting, electron microscopy 77—76425
TiO_2-Ga_2O_3 system, phase relations and microstructs. 78—3107
TiO_2-$LaCrO_3$-GaP photoelectrochem. reactor for materials synthesis using solar energy 80—45712
Tl $GaS_2(Se_2)$, optical and nonlinear optical props. *(Russian)* 79—51943
$TlGaS_2$, IR refl. spectrum., LO phonons *(Russian)* 77—40221
$TlGaS_2$, IR refl. spectrum, Kramer-Kronig analysis, transverse optical phonons 78—19489
$TlGaS_2$, optical and photoelectric exam. 79—11180
$TlGaS_2(Se_2)$ film, elec. and photoelec. props. *(Russian)* 78—52109
$TlGaS_2(Se_2)$, IR reflection spectra, lattice vibrs. *(Russian)* 77—85701
$TlGaS_2(Se_2)$, phase transforms. under hydrostatic press., Raman scatt. study 80—25366
$TlGaS_2(Se_2)$, Raman spectra, intralayer and interlayer modes 78—43876
$TlGaS_{2x}Se_{2(1-x)}$, layer solid soln., mixed one- and two-mode behaviour of optical phonons 79—47445
$TlGaS_{2x}Se_{2(1-x)}$, layer solid soln., long wave lattice vibrs., IR reflection spectra 80—11388
$TlGaS_{2x}Se_{2(1-x)}$, solid soln., fundamental optical absorpt. edge 80—25408
$TlGaS_xSe_{2-x}$, optical and photoelectric props., composition depend. 79—15183
$TlGaSe_2$, Raman and IR spectra, zone centre optical phonons 78—76462
$TlGaTe_2$, multilayer cryst., lattice vibr. symm., IR absorpt. and Raman scatt. selection rules 80—39231
$V_{1-x}Ga_xO_2$, M1→T phase transition, X-ray and mag. meas. 77—11692
$V_{1-x}Ga_xO_2$, phase transitions, semicond. metal transition, antiferromag. props. 77—11969
V_2O_5-$GaNbO_4$ system, interfacial reactions, efficient boundary conditions and solid state reactivity 80—76542
$(Y,Sm,Ga)_3(Fe,Ge,Si)_5O_{12}$ film, static and dynamic mag. props., 20-160°C 77—24725
$Y_{3-x}Bi_xFe_{5-y}Ga_yO_{12}$-PbO-$B_2O_3$-$Bi_2O_3$ system, crystn. fields 78—43996
$Y_{2.35}Eu_{0.65}Ga_{1.2}Fe_{3.8}O_{12}$, bubble translation vel., ion-implantation effects 78—68327
YEuTmGa garnet bubble film, dynamic diffuse wall deform. 80—54927
$Y_3GaFe_4O_{12}$, mag. props. meas. in high mag. fields, review *(Japanese)* 78—52303
$Y_3Ga_2Fe_{5-x}O_{12}$, garnet, computer simulation of temp. and field depend. of sublattice magnetisation and spin-flip transition 79—11300
YGaIG, magnetoelastic wave propagation time dispersion reduction 80—75836
$Y_3Ga_5O_{12}$:Tb^{3+}, fluoresc. and absorption spectra 77—32422
YIG, Ga-substituted, mag. birefringence rel. to sublattices 79—28723
YIG:Ga, films, ferromagnetic resonance, ion implantation effect 80—97145
$Y_{2.85}La_{0.15}Fe_{3.85}Ga_{1.15}O_{12}$ garnet, mag. props., ion implantation effect, Mossbauer study 80—97166
Y_2O_3-Fe_2O_3-Ga_2O_3-PbO-P_2O_5, primary crystallisation regions 77—44222
Zn-Ga-P-S quaternary system, p-type conductive alloys 78—39105
$ZnGa_2O_4$:$Fe^{3+}(Mn^{2+})$, EPR, spin Hamiltonian parameters 80—25195
$ZnGa_2S_4$, band struct., pseudopot. method 80—92816
ZnTe-Ga_2Te_3, phase diagram 78—35360
p-ZnTe-n-GaN, electroluminescent hetero-junctions, memory effect, I-V characts. *(Russian)* 77—40289

gallium phosphide light emitting diodes *see light emitting diodes*

galvanomagnetic effects
see also Hall effect; magnetoresistance; thermomagnetic effects
alloys, dil. mag., transport props. in mag. field, impurity-electron scatt. 80—65541
anisotropic solid with macroscopic inclusions, elec. consts. *(Russian)* 78—68002
$Bi_{1-x}Sb_x$ narrow band gap semiconductors, galvanomagnetic, optical and photoelectric props. 80—15544
cascade capture of charge carriers in quantised mag. field, appl. to many-valley semicond. *(Russian)* 79—4572
n-channel MOSFET, Si inversion layer, negative differential resistance 78—30996
continuous flow cryostat, for measurement in pulsed magnetic fields 78—37017
covalent semiconductors, low temp. galvanomag. effects, shallow attractive traps 80—88575

galvanomagnetic effects continued
- cubic metals, low-field galvanomag. transport coeffs., appl. to dil. Al-Ge alloys 79—91029
- degenerate semiconductor, diffusivity-mobility ratio under mag. quantisation, band non-parabolicity effects 77—20339
- degenerate semiconductor film, with different surfaces, transport effects in weak mag. fields 79—73607
- degenerate semiconductor with Kane dispersion rel., nonlinear effects 77—55553
- degenerate semiconductors and metals, cond. current and generalised Einstein rel. 77—15810
- disordered system, AC cond. tensor in mag. field 80—92870
- disordered system in mag. field, frequency dependence of conductivity tensor, theoretical investigation 80—70725
- ferrite-semiconductor structure, transverse galvanomag. effect *(Russian)* 77—24569
- ferroelectric ceramic, elec. and thermoelec. props. of grains and grain boundaries 78—43382
- ferromagnetic semiconductor, LF magnetostatic waves with discrete spectrum 77—89792
- ferromagnetic semiconductor, wide-gap, nonlinear galvanomag. effects 77—39862
- ferrometnatic metal slab, transmission of 24 GHz radiation, effect of diffuse surface scatt. of carriers, calc. 80—34780
- film, electronic props. in longit. mag. field 79—73603
- film, inhomogeneous, galvanomagnetic props. 79—69608
- galvanomagnetic-recombination field effect, theoretical model 78—43420
- gapless semiconductor, transport coeffs. in quantum limit 80—80302
- graphite, anomalous galvanomag. props. in quantum limit 80—39604
- graphite, anomalous galvanomagnetic properties, in strong mag. field 79—23986
- graphite, grain boundary scattering effect on temp. depend. of electroresistivity, galvanomagnetic effect *(Russian)* 78—56148
- graphite, low field data and free carrier densities 78—87986
- graphite, pyrolytic, galvanomag. effects, effect of fast neutron irradiation 80—34465
- graphite, thermoelec. and thermomag. props., cylindrical band model 80—39616
- graphite, trigonal warping of constant energy surfaces 78—87987
- graphite intercalation compounds, galvanomagnetic and optical data, electronic structure 77—51634
- Gunn diodes, domain instabilities in transverse mag. field 79—23981
- hopping conduction, master eqn. approach in presence of mag. field 80—103697
- impurity breakdown in mag. field 77—24564
- impurity scattering in quantised mag. field *(Russian)* 78—47752
- impurity scattering of current carriers in quantizing mag. field 78—51954
- n-InSb, acceptor effect of plastic bending 80—6885
- longitudinal magnetoconductivity, effect of multiple scatt. 80—96836
- magnetoconcentration effect in variband struct. *(Russian)* 78—60143
- many valley semiconductor, galvanomag. effects 79—11157
- many-valley semicond., size-induced changes in valley populations in strong elec. fields 80—6855
- many-valley semiconductor, current-voltage characts., in weakly heating elec. current and strong mag. field 78—26876
- many-valley semiconductor, new type of galvanomag. effect for hot electrons 77—32028
- measurement at pressures up to 27 kbar, using low-temperature hydrostatic pressure chamber 80—47069
- metal, acoustic breakdown, electron energy spectrum *(Russian)* 78—18948
- metal, compensated, transport of spatially inhomogeneous current under mag. fields, pot. and current distribs. 79—87081
- metal, compensated, transport of spatially inhomogeneous current under mag. fields, dynamical props. 79—87082
- metal, deformed, transfer phenomena *(Russian)* 77—35906
- metal, ferromag., antiferromag., magnetoelastic coupling effect on magnetoelec. reson. 80—75837
- metal, quantum theory, cond. rel. to migration of cyclotron orbit centres *(Russian)* 77—66153
- metal, surface scattering of conduction electrons and kinetic phenomena *(Russian)* 79—56210
- metal, transport coeffs. in strong mag. field, Wiedemann-Franz law and Mott rule 77—69303
- metal film, boundary scatt. indicatrix of cond. electrons, expt. data *(Russian)* 77—39969
- metallic glasses, transport properties, applicability of liq. metal theory 79—56179
- metals, conduction electron focusing by nonuniform mag. field *(Russian)* 79—99533
- metals, liq., viscosity effect on cond. meas. by rotating mag. field method *(Russian)* 77—57349
- metals, surface impedance in mag. field, theory *(Russian)* 78—6427
- metals, with open Fermi surfaces, galvanomag. effects, static skin effect *(Russian)* 80—29389
- metals and semimetals in strong mag. fields, EM excitations, review 77—8130
- MIM structure, zero-bias anomalies due to Kondo scatt., hopping model, mag. field effect 77—59334
- MOS inversion layer, hot electron effects in Landau levels 80—6998
- MOST, galvanomagnetic props., theory and expt. *(German)* 77—76926
- narrow band gap semiconductors, conference, Warsaw, Poland (Sept. 1977) 79—82582
- narrow band gap semiconductors, conference, Warsaw, Poland (Sept. 1977) 80—49703
- narrow band-gap semiconductor, energy depend. relax. time, EM response of electrons 78—60142
- narrow gap semiconductor, plasma frequency, effect of electron spin, in quantising mag. fields 79—95436
- negative differential cond. of hot electrons in mag. field due to carrier density nonlinearity 77—55540
- nondegenerate semiconductor electrons in strong elec. and quantizing mag. fields 78—10457
- nonlinear electronic system, series expansions calcs. 77—39814
- orthorhombic structures, weak field galvanomagnetic coeffs., calc. 79—99567
- Permalloy film, galvanomag. rotation characts., under uniaxial stress 78—84466
- Permalloy film, stripe domain struct., distrib. of magnetisation *(Russian)* 77—66396

galvanomagnetic effects continued
- piezoelectric semiconductor, plasmon enhanced sound amplification in mag. field 77—39900
- polar semiconductor, HF mobility in longitudinal quantising mag. field 79—51619
- polar semiconductor, high field quantum magnetotransport theory 78—30941
- polar semiconductors, anharmonicity influence on cond. in quantising mag. field 80—2406
- semiconductor, acoustomagnetoelectric effects in inelastic scatt. of electrons by optical phonons 77—4372
- semiconductor, carrier effective lifetime modulation, surface recomb. and mag. field effects 77—28193
- semiconductor, effect of effective lifetime modulation 78—47807
- semiconductor, effect of effective lifetime modulation 78—47808
- semiconductor, effect of overlap function on electron mobility in quantising mag. field 78—43374
- semiconductor, elec. cond. in quantising mag. field, and electron heating, mutual electron-phonon drag 77—69355
- semiconductor, electron transport phenomena, high-field transport and quantum transport in strong mag. fields *(Japanese)* 77—55526
- semiconductor, electron-electron relax. in ultraquantum mag. fields, electron-phonon interactions 77—4371
- n-semiconductor, electron-phonon drag in longit. quantising mag. field 77—76805
- semiconductor, excitation and amplification of weak helical waves by strong waves in strong mag. field 78—19077
- semiconductor, hot electron current voltage curves, transverse mag. field, phonon heating 78—6384
- semiconductor, hot electron distrib. in strong electric and quantised mag. fields 79—95417
- semiconductor, hot electron quantum magnetotransport, review 78—30940
- semiconductor, hot electron waves in transverse mag. field 77—4387
- semiconductor, intrinsic, quantum theory of transverse galvanomag. phenomena, model of two standard bands *(Russian)* 77—62945
- semiconductor, layered compound, collective electron cond. in strong mag. field 79—42525
- semiconductor, magnetoconcentration effect, use of Boltzmann formalism *(French)* 77—32025
- semiconductor, magnetodiode and magnetoconcentration effects, influence of field effect 80—107903
- semiconductor, measurement cryostat *(Hungarian)* 77—17986
- semiconductor, microwave magnetoconductivity in large quantising mag. field, effect of band non-parabolicity 79—47112
- semiconductor, mobility of hot electrons in mag. field 77—4368
- semiconductor, model, transport phenomena in presence of medium range disorder *(French)* 78—56162
- semiconductor, nondegenerate, magnetophonon reson. in acoustic relax. of hot electron energy 78—26892
- semiconductor, nonequilibrium fluctuations in quantized mag. field *(Russian)* 79—95426
- semiconductor, nonradiative multiphonon carrier capture by deep neutral traps 80—6871
- semiconductor, piezogalvanomagnetic effects measurement at low temps., apparatus with stabilised dynamic load 77—67458
- semiconductor, polar, mobility in mag. field, extreme quantum limit, iterative technique 78—2498
- semiconductor, polarity reversing control current magnet power supply with triangular waveform for meas. 79—12827
- semiconductor, quantum theory, cond. rel. to migration of cyclotron orbit centres *(Russian)* 77—66153
- semiconductor, relax. time energy depend. and surface galvanomagnetic props. 78—43459
- semiconductor, total separation of galvano- and thermomagnetic effects 77—55545
- semiconductor, weak heating of electrons, cyclotron reson. conditions, quantising mag. field 78—39141
- semiconductor and semimetallic thin films, dislocation superstructures and conduction electron kinetics, oscill. phenomena *(Russian)* 79—19678
- semiconductor crystal surface, nonequilib. electron effects due to chem. excitation 78—72239
- semiconductor electron plasma, EM wave propag. in external alternating mag. field 77—20350
- semiconductor gapless, nonlinear effects in transverse quantising mag. fields 77—69353
- semiconductor in mag. and US wave fields, electronic density of states *(Russian)* 78—72056
- semiconductor layers, double injection in transverse mag. field, theory 80—80421
- semiconductor materials testing, small 77 to 400K cryostat 77—30149
- semiconductor piezogalvanomagnetic effects at low temp., meas. installation 77—41625
- semiconductor stable electron-hole plasma, diffusion in magnetic field 79—24001
- semiconductor voltage and current transducers, Gauss effect compensation 78—77892
- semiconductor with deep traps, magnetodiode effect 78—6401
- semiconductors, electrical properties calculated from thermophysical and thermomagnetic effects 79—73535
- semiconductors, galvanomagnetic effects in high mag. fields, for electron scatt. by optical phonons 80—2405
- semiconductors, hot electron transverse escape galvanomagnetic effects *(Russian)* 80—80289
- semiconductors, liq., viscosity effect on cond. meas. by rotating mag. field method *(Russian)* 77—57349
- semimetal, degenerate, quantum theory of transverse galvanomag. phenomena, model of two standard bands *(Russian)* 77—62945
- semimetal, electric current distribution, by diffusion size effect 79—23987
- semimetal, longit. cond. in extremely strong mag. field 77—89779
- semimetal, mag. freeze-out of extrinsic carriers 77—59268
- semimetal or metal, magneto-quantum oscillations obs., new method 77—62946
- semimetals, exciton phase, transport effect in strong mag. fields 78—87977
- solid, time inversion symmetry and transport props. 77—89744
- space-time symmetry restrictions on transport coefficients 80—70662
- spatially inhomogeneous magnetic field effect on semiconductor carriers 80—92916
- TCNQ salt QCTCNO, strong Coulomb correlations 79—56203

galvanomagnetic effects continued
  thermoelectric materials, meas. under isothermal conditions *(Russian)* 78—56160
  TTT, dark cond. and photocond. effect of strong mag. field, at charge carrier injection *(Russian)* 79—69607
  TTT, dark injection current, sign inversion of low mag. field *(Russian)* 79—73602
  AgCl(Br), crossed elec. and mag. fields, hot electrons, streaming motion, population inversion 80—44649
  Ag_2Re films, galvanomag. props. and quantum size effects, obs. 80—70866
  α-Ag_2S, electronic and electrogalvanic props. *(French)* 78—84237
  Ag_2Se, electronic and electrogalvanic props. in α-phase region *(French)* 80—107820
  Al, quantum oscills. of thermal EMF under mag. breakdown conditions *(Russian)* 77—69305
  Al, Sondheimer oscillation 79—87085
  Al-Ge(Mg)(Zn)(Ga), dil., electronic transport coeffs. for point defect scatt., 4-OPW calc. 79—42531
  Be, low temp. elec. and thermal cond. in mag. field, use as heat switch 77—35923
  Be, quantum oscillations of thermal EMF under mag. breakdown conditions *(Russian)* 77—69305
  Bi alloy, mag. field depend. electron scatt. rates, de Haas-van Alphen meas. 78—10436
  Bi, electron specular refl. by binary plane, ang. depend., focusing by transverse mag. field *(Russian)* 77—80798
  Bi film, transverse mag. field depend. of thermoelec. power *(French)* 78—2587
  Bi, galvanomag. wave propag. obs. *(Russian)* 79—33301
  Bi, magneto-thermopower, weak-field, implication for scatt. mech. 80—49790
  Bi, magnetoplasma waves at 9 to 100 GHz microwave freqs. 79—78127
  Bi, magnetoplasma waves in strong mag. fields at 300 GHz 79—38116
  Bi, oscillations with short periods of collector voltage for transverse focusing of electrons *(Russian)* 77—47837
  Bi, polycryst., grain boundary scattering effect on temp. depend. of electroresistivity, galvanomagnetic effect *(Russian)* 78—56148
  Bi, surface potential under high mag. fields 78—26887
  Bi, thermoelectric power, electronic thermal cond., in mag. field 80—60015
  Bi, transport of spatially inhomogeneous current under mag. fields, dynamical props. 79—87082
  Bi-Sb, magnetoplasma waves in strong mag. fields at 300 GHz 79—38116
  Bi-Sb (0 to 6 at.%), semimetal, magnetoplasma waves at 9 to 100 GHz microwave freqs. 79—78127
  $Bi_{0.924}Sb_{0.076}$, doped, optical, oscillation and galvanometric effects *(Russian)* 77—85247
  $Bi_{1-x}Sb_x$, band inversion under press., Fermi surface anisotropy, galvanomag. meas. 77—51637
  $Bi_{1-x}Sb_x$, galvanomag. props., energy spectrum *(Russian)* 79—56248
  $Bi_{1-x}Sb_x$, semiconductor, anomalous conductance in strong electric and longit. quantised mag. field *(Russian)* 78—76084
  $Bi_{1-x}Sb_x$:Te(Sn), band struct., plasma refl. spectra and galvanomag. tensor 77—16315
  $Bi_{88}Sb_{12}$-Sn, current carrier energy spectrum *(Russian)* 78—60139
  $Cd_{0.24}Hg_{0.76}Te$, mag. quantum oscills. in photovoltaic effect 79—19619
  $Cd_xHg_{1-x}Te$, characts. of low temp. transport props. 78—39160
  $Cd_xHg_{1-x}Te$, current-voltage characts., pinch effect, mag. field effects 80—6858
  $Cd_xHg_{1-x}Te$, effects of electron heating at low temps. 80—49823
  n-$Cd_xHg_{1-x}Te$, in strong mag. field, current-voltage characts., current instabilities 78—87980
  $Cd_xHg_{1-x}Te$, variable-gap structures, galvanomagnetic effects 80—11014
  CdTe, compensated single cryst., impurity centre parameters, elec. cond. and galvanomag. props. *(Russian)* 77—47811
  CdTe, n- and p-type, elec. and galvanomag. props. 79—7830
  $Cd_{3-x}Zn_xAs_2$, cryst., two-band and impurity conduction, 1.8 to 370K 78—19057
  $CeAl_3$, effect of disorder on cond. transition into ground state 77—89755
  $CuSO_4$, aq. soln., electrolytic resistance variation in mag. field 80—11897
  Dy, longitudinal galvanomag. effect in single crysts. *(Russian)* 78—56132
  EuB_6, electrical transport under press. 79—87101
  EuB_6, growth by soln. method, struct., mech. and elec. props. 80—16168
  Fe_2O_3, hematite, weakly ferromag., transverse galvanomag. parity effects anisotropy *(Russian)* 80—49770
  Fe_3Pd, quenched, or annealed exam. of magnetostriction, galvano- and thermomagnetic props. *(Russian)* 79—19757
  B-Ga, metastable, elec. props. in normal and supercond. states *(Russian)* 80—65520
  GaAs, donor energy spectrum, mag. field effect, submm. photocond. meas. *(Russian)* 77—43666
  p-GaAs, influence of light holes on transport props. 77—4367
  n-GaAs, magneto-impurity effect, review 79—91081
  GaAs, n-i-n three layer struct., transmitted phonon effect in strong mag. fields 77—20341
  GaAs, semi-insulating, magnetophotoconductivity as function of etching time 79—56265
  n-GaAs, subject to crossed static elec. and mag. fields, microwave amplification 77—1440
  GaAs:Cr diode, high magnetosensitivity of negative resist. region 78—26946
  GaAs:S(Se), ion implanted, evaluation by contactless mobility meas. 79—1448
  n-GaSb, galvanomagnetic effects 78—72172
  Gd, longitudinal galvanomag. effect in single crysts. *(Russian)* 78—56132
  Gd-Dy alloy, longitudinal galvanomag. effect in single crysts. *(Russian)* 78—56132
  n-Ge, anomalously enhanced plasma diffusion transverse to mag. field 80—96931
  p-Ge, diffusion coeff. for hot holes in mag. field 80—39614
  Ge, donor energy spectrum, mag. field effect, submm. photocond. meas. *(Russian)* 77—43666
  Ge, electron-hole plasma, helical instability excitation in strong. mag. field *(Russian)* 77—69368
  p-Ge, energy spectrum of impurities and effect of mag. field *(Russian)* 77—47770

galvanomagnetic effects continued
  Ge, galvanomagnetic-recombination field effect, theoretical model 78—43420
  Ge, inhomogeneous mag. field effects on conductivity 77—4374
  Ge, magnetic field effects on hot-hole noise 77—4415
  Ge, magnetoconductivity meas. at 9.3 GHz, using three-wave interferometer *(French)* 77—47844
  Ge microconductor mag. field transducer, cast, galvanomag. recomb. effect 79—19609
  Ge, n- and p-type, magneto-impurity effect, review 79—91081
  Ge, oscillistor effect in strong mag. fields, ambipolar drift and breakdown 78—2511
  Ge, photocond., inversion of magneto-impurity oscills. 77—15913
  n-Ge:Au, current oscill. damping in weak transverse mag. field 77—4365
  Ge:Cu, low frequency oscillations 77—15872
  Ge:Ga, photoconductivity oscillation with respect to applied mag. field *(Russian)* 78—80026
  GeSe, galvanomag. meas., anisotropy, metal to semiconductor transition 80—6847
  $Hg_{0.85}Cd_{0.15}Te$, acceptor states, galvanomagnetic effects study 79—82560
  $Hg_{1-x}Cd_xTe$-type semimetals, kinetic props., local acceptor level effects 80—65557
  n-$Hg_xCd_{1-x}Te$, narrow band gap, Auger effect under high mag. fields 79—82609
  $HgCr_2Se_4$, ferromag. semicond., transport props. 78—68039
  $Hg_{0.98}Mn_{0.02}Te$, resonance acceptor level 78—23048
  HgTe, and ternary compounds, mag. field induced microwave transparency 80—49797
  HgTe, gapless, nonlinear effects in transverse quantising mag. fields 77—69353
  HgTe, quantum galvanomag. effects 80—49782
  p-In-Sb, effect of static mag. fields on transverse photocurrent spectrum 78—14766
  InAs surface accumulation layers, magneto-transconductance meas. 78—64137
  InAs surface accumulation layers, magneto-transconductance study 80—49948
  n-InP, magneto-impurity effect, review 79—91081
  InSB, impact ionisation, influence of external mag. field on recomb. radiation and I-V characts. 79—56864
  n-InSb, acoustomagnetoelec. effect, 20-120K, sign reversal obs., and Hall mobility 77—24592
  n-InSb, degenerate, acoustomagnetoelec. effect obs. 78—72207
  InSb, donor spectrum, effect of strong mag. field 79—7806
  InSb, elec. cond. in intense mag. field, freeze out, hopping 77—20338
  n-InSb electron heating and energy relaxation time in quantising mag. field 80—10996
  n-InSb film, galvanomagnetic meas. of surface layer carrier conc. and mobility 77—55628
  InSb film, magneto-concentration effects *(Russian)* 79—47113
  InSb, high field quantum magnetotransport theory 78—30941
  InSb, high-purity, electron irradiation effects on transport props. 79—23650
  n- InSb, hot electron energy relax. in quantizing mag. fields 78—31259
  n-InSb, hot electrons relax. in quantising mag. field *(Russian)* 80—6876
  InSb, impact-ionisation magnetoelec. effect 78—52016
  n-InSb, influence of mag. field on hot electron effects 78—2493
  p-InSb, influence of plastic bending on galvanomag. props. 79—28349
  InSb, intrinsic capacitance in transverse mag. field *(Russian)* 79—91070
  n-InSb, ionized impurity scatt. limited mobility, expt. 80—80274
  p-InSb, magnetoconcentration effect, negative differential conductance 80—70729
  n-InSb, mobility in mag. field, extreme quantum limit, iterative technique 78—2498
  n-InSb, phonon heating by hot electrons in quantising mag. field 77—4354
  n-InSb, photoconductivity meas. in crossed fields 79—7852
  n-InSb, plasma, nonequilibrium, magnetohydrodynamic instabilities, theory and expt. *(Japanese)* 78—10493
  p-InSb plate in crossed E and H fields, even magnetoconcentration effect *(Russian)* 77—85244
  InSb, polar semiconductor, impact ionisation in crossed elec. and mag. fields 79—28355
  InSb thin film element having non-linear galvanomagnetic effect 80—34534
  p-InSb:Ge, photocond. in quantising mag. field, uniaxial press. influence 77—15907
  InSb-Au Schottky barrier, photovoltaic spectra and magneto-optical transitions, Landau levels and excitons 77—47858
  InSb-NiSb system, anisotropic, acoustomagnetoelec. effect, theory 79—24021
  K, theory of residual resistivity anomaly 77—80765
  Mg, quantum oscills. of thermal EMF under mag. breakdown conditions *(Russian)* 77—69305
  Mn ferrites, photogalvanomagnetic effects 80—34483
  Mo, Fermi surface press. depend., surface impedance and US attenuation oscills. in mag. field 77—43476
  Ni film, polycrystalline, resist., conduction electrons and s-d exchange interaction 78—19021
  Pb, high-field thermal and elec. magnetoconductivities meas. 77—59279
  $Pb_{1-x}Sn_xSe$, ($x=0.125$), pressure induced band inversion, effect on energy spectrum *(Russian)* 78—39007
  $Pb_{1-x}Sn_xTe$:In, nonequilib. metallic state *(Russian)* 79—33300
  $Pb_{1-x}Sn_xTe$:In, semiconductor-metal-semiconductor transitions under press. 80—34491
  $(SN)_x$ crystal, galvanomagnetic effects meas. 77—85246
  $(SN)_x$, intrinsic cond. anisotropy from galvanomag. effect obs. 78—6369
  Si, amorphous, photoconductivity, mag. field depend. 78—80023
  n-Si, γ-irradiated, with layer inhomogeneity, quantum current oscillations 80—11010
  p-Si, inversion layer, screening effect and quantum transport in strong mag. fields 78—19155
  Si, magnetodiode effect, expt. *(Slovak)* 77—8186
  Si, many-valley semiconductor, linear galvanomag. effects of hot electrons 79—11154
  n-Si, multivalued Sasaki effect 80—107795
  n-Si, new type of galvanising effect for hot electrons 77—32028
  n-Si, noise and hot carrier diffusion in mag. fields 79—11193
  Si powder semicond., microwave propagation, Rayleigh limit 79—78126
  Si, powdered, microwave propag. 78—56175

galvanomagnetic effects continued
- Si surface doped channels, gate controlled, quantum galvanomagnetic effects 78−64134
- Si:Ir, magnetosensitive diodes, characts. 79−24069
- Si:P, heavily doped, metallic region, resist. decrease due to ESR 77−16178
- Sn, Fermi surface press. depend., surface impedance quantum oscills. in mag. field 77−47717
- SnTe-Tl$_2$Te, phase and elec. props. 77−48406
- Te, dislocations influence on galvanomag. props. 80−54722
- Te, Faraday-type microwave Kerr effect 79−23998
- Te, galvanomagnetic props., surface layer effects reduced by etching 77−51769
- p-Te, magneto-impurity effect, review 79−91081
- Te, photoconductivity in strong mag. fields, doping effects, impurity levels 80−75602
- Te, pure and Sb doped, impurity state and impurity cond., press. effect 80−54723
- U film, condensed on cold substrate, electronic props. *(Russian)* 79−7912
- W, Fermi surface press. depend., surface impedance and US attenuation oscills. in mag. field 77−43476
- YIG-Ge layered struct., anisotropy of EMF under nonlinear ferromag. reson. conditions 77−8417
- YIG-Ge structure, profile and position of reson. galvanomag. effect curve 78−72242
- Zn, bicrystals, galvanomagnetic phenomena at common boundary, electric field potential distribution *(Russian)* 80−29388
- Zn, quantum oscills. of thermal EMF under mag. breakdown conditions *(Russian)* 77−69305

galvanomagnetism *see electromagnetism*

galvanometers
- balance indicators appl. *(Polish)* 77−10064
- ballistic, magnetic props. meas. appl., calibration procedure *(Polish)* 79−71498
- ballistic galvanometer, error due to non-transient impulses, integral expression 80−86349
- beam-scanning rotating lens system, for laser fibre drawing 79−41463
- commercial large-scale laser displays using path-controlled galvanometers 77−17963
- DC galvanometer internal resistance meas. by potentiometer 77−13777
- deflection system, X-Y beam, accuracy and repeatability improvement 77−58480
- electromechanical deflector with quasi-time-optimal scanning control *(Russian)* 77−58431
- electromechanical type, scale charact. alteration method *(Bulgarian)* 77−61081
- GT8 galvanometer drive amplifier system for interface with multichannel UV chart recorders 79−63204
- harmonic oscillator demonstration for teachers, recording facilities 78−16606
- laser beam resonant chopper performance characteristics and limitations 80−64084
- laser galvanometer scanning system, CAD 77−58475
- light scanners, compensated moving-coil mirror galvanometer 77−58479
- Low-inertia mirrors for galvanometers 78−71191
- low-inertia scanner selection 77−58476
- oscillograph, construction for fast process recording 80−73346
- photoelectric colorimeter reconditioning methods 79−39618
- picture taking parameters display in amateur cameras, review 78−89578
- space applications of LF supercond. sensors inc. SQUID devices 80−56691
- UV recording techniques 79−93129

galvanothermomagnetic effects *see thermomagnetic effects*

game theory
- *see also information theory*
- assignment problem, mixed, strategy game, utility function maximisation, equilibrium points 80−68028
- differential encounter-evasion game, nonstationary, theorem on the alternative 80−68026
- differential games, control systems with aftereffect 80−68025
- differential games, stable position control 80−68024
- information distance and extent, knowledge distance, concepts evaluation 78−77687
- lumped system in conflict with environment, Liapunov type design 79−57498
- matrix games, monotonic iterative algorithm 79−12563
- nonanalogue Monte Carlo games, conditions concerning nonanalogue transition kernels and estimators 78−62594
- nonlinear mechanical system with time optimal condition, synthesis 78−54176
- nuclear material inventory differences interpretation 79−85744
- quandice, rel. to quantum non-locality detections 80−86143
- reservoir operation under conflicting objectives 77−73777
- stochastic search game 78−77689
- thermal power reactor, operations research 79−13396
- transport equations, Monte Carlo game, variance versus efficiency 80−27238
- two-person nonzero sum stochastic differential game with stopping time 77−53755

gamma fission reaction *see photofission*

gamma radiation *see gamma-rays*

gamma-ray absorption
- 6 MeV gamma photons, penetration through Al, concrete and graphite 80−5256
- absorbed energy distrib. in γ-irradiated layered target, Monte Carlo program 79−19279
- air-water slug flow in horizontal pipe, liquid holdup determination 79−46362
- attenuation method using variable-thickness filter, calibration 77−83110
- biological materials, extrapolation of linear attenuation coefficients from diagnostic energies to megavolt range 78−24145
- bone mineral content meas. using gamma-ray attenuation by pair prod. 77−44740
- bremsstrahlung influence on γ dose buildup factors rel. to penetration depth *(Russian)* 79−13542
- build-up factors for finite media 77−61623
- concrete, porosity determ. from combined US and gamma absorption meas., mech. props. 79−29295
- differential Compton scatt. cross-sections meas. 77−30731

gamma-ray absorption continued
- dose, bounded estimate using linear programming 78−37452
- dosimetry, restricted energy absorption coefficients 78−80971
- Fe, photon penetration, photon backscatt. incidence angle depend. 80−104008
- heavy element analysis through absorption jump in interfering element 78−85263
- intense photon flux absorbed dose meas. 78−41387
- LWR LOCA, fission product gamma-ray energy absorption in emergency cooling solns. 79−31052
- multiphase pipeline flows, measurement of component ratios 80−38513
- non-homogeneous materials, absorpt. coeffs. 77−34527
- nuclear, enhancement using radiation field of high-power laser, cross section determ. 79−59033
- organ doses from isotropic γ-ray fields, review 80−109026
- penetration in heterogeneous systems 79−18050
- PMMA, constancy of composition obs., dosimetry appls. 79−60286
- polystyrene, constancy of composition obs., dosimetry appls. 79−60286
- polystyrene, photon penetration, photon backscatt. incidence angle depend. 80−104008
- pulmonary oedema of intact dogs, meas. by transthoracic γ-ray attenuation 80−81787
- radiation absorbing bodies, temp. fields, Julich reactor expts., finite element calcs. *(German, English)* 77−82998
- radiation shields, gamma ray spectral penetration, review 80−5343
- radionuclide computed tomography, method for γ attenuation correction, reconstruction algorithm 78−40307
- reactor shielding materials, Pb and steel, 6 MeV γ penetration bremsstrahlung 78−58350
- self-absorption in vol. shaped source for NaI, detectors, Monte Carlo calc. 77−26909
- shielding, concrete wall cavities, compensation by Fe plates *(German, English)* 77−83109
- tissue attenuation factors for human body omnidirectional γ-irradiation 79−92383
- water as source medium, calc. of absolute photopeak efficiency 78−78558
- water irradiated by photons up to 2 MeV, initial energies of Compton electrons and photoelectrons 80−108320
- Ag-Cu-Pb coin chem. anal. by low energy γ-rays and neutron transmission meas. 80−35591
- Al, photon penetration, photon backscatt. incidence angle depend. 80−104008
- Mo, γ-ray attenuation meas. using Ge(Li) detector 78−17539
- Pb, γ-ray attenuation meas. using Ge(Li) detector 78−17539
- Pb-Bi, X- and γ-ray attenuation obs. 79−61457
- Pd concentration determ. by gamma-ray absorption from ^{119}Sn^{m} 80−108123
- ^{119}Sn^{i}, total mass absorpt. coeff. of gamma quanta, chem. binding influence, determ. using Mossbauer effect 80−99467
- Ta, γ-ray attenuation meas. using Ge(Li) detector 78−17539

gamma-ray angular distribution
- *see also gamma-ray spectra*
- angular correlation, intrasource absorpt. and scatt. effects 79−97958
- angular correlation techniques, Ge(Li)-NaI(Tl) and NaI(Tl)-NaI(Tl) *(Spanish)* 79−89525
- annihilation photon ang. distrib. meas., spectrom. control unit 79−49890
- asymptotic attenuation coeffs. in ang. correls. random perturbations 77−30507
- atmosphere, angle and energy distrib., 2-25 MeV 78−12033
- atmosphere, spectra and angular distrib. 0.3 to 10 MeV 77−49205
- backscattering from various barriers, characts. and spectral ang. distrib. 77−61621
- beam-tilted foil surface interactions, nuclear hyperfine interactions 77−23544
- bovine carbonic anhydrase, γ-ray perturbed directional correl. obs. of conform. change, active site ^{111}In ions 79−83700
- computer program for coeffs. for X-rays of mixed multipolarities from partially-aligned nuclei 78−86503
- continuum γ rays, multipolarity, enhanced ang. correlation meas., heavy ion-compound nucleus reactions 78−93963
- cosmic ray γ-rays in range 3.5 to 100 MeV, system for meas. ang. and energy distribs. 77−50324
- Coulomb excitation, accuracy of WKB approx. determ. 77−65216
- Cross sections for gamma-ray production by 14-MeV neutrons 78−21552
- CU ^{23}Na(n,2nγ), (n,n$'\gamma$), 14.6 MeV, γ-ray ang. distrib. *(Russian)* 77−88147
- E1-E2 direct-semidirect model for fast nucleon radiative capture, γ ang.-distribs. 78−62536
- fp-shell nuclei, high-spin states 78−12946
- gamma reactions initiated by polarised particles, Legendre polynomial coeffs. 80−73107
- ground state rot. band transitions and delayed feeding via (d,3n) for A=158-180 77−34211
- hadron-nucleus scatt., corrections to γ angular distrib. *(Russian)* 78−41683
- heavy ion induced reactions, γ-ray multiplicity, ang. momentum and struct. depend. *(Rumanian)* 78−89906
- heavy ion reactions, statistical γ-rays and ang. momentum alignment 79−67761
- heavy-ion induced fusion-evaporation, phenomenological restrictions for spin alignment attenuation factors 77−57686
- heavy-ion stopping in matter, study of nuclear and elec. mechanisms from Coulomb excitation expts. 77−10569
- hot nuclei with high angular momenta, γ-ray emission in heavy ion reactions, rot. bands 78−13133
- incoherent scattering from atoms 77−54538
- ion, free, aligned, static hyperfine interaction, gamma-ray ang. distrib. 79−9508
- ions, deceleration in polarised ferromag. media, transient field phenomena 78−72445
- isomeric A=48-50 nuclei, mag. moments and core polarisation 78−37274
- linear polarisation mixing coeffs. for mixed dipole and quadrupole γ-radiations, Compton polarimeter 80−73110
- neutron radiative capture, DSD capture model 78−89861
- nucleon radiative capture model, through collective M1 excitation, photon angular distrib. 78−58276

gamma-ray angular distribution continued
- oriented radioactive nuclei, JINR investigs. using SPIN equipment *(Czech)* 77−42220
- PAC experiments with complex perturbations, effective X-ray anisotropy 77−48103
- particle spectra line shapes after γ emission in flight 78−41665
- penetration in heterogeneous systems 79−18050
- photon backscattered ang. distrib. for oblique incidence *(Rumanian)* 80−47456
- photon-nucleus scatt., 5 to 30 MeV 77−79359
- polarised nucleus mixed parity radiation, third-order approxs. in ang. distrib. 77−6288
- positron+halide ion, competitive reaction in water, ang. correl. obs. 79−61846
- radiative capture of fast nucleons, γ-ray ang. distrib. 77−41964
- radiative particle capture, gamma ang. distrib. theory 79−93571
- relativistic electron+laser photon scatt., angular and energy distrib. *(Russian)* 79−3029
- spin-alignment attenuation factors in mass 61-67 nuclei populated by (α, n) and (α, p) reactions 79−26390
- streaming through annular cylindrical duct, dose computation at exit 77−65342
- vitamin B_{12}-^{181}Hf complex, γ-ray PAC expt., crystal and liq. 79−39341
- (α,α'), γ-α ang. correls., theoretical description including delay effects *(Russian)* 77−34329
- $e^+e^-\to 2\gamma$, ang. correl. meas. device *(German)* 78−86726
- $e^+e^-\to\nu_e\bar{\nu}_e\gamma$, gauge theory analysis, Weinberg-Salem model, ang. and energy distribs. 78−12894
- $(n,x\gamma)$ reactions, ENDF/B prompt γ-ray evaluations, models and data 77−26753
- π^- interactions in nucl. emulsions, 65 GeV/c, γ quanta production 78−13160
- $\pi^- p\to\gamma\gamma n$, near threshold, perturbation theory estimates, branching ratio and ang. distrib. 79−89183
- Ψ', neutral radiative decay, possible intermediate states 77−241
- ^{63}Cu+^{20}Ne, 168 MeV, gamma ray multiplicity distrib. in strongly damped oscills. 79−36266
- ^{105}Ag decay, γ-ray spectra, γ-γ coincidence and ang. correl. meas. 78−13007
- ^{109}Ag levels from ^{109}Pd decay, spins, γ cascades, mixing ratios 77−22930
- Al, radial distrib. of γ-rays from narrowly collimated source *(Russian)* 77−30549
- ^{24}Al, β-transitions, weak magnetism, nuclear struct., matrix elements 79−13253
- ^{27}Al$(n,n'\gamma)^{27}$Al, γ-ray prod. cross-section meas. 79−26434
- ^{32}Ar, high spin states from heavy-ion fusion evaporation reactions, decay schemes 77−2932
- ^{75}As$(n,n'\gamma)^{75}$As, deexcitation gammas, energy levels, branching ratios, spins, parities, excitation function meas. 78−89869
- ^{209}At high spin states from ^{206}Pb(^{6}Li, 3nγ), γ meas., neutron hole influence 77−2934
- Au, A=189, 191, 193, γ-ray ang. distrib. meas., particle-hole symm. 77−88074
- ^{197}Au+^{136}Xe, 1064 MeV, fragment spin orientation from continuum γ-ray anisotropy meas. 80−22853
- ^{197}Au(n,γ), ^{198}Au energy level spins 79−457
- ^{198}Au level spin assignments from γ ang. distrib. and circular polarisation from ^{197}Au(n,γ) 80−52570
- ^{9}Be$(d,p\gamma)^{10}$Be, 1.5 MeV, angular correlation meas. 78−94015
- ^{207}Bi, decay, time differential perturbed ang. γ-γ correl. meas. 78−17134
- ^{78}Br, in liq. metal target, in-beam γ-NMR-PAD 77−59465
- ^{12}C, β-transitions, weak magnetism, nuclear struct., matrix elements 79−13253
- ^{12}C(p,p'), 22-27 MeV, 1^+ state de-excitation γ-ray ang. distrib., tensor force effects, DWBA anal. 80−68580
- ^{13}C$(^3\mathrm{He},\gamma_2)^{16}$O, ang. distrib. and correlation meas. of 26.42 MeV resonance 77−61444
- ^{23}C$(d,\gamma)^{15}$N, 2.90-9.95 MeV, cross sections, ang. distrib. meas. 77−6395
- ^{A}Ca, A=44,46 excited states and transition ang. distribs. from Ti(^{14}C,^{16}O) 80−95308
- ^{40}Ca$(\alpha,\gamma)^{44}$Ti, 2.75-4.00 MeV, γ-ray ang. distrib. of reson. for spin parity values 77−65230
- ^{40}Ca$(n,\gamma_0)^{41}$Ca, 8,12 MeV γ-ray ang. distrib. 78−66279
- ^{41}Ca, deorientation of highly stripped ions recoiling in vacuo 78−37325
- ^{41}Ca, highly stripped ions, recoiling in vacuo, γ-decays of isomeric states obs. 78−50119
- Cd, A=104 and 105, populated in α+Pd reactions, high spin states 78−62484
- ^{A}Cd, static quadrupole moments determ. for A=111, 113, 115 78−37281
- ^{107}Cd, heavy ion nucl. alignment, recoil in vac., time-differential meas. 78−37304
- ^{110}Cd transitions following inelastic scatt. of fast reactor neutrons 77−6287
- ^{110}Cd(p,γ) γ-22 MeV differential cross-section meas. 79−93617
- ^{111}Cd, quadrupole interaction of 247 keV state in Te 78−48088
- ^{112}Cd transitions following inelastic scatt. of fast reactor neutrons 77−6287
- Cd$(n,n'\gamma)$, A=114,6, E=2.67 MeV, ang. distribs. meas., 3^- octupole states anal. 77−38275
- Cd$(n,n\gamma)$, γ spectra and ang. distrib., ^{114,116}Cd energy levels, spins, particles 77−88070
- Ce, A=137, 139, high spin levels, γ spectra, hole-core coupling 77−50063
- ^{141}Ce collective M1 excitation effects on γ-ang. distribs., direct semidirect model of ^{140}Ce(n,γ) 80−57733
- ^{252}Cf spontaneous fission, prompt γ-ray differential angular distrib. 80−102220
- Cl, A=35,36,37 high spin states from heavy-ion fusion evaporation reactions, decay schemes 77−2932
- ^{36}Cl, g-factor determ. from perturbed ang. distribs. 78−12970
- ^{50}Cr$(p,p'\gamma)$, 2.00-3.03 MeV, proton and γ-ray ang. distrib. meas., p-wave reson. obs. 77−41961
- ^{51}Cr, bands, levels, EM transitions, J^π, branching and mixing ratios from ^{48}Ti $(\gamma,n\gamma)^{51}$Cr and ^{51}V$(p,n\gamma)^{51}$Cr 80−52606
- ^{51}Cr, strongly deformed $K^\pi=1/2^-$ bands from γ meas., level transition parameters 79−3113
- ^{52}Cr, high-spin states populated by ^{50}Ti$(\alpha,2n\gamma)$, assignment from spectroscopic states 77−65190

gamma-ray angular distribution continued
- ^{131}Cs, gamma-ray spectra from ^{131}Ba decay 79−85400
- ^{133}Cs, quadrupole interaction of 81 keV state in Te 78−48088
- ^{61}Cu analogue states, γ-ray ang. distribs. obs. 77−82848
- ^{63}Cu, decay of analogues, γ-ray ang. distribs. and spins of resons. 78−13002
- ^{63}Cu(p,p') negative parity level excitation, gamma ray obs., test for core excitation model 80−68534
- ^{64}Cu, γ-spectra, J^π assignments via ^{64}Ni$(p,n\gamma)$ 2.75-3.75 MeV 77−18470
- ^{155}Dy, γ-ray angular correlations 79−6494
- ^{160}Dy, γ-ray intensity and ang. correl. meas. 77−10354
- ^{A}Er, A=154, 155, γ-ray spectra, ang. distrib., high spin states 79−9503
- ^{167}Er levels and transitions, spectroscopic factor bombarding energy depend. from ^{168}Er(d,t), 9-15 MeV 79−495
- ^{A}Eu, A=145, 147, 149, mag. moments of $11/2^-$ states 79−40846
- ^{18}F ions recoiling in vacuum, mag. decoupling of hyperfine interaction 78−37270
- ^{20}F, β-transitions, weak magnetism, nuclear struct., matrix elements 79−13253
- Fe, ferromag., transient mag. field for ^{13}C 79−47362
- ^{A}Fe(p,γ_0)Co, A=54,56, giant dipole resonance splitting, direct-semidirect capture model anal. 80−106055
- ^{53}Fe, strongly deformed $K^\pi=1/2^-$ bands from γ meas., level transition parameters 79−3113
- ^{56}Fe isobaric analogue resonances, γ ang. distribs., spin assignments, decay characts. 78−78342
- ^{56}Fe$(n,2n\gamma)$, $(n,n'\gamma)$, 14.6 MeV, γ-ray ang. distrib. *(Russian)* 77−88147
- ^{67}Ga levels below 2.5 MeV populated in ^{64}Zn$(\alpha,p\gamma)$ 77−88042
- ^{67}Gd, γ-spectroscopy of high-spin levels via ^{64}Zn$(\alpha,p\gamma)$, ^{53}Cr(^{16}O,pnγ) 78−93960
- ^{146}Gd, 1579 keV state, assignment of isospin and parity, using γ-ray ang. distrib. 78−21489
- ^{151}Gd, high spin states, gamma ray and conversion electron obs., level struct. 77−46130
- ^{153}Gd γ-directional distrib., levels, spin assignments from ^{153}Tb decay 79−13241
- ^{153}Gd, mag. moment meas. of 129.2 keV 77−82850
- ^{154}Gd levels from γ ang. distribs., populated by ^{152}Sm$(\alpha,2n\gamma)$ and ^{154}Tb decay 79−442
- ^{70}Ge level spin and parity assignments from ^{56}Fe(^{16}O,2pγ), ^{67}Zn$(\alpha,n\gamma)$, ^{68}Zn$(\alpha,2n\gamma)$ 79−3081
- ^{71}Ge, in liq. metal target, in-beam γ-NMR-PAD 77−59465
- ^{71}Ge, levels, studied via ^{68}Zn$(\alpha,n\gamma)$, 8 to 10 MeV, comparison with coupling model calcs. 78−8742
- ^{72}Ge levels pop. in ^{8}Zn(^{6}Li,pn), in beam gamma-ray spectroscopy 80−47343
- H_2O, radial distrib. of γ-rays from narrowly collimated source *(Russian)* 77−30549
- ^{178}Hf, g-factor for K=6, $J^\pi=6^+$ isomer, perturbed ang. distrib. meas. 78−37277
- ^{197}Hg energy levels from ^{195}Pt$(\alpha,2n)$, γ and conversion electron spectra, spins, parities 78−25149
- ^{203}Hg nuclei, optically pumped, anharmonic mag. resonance phenomena 79−94015
- ^{165}Ho$(p,xnyp\gamma)$, 60 MeV, n and γ energies and ang. distribs. 78−89872
- ^{166}Ho, internal hyperfine field obs. using β-γ directional correl. 80−32229
- ^{166}Ho, spin assignments to levels, using ^{165}Ho(n,γ) polarised target and projectile 79−59062
- ^{127}I$(n,n'\gamma)$, fast n, γ-ang. distribs., level ang. momenta 80−18224
- ^{132}I isotope, doubly odd, quadrupole moments, PAC meas. 78−37280
- ^{109}In high spin states, γ-transitions, ang. distribs. from ^{108}Cd$(\alpha,2np)$ 80−73783
- ^{111}In band structure and hole-core coupling, ^{109}Ag$(\alpha,2n\gamma)$, branching and mixing ratios 78−58249
- ^{113}In$(\alpha, 2n\gamma)^{115}$Sb, 20-30 MeV, high-spin states in ^{115}Sb anal. 77−41982
- ^{115}In(p,γ) γ-22 MeV differential cross-section meas. 79−93617
- ^{40}K, g-factor determ. from perturbed ang. distribs. 78−12970
- ^{41}K, highly stripped ions, recoiling in vacuo, γ-decays of isomeric states obs. 78−50119
- ^{41}K, populated by ^{38}Ar$(\alpha,p\gamma)$, levels props., shell model calc. 78−62588
- ^{41}K(p,p'), impurity in Co, hyperfine field calc. by gamma ray ang. corr. method 78−6340
- ^{42}K, yrast state J^π assignments via ^{26}Mg(^{18}O, pnγ) anal. at 25,34 MeV 77−57618
- ^{79}Kr, low lying levels from ^{79}Br$(p,n\gamma)$ 80−105972
- ^{138}La, magnetic moment of the first excited state, meas. using TDPAD 79−63589
- ^{7}Li$(^3\mathrm{H},\gamma)^{10}$Be, 0.4-1.1 MeV, excitation curves, ang. distribs. 78−33200
- ^{177}Lu, 150 keV state, mag. dipole moment, TDPAC 77−41886
- ^{24}Mg$(^{32}\mathrm{S},^{32}\mathrm{S}\gamma)^{24}$Mg, TIPAC obs. on first 2^+ states 77−67762
- ^{24}Mg$(d,\alpha\gamma)^{22}$Na, 7.75 MeV, ang. correl. meas. using tensor polarised deuterons 77−22934
- ^{26}Mg+^{18}O, 34 MeV, yrast states in ^{41}K, ^{41}Ca, spins, parities from γ meas. 78−58250
- ^{53}Mn fragmented $g_{9/2}$ isobaric analogue resonance, γ-spectra and excitation functions from ^{52}Cr(p,γ) 80−68627
- ^{95}Mo, first excited $3/2^+$ state, g-factor determ. 77−26574
- ^{12}N, β-transitions, weak magnetism, nuclear struct., matrix elements 79−13253
- ^{14}N, meas. of nucl. g-factor of 5.11 MeV 2^- state by recoil distance technique 78−37268
- ^{14}N(p,γ), 1.742 MeV, 8.92 MeV doublet and 8.98 MeV level in ^{15}O anal. 77−38243
- ^{15}N polarisation, spin alignment and excited state ang. distrib. from ^{88}Sr(^{16}O, ^{15}N) 79−67709
- ^{15}N$(\alpha,\gamma)^{19}$F, 2.8 to 4.0 MeV, ^{19}F reson. strengths and ang. distrib. 77−65211
- ^{15}N$(p,\gamma_{0,1,2})$, 6-22 MeV, ang. distrib. and correl. meas., ^{16}O excited state giant resonance 77−82926
- ^{15}N$(p,\gamma)^{16}$O, anal. of ^{16}O giant dipole reson. struct. 78−4942
- ^{A}Na, A=22, 24, β-transitions, weak magnetism, nuclear struct., matrix elements 79−13253
- ^{21}Na, mag. moment of first excited state, time differential plunger meas. 78−37271
- ^{23}Na$(n,n'\gamma)$, 0.52-4.23 MeV, cross-sections, ang. distribs., mag. substate populations meas. 78−13100
- ^{23}Na$(n,n'\gamma)$, cross-section near threshold 78−8808
- ^{93}Nb$(\alpha,2n\gamma)^{95}$Tc, 17 to 27 MeV, band struct. of high momentum states in TC 78−33109

gamma-ray angular distribution continued
^{97}Nb level structure from ^{97}Zr decay, spins, parities γ ang. correls. 78−29418
Nd, A=139, 141, high spin levels, γ spectra, hole-core coupling 77−50063
Nd, A=148, 150, ions recoiling in vac. or low press. He, nuclear deorientation, perturbation mech. model 77−50105
^{21}Ne, recoil into vacuum g-factor meas. of $5/2^+$ state, 0.350 MeV 78−37272
^{21}Ne*, produced in ^{2}H(^{20}Ne,p)^{21}Ne*, 351 keV $^{5}/_{2}{}^{+}$ state lifetime and mag. moment 78−41631
^{21}Ne(p,γ)^{22}Na, γ-ray ang. distrib. and mixing ratios, analogue resons. 78−62504
^{58}Ni(^{16}O,2pγ), 40-58 MeV, γ ang. distribs., coincidences, ^{72}Se yrast states, lifetimes 77−54176
^{60}Ni, 1173 keV transition M3/M2 mixing ratio meas. 80−52608
^{60}Ni high spin states, J^π, $T_{1/2}$, ang. distribs. and polarisations from ^{56}Fe(^{7}Li, p2nγ) 80−99116
^{60}Ni(α,nγ)^{63}Zn, 8-16 MeV, low-lying negative parity states of ^{63}Zn anal. 78−21521
^{62}Ni(α, nγ), 8-14 MeV, γ ray study of ^{65}Zn odd-parity states, energies, transitions 78−50120
Ni(α,nγ)Zn, 6.5-17 MeV, particle-vibr. coupling in ^{65,67}Zn 77−38241
O^{16}, in beam-foil system, γ-ray angl. distrib. spin rot. 77−23545
^{15}O, nucl. g-factor and lifetime of 5.24 MeV $5/2^+$ level 78−37269
^{16}O(n,$\alpha\gamma$), 7-10.5 MeV gamma-ray prod. cross sections meas. 78−37338
^{18}O(p,p′γ), 3-3.5 MeV, γ-ray ang. distrib., for ^{19}F reson. and bound levels 78−89790
^{31}P(p,γ)^{32}S, ang. distribs. of γ-rays from decay of ^{32}S reson. states 78−13085
^{204}Pb(n,n′γ), 1.5-3.1 MeV, levels, J^π, excitation functions and mixing ratios 80−102123
^{208}Pb(N, γ_0), γ-ray ang. distribs., giant E3 resonances, direct-semidirect model 79−67727
^{208}Pb(N,γ), 6 to 40 MeV, dipole/quadrupole interference, direct-semidirect model, γ ang. distrib. 78−93994
^{208}Pb(p, γ), γ ang. distrib., isovector giant quadrupole resonance, direct-semidirect model 79−63647
^{208}Pb(p,γ), γ-ray ang. distribs. asymmetry effects through IAR, direct-semidirect model 80−42581
^{208}Pb(p,γ) fast capture, direct-semidirect model excitation function calcs. 78−94004
^{102}Pd, meas. of Q($2_1{}^+$) by reorientation precession technique 78−12971
^{104}Pd, meas. of Q($2_1{}^+$) by reorientation precession technique 78−12971
^{147}Pm, level scheme and transitions following ^{147}Nd 80−83073
^{147}Pm, low-lying levels, spin-parity and multipole mixing ratios 77−88043
^{141}Pr, positive parity levels, gamma-ray yields and ang. distribs. 80−105962
^{143}Pr in Ce, Ce(NO$_3$)$_3$ soln., mag. dipole moment of 57 keV state, PAC meas. 77−46110
^{191}Pt energy levels, γ and conversion electron spectra, spins, parities 78−25149
^{183}Re, elec. quadrupole moment of 514 Nilsson state, TDPAC meas. 78−37276
^{103}Rh, β-γ-γ directional correl., J^π determ. 77−26628
^{103}Rh, quadrupole moments of $3/2^-$ and $5/2^-$ states, reorientation precession meas. 77−2905
^{210}Rn high spin states, decay and lifetimes, spin assignments from ^{204}Pb(^{9}Be,3n) 80−18168
^{95}Ru level scheme, low lying states, g-factor spin, parity 77−88071
^{100}Ru, negative parity bands obs. in ^{100}Mo(α,4n)^{100}Ru 77−6291
^{105}Ru, γ-γ ang. correl. meas., spin and γ-ray mixing ratios 78−21516
^{32}S, transient field g-factor meas. on $2_1{}^+$ states 78−37273
^{33}S, excited states, ang. correl. meas. 77−38239
^{33}S, state spectroscopy via ^{30}Si(α,nγ), E1,E2, J^π assignments <5 MeV 77−34227
^{34}S, transient field g-factor meas. on $2_1{}^+$ states 78−37273
^{34}S(p,γ)^{35}Cl, determ. of ^{35}Cl resonance level spin and multipolarity mixing coeff. 79−9552
^{34}S(p,γ)^{35}Cl, $E_p=700$ to 2100 keV, γ-ray angular distrib. 79−9466
^{119}Sb, γ-γ and γ-e directional correls. following ^{119m}Te decay, branching ratios 78−546
^{121}Sb, positive parity levels, Coulomb excitation obs. 78−21522
^{122}Sb→^{122}Te second 2^+ excited state, β-γ ang. correls., β-ray spectrum shape 77−38250
^{123}Sb, positive parity levels, Coulomb excitation obs. 78−21522
^{41}Sc, decay and partial widths of 2883 and 5037 keV levels 77−88077
^{45}Sc, low-lying negative parity levels, Coulomb excitation 79−93552
^{28}Si, prolate and oblate intrinsic states *(French)* 78−70482
^{28}Si(^{16}O,αpγ) or (^{16}O,2pγ), high spin states, in ^{39}K and ^{42}Ca from γ meas. 78−89787
^{144}Sm+^{86}Kr, 490 MeV, γ-ray multiplicity moments 78−54798
^{149}Sm, γ-γ ang. correl. meas., transition multipolarities, multipole mixing ratios 77−41910
^{151}Sm, low energy levels, spin values, ga gamma-gamma ang. correl. meas. 77−18398
^{152}Sm(n,n′γ) spectra and ang. distribs. anomalous excitation *(Russian)* 77−54224
Sn, single closed shell even mass nuclei, collective bands, spin, parity, from Cd(α,2nγ), γ meas. 78−54719
^{A}Sn, even A=116, to 124, $2_2{}^+\to2_1{}^+$ energy level transitions in (n,n′γ) reaction, pair interaction effects *(Russian)* 79−3114
^{112}Sn, determ. of multipole mixture values in $2_2{}^+\to2_1{}^+$ transitions *(Russian)* 79−89268
^{114}Sn, determ. of multipole mixture values in $2_2{}^+\to2_1{}^+$ transitions *(Russian)* 79−89268
^{120}Sn(^{12}C,3nγ)^{129}Ba, E=45-54 MeV, excitation of high-spin levels in ^{129}Ba 78−17104
^{88}Sr(n,γ), 7-11 MeV ang. distrib. from fast capture 78−54758
^{178}Ta, nucl. orientation in Fe 78−39412
^{181}Ta, 136 keV level, g-factor meas. 79−6387
^{181}Ta, anomalous M1-conversion, 482-keV transition, penetration parameter meas. 77−61382
^{181}Ta, elec. quadrupole interactions in 482-keV level, meas. using Ge detector 79−40842
^{148}Tb, high spin states, transitions J^π assignments from (Li,xn) and (^{10}B,xn) 79−49582
^{153}Tb low excited states, γ-ray angular distrib. in ^{153}Dy decay 79−6471
^{153}Tb, low excited states, lifetime meas. 79−6492

gamma-ray angular distribution continued
^{155}Tb, oriented in Gd, γ-decay ang. distrib., hyperfine splitting, moment and mixing ratios 79−45242
^{156}Tb, orientation in Gd matrix, γ-ray ang. distrib. anisotropy meas. 79−59031
^{160}Tb, perturbed ang. correl. determ. by one ang. meas. 79−17851
^{160}Tb→^{160}Dy, $A_2{}^\beta$ ang. correl. coeff., β-γ-γ ang. correl. studies 79−13255
^{160}Tb→^{160}Dy, γ-transitions and angular distributions 80−83060
^{96}Tc, high spin states, γ-energy, intensity, coincidence, ang. distrib. and electron conversion from ^{93}Nb(α,n) 80−52554
^{97}Tc E2/M1 mixing from 785 keV ^{97}Tc γ-γ correl. 77−54178
^{97}Tc, γ-γ ang. correl. study, E2/M1 mixing ratios, transition strengths 77−71584
^{99}Tc, 920 keV level spin, from ^{99}Mo beta decay gamma-ray obs., 0.1-1 MeV 77−54145
Te(n,n′γ), A=124-130, gamma-ray ang. distribs. 77−34316
^{A}Ti, A=48,50, excited states and transition ang. distribs. from Cr(^{14}C,^{16}O) 80−95308
^{46}Ti(α,nγ)^{49}Cr, gamma-ray ang. distrib., ang. correlation, linear polarisation and Doppler-shift attenuation meas. 77−82941
^{48}Ti+^{16}O, anisotropy of yrast γ-transmissions 79−93650
^{198}Tl rotational structure, studied via ^{197}Au(α,3n) using in beam γ-ray spectroscopy 77−54130
^{163}Tm, high spin rot. levels, studied via ^{165}Ho(^{3}He,5n) and ^{165}Ho(α,6n) reactions 78−8722
^{167}Tm, energy level scheme from ^{165}Ho(α,2nγ) *(German)* 80−68576
^{167}Tm(HI,xnγ), ang. distrib., multipolarities *(French)* 80−68575
^{169}Tm, studied via ^{169}Tm(^{32}S,^{32}S′γ), EM props. of ground state rot. band 78−8726
^{171}Tm, 635.4 keV level props., mag. moment from γ ang. correl. meas. 78−13017
^{51}V(^{16}O, p2nγ), lifetimes of ^{64}Zn levels 78−13019
W, produced in (^{16}O,xn) 78−37371
^{A}W, A=173, 175, high-spin states, single-particle structure 78−93922
Xe, γ-γ PAC following nucl. electron capture, cascades perturbed by hyperfine coupling 78−37303
^{89}Y excited state ang. distrib. from ^{88}Sr(^{16}O,^{15}N) 79−67709
^{89}Y high spin states from γ-ang. distribs. in ^{87}Rb(α,2nγ), 30-55 MeV 78−93941
^{99}Y(n,γ), 7-11 MeV ang. distrib. from fast capture 78−54758
^{161}Yb, produced in (^{16}O, xn), γ-ray spectra, dipole moment in yrast cascade 78−37371
^{176}Yb(d,xnγ), 14 MeV, γ-ray spectra angular distribs. and $\gamma\gamma$ coincidences 79−75838
^{176}Yb(p,xnγ), 66 MeV, γ-ray spectra angular distribs. and $\gamma\gamma$ coincidences 79−75838
^{63}Zn, $5/2^-$ 193 keV level, γ-ray ang. distrib. integral rot. 77−41912
^{63}Zn level scheme, spin and parity assignments from (p,d), (p,nγ), (α,nγ), (^{12}C,pnγ) 79−465
^{64}Zn, γ-ray studies of levels above 3.1 MeV 80−32238
^{67}Zn, populated in ^{64}Ni(α,n), level struct. below 2.0 MeV, γ-ray studies 78−62483
^{68}Zn(α,pnγ)^{70}Ga, high spin levels of ^{70}Ga 77−30611
Zn(p,γ)^{67,69}Ga, 3 MeV, γ-ray ang. distrib. 78−74353
Zr (^{13}C, 3nγ), 45-56 MeV, collective and two-quasiparticle excitation in Pd 77−18601
^{89}Zr high spin states, J values, γ ang. distrib. from (α, 2nγ) and (α, nγ) 79−89217
^{94}Zr(p,nγ)^{94}Nb, neutron escape cross section determ., 1.7-3.0 MeV 79−9551
^{96}Zr(^{16}O, 4nγ), 56 MeV, γ yields, polarisations, ang. distribs., ^{108}Cd decay scheme 78−66301

gamma-ray applications
see also radiation therapy
absorption thickness gauges, effect of scattered γ radiation on sensitivity 79−71411
air/water mixture mass flow meas. by drag devices and γ densitometer 80−79385
back scattering flaw detector and thickness gauge 78−44333
boiler tube corrosion investigation 77−9011
cerebral blood flow meas., use of ^{133}Xe and computer calc. 77−5098
commercial irradiation plant, Japan 77−59794
cryogenic liquid, density meas. using radio-isotopic γ-attenuation method *(Russian)* 77−37847
density meas. by radio-isotopic technique *(Russian)* 77−33976
density measurement, metals, 0-2000°C, automatic device using γ-ray transmission 79−87787
density measurement by high energy photon scatt., dynamic capabilities 77−7485
density meter using radioisotopes, calibration and temp. compensation *(Russian)* 77−49713
density of fluid meas., theory, practices and appl. 80−73325
density of liquids meas., food industry appl. 79−44903
element analysis, using nuclear-physical methods *(German)* 77−25347
ethylene-Co copolymers and -SO$_2$ copolymers prep. by catalysis and ^{60}Co γ-radiation, mech. props. 80−66841
fast diffusion meas., nondestructive, using positron emitter as tracer 78−54519
flaw detection, use of Kalman filter 79−5121
flaw detector, multichannel 77−90565
flaw detector with analogue data processing, design and error calc. 77−73406
flow of liquid in pipes, continuity determ. 79−94748
fluid meas. in mechanical engineering, conf., Johannesburg, South Africa, (Feb. 1979) 80−75016
geophysical prospecting, allowance for scattered gamma radiation *(Russian)* 80−105067
GUPS-1 immersion follower gamma-level gauge 77−67412
HTGR block fuel elements, fuel zone location meas. using gamma scanning *(German)* 79−67847
incoherent scattering of gamma rays, spectrometer for electronic momentum distribs. investigation *(German)* 77−41741
irradiation facility of Bulgarian Academy of Sciences *(Russian)* 77−38592
irradiation geometries for food preservation 77−70508
liquid metals, diffusion, isotope effect determ. using radioisotopes 79−95191
local defect detection by scattering 78−44331

gamma-ray applications continued
medical diagnosis imaging stochastic distributed filtering approach 77−13026
medical instrument presterilisation 77−81558
metals activation analysis for impurities appl. of 30 MeV microtron 77−66720
mineral deposit evaluation with Metalog anal. technique 77−64446
multibeam sonde, stand for adjusting 80−85103
multiphase pipeline flows, measurement of component ratios 80−38513
NDT flaw detector with analogue data processing, param. optimisation 77−81374
nuclear power plant components, acceptance tests, using X- and gamma ray images *(German)* 78−44297
nuclear reactor fuel burnup, nondestructive verification, γ-ray spectrometry 77−3137
perimeter security system using ^{137}Cs γ-ray beams 77−18713
polyethylene, irradiation, crystallinity and crosslinking efficiency 80−66843
polyethylene-glass fibre composites, gamma-irradiated filler 80−66840
polymer manufacture, radiation treatment of waste-water, feasibility *(Russian)* 78−46181
qualitative assessment, field assessment 78−85444
quartz dental composites, acrylic acid grafted on particles by gamma-radiation 80−66840
radioactive tracers, principles, techniques, appl. to engineering systems 77−65065
radiography, use of Se electroradiography plates 78−72978
rate meter-type flaw detector, measuring circuits 78−60963
rubber-metal facings, vulcanisation degree determ., γ-ray method 80−61043
seawater density determ. using gamma radiation *(Russian)* 77−82037
soil-water system, γ-ray transmission studies, calibration 80−26629
speed-granularity relations for X-ray and γ-ray exposures 79−21828
sterilisation, ^{60}Co plant design for developing countries 77−60246
sterilisation facilities, for medical products 77−70543
sterilisation facility, in Medicor Works' Debrecen Factory of Surgical Instruments, test dosimetry 78−40336
sterilisation of semi-synthetic penicillins 80−17064
TDPAC, appl. to chemistry and solid state physics, review 79−75665
teletherapy unit, radiation head, temp. distrib. 79−72790
thermometer and strain gauge for remote meas. 78−12694
thickness meas. of spacecraft equipment 78−66013
vaccine production, use of ^{60}Co-γ-irradiation, polymerisation conditions 78−40320
^{60}Co irradiation sterilisation processing unequal mass interchange model verification 79−26759
^{60}Co irradiation sterilisation processing, unequal mass interchange model 79−26758
^{60}Co irradiation sterilisation processing, nonstandard double carton simulation 79−26760
Nb-H, $\alpha+\alpha'$ region, precipitation morphology investigation by gamma ray diffr. 77−52333
RbI, single crysts., mosaic struct. changes, press. induced 412 keV γ-rays obs. 77−51507

gamma-ray astronomical observations
γ195+5, SAS-2 high-energy obs. 77−33688
B 1900+14, soft gamma-ray bursts obs. *(Russian)* 80−36742
background radiations in 0.03-4.1 MeV range, Kosmos 461 meas. *(Russian)* 77−33708
burst, 1979 March 5, evidence for periodicity 80−31389
burst events, Pioneer Venus orbiter obs. 80−46707
burst obs. at altitude of possible Cygnus source *(Japanese)* 78−61933
burst obs. from Helios 2, source directions 79−101218
burst obs. in 1978 November, ISEE 3 high-resolution spectroscopy 80−67907
burst source, 1979 March 5, error box 79−58441
burst source in Sculptor measured by Venera 11, 12 and Prognoz 7, identification attempt *(Russian)* 80−77520
burst source obs., 1976, Dec. 77−9821
burst source on 1976 August 16, balloon-borne obs. 78−54078
burst source registration by Prognoz 6 Sneg-2MP instrument *(Russian)* 79−21468
burst sources, ISEE 3 obs. and expt. 80−98546
burst sources distrib. over celestial sphere *(Russian)* 79−88766
burst sources of 1977 October 20 and November 10, position bands *(Russian)* 80−36738
bursts, intensity distrib., galactic origin *(Russian)* 79−16772
bursts of γ-rays obs. with Prognoz 6 and Sneg 3 satellites, localization of sources *(Russian)* 79−80371
3C273, COS B high-energy gamma-ray obs. 78−93454
3C 273, search for 1-20 MeV gamma rays, balloon-borne obs. of QSO 80−67912
Centaurus A, nuclear γ-rays detect. 77−13482
CG 135+1, evidence for nearby low-energy γ-ray emission 80−31392
CG 135+1, search for 1-20 MeV gamma rays, balloon-borne obs. of QSO 80−67912
CG 135+1, spectrum obs. 20 keV-25 MeV 80−105398
CG 195+4, 35-8737 keV gamma ray search in Geminga field 80−27012
CG sources, 100 MeV, very high energy gamma-ray emission search 79−40293
cosmic diffuse γ-ray flux, 2-25 MeV energy range 78−32309
cosmic gamma-ray burst source, position from Helios 2-Vela-Ariel 5 obs. 79−48956
cosmic gamma-ray bursts, obs. and new limits on distrib. 78−93465
cosmic gamma-ray bursts, preliminary results from Solrad 11 detectors 77−57108
cosmic gamma-ray bursts, Venera 11 and 12 CONUS expt. obs. *(Russian)* 79−58449
cosmic ray γ quanta, short-term fluctuations obs. 80−67483
cosmic rays, 0.511 MeV energy, meas. with balloon-borne Ge(Li) spectrometer 77−53373
Crab Nebula, final SAS-2 gamma-ray results 77−33688
Crab Nebula, low-energy gamma-ray obs. 77−29894
Crab Nebula, obs. by gamma-ray telescope with modulating anticollimator *(Russian)* 79−16832
Crab Nebula, possible γ-ray line detect. 77−49458
Crab Nebula, search for 400 keV γ-ray line 78−12345
V1500 Cygni, search for gamma ray lines 78−8013

gamma-ray astronomical observations continued
V1500 Cygni (Nova 1975), high-energy gamma-ray flux upper limit 78−36603
Cygnus, burst source observed at balloon altitude, position 78−41096
Cygnus X-1, obs. in energy range 100 keV-3 MeV 78−20907
Cygnus X-1 and X-3, search for 1-20 MeV gamma rays, balloon-borne obs. 80−67912
Cygnus X-3, 1974 EAS obs. of high-energy gamma-ray source *(Russian)* 77−64881
Cygnus X-3, γ-ray flux meas. above 10^{12} eV 77−53706
Cygnus X-3, Crab and Vela pulsars and galactic plane, high energy γ-ray spectra comparison 79−80368
Cygnus X-3, gamma-ray emission periodicity 79−62932
Cygnus X-3, gamma-ray obs. with 4.8 hr periodicity 77−26086
Cygnus X-3, periodic γ-ray emission obs. *(Russian)* 77−91672
Cygnus X-3, periodic gamma flux *(Russian)* 77−26090
Cygnus X-3, search for gamma ray emission 77−74159
diffuse galactic components and H I distrib. 80−41917
diffuse gamma radiation, SAS-2 obs. 78−8169
diffuse gamma-ray radiation, MeV excess in energy spectrum 78−73777
enhanced gamma-ray emission detect. by COS B satellite 77−17722
EXP 0520−66, flaring X-ray pulsar, recurrent gamma-ray bursts obs. *(Russian)* 80−36741
exploding black holes, search using atm. Cherenkov method 78−49473
fast intense gamma-ray transient (1979 March 5), detect. 80−73073
flaring X-ray pulsar in Dorado, gamma-ray bursts *(Russian)* 79−88765
galactic γ-ray lines, balloon investigation using Ge(Li) spectrometer 80−8677
galactic anticentre region sources, final SAS-2 results 77−33688
galactic background, structure from gamma ray obs. 80−98743
galactic centre and anticentre 79−62901
galactic centre direction, positron annihilation radiation at 511 keV 79−5902
galactic centre hard γ-rays and diffuse background, Kosmos 561 obs. 79−84597
galactic centre region, high energy gamma-ray emission 77−53704
galactic centre region, medium-energy gamma-ray emission obs. 79−9030
galactic disc, high-energy gamma-ray spectral characts., COS-B obs. 78−36695
galactic disc, obs. between $-45^\circ < l^{II} < 45^\circ$ in 80 keV to 8 MeV energy range 80−82540
galactic disc anticentre direction, localised high-energy γ-ray emission, COS-B obs. 77−49495
galactic gamma radiation in 0.03-4.1 MeV range, Kosmos 461 meas. 77−67144
galactic gamma-ray flux, 60 keV to 5 MeV range, from ensemble of point sources 79−53933
galactic gamma-ray lines, balloon obs. with high resolution Ge(Li) spectrometer *(Japanese)* 79−80353
galactic high-energy gamma-ray sources obs. by COS-B satellite 77−91670
galactic plane, search for 1.2 MeV γ-ray line 78−93475
gamma-ray burst, distance and spectrum of 1972 April 27 event 80−67903
gamma-ray source near 3U 0258+60, flux meas. 77−2497
implications for energetic particle acceleration 80−31390
isotropic metagalactic background in 0.03-4.1 MeV range, Kosmos 461 meas. 77−67144
LMC N 49, X-ray source 0525.9-66.1, gamma-ray burst obs. *(Russian)* 80−36739
Moon, regolith Ti composition, orbiting γ-ray expt. 80−17510
N49, SNR in LMC, Pioneer Venus Orbiter obs. of 1979 March 5 gamma-ray transient 80−77518
NGC 4151, search for 1-20 MeV gamma rays, balloon-borne obs. of Seyfert galaxy 80−67912
NGC 4151, Seyfert galaxy, gamma-ray energy spectrum *(Russian)* 79−88748
NGC 4151, Seyfert galaxy, low energy gamma-ray obs. 78−12368
NGC 4151, Seyfert galaxy, low-energy γ-ray spectrum 80−31370
Nova Serpentis 1970 search for gamma ray lines 78−8013
NP 0532, Crab pulsar, search for pulsed gamma-rays of energy 10^{13} eV 77−13373
observational test of cosmological particle production theories 80−109574
primordial black holes, search for high energy gamma ray bursts 78−54084
PSR 0531+21 (Crab pulsar), pulsed γ-ray emission, COS-B obs. 78−8033
PSR 0833-45, Vela pulsar, pulsed high energy gamma rays 80−41848
PSR 0833-45, Vela pulsar, radio and γ-ray pulses, relative phases 78−85966
PSR 0833-45, Vela pulsar, SAS-2 high-energy γ-ray obs. 77−49411
PSR 0833-45 (Vela pulsar), pulsed γ-ray emission, COS-B obs. 78−8033
PSR 1747−46, gamma-ray emission obs. by SAS-2 77−2450
PSR 1822−09, balloon-borne gamma-ray obs. 80−105269
pulsar NP 0532, COS-B satellite obs., appl. of X-γ synchronisation to non-parametric anal. 78−73729
pulsars, gamma-ray light curves, geometrical anal. 80−36653
pulsars, high-energy pulsed gamma rays obs. 78−45346
Scorpius X-1, low-energy γ-rays, Dec. 1974 balloon obs. in 0.2-5 MeV range *(Portuguese)* 78−57702
sky survey with fine energy resolution using Ge gamma-ray spectrometer 77−53701
solar flares, particle acceleration, X-ray and gamma-ray obs. 80−31265
solar spectrometric obs. from Prognoz satellites 79−21127
spiral galaxies, gamma-ray luminosity, contrib. to diffuse background above 100 MeV 78−93481
Sun, gamma-ray lines from flare, HEAO 1 obs. 80−67682
Taurus region, evidence for detect. of 1-10 MeV emission in 1971 August 77−45605
transient gamma-ray event of 1979 March 5, location 80−73074
4U 1206+39 (NGC 4151), hard X-ray variability of Seyfert galaxy 80−17647
ultra high energy gamma-ray bursts from celestial sources, unsuccessful search 80−67911

gamma-ray astronomy
see also gamma-ray sources (astronomical)
active aperture imaging for direction meas. of high energy γ-rays 80—62022
artificial satellite investigs. 79—53727
astrophysics review, new look at universe 79—80373
background radiation spectrum, effects of evaporation of primordial black holes 79—88695
balloon and satellite obs. of gamma-ray lines, appls. 78—45241
balloon obs., effect of multiple Compton scatt. in atmosphere 78—28352
burst sources, location via periodic slot collimator 77—64647
bursts, galactic origin and chronological catalogue 77—37672
Cherenkov atmospheric detectors, sensitivity 77—3232
Compton telescope, appl. of Anger camera principle, for gamma-ray astronomy 79—80223
conference, non-solar gamma-rays (Bangalore, India, May-June 1979) 80—77548
conference (La Jolla, CA, 12 to 14 September 1978) 79—53937
COS-B, instrument description *(Danish)* 80—82544
COS-B satellite, ESA extraterrestrial gamma radiation obs. project *(German)* 79—21151
cosmic gamma ray spectroscopy, review 80—67582
cosmic gamma-ray origin and obs., review 77—73912
cosmic ray origin and gamma-ray astronomy 79—29951
cosmic ray physics 80—46352
cosmic ray primaries meas., 10 to 100 GeV, using air showers Cherenkov light distrib., detector system 78—73597
cosmic ray studies, SAS-2 and COS-B satellite studies 78—7843
cosmic rays, review *(Korean)* 79—12368
cosmic rays in the galactic centre, predicted from high energy γ ray observations 80—72731
detector angular resolution 80—8539
detectors for gamma-ray burst astronomy, critical comparison 77—64648
diffuse background meas. using nondirectional detectors 77—73968
diffuse cosmic gamma-ray spectrum, Apollo data in 0.3-10 MeV region 77—33705
diffuse isotropic background, cosmological considerations 80—51923
double scatter telescope for medium energy gamma ray astronomy from a satellite 79—48676
drift chamber detector, performance figures, γ-ray astronomy appl. 79—48674
drift chamber detector for high resolution gamma-ray astronomy 77—9660
drift chamber telescope for gamma-ray astronomy 79—21185
drift chambers in high-energy gamma-ray telescope 80—41726
electron-positron pair track analysis in multilayer gamma-ray telescope 80—63469
energetic particle acceleration, gamma-ray obs. implications 80—31390
experimental basis, review *(Polish)* 78—96394
Franco-Soviet cooperation, in gamma-ray astronomy area *(Russian)* 78—40844
galactic background, structure from gamma ray obs. 80—98743
galactic emissivity, large scale structure 79—71116
galactic gamma-rays and origin 77—78584
galactic structure, models and theories based on gamma astronomy *(French)* 77—60829
galactic structure from gamma-ray data 78—16538
gamma-ray picture of sky, review *(Russian)* 78—41097
hard X-ray camera for study of gamma ray burst sources 79—25502
HEAO programme outline 77—78595
High Energy Astronomy Observatory (HEAO) programme 79—44368
hot accretion disks in galactic nuclei, pair production and gamma-ray luminosities 80—56930
imaging detector for hard X-rays/soft γ-rays 79—58250
imaging double Compton telescope for balloon obs. of MeV gamma radiation 79—25503
instrumentation, for low and medium energy ranges 79—25492
ISEE 3 experiment and obs. of burst sources 80—98546
large area gamma-ray telescope, coordinate-sensitive time-of-flight scintillation system 79—84676
large scale telescopes for high resolution obs. 78—93114
line emission sources, review 79—44641
Lixiscope, X-ray and gamma-ray telescope system 80—62020
maximum-entropy image processing in gamma-ray astronomy 79—48684
MISO low energy γ-ray telescope 79—25472
modulating anticollimator for low and medium energy gamma-ray telescope *(Russian)* 79—16832
Moon, geochemical mapping by orbital gamma-ray spectroscopy 77—25953
multilayer wide-gap spark chamber for a gamma telescope 79—76267
neutron star cyclotron line emissions meas. with Ge(Li) balloon borne spectrom. 80—41721
neutron stars, redshift determ. of X- and γ-ray lines rel. to strong principle of equivalence 78—40814
origin of gamma-rays in cosmic ray interactions with matter *(Polish)* 78—96571
Pioneer Venus Orbiter Gamma Burst Detector 80—67505
planetary surface elemental anal. via orbital gamma-ray spectroscopy 79—12412
point sources of 10^{11}-10^{14} eV gamma-rays using atmospheric Cherenkov technique 79—25422
present status, review 79—25763
proton interaction with lunar and planetary material, gamma-ray production, simulation 78—16318
pulsars, gamma-ray spectra 79—30083
remote sensing spectrometers, data analysis system for planetary mission appl. 79—12411
review 77—64888
satellite prospects, COS B rewards 80—21889
solar flares, pulsars, galactic disc and cosmic diffuse background obs., review *(German)* 77—60853
solar gamma ray emissions study, Solar maximum mission, detector assembly and electronic assembly 80—63476
Solar Maximum Mission, gamma-ray spectrometer 80—51657
Space Shuttles, Gamma Ray Observatory launch instrums. and operations 80—109365
spark-chamber, wide-gap chamber for gamma-ray astronomy, Soviet-French design 78—17503
spectra in 10 keV-100 MeV range, book 77—37673
spectrometers, cooled Ge, on P78-1 satellite 80—58019
spectroscopy and gamma-ray line production 80—31271

gamma-ray astronomy continued
stellar nucleosynthesis constraints from detect. of ^{26}Al gamma ray line 80—94780
superconducting superheated granules as X-ray and γ-ray imaging detectors 79—25504
telescope for high energy X-rays, large sensitivity, energy and angular resolution 80—62016
telescope for medium energy gamma-rays scintillation counter time-of-flight system 80—62017
telescope on satellite, axis orientation determ. 79—2479
time of flight directional coincidence telescope for gamma ray telescopes 77—390
time of flight telescope for high energy gamma-ray astronomy 80—31210
ultra-high energy γ-ray astronomy (10^{11}-10^{13} eV) 80—101649
Ge spectrometers, cooled, for X-ray and gamma-ray astronomy 77—5438
Ge(Li) balloon borne spectrom. for obs. of neutron star cyclotron line emissions 80—41721
Ge(Li) spectrom., balloon-borne, recent meas. 78—93107
Ge(Li) spectrometer, high resolution, appl. to galactic gamma-ray lines obs. *(Japanese)* 79—80353
NaI(Tl) large area multi-crystal detectors for X-ray and gamma-ray astronomy 77—22070

gamma-ray detection and measurement
see also gamma-ray spectrometers; radioactivity measurement
$4\pi\beta$-γ coincidence method for radioactive source standardisation *(Rumanian)* 77—46472
4 $\pi\beta$-γ coincidence counting, source prep. using AlCl$_3$ 78—838
140 keV γ position-sensitive multiwire proportional chamber characteristics 79—54749
acoustic detector for beta and gamma radiation *(German)* 79—63876
activated thick foil close to NaI detecting crystal, gamma counting and self-shielding efficiency 80—69043
activation of mica and plastic, neutron fluence meas. 78—13346
activity meter for nuclear medicine, ionisation chamber characts. 79—66558
air ionisation probe for α, β, γ hand and shoe monitor 80—58084
airborne γ-ray spectrometer calibration, altitude effects 80—18754
airborne gamma-ray detectors, fields of view 80—51555
airborne gamma-ray spectrometry data processing using multivariable statistical analysis 79—35004
airborne mapping and tracking system 77—38427
alarm device, portable, with audible/visual warnings 78—8390
analysis using ion induced gamma rays 79—5220
Anger camera dead-time, effect of window fraction 77—86598
Anger camera image digital filtering 77—9256
Anger scintillation cameras, state-of-the-art in suitable photomultiplier tubes 78—40304
angular correlation, intrasource absorpt. and scatt. effects 79—97958
angular correlation apparatus for materials science 77—74563
annihilation radiation measurement in activation analysis, specificity enhancement by triple coincidence 77—90687
annihilation spectra, two-component, resolution using count ratio technique 78—44424
Asama volcano, Japan, distrib. of gamma radioactivity 79—66696
Asama volcano, Japan, in situ gamma ray radiometry appl. *(Japanese)* 79—66824
associated gamma-ray technique for neutron fluence meas. 79—9978
astronomical Compton telescope, high ang. resolution, for 0.3-10.0 MeV gamma-rays *(Portuguese)* 78—85847
astronomy, high energy, γ-ray telescope, large sensitivity, energy and angular resolution 80—62016
astronomy medium energy gamma-ray telescope, scintillation counter time-of-flight system 80—62017
attenuation meas. using Ge(Li) detector for Pb, Ta, Mo 78—17539
automatic peak locating techniques 77—71731
autoradiographic inventory methods for nondestructive assay of reactor fuels and fuel assemblies 80—71875
back-scattering radiometry for concrete density meas. 77—36699
background correction algorithm for γ-γ coincidences 79—13616
backscattered photons number albedo meas. 79—36490
backscattering of γ-rays 77—88323
Bayesian deconvolution, appl. and algorithm implementation 78—70103
beam time saving technique for measuring excitation functions in heavy ion reactions 78—70721
benchmark γ-spectrometry, unfolding codes 79—26802
beta-gamma survey meter with numerical display 77—64134
betatron, radiation protection meas. 79—29636
biological and ecological samples *(French)* 78—5052
biomedical scintillation chamber, operating model 80—30848
bone-seeking radionuclide skeletal burden determ. from in vivo scintillation meas. of head 78—15915
borehole capture gamma-ray anal., optimal size ^{252}Cf neutron source 79—29890
borehole probe with LED for γ-ray spectrum stabilisation 79—45552
bremsstrahlung energy flux unit, 0.8 to 8 pJ, USSR special standard 77—30730
bulk sample gamma-ray assay, equipment specification 78—24158
BWR spent fuel safeguarding, nondestructive assay using gamma spectrometry 80—68802
BWR Vermont Yankee power station, external radiation field meas. 77—54368
calibration system standardisation for nationwide use 77—38583
calorimeter for high energy photons 79—36469
calorimetric dose meas. in ^{60}Co gamma field 77—40787
camera, 3-D particle track chamber using Compton interactions 77—86622
camera, electronically collimated, for single gamma emission computed tomography 78—44603
cameras, use of coded apertures with digital decoding 77—86620
capture gamma-ray detector, neutron sensitivity 80—18767
cellulose acetate detector, gamma-ray effect on light absorption used as dose meas. technique 78—13345
cellulose nitrate, effect of high γ-doses on etching characts., dosimetry appl. 79—31224
cellulose nitrate solid state nucl. track detector, gamma dose meas. 78—73247
channel-type reactors, γ-ray dose rate spatial distrib. over entire thickness of side shield 78—86697
charge plunger technique, nuclear lifetime meas. 78—29698

gamma-ray detection and measurement continued
chemical dosimeters, aq. solns., comparison for absorbed doses of 10-1000 rads 78—41885
chemistry applications of γ-γ perturbed ang. correl. meas. *(Japanese)* 78—40098
Cherenkov atmospheric detectors for gamma-ray astronomy, sensitivity 77—3232
Cherenkov counter, liq.-filled, for gamma-ray counting of large samples 78—53491
Cherenkov counter photomultiplier, sensitivity to gamma quanta 78—9032
Cherenkov ring imaging counter, single photon detectors 80—58036
coded aperture γ-ray imaging, multiplex noise *(French)* 77—90887
coded aperture imaging, signal to quantum noise ratio 78—37122
coded aperture imaging of gamma-ray sources, class of near perfect coded apertures 78—40300
coded-aperture configuration, gamma-ray imaging in Fourier space 79—17588
coincidence and sum method, appl. to ^{110}Cd spectra *(French)* 78—62675
coincidence meas. of α, X, and γ-rays 79—26851
coincidence method for Coulomb excitation studies of weakly populated vibr. like levels 78—70716
coincidence two-dimens. spectral data, offline treatment 79—97960
composite X-ray and γ-ray detectors 79—9890
Compton telescope, appl. of Anger camera principle, for gamma-ray astronomy 79—80223
computer assisted ring detector positron camera system for brain reconstruction tomography 78—40306
concrete, meas. of albedo number using ^{60}Co, ^{137}Cs sources 79—26768
constant fraction differential discriminator for use in fast timing coincidence systems 79—45580
cosmic gamma-ray burst astronomy, critical comparison of detectors 77—64648
cosmic ray γ-rays in range 3.5 to 100 MeV, system for meas. ang. and energy distribs. 77—50324
cryogenically pumped gas target for γ-ray ang. distrib. meas. 78—55076
crystal diffraction spectrometers 79—72183
curved crystal spectrometers, high precision γ-ray energies of fission products 79—93865
curved plunger for TDPAC meas. on recoil into gas 79—76313
defectoscope, multichannel, spectrometric method of recording γ-radiation in scintillation counter 78—53099
delayed coincidence summing, nucl. half life meas. 78—55088
detector calibration for extended sources 79—724
detector perturbations to neutron and gamma-ray spectra measurements in liquid air 79—59314
detector system for determ. of internal radiation exposure dose 79—5378
diamond tissue-equivalent dosimeter, for X-rays and gamma-rays 77—56477
diffractometer using ^{198}Au source at FRM reactor 78—54514
digital multidiscriminator for use in gamma-gamma coincidence experiments 78—70707
directional γ-ray detector for in-core fuel motion monitoring 78—37448
directional fully encapsulated gamma detector for in-core reactor meas. 80—63307
discrete and continuum γ rays from Cu(n,nγ) prod. cross sections 77—34293
distance meas. with coincident gamma-ray using positron lifetime spectrometer 79—12765
Doppler effect appl. in nucl. spectroscopy *(Hungarian)* 80—14036
dose intensity in dwelling places, dose conversion factors *(Hungarian)* 77—77990
dose meas. in d(80)+Be neutron beam 79—70648
dose rate meter, use as X- and γ-ray secondary protection-level standard 77—81579
dose rates in mixed beta-gamma fields, scintillation counter method 77—60254
dose-rate conversion factors for external exposure to photons and electrons, modifications to DOSFACTER code 80—104775
dosimeter, CdS with Cu traces, prod. and characts. 78—8999
dosimeter, clear Perspex effect of storage temp. on calibration 77—60256
dosimeter, differential microcalorimeter, 0.01-10 W *(Russian)* 78—85385
dosimeter, KG21, features 78—74509
dosimeter, Se, differential dosimetric characts. w.r.t. γ-radiation 80—32529
dosimeter calibration in terms of absorbed dose in water for ^{60}Co γ-radiation 80—18696
dosimeter neutron/gamma sensitivity determ., comparison of spectral difference and Pb filtration methods 77—90915
dosimeter system, transit type, for ^{60}Co rot. therapy, electronic modification 77—2053
dosimeter testing, effect of air scattered radiation 79—6774
dosimeters, energy relationship of effectiveness and error estimation 79—31225
dosimeters, integral, calibration for personal dosimetry *(Czech)* 80—27825
dosimeters, thermolum., supralinearity 77—10495
dosimeters for personnel monitoring, intercomparison 77—40781
dosimetry, effect of buildup factors 80—18698
dosimetry, irrad. vessel wall effects in chemical dosimeters 80—18697
dosimetry, using cholesteric liq. cryst. soln. colour transition 77—48877
dosimetry of n and γ from ^{252}Cf source with high emission, safety *(Czech)* 78—33296
dosimetry of sterilisation facility in Medicor Works' Debrecen Factory of Surgical Instruments 78—40336
Double Compton Telescope, background sensitivity to atmospheric neutrons 78—53827
double cylindrical 4π ionisation chamber for γ source nuclide activity 77—10536
double ionization chamber for the differential method 79—22552
double scatter telescope for medium energy gamma ray astronomy from a satellite 79—48676
drift chamber detector, performance figures, γ-ray astronomy appl. 79—48674
drift chamber telescope for gamma-ray astronomy 79—21185
dust samples, neutron activation anal. using high-rate loss-free gamma spectroscopy system 78—61129
EAS arrival direction distributions 78—28471
EBR-II active calorimeter design improvement 79—9967

gamma-ray detection and measurement continued
education, nuclear fallout radioactivity γ-ray detection and anal., Chinese fission bomb anal. 78—49596
eight-sensor low-energy γ topograph *(Russian)* 78—35932
electron and γ interaction ranges, Monte Carlo calc. *(Russian)* 79—12370
electron-photon cascades separation by scintillation counter system 78—78563
electronic lifetime meas. with Ge(Li) detector using centroid-shift method 79—6790
elemental analysis by neutron inelastic scatter gamma rays with a radioisotope nuetron source 80—30311
elemental sensitivity data modeling for in situ neutron capture gamma-ray experiments 79—61928
EM shower sampling counters, characteristics of plastic scintillator and radiator layers 78—58530
emulsion chamber for cosmic γ-ray detection 79—29959
emulsion chamber for cosmic γ-ray detection 79—29958
emulsion chamber measurements of ultrahigh energy γ-rays *(Chinese)* 77—10525
energy deposition measurement by thin film resistors 78—29719
environmental γ flux meas. method using NaI(Tl) scintillation counter and photomultiplier 78—21786
environmental gamma radiation in Norway, population doses 78—11745
environmental measurements using standard Ge(Li) detectors 77—38568
environmental source monitoring 77—38429
exposure rate and absorbed dose meas. for 6-7 MeV 79—26766
expsoure efficiency dependence on distance, theoretical interpretation *(Czech)* 80—850
fallout γ-ray spectra anal. using Ge(Li) detector, 19th Chinese nucl. test explosion *(Japanese)* 79—31219
FFTF element measuring system 79—9729
film photon and electron absorbed-dose detector 80—91379
fission and radiative capture cross sections ratio meas. in reson. region 77—50175
fission product activity ratios in RA used fuel element, γ-ray spectroscopy 79—41061
fission reactor loss of coolant studies, gamma densitometer detector comparison 80—57881
fission track-etch-cum-γ-spectrometry method for absolute fission yield meas. 80—27859
flash tube chamber, high press., γ-ray energy and spatial coords. meas. 77—57794
foil, surface density meas. method using back-scattered low energy γ-rays *(Czech)* 77—50323
gamma camera, Anger-type, time resolution *(German)* 77—13000
gamma camera, appls. for three-dimensional emission tomography using scattered photon information 80—98134
gamma cameras, state of art 80—3802
gamma radiation dosimeters, sensitivity of p-type channel MOS transistors 79—67966
gamma radioactive source measurement, in dynamic condition, error sources *(Rumanian)* 78—46243
gamma thermometer, developments for LWR power monitoring 79—45368
gamma-gamma coincidence 2-D analysis 77—18733
gamma-ray camera using Compton effect 78—10087
gamma-ray spectrometers; calc. of radioactivity induced during spaceflight 80—102382
gas flow detector, back-scatter-type, conversion electron Mossbauer spectrometry 80—37680
Geiger-Mueller counter γ dosemeters, fast neutron sensitivities, mixed field dosimetry 78—92705
Geiger-Muller gamma dosemeters, fast neutron sensitivities, 14.7 MeV 77—52880
graphite ionisation chamber with CO_2 filling, Monte Carlo anal. of fast neutron irradiation 78—82583
hardness dependence of glass dosimeters for photons with energy up to 6 MeV 80—846
high density proportional counter, medical imaging of e^+ radioisotope distrib. 79—5399
high energy, organic liquid scintillator appl. *(Japanese)* 77—46451
high energy interaction, effect on spectral peak centroid determ. 79—36468
high rate 4π β-γ coincidence counting system 79—45588
hodoscopic spectrometer, gamma-quanta coordinate meas. in NITsE scintillation spectrometer 78—78549
HTGR, at Peach Bottom, gamma scanning the primary circuit at end-of-life 77—46419
HTGR block fuel elements, fuel zone location meas. using gamma scanning *(German)* 79—67847
HTGR coated-particle fuel, irrad. performance determ. by irradiated microsphere gamma analyzer (IMGA) 79—54543
HTGR core, γ-spectroscopic exam. of fission product distrib. after shutdown 79—67909
human total-body counter 79—100728
hybrid MWPC gamma ray detecting system for applications in nuclear medicine 79—5397
image intensifier gamma camera using Si posn. sensitive strip detector 77—81565
image intensifier scintillation cameras for nuclear medicine 77—40732
imaging double Compton telescope for balloon obs. of MeV gamma radiation 79—25503
instrumentation, for low and medium energy ranges, astronomical appl. 79—25492
integral dosimetry, use of lyoluminescence *(Czech)* 79—67964
integral measurements, shielding cross section test 77—23305
integrating counting technique, appl. to ^{197}Au Mossbauer spectroscopy 78—25377
intense photon flux absorbed dose meas. 78—41387
intense proton beam current measurement via prompt γ rays from nuclear reactions 78—93784
ionisation chamber for X, gamma rays, performance monitoring of radiation shielding 79—6797
ionisation chambers, depth dose distrib. of 9 MeV photons, comparison with phantom results 77—32957
irradiated fuel rods, computer-controlled gamma scanning 79—9753
K-factors, correction of error 79—84278
Kodak Type II film badges, gamma dose meas. in presence of thermal neutrons 79—39517
leakage radiation meas., effective energy determ. 78—28089

gamma-ray detection and measurement continued
  - lignocellulose polymer composites as γ-dosimeters in the kilorad range 80—95465
  - liquid activity meas. instrumentation in Czechoslovakia 79—49873
  - liquid rare gases, ionisation and scintillation, review *(Japanese)* 78—35206
  - liquid scintillator determ. of dose rates from homogeneously distrib. β,γ- and EC,γ-emitters in phantom organs 78—53501
  - LMFBR fuel pins, computer anal. and control for nondestructive gamma scanning 79—9754
  - low-background system for neutron activation anal. 77—36843
  - low-energy photon sources, rel. to in vivo distrib. meas. 77—65377
  - luminescent detector efficiency for 600 MeV protons, mass stopping power calc. 80—99346
  - LWR, fuel reprocessing plant, NDT control methods 80—5314
  - LWR core, power shape determ., gain stabilized NaI(Tl) γ-ray detector system 78—33284
  - LWR irradiated fuel assemblies, nondestructive exam. using γ-ray and neutron techniques 80—66760
  - LWR spent fuel, nondestructive meas. and verification for materials safeguards 80—78420
  - lyoluminescence dosimetry in photon and fast neutron beams, using mannose 78—15902
  - lyoluminescence dosimetry using saccharides 77—52881
  - magnetic pair and Compton spectrometers 79—68130
  - marine gamma-spectrometric surveying problems 79—2390
  - Marinelli type vessel, geometry in γ-ray activity determ. *(Japanese)* 80—91409
  - medical detector, gaseous, good low-energy resolution for $\leq$50 keV imaging 80—3795
  - medical gamma-ray cameras of Anger type, optimisation *(French)* 80—26328
  - medical imaging instrument, positron emitting heavy ion beam injection 79—48329
  - megachannel gamma-gamma coincidence system using PDP-8/E computer and moving-head discs 77—57834
  - megachannel pulse height analyser for gamma-ray coincidence analysis 80—99430
  - metal convertors for γ-ray detection and mapping 77—3235
  - microdosimetric studies with low LET radiation using cylindrical walled and wall-less proportional counters 80—36140
  - MISO low energy γ-ray telescope 79—25472
  - mixed β-γ dosimetry, ionisation and scintillation counters 80—57975
  - mixed energy gamma radionuclide meas. using radionuclide calibrator 77—14319
  - mixed field, of fast neutrons and γ-rays, Fricke and $Ce_2(SO_4)_3$ dosimeter appls. 78—74514
  - mixed n-γ field microdosimetry and neutron/gamma discrimination *(French)* 80—12279
  - mixed neutron-gamma beam from IBR-30 reactor, beam characts., detectors props. *(Russian)* 77—67793
  - mixed neutron-gamma ray field, γ contrib. to proton recoil counter spectrum 77—88337
  - mixed-field γ meas. with nonhydrogenous Rossi counter 80—9430
  - mobile gamma camera with remote image processing computer system, for nuclear medicine 78—92700
  - monitoring beta and photon radiations for radiation protection purposes 78—15908
  - monitors testing, compact set-up with ^{60}Co reference gamma source 77—10494
  - Monte Carlo calcs. of external detector response to photon source in phantom's lungs 80—8132
  - Monte-Carlo calcs., number and energy albedo 79—31221
  - Mossbauer effect, inelastic scattering intensity meas. 80—71245
  - Mossbauer effect measurement apparatus for use at high press. and low temps. 77—67548
  - Mossbauer spectroscopy, fast detection systems 78—25376
  - MOST suitability as γ-ray dosimeter *(Czech)* 77—86636
  - multi-anode microchannel array detector tube, effects of 1 MeV gamma-rays 79—71582
  - multichannel focusing collimator, computation of efficiency distrib. functions 77—10519
  - multichannel gamma flaw detector 77—90565
  - multicrystal detection system for localisation and meas. of photon emitters without external collimation 77—32959
  - multidetector meas. of ang. correl. 79—41084
  - multilayer γ-telescope spark chambers, 5-200 MeV $e^{+}e^{-}$ pair track anal 80—63469
  - multilayer wide-gap spark chamber for a gamma telescope 79—76267
  - multiplane γ source image reconstruction using Fresnel zone plate aperture 77—52874
  - multiplicities of γ-rays from nuclear reactions, meas. with Ge(Li) and Na(I) detectors 77—88356
  - multiplicity meas., fast converging bootstrap method for data anal. 78—70730
  - multiwire proportional chamber characts. using matrix cathode 79—81136
  - multiwire proportional gamma camera for imaging ^{99}Tc^{m} radionuclide distribs. 78—53493
  - MWPC, γ-image blurring reduction by delay line readout 78—37492
  - MWPC, appl. to radiation localisation problems in medicine and biology, review 79—5432
  - MWPC on cube lattice 79—93875
  - MWPC positron camera, 3-D iterative reconstruction method 78—40302
  - MWPC with analogue read-out, high energy e^{-}/γ detection 79—13593
  - natural background, exposure rate variations in open air *(Czech)* 77—67900
  - natural soil radioactivity monitoring with portable gamma ray spectrum 80—31148
  - NDT flaw detector with analogue data processing, param. optimisation 77—81374
  - NE 213 liquid scintillator, decay under neutron and gamma excitation *(German)* 78—55097
  - NE 213 liquid scintillator, deuterated, decay mode *(German)* 78—55096
  - NE 238 fast liquid scintillator, scintillation decay and n-γ discrimination *(German)* 78—55101
  - NE-213 liquid scintillator, Monte Carlo calc. of response function 79—97926
  - neutron activation anal. of geological materials, coaxial, planar Ge detector appl. 77—81443

gamma-ray detection and measurement continued
  - neutron capture absolute yield calibration, saturated resonance technique 79—80935
  - neutron capture gamma and electron spectroscopy, instruments and techniques 80—37695
  - neutron collimated fast beam, radiation quality local distrib. 80—12247
  - neutron multiplicity for gamma rays from (particle, xnγ) reacts. 80—37689
  - neutron radiative capture cross section measurement techniques, review 77—26932
  - neutron-gamma discrimination in fission chamber *(German)* 77—88357
  - neutron-gamma pulse shape discrimination, digital technique 77—403
  - nondestructive assay of highly enriched spent fuel, using Ge(Li) detector and ^{235}U fission chambers 79—89522
  - nondestructive assay of irradiated nuclear fuel for safeguards, review 78—82495
  - nonhydrogenous organic liquid scintillator gamma-ray detector, sensitivity function calc. 78—78572
  - nuclear accident dosimetry system, Czechoslovakia 80—57978
  - nuclear accident dosimetry systems, comparison 79—22496
  - nuclear accident dosimetry systems, neutron and gamma-ray dose meas. 77—38425
  - nuclear energy level lifetime measurement using on-line computer and registration time shift compensation 80—68577
  - nuclear energy level lifetimes, new plunger device using Doppler effect and spectra, expt. testing 78—13375
  - nuclear excited states, 10^{-10} to 10^{-6} s, lifetime meas. by time spectrometer system 79—31313
  - nuclear explosion, time distrib. and anal. fallout particles from 1977 Sept. 18 Chinese detonation 79—25796
  - nuclear fuel burnup determination using Aragonic γ detector 80—63262
  - nuclear imaging of tumour, optimum detector spatial resolution performance study 78—73223
  - nuclear materials accountability, U and P NDA of crated waste by gamma-ray and neutron coincidence counting 80—83166
  - nuclear materials safeguarding, gamma spectrometric techniques and standards *(French)* 80—68811
  - nuclear medicine imaging principles, concepts and equipment 80—17113
  - nuclear picosecond lifetime meas., appl. to ^{207}Pb 78—55090
  - nuclear reactor criticality incident detect. with γ dose rate alarm 79—36423
  - nuclear spent fuel assembly, gamma dose rate distrib. meas. with TLD 80—47735
  - nuclide activity measurement, correlation factor for self-absorpt. 79—34401
  - nuclide mass yield identification following heavy ion induced reacts. 79—22531
  - ocean sedimentation rates determ. by nondestructive gamma-gamma coincidence spectrometry 78—85709
  - on-line data acquisition system for monitoring high resolution multidimensional spectra 78—58567
  - on-line gamma-ray meas., Ge(Li) spectra anal. 77—23395
  - on-line radiation monitoring at a nuclear fuel reprocessing plant 80—95469
  - optical γ-ray imaging device 77—5056
  - optimum recognition of transient increase in rate from constant background rate 77—82658
  - ore analysis by selective gamma-gamma method, elimination of geometrical effects 78—44425
  - oriented radioactive nuclei, JINR investigs. using SPIN equipment *(Czech)* 77—42220
  - paired LiF TLD 600, 700 technique, γ-dose in mixed n-γ radiation fields 79—45432
  - particle beam, relativistic, in medium, energy meas. by spontaneous γ-radiation emission *(Russian)* 78—29891
  - particle detectors, microprocessor-controlled data acquisition system for temporal/angular correl. between β- and γ-ray emission *(Spanish)* 80—106238
  - passive personnel portal detectors for nuclear materials diversion protection using gamma-ray and neutron detectors 80—78389
  - pattern recognition theory appl. to gamma-ray spectra identification 77—67931
  - peak areas and detection limits, digital calc. methods 78—50433
  - peak search and anal. of γ-ray spectra with very low statistics 77—54390
  - personal monitoring, effect of environmental radiation, thermoluminescent dosimeter *(Japanese)* 80—61707
  - personnel dosimetry, Czechoslovak comparison of methods 77—50302
  - personnel external gamma dosimetry, meas. of weighted average whole-body dose 80—26367
  - phosphate glass, appl. in gamma dosimetry *(Slovenian)* 80—32521
  - phoswich detector, field monitoring of alpha-emitting contaminants in environment 78—70646
  - phoswich detector for ^{147}Pm in-vivo meas. 78—28087
  - photographic film dosimetry by low energy photon transmission 79—45433
  - photon collimation problems, Monte Carlo anal. 78—70724
  - photon detection processes, statistics of radiation 77—65010
  - photon energy spectra estimation based on 34×34 matrix 79—41059
  - photon position monitors for CHESS synchrotron source, using split photoelectron detectors and ionisation chamber 80—91336
  - photon radiation meas. in nuclear power stations 80—63403
  - planar positron cameras, 3-D reconstruction using Fourier deconvolution of generalised tomograms 78—40295
  - plastic scintillator, neutral radiation incident spectrum determ. 77—54398
  - plastic scintillator excited by ^{60}Co γ-rays, absolute radioluminesc. yield meas. 80—2829
  - plastic solid state nuclear track detector, large γ dose meas. 77—38559
  - plastic track detectors, structural charges due to high dose γ-rays 80—95500
  - Poisson and Brockwell-Moyal freq. distribs., χ-square test 80—5430
  - polarimeter, 100 to 800 keV, high resolution 80—52839
  - polarimeters, linear systems, optimisation of geometrical factors 77—54478
  - polycarbonate plastic dosimeter, high exposures 79—63815
  - position determination using high press. flash tube chamber 77—57795
  - position sensitive detectors, read-out systems *(Japanese)* 78—33397
  - position sensitive detectors using resistive charge division readout 77—54420
  - position sensitive gamma ray detection system, 3-D, fabrication and efficiency 80—63483

gamma-ray detection and measurement continued
position sensitive high energy gamma-ray detector 77-83445
position sensitive semiconductor detector 77-54435
positron annihilation, 2-D Doppler broadened technique 78-70722
positron annihilation, Doppler broadened spectra, deconvolution using solid state detector 78-72631
positron annihilation, Doppler broadened spectra, parameters 78-72630
positron annihilation, spatial factors 77-54396
positron annihilation coincidence detection tomography, circular ring camera system 77-64124
positron annihilation detection, high resolution computed tomography 77-66837
positron annihilation in rare gases, Doppler broadening meas., electron mom. distribs. 78-55131
positron annihilation line broadening, Ge detector 77-16418
positron annihilation radiation at 511 keV from galactic centre 79-5902
positron camera, 3-dimens. imaging using Fourier techniques 77-32951
positron camera, $Bi_4Ge_3O_{12}$ as potential scintillation detector 78-3586
positron camera for brain imaging *(Swedish)* 78-28032
positron camera proportional chamber, Fourier deconvolution technique 78-40297
positron circular ring camera, in 3-dimens. radionuclide tomography 77-73566
positron emission transverse tomograph, PETT IV 78-40299
positron imaging device resolution limit 77-60243
positron imaging system using annihilation coincidence detection, model, design, performance 78-40303
positron ring, 280-crystal, design and construction for 3D imaging 78-28063
positron two-photon annihilation coincidence technique, difference mode 78-54516
prompt neutron correction for γ-ray detectors 79-93610
proportional counter, sectional flow, high background, for Mossbauer spectroscopy 79-727
proportional counter, spherical, with isotropic sensitivity, for soft γ-radiation 78-61732
proportional counter, toroidal, Mossbauer spectroscopy appl. 78-33364
proton accelerator beam scraper, photon dose rate calc. 80-99367
pulse shape analyser, effect of pulse pile-up on discrimination between neutrons and gamma rays 80-91402
pulse shape discrimination cct. for n and γ multidetector meas. 78-70709
pulse shape discrimination for alpha-gamma separation with trans-stilbene 78-13386
pulse shape discriminator for n,γ separation, appl. to TOF spectroscopy 79-6786
pulse-height response of NE-213 scintillation detector 78-17508
pulsed gamma-ray method for rocks density determ. theory *(Russian)* 79-39956
pulsed ruby laser, apparatus for registration of gamma secondary radiation 79-76303
pulsed source, distrib. of scattered γ-radiation, unsteady transport 80-27830
PWR, fixed in-core gamma thermometer for neutron flux meas. 80-717
PWR irradiated fuel, monitoring by gamma spectrometry nondestructive meas. *(French)* 80-63288
PWR steam generator, γ-dose rate distrib. meas. 80-5382
pyroelectric detector for dosimetry of pulsed γ-radiation 77-71725
pyroelectric receiver, gamma pulse meas. 78-860
Q-values of β^- decay, rapid meas. from electron and gamma energy decays 80-78220
radial distribution of γ-rays, coeffs. for calc. *(Russian)* 78-37528
radioactive cloud, external gamma dose model 79-85828
radioactive element conc. from γ-ray intensity meas., numerical method 79-18059
radioactive plume in atmosphere, depletion calc., and exposure from deposited activity 79-66561
radioactivity meas., fly-ash radioactivity meas., environmental protection *(Polish)* 77-14318
radioimmunoassay, automated on-line system, Gammaflow 77-9247
radioisotope camera performance comparison 78-44595
radioisotope gamma camera oscilloscope display, performance meas., computer simulation 78-7425
radioisotope hybrid scanner, design of detector and collimators 78-7423
radioisotope imaging, collimator design and fabrication, Pb hexagonal multihole type 78-11717
radioisotope meas., gamma detection using 4π ionisation chambers 79-85869
radioisotope scanning, three dimensional imaging using scintillation camera, expt. 78-11734
radionuclide activity, γ-radiating, comparison of measurement standards within COMECON framework 80-42899
radionuclide disintegration rates determ. for EC isotopes 77-57804
radionuclide radiation precision spectrometry using semiconductor detectors *(Russian)* 79-31305
radiopharmaceuticals, γ-emitting, in rat blood, continuous monitoring technique 79-2129
reactor core gamma dosimetry, solid state nucl. track detector appl. 80-95466
reactor dosimetry using TLD and Rh activation techniques 77-50301
reactor fuel burn-up and cooling time determ. using gamma spectrometry 80-63289
reactor fuel burn-up determination using gamma spectrometric nondestructive assay for IAEA safeguards 80-68806
reactor fuel burn-up determination using gamma spectrometry, IAEA safeguards experience in Czechoslovakia 80-63292
reactor fuel burn-up measurement using spatial power distrib. eval. and gamma spectrometry 80-68803
reactor primary coolant flow rate determ. using gamma/neutron ratio near primary line 77-65254
reactor spent fuel safeguards verification using gamma spectrometry 80-63290
real-time environmental α-β-γ radiation monitoring system 78-94152
recoil distance meas. in coincidence mode, corrections calc. 77-10565
reference material, based on silicate glass 80-78454
REM ratemeter for direct reading of dose equivalent rate 78-53502
resonance capture reactions with a total energy detector 80-37694
resonance gamma-ray absorpt. method 78-55089
review, cosmic gamma radiation, sources and detection 78-12059
rocks and soils, Ge(Li) detectors for γ-radioactivity meas. 80-67418
satellite Cosmos 954, estimating fallout on Great Slave Lake 79-85830

gamma-ray detection and measurement continued
scattered radiation from neutron collimator 77-48870
scintigram preprocessing and display by microcomputer *(Hungarian)* 78-15881
scintillation camera, ^{123}I imaging, detect. performance and quality factor 77-40743
scintillation camera, with 2 mm intrinsic resolution, biomedical appl. 77-70525
scintillation camera deadtime in meas. of left ventricle ejection fraction 79-62355
scintillation camera transfer function, statistical study 77-70541
scintillation camera with brightness amplifier *(French)* 77-37036
scintillation cameras, large-field-of-view 78-44596
scintillation cameras for radioisotope imaging *(Spanish)* 78-7428
scintillation counter, anomalies in charge collection effects on time resolution *(French)* 77-57801
scintillation counter, for gamma radiation, design calibration and construction *(Spanish)* 80-5437
scintillation counter multidetector arrangement for on-line meas. of neutron and γ-ray multiplicities 78-50440
scintillation detection, appl. of pulsed reference light source for photon counting systems 77-3640
scintillation detector in isotropic radiating medium, efficiency 77-30728
scintillation detector system of adjustable response for lung clearance studies 77-56451
scintillation pickups with plateau in counting characteristic, review 80-47811
scintillator detector, toluene based, Pb-foil radiator *(Japanese)* 78-90032
seawater γ-ray field, meas. system *(Russian)* 80-109268
segmented scanning device for gamma-ray meas. of Pu and Am in molten salt residues 80-83165
self absorption factor of gamma radiation in reactor fuel assemblies 80-63320
self-absorption in vol. shaped source for NaI detectors, Monte Carlo calc. 77-26909
self-powered detectors, reactor in-core monitoring *(Slovak)* 79-31322
self-powered detectors, review 79-45558
self-powered flux detectors, response characts. in CANDU reactors 78-82594
self-powered gamma-ray detector with directional discrimination 79-30895
self-powered threshold gamma-ray detector 79-59306
semiconductor detector active volume, determ. from gamma ray interactions, Monte Carlo method 80-63448
semiconductor detector for ionising radiation dosimetry, anisotropy of dose sensitivity 78-70705
semiconductor detectors, S/N ratio optimisation *(German)* 77-10534
semiconductor detectors, state of art and future prospects *(Hungarian)* 80-42890
semiconductor detectors for dosimetry in intense neutron-gamma fields 77-46460
SF5 lead glass Cherenkov counter, high energy photon position determ. 80-58032
shielded 3-detector system 77-75021
solid-liquid pipe flow, cross correlation method anal. 79-32638
solid-state nuclear track detectors, development and use for reactor phys. expts. 78-41886
source activity calculation from counting rates in single and coincidence photopeaks 78-13371
spacecraft instrumentation, induced background radiation 78-85821
spark chamber, electron-photon shower recording, single-particle background suppressing method 78-78573
spectral meas. of secondary neutrons and photons from 52 MeV proton irrad. of thick targets of C, Fe, Cu, and Pb 78-58282
spectral peaks, goodness of fit determ. using figure of merit 77-88360
spectral radiation detectors, calibration and error anal. 78-46177
spectrograph for single pulse detection 78-846
spectrometer for underwater gamma surveying, calibration 79-21066
spectrometer systems, portable, in situ field meas. applications 79-9958
spectroscopy processor X- and γ-ray, active zero-pole cancellation feedback loop 79-9972
spectrum 77-54397
spent nuclear fuel burn-up level determ., computerised equipment *(Polish)* 80-32582
spherical detectors, calc. of γ-ray recording efficiency 80-83236
stack gas monitor, β scintillation detector + Ge(Li) detector system, environmental γ dose *(Japanese)* 79-3246
statistical evaluation of gamma photopeaks in complex spectra from very low activity samples 79-76254
stilbene scintillator, ^{239}Pu, capture/fission cross-section ratio meas., 0.007 eV-12 keV 77-54266
subnanosecond lifetime measurements, system using microchannel plate photomultiplier 78-37520
subterranean gamma-ray in situ spectroscopy 77-57806
sum-coincidence spectra, pairs of extraneous peaks 78-70718
superconducting gamma camera, for clinical utilisation 79-63330
superconducting superheated granules as X-ray and γ-ray imaging detectors, astronomical appl. 79-25504
surface contamination meter 79-22494
survey meters for low γ-ray dose rate meas. 79-41081
tandem accelerators and nuclear phys. conf. 78-13349
telemetric system, with external storage, for detect. of radionuclide tracers in humans 77-12995
thermal neutron capture γ-ray meas. using neutron guide tube 80-58099
thermoelectret gamma radiation dosimeter, use of BeO 80-7270
thermoluminescence dosimeter, low dose meas. *(Japanese)* 78-86696
thermoluminescnece environmental monitoring methods and techniques at nuclear facilities 79-85819
three Ge(Li) Compton polarimeter with kinematic selection, for γ polarisation meas. 77-83456
three-dimensional scintigram processing algorithm 78-7446
threshold self-powered detector, use as reactor power monitor 77-65280
time-domain spectroscopy of recoilless gamma rays 79-26812
time-resolved coded aperture imaging system, for nuclear fuel motion HCDA conditions 78-45764
tissue equiv. medium, simultaneous meas. of neutron and gamma ray spectra 78-5058
TLD, use in high level photon dosimetry 78-74503
TLD measurement errors 80-18705

gamma-ray detection and measurement continued
TLD phosphors, sensitised, photon energy dependence 80—78498
TLD phosphors, use for high-level gamma-ray dosimetry 80—13934
TLD system, automated, for gamma radiation monitoring 80—57964
TLD with BeO, for low exposure of personnel, sensitivity, accuracy 77—29209
TOF meas. on spectra from N_2 sphere surrounding D-T source 77—38422
tomographic imaging by scintillation camera, algorithm 79—57773
transition energy standard value and accurate determ. *(Czech)* 80—22755
transverse-section emission tomography, description and potential of technique 77—86619
TREAT facility, pinhole imaging of test fuel element 78—21627
TRIGA core, gamma dose meas. by plastic detectors 80—9381
two-phase flow system, local density measurements, side-scatter gamma technique 80—569
vacuum emission detector sensitivity to γ-rays 77—54462
VIPER reactor, neutron leakage spectrum and dose meas. 79—3243
walk-free centroid method for lifetime meas. with pulsed beams 78—70715
weak γ-ray transitions observed in coincidence with summed cascades 79—76264
whole body counter, portable chair type for in vivo internal contamination monitoring 78—61260
whole-body counter, shadow-shielded, for detection, identification, and localisation of incorporated radionuclides *(German, English)* 78—20266
whole-body monitors, shadow-shield, accuracy of person internal contamination determ. *(Czech)* 78—35962
windowed ang. correl. method for positron annihilation params. meas. 77—34528
X-ray pellicle stack, γ-ray family from cosmic-ray hadron reactions, accelerated scanning method 78—78546
yrast isomer prod., pulsed beam meas. using plastic scintillation spectrum 80—27871
ZPPR at Argonne, gamma-ray response calc. for encapsulated solid-state dosimeters 77—46420
e-γ delayed coincidences using magnetic lens spectrometer and Ge(Li) detector 79—710
e^+ annihilation in solids, angular correl. meas. by proportional counter 79—4869
e^+e and 3-quanta annihilation, automatic spectrometer 77—88321
$e^+e^- \rightarrow 2\gamma$, ang. correl. meas. device *(German)* 78—86726
γ-emitting radioelements, meas. of weak doses *(French)* 80—91410
γ-γ coincidence techniques, lifetime meas. following fusion evaporation reaction 79—59318
γ-n mixed field, dose distrib. meas. on phantoms, TLD, solid-state, photoluminesc. detectors *(Russian)* 78—33297
(n,γ) thermal react. cross section meas. with liquid scintillation spectra 78—25382
p-γ coincidence expt., use of Ge(Li) detector near 400 MeV intense proton beam 80—5452
$^{110}Ag^m$ decay, precise γ-ray spectroscopy 78—58251
^{110m}Ag, gamma-ray intensities, precision meas. 80—102139
Al, meas. of albedo number using ^{60}Co, ^{137}Cs sources 79—26768
Al_2O_3 TLD for dosimetry after accidental gamma radiation release 78—57076
Al_2O_3 TLD phosphor 77—6637
AlSb as high-energy photon detector 77—75026
^{241}Am 60 keV γ backscatter meas. of solid powder mixture composition 77—52695
^{241}Am spectrometer for Compton scatt. studies 79—2899
Ar, liquid calorimeter γ-detector, 5 to 80 MeV 79—6799
Ar, liquid ionisation chamber with 4.5 cm gap 80—18761
^{41}Ar release from TRIGA reactor, comparison of γ-ray detectors 78—57309
^{198}Au, redetermination of γ-ray standards between 0.1 and 1.0 MeV 78—37472
BeO ceramic TLD, gamma ray response 80—23153
^{7}Be, 477.6 keV, Analytic fitting of full-energy peaks in Ge(Li) spectra at high count rates 80—99147
$Bi_4Ge_3O_{12}$, 38 mm scintillator, γ-ray response 80—58048
$Bi_4Ge_3O_{12}$ scintillators, appl. as high energy gamma detectors 80—47827
$Bi_{12}SiO_{20}$ photoelectret, in optical processing and X, γ ray imaging 80—23764
^{207}Bi, gamma-ray intensities, precision meas. 80—102139
CaF_2(Eu) Phoswich detector, evaluation for ^{90}Sr in situ anal. 80—58067
$CaSO_4$:Dy, α and γ thermoluminescence response comparison 79—85814
$CaSO_4$:Dy phosphor powder, effect of grinding on thermoluminescent sensitivity 79—33852
$CaSO_4$:Dy photostimulated luminesc. for dosimetry 77—90910
$CaSO_4$:Dy TLD, fading in high γ-dose region 78—90027
$CaSO_4$:Dy TLD, glow curve behaviour in ^{60}Co γ-exposure 79—49903
$CaSO_4$:Dy TLD, low exposure rate depend. meas. 80—102408
$CaSO_4$:Dy TLD, monitoring of environmental radiation levels 79—93839
$CaSO_4$:Dy TLD, temp. effect during UV and gamma irradiation 79—38684
$CaSO_4$:Dy TLD, thermal neutron and γ-ray meas. in mixed radiation field, activation and capture gamma technique 79—738
$CaSO_4$:Dy Teflon TLD discs, metal filters for compnesation of photon energy depend. 80—30901
$CaSO_4$:Dy thermoluminescence sensitivity and glow curves, 700° to 1300°C 79—85815
$CaSO_4$:Tm, Li, mixed field TLD 77—9263
$CaSO_4$:Tm composite TLD for γ-rays, X-rays, β-rays, and thermal neutrons 78—28076
CdS γ-ray dosimeters with elevated stability under irradiation 80—86995
CdTe, camera, medical appls. 79—49351
CdTe detector, resolution for 122 keV ^{57}Co and 59 keV ^{241}Am 77—75027
CdTe detector for personal radiation chirper 79—45557
CdTe detector for radionuclide tracer biotelemetry 77—86587
CdTe, detector grade semi-insulating crystals, determ. of product of mobility and carrier lifetime 80—39601
CdTe detectors, gamma and electron irradiation effects 78—41893
CdTe detectors, props. 77—61658
CdTe detectors, X-ray fluorescence escape peaks in X-ray spectra 80—9448
CdTe detectors with small volume, high gamma-ray sensitivity, 100 to 150 keV 79—63865
CdTe, film, theoretical models of impurity levels 79—82557

gamma-ray detection and measurement continued
CdTe gamma backscatt. assay meter 80—58070
CdTe gamma radiation detectors, operation, energy resolution, efficient and appl. 79—68156
CdTe, growth by travelling heater method, high resistivity charact., γ-ray detector appl. 78—84707
CdTe, high purity crystal, growth from soln., γ-ray detector appls. 77—14310
CdTe, irrad.-induced damage on γ-detector performance 80—23264
CdTe matrix γ-camera, biomedical appl. 80—76827
CdTe metal-semiconductor-metal γ-ray detector characts. 80—57451
CdTe photovoltaic mode γ- and X-radiation dosimeters 79—13594
p-CdTe:Cl, gamma-ray detector prep. and resolution 77—39802
CdTe:Cl, gamma-ray detector growth, travelling heater method improvement 77—40353
$^{139}Ce \rightarrow ^{139}La$, internat. comparison of activity meas. March 1976 79—13613
^{252}Cf, spontaneous ternary fission, multiplicity distrib. of prompt γ rays 78—21615
^{252}Cf(n,γ), neutron capture gamma expt. equipment designs 80—52832
^{56}Co, gamma-ray intensities, precision meas. 80—102139
^{56}Co, relative intensities of γ-transitions meas. 79—97930
^{60}Co, absorbed-dose standards comparison 78—74512
^{60}Co, exposure-rate calibration of small radioactive sources 78—41881
^{60}Co gamma radiation, filtration anal. of collimated beams 79—63861
^{60}Co gamma-rays, calibration in water vs. calibration in air for teletherapy units 77—21630
^{60}Co skyshine, continuous γ-spectra unfolding 79—81118
^{60}Co source, ionisation chamber beam standardisation, Monte Carlo calcs. of wall correction factors 79—3288
^{60}Co teletherapy head shutter irrad. timer 77—66836
CsI(Tl), params., of FEU-118 photomultiplier in operation with NaI(Tl), CsI(Tl) dets. 79—3284
CsI(Tl) well-detector for low background γ-spectrometry, comparison with NaI(Tl) 78—86724
^{134}Cs, gamma-ray intensities, precision meas. 80—102139
^{137}Cs distributions effects on γ-intensity in γ scan method for reactor fuel bundle *(Japanese)* 79—36342
^{137}Cs, exposure-rate calibration of small radioactive sources 78—41881
^{137}Cs gamma radiation, filtration anal. of collimated beams 79—63861
^{137}Cs gamma-ray spectra of spherical reactor fuel elements, burn-up determ. *(German)* 78—25299
^{A}Eu, A=152,154, gamma-ray intensities, precision meas. 80—102140
^{152}Eu, intercomparison of gamma ray emission rate meas., using Ge spectrometers 78—82568
^{152}Eu sources, international comparison of γ-ray emission rate meas. using Ge spectrom. 79—22529
$FeSO_4$-$CuSO_4$ dosimeter, intense γ-radiation field effects *(Spanish)* 77—48876
^{67}Ga-citrate images obtained with rectilinear scanner and large-field Anger camera 77—66841
Gd loaded large liquid scintillator, neutron radiative capture cross-section meas. 78—25380
Ge 2-D position sensitive orthogonal strip gamma-ray detector employing resistive charge division 77—10538
Ge camera, 2-detector, 512 element high purity prototype 78—40301
Ge coaxial detectors, n-type high purity, construction and performance 79—41075
Ge, Compton scatter, spatial spread meas., imaging with position-sensitive detectors 78—46214
Ge detector, delayed coincidence summing, nucl. half life meas. 78—55088
Ge detectors, automatic anal. of gamma-ray spectra 77—3246
Ge detectors, γ-γ linear polarisation direction correls., $^{110}Ag^m$ cascade decay *(Japanese)* 78—41903
Ge detectors, high purity, event timing, compared to Ge(Li) detectors 80—69018
Ge detectors, use at low temps. 77—65398
Ge detectors in space, computer spectral anal. of cosmic ray proton induced radioactivity 79—12413
Ge diodes, γ-radiometric appl. 78—33385
Ge gamma camera resolution loss at depth, elimination technique 79—49352
Ge γ-ray camera, calc. of picture element efficiency and side scatt. fraction 77—77968
Ge γ-ray detectors, materials props., appls., radiation damage 78—13392
Ge intrinsic detector, use in borehole sonde for U exploration 77—9547
Ge multidetector camera, biomedical appls. 79—49353
Ge p^+-ν-n^+ structures, large-scale trap characts. 80—92966
Ge radiation detectors, recording power at 4.2K 77—67936
Ge radiation detectors used for high resolution gas ray spectroscopy 79—6804
Ge semiconductor detector efficiency determ. using a standard Marinelli beaker geometry 80—63450
Ge shielded detector, cryostat cold-finger support 79—93868
Ge spectrometer, energy and efficiency calibration in 100 keV to 3000 keV γ-ray energy range 78—17464
Ge spectrum, precise γ-ray energies for calibration up to 3.5 MeV 79—31311
Ge:Li, determ. of drift parameters of Li 78—17509
Ge:O, intrinsic γ detector, deep level defect connection with O content *(Russian)* 78—43331
Ge-Li total efficiency calc., algorithm for small calculators 79—9938
Ge(Li) and HPGe detectors, coincident sum peaks 80—63447
Ge(Li), anomalies in charge collection effects on time resolution *(French)* 77—57801
Ge(Li) anticoincidence shielded spectrom. for environmental radionuclide meas. 79—6791
Ge(Li), calc. of finite angle correction coeffs. and linear polarisation sensitivity 79—736
Ge(Li) detector, absolute determ. of ^{238}U conc. in ore 77—13133
Ge(Li) detector, calc. of gamma-ray efficiency 80—37693
Ge(Li) detector, comparison with Ge(Li)-NaI(Tl) Compton suppression spectrometer for low level activity meas. *(Slovak)* 78—21814
Ge(Li) detector, for in situ anal. of river bottom sediments 77—87115
Ge(Li) detector, gamma pulse pileup, random summing losses 80—58023
Ge(Li) detector, gamma-ray activity of large vol. samples, determ. 77—90656
Ge(Li) detector, γ-spectra, noniterative method for fitting Gaussian to peaks 77—57840

gamma-ray detection and measurement continued
Ge(Li) detector, mathematical model of monoenergetic spectra 78−13372
Ge(Li) detector, Monte Carlo photon transport simulation 79−81122
Ge(Li) detector, relative ang. efficiency meas., Q_k factors and Doppler broadening 79−54750
Ge(Li) detector, use in activity determ. of gamma source with flat surface *(German)* 78−58528
Ge(Li) detectors, anal. of monochromatic γ-ray and annihilation spectra 78−50429
Ge(Li) detectors, commercial, time parameters 79−728
Ge(Li) detectors, energy meas. source position effect 79−13579
Ge(Li) detectors, gamma-ray intensity standards for calibration 80−74083
Ge(Li) detectors for environmental assay, calibration using NBS mixed-radionuclide gamma sources 77−38541
Ge(Li), determ. of gamma ray energy from naturally occurring ^{40}K and ^{138}La 80−52811
Ge(Li) gamma detectors, radial efficiency gradients 78−9034
Ge(Li) gamma-ray spectra analysis of fission products, automatic general-purpose program GSAP *(Chinese)* 80−69013
Ge(Li) gamma-ray spectrometer calibration for radioactive inert gas meas. 77−83442
Ge(Li) γ-ray spectra, effect of base line shape on peak unfolding 78−851
Ge(Li) in situ spectrometry, exposure rates due to rainfall 80−42873
Ge(Li), meas. of γ-ray elastic and Compton scatt. through small angles 79−718
Ge(Li), peaks in gamma spectra analysis, analytic approx. 80−102395
Ge(Li) semiconductor, used simultaneously with NaI(Tl) scintillation spectrometer, in neutron activation cross-section meas. 80−78485
Ge(Li) spectrom., precision energy meas. of gamma rays of ^{51}Cr, ^{103}Ru, ^{109}Cd, ^{144}Ce, and ^{203}Hg 78−58533
Ge(Li) spectrometry at low source-detector distances, coinc. summing corrections 79−22528
Ge(Li) well-type semiconductor detector, γ-ray spectrometry *(Japanese)* 79−89521
Ge(Li)-NaI(Tl), Compton suppression spectrometer for in-beam expts., design and performance 78−78553
Ge(Li)-NaI(Tl) Compton suppression spectrom. for low-level activity meas. 78−9022
Ge(Li)-NaI(Tl) Compton suppression spectrometer for low level activity meas., rel. to Ge(Li) detector *(Slovak)* 78−21814
^{73}Ge, Mossbauer gamma-ray detection with Si(Li) and Ge detectors 77−10530
He filled detector using thin foils to convert gamma rays to electrons 80−27872
^{3}He ionisation chamber, improved time resolution in n-γ coincidence meas. 80−99416
HgI$_2$, charge collection efficiency 80−32575
HgI$_2$ detectors, fabrication, appl. to X- and gamma-ray detection 77−83459
HgI$_2$, gamma radiation detectors, operation, energy resolution, efficient and appl. 79−68156
HgI$_2$ in vivo medical probe, DC and pulse counting meas. 78−44593
HgI$_2$ miniature probes for in-vivo medical appls., fabrication, spectroscopic evaluation 78−40308
HgI$_2$ nuclear detectors, bulk homogeneity, spectral response, performance 78−37524
HgI$_2$, room temp. detector, cryst. growth 78−39675
HgI$_2$, soft γ-ray detector fabrication and props. 77−3208
HgI$_2$, soln. grown crystals, low-energy gamma-ray cond. type detectors 80−97418
^{166m}Ho, relative intensities of gamma-rays 78−46201
^{123}I assays, coincidence counting of γ- and X-rays 77−14320
^{123}I source sumpeak calibration absolute activity 77−57785
^{123}I two-crystal coincidence counting 78−13394
^{125}I, variation of γ-counting efficiency with sample composition 80−83238
^{129}I coincidence counting, efficiency extrapolation technique, methane 4π counter efficiency 77−88354
In$_2$Te$_3$, photosensitivity on γ- and neutron-irrad., γ-ray dosimeter mat. applic. 77−85258
In$_2$Te$_3$ type semiconductors, basis of ionising radiation detectors 78−86743
^{192}Ir, gamma-ray intensities, precision meas. 80−102140
^{192}Ir, redetermination of γ-ray standards between 0.1 and 1.0 MeV 78−37472
^{192}Ir, specific γ-ray constant and exposure rate constant 79−36187
^{40}K natural gamma photon fluxes in long-distance runners 79−96729
^{40}K, natural radioactivity in building materials 77−38424
^{43}K evaluation for rectilinear scanner imaging using performance index technique 78−73226
^{140}La γ-ray intensities, meas. with coaxial Ge(Li) detector *(French)* 78−58534
Li$_2$B$_4$O$_7$:Mn, gamma ray response 80−23153
LiF TLD response to high-energy X-rays and electrons rel. to ^{60}Co photons 78−40332
LiF thin layers, effect of LET on thermolum. props. 78−73255
LiF:Mg,Ti detectors, depth dose distrib. of 9 MeV photons, comparison with phantom results 77−32957
^{3}Lif TLD, evaluation of γ-ray response calcs. 79−31229
^{7}LiF-Teflon disc TLD, determ. of neutron fluence and γ-dose distribs. 79−45434
NaI absolute photopeak efficiency, relationship between point- and extended source geometries 77−26944
NaI collimated detector response matrix generation 79−22553
NaI detector system, front end electronic, pulse height anal. 79−45587
NaI detectors, synthesis of response functions to gamma-rays 78−94158
NaI face-type detector efficiencies for 10 to 150 keV γ-rays 77−3215
NaI opposed detector/turntable γ counter for voluminous samples 79−100706
NaI position sensitive detector, test results 79−76288
NaI scintillation counter, sex-dependent calibration factor, ^{42}K whole-body content meas. 79−29593
NaI scintillation counter, calc. of self-shielding and detector efficiency 80−99419
NaI scintillation detectors, efficiency values, source gamma-ray track length 78−13387
NaI spectrometer, response matrix for 6 MeV γ-ray penetration meas., benchmark data 78−50432

gamma-ray detection and measurement continued
NaI, through well, well type detectors, comparison 78−90020
NaI:Tl, scintillation excitation mechanism 80−2857
NaI:Tl scintillator response, γ-ray, (X-ray) rel. $^{1}/_{2}$-width energy depend., undergrad. expt. 78−49600
NaI:Tl spectrometer meas. of activity of radioisotope emitting two gammas in cascade, geometrical effect 77−88320
NaI(Tl), anomalous intensity variation of backscattered gamma ray peaks 80−37691
NaI(Tl), background characts., appl. as low-level γ detectors 79−68144
NaI(Tl) crystals for volume cylindrical sources, efficiency of detection 80−63457
NaI(Tl) detectors, determ. of full energy peak efficiency 79−31318
NaI(Tl) detectors, response functions to terrestrial γ-radiation, computer program 80−83233
NaI(Tl) large area multi-crystal detectors for X-ray and gamma-ray astronomy 77−22070
NaI(Tl) large modularised detector, 50 MeV γ-ray meas. 79−76257
NaI(Tl) linear response photon counter 79−45567
NaI(Tl), params. of FEU-118 photomultiplier in operation with NaI(Tl), CsI(Tl) dets. 79−3284
NaI(Tl), pile up reduction in low intensity rad. counting, fractional charge collection technique 77−88345
NaI(Tl) Polyscin module detector arrays, Monte Carlo code for design, use in γ-ray spectroscopy 77−54436
NaI(Tl), pulse shape discrimination of high-energy neutrons and gamma rays 78−33395
NaI(Tl) right circular cylindrical crystal detectors, simple model for γ pulse-height spectra prediction 77−6611
NaI(Tl) scintillation counter, meas. of induced activity for ^{12}C+Ne^{10+} in polystyrene 77−3035
NaI(Tl) scintillation counter, γ-ray flux meas., appl. to environmental γ radiation anal. *(Japanese)* 77−71732
NaI(Tl) scintillation spectrometer, used simultaneously with Ge(Li) semiconductor, in neutron activation cross-section meas. 80−78485
NaI(Tl) scintillator, specific sensitivity in γ-ray recording from radioactive ores 78−81449
NaI(Tl) scintillator, electron detection efficiency for electrons and gamma-rays > few keV 79−36461
NaI(Tl) well type detector calib. for absolute counting of ^{85}Kr and ^{133}Xe 78−9036
NaI(Tl) well-type detector calibration 79−85858
NaI(Tl) well-type detectors, photopeak efficiency values, expts. and calcs. 80−63454
Na(Tl) scintillator detectors for neutron-gamma discrimination 80−102386
^{92}Nb, half life determ. by gamma spectroscopy, comparison of ^{92}Nb, ^{94}Nb activities and abundances 78−29423
Pb glass detectors for high-energy photons, Monte Carlo calc. of energy resolution 79−18072
Pb glass EM shower detector, test results 78−70689
Pb single convertor photon detection efficiency below 500 MeV, semi-empirical formula 80−27866
Pb-foiled plastic scintillator, γ-ray meas. *(Japanese)* 77−57825
Pb-glass Cherenkov detector for high-energy gamma rays 77−3222
Pb-glass hodoscope for 50 to 150 MeV photons 80−18758
Pb-scintillation counter, modular EM shower detector for CERN ISR 79−76275
Pt self-powered detectors, neutron/gamma sensitivity 78−78557
Pt self-powered flux detectors, charact. in HWR 77−65282
Pu holdup in glove-box exhaust filter, in-line monitoring by gamma ray detection 80−78458
Pu, isotope compositon, determ. using gamma spectrometry 80−66915
Pu, isotopic composition, determ. using precise absolute gamma spectroscopic meas. 80−66916
Pu safeguards, product soln. gamma-ray NDA using K-absorption edge densitometer 80−83162
Pu safeguards assay, isotopic meas. by gamma ray spectrometry using two-detector method 80−83161
Pu-Am survey instrument, β-α-γ-X-ray scintillation detect. probe 78−33376
Pu-island element, B304, gamma scanning of power and burnup distrib. 80−721
^{226}Ra, exposure-rate calibration of small radioactive sources 78−41881
^{226}Ra, natural radioactivity in building materials 77−38424
^{81}Rb evaluation for rectilinear scanner imaging using performance index technique 78−73226
^{88}Rb decay, γ-ray energy meas. 79−22530
^{222}Rn concentration in water, meas. by gamma counting 78−53733
^{222}Rn flux measurement using charcoal canister 77−6646
Ru isotopic axial distributions in EBR II (U, Pu)O$_2$ failed fuel pins, γ-scanning determ. 78−687
^{106}Ru 512 keV γ-ray, precise meas., Ge(Li) detector, comparison with positron annihilation radiation standard 77−6610
Sb determ. in biological and environmental samples by neutron activation anal. 79−53008
Si detector dosimeter, energy dependence of spectral sensitivity 79−68146
Si detector with p-i-n junction in pulse count mode for γ dosimetry 78−33386
Si diodes, γ-radiometric appl. 78−33385
Si microelectronic p-n junction photon detector 79−26815
Si solid state detector telescopes, neutral particle background effects 78−28472
n-Si-^{119}Sn resonant detector for Mossbauer spectroscopy 80−883
Si(Li) detector, improvement of time depend. instabilities by IR and γ-irradiation 79−36477
Si(Li) detectors, efficiency for 0.05-1.25 MeV γ-rays 78−86744
Si(Li), peaks in gamma spectra analysis, analytic approx. 80−102395
^{119}Sn, total mass absorpt. coeff. of gamma quanta, chem. binding influence, determ. using Mossbauer effect 80−99467
^{85}Sr, 514.0 keV, Analytic fitting of full-energy peaks in Ge(Li) spectra at high count rates 80−99147
^{181}Ta, elec. quadrupole interactions in 482-keV level, meas. using Ge detector 79−40842
^{181}Ta, Mossbauer gamma-ray detection with Si(Li) and Ge detectors 77−10530
ThBr$_4$, inorganic scintillator, use in nucl. and accelerated particle detection 78−58540
^{228}Th, precise γ-ray energy meas. with Ge(Li) detectors 78−13376
^{230}Th, precise γ-ray energy meas. with Ge(Li) detectors 78−13376

gamma-ray detection and measurement continued
^{231}Th, L2/L3 vacancy ratio for internal conversion by γ-X-ray coincidence technique *(Spanish)* 79—97682
^{232}Th, natural radioactivity in building materials 77—38424
U activity, liquid scintillation counting 80—27873
U, assay of natural samples, meas. of gamma- or neutron activity of short-lived fission products 80—61179
U exploration and assay, nuclear methods 77—41228
U ore bodies ground level radiometric surveys, overburden effects correction techniques 79—88485
U- and Th-series, secular equilib. investigation method 79—2381
U-bearing rocks, radioactive disequilib. determ., isotopes relative abundance meas. 78—57330
UO_2, γ attenuation coeffs. meas. for burn-up determ. correction *(Russian)* 78—82597
^{235}U fuel enrichment, nondestructive determination by Ge(Li) spectrometer *(Czech)* 77—46371
^{235}U isotopic content determ. of nuclear materials using gamma spectrometry 79—85756
Xe high pressure proportional, scintillation camera for X-and γ-ray imaging 80—99412
^{133}Xe, gaseous, absolute counting, calibration of well-type NaI(Tl)-detector 78—9036
^{88}Y, gamma-ray intensities, precision meas. 80—102139
^{88}Y solution, standardisation using efficiency extrapolation method, β-γ coincidence meas. 78—21832
Zr, γ attenuation coeffs. meas. for burn-up determ. correction *(Russian)* 78—82597
ZrO_2 TLD using stabilised single cryst., for high gamma doses 77—56476

gamma-ray diffraction
channelled charged particles, diffr. of emitted radiation 78—75699
combined neutron/gamma ray crystallography techniques, possibilities 79—46518
crystal structure 80—14972
graphite, pyrolytic, thermal diffuse scatt., Mossbauer γ-ray diffr. 80—40026
pentaerythritol, Bragg reflection, thermal diffuse scatt. meas. *(German)* 78—75509
phase transitions, twinned texture studies, domain structures 80—19678
quartz, gamma-ray diffr. props. and piezoelectricity 77—20801
quartz, struct. transitions, optical SHG and γ-ray diffr. results 78—14459
twinned crystals, γ-ray diffractometry study technique 79—68987
Al, energy release during annealing, Bragg diffr. expt. with Mossbauer γ rays 79—24546
Au, inner electron wavefunction, meas. using Bragg scatt. of 412 keV gamma-radiation 79—14734
^{198}Au, 412 keV γ-radiation, Compton scattering and Bragg diffraction, study of electron densities in solids 80—18059
Cu, single crystals, deformed, extinction, γ-ray diffractometry and neutron struct. refinement 77—84588
$FeBO_3$, suppression effect under hyperfine quadrupole splitting, Mossbauer study *(Russian)* 80—75906
Fe_3O_4 single cryst., Mossbauer γ-ray diffr. 77—84600
$FeRO_3$, enhanced nuclear resonance scattering in dynamical diffraction of gamma-rays 80—44982
KH_2PO_4, appl. of gamma-ray diffractometry for study of ferroelastic crystals 77—8533
KH_2PO_4, appl. of γ-ray diffractometry to twinned crystals study 79—68987
KH_2PO_4, ferroelectric-ferroelastic phase transition, γ-ray diffr. 78—43819
KH_2PO_4, struct. transitions, optical SHG and γ-ray diffr. results 78—14459
KH_2PO_4, tricrit. point, γ-ray and neutron diffr. 78—39516
LiF (200) Bragg peak, Mossbauer diffraction meas., calibration 79—82897
α-NbD_x, under hydrostatic press., γ ray diffr., Bragg refls. 78—75726
$PdH_{0.73}$, 50K transition, γ-ray and neutron diffr. study 79—14932
RbH_2PO_4, ferroelectric-ferroelastic phase transition, γ-ray diffr. 78—43819
RbI, single cryst., mosaic struct., gamma-ray diffr. study in metastable press. region 77—20065
$TbVO_4$, Jahn-Teller phase transition, γ-ray diffractometry 78—91205

gamma-ray effects
see also biological effects of gamma-rays; radiolysis
absorbed energy distrib. in γ-irradiated layered target, Monte Carlo program 79—19279
N-acetyle DL-methionine, γ-irradiated, radical cation EPR, ^{33}S hyperfine coupling 77—40559
adamantanc, γ-irrad., free radicals EPR and ENDOR 80—69170
agar, prop. change due to ionising radiation *(Korean)* 77—48699
alchohols, glassy, spectra shift of trapped electrons, after γ-irrad. 79—78709
alkali borate and silicate glasses, γ-irrad., paramag. SO_3^- radicals 79—42838
alkali halide, gamma irradiated, positron annihilation 79—23643
alkali halides, far IR reststrahlen spectra 77—40244
alkali halides, irradiated at room temperature, stored energy 80—79839
alkaline earth orthosilicates, gamma-irrad., ESR spectra 79—51853
alkaline glass: tryptophan (tyrosine), γ-irrad., electron traps, stimulated luminesc. 78—11536
alkane glass, γ-irradiated, charge trapping, isotope and mol. struct. effects 79—5164
aluminophosphate glasses, multicomponent, γ-irrad., EPR study 79—91290
amino acid formation by ^{60} Co to γ-ray irradiation of HCN solns. 77—37410
anthracene, γ-irrad., radical pairs EPR detection 78—31664
anthracene, γ-irradiated, temp. depend. of photolum. *(Russian)* 78—56511
anthracene, γ-irradiation influence on defects, luminesc. study *(Russian)* 80—55185
anthracene, irradiated, optical absorption and EPR meas., low temps. 78—68538
anthracene, structural defect, photolum., γ-irrad. and temp. depend. *(Russian)* 79—28797
anthracene single crystals, effect of γ-irrad. on photolum. *(Russian)* 80—2852

gamma-ray effects continued
aromatic ethers, comparative study of X-ray and γ-induced photolysis and radiolysis *(German)* 78—64854
aromatic polycrystals, γ-irrad., radical pair form., EPR meas. 78—80757
B-group vitamins in aqueous systems, decomposition by γ-rays in presence and absence of protective additives 79—2006
barium formate, γ-irrad., ESR of free radicals 79—65737
barytes concrete, gamma ray buildup factors 80—27823
benchmark gamma-ray skyshine expt. 79—59274
benzene, γ-irrad., radical pairs EPR detection 78—31664
borosilicate glass US attenuation temp. dependence rel. to γ irrad. 79—46755
borosilicate glasses, gamma irradiation effect on density, refractive index, thermal expansion 80—79838
bovine bone, degraded, ESR study 79—39432
β-brass, disordering under γ-irrad., elec. resist. meas. *(Russian)* 77—48429
1-bromoadamantane, orientationally disordered, γ-irrad. free radical defects, positron probe obs. 79—23647
building factors for photons in air, water, iron, moments method code 80—27828
buildup factors for mats. with very low atomic numbers 80—27822
n-butanol, gamma-irradiated, trapped electrons, conc. of mol. vacancies determ. 77—65948
cables insulated with Al_2O_3 and MgO, resistance to high-temp. and intense gamma radiation 78—25332
cadmium formate, γ-irrad., ESR of free radicals 79—65737
cellulose acetate, gamma-ray effect on light absorption used as dose meas. technique 78—13345
cellulose fibre, gamma-irrad., and storage effects on props. *(Russian)* 80—61121
cellulose nitrate, effect of high γ-doses on etching characts., dosimetry appl. 79—31224
cephalosporins, radiation-sterilisation 80—66822
charge deposition profiles, thin layers near irrad. material interfaces 77—27906
chloroform-paraffin system chem. changes after ^{60}Co γ-irradiation, dosimetry appl. 80—30258
cholesteric liq., cryst., selective reflection, temp. depend., γ-irrad. effects 77—43130
cholesteric liquid crystal soln., γ-irrad. induced colour transition, dosimetry appls. 77—48877
chromatographic support materials decomposition by ionising radiation *(German)* 78—92587
coherent laser detection system, radiation effects analysis 78—30056
concrete, gamma-ray buildup factors, Tchebycheff-fitted Berger coeffs. 79—31226
concrete Eisenhauer-Simmons γ-ray build-up factors, Taylor coeffs. 77—34394
n-decane-n-decane-d_{22}, γ-irrad., H_2/D_2 product ratio mass spectra, mechanism 77—40558
deposition profiles of irradiated materials interfaces, Monte Carlo calcs., photo Compton current 79—24383
di(2-ethylhexyl) phosphoric acid, organic extractant in liquid radwaste, gamma radiolysis 79—67879
diacel solid state track detector 79—750
2,6-N,N-diacetyldiaminopyridine elec. cond., γ dose and temp. (303-363K) effects 80—103696
2,6-N,N-dibenzoyldiaminopyridine elec. cond., γ dose and temp. (303-363K) effects 80—103696
dimethyl sulphoxide, UO_2^{2+} γ-irrad. frozen solns., radiothermolum. and temp. deactivation *(Russian)* 79—33854
2,4-dimethylpentane, glasses, γ-irrad., trapped electron yields, mol. struct. and temp. effects 77—40561
diphenylselenone crystals, gamma irradiation, ESR study of trapped phenylselenonyl radical 80—44917
doped-silica optical fibres, nuclear radiation effects 80—33172
elbaites, Zn-Fe, γ-irradiated, Mossbauer study 80—44990
endosseous implant material, radiation processed alumina-polyacrylic acid composite 77—60308
epoxy, for interference filter, γ-radiation effects on transmission 79—64297
epoxy resin, low temp. irradiation effects on mechanical props., use in superconducting magnets 78—60737
epoxy resin based composites, superconducting magnet insulators, gamma-ray radiation effects 80—24495
ethanol glass, 4K γ-irradiated, presolvated electron photoconductivity 78—47827
ethanol glasses containing anion radicals of fluorene and isologs, γ-irrad., optical absorpt. and EPR obs. after photobleaching 77—44491
ethanol-d_0, -d_1, -d_5, γ-irrad., trapped electron spin-lattice relax. 77—60089
ethylene propylene terpolymer, insulating materials, dose rate effect on degradation behaviour 79—99239
experimental radiation transport to large distances from a bare reactor 79—59275
FBR blanket facility, gamma-ray heating rate meas. in stainless steel and Pb 80—57912
ferroelectric, polarisation switching influence of mobile point defects 78—31165
ferroelectric ceramic, defect effects on mech. strength 78—64332
ferroelectric phase transitions, in $(NH_4)_2BeF_4$ *(Japanese)* 80—11349
fission reactor irradiation loop containing nonfissile material, optimality criterion based on γ-ray flux losses 80—63236
fission reactor materials, gamma heating-effects, meas. using calorimetric and dosimetric techniques 80—658
fission reactors, gamma-power of hot circuit, calc., effect of flow hydrodynamics of process materials 80—63235
fluorene:benz(f)indan(anthracene), single cryst., γ-irrad. rel. to luminesc. decay 77—12417
fluorene, γ-irrad., void form. 80—2068
fluorphlogopite, valence transition of Ti impurity, ESR and optical absorption data 77—16155
fusion reactor, radiation-induced degassing of cryopumps 79—85780
fusion reactor electrical insulators 78—95082
fusion reactor supercond. magnet insulation, gamma irrad. effects 80—34051
gas permselective membranes, irrad. effects on permeation and separation performances 78—29591
Geiger counter, self quenching, plateau characteristics improvement by γ-irradiation 78—13389

gamma-ray effects continued
geoelectric field, disturbed by nucl. explosion gamma-rays 79—70852
glass, for interference filter, γ-radiation effects on transmission 79—64297
glass, K-8, radiation coloured, msec laser pulse effects 77—16435
glass, Libyan Desert Glass, redox form. conditions, EPR obs. of as-received and irrad. samples 78—28228
glass fibre waveguide, γ-irrad., reversible optical bleaching of induced absorpt. 80—14462
glass fibre-reinforced polyethylene, ionising radiation effects on mech. props. *(Russian)* 77—59736
glass-epoxy laminate, superconducting magnet insulators, gamma-ray radiation effects 80—24495
glasses, aqueous soln., stabilising excess electrons, DTA at cryogenic temps. 78—76889
glutaric acid, γ-irrad. single crysts., free radical EPR obs. at 77K 80—81340
hexachlorobenzene, γ-irrad., ESR spectrum 79—65735
n-hexatriacontane, cryst. struct., γ-ray effects obs. 78—43048
high-speed cassette film fogging and shielding 78—8460
hydrocarbons, γ-radiolysis in glassy and polycryst. states, EPR spectra 77—52658
hydrocarbons, glasses, γ-irrad., trapped electron yields, mol. struct. and temp. effects 77—40561
1-hydronaphthyl radical, 4.2K absorpt. spectrum *(French)* 80—80809
III-V semiconductors, radiation-induced defects, review 77—80544
illumination systems using DRSh-1000 and PRK-7 Hg-quartz lamps 77—88879
insulating materials, high energy radiation effects 80—19835
β-iodophenylacetylene radical, PhC$_2$I$^-$, from γ-irrad. morpholine β-iodophenylacetylene complex, EPR obs. 77—52652
iron oxalate, γ-ray and neutron irrad. effects, Mossbauer spectra obs. 79—65778
isopropyl vinyl ether, chem. initiated soln. polymerisation and radiation-initiated bulk polymerisation 79—91952
Kapton (polyimide), insulators for superconducting magnets, effect of low temp. irradiation 80—25817
KCl, pure and Ba-doped, γ-irrad., point defect form. and interaction, X-ray and optical studies 79—65078
leucosapphire, large cryst., UV transmittance 77—88876
light flash excited by γ-quantum pulse without direct visibility of source 78—69457
lipid peroxide formation in irrad. synthetic diets, storage effects 80—101025
liquid crystal, encapsulated, appl. to dosimeter 77—38547
LWR, chemical factors controlling γ radiation fields around coolant circuits 80—5371
magnesium formate, γ-irrad., ESR of free radicals 79—65737
mannose, γ-irrad., EPR spectra 79—73814
metallic elements, gamma-ray irradiated, energy spectra of secondary electrons 78—84683
metallic mirrors for laser fusion reactors, neutron and gamma irrad. response calc. 80—23121
metals, degenerate electron gas, collective props. using electron knock-out processes 80—6758
metals, thickness meas. by backscatt. γ radiation 80—101781
meteorites, stony, gamma-ray induced thermoluminesc. gradients 77—74020
methanol-2-methyltetrahydrofuran mixed glasses, annealed, γ-ray produced electrons transfer from IR to bisible traps 80—11440
4-methyl 2,6 di-tertiary butyl phenol, gamma-irradiated, electron-methyl group dynamical interactions 77—43161
4-methyl-2,6-di-tertiary butylphenol, gamma-irradiated, effect of radiation damage on hindered methyl group rotation 77—35494
4-methyl-2,6-ditertiarybutylphenol, tunnelling methyl groups, EPR 79—4723
methylene diiodide, in 3-methyl pentane, γ-radiolysis 79—24776
12-methylpentane, γ-irrad. glass, trapped electron yield, elec. field effects 77—16848
mica, natural, high γ- and electron-irrad. doses effect on annealing behaviour, thermal decomp. resist. 80—60897
microwave generation in Zn by modulated γ beam *(Russian)* 78—2939
mixed fluoride crystals, nucl. radiation effects 80—80831
MOS capacitor, ionising radiation effect on mobile Na$^+$ current peaks 78—47876
MOS capacitors, radiation-induced increase of Na ions 78—26956
MOST struct., gamma irrad., interface states and carrier mobility 79—73593
Mylar (polyester), insulators for superconducting magnets, effect of low temp. irradiation 80—25817
naphthalene, γ-irrad., radical pairs EPR detection 78—31664
Nomex (nylon paper), insulators for superconducting magnets, effect of low temp. irradiation 80—25817
nuclear power reactor materials calorimetric validation of TLD-measured heating effects 80—63254
nuclear track detectors, effect of γ-radiation on bulk etching rate 80—885
octadecylacrylamide films, oriented ultrathin, radiation-induced solid state polymerisation 80—80128
oil, lubricating, radn. effects and radn. dosimetry appl. 80—2069
optical fibre, γ-irrad., differential interferometric meas. of refr. index changes 80—78952
optical fibre, γ-ray irrad., damage recovery by annealing 79—23078
optical fibre, gamma irradiated, radii and refr. index changes 80—1338
optical fibre, low-dose radiation damage growth and decay obs. 78—1398
optical fibre, neutron and gamma induced transient absorpt. and luminesc. 80—58763
optical fibres, radiation-induced optical loss, spectral dependence, 0.45-1.75 μm region 79—50421
optical materials, radiation induced transmission loss 79—94306
organic crysts., γ-irrad., positron lifetime rel. to free radical conc. 78—72635
organic insulating materials, dielect. parameters changes *(Hungarian)* 78—59836
oxide glasses, γ-irrad., CuO effects on EPR 80—84645
pentane:octane, γ-irrad., octane radical cations ESR 77—36765
perfluorocarbons, γ-irrad. solns., mag. field effect on fluoresc. 80—55677
personnel dosimetry, Czechoslovak comparison of methods 77—50302
PET fibre, irrad., radical yields 79—96343
phosphors, TLD, γ-induced sensitisation and residual thermolum. 79—28844

gamma-ray effects continued
photochromic glass, γ-ray effects on sensitivity *(Japanese)* 79—38583
photochromic glass, darkening effect due to γ-irrad. 80—96566
photoelastic modelling, suitability of materials under γ-irradiation *(German)* 79—33666
photographic film, fogging effects diagnosis, use of granularity meas. 79—47952
plastic fibre-optic waveguide, effect of ionising radiation on optical attenuation 78—63170
plastic scintillator excited by ^{60}Co γ-rays, absolute radioluminesc. yield meas. 80—2829
PMMA, neutron and gamma irradiation effects 80—66839
PMMA, thermoelectrets, γ-irrad., heterocharge stability, TSC spectra 78—72453
PMMA, visoelastic props., γ-irrad. influence *(Russian)* 78—88492
poly(dimethyl siloxane), networks formed by gamma irradiation, crystallisation 77—51330
poly(trioxane), γ-irrad. effects on melting behaviour 77—62620
poly-1,6-di-N-carbazolyl-2,4-hexadiyne, synthesis, thermal expansion, photocond., optical transition 78—76858
polybutadiene networks, cis-trans isomerisation, γ-ray induced 79—74374
polycarbonate, γ-irradiated, dielec. behaviour and glass transition 80—97182
polycarbonate, insulators for superconducting magnets, effect of low temp. irradiation 80—25817
polychloroprene and polychloroprene vulcanizates, γ-radiation effects on struct., physicomech. props. 77—1840
polydextran, γ-irrad. frozen gel, electron trapping, EPR and optical obs. 78—20030
polyethylene, γ-irrad., alkyl radicals ESR and hindered oscill. 78—85182
polyethylene, γ-irrad., asymmetric 002 X-ray line profiles, analysis 80—96567
polyethylene, γ-irradiated, effect of elec. field on TSC 79—65790
polyethylene, γ-irradiated, luminesc. in warming and cooling 77—32450
polyethylene, γ-ray polymerised, cold compacted films, mech. relaxations, mechanism 77—16631
polyethylene, γ-ray polymerised, dielectric loss reduction 77—24783
polyethylene, amorphised by γ-irrad., interchain ordering, X-ray obs. 78—30545
polyethylene, amorphised by γ-irradiation, radial distribution function anal. for degree of interchain ordering 79—23530
polyethylene, cross linking by energy rich radiation, mech. and elec. props. *(German)* 78—20035
polyethylene, cross-linked, insulating materials, dose rate effect on degradation behaviour 79—99239
polyethylene, high density, carrier trapping, X-ray induced TSC 80—11005
polyethylene, investigation of traps by photostimulated detrapping current analysis 77—15894
polyethylene, irrad., electrolum., 77K 77—32442
polyethylene, linear, γ-irrad., plastic deform. 79—56996
polyethylene, linear, γ-irradiated, crystallite size distrib. and lattice distortions 79—69157
polyethylene, linear, irrad. crosslinking and chain scission in extended chain and bulk films 77—60095
polyethylene, low density, γ irrad. effect on elec. cond. and temp. characts. 77—85221
polyethylene, low density, γ-irrad., unixial elongation effect on elec. cond. 80—25812
polyethylene, low-density, α-irrad., thermolum. mechanism biphenyl anions influence 80—2880
polyethylene, low-density, γ-irrad., spin trapping reaction 80—39873
polyethylene, single, polycryst., ^{60}Co-γ irrad., effect on melting behaviour 77—15548
polyethylene, ultra high molecular weight, wear limit, γ-irradiated and unirradiated *(Japanese)* 78—27649
polyethylene, vinyl group reactions during γ-irrad., crystallinity effect, absorbance obs. 80—81346
polyethylene crystal, highly gamma-irradiated, unit cell dimension meas. 77—76326
polyethylene films, elongated, γ-irrad., TSC meas. 80—11324
polyethylene films, low density, γ-irrad., elec. cond., effect of elongation 79—4564
polyethylene microspheres, deuterated, variable density, laser fusion targets, prep. 78—74468
polyethylene prostheses, radiation crosslinking improvement of shock- and abrasion-resistance 77—60307
polyethylene sorption properties, γ-ray effects in N$_2$O$_4$ medium *(Russian)* 77—72796
polyethylene terephthalate, exposed to aq. medium and γ-radiation, lifetime levels and fracture 80—40520
polyethylene terephthalate, irradiated with radiations with linear energy losses, peculiarities in chemical etching 78—39934
polyethylene terephthalate fibre, radiation grafting 79—96342
polyethylene terephthalate films, gamma radiation induced cond. under high elec. field 78—47798
polyethylene terephthalate under high elec. fields, γ-ray induced cond. 79—60840
polyethylene-glass pair, contact interaction under elastic strain, friction and γ-ray effects 80—40549
cis-polyisoprene, ^{1}H NMR of γ-induced cross-linked polymer 79—69739
polymer, chlorine-containing, dose rate effect on degradation behaviour 79—99239
polymer clad SiO$_2$ fibre, ionizing radiation effect on attenuation 78—42405
polymer films, superconducting magnet insulators, gamma-ray radiation effects 80—24495
polymethacrylates degradation obs., for PMMA, PBMA, PMA and PMA AN 78—27795
polymethylpentene, visoelastic props., γ-irrad. influence *(Russian)* 78—88492
polypropylene, gamma-irradiated, active centres recombination kinetics, ESR study *(Rumanian)* 79—19778
polypropylene, insulators for superconducting magnets, effect of low temp. irradiation 80—25817
polypropylene, stability under radiation sterilisation 77—60245
polypropylene fibres, γ-irrad., microstruct. changes in glassy-high elastic state transition *(Rumanian)* 80—49347
polypropylene fibres, EPR during glass transition, γ-irrad. 79—8445
polysytene, neutron and gamma-irradiation effects 80—66839

gamma-ray effects continued
polytetrafluoroethylene, degradation by electron or γ-ray bombardment in inert atmosphere *(German)* 80—19840
polytrifluoroethylene and copolymer, γ-irrad., Ar diffusion and solubility *(Russian)* 79—51315
polytrioxane, γ-irrad., layer-like void formation 78—22760
polyvinyl alcohol, γ-irrad., ESR of trapped free radicals 78—85183
polyvinyl difluoride, γ-irrad., low-temp. TSD obs. 77—63358
polyvinylidene fluoride, γ-irradiated, low temp. internal friction 78—83874
polyvinylidene fluoride, γ-ray irradiation effect on mech. props., in presence of triallyl trimellitate *(Japanese)* 77—86091
potassium antimonyl tartrate, neutral aq. soln., gamma radiolysis 80—101030
potassium hydrogen malonate, γ-irrad. cryst., ESR and ENDOR of trapped radical 79—78524
n-propanol, gamma-irradiated, trapped electrons, conc. of mol. vacancies determ. 77—65948
PTFE, γ-ray effects on 19 and 30°C phase transitions, Fourier transform IR spectroscopy 80—103387
PVC, plasticisers effect on behaviour under γ-irrad. *(Russian)* 79—87864
PVC, with stabiliser, dielec. and mech. characts. under γ-irrad., plasticisers effects *(Korean)* 77—81054
pyrene, single cryst., γ-irradiated, EPR and optical absorption meas. 78—72412
pyrimidine N_2O aq. solns., dimer formation in γ-radiolysis, chromatographic obs. 80—7785
pyroceramic end gauge, high-precision stability 79—76778
α-quartz:Ag^{2+}(Cu^{2+}), γ-irradiated, stabilisation of impurity atoms 79—8047
α-quartz:Al, thermal cond. below 10K 79—51320
quartz, absorpt. of γ-irrad. samples, comparison with absorpt. of electron irrad. samples 79—1779
quartz, comparison of different radiation effects 78—26596
quartz, crystalline, thermolum. sensitivity 77—90205
quartz, E_1' centre formation and regeneration, α and γ radiation efficiency 79—32992
α-quartz, EPR of E'_4-centre 79—73810
quartz, natural, gamma-irradiated, stress effect on thermolum. sensitivity 80—11482
quartz, natural, thermoluminesc. glow curves and spectral characts., γ-ray effects 78—2927
quartz, natural, virgin (γ-irradiated), polarisation effect on thermolum. sensitivity 80—11483
quartz, piezoelectric, var. of elastic consts. under gamma irradiation 77—36180
quartz, smoky, γ-irrad., electric dipolar echoes 80—20604
quartz, smoky, HF US relax. 78—71796
quartz, smoky, sp. ht. 78—71867
quartz, surface damage by X-rays, γ-rays, neutrons, SEM study 80—79837
quartz, surface space-charge layer form. on γ-irrad. 80—10575
quartz, TFTR diagnostic windows, radiation damage 80—34063
quartz, thermoluminesc., γ-irrad. sample, heat treatment 78—64418
quartz, thermoluminescence output intensity depend. on γ- and ξ-irrad. temp. 77—59623
quartz , fused and γ-irrad. 79—99770
quartz crystal, γ-irradiated, US shear wave propag., beat obs. 77—43283
quartz crystal, oscillating characts., nucl. and X-irrad. effects 79—78626
quartz glass, hydroxyl-free, for low-loss fibre waveguides, γ-irrad. effects 78—13773
quartz glass fibre waveguides, low-loss, radiation-optical stability 79—64345
radial clearance determ. for engine crankshafts by γ-ray method 78—53147
radial electric fields from air polarisation due to Compton electrons excited by γ-quanta pulse 80—21805
radiation dose rate calc. in building materials 79—18057
radiation processing, conf., Miami, FL, USA (Oct. 1978) 80—36772
radiation stability of 'nuclear class' ion-exchange resins 79—43609
radiation sterilization of medical products using electron accelerators and gamma sources 79—49870
ruby, γ-irradiated low temp. UV bleaching 79—23646
ruby, radiation-induced optical processes, impurity effects 80—66310
scintillator systems, liq., organic, energy transfer, fluoresc. intensity-max. solvent depend. 78—21966
semiconductor, Frenkel pair defect formation threshold energy during particle irrad. 79—90647
semiconductor, space charge region thickness, deep level props., determ. by γ-ray absorpt. 80—59995
semiconductor, threshold energy for displacement of atoms 78—47428
sewage sludge irradiation plant, dose and irradiation homogeneity 79—22489
n-Si, recombination centres and carrier lifetimes after γ-irrad. 80—60004
silica gel, effect of gamma-rays, electron scavenging by N_2O 79—24762
silica optical fibres, large core polymer clad, radiation response 80—33171
silicate glasses, effect of high-dose X-rays and reactor radiation 80—19838
silicone rubber biomaterial, filler free, radiation chemical and physical evaluation 79—39608
silicone-clad silica low-loss fibre radiation response obs. 78—1397
skyshine dose due to gamma-rays from nucl. power plant *(Japanese)* 79—29917
smoky quartz, thermal props. at very low temp. 80—24610
sodium metaphosphate glasses, γ-irrad., ESR 78—23339
SOS capacitors, ion-implanted with negative charge gamma radiation effects 79—23645
square cut irradiated rod-rod gap sparkover under nonstandard impulse voltage 78—67564
steel, austenite, γ and neutron irradiation, Mossbauer spectra anal. 78—692
steel, stainless, type 4301, radiation enhanced permeation of H_2 80—59732
steel, stainless type 304, radiation induced outgassing 80—624
styrene-methacrylic acid copolymer, ionomer radiothermoluminesc. 79—95856
sulphonated cool, gamma radiation breakdown 78—693
superconducting fusion magnets, radiation effects 78—50294

gamma-ray effects continued
superconducting magnet epoxy fracture after low-temp. irradiation 79—34147
superconducting magnet materials and components for high energy, phys. appl. 77—69012
superheated water, flashing kinetics, γ-radiation effects 80—92025
superlinear filling of traps in crystals due to competition during irradiation 79—33850
tartaric acid salts, and deuterated forms, irrad.-crysts., primary reactions, EPR obs. 80—3370
Teflon, gamma irradiated, free four-term analysis of positron lifetime spectra 80—76101
Teflon, non-destructive charge release 80—24946
teflon, positron lifetime spectra, low dose range 78—76550
Teflon-4, gamma irrad., wear resistance and antifriction props. 80—7691
tetrahydro-2-methylfuran glass, γ-irrad., spin trapping of radicals by BNB, EPR obs. 78—10776
TGS:Cr single cryst., lattice defect influence on critical behaviour 80—25315
TGS, γ-irrad., lattice defect effects on ferroelec. dispersion 79—51904
TGS, gamma irrad. effects on heat capacity, Curie temp., permittivity 78—67737
TGS, interaction of γ-irrad., induced defect electron microscope expts. 79—10876
TGS, pure and with lattice defects, elec. cond. 79—42538
TGS γ-ray irrad. cryst., heat capacity anomalies near phase transition *(Russian)* 80—49375
TGS crystals, thermal props., γ-radiation defects and inhomogeneity of domain deposition 79—46810
TGS crysts., effects of radiation induced defects on internal bias field 80—88941
TGSe, ferroelec., effect of gamma irradiation on dielec., piezoelec. and elastic props. 77—43943
thiourea monocrystals, γ-irrad. effects on dielec. props. 79—91391
thiourea single cryst., γ-irrad. effect on elec. permittivity 78—64311
thymidine monophosphate aqeous solution, gamma irrad. effect on base damage, phosphate release 80—89806
TLD-600, activation and damage effects after neutron pre-exposure 79—13540
trifluoromethylhalide radical anions, formation, ESR and struct. 77—32809
trimethylenemethane, ground state triplet, HFS, EPR obs. 80—50188
tris(trimethylsilyl)phosphine, gamma irrad., free radicals, struct. and EPR spectra 80—29623
n-vinyl carbazole, radiation induced polymerization ESH study 80—7817
n-vinyl carbazole-acrylamide, post radiation induced polymerisation 80—7818
n-vinyl carbazole-acrylamide, radiation induced polymerization, monomer crystallinity effects 80—7819
1-vinyl-o-carborane, orientationally disordered, γ-irrad. free radical defects, positron probe obs. 79—23647
viscoelasticity linear theory solns. by model γ-irradiation, polarisation-optical method 80—33485
vitamins, B group, γ-irrad. resist. 78—76890
zeolites, Y-type, γ-irrad., H_2O^- ESR 77—9099
zeolites, Y-type, EPR triplet assignment, NO_3^{2-} vs. H_2O^- 78—11534
Ag-Zn (24 at.% Zn), γ-irradiated, freely migrating defects, rate of production *(French)* 79—10877
AgBr emulsion, sub-image and latent image specks form. and props. 78—21245
$AgClO_3$, γ-irrad., ESR of O_3^-, ClO_2 and $(ClO_2\text{-}Cl)^-$ paramag. centres 77—9102
$AgClO_3$, γ-irradiated, resonant Raman effect of O_3^- centres 78—48178
Al, gamma-ray attenuation coeff. meas., 1115, 1173, 1332 keV 77—55303
Al gamma-ray dose buildup factor functions, polynomial parameters 79—54607
Al steel, austenite, martensite cryst. struct. changes on γ irrad. 79—90699
Al-Li alloy, dil., quenched and irrad., recovery, resist. and internal friction obs. 78—52848
$Al_xGa_{1-x}As$ epitaxial diode, neutron and γ-irrad. effects on cathodolum. in SEM 79—11473
Al_2O_3, $3d^4$ ion study by cross-relaxation 79—99755
Al_2O_3, corundum, γ-irrad., colour centres, growth method effect 77—1710
Al_2O_3, gamma irradiated single crystal, defect centres 79—65117
Al_2O_3, γ-irrad., hole centres, luminesc. and EPR obs. 77—32256
Al_2O_3, thermoluminescence, effect of heat treatment following gamma irradiation 77—59624
Al_2O_3:Si, Ti, pure and doped, luminescence, optical absorpt. and colour centres 79—87501
Al_2O_3:Si(Ti)(V)(Fe)(Co)(Ni), gamma-irrad., low temp., induced absorpt. spectra 79—56820
Al_2O_3:V, valency changes of V ions, γ irradiation, thermal cond. optical absorption and EPR meas. 77—80541
$AsS_{3.5}Te_{2.0}$ glass, gamma-irradiated, TSC meas. 77—66166
As_2Se_3, vitreous, effect of gamma-radiation on solution kinetics 77—19986
Au-Cr-GaAs Schottky-barrier diodes, effect of γ-radiation on current-voltage charact. *(Russian)* 80—2459
B_4C-Al(silicone)(graphite), neutron shielding materials, long term radiation effects 80—9413
B_4C-phenolic fibre reinforced composite for nuclear shielding appls. 80—102353
$Ba(ClO_3)_2H_2O$, γ-irradiated, resonant Raman effect of O_3^- centres 78—48178
$Ba(ClO_3)_2.H_2O$, Γ-irrad. defects, ^{35}Cl NQR, 77 and 300K 78—91981
BaF_2:RF_3, cryst., absorpt. spectra, γ-ray effects 77—12409
BaFBr, X- and γ-irrad., thermolum. and optical absorpt. spectra 79—95857
BaFCl crystals, F-centres, X- and γ-irradiation, thermoluminescence and optical absorption spectra 80—45155
$BaGeF_6$, Group IV hexafluoride anion radical γ-irrad., EPR spectra 78—72411
$BaPbF_6$, Group IV hexafluoride anion radical γ-irrad., EPR spectra 78—72411
$BaSO_4$, natural barite, thermoluminesc. glow curves after γ-ray irrad., low doses 77—63471
$BaTiO_3$, ferroelectric semicond. anomalous photovoltaic effect due to ionising radiation 80—29437

gamma-ray effects continued
- $BaTiO_3$, rare earth doped ceramics, thermolum. and microwave induced thermolum. fading 79—1792
- BeO discs, thermally stimulated exoelectron emission and thermolum. sensitisation 78—35277
- BeO, thermoelectret state, effect of gamma radiation 80—7270
- C fibre reinforced plastics with mixed fibres, exam. of fracture toughness and shear strength 79—20151
- C fibre reinforced polyethylene matrix, ultra high molecular weight, wear limit, γ-irradiated and unirradiated *(Japanese)* 78—27649
- C, gamma-ray attenuation coeff. meas., 1115, 1173, 1332 keV 77—55303
- C resistors as low temp. sensors in low temp. reactors, gamma, neutron irrad. investig. 77—45848
- $CaCO_3$, irrad. defects, absorpt. spectra obs. 77—63447
- CaF_2, low symmetry U^{5+} centres 78—76307
- CaF_2:^{57}Co, γ-irradiated, Mossbauer spectra 77—81036
- CaF_2:Dy dosimeter crystals, γ-irrad. dose effect on thermoluminesc. response 77—64135
- CaF_2:Er, γ-irrad., photostimulated luminesc. meas. 77—66538
- CaF_2:Na, γ-irrad. cryst., spontaneous and induced colour centre emission 79—7131
- CaF_2:RF_3, colour centre prod. by γ-irrad., absorpt. spectra obs. 78—72565
- CaF_2:U, γ-irrad., EPR and luminesc. studies of U^{5+} and U^{6+} centres 79—51854
- CaF_2:U^{5+}, charge compensation, struct. 79—15124
- $CaSO_4$, γ-irradiated, ESR and bleaching studies of radical ion centres 80—2637
- $CaSO_4$ phosphors:Ce(Eu)(Dy)(Tm), gamma-irradiated valency conversions in rare-earth ions 80—55198
- $CaSO_4$ with rare-earth and Y dopants, ESR, thermolum. correlation studies following gamma irradiation 77—59628
- $CaSO_4$:Dy, competing deep trap model for thermoluminescence 79—83039
- $CaSO_4$:Dy, γ-ray induced sensitization, competing trap model 80—2881
- $CaSO_4$:Dy, TLD phosphor, gamma-ray induced sensitisation 78—74542
- $CaSO_4$:Dy, thermoluminescent glow peaks, post γ-irrad. annealing study 80—89077
- $CaSO_4$:Dy phosphor powder, effect of grinding on thermoluminescent sensitivity 79—33852
- $CaSO_4$:Dy TLD, glow curve behaviour in ^{60}Co γ-exposure 79—49903
- $CaSO_4$:Dy TLD, temp. effect during UV and gamma irradiation 79—38684
- $CaSO_4$:Dy TLD phosphor, γ radiation changes in glow curve 80—60688
- $Cd(ClO_3)_2$, irrad., bleaching and annealing expts., EPR and optical absorpt. 79—91476
- $Cd(ClO_3)_2$ irradiated single crystal, ESR and annealing, trapped defect centre 80—55141
- $Cd_{1-x}Hg_xTe$(:Ag), impurity diffusion, gamma-ray effects 80—54441
- CdS:Mn gamma-irradiated ESR meas. 79—11342
- CdTe detectors, gamma and electron irradiation effects 78—41893
- CdTe, high-resistivity, irradiation effects on carrier transport and trapping process 78—2164
- CdTe, irrad.-induced damage on γ-detector performance 80—23264
- CdTe metal-semicond.-metal detectors, degradation characts. due to e and γ irradiation 79—45543
- p-CdTe:Cl, influence of gamma-irradiation on elec. props. 77—62951
- CdTe-HgTe, semicond. solid solns., effect of reactor irrad. on electrophys. props. 77—51744
- Co complex, 2,6-N,N-diacetyldiaminopyridine-Co(II) elec. cond., γ dose and temp. (303-363K) effects 80—103696
- Co complex, 2,6-N,N-dibenzoyldiaminopyridine-Co(II) elec. cond., γ dose and temp. (303-363K) effects 80—103696
- CoO-containing glass, effects of γ-rays, electron beam and neutron flux on transmissivity *(Japanese)* 77—73156
- ^{60}Co, polyethylenes loss tangent variation *(German)* 80—75266
- CrF_3, gamma-ray effects, absence of coloration 77—35586
- $CsAsF_6$:BiF_6^-, gamma irrad., BiF_6^{2-} prod., EPR meas. 78—19329
- CsBr, gamma irrad., EPR of Br_2^- ions 79—51838
- CsBr, impurity absorpt. spectra after γ-irrad., aggregated colour centres 79—4829
- CsBr(Cl):Cu^+, γ-irradiated, thermolum. emission 80—104001
- CsCl(Br)(I), F-centre ESR in relaxed excited state, isotropic superhyperfine interaction consts. 79—65733
- CsH_2AsO_4 crystals, dielectric radiation effects, γ-radiation 80—93234
- CsH_2AsO_4, influence of γ-radiation on dielec. props. 79—46703
- $CsNO_3$, single cryst., γ-irradiated, X-ray diffr. effects 79—46704
- ^{137}Cs deposition on plate glass surface, contamination *(Japanese)* 78—29654
- Cu, gamma-ray attenuation coeff. meas., 1115, 1173, 1332 keV 77—55303
- Cu(II) iminodiacetates in aqueous solution, gamma-ray radiolysis 80—35560
- D-D fusion reactor blanket, nucl. characts., summary 78—89973
- 1,6-di-(N-carbazolyl)-2,4 hexadiin, cryst. struct., luminesc., γ-ray polymerisation 78—18629
- Fe gamma-ray dose buildup factor functions, polynomial parameters 79—54607
- Fe-Al alloy, γ-ray effect on resistivity and configuration struct. *(Russian)* 78—43049
- Fe-Al-C, gamma irrad., crystal lattice parameter reversible changes *(Russian)* 80—10576
- Fe-Cr-Ni, austenitic, self-diffusion and swelling under irradiation 80—39343
- FeO-P_2O_5 glass, elec. props. effect of high energy γ-radiation 79—11173
- $FeSO_4.7H_2O$, γ-ray irradiated, Fe^{3+} formation, Mossbauer study *(Russian)* 78—84509
- GaAs, carrier lifetime, radiation induced changes, edge luminesc. spectra 77—8664
- GaAs, deep radiation centres from heat treatment, γ-irrad., deform., probability of nonradiative electronic transitions 80—50408
- GaAs, defect clusters induced by γ-rays and neutrons, effect on elec. props. 80—29408
- GaAs, electroluminescent study of irrad. induced struct. damage, athermal annealing 80—108280
- n-GaAs, electron and gamma ray irradiated, introduction and annealing of defects 78—67736
- n-GaAs, epitaxial film, defect clusters, charge-carrier mobility temp. depend. anal. 80—54701

gamma-ray effects continued
- GaAs, form. of defects, contrib. of inelastic nucl. reactions *(Russian)* 77—27905
- GaAs, gamma and electron irrad. defect formation depend. on interface, luminescence study 80—34057
- GaAs, low temp. gamma irrad., donor-acceptor pair formation 79—69158
- n-GaAs, luminescence emitted from deep centres, γ-irrad. induced changes in internal quantum efficiency 80—20701
- GaAs MIS Schottky barrier diodes, radiation effects 79—24078
- n-GaAs, nature of low temp. field generation of carriers, liberation from surface states 80—92960
- GaAs, radiation defect obs. using Schottky diode characts. 78—76024
- $GaAs_{0.65}P_{0.35}$ deep level study using DLTS and photocapacitance methods *(Japanese)* 80—49665
- GaP diodes, TSCAP and admittance spectroscopy of gamma-ray induced defects 77—89472
- GaP LED degradation, effect of γ-irradiation 78—95610
- GaP:Zn,O LED, 76K electrolum, spectrum, γ-irrad, and forward bias effects 79—78756
- GaSb film, gamma-irradiated, struct., TEM and SEM obs. 79—15033
- Ge, gamma irrad. above threshold, defect formation impurity ionisation mechanism 80—6433
- Ge, gamma irradiated, radiation defects, formation kinetics, successive capture of vacancies by impurities 79—10873
- Ge, gamma-irradiated, number of Frenkel defects 78—14377
- n-Ge, group V doped, point defect form. due to γ-ray irrad., carrier density, mobility meas. 78—71759
- n-Ge, γ-irrad., nonlinear steady-state recomb., nonequilib. carrier lifetime and density 80—20215
- n-Ge, γ-irrad. and subjected to arbitrary excitation and rate, recombination 79—38101
- n-Ge, irradiation induced compensation, elec. meas. 77—85225
- Ge, lattice defects formed on γ-irrad., effect on elec. props. 80—19839
- Ge, point defect formation 77—80501
- n-Ge, proton and γ irrad., minority carrier recombination 80—65591
- Ge:Ag(Ni), gamma ray effects on impurity states 80—96822
- Ge:Au, gamma-irradiated and electron irradiated, elec. props. meas. 77—62950
- Ge:Ba(Ca), elec. props. and effect of impurities on γ-radiation defect formation 78—10088
- p-Ge:Ga, cryst. defects due to γ-irrad., annealing 79—55779
- p-Ge:Ga, lattice defects induced by γ-irrad. 80—29051
- Ge:O, elec. props., O interaction with point defects 79—11081
- Ge:P(Sb)(Bi), γ-irrad., carrier trapping and recomb. at point radiation defects 80—107810
- p-Ge:Sb, cryst. defects due to γ-irrad. 79—55779
- Ge:Sb, γ-irrad., electron capture mechanism by radiation defects 78—26885
- n-Ge:Sb, γ-irrad. effects on donor conc. and compensation by acceptors 78—56106
- n-Ge:Sb, γ-irradiated, trapping and recomb. coeffs. 77—43616
- Ge-GaAs heterojunctions, effect of γ-radiation on current-voltage charact. *(Russian)* 80—2459
- p-Ge-nn$^+$-Si, heterojunction, γ-radiation effect on forward I-V characteristics *(Russian)* 78—72255
- GeO_2, gamma-ray generation of O vacancies and O diffusion 79—99358
- GeO_2, hexagonal and glassy, X and γ-irrad., thermolum. and paramag. centres 77—63472
- H_2O, gamma-ray dose buildup factor functions, polynomial parameters 79—54607
- H_2SO_4 glass, γ-irrad., trapped H ESR, vol. relax. effects 79—52703
- HfO_2, stabilised, low temp. induced centres, ESR meas. 78—72409
- HfO_2:M^{n+}, M=Ce, Pr, Tb, Eu impurity valence transitions 77—51694
- $Hg_{1-x}Cd_xTe$ photoconductors, gamma ray effects on surface props. and detector props. 79—17489
- HgTe(:Ag), impurity diffusion, gamma-ray effects 80—54441
- ^{125}I+methane, γ irrad. effects on organic iodide form. and decomp. *(Japanese)* 77—81418
- InGaAs, LED, 1.06 μm range, neutron and γ-irrad. effects 79—97433
- n-InP, γ-ray and electron irrad., annealing of radiation point defects, elec. cond. and Hall coeff. meas. 80—65051
- InSb, energy spectra of impurity atoms under 4.2K gamma irradiation 77—89471
- InSb film, gamma-irradiated, struct., TEM and SEM obs. 79—15033
- InSb, gamma irradiated, changes in energy spectrum of impurity spectrum 78—51937
- InSb MIS capacitors, gamma-ray radiation effects at cryogenic temps. 80—34517
- In_2Te_3, photosensitivity on γ- and neutron-irrad., γ-ray dosimeter mat. applic. 77—85258
- KBr, gamma-irrad., hologram recording by F-centre bleaching 80—78814
- KBr, NO_3^- centre form. by γ-bombardment in air *(Russian)* 78—31668
- KBr:Li(Na), low temp. radiation hardening mechanism, single halogen interstitials as hardening agent, Ha annealing 79—23634
- KCl, cryst. γ-irrad., holographic information recording appls. *(Russian)* 79—27218
- KCl, F-F′ conversion at room temp. 78—51539
- KCl, gamma irrad. relationship between thermolum. and deform. luminesc. 79—19942
- KCl, gamma-irradiated crystal, interrelation between V_2 and V_3 centres *(Russian)* 79—69862
- KCl, γ-irrad., F-centre absorpt., flash-stimulated changes 80—92524
- KCl, γ-irrad., photoplastic effect and internal friction aftereffect 80—24529
- KCl, γ-irrad. and doped, lattice relax., cold neutron scatt. obs. 77—7715
- KCl, γ-irradiated, photo- and thermoluminesc., F-centre interstitial recomb. 77—44036
- KCl, γ-irradiation effect on dielectric const. *(Japanese)* 79—51896
- KCl, γ-radiation effect on 10.6 μ absorpt. coeff. assoc. with F-aggregate centres 77—4661
- KCl, irradiated, determ. of molar extinction coeff. and oscillator strength of V_2-centre *(Russian)* 78—80384
- KCl, NO_3^- centre form. by γ-bombardment in air *(Russian)* 78—31668
- KCl, optical breakdown, γ-irrad. effects, rel. to appl. in high power lasers 77—8507
- KCl, perturbed M-centre triplet state, M-F centre exchange mechanisms 79—69884
- KCl, photo-induced F-centres, hologram recording 80—28174

gamma-ray effects continued
- KCl, pure and Ba doped, symm. of elastic fields due to defect displacements, diffuse X-ray scatt. 80−70256
- KCl, pure and Ba-doped, irrad. effects on intensity distrib. of diffuse X-ray scatt. 77−24329
- KCl:Ba, γ-irradiation, defect struct., X-ray and chemical etching exam. 77−84793
- KCl:Ba, structural changes due to γ-irradiation *(Russian)* 77−76460
- KCl:Eu^{2+}, γ-irrad., photostimulated low temp. recomb. luminesc. 80−11435
- KCl:Pb^{2+}, γ-irrad., rel. to props. 78−31262
- $KClO_3$, Γ-irrad. defects, ^{35}Cl NQR, 77 and 300K 78−91981
- K_2CrO_4, $KCrO_3Cl$, γ-irrad. single crysts., identification of paramag. centres 78−67994
- KF, deformation coloration 77−76397
- KF:U, EPR of U^{5+} centre charge compensation mechanism 77−90030
- KH_2AsO_4, γ-irradiated, free radicals, EPR and ENDOR study of consequences of ferroelec. transition *(French)* 80−93209
- $K(H_{1-x}D_x)_2PO_4$, single cryst., 77K, γ-radiation damage centres, and EPR obs. 78−68379
- KI(Br), irradiated at room temp., thermolum. and F-centre thermal stability 78−84669
- $KMg_3[AlSi_3O_{10}].F_2$ with excess Al, synthetic fluorphlogopite, radiation-induced paramag. O^- centres 80−60417
- KNO_3-$Ca(NO_3)_2$ glasses, radiation products and recombination 79−57261
- K_2O-B_2O_3 glass, γ- and UV- irrad., thermodecolorisation and thermolum. 80−20721
- K_2O-B_2O_3-Fe_2O_3, γ-irrad., Mossbauer spectroscopic study 80−108132
- KPF_6, γ-irrad., trapped free radicals EPR obs. 80−63683
- KPO_3-Fe_2O_3 glasses, γ-irrad., ESR 80−50182
- K_2SeO_4, symmetry determ. of commensurate and incommensurate phases by EPR of γ-irrad. crysts. 79−78525
- K_2SnF_6, Group IV hexafluoride anion radical γ-irrad., EPR spectra 78−72411
- LaF_3, gamma-irrad. induced coloration and role of impurities 77−35586
- LiCl, radiation effects on decay time of F-centre emission 80−93381
- LiCl single crysts., γ-irrad., thermolum. meas. 80−80880
- LiF crystal, gamma irradiated, shear stress depend. on oriented dipoles conc. 79−28013
- LiF crystals, in pile irradiation, nucl. reactions 78−29463
- LiF, dosimeter material, thermolum. non-linear response to sequential irrad. at different dose rates 79−1793
- LiF, γ-irrad. induced defects, positron capture and annealing obs. 80−60707
- LiF, γ-irrad. pure and Mg-doped, phonon scatt. and interstitial clusters 80−70254
- LiF, γ-irradiated, chemilum. during dissolution *(Russian)* 78−80427
- LiF, γ-irradiated, Huang diffuse scattering of neutrons 80−10544
- LiF, γ-irradiated crysts., dislocation retardation centre 79−95051
- LiF, irradiated and plastically deformed, thermoluminesc. defect centres 77−1740
- LiF, M-centre vibronic absorpt. spectra, elec. field, method of moments 78−27186
- LiF, powder, irradiated with ^{60}Co γ-rays 77−12504
- LiF, single crystal, neutron and gamma irradiation, SEM and Bragg profile anal. 80−15158
- LiF TLD phosphor, γ-irrad. induced sensitisation, UV effects 80−108286
- LiF TLD phosphor, incompatibility of sensitisation and dose re-estimation 78−40340
- LiF TLD phosphor, residual thermoluminescence effect on sensitisation 80−108287
- LiF, TLD phosphor, Z_3 centre, thermolum. and optical absorption spectra 79−24374
- LiF, thermoluminescence, γ-radn.-induced sensitization and supralinearity 79−91507
- LiF, thermoluminescence mechanisms following gamma irradiation 77−59625
- LiF, thermoluminescence response to gamma rays 77−59626
- LiF:Mg,Ti, (TLD-100), optical bleaching of defect centres 79−19911
- LiF:Mg,Ti, optically induced dichroism of Z_2-centres 79−28710
- LiF:OH:Mg, γ-irrad. induced oxyhydryl complexes 80−92555
- LiF:U, EPR of U^{5+} centre, charge compensation mechanism 77−90030
- LiF:U, X-ray and γ-ray irrad., EPR of U^{5+} centres 79−91295
- LiF:U_3O_8, irrad., U^{5+} luminesc. molecular centres, optical and ESR expts. 77−48224
- LiF-OH, γ-irrad., colour centre lasing at 0.84-1.13 μ at 300K 80−5739
- LiH, EPR line shape of Li colloids created by γ-irrad. 77−77097
- LiI crystal, irradiated at low temps., optical absorption spectra 80−45123
- $LiNbO_3$, γ-irradiated and annealed, elastic and piezoelectric props. 78−2807
- $LiNbO_3$, hologram recording, γ radiation effect 80−78812
- $LiNbO_3$, optically active centres, form. by electron and γ-irrad. 78−18642
- $LiNbO_3$:Fe, photorefraction, γ-irrad. influence, polarisation-optic and holographic obs. 80−11359
- $LiNbO_3$:Fe, X-ray and γ-ray irradiation effects on Fe charge state, Mossbauer study 80−40013
- $LiNbO_3$:Fe (0.05%), hologram recording γ radiation effect 80−78812
- Li_2O-Al_2O_3-SiO_2:Cd^+, glass, ESR study 80−103879
- Li_2O-TiO_2-Al_2O_3-SiO_2 glass, γ-irrad., struct. position of Ti, EPR study 80−84644
- $LiYO_2$:Nd^{3+}, absorption and luminesc. spectra, γ-irrad. induced colour centre form. 77−63441
- Mg, SiO_4:Th TLD phosphor, γ-ray induced sensitisation and phototransfer 79−33851
- $MgAl_2O_4$, γ-irradiated crystal, TSC, thermoelec. power, thermolum. and afterglow 80−75583
- $MgAl_2O_4$, spinel, γ-irrad. effect on optical absorpt. and thermolum. spectra 77−85759
- MgF_2, gamma- or neutron irradiated, ESR meas. on hole centres 77−12201
- MgF_2:Fe^{2+}, γ-irrad., F-centres, Fe^{2+} ion hole traps, absorpt. and EPR meas. 79−7598
- MgO, defect centres, thermolum. examination 78−15235
- MgO, γ-irrad. polycryst., isothermal luminesc., recomb. of electron from F_s^+ centres 80−34985
- MgO powder, vacuum UV induced thermoluminesc. in Γ-irradiated and non-irradiated samples 77−36302

gamma-ray effects continued
- MgO single cryst., γ-irrad. in presence of O_2, H_2 and H_2O adsorbates, thermostimulated surface cond. 80−34499
- MgO, single crystal, thermal and optical stimulation processes of V-centres *(Japanese)* 80−11485
- MgO:Ga, γ-irradiated, EPR and optical studies 79−73809
- MgO-Al_2O_3-SiO_2-NiO glass, gamma ray irradiated, exam. of ESR spectrum of Ni(I) 79−4719
- MgO-TiO_2-Al_2O_3-SiO_2 glass, γ-irrad., struct. position of Ti, EPR study 80−84644
- MnF_2, radiation damage, optical absorpt. and luminesc. expts. 78−2161
- $Mn_{1.77}Sn$, 170K transitions temp. in ferrimag. state, pressure and γ-irrad. effects 77−51902
- Mo, gamma irradiated defects, interaction with positrons *(Russian)* 80−97372
- Mo, gamma-ray irrad. positron annihilation during radiation defect annealing *(Russian)* 79−99970
- N_2, electric breakdown in long high-voltage gaps with gamma and alpha particle irrad. 79−18993
- NH_3, solid, gamma-irrad., cryostats development 77−45856
- $(NH_4)_2BeF_4$, γ-irrad., trapped H atoms, ferroelec. transition, EPR meas. 79−4724
- $(NH_4)_2BeF_4$, γ-irrad. cryst., F_2^- ions, ESR meas. 80−34770
- NH_4ClO_4, γ-irrad., trapping and motion of NH_3^+ radical in cryst. lattice 79−33538
- NH_4ClO_4, γ-irrad., motions of trapped NH_3^+ radical, ESR study 79−95648
- NH_4ClO_4, γ-irrad. single cryst., NH_3^+ EPR obs., g-tensor hyperfine splitting 78−2739
- $((NH_4)_{1-x}Cs_x)_2SO_4$ mixed cryst., EPR of NH_3^+ and SeO_3^- radicals 80−50190
- $((NH_4)_{1-x}Rb_x)_2SO_4$ mixed cryst., EPR of NH_3^+ and SeO_3^- radicals 80−50190
- $(NH_4)_2SO_4$, irrad., −50°C transition, librational mode softening, paramag. NH_3^+ probe obs. 77−20037
- NaCl, gamma irradiated, optical bleaching of colour centres, F-aggregate centre form. 79−95813
- NaCl, gamma irradiation, optical and thermal bleaching of colour centres, trapped electron centre form. 79−95814
- NaCl, gamma-irradiated, aquoluminescence spectra in presence of activators 77−69913
- NaCl, γ-irrad., F-centres form., energy storage 79−82264
- NaCl, γ-irrad., F-stimulated inversion of sign of dislocation charge 80−59475
- NaCl, γ-irrad., photoplastic effect and internal friction aftereffect 80−24529
- NaCl, γ-irrad. and doped, lattice relax., cold neutron scatt. obs. 77−7715
- NaCl, γ-irradiated, F→M phototransformation, effect on aquoluminescence 80−7418
- NaCl, γ-radiation effect on 10.6 μ absorpt. coeff. assoc. with F-aggregate centres 77−4661
- NaCl, internal stresses and dislocation mobility 78−48440
- NaCl, irrad., C-centres, positron ang. correl. obs. 78−22712
- NaCl, irradiated, determ. of molar extinction coeff. and oscillator strength of V_2-centre *(Russian)* 78−80384
- NaCl, M-centre prod. processes, in-beam studies, 15-95°C 79−55737
- NaCl, M-centre statistical prod. meas. 80−15097
- NaCl, optical strength, effect of irrad. in mechanically stressed state 80−80695
- NaCl:Ca, Z_1 centre thermoluminescence study 80−16109
- NaCl:Ca(Mg), X- and gamma-irrad., thermostimulated electrons and luminesc. 79−91505
- NaCl:Cd^{2+}, dielectric loss following plastic deform. 80−84690
- NaCl:Tl^+, γ-irrad., aquoluminesc. obs. 80−2856
- NaCl(:Ca), irrad. at room temp., stored energy rel. to thermolum. 80−10574
- NaCl(F), irradiated at room temp., thermolum. and F-centre thermal stability 78−84669
- $NaClO_3$, Γ-irrad. defects, ^{35}Cl NQR, 77 and 300K 78−91981
- $NaClO_3$, γ-irradiated, ESR of trapped O_3^- 79−29381
- $NaClO_3$, reson. Raman scatt. from metastable O_2 produced by γ-irrad. 78−60432
- $NaClO_3$ single crystals, change of elastic constants by gamma radiation 78−63800
- $NaClO_3$:O_3^-, form. by γ-irrad., reson. Raman scatt., temp. depend. 78−92062
- NaF, gamma irrad., colour centre stimulated emission, threshold pump power, tuning range 79−73971
- NaF, γ-irradiated cryst., relaxational damping of elastic waves and activiation energy of motion of defects 79−14891
- NaF, M-centre vibronic absorpt. spectra, elec. field, method of moments 78−27186
- NaF:K^+, γ-irradiated, $H_A(K)$ centres, EPR obs. 77−69689
- NaF:LiF, γ-irrad., colour centre form., reflectance and thermolum. meas. 79−55739
- NaF:U, EPR of U^{5+} centre, charge compensation mechanism 77−90030
- NaI colour centre formation and accumulation *(Russian)* 77−65978
- NaI(Tl) scintillation detectors, temp. depend. of radiation-induced coloration 79−72204
- $NaNO_3$, pure and Ca^{2+} doped, γ-irrad., damage species annealing 79−66324
- Na_2O-B_2O_3 glass, γ- or UV-irrad., laser and thermal bleaching of colour centre, absorpt. spectra 79−33744
- Na_2O-B_2O_3:Se, EPR, γ-ray effects *(Russian)* 78−31109
- Na_2O-SiO_2:CuO glass, gamma-irradiated, EPR and optical spectra 80−103885
- Na_2O-TiO_2-Al_2O_3-SiO_2 glass, γ-irrad., struct. position of Ti, EPR study 80−84644
- NaOH aqueous glassy systems, 77K, γ-irrad., struct. stabilisation 79−91976
- $Na_5P_3O_{10}$, γ-irrad., PO_3^{2-} EPR obs. 78−27091
- $NaReO_4$, EPR spectra of paramag. centres and free radicals 80−108072
- Nb_3Sn, proton and γ-irradiated, lattice dynamics from ^{119}Sn Mossbauer studies 78−39458
- Nd:glass laser, γ-ray induced absorbing layer form. in optical medium 77−50688
- Nd:glass laser, influence of neutron and γ irrad. on generating characts. *(Russian)* 80−69402
- NdF_3, gamma-irrad. induced coloration 77−35586

gamma-ray effects continued
  Ni complex, 2,6-N,N-diacetyldiaminopyridine-Ni(II) elec. cond., γ dose and temp. (303-363K) effects 80—103696
  Ni complex, 2,6-N,N-dibenzoyldiaminopyridine-Ni(II) elec. cond., γ dose and temp. (303-363K) effects 80—103696
  Ni, self interstitial migration and crowdion conversion, dislocation pinning expts. 77—84762
  Ni-Fe, 79 NM alloy, gamma and neutron influence on mag. susceptibility comparative study *(Russian)* 80—39751
  Pb, gamma-ray attenuation coeff. meas., 1115, 1173, 1332 keV 77—55303
  PbF_2, gamma-ray and neutron irrad. at low temps., EPR of Pb^{3+} ions 77—63262
  β-PbF_2, γ-irrad., F-band region spectrum, impurity effects 77—44026
  PbO-SiO_2 and Na_2O-PbO-SiO_2 system glasses, radiative paramag. and optical absorpt. centres 77—8402
  PbO-SiO_2 glasses, charge trapping and dielec. breakdown, radiation-induced, microphase separation 78—23399
  PbTe, diffusion of Ag, effect of gamma irradiation 80—59515
  PrF_3, gamma-ray induced coloration 77—35586
  Pt:^{181}Hf, interaction of implanted impurity with radiation induced lattice defects, TDPAC meas. 80—24494
  Pt-self-powered neutron detector, temp. and radiation tests 79—81132
  RbBr, suprapure, thermolum. glow and emission studies at room temp. 80—7423
  RbCl, F-centre ESR in relaxed excited state, isotropic superhyperfine interaction consts. 79—65733
  RbCl, undoped and Sn doped, γ-irrad. crysts., thermolum. and emission, 300 to 560K 79—15539
  RbCl:Eu, γ-irrad., thermoluminesc., EPR meas. 78—84670
  RbCl:Mg, γ-irrad., thermoluminesc. 79—47528
  $RbMnF_3$, radiation damage, optical absorpt. and luminesc. expts. 78—2161
  $RbNgF_3$, radiation defect F,M,R-centre absorpt., emission, excitation spectra 79—43000
  Rh-self-powered neutron detector, temp. and radiation tests 79—81132
  S, allotropic modifications and activity distrib. 80—70255
  SF_6, γ-irrad., SF_5 anisotropic ESR spectrum 77—21400
  $(SN)_x$, γ-irradiated, temp-depend. of elec. resist. and mag. susceptibility 77—51877
  $SO_2{}^+$ radical-ion formation 77—25285
  sapphire, TFTR diagnostic windows, radiation damage 80—34063
  Si based MOS device irradiation with γ-rays, minority carrier generation, CV characts. 80—88637
  n-Si, defect charge states, complex form., gamma-ray effects 80—96564
  Si depletion regions, radiation damage coeffs. for fission neutron and gamma-ray irrad. 80—34058
  Si, diffusion of impurities accelerated by γ rays 77—55394
  Si, divacancy charge states, photoconductivity spectra 77—15899
  Si dosimetry diode, irrad. by γ-rays and fast neutrons, lattice defect annealing *(Czech)* 79—45570
  Si extrinsic IR detectors, As doped, low-level γ-ray irrad. effects 80—37085
  n-Si, gamma ray irrad., impurity composition influence on recombination centre formation 80—6872
  Si, gamma-irradiated, number of Frenkel defects 78—14377
  n-Si, γ- and electron irradiated, influence of deform. on capture of electrons by divacancies 77—1449
  n-Si, γ-irrad, (E_{max}=100 MeV), carrier recomb. 78—56158
  n-Si, γ-irrad., galvanomagnetic effect anisotropy rel. to layer inhomogeneity 79—33299
  n-Si, γ-irradiated, with layer inhomogeneity, quantum current oscillations 80—11010
  n-Si, inhomogeneous impurity distrib., elec. props., effect of γ-irradiation 77—55550
  n-Si, irrad., elec. props., in strong elec. fields 79—95416
  Si, n^+-p diode, γ-radiation defects, annealing and recomb. props. 80—65045
  Si, neutron doped, γ-irrad. influence on elec. props. 80—6845
  Si p-n junction, negative annealing of γ-radiation defects 77—43246
  Si, photodiode, 1.06 μm range, neutron and γ-irrad. effects 79—97433
  Si, radiation defects, influence of dislocations on accumulation, elec. props. 80—92558
  Si:Au, precipitation of solid soln., effect of gamma irradiation 80—59515
  Si:Au diodes, diffused, influence of gamma irradiation, Au levels monitored 77—66199
  -Si:Fe, effect of γ-irradiation, photocapacitance meas., impurity centre conc. 78—18993
  p-Si:Gd, irradiated, elec. props. 79—51613
  Si:Gd, radiation defects effect on elec. props. 77—28184
  Si:Li P/N type solar cells, irradiation obs. 79—66406
  Si:Ni,Co,Mn, γ-irrad., interaction of deep-level impurity atoms with radiation defects 77—76457
  Si:S, γ-irrad. influence on elec. props. 80—6845
  n-Si-SiO_2, MOS structures, radiation states 80—103758
  Si-SiO_2 interface, anal. of fast surface states 79—42648
  Si-SiO_2 interface, γ-ray irradiated thin oxide, MOS struct. *(Russian)* 78—84302
  Si-SiO_2 interface of MIS structure, generation-recomb. characts., effect of γ-irradiation *(Russian)* 77—76938
  Si(:Au), gamma-induced trapping levels 79—87059
  $SiCl_4{}^-$, γ-irrad. of $SiCl_4$ in adamantane matrix, ESR spectra 79—27011
  SiH_3X^-, X=Cl, Br, I, and isotopic forms, EPR spectra, mol. struct. 79—94023
  Si(Li) detector, improvement of time depend. instabilities by IR and γ-irradiation 79—36477
  SiO_2, D-impregnated, vitreous, radiation induced isotope exchange 79—99240
  SiO_2, doped, fibre-optic waveguide, effect of ionising radiation on optical attenuation 78—63170
  SiO_2, fused, as-received and irrad., dielectric props. 79—65786
  SiO_2, fused, γ-irrad., O-associated trapped-hole centres, optical absorpt. and ESR spectra obs. 79—65729
  SiO_2, fused silica, KLR1, KLR2 and KU2, high-precision stability of end gauges 79—76778
  SiO_2 gel, irrad., adsorpt. of NH_3, neutron scatt. 79—33194
  SiO_2, glass, ^{29}Si hyperfine struct. of E′ centre, microwave saturation props. 80—7165
  SiO_2, glass, irrad., EPR of Al $E_1{}'$ centres 80—11268
  SiO_2, noncryst., radiation-induced defect centres, ESR spectra and struct. 78—23343

gamma-ray effects continued
  SiO_2 optical fibres, plastic clad, gamma-ray irradiated, signal level depend. of recovery rate 79—36997
  SiO_2 optical fibres, plastic-clad, short-term transient radiation effects 79—50420
  SiO_2, vitreous, grown from vapour, gamma ray irradiated, ESR and thermoluminescence exam. 78—88189
  SiO_2, vitreous, H impregnated, hydride, hydroxyl formation 79—87874
  SiO_2:Al gel, gamma rad. effects, depend. of H_2 adsorption and colour centre form. on Al content 79—69156
  SiO_2:Ge silica-core fibre-optic waveguides, effect of B, P and OH on radiation response 79—50419
  SiO_2:GeO_2/SiO_2, SiO_2/SiO_2:B_2O_3, glass fibre waveguides, γ-radiation optical stability 80—23799
  SiO_2:H(D), γ-irrad., hydroxyls and hydrides form., detect. by Raman scatt. 77—32817
  Sn, gamma-ray attenuation coeff. meas., 1115, 1173, 1332 keV 77—55303
  SrF_2:CeF_3(GdF_3)(TbF_3), absorpt. spectra of γ-irrad. cryst., 77K, 200-700 nm 78—84615
  SrO, hydrogenated, EPR and ENDOR meas. of γ-irradiated cryst. 77—8403
  SrO, irradiated, low temp. photocond. 77—39891
  SrO, trapped hole defects, ENDOR and EPR spectra of V-centres 77—32255
  SrO:D, γ-irrad., V_{OD} defects, EPR and ENDOR 78—27116
  Ti anode, with RuO_2-TiO_2 active film, Cl overvoltage, γ-irrad. effects 79—16005
  $TlCl_3$.$(TlCl)_3$, labelled, exchange of Tl ats. rel. to γ-irrad., heat treatment, grinding 78—92470
  TlSe.As_2Se_3, Tl_2Se.As_2Se_3, γ-irrad. effects on mech. props. 77—80567
  Xe, liq. and solid, γ-irrad., average energy expended per ion pair *(Russian)* 80—5438
  YAG:Ce, γ-irradiated elec. cond. meas. 77—43601
  YAG:Nd,Ce,Cr, effect of γ-rays, fast electrons on optical props., annealing and colour centre destruction 77—8608
  YIG, electron and γ-irrad., photomagnetic effect 80—103877
  ZnO, adsorption of Br_2 and I_2, γ-irrad. induced centres 80—54513
  Zr, gamma-ray attenuation coeff. meas., 1115, 1173, 1332 keV 77—55303
  ZrO_2, cubic single crystal, colour centres 77—15410
  ZrO_2, stabilised, low temp. induced centres, ESR meas. 78—72409
  $(ZrO_2)_{0.9}(Y_2O_3)_{0.1}$:Ti, γ-irrad., ESR of trigonal centres, attributed to Ti^{3+} at cation sites 77—24740

gamma-ray interactions
  see also gamma-ray scattering
  EAS, hadron interaction model and mass spectrum *(Russian)* 79—96873
  secondary radiation excited in air, meas. with ionisation chamber *(Czech)* 79—67967
  $\gamma d \to K^+ \Delta n$, differential cross section, influence of Δn interaction *(Russian)* 79—394
  γn to 5.3 GeV, multipion and strange particle prod., reson. 77—10261
  Ge, total pair prod. cross section near threshold, meas. using variable energy source *(French)* 79—85866

gamma-ray lasers
  collimated particles, gamma-ray lasing and radiation emission 79—27230
  computerised analysis, collaboration collection report 80—73106
  concepts, configurations *(German)* 78—1201
  electron-positron pair stimulated annihilation, coherent γ-emission 79—55104
  kinetics, quasi-classical approach *(Russian)* 80—74332
  micro-resonators, high flux, for X and γ-ray lasers 79—7151
  Mossbauer coherent γ-radiation generation, collective and stimulated processes *(Russian)* 78—9356
  Mossbauer effect in magnetised plasma, applic. to gamma-ray lasers 80—28186
  negative light absorption by medium with selective freq. modulation of quantum oscillators 80—106501
  neutron capture, direct pumping of gamma-ray laser 80—14310
  nuclear inversion coherent excitation by relativistic electron beam *(Russian)* 80—48206
  nuclear orientation techniques for directed emission 77—27268
  nuclei in intense laser fields, spontaneous-stimulated γ-ray emission 77—83843
  parametric non-threshold amplification, three-frequency interaction *(Russian)* 77—79902
  physical basis, technical configurations *(German)* 77—75530
  polarised nuclei use, laser threshold conditions 78—37868
  progress and problems *(Russian)* 79—36867
  quadrupole spin echo, gamma avalanche launching, ^{103}Rh numerical estimate 77—79794
  recoilless γ-rays, observation of stimulated emission, possibilities *(Russian)* 79—18383
  relativistic particle channelling in cryst., spontaneous emission of γ-quanta, new effect 78—15243
  superfluorescence kinetics for single-mode emission, single-passage mirrorless laser *(Russian)* 77—46714
  three-level Mossbauer gamma-ray lasers, two-stage pumping 80—78857
  two-photon annihilation stimulation of relativistic electrons and positrons 79—64195
  ^{161}Dy polarised nuclei system, nonthreshold and amplification *(Russian)* 79—98332

gamma-ray polarisation
  bremsstrahlung, circularly polarised, from longit. polarised electrons in single nonmag. crysts. 78—15242
  bremsstrahlung, coherent, polarisation at nonaxial collimation 77—20950
  circular polarisation in $np \to d\gamma$, test of weak neutral current models 78—41562
  eikonal approx., electron-oriented nucleus scatt., polarisation of e^-, nuclei and emitted γ rays 78—37331
  electron bremsstrahlung on thin diamond monocrystals *(Russian)* 77—6603
  hadron-nucleus scatt., corrections to circular polarisation of γ quanta *(Russian)* 78—41683
  linear polarisation direction correlation γ-γ meas., Ge detectors, $^{110}Ag^m$ cascade decay *(Japanese)* 78—41903
  linear polarisation enhancement of bremsstrahlung in crystals, spin effects 79—11359

gamma-ray polarisation continued

- longitudinal polarisation, of e,e^+ and γ-rays in e^+e^- annihilation in crystal 79−11482
- Mossbauer 14.4 keV gamma-ray source, design, calibration and polarimeter 80−86535
- oriented radioactive nuclei, JINR investigs. using SPIN equipment *(Czech)* 77−42220
- parity violating terms in nuclear EM operators and struct. effects 79−6482
- parity violation in nuclear processes with polarised neutrons 79−59008
- Rayleigh scattering spin depend., circ. polarised γ-rays on magnetised Fe-Co 77−59637
- template modulated coherent light for X- and γ-ray production, energy spectra, freq., polarisation 77−13833
- three Ge(Li) Compton polarimeter with kinematic selection, for γ polarisation meas. 77−83456
- $np \rightarrow d\gamma$, parity-nonconserving nucl. force 77−10333
- np radiative capture, triplet state effect, γ-ray circular polarisation meas. *(Russian)* 77−23009
- Ag+^{40}Ar deep inelastic reactions, γ-ray polarisation meas., neg. deflection angles 78−8845
- Ag+^{40}Ar(^{86}Kr), γ-ray circular polarisation meas. 78−54788
- ^{197}Au(n,γ), ^{198}Au energy level spins 79−457
- ^{129}Ba, γ-ray linear polarisation meas. from ^{120}Sn(^{12}C,3n) 78−50121
- Ca(n,γ), A=42, 44, γ circular polarisation meas. 78−62533
- Cd, A=105 to 109, parity assignments from linearly polarised γ-rays 78−41630
- ^{57}Co:Fe Mossbauer source linear polarisation rate meas. *(French)* 79−30633
- ^{64}Cu, γ-spectra, J^π assignments via ^{64}Ni(p,nγ) 2.75-3.75 MeV 77−18470
- e^-e^+ pair photoproduction in crystals by circularly polarised γ-quanta 78−17005
- ^{18}F, 1.08 MeV γ transition, circular polarisation affected by neutral weak currents 78−41663
- ^{18}F, 1.08 MeV γ transition, circular polarisation affected by neutral weak currents 79−13243
- ^{19}F(p,p′), 5.5 MeV; time differential obs. of perturbed γ linear polarisation distrib., Hanle effect 78−78360
- Fe(n,γ), A=56, 58, γ circular polarisation meas. 78−62533
- ^{1}H(n,γ), thermal, photon circular polarisation in parity violating capture 77−6375
- ^{1}H(n,γ), thermal calc. of γ-circular polarisation, p-nonconservation effects 77−18564
- ^{2}H photodisintegration and electrodisintegration, weak interaction and P nonconservation 78−89849
- ^{165}Ho, electron-oriented nucleus scatt., eikonal approx. calc. 78−37331
- ^{41}K, populated by ^{38}Ar(α,pγ), levels props., shell model calc. 78−62588
- ^{64}N(n,γ), γ circular polarisation meas. 78−62533
- ^{21}Ne, γ-ray circular polarisation, parity mixing 78−70443
- Ni+^{16}O, 100 MeV, deep inelastic, γ-circular polarisation and spin orientation 79−17848
- ^{58}Ni+^{16}O, 100 MeV, γ-ray circular polarisation meas. 78−54788
- ^{124}Sb, first forbidden β-transitions, β-γ circular polarisation correlations 79−9517
- ^{124}Sn(^{32}S,xn), continuum γ rays, linear polarisation, feeding high spin yrast states in ^{151,2}Dy 80−497
- ^{130}Te(^{32}S,xn), continuum γ rays, linear polarisation, feeding high spin yrast states in $^{156\text{-}8}$Er 80−497
- ^{46}Ti(n,γ), γ circular polarisation meas. 78−62533
- U linear polarisation of elastically scatt. γ-rays of 279 and 662 keV 77−6344
- ^{64}Zn, J^π assignments from γ-ray linear polarisation meas. from ^{59}Co(^{7}Li,2n) 79−6383
- ^{67}Zn, populated in ^{64}Ni(α,n), level struct. below 2.0 MeV, γ-ray studies 78−62483

gamma-ray production

- 4.43 MeV source, Am-Be or Pu-Be surrounded by hydrocarbon, for undergraduate laboratory 78−77648
- $\mu^+ \rightarrow e^+\gamma$, upper limit for decay 78−25030
- apparatus for low-temp./high pressure Mossbauer absorber study, modified 79−17591
- autonomous γ-irradiator, construction *(Bulgarian)* 78−78053
- bremsstrahlung energy deposition as function of converter foil thickness, optimisation 77−23388
- commercial irradiation plant, Japan 77−59794
- Compton experiment, with annular ^{241}Am source, momentum resolution and reliability meas. 80−312
- Compton scattering, electron momentum density studies 80−14028
- cosmic ray gamma quanta prod. by hadrons of tens of TeV energies, energy characts. 79−80148
- cosmic ray gamma-quantum families, atmospheric nuclear cascade characts. calc. 79−80157
- cosmic ray gamma-quantum families, hadron interactions transverse momenta at 10^{14} to 10^{15} eV 79−80170
- cosmic ray high-energy gamma-quantum and hadron families, Monte Carlo studies 79−80158
- cosmic ray-nucleus interactions, gamma ray-charged particle correlations, 20 TeV 78−45170
- Cross sections for gamma-ray production by 14-MeV neutrons 78−21552
- direct photon emission from excited bosons and e^+e^- collisions, relativistic oscillator model 78−37208
- dosimeter, thermoluminesc., calibration, γ-ray irradiator *(Japanese)* 78−66452
- electron-photon beams from proton accelerators, EM interaction investigation *(Russian)* 80−106214
- electron-positron annihilation in mag. field, neutron star 77−10236
- fusion reactor materials, 14 MeV neutron scatt. in extended samples of LiF and ^{56}Fe 77−57739
- gamma source with flat surface, activity determ. using Ge(Li) detector *(German)* 78−58528
- heavy ion induced reactions, γ-ray multiplicity, ang. momentum and struct. depend. *(Rumanian)* 78−89906
- high-energy cosmic-ray components in atmosphere, scaling features 78−93062
- inclusive γ production in pp collisions, quark parton model 79−429
- ion induced γ-rays, thick sample reaction yields, energies, appl. in prompt nuclear anal. 78−62502
- monochromatic and polarised photon beam at Frascati 80−23239

gamma-ray production continued

- monochromatic annihilation beam prod. from 2 GeV linear electron accelerator 77−50322
- monochromatic polarised photon source from Compton backscattered laser light on electrons 80−52800
- monochromatisation method based on Compton scattering *(Russian)* 79−89516
- Mossbauer 14.4 keV gamma-ray source, design, calibration and polarimeter 80−86535
- Mossbauer source preparation, tabulation, book contrib. 79−87366
- multiple Compton effect, cross sections, γ spectra and number *(Russian)* 79−370
- (n,γ) cross sections meas. for 22 elements between Z=3 and Z=82 77−26681
- N-16 source, exposure rate and absorbed dose meas. for 6-7 MeV photons 79−26766
- NBS positron annihilation in flight facility, positron beam calibration 79−31306
- neutron capture via nuclear reactor, review 80−14029
- nuclear explosions EM pulse, anal. 78−21771
- nuclear NDT methods, sensitivities and detection limits 77−32756
- nucleus+nucleus high energy studies at Berkeley Bevalac, expt. data, theoretical predictions 77−50144
- pair annihilation, 1γ and 2γ, in strong mag. fields 79−17704
- pair recombination in travelling wave struct., stimulated emission of γ-rays 78−37863
- polarised monochromatic beam prod., Ladon project at Frascati 77−83437
- polarised photon beam production, 100 GeV energy range 77−38522
- positron annihilation, 20-120 Mew quasi monochromatic beam at 600 MeV Saclay linac 80−5425
- proton interaction with lunar and planetary material, gamma-ray production, simulation 78−16318
- radiation protection at γ-irradiation installation, GOU-1 *(Bulgarian)* 78−82530
- radioactive γ-ray sources, comparison of characteristics of X-ray and γ-ray sources 80−14030
- secondary standard preparation for low activity gamma spectrometry 80−18701
- solar flares, 0.51 MeV gamma-ray line prod. 77−13292
- solid angle, self-absorption factors, evaluation by Monte Carlo method *(Rumanian)* 78−58526
- sources for Compton profile meas. 79−35907
- steel, stainless, fusion reactor shield, neutron induced activity and γ-ray source investigation 78−54872
- template modulated coherent light for X- and γ-ray production, energy spectra, freq., polarisation 77−13833
- Tomsk synchrotron, system of tagged photons 78−833
- Triga Mark III nuclear reactor, as intense gamma radiation source *(Spanish)* 80−83232
- tunable narrow band radiation production using laser saturation 80−57680
- $e^+e^- \rightarrow \gamma\gamma$ at 6.2-7.4 GeV CM, comparison with QED predictions 77−49942
- $e^+e^- \rightarrow \gamma\pi^0$, inclusive production, 4.9 to 7.4 Gev, cross sections 78−89723
- e^+e^+ annihilation monochromatic photon beam prod. at Frascati Linac Lab. 77−83438
- (n,γ), gamma-ray production cross sections for reactor materials 77−23067
- (n,γ) variable energy linearly polarised photon beam prod. 79−76248
- (n,n′γ), 14.2 MeV, meas. of gamma-ray production cross-sections 77−23070
- $N\bar{N}$ system, single γ and π emission rates, meson quantum number assignments 78−78208
- $\bar{\nu}N$ charged-current interactions, semi-inclusive γ prod. 79−71737
- (p,γ) resonance yield curves, from H_2^+ and H_1^0 beams on Al targets, materials anal. 79−3530
- pp collisions, real photon prod. at large p_T, cross section calc. 79−13149
- $pp \rightarrow \gamma X$, 24 GeV/c, inclusive π prod. 77−14003
- $\bar{p}p \rightarrow \gamma + X$, 4.6, 9.1 GeV/c, inclusive total, topological and invariant differential cross sections 79−408
- $\bar{p}p$ interactions, 100 GeV/c, inclusive distribs. for γ, K_s, Λ^0, $\bar{\Lambda}^0$ prod. 77−38213
- πp, real photon prod. at large p_T, QCD and CIM anals., jets 79−89185
- Υ decay, photon spectrum, branching ratios, leptonic-, hadronic widths, quarkonium model 79−3020
- ^{27}Al(n,n′γ)^{27}Al, γ-ray prod. cross-section meas. 79−26434
- Al(n,xγ)Al, E_n=5.3 MeV, γ prod. cross-section obs. 78−89863
- ^{241}Am, radioactive decay, 59.5 keV photon yield 77−6588
- ^{198}Au, 412 keV γ-radiation, Compton scattering and Bragg diffraction, study of electron densities in solids 80−18059
- ^{13}C(α,n), n and 6.13 MeV γ-ray emission for Ge(Li) detector calibration 79−13572
- ^{252}Cf, spontaneous ternary fission, multiplicity distrib. of prompt γ rays 78−21615
- ^{57}Co:Fe Mossbauer source linear polarisation rate meas. *(French)* 79−30633
- ^{57}CoO, compact single-line Mossbauer source preparation 77−10518
- ^{60}Co, 2505 keV gamma ray intensity in β-decay 79−13249
- ^{60}Co isotopic γ-ray source, quantum yield of electrons from cylindrical casing 79−31289
- ^{60}Co plant design for radiation sterilisation in developing countries 77−60246
- ^{60}Co spectrometry, for instrument calibration 77−6608
- ^{60}Co-charging of γ-irradiation installation *(Bulgarian)* 78−82558
- Cu, fusion reactor shield, neutron induced activity and γ-ray source investigation 78−54872
- Cu(n,nγ), 0.67-19.6 MeV, prod. cross sections, discrete and continuum γ rays 365 to 6620 keV 77−34293
- Cu(n,xγ)Cu, E_n=5.3 MeV, γ prod. cross-section obs. 78−89863
- ^{152}Eu, intercomparison of gamma ray emission rate meas., using Ge spectrometers 78−82568
- F+n, differential cross sections for prod. of low energy photons 77−23068
- ^{197}Hg source for Mossbauer studies 79−26796
- Mo, fusion reactor shield, neutron induced activity and γ-ray source investigation 78−54872
- N, neutron scatt. and gamma-ray prod., Monte Carlo anal. 77−26682
- ^{103}Pd decay, 357 keV γ:K X-ray abundance ratio obs. 79−498

gamma-ray production continued
- ^{237}Pu gamma-emitting isotope, prep. of tracer by ^{238}U(^{3}He,4n) 77−34497
- ^{153}Sm, reactor prod. of curie strength photon beam 78−86709
- Ta+n, differential cross sections for prod. of low energy photons 77−23068
- ^{182}Ta Mossbauer sources *(French)* 80−74064

gamma-ray scattering
- *see also Compton effect; gamma-ray interactions*
- albedo data, removal of negative albedo terms 80−5347
- anisotropic computations, selection of angular quadrature 77−37828
- area skyshine from radioactive waste, gamma-ray backscatt. photon spectra 80−31119
- atom, bound state Compton cross section, depend. and IR behaviour on binding and off-mass shell effects 79−63967
- atom, coherent and incoherent scatt. by bound electrons, 0.145-1.33 MeV 79−45680
- atom, photon-bound-electron scatt. meas. 77−14394
- backscattered photons number albedo meas. 79−36490
- backscattering, ^{60}Co source, sky-shine spectra 77−65341
- backscattering, survey of principal research 77−65340
- backscattering coefficients, Monte Carlo calcs. 77−61171
- backscattering from various barriers, characts. and spectral ang. distrib. 77−61621
- backscattering of γ-rays 77−88323
- bone, mineral content, coherent scatt. of photons 80−67238
- coal, ash content, determ. by forward-scattered γ-radiation, improved accuracy 78−7280
- collimator scattering of γ rays into detector, spectral distrib. analysis 77−57793
- Compton experiment, with annular ^{241}Am source, momentum resolution and reliability meas. 80−312
- Compton scatt. studies and spectrometers 79−74014
- concrete, density meas. by back-scattered gamma radiation 77−36699
- crystallographic structure measurements at MURR 80−13192
- densitometer meas., anal. of dynamic bias 80−27730
- densitometry, static error evaluation 80−27729
- densitometry side-scatter, dynamic bias, nuclear react. appl. 80−27728
- differential Compton scatt. cross-sections meas. 77−30731
- diffraction meas. in mosaic struct. of RbI in metastable press. region 77−20065
- diffractometry for study of ferroelastic crysts., appl. to KH_2PO_4 77−8533
- double-scattered γ energy spectrum simulation and expt. 79−9905
- dual gauging using penetrating and scattered photon fluxes 77−41551
- elastic and Compton scatt. through small angles, Ge(Li) meas. 79−718
- geophysical prospecting, allowance for scattered gamma radiation *(Russian)* 80−105067
- incoherent scattering of gamma rays, spectrometer for electronic momentum distribs. investigation *(German)* 77−41741
- inelastic scattering intensity meas. using Mossbauer effect 80−71245
- lung density, Compton scatt. meas., multiple photon interactions 80−67146
- media interface, calc. of gamma-ray backscattering 78−85106
- memointerference or vibrointerference phenomenon and application 78−55313
- Monte Carlo calculation of γ-ray backscatt., atomic number depend. 77−67734
- nuclear reactor, subchannel void fraction by gamma scattering 80−27726
- nuclear resonant scattering, body Fe stores meas. technique 79−83914
- organic binary system composition, determ. by γ-ray scatt. from low Z nuclei 79−87897
- photon, spectra of gamma rays backscattered by infinite air (skyshine) 80−101436
- PMMA, Rayleigh scatt. of Mossbauer γ-rays 79−73864
- pulsed source, distrib. of scattered γ-radiation, unsteady transport 80−27830
- quartz, piezoelec. and gamma-ray diffr. props. 77−20801
- resonant scattering, solid state properties of target 80−18060
- SCAP-BR, multilegged duct γ streaming computer program 79−9906
- singly scattered gamma radiation, albedo 79−40783
- steel, subsurface defect detection using gamma rays 78−85104
- steel slab, scattered radiation intensity of ^{192}Ir gamma rays 77−30673
- two-phase flow system, local density measurements, side-scatter gamma technique 80−569
- Z-depend. of elastic scatt., power law 78−45578
- $\gamma p \rightarrow \gamma p$, differential cross sections in 240 to 440 MeV range, Δ(1232) region 77−10255
- γp low energy scatt., one particle exchange model 78−33070
- ^{60} γ-ray scatt. in air, anal. by discrete ordinates transport codes 80−32525
- Ag, total at. cross-section, incoherent scatt., 45-1115 keV 79−13679
- Al, radial distrib. of γ-rays from narrowly collimated source *(Russian)* 77−30549
- Al, total at. cross-section, incoherent scatt., 45-1115 keV 79−13679
- Au, incoherent γ-ray scatt. by K-shell electrons 77−83560
- ^{198}Au, 412 keV γ-radiation, Compton scattering and Bragg diffraction, study of electron densities in solids 80−18059
- Bi, K-shell electrons, γ-ray inelastic scatt. cross-sections 77−14395
- C, total at. cross-section, incoherent scatt., 45-1115 keV 79−13679
- CaO, coherent/incoherent scatt. cross-sections of 136-278 keV γ-rays 78−70881
- ^{60}Co therapy for Hodgkin's disease, gonadal and eye doses 79−96665
- Cu, atom and ions, isoelectronic sequence, coherent photon scatt. cross section calc. 78−5177
- Cu, incoherent scatt. of 279, 322, 662 and 1115 keV gamma rays 80−40179
- Cu, total at. cross-section, incoherent scatt., 45-1115 keV 79−13679
- Fe, incoherent γ-ray scatt. by K-shell electrons 77−83560
- H_2O, radial distrib. of γ-rays from narrowly collimated source *(Russian)* 77−30549
- Ho, incoherent γ-ray scatt. by K-shell electrons 77−83560
- In complexes, formation in aq. solutions, perturbed γ-ray directional correlation 77−12847
- Li_3N, electron density study using Compton scattering 80−79750
- NaI:Tl scintillation crysts., analytic calc. of photofractions to monoenergetic γ-rays 79−52038
- Pb, elastic scatt. cross section for 279 keV γ-rays 79−26421
- Pb, elastic scatt. of 145 keV gamma rays 79−13680

gamma-ray scattering continued
- Pb, incoherent γ-ray scattering, differential cross-section determ. 78−43952
- Pb, incoherent scatt. of 279, 322, 662 and 1115 keV gamma rays 80−40179
- Pb, total at. cross-section, incoherent scatt., 45-1115 keV 79−13679
- Sm, total at. cross-section, incoherent scatt., 45-1115 keV 79−13679
- Sn, elastic scatt. cross section for 279 keV γ-rays 79−26421
- Sn, elastic scatt. of 145 keV gamma rays 79−13680
- Sn, incoherent γ-ray scatt. by K-shell electrons 77−83560
- Sn, incoherent scatt. of 279, 322, 662 and 1115 keV gamma rays 80−40179
- Ta, elastic scatt. cross section for 279 keV γ-rays 79−26421
- Ta, elastic scatt. of 145 keV gamma rays 79−13680
- Th, incoherent scatt. of gamma rays 77−79585
- Th, L-shell electrons, incoherent γ-photon scatt. cross-sections 78−62768
- W, total at. cross-section, incoherent scatt., 45-1115 keV 79−13679
- Zr, elastic scatt. cross section for 279 keV γ-rays 79−26421
- Zr, elastic scatt. of 145 keV gamma rays 79−13680

gamma-ray sources *see gamma-ray production*

gamma-ray sources (astronomical)
- 1-100 MeV gamma-ray background, spectrum rel. to cosmological cosmic rays and light elements prod. 78−12436
- γ195+5, SAS-2 high-energy obs. 77−33688
- γ195+5, X-ray emission obs. 79−97101
- accreting matter around neutron stars and black holes, nuclear γ-ray line emission 78−4403
- Apollo 16 gamma-ray burst, distance and spectrum of 1972 April 27 event 80−67903
- B 1900+14, soft gamma-ray bursts obs. *(Russian)* 80−36742
- background isotropic radiation excess at 1 MeV, possible Seyfert galaxy origin 80−77522
- background radiation origin 77−33703
- binary star containing eruptive star assoc. with pulsar *(French)* 78−20913
- binary stars, short period, X- and γ-ray bursts from mag. reconnection 78−81654
- black holes, accreting, gamma rays emission spectrum 78−32504
- black holes, evaporation of primordial objects and search for associated γ-rays 78−36633
- black holes, gamma rays from accretion 79−48841
- black holes, Penrose-powered, in Centaurus A, 3C 273 and NGC 4151, gamma rays emission 80−56925
- black holes in binary stellar systems, gamma emission during spherically symmetric accretion 80−17608
- burst, 1979 March 5, evidence for periodicity 80−31389
- burst, assoc. with radio pulse 77−64887
- burst events, Pioneer Venus orbiter obs. 80−46707
- burst from Cygnus observed at balloon altitude 78−41096
- burst obs. from Helios 2, source directions 79−101218
- burst obs. in 1978 November, ISEE 3 high-resolution spectroscopy 80−67907
- burst source, 1979 March 5, error box 79−58441
- burst source in Cygnus, high altitude obs. *(Japanese)* 78−61933
- burst source in Sculptor measured by Venera 11, 12 and Prognoz 7, identification attempt *(Russian)* 80−77520
- burst source obs., 1976, Dec. 77−9821
- burst source on 1976 August 16, balloon-borne obs. 78−54078
- burst source registration by Prognoz 6 Sneg-2MP instrument *(Russian)* 79−21468
- burst sources, distance limit for non-relativistic models 78−32612
- burst sources, galactic distrib. models 80−22117
- burst sources, location via periodic slot collimator 77−64647
- burst sources, optical counterpart identification using proper motion data 78−93457
- burst sources distrib. over celestial sphere *(Russian)* 79−88766
- burst sources of 1977 October 20 and November 10, position bands *(Russian)* 80−36738
- bursts, atmospheric fluorescence in near UV as means of detection 77−9663
- bursts, episodic gas accretion on neutron star 77−5600
- bursts, galactic origin and chronological catalogue 77−37672
- bursts, possibly from black holes in globular clusters *(Russian)* 77−17721
- bursts, Venera 11 and 12 CONUS expt. obs. *(Russian)* 79−58449
- bursts and cosmic fireballs 78−54087
- bursts of γ-rays obs. with Prognoz 6 and Sneg 3 satellites, localization of sources *(Russian)* 79−80371
- 3C273, COS B high-energy gamma-ray obs. 78−93454
- 3C273, gamma-radiation, X-ray source size limitations 79−30143
- 3C 273, gamma-ray emission from Penrose powered black hole 80−56925
- 3C 273, quasar, second-order Compton interpretation of X-rays and γ-radiation 80−22106
- C relativistic electrons, inverse Compton interactions rel. to astrophysical gamma-ray prod. 80−17448
- Cassiopeiae A supernova remnant and surrounding H II region, γ-ray generation 80−85989
- Centaurus A, gamma-ray emission from Penrose powered black hole 80−56925
- CG135+1, CG189+1, cosmic sources, identification with H II regions 77−91669
- CG195.5+4.5, upper limit to 59.35 s periodic radio emission at 18 cm 80−86018
- CG 135+01 (=LS I+61°303), X-ray emission detect. 80−105400
- CG 135+1, discovery of radio counterpart 78−24560
- CG 135+1, evidence for nearby low-energy γ-ray emission 80−31392
- CG 135+1, new highly variable radio source as possible counterpart 78−54095
- CG 135+1, possible identification with LS I +61°303 (OB star) 78−32473
- CG 135+1, possible X-ray counterpart identification 78−54092
- CG 135+1, spectrum obs. 20 keV-25 MeV 80−105398
- CG 135+1 (=GT 0236+610), absence of variability in optical counterpart (LSI+61°303) 78−49438
- CG 135+1 (LS I+61°303), radio, optical, X-ray, gamma-ray Be star, obs. 79−88755
- CG 176-7, 189+1 and 195+4, X-ray emission associated with γ-ray source 80−31393

gamma-ray sources continued
CG 195+4, 35-8737 keV gamma ray search in Geminga field 80−27012
CG 195+4, pulsating γ-ray source, no pulsed ratio emission at 325 MHz 78−65717
CG 195+4 (Geminga) pulsating γ-ray source, neutron star models 78−4402
CG 312−1, possible X-ray counterpart identification 78−54092
CG 327−0, possible X-ray counterpart identification 78−54092
CG 327-0, identification with X-ray source (25 1553−542) 78−28860
CG 353+16 not assoc. with ρ Ophiuchi region 80−94896
CG 78+1, nature from gamma-ray flux prediction from Cygnus X region 79−92895
CG sources, 100 MeV, very high energy gamma-ray emission search 79−40293
Circinus X-1 as gamma-ray source, eccentric orbit binary model 79−97100
close binary systems in quiet stage, detect. from γ-ray emission 79−67058
Compton emission models, constraints from gamma-ray data 80−67902
conference, non-solar gamma-rays (Bangalore, India, May-June 1979) 80−77548
COS B catalogue and identifications 78−73775
COS B sources, 26-1200 keV hard X-ray obs. of error boxes 78−73774
COS-B γ-ray sources, nearby faint X-ray sources detect. 78−54093
COS-B γ-ray sources, positional coincidences with compact supernova remnants 78−45435
cosmic, gamma-ray bursts, prod. by intergalactic relativistic dust grains 79−88764
cosmic burst, possible obs. at radio freqs. 77−9819
cosmic bursts, critical comparison of detectors 77−64648
cosmic bursts, models, rel. to solar flare physical mechanisms 77−17499
cosmic bursts, search with coincident balloon flights 77−49506
cosmic bursts, sources, models 77−9823
cosmic gamma ray bursts, size spectrum, idealised galactic distrib. of sources 78−65716
cosmic gamma-ray background, prod. by annihilation of primordial stable neutral heavy leptons 78−93479
cosmic gamma-ray burst sources, new limits on distrib. 78−93465
cosmic gamma-ray bursts, coincidences with X-ray bursts observed by OGO-5 77−13492
cosmic gamma-ray bursts, origin theories *(Czech)* 77−2490
cosmic gamma-ray bursts, preliminary results from Solrad 11 detectors 77−57108
cosmic gamma-ray bursts, rel. to accretion instabilities on rot. magnetised neutron stars 77−13377
cosmic soft gamma-ray pulses, prod. in high-temp. astrophysical plasmas 77−78736
cosmic X-ray sources, multiple Compton scatts. effects on X-ray emission spectrum 78−96389
Crab Nebula, final SAS-2 gamma-ray results 77−33688
Crab Nebula, low-energy gamma-ray obs. 77−29894
Crab nebula, model for pulsed γ-ray and X-ray emission 80−62230
Crab Nebula, obs. by gamma-ray telescope with modulating anticollimator *(Russian)* 79−16832
Crab pulsar, high-energy photon spectrum rel. to energetic particles momentum distrib. 78−73727
Cygnus X-3, 1974 EAS obs. of high-energy gamma-ray source *(Russian)* 77−64881
Cygnus X-3, γ-ray flux meas. above 10^{12} eV 77−53706
Cygnus X-3, cocooned X-ray binary pulsar model 78−36723
Cygnus X-3, Crab and Vela pulsars and galactic plane, high energy γ-ray spectra comparison 79−80368
Cygnus X-3, gamma radiation during radio outburst 77−64884
Cygnus X-3, gamma-ray emission from mag. accretion disc 77−78894
Cygnus X-3, hard X-ray spectrum obs. 80−31388
Cygnus X-3, periodic γ-ray emission obs. *(Russian)* 77−91672
dense clouds and diffuse production of gamma-rays 78−54011
diffuse background, rel. to D prod. by high energy particles 77−33709
diffuse gamma radiation, galactic and isotropic components 78−65725
diffuse gamma-ray emission from active galaxies 80−12806
diffuse gamma-ray radiation, MeV excess in energy spectrum 78−73777
discrete gamma-ray sources rel. to galactic cosmic ray distrib. *(Russian)* 78−65719
discrete sources, contrib. to galactic gamma rays 79−35436
discrete sources of 100 MeV gamma-rays, model 78−49558
dwarf stars, degenerate accreting, thermonuclear burst assoc. with chromosphere γ-ray emission 80−98684
enhanced gamma-ray emission detect. by COS B satellite 77−17722
EXP 0520−66, flaring X-ray pulsar, recurrent gamma-ray bursts obs. *(Russian)* 80−36741
exploding black holes, search using atm. Cherenkov method 78−49473
extragalactic sources, observational results review 79−25763
fast intense gamma-ray transient (1979 March 5), detect. 80−73073
flaring X-ray pulsar in Dorado, gamma-ray bursts *(Russian)* 79−88765
galactic γ-ray sources, number intensity relation rel. to galactic disc emission 80−46702
galactic anticentre region sources, final SAS-2 results 77−33688
galactic background, contrib. from energetic secondary electrons in interstellar clouds 77−33593
galactic burst sources, review of models 80−82494
galactic centre, annihilation radiation due to positron prod. by evaporating black holes 80−46599
galactic centre, gamma-ray emission rel. to high energy particle fluxes 80−36713
galactic centre, gamma-ray line emission 79−44641
galactic centre, positron annihilation rel. to gamma radiation spectrum 79-44309
galactic centre hard γ-rays and diffuse background, Kosmos 561 obs. 79−84597
galactic centre region, high energy gamma-ray emission 77−53704
galactic centre region, medium-energy gamma-ray emission obs. 79−9030
galactic disc, bremsstrahlung gamma radiation emissivity and local interstellar electron spectrum 79−25417
galactic disc, longit. distrib. rel. to gamma-rays origin 77−87213
galactic disc, non-thermal electron bremsstrahlung gamma-ray prod. 78−24414
galactic disc, obs. between $-45^\circ < l^{II} < 45^\circ$ in 80 keV to 8 MeV energy range 80−82540
galactic disc, pulsar contrib. to gamma-rays 77−67143

gamma-ray sources continued
galactic disc anticentre direction, localised high-energy γ-ray emission, COS-B obs. 77−49495
galactic disk, implications of gamma-ray obs. for galactic struct. studies 77−26083
galactic distribution rel. to pulsars and SNRs 79−71152
galactic gamma radiation, possible origin, data from COS-B and SAS-2 satellites *(French)* 78−85776
galactic gamma radiation in 0.03-4.1 MeV range, Kosmos 461 meas. 77−67144
galactic gamma ray obs. interpretation *(Polish)* 79−58451
galactic gamma rays, discrete source component 79−35436
galactic gamma rays sources, shock region between stellar wind and interstellar matter 80−77512
galactic gamma-ray emission, data rel. to new constraints on galactic halo size 78−12353
galactic gamma-ray emission, discrete source contrib. 78−69907
galactic gamma-ray emission, rel. to Galaxy cosmic rays and mag. field distrib. 80−4207
galactic gamma-ray flux, 60 keV to 5 MeV range, from ensemble of point sources 79−53933
galactic gamma-ray sources, unidentified, rel. to quasars and radio galaxies 79−25747
galactic gamma-rays, distrib. from diffusion model for nuclear component propag. 79−53678
galactic high-energy gamma-ray sources obs. by COS-B satellite 77−91670
galactic plane, cosmic ray diffusion influence 77−64854
galactic plane gamma-radiation 79−71105
galactic small-scale structure from obs. of discrete sources 80−98743
galactic sources, obs. with COS-B *(Danish)* 80−82544
galactic sources, observational results review 79−25763
galaxies, primeval, appearance in X- and γ-ray regions, contrib. to background rad. 80−8692
galaxies as gamma sources, electron-microwave interaction 80−22121
Galaxy, gamma-ray lines balloon obs. with high resolution Ge(Li) spectrometer *(Japanese)* 79−80353
Galaxy gamma-ray emission, fluxes determ. from cosmic ray electron spectrum 80−62257
γ Geminorum, companion to gamma-ray source CG195+4 78−32459
Helios 2-Vela-Ariel 5 gamma-ray burst source, position 79−48956
local interstellar cloud, possible detectability through gamma-ray emission 80−26953
interstellar grains, narrow gamma-ray line emission 77−13437
interstellar molecular clouds, cosmic rays exclusion rel. to gamma-ray fluxes 77−13190
interstellar radioactivity, nuclear gamma-ray transition detection in background 77−2501
isotropic metagalactic background in 0.03-4.1 MeV range, Kosmos 461 meas. 77−67144
Kerr black hole, low-freq. radiation from infalling particle 80−62176
line spectra, prod. by nonthermal ions 78−36725
LMC N 49, X-ray source 0525.9-66.1, gamma-ray burst obs. *(Russian)* 80−36739
location rel. to neutral pion production processes *(Polish)* 77−70999
magnetic white dwarfs, energy bursts, model *(Chinese)* 80−12831
Milky Way companion galaxy, 0.670 GHz synthesis obs. rel. to identification 77−29941
N49, SNR in LMC, Pioneer Venus Orbiter obs. of 1979 March 5 gamma-ray transient 80−77518
N49 SNR in LMC, X-ray obs. of gamma-burst field 80−27019
N49 supernovae remnant as source of March 1979 γ-ray burst 80−105270
neutron star, plasma interface, physical processes in strong gravit. field, electron-positron pair prod., γ-ray emission *(Russian)* 79−80333
neutron stars, accreting, thermonuclear burst assoc. with chromosphere γ-ray emission 80−98684
NGC 4151, gamma-ray emission from Penrose powered black hole 80−56925
NGC 4151, Seyfert galaxy, gamma-ray emission, Compton scatt. model 80−98711
NGC 4151, Seyfert galaxy, low energy gamma-ray obs. 78−12368
NGC 4151, Seyfert galaxy, low-energy γ-ray spectrum 80−31370
NGC 5128 (Centaurus A), gamma-ray line emission 79−44641
NP 0532, Crab pulsar, search for pulsed gamma-rays of energy 10^{13} eV 77−13373
NP 0532, Crab pulsar, X-ray and gamma-ray radiation 80−41885
optical counterparts search, supernova remnants 79−35429
primordial black hole explosions, gamma-ray bursts rate upper limit 77−29873
primordial black holes, gamma-ray bursts, upper limits 79−30085
protogalaxy formation age and γ-ray background 80−62325
PSR 0531+21, Crab pulsar, γ-ray obs. with COS-B *(Danish)* 80−82544
PSR 0531+21 (Crab pulsar), pulsed γ-ray emission, COS-B obs. 78−8033
PSR 0833−45, Vela pulsar, γ-ray obs. with COS-B *(Danish)* 80−82544
PSR 0833-45 (Vela pulsar), pulsed γ-ray emission, COS-B obs. 78−8033
PSR 1822−09, balloon-borne gamma-ray obs. 80−105269
pulsars, curvature radiation-pair prod. model for gamma-ray emission 79-5852
pulsars, gamma ray emission model 78−65641
pulsars, gamma-ray emission theory 78−53975
pulsars, gamma-ray production mechanism 80−77433
pulsars, high-energy pulsed gamma rays obs. 78−45346
pulsars, observability 78−81646
pulsars, pair form. above polar caps rel. to X-ray and gamma-ray emission 79−92790
pulsars, rotational energy loss, slowing down index and time derivs., gamma radiation 80−67762
pulsars and compact X-ray sources, gravit. redshifted γ-rays, neutron star mass constraints 78−4274
quasars, Comptonised spectrum, Monte Carlo simulation 80−90566
quasars nuclei, gamma-ray source model 79−25747
radio burst correlated with gamma-ray event 77−33668
radio galaxies, as source of 1-10 MeV gamma-ray background 77−87213
radio galaxies nuclei, gamma-ray source model 79−25747

gamma-ray sources continued
relativistic electron spectra, inference from meas. of inverse Compton radiation 80–90339
review, cosmic gamma radiation, sources and detection 78–12059
review, new look at universe 79–80373
review, of gamma-ray picture of sky *(Russian)* 78–41097
reviews, galactic and intergalactic astronomy *(Russian)* 77–57061
Scorpius X-1, low-energy γ-rays, Dec. 1974 balloon obs. in 0.2-5 MeV range *(Portuguese)* 78–57702
Seyfert galaxies, source of diffuse cosmic γ-ray background 78–57700
Seyfert galaxies contrib. to low-energy γ-ray background 78–86007
sky survey with fine energy resolution using Ge gamma-ray spectrometer 77–53701
SNRs as gamma-ray sources 79–92887
spatial pattern, anal. via spectrometer with various shaped scintillators 79–16831
spiral galaxies, gamma-ray luminosity, contrib. to diffuse background above 100 MeV 78–93481
supernova, nearby, UV and gamma radiation effects on terrestrial atmosphere 80–94584
supernova γ- and X-rays, recorded by Antarctic ice NO_3^- content 80–31314
supernova shells of young pulsars *(Russian)* 77–74077
supernovae, gamma-ray emission, continuum intensity and spectrum 80–101602
Taurus region, evidence for detect. of 1-10 MeV emission in 1971 August 77–45605
transient gamma-ray event of 1979 March 5, location 80–73074
transrelativistic plasmas, relevance of photon pair prod. 78–20632
3U 0258+60 region, γ-ray flux meas. 77–2497
ultra high energy gamma-ray bursts from celestial sources, unsuccessful search 80–67911
ultra-high energy sources (10^{11} to 10^{13} eV) 80–101649
Vela pulsar (PSR 0833−45), radiation model 80–94824
^{26}Al, in interstellar medium, galactic source of γ-ray line emission 77–33692
ρ Ophiuchi dark cloud complex, gamma-ray sources and particle acceleration 80–31345

gamma-ray spectra
see also gamma-ray angular distribution; gamma-ray spectra of liquids and solids; nuclear decay theory
^{173}Lu decay scheme determ. 77–82868
^{239}Pu(n,f), thermal, fission product yield 80–27678
γ-ray multiplicities meas. at beam energies 40 to 140 MeV 78–21585
γ-ray yield functions from high spin states, comparison with 79–93492
A=45 to 200, mass dependence for radiative capture of 14.1 MeV neutrons 78–13087
A≥208, accurate g-factor measurement using heavy-ion induced reactions 77–26572
accelerated fitting and nuclide identification by graphical and associative memory methods 79–9945
activation analysis, low-energy photon spectra, nonlinear least-squares fitting program 79–1987
activation analysis, photopeak integration, quality assurance of computer programs 79–1986
aerial radiometric data anal. using line-intensity estimation code MAZAS 79–62627
alpha-induced prompt gamma-ray spectrometry, developments in analytical uses 77–90686
analysis, software system VAT-69 79–9949
analysis program SAMPO, radioisotope identification subroutine IDENT 79–9953
analysis using computer programmes, for activation anal. 78–7287
annihilation radiation from point isotropic photon sources, numerical calc. 79–85096
annihilation spectra, two-component, resolution using count ratio technique 78–44424
atmosphere, spectra and angular distrib. 0.3 to 10 MeV 77–49205
automated spectrometry, original version of neutron activation analysis 79–11861
automatic anal., using nonlinear least squares fitting 77–23362
automatic analysis, fast program 79–9948
automatic peak locating techniques 77–71731
average energy and numerical buildup factors meas. 77–54397
background correction algorithm for γ-γ coincidences 79–13616
background subtraction, direct method 79–723
backscatter peak shape *(Czech)* 77–50303
backscattered gamma method, universal, based on computer interpretation of spectra 79–1984
biological systems interacting with high energy particles 80–108951
biparametric γ-γ coinc. method, γ-transition intensity meas. *(French)* 78–29697
bremsstrahlung contribution from low energy electrons to scattered gamma ray spectra 80–78192
bremsstrahlung spectrum of electrons, sharp γ-lines present 77–82846
calibration materials for X and γ-ray spectrometers, decay data 80–106221
CANDU fuel radioactive decay props., natural uranium fuel cycle 77–71655
chemical anal. with low-energy t and α particles, 0.1 to 100 ppm 79–8460
Chinese nuclear test explosion, September 1976, hot particle anal. from γ-spectra *(Japanese)* 78–82519
coal analysis by neutron-capture gamma-ray meas. in boreholes 79–52853
coal analytical assembly using capture gamma rays from accelerator neutrons 79–96401
Compton gamma-ray spectroscopy, for early detection of osteoporosis 78–11729
computer code for qualitative anal. 79–9943
computer interpretation of spectrometric information in instrumental neutron-activation analysis 79–31351
computer methodology for spectral data reduction and anal. 79–1988
computer processing code for large numbers of spectra 79–9942
computers in activation analysis and γ-ray spectroscopy, conference, Mayaguez, Puerto Rico (May 1978) 79–1983
Conference, nuclear materials, safeguards and accountability meas., Williamsburg, USA (May 1978) 79–81045
continuum γ-ray energy depend. multiplicities via (^{27}Al,xn) reactions 77–41916

gamma-ray spectra continued
cosmic gamma ray spectroscopy, review 80–67582
cosmic gamma-ray spectra, high energy, near top of atmos. detection+meas. by emulsion chamber 79–29958
cosmic ray γ-ray spectra at 30-500 TeV 77–64574
cosmic ray γ-rays in range 3.5 to 100 MeV, system for meas. ang. and energy distribs. 77–50324
cosmic ray γ-rays recorded by nucl. emulsion and X-ray film 77–64572
cosmic ray electrons, detect. by synchrotron radiation in geomag. and interstellar mag. fields 78–57412
cosmic ray fluxes meas. at 4370 and 4880 m above sea level 77–64551
cosmic rays, scaling and charge ratio at 1-10 TeV 77–64576
cosmic rays recorded in X-ray emulsion chambers, decascading 77–64578
cosmic-ray γ-ray and hadron spectra with $\Sigma E_\Gamma > 500$ TeV 77–64575
cosmic-ray γ-rays from hadron interactions above 2.5 TeV 77–64573
Coulomb-nuclear interference for high spin states 78–46097
Cross sections for gamma-ray production by 14-MeV neutrons 78–21552
data analysis, theoretical foundations 79–233
deformed nuclei fusion reactions, γ-multiplicities, collective and statistical γ-rays Monte Carlo calcs. 79–578
delayed fission product γ spectra following short neutron irrad. 79–9645
diffusion model of heavy ion induced reacts. 78–54789
Doppler-shift attenuation, γ-rays from slowing down of excited particles 77–26945
double-scattered γ energy spectrum simulation and expt. 79–9905
doublet resolving power and area determ. accuracy, comparison of computer programs 79–9944
doubly odd deformed nuclei, EM transitions, nanosec. lifetimes 78–62505
E2 α_k conversion coeffs. for $2^+ \rightarrow 0^+$ transition, review 78–17143
electron beam fusion, pellet and pellet-blanket neutronics and photonics 80–74006
electron capture to positron ratios, recent developments, review 77–18895
electronic lifetime meas. with Ge(Li) detector using centroid-shift method 79–6790
element analysis, role of neutron capture γ-rays 80–50926
elemental sensitivity data modeling for in situ neutron capture gamma-ray experiments 79–61928
ENDF/B data, processed, rapid spectral and decay heat calcs. 79–67797
energy spectrum of resonance gamma-rays obtained by time measurements *(Russian)* 79–19815
environmental, eval. of standard library spectra for use in least-squares resoln. 79–9915
environmental, least squares method for computing nuclide conc. 79–9914
environmental samples anal. for U, Th, neutron activation anal. data resolution for high throughput system 79–11848
error in total absorpt. peak location by linearization method 79–68125
evaluation, appl. of programmable calculators and minicomputers 79–9956
even-even nuclei, $58 \leq A \leq 150$, E2, M1 multipole mixing ratio, data survey 78–50118
excited nuclear states, 10^{-18} to 10^{-6} s, lifetimes, direct meas. 79–30804
exciton model of γ-emission in (N,γ) reactions 78–62539
factor analysis for gamma-ray spectrometry 78–7778
fast Fourier transform anal. *(Chinese)* 80–77762
fission fragment deexcitation, statistical model anal. of spin influence 79–17941
fission product γ-radiation intensity in short operation nuclear reactors 79–67823
fission product gamma-ray and half-life $29 \leq A \leq 69$, data collection 78–50134
fission products, estimation using nucl. systematics 78–70587
fission products from fast and thermal fission of U, Pu 77–23127
fission products in reactor coolant water, continuous radiochem. anal. 77–71652
fission reactor fuel, gamma-ray spectrometric determ. of fission product activity and activity ratios 78–37430
fission reactor spent fuel γ-ray spectrometry and chemical analysis 78–54841
fission track-etch-cum-γ-spectrometry method for absolute fission yield meas. 80–27859
fp-shell nuclei, high-spin states 78–12946
fuel element scanning, Ge(Li) gamma spectroscopy, ANGEL computer program 79–9755
fusion reactor materials, 14 MeV neutron scatt. in extended samples of LiF and ^{56}Fe 77–57739
fusion reactor radiation protection, shield integral expts. at ORNL 80–47709
gamma-gamma coincidence 2-D analysis 77–18733
gamma-ray peak fitting, fast approx. to complementary error function 79–93903
GASP, gamma-ray spectra analysis programme, user guide 79–6810
GCFR, Pu fuelled, fission products and secondary gamma-ray spectra 78–676
Ge(Li) spectrometers, set of computer programs SPECTRAN for anal. 79–9947
half-life vs. energy map for gamma-rays emitted by radionuclides, photon activation anal. 77–16883
(heavy ion, xn) reactions, higher moments of γ-ray multiplicity 77–18604
heavy ion collisions, continuous γ-ray spectra anal. 78–41747
heavy ion in-beam spectroscopy, selective population of high-spin states in 1$f_{7/2}$-shell 77–18374
heavy ion induced Coulomb excitation 79–79352
heavy ion induced reactions, information from γ-spectroscopy *(Rumanian)* 78–58300
heavy ion reactions, statistical γ-rays and ang. momentum alignment 79–67761
heavy ion-nucleus reactions, spectra anal. by interactive computerised system 79–9509
heavy nuclei, fission process gamma ray analysis *(Rumanian)* 79–40973
heavy-ion collisions, in-beam gamma-ray spectroscopy, nuclear shape and reaction mechanism *(French)* 79–560
high-spin states, means and methods of investig. 78–86722
HTGR block fuel elements, fuel zone location meas. using gamma scanning *(German)* 79–67847

gamma-ray spectra continued
HTGR core, γ-spectroscopic exam. of fission product distrib. after shutdown 79−67909
IFOM, a formula for universal assessment of goodness-of-fit of gamma ray spectra 80−27912
in-beam gamma-ray spectroscopy, book 77−83449
inclusive γ spectra from $\psi(3095)$ and $\psi'(3684)$ decays in e^+e^- colliding beams 77−57549
instrumental neutron activation anal., improvements to basic advance prediction program 80−14042
intense proton beam current measurement via prompt γ rays from nuclear reactions 78−93784
intensity from an activated cylinder 78−16761
internal conversion coefficients, $30 \leq Z \leq 104$, Hartree-Fock-Slater model calcs. 79−36199
interstellar radioactivity and gamma-ray energy spectra in 0.02-12.27 MeV range 77−2501
intrareactor spectrum measurement, calorimetric method 78−17293
ion induced γ-rays, thick sample reaction yields, energies, appl. in prompt nuclear anal. 78−62502
$K_L^0 \to \pi^+\pi^-\gamma$, branching ratios and γ-energy spectrum 80−47280
least squares peak fitting with very low statistics 78−74529
least-squares peak search algorithm, linear 79−754
light elements, γ-ray internal conversion coeffs. 77−82866
line production and astrophysical gamma-ray spectroscopy 80−31271
liquid air, calc. of neutron and gamma-ray energy spectra 78−29529
liquid air, transport of neutron and secondary γ-rays from 14 MeV source 78−50234
liquid N_2, calc. of neutron and gamma-ray energy spectra 78−29529
low-energy photon sources, rel. to in vivo distrib. meas. 77−65377
lunar surface elemental composition, analytical determ. from Apollo X-ray and γ-ray spectrometer data 79−2495
LWR, fission product activities, fuel survey 80−736
LWR fuel rods, power cooling mismatch induced failure, meas. fission product release 79−93772
LWR spent fuel elements, gamma spectrometric meas. of burnup U/Pu ratio and cooling time for materials safeguards 80−78423
Mars, cosmic-ray interactions with rocks and atmosphere, gamma-ray spectra 77−53448
massive transfer in heavy ion reactions on rare-earth targets, α-γ coincidence 78−70556
mathematical modelling for radionuclide gamma emission 80−32236
measurement standards, National Bureau of Standards (USA) 80−90807
meson condensation and two photon emission in hadron capture by nuclei and heavy-ion collisions 79−3109
metal targets 514, 661.6, 765.8, 1115.5 keV energies 79−72285
microprocessor system 79−9955
millisecond isomers, 38 MeV α-induced reactions, abs. cross-section determ. 79−9502
minicomputer-based gamma spectrum analysis system SAMPO78 80−14043
mobile computerised analysis and data processing system 79−9959
model uncertainty and bias in evaluation, smoothest consistent baseline theory 78−11591
moderately deformed nuclei, high-spin states studied in (heavy ion, $xn\gamma$) reaction 77−14180
monoenergetic, mathematical model of spectra from Ge(Li) detector 78−13372
Monte Carlo calcs. on cascades prod. at 10^{13} eV 77−61322
Mossbauer effect probability determ. using resonance detectors 78−94160
Mossbauer gamma-X-ray coincidence meas. 80−14041
multiple Compton effect, cross sections, γ spectra and number *(Russian)* 79−370
in multiple hadron prod., case for discrete fireball mass spectrum 77−57499
multiplet resolution, semiempirical approach 79−234
multiplicity distribution, shape, and low-fold coincidence probabilities 78−54779
multiuser minicomputer system for gamma-ray spectroscopy and laboratory programming 79−9952
nanosecond isomers, in-beam gamma spectroscopic investigation, Ge(Li) detector 78−86506
natural flux spectral distribution, analytical approx. 78−815
neutron activation anal., computer methodology, appl. to geological and environmental samples 79−11867
neutron activation anal., computer simulated γ-ray spectra 78−92577
neutron activation anal., computer-simulated gamma-ray spectra 79−1985
neutron activation anal., control software for high throughput system 79−11849
neutron activation anal., data processing system 79−11863
neutron activation anal., instrumental large-scale routine, computer aspects 79−11862
neutron activation anal., ion microprobe surface anal., control and data analysis software 79−11860
neutron activation anal., least squares deconvolution on minicomputer, NAALSQ program 79−11853
neutron activation anal. instrumental, in US Geological Survey (Reston) 79−11850
neutron capture, $l=1$, near 24 keV, width correlations 77−26765
neutron capture gamma spectra for neutron thermometry 79−30837
neutron collimated fast beam, radiation quality local distrib. 80−12247
neutron flux distrib. in nonhomogeneous samples, computational model for prompt gamma-ray analysis 80−14060
neutron irradiation short-lived products, rapid anal. using minicomputer based pulse height analyser 79−11866
neutron radiative capture, prompt gamma-ray spectra in keV region, rel. to reactor shielding 77−26761
neutron radiative capture cross section measurement techniques, review 77−26932
nonstatistical effects in neutron capture γ-ray spectra from target elements Ca to U 77−30569
NRX and process effluents, gamma ray spectrometric anal. 78−29656
nuclear continuum spectrum from disintegration by high energy particles, direct and resonant mechanisms *(Russian)* 79−30803
nuclear decay scheme computation on basis of γ-γ coincidence meas. 79−59295
nuclear fuels, nondestructive measurement of U and Th conc. and quantities using XFA and gamma spectrometry 80−71877

gamma-ray spectra continued
nuclear fusion α-induced, γ-ray spectra calcs. 79−36291
nuclear gamma-rays from energetic particle interactions 80−18219
nuclear isomers, 10^{-4} to 10^{-1} sec lifetime, decay spectra, meas. procedure 79−36167
nuclear isotopes far off stability line, production, props., review *(Hungarian)* 79−9927
nuclear materials, nondestructive element and isotope assay of Pu and U 80−71870
nuclear materials safeguards, inventory verification using high resolution gamma spectroscopy 80−69016
nuclear reactor fuel burnup, nondestructive verification, γ-ray spectrometry 77−3137
nuclear transitions, laser spectroscopic techniques involving atom, mol. excited states, book contrib. 78−9212
odd mass nuclei with 51 neutrons or 51 protons, radioactivity, expt. theory *(French)* 77−293
organ depth estimation by gamma-ray spectral comparison 77−86612
painting and artist identity, autoradiography and gamma-ray spectroscopy appl. 80−26073
particle beam, relativistic, in medium, energy meas. by spontaneous γ-radiation emission *(Russian)* 78−29891
particle spectra line shapes after γ emission in flight 78−41665
pattern recognition theory appl. to gamma-ray spectra identification 77−67931
peak areas, analytical results calc. 79−11851
peak areas observed with Ge(Li) detectors, least squares spectrum fitting method 79−85854
peak search and anal. with very low statistics 77−54390
peak shapes observed with Ge detectors, divergence from Gaussian, formula for peak fitting 79−85853
photomultiplier tube, solid-state, for improved gamma counting techniques 79−54748
photon energy spectra estimation based on 34×34 matrix 79−41059
photon showers produced by 150 MeV electrons 77−10563
planetary surface elemental anal. via orbital gamma-ray spectroscopy 79−12412
polyatomic molecule, nuclear γ-transitions, Franck-Condon principle *(Russian)* 79−59522
positron lifetime spectra, anal. using DBLCON version of POSITRONFIT with nonGaussian prompt 78−33359
prod. cross sections from shell model theory 78−62501
proton induced γ-ray emission, interference by neutron induced γ-ray emission 78−27868
proton induced γ-ray yields 80−45608
Pu nondestructive assay, gamma-spectrometric method 79−81068
pulse height analyser data, on-line method for peak area determ. 79−755
pulse height analysers, computerised, windowless stabilisation scheme 79−9976
pulse height analysis computer system 79−9975
R-A reactor fuel burnup, gamma-spectrometric determ. 78−50265
RA fuel burnup determ. from γ-ray spectrometry of ^{106}Ru, ^{134}Cs, ^{137}Cs 78−54848
RA reactor fuel, gamma-spectrometric determ. of fission product activity ratio 78−33269
radiation shielding materials, benchmark radiation transport data, air-over-ground neutron and gamma spectroscopy 80−23161
radioactive nuclides, quantum radiation, data handbook 80−94933
radioactive waste, control and accountability by gamma scan assay 79−9913
radiochemical analysis by coincidence spectrometry, minicomputer system 79−11864
radioisotope activities, quantitative analysis, gamma-ray spectrometry 77−18734
radioisotope identification and mass determination, using SAMPO programme with IDENT subroutine 78−48731
radionuclides, short-lived, gamma-ray spectrometry, correction for dead-time losses 80−42312
radionuclides in BWR cooling system, gamma spectra 79−9731
rapid reduction via desk-top calculator 77−53870
reactor shielding materials, Pb and steel, Γ leakage spectra, computer calcs. 78−58350
recoil corrections in electric gamma transitions 79−89263
relativistic electron+laser photon scatt., angular and energy distrib. *(Russian)* 79−3029
resonance gamma-ray absorpt. method 78−55089
rotational nuclear struct., moment of inertia, ang. momentum sel. using total γ-energies 79−89221
scattered spectrum, asymptotic solution of γ-ray transport eqn. 77−45810
secondary bremsstrahlung, contrib. in gamma quanta transport problems 79−40782
single full energy peaks, automatic examination program 78−82571
sky-shine spectra, ^{60}Co source 77−65341
source activity calculation from counting rates in single and coincidence photopeaks 78−13371
spectral analysis using FFT *(Japanese)* 78−90047
spectral parameter measurement for γ-rays using overtake effect 79−45436
spectrometry appl. in radiological protection meas., small computer system 79−9917
spent nuclear fuel cooling time determ. utilising gamma-ray meas. 80−63268
spontaneous emission by channelled charged particles *(Russian)* 77−52198
statistical evaluation of gamma photopeaks in complex spectra from very low activity samples 79−76254
streaming through ducts, spectral meas. 80−32523
superdense nuclei, search in reactor active zone 79−75824
TFTR neutral beam injectors, neutronics calcs. 79−59253
thermal neutron capture γ-ray meas. using neutron guide tube 80−58099
thermal-neutron activated samples, CERPL and CEREL codes for γ emitter automatic ident. and determ. 79−11852
time-dependence of reson. scatt. radiation 77−14060
Tokamak test reactor, neutron activation code REBATE 79−49852
twelve-program package for activation anal. and gamma spectrometry 79−9950
unfolding of spectra with continuum and discrete components 79−9946
VIPER reactor, neutron leakage spectrum and dose meas. 79−3243

gamma-ray spectra continued
weak γ-ray transitions observed in coincidence with summed cascades 79−76264
whole-body counter in vivo calibrations for quantitative retention estimation 78−3579
Wigner scheme, Γ-decay of analogue states, β-decay 77−41930
yrast isomers from delayed γ cascades in heavy ion reactions 78−8844
β-decay of fictional nuclide, Pandemonium, statistical model 78−8779
γ-γ coincidence techniques, lifetime meas. following fusion evaporation reaction 79−59318
(n,γ) gamma ray spectra calc. 80−52620
(n,γ) reactions with polarised thermal neutrons, spin state determ. *(Dutch)* 79−22290
$(n,\gamma\alpha)$, thermal n, systematic search, γ-spectra and selective state population 80−37390
$(n,\gamma p)$, thermal n, systematic search, γ-spectra and selective state population 80−37390
$(n,n'\gamma)$, excitation of low levels of ^{48}Ti, ^{56}Fe, ^{58}Ni, ^{92}Zr and ^{94}Zr isotopes, 1.57 to 2.8 MeV inelastic neutron scatt. *(Russian)* 78−41722
(n,p) at 14.7 MeV, on 48 stable nuclides 77−61417
(n,t) reaction, 14.6 MeV medium and heavy mass nuclei, production cross sections 79−49629
$(n,x\gamma)$ reactions, ENDF/B prompt γ-ray evaluations, models and data 77−26753
(p,γ), 50 MeV, giant dipole resonance, γ-emission spectrum from giant dipole resonance 79−59065
p+nucleus, 303 GeV/c, in emulsion chambers, high energy γ-rays 78−70521
p+nucleus reactions, 400 MeV, multi-nucleon removal, p-γ coincidence spectra 79−6549
$\bar{p}p$ annihilation, γ spectra, evidence for quasinuclear bound states 78−54642
$p\bar{p}$ annihilation at rest, γ-ray spectrum 78−21450
$\bar{p}p$ atoms, quasiatomic and very energetic γ-rays 80−42574
$pp\rightarrow\pi^0X$, scaling in the mean hypothesis and Feynman variable energy depend. 80−42501
(π^+, π^0) inclusive reacts., 100 MeV, π^0 detection from γ-ray spectra 78−33222
$(\pi,X\gamma)$ reaction at 70 MeV on s-d shell nuclei 78−29504
$\pi^-d\rightarrow 2n+\gamma$, n-n scatt. length from γ spectrum 78−62576
$\pi^-p\rightarrow\pi^0\pi^0n$, matrix element calc. and verification *(Russian)* 79−9396
$\pi^-p\rightarrow\pi^0\pi^0n(\pi^0\gamma n)$, 270 MeV, γ-ray spectra, cross-sections meas. *(Russian)* 77−22767
π^+p, anal. of reson. multipoles, γ-ray spectra calc. *(Russian)* 79−26346
ψ (3095) and ψ (3684) radiative decays, possible intermediate states from inclusive photon spectra 77−10246
Σ^0 decay, energies and emission angles of γ quanta *(Russian)* 78−46114
Ag, A=107, 9, +^{86}Kr, 618 MeV, γ-ray multiplicities and angular momentum fractionation 78−37370
Ag+^{20}Ne, 175 MeV, γ-ray multiplicities and energies, primary fragment angular momenta 78−46093
^{A}Ag, A=97, 98 and $99^{g,m}$ decay spectral meas. 78−93976
^{102}Ag$(e,\gamma)^{102}$Pd, 1592 keV E0 transition, half life measurement 80−22762
^{105}Ag decay, γ-ray spectra, γ-γ coincidence and ang. correl. meas. 78−13007
^{105}Ag, excited level struct. and transitions populated by decay of ^{105}Cd 79−97655
^{105}Ag, γ-transitions, level scheme via $(p,n\gamma)$ reaction *(Russian)* 77−74801
^{105}Ag, high spin states γ-single spectra, γγ coincidence, excitation functions, ang. distrib., polarisation meas. 78−21519
^{107}Ag$(n,\gamma)^{108}$Ag, coincidence meas. of low-lying states of 215.38 keV 78−12975
^{108}Ag, low-lying states and state distrib. following ^{107}Ag(n,γ) 78−50084
^{108m}Ag, γ-ray energies meas. for Ge(Li) detector calibration 80−27865
^{110m}Ag, gamma transitions to ^{110}Cd 79−85401
^{110m}Ag, gamma-ray intensities, precision meas. 80−102139
Al, reactions induced by ^{12}C and ^{19}F ions, γ-ray spectroscopy of induced activities 77−23107
^{24}Al, ^{24}Al^m, decay to γ-ray and α-particle emitting ^{24}Mg states 79−49607
^{24}Al, 1^+ isomer decay 79−85414
^{27}Al+^{12}C, 107, 155, 197 MeV, evaporation residue ^{39}K, prompt γ deexcitation 78−74395
^{27}Al+^{20}Ne, 120 MeV, prompt γ emission, reaction products deexcitation 78−74396
^{27}Al+^{28}Si, 72 MeV, multinucleon removal 78−41755
^{27}Al+hp, 400 MeV, multinucleon removal in quasifree process, p-γ coincidence expt. 78−37342
^{27}Al+π^-, γ-π^- coincidence spectra, 190 MeV 78−89913
^{27}Al$(p,\gamma)^{28}$Si, E_p=992 keV resonance, γ-ray intensity standard 78−17472
^{27}Al$(\pi,x\gamma)$, gamma ray coincidence spectra, nuclear surface clustering evidence 79−6707
^{27}Al$(\pi^-, px\gamma)$, 300 MeV, proton-gamma ray coincidence spectra 79−6704
^{27}Al$(\pi^\pm,\pi^\pm x\gamma)$, 300 MeV, pion-gamma coincidence spectra 79−6705
^{27}Al$(\pi^\pm,x\gamma)$, 300 MeV, gamma-ray coincidence spectra, clustering evidence 79−6706
Al(n,γ), γ-ray energies and intensities 78−89876
^{232}Am α-decay, absolute γ yields 78−86516
^{241}Am, α-decay low-energy γ-radiation *(French)* 78−74342
^{241}Am, gamma ray spectra of reactor fuels 80−42577
^{241}Am, γ-ray spectrum above 600 keV, Ge(Li) detector, ^{237}Np states 79−6480
^{241}Am(n,α) sources, characteristic gamma-ray spectra from light elements within sources 79−3269
^{243}Am, absolute yields of 43.5, 74.7 and 117.8 keV photons 80−32568
^{32}Ar, high spin states from heavy-ion fusion evaporation reactions, decay schemes 77−2932
^{40}Ar+^{58}Ni, deep inelastic collision at 280 MeV, fragment energy and spin 78−21599
^{41}Ar states from ^{40}Ar(d,p), lifetimes meas. by DSA method 78−78308
^{44}Ar β decay into ^{44}K, neutron rich isotopes, weak coupling predictions, γ-ray meas. 78−74336
^{46}Ar decay, gamma-ray spectra meas., half-life determ. 78−21513
^{68}As β-decay, γ coincidence and singles spectra, spin, parity assignments, half-life meas. 77−79333

gamma-ray spectra continued
^{75}As, stopped π^- absorption, in beam and activation γ-ray spectroscopy 79−40960
^{75}As, transitions populating and depopulating 279 keV level, δ(E3/M2) 77−82852
^{75}As(n,γ), 1.3-2.8 MeV, ^{75}As levels determ. 77−26611
^{75}As$(n,n'\gamma)^{75}$As, deexcitation gammas, energy levels, branching ratios, spins, parities, excitation function meas. 78−89869
^{85}As, investigation of beta-strength functions by neutron and γ-spectroscopy 79−45209
^{71,73}As, γ-spectroscopy of high-spin states via heavy-ion reactions 77−74795
^{206}At$\rightarrow^{206}$Po, EC-β^+ decay, Po excited levels 77−79340
^{209}At, gamma-ray spectra, produced by ^{209}Bi$(^3$He, $3n\gamma)^{209}$At, 28 and 26 MeV 78−74377
^{209}At high spin states from ^{206}Pb$(^6$Li, $3n\gamma)$, γ meas., neutron hole influence 77−2934
Au(Ar,X), 227 MeV, ang. momentum transfer in deep inelastic collisions 79−45281
Au$(^{63}$Cu,X), 365 and 443 MeV, ang. momentum transfer in deep inelastic collisions 79−45281
^{187}Au energy states from ^{187}Hg decay, parities γ-spectra, triaxial nuclear deform. *(French)* 78−33143
^{194}Au decay scheme, γ-spectrum, low-intensity transitions and level energies of ^{194}Pt 78−13003
^{194}Au, isomeric states anal. conversion electron and γ-ray spectra from ^{194}Pt(p,n) and ^{195}Pt(p,2n) 77−71582
^{197}Au +^{86}Kr, 618 MeV, γ-ray multiplicities and angular momentum fractionation 78−37370
^{197}Au, stopped π absorption, in beam and activation γ-ray spectroscopy 79−40960
^{197}Au+^{136}Xe, 1064 MeV, fragment spin orientation from continuum γ-ray anisotropy meas. 80−22853
^{197}Au$(^3$He, $3n\gamma)$, 24-28 MeV, level struct. in ^{197}Al anal. 77−46177
^{198}Au, radioactive decay, γ-ray energy meas. *(German)* 77−57633
^{198}Au, redetermination of γ-ray standards between 0.1 and 1.0 MeV 78−37472
Ba and rare-earth neutron deficient isotopes, β^+ strength $T_{1/2}$, X-ray, γ-ray spectra 77−34260
^{123}Ba, high spin levels and bands from ^{114}Sn$(^{12}$C, 3n$)^{123}$ Ba 79−45127
^{129}Ba, γ-ray linear polarisation meas. from ^{120}Sn$(^{12}$C,3n) 78−50121
^{131}Ba decay, ^{131}Cs level struct. obs. 77−10359
^{133}Ba decay data and standardisation 77−88081
^{134}Ba, inversion of 0^+ phonon states and γ softness 77−10364
^{138}Ba, 6^+ state, nucl. g-factor and nucl. spin relax. in Xe 77−22884
^{140}Ba, fission product, γ-ray emission probability 77−82862
^{143}Ba, nuclear spectroscopy of neutron rich A=143 nuclei 79−59039
^{7}Be, 477.6 keV, Analytic fitting of full-energy peaks in Ge(Li) spectra at high count rates 80−99147
^{7}Be, electron capture decay, internal ionisation 77−18892
^{7}Be$\rightarrow^{7}$Li, inner bremsstrahlung spectra, disintegration energies 77−54191
^{7}Be$\rightarrow^{7}$Li, total electron capture decay energy from inner bremsstrahlung spectrum, student experiment 78−24611
^{8}Be, ΔT=1 γ-decay from 16.6-16.9 MeV states 78−8771
^{9}Be π capture, two-photon emission obs. 79−26460
^{9}Be+^{12}C, 3.5 to 9.5 MeV, sub barrier, cross sections and optical model calcs. 78−8838
^{9}Be+^{16}O, 2 to 5.1 MeV, sub barrier, cross sections and optical model calcs. 78−8838
^{9}Be+^{16}O, 3.2-14.4 MeV, excitation functions from residual nuclei gamma-ray yield 79−49599
^{9}Be+^{19}F, 7 to 16 sub. barrier, cross sections and optical model calcs. 78−8838
^{9}Be(γ,γ'), 32 MeV, energy spectra, d prod. process *(Russian)* 80−91177
^{204}Bi, decay scheme 78−50122
^{207}Bi, gamma-ray intensities, precision meas. 80−102139
^{207}Bi, gamma-ray transitions following electron capture, 1.44 and 1.46 MeV γ-rays 79−85399
^{207}Bi, γ-γ coincidence spectra, Ge(Li) detect. 77−2930
^{207}Bi, spin and parity of states with J≤21/2, ^{205}Tl$(\alpha,2n)^{207}$Bi and ^{205}Tl$(\alpha,2n)^{207}$Bi 78−89788
^{209}Bi, pion capture, high spin states and neutron multiplicities meas. 78−54806
^{209}Bi, stopped π^- absorption, in beam and activation γ-ray spectroscopy 79−40960
^{209}Bi+^{12}C reaction, fission product charge distrib., 40 to 66 MeV 77−79406
^{76}Br, populated by ^{76}Se$(p,n\gamma)$, level scheme 78−50091
^{80}Br, level struct. determ. from thermal (n,γ) meas. 78−41667
^{80}Br, study of excited states from ^{79}Br(n,γ) and ^{80}Se$(p,n\gamma)$ *(French)* 78−29393
^{82}Br, level struct. determ. from thermal (n,γ) meas. 78−41667
^{82}Br, study of excited states from ^{82}Se$(p,n\gamma)$ and ^{81}Br(n,γ) *(French)* 78−29393
^{87}Br, investigation of beta-strength functions by neutron and γ-spectroscopy 79−45209
^{88}Br$\rightarrow^{88}$Kr, γ-ray spectrum, transitions 77−295
C+p, 52 MeV, spectral meas. of secondary neutrons and photons from thick targets 78−58282
CO_2, gaseous reactor coolant, monitoring of U, Pu and fission products by gamma spectrometry 79−89374
^{12}C gamma line Doppler broadening in ^{12}C$(n,n'\gamma)^{12}$C and ^{9}Be$(\alpha,n\gamma)^{12}$C, 4438 keV 80−91147
^{12}C, photodisintegration induced by 40 MeV γ-rays, correl. spectroscopy 77−6345
^{12}C, π capture, two-photon emission obs. 79−26460
$^{12}C_{2+}$ spin alignment using γ-decay in flight in ^{16}O$(^{12}$C,$^{12}C_{2+})^{16}$O and ^{12}C$(^{16}$O,$^{12}C_{2+})^{16}$O interactions 78−41767
^{12}C+^{12}C fusion, 2.5 to 6.2 MeV, γ-ray transitions and cross-section fluctuations 77−30628
^{12}C+^{12}C$\rightarrow^{12}$C$(2_1{}^+)$+^{12}C$(2_1{}^+)$, 15-45 MeV, obs. of molecular resonances 77−74867
^{12}C+^{14}N, fusion cross sections, struct. in γ-ray yields 79−9626
^{12}C+^{16}O, 12.8 to 18.2 MeV, reactions and inelastic scatt., resonance anomaly study by γ ray techniques 78−4955
^{12}C$(^{12}$C,$\gamma)^{24}$Mg, 5 to 11 MeV, γ yields, resonance features 78−54799
^{12}C$(^{16}$O, n$)^{27}$Si, 12.8 MeV resonance investig. by time-of-flight spectra and n-γ coincidence 79−9627
^{12}C$(\pi^-, \gamma)^{12}$B*, excitation of collective states, shell model 80−22652

gamma-ray spectra continued
^{13}C(d,γ_0)^{15}N, E_{exc}=17.7 MeV, 95° differential cross section resonance struct. 78−37351
^{14}C, photodisintegration induced by 40 MeV γ-rays, correl. spectroscopy 77−6345
^{23}C(d,γ)^{15}N, 2.90-9.95 MeV, cross sections, ang. distrib. meas. 77−6395
^{40}C(π,γX), short-range 4-N correls. 77−18613
^{40}Ca ions recoiling in vacuum, decoupling of hyperfine interactions 77−22931
^{40}Ca, weak s resonance γ-ray decay in negative parity low lying levels 80−27591
^{40}Ca+^{40}Ca, collective modes excitation 79−54448
^{40}Ca+$\pi^{\pm}$, multinucleon removal, prompt de-excitation γ-spectra obs. 79−6708
^{40}Ca(α,γ)^{44}Ti, lifetimes and spins of ^{44}Ti levels meas. 77−79328
^{40}Ca(μ,$\nu\gamma$),^{40}K,*, 85 MeV/c, radiative capture branching ratio, photon asymm. 77−79365
^{41}Ca, transverse decoupling of hyperfine interactions in free atoms 77−18468
^{43}Ca γ-ray spectroscopy, levels and decay scheme deform. 79−80896
^{44}Ca(p,γ)^{45}Sc, 1.62-2.18 MeV, e.m. decay of fragmented analogue states of Sc 77−2987
^{48}Ca+^{15}N(^{18}O) fusion-evaporation reaction, ^{59,60}Fe, ^{59,60}Co yrast decay scheme 78−13154
Cd, A=104 and 105, populated in α+Pd reactions, high spin states 78−62484
^{104}Cd quasirot. ground state band and γ-transition from ^{102}Pd(α,2nγ) 80−105955
^{106}Cd, high-spin states via γ-spectra populated in ^{105}Pd(α,2nγ) 77−30508
^{109}Cd, gamma-ray precision energy meas. 78−58533
^{109}Cd, low lying level struct. via γ-γ correls. following ^{109}In decay 77−30509
^{110}Cd, γ-ray spectra using coincidence and sum method *(French)* 78−62675
^{110}Cd, recoiling in Fe, enhanced transient fields 78−37284
^{110}Cd(p,γ) γ-22 MeV differential cross-section meas. 79−93617
^{111}Cd(p,nγ)^{111}In, E_p=6 MeV, γ-ray spectra and ^{111}In level scheme 78−13083
^{113}Cd, level scheme from ^{113}Ag 5.3 h β-decay 78−46028
^{115}Cd, level scheme from ^{115}Ag 20 min decay 78−46029
^{119g,m}Cd, decay schemes, half-lives, excited levels 77−296
Cd(n,nγ), γ spectra and ang. distrib., ^{114,116}Cd energy levels, spins, particles 77−88070
Cd(π^-, X), A=111, 112, 0 MeV, E2 nuclear resonance effects, γ and X-ray meas. 78−41774
Ce, A=136, 137, 138, from (α,xn) reactions, high spin states and isomers obs. using in-beam γ-spectroscopy 78−82309
Ce, A=137, 139, high spin levels, γ spectra, hole-core coupling 77−50063
^{A}Ce (A=149,150), fission product, γ-spectra, half-life meas. 77−38240
^{134}Ce, γ-ray emission, excited levels of ^{134}La determ. 77−6290
^{144}Ce, errors in activity ratio determ. in reactor RA used fuel element 79−41061
^{144}Ce, gamma-ray precision energy meas. 78−58533
^{139m}Ce, internal conversion of N=81 isotones 78−13027
^{250}Cf, spontaneous fission, mass distrib., radiochem. and γ-ray spectrometric meas. 77−67775
^{252}Cf, spontaneous fission, prompt γ-ray multiplicity distribs. 77−50174
^{252}Cf, spontaneous ternary fission, multiplicity distrib. of prompt γ rays 78−21615
^{252}Cf-^{235}U subcritical multiplier, computer-controlled cyclic activation anal. 79−11865
Cl, A=35,36,37 high spin states from heavy-ion fusion evaporation reactions, decay schemes 77−2932
Cl, short lived nuclear states, neutron activation anal. in aerosols of Otto carburettor engine *(German)* 77−12860
^{35}Cl(n,γ)^{36}Cl, E1 and M1 radiative strength functions 78−4940
^{37}Cl(n,γ)^{38}Cl, recoil energy spectrum calcs. 78−86531
Cl(n,γ), γ-ray energies and intensities 78−89876
^{245}Cm, from ^{249}Cf α-decay, γ-spectra and internal conversion spectra 79−6477
^{248}Cm, spontaneous fission, mass distrib., radiochem. and γ-spectrometric meas. 77−67775
^{56}Co, gamma-ray intensities, precision meas. 80−102139
^{56}Co, relative intensities of γ-transitions meas. 79−97930
^{56}Co standard source, relative γ-ray intensities 78−55069
^{57}Co, radioactive decay, γ-ray energy meas. *(German)* 77−57633
^{59}Co, stopped π^- absorption, in beam and activation γ-ray spectroscopy 79−40960
^{59}Co(^{7}Li,2n), E=18 MeV, high-spin states in ^{64}Zn 78−33145
^{59}Co(n,2n), (n,np), (n,d), 16.2 to 21.8 MeV, γ-ray prod. cross sections 78−13080
^{59}Co(n,2n), isomeric cross-section ratio and excitation function, mixed-powder method and gamma-ray spect. 80−47472
^{59}Co(n,α), excitation function, mixed-powder method and gamma-ray spect. 80−47472
^{60}Co gamma radiation, filtration anal. of collimated beams 79−63861
^{60}Co, high energy gamma spectra appl. of improved HgI_2 spectrometer 77−65378
^{60}Co, radioactive decay, γ-ray energy meas. *(German)* 77−57633
^{60}Co skyshine, continuous γ-spectra unfolding 79−81118
^{A}Cr(n,n$'\gamma$), A=50-54, 0.84-3.97 MeV, neutron inelast. scatt. cross-sections determ. 78−62529
^{51}Cr, gamma-ray precision energy meas. 78−58533
^{51}Cr→^{51}V, inner bremsstrahlung spectra, disintegration energies 77−54191
^{52}Cr, γ-spectra, levels, J^{π} via α+^{50}Cr reaction 77−74794
^{52}Cr, high-spin states populated by ^{50}Ti(α,2nγ), assignment from spectroscopic states 77−65190
^{52}Cr studied via (α,2nγ), high spin states, shell model calcs. 78−54675
^{52}Cr(n,n$'\gamma$), 0.5-10 MeV, γ-ray production cross sections 77−26762
^{52}Cr(p,γ)^{53}Mn, resonant react. appl. to Cr depth distribs. 79−33011
^{53}Cr, excited negative parity states to 2322 keV via (p,p$'\gamma$) and (α,$\alpha'\gamma$) 77−82851
^{56}Cr, yrast decay schemes for heavy-ion fusion evaporation reactions 77−82854
Cr(n,n$'\gamma$) 77−26767
Cr(π^+, π^0), 200 MeV, deexcitation γ spectra, transitions in ^{52}Mn 78−89912

gamma-ray spectra continued
Cs, A=114-118, neutron deficient isotopes, half lives, β^+,γ, delayed p and α meas. 78−70489
Cs, A=118,120,122, ground isomeric states, β-decay, $T_{1/2}$, γ- and CE-spectra 77−57601
^{123}Cs(^{123m}Cs), gamma and conversion electron radiation 80−106017
^{124}Cs, EC and β^+-decay, exam. of Xe nuclear level struct. 78−21498
^{126}Cs, EC and β^+-decay, exam. of Xe nuclear level struct. 78−21498
^{127}Cs, 66-keV decay, $T_{1/2}$, K conversion coeff. 77−54184
^{131}Cs, gamma-ray spectra from ^{131}Ba decay 79−85400
^{133}Cs,(n,γ)^{134}Cs, E_n=14.1 MeV, γ emission exciton model *(Russian)* 79−13302
^{133}Cs(N,γ)^{134}Cs, exciton model, γ spectra calc. 78−62539
^{133}Cs(n,n$'\gamma$), level scheme and deexcitation of excited ^{133}Cs levels 78−13004
^{134}Cs, gamma-ray intensities, precision meas. 80−102139
^{134}Cs, half-life, gamma-spectrometric determ. 78−93972
^{135}Cs, error in activity ratio determ. in reactor RA used fuel element 79−41061
^{137}Cs, errors in activity ratio determ. in reactor RA used fuel element 79−41061
^{137}Cs excited levels from ^{137}Xe β decay, γ spectra, coincidences, branching, logft values 77−54186
^{137}Cs gamma radiation, filtration anal. of collimated beams 79−63861
^{137}Cs, gamma source, Poisson and Brockwell-Moyal freq. distribs., χ-square test 80−5430
^{137}Cs, radioactive decay, γ-ray energy meas. *(German)* 77−57633
^{143}Cs, nuclear spectroscopy of neutron rich A=143 nuclei 79−59039
Cu, reactions induced by ^{12}C and ^{19}F ions, γ-ray spectroscopy of induced activities 77−23107
Cu+p, 52 MeV, spectral meas. of secondary neutrons and photons from thick targets 78−58282
^{63}Cu, level struct. from ^{63}Cu(p,p$'\gamma$) react. 78−78378
^{63}Cu+^{197}Au, quasi-fission, 443 MeV, γ-ray multiplicity 77−34330
^{64}Cu, autoionisation of K-shell following β-decay 78−13029
^{64}Cu, γ-spectra, J^{π} assignments via ^{64}Ni(p,nγ) 2.75-3.75 MeV 77−18470
^{65}Cu(p,p$'\gamma$), 5.25, 6.0 MeV, levels, transition energies, lifetimes, branching ratios determ. 77−41960
Cu(n,nγ), 0.67-19.6 MeV, prod. cross sections, discrete and continuum γ rays 365 to 6620 keV 77−34293
$^{148}Dy_{82}$ 10^+ isomer, $\pi h_{11/2}$ effective E2 charge 78−93964
^{153}Dy, populated in ^{153}Ho β-decay, lower excited states 80−22765
^{156}Dy, prompt transitions multipolarities, γ and conversion electron spectra, energy level bands, spin, parity 78−8768
^{160}Dy, quasi-continuum transitions multipolarities from ICC via ^{160}Gd(α,4n)^{160}Dy 77−82945
^{162}Dy, level scheme, γ-branchings following ^{162}Tb decay 77−34246
^{162}Dy+^{16}O, Coulomb-nuclear interference for high spin states 78−46097
^{164}Dy(^{32}S,^{32}S$'\gamma$), recoil distance lifetimes of ground state bands 78−8774
^{164}Dy(n,n$'\gamma$), γ spectrum, level populations 77−61406
^{165}Dy, γdecays obs., ^{165}Ho level determ. *(French)* 77−274
Dy(α, xn γ)Er, 90 MeV, preequilibrium and equilibrium de-excitation processes 78−50185
^{A}Er, A=154, 155, γ-ray spectra, ang. distrib., high spin states 79−9503
^{A}Er, A=166-170, α-particle Coulomb excitation of octupole vibr. states 78−41618
^{160}Er, produced in ^{124}Sn+^{40}Ar, γ-ray multiplicity spectra, nuclear shape at high angular momentum 78−37260
^{166}Er, Coulomb excitation with ^{4}He and ^{16}O ions 78−8839
^{166}Er+^{86}Kr, 5.99 MeV/N, are γ-ray multiplicity 78−82375
^{166}Er(^{86}Kr, X), 600 MeV, deeply inelastic, alignment of transferred ang. momentum, discrete γ-ray ang. correlations 80−47498
^{169}Er, β-decay half-life, γ-ray spectra 77−79330
^{170}Er(^{32}S,^{32}S$'\gamma$), recoil distance lifetimes of ground state bands 78−8774
^{252}Es, half-life, γ-ray decay obs. 78−4914
Eu, A=147, 149, 151, band struct. obs. via heavy-ion reactions 77−82855
^{A}Eu, A=152,154, gamma-ray intensities, precision meas. 80−102140
^{143}Eu^{m}, decay obs., struct. determ. 78−50130
^{150}Eu decay, ^{150}Sm nucl. struct. determ. *(Japanese)* 77−41888
^{151}Eu(^{16}O,^{16}O$'\gamma$), 25-42 MeV, energy levels, transitions, spin assignments determ. 77−38294
^{152}Eu, level scheme, low energy transitions, reaction data, Nilsson model interpretation 78−66215
^{152}Eu, radioactive decay, γ-ray energy meas. *(German)* 77−57633
^{152}Eu sources, international comparison of γ-ray emission rate meas. using Ge spectrom. 79−22529
^{153}Eu(n,X), gamma transitions and band levels *(Russian)* 79−67700
^{153}Eu(n,γ)^{154}Eu, thermal, ^{154}Eu level scheme 77−61374
^{141g}Eu, ^{141m}Eu β-decay props., J^{π}, decay energy, $T_{1/2}$ 77−82876
^{150m}Eu, 35.8 y, decay coincidence study, ^{150}Sm levels 77−82858
^{18}F, 5603 keV level, isospin mixing via (α,γ) and (p,γ) reactions 78−543
^{19}F, 3907 keV state, lifetime meas. by Doppler shift attenuation method 77−88079
^{19}F, hyperfine interactions of fast ions recoiling in noble gases 77−18469
^{19}F, produced in ^{15}N(α,γ)^{19}F, 5.2 to 8.4 MeV, resonances and gamma decay schemes 78−37358
Fe, gamma fields induced by ^{252}Cf neutrons 78−50240
Fe, high resolution fast neutron gamma-ray prod. cross sections 77−67745
Fe shield, meas. of neutron and gamma ray penetration 80−47730
Fe slab *(Japanese)* 80−18595
Fe+p, 52 MeV, spectral meas. of secondary neutrons and photons from thick targets 78−58282
^{20}Fe, β-γ directional correlation, second class current 78−50127
^{52}Fe, γ-spectra, levels, J^{π} via α+^{50}Cr reaction 77−74794
^{54}Fe, studied via (α,2nγ), high spin states, shell model calcs. 78−54675
^{55}Fe resonances, levels, J^{π}, valence capture γ-ray spectrum from ^{54}Fe(n,γ) 80−86852
^{56}Fe, recoiling in Fe, enhanced transient fields 78−37284
^{56}Fe(n,γ), 6-150 keV, shape anal. and width correlations 77−26766
^{56}Fe(n,n$'\gamma$), up to 14.6 MeV, radiation and neutron widths for highly excited levels *(Russian)* 78−605
^{57}Fe, γ-ray emission, test of time reversal invariance 78−29421
^{58}Fe high spin states from ^{55}Mn(d,pγ), decay props., γ-γ coincidence 78−21515
^{58}Fe(n,λ), resonance capture cross section s- and p-wave radiative widths 80−47476
^{59}Fe decay, sum-coincidence γ-spectrum, ^{59}Co level struct. 77−14063
Fe(n,γ), γ-ray energies and intensities 78−89876

gamma-ray spectra continued
^{67}Ga, levels, branching, mixing, T$_{1/2}$, via ^{67}Zn(p,nγ) 3.6-4.3 MeV 77−34247
^{72}Ga→^{72}Ge, gamma and beta-ray spectra, intensities, branching ratios, spin and parity assignments *(Korean)* 78−50128
Gd(^{35}Cl,^{35}Cl′γ), A=154, 6, 132-43 MeV, lifetime meas. of high spin states 78−13140
^{A}Gd, A=152, 154, γ-transition energy and intensity meas. from Eu decay 80−73818
^{A}Gd+α, A=154,160, reaction cross section meas., in beam γ-spectrometric technique 79−26445
^{A}Gd(n.γ), A=154,156-8, 2, 24 keV, resonance averaged γ-spectra, level and J$^{\pi}$ appls. 80−37347
^{67}Gd, γ-spectroscopy of high-spin levels via ^{64}Zn(α,pγ), ^{53}Cr(^{16}O,pnγ) 78−93960
^{146}Gd, 3^{-} 1579 keV first excited state 78−41670
^{146}Gd decay, γ- and internal conversion electron spectra 79−75916
^{146}Gd, lowest 2^{+} state and energy gap at Z=64 78−82310
^{147}Gd→^{147}Eu decay, γ-ray spectra obs. at small-source detector distance *(Russian)* 79−93520
^{151}Gd, 108 and 395 keV levels, mag. moments and half-lives, PAC 77−22883
^{151}Gd, high spin states, gamma ray and conversion electron obs., level struct. 77−46130
^{152}Gd populated in ^{152}Eu decay 80−22768
^{152}Gd(α,3nγ)^{153}Dy, 35-45 MeV, collective band struct. of ^{153}Dy anal. 77−61342
^{153}Gd, mag. moment meas. of 129.2 keV 77−82850
^{154}Gd (α,xn), deformed Dy quasicontinuum spectrum, M1, E1, E2 components 80−498
^{154}Gd, γ-γ directional correls., coincidence meas. 77−65212
^{156}Gd(n,γ), up to 2.24 keV, n resonances, spectra fluctuation, statistical theory test 79−36188
^{157}Gd(n,γ), γ and conversion electron spectra, ^{158}Gd collective bands 78−89819
^{160}Gd(α,xnγ), compound and precompound γ-ray entry lines from measured multiplicities and energies 79−6649
Ge detectors, automatic computer anal. for peak area and position 79−9941
Ge detectors in space, computer spectral anal. of cosmic ray proton induced radioactivity 79−12413
Ge(Li), analytic fitting of full energy peaks 77−71716
Ge(Li) and HPGe detectors, coincident sum peaks 80−63447
Ge(Li), automatic anal. of complex γ-ray spectra 78−33370
Ge(Li) detector, gamma pulse pileup, random summing losses 80−58023
Ge(Li) detector, γ-spectra, noniterative method for fitting Gaussian to peaks 77−57840
Ge(Li) detector, IAEA intercomparison of computer processing methods 79−9954
Ge(Li) detector, simple computer program (BASIC) for spectra eval. 79−9951
Ge(Li) detectors, anal. of monochromatic γ-ray and annihilation spectra 78−50429
Ge(Li) gamma-ray spectra, interfering peak anal., using resolution enhancement filters 78−11590
Ge(Li) γ-ray spectra, NUKLID program for automatic line identification *(German)* 78−58536
Ge(Li) spectra, effect of base line shape on peak unfolding 78−851
^{70}Ge(α, nγ) 10-18 MeV populating ^{73}Se high-spin states 77−10324
^{72}Ge, gamma-ray spectra, energy levels, spin and parity assignments, from ^{72}Ga beta-decay *(Korean)* 78−50128
^{72}Ge levels pop. in ^{8}Zn(^{6}Li,pn), in beam gamma-ray spectroscopy 80−47343
^{74}Ge(^{12}C,3n)^{83}Sr, high spin states and spin ordering, γ-ray excitation functions 78−66199
^{75}Ge, beta decay of 83 min ground state, decay characts. and scheme 79−67713
^{76}Ge(^{12}C,3n)^{85}Sr, high spin states and spin ordering, γ-ray excitation functions 78−66199
^{76}Ge(^{86}Kr,xn), 314-376 MeV, γ-multiplicity meas., Er compound nucleus formation 79−89320
^{2}H(^{40}Ar,nγ)^{41}K, ^{2}H(^{40}Ar,pγ)^{41}Ar, 56 MeV, γ-decays of low-lying states in ^{41}K, ^{41}Ar obs. 77−41986
^{3}H(^{35}Cl,pγ)^{37}Cl, γ-ray spectroscopy of ^{37}Cl 78−13013
$_{\Lambda}^{7}$He, prod. cross section calc., γ decay spectrum, shell model theory 78−62501
^{172}Hf rotation bands from ^{160}Gd(^{16}O,4n), high spin states, halflives 78−25217
^{177}Hf(n,γ), 1-165 eV, γ-ray spectra obs., level scheme determ. 77−50130
Hg, A=191,2,3,5,7,9, rot. aligned bands, high spin states, energy levels B(E2) values 78−70483
^{A}Hg, A=198-204, reorientation effect meas. on 2^{+} states 78−37282
^{A}Hg, A=200,202,204, oblate shape determ. 79−17792
^{180}Hg, T$_{1/2}$=3s decay chain, on-line γ-ray spectroscopy 78−13034
^{197}Hg (64 h) decay γ intensities, obs. 79−75922
^{197}Hg energy levels from ^{195}Pt(α,2n), γ and conversion electron spectra, spins, parities 78−25149
^{197}Hg source for Mossbauer studies 79−26796
^{198}Hg(α,2n), 30 MeV, levels of ^{200}Pb and isomers 78−66192
^{202}Hg(α,3nγ), 38.2 MeV, γ-spectra obs., ^{203}Pb decay scheme determ. 78−29489
^{203}Hg, gamma-ray precision energy meas. 78−58533
^{159}Ho, level scheme, γ-singles, conversion electron spectra via ^{159}Er decay 78−547
^{165}Ho +^{86}Kr, 618 MeV, γ-ray multiplicities and angular momentum fractionation 78−37370
^{165}Ho(p, xnyp γ), 60 MeV, preequilibrium and equilibrium de-excitation processes 78−50185
^{165}Ho(p,xnypγ), 60 MeV, n and γ energies and ang. distribs. 78−89872
^{166}Ho, beta decay 77−6310
^{166m}Ho, relative intensities of gamma-rays 78−46201
^{A}I, A=131-135, gamma spectra of radioiodines in reactor coolant 79−9732
^{123}I decay, gamma-ray spectra, ^{123}Te level scheme obs. 77−10361
^{123}I source sumpeak calibration absolute activity 77−57785
^{127}I γ cascade following ^{127}Te decay, 360.3-57.6 keV γ-γ directional correl. 78−25151
^{129}I energy levels populated in ^{129}Te decay, γ spectra, coincidence spectra 77−2935
^{129}I, γ-ray and X-ray radiation, internal conversion coeff. 79−6499

gamma-ray spectra continued
^{132}I decay, weak transition energies and intensities, γ-spectrum, ^{132}Xe levels 79−9521
^{136}I β-decay, ^{136}Xe levels anal. neutron particle-hole states 77−74811
^{137}I, investigation of beta-strength functions by neutron and γ-spectroscopy 79−45209
^{138}I, β-decay scheme, population of ^{137}Xe and ^{138}Xe levels, delayed neutron obs. 80−27600
In, A=109, 110, 111, low temp. orientation, γ-ray spectra 77−79327
^{A}In, A=104, 106, β-decay half lives and decay schemes 78−74333
^{106}In level scheme via ^{106}Sn decay 78−93971
^{108}In, level scheme determ. from ^{108}Sn decay and ^{108}Cd(p,n) 78−41636
^{108}In, levels, J$^{\pi}$ from ^{108}Sn decay γ- and conversion electron-spectra 77−71589
^{111}In band structure and hole-core coupling, ^{109}Ag(α,2nγ), branching and mixing ratios 78−58249
^{112}In, half-lives and mag. moments of two high spin states, γ-ray spectra 77−22940
^{115}In(^{12}C,4n)^{123}Cs, in-beam γ-ray spectroscopy, decoupled band in ^{123}Cs obs. 78−21520
^{115}In(p,γ) γ-22 MeV differential cross-section meas. 79−93617
^{119g,m}In, decay schemes, half-lives, excited levels 77−296
^{181}Ir, γ-ray spectra, half-life, decay scheme 78−41672
^{192}Ir, gamma-ray intensities, precision meas. 80−102140
^{192}Ir, redetermination of γ-ray standards between 0.1 and 1.0 MeV 78−37472
^{193}Ir, muonic, mag. hyperfine anomaly 77−83768
K, A=48, 49, 50, half lives, γ meas. 78−74341
^{38}K^{m}, β and γ spectra meas., determ. of isomeric ratios *(Russian)* 77−74771
^{39}K de-excitation, continuum γ-ray emission and ang. momentum dissipation 77−6293
^{40}K excitation energy, γ decay, of lowest T=2 state populated in ^{40}Ar(p,n) 78−8769
^{40}K, γ-ray energies meas. for Ge(Li) detector calibration 80−27865
^{40}K, naturally occurring, gamma-ray emission energies 80−52811
^{41}K states from ^{40}Ar(d,n), lifetimes meas. by DSA method 78−78308
^{42}K, yrast state J$^{\pi}$ assignments via ^{26}Mg(^{18}O, pnγ) anal. at 25,34 MeV 77−57618
Kr, A=90, 91, ^{232}Th fission products, yields, γ-ray spectra 78−74410
^{81}Kr low lying states populated in ^{81}Br(p,nγ), γ spectra, γ-γ coincidences 78−25195
^{82}Kr(α,n), 14-21 MeV, in-beam γ-ray spectra, high-spin states of ^{85}Sr obs. 77−41915
^{84}Kr(α,3n), 35-45 MeV, in-beam γ-ray spectra, high-spin states of ^{85}Sr obs. 77−41915
^{87}Kr energy levels from ^{87}Br β-decay, delayed neutrons, high energy γ spectra 78−25155
^{88}Kr level scheme and transitions, delayed neutrons from ^{88}Br β-decay 80−42600
^{93}Kr, γ-ray decay scheme, levels, J$^{\pi}$, logft values 77−54152
La, A=144-6, β-decay, γ-ray singles and coincidence meas. 78−4913
^{131}La→^{131} decay scheme, γ, X-ray and conversion electron spectra *(Russian)* 80−32241
^{134}La decay, ^{134}Ba level scheme obs. 77−10360
^{138}La, naturally occurring, gamma-ray emission energies 80−52811
^{138}La, radioactive decay meas., half life, γ energies 80−13418
^{139}La(n, γ), 10-70 keV, gamma-ray transitions 78−17185
^{139}La(n, γ), 2.5-90 keV, s- and p-wave resons. 78−17186
^{140}La, fission product, γ-ray emission probability 77−82862
^{143}La, decay, gamma-ray spectra *(French)* 77−30517
^{143}La, gamma-ray spectra, half-life 77−82859
^{144}La, radioactive decay meas., half life, ^{144}Ce levels 80−13417
^{6}Li, excitation energy of second excited state meas. in (p,p') and (p,α) 77−57619
^{6}Li, γ-ray spectra of stopped K^{-}, transitions in $_{\Lambda}^{4}$H and $_{\Lambda}^{4}$He 79−63621
^{6}Li(t,d)^{7}Li, 0.35 to 1 MeV, resonance struct. in compound nucl. excitation curves 78−17217
^{6}Li(t,γ)^{9}Be, 0.35 to 1 MeV, resonance struct. in compound nucl. excitation curves 78−17217
^{6}Li(t,p)^{8}Li, 0.35 to 1 MeV, resonance struct. in compound nucl. excitation curves 78−17217
^{7}Li, γ-ray spectra of stopped K^{-}, transitions in $_{\Lambda}^{4}$H and $_{\Lambda}^{4}$He 79−63621
^{7}Li(K^{-},π^{-} γ), hypernuclear γ-ray line 78−37377
^{7}Li(γ,γ′), 32 MeV, energy spectra, d prod. process *(Russian)* 80−91177
^{7}Li(n,n′γ)^{7}Li*, threshold to 5 MeV, absolute meas. of cross section 79−67751
^{7}Li(t,γ)^{10}Be, excitation functions and resonant struct. for 17.79 MeV state 78−13110
^{11}Li beta decay, γ activity 80−106018
Lu, A=162,4,5, from Eu(^{16}O, xn), gamma transitions, half-lives anal. 78−62509
^{172}Lu decay, identification of γ-spectra unplaced energies by delayed coincidence meas. 80−78221
^{172}Lu, decay scheme, γ-ray, conversion electron spectra 79−75913
^{172}Lu, γ-ray spectrum anal. 77−82847
^{172}Lu, radioactive decay, γ-ray spectra, internal conversion electron spectra 79−75912
^{173}Lu→^{173}Yb e.m. consts. of lower rot. bands of ^{173}Yb determ. 77−82802
^{176}Lu, reson. spins, secondary γ-transition intensity, from ^{175}Lu(n,γ) 78−21512
^{177}Lu, reson. spins secondary γ-transition intensity meas. in ^{176}Lu(n,γ) 78−21512
^{24}Mg, 11.86 MeV level, confirmation of J$^{\pi}$=8^{+} assignment from ^{12}C(^{16}O,αγ) 42 MeV 78−70445
^{24}Mg, T=2 state props., obs. in ^{23}Na(p,γ)^{24}Mg reaction 78−8767
^{24}Mg+p, 400 MeV, multinucleon removal in quasifree process, p-γ coincidence expt. 78−37342
^{24}Mg(α,nγ)^{27}Si, 12.60-16.35 MeV, ang. correl. and lifetime meas. 78−17224
^{24}Mg(d,pγ)^{25}Mg, particle-gamma and gamma-gamma coincidence, energies and branching ratios 77−22892
^{26}Mg+^{18}O, 34 MeV, yrast states in ^{41}K, ^{41}Ca, spins, parities from γ meas. 78−58250
Mn, A=54-6, yrast decay schemes from heavy-ion fusion evaporation reactions 77−82854
^{52}Mn, γ-spectra, levels, J$^{\pi}$ via α+^{50}Cr reaction 77−74794
^{52}Mn, high spin state spectroscopy via ^{39}K(^{16}O,2pnγ) 37-52 MeV 77−10321

gamma-ray spectra continued
^{55}Mn(α,α), 4.5 to 7 MeV, Coulomb excitation, search for 1.29 MeV 1/2$^-$ level 78−82360
Mo, A=103-5, half-lives and γ-ray energies of short-lived isotopes following ^{235}U fission 78−17137
Mo, reactions induced by ^{12}C and ^{19}F ions, γ-ray spectroscopy of induced activities 77−23107
Mo(A=94, 95, 96), nuclear reson. fluoresc., line profiles, level lifetimes 77−71586
^{A}Mo(n,γ) A=98, 100 resonance parameters, capture Γ-rays and reaction mechanism 80−18272
^{92}Mo in beam γ-spectroscopy, level, lifetimes and excitation functions from ^{90}Zr(α,Zn) 79−13240
^{93}Mo^{m}, low temp. nucl. orientation, γ-ray spectra 77−79327
^{94}Mo, level spins and multiple mixing ratios from γ-γ correlation meas. 78−21517
^{98}Mo(d,p), (d,n), (d,α), activation analysis, excitation functions 80−22842
^{99}Mo, short lived isomers from photonuclear reactions, internal conversion coeffs. 78−37308
^{91g}Mo, ^{91m}Mo, decay anal., half-life meas., γ-γ coincidences 77−2937
^{14}N(α,γ)^{18}F, hadronic nuclear-parity violation with change of isospin, γ spectrum search 78−94018
^{14}N(γ,γ'), 32 MeV, energy spectra, d prod. process *(Russian)* 80−91177
^{14}N(n,γ), gamma-field from monodirectional neutron source in air 77−67785
^{14}N(π^-,xγ), recoil momentum spectrum of ^{12}C* using deexcitation γ rays Doppler broadened 77−54256
NaI pulse height spectra for >1.5 MeV gamma-rays, model modification 79−36459
^{22}Na, isoscalar M2 transition, γ-ray spectra obs. 77−10363
^{23}Na, 2.8 keV and thermal neutron capture gamma-ray spectra 77−38263
^{23}Na(n,Xγ), 0.2 to 20 MeV, reaction cross sections 80−99172
Nb, A=90, 92, short lived isomers from photonuclear reactions, internal conversion coeffs. 78−37308
^{92}Nb, γ-spectra, level and decay scheme for states to 1.6 MeV excit. 77−30504
^{93}Nb(n,γ)^{94}Nb, E_n=14.1 MeV, γ emission exciton model *(Russian)* 79−13302
^{93}Nb(n,γ)^{94}Nb, exciton model, γ spectra calc. 78−62539
^{93}Nb(n,n$'\gamma$), 1.3-2.7 MeV, energy levels, decay scheme, de-excitation gammas 78−41710
^{93}Nb(n,n$'\gamma$), (n,γn$'$), 14.6 MeV, differential cross sections from nγ coincidence spectra anal. *(Russian)* 78−17209
^{93}Nb(n,n$'\gamma$), up to 14.6 MeV, radiation and neutron widths for highly excited levels *(Russian)* 78−605
^{94}Nb excited states from ^{94}Zr(p,nγ), spin, parity, γ-spectra 77−88125
^{95}Nb, K-shell autoionisation in β-decay 77−298
^{99}Nb, level schemes, from ^{99}Zr β-decay obs. 79−17863
^{133}Nb, high-spin levels, in-beam γ-ray spectra meas. *(French)* 77−61372
Nd, A=139, 141, high spin levels, γ spectra, hole-core coupling 77−50063
Nd(^{16,18}O, xnγ), 69-78 MeV, ^{161,162}Er high ang. momentum states, γ decay modes from multiplicity meas. 78−29419
^{144}Nd, neg. parity states, γ-transition multipolarity 79−40882
^{144}Nd(^{12}C,6n)^{150}Dy, 112 MeV, high spin isomers of ^{150}Dy, gamma-ray spectra 78−50075
^{144}Nd(n,γ), 0.04 to 11 keV, reson. γ-ray anal. 78−8823
^{146}Nd(^{12}C,8n)^{150}Dy, 118 MeV, high spin isomers of ^{150}Dy, gamma-ray spectra 78−50075
^{148}Nd from ^{148}Pr β-decay, low lying energy levels, quasi band description 80−5096
^{148}Nd(α,3nγ)^{149}Sm, 35-45 MeV, collective band struct. of ^{149}Sm anal. 77−61342
^{150}Nd+^{20}Ne, 128 to 172 MeV, γ-ray multiplicities in evaporation residues 77−14065
^{150}Nd(^{20}Ne, xnγ), multipolarities of yrast and statistical cascades, total γ conversion coeff. 78−70484
^{150}Nd(^{20}Ne,X), 115, 130 MeV, γ-continuum multiplicity distrib., yrast bump 80−9265
^{150}Nd(α,4n)^{150}Sm, 45 MeV, yrast bands in Sm anal. in interacting boson approx. 78−13124
^{180}Nd(^{12}C,xn), deformed Dy quasicontinuum spectrum, M1, E1, E2 components 80−498
^{141m}Nd, internal conversion of N=81 isotones 78−13027
^{20}Ne, form. in ^{19}F(p,γ) reaction, 668 keV, γ-ray transitions to ground state, rel. to stellar nucleosynthesis 78−17191
^{20}Ne, unnatural parity levels at high excitation, γ spectra from ^{12}C(^{12}C,$\alpha\gamma$) 77−2933
^{21}Ne, TDPAC obs. on ions recoiling in vacuum 77−22942
^{21}Ne*, produced in ^{2}H(^{20}Ne,p)^{21}Ne*, 351 keV $^5/_2{}^+$ state lifetime and mag. moment 78−41631
^{22}Ne, first excited 2$^+$ state, mag. moment determ. 77−18388
^{22}Ne($4_1{}^+$) from ^{4}He (^{19}F,pγ), lifetime meas. by high vel. coincidence DSA method 78−33148
^{22}Ne(α,nγ)^{25}Mg, particle-gamma and gamma-gamma coincidence, energies and branching ratios 77−22892
Ni+^{12}C, 107, 155, 197 MeV, evaporation residue Se, prompt γ deexcitation 78−74395
Ni+π, E_π=0, 45 MeV γ-ray spectra, prod. cross-section for residual nuclei meas. 78−649
^{A}Ni(n,γ), A=58, 60, 61, 6-150 keV, shape anal. and width correlations 77−26766
^{A}Ni(n,n$'\gamma$), A=58-64, <4 MeV, gamma prod. and inferred cross sections 80−525
^{A}Ni($n_{th}\gamma$)$^{A+1}$Ni (A=58, 60, 62, 64), γ-ray spectra, level schemes, M1 and E2 strength functions 77−57674
^{A}Ni($\pi^{\pm}$,xγ), 100-200 MeV, prompt and delayed γ spectra, nuclide yields 79−22332
^{58}Ni spallation by 1 GeV protons, reaction channels *(Russian)* 78−74370
^{58}Ni+p, 1 GeV, alpha-particle decay channels 80−22826
^{58}Ni(^{16}O, 2pγ), 54.5, 59.5, 64.5 MeV high spin and excitation energy regions in ^{72}Se, γ cascade 78−54795
^{58}Ni(^{16}O,2pγ), 40-58 MeV, γ ang. distribs., coincidences, ^{72}Se yrast states, lifetimes 77−54176
^{58}Ni(^{16}O,2pγ)^{72}Se, 54.5-64.5 MeV, high spin and excitation regions anal. 78−25226

gamma-ray spectra continued
^{58}Ni(d,$\alpha\gamma$), 7 MeV, mean lifetimes of ^{56}Co levels 78−4950
^{58}Ni(n,n$'\gamma$), 0.5-10 MeV, γ-ray production cross sections 77−26762
^{58}Ni(p,γ)^{59}Cu, γ-decay of ^{59}Cu analogue resons. 78−13005
^{59}Ni, levels and new γ-transitions following ^{59}Cu(β^+)^{59}Ni 77−22935
^{59}Ni, radiative capture of K-electrons, γ spectra anal. 77−61384
^{60}Ni, aero-phonon, $4_1{}^+ \rightarrow 2_2{}^+$ γ-ray transition 78−17136
^{60}Ni populated in ^{60}Co beta decay, 2506 to 2159 keV γ transition 77−22929
^{60}Ni+p, 400 MeV, multinucleon removal in quasifree process, p-γ coincidence expt. 78−37342
^{60}Ni+π, 70 MeV, γ+charged particle coincidence spectroscopy, cross section, p multiplicity 78−46111
^{60}Ni(n,n$'\gamma$), 0.5-10 MeV, γ-ray production cross sections 77−26762
^{60}Ni(p,γ)^{61}Cu, 1800 to 290 KeV, γ-ray spectra and j$^\pi$ assignments 79−59063
^{61}Ni, γ-spectroscopy above 2.2 MeV excit., J$^\pi$,$T_{1/2}$, branchings 77−54172
^{61}Ni(α,nγ)^{64}Zn, 7.8 MeV, γ-ray spectroscopy Zn levels below 3.1 MeV 78−21514
^{62}Ni(α, nγ), 8-14 MeV, γ ray study of ^{65}Zn odd-parity states, energies, transitions 78−50120
^{64}Ni(α,n), (α,2n), 17-25 MeV, level struct. of ^{66}Zn, ^{67}Zn determ. 77−46178
Ni(α,nγ)Zn, 6.5-17 MeV, particle-vibr. coupling in ^{65,67}Zn 77−38241
Ni(n,n$'\gamma$), 3-6 MeV, γ-ray prod. cross sections 77−26767
Ni(π^+, π^-), 200 MeV, deexcitation γ spectra, transitions in ^{58,60}Cu 78−89912
N(n,γ), 14 MeV neutron source, electron recoil spectra from gamma-rays anal. 77−26683
^{237}Np, gamma ray spectra of reactor fuels 80−42577
^{237}Np, gamma-ray spectra following ^{231}Am α-decay *(French)* 79−492
^{15}O, reson. widths and branching ratios meas. from ^{14}N(p,γ)^{15}O 77−38244
^{16}O, hyperfine interactions of highly stripped ions recoiling into H and He 77−22932
^{16}O ions, mag. hyperfine interactions, PAC meas. 80−95734
(^{16}O, xn), population of ^{174,175}W, ^{161}Yb, γ continuum spectra, yrast cascades, dipole component 78−54794
^{16}O^{8+}+Au K-shell ionis., δ-ray emission 77−79557
^{16}O+^{12}C, 15-72 MeV, gross struct. in γ-ray yields 78−78405
^{16}O(^{28}Si,X), 55-96 MeV, γ-ray yield functions from high spin states, comparison with ^{12}C+^{24}Mg 79−93492
^{16}O(π,γn), direct and resonance reaction unified shell model, n, γ spectra 80−52696
^{16}O(π^-,γn), γ-spectrum and γ-n ang. correlation function from continuum shell model 78−86551
^{16}O(π^-,γn)^{15}N, information from radiative π capture coincidence spectra 78−86550
^{18}O, 2$^+$ 1.98 MeV level lifetime and g-factor determ. from high velocity recoil in vacuum 77−18474
^{177}Os, decay, lower excited states of ^{179}Re obs. 78−17145
^{179}Os decay, lower excited states of ^{179}Re obs. 78−17145
^{185}Os, γ-ray spectra obs., first forbidden beta decay anal. 78−559
^{190}Os(n,γ), energy levels and spectra of ^{191}Os determ. 77−41917
^{192}Os(2n,γ)^{194}Os, level transitions, prolate-oblate transition 78−62540
^{192}Os(p,p$'$) and (d,d$'$), γ-ray spectra, energy level scheme 77−34243
^{194}Os beta decay, X-ray/gamma relative intensities, L_1 subshell yields 78−4919
P, A=30, 32, high spin states from ^{16}O+^{16,18}O reactions and ^{27}Al(α,n), γ-ray meas. 78−74386
^{31}P, precision Doppler-shift attenuation lifetime meas. from γ-ray lineshapes 79−36195
^{31}P(p,γ)^{32}S resonances below E_p=1.5 MeV 77−50141
^{243}P, γ-γ coincidence via (n,γ) reaction 77−6202
^{234}Pa isomers from ^{234}Th β^- decay, low energy γ-spectrum 78−70493
Pb, short lived nuclear states, neutron activation anal. in aerosols of Otto carburettor engine *(German)* 77−12860
Pb+p, 52 MeV, spectral meas. of secondary neutrons and photons from thick targets 78−58282
^{204}Pb populated by ^{204}Bi decay, isomeric transitions, J$^\pi$ assignments 78−50122
^{204}Pb yrast levels populated in ^{204}Hg (α,4n), spin, parity, γ spectra 78−12954
^{206}Pb, level scheme including conversion electrons $\lesssim$40 eV 78−21518
^{207}Pb, γ-γ directional correls. in ^{207}Bi decay, mag. perturbation obs. 77−74796
^{207}Pb(n,γ), primary E2 transitions to ^{208}Pb ground state 78−58284
^{208}Pb compound nucleus, γ-decay spectral function depend. on ang. momentum *(Russian)* 78−86467
^{208}Pb(n,γ)^{209}Pb, 11 MeV, gamma-ray spectra, role of two-particle one-hole states 77−26764
^{104}Pd, characts. of the levels excited in ^{104,104m}Ag decay 79−9515
^{105}Pd levels with large spin, γ spectra 79−6478
^{106}Pd, gamma-gamma ang. correlation meas. from decay of ^{106}Rh^{g} 77−79325
^{106}Pd, γ-γ directional correlations, mixing ratios 77−82853
^{109}Pd, ^{238}U fission product, gamma-ray spectra, half-life determ. 77−50084
^{109}Pd, level structure and half life 77−82827
^{110}Pd(^{12}C,xnγ), shell effects at high spin in the γ-continuum from Te evaporation residues 79−22165
^{111}Pd^{g,m} γ-ray decay, ^{111g}Pd half-life, ^{111}Ag levels and decay 78−541
^{112}Pd, ^{238}U fission product, gamma-ray spectra, half-life determ. 77−50084
^{109g}Pd, gamma-ray decay, gamma-gamma coincidences 78−29417
Pm, A=143, 144, 145, ICC, γ-spectra, multipolarities for low-lying levels 77−50081
^{145}Pm, form. in electron capture decay of ^{145}Sm, γ-transition decay rate and intensities 78−13030
^{147}Pm, γ-γ cascades angular correlations in ^{147}Nd beta decay 79−63624
^{147}Pm, level struct. via ^{148}Nd(p,2nγ) 12.1-20.2 MeV 78−510
^{148}Pm, ^{148m}Pm decay, struct. of ^{148}Sm determ. 77−67717
^{149}Pm$\rightarrow$^{149}Sm, beta decay matrix elements 78−70488
^{150}Pm, decay, ^{150}Sm nucl. struct. determ. *(Japanese)* 77−41889
^{152}Pm decay, β and γ rays, spins, half lives, ^{152}Sm levels 78−542
^{207}Po^{g} decay, spin from conversion electron meas., γ intensities 78−58252
^{208}Po, yrast two proton-two neutron hole states 78−78307
^{210}Po, alpha-decay, population of 0$^+$ of ^{206}Pb 80−22775
^{215}Po, excited states, half-life meas. *(French)* 79−97679

gamma-ray spectra continued
^{A}Pr (A=149,150), fission product, γ-spectra, half-life meas. 77—38240
^{141}Pr, ICC, γ-spectra, multipolarities for low-lying levels 77—50081
^{141}Pr(n,γ), circular polarisation, ang. distrib. meas. 80—32285
^{142}Pr, $2^{-}\rightarrow 2^{+}$ β spectrum, shape meas. 77—50083
^{146}Pr$\rightarrow^{146}$Nd, decay scheme and energy levels, log ft values 78—4912
^{150}Pr decay into ^{150}Nd vibr. levels 78—89817
^{191,193}Pt high-spin levels via ^{190,192}Os(α,3nα), triaxial rotor model 77—34213
^{191}Pt energy levels, γ and conversion electron spectra, spins, parities 78—25149
^{195}Pt(n,γ)^{196}Pt, low spin positive-parity states struct., O(6) limit of IBA model 78—33110
^{196}Pt (^{20}Ne, ^{20}Ne′), excited states, lifetime meas. using recoil-distance method 80—13413
^{196}Pt (^{58}Ni, ^{58}Ni′), excited states, lifetime meas. using recoil-distance method 80—13413
(Pu,U)O_2, low-enriched fuel assemblies, profiles of activity ratios of ^{134}Cs, ^{137}Cs and ^{106}Ru fission products 77—57713
Pu isotope ratios, γ-ray spectrometric determ. 77—6518
Pu, multigroup time-dependent delayed γ-spectra from fission and activation 78—13184
Pu nondestructive rapid isotopic anal. gamma-ray spectrometric method 79—81069
Pu safeguards, product soln. gamma-ray NDA using K-absorption edge densitometer 80—83162
Pu safeguards accountability, gamma-ray meas. of Pu and Am in molten salt residues 80—83165
Pu safeguards assay, isotopic meas. by gamma ray spectrometry using two-detector method 80—83161
^{A}Pu, A=238 to 241, gamma ray spectra of reactor fuels 80—42577
^{239}Pu(n,X), thermal n, gamma spectra from capture, fission and fission products 80—37352
π^{-}d$\rightarrow\gamma$nn, n-n scatt. length from photon spectra 79—67600
π^{-}p$\rightarrow\gamma$n, n-n scatt. length from photon spectra 79—67600
^{223}Ra decay chain, precise γ-ray spectroscopy 77—54175
^{223}Ra, excited states, half-life meas. *(French)* 79—97679
^{226}Ra decay chain, γ-ray energies meas. for Ge(Li) detector calibration 80—27865
^{226}Ra levels from ^{230}Th α decay, search for $K^{\pi}=0^{+}$ excited states 78—86504
^{226}Ra(p,f), 12 MeV, prompt γ-ray spectra meas. 78—13183
^{228}Ra-^{228}Ac decay and ^{228}Th decay chain, gamma ray energies 79—85857
^{213m}Ra, 2.1 msec. isomer, gamma and alpha decay meas. 77—14067
^{80}Rb, level struct., quasi-rot. bands, via ^{79}Br(α,3n) 30-55 MeV reaction 77—88028
^{85}Rb, single-particle estimate of γ-γ transition probability 78—13023
^{85}Rb, two-quantum γ-γ decay of 514 keV excited state 78—13009
^{87}Rb(p,nγ), 3.8 MeV ^{87}Sr excited levels, spin, parity, branching ratios, lifetimes 77—50076
^{88}Rb decay, γ-ray energy meas. 79—22530
^{90}Rb, β,γ, conversion electron spectra obs. 77—71583
^{93}Rb, γ-ray decay scheme, levels, J^{π}, logft values 77—54152
^{98}Rb, γ spectra and coincidence meas., deform. in ^{98}Sr anal. 78—12961
^{172}Re, isomeric states, γ-ray transition 79—9433
^{181}Re states and transitions, rot. bands and Nilsson states from ^{181}Ta(^{3}He,3nγ) 79—36152
^{183}Re, γ-ray spectra obs., first forbidden beta decay anal. 78—559
^{189}Re, beta-decay, ^{189}Os scheme 79—54388
^{99}Rh γ-ray cascade, obs. in ^{90}Zr+^{12}C, and ^{91}Zr+^{11}B 78—41762
^{99}Rh isomer, ($T_{1/2}$=4.5 hr.), decay, anticoincidence and integral coincidence spectra meas. 79—6479
^{100}Rh, γ-ray spectrum and ang. $\gamma\gamma$ correlations, ^{100}Ru level struct. study 79—6510
^{100}Rh, lifetime measurements in excited states 79—63631
^{103}Rh level scheme from fast n scatt., γ transitions, spins, parities, cross sections 78—78374
^{106}Rh^{g}, decay, excited states and transitions in ^{106}Pd 77—79324
^{108}Rh, level structure and half life 77—82827
^{109}Rh, 79.8 sec., β-decay to ^{109}Pd, γ and γ-γ meas. 79—3116
^{109}Rh, half-life and decay props. 78—25154
^{221}Rn, decay scheme, α-, β-, γ-spectra meas. 79—6507
Ru short lived isotopes, gas phase fast separation 77—23582
^{95}Ru level scheme, low lying states, g-factor spin, parity 77—88071
^{101}Ru, short lived isomers from photonuclear reactions, internal conversion coeffs. 78—37308
^{103}Ru, gamma-ray precision energy meas. 78—58533
^{103}Ru, level scheme determ. from ^{103}Tc β-decay 79—85413
^{105}Ru, γ-γ ang. correl. meas., spin and γ-ray mixing ratios 78—21516
^{105}Ru, level and γ-decay scheme determ. 78—82312
^{106}Ru, errors in activity ratio determ. in reactor RA used fuel element 79—41061
^{93g}Ru, ^{93m}Ru, decay anal., half-life meas., γ-γ coincidences 77—2937
^{32}S(π,γX), short-range 4-N correls. 77—18613
^{34}S(α,Γ)^{38}Ar, 2-3.5 MeV, reson. levels, mixing ratio 79—71859
Sb, A=108,109,110, gamma-ray meas., decay scheme calc. 77—18473
^{112}Sb, ^{114}Sb, 8^{-} states, half-life and mag. moment, γ-ray spectra 77—22941
^{114}Sb, 8^{-}, 210 μs state, mag. moment, PAC of liq. Sn:^{114}Sb 77—26609
^{121}Sb(n,γ), ^{122}Sb, low-lying state props., coupled neutron quasiparticle-proton model 77—61378
^{121}Sb(n,γ), γ and conversion electron spectra, ^{122}Sb energy level scheme 78—54721
^{123}Sb populated in ^{123}Sn^{m} decay, γ-ray, X-ray and electron spectra 77—88073
^{124}Sb, beta-decay to ^{124}Te, level struct. determ. 79—54387
^{125}Sb decay, gamma-ray spectra, ^{125}Te level scheme obs. 77—10361
^{131}Sb partial level scheme from ^{131}Sn beta decaying isomer, γ spectra 77—50091
^{135}Sb, investigation of beta-strength functions by neutron and γ-spectroscopy 79—45209
Sb(α,2nγ), collective excitations in ^{123,125}I, spin, parity, level schemes 78—4891
^{41}Sc, decay and partial widths of 2883 and 5037 keV levels 77—88077
^{45}Sc(α,pγ), ^{48}T excited states, level struct., lifetimes, from DSA and pγ coincidence meas. 78—74326
^{46}Sc, s- and p-wave radiative widths obs. in ^{45}Sc(n, γ) 78—17187
^{A}Se (A=85-8), fission product, γ-spectra, half-life meas. 77—38240
^{69}Se, decay, T=1/2 β-delayed proton precursor 77—88082

gamma-ray spectra continued
^{70}Se de-excitation, continuum γ-ray emission and ang. momentum dissipation 77—6293
^{75}Se decay, gamma transitions 78—13008
^{76}Se, level scheme from $\gamma\gamma$ coincidence meas. of ^{76}As decay 80—22754
^{82}Se(^{40}Ar,xnγ), shell effects at high spin in the γ-continuum from Te evaporation residues 79—22165
^{83m}Se, decay scheme refinement, ^{83}Br levels 78—17147
^{28}Si, 12917 and 12924 KeV level gamma-gamma directional correl. 79—536
^{28}Si, γ-spectra, isobaric analogue resonances via ^{27}Al(p,γ)^{28}Si 2.4-2.74 MeV 77—57646
^{28}Si p3/2 neutron resonance γ-decay, partial rad. widths from Si(n,γ) 80—52617
^{28}Si, precision Doppler-shift attenuation lifetime meas. from γ-ray line-shapes 79—36195
^{28}Si+^{16}O, fusion oscillations, evaporation residue gamma yields, cross section 80—42725
^{28}Si+p, 400 MeV, multinucleon removal in quasifree process, p-γ coincidence expt. 78—37342
^{28}Si(^{16}O,αpγ) or (^{16}O,2pγ), high spin states, in ^{39}K and ^{42}Ca from γ meas. 78—89787
^{28}Si(α,γ)^{32}S resonances below E_{α}=3.83 MeV anal. 77—50141
^{29}Si neutron resonance, γ-spectra, partial and total radiative widths from ^{28}Si(n,γ) 80—42578
^{29}Si(n,γ), evidence for neutron capture through doorway states 79—17909
Si(n,γ), 3.2-15 MeV, cross-section determ. 77—41962
Si(n,γ), A=28.9, E=31.7-67.7 keV, gamma-ray spectra, single particle effects obs. 77—6372
Sm, ion recoiling into gas and vac., hyperfine field and correl. time meas. 78—66240
^{144}Sm, produced in ^{100}Mo+^{48}Ca 78—37260
^{144}Sm+^{86}Kr, 490 MeV, γ-ray multiplicity moments 78—54798
^{146}Sm levels excited by ^{146}Eu decay, spin-parity assignment *(Russian)* 77—14062
^{149}Sm, γ-γ ang. correl. meas., transition multipolarities, multipole mixing ratios 77—41910
^{149}Sm(n,γ)^{150}Sm, neutron capture γ-ray spectra calcs. 78—94006
^{150}Sm, γ-spectra, levels in ^{150m}Eu, 35.8 y decay 77—82858
^{150}Sm, nucl. struct. from Coulomb excitation *(Japanese)* 77—41890
^{150}Sm(α,3nγ)^{151}Gd, 35-45 MeV, collective band struct. of ^{151}Gd anal. 77—61342
^{151}Sm, gamma spectra, energy levels *(Dutch)* 80—47430
^{151}Sm, populated in ^{151}Pm decay, level scheme, γ-ray spectra 77—74792
^{152}Sm, γ-transition energy and intensity meas. from ^{152}Eu decay 80—73818
^{152}Sm levels populated in ^{152}Pm decay, γ spectra 78—542
^{152}Sm, populated in ^{152}Eu decay 80—22768
^{152}Sm(^{35}Cl,^{35}Cl′γ), 132-43 MeV, lifetime meas. of high spin states 78—13140
^{152}Sm(n,n′γ) spectra and ang. distribs. anomalous excitation *(Russian)* 77—54224
Sm(d,3nγ)Eu, 18-25 MeV, band struct. in ^{149,151}Eu determ. 77—41913
S(n,γ), 3.2-15 MeV, cross-sections determ. 77—41962
Sn, photoactivation by 42 MeV bremsstrahlung, gamma transition energies and line intensities 78—13057
Sn, single closed shell even mass nuclei, collective bands, spin, parity, from Cd(α,2nγ), γ meas. 78—54719
^{A}Sn(^{40}Ar, xn), (A=116, 120, 122, 124), 161-236 MeV, γ-multiplicity meas., Er compound nucleus formation 79—89320
^{106}Sn decay, ^{106}In level scheme determ. 78—93971
^{11x}Sn, (x=3-6,8) quad. moment, γ-ray spectra of Cd:Sn 77—26571
^{120}Sn+^{86}Kr, 5.99 MeV/N, are γ-ray multiplicity 78—82375
^{120}Sn(^{12}C,3nγ)^{129}Ba, E=45-54 MeV, excitation of high-spin levels in ^{129}Ba 78—17104
^{122}Sn(^{40}Ar,4n)^{158}Er, high-spin yrast levels in ^{158}Er, second discontinuity obs. 77—61373
^{122}Sn(K^{-}, X), 0 MeV, E2 nuclear resonance effects, γ and X-ray meas. 78—41774
^{123}Sn^{m} decay scheme, γ-ray, X-ray and electron spectra, ^{123}Sb transitions 77—88073
^{124}Sn(^{32}S,xn), continuum γ rays, linear polarisation, feeding high spin yrast states in ^{151,2}Dy 80—497
^{124}Sn(^{40}Ar,xn)Er, 161-236 MeV, pre-equilibrium neutron emission 79—3169
^{132}Sn, energy levels, gamma transitions, spin and parity 80—9239
^{117m}Sn, half-life and γ-ray intensities 78—4916
Sn(n,γ), up to 20 keV, ^{123,125}Sn level schemes, spin-parity assignments, neutron separation energies 77—54215
Sn(p,2nγ)Sb, A=111, 3, 5, excited states of Sb anal. 77—2911
^{83}Sr, excited states struct. ^{83}Y β^{+} decay, γ-ray coincidence meas. 77—6309
^{85}Sr, 514.0 keV, Analytic fitting of full-energy peaks in Ge(Li) spectra at high count rates 80—99147
^{85}Sr, β-decay, γ-ray weak transitions, intensities 77—79326
^{85}Sr, lifetime DSA meas. in ^{85}Rb(p,nγ) 79—36196
^{86}Sr, 8^{+} state, nucl. g-factor and nucl. spin relax. in Kr 77—22884
^{91}Sr, decay scheme, gamma-ray spectra 77—71587
^{93}Sr, γ-ray decay scheme, levels, J^{π}, logft values 77—54152
^{48}T excited states from ^{45}Sc(A,pγ), level struct., lifetimes, from DSA and pγ coincidence meas. 78—74326
Ta, reactions induced by ^{12}C and ^{19}F ions, γ-ray spectroscopy of induced activities 77—23107
^{166}Ta, isotope identification in ^{159}Tb(^{16}O,9n) reaction, half-life and decay scheme 77—79331
^{173}Ta, levels, rot. parameters, γ-mixing 77—34248
^{176}Ta, isomeric states and rot. struct. anal., in-beam γ-ray spectroscopy 78—78312
^{177}Ta, γ-transition $55/22^{+}\rightarrow 77/22^{+}$, E2/M1 mixing, μ determ., $T_{1/2}$ 77—10355
^{181}Ta, pion^{-} capture, high spin states and neutron multiplicities meas. 78—54806
^{181}Ta(n,γ), 2-3 eV, γ-spectra, energy levels, J^{π} 78—602
^{181}Ta(n,γ), γ-ray spectral shape depend. on n energy diverging interval size 78—78373
^{151}Tb, positron decay, γ-ray coincidence spectra 79—9513
^{153}Tb excited states from Eu(α, xn), rot. bands, spin, parity, γ spectra 78—62552
^{159}Tb(^{14}N,αxn), 95 MeV, γ-multiplicities following fast α-emission 79—67770

gamma-ray spectra continued
^{159}Tb(^{14}N,αxn)$^{169-x}$Yb, 95 MeV, γ-ray identification 77−57697
^{159}Tb(n,γ), resonance parameters *(Russian)* 77−74850
^{159}Tb(n,γ)^{160}Tb, E_n=14.1 MeV, γ emission exciton model *(Russian)* 79−13302
Tc, A=93, 94, 95, low temp. nucl. orientation, γ-ray spectra 77−79327
Tc, A=98, 100, 101, short lived isomers from photonuclear reactions, internal conversion coeffs. 78−37308
^{93}Tc, g.m, γ-ray spectra 79−6476
^{96}Tc, low-lying levels, γ-transitions via ^{93}Nb(α,n)^{96}Tc 10.8, 14.0 MeV 77−2931
^{97}Tc, K-capture probability for β-transition to 216 and 324 keV levels 79−6511
^{103}Tc, decay scheme to ^{103}Ru 79−9470
^{104}Tc, β^- decay, γ-spectra, ^{104}Ru level scheme determ. 78−82313
^{91g}Tc, ^{91m}Tc, decay anal. half-life meas., γ-γ coincidences 77−2937
^{99m}Tc, supercond. effect on decay rate, lattice consts., transition temp. 78−41671
^{A}Te (A=135-7), fission product, γ-spectra, half-life meas. 77−38240
^{118}Te, produced in ^{82}Se+^{40}Ar, γ-ray multiplicity spectra, nuclear shape at high angular momentum 78−37260
^{125}Te, levels and transitions following decay of ^{125}Sb 79−71816
^{130}Te(^{32}S,xn), continuum γ rays, linear polarisation, feeding high spin yrast states in $^{156-8}$Er 80−497
^{119m}Te, electron capture decay, γ-ray spectra, ^{119}Sb level scheme determ. 77−50088
Th, prospecting method, using Ra accumulation in animal thyroid glands, anal. 78−27853
^{228}Th, precise γ-ray energy meas. with Ge(Li) detectors 78−13376
^{229}Th levels from γ-spectra following ^{233}U decay 77−26636
^{230}Th, precise γ-ray energy meas. with Ge(Li) detectors 78−13376
^{232}Th, vibr. states, Coulomb excitation 79−9432
^{A}Ti(n,γ), A=46 to 50, thermal capture, gamma ray spectra 79−93629
^{45}Ti, weak E1 transitions examined using γ-ray, γ-γ coincidence and n-γ coincidence techniques 80−57724
^{48}Ti(α,pnγ)^{50}V, high-spin levels obs. by in-beam γ-spectroscopic technique *(French)* 78−21572
^{49}Ti, polarised, T violation test, γ-ray directional correlation 78−62330
^{50}Ti, studied via (α,2nγ), high spin states, shell model calcs. 78−54675
Tl, A=195, 197, rot. bands, high spin states 78−62476
Tl, A=201,203, levels via (d,3nγ), J^{π},$T_{1/2}$, 9/2$^-$ band discovery 77−34207
^{186}Tl decay, γ, conversion electron spectra and coincidences, ^{186}Hg bands, shape coexistence 78−25156
^{205}Tl(α,3n), 35-51 MeV, ^{206}Bi high-spin states anal. 78−82368
Tl(α,xn)^{205}Bi, population of high spin states, γ and conversion electron spectra 77−30616
Tm decay, nucl. energy levels determ. of ^{157}Er and ^{155}Er *(French)* 77−57630
^{163}Tm decay, ^{163}Er excited state obs. 78−17146
^{163}Tm, high spin rot. levels, studied via ^{165}Ho(^{3}He,5n) and ^{165}Ho(α,6n) reactions 78−8722
^{165}Tm, levels excited by β-decay of ^{165}Yb 78−74334
^{169}Tm, anisotropic ang. correlation between γ-rays and K X-rays following internal conversion 77−6305
^{169}Tm, γ-ray transitions for level struct., obs. in ^{169}Yb electron capture decay 78−82307
^{169}Tm, high resolution meas. of anisotropic directional correl. between γ-rays and KX rays 80−32243
^{169}Tm, studied via ^{169}Tm(^{32}S,^{32}S$'\gamma$), EM props. of ground state rot. band 78−8726
^{170}Tm, precise γ-ray energies from radioactive decay 79−45525
^{171}Tm, 635.4 keV level props., mag. moment from γ ang. correl. meas. 78−13017
U gamma abundances 77−65270
U, multigroup time-dependent delayed γ-spectra from fission and activation 78−13184
U ore bodies, overburden effects correction in ground level radiometric surveys 79−88485
U, prospecting method, using Ra accumulation in animal thyroid glands, anal. 78−27853
U resource survey, NURAB system for processing neutron activated samples 79−11847
U well logging, gamma-ray spectra calc. using discrete ordinates transport code 79−53572
^{A}U(n,X), A=233, 235, thermal n, gamma spectra from capture, fission and fission products 80−37352
^{230}U decay chain, γ-ray single and coincidence meas., internal conversion spectra obs. 77−6319
^{232}U$\rightarrow$^{212}Pb decay chain, obs. of collective states fed by weak α-transitions 78−8786
^{233}U, gamma ray spectra of reactor fuels 80−42577
^{233}U, high-energy spin state obs. using Coulomb excitation 78−17102
^{235}U α decay and ^{231}Th β decay, γ-radiation study, energy level scheme *(Russian)* 78−17160
^{235}U fission product γ radiation for short irrad. times, energy distrib. 80−73929
^{235}U, radioactive series decay, computer simulation 80−102160
^{235}U/^{238}U isotopic ratio determination, by γ-ray spectroscopy 79−5240
^{235}U(γ, f), 12-70 MeV bremsstrahlung, product yields and γ-spectra 80−42716
^{235}U(n,f), thermal, fission product decay spectra calcs., comparison with expt. results 79−93674
^{235}U(n,γ)^{236}U, gamma-ray spectra study *(Russian)* 77−6392
^{238}U, neutron capture cross-section below 100 eV meas. 77−26680
^{238}U, radioactive series decay, computer simulation 80−102160
^{238}U, stat. model calcs. of neutron capture gamma-ray spectra 77−67742
^{238}U+^{40}Ar, Coulomb-nuclear interference for high spin states 78−46097
^{238}U(e,α)e$'$^{234}Th, cross section, α-spectra, γ-spectra of ^{234}Th decay 78−58262
^{238}U(n,f), second well gamma decay if subthreshold fission resonances 77−26800
^{238}U(n,γ), 2, 24 keV, resonance averaged γ-spectra, level and J^{π} appls. 80−37347
^{238}U(n,n$'\gamma$), 1.06 MeV, cross sections and γ spectra for various energy levels *(Russian)* 79−40883
V, A=52, 3, yrast decay schemes from heavy-ion fusion evaporation reactions 77−82854
^{50}V, half-life limits for β-decay and electron capture 77−79334
^{51}V, γ-strength function, γ-ray spectra, average resonance method from ^{50}Ti(p,γ) 80−9257

gamma-ray spectra continued
^{51}V(^{16}O,p2n), E=36-46 MeV, high-spin states in ^{64}Zn 78−33145
^{51}V(α,nγ)^{54}Mn, Doppler shift attenuation meas. of ^{54}Mn excited state lifetimes 78−17141
^{51}V(n,γ), circular polarisation, ang. distrib. meas. 80−32285
^{52}V, decay, γ-ray spectrum, energies and intensities, ^{52}Cr level scheme *(French)* 77−14066
W isotopes, A=182, 184, 186, Coulomb excitation with ^{4}He and ^{16}O ions 78−8839
W, produced in (^{16}O,xn) 78−37371
^{A}W, A=173, 175, high-spin states, single-particle structure 78−93922
^{182}W, level struct. determ. from (α,2nγ) and ^{182m}Re decay 77−41914
Xe, A=139, 140, ^{232}Th fission products, yields, γ-ray spectra 78−74410
Xe levels populated in ^{129}Cs, ^{133}I β decay energy level scheme, γ spectra meas. 77−2936
^{124}Xe, energy level scheme, ^{124}Cs decay 78−13033
^{127}Xe decay, absolute gamma-ray intensities 78−548
^{131}Xe, ang. correl. meas. of γ-γ cascades from ^{131}I decay 77−6292
^{136}Xe(n_{th},γ)^{137}Xe, spectra meas., ^{137}Xe level and decay scheme 78−13102
^{88}Y, gamma-ray intensities, precision meas. 80−102139
^{89}Y+^{40}Ar, 237 meV, γ-ray multiplicities and energies, primary fragment angular momenta 78−46093
^{89}Y(^{3}He, 3nγ), 20-28 MeV, in-beam γ-ray spectroscopy, ^{89}Nb levels determ. 77−41983
^{89}Y(^{40}Ar,X), 237 MeV, ang. momentum transfer in deep inelastic reactions 80−5156
^{100}Y, fission product, γ-spectra, half-life meas. 77−38240
^{171}Y populated in ^{171}Lu decay, level scheme, γ-transitions, spin-parity assignments 77−46133
^{90m}Y, ^{90g}Y decays, weak β transitions, γ-ray emission 77−34265
^{161}Yb, produced in (^{16}O, xn), γ-ray spectra, dipole moment in yrast cascade 78−37371
^{169}Yb, populated in ^{169}Lu decay, meas. of γ-ray and conversion electron spectra 80−22766
^{169}Yb populated in ^{169}Lu decay, γ-ray and conversion electron spectra 80−22767
^{169}Yb, precise γ-ray energies from radioactive decay 79−45525
^{172}Yb, β-decay of ^{172}Hf and ^{172}Lu 78−33140
^{174}Yb(^{32}S,^{32}S$'\gamma$), recoil distance lifetimes of ground state bands 78−8774
^{176}Yb(^{12}C,8n)^{180}Os, 120 MeV, continuous γ-ray spectra anal. 78−41747
^{176}Yb(d,xnγ), 14 MeV, gamma-ray spectra *(Russian)* 78−54720
^{176}Yb(d,xnγ), 14 MeV, γ-ray spectra angular distribs. and $\gamma\gamma$ coincidences 79−75838
^{176}Yb(p,xnγ), 66 MeV, γ-ray spectra angular distribs. and $\gamma\gamma$ coincidences 79−75838
^{176}Yb(p,xnγ), 6.6 MeV gamma-ray spectra *(Russian)* 78−54720
^{A}Zn(p,γ), A=64, 66, $g_{9/2}$ isobaric analogue resonances 79−63663
^{67}Zn, Coulomb excitation, gamma-ray spectra 79−9434
^{67}Zn, γ spectroscopy of low spin states from ^{64}N(α,nγ), 8.2 MeV 78−78303
^{67}Zn, populated in ^{64}Ni(α,n), level struct. below 2.0 MeV, γ-ray studies 78−62483
Zr (^{13}C, 3nγ), 45-56 MeV, collective and two-quasiparticle excitation in Pd 77−18601
Zr, A=86, 87, 88, high spin states 78−74383
^{A}Zr(n,n'γ), A=92, 94, 3-6 MeV, γ-ray prod. cross sections 77−26767
^{87}Zr, in-beam γ-ray spectroscopy of excited states 79−17852
^{89}Zr, electron capture to positron emission ratios determ. 77−18896
^{89}Zr high spin states, J values, γ ang. distrib. from (α, 2nγ) and (α, nγ) 79−89217
^{90}Zr, $\gamma\gamma$ directional correl. meas. 78−33144
^{90}Zr(n,γ)^{91}Zr, thermal neutron reactions, γ-ray line obs. 78−17190
^{91}Zr, nuclear reson. fluoresc., γ-ray spectra 78−588
^{91}Zr(p,nγ), 3.5-4.8 MeV, ^{91}Nb lifetimes, branching ratios, multipole mixing ratios 78−13011
^{92}Zr, gamma-gamma directional correl. study 78−29422
^{92}Zr(n,γ)^{93}Zr, thermal neutron reactions, γ-ray line obs. 78−17190
^{94}Zr, 2$^+$ state, recoiling in Fe, enhanced transient fields 78−37284
^{94}Zr(n,γ)^{95}Zr, thermal neutron reactions, γ-ray line obs. 78−17190
^{96}Zr(^{16}O, 4nγ), 56 MeV, γ yields, polarisations, ang. distribs., ^{108}Cd decay scheme 78−66301
^{96}Zr(n,γ)^{97}Zr, thermal neutron reactions, γ-ray line obs. 78−17190
^{98}Zr, level scheme determ. from β-decay of ^{98}Y 77−41934
^{100}Zr, fission product, γ-spectra, half-life meas. 77−38240
^{100}Zr, levels, J^{π} via ^{100}Y β-decay 77−82878

gamma-ray spectra of liquids and solids
see also Mossbauer effect
Allende, S content, neutron capture gamma-ray spectroscopy 80−94728
allowed β-γ angular correlations induced by mag. interactions 78−68419
angular correlation apparatus for materials science 77−74563
antiferroelectric structures, gamma-ray generation by fast electrons 78−76545
antiferromagnetic structures, gamma-ray generation by fast electrons 78−76545
biophysical appls. of perturbed gamma-ray angular correlations 78−44739
bremsstrahlung, secondary, generation by γ-quanta transport in matter *(Russian)* 77−63479
brute-force nuclear orientation 77−28452
channelled particles, emission of γ quanta *(Russian)* 79−8205
concrete, high-resolution gamma-ray spectra 77−50309
concrete, ultrasonic wave velocities and density, calc. and meas. 79−52545
crystal sources, geometrical coeffs. for interpretation of γ-ray perturbed angular correl. with quadrupole interactions 80−73109
crystals, electron spin correlation, gamma-ray and X-ray production 79−11486
diamond:^{111}In, ion implanted, intrinsic limitations of doping 80−34019
diamond:^{129}Xe, implanted, elec. quadrupole interaction, integral perturbed ang. correlation study 79−11364
diamond, channelled electrons, gamma emission 80−54293
diamond, channelling of 4.7 GeV electrons, γ-quanta yield *(Russian)* 79−69170
diamond, electron channelling, γ-ray spectra *(Russian)* 79−61280
diamond, electron channelling gamma-ray spectra 80−40023
diamond, implanted ^{129m}Xe, lattice location, combined Mossbauer and IPAC meas. 78−43733
diamond crystal, radiation of channelled 800 MeV electrons 79−61274
double γ-resonance, γ-ray scatt. 79−78593

gamma-ray spectra of liquids and solids continued
dual-parameter time and energy spectrometry for positron annihilation studies 77−34505
electric field gradient sign, possibility of obtaining from combined TDPAC and Mossbauer meas. 78−24907
electric field gradient sign, possibility of obtaining from combined TDPAC and Mossbauer meas. 78−24908
electric quadrupole interactions measured by nuclear orientation and NMR on oriented nuclei, review 80−92868
electron and positron relativistic channelled beams, X-ray and γ-ray emission 77−36304
electron gas, ang. correl. in positron annihilation 80−24821
enzyme, nucl. quadrupole interaction parameter related to structure-function 77−8472
ferromagnet:Ra, hyperfine field determ. 77−85622
fluorides, electric field gradient, time-differential-angular-distrib. method 80−60463
gamma resonance spectroscopy under HF excitation conditions, review 77−48113
generalised spin precession eqn., elec. quadrupole interaction sign 78−43744
graphite, electron channelling, γ-ray spectra *(Russian)* 79−61280
interference parameters in γ-ray optics 78−19395
intermediate state perturbation in low temperature nuclear orientation 80−97168
isomeric states, in-beam γ-NMR-PAD 77−59465
Knight shift for ions with $Z>83$ 77−12275
linear polarisation, elec. quadrupole interaction effects 77−12265
linear polarisation enhancement of bremsstrahlung in crystals, spin effects 79−11359
liquid metal, nucl. quad. relax. rate temp. depend. calcs. 77−12273
liquid metal targets, ^{71}Ge, ^{78}Br nuclear states, in-beam γ-NMR-PAD 77−59465
lunar rock, S content, neutron capture gamma-ray spectroscopy 80−94728
magnetic critical phenomena, hyperfine expts., selective review 78−43722
magnetic spin rotation in presence of weak quadrupole interactions 78−43345
metal, correlation of annealing temp. for radiation damage fields to melting point in DPAD expts. 78−43737
metal, positron annihilation, ang. correl. data analysis 78−52592
metalloenzyme, metal ion geometry and mechanism from PAC expts. 78−44449
metals, noncubic s-p, influence of impurities on solutes elec. field gradient 77−24770
metals, sp, elec. field gradient at ^{111}Cd, effects of high press., TDPAC meas. 80−25266
method and alloys, liquidus and solidus temperatures, determ. by γ-ray method 80−65193
molecular liquid, reorientation PAC, nonadiabatic effects 77−12274
Mossbauer effect-time dependent PAC technique, theory of combined method 79−28645
multipole transition, Hermitian intensity matrix 77−43911
neopentane, soln., positronium form. inhibition by organic iodide addition, momentum distrib. 77−90631
neutron activation analysis, gamma-ray spectra prediction, detection limits, computational procedure 78−85242
non-axially symmetric nuclear ensemble, gamma-ray emission, statistical tensors 79−95694
nuclear elec. coupling const. sign determ. from emitted γ-ray anisotropy meas. 77−12291
nuclear quadrupole alignment and low temp. systematics of elec, field gradients of ^{176}Lu^{m} and ^{177}Lu 79−78565
nuclear resonant Bragg scatt., symmetry radiant state 78−27122
ocean sediments, neutron activated, gamma-ray scanning for elemental profile distribs. 77−17079
ore Au content determ. 78−35076
PAC experiments with complex perturbations, effective X-ray anisotropy 77−48103
perovskite crystals, static and dynamic aspects of PAC meas. 78−88241
phase diagrams, construction, use of NMR, Mossbauer effect, and gamma ray perturbed angular correlation 79−8417
polyglutamic acid, helix-random coil transition observed by gamma-ray ang. correlation 78−80828
polyglutamic acid molecular dynamics in soln., γ-ray perturbed angular correl. 78−94960
positron annihilation, 2γ-annihilation radiation ang. correl., book contrib. 80−2893
positronium determination in matter, Compton profile comparison to γ-annihilation radiation ang. correlation *(Russian)* 77−55845
protein-solvent systems, dynamics investigation by nucl. gamma-resonance 79−62166
quantum beats from nuclei excited by synchrotron pulses 78−88239
radioactivation of shielding materials Fe, Benelex by fast neutrons, decay rates 79−682
rare earth, heavy, elec. field gradient, at ^{111}Cd impurities, temp. depend. 79−28642
rare earth alloys, $\mathrm{RIn_3(Sn_3)}$, ^{111}Cd quadrupole coupling consts. and valence states, PAC meas. 77−48102
rare earth ferromagnet, polarisation in external mag. fields, TDPAC 77−8462
rare earth garnets: $^{154}\mathrm{Gd}^{3+}$, hyperfine interactions, PAC 77−43909
recoil atoms of heavy ion reactions, local lattice damage, TDPAD meas. 80−84220
relaxation phenomena and magnetic hyperfine fields of isolated Ce ions in liquid and solid metals 80−108137
resonant γ-radiation, transmission through nonresonance absorber, time depend. *(Russian)* 79−19814
sea water, gamma-radiation from neutrons radiative capture rel. to chlorinity determ. *(Russian)* 78−77360
solid state studies, PAC method appls. *(German)* 80−2679
spin system orientation due to stimulated emission and absorpt. of radiation 77−52001
stochastic theories for hyperfine spectra in presence of relax. 78−43743
stratified crystal structs., strongly bound γ-rays 80−80895
stroboscopic resonance meas. of nucl. quadrupole interaction 77−85621
surface analysis, using SIMS, Mossbauer spectra and spectrometry 79−16050
symmetric ordered nuclear spin struct., gamma-ray emission at low temps. 79−95695

gamma-ray spectra of liquids and solids continued
TDPAC, appl. to chemistry and solid state physics, review 79−75665
TDPAC pattern depend. on principal axis orientation 80−39898
transferrin, ^{111}In labeled, perturbed angular correls. study 79−39342
transition metal, d-series, density of partially delocalised d electron from distrib. of γ-ray from positron-electron annihilation 79−14811
transition metal octahedral $(\mathrm{MeF_6})^4$, fluorine ion Sternheimer antishielding, PAC 78−10818
transition metal salts, antiferromag., ^{111}Cd hyperfine fields, PAC meas. 77−48104
ultrarelativistic particle radiation in cryst., γ-γ correlations obs. 80−71274
US modulation of γ-radiation 79−24249
vacancy induced hyperfine interaction detected by γ-ray PAD 77−43913
Ag alloy, dil., temp. depend. of elec. field gradient, impurity mass and conc. effects 78−48085
Ag, correlated radiation damage, TDPAC of ^{109}Cd and ^{113}Sn 78−43739
Ag host, electric field gradients created at ^{111}Cd nuclei by near neighbour impurities 78−39450
Ag, recoil implanted ^{111}In impurities, interaction with radiation damage, TDPAC meas. 79−11362
Ag, spin rotation amplitudes for ^{107}Cd and ^{109}Cd, comparison of temp. depend. 78−43738
Ag:^{111}Cd, hyperfine interaction, dose-rate depend. and annealing props. rel. to PAC obs. 77−27920
Ag-^{112}In, dil., ^{112}In nucl. alignment, radiation damage, γ-ray spectra 78−19398
Ag-Al(Ga) electric field gradient temp. depend., nearest neighbour impurity mass effect, TDPAC meas. 78−6612
Ag-Cd, dil., DPAD meas. on ^{107}Cd and ^{109}Cd, nucl. Larmor precession meas., role of hyperfine interactions 79−47363
Ag-Cu(Au)(Zn)(In)(Sn)(Bi), dil., elec. quadrupole interactions on ^{111}Cd probe nuclei, time differential PAC meas. 78−15066
Ag-Cu(Sn), dil. alloys, EFGs at impurities, ^{111}Cd TDPAC 77−16213
Ag-Cu(Zn)(In)(Sn)(Au), temp. depend. of elec. field gradient, TDPAC meas. 77−32304
Ag-In, dil., interaction between recoil implanted impurities and lattice defects, TDPAC meas. 78−39467
Ag-Mn, dil., nuclear orientation expts. 78−43713
Ag-Pd, dil., elec. field gradients due to Pd near neighbour configs., TDPAC obs. 78−19391
Ag-Pd, dil., elec. field gradient, conc. and temp. effects 78−68416
Ag-Pd(Pt), dil., electric field gradient temp. depend., TDPAC meas. 78−39451
Ag-Pd(Pt), dil., electric field gradient meas. by TDPAC method 78−39452
Ag-Pd(Pt), dil., TDPAC exam. of radiation damage 78−39464
Ag-Sn, dil., electric quadrupole interaction of ^{111}Cd probe nuclei, time depend. PAC 77−16229
$\mathrm{Ag_xAl_y}$, TDPAC meas. of ^{111}Cd 77−28492
$\mathrm{Ag_xCd_y}$, TDPAC meas. of ^{111}Cd 77−28492
$\mathrm{Ag_xZn_y}$, TDPAC meas. of ^{111}Cd 77−28492
Al, radiation damage with radioactive probes, TDPAC meas. 77−24336
Al:^{111}In, electron irrad., defect trapping at impurities 78−55892
Al-In, dil., vacancy trapping and detrapping at ^{111}In, PAC spectra 78−39461
Al-Y, dil., hyperfine interactions, ^{87}Y^{m} nuclear orientation meas. 78−43715
$\mathrm{Al_2La_xCe_{1-x}}$, low temp. mag. props. 80−20564
$^{27}\mathrm{Al}^{+}$ ion ranges in Ti(Ni)(Cu)(Mo)(Ag)(Ta)(W)(Au)(Pb), meas. by (p,γ) reson. broadening 79−46729
Au lattice location in Zn, gamma-spectral study 80−80227
Au-Ag-Cd, γ-ray PAC of ^{111}Cd, nearest neighbour contrib. to elec. field gradient 77−36161
Au-Fe, dil., contact charge density, internal conversion meas. 79−56630
Au-Mn, dil., ^{52}Mn γ-ray anisotropy down to 3 mK, Kondo and relax. effects 77−81034
Au-Mn, dil., nuclear orientation of recoil implanted ^{52}Mn 78−43716
Au-Mn(Cr)(Fe), dil., spin glass state and Kondo effect, nucl. orientation of ^{54}Mn 78−6514
Au-Y, dil., hyperfine interactions, ^{87}Y^{m} nuclear orientation meas. 78−43715
BN, ^{15}N zero point vibr. energy from nuclear photon scattering 80−59593
$\mathrm{BaCO_3}$, electric quadrupole interaction, TDPAC meas. 78−39455
$\mathrm{BaSO_4}$, electric quadrupole interaction, TDPAC meas. 78−39455
$\mathrm{BaTiO_3}$:Hf, crystal field distortion by stacking faults, PAC meas. 80−11306
Be, electric field gradients of recoil-implanted ^{19}F via ^{9}Be(^{12}C, np)^{19}F 77−8471
Be, quadrupole interaction for ^{100}Rh, ^{111}Cd, and ^{181}Ta, temp. depend. TDPAC obs. 77−20772
Be:^{100}Rh(^{111}Cd)(^{181}Ta), quadrupole interaction temp. depend. 77−8466
Be-Au, dil., quadrupole interactions and lattice location, ^{197}Hg TDPAC and Mossbauer expts. 78−43726
Be-Hg, dil., quadrupole interaction and lattice location for Hg 78−48086
Be-Ru, dil., quadrupole interactions at ^{99}Ru, TDPAC meas. 78−91996
$\mathrm{BeF_2}$ aqueous solns., mag. and quadrupole relax. 80−71226
$\mathrm{BeF_2}$, radiation induced defects, nuclear Hanle effect 78−43734
Bi, quadrupole interaction of ^{69}Ge, TDPAD expts. 78−48089
BiMn, ferromag., nucl. orientation of Bi isotopes 78−13010
$\mathrm{CaF_2}$, radiation induced defects, nuclear Hanle effect 78−43734
$\mathrm{CaHfO_3}$:Ta, electric field gradient temp. depend., TDPAC 77−20768
Cd complex, bis(thiosemicarbazide) Cd II sulphate, elec. field gradients, γ-ray PAC spectrosc. 79−65773
Cd conc. in kidney and liver, neutron activation anal., organ depth determ. 80−72321
Cd, electric field gradient press. depend., lattice vibrs. effect, PAC expts. 79−61267
Cd, lattice defects studied by gamma ray angular correlation 79−51895
Cd, quadrupole hyperfine interaction of ^{111}Cd, effect of radiation defect annealing 78−43741
Cd, quadrupole interaction of ^{107}Cd $11^{-}/2$ states 77−8468
Cd, quadrupole interaction for ^{129}I, ^{131}I, and ^{132}I, PAC expts. 78−48087
Cd:^{113}Sn, quadrupole interaction temp. depend. 77−8469
Cd:^{116}Sn, quadrupole interaction, radiation damage effects 78−43752
Cd:^{11x}Sn, (x=3-6,8), γ-ray spectra, quad. interaction, spin-rot. spectra 77−26571
Cd:^{67}Ge, elec. quadrupole interaction temp. depend., PAC meas. 79−42877

gamma-ray spectra of liquids and solids continued
Cd:^{67}Ge, quadrupole interaction temp. depend. 77−12264
Cd:^{67}Zn elec. quadrupole interaction temp. depend., PAC meas. 79−42877
Cd:^{99}Ru, quadrupole interaction temp. depend., PAC method, electric field gradients 77−73105
Cd-Hg, dil., anomalously high elec. field gradients below 0.05K 78−72442
Cd-perovskites, $CdXO_3$ (X=Ti,Zr,Hf,Sn), electric field gradient temp. depend. 78−39454
Cd-Sb, dil., loss of nucl. alignment of ^{115}Sb by radiation induced defects 78−43344
CdHg, electric field gradient temp. depend., TDPAD meas. 79−56647
$CdSiP_2$, PAC examination of deuteron irrad. damage, annealing effects 78−47446
$CdTiO_3$, perovskite, elec. quadrupole interactions, TDPAC meas. 78−31129
^{111}Cd, nucl. orientation coeffs. with axially symm. elec. field gradient 80−97168
Ce:^{143}Pr, mag. dipole moment of Pr 57 keV state, PAC meas. 77−46110
$Ce(NO_3)_3$:^{143}Pr, aqueous soln., mag. dipole moment of Pr 57 keV state, PAC meas. 77−46110
^{252}Cf, measured neutron and γ spectra in a tissue equivalent medium 80−3805
Co alloys, ferromag., 4d and 5d impurities, hyperfine fields 78−31133
Co, hyperfine mag. fields at ^{67}Ge, TDPAC meas. 78−43701
Co:Ga(Ge)(As), temp. anomalies of hyperfine fields 78−23265
Co:Lu, nuclear orientation meas., hyperfine field 77−32308
Co:Ra hyperfine field determ. 77−85622
Co-^{48}V, nucl. orientation of ^{48}V, γ-ray anisotropy obs. 80−97169
Co-Ru, dil., mag. hyperfine fields, TDPAC meas. 78−43702
CoO, paramag. shifts of ^{19}F at O 78−43719
$Co_{80}P_{20}$, amorphous, sign and magnitude of ^{60}Co hyperfine field, nucl. orientation 78−48100
Cr, antiferromag., mag. and non-mag. impurities, hyperfine interactions, ^{181}Ta and ^{100}Rh TDPAC meas. 78−43704
Cr, hyperfine interactions on ^{111}Cd-probe nuclei, TDPAC meas. 80−75904
Cr, spin density waves detected by Ta mag hyperfine field meas. 78−60364
Cr-Rh, dil., hyperfine fields meas. 79−47056
Cr-Ru, dil. absence of mag. hyperfine field, TDPAC meas. 80−50237
Cr-Ta, mixed SDW and Zeeman hyperfine interactions, TDPAC calc. 79−99797
$Cs_4Hf(C_2O_4)_4.nH_2O$, electric field gradient at metal site, γ-ray perturbed ang. correlation meas. 78−52380
^{137}Cs gamma-ray spectra of spherical reactor fuel elements, burn-up determ. *(German)* 78−25299
Cu, defect annealing around stage III, $\gamma\gamma$ ang. correlation expt. 79−14846
Cu, implanted ^{222}Rn TIPAC measurements 78−43732
Cu, ion-irradiated, impurity defect configuration, by DPAC-technique with ^{111}In 79−28021
Cu monocrystals, positron annihilation quanta ang. correl., point defect effects 77−76729
Cu, radiation damage with radioactive probes, TDPAC meas. 77−24336
Cu, radiation damaged, elec. field gradient, temp. depend. 78−39481
Cu, radiation damaged, temp. depend. of elec. field gradient, DPAC expt. 78−43727
Cu:^{69}Ge(^{67}Zn), nucl. alignment temp. depend. rel. to radiation damage during PAC obs. 77−27919
Cu-In, dil., point defect trapping after ion implantation, DPAC meas. 78−43728
Cu-Mn Kondo system, ^{54}Mn nucl. orientation 78−68421
Cu-Pd, dil, perturbed angular correlation exam. of Pd impurity, ^{111}Cd probe 79−78588
Cu-Rh (0.5 at.%), nucl. quad. relax. 79−82898
Cu_2MnSn(In), Heusler alloy, hyperfine field at ^{111}Cd, TDPAC meas. 78−43705
Dy:^{111}Cd(^{177}Hf), polycryst. ferromag., impurity hyperfine field polarisation, TDPAC and IPAC 77−73106
Dy:^{181}Ta, ferro- and antiferromag. phases, temp. depend. of mag. hyperfine field, TDPAC obs. 77−36165
Dy-Ta, dil., elec. field gradient at ^{181}Ta, temp. depend., TDPAC meas. 79−95689
Er-Ta, dil., elec. field gradient at ^{181}Ta, temp. depend., TDPAC meas. 79−95689
Er-Ta, dil., mag. hyperfine field determ., TOPAC meas. 79−91330
EuO:Sm^{3+}, hyperfine field at Sm, TDPAC meas. 80−93215
Fe, ^{56}Fe recoil, PAC, enhanced transient fields 77−15802
Fe aerosols in atmosphere, source determ. 77−41235
Fe alloys, ferromag., 4d and 5d impurities, hyperfine fields 78−31133
Fe, dynamic exponent, crossover obs., TDPAC Meas. 80−108021
Fe, effective mag. fields near ^{238,240}Pu and ^{248}Cm, PAC obs. *(Russian)* 77−4593
Fe, ferromag., transient mag. field for ^{13}C 79−47362
Fe, ferromagnetic, temp. depend. of hyperfine fields for F 80−20141
Fe foil, hyperfine interactions of implanted reaction products 78−48093
Fe, gamma fields induced by ^{252}Cf neutrons 78−50240
Fe, hyperfine mag. fields at ^{67}Ge, TDPAC meas. 78−43701
Fe, implantation of ^{197m}Hg, NMR of oriented nuclei 77−81020
Fe, mag. hyperfine field of K, Ca and Ti, TDPAD meas. 78−52389
Fe, magnetic hyperfine fields of Zr, DPAD meas. 80−39901
Fe, magnetic transient fields at N and O nuclei recoiling in external mag. field 77−12263
Fe, magnetised, nature of dynamic mag. fields acting on ^{82}Se, ^{56}Fe and ^{28}Si, gamma-ray spectra meas. 78−43697
Fe, nuclear orientation-mag. reson. of ^{48}V 79−61288
Fe, polarised, ferromag., evidence for K-shell polarisation of ^{12}C ions via mol. orbital promotion 80−71273
Fe, polarised, high vel. ion recoil, transient mag. fields 77−43910
Fe radiative detection of single- and multiple-pulse mag. reson. of oriented ^{60}Co radioactive nuclei 77−66437
Fe, stimulated spin echo obs. of oriented ^{60}Co nuclei 79−65780
Fe, transient mag. field, vel. and atomic number depend. 78−91999
Fe, transient magnetic field velocity and Z depend. 80−39904
Fe, transient magnetic low velocity field 80−80642
Fe, triple pulse reson. studies of ^{60}Co nuclei 78−43675
Fe:^{103m}Rh, γ-detected NMR of 40 keV metastable state, 0.5 to 14 kG external fields 77−59499

gamma-ray spectra of liquids and solids continued
Fe:^{105}Rh(^{95}Tc), nuclear orientation of nuclei, anisotropy of gamma-ray emission 77−46111
Fe:^{106}Rh, nuclear orientation and mag. moment 77−85623
Fe:^{110}In, nucl. orientation, nucl. mag. moment, γ-ray spectra 77−28485
Fe:^{119m}Te, mag. moment, nucl. orientation, γ-ray spectra 77−28486
Fe:^{12}C(2_1^+), PAC meas. of transient mag. fields 79−99800
Fe:^{131}Xe, negative parity states, nucl. orientation, γ-ray spectra 77−28487
Fe:^{169}Yb, hyperfine field of implanted Yb, annealing temp. depend., PAC meas. 77−48100
Fe:^{172}Yb, hyperfine mag. field, TDPAC meas. 78−52394
Fe:^{198}Hg, combined lattice-location hyperfine-interaction expt. on implanted Hg 77−20752
Fe:^{220}Rn(^{222}Rn), combined elec. quad. and mag. interaction, PAC 77−16214
Fe:^{60} Co, nucl. orientation-pulsed NMR obs., γ-radiation anisotropy 77−59490
Fe:^{82}Br, nucl. orientation 77−59486
Fe:^{93,94}Tc, γ-ray spectra, nucl. mag. moment determ. 77−28484
Fe:F, F lattice location, channelling and proton-induced nuclear reaction obs. 77−59041
Fe:K(Ar), mag. hyperfine interaction, temp. depend. 78−68420
Fe:Lu, nuclear orientation meas., hyperfine field 77−32308
Fe:Ra, hyperfine field determ. 77−85622
Fe:Xe, gyromagnetic ratios of first 2^+ states in Xe, implantation PAC 78−12966
Fe:Yb,O, interaction between impurities, perturbed ang. correlation meas. 77−1628
Fe-^{48}V, nucl. orientation of ^{48}V, γ-ray anisotropy obs. and NMR meas. 80−97169
Fe-Co-Cd(Sn), mag. hyperfine fields at Fe, Cd and Sn sites, Mossbauer and TDPAC meas. 78−60363
Fe-K(Ca)(Ti), dil., mag. hyperfine field, TDPAC meas. 78−43699
Fe-Ni alloy, disordered, short-range order study by time-depend. PAC method 78−6618
Fe-Y, dil., hyperfine interactions, $^{87}Y^m$ nuclear orientation meas. 78−43715
Fe_3C, cementite, modified by rare earth metal and alloying additions, thermal stability *(Russian)* 78−56663
$FeSn_2$, hyperfine mag. fields at ^{57}Fe, ^{119}Sn nuclei, under press. *(Russian)* 78−39486
^{57}Fe, Mossbauer effect-time dependent PAC technique, theory of combined method 79−28645
Ga amorphous film, elec. field gradient 80−25264
Ga, liq., Knight shift of ^{69}Ge 77−12271
Ga, orthorhombic, quadrupole interaction of $9^+/2$ states of ^{71}As and ^{73}As 77−8467
GaAS, positron annihilation, deep acceptor level props. 79−11485
GaIn, liq. alloys quad. relax. rates, 3-particle correls., ^{71}Ga and ^{115}Sn 77−12272
Gd, ^{161}Dy TDPAC, hard core correl. 78−10809
Gd alloys, ferromag., 4d and 5d impurities, hyperfine fields 78−31133
Gd, ferromag., transient mag. fields at stopping nuclei, stopping power 78−34555
Gd, ferromag., vel.- and Z-depend. of transient mag. fields 78−43698
Gd ferromagnet, enhanced transient fields acting on fast Gd nuclei 77−90081
Gd, ferromagnetic, temp. depend. of hyperfine fields for F 80−20141
Gd host matrix, hyperfine interaction of ^{188}Os, temp. depend. 78−48102
Gd, magnetic transient hyperfine fields, IMPAC obs. 77−8464
Gd, magnetised, nature of dynamic mag. fields acting on ^{82}Se, gamma-ray spectra meas. 78−43697
Gd:^{160}Tb, hyperfine interaction for ^{160}Tb *(Russian)* 77−63347
Gd:^{177}Hf, polycryst. ferromag., impurity hyperfine field polarisation, IPAC 77−73106
Gd:^{75}As, mag. hyperfine field determ. by PAC 77−8459
Gd:Ra, hyperfine field determ. 77−85622
Gd-Hg, dil., mag. hyperfine field, TDPAC meas. 78−52414
Gd-Sc, dil. alloy, ferromag. hyperfine field determ. 77−43919
Gd-Ta, dil., elec. field gradient at ^{181}Ta, temp. depend., TDPAC meas. 79−95689
Gd-Ta, dil., mag. hyperfine field and elec. field gradient at ^{181}Ta impurities, TDPAC meas. 79−47361
Gd_2O_3, ^{161}Dy TDPAC, hard core correl. 78−10809
$GdZrFe_2$, hyperfine field at Gd, TDPAC meas. 80−93214
Ge, α-particle damage, quadrupole nucl. interactions on ^{73}A nuclei, TDPAC meas. 77−36160
H_3PO_4-H_2O, superviscous and glass, relax., ^{111}Cd TDPAC obs. 80−15831
Hf complex, Hf-EDTA 80−34837
Hf complex, tetrakis (tropolonato) hafnium (IV), mol. interactions in solid, perturbed γ-γ ang. correl. obs. *(French)* 79−8076
Hf complex, with N-benzoyl N-phenyl hydroxylamine, mol. reorientation in soln. 77−16218
Hf-Ta, dil., hydrostatic and uniaxial compression, elec. field gradient at Ta, time differential PAC meas. 77−69739
HfC:Ta, perturbed ang. correlation spectra, elec. quadrupole interaction 80−15916
$HfCo_2$:Ta, perturbed ang. correlation spectra, elec. quadrupole interaction 80−15916
$HfFe_2$:Ta, perturbed ang. correlation spectra, elec. quadrupole interaction 80−15916
$HfGeO_4$, nuclear quadrupole interactions, TPDAC meas. 79−82902
HfNi, hyperfine critical exponents, TDPAC meas. of bulk meas. 77−8465
HfO_2, chem. induced elec. field gradient, perturbed ang. correl. obs. 78−80257
HfO_2-CaO(MgO) elec. field gradient at ^{181}Ta, TDPAC meas. 79−33577
$HfOCl_2$, aqueous solns., rotational diffusion, TDPAC study 80−34837
$HfO(H_2PO_4)_2.H_2O$, chem. induced elec. field gradient, perturbed ang. correl. obs. 78−80257
HfP_2O_7, chem. induced elec. field gradient, perturbed ang. correl. obs. 78−80257
$Hf(SO_4)_2$, elec. quadrupole interaction, TDPAC technique, coincidence system 80−93216
HfV_2O_7:^{181}Ta, EFG temp. depend., TDPAC 77−59488
Hf_xZr_{1-x}, elec. quadrupole interactions at ^{181}Ta impurities, TDPAC meas. 78−76364
Hg electric field gradients at different Be lattice sites, gamma-spectral study 80−80224

gamma-ray spectra of liquids and solids continued
Hg, quadrupole interactions in Zn, lattice location, gamma spectral study 80—80227
Ho, ^{111}Cd impurity electric quadrupole interaction temp. depend. 80—39900
^{165}Ho:^{166}Ho^{m}, gamma-ray emission from oriented nuclei in multiaxis nucl. spin system 79—82905
Ho-Au, dil., hyperfine interaction of Ho^{3+}, nuclear orientation expts. 78—43717
Ho-Ta, dil., elec. field gradient at ^{181}Ta, temp. depend., TDPAC meas. 79—95689
Ho-Ta, dil., mag. hyperfine field determ., TOPAC meas. 79—91330
HoVO$_4$, below 1K, nuclear orientation study of Van Vleck enhanced nuclear antiferromagnet 80—88899
^{181}Ho-^{181}Ta, dil., elec. field gradient at impurity, anomalous temp. depend., host 4f levels, γ-γ correls. 78—95272
In complexes, formation in aq. solutions, perturbed γ-ray directional correlation 77—12847
In, liq., PAC of ^{111}Cd 77—4584
In, nuclear quadrupole alignment of ^{114}In^{m} 78—48090
In, quadrupole interaction of ^{69}Ge, TDPAD expts. 78—48089
In:^{67}Ge, elec. quadrupole interaction temp. depend., PAC meas. 79—42877
In-Ag, dil., TDPAC technique appl. to diffusion model 79—78589
In-Bi alloy, liq., PAC of ^{111}Cd 77—4584
In-Cd, dil., elec. field gradient at Cd impurities, press. depend., TDPAC meas. 78—64302
In-Sb alloys, liq., spin relax. of ^{117}Sb and ^{115}Sn 77—16216
In-Te, elec. field gradient, at ^{111}Cd probes, temp. depend. 79—28643
In-Te, liq., nucl. spin relax. of ^{117}Sb 77—52004
InBi, quadrupole interaction precession frequency of ^{111}Cd, TDPAC meas. 77—16224
In$_2$Bi, quadrupole interaction precession frequency of ^{111}Cd, TDPAC meas. 77—16224
InP, recoil damage obs. by PAC with ^{111}Cd 77—89484
InSb, recoil damage obs. by PAC with ^{111}Cd 77—89484
In$_{1-x}$Sb$_x$, liquid, nucl. quadrupole relax. of Sb, time depend. PAD meas. 77—43899
^{111}In, nucl. orientation coeffs., nucl. mag. moment 80—97168
K content in natural samples, γ spectrometric determ. *(Russian)* 78—92562
KCl, delocalised positronium, 4.2K, direct obs. γ-spectra 78—88235
K$_4$Hf(C$_2$O$_4$)$_4$.nH$_2$O, electric field gradient at metal site, γ-ray perturbed ang. correlation meas. 78—52380
K$_3$HfF$_7$:^{181}Ta, elec. quad. interac., DPAC 77—32299
(La,Th)-Ce, dilute alloys, mag.-nonmag. transition of impurity moments, environment effects 77—40034
La:Eu^{2+}, liquid, γ-ray spectra observation of exchange interaction 80—84672
La$_{1-x}$Y$_x$ alloys, PAC obs. of hyperfine field fluctuation at ^{140}Ce, Kondo effect interpret. 77—20761
Lu, electric field gradient, at ^{181}Ta substitutional atoms, pressure dependence 78—52385
Lu, nuclear quadrupole alignment of ^{177}Lu 78—48090
Mg, quadrupole interaction of ^{181}Ta, gamma-spectral study 80—80228
MgO:Al^{3+}, positron annihilation meas. 77—8681
Mn-Tb, dil., hyperfine interactions, nuclear orientation 80—15929
MnCl$_2$.4H$_2$O, single cryst., mag. phases, obs. by ^{54}Mn nucl. polarisation 77—81031
MnO, ^{19}F isomer shift, time differential PAD 77—12280
Mo, deformed, ^{57}Fe doped, positron annihilation exam. 79—15556
Mo, irrad., defect configurations, PAC study 79—86817
Mo-Ni-Fe-Co-Zn alloys, Ni, Fe, Co and Zn distrib. using neutron-activation anal. 79—52531
MoO$_3$, electric quadrupole interaction, TDPAC meas. 78—39455
^{15}N$_2$ monolayer, adsorbed on Grafoil, reson. photon scatt. 80—34832
NH$_4$Cl, ^{15}N zero point vibr. energy from nuclear photon scattering 80—59593
(NH$_4$)$_4$Hf(C$_2$O$_4$)$_4$.nH$_2$O, electric field gradient at metal site, γ-ray perturbed ang. correlation meas. 78—52380
(NH$_4$)$_3$HfF$_7$, longitudinal decoupling of quadrupole interaction 78—39456
Na estimation in cotton clothing for use in neutron activation dosimetry 80—47729
Na$_4$Hf(C$_2$O$_4$)$_4$.nH$_2$O, electric field gradient at metal site, γ-ray perturbed ang. correlation meas. 78—52380
NaNO$_3$, N atom velocity, NO$_3{}^-$ vib. and orientation, nucl. reson. photon scatt. 78—68433
^{95}Nb, beta decay, K-shell electron ejection 77—18888
Ni alloys, dil., hyperfine field distribs., DPAC meas. 80—93222
Ni alloys, ferromag., 4d and 5d impurities, hyperfine fields 78—31133
Ni, critical exponent β for hyperfine fields, PAD techniques 78—19403
Ni, critical exponent meas. by PAC in Ni-^{100}Rh 77—20774
Ni dynamic exponent, crossover obs., TDPAC meas. 80—108021
Ni, ferromagnetic, temp. depend. of hyperfine fields for F 80—20141
Ni, hyperfine mag. fields at ^{67}Ge, TDPAC meas. 78—43701
Ni, lattice defect symmetry, time differential PAC meas. 78—15069
Ni, mag. hyperfine field at ^{140}Ce, TDPAC meas. 79—11363
Ni, magnetic hyperfine fields of Zr, DPAD meas. 80—39901
Ni, polarised, ferromag., evidence for K-shell polarisation of ^{12}C ions via mol. orbital promotion 80—71273
Ni quadrupole interaction of vacancy associated with Te impurity, β-γ TDPAC meas. 78—43730
Ni, self implantation damaged, crit. behaviour, perturbed ang. distrib. meas. anal. 80—60476
Ni:^{111}In, ion implantation damage, DPAC obs. 77—59052
Ni:^{172}Yb, hyperfine mag. field, TDPAC meas. 78—52394
Ni:^{192}Ir, NMR/ON, resonant freq. shift with applied field 77—28462
Ni:^{86}Y, mag. hyperfine field determ. by DPAC 77—8458
Ni:Cu, ^{62}Cu 390 keV state, ferromag. effect, spin assignment 77—2903
Ni:F, F lattice location, channelling and proton-induced nuclear reaction obs. 77—59041
Ni:F, ion-implanted, mag. hyperfine field, anomalous temp. depend., PAC meas. 79—4754
Ni:Lu, nuclear orientation meas., hyperfine field 77—32308
Ni:Ra hyperfine field determ. 77—85622
Ni-As, dil., temp. depend. of hyperfine field, TDPAD meas. 78—43700
Ni-Cu(Zn)(In), implantation damaged, crit. behaviour, perturbed ang. distrib. meas. anal. 80—60476
Ni-H, implanted film, resistivity and TDPAC meas. 78—39229
Ni-In, dil., symmetry of lattice defect, DPAC meas. 78—43729

gamma-ray spectra of liquids and solids continued
Ni-In, dil., uncorrelated radiation damage, TDPAC meas. 78—43343
Ni-In, elec. field gradient, at ^{111}Cd probes, temp. depend. 79—28643
Ni-In, ion-implanted, impurity defect interaction and diffusion, Rutherford backscatter and TDPAC expts. 80—34039
Ni-Ta, dil., crit. behaviour, ^{181}Ta PAC expt. 78—43723
Ni-Ta, dil., crit. behaviour of local magnetization, PAC and magnetisation meas. 78—48098
NiMnSb, hyperfine mag. field at Cd impurity, TDPAC study 80—39906
Ni$_{1+x}$MnSb, mag. hyperfine field on ^{111}Cd, TDPAC obs. 78—43709
Ni$_2$MnSn(In)(Sb), Heusler alloy, hyperfine field at ^{111}Cd, TDPAC meas. 78—43705
NiO, paramag. shifts of ^{19}F at O 78—43719
NiO:^{67}Zn, perturbed ang. correl. 78—95535
Pb, elastic scatt. cross section for 279 keV γ-rays 79—26421
Pb, energy of form. of monovacancies, positron annihilation obs. *(German)* 78—71721
Pb, liq., mag. relax. of excited ^{207}Bi 77—16217
Pb, perturbed angular distribution of ^{208}Po, temp. depend. 78—43735
Pb, perturbed γ-ray angular distrib. of ^{210}Po, temp. depend., radiation damage effects 78—43736
Pb-foiled plastic scintillator, γ-ray meas. *(Japanese)* 77—57825
Pb$_{1-x}$Ba$_x$ZrO$_3$, electric quadrupole interaction meas., by PAC 77—4591
PbHfO$_3$, elec. field gradient, crit. behaviour, DPAC meas. 78—80303
PbHfO$_3$, elec. quadrupole interaction, temp. depend., DPAC meas. 79—51884
PbZr$_{1-x}$Hf$_x$O$_3$, crystal field distortion by impurities, PAC meas. 80—11306
Pd, localised vacancies produced by thermal neutron capture recoil 78—26598
Pd:^{111}Cd, radiation damage in DPAD expts., quad. interaction 77—27917
Pd$_x$H-^{54}Mn, dil., nucl. orientation of ^{54}Mn 77—12257
Pd$_2$MnIn(Sn)(Sb), Cd impurities, hyperfine field meas. 78—15074
Pd$_{1+x}$MnSb Heusler alloys, magnetic hyperfine fields on ^{111}Cd, TDPAC and magnetisation meas. 80—93219
Pd$_2$MnSb and PdMnSb, Heusler alloy, hyperfine field at ^{111}Cd, TDPAC meas. 78—43705
Pd$_2$MnSn$_{1-y}$Sb$_y$-Cd, dil., Heusler alloy, hyperfine mag. field on Cd, TDPAC obs. 79—8075
PrIn$_3$, nucl. orientation of ^{144}Pm in singlet ground state, exchange interaction and cryst. field splitting obs. 80—71275
Pt, radiation damage with radioactive probes, TDPAC meas. 77—24336
Pt, s-electron densities at nucleus, meas. using internal conversion of 31 keV M1 transition in ^{195}Pt^{m} 78—27140
Pt:^{181}Ta, lattice defect induced elec. field gradient, PAC meas. 79—42878
Pt-^{95}Nb, nuclear orientation meas. 79—65644
Pt-In, dil., damage induced quadrupole interactions, DPAC exam. 78—39465
Pt-In, dil., radiation damage heating, TDPAC exam. 78—39466
Pt-Mn, dil., nuclear orientation exam. 79—61171
PtMnSb, hyperfine mag. field at Cd impurity, TDPAC study 80—39906
PtMnSn(Sb), Cd impurities, hyperfine field meas. 78—15074
Pu, determ. in soln., on-line γ-ray spectrometric meas. 79—11872
Pu, K-absorption edge energy, accurate determ. using γ attenuation 77—59642
Ra content in natural samples, γ spectrometric determ. *(Russian)* 78—92562
Rb, liq., nuclear spin relax. of 13.9 msec ^{88m}Y 77—12270
Rb$_4$Hf(C$_2$O$_4$)$_4$.nH$_2$O, electric field gradient at metal site, γ-ray perturbed ang. correlation meas. 78—52380
Re, nuclear quadrupole alignment of ^{183,184,186,188}Re in single cryst. at low temps. 78—48091
Re-Hg, dil., anomalously high elec. field gradients below 0.05K 78—72442
Rh$_2$MnGe, ferromag. Heusler alloy, hyperfine mag. field meas. by TDPAC technique 79—78580
Rh$_2$MnGe(Pb), hyperfine mag. field at Cd impurity, TDPAC study 80—39905
Rh$_2$MnSn, ferromag., mag. hyperfine fields, time differential PAC meas. 77—81040
Rh$_2$MnSn, ferromag. Heusler alloy, hyperfine mag. field meas. by TDPAC technique 79—78580
Rh$_2$MnSn, mag. hyperfine fields at Rh and Sn sites, and their temp. depend. 78—43708
Sb, quadrupole interaction of ^{69}Ge, TDPAD expts. 78—48089
Sb:^{111}Cd, quad. interac. temp. depend. 77—59487
Sb:Cd, electric field gradient temp. depend. for ^{111}Cd 79—51894
Sb-Hg, quadrupole interaction, time differential perturbed ang. correl. and nucl. orientation 79—24250
SbSn, ^{120}Sb elec. quadrupole interaction, temp. depend. 78—19399
Sc, Compton profile, electron momentum distrib., renormalised free atom model 77—1756
Sc, electric field gradient of ^{181}Ta substitutional atoms, press. depend. 78—52385
Sc-Ru, elec. field gradient and temp. depend. TDPAC meas. 80—60477
Se:Cd dilute liquid, perturbed ang.-correl. meas. of motional-correl. time 79—41930
Si, (p,γ) resonance broadening method 80—24646
Si, implanted ^{222}Rn TIPAC measurements 78—43732
Si, neutron transmutation doping, ^{31}P conc. meas. 80—19833
Si, relativistic electron channelling spectra 10-130 keV 80—24516
Si:In, clustering and precipitation, time-dependent perturbed ang. correlation meas. 80—65234
Si:In, ion implanted, annealing behaviour, time differential PAC obs. 77—89455
SiO$_2$, implanted ^{222}Rn TIPAC measurements 78—43732
Sm-Eu alloy, dil., mag. and elec. hyperfine interac., TDPAD obs., paramag. behaviour, exchange integral 80—103908
Sn, ^{69}Ge TDPAD, search for isotopic mass effect on quadrupole coupling consts. 78—43725
Sn, elastic scatt. cross section for 279 keV γ-rays 79—26421
Sn, elec. field gradient on Cd, press. depend., TDPAC expts. 78—48092
Sn, electric field gradients of recoil-implanted ^{19}F via ^{9}Be(^{12}C, np)^{19}F 77—8471
Sn, liq., quad. relax. of ^{114}Sb impurities 77—16215
Sn, quadrupole interaction of ^{69}Ge, TDPAD expts. 78—48089
Sn:^{114}Sb, PAC, mag. moment of 8^{-}, 210 μs state of ^{114}Sn 77—26609
Sn:^{117}In, quadrupole interaction temp. depend. 77—8470

gamma-ray spectra of liquids and solids continued
Sn:^{120}Sb, elec. qudrupole interaction, perturbed ang. distrib. method 79−99799
Sn:^{67}Ge, elec. quadrupole interaction temp. depend., PAC meas. 79−42877
Sn:^{67}Ge, quadrupole interaction temp. depend. 77−12264
Sn:^{99}Ru, quadrupole interaction temp. depend., PAC method, electric field gradients 77−73105
SrTiO$_3$:^{181}Ta, quadrupole interaction, $\gamma\gamma$ cascade PAC meas. 77−81042
Ta, elastic scatt. cross section for 279 keV γ-rays 79−26421
TaS$_2$, 2H polytype, Li intercolation kinetics PAC hyperfine spectrosc. 79−87337
TaS$_2$ intercalated with NH$_3$, charge transfer, PAC meas. 78−76366
TaS$_2$, TDPAC meas., CDW, structural and charge transfer effects 78−39468
TaS$_3$(1T), inequivalent lattice sites in charge density distorted phases 80−15835
TaS$_2$(1T)(2H), nucl. quadrupole interactions, high press. effects 78−35072
Tb-Ta(Cd), elec. quadrupole interaction, temp. and press. depend., TDPAC meas. 80−60469
TbFeO$_3$ static effective mag. field acting on ^{160}Dy nucleus 77−90074
TbO$_2$:Dy^{3+}, mag. hyperfine interaction, PAC expt. 78−35069
TbSi$_2$, γ-γ ang. correl. obs. of polymorphic transition, 200-900°C 80−29653
^{99m}Tc, point source depth, meas. from γ-ray spectra 79−39492
Te, elec. field gradient and lattice location of Sn, TDPAC and Mossbauer effect meas. 78−52395
Te, quadrupole interaction for ^{129}I, ^{131}I, and ^{132}I, PAC expts. 78−48087
Te, quadrupole interaction of 81 keV state of ^{133}Cs and 247 keV state of ^{111}Cd, TDPAC expts. 78−48088
Te:^{111}Cd, quad. interac. temp. depend. 77−63324
Te:^{125}Te, PAC, quad. moment of $9/2^{-}$, 321 keV level of $_{52}{}^{125}$Te$_{73}$ 77−28488
Te:Ta, quadrupole interaction at ^{181}Ta, TDPAC meas. 80−20521
TeSn, ^{115}Te elec. quadrupole interaction, temp. depend. 78−19399
Th content in natural samples, γ spectrometric determ. *(Russian)* 78−92562
Ti, deform. and H$_2$ inclusion effect on annihilation γ-ray ang. correl. curve shape 78−31273
Ti:^{57}Fe, quadrupole interaction, Mossbauer and PAC meas. 77−48101
TiO$_2$:^{44}Sc, gamma-gamma directional correlation 77−20775
Tl, liq., mag. relax. of excited ^{207}Bi 77−16217
Tl, quadrupole interaction of ^{69}Ge, TDPAD expts. 78−48089
Tl-Cd, dil., quadrupole interaction, γ-γ ang. correl. meas. 79−56629
U, assay in fuel rods, by passive gamma-ray spectrometry 78−92576
U content in natural samples, γ spectrometric determ. *(Russian)* 78−92562
U, electric field gradient, of ^{181}Ta substitutional atoms, press. depend. 78−52385
U$_3$O$_8$ enrichment standards, gamma-ray spectra 80−78378
^{235}U, nondestructive determ. of content in fuel elements using passive gamma ray spectrometry 80−18418
WC recoil implantation damage, PAC obs. 77−85620
WO$_3$, recoil implantation damage PAC obs. 77−85620
Y-Cd, dil., electric field gradient, γ-ray ang. correl. meas. 79−56632
Y-Ru, elec. field gradient and temp. depend. TDPAC meas. 80−60477
YIG:Gd^{3+}, mag. relax., hyperfine field interactions, PAC expts. 78−27128
Zn, EFG sign at ^{69m}Zn site 77−59492
Zn, elec. field gradient on Cd, press. depend., TDPAC expts. 78−48092
Zn, electric field gradients of recoil-implanted ^{19}F via ^{9}Be(^{12}C, np)^{19}F 77−8471
Zn, nuclear quadrupole alignment of ^{69}Zn^{m} 78−48090
Zn, positron annihilation, external electric field effect on ang. distribs. 77−77317
Zn, quadrupole interaction of ^{67}Ge and ^{71}Ge, TDPAC meas. 78−43740
Zn, quadrupole interaction for ^{129}I, ^{131}I, and ^{132}I, PAC expts. 78−48087
Zn, quadrupole interaction at ^{181}Ta, TDPAC meas. 78−52392
Zn:^{115}In, 828 keV state, elec. quadrupole interaction meas. 77−8484
Zn:^{67}Ge, elec. quadrupole interaction temp. depend., PAC meas. 79−42877
Zn:^{67}Ge, quadrupole interaction temp. depend. 77−12264
Zn:^{69}Ge, quad. interac., rad. damage effs. during PAC obs. 77−27918
Zn:^{99}Ru, quadrupole interaction temp. depend., PAC method, electric field gradients 77−73105
Zn-^{54}Mn, nuclear orientation meas. 79−65644
Zn-Ag, dil., elec. field gradient, temp. depend. 78−39481
Zn-Hg, dil., anomalously high elec. field gradients below 0.05K 78−72442
(Zr,Hf)Fe$_2$, mag. hyperfine field at Hf sites, TPDAC meas. 79−82901
Zr, elastic scatt. cross section for 279 keV γ-rays 79−26421
ω-Zr, electric field gradients at substitutional Ta atoms, TDPAC high-pressure study 78−52384
ZrH$_{1.97}$, FCT, elec. quadrupole interaction at ^{181}Ta, TDPAC obs., 20-588K 79−33574

gamma-ray spectrometers
see also gamma-ray spectra
$4\pi\beta$(CP)-γ coinc. counter for radioactive source calibration 77−38545
412 keV Compton spectrometer 80−14037
airborne, effect of altitude on calibration constants 80−18754
annihilation photon ang. distrib. meas., spectrom. control unit 79−49890
annihilation photon energy spectroscopy, stability problems 80−29821
anti-Compton spectrometer with Ge(Li) semiconductor detector 79−26804
artificial satellite gamma telescope, Kosmos-461 79−97480
automated complex, Mossbauer spectra information retrieval and processing *(Russian)* 78−82091
automated correlation spectrometer with two Ge(Li) detectors 78−82562
benchmark γ-spectrometry, unfolding codes 79−26802
body radioactivity measurement, SABRE 3 computer system 78−85425
burnup meter for fast reactor fuels using γ-ray spectrometer with minicomputer *(Japanese)* 77−50206
calibration problems in automatic processing of gamma spectra obtained with Ge(Li) detectors *(Rumanian)* 80−5431
CAMAC system for use in gamma spectroscopy system 78−37531
Cherenkov multichannel spectrom., energy reconstruction of events 79−76259
Cherenkov shower total absorption spectrometer 77−46448
coal 79−48015

gamma-ray spectrometers continued
collimator system, for high intensity, accurate Compton profile meas., construction 78−90013
Compton polarimeter for gamma rays 79−76317
Compton recoil gamma-ray spectroscopy, current status 80−47808
Compton scatt. studies and spectrometers 79−74014
Compton spectrometer, study of electron densities in solids 80−18059
Compton spectrometer for elec. momentum density studies 79−21885
Compton suppression spectrom. for in-beam gamma-ray spectrometry 79−76261
Compton telescope, appl. of Anger camera principle, for gamma-ray astronomy 79−80223
Compton-suppression spectrometer, Ge control detector, dead layer minimisation 80−99400
computer controlled gain stabilizing system for scintillation spectrometer using LED, processor in feedback 78−17473
computerised gamma spectrometer system for meas. isotopic and total Pu conc. in solns. 80−63363
computers in activation analysis and γ-ray spectroscopy, conference, Mayaguez, Puerto Rico (May 1978) 79−1983
cosmic gamma-ray telescope in 10-30 MeV range 78−73638
crystal diffraction spectrometers 79−72183
curved crystal spectrometers, high precision γ-ray energies of fission products 79−93865
differential signal channel pulse stream statistics *(Russian)* 78−17474
digital based triangular wave generator for Mossbauer spectroscopy 78−55113
double Compton gamma-ray telescope, calibration in neutron beam 78−53827
double Mossbauer spectrometer for small resonance line shift meas. 78−82560
drift chamber detector for high resolution gamma-ray astronomy 77−9660
drift chamber telescope for gamma-ray astronomy 79−21185
dual-parameter time and energy spectrometry for positron annihilation studies 77−34505
electro-optical stabilisation of subnanosecond lifetime spectrom. 77−34508
electronic control block for moving system of spectrometer 77−38075
EM shower sampling counters, characteristics of plastic scintillator and radiator layers 78−58530
emulsion chamber measurements of ultrahigh energy γ-rays *(Chinese)* 77−10525
fine γ spectrometry and release meas. *(French)* 79−3258
fission materials nondestructive analysis development, for EURATOM (CEC) Safeguards Directorate 79−85693
flash tube chamber, high press., γ-ray energy and spatial coords. meas. 77−57794
flash tube chamber, high press., γ-ray position and energy determ. 77−57795
four-detector counting system, computer controlled 79−9957
four-window for airborne meas. of terrestrial radioactivity, natural, estimates of ground concentration 79−53575
gamma resonance phase anal., background allowance using total resonance absorpt. filter 78−33363
gamma-ray spectrometric logging and surface exploration equipment calibration 78−85706
gas flow detector, back-scatter-type, conversion electron Mossbauer spectrometry 80−37680
gaseous release monitoring and γ spectrometric analysis *(French)* 79−3259
geochemical sample anal. by gamma-spectrometry, data bank system 80−31120
high-rate spectroscopy system using low noise DC coupled prefilter 77−10527
highly stable gamma-resonance spectrometer, simple circuit 77−65384
hodoscopic spectrometer, gamma-quanta coordinate meas. in NITsE scintillation spectrometer 78−78549
human total-body counter 79−100728
in vivo low-level gamma spectrometry, optimum detector size and position 78−28075
in-beam Ge(Li)-NaI(Tl) Compton suppression spectrom. 77−88325
incoherent scattering of gamma rays, spectrometer for electronic momentum distribs. investigation *(German)* 77−41741
integrating counting technique, appl. to ^{197}Au Mossbauer spectroscopy 78−25377
International Committee for Radionuclide Metrology, report 77−23357
intrareactor spectrum measurement, calorimetric method 78−17293
large capacity sample changer for fully automated gamma ray spectroscopy 80−58021
liquid scintillation spectrum, (n,γ) thermal react. cross section meas. 78−25382
low-background system for neutron activation anal. 77−36843
magnetic Compton spectrometer free of second-order aberration 79−36457
magnetic pair and Compton spectrometers 79−68130
MOS diode as low energy Xand γ-ray spectrum 79−36462
Mossbauer, drive system, low cost, using μA747 ICs 79−89049
Mossbauer, fast γ-ray detection systems 78−25376
Mossbauer, piezoelec., with fast channel advance rates 78−24904
Mossbauer absorpt. spectra determ. with resonance detectors 77−79502
Mossbauer apparatus for resonance studies at high press. and low temps. 78−49943
Mossbauer CAMAC data acquisition system 79−30439
Mossbauer const. velocity spectrometer, control circuits 79−93866
Mossbauer data calibration using laser interferometer 77−88326
Mossbauer furnace for amorphous alloy investigations 80−98916
Mossbauer low temp. high field spectrometer using Bitter magnets 79−51888
Mossbauer microprocessor controlled spectrom. 79−97931
Mossbauer spectrom., velocity nonuniformity meas. 78−848
Mossbauer spectrom. system with data processing capability 77−30699
Mossbauer spectrom. with 2-4 T electromagnet 78−847
Mossbauer spectrometer, absolute vel. control via laser interferometer 77−71715
Mossbauer spectrometer, constant acceleration, with spring reaction compensation, circuit and construction 80−47158
Mossbauer spectrometer, design and construction 79−75668
Mossbauer spectrometer, high field, with Bitter magnets, arrangements, problems 78−89608
Mossbauer spectrometer, microcomputerised 79−67447

gamma-ray spectrometers continued
- Mossbauer spectrometer and its applications *(Chinese)* 79—35913
- Mossbauer spectrometer design, use of resonance and selective ionisation chambers 77—48094
- Mossbauer spectrometer NP 255, measuring capacity enlargement *(Czech)* 80—73558
- Mossbauer spectroms., multi-purpose velocity transducer 77—38544
- Mossbauer spectroscopy, new directions, workshop, Argonne, USA (1977) 78—24903
- Mossbauer spectroscopy, spherical electrostatic electron spectrometer 78—25378
- Mossbauer systems, synchronous digital triangle generator and servo loop pre-amp 77—88351
- multi-channel analyser, portable microprocessor controlled, accessories, data acquisition 80—63474
- MWPC, γ-image blurring reduction by delay line readout 78—37492
- MWPC, design and construction, for high count rate, Mossbauer spectroscopy 79—13580
- MWPC positron camera, 3-D iterative reconstruction method 78—40302
- NE 213 liquid scintillator, decay under neutron and gamma excitation *(German)* 78—55097
- NE 213 liquid scintillator, deuterated, decay mode *(German)* 78—55096
- NE 238 fast liquid scintillator, scintillation decay and n-γ discrimination *(German)* 78—55101
- NE-213 liquid scintillator, Monte Carlo calc. of response function 79—97926
- Ne-213 organic liquid scintillator appl. *(Japanese)* 77—46451
- neutron and γ-ray spectra meas. on radial shielding model of KS-150 reactor *(Slovak)* 78—21624
- neutron capture gamma and electron spectroscopy, instruments and techniques 80—37695
- ninety-channel Cherenkov mass spectrometer for high-energy electrons and gamma quanta (the 'photon' installation) 80—91362
- nuclear excited states, 10^{-10} to 10^{-6} s, lifetime meas. by time spectrometer system 79—31313
- nuclear oil well logging using 14 MeV neutron-excited gamma-ray spectrometry 79—48581
- nuclear studies with tagged photons 80—23245
- on-line system, automatic sequencing using microprocessor controller 77—54393
- pair spectrum, high resolution for medium energy photons 79—31312
- peak areas and detection limits, digital calc. methods 78—50433
- Pioneer Venus Orbiter Gamma Burst Detector 80—67505
- planar positron cameras, 3-D reconstruction using Fourier deconvolution of generalised tomograms 78—40295
- plastic detector, large-volume, for aerial gamma-ray spectroscopy 79—58126
- plastic phosphor, appl. to in situ subterranean gamma-ray spectroscopy 77—57806
- portable, in situ field meas. applications 79—9958
- portable 1024-channel instrument 77—57792
- position sensitive high energy gamma-ray detector 77—83445
- position sensitive target counter for photons above 50 MeV 79—76285
- positron lifetime spectrom., improved time resolution in liquid scintillator NE 238 78—29696
- positron lifetime spectrometer 78—29695
- preamplifier modernisation by input FET operating regime control 80—32579
- proportional counter, sectional flow, high background, for Mossbauer spectroscopy 79—727
- proportional counter, toroidal, Mossbauer spectroscopy appl. 78—33364
- proportional counter for efficient backscatter Mossbauer effect spectroscopy 79—76289
- protection and operation simplification, by relay device attachment 80—57447
- pulse selection to improve energy resolution of spectrometers with CdTe detectors 79—22533
- pulse shape analyser, effect of pulse pile-up on discrimination between neutrons and gamma rays 80—91402
- radionuclide concentration determ. in ground level air 79—24927
- remote computer-controlled, for nuclear power plant monitoring 79—9916
- remote sensing, data analysis system for planetary mission appl. 79—12411
- resonance capture reactions with a total energy detector 80—37694
- response function interpolation by splines 78—82561
- river water pollution detection, multielement anal. 78—69511
- scattering by collimator into detector, spectral distrib. analysis 77—57793
- scintillation, with stilbene crystal, separation of neutron and gamma-ray spectra in mixed field *(Czech)* 77—50327
- scintillation counter, NE 213, Munich pulse shape discrimination cct., low energy performance 78—46233
- scintillation counter arrays, testing with computer controlled LED flashing system 77—57802
- scintillation counter multidetector arrangement for on-line meas. of neutron and γ-ray multiplicities 78—50440
- scintillation counters, in-beam γ-ray spectroscopy at tandem Van de Graaff accelerators 78—13373
- scintillation counters, temperature characteristics of α-datum stabilizers 79—26808
- scintillation detector, gain stabilising scheme, gated radioactive source and broad digital window 80—63453
- scintillation spectrometer, photomultiplier gain stabilization, computer control software 78—13369
- scintillation time-of-flight telescope for cosmic γ-ray preselection 78—82572
- scintillator, NE213, organic liquid, Monte Carlo calcs. of electron energy loss spectrum for incident gamma-rays 77—6613
- scintillator material activation during spaceflight, data for assessment 77—23382
- scintillator response, pulse height spectra unscrambling, computer program 78—55092
- scintillators with various shapes, for gamma-ray spatial pattern anal. 79—16831
- self-stabilising peak detector *(Russian)* 79—26814
- semiconductor detectors, use in high energy physics *(Russian)* 77—50325
- shielded 3-detector system 77—75021
- SIN pairspectrom., meas. on $^{12}C(\pi^-,\gamma)$ 77—10523
- single-channel γ-spectrometer transformation to computer controlled multi-channel analyser 79—57765

gamma-ray spectrometers continued
- spark chamber telescope for range 10-100 MeV 78—36459
- spark-chamber, wide-gap chamber for gamma-ray astronomy, Soviet-French design 78—17503
- spectrograph for single pulse detection 78—846
- spectroscopy processor X- and γ-ray, active zero-pole cancellation feedback loop 79—9972
- spent fuel verification by gamma-ray spectroscopy for materials safeguards 80—78422
- stabilized spectrometer for scattered γ-radiation, analysis of operating quality 80—69009
- standard sources using complex decay schemes 80—9081
- subnanosecond lifetime measurements, system using microchannel plate photomultiplier 78—37520
- thermal neutron induced capture gamma-ray spectrometry 79—52836
- time dependent deadtime and pile up corrections, γ-ray spectroscopy 77—23385
- time of flight directional coincidence telescope for gamma ray telescopes 77—390
- time-domain spectroscopy of recoilless gamma rays 79—26812
- TLD, graded-Z flash bremsstrahlung depth-dose spectrum 77—391
- total absorption Cherenkov spectrometer, characteristics for electrons and gamma quanta 78—5092
- underwater gamma surveying, calibration 79—21066
- unfolding codes for benchmark gamma spectrometry, tests 80—47807
- β-γ-γ coinc. spectrom. using GM-Ge(Li)-Na(Tl) counter combination 78—46210
- e-γ coincidence spectrometer 77—23390
- e^+e and 3-quanta annihilation, automatic spectrometer 77—88321
- ^{241}Am spectrometer for Compton scatt. studies 79—2899
- Ar, liquid ionisation chamber with 4.5 cm gap 80—18761
- CdTe, characterisation by light spot scanning 78—41894
- CdTe, Cl compensated detectors, polarisation suppression methods 77—61661
- CdTe crystal growth for γ-ray detectors 78—41889
- CdTe, detection characteristics 78—41888
- CdTe detector, Cl doped, for reentry vehicle appl., development electronics 77—45288
- CdTe detector, performance compared to HgI_2 detector 80—58062
- CdTe detector, use in γ-ray spectrometric study of VVER reactor spent fuel rods 79—76094
- CdTe detectors, finite solid angle correction factors for 100 keV to 10 MeV γ-rays 77—61659
- CdTe detectors, gamma and electron irradiation effects 78—41893
- CdTe detectors, geometry variations 77—61663
- CdTe detectors, international workshop 78—41887
- CdTe detectors, use in spectrometers, physical and electronic factors *(Czech)* 80—23259
- p-CdTe diodes, X-ray escape peak variations 77—71723
- CdTe gamma radiation detectors, operation, energy resolution, efficient and appl. 79—68156
- CdTe γ spectrometer, use in monitoring activity deposited in nuclear power stations 77—42193
- CdTe n-type low resistivity detectors, advantages and limitations 78—41890
- CdTe sensors, review of medical appl. 77—64147
- CdTe, single carrier charge collection 77—61657
- n-CdTe surface barrier detectors, energy resolution 77—71724
- ^{252}Cf(n,γ), neutron capture gamma expt. equipment designs 80—52832
- CsI(Tl), characteristics of γ-emission scintillation detection units 78—33365
- CsI(Tl) well-detector for low background γ-spectrometry, comparison with NaI(Tl) 78—86724
- ^{57}Fe Mossbauer spectroscopy, added precision 77—88327
- Ge camera, 2-detector, 512 element high purity prototype 78—40301
- Ge detectors, automatic anal. of gamma-ray spectra 77—3246
- Ge detectors, calibration using precise relative γ-ray intensities 78—17469
- Ge detectors, calibration using ^{152}Eu source uncertainties in peak area determ. 80—5436
- Ge detectors appl., high-purity, preparation and properties 78—86723
- Ge, efficiency calibration in range 122-412 keV 80—37682
- Ge, high parity detectors, 6 GeV/c proton irradiation 78—37508
- Ge, high resoln. spectrometry for uranium assay in boreholes 79—53571
- Ge hyper-pure closed and coaxial spectrom., pulse height depend. on source position 77—54403
- Ge, intrinsic, detection of Mossbauer gamma-rays from ^{73}Ge and ^{181}Ta 77—10530
- Ge intrinsic diodes, appl. to in-situ subterranean gamma-ray spectroscopy 77—57806
- Ge planar detectors, high-resolution charged particle spectroscopy 77—54401
- Ge radiation detectors, high-purity, ion implanted n-type contact 77—54416
- Ge spectrom., intercomparison of ^{152}Eu gamma-ray emission rate meas. 78—82568
- Ge spectrometer, energy and efficiency calibration in 100 keV to 3000 keV γ-ray energy range 78—17464
- Ge spectrometers, cooled, for X-ray and gamma-ray astronomy 77—5438
- Ge spectrometers, cooled, on P78-1 satellite 80—58019
- Ge spectrum, precise γ-ray energies for calibration up to 3.5 MeV 79—31311
- Ge wide range spectrometer for on-line meas. of reactor cooling water activity 77—65381
- Ge-Li spectrom., re-evaluation of precise γ-ray energies for calibration 78—90015
- Ge(I) gas cooled high resolution mini-probe 79—22550
- Ge(Li) 50 cm^3 detector, energy response for 4 to 10 MeV photons 78—46211
- Ge(Li), analytic fitting of full energy peaks 77—71716
- Ge(Li) anticoincidence shielded spectrom. for environmental radionuclide meas. 79—6791
- Ge(Li), appl. to in situ subterranean gamma-ray spectroscopy 77—57806
- Ge(Li), automatic anal. of complex γ-ray spectra 78—33370
- Ge(Li) balloon borne spectrom. for obs. of neutron star cyclotron line emissions 80—41721
- Ge(Li), calibration for radioactive inert gas meas. 77—83442
- Ge(Li) coaxial detector, triple const. fraction discriminator evaluation 78—70708
- Ge(Li) detector, calibration using linearly varying amplitude pulse generator 77—10526

gamma-ray spectrometers continued
Ge(Li) detector, use in activity determ. of gamma source with flat surface *(German)* 78—58528
Ge(Li) detector, use near 400 MeV proton beam in p-γ coincidence expt. 80—5452
Ge(Li) detector, well type, spectrum interpretation problems due to self absorption variations 79—31307
Ge(Li) detector efficiency determ. for gas bomb geometries 80—78486
Ge(Li) detector for precise meas. of ^{106}Ru 512 keV γ-ray 77—6610
Ge(Li) detector pulse formation, Monte-Carlo anal. of multiple interaction processes 77—399
Ge(Li) detectors, anal. of monochromatic γ-ray and annihilation spectra 78—50429
Ge(Li) detectors, efficiency calibration using continuous external bremsstrahlung 78—46228
Ge(Li) detectors, energy meas. source position effect 79—13579
Ge(Li) detectors, relative γ-ray intensities for calibration 79—49896
Ge(Li) detectors, use of annihilation radiation for precision energy calibration 77—10528
Ge(Li) detectors for γ-radioactivity in rocks and soils 80—67418
Ge(Li) efficiency, effect of counting rate and source-to-detector distance 79—68122
Ge(Li), γ-ray energies of ^{40}K, ^{108m}Ag and ^{226}Ra decay chain 80—27865
Ge(Li) γ-ray spectra, effect of base line shape on peak unfolding 78—851
Ge(Li) γ-ray spectra, NUKLID program for automatic line identification *(German)* 78—58536
Ge(Li) γ-ray spectrometer for neutron activation anal., modification and appl. of SPECTRA program 78—20107
Ge(Li) high-resolution detector, role in neutron activation anal. of water 77—56324
Ge(Li) in situ environmental spectrometer, spectrum-to-exposure rate conversion function 77—65379
Ge(Li), in situ meas of fission product plateout in HTGR 80—73881
Ge(Li), in-beam γ-ray spectroscopy at tandem Van de Graaff accelerators 78—13373
Ge(Li) large detectors, timing improvement by pulse shape selection method 77—54457
Ge(Li), meas. of γ-ray elastic and Compton scatt. through small angles 79—718
Ge(Li) photon detectors, analytic fitting of full energy peaks 79—36458
Ge(Li) planar detector, in γ-γ polarised directional correlations set-up 77—34530
Ge(Li) semiconductor, used simultaneously with NaI(Tl) scintillation spectrometer, in neutron activation cross-section meas. 80—78485
Ge(Li) spectrom., balloon-borne, recent meas. 78—93107
Ge(Li) spectrom., precision energy meas. of gamma rays of ^{51}Cr, ^{103}Ru, ^{109}Cd, ^{144}Ce, and ^{203}Hg 78—58533
Ge(Li) spectrometer, high resolution, appl. to galactic gamma-ray lines obs. *(Japanese)* 79—80353
Ge(Li), spectrometer efficiency, dead time and pulse pile-up correction 78—50442
Ge(Li) spectrometry, pulser method limitations in pile-up and dead-time corrections 77—23384
Ge(Li) spectrometry at low source-detector distances, coinc. summing corrections 79—22528
Ge(Li) spectrum, ^{236}Ra as calibration standard 77—38543
Ge(Li) summing-up effects, optimisation of detector-target geometry for in-beam γ-spectroscopy 80—74070
Ge(Li) upward looking dip-stick type spectrom., in-situ environmental γ-ray meas. 78—37480
Ge(Li), use of 2046 keV ^{27}Al(p,γ) as gamma ray intensity calibration standard 77—30698
Ge(Li), well-type detectors for low-level radiochemical analysis 78—37119
Ge(Li) well-type semiconductor detector, γ-ray spectrometry *(Japanese)* 79—89521
Ge(Li)-NaI(Tl), Compton suppression spectrometer for in-beam expts., design and performance 78—78553
Ge(Li)-NaI(Tl) Compton suppression spectrom. for low-level activity meas. 78—9022
He filled detector using thin foils to convert gamma rays to electrons 80—27872
HgI_2, characterisation by light spot scanning 78—41894
HgI_2, charge collection efficiency 80—32575
HgI_2 detector, performance compared to CdTe detector 80—58062
HgI_2 detectors, fabrication, appl. to X- and gamma-ray detection 77—83459
HgI_2 detectors, γ- and X-ray detection, solution grown crystals 80—63452
HgI_2 detectors, international workshop 78—41887
HgI_2, detectors, novel pulse processing system 78—41902
HgI_2 detectors, state-of-art crystal growth and nucl. spectroscopic evaluation 78—41895
HgI_2, effects of dislocations and crystal defects on energy resolution and reponse uniformity 77—54412
HgI_2, energy response to ^{137}Cs photons, appl. to medical imaging 78—44592
HgI_2, gamma radiation detectors, operation, energy resolution, efficient and appl. 79—68156
HgI_2, high energy gamma spectrometers, room temp., appl. to ^{60}Co 77—65378
HgI_2, single carrier charge collection 77—61657
Mn nodule mining and processing with nuclear meas. 77—4975
Na I (Tl) detector for gamma-ray from fast neutron radiative capture 77—26925
NaI 4γ multidetector system for exam. of nuclear struct. and reactions at high ang. momentum, theory 80—74071
NaI detector absolute photopeak efficiency calc. for water as source medium 78—78558
NaI detector calibration using large diam. sources 78—33396
NaI detector efficiency for 10 to 150 keV gammas, 4π geometry vs. well- and face-type cryst. 77—3214
NaI detectors, synthesis of response functions to gamma-rays 78—94158
NaI face-type detector efficiencies for 10 to 150 keV γ-rays 77—3215
NaI gamma spectrometer with ^{6}LiH shielding for neutron background reduction 78—90012
NaI, meas. of fast neutron capture cross sections 78—74530
NaI pulse height spectra for >1.5 MeV gamma-rays, model modification 79—36459

gamma-ray spectrometers continued
NaI scintillation spectrometer, gamma-ray energy released from fission products, response matrix *(Japanese)* 80—42888
NaI spectrometer, response matrix for 6 MeV γ-ray penetration meas., benchmark data 78—50432
NaI well-type detectors, efficiency values for 10 to 150 keV gammas, point and needle sources 77—3213
NaI:Tl scintillator response, γ-ray, (X-ray) rel. $^1/_2$-width energy depend., undergrad. expt. 78—49600
NaI:Tl spectrometer meas. of activity of radioisotope emitting two gammas in cascade, geometrical effect 77—88320
NaI(Tl), anomalous intensity variation of backscattered gamma ray peaks 80—37691
NaI(Tl), appl. in NBS positron annihilation in flight facility 79—31306
NaI(Tl), appl. to in situ subterranean gamma-ray spectroscopy 77—57806
NaI(Tl) array, calibration using 500 keV Van de Graaff proton accelerator 79—45524
NaI(Tl) double crystal gamma ray spectrom., efficiency calibration 79—717
NaI(Tl), elemental analysis by neutron inelastic scatter gamma rays with a radioisotope nuetron source 80—30311
NaI(Tl) large modularised detector, 50 MeV γ-ray meas. 79—76257
NaI(Tl), portable, natural soil radioactivity monitoring 80—31148
NaI(Tl), pulse shape discrimination of high-energy neutrons and gamma rays 78—33395
NaI(Tl) right circular cylindrical crystal detectors, simple model for γ pulse-height spectra prediction 77—6611
NaI(Tl) scintillation spectrometer, used simultaneously with Ge(Li) semiconductor, in neutron activation cross-section meas. 80—78485
NaI(Tl) well type detector, efficiency determ. 78—55087
Na(Tl), circular ring transaxial positron camera, coinc. electronics 78—31953
Pb glass detectors for high-energy photons, Monte Carlo calc. of energy resolution 79—18072
Pb-glass hodoscope for 50 to 150 MeV photons 80—18758
Pu, isotopic composition, nondestructive anal. using gamma spectrometry 80—63392
^{241}Pu in ^{241}Am, determ. by γ spectrometry 79—52808
Si bent crystal gamma diffractometer, X-ray topographic study of large crystals 77—57805
Si(Li), detection of Mossbauer gamma-rays from ^{73}Ge and ^{181}Ta 77—10530
Si(Li) detector, improvement of time depend. instabilities by IR and γ-irradiation 79—36477
Si(Li) gas cooled high resolution mini-probe 79—22550
Si(Li), in-beam γ-ray spectroscopy at tandem Van de Graaff accelerators 78—13373
Si(Li) photon detectors, analytic fitting of full energy peaks 79—36458
$ThBr_4$, inorganic scintillator, use in nucl. and accelerated particle detection 78—58540

gamma-ray transport *see photon transport theory*

gamma-rays
atmosphere, angle and energy distrib., 2-25 MeV 78—12033
atmospheric gamma-rays, north-south anisotropy at balloon altitudes 77—29608
coastal sediments, English Channel, distribution of fission products (1976-78) *(French)* 79—84219
cosmic γ-ray spectrum from pp collisions, fireball model 77—18364
cosmic γ-rays, energy and flux meas., emulsion chamber detection *(Japanese)* 78—20595
cosmic bursts, stellar superflare model *(Chinese)* 77—22021
cosmic diffuse γ-ray background from galactic halo 77—53711
cosmic gamma-ray origin and obs., review 77—73912
cosmic gamma-rays, originating from external galaxies, electron-microwave interaction 80—22121
cosmic ray bursts, sources, models 77—9823
cosmic rays, 0.511 MeV energy, meas. with balloon-borne Ge(Li) spectrometer 77—53373
cosmic rays gamma-rays, traversing cosmic blackbody photon gas, effective penetration distance 79—5742
diffraction meas. in mosaic struct. of RbI in metastable press. region 77—20065
diffraction properties of quartz and piezoelectricity 77—20801
diffractometry for study of ferroelastic crysts., appl. to KH_2PO_4 77—8533
diffuse cosmic and atmospheric MeV γ-rays, balloon obs. 78—4048
diffuse cosmic gamma-ray spectrum, Apollo data in 0.3-10 MeV region 77—33705
environmental γ radiation, variation during rainfall *(Japanese)* 78—36240
extended sources, energy distrib. calc., rel. to remote spectroscopy, of Earth surface 78—61586
galactic centre γ-rays from trapped cosmic rays 77—87212
precise γ-ray standards 80—36973
radiation field induced in air by fast neutrons, intensity and absorbed energy calc. method 77—50310
radiation of relativistic channelled particles 78—22779
supernova remnants, cosmic rays in dense shell 77—33599
upper atmosphere γ-ray flux above 40 MeV 77—53257

gamma transition *see glass transition*

Gamow-Teller transitions *see beta-decay*

garnets
includes ferrimagnetic insulators, $M_3Fe_5O_{12}$; for rock-type garnets, $MM'(SiO_4)_3$, see minerals
see also ferrimagnetic properties of substances
antiferromagnetic garnets, review 77—80952
bubble device materials, single-layer, ion-implantable small, design and development 79—82844
bubble domain, empirical relation for saturation vel. 78—95496
bubble domain lattice collapse characts. in alternating mag. field 80—54932
bubble domain memory appls., growth requirements 77—20660
bubble domain structure, mag. contrast in SEM 78—18511
bubble domains, wall oscill. and overdamped motion in mag. bubble domains 78—6550
bubble film, anisotropy field and nonmagnetic regions in implanted layers, ferromag. reson. study 79—99774
bubble film, ellipsometric meas. of thickness and refr. index 79—78463
bubble film, fuzzy walls obs. 79—99738

garnets continued
bubble film, high g, two resonant peaks 78—68388
bubble film, ion-implanted propag. patterns, cryst. symm. effects, roof-top designs 80—15768
bubble film, LPE growth reproducibility 79—1830
bubble film, magnetoelastic interactions 80—65976
bubble film, quenching of coercive force by domain wall restoring forces, theory and expt. test 79—78460
bubble film, with induced anisotropy, domain wall energy 79—19750
bubble film, [111]-oriented simple method of meas. cubic anisotropy const. 78—19285
bubble film LPE with high Pb content 79—38750
bubble garnet, domain-wall dynamics in in-plane field 79—87296
bubble garnet, ion-implanted, gradientless propulsion for $S=1$ bubble 79—78470
bubble garnet film, non-implanted, surface mag. struct. 80—84628
bubble garnet film, saturation velocity, in-plane field effects 80—108041
bubble material, coherent precession mode of twisted wall 79—78468
bubble materials, low loss, mag. domain wall dynamics 78—10738
bubble-collapse and stripe-chop mechanism 77—80975
Ca,Ge-substituted, LPE growth atm. effects on bubble props. 77—20655
cation site distrib. and valence states 79—99167
charged wall behavior in 1-μm bubble implanted structures 78—91892
chemical site preference of rare earth ions 77—68936
composite garnet ferrite epitaxial film ferromag. resonance obs. 77—85578
concentrational inhomogeneities, appl. of vacuum decoration method 79—14835
contiguous disc bubble patterns utilising intrinsic crystalline anisotropy 80—2611
crystal and static mag. props. 79—99166
crystal growth, flow transitions and interface shapes in Czochralski growth 77—24949
crystal growth for mag. appl., book 79—69967
crystal structure, body-centred cubic cylinder packing 77—62497
crystal symmetry, X-ray diffr. data 79—42024
cubic ferr-te garnet, diffracted light polarisation characts., spin and magnetoelastic waves 80—20614
Czochralski bulk flow in the growth of garnet crystals 80—38979
domain, wall motion, one-dimens., static in-plane field-biased, dynamic characts. *(Japanese)* 79—73767
domain boundary mobility, effect of easy magnetization axis inclination 78—19293
domain wall oscillations, bubble domain wall motion 80—108042
domain wall structure and phase diagram near compensation point *(Russian)* 77—12149
domain-wall behaviour in ion-implanted layers for 1-μm bubble devices 80—2613
doped, site symm. exam., ang. variation of induced linear dichroism 78—95429
doped magnetic, ang. variation of induced anisotropy, symm. of centres 78—2676
double layer prod. for magneto-optical devices, LPE 77—21043
dynamic collapse expt., in presence of inplane field 77—85479
epilayers, domain structure, technique for observation 78—91914
epitaxial ferrite garnet film growth, automatic machine 78—27418
epitaxial ferrite-garnet films with inversion layers, behaviour of cylindrical mag. domains, visual tracking method 80—71139
epitaxial film, anisotropy consts. from reciprocal of susceptibility meas. 77—73057
epitaxial film, damage prod. by multiple ion implantation, ferromag. reson. obs. 80—34703
epitaxial film, easy magnetisation axis inclination temp. depend. 79—65699
epitaxial film, elastic surface wave propag., magnetoelastic effect 77—20669
epitaxial film, Faraday effect and magnetometrical meas. 78—52317
epitaxial film, mag. bubble props., permanent local modification by laser annealing 80—2612
epitaxial film, physical thickness and refr. index meas. 77—77309
epitaxial film, stress induced magnetocrystalline anisotropy 80—71013
epitaxial film, X-ray topographic measurement, local variations in spacing and orientation of lattice plane *(Japanese)* 78—38585
epitaxial films, easy magnetisation axis orientation 80—60383
epitaxial garnet film, mag. domain wall damping, vel. depend. 77—85517
epitaxial garnet films, technique for magnetostriction coeff. meas. 80—243
epitaxial layer, decomposition caused by annealing 78—18918
epitaxial layer/substrate lattice mismatch meas. using X-ray double-crystal method 79—28235
epitaxial layers, growth kinetics and struct. as functions of cryst. lattice parameter mismatch 80—6677
epitaxial thin films, for mag. bubble memories *(Czech)* 78—88147
Faraday element fabrication for intracavity laser appls. 78—66852
ferrite, optic axes determ. using two sublattice model mag. birefr. 77—8555
ferrite epitaxial layer, flaw detection method 78—2719
ferrite film, local conc. of effective mass of domain boundaries *(Russian)* 77—12179
ferrite garnet film, ion-implanted, hard mag. bubble suppression mechanism 80—44890
ferrite-garnet film, waveguide light propag. charact., integrated optics appl. *(Russian)* 78—1346
ferrite-garnet film thickness meas. with UM-2 monochromator interference attachment 78—3035
ferrogarnet crystal, surface layer damage thickness meas. 79—5106
ferrogarnets, monocrystalline films, mag. anisotropy 80—2609
film, 79—99727
film, 180° capped double layer LPE film, bubble wall states coding 80—34716
film, 1 μm bubble contiguous-disk device, orientation depend. of propagation margin 79—82846
film, Bi substituted, LPE growth 77—1798
film, bubble domain stability, spin precession effects 77—32226
film, bubble motion due to closure domain interaction with loop current 77—85525
film, complementary σ-bubbles in bubble automation 79—78465
film, depth profiling using raster scanning SIMS 77—16441
film, domain obs. by SEM 77—69646
film, domain wall displacement in pulsed field 77—16129
film, domain wall dynamics, time depend. effects 77—12168

garnets continued
film, double heteroepitaxy, magneto-optical devices for phase matching *(French)* 77—3675
film, dynamic behaviour of domain walls and bubbles 78—52321
film, dynamic charges in bubble domain lattice 78—60325
film, gradient bubble propag. ballistic overshoot 77—12170
film, gradientless propulsion of bubbles 77—4535
film, growth rate depend. of growth-induced anisotropy 78—14992
film, ion implanted, bubble propag., wall states 77—16128
film, ion implanted bubble circuits 79—78473
film, ion-implanted, bubble collapse field, in-plane mag. field effect 77—73060
film, ion-implanted, controlled generation and discrimination of χ_+ and χ_- bubbles by single bias pulse 79—51826
film, ion-implanted, crit. curves for determining magnetisation directions 79—91263
film, ion-implanted, discrimination of $S=1$ and $S=0$ bubbles by dynamic bubble collapse 79—51825
film, ion-implanted, domain wall mobility 78—95495
film, low freq. excitation spectra, mobility of domain boundaries 79—42815
film, LPE, growth-induced anisotropy, magnetostriction theory 79—95624
film, LPE, high speed bubble domain motion, time resolved obs. system 77—40096
film, LPE, stripe domain, time resolved obs. of contracting motion 77—85519
film, LPE, time resolved obs. system for domain dynamics, appl. to contracting motion of stripe domains *(Japanese)* 79—47312
film, LPE bubble, growth-induced anisotropy, effects of La 77—85514
film, LPE technique, difficulties and advantages 79—28958
film, mag. bubble domain, annealing by laser pulse 80—15769
film, magnetic bubble materials, review 80—50153
film, magnetic rag-domains, appl. to magneto-optical displays 78—91912
film, magnetoelastic energy of stripe domain patterns 78—68334
film, minimum bubble drive field, ion implantation effect 77—24721
film, motion of mag. bubble domains near point defect 79—28575
film, numerical display element exploiting rag domains 78—68339
film, Permalloy-coated, bubble vel. and stability, influence of planar domains 80—39831
film, uniaxial, cubic anisotropy effect 77—89998
film, wall velocity at high drive fields 77—85518
film bubble material, high peak velocity 77—85513
film containing Lu, Curie temp. and flux spin-off, melt comp. effect 77—85515
film in mag. field, domain dynamics *(Russian)* 79—4711
film ion implanted contiguous disk structure dynamics of 1 μm bubbles 79—78474
film LPE growth, for bubble memory appl., review, book contrib. 79—70009
film preparation, single crystal, for magnetic bubble domain appl. 78—60588
film waveguide, magneto-optical effects 77—54802
film waveguide, magnetooptical effects 77—3650
films, (111)-oriented, cubic anisotropy meas. 80—54924
films, bubble statics, dynamics *(Japanese)* 78—52326
films, containing Ca and Ge, refr. index meas., 0.56-0.97 microns 77—52192
films, LPE growth, oxidic high temp. solns. struct. 80—10808
films, meas. of Faraday effect and susceptibility using magnetooptical apparatus 80—105680
films for fast bubble devices 80—25168
films with orthorhombic anisotropy, domain wall motion 80—80580
flux-grown magnetic garnets, comp. anal. by AAS 78—92585
garnet:Nd^{3+}, doped, Schottky specific heat and mag. susceptibility calcs. 79—51759
garnet:Nd^{3+}, spectral, structural regularities, anal: 78—51948
garnet bubble films, 111 orientated, mag. anisotropy predictions, model 78—68326
growth from solution, freezing point depression of PbO solvent by oxide cpds. 80—24393
growth induced anisotropies, large, arising from preferential occupation of Ir^{4+} and Mg^{2+} on Fe sites 80—75754
gyromagnetic ratio determ. by magneto-optical method *(Russian)* 77—32356
heavy ion-solid surface collision cascade theory and expt. *(Japanese)* 80—11527
hydrothermal crystallisation, for mag. appl., review, book contrib. 79—69974
ion-implanted bubble film, vel. asymmetry during stripe head propag. 80—39834
ion-implanted film, large automotion of $S={}^1/_2$ bubble 79—24203
IR reflectivity, ATR, Voigt and Faraday expts. 80—66180
isolated steps on vicinal faces, rate analysis of growth parameters 80—10805
large growth-induced anisotropy to preferential occupation of Fe sites 80—75754
laser crystal matrices, development aspects, spectral generation data survey 77—10928
low loss bubble material, wall struct. changes 77—89994
LPE, liquidus, temp. and growth-dissoln. kinetics 79—51028
LPE film, bubble technology *(Polish)* 77—77076
LPE film, domain dynamics in microwave field 77—20663
LPE film, laser beam deflector 77—54803
LPE film growth thermally induced substrate fracture 78—68639
LPE garnet bubble films, capping layer upper cap-switch field, model 78—95498
LPE growth, using horizontal dipping, exam. of growth kinetics 78—60039
LPE growth 77—89673
LPE layers, bubble collapse field meas., new method 78—56356
LPE layers, growth rate depend. on supercooling, induced striation expt. 79—24453
LPE layers, SIMS in-depth conc. profiling 77—24489
magnetic, cryst. growth from high-temp., solns., book contrib. 79—69973
magnetic, Internat. School of Phys. 'Enrico Fermi', Varenna on Lake Como, Italy, (June-July 1977) 79—99668
magnetic anisotropy and magnetostriction 79—99748
magnetic bubble dynamic props. rel. to bias-field-determined bubble size 78—91915

garnets continued

- magnetic bubble garnet epitaxial film multilayer structures, interphase boundary rearrangement obs. 79—78489
- magnetic bubble materials, props. and preparation models, review *(Rumanian)* 80—93149
- magnetic bubble stability in ion implanted channels, model 78—68320
- magnetic bubble state stability in rot. field 78—68317
- magnetic domain structure obs. by birefringence of mag. colloid 79—51809
- magnetic domain wall and bubble dynamics 77—69599
- magnetic domain wall mobility, computer simulation and meas. 77—12148
- magnetic domains, skew, cylindrical, light modulator appl. anal. 79—38360
- magnetic excitations 79—99695
- magnetic films, (111) oriented susceptibility, uniaxial anisotropy field 80—54930
- magnetic ordering of S-ions *(Russian)* 79—95579
- magnetic properties and applications, structural props. 80—65760
- magnetic properties of V^{4+} ion, effect of covalency 78—64010
- magnetic relaxation phenomena 79—99776
- magnetic structure, neutron diffraction patterns, group theoretical, exchange Hamiltonian symm. anal. *(Russian)* 79—65648
- magneto-optical expts., MG field production and appls. 79—71491
- magneto-optical photoconductor sandwich 77—40213
- magneto-optical properties 79—99859
- magnetoelastic symmetry, growth-induced lowering 78—64255
- magnetostriction effects from Mn^{3+}, Co^{2+} and Fe^{2+} ions 79—91277
- manufacture, modified technology development *(German)* 77—21073
- Mossbauer effect, electric field gradient of ^{57}Fe 79—1732
- Mossbauer spectra of ^{57}Fe and ^{119}Sn 80—20568
- optical waveguide with high Faraday rotation, mode degeneracy 78—94454
- orthoferrite garnet, mag. bubble lattice nucleation obs. 78—76283
- oxide and fluoride garnets, relation between lattice parameters and ionic radii 80—1986
- Permalloy-coated garnet films, bubble properties 78—2715
- photoinduced phenomena 79—99718
- photomagnetic effects, irreversible 79—99719
- preparation and imperfections, rel. to props. 79—100031
- pretransition phenomena and long-range ordering 79—99151
- rare earth compounds and alloys, spin-reorientation transitions, review 77—36073
- rare earth Fe garnet, difference in comp. between targets and sputtered films, expt. 78—6848
- rare earth ferrite garnet single crystals, spin reorientational phase transitions *(Russian)* 78—39349
- rare earth ferrite garnets, phase transitions, field-induced spin-orientational 80—75767
- rare earth ferrite-garnets, compensation temp., rare earth ion influence 79—51775
- rare earth gallium garnet, growth of crystals from $50PbO.40PbF_2.10B_2O_3$ flux 77—21014
- rare earth garnet prep., novel Li_2MoO_4-$R_2(MoO_4)_3$ flux system 77—48359
- rare earth garnet substrate films, substituted, and LPE fims for magneto-optic appls. 78—31351
- rare earth garnets: $^{154}Gd^{3+}$, hyperfine interactions, PAC 77—43909
- rare earth garnets, appl. of superposition model to cryst. field 78—68132
- rare earth garnets, cryst. field depend. on coordination of dodecahedron 79—73475
- rare earth garnets, Debye charact. temp. and reciprocal lattice consts. 80—29144
- rare earth garnets, field depend. magnetocryst. anisotropy 77—69543
- rare earth garnets, prep. and props. book contrib. 80—44193
- rare earth garnets, preparation, substrate and epitaxial layer surface quality control, X-ray topography *(German)* 77—55432
- rare earth garnets, RIG, (R=Tb, Dy, Ho, Er), spontaneous Faraday rot. rel. to sublattice magnetisation 80—66159
- rare earth garnets-$R_xR'_{3-x}Fe_{5-t}M_tO_{12}$, R,R′-rare earths, on Y ions, Mp=Al^{3+}, $Ga^{3+}Sc^{3+}$, In^{3+}, effect of ion replacements on lattice constant 79—1408
- rare earth iron, two-sublattice ferrimags., mag. polaritons 80—65845
- rare earth iron garnet, Faraday rotation from empirical scaling model 77—81083
- rare earth iron garnet single crystal films, synthesis and props., reviews 78—48013
- rare earth iron garnets, (Ca,Ge)-substituted, flux growth in regular soln. approx. 79—78907
- rare earth iron garnets, anisotropic, mag. props., high field and low temp. 80—75801
- rare earth iron garnets, contribution of Fe ions in noncubic magnetostriction from crystal field model 78—43622
- rare earth iron garnets, level intersection and instability of mag. struct. *(Russian)* 77—43816
- rare earth iron garnets, magnetic relaxation phenomena 79—99776
- rare earth iron garnets, mol. field coeffs. 77—1544
- rare earth iron garnets, site ordering and magnetostriction 77—90007
- rare earth iron garnets, spectra calc. using exact microscopic Hamiltonian 77—8553
- rare earth thin films, macroscopic mag. props., magneto-optical expts. 80—46764
- rare earth-transition metal garnets, $R_3M_5O_{12}$, amorphous films for mag. bubble memories, materials review *(Polish)* 80—34715
- rare-earth Fe garnets, solubility model in PbO/B_2O soln. 79—46807
- regular domain structs., magneto-optical characts., optoelectronics appls. 80—40098
- small-bubble-diameter mag. memory materials, past, present and future requirements 79—78458
- specific heat meas., elastic type of antiferromag. ordering *(Russian)* 77—55686
- spin Hamiltonian and mag. anisotropy appl. to $3d^4$ and $3d^6$ ions 79—99669
- Stockbarger-grown, impurity capture and distrib. 77—28713
- stripe head vel. meas. using magnetoresist. signal 78—68316
- structural parameters, appl. of Poix formula 78—67701
- substituted polycryst., low FMR linewidth, relax. processes 77—20718
- superexchange operator and cryst. field interactions 80—59931
- transparent, wave props. of domain wall 78—48011
- transparent magnetic materials *(Japanese)* 80—11369
- two-layer mag. structures, thermomag. recording 80—100588

garnets continued

- YAG, crystal orientation determ. by Laue method, computer calc. *(Chinese)* 79—32853
- YAG, single crysts., melt growth using heat exchange method 79—52106
- YAG crystals, EPR spectra of V^{2+} ions, ion energy levels 80—7157
- YAG synthetic, cryst. growth, review *(German)* 79—33926
- YIG, bulk, convolution with magnetoelastic Rayleigh waves 79—64404
- YIG, cryst. growth from high-temp. soln., book contrib. 79—69973
- YIG, energy location of mag. Fe levels, spin polarised photoemission 79—24413
- YIG, hot spraying to give fine, free flowing, sinterable powder 80—20865
- YIG, optical absorption and magneto-optic spectra 79—99860
- YIG, reson. magnetostatic modes, spectrum in inhomogeneous mag. field 79—28621
- YIG, thermal cond. at low temps. 80—2222
- YIG films, spin wave dispersion eqn. for delay lines *(Russian)* 80—88736
- $(YSmEuCa)_3(FeGe)_5O_{12}$, garnet film, ion implanted, bubble domain props. 78—88152
- $3Y_2O_3.5Al_2O_3$, garnet, synthesis by firing mixed oxides 79—61545
- Bi garnet-MnBi film structure, thermomag. information recording appls. *(Russian)* 78—23305
- Bi:garnet thick layers, regular domain structure, magnetooptical diffr. of light 80—108188
- $Bi_{3-2x}Ca_{2x}$ $Fe_{5-x-y}In_yV_xO_{12}$, growth and mag. props. of single crystals *(Chinese)* 77—40056
- $Bi_{3-2x}Ca_{2x}Fe_{3-x}V_xO_{12}$, crystallization in $Bi_{0.7}Ca_{2.3}Fe_{3.85}V_{1.15}O_{12}$-$Bi_2O_3$-PbO 77—48330
- BiIG, transparent, domain struct. realignment in external mag. field 78—10739
- BiTm ferrite garnet coating on $LiNbO_3$:Ti optical waveguide *(Russian)* 77—42623
- $(BiTm)_3(FeGa)_5O_{12}$ ion implanted epitaxial garnet film, bubble domains, cryst. struct. disorder 80—93150
- $(BiTm)_3(FeGa)_5O_{12}$, monocrystalline films, mag. anisotropy 80—2609
- $(BiTm)_3(FeGaTm)_3O_{12}$, layer separation of domain struct. 80—44857
- $Ca_3Al_2Ge_3O_{12}:Fe^{3+}$, spin Hamiltonian parameters, g-factors, temp. depend. EPR obs. 77—48038
- $Ca_{2x}Bi_{3-2x}Fe_{5-x-y}V_xIn_yO_{12}$, ferromagnetic relax. meas., 4.2-300K 80—44923
- $Ca_{2x}Bi_{3-2x}V_xFe_{5-x}O_{12}$ ferrogarnet, magnetis. distrib., correl. with morphological habit 79—42802
- $Ca_3Cr_2Ge_3O_{12}$, and $Ca_3Cr_2Si_3O_{12}$, absorpt. and luminesc. spectra, cryst. field and exchange interactions 77—73154
- $Ca_3Fe_xCr_{2-x}Ge_3O_{12}$, antiferromagnetic order below 12K, Mossbauer study 80—39945
- $Ca_3Fe_2Ge_3O_{12}$, antiferromagnetic reson., anisotropy and magnetoelastic interaction effects *(Russian)* 77—69712
- $Ca_3Fe_2Ge_3O_{12}$, antiferromag. single crystal garnet, magnetostriction *(Russian)* 79—8027
- $Ca_3Fe_2Ge_3O_{12}$ garnet, light absorpt. spectral study 80—93322
- $Ca_3Fe_2(Mn_2)Ge_3O_{12}$, single magnetic sublattice antiferromagnetic garnets 78—52652
- $Ca_3Fe_2Si_3O_{12}$, andradite, hyperfine parameters, Huckel theory calc. 80—39542
- $Ca_3Fe_{3.5}V_{1.5}O_{12}$, crystallisation field in CaO-V_2O_5-Fe_2O_3-PbO system 77—16548
- $Ca_3Ga_2Ge_3O_{12}$, appl. as substrate for mag. bubbles 77—28418
- $Ca_3Ga_2Ge_3O_{12}$, substrate, electron examination of microstruct. and microsegregation 78—67919
- $Ca_3Ga_2Ge_3O_{12}:Nd^{3+}$, stimulated emission at 300K 80—38019
- $Ca_3Ga_3Ge_3O_{12}:Fe^{3+}$, spin Hamiltonian parameters, g-factors, temp. depend. EPR obs. 77—48038
- $Ca_3Mn_2Ge_3O_{12}$, antiferromagnetic garnet, neutron diffr. study in mag. field 80—50060
- $Ca_3Mn_2Ge_3O_{12}$, crystal struct. distortion due to cooperative Jahn-Teller effect *(Russian)* 77—1119
- $Ca_3Mn_2Ge_3O_{12}$ garnet, metamagnetic transition, high anisotropy peculiarities *(Russian)* 80—60274
- $Ca_3Mn_2Ge_3O_{12}$, highly anisotropic garnet, neutron diffr. obs. of mag. struct. 78—68168
- $Ca_3Mn_2Ge_3O_{12}$, mag. struct. study 80—2554
- $Ca_3Mn_2Ge_3O_{12}$, neutron diffr. in mag. field, metamagnetism, antiferromag. ordering 79—65651
- $Ca_3SbSnFe_3O_{12}$, mag. ordering and bond geometry rel. to tetrahedral Fe^{3+} 77—32163
- $Ca_3SbSnFe_3O_{12}$, neutron diffr. patterns, group theory approach for determ. of mag. struct. *(Russian)* 79—51749
- $Ca_3Ti_{2x}V_{1.5-}xFe_{3.5-x}O_{12}$, mag. and neutron diffraction investigation 77—16044
- CaV ferrite garnet, large grained, mag. props. 78—64222
- CaVG, polycryst. IR transmission spectra rel. to Faraday rotator and modulator appl. 78—10900
- $Ca_3Y_2Ge_3O_{12}:Eu^{3+}$, garnets, prep., struct., luminesc., absorpt. spectra, Eu^{3+} localisation 77—69884
- $CaY_2Mg_2Ge_3O_{12}$:Nd, CW room temp. laser operation, 0.941 and 1.059μm 78—66842
- $CaY_2Mg_2Ge_3O_{12}:Nd^{3+}$, optical absorpt. and fluoresc. intensities 80—29793
- $Ca_3ZrSbFe_3O_{12}$, mag. ordering and bond geometry rel. to tetrahedral Fe^{3+} 77—32163
- $Cd_3Cr_2Ge_3O_{12}$, absorpt. and luminesc. spectra, cryst. field and exchange interactions 77—73154
- $Cd_3Cr_2Ge_3O_{12}$, antiferromagnetic ordering of Cd^{3+}, sp. ht. and mag. susceptibility meas. 77—16062
- $Cd_3Cr_2Ge_4O_{12}$, antiferromagnetic reson., anisotropy and magnetoelastic interaction effects *(Russian)* 77—69712
- $Cd_3Ga_5O_{12}$ melt, simulation of fluid flow 78—31321
- DyAG, adiabatic magnetisation, optical obs. 78—88283
- DyAG, antiferromag., induced staggered mag. fields 80—65810
- DyAG, antiferromag., induced staggered magnetic fields, microscopic mech. 80—80527
- DyAG, crit., tricrit., and crossover phenomena, light scatt. 78—68251
- DyAG, cubic antiferromagnet, multiaxis phase transitions 79—78377
- DyAG, electrostatic model of cryst. field 80—59945
- DyAG, forced magnetostriction meas. 78—68349
- DyAG, induced staggered mag. fields and order parameters 77—63099
- DyAG, light scatt. from metamag. domains, crit. exponent determ. 77—66482
- DyAG, magnetic tricriticality nonuniversality 79—78392

garnets continued
DyAG, single cryst. growth by Czochralski method 78−95690
DyAG, tricritical crossover exponent 77−4239
DyAg, neutron diffr. expts. in external mag. field, temps. below 1.2K 79−61067
DyAlG, tricrit. wing exam. 77−73026
$Dy_3Al_5O_{12}$, antiferromag., optical birefringence in fields along [111] meas. 77−28540
$Dy_3Al_5O_{12}$, magneto-optical rotation in transverse field 79−73902
$Dy_3Al_5O_{12}$, magnetostriction, role of order parameter 79−73796
$Dy_3Al_5O_{12}:Ca^{2+}$, optical absorpt. spectrum, strong crystal field of tetragonal symm. 77−32410
$Dy_3Fe_5O_{12}$, formation mechanism from metallic oxides 77−48376
$Dy_3Ga_5O_{12}$, crystal field effect on paramag. props. of Dy^{3+} ion 80−50040
$Dy_3Ga_5O_{12}$, dipolar magnet, sp. ht. and magnetisation meas. 80−60344
$Dy_3Ga_5O_{12}$, sp. ht. meas., 0.4-90K 77−55680
$Dy_3Ga_5O_{12}$, sp. ht. meas, 37mK-2K 77−85476
$Dy_3Ga_5O_2$, induced staggered mag. fields, neutron diffr. study 80−60196
DyIG, mag. and magnetooptical props., temp. and field depends. 77−89927
DyIG, magneto-optical absorption, near IR 80−40094
DyIG, mol. field coeffs., magnetisation and mag. susceptibility anal. 78−95406
DyIG, non-cryst., Mossbauer and magnetisation studies 80−44979
DyIG, noncrystalline, Mossbauer and magnetisation data 80−34828
DyIG, thermoelectric power, elec. cond. charge carrier conduction mechanism 80−34441
DyScFe garnets, mag. props. 77−47979
EUIG:Pb, valence of Pb in Fe-garnets 77−47480
$(Er,Tb,Gd_3)Fe_5O_{12}$ plate, pseudouniaxial, domain struct., magneto-optical obs. 80−11221
ErAG, facet formation 78−63687
ErAG, rare earth impurity, spectral probe of stoichiometry variations 77−85790
$ErAG:Er^{3+}$, 3 μm stimulated emission at room temp. 77−42541
ErAlG:Ho, Tm, Et⇄Ho and Er⇄Tm energy transfer, fluorescence meas. 78−27305
$(ErEu)_3(FeGa)_5O_{12}$ film, for mag. writing and magneto-optical displays 78−6549
$Er_2EuFe_{5-x}Ga_xO_{12}$, rag-domain garnet film, controlled variation of props. under O_2 annealing 79−15328
$Er_3Fe_{5-x}In_xO_{12}$, lattice consts., T_c, mag. saturation, K-absorpt. and Mossbauer spectra, 80K *(Russian)* 77−20954
$Er_3Fe_5O_{12}$, low temp. CVD epitaxial film growth and mag. props. 79−42406
ErGG, rare earth impurity, spectral probe of stoichiometry variations 77−85790
ErGa garnet, crystal field theory of Er^{3+} ion behaviour 77−8259
ErIG, high-field magnetisation, low temp. mag. anisotropy 80−75802
ErIG, magnetic props. of single cryst., 4.2-600K 79−78341
ErIG, superexchange operator and cryst. field interactions 80−59931
$Er_xY_{3-x}Fe_5O_{12}$, garnet, mag. anisotropy and magnetostriction 80−11189
$Er_xY_{3-x}Fe_5O_{12}$, spin reorientation transitions 78−2686
$(Eu,La,Ca)_3(Fe,Ga,Al)_5O_{12}$ film, LPE growth and induced orthorhombic anisotropy 77−20652
$(Eu,Lu)_3(Fe,Al)_5O_{12}$ film, epitaxial, increased domain wall velocities, due to orthorhombic anisotropy 77−20653
$(Eu,Lu)_3Fe_5O_{12}$ epitaxial film, induced orthorhombic anisotropy 77−69640
$(Eu,Lu)_3Fe_5O_{12}$, epitaxial film, orthorhombic mag. anisotropy 78−19290
$(Eu,Lu)_3Fe_5O_{12}$, submicron bubble films on rare earth-Ga garnet substrates, prep. and mag. props. 78−91909
$(Eu,Lu)_3Fe_5O_{12}$:Ga(Al)(Ca,Ge), bubble material, dynamic characterisation, comparison between transport and FMR methods 80−39833
$(Eu,Y)_3Fe_5O_{12}$, low temp. CVD epitaxial film growth and mag. props. 79−42406
$(Eu,Yb)_3Fe_5O_{12}$, low temp. CVD epitaxial film growth and mag. props. 79−42406
Eu-Ce(Pr)-Fe-O system, solid solns. of ferrogarnet and ferroperovskite type 78−27488
Eu-Fe garnet, light mag. linear birefringence and dichroism near absorption band *(Russian)* 80−55063
$Eu_{3-x}Ca_xSi_xFe_{5-x}O_{12}$, bubble film, LPE growth induced anisotropy 77−20659
$EuEr_2Ga_{0\,7}Fe_{4.3}O_{12}$, garnet thin films, magnetisation orientation, temp. depend. 80−71125
$Eu_3Fe_5O_{12}$, thermodyn. props. 77−84947
$Eu_3Fe_5O_{12}$, thermodynamic stability 77−52662
$Eu_3Ga_5O_{12}$, sp. ht. meas., 0.4-90K 77−55680
EuGaYIG film, bubble dynamics, anisotropy depend., ferromag. reson. expts. 77−63240
EuGaYIG:Cr, epitaxial garnet film, interaction pot. of domain walls with localised stress fields 80−44889
EuIG bubble domain film, magnetocrystalline anisotropy coeff. reduction, by Pb addition 79−11329
EuIG, non-cryst., Mossbauer and magnetisation studies 80−44979
EuIG, noncrystalline, Mossbauer and magnetisation data 80−34828
EuIG:Ga(Al), pure and doped, mag. anisotropy, magnetisation meas. 80−60240
EuIG:Pb film saturation magnetisation improved by Sb^{5+} substitution 80−54926
EuIG:Sb(Ca)(Ti), growth from $PbO-B_2O_3$ based flux, prop. depend. on Pb content 80−39824
EuIG:Si, magnetoresistance meas. 79−78120
EuIG+Pb, (100) LPE film, magnetocryst. anisotropy and lattice mismatch 77−20647
$(EuLu)_3(FeAl)_5O_{12}$, film epitaxial growth on Gd_3GaO_{12} substrate, mag. props. 80−65402
$(EuLu)_3Fe_5O_{12}$, Ga, Al or (Ca,Ge) substituted, mag. props. and growth of 2 μm bubbles 78−91910
$Eu_{2.9}Lu_{0.1}Fe_5O_{12}$:Si magnetoresistance meas. 79−78120
EuTm-CaGe, magnetic FE garnet film, LPE growth and composition 78−23634
$EuTm_2Fe_5O_{12}$ film , CaGe substituted, LPE growth kinetics 78−31349
$(EuY)_3(FeGa)_5O_{11}$, ferrite garnet film, mag. bubble motion delay 79−91269
$Eu_{0.6}Y_{2.4}Ga_{1\,26}Fe_{3.74}O_{12}$ garmet film, Walker oscills., detection by dynamic bubble collapse 78−68318
$Eu_{0.6}Y_{2.4}Ga_{1.26}Fe_{3.74}O_{12}$ garnet film, dynamic bubble-collapse determ. of domain wall motion oscillation 79−78454

garnets continued
$Eu_zY_{3-z}Ga_tFe_{5-t}O_{12}$, epitaxial garnet films, props. at compensation points 80−39823
EuYIG:Sb, growth from $PbO-B_2O_3$ based flux, prop. depend. on Pb content 80−39824
Fe garnet, Bi substituted, epitaxial film, magneto-optical controlled transparencies 78−50932
Fe garnet, Bi-substituted, film, domain boundary transform. into canted phase at compensation point 77−24724
Fe garnet, ferrimagnetic, sublattice magnetisation calc. 77−16063
Fe garnet, optical radiation interaction with magnetostatic waves 80−76009
Fe garnet epitaxial film, thermomag. data recording by electron beam heating 78−27066
Fe garnets, sublattice magnetisation curves, Mossbaeur study 80−75808
with Fe^{3+} ions in tetrahedral sublattice, mag. ordering and bond geometry 77−32163
Fe^{3+} ligand field spectrum 79−78701
$FeBO_3$, spin waves, Brillouin scatt. studies 79−99696
GGG, GGG-ErGG, rare earth impurity, spectral probe of stoichiometry variations 77−85790
Ga substituted garnet films, mag. prop. control during LPE growth and processing 78−68638
Ga-YIG, accelerated crucible rotation technique effect on cryst. growth by induced striation method 77−63553
GaYIG, magnetoelastic surface wave attenuation 77−20667
$(Gd, Bi)_2$ $(Fe, Ga)_5O_{12}$ magneto-optic LPE garnet films, high-energy heavy ion irrad., props. 80−71390
$(Gd,Bi)_3,(Fe,Al,Ga)_5O_{12}$ LPE film, 180° Bloch wall pinning at etched nucl. tracks 78−39376
$(Gd,Bi)_3(Fe,Ga)_5O_{12}$ magneto-optic film, ion irrad. effect on storage props. 78−52324
$(Gd,Bi)_3(Fe,Ga)_5O_{12}$, LPE film, coercivity, influence of nuclear tracks 79−51829
$(Gd,Bi)_3(Fe,Ga)_5O_{12}$ epitaxial garnet film, nucl. tracks effect on mag. props. 80−11234
$(Gd,Lu)_3(Fe,Mn,Al)_5O_{12}$ epilayer with orthorhombic anisotropy, domain wall vel. 78−52322
$(Gd,Tm,Y)_3(Fe,Ga)_5O_{12}$ film, magnetocrystalline anisotropy 79−78450
$(Gd,Tm,Y)_3(Fe,Ga)_5O_{12}$ LPE garnet thin films, magnetocrystalline anisotropy 80−93147
$(Gd,Tm,Y)_3(Ga,Fe)_5O_{12}$, bubble domain gradient propag., elliptical distortion and bias compensation 78−19292
Gd-Ga garnet growth, effect of buoyancy parameter of Czochralski bulk flow 79−61512
GdAG, electrostatic model of cryst. field 80−59945
$Gd_3Al_5O_{12}$ phase obtained by crystallisation of amorphous $Gd_2O_3.5/3Al_2O_3$ by quenching 78−92224
GdCa garnets, solid soln., mag. and cryst. chem. props. 77−16057
GdFe garnet, thermomagnetic recording on magnetised single cryst. plate 79−47285
$Gd_3Fe_3O_{12}$, electron irrad., primary-ion charge compensation using SIMS 79−57322
$Gd_3Fe_5O_{12}$, formation mechanism from metallic oxides 77−48376
GdGa garnet, appl. as X-ray monochromator for high-angle double-cryst. diffr. 77−43111
GdGa garnet, Czochralski grown, substrate material dislocation propagation 78−59771
GdGa garnet single cryst. substrate surface quality *(Russian)* 77−44371
GdGa, microwave losses 77−4531
$Gd_3Ga_{5-x-y}Mg_xZr_yO_{12}$, cryst. growth, coupled substitution of Ga by Mg and Zr 78−31325
$Gd_2Ga_5O_{12}$, cryst. growth by Czochralski technique, dissociation products calcs. 79−47615
$Gd_3Ga_5O_{12}$, brilliance, sparkliness and fire of diamond simulants 78−90363
$Gd_3Ga_5O_{12}$, Ca, Zr and Mg substituted artificial garnets, track registration props. 78−62679
$Gd_3Ga_5O_{12}$, chem. binding, 4d X-ray spectra obs. 79−69910
$Gd_3Ga_5O_{12}$ crystal growth from melt, X-ray topography meas. *(Hungarian)* 80−11556
$Gd_3Ga_5O_{12}$, Czochralski grown, effect of melt flow phenomena on perfection 78−88419
$Gd_3Ga_5O_{12}$, decorated dislocations, large interstitial climb loops round precip. particles 77−19960
$Gd_3Ga_5O_{12}$, dielectric constant, effect of degree of purity and perfection 77−48117
$Gd_3Ga_5O_{12}$ dislocation anal. at inclusions by repeated etching technique 80−29024
$Gd_3Ga_5O_{12}$, elec. cond. meas. 79−23961
$Gd_3Ga_5O_{12}$, flux growth and nucleation temp. determ. *(Chinese)* 80−60761
$Gd_3Ga_5O_{12}$, garnet substrate, surface polishing, damage, abrasion, brittle fracture model *(German)* 77−73357
$Gd_3Ga_5O_{12}$, garnet substrate surfaces, working damage, electron microscope investig. 77−77605
$Gd_3Ga_5O_{12}$, garnet-perovskite transform 80−15239
$Gd_3Ga_5O_{12}$, grown by automatic diameter control, growth striae 77−69979
$Gd_3Ga_5O_{12}$, growth of 3″ diameter crystals 78−68616
$Gd_3Ga_5O_{12}$, high energy heavy ion irrad., lattice strain 80−49278
$Gd_3Ga_5O_{12}$, IR refl., ATR, Voigt and Faraday expts. 80−66180
$Gd_3Ga_5O_{12}$, interface processes with $(YSm)_3(FeGa)_5O_{12}$ film, LPE, horizontal dipping obs. 80−49552
$Gd_3Ga_5O_{12}$, mag. phase diagram, AC susceptibility meas. 80−60265
$Gd_3Ga_5O_{12}$, magnetic interactions and short range order 79−78401
$Gd_3Ga_5O_{12}$, opt. dispersion 78−64343
$Gd_3Ga_5O_{12}$, optical birefringence images of edge dislocations 77−1129
$Gd_3Ga_5O_{12}$, planar defects, X-ray topography obs. *(French)* 80−2008
$Gd_3Ga_5O_{12}$, precipitates assoc. with dislocation climb trails *(German)* 77−35567
$Gd_3Ga_5O_{12}$, single cryst., helical dislocation obs. by etching 77−11558
$Gd_3Ga_5O_{12}$ single crystal polishing characteristics, comparison chemical, mechanical methods, magnetic bubble device appl. *(Japanese)* 79−5067
$Gd_3Ga_5O_{12}$, single cryst. growth for mag. appls., book contrib., review 79−69968
$Gd_3Ga_5O_{12}$, substrate, electron examination of microstruct. and microsegregation 78−67919
$Gd_3Ga_5O_{12}$, synthetic, cryst. growth, review *(German)* 79−33926

garnets continued
$Gd_3Ga_5O_{12}$, X-ray topography and double-crystal diffraction 80–92534
$Gd_3Ga_5O_{12}:Ho^{3+}$, stimulated emission at low temps. 80–106526
$Gd_3Ga_5O_{12}:Ho^{3+}(Er^{3+})$, stimulated emission and Ho^{3+} cascade laser action 79–91466
$Gd_3Ga_5O_{12}:Nd^{3+}$, cryst. field anal. 78–64013
$Gd_3Ga_5O_{12}:Nd^{3+}$, optical absorpt. and fluoresc. intensities 80–29793
GdIG, amorphous, Mossbauer specfra, mag. props. 80–15849
GdIG, empirical formula for lattice const. calc. 79–27968
GdIG, expts. on chem. equilib. for possible appl. in CVD 80–24750
GdIG, IR refl., ATR, Voigt and Faraday expts. 80–66180
GdIG, local mag. anisotropy in stress field of single dislocation 80–88744
GdIG, mag. props. meas. in high mag. fields, review *(Japanese)* 78–52303
GdIG, one-magnon light scatt. with and without compensation temps. 78–31062
GdIG single crystal plates for magnetooptical information storage 79–7997
GdIG, spin struct. by Faraday rotation expts. in fields up to 200 T 77–69809
GdIG, spin wave intrinsic relaxation, magnon damping at low temps. 80–29543
GdIG, spin-orientation phase transitions, magneto-optic and visual exam. 77–24675
GdIG, thermal effect on re-entrant hysteresis loop and coercive force 78–2702
GdIG, thermoelec. power, elec. cond., 500-1200K, ferrimag. Curie temp. 79–99543
Gd_2O_3-Fe_2O_3-PbO-B_2O_3, primary crystallisation regions 77–12604
$(GdPrBi)_3(FeGaIn)_5O_{12}$, pure and In^{3+} doped, near IR absorpt. and Faraday rot. 78–95580
GdScFe garnets, mag. props. 77–47979
GdTmGa garnet bubble film, ion implanted, pot. wells under charged wells 80–34717
$Gd_{0.9}YTm_{1.1}1Ga_{0.44}Fe_{4.56}O_{12}$, ion implanted, ferromag. reson. meas. 78–68385
Ge substituted garnet films, mag. prop. control during LPE growth and processing 78–68638
Ho-YIG, magnetic props. in strong fields at low temp., Ising approx. calcs. *(Russian)* 80–54920
$Ho_3Fe_5O_{12}$:Pb film, grown from fluxed metals by LPE 77–24972
HoGa garnet, mag. ordering induced by hyperfine interaction, neutron diffr. meas. 77–66265
$Ho_3Ga_5O_{12}$, hyperfine interac. induced antiferromag. order *(French)* 77–59392
HoIG, anomalous Faraday behaviour, mag. props. 79–82955
HoIG, Faraday rotation, mag. field depend., 4.2 to 300K, magneto-optical coeffs. 78–95577
HoIG, mag. permeability, Faraday rotation expts. 77–16287
HoIG, mol. field coeffs., magnetisation and mag. susceptibility anal. 78–95406
HoIG, spin reorientation from Faraday effect meas. 79–51780
HoYIG, level intersection and instability of mag. struct. *(Russian)* 77–43816
La-Sm-Lu iron garnet film grown as NdGaG substrates, mag. props. 80–44888
$(LaLuSm)_3(GaFe)_5O_{12}$ bubble garnet film, coercivity 79–78459
$(LaTmCa)_3(FeGe)_5O_{12}$, mag. loss and domain wall mobility 80–65980
$(LaTmCa)_3(Fe_{5-x}Ge_x)O_{12}$ film, high g, for mag. bubble applics. 77–85529
$(Lu,Bi)Fe_5O_{12}$, magneto-optic colour effects 78–23308
$(Lu, La, Y, Ca)_3(Ge, Fe)_5O_{12}$, temperature compensated high mobility bubble garnet, LPE and props. 77–20656
LuAG, electrostatic model of cryst. field 80–59945
LuAG:Nd^{3+}, cryst. field anal. 78–64013
LuAl garnet:Mo^{3+}, single crysts., EPR *(Russian)* 77–63267
$Lu_3Al_5O_{12}:Er^{3+}$, 3 μm stimulated emission at room temp. 77–42541
$Lu_3Al_5O_{12}:Er^{3+}(Ho^{3+})$, stimulated radn., electron-phonon interaction *(Russian)* 77–8605
$Lu_3Al_5O_{12}:Ho^{3+}$, stimulated emission at low temps. 80–106526
$Lu_3Ga_5O_{12}:Nd^{3+}$, cryst. field anal. 78–64013
LuTb garnet film, scratch-modified mag. domain patterns 78–48007
Mn-substituted garnet film, growth characts. and mag. props. 80–39826
$Mn_3Al_2Ge_3O_{12}$, garnet, mag. ordering, neutron diffr. patterns 78–19220
$Mn_3Al_2(SiO_4)_3$, Mossbauer spectra and absorpt. bands 80–55144
$Mn_3Cr_2Ge_3O_{12}$ garnet, antiferromag. ordering *(Russian)* 78–80146
$Mn_3Cr_2Ge_3O_{12}$, magnetically ordered Mn^{2+} and Cr^{3+} ions *(Russian)* 77–8281
$NaCa_2Cu_2V_3O_{12}$, crystal struct. distortion due to cooperative Jahn-Teller effect *(Russian)* 77–1119
$NaCa_2Mn_2V_3O_{12}$, antiferromag., spin wave contrib. to sp. ht., λ-anomaly at 25.05K T_N 77–77068
$NaCa_2Sb_2Fe_3O_{12}$, mag. ordering and bond geometty rel. to tetrahedral Fe^{3+} 77–32163
$NaCa_2Sb_2Fe_3O_{12}$, neutron diffr. patterns, group theory approach for determ. of mag. struct. *(Russian)* 79–51749
$Na_3M_2Li_3F_{12}$, M=Al, Fe, fluoride garnets, high press. form 77–76554
$Na_3Sc_2V_3O_{12}:(Fe^{3+}, Mn^{2+})$, spin Hamiltonian parameters, g-factors, temp. depend. EPR obs. 77–48038
$Na_3Te_2Fe_3O_{12}$, mag. ordering and bond geometry rel. to tetrahedral Fe^{3+} 77–32163
$Na_3Te_2Fe_3O_{12}$, neutron diffr. patterns, group theory approach for determ. of mag. struct. *(Russian)* 79–51749
$Nb_xY_{3-x}Fe_5O_{12}$, low-temp. magnetocrystalline anisotropy study 79–95586
Nd:YAG, high repetitive picosecond laser system and broad range wavelength tuning *(Japanese)* 79–3698
Nd:YAG, solid-state formation 80–35121
Nd:YAG mode-locked laser picosecond pulse profile and power meas. 77–7112
$NdGa_5O_{12}$ wafer, dislocations, etch pits and birefr. obs. 78–83818
$Nd_3Ga_5O_{12}$, elastic and thermoelastic consts., US meas. *(German)* 77–59061
$Nd_3Ga_5O_{12}$, floating zone method growth, interface shapes 80–60775
$Nd_3Ga_5O_{12}:Nd^{3+}$, radiationless decay processes, laser photoacoustic spectroscopy meas. 80–84766
NdScFe garnets, mag. props. 77–47979
$Pr_3Ga_5O_{12}$, sp. ht. meas., 0.4-90K 77–55680
$(PrGdYb)_{3-x}Bi_x(FeAl)_5O_{12}$ system, LPE growth and magnetooptical props. 79–65842

garnets continued
$Pr_xY_{3-x}Fe_{5-y}O_{12}$ film, IR absorpt. and Faraday rot. spectra 77–52093
$(Sm,Er)(Ga,Fe)_5O_{12}$, LPE, non-grooved film, thermomag. writing 78–76278
$(Sm,Lu)_3Fe_5O_{12}$, submicron bubble films on rare earth-Ga garnet substrates, prep. and mag. props. 78–91909
$(Sm,Y)_3(Fe,Ga)_5O_{12}$, epitaxial mag. layer, LPE, growth rotation rate, effect on props. 78–56053
Sm-YIG garnets, implanted and Permalloy coated, comparison between planar domain walls in bubbles 77–85520
SmCaGe garnet LPE bubble film, coercivity, thickness depend. 78–68324
$Sm_3Fe_5O_{12}$, spin-reorientation phase transition, NMR spectra and anisotropy consts. meas. 77–28458
SmGa garnet film, scratch-modified mag. domain patterns 78–48007
$Sm_3Ga_5O_{12}$, elastic and thermoelastic consts., US meas. *(German)* 77–59061
$Sm_3Ga_5O_{12}$, garnet-perovskite transform 80–15239
SmIG, hysteresis in spin-orientation phase transitions 79–73761
SmIG, mag. phase transitions, Mossbauer spectroscopy obs. 80–80509
$(SmLu)_3(FeAl)_5O_{12}$, film epitaxial growth on $Gd_3Ga_5O_{12}$ substrate, mag. props. lattice mismatch 80–65402
$Sm_{0.3}Lu_{0.2}Tm_{0.2}Y_{1.45}Ca_{0.85}Fe_{4.15}Ge_{0.85}O_{12}$, LPE growth, saturation magnetisation, collapse field, bubble diameter 78–95703
$(SmLuYCa)_3(FeGe)_5O_{12}$ film, ion implant profile 79–78477
$(SmTm)_3(FeGa)_5O_{12}$, small-bubble appl. 79–82845
SmTmIG, epitaxial layer with submicron bubbles, mag. props. 77–12172
$(SmYCa)_3(FeGe)_5O_{12}$ epitaxial layer, growth kinetics and struct. as functions of cryst. lattice parameter mismatch 80–6677
$Sm_{0.1}Y_{1.9}CaFe_4GeO_{12}$, LPE growth, saturation magnetisation, collapse field, bubble diameter 78–95703
$(SmY)_3(FeGa)_5O_{12}$, LPE on $Gd_3Ga_5O_{12}$, growth kinetics, 920-980°C 78–3064
$Sm_{0.4}Y_{2.6}Fe_{3.8}Ga_{1.2}O_{12}$, LPE. improved method of stirring 78–68641
$Sm_{0.4}Y_{2.6}Fe_{3.8}Ga_{1.2}O_{12}$ epitaxial films, uniaxial mag. anisotropy, ferrimag. reson. study 80–80577
$Sm_xY_{3-x}Fe_5O_{12}$, mag. anisotropy, meas. temp., depend. 78–19247
$Sm_xY_{3-x}Fe_5O_{12}$, magnetostriction comp. depend., 78 to 300K 77–77082
$Sm_xY_{3-x}Fe_5O_{12}$, spin reorientation transitons 78–2686
SmYGa garnet, bubble motion depend. on wall pinning 79–78455
$Sm_{0.4}Y_{2.6}Ga_{1.1}Fe_{3.9}O_{12}$, LPE, growth rate anisotropy and kinetic coeffs. of vicinal faces 78–51846
$Sm_{0.4}Y_{2.6}Ga_{1.2}Fe_{2.8}O_{12}$, H^+ implanted film, epitaxial, mag. bubbles, walls and fine struct. 77–63241
SnCaV garnet polycrystal, ferrimag. resonance loss rel. to grain size 77–85581
Tb compounds with garnet and zircon structure, anisotropic magnetoelastic props. 77–69660
TbAG, reson. electronic Raman effect, interferences, lifetime meas. 80–93294
$Tb_{0.7}Er_{1.3}Gd_{1.0}Al_{0.2}Fe_{4.8}O_{12}$, garnet plate, domain struct. 80–2602
$TbFeO_3$, thermodynamic props. 77–36078
$Tb_3Fe_5O_{12}$, Faraday rotation in high transient mag. fields 77–69810
$Tb_3Fe_5O_{12}$, mag. phase transition exam. 79–19736
$Tb_3Fe_5O_{12}$, quasiantiferromag. state magnetised along two-fold symmetry axis, mag. phase diagram 77–69564
$Tb_3Fe_5O_{12}$, weak field mag. transition, magneto-optical and magnetisation meas. 77–69551
TbGa garnet, mag. ordering induced by hyperfine interactions, neutron diffr. meas. 77–66265
TbGa garnet, Verdet const. meas. with pulsed mag. field 78–68486
$Tb_3Ga_5O_{12}$, hyperfine interac. induced antiferromag. order *(French)* 77–59392
TbIG, [111] magnetoelastic props., rel. to Cotton-Mouton birefringence, 90-500K 80–103876
TbIG, anisotropic forced magnetostriction meas. 78–64251
TbIG, anisotropic garnet, mag. struct., magnetisation and Faraday rotation obs. 78–68169
TbIG, anisotropic linear mag. birefr., light modulation 77–8548
TbIG, appl. of superposition model to cryst. field 78–68132
TbIG, Faraday rot., temp. and high mag. field depend. 79–95736
TbIG, Faraday rotation and transition of spin config. at high mag. fields 80–39776
TbIG, hyperfine interaction determ. from Mossbauer spectra in applied mag. field 77–28497
TbIG, mag. birefringence rel. to sublattices 79–28723
TbIG, mag. linear double refr., two-sublattice model *(Russian)* 79–28728
TbIG, magnetisation and mag. susceptibility meas. along (111) direction, 4.2-295K 77–80917
TbIG, mol. field coeffs., magnetisation and mag. susceptibility anal. 78–95406
TbIG, neutron depolarisation near mag. compensation point 77–24709
TbIG, refr. index, higher-order anisotropic mag. contrib. 77–69808
TbIG, X-ray topographic obs. of domain evolution in mag. field 77–69600
TbIG:Si magnetoresistance meas. 79–78120
$Tb_2Lu_1Fe_5O_{12}$ film, magnetostriction meas. using double cryst. X-ray diffractometry 78–84468
TbScFe garnets, mag. props. 77–47979
TbY ferrite garnet, Tb^{3+} energy level inversion, Faraday effect *(Russian)* 79–47418
$Tb_{0.2}Y_{2.8}Fe_5O_{12}$, Mossbauer investigation of spin-reorientation transition 78–88243
$Tb_{0.26}Y_{2.74}Fe_5O_{12}$, anomalous props., 200-250K 79–28527
$Tb_{0.26}Y_{2.74}Fe_5O_{12}$ garnet, mag. transition, mag. props. anomaly 80–93120
$Tb_xY_{3-x}Fe_5O_{12}$ hysteresis in spin-orientation phase transitions 79–73761
$Tb_xY_{3-x}Fe_50_{12}$, anomalies of magnetisation and magnetostriction obs. in strong fields, 4.2K 77–1581
Ti garnets, synthetic, IR spectra, Ti struct. role 80–7346
Tm ferrogarnet film, cylindrical mag. domain motions, domain boundary oscills. *(Russian)* 80–71140
TmAG, Mossbauer study of crystal field props. 80–66082
$Tm_{2.2}Bi_{0.8}Fe_{3.5}Ga_{1.5}O_{12}$ epitaxial film, Faraday effect and domain struct. near compensation point 77–20838
$Tm_{2.7}Bi_{0.3}Ga_{0.3}Co_xFe_{4.7-x}O_{12}$, Co ion concentration effect on mag. props. close to mag. compensation point *(Russian)* 79–73788
$Tm_3Fe_5O_{12}$, mol. field coeffs., mag. moment/temp. relations 80–50067
$Tm_3Ga_5O_{12}$, Mossbauer study of crystal field props. 80–66082

garnets continued
$Tm_3Ga_5O_{12}$:$Cf^{3+}(Yb^{3+})(Gd^{3+})$, Van Vleck paramagnet, EPR g-shifts and linewidths, temp. depend. 77—66419
UIG, Ga-substituted, computer simulation of temp. and field depend. of sublattice magnetisation and spin-flip transition 79—11300
$(Y,Ca)_3(Fe,Ge)_5O_{12}$ LPE layer, exchange stiffness coeffs., 30-300K 79—78464
$(Y,Ca)_3(Fe)_2(FeGe)_3O_{12}$ film, exchange const., ferromag. reson. meas. 79—8023
$(Y,Eu,Lu,Ca)_3(Fe,Ge)_5O_{12}$, bubble memory chip, dynamic conversion comparison with $(Y,Sm,Lu,Ca)_3(Fe,Ge)_5O_{12}$ 78—68319
$(Y,Eu,Sm)_3(Ga,Fe)_5O_{12}$ film, mag. loss and bubble dynamics 77—8371
$(Y,Eu,Tm,Ca)_3(Fe,Ge)_5O_{12}$, Ca, Ge substituted garnet LPE films, elec. props., charge imbalance, Seebeck effect 78—68101
$(Y,Eu,Tm,Ca)_3(Fe,Ge)_5O_{12}$ garnet film coercivity, new annealing method 78—84459
$(Y, Eu, Yb, Ca)_3(Ge, Fe)_5O_{12}$, bubble film, LPE on $Gd_3Ga_5O_{12}$, mismatch and faceting 77—20657
$(Y,Eu)_3(Fe,Ga)_5O_{12}$, epitaxial, cylindrical mag. domain struct., radial wall motion effect *(Russian)* 77—8373
$(Y,Eu)_3(Fe,Ga)_5O_{12}$, LPE growth from molybdate fluxes, bubble props. 78—68322
$(Y,Eu)_3(Ga,Fe)_5O_{12}$ film, bubble wall state stability obs. 77—20651
$(Y,Gd,Tm)(Fe,Ga)_5O_{12}$, cylindrical mag. domain behaviour in external mag. field *(Russian)* 78—6553
$(Y,Gd,Yb,Bi)_3(Fe,Al,Ga)_5O_{12}$ films, magnetic bubble domains, domain wall motion examined 78—19294
$(Y,Gd,Yb,Bi)_3(Fe,Al)_5O_{12}$ film, nonreciprocal effects in domain boundary motion in inhomogeneous field 77—24726
$(Y, Gd, Yb, Bi)_3(Fe, Al)_5O_{12}$ epitaxial film, domain wall motion and oscill. 80—2616
$(Y,Gd,Yb,Bi)_3(Ga,Al,Fe)_5O_{12}$, bubble conversion to anomalous behaviour 78—23309
$(Y,Gd,Yb)_{3-x}Bi_x(Fe,Al)_5O_{12}$, garnet single cryst. film, possible bubble appl. 78—6552
$(Y,Gd,Yb)_{3-x}Bi_x(Fe,Al)_5O_{12}$, LPE, for magneto-optical appls. 78—48341
$(Y,Gd,Yb)_3(Fe,Ga)_5O_{12}$ film, magnetisation processes and domain struct. near compensation temp. 78—14996
$(Y,Gd)_3(Fe,Ga)_5O_{12}$, thin film lightguide, noninteracting mode conversion *(Russian)* 78—1347
$(Y,Lu)_3(Fe,Sc)_5O_{12}$ LPE layer, exchange stiffness coeffs., 30-300K 79—78464
$(Y,Re)_{3-x}Ca_xGe_{5-x}Ge_xO_{12}$, garnet films, LPE growth for bubble memory appls. 77—11813
$(Y,Sm,Ca)_3(Fe,Ge,Si)_5O_{12}$ single-crystal films, props. 78—64247
$(Y,Sm,Ca)_3(Fe,Ge)_4O_{12}$, garnet thin film, mag. anisotropy, Faraday effect meas. 79—42812
$(Y,Sm,Ca)_3(Fe,Ge)_5O_{12}$, domain wall, radial motion, method of dynamic collapse of mag. bubbles 79—8026
$(Y,Sm,Ca)_3(Fe,Ge)_5O_{12}$ epitaxial films, mag. props., growth condition effects 80—97124
$(Y,Sm,Ca)_3(Ge,Fe)_5O_{12}$ film, bubble wall state stability obs. 77—20651
$(Y,Sm,Ga)_3(Fe,Ge,Si)_5O_{12}$ film, static and dynamic mag. props., 20-160°C 77—24725
$(Y, Sm, Lu, Ca)_3(Fe, Ge)_5O_{12}$:$Ne^+$, film, $S=1$ bubbles dynamic props., temp. depend. 77—20658
$(Y,Sm,Lu,Ca)_3(Fe,Ge)_5O_{12}$, bubble memory chip, dynamic conversion comparison with $(Y,Eu,Lu,Ca)_3(Fe,Ge)_5O_{12}$ 78—68319
$(Y,Sm,Lu,Ca)_3(Fe,Ge)_5O_{12}$ garnet film coercivity, new annealing method 78—84459
$(Y,Sm,Lu,Ca)_3(Fe,Ge)_5O_{12}$ bubble magnetic garnet film, LPE grown, props., $CaCO_3/GeO_2$ molar ratio influence 80—50152
$(Y, Sm, Lu, Ca)_3(FeGe)_5O_{12}$ LPE films, factors affecting coercivity 79—91267
$(Y,Sm,Lu,Ca)_3(Ga,Ge,Fe)_5O_{12}$, film growth and mag. props. for bubble-memory appl. 79—87297
$(Y,Sm,Lu,Cu)_3(Fe,Ge)_5O_{12}$, ion implanted, hard bubble suppression 80—11238
$(Y,Sm,Lu,Tm,Ca)_3(Fe,Ge)_5O_{12}$, epitaxial garnet film, temp. depend. mag. props. 80—39825
$(Y,Sm,Lu)_3(Fe,Ga)_5O_{12}$, LPE mag. film, suitability for 1 to 3 micron bubble devices 78—68323
$(Y, Sm, Tm)_3(FeGa)_5 O_{12}$ LPE films, factors affecting coercivity 79—91267
$(Y,Sm)_3(Fe,Ga)_5O_{12}$ film, static and dynamic mag. props., 20-160°C 77—24725
$(Y,Sm)_3(Fe,Ga)_5O_{12}$, garnet LPE films, growth rate anisotropy 80—54558
$(Y,Sm)_3(Fe,Ge)_5O_{12}$, Ca, Ge substituted garnet LPE films, elec. props., charge imbalance, Seebeck effect 78—68101
$(Y,Sm)_3(Ga,Fe)_5O_{12}$ epitaxial layers, annealing effect on mag. props. 79—61191
$(Y,Sm)_3(Ga,Fe)_5O_{12}$ film, domain boundary mobility, effect of easy magnetization axis inclination 78—19293
$(Y,Sm)_3(Ga,Fe)_5O_{12}$ films, growth from melt, growth property control 78—27395
$(Y,Sm)_3(Ga,Fe)_5O_{12}/(Eu,Er)_3(Ga,Fe)_5O_{12}$ double-layer self-biasing garnet films, dynamic behaviour of domain walls 80—34722
$(Y,Gd,Yb)_{3-x}Bi_x(Fe,Al)_5O_{12}$ film growth on $Gd_3Ga_5O_{12}$ substrates 79—78623
Y ferrite-garnet, porous polycrystal, law of approach to saturation *(Russian)* 78—47956
Y garnet, inhomogeneous collective magnon oscill. excited by RF field *(Russian)* 80—100582
Y, magnetoelastic wave propagation characts. obs. 77—40107
Y-Sm ferrogarnet *(Russian)* 80—71140
YAG, as substrate for $Er_3Al_{5-x}Ga_xO_{12}$ LPE film for solid laser 80—93419
YAG, brilliance, sparkliness and fire of diamond simulants 78—90363
YAG brittleness anisotropy, microcrack formation due to surface treatment 80—40526
YAG, colour centres conceived as bound polarons 78—63990
YAG crystal with rare earth ion impurities, active medium reson. pumping method for Nd laser freq. conversion 80—1206
YAG, crystallization kinetics and growth mechanism on oriented seeds in melt-solns. 79—14717
YAG crystals, dislocations and inclusions, birefringence topography obs. 80—107248
YAG, Czochralski grown crystals, interface shape change 78—83760
YAG Czochralski grown crysts., growth of facets and vicinal interfaces *(Chinese)* 79—90578

garnets continued
YAG, electrostatic model of cryst. field 80—59945
YAG, exposed to ultrasoft X-rays, thermal luminesc. and electron emission 79—8192
YAG, facet formation 78—63687
YAG, for electron microscopy, using auto emission gun *(Czech)* 78—21280
YAG, high temp. soln. growth using accelerated crucible rotation 79—100039
YAG, high-resolution many beam lattice image anal. 80—14979
YAG, influence of facial growth effect on Yb ion incorporation 79—10822
YAG, interrelationship between mech. props. and elec. relief on surface layer 79—23821
YAG laser, resonator length effects on loss coeffs. and ouptut energy *(German)* 78—66849
YAG, melting behaviour and metastability determ. by optical DTA 80—92648
YAG, molten, complexity in solidification behaviour, SEM electron images 79—43229
YAG, neutron diffr. determ. of O coordinates 77—1117
YAG, optical absorption of hole centres, polaron model 80—97314
YAG, optical films, high quality growth 79—46984
YAG, phonon spectrum, incoherent inelastic neutron scatt. meas. 77—66006
YAG, production of densely sintered ceramic, exam. of recrystallisation during sintering 80—11609
YAG, rare earth impurity, spectral probe of stoichiometry variations 77—85790
YAG rods, thermally induced birefringence in (001) direction, transmission loss *(Chinese)* 77—77166
YAG, simulated mol. images, point models and kinematical struct. amplitudes 80—103223
YAG single crystal growth by flux method *(Japanese)* 78—19655
YAG single crystal growth, by vertical directed crystn., thermal characts. 80—2944
YAG single crystals, derivation of cryst. parameters and orientation by X-ray topography *(Chinese)* 79—46622
YAG, single crysts., kinetic characts. of growth from melt-solns. on oriented seeds 79—14719
YAG, solubility in solvent $PbO_{-x}PbF_2$, phase form. in system Y_2O_3-Fe_2O_3-PbO-PbF_2-B_2O_3 78—95247
YAG solution, in $PbO/PbF_2/B_2O_3$ solvent systems, density, surface tension and expansivity data, effect of B_2O_3 conc. 79—19985
YAG, stress fields of dislocation arrays *(German)* 79—23615
YAG, surface grating relief pattern profile altering, oblique shadow deposition technique 79—68451
YAG, temp. distribution in growth from Czochralski method 79—65998
YAG, transient colour centres caused by UV radiation 77—84744
YAG, traps, energy spectra, X-irrad. effects and thermoluminesc. *(Russian)* 77—20940
YAG, undoped and Ce^{3+}-doped, cathodolum. intensity and decay time, 10-480K 79—99952
YAG, Yb^{3+} crystalline field, Schottky specific heat, paramagnetic susceptibility temp. depend. 77—11882
YAG:Ce, γ-irradiated elec. cond. meas. 77—43601
YAG:Ce phosphors, luminesc. efficiency, prep. and dopant effects 80—45151
YAG:Ce^{3+}, new fast scintillator for SEM 78—86394
YAG:Ce^{3+}, photoluminescence excitation energy, crystal field and temp. effects 80—11460
YAG:Ce^{3+}, scintillation detector, in SEM, electro-optical props. 80—52819
YAG:$Ce^{3+}(Eu^{3+})(Gd^{3+})(Tb^{3+})$, cathodoluminesc. efficiency rel. to activator conc. 80—11479
YAG:$Ce^{3+}(Tb^{3+})$, recomb. processes, spectral, kinetic and relative quantum intensity meas. 79—61443
YAG:Cr, optical detection of phonons 80—92630
YAG:Cr^{3+}, absorption and luminesc., spectra, Cr conc. depend. 77—12435
YAG:Cr^{3+}, electronic states interactions with crystal odd vibrs., R-lines vibr. recurrences 78—84639
YAG:Cr^{3+}, optical absorption, cryst. field pot. expansion 77—36268
YAG:Cr^{3+}, radiation colour centres, absorpt. and thermolum. spectra 78—48206
YAG:Cr^{3+} 80—2740
YAG:Dy(Er)(Tm)(Tb)(Yb), US attenuation 77—89500
YAG:Er, elastic wave damping, 300 to 1500 MHz, impurity effects 80—92602
YAG:Er^{3+}, 3 μm stimulated emission at room temp. 77—42541
YAG:Er^{3+}, crystal field theory, Er^{3+} behaviour in tetragonal field 77—8259
YAG:$Er^{3+}(Ho^{3+})$, stimulated radn., electron-phonon interaction *(Russian)* 77—8605
YAG:$Er^{3+}(Ho^{3+})(Tm^{3+})$, oscillator strengths of impurities, 5000 to 30000 cm^{-1} 79—4830
YAG:Eu^{3+}, reson. fluoresc. spectra, showing multiple Eu^{3+} sites 80—2812
YAG:Gd^{3+}, EPR absorpt. spectrum 78—76305
YAG:Ge^{3+}, excited state absorpt. loss, 5d→4f rare earth lasers 78—90417
YAG:Ho^{3+}, low-lying cryst. field levels 79—91007
YAG:Ho^{3+}, spectroscopy, stimulated emission 80—93374
YAG:Ho^{3+}, stimulated emission at low temps. 80—106526
YAG:M^{3+}, ESR absorption spectra, line broadening of Fe^{3+}, Cr^{3+}, Gd^{3+} 78—91940
YAG:Mn, impurity-induced O^- colour centres, absorpt. and fluoresc. spectra 77—1709
YAG:Nd, heat capacity and thermal diffusivity meas. 80—19956
YAG:Nd, laser cryst., dislocations density and propag., rel. to Czochralski growth *(Chinese)* 77—11552
YAG:Nd, laser material, linear expansion coeff. and r.i., temp. depend. 77—733
YAG:Nd, pumped laser rod, quantum efficiency 77—88724
YAG:Nd, single crysts., melt growth using heat exchange method 79—52106
YAG:Nd, with improved fluoresc. lifetime of $^4F_{3/2}$ state 77—687
YAG:Nd,Ce,Cr, effect of γ-rays, fast electrons on optical props., annealing and colour centre destruction 77—8608
YAG:Nd crystal, orientation influence on thermally induced birefringence *(Chinese)* 80—88958

garnets continued
- YAG:Nd laser, crystal defects influence on energetic effectiveness obs. *(Czech)* 78—79022
- YAG:Nd laser, kinematic mode synchronisation *(Russian)* 77—34892
- YAG:Nd laser, radiation characts. rel. to pumping intensity in long-time operation *(Russian)* 77—68214
- YAG:Nd laser pulses, mutual exchanges with plasma *(German)* 80—48918
- YAG:Nd^{3+}, Ce^{2+}, sensitisation, luminesc., absorpt. and emission spectra *(Russian)* 78—10982
- YAG:Nd^{3+}, cryst. field parameters calc., exchange charge model 78—47747
- YAG:Nd^{3+}, cryst. field anal. 78—64013
- YAG:Nd^{3+}, energy transfer between Nd^{3+} ions, laser-excited time-resolved site-selection spectroscopy 79—95839
- YAG:Nd^{3+}, many-phonon nonradiative transition probabilities 79—95842
- YAG:Nd^{3+}, nonradiative multiphonon relaxation of isolated impurity level, transition probability calcs. 79—56853
- YAG:Nd^{3+}, photon echo form. 77—23720
- YAG:Nd^{3+}, radiationless decay processes, laser photoacoustic spectroscopy meas. 80—84766
- YAG:Nd^{3+} and free Nd^{3+} ion, energy levels, absorption spectra 79—11076
- YAG:Nd^{3+} crystal, zero-phonon linewidths, in $^4I_{9/2}\rightleftarrows{}^4F_{3/2}$ luminesc. band calc. 79—28834
- YAG:R^{3+}, CRT and X-ray phosphor lattice-activator energy transfer model 78—6792
- YAG:R^{3+}, R=Nd, Er, (Er, Ga), LPE and luminesc. 78—64408
- YAG:rare earth, phonon impurity scatt., lattice thermal cond. and US attenuation meas. 78—87748
- YAG:rare earth metal, US absorpt. meas., relax. model 80—24539
- YAG:Ti, crysts., colour centres, optical absorpt. spectra 79—65080
- YAG:Ti, growth conditions from melt 79—95924
- YAG:V_2O_5, CaO, V^{4+} ion impurity spectral anal. 79—78719
- YAG-Ce^{3+}(Eu^{3+})(Tb^{3+})(Gd^{3+}), cathodolum. intensity, temp. depend., comparative study 79—99953
- YAG-Ti, polarised luminescence 79—95843
- $Y_3(Al,Fe)_5O_{12}$, optical anisotropy and stress birefringence assoc. with growth striations 79—42940
- $Y_3(Al_{0.5}Ga_{0.5})_5O_{12}$:Nd^{3+}, radiationless decay processes, laser photoacoustic spectroscopy meas. 80—84766
- $Y_3(Al_{1-x}Ga_x)_5O_{12}$:Nd, fluoresc. energy transfer and radiationless relax. 79—38625
- $Y_3(Al_{1-x}Ga_x)_5O_{12}$:Nd^{3+}, time-resolved site-selection spectroscopy, energy transfer 80—2814
- $Y_3Al_3O_{12}$ crystal growth from melt, gas bubble capture theory 80—64941
- $Y_3Al_5O_{12}$ crystals, variation of microhardness anisotropy with heat treatment 79—56053
- $Y_3Al_5O_{12}$, laser cryst., struct. inhomogeneity obs. by vac. decoration 77—35701
- $Y_3Al_5O_{12}$, layer structuresrevealed by decoration method and electron microscopy 77—27902
- $Y_3Al_5O_{12}$:Nd^{3+}, single crystal, $^4F_{3/2}$ level splitting and spectra dependence on press. *(Russian)* 77—52183
- $Y_{1.6}Bi_{1.0}Ca_{0.4}Fe_{4.4}In_{0.4}V_{0.2}O_{12}$, cation distrib. 79—19211
- $(YBiEr)_3(FeGa)_5O_{12}$ ferrite-garnet film, micron cylindrical mag. domains, high recording density 80—65978
- $Y_{1-4}BiFe_{3.8}Ga_{1.2}O_{12}$ garnet films, bistable bubble domain 79—15331
- $Y_2BiFe_{3.8}Ga_{1.2}O_{12}$ film, colour contrast between different domains 77—12166
- $Y_2BiFe_{3.8}Ga_{1.2}O_{12}$ film, magnetooptic interference of light 77—32458
- $Y_2BiFe_{3.8}Ga_{1.2}O_{12}$, film, dynamics of domain walls 78—27065
- $Y_{2.7}Bi_{0.3}Fe_{3.8}Ga_{1.2}O_{12}$ epitaxial film, mag. domains in microwave mag. field, Faraday obs. 78—19295
- $Y_{3-x}Bi_xFe_{5-y}Ga_yO_{12}$, epitaxial film, domain wall dynamics *(Russian)* 78—2718
- $Y_{3-x}Bi_xFe_{5-y}Ga_yO_{12}$-PbO-$B_2O_3$-$Bi_2O_3$ system, crystn. fields 78—43996
- $Y_2BiFe_5O_{12}$ garnet films, magnetooptical interference 79—28724
- $Y_{3-x}Bi_xFe_5O_{12}$, ferrite-garnet formation 78—52737
- $(YBiSmCa)_3(FeGe)_5O_{12}$ epitaxial layer, growth kinetics and struct. as functions of cryst. lattice parameter mismatch 80—6677
- $(YBi)_3.(FeGa)_5O_{12}$ film, interaction between Bloch walls and dislocations *(Russian)* 79—61196
- YCa garnets, solid soln., mag. and cryst. chem. props. 77—16057
- $(YCaEuYb)_3(FeGe)_5O_{12}$, LPE, stripe end motion, effect of in-plane field 78—68330
- $Y_{3-x}Ca_{2x}Fe_{2-y}In_yFe_{3-x}V_xO_{12}$, first magnetocryst. anisotropy const., ferrimag. reson obs. 78—68218
- $(Y_{3-x}Ca_x)(Fe_{2-x}Sn_x)(Fe_3)O_{12}$, long and short range magnetic order 79—38419
- $Y_{3-2x}Ca_{2x}Fe_{5-x}V_xO_{12}$, single cryst., Faraday effect and opt. props. 77—1660
- $Y_{3-y}Ca_yFe_{2-y}Zr_yFe_3O_{12}$, first magnetocryst. anisotropy const., ferrimag. reson obs. 78—68218
- YCaSmTmGeIG, epitaxial layer with submicron bubbles, mag. props. 77—12172
- $YCa_3Zr_2Fe_{2.75}Ga_{0.25}O_{12}$, mag. ordering and bond geometry rel. to tetrahedral Fe^{3+} 77—32163
- $(Y_{3-x}Ca_x)[Fe_{2-x}Sn_x](Fe_3)O_{12}$, Mossbauer spectra of Fe^{27} and Sn^{119} nuclei 79—95578
- $Y_{3-x}Ca_x[Fe_{2-x}Sn_x]Fe_3O_{12}$, Mossbauer spectra, Sn hyperfine mag. field 80—15893
- $(YCdYbBi)_3(FeAl)_5O_{12}$, cylindrical domain wall vel. anisotropy *(Russian)* 77—59440
- YE+AG:Er^{3+}, laser material, radiative and nonradiative transitions, conc. quenching 77—16391
- $(YErCa)_3(Fe\ Ge)_5O_{12}$, mag. loss and domain wall mobility 80—65980
- $(YErCa)_3(Fe_{5-x}Ge_x)O_{12}$ film, high g, for mag. bubble applics. 77—85529
- $(YEuCa)_3(FeGeSi)_5O_{12}$, mag. loss and domain wall mobility 80—65980
- $(YEuErCa)_3(GeFe)_5O_{12}$: H, Ne, Ar ion-implanted, threefold symmetrical bubble properties 78—64243
- $(YEu)_3(FeGa)_5O_{12}$ rigid magnetic bubble transition to normal behaviour 78—95501
- $(YEu)_3(FeGa)_5O_{13}$, LPE growth, uniaxial magnetocryst. anisotropy 77—8766
- $Y_{2.45}Eu_{0.55}Fe_{3.8}Ga_{1.2}O_{12}$, hard bubble conversion in in-plane field 78—14998

garnets continued
- $Y_{2.35}Eu_{0.65}Ga_{1.2}Fe_{3.8}O_{12}$, bubble translation vel., ion-implantation effects 78—68327
- $(YEuLuCa)_3(FeGe)_5O_{12}$ film, stable state of bubbles containing Bloch lines 78—76281
- YEuLuCaGe garnets, 7 μm-period bubble devices 80—44887
- YEuLuGa garnets, 7 μm-period bubble devices 80—44887
- YEuTmCa garnet bubble films, domain wall transition 79—56584
- $(YEuTmCa)_3(FeGe)_5$ bubble garnet films, ion-implanted, mag. susceptibility meas. 79—47311
- YEuTmCaGe garnets, 7 μm-period bubble devices 80—44887
- $(YEuTmCa)_3(GeFe)_5O_{12}$ film, Bloch loop punch-through in mag. bubbles 77—59437
- $Y_{1.52}Eu_{0.3}Tm_{0.3}Ca_{0.88}Ge_{0.88}Fe_{4.12}O_{12}$, bubble translation vel., ion-implantation effects 78—68327
- $(YEuTm)_3(FeGa)_5O_{12}$ film, dynamic props. of bubble domains by high speed photography 80—15771
- $(YEuTm)_3(FeGa)_5O_{12}$ garnet film, bubble domain steady state motion on a circle 80—29589
- YEuTmGa garnet bubble film, dynamic diffuse wall deform. 80—54927
- YEuTmGa garnets, 7 μm-period bubble devices 80—44887
- $(YEuTm)_3(GaFe_5)O_{12}$ ferrite garnet films, mag. bubbles, translational motion, mechanism for inertial effects 80—100606
- $Y_{1.57}Eu_{0.78}Tm_{0.65}Ga_{1.05}Fe_{3.95}O_{12}$, bubble garnet, low drive stripe head vel. 77—32225
- $Y_{1.57}Eu_{0.78}Tm_{0.65}Ga_{1.05}Fe_{3.95}O_{12}$ film, gradient propagation, overshoot and creep 78—19291
- $(YEuYbCa)_3(FeGe)_5O_{12}$, ion-implanted, in-plane mag. field effects on bubble props. 77—85521
- $(YEuYbCa)_3(FeGe)_5O_{12}$ film, mag. σ-bubbles, automation props. 78—88150
- $(YEuYbCa)_3(FeGe)_5O_{12}$ bubble films, Ne$^+$-implanted, cryst. and mag. props., X-ray diffr. obs. 79—38362
- $(YEuYbCa)_3(FeGe)_5O_{12}$ film, isolated straight stripe domain dynamic props. 79—33514
- $(YEuYbCa)_3(FeGe)_5O_{12}$, garnet film, isolated straight stripe domain, dynamic behaviour 80—39809
- $(YEuYbCa)_3(GeFe)_5O_{12}$ bubble film with ion-implanted layer, FMR study 80—2643
- $(YEuYbCa)_3(GeFe)_5O_{12}$: H, Ne, Ar ion-implanted, threefold symmetrical bubble properties 78—64243
- $(YEuYb)_3(FeGa)_5O_{12}$, LPE, stripe end motion, effect of in-plane field 78—68330
- $Y(Fe, Ga)_5O_{12}$, garnet film, strip domain struct. behaviour in applied field 78—68341
- $YFe_{5-x}Al_xO_{12}$, impurity redistrib. kinetics, temp. depend., vacancy effects 80—75263
- $Y_3Fe_{5-x}Al_xO_{12}$, linear expansion 77—48024
- $Y_3Fe_{5-x}Al_xO_{12}$, permeability spectra rel. to microstruct. 80—71100
- $Y_3Fe_{5-z}Al_zO_{12}$, mixed garnet, cation distrib., temp. depend., magnetisation study 80—79831
- $Y_3Fe_{5-x-y}Co_xGe_yO_{12}$, anisotropy and magnetostriction, ferromag. reson. expts., 4.2-500K 78—27030
- $Y_3Fe_{5-x}Co_{x/2}Si_{x/2}O_{12}$, spin reorientation, NMR and ferromag. reson. meas. 80—65890
- $YFe_{4.5}Ga_{0.5}O_{12}$ domains, neutron dpolarisation and Faraday rotation study 80—93137
- $YFe_{5-x}Ga_xO_{12}$, impurity redistrib. kinetics, temp. depend., vacancy effects 80—75263
- $Y_3Fe_{4.2}Ga_{0.8}O_{12}$, LPE grown thin film, ferromag. reson. 78—35041
- $Y_3Fe_{4.5}Ga_{0.5}O_{12}$, domain struct., neutron depolarisation and Faraday rot. 80—71084
- $Y_3Fe_{4.6}Ga_{0.4}O_{12}$ film, surface spin wave reson. 77—85576
- $Y_3Fe_{5-t}Ga_tO_{12}$ garnet, spin wave parametric excitation threshold anisotropy in second region 80—29542
- $Y_3Fe_{5-x}Ga_xO_{12}$ epitaxial layers grown from soln., prep. and props. *(German)* 78—52691
- $Y_3Fe_{5-x}Ga_xO_{12}$, garnet, magnetically inequivalent positions of cations in external mag. field 80—11307
- $Y_3Fe_{5-x}Ga_xO_{12}$, inhomogeneous stress effect on ferromagnetic resonance 79—24219
- $Y_3Fe_{5-x}Ga_xO_{12}$ layers, current-induced soln. growth 77—48358
- $Y_3Fe_{5-x}Ga_xO_{12}$, mag. domains and cryst. defects 80—75789
- $Y_3Fe_{5-x}Ga_xO_{12}$, refr. index spectrum, visible region 79—73894
- $Y_3Fe_{5-x}Ga_xO_{12}$, substituted garnet, floating zone grown, FMR line width, saturation magnetisation 80—29626
- $Y_3Fe_{5-z}Ga_zO_{12}$, mixed garnet, cation distrib., temp. depend., magnetisation study 80—79831
- $Y_3Fe_{5-x}Gd_xO_{12}$, permeability spectra rel. to microstruct. 80—71100
- $Y_3Fe_{5-x}In_xO_{12}$, K absorpt. and Mossbauer spectra *(Russian)* 77—32467
- $Y_3Fe_5O_{12}$, formation mechanism from metallic oxides 77—48376
- $Y_3Fe_5O_{12}$ LPE growth on $Gd_3Ga_5O_{12}$ substrates, substrate orientation effect 80—66438
- $Y_3Fe_{5-x}Sc_xO_{12}$, garnets, magnetooptical spectra, 15000-21000 cm^{-1} 77—90131
- $Y_3Fe_{5-x}Si_xO_{12}$, photoinduced jumps of permeability 79—28564
- YGG, YGG-ErGG, rare earth impurity, spectral probe of stoichiometry variations 77—85790
- YGa garnet, Yb^{3+} crystalline field, Schottky specific heat, paramagnetic susceptibility temp. depend. 77—11882
- $Y_3GaFe_4O_{12}$, mag. props. meas. in high mag. fields, review *(Japanese)* 78—52303
- $Y_3Ga_xFe_{1-x}O_{12}$, film growth conditions rel. to memory element props. 77—66399
- $Y_3Ga_xFe_{5-x}O_{12}$, Faraday rot., 1.06 μm, 100-300K 77—52059
- $Y_3Ga_xFe_{5-x}O_{12}$ film, growth kinetics of film with cylindrical mag. domains 77—1577
- $Y_3Ga_xFe_{5-x}O_{12}$, HF Faraday light modulator, optical characts. crystal struct. depend. 77—39052
- $Y_3Ga_xFe_{5-x}O_{12}$, spin struct. obs. by Faraday rotation expts. in fields up to 200 T 77—69809
- YGaIG, magnetoelastic wave propagation time dispersion reduction 80—75836
- $Y_3Ga_5O_{12}$, rare-earth doped garnet, high temp. mag. susceptibility 79—78347
- $Y_3Ga_5O_{12}$:Fe^{3+}, impurity absorpt. spectra to 5.5 eV 77—20892
- $Y_3Ga_5O_{12}$:Fe^{3+}, spin Hamiltonian parameters, g-factors, temp. depend. EPR obs. 77—48038
- $Y_3Ga_5O_{12}$:Ho^{3+}, low-lying cryst. field levels 79—91007
- $Y_3Ga_5O_{12}$:Nd^{3+}, cryst. field parameters calc., exchange charge model 78—47747

garnets continued
$Y_3Ga_5O_{12}$:Nd^{3+}, cryst. field anal. 78—64013
$Y_3Ga_5O_{12}$:Nd^{3+}, energy transfer between Nd^{3+} ions, laser-excited time-resolved site-selection spectroscopy 79—95839
$Y_3Ga_5O_{12}$:Nd^{3+}, radiationless decay processes, laser photoacoustic spectroscopy meas. 80—84766
$Y_3Ga_5O_{12}$:Tb^{3+}, fluoresc. and absorption spectra 77—32422
$Y_3Ga_5O_{12}$:Tb^{3+}, luminesc. 77—48251
$Y_3Ga_5O_{12}$-$Y_3Fe_5O_{12}$ garnets, EPR spectra of ferric ions 77—66414
$Y_3Gd_3Bi_3(FeAlGa)_5O_{12}$, epitaxial film, thermomag. recording *(Russian)* 77—1571
$Y_{1.4}Gd_{0.6}BiFe_{3.8}Ga_{1.2}O_{12}$ film, bistable bubble domains, static, dynamic and optical props. 79—28574
$Y_{3-3x-2z}Gd_{3x}Ca_{2z}Fe_{5-z-u}V_zSi_uCo_uO_{12}$, mag. props., effect of V substitution 77—20582
$Y_{2.3}Gd_{0.6}Fe_{4.7}Al_{0.4}O_{12}$ garnet, effect of Gd on magnetite exsolution in a garnet matrix 79—11624
$Y_{3-x}Gd_xFe_{5-y}Al_yO_{12}$, solid solns., IR absorpt. spectra, physical props. 80—55082
$Y_{2.6}Gd_{0.4}Fe_{3.9}Ga_{1.1}O_{12}$, epitaxial uniaxial film, mag. phase diagram, optical expts. *(Russian)* 77—48022
$Y_{2.01}Gd_{0.99}Fe_{4.925-x}Mn_xO_{12}$, comp. depend. of mag. props., and stress sensitivity control 78—27057
$Y_{3-x}Gd_xFe_5O_{12}$, FMR, influence of Gd^{3+} substitution on linewidth 77—8416
$Y_{3-x}Gd_xFe_5O_{12}$, field depend. of susceptibility *(Russian)* 78—68176
$Y_{3-x}Gd_xFe_5O_{12}$, linear expansion 77—48024
$Y_{3-x}Gd_xFe_5O_{12}$, mag. phase diagrams, mag. transitions, exchange interaction *(Russian)* 80—54896
$Y_{3-x}Gd_xFe_5O_{12}$, solid solns., IR absorpt. spectra, physical props. 80—55082
$(YGd)(GaFe)_5O_{12}$ epitaxial film, nonlinear magnetoelastic effects *(French)* 80—34745
$Y_{2.55}Gd_{0.45}GaFe_4O_{12}$, garnet thin films, magnetisation orientation, temp. depend. 80—71125
YGdIG, with various domain wall orientations, natural spin reson. 80—66040
Y_2GdIG film, amorphous, mag. bubbles obs. and structural transformation 80—75824
$YGdTmFe_{4.3}Ga_{0.7}O_{12}$ epitaxial films, bubble-domain lattices with specified parameters 80—60386
$(YGdTm)_3(FeGa)_5O_{12}$ epitaxial film, formation of lattice of cylindrical mag. domains from stripe domains *(Russian)* 80—80579
$(YGdYbBi)_3$ $(FeAl)_5O_{12}$ epitaxial film, diffuse domain wall, bubble domain expansion 80—25170
$Y_{0.9}Gd_{1.1}Yb_{0.7}Bi_{0.3}Al_{0.9}Ga_{0.2}Fe_{3.9}O_{12}$ films, cylindrical mag. domain form. *(Russian)* 77—40098
$(YGdYbBi)_3(FeAl)_5O_{12}$, epitaxial garnet film, with mag. compensation point, behaviour of 'compromise' phase boundary 78—60321
$(YGdYbBi)_3(FeAl)_5O_{12}$, garnet, epitaxial film, interior domains 79—91268
$(YGdYbBi)_3(FeAl)_5O_{12}$, epitaxial film, 360° domain walls with periodically distrib. Bloch lines 80—7127
$(YGdYbBi)_3(FeAl)_5O_{12}$ ferrite-garnet films, effect of in-plane field on dynamics of domain walls 80—65979
$(YGdYbBi)_3(FeAl)_5O_{12}$ epitaxial garnet film, uniaxial ferromagnet domain struct., phase transition *(Russian)* 80—108044
$(YGdYbBi)_3.(FeAl)_50_{12}$ films, substrate orientation influence on max. vel. of domain boundaries 79—15330
$Y_{1.3}GdYb_{0.7}GaO_{12}$, epitaxial film, ferromagnetic reson. exam. 77—85579
YIG, Al substituted, transferred hyperfine fields, Mossbauer effect meas. 79—1726
YIG, Al- and Ga-substituted, floating zone method growth, interface shape and horizontal variations of Al and Ga contents by electron pulse anal. 79—33929
YIG, amorphous, ionic glass, hard-sphere random-packing model 80—24369
YIG, and Ga-substituted YIG, mag. birefringence rel. to sublattices 79—28723
YIG and Ga-substituted YIG, high energy heavy ion irrad., lattice strain 80—49278
YIG, anisotropic elastic waveguide normal-mode anal., appl. to Rayleigh-Love wave mode converter 79—23113
YIG, anisotropic linear mag. birefr., light modulation 77—8548
YIG, anomalous subsidiary absorpt. butterfly curves at 9.16 GHz and 300K 79—82875
YIG, Barkhausen effect *(German)* 78—14986
YIG, Bi-substituted, LPE film, optical absorpt. changes due to impurity incorporation 77—1702
YIG, Bi-substituted, LPE, domain wall reson. 80—60387
YIG, Bloch line mass and mobility in a domain boundary *(Russian)* 80—93138
YIG, Bloch wall mobility, effect of dynamic change in wall struct. *(Russian)* 78—2698
YIG, Brillouin-Mandelstam scattering from thermal and excited magnons 80—70980
YIG bubble films, light scatt. from spin waves, hysteresis meas. by Voigt effect 80—15770
YIG, bulk, low mag. domain wall mobility 78—95463
YIG, CVD defect free epitaxial growth, conditions depend. 77—16502
YIG, cation sites distrib. and valence states 79—99167
YIG ceramic, transient flash effect on permeability 78—27024
YIG, computer optical isolator for near IR region 78—83104
YIG, corrugated slab, magnetostatic surface wave propagation 78—27072
YIG, crit. behaviour, Mossbauer and magnetisation meas. *(Russian)* 79—61106
YIG crystals, bulk growth from high temp. solns., props. 80—66413
YIG, cylindrical mag. domains, translational motion 80—108043
YIG, deformed at high temp., subgrain boundaries and dissociations of dislocations, TEM obs. 79—90658
YIG, demagnetising factor meas., magnetoelastic Rayleigh wave convolution 77—10072
YIG, diamagnetic substituted, anal. of polar Kerr rot. spectra 78—68485
YIG, diamagnetically substituted, annealing effects on cation distrib. 79—1455
YIG dielectric layered struct. magnetostatic bulk wave steering 80—25166
YIG, diffr. of laser radiation by parametrically excited elastic and magnetoelastic waves 78—19338
garnets continued
YIG, dilute, magnetoacoustic surface wave excitation by RF field on Bloch walls 80—25178
YIG, dissociation press. and Gibbs energy of form. 79—11816
YIG, distrib. of easy magnetisation axes near edge dislocation *(Russian)* 80—44891
YIG, domain boundary nuclear spin echo excitation, NMR domain freq. capture effect *(Russian)* 80—44955
YIG, domain wall mobility and mass meas. method *(Russian)* 80—108033
YIG, domain wall size and mag. losses in freq. spectra 77—85481
YIG, double layer struct., LPE growth from molybdate and Pb borate fluxes 80—39827
YIG, dynamic characts. of domain walls, low temp. behaviour 77—69598
YIG, elastic and thermoelastic consts., US meas. *(German)* 77—59061
YIG, elec. props. 79—99552
YIG, elec. props. meas., 600-1500K 77—8098
YIG, electron and γ-irrad., photomagnetic effect 80—103877
YIG, electrostatic model of cryst. field 80—59945
YIG, empirical formula for lattice const. calc. 79—27968
YIG, energy dispersive X-ray microanalysis, improved reproducibility by normalization to the background 78—48727
YIG, epitaxial, temp. stabilisation of ferrimag. reson. field by Ga, La substitution 77—77104
YIG epitaxial film, strong in-plane ang. depend. of spin-wave intensities 77—69521
YIG epitaxial film, magnetostatic volume wave propag. 78—10736
YIG epitaxial film and cryst., bound magnetostatic waves controlled by field gradients 78—95425
YIG epitaxial films, substituted, floating bubble domains, effect of structural stratification 80—2615
YIG, epitaxial layer, n and p-type, UPS, elec. struct. 77—4710
YIG epitaxial layers grown from soln., prep. and props. *(German)* 78—52691
YIG, FMR line broadening, two-magnon scatt. contribs. 77—20711
YIG, Faraday effect, influence of mag. field on sublattice contributions 80—88975
YIG, Faraday effect and IR radiation modulation 79—10403
YIG, Faraday rot. rel. to sublattice magnetisation 79—33675
YIG, ferromag. film on nonmag. substrate, magnetoelastic wave propag. 79—99744
YIG, ferromag. reson. of unclamped specimen, magnetoreson. force effects *(Russian)* 77—32264
YIG, ferromag. reson., press. up to 6.5 kbar 77—51956
YIG ferromagnetic film, quasi surface spin wave giant oscills. *(Russian)* 80—15767
YIG, ferromagnetic resonance and magnetostatic waves in inhomogeneous internal field *(Russian)* 80—54954
YIG film, Ca, Ge-substituted, having mag. bubbles, LPE growth 78—31350
YIG film, calc. of magnetostatic mode freq. 78—68313
YIG film, dielec. layered struct., magnetostatic volume wave propag. 78—95426
YIG film, dielec. layered struct., magnetostatic bulk wave power flow and energy distrib. 80—34610
YIG film, domain struct., influence of planar anisotropy 79—78472
YIG film, ferrimag., determ. of freq. of magnetostatic modes 77—36104
YIG, film, LPE, annealing-induced relief of compressive misfit strain 78—2386
YIG film, low field microwave excitations of mag. domain walls 79—78456
YIG, film, magnetostatic surface wave refl. at shallow groove 78—19283
YIG film, magnetostatic surface wave propag. 79—4661
YIG film, magnetostatic forward volume wave excitation 79—82775
YIG film, magnetostatic surface wave propag. in nonuniform mag. field, anal. 80—20437
YIG film, magnetostatic surface and forward volume wave oblique incident at shallow groove 80—34704
YIG film, magnetostatic surface wave propag. in nonuniform mag. field 80—80574
YIG film, microwave generation and manipulation of magnetic domains 78—39378
YIG film, oblique incidence of magnetostatic waves on metallic grating 78—19229
YIG film, on GdGaG, mag. excitations, diffusion layer effects 78—31112
YIG film, periodically corrugated, insertion loss, reson. linewidth effect 80—80614
YIG, film, photoinduced mag. surface anisotropy spin wave reson. 77—4560
YIG film, shallow groove, magnetostatic surface wave reflectivity 77—73055
YIG film, shallow groove effect on magnetostatic forward volume wave reflection 78—84473
YIG, film, spin wave reson., complex mag. surface energies 77—4561
YIG, film, spin-wave spectra in terms of mag. boundary conditions 79—78532
YIG film, stripe domain struct. with two periods 79—69706
YIG film, surface effects in spin wave reson. 77—16182
YIG film, surface pinning parameter, symm. props. 79—28570
YIG film, tangentially magnetised, magnetoelastic Lamb wave propag. 79—82856
YIG film, with periodic mag. struct., dispersion characts. anal. *(Japanese)* 79—42809
YIG film filter, theory of characts. 79—42808
YIG film tangentially magnetised, magnetostatic surface wave excitation 80—29586
YIG, film waveguide, magnetooptical effects 77—3650
YIG film-dielectric layer-conductor struct., magnetostatic bulk wave propag. dispersion relations 80—54925
YIG films, deposition by DC sputtering from two facing targets 78—31341
YIG films, MCD spectrum 79—28722
YIG, floating zone method growth, interface shapes 80—60775
YIG, forced magneto-optical rot. 79—61347
YIG, Ga and Al substituted, single cryst. growth by the travelling solvent float zone technique 79—43138
YIG, garnet, high temp. solns., shear viscosity meas., rel. to LPE 80—10697
YIG, growth from molten soln., improved crucible shapes *(German)* 77—1800

garnets continued

- YIG, heat transport by magnons, effect of magnon-phonon thermal relax., calc. 77−39705
- YIG, Hf response and thermodynamic props. *(Russian)* 78−72338
- YIG, high field magneto-optical study 77−85749
- YIG, homogeneous crit. relax. in dipole region *(Russian)* 78−10782
- YIG, homogeneous mag. relax. near phase transition *(Russian)* 78−23351
- YIG, hyperfine interaction determ. from Mossbauer spectra in applied mag. field 77−28497
- YIG, hyperfine parameters, Huckel theory calc. 80−39542
- YIG, impurity absorpt. spectra to 5.5 eV 77−20892
- YIG, in multilayer planar structure, magnetostatic propag. 77−16120
- YIG, influence of X-ray radiation on mag. props. 77−8337
- YIG, interaction force between 180° domain wall and edge dislocation 77−28408
- YIG, intrinsic microwave emission, coupling to waveguide system, magnon system cooling 77−24912
- YIG, LPE and CVD films, boundary effects, spin wave reson. meas. 79−78447
- YIG, LPE film, magnetostatic wave to exchange resonance coupling 79−82774
- YIG, LPE film, non-Ohmic currents 78−68099
- YIG LPE film, optical waveguide in mag. strip domains *(French)* 77−83979
- YIG, LPE grown, FMR linewidth, Pb incorporation effects 77−8407
- YIG, La- and Ga-substituted, inhomogeneous epitaxial films, spin wave reson. 79−99773
- YIG, light diffr. by banded domain struct. *(Russian)* 78−15150
- YIG, light scatt. by parametric spin waves with longit. pumping *(Russian)* 78−43648
- YIG, localised high-Q ferromag. reson. in nonuniform mag. fields 77−85575
- YIG, MCD meas. by retardation modulation technique 80−16014
- YIG, MW dielectric losses, causes and reduction *(Chinese)* 80−75930
- YIG, mag. and magneto-optic props., temp. and exchange field depend. 77−24824
- YIG, mag. domain walls, Lorentz microscopy 79−91249
- YIG, mag. linear double refr., two-sublattice model *(Russian)* 79−28728
- YIG magnetic bubble domain grating, light diffr. *(German)* 79−95737
- YIG, magnetic domain wall motion in high drive fields 80−65955
- YIG, magnetic relaxation phenomena 79−99776
- YIG, magnetisation density, polarized neutron expts. 78−52215
- YIG, magnetised in raised cosine profile magnetostatic surface wave propag. 80−2567
- YIG, magneto-optical coeffs. induced by elec. and mag. dipole transitons 77−52060
- YIG, magneto-optical Kerr effect, reflectivity spectra 80−66157
- YIG, magnetocrystalline surface anisotropy energy, one-ion mechanism 79−42756
- YIG, magnetocrystalline surface anisotropy energy, one-ion mechanism 79−78362
- YIG, magnetoelastic wave dispersion rels. and normal modes 77−55694
- YIG, magnetoelastic wave propagation time dispersion reduction 80−75836
- YIG, magnetooptical spectra, polar Kerr rotation, dielectric tensor elements spectra 80−40091
- YIG, magnetoresistance of bulk and epitaxial films 78−91706
- YIG, magnetostatic precession modes, optical investigation 78−19337
- YIG magnetostatic surface wave dispersion rel. to mag. saturation diffusion 78−2671
- YIG, magnetostatic volume waves, magnetocrystalline anisotropy effects, group delay 79−78355
- YIG, magnetostatic wave linewidth, wave no. depend., mag. relax., rods and films *(Russian)* 78−2667
- YIG, magnetostriction meas. with recording rot. field magnetostrictometer 78−12733
- YIG, magnon high amplitude collective oscills., double parametric reson. *(Russian)* 77−28451
- YIG, monocrystal film growth by chem. transport in closed system 77−77392
- YIG monocrystals, echo of magnetoelastic waves 77−55697
- YIG, mulitiple mag. layer structures, magnetostatic surfacewave propag. 80−88839
- YIG multilayered film, magnetostatic spectrum 78−23350
- YIG, Neel point behaviour in stoichiometry vicinity 80−88750
- YIG, nonreciprocal attenuation of elastic surface waves 77−55696
- YIG, nonreciprocal attenuation of magnetoelastic Rayleigh waves 80−60399
- YIG nonreciprocal thin film acoustic device, design, appl. of cct. theory of elastic waveguides 77−85042
- YIG, nonstoichiometry and electronic defects, thermogravimetric expts. and anal. of elec. data 78−6050
- YIG, normally magnetised disc, reson. modes of magnetostatic waves 77−81015
- YIG octa- and tetra-sublattices, anisotropy of effective mag. field at ^{57}Fe *(Russian)* 80−10929
- YIG, one-magnon light scatt. with and without compensation temps. 78−31062
- YIG, one-magnon Raman scatt., Faraday rot. 80−66156
- YIG, open die hot pressing, spin wave and FMR line width 80−89170
- YIG, optical detection of scatt. of homogeneous precession of magnetisation by defects 79−69728
- YIG, optical spectroscopic exam. of ferromag. reson. *(Russian)* 77−48057
- YIG, parallel microwave pumping threshold, RF modulation of mag. field 78−88195
- YIG, parametric excitation of spin waves in single-domain and polydomain states 77−12206
- YIG, parametrically excited spin waves, spectral density *(Russian)* 79−4667
- YIG, parametrically excited reson. magnetostatic modes of spin, elastic and magnetoelastic waves 79−56523
- YIG, parametrically excited wave discrete structure obs., light diffr. and modulation *(Russian)* 79−95650
- YIG periodic film layer, magnetostatic surface wave propag. 80−2607
- YIG, permeability, domain rot. and wall displacement contrib. 80−80564
- YIG, permeability spectra rel. to microstruct. 80−71100

garnets continued

- YIG, perpendicular pumping, spin wave instabilities, laser probing 77−43889
- YIG, phonon inelastic scatt. by magnons 77−20570
- YIG, phonon viscosity effect on dislocation motion 80−24450
- YIG, photomagnetic effects, irreversible 79−99719
- YIG, plastic deform. and mag. props 77−40087
- YIG, plastically deformed, TEM, dislocation Burgers vectors 77−11557
- YIG, polar Kerr rotation spectra, 2-5.7 eV, comparative study with $Li_{0.5}Fe_{2.5}O_4$ 79−47413
- YIG, polarised neutron diffr. and extinction models 77−1046
- YIG, polarised neutron expts., extinction models 80−24322
- YIG, polariser neutron study of covalency effects 80−2552
- YIG, polycryst., initial and reversible parallel susceptibilities, hydrostatic press. effects 80−75835
- YIG, polycrystalline, microwave relax. at low power levels 78−39409
- YIG, polycrystalline, microwave relax. at high power levels 79−61231
- YIG, porous, parallel-pump spin-wave instability temp. depend. 79−78531
- YIG, porous and fine grain polycrystalline, temp. depend. of effective linewidth 77−85574
- YIG, precipitation of Fe_3O_4 78−84815
- YIG, prep. and imperfections, rel. to props. 79−100031
- YIG, press. depend. of effective mag. fields on ^{57}Fe nuclei 78−52383
- YIG, pseudo-surface magnetoelastic waves, damping *(Russian)* 78−23320
- YIG, pure and Ga-substituted diffuse refl. and thermorefl. spectra near Curie point 80−40131
- YIG, refr. index, isotropic exchange and higher-order anisotropic mag. contribs. 77−69808
- YIG, relax. after spin wave excitation in ferrite *(Russian)* 79−19783
- YIG, resonant phonon-magnon scatt., phonon spectroscopy obs. 79−65150
- YIG rod, inhomogeneously magnetised, propag. characts. of magnetoelastic wave 78−15006
- YIG, SAW transducers, approximate theory 79−68533
- YIG sandwiched between grounded dielectric layers, magnetostatic bulk wave propagation 80−60380
- YIG, second group of spin waves, parametric excitation 79−99694
- YIG, Si substituted, spin reorientation, Mossbauer spectroscopy obs. 80−44989
- YIG, single cryst., Neel lines, Faraday effect obs. 78−64216
- YIG, single cryst., spin-wave linewidth influence on spin wave propagation direction for parallel pumping 79−1660
- YIG, single cryst. film, pinning effects on magnetostatic modes 78−31111
- YIG, single cryst. growth by floating zone method 78−19656
- YIG, single cryst. growth from high temp. soln. 78−31315
- YIG single crystal growth in Na_2O-B_2O_3 flux system in air 77−81207
- YIG, single crystal., domain wall struct. and cryst. orientation 77−16104
- YIG single crystals, liq. flux growth, obs. 80−66416
- YIG, single crysts. grown by floating zone method, quality eval. of etching and optical microscopy, ferromag. resonance linewidth meas. 79−19990
- YIG slab, corrugated, magnetostatic surface-wave propagation 78−19228
- YIG slab, magnetostatic forward vol. waves delay characts. 79−99691
- YIG slab, partially magnetised, expt. obs. of group delay of magnetostatic waves 80−7100
- YIG, sound vel., temp. depend., phonon scatt. processes 80−96598
- YIG spheres, anomalously low saturation threshold of magnetostatic modes 79−69729
- YIG, spin and magnetoelastic waves on longit. mag. pumping, optical obs. *(Russian)* 80−29727
- YIG, spin struct. obs. by Faraday rotation expts. in fields up to 200 T 77−69809
- YIG, spin wave and magnetostatic wave echo 77−43887
- YIG, spin wave instability, parametrically excited spin waves distribs. *(Russian)* 79−38317
- YIG, spin wave instability theory 79−73825
- YIG, spin wave parametric excitation threshold at low temp. 80−97084
- YIG, spin waves, nonlinear spectroscopy studies 79−99696
- YIG, spin-wave and magnetostatic mode attenuation, double-pulse echo method 79−82874
- YIG, spinwave dispersion curves 78−19230
- YIG, subsidiary absorpt. spin-wave instability threshold, anomalous struct. 80−34776
- YIG, substituted, effect of electron bombardment on mag. and elec. props. 79−42103
- YIG, substituted, magnetite nucleation in transitional zone, ionic process, lattice imaging 80−107424
- YIG substituted film waveguides, TE→TM mode conversions 78−66904
- YIG substrate magnetoacoustic modes, meander-line excitation 77−20670
- YIG substrates, magnetoelastic surface waves, magnetostatic reson. anal. 80−20441
- YIG, superexchange and applied field depend. of Faraday rot. induced by elec. dipole transitions 77−36206
- YIG, surface spin waves, microscopic theory, mag. field effects 78−35044
- YIG target and DC glow discharge sputtered film compositions compared 77−55886
- YIG, thermal attenuation of US waves, 500-1000 MHz 77−84854
- YIG, thermodynamic props. 77−36078
- YIG, thermomag. anal. by electron diffr. 80−108035
- YIG, thermoreflectance spectra 80−20616
- YIG, thick epilayer, unpinned magnetostatic modes 77−63290
- YIG, thin ferromagnetic resonators, intermodulation distortion, spin waves 78−48048
- YIG, thin ferromagnetic film, exchange interaction constant, from paramag. resonance spectra of spin waves 79−42811
- YIG, thin film, Brillouin scattering from spin waves 80−65843
- YIG thin film, metal film effect on mag. boundary conditions, spin wave reson. obs. 79−78527
- YIG thin film gyromag. waveguide, on GGG substrate, optical propag. props. Faraday effect 80−74513
- YIG, thin films, magnetostatic modes at Q-band freq. 80−65828
- YIG, transparent, domain struct. realignment in external mag. field 78−10739
- YIG, universal hysteresis loop for soft ferrimag. polycryst. 77−69620
- YIG, vitreous electric-field-gradient distrib., Mossbauer quadrupole splitting meas. 80−75901

garnets continued
YIG: Ca,(Mg), films, microwave losses induced by Fe^{4+} ions, ferromag. reson. study 79−1715
YIG: Ca^{2+} epitaxial films, Fe^{4+} centres, MCD, optical absorpt., and thermoelectric power meas. 78−95595
YIG: Si single crysts., mag. props. 80−107981
YIG:B,Pb, IR spectrum, localised modes, rel. to impurities and O vacancies 80−50377
YIG:Be^{2+} LPE film, microwave relaxation props. 79−65741
YIG:Ca, epilayer, reversible oxidation, ferromag. reson. 78−76781
YIG:Ca, O diffusion depend. on defect conc. 78−67857
YIG:Ca, oxidising effects of high temp. annealing in reducing atmosphere 80−66696
YIG:Ca eddy current damping 80−39876
YIG:Ca film, strong mag. reson. of Fe^{4+} 78−48047
YIG:Ca films, rapid O diffusion at 25 to 250°C 77−85120
YIG:Co film, influence of stress induced anisotropy on domain struct. 80−100605
YIG:Co LPE films, with rectangular bubble domains, prep. and props. 79−82848
YIG:Co^{2+}, mag. permeability, illumination and impurity depend. *(Russian)* 78−64220
YIG:Fe^{2+}, magnetocrystalline anisotropy, effect of high hydrostatic press. 77−43831
YIG:Fe^{2+}, magnetostriction const. temp. depend., ferromag. reson. meas. 77−40103
YIG:Ga, crystal growth from high temp. soln., induced striation method 77−1802
YIG:Ga(Sc), magneto-optical Kerr effect, reflectivity spectra 80−66157
YIG:Gd, Ga, optical probing of magnetoelastic Rayleigh waves 79−78495
YIG:Gd^{3+}, mag. relax., hyperfine field interactions, PAC expts. 78−27128
YIG:Ho(Er), magnetisation anomalies in strong mag. fields *(Russian)* 77−43854
YIG:Ir, Ir on tetrahedral sites, contrib. to mag. anisotropy, optical absorpt. meas. 77−69867
YIG:La, Ga, horizontally dipped LPE film, inhomogeneities, spin wave reson. meas. 79−91298
YIG:La,Ga, film, LPE-grown, Ga incorporation, depend. of magnetisation on growth rate 80−84627
YIG:La,Ga film, uniaxial anisotropy, variation along growth direction 77−28416
YIG:La film, for microwave applics., growth and ferromag. reson. meas. 78−3008
YIG:La(Ga) films, ferromagnetic resonance, ion implantation effect 80−97145
YIG:Nb, tetrahedral Fe^{2+} detect. by induced anisotropy ang. variation 79−11311
YIG:Pb, valence of Pb in Fe-garnets 77−47480
YIG:Pb(Si) film, (111) LPE, in-plane mag. anisotropy and ferromag. reson. meas. 78−2706
YIG:Pr^{3+} influence of Pr^{3+} ions on spin-wave damping 79−28625
YIG:Ru, optical absorpt. and MCD obs. of Ru^{4+} site occupancy 80−71456
YIG:Ru(Ru,Zn), mag. anisotropy 77−69544
YIG:Si, EM wave effects on mag. and optical props., lecture 78−27031
YIG:Si, enhanced photoinduced mag. circular and linear dichroism 77−52053
YIG:Si, photo-induced low freq. mag. permeab. *(Russian)* 78−39368
YIG:Si, relative Fe^{2+} ion conc. depend. 77−48150
YIG:Si, thermomagnetic processing and illum. effects on mag. props. *(Russian)* 77−8410
YIG:Si^{4+}, mag. permeability, illumination and impurity depend. *(Russian)* 78−64220
YIG:$Si^{4+}(Ti^{4+})(Zr^{4+})$, X-ray induced change in initial permeability 78−19280
YIG:Si(Ge), effects of nontrigonal cryst. field on spectroscopic props. of Fe^{2+} ions 80−92864
YIG:Si(Ge), Fe^{2+} spectroscopic props., nontrigonal cryst. field effects 80−44553
YIG:Sm^{3+}, mag. anisotropy, effect of Sm^{3+} ferromag. reson. study 80−80615
YIG:Sn, IR absorpt. and MCD 78−19447
YIG:Sn, mag. circular dichroism orientation depend., optical absorpt. 79−99914
YIG:Tb garnet, Faraday effect in strong mag. field *(Russian)* 80−100651
YIG:V, mag. anisotropy and magnetostriction, effect of V 78−27029
YIG:Yb, magnetoelastic coupling of Yb ions, ferromag. reson. meas. 77−69698
YIG:Zr, near IR absorpt. and magnetic circular dichroism 80−60580
YIG/n-GaAs layered structure, magnetostatic surface wave amplification 78−88107
YIG-dielectric layered structure, magnetostatic surface wave propag., finite width effects 77−20668
YIG-Ge layer structure, amplification of bulk magnetostatic waves 78−34972
YIG-Ge structure, profile and position of reson. galvanomag. effect curve 78−72242
YIG-InSb system, surface magnetostatic wave interaction with drift electrons *(Russian)* 77−12185
YIG-LiF film system, ATR, substrate surface polaritons reson. effect *(Russian)* 77−32384
YIG-rare earth garnet solid solutions, magnetisation temp. depend. calcs. 80−20388
YIG-semiconductor coupled systems, energy anal., magnetostatic surface wave amplification 77−55699
YIG-semiconductor coupled system, magnetostatic surface wave amplification, ferromag. loss 77−85434
YIG-semiconductor-dielectric-metal layered structure, amplification characts. of magnetostatic surfaces waves 78−23321
YIGaG, magnetoelastic wave propag. time and total loss, freq. depend. *(Russian)* 77−43859
$(YLaBi)_3(FeGa)_5O_{12}$, pure and In^{3+} doped, near IR absorpt. and Faraday rot. 78−95580
$Y_{2.85}La_{0.15}Fe_{3.75}Ga_{1.25}O_{12}$ epitaxial film, magnetostriction consts., microwave reson. meas. 77−24716
$Y_{2.85}La_{0.15}Fe_{3.75}Ga_{1.25}O_{12}$, inhomogeneous bubble film, spin wave reson. 77−32265

garnets continued
$Y_{2.85}La_{0.15}Fe_{3.75}Ga_{1.25}O_{12}$ epitaxial film, spin wave reson. spectrum 77−69703
$Y_{2.85}La_{0.15}Fe_{3.75}Ga_{1.25}O_{12}$ LPE films, ion implantation effect on spin waves 80−71124
$Y_{2.85}La_{0.15}Fe_{3.85}Ga_{1.15}O_{12}$ garnet, mag. props., ion implantation effect, Mossbauer study 80−97166
$Y_{3-x}La_xFe_{5-y}Ga_yO_{12}$, mag. bubble film, low freq. ferrimag. reson. 78−31110
$Y_{3-x}La_xFe_{5-y}Ga_yO_{12}$ film, horizontally dipped LPE grown, FMR, anisotropy field obs. 79−78449
$Y_{3-y}La_yFe_{5-x}Ga_xO_{12}$, garnet film, radial oscillation of bubble lattice 79−73787
$Y_{3-x}La_xFe_5O_{12}$, mag. props. rel. to ionic struct. 80−75756
$(YLuSmCa)_3(FeGe)_5O_{12}$ garnet film, bubble domain expansion, fuzzy wall struct. 80−71128
$(YLuSmCa)_3(GeFe)_5O_{12}$ bubble garnet film, coercivity 79−78459
$(YLuSmCa)_3(GeFe)_5O_{12}$ garnet films, bubble expansion saturation vel., sampling optical photography 80−75820
Y_2O_3-Fe_2O_3 systems, solid-phase reacts., $Y_3Fe_5O_{12}$ form. 78−44062
Y_2O_3-Lu_2O_3-Eu_2O_3-CaO-GeO_2-Fe_2O_3-PbO-B_2O_3 system, garnet crystn. fields 78−43995
$Y_{2.5}Pr_{0.5-x}Ca_xFe_5O_{12}$, magnetic aftereffect exam. 78−23304
$Y_{2.8}Pr_{0.2}Fe_5O_{12}$, magneto-optical props. 78−72489
YRBiFe garnets, epitaxial films, R=Gd+Yb, Faraday effect and phys. props. 77−69928
$(YRBi)_3(FeAl)_5O_{12}$ films, R=Gd, Yb, Faraday effect in transverse mag. field, orientation depend. 80−88971
$(Y_{1-x}R_x)_3Fe_5O_{12}$, photoinduced decrease in permeability, 77K 77−85497
$Y_3Sc_2Al_3O_{12}$:Nd^{3+}, cryst. field parameters calc., exchange charge model 78−47747
YScIG, expitaxial film, magneto-spatial interaction, conversion coeffs. 77−55774
$Y_{1.62}Sm_{0.21}\ Lu_{0.27}Cu_{0.9}Ge_{0.9}Fe_{4.1}O_{12}$, implanted bubble garnet, anisotropy profile, FMR study 80−7103
$(YSmCa)_3\ (FeGe)_5O_{12}$ mag. bubble garnets, ion implantation induced stress influence on props. 79−91274
YSmCaFeGe, mag. garnet films, segregation of Ca and Ge in LPE growth 80−29959
$(YSmCa)_3(FeGe)_5O_{12}$ LPE films, optimum growth conditions for low coercivity 78−95499
$(YSmCa)_3(FeGe)_5O_{12}$ LPE film, growth and coercivity 79−4707
$(YSmCa)_3(FeGe)_5O_{12}$ films, cc $(YSmLuCa)_3(FeGe)_5O_{12}$ films, mag. bubble props. mag. bubble props. and LPE conditions 79−74107
$(YSmCaLu)_3(FeGe)_5O_{12}$, bubble film inhomogeneity, spin wave reson. meas. 80−44439
$Y_{2.2}Sm_{0.4}(Fe,Ga)_5O_{12}$, garnet film, strip domain struct. behaviour in applied field 78−68341
$(YSm)_3(FeGa)_5O_{12}$ film, LPE on $Gd_3Ga_5O_{12}$, interface processes, horizontal dipping obs. 80−49552
$(YSm)_3(FeGa)_5O_{12}$, growth rate anisotropy and kinetic coefficients of vicinal faces 78−63954
$Y_{2.6}Sm_{0.4}Fe_{3.8}Ga_{1.2}O_{12}$, garnet films, LPE growth, mag. anisotropy field control 77−69642
$Y_{3-y}Sm_yFe_{5-x}Ga_xO_{12}$ film, LPE process exam. by induced striation 77−69643
$Y_{3-y}Sm_yFe_{5-x}Ga_xO_{12}$ film, LPE growth induced mag. anisotropy 78−2709
$Y_{3-y}Sm_yFe_{5-x}Ga_xO_{12}$ epitaxial layers grown from soln., prep. and props. *(German)* 78−52691
$Y_{2.6}Sm_{0.4}Fe_{5-x}Ga_xO1_2$, epitaxial, domain wall crit. vel., effect of material parameters 79−99740
$Y_{3-x}Sm_xFe_5O_{12}$, cubic and induced anisotropy, temp. depend., 100-300K, ferromag. reson. obs. *(Russian)* 78−39313
$Y_{3-x}Sm_xFe_5O_{12}$:^{57}Fe film, ion implanted, Mossbauer conversion spectra study 80−80663
$Y_{2.6}Sm_{0.4}Ga_{1.2}Fe_{3.8}O_{12}$ film, ion-implanted, bubble domain behaviour 77−12177
$(YSm)_3(GeFe)_5O_{12}$: H, Ne, Ar ion-implanted, threefold symmetrical bubble properties 78−64243
$(Y_{1.5}Sm_{0.3}Lu_{0.3}Ca_{0.9}\ )(Fe_{4.1}Ge_{0.9})O_{12}$, growth reproducibility, static bubble props. 77−16130
$(YSmLuCa)_3(FeGaGe)_5O_{12}$, reproductibility in bubble garnet LPE growth 78−92204
YSmLuCaFeGe garnets, growth and temp. characts. of small bubbles 78−80183
$(YSmLuCa)_3(FeGe)_5O_{12}$, mag. props. and growth of 2 μm bubbles 78−91910
$(YSmLuCa)_3(FeGe)_5O_{12}$, LPE growth, growth reproducibility of bubble props. 78−92208
$(YSmLuCa)_3(FeGe)_5O_{12}$ films, mag. bubble props. and LPE conditions 79−74107
$(YSmLuCa)_3(FeGe)_5O_{12}$ film, bubble propagation direction effects on high frequency bias margin 79−78480
$(YSmLuCa)_3(FeGe)_5O_{12}$, double layer struct., LPE growth from molybdate and Pb borate fluxes 80−39827
$(YSmLuCa)_3(FeGe)_5O_{12}$, bubble material, dynamic characterisation, comparison between transport and FMR methods 80−39833
$(YSmLuCa)_3(FeGe)_5O_{12}$, mag. loss and domain wall mobility 80−65980
$(YSmLuCa)_3(FeGe)_5O_{12}$, epitaxial films, LPE grown, annealing effects on mag. anisotropy 80−66548
YSmLuCaGe garnets, 7 μm-period bubble devices 80−44887
$(YSmLuCa)_3(GeFe)_5O_{12}$, garnet film, refractive index dispersion 78−88273
$(YSmLuCa)_3(GeFe)_5O_{12}$, LPE low defect density films, prep. for mag. bubble device fabrication 79−87590
$(YSmLuCa)_3(GeFe)_5O_{12}$, stripe domain wall, form. and punch-through of horizontal Bloch line 79−99723
$(YSmLuCa)_3(GeFe)_5O_{12}$: H, Ne, Ar ion-implanted, threefold symmetrical bubble properties 78−64243
$YSm_{0.5}Lu_{0.7}Ca_{0.8}Ge_{0.8}Fe_{4.2}O_{12}$ film, magnetic bubble propagation with 8 μm period ion implanted propagation patterns 79−78475
YSmLuCaGeIG, mag. props. and defects, depend. on B_2O_3 conc. on growth in PbO-B_2O_3 solvents 78−68321
YSmLuCaGeIG films, epitaxial growth with 3 μm magnetic bubbles 79−61518
$(YSmLu)_3(FeGaSc)_5O_{12}$, submicron mag. bubble garnet 80−54929
YSmLuGa garnets, 7 μm-period bubble devices 80−44887
YSmTmCaGe garnets, 7 μm-period bubble devices 80−44887
$(YSmTmCa)_3(GeFe)_5O_{12}$ film, YY pattern racetrack discrimination and state stability of S=1 and 0 bubbles 78−91908

garnets continued
  $(YSmTm)_3(FeGa)_5O_{12}$, small-bubble appl. 79−82845
  YSmTmGa garnets, 7 μm-period bubble devices 80−44887
  $Y_{1.5}Tb_{1.5}Al_{0.65}Fe_{4.35}O_{12}$, garnet thin films, magnetisation orientation, temp. depend. 80−71125
  YbAG, cryst. field parameters calc., exchange charge model 78−47747
  YbAG, electrostatic model of cryst. field 80−59945
  YbGaG, mag. props. between 44-600 mK 80−80517
  $Yb_3Ga_5O_{12}$, dipolar magnet, sp. ht. and magnetisation meas. 80−60344
  YbIG, H parallel to (100), transition between canted phases, liquid-vap.-like critical point 77−80938
  YbIG, IR Faraday rotation meas. 77−43978
  YbIG, mag. permeability, Faraday rotation expts. 77−16287
  YbIG, mag. transitions at low temp., soft mode existence 77−69557
  YbIG, mean field phase diagrams 78−23269
  YbPrBiIG, wave props. of domain wall 78−48011
  YiG-Bi layer struct., Landau electron absorpt. mechanism, spin wave amplification 78−72344
gas *see gases*
gas analysis *see chemical analysis*
gas blast circuit breakers
  see also air blast circuit breakers
  arc, very high current, local voltage and cross-sectional area correlation in air and SF_6 80−38779
  arc boundary in nozzle throat section, arc diameter, RF technique 78−87528
  arc model, current zero period, boundary layer integral method 78−87522
  arc quenching, plasma turbulence effects 79−27861
  arcs, radiative transfer investigation 79−27864
  circuit breaking arcs, radiative energy transfer 80−1416
  conference, Liverpool, England, Sep. 1978 78−87521
  DC arc in blocked nozzle, boundary layer integral method anal. 80−6295
  DC arc in supersonic nozzle flow, appl. to gas blast circuit breaker 79−23469
  detonation products of condensed explosives elec. stability 79−86635
  fusible shunts for 100 kA circuit breaker 77−10050
  hot gas surrounding arc core, thermal disturbances 78−87529
  HV, arc mechanism and control 80−92409
  nozzle gas blast flows with arc heating 79−46502
  thermal disturbance prod. by arc 79−60208
  three nozzle arc models, review 79−27862
  Tokamaks, gas breakers for ohmic heating circuits 78−66396
  SF_6, 20 kA arc, electrode vap. contamination, time depend. energy balance 78−87525
  SF_6 arc model, convection-loss dominated 78−87519
  SF_6, clogging transition 78−87530
  SF_6, electron temp. at current zero, 3 kA arc 78−87526
  SF_6, energy clogging, current and voltage meas. at different press. 78−87531
  SF_6 equivalent thermal conductivity determ. *(Czech)* 80−53911
  SF_6 gas blast breaker, current zero meas. 80−38795
  SF_6 high-current arc props., influence of electrode material 78−71592
  SF_6, high-temp. circuit-breaking arc, axial and radial heat transport 79−19105
  SF_6, high-voltage, low-noise, meas. of impulse sound levels, comparison with oil type *(German)* 79−94401
  SF_6, particle densities in decaying plasma 78−75442
  SF_6, very high current arcs, elec. conductance of arc gap 78−87524
gas breakdown *see electric breakdown of gases*
gas bubbles *see bubbles*
gas discharge lamps *see discharge lamps*
gas-discharge tubes
  see also ion sources; mercury arc rectifiers; thyratrons
  AC display discharge, charge modes, between insulated glass electrodes *(German)* 77−43087
  AC plasma display panel wall charge magnitude and distribution probe 78−67487
  AC plasma panel, phase change meas. $<10^{-5}$Å, laser interferometer 77−18087
  AC-operated plasma display panels, optimum composition of dielectric materials, CaO and SrO 80−14945
  Bruce electrode, surface elec. field 77−75359
  cataphoresis laser oscillators, Al_2O_3 ceramic discharge tubes 77−75551
  cathode region transfer process simulation, Monte Carlo method 78−71600
  cathode spot excitation, dielectric stimulator, pulsed gas discharge switch 77−19802
  cold-cathode controlled gas discharge switch 78−86300
  colour display panels, comparison of light output *(Japanese)* 78−62191
  Converse hodoscopic tubes combined with streamer chamber for ν detection 80−63455
  crossed field tube for high power on-off switching 77−24222
  double-section, for pulsed 722.9 nm Pb laser 80−9902
  EM MM-wave detection properties, in mag. field 80−70059
  filling of dischargers with mixture of SF_6 and N_2 80−105668
  gas supply generator 79−88927
  gas-filled diode, rarefied gas breakdown time delay statistics 78−87571
  getter action of Ti, for H_2 and N_2 80−10796
  glow discharge, breakdown and extinction, tube wall role 80−44002
  glow discharge, detector for millimeter rad., cyclotron reson. effect on sensitivity 78−62222
  glow discharge, tube impedance with and without metal cover 78−67508
  glow discharge breakdown, temporal development of electrode pot. 80−44003
  grid controlled switching element, stationary conducting state 79−77430
  grid controlled switching element, stationary conducting state, arc conditions 79−77431
  high-pressure, device for filling and sealing 79−35772
  hollow cathode tube, high current metastable atoms production 80−10445
  hollow cathode type, with conical bottom, spectroscopic and elec. characts. 80−31891
  hollow-cathode discharge, external cathode type, morphologic study 79−60207
  inert gas ion laser discharge, energy balance 78−74884
  inert gas ion laser ion-acoustic wave excitation 78−74885
  information display technology, symposium, San Francisco (1978) 79−9209
gas-discharge tubes continued
  inplatron, sensitivity and resolution, LF noise fluctuation 77−19779
  intensity modulated vacuum UV source 77−39009
  laser triggered Krytron-Blumlein electro-optic switch 78−9450
  light sources, UV, comparison of sources for 120 to 200 nm range *(German)* 79−85186
  magnetic discharge cells with nonuniform periodic magnetic field 80−101799
  magnetron geometry, mag. field and press. effects 77−43090
  metal halide vapour lasers using gas-discharge tubes 79−64251
  metal ion, gas-discharge source 79−36448
  microwave discharge source for production of supersonic atom and free radical beams 79−80720
  optical chambers in mode of pulsed proportional amplification 79−726
  phototube, gas-filled, rise time spectral depend., appl. to EM radiation detector miniaturisation 78−86318
  planar display, digital panel meters appl. 77−37867
  plasma interaction with thin quartz glass layer *(Russian)* 78−14178
  plasma sheath, metal probe-gas discharge plasma boundary, impedance parameter variations 77−58869
  plasma-filled fast-opening switch for use with relativistic electron beam diode 77−47275
  plasmatron thermal cathode, emission cooling *(Russian)* 80−54052
  plasmatrons, mono- and duo-, anode space-charge sheath characts. rel. to ion source 79−55576
  secondary electron emission at wall 77−27762
  secondary electron emission in cathode fall region of tube wall 80−44001
  shape, flow velocity, effect on electron temp. of medium pressure positive column 79−64941
  subnormal glow discharge detection of microwaves, internal signal gain 78−16843
  temperature, effect of bulk absorpt. of radiant energy *(Russian)* 80−43422
  thermionic diodes, planar low press. gas discharges, plasma regime, plasma characts. 79−77435
  thermionic diodes, planar low press. gas discharges, space charge regime, volt-ampere characts. 79−77434
  thermionic emission triode, with auxiliary discharge, rectifying parameters 79−64925
  transparent hollow cathode, discharge tube 79−1368
  vacuum-deposited layers formation, use of borosilicate glass intermediate layer 80−80979
  Ar-air, transformer plasmatron, LF discharge, electrical and energy props. 80−103200
  CO_2 laser, Lamberton and Pearson type, shock wave detect. 79−36946
  CO_2 waveguide laser, dynamic gain, discharge tube depend. 80−23668
  CO_2 waveguide laser amplifier with strong discharge tube 80−74398
  Cr film vacuum deposition on glass display panels 78−39694
  Cs, thermionic converter, ion species mass anal. 77−89344
  H atomic source, for electron scatt. expts. 78−94332
  H, diffusion coeff., in H_2, luminesc. intensity meas. 80−103098
  H_2 laser, VUV, with sealed gas-discharge tube 80−74399
  He-Cd, hollow cathode discharge tube, voltage, ion spectral line intensities and metastable states 79−46505
  He-Cd plasma, in discharge tube, excitation mechanism obs. 78−30479
  He-Ne laser discharge tubes, design and technology, review *(Czech)* 79−72586
  Hg-A positive column, scaling towards display cells 77−84565
  Ne, meas. of high intensity microwave elec. field using Ne gas-discharge tube 80−9006
  Ne-Ar (0.1%) mixture, AC plasma panel, Paschen breakdown curves 77−11418
gas discharges *see discharges (electric)*
gas dynamics *see aerodynamics*
gas ionisation *see ionisation of gases*
gas lasers
  see also chemical lasers; excimer lasers; gasdynamic lasers; ion lasers
  3.39 μm He-Ne laser frequency stabilisation without FM 79−55152
  100 kJ CO_2 laser, Antares, for fusion reactor ignition, status report 80−64075
  ^3He-^{20}Ne stabilised transverse Zeeman laser, tuning characts., freq. fluctuation 80−48273
  acetic acid, active medium of optically pumped submm laser, double reson. 79−18215
  acetonitrile, far IR laser gas absorption obs. with and without DC field 79−31870
  acetonitrile, submillimeter rotational spectrum, laser generation line identification 79−64210
  acetonitrile sub mm laser, generation lines identification *(Russian)* 78−82952
  acetylene, CO-C_2H_2 energy transfer, e-beam controlled discharge excitation 77−27277
  acetylene-d_2, 17 to 21 μm laser lines generated using CO_2 laser pump 80−69375
  amplification depend. on geometry of discharge cross section 79−64203
  amplification of incoherent radiation 78−55334
  amplifier, quasi-Gaussian pulse propagation, effect on line-shape parameter anal. 78−55333
  anisotropy due to saturating fields 78−55337
  annular gas laser, with anisotropic resonator, longit. mag. field effects 79−27293
  annular HSURIA resonators, testing with CO_2 laser, polarisation effects 80−58599
  Antares, a 200 TW CO_2 laser for fusion reactor ignition 80−32502
  Antares CO_2 laser power amplifier, design 80−69423
  Antares laser, for laser fusion expts., energy storage system design 78−55030
  apparatus and applications *(Japanese)* 77−61961
  applications and laser principles *(French)* 80−83590
  atomic and ionic lasers, excitation mechanisms and characts., book contrib. 80−106512
  atomic and molecular lasers appl. to collision physics 80−63596
  atomic collisional gas-discharge laser feasibility 80−91779
  atomic constants and collision cross sections determ. by level crossing 78−50763
  autodyne effect 79−81404
  automatic adjustment system for lasers with unstable cavities 77−50693
  automatic frequency control system, long-term instability and irreproducibility of freq. 79−45962

gas lasers continued
Blumline type discharge laser, single switch operation 78—13727
book, gaseous electronics and gas lasers 80—73120
book, principles of laser plasmas, for graduate students and researchers 77—50647
book, quantum electronics 80—105442
Brillouin laser, high efficiency, wavefront reversal influence on operation 79—23026
bromotrifluoromethane, CW optically pumped, FIR laser action obs. at 823, 883 μm 80—14321
bromotrifluoromethane 823 laser line, simple accurate method for wavelength meas. 80—106554
capacitive mesh output couplers for optically pumped far IR mol. lasers 78—74916
carbon tetrafluoride, laser parameters with optical pumping 79—72557
carbon tetrafluoride, lasing action, spectroscopy of features near 9 μm lines 79—22944
carbon tetrafluoride 16 μm laser, radiance enhancement 78—87045
carbon tetrafluoride $^{12}CF_4$ laser, Doppler-limited absorption spectroscopy 80—74347
carbon tetrafluoride $^{12}CF_4$ optically pumped laser efficiency 80—74348
carbon tetrafluoride laser, CF_4 molecule $\nu_3+\nu_4$ band optical pumping 80—74349
carbon tetrafluoride laser, emission spectrum in 16 micron range, CO_2 laser stimulation 80—9870
carbon tetrafluoride laser, frequencies of pump and laser transitions 79—94218
carbon tetrafluoride laser, high energy output in 16 μm region, CO_2 laser pump 79—89927
carbon tetrafluoride laser, optically pumped, freq. tuning 80—28208
carbon tetrafluoride laser, weakly forbidden vibr.-rot transitions 79—55121
carbon tetrafluoride laser oscillator amplifier meas., small signal gain and self-absorpt. 79—59683
carbon tetrafluoride laser with optical pumping, freq. tuning and stabilisation 80—99706
carbon tetrafluoride optically pumped laser, pulse-periodic operation, 0.2 W average output power 79—27247
carbon tetrafluoride optically pumped laser, spectroscopic characts. 79—89896
carbon tetrafluoride optically pumped laser, stimulated emission stabilisation and tuning 80—9866
carbon tetrafluoride pulsed laser characts., optically pumped by CO_2 laser 80—91778
cascade, transitions gain coeff. maximal meas. method 77—31104
cataphoresis laser oscillators, Al_2O_3 ceramic discharge tubes 77—75551
cavity, universal unit for beam extraction 80—1230
cavity light intensity optimisation for three-mirror system utilising Fabry-Perot resonators 80—48305
cavity unit for radiation lead-out *(Russian)* 78—90433
[cc] He-Ne laser scanning system, for video record player, information identification *(German)* 80—106557
cell for high temp. transverse discharge 77—38914
chlorodifluoromethane subMM wave laser, optically pumped 80—87376
chloroform, energy transfer from D_2, 4-5 μm 77—88701
closed-cycle high-energy pulsed lasers, investigation and management of acoustic waves 80—38153
CO_2 laser construction as student project, design and building methods 79—97166
CO_2 laser gas mixture 80—78829
CO_2 laser system, compact 0.1 TW design 80—87370
CO_2 lasers, CW, high-power appl. of photoinitiated impulse-enhanced electrically excited discharge 78—50785
CO_2 waveguide laser design 80—33025
CO_2-N_2, highly efficient gas for nanosecond pulse CO_2 laser system *(Japanese)* 80—48214
coaxial cable pulse forming network as rare gas halide laser pump 80—69424
coherent and nonlinear optics, conf., Leningrad, USSR (Jun. 1978) 80—98753
combined discharge in average press. gas using two HV pulse sources, gas laser development 80—44027
compact high-pressure electron beam controlled laser system 78—5496
complex organic vapor lasers, new active media, buffering gas influence 79—94213
computer model for CW optically-pumped submm laser performance prediction 78—87041
computer modelling, at. and mol. processes 80—23661
conference, Dresden, Germany (Mar.-Apr. 1977) 77—83881
conference, inertial confinement fusion, San Diego, USA, (Feb. 1978) 78—46171
conference, laser and electro-optical systems, San Diego, CA, USA (Feb. 1980) 80—62392
conference, laser engineering and appls., Washington, USA (May-June 1979) 80—1216
conference, Novosibirsk, USSR (June 1975) 77—693
conical laser plasma tube, electron density distrib. 78—58981
corrosive gas laser systems, capacitance manometer design and perform. 79—36909
coupled transitions with arbitrary polarization of radiation 80—78827
coupling modulated, mode coupling distortions minimisation anal. 78—55384
CW, small power-radiation instability levels meas., using photodiode circuit 80—23704
CW FIR laser, optically pumped, analysis of efficiency 79—76667
CW flowing gas lasers, mode medium interaction 79—36876
CW laser appls. 80—58550
CW laser radiation power stabilisation by external control element 80—91832
CW lasers, homogeneously broadened, with uniform distribution loss, exam. of output power 78—55332
CW optically pumped far IR laser performance, determinative molecular parameters 80—69377
CW optically pumped far IR waveguide lasers, high-power operation and scaling 77—38949
1,4-di(2-(5-phenyloxazolyl))-benzene, vap., lasing kinetics calcs. *(Russian)* 79—13778
dichloromethane, CD_2Cl_2, CW optically pumped, submm. laser action, 100 to 900 μm 79—929
dideuteroacetylene, optically pumped laser action, 17.4 to 20.5 μm 79—935

gas lasers continued
diffraction limited CW optically pumped far IR lasers 77—54727
diffraction-limited CW optically-pumped far IR lasers, beam characts. 77—38953
diffusion of fast electron in presence of mag. field 77—84408
1,1-difluorethane, optically pumped, use of optoacoustic effect to discover CW far IR laser lines 77—79803
cis-1,2-difluoroethene, CO_2 laser pumped, CW far IR laser lines 80—69372
difluoroethylene, absorption coeff. at 10.6 μm 77—23654
1,1-difluoroethylene, optically pumped, complete freq. coverage for submm. laser spectroscopy 78—25860
1,1-difluoroethylene, optically pumped, far IR laser line assignment 79—31865
difluoroethylene, optically pumped sub mm laser design 77—14757
difluoroethylene, optically pumped submm. wave amplification 78—29941
1,1-difluoroethylene, submillimetre laser molecules, Stark and ODR spectroscopy 79—31864
cis-1,2-difluoroethylene laser, far IR CW optically pumped 80—69368
1,1-difluoroethylene mm laser, waveguide cavities comparison, CW props. 78—42328
1,1-difluoroethylene submillimetric wave emission assignments 80—102708
difluoromethane, optically pumped, CW far IR laser line frequencies 80—102706
difluoromethane, optically pumped, efficient CW far IR laser action obs. 79—928
difluoromethane, optically pumped by CO_2 laser, new CW FIR lines 79—94219
difluoromethane far IR laser gas, CW laser pumped, gain 80—69367
difluoromethane laser, optically pumped, FIR lines, performance efficiency 79—94220
2,5-diphenylfuran vapour, spectral, fluoresc., photochem. and laser props. 80—106344
dipolar media, semiclassical theory, appl. to gas laser 80—83586
direct nucl. pumped laser for feedback laser fusion 78—58445
discharge, high-power, stabilisation with mag. field 80—99739
discharge, pulsed, density perturbations, laser beam diagnostics 79—7498
discharge in gas stream, stability conditions 78—18480
discharge interaction with gas flow 78—42319
discharge pumped generic wavelength system for fusion reactor ignition 78—58423
discharge pumped multiwavelength lasers *(Chinese)* 80—102703
discharge tube, chemical reactions, computer generation, REACS 80—48844
discharge tube, plasma chem. species, number density variation with time, numerical model, PLASKEM 80—48845
distributed spark discharge for volume photoionization laser appls. 79—14634
dynamic atmospheric pressure discharge, electron beam excitation 77—27764
dynamic power supplies for TEA lasers 79—7136
electrically excited preionisation unit with electron beam energy recuperation 78—59013
electrically pumped, breakdown delay 77—27270
electroionisation lasers, closed gas-flow cycle without mech. elements 78—94401
electron accelerator, high-current, for optical pumping of gases 80—32544
electron beam accelerator design principles 78—13720
electron beam and discharge technologies for laser pumping, kinetics and design 77—34897
electron beam controlled, electron beam parameter optimization and choice of foil 80—48269
electron beam controlled laser, space-time evolution of cathode layer 79—10288
electron beam excitation 77—711
electron beam excited laser vapour cell designs 79—13951
electron beam ionised lasers, book contrib. 77—50664
electron beam pumped, gas pumping arrangement 77—701
electron beam pumped laser cells, spatial energy deposition by press. meas. 80—78835
electron beam sources for pulsed lasers 79—36913
electron beam stabilised discharge in flowing medium, numerical calc. 78—94943
electron beam stationary recombination laser, feasibility study *(Russian)* 78—13694
electron beam sustained discharge, electron neutral inverse bremsstrahlung, rel. to high-press. IR lasers 78—63604
electron density and temp., spectroscopic diagnostics, book contrib. 77—51242
electron powered gas laser, electron-neutral energy exchange in AC field 77—42519
electron-beam sustained gas discharge/pulse forming network 78—5481
electron-beam-controlled, angular divergence, gasynamic motion influence during pump pulse 79—59668
electron-beam-excited high-press. laser research, appl. of electron-photon cascade model 77—68157
electron-beam-sustained discharge, plasma contraction by mag. field of current 80—100115
electronic transition lasers, conf., Snowmass Village, USA (Sept. 1976) 78—63076
energy characteristics, field and amplifying medium spatial inhomogeneity effect 77—75483
energy storage and nonstoring advanced lasers for fusion appls. 78—79027
engineering aspects, colloquium, London, England (Nov. 1978) 79—31940
ethyl iodide submillimeter wave laser, optically pumped 80—87376
ethylene, off-reson. IR laser action without population inversion, Raman type transition 77—10891
excimer, book contrib. 77—50665
excitation by fission fragments, preparation method for supported U_3O_8 foils 77—68218
excitation degree determ., modulation method 78—1285
excitation processes, new lasers investigation *(Chinese)* 79—81406
externally maintained discharge with gasdynamic window for low energy electron beam 79—32843
Fabry-Perot cavity, gas filled, optical bistability described by stochastic master eqn. 79—76652

gas lasers continued
- Fabry-Perot cavity acoustooptic modulator for internal laser modulator *(Japanese)* 77−88814
- far infrared, electrically tuned, time, frequency standard appl. 78−174
- far IR, common resonator with CO_2 pump laser 77−38950
- far IR, high speed freq. modulation using Stark effect 77−72010
- far IR, present and future problems 78−5466
- far IR CW lasers, optically pumped, review 78−46588
- far IR CW optically pumped lasers, simple accurate method for wavelength meas. 80−106554
- far IR CW waveguide laser, CO_2 laser pumped, efficiency high-power operation 77−10937
- far IR gas laser pump line, optoacoustic determ. 79−31872
- far IR laser, intracavity pumped by TE CO_2 laser 80−87382
- far IR laser, optically pumped, electronic tuning and phase-locking 78−59055
- far IR laser, optically pumped, injection phase locking 80−69431
- far IR laser, pump radiation self-focusing and defocusing 78−79003
- far IR laser gas absorption obs. with and without DC field 79−31870
- far IR laser gases, CW laser pumped, saturated and small-signal gain calc. 80−58521
- far IR laser line frequency meas. by klystron harmonic comparison 77−7113
- far IR laser lines, optically pumped, atm. transmission 77−19237
- far IR laser monitoring by piezoelec. transducers 80−102729
- far IR laser stabilisation servo electronics 77−38928
- far IR lasers, optically pumped, frequency modulated noise measurements 78−55392
- far IR optically pumped lasers, uniform transmission Si Fabry Perot couplers 80−69404
- far IR oscillator, optically pumped, parametric study 80−95862
- far IR pulsed lasers, optically pumped 78−46589
- far IR receiver optical preamplifier 77−39068
- far IR systems, for plasma studies 78−47185
- far IR technology and applications, conf., Reston, USA, (Apr. 1977) 78−45711
- far IR waveguide laser, Stark modulation 77−54744
- far IR waveguide laser cavity design criteria 77−38951
- far IR waveguide laser Stark effect obs. 77−38875
- far-IR, optically pumped, operation, appl. of opto-acoustic effect 77−31105
- fast discharge-pumped visible and UV lasers *(Chinese)* 79−72559
- FIR laser, optically pumped, nearly transparent power monitors 80−5773
- flow through laser with closed gas-circulation system, use of diametral blower 80−23701
- fluctuations of intensity and freq., single-mode laser with absorpt. cell 78−17993
- fluctuations of laser beam diameter of single-mode laser, lens effect 80−64090
- fluoromethane, 496 μm high-power smooth-pulse laser systems 77−19332
- fluoromethane, 496 μm transition, laser pumped mol. laser theory 79−36868
- fluoromethane, $^{12}CH_3F$, far IR CW laser emission by optical pumping 79−3687
- fluoromethane, and other optically pumped lasers, dynamic Stark effect 78−17911
- fluoromethane, angular correlation between far IR emission and CO_2 pump radiation, Dicke superradiance theory 79−41370
- fluoromethane, excited state rot. spectroscopy and kinetics, appl. of tunable sub-MM sources 80−14162
- fluoromethane, far IR laser, electronic tuning and phase-locking 78−59055
- fluoromethane, far IR laser, pump radiation self-focusing and defocusing 78−79003
- fluoromethane, laser pumped molecular lasers, sub MM laser expts. 80−1192
- fluoromethane, laser submillimetre with optical pumping energy yield, emission pulse delay time depend. on pumping pulse *(Russian)* 78−71088
- fluoromethane, near-MM-wave laser synchronous pumping, ultrashort pulse generation at 496, 193 μm 80−102705
- fluoromethane, optical pumping of far-IR molecular lasers by CW CO_2 waveguide laser 80−83615
- fluoromethane, optically pumped laser, IR-FIR transferred Lamb dip spectra 80−1193
- fluoromethane, pulsed optically-pumped submillimetre-wave amplifier theory 79−31868
- fluoromethane, pulsed submm. laser, high intensity, narrow bandwidth, for plasma diagnostics 77−19307
- fluoromethane, single-mode optical pumping, superradiant far IR emission 78−42329
- fluoromethane, submillimetre laser Thomson scatt. system for plasma diagnostics 77−84526
- fluoromethane, synchronous mode-locked pumping, mode-locked far IR pulse generation 79−27271
- fluoromethane, two photon generated lasing, effect of pressure 77−88703
- fluoromethane, unstable-resonator laser performance at near MM wavelengths 80−58607
- fluoromethane+$SF_6(CS_2)$, fluoromethane laser, buffer gases collisional narrowing 80−99710
- fluoromethane DFB gas laser, construction and operation 80−23715
- fluoromethane far IR CW laser, Stark effect, large freq. tuning and resolved structures 79−45931
- fluoromethane far IR laser FM and stabilisation by Stark effect 78−59056
- fluoromethane far IR Stark laser using rectangular metal-dielec. waveguide 79−27245
- fluoromethane for IR laser, evidence for Stark induced freq. shift 77−58358
- fluoromethane high-power laser, tuning behaviour 80−63994
- fluoromethane laser, optically pumped far-IR waveguide, output, temp. depend. 80−58512
- fluoromethane laser, synchronously pumped, subnanosec. transients 79−89891
- fluoromethane laser diagnostics using two CO_2 laser pump pulses 79−31869
- fluoromethane laser emission from unstable resonator 79−22983
- fluoromethane molecular laser operating in 16 μm region 77−50656

gas lasers continued
- fluoromethane optically pumped far IR lasers, 604 GHz, developments 77−83882
- fluoromethane optically pumped molecular laser, relax. oscills. 80−95875
- fluoromethane TEM_{00} far IR laser with integrated pump laser 80−43348
- fluoromethane TEM_{00} far IR laser with integrated pump laser 80−58578
- fluoromethane waveguide laser, tunable, for far IR freq. synthesis in 500-70 μm region 78−90439
- fluoromethane-^{13}C, pulsed far IR emission 80−69370
- fluoromethane-^{13}C optically pumped molecular laser, relax. oscills. 80−95875
- fluoromethane-SF_6 496-μm optically pumped laser, energy-transfer mechanisms 80−99712
- foilless anode electron-beam laser with chopper-wheel gas pulser 78−63122
- formaldehyde, D_2CO, HDCO, CW optically pumped laser action 77−88700
- formaldehyde-d_2 733 μm line, Autler-Townes effect in laser interacting with RF field 80−53269
- formaldehyde-d_2 vapour, far IR laser emissions 78−63072
- formaldehyde-d (d_2) submillimetre lasers, optically pumped, assignment of laser lines 80−58513
- formic acid, and isotopic species, CW CO_2 laser pumped, far IR lines accurate meas. 77−88714
- formic acid, CW submm. laser assignment 79−27244
- formic acid, far IR laser gas absorption obs. with and without DC field 79−31870
- formic acid, laser transitions near 5.6 μm, HF laser optical pump 78−58995
- formic acid, optically pumped by pulsed HF laser, emission obs. at 5.7μm 79−50283
- formic acid, optically pumped sub mm laser design 77−14757
- formic acid, vap., laser lines identification 78−1222
- formic acid laser 311 μm line, freq. meas. by mixing with HCN laser 79−76728
- formic acid laser far IR pulse generation by Q-switched CO_2 laser pump source 80−69383
- formic acid submillimetre laser CW lines *(French)* 77−725
- formic acid-d_0,-d_1,-d_1,-d_2, submillimetre laser appls. 77−27282
- Freon 14, optically pumped roto-vibr. mol. laser, low temp. operation and performance 79−50315
- Freon 14, roto-vibr. mol. laser, low-temp. performance 80−9871
- freq. meas. in submm. and IR regions 80−99698
- frequency modulated, threshold conditions for gain and freq. 77−88816
- frequency multiplication to 88 THz 80−99701
- frequency noninteraction of oppositely travelling waves in gas ring laser 80−38043
- frequency selection, using Faraday effect in active medium 78−1257
- frequency stabilisation *(Japanese)* 80−9891
- frequency stabilisation using ultranarrow resonance 79−59775
- frequency stabilised by saturated absorpt., synthesis and measurement of optical frequencies, review *(French)* 79−31966
- frequency stability, reference freq. and resonator length fluctuations effect 77−3619
- frequency stability measurement techniques, mass-production appl. 78−90444
- frequency stabilization method, comparative anal., using mobile and fixed Lorentzian resonances 78−33761
- fusion reactor study, SOLASE, laser, optics and pellet design 78−58426
- fusion reactor study, SOLASE 78−58424
- fusion system beam quality, Laser Optical Train Simulation code 80−78886
- gain-switched laser oscillators, analytic modelling 77−7052
- gas DFB laser waveguide precision calc. and pulse energy obs. 80−58577
- gaseous electronics, conference, Pittsburgh, PA, USA (Oct. 1979) 80−22142
- Gaussian laser beams, geometric props. 77−19276
- glow discharge infinite, dense gas homogeneity, theory 77−51253
- glow discharge lasing process, excitation freq. calc., electron upflux, book contrib. 77−50648
- glow discharge stability, high-power mol. laser, book contrib. 77−50650
- glow discharges, high-pressure, electro-optical meas. of current and voltage 78−37033
- halogen hydride lasers, vibr. energy transfer, from metastable diatomic molecules 79−31882
- halogen-metal vapour lasers, average lasing power 79−936
- He-Ne, automatic frequency trimming circuit *(Russian)* 80−1217
- He-Ne laser discharge, dynamic characts. 79−98341
- He-Ne methane saturated absorpt. stabilised lasers *(Chinese)* 79−59718
- Helios gas laser system for laser-induced fusion reactor ignition 80−32501
- high energy gas laser facility, distributed microcomputer control system 77−61975
- high energy gas laser facility, energy storage system design 78−55030
- high intensity, multimode standing-wave operation, matrix formalism 77−19229
- high intensity modes competition for different polarisations 77−58311
- high intensity single-mode laser theory 77−88691
- high power industrial gas laser system design, 1 kW 77−19321
- high power lasers and their applications 78−87092
- high power lasers for practical appls., conference, Reston, Va., USA (Mar. 1976) 77−34895
- high pressure laser media excitation by discharge through an insulator 79−27273
- high-efficiency, high-power lasers for fusion appl. *(Japanese)* 78−5486
- high-power, model for stable high-density discharges 79−13943
- high-power lasers and appls., conf., Munich, Germany (June 1977) 79−964
- high-power submillimetric laser oscillator-amplifier system design 77−38927
- high-pressure ioniser-sustainer lasers, far IR absorpt. determ. of electron densities 77−14695
- high-pressure laser cell with a transverse excitation scheme 80−78859
- high-pressure metal-vapour/inert-gas mixture discharge peculiarities 78−71620
- hollow cathode, short, expt. *(Japanese)* 77−88736
- hollow cathode discharges for gas lasers, review 80−99717
- hollow cylindrical anisotropic dielectric guide, propagation 79−32047

gas lasers continued
holographic method for laser radiation divergence reduction *(Russian)* 78—63147
homogeneously broadened laser, two mode operation, analytical string signal analysis 78—55331
induced polarisation anisotropies, direct meas. 77—19234
inert gas, electron beam pumped, visible absorpt. rel. to visible laser development 78—63057
inert gas, highly ionised, vacuum UV lasing obs. 77—79798
inert gas atomic transition lasers, excitation by discharge through an insulator 79—27273
inert gas halide high-efficiency UV lasers 77—54706
inert gas halides, laser mechanism, excitation methods and appls. 80—95871
inert gas halogen, isotope separation appl., system requirements 77—46405
inert gas hydride laser, use two-step nucl. fusion dissipative confinement of doubly isotopic boron hydrides 78—82506
inert gas IR lasers pumped by U fission fragments 80—28198
inert gas oxide, electron beam pumped, system requirements for fusion appl. 77—46403
inert gas-halogen mixture, ion form., collisions, rel. to excimer laser operations 77—61841
inert gas-SF_6 mixture, formation of inert gas fluorides in AC discharge 80—64817
infrared multiphoton processes, apparent step cross-sections, pulse spatial structure, irradiation techniques 80—32792
infrared multiphoton processes, reaction rate, scale factors, pulse structure 80—32791
inhomogeneous active medium gain 79—22930
interferometric correction of output charact. *(Russian)* 77—79855
interferometric optical anal. of laser systems 80—87401
internal modulation by acoustic surface waves 78—25901
iodomethane, and deuterated, optically pumped submm. wave amplification 78—29941
iodomethane, laser characts. with transverse optical pumping *(Russian)* 79—50286
iodomethane, laser submillimetre with optical pumping energy yield, emission pulse delay time depend. on pumping pulse *(Russian)* 78—71088
ionisation by low energy electron beam, non-self-maintained discharge *(Russian)* 77—11428
ionised-gas lasers, refr. during pump pulse due to gasdynamic motion 79—3723
IR generation, tunable, from four-wave mixing in room temp. Ge 80—9940
IR laser optical pumping 77—58348
IR physics, conference, Zurich, Switzerland (Mar. 1979) 80—4783
IR tunable for remote meas. of atmospheric gases 77—49199
IR waveguide and mini-TEA lasers, operation 1.25 to 10.6 μm 77—88752
isotope, opposing waves competition at lasing line centre 80—1187
kinetics, proton excited gas mixture obs. 79—48013
kinetics simulation of high-power gas lasers 79—59676
Lamb dip, transit time broadening, perturbation theory calcs. 77—647
large-bore CW high-energy, holographic interferometry during power extraction 80—28172
laser modulator 80—48311
LG-36A (USSR), synchronisation with SRF-2M camera 80—73489
linearly polarized waves, interaction with longitudinal mag. field 80—95936
long pulse electron beam accelerator 77—23321
longitudinal flow, effect of flow on output power 78—58975
magnetooptical switch for synchronization of CO_2 and red laser beams 80—58615
metal atom lasers, finely dispersed metal particle active medium 80—91777
metal halide vapour lasers, kinetic model 79—94222
metal halide vapour lasers using gas-discharge tubes 79—64251
metal pure vapours, apparatus for stimulated emission obs. from transverse discharges 79—13954
metal vapour, explosively formed, apparatus for stimulated emission obs. 78—50764
metal vapour, hollow cathode, review *(Rumanian)* 80—87409
metal vapour, laser operation by dissoc. of halides, alkyls and carbonyls 77—54702
metal vapour laser, afterglow electron energy balance 79—76678
metal vapour laser, upper and lower laser states population densities, simultaneous determ. method 78—87042
metal vapour lasers excited by pulse trains 79—13955
metal vapour pulsed lasers, quantum amplifiers, image distortion 79—18433
metal vapour transverse separation in cataphoretic lasers 77—50659
metal-vapour recombination lasers using segmented plasma excitation 80—74370
metastable states, at. and mol. vibr. and electronic, book contrib. 77—50653
methane, continuous coherent radiation obs. in spatially spaced fields *(Russian)* 78—9372
methane, line profile of coherent radiation in separated fields due to $F_2^{(2)}$ transition 80—37835
methane stabilised laser, stability evaluation *(Japanese)* 78—90437
methanol, 118 μm, diagnostic experiments and modelling 80—58515
methanol, and deuterated, laser far IR pulse generation by Q-switched CO_2 laser pump source 80—69383
methanol, CD_2HOH, CH_2DOH, CW optically pumped, submm. laser action, 100 to 900 μm 79—929
methanol, CH_3OH and CD_3OH, far IR laser lines, optically pumped by CO_2 laser 78—90415
methanol, CW far IR optically pumped, anisotropic gain 77—61944
methanol, far IR laser, intracavity pumped by TE CO_2 laser 80—87382
methanol, far IR laser gas absorption obs. with and without DC field 79—31870
methanol, far IR laser line obs. and assignment 79—31867
methanol, far IR laser lines pumped by CO_2 laser sequence lines 78—9369
methanol, far IR laser resonator for TEM_{00} mode operation 78—66847
methanol, high power optically pumped CW laser, line assignments 77—54701
methanol, in submm. interferometer system, for plasma density meas. 77—7586

gas lasers continued
methanol, optical pumping of far-IR molecular lasers by CW CO_2 waveguide laser 80—83615
methanol, optically pumped, assignment of weak FIR laser lines 80—14320
methanol, optically pumped, far IR gain meas. 78—22114
methanol, optically pumped, far IR laser lines meas. and assignments 79—22939
methanol, optically pumped, laser line assignment 77—54698
methanol, optically pumped CW far IR laser frequency characteristics 77—38873
methanol, optically pumped CW for IR laser lines, freq. meas. 80—58514
methanol, optically pumped CW subMM emission lines 80—95876
methanol, optically pumped laser, IR-FIR transferred Lamb dip spectra 80—1193
methanol, optically pumped sub mm laser design 77—14757
methanol, optically pumped submm. wave amplification 78—29941
methanol, pumping by narrow band CO_2 TEA laser 77—54729
methanol, submillimetre laser molecules, Stark and ODR spectroscopy 79—31864
methanol 118 μm laser line, simple accurate method for wavelength meas. 80—106554
methanol 70 and 118 μm laser line diagnostic expts. 80—69387
methanol CW optically pumped waveguide far IR laser, 10 to 100 mW, design and perform. 79—31934
methanol far IR CW laser, Stark effect, large freq. tuning and resolved structures 79—45931
methanol far IR laser, CW laser pumped, saturated and small signal gain calc. 80—58521
methanol far IR laser, optically pumped, Stark effects 79—72552
methanol far IR laser, twin optically pumped, for plasma diagnostics 80—59306
methanol far IR laser emission spectroscopy 80—58524
methanol far IR laser gas, CW laser pumped, gain 80—69367
methanol far IR laser line Stark splitting obs. 80—58313
methanol far IR Stark spectroscopy and 9-P(34) CO_2 laser line 80—69145
methanol far-IR laser, optically pumped, intracavity polarization modulation 80—23726
methanol laser, CW, optically pumped, 170-μm emission, press. shift 80—106510
methanol laser, optically pumped, use of crystalline reflector in cavity 80—64080
methanol laser, twin optically pumped far IR, use in plasma diagnostics 80—54049
methanol optically pumped 118.8 μm laser line, Stark splitting obs. 80—102710
methanol optically pumped laser, frequency instability meas. at 70.5 and 118 μm 80—1254
methanol subMM laser line obs. 80—58523
methanol twin optically pumped far IR laser for plasma diagnostics 80—103189
methanol waveguide laser radiation modulation by Stark cell 77—38962
methanol-d_1, CH_2DOH optically pumped CW far IR laser lines and frequencies 80—102707
methanol-d_1, CO_2 laser pumped, CW far IR laser lines 79—76672
methanol-d_3, CO_2 laser pumped, CW far IR laser lines obs., 34.5 to 287 μm 78—71082
methanol-d_3, optically pumped, CW far IR laser lines obs. 78—79005
methanol-d_x, optically pumped, new FIR laser lines 79—72553
methanol-d, CO_2 laser pumped, CW laser lines obs. 80—53272
methanol-d, optically pumped CW subMM emission lines 80—95876
methyl alcohol, and deuterated forms, complete freq. coverage for submm. laser spectroscopy 78—25860
methyl alcohol, assignment of submillimetre transitions 79—22943
methyl alcohol, optically pumped, far IR laser line assignment 77—38869
methyl alcohol, optically pumped, new CW FIR laser lines meas. and assignments 80—48224
methyl alcohol, optically pumped far IR laser, spectroscopy appl. 77—5932
methyl alcohol high-power optically-pumped CW laser line assignment 77—38868
methyl alcohol IR absorption, diode laser obs. 79—31518
methyl alcohol IR transitions, saturated absorption spectroscopy 77—38874
methyl alcohol laser, freq. meas. at 4.25 THz using Josephson harmonic mixer and phase lock techniques 80—95078
methyl alcohol submm wave laser, optically pumped, intracavity double resonance obs. 80—58522
methyl alcohol-CO_2 far i.r. laser with metal-dielectric waveguide, Stark effect obs. 77—700
methyl alcohol-d, optically-pumped laser line freqs. 78—55345
methyl bromide, optically pumped submillimetre laser characts. *(Russian)* 79—68384
methyl bromide, submillimeter rotational spectrum, laser generation line identification 79—64210
methyl bromide sub mm laser, generation lines identification *(Russian)* 78—82952
methyl chloride optically pumped submillimetre laser characts. *(Russian)* 79—68384
methyl cyanide, far IR laser line assignments 80—69380
methyl cyanide, intracavity pumped submm wave laser, CW 77—88741
methyl cyanide submillimetric waveguide laser amplifier design and operation 77—38926
methyl cyanide-CO_2 far i.r. laser with metal-dielectric waveguide, Stark effect obs. 77—700
methyl fluoride, 496 μm line, freq. meas. 77—42557
methyl fluoride, $^{13}CH_3F$, high-power pulsed laser 80—69386
methyl fluoride, CW optically pumped far IR laser with variable output Michelson coupler 78—55372
methyl fluoride, deuterated, optically pumped near-MM laser 80—69379
methyl fluoride, double-ended unstable resonator submillimetre laser characts. 79—81461
methyl fluoride, high-power narrow-linewidth linearly pumped oscillator-amplifier system 77—54726
methyl fluoride, optically pumped mirrorless laser at 496 μm 79—31871
methyl fluoride, stimulated emission at 9.75 μm following two-photon excitation 78—42323
methyl fluoride, tunable diode laser spectroscopy, 9-10 μm 77—54558

gas lasers continued
methyl fluoride laser far IR pulse generation by Q-switched CO_2 laser pump source 80—69383
methyl fluoride laser pumped with continuously tunable multiatm. CO_2 laser 80—69421
methyl fluoride pulsed high-power laser development 77—38872
methyl fluoride-d_3, optically pumped sub-MM wave laser 80—23676
methyl halides, candidate transition identification for optically pumped far IR lasers 79—931
methyl iodide, and deuterated, pulsed subMM lasers pumped by CO_2 laser 80—106511
methyl iodide, optically pumped sub mm laser design 77—14757
methyl mercaptan, CW subMM emission lines, optical pumping 80—87381
methyl nitrile CW for IR mol. laser, optical pumping with $^{16}CO_2$ and $^{18}CO_2$ lasers 80—74343
methylfluoride, CW for IR mol. laser, optical pumping with $^{16}CO_2$ and $^{18}CO_2$ lasers 80—74343
methylfluoride laser, CW, 496 microns, rate equation model, review 78—55343
microwave gas discharge problems in lasers *(Russian)* 80—14345
millimetric-wave high-power optically-pumped laser performance and applic. 78—5469
millimetric-wave optically-pumped laser CW performance 78—5468
minicomputer-controlled diagnostic and display system for high-energy lasers 79—36915
mode interaction, transition level degeneration effects *(Russian)* 77—61940
mode interactions in longit. mag. field, active medium dispersion effects 80—63967
mode locked ring-laser with two isotope medium, two-mode emission 78—1278
mode-locked binary laser oscillator, bistability induced by optical nutation 79—31958
mode-locking operation using modulator with acoustic Fabry-Perot resonator 79—45976
modulation method, for relative excitation level, cavity bandwidth and at. temp, appl. to He-Ne laser 80—5771
modulation spectroscopy using solid-state and gas lasers 79—30572
molecular amplifier, vibr. relax. effect on laser pulse energy characts. 78—17921
molecular FIR laser design, freq. tunable by Stark effect 80—5750
molecular gas lasers, pulsed high press. transversely excited, design 79—31946
molecular laser, optical pumping in damped photodissoc. wave propag. in dense gas 80—99714
molecular laser processes, mm. and submm. microwave spectroscopy 78—13685
molecular lasers, IR-FIR transferred Lamb-dip, standing wave saturation effects 80—58520
molecular lasers, laser pumped, theory 79—36868
molecular lasers, laser pumping, dispersion 80—87375
molecular lasers, optically pumped, polarisation phenomena appl. 80—87384
molecular lasers with gas pumping, temp. field calc. 79—76673
molecular mixture, strongly excited, vibr. relax. 80—102555
molecular modern laser types, high output and efficiency *(German)* 77—7133
moving striations, conditions for self-excitation 80—69358
multichannel surface spark gaps 79—18436
multifrequency emission, atomic states interference effect on polaris, characts. 79—27235
multigas electron beam pumped lasers 78—94396
multimode, active medium polarisation with excitation modulation 78—82942
multimode high-intensity laser dynamics theory 79—41363
near MM wave laser synchronous pumping, ultrashort pulse generation 80—69385
neutral gas lasers, empirical scaling laws derived 77—14693
neutral gas recomb. laser, CO_2-laser-produced plasma-initiated 80—48286
noise, low frequency 80—69364
non-self-maintained discharge, three-body electron attachment to O_2, plasma decay obs. 80—43844
non-self-sustained discharge plasma, thermal instability development, laser appls. 78—71611
non-self-sustaining discharge, mag. mirrors *(Russian)* 80—106530
nonequilibrium gas relaxation in supersonic nozzle, analysis method 80—74941
α-NPO-Ar mixture, vapour phase laser, electron beam pumping 78—63097
nuclear laser reactors, characts. of produced laser pulse estimated 77—65592
nuclear pumped laser reactors 80—23117
nuclear pumped laser simulation experiments 80—64042
nuclear pumping by vol. source of fission fragments 79—36879
operation, fast electron beam irrad. effects *(Russian)* 78—74878
optical inhomogeneity of laser medium, phase front meas. of output radiation 77—79841
optically pumped CW far IR lasers, quantum mechanics 77—54700
optically pumped CW far IR waveguide lasers, high power, scaling 77—54731
optically pumped far IR laser design and performance, review 79—31917
optically pumped far IR laser output power, temp. depend., four-level model 79—59674
optically pumped far IR lasers, freq. and power meas. and LMR spectroscopy 77—54725
optically pumped FIR laser with variable Fabry-Perot output coupler 77—68220
optically pumped for IR lasers for spectroscopy 78—4713
optically pumped IR lasers, book contrib. 77—46718
optically pumped laser three-photon transition theory 80—102690
optically pumped lasers utilizing self-terminating transitions, CW stimulated emission possibility 80—14329
optically pumped mid-IR lasers 79—22961
optically pumped sub mm lasers 77—54699
optically pumped sub mm wave regenerative amplifier 77—54728
optically pumped submillimetre lasers, collisional contrib. to dynamic Stark effect 79—13765
optically pumped submillimetric laser models and rate eqns. 77—38871
optically pumped waveguide gas lasers 78—5490

gas lasers continued
optically pumped waveguide laser characteristics 77—38870
optically-pumped submillimetre oscillator, for plasma diagnostics 78—47184
organic compound laser, limiting length, stimulated radiation reabsorpt. by unexcited and excited singlet mols. 80—48240
organic dye attachment for wavelength conversion within 340 to 1200 nm 79—7147
organic molecules, far IR laser active, optoacoustic spectra 79—59448
organic seedants for UV preionised lasers, photoionisation and photoabsorpt. characts. 78—13688
organic vapour phase laser, electron beam pumping of inert gas-organic vapour mixture 78—63097
organic vapours, lasing characteristics 80—99716
oscillations in gas laser discharge, review 78—55339
output characts., effect of spatial and temporal modulation of excitation 79—3681
output power external stabilisation using Faraday effect, control unit design *(German)* 79—18455
output power profile collision induced asymmetry, simplified model 80—87366
partially homogeneously broadened gas laser amplifier, wave impedance formulation 77—75468
phase locking by mechanical cavity length modulation 78—46571
photoionisation, multiple, infrared laser 80—69194
plasma dispersion function 78—17894
plasma lasers in molecular medium, thermal ionisation and recomb. *(Russian)* 78—22118
plasma UV, rel. to influence of vibrational kinetics on shortwave emission of dissociating molecules 77—42395
polarisation effects, theory 80—23660
polarisation effects 80—58605
polarisation of output radiation, two-mode laser with resonator weak phase anisotropy 79—64264
polarisation states of gas laser with internal mirrors 77—50701
polyatomic molecules excited by CO_2 laser pulses, stimulated emission *(Russian)* 79—94214
power as function of level of optical signal synchronisation 80—69359
precise elec. meas., conf., Brighton, UK (Sep. 1977) 77—82551
precision EM measurements conference, Boulder, Colorado (June 1976) 77—18010
preionisation by ^{241}Am radioactive source 78—29963
preionisation by electrodeless capacitative pulses, pulse-periodic operation regime 79—31937
propynal, CW for IR mol. laser, optical pumping with $^{16}CO_2$ and $^{18}CO_2$ lasers 80—74343
pulse duration increase in self-limiting transitions *(Russian)* 78—33719
pulsed atomic gas laser, time and energy characts. in mag. field *(Russian)* 78—22108
pulsed collinearly pumped far IR amplifier, rate analysis 79—81408
pulsed laser with unstable resonator, beam shaping 78—17987
pulsed lasers pumped by LC inversion cct. made of $BaTiO_3$ and $SrTiO_3$ series ceramic capacitors 80—99779
pulsed light source with thin-film modulator, fabrication and characts. 80—43467
pulsed N_2 laser, with plane parallel plates 79—86170
pulsed optically-pumped submillimetre-wave amplifier theory 79—31868
pulsed plasma laser, falloff rate of field 78—82944
pulsed submillimeter, with optical pumping, construction and expt. parameters 80—58565
pumping, quasi-reson. energy and charge exchange processes, new transitions 80—58526
pumping by electron accelerator, design principles 78—5483
pumping oscillator for transverse excitation lasers 78—5488
pumping using self-sustained electron-photoionization discharge, high power laser 80—33013
Q-switched operation *(Japanese)* 77—691
radially converging electron beam accelerator for gas laser excitation 78—9391
radially pumped UV laser, space charge limited current flow 77—39477
radiation synchronisation with quantum RF standard 77—68226
radioactive source preionisation of visible and UV discharge lasers 78—63096
rare earth halide vapour, discharge, potential fusion laser systems 78—63074
rare earth lasers, book contrib. 80—53306
recombination lasers using elemental vap., metal ion transitions 78—17923
recombination lasers using elemental vap.; stimulated emission conditions 78—17922
recombination processes, book contrib. 77—50663
regeneration mode with saturation effect taken into account 77—650
relaxation parameters and performance, Lamb theory 77—75467
resonance in output of laser with nonlinear absorber, freq. stabilisation 77—83854
resonant amplification, transient and spatially inhomogeneous excitation 77—652
resonant pumping, high-power, of molecular systems *(Russian)* 77—54690
resonant vibrational excitation, by electron impact, low energy, book contrib. 77—50662
resonant-pulse propagation method for line-shape parameters analysis 79—55168
resonantly excited laser media, possible use in wavefront reversal 79—94281
resonating structure loss reduction, wave propag. in hollow rectangular anisotropic guide 78—83084
resonator filled with flowing medium, EM anal. 77—79856
resonator parameters effect on mode volume *(Hungarian)* 80—58603
resonators, simple method of adjusting mirrors 80—19054
retroreflecting mirror for dynamic compensation of optical inhomogeneities 79—31970
review, neutral atom, ion, metallic vapour and mol. lasers 77—38866
review 77—7099
review of lasers with wide-band optical pumping 79—31885
review of systems and appls., book contrib. 77—50680
ring, limiting characts. of power resonances 80—19058
ring, nonlinear interaction of opposing beam waves with arbitrary polarisation, anal. *(Russian)* 78—82993
ring gas laser, freq. synchronisation region of colliding waves 80—83620

gas lasers continued
ring gas laser interaction of elliptically polarised opposing waves 80—38044
ring laser, effect of elastic collisions on drift splitting of opposite wave frequencies 80—14370
ring laser, emission spectrum control by mag. field induced phase anisotropy of active medium 79—94264
ring laser, mode self-locking 78—1283
ring laser, multimode, high-Q power resonances 78—82997
ring laser, nonlinear polarisability of two-isotope active medium 80—14369
ring laser, nonlinear Zeeman effect 78—71123
ring laser, opposite wave freq. difference, mag. field 79—7156
ring laser, relativistic Doppler effect, two-wave mode instability and optimum tuning 77—38940
ring laser, reson. radiation trapping and nonlinear interaction of waves 79—18452
ring laser, resonance phenomena with saturated absorpt. *(Russian)* 78—59048
ring laser, saturating opposite waves interaction 77—50695
ring laser, scale factor for saturating oppositely travelling waves 80—9910
ring laser, synchronous four-wave regimes boundary 77—721
ring laser characteristics, influence of radiation interaction with reflector material 79—13993
ring laser gyro, dispersion and gas flow effects 80—1267
ring laser output characteristic coefficient determ. 77—7123
ring laser power resonances shape 77—58355
ring laser under gain modulation conditions 77—72011
ring two-mode laser with two-isotope active medium, freq. characts. 77—79864
rotating anharmonic oscillators in resonator, stimulated emission power 80—99689
roto-vibrational molecular laser, optically pumped, rate eqn. model 78—37874
roto-vibrational molecular laser scaling, CO_2TEA laser pumped 80—5728
saturation, polarisation and spectral inhomogeneities, relax. consts. 77—50652
scattered radiation reception by optical quantum amplifier 78—17946
short resonator, single freq. emission condition 77—58356
single mode, mode polarisation in transverse mag. fields 78—22107
single-mode, autodyne effect *(Russian)* 79—925
single-mode, in transverse mag. field, polarisation props. 79—7167
single-mode gas laser with slightly anisotropic resonator, output polarization stability 80—43370
single-photon counting system for measuring laser parameters 79—89915
skimming discharges for pulsed gas-discharge laser preionisation, spectral characts. 80—99740
solar excitation *(Russian)* 77—83847
spatial coherence increase, new method *(Russian)* 78—37928
spatial gain distrib., in i.r. lasers, meas. technique 77—696
spatially coherent laser beam form., phase transitions 78—17898
spontaneous coherent pulsations in laser oscillators 79—921
stabilised two-frequency laser, use in ellipsometry 80—101820
Stark effects in optically pumped far IR lasers 77—38963
startup system for magnetic fusion 77—18704
steady state, parametric relation investigation 79—76677
stimulated reactive oscillations, laser-elec. circuit Q 77—58315
sub mm media, lasing performance, low-mol.-wt. alkanes and cavity temp. effects. 78—42328
sub-mm CW optically pumped laser, scaling 78—55341
submicrosecond pulses, use in laser gas dynamics *(Russian)* 78—29940
submillimetre, optically pumped, two-photon transitions 78—22112
submillimetre, optically pumped lasers 78—46587
submillimetre CW laser, amplitude stability improved by phase modulated pumping 79—22967
submillimetre laser molecules, Stark and ODR spectroscopy 79—31864
submillimetre laser output and efficiency, rel. to pump frequency displacement 79—31866
submillimetre laser sources for magnetic resonance spectroscopy, standard frequencies 77—13788
submillimetre optically pumped lasers, design optimisation 77—14757
submillimetre wave laser operating in CO_2 laser cavity 77—83885
submillimetre wave laser waveguides 78—5505
submillimetre wavelength tables, 34 μm to 1.965 mm, Co_2 laser pumping 77—7095
submillimetre waves and applications, conference, Guildford, England (1978) 79—31916
submillimetric pulsed laser with optical pumping, characts. rel. to vapour pressure *(Russian)* 79—94215
submillimetric waveguide laser for gas spectroscopy 80—33022
submillimetric-wave laser waveguides 77—38952
supersonic boundary layer, density distrib., cathode emanation perturbation, gas laser appl. 77—84544
supersonic flow electronic transition lasers, low-temp. and high-pressure, pulsed blowdown and electron gun facility 79—59723
surface discharge, use for gas preionisation 79—46504
surface spark discharges high current, light emission props. and appls., book contrib. 79—77449
tapered tube design 77—10940
TEA laser discharges, inhomogeneities 77—14687
TEA-CO_2 laser, transverse profile pulse evolution 79—98425
technology advances, conf., Washington, USA (Mar. 1978) 79—36911
tetrafluoromethane, optically pumped laser, 11-17 μm 78—46581
tetrafluoromethane laser, pulsed, high repetition rate, average power limitations at 10.6 and 16 μm 80—58503
tetrafluoromethane molecule, laser spectrosc. and optical pumping from CO_2 laser 80—74202
tetrafluoromethane optically pumped laser, tuning and stabilisation 79—13985
three body recombination processes for high power c.w. visible output 77—651
three level molecular system interaction with two laser fields 77—54685
three-level gain medium, semiclassical theory, population pulsations and interf. effects 80—95863
three-level molecular laser pumping and dispersion eqns. 80—69384
thyratron ignition of gas lasers *(German)* 79—64245
thyratron pulser, high-power, HF, for photo-impulse ionised lasers 79—18444
transverse electromagnetic, spatial control of pulsed high-pressure preionisation stabilised glow discharges 80—79606

gas lasers continued
transverse mode struct., laser field transformation *(Russian)* 78—37934
travelling wave amplifier, spontaneous radiation channelling 79—27294
travelling wave cross-saturation asymmetry 80—43371
travelling-wave Zeeman gas laser operating at high radiation intensities, theory 80—9912
trifluoroiodomethane, high press., selective isotope dissociation with pulsed CO_2 laser 79—72370
trifluoroiodomethane, optically pumped laser, 11-17 μm 78—46581
trifluoroiodomethane nuclear pumped lasers, electron impact cross section meas. 80—63985
trioxane, D_2CO, HDCO, CW optically pumped laser action CW optically pumped laser action 77—88700
tunable high power lasers for isotope separation 77—34904
tunable high-pressure molecular gas lasers in IR, saturation behaviour *(German)* 77—23650
tunable IR lasers, principles and operating characts., review 79—98376
tuning using SAW light diffraction grating *(Russian)* 78—33759
two-level molecular systems, optically pumped, increased inversion efficiency 80—23657
two-mode, with smooth variation of mode separation, freq. characts. 80—53264
two-mode emission in strong field, limits of stability 77—14685
two-mode gas laser, strong coupling, transients 79—55114
two-mode oscill. gas laser, saturation-induced polaris. preferences 79—22929
two-photon spatially periodic pumping, excitation threshold and output power *(Russian)* 78—13693
unstable confocal resonator operating point choice 79—36938
unstable confocal resonators, operating point choice 79—59727
unstable resonator properties, small-scale phase inhomogeneity influence 78—59050
UV laser *(Japanese)* 79—3686
UV lasers, Blumein circuit transient anal. for effective operation 77—68230
UV/visible gas lasers, appls. in commercial photochemical processes, review 79—55123
vacuum UV, travelling wave source pumping, numerical anal. 77—83864
vacuum UV tunable coherent radiation generation by lasers 77—54705
vapour laser assembly 80—9896
velocity measurement, laser Doppler anemometer, reflecting objects and fluid flow *(Russian)* 79—82009
vibration immunity for interference work 78—5489
vibrational interaction of diatomic and triatomic mols., theory 77—23670
visible and IR stabilised lasers, wavelength intercomparison 77—7114
visible and UV lasers for diverse appls., new families 79—59705
volume discharge excited by electron beam, mag. field influence 79—27241
volume high-pressure discharge with photoionization for laser pumping 80—54058
volumetric nuclear pumped lasers 78—5457
waveguide, laser, pump efficiency, saturation effects 78—17981
waveguide, miniaturised, communication appl. 79—31936
waveguide laser, construction and operation characteristics *(Rumanian)* 78—59049
waveguide laser, mode comp. of radiation 80—28192
waveguide lasers, operation under multimode conditions, relative efficiency of cavities, comparison 79—55158
waveguide lasers, props. and current-voltage characts. of discharges 78—1208
white light lasers, two types *(Russian)* 77—27303
X-ray preionisation for elec. discharge lasers 79—64205
Zeeman linearly polarised laser, Izsing atom susceptibilities, first and third order approx. *(Japanese)* 78—71071
Zeeman linearly polarised laser, mag. field reson. on laser output, freq. stabilisation *(Japanese)* 78—66798
Ag-He CW mW-level laser source at 224 nm 80—43352
Ar, CW UV emission, power enhancement 78—17906
Ar, discharge current control using thyristor convertor 77—14747
Ar, fission fragment energy deposition kinetics rel. to nucl. pumped laser 77—23652
Ar I, high press. tunable laser emitting at 0.91 μm 78—50755
Ar laser, longit. mode locking in three mirror cavity 79—55164
Ar laser, new IR laser transitions, 3.725 to 17.233 μm, 5.804 μm laser line identification 80—87374
Ar, laser oscill. obs. in transversely initiated laser-produced plasma 77—88696
Ar laser power supply for discharge current and output power control 77—38912
Ar, recomb. laser in expanding CO_2 laser prod. plasma, 1.79 μm laser oscill. 77—88698
Ar, simple high-power TEA laser operating in near IR 79—94251
Ar, wavelength measurement using digital interferometer 80—37079
Ar-Kr white light lasers *(Russian)* 77—27303
Ar-N_2, UV emission, 100-500K, kinetic model 77—58321
Ar-N_2 mixture, fission fragment energy deposition kinetics, rel. to nucl. pumped laser 77—23652
Ar-$N_2(Cl_2)(F_2)(H_2O)$ laser, energy pathways by proton excitation 78—5459
Ar-Xe, low-threshold nuclear pumped laser, generation characts. 80—19018
Ar-Xe high press. transverse discharge laser using Xe IR transitions 80—63978
Ar-Xe high-press. neutral IR laser emission from Xe 79—86159
Ar-Xe IR laser pumped by electron beam stabilised discharge, lasing parameters 80—102698
Ar-Xe-tetrachloromethane, self-sustained electrophotoionised discharge in compressed gas 80—38003
ArF, laser spectra, absorpt. lines 80—9604
$Ar^*(4p),(5p)$ states, lifetimes and two-body rate consts. meas. 78—63058
Au vapour, discharge excitation, pulse stimulated emission in visible and UV 77—79810
Au vapour brightness amplifier at 627.8 nm, for projection microscope 80—83616
Au vapour laser, 627.8 nm UV emission, average output power and efficiency 79—45933
Au-He CW mW-level laser source at 280 nm 80—43352
Ba, discharge heating, power and performance 78—46580
Ba, discharge-heated, 1.5 μm, improved performance by vol. scaling 77—88778
Ba, high average output power 79—72593

gas lasers continued
Ba, vap. in heat pipe oven, 1.5 μm monomode emission *(French)* 77—3570
Ba vapour gas discharge laser excited by dual-pulse, lasing characts. 79—89895
Ba vapour laser, energy characts. at 1.5 μm 79—13953
Ba vapour laser, pulse repetition frequency scaling law 78—82954
Ba vapour laser, pulsed lasing due to 1.13, 1.5 μm atomic transitions 80—53276
Ba-Tl laser optically pumped by pair-absorption transitions, 1.5 μm emission obs. 80—58517
Bi atom, pulse stimulated emission of 472.2 nm line 78—17920
Bi pulsed laser, stimulated emission mechanism at 472.2 nm 80—19022
Br_2, optically pumped at 532 nm, lasing obs. in visible and near IR 78—63094
Br_2-CO_2 IR laser with $Br^* \rightarrow CO_2$ electronic-vibr. energy transfer as pump mechanism 80—53260
Br_2+CO_2 mixture, Raman laser optical excitation, electron phototransition theory *(Russian)* 80—99711
C afterglow laser, recombination-pumped 77—50657
C, atomic. in He-CO(CO_2) mixtures, direct nuclear pumped, laser action obs. 78—5460
C nuclear pumped lasers employing Ne(He)-CO(CO_2) mixtures, energy storage 80—63996
CF_4, for 16 μm range, review *(Rumanian)* 80—87408
CO, 600-W convective flow laser, characts. 78—17969
CO, absorption of radiation in 5 μ region by water vapour, optoacoustic meas. 77—2241
CO, acetone decomposition, near IR laser action 78—63055
CO, atm. press., emission spectrum spectral and temporal characts. 77—670
CO, CO_2 lasers, appl. to atmospheric pollutants selective quantitative meas. 78—69526
CO CW 80-kW supersonic elec. laser, elec. and laser diagnostics 79—98399
CO CW electric discharge laser, saturation parameter expt. determ. 78—50762
CO, CW electric laser, anal. model 78—25862
CO CW laser emitting dominant spatial mode, output power stability rel. to CO_2 laser 80—32965
CO CW lasers, effect of Xe addition on room temp. operation 79—18407
CO, CW output spectral content meas. with scanning Fabry-Perot interferometer 77—27292
CO, continuous flow longit. discharge high specific output energy 78—46585
CO cooled electron-beam-controlled laser, two-quantum transitions 79—45935
CO discharge, low-pressure laser striation obs. 78—66814
CO discharge lasers, low transitions, theory and expt. 77—3568
CO, discharge plasma, C combustion effect on vibr. excitation 77—50666
CO, efficient self-sustained pulsed laser 78—55377
CO, elec. excited overtone bands lasing at 2.7 to 3.1 μm 78—13684
CO electric discharge laser using single vibr.-rot. transition, laser line selection 79—59687
CO electric discharge laser, system efficiency *(Japanese)* 79—64206
CO electric discharge lasers, vibr. kinetics, modelling and expts. 80—69374
CO electric discharge supersonic laser, pulser-sustainer, construction and performance 78—25888
CO electric discharge unstable resonator laser, computer model 78—58988
CO electrical discharge laser, vibr. excitation rate levels and energy balance 79—81413
CO, electroionisation laser, generation efficiency *(Russian)* 77—58313
CO electron beam controlled laser, stimulated emission characts. 78—1221
CO electron beam controlled laser, energy and spectral characts., NO admixtures effect 80—9867
CO, electron impact, vibr. levels stepwise excitation 78—1095
CO, electron-beam-controlled, short high-power pulse generation 78—25863
CO, far IR difference freq. generation 77—19366
CO, flowing plasma, spontaneous emission, A coeffs. 77—7070
CO gas discharge laser, optimisation of active media comps. and working parameters 79—64216
CO, high power discharge lasers, operational principles and design constraints 77—38931
CO, high press. pulsed elec. laser 77—79847
CO, high-press. electroionisation laser, lasing action *(Russian)* 77—7127
CO laser, analytical theory, multilevel cascade emission *(Chinese)* 80—102702
CO laser, CW, with RF excitation in supersonic flow 80—74375
CO laser, chem. composition of plasma, room temp. 77—83866
CO laser, cooled electron-beam controlled, characteristics 80—19023
CO laser, cooled electroionisation type, in nucl. reactor active zone 80—64066
CO laser, externally sustained discharge, energy characts. 80—28207
CO laser, liq. N_2 cooled, extended spectral distrib. of lasing transitions 79—89894
CO laser, multiphoton amplification, HF removal of forbiddenness *(Russian)* 80—53262
CO laser, radiation power, generation line selection influence *(Russian)* 77—83865
CO laser, sealed-off, output power and efficiency meas. 80—99743
CO laser, simple model for power and spectra 79—7119
CO laser, steady state operation, vibr. distrib., numerical calc. 79—36884
CO laser, water-sealed, efficiency increase by reducing resonator losses 80—64081
CO laser driven spectrophone, humidity trace detection in H_2 and air 79—20477
CO laser lines, spectral coincidences with NO absorpt. lines 79—86162
CO, laser mag. resonance detect. of NO_2 in N_2 77—12855
CO laser output power, active species and buffer He isotope effects *(Russian)* 80—63986
CO laser pumping with high-energy particles 79—64211
CO laser with selective resonator, gain saturation law, lasing transition efficiency 80—48227
CO lasers, scaling laws 80—95878
CO, longit. discharge lasers, aerodynamically stabilised cathode 77—10955

gas lasers continued
CO low-press. laser discharge, effects of O_2 78—17914
CO, mass spectra of positive ions in discharge plasma 77—89315
CO nuclear pumped laser, fission fragment excited with gas cooling, performance obs. 80—63997
CO, overtone generation, by pumping in elec. discharge *(Russian)* 78—22116
CO, pulsed laser, characts. 80—43325
CO pulsed laser, stimulated emission dynamics, transition lines for isotope enrichment 80—48225
CO pulsed laser emission with line selection, analytical theory 80—53277
CO pulsed TE laser and pulsed CS_2/O_2 chemical laser, comparative study 79—31876
CO pump laser, multiline operation producing SFRL multiline output, CO laser lines 79—7132
CO, review theoretical, experimental developments *(Japanese)* 78—25857
CO room temperature nuclear pumped laser, parameter optimisation and spectral props. obs. 80—63995
CO sealed laser, approximate analytic theory 78—58994
CO, sealed TE laser, UV preionisation 78—17966
CO, simple high energy TEA laser 79—3714
CO, simple high-power TEA laser operating in IR 79—94251
CO, stable CW, step-tunable, pumping of external-resonator controlled Raman laser 80—9624
CO, supersonic laser mixture, double discharge stabilisation 78—5461
CO supersonic lasers, CW double elec. discharge performance 80—69416
CO, variable attenuator for Gaussian laser beams 79—22987
CO, vibr. relax. at glass surface, glow discharge meas. 79—18409
CO waveguide CW laser, 280-290K *(Russian)* 77—71975
CO, waveguide laser operating near room temp., design and construction 78—22144
CO, window materials, absorption props. 77—46770
CO, $X^1\Sigma^+$ state elec. dipole moment function, transitions, vibr.-rot. band calcs. 77—14410
CO-^{3}He nuclear pumped laser, optimisation with 2 MeV protons 80—64000
CO-Ar(-N_2), high press., arc assisted elec. discharges 77—3606
CO-CS_2, interaction between vibr. states, theory 77—23670
CO-He, plasma-injection-stabilised discharges at low temp. 78—17959
CO-He low press. mixture, CO vibr. distrib. to high level 78—58985
CO-He nuclear pumped laser, high energy beam deposition 80—63999
CO-He-O_2 gas discharge laser plasma, positive ion generation mechanism *(Russian)* 79—99005
CO-He-O_2-H_2O laser discharge, stability, influence of recombination and ion chem. 78—17915
CO-He-Xe, Xe effect on gas temp. 77—19238
CO-N_2 and CO lasers, energy and spectral characteristics 80—14327
CO-N_2 discharge, energy balance influence of N_2 rot. level reson. excitation 78—17903
CO-N_2-^{3}He, laser mixture, excitation in externally maintained discharge in reactor core 80—28193
CO-N_2-^{3}He, nucl. reactor active zone, plasma and sustained discharge props. 80—5729
CO-N_2-He laser, cooled electron-beam-controlled, characteristics 80—19024
CO-UF_6 nuclear pumped laser, expansion cooled, vibr. excitation distrib. 80—63997
CO-Xe-N_2-He gas laser power rel. to mixture composition *(Russian)* 79—7114
CO+ perfluoroalkyl halides, collisional relax. 79—13799
CO_2, 1 mJ line tunable optically pumped laser 78—66840
CO_2 1KJ laser system for laser-plasma interaction expts. 78—5502
CO_2 10 kJ laser for fusion research, automated alignment 79—76703
CO_2, 100 kJ laser, optical design and components 78—82990
CO_2, 10.17 μm R(32) transition, appl. to He-Ne laser freq. meas. 77—31113
CO_2, 10.6, 9.4 μm laser bands high-press. absorpt-spectra 78—66543
CO_2, 10.6 μm, $LiNbO_3$-Ge acousto-optic modulator 80—99776
CO_2 10.6 μm laser, freq. modulation and demodulation 80—43378
CO_2, 16 μm, kinetic mechanisms, model simulation 79—98338
CO_2 16 μm laser, pumped optically in 4.3 μm, 9.6 μm bands, energy characts. 79—18398
CO_2, 16.5 micron band generation, HF laser pumped, threshold characts. *(Russian)* 77—83846
CO_2, 200 J TEA laser, injection mode locking 78—79049
CO_2, 30 ps pulse generation by free induction decay 77—14738
CO_2, 300 Mb/s communication terminal 77—19441
CO_2 9 μm band laser amplifier, using saturable gas absorber 79—76709
CO_2 ANTARES device, target-induced parasitic oscills. 78—59072
CO_2, absolute transition freqs. by multiplication of difference-freqs. 78—90445
CO_2, acetone decomposition, near IR laser action 78—63055
CO_2, adaptive resonator expt. config. 78—55386
CO_2 amplifier, method for radiation pulse shape control 80—43367
CO_2 amplifier, pulsed, large-vol., small-signal gain meas. 80—91772
CO_2 amplifier, spatial and temporal fluctuations of nanosecond radiation pulses 79—14009
CO_2, amplifier with UV preamplification 80—48284
CO_2 Antares laser amplifier, large-area cold-cathode grid-controlled electron gun 80—68955
CO_2 Antares laser system, Optical Evaluation Laboratory for laser fusion 80—14346
CO_2 Antares laser system, Cu plated substrate mirrors 80—14349
CO_2, atm. press. laser pulse duration reduction by stimulated emission quenching 79—18400
CO_2, atmospheric sealed CW laser, gain characts. 79—36871
CO_2, α-crystal quartz mirror 79—36908
CO_2 beam alignment by Seebeck effect position sensor 80—5772
CO_2, beam compensation using phase plate 77—42556
CO_2, beam shaping with computer generated hologram 77—14726
CO_2, beam steering, using hole grating attenuator 78—59071
CO_2, CW, surface modification and welding appl. 79—15879
CO_2, CW, transverse mode suppression by cavity length control 77—14762
CO_2, CW and pulsed, unstable resonator props. with field rotation 80—53343
CO_2 CW capillary waveguide laser for optically pumping D_2O 80—48278
CO_2 CW closed-cycle technological laser with 6 kW output power 79—27291

gas lasers continued
CO_2 CW coaxial discharge laser, props. and advantages 79—81442
CO_2 CW continuous flow laser, unstable resonator props. using dihedral corner reflector 78—29983
CO_2, CW electric discharge lasers, mode medium interaction 79—36876
CO_2 CW electric discharge laser, output beam props. 79—36877
CO_2 CW high power lasers, appls. for metal working 78—79026
CO_2, CW high power recycled electric discharge laser *(Chinese)* 79—98410
CO_2, CW high power TE electron initiated laser, small signal gain profile calcs. 79—72550
CO_2 CW laser, axial gain distribution 80—58502
CO_2 CW laser, electron-beam-controlled, closed-cycle 80—14315
CO_2 CW laser, sealed-off design, NaCl Brewster angle mirrors 78—55370
CO_2, CW laser, tunable simultaneous double wavelength operation 79—72583
CO_2 CW laser, vibr. temp., dissoc. and gain limitation determ., new technique 80—87369
CO_2 CW laser emitting dominant spatial mode, output power stability rel. to CO laser 80—32965
CO_2 CW laser model, electron beam ionisation 80—32954
CO_2 CW laser radiation, freq. conversion in Tl-Cs vapour mixture 80—74438
CO_2 CW laser radiation coupling coeffs. on stainless steel 80—84811
CO_2, CW laser spectroscopy of hexafluorides 80—83367
CO_2, CW sequence band laser, optical pumping of $^{15}NH_3$ far IR laser 78—46578
CO_2 CW sequence laser lines generated using incavity NH_3 cell 79—18438
CO_2 CW waveguide laser, freq. stabilised, operation and performance characts. 78—42349
CO_2, CW waveguide laser, anodised Al waveguide construction 78—55376
CO_2, CW waveguide laser, nearly atm. press., using plasma injection technique 78—74925
CO_2, cavity dumping using antiresonant ring 77—88792
CO_2, closed cycle CW electrodeless pulse ionisation discharge *(Russian)* 77—75474
CO_2, coherent optical pulse generation with up to five independent lasers 77—38907
CO_2, coherent optical pulse synthesis using phase-locked lasers and non-linear optical processes 79—76724
CO_2, compact cold cathode electron beam gun *(German)* 80—86501
CO_2, compact cylindrical TEA laser 77—703
CO_2, compact electro-ionising laser, 1 kJ radiation energy *(Russian)* 77—19316
CO_2, compact flowing gas system for waveguide lasers 78—87067
CO_2 compact high PRF TE laser 78—46643
CO_2, compact high-repetition-rate double-discharge TEA 77—23693
CO_2 compact pulse-periodic laboratory laser 80—9903
CO_2, compact pulsed double transverse discharge 80—53324
CO_2 compact repetitively pulsed superatm. press. laser with high output power density 80—102731
CO_2 compact sealed TEA laser, single mode operation 79—968
CO_2 compact sealed waveguide laser, design, construction and performance data 77—10947
CO_2 compact TEA laser with ladder-type preionization discharge *(Japanese)* 77—23694
CO_2, computer modelling, book 79—41364
CO_2, construction, industrial appls. *(German)* 77—88731
CO_2, construction and excitation circuit 79—22968
CO_2, continuous, vibrational control in stabilisation of ionisation-thermal instability 77—19302
CO_2, continuously tunable multiatom. laser, real time linewidth meas. 78—9405
CO_2, continuously tunable high press. monochromatic laser for spectroscopy 80—5762
CO_2 continuously tunable laser, optical pumping of NH_3 laser 80—83596
CO_2, controlled multiline oscillator 78—1259
CO_2 convection laser discharge, negative ion effects 78—55335
CO_2, coupling modulation near intermode spacing freqs., freq. response 77—38956
CO_2 cross-flow CW laser output and gain rel. to discharge instability 78—46563
CO_2, cutoff filter 77—88938
CO_2, development of miniature high-power high-press. UV and IR lasers 78—46642
CO_2, difference freq. mixing for far IR generation, book contrib. 77—46763
CO_2 doped TEA laser, Penning ionisation 79—3678
CO_2 Doppler-tuned CW IR radiation for highly excited atomic beam source 77—27204
CO_2, double discharge and photopreionisation types, comparison *(French)* 79—31855
CO_2 dual beam laser system for fusion ignition *(Japanese)* 79—81456
CO_2, dual beam module for nuclear fusion expts. 77—19336
CO_2, E-beam sustained large amplitude discharge, for fusion appls. 78—55382
CO_2, efficiency at 14 and 16 μm 79—59670
CO_2 eight beam 10 kJ laser fusion system, SF_6 saturable absorber effects on optical performance 80—106577
CO_2 eight-beam laser, Helios, evaluation of single-point diamond-turned Cu mirrors 79—23044
CO_2, eight-beam system, power amplifier stabilisation by saturable absorbers 78—46619
CO_2 electric discharge excited 16 μm laser for isotope separation meas. 77—88746
CO_2, electric discharge convection laser, saturation characts. *(Chinese)* 78—90408
CO_2 electric discharge laser, free oscill. stimulated emission, nanosecond pulse duration 79—31860
CO_2 electric discharge CW laser beam properties 79—76736
CO_2 electric-discharge mixing laser, 30 kW output, 9% efficiency 80—87410
CO_2, electro-optical shutter, for ns pulse generation 78—37926
CO_2, electrodeless discharge closed cycle laser theory *(Russian)* 77—75475
CO_2 electroionisation laser plasma mirror, soft X-ray emission for biological radiography 79—43983
CO_2, electroionisation pulsed laser 79—89922

gas lasers continued
CO_2, electron beam controlled, pulse interaction with Al in air 77—35370
CO_2, electron beam controlled, plasma mirror 78—17976
CO_2, electron beam controlled laser, with grid-controlled electron gun 78—46635
CO_2, electron beam controlled laser with plasma mirror, stimulated emission dynamics 78—50799
CO_2 electron beam controlled laser, plasma mirror refl. characts. 78—59064
CO_2 electron beam controlled laser, emission pulse synchronisation with plasma mirror 79—89930
CO_2, electron beam pulsed, laser solenoid for fusion power 77—47250
CO_2, electron energy distrib., exp. 80—37989
CO_2, electron-beam-controlled closed-cycle laser, pulse periodic conditions 78—46632
CO_2, electron-beam-controlled laser, operation characts., 1 to 10 atm range 78—71118
CO_2, electron-beam-controlled laser, pulse forming network power source 78—74928
CO_2, electron-beam-controlled, angular divergence, gasdynamic motion influence during pump pulse 79—59668
CO_2, emission power stabilisation system 80—106536
CO_2, excitation by discharge through an insulator 79—27273
CO_2 excitation by RF discharge with rot. elec. field, linear and circular polarisation 80—37991
CO_2, far IR difference freq. generation 77—19366
CO_2 fast flow laser, combined pulse and DC discharge as pump 78—71117
CO_2, fast flow laser, meas. of N_2 vibr. temps. 80—32955
CO_2, fast modulator using CdS two-photon magnetoabsorpt. 77—88805
CO_2, fast transverse flow discharge laser, stimulated emission stability 77—75478
CO_2, fast-flow, elec. discharge chamber characts. 77—79854
CO_2, fast-flow CW laser using atm. air-CO_2 mixtures 77—75559
CO_2 fast-flow CW laser characts., DC self-sustained excitation 80—53259
CO_2 fast-flow closed-cycle laser, output power, medium comp. effect 80—48213
CO_2 fast-flow electric-discharge laser, dynamic characts. 80—32956
CO_2, fast-flow laser, pumping efficiency by AC discharge 78—50801
CO_2 fast-flow laser with nonself-sustained discharge, active medium characts. 80—28194
CO_2, for 16 μm range, review *(Rumanian)* 80—87408
CO_2, for communications, Stark cell applications 77—19444
CO_2, for fusion, comparative review of Nd:glass, CO_2, HF and I lasers 77—7062
CO_2, for optically pumped CW FIR lines from $^{15}NH_3$, CD_3OH and CH_3OH 78—90415
CO_2, for selective interactions with matter 77—27296
CO_2, forced air convection cooled waveguide laser 77—38921
CO_2, forced laser oscill. by injection of weak external optical signal 77—19347
CO_2, freq. stabilisation expts. *(Japanese)* 77—68225
CO_2, freq. stabilisation through saturated absorption in SF_6 77—75556
CO_2, freq. stabilisation using OsO_4 narrow resonance, expts. *(Russian)* 78—33747
CO_2, freq. stabilised laser with OsO_4 absorber, output freq. reproducibility 78—50800
CO_2, freq. stabilization by fluorescence of CO_2 gas 80—102693
CO_2 freq.-tunable laser for photoreceiver characts. meas. 77—14728
CO_2, frequency control by spectrally depleted destructive two-beam interf. 78—74941
CO_2, gain spectra meas. using $Pb_{1-x}Sn_xTe$ diode laser *(Japanese)* 79—49306
CO_2, gain spiking and mode-beating control by signal injection 77—71999
CO_2, gas discharge laser, 14 and 16 μm emission *(Russian)* 77—10885
CO_2 gas flow laser, vibr. and translational temp. fields, panoramic spectrosc. obs. *(Russian)* 79—12868
CO_2 gas laser, glow discharge electron irrad. rel. to output characts. 79—64198
CO_2, gaseous saturable absorber cell to suppress parasitic oscillations 78—87066
CO_2, He recovery system 78—82974
CO_2, helical TEA laser, spectral output, charging voltage depend. 77—61936
CO_2, helical TEA laser, output power as function of discharge inductivity 79—10278
CO_2 Helios fusion laser alignment system 80—33070
CO_2 Helios fusion laser, alignment accuracy 80—33071
CO_2, high flow rate, gain and discharge characteristics 77—38855
CO_2, high power, appl. of SF_6 based broadband isolator 78—42339
CO_2, high power, CW, electron beam sustained, performance, theory and expt. 78—71074
CO_2, high power, design and fabrication for laser applications 77—46732
CO_2, high power, transmissive optical components 78—79057
CO_2, high power amplifier, energy and time characts. 77—79797
CO_2, high power CW output meas. from temp. rise of Al slab power meter 79—59739
CO_2 high power elec. discharge laser, multielement cathode design and operational characts. 78—82983
CO_2, high power electrical laser technology 77—88777
CO_2, high power electron beam controlled laser for fusion research 77—709
CO_2 high power laser beam monitor 78—74943
CO_2, high power laser optics with KCl single crystal 78—22181
CO_2, high power pulse, single-stage, electroionisation laser, tens of gigawatts 79—3704
CO_2, high power pulse laser with unstable resonator 77—75564
CO_2, high power system, prepulse elimination 77—19337
CO_2, high press., continuous tuning, electron beam controlled 77—713
CO_2, high press., pulse temporal struct. using up-conversion 77—3603
CO_2, high press. sealed-off laser amplifier characts. 79—18397
CO_2, high press. stabilised discharge 78—17904
CO_2, high repetition rate hybrid TEA laser freq. and amplitude characts. 78—37897
CO_2, high repetition rate TEA laser, sealed operation 78—46623
CO_2, high repetition rate mini-TEA lasers design 80—58571
CO_2 high stability CW waveguide laser, for high resolution saturation spectroscopy 78—71112

gas lasers continued

- CO_2, high temp. absorpt. meas. in 10.4 μm laser band 79—36870
- CO_2, high voltage microsec. pulse-forming network 78—5494
- CO_2, high-power, multi-atmosphere, photoionization stabilized system 77—38919
- CO_2, high-power discharge lasers 77—34872
- CO_2 high-power elec. discharge laser, holographic interferometry during power extraction 80—28172
- CO_2, high-power high-energy, using an absolute calorimeter 78—93686
- CO_2, high-power multibeam CW laser, parallel packed tubes in common resonator 79—13984
- CO_2 high-power pulsed laser continuously tunable over wide freq. range 79—45925
- CO_2 high-power pulsed laser, wave-optical resonator modelling, gain saturation law 80—99693
- CO_2 high-power pump laser, direct narrow-line tuning 80—58579
- CO_2, high-power rapid flow CW laser with combined-discharge pumping, I-V characts. 80—14318
- CO_2, high-power tunable laser for 9 to 12.5 μm range 77—83884
- CO_2, high-press. cathode preionis. pulse type, design 77—65596
- CO_2, high-press. laser, gain contribs. from 00°2 and 00°3 sequence bands, theory 78—46565
- CO_2 high-press. laser with cascade discharge 79—68407
- CO_2, high-press. tunable IR lasers 78—59030
- CO_2, high-pressure, pulsed ionisation using cold-cathode glow discharge electron gun 79—27269
- CO_2 high-pressure discharge, sequence-band lasing 78—46570
- CO_2 high-pressure Q-switched electron-beam-controlled laser characts. 79—59669
- CO_2 high-pressure reinjection oscillator design and performance 80—78867
- CO_2 highly multimode pulsed electron beam laser, beam divergence 79—3731
- CO_2 hybrid laser, operating regimes 79—22932
- CO_2 hybrid laser, transverse mode struct., effect on laser induced acoustic waves in liq. 79—77683
- CO_2 hybrid laser operation 79—64246
- CO_2 IR laser, line tunable and optically pumped 77—88747
- CO_2 IR laser, transients obs. by modulation of intracavity absorber 78—74933
- CO_2, IR luminesc. of active layer *(Russian)* 79—31862
- CO_2, impulsive and continuous heating of thin metallic layer 77—40311
- CO_2, in-cavity hot cell 78—5495
- CO_2, influence of added gases on laser action *(Rumanian)* 77—27273
- CO_2, intense annular beam, optical breakdown of gas, flow-concentration effects 79—64886
- CO_2, intense high-press. sequence-band 78—33749
- CO_2, intermode beats, use in automatic frequency control system 80—48209
- CO_2 intracavity CdTe electro-optical modulator 77—19443
- CO_2, inversion transitions in aerodynamic cooling region *(Russian)* 77—34869
- CO_2, inverted, on-resonant phase-conjugate refl. and amplification at 10.6 μm 79—64275
- CO_2, inverted, wavefront reversal, high efficiency 80—74436
- CO_2 isotope laser transitions, absolute freq. calibration, heterodyne technique 77—19230
- CO_2, KCl laser windows at 10.6 μm, optical distortion parameter 78—79036
- CO_2, kinetic cooling of beam 77—62018
- CO_2 Lamberton and Pearson type, shock wave detect. 79—36946
- CO_2 large aperture TEA laser, injection mode locking 77—14737
- CO_2, large-volume pulsed laser amplifier 79—64253
- CO_2 laser, 10 ns pulse generation, rotating mirror technique 80—33042
- CO_2, laser, 16 GHz tunable sideband generation 78—90428
- CO_2 laser, absorption of laser radiation in Stark tunable mol. gases *(Rumanian)* 79—86157
- CO_2 laser, accurate frequency meas. *(Japanese)* 80—9850
- CO_2 laser, alkali halides, behaviour as materials for optical components *(Rumanian)* 79—18462
- CO_2 laser, Antares system, 100 kJ, for fusion expts. 78—46665
- CO_2 laser, atmospheric pulsed photoionisation, active medium optical homogeneity 80—58508
- CO_2 laser, broadband electronically tunable resonant microwave modulators 79—64256
- CO_2 laser, CW, construction and power calibration *(Korean)* 78—17961
- CO_2 laser, CW, electrically excited *(Japanese)* 79—3676
- CO_2 laser, compact single-mode design 80—23664
- CO_2 laser, continuous, fast flowing, thermal discharge contraction *(Russian)* 79—99009
- CO_2 laser, detuning effects of FM mode-locking 80—69434
- CO_2 laser, double transverse pulsed discharge characteristics 78—71617
- CO_2 laser, Faraday effect optical isolation at 10.6 μm using chalcogenide spinels 78—50816
- CO_2, laser, freq. tripling in DCl gas 79—76751
- CO_2 laser, frequency stabilisation method, phase-locking 80—74401
- CO_2 laser, Gaussian beams energy profile 79—64247
- CO_2 laser, glow discharges at high press., voltage-current characts. 78—87036
- CO_2 laser, high performance, appls. in drilling, welding, cutting definite abrasion and surface treatment *(German)* 80—108608
- CO_2 laser, high press. with nonself-sustaining discharge 79—98339
- CO_2 laser, high pressure, passive mode-locking characteristics *(Japanese)* 80—14357
- CO_2 laser, high repetition rate-pulsed, weak shock wave effect 78—90409
- CO_2 laser, high-field preionised discharge for transversely excited waveguide laser 77—83844
- CO_2 laser, high-power photopreionisation stabilised, operation at press. up to 13 atm. 78—63131
- CO_2 laser, high-press., homogeneous self-sustained discharge 80—9852
- CO_2 laser, high-press. ns pulse generation *(Russian)* 77—75581
- CO_2 laser, high-press. CW, output power fluctuations 80—74333
- CO_2 laser, IR freq. absolute meas. *(Russian)* 80—9851
- CO_2 laser, influence of tripropylamine admixtures 80—23669
- CO_2, laser, internal modulation 80—23728
- CO_2 laser, intracavity IR absorpt. of vinyl chloride, ethylene, and propylene 78—78835
- CO_2 laser, long and short pulse formation, optimum conditions 78—87037
- CO_2 laser, mode locking obs. by intracavity plasma injection 80—83624

gas lasers continued

- CO_2 laser, modulation and freq. stabilisation by Stark effect in difluoroethane 79—59667
- CO_2 laser, multiphoton amplification, HF removal of forbiddenness *(Russian)* 80—53262
- CO_2 laser, N_2 electron beam-ionis. optical pumping characts. 77—75477
- CO_2 laser, nsec pulse amplification at efficiencies greater than 20% 78—50818
- CO_2 laser, optical isolation by flowing gaseous saturable absorbers 78—59096
- CO_2 laser, output characts. at high pump levels 80—58509
- CO_2 laser, p-Ge broadband passive isolator, pulse shaping 78—46662
- CO_2 laser, passive Q-switching using heated CO_2 saturable absorber 78—25900
- CO_2 laser, periodically pulsed, heating of oxidising metal 80—7445
- CO_2 laser, periodically pulsed, power supply inductive pulse shaping 80—53311
- CO_2 laser, pulse flow stretching *(Chinese)* 78—90435
- CO_2 laser, pulsed, high repetition rate, average power limitations at 10.6 and 16 μm 80—58503
- CO_2 laser, pulsed transverse electrodeless discharge excitation 79—45958
- CO_2 laser, Q-switched, single rot. line-selection *(German)* 78—46562
- CO_2 laser, radiation duration control, expts. and devices 78—22156
- CO_2 laser, SF_6 intracavity hysteresis, bistability, critical behaviour onset and extinction of lasing 79—98336
- CO_2 laser, saturable absorber using doped KCl 79—10363
- CO_2 laser, selected two-colour operation for length meas. scheme 80—99747
- CO_2 laser, stabilized, meas. of freq. 80—99699
- CO_2 laser, successively excited sections, duration of emission pulses 79—94257
- CO_2 laser, TEA, double helical, computer simulation study of dynamics *(Chinese)* 80—74390
- CO_2 laser, TEA, single longit. mode, various prod. techniques 80—106547
- CO_2 laser, target bombardment, plasma shock wave production and propagation 79—64885
- CO_2 laser, thermally excited quantum oscillators and second law of thermodynamics 77—34863
- CO_2 laser, thermodynamic approach *(Rumanian)* 79—7109
- CO_2 laser, transitions, linewidth, temp. depend. 80—69360
- CO_2 laser, transverse double-discharge, spectral characts. *(Russian)* 77—656
- CO_2 laser, transverse mode-medium instability anal. 79—76662
- CO_2 laser, tri-n-propylamine in working gas 79—22935
- CO_2 laser, tripropylamine additive on amplification characts., CO_2+N_2+He gas *(Russian)* 78—25848
- CO_2 laser, use for extension of visibility range of He-Ne laser beacon in fog 80—101434
- CO_2 laser, vac. UV preionisation source spectral characts. 79—31938
- CO_2 laser, variable pulse width generation, 100 ps to 1 ns range 78—46691
- CO_2 laser, with anisotropic resonator, radiation polarisation *(Russian)* 79—27309
- CO_2 laser, with anisotropic resonator, output polarisation 80—28253
- CO_2 laser action on wateraerosol, efficiency, optical thickness, water content 77—66774
- CO_2 laser active medium study using heterodyne photoreceiver 80—95868
- CO_2 laser amplifier, double-discharge at 1800 torr 78—50815
- CO_2 laser amplifier, high power large aperture electron beam controlled, development *(Japanese)* 78—66846
- CO_2 laser amplifier, short pulse amplification calcs. 78—58979
- CO_2 laser amplifier, short pulse propagation calcs. 79—76730
- CO_2 laser amplifier chain, laser plasma isolator for retropulse 79—22959
- CO_2 laser amplifier design, IR laser optical pumping appl. 78—63133
- CO_2 laser amplifier isolation from target reflection 77—19288
- CO_2 laser amplifier multipulse energy extraction 80—78832
- CO_2 laser amplifiers, porous tube generated flow field, heat and mass diffusion 80—63969
- CO_2 laser Antares fusion system power amplifier optics 80—74394
- CO_2 laser Antares fusion system beam alignment 80—74422
- CO_2 laser Antares fusion system, mirror quality specifications 80—74423
- CO_2 laser Antares fusion system optical diffraction computation 80—74424
- CO_2 laser Antares system, power amplifier module 78—46666
- CO_2 laser Antares system, optical design and anal. 78—46667
- CO_2 laser Antares system, energy extraction, pulse shaping 78—46668
- CO_2 laser beam, intensity fluctuations, spatial distrib. 79—18458
- CO_2 laser beam Al target interaction, pulse shape importance 80—108307
- CO_2 laser beam alignment, accuracy, Snout test 78—59073
- CO_2 laser beam meas. using pyroelectric vidicons 78—49907
- CO_2, laser beam parameters meas., potential use of wire diffraction grating 77—730
- CO_2 laser beam-diagnostics techniques, laser beam parameter monitoring 80—64089
- CO_2 laser beats, technical line width, acoustic interference and current fluctuations influences obs. 80—48210
- CO_2 laser bimetallic mirror coating vacuum sputtering technology 80—35086
- CO_2 laser cavity and Ge phase-conjugate 10 μm reflection expts. 80—78894
- CO_2 laser compact wideband ring modulator 77—88803
- CO_2 laser control using Ge and InSb 78—1203
- CO_2 laser discharge, positive ion processes, mass spectrometric obs. 77—89337
- CO_2 laser discharge, special case of effect of initial conditions on homogeneous discharge development 78—63613
- CO_2 laser discharge, TEA, glow form. and glow-to-arc transitions, high speed camera obs. 78—25846
- CO_2 laser discharge tube, phase distortions due to heating differential 80—95865
- CO_2, laser discharges, determ. of recombination coeff. 78—90407
- CO_2 laser discharges, electrode surface field and preionisation effects on spatial distrib. of arcs 78—63054
- CO_2 laser Doppler system atmospheric attenuation 77—75601
- CO_2, laser electron beam pulsed, sealed electron guns 78—71119
- CO_2 laser emitters, antenna characts. of heterodyne receivers 77—67498
- CO_2 laser excited by capacitative AC discharge, expt. model 80—9853
- CO_2 laser freq. and wavelength meas., speed of light determ. 77—49708

gas lasers continued
CO_2 laser freq. stabilization for far IR laser pumping 77—68223
CO_2, laser frequency measurements: a review, limitations, extension to 197 THz (1.5 μm) 78—81952
CO_2 laser frequency tripling by molecular gas vibrational nonlinearity *(Russian)* 79—72618
CO_2 laser fusion development 79—49859
CO_2 laser fusion effort at Los Alamos Scientific Lab. 78—33290
CO_2 laser fusion electron-beam gun, design principles 78—9390
CO_2, laser fusion system, metal mirror considerations 78—5476
CO_2 laser fusion systems, optical design approach for design and assembly 79—86193
CO_2 laser fusion system optical design and analysis 80—74391
CO_2 laser fusion system alignment by IR Smartt interferometer 80—74425
CO_2 laser fusion system wavefront correction, deformable mirror design 80—74427
CO_2 laser fusion system phase conjugation 80—74429
CO_2 laser fusion system, optical design considerations 80—78868
CO_2 laser fusion target alignment 78—46706
CO_2, laser gain isolation by saturable absorber gases 78—59095
CO_2 laser gain switch, pulse characts., approx. evaluation 80—58504
CO_2 laser gas mixture, vol. photo-preionisation by VUV radiation 80—87966
CO_2 laser Gemini fusion system optical performance 80—74392
CO_2 laser Gemini fusion system, wavefront error correction by deformable mirror 80—74426
CO_2, laser generation by pulsed microwave excitation 78—74879
CO_2 laser Helios fusion system, multicomponent gaseous saturable absorber optimisation 80—74393
CO_2 laser Helios fusion system, beam simultaneity system 80—74419
CO_2 laser Helios fusion system alignment 80—74420
CO_2 laser Helios fusion target positioning with orthogonal telescopes 80—74421
CO_2 laser Helios fusion system beam diagnostics 80—78882
CO_2 laser heterodyne spectrometer for examining wave-number stability of laser diode mounted in closed-cycle He refrigerator 80—31906
CO_2, laser hot-band transitions, heterodyne freq. meas. 77—88695
CO_2 laser implosion of polyethylene shell into D-filled conical region, neutron generation 78—87468
CO_2, laser intensity distrib., hot spot detect. using Ag halide film 78—82945
CO_2 laser intracavity freq. modulation, transient behaviour 80—14374
CO_2 laser intracavity phase error correction adaptive resonator 79—59729
CO_2 laser irrad. of SF_6 molecule, IR absorpt. *(Russian)* 80—986
CO_2 laser light pulse amplification calc. Fortran program PULSAMP 77—58312
CO_2 laser line, electro-optic frequency shift *(Chinese)* 80—43379
CO_2, laser line selection using metal film reflection filter 78—55368
CO_2, laser lines, 12 GHz continuous tuning in integrated electro-optic modulator 77—83907
CO_2 laser long-path absorption system, computer automation, air pollution monitoring 78—92971
CO_2 laser mixtures, high press. glow discharge, collision freq. 77—55184
CO_2 laser modulation, plasma injection into cavity 80—83626
CO_2 laser modulation by Si p-ν-n diode, temp. and switching characts. 79—81467
CO_2 laser modulation Si diode characteristics 78—42364
CO_2 laser multiwavelength interferometry, absolute distance meas. 79—31974
CO_2 laser nanosecond pulse coherent interactions with amplifying media *(Russian)* 80—14314
CO_2 laser operating under free-oscillation conditions, nanosecond pulse emission 79—22933
CO_2 laser plasma, electron beam spreading, field variations 78—5446
CO_2 laser possibility of hitting high speed targets, shield piercing 77—68235
CO_2 laser power variation detection via plasma tube impedance changes 80—69437
CO_2 laser processing of materials, interfacing with modern prod. engng. technology 78—33767
CO_2 laser produced plasma, nonlinear scattering of laser radiation by fast ion waves in plasma 80—106916
CO_2 laser pulse, nonlinear propagation, computer simulation *(Japanese)* 80—95963
CO_2 laser pulse, nonlinear propag. characts., computer simulation 80—106575
CO_2 laser pulse compression and mode locking using KCl:ReO_4 nonlinear absorpt. 80—74443
CO_2 laser pulse duration discrimination, transient versus steady-state mol. absorption 77—79865
CO_2, laser pulse generation, cavity dumping by NH_2D Stark active mol. 77—88800
CO_2 laser pulse meas., single sweep 5 GHz oscilloscope detector system 77—88817
CO_2 laser pulse meas., pyroelectric detector development 80—78884
CO_2, laser pulse mode quality, effect on multiple photon absorpt. 78—66615
CO_2 laser radar used to measure average atmospheric temp. 80—90225
CO_2 laser radiation, saturated absorpt. by SiF_4 mol. 80—37811
CO_2 laser radiation, single pulse, thermal blooming 80—19080
CO_2 laser radiation two photon pumped InSb laser 79—86182
CO_2 laser range finder, performance in radiation environments 80—38054
CO_2 laser rangefinder using heterodyne detect., acousto-optic modulator 80—102825
CO_2 laser resonator, intracavity deformable mirror adaptive optical system 78—87078
CO_2 laser self-sutained discharge, effect of low-ionisation-potential additives 78—71616
CO_2, laser sequence lines, pumping of methanol far IR laser lines 78—9369
CO_2 laser short pulse diagnostics, using upconversion linearity in Ag_3AsS_3 79—27304
CO_2 laser short pulse propagation and energy extraction 80—74335
CO_2 laser small-signal gain coefficient calc. 80—78831
CO_2 laser stability and heterodyne frequency calibration 78—59031
CO_2 laser stabilization for use in far IR laser pumping 79—72551
CO_2, laser start-up system for mag. mirror fusion 77—62383

gas lasers continued
CO_2 laser subnanosecond pulse generation by Pockels cell modulator 77—19357
CO_2 laser system, broadband gas isolator mixes 78—46663
CO_2 laser system, eight beam, optical anal. 78—50814
CO_2 laser system, multipass power amplifier stabilisation using saturable absorbers 78—46664
CO_2, laser system, p-Ge saturable absorption isolator 77—19284
CO_2 laser system, pulsed, for fusion research 80—58556
CO_2 laser system, zero small signal gain 80—48271
CO_2 laser systems, Faraday rotator technology using $CoCr_2S_4$ 78—95579
CO_2 laser systems, multiline oscillator 79—72584
CO_2 laser systems for laser fusion appls. 78—50817
CO_2 laser transition absolute freqs. by multiplication of difference freqs. 80—37992
CO_2 laser transitions, absolute freq. meas. by multiplication of CO_2 difference freq. 80—105618
CO_2 laser velocimeter, optical design for long-range anemometry 78—36333
CO_2 laser waveguide, photoionisation stabilisation using Blumlein-type pulser 77—54734
CO_2 laser wavelength standards 77—17945
CO_2 laser with partial population inversion, 16 μm steady state action 79—36873
CO_2 laser with single crystal CdTe window 77—75566
CO_2 laser-diode laser heterodyne spectrometer, meas. of 2sQ(1,1) in NH_3 2ν-ν_2 79—75626
CO_2 laser-heated electron emission from C-coated metal surface, appl. to emissive probe meas. 80—6270
CO_2 laser-plasma amplifier, 11-16 μm range 78—22173
CO_2 lasers, high-power, book contrib. 77—50651
CO_2 lasers, IR saturable absorpt. in benzene, chlorobenzene and bromobenzene 80—69465
CO_2 lasers, optically pumped, use of crystalline reflector in cavity 80—64080
CO_2 lasers, radiation detection using CdHgTe detectors 79—40615
CO_2 lasers used in compressive plasma fusion of D-T macrosamples 78—82507
CO_2, line-selectable waveguide laser, optoacoustic detect. of ethylene 78—56947
CO_2 long-pulse 2 GW single longit. mode source for laser-matter expts. 80—78860
CO_2, longit. pulsed, appl. in TEA lasers single-mode operation 77—68229
CO_2, longitudinal excited, double pulse discharge excitation scheme 77—19319
CO_2, low energy output meas. with absolute calorimeter 78—55396
CO_2, machinery appl. feasibility study *(Czech)* 77—19274
CO_2, materials processing appls. *(German)* 78—1294
CO_2, microsurgery and laryngology applics. 78—35905
CO_2, mirror grating mount, compact stepping motor design 80—87402
CO_2 mixed isotope multiatmosphere laser, lasing action 80—19016
CO_2 mode-locked hybrid TEA laser, variable width stable pulse prod. 79—76726
CO_2, modulation by electrooptical waveguide 77—27349
CO_2, modulation using p-ν-n diode 77—79873
CO_2, molecular discharge, externally sustained, thermal instability 77—58915
CO_2, multi-atm. TE laser, 10.6 μm ultrashort pulse generation by injection mode-locking 77—88799
CO_2, multi-kilowatt, for industrial applications, survey 77—46731
CO_2 multi-rotational line TEA laser, theoretical model 80—69361
CO_2 multiatmosphere laser, mode-locked pulses 80—1248
CO_2 multiatmosphere laser tuning for methyl fluoride laser pumping 80—69421
CO_2 multiatmosphere UV preionized laser, elec. and gain characts. 80—14313
CO_2 multiatmospheric UV-preionised lasers 78—50805
CO_2, multimode, fluctuating polarisation, correct use of beam splitters 77—79884
CO_2 multistage laser, amplifier module, discharge and optical characts. 80—28248
CO_2, NASA high power system for laser appls. 78—5493
CO_2, narrow band TEA laser for far IR laser pumping 77—54729
CO_2 needle laser improvements, preionization influence 79—31926
CO_2, neutron flux preionised laser, operation in nuclear reactor active zone 78—17975
CO_2, noise, fluctuations and output power stabilisation, 1 Hz to 150 kHz *(Polish)* 78—5447
CO_2, non-self sustaining discharge for CW laser excitation, review 78—42849
CO_2, optical coupling modulation in travelling-wave cavities 77—42553
CO_2, optical data communication for Earth sensing satellite 77—19427
CO_2 optical gain in TE channel waveguides, discharge-related limitations 78—17951
CO_2, optical pump source for high-energy NH_3, CF_4 lasers 79—89927
CO_2, optical pumping in stimulated Raman scatt., tunable laser emitting at 14,16 μm, theory 78—46568
CO_2, optical suitability of laser window materials 77—58361
CO_2, optically pumped laser, simultaneous lasing in bands of sequence 80—5725
CO_2 optogalvanic stabilised laser 79—89923
CO_2 oscillating laser transition, band width meas. 79—3677
CO_2 oscillator, high power nsec. pulse selection 79—98382
CO_2 oscillator, multiatm. injection mode-locking, high-power subnanosec. pulses 78—29988
CO_2, output power stabilisation by external control element 80—91832
CO_2, p-type Te photon drag detectors 77—5911
CO_2, PRF control by BCl_3 gaseous phototropic shutter 78—50833
CO_2, parametric frequency conversion, by radiation mixing with dye laser radiation *(Russian)* 78—22175
CO_2, passive Q-switching by CH_3F 78—9402
CO_2, passive Q-switching by FIR laser gas CH_3I 80—1246
CO_2, periodically operated laser, pulse repetition freq. limits 78—50750
CO_2, periodically pulsed, metal, semiconductor and oxide thin film deposition 79—28926
CO_2 periodically pulsed laser, appl. isotope separation 79—27287
CO_2, photoinitiated impulse-enhanced elec. excited struct., operational characts. 79—27283
CO_2, photoionis. TEA type, output pulse characts. calc. 80—32953
CO_2, photoionisation, atm. press., high sp. energy output 78—29975

gas lasers continued
CO_2, photoionisation and photoabsorpt. characts. of organic seedants 78—13688
CO_2 photoionisation laser, elec. and stimulated emission characts. 77—71971
CO_2 photoionisation laser with 300 J output energy 79—31939
CO_2 photoionisation laser, breakdown effect on output 79—68379
CO_2 photoionisation TEA laser, characteristics calculation using computer model *(Russian)* 80—83589
CO_2 pin-bar TEA laser, internal arcing, ultra high speed photography 78—9357
CO_2, planar hollow-core doubling grating DFB laser, characts. 78—46673
CO_2, plasma focus as laser pulse clipper and optical isolator 77—65601
CO_2, plasma-sheet pulsed laser 77—23696
CO_2, possible freq. stabilisation using 1-1 difluoroethane in external Stark cell 79—94266
CO_2, power meas. by new thermoelec. detector *(French)* 77—58365
CO_2, power stabilisation *(Russian)* 78—22145
CO_2, preamplifier capabilities for low level 10.6 μm direct detectors 77—53976
CO_2, preionisation effect on discharge characts. 77—61938
CO_2, preionization by pulse electron accelerator 77—88780
CO_2, processing appls., behaviour of various materials 77—5820
CO_2, Pt-catalysed recombination of CO and O_2 in sealed TEA lasers 78—46566
CO_2, pulse evolution 77—10884
CO_2, pulse laser, UV photoionisation, impurities effect 78—1206
CO_2, pulse periodic laser with non-self-sustaining discharge 78—1263
CO_2, pulse periodic open cycle laser, 500 W average output power 77—61974
CO_2, pulse type, transversally controlled, discharge electric circuits parameters design *(German)* 77—75473
CO_2 pulse-periodic laser, preionisation by electrodeless capacitative pulses 79—31937
CO_2 pulse-periodic laser utilising air-CO_2 mixture, emission characts. 79—89886
CO_2 pulse-periodic laser, gas stream gasdynamic perturbations, heated gas convective removal 79—94207
CO_2 pulse-periodic laser, gas stream gasdynamic perturbations, acoustic waves 79—94208
CO_2 pulse-periodic laser, multiphoton molecular dissociation 80—9931
CO_2 pulse-periodic TEA laser freq. stabilisation by low press. CW laser signal injection 80—74408
CO_2, pulsed, broadening of lasing spectrum 79—94205
CO_2, pulsed, design improvements for machining appl. 77—46733
CO_2, pulsed, elec. field distrib. in vol. discharge controlled by electron beam 80—58505
CO_2, pulsed, electric-discharge, with stable parameters 80—48283
CO_2 pulsed, high-press., high-power, electron-beam-controlled, continuously tunable laser 80—64065
CO_2, pulsed, laser induced medium perturbation 78—58977
CO_2, pulsed, with transverse discharge operating at atmos. press., energy characts. of emission 77—42520
CO_2, pulsed elec. discharge laser, UV ionisation at atm. press. 78—46630
CO_2 pulsed electroionisation laser with controllable emission parameters 80—78865
CO_2, pulsed electron-beam-controlled laser, parameters optimisation 78—71116
CO_2 pulsed gas discharge laser, emission on molecular transitions at 14, 16 μm 80—53261
CO_2, pulsed gas-discharge laser, skimming discharges for preionisation 80—99740
CO_2, pulsed laser, 23 J, Lamberton-Pearson config., parameters 77—19317
CO_2 pulsed laser, damage resistance of coated optics 79—45989
CO_2, pulsed laser, high power, oscill. spectrum expansion *(Russian)* 78—74882
CO_2 pulsed laser beam, thermal coupling 78—63145
CO_2, pulsed laser characts., UV preionisation 77—7059
CO_2 pulsed laser output, spatial distrib. meas. by photographic device 79—14008
CO_2 pulsed laser radiation field, energy density distrib. recording 78—1292
CO_2, pulsed laser radiation action on polydisperse water aerosols 80—14378
CO_2 pulsed laser system, acoustic suppression 80—74378
CO_2 pulsed laser with combined current discharge 77—14689
CO_2 pulsed laser with continuously tunable radiation frequency 80—48292
CO_2 pulsed laser with transverse electric discharge 77—38913
CO_2, pulsed low-pressure far IR, for use in plasma diagnostics 80—53332
CO_2, pulsed TE laser, tunable single-mode operation by means of selective absorbers 79—36940
CO_2, pulsed TEA, tuning by 9.55 μm CO_2 laser radiation injection 77—38908
CO_2 pulsed transversely excited waveguide laser design 79—27280
CO_2, pulser-sustained, gain and optical extraction meas. 79—27284
CO_2, pump for submillimetre gas lasers, wavelength tables 34 μm to 1.965 mm 77—7095
CO_2, pump laser for far IR gas laser in common resonator 77—38950
CO_2, pumped by energy transfer from Br, line tunable 78—5448
CO_2, pure and CO_2-He mixture, optically pumped continuously tunable lasers 78—13678
CO_2 Q-switched laser pump source for CH_3OH/D, CHOOH and CH_3F lasers 80—69383
CO_2 quantum amplifier, high power radiation pulse generation, efficiency 78—13680
CO_2, radiation absorpt. by propane and propane-N_2 gas mixture 77—58366
CO_2, radiation attenuation using multilayer Dacron filters 80—58616
CO_2, radiation density quantitative estimation using PVA-I_2 film 77—58368
CO_2, radiation detection by PbSnTe detector and preamplifier modules 78—32875
CO_2 rapid discharge TEA laser, construction and performance characts. 79—3710
CO_2 repetitively pulsed electron beam laser operation 79—31943

gas lasers continued
CO_2 rotating-mirror Q-switched TEA laser, mode sweeping effects 80—99769
CO_2, saturation parameter from gain meas. 78—66797
CO_2 sealed high-pressure pulsed laser, gas equilibrium chemical comp. 80—63972
CO_2 sealed photoionisation TEA laser, limiting processes 78—82946
CO_2 sealed TEA lasers, with external control of gas chemistry 77—88738
CO_2 sealed type laser using metal construction *(Chinese)* 79—81459
CO_2, sealed UV-preionization TEA laser 78—46627
CO_2, sealed-off, parameter meas. 77—3614
CO_2 sealed-off TEA lasers, size reduction and improved efficiency 79—31942
CO_2, seeded mixture, photoabsorption and ionisation cross sections 77—23645
CO_2, self sustaining discharge, medium effect on output energy 77—14690
CO_2, self-focusing parallel-plate waveguide, transverse excitation 77—7139
CO_2, self-modulation by means of nonlinear absorbing filters, anal. 78—37925
CO_2 self-pumping on pulsed periodic energy input *(Russian)* 80—106506
CO_2 self-sustained laser system, electron avalanche and electron-ion recomb. coeffs. meas. 80—102694
CO_2, semi-self-sustained discharge, optical homogeneity, mol. gas heating 80—37990
CO_2, sequence band transitions, heterodyne freq. meas. 77—71970
CO_2, sequence bands, laser power and gain meas. 77—79795
CO_2 Sharplan 791, for clinical surgery 78—35904
CO_2, short pulse generation from intracavity laser breakdown plasmas 78—37924
CO_2, short pulse laser, efficiency rel. to discharge parameters 77—708
CO_2, short-pulse high-energy operation 77—88758
CO_2 short-pulse laser high-pressure amplifiers, design engineering 79—36936
CO_2, short-pulse oscillator, variable pulse repetition freq., pulsewidth and wavelength control 77—88801
CO_2, signature curve anal. 77—654
CO_2, simple high-power TEA laser operating in IR 79—94251
CO_2, simple preionised waveguide TE laser with continuous discharge electrodes 77—54721
CO_2, single axial mode laser, digital feedback stabilization 79—89928
CO_2, single freq. atmospheric press. laser 78—13728
CO_2, single mode, internal freq. modulation up to 350 MHz 77—19308
CO_2, single mode locked pulse selection, semicond. refl. switching 77—3609
CO_2, single ultrashort pulse generation in Fabry-Perot interferometer 78—29996
CO_2 single-discharge self-sustained laser, 5 cm gap distance, high power output 80—102735
CO_2, single-frequency, using unstable resonator 77—38939
CO_2, single-mode laser freq. modulation 78—13737
CO_2 single-pulse laser, emission spectrum photographic recording by parametric conversion 79—10357
CO_2, sliding-spark arrays for laser pre-ionization 77—46726
CO_2, small high press. UV preionised laser, continuous tuning characts. 79—59722
CO_2, small-gap multiatm. press. system 78—74921
CO_2, smooth high power pulse form. 78—17990
CO_2, spark photoionisation, tripropylamine additive 78—13679
CO_2, split beam system, for optical fibre drawing heat source 77—19465
CO_2, split-mode unstable resonator, phase locking 77—58351
CO_2, spontaneous emission probabilities and collisional broadening of $00^{0}1$-$10^{0}0$ lines 77—23649
CO_2, stabilisation using 4.3 μm fluorescence technique 77—75557
CO_2, stability of parallel pin electrode laser discharges, theoretical investigation 80—83588
CO_2 stable grating controlled laser design 80—64063
CO_2, Stark cell noise reduction 78—59059
CO_2, Stark effect modulation by iodomethane 78—17992
CO_2, submillimetre wave laser operating in passive Q-switched intracavity pump mode 77—83885
CO_2, surgical appls. 77—9297
CO_2, systems for nucl. fusion expts. 77—19335
CO_2, TE, injection mode locking, press. up to 8 atm. 77—10883
CO_2 TE laser, high-pressure O_2 contaminated, excitation 79—89882
CO_2 TE laser, longit. mode control using intracavity gas-phase absorbers 79—72579
CO_2 TE laser, passive mode locking using p-Ge saturable absorber 78—71127
CO_2 TE laser, performance improvement with tripropylamine additives 78—78991
CO_2 TE laser, waveguide, role of elec. field to press. ratio 78—17901
CO_2 TE laser amplifier, characts., with different UV preionisation at superatmospheric press., tripropylamine doped 77—14686
CO_2 TE laser pumped NH_3, IR and far IR laser emissions 79—934
CO_2, TE multiatmos. laser, 10 μm pulse generation and amplification 79—45981
CO_2 TE pulsed 4.3 μm laser 79—89926
CO_2 TE unstable resonator laser, operation using additives 79—98403
CO_2 TE waveguide laser, operation using pulser-sustainer method 80—38029
CO_2, TEA, 4.3-μm radiation pulse generation 80—5724
CO_2, TEA, attachment loss of photoionisation electrons 78—5450
CO_2, TEA, equilib. gas temp. and its distrib. 77—54691
CO_2, TEA, field uniformity requirements 79—3675
CO_2, TEA, freq. chirp reduction, improved stability 77—10959
CO_2, TEA, injection-locked single mode, IR absorpt. meas. of SF_6 80—9665
CO_2, TEA, mode characts. using unstable resonators 79—3719
CO_2, TEA, multifreq. injection locking, resonator config. 77—7141
CO_2, TEA, multiline oscill. temp. control., intercavity etalon method 79—98337
CO_2, TEA, pulse stretching by CO addition 77—14754
CO_2, TEA, pulse-forming and line-broadening in AM mode locking 77—54743
CO_2, TEA, self-sustained discharge, excitation 77—7061
CO_2, TEA, tunable simultaneous double wavelength operation 77—61970
CO_2, TEA, with seed gas, Penning ionisation 78—5449

gas lasers continued
- CO_2 TEA amplifier, gain meas. on sequence bands 78−78990
- CO_2, TEA and superatm. press., design and operation 79−31946
- CO_2, TEA discharge, arc suppression 77−7056
- CO_2 TEA far IR laser, optimum spectral matching 79−31857
- CO_2 TEA helical laser, axial mode behaviour 79−55108
- CO_2 TEA high-power tuned laser using three-mirror confocal unstable resonator 80−23719
- CO_2, TEA injection laser, single-mode pulse prod. 77−54722
- CO_2 TEA laser, actively modelocked multiline, controlled by NaCl etalon 80−23713
- CO_2, TEA laser, catalytic control of gas chemistry 79−76663
- CO_2 TEA laser, compact sealed single mode operation 78−50810
- CO_2 TEA laser, compact sealed photopreionised, without heterogeneous catalysis or gas recycling 79−59709
- CO_2 TEA laser, construction and optimisation with pin electrodes *(German)* 77−23697
- CO_2, TEA laser, energy extraction improvement in multiline double band mode 78−63129
- CO_2 TEA laser, fine freq. tuning 79−98405
- CO_2 TEA laser, high power, construction and performance 77−3566
- CO_2 TEA laser, homogeneous discharge development, preionisation conditions influence 79−18399
- CO_2 TEA laser, injection mode locking on P and R transitions in 9, 10 μm bands 79−89883
- CO_2 TEA laser, injection tuning and mode locking on low gain rot. lines 80−95928
- CO_2, TEA laser, intense pulsed lasing at lines of P and R branches of $00^02\text{-}(10^01,02^01)_{I,II}$ 79−89887
- CO_2 TEA laser, isolation between amplifiers using absorbing gases 80−95911
- CO_2 TEA laser, laser output depend. on initial photoelectron density 80−43320
- CO_2 TEA laser, mode-locked, cavity-dumping 80−87415
- CO_2 TEA laser, multiline operation with CO_2 as intracavity absorber 79−94206
- CO_2 TEA laser, optimum operational conditions with double discharge at atm. pressure *(Bulgarian)* 78−33720
- CO_2 TEA laser, photochemical reaction induction 79−57257
- CO_2 TEA laser, picosecond pulse generation using Ge optical switch 79−7159
- CO_2 TEA laser, production of striated filamentary sparks 80−24288
- CO_2, TEA laser, pulse shape and duration, excitation method *(German)* 78−83010
- CO_2 TEA laser, pulse shaping by independent excitation of coaxial discharge systems 79−7150
- CO_2 TEA laser, pulse shape and gain 80−1181
- CO_2, TEA laser, self sustained discharge excitation, efficiency 77−655
- CO_2 TEA laser, sequence band effect on 10.4 μm band multiline oscillation 80−74334
- CO_2 TEA laser, shortening of pulses *(Rumanian)* 79−86199
- CO_2 TEA laser, tri-n-propylamine doped, parametric meas. 80−78830
- CO_2 TEA laser, UV preionisation, parametric studies 80−64040
- CO_2 TEA laser, UV preionised, characts. 80−69414
- CO_2, TEA laser amplifier, high power short-pulse, efficiency enhancement 79−36872
- CO_2 TEA laser design and construction *(Italian)* 78−55360
- CO_2 TEA laser discharges 77−14687
- CO_2, TEA laser discharge form., electrode and preioniser geometry effects 77−27269
- CO_2 TEA laser discharge, influence of additives and contaminants evaluated by electrical meas. 78−94388
- CO_2 TEA laser electrical excitation rates, theory and expt. 78−71078
- CO_2, TEA laser emission on sequence bands 78−71075
- CO_2 TEA laser injection locked, tunable single longitudinal mode operation, O_3 absorpt. spectra 80−33018
- CO_2 TEA laser mode locked by positive Ge, pulse shape meas. 78−46694
- CO_2 TEA laser operation, effect of low-ionisation gas additive along with UV photopreionisation 77−50683
- CO_2 TEA laser oscillator, longit. mode rejection, cavity length tuning effect 79−86189
- CO_2 TEA laser oscillator, transverse mode locking by short pulse injection 80−38045
- CO_2 TEA Laser pulse, PCM with CdTe crystal Pockels modulator 80−102742
- CO_2 TEA laser pulse forming network 78−9389
- CO_2, TEA laser pumping efficiency increased by longitudinal mode control 77−38924
- CO_2 TEA laser sensing of methanol in He, phase fluctuation optical heterodyne spectroscopy 80−68266
- CO_2 TEA laser stability 77−38935
- CO_2 TEA laser system, 20-J nanosecond pulse, based on injection-mode-locked oscillator 80−99752
- CO_2, TEA laser transverse discharge electrode system, relax. and plasma homogeneity 77−23648
- CO_2, TEA laser tube, helical electrodes, convergent lensing effect *(French)* 77−75472
- CO_2 TEA laser with long optical resonator, mode-locked operation 78−79041
- CO_2 TEA lasers, one-step photoionisation, preionisation discharge effect on electron density 80−53256
- CO_2 TEA lasers, SF_6 dissoc. processes 78−74713
- CO_2, TEA lasers using amine additives, cyanide deposits prod. 77−71991
- CO_2, TEA oscillator, injection locking, mode selection 77−653
- CO_2 TEA oscillator, injection mode-locking using N_2 laser-controlled semicond. switching of 10-μm radiation 80−1247
- CO_2 TEA oscillator, simultaneous freq. stabilisation and injection 78−55362
- CO_2 TEA pulse-periodic laser, utilisation efficiency of gas flow 79−64201
- CO_2 TEA pulsed, UV preionized, high power laser, development and performance 80−106539
- CO_2, TEA pulsed laser rangefinder 78−46760
- CO_2 TEA pulsed laser with gas recirculation system, use of $^{13}CO_2$ 80−1182
- CO_2, TEA sealed laser, seed gas compatible system with unheated oxide catalyst 78−63130
- CO_2 TEA single longit. mode laser with tilted intracavity etalon 78−5484

gas lasers continued
- CO_2 TEA UV preionized laser, non-dispersive tuning 79−31856
- CO_2 TEA waveguide laser, high power 80−91814
- CO_2, TEA with high repetition rate *(Italian)* 79−27276
- CO_2 technological closed-cycle laser optimisation to 10 kW power 79−94254
- CO_2, therapeutic appls. and results 80−56155
- CO_2 thermally pumped laser, He and Ar gas addition effect on small signal gain 79−22931
- CO_2, tilted mirror unstable resonator laser cavity 78−29979
- CO_2 transition, $10^\circ0 \rightarrow 01'0$ 13.9 μm, in pulsed elec. discharges, laser emission 77−88692
- CO_2, transition strength of $00^\circ2$ 9.4 μm sequence band, appl. to IR isotope anal. 79−18395
- CO_2, transverse discharge, spatial gain distrib. meas. 77−696
- CO_2 transverse discharge flow type laser, theoretical model *(Chinese)* 80−53255
- CO_2, transverse flow CW, glow discharge stabilisation 78−37900
- CO_2 transverse flow CW laser, modelling and props. meas. 80−43321
- CO_2, transversely excited, advances in control 77−88748
- CO_2, transversely excited waveguide laser, high field preionisation, design considerations 77−88751
- CO_2 transversely excited miniature laser, freq. characts. 79−98335
- CO_2, tunable, appl. to remote meas. of gases 77−87118
- CO_2, tunable 2.75 GHz IR source 77−14786
- CO_2 tunable dual-line laser for atmospheric spectroscopy and pollution monitoring 78−3977
- CO_2 tunable high-press. waveguide laser, spectroscopy of OsO_4, SF_6 mols. 80−43054
- CO_2, tunable linearly polarized TEM_{00} operation, concave diffr. grating 77−19344
- CO_2, tunable stabilised single-mode TEA 78−5485
- CO_2 tunable waveguide laser 79−64249
- CO_2 UV preionised laser discharge, large scale, aero-acoustic effects 79−36875
- CO_2 UV preionised TEA laser, parametric study 80−102738
- CO_2 ultrashort pulse generation by free-induction decay in $KCl{:}KReO_4$ 80−74444
- CO_2, unstable resonator, gain, spatial inhomogeneity effect 77−34870
- CO_2 unstable resonator laser pump for high energy density NH_3 laser 80−53327
- CO_2 upper hybrid and whistler mode laser radiation anomalous penetration in overdense magnetoplasma 79−77386
- CO_2, upper laser level population, active medium gain in waveguide discharge channel 79−86158
- CO_2, used in feedback-stabilized fractional fringe interferometer for plasma density measurements 79−75582
- CO_2, using BeO waveguide, long-term operation 77−10956
- CO_2, using CdS fast optically controlled modulator 78−13736
- CO_2, versatile high-power industrial system 78−55380
- CO_2 versus semiconductor diode lasers for long path monitoring of ambient gases 79−16682
- CO_2, vibr. distrib., effect of laser radiation 77−34868
- CO_2, vibr. distribs., O_2 addition effect 78−50757
- CO_2, vibr. energy transfer by current modulation 78−1204
- CO_2, volume discharge excited by electron beam, mag. field influence 79−27241
- CO_2, wavefront analyser for diagnosing high-energy lasers 79−59740
- CO_2 waveguide amplifiers, temp. depend. of small signal gain and saturation power 78−46569
- CO_2 waveguide high press. laser, line selection and tunability 78−59026
- CO_2 waveguide laser, CW, optical pumping of far-IR molecular lasers 80−83615
- CO_2 waveguide laser, design and performance characts. 80−9909
- CO_2 waveguide laser, dynamic gain, discharge tube depend. 80−23668
- CO_2 waveguide laser, electrooptically Q-switched 79−98416
- CO_2 waveguide laser, for space link transceiver 77−19322
- CO_2, waveguide laser, gain calcs. 78−25849
- CO_2 waveguide laser, gain and saturation *(Rumanian)* 80−23667
- CO_2, waveguide laser, low prime power, gain and discharge power meas. 77−88749
- CO_2 waveguide laser, multibeam, excited by AC discharge 80−99754
- CO_2 waveguide laser, parameters meas. 79−31859
- CO_2 waveguide laser, performance characts. *(Japanese)* 77−19318
- CO_2, waveguide laser, population and gain, kinetic eqn. soln. 79−64200
- CO_2 waveguide laser, pulsed operation 78−42353
- CO_2 waveguide laser, saturation intensity, effect of wall deexcitation 79−924
- CO_2 waveguide laser, saturation parameter 79−94209
- CO_2 waveguide laser, saturation parameter 80−9856
- CO_2 waveguide laser, saturation parameter meas. method 80−87372
- CO_2 waveguide laser, small signal gain, saturation intensity and volumetric output power 78−74880
- CO_2 waveguide laser, transversely excited multiatmosphere, construction and characts. 77−79845
- CO_2 waveguide laser, transversely RF excited 78−63127
- CO_2 waveguide laser, tunability calc. *(Rumanian)* 80−87371
- CO_2 waveguide laser 79−98380
- CO_2 waveguide laser amplifier, using short BeO ceramic discharge tube, gain meas. 80−33027
- CO_2 waveguide laser amplifier with strong discharge tube 80−74398
- CO_2 waveguide laser and appls. 77−75568
- CO_2 waveguide laser discharge, cooling, gas temp. meas. 78−17958
- CO_2 waveguide laser pulse shaping on multiple rot. lines 80−78879
- CO_2, waveguide laser structures, design, construction and performance 77−88750
- CO_2, waveguide laser with BN channel 77−14743
- CO_2 waveguide laser with plane parallel mirror resonator 79−3715
- CO_2 waveguide laser with pulsed high-freq. discharge 80−99755
- CO_2 waveguide lasers, engineering aspects 79−31941
- CO_2 waveguide lasers, high stability 77−3615
- CO_2 waveguide lasers, high-power, high-press., photoionisation-stabilised 78−46641
- CO_2, waveguide TE laser, modes of operation 79−81451
- CO_2, wavelength, comparison of 2 beams, two-wave interference, book contrib. 78−9408
- CO_2 wavelength and freq. meas., speed of light determ. 77−45822
- CO_2, weak laser lines around 10.6 μm, wavenumber meas. 78−17998
- CO_2, weak transitions, freq. and gain meas. using diode laser 77−88693
- CO_2 whispering-gallery CW laser, design and operation 79−81447
- CO_2, wideband modulation of R(18) with NH_3 Stark cell 77−23704

gas lasers continued
CO_2, window materials, absorption props. 77—46770
CO_2 wire-triggered high press. pulsed laser 79—89935
CO_2, with foreign gas additives, time delay in pulsed operation 77—7058
CO_2, with intracavity Stark cell, for pulsed and Doppler laser radar 77—19320
CO_2, with transverse excitation and preliminary photoionisation 78—1254
$^{12}C^{18}O_2$, double-discharge Pyrex waveguide CW laser 78—9393
$^{13}C^{16}O_2$ laser, isotopically enriched, appl. in optically pumping far IR laser 80—58507
CO_2:N_2:He plasma, lasing action, gain limiting attainment possibility 79—89884
$CO_2/^{192}OsO_4$ laser, absolute light oscill. freq., universal const. variation meas. possibilities *(Russian)* 80—5723
CO_2-air, open cycle laser, generated power depend. on pulse repetition freq. *(Russian)* 77—19231
CO_2-Br laser, pulsed, electron-vibr. energy exchange from Br* 78—29930
CO_2-Br_2-He mixture, possible gas lasers with solar excitation 80—99695
CO_2-CO, He free TE laser, variable pulse length. operational characts. 78—22151
CO_2-DF-He CW optically reson. pumped transfer laser 77—75471
CO_2-H_2-He 10.6 μm scan laser with programmable VO_2 mirror 80—38026
CO_2-He UV photopreionisation TEA laser, role of He excited atoms 78—17902
CO_2-N_2 electroionisation laser mixture, ionisation instability of semi self maintaining discharge 80—63971
CO_2-N_2 fast-flow laser with unstable resonator, self-oscillation instability 80—95870
CO_2-N_2 laser, high-pressure, numerical optimisation 77—10882
CO_2-N_2 mixture, strongly excited, vibr. relax. 80—102555
CO_2-N_2-^{3}He, laser, plasma diagnostics of media capable of lasing in nucl. reactor environment 79—10279
CO_2-N_2-^{3}He laser, nonautonomous continuous discharge due to thermal neutrons from reactor 78—29929
CO_2-N_2-^{3}He laser mixture, excitation in externally maintained discharge in reactor core 80—28193
CO_2-N_2-H, laser discharge circuit parameters, effect on energy imput mode 77—75476
CO_2-N_2-H_2 electron beam controlled laser, efficiency and output energy depend. on H_2 78—58978
CO_2-N_2-H_2O fast flow discharge laser, output power time depend. 80—99697
CO_2-N_2-H_2O gasdynamic laser, small signal gain and vibr. wall accomm. 79—98340
CO_2-N_2-He, fluorescent IR radiation from glow discharge 78—94386
CO_2-N_2-He, pulse-periodic operation of electron-beam-controlled discharges, energy characts. changes 80—102695
CO_2-N_2-He, transverse combined discharge laser, 10-20 kW *(Russian)* 77—54703
CO_2-N_2-He discharge, energy balance, influence of N_2 rot. level reson. excitation 78—17903
CO_2-N_2-He electroionisation laser, freq. mode, lasing conditions 80—63970
CO_2-N_2-He flowing gas mixture, glow discharge produced population inversion 78—78992
CO_2-N_2-He laser, civr. temp. approx. for N_2, applicability limit 78—5452
CO_2-N_2-He laser, pulsed microwave discharge pump, skin effect and gain 79—13945
CO_2-N_2-He laser, vibr. population distrib. of N_2, vibr. temp. determ. 77—14688
CO_2-N_2-He laser media excitation by electron beams admitted through gasdynamic windows 80—99694
CO_2-N_2-He laser mixtures, self-sustained glow discharges, low ionisation pot. organic additives effects *(French)* 77—88694
CO_2-N_2-He laser mixtures, electron swarm parameters, Boltzmann eqn. anal. 79—18396
CO_2-N_2-He laser mixture in nonself-sustained discharge, direct heating mechanism 80—28195
CO_2-N_2-He pulsed transverse discharge, investigation of gain 80—9855
CO_2-N_2-He self-sustained TEA discharge laser, config. for high beam qualtiy 77—14753
CO_2-N_2-He system, CO_2 TEA laser discharge development, high-speed-camera investigation 79—55109
CO_2-N_2-He volume discharge, self-sustained, with UV preionis. 79—60211
CO_2-N_2-He-CO, electron diffusion perpendicular to elec. field, second order theory 80—43322
CO_2-N_2-He-CO mixture, electron motion anal. 79—64199
CO_2-N_2-He(H_2) laser mixtures, composition effect on excitation efficiency in dicharge 78—5453
CO_2-N_2-Ne-H_2O mixture IR laser *(Russian)* 79—10323
CO_2-N_2O, optical pumping in 4.3 μm band 77—7060
CO_2-OsO_4 laser frequency meas., D_2O laser phase locking to freq. standard 80—95080
CO_2-Xe, sealed-off, high efficiency, low impedance 77—3614
CO_2+ perfluoroalkyl halides, collisional relax. 79—13799
CO_2+COS mixture, Raman laser optical excitation, electron phototransition theory *(Russian)* 80—99711
CO_2+H+Xe plasma, elec. parameters, Xe effects *(Russian)* 77—84507
CO_2+monobromomethane mixture, Raman laser optical excitation, electron phototransition theory *(Russian)* 80—99711
$^{13}C^{16}O(^{12}C^{18}O)$, freqs. relative to $^{12}C^{16}O$, by Stark spectroscopy of formaldehyde 77—75150
CO_2laser, N_2-O_2 effects on plasma current establishment/relax. processes *(Russian)* 79—99011
CS_2, for 16 μm range, review *(Rumanian)* 80—87408
CS_2, HV pulser development 80—23707
CS_2, high-power tunable laser for 9 to 12.5 μm range 77—83884
CS_2, laser transition, rel. dipole strengths calcs. 77—61937
$^{13}CS_2$, laser emission at 6.9 μm, HF laser optical pump 78—58995
$^{13}CS_2$, optically pumped by pulsed HF laser, emission obs. at 6.9 μm 79—50283
CS_2/O_2 additive flame laser, design and performance 80—78870
CO_2 CW laser, unstable resonator with small-scale phase inhomogeneities, props. 80—19057
Ca, pumped via collision-induced absorpt. in Ca-inert gas mixture 79—7117
Ca-H_2, single freq. laser, 5.54 μm emission, mag. field tuning 78—46634
Cd, CO_2 laser produced plasma evolution, laser possibility 77—80325

gas lasers continued
Cd, cataphoretic laser, transverse separation dynamics 77—38865
Cd plasma, laser action via recombination process 79—94217
Cd vapour laser LG-70, specification 78—74889
Cl_2+N_2 mixture, Raman laser optical excitation, electron phototransition theory *(Russian)* 80—99711
ClO_2, CW for IR mol. laser, optical pumping with $^{16}CO_2$ and $^{18}CO_2$ lasers 80—74343
Cn, vapour laser excited by single elec. pulse, lasing characts. 80—87386
Co, cataphoretic at. distrib. in $CoCl_2$-He discharge 77—31092
Co_2 injection mode-locked TEA laser, extra-cavity feedback into unstable resonators 79—72601
Co_2, wavefront analyzer for diagnosing high-energy lasers 79—59738
Cr vapour, laser transitions in near IR 80—99704
Cs vapour heat pipe discharge tube pumping for 823 cm^{-1} tunable IR laser 78—63069
Cs-Xe vapour mixture, possibility of solar direct energy conversion into laser radiation 79—59688
Cu, 40 kV discharge, pulsed 400 $\mu J/cm^3$ output *(Russian)* 77—10895
Cu atom lasers, finely dispersed metal particle active medium 80—91777
Cu atom pulse stimulated emission, discharge excitation in $CuBr_2$, $CuCl_2$ 77—23663
Cu atoms in halide vap. transverse discharge 77—88716
Cu, blue-green laser technology for ocean optics 77—78458
Cu, comparison of CuCl, CuBr and CuI lasants 77—34875
Cu, continuously pulsed halide lasers, kinetic processes 77—88702
Cu, CuBr lasant, continuously pulsed, long duration, high efficiency operation 78—79029
Cu, Doppler-free laser spectroscopy in hollow cathode discharge 80—9537
Cu, electron temp. meas. using a microwave radiometer 77—7072
Cu, exploding wire *(Russian)* 77—38863
Cu, for pumping jet dye laser 77—7128
Cu halide, continuously pulsed, degradation due to axial cataphoresis effects 77—31093
Cu halide, Cu laser lines, broadening, induced emission cross-sections 79—26928
Cu halide, transverse excitation, large active volume 78—59021
Cu halide laser, pumping efficiency 79—68385
Cu halide laser, rapid differential decay of Cu metastable populations 80—53270
Cu halide laser driving ccts., parametric study 80—83610
Cu halide laser systems, high average power pulser design 78—5497
Cu halide vapour laser, kinetic model 79—94222
Cu, high repetition rate discharge-heated discharge circuitry 78—5479
Cu I lines, superradiance obs. in pulse vaporisation of pulverised Cu_2O, CuO 79—45934
Cu II laser, UV, operating period extension by Ar admixture 80—74342
Cu, in radial transverse discharge, stimulated emission 77—50658
Cu, laser action at 5106 Å and 5782 Å, using copper acetate lasant 78—25854
Cu, laser action on 5106, 5782 Å lines in copper acetylacetonate, $Cu(NO_3)_2$ vapours 77—88712
Cu laser line structure at 510.6, 578.2 nm 80—53274
Cu, long lived sealed off halide discharge 77—88770
Cu, nanosecond pulsed laser, Milan-1, technical specification 78—17979
Cu, optically pumped lasers utilizing self-terminating transitions, CW stimulated emission possibility 80—14329
Cu, pulsed emission at elevated powers 78—25895
Cu, pulsed laser with unstable resonator, beam shaping 78—17987
Cu, pumping of efficient high average power dye amplifier 77—88755
Cu, self heating, optimum discharge parameters 77—75563
Cu, single pulse spectral distrib. meas. 79—3732
Cu, steady multiply pulsed discharge heated vap., halide lasant 77—38911
Cu, time depend. of electron density, resist. and interferometric meas. 78—25864
Cu transversely excited pulsed vapour laser, gas discharge parameters influence 79—10291
Cu, used for single crystal impurity luminesc. attenuation in Raman spectra 79—15467
Cu, using Cu acetylacetonate as Cu atom donor 78—82956
Cu, using CuCl, double pulse, output characts. at small pumping pulse delays 78—13690
Cu, using $Cu(NO_3)_2$ as working substance 79—79244
Cu vapour, comparison of copper acetate, acetylacetonate and CuCl lasants 79—31875
Cu vapour, discharge heated longit., scaling 78—50790
Cu vapour, discharge-heated high-power high-pressure 79—81453
Cu vapour, excited in pulsed radially transverse discharge, efficiency 80—14331
Cu vapour, explosively formed, apparatus for stimulated emission obs. 78—50764
Cu, vapour, gas temp. meas. using Doppler broadening of Ne buffer gas lines 80—19020
Cu vapour, He buffer gas effect on output parameters 78—9368
Cu vapour, mode-locked, high pulse rate operation 77—61967
Cu, vapour, pulse repetition freq. up to 100 kHz 77—669
Cu vapour, using CuCl metal source, Cu ground state and metastable level population densities 77—83860
Cu vapour 78—46584
Cu, vapour annular discharge laser, laser powers, device efficiency 80—19043
Cu vapour coaxial laser, operation at above atm. buffer gas press. 79—59690
Cu, vapour electron energy distrib. function computation 78—71091
Cu vapour laser, characts. comparison with CuBr(Cl) lasers 80—102711
Cu vapour laser, coherent props., dynamic holography in VO_2 films 79—13929
Cu vapour laser, discharge-heated 79—7149
Cu vapour laser, electron energy distribs. in Cu-Ne(He) mixtures 79—13956
Cu vapour laser, energy conversion efficiency, reson. levels excitation 80—99715
Cu vapour laser, fabrication, green and yellow emission *(French)* 80—43360
Cu vapour laser, for optical systems with brightness amplifiers *(Russian)* 79—98498
Cu vapour laser, induced emission, spectral comp., time evolution 80—74344
Cu vapour laser, non heated, kinetic processes 80—37999

gas lasers continued
  Cu vapour laser, optimisation of excitation conditions 80—9900
  Cu vapour laser, population inversion kinetics, modified hook method meas. 80—53275
  Cu vapour laser, preionisation effect 80—87377
  Cu vapour laser, rate processes, computer simulation 80—69371
  Cu vapour laser, service life and efficiency 79—27292
  Cu vapour laser, unstable resonator oscillator and oscillator-amplifier characts. 80—23720
  Cu vapour laser as image amplifier for transmitted-light laser projection microscope 80—73446
  Cu vapour laser discharge, power deposited, pump pulse repetition freq. influence 80—74350
  Cu, vapour laser emission, pulse characteristics rel. to plasma parameters 78—71090
  Cu vapour laser excited by transverse discharge 80—53280
  Cu vapour laser optical pumping for I_2 molecule B-X electron transition *(Russian)* 80—78845
  Cu, vapour laser output conversion by dye solution to 5782 Å 80—48241
  Cu vapour production, in sputtered Cu_2O and CuO pulse discharge *(Russian)* 77—84556
  Cu, vapour production method, hollow cathode arc, Ar buffer gas 78—86981
  Cu vapour pulsed laser, spectral comp. of superradiance, stimulated and spontaneous radiation 80—102713
  Cu vapour pulsed laser, stimulated emission mechanism 79—64213
  Cu vapour sealed laser, operation at buffer gas atm. press. 80—38033
  Cu/CuCl double pulse laser, continuous glow discharge appl. 80—1190
  Cu/CuCl double pulse laser, pumping pulse and output pulse characts. 80—87380
  Cu/CuCl double pulse laser, dissoc. pulse, afterglow, and laser pulse model 80—91775
  Cu/CuCl double pulsed laser, extrema by electron density and output pulse energy 79—10283
  Cu-Ne, hollow cathode laser discharge, spectroscopic temp. meas. 79—7490
  Cu-Ne CW mW-level laser source at 250 nm 80—43352
  Cu-Ne laser, spectral lines emission of gas-discharge pulse plasma 79—31883
  Cu-Ne mixture, 3-20 kHz pulse discharge obs. 78—71092
  Cu-vapour-He laser discharge, metastable decay rates 79—86164
  CuBr, continuously pulsed laser, cable-capacitor Blumlein discharge circuit, expt. characts. 78—82981
  CuBr laser, bubble gas effects on ground and metastable populations 78—82955
  CuBr laser, burst-mode, laser power variation and time depend. of populations 79—50284
  CuBr laser, tunable dye laser radiation, gas temp. atomic density meas. technique 79—82037
  CuBr, rapid differential decay of Cu metastable populations 80—53270
  CuBr vapour laser, characts. comparison with Cu, CuCl lasers 80—102711
  CuBr-He-Ne pulsed discharge, Cu I relax. processes 78—25865
  CuCl, continuously pulsed laser, cable-capacitor Blumlein discharge circuit, expt. characts. 78—82981
  CuCl, dissoc. pulse cct. inductance effect 78—29936
  CuCl, double pulsed laser, scaling to 10 mJ 78—46624
  CuCl, double-pulse, addition of HCl 77—50654
  CuCl double-pulse laser, weak axial mag. field effects on energy output 78—42327
  CuCl, double-pulsed, parametric study 77—50681
  CuCl, double-pulsed laser, energy output, initial current rise effect on pumping 78—13687
  CuCl, hollow cathode laser using metal tube 77—14742
  CuCl, laser gas-discharge tubes, output characts. 79—64251
  CuCl, metal vapour lasers excited by pulse trains 79—13955
  CuCl, potential, high-energy large vol. device 78—50807
  CuCl pulsed laser, time depend. of Cu-atom conc. in ground and metastable states 78—66806
  CuCl vapour laser, characts. comparison with Cu, CuBr lasers 80—102711
  CuCl vapour laser, output power limiting processes 80—91776
  CuCl vapour laser, use for image amplification in projection microscope system 79—98407
  CuI-He-Ne pulsed discharge, Cu I relax. processes 78—25865
  DCN, 250 mW continuous discharge laser at 195 μm 79—31949
  DCN, CW submm. waveguide laser, high volumetric efficiency 78—42351
  DCN waveguide lasers, optimised 190/195 μm, amplifying medium characts. 80—99709
  DF, pulsed laser induced damage to optical materials 77—46751
  D_2O, 385 μm transition, laser pumped mol. laser theory 79—36868
  D_2O 385-μm laser, CO_2 laser pumping, dispersion 80—87375
  D_2O, angular correlation between far IR emission and CO_2 pump radiation, Dicke superradiance theory 79—41370
  D_2O, candidate transition identification for optically pumped far IR lasers 79—931
  D_2O FIR lasers, reststrahlen laser resonator for 66 μm line 78—55385
  D_2O, far IR CW laser emission by optical pumping 79—3687
  D_2O, far IR laser, intracavity pumped by TE CO_2 laser 80—87382
  D_2O, far IR laser, tunable single mode optical pumping 77—42526
  D_2O far IR laser pulses, real-time spectral anal. using SAW dispersive delay line 79—45983
  D_2O, far IR laser system, high power optically pumped 77—54724
  D_2O, far IR superradiant laser action 77—663
  D_2O, far IR superradiant laser, 114, 66 μm emission, time-resolved pulse and wavelength meas. 77—88715
  D_2O, heterodyne meas. of IR absorpt. freqs. 78—55175
  D_2O laser, 66 μm, with unstable reststrahlen resonator 80—83619
  D_2O, laser, emission characteristics at 50, 66, 83, 111 and 116 μm 80—58525
  D_2O laser, pulsed, optically-pumped, development for Tokamak plasma diagnostics, review 80—24242
  D_2O laser, synchronously pumped, subnanosec. transients 79—89891
  D_2O laser, zigzag-pumped, oscillator and superradiance characteristics 79—31873
  D_2O laser phase locking to freq. standard, CO_2-OsO_4 laser freq. meas. 80—95080
  D_2O, laser pumped molecular lasers, sub MM laser expts. 80—1192
  D_2O, laser submillimetre with optical pumping energy yield, emission pulse delay time depend. on pumping pulse *(Russian)* 78—71088

gas lasers continued
  D_2O, optically pumped, superradiant line obs., 235, 280, 97 and 98 μm 78—1215
  D_2O optically pumped mirrorless laser at 385 μm 79—31871
  D_2O oscillator, zigzag pumped, superradiant 66 μ emission 78—33743
  D_2O, oscillator-amplifier laser system, high power, narrow linewidth, at 384.6 μm 77—10894
  D_2O, pulsed laser-pumped submm amplifier, gain spectrum 78—79000
  D_2O, single-mode optical pumping, superradiant far IR emission 78—42329
  D_2O, submillimetre laser Thomson scatt. system for plasma diagnostics 77—84526
  D_2O superradiant laser, Raman shifts of 99 μm output, Fabry-Perot freq. meas. 79—55120
  D_2O, synchronous mode-locked pumping, mode-locked far IR pulse generation 79—27271
  D_2O tunable vapour laser, optically pumped with single-mode CO_2 TEA laser 79—55145
  D_2O, vap., 9.7 μm radiation absorption rel. to laser design 77—31098
  D_2O vapour high-power 385 μm laser oscillator 80—69422
  D_2O vapour high-power optically-pumped submillimetric laser system 77—38925
  D_2S, CO_2 laser pumped, high power far IR superfluorescent emission 79—27243
  D_20, near-MM-wave laser synchronous pumping, ultrashort pulse generation at 385, 66 μm 80—102705
  Eu atoms and ions, self-terminating lasers, energy and time characts. 77—75493
  F atomic laser, doublet and quartet transitions, spectral press. depend. 77—58318
  F atomic laser produced by He-NF_3 fast pulsed discharge, pumping mechanism 79—81410
  F hollow-cathode laser, using He-$NF_3(SF_6)$ mixtures 80—48289
  F, simple high-power TEA laser operating in visible and near IR 79—94251
  F_2-He, high-press. mixture, neutral atomic F laser lines 79—86167
  FCN, CW for IR mol. laser, optical pumping with $^{16}CO_2$ and $^{18}CO_2$ lasers 80—74343
  Fe, pumping using KrF laser, vap. form. by flash and discharge decomp. of $Fe(CO)_5$ 78—74890
  Fe vapour laser, 4529 Å emission 79—10282
  $Fe(CO)_5$ photodissociation laser 78—74886
  fluoromethane 496-μm laser, CO_2 laser pumping dispersion 80—87375
  H, inverted, optical gain at Lyman-α spectral line 80—95880
  H-like plasmas for short-wavelength lasers, population inversion 78—34277
  H_2, compressed, Raman laser, axial mode self-locking 79—94223
  H_2 compressed high-power tunable Raman lasers and applications 77—54709
  H_2, efficient tunable Raman laser 80—28245
  H_2 high power tunable IR compressed laser, for spectroscopy 80—48277
  H_2 laser, stimulated Raman scatt., appl. to holography 80—91782
  H_2 laser, tunable IR waveguide Raman type pumped by dye laser, 0.7-7 μm range 79—45959
  H_2, Raman gain dependence on pump laser bandwidth 79—81483
  H_2 Raman laser, for efficient coherent summation of Nd laser nanosecond pulses 80—23718
  H_2 Raman laser, multiple-pass-cell, controllable pulse compression 80—91825
  H_2, Raman laser, use of waveguide for improved conversion efficiency 77—658
  HBr high-energy laser, parametric and engineering studies 79—41391
  HCCF, CW for IR mol. laser, optical pumping with $^{16}CO_2$ and $^{18}CO_2$ lasers 80—74343
  HCN, 2m CW, design and characts., brown deposit 77—3605
  HCN, 337 μm tunable radiation in laser-klystron link through Schottky diode or metal-semicond. point contact 78—46714
  HCN, CW 337 μm laser, spatial coherence meas. 77—3595
  HCN, CW 337 μm waveguide laser, scaling laws 77—19300
  HCN CW compact laser, output characts. expt. 80—38035
  HCN CW laser, auxiliary DC discharge effects 79—31925
  HCN CW laser, output characts. *(Japanese)* 80—9863
  HCN CW laser gain in hollow dielec. rectangular discharge tube 79—72554
  HCN, CW power characts., 337 μm, 0.3-0.8 A current 77—3604
  HCN, CW source for magnetospectroscopy and plasma diagnostics *(German)* 77—10948
  HCN compact CW laser optimisation 78—59022
  HCN compact CW laser, output increased by He, Ar, air and O_2 buffer gases 79—10293
  HCN, $H^{15}CN$, far IR laser transition assignments 78—46579
  HCN laser, power output, temp. and gas flow *(French)* 78—13686
  HCN laser, transversely excited double discharge 80—5749
  HCN, laser plasma, microwave spectra of excited vibr. states 78—17656
  HCN laser processes, mm. and submm. microwave spectroscopy 78—13685
  HCN, laser translator of standard freq. to submm. range 78—17973
  HCN, plasma effects, radial gain and refractive props. 77—61942
  HCN, short 337 μm CW laser, output characts. 79—36882
  HCN, temporal coherence meas., comparison of TGS pyroelec. detector with W-C point contact diode 80—31871
  HCN, transversely excited waveguide laser with UV preionisation 77—54730
  HCN waveguide and Fabry-Perot CW laser power scaling laws 79—76715
  HCl-He, discharge, possible laser action on vibr. transitions 80—14332
  HD, vibr.-rot. transitions, possible laser appl. 79—55122
  HDS, CO_2 laser pumped, high power far IR superfluorescent emission 79—27243
  HF-DF, 10 W repetitively pulsed closed cycle system, elec. excitation 77—88753
  HN_3 high energy density laser using unstable resonator CO_2 laser pump 80—53327
  H_2O, CW laser, characts. at 118 and 28 μm 79—81411
  H_2O, electronic-vibr. energy transfer from $Br(4^2P_{1/2})$, 12 laser transitions 7 to 7.7 μm 77—31094
  H_2O, IR ellipsometer for Si epitaxial layers meas., expt. 78—62219
  H_2O laser meas. of H_2O, D_2O far IR absorpt. coeffs. by H_2O laser meas. 80—9599
  H_2O, pulsed oscill., elongation by admixture of He 78—87039

gas lasers continued
H_2O vapour, 118.6 mm radiation absorption by H_2O vapour, temp. and press. effects meas. 78−75255
H_2O vapour laser, CW 28 μm, operating characts. and discharge conditions 80−69369
He, energy pathways by proton excitation 78−5459
He, gain coeffs. for fission fragment generated plasma 77−31488
He, high press., laser plasma optically pumped by focusing CO_2 laser beam with axicon 79−32792
He I slot cathode discharge, laser action 77−61943
He, nucl. pumping by fission fragments, plasma electron distrib. function 77−23653
He, positive column, with diffusion loss to wall, axial elec. field effects *(Japanese)* 78−47196
He-^{20}Ne-^{22}Ne, orthogonally polarised laser mode interactions *(Russian)* 77−19235
He-Ar, Ar I TEA lasers, energy characteristics 80−63977
He-Ar hollow cathode discharge, CW laser oscill. obs. 78−5454
He-CO_2, nuclear pumped laser, use of fast burst Caliban reactor *(French)* 79−89889
He-CO_2 atomic C nuclear pumped laser collision processes, output delay 80−38002
He-CO_2 pulsed atomic C laser, time and energy characts. in mag. field *(Russian)* 78−22108
He-CO_2-Xe electrical discharge laser pumped by crossed electric and mag. fields 78−42320
He-Cd vapour laser, continuous wave, intensity fluctuations investig. 80−83593
He-Cd(Zn) hollow cathode laser, upper level decay rate, mag. field tuning dip meas. 78−87043
He-F, doublet series laser lines near 700 μm, hyperfine splitting and broadening meas. 78−63070
He-F gas mixture, electron drift velocities, laser modelling 78−63061
He-F laser, press. depend. of atomic F laser transition intensities 77−659
He-F_2, dissociative electron attachment, rate coeffs., appl. to lasers 78−46575
He-Hg direct nuclear pumped laser, optimum conditions for lasing 77−50655
He-Hg nuclear pumped laser, charge exchange pumping 80−63996
He-Hg plasma, prod. by nucl. radiation, charge exchange effects 77−24103
He-Kr, Kr I TEA lasers, energy characteristics 80−63977
He-metal vapour hollow cathode lasers, negative glow electron energy distrib. appl. 77−19790
He-N_2, pulsed atomic N laser, time and energy characts. in mag. field *(Russian)* 78−22108
He-N_2 laser, energy pathways by proton excitation 78−5459
He-N_2-CO_2 mixture, IR laser output from elec. discharge after X-ray preionisation 79−64205
He-NF_3 laser, F* relax., generating 250 kW at 0.6-0.75 micron, for 2-3ns *(Russian)* 78−1219
He-Ne, $^{127}I_2$ frequency stabilisation, 612 nm and 640 nm 78−66871
He-Ne, $^{127}I_2$ stabilised, absolute wavelength measurements 78−73971
He-Ne, $^{127}I_2$ stabilised, freq. shifts, limitations 78−90440
He-Ne, 0.63 μm emission intensity fluctuations, spectral correl. 78−1212
He-Ne, 0.633μm line freq. stabilisation with 3.39μm line locked to CH_4 80−28258
He-Ne, 1.15 μm laser line, 260 THz freq. synthesis using $CdGeAs_2$, Ag_3AsS_3 crysts. 79−64263
He-Ne, 2 mW and 5 mW, reliability 80−95913
He-Ne, 3.39 μm, polarisation capture *(Russian)* 78−5456
He-Ne, 3.39 μm laser, actively mode-locked oscill., modulation freq. depend. 77−61983
He-Ne, 3.39 μm laser with internal absorpt. cell, inverted Lamb dip contrast 77−14765
He-Ne, 3.39 μm laser with no freq. modulation, freq. stabilisation rel. to methane saturated absorpt. 79−76700
He-Ne, $3s_2$-$2p_4$ and $3s_2$-$3p_4$ coupled transition sensitivity to discharge current fluctuations 77−75484
He-Ne, 6328 Å, single-mode collapse 78−94404
He-Ne, 632.8 nm, energy characteristics, spatial inhomogeneity effect 77−75483
He-Ne, Al cold cathode performance improvement, vapour deposited, by Cu addition 80−5748
He-Ne, anisotropic ring laser cavity, polarisation characts. 79−59726
He-Ne, anisotropy due to saturating fields 78−55337
He-Ne, application to optics experiments 77−27246
He-Ne, average output power, resonator losses, freq. modulation 77−34901
He-Ne, beam compensation using phase plate 77−42556
He-Ne, beat freq. generation between CW dye laser with 80-GHz freq. offset 80−1253
He-Ne, cell for laser stabilised by saturation absorption in $^{127}I_2$ 78−17971
He-Ne, circuit for prod. and recording pulse flashes 15 to 400 μsec *(Russian)* 80−1235
He-Ne, complex resonator laser, stabilisation by freq. offset-lock 77−31107
He-Ne, diffr. patterns prod. by red blood cells, diameter meas. 77−86582
He-Ne, discharge current rel. to optical power, automatic control of radiation level *(Russian)* 77−46716
He-Ne, discharge reson. props. effect on radiation fluctuations, expt. 78−74883
He-Ne, discharge tube design and construction *(Czech)* 79−76702
He-Ne, factors affecting service life *(German)* 78−90424
He-Ne, field autocorrelation function, in threshold region, fine struct. 79−3683
He-Ne, fine structure of radiation, Fabry-Perot scanning interferometer meas. 77−54749
He-Ne, fluctuation spectra of freq. and amplitude 78−82950
He-Ne, for original equipment manufacturer, aligning, recording and meas. appls. 77−75597
He-Ne, freq. characts. under two-mode generation 80−53264
He-Ne, freq. selection, using Faraday effect in active medium 78−1257
He-Ne, freq. stabilised, use as freq. and length standards *(French)* 79−31935
He-Ne, freq. stabilised by ref. to I and methane absorption transitions 77−83913
He-Ne, freq. stability improvement with hot wall I cell 77−83914

gas lasers continued
He-Ne, frequency spectrum control, phase polarisation method 77−75583
He-Ne, gain probing by intracavity dye laser spectroscopy 77−7092
He-Ne, gain saturation, polarisation and spectral inhomogeneities, relax. consts. 77−50652
He-Ne, generation by hollow cathode discharge excitation, mechanism *(Russian)* 77−10888
He-Ne, HF discharge, electron energy distrib. 77−34874
He-Ne, high stability, single freq., 3.39 μm 78−71121
He-Ne, hot wall I cell freq. stabilisation using saturated absorpt. peak 77−65598
He-Ne, I_2, hyperfine component classification, suitability for laser wavelength stabilisation 78−86965
He-Ne, I_2 stabilised, design construction and performance 79−13978
He-Ne, I_2 stabilised, freq. shifts 77−50697
He-Ne, I_2 stabilised, freq. stability and reproducibility 78−13726
He-Ne, I_2 stabilised, reproducibility limitations 77−46740
He-Ne, I_2 stabilised, saturated absorption signal props. 77−75481
He-Ne, I_2 stabilised, wavelength intercomparison 77−19305
He-Ne, I_2 stabilised, with improved performance 79−22964
He-Ne, I_2 stabilised laser, wavelengths comparison by two-beam interferometer 78−86326
He-Ne, I_2 stabilised lasers, conf., Germany (Feb. 1977) 78−87069
He-Ne, I_2 stabilised laser design, freq. reproducibility 78−87070
He-Ne, I_2 stabilised laser research 78−87071
He-Ne, I_2 stabilised laser with hot wall I_2 cell 78−87073
He-Ne, I_2 stabilised lasers, length metrology *(French)* 78−87074
He-Ne, I_2 stabilised laser, spectral profile modulation broadening 78−87083
He-Ne, I_2 stabilised laser, instrumental freq. offsets 78−87084
He-Ne, I_2 stabilised lasers, international intercomparison meas., hyperfine struct. spacings 78−87088
He-Ne, I_2 stabilised lasers, beat frequency, international comparisons *(French)* 78−87090
He-Ne, intensity fluctuations produced by multimode lasers in combination with dielectric beam splitters 78−22160
He-Ne, intensity fluctuations meas., comparison with He-Cd laser 78−71087
He-Ne, intensity oscillation spectrum obs. for external modulating signal on discharge plasma 77−7066
He-Ne, internal mirror, polarisation props. of output beam 77−46744
He-Ne, internal modulation by acoustic surface waves 78−25901
He-Ne, intracavity laser modulation by elec. controllable diffr. grating 77−58357
He-Ne, iodine- and methane-stabilised, reproducibility comparison 77−7135
He-Ne, kinetics calcs. using electron distrib. function *(Russian)* 77−61941
He-Ne, LG-56, radiation power stabilisation 78−17970
He-Ne, LG-75-1 laser 79−94256
He-Ne, laser beam diffraction focusing by sequence of irises 79−50332
He-Ne, laser frequency measurements: a review, limitations, extension to 197 THz (1.5 μm) 78−81952
He-Ne, laser power as function of level of optical signal synchronisation 80−69359
He-Ne, laser pumping transition, mol. beam obs. 77−7064
He-Ne, laser revived by running in He atm. 78−46614
He-Ne, laser single frequency generation model and expt. *(Russian)* 77−58314
He-Ne, laser system for 3.39 μm freq. synthesis 78−18001
He-Ne, laser transfer printing, microfilm 78−65994
He-Ne, lasing spectrum, modulation freq. of resonator losses 77−34902
He-Ne, longit. mode locking using Fabry-Perot etalon 79−50318
He-Ne, low noise manufacturing 78−79038
He-Ne, low power, for particle size spectrometry 77−78485
He-Ne, low-power, using cold-cathode plasma tube, educational demonstrations and experiments appl. 78−45448
He-Ne, low-power low-cost design and manufacture 77−19329
He-Ne, mag. polarised, performance 77−14750
He-Ne, manufacturing problems with low noise specification 78−59047
He-Ne, methane and I_2 stabilised lasers, wavelength intercomparison using Michelson interferometer 78−87089
He-Ne, methane stabilised, intercomparisons 77−19304
He-Ne, methane stabilised, freq. fluctuation analysis 77−31108
He-Ne, methane stabilised, 3.39 μm freq. meas. relative to 10.17 μm CO_2 laser 77−31113
He-Ne, methane-stabilized, low noise laser tube characts. *(Japanese)* 78−25891
He-Ne, microwave pumping advantages 78−50754
He-Ne, mobile resonances, appl. to freq. stabilisation and tunability 77−7138
He-Ne, mode coupling, nonlinear effects *(German)* 77−19233
He-Ne, mode locking, phase interferometer control 77−72009
He-Ne, mode selection and mode locking, effect on two-photon absorption efficiency 78−83023
He-Ne, mode stabilisation by axial mag. field, long resonator case 77−7143
He-Ne, narrow linewidth frequency scannable 3.39 μm laser, appls. 77−88757
He-Ne, Ne $3s_2$-$2p_4$ transition, relaxation characts. of degenerate states obs. using polarisation spectroscopy *(Russian)* 80−27348
He-Ne, Ne absorber induced features in AC response 77−3613
He-Ne, near IR emission characts., coupled transitions 77−27275
He-Ne, operating on 0.63, 3.39 μm coupled transitions, intensity modulation 80−69365
He-Ne, optimal conditions for microwave pumping 80−32961
He-Ne, Original Equipment Manufacturer applics. 78−33765
He-Ne, oscills. in laser discharge 78−55339
He-Ne, population inversion radial distrib. in active element, excitation conditions effect 78−71079
He-Ne, power characteristics obs., with CH_4 cell, at $\lambda=3.39$ μ *(Russian)* 78−1207
He-Ne, pulsed atomic Ne laser, time and energy characts. in mag. field *(Russian)* 78−22108
He-Ne, radial profiles of upper and lower level emission 77−31088
He-Ne, radiation field spatial distrib. distortions due to multilayer dielectric mirrors 77−38970
He-Ne, reliability calcs. rel. to system's operating life 77−10932
He-Ne, ring laser, difference freq. depend. on active medium gain 77−722

gas lasers continued
He-Ne, ring laser, rapidly pumped, competition between opposite waves 78—17985
He-Ne, ring laser, Zeeman effect, influence of reson. radiation trapping 77—75574
He-Ne, rotating ring laser, output characts. 78—29982
He-Ne, scheme for automatic fine frequency tuning along the Lamb depression 80—74385
He-Ne, sealed, nondestructive analysis using spectral emission methods 80—1210
He-Ne, self-locked, pulse velocity, power and mode phase 77—61939
He-Ne, short pulses, self mode-locking *(Rumanian)* 79—13995
He-Ne, simultaneous oscillation at 0.63 and 3.39 μm, output power depend. on loss in mag. fields *(Japanese)* 80—32959
He-Ne, single mode laser, mode polarisation in transverse mag. fields 78—22107
He-Ne, single mode laser, emission zone nonlinear active lens effect 80—32960
He-Ne, single transverse mode radiation, spatial coherence 77—14733
He-Ne, single-mode, autodyne effect *(Russian)* 79—925
He-Ne, six new transitions near 1.49 μm 77—38856
He-Ne, stabilised by I_2 saturated absorpt., technological principles *(French)* 78—87075
He-Ne, stabilised by saturated absorption in I_2, wavelength meas. 80—28264
He-Ne, stabilizer two freq. 0.63 μ laser 79—94243
He-Ne, stable laser with methane absorpt. cell, 7 Hz width 3.39 μm line emission 78—17974
He-Ne, standard wavelength sources 78—74957
He-Ne, standing wave, two-mode locking *(Russian)* 77—79874
He-Ne, stimulated emission, vel. to striation 80—37994
He-Ne, three mode stimulated emission 77—75485
He-Ne, three-mode, for small displacement meas. 80—77748
He-Ne, three-mode, total intensity under mode locked conditions, freq. stabilisation 77—83853
He-Ne, transition probabilities of Ne spectral lines at 352, 363, 345 and 543 nm 78—25851
He-Ne, two-mode ring laser, stimulated emission regimes 77—657
He-Ne, unstable telescopic resonator adjustment precision *(Russian)* 80—38040
He-Ne, waveguide resonator, oscill. modes 77—27311
He-Ne, wavelength, comparison of 2 beams, two-wave interference, book contrib. 78—9408
He-Ne, wavelength meas. appl., reference standard use of neon or iodine cell 77—7124
He-Ne, wavelength switching using var. methane pressure 77—19312
He-Ne, weakly anisotropic resonator laser, natural polarisation fluctuations of emission 77—79801
He-Ne, with $^{127}I_2$ weakly saturable absorber, high contrast power reson., freq. stabilisation 78—29976
He-Ne, with methane absorber, reson. obs. in output, freq. stabilisation 77—83854
He-Ne, with methane absorpt. cell, reson. freq. shift with methane press. 77—50687
He-Ne, with methane absorpt. cell, hyperfine struct. influence on freq. reproducibility 78—50864
He-Ne, with photodiode, for angular displacement recording 77—49712
He-Ne, with transverse microwave discharge, use of secondary electrons 80—9899
He-Ne, with ZnS diffraction mode selector 79—89951
He-Ne, zero beat AFC system, two laser injection locking system 77—88737
He-Ne $^{127}I_2$ stabilised laser, laser induced line narrowing for Ne $3s_2-2p_4$ line wavenumber determ. 79—76385
He-Ne $^{127}I_2$ stabilised laser source for Michelson interferometer, optical feedback obs. 80—106545
He-Ne 3.39 μm laser, FM eliminated CH_4 locked freq. stabilisation in dual feedback control 80—99772
He-Ne 3.39 μm laser mode-locking for ultrashort pulse generation 77—83909
He-Ne ($^{127}I_2$) laser freq. stability, expt. 77—83915
He-Ne CH_4 locked laser, freq. stability meas. 80—87422
He-Ne CW laser nuclear pumping demonstration 79—13949
He-Ne CW TEM_{00} laser, birefringent material stress determ. in single hologram exposure 80—106770
He-Ne coherent laser, resonators filled with inhomogeneous material, longitudinal modes 79—81463
He-Ne commercial multimode low power laser, conversion to single mode laser 80—53325
He-Ne compact LG-78 laser 79—7148
He-Ne complex resonator laser, stabilisation 78—55374
He-Ne discharge, 3071, 5665 and 10353 nm. laser transitions 77—54692
He-Ne double mode laser in axial mag. field. *(Russian)* 79—86160
He-Ne dual mode laser, injection modulation in coupled laser oscillators 80—99773
He-Ne gas laser, anisotropic resonator, linear polaris. freq. depend. 77—10961
He-Ne gas laser, behaviour in nonsynchronous frequency modulation regime *(Russian)* 79—7161
He-Ne gas laser, glow discharge electron irrad. rel. to output characts. 79—64198
He-Ne gas ring laser, unidirectional two-mode lasing, stability region width 79—76721
He-Ne glass-sealed laser tubes, Toshiba manufacture 77—14760
He-Ne I_2 stabilised laser, practical approach to design and construction 80—19051
He-Ne I_2-stabilised, with long path interferometer, optical feedback effect 77—9544
He-Ne IR laser, internal modulation of polarisation 77—19350
He-Ne internal mirror lasers, polarisation in mag. field 78—17907
He-Ne internal mirror laser, degeneration of longitudinal modes and freq. stabilisation *(Japanese)* 78—90426
He-Ne laser, $^{127}I_2$ saturated absorption stabilised, wavelength meas. *(Russian)* 79—22996
He-Ne laser, $^{127}I_2$ stabilised, length or freq. standard 80—106544
He-Ne laser, 3.39 μm, in-resonator losses, effects on power *(Russian)* 78—5455
He-Ne laser, 60 mW, perturbation spectroscopy *(Rumanian)* 78—50752
He-Ne laser, 6328 Å, output power, using intracavity rot. reflector 79—7113
He-Ne laser, 6328 Å power fluctuations due to striation noise 80—78834

gas lasers continued
He-Ne laser, autodyne effect 79—81404
He-Ne laser, beat freq., high displacement sensitivity meas. 80—95926
He-Ne laser, cavity losses, phase polarisation method in lasing regime 80—87413
He-Ne laser, compact, transverse microwave discharge, energy characts. 80—64064
He-Ne laser, competitive oscillation mode frequency stabilisation *(Russian)* 79—22962
He-Ne laser, Doppler-free intracavity polarization spectroscopy using elliptically polarized light 80—5537
He-Ne laser, double reson., RF mag. field strength and g-value depend. *(Japanese)* 78—9359
He-Ne laser, doubly resonant intracavity SHG of 1153 nm radiation with stabilization on HFS components of $^{127}I_2$ 80—33077
He-Ne laser, elec. parameters of active element 79—3682
He-Ne laser, field distrib. and spatial coherence of superluminescence at 3.39 μ transition *(Russian)* 78—13682
He-Ne laser, Fraunhofer diffraction and interference, He-Ne laser 77—60878
He-Ne laser, freq. conversion in Na vapour *(Russian)* 78—33776
He-Ne laser, I_2 stabilised, realisation of length unit 78—87068
He-Ne laser, I_2 stabilised, saturated absorpt. lines press. and power broadening 79—76765
He-Ne laser, IR lasing lines, anomalous competition effects *(Russian)* 77—68202
He-Ne laser, in axial mag. field, output power dependence of mode locking phenomena 78—71129
He-Ne laser, internal pulse-code modulation, 0.6328 μm at 150 Mbits s^{-1} 79—76725
He-Ne laser, intracavity saturable Ne absorber, response enhancement 77—65602
He-Ne laser, methane-stabilized at 88 THz 80—73304
He-Ne laser, methane-stabilized, meas. of freq. at 88 THz accurate to ±3 parts in 10″ 80—99700
He-Ne laser, mode interaction, transition level degeneration effects *(Russian)* 77—61940
He-Ne laser, Ne $3s_2$-$2p_4$ transition relax. consts. using cross saturation of travelling waves 79—76374
He-Ne laser, optical freq. standard, freq. stabilised by warm walled I_2 cell *(French)* 78—42343
He-Ne laser, optical heterodyning of spontaneous emission 78—29995
He-Ne laser, output power, unsaturated gain distrib. 78—50751
He-Ne laser, population changes of Ne levels, laser action in intermediate IR 78—29933
He-Ne laser, refl. anisotropy of 6320 Å mirrors 79—98413
He-Ne laser, rejuvenation methods 77—37687
He-Ne laser, spatial anisotropy induced by cascade laser transitions 78—29931
He-Ne laser, stabilised by $^{127}I_2$ saturated absorpt., wavelength international comparisons 80—95872
He-Ne laser, stabilized, meas. of freq. 80—99699
He-Ne laser, thermal effect of penetrating radiation *(Russian)* 78—22109
He-Ne laser, two-mode ring laser power resons. 78—1211
He-Ne laser, two-photon amplification on cascade-transitions, power tuning curve meas. 80—48219
He-Ne laser, two-photon correls. in amplified light 79—76670
He-Ne laser, type 300.1 TEM_{00} *(Rumanian)* 80—9898
He-Ne laser, unmodulated, stabilizing to $^{127}I_2$ hyperfine component, preliminary expt. 79—50328
He-Ne laser, use at 0.63 μm, intensity fluctuations at quantum level 77—27274
He-Ne laser, used in Sagnac fibre-ring interferometer gyro with electronic phase sensing 79—17472
He-Ne laser 10kV/1.5kV power supply 79—36906
He-Ne laser beacon, visibility range extension in fog using coaxial CO_2 laser beam 80—101434
He-Ne laser beam, intensity fluctuations, spatial distrib. 79—18458
He-Ne laser discharge tubes, design and technology, review *(Czech)* 79—72586
He-Ne laser energy characteristic control, by discharge current modulation 77—79800
He-Ne laser freq. determ., interferometric comparison with upconverted CO_2 laser radiation 78—55395
He-Ne laser frequency stabilisation using mag. field tuning dip 79—55153
He-Ne laser IR applications 79—94275
He-Ne laser interferometer, microtremor meas. *(Japanese)* 80—9025
He-Ne laser light polarisation in transverse mag. field, Zeeman effect *(Dutch)* 78—29997
He-Ne laser line, diffraction losses for symmetrically tilted plane reflectors in open resonators 80—58598
He-Ne laser modal configuration, interference spectrometer study *(Spanish)* 80—86458
He-Ne laser mode locking by three-level reson., Zeeman tuning of intracavity Ne absorber 79—89943
He-Ne laser model LG-10, design *(Rumanian)* 80—87407
He-Ne laser near threshold, intrinsic third-order intensity correlation 77—10887
He-Ne laser photon statistics variation with cavity length 80—53265
He-Ne laser plasma, line profiles meas. by optogalvanic spectroscopy 78—62233
He-Ne laser plasma, metastable at. and electron density diagnostics 77—84499
He-Ne laser pulsed internal modulation 77—61985
He-Ne laser radiation, spatial and temporal correlation of intensity fluctuations 79—81473
He-Ne laser radiation freq. conversion 1.15 μm to 377.6 nm in Tl vapour 80—95948
He-Ne laser radiation intensity rel. to striations and oscillations 77—83852
He-Ne laser rangefinder and profilometer, high-resolution 80—102754
He-Ne laser retinoscope 80—41159
He-Ne laser saturation resonance in static magnetic field 77—54693
He-Ne laser stabilisation, I_2 absorption cell power densities 80—99767
He-Ne laser stabilisation and performance for dimensional meas. 80—19049
He-Ne laser stabilisation by I_2 612 nm saturated absorption 80—99765
He-Ne laser stabilisation by I_2 611.8 nm saturated absorption 80—99766
He-Ne laser stabilised by saturated absorpt. in I_2 at 612 nm 79—59730

gas lasers continued
He-Ne laser stabilised by methane E-component saturated absorpt., quantum freq. standard 80—9901
He-Ne laser stabilised by methane E-component, reference source freq. reproducibility 80—106507
He-Ne laser stability and I cell gaseous impurity detection *(French)* 77—73496
He-Ne laser status, I_2 vapour stabilised 78—87072
He-Ne laser tube, laser module LGK 7621, construction 80—53314
He-Ne laser tube construction and cost analysis 77—65599
He-Ne laser tube LGR 7621 using coaxial glass technology 77—3567
He-Ne laser tube reconditioning 77—78933
He-Ne laser tubes, salvaging technique 79—94247
He-Ne laser two-beam interferometer phase errors *(Russian)* 79—6166
He-Ne laser unconventional recording materials 80—18040
He-Ne laser wavelength drift 80—67978
He-Ne laser wavelength stabilisation on I_2 *(Czech)* 78—87061
He-Ne laser wavelength stability, calibration and traceability 80—19050
He-Ne laser with anisotropic cavity, fluctuations of field polaris. 79—27242
He-Ne laser with external optical resonator, SHG 79—27326
He-Ne laser with I_2 absorpt. cell, nonlinear resonances at 0.63 μm *(Russian)* 79—59672
He-Ne laser with internal mirrors, mode polarisation props. 80—23672
He-Ne laser with methane nonlinearly absorbing cell, freq. self-stabilisation effect 79—98420
He-Ne lasers, I_2 stabilised, 633 nm line, performance improvement 78—90429
He-Ne lasers, I_2 stabilised development, laser freq. locking 79—68380
He-Ne lasers, in hollow Cu cathode, 632.8 nm output characts. 80—63975
He-Ne lasers, life time depend. on impurity gases *(Chinese)* 79—36881
He-Ne lasers, population changes of Ne levels, laser action in intermediate IR 78—29932
He-Ne lasers, stabilised by saturation absorpt. in I_2 78—1270
He-Ne lasers, transverse microwave freq. gas-discharge pumping 80—74339
He-Ne lasers levels, modulation spectroscopy 78—46572
He-Ne lasers with Brewster windows in static magnetic field, detuning, polarisation properties 77—83850
He-Ne lasing medium, evaluation of population changes of Ne levels 78—25855
He-Ne low cost integrated construction 77—79843
He-Ne low noise tube, completely glass sealed, noise characts. 77—38920
He-Ne low-gain laser amplifier, phase control 80—64059
He-Ne methane stabilised laser, confirmation of speed of light value 299,792,458 m/s 80—37002
He-Ne methane system, narrow nonlinear resonances in three level system *(Russian)* 80—78898
He-Ne mixture, electron beam prod. plasma decay, appl. to laser pumping 79—41847
He-Ne mode locked laser for very wide band communication system 78—17994
He-Ne modes self-selection based on Zeeman effect *(Russian)* 80—1251
He-Ne monochromatic directed radiation source, long-life 80—33021
He-Ne multimode and single-mode lasers, phase locking to very high coherence degree 79—76710
He-Ne nuclear-pumped CW lasing 80—48216
He-Ne optical waveguide amplifier, operation 80—43363
He-Ne parallel plate development 80—1224
He-Ne ring laser, 0.6328 μm, self-pulsing conditions 80—87414
He-Ne ring laser, absorbing medium press. influence on power resonance characts. *(Russian)* 80—23725
He-Ne ring laser, freq. shift of 3.39 μm methane transition 79—27298
He-Ne ring laser, influence of pressure on Zeeman effect 80—19056
He-Ne ring laser, methane absorber narrow nonlinear resonances at low press. *(Russian)* 79—76722
He-Ne ring laser, methane stabilised, nonlinear resonance freq. shift due to back scatt. *(Russian)* 80—78874
He-Ne ring laser, Ne isotopic composition changes during prolonged discharge *(Russian)* 78—22110
He-Ne ring laser, nonlinear polarisation interaction of opposite waves 78—50828
He-Ne ring laser, nonlinear Zeeman effect 78—71123
He-Ne ring laser, nonlinear spectroscopic technique 80—91819
He-Ne ring laser, nonreciprocal effects on appl. of transverse mag. field to active medium 80—53341
He-Ne ring laser, nonreciprocal effects with transverse mag. field applied to active medium 80—91820
He-Ne ring laser, operating well above lasing threshold Zeeman effect 80—33039
He-Ne ring laser, opposing waves competition at lasing line centre of Ne isotope 80—1187
He-Ne ring laser, opposite waves competition dynamics 77—72008
He-Ne ring laser, unidirectional, modes 80—91818
He-Ne ring laser beat frequency deviation rel. to dispersion and modulation 79—68410
He-Ne ring laser placed in longit. mag. field, nonlinear nonreciprocity effects 80—43377
He-Ne ring laser with methane absorpt. cell, power reson. characts. 80—28255
He-Ne ring laser with nonlinear absorber, competition of orthogonally polarised modes 78—17984
He-Ne ring Zeeman laser, interaction of modes characterized by orthogonal circular polarizations 80—48306
He-Ne rotating ring laser, freq. characts., mode composition effects 77—54741
He-Ne single mode lasers, meas. of intensity of sources of inherent fluctuations 80—32958
He-Ne stabilised by I_2 saturated absorpt., performance characts. *(Chinese)* 79—59717
He-Ne stabilised transverse Zeeman laser, light source for optical meas. 80—48272
He-Ne stable gas laser with 0.4 Hz line width 80—48294
He-Ne travelling wave laser, spontaneous emission spectra, 3.39 μm region 80—37995
He-Ne two mode ring laser for interferometry 78—1260
He-Ne two-mode gas laser, strong, coupling, transient 79—55114
He-Ne two-mode laser with methane absorbing cell, freq. stability and reproducibility 79—89934
He-Ne two-mode travelling-wave laser, Zeeman beats 78—50827

gas lasers continued
He-Ne waveguide laser, discharge plasma theory, max. output intensity depend. on discharge tube radius 79—55110
He-Ne waveguide lasers, HF discharge stability 79—18401
He-Ne waveguide lasers, props. and current-voltage characts. of discharges 78—1208
He-Ne wavelength measurement using digital interferometer 80—37079
He-Ne with Brewster windows, simultaneous oscillation at 0.63 μ and 3.39 μ in mag. field 79—68381
He-Ne Zeeman laser, two-transitions with common upper level *(Japanese)* 79—55112
He-Ne/CH_4 FM eliminated laser, freq. stability meas. 80—87423
He-Ne/CH_4 laser, IR freq. absolute meas. *(Russian)* 80—9851
He-Ne-laser tube, using coaxial glass technique, LGR 7627 78—90410
He-Ne-methane ring laser, frequency stabilized, operating charact. 80—14366
He-Ne-methane ring laser, power resonances 80—99761
He-Ne-methane ring laser, freq. synchronisation interval for oppositely directed waves 80—99762
He-Ne-methane stabilised ring laser, freq. stability calcs. *(Russian)* 78—9401
He-Se, cataphoretic effects in power output 77—83863
He-Se, noise props. 77—83857
He-Se, vapour laser, continuous wave, intensity fluctuations investig. 80—83593
He-Xe, H_2CO-stabilised laser, freq. stability in axial mag. field 79—22991
He-Xe, high-press. neutral IR laser emission from Xe 79—86159
He-Xe, low-threshold nuclear pumped laser, generation characts. 80—19018
He-Xe, unstable resonators for annular gain vol. lasers 78—46672
He-Xe, Xe I TEA lasers, energy characteristics 80—63977
He-Xe 3.51 μ laser mode competition in axial mag. field 80—63974
He-Xe laser, 3.51 μm, mode competition in axial mag. field 78—25850
He-Xe laser, freq.-offset-locked at 3.51 μm 79—98400
He-Xe laser, nuclear pumping by vol. source of fission fragments 79—36879
He-Xe laser, Zeeman tuned *(Korean)* 79—7145
He-Xe optical amplifier, high gain coeff., noise characts. 80—43365
He-Xe optical amplifier, striation form. for DC discharge plasma, noise anal. 80—43366
He-Xe recombination lasers, CO%d2 laser-produced plasma-initiated 80—48286
He-Ze laser, freq. stability at 3.51 μm 79—98401
He-Zn and He-$ZnCl_2$ hollow cathode laser discharges, comparison 80—28203
He-Zn hollow cathode laser discharge, radiative cascade excitation effect on upper laser levels 80—102697
^{3}He direct nucl. pumped laser, power density 78—58980
^{3}He laser, direct nuclear pumped, power density 78—9362
^{3}He-^{20,22}Ne/$^{127}I_2$, 0.63 micron laser generated contrasting power resons. *(Russian)* 77—23651
^{3}He-^{22}Ne 0.63 μm laser stabilised with $^{129}I_2$ nonlinear absorpt. cell, freq. characts. 80—53333
^{3}He-^{22}Ne laser, interaction of orthogonally polarised modes with various transverse distribs. *(Russian)* 77—27276
^{3}He-^{22}Ne laser with I_2 absorption cell 77—79867
^{3}He-Ar (Xe)(Kr)(Cl), volume pumped nuclear laser, survey of lasing 80—63979
^{3}He-Ar volumetric nucl. pumped laser, dominating processes and reaction physics 80—63981
^{3}He-Ar(Xe)(Kr)(Cl), nucl. lasing, population inversion mechanism 80—63980
^{3}He-Ar(Xe)(Kr)(Cl) direct nuclear pumped lasers using ^{3}He(n,p)^{3}H reaction 79—31863
^{3}He-Kr, nucl. pumping by volumetric ^{3}He(n,p)^{3}H reaction 77—10886
^{3}He-Ne stabilised by saturated absorption ^{127}I, laser wavelength standard development appl. *(German)* 78—79034
^{3}He-Xe, direct nucl. pumping via ^{3}He(n,p)^{3}H 77—71972
^{3}He-Xe, nucl. pumping by volumetric ^{3}He(n,p)^{3}H reaction 77—10886
^{3}He-Xe laser, direct nuclear pumping by protons and tritons 78—5458
^{3}He-Xe nuclear pumped laser, small signal gain coeff. and power output, theory comparison with expt. 80—63983
^{3}He-Xe nuclear pumped laser, electron distrib. function role 80—63984
^{3}He(n,p)^{3}H direct nuclear pumped laser 77—83851
Hg, cataphoretic laser, transverse separation dynamics 77—38865
Hg, lifetimes and cross sections of depolaris. collisions of laser working levels 79—76387
Hg, optically pumped, saturable absorber overlap of ^{127}I 77—83932
Hg vapour laser, optically pumped, gain and output power 78—66843
Hg-N_2, optical pumping, vibr. excitation, laser theory 78—66517
Hg-N_2, optically pumped pulsed 546.1 nm laser emission 79—13952
I, dye laser pumped to dissoc. point of I_2, laser action 78—63064
I I,II, radiative lifetime meas., rel. to I and He-I$^+$ laser transitions 79—54810
I metastable atoms prod. from He-I_2, quenching rate const. by I_2 mols. 78—13691
I, recomb. laser, possible use of alkali metals to obtain population inversion 79—94221
I_2, flashlamp excited photodissociation laser 79—72558
IBr-CO_2 IR laser with Br*→CO_2 electronic-vibr. energy transfer as pump mechanism 80—53260
K, atomic Rydberg state 16 μm output 77—54696
K atomic Rydberg state tunable subMM laser 80—69378
Kr, CW UV emission, power enhancement 78—17906
Kr, energy pathways by proton excitation 78—5459
Kr laser, new IR laser transitions, 3.725 to 17.233 μm 80—87374
Kr, laser, tunable, Lyman alpha radiation, nonlinear generation 78—87038
Kr, laser oscill. obs. in transversely initiated laser-produced plasma 77—88696
Kr, recomb. laser in expanding CO_2 laser prod. plasma, 3.07 μm laser oscill. 77—88698
Kr, single pulse extraction from mode locked train using dye amplifier 77—19314
Kr, wavelength measurement using digital interferometer 80—37079
KrF laser, excitation by double-sided electron beam generator, fusion appl. 80—68956
KrF, laser spectra, absorpt. lines 80—9604
Li I laser, 207 Å, oscillator strengths 80—83598
Li laser, 207 Å, proposal for construction 80—43324

gas lasers continued
- Mn atom lasers, finely dispersed metal particle active medium 80—91777
- Mn, cataphoretic at. distrib. in $MnCl_2$-He discharge 77—31092
- Mn, optically pumped lasers utilizing self-terminating transitions, CW stimulated emission possibility 80—14329
- Mn, self-terminating vapour laser, max. pulse repetition freq. 80—23677
- Mn vapour, high pulse rate, self heating with He buffer gas 77—23664
- Mn vapour, use in laser projection microscope with image-brightness amplifier 80—106541
- Mn-He, stimulated emission mechanism, energy characts. 77—3571
- $MnCl_2$ vapour laser, output spectrum as function of excitation conditions 79—68387
- $MnCl_2$-inert gas laser, energy characts. *(Russian)* 77—665
- N afterglow laser, recombination-pumped 77—50657
- N I, laser transition obs. at 9064 Å in He-N_2 afterglow 78—74891
- N_2, Blumlein-driven, low-inductance spark gap switch 80—33010
- N_2, double-channel laser 80—19046
- N_2, high average power and longitudinal discharge 79—94244
- N_2, IR laser transition, excitation mechanism *(Japanese)* 80—83594
- N_2 laser, power investig. using Crookes radiometer 79—62978
- N_2 laser near-threshold IR enhancement by He additive *(Japanese)* 80—14324
- N_2 laser pump for pulsed dye laser, optical resonator 79—94260
- N_2 laser UV-IR pulse time lag theory *(Japanese)* 80—14325
- N_2, TEA, used in Mach-Zehnder four-framing laser interferometer system 80—4761
- N_2-Ar, laser high power, energy and power output *(Russian)* 77—7065
- N_2-CO_2 mixture, electron drift vels., time-of-flight meas. 80—28855
- NH_3, 1 mJ output energy at 16 μm, optical excitation of mol. levels 77—88707
- NH_3, 12.08 μm emission, CO_2 laser pumped, temp. depend. 78—46582
- NH_3 12.8 μm laser, 60% efficient SHG in Te cryst. 80—83640
- NH_3 81.5 μm subMM laser, freq. meas. by CO_2 laser difference freq. comparison 80—74415
- NH_3, CW efficient optically pumped far IR waveguide laser 77—72001
- NH_3 CW far IR laser lines, CO_2 laser pumping and Stark tuning 80—69382
- NH_3 CW far IR laser lines, CO_2 laser pumping and Stark tuning 80—106508
- NH_3, compact, high-efficiency, optically pumped 78—5492
- NH_3, efficient energy extraction by superradiant emission 80—53271
- NH_3, excited state population decay time meas., press. depend. 77—75489
- NH_3, far IR CW Raman lasing 80—83595
- NH_3, far IR cascade emission 77—38867
- NH_3, far IR emissions by IR pumping using N_2O laser 80—74345
- NH_3, far IR emissions from forbidden transitions, using Stark effect with CO_2 laser pumping 79—86168
- NH_3, for 16 μm range, review *(Rumanian)* 80—87408
- NH_3, high power, 12.08 μm, optically pumped, for appl. to UF_6 isotope separation 78—74923
- NH_3 high power laser, improved optical pumping geometry in Littrow cavity config. 79—22973
- NH_3 high power laser characts. 77—79806
- NH_3, high power pulse laser pumped optically by CO_2 laser radiation 78—46631
- NH_3, hot band lasing transitions 80—1191
- NH_3, IR and far IR laser emissions, using TE CO_2 laser pump 79—934
- NH_3 inverse level doubling mol., space and combined parity nonconservation *(Russian)* 80—52879
- NH_3 laser, high energy output in 13 μm region, CO_2 laser pump 79—89927
- NH_3 laser, high-power efficient optically pumped, tunable over 770 to 890 cm^{-1} range 80—91780
- NH_3 laser, optically pumped, multiwatt, laser operation in 12-13 μm range 79—7141
- NH_3 laser, optically pumped 12 μm, for UF_6 isotope separation, parametric study *(Japanese)* 79—81414
- NH_3 laser, optically pumped, freq. tuning 80—28208
- NH_3 laser, optically pumped, wide range line-tunable oscill. 80—53267
- NH_3, laser action 11-13 μm, optical pumping by continuously tunable CO_2 laser 80—83596
- NH_3, laser submillimetre with optical pumping energy yield, emission pulse delay time depend. on pumping pulse *(Russian)* 78—71088
- NH_3 laser transitions, CW, two-photon pumped 80—99702
- NH_3 laser with focusing-prism raster and light-guide pump system 80—9905
- NH_3, multiline IR emissions, appl. for InSb Raman laser pumping 79—94216
- NH_3, near-MM-wave laser synchronous pumping, ultrashort pulse generation at 151 μm 80—102705
- NH_3, off-reson. IR laser action without population inversion, Raman type transition 77—10891
- NH_3, optically pumped, multi-line, 9.3-13.8 μm 77—14751
- NH_3, optically pumped by CO_2 laser, high power emission at 12.812 μm 77—38864
- NH_3, optically pumped laser, 11-17 μm 78—46581
- NH_3, pumped by two CO_2 lasers *(Russian)* 79—68386
- NH_3, resonantly pumped, for spectroscopy 80—48277
- NH_3, stimulated hyper-Raman scatt. via 3-photon process to obtain IR and far IR radiation 80—58633
- NH_3, sub mm output, optical pumping, Michelson interferometric output coupling 77—14744
- NH_3, two photon excited 16 μm laser 78—58986
- NH_3, two photon generated lasing, effect of pressure 77—88703
- NH_3, two-photon-excited, 16μm emission, wavelength meas. technique 78—71085
- $^{14}NH_3$, CW far IR lasing using Stark tuning 79—81407
- $^{14}NH_3$, Doppler free spectroscopy, 16 micron generation applications 79—94049
- $^{14}NH_3$, far IR CW laser emission by optical pumping 79—3687
- $^{15}NH_3$ far IR laser emission at 153, 375 μm, optically pumped by $^{13}C^{16}O_2$ laser 80—58507
- $^{15}NH_3$, optical pumping by HF laser, press. and temp. depends. 78—29939
- $^{15}NH_3$, optically pumped by CW sequence band CO_2 laser, far IR laser emission 78—46578
- NO, electronic-vibr. energy transfer from $Br(4^2P_{1/2})$, 5.5 μm transition 77—31094
- N_2O, electronic-vibr. energy transfer from $Br(4^2P_{1/2})$, 10.9 μm transition 77—31094

gas lasers continued
- N_2O, high-power tunable laser for 9 to 12.5 μm range 77—83884
- N_2O IR laser, transients obs. by modulation of intracavity absorber 78—74933
- N_2O isotopes, laser transitions near 4.6 μm, HF laser optical pump 78—58995
- N_2O laser as IR pump for obtaining far IR emissions in NH_3 80—74345
- N_2O, mass spectra of positive ions in discharge plasma 77—89315
- N_2O, new lines in 10 μm region, rot.-vibr. transitions in $(00^02\text{-}10^01)$ band 77—27281
- N_2O, simple high-power TEA laser operating in IR 79—94251
- N_2O stable grating controlled laser design 80—64063
- N_2O waveguide laser design 80—33025
- $^{15}N_2O$, $^{14}N^{15}NO$, $^{15}N^{14}NO$, optically pumped by pulsed HF laser, emission obs. at 4.6 μm 79—50283
- N_2O-CO_2, optically pumped transfer lasers, continuously tunable 78—13678
- NOCl, for 16 μm range, review *(Rumanian)* 80—87408
- NOCl, molecular laser operating in 16 μm region 77—50656
- NOCl, optically pumped laser, 11-17 μm 78—46581
- $^{14}NH_3$, laser emission at 16 μm by two-quantum excitation of $2\nu^-{}_2(7,5)$ state 79—86165
- $^{14}NH_3$, laser generation on two-photon excitation, 6 to 35 μm 77—10890
- $^{14}NH_3$, two-photon pumping for 12.16 μm radiation for isotope separation 78—90414
- $^{15}NH_3$, far IR laser lines, optically pumped by CO_2 laser 78—90415
- $^{15}NH_3$ far IR CW laser, optically pumped with $^{13}C^{16}O_2$ laser 80—78866
- Na, in shock heated salt vapour, anomalous emission from atomic lines 78—63089
- NaI, inversion and superfluoresc. emission of Na reson. line by selective photodissoc. 78—87040
- Nd complex, Nd(2,2,6,6-tetramethyl-3,5-heptanedione), vapours, excited-state kinetics and fusion laser media prospects 79—64243
- $NdCl_3$-$AlCl_3$ vapour complex, optical gain at 1.06 μm 78—33742
- Ne 6328 Å laser transition, homogeneous saturation due to collisions, weak collision model 78—78995
- Ne, atomic deexcitation effects of X-rays, X-ray preionisation in TEA lasers 79—793
- Ne, Lamb-dip structure anal., linear and helicoidal polaris. 78—25852
- Ne, population inversion mechanism between 4p→3d, laser generation conditions 80—1185
- Ne, population of $5s'[1/2]_1{}^0$, $4p'[3/2]_2$ levels interacting with laser radiation 80—23670
- Ne, positive column, with diffusion loss to wall, axial elec. field effects *(Japanese)* 78—47196
- Ne ring laser, two-mode, oppositely travelling waves, beat freq. obs. 77—10963
- Ne-He lasers, gynaecological cancer care appl. *(German)* 78—24176
- Ne-N_2, atomic N nuclear pumped lasers, surface effects 80—63996
- Ne-N_2, energy transfer, H^+ ion beam produced plasma, ion density and temp. 80—38539
- Ne-N_2 laser, energy pathways by proton excitation 78—5459
- ^{20}Ne, 260 THz, 1.15 μm SHG in $LiNbO_3$ crystal, absolute freq. meas. in visible region 79—93104
- Ni, cataphoretic at. distrib. in $NiCl_2$-He discharge 77—31092
- O atoms, two-photon absorpt., auroral transition relax. obs. *(Japanese)* 80—47954
- O, high power system for nuclear fusion 77—19338
- OCS, for 16 μm range, review *(Rumanian)* 80—87408
- OCS, optically pumped roto-vibr. mol. laser, rate eqn. model 78—37874
- OCS, optically pumped roto-vibr. mol. laser, low temp. operation and performance 79—50315
- OCS, optically pumped CW subMM emission lines 80—95876
- OCS, roto-vibr. mol. laser, low-temp. performance 80—9871
- OH, potential u.v. laser, proton beam excited Ar-H_2O mixture 77—662
- OH + Ar, pure rot. collisionally pumped laser, vibr.-rot. transfer 77—42523
- $O(^1S)$, absolute quantum yield meas. by XeO luminesc. in CO_2, N_2O photolysis 80—35561
- PH_3, laser emission 83 to 223 μm region, laser line assignments 78—71084
- Pb, discharge-heated, 0.723 μm, improved performance by vol. scaling 77—88778
- Pb, long life operation at 7229 Å 78—79037
- Pb, optimum working conditions and characts. *(Russian)* 78—13723
- Pb pulsed 722.9 nm laser with double-section gas-discharge tube 80—9902
- Pb pulsed lasing by discharge in $PbCl_2$ vap. 77—79812
- Pb self-terminating vapour laser, max. pulse repetition freq. 80—23677
- Pb vapour, long-lived sealed-off laser design, 7229 Å emission 78—50808
- Pb vapour, use in laser projection microscope with image-brightness amplifier 80—106541
- Pb vapour pulsed laser, with <20 kHz repetition freq. 78—9374
- Rb, in shock heated salt vapour, anomalous emission from atomic lines 78—63089
- Rb vapour, dynamic Stark tuned far IR laser 78—63126
- S, IR transitions in SF_6-He discharge 77—79805
- $S_2 + N_2$ *(Russian)* 80—99711
- SF_6, for 16 μm range, review *(Rumanian)* 80—87408
- SF_6-R-He(Ar) ternary mixtures, formation of inert gas fluorides in AC discharge 80—64817
- Se photolytic fluorescence pumped gas laser system 78—62606
- Sn hollow cathode laser, emission obs. from Sn II, I transitions 80—106509
- Sr atom, laser action mechanism due to 3066.2, 3011.1 nm $4d^3D_{1,2}\text{-}5pP^0{}_2$ transitions 80—9869
- Sr vapour pulsed laser, power characts. of laser transitions in Sr I, II 79—10290
- Tb complex, Tb(2,2,6,6-tetramethyl-3,5-heptanedione), vapours, excited-state kinetics and fusion laser media prospects 79—64243
- Tb-Al-Cl vapour complex, fusion laser gain medium 78—63073
- $TbCl_3$-$AlCl_3$, vap., high-energy laser medium props., for fusion ignition 78—63075
- $TbCl_3$-$AlCl_3$ complex, fluoresc. spectrum and gas-phase lasing 77—83861
- $TbCl_3$-$AlCl_3$ vap. complex, kinetics and laser fusion pot. 79—98343
- Tl, $6^2P_{3/2}\text{-}6^2P_{1/2}$ transition, population inversion 80—950
- Tl, UF_6-TlF-F_2 nuclear-reaction laser, possible steady-state operation 77—42527
- TlF-F_2 recombining plasma, light amplification possibility 78—17924
- UF_6 admixture effect on N_2 and Ar excited state lifetimes 79—10281
- UF_6, nucl. lasing, population inversion mechanism 80—63980

- **gas lasers** continued
  - UF_6 nuclear pumped lasers, electron impact cross section meas. 80—63985
  - UF_6-He fission pumped nucl. laser, power deposition 78—58987
  - Xe 3.5 μm self-mode-locked laser pulse, waveform analysis 78—1290
  - Xe, 3.5 μm transition, quasi-Gaussian pulse propagation, effect on line-shape parameter anal. 78—55333
  - Xe 3.51 μm laser amplifiers, spectral narrowing and saturation induced rebroadening optical heterodyne obs. 80—63976
  - Xe, 3.51 μm laser transition, phase-changing broadening, inert gas perturbers 78—82949
  - Xe, $5d_{7/2} \rightarrow 6p_{5/2}$ transition struct., laser spectrosc. and double reson. obs. 78—1210
  - Xe, Autler-Townes effect, i.r. laser transitions 77—425
  - Xe, discharge tube, radial variation meas. of 3.51 μm gain 77—54694
  - Xe, electron beam excited, form. of multiply-charged ions *(Russian)* 78—25853
  - Xe, high gain, ang. multiplexing for short pulse amplification 79—36924
  - Xe laser, and associated high gain phenomena, expt. and theory 79—10280
  - Xe laser, new IR laser transitions, 3.725 to 17.233 μm 80—87374
  - Xe, laser oscill. obs. in transversely initiated laser-produced plasma 77—88696
  - Xe, lifetimes and cross sections of laser levels, Hanle effect 77—75480
  - Xe, optical strength of LaF_3-MgF_2 multilayer mirrors 77—27294
  - Xe, pumping by relativistic electron beam, energy transfer theory 77—31089
  - Xe, recomb. laser in laser prod. plasma, 2.03, 2.65, 3.43 and 3.65 μm laser oscills. 77—88698
  - Xe-He, 3.51 μm laser amplifiers, spectral narrowing and saturation induced rebroadening optical heterodyne obs. 80—63976
  - XeF*(B), nuclear pumped laser, buffer effects 80—37617
  - ^{136}Xe laser amplifier, pressure shifts of 3.51 μm line 79—76669
  - Zn, cataphoretic laser, transverse separation dynamics 77—38865

- **gas permeability** *see permeability*

- **gas phase electron diffraction**
  - S,S′-dimethyldithiocarbonate, pot. for rot. about $C(sp^2)$-S bonds, electron diffr. obs. 80—23572
  - analysis, use of spline functions, program description 79—89810
  - basketene, electron diffr. determ. of struct. 78—37764
  - benzene, electron diffraction cross-section, finite scatt. geom. in mol. beam expt. 78—74803
  - benzyl fluoride, mol. struct., NMR and gas electron diffraction obs., ab initio and mol. mechanics calcs. 80—23574
  - bicyclo [4.4.0] dicane, cis and trans forms, mol. struct., electron diffr., mol. mechanics 78—50658
  - bicyclo[3.1.0]hexane, zero-point average struct., microwave spectra and electron diffraction 78—25738
  - bis(trimethylstannyl)-acetylene, mol. struct. determ. from gas phase electron diffr. 78—25740
  - bromochlorofluoromethane, struct., vibr. amplitudes, gas phase electron diffr. obs. 79—31690
  - bromotrifluoromethane, mol. struct., electron diffr., microwave spectra, CNDO/2 calcs. 78—37766
  - bromtrinitromethane, electron diffr. study of gas phase mol. struct., rot. isomerism 78—1080
  - carbon tetrachloride, internucl. parameters meas. using total scatt. of fast electrons 80—32857
  - channel electron multiplier appl. for fast expts. 78—83684
  - 2-chloro-3-fluoro-1-propene, struct. and conformers, force field and vibr. amplitudes 78—25747
  - chlorobenzene, gas phase electron diffr. struct. determ. 80—69251
  - p-chloronitrobenzene, struct., influence of NO_2 group on C-Cl bond 80—69251
  - chlorotrifluoromethane, mol. struct., electron diffr., microwave spectra, CNDO/2 calcs. 78—37766
  - chlorotrinitromethane, electron diffr. study of gas phase mol. struct., rot. isomerism 78—1080
  - cycloheptane, geom. struct. by electron diffr. 79—31682
  - 1,2,6-cyclononatriene, mol. struct. and conformation, gas phase electron diffr. 80—106400
  - cyclopentadienyl cobalt dicarbonyl, mol. stuct., gas phase electron diffr. obs. 79—31688
  - di-2-pyridyl sulphide, mol. struct. gas phase electron diffr. obs. 79—81296
  - diatom, probability distrib. function calc. from diffr. data, non-parametric estimation method 79—86066
  - 1-10-dicarba-closo-decarborane (10), mol. struct., vibr. and shrinkage corrections calc. from force field 80—95739
  - dimethyl ethyl amine, mol. struct. determ. by gas phase electron diffr. 80—95743
  - ethylbenzene, vapour, conform. and struct. obs. 80—69247
  - evaporator design, with continuous control of vapour pressure 80—57424
  - formyl fluoride, and isotopic forms, mol. struct., from electron diffr. and microwave data 80—23570
  - furan-2-aldehyde, mol. struct., electron diffr. and IR spectroscopic examination 79—10106
  - hexafluoropropene, mol. struct. by electron diffr. of gas phase 79—59572
  - high-temperature, review 80—52237
  - internuclear parameters measurement method using total scatt. of fast electrons 80—32857
  - iodotrifluoromethane, mol. struct., elcctron diffr., microwave spectra, CNDO/2 calcs. 78—37766
  - metal cluster generator for gas-phase electron diffr., variation of microcryst. with size 78—63645
  - methyl vinyl sulphide, syn-gauche equilib., force field and ab initio calcs., microwave and Raman spectra 80—23573
  - molecular beam scattering, effect of finite scatt. geom. 78—74802
  - molecular configuration, torsional vibr. effect on determ., pot. barrier height estimation 78—25743
  - molecular geometric molecular geometry, computer generated backgrounds 79—97368
  - multicentre molecules, intratarget diffr., extended Glauber theory 80—58380
  - partial wave electron scatt. factors evaluation 78—86963
  - photometry of diffraction patterns of mols. via IFO-451 microphotometer 77—27201
  - polyatomic molecules, bond distribution functions, anharmonicity effects of electron diffr. pattern 80—69234

- **gas phase electron diffraction** continued
  - pyrazine, mol. struct. determ. from gas phase electron diffr., r_α struct. 78—25739
  - quadrupole mass spectrometer attachment to EG-100 A electronograph for vapour composition monitoring 79—94108
  - quinuclidine struct. determ. by gas phase electron diffr. 80—95742
  - tetrabromoformaldazine, mol. struct., electron diffr. determ. 79—45858
  - 1,1,1,2-tetrafluoroethane, mol. struct. studied by gas-phase electron diffr., vibr. amplitudes, bond angles and lengths calc. 80—95740
  - tetrafluoromethane, electron diffraction cross-section, finite scatt. geom. in mol. beam expt. 78—74803
  - tetrakis(trifluoromethyl)germane, gas phase electron diffr. struct., torsional force consts., CNDO/2 calc. 79—31687
  - tetrakis(trifluoropropynyl)-tin, mol. struct. determ. from gas phase electron diffr. 78—25741
  - tetravinyltin, electron diffr. determ. of struct. 78—37763
  - 1,1,2-trifluoroethane, mol. struct., gas phase electron diffraction, rotamer abundance 79—76514
  - 1,1,1-trimethoxyethane, mol. struct., electron diffr., vibr. spectra 78—37765
  - trinitromehtane, electron diffr. study of gas phase mol. struct., rot. isomerism 78—1080
  - tris(trimethylstannyl)amine, gas phase electron diffraction 80—106401
  - vapours,, high-temp., photographic plate for electron diffr. studies 77—39516
  - vinyl bromide, mol. struct., from gas-phase electron diffr. and microwave data 80—23571
  - vinylchloride, mol. struct., gas-phase electron diffraction and microwave spectra, vibr. amplitudes 79—76421
  - vinylfluoride, gas phase electron diffr. and microwave spectra, rot. consts., struct., isotope shifts 79—31686
  - p-xylene, mol. geom. struct. and ring distortion, gas-phase electron diffr. 79—59573
  - $AsBr_3$, gas-phase electron diffr., mol. struct., force consts., vib. unharmonicities 77—546
  - BrF_5, gas phase electron diffraction and microwave rot. consts. data anal., mol. struct. 79—76363
  - CO ($^1\Sigma^+$), X-ray and electron diffr. scatt. intensities, electron correlation effects 78—17577
  - CO_2, electron diffraction cross-section, finite scatt. geom. in mol. beam expt. 78—74803
  - CaI_2, mol. struct. parameters and geom. config., gaseous electron diffr. obs. 80—37883
  - $(CrO_3)_4$, identification of polymer species by vapour phase electron diffraction 80—53135
  - $FBrO_3$, gas-phase electron diffr., mol. struct., force field, vib. amplitudes 77—547
  - $FeBr_2$, electron diffr. determ. of mol. struct., evidence for Fe_2Br_4 species 78—37767
  - $FeCl_2$, electron diffr. determ. of mol. struct. 78—37767
  - $GeCl_2$, combined electron diffr. and mass spectra mol. struct. determ. 79—89783
  - $HCo(CO)_4$, mol. struct., gas phase electron diffr. expt. 78—13623
  - $H_2Fe(CO)_4$, mol. struct., gas phase electron diffr. expt. 78—13623
  - $HMn(CO)_5$, mol. struct., gas phase electron diffr. expt. 78—13623
  - HgI_2, mol., gas-phase electron diffr. for geom. struct. 79—97368
  - HgI_2, mol. struct. and vibr. pot. function, gas-phase electron diffr. obs. 79—31689
  - I_2, electron diffr. data for geom. struct., non-parametric estimation method 79—86066
  - I_2, electron diffraction parameters, spectrosc. calc. 78—70932
  - I_2, mol., gas-phase electron diffr. for geom. struct. 79—97368
  - IF_5, gas phase electron diffr. and B_0 rot. const., struct. determ. 79—89782
  - Li_2F_2, struct., internuclear-distances and mean amplitude of vibr. determ. by electron diffr. 80—69252
  - $MgCl_2$, mol. struct. parameters, average values, geom. config., gaseous electron diffr. obs. 80—37904
  - $NbCl_5$, mol. struct., vibr. assignments, barries to pseudorotation 78—29858
  - $Ni(CO)_4$, mol. struct. by gaseous electron diffr., quadratic force field refinement 79—64115
  - O_2, electron diffraction parameters, spectrosc. calc. 78—70932
  - Pb microclusters, mol. beam electron diffr., amorphous struct. 78—66703
  - $PbCl_2$, mol. struct. determ. from gas phase electron diffr. 78—25742
  - $RbBO_2$, mol. struct. determ. by gas phase electron diffr. 79—10227
  - SF_6, hot, vibr. anharmonicity, electron diffr. study, 298-10^3K 79—68316
  - SF_6, laser pumped, mol. vibr. amplitude changes, gas phase electron diffr. obs. 79—76513
  - SF_6, struct. by electron diffr. 78—29859
  - SrI_2 mol. struct. parameters and geom. config., gaseous electron diffr. obs. 80—37883
  - $TaCl_5$, mol. struct., vibr. assignments, barries to pseudorotation 78—29858
  - TeF_6, gas phase electron diffr. patterns, mol. struct., three-at. scatt. 78—66662
  - TiF_4, equilib. config., force field, Coriolis consts., vibr. freqs. and amplitudes 80—32835
  - $TlBO_2$, mean geom. config., gas-phase electron diffr. 77—83759
  - VBr_4, mol. struct., vibronic interactions, dynamic Jahn Teller effect, gas phase electron diffr. 79—31711
  - $(WO_3)_3$, identification of polymer species by vapour phase electron diffraction 80—53135
  - WOF_4, gas phase electron diffr., mol. struct. 77—34775
  - Xe, electron elastic scatt. 79—857
  - ZrF_4, mol. struct. and vibr. freqs., gaseous electron diffr. obs. 80—32836
- **gas pressure cables**
  - SF_6-N_2, horizontal cylindrical power cable, convective heat transfer, simulation *(Russian)* 77—58676
- **gas-surface interactions** *see sorption*
- **gas technology, natural** *see natural gas technology*
- **gas turbine power stations**
  - coal, fluidised bed gasification, power generation fuel gas manufacture for combined cycle gas turbines 80—26104
  - coal gasification/combined cycle power generation test facility, preview 80—16773
  - compressed air energy storage power plant using coal-fired fluid bed combustor, technical assessment 80—30573
  - hybrid solar-fossil power generation, combined cycle system 80—30406
  - ocean thermal energy conversion, design of NH_3 turbine 80—30503

gas turbine power stations continued
off shore, electricity generation, off shore gas utilisation 80—21360
solar receiver, central, heat pipe, 10 MWe plant conceptual design 79—52910
waste heat utilisation for elec. energy generation and desalination *(German)* 79—87936

gas turbines
see also gas turbine power stations; turbogenerators
airfoils, protective coatings, degradation characts. and methods of application 79—24670
annular axial compressor nonaxisymmetric flow anal. 79—32679
annular vortex shedding acoustic resonance analysis *(Japanese)* 80—14526
asymmetric swirling flow anal. 79—27694
blading high-temperature corrosion protective coating by plasma spraying, description 77—12728
blading overspeed vibrations meas. optical methods 77—74387
cascaded blades with injection or suction, boundary layer theory and cascade tests 79—18878
ceramic material fracture mechanics, n review 80—45373
ceramic turbine disc, subjected to centrifugal stresses, failure probability, photoelastic model 79—18816
closed Brayton cycle, for fusion power generation, design study 77—38395
closed cycle, internal forced convection of inert gas mixtures 77—47005
combustion chamber, isothermal model, bluff body, recirculation phenomena in primary zone 79—47925
combustion chamber flow three-dimens. calc. 80—79405
combustion region, perturbations produced by unsteady combustion and heat addition 80—53764
diffusion barrier between Ni-Cr-Al coatings and Ni eutectic alloys in gas turbines 79—24673
energy conversion, Conf., San Diego, CA, USA (Aug 1978) 79—48038
engine, substitution of ceramics for high temp. alloys 80—97678
exhaust gas diffuser flow anal. 77—75884
exhausts, core noise 78—13850
expansion turbines, review 77—5847
gas turbine-HTGR system heat exchanger design 78—739
GCFR, transient analysis of closed gas turbine cycles, TUGSIM-10 computer code 77—18675
high pressure gaseous flow in nozzles *(Spanish)* 79—98781
high speed unequally spaced fan rotor acoustics and performance anal. 80—96163
high-temperature heat conversion efficiency enhancement using coolant with particle suspension *(Russian)* 79—68549
high-temperature materials, technological requirements, R and D, report 80—45222
holes rows adiabatic wall temp. and heat transfer anal. 79—7376
HTGR, with direct cycle gas turbine, project development in Germany 77—46389
jet engine noise meas., flowing duct sound separation probe 78—13878
jet mixing, secondary zone characteristics *(Russian)* 77—84292
measurement of fan vibration using double pulse holography 79—30462
noise, acoustic disturbance propagation in gas stream anal. *(Russian)* 79—32131
noise source mechanisms, expt. determ. in gas turbine combustors 80—69597
rotor vibration contactless meas. system *(Russian)* 80—8982
solar energy conversion, aqua-ammonia unit development, for farm power needs in India 79—62024
solar gas turbine, thermal cycle with gas reheating 79—92064
solar gas turbine plant, N_2O_4 as chemically reactive working fluid 79—39316
solar receiver, central, using liquid metal heat pipes 79—48096
stator heat transfer rate meas. method 79—98731
steam-gas power stations using multi-stage high-sulphur residual fuel oil combustion 77—9487
temperature gradient along cooling channel surface, heat transfer in initial hydrodynamic section, effects 79—18892
turbine-vane passage velocity meas. using laser Doppler velocimeter 80—95086
uncooled radial, heat transfer anal. 79—4010
vibration and noise review, central power station large turbomachinery 80—23835
vibration-acoustic diagnostics, random signal patterns recognition, with aid of computer *(Slovak)* 79—18612
wideband combustion noise obs. *(Japanese)* 80—11890
Ar isotope separation by axial flow turbomachine model 78—78500
Co-Cr-Al-Y protective coating for combustion turbines, hot corrosion evaluation 80—40608
H production from radioactive waste heat and utilisation in gas turbines 80—30326
NH_3 turbine design for ocean thermal energy conversion 80—30503
Ni-Co-Cr-Al-Y protective coating for combustion turbines, hot corrosion evaluation 80—40608
Ni-Cr-Al-Y/ZrO_2-Y_2O_3, NASA two-layer thermal barrier coating, for gas turbine engines, test results 80—40617
NiAl, gas turbine material, oxidation, effect of gaseous NaCl 78—95853
(NiCo)-Cr-Al-Y/ZrO_2-Y_2O_3 plasma sprayed ceramic coating for turbine engine components 80—40616
Si-B based CVD coating for gas turbine blading, props. 80—40615
ZrO_2, stabilized, thermal barrier coating system, spectral emission and absorpt., 300 to 1590K 79—24672
$ZrO_2Y_2O_3$/Ni-Cr-Al-Y, NASA two-layer thermal barrier coating, for gas turbine engines, test results 80—40617

gasdynamic lasers
amplification index variation 77—15137
benzene-air combustion products for CW laser, gain values 77—75494
cavity design, plane flows in presence of weak supply of energy *(Russian)* 79—32498
channel flow, unsteady, of compressible gas with shock waves, appl. to gasdynamic laser 77—72327
CO_2, CW operation, specific output energy and efficiency 80—48212
confocal unstable resonators, near- and far-field laser modes, free space and saturable gain media 78—46674
convective cooled fast flow high repetition rate CO_2 laser, pulse discharge stability 78—94389
CW supersonic chemical laser, porous nozzle, chemically reacting boundary layer 80—100022

gasdynamic lasers continued
Fabry-Perot resonator of gasdynamic laser, collisional relax. effect on fundamental mode 79—31948
flow generated by an array of eccentric porous tubes 79—965
high energy laser system, optical distortion sources 78—83018
high speed, freq. stability mode struct., and output power characts. *(Chinese)* 79—31854
high speed flow lasers, stable oscillation condition mode struct., output power characters 79—76660
improved free-vortex, subsonic aerodynamic window 80—23663
intensity fluctuation magnitude in fast flow laser 80—53257
MHD laser, admixture atom conc., automatic meas. system *(Russian)* 78—73123
microwave discharge, supersonic flow in waveguide, electron densities, possible laser 80—38842
molecular beams, sources, gasdynamic, use of lasers, time-of-flight and detection techniques 80—69264
multiatomic gas kinetics in presence of radiation field 80—102714
multipass CW gasdynamic laser cavity, simplified theory 78—63140
nozzle flowfield props. boundary layers 80—24027
numerical analysis, laser utilizing selective thermal excitation and supersonic mixing 79—64202
optically inverse media, improved GDL perform. by selective thermal pumping 79—31858
partial population inversion laser, quasireson. V-V exchange effects 79—55125
pulsed gasdynamic shock-tube laser, working time extension 80—99696
resonator cavity, flow fields and amplification coeffs., 2-D calc. 80—5722
supersonic flow, amplification coefficient, effect of mixing conditions in a laval nozzle 80—6085
supersonic flow over deep cavity, flow disturbances, laser appl. 79—98748
thermal, energy parameters, analytic calc. method 77—75479
thermal excitation and mixing in ultrasonic flow, output power and resonator efficiency *(Russian)* 77—23646
thermal nonequilibrium heating of active medium by elec. arc 80—53258
two-phase media, mol. vibr. relax. in gas-aerosol system 79—45807
Ar plasma MHD arcjet, recombination lasing 77—65588
CO CW, gain and population inversion 77—27278
CO, CW preexcited supersonic laser, performance 77—14741
CO, elec. excited, with closed-cycle gas flow, operation 80—102732
CO, electrically excited, operation and performance *(German)* 78—33754
CO, electrically excited, closed cycle operation *(German)* 80—43362
CO, energy characts. calc. 78—9367
CO, fast flow continuous-wave laser, with longit. elec. discharge 78—9373
CO, gasdynamic laser working media, energy characteristic 80—14319
CO, increase of specific energy 77—31090
CO, optimum energy characts. 80—23665
CO, vibr. relax. in CO-Ar supersonic stream 77—14697
CO, weak signal gain, calibration loss method meas. 78—17919
CO-Ar, output power, specific output energy and efficiency 78—46583
CO-N_2-Ar mixture, supersonic expansion, CO vibr. level populations, gasdynamic laser appl. *(French)* 77—23659
CO-N_2O gasdynamic laser, CO_2 vibr. level superequilibrium chem. pumping, mixture composition, He effects 79—76666
CO_2, active medium obs. using heat camera system 80—1257
CO_2, bipropellant, advanced fuel-rich and screen mixing gasdynamic laser concepts, performance 79—36878
CO_2 CW burning CO in air for pump energy, saturation parameters 78—71077
CO_2 CW gasdynamic laser, determ. of saturation parameter 78—37871
CO_2 CW gasdynamic mixing lasers, pumped by N_2 or air, low stagnation temp. characts. 78—63053
CO_2, combustion driven, effect of residual CO on small signal gain 80—63973
CO_2, combustion driver, thermally pumped 77—34871
CO_2, combustion gasdynamic laser, working cpds. simulation *(Russian)* 79—27239
CO_2, combustion-driven, contaminants effect on gain and power 78—25847
CO_2, combustion-driven gasdynamic laser, effect of N_2 preheat 77—38854
CO_2, conical optics for radiation conversion from laser with unstable resonator 80—91831
CO_2, discharge and power extraction characts. *(Rumanian)* 80—95869
CO_2, effect of supersonic nozzle 78—46564
CO_2, electric discharge gasdynamic 16 μm laser, high average power, high repetition rate 78—55381
CO_2 electron-beam-controlled gas-flow laser, CW and pulse periodic lasing 79—7111
CO_2 fast flow laser, active medium parameter input fluctuations, intensity response 80—53257
CO_2, flow inhomogeneity effect on gain distrib. 78—1205
CO_2, gas heating by electrically induced explosion, parameter optimization 79—64250
CO_2 gas transport laser with cylindrical geometry 79—7108
CO_2 gasdynamic 16 μm laser, performance determ. using multipass cavity 79—81443
CO_2 gasdynamic laser, 16 μm radiation, modified Anderson's time-depend. anal. 80—106505
CO_2 gasdynamic laser, depopulation of lower active level by CO_2+NO collisions 80—74336
CO_2 gasdynamic laser, energy characts. calcs. 80—95866
CO_2 gasdynamic laser, gain prediction, comparison of vibr. models 78—29928
CO_2 gasdynamic laser, gain supersonic flow heating effect, condition optimisation 78—82947
CO_2, gasdynamic laser, optimisation of gain coeff. in nozzle stream *(Russian)* 77—27272
CO_2 gasdynamic laser, population inversion, press. effect 80—102692
CO_2 gasdynamic laser power, free-piston shock tube expts. *(Japanese)* 79—76661
CO_2 gasdynamic laser with partial inversion at 16 μm, gain calcs. 80—78833
CO_2 gasdynamic lasers, amplifying characteristics, combustion product utilisation 79—27240
CO_2 gasdynamic lasers, multicomponent working media, energy characts. calcs. 80—95867
CO_2, HCl, HF, DCl and DF effects on physical kinetics 78—5451

gasdynamic lasers continued
CO_2, IR spectroscopic determ. of vibr. level populations 80—32952
CO_2, in burnt gases of combustion engines, laser action 79—45924
CO_2 injection into supersonic stream containing CO, gain 79—31861
CO_2 laser, 14-μm and 16-μm, CW and improved pulsed operation 78—17900
CO_2 laser, effect of H_2 addition on gain coeff. in expanding CO_2-N_2 stream *(Russian)* 77—27271
CO_2 laser, thermally pumped, output power enhancement by Ar gas addition 78—55336
CO_2 laser energy characts., CO_2 aerosol/hypersonic air stream interaction 80—48211
CO_2 laser resonator, gasdynamic, optimal parameters determ. from vibr. energy exchange kinetics 80—14317
CO_2 mixing gasdynamic laser 78—71073
CO_2, mixing-type, simplified model for cavity flow, population inversion calc. 78—46567
CO_2, operating on combustion products, gain coeffs. of complex working media 80—58506
CO_2, peak small-signal gain, closed-form correl. 77—42518
CO_2 pulse-periodic elec. pumped gasdynamic laser, possibility of spontaneous circulation 79—45926
CO_2, rapid wavelength switching probe laser, J-line scan gasdynamic laser diagnostic 78—59044
CO_2, resonator action, output power 78—13681
CO_2, resonator design, lasing medium model 78—29984
CO_2, specific power optimisation 77—712
CO_2 supersonic-after-mixing-type, gain charact. *(Japanese)* 77—23647
CO_2, thermally pumped gas-dynamic laser based on deformation and symmetric modes 79—36874
CO_2, transitions between levels of paired modes, vibr. relax. kinetics 79—89885
CO_2, two-stage expansion of N_2, supersonic nozzle 78—71076
CO_2, unstable resonator selection 77—23701
CO_2, using methane-O_2-N_2-Cl_2 mixture combustion products 77—50649
CO_2, vibr. temp. meas. method 80—9854
CO_2 vibrational temperature determ. in gasdynamic laser with $CO_2+N_2+H_2$ mixture 80—9849
CO_2 vibrational temps. in reaction products of $CO+N_2O$ under gasdynamic laser conditions 80—21276
CO_2, with gas mixing, excitation efficiency 79—22934
CO_2-F_2-Ar mixture, vibr. relax. in shock wave, 4.3 μm radn. 78—1062
CO_2-gas dynamic laser, combustion-type, effect of residual CO on performance 79—68378
CO_2-He-N_2, gas dynamic laser, gain coeff. numerical estimates, book contrib. 80—1183
CO_2-N_2, CW gasdynamic laser, qualitative comparison with N_2O-N_2 laser 78—25856
CO_2-N_2, CW mixing gasdynamic laser, saturation parameter and small signal gain 79—45923
CO_2-N_2, gasdynamic laser mixture, vibr.-nonequilib. nozzle flows, numerical and approx. solns. 78—74881
CO_2-N_2, gasdynamic laser, gain-optimisation, theory 79—76664
CO_2-N_2, gasdynamic laser, theoretical gain-optimisation, parametric study 79—76665
CO_2-N_2, performance for various injection techniques 77—38917
CO_2-N_2, thermal nonequilibrium heating of active medium by elec. arc 80—53258
CO_2-N_2 downstream mixing gasdynamic laser, Navier Stokes eqns., laminar mixing flows 80—23662
CO_2-N_2 gasdynamic laser, amplification coeff. rel. to water vapour content *(Russian)* 77—7057
CO_2-N_2 mixture gasdynamic laser, energy characts. 80—69362
CO_2-N_2-H_2O, nonequilib. flow calc. by relaxation formula *(Chinese)* 79—31853
CO_2-N_2-H_2O, water vapour condensation and mol. relax. processes 79—13946
CO_2-N_2-He, gasdynamic laser, effect of weak flow perturbations on gain 80—14316
CO_2-N_2-He, laser utilizing selective thermal excitation and supersonic mixing, numerical analysis 79—64202
CO_2-N_2-He, supersonic nozzle flow, cooling, population inversion *(Russian)* 77—7412
CO_2-N_2-He (H_2O) gas mixture, method for obtaining vibrational population inversion 79—94210
CO_2-N_2-He CW gasdynamic laser, closed-cycle, construction and operating parameters 80—23717
CO_2-N_2-He mixture in gas-dynamic system with independent thermal excitation, population inversion in two-step mixing 79—89888
CO_2-N_2-He mixture supersonic adiabatic expansion, population inversion and gain 80—19017
CO_2-N_2-He nozzle flows with boundary layer, gain coefficients 80—14312
CO_2+D_2, near reson. V-V exchange 77—27165
CS_2, increased efficiency, 11.4-117 μm emission 77—27283
Co_2 laser radiation amplification in reaction products of $CO+N_2O$, nonequilib. chem. pumping effects 77—83848
D_2-CO_2, interaction between vibr. states, theory 77—23670
D_2-HCl electric discharge gasdynamic laser, turbulent mixing characts. 78—9366
D_2-HCl-Ar(He) gasdynamic lasers, gain 79—64217
H plasma, freely expanding, population inversion obs. 80—95877
H, recombination dynamic plasma, freely expanding, from supersonic nozzle 77—19240
HCl-D_2-He mixture 78—50761
H_2O-H_2 cooling in supersonic nozzle, submillimetre wave generation 80—48229
H_2O-H_2 mixtures, vibr. energy transfer in shock waves, population inversion 80—37996
He-CO_2-Cs mixture in rapidly circulating laser, interaction rate of Cs and CO_2, gasdynamic parameters 79—86173
He-CO_2-Xe, supersonic elec. discharge TEA laser, mag. field effects 79—7110
Li plasma dynamic laser, using supersonic nozzle, population inversion, excitation cross section 78—50760
N_2, gas with clusters, free expansion, upper rot. levels population *(Russian)* 78—33581
N_2 gasdynamic laser, active medium increased lifetime 79—68388
N_2-CO_2-H_2O gasdynamic laser mixture, electron beam diagnostics 77—83845

gasdynamic lasers continued
N_2O, CW, thermally excited and selectively-pumped mixing, comparison with CO_2 laser 77—42521
N_2O CW gasdynamic mixing lasers, pumped by N_2 or air, low stagnation temp. characts. 78—63053
N_2O, flow inhomogeneity effect on gain distrib. 78—1205
N_2O, gasdynamic laser, population inversion mechanism, kinetics 77—7074
$N_2O/N_2/H_2O$, CW, numerical anal. 78—29935
N_2O-CO-He mixture, radiation amplification factor in supersonic expanding stream of gas 77—10896
N_2O-N_2, CW gasdynamic laser, qualitative comparison with CO_2-N_2 laser 78—25856
N_2O-N_2, CW mixing gasdynamic laser, saturation parameter and small signal gain 79—45923
N_2O-N_2-He, gasdynamic laser, effect of weak flow perturbations on gain 80—14316
N_2O-N_2-He, population inversion of N_2O vibr. levels behind shock wave front 79—31886
N_2O-N_2-He mixture, radiation amplification factor in supersonic expanding stream of gas 77—10896
Na-CO_2 mixing-type gasdynamic laser, experimental and theoretical studies *(Japanese)* 80—23666

gases
see also aerodynamics; compressibility of gases; density of gases; dielectric properties of gases; diffusion in gases; electric breakdown of gases; electrical conductivity of gases; equations of state of gases; ionisation of gases; kinetic theory of gases; liquefaction of gases; luminescence of gases; Scott effect; Senftleben-Beenakker effect; specific heat of gases; thermal conductivity of gases; thermal diffusion in gases; viscosity of gases
diatomic, spherical source expansion 80—58356
dilute gases, transport props., softness expansion for inverse power pot. 80—28589
light scatt. induced by two-body collisions, memory function approach and mol. dynamics 78—25658
polyatomic, transport coefficients, multilevel description 79—55436

gauge field theory
see also Weinberg model; Yang-Mills theory
0(3) gauge theory, uniqueness of 't Hooft-Polyakov magnetic monopole soln. 77—2747
1/N expansion in two-dimensional lattice gauge theory 80—86559
γ-W^0 mixing as an alternative to unified weak-electromagnetic gauge theories 79—2966
$\eta\phi^6$ theory, 1/N expansion and instantons, gauge theory extension 80—47180
θ-vacua energy depend., P and T conservation in the presence of instantons 78—89628
θ-vacua in two-dimensional quantum chromodynamics 79—67499
σ model, supersymmetric nonlocal conservation laws 80—46938
σ models, nonlinear, soft mass renormalisation of 1/N expansion 80—47164
σ-model, nonlinear, sypersymmetric, Ricci-flat Kahler manifolds and supersymmetry 80—90994
σ-models, nonlinear, generalisation with gauge invariance 80—57469
$(\phi^3)_6$ theory, IR behaviour, gluon confinement mech., nonperturbative approach 78—24954
ϕ^4 lattice field theory as an asymptotic expansion about Ising limit 80—31967
ϕ^4 scalar field theory and exact solns. to classical SU(2) gauge theory 77—45949
ϕ^4-model, dimensional regularisation and instantons, scalar field theory model 80—4830
ϕ^4-theory, soliton soln., fluctuation renormalisation and extended particles 77—5996
't Hooft's disorder parameter, meson like configurations contribution, confinement phase 80—86574
't Hooft monopoles, interaction energy in Prasad-Sommerfield limit 79—12950
't Hooft Polyakov monopoles, force between widely separated interacting monopoles 77—87895
$A_0=0$ gauge canonical formalism, gauge degrees of freedom, external charges, quark confinement 79—2936
Abelian, canonical approach to instantons, multiple vacua and vacuum tunnelling 77—49855
Abelian and non-Abelian gauge theories, mass generation, renormalisation, chiral and unified theories 80—4871
Abelian gauge field, $A_0=0$ gauge, canonical and path-integral quantisation 78—70277
Abelian gauge model, perturb. anomaly compensation 77—13843
Abelian gauge theories, (1+1) dimens., instanton effects 79—261
Abelian gauge theories, charge screening and mass spectrum, form factor anal. 79—75686
Abelian gauge theories, dual transformation 79—63370
Abelian gauge theories, QED_2 generalisation, quark confinement 79—71605
Abelian gauge theories, renormalization using BRS symmetry 79—54257
Abelian gauge theories with dynamical symmetry breaking, effective pot., scale and chiral invariance *(Russian)* 80—57503
Abelian gauge theory supersymmetric aspects, Becchi-Rouet-Stora supertransformation, QED reformulation 77—34103
Abelian Higgs and Goldstone models, no-hair theorems for black holes 79—17016
Abelian Higgs Kibble model, generalised Slavnov invariance, supersymm. struct. 78—78070
Abelian Higgs model, lattice version, phase transitions and confinement 79—49398
Abelian Higgs model, two dimens., multiple vacs. in lattice formulation 78—54543
Abelian Higgs model, two dimens. quark confinement 79—263
Abelian Higgs model relation to spontaneously broken massless scalar electrodynamics 77—54057
Abelian Higgs-Kibble model on lattice, spontaneous magnetisation 78—57870
Abelian lattice gauge field theory, 2+1 dimens., phase transition 78—24963
Abelian lattice gauge theories, θ-vacua construction in compact gauge theories 79—58874
Abelian lattice gauge theories, Monte Carlo anal. 80—18079
Abelian lattice gauge theories, phase transitions 78—12812

gauge field theory continued
- Abelian lattice gauge theory, quark confinement 78—66040
- Abelian monopole equivalence to non-Abelian stringless counterpart by method of sections 77—49856
- Abelian self-dual multimonopoles, covariant Laplace operator Green function 80—77969
- Abelian spontaneously broken gauge model, perturbation expansions *(Chinese)* 78—8500
- Abelian theory, stability of solns. with dynamically broken symm. *(Russian)* 77—38093
- Abelianizable field, duel charged soln., gauge field decomposition and reduction 79—26245
- ACD off light-cone, transverse momentum cut-off 78—381
- algebraic models with non-Abelian gauge group U(1) and superselection rates 77—30266
- amorphous state analogy 79—54370
- angular momentum in non-Abelian gauge field theory 77—71446
- anharmonic oscillator, calculation of instanton-anti-instanton contributions in quantum mechanics 80—68078
- anisotropic nonlinear σ-model, two dimens., instanton quantum fluctuations *(Russian)* 80—86600
- anomalies, unitarity and renormalization, book contrib. 80—42352
- anomalies in gauge models, cancellation by regularisation independent renormalisation scheme 80—77931
- anomalies of higher-dimension composite fields 80—95218
- anomalous currents in curved space 78—62336
- antisymmetric tensor gauge field, action principle quantisation 79—71623
- antisymmetric tensor gauge fields, covariant quantisation, Faddeev Popov ghosts 80—27406
- antisymmetric tensor gauge fields, local supersymmetry without gravity 80—46910
- approximation algorithm for functional integrals, and the instanton gas 79—85235
- asymptotic dynamics for gauge theories 79—21949
- asymptotic estimates in perturbation theory and complex instantons 79—6273
- asymptotic free field anal. of μ-p deep inelastic scaling violations 78—4863
- asymptotic freedom and local duality 77—71518
- asymptotic freedom predictions for neutral and charged current neutrino interactions 78—8581
- asymptotically free, higher order effects 77—38092
- asymptotically free, higher-order effects for coupling const. 77—34095
- asymptotically free, mass corrections in deep inelastic scatt. 77—61297
- asymptotically free colour gauge theory, electroprod. local duality and precocious scaling 77—22630
- asymptotically free field theories, operator mixing and scaling deviations 77—18181
- asymptotically free gauge theories, deep inelastic scatt. beyond the leading order 79—21937
- asymptotically free gauge theories, higher twist effects, four quark operator anomalous dimensions 80—105848
- asymptotically free gauge theories, higher-order effects, anomalous dimensions of Wilson operators 78—4771
- asymptotically free gauge theories, massive lepton-pair prod. 77—74734
- asymptotically free gauge theories, scaling violations in leptoproduction 78—4769
- asymptotically free gauge theories predictions, comparison with high energy deep inelastic scatt. data 77—49974
- asymptotically free gauge theory, effective coupling constant 78—21333
- asymptotically free parton model, struct. function transverse momentum behaviour, SU(3) gauge model 80—27469
- asymptotically free SU(2)×SU(2)×SU(4) model of unified interactions 78—16968
- asymptotically free theories structure, renormalisation group appls. 77—57461
- Atiyah-Singer index theorem, local version for vector fields 78—58128
- Atiyah-Singer theorem, classical anomalies 78—382
- atoms, handedness and parity non-conservation 78—29757
- automorphic fields on flat space-times, vacuum stress tensor 80—22510
- automorphic theory, mathematical issues 80—22509
- axial anomaly and Atigah-Singer theorem 78—377
- axial anomaly and meron configurations in 2-dimens. Euclidean Schwinger model 80—86545
- axial current in dimensional regularization 80—13233
- axial gauge, canonical quantisation of non-Abelian gauge theories 78—70279
- axial gauge, QCD, differential identities and soft-gluon singularities 77—74585
- axial gauge for unified gauge models, renormalisation constants 79—12930
- axial symmetry in lattice theories 79—9280
- axial vector anomalies, weak-EM interactions nonrenormalisability 80—62859
- axial vector current anomaly in gauge field theory Green's function calc. *(Russian)* 80—27412
- axial-vector currents, chiral and gauge invariant regularisation 80—4956
- axially gauge-covariant electrodynamics 79—17644
- axion emission in decay of excited nucl. states 78—49975
- axion mass in extended SU(2)×U(1) colour gauge theory 78—78080
- b-quark, horizontal gauge symmetry, Cabibbo universality and fermion masses 80—22583
- back reaction of quantised field in gauge treatment of gravity 78—16711
- background field gauge in supergravity 80—46912
- background functional renormalisation, in non-abelian gauge theories 79—30663
- Backlund transformations describing SU(2) mag. monopoles 79—2915
- Backlund transforms. for mag. monopoles in SU(2) gauge theory 79—2916
- Bargmann-Wigner and Weyl spin-3/2 fields, spinors, chiral operator 80—31981
- baryon bound state in two-dimens. SU(N) gauge theory 77—13918
- baryon dynamics description in dual and gauge theories 77—65138
- baryon-lepton symmetry model, μ-number and flavour nonconserving neutral currents 78—66069
- basis and gauge sets for EM interaction representation 80—42371
- Becchi-Rouet-Stora transform. for gravitational field 78—93590
- Bethe-Salpeter eqn. for two fermion EM bound state systems 78—78058
- Bhabha-Gupta field coupled to external EM and gravitational fields, causality 78—4767
- Bianchi identities for supersymmetric gauge theories 78—62299

gauge field theory continued
- Bianchi IX metrics, self-dual asymptotically Euclidean, quantum gravity 78—65857
- bilocal fields for study of quantum corrections to dynamically broken symmetries 78—16985
- bilocal gauge field theory 80—31986
- bilocal models of hadrons, relative time depend. as gauge freedom 77—74584
- Bogomolny-Prasad-Sommerfield monopole, multiinstanton ADHM generalisation 80—52407
- Bogomolny-Prasad-Sommerfield one-monopole soln. by Backlund transformation 80—99059
- Born helicity amplitudes and cross-sections 77—2777
- boson system, superfluid flow rel. to local gauge invariance 80—54450
- bound states from instantons 78—78087
- box diagrams with nonvanishing external four-momenta 80—22525
- BPS one monopole generation by Backlund transform 80—77980
- bremsstrahlung production of high-energy lepton pairs in QCD, gauge invariance effects 77—74650
- broken colour gauge theories, effective weak vertex, colour contrib. 79—40750
- broken SU(3) gauge model of strong and EM interactions, scatt. lengths, baryon mag. moments 78—74133
- broken supersymmetry theories, parity conservation 77—41785
- BRS supersymmetry, non-trivial realisation 80—82882
- C* algebra, gauge transformation formulation for EM field 79—6307
- Cabibbo angle, CP violation quark masses 78—33016
- Cabibbo angle and CP violation in a gauge model with discrete symmetry 79—45028
- Cabibbo angle and discrete symm. 78—29288
- Cabibbo angle calc., SU(2)×SU(2)×U(1) gauge theory 78—4776
- Cabibbo angle formula, discrete flavour symm. 78—417
- Cabibbo angle in six quark $SU(2)_L \times SU(2)_R \times U(1)$ gauge model 79—17683
- Cabibbo current and CP violation in a six quark gauge model 78—70329
- Callan-Gross relation, instanton violation, nonperturbation correction asymptotic behaviour 80—27409
- Callan-Symanzik $\beta(g)$ function in perturbation theory around gauge theory instanton 79—2931
- caloron space of moludi at finite temps., gauge theory vacuum struct. 79—21947
- canonical anticommutation relations with compact gauge group, quasilocal algebra 79—89069
- canonical field theory, quark binding 78—32994
- canonical field theory, quark-binding 78—29264
- canonical formalism, appl. to monopole solns. 77—206
- canonical neutral-current predictions from the weak-electromagnetic gauge group SU(3)×U(1) 80—95242
- canonical quantisation in axial gauge with indefinite metric, perturbation calc. 80—101928
- canonical quantisation of gauge fields, gravitational field *(Chinese)* 80—22266
- canonical quantization of massless and massive spin 3/2 field in general covariant gauges 79—71334
- canonical struct. of Abelian gauge theories 79—40666
- Caratheodory's canonical theory for fields, quark confinement 77—87941
- CERN School of Physics, Austerlitz-Zeist, Holland (June 1978) 79—30857
- changed field, electromagnetic self-energy, in non-minkowskian spacetime, gauge depend. of mass renormalisation 79—85214
- charge conservations as concomitant of conformal motions coupled to gauge transforms 80—62835
- charge-monopole composites, system of identical particles, statistics 78—93796
- charge-monopole duality and nonAbelian gauge theory phases 79—71625
- charge-monopole duality in spontaneously broken gauge theories 79—267
- charged Higgs boson in SU(2)×U(1) gauge field theory, production and decay 79—13015
- charged particle, soft photon contrib. to Green's function, IR asymptotics, gauge transform. *(Russian)* 77—57438
- charged particle interaction, mag. field energy, spatial distrib. of interaction contrib. 80—73625
- charged particle scattering by mag. monopoles, SO(3), gauge theory 77—13907
- charged particles interacting with EM field, line-integral Lagrangian 79—81346
- charged spin-1 gluons, integer charged quarks, e- and ν- prod. 77—49894
- charges, vortices and quark confinement, confinement phase transition 79—36004
- charm particles and observable quantities 77—34099
- charmonium, rel. to gluons, quantum chromodynamics theory 78—62362
- charmonium and asymptotic freedom in QCD 79—6327
- charmonium spectrum, relativistic and nonrelativistic theory 78—50010
- Chern classes, Pontrjagin forms and classification of gauge fields 79—67461
- chiral (γ_5) symmetry of massless fields, neutrino theory of photons 78—411
- chiral field on path, integrability 79—97492
- chiral fields, two-dimens., hidden symm. 78—29243
- chiral fields on loop space, colour-electric flux rings 80—42327
- chiral gauge invariant Lagrangian, relationship to strong interactions *(Chinese)* 79—21968
- chiral gauge spinor superfield as scalar multiplet 79—85241
- chiral gauge symmetry without anomalies 77—6005
- chiral Gross-Neveu model embedded in U(1) gauge theory, fractional winding 80—86569
- chiral symmetry spontaneous breaking, using vacuum stability condition 79—35986
- chiral U(1) symmetry and CP invariance in presence of instantons 78—78075
- chirally extended supergravity, Maxwell-Einstein supergravity, auxiliary field struct. 78—78126
- classical electrodynamics, nonlinear gauge approach, charged particle solns. 78—32695
- classical eqns. exact cylindrically symmetric solns. from compact Lie groups *(Russian)* 80—42317
- classical field theories, non-signification of super gravitation 80—27193
- classical gauge field theory eqns. with arbitrary value of topological charge 79—21954
- classical gauge fields on coset spaces 78—45781

gauge field theory continued
classical interacting strings, dimensional reduction, Abelian gauge fields 80—73685
classical interactions of 't Hooft monopoles 78—78233
classical multimeron solutions of generally invariant gauge theories 78—37142
classical particle interaction with external non-Abelian gauge field 77—65098
classical supersymmetric particles 80—86560
classification, Lorentz and gauge invariants 79—30648
classification by spinors and Lorentz invariants rank 79—259
classification of non-Abelian fields 80—31976
closed vortices and Hopf index in Abelian and non-Abelian Higgs model, and nonlinear σ model 79—12960
coherent beam interference, phase shift in gauge and grav. fields 80—4627
color embeddings, charge assignments, and proton stability in unified gauge theories 79—6309
colour and flavour in QCD and QFT 80—91011
colour confinement, possible mechanism gauge invariance 79—54311
colour gauge groups, quark line rule 78—29305
colour gauge models, symmetry breaking and asymptotic freedom 77—13917
colour gauge theory, quark elastic scatt. and large transverse mom. hadron prod. 78—8610
colour model of hadrons, SU(6), review 77—82702
colour screening, SU(3) gauge fields 78—82102
colour-flavour symm., renormalisation effects in guage theories 78—33018
coloured quark model 77—71482
compact gauge groups for unified weak and EM interactions, representations and classifications 79—22008
compact group gauge fields, breaking of symmetry and dual charges *(Chinese)* 79—35918
complete Lorentz covariant gauge condition for Abelian and non-Abelian gauges 80—47182
complex structure of monopoles, instanton techniques, classical monopole eqns. 78—54537
composite fields, renormalisation group eqn. using Green's functions generating functional *(Russian)* 78—16934
Compton scattering, deep-inelastic, manifestation of colour effects 78—37215
conference, group theoretical methods in physics, Austin, Texas, USA (Sep. 1978) 80—4474
conference, lepton-hadron physics, Karlsruhe, Germany (Sep. 1978) 80—73098
conference, Schladming, Austria (Feb.-Mar. 1978) 79—26203
conference on hadron struct. and lepton-hadron interactions, Cargese, France (July 1977) 80—4473
configuration space renormalisation to phase space, gauge coupling 80—18074
confinement criteria for gauge invariant, lattice, and Abelian models 79—22023
confinement in colour SU(N) gauge theory 78—8592
confinement in SU(N) lattice gauge theories 80—57493
confinement in Z_n lattice gauge theories implies confinement in SU(n) lattice Higgs theories 79—58930
confinement model for gauge theories 79—89109
confining gauge theories, quark correlation functions in massive QED_2 80—105845
confining theories, chiral symmetry breaking in gauge theories 80—95244
conformal and gauge spontaneous symm. breaking, cosmology quantum effects 80—37185
conformal gravity as a gauge theory 79—49144
conformal gravity in SO(4,2) gauge *(Chinese)* 79—93027
conformal invariance and gauge vacuums 78—8530
conformal mapping 78—4784
conformal phase gauge field, coupling with complex scalar field 80—82875
conformal relativity, bare mass theory 80—27417
conformal relativity, gauge theories of interaction 79—9281
conformal relativity, kinematic theory of mass 78—77706
conformal relativity, special, theory of mass 78—77707
conformal spinor current anomalies 78—8520
conformal spinor current anomaly from symmetry arguments 78—4803
conformal supergravity, constraints and invariance 80—46917
conformal supergravity, curvature constraints for dependent gauge fields 79—67209
conformal supergravity, props., gauge theory 78—78085
conformal supergravity on basis of SO(4,2) gauge *(Chinese)* 79—93021
conformal transformations, gauge covariant 79—12946
conformally flat space, strong gravity field coupled to SO(3) gauge field 80—62563
conformally invariant σ-model in four dimens., instantons 80—95215
connection in vector bundle theory, identity of theories 77—18184
conservation laws of general relativity, gravit. gauge group $SL_{2,C}$ 77—22456
conservation laws of lepton flavours, unified gauge theories, new neutral lepton 77—54095
constant SU(2) non-Abelian gauge pot., vacuum polarisation by fermions, integral representation 80—22543
constrained Hamiltonian systems, canonical treatment of noncanonical gauges 77—49832
continuous gauge transformation, SU_2 as an example which cannot be continuously lifted to Lie algebra 80—52396
continuous three states model, mean field cluster expansion convergence, phase transitions existence 79—12922
convolution regularisation and gauge invariance 77—57446
copies, perturbation theory, Abelian and non-Abelian cases 80—47170
correlation inequalities for lattice gauge fields 77—45940
cosmological baryon excess, finite temp. gauge theory effects, entropy 80—51933
cosmological constant, broken gauge theories and 3K black-body radiation 78—28870
cosmological models, spontaneous symmetry breakdown, open and closed Friedmann model 80—51929
Coulomb and Landau gauges interpolation in Hilbert space of free QED 78—24987
Coulomb gauge fixing degeneracy, gauge transformation group in square integrable space 80—62846
Coulomb gauge vac. degeneracies in (2+1) dimensions 79—2928

gauge field theory continued
Coulomb gauge vacua of SU(3) gauge theory 80—47188
Coulomb scattering, Lee-Nauenberg theorem analysis 78—54595
Coulomb-like quantization of the electromagnetic field on spacelike hyperboloids 79—306
coupled Einstein SO(3) gauge field eqn. solns. 79—274
coupled Einstein Yang Mills eqns. for massless and scalar fields, stationary solns. 78—12621
coupled Einstein-Higgs field, mag. monopole and dipole soln. *(Chinese)* 78—82112
coupling constant renormalisation anal. in unified theories, generalised gauge hierarchies 79—97556
coupling parameter trajectories 78—8519
coupling strengths and renormalization scale parameter in QCD by dimensional transmutation 79—6316
covariance problems in two-dimens. QCD 80—22575
covariant 'in-out' formalism for creation by external fields 79—107
covariant inverse problems of variational calculus 77—74278
covariant quantisation of gauge theories with open gauge algebra 79—12947
covariant quantisation of solitons in gauge theories 78—16916
covariant theory of gravitation, curvature quantities, Yang-Mills type field *(German)* 77—53816
CP^{N-1} σ-model, N-component scalar QED model, renormalisation group functions 79—97500
CP^{N-1} model, instanton and large-N methods, QCD similarity 80—77963
CP^{N-1} model, QCD toy model, instantons θ vacua and confinement 80—9138
CP^{n-1} model with non-Abelian gauge symmetry, generalisation in $2+\varepsilon$ dimensions 80—77953
CP^{N-1} model with unconstrained variables, Lagrangian and Hamiltonian formulations 80—105780
CP^{N} model, generalisation with gauge invariance 80—57469
CP(N) ($N\geq2$) chiral theory, 2-dimens., non-selfdual instantons 80—86585
CP invariance, microweak violation 77—71456
CP violation, radiative symm.-breaking, fermion and Higgs boson masses 78—41435
CP violation, superweak model gauge theory 77—10194
CP violation and off-diagonal neutral currents 79—13008
current induced reactions, conf. 77—34106
current nonconservation in light-cone quantisation of scalar field 80—47220
current trends in the theory of fields, conf., Tallahassee, Florida, 6-7 April 1978 79—12923
currents and continuous symmetry restoration in two dimens., perturbation theory 79—21910
currents in Su(5) and E_7 unified gauge theories 78—54600
cut vertices and dimensional renormalization in non-Abelian gauge theories 80—57484
cylindrical gauge field configurations, confinement in QCD 78—12870
cylindrically symmetric instantons for the gauge groups of rank 2 (SU(3), O(5) and G_2) 79—58877
de Sitter gauge invariance based unified field theory 80—22255
de Sitter gauge theory for gravitation *(Chinese)* 79—80487
de Sitter gauge theory of gravitation 79—97285
de Sitter invariant Lagrangian 80—82868
deep inelastic electroproduction struct. funct., Abelian gauge field effects 79—71754
deep inelastic lepton-hadron interactions, scaling deviations 78—32991
deep inelastic lepton-hadron scatt. in massive vector gauge models 78—74262
deep inelastic leptoproduction data, Wilson coeffs. from struct. functions 77—61292
deep-inelastic leptoproduction off nucleons, struct. function model in asymptotically free gauge models 79—40786
deep-inelastic neutral-current cross-sections 78—66074
defect dynamics, gauge transforms. in vector field theory 79—27981
degenerate (non)quadratic functional, partition function 79—67458
dense matter, U(1) symm. gauge model, eqn. of state 78—62500
dense neutron star matter eqn. of state, QCD instanton effects 79—92796
dense quark matter, thermodynamic functions, instanton contrib. 80—52464
dense stellar matter in asymptotically free gauge theories, high density limit 77—53421
Dicke model with classical spins, phase operator and phase transition 77—82448
differential geometry methods in gauge and gravitational theories 80—90768
dimensional regulation, SU_2 gauge theory, instantons 80—18066
dipole ghost gauge theory as gluon model, confinement 78—66079
diquark-antidiquark states, mass difference in lattice gauge theory 79—2985
Dirac's monopole, generalisation to SU(2) gauge field theory 78—32975
Dirac's monopole and the Hopf map 80—27402
Dirac's monopoles and action-at-a-distance theory: classical dynamics 80—95210
Dirac's test, augmented algorithm for the Hamiltonian 80—82905
Dirac conjecture and test, example of failure 80—77976
Dirac eqn. De Sitter gauge transformation, gravit. field interaction 77—67563
Dirac Hamiltonian in presence of instanton and meron fields, fermion zero modes and level crossing 79—21927
Dirac massless field theory, pot. method anal. 77—82668
Dirac particle, charged scalar field, strong coupling theory 78—16976
Dirac particles, creation in general relativity with torsion and electromagnetism, general formalism 79—88856
Dirac spinor, relativistic exact bound states with gauge monopole 79—268
Dirac string Lagrangian in A^0-0 gauge, path integral quantisation 80—32007
direct interactions between membranes, gauge invariant theory 78—4551
disconnected gauge groups and the global violation of charge conservation 78—78086
discrete Abelian spin and gauge systems, phase struct. 79—85232
discrete and Abelian lattice gauge theories 79—9279
discrete finite nilpotent Lie analogs: new models for unified gauge field theory 78—66025
discrete lattice gauge fields, duality transformation, review 79—26236

gauge field theory continued
- discrete lattice gauge theories with matter fields, 1/N expansions phase diagram 80—73603
- discrete symmetries, Cabibbo universality, flavour mixing angles, in gauge model with six quarks 78—62346
- dislocations and gauge invariance 79—27980
- disorder×order operator combination, quark confinement and gauge theories 79—85270
- distorted gauge invariant theory, renormalisation props. 77—45967
- double counting, collective coordinate resolution of identity of unity 80—68359
- Drell-Yan annihilation processes, transverse momentum distribs., gauge theory predictions 79—97585
- Drell-Yan process as a probe of color excitation 79—36021
- dressed fermions in Abelian gauge theories 78—82093
- dressed quark-gluon vertices, instantaneous approx. 78—78091
- droplet model for quark confinement phase transition, reduction to string statistical mechanics 79—2991
- dual charge and principle bundles structure *(Chinese)* 77—71438
- dual charge of nonAbelian gauge groups, mag. monopoles *(Chinese)* 77—34076
- dual charged solution in curved space time, Dirac quantisation, $SU(2)\times U(1)$ gauge theory 78—12827
- dual charges, U_1 gauge field in SU_N gauge field *(Chinese)* 78—86417
- dual electromagnetism and neutral-current interactions 79—71678
- dual resonance model, conformal invariance, spontaneous symm. breaking 77—6092
- dual strings condensate, gauge fields as phonon excitations 79—35934
- duality for non-abelian lattice fields 80—42431
- duality rotations in EM charge space, secondary symmetry, magnetic current conservation 80—27431
- duals of gauge field tensors, representations 79—89057
- Duffin-Kemmer formulation of gauge theories 79—97511
- dynamic charges in field theories 79—54251
- dynamic torsion, space-time dependent coupling 79—45017
- dynamical Higgs mechanism, weak $\Delta I=1/2$ rule, sum rules, heavy quarks and leptons 80—27442
- dynamical symmetry breakdown at the two-dressed-loop level and beyond 79—294
- dynamical symmetry breaking, improved effective-pot. formalism for composite fields 77—6033
- dynamically broken chiral symmetry and the gauge technique for Ward identities 80—47211
- dynamically broken gauge model, 4-fermion interaction 77—71442
- dynamically broken gauge models, natural mass hierarchy, unification 80—68409
- dynamically broken-gauge theories, P and T violation in QCD 80—9093
- dynamically spontaneously broken symmetries of gauge theories *(Chinese)* 79—80740
- dyon solution of non-Abelian gauge theory with surface terms 77—74592
- Dyon solutions, existence, rigorous results 80—73595
- dyons, spin statistics connection 79—54248
- E6 unified gauge model, breaking patterns, quark-lepton symmetry and mass scales 78—86434
- E7 gauge model, multilepton prod. by ν, heavy leptons 77—74588
- E_6 unifying gauge symmetry, strong, weak and EM model embedding 79—9325
- E_7 gauge model, lepton assignments and trimuon events in neutrino scatt. 79—17709
- E_7 gauge model of weak interactions, neutrino prod. of neutral heavy lepton 79—17710
- E_7 gauge theories with proton stability *(Russian)* 79—17659
- E_7 grand unification, neutral currents problem in $SU(2)\otimes[U(1)]^3$ gauge theory *(Russian)* 80—62913
- E_7 grand unification using $SU(3)\times(U(1))^3$ gauge group, neutral currents 80—27444
- E(6) gauge theory, dynamical symmetry breaking 80—86580
- E based vector-like unified theory, group theoretical anal. of symm. breaking 77—87929
- early Universe, gauge theories, grav. constant time depend. and antigravity 80—90591
- echo hadrons, colour confinement and fractionally charged states 79—67506
- education, EM wave interaction with matter, gauge invariant formulation 78—62006
- education, gauge invariance, analogy with relativity, particle internal symmetry 78—49595
- education, gauge symmetry breaking, geometrical approach, superconductivity and spontaneous symmetry breaking 80—57028
- effective Lagrangian in spontaneously broken gauge theories 79—17653
- effective potential for non-Abelian gauge theories and spontaneous symmetry breaking 80—4863
- effective potential for spontaneously broken gauge theories and gauge hierarchies 80—18080
- effective potential of Coleman-Weinberg Lagrangian, simple computation 78—8543
- effective potentials in gauge field theories containing scalar bosons 78—21330
- eight quark model, CP violation, heavy quark degeneracy, explanation of $K_L\to 2\pi$ 77—26490
- eight quark model based on $SU_w(2)\times U_w(1)$ gauge theory, ν reactions and e^+e^- annihilations 78—16982
- eight quark model by adding horizontal SU(2) gauge to Weinberg-Salam model 79—71682
- Einstein's impact on theoretical physics 80—77677
- Einstein symposium, Berlin, Germany (Mar. 1979) 80—90596
- Einstein theory of gravity, quantized, test of gauge invariance and unitarity 77—13673
- Einstein vacuum and Einstein-Maxwell space-times, infinitesimal holonomy group structure and geometrization 80—73252
- Einstein-Cartan theory, with anticommuting variables, quantisation in Diracs Hamiltonian formalism 79—93017
- Einstein-Cartan theory as Poincare symmetry gauge theory 77—22463
- Einstein-Maxwell, field theory with teleparallelism and Dirac electron *(German)* 79—9168
- Einstein-Maxwell equations: gauge formulation and solutions for radiating bodies *(German)* 80—27194
- Einstein-Yang-Mills theory, gauge theory and symmetry 77—22464
- Einstein-Yang-Mills theory, grand unified schemes and spontaneous compaction 77—87896
- Einsteins gravitation theory as a gauge field 79—26209

gauge field theory continued
- electric and magnetic charges as extra components of four momentum 79—71603
- electric charge possible nonconservation in spontaneously broken gauge model 79—71620
- electric dipole radiation interactions, implications of gauge invariance 79—30268
- electrodynamics, field intensity and relativistic considerations in choice of gauge 79—54287
- electrodynamics, quantisation, gauge invariance and mass without spontaneous symmetry breaking 79—89088
- electromagnetism and conformal phase group 77—67360
- electromagnetism without monopoles, in nontrivial U(1) fibre bundles 80—12920
- electron anapole moment, static parity violating coupling to EM field, unified gauge theory 80—68390
- electron gas, relativistic, ground-state energy 78—8536
- electron mass, truncated, gauge dependence 80—22542
- electron-monopole system dynamics in U(1) gauge theory 79—54247
- electrons and gravitational instantons 79—25961
- electroweak gauge models with heavy W bosons, $SU_2\times U_1\times U_1'$ scheme *(Russian)* 80—86652
- electroweak gauge models with sequential W and Z bosons 80—101971
- electroweak interaction model based on $U_L(2)\otimes U_R(2)$ left-right symmetric gauge group 80—57544
- electroweak interactions, dynamically broken gauge theories, CP nonconservation without elementary scalar fields 80—86613
- electroweak interactions beyond Z pole 79—97568
- electroweak theory in $SU(2|1)$ 79—63402
- elementary particle appl. *(Chinese)* 79—63338
- elementary particle classification and quark model, symmetry breaking gauge theories, unified theories 79—346
- elementary particle interactions, unification rel. to origin of baryons in Universe 79—62938
- elementary particle interactions, unified theories from non-Abelian gauge theories 80—62903
- elementary particle symmetries, axiomatic approach 79—21897
- elementary particle theory, mathematical method, conf., Liblice, Czechoslovakia (June 1978) 79—21891
- elliptic meron-antimeron soln. of Minkowski SU(2) gauge theory 80—337
- EM and weak interaction unification, bearing of Weinberg model and gauge invariance *(German)* 80—32054
- EM field algebraic quantisation 79—63391
- EM field without indefinite metric, relativistic invariance 78—8565
- EM four pot., transformation properties, gauge invariance 80—91002
- EM interactions, gauge formulation, $SU_\tau(2)$ internal symmetry and P- and CP-violation *(Russian)* 80—42368
- EM potential, two degrees of freedom quantisation for any gauge 77—22670
- EM theory, quantisation 77—61176
- embeddings of gauge groups in Yang-Mills theory, SU(3) case 78—93802
- energy density commutator for massless spin 3/2 field in a covariant gauge 79—71335
- energy-momentun tensor, renormalisation of gauge invariant operators 77 205
- equivalence theorem, validity in nonperturbative context 79—26214
- Euclidean field theory, nonclassical configs. as minima of constrained systems 78—70256
- Euclidean gauge theory, four dimens. QCD, quark confinement mechanism 77—30321
- Euclidean gravity, asymptotically flat self-dual solns. 78—45834
- Euclidean Green functions, quantum fluctuations of instantons 79—26220
- Euclidean Higgs fields, topology 78—4759
- Euclidean lattice gauge theory, selfadjoint, strictly positive transfer matrix 77—65071
- Euclidean light cone gauge, 1/N expansions with non-isoscalar gluons 80—47169
- Euclidean manifolds, N-dimensional instantons and monopoles 80—42321
- Euclidean QED_2 on lattice, continuum limit, Schwinger functions, vacuum expectation values 80—73624
- Euclidean QED_2 on periodic lattice, continuum limit 80—18092
- Euclidean quantisation of gauge theories, Weinger integral and nonstandard analysis 80—68358
- Euclidean R^4, nonAbelian gauge field theory, instanton solns., role of scalar fields 77—82671
- Euclidean space, spherically symmetric self-dual eqns., representation theory and integration 80—77936
- exact classical solutions of the massless α-model with gauge fields in Minkowski space 79—17619
- exact SU(n) instantons with cylindrical symmetry, SO(3) symmetric 79—9290
- exceptional gauge groups and quantum theory 79—35983
- exceptional gauge theories in 3×3 matrix formalism 78—70248
- exceptional groups and elementary particles 77—18191
- existence near instantons *(Russian)* 80—27414
- exponential loop integrals, functional equation 79—35935
- extended hadrons, de Sitter fibre bundle, gauge theory of strong interactions 77—18189
- extended hadrons and quark confinement, description using nonlinear De Sitter symmetry 78—58140
- extended hadrons in geometrically formulated gauge dynamics with fibre bundles 80—9141
- extended $N=4$ supersymmetric gauge theories, off-mass-shell formulation 80—77959
- extended object field geometry 80—57499
- extended objects, gauge theory, Lagrangian formation, eqns. of motion 79—97508
- extended structures described by Z(N) spin and gauge models, applications 79—67479
- extended supergravity, eqns. of motion in terms of geometrical quantities in superspace 78—65856
- extended supergravity, gauge internal symmetry 77—38115
- extended supergravity, $N=3,4$, meson type classical solns. 80—90755
- extended supergravity, three loop counterterms, nonrenormalisability 78—65854
- extended supersymmetric theories, spontaneous generation of massive multiplets and central charges 79—35958

gauge field theory continued
  - extended supersymmetry and gauge theories, superfields formulation 78—41410
  - factorised gauge solitons for compact gauge groups in n dimens. 79—21944
  - Faddeev Popov ghost fields, secondary and higher generation ghosts 80—73578
  - Faddeev Popov ghost fields, vanishing norm 78—8523
  - Faddeev-Popov ghost field, explicit classical construction, Yang-Mills field 80—82874
  - Faddeev-Popov procedure and Gribov copies in gauge theories, QCD appl. 78—32979
  - Fermi quantisation of Landau gauge 78—54591
  - fermion and boson fields interacting with gravitational fields 78—86208
  - fermion fields, spin 1/2, 3/2, accelerated states, stress-energy tensor vac. expectation value 78—70313
  - fermion fields, vanishing theorem, harmonic spinors 78—62314
  - fermion mass, unified gauge model based on E6 80—32053
  - fermion mass generation, regularisation 80—9090
  - fermion masses, short distance chiral invariance *(Russian)* 77—10187
  - Fermion number violation in the presence of instantons 79—12949
  - fermion theories, path integral 80—82896
  - fermion zero modes in soliton fields 78—8517
  - fermionic solitons in gauge theories and their quantum corrections 80—101927
  - fermions, charge density phase transitions in gauge theories with spontaneous symmetry breaking *(Russian)* 79—2969
  - fermions, massless, isospin 3/2, coupled to N-particle field 79—6298
  - fermions and vortex solutions in Abelian and non-Abelian gauge theories 79—12959
  - fermions coupled to pseudoparticle gauge field, Dirac operator eigenvalues 77—67569
  - fermions on the hypertorus 78—74149
  - Feynman path integral and gauge invariance 80—82601
  - Feynman rules for lattice gauge theory of quark confinement, Green's functions, review 78—93850
  - fiber bundle analysis of global feature of gauge field theory 79—71616
  - fiber bundle structure of gauge field and reduction by the Higgs mechanism 80—82885
  - fibre bundle analysis of topological charges in spontaneously broken gauge theories 79—2910
  - fibre bundle techniques in gauge theories 78—54573
  - fibre bundle with Cartan connection, group contraction 77—74573
  - fibre bundles, gauge theory of strong and EM interactions 78—54574
  - fibre bundles, internal affine symm. of Dirac fields 78—24697
  - fibre bundles, mag. monopoles and gauge fields *(Chinese)* 79—80741
  - fibre bundles and topology 80—105793
  - fibre-bundle approach to gauge field theory 78—58130
  - field operator quantisation rules 78—41405
  - field strength and dual variable formulations 79—35946
  - fine structure constant, estimate in unified theories with unstable proton 80—9133
  - finite temp. gauge theory, Euclidean solns. 77—71423
  - Finsler spaces, physico-geometrical remarks on theory of physical fields 77—22394
  - flavour mixing in ambidextrous $SU(2)_L \times SU(2)_R \times U(1)$ gauge theory 78—12805
  - flavour singlet Wilson operators and coeff. functions in asymptotically free gauge theories 79—67501
  - flavour-changing neutral-current process in gauge models and strong interactions 78—8541
  - fluxon solutions in non-abelian gauge models 79—9287
  - Fock quantisation for indefinite metric gauge fields 80—77942
  - Foldy-Wouthuysen time-depend. transformations, gauge invariance and Pauli Hamiltonian 77—41762
  - forbidden ghost states in non-Abelian gauge theories 79—2929
  - forces between leptons and quarks, a gauge field phenomena 80—91008
  - formulation in quantum field theory framework 79—21908
  - four dimensional gauge theories, classical mass spectrum quantum corrections using supersymmetry algebra 78—89630
  - four flavour $SU(2)_L \times U(1)$, gauge model with unconfined colour, $\Delta I = 1/2$ rule, GIM currents 77—82708
  - four-quark model, $SU_{2L} \times SU_{2R} \times U_1$ gauge group, Cabibbo angle and quark masses 78—25002
  - free automorphic quantum field theory, gauge transformations and field algebras 80—86546
  - free EM field quantisation, gauge invariant fields 80—105817
  - free photon field, generalised Coulomb gauges 77—26466
  - free relativistic particle, Lagrangian approach to quantum theory 79—58867
  - free tensor potential equivalence in QED 80—73579
  - functional bridge between gauge theory and strings in two dimens. 77—45966
  - fundamental length hypothesis, concept in gauge vector field theory 78—93836
  - fundamental length hypothesis in a gauge theory context 80—9101
  - fundamental monopoles and multimonopole solutions for arbitrary simple gauge groups 80—77952
  - G_1, spin depend. struct. function, scaling violations 78—93880
  - gauge ambiguity in $n.A^a = C_2{}^a(x)$ 79—75679
  - gauge Bosons struct., quark-antiquark pair 77—30308
  - gauge conditions *(Chinese)* 79—93281
  - gauge dependence of spectral functions 80—37191
  - gauge equivalent fields, existence near instantons *(Russian)* 80—62865
  - gauge field copies 79—63362
  - gauge fixing in Abelian and non-Abelian theories 79—97493
  - gauge hierarchies beyond the tree approximation 79—67470
  - gauge hierarchy in presence of discrete symmetry, $U(1)_L \times U(1)_R$ and $SU(2)_L \times SU(2)_R \times U(1)$ 80—9094
  - gauge hierarchy problem, proposal for elimination in unified theories 79—75707
  - gauge independ. two body amplitudes, VDM of EM form factors 77—74645
  - gauge independence as a consequence of gauge covariance 79—6274
  - gauge invariance, minimal coupling, and torsion 78—78084
  - gauge invariance and pseudoperturbations 80—22545
  - gauge invariance in operator-product expansion in non-Abelian gauge theory 77—2751
  - gauge invariance in second quantisation, Hartree-Fock and random phase approximations 79—75395

gauge field theory continued
  - gauge invariance of spontaneously broken non-Abelian theories in Bogoliyubov-Parsyuk-Hepp-Zimmermann method 77—49861
  - gauge invariance of transition probabilities 79—97487
  - gauge invariance with massive gauge bosons 80—9107
  - gauge invariant operators, renormalisation, S-matrix elements 79—256
  - gauge lattice systems, transition, duality 79—262
  - gauge supersymmetry, spontaneous breaking, supergravity gauge invariance 79—9277
  - gauge symmetry, dynamical symmetry breakdown, appl. to intermediate vector boson mass relations 79—54269
  - gauge sypersymmetry eqns., spherically symm. soln. 78—4532
  - gauge theories, an introduction for experimental particle physicists 78—82119
  - gauge theories without anomalies 77—2756
  - gauge variables and singular Lagrangians 78—78063
  - gauged $N>4$ supergravity, vanishing one loop β-function, infinite renormalisation 80—86186
  - gauging SU(n/m) 79—67467
  - Gaussian fluctuations: 't Hooft's method and an approximate method 79—85236
  - general approach to the computation of instanton effects 79—12961
  - general gauge graviton loop calculation 80—27204
  - general relativity, gauge field theory 78—36898
  - general relativity, monad method and canonical formalism 78—36896
  - general relativity, quantum field theory, vierbein formalism 80—22263
  - general relativity, superspace, local supersymmetry, superfibre bundle theory 78—77782
  - general relativity 78—36897
  - general relativity reformed as gauge theory in spinor affine space-time 77—22470
  - general self-dual nonAbelian plane waves, R-gauge formulation 80—52408
  - general-relativistic and gauge field theories 78—86212
  - generalised 't Hooft monopole solns. in gauge theories 77—13854
  - generalised Federbush model, current definition, perturbation calcs., gauge transformations 79—6297
  - generalised local gauge symmetry, Ward identities in unified field theories 77—10171
  - generalized dual loop expansion of $U(N_c)$ gauge theory 79—93385
  - generalized gauge field copies with higher order curvature covariants 79—93294
  - generating functional for gauge-invariant Green's functions 79—63355
  - generators, Cawley's counter example to Dirac conjecture 80—13225
  - geodesic in gauge supersymm. 78—12634
  - geometric gravity Lagrangian, SP(4) and general coord. transforms. 78—70039
  - geometric quantisation and internal symm. in gravit. 77—79022
  - geometric quantization and internal symmetry 80—42089
  - geometrical gauge theory of gravit., strong interactions, EM interactions 78—70041
  - geometrical models from fibre bundles in gauge fields 79—21899
  - geometrical unification of gauge and Higgs fields 80—99077
  - geometrodynamical model of extended baryons 77—79251
  - geometrodynamics for quarks and hadrons, currents and gauge invariance 78—45809
  - ghost free non-Abelian, mixing of gauge invariant operators 77—67559
  - ghost-free axial gauge in supergravity 80—57162
  - ghost-free string models, systematic search, struct. constants in gauge superalgebra 79—30719
  - Gibov vacuum copies in terms of harmonic maps for SU_2 gauge theories 80—57488
  - Glashow-Weinberg theorem, neutral currents 78—8582
  - global equivalence of Euclidean gauge and Higgs fields 78—8527
  - global SU(2) conformally invariant theory, pseudoparticle-antipseudoparticle config. 78—24975
  - global U(1) gauge theory, commutational relation *(Chinese)* 79—35919
  - glueball spectra, prod. and decay for QCD and SU(n) gauge theories 80—62941
  - gluon collective excitations, nonabelian gauge theories, effective chiral Lagrangian 79—22034
  - gluon distrib. function, tests of QCD 78—45796
  - gluon mass, lower bound in integer-quark-charge model 80—78042
  - gluon mass shell Ward identities verification in axial gauge 79—13037
  - Goldberger-Treiman relation, corrections, unified gauge-field model 78—16969
  - grand unification from neutral currents in gauge models 80—78009
  - grand unification gauge groups, const. 79—71338
  - grand unification theories and monopoles 77—74580
  - grand unified gauge theories, running coupling constants and unifying mass scale 80—91029
  - graphical gauge transformations, using path-integral proof of gauge invariance 79—35950
  - Grassman number systems, Hamiltonian formalism, canonical quantisation by Feynman path-integral 80—77697
  - gravitation, appl. of Palatini-type variational principle to SL(2,C) gauge invariant Lagrangian density 78—78059
  - gravitation, gauge covariant theory, cosmological constant 79—88865
  - gravitation, gauge field actions and their principle bundle formation *(Chinese)* 79—71331
  - gravitation, gauge formulations, relationship to Riemannian holonomy struct. 80—42131
  - gravitation, gauge theory, special relativistic limit 80—22256
  - gravitation, generalised Gupta program, review 80—12957
  - gravitation, local scale invariant theory, Hamiltonian formalism 78—29033
  - gravitation, Mansouri-Chang gauge theory of gravitation comparison with general relativity 78—36919
  - gravitation, metric-affine theory as gauge theory of affine group 78—32746
  - gravitation, spinor formalism 80—90762
  - gravitation as gauge theory of Poincare group 80—86189
  - gravitation duality in quantisation problem 79—30344
  - gravitation theory, de Sitter gauge invariance and spinor calculus 80—12978
  - gravitation theory with alternative to black holes 80—57168
  - gravitational bubbles, radiative corrections to covariant massless quartically self-interacting meson theory 80—62826
  - gravitational considerations and red shift *(Japanese)* 79—80484
  - gravitational energy, torsion of spacetime included in a quadratic Lagrangian 78—8316

gauge field theory continued
gravitational energy from quadratic Lagrangian with torsion 78—115
gravitational eqns. of Bianchi identity type vac., variational principle 80—4599
gravitational field eqns., gauge covariant, exact one body soln. 78—36899
gravitational field gauge theories, review 80—98848
gravitational field quantised using Feynman path integral 78—73914
gravitational field theory, renormalisable, and cosmological implications 79—44839
gravitational gauge theories 79—80493
gravitational gauge theory, restrictions 77—17893
gravitational gauge theory with no black holes 80—82702
gravitational instanton, CP^2 props. compared with SU(2) Yang-Mills instanton 78—81909
gravitational instanton symmetries, classification 79—63110
gravitational instantons and universal spin structs. 78—78128
gravitational interaction of spin-1/2 particles, Lorentz invariant theory 80—22257
gravitational multi-instanton scalar fields, Greens functions 79—85050
gravitational multi-instantons 79—2693
gravitational theory of symmetry breaking of transformation intransitive groups 80—36912
gravitationally coupled classical fields, decomposition method extension 78—127
gravitino, axial current anomaly, Faddeev-Popov ghosts 80—68120
graviton scatt. amplitude, gauge invariance 80—82700
gravity, broken symmetric theory, unified gauge field breaking 79—30343
gravity, locally scale invariant Weyl theory, conformal and superconformal group 77—74300
gravity, strong-gravity solution, stability under perturbation, Hamiltonian formalism 80—52453
gravity and spin 1 gauge fields 79—21923
gravity and supergravity, conformal, Yang-Mills-like Lagrangians 80—62560
gravity and supergravity on a group manifold, gauge theory 79—21635
gravity as a Goldstone field in the Lorentz gauge theory 80—31655
gravity as gauge theory of de Sitter group, fundamental length parameter 77—64990
Green's exponential functions, chiral and gravitational 79—97490
Green's functions, nonperturbative generating functionals 80—73588
Gribov's ambiguities and horizons 79—71639
Gribov ambiguity, gauge transform. on set of all connections of principle bundle 78—58108
gribov ambiguity, perturbation theory, and confinement 79—21934
Gribov ambiguity, same origin as spin 3/2 field problem 78—93808
Gribov ambiguity in general relativity, solns. in Coulomb gauge 79—54023
Gribov ambiguity without topological charge 80—4864
Gribov copying, effect on gauge theory functional integral 79—93288
Gribov degeneracies, Coulomb gauge, conditions and initial value constraints 79—58864
group weight and vanishing graphs 80—57482
guage fixing problem around classical solns. of Yang-Mills theory 78—70260
H spaces admitting a Killing vector, classification 80—105
hadron decay, ν sources, right hand weak currents and direct neutrinos *(Russian)* 77—82699
hadron mass, instanton effects on light quark spectroscopy, MIT bag model 78—62372
hadron mass spectrum in lattice gauge theory 78—74139
hadron states, quark sea and non-Abelian gauge field contrib. 79—327
hadron superconducting quark model quantum corrections 77—6082
hadronic bag quark confinement through tensor gauge fields, de Sitter microuniverses 79—22045
hadronic gauge couplings in meson decays 80—102037
hadronic neutral current struct. 78—24994
hadronic reactions, trajectory slopes in gauge-dual-topological approach 80—18142
hadronic transitions between $q\bar{q}$ bound states, colour gauge field theory 78—37181
hadronic wave eqns. from lattice gauge theory, breathing modes 79—97586
hadrons, QCD model, asymptotically free field theory, anomalous dimensions of composite particles 80—73665
Hamilton-Jacobi formalism for strings, string-gauge theory link 80—78048
Hamiltonian classical mechanics, EM and gravitational fields 80—13202
Hamiltonian classical mechanics, gauge theory for long range fields 80—86077
Hamiltonian dynamics, interacting gravit. gauge and Higgs fields, spherical symm. appls. 77—54051
Hamiltonian dynamics of particles with gauge degrees of freedom 79—75330
Hamiltonian form for massless higher-spin fermions 80—52412
hamiltonian formulation of non-Abelian gauge fields and nonrelativistic bound states 78—70280
hard-soft renormalization of massless fields 80—13214
Hausdorff dimensions and gauge theories 79—35942
heavy Higgs scalars, in $SU(2)_L \times SU(2)_R \times U(1)$ gauge theory, no decoupling at low energy 79—13018
heavy Higgs scalars and the renormalization of spontaneously broken gauge theories 79—71607
heavy lepton model of rare μ and K decay modes 78—45898
heavy leptons, weak gauge boson and neutrino trimuon prod. 78—4851
heavy quark pot., instanton effects, effective Hamiltonians 79—22048
heavy quark potential, non-perturbative contrib., appl. to QCD 79—13025
heavy quarkonium decay in the presence of instantons 79—85296
heavy stable neutral lepton, astrophysical consequences of existence 78—93091
Heisenberg equations of motion in a nonabelian gauge theory *(German)* 80—27387
Heisenberg spin systems, two-dimensional, phase diag., renormalisation group approach to phase diag. 80—4847
hidden gauge symmetry, appl. to elementary particle fundamental interactions 79—30658
hidden ghosts in antisymmetric tensor gauge fields coupled to gravity 80—82889
hidden global symmetry apparent after local symmetry breakdown, possible spin-zero leptons 77—57453

gauge field theory continued
Higgs and gauge fields, group actions on principle bundles and dimensional reduction 80—105770
Higgs boson, charged and trimuon events in neutrino reaction 78—21413
Higgs boson, spontaneously broken gauge theory phenomenon, possible weak interaction model 78—74200
Higgs boson couplings, charged, K_L-K_S mass-differences 80—62917
Higgs boson mass and weak interaction strength at very high energies 77—46013
Higgs Boson nature, test in $e^+e^- \to$ HHZ 79—63405
Higgs bosons, effects on experimental observables, and fermion mass scale 80—32061
Higgs bosons, masses, gauge hierarchies, SU$_5$ model 80—47236
Higgs bosons from two-gluon annihilation in pp collisions 78—41501
Higgs bosons in gauge models with right-handed charge currents 77—49892
Higgs bosons in $SU(2) \times SU(2) \times U(1)$ left-right gauge field, coupling strength 79—13017
Higgs exchange in guage models with right-handed charged currents P and CP invariance 78—12824
Higgs field zeros for axially symmetric multi-monopole configurations 80—82887
Higgs fields and the determination of the Weinberg angle 79—40709
Higgs mechanism, spontaneous symm. breaking in local gauge quantum field theory 78—396
Higgs mechanism and non-linear realisation for extended supersymmetry 78—16941
Higgs mechanism and the inverse Einstein-Infeld-Hoffman problem 79—63100
Higgs mechanism in temporal gauge 78—70278
Higgs meson prod., muon-number violation 78—41422
Higgs meson prod., possible signals in high energy collisions, gauge groups 78—89649
Higgs model, 1+1 dimensional, charge confinement and vacuum struct., instantons 80—341
Higgs self coupling effects on asymptotic freedom 79—266
Higgs-Boson mass, weak interactions at very high energies 78—8540
Higgs-Kibble mechanism, superfield theoretical treatment 78—89616
Higgs-Kibble mechanism and electron-muon mass ratio 78—66065
high spin fields with antisymmetric tensor-spinors and Maxwell-like field equations 80—105772
high temperature behaviour, symmetry restoration, renormalisation group methods 80—31996
high-energy physics, particles and interactions, accelerators 80—77944
higher spin gauge fields, beyond 3/2, systematics 80—46937
history of quantum field theory, search for unity 78—28904
homogeneous isotropic universe, closed type, spontaneous breaking of guage symmetry *(Russian)* 77—45979
homoheneous isotropic universe, influence of extra dimensions 80—51928
horizontal gauge symmetry as a natural CP-violation source at the two-generation level 79—93310
horizontal symmetries dynamical symmetry breaking and neutrino masses 80—105830
horizontal-quantum-flavor-dynamics approach to the fermion mass spectrum in $[SU(2) \times U(1)]_{WS} \times U'(1)$ gauge 80—52474
hypercomplex quark fields and quantum chromodynamics 79—93344
indefinite metric quantum field theory of general relativity 78—65853
indefiniteness of gravitational action, path integrals convergence, one-loop approx. 78—70318
index theorem boundary terms for gravitational instantons 80—123
index theory and axial current anomaly in two dimens. 78—4778
induced spontaneous sypersymmetry breaking in first order 77—211
infinite conservation laws for EM and asymptotic gravitational fields 79—21613
infrared attractive fixed points, gauge symmetries, QED and anti-grandunification 80—95213
infrared divergences in non-Abelian gauge theory 77—6001
infrared regularizations in a model gauge theory 79—30700
infrared singularities of self energy functions in axial gauge 77—2746
infrared unstable, low-energy spectrum, appl. to quantum chromodynamics 77—2793
inhomogeneous local gauge transformations in spacetimes with torsion 79—71330
instanton, group theoretical aspects 79—97494
instanton distribution, external field effects in SU(2) gauge field 80—4849
instanton effective size estimate from gluon field strength tensor vacuum expectation value 78—70326
instanton effective size in dilute gas model, $q\bar{q}$ spin exchange force 79—6258
instanton effects in bound state dynamics, quark-antiquark binding, gluon-instanton interactions 79—6280
instanton effects in finite density and temperature OCD 80—9139
instanton effects on axion mass 78—58127
instanton effects on static $\bar{Q}Q$ potential 79—9333
instanton Green functions and tensor products 79—54252
instanton interactions, inequivalent embedding of SU(2) 77—10180
instanton interactions and Riemannian geometry 77—71447
instanton interactions at one-loop level in non-Abelian gauge theory, topological charge 79—6282
instanton phenomena, real time approach, multidimens. potential with continuous symmetry 79—2922
instanton poles and jumping lines of algebraic vector bundles on P^3 79—97520
instanton singularities, Borel summing, method introduction 79—71624
instanton soln., Dirac eqn. 78—82100
instanton solns. for coupled nonlinear scalar and fermion fields 77—79220
instanton solution symmetry *(Russian)* 77—38094
instanton solutions in Euclidean space, geometrical interpretation 79—40672
instanton solutions on arbitrary four dimens. compact manifolds, no. of parameters 78—41406
instanton system weakly interacting with anti-instanton system, external electric fields, structure and stability 80—77956
instantons, dynamical role in quarkless chromodynamics, bag model test 80—47246
instantons, generation of meson mass spectrum, current algebra, mixing angles 80—86567
instantons, gravitational, flavour currents of QCD, Green's functions, foam-like structure of space-time 80—62825

gauge field theory continued
instantons, high-dimens., topological charges in SU(3) group 79—30638
instantons, numerical significance at short distances 78—70339
instantons, relationship to confinement, one-dimens. quantum mech. model anal. 79—12962
instantons, the quark model, and the 1/N expansion 79—36005
instantons and embeddings in gauge field configurations, group theoretic study 80—4878
instantons and fermions in the field of instanton 79—26217
instantons and Higgs fields 79—21957
instantons and infrared divergences 78—70284
instantons and Kahler manifolds 79—12925
instantons and quark-mass generation—the how of spontaneous chiral symmetry breaking 80—4963
instantons and restoration of symmetries 78—66033
instantons in $N \to \infty$ limit, weak and strong coupling β-functions 80—95217
instantons in non-perturbative QCD vacuum 80—47243
instantons in nonAbelian gauge theories and QCD mesons 80—105777
instantons in quark plasma, multibaryon hadrons and neutron stars 79—40733
instantons in U(1) lattice gauge theory, Coulomb dipole gas 78—8351
instantons on line, gauge equivalence to fields 78—62310
intense field electrodynamics, Goppert-Mayer gauges 80—99075
interacting instanton-antiinstanton system under external colour mag. fields in SU(2) gauge 80—101920
interaction of scalar field with nonstationary vector field, spontaneous breaking of gauge invariance 78—8545
interaction potentials for multiquark states from instantons and other background gauge field configurations 80—101995
internal gauge symmetry theory 79—12958
internal symmetry origin 77—45959
interquark potential, instanton contrib. in dilute gas approx. 80—37220
invariant integration over SU(N) 79—243
invariant supersymmetry space integrals using nonmetric formalism 78—4796
invariants of equivalent Lagrangians 79—40654
IR singularities in gauge theories, renormalisation group method, coupled massless field theories 78—54538
Ising model-gauge field analogues, universality 80—18068
isofermion Dirac particles, energy spectra in 't Hooft Polyakov monopole field 78—24965
isotopic breaking of gauge symmetry 79—97517
isotropic cosmological models, vacuum stress energy tensor and particle creation *(German)* 80—94901
jet processes in QCD 78—82104
jet struct. of hadronic final states, Bose-Einstein effect 78—16994
K-M matrix calc. using horizontal gauge *(Chinese)* 80—101931
kerr-Schild geometry, spinors, and instantons 79—35601
Killing vectors in gauge supersymmetry 79—131
kinetic energy trajectories, decomposition of vac. manifold 78—24951
Kugo-Ojima formalism for gauge theories, unitary proof validity 80—37164
Lagrangian formalisms with CPT violation, causal Lagrangian, gauge theories 78—62303
Lagrangian formulation for gauge theory of strong+EM interactions defined on Cartan bundle 78—16964
Landau gauge, commutators for integer spin fields 78—93807
Landau gauge formalism for non-Abelian gauge theories, Lagrangian gauge fixing term 79—6285
Landau gauge realisation in QED 77—22672
large transverse momentum behaviour of Compton scatt., Moller scatt., and quark-quark scatt. 77—71429
large-N lattice gauge theory, third-order phase transition 80—52418
lattice Abelian gauge fields, approx. scheme 77—41547
lattice and continuum gauge theories, rigorous results 80—4880
lattice confinement, gauge fixing and transfer matrix 77—41766
lattice Coulomb gas representations of two-dimensional problems 78—70068
lattice Coulomb-gas representation of two-dimensional problems 79—58650
lattice Dirac eqn., spectral degeneracy as function of lattice shape 78—376
lattice fermions, Dirac fields and Thirring fields, spontaneous breaking of chiral symm. 78—24962
lattice field theory Dirac eqn. 78—24924
lattice formulation of general relativity 79—40426
lattice gauge field theories in 2-dimens., continuum limit 77—41765
lattice gauge fields, review 78—45797
lattice gauge models in strong coupling regime, quark confinement 77—49835
lattice gauge theories, boxiton scatt. cross section 80—82890
lattice gauge theories, chiral symmetry dynamical breaking 80—99061
lattice gauge theories, effective actions 78—29239
lattice gauge theories, extrapolation to continuum limit 80—349
lattice gauge theories, selfduality and topological-like props. 80—22506
lattice gauge theories, strong coupling phase large space-time dimension, Ising model 80—27397
lattice gauge theories, two dimens., static quark confinement 79—35916
lattice gauge theories, U(N) and SU(N), non-planar diagrams in large N limit 80—47187
lattice gauge theories, vortex free energy, strong and intermediate coupling string tension 80—105786
lattice gauge theories, Z(N) system phase struct., dual variables 80—62848
lattice gauge theories with fermions, cluster expansion 78—58119
lattice gauge theories with fermions, phase transitions and renormalised struct. 78—82105
lattice gauge theories with Higgs fields, phase diagrams 79—85231
lattice gauge theory, 4-D Z_2 gauge, verification of first order phase transition 79—58876
lattice gauge theory, constructive method for gauge invariant actions, strong and weak coupling 79—6284
lattice gauge theory, coupling consts. and meson two-body decay amplitudes 77—34126
lattice gauge theory, extreme environments and duality transform., review 79—13024
lattice gauge theory, gauge-fixing and mass renormalisation 78—24949
lattice gauge theory, local struct. Kirkwood-Salzburg eqn., recursive eqns., critical behaviour 79—26207

gauge field theory continued
lattice gauge theory, map between corner and link operators, QCD relation 79—35926
lattice gauge theory, phase transitions, recursion relations 78—24953
lattice gauge theory, string model, hadron spectrum, Regge trajectories 77—57452
lattice gauge theory, strongly coupled, confinement of fermions 79—2905
lattice gauge theory, Z_N Abelian group, phases, duality 80—42323
lattice gauge theory *(Chinese)* 79—63336
lattice gauge theory and spin systems, review 80—22528
lattice gauge theory continuum limit, renormalised perturbation theory, lattice Lagrangian 79—6283
lattice gauge theory with fermions, renormalised phases, vacuum polarization 80—13198
lattice Hamiltonian, strong-coupling calcs. and Pade approximants 78—4762
lattice massive Schwinger model, renormalisation group approach 77—30246
lattice nonlinear $O(2)_3$ model, phase transition between broken/unbroken symmetries 79—9147
lattice QCD_2, Wilson's loop eqn. soln. for large N limit 80—78030
lattice QCD, mass levels of boxiton (glueball) states 79—54259
lattice regularised field theory, renormalised and bare coupling constants 80—77960
lattice Schwinger model, form factors of dipole states 78—66029
lattice SU(N) gauge theory, vacuum structure, large-scale 80—57470
lattice theory, reconstruction of Euclidean fields from plane rotator models 79—97509
lattice theory, space-time symmetries of (2+1) dimens. Dirac eqn. 78—4799
lattice theory of SU(N) gauge fields, non-convergence of 1/N expansion 77—71427
lattice U(1) gauge fields, quark trapping 77—18175
leading IR divergences in quantum chromodynamics, behaviour in axial gauge 77—13924
left-right symm. gauge model, neutral gauge boson 78—29289
left-right symm. gauge theories, CP violation, absolutely stable hadrons 78—74155
left-right symmetric gauge models, parameter constraints from neutral current data 80—86588
left-right symmetric gauge models, $SU(2)_L \times SU(2)_R \times U(1)_L \times U(1)_R$, weak currents, Z^0 prod. and mass 79—253
left-right symmetric $SU(2)_L \times SU(2)_R \times U(1)$ gauge theory, atomic P violation 78—74144
left-right symmetric $SU(2)_L \times SU(2)_R \times U(1)$ theory, atomic parity, e^+e^- collisions asymm. at PETRA, PEP energies 78—12820
left-right symmetric SU(N) gauge models, parity violation in atoms 79—21966
left-right-symm. unified theory of quarks and leptons 78—41466
left-right-symmetric theory of weak interactions in unified gauge theory, constraints on phenomenology 78—21369
Lehmann-Symanzik-Zimmermann formulas in a gauge-independent path-dependent formalism 79—21942
lepton number nonconservation with scalar bosons 78—4798
lepton pair prod., hard-scatt. expansion 78—66091
lepton pair production in two-dimens. QCD 77—74644
lepton structure, SU(2)×U(1) gauge theory 77—82691
lepton structure model 80—91063
lepton-hadron deep inelastic scatt., massive vector gauge model *(Russian)* 78—89720
lepton-quark and space-time symmetry 78—16967
leptonic exotic decays of muon and heavy leptons in gauge theories 77—49939
leptonic interaction gauge model in SU_3 with 30° Weinberg angle 80—4903
leptons, SU(3) electroweak theory 80—86638
leptoquark bosons, confinement in SU_4 theory 79—45052
lh theory of leptons and hadrons, unification in $GA_{4,R}$ gauge 80—86639
Lie algebras, BRS transform. 78—93591
Lie-admissible deformation of self-adjoint systems 80—101941
light cone gauge theories, singlet gauge operator nonconservation, QCD flavour charge operators 80—52462
linear deformations of the Prasad-Sommerfield monopole 80—52419
linear gauge theory algebraic struct., spontaneously broken symmetry, quantisation, massive gauge field 79—2906
linearised GL(4) gravities, dynamical structure 78—65846
linearised gravitational pot., Euclidean and Minkowski space formulations 80—121
local covariant gauge quantum field theories, cluster property 78—70265
local determination by field strength and gauge derivative *(Chinese)* 77—67579
local field theory and superselection rules 77—18190
local field theory of solitons 79—12953
local gauge symmetry, dynamical stability and large distance behaviour 80—90991
local operator products, gauge invariance and renormalisation 78—358
local operator products 78—12804
local structure of functional spaces and dynamical variables of gauge-invariant fields 80—9099
local symmetry groups and fermion families 79—13030
local Z(2) lattice gauge theory, gauge and matter screening 79—89065
locally supersymmetric theories with model-independent transformation laws 78—93819
long distance behaviour of singlet current correlation functions of gauge theories on lattice 77—13858
secret long range force in QFT with instantons 79—9283
long-range quantum effects in IR stable Yang-Mills system 77—67565
loop phase factor approach, equivalence problem, space-time symm. *(Chinese)* 78—82110
loop-space representation and the large-N behavior of the one-plaquette Kogut-Susskind Hamiltonian 80—99060
Lorentz covariance and EM props. of elementary systems 80—32037
Lorentz gauge field in Riemannian space, spherically symmetric static exact solns. 80—4596
Lorentz invariance of quantum field theory of electric and mag. charge 78—33010
lorentz transformations of observable and ghost particle states in quantum electrodynamics and in a massive gauge theory 78—66061
low energy light particle processes in spontaneously broken gauge theories, heavy particle effects 80—22521

gauge field theory continued
- macroscopic gauge theory of gravity, uniform gravitational collapse, lepton pair creation 78—81724
- magnetic charge in SU_2 and global U_1 gauge theory *(Chinese)* 77—71437
- magnetic charge of Yang-Mills fields, in terms of Higgs fields, SO(4), SU(4) 77—45935
- magnetic charge operator 77—79215
- magnetic charges, quantum strings and gauge invariance 78—33009
- magnetic field effect on particle, gauge variance 80—47167
- magnetic flux metamorphosis in spontaneously broken gauge theories 80—99047
- magnetic monopole, energy tension and gravitational field *(French)* 80—52075
- magnetic monopole long range interactions in non-Abelian gauge fields 80—22520
- magnetic monopole soliton solns., gauge particles 78—16920
- magnetic monopole solutions to SU(3) gauge model 77—6047
- magnetic monopoles, gauge theory 77—64950
- magnetic monopoles and topological lines 78—16907
- magnetic monopoles in broken SO_3 and SU_2 gauge theories *(Chinese)* 78—86459
- magnetic monopoles in classical field eqns. with a mag. charge 80—4872
- magnetic monopoles in compact simple Lie groups, quantisation condition 77—13869
- magnetic quark confinement, flux tube in gauge field model 77—6084
- magnetically extended Lagrangian theory, 0(3) gauge theories with spontaneous symm. breaking, shared photon sector 78—62306
- Majorana fields and right-handed weak currents in gauge models 77—22643
- Mandelstam-'t Hooft duality in Abelian lattice models 78—78057
- manifestly conformally covariant field equations and a geometrical understanding of mass 80—105788
- many-dimensional solitons, gauge invariant theory of nonlinear chiral field 77—34082
- many-instanton problem, Euclidean supersymmetry 77—74615
- mass corrections to some instanton effects 79—71604
- mass singularities and coherent states in gauge theories, QED and QCD results 79—12948
- mass spectrum for integral isospin monopoles, bag model as high isospin limit 78—24935
- massive, with instantons, wave functions, energies, vacuum and heavy quarks, WKB Schrodinger eqn. 79—35951
- massive gauge fields, complete spontaneous symm. breaking, asymptotic freedom, symplectic and G_2 groups 78—62305
- massive propagators in instanton fields, Green's functions, quantum chromodynamics 79—49390
- massive QED, gauge invariant subtraction scheme 79—21993
- massive scalar field with scalar electrodynamics, spontaneous symmetry breaking 77—61214
- massive Schwinger model, asymptotic completeness and confinement 78—66028
- massive Schwinger model, canonical formalism, dynamical surface terms 77—79221
- massive Schwinger model, consistency and Lorentz invariance 78—89613
- massive Schwinger model, fields and observables 77—45968
- massive Schwinger model, saturation, fermion confinement and instantons 80—47175
- massive Schwinger model, vacuum degeneracy and confinement 78—78090
- massive Schwinger model in infinite momentum frame, phys. particles spectrum 77—49886
- massive spin-zero particles, consistent formulation of relativistic dynamics in external fields 79—21977
- massive supergravity, from spontaneous breaking orthosymplectic gauge symmetry 78—77787
- massive supergravity nonlinear realisation of orthosymplectic gauge symm., coupling to spin 1/2 spin 1 multiplet 78—33019
- massive vector boson field theory with spontaneous symmetry breaking 80—52443
- massive vector fields without scalar fields, renormalisation 78—8528
- massless 't Hooft model, tachyonic modes, vanishing of scalar density 80—77949
- massless Abelian gauge theory, infrared problem and boson suppression 77—2742
- massless Abelian theory, IR singularities and boson suppression *(Russian)* 77—61203
- massless antisymmetric tensor gauge fields, second rank, free field theory quantisation 79—257
- massless BPHZ renormalised QED, IR finiteness 77—74623
- massless fermion coupled to single axial vector field in U(1) model, AAA triangle diagram 79—35965
- massless fermion effective action with instantons perturbation theory vacuum for QCD 79—71608
- massless fermion representations in grand unified gauge theories 79—97553
- massless field supermultiplets with arbitrary spin, gauge transformations and Lagrangians 79—85240
- massless field theory observables, infrared finiteness proof for all perturbation theory orders 79—21917
- massless fields with half-integral spin 79—21926
- massless fields with integer spin 79—21925
- massless gauge theories, supersymmetric extension, supercurrent construction principle 79—40664
- massless non-Abelian fields, study of state vectors using Schrodinger equation *(Russian)* 79—30667
- massless QCD, instanton contribs. to fermion Green's functions 79—22037
- massless QCD 78—78093
- massless QED, dimensional regularisation of gauge fields in spherical spacetime, free field trace anomalies 79—40699
- massless Rarita Schwinger field, axial current quantisation, chiral charge of ghosts 79—2918
- massless Rarita-Schwinger field, covariant canonical quantisation 79—97280
- massless spin 3/2 field, covariant canonical quantisation in general covariant gauges 79—40440
- massless spin 3/2 field, irreducibility 79—35620
- massless spin 3/2 theory, unmixed spinor representationof Lorentz group 77—18163

gauge field theory continued
- massless spin two field, covariant quantisation in general covariant gauge 78—66027
- massless $[g\phi^4]_4$ theory, functional integrals, complex instantons and asymptotic perturbation series 80—86571
- mathematical formulation of gauge theory 79—40656
- mathematical idea in gauge theories 79—26204
- matter couplings in supergravity theory 77—17895
- Maxwell's equations in axiomatic QFT, field tensor and pots. 77—71421
- Maxwell field quantisation in linear conformal invariant gauges 79—71666
- Meissner effect in gauge fields 78—29250
- membrane models and generalized Z_2 gauge theories, renormalisation props. 80—86587
- meron and meron pair analogs in XY model 80—32010
- meron configurations in two dimens. O(3) σ model 78—32983
- meron solutions in a non-Abelian, conformal invariant Higgs model 79—17610
- meronic solution class for charged particle conformal invariant interaction 80—90983
- merons and other field configurations, SU(2) theory *(Chinese)* 79—63335
- meson mass generation in chiral flavour U(3)×U(3) symmetry by instantons 79—89121
- meson masses in gauge theory with harmonic oscillator pot., coloured quark-gluon model 79—350
- meson spectrum calc. from quark model 77—71485
- meson wave functions in 1+1 dimens. QCD 78—54559
- meson-mass generation by instantons in coloured gauge field theory 79—54321
- metastable vacuum states in SU(2) Yang-Mills theory, quantisation in $A_0=0$ gauge 79—250
- metric existence in 2-D affine manifolds 79—85039
- metric-affine unification of gravity and gauge theories 79—63109
- milliweak gauge models of CP violation 80—73633
- minimal anomaly-free electroweak model for several generations 80—4906
- minimal gauge theory of leptons, new heavy lepton, associated neutrino, muon number nonconservation 77—54096
- minimal surfaces in pseudo-Euclidean space, correl. with instantons, SU(2) gauge field solns. 79—21936
- mixing of leptons with different quantum numbers in gauge theories of weak and EM interactions *(Russian)* 78—54601
- mixing of states containing heavy quarks 78—422
- model of weak and EM interactions with SU(3)xU(1) symm. *(Russian)* 77—6074
- model U(N) lattice gauge theories, exactly soluble, $N=\infty$ phase transition 80—86583
- model with spontaneous P-violation, anal. of spontaneous CP violation 77—38113
- models of dynamically broken gauge theories 80—77974
- modified supersymmetries 79—45024
- molecules under static mag. field, gauge invariance 80—102587
- momentum subtraction scheme, quark mass depend. cancellation in anomalous dimens. 80—77965
- monopole, accelerated, field strength determ. *(Chinese)* 78—77740
- monopole bound states, SU(4) spontaneously broken 77—82679
- monopole classification in SU(2) and SU(3) gauge field theory 77—38082
- monopole concept and elementary theory 79—49366
- monopole soln. uniqueness 77—41760
- monopole solns., Lorentz transformations, Poincare group algebra representation 78—16925
- monopole solns. in spontaneously broken SU(n) gauge theory 78—82103
- monopole solutions for strong gravity coupled to SO(3) gauge fields 80—4621
- monopole theories, geometrical aspects 77—74591
- monopole-dyon system in nonAbelian gauge theories, Georgi-Glashow model 77—79213
- monopoles, topology and symmetry 79—49370
- monopoles 't, Hooft type, time depend.-generalizations, gauge theory solns. 77—6023
- moving nonAbelian charge, radiation emission, nonAbelian gauge theory solns. 80—52405
- multi-instanton determinants for covariant laplacian D^2, 't Hooft solution extension 80—13216
- multicomponent chiral and gauge models, stationary solns. 79—85213
- multiple vacua for non-Abelian lattice gauge theories 79—35929
- muon g-factor anomaly, review of theoretical contribs. 77—30384
- muon number nonconservation effects in gauge theory with V+A currents and heavy neutron leptons 78—8573
- mutually interacting charge fields, gauge theoretical formulations of elementary particle processes 78—58122
- N=2 supergravity with gauged central charge 78—62349
- n=4 supergravity theory with local SU(2)×SU(2) invariance 78—66067
- N=8 spontaneously broken supergravity, mass matrix, gauge couplings 79—97281
- $n\neq4$ axial vector anomaly, noncontribution 80—62858
- N-dimensional higher order metric space, gauge field theoretical aspects 78—45779
- N-O model, quantum expansion around vertex type soln., energy eigenvalue *(Chinese)* 78—82111
- Nambu-Jona-Lasinio type model for gravity, effective Lagrangian 77—74628
- Nambu-Jona-Lasinio type unified model for gravitational and EM forces 78—65850
- natural flavour conservation in neutral weak interactions, SU(5) and SO(10) unified models 78—4817
- natural lepton models for rare μ decays, doubly charged leptons 77—34143
- neutral current constraints on gauge models of weak and EM interactions 78—45831
- neutral current effects in charged-lepton-nucleon elastic scatt., polarisation asymm. 78—33071
- neutral current expts., left-right symmetry for $SU_L(2)\times SU_R(2)\times U(1)$ gauge group 78—21375
- neutral current scattering expt., test of nonconfinement, gauge theory of physical colour 77—46017
- neutral currents, Higgs flavour-changing, suppression in $SU(2)_L\times SU(2)_R\times U(1)$ left-right symmetric gauge theory 80—78016

gauge field theory continued

- with neutral currents, high-density and high-temp. effects on symmetry breaking 77—22664
- neutral currents and gauge theories, review 79—13011
- neutral currents and quark charge origin 78—21373
- neutral currents in generalised SU(2)×U(1) gauge models 78—45832
- neutral currents in left-right symmetric unified gauge models 79—45044
- neutral currents properties and structure, gauge theory predictions, obs. 78—12856
- neutral gauge bosons props. in weak electron theories with natural parity conservation 79—321
- neutral spinless meson exchange, suppression of flavour changing effects 79—40716
- neutral weak currents at high energy, SU(6) model of weak interactions *(Russian)* 78—45836
- neutrino mass problem, gauge hierarchy 80—90989
- neutrino neutral current couplings in SU(2)×U(1) gauge theories, natural relations, flavour dynamics 79—89095
- neutrino physics and gauge theory, book 79—30726
- neutrino processes, deep inelastic *(Russian)* 77—49943
- neutrino scattering scale breaking models 79—13107
- neutrinos, gauge theories, EM props., forbidden processes and currents with anomalous Lorentz struct. 78—54599
- neutron matter-quark matter phase transition, QCD and extended Higgs model, instantons 80—91062
- neutron oscillation phenomenology in gauge model with spontaneously broken B-L symmetry 80—90996
- Neveu Schwarz Ramond model, complete action for spinning string, field eqns., constraints 77—13943
- new gauge transformation for a generalized quantum representation 80—86136
- new general relativity, geometry translation group gauge theory 77—79020
- new physics from experiments above 100 TeV, appl. to QCD, weak interaction, and gauge theory 79—63564
- Newtonian gravitational theory, continua and particle dynamics 79—6038
- Nielsen Olesen vortex stability in SO(3) Georgi-Glashow guage model 79—49391
- Nielsen-Olesen vortices in coherent state approx., creation and annihilation operators 79—9284
- non abelian gauge fields, conserved axial vector currents 77—30264
- non Abelian gauge theories, relation between fields and pot. 80—22529
- non Abelian gauge theories in external electromagnetic fields *(Russian)* 80—57533
- non-Abelian, 2-D, field strength method and Gribov ambiguity 79—49371
- non-Abelian, asymptotic field theory approach to quantisation 77—22653
- non-Abelian, exponentiation of vector vertex and vector-current coupling 77—13860
- non-Abelian, field strength potential 79—17617
- non-Abelian, gauge fixing and canonical quantisation 79—35947
- non-Abelian, group theoretical weights attached to Feynman diagrams 77—6004
- non-Abelian, Pomeranchuk singularity *(Russian)* 77—30342
- non-Abelian, power counting theorem for infrared logarithms 77—45964
- non-Abelian, quantum effects of pseudoparticle size 77—22648
- non-Abelian, Schrodinger representation 77—2757
- non-Abelian, spontaneous breaking of supersymmetry 77—49878
- non-Abelian asymptotically free theories, composite operator renormalisation 77—65105
- non-Abelian defined on S^4, use of holonomy group in problem of embedding 79—45016
- non-Abelian dyons, Nambu mechs. descript. 78—41490
- non-Abelian fields, canonical quantisation, Lorentz and gauge invariance 77—49852
- non-Abelian fields, transversal quanta 79—85217
- non-Abelian gauge field theory, infrared struct. 78—8534
- non-Abelian gauge field theory, local gauge invariance 78—12813
- non-Abelian gauge fields, canonical quantisation, Lorentz and gauge invariance 77—49852
- non-Abelian gauge fields, hidden singularities 80—52398
- non-Abelian gauge fields, physical degrees of freedom 80—105778
- non-Abelian gauge fields, prepotentials 77—87912
- non-Abelian gauge fields, quantisation and renormalisation, Fadeev-Popov ghosts 77—5979
- non-Abelian gauge fields, symmetry conditions 78—32977
- non-Abelian gauge fields and nonrelativistic bound states 77—71425
- non-Abelian gauge group theory, relationship with solitons 80—4549
- non-Abelian gauge potential, decomposibility in Cartan geometry with zero torsion *(Chinese)* 79—17624
- non-Abelian gauge theories, cancellation of IR divergences 77—13849
- non-Abelian gauge theories, canonical methods, renormalisation 77—41764
- non-Abelian gauge theories, chiral U(1) current 79—85216
- non-Abelian gauge theories, constraints on finite energy solns. 78—58117
- non-Abelian gauge theories, coupling constant IR props., colour confinement 79—93293
- non-Abelian gauge theories, coupling constant IR props., glue propagator 80—31999
- non-Abelian gauge theories, dual transformation, SU(2) Higgs-Kibble models 79—85234
- non-Abelian gauge theories, high energy behaviour, reggeon field theory, QCD 80—62822
- non-Abelian gauge theories, IR behavior 77—67570
- non-Abelian gauge theories, local covariant operator formation, quark confinement 80—47190
- non-Abelian gauge theories, triangle anomalies and renormalisation 77—49837
- non-Abelian gauge theories and mag. monopoles, strong interaction models and quark confinement 79—49367
- non-Abelian gauge theories and quark confinement 79—13022
- non-Abelian gauge theories in a background field, Green's functions 79—75689
- non-Abelian gauge theory, asymptotic of fermion inelastic form factor *(Russian)* 78—45883
- non-Abelian gauge theory, colour model, high-energy hadron interactions 77—45973
- non-Abelian gauge theory, colour-singlet quark form factor anal. 77—65084

gauge field theory continued

- non-Abelian gauge theory, high energy behaviour, T_{n-m} in leading ln s approx., pomerons 79—49374
- non-Abelian gauge theory, nonplanar skeleton graph, vanishing graphs, planarity and Reggeisation 79—97504
- non-Abelian gauge theory, relation between field strength tensor and current 78—24923
- non-Abelian gauge theory in a nonlinear gauge, charged current description 79—12937
- non-Abelian gauge theory of quarks and gluons in two dimens. 79—30654
- non-Abelian gauge theory of strong interactions, EM current renormalisation 79—63350
- non-Abelian gauge theory with many flavours, high energy processes, asymptotical behaviour *(Russian)* 80—101935
- non-Abelian group spontaneous violation, gauge models and external currents *(Russian)* 77—207
- non-Abelian group SU(2) mag. monopole *(Chinese)* 78—78096
- non-Abelian lattice fields, duality 79—93280
- non-Abelian lattice gauge theories, composite hadrons anal. 77—13852
- non-Abelian mag. charge and gauge invariance 77—6011
- non-Abelian mag. charges, quark confinement 77—49849
- non-Abelian massive gauge theory high energy behaviour via Regge field theory 77—61197
- non-Abelian plane EM wave analogues 77—87904
- non-abelian plane-fronted waves 79—67468
- non-Abelian quark-gluon theory, energy-momentum tensor 77—38122
- non-Abelian static forces and the permutation group 79—49382
- non-Abelian symmetries, spontaneous breaking in SU(2) and SU(2)×SU(2), observable consequences 79—26252
- non-Abelian symmetry, Dirac strings and monopoles 77—41773
- non-Abelian theories, dual formulation 80—82902
- non-Abelian theories, struct. of leading IR divergences 78—4785
- non-Abelian theory, axial gauge canonical quantisation 77—22644
- non-Abelian two-dimens. theories, novel inconsistency, quantum chromodynamics 77—65097
- non-Abelian vortex-bond model of hadrons 78—4827
- non-analytic mass behaviour, renormalisation group 77—67558
- non-asymptotically free theories, scaling in deep inelastic processes 77—67568
- non-inertial framed space-time configurations, gauge theory appl. 80—22262
- non-integral gauge theories 79—12675
- non-Riemannian generalised super-gauge formalism, corresponding invariant physical theory 78—82122
- non-self-dual gauge fields 79—9282
- non-self-dual static gauge fields 80—52421
- non-semisimple gauge models, classical theory, ghost state props. 79—6253
- non-semisimple gauge modes, renormalization 79—6254
- nonAbelian, charge sectors of QED, local observables framework 79—58908
- nonAbelian, elastic and inelastic processes involving fermion exchange *(Russian)* 77—61204
- nonAbelian gauge condition ambiguity in the vicinity of instantons, ghost operator *(Russian)* 79—40677
- nonAbelian gauge field, gauge-invariant conserved current *(Chinese)* 78—12806
- nonAbelian gauge field monopole, ang. momentum operator *(Chinese)* 79—58865
- nonabelian gauge fields, soln. of finite string type *(Russian)* 78—391
- nonAbelian gauge groups, dual charge (mag. monopole) problem 79—63376
- nonAbelian gauge model, Becchi-Rouet-Stora invariant, superfield struct. 78—74121
- nonAbelian gauge model, radially separated monopole solns. 77—74593
- nonabelian gauge theories, coherent state approach to IR behaviour 78—82107
- nonAbelian gauge theories, electric and mag. flux props., Georgi-Glashow IR struct. 79—71606
- nonAbelian gauge theories, Euclidean instanton solns. 78—373
- nonAbelian gauge theories, Faddeev-Popov ghost decoupling, QCD gauges and gluons 80—52406
- nonAbelian gauge theories, gauge fixing degeneracies, confinement 78—54545
- nonAbelian gauge theories, path depend. phase factors, point splitting 78—49959
- nonAbelian gauge theories, quantisation 78—78066
- nonAbelian gauge theories, topological configurations, magnetic poles on flux strings 79—49368
- nonAbelian gauge theories with Higgs fields, classical Euclidean pseudoparticle solns. 78—24961
- nonAbelian gauge theory, construction of planar diagrams 77—6031
- nonAbelian gauge theory, Higgs couplings and asymptotic freedom 79—21948
- nonAbelian gauge theory, light quarks and instantons, chiral symmetry breaking 79—63332
- nonAbelian gauge theory, quark and parton phys., introduction, book 79—85276
- nonAbelian gauge theory, spherically symm. monopoles 77—61191
- nonAbelian gauge theory, spontaneous breaking of scale invariance *(Russian)* 77—74604
- nonAbelian gauge theory, spontaneous symm. breaking without scalar mesons 77—30250
- nonAbelian gauge theory, topological symmetry breakdown and quark confinement 79—71611
- nonAbelian gauge theory, transformation into Abelian gauge theory 80—99041
- nonAbelian gauge theory, unification of weak and EM interactions 77—18188
- nonAbelian gauge theory quantisation, nonclassical field configs., broken symmetries, gauge copies 79—49373
- nonAbelian lattice gauge theories, phase structure critical temp. 80—86592
- nonAbelian SU(2) gauge field, dual charge *(Chinese)* 77—34077
- nonAbelian theories with nontrivial gauge transforms., topological tunnelling, Goldstone gluons 78—24956
- noncompact group, soluble gauge theory 80—32013
- noncompletely reducible representations of the Poincare group associated with the generalised Lorentz gauge 78—70249
- noncontinuous gauge potentials without magnetic monopoles 79—93278

gauge field theory continued
- noncovariant effects in the perturbation theory of two-dimensional gauge theories 80—57495
- nonleading logarithm struct. in terms of β-function and anomalous dimens. 80—77964
- nonleptonic decays of ordinary and charmed hadrons, gauge model with right handed current 78—41545
- nonlinear σ model, 2-D, topology and higher symmetries 79—26241
- nonlinear σ-model, Hamiltonian lattice formulation 77—10183
- nonlinear σ-model and classical solns. of instanton and meron type 79—21905
- nonlinear chiral models, modification using non-Abelian gauge fields 78—4792
- nonlinear gauge fields and the structure of gravity and supergravity theories 78—77791
- nonlinear Lagrangians and spontaneous symm. breaking 78—70303
- nonlinear models, gauge theory formulation 79—71627
- nonlinear O(N) σ-model with gauge interactions, two-dimens., phase transitions 77—6029
- nonlinear realisation, unified interaction, spontaneous symmetry breaking 79—13010
- nonlinear realizations of compact and noncompact gauge groups, grand unification 80—47183
- nonlocal properties of fermionic matter in strong gravitational fields 79—26210
- nonlocalization concept 78—21324
- nonperturbative gauge technique soln. for Schwinger model of 2-dimens. electrodynamics 78—78120
- nonperturbative QCD, large N_c, QCD bag model, instantons and η' mass 80—57559
- nonrelativistic algebraic models, gauge invariance, causality props. 78—62319
- nonrelativistic gauge theories, massive fields with nontrivial field eqns. 80—105773
- nonuniqueness of gauge field potentials 77—13861
- nonzero vacuums in non-Abelian gauge theory and infrared divergence 80—52420
- normal-product methods, functional formalism 78—29252
- nuclear force, strong short-range repulsion 78—12880
- nuclei, transitional, pairing rotations and quadrupole modes 80—18165
- nucleon structure function, asymptotically free gauge theory 78—50036
- null gravidynamics, initial value problem and Dirac-bracket relations 78—77781
- O(10), SU(4) colour subgroup, fractional charged gauge boson, proton half-life 80—73644
- O(2) Heisenberg gauge invariant model, eigenfunctions and energy spectrum 79—58875
- O(3) σ-model, nonlinear, quantum fluctuations of instanton solns. *(Russian)* 78—74161
- O(3) model, correct criteria for gauge hierarchies 80—27405
- O(3) nonlinear δ-model, instanton-anti-instanton interactions, fermion theory *(Russian)* 80—47193
- O(3) nonlinear σ-model, mass generation in dense instanton gas approx. 80—82880
- O(4)×U(1) gauge model, restrictions from νN expt. data 77—71477
- O(4)⊗U(1) gauge model for weak and EM interactions 79—71681
- O(5) gauge field coupled system with massless scalar fields in Euclidean space, exact classical solns. 79—97499
- O(5) nonlinear σ-model as a SU(2) gauge theory 79—35937
- observability differences between classical EM and gravitational gauge fields 80—36925
- observable phase factors and symmetry of electric and magnetic charges 78—86428
- octonions in quantum mechanics 80—27479
- one dimensional gauge field theories, at finite temp. and densities, props. and quark confinement 79—49468
- one loop equivalent gauges, one loop infinities and renormalisation constants 80—62842
- one loop finiteness of quantum gravity off mass shell 78—62142
- one-loop counter terms, system with derivative couplings to fermions 79—249
- operator formalism of statistical mechanics of gauge theory in covariant gauges 80—86591
- operator mixing in asymptotically free theories, deep inelastic scattering 78—37145
- operator ordering, gauge fixing in non-Abelian theories 80—77975
- operator ordering and Feynman rules in gauge theories 80—101926
- operator products near light cone, expansion in terms of regular bilocal operators 77—87899
- order-disorder transitions in gauge and spin systems 78—70072
- order/disorder quantum field operators associated with 2—D Ising model in continuum limit 79—9276
- ordered media containing defects, gauge-like variables 79—88889
- $P(\phi)_2$ gauge invariant massive theory 78—41403
- P and T invariance in colour gauge theory of strong interactions 78—37153
- P and T violating electromagnetic interaction of the quark in the instanton field 80—52430
- parity symmetric, consequences for $\mu \to e\gamma$ rate 77—49941
- parity violating asymmetries in polarized electron scattering from p, d, e 80—9111
- parity violating internucleon potential due to vector meson exchange, asymptotically free theories 77—10210
- parity violating neutral currents, radiative corrections, Weinberg-Salam and left-right symmetric models 80—52451
- parity violation in atoms, SU(2)×U(1) models, higher-order corrections 78—45807
- parity-violating nucleon-pion amplitude in unified gauge-invariant models 77—6070
- particle and field equations for gauge theory based on SO(4,1) de Sitter group 79—58868
- particle creations in the pseudoparticle gravitational fields 79—2704
- particle-like solns. of gauge theories 77—41779
- particles, creation in general relativity with torsion and constant electric field 79—88857
- particles in curved space-time, group of parallel transports 78—54602
- partition function of degenerate quadratic functional and Ray-Singer invariants 78—54531
- parton distributions, Q^2 depend., using asymptotically free gauge theories 78—33034

gauge field theory continued
- path dependent formulation and origin of field, copies in non-Abelian case 80—86594
- path group appl. to gauge theory and quarks 80—31985
- path-depend. approach to coloured mag. monopoles 78—37127
- path-integral in collective fields and its application to nuclear and hadron physics *(Russian)* 79—93277
- path-integral measure for gauge-invariant fermion theories 79—54267
- pathological lattice field theory for interacting strings 80—47186
- Pati-Salam model, higher order parton transition effects in deep inelastic scatt. 80—78008
- Pati-Salam neutral vector gluons, possible expt. search in e^+e^- collisions 80—37202
- Pati-Salam $SU(2)_L \times SU(2)_R \times SU(4)$, gauge-c 78—12851
- Pauli-Villars regularization for non-Abelian gauge theories 79—21956
- PCAC, dimensional derivation of gravitational correction 78—21371
- periodic potential energy levels, late terms, asymptotic expansions 79—25895
- periodic solns. to scale invariant classical field theories 77—67305
- periodic vacuums, functional integrals, classical sine-Gordon solns., Coulomb gas props. 79—26226
- periods on manifolds, quantisation, gauge, comments on Kiehn's work 78—8508
- periods on manifolds, quantisation, gauge, topological props. of phys. theories 77—49826
- perturbation expansion, renormalisation, Ward-Takahashi identities, lecture series 77—57460
- perturbation expansion of quantised composite field theory, gauge invariance *(Chinese)* 78—82156
- perturbation theory, gauge symmetry hierarchies upper bounds 80—77958
- perturbative QCD, jets, inelastic distribs., colourless clusters, scaling, multiplicity and tree evolution 80—52459
- perturbative QCD and exptl. signatures of weak bosons 78—93916
- perturbative QCD in a covariant gauge, moments of struct. functions 80—32073
- phase diagrams, dynamic mass generation and renormalisations 80—68365
- phase transition in nonAbelian quantised gauge field theories, permanent quark confinement 78—70322
- phase transition with symmetry restoration 77—5984
- phase transitions, first-order, in spontaneous broken gauge theory 78—24943
- phases, anal. in Ising model, Z_2-theory, order, disorder, lattice duality and non Abelian theory 79—97486
- photon structure functions, QCD predictions in asymptotically free gauge theory 79—30736
- photon-photon, dimensional scatt. amplitude and gauge invariance in lowest order 77—71471
- photon-photon scatt. anomalous cross section 77—38169
- physico-geometrical remarks on unified gauge field and supersymm. concepts 78—37167
- pion production by weak neutral currents, gauge theory model predictions 79—13014
- pionisation region gauge invariance violation for hadrons, K and γ in EAS *(Russian)* 79—40676
- planar approx. to field theory through limit of large internal symmetry group 78—45519
- planar Feynman diagrams in perturbation theory 77—61189
- planar model electrodynamics, phase diagram, continuum limit, and mass spectrum 79—63426
- Poincare covariance of free massive two dimens. quantum string 77—6048
- Poincare gauge invariance, conservation laws for particle, string and membrane systems 79—55
- Poincare gauge theory of gravitation, translational part of Lagrangian 79—2710
- Poincare gauge theory of gravitation 79—75434
- Poincare gauge theory with Weyl-type Lagrangian and gravitation 78—4545
- Poincare group gauge theory, geometric meaning, equivalence to Einstein-Cartan gravitation 80—62845
- point electric and mag. charge, nonAbelian gauge invariant classical Lagrangian formalism 79—12627
- polarised lepton scatt., gauge model of weak and electromag. interactions 78—45901
- Polyakov-'t Hooft monopole and dyon, quantum theory *(Russian)* 78—392
- positronium hyperfine splitting, anomalous contribs., radiation gauge 77—83771
- post-Newtonian approximation of the Poincare gauge theory of gravitation 80—52115
- potential scatt., amplitude, quasiclassical asymptotic behaviour, quantum correction 78—62325
- pre-quarks and fractional charges 80—91048
- precocious chiral grand unification based on $SU(8)_L \times SU(8)_R$ semi-simple gauge group *(Russian)* 80—42382
- preon model for hadron and lepton struct. 78—78124
- presymplectic Hamilton and Lagrange systems, gauge transformations and the Dirac theory of constraints 80—9106
- primordial magnetic monopoles in unified gauge theories 80—91035
- proceedings of the 1977 CERN-JINR School of Physics, Nafplion, Greece (May-June 1977) 78—81726
- projective invariance in general space times with spinor, torsion and Yang-Mills fields 78—57832
- projector valued field formulation 79—49379
- pseudo-Goldstone bosons in Pati-Salam model 77—87933
- pseudoinvariant gauge Lagrangians for Einstein gravity and supergravity 79—12680
- pseudoparticle, four-dimens., quantum effects calcs., SU(2) gauge theory, chiral symm. breakdown 77—30247
- pseudoparticle field propagators 78—8513
- pseudoparticle fields, propagation functions 78—54556
- pseudoparticle fields, propagator functions calc. 77—87906
- pseudoparticle fields, role of fermionic zero modes 78—74159
- pseudoparticle fields with massless excitations, Dirac eqn. equivalence for spinor with chirality 78—4788
- pseudoparticle solns., classification in gauge theories 78—4789
- pseudoparticle solutions in gauges with unique pots., physical interpretation 77—79222

gauge field theory continued
- pseudosymmetry, weak decays and gauge group $U(1)\times SU(2)\times SU(2)\times U(1)$ 77−18214
- pure gauge fields on coset space 79−40673
- pure vacuum copies, gauge ambiguities, zero modes and classification of field size 79−97507
- $Q^2\bar{Q}^2$ states, mass levels in (3+1) dimens. lattice gauge theory 79−58942
- QCD, 2-dimens., IR structure, EM form factors and inelastic struct. functions *(Chinese)* 79−58935
- QCD, μ pair transverse momentum distrib. in Drell-Yan processes 78−62374
- QCD, anomalous dimensions of gauge-invariant three-fermion local operators of twist three 80−86662
- QCD, axial gauge, mass shell behaviour 78−49966
- QCD, coloured cuts and mass gaps 79−9335
- QCD, decays of heavy leptons and intermediate weak bosons 78−8524
- QCD, dense quark gas, colour magnetic stability 79−71709
- QCD, dynamical props. 78−70332
- QCD, E_7 model, quark and lepton assignments 78−8590
- QCD, e^+e^- annihilation energy, asymptotically free perturbation theory 78−66045
- QCD, electric field representation without gauge field constraints 78−93846
- QCD, energy levels of 1+1 dimensional lattice gauge theory 78−4828
- QCD, exclusive quark form factor leading IR behaviour 77−54074
- QCD, expt. test 78−8601
- QCD, failure of U(12) 77−67576
- QCD, field strength and action copies in any axial-like gauge 78−82143
- QCD, field theoretical aspects, perturbative effects 79−26286
- QCD, gauge field propagator and the number of fermion fields 80−62928
- QCD, gauge independence of IR cancellation, fermion-fermion scatt. 78−50006
- QCD, gauge invariance and perturbative calcs. 79−63417
- QCD, gauge invariance and the quark-antiquark static potential 79−97587
- QCD, gauge invariant quantum variables, $SU(N)_1\otimes SU(N)_2\otimes SU(N)_3$ algebra 79−30705
- QCD, Gell-Mann-Low function in 3 loop approx., nonAbelian gauge theory with fermions 80−86675
- QCD, gluon colour screening by Higgs mechanism 78−93861
- QCD, hadron prod. at large transverse momentum 77−87949
- QCD, hard processes, universality of mass singularities 78−82101
- QCD, infinite-mass limit determ. 78−66039
- QCD, infrared, near-mass-shell, behaviour of non-Abelian gauge theories 78−24947
- QCD, infrared behaviour, colour-singlet quark form factor 78−24948
- QCD, instanton induced interactions 79−71698
- QCD, jets, deep inelastic scatt., renormalisation group 79−26287
- QCD, lattice and continuum, Λ parameters connections 80−82945
- QCD, lattice-gauge theory calc. of π and ρ-meson decay consts. 78−74154
- QCD, long-range correl. in forward quark-quark scatt. 78−4779
- QCD, Migdal's regularisation scheme, hadron struct. 78−4782
- QCD, new quarks and hadrons 78−8591
- QCD, parton and gluon distribs. 78−16981
- QCD, parton distrib. function, transverse momenta, axial gauge ladder model 80−27467
- QCD, perturbative, energy flow and energy correlations in deep inelastic scattering, infrared safety 80−27465
- QCD, quantised electric flux tubes 78−45844
- QCD, review 78−37146
- QCD, stagnant gauge for gluon propagator 80−57554
- QCD, static potential $Q\bar{Q}$ model in weak coupling expansion 77−74647
- QCD, strong interaction gauge theory, SU(3) colour gauge vector mesons, confinement 78−78136
- QCD, two dimens., bound state eqns. on null planes, Hamiltonian approach 78−37137
- QCD, two dimens., hadron scatt., leading order calcs., meson-meson scatt. 78−4831
- QCD, two dimens., renormalisation group functions 78−29242
- QCD, two dimens., with SU(N) gauge symm., $N\to\infty$ limit 78−41489
- QCD, two dimens. light-like gauge formulation, hadronic reactions 78−21388
- QCD, two-dimens. extrapolation to four-dimens. 78−78081
- QCD, unconfined quarks and gluons 78−45850
- QCD and polarised quarks *(Russian)* 78−74217
- QCD and QED IR equivalence in non-perturbative solns. 77−74579
- QCD and the string model 79−26292
- QCD axial gauge, $O(\alpha_s)$ infra-red divergences, deep inelastic quark struct. function 80−86676
- QCD calc. of three-jet processes in leptoprod. and hadronic μ-pair prod. 78−21338
- QCD conf. La Jolla, CA, USA, 1978 79−97592
- QCD effects, parton transverse momenta, large-p_T hadron prod. 78−66083
- QCD estimates for heavy-particle prod. 78−82108
- QCD gluon contribs. to large p_T reactions 78−41504
- QCD in axial gauge, boundary terms and Poincare invariance, asymptotic gauge pots. 79−329
- QCD in two colours, virtual quark-quark scatt. in pseudoparticle background 78−12823
- QCD invariant charge, study of gauge theory by Lipatov's method *(Russian)* 78−74220
- QCD IR divergences exponentiation 78−41492
- QCD lattice gauge theory, matrix Pade approximants, ratio of hadron to nucleon mass 80−4928
- QCD of highly condensed matter 78−70267
- QCD on mass shell, Ward identities 78−16913
- QCD renormalisation in two loop approx. in arbitrary gauge 80−102002
- QCD spectrum calcs. in lattice gauge theory using Wilson's fermion method 79−367
- QCD theories of interactions, CP conservation, in presence of pseudoparticles 78−16923
- QCD theory for the strong interaction 80−4962
- QCD transverse lattice theory, confinement and hadron bound states 80−4961
- QCD two-dimens. 't Hooft Hamiltonian spectrum 77−65106
- QCD vacuum, effects on hadronic currents, instantons, e^+e^- annihilation and precocious scaling 79−332

gauge field theory continued
- QCD vacuum, quantum liq. model, gauge and rotational invariances of colour fields 80−13283
- QCD vacuum of background SU(2) gauge field, colour mag. permeability 80−78023
- QCD with heavy quarks, effective qauge theories 80−52467
- QDD, quantum dath dynamics, SU(3) model for composite quarks and leptons 80−91055
- QED, $A_0=0$ gauge, propagation of fermions 79−71669
- QED, conformal-invariant, Ward identity of dilation current 80−68401
- QED, covariant, renormalised transition amplitudes, gauge independence, Green functions 80−57530
- QED, Euclidean formulation, H-like energy levels for scalar and spinor fields 77−88378
- QED, gauge covariant approx., Dyson-Schwinger eqns. i.r. behaviour 78−16918
- QED, gauge invariant formulation using local currents 77−45997
- QED, perturbation series, asymptotic estimates and guage invariance 77−87925
- QED, relativistic two particle bound state energy levels, gauge invariance 80−77989
- QED appl. of gauge technique 79−35925
- QED in nonlinear gauge, for processes involving soft photons 77−79236
- QED treatment of scalar and longitudinal photons, EM field quantisation, Lorentz gauge 77−34111
- quadratic lagrangians in a space with torsion and the theory of the spinor gauge field 80−91006
- quadratic Poincare gauge theory of gravitation, short range confining component 78−89388
- quantisation, renormalisation, and fluctuations 79−30670
- quantisation, using path integral procedure, physical state Hilbert space construction 78−82106
- quantisation in finite volume without constraints or A_0 ambiguity 80−73605
- quantisation of relativistic systems with first-and second-class constraints 78−21337
- quantisation procedure avoiding path-integral formalism 77−13863
- quantised field construction, lattice approx. convergence 80−37156
- quantised gauge theories, canonical, large time behaviour, asymptotic anal. 80−27395
- quantised gravitational wave perturbations in Robertson-Walker universes 78−12636
- quantised lattice gauge field construction, mass generation and Abelian Higgs models 80−4831
- quantised SU(2) gauge theory, Monte Carlo study 80−77973
- quantum chromodynamics, IR struct. perturbation theory calcs. 77−74577
- quantum chromodynamics, nonperturbative approach 77−67617
- quantum chromodynamics, scale violation in presence of instantons 77−61196
- quantum chromodynamics, strong interaction theory, review 79−67498
- quantum chromodynamics, two dimens. U(N) invariant, 't Hooft bound state eqn. 77−26495
- quantum chromodynamics, unified approach to gauge, dual, Gribov theories 77−18223
- quantum chromodynamics in two dimens. 77−74590
- quantum contour field equations, renormalisation and string like eqn. 80−86581
- quantum electrodynamics in the temporal gauge 79−49425
- quantum flavour dynamics, renormalisability conditions 80−42404
- quantum fluctuations of instantons 78−54530
- quantum fluctuations of multi-instanton solutions 79−58878
- quantum fluctuations of pseudoparticles, O(5) Casimir operators 77−65083
- quantum gauge anomalies axial vector current derivation method calcs. *(Russian)* 80−62863
- quantum gauge supersymmetry, props. of globally supersymmetric Green's functions 79−63352
- quantum gravity, topological invariants 77−5729
- Quantum inequivalence of different field representations, supergravity appl. 80−95214
- quantum SU(2) gauge theory, vacuum stability, dynamical symmetry breaking 80−32000
- quantum vortex soliton operators in canonical formalism, gauge theory superselection rules 79−49386
- quark and string interacting system, gauge theory for 2-D statistical mechanics 79−30713
- quark binding, QCD and perturbation theory 77−71444
- quark confinement, asymptotically free nonAbelian gauge theory 77−2794
- quark confinement, dynamical and topological considerations, review 79−26296
- quark confinement, infrared struct. of QCD, perturbation theory 77−71443
- quark confinement and field theory, conf., Rochester, USA, (June, 1976) 77−71440
- quark confinement and lattice calculation, by Monte Carlo methods 79−13023
- quark confinement equation, gauge field theories, Hamiltonian formalism 78−41488
- quark confinement for gluon generation 78−25008
- quark confinement in 2-D lattice Higgs-Villain model 79−26289
- quark confinement in (1+1) dimensions and fermions 79−63422
- quark confinement in condensate of non-Abelian vortices 78−70328
- quark electric dipole moment from CP noninvariant gauge theory, left handed currents *(Russian)* 78−74218
- quark form factor, non leading contribs. to asymptotic behaviour 78−8586
- quark form factor and jet cross sections, high energy asymptotics 80−32112
- quark fragmentation in gauge theories 78−21340
- quark gas, nonAbelian gauge field theory 78−21341
- quark gas, relativistic, ground-state energy 78−8537
- quark hyperfine interactions in negative parity baryons, QCD 78−16984
- quark mass dependence ambiguities in gauge theory renormalisation 79−21913
- quark mass shell gauge in Kondo-Yang-Mills theory 77−30309
- quark masses and Cabibbo angles 79−9332
- quark masses and structure functions 80−22585
- quark masses in QCD, one loop approx. calc. in axial gauge 79−58925
- quark model, integral versus fractional charges 77−18226

gauge field theory continued
- quark model, weak interactions, quark masses, spontaneous violation of parity 77−6054
- quark structure model 80−91063
- quark-antiquark pot., charmonium model modifications, spin forces and instantons 78−93842
- quark-gluon coupling constant renormalisation, unified gauge theories containing Pati-Salam model 77−6072
- quark-lepton correspondence, multigeneration $SU(2)_L \times U(2)$-based model 80−22584
- quarkonium mass spectra, one gluon exchange corrections, gauge invariance and choice 80−52483
- quarks, flavour number determination using Higgs scalar particle 80−13288
- quarks and leptons, EM and weak interactions, flavour $SU_3 \times U_1$ gauge model 79−97554
- quarks and leptons, fermion physics in terms of $SU(2) \times SU(1)$ gauge theory 78−74197
- quarks high energy scattering in gauge theories, QCD IR struct. 77−74649
- quarks with more than three colors in a class of asymptotically free gauge theories 80−394
- quasiconfinement in colour gauge symmetry, unconfined quarks and gluons 80−86686
- quasiperiodic boundary conditions, vac. struct., in gauge theories, quantum mech. analogue 78−70255
- quaternion model, gauge theory for leptons and quarks *(Russian)* 78−62315
- quaternionic multi $S^4 \approx HP(1)$ gravitational and chiral instantons 80−31656
- radiation gauge static pot. between fermion and antifermion, non Abelian gauge fields 78−89621
- radiation theory, multipolar Hamiltonian QED and quantum optics 80−86634
- radiative corrections in gauge theories, QCD current algebra formulation, weak interaction universality 78−93883
- radiative corrections to parity violation in atoms in $SU(3) \times U(1)$ gauge theory 78−62402
- random magnetic systems, gauge symmetries, Ising and X-Y models anal. 79−38295
- random spin systems, gauge symm., phase transitions *(Russian)* 80−77929
- real-time approach to instanton phenomena, multidimensional pots. with degenerate absolute minima 78−78067
- reciprocal effects and other quark theories, charm quarks, J/ψ discovery, gauge theories *(Danish)* 79−30698
- recursion eqns. for renormalisation group transforms. in lattice gauge theories including fermion variables 78−62298
- Regge behaviour of electroproduction structure functions in asymptotically free theories 78−25025
- Regge behaviour of spontaneously broken non-Abelian gauge theory 78−70287
- reggeisation in theories with broken global symmetries, nondegeneracy of vector meson masses, non-trivial mixing 80−13236
- Reggeisation of meson trajectories quark-gluon gauge theories 78−25005
- Reggeization of elementary fermions in arbitrary renormalizable gauge theories 80−68367
- Reggeization of gauge vector mesons and unified theories 79−97562
- reggeization of vector mesons for non-Abelian theories with arbitrary symmetry 77−2740
- regular N-instanton fields and singular gauge transformations 78−4772
- regularity constraints and quantised actions 80−73601
- relativistic constrained system, compensating functional and quantisation, S-matrix 79−97527
- relativistic nuclear field theory with π and ρ, cold nuclear matter calcs. 79−93527
- relativistically invariant two-dimens. models, classification method *(Russian)* 78−70291
- renormalisation group eqns. for gauge field theory with multiple coupling consts. 78−360
- renormalisation group techniques and infrared behaviour 77−45965
- renormalisation of Abelian and non-Abelian gauge theories 77−13851
- renormalisation of Spontaneously broken gauge theories 79−12945
- renormalisation theory, perturbative, general features, quantum action principles, pure Yang-Mills theory 80−105794
- renormalizable interactions in two dimensions and sharp-time fields 78−81882
- renormalization of gauge theories *(Chinese)* 79−63337
- restricted theory as subset of nonAbelian gauge theory 80−62851
- review of gauge theories for space-time symmetries 77−2723
- review of gauge theories of weak, EM and strong interactions 77−13835
- riemannian spaces with local duality and gravitational instantons 79−25938
- right handed neutrino interactions in gauge theories 79−35941
- right translation invariant metrics and variational principles on principal bundle, gauge theories *(Chinese)* 80−101743
- Rohrlich string, classical, gauge mapping theorem 78−17001
- S-matrix, gauge singlet operators instead of bound states 80−99063
- saturation of gauge invariant Schwinger model correlation functions by instantons 77−30296
- scalar and SO(3,1) gauge Minkowskian field theory, instanton solns. 78−49956
- scalar electrodynamics, gauge invariant approx. 77−71469
- scalar Higgs eqn., particle-like solns. *(Russian)* 78−12829
- scalar loops consequences on gauge symm. hierarchies 79−2930
- scalar QED on lattice, correl. inequalities, infinite vol. limit 77−61233
- scalar quantum field in an external gauge field 79−97489
- scalar-field algebraic chromodynamics 80−52423
- scalar-spinor instanton, systematic quantisation 78−21331
- scalar-vector instantons in n-dimens., surface terms 78−49958
- scale dependent quark mass in colour gauge theory, $e^+e^- \to$hadrons anal. 77−30320
- scale invariant gauge theories, instanton role, short distance limit 80−101924
- scale-invariant gauge theories, instanton role in QCD, QED and $CP^{(N-1)}$ 80−27400
- scaling, asymptotically-free field theory 77−18182
- scaling violation in infinite-momentum frame 78−70286
- Schrodinger electron-photon interaction, gauge and hybrid transforms. 80−22544

gauge field theory continued
- Schwinger mechanism for chiral breaking dynamical fermion mass generation 77−41789
- Schwinger model, $A=0$ gauge, breaking of chiral symm. 78−62307
- Schwinger model, canonical surface formalism, axial anomaly, chiral symm. breaking 78−12816
- Schwinger model, chiral symm. breaking and vac. struct. 78−89615
- Schwinger model, new and local Lorentz-covariant soln. for arbitrary gauge 79−40668
- Schwinger theory, vacuum struct. generators in Lowenstein-Swieca gauge 79−6259
- Schwinger-Dyson equation for massless vector theory, absence of fermion pole and cut 77−13855
- self dual Euclidean gauge fields, semisimple groups, Lie algebra, SU(2) and SU(3) fields 79−6278
- self-dual equations for SU(n) theory, props. 79−17607
- self-dual gauge field, Green function 78−82099
- self-dual gauge fields and space-times 80−9108
- self-dual guage field, correspondence to complex vector bundles 77−45947
- self-dual sector, field strength formulation 78−29256
- self-dual SU(2) fields in Eguchi-Hanson space 80−57483
- self-dual SU(2) gauge field, Pontryagin density 78−66044
- self-dual SU(2) gauge fields, Backlund transform. and Atiyah-Ward ansatze 78−21339
- self-dual SU(2) gauge fields, symmetries 79−21935
- self-dual Z(N) gauge theories, critical temp. 79−49375
- self-duality condition for SU(2) gauge fields on Euclidean four dimens. space 77−61195
- self-duality eqns. for SU(3) gauge theory 77−65082
- self-generating discrete-space structure, lattice model in QFT 79−93276
- semiclassical QCD, regularisation and renormalisation 80−4925
- semiinfinite plasma interaction with charged nonrelativistic particle 77−38110
- semisimple unified gauge theories 78−70282
- seven lepton model, quantum flavour dynamics, mixing angle, masses, spontaneous symmetry breaking 78−89652
- sine-Gordon equation, discrete, on SU(2) lattice, group theory aspects 80−57486
- single scalar semiclassical theory, effective interaction local minima decay 77−65108
- singletons and massless, integral-spin fields on de Sitter space 80−110
- singular gauge fields, effect on inclusive differential cross sections 80−105782
- singular gauge instanton field, gauge zero modes, instanton determinants, and quantum-chromodynamic calculations 79−71635
- singular gauge transform. in non-Abelian gauge theory 79−2927
- singular gauge transformations, monopole vortex line systems, Nielsen Olsen SU(2) Higgs model, Nambu model 78−66034
- singularities and noninteger topological charge 80−9088
- six-quark model, $SO(4) \times U(1)$ gauge group 77−49905
- six-quark model of quantum flavourdynamics, Cabibbo angle and quark masses 78−33017
- sixth quark mass in $SU(2)_L \times SU(2)_R \times U(1)$ gauge group 79−26291
- Skyrme gauge model, topological solitons 80−9086
- $SL_{2,C}$ gauge theory of gravit., Lagrangian approach 78−77777
- SL_{2C} gauge formulation of general relativity, geometry 78−41211
- Sl(2,R) non-compact group for Dirac eqn. 80−22503
- Slavnov-Taylor identities, gauge conditions *(Chinese)* 78−24916
- SO_2 extended supergravity, geometrical interpretation 77−49660
- SO_4, $SL_{2,C}$ classical gauge field eqns., isotropic and solitary-wave solns. 78−93795
- SO(1,3)-gauge theory of gravity 79−129
- SO(2) linearised supergravity, multiplets 79−80488
- SO(3,2) de Sitter symmetry, spontanously broken, gravitational holonomy group 80−57149
- SO(3, 1) gauge field, Einstein-Weyl-Yang system, strong gravity model 78−86201
- SO(3) field coupled to strong gravity, particle like soln. 78−4758
- SO(3) gauge group, monopoles, spontaneously broken gauge theory 77−2753
- SO(3) gauge invariant theory, quantisation, spontaneous broken gauge theory, S-matrix gauge independ. 79−269
- SO(3) Georgi-Glashow model, field-strength description of non-Abelian gauge theories 80−62856
- SO(3) isotropy subgroups and Higgs pots. 78−37132
- SO(3) non-Abelian gauge theory, configurations of monopoles with multiple magnetic charge 77−2745
- SO(4,1) gauge field eqns., de Sitter plane wave solns. 79−30646
- SO(4,1) sourceless gauge field eqns., classical solns. 79−2921
- $SO(4) \times U(1)$ model of weak and electromagnetic interactions 79−13009
- SO(4n+2) gauge theory, dynamical symmetry breaking 80−86580
- SO(N) grand unified gauge theories, eigenvalue conditions and asymptotic freedom 79−22010
- soft CP violation, renormalisable gauge model for strong, weak and EM interactions 78−74196
- soft CP-invariance violation at high temperature 79−75697
- soft graviton emission in scatt. processes, linearised gauge theory 78−49746
- soliton solutions, quantum expansion generalisation *(Chinese)* 78−24915
- soliton solutions of nonAbelian gauge fields *(Chinese)* 78−24917
- solitonlike fields, gauge phase factor operators, extended Higgs models and 't Hooft algebra 80−42324
- solitons, nontopological, in three dimens. space, SU(2) gauge field + spin-0 field 77−18167
- solitons in 2+1 dimens., Coleman's rules 77−82678
- sourceless, gauge fields, natural connections on Stiefel bundles 78−58118
- sourceless, impossibility of geon analogues 78−361
- sourceless quantum EM field in multiply connected asymptotically flat background metric 79−25946
- $Sp(4) \times U(1)$ gauge symm. for weak interaction, $\Delta I = {}^1/_2$ rule 77−34093
- $Sp(4) \times U(1)$ theory of weak and EM interactions, little groups and discrete symmetry 79−26283
- space translation, gauge invariant, spinor field-electromag. pot. (quantised or unquantised) interaction 78−62296
- space-dispersion approach to the explanation of the Higgs-mechanism 80−90975
- space-time inversion in gauge theory, classical approach 78−41416
- space-time symmetry, Higgs model 80−52385
- spherically nonsymmetric instantons in scalar field theories *(Russian)* 79−93298

gauge field theory continued
  spherically symm. monopole soln. 78–8539
  spherically symm. monopoles anal. 77–71417
  spherically symmetric eqns. in gauge theories for arbitrary semisimple compact Lie group 79–9289
  spherically symmetric solitons for nonlinear or scalar field-gauge field interactions 79–97521
  spherically symmetric SU(2) gauge fields and monopoles *(Chinese)* 77–74568
  spin 1/2, gauge invariant antisymmetric tensor spinor field 80–47184
  spin 3/2 field, axial and trace anomalies 79–2690
  spin 3/2 field and Cartan's geometry 78–16712
  spin 3/2 fields, gauge quantisation 77–2735
  spin 5/2 fields, gauge theory 80–73583
  spin-1/2 particle in monopole field 78–4766
  spin-3/2 theory of gravitation 79–49148
  spin-5/2 gauge fields 79–63363
  spin-$^{1}/_{2}$ particle, energy in constant coloured mag. field 79–80742
  spin-couplings 3/2, consistency 79–44824
  spin-glasses, Landau-Ginzburg gauge model 79–42772
  spin-mass trajectories and QED in null plane, free field theories 78–29259
  spin-orbit terms of the heavy-quark potential in the presence of instantons 79–71710
  spinning particle in metric-torsion field, eqn. of motion 80–62543
  spinor electrodynamics, anomaly free and axially coupled, bilinear gauge renormalisation 79–307
  spinor fields, nonlocal, physico-geometrical gauge field theory 78–37134
  spinor fields in four dimensional space-time 79–6271
  spinor gauge field in spinor space-time formalism 78–41401
  spinor monopole soln. *(Chinese)* 78–78097
  spinor theories in curved space-time, nonlinear invariances 79–54029
  spinor theory of general relativity, without elementary gravitons 78–8321
  spontaneous breakdown, grand unification of QCD and $SU(2)\times U(1)$ 79–49380
  spontaneous breaking of gauge symmetry in a nonstationary isotropic metric 79–21643
  spontaneous compactification, mag. monopoles in higher dimens., Wu Yang global gauge descript. 79–2920
  spontaneous compactification of arbitrary space-time dimens., SO(N) gauge group 77–22458
  spontaneous origin of Newtons const., modified Einstein eqns., matter interactions in weak gravit. fields 78–12853
  spontaneous symmetry breakdown, nonsingular cosmology as vacuum effect 79–53947
  spontaneous symmetry breakdown 77–34083
  spontaneous symmetry breaking 77–74574
  spontaneous symmetry breaking and gauge interaction hierarchy 79–17621
  spontaneous symmetry breaking and particle spectrum in $SU(2)_L\otimes U(1)\otimes U(1)$ model 77–30257
  spontaneous symmetry breaking of $U_1(M)\otimes U_2(M)\otimes U_3(M)$ with coloured Higgs particles 77–79209
  spontaneous symmetry breaking theories *(Russian)* 77–6038
  spontaneous symmetry breaking with quaternionic scalar fields, $Sp(1,Q)\otimes U(1)$ group for unified gauge theory 77–61236
  spontaneously broken gauge theories, 1-loop corrections, 2-point functions and fermion masses 79–17599
  spontaneously broken gauge theories, 3- and 4-point functions and renormalisation consts. 79–17600
  spontaneously broken gauge theories, general struct. and renormalisation 79–17598
  spontaneously broken gauge theories with heavy Higgs bosons 80–13209
  spontaneously broken gauge theory model, ρ' vector meson, e^+e^- colliding beam data 77–2845
  spontaneously broken local gauge supersymm. struct., real gravit. interactions 77–49843
  spontaneously broken nonAbelian gauge theory, Regge behaviour 78–41438
  spontaneously broken SU(2) gauge theory, nonexistence of spherically symmetric monopoles with multiple mag. charge 77–6010
  spontaneously broken symmetry restoration in mag. field, massive charged vector meson effects *(Russian)* 78–74178
  spontaneously broken Yang Mills theories, high-energy gauge meson exchange reactions, factorisation, Reggeisation 77–18172
  stability and supersymmetry, general formalism, explicit two-loop appls. 77–79228
  stability and supersymmetry, models with local gauge symmetry, renormalisation group anal. 78–70296
  stability subgroup of vacuum in nonlinear realization 78–390
  stable heavy neutrinos, dynamical interactions and astrophys. effects 79–5743
  standard electroweak gauge model with light W and Z bosons 80–95236
  standard weak-EM gauge model, six-quark phenomenology and Grand Unification 80–37204
  static colour change screening in classical gauge theories 79–45050
  static confinement conditions, two-dimens. anal., SO_2 mesons 80–13262
  static finite energy solns. of gauge fields with separated radial variable 77–45956
  statistical mechanics of field theories with broken, global, and local SU(3) gauge symmetries 79–58881
  stepwise breaking of gauge and discrete symm. 78–29269
  stochastic quantisation processes, review, Markov processes, Martingales, quantum dynamics 80–94969
  strangeness changing neutral currents, avoidance in gauge theories of weak and EM interactions 79–22005
  strangeness changing processes, gauge models with V+A currents, high order effects 77–22677
  stress tensor in gauge theory class, Lagrangian density, massless Rarita-Schwinger theory 79–2939
  string, relativistic, $SU_{3,1}$ in orthornormal gauge 78–437
  string direct interaction, gauge-invariant theory, gravit. interaction 77–41804
  string representation of gauge fields, chiral field topological props. 80–52410
  string representations and hidden symmetries for gauge fields 79–49378
  string tape solns., in classical gauge field theories, broken gauge symmetry 78–62317
  strings, vortices, gauge fields 77–71493
  strings as collective field theory of U(N) gauge fields 80–62849

gauge field theory continued
  strings in non-Abelian gauge theories 80–52403
  strong coupling theories, fermions and gauge fields on lattice 77–6009
  strong gravity, field equations, strong interactions, de Sitter microsphere idea of hadrons 80–68111
  strong gravity, supersymmetric theory for f- and g-gravitons and massive gravitinos 78–62141
  strong interaction theory based on fibre bundle geom., currents 77–79204
  strong P and T noninvariance, natural suppression in $SU(2)_L\times SU(2)_R\times U(1)_{L+R}$ gauge model 79–9303
  strong P and T noninvariances and neutron electron dipole moment 79–63372
  strong-coupling limit of gauge theories, Fermion-Boson decoupling, quark confinement 79–35924
  strongly interacting Higgs bosons, gauged nonlinear σ-model, $SU(2)_L\times U(1)$ extension 80–86656
  SU_2 gauge field theory, possible construction with non-Yang-Mills field eqns. 79–93307
  SU_2 gauge model, light neutral gauge boson, consequences for e^+e^- and pp($\bar{p}$) reactions 78–58154
  SU_2 gauge theory, exact dyon solns. 79–80745
  $SU_3\times U(1)$ gauge models and neutral current reacts. 78–89648
  SU_5 theory, superheavy particles, decoupling at low momenta 80–52431
  $SU_L(2)\times SU_R(2)\times U(1)\times[SU(3)\times SU(3)]_c$ gauge model, chiral colour symmetry breaking 80–47234
  $SU_L(2)\times U(1)$ and $SU_L(2)\times SU_R(2)\times U(1)$ predictions at high Q^2, neutral currents, Z-bosons 80–63029
  $SU_L(2)\otimes SU(2)_R\otimes U(1)$ and $SU(2)\otimes U_L(1)\otimes U_R(1)$ gauge theories, neutral current constraints 79–277
  $SU_L(3)\times SU_R(3)$, leptonic nonet anal. 77–87908
  $SU_L(3)\otimes U(1)$ gauge model, exact Cabibbo universality, τ^- and X^- 80–4852
  $SU_L(4)\times SU_R(4)\times U(1)$ model, generation of u- and d-quark masses 79–63419
  $SU_L(4)\times U(1)$ as gauge symm. for quark, lepton quartets, weak and EM interactions, weak currents 78–74174
  SU_N gauge group uniqueness in grand unified model, U_1 color, proton stability 79–316
  SU_N/Z_N gauge invariant theory, phase factor operators and soliton fields 80–77947
  $SU(2)_L\times(T_3)_R\times U_V(1)$ gauge group, grand unification, symmetry breaking and Z bosons 80–73641
  $SU(2)_L\times(T_3)_R\times U_V(1)$ gauge unified model, neutral current interactions, ed and ν scatt. 80–18107
  $SU(2)_L\times SU(2)_R\times U(1)_L\times U(1)_R$ gauge models, parity violation in SLAC neutral current expt. 79–9305
  $SU(2)_L\times SU(2)_R\times U(1)$ based L-R symmetric gauge theory, spontaneous breakdown of parity 79–75681
  $SU(2)_L\times SU(2)_R\times U(1)$ gauge group axial-vector isosinglet neutral hadronic current coupling to ν and e 79–63371
  $SU(2)_L\times SU(2)_R\times U(1)$ gauge model, possibility of b-quark weak interactions 79–26285
  $SU(2)_L\times SU(2)_R\times U(1)$ gauge model for weak/EM interactions, u-d quarks mass difference 78–12850
  $SU(2)_L\times SU(2)_R\times U(1)$ gauge models, neutral currents, P-violation 79–54293
  $SU(2)_L\times SU(2)_R\times U(1)$ gauge models, parity violating effective interaction 79–9304
  $SU(2)_L\times SU(2)_R\times U(1)$ gauge symm., Higgs particles, parity conservation 78–70305
  $SU(2)_L\times SU(2)_R\times U(1)$ gauge theory, left-right symm., neutral current struct. 78–41420
  $SU(2)_L\times SU(2)_R\times U(1)$ gauge with permutation symmetry, quark mass and Cabibbo angles 80–47232
  $SU(2)_L\times SU(2)_R\times U(1)$ Higgs scalars, vacuum expectation values, quark mass ratios 79–49404
  $SU(2)_L\times SU(2)_R\times U(1)$ model, weak and EM interactions, Higgs scalars, vac. instability 79–317
  $SU(2)_L\times SU(2)_R\times U(1)$ six quark gauge models, flavour violation 80–4951
  $SU(2)_L\times U(1)$, strong CP-violating phase, one-loop corrections, Higgs particles 80–62910
  $SU(2)_L\times U(1)\times SU(2)_R$ model for lepton decay and neutrino lifetime 78–62331
  $SU(2)_L\times U(1)$ gauge model, mixing angles and CP violation 80–73648
  $SU(2)_L\times U(1)$ gauge model with off-diagonal neutral currents, anomalous lepton events 79–2923
  $SU(2)_L\times U(1)$ gauge theory, four flavours, Cabibbo angle natural relations and bounds 80–57550
  $SU(2)_L\times U(1)$ gauge theory, weak interactions of ultra-heavy fermions 79–75713
  $SU(2)_L\times U(1)$ gauge theory of weak interactions, universal lepton mixing and mixing angles *(Russian)* 79–54298
  $SU(2)_L\times U(1)$ primitive particle model 79–40708
  $SU(2)_L\otimes SU(2)_R\otimes U(1)$ gauge models confronting neutral current data 79–22013
  $SU(2)_L\otimes SU(2)_R\otimes U(1)$ model, implications of absence of parity nonconservation in atomic physics 77–41758
  $SU(2)_L\otimes U(1)$ models, implications of absence of parity nonconservation in atomic physics 77–41758
  $SU(2)_L$ x $SU(2)_R$ x $U(1)$ gauge models, neutral current sector, natural parity conservation 79–9324
  $SU(2)_w\times U(1)$ gauge theory models, in inelast. neutrino-nucleus scatt. 77–14117
  $SU(2)+U(1)$ gauge models, constraints from neutrino interaction data 77–30251
  $SU(2)\times SU(2)\times U(1)$ supersymmetric gauge model, atomic parity violation and neutral current predictions *(Russian)* 79–54294
  $SU(2)\times SU(2)$ chiral symmetric Lagrangian description of low energy πN and NN scatt. 79–26251
  $SU(2)\times U(1)$, gauge theory of weak interactions 78–21328
  $SU(2)\times U(1)$, P and T invariance violation suppression, quark mixing angles 79–54278
  $SU(2)\times U(1)\times G$, hadronic neutral current in neutrino interactions and single Z-boson hypothesis 79–54295
  $SU(2)\times U(1)\times G$ expanded gauge models of neutral currents, propagator momentum transfer 80–47237
  $SU(2)\times U(1)\times SU_F(2)$ gauge symmetry, CP violation, neutron elec. dipole moment, muon number changing process 79–89091

gauge field theory continued
SU(2)×U(1)×U(1) gauge model, quark-lepton correspondence in neutral and charged current interactions 79—54296
SU(2)×U(1)×U(1) gauge models, neutral current struct., parity nonconservation 79—292
SU(2)×U(1)×U(1) gauge theory of weak and EM interactions in unified SU(6) scheme 78—41465
SU(2)×U(1) gauge group in (V-A) model, mixing between ordinary and heavy leptons 78—41472
SU(2)×U(1) gauge model, chiral SU(2)×SU(2) symmetry and electron mass 80—57542
SU(2)×U(1) gauge model, eigenvalue condition for Weinberg mixing angle, new leptons and quarks 78—41463
SU(2)×U(1) gauge model, muon anomalous mag. moment, charged Higgs boson contrib. 80—78011
SU(2)×U(1) gauge model, right-handed charm current, CP violation 78—45795
SU(2)×U(1) gauge model, symmetry breaking pattern with two Higgs doublets 79—12978
SU(2)×U(1) gauge model and parity violation in atoms 78—4775
SU(2)×U(1) gauge model predictions for neutral current reactions 77—71424
SU(2)×U(1) gauge models, CP violation origin, Yukawa interaction 79—40712
SU(2)×U(1) gauge models, with diagonal neutral currents 77—71433
SU(2)×U(1) gauge models with lepton doublets and singlets, exact consequences of universality 77—54065
SU(2)×U(1) gauge theories, successes and current issues 80—18064
SU(2)×U(1) gauge theories of leptons, T violation, leptonic decay and dipole moment 79—299
SU(2)×U(1) gauge theories of weak and EM interactions, neutral current contraints 78—70272
SU(2)×U(1) gauge theory, μ-e mass ratio and CP violation as quantum effect 79—30691
SU(2)×U(1) gauge theory, charged heavy lepton and neutrino 78—45794
SU(2)×U(1) gauge theory, natural suppression of CP violation 78—41421
SU(2)×U(1) gauge theory of weak, EM and dual EM interactions 80—52448
SU(2)×U(1) gauge theory of weak and EM interactions, quark model 77—26458
SU(2)×U(1) model, fermion and Higgs multiplet structure, universality 80—62909
SU(2)×U(1) six quark model, uniquely determined discrete symmetry 79—93360
SU(2)×U(1) theories, weak isospin breaking, higher order corrections 80—95235
SU(2)×U(1) unified gauge field, Euclidean space and O$_4$ invariance 80—91031
SU(2)×U(1) unified gauge theories, implications of parity violating obs. on heavy atoms 77—46006
SU(2)×U(1) unified gauge theory, mech. for nonconservation of muon number, $\mu \rightarrow e+\gamma$ appl. 77—30303
SU(2)×U(1) unified gauge theory threshold effects 78—82098
SU(2)×U(1) vectorlike model: new leptons, quarks, and the axion question 79—40711
SU(2)×U(1) Weinberg-Salam model, weak mixing angle, grand unified gauge theories 79—89093
SU(2)×U(1) with very heavy quarks, maximal CP violation, kaon decays 77—38123
SU(2)⊗U(1)$_y$⊗U(1)$_c$ gauge model, neutral current and $\Delta I=1/2$ rule 79—6257
SU(2)⊗U(1)⊗U′(1), anal. in neutral current interactions, parity nonconservation in ed scatt. 79—17731
SU(2)⊗U(1)⊗U(1)′ gauge model of weak interactions, $\Delta I=1/2$ enhancement 77—6073
SU(2)⊗U(1)⊗U(1)′ gauge theories and extensions, one-loop generated CP violation 79—89078
SU(2)⊗U(1)⊗U(1) gauge model without parity violation in heavy atoms 78—82097
SU(2)⊗U(1) gauge group theory tests from neutral current phenomena 78—24992
SU(2)⊗U(1) gauge model, strange baryon weak radiative decays and CP violation 79—6260
SU(2)⊗U(1) gauge model of EM and weak interactions, fermion mass restriction *(Russian)* 78—89650
SU(2)⊗U(1) gauge models, neutral current couplings 79—40715
SU(2)⊗U(1) gauge models of weak and electromagnetic interactions and the μe universality *(Russian)* 80—13257
SU(2) and SO(2) gauge fields in 4-, 5- space-time dimens., confinement, critical dimensionality 79—89064
SU(2) classical gauge field with sources 80—52416
SU(2) coupling model with tachyon fields *(Korean)* 77—49844
SU(2) gauge field, ground state wave functionals 78—74142
SU(2) gauge field, Hamiltonian formulation in interaction with external source 80—62850
SU(2) gauge field, spinorial classification 79—260
SU(2) gauge field, static spherosymmetric sourceless soln., selfduality and induced charge current *(Chinese)* 79—80755
SU(2) gauge field classification, Lorentz invariant versus gauge invariant schemes 79—85228
SU(2) gauge field configuration in curved spacetimes 80—18077
SU(2) gauge field struct. *(Chinese)* 77—57434
SU(2) gauge field theory, nonlinear scalar field eqn., spherical symmetric exact solns. *(Chinese)* 80—62886
SU(2) gauge fields, classification 78—70281
SU(2) gauge fields, eigenspinor-eigenvalue eqn. 78—78076
SU(2) gauge fields, interaction Hamiltonian for quark source interactions 79—67466
SU(2) gauge fields, singular Wu-Yang soln. 77—65086
SU(2) gauge fields, sourceless solns. of static monopole systems *(Chinese)* 78—86418
SU(2) gauge fields coupled to strong gravity, Coulomb like solutions . 80—82701
SU(2) gauge fields in interaction with static extended quark sources 79—30709
SU(2) gauge fields in Minkowski space-time reparametrisation invariant formulation 78—70257
SU(2) gauge fields over 4-dimens. sphere, topological charge concentrated at a point 79—85224

gauge field theory continued
SU(2) gauge group, magnetic monopole as finite energy smooth soliton soln., review 78—89625
SU(2) gauge group, solns. for Yang-Mills eqns. *(Russian)* 77—79226
SU(2) gauge model, classical soln. instability 78—93806
SU(2) gauge supermultiplet, classical solns. 78—8549
SU(2) gauge theory, equivalence of massive and dimensional regularisation in the infrared 79—71612
SU(2) gauge theory, exact monopole and dyon solns. for arbitrary semi-simple compact group 79—71599
SU(2) gauge theory, external charges, topological classification for Yang-Mills eqns. 80—90977
SU(2) gauge theory, Mobius invariance and classical solutions, generalised and excited merons 79—6265
SU(2) gauge theory, polarised eN scatt. anal. 78—58193
SU(2) gauge theory, resonances, particle motion, metastable states, interaction with monopole 77—74595
SU(2) gauge theory, sypersymm. breaking by pseudoparticles, supergravity implications 78—24959
SU(2) gauge theory instanton solns., duality condition, Lie group interpretation, quasiparticle soln. 79—6261
SU(2) gauge theory solns. 79—9285
SU(2) group potentials *(Chinese)* 78—78098
SU(2) instanton, physical interpretation of degrees of freedom 78—62312
SU(2) magnetic monopole solns., parameter counting in Prasad Sommerfield limit 80—352
SU(2) monopoles in non-Abelian gauge theory, Bogomolny eqn. for interacting monopoles 79—85225
SU(2) pseudoparticle field, scalar propagator calc. 78—29253
SU(2) self dual gauge fields, static axially symmetric solns. 79—35603
SU(2) spontaneously broken gauge theory, canonical quantisation *(Chinese)* 79—49406
SU(2) symmetry, classical quark confining solns. incorporating colour 79—339
SU(2) theory, asymptotic freedom scales calc. using Monte Carlo methods 80—90988
SU(2) theory, self-dual solns. 78—41402
SU(2) vacuum gauge field, chiral connection with ferromagnetism and axisymmetric gravitational problem 78—70258
SU(2) x U(1) gauge group, neutral current couplings 77—67567
SU(2) Yang's monopole, quaternionic gauge fields on S^7 80—57473
SU(2)-flavour Schwinger model on the lattice, Hamiltonian lattice perturbation exam. 78—16747
SU(3)$_{colour}$×SU(2)×U(1) gauge, full operator structure of the nonleptonic $|\Delta S|=1$ weak Hamiltonian 80—99089
SU(3)$_L$×SU(3)$_R$ as gauge groups of weak and associated charges, symm. breaking 78—74175
SU(3)×SU(3) chiral renormalisable gauge model, nonleptonic decays 78—24938
SU(3)×U(1)×U(1) symmetry, gauge model of weak and electromag. interactions *(Russian)* 78—45838
SU(3)×U(1) electroweak model, strong extension, flavour and colour gauge exchange symmetries *(Chinese)* 80—101975
SU(3)×U(1) gauge model of weak interactions, quark triplets, charmed hadron decay 77—2789
SU(3)×U(1) gauge models, generalised mixing and CP violation in hadron decays 78—41473
SU(3)×U(1) gauge theory, charged intermediate boson mixing 77—87910
SU(3)×U(1) gauge theory, electro-weak interaction, helicity mixed representation 80—78013
SU(3)×U(1) gauge theory of weak and EM interactions 78—70317
SU(3)×U(1) low-energy symmetry within the unifying SU(4)$_F$×SU(4)$_C$ gauge group 79—67489
SU(3)×U(1) models, exam. of weak currents and associated features 78—16975
SU(3)×U(1) modified model, quark and lepton mass hierarchy 78—89653
Su(3)×U(1) unified gauge theory without μ-e universality 79—26274
SU(3)⊗U(1) gauge model of trimuon prod. in neutrino interactions 77—74671
SU(3)⊗U(1) theory of weak and EM interactions 77—57481
SU(3) colour gauge group, coloured monopoles 80—68360
SU(3) colour gauge theory, effective scale depend. quark masses in chiral limit 77—18222
SU(3) gauge field nontopological soliton in three dimens. space 77—18168
SU(3) gauge model of weak and EM interactions, Weinberg angle, Han-Nambu quarks 80—52452
SU(3) gauge theories without scalars, mag. monopoles, dyons, other topologically stable solns. 77—49819
SU(3) gauge theory, gauge fixing conditions 79—97505
SU(3) gauge theory, leptonic octets and heavy lepton decays 77—34094
SU(3) instantons with cylindrical symmetry, Pontryagin indices 79—286
SU(3) non-Abelian gauge theories, gauge fixing ambiguities in axial and Coulomb gauges 79—21945
SU(3) theory, asymptotic freedom scales calc. using Monte Carlo methods 80—90988
SU(3)-symmetric gauge theory, static gluon pots., appl. to fermions 79—12967
SU(4|N) gauge transformations, determ. of Lagrangian for supertheories 79—63118
SU(4)$_L$×SU(4)$_R$×U(1) gauge, lepton weak interaction, right currents, effective Fermi interaction const. universality *(Russian)* 79—58921
SU(4)$_L$SU(4)$_R$×U^Y(1) gauge group for lepton and quark weak interactions *(Russian)* 79—97566
SU(4), magnetic monopoles 78—24918
SU(4)×U(1) gauge theory, Cabibbo mixing, new approach, CP nonconservation calc. 79—71657
SU(4)×U(1) unified gauge theory, CP nonconservation 79—71656
SU(4)×U(1) unified gauge theory, muon number conservation 79—71655
SU(4)⊗U(1) broken gauge theory, muon number nonconservation 77—74638
SU(4) σ model with massive gauge fields 77—10184
SU(4) broken lattice gauge theory spectrum 79—49474
SU(4) gauge fields, pseudoparticle solns. *(Chinese)* 78—74128
SU(4) gauge theories, instantons 77—30243
SU(4) theory of interacting monopoles, classical solns. 77—67574
SU(5|1) superunified model in 6-dimens. 79—97557
SU(5), gauge invariance and fermion mass dimensions 80—62907

gauge field theory continued
SU(5), symmetry breaking patterns, Higgs fields 80−101953
SU(5) gauge model, masses, mixing angles, CP violation and b-quark decay 80−78006
SU(5) grand unified theory, flavour number limit from fermion mass higher order corrections 80−4904
SU(5) model, gauge hierarchy for grand unified theory prototype 79−75711
SU(5) unified gauge theory, non-Abelian electric and mag. flux 80−57545
SU(6) based renormalisable unified gauge model with calculable masses 78−89647
SU(6) based vector-like gauge theory, unified theory with right handed currents, proton stability 77−49890
SU(6) exotic gauge model, lepton-quark symm., CP-violation and $\mu \to e\gamma$ decay 78−12875
SU(6) quark model of hadron struct., field theory treatment 79−49483
SU(6) unified gauge field theory of weak, EM and strong interactions 79−17658
SU(6) unified gauge group, neutral current coupling to ν_μm and ν_e 78−54626
SU(6) unified gauge model, based on SU(3)×U(1) and colour SU(3) subgroups 78−12847
SU(8) grand unification, natural embedding of SU(3) horizontal symmetry 80−86646
SU(N+1) gauge theory, exact monopole solns. with spherical symmetry 79−71626
SU(n), instantons, geometrical description of parameter space 79−30653
SU(N) Coulomb and Landau gauge theories vacuum struct., Gribov ambiguities, harmonic anal. 80−68363
SU(N) gauge groups, N=2,3,4, meron and meronlike configurations 79−71636
SU(N) gauge models, symm . of Higgs pot. 78−32980
SU(N) gauge theories, 1/N expansions, singular integral operator 80−57511
SU(n) gauge theories, directions of spontaneous symmetry breaking 80−13228
SU(n) gauge theories, spontaneous symmetry breaking pattern 80−95228
SU(N) gauge theory consistency in two Euclidean spacetime dimens., quark-gluon theory 77−74598
SU(N) gauge theory with scalar fields, effective Lagrangian 80−82897
SU(N) group, quantum fluctuations in vicinity of an instanton, quadratic Lagrangian 79−6266
SU(N) lattice gauge theories, weak to strong coupling crossover 80−95212
SU(n) Lie gauge group, triangular anomaly 78−29270
SU(N) spontaneously broken to U(1), composite magnetic monopoles 77−2765
SU(N) symmetric quantum dynamical systems, $N \to \infty$, energy spectrum for singlet and adjoint states 80−62880
SU(N) theories, order and disorder parameter inequalities 80−99051
SU(N) theory, current synchrospherical symmetrical monopole in multi-synchrospherical symmetrical case *(Chinese)* 80−22527
SU(N) unification of extra strong interactions, no-go theorem 80−32056
super-dense matter, phase transitions in gauge theories and cosmology, review 79−44654
super-gauge symmetry in general relativity, Einstein's A transformation *(German)* 78−86199
superconducting early Universe, cosmological baryon prod., CP invariance grand unification 80−90592
superconductivity, gauge invariant model, local, collective excitations 77−87902
superconformal gravity, local geometry 79−44836
superconformal supergravity and internal symm., proliferation of gauge fields 77−54056
superconformal transformations and six-dimensional spacetime 80−27196
superconformal unified field theory 78−12848
superdense matter, symm. breaking 77−45955
superdiagram technique for gauge theories, renormalisation 77−30267
superfield eqns. of motion 78−8503
superfield perturbation theory, loop calculations 80−13229
superfield supergravity with symmetry 80−8891
superfields in higher-dimensional spacetime 79−17316
supergauge, differential forms on supermanifolds *(Russian)* 80−4889
supergauge and gauge transformations, spinor equation admitting an infinite group 79−71645
supergauge theory, geometric aspects, broken gauge invariance 78−8506
supergrand exceptional unification and quark-lepton constituents 80−91030
supergrand unification in E_8, quark-lepton assignments, symmetry breaking scheme 80−68408
supergraph anal., gauge supersymmetry, S-matrix 80−27422
supergraph formalism UV finiteness in gauge supersymmetry 80−46913
supergravity, 2-loop divergence, with external gravitons on-shell cancellation 77−49659
supergravity, auxiliary fields 79−17315
supergravity, auxiliary fields for closed algebra using S-matrix 78−81911
supergravity, classical solns. 78−122
supergravity, constraint-free superfield formalism 79−17309
supergravity, covariant quantisation 78−41470
supergravity, extended, with gauge internal symmetry in de Sitter space 77−79021
supergravity, geometry of superspace, vector-spinor matter 78−49744
supergravity, ghost counting on one-loop level of Rarita-Schwinger field, gauge fixing 78−93589
supergravity, locally invariant supersymmetric gauge field theory 78−49742
supergravity, minimal set of auxiliary fields, gauge algebra closure 78−49743
extended supergravity, N=2, auxiliary fields in 5, 6 space-time dimens. 79−30339
supergravity, Poincare and conformal, multiplication rule and supersymmetric densities for multiplets 78−70037
supergravity, Poincare and conformal models with closed algebra 78−74198
supergravity, relation between vector and scalar multiplets and gauge invariance 79−12684
supergravity, status as unified gauge theory 80−46925
supergravity, superfield Lagrangian 78−41468

gauge field theory continued
supergravity, supersymmetric generalisation of differential geometry tensors 78−45546
supergravity, surface integrals as symmetry generators 77−74634
supergravity, trivial solution identification, gauge transformation to Einstein vacuum soln. 80−68115
supergravity, unitarity in general covariant gauge 79−75428
supergravity, Weyl and Einstein, unified approach to matter coupling 78−54275
supergravity and gravity unified geometric theory 77−41521
supergravity as gauge theory of supersymmetry 78−8576
supergravity as limiting case of gauge supersymmetry 77−2593
supergravity geometrization in superspace and local supersymmetry 80−8890
supergravity in 11 dimens., action and transform. laws 78−70038
supergravity in superspace, algebraic approach 79−17314
supergravity structure, gauge actions, multiplets 79−2971
supergravity supergraphs, perturbation theory description from globally-supersymmetric gauge breaking 79−67203
supergravity with axial-gauge invariance 77−41790
supergravity with complex spin-3/2 gauge fields, invariant under local complex supersymm. 77−5731
supergravity with Majorana spin 3/2 gauge fields and supersymmetry 77−17894
supergravity without cosmological constant, spontaneous symmetry breaking and Higgs effect 79−17310
superrenormalisable abelian gauge model with confinement in four dimens. 80−31998
superrenormalisable interactions, struct. of infrared divergences 79−40663
superspace, generally covariant theories of gauge fields 78−54568
superspace, new class of superalgebras and local gauge groups 78−29230
superspace 80−22264
superspace formulation for supergravity, book contrib. 80−22261
superspace formulation of supergravity using vierbeins 79−2972
superspace gauge theories, superspace Maxwell and Yang-Mills actions 80−86582
supersymmetric, charge renormalisation vanishing 78−24930
supersymmetric and nonsupersymmetric, regularisation by dimensional reduction 80−77951
supersymmetric gauge models of weak and EM interactions 78−58106
supersymmetric gauge theories, invariant regularisation 79−71646
supersymmetric gauge theories and their possible applications to the weak and electromagnetic interactions 79−49419
supersymmetric nonAbelian gauge theory, supercurrent anomaly 78−24958
supersymmetric nonlinear σ-model in 4-D, coupling to supergravity 78−49981
supersymmetric QED, supercurrent gauge invariance, α-independ. 80−95233
supersymmetric vector-like model of lepton interaction 78−412
supersymmetrical field theories, mathematical base *(Russian)* 79−67478
supersymmetry, algebraic props., applic. to particle physics 77−87918
supersymmetry, physico-geometrical comments, unified field theories and supergravity, gauge transformations 80−364
supersymmetry, spontaneous breaking, unified gauge models appl. 77−71452
supersymmetry, spontaneously broken, quantum loops UV finiteness 79−21919
supersymmetry algebras with central charges, SU(4) invariance, gauge theory 78−70301
supersymmetry and developments in gauge theory *(Chinese)* 80−77978
supersymmetry and gauge theories of weak and electromagnetic interactions 79−26208
supersymmetry and Lagrangian field theory 77−6041
superunified field theories, geometrical transformation laws 79−63117
superunified theories, geometry of gauge invariance 78−24723
superunified theories in superspace 80−8886
superweak gauge theory of CP-invariance violation 79−75710
superweak gauge theory without charm, CP violation 77−10195
Symanzik's approach to nonrenormalizable theories for massless models 79−26212
symmetric gauge fields 78−362
symmetry breaking and space-time geometry 78−54533
symmetry breaking perturbation technique, tensor operators 79−12975
symmetry definition for gauge theories 78−32973
symmetry hierarchies, tree approx. 77−2758
symmetry violation natural suppression, muon and electron lepton number nonconservation 78−8574
systematics of higher-spin gauge fields 80−57478
T*-product convention, quasilinear systems and transverse nonAbelian fields 79−97498
T-baryonium system, four-body potential in multiquark states 80−101996
taming of the dipole ghost in relativistic quantum field theory 78−66035
temporal gauge $A_0=0$ 80−90984
tensor gauge theory, Kerr type exact soln. 79−21631
tensor gauge theory with steeply-rising pot., rising Regge trajectories 77−49858
tetrad gravitational field, weak principle of equivalence and gauge theory *(Russian)* 78−62135
tetrad Palatini formalism and quadratic Lagrangians in gauge theory of gravitation 79−2697
thermal props. of gauge fields and quark liberation 78−24936
thermodynamic pot. at finite temp. and density, QED and QCD 78−8535
Thirring and Schwinger models, asymptotic field operator solns. 77−49847
three-loop charge renormalization effects due to quartic scalar self-interactions 80−57489
time dependent Hamiltonian, scale gauge transforms., adiabatic approx. principle, suitability for teaching 78−45506
topless model for grand unification 80−73653
topological charge, effects in gauge theories 79−26205
topological charges for N=4 supersymmetric gauge theories and monopoles of spin 1 79−63364
topological excitations in Abelian Higgs model 78−70275
topological fluctuations and chiral breaking in gauge theories involving massless fermions 77−38088
topological invariants of gauge fields with several vacua *(Russian)* 77−37786

gauge field theory continued
  topological methods for gauge theories, winding numbers, euclidean Dirac eqn. 79—26206
  topological problems in gauge theories, appl. to quark confinement 79—63351
  topological solitons and instantons 79—12924
  topology, and quark confinement 77—41808
  trace and dilatation anomalies in gauge theories 78—4790
  transformations and symmetries 80—4833
  translational gauge theory of gravity: post-Newtonian approximation and spin precession 80—46945
  translations as gauge transformations using fibre bundles formalism 78—12808
  transverse pure gauge fields and nonlinear chiral solitons, Coulomb condition 78—78068
  trimuon production by neutrinos, heavy lepton cascade mechanism using SU(2)×U(1) gauge model 78—58180
  tumbling gauge theories with chiral fermion fields, symmetry breaking 80—99042
  twisted lattice gauge fields, local order parameter, phase transitions 80—77966
  two dimensional field theories with infinite number of conservation laws and Backlund transformations 80—9095
  two dimensional space time, gauge theory path ordered operator formalism 80—77967
  two loop calculation about quantum mech. instanton, test of tunnelling 78—58126
  two-current two-particle amplitude, narrow-reson. model, gauge invariance and scaling 77—74576
  two-dimens., high-energy scatt. anal. 77—13933
  two-dimens. SU(N) gauge theory for mesons 77—49840
  two-dimens. U(1)-Goldstone model, QFT on lattice 78—74158
  two-dimensional gauge model perturbation theory, Schwinger and massive vector meson models 79—6269
  two-dimensional massive QED in unitary gauge as renormalisable theory 77—57478
  U_3(W), charged heavy muonic lepton production, explanation of Kolar events in ν_μN collisions 79—9364
  U_3(W) gauge models, neutral currents 79—49443
  $U_L(1)\times U_R(1)\times R_R$ group, mass ratio and symmetries of electron and muon, model 79—58917
  U(1)×SU(2) unified gauge field theories, field function O(4) invariance 80—37201
  $U(1)\times SU(4)_L\times SU(4)_R$ based weak-EM synthesis with manifest left-right symm. 78—8571
  U(1) as the minimal horizontal gauge symmetry, fermionic generations 79—80753
  U(1) chiral symmetry breaking from SU(1) gauge theory 80—86617
  U(1) gauge theories, fibre bundles in two-dimens. 78—24941
  U(1) Goldstone boson, anal. of BRS invariance in nonAbelian gauge theories 79—80798
  U(1) lattice gauge model, phase transition in four-dimensional compact QED 80—105820
  U(1) lattice gauge theory, four dimens., nonconfining phase, existance proof 80—73602
  U(1) problem in generalised θ-vacua, Goldstone boson and QCD 80—52399
  U(1) without instantons 80—13265
  U(N) gauge theory, Nambu-Gato string like equation 80—105785
  U(N) lattice gauge QCD, complete integration in large-N limit 80—42338
  U(N) lattice gauge theories with quarks, string eqns., Dyson-Schwinger eqns. 80—4857
  U(N) lattice gauge theory, string representation, Wilson loop amplitudes 80—4856
  U(N) lattice gauge theory as $N\to\infty$, planar diagram sums in terms of statistical ensembles 80—99052
  U(N)-symmetric gauge theory in 1/N expansion, dynamical symmetry breaking 77—6006
  U gauge in Abelian and non-Abelian gauge theory, Gribov ambiguities 78—45788
  U-gauge Green's functions construction, with spontaneous symmetry breaking and Slavnov identities 79—235
  unambiguous field-strength formulation and dual potentials for gauge theories 79—35938
  unconfined unstable quark, unified gauge theory predictions, selection rules 77—61253
  unconfined unstable quarks in unified gauge theory 77—13916
  unification mass and gauge hierachies for O(10), E_6 and $[SU(4)]^4$ models 79—80782
  unification of elementary forces of nature 77—65067
  unification of fermions and bosons, interacting model 79—21629
  unification of fermions and bosons, math. structures and phys. questions 79—21630
  unification of fermions and bosons, physical foundations of local (algebraic) approach 79—21628
  unification of fundamental forces, review 80—95238
  unification of Maxwell, Dirac and Yang-Mills eqns., octave algebra 79—2967
  unified, rel. to nonlocality 77—82673
  unified actions for gauge fields and gravitation *(Chinese)* 79—17305
  unified affine gauge theory of gravity and strong interactions, GL(4,R) spinor fields 79—93331
  unified field theory, geometrical consideration 78—12809
  unified field theory bounds on number and masses of quarks and leptons 78—58151
  unified gauge field theories and coupling constant trajectories 77—22675
  unified gauge field theory with torsion, symmetries 78—89386
  unified gauge field underlying supersymmetry space, physico-geometrical remarks 79—13007
  unified gauge theories, grand, asymptotic freedom constraints 80—62914
  unified gauge theories and gravitational cut-off, renormalisation group method 77—18213
  unified gauge theories and Higgs bosons 77—45948
  unified gauge theories and the baryon number of the universe 78—85842
  unified gauge theories of weak and electromag. interactions, review *(Russian)* 79—26278
  unified gauge theory, improved Pati-Salam model for strong+EM+weak interactions 79—318
  unified gauge theory, low energy neutral current struct. 79—2975
  unified gauge theory of gravit., e.m., mag. monopole fields 77—57263

gauge field theory continued
  unified gauge theory with Abelian massless gluons, binding of fractionally charged quarks 78—29296
  unified Lagrangian formulation for massive and massless tensor fields 79—12686
  unified lepton-quark model of Nambu-Jona-Lasinio type for weak, EM and strong forces 77—30304
  unified model for atomic parity violation and neutral currents in gauge theories 80—4912
  unified model of weak and electromagnetic interactions based on the gauge group SU(3)×U(1) 79—22003
  unified scalar-free theory, order-R vacuum functional, with spontaneous scale breaking 80—78003
  unified SU(3)×U(1) gauge theory with different muon and electron neutral currents 78—58152
  unified SU(6) gauge theory, hierarchy of gauge symm. and CP nonconservation 78—41464
  unified superconformal gauge theories for gravity+other gauge interactions 77—87928
  unified theories, gauge hierarchies, book contrib. 80—42384
  unified theories, quantised Grassmann variables, colour and flavour degrees of freedom 77—49891
  unified theories, restrictions on possible supergroups and flavour groups 77—65129
  unified theories 80—73652
  unified theory of direct interaction between particles, strings and membranes 78—86433
  unified theory of EM and weak interactions, local gauge invariance 80—82928
  unified theory of gauge fields and supersymmetry 78—58150
  unified theory of gravitation, particle masses, instantons 78—37168
  unified theory of weak interactions of leptons and quarks, gauge model 80—22556
  unified U_3 theory of weak and EM interactions, six quark flavours and lepton types 77—18215
  unified vectorlike gauge theory based on group SU(6) for quarks+leptons 78—4818
  unified weak and EM interactions, semi simple SU(3l) gauge groups for hadrons 78—74195
  unifying mass scales without intermediate schiral colour symmetry 80—22555
  uniqueness of the Weinberg-Salam gauge model 79—35989
  unitarising high energy scatt. amplitudes in field theory QED 78—62341
  unitarity and renormalized 't Hooft identities 80—13205
  unitarity of S-matrix in Yang-Mills theory 77—82681
  unitarity proof for theory with Faddeev ghost 77—13842
  unitary and renormalisation gauge, point transformations 77—41763
  unitary field theory, preliminaries and recent developments, review 79—35613
  unitary gauge, ambiguities and breakdown configs. 78—93798
  unitary gauge in SU(2) Yang-Mills-Higgs system 77—30229
  universal CP noninvariant superweak interaction and baryon asymmetry of the universe 78—66072
  V_3(W), spontaneous symm. breaking, parity violation in atomic physics 77—71476
  V+A currents coupling old quarks to new quarks 77—26486
  V-A gauge model, muon and electron number nonconservation 77—74667
  vac. struct. of two-dimens. Higgs model, quark pair prod. 78—29254
  vaccuum tunnelling, fluctuations around a most probable escape path in Minkowski space 79—2935
  vacuum copies and perturbation theory 79—17612
  vacuum copies and perturbation theory in the 't Hooft-Veltman gauge of QED 79—21989
  vacuum instability, appl. to Goldstone and Weinberg models 77—65107
  vacuum instability and Higgs scalar mass, appl. to Weinberg model 77—10178
  vacuum manifolds, gauge groups and topological invariants 79—237
  vacuum polarisation induced by intense gauge field, renormalisation group method 78—49994
  vacuum polarization about instantons 79—21928
  vacuum polarization effects in lattice gauge theories 80—13211
  vacuum polarization in uniform non-Abelian gauge fields 80—4898
  vacuum spacetimes, stationary and axially symmetric, homogeneous Hilbert problem, Kinnersley-Chitre transformations 80—68349
  vacuum states for pure gauge fields on coset, topological props. 80—68372
  vacuum structure in gauge theories, strong CP violation and cosmology 80—86578
  vacuum structure of SU(3) gauge field theory in Coulomb gauge 78—62311
  vacuum symmetries of gauge supersymmetry, quantum effects 79—17634
  vacuum tunneling in spontaneously broken gauge theory 79—40703
  vacuum tunnelling of gauge theory in Minkowski space 78—41425
  vector boson and graviton propagators in the presence of multipole forces 79—85207
  vector boson model from SL(2,C) gauge theory of gravitation and Yang-Mills theory 79—322
  vector bundles theory *(Chinese)* 78—32978
  vector field with bare mass and Higgs mechanism 77—5998
  vector gauge theories, Higgs boson signature, trilepton prod. in μN reactions 77—61237
  vector meson masses, possible bounds on their ratios in gauge hierarchies 78—93791
  vector superfield as Abelian gauge field, Lagrangian density 77—18170
  vector-like theory with Majorana particles, lepton masses 77—18366
  vectorlike SU(3)×U(1) gauge model of weak interact. $\bar{\nu}$ reactions, neutral currents 77—41805
  vertical-horizontal symmetric minimal grand-unification 80—47229
  vortex condensation mechanism for static quark confinement, Abelian gauge theories 80—52457
  vortex strings, mag. monopoles in gauge field theory 78—70283
  vortex-line theories, field eqn. reduction, saturated bounds 77—41767
  vortices topology of unified intrinsic field quantities for elementary particle systems 79—40653
  VV+AA gauge model 78—29246
  VV+AA type gauge models, effective ν interactions 78—66038
  Ward identities in the axial gauge, self-coupled non-Abelian theory 77—65096
  Ward Takahashi identities soln. 79—241

gauge field theory continued
Ward-Takahashi identities for gauge-ghost field proper vertices *(Chinese)* 80−99062
wave function renormalisation constants, gauge independ. in gauge field theories 80−82883
wave mechanics, gauge invariant and Power-Zienau-Woolley transformation 80−99073
weak, EM, and strong interactions, book contrib. 79−30694
weak and EM interactions, quantisation and renormalisation of gauge theories, book contrib. 79−30669
weak and EM interactions with SU(3)×U(1) symmetry 78−58153
weak and EM phenomenology, gauge theoretical prospective, charm and flavour conservation 80−4916
weak coupled gauge field formulation using quaternions and p, n, λ quark fields 79−63349
weak external gauge fields, energy levels, modified functional measure 78−49973
weak gauge boson doubling in standard SU(2)⊗U(1) model, W, Z bosons 80−62916
weak hypercharge embedding in strong gauge groups 79−30692
weak interaction model with left-handed 8 quarks and 8 leptons 77−18218
weak interactions, renormalisable model on gauge group $SU(2)\times SU(2)_R\times U(1)$ 78−12855
weak interactions and gauge theories, review 77−26479
weak interactions of ultra heavy fermions 78−93838
weak interactions second threshold related to Higgs mechanism 77−57483
weak interactions vectorlike model with six quarks, gauge theory, SU(2)×U(1), νN appl. 77−57480
weak intermediate boson mass bounds in spontaneously broken gauge theory 77−46007
weak quark and lepton chiral symmetries, dynamical breaking gauge interaction 80−47215
Weinberg's model of CP violation in gauge theories, valence quark hypothesis 79−12940
Weinberg model, universality and weak isospin leptons, nucleons, quarks 78−70273
Weinberg-Salam model, gauge ambiguity effects 80−4908
Weinberg-Salam SU(2)⊗U(1) gauge theory effective Lagrangian, neutral current results 79−35992
Wess-Zumino model, massive, dimensional regularisation, supersymmetry 80−27398
Weyl's gauge field and spin 1/2 particle coupling 77−49846
Weyl gauge field, positive energy density and spin 1/2 noncanonical spinor field interaction 79−54258
Wilson's lattice, local chiral symmetry for gauge theories 80−105774
Wilson loop critical point behaviour in gauge and lattice guage theories 80−90993
Wilson loop expectation value, area low and loop wave eqn., quark confinement 80−47185
X-Y model, gauge theory analogue, 4-D self-dual gauge model, phases and transitions 80−27399
Yang's gravitational gauge field, plane wavelike solns. *(Chinese)* 79−80486
Yang Mills field strengths and gauge potentials *(Chinese)* 77−71436
Yang-Mills, dyon solns. and symmetry, elec. and mag. charge conservation 77−26183
Yang-Mills and gravitation, quantisation, Ward identities and Green's function eqns. 77−67552
Yang-Mills classical field classification using spinor methods 77−78990
Yang-Mills classical SU(3) theory, dyons and new topologically conserved quantity 77−6014
Yang-Mills classical theory, glueball non-existence 77−74569
Yang-Mills continuum field, gauge invariant freq. splitting 77−87905
Yang-Mills field equation, soln. 77−30265
Yang-Mills gauge theory of gravity, SO(1,3), self-gravitating cosmons 77−82431
Yang-Mills lattice gauge theories, comparison with gauge groups SU(2) and Z_2 80−31966
Yang-Mills sourceless SO(4) and SO(3,1) eqn. spherically symmetric soln. 77−65103
Yang-Mills SU(2) high-energy scatt. amplitudes to arbitrary perturbative orders 77−67571
Yang-Mills theory, field strength and gauge pot. *(Chinese)* 77−13841
Yang-Mills theory, nonleading IR divergences in QCD, renormalisation group function 77−71422
Yang-Mills theory renormalisation in two-loop approx. for arbitrary gauge *(Russian)* 77−49865
Yang-Mills two-dimens. pseudoparticles and sine-Gordon solitons, transformations 77−65100
Yang-Mills-Einstein eqn. pseudoparticle solns., gravit. effect on Yang-Mills topology 77−82682
Z_2 lattice gauge Higgs theories, Monte-Carlo calcs. 80−86593
Z_n four dimensional lattice gauge theories, series anal. 80−99050
Z_n lattice gauge theory coupled to Higgs field, phase diagrams 80−57485
Z_N symmetric models phase transitions 80−101922
Z(2) gauge theories, hidden fermions 80−82899
Z(2) gauge theory, phase transition, variational calcs. 80−99049
Z(2) gauge theory, renormalisation group calc. 80−22514
Z(2) lattice gauge theory, variational approach, two phase struct., phase transition 80−68361
Z(2) lattice gauge theory in 2+1 dimens., fermion representation 80−82900
Z(N) and U(1) lattice theories in three-dimens., phase diagram 80−82901
Z(N) gauge theories, phase transitions 80−73609
Z(N) gauge theories, self duality 79−2919
Z(N) lattice gauge theories, Hamiltonian approach 79−85233
Z(N) spin and gauge models, extended structs. appls. 79−85222
Z(N) strings and hadron structure 80−86572
Z-boson and two-boson models, neutral current phenomena, μ-e universality 80−18109
zero energy fermions in U(1) pointwise monopole field *(Chinese)* 80−42345
zero-mass limit for gauge singlet prod. amplitudes 78−37139
b-quark interaction with τ^--lepton, gauge model 79−40738
Δ(1236) isomer production, by charged and neutral currents 79−17711
e:μ mass ratio, EM coupling const., flux quantization model 77−79240

gauge field theory continued
e/μ mass ratio, extended Weinberg model with heavy leptons, discrete symm. appls. 77−57482
e-μ permutation symm., lepton number conservation in gauge theories 78−4777
e-μ universality possible violation in gauge theories with heavy leptons 77−2739
e-μ-τ spontaneous symmetry breaking and rare τ decays 79−9301
e^- +nucleus parity violating neutral current interaction, gauge theory predictions, radiative corrections 78−86436
ed, polarised e, elastic scatt. asymmetries in SU(2)×U(1) gauge theory 79−40781
e^+e^- annihilation, neutral weak current effects, gauge model anal. 77−61243
e^+e^- annihilation channel, differential dispersive theory of ψ/J 78−45933
e^+e^- annihilation cross sections, operator approach, one-photon approx. 80−47315
$e^+e^-\rightarrow F\bar{F}$, with polarised particles, weak asymmetries, unified gauge theory anal. 78−8636
$e^+e^-\rightarrow\gamma\gamma$, weak interaction effects, QED tests, SU(2)×U(1) gauge theory 79−40767
$e^+e^-\rightarrow$hadrons, asymptotically free quark model predictions in complex plane 77−71522
e^+e^- inclusive annihilation, leading logarithm sum for struct. functions in QCD 79−71735
$e^+e^-\rightarrow\nu_e\bar{\nu}_e\gamma$, gauge theory analysis, Weinberg-Salem model, ang. and energy distribs. 78−12894
$e^+e^-\rightarrow U^+e^-$, SU(2)⊗U(1) gauge models 77−71502
en, polarised e, elastic scatt. asymmetries in SU(2)×U(1) gauge theory 79−40781
eN deep inelastic scattering asymmetries, gauge theory predictions 79−22104
$eN\rightarrow eX$, $SU(2)_L\times U(1)$ gauge theory distinguished from $SU(2)_L\times SU(2)_R\times U(1)$, neutral currents, z-bosons 80−62908
$en\rightarrow en\pi$, pol. e, P-odd asymmetry and cross sections, SU(2)xU(1), SU(3)xU(1) calcs. *(Russian)* 80−62998
eN interactions, parity nonconservation, $SU(2)_L\times SU(2)_R\times U(1)$ gauge model anal., Z boson decay widths 80−47302
eN scatt., polarised e, testing unified gauge theories prediction 79−17732
$e^-N\rightarrow e^-\Delta(3/2, 3/2)$, P-odd asymmetry, P nonconserving neutral current interaction 80−57611
eν interaction, local conservation law from neutrino massless, gauge invariance 80−42355
ep, polarised scattering, asymmetries, gauge models 80−62991
e^-p, polarised e, elastic scatt. asymmetries in SU(2)×U(1) gauge theory 79−40781
$e^\pm p\rightarrow e^\pm\gamma+X$, deep-inelastic bremsstrahlung, quark charges, colour gluon mass 78−74216
η or η′ meson, tunnelling effects, phase coherence and mass in non-Abelian gauge theory 79−93287
η′, QCD sum rules for mass, possible pseudoscalar gluonium, instanton effects 80−388
$F_1\rightarrow F_2\gamma$, nondiagonal transition amplitude for arbitrary fermion charges *(Russian)* 80−86722
γν weak interaction, spontaneous breakdown of γ and gauge symm. at finite temp. 78−70299
$\gamma p\rightarrow hX$, SU(3)×SU(3) invariant interaction of quarks, large p_T, gluon bremsstrahlung 78−33072
$K_L\rightarrow 2\gamma$ or $\pi^+\pi^-\gamma$, Weinberg-Salam model, weak radiative decays, large dist. contribs. *(Russian)* 77−82740
μ, (g−2) value, second order weak correction in arbitrary gauge models 78−62301
μ anomalous mag. moment, weak correction in gauge models 78−16965
μ anomalous mag. moment in SU(3)×U(1) gauge model 79−3026
$\mu\rightarrow e\gamma$, and other rare decays, in SU_6 superunified gauge theory 78−21408
$\mu\rightarrow e\gamma$, gauge theory with lepton mixing, decay probability, neutrino oscillations 77−49940
$\mu\rightarrow e\gamma$, SU(2)×U(1) unified guage theory 78−8643
μ number nonconservation, gauge model with left-handed lepton doublets 78−8542
$\mu\rightarrow\bar{\nu}_\mu x^+$, hypothetical, search for scalar charged boson, apparatus and theoretical aspects 78−58177
μ pair prod., QCD ang. correl. 78−49976
μ-e universality and spontaneous μ-e mass splitting 77−30302
μ-e universality constraints, implications for SU(2)×U(1) gauge models of π decay 79−9368
μ^- +nucleus→e^- +nucleus reaction rate calc. using gauge theory models 77−65157
μe universality breakdown of neutral weak currents in $SU_2\times U_1$ gauge *(Russian)* 79−75712
μμ, fourth order contrib. in gauge theory of weak interactions 77−38117
$\mu^-\mu^-\mu^+$ events in ν_μ reactions, SU(3) gauge models 77−74674
$\mu^-\mu^-\mu^+$ prod. in neutrino interactions, gauge theory, heavy leptons 77−65085
μN deep inelastic scatt., asymm., quark proton model evaluation, gauge theories test 78−62408
n electric dipole moment, CP violation in gauge theories 80−91041
NN elastic scatt. in spontaneously broken gauge field theory 79−36091
NN P-violating interaction in Bars-Halpern-Yoshimura gauge model 77−22758
$np\rightarrow d\gamma$, γ-polarisation, NN weak pot. in simple gauge model 78−54644
$np\rightarrow d\gamma$, parity nonconservation effects due to $\rho^\pm\rightarrow\pi^\pm\gamma$, short dist. contrib. to γ circular polarisation 77−41855
np mass difference in gauge models 77−61285
ν, massless, left-right symmetric gauge models, $SU_{2,L}\times SU_{2,R}\times U_1$ 80−27461
$\bar{\nu}$ anomalies and right-handed currents 78−8654
ν data, exotic quarks and high gauge groups 77−74583
ν decay in gauge theory of weak and EM processes *(Russian)* 79−22087
ν interactions involving weak neutral currents, expt., theory, gauge models 77−49901
ν magnetic moment calc. in SU(2)×U(1) gauge model 77−18180
ν neutral current data, elastic and deep inelastic, gauge model constraints 79−40718
$\nu(\bar{\nu})e$, differential cross-section calc. in gauge theories, W-boson exchange 77−82728

gauge field theory continued
  $\nu(\bar{\nu})p$ elastic scatt., final state polarisations, test for T-invariance and 2nd class currents 79—63466
  ν oscills., weak-interaction-induced, gauge models 78—70359
  ν-nucleus reactions, multimuon events, QCD predictions for associated prod. of charm 78—25034
  ν_μ, transition magnetic moment 78—78168
  ν_μ mass limit in absence of muon-lepton-number conservation, unified gauge theories 78—21368
  $\nu_\mu(\bar{\nu}_\mu)p \to \nu_\mu(\bar{\nu}_\mu)p$ hadronic neutral current, final-proton polarisation 78—82200
  $\nu_\mu e$, scatt. meas., interaction gauge models *(German)* 80—37251
  νN, heavy-quark production, t and b-quarks, $SU(2)\times SU(2)\times U(1)$ gauge group mixing angles 80—68445
  $\nu N \to \nu X$, $SU(2)_L\times U(1)$ gauge theory distinguished from $SU(2)_L\times SU(2)_R\times U(1)$, neutral currents, z-bosons 80—62908
  p electroprod. struct. function and constituent-particle scatt. 78—45931
  $p+N\to\mu^-\mu^+X$, 400 GeV, charged gluon effects, broken colour gauge model study 79—49473
  $pp\to\pi X$, large-P_T reactions in broken color gauge theory 80—95292
  π mass difference, Bars-Halpern-Yoshimura unified gauge model, perturbative calc. 77—10251
  π prod. by weak neutral current, comparison of gauge theory models 78—82139
  π struct., gauge model, confinement scheme 78—45841
  QCD, $\bar{q}$ polarisation in quark sea of proton 78—12867
  $q\bar{q}$ non Abelian gluon interactions, long distance behaviour of chromostatic potential 79—17676
  $\rho\pi$ scatt. in Bardakci-Halpern model 1^+ channel, N/D anal., A_1 status 79—40688
  $\sigma(e^+e^-\to\text{hadrons})/\sigma(e^+e^-\to\mu^+\mu^-)$, asymptotic freedom predictions leading to paradox 77—49988
  τ particle properties, QCD type gauge theories, absence of $\tau^+\tau^-$ resonance in e^+e^- annihilation 78—37144
  $\Upsilon(9.4)$ family, gauge theory mass anal., harmonic oscillator pot. 78—82186
  $\Upsilon(9.5)$ hadronic prod., parton distrib. and QCD 78—78142
  Υ (9.5), implications of Υ for ν interactions in weak gauge theories 78—70271
  $Z\to H\gamma$, decay rate determ. in $SU(2)\times U(1)$ gauge theory 79—40717
  $Z\to l^+l^-$, deviations from lepton universality in renormalisable gauge models 80—91122
  H parity violations, fundamental struct. of weak current, unified gauge theories 78—12849
  ^{3}He, superfluid, gauge group and p-wave phases 79—23798
  ^{3}He, superfluid, gauge groups and phases 79—55992
  ^{3}He, superfluid, Ginsburg-Landau region, phase equilib. in Lie group method 79—23799

Gaussian noise *see random noise*

Gaussian orbital calculations *see GO calculations*

Gaussian-type orbital calculations *see GTO calculations*

Ge-Si alloys
  amorphous, freshly evap. and ion-bombarded, struct. differences 79—55666
  amorphous, solar cells, multijunction structure, increased conversion efficiencies, low cost 80—45677
  amorphous, solar cells, tandem multiple gap 80—94029
  amorphous film, crystn. transform. kinetics 78—22653
  amorphous film, effects of annealing and crystn., ESR microstruct. and elec. meas. 78—26790
  amorphous semiconductor characterisation for solar cell applications 79—61983
  composition, determ. using ellipsometric method 80—35615
  crystal growth, equilib. gas phase comp. in Si-Ge-Br heterogeneous system 79—10820
  crystal growth by electron-beam zone melting without crucible 79—4917
  defect modes and optical spectra 80—11413
  diffused p-n junction, elec. and photoelectric props. 80—101095
  dilute, impurity concentration effects 78—75777
  dilute, IR absorpt. and first-order Raman scatt. due to single and paired impurity atoms 79—82976
  dopant inter-reactions, Au+Sb 77—84774
  doping characts. 78—22745
  electron irrad.-induced defects, DLTS meas. 80—24499
  electronic struct. comp. depend., X-ray spectral obs. 77—81178
  electronic structure, short-range order effects, calc. 80—92861
  epitaxial growth by getter sputtering, characts. 79—28915
  film, amorphous, ESR line intensity anal., rel. to cond. mechanism 78—43645
  film, amorphous, ferromagnetic interaction between spins 78—2710
  heat treated, carrier heating by strong microwave elec. field 77—69366
  heavily doped, hot pressed p-type alloys, high temp. phonon thermal cond. *(French)* 78—43190
  heavily doped, reversal of precip. 80—2409
  heteroepitaxial layers on Si substrate, lattice const. meas. 79—69382
  hot-pressed, fine-grained, boundary scatt. of phonons, lattice thermal cond. 80—107583
  hot-pressed, fine-grained, boundary scatt. of phonons, theory 80—107584
  IR spectra, calc. for imperfect homopolar crysts., lattice dynamics 80—59601
  jet thinning apparatus for foil prep. 78—88589
  lattice energy and consts., virtual cryst. approx., pseudopot. calc. 80—44166
  lattice thermal conductivity rel. to grain size and carrier conc. 78—91495
  long wavelength optical vibr. 78—6135
  n-type, phonon thermal cond. of hot pressed alloy, 300-1100K 78—91494
  n-type, phosphorous doped, precipitation effects due to heat treatment 80—107833
  p-n junction, Sb-diffused, TSC 80—20289
  phase diagram, lattice const. var. effects 80—97470
  phase diagrams near melting point, Helmholtz free energy, heat of solution 80—70379
  phonon boundary scatt., reduction of lattice thermal cond. 78—55921
  photoconductivity, of single crysts. 79—87126
  photoconductivity and optical props. of samples fabricated by Si implantation 79—24014
  photoconductivity of single crystals in intrinsic region *(Russian)* 79—11170
  photofield emission cathode, multitip, fabricated by crystn. from vapour, emission characts. 78—2975

Ge-Si alloys continued
  solubility of Au, thermodynamic calcs. 79—86890
  thermal neutron monochromators 80—49053
  thermoelectric alloys, phase diagrams, and imperfection chemistry 80—108422
  thermoelectric material, p-type cond., stoichiometry 78—30945
  thermoelectric materials, high temperature 80—89659
  thermoelectric performance improvement, by GaP additions 79—47115
  vacuum hot pressing, effect on thermal, electrical props. 80—25594
  variable-gap cryst. made from solid soln. 79—66003
  vibrational and Raman-scattering props. 78—10884
  X-ray scattering, diffuse, phase diagram determ. *(German)* 78—30517
  $(Ge,Si)_{1-x}Y_x$, $Y=H,F,B,P,\ldots$, amorphous struct., kinetically determined topological model 79—55666
  Ge-Si alloy, quenching from high temp., thermal electric parameters, obs. 77—28165
  Ge-Si single crystals, heat treated, hot carrier thermo-EMF 77—24575
  Ge-Si:Sb, energy spectrum of Sb 80—34382
  Ge-Si:Sb, prepared in Universal Furnace expt. in Soyuz-Apollo programme, melting and crystn. 80—19737
  Ge-Si:Te, solid solns., donor states energy spectrum 80—88516
  Ge-Si-Sb, segregation of Si,Sb due to barometric mol. diffusion in gravitational, centrifugal fields 78—14472
  Ge-Si-Sb solid soln., prod. by ‘Universal Furnace’ expt. Sb and Si distrib. *(Russian)* 78—23692
  Ge-Si-Sb solid soln., struct. peculiarities and mech. props. under weightlessness *(Russian)* 78—23693
  $GeSe_2$, far IR reflectivity meas. 77—28565
  $Ge_{0.8}Si_{0.2}$, elec. cond., density of states, impurity and temp. depend 80—65568
  p-$Ge_{1-x}Si_x$, $0.004\leq x\leq 0.08$, hole mobility and hopping cond. rel. to composition fluctuations 77—76819
  $Ge_{1-x}Si_x$:Ga,As, interimpurity radiative recombination, composition depend. 79—11465
  $Ge_{30}Si_{70}$, hot press sintering 80—50572
  Ge_xSi_{1-x}, Si X-ray emission spectra obs. *(Russian)* 77—1767
  Ge_xSi_{1-x}:Cu, solid soln., single cryst., photocond. spectra 79—24015
  $NiMnGe_{1-x}Si_x$, mag. props., neutron diffr. and magnetometric meas., 80-600K 80—65793
  Si/Si-Ge junction, elec. and photoelec. props. 78—10545
  Si-Ge, heavily doped vacuum hot-pressing, thermal and electrical props. 77—40400
  Si-Ge (22 at.%) alloy, thermoelec. props., time and temp. dependence 78—91712
  Si-Ge heteroepitaxial layers, Ge/Si ratio transfer curve from gas phase to solid phase obtained by epitaxial growth 77—73234
  Si-Ge solid solns., p-n junctions, photoelec. props. obs. 77—1471
  Si-Ge:Al, B, P, hot-pressed alloy, thermoelec. props. 78—91711
  SiGe, matrix isolated cluster, optical absorpt. 80—16045
  $Si_{0.92}Ge_{0.08}$ film on Si, elastic strain, misfit dislocation density 77—85119
  Si_xGe_{1-x}, Ge distrib. in single crysts. grown by zone refining without crucible 78—22754
  Si_xGe_{1-x}:H, amorphous, photoinduced optical absorption 79—82973
  Si_xGe_{1-x}-GaAs, heterojunction, elec. and recomb. props., interface defect effects 80—80365
  Si_xGe_{1-x}-GaAs, p-nn^+ junction, I-V characts., inverse branch, effect of dislocation defects *(Russian)* 79—15217
  Si_xGe_{1-x}-Si(GaAs) heterodiodes, interfacial structural defects effect on avalanche breakdown 79—42644
  Si_xGe_{1-x}(H) amorphous alloys, from glow discharge, optical properties 78—19510

gegenschein *see zodiacal light*

Geiger counters
  additional RF voltage characteristics, Geiger threshold voltage anal. *(Chinese)* 80—42896
  background determ. by hard cosmic radiation 80—69027
  CANDU, development of irrad. fuel bundle counters for reactor safeguards systems 78—94119
  CANDU 600 MW, spent fuel bundle counter, safeguard design 79—13495
  Chinese nuclear weapon tests, fresh fallout anal. using beta counting technique 79—92106
  circuit simple and inexpensive 79—63866
  compensated count rate cct. for portable survey meter 80—99426
  coordinate counters for UV and X-ray photons 80—69026
  counting loss correction using anticoincidence gated scaler and a live timer 78—86737
  dead time, two radioactive source method, optimum meas. 79—85868
  dekryptonation thermal anal. using flow type GM detector 77—66786
  dosimeter for mixed n-γ dosimetry 78—25394
  EHT inverter for Geiger-Muller tubes, cct. 79—81120
  end window type for millisec. β activity cross section meas. 80—27880
  fast neutron sensitivities of Geiger-Mueller counter γ dosemeters, mixed field dosimetry 78—92705
  gamma dosemeters, fast neutron sensitivities, 14.7 MeV 77—52880
  gas-chromatography, beta radio effluents, window flow counter 80—93824
  Geiger counter, self quenching, plateau characteristics improvement by γ-irradiation 78—13389
  hodoscope, protection from spark chamber noise 77—18742
  liquid effluent beta monitor 77—61656
  needle counter, small size low-level 80—58075
  neutron calibration technique for detectors with low neutron/high photon sensitivity 79—31344
  nonlinearity due to dead time loss, method of correction 79—54742
  organic, suppression and utilisation of spurious pulses 79—22547
  photosynthesis measurements, applications *(German)* 77—70436
  pocket Geiger counter for β detection *(Spanish)* 80—14051
  pulsed radiation intensity meas. by counting delayed pulses produced in Geiger-Muller counter 77—46407
  radiation overload warning system for Geiger-Muller detectors 80—78492
  self-quenching, anode surface changes with ageing 80—58025
  windowless Geiger-Muller gas flow counter, design for thermally stimulated electron emission 77—79505
  β-decay surface contamination, comparison of counter efficiency 78—25398
  β-γ-γ coinc. spectrom. using GM-Ge(Li)-Na(Tl) counter combination 78—46210
  $\beta\gamma$ survey meter with numerical display 77—64134

Geiger counters continued
- Ag-activated Geiger counter calibration for neutron yield determ. in Frascati plasma focus expt. 80—99409
- ^{41}Ar release from TRIGA reactor, comparison of γ-ray detectors 78—57309
- HCN, gaseous, radioactivity meas. by internal counting method 79—36483
- ^{125}I surface contamination meas., sensitivity comparison with other detectors *(Czech)* 79—34673

Geiger Muller counters *see Geiger counters*

gelatin
- *see also gels*
- adsorption on single AgBr crystals, ellipsometric investigations 79—24779
- aqueous, crystn. and melting 79—61914
- bubble formation, model for decompression sickness 77—13051
- chromatised gelatin layers, processing for holographic recording *(Russian)* 80—91762
- coating swelling meas. by real-time holographic interferometry 79—98316
- contact interaction between spherical surfaces under press. in various media *(Russian)* 77—7958
- crosslinking by formaldehyde, ^{13}C NMR obs. 79—5187
- diazo salt sensitised gelatin for holographic recording, grating form. 80—78798
- dichromate gelatin, holographic information recording *(German)* 79—27207
- dichromated, for holographic optical element fabrication 79—89865
- dichromated, methylene blue sensitised, Lippmann colour hologram recording 79—94196
- dichromated, methylene blue sensitised, methods of increasing sensitivity 79—94184
- dichromated gelatin as holographic storage medium 80—43303
- film, deuterated, IR absorpt. spectra, heat treatment and ageing *(Russian)* 78—39621
- film, dielectric losses and breakdown, struct. effects *(Russian)* 77—52017
- film, internal stresses, 20-240°C *(Russian)* 79—87645
- film, orientating action of solid substrates, on liq. cryst. layer exam. 80—44111
- films with Fe,Cu,Ag and S containing compounds, IR spectra *(Russian)* 78—49928
- fine-grained bleached emulsion scatt. model and expt. 80—102670
- gelation and phase separation, H_2O-methanol as gel fluid 79—66373
- gels, coloured component addition, struct. form., dynamic shear modulus, viscosity meas. *(Russian)* 80—7871
- gels, in water and glycerol/water mixtures, dynamic viscoelastic props. 80—64508
- hardened layer structuralisation, kinetic anal. using swelling 78—62255
- holographic optical element fabrication using dye-sensitised dichromated gelatin 78—63043
- IR absorption spectra of pure layers and layers with AgBr emulsion layer *(Russian)* 80—62776
- IR spectroscopic study of effects of impurities and other actions, fine struct. *(Russian)* 78—58083
- layer, dry, aqueous soln. penetration 80—85221
- layers, swollen, electrolyte diffusion 78—32910
- metal-gelatin-n-GaAs struct., C-V characts. and gelatin-semiconductor interaction rel. to photographic process *(Russian)* 80—49944
- nuclear photoemulsion, effect of pulsed elec. field on physical and mech. props. *(Russian)* 78—869
- optical matched filter correlator memory techniques and capacity 80—43280
- phosphorescence kinetics curves of gelatin layers with and without $AgNO_3$ *(Russian)* 80—62776
- photographic developer, effect of diffusion on swelling of gelatin layers *(Russian)* 79—97461
- photographic emulsion 78—16866
- photographic emulsion gelatin enzymic hydrolysis expts. 79—79311
- photographic emulsions, weakening of colloid protection by gelatin 78—32906
- photographic gelatin, gel-sol transition, gel characts. 78—35724
- photographic gelatin classification problem 79—100448
- photographic layers, permeation of photographic developer, potentiometric exam. *(Russian)* 80—73500
- polymer, brittle photoelastic, use of gelatin gels in prep. for optical polarization stress study 80—40325
- reflection holograms in dichromated gelatin 80—19006
- swollen gel layer, solute penetration times 78—16867
- thiosulphate determ. in photographic gelatine, spectrophotometric method *(Hungarian)* 80—66905
- tissuelike medium α trajectory production of δ-rays 80—9465
- water molecules state, NMR meas. *(Russian)* 79—52790
- Ag halide film physical props., effect of gelatin structure 80—97715
- Ag halide hydrosol models of photographic emulsions 79—20470
- Ag halide sensitised gelatin processing, phase volume hologram form. 80—78797
- AgBr cryst. growth mechanism in gelatin solns. 77—54004
- AgBr, photographic gelatin dispersion, cryst. habit. rel. to Br$^-$, cyanine absorpt. 78—32908
- AgCl electrode, electrochem. dye spectral sensitization, gelatin addition *(Japanese)* 79—57262
- Al-gelatin-GaAs, C-V characts., irrad. effects *(Russian)* 77—51823
- Al-gelatin-GaAs, capacitance-voltage characts. after and before incorporation of $AgNO_3$ 79—51684
- Fe, corrosion pitting in acid, alkaline solution, gelatin effect 78—95838

gels
- acrylamide gel, spinodal line and critical point, light scatt. meas. 79—79315
- acrylic, US observation of critical behaviour *(French)* 79—29414
- acrylonitrile Na methallylsulphonate copolymer electrolytes in dimethylformamide, gel permeation chromatography appl. 80—21345
- agar, prop. change due to ionising radiation *(Korean)* 77—48699
- agargel electrophoresis, protein transport, stochastic model 77—77769
- agarose gels, bubble prod., stabilisation by nonionic surfactants 80—76562
- agarose gels, $H_2{}^{17}O$ enriched, ^{17}O NMR, hydration anal. 77—81426
- agarose-water gels, stability, conc. and isotope effects, photometric obs. 79—66362
- agarose-water systems, gel-sol transition, thermal hysteresis and reversibility 79—66361

gels continued
- alumina gel, hydrated, prep. by homogeneous precipitation method, phase change by heating *(Japanese)* 77—25046
- amylopectin, glycerin impregnated, dynamic viscoelasticity *(Japanese)* 80—104203
- amylose, glycerin impregnated, dynamic viscoelasticity *(Japanese)* 80—104203
- biopolymer negative resistance, rel. to living cell props. 78—64923
- bolus material of shredded-gel for use with EMI CT 1010 brain scanner 80—41173
- branched polymers near gelation threshold, field theory statistics 78—91220
- butadiene acrylonitrile copolymer, raw elastomer, containing crosslinked particles, flow behaviour 79—37359
- calcium alginate gels, Raleigh scatt., spectral broadening, density fluctuations 79—1776
- cellulose acetate-dimethylphthalate gel, mech. props., substitution effect *(Russian)* 79—23291
- cellulose trinitrate, in soln., gel-like aggregate form. rel. to configuration 77—31036
- cement paste, hardened, physics and chemistry 78—73013
- Cl ThO_2 glasses, thermal anal. *(French)* 78—14282
- contact lens gel materials for extended wear, water flow cond. 78—81062
- contractile polymeric structures, deformative props., artificial muscles 77—25595
- correlated percolation, ϵ expansion, appl. to gels 80—77714
- critical concentration fluctuation dynamics, near phase separation 78—56921
- cylindrical gel, in silicone oil, method for viscoelastic consts. meas., longit. vibrs. 77—73619
- defibrillator electrode gel testing, meas. of impedance to transthoracic DC discharge 78—57056
- diepoxide-diamine network polymers, chem. props. and average mol. wt. 80—37915
- diepoxide-diamine network polymers, reaction mechanism investigation using gel permeation chromatography 80—40789
- N,N-diethylacrylamide, cross-linked copolymer, improved mech. props. 80—61091
- diffusion in glassy polymer sheets and spheres, with discontinuous swelling 80—44354
- dioxane based, scintillation yield and mechanisms involved study *(French)* 80—52816
- dipalmitoyl lecithin bilayer, mol. tilt, X-ray diffraction obs. in gel phase 80—84059
- dipalmitoyl phosphatidyl choline, deuterated gel phase lipid bilayer, neutron scatt. sudy 79—43829
- dipalmitoyl phosphatidylcholine, gel and liquid crystalline phases, deuterium mag. resonance obs. 79—91308
- dynamic light scattering theory 78—60475
- elastic response under strong deform., non-linear behaviour 78—7240
- electrocapillary acceleration meters with electrolyte in gel form 80—73330
- electrophoresis, 2-dimens., in study of somatic cell differentiation 80—46114
- ethidium bromide E-DNA, intercalated birefringent fibres, microspectrophotometric investig. *(German)* 80—57392
- ethylene-vinyl acetate copolymer, powdered, prep. by emulsion polymerisation *(Japanese)* 80—104110
- Ficoll, bacterial movement in viscous environments 79—43840
- finite polycondensing system, mean chain length distrib., probabilistic theory 79—70324
- fission product and actinide adsorption on silica gel, for urinary gross α activity determ. 79—88155
- Fresnel lens film prep. by electron beam irradiated mould polymerisation 79—98515
- gas cavitation nuclei, physical props. of surrounding nonionic surfactants 79—100444
- gel-chromatogram processing technique allowing for spreading, Friedholm eqn. soln. *(Russian)* 79—24880
- gelatin, layers, swollen, electrolyte diffusion 78—32910
- gelatin, with H_2O-methanol as gel fluid, phase separation and gelation 79—66373
- gelatin gels, in water and glycerol/water mixtures, dynamic viscoelastic props. 80—64508
- gelatin sol-gel transition, viscosity meas. method 80—85219
- gelatin-Pd II complex formation, circular dichroism and absorpt. spectra meas. 79—61881
- gels, dynamic light scattering in poor solvent 78—88318
- glass, surface layer, structure and processes *(German)* 80—38928
- glasses, refractory, obtained by hot pressing of gels, crystallisation *(French)* 78—11193
- glassy polymer multi-phase Stefan problem describing swelling and dissolution 78—2263
- graph-like state of matter, electrical cond. of random networks, gelation and elasticity 78—65875
- haemoglobin, deoxygenated sickle cell, gels, liq. cryst. props. 78—3445
- heterogeneous two-phase, permeability 80—76563
- hydrogel coatings, and impregnations in silastic, dacron and polyethylene 79—20719
- hydrogel of high water content as a material for the soft contact lens *(Japanese)* 80—12300
- hydrogel pilocarpine release rate control by plasma polymerisation 77—60284
- hydrogels, two-component, elasticity theory and compress. meas. 80—44246
- ionomer solutions, in water, gel form. and demixing transition 80—61172
- isotactic polystyrene, anomalous X-ray diffraction effects, rel. to chain conformation and isomeric homogeneity 77—50576
- jelly-filled optical fibre cable fabrication and characteristics 80—53490
- lecithin surface films, equilib. and metastable states rel. to use as biological model 77—60188
- light modulating media, controlled gelatinous, dynamic deform obs. by laser interferometry 79—32072
- light scattering, dynamic behaviour obs. 80—55727
- lipid phase transition, cluster model, appl. to bilayer mol. passive permeation and struct. relax. 78—53346
- LKB Multiphor, universal system for electrofocusing, electrophoresis, immunoelectrophoresis and isotachophoresis 80—7888
- macromolecular solution, gel conc. and diffusivity at gelling determ. by ultrafiltration 80—21325
- macromolecular system, critical branching, a statistical theory 80—3413

gels continued

- medical US phantoms, water-based gels 80—81671
- mesomorphic monolayers, quasitwo dimens., theoretical models 80—76713
- methyl methacrylate+diallyl phthalate, two-step copolymerisation, light focusing plastic rod prep. *(Japanese)* 79—37064
- methylcellulose, bacterial movement in viscous environments 79—43840
- micro-organism electroretention effectiveness rel. to electrode type *(Russian)* 80—26419
- multidimensional system of order II, gel point determ. 77—32834
- nylon-6 dilute soln., gelation and crystallisation, struct. determ. 79—37635
- ovalbumin aqueous soln., macromol. gel layer formed on ultrafiltration tubular membrane, charact. 80—14260
- particle porosimetry by inverse gel permeation chromatography 77—90659
- partition/permeation chromatography using n-alkane solutes 78—44429
- PET, filament form. from gels 78—80508
- photographic gelatin, gel-sol transition, gel characts. 78—35724
- photoresists, crosslinking efficiency, exptl. determ. 77—87862
- PMMA gels, neutralised cross-linked, selective uptake of ions 78—35719
- poly(γ-benzyl L-glutamate), soln. and film, light scattering study 79—66374
- poly(dihydroxypropyl methocrylate), surface charact., by contact angle methods 80—61140
- poly(ethylene-but-1-ene) copolymer, gelation and precipitation from solutions, NMR exam. 79—43641
- poly(hydroxyethyl methacrylate), surface charact., by contact angle methods 80—61140
- poly(m-xylylene adipamide), molten, gel form. kinetics *(Japanese)* 80—108757
- poly(methacrylic acid), aq. soln., gelation kinetics under shear stress 78—3387
- poly(methoxyethyl methacrylate), surface charact., by contact angle methods 80—61140
- poly-2-hydroxyethyl methacrylate gel, thermoelasticity 77—84205
- polyacrylamide, audiofrequency very slow propagating mode 79—74429
- polyacrylamide, automated scanning of ^{14}C 80—17221
- polyacrylamide, gels and single chains, phase transitions and crit. behaviour 80—40759
- polyacrylamide, network density fluctuations, crit. behaviour 77—44518
- polyacrylamide gel and single chain in soln., laser light scatt. obs. near phase transitions 80—93808
- polyacrylamide gel structure inhomogeneity from permeability and viscoelasticity 77—89384
- polyacrylamide gels, structural collapse in solvent, crit. endpoint 78—48702
- polyacrylamide-water, translational and collective diffusion 79—52787
- polyacrylamide-water gels, copolymerised with N,N-methylene bisacrylamide, dynamic light scatt. 78—60477
- 1,2-polybutadiene, crosslinked in states of strain, entanglement networks, swelling anisotropy obs. 80—79666
- polybutadiene networks, cis-trans isomerisation, γ-ray induced 79—74374
- polydimethylsiloxane chains, end-linked, swollen model networks, stress/strain isotherms and elastic modulus 80—79668
- polyether-urethane elastomers, crosslinked, three dimensional polymerisation, kinetics, gel. form., mech. props. *(Russian)* 80—7792
- polyethylene terephthalate-co-isophthalate, gelation and crystallization 80—24377
- polymer, brittle photoelastic, use of gelatin gels in prep. for optical polarization stress study 80—40325
- polymer, crosslinked, probabilistic theory of structural and physical characteristics 80—5649
- polymer, reactivity and gelation, intrinsic reactivity 79—100363
- polymer, reactivity and gelation, substitution effect 79—100364
- polymer adsorption on small spheres, scaling approach 78—3377
- polymer gel, quasielastic laser light scatt. theory 79—82986
- polymer gelation, crit. percolation probabilities, appl. to hard sphere packing expt. 78—61063
- polymer gelation, site-bond percolation, low-density series anal. of uncorrelated limit 80—4657
- polymer gelation, statistical mech. model, site-band correl. 79—34368
- polymer gelation theory *(Chinese)* 79—74379
- polymer gels, comb-like, dielec. polarisation *(Russian)* 77—48698
- polymer gels, thermodynamic props., review *(German)* 78—20073
- polymer gels, with liq. cryst. solvents, theory 80—11963
- polymer network, crystn. and form. through crystn., crystallinity influence on radiation induced form. 80—38964
- polymer network formation, pre-gel intramol. reaction and gelation, shear moduli and glass transition 80—45501
- polymer network in solution, free energy of deform. 80—38900
- polymer solutions, microgel-containing, physico-chem. and rheological props., light scatt. obs., review *(Polish)* 78—50704
- polymer solutions and networks at equilib. swollen state, inelastic light scatt. by gel modes 78—1972
- polymer statistics of long chains in solns. or melts 79—31758
- polymeric, light scatt. intensity, network struct. effects 79—70381
- polymethacrylic acid, swollen networks, viscoelastic photoelastic behaviour 80—59366
- polymethylsiloxane-toluene gels, light scatt., compression moduli, cooperative diffusion 78—23970
- polysaccharide, anomalous behaviour of PMR line width of water *(Russian)* 80—11962
- polysaccharide gels, spectral broadening of Rayleigh scattering 78—31771
- polysaccharide gels and sols, PMR relax. times rel. to temp., pH and conc. 78—56952
- polystyrene, conform. and near all-trans extended-chain model relevant in gels, X-ray diffr. patterns interpret. 80—79707
- polystyrene, isotactic gel film, Fourier transform IR spectrum 80—104465
- polystyrene, low mol. wt., conc. transdecalin soln., hydrodynamic and gel modes light scatt. obs. 79—73085
- polystyrene, porous gel, solute elution behaviour in high performance liq. chromatography 78—92524
- polystyrene hydrophobic gel beads, gel permeation chromatography behaviour 79—66386
- polystyrene networks swollen in cyclohexane, swelling equil. and light scatt. at theta conditions 80—107036
- polystyrene-co-divinylbenzene microgels in dimethylformamide, diffusion coeff., viscosity and mol. wt. meas. 80—30286

gels continued

- polysulphonamide solutions, mech. props. during gelling *(Russian)* 77—19579
- polyuranate gels, changes in pore structure during reduction and sintering 77—71685
- polyvinyl alcohol networks, swelling equil. with dil. salt solns., thermoelastic behaviour, hydroxyl group interact. 80—79667
- polyvinyl-pyrrolidone/polyethylene glycol oligmers, elasticity theory, and compression meas. 80—44246
- polyvinylacetate and polyvinylacetate—microgels, light scatt. 80—20652
- polyvinylalcohol, macromol. gel layer formed on ultrafiltration tubular membrane, charact. 80—14260
- porous 80—11955
- precipitation, spontaneous pattern formation, symmetry breaking instabilities 78—80792
- PVA hydrophobic gel beads, gel permeation chromatography behaviour 79—66386
- rheological properties, Weiler-Rhebinder method, polymer conc. *(Russian)* 78—53274
- rodlike macromolecules, nonlinear elasticity in condensed state 80—104199
- rods, elastic dilatational mode, light beam positional modulation 80—64167
- scanner for location of proteins separated by isoelec. focusing 80—30953
- sickle haemoglobin gelation, reaction order and crit. nucleus size 78—76983
- silica, appl. to $BaMoO_4$ and $BaCO_3$ cryst. growth 77—36379
- silica, elec. cond. on surface, effect of impurity adsorption *(German)* 78—30971
- silica, ion exchanger, isotope separation appls. 78—86961
- silica, naphthalene adsorption, biphasic photochemistry, time-resolved spectra 80—30252
- silica, pyrene adsorption, biphasic photochemistry, time-resolved spectra 80—30252
- silica, thermodynamics of adsorption from perfect binary liq. mixtures 80—44428
- silica (metallised) gels, thermal cond., 10-200K, cryogenic appls. 78—79828
- silica gel, adsorption from soln. of benzene-cyclohexane mixtures 79—23826
- silica gel, effect of gamma-rays, electron scavenging by N_2O 79—24762
- silica gel, fixed substance identification using Raman spectroscopy *(French)* 78—88664
- silica gel, infrared absorpt. spectra *(Russian)* 77—55794
- silica gel, IR spectra of dry transparent plates, surface struct. study 79—87884
- silica gel, microporous amorphous toroidal, spectroscopic and thermal analysis, adsorption properties 79—57305
- silica gel, Mn^{2+} adsorption rel. to H_2O adsorpt., EPR study 79—5180
- silica gel, polymer adsorption into surface pores, computer simulation, phase transition *(Russian)* 78—51824
- silica gel, pore struct., effect of washing with aq. solns. containing Mg^{2+}, Ca^{2+} ions 79—52786
- silica gel, skeletal struct. modification with alcohols and water vap., thermal analysis obs. 78—88659
- silica gel, struct., dielec. polarisation, IR spectral investigs. *(French)* 77—81427
- silica gel, thermal conductivity rel. to moisture content *(Russian)* 77—54864
- silica gel for low temp. regenerator of cryogenic refrigerator 77—17994
- silica gel regeneration by adiabatic desorption mathematical model 79—1967
- silica gel with benzene submonolayer PMR and DMR dynamics and surface heterogeneity 79—69735
- silica gels, surface treatment, adsorption properties *(Japanese)* 78—95855
- silicaalumo, Na-K, crystn. and characts. of A-type zeolites 79—52780
- silicate gardens, growth morphology, mechanisms 80—100765
- silicic acid sol., gel formation, characteristics of light scattering 78—53269
- silicon tetramethoxide, prep. from metal alkoxide, props. as precursor of oxide glass 78—48700
- sol-gel transition, incoherent light scatt. 79—61915
- sol-gel transition, sol viscosity, Rouse approx. *(French)* 78—61054
- sol-gel transition, theory, polycondensing system, mol. size 79—57303
- sol-gel transition, US attenuation meas. 80—101043
- sol-gel transition kinetics 80—85218
- solgel scintillators for liq. scintillation counting of aqueous and non-aqueous samples 77—38546
- soya protein gels and sols, PMR relax. times rel. to temp., pH and conc. 78—56952
- starch, glycerin impregnated, dynamic viscoelasticity *(Japanese)* 80—104203
- starch gelatinisation investigation using small-angle light scatt. photometer with solid-state photodetector 77—86382
- styrene copolymer, props. rel to composition *(German)* 79—66291
- swelling kinetics, device 80—21210
- swelling kinetics theory, polyacrylamide gel obs. 79—39214
- thin-layer gel apparatus for chromatography in organic solvent systems 78—27873
- thoria sol-gel processes for nucl. fuel fabrication 79—13503
- tissue mimicking materials for ultrasound phantoms 79—5333
- tracheal mucus gel props., changes induced by divalent cations 80—51142
- with trapped polymer chain, relaxation *(French)* 77—62483
- unsaturated polyester resins, gelation, viscosity meas. *(Polish)* 80—59690
- uranyl gel microsphere characterisation by emanation thermal anal. for UO_2 fuel prep. 80—95391
- viscoelastic properties, appl. to meas., at small constant shear stresses 79—54123
- Al_2O_3, derived from gels, sintering behaviour, microstruct. 80—20875
- Al_2O_3 gel, prep. of ultra-fine particles, from $Al(OH)_3$ colloidal soln. 79—74431
- Al_2O_3 hydrated gel synthesis by homogeneous precip. method using $NaAlO_2$, phase change by heating *(Japanese)* 78—68937
- Al_2O_3, transparent, polycrystalline, prep. by sol-gel method *(Japanese)* 78—19698
- Al_2O_3 ultrafine gel particle form. from NH_3-$AlCl_3$ solution 80—93807
- $Al(OH)_3$, coprecipitated with $Cr(OH)_3$ gel, magnetic, optical studies, calcination 79—47995

gels continued
B_2O_3-SiO_2, glass synthesis by hot pressing of gels 79—15637
$Bi_2(SeO_4)_3$, single cryst. growth in silica gels, X-ray diffr., IR and emission spectroscopy study 79—74075
C-S-H gel, formed in hydration of C_3S pastes, chem. comp. 79—79346
$CaHPO_4.2H_2O$, cryst. growth in silica gel, etch pits obs. on as grown faces 79—73169
$Cr(OH)_3$, coprecipitated with $Al(OH)_3$ gel, magnetic, optical studies, calcination 79—47995
Fe (III), magnetisation vector diffusion coeff., anisotropy energy, vol. distrib. of particles by Mossbauer effect 78—48099
$Fe(OH)_2$, gel, coprecipitation of divalent metal ions in soln. *(Japanese)* 78—31714
FeOOH, ferric hydroxide gel, struct. determ. 79—11832
FeOOH gels, Mossbauer spectra, mag. props. 80—11303
La_2O_3-SiO_2, gels, microstruct. and crystallisation, prep. method and thermal treatment effect 79—61913
La_2O_3-SiO_2, glass synthesis by hot pressing of gels 79—15637
Na_2O-CaO-SiO_2-H_2O system gels, metastable nature 80—71952
Nb_2O_5, hydrated gel, prep. conditions on pore struct., adsorpt. meas. 78—3068
^{233}Pa removal from ^{237}Np by coprecipitation with MnO_2 or sorption on silica gel 79—52733
$PbMoO_4$, cryst. growth from gel soln., habit modifications 78—2043
SiO_2, amorphous forms, surface struct. ESCA, X-ray line shift meas. *(Russian)* 77—66775
SiO_2 gel, adsorption curves of O_2, EPR *(Russian)* 79—52776
SiO_2 gel, $BaMoO_4$ crysts. grown under influence of elec. field 80—93469
SiO_2 gel, internal and surface struct. by X-ray scatt. 80—84074
SiO_2 gel, irrad., adsorpt. of NH_3, neutron scatt. 79—33194
SiO_2 gel, meso-porous, SCI/IUPAC/NPL surface area standard, pore meas. 77—4941
SiO_2, gel, pyrolysis, for low-temp. silica glass synthesis 79—43194
SiO_2 gel, sintering 77—85980
SiO_2 gel, steam treatment, struct. changes 80—35579
SiO_2 gel. struct., IR spectra obs. 78—88297
SiO_2 gels, heats of immersion, effects of pore narrowing 79—11833
SiO_2, glass synthesis by hot pressing of gels 79—15637
SiO_2 macroporous modification of surface by adsorption of thin layer of polymer 80—6624
SiO_2:Al gel, gamma rad. effects, depend. of H_2 adsorption and colour centre form. on Al content 79—69156
SiO_2-Al_2O_3, coprecipitated gel, Si-Al spinel formation during transformation on heating 79—78958
SiO_2-water system, inorg. polymer struct. form., globular crystn. 80—101042
SiO_2-ZrO_2 adsorbents, coprecipitated, porous struct. rel. to form. conditions 78—53263
SnO_2, hydrous, gel, chemisorption of organic compounds, transmission IR spectroscopy 77—55465
Ta_2O_5-H_2O_n, influence of preparation on pore structure and ion exchange props. 79—1970
$(Th,U)O_2$ microspheres, fabrication 80—801
ThO_2 gel, morphology relations during bulk transport sintering 77—70015
ThO_2, sol-gel, for nucl. applics., sorption of water, CO_2 and N_2 77—4940
$Ti(OH)_4$, polyacrylamide gel, adsorption of U (VI) from sea water *(Japanese)* 77—54347
U kernels preparation by external gelation process 79—26663
U^6 xerogels, calcination, UO_2 preparation, thermal treatment modelling 79—49813
UO_2 microspheres, Gel-Sphere-Pac process 80—13764
UO_2, sintered, production by gel calcination and drying, thermal anal. *(Czech)* 80—45260
UO_2 sintering, thermal anal., hexavalent uranium xerogel drying, thermal treatment modelling *(Czech)* 79—36378
UO_2 sol-gel particles, low temp. sintering and props. 79—100101
U(VI) gel, prep. by internal gelation, determ. of region of existence 77—9136
Zr gels, thermal and related studies 80—71937
ZrO_2 gels, calcination 80—11964
ZrO_2-SiO_2(-Na_2O) glass fibres, prep. from metal alkoxides, resistance to NaOH soln. 80—97454

general relativity
see also cosmology; gravitation; gravitational red shift; Schwarzschild metric; space-time configurations; unified field theories
1919 eclipse test and preceding events and discussions, book contrib. 80—22249
μ-space, vector and multivector fields 80—4594
Ψ collapse and relativistic covariance *(French)* 80—82682
$\mathcal{M}$-space formalism 78—21018
absolute space, soln. 79—58514
accelerated detectors, thermal like behaviour, quantum noise 79—139
acceleration of freely falling particle in stationary gravit. field *(Russian)* 77—53808
acceptance in Canada 80—68012
aether drag and radiation press. in dispersive medium 79—35124
algebraic computations by CAMAL 80—94998
algebraic type of space-times possessing a nonsingular killing horizon 78—62126
almost contact manifold, generalised S-curvature like tensor field 80—36909
angular momentum, rot. black hole perturbations 77—53623
angular momentum in general relativity, defn., asymptotic behaviour 77—49650
angular momentum of stationary gravitating systems 79—88851
anholonomic Cauchy problem in general relativity 80—86166
anisotropic Bianchi II cosmological models with matter and electromagnetic fields 79—48976
anisotropic cosmological solutions in theory with quadratic invariants *(Russian)* 77—91673
anisotropic fluid in spherical space-time, high freq. null radiation state 78—21016
anisotropic fluids with two-perfect-fluid components, Einstein eqn. soln. 80—105554
anisotropic incoherent fluid cosmological model in general relativity 79—40303
anisotropic spheres, adiabatic contraction in general relativity 80—36489
anisotropic uniform model universes with cosmical const., flat space 78—73788

general relativity continued
anisotropy damping through quantum effects in early universe 78—57708
anomalous currents in curved space 78—62336
approximation methods 80—73235
arbitrary pseudo-Euclidean space, real and complex boosts 78—113
Arnowitt-Deser-Misner energy and g_{00} 79—17297
artificial satellite tracking, relativistic Doppler shift meas. 80—46951
aspherical gravitational collapse, matter associated perturbations, linear Einstein field and conservation eqns. 79—5843
astronomical tests 80—36934
asymmetric Maxwell theory, additional universal inverse square forces 80—27149
asymptotic structure of isolated systems 80—73230
asymptotic symmetries, energy-momentum and angular momentum at future null infinity 80—73231
asymptotically flat gravit. field, Hertz pot. and radiation fields 77—60994
asymptotically flat initial data for vacuum spacetimes 78—16702
atomic clocks in relativity expts. 80—46950
axial solutions to eqns. *(Russian)* 78—4531
axial symmetric space-times, canaonical forms 80—105545
axially symmetric Brans-Dicke solutions for Einstein's field eqns. 80—90753
axially symmetric electrovac fields from empty space gravit. fields 78—16700
axially symmetric stationary perfect fluid solns. of Einsteins field eqn. 80—86157
axially symmetric two body problem, free fall, gravit. energy flux 77—71254
axially symmetric two-body problem, Bondi mass loss, quadrupole formula failure 80—42120
axially symmetry gravit. vacuum configs., theorem *(French)* 77—67341
axisymmetric gravit. fields, review 77—17881
axisymmetric gravitational collapse with escaping neutrinos, Einstein's field eqns. 80—26888
axisymmetric gravitational fields, internal symmetries 79—88849
axisymmetric scalar-tensor gravit. field, galaxies, oblate bodies 77—33917
b-boundaries of special space-time models 80—31602
b-boundary definition, modifications 80—31606
b-boundary of S^1 with const. connection 77—37802
Bach field equations, jump relations and associated transport equations *(German)* 79—9162
Bach-Lanczos identity derivation from modified Hilbert variational principle 78—32737
Backlund transformations of axially symmetric stationary gravitational fields 79—40421
Barotropic fluid in semi-Riemannian manifold, classical and relativistic vorticity 78—65842
Bel-Petrov field classification, algorithm 78—93566
Bel-Robinson superenergy tensor, tetrad description of gravit. field 77—57236
Bel-Robinson tensor, stationary solns., positive energy problem 78—100
bell's inequalities from the field concept in general relativity 80—105771
Bells inequality, quantum generalisations for different space-time regions 80—101728
Bertotti-Robinson EM universe 78—36741
Bertotti-Robinson metric, pair production, semi-classical treatment 79—2702
bi-metric theory of gravit. 77—17889
bi-recurrent Finsler space, basic props. 80—12958
bi-scale theory of gravitational and strong interactions 79—12696
Bianchi cosmologies, singularities, Einstein eqn. solns., review 80—12837
Bianchi IV cosmological model, exact solns. 77—67151
Bianchi IV metric with electromagnetic field, Einstein eqn. exact solns. 80—22247
Bianchi model Lie groups, automorphisms 79—30313
Bianchi type II exact cosmological model with matter and EM field 80—105560
Bianchi type V model, matter dynamics, horizon and singularity problems 80—36749
Bianchi type VII homogeneous cosmological models 77—17734
Bianchi type-I cosmologies and spinor fields 80—62347
Bianchi type-I universe, entropy per particle in early stage 77—17732
Bianchi type-I universes, entropy prod. and viscous dissipation 78—8179
Bianchi V LRS dust space-times, intermediate singularities, whimpers, instability 80—36750
Bianchi VI_0, VII_0 cosmological models with spin and torsion 80—46720
Bianchi VIII/IX cosmological models, anisotropic, with matter and EM fields 78—73784
bifurcate Killing horizons 79—88850
big bang model, hot, observational cosmology 78—12444
bimetric general relativity theory, space-times 79—67198
bimetrical formalism and observables, gravitational field description *(Russian)* 77—45750
binary pulsar, PSR 1913+16, post-Newtonian, timing effects 78—4261
binary stars, gravit. waves interaction, tidal reson. 78—93089
binary system with compact objects, static two-body problem and attraction law 78—93574
binary systems with compact objects, static two-body problem and attraction law, post-post Newtonian approx. 79—117
Birkhoff's theorem generalisation 80—27187
black hole, charged, plasma horizons 78—12282
black hole, definition 79—2555
black hole, definition for any causal space-time 80—31620
black hole, dissipative test EM fields in black hole background 79—25627
black hole, Kerr-Newmann, spontaneous discharge 78—12288
black hole, wave fronts 78—8282
black hole collisions, generation of gravitational radiation 77—13663
black hole evaporation in projective relativity 79—17014
black hole fields, MHD relativistic processes 78—12280
black hole formation, effect of zero point fluctuations 78—12286
black hole interactions, gravitational radiation emission 79—125
black hole MHD 78—12281
black holes, arguments against existence 79—75243
black holes, construction of metric and vector pot. perturbations 80—8647
black holes, energy states, classical and quantum 78—12285
black holes, exploding, instantaneous Cauchy surfaces topological change 78—12087

general relativity continued

- black holes, gravitation, charges, cosmology and coherence, elementary particles and Dirac large numbers 79—2477
- black holes, gravitational aspects *(Hungarian)* 80—46894
- black holes, Hawking's effect, quantum field theory applied in curved space-time 78—12268
- black holes, high-freq. EM waves propag. through magnetised plasma in curved space time 80—48894
- black holes, in quasi-isotropic Tolman soln. *(Russian)* 77—91561
- black holes, magnetic 78—12283
- black holes, massive, rotating, charged, phenomena based on Schwarzschild and Kerr-Newman metric solns. 79—71064
- black holes, perturbations, potential barriers with equal reflection and transmission coefficients 80—27191
- black holes, primordial, radiation accretion in early Universe 80—67918
- black holes, primordial, self-similar growth for general sound speed case 79—5856
- black holes, relativistic accreting discs hydrodynamic struct. 78—36632
- black holes, Robinson's identity, EM generalisation 78—81649
- black holes, rotating, electromagnetic perturbations 78—12279
- black holes, small, quantum mechanical approach 78—16453
- black holes, small mass, spin effects on formation in Einstein-Cartan theory 77—71125
- black holes, spherically symmetric, perturbations, linearised Einstein-Maxwell eqns. 80—72992
- black holes, stationary, uniqueness theorems 78—96500
- black holes, test particle motion in crossing Schwarzschild surface, book contrib. 79—44816
- black holes, thermally evaporating, Raychaudhuri eqn. 80—109457
- black holes, vacuum uniqueness theorem and generalisations 78—12278
- black holes, white holes and wormholes, review 77—17610
- black holes and particle detectors 78—12287
- Bochner curvature tensors, Kahler manifolds *(Japanese)* 79—12663
- Bondi formalism, evolution of isometries 77—45758
- Bondi vector, Seliger and Whitham variational principle for matter fields 79—93013
- Bondi-Metzner-Sachs group, lifting of projective representations 78—21028
- Bonnor electrovac counterparts of Tomimatsu-Sato solns. of Einstein eqn. 78—57835
- Bonnor transform. extension 80—31643
- book, relativistic theories of materials 78—81907
- bound state, two charged media interaction, self-consistent field theory 78—16667
- bound states of nonlinear scalar field in general relativity 78—77778
- boundary definitions for space time configurations 80—31605
- bounded system of extended bodies, relativistic eqns. of motion 78—73898
- Brans Dicke's scalar field, geometrisation 78—54258
- Brans-Dicke axisymmetric stationary vacuum fields 77—33921
- Brans-Dicke cylindrically symmetric fields, singularity of solns. 79—2669
- Brans-Dicke fields generated from Einstein's vacuum fields, 'rod solution' 79—71326
- Brans-Dicke static spherically symmetric field, EM potential of test point charge 79—85041
- Brans-Dicke theory, EM solns. 78—57841
- Brans-Dicke-Jordan theory connection, general relativity extension 80—62547
- bundle boundaries, Schwarzschild and F-R-W solns. 77—57248
- bundle boundary for the Schwarzschild and Friedmann solutions 80—31603
- bundle completion for parallelisable space-times 80—31604
- C-metric black hole solution to vac. Einstein field eqns. 78—89216
- calibration theory and gravitational const. variation in early universe *(Russian)* 80—17706
- canonical coordinates in stationary axial symmetry *(French)* 79—25918
- canonical decomposition of the general relativistic initial value problem 79—71304
- canonical formulation by analogy with elementary particle string model 78—8287
- canonical formulation of gravitational theory, generally covariant space-time separation *(Russian)* 77—41513
- canonical vierbein form 77—13659
- Cartan space, scalar and massless vector fields 77—9931
- cartesian operator algebra for expansion of tensor quantities and equations in a spherically symmetric background 79—44821
- Casimir cancellations in half an Einstein universe 80—86161
- Cauchy problem for general relativistic perfect magnetofluid 78—70024
- Cauchy problem formulation for Einstein eqns., coordinate conditions, reference frame theory 80—57150
- Cauchy problem on a manifold, Einstein eqn. solns. *(French)* 79—25920
- Cauchy surface topology restriction in general relativity 77—9921
- Cauchy surfaces, determ. from intrinsic props. 78—70023
- causal universe, cosmological matter creation 79—53945
- causality structure, relativistic, representations by operator density current 77—45767
- caustics and singularities, gravitational converging effects 80—77654
- caustics and WKB approx. 77—45757
- caustics in general relativity, Hamilton-Jacobi function in phase space coords. 77—79007
- cavity, vanishingly small, gravitational field inside matter 80—95012
- celestial mechanics, astron. meas. and coord. systems 80—36481
- celestial mechanics, periodic solns. in Hill's relativistic problem 78—40804
- central field, general relativity without tensors 78—12616
- characteristic initial-value and mixed problems 77—71246
- charge in cosmological models, effect on curvature parameter 78—69921
- charged black hole, perihelion precession for two body problem 77—78626
- charged black holes, total charge, energy and size relationship, cosmic censorship validity 80—113
- charged bodies, lower size limits 80—22245
- charged body free fall motion in gravit. field, field energies and equivalence principles 78—49740
- charged elastic fluid sphere, Einstein's field eqns. soln. 80—111
- charged elastic fluid sphere, interior soln. 77—9929
- charged fluid, general relativistic pulsation eqn. 77—5711
- charged fluid, orthonormal tetrads in general relativity 78—54269
- charged fluid sphere, anal. of Krori Barua soln. 77—26213
- charged fluid sphere, exact interior solns. of Einstein-Maxwell field equations 78—62122

general relativity continued

- charged fluid sphere, general relativity soln., Einstein-Maxwell eqns. 80—68088
- charged fluid sphere, gravitational collapse 80—31637
- charged fluid sphere, soln. for interior metric 77—2571
- charged fluid spheres, regular solns. to Einstein field eqns. 79—92998
- charged fluid spheres, relativistic field eqn. soln. 80—31641
- charged homogeneous cosmologies, theory 79—25767
- charged Kerr-Tomimatsu-Sato family of solns. 78—62130
- charged media, general relativistic Lagrangian dynamics *(Russian)* 78—7874
- charged particle, gravitational mass derivation 80—4597
- charged particle dynamics, symmetries 77—45742
- charged particle motion, charged Robinson Trautman soln. 78—62124
- charged particle motion in an electromagnetic field on Kerr background geometry 79—9167
- charged particle orbits in Kerr geometry with EM fields 80—52096
- charged particle trajectories in mag. field in Schwarzschild geometry 77—41296
- charged particle trajectories in static Ernst space-time 79—17291
- charged particles, motion in relativistic fields 80—57146
- charged particles in Newtonian and post-Newtonian approximation, dynamical motions in general relativity 79—80480
- charged perfect fluid distrib., spherical symmetry 79—12668
- charged point particles with magnetic moment in general relativity 79—44811
- charged rotating bodies, generation of metrics 78—49735
- charged singularities, repulsive effects 80—90731
- charged sphere, freq. shift of radiation from moving surface 77—57260
- charged stationary axially-symm. metric 78—62131
- charged top in Kerr-Newman bcakground, Lagrangian method 77—64978
- charged universe, general relativistic cosmological model 79—25766
- charged Weyl rod, Curzon metrics 78—45539
- chirally extended supergravity, Maxwell-Einstein supergravity, auxiliary field struct. 78—78126
- Christoffel symbol, generalized, extension to projective quaterion space *(Rumanian)* 78—81892
- chronogeometry and dyadic method *(Russian)* 78—65826
- chronos principle and interactions of fields of spin 0 and 1 78—8286
- circular geodesics, non-equatorial, with constant latitude in Kerr metric, non-existence 79—25930
- classical field theory in reference frames space, Einstein's gravit. theory, Maxwell's EM theory appls. 78—41173
- classical fields with spin 78—8298
- classical pseudoparticle solutions in general relativity 78—89390
- classical quark confinement from general relativity 78—45842
- classical quark confinement from general relativity 78—58162
- classical scalar and vector field evolution in spaces with Killing vectors 80—4608
- classification scheme for non-rotating inhomogeneous cosmologies 80—8726
- Clebsch representations and relativistic dynamical systems 79—93001
- Clifford algebra and Dirac matrices in a tensor formulation *(Russian)* 80—12966
- Clifford-Klein space times, effective Lagrangian and vac. stress-energy tensor 79—2674
- clock paradox as cosmological problem 78—36907
- clock synchronization in a rotating frame 79—49037
- closed Friedmann cosmos, entropy prod. density for chem. reactions *(German)* 77—26101
- cold relativistic neutron gas, study of massive neutron cores 79—35292
- collapse of axially symmetric star, initial data 80—85960
- collapsing relativistic stars, linearised odd-parity radiation 78—93297
- collapsing star, neutrino ang. momentum loss by Poynting-Robertson effect 79—16928
- colliding plane gravitational waves 79—40431
- colour geometrodynamics, eightfold way, review 80—95243
- coloured cosmological black holes, soln. of Einstein-Yang-Mills system 79—12492
- combined Dirac-Einstein-Maxwell field eqns., tetrad field variation 78—4536
- commutation relations in vierbein formalism 80—27205
- compact rotating gravitational instanton from Einstein eqn. solns. 79—9161
- compact spacelike submanifolds in Euclidean spaces 77—53750
- comparison with time varying pot. theory 79—30305
- compatibility relations, derivation from gedanken expts. *(German)* 77—22465
- complex line bundles 78—49732
- complex pot. eqns., appl. to general relativity 77—13655
- complex space-time real slices 77—60992
- computer language FORMAC, use in general relativity 77—41522
- concentric shells, relativistic spin-spin interactions, appl. to Earth and pulsar physics 80—46148
- conference, group theoretical methods in physics, Austin, Texas, USA (Sep. 1978) 80—4474
- conference, singularities in general relativity, Waterloo, Canada (Aug. 1977) 80—31405
- conference, Trieste, Italy, 1975, July 78—8285
- conformal electrodynamics in Einstein spacetime 80—31644
- conformal field equations 80—46881
- conformal gravity in SO(4,2) gauge *(Chinese)* 79—93027
- conformal invariance, black hole nonexistance 79—25929
- conformal invariance, effect on field equations 79—25928
- conformal invariance 80—90736
- conformal invariant model of localised spinning test particles 78—49729
- conformal Killing horizons 79—49123
- conformal relativity, based on $SO_{4,2}$ 78—8311
- conformal relativity, classification of metric bosons 78—93803
- conformal relativity, general theory 79—54022
- conformal relativity, Klein-Kaluza scheme 77—74297
- conformal relativity, particle species classification, symms., space time origin of isospin 78—93815
- conformal relativity, unified description of bradyons and tachyons based on dynamical SO(4,2) 77—67352
- conformal trace anomalies of stress-tensor 78—29023
- conformal transformation, eqn. of motion, strong principle of equivalence 77—13653
- conformal transformations, props., appl. to MHD and thermodynamic perfect fluid *(French)* 80—101

general relativity continued
conformal two-structure as the gravitational degrees of freedom in general relativity 79−17292
conformally flat non-static plane symmetric perfect fluid distributions 79−30311
conformally flat non-static spherically symmetric perfect fluid distributions in general relativity 79−21599
conformally flat space-time, space tensors, trace anomalies 78−12623
conical singularities, struct. of curvature tensor 78−32742
conjectures on Einstein's theory of gravit. 78−104
conservation equations and the gravitational symplectic form 79−2679
conservation laws and invariant quantities *(Russian)* 77−9932
conservation laws and sources of plane symm. gravit. field *(Czech)* 79−12654
conservation laws for general relativistic plasma MHD, black hole rot. energy 79−2685
conservation laws for geometrical optics in general-relativistic refractive media 79−54021
conservation laws of general relativity, gravit. gauge group $SL_{2,C}$ 77−22456
conserved quantities for self gravitating system 79−63098
consistent factor ordering of general-relativistic constraints 80−109
constitutive theory of general relativistic EM fluids 78−57843
constraint equations on noncompact manifold, asymptotically flat solns. *(French)* 77−67343
continuity of soln. through singularity, direct variatonal theory *(Russian)* 78−12610
continuous creation cosmologies and large number hypothesis 77−78902
continuous media with spin 78−57845
continuous medium and grav. field, eqns. of state from variational method 80−42122
contracted Ricci collineations, timelike mapping characterisation 77−67345
convergent and asymptotic iteration methods in general relativity 79−93002
coordinate identification in line elements, isometries, Killing solns. 78−54252
correspondence principle, energy aspect, in gravitational theory *(Russian)* 77−2576
cosmic betatron model, general relativistic induction accelerator 77−37793
cosmic betatron model *(Rumanian)* 78−49315
cosmic censorship, black holes, and particle orbits 79−44802
cosmic censorship, mathematical formulations 80−31619
cosmic censorship and test particles, black hole destruction 80−105552
cosmic censorship hypothesis 80−31616
cosmic censorship hypothesis and the positive energy conjecture 80−31618
cosmic microwave background spectrum, G-varying cosmology 80−86020
cosmological const., physical interpretation *(French)* 77−87580
cosmological const. modification from correspondence limits of general relativity 78−24581
cosmological model, with gravit. and scalar waves 79−53949
cosmological model without big-bang, gravitational origin for universal red shift *(German)* 80−51927
cosmological models, homogeneous, using Einstein's theory of gravitation 79−12547
cosmological models with Hoyle's hypothesis 78−86045
cosmological objects in nonradial motion, redshifts, special and general relativistic anal. 79−80212
cosmological principle, new look 78−86042
cosmological rotating metrics, scalar perturbations 80−62348
cosmological singularities, specific examples 80−36748
cosmological tests, using derivatives of scale factor 77−49662
cosmologies with synge gas and blackbody radiation 80−36751
cosmologies with varying gravity, theories and effects 77−60858
cosmology, adiabatic density perturbations evolution 79−25769
cosmology, anisotropic MHD model 79−35437
cosmology, differences of Brans-Dicke and relativistic theories *(Polish)* 80−27024
cosmology, Einstein's field eqns., inhomogeneous soln., for $p = \mu$ eqn. of state 79−12666
cosmology, general relativity, big bang model, nucleosynthesis, scale covariant theory, review 78−73789
cosmology, generalised principle in Newtonian and relativistic theories *(Polish)* 80−27025
cosmology, initially inhomogeneous model, rel. to QSOs number density excess 79−2576
cosmology, Lagrangian or Hamiltonian formulations, shift vector field restrictions, symmetry group 80−67923
cosmology, magnitude-redshift and ang. dia.-redshift relations for matter and radiation filled universes 78−20917
cosmology, relation between homogeneity of universe and dimensionality of space 77−64893
Coulomb interaction in Riemann space 80−90737
counter-orbiting drag-free satellites in Earth polar orbit, general relativity test and geodetic meas. 77−22047
counter-orbiting polar satellites, geodesy information in modified relativity mission 79−62426
coupled Einstein SO(3) gauge field eqn. solns. 79−274
coupled Einstein Yang Mills eqns. for massless and scalar fields, stationary solns. 78−12621
coupled EM and scalar fields, in cylindrically symm. space-time 79−85035
coupled inertial and gravitational effects in the proper reference frame of an accelerated rotating observer 79−93007
coupled scalar-vector-tensor eqns., axially symmetric soliton solns. 80−31635
covariance principles, Einstein study, 1912 to 1916 79−40343
covariant conservation eqns., relation to energy-momentum concept in general relativity 79−25933
covariant CP^2 non-linear σ-model, classical solns. 79−54020
covariant eqns. of relativistic electrodynamics of continua 78−57842
covariant perturbed wave equations in arbitrary type-D backgrounds 79−30314
covariant quantisation 78−8327
creation and gnosiological lessons 80−98780
curvature collineation for the field of total radiation 79−21606
curvature invariants and space-time singularities 77−57249
curved space-time, propag. of photons and neutrinos 77−79011

general relativity continued
cut points, conjugate points and Lorentzian comparison theorems 79−93009
Cygnus X-1, rotating black hole existence, obs. test from relativistic calc. 77−33699
cylindrical general relativistic collapse, numerical study results 78−93585
cylindrical soln. of disordered e.m. radiation 78−8306
cylindrical systems, numerical codes 80−67549
cylindrically symm. solns., static distrib. of fluid 77−71258
cylindrically symmetric self gravitating fluids, with press. equal to energy density 79−58591
cylindrically symmetric self-gravitating fluids with pressure equal to energy density 79−21612
cylindrically symmetric stationary fields 79−44812
cylindrically symmetric universe in general relativity, Petrov type I degenerate 80−17705
D(1,0) Killing structs. and ϵ-potentials 77−71252
D-type nondiverging and nontwisting electrovac soln. with λ 80−115
de Sitter metric, elliptical space temporal closed Universe 80−109570
decomposable differential operators in cosmological context 78−57825
Dedekind ellipsoids, deformed figures in post-Newtonian approximation to general relativity 78−32734
deformations of the embedded Einstein spaces 78−54254
deformed Lie groups 79−121
degenerate Killing horizons, red-shift and stability props. 79−97268
Derrick's theorem in curved space 79−12658
dielectric tensor and magnetic permeability in the weak field approximation of general relativity 80−90751
differential conservation laws in metric, tetrad and bimetric formulations *(Bulgarian)* 78−32735
differential conservation laws with generalised Lagrangian *(Bulgarian)* 79−9153
differential eqns., strength concept review, appl. to Einstein-Maxwell eqns. 78−16706
differential eqns. of motion for systems of free gravitating particles 79−44806
differential forms, complex vectorial formalism 80−57144
differential forms in general relativity 79−44818
differential geometry, math. model 78−69968
differential geometry in infinite dimens., dynamical formulation of general relativity 78−93582
dimensional analysis in relativistic gravitational theories 77−30067
Dirac's generalised Hamiltonian system 80−31650
Dirac's multiplicative cosmology, stellar clusters theoretical isochrones with decreasing gravit. const. 78−16586
Dirac electron mean motion in gravit. field 77−22478
Dirac equation, reduction to Pauli-type equation, metric and EM field theory *(German)* 77−9894
Dirac equation, reduction to Pauli-type equation *(German)* 77−57
Dirac equation and higher symmetries 79−25931
Dirac equation as basis for unified treatment of electromagnetic and gravitational theory 78−8314
Dirac fields in Riemannian space time, geom. props. 79−75430
Dirac fields in Riemannian space-time, geom. props. 79−75431
Dirac particles, creation in general relativity with torsion and electromagnetism, general formalism 79−88856
Dirac particles, creation in general relativity with torsion and constant electric field 79−88857
Dirac-Pauli particle, underlying classical model 77−45743
direct interactions between membranes, gauge invariant theory 78−4551
discontinuity surface, local interior-exterior distinction 78−70030
discrete space-time, geometric formulation of electrodynamics and general relativity 77−26184
disordered EM radiation with planar symmetry, exact relativistic soln. 77−87676
distributional geometry, appl. to black holes in general relativity 79−93006
divergence free tensor densities in 3-space 80−103
divergence free tensors, struct., Einstein field eqns. 79−17293
diverging type-D metrics 77−45761
Doppler effect, gravitational, explored using geostationary satellite 80−109351
Doppler effect and aberration of light via principle of equivalence 79−17286
Dopplers, Hα line freq. depend. general relativistic formula, appl. to (SS 433) 79−97010
dual charge 78−36906
dualism of field and matter in the general theory of relativity *(German)* 80−90748
dually charged perfect fluid, stationary gravitational fields 77−49654
dust, charged, rotating, cylindrically symmetric interior soln of Einstein-Maxwell eqns. 80−82688
dust cylinders in static spacetimes 80−42126
dust equations, non-radiative solns. 77−13643
dynamical equations, new Hamiltonian structure 77−45745
dynamics, Hamiltonian approach 80−73236
dynamics of test particles and systems of reference of single observer *(Russian)* 77−53812
early Universe, EM and gravit. Green's functions 78−73786
Earth artificial satellites motion, relativistic effects 79−2465
education, Bohr-Einstein weighing of energy debate, time and gravity 79−97152
education, Einstein's General Theory of Relativity and press reaction 80−57075
education, Mach's principle, Einstein's equation and classical physics anal. 77−49524
education, relativistic rot. disc circumference 77−87603
education, speed, Galilean and Einsteinian concepts, vel., rapidity and celerity 80−73130
education, two-, three-dimens. space times 78−5
education, uniformly accelerated reference frame 78−36747
education Einstein's principle of equivalence, source of confusion 77−45646
Ehlers-Rindler problem in cylindrical symmetry 79−63094
Ehlers-Rindler problem in cylindrical symmetry 79−92999
Einstein's 1907 essay, discussion 78−12454
Einstein's contribution to cosmology 80−77530
Einstein's contribution to development of science *(Russian)* 79−84926
Einstein's contribution to relativity and cosmology *(Norwegian)* 80−4598

general relativity continued
Einstein's cosmological constant, lunar ranging data anal. by Seelinger's theory 79—6040
Einstein's eqn., exact vac. solns. from linearised solns. 78—65833
Einstein's eqns., algebraically special one Killing vector solns. 79—9160
Einstein's eqns., characterisation of Tomimatsu-Sato stationary solns. 78—65835
Einstein's eqns., one Killing vector solutions, Ricci rotation coeff. 77—64974
Einstein's eqns., recently found solns. 79—93014
Einstein's eqns. for stationary axisymmetry 79—71311
Einstein's eqns. soln. for line mass of perfect fluid 79—58592
Einstein's equation, technique for generating stationary axisymm. solns. 79—30319
Einstein's equations, exact solns. for spinning mass 80—105548
Einstein's equations, special exact cosmological solns. 77—41516
Einstein's equations, spherically symmetric case, orthonormal tetrads 80—68095
Einstein's equations, stationary axially symmetric case, Painleve's transcendental functions *(French)* 80—73218
Einstein's equations, stationary axisymmetric soln. 80—95005
Einstein's equations and tetrad formalism 80—42117
Einstein's field eqns., algebraically pure radiation field solns. from vacuum 79—71307
Einstein's field eqns., information on local physical conditions 78—21017
Einstein's field eqns. for zero rest mass scalar fields, nonstatic plane symmetric soln. 77—2570
Einstein's field equations, exact solns., nonstatic charged fluid spheres 78—89370
Einstein's field equations, homogeneous solns. 78—65824
Einstein's field equations, solns. for static fluid spheres, relativistic polytrope anal. 79—12669
Einstein's field equations for charged static spheres of fluid, exact interior solns. 78—73892
Einstein's field equations with zero-rest-mass scalar fields, wave solns. 78—89373
Einstein's field theory with teleparallelism and Dirac's electrodynamics *(German)* 79—40418
Einstein's gravitational field eqns., finite element method soln. 80—86177
Einstein's impact on theoretical physics 80—77677
Einstein's matter free theory of gravit. construction using Yang Mills theories 78—70026
Einstein's non-symmetric unified field theory, universal symmetry and Klotz metric 80—62555
Einstein's route to general relativity theory *(Czech)* 80—27096
Einstein's theories extended, book 80—22164
Einstein's theory of gravitation, review 80—90745
Einstein's theory of gravitation, Shirokov's new effect, in Kerr field 77—82421
Einstein's theory of gravitation generalised using tetrad field to avoid singularities 78—57833
Einstein's theory of gravity, special formulations *(German)* 79—58605
Einstein's unified field theory, axially symm. approx. solns. 77—67365
Einstein's unified field theory eqn. soln. 77—82429
Einstein's universe, radiating charged particle 79—17302
Einstein's vacuum equations, class of self-dual solns. 78—81900
Einstein's vacuum field eqns., axially symmetric stationary exact solns. 79—35594
Einstein's vacuum field eqns., general static soln. 77—49649
Einstein's vacuum field eqns. classification, Sachs' lemma 78—16699
Einstein's vacuum field equations, axially symm. stationary solns. 79—17283
Einstein 4-D manifolds, characteristic classes 80—46886
Einstein action of Riemannian metrics, rel. to quantum gravity and thermodynamics 77—45778
Einstein and general relativity, historical perspectives 79—40316
Einstein axially symmetric stationary eqns., general integral 80—31622
Einstein dynamics without special-relativistic kinematics 80—77657
Einstein effect (gravitational deflection of light), obs. at solar eclipse (1981 July 31) *(Russian)* 80—51651
Einstein effects rel. to post-Newtonian effects in gravodynamics *(German)* 78—16286
Einstein eqn. soln., stability of asymptotic simplicity 78—45536
Einstein eqn. spherically symm. solution in presence of conformally invariant scalar field 80—17846
Einstein eqns., classification system for one Killing vector solns. 78—93579
Einstein eqns., exact classical wave solns. 80—8864
Einstein eqns., linearisation stability and space-time symmetries 77—73
Einstein eqns., plane wave solutions 78—70022
Einstein eqns., reln. to Yang-Mills eqns. 78—8521
Einstein eqns., soln. with scalar zero-mass source 78—36900
Einstein eqns. derivation from Lagrangian with internal symm. 77—64976
Einstein eqns. for one Killing-vector five-space 77—49651
Einstein eqns. for spherically symmetric elastic body, exact solns. *(Russian)* 79—88854
Einstein eqns. Kerr-Schild solns. and cosmological const. 77—30059
Einstein eqns. new family of solns., connection with spinning mass fields 77—30061
Einstein eqns. with stiff eqn. of state, exact soln. 79—2677
Einstein equation, 79—30321
Einstein equation, exact solns. *(Russian)* 78—65825
Einstein equation, with energy-momentum tensor of ideal liq., conformal mapping method and new solns. *(Russian)* 77—53813
Einstein equation dynamics modified by fourth derivative terms, radiation from charged test particles 78—41216
Einstein equation in lifted Finsler spaces 80—77665
Einstein equations, classes of exact solns., for space $T_{(2,1)}$ *(Russian)* 77—64972
Einstein equations, general cosmological solution, singularity problems 80—82686
Einstein equations, generalised de Sitter solution 77—26100
Einstein equations, harmonic soln. *(Russian)* 77—13651
Einstein equations, plane-symmetric solns., dynamical consequences 80—31639
Einstein equations, some classes of accurate solns. *(Russian)* 77—30060
Einstein equations, supersymmetry, and flat limits of curved superspace 79—25932
Einstein equations, $[(2+1)+1]$-formalism, apparent horizons in space-time with rotational Killing vector 80—73222

general relativity continued
Einstein equations with zero-rest-mass scalar meson field 78—70021
Einstein field eqns., exact soln. for metric with rotation in presence of matter *(Russian)* 77—74275
Einstein field eqns. for rotating isentropic perfect fluid, cylindrically symmetric solns. 79—40427
Einstein field eqns. of gravitation from general principle of relativity *(German)* 80—68086
Einstein field equations, characteristic initial value problem in general relativity 80—73238
Einstein field equations, exact soln., group theory role, recent developments 80—8875
Einstein field equations, homogeneous solns. 80—8878
Einstein field equations, nonstatic spherically symm. isotropic solns., perfect fluid 78—36892
Einstein field equations, plane symmetric static and homogeneous vacuum solns. 80—86164
Einstein gravit. field eqns., static solns. and Birkhoff's theorem 79—71340
Einstein gravitational eqns. and nonlinear scalar field, time-depend. solns. with localised energy 80—46888
Einstein Lagrangian as translational Yang-Mills Lagrangian 77—13660
Einstein linearized tensor, massive spin two fields 78—36890
Einstein Maxwell eqns., stationary, solns. 78—41208
Einstein Maxwell equations, class of exact interior stationary solns. 77—26215
Einstein Maxwell equations, source-free EM field plus pure radiation 80—77678
Einstein Maxwell equations, static axisymmetric interior soln., mag. support against gravit. collapse 78—16288
Einstein Maxwell field eqns., generalised, static spherically symm. solns. 78—41213
Einstein Maxwell field eqns., null field, propagation and polarisation vectors 78—29025
Einstein Maxwell field eqns., superposition of static cylindrically symm. solns. 78—12620
Einstein Maxwell field with null fluid present 80—77668
Einstein Maxwell space-times with symms., nonnull EM fields 78—65823
Einstein Maxwell static field eqns. 79—58594
Einstein pseudotensor, gravitational energy-momentum 80—98833
Einstein space physical interpretation, gravitational field potential, Keres' method 80—36919
Einstein space times, dynamical properties admitting Gaussian foliation 79—88845
Einstein spaces and homothetic motions 80—31630
Einstein spaces and homothetic motions 80—46883
Einstein static universe, generalised, equilib. configs. for perfect fluids 77—45748
Einstein stationary axially symmetric eqns., complete integrability 79—63099
Einstein symposium, Berlin, Germany (Mar. 1979) 80—90596
Einstein theory of gravity, quantized, test of gauge invariance and unitarity 77—13673
Einstein unified field theory, wave solns. *(Italian)* 79—49147
Einstein unitary field theory with tele-parallelism, Dirac's classical theory of electrons 79—12685
Einstein Universe, with source-free EM field 79—85036
Einstein vacuum field, generation of Brans-Dicke field 79—30308
Einstein vacuum field eqns., Taub-NUT family of solns. 79—12665
Einstein-Cartan, Friedmann-like cosmological models without singularities 78—77632
Einstein-Cartan's theory with anticommuting variables in Dirac's Hamiltonian formalism 79—49125
Einstein-Cartan and Einstein theories of gravity, effective equivalence 78—24703
Einstein-Cartan cosmology and singularity prevention *(Polish)* 77—71162
Einstein-Cartan dust spheres, spin 78—4538
Einstein-Cartan equations, solns. 78—8299
Einstein-Cartan equations with motion of matter, incompleteness of solns. 77—33915
Einstein-Cartan first order invariant variational structures 79—44809
Einstein-Cartan generalised field eqns., spin field 77—22472
Einstein-Cartan theories, first-order, classification problem, generally invariant Lagrangians *(Czech)* 80—42129
Einstein-Cartan theory, bounce of spheres 78—93572
Einstein-Cartan theory, charged static fluid spheres 77—87667
Einstein-Cartan theory as Poincare symmetry gauge theory 77—22463
Einstein-Cartan theory of gravitation in a Hamiltonian form 78—93581
Einstein-Cartan theory stationary cylindrically-symmetrical solns. of eqns. *(Russian)* 77—53811
Einstein-de Sitter model, singularity problem, book contrib. 80—46891
Einstein-de Sitter universe, classical predictive electrodynamics 80—86175
Einstein-Dirac equation, new soln. 80—90742
Einstein-Dirac equation, soln., neutrino representation 79—58596
Einstein-Godel universe 79—2583
Einstein-Godel Universe with EM field 79—80376
Einstein-Kaehlerian conharmonic recurrent spaces 79—63096
Einstein-Kaufman generalised theory, EM tensor 77—79017
Einstein-Klein-Gordon eqn. solns. in stationary axially symmetric space-time *(French)* 79—25921
Einstein-Klein-Gordon equations, Killing field vectors, theorem *(French)* 79—30340
Einstein-Lichnerowicz eqns., spatially homogeneous solns. 78—16708
Einstein-massless-scalar field eqns., conformally flat solns. 77—64979
Einstein-Maxwell, plane symmetric fields, comments on other solns. 77—30062
Einstein-Maxwell axially symmetric stationary electrovac solutions 80—52101
Einstein-Maxwell eqn., N soliton solutions *(Russian)* 80—105556
Einstein-Maxwell eqn., quasistationary systems without rot. *(Russian)* 77—49653
Einstein-Maxwell eqn., static electrovac soln. 80—31642
Einstein-Maxwell eqn. admitting G_7 automorphism group, soln. *(Italian)* 77—64968
Einstein-Maxwell eqn. parametric type-D solns. in left-degenerate representation 77—67346
Einstein-Maxwell eqn. soln. for spherical shell charged dust distrib. 77—2574
Einstein-Maxwell eqns., axially symmetric stationary solns. 78—93576

general relativity continued
Einstein-Maxwell eqns., class of approx. stationary solns. 77—13646
Einstein-Maxwell eqns., EM radiation recoil 77—57244
Einstein-Maxwell eqns., exterior stationary axisymmetric solns. 79—21622
Einstein-Maxwell eqns., infinite parameter symmetry group 77—74280
Einstein-Maxwell eqns., Killing vectors and invariance transformations 77—13656
Einstein-Maxwell eqns., Robinson, Schild and Strauss soln. 80—46901
Einstein-Maxwell eqns., soln. admitting nonsingular EM field 77—22452
Einstein-Maxwell eqns., solns. for cylindrically symmetric space-time 79—12657
Einstein-Maxwell eqns., some exceptional electrovac type D metrics with cosmological constant 79—75419
Einstein-Maxwell eqns., static stationary solns. 80—4617
static Einstein-Maxwell eqns., three parameter soln. 79—58593
Einstein-Maxwell eqns. for homogeneous cosmological type IX model with EM field, Hamiltonian formalism 77—53716
Einstein-Maxwell eqns. for non null EM fields, general solns. 77—2569
Einstein-Maxwell eqns. for T-spheres with homogeneous mag. and elec. fields *(Russian)* 77—60993
Einstein-Maxwell eqns. soln. for cylindrically symm. fluid distrib. and mag. energy 79—30312
Einstein-Maxwell eqns. with axial symmetry, exact solns. 80—118
Einstein-Maxwell equations, coupled, general soln., Ernst-Maxwell eqn. depend. on arbitrary harmonic function 77—74
Einstein-Maxwell equations, exact cylindrical solns. 79—97274
Einstein-Maxwell equations, exact soln. 79—49113
Einstein-Maxwell equations, family of solns. 78—89375
Einstein-Maxwell equations, inhomogeneous stationary cosmological solns. 80—62556
Einstein-Maxwell equations, solns., causality violation in rotating universe 79—44828
Einstein-Maxwell equations, some Robinson-Trautman solns. 78—89374
Einstein-Maxwell equations, static electrovac solns., complexification technique 80—68114
Einstein-Maxwell field, stationary, axisymmetric generation method 78—86202
Einstein-Maxwell field eqns., and charge conservation 77—5716
Einstein-Maxwell field eqns., asymmetric connection treatment 79—97266
Einstein-Maxwell field eqns., new solns. from electrovac space times with isometries 78—62128
Einstein-Maxwell field eqns., stationary axisymmetric, exact solns. 77—22455
Einstein-Maxwell field eqns., symmetries, null field case 77—13648
Einstein-Maxwell field equations, bivector field theories, divergence-free vectors 77—71251
Einstein-Maxwell field equations, connection approach 79—88860
Einstein-Maxwell field equations, non-null, algebraically general, class of solns. 77—2578
Einstein-Maxwell field equations in vacuo, consideration of axially symm. metric 79—85034
Einstein-Maxwell field theory, generalised mull EM fields 79—58606
Einstein-Maxwell fields, equilib. and global integrability conditions 77—30070
Einstein-Maxwell fields, solns. determ. 77—45756
Einstein-Maxwell fields, static and axially symmetric, comment on soln. 79—71339
Einstein-Maxwell fields, SU(2,1) symmetry 77—53821
Einstein-Maxwell fields, with null Killing vector 78—65821
Einstein-Maxwell fields for massless charge 79—44804
Einstein-Maxwell generalised eqns., Birkhoff's theorem and mag. monopole solns. 78—45535
Einstein-Maxwell generalised field theory, pp-wave soln. 79—6034
Einstein-Maxwell homogeneous fields 78—65829
Einstein-Maxwell massless scalar fields eqns., stationary axially symmetric solns. 77—74276
Einstein-Maxwell non-static field eqn. solns. 80—42128
Einstein-Maxwell null fields in Newman-Penrose formalism 80—17853
Einstein-Maxwell scalar fields, stationary axially symmetric solns. 77—67361
Einstein-Maxwell space times, momentum and angular momentum in H-space 79—49137
Einstein-Maxwell static axially symmetric fields 77—87670
Einstein-Maxwell static axially symmetric fields 77—87671
Einstein-Maxwell stationary axisymmetric eqns., exact solns. 78—93578
Einstein-Maxwell stationary eqns., symmetries 80—31627
Einstein-Maxwell stationary eqns., transforms. preserving asymptotic flatness 79—118
Einstein-Maxwell stationary equations, global integrability conditions 80—4604
Einstein-Maxwell stationary field eqns., symmetries 77—74279
Einstein-Maxwell stationary field eqns. 80—31626
Einstein-Maxwell system, linearisation stability 77—49656
Einstein-Maxwell-Yukawa fields, static and time-depend. solns. 78—97
Einstein-Petrov eqns., type I complete integrability conditions 77—71249
Einstein-Petrov type I spaces, eqns. 80—36913
Einstein-Proca field representation by A_4^* 79—75418
Einstein-Straus unified field theory, cosmological appl. 79—67123
Einstein-Yang-Mills equation, soln. for gravity coupled to non-Abelian plane waves 79—35602
Einstein-Yang-Mills system in six dimensions, static solution 80—8883
Einstein-Yang-Mills theory, gauge theory and symmetry 77—22464
Einsteinian relativity, rel. to gravit. const. and cosmic large numbers 79—48969
Einsteinian sub-struct. separation 78—32736
Einsteins assembly of test particles, reconstruction in Minkowski space-time 79—30303
Einsteins eqns. of general relativity, cosmological soln. 78—12617
Einsteins equations, harmonic solns. 80—90744
Einsteins gravitation theory, use of exterior forms 80—17845
Einsteins gravitational equations, non-static source of Taub solns. 78—4537
elastic media, dissipative, relativistic electrodynamics 80—73219
elastic medium, gravit. and acoustic waves, relativistic eqns., neutron star appl. 78—24712
elastic solids, constitutive theory 78—57844
elastic solids, initially stressed, infinitesimal discontinuities 77—45775
elasticity, stress-deformed state of rot. neutron star *(Russian)* 77—37612

general relativity continued
elasticity and electro-magneto-elasticity 78—70025
elastomechanics, compatibility relations *(German)* 78—81902
electric charge quantisation in elementary matter, generalized quaternion struct. of general relativity 78—29013
electric dipole at centre of spherical shell, EM radiation *(French)* 77—5709
electrically-conducting fluid, mag. flux linkage, relativistic case, planetary dynamo theory 80—12655
electro-gravitational induction, relativistic theory 79—85040
electrodynamic and gravitational effects of Proca stresses in astrophys. 78—93098
electromagnetic fields conformal to non-empty space-times 79—30331
electromagnetism and conformal phase group 77—67360
electron classical model based on Penney's balanced field eqns. 78—21031
electron mass change effect on mass-radius relations for cold spherical body 80—26730
electron pair production by photons in constant electromagnetic field in general relativity 78—8568
electron relativistic self-field interaction, particle-like solns. 78—16666
electrostatics in certain axially symmetric static spacetimes *(French)* 79—49112
electrovac solns., axially symm., source of gravit. and EM fields 77—60987
EM fields in Godel universe 80—42125
EM fields in space-times with local rotational symmetry 80—82694
EM fluid flows, geometry 79—58601
EM fluids and Ricci collineations 79—35605
EM null point source intensity in stationary spherically symmetric space-time 78—57839
EM polarisation tensors, calc. by Fokker's method *(French)* 78—24695
EM polarisation under frame dragging, dispersive rot., Mach's principle 77—26217
EM propagation between physical source and constant vel. receiver in vacuo 80—105502
EM radiation, polarisation plane rot. induced by non-Minkowskian space-time 79—35115
EM system free fall, equivalence principle, red-shift and Eotvos expt. 77—64982
EM tensor fields in space-time V_4 of general relativity 80—77674
EM wave transmission from isolated system 80—73247
empty space Einstein eqn. solns., Mach's principle in spatially homogeneous spacetimes 79—17295
empty space-times, four-parametric set of solutions to $G_{\mu\nu}=0$ 80—95007
energy and momentum, Landau Lifshitz, complex 80—4600
energy conditions and space-time singularities 80—31608
energy loss in scattering problems, Einstein quadrupole formulae 78—89379
energy momentum tensor for vector-tensor theory of gravity and electromagnetism 78—12633
energy momentum tensor symmetries, concomitant conservation laws, Einstein massless scalar meson field appl. 78—86205
energy problem, struct. of gravitational field *(Russian)* 79—21598
energy tensor definition for system of charged particles and EM fields 78—77734
energy-momentum in general relativity 78—54263
energy-momentum in general relativity 79—75423
energy-momentum quantised field tensor vacuum means 80—73227
energy-momentum tensor, effect of motions, meson field and perfect fluid 78—73903
energy-momentum tensors in locally isotropic space-times 80—31631
energy-momentum tensors in theory of EM fields admitting electric and mag. charge distribs. 77—74294
entropy and Einstein's theory of gravitation 78—12638
equation of motion of self-interacting massive charged particle, charged Robinson-Trautman soln. 79—93003
equations $\delta R^2/\delta g_{ij}=0$, transformability to 5 dimens. eqns. 79—12655
equations of motion and radiation reaction 80—73232
equations of motion for a class of space-time singularities 79—49114
equations of motion from generalised Einstein eqn. 80—90738
equations of motion in linearised gravity, introduction of external fields 79—93005
equatorial geodesic motion in Kerr and first Tomimatsu-Sato metrics 79—49110
equilibrium of slowly rotating relativistic fluids 80—46898
equilibrium states of relativistic charged gases *(Russian)* 77—13661
equivalence of active gravitational mass to inertial mass 79—44808
equivalence of reciprocity theories and general relativity 77—74304
equivalence of vacuum Yang-Mills gravitation and vacuum Einstein gravitation 79—25924
equivalence principle, gravitational collapse, and the classical particle problem 79—25927
equivalence principle, test using neutron elec. dipole moment 77—57265
equivalence principle, virtual quanta method as probe 78—36913
equivalence principle test using space-borne clock 79—49152
equivalence principle tests in Earth orbit 78—45551
equivalence principles, logical status 77—68
Ernst's eqn., three parameter soln. 78—41207
Ernst equation, Backlund transformation, pseudophysical method 79—123
Ernst equation, vacuum soln. family 80—62551
etergy-momentum tensors, characterization in gravitational field eqns. 79—88846
ether, cause of relativistic effects, and one-way velocity of light, discussion 79—30306
ether, relativity, and the wave nature of matter 79—25926
ether existence, geometry of inertial frames 80—42109
ether theory, compatibility with relativity 79—30307
ether-relativity polemic, nominalism and realism 80—42110
Euclidean Einstein gravity eqn. solns., for infinitely many instantons 79—71312
Euclidean gravity, asymptotically flat self-dual solns. 78—45834
Euclidean Taub-NUT metric, topological invariants, absence of axial anomaly 78—41218
evolution equations, appl. of well-posed quasi-linear second order hyperbolic systems 77—53743
evolution equations for Killing fields, vac. and Einstein Maxwell space-times 78—8279
evolution from equivalence principle 80—98779
evolving flowless drainhole, nongravitating particle model 79—44803

general relativity continued
- exact geodesics of Erez-Rosen metric 79—6027
- exact solutions to Einstein field eqns. yielding separable Hamilton-Jacobi eqns. 77—45747
- expanding shearfree spatially homogeneous universes, nonsynchronous time coord. 78—36740
- expanding spherical radiosources, flux vars. 79—17112
- expanding universe effect on quantum mechanics of electromag. bounded spin 1/2 particles 78—54271
- experimental precision, gravitation and general relativity 78—8333
- experimental testing, results *(German)* 80—73255
- experimental tests, mag. torque on shielded supercond. gyroscope 77—13678
- experimental tests, present evidence, future expts. 79—93031
- experimental tests, successes and limitations *(Danish)* 77—64985
- experimental tests of quantum effects in gravit. 77—87684
- experimental verification, planetary orbit and gravity wave searches *(Russian)* 77—9941
- experimental verification of the general theory of relativity 80—98850
- experiments with closed path signals 79—67215
- extended bodies, accel. and weight in relativity theory 77—33746
- extended bodies, description and motion 80—73233
- extended body dynamics, centre of mass description and quasirigidity 77—67359
- extended body dynamics, centre-of-mass, zero-linear-momentum vector field 79—85017
- extended body dynamics, centre-of-mass line uniqueness 79—85018
- extremal surfaces, uniqueness, maximizing props. in Taub type universe 79—6026
- falling through black hole into another universe, theory 78—32748
- Faraday's EM inductron prop. in Einstein's unified field theory 80—117
- faster than light phenomena in special and general relativity, book contrib. 79—44817
- Fermi normal coords., expansions of the affinity, metric and geodesic eqns. 80—104
- Fermi universal coupling and gravit. in general relativity 77—79
- fermion thermal radiation from an accelerated wall 79—54265
- Ferraro's law of isorotation, relativistic analogues 78—21035
- Ferraro's theorem, validity in non-flat space time 80—4247
- fibre bundles with Ricci curvature on Riemann manifolds *(French)* 79—21594
- field action, variational principle, with torsion and non-metricity 77—67347
- field eqns. exact soln. 77—78
- field equations for spatially homogeneous space-times 80—52083
- field equations with torsion, Palatini and Hilbert variational approach 77—22460
- field theory approach to gravitation 78—81910
- finite body, mass-energy invariant 78—24700
- finite rotating body in general relativity, anisotropic interior soln. of Kerr metric tensor 79—63104
- Finsler* space, remained affine motion 80—8869
- Finsler relativity theory, basic principles 80—73226
- Finsler space, scalar curvature, Einstein tensor 80—77655
- Finsler space, second curvature tensor 79—17318
- Finsler space and affinities for external EM fields 77—57256
- Finsler spaces, field theory, physico-geometrical features 79—58595
- Finsler spaces, gravitational field theory 80—12962
- Finsler spaces, physical aspects underlying the field theory 80—101745
- Finsler spaces, structurological remarks on field theory 79—12660
- Finsler spaces preserving killing vector fields 80—12961
- Finsler spaces with recurrent pseudocurvature tensor 80—52082
- Finsler theory of relativity, basic principles 80—73228
- Finslerian fields, deviations from gravitational field 80—8870
- Finslerian relativity, development and basic theoretical principles review 79—35596
- Finslerian space-time with absolute parallelism, scalar and EM fields 79—40436
- five-dimensional theory, conditions of existence of horizons 78—73907
- flat space time, conservation laws based on traceless energy momentum tensors 80—52085
- fluid ball problem, global anal. 80—98834
- fluid bodies, rapidly rotating, struct. and stability in general relativity beyond ang. vel. peak 79—101139
- fluid cylinders, static, and plane layers, general relativity solns. 80—68090
- fluid dynamics, macroscopic relativistic approach to numerical simulation 79—9122
- fluid sphere, interior soln. with variable gravit. mass density 77—69
- fluid spheres, charged, exact solutions 77—30069
- fluid spheres, physical solns. 79—21169
- fluid spheres, time-depend., obeying eqn. of state non-existence 78—45526
- fluids, rot. and non-rot., initial-value problems and singularities 78—112
- foliations from quadratic and Hermitian differential forms, Riemannian manifolds 79—93000
- form factors α and β product asymptotic limit for celestial bodies 79—84653
- formalism of external forms and non-inertial reference systems *(Russian)* 78—81894
- formulation in geometric picture 80—36895
- four-body forces and red-shift, gravit. clocks 77—61001
- fourth-order field eqns., Weyl-Eddington theories 78—121
- fractional winding numbers and surface effects 78—8579
- free falling body in field of black hole, superluminal speeds, tachyons 77—78816
- free particle propagator covarient WKB expansion in Riemannian space 80—68100
- frequency solutions of massive vector field eqns. in curved static space-time 78—36909
- Friedman models, the cosmological constant 77—64896
- Friedmann cosmological models, relativity of space finiteness-infiniteness 78—96582
- Friedmann cosmological models, relativity of spatial and temporal finiteness and infinity 79—62941
- Friedmann model, expanding Universe, nonlinear acoustic effects *(French)* 80—67921
- Friedmann universes, distance functions for Coriolis interaction 80—51925
- fundamental group unitarity *(Russian)* 77—53739

general relativity continued
- fundamentals of relativity, general, special and cosmological, book 78—29007
- G-structures, general theory and algebraically degenerate spaces 79—17299
- galaxies and quasars paradoxical redshifts compatibility with gravitation theory 78—73757
- galaxy clusters, as relativistic spherically-symmetric inhomogeneities 77—71147
- galaxy formation and vacuum quantum fluctuation of the gravitational field 79—30156
- galaxy formation in Eddington-Lemaitre universe 79—62909
- Galilean invariant Schrodinger eqn., relativistic wave eqn. derivation, Lie algebra 80—105555
- gas expansion, thermodynamics and cosmology 77—64892
- gauge conditions anal. 78—70031
- gauge covariant field eqns., exact one body soln. 78—36899
- gauge field theory, gravitational considerations and red shift *(Japanese)* 79—80484
- gauge field theory in general relativity 78—36897
- gauge field theory in general relativity 78—36898
- gauge group deformations, generalised Gupta program, review 80—12957
- gauge sypersymmetry eqns., spherically symm. soln. 78—4532
- gauge theory reformulation in spinor affine space-time 77—22470
- gauge theory with no black holes 80—82702
- gauge-invariant perturbations on most general spherically symmetric space-times 79—71322
- gauge-theoretical struct. and conserved current 77—57254
- Gauss-Hertz principle continuum form, derivation of general relativity in time domain 78—73851
- general flat four-dimensional world pictures and clock systems 79—17288
- general relativistic nonlinear field, kink soln. in generalised geometry 79—21922
- general relativity conference, Trieste, Italy, 1975, July 78—8285
- generalised axisymmetric spacetimes, Einstein vacuum eqn. solns. 80—22243
- generalised Einstein eqn., field eqn. for EM field and Yang-Mills instantons 80—8872
- generalised equations of motion for test particle 79—35593
- generalised field theory of general relativity, field eqns. 77—79013
- generalised Goldberg-Sachs theorems in complex spactimes energy-momentum and conformal tensors 79—71300
- generalised gravitation theory, with electromagnetism, derivation of conservation laws 79—49146
- generalised metric, invariant theories 77—9924
- generalised Peres space-time plane wave-like solns. of weakened field eqns. 78—57827
- generalised Rarita-Schwinger equations *(French)* 77—37790
- generalised Takeno space-time, coupled EM and zero-rest-mass scalar meson fields 78—70020
- generalized Einstein-Maxwell field theory, asymptotic behaviour 80—86184
- generalized macro-causality in relativity theory 79—85021
- generally invariant Lagrangians for the metric field and other tensor fields 79—71317
- genesis of general relativity 80—90747
- geodesic property of general space time *(French)* 78—16701
- geodesic triangles and expansion of metrics in normal coordinates 79—80476
- geodesically complete space time, topology change of edgeless acausal spacelike hypersurface 79—6029
- geodesics in rotating systems 79—6028
- geodesics in rotating systems 80—46882
- geodetic lines associated with space of plate stretched and compressed *(Ukrainian)* 79—97199
- geometric formalisation of classical dynamics *(Russian)* 79—9105
- geometric quantisation and general relativity 78—8288
- geometrical approach to general-relativistic cosmology 77—5606
- geometrical optics in general relativistic dispersive media 79—40435
- geometrical spacetime perturbation theory: regular first-order structures 79—2678
- geometrised gravitational theory, energy-momentum tensor 79—25958
- geometrodynamics and Gauss-Codazzi eqns. in affine 5-space 79—35595
- geometrodynamics with tensor sources 77—74282
- geometry of space-time at coordinate infinity 79—49111
- GF-hypersurfaces in a K-manifold 79—63097
- ghost free axial gauge, infrared gravitons 79—67214
- ghost free gravity Lagrangians with propag. torsion 80—86173
- global coordinate time scale, practical implications of relativity 80—47030
- global qualitative mathematical techniques for Einstein eqn. soln. 79—93012
- global relativity, recent advances 80—90746
- global superenergetic quantities, uniqueness in general relativity and Einstein-Cartan theory 80—4595
- globally hyperbolic spacetimes, conformal deform., Ricci curvature and energy condition 79—9159
- Godel metric, world function 80—31624
- Godel universe, scalar perturbations 78—57709
- gravi-inertial reference system, props. *(Russian)* 77—53810
- gravitating gas in presence of strong shock, spherically symm. motion 78—12629
- gravitation, canonical many-time quantisation 78—8328
- gravitation, metric theory, without minimal coupling of matter and gravitational field 77—13671
- gravitation, modified theory with regular solns. *(German)* 79—88844
- gravitation, relativistic corrections and radiation damping 79—97272
- gravitation, relativistic theory, static solutions and Poincare press. 80—31648
- gravitation and dynamical space, geometrical framework, Mach's principle 80—95001
- gravitation and inertia corpuscular model, geophysical consequences *(Russian)* 79—40439
- gravitation and inertia in general relativity 78—8317
- gravitation and space-time, general relativity 80—68104
- gravitation as gauge theory of Poincare group 80—86189
- gravitation experiments, relativity effects on some modern technological developments *(German)* 79—58615
- gravitation field quantisation procedure avoiding path-integral formalism 77—13863

general relativity continued
gravitation theories derived from nonlinear Lagrangian with limiting curvature 78—81897
gravitation wave propagation in expanding universe 78—73787
gravitation with torsion field, propagation eqns. for bodies with spin and rotation 80—77670
gravitational analogue of mag. monopole, Mandelstam path-dependent formalism 78—81898
gravitational and EM field interactions 78—41219
gravitational and EM shock waves and detection 77—5710
gravitational bremsstrahlung, post-Newtonian theory 78—40811
gravitational bremsstrahlung in post-linear fast-motion approximation 80—62549
gravitational collapse, bimetric general relativity theory 80—85853
gravitational collapse, classical and quantum problems *(Russian)* 77—56822
gravitational collapse, Einstein's gravitational equations, local and global modifications 78—61719
gravitational collapse to neutron stars and black holes, computer generation of spherical spacetimes 80—46385
gravitational conductors, waveguides, and circuits 80—36920
gravitational constant variation with time, Dirac's extension of general relativity *(Norwegian)* 78—69674
gravitational continuum field theory, convergence to general relativity 80—46875
gravitational coupling between laser beams, general relativistic treatment 79—85023
gravitational curvature, Einstein's theory, an introduction, book 80—22161
gravitational energy from quadratic Lagrangian with torsion 78—115
gravitational energy loss in scattering problems 80—73244
gravitational energy momentum localisation, general theory 77—9928
gravitational experiments in space, review 79—6042
gravitational field, axially symm., covariant decomposition of field eqns. *(German)* 79—80473
gravitational field, spherical symmetric, spin ang. momentum tensor calc. 80—42107
gravitational field and arbitrary gauge field, equations of motion, Heisenberg and classical, force term, spin-curvature coupling 80—57158
gravitational field at spatial infinity asymptotically Minkowskian spacetimes 80—46885
gravitational field energy, local eqn. 79—30323
gravitational field energy localisation, logic 78—49728
gravitational field eqn., higher order derivs. and spherically symmetric static solns. *(Chinese)* 80—42108
gravitational field eqn. solution by functional method 80—17847
gravitational field eqns., symmetries and solns. 77—5712 .
gravitational field struct. at spatial infinity, asymptotically Euclidean spaces 80—46884
gravitational field with absolute parallelism struct., integrable covariant energy-momentum conservation law 80—8873
gravitational field with flat spacetime, extended body weight, Einstein eqn. soln. 79—85015
gravitational fields, axially symmetric, Weyl's class of static vacuum solutions 80—68089
gravitational fields, spinor fields, and groups of motions 80—98832
gravitational inertial field and critical systems, free motion 78—93484
gravitational inertial field eqns., Lagrangian density, Hubble law 78—93483
gravitational instanton symmetries, classification 79—63110
gravitational instantons, soln. of classical Einstein eqns. 77—30066
gravitational interaction, spin, rotation and quantum effects, review 80—37203
gravitational interaction of spin-1/2 particles, Lorentz invariant theory 80—22257
gravitational mass change in two point charges system, for teaching 79—35460
gravitational mass defect in Reissner-Nordstrom metric *(Chinese)* 80—27186
gravitational Michelson-Morley expt., proposed, experimental and Schwarzchild metrics, black holes 79—97289
gravitational monopoles, path depend. approach for Einstein's eqn. 80—77682
gravitational potential, relation to mass-energy 80—22239
gravitational radiation, collapsed objects and exact solns., Einstein Centenary Summer School, Perth, Australia, 1979 January 80—105434
gravitational radiation, relativistic corrections and spectrum fine structure for binary stars 80—90479
gravitational radiation and invariants of curvature tensor in general relativity 78—57836
gravitational radiation flux from n-body system 77—22468
gravitational radiation from freely-falling bodies 77—41518
gravitational radiation from orbiting point masses, post-Newtonian theory 77—13226
gravitational radiation from spatially compact source, retarded soln. 77—5723
gravitational radiative corrections as the origin of spontaneous symmetry breaking 80—86192
gravitational redshift and principle of equivalence 77—9944
gravitational shear free collapse 79—97013
gravitational shift due to Earth's rot., verification 77—2579
gravitational shock waves 78—116
gravitational singularities, effect of self-induced torsion of Dirac sources 79—21626
gravitational theory based on Weitzenbock space-time 79—85022
gravitational theory of symmetry breaking of transformation intransitive groups 80—36912
gravitational theory with nonmetric connection, integrability conditions 80—105546
gravitational wave detection, astrophysical sources, resonant mass, laser interferometer and Doppler ranging methods 80—68122
gravitational wave energy in Einstein theory 80—4610
gravitational wave field, conformal coupling to curvature 80—68105
gravitational wave generation, linear momentum flux to higher orders 77—57258
gravitational wave generation, postlinear formalism 78—114
gravitational wave pulse in a spatially homogeneous universe, Einstein eqn. soln. 80—42121
gravitational waves, Bianchi type-I universe, tensor perturbation equations, derivation 79—124

general relativity continued
gravitational waves, generation of harmonics, plane-wave solns. of Einstein eqns. 77—13664
gravitational waves, interaction with elastic body, refractive index *(Russian)* 77—2584
gravitational waves, plane without singularities, collisions 80—31640
gravitational waves detector, appl. of photon-graviton resonance, technical problems, expt. possibilities 78—73905
gravitational waves energy-momentum 79—21607
gravitational-inertial field of Universe, generalised metric tensor theory 78—89275
gravitationally coupled classical fields, decomposition method extension 78—127
gravitationally nondegenerate Bianchi type I cosmological model 78—93490
gravity, microscopic, as Yang-Mills field 79—44829
gravity as a Goldstone field in the Lorentz gauge theory 80—31655
gravity in ray gauge 78—8313
gravity theories with propagating torsion 80—57161
Gribov ambiguity in general relativity, solns. in Coulomb gauge 79—54023
group structure of space and field *(Russian)* 77—13650
growth of curvature near a space-time singularity 80—31612
gyro precession and Mach's principle 80—36911
gyroscope, Earth orbiting, rot. motion according to general relativity 79—84651
gyroscope, geodesic deviation, detection possibility 78—45550
gyroscope experiment, high accuracy all angle readout using quantised flux 77—26223
gyroscope expt., high accuracy test facility 77—30077
gyroscope precession in Kerr geometry 80—42115
H space, the manifold of complex asymptotically shear free light cones 78—8292
H spaces admitting a Killing vector, classification 80—105
H-space, metric and curvature props. 78—89376
H-space of Robinson-Trautman type II soln., world-line 77—79010
hadron strong interactions, theory from general relativity 79—49143
Hagedorn temperature and Dirac's large numbers hypothesis 80—105410
Hamilton-Jacobi eqn., separable, in empty space-times 77—45755
Hamilton-Jacobi eqn. separation 78—110
Hamilton-Jacobi equation for free particle in Riemann space *(Russian)* 78—73901
Hamilton-Jacobi generalised theories 79—2681
Hamiltonian formalism for self gravitating relativistic perfect fluid, Lagrangian variational principle 78—16289
Hamiltonian n-particle systems, advanced retarded polarisation 78—29017
harmonic mappings of Riemannian manifolds to gravit. fields 77—49648
Hauser space-time in General Relativity *(French)* 79—25919
Hawking effect, temp. relativity, axiomatic field theory 80—109456
Hawking effect and Euclidean QFT 78—73732
heavens and their integral manifolds 77—57251
Helmholtz flat space eqn., non orthogonal separable coordinate systems 79—75416
DI Herculis, eclipsing binary, relativistic motion of periastron 80—94830
Hertz-Bromwich-Debye-Whittaker-Penrose potentials in general relativity 79—88858
hierarchical cosmology, exact model 78—69917
hierarchical cosmology, mathematical formalism and Einstein eqns. 80—82555
Higgs mechanism and the inverse Einstein-Infeld-Hoffman problem 79—63100
high energy stability and renormalisability of gravitation, Einstein Lagrangian supplement 79—25935
high frequency gravitational and electromagnetic wave coupling 78—8304
Hilbert's metrical matter tensor generalisation of Einstein's field eqns. 78—21040
historical development *(Hungarian)* 77—26224
history, 1907 to 1915 *(Russian)* 79—84934
homogeneous elastic sphere in its own gravit. field, general relativistic calc. 77—67344
homogeneous space-times of the Godel type 80—105553
homoheneous isotropic universe, influence of extra dimensions 80—51928
homothetic Killing trajectories, stationary limit surface geometry 79—40424
homothetic maps of the space-time distance function and differentiability 79—116
horizon stability in asymptotically flat spacetime 78—29021
hot hadronic matter in early universe, relativistic eqn. of state 78—45438
Huygens, principle on curved space-time, validity 78—21024
hydrodynamics of stellar cores, adiabatic collapse 79—96903
hypermomentum and Riemann constraint microscopic violation in general relativity 77—87678
ideal fluid, general relativistic dynamics *(Russian)* 77—49287
ideal fluid sphere moving in gravitational background, eqn. of motion, gravitational radiation 79—85026
ideal liquid, general theory of relativity, introduction of canonical variables in hydrodynamic eqns. 78—63510
impulsive gravitational waves collision, vac. Einstein eqns. soln. 78—21029
incompressibility definition consistent with general relativity principles 77—9930
incompressible minimal surfaces, 3-dimens. manifolds with nonneg. scalar curvature, positive mass conjecture 79—30318
indefinite Finsler type metrics and their peculiar properties 79—97265
indefinite metric quantum field theory, Poincare generators 79—35618
indefinite metric quantum field theory of general relativity 78—65853
indefinite metric theory, supplementary remarks 80—42133
indefinite-metric QFT of general relativity 78—89391
induced forces on mass particle in gravit. field 80—22240
induced rotational effects 77—2568
inertial forces, modified Thirring shell model 79—12667
inertial induction in open universe 77—57255
inertial induction of mass in general relativity 78—111
inertial navigation equations based on relativistic effects 77—67276
infinite charged filament, Kasner-type naked singularities *(Russian)* 79—58557
inhomogeneous cosmological model solns. of Einstein eqns. for perfect fluid 78—24585

general relativity continued
inhomogeneous cosmological models containing spacelike and timelike singularities alternately 78—69925
inhomogeneous cosmologies, exact solns. to Einstein field eqns. for perfect fluid 77—74285
inhomogeneous cosmologies as algebraically, special spacetimes, rot. dust soln. generalisation 77—49646
inhomogeneous local gauge transformations in spacetimes with torsion 79—71330
inhomogeneous models of early universe 77—17736
inhomogeneous perfect fluid cosmologies 77—74284
inhomogeneous Universe, gravitational wave effects, on orbital motions 80—61998
initial value formulation, anti-Machian formulation 78—8276
initial value problem of general relativity, conformal changes of metrics 77—79009
instanton solutions on arbitrary four dimens. compact manifolds, no. of parameters 78—41406
interacting EM and massless neutral scalar field *(Russian)* 78—4530
interacting EM waves in general relativity exact solns. of Einstein-Maxwell eqns. 77—60985
interacting relativistic particles in phase space, manifestly covariant theory, central force system 79—6031
interaction between plane strong EM wave and weak gravit. wave *(Russian)* 77—45774
interaction theory formalism 80—90735
interiors with relativistic dust flow 79—17290
interstellar flyby missions, relativistic effects 78—61729
intrinsic symmetries 80—12955
inverted black holes, anisotropic collapse, static vacuum, electrovacuum field struct. 80—67776
irreducible mass for the Tomimatsu-Sato space-times 79—49133
isentropic perfect fluids, integration of relativistic equations of motion 78—7872
isolated gravit. systems, energy-momentum and ang. momentum 78—73900
isolated gravitatineg systems, summer schooly, Varenna on Lake Como, Italy (Jun-Jul 1976) 80—73089
isolated N-body system, gravitational radiation in higher multipole moments 80—42119
isolated system, ang. momentum flux in higher multipole moments 79—80474
isolated system, supertranslation invariance of spin vectors 79—6030
isolated systems, integral conservation laws, privileged vector fields method, general relativity, external Kerr metric *(German)* 78—16698
isometry Lie algebras, new technique for struct. anal. 78—65831
isothermal-Kruskal coordinates and Einstein's equations 79—63106
isotopic spin sources, motion, gauge theories 80—12977
isotropic and pseudoisotropic subvarieties of n-dimensional hyperbolic variety *(French)* 77—53818
isotropic cosmological models without singularity, Einstein eqn. solns., Universe description 80—56988
isotropic Finsler spacers, const. sectional curvature in Berwald's connection *(French)* 79—44801
isotropic models of Universe, regularisation of fermion stress-energy tensor 78—81725
isotropic universe, gravit. perturb. propag., using general relativistic kinetic theory 78—20920
isotropy of relict radiation, coherence of Universe *(Russian)* 79—85024
Jacobi fields, four-dimens. Riemannian manifold 77—60983
Jacobi fields and geodesic spheres 79—63105
jacobians and curvilinear metrics, for teaching 79—62961
jet bundles and path structures 80—82684
K3 gravitational instanton, physical interpretation 79—17320
Kaehlerian S-recurrent spaces with Bochner curvature tensor 79—75415
Kaluza-Klein bundle, unified theory 80—37153
Kantowski-Sachs cosmological model, global struct. 78—24584
Kasner spacetime, conformal energy-momentum tensor trace anomaly calc. 79—21603
Kasner type solns. to Einstein eqns. 80—4603
Kasner type solns. to field eqns. generated by square of secular curvature 78—54256
KdV eqn., particular N-soliton soln. 80—31971
Kerr and Tomimatsu-Sato metrics from group transformation, rot. vacuum soln. 78—65838
Kerr associated metric, solution of Einstein's eqns. 77—5713
Kerr black hole, gravit. perturbations in spin coeffs and Weyl tensor components 78—12273
Kerr black hole, gravit. perturbations of quantities finite in stationary state 78—12274
Kerr black hole, gravitational perturbations 79—44819
Kerr black hole, high-freq. radiation from falling particle 78—16452
Kerr black hole, orbiting fluid discs analytic theory 78—36631
Kerr black hole, weak EM field of point charge on symm. axis 77—53624
Kerr black hole in thermal equilibrium and the ν vacuum 79—97022
Kerr black hole symmetries, Petrov type D Einstein Maxwell fields 78—12269
Kerr black holes, charged current loop field and pot. 78—40988
Kerr field, spherical motion parameters 80—46889
Kerr metric, causality violation 79—80479
Kerr metric, null trajectories 79—25925
Kerr metric, stationary axisymmetric test fields 77—41515
Kerr metric, stationary axisymmetry EM fields 79—58603
Kerr metric, test particle motion *(Russian)* 77—45752
Kerr metric, vector solns. to generalised almost Killing eqn. 78—65830
Kerr metric, vortical type geodesics, causality non-violation 78—54251
Kerr metric and stationary axisymm. gravit. fields 78—12272
Kerr metric effect on EM wave plane of polarization 80—94827
Kerr metric in cosmological background, event horizon radius 77—74082
Kerr metric sources, ellipsoidal space-times 78—54249
Kerr naked singularity, classical instability 78—57834
Kerr solution, new form 77—33914
Kerr solution superposition, Tomimatsu-Sato solution 80—31634
Kerr-Newman background space, nonstatic nuclear forces, meson field at black hole event horizon 78—61880
Kerr-NUT metric 77—9925
Kerr-Schild congruences and Kerr's theorem 77—60989
Kerr-Schild generalised metric and Einstein-Maxwell fields 78—77783
kerr-Schild geometry, spinors, and instantons 79—35601
Kerr-Schild metric, generalised, for gravit. waves *(French)* 77—71255

general relativity continued
Kerr-Schild metric, Maxwell-Hamilton-Jacobi-, and Dirac-eqns. Minkowski covariance 77—64977
Kerr-Schild metric singularities 79—80477
Kerr-Schild-Vaidya fields with axial symmetry 80—95000
Kerr-Taub-NUT soln. generalisation 78—49734
Kerr-Tomimatsu-Sato family of solns. with nonintegral distortion parameter 78—86204
Kerr-Tomimatsu-Sato family of spinning mass solutions 78—29012
Kerr-Tomimatsu-Sato generalised metric, infinite red shift surfaces 79—58602
Kerr-type particle, uniformly accelerating and rotating, Schwarzschild, Rindler and Kerr surfaces of red shift 80—85855
Killing fields, evolution for dust matter space time *(French)* 79—21617
Killing fields determ. from Cauchy data *(French)* 77—45744
Killing horizon as event horizon, a necessary condition in general relativity 78—8295
Killing horizons and dragging of the inertial frame about a uniformly accelerating particle 80—52084
Killing spinors, basic props. 77—22453
Killing tensors, symmetric and skew symmetric 78—93573
killing vectors and maximal slicing 80—77667
Killing vectors in plane HH spaces 78—54104
kinematics of relativistic ejection *(French)* 77—73943
kinematics via principle of equivalence 79—17285
kinetic equation of gases 80—21914
kinetic theory, scalar proper time and vectorial relativistic entropy 77—22461
kinks and cobordism in field theories, general relativity fermions 80—98835
Kinnersely-Chitre transforms for spinning mass solns. to Einstein eqns., integral eqn. method 79—97267
Kinnersley-Chitre spinning mass field 80—105550
Kinnersley-Chitre transformations, integral eqn. method 80—17844
Klein paradox and vacuum polarization 78—8329
Klein-Gordan field in static manifolds, canonical theory expressed in Feynman Green's functions 77—5718
Klein-Gordon eqn. in stationary space times, positive and negative frequency solns. 78—29002
Klein-Gordon system, gravit. equilib. 78—24719
Kruskal space time, algebraic isometric embedding 79—80478
Lagrange differential 77—53751
Lagrangian dynamics of polarised media with internal spin in general relativity 79—72962
Lagrangian eqns. of motion, with constraints 77—57252
Lagrangian formalisms in scalar pregeometry, quantum mechanical equivalence 79—54024
Lagrangian models of scalar fields, extended particles in two space dimens. 77—5995
Lagrangians in flat space-time 80—86169
Landau Lifshitz complex, covariant formulation 80—46879
Lane-Emden equation, spherically symmetric soln. 80—46890
large numbers hypothesis and the Einstein theory of gravitation 79—21477
lattice formulation of general relativity 79—40426
length prescription for generalised radial observer, Schwarzschild and Reissner-Nordstrom line elements 80—73223
Lense-Thirring effect and satellite relativistic nodal precession meas., covariance anal. 78—126
Lense-Thirring effect relativity test, counter-orbiting satellites 78—45554
leptons and quarks, unification within conformal relativity 79—93343
Lewis metric and flat space-time 80—46877
Lichnerowicz equation, global solns. on asymptotically Euclidean complete manifold 80—101738
Lichnerowicz equation soln. on an asymptotically euclidean manifold *(French)* 79—71302
Lie algebras, BRS transform. 78—93591
Lie derivatives and deviation equations in Riemannian spaces 80—46876
Lie group broken symmetry of transformation generating general relativistic theories 80—98836
Lifshitz-Khalatnikov time functions in gravitational collapse 80—31615
light bending by eclipsed Sun, star field obs. *(French)* 78—20634
light deflection by Sun, principle of equivalence calcs. 78—81729
light deviation in invariant mechanics *(French)* 80—90740
light propagation in Kerr metric, geometrical optics appls., analytical results 77—29637
light ray and particle paths on rotating disc 79—40422
line sources, ring singularity of Kerr metric 77—45763
linear density perturbation, relativistic cosmologies 77—22336
linear stellar structure model in general relativity 80—94709
linearisation stability and globally singular change of variables 80—31629
linearisation stability of Yang-Mills and Einstein-Yang-Mills eqns. 79—49142
linearised Einstein field eqns., initial value problem 77—57208
linearised gravitational radiation field, mag. components, measurability anal. 80—36921
linearised gravity, eqns. of motion, charged rotating sources 80—77663
linearised gravity, eqns. of motion, uniform acceleration, Robinson-Trautman fields 79—71308
linearised gravity, equations of motion, four momentum radiation 80—77662
linearised gravity eqns. of motion, run away sources 79—71309
local mass problem soln. 77—13644
local relative motion in general relativity 80—42123
local scale invariant theory, Hamiltonian formalism 78—29033
local simultaneity in general relativity 80—86167
long-range scalar field in conformally flat space-time 79—71303
longitudinal momentum of spherically symmetric source 80—46878
Lorentz gauge field in Riemannian space, spherically symmetric static exact solns. 80—4596
Lorentz symmetric spaces, conformal completion 77—64989
Lorentz transformation, generalised, and behaviour of physical quantities at R- and T-region boundary *(Russian)* 78—49725
Lorentzian manifold, Kahler-metrics 80—73251
Lorentzian manifold, stability of max. space-like hypersurfaces *(French)* 77—82420
M_4 factorisation, spinor algebra, Dirac equation geometrical, interpretation 80—62838
Mach's principle, modification of general relativity theory *(German)* 79—88843

general relativity continued
  Mach's Principle, relative motion and fundamental numbers 77—9943
  Mach's principle, the cosmological constant, and the scale-covariant theory of gravity 79—25774
  Mach's principle and general principle of relativity, elementary physical approach and observational basis 80—52080
  Mach's principle and the relation $GM=Rc^2$ 80—52078
  Mach principle, in conformally flat space, integral formulation, book contrib. 80—46892
  Mach principle, vacuum concepts, Lie group representations, Newman-Penrose method, book 80—46741
  mach principle and the quantal response of the Universe 79—12549
  Machian effects in compact rapidly spinning shells 79—2684
  macroscopic electrodynamics, forces and energy-momentum tensor 77—5675
  magnetisable media, relativistic models, and energy-momentum tensor of EM field *(Russian)* 80—86180
  magnetised cylinders in general relativity 79—25936
  magnetised relativistic continuum, shock invariants *(French)* 79—25944
  magneto-dipole configurations 80—67539
  magnetofluid, self-gravitating, local behaviour of congruences 78—89384
  magnetofluid, self-gravitating 78—36905
  magnetofluid flows, geometry 80—46895
  magnetofluid space-times, imperfect, spacelike, family of contracted Ricci collineations symmetry mappings 80—51650
  magnetofluids, self-gravitating, collineations and motions 77—51135
  magnetoviscous fluid cosmological models in general relativity 79—63095
  many-body equilib. of dual charged sources 78—29020
  many-body systems, relativistic effects, binary star appl. 80—8863
  marginally bound dust collapse, time functions in numerical relativity 79—71321
  mass integral formulation, cosmological solns. 78—12618
  mass quadrupole moment, eqns. of motion of a particle *(Russian)* 77—2577
  mass splitting in high dimens. extensions 78—89371
  massive particle finite motion in Kerr and Schwarzschild fields *(Russian)* 79—8833
  massive quantum field theory in two-dimensional Robertson-Walker space-time 79—25962
  massive scalar field in Einstein universe, vacuum stress tensor, finite-temp. effects 77—41769
  massive spheres, maximum central gravit. redshift 77—13229
  massive spheres, non-rigid with slowly varying density, eqn. solns. 80—101612
  massive spheres with an isothermal core 80—82405
  massless free fields, global properties 77—74303
  massless particle pole-dipole approx. 77—74289
  massless vector particles in general background metric, stress energy tensor trace anomaly 78—86200
  mathematical origins of general relativity and of unified field theories 80—95009
  matter and light wave interferometry in gravitational fields 80—94997
  matter field equation, covariant with semisimple Lie groups in general relativity 80—8876
  matter field spacetimes, symm. mappings satisfying vanishing contraction of Lie deform. of Ricci tensor 79—113
  matter tensor from Hilbert variational principle 77—22462
  matter terms in gravit. theory, minimal prescription method 79—25916
  matter-filled universe, relativity of space and time finiteness-infiniteness 78—96581
  matter-vacuum matching 78—21032
  maximal extension of nonsingular soln. in generalised theory of gravit. 78—41214
  maximal hypersurfaces, boundary valve problem 80—82687
  maximal hypersurfaces and positivity of mass 80—73237
  maximal surfaces in closed and open spacetimes 78—8294
  maximally symmetric space with torsion 79—115
  Maxwell's eqn. soln. for any static axisymmetric vac. space time 79—25874
  Maxwell's equations derivation, in general relativity space, based on principle of minimum paths 77—53791
  Maxwell's equations in anisotropic space 79—44758
  Maxwell equations, in Minkowski space-time and Poincare group 79—30301
  Maxwell equations covariance, comparison of electrodynamic systems 77—87680
  Maxwell fields, time depend., in stationary geometry 78—8308
  Maxwell-Einstein theory, local supersymmetry 77—2582
  measurement theory, interrelation of quantum theory and gravitation 78—54235
  mechanical oscillator, relativistic spin quadrupole gravitational effect *(Russian)* 80—68103
  mesonic test fields and spacetime cohomology 78—78065
  meta universe, tachyon energy and momentum, contribution to gravitational field 77—45760
  metric affine variational principles, Riemannian space time 79—21596
  metric fields, generally invariant Lagrangians 77—71247
  metric tensor and energy-impulse tensor, components at boundary between R- and T-regions *(Russian)* 78—49726
  metric tensor components interpretation, astrophys. implications 78—93097
  metric-affine gravit. theory, vol. preserving and canonical transform. 79—44826
  metric-torsion gravitational theories 77—87668
  metrical connection in space-time, Newton's and Hubble's laws 78—57435
  metrics for moving reference frame, teaching approach 77—67337
  MHD, definite material scheme 79—25943
  MHD, relativistic, shock waves 78—9770
  micro- and macro-gravitational fields, relationships, physico-geometrical remarks 79—63103
  microscopic and macroscopic models correspondence *(French)* 77—45786
  microwave background radiation polarisation, anisotropic cosmological expansion 78—73778
  miniphantom geometrodynamics for 2+2 resolution of space-time 78—62132
  Minkowski-Abraham-Eckart unified energy-momentum tensor 80—22253
  Minkowskian hypersurface, n-dimensional Finsler space set transformation 80—8868
  Minskowski space time, real analytic local extension 80—77656

general relativity continued
  MIT bag with de Sitter geometry 79—2988
  modified vortex sponge model 79—88848
  momentum and angular momentum of two gravitating particles 79—71310
  momentum transfer in gravitation theory 80—4601
  monad method and canonical formalism of general relativity 78—36896
  Morse theory on timelike and causal curves 77—13649
  motion of continuous medium in given space-time, four-velocity 80—68091
  motion up to second post-Newtonian approx. in general relativity 79—75079
  multiply-connected space-time, black holes and tachyons 79—30315
  multipole moments in general relativity 79—71306
  multipole struct. of static continuous matter distrib. 78—118
  N twisting gravitational field soln. to Einstein eqn., integrability conditions 78—86203
  naked singularities and cosmic censorship, current situation 80—31621
  naked singularities in Kerr metric, relationship to black hole 79—21600
  naked singularity solutions, gravit. collapse with axial symm., geodesics, particle orbits 78—41215
  Nariai's boundary condition in general relativity 80—57148
  natural theory of continuous media 79—25917
  Navier-Stokes equations, relativistic conductive additional terms 77—45746
  negative mass and positive mass matter, hypothetical coexistence, causal paradoxes 80—82685
  neutrino fields in axially and reflection symmetric space-times 79—40425
  neutrino radiation soln. 78—54261
  neutrino systems, relativistic kinetic theory of transport processes 80—73283
  neutrino trapping in rotating matter 79—2673
  neutron flux, gravitational interaction *(Russian)* 78—36901
  neutron interference, gravity and inertial effects, principle of equivalence at quantum level 80—77669
  neutron interferometer expt., role of gravity in quantum theory 80—86176
  neutron stars, electrodynamics in curved space 80—90465
  neutron stars, nonrotating, mass and moment of inertia bounds 79—2551
  neutron stars, nonuniform rotating struct. and mass *(Russian)* 77—91559
  neutron stars, relativistic elasticity 78—12267
  neutron stars, relativistic fluid spheres appl. 79—5855
  neutron stars, relativistic slowly rotating stars 79—21321
  neutron stars mass upper limit for stability against black hole form. 78—96498
  neutron stars structure and evolution, relativistic eqns. 77—33471
  Newman-Penrose formalism and its application in general relativity, review *(Russian)* 79—21595
  Newman-Penrose method, review, book contrib. 80—46905
  Newman-Penrose spin coeff. formalism, spherically symm. Einstein-Maxwell problem 77—33912
  Newman-Penrose spin coeff. formalism, vac. spherical symm. soln. 77—33911
  non-compact maximal submanifolds of Lorentzian manifold 77—74287
  non-linear coupling of quantum theory and classical gravity 80—27389
  non-linear wave equations in a curved background space 78—65827
  non-Riemann geometrizable effects in the gravitational one-body problem 79—85016
  non-static charged fluid sphere in general relativity 79—71299
  noncanonical vacuum metrics with two commuting Killing vectors 79—30320
  noncrossing timelike singularities of irrotational dust collapse 80—31617
  nondiverging algebraically special H-spaces, complexified spin coeff. formalism 77—45749
  noninertial coordinate system, moving media electrodynamics, ring cavity appl. 79—53990
  noninertial reference system, electrodynamics eqns. *(Russian)* 78—81895
  nonlinear, electromagnetic and gravitational Hertz potentials 79—2680
  nonlinear Einstein field eqns., numerical soln. algorithm 79—93011
  nonlinear electrodynamics, Birkhoff's theorem analogue *(Russian)* 78—54273
  nonlinear electrodynamics, new variant *(Russian)* 79—5990
  nonlinear electrodynamics, photon-gravitation coupling 79—97276
  nonlinear field theories, exact classical solutions 78—21327
  nonlinear graviton unprimed spinor description 80—8892
  nonlinear graviton-photon interaction in Einstein-Maxwell space-time 79—30338
  nonlinear Lagrangians and Einstein spaces 80—36915
  nonlinear Markov processes, curved phase spaces, path integral soln. Lagrangian, appl. to general relativity 77—26216
  nonlinear scalar field, general relativistic kink soln. props. 79—85226
  nonlinear scalar field theory in isotropic homogeneous space-time 79—2676
  nonlocal fields characterized by internal variables, geometrical theory 78—29014
  nonlocal spinor field theory of matter 79—49141
  nonlocal theories satisfying Bell's inequality 79—12642
  nonrotating neutron stars, integral eqns. for even parity perturbations 78—36628
  nonstandard vector connections given by nonstandard spinor connections 77—57250
  nonstatic charged fluid sphere, collapse or bounce 77—66
  nonstatic gravitational fields of an ideal fluid without shear and rotation 80—90741
  nonsymmetric field theories, Mach's principle 77—9920
  nonuniform configuration, classical and quantum gravitational collapse *(Russian)* 78—7873
  nonuniqueness of solutions to Einstein's equations, symmetries in T_{ij} 80—12953
  nonvacuum stationary Einstein space-times, analyticity 77—71
  Nordstrom field timelike and null geodesics 77—67350
  Nordstrom Reissner metric, generalised, exact soln. 77—82430
  Novikov coordinates, equivalent to Kruskal, transformaton from Schwarzschild coordinates 80—68098
  NP 0531, Crab pulsar, distrib. modelling of rotating matter and gravit. field *(Ukrainian)* 80—12775
  null hyperspace initial data 80—101740
  null hypersurface locally imbedding in Riemannian manifold, Cauchy problem 79—49124
  null tetrad formulation, notation and sign conventions 78—36910

general relativity continued
NUT metric in background of Einstein's static universe 78—93565
observability differences between classical EM and gravitational gauge fields 80—36925
observability of physical quantities, inertial mass, gravitational constant, planetary motion 80—56700
odd-parity perturbations, junction conditions on spherically symmetric space-times 80—42127
optical coordinates in general relativity, axiomatic approach 78—86207
optical ordinates, problem of distance 79—21601
orbital equations in the relativistic two-body problem 79—44805
origin of matter in the Universe 77—26096
oscillations, Einstein's field eqns. 80—73217
oscillatory collapse, exact soln. *(Russian)* 77—87256
Palatini method of variation, equivalence with Hilbert action principle 78—41209
Papapetrou eqn. of motion of spinning particles, Wigner-Lubanski integral 78—108
parallel vector fields and Betti number in Riemannian manifold 79—44810
parametrized post-Newtonian approx., Rastall's gravit. field eqns. 78—36894
parity violation in the neutron's gravitational interaction 79—58617
part-Newtonian hydrodynamics, centre-of-mass theorem 77—75
particle cloud surrounding massive rotating nucleus, relativistic dynamics 79—114
particle clusters, isotropic, spherical, exact solns. of eqns., internal geodesics 77—41514
particle creation and geometry 78—12442
particle creation by black hole due to Casimir effect 79—35607
particle creation by singularities in asymptotically flat spacetime 78—54260
particle creation in curved space-time, covariant treatment 78—12443
particle creations in the pseudoparticle gravitational fields 79—2704
particle emission in the de Sitter universe for massless fields with spin 79—40434
particle models, and effective radius *(German)* 78—86198
particles in external gravitational fields, relativistic dynamics *(Russian)* 78—12614
particles with internal structure, description in general relativity 80—8879
path structures on manifolds, analytic characterisation 78—4535
path-integral formulation, DeWitt-Morette measures 78—123
Pauli effect in relativity, force term in Einstein eqns. 79—49127
Peres space-time, generalised, algebraic props. and solns. 80—106
perfect fluid, interior soln., existence of horizons in gravit. theory with scalar field *(French)* 77—67340
perfect fluid cosmology with geodesic world lines 80—67924
perfect fluid in a conformally flat space time 80—27188
perfect fluids, Hamiltonian formalism 80—82689
perfect magnetofluid, matter tensor, convective deformations 80—36922
periastron advance in the second post-Newtonian approximation in general relativity 79—75078
perihelion anomaly, general relativity and quantum gravity 77—22473
perihelion precession rate in system of two charged masses 78—73897
periodic gravitational waves, focusing effects *(Russian)* 79—6032
perturbations of analytic background metric 78—8302
perturbations of general type-D metrics, separation of wave eqns. 77—64975
Petrov homogeneous vacuum space time source 80—31632
Petrov type {3,1} vacuum solns. with twist, Killing struct. of family 78—54253
Petrov type II twist free metrics, solns. to Einstein Maxwell eqns. 79—49115
Petrov type N vacuum metrics and homothetic motions 79—75421
phase locked cavity, inertial mass and anomalous ang. momentum, fermion model 80—86159
phase space and Liouville theorem of classical statistics, relativistic analoga 80—27184
phenomenological relativistic gravitational model 78—8319
philosophical aspects, ideas of Eastern and Western cultures 79—44699
photon emission from gravitationally intense cylindrical bodies 78—57840
photon motion in gravitational field of rotating cylinder 79—25937
physical equivalence of theories, distinction between general relativity and Brans-Dicke theory 77—57240
physical singularities and big bang theory *(Russian)* 78—81893
physicists' reactions and popular attitudes, historical account 80—77602
pinching theorem and laplace operator first eigenvalue estimate on Riemannian manifold *(French)* 80—27185
plane electromagnetic-gravitational waves, interaction general relativity soln. *(Russian)* 79—21605
plane symmetric space-time of class-1 and electromagnetism 80—22252
plane wave collisions, gravit., EM and neutrino waves 77—17886
plane wave solutions stationary generalisation *(Russian)* 80—12968
plane-symmetric cosmological model, Einstein eqn. solns. for dust 78—49733
planet, internal structure is general relativity 78—57477
planetary observations to test theory, astrometric and radiometric methods 78—45552
Plebanski classification of the tensor of matter 80—101737
Poincare's retention of Euclid on apparently adverse parallactic findings 79—40429
Poincare's thesis, stellar parallax, compatibility with Euclideanism of astronomical 3-space 79—40428
Poincare cycle, general relativity, cosmology and thermodynamics 79—80378
point source of scalar field, equation of motion 79—88853
Poisson sphere, global dynamics eqns. *(French)* 79—30324
polarisable media, relativistic models, and energy-momentum tensor of EM field *(Russian)* 80—86180
polarisation dynamics, fully relativistic kinetic model 78—62134
polytropic fluid spheres with negative index, struet. and stability *(Chinese)* 80—57143
positive action conjecture, complete manifolds with nonnegative scalar curvature 80—12964
positive energy conjecture and cosmic censor hypothesis 77—29640
positive energy conjecture for isolated systems 79—40419
positive mass conjecture proof for general relativity 79—40420
positive-action conjecture, proof 79—30322
positivity of energy 78—57830
positivity of energy functional shown 78—32741

general relativity continued
post Newtonian relativistic stellar dynamics, tensor-virial eqns. 78—4298
post Newtonian two-body problem, static balance conditions 77—64973
post-Newtonian charged n-body problem, centre of inertia and coord. transforms. 79—93025
post-Newtonian eqns. of motion, one-parameter class derivation from Einstein field eqns. *(Russian)* 79—71301
post-Newtonian two- and n-body problems with electric charge 78—8277
post-post-Newtonian approximation, conditions for static balance 78—12619
potential blue shift, Cs beam clock meas. as theory test 79—12704
Prasad-Sommerfield monopole, time depend. soln. of SU(2) Yang-Mills-Higgs system 79—273
predictive relativistic mechanics of gravitating masses 79—25914
pregeometry, gravity with composite metric 79—35619
prestressed relativistic elastic body, principal infinitesimal waves *(French)* 77—67294
primordial black holes formation 80—12776
principle of equivalence, expt. test *(Russian)* 78—77795
principles of equivalence 78—12455
problem of motion, Infeld theory *(Polish)* 79—35513
projection tensor hydrodynamics: generalized perfect fluids 79—85029
projective invariance in general space times with spinor, torsion and Yang-Mills fields 78—57832
projective relativity and MHD, MHD tensor struct. 79—85030
propagation of the general relativistic blast wave 80—105549
propagators for quantised scalar field in static closed Universe 79—35597
pseudoinvariant gauge Lagrangians for Einstein gravity and supergravity 79—12680
pseudoriemannian manifold, differential forms as spinors 79—25915
pseudorigid motions, Born rigidity 80—4612
pseudospherically symmetric tachyon perfect fluids 79—35599
PSR 1913+16, binary pulsar, general relativistic effects meas. 79—35286
PSR 1913+16, binary pulsar, orbit rel. to general relativity testing, progress report 79—75234
PSR 1913+16, binary pulsar, relativistic observable effects 80—77438
PSR 1913+16, binary system, test of relativistic effects *(Dutch)* 80—62172
pulsars and gravitational spin precession 78—12264
pure massless scalar geon from Einstein scalar field eqns. 80—86174
pure radiation fields and gravitational waves 80—77673
quadratic Lagrangians and Palatini's device 79—75417
quadrupole test particle as detector of gravit. waves, eqns. of motion in general relativity 77—82426
quantised scalar field vacuum, effective Lagrangian anal. 77—45762
quantum cosmology, non-singular model 79—30158
quantum effects and evolution of cosmological models 77—17735
quantum effects in the Bertotti-Robinson space-time 79—35930
quantum field theory, indefinite-metric, boson field, equal-time commutator 80—68119
quantum field theory, Lagrangian formulation, conservation laws, relativistic gravitation *(Russian)* 80—68337
quantum field theory, symmetry aspects 78—62139
quantum field theory, vierbein formalism 80—22263
quantum field theory for rotating observer 79—12941
quantum gravity, choral of symmetries in general relativity 80—105565
quantum linearization instabilities 79—44835
quantum many-particle systems in curved spacetime 80—98751
quantum mechanical one-particle state, interfering neutron beam expt. 80—95025
quantum mechanics in non-inertial reference frames *(German)* 77—45720
quantum spinors and singularity theorems 78—70027
quantum theory, gauge fields 78—86212
quantum vacuum cosmology 77—5728
quantum version, spin-spin contact interactions, comparison with Einstein-Cartan-Sciama-Kibble theory 77—5719
quark confinement, event horizons around a particle surrounded by a static confinement potential 78—66075
quasistationary conc. systems without rotation, gravitational field *(Russian)* 77—45768
radiating Demianski-type space-times 79—30309
radiating fluid spheres, interior solns., boundary conditions 80—77672
radiating fluid spheres in general relativity 79—71323
radiating Kerr-Newman metric 79—63107
radiating non-twisting charged systems, gravitational field 79—40430
radiating systems, gravit. field, twisting free type II metrics 77—71256
radiating Weyl metric, nonstatic soln. generalisation, neutrino and EM fields 78—41210
radiation damping, solvable model 80—73243
radiation damping in general relativity 78—8310
radiation from moving mirrors and from black holes 77—67372
radiation time symmetric advanced and retarded solns. 77—57259
radiative transfer for polarized light, eqn. soln. method in relativistic cosmology 78—73781
radio signal retardation by solar gravity, Viking expt. results 80—36933
radiosources, compact extragalactic, super-luminal expansion 77—53695
radiosources, nonthermal, evolution, relativistic expansion 78—41067
radiosources, superlight flux vars. in relativistically expanding sources, models 78—4377
radiosources cosmological evolution, free-form analysis, self-consistent luminosity function 80—46716
Rayner model, elastic sphere in general relativity theory *(Russian)* 79—92671
recurrent Finsler space, infinitesimal affine motion 79—71305
recurrent Finsler space, projective motion 79—30327
recurrent Finsler space, projective motion 80—12960
recursive calculation of axially symmetric stationary Einstein fields 80—77661
red-shift second-order effect, possible expt. 77—22477
redshift related to light crossing clusters of galaxies 77—17685
Reissner Nordstrom metric, static sources 78—93575
Reissner-Nordstrom black hole, metric perturbations 79—71319
Reissner-Nordstrom black hole, perturbation treatment using Newman-Penrose formalism 79—44820
Reissner-Nordstrom geometry, forced perturbations 78—8303
Reissner-Nordstrom geometry, scalar waves, approx. scheme 80—52089
Reissner-Nordstrom manifold, maximally extended, with cosmological const. 78—29022

general relativity continued
  Reissner-Nordstrom perturbations, coupled Einstein-Maxwell eqns. 80—68108
  Reissner-Nordstrom soln., geometrical mass determ. 78—24704
  Reissner-Nordstrom spacetime, spin coeffs. and electromagnetism 78—8309
  Reissner-Nordstrom-de Sitter metric, the third law, and cosmic censorship 79—35609
  relative motion detection in gravitational field 79—75422
  relativistic astrophysics, Einstein's theory *(German)* 79—80213
  relativistic astrophysics, pulsars, supernovae, and X-ray sources *(German)* 79—101060
  relativistic EM fluid flows 80—52094
  relativistic gas stationary macroscopic motions, relations to gravitational field symm. 80—62552
  relativistic gravitation from massless systems of scalar and vector fields 80—12969
  relativistic Kepler problem, field asymptotic behaviour in infinite past 79—88575
  relativistic Kepler problem, orbits with gravitational radiation damping, behaviour in distant past 79—88574
  relativistic magnetofluids and symmetry mappings 79—27700
  relativistic magnetofluids and symmetry mappings 79—23379
  relativistic magnetofluids and symmetry mappings. II 79—27701
  relativistic massive particles, gravitational deflection, general relativistic anal. 80—46767
  relativistic particle classification, representation theory, 8 nonisomorphic simply connected covering groups of O(3,1) 77—46008
  relativistic particle EM interaction using universal laboratory time 79—71672
  relativistic particles, gravitational scattering, post-linear approx. 80—27190
  relativistic rotating fluid cylinder, field eqns. 79—50815
  relativistic star clusters, unphysical distrib. functions 78—8066
  relativistic stellar dynamics, energy integral 78—4299
  relativistic wave equations in curved spacetime 79—21962
  renormalisation of the quantum stress tensor in curved space-time by dimensional regularisation 79—40423
  repulsive gravitational forces, possible clustering mechanism 77—37674
  restricted three body problem, appl. of Gauss method to periodic solns. form. 77—13215
  review, QED and general relativity, physics of strong fields 78—8561
  Ricci tensor, classification in space-times with four parameter group of motions 80—77660
  Ricci tensor, invariant two spaces and canonical forms 79—12659
  Ricci tensor classification in space-times admitting four parameter group of motions 80—77659
  Riemann curvature tensor, expressed as third-order potential tensor with symmetry props. *(Italian)* 79—49129
  Riemann space-time metric construction for given props. of trial particle motions 79—85025
  Riemann spaces, conformal correspondence tensor *(Russian)* 77—53814
  Riemann-Cartan space-time with cosmological principle, torsion tensor 80—31633
  Riemannian curvature and classification of Riemann and Ricci tensors in space-time 80—36914
  Riemannian manifold, harmonic forms of curvature type *(French)* 78—86124
  Riemannian manifolds, symmetric vectors and algebraic classification 80—68094
  Riemannian metrical tensor, coord. conditions reln. to kinematic invariants *(Russian)* 77—9933
  Riemannian space-time cut locus 80—36910
  Riemannian spaces, connections and spinor connections associated with finite groups of transformations 79—44842
  Riemannian spaces, linear connections *(Rumanian)* 77—74274
  Riemannian spaces, three-dimens., of second class of imbedding 77—82425
  riemannian spaces with local duality and gravitational instantons 79—25938
  riemannian-Maxwellian invertible structures in general relativity 80—4618
  rigidly rotating relativistic dust cylinder, Riemann tensor, ultrarelativistic case 80—86158
  Rindler, de Sitter and Schwarzschild spaces, Greens function thermal props., renormalisation 79—2686
  Robertson Walker solns. for various types of energy momentum tensor 77—13645
  Robertson-Walker and Petrov G_4 VIII cosmologies, general relativistic kinetic theory 78—24586
  Robertson-Walker metric, covariant point-splitting regularisation for scalar quantum field 77—82434
  Robertson-Walker metric, elementary particles in homogeneous isotropic universe 77—5734
  Robertson-Walker metric and symmetries belonging to contracted Ricci collineations 78—24580
  Robertson-Walker spacetime, energy-momentum tensor and particle state definition 79—25934
  Robertson-Walker type solutions in unitary theory *(French)* 79—17287
  Robertson-Walker universe, density constraint on local inhomogeneities 78—8281
  Robertson-Walker universe, finite temp. effects 78—45440
  Robertson-Walker Universe, quantum statistics 79—88769
  Robertson-Walker universes, field interaction effects on particle creation 80—42130
  Robinson's theorem, shear free condition 78—93586
  Robinson-Trautman space-times, cosmic time functions 80—42113
  rotary solid sphere, gravitational mass defect, rotation mass effect in general relativity *(Chinese)* 80—52074
  rotating black holes, superradiance, spin thermodynamic explanation 80—86179
  rotating body, initial value eqns. 78—95
  rotating body, motion, in linearised gravity 79—85020
  rotating body metrics, Einstein vacuum field eqns. solns. using local symm. 78—54257
  rotating charged dust, Newtonian and general relativistic treatments 78—73908
  rotating charged dust in general relativity 79—71320
  rotating disc, light ray and particle paths 79—2670
  rotating disc, light-ray and particle paths 79—2671
  rotating dust cloud, stationary exact soln. 77—87675

general relativity continued
  rotating dust cylinders 77—61000
  rotating dust sphere, slow rotation limit, maximal slicing condition 80—73246
  rotating fluids, central behaviour, tetrad formalism 80—53888
  rotating fluids, Killing inequalities 77—64981
  rotating infinite cylinder, exterior solns., everywhere singular metric 77—60986
  rotating model for radiation and radiation-reaction force of free-falling charge 78—8301
  rotating neutron stars, general relativity, exact solns. for slow rot. 79—75239
  rotating plane-fronted waves and their Poincare-invariant differential geometry 80—332
  rotating pressure-free space-time, thin self-similar disc config. 78—96387
  rotating radiating body, nonstationary soln. of Einstein eqns. 77—22450
  rotating relativistic polytropic stars, integral characts. and internal struct. *(Russian)* 77—91513
  rotating relativistic stars, generic instability 78—93567
  rotating soln. of Einstein's eqns. 77—17880
  rotating sources, eqns. of motion in linearised gravity 79—93004
  rotating sphere, internal gravit. field in weak-field approx., appl. to astrophysical objects *(Russian)* 79—25939
  rotating stars stability and gravit. radiation 78—93210
  rotating steady state configs., axial 77—49647
  rotating steady-state configurations 78—73899
  rotating system of observers, covariant decomposition *(German)* 78—49724
  rotating systems, Einstein equations 80—68101
  rotating universe, stability 79—17146
  rotating universe with successive causal and noncausal regions, solns. to Einstein eqns. 79—67200
  rotating very compact stars, existence of ergoregions 78—24523
  S_2 separable space-times, algebraic props., Weyl tensor 79—63093
  S-PRF_n-space of first kind 79—17294
  s-recurrent Finsler space, tensor field props. 80—12959
  s-recurrent Finsler space 79—30326
  satellite, orbits near Jupiter and Saturn, post-Newtonian effects 79—101054
  scalar field, anisotropic, with cosmical time 79—88847
  scalar field, exterior case, identification of variational principles *(French)* 80—73220
  scalar field, gravitational peculiarities 80—31623
  scalar field, modified stationary action principle, field eqns. for perfect fluid *(French)* 80—52076
  scalar field and gravitational instability 80—52079
  scalar field gravitational theory for perfect fluid, second approx. of internal soln. *(French)* 77—67342
  scalar fields, non-null eigenvalues 79—21623
  scalar fields, self-interacting, with geometrical interpretations 80—31397
  scalar meson fields in conformally flat space 78—8278
  scalar nonsingular sources 78—36908
  scalar pot. and event horizon 78—101
  scalar tensor gravitation theory in Lyra manifold, spherically symmetric solns. 80—22244
  scalar tensor theories, plane wave solns. in Einstein-Maxwell theory 77—33919
  scalar tensor theories and variable rest masses 80—36916
  scalar-particle prod. near anisotropic universe singularity due to gravit. field 77—91421
  scalar-tensor cosmology of Jordan-Brans-Dicke, influence of massless EM fields 77—45617
  scalar-tensorial field eqns. models 77—57241
  scale covariant gravity theories, astrophysical tests 80—73216
  scale covariant Lagrangians and spaces reciprocal to static Einstein spaces 80—27189
  scale covariant theory of gravitation, astrophys. appls. 78—16710
  Schrodinger's contribution 77—45659
  Schwarzschild black hole, $\gamma>5/3$ gas accretion 79—17011
  Schwarzschild black hole in ext. mag. field, radiation emitted by relativistic particles 78—96501
  Schwarzschild space time, algebraic embeddings in R^7 space *(Italian)* 79—17284
  Schwarzschild space-time parallel transport of vector along circular orbit 79—71313
  Schwarzschild space-time zero rest mass scalar wave eqn. solns 79—93010
  second law of black hole physics and tachyons 79—49117
  second order field equations for grav. field theory 80—27203
  self gravitating fluids with cylindrical symmetry 80—12970
  self-dual metrics with self-dual Killing vectors 80—108
  self-gravitating elastic sphere, critical radius *(French)* 79—54027
  self-gravitating irrotational barotropic fluid in conformally flat space 78—45542
  self-similar solutions with spherical shock waves *(Russian)* 78—8284
  self-similar space-times, perturbation scheme 78—54099
  self-similar space-times, solutions to general relativity eqns. 78—54098
  selfgravitating systems, strongly interacting, perturbation methods 80—73234
  semiclassical relativity, weak field limit 80—57169
  semiclassical theory of scalar field in globally hyperbolic universe 78—54250
  separability structures, appl. to vacuum space-times with two Killing vectors 79—49121
  separable coords. in four-dimens. Riemannian spaces 78—57826
  set of nonreflecting points, props. 79—49120
  seven-dimensional relativity, 4-D gravity coupled to Yang-Mills fields 80—82699
  shear hell holes and anisotropic universes 80—95011
  shock wave propagation, stationary approx. 80—86172
  shock waves, divergent and collapsing self-similar solns. *(Russian)* 77—74290
  shock waves in general relativity, geometrical struct. 79—71297
  short range scalar field 79—44813
  single soliton cosmological waves, Friedmann cosmological model background *(Russian)* 80—17708
  singular hypersurfaces, asymptotic regularisation as alternative to distrib. 80—36923
  singular points and projective limits 80—52077
  singular space times, classification scheme 80—31609
  singular spin harmonics 79—97529

general relativity continued
- singularities, in static axially symm. coupled fields 78−65822
- singularities, incompleteness and the Lorentzian distance function 79−30317
- singularities, native and classes 80−31610
- singularities, need for new principles *(Russian)* 77−26212
- singularities, review 77−57238
- singularities, upper bound to growth rate of Ricci curvature 77−45764
- singularities and causality violation 77−87666
- singularities and causality violation 80−31607
- singularities and invariants 80−31611
- singularities and rule of unanimity 78−4529
- singularities at real points of H space 80−98831
- singularities in general relativity theory 79−35591
- singularities in spatially homogeneous cosmologies 80−36747
- singularities in stationary, cylindrically symmetric dust solutions 80−31613
- singularity problems in gravitational theory, soln. modification of Einstein's eqns. 80−8534
- singularity-free extended particle model in general relativity 78−54255
- SL$_{2,C}$ gauge theory of gravit., Lagrangian approach 78−77777
- SL$_{2C}$ gauge formulation of general relativity, geometry 78−41211
- SL(2,C) gauge invariant Lagrangian density 77−5721
- SL(2,C) Lorentz group, relativistic equations and indecomposable representations 79−30298
- SL(2,C)Yang-Mills field theory description, in curved twistor space 79−21602
- slow-motion approximation in radiation problems 80−73242
- slowly pulsating axisymmetric systems, computation 77−5715
- slowly rotating nonhomogeneous bodies, quasistationary gravit. collapse 77−49289
- SO(3,2) de Sitter symmetry, spontanously broken, gravitational holonomy group 80−57149
- SO(3,2) gauge theory, geom. of Einsten-Cartan theory 79−75425
- SO(3, 1) gauge field, Einstein-Weyl-Yang system, strong gravity model 78−86201
- SO(4,1) de Sitter gauge theory, general relativity as gauge theory limit 79−58598
- solar angular momentum flow, rel. to oblateness and Brans-Dicke theory 77−45396
- solution generating theorem, appl. to general relativity 78−21027
- some electrovac models of homogeneous gravitational force fields in general relativity 80−95014
- source energy change for gravitational wave emission in Einstein theory 79−21608
- space and time, influence of matter *(German)* 79−67197
- space time curvature tensor, Newman Penrose formalism, CAMAL program calcs. 78−24701
- space-like infinity, conformal structure 78−8293
- space-matter spinor 79−30310
- space-matter tensor, algebraic classification 78−29009
- space-matter tensor algebra 79−12656
- space-time configurations, pseudo Riemannian manifold, maximal submanifold props. 78−12624
- space-time events, nonlocalisability 80−94972
- space-time experiments, potential of an orbiting interferometer 79−35624
- space-time homogeneous models with torsion 79−58607
- space-time manifold geometrical singularities, edge geometry 79−44807
- space-time properties, local and global, Einstein's eqns., Universe matter density 78−61942
- space-time properties of supergravity 80−8887
- space-time singularities and conformally invariant gravit. theory 77−74286
- space-time singularity, quantum fluctuations 80−8893
- space-time systems with Killing's property *(French)* 80−31601
- space-times, co-ordinate dependent investigation of limits 80−95003
- space-times with a group of motions on null hypersurfaces 80−42111
- space-times with four-parameter groups of motions acting on null hypersurfaces 77−57247
- spacelike geodesics in the Nordstrom geometry 79−88852
- spacelike motions admitted by the magnetofluid space-times 79−80481
- spacetime, extended conformal, interactions and dynamical groups of elementary particles 78−8290
- spacetime foam, mathematical framework 79−9172
- spacetime geometry 78−36895
- spacetime singularities 78−8291
- spacetime structure probed by spin 1/2 elementary particles, Riemann geometry with torsion 77−41517
- spacetime structure theory at very short distances, nonlinear sigma model 80−12979
- spatial conformal flatness in homogeneous and inhomogeneous cosmologies 78−69924
- spatial tensor anal. 78−93571
- spatially homogeneous and inhomogeneous cosmologies with equation of state $p=\mu$ 79−49122
- spatially homogeneous cosmology, dynamical degrees of freedom 79−30155
- spatially homogeneous universes 78−8318
- spatially homogeneous universes which admit source-free magnetic fields 80−12973
- spatially homothetic space-time, intrinsic scalar curvature *(French)* 78−36893
- special birecurrent Finsler space, props. 79−30325
- spectral shifts, variational study, relativistic aspects *(French)* 80−21909
- spheres filled with isentropic magnetofluids, exact solns. 77−82419
- spherical counter rotating dust bodies, relativistic dynamics 77−67358
- spherical multicomponent fluid, hydrostatic equilib., thermodynamic interpretation, 3-component neutron star 79−49135
- spherical rigid body, pole-dipole singularity idealised description 79−2683
- spherical stars, reformulations of Einstein eqn. solns. 78−49731
- spherical static fluid, interior solns., appl. to collapsed stellar objects 77−57245
- spherical stellar models, stability and normal modes 79−29983
- spherical symmetry in a 4-dimens. space-time 79−35590
- spherically symm. mass, eqn. of motion and gravit. radiation 77−17879
- spherically symmetric charged dust distrib., Brans-Dicke theory, Schrodinger eqn. soln. 79−12693
- spherically symmetric charged dust distrib., Einsteins theory generalised to Brans-Dicke theory 79−2694

general relativity continued
- spherically symmetric distrib. of matter with press., Einstein eqns. soln. 78−32617
- spherically symmetric fluid, general relativity, equation of state, no slow uniform contraction 80−62544
- spherically symmetric relativistic spheres, noncomoving coords. 77−87673
- spherically symmetric self-similar universe, theory 80−8727
- spherically symmetric space-times, even parity junction conditions for perturbations 80−31628
- spherically symmetric space-times with vanishing curvature scalar 80−68096
- spherically symmetric surface layers, error correction 79−49134
- spherically symmetric vacuum manifold, effect of nonvanishing cosmological const. 77−74288
- spin coefficient equations with nongeodesic eigenrays 79−25941
- spin frame independent variables, Newman-Penrose formalism 77−45759
- spin precession in the relativistic two-body problem 79−49118
- spin via square root procedure, supersymmetry 77−82437
- spinless EM charge, geom. theory 78−45533
- spinless particles, equations of motion using a general energy-momentum tensor 78−36891
- spinning mass, on Kerr and Tomimatsu-Sato solns. 77−87677
- spinning masses, generalisation of Tomimatsu-Sato solns. 77−49652
- spinning masses, metrics solns. 78−8297
- spinning particle in a gravitational field, field eqns. 80−31636
- spinning particle in grav. field with torsion, eqns. of motion *(Chinese)* 80−62546
- spinning particle in metric-torsion field, eqn. of motion 80−62543
- spinning particle paths as geodesics of an Einstein connection 77−87674
- spinning particles, eqn. of motion in post-Newtonian approx. of Einstein-Cartan theory 79−25954
- spinning test particle motion in Vaidya's radiating metric 77−45766
- spinor connections, almost product struct., Riemann spaces *(Rumanian)* 79−30297
- spinor covariant derivatives, geometric significance 77−26450
- spinor field in Riemann space time, energy-momentum tensor symmetrisation *(Russian)* 77−82422
- spinor fields in an Einstein universe, finite temp. effects 79−21614
- spinor Green's function in Einstein universe, vac. averaged stress-energy tensor 78−41217
- spinor space, quantum phenomena 79−17192
- spinor theory without elementary gravitons 78−8321
- spinorial structure of hyperheavens, Einstein's vacuum eqns. fracture 77−22454
- spontaneous compactification of arbitrary space-time dimens., SO(N) gauge group 77−22458
- spontaneous origin of Newtons const., modified Einstein eqns., matter interactions in weak gravit. fields 78−12853
- spontaneous particle creation in strong gravitational field, semiclassical theory 78−54281
- stability of initial data *(French)* 79−54019
- Stachel string cloud model in general relativity 80−4607
- standard hot big bang model of Universe, dynamics 78−69922
- star, cold, massive rest-mass density and redshift 80−56859
- star, spherical, emitting neutrinos, relativistic model 78−73705
- star clusters, relativistic, with high central redshift 80−105293
- star clusters, variational principle for perturbations 79−53860
- star with neutron core, gravitational equilib. relativistic treatment 78−57570
- starlight deflection by Sun, daytime obs. by photographic astrometry 79−8797
- stars, relativistic collapsing, radiation, linearized even-parity EM and gravit. radiation 79−75228
- stars, rigidly rotating, secular instabilities in general relativity, theoretical formalism 80−4341
- stars, rigidly rotating, secular instabilities in general relativity, numerical results 80−4342
- stars, rotating Newtonian, secular instability to gravit. radiation and viscosity 78−53922
- static and stationary axially symmetric fields, Kerr, NUT and Bardeen metrics *(German)* 80−52073
- static charged gas spheres, field eqns. solns. 80−101739
- static electric spherically symmetric field, particle soln. in Bonner unified field theory 79−67205
- static field, Einstein vacuum field eqns. 78−65836
- static fluid charged sphere, field equations, singularity force solution 79−97273
- static fluid cylinders and plane layers 79−17289
- static general relativistic stellar models, props. 80−86165
- static gravitational solitons, singularities, horizons, field behaviour at infinity *(Russian)* 80−73229
- static spherical shell of matter, line element calc. 77−30065
- static spherical sources of scalar, EM and gravitational fields *(Russian)* 78−12613
- static spherically symmetric distrib. of charge, complete field, charged dust appl. 78−21026
- static stars, mathematical curiosities 77−74045
- static stars, spherical symmetry in general relativity 77−45397
- static Universe model with two centres, red shift explanation 78−57706
- stationary axially symmetric Einstein eqns., linear eigenvalue problem, complete integrability 78−77780
- stationary axially symmetric gravitation fields, covariant eqns. and conservation laws 79−92997
- stationary axially symmetric vacuum metrics maximality of the local symmetry group 79−12664
- stationary axially symmetric vacuum solns. *(German)* 78−81903
- stationary axisymmetric gravit. fields, Tomimatsu-Sato solns. 77−79012
- stationary axisymmetric vacuum gravitation field equations, separable solutions 79−9156
- stationary axisymmetric vacuum gravitational field equations, new formulation 79−9155
- stationary Einstein Maxwell field equations, pots., nonlinear symm. transforms. 78−86206
- stationary Einstein-Maxwell equations, gravitational and EM potentials 80−86185
- stationary Einstein-Maxwell fields, electrovacuum solution 80−73225
- stationary gravit. fields, general electrovacuum *(Hungarian)* 77−22469
- stationary solutions and positivity of energy 77−33916
- stationary spherically symmetric clusters of particles, relativistic models 79−71298

general relativity continued
statistical formulation of gravitational radiation reaction 80−90749
statistical mechanics, BBGKY hierarchy and Boltzmann eqn. 79−63127
stellar aberration, classical rel. to relativistic theory 80−67517
stellar dynamics, stability of spherical systems, binding energy criterion 80−94837
stellar equilibrium statistical mechanics of relativistic systems with energy cutoff 78−93327
stellar evolution code 79−58317
stellar relativisitc clusters, steepest descent technique and stellar equilib. statistical mechanics 77−49444
stochastic parallel displacement of tensors, geodesic correction 80−8920
stochastic properties of complex nonlinear oscillation regimes 80−8919
stress tensor of conformally invariant field in conformally flat spacetime, axiomatic renormalisation 78−29034
stress-energy tensor for two-dimens. evaporating black hole 78−24706
stress-energy tensor regularization for particles propag. in general background metric 77−79006
stress-energy tensors 77−87672
string thickening, null-string dust, bivector field 80−77671
string thickening, perfect dust, timelike bivector field 80−90732
string-like model, gauge depend. problems 77−22471
strings and Maxwell fields of rank 2, local correspondence 80−73245
strong Backlund transformations, generalisation and existence in ≥ 4 dimens. 79−30316
strong gravitational field and general relativity 80−67548
strong gravity and elementary particle theory in general relativity 78−8315
strong gravity model, energy-momentum complex construction 77−9939
strong gravity with cosmological const. for quark binding 78−4820
strong principle of equivalence, test using redshift of X- and γ-ray lines of neutron stars 78−40814
strong spin-two interaction and general relativity, review 79−45046
strong-gravity solns. for Einstein's eqns. 78−24705
SU(1,1) spin coefficient equations with nongeodesic eigenrays 79−25942
SU(2,1) generation of electrovacs from Minkowski space 79−75427
SU(2,1) symmetry of the Einstein-Maxwell fields. II 78−93577
SU(2) harmonic analysis as basis for quantisation 80−9116
SU(2) self dual gauge fields, static axially symmetric solns. 79−35603
SU(4|N) gauge transformations, determ. of Lagrangian for supertheories 79−63118
super-gauge symmetry in general relativity, Einstein's A transformation *(German)* 78−86199
super-Hamiltonians, equiv. of parabolic and hyperbolic forms 78−32739
superconducting current variation with gravitational field variation, general relativistic phenomenological theory 80−54827
superconducting gyroscope to test Einstein's general theory of relativity 80−8897
superconductivity, general relativistic phenomenological theory 80−2518
superconformal group in flat superspace 77−2763
superdense neutron matter, relativistic theory and eqn. of state 78−45349
superenergy tensors and supertensors 77−30081
supergauge extensions, geometric backgrounds, supermanifolds 78−73891
supergravity, geometry of superspace, vector-spinor matter 78−49744
supergravity, space-time spin struct., and Hamiltonian constraint square roots 77−49663
supergravity, supersymmetric generalisation of differential geometry tensors 78−45546
superluminal frames and tachyons 79−58543
superluminal phenomena and frames in special and general relativity 78−36825
supermassive star, expanding, and contracting dust shell, Einstein's theory of gravit., black hole formation 78−12088
supermassive star collapse to black hole, Einstein eqns., numerical soln. 80−41851
supermassive stars, general relativistic stability towards non-adiabatic perturbations 77−41376
supermassive stars, possible dynamical stabilization by shadow gravitational potential 77−33338
supernovae and black holes analytic models, Einstein eqn. solns. 78−4258
superpotential forms and total energy/momentum vanishing in closed forms 80−98828
superspace, local supersymmetry, superfibre bundle theory 78−77782
surface deformations, their square root and the signature of spacetime 80−8874
symmetric and traceless tensors on Minkowski space 79−17298
symmetric vectors and Ricci directions 80−8725
symmetries and vacuum Maxwell's equations 80−86178
symmetries of energy momentum tensor, concomitant conservation laws 78−57831
symmetry breaking and space-time geometry 78−54533
symmetry mappings, particle number conservation, baryon number conservation 77−30063
symmetry of charged rotating body metrics 78−77776
symmetry properties of embedded space-times 79−44814
symplectic form, geometric construction 78−8289
symplectic formulation of relativistic particle dynamics 77−57237
symplectic struct. on Einstein metrics, general relativity, canonical formalism 77−9922
synchronous reference system, metric tensor components at R-T boundary *(Russian)* 78−45531
Synge's equations of motion applied to a perfect fluid 79−40433
syntopic spacetime meas., time dilatation and Lorentz contraction meas. 78−73896
tachyon dust universe 78−24583
tachyon emission from white holes 77−33718
tachyon observations in nucl. emulsions possibly overlooked 80−12963
tachyon quasi-catastrophe theory, tachyon existence, imaginaries, and causality, book contrib. 79−44815
tachyon solns. in classical relativity 80−36917
tachyons, absence in supergravity and classical Einstein gravity 79−67208
tachyons, charged, detect., theory, rel. to general relativity 78−41614
tachyons, monopoles and related topics, book 79−44718
tangent bundle, geodesics, correspondence with spinning particles 80−68099
tangentially stressed cylinder, general interior soln. of Einstein's field eqns. 77−17882
Taub's metric non-empty space-times *(French)* 78−45527

general relativity continued
Taub's type solns. *(French)* 77−64969
Taub-NUT congruence construction, Einstein's vac. field eqns. 77−33910
Taub-NUT instanton with an horizon 78−89392
teaching demonstration of curved space 77−57130
telescopic principles in the theory of gravitation *(German)* 79−40416
tensors, spinors and functions on unit sphere 77−13647
test, precision ring laser interferometry technique 80−52117
test by Viking relativity expt. 78−16716
test particle mass in gravitational field, rel. to Mach's principle 79−12670
test particles, dynamics of relative motion, variational principles 78−45525
test particles, kinematics of relative motion, geodesic deviation 78−45524
test particles, with internal struct., conservation laws 77−67338
tests at quantum level 80−98849
tetrad formalism for Einstein-Dirac eqns. and spinor Lagrangian 78−102
tetrad formalism of Maxwell equations with effect of gravitation. II 78−77784
tetrad formulation, localised Poincare group requirements *(Russian)* 78−12615
tetrad formulation, weak conservation law covariant consequences 80−17848
tetrad gravitational field, weak principle of equivalence and gauge theory *(Russian)* 78−62135
tetrad potentials gauge, reference systems with Newtonian time *(Russian)* 78−89378
theory of motion, electromagnetism, gravitation 80−105500
theory testing by lunar laser ranging and planet radar ranging 77−53823
thermal propagators and accelerated frames of reference 79−67211
thermodynamic equilib. of gravitating sphere in Lyra's geom. 78−65840
thermodynamics, density, momentum and energy laws 77−82424
thermodynamics, entropy law 78−8373
thermodynamics, laws and macroscopic quantities 77−82423
thermodynamics, relativistic, and temperature 79−63182
thermodynamics, relativistic, nonstationary, hidden variable approach 80−68097
thermodynamics in multiply connected spaces 80−4606
thin cylindrical shell of dust under rigid rotation in general relativity 80−42124
'thin sandwich conjecture' in general relativity initial value problem 78−4539
thin sandwich problem, geometry 80−73239
thin spherical time like shells, eqn. of motion from Lanczos eqns. 79−67199
tidal fields, d'Alembert's principle and test rigid rod 78−40812
tilted Bianchi type-III cosmologies 79−53948
time, length and mass changes in gravitational field 80−8871
time, uniform scale in astronomy rel. to relativity and Ephemeris time 77−53402
time's arrow and the structure of spacetime 79−97173
time analysis, universal and relativistic time 79−30299
time and frequency, conf., Helsinki, Finland (Aug. 1978) 80−46728
time travel conceivability 80−27192
time-machines 79−2672
Tolman-Omer and Godel universes, closed conformal transforms. *(French)* 77−71159
Tomimatsu Sata space-times, Einstein eqns. soln., effective pot. for equatorial motion 78−32621
Tomimatsu-Sato $\delta=3$ metric, Weyl conform tensor, invariants 80−68087
Tomimatsu-Sato family, exact soln. 78−89377
Tomimatsu-Sato family for stationary axisymmetric gravit. fields, exact solns. 80−8877
Tomimatsu-Sato generalised gravitational fields, limits 78−21022
Tomimatsu-Sato soln., symmetry axis extension 77−72
topological charge of singularity 79−12661
toroidal black holes 79−97023
torsion effect on macroscopic gyroscope 80−98830
torsion gravitational theories, spinning particle motion, Lagrangian theory 79−12692
torsion of spacetime included in a quadratic Lagrangian 78−8316
torsions in Riemann Cartan space times, U_4 reinterpretation, gravit. radiation solns. 78−45537
torsions in Riemann Cartan space-times, physical props., torsion classification scheme 78−45538
torsions in Riemann-Cartan spacetime, U_4 reinterpretation of null EM Einstein eqns. solns. 78−41212
total mass positivity of a general spacetime 80−12965
total superenergy tensors in general relativity, Einstein Cartan theory, closed system 78−45528
transport processes, relativistic generalisation in continuum *(Hungarian)* 78−89383
trapped null geodesics in rotating interior metric 77−9926
Trautman's radiation condition 80−73241
trial particle relative dynamics nonlinear effects, small perturbing forces effect 80−4609
trichromatic theory and time vector in relativity theory *(French)* 78−57006
twin paradox, round trip, gravitational field eqns. and geodesic eqns. of motion 79−58463
twin paradox in a Kerr matric 77−22449
twisted quantum fields in a curved space-time 78−73913
twisted scalar field, vacuum solns. 78−93804
twisting type-N solutions 80−73221
twistor connection and normal conformal Cartan connection 77−79008
twistor field equations 80−57145
twistor Hamiltonian anal. of massive scatt. 77−37792
twistor surfaces and right-flat spaces 79−49119
Twistor theory, symplectic forms 78−4468
twistor theory of space-time 80−17843
twistors and multipole moments 78−16705
two-body problem, nonlinear effects 79−8799
two-body problem in linearised gravity 80−86160
two-body relativistic interactions, Hamiltonian formalism 80−77666
two-body restricted problem, almost circular orbits in general relativity *(Ukrainian)* 79−101056
two-dimens. space-time, neutrino stress tensor regularisation 77−67561
type-N gravitational field with twist 78−45534
U_4 theory, positive energy 78−8296

general relativity continued
unification of gravitation and matter, crossing terms in Einstein's eqns., singularity 78—21039
unified field theory, five-dimensional theory of interacting scalar, electromagnetic, and gravitational fields 80—105833
unified field theory, nonsymmetric, metric hypothesis, spinor analysis 80—68404
unified fields in pentadimensional theory 79—44832
unified gauge field theory with torsion, symmetries 78—89386
unified gauge theory of gravitational and strong interactions 80—95016
unified treatment of null and spatial infinity 78—65848
uniform electrovacuum space time, observer dependent effects, Bertotti-Robinson line element 79—122
uniform field metric derivation without field eqns. 80—90739
uniform rotating sphere, five parameter internal gravit. field family *(Russian)* 80—95008
unit vector fibre bundle tangential to Finslerian manifold, elliptic operators *(French)* 80—22242
unitary interpretation of quantum physics and relativity 77—87641
universal atomic standard, Einstein field eqn. considerations 80—107
Universe, spatial homogeneity, philosophical problems 80—56984
universe model, Brans-Dicke theory, props. 78—45446
universe with variable G and c, initial conditions 79—48977
vacuum cosmologies, repulsive and attractive timelike singularities 79—92901
vacuum Einstein eqns., new Lagrangian and tetrad form 79—49116
vacuum energy of quantised field in closed universe 77—22479
vacuum field equations, fifth dimension, ratio of EM to gravitational force 80—77679
vacuum metrics, with two Killing vectors, twisting type II and III solns. 79—17296
vacuum stresses induced by accel. of infinite plane cond. for massless scalar and EM fields 77—30071
vacuum superfluidity near anisotropic singularity, phase transitions *(Russian)* 80—94905
Vaidya's metric, complexification, radiative and nonradiative, parts of energy-momentum tensor 80—68093
van Stockum metric, axially symmetric gravitational fields of bounded sources 79—21597
variable rest mass field theory and the cosmological singularity models 80—77525
variable rest masses, black hole solutions and neutron star models 79—30162
variable rest masses, relativistic theories, tests and consequences 80—31396
variational aspects of relativistic field theories 77—82417
variational principle and gravitational field energy 79—25923
variational principle for perfect and imperfect fluids in general relativity 80—90733
variational principle giving superpotentials, affine connection Riemann tensor, field eqns. 78—107
variational principles of relativistic theories involving torsion 77—60990
vector field with zero covariant deriv., general metric 80—68092
vector spherical harmonics of unit hyperboloid in Minkowski space 78—32732
velocity composition law 79—93008
velocity matrix in six-dimensional space-time 80—86171
velocity of light, Mossbauer meas., isotropy 80—95026
virial theorem in general relativity, consequences for spherical symmetry stability 79—21593
viscous fluid cosmological model in general relativity 78—61944
Vlasov-Einstein eqns. in spherical symmetry, self-similar analysis 80—67535
wave propagation in prestressed nonlinear elastic solids, relativistic theory 79—1124
weak conservation law covariant formulation 80—73224
weakened field eqns. 78—29008
Wentzel-Kramers-Brillouin method, self-gravitating, charged scalar fields 78—117
Weyl's theory and principle of least action, Riemannian manifold laws of motion *(French)* 80—62542
Weyl and Papapetrou axisymmetric space-time as geodesics of hyperbolic complex plane 79—49126
Weyl metrics, pseudo 80—95002
Weyl singularities, stability of nakedness 80—46896
Weyl solns. of Einstein vac. field eqns. 78—93580
Weyl space, proper time measurement by geometric clocks 79—30300
Weyl tensor in gravitational field, vector fields and ideal reference frames 80—36918
Weyl-type vacuum space-time, new solns. of Einstein eqns. 77—22459
whimper space-time solns. to Einstein eqn. 80—31614
white dwarfs, degenerate magnetic, critical parameters estimation, general relativistic corrections 78—65622
white dwarfs, rigidly rotating, critical ang. vel. and equilib. configurations 77—5525
white holes, angular appearance 78—45352
white holes, optical appearance 79—21323
X-ray bursters, radius and mass, general relativistic effects 80—8712
X-ray radiation emitted near black holes, relativistic radiative transfer and polarisation features 80—46700
Yang-Mills gauge symmetry, max. 4-dimens., and general covariance, implications 79—63115
Yang-Mills struct. of gravit. final state of collapsing matter 77—60984
Yang-Mills-Einstein eqn. pseudoparticle solns., gravit. effect on Yang-Mills topology 77—82682
Yano vector fields and conformally related spaces 80—98829
Yukawa spherical diffuse massless sources in relativity 77—87931
zero mass surfaces, rel. to cosmological singularities 79—25772
zero-rest-mass fields, boundary conditions at past null infinity 78—24661
zitterbewegung, atoms with point particles 80—57147
Zorn algebra in general relativity 79—63101
ν radiation, Einstein-Dirac eqns. *(Russian)* 78—49727
π inertial mass, quaternion field theory of matter 78—24702
π lifetimes, ratio of neutral to charged 79—49513

generator coordinate method
see also nuclear structure theory
adiabatic time-depend. Hartree Fock, relation to generator coordinate method, conjugate parameters 78—86498
amplitude evaluation using spherical Bessel functions, ^{6}Li(α,α) appl. 77—54194

generator coordinate method continued
Bose system, Jastrow wavefunction, hypernetted chain method 80—17866
Brueckner-generator-coord. method, α-α scatt. 78—62487
cluster systems, normalisation kernels, SU(3) prop., generator coordinate theory 80—73814
collective Hamiltonian quantisation in adiabatic expansion 79—85388
collective subspace of many-body Hilbert space, generator coord. approach, kinematics 78—70055
collective vibrs., double perturbation theory 77—79031
complex nuclei scatt., variational method in RGM based on GCM kernel 78—564
complex-generator-coord. technique in resonating-group calcs. 77—67705
composite particle scattering, generator coord. method, Kohn-Hulthen variational principle 77—2957
coupled channel variational method for microscopic study of reactions between complex nuclei 79—13263
deformed nuclei, giant quadrupole reson splitting 78—4924
deformed nuclei, heavy-ion scatt., generator coord. method 78—12960
discretisation techniques, mathematical foundation 80—5079
double folding pot. for inelastic scatt. between nuclei 80—13425
effective nucleus-nucleus pot., generator coord. method 78—13139
even parity states in ^{19}F, ^{21}Ne, ^{23}Na, generator coord. method, projected Hartree-Fock, and complete diagonalisation calcs. comparison 78—89796
exchange kernels, analytical derivation methods 79—13228
Fermi system, Jastrow wavefunction, hypernetted chain method 80—17866
ferromagnetism, generator coordinate method for boson representation of energy of $S={}^{1}/_{2}$ ferromag. 80—25066
giant resonance description, RPA, GCM, and semiclassical theories unification 78—54671
Griffin-Hill-Wheeler equation soln. for scatt. problems 80—73813
Griffin-Hill-Wheeler spaces, 1- and 2-conjugate parameter generator states, giant resonances and scatt. 80—42618
heavy ion interactions, generator coordinate method, microscopic treatment 78—66304
isovector pairing collective motions and transition rates, projected BCS solns., generator coordinate simplification 80—22654
kernels of GCM, RGM and OCM and their calculational methods 79—13227
large amplitude collective motion, collective subspaces and generator coordinate method 80—9199
matrix elements between arbitrary single particle wavefunctions, generator coordinate method 80—57751
multi-channel scatt., microscopic R-matrix theory 78—13041
in natural state formalism, appl. to harmonic oscill. 77—17831
nuclear collective dynamics generator coordinate Peierls-Yoccoz method, applicability 77—67708
nuclear collisions, two-centre generator coordinate basis for microscopic theories 78—13038
nuclear reactions with unequal fragments, generator coordinate and resonating group methods 77—18490
pairing vibrational and isospin rot. states in particle number and isospin projected GCM 78—54696
pf-shell nuclei, Hermitian operator method calcs., energy levels, transitions 78—54702
projection of wave functions on states with definite ang. momentum 78—12590
quartic anharmonic oscillator, symmetry properties in generator coord. method 78—49699
Rayleigh-Ritz principle in generator coordinate method, optimal TDHF solns. 80—42569
reaction matrix approach to the cluster state, Brueckner generator coordinate method, appl. to α-α scatt. 80—9250
resonating-group method for nuclear many-body problems, matrix elements calc. by GCM 79—9497
theory of resonating group method and generator coordinate method, and orthogonality condition model 79—13226
trial function regularisation and generator coord. amplitudes 77—14081
two-centre generator coordinate method for complex nuclear collisions 77—14080
two-centre generator coordinate model functions, ang. momentum eigenstates projection 78—12994
two-centre molecule-like states, generator coordinate wave function projection 78—12995
α-α scattering, appl. of generator coordinate formalism 77—18584
α-decay, Gamov states anal. 77—14075
^{8}Be collective excitation spectra from generalised hyperspherical functions method *(Russian)* 80—91133
^{8}Be low lying states, Sp(2, R) model with generator coordinate method 79—45169
^{9}Be, $1/2^{+}$ resonance state at 1.68 MeV 79—6398
^{9}Be, molecular model, ground state props. via HF and GCM calcs. 77—54137
^{9}Be, struct., size, quadrupole moment, generator coord. method calc. 79—71788
^{12}C, excited state struct., anomalous α-decay props. 3-cluster GCM model 79—6399
^{12}C+^{12}C, low energy, HFB and generator coordinate self consistent microscopic approach 80—42679
^{12}C+^{12}C system, dynamical struct. change during scatt. process and mol. resonances 79—13321
^{12}C+^{16}O elastic scatt., generator coord. calc., reson. spin assignments 77—57685
^{12}C(α,α'), generator coordinate multichannel calc., levels and resonances 80—78149
^{12}C(n,n), $<$17 MeV, resonating group calcs., phase shifts and differential cross sections 80—32275
^{14}C+^{16}O scatt., molecular resonances, generator coordinate study 79—36216
^{40}Ca, giant isoscalar monopole state energies in generator coordinate method 80—37317
^{40}Ca(^{16}O,^{16}O), rot. band of molecular resonances, generator coordinate model 80—13428
^{40}Ca(^{40}Ca, ^{40}Ca), generator coordinate study, rot. band of molecular resonances 79—75948
^{40}Ca(α, α), generator coordinate method for arbitrary cluster widths 77—18581
^{40}Ca(α,α), back-angle anomaly, RGM and GCM 78—616
^{19}F, even parity state, EM props., collective struct., generator coord. method, HF method anal. 79—89220

generator coordinate method continued
^{19}F, low-lying excited states calc. by generator coordinate method 78—12974
^{19}F, transition probabilities and multipole moments between states calc. by generator coordinate method 78—13022
^{54}Fe(p,p′), testing self consistent models of collective and single particle struct. 78—82300
H atom, variations, quantum theory calcs., generator coord. calcs. 80—41987
^{4}He(α,α), composite particle scatt., generator coordinate and natural boundary condition methods 80—13489
^{4}He(α,α), natural boundary condition methods for the microscopic treatment of composite-particle scattering 79—63680
^{4}He(α,α), s-wave, Coulomb amplitudes from generator coordinate theory 80—83107
^{4}He(α,α), size change of α effect on phase shift, generator coordinate and variational methods *(Chinese)* 80—68683
^{4}He(t,n)^{6}Li, cross section using var. calcs. in generator coordinate method 78—13122
^{4}He(t,t)^{4}He, cross section using var. calcs. in generator coordinate method 78—13122
^{4}Li, cluster model study using generator coord. method on ^{3}He+p scatt. 80—27581
^{6}Li(α,α)^{6}Li, cross section using var. calcs. in generator coordinate method 78—13122
^{23}Mg, even parity state, EM props., collective struct., generator coord. method, HF method anal. 79—89220
^{25}Mg, low-lying excited states calc. by generator coordinate method 78—12974
^{A}Na, (A=21, 23), even parity state, EM props., collective struct., generator coord. method, HF method anal. 79—89220
^{23}Na high spin positive parity state, approx. microscopic methods, shell model comparison 79—85352
^{23}Na, low-lying excited states calc. by generator coordinate method 78—12974
^{23}Na, transition probabilities and multipole moments between states calc. by generator coordinate method 78—13022
^{A}Ne, (A=19,21) , even parity state, EM props., collective struct., generator coord. method, HF method anal. 79—89220
^{21}Ne, low-lying excited states calc. by generator coordinate method 78—12974
^{21}Ne, transition probabilities and multipole moments between states calc. by generator coordinate method 78—13022
^{58}Ni, HFB and dynamic anal., collective motion, zero point energy correction 80—18161
^{16}O, giant isoscalar monopole state energies in generator coordinate method 80—37317
^{28}Si, generator coord. calc. 77—50073

generator protection *see machine protection*

generators, acoustic *see acoustic generators*

generators, electric *see electric generators*

geochemistry
see also Earth structure; geology
acid rain, neutralization in Hubbard Brook ecosystem 79—74922
N.Adriatic Sea, trace element analysis of seawater and sediment by neutron activation 77—21801
Aegean region, geochemistry rel. to dynamic model of Hellenic Arc 77—21734
S.African kimberlites, phlogopites excess ^{40}Ar distrib. rel. to K 79—34769
almandine-pyrope-grossular garnet, exsolution obs. 78—32074
Alpine meltwaters, ion exchange influence on dissolved load 78—81228
andesites, Andean region, petrogenetic composition variations 80—8313
andesites from S.America, Nd and Sr isotope data 79—29726
anorthosite gneisses, trace element comp. rel. to petrogenesis 78—65224
anorthosite massif of Labradors Nain complex, Proterozoic magma origin 80—94500
Antarctic dry areas geochemical problems 79—79844
Antarctic Peninsula igneous rocks, transverse geochemical vars. rel. to calc-alkaline magmas genesis 80—56466
Antarctic saline lakes—stable isotopic ratios, chemical compositions and evolution 79—74911
Antarctic snows, trace metals contents (1914 to 1974) 79—34867
Antarctic waters, effect of glacial weathering on Antarctic waters silica budget 78—20436
anthophyllite, kinetics of Fe-Mg exchange reaction, rock cooling rates calc. 77—81875
apatite in ijolitic and carbonatitic igneous rocks, comp. vars. 79—57929
apatite solubility in magma, laboratory expts. 80—72504
Aphebian alkaline plutonic and hypabyssal rocks, Great Slave Lake 79—84255
aqueous metals, adsorption on inorganic minerals 78—49006
Archaean mantle, siderophile and lithophile trace element evolution 80—46147
Archaean metasedimentary rocks from Kambalda, Western Australia, rare earth element geochemistry 80—109143
Archaean plutonic rocks, Pb isotope comp. 78—65223
Archaean precious-metal hydrothermal systems, Ontario, alteration patterns and metal distrib. 80—12382
Archaean precious-metal hydrothermal systems, Ontario, rare earth element and 0 isotope relations 80—12383
Archaean sialic crust, southern West Greenland, chemical and thermal evolution 80—31016
Archean continental crust, magma genesis by crustal anatexis, garnet-pyroxene thermometry and barometry 78—65236
Archean ultramafic rocks, discrimination between extrusive and intrusive on chemical basis 79—84256
Arctic aerosol and snow compositional differences 79—88377
arid terrain, soil zone chemistry in cyclic wetting and drying 79—62529
Asama Volcano, Japan, joint geophys. and geochem. obs. in 1977 *(Japanese)* 79—70771
ash-flow tuffs, Lake Precambrian in E. Newfoundland 79—84258
N.Atlantic basalt geochemistry rel. to mantle heterogeneity 79—29745
N.Atlantic mantle, chemistry and Pb, Nd, Sr isotopic correl. 80—90023
Central Atlantic Ocean, phosphate content rel. to underwater irradiance meas. *(Russian)* 78—77257
Atlantic Ocean waters, As and Sb content *(Russian)* 77—60428
Mid Atlantic Ridge, 22 to 30°N, magmatic process var. and upper mantle heterogeneity 79—88334

geochemistry continued
Mid Atlantic Ridge crest, geological and geophys. investigations 80—8284
azaarenes, presence in marine sediments 77—37181
Baikal rift zone, petrochem. of Cenozoic basalts and assoc. rocks 78—36171
Baja California, ancient lithospheric lherzolite xenolith in alkali basalt 77—81888
Barberton region, South Africa, Archaean granitic rocks, trace element geochemistry 78—11895
barite, in Devonian carbonate rocks, NE British Columbia, origin hypothesis 79—25240
barite rare earth composition rel. to formation conditions 80—41439
basalt, deep-sea, Mossbauer study of core-to-rim alteration 79—66688
basalt, hydrothermal alteration by seawater, chemical exchange exptl. results 79—20828
basalt, oceanic, Pb isotope comp., rel. to mantle evolution 78—65217
basalt from DSDP Leg 34, cooling rate effects on pyroxene chemistry 79—44148
basalt of back-arc basin, compositional evolution of mantle source 80—72471
basalt petrogenesis, role of dynamic partial melting 80—46179
basalt-seawater alteration reactions, studies via dynamic hydrothermal experimental system 79—5686
basalt-seawater interaction, trace element and Sr isotopic vars. in glassy basalt 80—8286
basaltic and gabbroic rocks from W. Mariana basin and Mariana trench 78—65254
basaltic magmas classification, use of Ti, Zr, Y, Sr, K, P and Nb distribs. 77—5150
basalts, deep sea, statistical anal. of clinopyroxenes 78—88828
basalts, from Central North Atlantic, Sr isotope geochemistry and Azores mantle plume 77—5179
basalts, from Pacific Ocean Basin, Sr isotope comp. rel. to mantle comp. 78—65218
basalts, oceanic, noble gas abundance patterns controlling factors 78—65220
basalts, open system cryst. fractionation and incompatible element var. 77—66916
basalts, Palaeocene, of Mull and Skye, immobile trace elements rel. to palaeotectonic affinities 79—34816
basalts from DSDP Leg 37 and FAMOUS area, compositional and petrogenetic comparisons 77—91077
basalts from DSDP site 332, geochemical characts. and evolution 77—91126
basalts from Mid-Atlantic Ridge in central N.Atlantic 79—39675
basalts from mid-ocean ridge, major and trace element data 79—88316
basalts from Project FAMOUS area, petrogenesis from 0 to 15 kbars exptl. study 79—29768
basalts geochemistry from back-arc spreading centre, East Scotia Sea 80—3989
belemnites, trace elements geochemistry rel. to post-depositional alteration and ^{18}O palaeotemps. 77—29455
Bering Sea shelf sediments, denitrification estimates 80—12433
big river sands, modern, petrology and chemistry 79—25274
biogeochemical cycles, role of atmosphere 79—79427
biotite+apatite system, thermochemical data rel. to use as geothermometer 78—85704
Black Sea, H_2S and O_2 zone boundaries rel. to water mass dynamics *(Russian)* 80—12435
Black Sea sediment cores, organic geochemistry 78—49040
Black Sea water, F content 78—32118
Bouvet triple junction, S.Atlantic Ocean, geochem. and petrology of dredged basalts 78—11877
bulk chemical anal. calc. from mineral phases obs. in thin section, BULK computer program 79—2378
Bushveld Complex, spheroidal pyroxenite aggregates chemistry rel. to silicate liq. immiscibility 79—88351
bytownite megacrysts., study of trapped basaltic melts, petrogenetic process study 78—95688
calc-alkaline volcanic rocks of Cerro Galan, NW.Argentina, Sr isotope evidence for crustal contamination 80—98318
calcite dissolution by fossil fuel CO_2, effect of sediment mixing 78—81212
calcite-depositing spring, chemical vars. and calcite precipitation 79—44202
calcrete deposits from Europe, Africa and India, isotopic comp. 78—73368
Caledonian granites in Britain, geochemical and geophysical evidence on geothermal pot. 79—74486
Caledonian granites petrogenesis, isotopic evidence for continental crust provenance 80—109146
Canadian Shield tholeiitic basalt-rhyolite magmatism and massive sulphide deposits 80—36298
Cantal continental volcanic system (France), ^{87}Rb-^{87}Sr constraints on genesis and evolution 79—88327
carbonate, (Si, Cl)-bearing from limestone-granite contact zone near Ikizdere, Turkey *(French)* 78—69339
carbonate chemistry of chalk water from Givendale, E.Yorkshire 79—66719
carbonate rocks, dissolution kinetics, lithology effects 77—78172
carbonatites, origin by liq. immiscibility 79—57928
E.Carpathians volcanic rocks, rare earth elements concs. and mock origin 77—5151
Caspian Sea, biogenous elements balance during period of regulated streamflow runoff 80—31073
cave waters, stable isotope geochemistry rel. to climatic change, 230000 to 100000 BP 79—2234
charcoal assimilation into deposits since post-Devonian times 80—51542
charnockites from Sao Paulo State, Brazil 79—44145
chemical speciation of Cd, Cu, Pb and Zn in mixed freshwater, seawater and brine solns. 78—20409
chert, Ce as indication of form. in marine environment 77—37200
cherts, deep sea, stable isotope geochem. 77—5182
Chesapeake Bay, pollution history 79—34445
N.Chilean ignimbrites, REE data and Sr isotopes rel. to petrogenesis 79—44146
classification of radiolarian cherts and siliceous sediments *(French)* 78—96319
clinopyroxenes, in Mesozoic pillow lavas from French Alps, comp. trends, cooling rate effects 77—5154

geochemistry continued
clinopyroxenes from deep-sea basalts, statistical anal. of chemistry 80—41437
coastal marine sediments and seawater, ^{134}Cs, ^{137}Cs, ^{210}Pb, ^{226}Ra and ^{228}Ra concs. determ. 79—88370
coastal zone, particulate U, Pu, and Po in biogeochemistries 79—29787
composite dike, geochemistry of co-existing acidic and basic melts 79—2233
composite dike geochemistry, magmas commingling model for coexisting acidic and basic melts 80—12391
contamination of marine sediments, trace metals from wastewater 79—83643
continent to ocean fluxes of water-soluble K, Ca and Mg, contribs. of atmospheric aerosols 80—72598
continental crust, evolution age and isotope evidence 78—65233
continental crust, heat-producing radioactive elements distrib. and redistrib. 78—65232
continental crust, radioactive elements effects on heat flow-age relation 77—21696
core, chemical differentiation rel. to energetics and geomag. field generation 77—73638
core formation effects, model 78—61368
Cretaceous kimberlites and mantle xenoliths from Southern Africa, Pb and Sr isotopes 77—60372
Cretaceous oceanic crust, isotope study of petrogenesis and hydrothermal alteration 80—46177
Cretaceous-Tertiary boundary event, Os and Ir enrichment of sediments 80—76976
crust and mantle chemical evolution from Early Archaean rocks comp. 78—65222
crustal evolution and sedimentary recycling, evidence from Th and U abundances in sedimentary rocks 80—85654
crustal geological-geophysical zoning possibility 78—57342
crystal settling in upper mantle magmas, high-press. viscosity expts. 77—29291
crystallization at inner core boundary under isochem. conditions, causing changes in dimens., stress and gravit. energy 79—84191
Dalradian metabasaltic rocks, petrochemical affinities 77—5202
Dalradian metabasaltic rocks, petrochemical affinities 77—5203
data bank design and use 77—9508
data management and analysis systems for hydrogeochemical reconnaissance 78—20520
data management and processing 78—57324
deep seismic zone, Tohoku, Japan, freq.-magnitude obs. rel. to geochem. changes 80—72447
deep-sea basalts, He and Xe as measure of magmatic differentiation 80—31040
deep-sea sedimentation, time scales and dynamic models 78—15988
Denchai Basalt, N.Thailand, paleomagnetism, age and geochemistry 80—41421
Derwent Reservoir, N.England, Zn, Cd and Pb in water, sediments and submerged plants 79—25286
diamonds from S.Africa, elemental concs. and Pb and Sr isotopes 79—34775
differentiation history revealed by mid-ocean ridge isotope abundances 80—36277
differentiation of Earth material, as energy source for continental tectonics and seismicity 79—44160
diopsides from kimberlite nodules mantle Nd and Sr composition 80—51363
DSDP interstitial waters, Ca and Mg profiles 77—5177
DSDP Leg 34 basalt, clay mineral form. 79—29767
DSDP Leg 35, Bellingshausen Abyssal Plain, interstitial water profiles and diagenetic reactions 77—5178
DSDP Leg 37 basalts, trace elements and petrogenesis 77—91076
DSDP Leg 37 rocks, O isotope geochemistry 77—91072
Earth's mantle, chemical evolution, nature and timing of mantle's differentiation 80—90043
Earth chemical history, rel. to Moon and parent body of achondrites 77—60639
Earth composition, comparison with Venus 77—29680
Earth crust, chemical balance 77—86831
earthquake prediction, changes in chemical composition, subterranean waters and gases *(Russian)* 79—84163
El Tatio geothermal field waters, N.Chile, isotopic comp. rel. to sources 79—16525
English Channel, actinide concs. and transfer into S.North Sea 79—48519
enstatite, low solubility of Al_2O_3, palaeogeotherm uncertainties 78—65283
environment evolution, available elements during Earth history rel. to life evolution 79—80030
Espanola Formation, Huronian sequence, Canada, carbonate-rich, element abundances 79—92533
estuaries, nontidal, natural and artificial hydrographic and hydrochemical changes 79—29792
estuarine tidal front, trace metal enhancements in biotic and abiotic components 79—2265
feldspar/water O isotope exchange, effect of fluid press. 78—57204
feldspars, superplastic flow and cryst. chemistry changes 79—79831
field configurations, analytical description in terms of differential geometry *(Russian)* 79—74986
Florida, water chemistry and mass transfer in artesian aquifer 78—49057
Floridan Aquifer rocks, dolomitisation 79—53346
fluorite, solubility equilibria in geothermal waters 77—60368
forested watershed Oesling, Luxembourg, chemical erosion 77—81930
formation waters from deep drillings in S.Israel, isotropic comp. 77—86945
forsterite-anorthite assemblage limits, results from peridotite hornfelses 77—5184
fractional crystallisation of periodically refilled magma chamber, geochemical evolution 77—41016
fractionation of Co and Sc versus Fe content for crystalline phases of ultramafic nodules 78—65306
Fraser River (British Columbia) deltaic sediments, heavy metals content 77—33048
Galapagos Rift hydrothermal fluids, chemistry rel. to hydrothermal mounds development 80—51383
Galapagos Rise hot spring field, radionuclides chemistry rel. to clam growth rate determ. 79—84300

geochemistry continued
Galapagos spreading centre, hydrothermal deposits and assoc. basement rocks 79—29750
Galapagos spreading centre, volcanic rock differentiation trends 80—104937
gamma-spectrometric anal. of geochemical samples, data bank system 80—31120
garnet, from Gassetts schist, Vermont, prograde reaction histories from compositional zonation and inclusions 78—36159
garnet and clinopyroxene solid solns., geothermometry based on Fe-Mg distrib. 80—46151
garnet lherzolite, high-press. phase equilibria and Mg^{2+}-Fe^{2+} partitioning among constituent minerals 79—66687
garnet pyroxene equilibria in $CaSiO_3$-$MgSiO_3$-Al_2O_3 system 77—2143
garnets, comp. and zoning rel. to metamorphism temp. and press. 77—2148
garnets from Grassy granodiorite aureole, chemistry and thermal history from fluid inclusion data 80—4012
gas-mineral equilibria and Earth interior chemical model 77—9411
geochemical specimens, energy dispersive X-ray fluoresc. anal. 77—48702
geological samples, trace element characterisation, by instrumental neutron activation anal. 78—73116
geothermal resources, nucl. techniques in geochemical studies 78—85746
geothermal steam samples from Lanzarote (Canary Islands) isotopic comp. 77—49048
geothermal vapour dominated field, Larderello, Italy, gases and H_2O isotopes content of steam 79—74920
geothermal vapour dominated field, Larderello, Italy, noble gas concs. 79—74919
geothermal water-rock association in Massif Central, France, ^{87}Rb-^{87}Sr systematics 77—60373
global processes, sedimentary cycling models 78—16162
Gondwanaland lithosphere, vars. in chemistry from Rb-Sr mantle isochrons 78—28201
granitic magma of Bushveld Complex, trace element abundances rel. to crystallisation history 80—109145
granitoid rocks, Nd-Sr isotopic relationship and continental crust development, chemical approach to orgogenesis 80—94522
granulite xenoliths from Lesotho kimberlites, chemistry rel. to lower continental crust comp. 78—24268
granulitic rock outcropping, trace elements determination by thermal and epithermal neutron activation *(Portuguese)* 80—7874
Great Lakes, sediment chemical composition, anthropogenic loadings 77—37256
groundwater, correction to C isotopic comp. for CO_2 outgassing effects during pH meas. 79—66718
groundwater, Giji and Kian, watersprings in southern Okinawa, Japan *(Japanese)* 79—96783
groundwater, movement of solutes through aqueous fissures in porous rocks 80—94553
groundwater in Hawaiian geothermal areas, compositions 77—64331
groundwater of Milk River aquifer, Alberta, isotope and ion geochemistry 80—8351
groundwater physicochemical characts. vars. around Asama Volcano, Japan, rel. to volcanic activity *(Japanese)* 79—70814
Gulf of Mexico, aromatic hydrocarbons concs. in seawater at proposed deepwater port sites 78—44880
Gulf of St. Lawrence and estuary, geochem. of Zn, Cu and Pb in sediments 78—92855
gypsum, hydration water isotopic comp. rel. to form. and water exchange 79—20829
haematite, reduction to magnetite under natural and laboratory conditions 78—65277
Harp dikes rel. to Helikian geological record in central Labrador 78—61411
Hawaii Geothermal Project, groundwater geochem. study 80—72567
Hawaiian basalt, petrologic data from silicate melt and other inclusions in olivine 77—2146
Hawaiian lavas, contamination evidence from ^{230}Th-^{238}U data 77—5166
heavy metals, distrib. and speciation in aquatic systems, analytical techniques 78—69390
Hepworth carboniferous sediments, Fe minerals and concretions origin 80—17262
high-pressure metamorphism in New Caledonia, phase equilib. in Ouegoa district 78—44811
Holocene soils and soil-geomorphic relations, in semiarid region of S New Mexico 77—78184
hot brines from French Dogger. metastable S species and trace metals 79—62527
hot spring water chemical constituents, Mt. Akagi region (Japan) *(Japanese)* 78—16072
hydrocarbons, light, in Recent Texas continental shelf and slope sediments, origin 79—2213
hydrometeorology, atmospheric contrib. to water systems chemical budget 78—96240
hydrothermal alteration of hot spring deposits 80—76974
hydrothermal Mn in deep sea, scavenging residence time and Mn/^{3}He relationships 78—32121
hydrothermal mounds near Galapagos Rift, chemistry 79—29739
hydrothermal solutions experimentation, new reaction cell 80—41555
hydrothermal system, temp. measurement scale based on chem. comp. of gas fraction 80—98277
Iceland, basalts of Reykjanes Peninsula, Mantle heterogeneity 80—21725
Iceland, Hg natural conc. 77—64244
Iceland, Skagi and western neovolcanic zones, geochemical vars. 78—96171
Iceland high-temperature geothermal systems, aquifer chemistry 78—96245
Icelandic basalts, general mixing eqn. appl. 78—53625
Icelandic rhyolites, generation by melting of plagiogranites in oceanic layer 77—86885
igneous rocks, granitic comp., trace elements appl. to petrogenesis 78—65215
immiscible picritic liquids, Ni partitioning 78—32069
Immiter Gabbroic Complex, Morrocan Atlas Mts., petrography and geochem. 80—41442
Indian Ocean, bottom sediments geochem. studies 79—20808
W.Indian Ocean, mantle uplifted block 79—25228
Indian Ocean, model of evolution rel. to breakup of Gondwanaland 80—41428

geochemistry continued
- Indian Ocean, physicochemical studies of coastal pollution off Bombay 80—104522
- SE.Indian Ridge, seafloor mag. anomalies rel. to chem. of mid-ocean ridge basalt 80—109102
- Indian rivers, chemical and sediment load input into world oceans 79—34870
- intrusive granitoids chem. comp. influence on mag. props. *(Russian)* 78—85535
- ionic diffusion in naturally-occurring aqueous solns., use of activity coeffs. in transition-state models 78—57224
- ionic exchanges at water-sediment interface in Norwegian Sea and Intertropical Atlantic *(French)* 79—62523
- Isla Tortuga volcanics, trace element and $^{87}Sr/^{86}Sr$ characts. 79—66657
- island arc lavas, sources as indicated by Nd and Sr isotopic studies 78—32044
- isotopic equilibrium, regional and local, in mantle, from volcanic rocks comp. 78—65216
- Isukasia, Greenland, C isotope comp. of graphite and carbonate minerals from metamorphosed sediments 78—11896
- Izu Peninsula, Japan, groundwater geochem. in crustal uplift area, rel. to earthquake prediction *(Japanese)* 78—96242
- NE.Japan, Quarternary magmas H_2O contents lateral vars. 79—57899
- Jordan-Dead Sea Rift Valley warm springs, correl. between SiO_2 conc. and orifice temp. 80—41464
- Juan de Fuca-Gorda Ridge area, origin of Fe-Ti rich basalts 77—29242
- Jurassic seafloor, Point Sal, California, rare earth and trace element geochem. 78—32094
- Karroo rhyolites, Swaziland, isotopic evidence of crustal contamination 80—21666
- Kauai shield-building volcanism, age and Hawaiian Island chain volcanism linear migration 80—36281
- Kerguelen igneous rocks, petrology and isotopic geochemistry rel. to continental or oceanic character 79—57924
- Kerguelen Islands igneous rocks origin, role of enriched oceanic mantle sources 80—98319
- KEYBAM interactive computer programs for use with PETROS petrochemical data bank 78—20523
- Kilauea volcano, incrustations and fumarolic condensates 77—29271
- kimberlite and kimberlitic intrusives of SE.Australia, review 80—51392
- kimberlites and garnet lherzolite inclusion minerals, Sm-Nd systematics 80—51397
- Kimmeridgian black shales, N Atlantic region, rare earth elements distrib. 79—44187
- komatiites and high-MgO lavas, origin, crystallisation 78—65312
- komatiitic lavas, Ni partitioning between magma and cryst. phases 77—49061
- La Perouse layered gabbro, Fairweather Range, Alaska, zoned spinel 77—5204
- Lac Seul region, English River Gneiss Belt, petrology, chemistry and metamorphism 77—5199
- Laccadive Sea, chemical oceanography 80—104995
- Laccadive Sea, trace metals concs. 80—104997
- Laccadive Sea waters, total Hg concs. 80—104996
- lacustrine sediments, selective chem. extraction of CO_3^{2-} associated metals 78—65406
- Lake Assal (FTAI), geothermal zone, geochemical and expt. studies 78—69314
- lake chemistry, geology and physics, book 79—44215
- Lake George, New South Wales, water levels, balance and chemistry 79—84332
- Lake Lisan-Dead Sea system, Pleistocene geochemical evolution 78—49047
- Lake Magadi basin (Kenya), hydrochemistry 77—49098
- Lake Michigan, surface microlayer and subsurface element concs. 80—77022
- Lake Monona, Wisconsin, Cu environmental chemistry 79—44214
- lake sediments, E_h meas. reliability conditions 79—48528
- lake studies, isotope techniques appl., advisory group meeting, Vienna (1977 August 29 to September 2) 80—41950
- Larderello field, secondary changes in composition of geothermal fluids 78—69387
- Late Cretaceous granodiorites, Jamaica and Haiti, Greater Antilles, Sr isotope geochemistry 79—57927
- late Precambrian mafic dykes, Montana, geochemistry and Rb-Sr geochronology rel. to Belt tectonics 78—77196
- Lehmann discontinuity, mantle props. beneath continents 80—56425
- Lesser Antilles volcanic island arc 78—7598
- lithosphere, present struct. and struct. evolution *(Russian)* 80—81857
- Loc Uisg granophyre, Isle of Mull, isotopic and chem. evidence for origin 78—65303
- lodestones, oxidation rel. to microstruct. and mag. props. 78—16004
- Lonar Crater, India, chem. study of impact glasses and basalts 79—20836
- Long Island Sound, ^{210}Pb balance 79—20861
- Louvem volcanogenic Cu deposit, Quebec, lithogeochem. anomalies 79—5480
- Lower Palaeozoic carbonate sequence, Arctic Canada, palaeosalinity and dolomitization 79—25241
- Mackenzie, N.W.T., Canada, Devonian-Cambrian stratigraphic differentiation by S isotopes in gypsum 78—61413
- magma, ascending, heat and mass transfer 79—34768
- magma chamber, fluid dynamics model of differentiation and layering 80—76939
- magma mixing at mid-ocean ridges, DSDP data 78—77209
- magma mixing at mid-ocean ridges, evidence from Mid Atlantic Ridge basalts 79—88335
- magma series erupted in different marine tectonic settings, trace element anal. 80—21667
- magmas, influence of volatile components 80—41418
- magmas, thermal history, low press. reference point 78—65244
- magmatic differentiation models, computer program for interactive testing 79—2377
- magmatic rocks, anchieutectic comp. 80—12381
- magnetic spherules in marine sediments, K and Ca isotopic comps. 79—44423
- Malartic Group, Abitibi, Archaean volcanism, petrography and geochemistry of lavas 80—17258
- Manicouagan impact melt, Quebec, chemical interrelationships with basement rel. to form. processes 78—81165

geochemistry continued
- mantle, evolution rel. to Earth comp. and Archaean mantle chemical heterogeneity 78—11844
- mantle, lithophile elements depletion rel. to continental crust comp. and nature of lower crust 80—94498
- mantle, mineralogy and chemistry above 1000 km 77—33015
- mantle, $NaAlSiO_4$ Ca ferrite isotype as Na host phase 77—64270
- mantle and crust chemical evolution, mean age of reservoirs 80—51359
- mantle chemical heterogeneity, evidence, conf., Nov. 1978, London 80—85623
- mantle chemical stratification 80—21687
- mantle closed geochemical systems, effects of finite deformation during fluid flow 79—92519
- mantle differentiation and crustal growth, geochem. model 80—21684
- mantle evolution, implications from Sm-Nd isotopic investigations of Isua supracrustals 78—36129
- mantle fluid comp. buffered by carbonates in peridotite-CO_2-H_2O 77—70644
- mantle Nd and Sr isotopes, differentiation occurring in episodes 80—67352
- mantle peridotite, petrogenetic grid, extension from siliceous dolomites 77—5137
- mantle xenoliths, equilibrated Nd and unequilibrated Sr isotopic comp. meas. 80—98321
- marble in Pikikiruna Range karst, solution processes 79—74906
- Marda calc-alkaline suite, rare earth elements, Archean geochem. analogue of Andean-type volcanism 78—11898
- marine environment of Straits of Malacca, radioactivity 79—12135
- marine mineral suspensates and geochemical exploration 78—88936
- marine plankton, C isotope ratio rel. to surface water masses 79—29783
- marine sediments, methane prod. and consumption rel. to conc. profiles meas. 80—12373
- marine sediments diffusion coefficients determ., resistivity techniques validity 79—92601
- marine sediments from W Indian coast, geochem. of Th and daughter products 77—41019
- marine sediments interstitial solns. comp. and diagenesis, seawater-sediment interface fluxes 80—3988
- marine sediments interstitial waters, dissolved organic matter nature and reactions 78—49039
- Massif Central hot springs, France, alkaline earth ions acquisition, rel. to geothermometry *(French)* 79—29788
- E.Mediterranean Sea, T and O_2 profiles 80—17298
- Mesozoic tholeiites from Antarctica, ^{40}Ar redistrib. rel. to $^{40}Ar/^{39}Ar$ age spectra 77—49047
- Mesozoic volcano-tectonic rift zone and back-arc basin development, South America 79—29762
- metabasalt block from Mid Atlantic Ridge, metamorphic mineral data 77—64279
- metabasalts from Point Sal ophiolite, California, rare earth and trace element geochemistry 78—32092
- lower metadiabase from Michigan Basin basement, chemical changes during metamorphism 80—4009
- metal enrichment of sediments, partitioning of metals, Ranafjord N. Norway 79—83641
- metal-rich deposits at ocean ridge crests, form. 80—41430
- metalliferous sediment components, microprobe study 79—34792
- metallogenesis along fossil oceanic fracture zone Arakapas fault belt, Troodos Massif, Cyprus 79—29769
- metamorphism, bathozones and bathograds as measure of regional scale post-metamorphic uplift 78—81113
- metamorphism, rate laws 79—16467
- metavolcanic rocks, Montauban-Les-Mines, Quebec, geochem., mineralization 78—36161
- micaceous kimberlites, micas chemistry 79—16465
- Michigan Basin deep hole metagabbro, mineralogy and geochemistry compared to seawater hydrothermal alteration 79—39710
- microtektites, chemical comparison of bottle-green and normal microtektites and tektites 77—82179
- Mid-Atlantic Ridge basalts, geochem. variation along length of ridge 80—90027
- Mid-Cayman Rise spreading centre, basalt glasses geochemical var. and petrogenesis 80—101364
- mid-ocean ridge basalts, composition restrictions 80—90025
- mid-ocean ridge basalts, density var. rel. to magma mixing and primitive lavas scarcity 80—56460
- midocean ridge basalts, source evolution from Bay of Islands ophiolite complex Nd and Sr isotopic study 80—85651
- mineral, dissolution under Earth surface conditions, rate control 79—20817
- mineralogy and petrology of French Western Alps, rel. to Alpine metamorphism 78—36157
- minerals, magnetic trends on alkali-Fe-Mg diagrams 78—85551
- minerals, metal-rich deposits in oceanic lithosphere, origin 78—53634
- minerals, weathering profile evolution simulation by aq. soln. *(French)* 77—60438
- minettes, REE and trace element contents and origin 79—74864
- Mistastin Lake crater, Labrador, Sr isotopes and trace element geochem. of impact melt 78—32105
- mixing models for geothermal systems and chemical geothermometers 78—69503
- mud volcanoes, Copper River Basin, Alaska, composition of emitted gases 79—84308
- muscovite in medium to high grade metapelites of NW.Maine, comp. var. 79—62493
- Nasu zone, NE.Japan, trace element vars. in volcanic rocks 79—88317
- natural waters, radiotracer methods for speciation study 79—88490
- natural waters, U content meas. technique 78—85705
- neutron activation anal., geochem. of genesis of ore deposits *(German)* 80—30301
- neutron activation anal. technique for Na/K ratios in fluid inclusions determ. 78—61568
- New Hebrides, geochemisty and origin of Quaternary volcanism 78—20375
- Newfoundland, Hercynian activity from geochemical data 77—29263
- NW.Nigeria, calc-alkaline volcanics and possible Pan-African suture zone 78—32086
- N.North Sea, actinide activities in inflowing water 79—16520
- Norwegian Sea pycnocline, T vertical distrib. rel. to apparent vertical eddy diffusion rates 78—81185

geochemistry continued
Nova Scotia southern plutons, geochemistry of tonalitic and granitic rocks 77—49064
nucleon stability, geochem. test independ. of decay mode 78—8667
nucleon stability testing, radiochemical and geochemical method limits 79—22093
obsidian, hydration 79—8629
ocean, confusion of mathematical notation for element residence times 77—86937
ocean, Fe removal mechanism in estuaries 78—20437
ocean, multiple components transport through thermohaline diffusive interfaces 80—12396
ocean basalt-seawater reactions chemical exchange, Fe, Mn, and S species results 80—17294
ocean chemistry, photopeak processing method for gamma-spectra *(Russian)* 77—60487
ocean chemistry, role of ridge crest hot springs 80—98304
ocean floor basalts and ferromanganese deposits, Pb, Nd and Sr isotope comp. 78—61395
ocean floor spilites, seawater/basalt ratio effects on chem. and mineralogy 78—92819
ocean major and minor elements balances, role of ridge crest hydrothermal activity from Galapagos data 80—41459
ocean N cycle, implications of N_2O meas. in tropical E.Pacific Ocean 80—94542
ocean phosphate budget, P accumulation rates in metalliferous sediments on E.Pacific Rise 77—60364
ocean ridge basalts, trace elements, rel. to mantle comp. 78—65219
oceanic basalts, differential Sm/Nd evolution 78—61391
oceanic basalts, hydrothermal alteration by seawater at high temp. 78—69327
oceanic basalts, titanomagnetites low-temp. oxidation rel. to mag. anomalies statistical anal. 80—36233
oceanic basalts, trace element mobility during hydrothermal alteration 78—69328
oceanic crust, automated X-ray spectrometer appl. 79—16711
oceanic crust, geochem. rel. to seafloor spreading mag. anomalies 80—56345
oceanic crust layer 2, low-temp. seawater-basalt interaction rel. to S distrib. 80—41432
oceanic crustal layer 2, oxidation rel. to magnetisation 77—91071
oceanic layer 2 basalts, DSDP Leg 37, low-temp. fluid lateration 77—91102
oceanic phosphorites, Fe, Ti and Al behaviour during initial form. stages 80—31029
oceanic suspended matter, trace metal chemistry, atmospheric input 79—44199
oceanic upper mantle, depletion by partial melting rel. to Owen fracture zone ultramafics petrology 80—94519
oceans, ^{226}Ra flux from estuarine and continental shelf sediments 78—32061
oceans, origin of Cl and Br 78—65342
oil and gas exploration, information content of geochem. parameters *(Russian)* 79—39957
oil shales of Green River, USA, thermal decomposition rel. to elec. cond. obs. 80—104495
oilfield brines from Kansas and Colorado, Sr isotopic comp. 78—57225
Oklo natural fission reactors geological environment, tectonic anal., petrography, geochemistry *(French)* 80—21742
Oklo natural reactor, rare earth elements behaviour 78—49019
olivine, point-defect chemistry, effect of enstatite activity and O_2 partial pressure 78—40549
olivine-sulphide assemblages, metamorphosed, from W. Australia, Fe/Ni partition 77—5185
olivine/liquid distrib. coeffs. and test for crystal-liquid equilib. 77—81889
Omo River project (Ethiopia) data management system appraisal 78—57326
Ontario Precambrian diabase dike, trace element geochemistry 78—61414
ophiolite petrogenesis in oceanic crust, Nd and Sr isotope study 80—61782
ophiolite suite, Bay of Islands, Newfoundland, petrology and geochem. 80—21726
ophiolites, geochemistry rel. to tectonic regimes of genesis 79—57898
ophiolitic sulphide deposits in Cyprue, ^{87}Sr enrichment confirms ore form. by circulating seawater 77—81887
Upper Ordovician volcanics, geochemistry and tectonics in E. and SE.Ireland 79—44144
ore prospecting, and mining research, examples of mineralogy contrib. *(French)* 79—5475
ore-deposition through geological time, review 78—77235
organic geochemistry and post-glacial palaeo-oceanography of Emerald Basin, Nova Scotia 77—5218
orogenic lherzolite petrogenesis in oceanic crust, Nd and Sr isotope study 80—61782
oxide minerals in Turnagain ultramafic complex, NW. British Columbia 79—84247
Pacific Ocean, Cd distrib. in bottom sediments surface layer 79—20809
Pacific Ocean, T transport models source function 78—32122
N Pacific Ocean waters, densities rel. to comp. and eqn. of state 78—73391
Pacific Ocean waters, nitrate N distrib. 80—31065
E.Pacific Rise, hydrothermal vents on seabed issuing H_2 and methane 80—41422
E.Pacific Rise geothermal system, limits on geothermal fluid temp. rel. to metal transport and sulphides deposition 80—101362
palaeoenvironmental conditions of sedimentation, organic geochemical indicators 78—40539
Palaeozoic granitoid plutons from contrasting tectonic zones, NE. Newfoundland, geochem. 78—57201
pegmatite ores in Tanco mine area, SE.Manitoba, in Canada, geochemical exploration 79—48577
pelitic sediments, Sr and Ar isotopic homogenisation during low grade regional metamorphism 79—62511
peralkaline rhyolites, assoc. with andesitic arcs of SW.Pacific 78—32043
Perch Lake Basin, Ontario, hydrological and geochemical studies conference, Chalk River, 1978 April 25 to 26 80—51955
peridotite, equilibration conditions in upper mantle 77—2130
peridotite, from upper mantle, rare earth fractionation patterns in partial melts 77—37198

geochemistry continued
Peru-Chile Trench basalts, fractionation and mantle heterogeneity 78—53626
PETPAK, computing package for petrologists 78—57323
petrogenesis of xenolith-bearing basalts from S.E. Arizona 80—8303
petrogenetic mixing models and Nd-Sr isotopic patterns 80—3965
petroleum generation in SW block of Los Angeles Basin, rel. to thermal subsidence 80—3967
petrology rel. to extreme metamorphism, symposium (Sydney, August 1976) 78—44821
phenocrysts and megacrysts in basalts of Pinacate volcanic field, textures and genesis 77—81881
phosphatic nodule beds in Victoria, geochemistry and rel. to late Miocene-Pliocene eustatic event 79—12105
phosphorites from Spanish continental margin, geochemistry and mineralogy *(French)* 78—65258
plagioclase, zoned, of different magmatic environments, preliminary ion-microprobe anal. 79—34815
plagioclase fractionation in igneous rocks, influence of augite 80—12390
plagioclase-garnet-Al_2SiO_5-quartz assemblage, pot. geobarometer-geothermometer 77—2147
plateau lavas from S.America, Nd and Sr isotope data 79—29726
Pliny Range, New Hampshire, intrusive complex, mineralogy and petrology 78—36158
plutonic granitic rocks, O and H isotope comps. 78—65221
polar desert pond, dynamic chemical equilib., as sensitive index of meteorological cycles 80—12441
potassic igneous rocks from Roccamonfina volcano, Roman comagmatic region, Italy,, O isotope geochemistry 80—41420
prebiological compounds, form. in volcanic processes 78—40667
Precambrian basement of W.Canada, Hg and As distrib. and abundance 80—56419
Precambrian Fe formations, rare earth elements evidence for changing oxidation states 77—64284
Precambrian solution photochemistry, inverse segregation, and banded iron formations 79—20863
primitive Earth, volcanic processes role in organic compounds evolution 78—32230
prospecting, effectiveness of geophysical and geochemical methods, evaluation *(Spanish)* 77—9552
prospecting, induced polarisation method, in situ soln. chemistry effects 78—3964
Proterozoic iron-formation, Labrador Trough, Canada, regional metamorphism rel. to mineralogy and chemistry 79—57916
Proterozoic low-potash, high Fe charnockitic Tromoy gneisses, chemistry and origin 77—86882
proton activiation analysis of B and Li local levels in minerals, rocks and ores 79—74477
pyroxene geotherms, thermodynamics 78—65282
pyroxenes in $CaO-MgO-Al_2O_3-SiO_2$ system, subsolidus phase relations rel. to geothermometry and geobarometry 79—16440
quantitative ion-microprobe analysis, geochem. appls. 79—34976
radioactive elements, migration rel. to Earth interior convective stability 77—9381
radioactive waste, geochemical aspects of radionuclide migration from waste repositories 80—13711
radioactive waste, geological disposal, chemical factors controlling environmental actinide sorption 80—13713
radioactive waste, geological storage, experience gained at Oklo natural fission reactors 80—21773
radionuclide disposal, GARD computer program for geochemical assessment 79—31068
rainwater over India, during summer monsoon, sea salt desposition 79—53473
rare earth element, abundances in layered Komatiite lava flow, Ontario, Canada 79—29764
rare earth elements, partitioning between hydrous silicate melt, amphibole and garnet peridotite 79—20775
rare earth geochemistry and mineralogy, book contrib. 80—46157
rare earth geochemistry of Late Cainozoic alkaline lavas from Antarctica 77—41030
rare gases in volcanic rocks, isotopes mass fractionation as indicator of gas transport to or from magma 80—98292
Red Sea brine, thiocyanate detect. and implications 79—57975
Red Sea brines origin, new isotopic evidence 78—96236
Red Sea geothermal system, ore transport and deposition 78—32096
resource potential, geochemical surveys of large areas in USA and Alaska 79—30924
rhyolitic ignimbrites origin, Batopilas area, Mexico, Sr isotope study 80—94501
River Main, County Antrim, N and P loads meas. by discrete and intensive sampling 79—44213
rivers, dissolved Fe, Mn, organic matter, estuarine mixing implications 80—17296
rivers, dissolved humic acids and Fe removal during estuarine mixing 79—34830
rivers, evidence for higher natural U content 79—44208
Roccamonfina volcano caldera wall, petrochem. of pumiceous layers *(Italian)* 77—49051
rock, assay-activation analysis, use of Au and Ag standards based on phenol formaldehyde resin 78—3419
rock magnetism, comparative anal. of chemical and thermoremanent magnetisation 77—81870
rock melts, prediction of major element mineral/melt equilibria 80—109125
rock samples, Sn determ. by neutron activation method 78—85258
rocks, ancient metamorphic, appl. of geophysical and geochemical data combined anal. *(Russian)* 79—8630
rocks, rare earth elements determination, neutron activation analysis, optimum method 79—88491
rocks, Sc determination by neutron activation analysis using ^{46m}Sc 79—79356
rocks and minerals, rare earth elements determ. by neutron activation analysis 79—88492
Roosevelt Hot Springs thermal area, Utah 79—84260
Roosevelt Hot Springs thermal area, Utah hydrothermal alteration prod. minerals, mass abundance 80—90008
Sabaloka Igneous Complex, Sudan, petrography and chem. analyses 78—32097
Saguenay Fjord, suspended particulate matter geochemistry 78—92852

geochemistry continued
Saguenay fjord sediments, distrib. and partition of Co, Ni, Cr and V 77−33100
salt deposits, Upper Traissic, of N.Atlantic region, lateral fractionation model for comp. var. 80−94516
sandstones of Southland syncline, New Zealand, zeolite facies alteration and geochemistry 78−32084
Saskatchewan and Manitoba, Boundary intrusions petrogenesis 77−66914
Scandinavian rocks, giant and dwarf haloes geochemistry rel. to unknown radioactivity 78−81157
E.Scotia Sea, back-arc basin, volatiles in submarine volcanic rock 80−67353
Scotia Sea Island arc and back arc tholeiites, geochemical study 78−11872
NW Scotland Tertiary continental volcanics, Nd and Sr isotope evidence for crustal contamination 79−66693
sea ice chemistry 79−12128
Sea of Okhotsk, water-soluble gases conc. meas. 79−2291
sea-floor basalt, rare earth elements behavior during weathering 79−57910
seashells, B loss during weathering rel. to palaeosalinity determ. 77−78204
seawater, electrochemical potential of pure metals *(Chinese)* 80−31062
seawater, hydrochemical characts. distrib. rel. to transparency 80−31057
seawater, organic chemistry of particulate matter 78−65344
seawater, radioactivity, and salinity changes with advection of water masses *(Russian)* 78−77275
secondary minerals in basaltic rocks from DSDP Leg 37, geochemistry 77−91127
sediment-water interface, chemical exchange 79−5505
sedimentary organic matter, subaerial weathering effects 78−57206
sediments, environments and processes involving an aqueous phase 77−86888
sediments, H_2S contaminated, stagnation coeff. and appl. in palaeogeographic reconstruction 80−36291
sediments, Recent unconsolidated lacustrine, organic geochemical analysis 78−49016
sediments from NW.Atlantic Ocean, sterol geochemistry 79−74885
SELLO, FORTRAN IV program for skewed distributions for normality transform 77−9502
serpentinisation, modern low temp., in New Caledonia, Oman and Yugoslavia 78−69344
Severn estuary, seasonal and spring neap tidal depend. of axial dispersion coeffs. 80−94534
shelf sediments off Bombay, geochem. study 79−48449
E. Sicily, genetic implications of isotope and trace element variations 78−11893
Silica Springs, New Zealand, spring water and alumino-silicate deposit anal. 78−32124
silicate content of anoxic pore waters, effects of oxidation during sampling 78−61394
silicate liquids high-temp. props., rel. to basic magma equilib. and ascent 77−86868
silicate rocks, chem. denudation rates in tropical catchments 78−73414
silicate rocks, X-ray spectral fluoresc. anal. 78−3762
silicate-K-(Fe-S liquid) equilibria and K solubility, in Fe-S liq., planetary implications 78−11843
silicic volcanics, Jurassic, from Nevada, USA, thermochemical remanent magnetisation 80−98310
sillimanite-andalusite-kyanite (Al_2SiO_5 polymorphs) thermal expansion and high-temp. cryst. chemistry 80−39319
silt-clay, physicochemical processes saturated gouge 78−40547
Singhbhum thrust belt (India), radioactive elements content rel. to heat flow 77−49050
Siqueiros transform fault and East Pacific Rise, basalt petrology and chemistry 77−33050
E.Sivash waters, ^{90}Sr content and salinity vars. *(Russian)* 78−77282
Skaergard intrusion, E.Greenland, Sr, Pb, O isotopic anal. 79−29763
soil, U and Ac series nuclides radioactive disequilibrium 80−4014
soil Al leaching response to acid precip., effects on high-elevation watersheds in NE. United States 80−12442
soil convective-dispersive solute transport with combined equilib. and kinetic adsorption model 77−64356
soil development models and slope models 77−81933
soil pollution elemental deposition downwind of coal-fired power plant 79−20838
soil potential as natural sink for atm. N_2O 77−21772
soil weathering, geochemical study and elemental redistrib. 78−7634
soils, multielement determ. by computerised instrumental neutron activation anal. 77−44546
Sokoman Fe Formation, trace element geochemistry 77−81884
South Africa, kimberlites, rare gases in phlogopite and phlogopite bearing nodules 78−11894
spark source mass spectrography, geochemical appl., element sensitivity, precision and accuracy 78−20544
speleothems, stable isotope geochemistry rel. to climatic change, 230000 to 100000 BP 79−2234
sphalerite, FeS content as geobarometer, experimental extension to 10 kbar 78−85703
spilite and keratophyre from Permo-Triassic volcanic arc terrane, Oregon-Idaho, petrogenesis 79−20826
spilitic rocks, rare earth element mobility and geochem. charact. 77−86887
spilitic rocks from Michigan Basin deep drill hole, petrology 79−39711
spinel lherzolite nodules from Pleistocene cinder cone, upper mantle origin 78−65299
spinel lherzolite xenoliths, implications of texture composition depend. 79−25244
spring water chemistry determ., Teels Marsh, W.Nevada 77−9455
Sr isotopic equilibration, soln. to paradox 77−41026
stable isotope abundances in natural compounds, meas. standards 78−32246
Stillwater complex, USA gabbro Sm/Nd age and mantle evolution curve of Nd 80−41410
streams, chem., hydrological, thermal characts., Haney, British Columbia 80−8350
submarine basalts, sea water weathering effect on K-Ar age 77−86830
submarine lithosphere, geophys., geochem. and petrological model 80−3994

geochemistry continued
submarine pillow balsalts, mag. minerals oxidation rel. to geomag. palaeointensities determ. 80−3927
submarine pillow basalts, abundance and distrib. of H_2O, C and S in glassy rims 79−12111
subsurface water chemistry study, coring and squeezing technique 78−57332
Sudbury dykes, Grenville Front region, palaeomag., petrochem., K-Ar ages 78−7633
sulphate deposits, stable isotopic comp. and early Archaean origins 79−20832
sulphide deposits from E.Pacific Rise near 21°N, mineralogy and geochemistry 80−101361
sulphide minerals in Mid-Atlantic Ridge drill core, comp. 77−91122
sulphide ores, disseminated, electrochemical model of induced-polarisation phenomena 79−92526
sulphides and sulphates from DSDP Leg 37, geochemistry rel. to S isotope comp. 77−91101
surface water chemistry and weathering processes, Absaroka Mts., Wyoming 78−32125
surface water on granite, dissolved elements and Al solubility *(French)* 77−41029
suspended sediments of Amazon river, reaction with seawater, cation exchange characts. 80−8337
Susquehanna River system, heavy metals behaviour, use of ^{210}Pb tracer 78−49046
synthetic phlogopite, Fe content as function of growth rate 78−32089
Tanzawa plutonic complex, Japan K, Rb, Sr in granitic and gabbroic rocks 77−17100
tetraalkyllead in air, natural source 79−2367
thermal fluids of Abano region, N.Italy, sources, circulation paths and geochemistry 79−20883
thermobarogeochemistry of inclusions *(Russian)* 80−104954
tholeiitic basalts, rare earth elements behaviour during submarine weathering 78−73369
tholeiitic basalts from Japan, geochemical types 78−96206
Tilting Harbour igneous complex, Fogo Island, Newfoundland, petrology 78−77230
trace element behaviour in magmatic processes, quantitative models 78−65214
trace element geochem. of peridotite-gabbro-basalt suite, DSDP Leg 37 site 79−34793
trace element meas. by neutron activation and atomic absorption methods *(French)* 77−41238
trace element separations, possible diffusional effects 77−41008
trace elements partition patterns in sediments from DSDP Site 219 78−36143
transitional basalts and tholeiites from E.Pacific Rise at 9°N 79−84218
transparency at 30 m depth in tropical Atlantic *(Russian)* 77−64307
Troodos ophiolitic complex, major oxide geochemistry and origin 80−98317
tschermakitic clinopyroxenes, mixing props. 77−2149
Tuscany hot springs, geochemical and isotopic abundances rel. to geothermal areas location 77−49049
Tyrrhenian Sea, oceanic floor basalts 79−53329
ultramafic inclusions, petrogenesis, geochem. and petrologic data 78−65301
ultramafic rocks, geochemistry rel. to mantle thermal gradients estimation 77−5138
ultramafic xenolith petrology and upper mantle processes, Kapfenstein, Austria 80−76973
ultramafic xenoliths/basanite magma reaction in Tahiti lava, implications for magma crystallisation 80−90086
ultrametamorphism and granitoid genesis 78−44808
undifferentiated Earth, chemical reactions thermal effects 79−25218
upper mantle, diffusion of Ca, Sr, Ba and Co in basalt melt 78−28223
Urach region, Germany, geochemical obs. rel. to temp. field investigation at great depths 79−48440
uraninite in Oklo natural fission reactors, geochemistry of insoluble organic material *(French)* 80−21748
US Geological Survey RASS-STATPAC system for mangement and statistical reduction of geochemical data 78−20522
Vellar estuary, Fe precipitation, conc. determ. 80−77015
volcanic material alteration in marine sediments, SE.Pacific Ocean 80−3990
volcanic rocks, altered, at Matagami, Quebec, geochemistry and geothermal model for massive sulphide genesis 78−77231
volcanic rocks, relation between major element chemistry and tectonic environment 78−16006
volcanic rocks, Tetagouche Group, Canada, geochem. rel. to origin 78−65298
volcanic rocks, W abundances 79−16468
volcanic rocks classification using Irvine and Baragar classification scheme, FORTRAN IV program 78−57203
volcanic rocks evolution in island arc, batch fractionation model, example from Japan 79−34818
volcanics from Archaean Prince Albert Group, Melville Peninsula, N.W.T. 79−53324
volcanosedimentary levels, S.Pacific, neoformation and weathering *(French)* 78−73353
Vulcano Island neighbourhood, heritage and neoformation in volcanic and hydrothermal sediments *(French)* 79−62482
Wabigoon belt, NW.Ontario, felsic rock geochronology and geochemistry 80−31004
Wairakei thermal region, thermal water transport of major rock constituents 77−81844
water and magmas, appl. of Gibbs-Duhem eqn. 78−57205
water from geothermal wells at geothermal well water, chemical analyses 80−90104
water-rock partition coefficients, correl. with seawater and river water comp. 79−44200
waters from high altitude region north of Jolma Longma mountain, geochem. characts. of isotopic distrib. *(Chinese)* 79−2304
watershed geochemistry, aqueous solns. control by soil materials 78−20445
Willyama Complex, New South Wales, cyclic reactions between andalusite, sericite and sillimanite 80−26508
X-ray radiometric methods applic. in geochem. haloes analysis 77−53231
Yellowknife, Northwest Territories, Canada, Archaean granite, rare earth and trace element data 80−4007

geochemistry continued
Zhamanshin impact structure, USSR, impact glass chemically similar to tektites 80−51358
zone regining below lithospheric plates, steady state astheriosphere model 79−88326
zoned steady-state magma chamber comp. var., evidence from Mid Atlantic Ridge 79−88336
Al$_2$O$_3$, solubility in orthopyroxenes in spinel and plagioclase peridotites and spinel pyroxenite 77−5186
^{241}Am from nuclear weapons testing, evidence for delayed fallout from concs. in ocean sediments 80−98303
Ar depletion on Alpine fault, New Zealand, rel. to frictional metamorphism and tectonic stress 80−41440
^{40}Ar, excess, in Alpine biotites, evolution from ^{40}Ar-^{39}Ar anal. 80−94521
^{40}Ar excesses in igneous minerals, identification by ^{40}Ar/^{39}Ar age spectrum technique 77−5152
^{40}Ar/^{36}AV in Devonian atmosphere, isotopic ratio from Rhynie chert 77−66917
As, inorganic, in freshwater environment, stability and solubility theoretical aspects 79−16553
As, migration capacity, effect of acid-alkaline conditions on hydrogeochem. 77−37244
B abundance determ. in rocks, soils, plants, waters and fertilisers 78−85559
B, content in bottom sediments interstitial waters on trans-Pacific profile 80−36289
B, inorganic, in St. Lawrence Estuary, determ. *(French)* 78−77274
Ba, non-conservative behaviour during mixing of Mississippi River and Gulf of Mexico waters 78−32120
^{10}Be geochemistry in North Pacific during Pliocene 80−101356
^{10}Be in 1000 and 5000 yr old Antarctic ice, meas. 79−2305
C cycle, atmosphere response to deep-sea injections of fossil-fuel CO$_2$ 80−31090
C isotope geochemistry of small groundwater system, NE. Ontario 79−84324
C, mass transfer and isotope evolution in natural water systems 79−20882
CO$_2$ content of ocean water, gradual increase 79−29786
CO$_2$ in upper mantle, fugacity at high temps. and press. from decarbonation reactions 79−16439
CO$_3^{2-}$ chemistry of groundwater from tropical tower karst, S.Thailand 79−79906
C0$_2$ solution in ocean surface waters, role of homogeneous buffer factor 80−21783
^{13}C, Isua sediments, W.Greenland, isotope averages and Archaean C and O cycles 79−84262
^{14}C, concs. in Florida annual coral rings 79−16513
Ca excess in snow and rain samples, Japan, from calcite source 79−39766
Ca, isotope fractionation on Earth and other solar system materials 79−20835
Ca^{2+} in seawater 80−31064
Ca-rich clinopyroxenes, intracrystalline Fe^{2+}-Mg equilibria 77−2145
CaCO$_3$ dissolution rates in deep ocean, in situ expt. in N.Atlantic 79−34853
Ca$_2$HPO$_4$SO$_4$.4H$_2$O, synthetic, cryst. struct. and relation to brushite and gypsum 78−83785
CaO, solid, phase transition at high-press., lower mantle implications 80−79876
CaO-Al$_2$O$_3$-SiO$_2$-H$_2$O system, margarite stability and compatibility relations 77−5183
Cd determination in sedimentary rocks and stream sediments 78−36170
Cl, Br, degassing by volcanism along Reykjanes Ridge and Iceland 78−36136
Cl$^-$ diffusion in marine sediments, hydrostatic press. effect, in situ expt. 78−44878
Cr content of magnetite from Bushveld Complex upper zone, vars. rel. to magma chambers heterogeneity 80−56421
Cr-rich pyroxenes of peridotite xenoliths, Nevada, comp. rel. to formation press. and temps. 77−5139
Cu, inorganic speciation in estuarine environments 78−69371
Cu-Ni enriched ferromanganese nodules and crusts from Bauer Basin, mineralogy and chemistry 77−86851
D/H ratios of natural serpentines, rel. D/H fractionation factors between serpentine and water at 100-500°C 79−34803
F, outgassing from basalts of Iceland and Reykjanes Ridge 79−57900
Fe, characterisation in environmental samples by Mossbauer technique 79−66433
Fe containing minerals, basalt rocks, Mossbauer spectroscopy identification 80−8302
Fe diagenesis in sulphide-rich sediment core, Mossbauer spectral studies 79−74917
Fe-Mn deposits on abyssal sea floor, geochem. 79−12107
Fe-Mn nodules from Pacific Ocean, sorption processes 79−16435
Ge/Si and Ga/Al ratios vars. along Reykjanes Ridge and Iceland 79−8617
Ge-Si and Ga-Al fractionation in Hawaiian volcanic rocks 79−12112
H isotope exchange between clay minerals and seawater 78−69329
H$_2$O, concs. in hypersthenic magmas rel. to juvenile outgassing and transport 80−72507
He in Earth interior, incorporated from immature Sun *(Russian)* 80−81856
He spots caused by diapiric magma from upper mantle, Matsushiro fault zone, Japan 79−8618
Hg, average content of oceans and European air, soil, and river sediments 79−8687
Hq, abundance in Greenland Ice Sheet 78−65349
I and Br geochem. behaviour in recent sediments from Namibian shelf 78−32062
K deficiency of ocean ridge silicic rocks, by vap. phase transport 80−81877
Li in Keweenawan rhyolites, anomalous abundance 79−84252
Li, needs and resources, conf., Corning, USA (Oct. 1977) 79−48473
Li, occurrence in flint clay and related rock types in United States, preliminary survey 79−48475
Li ores in Horse Spring Formation Miocene rocks, Clark County, Nevada, report 79−48474
Li, ores in United Kingdom, brief assessment 79−48476
Li rich brines in SW.Bolivia, chemical composition and distribution 79−48479
Li rich pegmatites, petrogenesis 79−57918

geochemistry continued
Mg mass balance in continental runoff 79−34859
Mg removal from interstitial waters in reducing environments 79−66673
Mn deposition and nodule growth in Jervis Inlet, British Columbia, effect of sediment-water exchange 78−96187
Mn, dissolved, in river water, rapid precip. rel. to estuarine Mn distribs. 79−62516
Mn, distrib. in Pacific Ocean 80−56494
Mn nodules, deep-sea, diffusion-controlled growth model 79−2212
Mn nodules, deep-sea, Ni and Cu accumulation as essential elements in 10-Å manganite 79−66674
Mn nodules, mineralogy and comp. changes from long-term seafloor mineral exposure expts. 79−5471
Mn nodules, oceanic, Th chemistry rel. to U series dating 77−29280
Mn nodules from N equatorial Pacific, post-depositional internal metal enrichment processes 79−34791
Na-selective electrodes in marine geochemical studies 79−12312
Nd and Sr geochemistry of volcanic rocks, Grenada, Lesser Antilles 80−21724
Nd, Sr isotope geochemistry of hydrous mantle nodules and host alkali basalts, rel. to mantle heterogeneities 80−56420
Nd-Sr isotopic correlation in mantle materials, geodynamic consequences 79−92512
O, in palaeoaquatic environment 78−44879
O isotope fractionation in decarbonation metamorphism, Mottled Zone Event 78−65307
O isotope geochemistry of cherts from South Africa 79−34820
O isotope stratigraphy and Late Pleistocene coral terraces in Barbados 77−78182
O isotopes in dissolved sulphate and water from hot springs and drill holes, reservoir temp. indicators 78−69382
δ^{18}O scales, proportional vars., interlaboratory comparison 78−69326
^{17}O+^{16}O, fractionation by chemical equilib. 80−89513
^{18}O+^{16}O, fractionation by chemical equilib. 80−89513
O$_2$ self-diffusion in feldspars, ion microprobe determ. 78−69325
^{18}O composition of metamorphosed chert and Fe formation from W.Greenland 78−81155
^{18}O distrib. among mineral triplets in igneous and metamorphic rocks 78−32071
^{18}O, Isua sediments, W.Greenland, isotope averages and Archaean C and O cycles 79−84262
P, atmosphere contrib. to aquatic system 79−100545
P determination in surface fresh waters, automated procedure 80−81517
P transport in sandy soils, expt. and simulation 77−66940
PO$_4^{3-}$ adsorption equilibria in lake sediments 79−66354
Pb in environment 79−34443
Pb-Zn occurrences, carbonate-hosted, in NE British Columbia, mineralisation processes 79−62494
^{206}Pb/^{204}Pb evolution during crust development, rel. to U, Th and Pb fractionation 79−57879
Pu, in Irish Sea, oxidation state 79−16516
Pu isotopes, in soil, determination using alpha-spectrometry 80−45601
^{241}Pu from nuclear weapons testing, evidence for delayed fallout from concs. in ocean sediments 80−98303
Ra monitoring for earthquake prediction *(Japanese)* 78−28181
^{226}Ra, behaviour in Pee Dee River−Winyah Bay estuary, S.Carolina 80−98360
^{226}Ra leaching from contaminated soils, investigation of Ra bearing soils from Port Hope, Ontario 79−20900
Rb-Sr isotopic systems, geologically meaningless total rock isochron prod. by secondary alteration 80−31014
^{87}Rb/^{87}Sr studies of waters in geothermal area, Cantal, France 78−61443
Re-Os geochemistry, rel. to use of Os isotopes as petrogenetic and geological tracers 80−89989
Rn concentration in underground waters from landslide zone, Narao district, Japan 78−11918
^{222}Rn in Hudson River estuary, distrib. and transport across sediment-water interface 78−16064
Ru determ. in silicate rocks, preseparation procedure for neutron activation anal. 77−44547
S cycle, sources in rain collected below wheat canopy 77−56698
S cycle of NE United States, role of man-made S sources 80−26178
S isotope exchange between sulphate and sulphide in acid solns., expt. determ. at 300°C and 1000 bars 78−62937
^{34}S/^{32}S ratio meas. using SO$_2$ and SF$_6$ methods, discrepancies 78−65405
Si-O bonds, cryst. chem. at high press., rel. to Earth mantle mineralogy 79−48470
Sn determ. in rocks by thermal neutron activation anal. 77−44552
Sr evolution in W.Greenland-Labrador craton, early Rb depletion in mantle 78−69304
Sr isotope comp. of Alpine tectonite lherzolites, evidence for mantle origin 78−65302
Sr, Pb, isotope geochemistry rel. to catastrophic or continuous core form. 78−57178
^{87}Sr/^{86}Sr ratio reduction during hydrothermal alteration of basalts 79−16446
^{87}Sr/^{86}Sr ratios of interstitital waters from DSPD sites rel. to sediment geochem. 79−34794
Th, analytical geochemical prospecting methods 80−72635
U, analytical geochemical prospecting methods 80−72635
U extraction from natural seawater, by sorption techniques 79−29902
U, geochemical cycle 79−84275
U in marine basalts, implications of conc. and distrib. 77−81886
U in oceanic rocks of DSDP Leg 37, concs. rel. to oceanic crust form. 77−91075
U, isotope fractionation in Edwards carbonate aquifer, Texas, rel. to aquifer oxidation/reduction state 80−98362
U isotopes, in soil, determination using alpha-spectrometry 80−45601
U prospecting, geochemistry of inclosure radioactivity 80−85766
U, regional geochemistry and deposit formation, N.Scotland 79−84269
U resource evaluation by neutron activation anal. 78−85741
U resource research using Pennsylvania State Univ. reactor 79−12159
U series disequilibrium, mechanisms involving recoiling alpha-emitting nuclei 79−16466
U series nuclide conc. in soil particles rel. to their size 77−33073

geochronology
see also radioactive dating
Abitibi dike, ^{40}Ar/^{39}Ar study 80−17237

geochronology continued
- Adelaide Geosyncline, Australia, Late Precambrian palaeomagnetism 80—101325
- S.African kimberlites, ^{40}Ar/^{39}Ar anals. of phlogopite nodules and phlogopite-bearing peridotites 79—34769
- Aiyansh Volcano, British Columbia, ages of eruptions 78—92811
- SWAlaksa, episodic accretion and plutonism 80—101346
- Alcaparrosa Formation (Upper Ordovician), Argentina, palaeomagnetism and K-Ar age 78—96135
- Alpine fault, New Zealand, frictional metamorphism and Ar depletion chronology and tectonic stress 80—41440
- Alpine metamorphism in internal French Western Alps, mineralogy, petrology and chronology 78—36157
- Alps, tectonic progradation rel. to plate tectonic evolution 80—56452
- N.America, climate vars. since 1602, reconstruction from tree rings 80—51528
- N.America, Lower Palaeozoic tectonics rel. to New Brunswick rock units palaeomagnetism 79—100809
- N.America, Pleistocene stages terminology reconsidered in light of Plio-Pleistocene continental glaciation 79—62470
- N.American Cordillera near Fortieth Parallel, tectonics and chronology 78—81138
- amino acid racemization, appl. to geochronology and geothermometry 78—20341
- ancient dykes in Sand River area, Limpopo Mobile Belt, Rb/Sr ages and geological setting 77—56611
- ancient rocks rel. to continental crust evolution 77—64255
- Antarctic glaciation, Cenozoic evolution rel. to circum-Antarctic Ocean and global palaeoceanography 78—16063
- W.Antarctic ice sheet, fluctuations in Antarctic Peninsula area 80—94549
- Antarctic igneous rocks, palaeomag. and K-Ar age 80—12332
- E.Antarctica, age from Rayleigh wave dispersion meas.; Precambrian shield 79—92513
- Antarctica, deep ice age and Holocene/Pleistocene climatic record from ice cryst. size 80—94544
- Antarctica, subglacially erupted rocks of Early Miocene 80—98287
- Anti-Atlas, Morocco, Pan-African province geodynamic interpretation from geology and geochronology *(French)* 80—76952
- apatite, Indian, fission track dating and annealing, U content determ. 79—57891
- apatite fission track ages, from Himachal Himalaya, India, tectonic interpretation 78—57182
- Appalachian Orogen in Canada 80—8304
- Archaean basic and ultrabasic volcanics Sm-Nd dating 78—11848
- Archaean layered greenstone from Pilbara Block, age of volcanics 78—53627
- Archaean lithospheric/crustal thickness from volcano spacings 78—65225
- Archaean migmatites in Lofoten-Vesteralen, Norway, Nd, Sr and Pb isotope data interpretation 79—34773
- Archaean rocks of E.Lac Seul region, English River subprovince, NW.Ontario, Rb-Sr isotopic study 80—94486
- Archaean sedimentary basins, time history rel. to lithosphere thickness 80—89986
- Archaean sialic crust, southern West Greenland, chemical and thermal evolution 80—31016
- archaeomagnetic field magnitude, rapid changes, 100 BC to (AD 300) 79—74830
- Archean greenstone belt, NW. Ontario, Zr-U-Pb geochronology 80—98272
- Arctic Basin, tectonic evolution, Jurassic to present 79—48446
- Arendal orthogneiss, geologically meaningless Rb-Sr total rock isochron 80—31014
- Armenian territory foundation, new struct. and age data *(Russian)* 79—74874
- Arran dykes of British Tertiary igneous province, palaeomagnetism and ages 78—73306
- S Atlantic Ocean, age of opening from palaeomag. of Cretaceous Pirgua Subgroup (Argentina) 77—90998
- S Atlantic Ocean, depositional history during last 125 million years 78—44798
- Atlantic Ocean, history of growth and topography of ocean bottom 80—3993
- S.Atlantic Ocean, opening chronology from equatorial fracture zone trends 78—85527
- atmosphere O$_2$ conc. evolution chronology, rel. to palaeoatmospheric O$_3$ effect on surface temp. 79—96807
- N.Australia Precambrian shields and platforms, cratonisation time rel. to tectonic style 80—3982
- Azores, K-Ar age of oldest volcanics, volcanic history 80—46158
- Baie d'Audierne (Brittany) basic-ultrabasic complex, age and tectonic implications 78—11852
- Baltic Ice Lake levels, dating rel. to S.Finland Salpausselka moraines 79—20872
- basalt, erupted at Reykjanes Ridge crest, vesicularity 78—73351
- basalts, Lower Silesian, K-Ar ages, Tertiary polarity events 78—53614
- basalts from DSDP Leg 37 cores, U and Pb abundances rel. to multi-stage history 77—91123
- basement slice in Appalachian orogen western margin, Saint-Malachie, Quebec, Grenvillian age 79—20824
- batholith between Princeton and Okanagan Lake Sr isotope study 77—17096
- Bay of Biscay, sedimentary sequences rel. to rifting, crustal attenuation and subsidence 79—2209
- Bay of Islands ophiolite complex, Sm-Nd age and Nd and Sr isotopic study 80—85651
- beach deposits near Al Jubail, Saudi Arabia, ^{14}C ages rel. to recent coastal uplift 79—79799
- beach ridges in S.Australia, palaeomag. chronology rel. to Milankovitch theory of ice ages 80—98307
- Benue Trough, stratigraphic evolution and implications for W.Africa Upper Cretaceous palaeogeography 79—2230
- Bergell region, uplift history of Alps, apatite fission track age 80—21727
- Bering Sea and NW.Pacific Ocean, Cretaceous age province rel. to S$_n$ waves propag. 80—51346
- biostratigraphic correlation within IGCP Project 148 79—62501
- biostratigraphic data quantification 79—62593
- biostratigraphical correlation 79—62503
- biostratigraphical logging methods 79—62594
- biostratigraphy, range charts and no-space graphs 79—62504
- biostratigraphy, temporal range charts 79—62595

geochronology continued
- biostratigraphy methods, comparison 79—62502
- Black Sea, mantle material intrusion age rel. to mag. anomalies nature *(Russian)* 78—85473
- Black Sea, Upper Quaternary deep-sea sediments stratigraphy 79—20811
- blueschists, from Ile de Groix, France, isotopic ages, metamorphic episodes determ. 77—66896
- Bolivia, evidence for glaciation 3.27 Myr BP 79—34865
- Boothia Uplift, Canada 79—57846
- Brezovica peridotite base, Jurassic metamorphism 78—96169
- British Columbia, S central, late Pleistocene stratigraphy 78—92804
- British geomagnetic master curve 10000-0 yr B.P. for dating European sediments 79—70740
- SE.Bulgaria, age of Upper Cretaceous resedimentation phenomena in NE.Strandja 78—36160
- Burlington Peninsula, Newfoundland, U-Pb ages of crystalline rocks, Fleur de Lys metamorphism age 78—28188
- Butte mining district, Montana, palaeomagnetism, rock magnetism and aspects of structural deform. 80—101326
- calcite dating, appl. of luminesc. under N$_2$ laser excitation 80—60685
- Canada, P-wave residuals rel. to tectonic age 77—91037
- Canadian Cordillera, geodynamic evolution 80—8276
- Canadian Rocky Mountains, Holocene glacial advances 80—8341
- NW Canadian Shield, geochronology of granitic rocks along Bear-Slave provinces boundary 77—91080
- Canary Islands, age and crustal struct. 80—67355
- Cantal continental volcanic system (France), ^{87}Rb-^{87}Sr ages and geochemistry 79—88327
- Capraia, Italy, volcanic rocks 79—16418
- Carboniferous Andacollo series (Argentina), palaeomagnetism, K-Ar dating and hydrothermal overprinting age 79—29698
- S.Carolina coastal plain, ages for basalt and sedimentary red beds 79—74879
- E.Carpathians, crystalline nucleus evolution, radiometric dating *(Rumanian)* 77—33029
- cave waters, stable isotope geochemistry, ages and climatic change, 230000 to 100000 BP 79—2234
- cavern, dating with ESR and thermolum. *(Japanese)* 77—44955
- early Cenozoic Atlantic Ocean, climatic fluctuations chronology from calcareous plankton palaeobiogeography 78—16143
- Cenozoic volcanic rocks, SE.California, regional stratigraphy, K-Ar ages and tectonics 79—70798
- Central Alps, structural zones history and continental collision 78—81124
- Chamita Formation stratotype (Mio-Pliocene) of northcentral New Mexico, mag. polarity stratigraphy 77—78087
- Chesapeake Bay, pollution history 79—34445
- Chibougamau pluton, Quebec, Precambrian Rb/Sr geochronology 80—98273
- Chile, Camaraca Formation of Middle Jurassic, palaeomag. and plate rotation 80—85586
- cirque glaciations, Holocene and latest Pleistocene, in Shuswap Highland, British Columbia, ages 78—92856
- climatology, 30000 yr isotope climatic record from Antarctic ice core 79—92586
- Coast Plutonic Complex, British Columbia, geochronology and thermal history 80—12351
- Coast Plutonic Complex, British Columbia, Rb-Sr geochronometry 80—12350
- Columbia Plateau, E.Washington, age of last major scabland flood 79—66726
- continental crust, evolution age and isotope evidence 78—65233
- continental growth and emergence timing 78—11867
- continental mantle, heat flow var. with age, appl. to lithosphere thermal models discrimination 79—70764
- continental plates, ages rel. to P-wave travel time residuals 79—62439
- W.Cordillera of N.America, oroclinal deform. chronology and plate linkage mechanism 77—66901
- Cordilleran Benioff zones 78—11866
- core formation, chronology from Sr and Pb isotope geochemistry constraints 78—57178
- Cornwallis Fold Belt, Canada, history and mechanism of basement uplift 77—91091
- Corsican granite, deformation effects on ^{39}Ar-^{40}Ar systematics 79—53347
- Coso Range, California 80—90049
- Cretaceous kimberlites and mantle xenoliths from S.Africa, Pb isotopic comps. and age 77—60372
- Cretaceous section of Chilean Andes, palaeomag. and K-Ar age 80—85585
- Cretaceous Tekenika Beds of Tierra del Fuego, age and tectonic significance 77—44996
- Cretaceous-Tertiary boundary (Z coal), Hell Creek, Montana, Rb/Sr age 80—94487
- Cretaceous-Tertiary boundary sediments, Red Deer Valley, magnetostratigraphy, biostratigraphy and geochronology 79—57888
- crustal age, correl. with lateral heterogeneity of upper mantle, multiple ScS meas. 77—29259
- Cumberland Peninsula, Baffin Island, hornblende grain etching, age and palaeoclimate indicator 80—8307
- Cuvier Basin, off W.Australia, crust form. by rifting, seismic study 80—12368
- cyclospectrometry, ^{10}Be conc. criterion for dating geochemical remains *(French)* 80—21859
- dating techniques, effects of thermal annealing on track etching rate of sphene, CaTiSiO$_5$ 78—65435
- dating using ESR *(Japanese)* 79—48437
- Deccan traps age from palaeomag. studies 77—48992
- Deccan Traps volcanic rocks, India, ^{40}Ar/^{39}Ar date and volcanic history 80—46178
- Dedham granodiorite, E.Massachusetts, Rb-Sr whole rock age determs. 77—81835
- deep sea carbonates, thickness and ^{14}C age of mixed layer 79—29742
- deep sea cores from Project FAMOUS, radiocarbon and ^{210}Pb distrib. 77—37179
- deep sea sediment core from E.Mediterranean, chronology and palaeoclimatic record 78—57294
- deep-sea cores, ^{231}Pa dating via ^{227}Th counting 78—32238
- deep-sea sediment core, thermoluminesc. dating 79—74871
- deglaciation, of Rannoch Moor, Scotland, radiocarbon dates 77—13115

geochronology continued
  Dellwood knolls, volcanic activity age rel. to role in triple junction tectonics off northern Vancouver Island 80—90067
  Denali fault system, geological history rel. to S.Alaska tectonic development 78—81137
  Denchai Basalt, N.Thailand, paleomagnetism, age and geochemistry 80—41421
  dendrochronology, Japanese cedar record of air temp. 77—21880
  Devensian glaciation in Britain, effects on water balance, 50000 yr BP to present day 80—72566
  Devonian Onondaga limestone (New York), palaeomagnetism chronology 80—3928
  diabase pebbles of val d'Illiez conglomerates (Haute-Savoie), geochronology *(French)* 78—92810
  Donegal granite, Ireland, emplacement age by isotope chronology 80—67356
  Duncansby volcanic neck, NE.Scotland, palaeomag., K/Ar ages, tectonic implications 78—61369
  Duxbury massif (2.5 Ga), Quebec, remobilised piece of pre 3.0 Ga sialic basement 80—76970
  Early Precambrian rocks of W.Greenland and Minnesota River Valley, U-Pb ages on single zircons 78—11845
  Earth, implications of initial Pb in Amitsoq gneiss, W.Greenland 78—20371
  Earth chemical evolution, mantle and crustal reservoirs mean age 80—51359
  Earth early history, review 79—20739
  Earth-Moon system history, palaeontological data 80—17224
  earthquake ages, determ. in central Asia via lichenometry 79—92505
  Eifel volcanic fields, pliocene and quaternary volcanic phases, K/Ar age determ. 80—46160
  NE Ellesmere Island, NWT, Canada, glacial geology and chronology 78—77233
  Ellsworth Mtns. crustal fragment, Antarctica, age and tectonic posn. 77—29262
  Elsonian magmatism in Labrador, age, characts. and tectonic setting 78—73365
  environment evolution, available elements during Earth history rel. to life evolution 79—80030
  Eocene terminal event, formation of ring system around Earth 80—76890
  SW.Ethiopia, dating of volcanic and rifting history 80—51369
  ferromanganese concretions in Baltic Sea, trace metal distrib., ages and accretion rates 77—81864
  ferromanganese nodules, oriented, U-Th series nuclides rel. to growth rates and turnover times 79—29740
  Fiordland, New Zealand, crustal struct. and ages 79—88325
  fission track annealing characteristics of epidote, appls. to geochronology, geol. 78—94038
  fission track dating and estimation of U in garnets 78—94039
  fission track dating technique 80—36417
  fission track dating using U glasses, error analysis 80—95503
  fission track retention in minerals, closing temp. rel. to dating 77—64268
  fission Xe isotope dating technique 79—21043
  Flandrian sea level changes in Thames Estuary, stratigraphy and chronology rel. to land subsidence 78—24304
  Fleur de Lys terrain, Newfoundland, minerals ^{40}Ar/^{39}Ar age spectra, rel. to metamorphism 77—70657
  fluorites, colouring, effect of impurities on absorpt. spectra, rel. to geochronology 79—56822
  Frontenac Axis dikes, Ontario, ^{40}Ar/^{39}Ar dating and implications for Grenville palaeomagnetism 79—62466
  Gaspe, Quebec, age and style of mesostructures 77—17094
  geochronology and cosmochronology, convention on use of decay consts. 78—28189
  geologic evolution of terrestrial planets 77—53442
  geomagnetic field reversal time scale back to 13 Myr BP 79—44085
  geomagnetic polarity time scale, revised, for interval 0 to 5 m.y. BP 79—57851
  geophysical timescales from absolute-dated ice cores from Greenland *(Danish)* 79—34776
  Gettysburg Bank, N.Atlantic Ocean, K-Ar data for age and evolution 79—88322
  Gippsland, Victoria, Pliocene eustasy and sand barrier form. onset 79—74886
  Glacial Lake Whittlesey, ice frontal position in eastern Erie basin 80—12436
  Glacier Peak tephra in North Cascade Range, stratigraphy, distrib., rel. to glacial events 79—25247
  glauconite group minerals, Norwegian-Greenland basin, age determ. by EPR and Mossbauer spectra 80—26467
  global plate reorganization during early Cenozoic 79—34788
  Goat Paddock cryptoexplosion crater, W.Australia, Eocene age determ 80—98322
  Godthaabsfjord area, W.Greenland, U-Pb dates on zircons from early Precambrian rocks 77—29256
  Gondwanaland, breakup rel. to evolution of Indian Ocean 80—41428
  Gondwanaland Mesozoic tholeiites, Rb-Sr mantle isochrons and lithosphere chemistry vars. 78—28201
  NW Gondwanaland Proterozoic tectonics, new evidence from E Newfoundland 79—57908
  granite-greenstone terrains of Rhodesian Archaean craton, age determs. 78—24288
  granites, Nanling region, southern China, K-Ar and U-Pb dating 77—2132
  granitic plutons, 325-265 Myr old, in Piedmont of SE. Appalachians 79—70797
  granitic plutons, E. Newfoundland, ages rel. to Appalachian evolution 77—66894
  N.Great Barrier Reef, ^{14}C dating 79—84225
  E Greenland, chronology and struct. of coastal dyke swarm and assoc. plutonic intrusions 80—56467
  E.Greenland, Jurassic basin evolution, chronology and sedimentation 78—73344
  E Greenland, southern Caledonian fold belt polyorogenic nature from isotopic age study 80—76938
  S.E.Greenland continental margin, struct. and age 77—33014
  Grenville and adjacent Palaeozoic formations Pb isotope ratios 77—44941
  Grenville basement rocks, SW Newfoundland, ^{40}Ar/^{39}Ar ages rel. to Proterozoic-Palaeozoic thermal history 79—20771

geochronology continued
  Grenville Belt magnetisation age, Rb-Sr and palaeomag. evidence from Swedish dolerites 77—81839
  Grenville orogeny, palaeomag., Rb-Sr ages from dolerites, Canada and Greenland 79—34772
  Grenville series of Ontario, palaeomag. rel. to Ar isotope dating 80—98232
  Grenvillian palaeopoles, calibration by ^{40}Ar/^{39}Ar dating 79—20778
  Gulf of Mexico-Caribbean area, Permian-Triassic continental reconstruction 80—56431
  Gulf Stream, vel. fluctuations during Late Cenozoic rel. to climate 80—12432
  Gulquac Lake area, New Brunswick, Rb-Sr ages 80—31006
  Hawaiian alkalic basalts, thermoluminescence dating 77—86832
  Hawaiian glaciation chronology, K/Ar and ^{14}C ages 77—33113
  Hebridean continental margin, seismic evidence for Mesozoic age sedimentary troughs 78—53643
  W. Hellenic Trench, high sedimentation rates and variable dispersal patterns 78—57193
  Hellroaring Plateau area, Beartooth Mountains, Montana 80—17238
  N.Hill End Trough, NSW, time-relationships between metamorphism and deform. in metasediments 80—26510
  Himalaya, uplift and cooling rates from geochronological data 80—85627
  Himalayan muscovites, fission track dating 78—3736
  Holocene glacial and tree-line vars. in Alaska and Yukon, ages 77—78251
  Holocene retreat of W.Antarctic ice sheet, model 79—66725
  Huronian polar wander and Thessalon volcanics palaeomag. 79—5444
  Iapetus Ocean, evidence for Cambrian opening 80—98299
  ice-wedge casts in NE county Wicklow, distrib., struct. and age 78—69379
  SW Iceland, K-Ar ages, stratigraphy and palaeomagnetism of Esja, Eyrarfjall and Akrafjall mountains 80—89950
  N.Iceland, lava succession, K-Ar dating, geological and palaeomagnetic obs. 80—109096
  E.Iceland lava, ^{40}Ar/^{39}Ar dates and ocean ridge growth 80—36273
  Iceland Plateau, history from sea floor morphology and mag. anomalies N of Iceland 80—89953
  Iceland-Faeroe Ridge, subsidence history rel. to Lower Tertiary laterite and Thulean land bridge 78—85514
  Imataca Series, Venezuela, total-rock U-Pb and Rb-Sr systematics 78—96168
  inclined seismic zones rel. to age-length depend. of subducting margin 78—57175
  S.Indian Craton, Archaean gneiss Rb-Sr date of 3360 Myr old 80—46155
  Indian Ocean crust, age rel. to geothermal convection through crust and sediments 79—79812
  Indo-Australian plate, internal deform. chronology rel. to Himalayan orogenic stage 80—109134
  Innuitian Province, Arctic Canada, tectonic history 80—8275
  insular phosphorite from Ebon atoll, Micronesia, U series dating 78—81121
  interglacial chronology, Rocky and Mackenzie Mountains, ^{230}Th-^{234}U dating of calcite speleothems 78—36120
  interstadial sea level of −40 m at 30000 yr BP, ^{230}Th/^{234}U age support 79—16504
  Ionian Sea, sapropels distrib. and ages E.Mediterranean Sea late Quaternary palaeoceanography 78—73350
  Iranian Makran, Recent faulting episode 78—32038
  central Israel, evidence for pre-Late Jurassic east-west fossil continental margin 79—34766
  Isua conglomerate boulder (W.Greenland), oldest dated rock, U-Pb ages on single zircons 78—11845
  Isua supracrustals, Greenland, Sm-Nd isotopic investigations and implications for mantle evolution 78—36129
  Japan, late glacial age chronolgy from morainic features and Lake Biwa sedimentary sequence 79—34872
  Japan, uplifted terraces ^{14}C dating rel. to large earthquakes time-predictable recurrence model 80—85598
  W.Karakorum, absolute age of granitoid rocks between Hindu Raj and Gilgit River 79—100818
  Karroo rhyolites, Swaziland, isotopic evidence of crustal contamination 80—21666
  KBS Tuff, E.Turkana, Kenya, K-Ar age estimate 80—56433
  KBS Tuff, N.Kenya, fission track age and assoc. hominid remains 80—56432
  Kerguelen ring complexes, chronology and geochemistry rel. to continental or oceanic character 79—57924
  King Island, Australia, fission track ages rel. to continental rifting 78—53628
  Klamath Mountains, Oregon, Rogue and Galice formations petrology, Jurassic island arc seqeunce identification 79—100836
  Koobi Fora and Shungura Formations, E.Africa, tuff correls. and ages 79—57930
  Korostenian pluton gabbro-anorthosites, form. time from palaeomag. meas. *(Russian)* 79—8599
  La Boca Formation, N.Mexico, palaeomag. pole position and age 77—2099
  Labrador, Archean gneiss dating using zircon data 80—3959
  coastal Labrador, granite intrusions, Rb-Sr ages and tectonics 77—81836
  Lac Seul region, English River Gneiss Belt, geochronology 77—5148
  Lake Bogoria, Kenya Rift Valley, radiocarbon date 79—44207
  lake level fluctuations since 30000 yr BP, global maps 80—51447
  Lake Mungo aboriginal fireplaces as geomagnetic records, dating 77—21679
  Lake Ontario, Late Wisconsin sediments, aspartic acid racemisation and ^{14}C dating 78—73415
  Lake Ontario, sedimentation rates determ., ^{210}Pb dating method 78—73408
  lake sediment sequences, pre-Pinedale, Yellowstone National Park, geology, palynology, climatology 79—66727
  lake sediments, radionuclide geochronology and pollution history 78—61451
  Lake Tahoe, California-Nevada, sediments, ages rel. to palaeomagnetism 80—41371
  Lakes Ontario and Erie, comparative ^{210}Pb, ^{137} Cs and -pollen geochronologies of sediments 79—66728
  Laschamp geomagnetic polarity reversal, K-Ar and ^{40}Ar/^{39}Ar age 78—81105
  Laschamp palaeomagnetic excursion age reconsidered 79—44091

geochronology continued
last (Eemian) interglacial, abrupt end in NE.France 80—21818
Late Brunhes polarity episodes, palaeomagnetism and radiochemical age estimates 78—11797
Late Holocene tectonic activity along Sinai subplate margins, chronology 79—57907
Late Palaeozoic slate belt, deform. chronology and plate tectonic significance 78—81140
Late Precambrian glaciations, Africa, nonsynchroneity 77—81940
late Precambrian mafic dykes, Montana, geochemistry and Rb-Sr geochronology rel. to Belt tectonics 78—77196
Late Quaternary uplift in New Hebrides, U series ages 78—3741
Late Tertiary Verde Formation, Arizona, magnetostratigraphy 78—65179
Lepontine Alps, chrontours rel. to heat-flow distrib. temporal changes assoc. with metamorphism 80—101347
Lewisian gneisses, Sm-Nd systematics and implications for granulites origin 79—20777
lithostratigraphic correl. of subsurface sequences in FORTRAN IV 79—62509
lithostratigraphic correlation, automatic, pitfalls 79—62506
Loch Lomond, Scotland, palynology, palaeomag. and ^{14}C dating of Flandrian marine and freshwater sediments 78—81234
Loch Lomond Stadial in British Isles 79—79887
S.Long Island, New York, Holocene submergence history 79—74881
Lower and Middle Cambrian sedimentary rocks, Desert Range, Nevada, palaeomag. rel. to polar wander 80—21620
Lower Ordovician rocks of NW.Argentina, paleomag. and K-Ar age 80—89938
Loyality Islands uplift rates, ^{230}Th/^{234}U dating of raised coral terraces 78—73347
Makapansgat Formation (South Africa), palaeomag. results and age 77—25637
Mamontova Gore silt, Siberia, radiocarbon dates and late Quaternary nonglacial stratigraphy 78—44819
Manicouagan melt sheet, Rb-Sr isochron age 78—81168
Marcus-Necker Ridge, volcanic rocks comp. and stages of development 80—36282
marine, sediment, ^{230}Th age, α-scintillation counting method 80—72636
marine inundation of USSR and N.America during Phanerozoic, secular changes 78—3735
Massif Central, upper mantle regional struct. and geodynamics chronology 78—81120
Massif central volcanism, age rel. to upper mantle struct. and geodynamics *(French)* 79—48424
Matuyama epoch, short geomag. episodes ages 79—66616
Mehone Bay, Nova Scotia, Late Quaternary geological history 78—77232
Messejana Dolerite fault-dike system (Iberia), age and origin rel. to N.Atlantic Ocean opening 79—2198
Messina Layered Intrusion, Limpopo Mobile Belt, S.Africa, tectonic setting, geology and age 80—76969
metagabbro at bottom of Michigan Basin deep drill hole, Rb-Sr geochronologic anal. 79—39680
metamorphic rocks, thermal overprinting of NMR and K/Ar ages 78—65278
metasomatic anhydrite in Mississippian reservoir carbonates, age determ. 78—73328
meteorites Earth residence times, determ. from thermoluminesc. 80—31262
Michigan Basin borehole, igneous and sedimentary rocks palaeomagnetism rel. to ages 79—39636
Michikamau Intrusion, Labrador, palaeomag. pole position and age 77—5130
Mid-Atlantic Ridge at 37°N, mag. anomalies rel. to ages and spreading rates 77—91070
Midland Craton of England and Wales, Precambrian polar wander path from palaeomag. study 79—66617
mineral fission fragment track annealing characteristics 79—100827
late Miocene shallow marine sediments, New Zealand, C isotope stratigraphy appl. 80—26479
Miocene-Pliocene lava sequence at Bassastadaa, E.Iceland 77—17046
montmorillonite group minerals, Norwegian-Greenland basin, age determ. by EPR and Mossbauer spectra 80—26467
Morarian age fcr younger Moines, central and W.Scotland 79—53328
Mossbauer spectroscopy, possible appl. to geochronology 80—41416
Munster Basin, NW.Germany, Upper Cretaceous limestones magnetisation age and Cretaceous pole position 80—89949
Murrumbidgee granite batholith, Rb-Sr isochrons and Sr isotopic equilibration 77—41026
muscovites, Himalayan, fission track dating and U conc. estimation 78—40524
S Nain complex, Labrador, anorthosite and assoc. plutons relative ages 79—20825
Nanling mesozoic granites *(Chinese)* 79—62468
Nazca group volcanic rocks, Peru, volcanic history 80—12357
Neogene relative motion between Pacific plate, mantle and Earth spin axis 79—44167
Neogene strata of Pakistan, geology and palaeontology 78—24269
nepheline syenite, dating, Rb-Sr internal isochron, ^{39}Ar-^{40}Ar plateau age methods *(French)* 78—32031
N.Central New Brunswick, age of deformed granitic rocks 77—81837
central New England, denudation rate over past 13700 yrs from estuarine sedimentation 79—92550
New England submarine canyons, bedrock geology 78—73356
Newark trend basins, USA, diabase intrusion geochronology by Ar isotope 80—51350
W.Newfoundland, ^{40}Ar/^{39}Ar ages and ophiolite obduction 77—33034
Newfoundland, Early Palaeozoic plate tectonic model 80—94509
Newfoundland, Hercynian activity, geochronology 77—29263
Newport granite, age, geological setting, rel. to NE.Newfoundland geology 79—92534
Nordlinger Ries giant meteorite impact crater, K-Ar and fission track dating 78—28236
North Mountain Basalt, Nova Scotia, K-Ar isochron age, ^{40}Ar/^{36}Ar ratio 80—3960
Norwegian eclogites, Caledonian Sm-Nd ages and crustal origin 80—76978
obsidian, hydration profiles meas. by sputter-induced optical emission, rel. to dating technique 79—24871
ocean basins, ages rel. to palaeobathymetry of spreading ridges crests 78—11869

geochronology continued
ocean floor bathymetry and heat flow vars. with age 77—33051
oceanic aseismic ridges, sedimentary history rel. to subsidence rates 77—37162
oceanic basalts, differential Sm/Nd evolution 78—61391
oceanic crust, hydrothermal alteration age 79—34798
oceanic lithosphere age-dependent subduction beneath western South America 79—2211
Okanagan Valley, British Columbia, Holocene peat core palynology and palaeoclimatology 77—5146
Olby-Laschamp geomag. polarity event, age 79—12067
Oligocene unconformities, oceanic and continental, in Australian region, chronologies 78—73370
Ontario, Pleistocene glaciation chronology rel. to geothermal regime perturbation 79—57883
Onverwacht Group Volcanics, southern Africa, Sm-Nd dating 79—62469
ophiolite complex, early Caledonain age, on Karmoy island, Norway 79—2235
ophiolites of Zagros and Makram, Iran, Ar isotope age, Jurassic tectonics 80—46156
ore mineralisation in Erma River Area, Bulgaria, age, genesis, Pb isotope and K-Ar investigs. 78—81115
ore-deposition through geological time, review 78—77235
orogenic episodes, dating from global sea-level changes 79—29743
Oxford Lake-Knee Lake greenstone belt, N.Manitoba, Rb-Sr ages 80—94485
Central Pacific Basin, ^{40}Ar/^{39}Ar ages of diabase sill and basalt, rel. to ocean floor history 77—66897
SW.Pacific basin crust, reverberant subbottom layers distrib. and age 80—8290
Pacific Basin mantle, age rel. to shear-wave polarisation anisotropy 77—49018
W Pacific guyots, ^{40}Ar/^{39}Ar ages and evolution 78—11876
Pacific island and seamount ages rel. to volcanic chains origin 77—64242
Pacific Ocean crust, layer 2A seismic props. rel. to plate age 77—29260
Pacific plate absolute motion, early Cainozoic change prod. by change in boundaries 78—85529
Pacific Pleistocenes palaeoclimatic stratigraphies, comparative anal. of results 78—57295
circum-Pacific region, timing of geological events 77—64233
E.Pacific Rise, equatorial, tectonic history and regional shape 78—44800
Paganzo Group (Argentina), red beds palaeomagnetism and correl. of Upper Palaeozoic-Lower Mesozoic rocks 77—90999
palaeobathymetry of spreading ridge crests rel. to age of ocean basins 77—29282
palaeoclimate marine-continental correlation, 150000 yr O isotope-pollen record from N.Pacific 79—80008
palaeoclimatic research, chronological control rel. to status and opportunities 80—51527
palaeoclimatology, abrupt events time scales and causes 80—51531
palaeoclimatology, in world climate conference, Geneva (1979 February 11 to 23) 80—46727
Palaeogene revised polarity time scale 78—77201
palaeomagnetic secular variation, recent, in lake sediments from New Guinea Highlands 79—12069
palaeomagnetic stratigraphy of Meadowcliffe Till, late Pleistocene excursion evidence 79—70745
Palmahim structure in SE Mediterranean off Israel, continuous tectonic activity since Upper Miocene 79—34790
SE.Pamir Mountains, geology and geochronology *(Russian)* 80—12392
Panamint Valley fault zone, W.Basin and Range province, California, Holocene offset and seismicity 79—79802
Parece Vela Basin, E.Philippine Sea, evolution and chronology 80—41431
Pearson Formation (Great Slave Supergroup, NWT), palaeomagnetism age and Coronation polar loop 78—77179
pelitic sediments, Rb-Sr and K-Ar dating rel. to Sr and Ar isotopic homogenisation during metamorphism 79—62511
Permo-Triassic and Jurassic ^{40}Ar-^{39}Ar ages from Greek igneous rocks rel. to rifting 79—74872
central Peru, Eocene uplift and unroofing of coastal batholith near Lima 79—2199
Phanerozoic palaeomagnetic restructurings, chronological distribution curves 79—53302
Philippine Sea origin and development, ^{40}Ar-^{39}Ar ages from DSDP Leg 31 77—64254
phlogopite, fission track etching and annealing, chronological application 79—84230
phosphatic nodule beds in Victoria, correl. with late Miocene-Pliocene eustatic event 79—12105
Pinchi Fault Zone, central British Columbia, geology and evolution 77—91129
plate tectonics in Phanerozoic 78—92812
Late Pleistocene glaciology effects, study of Taylor Valley, Antarctica 80—8343
Pleistocene magnetic stratigraphy of New England tills 79—70744
Pliocene and Pleistocene glaciations chronology, evidence from bottom of Barents Sea 78—57227
Pliocene Centerville Beach section (N.California) age and palaeomag. stratigraphy 77—60346
Pliocene-Quaternary deposits in Ukrainian SSR, model of regional magnetostratigraphic scale *(Russian)* 77—44916
Pliocene/Pleistocene boundary age estimate and palaeoclimatology 77—91133
Precambrian basement rocks of N Saskatchewan, lithology and tectonometamorphic relationships rel. to chronology 77—91132
Precambrian Gardar lavas, S.Greenland, mag. stratigraphy and mag.-petrologic props. 77—40973
Precambrian metavolcanics in Orange River region, S.Africa, isotopic study 79—44147
Precambrian terrain, multiply deformed, discrete structural-metamorphic events geochronology 79—57895
Precambrian zircons, metamictization and U-Pb systematics by IR absorpt. spectrometry 77—17099
Precambrian-Cambrian boundary, from Jbel Boho volcano zircons *(French)* 78—61359
Precambrian-Cambrian boundary problem, palaeomag. directions from Amadeus Basin, Central Australia 79—29697
pumice from KBS Tuff, East Rudolf, Kenya, ^{40}Ar/^{39}Ar dating 77—5160
pumice from KBS Tuff, East Rudolf, Kenya, fission track dating 77—5159

geochronology continued
N Pyrenean metamorphism, age and tectonic implications 79—34819
Pyrenees, history in subduction and collision model 77—81854
Quaternary deposits of Corsica (France), props. and chronological concls. 78—57234
Quaternary faulting along Caribbean-North American plate boundary, chronology 79—79804
Quaternary glaciations along Qinghai-Xizang Highway *(Chinese)* 79—92538
Quaternary glaciations and stratigraphical positions in China *(Chinese)* 79—79885
Quaternary glaciolacustrine sediments in Val Tresa, age and collapse dislocations origin *(Italian)* 79—8647
Quaternary loess deposits of Banks Peninsula, New Zealand, radiocarbon dating 78—24271
Quaternary of Chile, chronology of climate and sea level changes, tectonics and volcanism 78—44980
Quaternary palaeoclimate temp. and precip. chronology for N.America NW. coast region 80—98438
Quaternary sediments and stratigraphy, continental shelf, N.Norway, chronostratigraphic investigation 79—84228
Quipungo mobile belt, Western Angola, geological evolution *(Portuguese)* 79—70796
radiochronology of the Francevillian series using K-Ar methods *(French)* 80—21692
Red.Sea, crustal age and extent 77—29284
Red Wine alkaline province, central Labrador, chronology 78—11842
Reykjanes Ridge, heat flow survey, age and heat flow relation 79—79768
Rhodesian Archaean, 2.9 Myr BP event 79—66658
Ries impact crater, thermal events, age and intensity 79—79760
rinneite, Rb-Sr dating of potash salt deposits 80—67429
Roberts Arm Group, Newfoundland, age rel. to phases of volcanism 80—12354
Robinson's Head moraine, W.Newfoundland, ^{14}C dating, rel. to postglacial sea level changes 78—20401
Roccamonfina Volcano, geochronology and palaeomag. *(Italian)* 77—49036
Roche d'Enval syenodiorite, ^{87}Rb-^{87}Sr systematics and age 77—60373
rock glaciers in Jasper National Park, Alberta distrib. and ages 78—77276
Romanche fracture zone, equatorial Atlantic, Neogene crustal emersion and subsidence 78—11857
Ross Ice Shelf, Antarctica, artificial radionuclides depositional history 79—88027
Rostherne Mere, Cheshire, ^{137}Cs dating confirmation by algal stratigraphy 79—12156
Saglek area, Labrador, Uivak II gneiss, zircon age meas. 80—3958
Sahara plateau, petrographic and radiometric dating *(Italian)* 78—7595
lower Saint Lawrence estuary sediments, clay-sand sequence chronology in Rimouski shelf region 79—62530
Salpausselka moraines, S.Finland, dating rel. to Baltic Ice Lake levels 79—20872
salt deposits, Upper Triassic, of western N.Atlantic, stratographic age 80—94516
Samail oceanic crust, isotope study of petrogenesis and hydrothermal alteration 80—46177
sand deserts, age and extent during glacial maximum and climatic optimum 78—36259
Santorini (Thera) eruption, 1450 BC, archaeological dating for tephra discovered at Rhodes 80—109129
Sao Miguel, Azores, quantitative study of volcanism, tephrochronology 78—61382
Sao Vicente, Mato Grosso, geology and geochronology of granite *(Spanish)* 77—70652
NW.Scotland, Pb isotope meas. from oldest recognised Lewisian gneisses 77—70625
SW. Scottish Highlands, chrontours, rel. to heat-flow distrib. temporal changes assoc. with metamorphism 80—101347
Searles Valley, California, lacustrine sediment core chronology from palaeomagnetic data 80—89955
Sebakwian group, Selukwe, Rhodesia, Early Archaen age 77—13067
sediment core from Gulf of California, varve chronology rel. to ^{32}Si half life determ. 80—91153
sedimentary basins, heat flow and subsidence histories with finite crustal extension rates 80—89987
sedimentation rates determ. in rapidly accreting salt marsh by ^{137}Cs dating 78—96247
sediments baked by lava flows, Chaine des Puys, France, ages and palaeomag. field strengths 79—44100
Shackleton Range Metamorphic Complex, Antarctica, Rb-Sr dating study 80—46180
Shuswap Metamorphic Complex, B.C., Rb-Sr dates for granodiorite intrusions 77—81838
Sibley Group, Thunder Bay district, Ontario, Canada, stratigraphy and depositional setting 80—94517
Siebengebirge, Germany, K-Ar age of Tertiary volcanics 80—98280
Sierra Nevada, California, glacial deposits, relative dating techniques from weathering 80—8451
Sierra Nevada-Walker Lane region, recent crustal movements, rate and style of deform. 79—79838
silicic igneous rocks, Burlington Peninsula, Newfoundland, Rb-Sr ages, deform. 78—65212
Upper Silurian rocks from N Somerset Island, Arctic Canada, stratigraphy and sedimentology 77—91131
Silurian-Devonian rocks of NW.Argentina, paleomag. and K-Ar age 80—89938
Siwalik Group, Dhok Pathan, Potwar Plateau, Pakistan, mag. polarity stratigraphy and age 79—29725
slates age studies, ^{40}Ar/^{39}Ar stepwise outgassing method applicability 79—29721
Snares and Auckland Is., Campbell Plateau, radiometric ages 77—29281
soil, weathering age from U and Ac series nuclides radioactive disequilibrium 80—4014
South China Sea basin, development chronology from profiler-sonobuoy meas. 80—8291
South Fork Mountain Schist (N Coast Ranges, California), early Cretaceous metamorphic age 78—81114
South Island, New Zealand, Late Pleistocene tephra, identification and significance 80—8306
speleothems, in N. America, late Pleistocene palaeoclimates chronology 78—57297

geochronology continued
speleothems, stable isotope geochemistry, ages and climatic change, 230000 to 100000 BP 79—2234
speleothems from Britain, palaeoclimatic and geomorphic implications of ^{230}Th/^{234}U dates 78—36128
Spor Mountain, Utah, USA, U-Pb age of uraniferous opals and mineralisation processes 80—46149
St. Helena Is., seamount age and bathometry 79—16436
stalactite, from Akiyoshi cave, thermoluminescence and ESR dating comparison 78—88807
stalagmite, New Zealand, ^{14}C dating rel. to temps and climate change during last millennium 79—62574
stalagmite deposits, palaeomagnetism and ages 79—84107
Stillwater complex, USA gabbro Sm/Nd age and mantle evolution curve of Nd 80—41410
stratigraphic correlation conf. Syracuse, NY, USA (Oct. 1977) 79—62500
stratigraphic section correl. by continuous variables 79—62505
stratigraphic units, lateral tracing in FORTRAN 79—62510
structural characts. and tectonisms around microcontinent Japan Paleorzoic-Mesozoic geosyncline 78—81139
Sudbury dykes, Grenville Front region, palaeomag., petrochem., K-Ar ages 78—7633
Suess Wiggles and ^{14}C calibration curve for dendrochronology 79—74952
Sulawesi (E Indonesia) western arc, palaeomag. studies and fission-track dating rel. to tectonic history 80—89957
sulphide minerals, K-bearing, age meas. by ^{40}Ar/^{39}Ar technique 79—29720
Sumatra, explosive volcanism ages rel. to late Cenozoic clockwise rot. 77—60363
supracrustal rocks, Isua area, W.Greenland, least radiogenic Pb occurrence 78—44816
Swaziland Ancient Gneiss Complex, Rb-Sr age and source of bimodal suite 80—51395
Swedish rapakivi suite, palaeomag. study rel. to Proterozoic tectonics of Baltic Shield 80—56346
tektites, fission-track plateau dating evidence of australites older than indochinites 80—56780
E.Tennessee, Ordovician polar wander from Moccasin, Bays and Chapman Ridge Forms. palaeomagnetism 79—57854
tephra deposits, dating of ancient events 80—36283
Tertiary basalts, of E.Greenland continental margin, biostratigraphic ages, plate tectonics implications 77—5153
Tertiary palaeo-geothermal gradients in Upper Rhine Graben, determ. from coal metamorphic rock 79—70800
thermoluminescence and age determination *(German)* 80—105076
thermoluminescence dating of Quaternary calcite 79—84231
thermoluminescence dating of sediments baked by Chaine des Puys lava flows 78—92808
thermoluminescent dating of geological objects, appl. of natural quartz dosimetric props. 79—12288
Thompson Ni belt, Manitoba, geological and geochronological relationships 77—5196
till on Lake Huron E coast, mag., physical and lithologic props. and age 77—33057
Toba, N. Sumatra, late Pleistocene eruption K-Ar age 79—16427
Tokyo Bay, central Japan ages of recent formations and buried topography surfaces 78—44818
travertine from archaeological sites, Nahal Zin, Israel, U series dating 79—34781
tree ring ^{13}C records, interpretation problems 79—62573
tree-ring evidence of past climatic variability 79—16642
trondhjemitic basement enclave, near Favourable Lake volcanic complex, NW.Ontario, Canada, age 80—94518
Troodos ophiolitic sheeted complex 78—61365
Tuscan anatectic magmatism, eastward migration due to Apennines anticlockwise rot. 79—16428
Twillingate Granite and Herring Neck Group, Notre Dame Bay, Newfoundland, geochronology 77—17049
Umfraville Gabbro, Ontario, palaeomag. study and K-Ar age 80—12330
W United States, Cenozoic magmatism chronology rel. to plate interaction and absolute motion 79—2207
Upper Cenozoic volcanism, central Andes, ages and volumes 79—29730
Upper Cretaceous palaeomagnetic stratigraphy at Moria (Umbrian Apennines), verification of Gubbio section 78—96132
upper Mesorzoic subduction complexes along N.America west coast, distrib. and character 78—81136
Upper Palaeozoic-Lower Mesozoic red beds and igneous rocks, Argentina, palaeomag. 79—84098
Upper Precambrian sedimentary rocks, Desert Range, Nevada, palaeomag. rel. to polar wander 80—21621
Upper Proterozoic apparent polar wander, analogous loops from Laurentia, Fennoscandia and Africa 80—56360
Vancouver Island, Wisconsin stratigraphy, climate reconstruction 80—8267
vermiculite, fission track annealing and dating 80—81885
volcanic plagioclases, thermoluminescence dating 80—98475
volcanic rocks in Lesser Antilles island arc, palaeomagnetic survey and age determ. 80—8265
volcanism, continental, role of ancient lithosphere 77—2133
volcanosedimentary levels, S.Pacific, neoformation and weathering *(French)* 78—73353
Wabigoon belt, NW.Ontario, felsic rock geochronology and geochemistry 80—31004
Wascana Creek Ash, Canada, characterisation, source, fission track age, palaeomag., stratigraphy 77—66913
White Mountains intrusives, New Hampshire, Vermont and Maine, ages 77—78129
Whitehorse map area, Yukon, plutonic rock dates 80—31005
Wisconsin reef on Daito Ridge, Philippine Sea, isotopic evidences, Late Quaternary tectonic history 79—84227
Wollaston Lake Belt, Saskatchewan, Rb/Sr dating 77—17051
N.Wolverine Complex, British Columbia, geochronology and tectonics 80—3961
SE Yukon, unique stratigraphic record of late Tertiary-Quaternary events 79—62499
coastal Zagros, Mountains near Bandar Abbas, Iran, Holocene folding rates 79—48445
zircon, Indian, fission track dating and annealing, U content determ. 79—57891

geochronology continued
zircons, detrital, in N.Africa, no evidence of 500 Myr ages or Pan-African mountains 79−84213
^{26}Al, decay in marine sediments, meas. with cyclotron, dating technique 79−71819
Ar-K isotopic dilution method for absolute age determ. *(Rumanian)* 78−20562
^{39}Ar-^{40}Ar dating, K-feldspar importance in polyorogenic areas 79−44152
^{40}Ar/^{39}Ar dating, appl. of isochron diagrams 79−29873
^{40}Ar/^{39}Ar studies of deep-sea igneous rocks 79−53325
^{40}Ar-^{39}Ar geochronological studies on submarine rocks from W.Pacific 77−17075
^{40}Ar-^{39}Ar stepheating analyses of clay concentrates in Irish orebodies 79−66684
^{40}Ar-^{39}Ar systematics, temp. and pressure effects 79−44178
^{10}Be, mass spectrometric meas. with cyclotron, geochronological appl. 79−57338
^{13}C/^{12}C dating of New Zealand kauri cellulose for last millennium 80−21819
^{14}C beam prod. from natural sample, radioactive dating 79−25352
^{14}C dating, beta rel. to ion counting 79−74992
^{14}C dating, principles and disagreements with geophysical data *(French)* 77−37434
^{14}C dating, thermal diffusion enrichment, N. American glacial history extended to 75000 yrs ago 78−77284
^{14}C dating, time scale extension by thermal diffusion enrichment, appl. to NW. Europe climatology 78−77314
^{14}C dating of CO_2 sample with accelerator, blind meas. 79−25362
^{14}C dating of geological and archaeological samples 78−92993
^{14}C dating of mg geological samples with electrostatic accelerators 79−25361
^{14}C dating rel. to magnetic and other dating methods 78−57359
^{14}C radioactive dating, determ. of ^{14}C/^{12}C ratio, review of methods *(Hungarian)* 79−48578
^{14}C time scale changes and Late Pleistocene geomagnetic var. 79−62433
Fe ore, Calicut area, associated biotite pegmatite dating by fission track 77−13066
K-Ar ages for basalts from Great Meteor and Josephine seamounts 77−9399
K-Ar dating method for argillaceous sediments 79−8716
K-Ar dating of intrusion gas and scheelite mineralisation, Cantung, Canada 79−5460
K-Ar dating using three-dimens. plots 79−62601
K-Ar geochronology of Poohbah Lake alkaline complex, NW Ontario 77−17047
^{40}K-^{40}Ar mineral ages for rocks in SW.Brooks Range, Alaska 80−26469
Mn nodules, from Pacific Ocean growth rates from U series and hydration-rind dating 77−29280
O isotope palaeotemperatures, from Tertiary period in North Sea area 78−88903
O isotope stratigraphy and Late Pleistocene coral terraces in Barbados 77−78182
^{18}O in equatorial Pacific core, glacial time scales and climate 80−21817
Pb isotope studies of ore deposits of circum-Kisseynew volcanic belt, Canada, ages 79−5479
Pb isotopes struct. of basic-ultrabasic layered complex 80−81847
Pb sulphides, isotopic composition, mineralisation time determ. 78−73372
$^{206/207/204}$Pb ratios rel. to Earth age and chemical evolution 79−88315
^{210}Pb chronologies of lake and marine sediments, problems 78−81122
^{210}Pb chronology of Long Island Sound sediment core, biological mixing effects 79−66672
^{210}Pb dating, results from Lake Ipea and Lough Erne sediment cores 78−28202
Po haloes in rocks and geochronology 80−56468
Rb/Sr chronology, Rainy Lake Archean granitoid batholith 79−84188
Rb/Sr whole-rock systems and chemical control 78−61366
Rb-Sr, ratio determ., by X-ray fluoresc., for radiometric age meas. 77−70356
Rb-Sr ages of early Archean supracrustal rocks and Amitsoq gneisses Isua, Greenland 78−16013
Rb-Sr ages of rocks, Hopei, China *(Chinese)* 79−20776
Rb-Sr ages of weathered and stream transported quartz grains from Harney Peak Granite, S.Dakota 79−74865
Rb-Sr and Nd-Sm ages, appl. to Earth chemical history 77−60639
Rb-Sr chronology of central Australian granulites 79−53326
Rb-Sr dating of transect of Chilean Andes, latit. 45-46°S 79−29723
Rb-Sr whole rock dating of metamorphic events, Iglesian Complex, Venezuelan Andes 77−81894
Rb-Sr whole rock isochron, Newry Granodiorite, N.E.Ireland 77−5162
Rb-Sr whole rock isochron age from Kangamiut dykes rel. to Hudsonian orogeny in W.Greenland 79−5459
Rb-Sr whole-rock isochron age, 2390 Myr, for Scourie dykes, NW.Scotland 79−39690
Sm-Nd and Rb-Sr chronology of continental crust formation 79−12100
U minerals in Witwatersrand Triad, geochronology 77−86892
U ore dating from meas. of ^{238}U and Ru conc. 80−21863
U series dating, open system model appl. 79−29874
U-Pb ages of pegmatites in Enderby Land, Antarctic 80−76946
^{238}U, determ. of time since arrival in matrix existing at time of discovery in Pakistan 79−34822

geodesy
see also gravity
30th order harmonics from resonant inclination variations of ten satellites 79−84071
accuracy with transportable lunar laser ranging station 77−48988
actual gravity field isoparametric and isozenithal type representations 79−53297
adjusted straight line, strict determ. from correlated obs. via least squares method *(German)* 77−86751
aerial photography for densification of urban geodetic nets 77−78462
Afar region rifting, geodetic evidence and elastic-brittle model 80−21697
Afar triangle, geodetic evidence for rifting, model for vertical displacements 80−98295
altitude and gravity variations, meas. via N.W.Europe gravity base network *(German)* 78−15948
altitude observations, Fourier transform. *(German)* 78−61312
N American horizontal datum, new adjustment 77−2079
Ancona geodetic network, design problem 80−85578

geodesy continued
anomalous potential approx., choice of norm using least squares collocation 77−90985
Antarctica, geodetic and meteorological meas. 77−87073
antipodal normal section 79−29691
approximate ellipsoidal-Earth equations for mapping and fix-taking calculations 78−73303
array algebra for multilinear least squares prediction and filtering 78−69470
array algebra techniques in multilinear least squares problems 78−36296
artifical satellite geodesy techniques *(German)* 77−64190
artificial satellite geodesy and geophysics appls., review 77−64183
artificial satellite geodetic meas., ionosphere refr. influence *(French)* 79−58133
artificial satellite laser ranging, geodetic appls., San Andreas fault 77−64185
artificial satellite laser ranging, high precision, earthquake anal. 80−98215
artificial satellite laser ranging, oceanographic appls. 77−64484
astronomical azimuth determ., accuracy, geodetic networks orientation control appl. 78−92774
astronomical azimuths of terrestrial objects, as indicators of continental blocks rot. 78−53613
astronomical latitude, azimuth and longitude, simultaneous determ. method 77−60339
N.Atlantic, gravimetric geoid confirmation of sea surface topography by Skylab 77−17014
N.Atlantic Ocean, detailed gravimetric geoid 79−62422
NW.Atlantic Ocean, oceanic geoid and tides derived from Geos 3 satellite data 80−3901
atmosphere pressure deforming Earth shape, seasonal var. 80−21609
atmospheric phase path corrections for very long baseline radio interferometry, mathematical modelling techniques 77−78637
atmospheric processes, effect on tiltmeter and gravity obs. *(Russian)* 78−48957
automatic drafting system, appl. to problems of geodesy *(German)* 78−15952
automtic optical plumbline requirements and design *(German)* 77−70877
aviation gravimetric systems, sensitive element comparison *(Russian)* 77−73625
azimuth of nearly antipodal geodesic, soln. for lines for which azimuth is nearly 90° 77−60335
azimuth-dependent statistics for data interpolation 77−90982
base line estimation, using single passes of laser data 80−3910
base-free geodetic intersections method, theory *(Russian)* 79−96731
Blue Ridge and Piedmont provinces, levelling surveys rel. to Recent vertical crustal movements 79−79794
Bouguer formula of 1749, appl. to gravity corrections derivation 79−29692
boundary value problem, soln. 79−62424
boundary value problem 80−30975
British Isles 80−109086
bubble levels, apparatus for testing bubble vials 79−29871
cadastral survey administration, Bavaria, centralised and decentralised data processing *(German)* 77−2288
S.California, geodetic levelling rel. to Peninsular Ranges early 20th century uplift 79−79796
California coast, 1941-1978, land and sea level changes 80−21610
S.California uplift, geodimeter meas. of strain 79−48434
S.California uplift area, geodetic relevellings anal. for Recent vertical movements modelling 79−80055
Canada, N.W.T., astronomical surveying and midnight Sun 77−13052
cavity effect in tunnels of various cross-sections, theory *(Russian)* 78−88784
NE China, propagating deform. front rel. to Haicheng earthquake prediction 77−49028
China, Zhang Sui and first astronomical geodetic survey *(Chinese)* 77−64911
Clairaut eqn., connection to satellite geodesy and Jupiter 78−11795
co-geoid, appl. to interpolation of vertical deflection and to geoid determ. *(German)* 77−9323
collocation, with help of Gaussian algorithm *(German)* 79−79730
collocation method, theoretical foundation *(German)* 77−86748
contributions to geodynamics *(German)* 78−81101
control networks, strength analysis 77−44886
coordinate systems, time and reference frames 78−69272
counter-orbiting drag-free satellites in Earth polar orbit, general relativity test and geodetic meas. 77−22047
counter-orbiting polar satellites, geodesy information in modified relativity mission 79−62426
criterion matrices, appl. to design of homogeneous isotropic geodetic networks *(German)* 79−100983
crustal deformation analysis, models for estimation of parameters *(German)* 80−101319
crustal movement measurement, instrumentation trends and prospect 79−29738
crustal movements, conf., Palo Alto, California, USA (July 1977) 79−79785
cylindrical body of finite length, gravity pot. *(French)* 77−78079
data analysis by collocation method 80−77130
data base, basic entities definition 78−65392
data inversion, mathematical formulation for fault-plane solns. 78−12016
data inversion and model of 1927 Tango earthquake conjugate fault system 78−88779
deep asymmetry of Earth, inertia rel. to convection currents 80−98269
deflection of the vertical at Tokyo 80−17228
deflections of the vertical, from discrete soln. of geodetic boundary value problem 78−3702
densification of ground control networks, computer program package *(German)* 80−94452
Diablo Plateau region, W.Texas, new evidence for tectonic uplift 80−72481
digital correlation of complex exponentiated data *(German)* 79−44279
Digital Terrain Model, use of electronically controlled drawing machines *(German)* 78−20348
direct and reverse problems, closed formulae 77−44882
direct gravity formula for 1967 Geodetic Reference System 78−92775
Dirichlet problem, correl. functions on upper half space 77−90986
displacement meas., small, using three-mode laser 80−77748

geodesy continued
Doppler satellite positioning in Canada, review 77—44883
Earth deformation, mag. field effects 80—109085
Earth equilibrium figure, integro-differential eqns. 79—44077
Earth excitation pole, annual motion, vars. and periods *(Russian)* 78—40461
Earth figure and gravit. field determ., least-squares collocation method 79—48392
Earth free oscillations, rot. and elliptical splitting 79—88257
Earth pear-shaped section, improved longitude-averaged meridional profile 80—94450
Earth station geodetic coordinate transformation and datum definition 77—17015
Earth surface tidal tilts, influence of atmospheric press. fluctuations *(Russian)* 78—88790
Earth tide observations processing, individual monthly sets weightings *(Russian)* 78—88789
earth tides, long water-tube tilt meter 79—100959
earthquake prediction based on tilt anomaly 80—104917
ellipsoid, bi-axial, long geodesics computation through Gaussian quadrature 79—100806
ellipsoid orientation in geodetic networks 78—48955
ELWAAG automatic hydrostatic system for geodetic height meas. *(German)* 79—88511
EM distance measurement (EDM), single-wavelength, data ratios rel. to line length changes resolution 80—4143
Ethiopian rift geodimeter survey 77—70633
flat Earth upward continuation 79—84078
fracture zones, geoid anomalies rel. to oceanic lithosphere thickness 79—88231
free nets, modification of Helmert-Wolf's soln. *(German)* 80—94453
future role of astrometry *(German)* 77—17332
Gauss, Carl Friederich, correspondence on heliotrope and geomag. meas. *(German)* 77—67168
Gauss-Helmert model, singular covariances, least-squares adjustments *(German)* 80—56340
Gauss-Helmert model for least-squares adjustment, props. *(German)* 78—61309
generalised Laplace condition 78—69271
geocentric position variation due to terrestrial fluid mass motion 80—76894
geodetic astronomy and astrometry, international colloquium (Dresden, Germany, 1978) *(German)* 80—36223
geodetic elasticity theory, matter and appl. 77—60338
geodetic observations goodness, concept restatement rel. to recent crustal movements studies 79—57840
geodynamical changes, evaluation of Doppler satellite obs. 80—76893
geoid, rel. to single-cell mantle convection 77—60362
geoid, rel. to subduction and lower mantle convection 80—31023
geoid and global heights in Europe, collocation method analysis 80—76896
geoid and potential coeff. determ. from gravity data, atmospheric correction 77—17017
geoid anomalies, interpretation techniques 80—3897
geoid anomalies and lithospheric thickness 79—84077
geoid computation, effects of deviations of sea surface from geoid 77—64177
geoid depression and elevation obs. *(German)* 79—5442
geoid figure determ., dynamic method 78—16175
geoid height, spherical harmonic potential coeffs., use of area means 80—94449
geoid heights along Hawaiian-Emperor seamount chain, Geos 3 altimeter data results 80—3899
geoid heights in global soln. of gravity field 80—3914
geoid improvement in local areas, satellite to satellite tracking appl. 79—62423
geoid improvement in local areas by satellite gradiometry 78—36295
geoid major undulations, possible thermal nature 77—81784
geoid shape anomalies *(Hungarian)* 78—15944
geopotential, 15th-order resonance effects of Nimbus 1 rocket (1964-52B) 78—65168
geopotential, algorithms for computation using simple density layer 77—5128
geopotential, evaluation of 14th order harmonics 79—29694
geopotential, Neuman problem stable soln. 77—52964
geopotential 14th order harmonics evaluation from satellite resonant inclination vars. 78—48954
geopotential 29th order harmonics from Ariel 1 orbit at 29:2 reson. 77—56572
geopotential appls. of $\beta/2$ orbital reson. of artificial satellites 79—53296
geopotential calc., Hansen's coeffs. in satellite theory 77—49276
geopotential coefficients, 31st order, from Proton 4 satellite orbit determ. 77—64632
geopotential determ. by satellite laser tracking 77—64184
geopotential determination, upward and downward continuations, geodesy and topography effects 80—21603
geopotential expansion in nonsingular orbital elements 77—90988
geopotential from gravity measurements, levelling data and satellite results 80—101313
geopotential harmonic coefficients, determ. from China 2 rocket (1971-18B) orbit 80—4231
geopotential harmonics, mantle convection and stress field under Pacific plate calc. 77—9393
geopotential improvement from satellite and surface data (Goddard Earth Models 7 and 8) 77—32977
geopotential models, accuracy 79—25183
geopotential representation 77—44885
geopotential resonance, Skylab 1 rocket, 1973-27B, orbit determ. and anal. 80—67515
geopotential resonances on Vanguard orbits 77—32978
Geos 3, altimeter data anal. in Tasman and Coral seas 80—3903
Geos 3, altimetry data appl. to orbit determ. expt. 80—4226
Geos 3, calibration and evaluation of STDN S-band stations, using Doppler and laser ranging data 80—4228
Geos 3 altimeter data, processing for recovery of geoid undulations and gravity anomalies 80—3896
GEOS 3 altimetry data eval. using spherical functions expansions *(German)* 78—3708
Geos 3 laser tracking sites, base lines determ. from satellite-satellite tracking data 80—3911

geodesy continued
Geos 3 orbit determination expt., results of Geos 3/ATS 6 satellite-to-satellite tracking 80—4225
GEOS-3 altimetric data, short arc reductions 77—70583
German Bight, geoid determ. by gravimetric levelling *(German)* 78—3813
global coordinate systems geocentric origins, comparison from uniformly distributed data 79—57839
global correl. of topographic heights and gravity anomalies 78—15953
global covariance function, nonhomogeneity, least squares collocation 78—3699
global gravity field compared to geomagnetic potential 80—104854
Global Positioning System NAVSTAR connection to World geodetic system of DOD 79—25378
Goddard laser systems and their accuracies 77—64482
gravimetric geoid over Alps, and tectonic interpretation *(French)* 79—66600
gravimetric geoids. comparison with Geos 3 altimetric geoid 80—3898
gravimetric networks, adjustment *(German)* 79—44084
gravitational spectra from direct measurements 80—30978
gravity anomalies at Earth topographic gravity anomalies at Earth topographic surface, determ. by cosmic methods 80—56337
gravity anomaly reduction to a sphere *(Russian)* 77—86744
gravity field, soln. of downward continuation problem by initial value method *(German)* 77—86750
gravity model improvement using Geos 3 (GEM 9 and 10) 80—3909
gravity networks, optimisation *(German)* 78—15950
gravity new system, changes in international gravity base values and anomaly values 80—51317
gravity perturbation due to ocean tide, series computation 80—104857
gravity perturbing potential, calc. by Stokes eqn. 79—62428
gravity vector and geodetic position survey, inertial navigation system appl. 79—29914
Great Britain, Earth strain tides survey 79—44080
ground control networks, computer calculation of approximate co-ordinates *(German)* 79—84088
ground control networks, computer program for reliability estimation *(German)* 79—84089
ground tilt, measurement via borehole long-period seismometer (BELS type 79) with stable period *(Japanese)* 80—67417
Gulf Stream, large-scale frontal study using Geos 3 radar altimeter data 79—5488
Haystack-Westford base line vector, geodetic meas. comparison with radio interferometry obs. 80—89929
height and gravity, vars. with time *(German)* 78—15949
height meas. from satellite images using zoom height finder 78—36308
height vars., basic determ. problems *(German)* 79—34725
horizontal networks, height-controlled three-dimens. adjustment 80—101444
horizontal pendulum tiltmeters, recording device 78—40679
hydrostatic ellipticity calculation algorithm 80—62055
hydrostatic figure and related props. of Earth 79—66603
hydrostatic levelling, automatic precision instrument for geodesy *(German)* 77—29514
N Iceland, gravity and height vars. during present rifting episode 80—90060
NE Iceland rift zone, geodetic meas. and horizontal crustal movements 80—89930
Indian Ocean, 1×1° gravimetric geoid compared with GEOS-3 radar altimeter geoid profiles 79—16365
indirect effect (geoid undulation effect), considerations in marine gravity modelling 80—3907
inertial rotation sensors for surveying and geophysical meas. 80—12571
inertial surveying systems, geodetic appls. *(German)* 80—56656
inner structure and static deform., caused by external forces *(Hungarian)* 80—21606
integral computation over sphere, summation formula 79—29689
integral formulas for heterogeneous data 80—41363
interference distance meas. using semicond. lasers 80—77175
interpolation method using multiquadratic eqns. *(German)* 78—15951
inverse isostatic problem, global soln. for Pratt and Airy hypotheses 80—3893
inverse problem, unified least-squares method 77—73872
IR distance meas. instrument 77—49201
isostatic geoid anomalies 79—20742
Japan, astrogeodetic geoid 77—70584
Japanese Islands region, topography and gravity anomalies data compilation *(Japanese)* 80—67332
Kerguelen Islands area, geoid determ. from Geos 3 altimeter data 80—3900
Krafla Caldera, NE Iceland, gravity and elevation changes caused by magma movement 80—90052
Krafla volcano area, N. Iceland subsidence events, (1975 to 1979) 80—90053
LAGEOS, time digitiser for laser ranging, ps. resolution, built in CAMAC minicrate 78—36301
Lageos for crustal movement meas. 78—65441
LAGEOS high-mobility ranging station, geodesy appl. 79—79723
LAGEOS orbit, long-term evolution 80—94676
Lake Lugano, bathymetric map 78—96252
Landsat MSS points location on maps, methods and accuracy 79—2389
Laplace's expansion, generalisation to Earth's surface 77—60337
laser location *(Polish)* 79—27311
least squares adjustment and collocation 77—90984
level surveying, atoms. refr. correction *(Russian)* 80—77127
level testing, vertical and horizontal settings 77—29489
levelling, influence of temp. in Telyvel electronic system *(German)* 78—45037
levelling, systematic errors of compensator levels, new instrumental developments *(German)* 77—2289
levelling data, anal. for vertical crustal movements interpretation in time-space domain 79—80056
levelling data, automatic evaluation prospects *(German)* 78—32258
levelling data, time-space domain representation, computer program 78—88932
levelling survey data, math. anal. for assumed const. vertical vel. *(German)* 80—82081
literature survey for the year 1976, appendices *(German)* 77—90993
local physical frames transformation, decomp. theorem, geodetic interest 77—78082

geodesy continued
local vectors connection in actual gravity field of Earth, model field, disturbing pot. 78−61297
Love number determ. by satellite obs. 77−91410
magnetostriction appls. in geodesy and instrumental geophysics *(French)* 78−12004
mantle (lower), density anomalies derived from geophys. data 80−89927
marine boundary delineation, geodetic aspects *(German)* 77−91155
marine geodesy, geometrical problems *(German)* 78−3709
marine geoid spectrum, determ. from satellite altimetry 80−3904
mean geoid heights and mean gravity anomalies (550 km squares) 79−88233
measurement and instrumentation techniques *(German)* 77−33219
Molodensky's problem in gravity space, existence and uniqueness of soln. by Newton's method 79−12061
Molodensky's problem in gravity space, review of results 78−65173
mountain territories, formal morphostructural zoning 77−73876
multibaseline, geodetic meas. technique, precision ground based 79−34987
navigation and geodesy convergence 79−25186
NAVSTAR, satellite Global Positioning System 79−101042
NAVSTAR Global Positioning System satellites Doppler meas., geodetic solns. accuracy 79−100803
network adjustment, sparse symmetric matrices profile improvement algorithm 77−48989
network connection problems, siffening problem, error anal. 80−81799
networks, equiv. of estimable quantities and invariants 77−32980
networks, physical model of notion-system of information 77−64176
networks, three dimensional calculation *(German)* 79−84090
networks design for crustal movements study *(German)* 80−76897
normal ellipsoidal three-dimens. field, first-order numerical calc. 77−52960
North Island, New Zealand, axial tectonic belt 79−2173
Nova Scotia, gravity and tilt obs. rel. to improved ocean tide models 78−92821
observatory at Graz-Lustbuhel, Austria, work and projects 80−77117
ocean, geoid and topography via Seasat-A experimental oceanographic satellite 78−77455
ocean, sea level transients obs. by Geos 3 coincident orbits 80−72535
ocean geoid, determ. from Geos 3 altimetry data 80−3905
ocean geoid, Geos 3 investigation 80−3906
ocean geoid near Blake Escarpment, estimation using Geos 3 satellite altimetry data 80−3902
ocean tides mapping with satellites, computer simulation 79−39880
ocean topography, computations and obs. comparison 78−77250
oceanic geoid., satellite obs. 77−25635
oceanic geoid computations, accuracy 80−21608
oceanic geoid determination, via satellite altimetry short arc adjustment model technique 80−21830
oceanic loading on European laser-ranging sites 78−85462
oceanic tides, semidiurnal waves determ. via obs. of artificial satellites trajectories *(French)* 79−8634
oceanographic measurements, radio interferometer techniques appl. 79−53559
odd zonal harmonics determ. using modified equations 78−92773
offshore surveys, accurate positioning at distances to 400 km 80−12328
optical centering devices, vertical collimators, for geodetic appl. 78−13807
optical systems, high-precision compensated levels, geodetic appl. 80−101813
NW Pacific Ocean, gravimetric geoid 77−73624
Pacific sea-floor topography and isostatic compensation mechanism (Hawaii region) 80−104945
parameter accuracy, improvement by choice and quality of obs. 79−44078
periodic errors in measuring instruments, determ. via spectral anal. *(German)* 77−87131
Phlegrean Fields, Naples, geodetic and geophys. meas., elevation changes 79−29734
photogrammetry, use in network densification and land register surveying *(German)* 79−92633
physical and biological science conf., Japan (Feb. 1979) 80−12846
physical geodesy and surveying, objectives, meas. techniques and data processing methods *(German)* 80−101317
planetary dynamics obs. by satellite geodesy 77−81785
polar motion analysis by radio interferometric surveying, POLARIS project 79−79721
pole secular motion, global plate tectonics effects on Earth axis of figure 78−65172
position location and navigation, conf., San Diego, CA, USA, Nov. (1978) 79−25374
positive geoid height anomalies, correl. with subducted lithosphere and hotspots 80−90056
potential field anomalies, transformation error functional minimisation *(Russian)* 77−13053
potential field data, wavenumber domain methods 80−51559
potential fields, statistical interpretation with covariance functions 77−73873
potential function on Earth's surface, analytical collocation with kernel functions 80−36220
prospecting procedures and geodetic problems *(German)* 77−70588
radar altimetry data, smoothing processes for Geos-3 data 80−4144
radio interferometric differential baseline meas. comparison with conventional geodesy 79−79722
radio interferometric systems appl. 79−25375
radio interferometric technique, 1.24 km base line vector determ. 78−40686
radio methods, quasi-single freq. Doppler-Faraday technique 80−77128
rating net accuracy from angular geodetic cross bearings *(Russian)* 79−92476
recent crustal movements as determined by geodetic meas. 77−44960
recurrence relations for integrals of associated Legendre functions 79−29690
reference and coordinate system for global geodetic methods, subdecimetric precision range *(German)* 78−81102
reference frame establishment in geodynamics and geodesy 80−21601
reference systems for crustal motion studies 79−79720
regularisation technique, identical to least squares collocation 80−41364
review, geodesy as ordering factor in society *(German)* 77−60344
N.Upper Rhine Graben, negative height change causes *(German)* 79−34727

geodesy continued
Upper Rhine Graben, repeated levellings, errors *(German)* 79−34726
Upper Rhine Graben and Rhine Shield, levelling data, multivariate analysis *(German)* 79−34728
Rhinegraben, geodetic high-precision meas. in active tectonic area 79−79788
Riemann curvature tensor and closed geodesic paths, for teachers 78−24600
San Andreas and Calaveras fault region, crustal deformation, 1971-8 obs. 80−56428
San Andreas fault, California, short-period nonseismic tilts rel. to episodic slip 77−29276
satellite, geodesy, appl. to GRIM 2 gravit. pot. model determ. and evaluation *(French)* 79−8587
satellite altimeter data analysis, role of orbit determ. 78−77177
satellite altimetry, algorithm for subsatellite point position vector length determ. 79−29869
satellite altimetry, refinement of short arc adjustment model 77−60336
satellite altimetry data anal., combination solns. 80−76895
satellite altimetry geoids, correlated errors for GEOS-3 78−28152
satellite and lunar ranging, future developments 77−64483
satellite cameras, sidereally driven, numerical corrections 78−40678
satellite data application to regional anomaly surveys 80−51558
satellite determined gravity results, geophys. and geodetic appls. 77−25634
satellite Doppler techniques, geocentric positioning of triangulation of Great Britain 79−29695
Satellite Emission Radio Interferometric Earth surveying (SERIES), GPS geodetic system 79−100804
satellite geodesy, geometrical and dynamic methods, development *(Polish)* 78−88780
satellite geodesy, review *(German)* 77−44905
satellite laser ranging system, 2cm accuracy, for geodetic research 77−21932
satellite laser tracking data, ray tracing evaluation of refraction errors 79−8588
satellite location by tone-code trilateration 77−9653
satellite orbit, time regularisation of Adams-Moulton-Cowell algorithm 78−45208
satellite orbital elements and station coords. determ. by least-squares collocation *(Russian)* 78−49296
satellite photogrammetry, dynamical constraints 78−15943
satellite ranging, picosec. pulse freq. doubled Nd:YAG laser system 77−21933
satellites gravity measurements, basic mechanical principles of gravimeters and gravity gradiometers *(German)* 80−101461
scale and orientation in combined Doppler and triangulation nets 80−101311
sea surface topography, altimeter data analysis by sequential filter 80−4145
sea surface topography, four dimensional reference system realisation for ocean dynamics 78−77176
sea surface topography obs. with Geos 3 altimeter data 80−3908
sea-mount loads affecting crust, isostatic compensation and geoid anomalies 80−109132
SEASAT radar altimeter, resolution capability preliminary estimates 80−72645
SEASAT radar altimeter 80−56613
SeaSat-1 North Sea expt. *(German)* 80−81805
second-order derivatives in spheroidal and spherical coords. 80−101315
sequential solutions, with bandtype system of obs. eqns. 78−65169
SFB 78 Satellite Geodesy, GEOS-III obs. contrib. in 1975-76 period *(German)* 77−70591
Sierra Nevada, California, repeated geodetic levelling data rel. to recent crustal movement 79−79795
singular compensation problems, hypothesis tests *(German)* 78−44758
Smithsonian Astrophysical Observatory laser tracking systems 77−64481
smoothing function recurrence relation 80−98213
space geodesy, time synchronization requirements *(French)* 79−58233
space geodesy, twin probes method 79−25443
spherical harmonic coefficients of Earth's field, orthogonality 80−104881
spherical harmonic potential coeffs., use of area means 80−94449
spherical harmonics of gravitational potential, free boundary value problem, uniqueness 80−30973
spherical triangles, numerically stable computation *(German)* 78−88793
Starlette satellite, precision orbit computation 78−65478
station geocentric coordinate determination, artificial satellites, short arc station coordinate method 77−44902
statistical geodesy, engineering perspective 78−81099
statistical geodesy 79−29696
stereoplotter, TOPOCART B, accuracy and performance study 78−81436
stochastic parallel displacement of tensors, geodesic correction 80−8920
strain measurements, in Ancona (Italy) area 77−86742
subsoil behaviour in Potsdam rel. to storms and atmospheric pressure *(German)* 79−62425
surface deformation detect., 500-m base laser interferometer 80−105087
Surkhob fault zone, rel. to Garm region geodetic data 78−15979
systematic errors detection, hypothesis tests using adjustment in sections *(German)* 79−44083
tangent bundle, geodesics, correspondence with spinning particles 80−68099
Taylor expansion of theoretical gravity formula 79−100807
telluroid, definition 78−65171
tesseral harmonic, counter-orbiting satellites testing general relativity 78−45554
Theo 002 Universal Theodolite for geodetic astronomy 77−82028
thermoelastic strains and tilts, anal. of coupling between thermal boundary layer and topography 78−20346
three dimensional geodesy, datum problem 78−61310
three dimensional test net, investigations in Stuttgart area *(German)* 79−79731
three-dimensional geodesic mapping eqns., rel. to Earth best-known figure determ. *(German)* 78−73304
tidal tilts, parallel recording through digital print-out and photorecording channels *(Russian)* 78−88785
tides in solid Earth, review *(Chinese)* 80−89925
tilt measurement, halfsecond levels investigation *(Russian)* 78−40675
tilt meter observations at Berezovaya Rudka station, results *(Russian)* 78−88783

geodesy continued

- tilt meter observations harmonic anal., influence of S_1 diurnal meteorological wave *(Russian)* 78—88788
- topography and backscatter analysis of Geos 3 data 80—3915
- transatlantic long base line interferometry at 10680 MHz 79—48390
- TRANSIT satellites' contribution to navigation and geodesy 78—57161
- triangulation network adjustment to new European system *(German)* 77—70590
- trigonometric networks calculation, development and form. *(German)* 78—15947
- trilateration network, adjustments to account for meteorological conditions 80—77131
- undulation and anomaly estimation using Geos-3 altimeter data without precise satellite orbits 77—64178
- undulations of geoid implied by gravity anomalies on sphere 80—21614
- E.United States, geodetic levelling rel. to nearshore currents off Long Island 77—45014
- University of Hawaii lunar ranging expt., geodetic-geophysics support programme 77—56569
- W.USA, vertical crustal movement, anal. of levelling survey 80—72409
- variance-covariance-component estimation of Helmert type, introduction 80—101318
- variational formulation of geodetic boundary-value problem 78—92772
- Venice historical centre, altimetry rel. to defences against high water and subsidence *(Italian)* 77—86740
- vertical crustal movements, solvability and multiquadric anal. appl. 79—79787
- Very Long Baseline Interfereometry appl. to geodesy 80—109274
- Very Long Baseline Interferometry (VLBI), foundations and geodetic appl. *(German)* 78—45036
- very long baseline interferometry appl. to geodesy and geodynamics 77—56767
- VLBI appl. to geodesy, Earth rot. and network geometry optimisation 78—92996
- VLBI Earth surveying, miniature radio interferometer terminals 79—100805
- VLBI using geostationary satellite link 79—29968
- Walvis Ridge, compensation mechanism 80—94448
- water levels, obs. via electrooptical distance meas. *(German)* 78—69280
- Western Harz test net, height and geoid determ. *(German)* 77—70592
- window functions, influence on prediction in geodesy *(German)* 77—86749
- zenith telescope geodetic meas. 80—98550

geodetics *see geodesy*

geoelectricity *see terrestrial electricity*

geography

- NW Africa, Late Palaeozoic-Early Mesozoic palaeogeography 77—70659
- barrier islands, global distrib. in terms of tectonic setting 79—2214
- cultural and landscape interpretation from remotely sensed data 77—56782
- distributed data bases for structured data 77—53200
- East Berlin Formation, Connecticut Valley, palaeogeography 77—44983
- England, surface landforms ages from ^{230}Th/^{234}U dates on speleothems 78—36128
- estuaries, nontidal, hydrographic network changes under influence of natural factors and water management measures 79—29792
- geomorphology, land exploitation organisation Svencionys upland structure and development *(Russian)* 78—20423
- impact structs., so called, non-random geographical distrib., implications 79—34825
- information systems, conference, Dedham, Massachusetts (16 to 21 October 1977) 79—74826
- Iranian earthquakes, instrumental and relocated epicentres evaluation 79—88258
- ISO FORTRAN IV program for generating isopleth maps on small computers 78—57157
- Jordan, land system classification using Landsat imagery 79—2388
- land distribution, effects of continental drift on albedo contrast and glaciation 79—74950
- Musos Tyrelis (N.Lithuania) bog stratigraphy and palaeogeography *(Russian)* 78—49054
- S.W. Nigeria, Albian-Cenomanian, palaeogeographic implications, Africa-S.America land connection 79—84276
- north magnetic pole, 1975 position analytical determ. 78—92778
- orography, effects on global atmosphere electricity quasi-state model 79—96799
- palaeogeographic reconstruction, H_2S levels stagnation coeff. appl. 80—36291
- Palaeozoic base maps, palaeogeography and plate tectonics 80—41441
- quantitative cartographic analysis, SYMAP auxiliary programs, geoenvironmental appls. 79—70469
- remotely sensed data acquisition and processing, developing countries appl. 79—34963
- seismic zoning map, new elements 79—44105
- Spit of Kursiu Nerija, morphodynamical characteristics of protectional dune ridge *(Russian)* 78—20389
- Sulawesi, Indonesia, palaeomag. data rel. to palaeogeographic reconstructions 78—61330
- SE Sumatra coastal environment, remote sensing appls. 79—53556
- surface patterns in theoretical geography 78—57156
- Villalvernia-Varzi-Bobbio Line (N.Apennines), geomorphological evidence of neotectonic deform. *(Italian)* 79—8624
- world soil map 79—57937
- Yellow Sea, palaeogeographical environment evolution since Late Pleistocene *(Chinese)* 79—96766

geology

- *see also rocks*
- Abano region, N.Italy, geology rel. to thermal fluids sources and circulation paths 79—20883
- accretion at trenches, model, rel. to subduction complexes tectonic evolution 79—20797
- acoustic fluidisation, new geological process, theory and appls. 80—85653
- Adelaide Geosyncline, Australia, Late Precambrian geology and palaeomagnetism 80—101325
- Afar depression, Ethiopia, an Atlantic type continental margin in the making 77—21692
- Afar region, geological evolution and geophysics 79—5468
- Afghan Pamir, geology and tectonics of Himalayas 80—72513
- E.Afghanistan, Logar ultrabasite massif, geology and geomag. 80—72512
- NE Africa, geologic evolution and Pan-African belt plutonism 78—65305

geology continued

- SW.Africa, geology rel. to geodynamic model for evolution of continental margin 77—21740
- NW Africa, Late Palaeozoic-Early Mesozoic palaeogeography 77—70659
- W.Africa continental margin, subsidence and uplift, DSDP Leg 41 geological results 77—21754
- African plate, geology rel. to mantle convection pattern and stress system 77—81859
- Al Jubail, Saudi Arabia, evidence for recent coastal uplift 79—79799
- Alabama Piedmont, structural development 78—65290
- SE Alaska, megalineament marking Coast Range batholithic complex SW edge 79—62495
- Alaska, meteorite impact crater discovered with LANDSAT imagery 77—91136
- Alberta, Canada, crustal stress evidenced by bore hole asymm. 80—21671
- albrittonite, new mineral from Llano County, Texas 78—65286
- alluvial ground surface dislocation due to buried fault movements *(Japanese)* 80—21723
- Alpine fault, New Zealand, frictional metamorphism, Ar depletion and tectonic stress 80—41440
- Neo-Alpine orogenesis, thin-skinned plate tectonics 79—84207
- Alpine tectonite lherzolites, Sr isotope comp., evidence for mantle origin 78—65302
- Alps, stratigraphy and microfacies of Upper Triassic and Lias at Champ Fleuri *(French)* 78—24283
- Alps, tectonic progradation rel. to plate tectonic evolution 80—56452
- N.America, Plio-Pleistocene glacial sediments rel. to Pleistocene stages terminology 79—62470
- N America, Precambrian geology rel. to possible Proterozoic plate boundary 77—91079
- N.America west coast, upper Mesozoic subduction complexes distrib. and character 78—81136
- N.American continental margin in Nevada during Late Cambrian 79—48472
- N.American intra-plate crustal deformation, implications of VLBI meas. 80—51379
- ancient deep-sea fan in Cantabrian Mountains, growth 78—44813
- ancient metamorphic rocks, geophysical and geological data combined anal. technique *(Russian)* 79—8630
- Ancona region, Italy, geological survey rel. to seismo-tectonic considerations *(Italian)* 78—40492
- Andean andesites, petrogenetic composition variations 80—8313
- andesitic and alkaline provinces in Mexico and central America 79—57880
- Andrew's Point, Cape Ann, Massachusetts, localised fenitisation 77—64276
- Annual review of Earth and planetary sciences, vol.5 77—64174
- Antarctic Peninsula igneous rocks, transverse geochemical vars. rel. to calc-alkaline magmas genesis 80—56466
- Antarctica, subglacially erupted rocks of Early Miocene 80—98287
- Anti-Atlas, Morocco, Pan-African province geodynamic interpretation from geology and geochronology *(French)* 80—76952
- apatite solubility in magma, laboratory expts. 80—72504
- NW.Apennines, surface structs. rel. to seismicity 79—34749
- Aphebian alkaline plutonic and hypabyssal rocks, Great Slave Lake 79—84255
- Appalachian Orogen in Canada 80—8304
- Appalachian orogen western margin, basement slice at Saint-Malachie, Quebec 79—20824
- Appalachian salients and recesses, Lake Precambrian continental breakup and Iapetus Ocean opening 77—17057
- folded Appalachians, geology rel. to thermal springs origin and heat flow meas. 80—41414
- Appalachians, recent thrusting 79—79836
- Appalachians, structural trends NE of Newfoundland and Trans-Atlantic correlation 80—85656
- N Appennines, geology rel. to collisional orogen model 79—92515
- Apuane Alps structural evolution, continental margin deform. in N.Appennines, Italy 79—25245
- Arakapas fault belt, Troodos Massif, Cyprus, metallogenesis along fossil oceanic fracture zone 79—29769
- Archaean basin-craton complexes, critical appraisal, Canada 79—5481
- Archaean Dalembert tuff, Rouyn-Noranda, Quebec, Canada, petrography, and eruption mechanism 79—62472
- Archaean granite-greenstone terrains rel. to mafic dikes 79—57881
- Archaean greenstone belt, Island Lake, Manitoba, diapiric structs. and regional compression 79—57922
- Archaean greenstone belt, Yellowknife, Canada, structs. induced by granite diapirs, rel. to tectonics 77—81892
- Archaean migmatites in Lofoten-Vesteralen, Norway, Nd, Sr and Pb isotope data interpretation 79—34773
- Archaean peridotitic komatiites in La Motte Township, Quebec, emplacement 78—77234
- Archaean precious-metal hydrothermal systems, Ontario, alteration patterns and metal distrib. 80—12382
- Archaean precious-metal hydrothermal systems, Ontario, rare earth element and 0 isotope relations 80—12383
- Archaean rocks of E.Lac Seul region, English River subprovince, NW.Ontario, Rb-Sr isotopic study 80—94486
- Archaean rocks of Limpopo Mobile belt, showing early high-grade metamorphism 80—94502
- Archaean sedimentary basins, geology rel. to lithospheric thickness 80—89986
- Archaean supracrustal relics of Sierra Leone, Liberia, Guinea and Ivory Coast, zonation 78—44815
- Archaean terrains, press.-temp. data rel. to continental geotherms 79—34780
- Archean continental crust, magma genesis by crustal anatexis, garnet-pyroxene thermometry and barometry 78—65236
- Archean greenstone belt, NW. Ontario, Zr-U-Pb geochronology 80—98272
- Archean greenstone belts, Nyanzian System, W.Kenya, trace element model study 77—60375
- Archean sedimentary rocks, Kalgoorlie, Australia, rare earth elements and crustal evolution 77—60374
- Archean supracrustal Rb-Sr ages, Rocks and Amitsoq gneisses, Isua, Greenland 78—16013
- Arctic seafloor studies with Tethered Remote Operated Vehicle 78—61576
- area and centre of mass rapid computation 77—9507

geology continued
- arfvedsonite, sodic amphibole occurrence in basalt dykes, Newfoundland 78—65287
- SE.Arizona, Laramide folding and faulting, basement cored uplift model 80—8272
- S.E. Arizona, lava flows, xenolith bearing basalt form. 80—8303
- Arizona, palaeomag. poles and polarity zonation from Cambrian and Devonian strata 78—28156
- Armenian territory foundation, new struct. and age data *(Russian)* 79—74874
- Armorican Massif, occurrences of antimony minerals from ile de Sein and cap Sizun *(French)* 78—11888
- Arran dyke swarms, British Tertiary igneous province, palaeomagnetism 78—73306
- Arunta Block, Australia, sapphirine-bearing rocks with sedimentary and volcanogenic protoliths 79—44185
- ash-flow tuffs, Lake Precambrian in E. Newfoundland 79—84258
- E. and SE.Asia, evolution of marginal basins and adjacent shelves 78—32055
- Askja Caldera, Iceland, imaging radar obs. rel. to surface roughness 79—16426
- astrons, cosmic impact features, role in geological evolution 77—56632
- asymmetric folding and monoclinal kinking of compressible elastic multilayers 77—17093
- Athabasca Oil Sands area, Alberta, geology rel. to groundwater temps. 79—62465
- N.Atlantic, Mesozoic and Cainozoic, calcareous sediments depth distrib. 80—81866
- Atlantic continental margins, obs. and ideas 77—21691
- S Atlantic Ocean, depositional history during last 125 million years 78—44798
- S.Atlantic Ocean, palaeoenvironment of anaerobic sediments in Late Mesozoic 77—17074
- Atlantic Ocean, sedimentary distrib. relation to climate in last glaciation 80—8308
- Atlantic-type continental margins, post-Permian, sedimentary histories 77—21738
- Australia, tectonic, igneous and metallogenic provinces rel. to mantle convection and subcrustal stresses 80—72484
- Australia and Timor Trough, facies rel. to topographic wave migration during past 3 million years 78—49018
- Australia continental slope and shelf, sedimentary basins evolution from Mesozoic times 78—96175
- N.Australia Precambrian shields and platforms, struct. and tectonic style 80—3982
- Australian region, contrasts between oceanic and continental Oligocene unconformities 78—73370
- Australian Zn-Pb-Ba deposit, primitive Pb determ. 78—11900
- autocorrelation coeffs. from irregularly spaced areal data, in FORTRAN 77—33191
- automatic contouring of geological data, review 78—7820
- Avalon zone, Atlantic Canada, extent determ. from mag., seismic and gravity data 80—12384
- Badra area of Iraq, gravity investigation rel. to geological structs. 79—34729
- Baie d'Audierne (Brittany) basic-ultrabasic complex, age and tectonic implications 78—11852
- Baikal region hot springs *(Russian)* 80—94551
- Baikal rift zone, relationships between geologically young and ancient structures 78—36133
- Baja California, ancient lithospheric lherzolite xenolith in alkali basalt 77—81888
- Baltic Shield, geological and tectonic implications of Swedish rapakivi suite palaeomagnetism 80—56346
- banded deformation structures description and origin, regional strain, local perturbs. 78—7629
- Banks Island, Canada, deposits and aeolian processes *(French)* 78—36163
- Barbados, Late Pleistocene coral terraces and O isotope stratigraphy 77—78182
- barite rare earth composition rel. to formation conditions 80—41439
- Barnum Lake Pluton, Thunder Bay, Ontario, struct., petrography, geochem. 78—20403
- barrier island migration computer simulation 78—20384
- basal hills in Darling Downs, SE.Queensland, slope profiles of cycloidal form 78—44820
- basalt of back-arc basin, compositional evolution of mantle source 80—72471
- basalt petrogenesis, role of dynamic partial melting 80—46179
- basalt sheets, thermal effect on adjacent rock, heat flow model 80—46181
- basaltic andesite dykes, Iritono, central Abukuma plateau, plagioclase grain size 78—7618
- basaltic bodies, flow and emplacement direction from mag. susceptibility anisotropy meas. 79—29766
- Bashkir platform, oil and gas-bearing sites, mathematical selection methods *(Russian)* 77—9560
- basic intrusions emplacement mechanism 78—61374
- basic-ultrabasic layered complex, Pb isotope composition 80—81847
- Bay of Islands ophiolite complex Nd and Sr isotopic study rel. to midocean ridge basalts source evolution 80—85651
- Bay of Islands ophiolite suite, dynamothermal aureole 80—51355
- Bay of Islands Ophiolite Suite, evidence for oceanic crust hypothesis 78—81117
- Bear Valley Strip Mine, Pennsylvania, structural stages of Alleghany orogeny 79—88348
- bedrock topology, gravity exploration in glaciated areas 77—91289
- Belchertown pluton, W. central Massachusetts, palaeomag. evidence for tectonic rot. 77—44919
- Belingwe Greenstone Belt, Rhodesia, petrogenesis of peridotitic komatiites 78—32087
- Benin Gulf, Africa, struct. and sedimentation of continental margin 77—21693
- Benue Trough, Nigeria, early Cretaceous basalt volcanism and initial continental rifting 78—61417
- Benue Trough, stratigraphic evolution and implications for W.Africa Upper Cretaceous palaeogeography 79—2230
- biostratigraphic correlation within IGCP Project 148 79—62501
- biostratigraphic data quantification 79—62593
- biostratigraphical correlation 79—62503
- biostratigraphical logging methods 79—62594

geology continued
- biostratigraphy, range charts and no-space graphs 79—62504
- biostratigraphy, temporal range charts 79—62595
- biostratigraphy methods, comparison 79—62502
- Black River-Trenton boundary, deposition and revised stratigraphy 77—64277
- Black Sea, large rockslide formations rel. to Cenozoic sedimentation 78—3751
- Black Sea continental slope, Cretaceous rock outcrops 79—44173
- Black Sea depression basin as young trough *(Russian)* 78—88830
- Black Sea NW shallow, lithology and stratigraphy from seismic multidimensional vel. generalisation *(Russian)* 80—105068
- Black Sea transverse rise, geological and geophysical data 78—3754
- block faulting mechanism, geological and expt. studies 79—66692
- block tectonics analysis in Mongolia, appl. of two-dimensional autocorrelation anal. 80—56469
- blueschists, from Ile de Groix, France, isotopic ages, metamorphic episodes determ. 77—66896
- blueschists at Shangla Pass, N.Pakistan, early Tertiary, evidence for subduction 79—2229
- Bogoslof Island, E.Aleutian arc, alkalic rock suite 77—70660
- Bohus granite area, SW Sweden, geothermal investigations 80—85631
- Bolivia, evidence for glaciation 3.27 Myr BP 79—34865
- Bonnet Plume Basin, Yukon Territory, Canada, gravity profile anal. as aid to coal basin evaluation 80—76898
- borehole temp. gradient logs and lithology correlation 78—61416
- Boston Bay Group, Massachusetts, origin and significance of cylindrical sandstone structs. 78—69343
- Botswana, dyke swarm interpretation as failed Gondwana spreading axis 78—57180
- Botwood Group and Mount Peyton Batholith, Newfoundland, orogenic history, palaeomagnetic study 80—3917
- boudinage structures, displacement and stress distrib., finite element method 78—32078
- boudins, Precambrian terrain, India, geometric analysis 79—29771
- boxed sets of rock and minerals from Geological Survey of Canada 77—37203
- Brazil, coastline Quaternary formations, littoral zone evolution 77—21755
- NE.Brazil, Post-Palaeozoic volcanism and tectonic significance 77—21735
- Brazil, surface geology rel. to tropical weathering effect on elec. and EM meas. 79—88246
- Brazil, Uruguay and Argentina continental margin geology and tectonics, rel. to S.Atlantic opening 77—21704
- SE.Brazil and SW.Africa, geotectonic features correl. 77—21703
- N.Brazil continental margin, evolution, sediment distrib. and hydrocarbon potential 77—21697
- E.Brazil continental margin, salt distrib. and crustal models 77—21698
- N.Brazil continental margin, sedimentation 77—21748
- Brazilian Continental Margin, Panafrican thrusting and melting 77—21769
- S.Brazilian continental margin, preliminary structural study 77—21694
- Brevard ductile deformation zone, N.Carolina, struct. and seismic refl. study 78—65289
- N.Britain, crustal layering, rel. to seismic vels. of Lewisian metamorphic rocks at high press. 79—84137
- N.Britain, crustal struct. from Lithospheric Seismic Profile in Britain (LISPB) 78—73329
- British coalfields, geological aspects, resources and reserves 79—57931
- NE British Columbia, carbonate-hosted Pb-Zn occurrences, Robb Lake deposit 79—62494
- British Columbia, geology rel. to geotectonics of Cretaceous and Eocene plutons 77—91090
- British Columbia, S central, late Pleistocene stratigraphy 78—92804
- British Columbia, Shuswap Metamorphic Complex, Cariboo Mtns. 77—81838
- S.British Columbia, tectonics rel. to Mesozoic-early Cainozoic activity 77—81852
- S.W.British Columbia, Wisconsin lithostratigraphic units 77—81882
- British granites, Caledonian suture zone, geophys. correl. 80—17259
- British Isles, 1978 guide to information sources 78—88922
- British Isles, evidence for Cambrian opening of Iapetus ocean 80—98299
- SW.Brooks Range, Alaska, history from ^{40}K-^{40}Ar mineral ages 80—26469
- Bucegi Conglomerate, Romanian Carpathian submarine slope deposit 79—8632
- Bulgaria, plate tectonic theory of geological evolution 77—78148
- SE.Bulgaria, Upper Cretaceous resedimentation in NE.Strandja mountain 78—36160
- Bulgarian mid-Rhodopes massive, depth struct. metallogeny and main formation tendencies *(Bulgarian)* 79—34812
- Bulgarian Staro-Planina mountain range, metasomatic displays, geology, struct., form. of granitoids *(Russian)* 79—5476
- Bulong Complex, W.Australia, igneous layering due to fractionation of Archaean ultramafic magma 77—56626
- Burlington Peninsula, Newfoundland, U-Pb ages of crystalline rocks, Fleur de Lys metamorphism age 78—28188
- Bushveld Complex, geology, eastern compartment emplacement model 80—94505
- Bushveld Complex, spheroidal pyroxenite aggregates as special case of silicate liq. immiscibility 79—88351
- Bushveld Complex upper zone, magnetite Cr content vars. rel. to magma chambers heterogeneity and convection 80—56421
- Butte mining district, Montana, palaeomagnetism, rock magnetism and aspects of structural deform. 80—101326
- CAI, conf., Syracuse, USA (Nov. 1975) 77—15
- CAI, interactive computing with graphic display 77—21
- CAI, interactive CRT display of Bouguer gravity models 77—22
- CAI, PLATO system 77—20
- CAI 77—16
- Cainozoic intra-plate convection, rel. to mantle convection 80—98293
- calc-alkaline rocks from the East Carpathians, K, Rb and Sr distrib. 78—85555
- calc-silicate isograds, Riondel area, SE British Columbia 77—5197
- calcrete deposits from Europe, Africa and India, isotopic comp. 78—73368
- calcretes of Botswana and S.Africa, pseudo-anticlines and other structures 77—70656
- Caledonian blueschist from Irish Dalradian 79—53348

geology continued
California, geology rel. to geometry of triple junctions related to San Andreas transform 79—57904
Cambrian greenstone belts, Australia, marginal sea crust slices in Lachlan Fold Belt 79—29765
Cambrian slate belt of N Wales, mag. susceptibility anisotropy and correl. with strain 79—79832
Canada, U occurrences and mode of origin, N.Saskatchewan 79—84272
Canada Maritime Provinces, geology rel. to heat flow values 79—100819
Canadian Cordillera, geodynamic evolution 80—8276
Canadian Cordillera, Mesozoic-Tertiary basin models, geological constraints 78—28232
Canadian mineral occurrence index 77—53205
Canadian Shield, structure of Archean basin-craton complexes 78—61412
Canadian Shield tholeiitic basalt-rhyolite magmatism and massive sulphide deposits 80—36298
Canary Islands, palaeomagnetism and early magmatic history 80—72431
Canning Basin, W.Australia, hydrocarbon potential of Palaeozoic rocks 80—46176
CaO-SiO$_2$-CO$_2$, subsolidus and liquidus phase relationships to 30 kbar 80—85643
Cape Breton Is., Canada, post-Mississippian thrust faulting 78—61360
carbonate mineral identification by CO$_2$ evolution on heating 80—90248
Caribbean Basin, geology rel. to transitional intercontinental sutural geostructure model 80—31015
S.Carolina coastal plain, ages for basalt and sedimentary red beds 79—74879
Carpathian Mountains, disjunctive dislocations revealed by interpretation of space television photographs *(Russian)* 80—104958
Carpathians internal region, geology rel. to lithosphere dynamics and tectonic movements *(Russian)* 79—48444
S.Caspian depression, density variation in Upper Neogene deposits *(Russian)* 77—70661
cathodoluminescence, bibliography of papers till 1977 79—21482
Cavendish sulphide zone, Ontario, audio-frequency magnetotelluric sounding 80—51324
Cenozoic volcanic rocks, SE.California, regional stratigraphy, K-Ar ages and tectonics 79—70798
Central Mineral Belt of Labrador, a major Aphebian Helikian unconformity 79—84249
Cerro Galan Caldera, NW.Argentina, volcanic history rel. to plate tectonics setting 78—85523
Cesano geothermal field, Italy, geological study 80—76975
chalk of S.E. England, soils and geomorphology 77—44993
charcoal deposits since Lower Carboniferous, palaeoatmos. O$_2$ content 80—51542
Charleston-Summerville area of South Carolina, Geological and geophysical studies of seismicity 78—11837
Charlevoix structure, Quebec, shock produced mosaicism in plagioclase 77—44988
charnockites from Visakhapatnam, India, allanite occurrence 78—65285
chelogenic cycles in continental crust evolution *(Chinese)* 80—89984
chemical microanalysis of geological samples by X-ray microscopy near absorption edge with synchrotron radiation 78—20527
Chibougamau pluton, Quebec, Precambrian Rb/Sr geochronology 80—98273
Chilkat Peninsula, Alaska Upper Triassic rocks, regional implications 80—98271
SW.China, tectonic evolution 78—32054
Christmas Mountains, Texas, high-temp. metamorphism of carbonate rocks 77—2128
circular magmatic structures, Russian platform, rel. to circular magnetic anomalies *(Russian)* 79—88251
circular structures of large scale and great age, possible meteorite impact craters 78—28237
cirques in Bear River Range, north-central Utah, numerical anal. 80—72510
CLAIR data system overview 78—57325
clay bed, slope form and bedding dip correl., computer calc. *(German)* 77—64282
clay minerals, appl. of high resolution electron microscopy *(French)* 78—26396
cliff erosion, wave induced rel. to erosive force of waves 78—20388
Clyde Foreland, Baffin Is., last interglacial-glacial cycle, stratigraphy, biostratigraphy and chronology 78—61536
coal, from S.Wales coalfield, mag. susceptibility anisotropy meas., coalification process indicator 79—53340
coal, permeability to methane, influence of temp., geostatic and stratal press. *(Russian)* 79—66695
coal banding-plane indicator, magnetic susceptibility anisotropy meas. 78—77221
coal basins origin by salt solution 78—11899
coal fields of India, seam thickness by elec. and γ-logging 80—51394
Coal Measures of Westphalian B, NE.England, braidplain facies model 80—51396
coal seams, approx. seismic wave diffrac. theory for transparent half-planes 80—89974
Coast Plutonic Complex, British Columbia, geochronology and thermal history 80—12351
Coast Plutonic Complex, British Columbia, Rb-Sr geochronometry 80—12350
Coast Plutonic Complex of S.British Columbia, Canada, possible geothermal resources 79—70429
Coldbrook Group in Caledonia Highlands of S New Brunswick, stratigraphy, palaeogeography and tectonic setting 77—91128
Colombia, Laguna de Fuquene area, petrography of Quaternary volcanic ashes 79—84206
Columbia Plateau, basalt flow, contact zone remanent magnetisation 80—81881
COMOD, program for standardizing mineral resource commodity data 78—20524
compositional data Q-mode factor analysis, extended CABFAC and QMODEL programs 77—9504
compositional data Q-mode factor analysis 77—9503
computation from field survey and map data 77—9522
computer constructed optical-rose diagrams 77—9505
computer program for crystallographic data Cartesian translation 77—37196
computer simulation of geologic processes, for teaching 77—17
computer simulation of geologic strata, for teaching 77—18

geology continued
computer-assisted lineaments photointerpretation, perception method 78—7639
conference, natural fission reactors, Paris, France, 1977 80—17716
continental margins, sedimentary basins rel. to oceanic fracture zones, appl. to Equatorial Atlantic 77—21695
continental platform subsidence mechanisms and eustatic sea level changes 77—21718
continental rift fault patterns, analytical model 79—79805
continental shear zones, geological aspects of deform. 78—3768
Coosa Valley, Alabama, struct., folding and thrust faulting 78—65291
Cornwallis Fold Belt, Canada, history and mechanism of basement uplift 77—91091
Cornwallis Pb-Zn District, Canada, Mississippi Valley-type deposits controlled by stratigraphy and tectonics 77—91130
Cornwallis Pb-Zn district, deposits controlled by stratigraphy and tectonics, discussion 78—73366
Cos θ similarity coefficient, approximate levels of significance 77—86877
Coso Range, California 80—90049
Cretaceous magntic stratigraphy from Cismon section, N.Italy 79—44086
Cretaceous oceanic crust, isotope study of petrogenesis and hydrothermal alteration 80—46177
Cretaceous species extinction explained by cometary impact 80—76977
Cretaceous Tekenika Beds of Tierra del Fuego, tectonic and sedimentary significance 77—44996
Cretaceous-Tertiary boundary, plankton extinction and geochem. indicating extraterrestrial event 80—76976
Cretaceous-Tertiary boundary (Z coal), Hell Creek, Montana, Rb/Sr age 80—94487
Cretaceous-Tertiary boundary sediments, Red Deer Valley, magnetostratigraphy, biostratigraphy and geochronology 79—57888
E.Crimea, geological data rel. to deep crustal struct. *(Russian)* 80—104933
crustal fractures and photogeology 77—44954
crustal geological-geophysical zoning possibility 78—57342
cryptoexplosion structures, shatter cones geometry and description procedure 80—51398
crystallisation in layered intrusions formation simulation, in FORTRAN 77—33069
N.Cuddapah basin, granite domes on eastern margin 77—53019
Cundeelee area, W.Australia, regional geology and gross structure 79—2194
cylindrical shell, thin, instability rel. to mechanical anal. of geologic structs. *(Chinese)* 78—73364
Cyprus, ophiolitic sulphide ore deposits prod. by hydrothermal convection 79—29761
Dahomeyide orogenic belt, geology and struct. correl. with Volta Basin 80—109121
data bank model, appl. to geological data 77—53199
data management, conf., 1975, Nov., Paris, France 77—53198
data management and processing 78—57324
data management systems in economic geology 77—53201
Death Valley, California, radar discrimination of geological units 79—12293
Deccan lavas, mag. anomaly rel. to local geomag. secular var. 77—86768
Deccan Traps volcanic rocks, India, ^{40}Ar/^{39}Ar date and volcanic history 80—46178
deep geological structure, appl. of Bouguer regional anomalies reduction *(Russian)* 78—48958
deformational history of the Delhi rocks around Biliawas, Central Rajasthan 79—25246
deformed rocks, solid-body rot. natural indicators 79—79842
Delaware River, evidence for former extension to Wilmington Submarine Canyon 77—37255
Denali fault system, geological history rel. to S.Alaska tectonic development 78—81137
dendrogram association analysis, FORTRAN IV program 77—5326
depositional facies interpretation from seismic date 80—4122
S. Derbyshire, Pleistocene physiographic evolution 78—20422
desert features created by wind, Western Desert of Egypt compared with Mars 80—72815
desert regions, comparison with Mars 77—9688
Devonian alkalic basalt dykes, NE.Newfoundland, tensional environment 78—88826
Devonian carbonate rocks, NE British Columbia, barite origin hypothesis 79—25240
Devonian metamorphism, in the Bas-Limousin areas (Massif Central, France) 78—96204
Devonian Millboro Shale, Appalachian Plateau, slip planes, discfold anal. 78—65293
Deweras Group sedimentary environment, Rhodesia, palaeorift system 78—53650
Dezadeash flysch sedimentology rel. to strike-slip faulting along Denali Fault 77—17098
diabase intrusions, Newark trend basins, Ar isotope geochronology 80—51350
diamond with garnet inclusion, expt. crystallisation conditions study 80—46172
dictionary of geological terminology (3 vols.) *(Russian)* 80—22150
Dinaride central ophiolite zone, Yugoslavia, ultramatic modes 78—20411
Dinarides, tectonic framework and evolution 78—32053
Dinarides, Yugoslavia, middle Triassic volcanism rel. to peri-Mediterranean tectonics 78—77238
diopsides from kimberlite nodules mantle Nd and Sr composition 80—51363
Disko Island, Greenland, native Fe occurrences 77—81893
distributed data bases for structured data 77—53200
diversity indices computation, FORTRAN program 77—33076
Dnieper navigable lock, V.I. Lenin hydroelectric power station, geological problems *(Russian)* 77—86883
Dnieper-Donets depression, development rel. to Mohorovicic relict discontinuities *(Russian)* 77—44947
Dnieper-Donets depression, sedimentary cover struct. along Jagotin-Baturin profile *(Russian)* 78—92806
Dobrogea, Rumania, geophysics and geology *(Rumanian)* 78—20419
dolerite sills, 'Twin Sisters', Baluchistan, Pakistan, petrology 79—44188
Don Basin, deep struct. investigation via combined gravity and seismic methods *(Russian)* 79—74987
Donegal granite, Ireland, emplacement age by isotope chronology 80—67356

geology continued
- Dong-Xing Oil Field, seismic survey, three-dimens. interpretation of complex fault struct. *(Chinese)* 79−100833
- ductile deformation zones, mechanical processes involved in crystalline basement rocks deform. 79−53344
- dunite complex, S.Shetland Islands, deform., serpentinisation and emplacement rel. to fracture zone tectonics 78−44814
- Dunnage Melange, Newfoundland, regional geology 80−81875
- Duxbury massif (2.5 Ga), Quebec, remobilised piece of pre 3.0 Ga sialic basement 80−76970
- dyke injection direction determination, new criterion based on wall minerals ang. relations 79−79843
- dynamic clustering and strong patterns recognition, automatic classification appl. 78−28322
- Early Archaean rocks comp. rel. to crust and mantle chem. evolution 78−65222
- Earth deceleration evidence from geological time considerations 80−3916
- Earth resources satellite data information processing *(French)* 79−53526
- earthflow slope formation in Hong Kong 80−109144
- earthquake precursors, charact. time of tile and strain changes 79−88264
- earthquakes max. accel., max. vel. and source distance rel. to local geological conditions 77−9360
- East Berlin Formation, Connecticut Valley, palaeogeography 77−44983
- education, physics joint honours degree course at Manchester University 79−35456
- elastic dykes, pre-cleavage, at New Paltz, New York, redistrib. by folding 79−100837
- Elberton pluton, Georgia, USA, palaeomag. of granite 80−72423
- electron microscopy, use in Earth sciences 80−105091
- electronic communication methods, review 77−17252
- NE Ellesmere Island, NWT, Canada, glacial geology and chronology 78−77233
- Elsonian magmatism in Labrador, age, characts. and tectonic setting 78−73365
- Elta River reservoir, rock slide stability, geological survey *(German)* 78−7636
- Eltanin fault zone, Pacific Ocean, crustal struct. from petrographic data 80−12376
- NW England, Permotriassic arenaceous aquifers, matrix conduction props. 77−64347
- English Peak District, geological mapping, EM prospecting method 80−3924
- English River gneiss belt, Superior Province, aeromagnetic anomaly pattern 80−30981
- w. English River subprovince subdivision 77−81883
- epidote amphibolite masses, Mt. Higashi-akaishi region, Japan, megascopic textures 77−70663
- Espanola Formation, Huronian sequence, Canada, carbonate-rich, element abundances 79−92533
- SW.Ethiopia, magnetostratigraphy of Shungura and Usno Formations 78−85470
- Europe, hydrogeology rel. to local heat flow patterns from preliminary map 79−70765
- E.European platform, peculiarities of geoelectrical section and zonation of Volyn-Podolian margin *(Russian)* 78−48964
- evaporite deposition from groundwater mobilised salt, coastal sabkhas, Libya 80−81883
- evaporites from lower Proterozoic, East Arm, Great Slave Lake 77−78181
- evolution of surface features of Earth, endogenic and exogenic forces 80−3972
- Executive system for processing geological data 77−53212
- extension veins of deformed rock, crack-seal mechanism 80−61798
- fault gouge, structural changes during stable sliding and stick-slip 78−32079
- fault gouge composition effect on frictional sliding stability 78−3759
- fault termination deformation, a clay expt. 80−21734
- faulting analysis in three dimens., strain field 78−77225
- faulting in southcentral Arizona, caused by groundwater extraction 79−57979
- faulting process, cryst. defect theory approach 80−21731
- faults and other linear features, detect. from LANDSAT images 80−77177
- faults and shear zones, assoc. deep focus earthquakes 80−61786
- Favourable Lake volcanic complex (Archaean), NW.Ontario, Canada, trondhjemitic basement enclave 80−94518
- Fennoscandian Shield and Danish Embayment, crust and upper mantle geothermal models 77−49044
- field configurations, analytical description in terms of differential geometry *(Russian)* 79−74986
- N.Finland, magnetotelluric expts. rel. to geology 79−44093
- Fiordland, New Zealand, geology rel. to crustal struct. 79−88325
- Fishguard Volcanic Group, SW.Wales, rhyodacitic pillow lava and isolated-pillow breccia 80−12389
- Fleur de Lys terrain, Newfoundland, minerals ^{40}Ar/^{39}Ar age spectra, rel. to metamorphism 77−70657
- Floridan Aquifer rocks, dolomitisation 79−53346
- fluorite mineralisation of carbonate bearing rocks, dynamic model 80−81876
- fold shape analysis, expansion of dip isogons use and preliminary investigations implications 79−39986
- folding process, laboratory expt. and theory 80−21733
- folds and gravity tectonics in ice and rocks 77−70658
- formation anisotropy, effects on resistivity-logging meas. 79−92611
- FORTRAN program for lateral tracing of time-stratigraphic units based on faunal assemblage zones 79−62510
- fossil record of solar day and synodic month vars. rel. to Earth contraction 78−11794
- Fourier amplitude spectra of strong ground acceleration rel. to MMI and geology 79−62442
- fractional crystallisation of periodically refilled magma chamber, geochemical evolution 77−41016
- France, Ariege, layered pyroxenites in ultramafic complexes, petrology, comp., equilib. conditions *(French)* 77−86874
- France, Ariege, layered pyroxenites in ultramafic complexes, petrogenesis 77−86875
- Francevillian series, K-Ar radiochronology *(French)* 80−21692
- Franciscan formation, California, pedestrians guide to rock exposures 80−81849

geology continued
- Franciscan melanges, comparison with olistostromes of Taiwan and Italy 78−81159
- Frankische Alb, slope forms in Al(1) clay, statistical investigation *(German)* 78−57211
- French Western Alps, internal mineralogical and petrological investigations of Alpine metamorphism 78−36157
- Friuli, earthquake stricken zone, geological emergency interventions 78−24287
- Friuli, geology survey following 1976 May 6 earthquake 78−24249
- Friuli, safe areas following 1976 earthquakes, survey 78−24285
- Friuli area, LANDSAT-2 imagery of linear features 78−24284
- Frontenac Axis dikes, Ontario, ^{40}Ar/^{39}Ar dating and implications for Grenville palaeomagnetism 79−62466
- gabbro weathering, Quebec, geomorphological conditions 78−28230
- Galapagos spreading centre, volcanic rock differentiation trends 80−104937
- Gander-Avalon Zone boundary, SE Newfoundland, petrography 77−5198
- GARNET, graphic analysis of resources by numerical evaluation techniques 78−20525
- garnet and clinopyroxene solid solns., geothermometry based on Fe-Mg distrib. 80−46151
- garnet peridotites, fertile and sterile, density meas. 77−5193
- garnet-cordierite gneisses, geothermometry of granulite facies rocks from Rogaland, Norway 78−96193
- Garon Lake Archaean geothermal system, Matagami rock-water interaction 80−98283
- gas deposits, distribution related to Earth's rotation and local geological conditions *(Russian)* 79−83545
- gas-bearing strata, penetration zone break-up theoretical study *(Russian)* 79−39713
- gas-oil-source rock masses, lithogenesis *(Russian)* 80−4006
- Gaspe, Quebec, age and style of mesostructures 77−17094
- general objective data base system for distributed cooperative researcher files 77−53213
- GEOLOG computerised technique for field observation recording and interpretation 78−7774
- geological computer design 77−53211
- Georges Bank Basin, stratigraphy, seismic correl. to W.Scotian Shelf 78−28231
- Georgia Inner Piedmont, hornblende and biotite ^{40}Ar/^{39}Ar ages, rel. to tectonothermal history 78−48990
- Geos 3 project, review 80−4224
- GEOSAT, geological industry reommendations on remote sensing from space 78−69495
- geothermal energy potential 79−70427
- geothermal research in Netherlands *(Dutch)* 78−61415
- Geotraverse Rhenoherzynikum, fault zones investigation by seismic refl. and refr. studies 80−90046
- N.German sedimentary basin, cond. distrib. from widely spaced areal magnetotelluric meas. 79−74833
- Gilbert, Grove Karl, 1843-1918, life and contribs. to geomorphology 78−45451
- Gippsland, Victoria, Pliocene geology rel. to eustasy and sand barrier form. onset 79−74886
- glacial continental shelves, marginal longit. channels struct. and origin 77−64261
- glacial sediments of English Lake District, pre-Devensian till 80−94523
- glacial till minerals of Great Lakes region, glacial lobe indentification 80−56465
- Glacier Peak tephra comp. var. rel. to stratigraphy 79−57897
- Glacier Peak tephra in North Cascade Range, stratigraphy, distrib., rel. to glacial events 79−25247
- glossary 78−88833
- gneiss domes structural analysis, Saint Malo massif example *(French)* 78−7627
- Goat Paddock cryptoexplosion crater, W.Australia struct. and shocked rocks petrology 80−98322
- Gondwana basin, India, igneous activity, geomorphism around Pachmarhi 77−21771
- Gondwanaland, Precambrian lineaments rel. to India and Madagascar fit 79−62477
- Gore Range (Summit County, Colorado), Quaternary geology, and reported surface faulting 79−2238
- Gorringe Bank, oceanic mantle and crust, geological survey 78−53632
- grabens of Canyonlands National Park, Utah, geometry, mechanics, kinematics 80−21728
- Grand Banks and J-anomaly ridge, geological comparison 78−15983
- granite-greenstone terrains of Rhodesian Archaean craton, age determs. 78−24288
- granitic plutons, 325-265 Myr old, in Piedmont of SE. Appalachians 79−70797
- granitic plutons, E. Newfoundland, ages rel. to Appalachian evolution 77−66894
- granodiorite, late Precambrian, strain anal. of shear zone 78−77223
- Grassy granodiorite, Tasmania, thermal history meas. using garnet fluid inclusion data 80−4012
- gravel, ice-thrusting, shear deform. 78−65347
- gravity anomalies, geological reduction *(Russian)* 78−40467
- gravity corpuscular model, geological and geophysical consequences *(Russian)* 77−67367
- gravity interpretation, simple gradient method for geological contact 78−28332
- gravity vertical gradient meas. for detect. of small geological and anthropogenic forms, discussion 78−61575
- N.Great Barrier Reef, ^{14}C dating 79−84225
- Great Barrier Reef, Bewick and Stapleton cays, drilling investigation 79−84223
- Great Barrier Reef, general nature and environment, 1973 expedition 79−84221
- Great Barrier Reef, geological history and structure from seismic profile 79−84222
- Great Barrier Reef, sedimentation trends in lee of ribbon reefs 79−84224
- W.Great Kabylia (Algeria), granite, deform. by ductile shear *(French)* 79−39716
- Great Slave Lake, Canada, early history and tectonics of East Arm graben 78−49017
- Greatlakean Substage replacing Lake Michigan basin Valderan Substage 77−17104

geology continued
W.Greenland, ^{18}O composition of rocks 78—81155
W.Greenland, Archaean sialic crust chemical and thermal evolution 80—31016
SW Greenland, Fiskenaesset, Archaean aluminous ultrabasic rocks 78—11892
W Greenland, geology rel. to continental margin, Mesozoic and Cenozoic sediments provenance 79—62479
E.Greenland, Jurassic basin evolution 78—73344
E Greenland, struct. of coastal dyke swarm and assoc. plutonic intrusions 80—56467
W.Greenland Cretaceous-Tertiary volcanic region, magma traps theory appl. 79—70776
greenstone belts, ancient marginal basins or ensialic rift zones 78—61418
greenstone belts, Archaean, thermal modelling rel. to komatiite generation 79—70762
greenstone belts, numerical models of vertical Archaean tectonism 80—81861
greenstone belts from Superior Province in Manitoba, tectonic evolution 79—62497
Grenada, Lesser Antilles, volcanic rock Nd and Sr geochem. 80—21724
Grenville basement rocks, SW Newfoundland, ^{40}Ar/^{39}Ar ages rel. to Proterozoic-Palaeozoic thermal history 79—20771
Grenville Front Zone, Precambrian geological struct. of Labrador 80—98274
ground cracking, instrumentation and field monitoring 79—79729
ground exploration and geological evaluation using remote sensing from space platforms 78—40682
groundwater exploration, geomorphological studies in Rajasthan desert 79—53375
Guatemala earthquake, 1976 February 4, tectonic aspects 77—2137
Guaymas Basin, Gulf of California, basaltic sill intrusion into sediments, hydrothermal activity 80—46154
W.Gulf of Mexico, sedimentary section, multichannel seismic refl. results 77—21749
Gulf of Mexico-Caribbean area, geology rel. to Permian-Triassic continental reconstruction 80—56431
W.Gulf of Oman, land and submarine geology rel. to tectonics 80—8279
Gulf of Sidra (Mediterranean Sea), platform upper sediment mantle geological struct. 80—36290
Hackett River greenstone belt, Slave Province, NWT, regional deforms. and granitoid plutons emplacement 79—100834
halokinesis and thermal convection 78—65308
Haramosh-Nanga Parbat structure and Karakorum range junction, geological notes 78—85553
Hare Bay Allochthon, NW Newfoundland, assoc. suite of alkali basalts and gabbros 77—66912
Hare Bay metamorphic aureole, ^{40}Ar/^{39}Ar ages and ophiolite obduction in W.Newfoundland 77—33034
Harp dikes rel. to Helikian geological record in central Labrador 78—61411
harzburgite xenolith, evidence for upper mantle multiple spinel-garnet peridotite transitions 78—65309
Haute-Savoie, France, metamorphic events ages from conglomerate diabase pebbles geochronology *(French)* 78—92810
hazards warning, US Geological Survey's role 79—84488
heated rock contact, appl. of stepwise remagnetisation method to palaeomag. field intensity, determ. 80—21619
Hellenic Arc, recent Quaternary tectonics from geological obs. on land 79—79797
W. Hellenic Trench, high sedimentation rates and variable dispersal patterns 78—57193
Hepworth carboniferous sediment, Fe minerals and concretions origin 80—17262
heterogeneous formations, pulse neutron logging data interpretation theoretical bases *(Russian)* 79—44273
heterogeneous media, mathematical models *(Russian)* 78—11897
Hidaka metamorphic belt, Japan, migmatite tectonics 80—8310
Higashi-Izu monogenetic volcano group, Japan, geology *(Japanese)* 78—96176
N.Hill End Trough, NSW, time-relationships between metamorphism and deform. in metasediments 80—26510
W.Himalaya, Central Crystallines, geology and tectonics 80—72516
Himalaya, its rise and plate tectonics 79—53334
Himalaya, Tethyan and Higher, geological description 80—72515
Himalaya and Indo-Gangetic Plains, geology and pre-Mesozoic orogeny 80—72514
Himalaya geological structure study using satellite imagery *(German)* 77—66907
Himalayan geothermal belt *(Chinese)* 79—79759
Himalayan mountain range central portion crustal struct. and geological significance *(Chinese)* 77—91066
Himalayas region, conf., Mar. 1978, Katmandu, Nepal 80—72523
Hinterland Belt, Canadian Cordillera, deformation episodes 78—88825
history, methodologies of Gilbert and Chamberlin 79—17182
Holocane aeolian landforms in Belarabon area, NSW, dunefield 77—53054
Holocene alluviation in meltwater channels near Calgary, Alberta 77—81921
Holocene climatic change effects on tropical geomorphic processes 77—64418
Late Holocene marsh deposits rel. to prehistoric large earthquakes on San Andreas fault 79—2188
Holocene stratigraphy in flood frequency analysis 79—53390
Hong Kong badlands, slopewash patterns and rates 78—20441
horizontally stratified medium as reference large scale system 77—87093
hornblende, grunerite and garnet comp. in Archean Fe formation, Canada 78—7630
human interference with geological medium, investigating methods 80—85323
Hungary, petroleum deposits rel. to sandstone litho-stratigraphy 77—86884
Huronian sedimentary rock outlier, Goulais River area, Ontario 79—25243
hydrogeological database characts. *(Italian)* 80—109255
hydrogeological problems, geologic concept in geophysical research 77—9451
hydrothermal alteration of hot spring deposits 80—76974
Iapetus Ocean suture location in Newfoundland 77—66915
Iberian margin ocean-continent boundary struct., discovery of serpentinite diapir W. of Galicia Bank 80—94489

geology continued
Iceland, crust of oceanic affinity, borehole results 80—8264
NE Iceland, dyke swarms rel. to geomag. anomalies (ΔZ) 80—89951
Iceland, geothermal activity rel. to geological struct. 78—61376
N Iceland, results of height meas., (1965 to 1977) 80—89931
SW Iceland, stratigraphy and palaeomagnetism of Esja, Eyrarfjall and Akrafjall mountains 80—89950
Iceland position and plate tectonics 77—33041
identification, numerical taxonomy methods 79—84494
Iglesian complex, Venezuelan Andes, Rb-Sr whole rock dating of metamorphic events 77—81894
igneous dikes, depth estimation via mag. anomaly sounding *(Russian)* 80—105069
igneous layered rocks, magma double-diffusive crystallization 80—90081
igneous rocks, major element analyses, PETROS data bank 77—2249
imagery interpretation and geological lineament reproducibility 77—53250
Immiter Gabbroic Complex, Morrocan Atlas Mts., petrography and geochem. 80—41442
impact structs., so called, non-random geographical distrib., implications 79—34825
India, peninsular, fan faults rel. to origin of Himalayas 80—85630
S.Indian Craton, Archaean gneiss Rb-Sr date of 3360 Myr old 80—46155
S.Indian craton, tectonic-framework deduced by LANDSAT imagery 80—98290
Indian intra-cratonic sedimentary basins, deep struct. features and evolution 77—21728
Indian Shield, geological struct. rel. to crust deep seismic struct. 80—12358
Indo-Australian plate, deformed oceanic crust rel. to plate internal deform. 80—109134
Indo-Gangetic Plains and Himalaya, geology and pre-Mesozoic orogeny 80—72514
information services, conf., April 1978, London 80—46183
intraplate volcanism, geological and geophysical parameters 78—65243
Ionian Sea, sapropel distrib. and E.Mediterranean Sea late Quaternary palaeoceanography 78—73350
IR multispectral aircraft scanner data, image processing 80—98454
Iraq, subsurface geology in W.Karbala, gravity interprets. 77—73731
Isle of Skye granites, rare earth elements and origin 78—11890
central Israel, stratigraphic thickness rel. to pre-Late Jurassic east-west fossil continental margin 79—34766
Isua supracrustal belt (Early Precambrian), W. Greenland, cosmic grains discovery in Fe formation 80—72508
Italian W. Alps, mineral parageneses of mafic metamorphic rocks 79—16464
Italy, heat flow meas. rel. to main geological features 79—70769
NE.Italy, surface geology rel. to seismically active tectonic structures 78—24286
N.Italy area, geological struct. rel. to earthquakes max. magnitude prediction 78—40493
Itapicuru greenstone belt, survey for ore bodies in Brazil 80—81879
Jamaican blueschists, coaxial pure shear rel. to deform. assoc. with subduction 79—2236
Jan Mayen Ridge, Cepan 1 1975 survey 78—96184
Japan, granitic rocks rel. to country rocks 78—81119
S.W.Japan, Outer Zone, granitic rock emplacement 78—3767
Japan, Permian greenstones, geological significance 80—21629
Japan, subduction tectonics rel. to geology 78—20377
Japan Trench, continental rocks discovery rel. to eastward extension of Honshu *(German)* 79—84200
Japanese islands, lateral var. of phenocryst assemblages in volcanic rocks 77—86886
Jharia coalfield of India, survey of struct. and geol. 80—76972
Jharia Gondwana sedimentary basin, India, geology rel. to geothermal meas. 80—98276
Job's Hill, Jamaica, geology rel. to dickite ordered and disordered varieties 78—83786
jointing, distinguishing of regional directions from joint sets assoc. with individual structs. 77—86876
Jose Fernandes intrusive body Brazil, mineralogical and petrological aspects *(Spanish)* 77—70651
josephinite, Widmanstaetten patterns as evidence of mantle origin 80—81887
Jotunheimen Caledonian structure, geological evidence 79—25222
Jura folds, geometrical adjustments during limb rot. 77—21747
Jura mountains, stratigraphy and tectonics, rot. tectonics on laramide fault pattern *(French)* 79—34785
Kalka Intrusion (central Australia) plagioclase flotation and remelting rel. to anorthosite genesis 77—60371
Kambalda (W.Australia) komatiite sequence, precious metals values in interflow sedimentary rocks 79—20830
W.Karakorum, absolute age of granitoid rocks between Hindu Raj and Gilgit River 79—100818
karst depressions, areal growth rates, ages 79—48484
karst landscapes, origin of labyrinth and tower styles, necessary climatic conditions 78—96208
Keolu Hills, Oahu, Hawaii, hydrothermal mineralogy 77—73730
Keweenawan turbidites in Michigan, foundered basin sequence developed during protoceanic rift system evolution 79—39712
KEYBAM interactive computer programs for use with PETROS petrochemical data bank 78—20523
kimberlite nodules, upper mantle petrology and geotherms 78—65310
kimberlite pipes, exploration geophysics appl. 80—51393
kimberlites, South Africa, palaeomag. determ. of emplacement temp. 77—78180
kimberlites and garnet lherzolite inclusion minerals, Sm-Nd systematics 80—51397
Klamath Mountains, Oregon, Rogue and Galice formations petrology, Jurassic island arc seqeunce identification 79—100836
komatiite-derived tholeiites in Proterozoic of New Quebec 80—8305
komatiites and high-MgO lavas, origin, crystallisation 78—65312
Koobi Fora and Shungura Formations, E.Africa, tuff correls. and ages 79—57930
Krivoj Rog basin (Krivbas), geological bodies rel. to gravity anomalies interpretation *(Russian)* 78—85466
S.Kyushu, Japan, pyroclastic deposits correl. by Ca-Mg-Fe ratios of phenocrystic minerals *(Japanese)* 77—64278
L-S fabric scheme appl. to structural mapping and palaeostrain anal. 77—78176

geology continued
La Perouse layered gabbro, Fairweather Range, Alaska, zoned spinel 77—5204
Labrador, Archean gneiss dating using zircon data 80—3959
Labrador, geology rel. to continental margin, Mesozoic and Cenozoic sediments provenance 79—62479
Labrador, S.Nain complex, anorthositic dikes 79—84246
Labrador Trough, Canada, early recumbent folds in northeastern part 78—65300
Lac Seul region, English River Gneiss Belt, petrology, chemistry and metamorphism 77—5199
Laccadive Ridge, DSDP Site 219 results 77—73707
Lachlan Fold Belt in New South Wales, description, tectonic history 78—96211
lake chemistry, geology and physics, book 79—44215
lake sediment sequences, pre-Pinedale, Yellowstone National Park, geology, palynology, climatology 79—66727
land-ice slide, glacier-initiated, near Pylon Peak, British Columbia 78—36208
LANDSAT data for geological studies in India, digital anal. 77—78511
LANDSAT imagery appls. 77—91321
LANDSAT imagery geologic processing software 78—20521
Landsat views of Earth, book 78—7643
LANDSAT-1 imagery for N. Carolina coastal plain 77—33211
landslide mechanisms 79—96762
landslides on Ryuohzan Mountain, Japan, geology, model *(Japanese)* 78—96217
large impact craters, meteoritic material detect. and chemistry 78—57208
Late Cretaceous fore-arc basin, N. and Central California, petrofacies and petrologic evolution 79—2232
late Jurassic giant sabkhas of Arabian Tethys 77—66918
Late Palaeozoic slate belt, structural succession and tectonic significance 78—81140
late Precambrian mafic dykes, Montana, geochemistry and Rb-Sr geochronology rel. to Belt tectonics 78—77196
Late Quaternary African stratigraphy from Lake Abhe evolution study 77—21770
Late Quaternary deposits lithobiostratigraphic characteristics, Baltic Sea *(Russian)* 79—88332
lava flows, thick layered peridotite-gabbro, Munro Township, Ontario 78—36168
Laxfordian deformation in Carloway area, Isle of Lewis, Scotland 78—7638
Lepontine Alps, metamorphism rel. to heat-flow distrib. temporal changes 80—101347
Lesser Antilles island arc, volcanic rock, paleomagnetic and geochronological survey 80—8265
Liguro-Piemontes Alps, struct. anal. from terrestrial mag. field *(French)* 79—57896
limestone cave deposits, O isotopes for palaeotemp. of mid-Wisconsin 80—82069
limestone cave systems, development in dimensions of length and depth 79—62531
Limpopo Mobile Belt, Rb/Sr ages and geological setting of Sand River ancient dykes 77—56611
lineament, joint and drainage densities, rapid determ. method 78—32255
lineament interpretation, multi-attribute method 79—2399
lineaments, human perception from remote imagery, model 79—2400
lithostratigraphic correl. of subsurface sequences 79—62509
lithostratigraphic correlation, automatic, pitfalls 79—62506
lithostratigraphy, parametric interpolation of digitized log segments 79—62507
N.Lithuania, surface karst craters and lakes *(Russian)* 78—49053
Lithuanian inter-river relief, kames structure *(Russian)* 79—48486
Loc Uisg granophyre, Isle of Mull, isotopic and chem. evidence for origin 78—65303
local inhomogeneities determ. by reflected-wave probing method *(Russian)* 79—39947
loess geological environments, China *(Chinese)* 78—81156
loess profile near Einbeck, W.Germany, stratigraphic arrangements and material *(German)* 79—20823
central London, Quaternary pingo remnants 80—56502
Long Valley Caldera, California, implications of mag. model 77—86846
longitudinal folds, high-amplitude, form. and stress state 77—9382
Longonot volcano, Central Kenya, geology, question of volumes of volcanic products 80—85633
Los Angeles Basin SW block, sedimentary record rel. to thermal subsidence and petroleum generation 80—3967
Los Pinos pluton, S.California, petrology and emplacement 77—5200
Louvem volcanogenic Cu deposit, Quebec, lithogeochem. anomalies 79—5480
Lower and Middle Cambrian sedimentary rocks, Desert Range, Nevada, palaeomag. rel. to polar wander 80—21620
Lower Palaeozoic black shales rel. to geologic-oceanographic model 78—61436
Lower Palaeozoic carbonate sequence, Arctic Canada, palaeosalinity and dolomitization 79—25241
LWR spent fuel elements, disposal in geologic isolation, feasibility study report 80—106140
Mackenzie, N.W.T., Canada, Devonian-Cambrian stratigraphic differentiation by S isotopes in gypsum 78—61413
Mackenzie River, Canada, ice-push features stability 78—28247
mafic belts along margins of Japanese Islands, origin, geophys. survey 78—32100
Magadi volcanics, Kenya, palaeomag. results 79—79740
magma chamber, fluid dynamics model of differentiation and layering 80—76939
magmatic environments, zoned plagioclase anal. by ion-microprobe technique 79—34815
magnetic and gravity anomalies extrapolation, equivalence principle and geological interpretation *(Russian)* 79—39926
magnetic interpretation for geological contact and thin dike 78—28333
magnetic profiling of geological contact, harmonci inversion method 80—77137
magnetic stratigraphy of sediments using susceptibility meas. 79—84520
magnetostratigraphy of San Juan Basin, Cretaceous-Tertiary boundary 77—53055
NW.Maine medium to high grade metapelites, muscovite comp. var. 79—62493

geology continued
Makran coast, Iran and Pakistan, seismic harzards, regional tectonics and geology 79—88295
Manic 3 reservoir, Quebec, structural and lithological inhomogeneities rel. to induced seismicity 79—66636
Manicouagan structure, Quebec, central mag. anomaly rel. to mafic rock uplift 78—81169
Mantaro landslide, Peru, seismological and geological aspects 78—96248
mantle thermal gradients estimation, geological problems 77—5138
mantled gneiss domes of E.Finland, cluster pattern implying gravit. instability of Proterozoic crust 80—81848
map automatic compilation system design *(Russian)* 77—41025
mapping, thermal inertia method 80—8344
maps updating, index, using computerised file system 77—2252
Marcy (New York) and Morin (Quebec) anorthosite complexes, rare earth element abundances 77—78177
marginal basins, diffuse magnetic anomalies and their tectonic and petrologic significance 78—32064
Mariana Island arc and trough, volatiles content of submarine volcanic rocks 79—92535
marine geology, habitable submarine devices *(Russian)* 79—88902
marine geology and geophysics, 1967-77 review 77—64260
Marydale Formation, Kheis Group, South Africa, Rb-Sr age 78—32088
Marysville aureole, Montana, progressive metamorphism 77—33053
Massachusetts, garnet comp. and zoning rel. to metamorphism temp. and press. 77—2148
Massif Central, France, Rb-Sr systematics of geothermal water-rock association 77—60373
materials, multielement trace anal., solvent extraction-flame AAS method 78—7259
measurement errors of oblique and vertical joints 77—64280
Mediterranean Alpine Belt, geodynamics of eastern region 77—13071
Mediterranean area, clinopyroxene comp. ophiolitic metabasalts 79—57925
Mehone Bay, Nova Scotia, Late Quaternary geological history 78—77232
Mentese region, SW Turkey, LANDSAT imagery appls. 78—77236
Mesozoic volcano-tectonic rift zone and back-arc basin development, South America 79—29762
Mesozoic-Cainozoic sedimentary basins development in W. North America 77—5169
Messejana Dolerite fault-dike system (Iberia), age and origin rel. to N.Atlantic Ocean opening 79—2198
Messina Layered Intrusion, Limpopo Mobile Belt, S.Africa, tectonic setting, geology and age 80—76969
metabasites, geothermometry of granulite facies rocks from Rogaland, Norway 78—96193
metadolerite dykes and assoc. folds, Caledonides of Finnmark, Norway 78—61375
metallic mineral deposits of Australia mag. induced polarisation survey results 80—98223
metamorphic sodic amphibole from Newfoundland Appalachians, tectonic implications 77—29298
metavolcanic rocks, Montauban-Les-Mines, Quebec, geochem., mineralization 78—36161
meteorite crater field formation, effects of meteoroid atmospheric breakup 80—94760
meteorite crater structures, Kola Peninsula 79—70802
meteorite craters, form., props. and catalogue 78—96411
methods for evaluating shallow platform structures *(Russian)* 79—62623
Michigan Basin basement, lower metadiabase preliminary petrological study 80—4009
Michigan Basin deep drill hole, spilitic rocks petrology 79—39711
microseisms obs. at New York Rayleigh and Love wave characts., geologic control 80—26462
Mid Atlantic Ridge, geophysical significance of plagiogranite 78—16007
Mid-Atlantic Ridge, geology of submarine hydrothermal field at 26°N latit. 80—85641
Middle Jurassic magnetic polarity, from Summerville and Curtis Formations, Utah 78—65180
Middle Ordovician formations, E.Tennessee, tectonic significance of distal turbidites 78—65296
Midland Craton of England and Wales, Late Precambrian rocks palaeomag. study 79—66617
mineral discovery probability, quantitative fall-backs of naturalist classifications 77—53204
mineral exploration, computer uses, limitations and requirements 77—53207
mineral identification in rocks, mag. rot. hysteresis loss meas. 80—67428
mineral resource data bases 77—53203
minerals diogenesis, plate tectonic controls 80—12387
Minnesota, crustal struct. and seismicity, rel. to historic earthquakes 78—11840
Miocene-Pliocene lava sequence at Bassastadaa, E.Iceland 77—17046
Miramichi Bay, New Brunswick, Canada, echo sounder and seismic profiling survey 78—61390
models and interval vel. estimation error 77—86790
Moenkopi formation, SE.Utah, USA, magnetostratigraphy 80—72422
Moine thrust zone, differential stress determ. from deformation-induced microstructs. 80—85652
Moine Thrust Zone, Eriboll, Scotland, palaeostress estimates 79—79835
molasse and nonmarine-paralic sedimentary basins, tectonics and deformation 79—57902
molasse basin formation simulation 77—9428
Mole (Haute-Savoie, France), geological profile of south flank rel. to struct. and tectonics *(French)* 78—69348
montmorillonite neoformation by post-depositional subsurface weathering in slope deposit 78—73367
Morarian age for younger Moines, central and W.Scotland 79—53328
Mouana, Gabon, uraniferous deposits organization *(French)* 80—21741
mountain territories, formal morphostructural zoning 77—73876
mudboils nature and genesis, Keewatin, Canada 79—5478
multilevel syntax analysis for geological data compression 79—48569
multispectral imaging, principal components 79—34823
Murray-Darling river system, Australia, symposium (Melbourne, 13 October 1977) 79—92556
muscovite of regional metamorphic rocks in Xizhang, b_0 value and geological significance *(Chinese)* 79—74890
mylonites formation, mechanical processes involved in crystalline basement rocks deform. 79—53344

geology continued
Nain anorthositic complex, Labrador, examples of contrasted magmas commingling in plutonic environment 80−104959
S Nain complex, Labrador, anorthosite and assoc. plutons 79−20825
N.Namibia (SW.Africa) upper Damara sequence, Sr and Ar isotopic homogenisation of pelitic sediments 79−62511
Narao district, Japan, landslide rel. to Rn conc. in underground waters 78−11918
Narosura volcanics, Kenya, palaeomag. results 79−79740
National Coal Resources Data System of US Geological Survey 77−53208
natural gas, He conc. periodic vars. determ., algorithm 79−62608
Naxos island, Greece regional metamorphism, petrology and geothermal gradients 77−44985
Nazca group volcanic rocks, Peru, volcanic history 80−12357
Nelson River gravity anomaly, SE.Saskatchewan, seismic survey 78−28153
Nemaha Uplift in Oklahoma, Kansas and Nebraska, geological survey of seismicity and tectonic rels. 78−7589
Neogene-Quaternary volcanogenic formations, Dzhavakhet highland, palaeomag. 79−74834
Nepal, basic intrusions of volcanic origin 80−72477
Nepal Himalaya, struct. geology of Kusma-Sirkang section 80−72478
Neumann problem for potential in toroidal coords. for axial symmetry 77−64182
neutron activation analysis of geological materials 80−16747
Nevada, interpretation of gravity surveys in Grass and Buena Vista Valleys 80−41365
Nevada Test Site, geology effect on absolute travel-time residuals 79−16391
N.Central New Brunswick, age of deformed granitic rocks 77−81837
SW New Brunswick and SE Maine, stratigraphy and tectonic setting of Palaeozoic sedimentary rocks 78−57199
New Caledonia, Oman and Yugoslavia, modern low temp. serpentinisation 78−69344
New England submarine canyons, bedrock geology 78−73356
New Zealand continental and orogenic volcanism, magma traps theory appl. 79−70776
Newcastle-Port Stephens area of Australia late Quarternary deposits 79−88352
E. Newfoundland, aborted Proterozoic rifting 78−57200
central Newfoundland, folded thrust faults 77−33068
Newfoundland, geology rel. to Early Palaeozoic plate tectonic model 80−94509
SW.Newfoundland, geomorphology and Quaternary geology 78−20400
NE Newfoundland, geophysical and geological trends on continental shelf 77−5145
E Newfoundland, new geological evidence rel. to NW Gondwanaland Proterozoic tectonics 79−57908
SW Newfoundland, ophiolites rel. to tectonic models 77−17103
Newfoundland fjords, gravel clasts rel. to glacial erosion of bedrock 77−17148
Newport granite, age, geological setting, rel. to NE.Newfoundland geology 79−92534
Nias Island, Indonesia, sedimentology and palaeobathymetry of Neogene trench-slope deposits 80−104950
Nias Island, Indonesia, structural geology implications for subduction zone tectonics 80−109120
S.W. Nigeria, Albian-Cenomanian, palaeogeographic implications, Africa-S.America land connection 79−84276
N.Nigeria, pipe in schist belt, geophys. anomaly study 80−76971
W.North American plate, intraplate tectonics 77−41017
North Sea basin, subsidence in post-mid-Cretaceous 80−109133
N.Norway, Quaternary sediments and stratigraphy, continental shelf 79−84228
Norwegian Caledonides Trondheim Nappe melange and tectonic model 80−3985
Norwegian gneiss eclogites, giving evidence for Precambrian continent-continent collision 77−49057
nuclear power plant siting, US midcontinent 78−85501
nuclear raw materials prospecting, isotopic dating methods *(Russian)* 79−30925
nuclear waste disposal, migration in geologic formations 78−4994
ocean spreading ridge, silicic rocks, late-magma vap. transport of K 80−81877
oceanography, geological, book 78−92845
oil and gas deposits in low amplitude struct., parameters from gravity test data *(Russian)* 79−44271
oil and gas formations, prediction prior to drilling *(Russian)* 79−39970
oil and gas well profiles, appl. of combined well-logging techniques *(Russian)* 78−40705
oil bearing beds in inhomogeneous geological sections, pattern recognition methods *(Russian)* 78−28337
Oita, Japan, tectonic topography rel. to 1975 April 21 earthquake *(Japanese)* 77−2109
Oklo natural fission reactor, petrography of organic matter *(French)* 80−21749
Oklo natural fission reactors, review *(French)* 80−21770
Oklo natural fission reactors, review of French geological research *(French)* 80−21744
Oklo natural fission reactors geological environment, tectonic anal., petrography, geochemistry *(French)* 80−21742
Oklo natural nuclear reactor, discovery and reactor parameters, geological formation 79−2240
Oklo natural reactors, mining, geology and tectonics *(French)* 80−21743
Oklo natural reactors, review of mineralogical and petrographic studies at Strasbourg *(French)* 80−21745
Olinghouse fault zone, Nevada, strike-slip fault 79−79840
Omo River project (Ethiopia) data management system appraisal 78−57326
onshore borehole records, data bank system 77−53214
NW.Ontario, granitoid complexes and Archaean tectonics 80−31019
Ontario, Pleistocene geology rel to climatic vars. effect on geothermal regime 79−57883
Onverwacht Group, Transvaal, sedimentology rel. to early Earth characts. and evolution 78−44812
Onverwacht Group Volcanics, southern Africa, Sm-Nd dating 79−62469
ophiolite belts and island arc collisions, Arabian Shield 78−20421
ophiolite complex, early Caledonain age, on Karmoy island, Norway 79−2235

geology continued
ophiolite complexes, effects of alteration on NRM and implications for oceanic crust 78−65280
ophiolite fractionation trends, Bay of Islands, Newfoundland, polycyclic cumulate sequences 77−78179
ophiolite nappes emplacement, Mesozoic-Cenozoic examples 77−41012
ophiolite petrogenesis in oceanic crust, Nd and Sr isotope study 80−61782
ophiolite suite, Bay of Islands, Newfoundland, petrology and geochem. 80−21726
ophiolite suites, upper mantle origin rel. to oceanic lithosphere generation 78−65311
ophiolites, Chilean, hydrothermal metamorphism vars., ocean floor metamorphism implications 79−88354
ophiolites, N.W.Syria, rel. to Tethyan oceanic crust evolution during Mesozoic 77−81896
ophiolites, seismic vels. and oceanic crustal struct. 78−77226
ophiolitic breccias in E. Ligurian Apennines, comparison with rifted oceanic ridges 77−86881
ophiolitic melange, significance in Fleur de Lys Supergroup, N.Appalachians 77−78175
ophiolitic melange of Late Precambrian, Egyptian desert, formation process 80−81884
ophiolitic peridotites structures, role of young lithosphere thrusting in subduction zones 80−56446
ophiolitic rocks tectonic emplacement in Precambrian Mona Complex, Anglesey 79−8631
Ordovician basalt assoc. with Fe-rich deposits, in Scotland, ancient mid-ocean ridge? 80−81878
Ordovician Cap des Rosiers Formation, Quebec, deposits on submarine fan 79−25242
Ordovician lamprophyres Taylor Valley, Antarctica, palaeomag. pole position 78−32010
Ordovician sandstones from Tourelle Formation, Quebec rel. to Taconic orogeny 79−57919
Ordovician volcanic rocks, N.Maine, magmatic affinity and tectonic significance 77−44984
ore mineralisation in Erma River Area, Bulgaria, age, genesis, Pb isotope and K-Ar investigs. 78−81115
ores, sediments and metamorphism 77−86889
orientation data fitting to von Mises distribution, in FORTRAN 77−5201
orogenic lherzolite petrogenesis in oceanic crust, Nd and Sr isotope study 80−61782
Otago schist megaculmination, origins and tectonic significance in New Zealand Rangitata Orogen 78−81142
Otway Region, S.Victoria, Australia 78−20416
Otway region, S.W.Victoria, conf. (Melbourne, 1975 October 9) 78−20415
overburden stratification, effect on basement seismic vel. determ. *(Russian)* 79−39961
overthrusting, model of const. thickness overthrust on visco-plastic sole 80−51378
Oxford Lake-Knee Lake greenstone belt, N.Manitoba, Rb-Sr ages 80−94485
P-wave abnormal delays in The Geysers-Clear Lake geothermal area, California 79−74860
P-wave initial pulse widths rel. to anelastic props. and surface geology, central California 78−44778
Pabbi Hills, Pakistan, Upper Siwalik deposits, magnetic polarity stratigraphy 78−11798
S.Pacific, DSDP site 284, Late Cainozoic isotopic history 79−48516
SW.Pacific basin, reverberant subbottom layers distrib. 80−8290
Pacific basin, sedimentation rates and sea levels 79−88365
Pacific Margin, Vancouver Island and adjacent regions, tectonic-stratigraphic evolution 78−20399
E.Pacific Rise, geology of hot springs areas 80−101360
Paganzo Group (Argentina), red beds palaeomagnetism and correl. of Upper Palaeozoic-Lower Mesozoic rocks 77−90999
Pakistan, geology and palaeontology of Neogene strata 78−24269
Pakistan, northeast, near Skardu, structural geology 77−86872
palaeocontinental maps for Early Phanerozoic and Proterozoic 79−44150
palaeocontinental slopes of East Coast Geosyncline, Canadian Atlantic Margin 78−36141
palaeontology, statistically oriented teaching approach 77−19
Palaeozoic base maps, palaeogeography and plate tectonics 80−41441
Palaeozoic granitoid plutons from contrasting tectonic zones, NE. Newfoundland, geochem. 78−57201
palaeozoic sequences palaeobathymetric anal., rel. to basin tectonics 78−69341
Paluzu Mare (Rumania), mag. anomaly and core samples, struct. geology *(Rumanian)* 80−8309
SE.Pamir Mountains, geology and geochronology *(Russian)* 80−12392
Pamir-Himalayan deep fault zone description 79−39676
Pamir-Himalayas region, International working conf. on geological and geophysical studies *(Russian)* 77−73734
NE.Pannonian Depression, seismogeological study *(Rumanian)* 79−57877
Papuan Ultramafic Belt, mode of emplacement 79−84214
Paradox Basin, geological studies for nucl. waste repository siting 80−37485
parallel metamorphic belts in NW Himalaya 78−57207
pattern recognition, automatic, cartography applic. 77−21953
Pau D'Albo struct., Sao Paulo, Brazil, form. mechanism 79−48441
peridotite compositional layering, evidence of press. soln. creep in mantle 80−56471
Permo-Triassic and Jurassic ^{40}Ar-^{39}Ar ages from Greek igneous rocks rel. to rifting 79−74872
central Peru, Eocene uplift and unroofing of coastal batholith near Lima 79−2199
S.Peruvian coast, two-billion-year granulites in Late Precambrian metamorphic basement 78−28204
Peruvian Coastal Batholith, ring complexes, subvolcanic regime 77−5143
PETPAK, computing package for petrologists 78−57323
petroleum deposits and gas wells *(Russian)* 77−64281
petroleum traps, synthetic seismic sections 79−53311
petrologic modelling with extended Q-mode factor analysis, interactive computer program 77−33070
petrophysical props. of ultramafic rocks, using factor analysis 80−90087
Peyto glacier, geological features *(French)* 77−37199

geology continued
Phanerozoic sedimentary basins, Australia, tectonic implications 78—96174
phengite and eclogite in Xingyang metamorphic belt, tectonic significance *(Chinese)* 79—84264
photolineaments semi-quantitative interpretation 78—3766
E.Pilbara Block, W.Australia, Archaean shallow-water volcanic-sedimentary facies 79—57926
Pinchi Fault Zone, central British Columbia, geology and evolution 77—91129
Pine Mountain block thrust sheet, USA, energetics of driving force 80—21730
plate tectonics rel. to evolution of ideas in geological sciences 78—7605
Pliny Range, New Hampshire, intrusive complex, mineralogy and petrology 78—36158
Pliocene-Quaternary deposits in Ukrainian SSR, model of regional magnetostratigraphic scale *(Russian)* 77—44916
Pliocene/Pleistocene boundary age estimate and palaeoclimatology 77—91133
plutonic intrusions, influence of temp. on deep magmatic diapir folds *(Russian)* 80—104957
Pokiok Pluton, New Brunswick, pre-Acadian deform., metamorphism and intrusion 78—7631
Polesine area, surface subsidence study 78—28233
polynomial and Fourier trend surfaces computation 78—32245
potential fields, anal. of characteristic-components method in interface construction 77—44901
pre-carboniferous basement near Trail, British Columbia 79—84253
pre-Tertiary system, Shimokita Peninsula, NE Japan, geological structure 77—5163
Precambrian, time divisions in South America, chronotectonic boundaries 79—48442
Precambrian and Palaeozoic geological events, rel. to global tectonics, palaeomag. cycles and polar paths 79—66618
Precambrian basement, W.Canada, U and Th conc., petrologic and tectonic controls 80—17257
Precambrian basement of W.Canada, Hg and As distrib. and abundance 80—56419
Precambrian development rel. to geophysical evolution 78—53651
Precambrian dykes, preferred orientation of intrusion 78—88829
Precambrian Earth crust, seismic refls. rel. to geology 78—32034
Precambrian Fe formations, rare earth elements evidence for changing oxidation states 77—64284
Precambrian Fe formations, Schefferville, Canada, vertical mag. contouring 77—64495
Precambrian geologic history 77—2131
Precambrian high grade metamorphic terrains, interplate deform. rel. to SE Asian neotectonics 78—65250
Precambrian metamorphic rocks of Neumayerskarvet area, W Dronning Maud Land, Antarctica 77—86894
Precambrian schist belt, Karnataka, India, aeromag. anomaly harmonic inversion 79—44094
Precambrian strike complexes, structural map construction *(Russian)* 78—12014
Precambrian terrain, multiply deformed, discrete structural-metamorphic events geochronology 79—57895
Preslav anticline, oil and gas prospecting data anlaysis *(Russian)* 78—32085
prospecting data processing system, Poland *(Polish)* 78—88929
Proterozoic anorthosite massif of Labrador's Nain complex, magma origin 80—94500
Proterozoic iron-formation, Labrador Trough, Canada, regional metamorphism rel. to mineralogy and chemistry 79—57916
Proterozoic sequences, central Australian, magnetostratigraphic tests 79—84112
Pyramid Lake fault zone, Walker Lane, strike-slip fault 79—79839
Pyrenees, central southern region, gravity gliding and compressive nappes 78—69342
pyroxenes from planetary basalt, silicate mineralogy study 80—72802
quartz cryst. axes orientation, in metamorphosed volcanic sediment 80—85655
quartzites, microscopic deform. and flow laws, South Mountain Anticline 78—77220
Quaternary buried palaeosols, review 77—2151
Quaternary climatic change, physical evidence 77—64417
Quaternary glaciations along Qinghai-Xizang Highway *(Chinese)* 79—92538
Quaternary lavas, Snake River Plain, Idaho, mineralogy and petrology 78—20402
Quaternary loess deposits of Banks Peninsula, New Zealand, radiocarbon dating 78—24271
Quaternary succession near Ottawa, mass flow deposits 77—53050
Quebec, LG-3 dam fault average net slip, dome and basin structs. *(French)* 77—73732
S.Quebec ophiolites and Betts Cove type oceanic crust 77—81885
Quipungo mobile belt, Western Angola, geological evolution *(Portuguese)* 79—70796
Quottoon pluton, British Columbia, thermal effects of igneous intrusion and uplift 80—12352
radioactive waste disposal, high-level and long-lived, burial processes 78—29610
radioactive waste disposal in geologic formations, site selection criteria 80—106142
radioactive waste disposal into salt deposits, fault tree anal. appl. to safety assessment 78—55046
Raft River geothermal area, Idaho, seismic refr. study 80—3963
Rayleigh wave microseisms, geological control on three-component spectra 79—84122
Red Wine alkaline province, central Labrador, chronology 78—11842
redbeds of Great Slave Supergroup, Canada, mag. susceptibility anisotropy 77—78160
regional gravity anomalies, interpretation via mechanical modelling of crustal structs. form. *(Russian)* 78—49154
regression eqns. connecting geological and geophysical parameters *(Russian)* 77—73733
remote sensing, geological interpretation from composited radar and Landsat imagery 80—56647
remote sensing application 80—109279
remote sensing of natural resources using satellite and aircraft scanner data for Finland 79—100988

geology continued
remote sensing principles, concepts and philosophical problems 77—56772
remote sensing surveys in geologic exploration 77—56631
replicated diversity indices computation for random samples of specified size 77—37197
resedimented conglomerates of Huronian age, Lake Huron north shore, deposition from sediment gravity flow 78—36164
reservoir properties estimation for lithologies *(Russian)* 77—70662
residual gravity anomalies interpretation *(Russian)* 79—88232
Rhodesian Archaean, 2.9 Myr BP event 79—66658
rhyolitic ignimbrites origin, Batopilas area, Mexico, Sr isotope study 80—94501
rifts at high angles to orogenic belts, origin, Upper Rhine Graben example 78—48989
ring structures nature and origin in USSR *(Russian)* 78—16018
rinneite, Rb-Sr dating of potash salt deposits 80—67429
Rio Grande rift, New Mexico, transient heat flow model 79—34771
S.Rio Grande Rift, underlying oceanic mantle discovery 79—29724
Ririwai ring complex, Nigeria, heat flow meas. 79—57894
Roberts Arm Group, Newfoundland, age rel. to phases of volcanism 80—12354
rock chem. weathering rate 80—77142
rock cleavage, morphological classification 80—21736
rock deformation, elliptical particles non-coaxial deform. 79—79829
rock formation and penetration zone elec. parameters determ., probes number and type *(Russian)* 79—39969
rock fracture measurement in laboratory, under geological conditions 80—46171
rock joint orientation meas. evaluation in terms of regional stress 77—64487
rock joints, mapping via photogrammetry and EDP appl. 80—56470
rock joints filled with wet clay, shearing at high-press. 80—41438
rock strain determination using randomly oriented strain markers 78—3765
rock type discrimination using enhanced Landsat imagery 80—41568
Rockall Trough near-bottom traverse, hydrographic and geological inferences 79—62483
rockfall from cliff face, seasonal variation obs. in N.Ireland 80—105001
rocks and minerals spectral refl. data, lab. and remote obs. comparison 77—17251
Rocky Mountain foreland, drape folds modelling expts. under confining press. 79—58127
N.Rocky Mountains, British Columbia, Canada, structural interpretation 79—100835
Romanche fracture zone, limestones rel. to Neogene crustal emergence and subsidence 78—11857
Roosevelt Hot Springs thermal area, Utah 79—84260
Rubble Creek landslide, British Columbia, during 19th century, potential slide area 79—5477
Rumania, geological models rel. to plate tectonics *(Rumanian)* 77—33040
Sabaloka Igneous Complex, Sudan, petrography and chem. analyses 78—32097
Sahara plateau, petrographic and radiometric dating *(Italian)* 78—7595
salt deposit formation *(Russian)* 79—2237
salt deposits, Upper Triassic, of western N.Atlantic, obs. from Newfoundland Grand Banks 80—94516
salt dome evolution, fluid dynamics model 78—77237
salt domes, N.Louisiana, imaging radar mission 79—66833
salt glaciers, flow 79—84261
San Andreas Fault, geodetic tilt obs. 80—81800
San Andreas fault system, local stress field and kinematics modelling 79—79778
San Andreas fault zone, constitution at depth 79—12097
San Andreas fault zone, geology rel. to in situ seismic vels. at Sonte Canyon well 79—57865
San Francisco Bay region, landslide hazard 77—70665
sandstones, Indian east coast, post-Pleistocene age 79—48485
W.Santa Ynez fault system in S.California, geology rel. to struct. and neotectonics 79—79774
Santos Basin, Brazil, geology of bordering continental rifts system 77—21768
Sao Paulo Plateau, Brazil continental margin, struct. and comparison with S Angola margin 77—21750
Sao Vicente, Mato Grosso, geology and geochronology of granite *(Spanish)* 77—70652
S.Saskatchewan, composition study of sands 79—84254
S.Saskatchewan, geology rel. to seismotectonics 79—20757
N Saskatchewan, var. in lithology and tectonometamorphic relationships in Precambrian basement 77—91132
Saskatchewan and Manitoba, Boundary intrusions petrogenesis 77—66914
satellite imagery, linear features enhancement by rotational exposure 79—35874
satellite remote sensing appls. 77—25788
Saudi Arabia, late Proterozoic ophiolite complex at Jabal Ess, rel. to plate tectonics 79—70799
Scandinavian Caledonides, gabbro complex palaeomag., plate rot. or polar shift theories 80—21615
Scandinavian Caledonides, nappe displacement 78—81143
Scandinavian Caledonides, tectonic model, comments 77—66911
Scotland, imbricate thrust model of Southern Uplands 77—53031
NW.Scotland, Lewisian Units subsurface geology from seismic vel. depth depend. 79—44179
Scotland, magnetotelluric study, geophys. and tectonic implications 79—29706
N.Scotland, regional geochemistry rel. to U deposit formation 79—84269
SW. Scottish Highlands, metamorphism rel. to heat-flow distrib. temporal changes 80—101347
scree slope rockfall model 77—44990
seafloor, petroliferous structs. rel. to temp. anomalies, surface geothermal survey results *(Russian)* 78—40527
section prediction, appl. of seismic waves integral spectrum parameters *(Russian)* 79—8705
sediment of continental shelf, anomalous declination due to slumping 80—76964
sedimentary basins, development and evolution 79—29719
sedimentary deposits, welding out zones separation via multiple seismic waves freq. selection *(Russian)* 79—8706

geology continued
- sedimentary deposits composition, geological records coding mech. *(Russian)* 80—17383
- sedimentary geochemistry, environments and processes involving an aqueous phase 77—86888
- sedimentary rocks of Upper Rhine Graben, organic matter metamorphism as palaeo-geothermometer 79—70800
- sediments of old coast formations of E.Lithuanian upland *(Russian)* 78—16012
- seismic depth section, algorithm for tracing horizons *(Russian)* 77—66891
- seismic exploration problems of complicated basins, S.China appl. *(Chinese)* 79—100961
- seismic microzonation, geological considerations 79—88272
- seismic recording station geology rel. to strong ground motion duration 77—91036
- seismic waves interference effects in thin layers 78—92780
- seismicity from geological structure, seismic risk studies 79—92491
- seismite, occurrence in Precambrian rocks, Rajasthan, India 78—77227
- seismoacoustic activity distrib. near coal bed face 78—73320
- Sekwi formation, NWT, evidence for submarine sediment gravity flows 79—84259
- SELLO, FORTRAN IV program for skewed distributions for normality transform 77—9502
- sequential deformation in central Appalachians 78—65294
- serpentinization at Burro Mountain, California, magnetic study 79—79814
- Shackleton Range Metamorphic Complex, Antarctica, Rb-Sr dating study 80—46180
- Shap granite, English Lake District, constraints on struct. and emplacement, gravity and mag. survey 78—44817
- Shebandowan Lakes, Ontario, ferromanganese concretion deposits 79—84257
- shore platform formation on SE. coast of Izu peninsula, Japan 78—81147
- Shuswap Complex, S.Okanagan, British Columbia, recumbant folding, mechanism and geometry 80—4008
- SE Siberia, crust struct. and role of Archean folded ovals 80—101349
- E.Siberia, geological history determ. from amethysts *(Russian)* 80—12393
- Sibley Group, Thunder Bay district, Ontario, Canada, stratigraphy and depositional setting 80—94517
- Siebengebirge, Germany, K-Ar age of Tertiary volcanics 80—98280
- Sierra Nevada, California, crustal movement rel. to regional geology and tectonics 79—79795
- Sierra Nevada, California, glacial deposits, relative dating techniques from weathering 80—8451
- Sierra Nevada-Walker Lane region, recent crustal movements, rate and style of deform. 79—79838
- SIGMI, user-oriented file-processing system 77—9506
- silicate glasses of geologic interest; Mossbauer absorpt. of Fe III, effect of glass chem. comp. *(French)* 80—80658
- silicate liquids high-temp. props., rel. to basic magma equilib. and ascent 77—86868
- silicic igneous rocks, Burlington Peninsula, Newfoundland, Rb-Sr ages, deform. 78—65212
- single layer folds arc lengths, comparison between theory and obs. 79—53345
- single-layer folds, shape at small but finite amplitude 80—56473
- Siqueiros transform fault and East Pacific Rise, basalt petrology and chemistry 77—33050
- Siwalik Group, Dhok Pathan, Potwar Plateau, Pakistan, mag. polarity stratigraphy and age 79—29725
- Slate belt, volcanic evolution, possible primitive oceanic island arc 78—81125
- slaty cleavage, development Fleurieu Peninsula 80—21735
- slaty cleavage development across Nackara Arc, Adelaide Geosyncline 79—66694
- slaty cleavage development in French Alps 77—73736
- slope recession in Onefour Badlands, Alberta, Canada, rel. to moisture regimes 79—92552
- small amplitude structures, gravity prospecting, meas. spacings and contour intervals *(Russian)* 79—44272
- snad grain surface texture rel. to wind vel. conditions 80—41443
- Snake Bay-Kakagi Lake greenstone belt, NW.Ontario, expanding spread seismic refl. survey 80—12356
- soil resistance meter, geological and archaeological applications *(German)* 78—57361
- Sokoman Iron Formation near Ardua Lake, Quebec, mineralogy and petrology 78—77228
- N Somerset Island, Arctic Canada, Upper Silurian rocks stratigraphy and sedimentology 77—91131
- Somerset Island Formation, intertidal/supratidal succession 78—65297
- sonoprobe survey, automatic recognition of submarine sediments *(Japanese)* 79—39985
- South Africa, kimberlites, rare gases in phlogopite and phlogopite bearing nodules 78—11894
- South Island, New Zealand, Late Pleistocene tephra, identification and significance 80—8306
- South Mayo Trough, W.Ireland, possible Ordovician marginal basin 78—36162
- South Prebetic Sierra de la Puerta, Spain, Middle Eocene to Miocene sequence 77—66920
- southern continents, geology rel. to revised reconstruction 78—92805
- Southland syncline, New Zealand, zeolite facies alteration of sandstones 78—32084
- S.Spain, folding of sedimentary rocks, Malaguide Complex, Spain 80—8312
- Spain, geomagnetic anomalies, geological interpretation *(Spanish)* 79—29710
- S.Spain, high-temp. peridotites contact relations in Serrania de Ronda 77—73737
- Spain, residual gravity anomalies rel. to geology *(Spanish)* 78—88781
- Spanish continental margin of phosphorites *(French)* 79—79837
- spent nuclear fuel stored in basalt, chances of reintroduction into biosphere, analysis 80—106144
- sphalerite geobarometry in Balmat-Edwards district, New York 78—65261
- spinel lherzolite nodules from Pleistocene cinder cone, upper mantle origin 78—65299

geology continued
- Spor Mountain, Utah, USA, U-Pb age of uraniferous opals and mineralisation processes 80—46149
- Stavelot massif, pyrophyllite, dickite and kaolinite in quartz veins 79—34813
- stereograms production, FORTRAN program 77—9521
- Stillwater complex, USA gabbro Sm/Nd age and mantle evolution curve of Nd 80—41410
- stochastic models 77—81890
- strain patterns in crestal region of immature diapirs 79—29752
- strained rock units, stratigraphic thickness determ. 79—21034
- Strait of Juan de Fuca, magnetic and gravity anomalies, geology 77—52973
- Strandja Mountain, Bulgaria, new facial type of Triassic 78—81154
- strata-bound ore deposits rel. to chemical speciation of Cd, Cu, Pb and Zn in freshwater-brine solns. 78—20409
- stratified homogeneous formations, common depth point effective velocities, critical values *(Russian)* 79—39668
- stratigraphic correlation by principal components, effects of missing data 79—25350
- stratigraphic correlation conf. Syracuse, NY, USA (Oct. 1977) 79—62500
- stratigraphic data, support for astronomical theory of climatic fluctuations 80—72509
- stratigraphic interpretation, appl. of synthetic sonic logs 79—88483
- stratigraphic section correl. by continuous variables 79—62505
- stratigraphic sequences, differentiation by statistical anal. of seismic data 79—92503
- stratigraphic units correlation from geological maps 79—62508
- stratigraphy of deep sea sediments rel. to Eemian intergalcial 79—29770
- stratum sounding by UHF radar *(German)* 79—8702
- structural and vibr. bedrock props. in Sweden, seismic events 79—16402
- structural geology, conf. (1978), Toronto, Canada 80—101666
- structural geology, graphical methods for plane intersection line orientation determ. 79—58103
- structural geology, LANDSAT data anal. *(Italian)* 80—109281
- students' success rel. to spatial abilities, aptitudes and attitudes 77—5611
- Sub-soil Data Bank objectives *(French)* 80—21826
- subduction zone, thermal and geological effects of spreading ridge subduction 79—88321
- subduction zones, material transport within accretionary prisms and 'knocker' problem 80—101353
- submarine survey for Mont Saint-Michel Bay 77—25675
- Sudbury Ni Irruptive and Superior Province granites, ages 78—36126
- S.Sulaiman Range, Pakistan, struct. and seismicity rel. to tectonics 79—39715
- Sulawesi, Indonesia, past and present geotectonic position 78—32056
- sulphate evaporites, Middle Proterozoic, at Mount Isa mine, Australia 78—73371
- sulphide prospect in California copper belt, broadband EM study 80—72503
- Superior Geotraverse symposium (Toronto, 1978 October 23-26) 80—27029
- Superior Province, Canada, geology rel. to crust resistivity, audio freq. magnetotelluric results 79—57882
- supernova created sediment, γ-ray ablation of Moon 80—56731
- supracrustal rocks, Isua area, W.Greenland, least radiogenic Pb occurrence 78—44816
- surface geology, remote sensing by Heat Capacity Mapping Mission 79—5640
- surface geology of glaciated area of USA, ground mode radiowave propag. 80—76979
- central Sverdrup Basin, regional geological struct. correl. with crustal struct. 80—12355
- Swaziland Ancient Gneiss Complex, Rb-Sr age and source of bimodal suite 80—51395
- Sweden, deep-seated fracture zones in crust 79—66666
- N.Sweden, evolution of U province 79—84271
- S.W.Sweden, Permian multiple intrusion dykes in Bohuslan, mag. studies 80—36228
- Sweden, Proterozoic rocks indicating subduction zone 80—46162
- symmetrical folds, simple derivation of straight limbs shortening/rot. relation 79—79841
- Taconic unconformity, structural and metamorphic history 79—84248
- talus slopes angles, repose angles and shearing resistance angles 78—20405
- talus slopes angles, repose angles and shearing resistance angles, comment 78—20406
- Tanzawa plutonic complex, Japan K, Rb, Sr in granitic and gabbroic rocks 77—17100
- Tasman Fold Belt System in New South Wales, description 78—96210
- Tasman Fold Belt System in Tasmania, description 78—96209
- Tasman Fold Belt System in Victoria, evolution, tectonics, deform. 78—96212
- Tasman Orogenic Zone, description of eastern part 78—96214
- Tasman Orogenic Zone, Thomson Orogen, tectonically active area 78—96213
- tectonic dislocations prospecting in complex media, appl. to seismic surface waves correl. method *(Russian)* 79—8605
- Tehilla igneous complex, Sudan, petrology and evolution 77—81891
- temp. gradient distrib. and geological struct. Izmir-Seferihisar geothermal area, Turkey, relation between temp. gradient distrib. and geological struct. 80—56441
- E.Tennessee, palaeomag. results from Ordovician Moccasin, Bays and Chapman Ridge Forms. 79—57854
- E.Tennessee, palinspastic map 78—65295
- Tennessee Valley and Ridge, folding 78—65292
- tephra, late Holocene, from British Columbia and Alberta, identification 78—36167
- terrain evaluation methods, Mackenzie Transportation Corridor, Canada 78—20344
- terrestrial planets, geologic evolution 77—53442
- Tertiary basalts, of E.Greenland continental margin, biostratigraphic ages, plate tectonics implications 77—5153
- S. central Texas, effect of Balcones Faults on groundwater movement 78—53672
- Texas, geological interpretation of National Uranium Resource Evaluation (NURE) aerial radiometric survey data 80—101438
- Thalle Area, Baltistan, Karakorum, Central Asia, structural geology 77—81879
- thermal IR scanning appls. 79—8723

geology continued
- thermal model of Earth's surface for geological mapping by remote sensing 77−53056
- thermodynamics, proc. of NATO Advanced Study Inst. (Oxford, 17-27 Sept. 1976) 78−32103
- Thetford Mines ophiolites, Quebec, palaeomagnetism 80−61757
- Thompson Ni belt, Manitoba, geological and geochronological relationships 77−5196
- tidal strain, topography, geology and cavity effects 77−44896
- W.Tien Shan, crustal movements from geology of palaeomagnetic data 77−9392
- Tien Shan region, field data rel. to contemporary tectonics 79−29733
- till along Lake Huron east coast, age, mag., physical and lithological props., discussion 78−20404
- Tilting Harbour igneous complex, Fogo Island, Newfoundland, petrology 78−77230
- Timmins Mining area, Ontario, structural intepretation 77−78178
- Tirumalai hill range AP, porphyritic granite fracture pattern interpretation 79−44156
- Tokyo Bay, central Japan, recent formations and their basal topography 78−44818
- Torlesse Terrane, New Zealand, exceptionally large steeply plunging folds origin 80−12388
- tracer theory, nonsteady state systems 79−5646
- transversal bent fold, stress and strain rate, stress relax. effect 79−66651
- trappean terrain of Sholapur district, Maharashtra, groundwater occurrence 79−8649
- Triassic clay assemblages of Europe 79−12118
- Triassic Nikolai Greenstone, Alaska, palaeomag. 78−36166
- TRIPLOT, APL program for plotting triangular diagrams 78−57335
- SW.Tunguska syneclise, platform structure from gravity surveys 80−98289
- Turkish-Iranian Plateau, post-collisional tectonics, comparison with Tibet 80−3986
- Tweeddale Granite, newly discovered batholith in Southern Uplands 79−92541
- NW Ukrainian Shield, mag. props. of rocks of sulphide mineralisation zones *(Russian)* 79−96758
- Ukrainian Shield, petrovelocity crustal model and nature of M discontinuity *(Russian)* 77−44948
- Ukrainian Shield, regularities in distrib. of dike complexes *(Russian)* 77−44995
- ultramafic bodies in S.Appalachians, review 78−65288
- ultramafic inclusions, petrogenesis, geochem. and petrologic data 78−65301
- ultramafic nodules, from Kimberley pipes, South Africa 79−34821
- ultramafic xenolith petrology and upper mantle processes, Kapfenstein, Austria 80−76973
- ultramafic xenoliths, Baja California, textures, microstructs., deform. 78−20420
- Umfraville Gabbro, Ontario, palaeomag. study and K-Ar age 80−12330
- W United States, Cenozoic igneous activity rel. to plate interaction and absolute motion 79−2207
- United States, geological data appl. in seismic hazard maps 79−44110
- E.United States, geology rel. to low-temp. geothermal resources 80−85264
- United States Atlantic continental shelf, US Geological Survey core drilling 80−72511
- univariant curves, config. and extensions around invariant point on P-T diag. 78−20412
- Upper Cretaceous palaeomagnetic stratigraphy at Moria (Umbrian Apennines), verification of Gubbio section 78−96132
- Upper Jurassic pyroclastic rocks in Skye, W.Scotland 77−29297
- upper Palaeozoic rocks of W.Canadian Cordillera rel. to Cordilleran evolution 78−7632
- Upper Palaeozoic-Lower Mesozoic red beds and igneous rocks, Argentina, palaeomag. 79−84098
- Upper Precambrian sedimentary rocks, Desert Range, Nevada, palaeomag. rel. to polar wander 80−21621
- US, Missouri and S.Carolina seismic areas 78−85505
- US Geological Survey RASS-STATPAC system for mangement and statistical reduction of geochemical data 78−20522
- USA, East-Central, geological perspectives of earthquake hazards 78−11834
- N.E.USA, rel. of seismicity to geology 78−11836
- W.USA Cenozoic geodynamics rel. to Columbia-Snake River-Yellowstone region magmatism 77−73738
- SW.Utah, geology rel. to two areas of probable Holocene deform. 79−79803
- Varanger peninsula, Norway, Late Precambrian dolerite dykes 80−30989
- Vardar zone, mafic and ultramafic rocks assoc. with granites 78−7635
- Velez Blanco, Spain, Late Burdigalian folding in Subbetic rocks 77−66919
- Vempalle dolomite, Andhra Pradesh, India, petrography and thermolumineso. characts. 77−17088
- Ventersdorp lavas, Ni partitioning between immiscible picritic liqs. 78−32069
- vertical crustal movements in Atlantic coastal plain, USA 79−79790
- Victoria Island, Canada, tide-influenced delta complex in upper Proterozoic Shaler Group 78−28229
- visual observation from space, by Salyut-5 astronauts *(Russian)* 78−40796
- volcanic rocks, Tetagouche Group, Canada, geochem. rel. to origin 78−65298
- Volta Basin, geology and struct. correl. with Dahomeyide orogenic belt 80−109121
- Vredefort Dome, S.Africa, coesite and stishovite discovery 78−53653
- Vredefort structure, S.Africa, comp. of spherules on shatter cone surfaces 79−29773
- S.Wales, deep geologic struct. by explosion seismology 80−36261
- Wascana Creek Ash, Canada, characterisation, source, fission track age, palaeomag., stratigraphy 77−66913
- Washington, DC, Landsat reconnaissance 80−41444
- water-bearing rock formations, evaluation via DC resistivity sounding method 78−40474
- Wesleyville area, Bonavista Bay, Newfoundland, plutonic evolution 77−17095
- Western Australia, pre-greenstone sialic basement, tectonic reactivation 77−17101
- Western Australian Shield, struct. and tectonic style 80−3983

geology continued
- Western Desert of Egypt, wind pitted and fluted rocks compared with Mars obs. 80−72816
- Western Minas Gerais State, Brazil, Phanerozoic tectonic evolution 77−70630
- White Mountains intrusives, New Hampshire, Vermont and Maine, ages 77−78129
- Willimantic fault, Connecticut, pelitic lithologies 79−84245
- Willyama Complex, New South Wales, cyclic reactions between andalusite, sericite and sillimanite 80−26508
- late Wisconsinan till sheets, Brantford-Woodstock area, S.Ontario, trend surface anal. 78−92858
- Wolf Creek crater, Western Australia, gravity investigation 79−100838
- N.Wolverine Complex, British Columbia, geochronology and tectonics 80−3961
- Woodroffe thrust, deform. and fold axes reorientation in ductile mylonite zone 78−32101
- Woodroffe Thrust mylonite zone, biotite deform. and recrystallisation 80−21739
- Wrangellia, displaced terrane from Vancouver Island to S.Central Alaska 78−36165
- Yakuwa River sediments, petrography *(Japanese)* 77−70694
- Yellowknife mineralisation, vein geometry and hydrostatics 79−57920
- Yellowknife supergroup, Northwest Territories, volcanic rock density determ. from gravity obs. 80−98320
- Yellowstone Park hot spot, volcanic and tectonic evolution 80−56472
- Yellowstone volcanic plateau, conf., USA (1974) 78−49004
- Yerington mine, Nevada, geology rel. to induced polarisation and mag. susceptibility meas. 80−51323
- SE Yukon, unique stratigraphic record of late Tertiary-Quaternary events 79−62499
- Zagros Mountains, geological comparison with island arcs 79−2231
- zones of influence of linear geological structures, computation program 78−57202
- Fe ore band associated with meta- acidic intrusive, Himalayas, Mossbauer meas. 79−79821
- Fe ore formation, Addatigala, India, mag. profiles 79−34808
- Fe-Ni sulphide deposits, possible volcanic-exhalative origin 77−17097
- Li concentrations in McDermitt Caldera, in Nevada and Oregon, geological survey 79−48478
- Li deposits and potential, Quebec and Atlantic Provinces, in Canada, report 79−48481
- Li, needs and resources, conf., Corning, USA (Oct. 1977) 79−48473
- Li, occurrence in flint clay and related rock types in United States, preliminary survey 79−48475
- Li ores in Horse Spring Formation Miocene rocks, Clark County, Nevada, report 79−48474
- Li, ores in United Kingdom, brief assessment 79−48476
- Li ores resource evaluation, United States Geological Survey role 79−48477
- Li pegmatite ores in Western Superior Province, in Canadian Shield, distribution and petrogenesis 79−48480
- Li resources, Yellowknife area, in NW.Canada, report 79−48482
- Li resources and potentials, NW.Ontario, Manitoba, Saskatchewan, in Canada, estimation 79−48483
- Mn nodule undersea mining data file, management and statistical anal. 77−53206
- Mn nodules, accumulation rates from alpha track method 78−7610
- Mn nodules, geological history 77−25674
- Pb and Zn layers in South Niger, geological features *(Croatian)* 79−29772
- Po haloes in rocks and geochronology 80−56468
- Rn mapping in U exploration, exclusion of ^{220}Rn signal 80−61916
- U abundance in Himalayan plants, fission track method 80−101305
- U deposit, Saima alkaline massif, NE China 79−16470
- U, deposit distribution patterns and formation investigation *(Russian)* 79−30926
- U exploration, LANDSAT data merged with geol. and geophysics data 80−56651
- U, genesis of Proterozoic deposits, Australia 79−84270
- U in geological samples, rapid determ. using X-ray fluorescence anal. methods 79−88479
- U mineralization of Witwatersrand and Dominion Reef systems 77−86890
- U minerals in Witwatersrand Triad, geochronology 77−86892
- U ore bodies, overburden effects correction in ground level radiometric surveys 79−88485
- U ore deposit, H_2 as reducing agent 78−36169
- U ore deposits in collapse calderas, structural-geological features 77−25681
- U ore systems, morphogenetic grouping 78−81158
- U prospecting, pattern recognition appl. 77−66999
- U, review of Australian resources 79−87941

geomagnetic storms *see magnetic storms*

geomagnetic variations
- *see also micropulsations*
- 20 year variations, space and time distrib., interpretation 77−60352
- 20 year variations rel. to Earth diurnal rot. vel. and sunspot numbers 78−32005
- 60-year variations of geomag. field and mantle elec. cond. 79−8596
- ΣKp parameter, rel. to nighttime electron content of mid-latit. plasmasphere, 1974 August to November 80−94642
- A_2 index, sunspots and global weather data, cross-spectral anal. 77−78313
- A_p index in winter, influence of interplanetary mag. field sector struct. 80−8510
- A_p index rel. to weather and solar activity, spectral anal. 77−5308
- a_p magnetic index, neutral atmosphere response to major magnetic storm 77−9582
- A_p-index, 1964-1976, rel. to geomag. field and interplanetary field states 80−104866
- A_p-index, correl. with F-lacunae occurrence freq. 80−4193
- A_p-index, correl. with microearthquakes 79−66638
- A_p-index, correl. with solar activity and Jupiter decametric radio emission 79−21222
- A_p-index effects on atmospheric press. geopotential 80−4067
- aa annual index, appl. to solar cycle 21 max. intensity and date prediction 78−73696
- aa index, maximum entropy spectral anal. over 107 year interval 77−87187

geomagnetic variations continued
aa index rel. to solar dipole mag. field and interplanetary sector struct. *(Russian)* 79—21261
abnormal quiet days occurrence at Kodaikanal, India, 1950-75 period 79—53304
activity, effect on radar meteor rate 80—67662
activity and ionospheric absorpt. rel. to solar electron fluxes increase after flares 79—75175
activity correl. with heart attacks 77—13049
activity indexes rel. to interplanetary magnetic field *(Russian)* 78—16249
activity indices, anal. of 100-year series, components of annual wave at subauroral latits. *(French)* 78—40469
activity indices, anal. of 100-year series, positive conservation and mean values *(French)* 77—32981
activity indices, correl. with interplanetary scintillation indices assoc. with plasma turbulence 79—92645
activity indices, magnetospheric modulation, harmonic anal. of Km, Kn and Ks 78—40468
activity recurrence tendency during 20th solar cycle 79—25196
Adirondacks, geomag. fluctuations gradient anal. 80—89947
AE and D_{st} indexes, rel. to Earth currents short period oscills. *(Russian)* 77—44914
AE index, dusk-dawn asymmetry in magnetosphere response to interplanetary mag. field B_z component 77—2310
AE index, influence of substorms appearing N of Cambridge Bay 79—75054
AE index fluctuations, modulation by solar surface oscills. 79—8777
AE index levels occurrence, appl. to geomag. quietest days in year selection 79—66877
AE-index, correl. with rapid subauroral ion drifts obs. by Atmosphere Explorer C 80—4188
aeromagnetic data, diurnal drift removal by least squares 79—53529
amplitude variation of 27 day period in activity during 19th and 20th solar cycles 77—66886
annual and quasi-biennial waves, effects of dynamo region long period winds 77—2090
annual line in geomag. field elements, components 79—20752
annual line in geomag. spectrum 78—40470
annual progression of geomagnetic solar and lunar daily variations at Alibag 79—84091
annual variation for 1957-61 period 77—9327
antisymmetric S_q-variations, appl. of plasmasphere dynamo electric field-aligned currents theory 78—81499
Ap index and solar wind speed long-term averages correl. 77—60564
Ap index correl. with ionospheric daytime slab thickness 77—21992
Ap index of geomag. activity, correl. with Hale sector boundary of interplanetary mag. field 79—75055
ap indices, daily vars., determ. of interplanetary mag. field sector struct. 78—93066
aperiodic variation during sporadic mag. storm, approx. expressions 77—67012
archaeological ceramics, Peru, geomag. variations over last 2000 yrs. 80—94455
archaeomagnetic data compared with analytical representation of geomag. field for last 2000 years 78—73305
archaeomagnetic field determ. and secular var. in Caucasus 78—73309
archaeomagnetic field magnitude, rapid changes 79—74830
archaeomagnetic field strength, Egyptian adobe bricks (3000-0BC) 80—104862
archaeomagnetic polaeointensity study of Hohokam potsherds from Snaketown, Arizona 78—44769
archaeomagnetic polarity excursion, aboriginal fireplaces, thermoluminescent dating 77—21679
Arizona, Curie point isotherm from magnetic total intensity anomalies 78—61315
Middle Asia seismoactive regions, geomag. investigations 80—26464
Astronomical Netherlands Satellite, orbit prediction, geomag. disturbances effects 79—21139
E.Equatorial Atlantic, magnetic anomalies, Jurassic spreading and reversals 77—64253
N.Atlantic Late Cretaceous magnetic anomalies 77—81788
Mid Atlantic Ridge, palaeomag. studies, direct test of Vine-Matthews hypothesis 79—34734
atmospheric mag. field induced by sea waves, attenuation 77—13058
auroral disturbances, rel. to midlatit. F-region quiet time depressions 78—36385
auroral electrojet, nonpotential waves rel. to geomag. vars. 77—49212
auroral field lines, mag. perturbations assoc. with region of intense plasma wave turbulence 77—45228
auroral geomagnetic disturbances, role of ionospheric Birkeland currents *(Norwegian)* 80—31158
auroral luminosity rel. to geomag. field changes 80—77187
auroral oval, mag. fluctuations prod. by ionospheric Hall current 80—98501
auroral oval and polar cap mag. field perturbs., rel. to charged particles and interplanetary mag. field 78—45160
auroral particle instantaneous energy deposition rate, var. with mag. activity 78—81491
auroral zone, field-aligned currents and electrojets rel. to nightside auroras distrib. 78—32267
auroral zone, geomag. vars. rel. to elec. currents induction in Alaska pipeline 79—39645
auroral zone, ground-based obs. of elec. currents using two-dimensional magnetometer array 80—90245
auroral zone, magnetostatic model of electrojet 77—13163
auroral zone magnetic indices, correl. with dayside magnetosphere mag. flux transfer 78—96355
auroral zone modification due to geomag. excursions, minimum-effect model 77—78101
Australia, magnetic obs. during 1976, October 23 total eclipse 77—49000
S.E. Australia, recent secular variation and dipole wobble 78—11800
automatic digital magnetic recording system in Tihany Observatory 79—39989
Basque Provinces, Pyrenean folding, deep geomagnetic sounding *(French)* 80—67351
bay phenomena, theory of equivalent current systems including ground induction 80—41610
bays, frequency of appearance *(Russian)* 78—15956
bays, rel. to auroral and geomag. activity and interplanetary mag. field in (1968) 79—53654

geomagnetic variations continued
bays morphological features at high latits. 78—49232
bays observed at coastal observatory, effect of induced currents in sea 78—65462
Beaufort Sea sediment cores, NRM, geomag. excursion record 78—20349
Belgium, magnetic elements and variations since 1828 *(French, Flemish)* 77—32996
biotropicity, due to atmospheric Rn radioactivity increase induced by geomag. vars. 79—96621
Boso Peninsula, Japan, repeated mag. survey of total force intensity, 1968-76 period *(Japanese)* 77—60345
bow shock, mag. pulsations in quasi-parallel, quasi-laminar shock 77—37484
British Isles region, EM induction by analogue model 80—56368
Brunhes epoch palaeosecular var. studies in volcanic province, Germany 79—25198
Brunkes epoch, subdivisions rel. to regional magnetostratigraphic scale in Ukrainian SSR *(Russian)* 77—44916
Butkin anomaly of secular var. in Urals 78—69288
Cainozoic field inversions, W.Turkmenian data 79—44098
S.California downwarping, tectonomagnetic anomaly and seismicity 80—21626
Canada, secular change for 1975 78—65177
Caspian centre of secular geomag. field vars., dynamics 79—57848
central anomaly magnetization high and sea floor spreading, comments 77—5133
Ci index (1906-1976), solar eclipse perturbations 79—100811
climatic var. induced by magnetic field screening of cosmic rays 77—78398
coast effect, review 80—94458
coast effect in S.Australia 79—66610
conducting channel between India and Sri Lanka, effects on equatorial electrojet 79—25189
correlations of changes in geomag. field, climate and weather 79—39648
counter-electrojet afternoon events over India 78—12044
crochet, two-layer current model 79—44300
crochet associated solar microwave bursts, nature 78—69772
crochet type disturbances current systems and elec. fields in polar cap ionosphere 78—40733
crustal dilatancy and short-period var. 77—2096
cyclicity of geomag. activity rel. to solar wind velocity 79—79732
D_{st}, contrib. to aurora equatorward shift 79—75013
D_{st} index, annual and daily vars. 78—96351
D_{st} index, correl. with ring current growth and interplanetary quantity ε 79—75057
D_{st} index, negative change assoc. with whistler ducts formation 80—94659
D_{st} index, rel. to current fields at magnetopause and in radiation zone 79—53658
D_{st} index, standard reference level 77—29246
D_{st} variations, influence of solar wind parameters 79—40054
D_{st} variations analyses, comparison using distortion free filter 80—17419
D_{st} variations field, rel. to pulsations of decreasing period 79—53655
D-component variations at high latits., discrepancy with overhead horizontal current 79—75037
daily field variation in equatorial region and sector boundary passage 78—20355
daily mag. variations meas. in Alaska, atmos. current system 80—85590
daily magnetic variations influenced by interplanetary field 80—85591
daily pattern and equivalent current pattern, Alaskan 1978 obs. 80—41374
daily variation at equator affected by N. and S. hemisphere Sq currents 80—76904
daily variation in low latits., anal. 78—36098
daily variation of geomag. vertical intensity at Marion Island, phase shifts 78—81107
daily variations (lunar and solar) 80—109104
deep magnetic-variation sounding, geoelectric and geothermal interpretation of results 78—44765
detection by fish, expt. evidence 79—39381
dipole field vars. and length of day fluctuations, spectral line similarities 77—32993
disturbance accompanying seismic wave propag. *(Chinese)* 79—88238
disturbances, high-latit., generation rel. to ionospheric field-aligned currents 80—41631
disturbances, prediction from interplanetary scintillation obs. 79—58215
disturbances, prior to earthquakes, appearance time rel. to earthquake energy 77—13061
disturbances, rel. to occurrence of forenoon bite-out in F_2-layer critical freq. 78—65453
disturbances, solar wind-induced, rel. to interplanetary scintillation activity 79—58214
disturbances and 10 mbar surface geopotential fields characts. comparison 77—13055
disturbances intensity vars. rel. to polar E-region ionisation vars. 77—13151
disturbances prod. by meteoroids ballistic shock waves and explosion 77—13139
disturbances produced by large meteoroids shock waves 77—49231
disturbances rel. to nocturnally migrating bird orientation 77—66820
diurnal and UT variation in equivalent systems 80—51330
diurnal variation of horizontal field component, correl. with ionospheric equatorial anomaly 80—109301
diurnal vars. across Canada, coast effects 80—12331
double substorm in midnight sector, mid-latit. mag. signatures 77—53330
DP11-variations in polar cap 79—62677
DS latitudinal variation abnormalities 79—84591
Dst index levels occurrence, appl. to geomag. quietest days in year selection 79—66877
Dst space-time patterns during individual mag. storms 77—13184
Dst time derivative, rel. to ring current development and midlatit. convection elec. fields 78—57395
Dst variation rel. to interplanetary proton flux 77—67018
Dst variations and interplanetary B_z component vars., time displacement 79—101032
E-region, electron density variations during geomag. disturbances 78—69567
E-region, mag. disturbances rel. to cross polar cap horizontal currents and elec. fields 78—77405
E-region drift meas. and geomag. field vars. at tropical latits. 79—88528

geomagnetic variations continued
Early Triassic field reversal 77—60353
Earth's orbital eccentricity correl. with palaeoclimate and palaeomagnetism 77—78093
Earth-ionosphere waveguide channel parameters, influence of geomagnetic activity and statistical props. of VLF signals 79—88452
earthquake precursors, rocks stress cycling and inelastic volumetric strain rel. to remanent magnetisation 78—88820
earthquake precursory field changes, Nov. 1974 Hollister 'quake, California 80—104912
East Pacific Rise at 31°S, local axial migration and spreading rate variations 77—29274
effect of interplanetary mag. field on geomag. activity *(Hungarian)* 79—25544
effects on cancer deaths, glaciers and incident cosmic radiation 78—53615
effects on road accidents in Ahmedabad city (1972-5) 78—15958
electrokinetic effect and spring water discharge rel. to local var. 77—2097
EM field, conf., Hurbanovo, Czechoslovakia (Oct. 75) 79—39646
EM induction, transfer functions at pulsation periods 80—72417
EM induction for island-continent ocean channels, analogue model study for H-polarisation 77—81795
EM induction in Earth, by moving ionospheric current systems 79—16370
EM induction transfer functions at mid-latits., source field effects 79—74831
equatorial counter-electrojet, geomag. aspects review 78—36367
equatorial electrojet, bay type disturbances rel. to ionospherc dynamo regions global coupling 79—44297
equatorial electrojet, India, internal induction field from surface and satellite geomag. obs. 77—60535
equatorial geomagnetic field, daily variations, effect of sector boundary passage 80—67335
equatorial ionosphere, mag. vars. rel. to interplanetary mag. field vars. 78—77413
equatorial region bays, interplanetary mag. field sector polarity influence 80—8489
equatorial spread-F configs. correl. with geomag. activity 79—101007
equatorial zone, causes of daytime and nighttime vars. 79—66611
equivalent linear amplitude geomagnetic indices, evidence for strong artificial components 78—89008
SE.Europe, geomagnetic field variations between 6500 and 100 BC 78—32003
central Europe, upper mantle conductivity anomaly rel. to geomagnetism and secular var. *(German)* 78—7565
S.E.Europe, variations during last 8000 years 80—56351
evening sector eastward electrojet, ground-based magnetometer data 80—46341
excursions and palaeomag. record 77—86779
excursions and Pyramid Lake, Nevada palaeomagnetic record 80—101321
exosphere, mag. activity effects on temps. at high latits. 80—109286
F-region, mag. activity rel. to wind southward midnight surge 77—33233
Falkland-Agulhas Fracture Zone, ridge-crest offset history 80—26490
field disturbances produced by interplanetary mag. field B_z-component pulses 78—73583
field intensity variations during last 2500 years in Abkhazia 78—44762
field potential vars. separation into external and internal parts for mag. profiling *(Russian)* 79—39991
field reversal time scale back to 13 Myr BP 79—44085
field reversals, nature of transition periods 79—8598
field reversals, results from mag. prehistory of mountain rocks *(Russian)* 77—44917
field reversals, steady dynamos bifurcation from oscillating dynamos in nonlinear dynamo theory 78—49306
field reversals of steady dynamos rel. to geodynamo 80—51645
field variations during geomagnetically quiet conditions, spectral characts. 77—87179
field vector counterclockwise precession, prod. by non-dipole field westward drift 79—57853
Galapagos hot spot, bathymetry, magnetic anomalies and basalt magnetization 77—5132
Gazli earthquake, 1976 May 17, geomag. field vars. obs. 79—57859
Geomagnetic Meridian Project, magnetic var. of auroral electrojets 79—29936
geomagnetic moment second derivative, Sun-induced vars. 77—90981
geomagnetic storm sudden commencement preliminary reverse impulse, ionosphere transient response theory 80—8477
global characts. of main field for 1500-1970 period *(Russian)* 77—32989
global lunar semidiurnal geomagnetic var., seasonal changes 79—53598
global magnetic field, northward and westward drifts, theory *(German)* 79—16375
Gothenberg reversal, rejection of evidence from New Zealand 78—32007
Gothenburg geomagnetic excursion, global climatic change 77—29251
Grampian orogeny in Scotland: arc-continent collision and polarity reversal 79—39696
Gregory Rift Valley, Kenya, magnetotelluric and magnetovariational study 77—91000
H-component regular daily var. at Alibag, solar cycle depend. 79—8593
H-field quiet day variation at low latitudes 77—78102
H-polarisation, induction model for sea-floor coast effect 77—2104
harmonic analysis of vars. in 13-30 year period range 78—15962
Hawaii Island, mag. induction fields rel. to oceanic mantle elec. cond. struct. 78—40477
heart attack as biological effect of geomag. fluctuation 79—83812
heart attacks correl. with geomag. activity 79—39424
hemispheric geomagnetic activity, annual wave 79—66615
high-latitude, review 77—91381
high-latitude magnetic activity, comprehensive steady state model current system 79—92636
high-latitude variations, coupling to ionosphere equatorial elec. field 78—93029
horizontal field variations in Indian peninsula, induction at short periods 77—86773
Iberian Peninsula, cond. anomalies, continuous cond. channel from Mediterranean to N.Morocco *(French)* 77—86756
inclination and intensity vars. from archaeomag. investigation in Mongolia 77—48997
India, induced magnetic vars., regional charact. 79—39639

geomagnetic variations continued
India and Sri lanka coastline config. effects on induced field at short period 80—12337
Indian equatorial region, lunar magnetic tides 77—87154
induced magnetic fields at coastlines, EM scale model expts. 77—64205
induced var. in ground due to magnetospheric and ionospheric currents 77—70594
induction relationship, sufficient conditions 79—79739
induction vectors, local time var. 78—85477
intensity variation, over last 10000 years, archaeomagnetic record 80—36237
internal variations, screening by mantle when elec. cond. is concentrated near core boundary 79—12064
interplanetary mag. field caused by cyclical nature 80—81813
interplanetary mag. field variations correl. to mag. storms 80—41642
interplanetary magnetic field B_z component influence 79—62689
interplanetary magnetic field polarity, solar wind speed and geomagnetic index 77—78593
interplanetary magnetic fields affecting N.polar cap region fields 80—41644
interplanetary magnetic fields effect on activity *(Hungarian)* 77—74010
ionosphere, field var. at low and equatorial latitudes spectral characts. 78—36379
ionosphere, HF signals arrival angles depend. on mag. activity 77—91351
ionosphere, large-scale elec. field rel. to geomag. activity 77—87159
ionosphere, mag. activity correl. with S. hemisphere mid-latit. gravity waves obs. 79—21096
ionosphere, main valley electron temp. behaviour depend. on geomag. activity 80—4170
ionosphere, transitional electrodynamic processes rel. to geomag. disturbances 77—60515
ionosphere current system inducing currents in model Earth 80—30985
ionosphere disturbance, 1960, April 1, electrodynamic interaction between ionosphere and magnetosphere 78—28372
ionosphere F-region, equatorial stratified irregularities movement, time and magnetic dependence 80—8470
ionospheric current determ. from surface geomagnetic obs. *(Japanese)* 78—24406
ionospheric currents from Arecibo radar obs., rel. to mag. vars. and elec. fields 77—87166
ionospheric scintillation effect, obs. at Lunping Observatory 79—88545
Iran, mag. field intensity spatial vars. on N-S profiles, 1970 IGRF comparison 77—48999
Izu Peninsula, Japan, earthquake related short-period variations *(Japanese)* 80—41396
Izu Peninsula, Japan, geomag. force intensity vars. in crustal uplift area *(Japanese)* 78—96128
Izu-Oshima-kinkai earthquake, Jan. 1978, precursory mag. field changes *(Japanese)* 80—41395
Izu-Oshima-kinkai earthquake, Jan. 1978, precursory mag. variations and electricity *(Japanese)* 80—41397
Japan, secular change anomalies rel. to tectonic activities 77—2091
K_p and a_p indices, recalibration for universal time vars. 77—9333
K_p index, correl. with ELF emissions obs. at Moshiri, Japan 78—24413
K_p index, rel. to F-region diffusion-recomb. parameters 77—13156
K_p index, rel. to temp., density and comp. in disturbed thermosphere 77—37468
K_p index rel. to interplanetary mag. field intensity *(Russian)* 79—40055
K_p indices during magnetic storms, rel. to vertical motions of low-latit. F_2-layer 77—37479
K_p-index, 27-day variations, amplitude modulation 80—26703
K_p-index, correl. with mid-latit. charged particle precip. 79—44291
K_p-index, daily vars. correlated with heart attacks 80—21482
K_p-index, ionosphere, relation to spread-F parameters 80—8471
K_p-index, rel. to Pc 5 pulsations characts. at Indian equatorial station, Trivandrum 77—91379
K_p-index, vars. within 10-100 years range rel. to Earth rot. rate and sunspots relative numbers 77—90980
K_p-index (1956-66) rel. to spread-F at Kodaikanal, India 79—88542
K_p-index during August 1972, correl. with cosmic rays north-south anisotropies 78—89018
k_p-index influence on equatorial Pi 2 pulsations fine struct. 80—72721
K-index 3-hr range, geophys. meaning 80—82143
K-index estimation by computer 78—36305
Kansu Province, short period geomag. var. rel. to cond. belt *(Chinese)* 79—20745
S Karelia, elec. cond. anomalies from magnetovariation and magnetotelluric data *(Russian)* 79—96737
S Karelia, Onega mould schungites rel. to elec. cond. anomalies *(Russian)* 79—96737
Kenya Rift, mapping of induced currents, comparison of techniques 77—73628
Kp and AE-indices, geomag. activity effects on ionospheric F-region 80—8480
Kp variation at interplanetary mag. field sector boundaries 77—64202
Kp-index, correl. with midlatit. spread-F occurrence 78—36389
lake ground loading during filling, piezomagnetic effect 80—8346
Laschamp geomagnetic polarity reversal, K-Ar and ^{40}Ar/^{39}Ar age 78—81105
Laschamp magnetic reversal *(French)* 79—48401
Late Cretaceous polarity sequence, Scaglia Rossa limestone, Italy, rock and palaeomag. studies 78—11803
Late Tertiary field reversal, palaeomag. record in Tatoosh intrusion 78—48962
linear range activity indices, artificial components 77—87196
local daytime energy spectra, depend. on solar wind vel. and interplanetary mag. field direction 80—67476
local geomagnetic field changes determ., noise reduction techniques 80—26636
local variations assoc. with earthquakes dilatancy-magnetic effect *(Chinese)* 78—61333
long-period variations, spectra anal. methods *(Russian)* 79—34743
long-term variations rel. to solar wind speed vars. during 20th solar cycle 77—87361
low latitude field disturbance, effect of interplanetary mag. field 79—35090
low latitude geomagnetic activity response to sector boundary passage 77—64206
low latitude geomagnetic field, diurnal and seasonal vars. of effect of interplanetary mag. field Y-component 80—56354

geomagnetic variations continued
- low latitude positive bays occurrence rel. to interplanetary mag. field sector polarity 77—40982
- low latitudes, fluctuations correl. with interplanetary mag. field N-S component vars. 78—44772
- lunar daily geomagnetic variations at Sabhawala and Hyderabad, harmonic anal. 79—44097
- lunar daily geomagnetic variations at Tucson, anal. for M_2-tide 78—96136
- lunar daily var. at Alibag, oceanic and ionospheric dynamos contrib. 80—26444
- lunar daily variation, Sanae, Antarctica 79—12070
- lunar daily variation at Alibag, O_1 tide component detect. and contamination by M_2 component 80—56355
- lunar harmonic data analysis, least squares method 80—51327
- lunar semidiurnal tidal line width in geomag. spectrum, filtering methods 77—21678
- lunar tidal variation in Indian region 77—60541
- lunar tides seasonal var. 80—26445
- Lunping, Taiwan, solar and lunar daily variations, 1966 to 1976 period 80—72416
- mag. storms, vars. rel. to elec. field in equatorial ionosphere 77—78578
- magnetic activity, rel. to Pc 5 pulsations features during solar cycle 78—36406
- magnetic noise of low-freq., generated on auroral field lines 80—101494
- magnetic storms, delineation of cosmic ray flux, Earth mag. field *(German)* 80—51609
- magnetic tail, field vars. rel. to plasma flow pulsations 78—77436
- magnetometer for sea-floor mag. fluctuations, ULF-ELF 80—77152
- magnetosheath, mag. field strength vars. at dayside magnetopause rel. to plasma depletion 79—66876
- magnetosheath, microscale mag. fluctuations during quiet conditions, probability distrib. functions 78—4053
- magnetosheath and magnetosphere, mag. fluctuations anal. rel. to Pc pulsations reson. theory 79—80092
- magnetosphere, geomag. field fluctuations power spectra at synchronous orbit 78—96358
- magnetosphere, geomag. fluctuations obs. by new space-borne ring-core type magnetometer *(Japanese)* 80—94671
- magnetosphere, geomagnetic field fluctuations at synchronous orbit rel. to particles radial diffusion 78—96359
- magnetosphere, large scale elec. fields and currents, related geomag. vars., review 80—105121
- magnetosphere, mag. activity rel. to electron density meas. by (GEOS-1) 79—35071
- magnetosphere, mag. pulsations during early August (1972) 77—25888
- magnetosphere, plasma density depend. on mag. activity, GEOS-1 relaxation sounder obs. 79—35072
- magnetosphere current systems, N.polar cap mag. variations associated with interplanetary field 80—41645
- magnetosphere dayside cleft, mag. field perturbations rel. to interplanetary mag. field 79—40023
- magnetosphere substorm-associated long-period hydromagnetic waves, longit. extent 78—40772
- magnetosphere substorms, geomag. vars. rel. to plasma sheet radial dynamics 77—25871
- magnetosphere substorms, statistical mag. signature 78—49237
- magnetospheric modulation of geomag. activity, harmonic anal. of am, an and as indices 79—66605
- magnetotail, distant, lower-hybrid-drift wave turbulence 79—25399
- magnetotail, mag. field meas. rel. to plasma waves 77—29592
- magnetotelluric fields in E.Canada tectonically active region, time depend. 80—26451
- magnetotelluric investigation at Ronde, vars. due to atmospheric discharges and ionosphere elec. currents *(Danish)* 80—8250
- magnetotellurics, crustal resistivity and conductivity variations, thin sheet anal. 80—51329
- mantle, conductivity in deep regions, geomagnetic impulses 78—28200
- marine geomagnetism, plate tectonics, plate boundaries and mag. field reversals *(French)* 79—66621
- marine magnetic anomalies, Atlantic Ocean, palaeomag. field anomalous behaviour 79—29699
- marine magnetic anomalies, source shape and nature 77—17021
- Lower Matuyama epoch, geomagnetic events from palaeomag. obs. in SW Iceland 80—89950
- Matuyama epoch, short geomag. episodes meas. 79—66616
- McIntosh effects in geomagnetic activity, Boller-Stolov effect 77—49241
- measurement and data processing, new methods 79—39988
- Melanesia Basin deep-sea sediments, palaeomag., polarity reversals 78—36102
- mesosphere, day-night depend. of geomag. activity effects on temp. 77—21835
- meteor radar rates correl. with geomag. activity and solar wind sector struct. 78—65553
- Mid Atlantic Ridge crest at 26°N, magnetic anomaly patterns, spreading rate 77—32991
- midlatitude disturbances, assoc. VLF radio wave phase anomalies 80—56671
- Mio-Pliocene secular variations, palaeomag. results from Narosura and Magadi volcanics, Kenya 79—79740
- modulation of lunar component var. by interplanetary sector field polarity 78—15963
- Mono Lake geomagnetic excursion 79—48397
- monthly mean lunar daily geomag. vars. at Kakioka, Memambatsu and Kanoya, Japan (1958-1973) 79—96739
- N.Morocco, geomag. vars. recording, cond. anomaly existence *(French)* 77—86755
- negative bay, precipitating electron intensity modulation in auroral zone and coincident Pi 2 77—60539
- nondipole field component, westward drift rate determ. 79—12065
- north magnetic pole, 1975 position and secular and diurnal vars. 78—92778
- ocean currents due to geomag. field, theory 80—104962
- ocean electric current induced by Sq, around land masses 80—72413
- ocean internal waves causing geomagnetic gradient fluctuations 80—56491
- ocean wave effects, meas. using supercond. mag. gradiometer 77—33203
- ocean wave induced variations, analogue model 77—49003
- ohmic region effect on vars. *(German)* 79—29708
- Olby-Laschamp geomag. polarity event, age 79—12067

geomagnetic variations continued
- Oshima Island, Japan, anomalous secular variation, rel. to earthquake or volcanicity *(Japanese)* 80—41369
- palaeointensity secular variation, meas. on postglacial lavas from Iceland 80—89952
- palaeomagnetic data analysis, elimination of secular variation 80—61755
- palaeomagnetic secular variation, recent, in lake sediments from New Guinea Highlands 79—12069
- palaeomagnetism, revised polarity time scale for interval 0 to 5 m.y. BP 79—57851
- palaeomagnetosphere, third type of planetary magnetosphere during polarity reversals and geomag. excursions 78—61683
- palaeosecular variation, directional data sets shape 79—39881
- palaeosecular variation from W.Iceland lava flows palaeomag. anal. 77—56575
- palaeosecular vars. in Afar depression, meas. of lavas from axial zone 77—37126
- Pc 5 micropulsations, mag. vars. prediction from ionospheric reson. region radar obs. 78—65454
- piezomagnetic variations, response depth depend. rel. to tectonomagnetism as earthquake precursor 80—26465
- planetary pulsation indices of geophys. activity 79—40041
- plasmapause, position depend. on geomag. activity, Explorer 45 obs. 77—53285
- polar cap, mag. field signature rel. to empirical models of high-latit. elec. fields 77—45255
- polar cap and low latitude bays during substorms, ionospheric current systems 77—17300
- polar cap field, responses to solar sector changes 77—5134
- polar cap magnetic activity during undisturbed periods, characts. 77—33295
- polar cap magnetic disturbances, rel. to horizontal E-region currents 77—45230
- polar cap variations rel. to interplanetary mag. field transverse component 78—20733
- polar region seasonal dependences rel. to annual vertical component variation 80—41376
- polar regions, small-scale transverse magnetic disturbances 78—77423
- polar substorms, temporal and spatial changes rel. to auroral infrasonic wave emissions 79—100996
- polarisation anomaly at South Georgia 79—74835
- polarity reversals, role of fluid core dynamics with inward growing boundaries 80—76934
- polarity transition, evidence for strong intermediate palaeofield magnitude 77—44911
- polarity transition, palaeomag. field magnitude and direction 77—37429
- polarity transition, palaeomag. non-dipole field intensity and direction changes 77—37134
- polarity transition records and geomag. dynamo 77—91007
- polarity transitions, in two oriented sediment cores from NW.Pacific Ocean 79—88243
- pole-tide signal at low-latitude coastal station 78—61322
- positive bays in auroral zone rel. to reverse currents in electrojets *(Russian)* 78—4037
- potential variations, effects of bumpy core-mantle interface 79—79771
- power spectrum anal. of time series 79—16705
- Precambrian field reversals, Gardar lavas (S.Greenland) meas. 77—40973
- Precambrian geomagnetic reversal, from Korostenian pluton gabbro-anorthosite rocks NRM *(Russian)* 79—8599
- Proterozoic Belt Supergroup in Montana and Idaho, palaeopoles and polarity zonation 80—72420
- Ps 6 magnetic disturbances, seasonal and diurnal var. 80—67477
- pulsations before solar proton flares *(Russian)* 78—69291
- N.Pyrenees, anomalous field temporal var. 77—56574
- Q-index, correl. with large-scale inhomogeneities of auroral ionosphere E_s-layer 80—4171
- quasi-biennial geomagnetic variation, correl. with solar activity 78—32006
- quasibiennial variation caused by Sun 77—21677
- SW.Queensland, telluric currents assoc. with anomalous geomag. vars. 80—109089
- quiet and disturbed intervals, annual var. rel. to interplanetary mag. field sector polarity 77—86767
- quiet time field at successive universal times 78—61325
- quiet time var. rel. to interplanetary mag. field, autocorrel. effects 78—61697
- quiet time vertical magnetic field component over India 78—61326
- radionuclide survey of USA, ERDA aerial radiometric and magnetic survey 78—12027
- rapid field change in Permian during Zechstein marine transgression 78—15964
- real-time magnetometer data transmission via telephone lines 77—13126
- Red Sea area, geomag. secular var. and secular accel. 79—88248
- regular daily variation, magnetospheric and night-time induced effects 77—9627
- remote sensing at mesospheric heights 80—77124
- response to long-period geomagnetic fluctuations, phase 79—88239
- reversal, ^{10}Be conc. vars. search in marine sediment core 80—26511
- reversal chronology from Arizona volcanic sequence rel. to ocean floor polarity record 80—72419
- reversal during Wisconsinan Ice Age, evidence from Iceland 78—61327
- reversal sequences, statistics time var. and asymm. 77—32994
- reversal transition widths and fast spreading centres 77—17022
- reversals, correl. function anal. 80—21622
- reversals, transitional field configs. 78—65182
- reversals, virtual pole position peculiarities 77—73634
- reversals and climatic change, statistical correl. 78—61537
- reversals at central European locations 79—39652
- reversals rel. to magnetopause altitude 77—22019
- reverse equatorial electrojet events, mag. vars. at other latits. 78—36368
- Rhinegraben mag. anomaly, responsible elec. currents 80—46124
- S_q^p obs. from Alaskan meridian chain, ionosphere and magnetosphere currents 80—85813
- S_q variation, magnetosphere or ionosphere dynamo? 80—109090
- S_q variation at mag. conjugate points and interplanetary mag. field var. 78—69287
- S_q variation currents, day to day variability over Europe 79—44299
- S_q variation electric fields, rel. to F_2-layer global electron density distrib. 77—64514
- S_q variations field, magnetically conjugate structs. variability 79—58191

geomagnetic variations continued
S_q variations in San Jose, mag. activity at S_q current system focus 78—44763
S_q variations phase and amplitude at mag. conjugate points 78—40479
S_q variations seasonal pattern at solar activity minimum 77—60351
S_q-field, seasonal and latit. vars. deduced via natural nonorthogonal functions method 78—36359
San Andreas fault, local mag. field meas. rel. to fault creep obs. 80—85629
San Andreas fault, local mag. field vars. and stress changes near slip discontinuity 80—26448
San Andreas fault (central California), mag. field local vars., creep rate changes and local earthquakes 80—26450
sea floor temporal mag. variation meas. using magnetometer 80—51581
secular acceleration, spherical harmonic model 79—88249
secular change determ. by tridipole model, 1942-1950 period 79—5443
secular changes effects on cosmic ray variational coeffs. 78—93058
secular departures from International Geomagnetic Reference Field 78—40481
secular geomagnetic field variations in Carpathians, characts. 79—53301
secular impulse rel. to deep mantle conductivity 80—98236
secular trends in daily mag. variations 80—109103
secular var. anomalies around Sverdlovsk magnetic observatory 78—61319
secular var. from palaeomagnetism of varved sediments from W.New England 79—70739
secular variation, 1947-1977, implications for mantle elec. cond. 80—61754
secular variation, 1966-1975, obs. at Ulan-Bator observatory 78—44767
secular variation, dynamo theory frictional damping of Hide's mag. waves 80—98218
secular variation, EM induction of core source in rot. cond. Earth 78—44764
secular variation, mathematical-physical anal. and interpretation *(German)* 79—34742
secular variation, modelled on mantle elec. cond. inhomogeneity *(German)* 80—81806
secular variation, palaeomag. record from Lake Michigan sediment cores 77—60347
secular variation, repeated obs. appl. to elec. cond. anomalies detect. *(Russian)* 79—96736
secular variation, solar cycle depend., Rumanian data 80—56366
secular variation anomalies, external and normal fields *(Russian)* 77—73630
secular variation anomalies in Europe 79—39650
secular variation anomalies in GDR, meas. 80—26449
secular variation anomalies in Urals, rel. to aseismic geodynamics 80—26447
secular variation correl. with cosmic ray threshold rigidity 77—53368
secular variation for 1965, definitive model derivation and comparison with IGRF 78—96133
secular variation in Europe, analytical representation on basis of observatory data 80—101323
secular variation in Finland, 1650-1970 period 80—67336
secular variation in India, regional and local features 77—86768
secular variation of International Geomagnetic Reference Field in Europe 77—86763
secular variation of mag. declination in Belgium *(French)* 77—17019
secular variation of mag. field in San Jose las Lajas (Cuba) 79—57849
secular variation of northward component correl. with solar cycle 77—73635
secular variation periods, spectral anal. of archaeomagnetic data 80—41372
secular variation rel. to Earth internal struct. 79—39647
secular variation since 8500 BP 80—104865
secular variations, correl. with Earth daily rot. vars. 78—73302
secular variations, dynamics rel. to Earth core elec. cond. 79—12066
secular variations, geomag. field models comparison with obs., rel. to broad scale anomaly studies 80—72425
secular variations, short period, meas. from palaeomag. records of N.Poland Holocene lake sediments 80—98221
secular variations, space-time separation into fields of separate centres *(Russian)* 79—96738
secular variations, spherical harmonic anal. using internal coeffs. 77—78104
secular variations during last 250000 years, results from rapidly deposited sediments 77—32983
secular variations from Iceland lava flour data, model 80—104871
secular variations meas. in Bashkiriya, anomalies 77—91004
secular variations of vertical component, morphological characts. 77—91003
secular variations on historical time scale 80—36236
secular vars. recorded in Loch Lomond sediments 79—44088
seismo-magnetic effect in 1964 Niigata earthquake 77—2093
seismomagnetic earthquake precursors, uniaxial stress effects upon rocks remanent magnetisation 80—26505
seismomagnetic effect during Gazly, 1976 May 17, earthquake, unsuccessful search 80—26463
separation into quiet and disturbed components by natural orthogonal components method 80—3922
SFE and SSC at Hyderabad, diurnal var. 77—70922
short period variations in EM field, anal. for wave type and propag. direction determ. *(Russian)* 78—85474
short-period anomaly over Imandra-Varzuga structure (Kola Peninsula) *(Russian)* 80—85589
short-period field variations, electromechanical effects 79—57847
short-period variations, changes in direction of mag. vector before 1972 Sitka, Alaska, earthquake 80—76923
simultaneous high and low-latitude vars., polar elec. fields transmission to Equator 78—65456
small bay disturbances, possible correl. with VLF hiss emissions 78—81509
solar and lunar daily vars., long-term variability 77—60350
solar coronal holes, solar wind streams and geomag. activity during 1976-77 period 79—25570
solar cycle modulation at Alibag 77—60354
solar cycle variation, of geomag. external spherical harmonic coeffs. 80—85592
solar cycle variations, of first-degree spherical harmonic components of geomag. field 80—85593

geomagnetic variations continued
solar daily geomagnetic variations at Sabhawala and Hyderabad, harmonic anal. 79—44097
solar eclipse, 1976, October 23, mag. obs. in Australia 78—81498
solar flares effects 79—84764
solar high latitude field rel. to geomagnetic activity 79—44308
solar polar coronal holes, rel. to geomag. activity and solar cycles 80—21979
solar wind high-speed streams, influence, on geomag. activity 77—37487
solar wind long-term average speed, correl. with geomag. activity 78—32301
solar wind parameters depend. of geomag. activity, statistical anal. 79—48402
solar wind velocity rel. to geomag. activity 79—100813
Soviet Carpathians, deep magnetotelluric S_q-variation profiling *(Russian)* 80—30987
spatial distrib. of spectral composition for disturbed days 77—78103
spectral analysis, rel. to correl. with solar oscills. 78—89013
spread-F occurrence following geomag. activity, time delay latit. depend. 80—8481
Sq and EM induction of oceans, during IGY 80—72428
Sq at low latitude, hourly study of secondary effect 80—56362
Sq current distrib., equatorial F-region ionisation motions determ. 77—21981
Sq current system during International Geophysical Year 77—45219
Sq current system in E-region, electrodynamic effects of solar tides 77—9610
Sq effect at satellite altitudes, correction for Magsat data analysis 79—75015
Sq variation at Addis Ababa, 1958-1973 period 77—52982
Sq variation near mag. equator, solar control, obs. at Huancayo 1922-73 period 79—2181
St. Vincent's Gulf, South Australia, Island and coast effect in geomag. vars. 80—72426
stable solar wind and geomagnetic activity 79—53696
strong disturbances, correl. with lower atmosphere instability at different seasons 80—61881
strong disturbances, correl. with vars. in surface atmospheric press. field 78—36245
substorm variation field modeling, current system anal. 80—105130
substorms, comprehensive model current system for high-latit. mag. activity 79—92640
substorms, high-latit., mag. vars. characts. 80—109315
substorms, negative bays rel. to electron flux vars. in inner radiation belt near trapping zone boundary 80—67470
substorms, rel. to magnetotail hot tenuous plasmas, fireballs and boundary layers 78—32300
sunspot cycle influence on geomag. field 77—78090
Switzerland survey methods, instrumentation *(French)* 78—40490
Tajikistan, tectonomagnetic studies 80—26446
Tangshan earthquake, China, related geomag. field variations *(Chinese)* 80—56372
tectonic stress origin, theory of electrokinetic-mag. anomalies 80—21627
tectonomagnetic effects in N.W. Turkey 77—2094
tectonomagnetic events, detect. using empirical transfer functions 79—16374
tectonomagnetic experiments, noise reduction by multivariate linear regression 79—84515
tectonomagnetics and small scale secular variation, symposium, Seattle, Washington (1977 August 22) 80—22133
tectonomagnetism, implications of magnetite mag. susceptibility under hydrostatic press. 80—26504
tectonomagnetism, improved signal discrimination and volcanomag. effect at Kilauea, Hawaii 79—92629
tectonomagnetism, rocks NRM stress sensitivity meas. using cryogenic magnetometer 80—26506
tectonomagnetism in western USA 77—2092
terrain induced aeromagnetic anomalies, reduction by parallel surface continuation 78—61316
thermosphere, magnetic activity effects on winds in N.Polar Cap 80—67445
thermosphere, midlatitude winds rel. to storm time disturbance change rate 79—12323
thermosphere, zonal mean circulation vars. rel. to geomag. activity 78—32262
thermosphere and exosphere, neutral temperature and winds, geomag. disturbances effects 80—26658
thermosphere temperatures depend. on geomag. activity, incoherent scatter data comparison with global models 80—8467
tides, anal. methods 77—87079
tides, ocean effects 77—86752
Tien-Shan seismic zone, secular geomagnetic variations *(Russian)* 77—86777
total intensity secular trend at Bombay (1848-1967) rel. to sunspot nos. 80—81811
transient irregular variations, morphological classification, statistical laws 79—66606
Turkey, local magnetic constant var. rel. to seismicity 77—2095
twelve month wave in an and as activity indices 80—72427
upper atmosphere tidal effects on geomagnetic and ionosphere variations 77—87137
upper atmosphere-ionosphere, seasonal vars. in response to mag. activity 77—53289
Vancouver Island region, analogue model study of EM induction 80—56356
Vancouver Island region, electromagnetic induction model 80—56367
Vancouver Island region, terrestrial EM induction 80—104879
vertical component daily vars. phase relation at two stations *(Chinese)* 79—88236
volcanomagnetic effect, piezomag. field assoc. with Mogi model for surface displacements 80—67334
vorticity area index at 500 mb, geomagnetic disturbance effects 80—61873
weak global magnetic disturbances, characts. and origin 79—53660
weekend increase in geomagnetic activity, power line harmonic radiation effects 79—79738
westward drift of Earth magnetic field 77—81794
Yellowstone and Jackson Lakes, mag. props. and secular var. in sediment cores 78—48968
Yoldia Clay sequence from Denmark, 14-40000 yr B.P., geomag. variations 80—94454

geomagnetic variations continued
^{14}C concentration in Earth's atmosphere, corrections with astrophysical and geophysical phenomena 78−61477
^{14}C concentration in Earth's atm. with variations of geomag. field, spectral anal. 78−61478
^{14}C in atmosphere content variation, past geomagnetic and cosmic ray intensity variations 78−61691

geomagnetism
see also geomagnetic variations; magnetic storms
1972, Canadian magnetic observatories, annual report 77−9329
activity indices, analysis of 100 year series, log-normal freq. distrib. *(French)* 77−52969
activity rel. to occurrence of E_s-layer with group delay 77−29545
Adirondak mountains, mag. field components, fluctuation anal. 80−89946
aeromagnetic anomaly from remanently magnetised Precambrian schist belt, Karnataka, India harmonic inversion 79−44094
aeromagnetic control network construction in USSR, metric principles 77−21676
aeromagnetic data from different times with varying specifications, integration method 80−4127
aeromagnetic surveys, bicubic spline interpolation 80−17405
E.Afghanistan, Logar ultrabasite massif, geology and geomag. 80−72512
African plate, evidence for western sector N-S shift from mag. anomaly study 77−53035
African plate, mag. features rel. to mantle convection pattern and stress system 77−81859
Agulhas Basin of S.Atlantic, seafloor spreading history, geomag. study 80−21696
airborne EM mapping, aircraft altitude and displacement currents effects 77−52975
albedo particles ionization losses calc. with allowance for geomag. field 79−53621
E.Alps, gravity and mag. field transformations *(German)* 79−70735
E.Alps, mag. and gravity anomalies correls. *(German)* 79−53327
alternating EM field perturbs. by cond. inhomogeneities 79−39653
N.America, E. coastal region, EM induction model 80−98235
S.American geomagnetic equator, EM induction from ionospheric current meas. 79−75021
ancient planetary magnetic field investig. using cosmic ray latitude depend. cutoff 77−45269
ancient shields, crustal magnetic model construction problems *(Russian)* 77−32985
animal sensitivity to geomag. field, ferromag. coupling to muscle receptors as basis 80−72185
anisotropic inhomogeneities oriented along geomagnetic field, radiowave scattering 78−53771
anomalies, approx. theory *(Russian)* 78−28338
anomalies, Atlantic Ocean, statistical anal. 79−44101
anomalies, comparison with Moon 78−4122
anomalies, conformal deform. method for singular points determ. *(Russian)* 79−39934
anomalies, Czechoslovakia *(Russian)* 79−39655
anomalies, deep sounding data interpretation, use of equivalent current systems 79−25190
anomalies, derivative harmonic function restoration *(Russian)* 80−85577
anomalies, Falkland escarpment and Agulhas fracture zone, boundary between oceanic and continental basement 77−21700
anomalies, interpretation, Kolmogorov-Wiener least-squares filters appl. 78−61580
anomalies, interpretation by singular point method 77−53229
anomalies, interpretation with end-corrected Fourier-transforms 78−65418
anomalies, linear anal. *(Russian)* 78−53755
anomalies, magnetic and gravitational equivalence of extrapolation *(Russian)* 79−39926
anomalies, new interpretation theory 79−84509
anomalies, numerical interpolation schemes *(Russian)* 79−62622
anomalies, quantitative interpretation 80−26652
anomalies, satellite data inversion 80−12563
anomalies, source depth estimation, spectral method 79−92631
anomalies, spectrum of 2-D and 3-D bodies rel. to gravity anomalies *(Chinese)* 80−56342
anomalies, total, of step model, spectral anal. 79−5450
anomalies across Campbell Plateau, New Zealand 79−29700
anomalies analysis, regional background separation *(Russian)* 78−40703
anomalies assoc. with dilatant regions in layered Earth rel. to earthquake prediction 79−39658
anomalies at mouth of Gulf of Kutch 79−25195
anomalies calc. for regular homogeneous perturbing bodies *(German)* 78−69478
anomalies caused by alkaline rocks, spectral anal. in geophysical prospecting *(Rumanian)* 80−12338
anomalies caused by long horizontal cylinders, direct interpretation method 77−52971
anomalies caused by two-dimens. vertical faults, direct interpretation method 78−77181
anomalies due to homogeneous polyhedral bodies, analytical expressions 80−3894
anomalies due to rectangular prismatic bodies, spectral anal. 77−53222
anomalies due to subsurface features, rel. to sloping contacts interpretation 80−98222
anomalies in Altai Sayan folded region USSR, due to deuteroorogenic stage complexes 80−101327
anomalies in crustal abyssal zones *(Russian)* 77−73631
anomalies in satellite data, reduction and treatment 77−86766
anomalies interpretation, separation from gravity anomalies of comparable horizontal dimensions 80−94606
anomalies interpretation, Tikhonov's regularization method 78−49163
anomalies of arbitrary bodies, FFT method for rapid computation 77−41186
anomalies of cylindrical bodies, separation of gravity and magnetic effects *(Russian)* 77−9325
anomalies of mag. and gravity field, anal. by unitary method 80−89932
anomalies of polygonal prisms, mag. terrain corrections appl. 77−2082
anomalies over three-dimens. objects, inverse problem soln. 80−89939
anomalous EM fields from different sources over polarized sections *(Russian)* 77−86776
anomalous field, nature and interp. 77−86762

geomagnetism continued
anomalous field, statistical props. rel. to crustal struct. 77−86761
anomalous magnetic field in E. Mongolia, two-dimensional autocorrel. anal. rel. to block tectonics 80−56469
anomalous magnetic fields interpretation, computer modelling 79−34971
anomaly, direct computation by equiv.-point method and simplified cubic spline 78−7780
anomaly depth determ. and inverse problems 77−45165
anomaly due to 2-D assym. triangular prism, expression for total field 80−94457
anomaly due to arbitrarily shaped mag. body, rapid computation 80−36226
anomaly due to inhomogeneous density distrib., computation 78−7779
anomaly due to magnetic body, parameters of body from pot. data 80−85581
anomaly due to vertical right circular cylinder with arbitrary polarisation 78−77180
anomaly field vertical intensity, autocovariance function analytic derivation for sources statistical distrib. *(German)* 79−34746
anomaly interpolation to regular network nodes *(Russian)* 78−15945
anomaly interpretation, pot. fields linear anal. *(Russian)* 79−35011
anomaly interpretation using statistical algorithms 77−70856
anomaly intrepretation, bidimensional inhomogeneous problem soln. via Cauchy integrals *(Russian)* 79−35013
anomaly inversion, generalised multibody model 80−98226
anomaly of thin dike, curve fit by calculator program 80−98228
anomaly reduction to mag. pole *(Chinese)* 79−100963
anomaly sounding, estimation of cover thickness above magnetised mass *(Russian)* 80−105069
anomaly source models, statistical parameters rel. to pot. fields obtained by superposition *(German)* 79−34783
anomaly sources in crust of Siberian platform *(Russian)* 77−32987
anomaly survey data analysis, curve-matching optimisation method *(Chinese)* 80−89935
E Antarctic craton sedimentary basins from seismic, mag., gravity and radar obs. 77−21733
anticlinal thin bed and thin dipping dike equivalence 77−40975
apparent source depth of mag. field, appl. to planetary fields and internal struct. 78−57478
arbitrarily shaped three dimensional body 77−44908
Archean shield of Manitoba and Ontario, surface magnetisation distrib. 80−26439
Arctic Basin, detailed aeromag. survey, rel. to tectonic evolution 79−70746
Arctic Ocean, mag. anomalies rel. to evolution 79−48398
Arctic Ocean, magnetotelluric soundings rel. to sediment thicknesses and upper mantle temps. 79−48454
areal magnetovariation studies, Russian Platform 79−62432
Argo Abyssal Plain, mag. anomalies, bathymetry and seismic struct. 79−29741
artificial premagnetization method, theory, ore prospecting appl. 79−39876
Asama Volcano, Japan, amg. and elec. obs. *(Japanese)* 79−70736
central Asia, variable geomagnetic field anomaly 79−62431
asthenosphere under NE.Pacific, magnetotelluric sounding obs. 80−46123
N. Atlantic, sea floor spreading and early opening, mag. and gravity data 78−65247
S Atlantic anomaly, working group of Antarctic and Southern Hemisphere Aeronomy Year (ASHAY) 77−87210
S.Atlantic anomaly region, aeronomic and geophysical indicators anal. 79−58187
Atlantic bottom topography and magnetic field of elevated area *(Russian)* 78−85531
Atlantic Ocean, history of growth and topography of ocean bottom 80−3993
N.Atlantic Ocean, mag. anomalies 77−49001
S. Atlantic Ocean, mag. lineaments rel. to seafloor spreading south of Agulhas Fracture Zone 78−24277
Atlantic Ocean south of Bermuda, geophys. survey within Mesozoic mag. anomaly sequence 80−26492
S.Atlantic oceanic crust in Mesozoic and subsequent evolution, mag. and gravity data 80−21699
Mid Atlantic Ridge crest, geological and geophys. investigations 80−8284
Atlantic S.E. of Azores, crustal struct. rel. to mag. anomalies and bathymetry 80−51384
Atlantic type continental margins, struct. from geophysical meas. 77−21702
atmosphere, DC source in continuously var. conductivity, electric and magnetic fields 77−49140
atmosphere electrodynamic state, horizontal mag. field component influence *(Russian)* 78−73556
atmospheric ionization inhomogeneities advected neutral gas motions, geomag. field effects 80−26677
atmospheric showers, γ-ray initiated, computer simulations, Cherenkov radiation, geomag. field effects 77−49254
audiomagnetotelluric investigations in geothermal areas 79−84097
auroral forms, magnetic field aligned electric fields rel. to downward electron energy fluxes 79−53606
auroral phenomena, role of mag. mirroring 78−20572
central Australia, geomag. induction 80−72424
Australia, geophysical profile along 29°S 80−72460
Australian magnetic observatories 80−72632
Avalon zone, Atlantic Canada, extent determ. from mag., seismic and gravity data 80−12384
Baikal rift zone, mag. anomalies rel. to continental rift form. *(Russian)* 80−12364
Baikal rift zone and adjacent area, mag. anomalies 78−36103
balloon obs., high altitude, at Northeastern Japan *(Japanese)* 77−82019
basement rock type determ. using magnetic anomalies 77−45166
Bathurst and McDonald faults, N.W.T., aeromagnetic anomalies 77−5168
bays rel. to geomagnetic activity and 1972 interplanetary magnetic field 80−105124
Belgium, magnetic elements and variations since 1828 *(French, Flemish)* 77−32996
Bengal fan, aeromagnetic anomalies 77−73632
Benin Gulf, Africa, mag. survey of continental margin struct. 77−21693
Bielsko, Poland, mag. field components meas. by proton magnetometer *(Russian)* 79−39656

geomagnetism continued
Black Sea, nature of mag. anomalies *(Russian)* 78−85473
Bode's law of planetary magnetism, re-evaluation 78−40853
bow shock, DC mag. field obs. 80−90306
bow shock, ISEE magnetic field profiles 79−58196
Brazilian geomagnetic anomaly, E_s-layer phenomena rel. to regular particle ionisation source 77−78558
Brunkes epoch, subdivisions rel. to geomag. field origin and Ukraine palaeomag. stratigraphy *(Russian)* 77−44916
Canada, 1975 annual report for magnetic observatories 78−61323
central Canada, 3-component aeromagnetic survey 78−96138
Canada, annual report of geomagnetic observatories 77−78094
Canada, geomag. field models comparison with obs., rel. to broad scale anomaly studies 80−72425
Canada, long-wavelength mag. anomalies determ. using polynomial and upward continuation techniques 80−85594
Canada, magnetic observatories annual report (1977) *(French, English)* 80−72418
Canada, main geomag. field for 1975, analytical model 77−66887
E. Canada, sedimentary cover thickness meas. by aeromag. survey 80−77138
W Canada, three-component aeromag. survey 77−32990
Canadian Cordillera geomag. transition anomaly, lateral cond. changes 77−64200
Canadian magnetic observatories, annual report for 1973 77−45183
Cape Verde archipelago, underlying crustal struct. from seismic, mag. and gravity data 77−17052
Caspian Sea, Turkmenian sector, magnetotelluric sounding results 77−40980
Cayman Trough, mag. anomalies inversion and sea floor spreading 79−34789
Chagos-Laccadive Ridge (Indian Ocean), mag. anomalies rel. to struct. 77−44952
charged particles motion in one-dimens. mag. current sheets 78−65464
circular electric current loop field representation of Earth's mag. field 80−12329
circular lamina, mag. anomaly 79−88247
circular magnetic anomalies, Russian platform, rel. to circular magmatic structures *(Russian)* 79−88251
closed field lines and auroral forms 78−36356
coal banding-plane indicator, magnetic susceptibility anisotropy meas. 78−77221
coal seam thickness meas. using resonant loop as EM sensor 78−57366
Colorado, field gradient meas. and noise reduction techniques 77−29249
Colorado, tectonomag. study using field difference method 80−21850
Columbia Plateau, basalt flow, contact zone remanent magnetisation 80−81881
composite magnetic fields in three-dimensional space, singular points numerical characts. determ. *(Russian)* 79−96833
conducting sphere in mag. dipole field, general soln. 80−3921
conductive cylinder, anomalous mag. field, induced by elec. current *(Chinese)* 80−104858
conductivity anomalies, magnetotelluric calcs. 79−53299
conductivity anomaly, response to inducing source fields, lab. model 78−36100
contact surface parameters, determ. using space domain filter method *(Chinese)* 80−89933
contour map aeromagnetic data computer processing 78−7819
contouring irregularly spaced data 77−64180
cooling orogen, magnetic and isotopic blocking temps. 78−65226
cooling orogen, magnetic blocking temp. 78−65227
coordinate system, high latitude station location, error determination 80−4202
Coral Sea basin tectonic evolution from marine mag. anomaly data 80−21698
core, magnetic waves and Braginsky's stability conditions, comments 78−44770
core boundary irregularities influence on liquid vel. and mag. field 77−13065
core energetics, rel. to geomag. field generation and heat flow 77−73638
core fluid vel. and mag. field bounds imposed by MHD $\alpha\omega$-dynamo 78−36101
core physical characts. from geomag. data 79−79765
core thermal evolution 80−21674
core-mantle boundary, magnetic contour map 80−104880
core-mantle boundary irregularities, effect on fluid speed and geomag. field 78−73333
core-mantle boundary irregularities, effects on fluid vel. and mag. field 78−44792
core-mantle EM interaction when elec. cond. concentrated near core boundary 77−91001
core-mantle interface radial dipoles, resolution of secular vars. into fields of separate centres *(Russian)* 79−96738
core-mantle system, conductivity profile 80−36238
cosmic ray electrons, detect. by synchrotron radiation in geomag. and interstellar mag. fields 78−57412
Coso Range, California, aeromagnetic and gravity surveys 80−89943
crust, nonparallel stratified models, scattered EM radiation field 78−44773
crust, nonparallel stratified models, scattered surface wave 78−40489
crustal magnetic model under Ukrainian Shield 78−61313
Cuddapah basin, India, regional mag. profiles 78−85476
Curie depth determination from aeromag. spectra, W.USA 77−60349
current loop models 80−21623
D- and F-region ionisation, geomag. control and possible coupling mechanism 77−9598
damping of satellite rotation, magnetic field effects 78−69645
damping of satellite rotation, shielding effects 78−69646
data reduction and analysis, data from satellite magnetometer 80−77141
data reduction on arbitrary surface in regions of high topographic relief 78−61298
Dead Sea Rift and N.Israel, mag. and gravity obs. and interpretation 80−98233
declination field near Earth surface, error in analytic representation 78−73307
deep crustal magnetic anomalies, mineralogical constraints on Curie isotherms 78−44805
deep crustal struct. inferred from mag. anomalies of long-wavelength 80−72430
deep EM sounding and profiling 77−9326

geomagnetism continued
deep magnetotelluric and magnetovariational sounding results in Ciscaucasian area 77−78096
deep magnetotelluric sounding, model of geoelectric section 78−44768
deep magnetovariation sounding curves, resolution of elec. cond. model parameters 79−53300
Dellwood knolls, mag. anomalies rel. to role in triple junction tectonics off northern Vancouver Island 80−90067
differential geomagnetic sounding 77−53225
digital recording field system for geomagnetic telluric-array studies 79−62605
dipole axis precession rel. to auroral activity equatorial latitude 80−98499
dipole field, comparisons with cosmological expectations 80−67337
dipole tilt angle influence on auroral electrojet development 79−16744
direct and inverse problems soln. using approximate equivalence method *(Russian)* 77−70586
disturbances effect on tropospheric processes 77−29361
Djibouti Republic, magnetic anomaly map and tectonic interpretation 80−61753
Dnieper-Donets depression, magnetotelluric sounding data rel. to deep struct. *(Russian)* 78−96170
DSDP Leg 37 samples, magnetisation rel. to surface mag. anomaly 77−90996
dual-spin satellite magnetic attitude control system, geomag. field effects 78−65484
dykes magnetic anomalies interpretation using Fourier transforms 79−58106
dynamo, ^{40}K fractionation in Fe-S liq. outer core, experimental evidence 78−11843
dynamo, rel. to model for terrestrial planets internal struct. and mag. fields 78−12125
dynamo, stationary kinematic theory 77−13054
dynamo action, helical symm. in unbounded fluid conductor 80−10315
dynamo action, helical symm. in unbounded fluid conductor 80−10316
dynamo action in rotating shell 80−81807
dynamo integrals, numerical evaluation code 79−34733
dynamo macrodynamics of rotating stratified fluid 80−36245
dynamo model, cylindrical convection in rotating gravitational sphere *(German)* 77−25638
dynamo model of magnetic field, self-consistent treatment 80−81808
dynamo models, driven by convection 80−36241
dynamo problem, dynamics of fluid core with inward growing boundaries 80−76934
dynamo problem, hydromag.-intertial-gravity waves propag. in mag.-vel. shear 79−55422
dynamo strength, scaling law test rel. to planetary mag. moments predictions 80−21934
dynamo theorems 80−81810
dynamo theory, core formation and evolution model 80−51367
dynamo theory, core paradox reconsidered 80−90033
dynamo theory, MHD, book contrib. 78−61331
dynamo theory, observational constraints 78−40478
dynamo theory, spherical dynamo with anisotropic α-effect 80−81809
dynamo theory *(German)* 78−40852
dynamo theory 79−74837
dynamo theory based on mean field electrodynamics 80−36243
dynamo theory for Earth mag. field prod. *(German)* 77−17026
dynamo theory of Earth's mag. field, using mean-field electrodynamics 77−73636
dynamos in interior driven by gravitational settling 80−36246
E-layer crit. freq., geomagnetic east component, and sunspot number relationships 78−65461
E-polarisation, numerical soln., improved geomagnetic boundary conditions 78−77182
Earth core electric current and zonal mag. fields, theory 80−36240
Earth core magnetic field strength 80−36239
Earth deformation, mag. field effects 80−109085
Earth interior, Love waves propag. in stratified magnetoelastic solid with material boundary 78−32015
earthquake assoc. changes, piezo-mag. or dilatancy-mag. effects *(Chinese)* 80−56374
eddy current torques, air torques, and spin decay of orbiting cylindrical rocket bodies 78−93074
effects on cosmic rays, development of studies 77−17308
electric current circular loops model 79−39635
electrically conducting fluid core location from external mag. obs. 78−32248
electrically conducting rot. sphere behaviour in time-independ. homogeneous external mag. field 78−49309
electrically-conducting fluid, mag. flux linkage, relativistic case, planetary dynamo theory 80−12655
electrometry inverse problems, soln. via variational method *(Russian)* 77−44915
EM airborne profiles, sphere model for interpretation 77−45171
EM anomalies in Abitibi Clay Belt 77−81789
EM depth sounding interpretation, master tables, book 80−86043
EM depth sounding systems, detectability analysis 77−91295
EM exploration, target near dipping contact, response modelling 79−8595
EM field, conf., Hurbanovo, Czechoslovakia (Oct. 75) 79−39646
EM field above two-dimensional inhomogeneous struct., boundary conditions 80−85595
EM field build-up sounding method, resolution 78−16176
EM field formation method in conducting half space *(Russian)* 79−84110
EM field of infinitely long cable, diffr. over wedge-shaped conducting media *(Russian)* 78−40484
EM field rel. to conductivity anomaly, perturbation and induction arrow calc. 77−49004
EM field short period variations, anal. for wave type and propag. direction determ. *(Russian)* 78−85474
EM field sounding, appl. of composite obs. patterns in near field *(Russian)* 79−44270
EM field variations assoc. with sea waves, possible origin 78−44834
EM fields, about horizontal electric wire source of abritrary length 79−27130
EM fields, refl. in in situ gasified coal seam 77−41212
EM fields, topographic effect in three-dimensional cond. model 77−25639

geomagnetism continued
EM fields in halfspace with ore body, local element transformation 79—66828
EM fields of vertical mag. dipole over thin conductive overburden 78—65183
EM frequency sounding, crustal struct. determ. 78—49167
EM frequency sounding in horizontal coils system, field test 77—49182
EM frequency soundings, exptl. study 79—58129
EM ground waves, elec./mag. field ratios in realistic terrain 78—88795
EM induction, freq. and transient responses of EM fields created by currents in confined conductors 79—29702
EM induction, H-polarisation problem soln. by wavenumbers integral eqn. method 77—44913
EM induction, in rot. conductive Earth 78—44764
EM induction, one-dimens. problem, Frechet derivative 77—48996
EM induction, source field effects on transfer functions at mid-latits. 79—74831
e.m. induction, two-dimens., finite difference soln. 77—2101
EM induction, two-dimensional, in thin surface sheet of variable integrated cond. 79—16372
EM induction effects of ocean coast 80—76908
EM induction for island-continent ocean channels, analogue model 77—9336
EM induction for island-continent ocean channels, analogue model study for H-polarisation 77—81795
EM induction in conducting stratified medium, numerical analysis 79—34740
EM induction in Earth and Moon, workshop proc. (Murnau, W.Germany, 1978 September 7-13) 79—79741
EM induction in thin sheets, statistical theory 77—86769
EM induction in three-dimens. struct. for various source fields 79—66609
EM induction one-dimensional problem, model refinement 79—44096
EM induction over perfectly conducting ocean edge, H-polarisation 77—44912
EM inverse interpretation, trend influence 78—81103
EM lateral waves, Earth-sounding radar obs. 77—44909
EM logging in inhomogeneous media, axisymm. problem 79—39877
EM methods with distant source, terrain relief effects 79—79735
EM modelling, finite element program package 77—73874
EM probing of permafrost terrain, theory 78—28323
EM prospecting, harmonic and transient fields behaviour on surface of two-layer medium 79—92478
EM prospecting, inverse problem 79—53583
EM prospecting, kernel function for horizontally stratified Earth 77—21918
EM response of conducting cylinder inside conducting shell 77—64198
EM response of conductive inhomogeneity in layered Earth 77—40976
EM scattering from buried wires, fast Fourier transform 79—16369
EM shielding of sources within metal-cased borehole 77—40979
EM sounding, analogue model meas. for horizontal mag. dipole embedded in conducting medium 79—12068
EM sounding, appl. to shallow permafrost mapping 79—16694
EM sounding, computation of multilayer response 79—92618
EM sounding, induced polarisation effect on near-field form. *(Russian)* 79—39641
EM sounding, interpretation of transients in Laplace space representation *(Russian)* 78—40483
EM sounding, iterative ray tracing between boreholes for underground image reconstruction 80—98466
EM sounding, multicoil II airborne system 80—51554
EM sounding, numerical modelling of new multi-freq. system 80—56623
EM sounding, of asthenosphere of E.European Platform 77—53021
EM sounding, VLF-EM profiles, topographic correction based on model studies 80—101452
EM sounding methods, theoretical principles 78—49166
EM sounding of glaciers and permafrost 79—62768
EM sounding of kimberlite pipes, prospecting techniques and EM signature 80—51393
EM sounding of ocean floor near Californian coast, interpretation 77—9383
EM sounding over horizontally layered media, total field resistivity mapping 79—16693
EM sounding over permafrost region, computer-assisted anal. 77—2086
EM sounding with mag. susceptibility in layered Earth model parameters 77—53226
EM soundings, multifrequency, topographic and misorientation effects study 80—101451
EM subsurface profile from HF meas., reconstruction technique algorithms appl. 77—45199
EM time-domain sounding of multilayered Earth 79—57850
EM transient response of vertical elec. dipole in homogeneous anisotropic medium *(Polish)* 77—52970
EM transients over low-resist. polarisable Earth, formulae *(Russian)* 79—39644
EM wave excitation by dipole emitters buried in stratified media 78—48966
EM waves, lateral-wave propag. in oceanic lithosphere 79—92482
EM waves and antennas above and below Earth surface, theory 79—66620
energy propag. of EM field of dipole source on conducting halfspace 77—9330
English Channel, deep structs. and mag. anomalies, possible hidden suture NW of Brittany 78—61397
English River gneiss belt, Superior Province, aeromagnetic anomaly pattern 80—30981
Eolian Islands, S. Thyrrenian Sea, basement structural trends from aeromagnetic and gravimetric data 78—40519
equatorial field and ionosphere, interplanetary magnetic field polarity effects 78—36416
equivalent linear amplitude geomagnetic indices, evidence for strong artificial components 78—89008
evolution of life, mechanism for influence of geomag. field 77—90977
evolution of life, role of Earth's magnetic field and steady ozone layer 80—104883
external mag. field, analytical extrapolation into two-dimens. magnetised body *(German)* 79—48393
external spherical harmonic coeffs., solar cycle var. 80—85592
F_2-layer field-aligned and field-perpendicular vels. theory 78—85760
F-region, geomag. control of low-latit. annual periodicity of (NmF2) 77—53306

geomagnetism continued
F-region low-latit. geomag. anomaly, topside and bottomside struct. 78—36373
ferromagnetic materials, demagnetisation level determination, after NDT 79—49261
field computation, accuracy of construction of external Dirichlet problem boundary condition 78—44766
field definitive model and secular variation for 1965, derivation and comparison with IGRF 78—96133
field effects on charged particles in ocean *(Russian)* 77—60416
field expansion using orthonormalised polynomials, for mag. mapping 77—29248
field generation by battery effect in core, comparison with Ap-type stars *(Russian)* 77—17591
field in multilayer medium with periodic conductivity var. *(Russian)* 77—44922
field intensity modulus, repeated obs. appl. to elec. cond. anomalies detect. *(Russian)* 79—96736
field intensity vector, components determ. from absolute value 79—53534
field intensity vector components, determ. from magnitude, error estimate 78—73308
field interpretation, optimal computing scheme construction 77—33201
field line merging and slippage in auroral arcs 78—77393
field line reconnection in magnetotail 79—80102
field line reconnection mechanisms in collisionless plasma 79—77352
field longitudinal dependence, rel. to loss cones asymmetry in pitch-angle diffusion 77—13162
field meas., magnetotelluric sounding technique using SQUID devices 78—96322
field models based on total intensity meas., effect of obs. errors 77—9335
field over cylindrical basement uplift or depression *(Russian)* 77—70598
field palaeohistory, nature of transition periods during reversals 79—8598
field reconnection in magnetopause, plasma acceleration evidence 80—26701
field reduction to pole, fast Fourier series algorithm 77—5333
field representation as circular current loop 79—84105
field reversals, relaxation model 78—85480
field reversals 79—2182
field structure and secular variation, mathematical-physical anal. and interpretation *(German)* 79—34742
field tipping, nonlinear differential eqns. *(Hungarian)* 79—16368
field vector counterclockwise precession, prod. by non-dipole field westward drift 79—57853
fields space-time filtering 77—49178
N.Finland, magneto-telluric expts. 79—44093
Fiordland, New Zealand, mag. anomalies rel. to crustal struct. 79—88325
first-degree spherical harmonic components, solar cycle vars. 80—85593
flux ropes and sheets, alpha-effect 80—36244
fluxgate magnetometry, review 79—35800
folds, magnetic fabric 78—85481
Fourier analysis of gravimetric and magnetometric anomalies *(Rumanian)* 79—58123
fracture zones mag. features 77—78092
frequency EM sounding, anomalous high cond. bands discovery in crystalline foundation *(Russian)* 78—96137
Galapagos Islands, t, spreading centre jumps 80—104877
Gauss, Carl Friederich, correspondence on heliotrope and geomag. meas. *(German)* 77—67168
geodynamo and field reversals of steady dynamos 80—51645
geodynamo behaviour during reversal, model 79—88240
geoelectric inhomogeneities, position determination by variable geomag. field method 80—89956
geological contact and thin dike, simplified magnetic interpretation 78—28333
geological contact magnetic profiling, inverting by harmonic method 80—77137
geophysical potential fields on sphere, stochastic props. study 80—56338
geopotential fields singularities localization in three dimens. space 79—74968
geothermal energy prospecting by geophys. methods, review 78—7803
N.German sedimentary basin, widely spaced areal magnetotelluric meas. rel. to cond. distrib. 79—74833
N.Germany, magnetotelluric meas. of nearly circular salt dome 77—64201
global field, solid core motion effect 79—84104
global geodynamics, Canadian contribs., 1971-79 period. 80—8262
gradient magnetotelluric marine sounding method 79—62599
gradients from ocean waves, meas. using supercond. mag. gradiometer 79—29867
gradiometer data integration in geomagnetic surveying 80—105064
gravimagnetic anomalies, interpretation on basis of pots. classes with inverse problem finite form 80—21847
gravimagnetic fields, anomalous pot. fields appl. to Earth interior mass distribs. modelling 79—96750
gravitational and geomag. fields correl., rel. to bumpy core-mantle interface 77—2085
gravitationally powered dynamo, thermal consequences 79—39687
gravitationally powered dynamo model 79—84102
ground magnetic effect of vertical currents connected with Pedersen currents in uniform-conductivity ionosphere 77—29579
ground magnetic perturbations rel. to interplanetary magnetic field vars. 78—77431
ground subsurface, EM transient response 78—57166
groundwater exploration in hard rock terrain, total field meas. 77—41075
Gulf of Aden, mag. survey, seafloor spreading phases determ. 78—32049
Gulf of Aden and Afar, mag. anomaly map and plate tectonics 80—56364
Gulf of Valencia, W.Mediterranean, aeromagnetic survey *(French)* 77—29243
H-polarisation induction over ocean edge coupled to mantle by conducting crust 77—48994
H-polarization induction in two thin half-sheets 79—34737
HF EM induction profiling, of boreholes in underground mines *(Polish)* 80—51547
HF radiowave propagation at high latitudes, geomagnetic activity influence *(Russian)* 77—29551
horizontal component, sudden storm commencement, negative impulse at equatorial stations 79—16768
horizontal component of field, absolute value determ. method 78—81420

geomagnetism continued
horizontally stratified media sounding, geophysical problems unification 80—56622
hydromagnetic dynamo, axially symmetric model 79—62430
hydromagnetic dynamo of atmosphere 78—96335
NE.Iceland, elec. resist. model from magnetotelluric obs., correl. with temp. 80—89954
NE Iceland, mag. anomalies (ΔZ) and interpretation based on rock magnetic investigations 80—89951
Iceland, mag. anomalies rel. to mag. layer concept 77—60365
Iceland, magnetostratigraphy 77—66885
Iceland, magnetotelluric investigation of lower crust and upper mantle 79—66612
Iceland, sea floor morphology and mag. anomalies N of Iceland 80—89953
W.Iceland shelf, central volcanoes, magnetic and gravity evidence 77—37180
S.Iceland shelf, marine magnetic survey 77—37128
India, anomalies due to geological structs., equatorial region 80—41375
SW Indian coast, seismic and magnetic obs. 77—41018
Indian Ocean, anomalous geomag. field, statistical model 77—78105
Indian Ocean, mag. anomalies rel. to evolution and breakup of Gondwanaland 80—41428
N.W.Indian Ocean, mag. inhomogeneity of basin floors 77—49002
SE.Indian Ridge, seafloor mag. anomalies rel. to chem. of mid-ocean ridge basalt 80—109102
induced polarisation sounding, freq. depend. of measured parameters *(Russian)* 79—74836
induced polarisation technique for prospecting 78—69473
induction, in arbitrarily shaped ocean of finite conductivity 79—16371
induction in arbitrarily shaped infinitely conducting oceans 78—61318
induction sounding of stratified media using vertically displaced sensors *(Russian)* 79—58119
induction vectors, local time var. 78—85477
inductive magnetisation sounding, inverse mag. problem numerical soln. *(Russian)* 79—34747
intensity rel. to climate, historical records 79—39638
interference fields separation, statistical algorithms *(German)* 77—29462
interior structure inferred from surface mag. field 80—36528
International Geomagnetic Reference Field 1975, comparisons 78—40481
international reference field 1975, adoption and coeffs. table 77—9332
interplanetary magnetic field, impulse response of Earth's field 80—51622
interpretation of time-domain airborne electromagnetic (INPUT) anomalies 79—2383
invariant coordinates for epoch 1977.25, global maps 77—56798
inverse log.-potential problems, integral and functional eqn. analysis 77—40968
inverse problem, appl. of linear programming, basic numerical techniques 79—53581
inverse problem, interval estimation of geophysical parameters via identification methods 77—82024
inverse problem of gravit. and mag. prospecting, approximate soln. *(Russian)* 79—39927
inverse problems, stable soln. in a class of convex bodies 77—64181
ionosphere, cleft currents determined from magnetic and electric fields 79—35036
ionosphere, elec. currents and mag. field vector obs. by S-310-5 rocket *(Japanese)* 80—94635
ionosphere, evidence for closed field lines in dayside auroral region 78—77391
ionosphere, field parameters rel. to radiowave magnetoionic components lateral deviations 79—8747
ionosphere, field-aligned equatorial bubbles obs. by topside sounder 79—16737
ionosphere, geomag. control of mesosphere NO concs. from D and F region ionisation meas. 79—8651
ionosphere, mag. field obs. by Atmosphere Explorer C rel. to field-aligned currents and plasma drift vels. 80—72681
ionosphere, mag. field orientation rel. to intersatellite whistler-mode pulses propag. 78—69605
ionosphere, mag. field rel. to reson. coupling of ionisation waves and acoustic gravity waves 77—25832
ionosphere bottomside, fictitious surface admittance for arbitrary geometric field 79—84565
ionosphere electrostatic field structure in wake of disc, external mag. field effect 79—10648
ionosphere inhomogeneities drift, ionospheric wind influence *(Russian)* 79—29926
ionosphere plasma stream propag., geomag. field effects in controlled rocket-borne expt. 78—57424
ionosphere source, for geomag. field elements annual line component 79—20752
ionosphere unstable polar cap, mag. fields meas. rel. to electrostatic waves 79—29927
ionosphere-magnetosphere small-scale dynamo, multiple layer model 79—53612
ionospheric currents used in calc. of Earth surface field 80—41615
ionospheric modification, mag. field effects on electrons 77—60531
ionospheric records over Shanghai, March 1953 to June 1955, Earth mag. field intensity *(Chinese)* 80—77192
central Israel, crustal structure for magnetotelluric data inversion 79—2196
central Israel, mag. evidence for pre-Late Jurassic east-west fossil continental margin 79—34766
Italy, anomalies from regional magnetic survey 78—65175
Itapicuru greenstone belt, Bahia, Brazil, mag. survey for ore bodies 80—81879
Iturup Island, magnetotelluric soundings, geoelectric horizon and sedimentary layer 80—3925
Juan de Fuca-Gorda Ridge area, mag. anomalies and basalt comp. 77—29242
S Karelia, elec. cond. anomalies from magnetovariation and magnetotelluric data *(Russian)* 79—96737
Karelia magnetic anomalies rel. to crustal structure *(Russian)* 77—32986
Kenya rift valley, geophysics 77—86825
kinematic α-effect dynamo eigenvalues 77—44906
kinematic dynamo of three spherical eddies, model 78—69286
kinematic dynamo of three spherical eddies, model 79—8597

geomagnetism continued
kinematic dynamo problem, role of mean circulation in parity selection 78—7566
Kirovograd anomaly/Dnieper-Donets depression intersection, magnetotelluric sounding *(Russian)* 79—20748
Kokchetav mountain massif, magnetotelluric soundings 77—40981
Kusatsu-shirane Volcano, Japan, 1976 steam explosion, geophys. obs. *(Japanese)* 79—70773
Kusatsu-shirane Volcano area, Japan, geomag. total force intensity meas. *(Japanese)* 79—70737
Lake Mungo palaeomagnetic excursion, geomag. source models and their implications 77—86771
Lau Basin, magnetic anomalies and crustal dilation 77—5131
Leon province, Spain, mag. anomalies *(Spanish)* 80—36247
lightning direction finding, by mag. method 80—77078
Liguro-Piemontese Alps, mag. field intensity anomalies rel. to struct. *(French)* 79—57896
local distortions in sounding, exclusion method *(Russian)* 77—45196
local field separation theory *(Chinese)* 79—88237
local field sources, rel. to short-period geomag. vars. and electrochemical effects 79—57847
Long Valley Caldera, California, implications of mag. model 77—86846
long-period fluctuations, anal. rel. to Earth global elec. cond. qualitative character 80—17231
long-term behaviour, thermal interaction at core-mantle boundary 77—52981
low latitude geomagnetic field, diurnal and seasonal vars. of effect of interplanetary mag. field Y-component 80—56354
mafic belts along margins of Japanese Islands, origin, geophys. survey 78—32100
magnetic depth sounding, use of vertical component 77—91290
magnetic field effects on ionospheric EM pulse time dispersion 78—45116
magnetic field effects on surface waves in stressed conducting media, theoretical study 80—8253
magnetic field reconnection with interplanetary mag. field, untenability of models 77—22007
magnetic induced polarisation techniques, effect of large cond. contrasts 80—98461
magnetic induced polarization method, theoretical problems *(Chinese)* 79—100962
magnetic moment correction for atm. inhomogeneity 77—29247
magnetic potential compared to global gravity anomaly field 80—104854
magnetic prospecting, inverse problem soln., decomposition iteration method *(Russian)* 80—4134
magnetic prospecting, optical filtering of airborne and ground data 77—25797
magnetic prospecting inverse problem, linear programming *(Russian)* 78—15955
magnetic variation soundings above inhomogeneities of Earth spherical model 77—13056
magnetized buried object, depth determ. errors *(Russian)* 79—20750
magneto-telluric response dispersion relations, inversion problem theory 80—104861
magnetometric and electrometric methods for landslide dynamics investigation 77—87091
magnetometric resistivity method field test on plateau 77—40977
magnetometric resistivity methods, theory 79—53531
magnetopause, compressible reconnection model 77—37485
magnetopause, mag. merging, dayside cusp proton acceleration 78—12054
magnetopause structure, obs. and implications for mag. reconnection 79—80103
magnetopause structure from Ogo 5 obs., classical reconnection model 79—58195
magnetosheath, high latit., mag. field lines rel. to $\lesssim 2$ MeV electrons transport 80—90296
magnetosphere, adiabatic modulation of equatorial pitch angle anisotropy by mag. field 78—89003
magnetosphere, assoc. elec. field, mag. field and electron precip. fluctuations 78—81507
magnetosphere, current fields at magnetopause and in radiation zone 79—53658
magnetosphere, current instability in reconnecting current sheets 77—37486
magnetosphere, D_{st} contrib. to tail mag. flux and aurora equatorward shift 79—75013
magnetosphere, dayside, particle meas. and mag. perturb. rel. to interplanetary mag. field 79—75044
magnetosphere, dayside mag. flux transfer assoc. with expansions and contractions 78—96355
magnetosphere, dayside magnetopause mag. merging and polar cusp geometry 79—66884
magnetosphere, diamag. effect of solar wind filamentary plasma elements penetration 77—78581
magnetosphere, dynamics of protons trapped in geomag. field 79—16756
magnetosphere, elec. and mag. fields at high latits. 78—12057
magnetosphere, elec. currents and mag. field in hot adiabatic plasma 78—89002
magnetosphere, elec. field around rot. mag. dipole 78—45141
magnetosphere, energetic electrons distrib. in geomag. field 77—22006
magnetosphere, equilib. mag. flux distrib. in moving force tube 78—69618
magnetosphere, field line convection rel. to lower ionosphere current and wind systems 77—5386
magnetosphere, field line MHD torsional oscill. rel. to mini-substorm and long-period Pi 2 event *(Japanese)* 80—94653
magnetosphere, field-line reconnection, static-state model 78—61677
magnetosphere, force tube width rel. to turbulence development in longit. currents 80—67469
magnetosphere, frontside boundary layer obs. and reconnection problem 78—89010
magnetosphere, geomag. tail topology 77—53331
magnetosphere, geomagnetic diagnosis, book 78—89015
magnetosphere, interplanetary plasma flow field line reconnection rel. to Pc 1 pulsations 78—45142
magnetosphere, local electron density and mag. field meas. via JIKIKEN (EXOS-B) satellite stimulated plasma wave expts. *(Japanese)* 80—94649
magnetosphere, mag. curl in front of magnetosphere boundary 80—85804

geomagnetism continued
magnetosphere, mag. energy accumulation and transfer during substorms 79—12343
magnetosphere, mag. energy accumulation due to solar wind EM field interaction 78—28419
magnetosphere, mag. field and plasma dynamics laboratory simulation 79—16757
magnetosphere, mag. field models rel. to drifting energetic protons pitch angle dispersion 78—77428
magnetosphere, mag. field tension rel. to plasma sheet press. anisotropies 78—89009
magnetosphere, mag. flux tubes interchange rel. to irregularities form. and evolution 80—21876
magnetosphere, mag. reconnection as energy source, comparison with Jupiter magnetosphere 79—58201
magnetosphere, magnetic field, quantitative models evaluation 77—9629
magnetosphere, magnetic field models 80—41640
magnetosphere, MHD wave energy, effect of geomag. latitude 77—25889
magnetosphere, open and closed models, expt. evidence 79—8771
magnetosphere, plasma instability, reunification of mag. field in plane layer *(Russian)* 77—58860
magnetosphere, plasma mantle and ionospheric plasmas, field aligned distrib. 78—57406
magnetosphere, quadrupole shape 80—101492
magnetosphere, scalar field meas. rel. to magnetospheric currents density evaluation 77—13186
magnetosphere, simulation of plasma beam-mag. dipole interactions 77—7585
magnetosphere, substorm-assoc. particle-flux vars. due to drift in geomag. field 79—35067
magnetosphere, tail mag. field splitting rel. to configuration energy in two-dimensional model 77—91370
magnetosphere, two-sheet configuration rel. to reconnection of lines of force 78—45140
magnetosphere, VLF transmitter induced field rel. to hiss emissions quiet bands 79—66878
magnetosphere and ionosphere, elec. and mag. fields, rel. to coupling 79—66870
magnetosphere boundary, mag. field from laboratory simulation data 78—57396
magnetosphere dayside cusp, mag. reconnection rel. to solar wind plasma injection 78—40775
magnetosphere geomag. tail, distrib. of B_y 79—80091
magnetosphere low altitude polar cusp, correlated elec. field and low-energy electron meas. 78—40770
magnetosphere near-Earth plasma sheet, search for mag. neutral line 77—25872
magnetosphere neutral points position in two-dimens. model 77—25865
magnetosphere neutral sheet, mag. field rel. to auroral particles adiabatic movement 78—28421
magnetosphere plasma sheet, mag. field parameters rel. to particle dynamics 79—66879
magnetosphere plasma sheet, variability of mag. field and dynamics during substorms 80—98518
magnetosphere reconnection models, criticism 78—49233
magnetosphere source, for geomag. field elements annual line component 79—20752
magnetosphere tail, explosive tearing mode reconnection 78—88992
magnetosphere tail lobe, field vars. rel. to substorms statistical mag. signature 78—49237
magnetosphere-solar wind interaction, Chapman-Ferraro image method graphs correction 80—12620
magnetostatic field problem, soln. in high susceptibility case via method of subsections 80—105065
magnetostratigraphy of San Juan Basin, Cretaceous-Tertiary boundary 77—53055
magnetotail, adiabatic particle motion in nearly drift-free mag. field 78—57399
magnetotail, expected reconnection signatures 78—96361
magnetotail, field struct. rel. to hot tenuous plasma, fireballs and boundary layers 77—29588
magnetotail, lower-hybrid-drift instability and mag. field line reconnection 77—45254
magnetotail, mag. merging obs. and form. of plasma sheet 77—87189
magnetotail, magnetic merging obs., appl. to solar flares 77—17301
magnetotail, neutral sheet, particle accelerations 80—72696
magnetotail, unsteady mag. reconnection rel. to plasma flow pulsations 78—77436
magnetotail boundary layers, mag. merging, hot tenuous plasmas and fireballs 78—77438
magnetotail configuration near midnight during quiet and weakly disturbed periods, mag. field modelling 78—96354
magnetotail magnetic current sheets, effect of press. anisotropy on equilib. struct. 79—12354
magnetotail magnetic field 79—80089
magnetotail neutral sheet southward mag. field rel. to energetic electrons distrib. and substorms 80—26695
magnetotail neutral sheet wavy profile, Imp 5 meas. 78—61665
magnetotelluric analysis for layered Earth, matrix relation 78—32008
magnetotelluric and geoelectrical prospecting, thin-layer problem 79—44095
magnetotelluric and geothermal surveys in NW Germany, comparisons 80—12336
magnetotelluric and magnetic variational sounding, 3-dim. modelling 78—7563
magnetotelluric and magnetovariation methods, elec. cond. functions 77—32982
magnetotelluric and telluric parameters, cross-correlation estimates 79—92484
magnetotelluric anisotropic data, inversion technique 77—60475
magnetotelluric data analysis: removal of bias 79—53530
magnetotelluric diagrams 77—2087
magnetotelluric field in homogeneous layer with cylindrical inclusion *(Russian)* 78—53617
magnetotelluric field of electrical currents in bottom and shore of Barents Sea 80—104864
magnetotelluric field over gently sloping elongated structures *(Russian)* 79—84111
magnetotelluric field over graben *(Russian)* 77—91006
magnetotelluric field over graben containing high-resist. intercalation, calc. and anal. *(Russian)* 78—48965

geomagnetism continued
magnetotelluric fields, calc. in horizontally-inhomogeneous media using finite differences method *(Russian)* 79—44102
magnetotelluric fields modelling above heterogeneities in conducting base 77—52979
magnetotelluric impedance function estimation 78—85731
magnetotelluric investigations, induction effects detect. methods appl. in Sakhalin and Yakutia *(Russian)* 79—39642
magnetotelluric meas. over horizontally stratified formations, stratigraphic interpretation method *(Russian)* 79—62620
magnetotelluric meas. using SQUID magnetometer, remote reference technique 79—29866
magnetotelluric measurements, using lock-in signal detect. 78—81104
magnetotelluric measurements, with remote mag. reference 79—88245
magnetotelluric method for investigation of media with monotonically changing cond. 77—78439
magnetotelluric monitoring of geoelectrical resistivity changes 77—2103
magnetotelluric probing, data interpretation, reliability estimate *(Russian)* 79—39949
magnetotelluric probing, input impedance determ. accuracy, noise effects *(Russian)* 79—39950
magnetotelluric probing in complex geoelec. conditions, data interpretation *(Russian)* 79—39932
magnetotelluric probing phase curves, horizontally inhomogeneous medium *(Russian)* 79—39931
magnetotelluric profiling of vertical conductors 77—52983
magnetotelluric rapid profiling across Berici-Euganean ridge eastern edge 77—48998
magnetotelluric signals digitization equipment *(French)* 77—87092
magnetotelluric sounding, affected by resistivity freq.-dispersion 80—41368
magnetotelluric sounding, audio-frequency, case history at Cavendish geophysical test range 80—51324
magnetotelluric sounding, direct problem soln. for ideally conducting hemisphere with point source *(Russian)* 79—34745
magnetotelluric sounding, effect of primary field inhomogeneity *(Russian)* 77—86774
magnetotelluric sounding, expt. study of edge effect 77—78441
magnetotelluric sounding, fields of vertical mag. dipole over vertically inhomogeneous Earth 79—34736
magnetotelluric sounding, fundamental model 80—77167
magnetotelluric sounding, high-resistance horizons in laminated medium *(Russian)* 78—69290
magnetotelluric sounding, input impedance function for horizontally stratified Earth 77—21918
magnetotelluric sounding, inverse problems soln. 78—49162
magnetotelluric sounding, natural source obs. one-dimensional inversion 79—92479
magnetotelluric sounding, plane EM field over polarized section *(Russian)* 77—86775
magnetotelluric sounding curve distortion rel. to diurnal surface dip *(Russian)* 79—84109
magnetotelluric sounding curves in nonuniform field of linear sources, comparative anal. *(Russian)* 79—48395
magnetotelluric sounding localization and accuracy improvement *(Russian)* 78—53754
magnetotelluric sounding method development in USSR 78—49169
magnetotelluric sounding over models of continuously varying conductivity 78—32009
magnetotelluric soundings, analogue modelling 77—33197
magnetotelluric soundings, effect of field vertical components on impedance determ. *(Russian)* 78—48963
magnetotelluric studies in Central Urals and Transurals 79—25194
magnetotelluric studies in USSR, review 78—49168
magnetotelluric study, S.Scotland, fieldwork, data anal. and results 79—29705
magnetotelluric study, S.Scotland, Monte-Carlo data inversion, geophys. and tectonic implications 79—29706
magnetotelluric tensor analysis, appl. to two-dimensional geological structs. 78—40471
magnetotelluric two-dimensional inversion 77—73629
magnetotelluric vars. in 10-1000 sec. range, processing *(Russian)* 79—84535
magnetotellurics, automatic data processing 79—80041
magnetovariational sounding curves, effect of relief of high-impedance basic horizon 78—85475
Magsat data analysis, Sq. var. correction 79—75015
Manicouagan structure, Quebec, central mag. anomaly 78—81169
marginal basins, diffuse magnetic anomalies and their tectonic and petrologic significance 78—32064
marine gradient magnetic sounding method 79—62598
marine magnetic anomalies, implications from Troodos ophiolite metamorphism 80—81812
marine magnetic anomalies, validity of geological interpretations 77—60348
marine magnetic anomalies origin, implications of palaeomagnetism of Thetford Mines ophiolites, Quebec 80—61757
marine magnetic anomalies source, dredged oceanic gabbro mag. props. 79—16437
marine magnetotelluric investigations, tidal currents effects 77—78095
marine short-wavelength mag. anomalies coherence, effect of random crustal magnetisation 80—36225
marine waves, nonstationary, theory of EM field 78—44833
Martinique, aeromag. survey, conductivity anomaly existence *(French)* 77—86754
measurement, accuracy of vector aeromagnetometer instrument set in bench tests 78—45016
Mesozoic sea floor off Dronning Maud Land, Antarctica, magnetic mapping 78—3715
metallic mineral deposits of Australia mag. induced polarisation survey results 80—98223
meteor plasma diffusion, geomagnetic field effect expt. *(Russian)* 78—61814
trans-Mexican volcanic belt, seismic refl. and geomag., leg 17 of project CICAR *(Spanish)* 80—36280
Mezen' Bay (White Sea), marine tides EM fields 78—73378
MHD convection in rapidly rot. fluid layer, stability, rel. to geomagnetism 79—50808
MHD dynamo theory of mag. field *(French)* 79—35161
MHD flows, diffusive instability, rel. to geomag. field 79—50807

geomagnetism continued
MHD waves in upper atmosphere, absorpt. rel. to neutral atmosphere heating 79—53588
microstructure separation, digital filtering methods 78—69480
Mid-Atlantic Ridge at 37°N, mag. anomalies in DSDP Leg 37 drilling area 77—91070
mineral exploration, effect of tropical weathering on elec. and EM meas. 79—88246
mirroring, classical surface of section determ. 77—13231
Moho, magnetic boundary 79—96748
Monastyrishche magnetic anomaly, in Dneiper-Donets depression, USSR *(Russian)* 80—36231
Moon recording Earth mag. field on fission origin from mantle 80—101537
Mount Carmel, struct. and extension into E.Mediterranean, marine geophys. survey 77—33026
Mount Shasta, magnetisation implications for virtual geomag. poles determ. from seamounts 79—39637
Mozambique Basin, Mesozoic magnetic lineations 79—66608
Narmada-Son lineament, extension towards Murray Ridge 78—15985
near-Earth plasma, elec. fields penetration along geomag. force lines, electrostatic approach applicability 80—4178
near-Earth plasma sheet, mag. neutral line search, obs. at lunar distance 78—16250
Newfoundland, geomag. sounding near northern termination of Appalachian System 78—61314
NE Newfoundland, geophysical and geological trends on continental shelf 77—5145
Newfoundland Basin, mag. survey rel. to Mesozoic evolution 78—32045
NE.Newfoundland continental shelf, mag. survey rel. to Charlie Fracture Zone 77—25664
non-dipole field, origin rel. to secular vars. during last 25000 years 77—32983
nondipole field component, westward drift rate determ. 79—12065
nonharmonic EM induction in two-layer spherical Earth 79—100812
nonlinear α-effect dynamo eqns., numerical solns. 77—56576
nonlinear analytical prolongation method, survey inverse problem appl. *(Russian)* 79—21037
nonlinear core dynamo action, example 77—73637
nonlinear magnetic dynamos, bifurcation of steady dynamos from oscillating dynamos 78—49306
nonperiodic EM induction in conducting Earth 78—44761
Nootka Fault Zone, new plate boundary off W.Canada, mag. anomalies 79—92518
normal and observed mag. field, separation method 78—69479
north magnetic pole, 1975 position analytical determ. 78—92778
north-south asymmetry of time averaged field, evidence and dynamo theory 80—36235
ocean, EM field of wide current for arbitrary direction of permanent mag. field 79—57946
ocean current induced EM fields, theory 80—61805
ocean current of finite width, EM field 79—53351
ocean dynamo and lunar geomagnetic tides 78—36099
ocean floor, geomag. provinces boundary determ. method 77—64480
ocean floor, implications of magnetisation of crustal layer(2) 77—91071
ocean floor magnetic records rel. to sea floor spreading 77—9337
ocean ridge anomalies, mantle thermoconvective wave explanation 80—90064
ocean wave geomag. fields, towed magnetometer investigation 80—3923
ocean-coast model, EM response to E-polarisation induction 78—61321
ocean-wave induced magnetic fields for nonuniform depths and sea-land interfaces. model study 79—66807
oceanic crust, borehole magnetometer data interpretation 80—21625
oceanic crust, geochem. rel. to seafloor spreading mag. anomalies 80—56345
oceanic crust mag. props., DSDP Leg 34 results from Nazca plate 77—17024
oceanic crust magnetic reversal boundary, three dimens. modeling inversion of deep sea tour obs. 80—109098
oceanic crust magnetic signal, simulation of long-term changes 77—90995
oceanic crust magnetisation 77—2088
oceanic induction and spectrum shifting method 78—20353
oceanic magnetic anomalies recorded during deep-water mag. surveys, statistical anal. 80—36233
oceanic magnetized layer, lower bound on thickness 78—28162
offset dipole and zonal nondipole field models, comparison using Icelandic palaeomag. data 79—57852
orbit design for geomagnetic tail mission 79—92647
origin of mag. field, conf., Nov. 1978, Texas USA 80—36234
origins, homogeneous axisymmetric generator based on Nernst effect 80—8251
orogenic regions deep crustal probing by natural EM fields surface impedance vars. 77—13060
Pabbi Hills, Pakistan, Upper Siwalik deposits, magnetic polarity stratigraphy 78—11798
N. central Pacific, ocean floor magnetotelluric sounding 77—86772
W.Pacific marginal basins, sea floor spreading evidence 77—37177
E.Pacific Rise, mag. gradiometer meas. rel to marine mag. anomalies origin 80—101360
E.Pacific Rise—Gapalagos Rise system, magd mag. anomalies and rock magnetism 78—73331
palaeointensity, determ. at heated rock contact by stepwise remagnetisation method 80—21619
palaeointensity determination, ARM correction method 79—34968
palaeomagnetic field configuration during Permian period, rel. to reconstruction of Pangaea 77—56577
Paluzu Mare (Rumania), mag. anomaly and core samples, struct. geology *(Rumanian)* 80—8309
Parece Vela Basin, E.Philippine Sea, mag. anomalies rel. to evolution 80—41431
passive continental margins, mag. anomaly rel. to ocean-continent boundary evolution 77—81777
periodic motions totality in meridian plane of mag. dipole 78—12052
permafrost mapping by audiofrequency magnetotellurics 79—58102
perturbed Stormer problem, long periodic solns. families 80—17440
piezomagnetic anomaly field, Kilauea volcano, Hawaii 77—2089
piezomagnetic field, assoc. with Mogi model of surface displacements around volcanoes 80—67334
plasma sheet, near-Earth, search for mag. neutral line from Imp 6 mag. field obs. 78—89007

geomagnetism continued
plasma sheet, plasma flows and mag. field vectors during substorms 78—96357
plasma sheet mag. neutral line, IMP 6 obs. 77—53325
plasma sheet outer boundary, satellite meas. and field-line mapping during substorms 78—88990
plasmasphere, Coulomb collision-induced photoelectron trapping by geomag. field 79—8739
plasmasphere, cyclotron instability, mag. field longit. inhomogeneity effect *(Russian)* 77—3929
plasmasphere, mag. field effects on plasma density distrib. 77—17288
Poland, geomag. reference field *(Polish)* 78—3710
polar coupling coeffs. for cosmic ray multiple neutrons up to 15 GeV 77—70954
polarity changes, skin effect of electrically conducting spherical shell 80—46389
polarity in magnetotail neutral sheet, statistical determ. 80—72717
Poplar Bay, Lac du Bonnet, Manitoba, possible meteorite impact crater 77—17150
potential, series expansion in spherical functions at surface of ellipsoid 77—13057
potential field anomalies geodynamic interpretation, physically based source models *(German)* 79—34782
potential field data, wavenumber domain methods 80—51559
potential field data interpretation, generalized matrix inversion method 77—87087
potential field modelling, end corrections 80—85580
potential fields, accuracy of linear transformations in presence of interference 77—44900
potential fields, anal. of characteristic-components method in interface construction 77—44901
potential fields, analytic continuation for plane problem 77—56568
potential fields, statistical interpretation with covariance functions 77—73873
potential fields, two-dimens. and three-dimens., in freq. domain, equivalence theorem *(Chinese)* 79—88478
potential fields due to vertical circular cylinder and dike, statistical anal. 79—34972
potential fields extrapolation numerical techniques *(Russian)* 79—74988
potential fields from arbitrary 2-, $2^{1}/_{2}$- and 3-dimensional bodies, wavenumber domain expressions 79—5634
potential fields inclined dykes interpretation in wavenumber domain 79—92630
potential fields interpretation, statistical algorithms *(German)* 77—29461
Precambrian Fe formations, Schefferville, Canada, vertical mag. contouring 77—64495
prospecting, 3-D anisotropic body mag. field calcs. and algorithm 80—4141
prospecting problems, approx. anal. *(Russian)* 79—84108
quartz H magnetometer, calc. formula for horiz. component 80—105062
quasi-static EM fields of horizontal electric dipole on polarisable half-space surfaces 78—69283
Quebec City, geomagnetic and telluric var. in seismic region 77—52974
quiet magnetotail, self-consistent theory in three dimensions 77—33286
Raft River Valley, Idaho, surveys of geothermal system 79—84307
regional and local mag. fields, local function representations 80—98225
regional anomalies in Soviet Union, statistical processing *(Russian)* 79—84081
regional anomalies interpretation procedure *(Russian)* 77—33199
regularization method and uniqueness problems in study of regional flat-layered structs. 78—49161
remote reference magnetotellurics, random error derivations relating to impedance 80—12335
research, international collaboration in early 19th century 78—4450
reversals, low order moments of alpha dynamo eqns. 77—44921
reversals, possible influence of ice ages on Earth rotation 77—56578
Reykjanes Ridge, mag. anomalous south of 60°N rel. to evolution between 40 and 12 Myr BP 80—90069
Rhinegraben, differential geomag. sounding 79—74832
ring anomalies rel. to ancient crustal structure *(Russian)* 77—33019
ring current magnetic field at magnetically quiet geomagnetic equator 80—105123
ring current magnetic field characts., spherical harmonic analysis 80—101493
river sediments, source identification, mag. meas. techniques 80—8348
Roosevelt Hot Springs, resistivity sounding, EM and Schlumberger 79—84095
San Andreas fault zone, Earth crust magnetisation rel. to local mag. field vars. near slip discontinuity 80—26448
Sanriku, geomag. obs. by (B_5-79) *(Japanese)* 79—79733
satellite data application to regional anomaly surveys 80—51558
satellite measurement of field from near-Earth orbit, review of obs. 80—56347
scale model of core, transient magnetic effects 78—48969
sea waves, mag. field exptl. obs. 79—53350
secular variation sources, evidence from New Guinea Highlands lake sediments palaeomagnetism 79—12069
seismomagnetic effects, space correl. method rel. to earthquake prediction *(Chinese)* 78—3719
Sendai, Honshu, balloon-borne magnetic survey during 1978 June 12 earthquake *(Japanese)* 80—30990
Seychelles-Mauritius Plateau, mag. anomalies, sediment thickness 78—3750
Shap granite, English Lake District, constraints on struct. and emplacement, gravity and mag. survey 78—44817
SI units *(German)* 78—65391
W Sicily, mag. survey, site for geomag. observatory 77—86757
singular points in mag. field models 78—69289
Skeleton Lake, Ontario, Canada, evidence for Palaeozoic impact crater 79—92553
solar eclipse effects on geomag. field, 1968 Sept. 22 *(Chinese)* 77—22154
sounding data, upward and downward continuation as inverse problems 79—44262
Souss Basin, S.W. Morocco, mag. survey and crustal struct. 80—89958
space-time structure of main field for 500 year period 77—25636
Spain, geomagnetic anomalies, geological interpretation *(Spanish)* 79—29710
spatial analysis of upward continuation of potential field data 79—74828
spectrum spatial analysis method for geomagnetic field *(Russian)* 77—91292

geomagnetism continued
spherical dynamo theory results 80—36242
spherical harmonic analysis appl. 78—49164
spherical harmonic coefficients of Earth's field, orthogonality 80—104881
spherical harmonic spatial power spectra, for crust and core fields 80—104882
spherical ore mass, interpretation of vertical anomalies 78—40476
static potential data inversion, generalized linear inverse 77—40967
static potential fields data inversion, generalised inverse appl. 78—77350
Stormer problem, effect of perturbation on periodic solns. 78—20582
Strait of Juan de Fuca, magnetic and gravity anomalies, geology 77—52973
subsurface EM field propagation from horizontal elec. dipoles, comprehensive study 80—98229
subsurface Em response of conducting-sphere in two-layer conductor 78—15961
Superior Province, Canada, shallow crustal sounding by audio freq. magnetotellurics 79—57882
Superior-Churchill boundary zone extension into S.Canada 80—26468
surface field components, effects of dynamo region long period winds 77—2090
surface of Earth with variable conductance, 3D-model of EM induction 80—30983
surface vertical component from aeromagnetic survey, computational method 80—105061
surveying using horizontal gradient vectors 78—28334
Switzerland geomagnetic survey instrumentation and results *(French)* 78—15966
Tangshan earthquake, China, related geomag. field variations *(Chinese)* 80—56372
Tasman Sea evolution, marine magnetic data 78—11870
tectonomagnetism and tectonoelectricity, symposium (Japan, 1975, September 5) 77—2084
telluric and magnetotelluric methods, comparison for sedimentary structures 78—3713
thermomagnetoelastic model of earthquake source mechanism 79—70758
thermosphere, polar airglow mag. ordering 78—57378
three-dimensional potential fields conversion and pseudo-gravit. field computation 77—82026
three-frequency computational method for two-layer CFS data 79—16688
time-domain EM method, optimum pulse shape selection 77—45167
Tohoku District mag. anomalies, high-altitude meas. by balloon-borne ring-core magnetometer *(Japanese)* 80—94608
total field mag. anomalies of spherical ore-bodies, interpretation via zero-line method 79—39973
total intensity anomalies, charts for quick determ. using horizontal plates *(Spanish)* 79—100982
transient EM field due to point source above surface of two-layered medium *(Polish)* 77—73627
transient EM fields, two-layer polarizable Earth 77—64199
transient EM prospecting using interactive minicomputer 79—62604
transient EM response from irregular surface models 78—57165
transient EM response of anisotropic rock to vertical electric dipole *(Polish)* 80—41367
transient EM response of sphere, conductive overburden effect 77—64197
transient EM sounding records computer processing, meas. errors anal. *(Russian)* 79—44269
transient field curves in proximate zones, regularities *(Russian)* 79—62434
Trivandrum, crust-mantle structure from Indian geomagnetic data 78—85520
turbulent diffusion regimes along the pitch angle in a geomagnetic trap *(Russian)* 79—55534
turbulent thermal convection in presence of rot. and mag. field, stellar and planetary dynamos appl. 80—6042
twelve month wave in an and as activity indices 80—72427
two-dimensional gravimetric and magnetometric problem, analytic construction based on Poincare sweep model 80—21846
Ukrainian Precambrian Shield, deep fractures analysis *(Russian)* 79—20773
Ukrainian Shield, rock mag. props. map rel. to composition and metamorphism 80—17229
ULF/ELF EM fields generated above finite depth sea by submerged vertical mag. dipole 79—48400
underground quarries, EM transmission meas. 78—57365
unipolar generator expt., rel. to geomag. field 77—9334
NE. United States and White Mountain heat flow anomaly 79—8594
Urach region, Germany, geomag. obs. rel. to temp. field investigation at great depths 79—48440
$V_{zz}(V_\Delta, Z_a)$ anomalies over stratified bodies, interpretation analytic method *(Russian)* 79—39968
Vancouver Island region, analogue model study of EM induction 80—56356
variable EM field, effect of conductivity irregularities in layer 78—20354
variable geomagnetic and gravitational potentials, effects of bumpy core-mantle interface 79—79771
VLF signals in ionosphere-Earth waveguide, geomag. activity effects *(Russian)* 79—2426
VLF-EM prospecting method, model study 77—49181
Waipipi ironsands in New Zealand, technique for titanomagnetite assessment 80—17254
Weddel Sea, geomagnetic, bathymetric and seismic obs. of crust 80—104929
world-wide belts in geomag. field, rel. to tectonic features 79—39651
Yellowstone Lake, submerged hydrothermal explosion crater in Mary Bay, bathymetry, seismic and mag. surveys 78—49050
Yerington mine, Nevada, in situ induced polarisation and mag. susceptibility meas. 80—51323
Yermak hot spot in Arctic Basin, magnetic and bathymetric evidence 79—88313
Yoshioka-Shikano Fault, seismically active fault along Japan Sea coast, geomag. induction study 80—26475
zonal nondipole and offset dipole field models, comparison using Icelandic palaeomag. data 79—57852
Fe ore deposit integral characts. determ. from magnetic anomalies *(Russian)* 79—62621
Fe ore deposits from gravity and magnetic anomalies, determ. accuracies *(Russian)* 79—84536
Fe ore prospecting, magnetic anomaly detect. *(Russian)* 78—16009

geometric programming
regional water quality management, optimisation model using geometric programming 77—66945
^{3}H breeding ratio maximisation 79—9879
T breeding in fusion-fission Tokamak, optimisation with geom. program 78—74477

geometrical optics
aberration-free lens, near focus intensity distribs. for Gaussian and const. intensity beams 77—615
acoustic target recognition, 2 theoretical techniques using geometrical optics and physical optics theories *(French)* 80—53509
acoustic wave amplitude variance in random medium with nonuniform background 78—38104
acousto-optical modulator, geom. optics model in low scatt. efficiency limit 77—34935
aerosol medium bleached zone, probe radiation propag., intensity and phase fluctuations 80—67411
AM/FM radio signal diffraction in homogeneous dispersive medium, space time geometric theory 79—4149
analogue model, light reflection and refraction, teaching 80—67948
anisotropic-isotropic interface, ray tracing in uniaxial and biaxial media 77—602
antipodal focusing, simple correction formula *(German)* 78—4034
apparent depth, viewing angle depend., ray tracing expts. 78—12475
arrival position fluctuations, geometric optics analysis limitations 78—46530
aspheric reflecting systems, geometrical design 80—38083
astronomical telescope resolution explanation *(Spanish)* 79—40075
automatic correction of optical systems by accurate ray tracing *(Spanish)* 80—53401
automatic correction of optical systems by accurate ray tracing *(Spanish)* 80—53402
beam positioning and focusing system combination in optical memory system *(Russian)* 79—7194
beam splitting device for use with smoke chamber ray optics demonstrations 80—67990
beam wave, propag. through weak turbulence, frequency spectra 78—78911
bent multimode waveguide, loss calcs., geometric optics method 79—37013
binocular vision, artificial aniseikonia, geometrical explanation of induced size effect 80—72173
bipolar spatial filtering, incoherent, review 80—102822
catadioptric systems, matrix optics 79—94167
catastrophe and fractal regimes in random waves 80—8811
caustic, phase shift, WKB approx. 77—19166
caustic patterns for melt zones in solidified glass samples, asymmetric cases 79—22893
caustic patterns for melt zones in solidified glass samples, symmetric cases 79—22892
caustic point displacement due to generalised bending, third-order approx. 80—83656
caustic surface calcs. and analytical illuminance 77—3643
caustics, crit. exponents from catastrophes, focusing and twinkling 78—22084
caustics from rippling water 79—18345
Cherenkov radiation, in inhomogeneous medium, geometric optics description 78—66766
circular cylinders, single scatt. phase matrix, ray optics and wave theory comparison 80—102610
circular symmetrical reflector with laterally defocused light source, axial ray trace equations *(Russian)* 78—90365
collimator, single element gradient index design 78—9426
commutator relation of ray operators and wave equation, relation 80—36877
complex ray analysis for plasmas 80—83902
compound elliptical concentrator, geometrical vector flux field 80—33119
compound parabolic concentrator, derivation of 79—72651
concentrator, compound parabolic, phase space conservation for incoherent propag. 80—69491
condensing light pipes and reflecting baffles, skew rays 77—3648
cone collectors for finite sources 78—46742
conic reflectors, basic props. of meridional and sagittal caustics 78—25948
conical light guide, theory, divergence reducing props. *(German)* 79—14090
conservation laws for geometrical optics in general-relativistic refractive media 79—54021
contemporary optics, book 79—81353
continuous system without symm., Lagrangian aberration theory 77—34815
continuously varying refracting media, CUPID ray tracing program 80—18990
corner diffraction, Albertsen's coeff. testing via spectral domain approach 80—87304
crystal inhomogeneous in optical anisotropy due to stress distrib., light propag. eqns. 79—13897
curved 4-space interpret. of classical light propag. 77—58253
curved multimode waveguide, geometrical optics shape of nonmeridional rays *(German)* 78—5566
cylindrical lenses, rotation of parallel fan of light, matrix representation 80—38089
deflectors using electro-optically controlled interference 79—1007
differential mode delay rel. to refr. index profile, geometrical optics treatment 80—69529
diffraction, geometrical theorem and Keller's diffr. coeff. *(French)* 79—41307
diffraction and aberration effects, wave optical calc. 80—83549
diffraction by semi-infinite complex structures, modified geometrical theory/moment method 77—75379
diffraction catastrophes, caustics 80—9801
diffraction grating, geometric optical theory 80—32904
diffraction grating geometrical aberration theory 79—55068
diffuse light collection onto extended absorber, mirror designs 78—22186
directional coupling device of two glass prisms, geometrical optics *(German)* 79—18524
dispersive anisotropic media, quasioptics 80—38567
dispersive media, derivation from Maxwell's eqns. 77—61917
double phase-matching function 79—41332
doubly curved crystal point focusing X-ray monochromator 77—82657

geometrical optics continued
doubly-curved narrow-beam reflectors 79—23040
eccentric system, paraxial approx. 79—98459
education, cornea, radius of curvature, quantitative geometric optics expt. 78—62004
education, description of unusual lunar halos 77—45634
education, lens Fourier transform properties 80—57024
education, matrix optics, principal plane concept generalisation 80—73140
education, perspective distortion in photography, eye as simple lens 80—17734
education, the principal plane, its pedagogic role 79—97150
education diffraction pattern classroom anal., image-space method 80—51983
education hyperbolic mirrors, holography and Fermat's principle, geometrical anal. 77—45647
elastic contact of two discs, method of caustics study 79—59948
electron optics, charged particle trajectory calc. in electrostatic field, teaching 80—90635
elliptic umbilic diffraction catastrophe 79—50213
elliptical multimode fibres, whispering and bouncing mode evaluation 80—10015
ELMO Bumpy Torus, ray tracing near electron cyclotron freq. 80—83975
EM scattering from dielectric coated conducting cylinder, ray optical anal. 80—83542
EM wave absorption in medium with smooth space-time fluctuations, statistical characts. 79—81339
EM wave diffr. on convex, smooth, ideally conducting and electrically large surface 78—94363
EM wave diffraction by plane angular sector, geometrical theory 79—45896
EM wave diffraction theory, book 77—3524
EM wave generated by long-narrow slit, EM field estimation 78—46494
EM wave propag. in birefringence medium, geometrical optics approx. *(Russian)* 77—68167
EM wave propag. in inhomogeneous three-dimens. anisotropic media, geometric optics method 80—43235
EM wave reflection from nonhomogeneous plane stratified plasma 78—87453
EM waves in medium with ellipsoidal inhomogeneities and regular refr., ray statistics 78—25773
extraparaxial region, laser beam self-focusing/defocusing, geom. optics approx. 78—5529
extremal problems, theory, book 79—63001
Fermat's principle, student expts. 79—30178
Fermat's principle and real space-time rays in absorbing media 77—88636
fibre, graded index, mode coupling due to perturbation of index profile 80—106598
fibre, graded-index, geometric optics approach to light acceptance and propag. 77—23756
fibre, multimode, step or graded index, ray analysis *(French)* 77—79915
fibre, spherical-ended, efficient coupling to LED, geometrical optics anal. 78—83086
fibre, unclad, backscattered light, approx. ray theory 77—7177
fibre excitation by partially coherent sources, geometric optics theory 77—79948
fibre in circular arc, meridional rays *(German)* 77—39048
fibre light propagation *(Czech)* 78—74997
fibre scattering, ray theory 80—69528
fibre tapered sections, ray trajectories 79—18508
fibre-optic scattering loss dependence on launching condition, lossy-layer model 78—5577
fibres, elliptical step-index multimode fibre, rays and modes 80—14442
fibres, randomly bent, ray theory 78—66921
fibres, theory of propagation, ray approach *(French)* 77—79916
flux concentrators, approach to ideality 78—66885
focal length of thin lens under water, determ., teaching appl. 79—44676
focused beam ray tracing for laser fusion 80—83218
focused field, symmetry props. 80—83550
focused light beams, phase anomaly, intuitive explanation 80—99622
focused radiation scintillations, freq. correl. by speckle interferometry 79—94153
Fresnel's classical papers, history and present appls. *(French)* 78—37800
funnel concentrator optics, ray tracing 78—58900
gasdynamic high speed lasers, optical cavity anal. using geometrical optics methods *(Chinese)* 79—31854
Gaussian beam propagation in 3-layered dielec. medium *(Japanese)* 80—87306
Gaussian optics parameters, HP-67 calculator program 80—106439
general nonhomogenous cylindrical medium ray tracing 79—94335
general optical concentrator, max. radiant power density at receiver 80—102794
general relativistic dispersive media 79—40435
generalised radiance propag. through lenses 79—27359
generalised ray tracing, caustic surfaces, bending and merit function for optical design 80—102612
geodesic lens, axially symmetric, geometrical theory 80—33238
geodesic waveguide lens anal., ray tracing 78—13778
graded index waveguide problem soln., comparison of wave and ray techniques 78—59140
graded-index fibre modal power distrib. determ. from near-field patterns 79—81518
graded-index fibre propag., ray optics approach 79—76849
graded-index non-circular fibres, ray theory 79—55229
graded-index noncircular fibres, geometric optics analysis 79—55231
graded-index optical fibres, ray optical paths and relative delays, calcs. 79—89987
gradient index imaging system theory 80—14294
gradient-index imaging, theory 80—69331
graphical ray tracing for conic surfaces 80—5683
grating equation, Hilbert's independence integral 79—899
gravitational lens effect, focusing by slowly rotating relativistic spherical mass 80—105155
gravitational lenses, high-intensification regions 79—25463
group theory in geometrical optics 78—25944
HF radiation from impedance surface on conducting circular cylinder 77—75380
HF surface fields excited by point source on concave perfectly conducting cylindrical boundary 79—64146

geometrical optics continued
holograms, 2-dimens. volume, power conservation theorem 77—3550
holographic grating arbitrarily oriented in space, ray path calc. 80—99677
holographic imaging, geometrical analysis 80—43291
holography, two-dimensional volume, coupled wave differential eqns. derivation 78—55317
homogeneous medium, Gaussian light beam propag., diffr. effects described using complex-ray method 80—78770
Huygens-Fresnel integral in circular coords., asymptotic soln. 78—87013
ice crystals, atmospheric, ray tracing rel. to origin of 46° halo and its arcs 80—82065
ideal concentrators, three dimens., for distant sources 79—41334
illumination, relative, easy calc. 80—63920
illuminator using laser light source, geometrical optical anal. *(Russian)* 78—79094
inhomogeneous anisotropic medium, linear wave transformation *(Russian)* 77—3518
inhomogeneous media, phase fluctuations, strong scintillations *(Russian)* 77—75417
inhomogeneous plane wave shadowing by an edge 78—90356
inhomogeneous waveguide lens anal. 78—5561
integrated optical systems, EM surface-wave modes ray theory 79—64360
interferometer, real-time shearing, quality factors testing appl. 80—37081
interferometric length measurement with curved wavefronts *(German)* 80—77752
interferometry, real-time digital heterodyne, for optical path difference maps 80—37076
ionosphere waveguide propagation, excitation by ground based sources *(Russian)* 78—32283
laser adjustment technique based on laws of geom. optics 78—5475
laser beam, diffractive ray tracing 77—27291
laser beam, far-field profile, focal plane technique 78—87087
laser beam distrib. near lens focus 80—1290
laser beam divergence influence on axicon axial intensity distrib. 80—95934
laser beam focusing, geometrical optics model, focusing system design 77—7109
laser beam propag. in evap. liq. drop medium, wind refr. 77—5322
laser beams, Gaussian, geometric props. 77—19276
laser beams, spatial structure 78—83014
laser cavities with two foci, stability conditions 78—66850
laser cavity, focal length of thermal lens 77—61977
laser Doppler anemometry, image form., wall scatt. effect on S/N ratio 79—89953
laser far IR waveguide cavities, coherently pumped, geometrical design criteria 77—54739
laser radiation absorption by spherical plasma, geometrical optics 80—59189
launching and propagation of light in optical fibres 80—69504
least-squares wave front errors of minimum norm 80—48137
lens, gradient-index rod, aberrations in multimode optical fibre devices 80—69487
lens, multi-element, defective surfaces, tilt meas. 78—66886
lens maker's equation, teaching 79—44683
lens paraxial eqn. dimensional analysis 80—74462
levitation of spheres by laser beam *(French)* 79—98428
lidar system, geometrical optics anal., atmospheric backscatt. 78—37936
light flux leaving a hollow cylinder 80—32909
light propagation in noninertial reference system *(Russian)* 79—897
light pulse propagation in pipes, model 78—30068
light ray reflection at dielectric-vacuum interface, exam. using Fermat's principle and evanescent waves 78—58902
lightguide transmission, radiance diminution, Hamiltonian ray optics analysis 78—46787
lightguides with oblique input endface, geometrical optics relations 77—68271
lightpipe, cylindrical, steady and transient radiation transport, exact soln. 77—27365
linear Fresnel lens with grooves of finite size, solar radiation concentration 80—106592
linear systems, Fourier transforms and optics, book 79—41350
liquid crystal optics, Poincare sphere analysis 77—85690
loaded unstable resonators with centered or corner obscurations, far field energy 77—72006
localised wave fields, nonlinear geometric optics *(German)* 80—69448
long optical fibres with random inhomogeneities, output pulse shape 79—3791
lower hybrid waves in nonuniform plasmas, geometric optics 80—83924
Maxwell fish-eye theory, formal equivalence with Kepler problem 78—81733
MHD wave propagation in inhomogeneous media, calc. allowing for finite cond. *(Russian)* 78—63553
microcapillary gas-dielectric filled waveguide with azimuthally asymmetrical cross-section, attenuation calcs. 78—83105
Mie scattering efficiencies, asymptotic behaviour 80—106452
mirror lens systematisation according to extent of central obstruction *(German)* 80—102795
models of optical systems 80—9821
moire depth contouring of surface 79—75488
moire pattern calculations 77—19164
Moire projection topography accuracy and sensitivity 78—45677
molecular pumping, thermal lens phenomena, time-resolved geom. optics approach 80—9708
mountain shadow phenomena, spike seen by off-summit observer 80—78761
mountain shadow phenomena theory 79—36831
moving object imaging, anticausal behaviour 79—81381
multimodal optical fibre, excitation anal. by ray optic method 79—81550
multimode fibres, arbitrary index profile, propag. mode anal. using ray optics adiabatic approx. 80—53418
multimode fibres of arbitrary refr. index profile, pulse dispersion 80—74475
multimode GRIN fibre, power launching theory 77—7179
multimode step-index fibre, OTF, geometrical optics calc. 77—65637
multimode telecommunications fibre scatt., geometrical analysis 77—23748
multimode waveguide core-cladding interface, macroscopic roughness effect 79—18523

geometrical optics continued
- multimode waveguide with elliptical cross-section, geometrical optics analysis *(German)* 79−76844
- multiple integrals in waveguide scatt. problems 79−3796
- multiple lens experiment 80−82596
- multiply reflected Gaussian beams in circular cross section 79−18343
- near field speckle statistics 77−19182
- non-coaxial aspherical IR optical system, automatic design *(Chinese)* 80−5810
- nonimaging concentrators and geometrical vector flux 79−72650
- nonlinear Schrodinger equation, exact solution, localised wavefield evolution 80−53191
- nonmeridional rays in multimode optical waveguides, transmission characts., multimode propag. *(German)* 77−54799
- nonrelativistic particle trajectory, analogy with optical ray trajectory 77−14657
- nonsymmetrical optical system, matrix representation 80−64130
- ocean waveguide, stochastic ray tracing 77−3694
- optical channel transmission calc., matrix method 78−18033
- optical fibre, power-law refractive index profile, scalar modal eigenvalues and group delays 80−28322
- optical fibre, side illuminated, noncircular cross section effect on forward scatt. pattern 80−33150
- optical fibre coating concentricity meas. and anal., ray theory 77−88898
- optical microdevice with square law media, Gaussian beam characts. by wave optics 79−81360
- optical paths in refractive medium, global existence, smoothness and nonfocusing 78−29898
- optical system, geometrical optics field 79−81503
- optical system design method 79−36974
- optical systems with spherical and nonspherical diopters, in three-dimens. space, calc. method *(Rumanian)* 79−13898
- optical waveguides, multimode, variable dia., light propag. 78−33894
- parabolic index fibre, theory of helical bends 77−88951
- parabolic index fibres, light propag. along helical bends 77−7183
- parabolic index glass rods and fibres, imaging props. 77−42599
- parabolic-profile splices with unequal core diameters, transmission vs. transverse offset 77−3652
- paraxial air angles between cemented surfaces, calc. 79−76799
- paraxial approximation to scalar Helmholtz eqn., discrete eikonal and ray eqns. 78−90360
- paraxial optical systems, nomographic diagrams for design and anal. 80−48377
- phase fluctuation effect on deform. of caustic surfaces 79−94152
- phase retrieval from intensity meas., uniqueness question 79−13915
- photoelastic materials and crystals, light wave propag. 79−898
- plane plates, two sets of different physical props., energy flux splitting *(German)* 79−18500
- plane waves in strongly turbulent media, two-frequency mutual coherence function 77−21907
- planetary atmospheres, complex geometric optics of radiowave propag. under superrefraction *(Russian)* 78−49353
- plasma, formalism 80−83925
- plastic rectilinear waveguide with core/cladding and cladding/surrounding interface *(German)* 77−34941
- plate, rectangular, deformed, light ray propag., geometrical effects, nonclassical behaviour *(Russian)* 78−22080
- point eikonal coeffs. calc. from angle eikonal coeffs. 77−34817
- point spread function synthesis, geometrical optics approach, transaxial tomograph processing 79−94163
- polarised light, extension of geometrical optics, optics field spinor formalism 79−50210
- polymer lightguide, light propag., nonlinearity, quasi-optical approx. 80−99837
- principles, w.r.t. electronics engineer appl. 77−83818
- principles for electronic engineers *(Japanese)* 80−9799
- propagation through plane layers 80−53194
- proximate ray tracing and wave aberration coeffs. 77−597
- quasi-homogeneous sources and geometrical optics 80−23620
- quasi-Ronchigrams for interpreting wave-front and glass-error slopes 80−37078
- quasioptics in anisotropic and dispersive media 80−91943
- radiation flaw detection, correction of shadow images 80−89456
- radio source radiation in presence of smooth convex bodies, diffr. geometrical theory 79−64151
- Raman-Nath acousto-optical interaction, geometrical interpretation of image form. *(French)* 77−34836
- random inhomogeneous media, Lagrangian and Euler description *(Russian)* 77−3537
- random phase screens, probability density for intensity of plane waves 80−87317
- randomly bent multimode fibres, ray theory 78−79129
- randomly inhomogeneous medium, fluctuations in phase arrival angle and freq. correl. of spherical waves 80−106456
- ray and wave optics of integrable and stochastic systems, WKB method 80−59244
- ray equations for absorbing media, uniqueness of solns. 77−3521
- ray optics, theory of light field, statistical optics, light meas., photometry, polarimetry 77−79748
- ray paths in a fluctuating environment 79−9129
- ray paths in nonuniform axially symmetric medium 79−7076
- ray paths in refractive scattering medium 77−68175
- ray statistics of multimodal optical fibres 78−94450
- ray surface equation and Fermat's principle, in moving anisotropic media 80−106425
- ray trace code for glass microbubbles 77−18702
- ray trace program, TI59 calculator 79−32023
- ray trace program for TI-59 calculator with PC100A printer 79−89985
- ray tracing, generalised, caustic surfaces 79−23043
- ray tracing, programmable pocket calculator appls. 79−58468
- ray tracing algorithm for programmable pocket calculator 79−81508
- ray tracing in general index distributions 80−14279
- ray tracing through tilted and decentred optical surfaces, computer program 80−33120
- ray-optical analysis of unstable resonators with spherical mirrors 80−14415
- real space-time rays in absorbing media, Fermat's principle 79−3628
- reduced wave eqn., parabolic approx., asymptotic solns. 78−78908
- reflectance, geometrical considerations and nomenclature 78−29146
- reflector design using complex coordinates 77−19380

geometrical optics continued
- reflector surface design by numerical method, bivariate beamshaping in elliptic case 77−27225
- refracting sphere system, skew ray tracing *(German)* 78−9322
- refraction, generalised ray tracing 77−27249
- refractive index distribution for prescribed two-dimens. ray path. 79−59633
- resonator, sensitivity to misalignment, anal. by ray contour method 80−58602
- resonators, cylindrical unstable, ray-optical anal. 79−72652
- retroreflection from rough surfaces 79−10258
- RF EM plane wave incident on a man model, energy absorpt. by and fields in calcs. 80−56115
- RF higher-frequency energy absorpt. by biological models, geometrical optics calcs. 80−56116
- rhomb laser beam sampler, two-grating, inherent aberration correction, inverse filter description 80−37954
- ring laser, perturbed cavity calcs. 80−102739
- rod, tapered gradient-index, geometrical optics 80−69322
- Rowland circle, corrected, least-squares method derivation 80−64161
- scalar diffraction model for small apertures *(Spanish)* 79−59629
- scattering by ice crystals, geometric ray optics anal. *(Russian)* 80−94601
- scattering from inhomogeneous particles, glory ray and rainbow 77−29430
- scattering of ultrashort laser pulse by large spherical particle 79−906
- seismic ray tracing, three-dimens. methods 77−73870
- seismic surface-wave ray tracing, appls. 79−66630
- short wave radiation problems in inhomogeneous media, book 77−10840
- single lens, longitudinal-chromatic and spherical aberrations, ray-tracing method estimation 78−1311
- single strip diffr., Kirchhoff, geometrical theories and Maxwell eqn. exact soln. 77−6975
- skew ray tracing, trigonometric formulae *(German)* 77−61913
- skew ray tracing through plane surfaces *(German)* 79−900
- skew ray tracing with the TI-59, programmable calculator 80−48141
- slab waveguide, modified zigzag ray model 77−39035
- smooth convex surface HF scatt., transform-domain Galerkin soln. 77−38783
- solar collector, fixed spherical, geometrical optics *(French)* 77−83945
- solar concentrator using catenary curve reflecting surfaces 78−46744
- solar tower concept, ray trace approach 78−5571
- solid bodies, optic-geometric method calc. of diffraction patterns *(Russian)* 80−91746
- source dimension estimation from diffraction image using Chebyshev approx. *(Russian)* 78−82903
- speckle, affine geometry, tilt topology 77−19176
- speckle photography and holographic interferometry, scatt. geometry, topology, vector fields, theory 80−87347
- sphere, force exerted by laser beam, stable optical levitation conditions 79−76733
- spherical particle velocity and size meas., crossed-beam light scatt. interferometry 80−47011
- spherical surfaces, extrameridional aberrations anal., with large decentring angles 77−68181
- spot diagram automatic computation and plotting program 79−72645
- square law medium, incident Gaussian beam field distrib. 78−74840
- step index fibre, pulse widths, Goos-Hanchen shift effects 77−83952
- stigmats using two curved Fresnel surfaces 80−38084
- stray light phenomena, GUERAP III Monte Carlo simulation 78−58907
- stray light simulation with advanced Monte Carlo techniques 78−58906
- stray radiation analysis using first-order deterministic APART program 78−59116
- structural stability in physics (conference, Tubingen, Germany, May and Dec. 1978) 80−8739
- surface representation in cartesian coordinates, optical path calc. appl. *(German)* 78−78902
- surface waveguide electrooptical deflector, high-resolution, prism model 80−48454
- synchrotron radiation from electron storage ring, focusing condition 77−42584
- tapered cylindrical optical fibre, radiation characts. 79−10388
- tapered gradient index rod, geometrical optics and imaging props. 80−14280
- teaching, handling of spherical mirrors and lenses *(Hungarian)* 78−12449
- teaching, paraxial and nonparaxial approx., matrix methods 78−77638
- teaching to engineers, matrix algebra methods 80−62415
- telescope, image vergence variation with object distance change, general case 80−63934
- telescope-spectrometer combination, optical props. 80−87455
- telescopic systems, practical approach to parallax problems 80−99818
- terminology of transmission, refl., scatt., and emission 78−37044
- thermal lens, time-resolved geometrical optics 79−12795
- thin lenses formulae for teaching purposes 79−35509
- time-dependent, Fermat's principle 77−605
- Tokamak, Vlasov plasmas, geometrical optics approach to electron-cyclotron frequency heating 80−14917
- Tokamak machines, Vlasov plasmas, geometrical optics approach, Tokamak appl. 80−14902
- total internal reflection, boundary type soln. 78−42272
- total internal reflection, focal shift, ray model 77−34809
- trajectories of reflected and transmitted beams in oblique tunnel effect 78−78903
- transparent hollow sphere, radiation pressure in cylindrical beam *(French)* 78−29896
- tunnelling ray attenuation in fibres, generalised parameters 78−66908
- turbulent medium with smooth space-time fluctuations, absorpt. effects on statistical characts. *(Russian)* 79−18330
- uniaxial crystals interface, EM wave refl. and refr. laws, tensor derivation 78−71029
- unstable resonator analysis, ray transfer matrix approach 79−50322
- unstable resonator laser, intensity distribs., simple geom. model 77−50691
- unstable resonators with rounded edges, mode losses 78−79039
- volume phase holograms, 3-D vectorial theory 79−81385
- volume phase holography, vector differential equations solns. 79−81386
- wave propagation, in randomly inhomogeneous medium, frequency correlation *(Russian)* 77−88623
- wavefront aberration polynomial, calc. 80−102614

geometrical optics continued
  wavefront estimation from wavefront slope meas., least-squares curve fitting model 80–106467
  waveguide, parabolic index with random dielectric constant gradient, Gaussian beam propag. 80–58698
  weakly nonlinear media, spatial and temporal self-focusing, ray theoretic anal. 78–18026
  whispering-gallery waves, polarisation and losses along twisted trajectories 80–9798
  white holes optical appearance in geometrical optics framework 79–21323
  wide aperture optical systems, irradiance field formation, comparative analysis 78–90479
  Wigner distrib. function and Hamilton's characts. 80–1143
  Wigner distribution function, transport eqns. 80–32907
  Wigner distribution function, transport equations, inhomogeneous dispersive medium 80–53214
  Wigner distribution function and its application to first-order optics 80–37958
  Wigner distribution function applied to optical signals and systems 78–50713
  X-ray interferometer, LLL type, interfering beam phase rels. 80–90973
  HF CW chemical laser, spatial homogeneity of radiation improvement using telescopic resonator 80–106549
  Na vapour lamp reflector design *(Spanish)* 79–23042
  WO$_3$, antireflection coating on W dendritic surfaces, reflectance, geometrical study 79–91511

geometry
  see also space time configurations
  σ-models, conservation laws, infinite series, differential geometric content 80–62841
  acoustic wave refl. from general surface, geometric props. 77–84026
  algebra generated by Hodge's star and external differential 79–92926
  amorphous spaces, affinely-rigid motion 77–60991
  angular structure of unique spherical shells, appl. to ang. momentum quantisation 78–73873
  area of intersection of n equal circular discs, appl. to hard-disc fluid model 78–57755
  astroarchaeology, Avebury, geometry and metrology of ring, new accurate survey results 77–33359
  astroarchaeology at Kerlescan megalithic stone alignments, alternative geometry 77–41321
  Bachlund problem, Lie algebra bundles *(French)* 80–18085
  Backlund transformations in several variables, differential geometric anal. 80–86073
  Banach manifolds, affine transformations 78–31
  Bianchi model universes, hypersurfaces of transitivity, Riemann curvature 80–67922
  big bang model, hot, observational cosmology 78–12444
  boundary-value problems, variational principles and hypercircle 78–57749
  bundle boundaries, Schwarzschild and F-R-W solns. 77–57248
  chronos principle and interactions of fields of spin 0 and 1 78–8286
  classical field theory geometrisation, applied to Yang-Mills field theory 80–46841
  closed geodesics on Finsler manifolds, arithmetic theory 78–12536
  coincidence site lattice, differential geometry 79–28000
  compact Riemannian manifold with no conjugate points, spectral function of the Laplacian *(French)* 77–5639
  compact spacelike submanifolds in Euclidean spaces 77–53750
  complex space-times, real geom. 78–77684
  configuration space geometrization using projective geometry 77–71192
  conformally symmetric spaces with positive definite metric forms 77–49574
  conformally-recurrent Ricci-recurrent spaces, existence 77–49573
  conharmonic curvature tensor, Kahler space 78–54146
  constant mean curvature and canonical time, concept generalisation 78–98
  contracted Ricci collineations, timelike mapping characterisation 77–67345
  control moment gyroscopes, single-gimbal, geometric theory 79–21738
  coordinate transformation of Laplace operator in 2-D, for teachers 78–61999
  cosmology, geometrical approach 77–5606
  coupled harmonic oscillators, natural freqs. from anal. geometry, for teaching 79–25806
  curvature of bidimensional orientations from a point in a four dimens. space *(Italian)* 77–13582
  cyclic pursuit in a plane 80–12896
  differential, appl. to continuum mechanics 78–12566
  differential, appl. to mechanics, math. model of general relativity 78–69968
  differential, of wedge disclinations, simple cubic crystals 77–59011
  differential forms in mathematical physics, book 78–81810
  differential geometry, appl. to geophysical fields configurations analytical description *(Russian)* 79–74986
  differential geometry, appl. to mechanical systems, gyroscopic forces *(Russian)* 79–63016
  differential geometry, nonlinear realisation of symm. groups. 77–60899
  differential geometry methods in gauge and gravitational theories 80–90768
  differential geometry of deformed crystals 80–19867
  dimensionality of physical space, assumption of three-dimensionality 78–93515
  distributional geometry, appl. to black holes in general relativity 79–93006
  divergence free vector fields and Bochner's theorems 79–63003
  diverging type-D metrics 77–45761
  dynamical systems, symmetries, first integrals and differential forms 80–77983
  edge notches, conformal transformations 80–27128
  Einstein space, symmetric 2-tensor with divergence zero *(French)* 77–17783
  Einstein-Cartan equations, solns. 78–8299
  Einstein-Cartan gravitation theory, junction conditions 77–30058
  Einstein-Yukawa theory, unified 78–29240
  elliptic space as unit sphere in Euclidean vector space *(German)* 77–60909
  Euler-Lagrange differential in fibred manifolds 78–45469
  Eulerian and Lagrangian coordinate systems, for teachers 79–21491

geometry continued
  faceless linear cones, orders, gauge, and distance, appl. to continuum mechanics and special relativity 78–57753
  fibre bundle techniques in gauge theories 78–54573
  fibre bundles, gauge theory of strong and EM interactions 78–54574
  fibre bundles, pseudoconvexity 77–29998
  fibre bundles and relativity principles 80–8783
  fibre-bundle approach to gauge field theory 78–58130
  field theory in Finsler spaces, nonlocalisation, internal variable 78–49963
  fifteen parameter conformal group, geometry and isomorphism 79–9154
  Finsler spaces, physico-geometrical remarks on theory of physical fields 77–22394
  Finsler spaces, recurrent spaces of second order 77–67230
  fixed points of cyclic group actions on disks 79–62994
  fuzzy spaces, direction and particle interactions 77–22395
  Gauss-Codazzi-Ricci eqns. of local isometric embedding 77–57162
  Gaussian random surfaces, umbilic points 78–4467
  general relativity, dynamical formulation using infinite dimensional differential geometry 78–93582
  general relativity, superspace, local supersymmetry, superfibre bundle theory 78–77782
  general relativity, symplectic form, geometric construction 78–8289
  general relativity, U$_4$ theory, positive energy 78–8296
  general relativity conference, Trieste, Italy, 1975, July 78–8285
  generating forms of K-generalised Lagrangian and Hamiltonian systems 78–4475
  geodesic balls, volume, and geometry of Riemannian manifold *(French)* 80–68085
  geometric quantisation, book 77–41510
  geometric quantization and quantum mechanics, book 80–94908
  global differential geometry anal. of construction leading to classical Hamiltonian or Lagrangian dynamics 77–33861
  global first integral for dynamical systems, importance of div. 77–82374
  grain boundaries, differential geometry 77–27893
  gravitation, canonical many-time quantisation 78–8328
  gravitation and inertia in general relativity 78–8317
  gravitational axial superfield and the formalism of differential geometry *(Russian)* 80–57164
  gravitational curvature, Einstein's theory, an introduction, book 80–22161
  gravitational index theorems and super theorems 79–75432
  gravity, quantisation of space-time 77–33924
  H space, the manifold of complex asymptotically shear free light cones 78–8292
  Hamilton's Principle, geometric formulation, spin particles 78–45482
  Hamilton G-spaces, quantisation of A-bundles 77–26139
  Hamilton-Jacobi theory, differential geometrical methods 78–45471
  Helmholtz, H. von, evolution of empiricism, study of a universalist 78–8212
  Hilbert space affine connection, quantum geometrodynamics 77–60962
  Hochschild cohomology within transitive Lie pseudogroups, appl. to deform. theory *(French)* 77–67227
  holomorphic vector bundles, exact complex symplectic or unimodular structures *(French)* 77–26140
  holomorphically subprojective Kahlerian manifolds 77–87630
  indefinite Finsler type metrics and their peculiar properties 79–97265
  information processing and origin of pure geometry 77–44624
  instantaneous invariants in three-dimensional kinematics 79–18698
  instanton interactions and Riemannian geometry 77–71447
  integrable equations and differential geometry 79–75407
  integral geometry and geometric probability, book 77–60910
  intrinsic geometry of quantum mech. phase space Hamiltonian systems, correspondence principle 79–83
  intrinsic metrics on continuous spatial manifolds 77–41459
  invariant measures for manifold families in M$_2$ space *(Rumanian)* 78–20944
  inverse power law potentials about polygonal prisms and in polygonal cavities 78–95232
  inverse scattering and solitons, geometric considerations 80–4550
  isometric folding of Riemannian manifold 78–77685
  Jacobi manifolds and associated Lie algebras *(French)* 78–28919
  jacobians and curvilinear metrics, for teaching 79–62961
  Kerr metric, vortical type geodesics, causality non-violation 78–54251
  Kerr-Schild congruences and Kerr's theorem 77–60989
  Killing spinors, basic props. 77–22453
  Killing trajectories, intrinsic geometry, n-dimens. Riemannian space 77–22393
  Kostant-Souriau geometric quantization of nuclear collective models 80–9247
  L-equivalence classes of submanifolds in complex projective spaces 79–75323
  Lagrange differential 77–53751
  Lagrangian field theory, vector bundles, rth order Noether invariants and canonical symmetries 78–86409
  Lane-Emden eqn. of index 5, geometric technique for M-solns. 78–61851
  Lee's derivative of geometrical objects, tetradic transform. *(Russian)* 79–93024
  left-flat space-times, null tetrad and restrictive conditions 80–62545
  Legendre transformation, geometric definition 78–24640
  Lie algebra, class of representations on vector field, partial differential operators *(French)* 77–67228
  Lie group, path integral and quasiclassical asymptotic behaviour 78–54230
  Lie groups, left-invariant differential forms and systems *(French)* 77–5620
  Lobachevskii space vector and relativistic kinematics 78–62076
  London equations in Riemann space 77–15989
  Lorentz manifolds, potentially umbilical, structured by parallel spatial connection *(French)* 78–49646
  Lorentzian manifold, Kahler-metrics 80–73251
  matrix representation of unbounded operators 79–97231
  matter field spacetimes, symm. mappings satisfying vanishing contraction of Lie deform. of Ricci tensor 79–113
  maximal surfaces in closed and open spacetimes 78–8294
  Maxwell fields, time depend., in stationary geometry 78–8308
  mechanical theorem-proving in elementary differential geometry *(Chinese)* 79–35535
  MHD, in transverse mag. field, streamline orthogonal-net anal. 79–37417

geometry continued
- monopole theories, geometrical aspects 77—74591
- Nelson's stochastic mechanics on Riemannian manifolds, classical dynamical system 78—57860
- new general relativity, geometry translation group gauge theory 77—79020
- Newtonian mechanics, linear connection and curvature 77—5733
- Newtonian mechanics, time-dependent transformation, relativity of force, geometrical viewpoint 77—57177
- non-Euclidean geometry and physical basis, Galilean geometry and relativity, book 79—62989
- non-Euclidean geometry and structures prior to Einstein, speculations *(German)* 80—90651
- nonholonomic mech. systems of second order, geometrisation of motion 78—57771
- nonintegral dimens. spaces, axioms, measures, topology, physical implications 77—64929
- nonlinear σ model in two dimensions, geometry 77—41496
- nonlinear string dynamics, rigid body motions, space curves, prolongation structures, fiber bundles, and solitons 79—97213
- nonlocal fields characterized by internal variables, geometrical theory 78—29014
- nuclear potential, effect of geometry 78—4900
- null strings, geometry in complex space-times 80—22241
- orbital motion of three bodies, Hill's curves, geometric prop. 78—77474
- pairs of focal curves in orthogonal planes and movable bar frames *(German)* 77—60927
- particle creation and geometry 78—12442
- Pauli principle in Euclidean geometry, for teaching 80—17768
- physical geometry, axiomatic characterisation, book 80—41970
- physics, algebras, manifolds and fibre bundles 79—44709
- pinching theorem and laplace operator first eigenvalue estimate on Riemannian manifold *(French)* 80—27185
- Poincare's conventionalism of applied geometry 78—86110
- point-surface distance meas. adjustment, geometrical aspects *(German)* 80—86255
- prequantum bundles and projective Hilbert geometries 78—36799
- presymplectic Hamilton and Lagrange systems, gauge transformations and the Dirac theory of constraints 80—9106
- quantisation, geometric, representation spaces 78—36869
- quantisation using geometry and general relativity 78—8288
- quantum systems, multiparticle, geometric methods and appl. to bound state spectrum 77—82452
- quantum theory, physical geometry, group manifold 80—105522
- Randers space of scalar curvature 78—4469
- Reissner-Nordstrom geometry, forced perturbations 78—8303
- Reissner-Nordstrom spacetime, spin coeffs. and electromagnetism 78—8309
- relational theory of physical space 77—74184
- relativistic particles, with isotopic spin, kinematics, geometric quantisation 80—62871
- relativity, general, differential forms, complex vectorial formalism 80—57144
- Riemann curvature of conservative systems in classical mechanics 78—89332
- Riemannian manifold, harmonic forms of curvature type *(French)* 78—86124
- Riemannian manifold, Harnack's constants, upper bound of the heat connection *(French)* 77—26141
- Riemannian manifold with quasi-concurrent vector field 77—26142
- Riemannian manifolds, separability structures, Killing 2-tensors 78—45470
- Riemannian manifolds admitting an infinitesimal conformal transformation 77—67231
- Riemannian metrics of nonnegative curvature on fibre bundles 77—49575
- Riemannian spaces, linear connections *(Rumanian)* 77—74274
- Riemannian spaces, three-dimens., of second class of imbedding 77—82425
- rigid body with fixed point, Riemannian struct. of continuum of configs. *(Italian)* 78—12548
- Rosen's bimetric theory of gravity, orbital topoography and other astrophysical consequences 78—54274
- rotating plane-fronted waves and their Poincare-invariant differential geometry 80—332
- rotational frames and Euclidean connection 77—60907
- second order symm. tensors in compact Riemannian manifold, compatibility and orthogonal decomp. 77—57161
- segmented structures, space-time point segment 78—32
- semiclassical theory of scalar field in globally hyperbolic universe 78—54250
- simplex volume in constant-curvature spaces, integral representation *(German)* 77—57163
- Sine-Gordon eqns., differential geometry appls., soluble relativistic field theories *(Russian)* 78—74162
- single elastic body point, geom. of motion 78—49662
- singular spin harmonics 79—97529
- smooth vector fields, geometrical generalization of relation between limit cycles and symms. 78—54163
- solar hour angle, formula rel. to latit.-independ. sundial construction 78—81549
- some thermodynamical remarks on the theory of gravitational field 78—81899
- space derivatives, scalar and vector fields 77—37785
- space-field geometry anal., fundamental eqn. soln. *(Russian)* 77—53752
- space-time manifold geometrical singularities, edge geometry 79—44807
- space-time structures, classification 77—30057
- spacetime geometry 78—36895
- spacetime singularities 78—8291
- spacetime structure probed by spin 1/2 elementary particles, Riemann geometry with torsion 77—41517
- spatially homogeneous universes 78—8318
- special relativity, rotating frames anal. 78—36824
- sphere, largest possible inscribed between four spheres *(French)* 77—60906
- sphere, surface arrangement of points, unit charges, equilib. configs., stereochem. appl. 77—79552
- spinor fields, nonlocal, physico-geometrical gauge field theory 78—37134
- spinor Lie derivative, geometric significance 78—73826
- spontaneously broken symm. projective geometry and group contraction 78—8551
- stable tangent bundle in differential geometry and unified field theory, generating method 79—5974
- statistical physics, scaling and fractals 79—58625
- strong gravity and elementary particle theory in general relativity 78—8315
- SU(2,2) homogeneous symplectic manifolds, conformal Lie algebra 78—45808
- supergauge theory, geometric aspects, broken gauge invariance 78—8506
- supergeometry mathematics, supersymmetries 78—73891
- supergravity, curvature in terms of torsion and convariant derivatives, Bianchi identities 80—62561
- supergravity, geometry of superspace, vector-spinor matter 78—49744
- supergravity, supersymmetric generalisation of differential geometry tensors 78—45546
- superspace, generally covariant theories of gauge fields 78—54568
- superspace with Fermi and Bose coords., appl. to graded Lie bundles and supergravity 77—26143
- supersymmetry, geometric model 78—54579
- surface shape factors determ., luminous flux transfer meas. 77—31147
- symplectic geometry and second quantisation, field theory 77—45977
- teaching, insight and intuition appl. to geometrical problem 79—80397
- thermodynamics, irreversible, near equilib., metric geometry 80—62604
- thermodynamics, phenomenological theory, differential geometrical methods 78—45471
- 'thin sandwich conjecture' in general relativity initial value problem 78—4539
- transitive Lie pseudogroups, normalisers *(French)* 77—67229
- transitive mechanical systems, param. determ. from co-adjoint action 78—12554
- twist disclinations, differential geom. 79—14805
- Twistor theory, symplectic forms 78—4468
- twistor theory and particles, book 79—97485
- twistors and SU(2,2) induced representations 78—8229
- unified field theory, geometrical consideration 78—12809
- variational principles on rth order jets of fibre bundles in field theory 78—86168
- vector fields tangent to sub-manifold, Lie algebra derivation *(French)* 79—53965
- wave fronts defined by eikonal equations, structural stability, elementary catastrophes 80—73187
- Yang-Mills theory, instantons and algebraic geometry 77—74570

geons *see gravitons*

geophones *see seismometers*

geophysical aspects of cosmic rays
- 11 year variations during 19th and 20th solar cycles 79—84602
- 1972, August cosmic ray storm, north-south anisotropies and related phenomena 78—89018
- air showers impact on water surface, acoustic pulses generation and detect. 79—66901
- albedo determ. from meas. in stratosphere 79—80134
- altitude differences and geomag. field secular changes effects on variational coeffs. 78—93058
- amplitude modulation in 27-day variations 80—26703
- annnual and semiannual vars. 80—26704
- Antarctic ice as supernovae recorder, NO_3 produced by γ- and X-rays 80—31314
- antiproton spectrum, at top of atm., scaling law 79—12365
- atmosphere, ion-pair production rate above 18 km altitude, parametrisation 78—65469
- atmosphere mean-mass temp. vars. determ. from cosmic ray intensity data 77—91387
- atmosphere medium-energy gamma-rays, spectrum meas. 79—9030
- atmosphere MeV gamma radiation, theoretical zenith angle distrib. at high balloon altitudes 77—45208
- atmosphere prompt high-energy neutrinos, rel. to cosmic neutrinos diffuse fluxes 79—44327
- atmosphere prompt neutrinos, W-bosons prod. 79—3014
- atmosphere ultrahigh-energy neutrinos, fluxes and detect. techniques 78—49264
- atmospheric Cherenkov pulse duration, depend. on cosmic ray shower parameters 78—89025
- atmospheric electrical conductivity, cosmic ray effects rel. to global electricity, quasi-static model 79—96799
- atmospheric electrons, MeV range registration instrument 79—5645
- atmospheric gamma ray angle and energy distrib., 2-25 MeV 78—12033
- atmospheric gamma-rays, north-south anisotropy at balloon altitudes 77—29608
- atmospheric high-energy neutrons, flux and energy spectrum meas. at balloon altitudes 77—21836
- atmospheric neutron and gamma ray fluxes and energy spectra 79—75063
- atmospheric nuclear cascade characts., calc. for Pamir expt. 79—80157
- atmospheric showers, muon energy spectra at large zenith angles, 0.28 to 35 TeV *(Russian)* 77—9639
- atmospheric X-rays, separation from primary diffuse X-ray component using growth curves 79—25512
- auroral proton source in magnetosheath 77—33240
- bow shock, origin of 30-100 keV protons in upstream region 79—48622
- charged hadrons, negative/positive ratio, 3220 m above sea level *(Chinese)* 79—12369
- charged particle fluxes meas. on geostationary orbit 79—80082
- clean atmospheric jet, 878 TeV, cascade degradation absence 79—35084
- climatic var. induced by magnetic field screening of cosmic rays 77—78398
- conference, Yakutsk, USSR (Jun. 1977) 79—80110
- cosmic rays, velocity diffusion, turbulent mag. field, Monte Carlo calc. 78—53777
- cosmogenic isotope production in Earth atmosphere, secular vars. 79—53686
- cutoff rigidity decrease over Europe, 1973, April 1, neutron results *(German)* 77—13194
- cutoff rigidity vars. during mag. storm, magnetospheric ring current radii determ. 79—62685
- D-region, effects of cosmic ray modulation by interplanetary mag. field 77—33272
- D-region, ionisation effects from cosmic X-ray sources 79—35048
- daily intensity variation, depend. on mag. storms, sunspot no., and solar flux 79—35082

geophysical aspects of cosmic rays continued
Dhajala meteorite shower atmospheric fragmentation and ablation based on cosmic ray track obs. 77−82188
difference coupling coefficients, method for cosmic rays 78−28461
differential, ionospheric and ^{14}C coupling coeffs. for investigation of variations 79−80142
diffusion equations for nucleon and charged pions in atmosphere 79−70936
diffusion in random magnetic field, weak particle-field interaction theory validity 79−21109
diurnal anisotropy, anal. of 80−94660
diurnal anisotropy energy spectrum in 1971-75 period 79−80136
diurnal variation, fundamental and second harmonic 77−53363
diurnal variation, power spectrum anal. 79−25416
diurnal variation of cosmic ray intensity, interplanetary diffusion coeffs. calcs. 79−29952
diurnal variation of cosmic ray intensity, two approaches to study 79−29953
doubly scattered electron fluxes in atmosphere 77−53358
dynamic processes on Earth, extraterrestrial causes, rel. to extinction of life 78−92820
EAS, atmospheric elec. field, rapid vars. connected with high energy primary particles 79−66739
EAS, detectors pulse profiles studies 79−25421
EAS, upper troposphere, balloon obs., nuclear reactions, 10^{15} eV energy particles 79−80161
EAS and radiowaves produced from secondary electrons in geoelectric field, 10 kHz-10 MHz 79−21118
EAS radio emission, field strength at 44, 60 and 80 MHz 80−8505
EAS radio pulses, correlation at 60 and 80 MHz 80−8504
electrons and γ-rays, short-period fluctuations, in upper atm., correl. with solar diameter vars. 79−21115
electrons and protons quasiperiodic pulsations in stratosphere 79−80133
electrons in 100 MeV-100 GeV range, Interkosmos 17 spectrometer study 80−8503
electrons in atmosphere, energy spectra evolution allowing for secondary electron production 80−41676
EM cascade, particle-induced, in water, thermoacoustic effect, neutrino detection appl. 79−29960
EM cascades in air, caused by 10-100 GeV electrons and photons 79−21120
energetic particles in magnetosphere, investigation using Sambo programme of balloon expts. 79−80081
energetic solar protons, auroral zone precip. assoc. with storm sudden commencements 77−82081
environmental radiation fields prod. by cosmic rays 80−51630
environmental radiation measurements, atmospheric cosmic-ray components altitude depend. *(Japanese)* 79−80144
equator-pole symmetrical anisotropy during unusual cosmic ray storm 78−89020
fast electrons long-term vars. in Earth's outer radiation belt 78−49226
flare proton intensity north-south asymm. rel. to plasma sheet and daytime polar cusp dynamics 77−17297
fluctuations at 250 GV, spectral analysis 79−75062
flux in atmosphere, primary and splash albedo components, polar orbiting satellite meas. 79−25415
flux variations meas., Elbrus spectrographic system appl. 79−84605
forbush decreases: origin and development in the interplanetary space 79−75059
Forbush decreases and geomagnetic storms rel. to interplanetary parameters 77−70956
galactic cosmic rays, inside magnetosphere, local energy spectra calc. *(Russian)* 78−16258
gamma rays, 6.13 MeV, detect. within and at top of atm., extraterrestrial source hypothesis 80−46354
gamma rays in 10^{11}-10^{14} eV range using atmospheric Cherenkov technique 79−25422
gamma-ray angle and energy distrib., sea level to 39 km altitude 2.25 meV 80−26705
gamma-ray bundles, high transverse momentum estimated from RE distribs. 79−40046
gamma-ray bursts, balloon obs., effect of multiple Compton scatt. in atmosphere 78−28352
gamma-ray lines observed in balloon flights at high rigidity, extraterrestrial line flux upper limit 80−21882
gamma-ray meas. with Aryabhata satellite 77−22023
gamma-ray prod. spectra for high energy reactions in graphite 79−29959
gamma-ray spectra, high energy, near top of atmos. detection+meas. by emulsion chamber 79−29958
gamma-rays, 0.511 MeV energy, meas. with balloon-borne Ge(Li) spectrometer 77−53373
gamma-rays, hard intensity radiation pulsations in the atmosphere *(Russian)* 80−17454
gamma-rays, quasi-periodic intensity variations in stratosphere *(Russian)* 80−90177
geomagnetic and solar disturbance effects on cosmic rays and neutrons 77−13195
geomagnetic effects on incident cosmic radiation 78−53615
geomagnetic field effects, development of cosmic ray studies 77−17308
geomagnetic field effects on cosmic monopoles *(Chinese)* 80−46358
geomagnetic field interaction, influence of partially magnetospheric current systems on cosmic ray flux *(German)* 80−51609
geomagnetic secular variation correl. with cosmic ray threshold rigidity 77−53368
geomagnetic shielding of artificial satellite, cutoff probability for nuclei 80−12626
ground level enhancements, comparison of 1977 Nov. 22 and 1969 Feb. 25 events 79−40042
ground level enhancements during 21st solar cycle 79−12361
ground level event of 1977 November 22, solar flare increase of cosmic ray intensity 79−48629
hadron spectrum, ground level, 30 to 1000 GeV 79−75064
hadronic interactions, 10^{12} to 10^{15}eV, and cosmic ray components in atmosphere 79−62708
hard X-rays, cosmic ray and electron-induced background, HXX results from ANS in Earth orbit 78−81716
heavy nuclei penetration into atmos., calc. 80−85826
high energy interactions and cosmic ray components in the atmosphere 79−62707

geophysical aspects of cosmic rays continued
high-energy cosmic-ray components in atmosphere, scaling features 78−93062
high-energy event analysis at Yunnan Cosmic Ray Station *(Chinese)* 79−96872
historical high-altitude meas. on balloons 79−80141
inclined muon monitors, muon spectra, generating functions, rel. to diurnal variation at Kiruna 78−85783
induced neutron background sources 78−40781
intensity fluctuations, sudden increases and sharp decreases 77−70955
intensity var. from tree ring stable isotope conc. 78−61692
intensity variations of interplanetary, magnetospheric and atmospheric origins, Sayan spectrograph data 79−84606
intenstiy variations in midlatit. stratosphere, total solar mag. field effect 79−62696
interplanetary magnetic field related variations, rel. to lower ionosphere and lower atmosphere 80−8510
ionisation events in stratosphere, effects on NO_2, O_3 and climate, rel. to life extinction 78−96273
large air showers, Cherenkov radiation image reconstruction 79−25420
latitude course of nucleon component, meas. with mobile system 77−53372
latitude dependent cutoff use in ancient planetary magnetic field investig. 77−45269
latitude distribution var. with time of cosmic rays in atm. 79−84601
LF radio waves, signal vars. with cosmic rays and sunspot cycle 77−78560
magnetosphere, asymm. periodic oscills. in Stormer problem 77−78586
magnetosphere, particles distrib. above 400 km altitude beneath radiation belts 78−49227
magnetosphere, relativistic electrons interaction with Alfven waves *(Russian)* 78−49229
magnetosphere and interplanetary space, fast electron intensity 77−33282
magnetosphere cosmic noise absorption during substorms 80−72727
meteorological and geomagnetic vars., separation via spectrographic instrument set 79−12404
meteorological conditions determ. from cosmic ray obs., spectrographic method 78−69627
middle atmosphere chemical comp., importance of energetic particle precip. 80−109213
multiple scatt. by Pb nuclei at sea level, anomalous scatt. distrib. 78−7851
multiple scatt. by Pb nuclei at sea level, Rainwater-Cooper theory, 230 MeV/c muons 78−7850
muon charge ratio, sea level, phenomenological model 80−67487
muon intensity in atmos., solar activity affecting height depend. of intensity 80−41675
muon lateral distribution at different altitudes in atmosphere 80−26708
muon spectra at different altitudes, Bose-type model calcs. 79−44326
muon spectra at sea-level, solar modulation at geomag. equator 79−16775
muons, meteorological coeffs. computation for scintillation supertelescope 77−13202
muons, parent nucleons, energy distrib., at sea level and underground, phenomenological model 80−61974
muons, radiative energy losses in ground 79−84619
muons, scaling and charge ratio 79−12371
muons, sea-level spectrum, Dao scaling model for pp$\rightarrow\pi^-$X 78−61694
muons, vertical integrated momentum spectra, 3220 m above sea level *(Chinese)* 79−12372
muons and neutrinos detect. in deep sea using manned submersibles 78−81510
muons integral intensity meas. at low latit. station 79−53690
Musala expt. rel. to cosmic ray vector and tensor anisotropy 77−17302
near-Earth supernova, cosmic ray effects on Cretaceous-Tertiary environment 78−32499
neutron albedo flux meas. with Aryabhata satellite 77−22023
neutron component vars. during September 1977, Mirny and Moscow obs. 80−105137
neutron integral generation factors rel. to atmospheric depth 77−53380
neutron intensity variations, hysteresis, fluctuations and barometric and ionospheric effects 79−84604
neutron monitor diurnal anisotropy, effects of fluctuations and noise 77−45264
neutron monitor total vector anisotropy 79−53685
neutron sea level spectra meas. with anthracene scintillator 77−5405
neutron transport in upper atmosphere, Monte Carlo calcs. 80−8468
neutron/proton ratio and neutron spectrum, calc. from primary nucleon spectrum 80−8499
neutrons at aircraft altitudes, Ames collaborative study on mid-latitude flights 78−53538
nonstationary modulation theory, self-similar solns., rel. to vars. obs. on Aragats Mountain 79−80143
north-south anisotropy of intensity pulses 80−56687
north-south asymmetry, interplanetary mag. field sector polarity determ. 79−30009
nucleon cascade in atmosphere 79−12363
nucleon spectrum meas. at GSFC, vertical sea-level meson-neutrino spectrum determ. 78−85782
nucleonic component of cosmic rays, diurnal variation coeff. 79−75060
nucleons, altitude variation, Feynman scaling hypothesis calcs. 80−77245
particle flux variation, correlation with atmospheric variables 77−22030
particle trajectory, in geomagnetic field 77−68155
penetrating-particle beams, locally generated, at air equivalent depth 200 m 79−84603
pion spectrum, at top of atmosphere 78−53780
polar cap absorption intensity and solar cosmic rays north-south asymm., riometer data 78−69629
polar cap riometer absorpt. and solar protons, night and day relationships 78−28413
polar coupling coeffs. for multiple neutrons up to 15 GeV 77−70954
primary heavy nuclei diffusion in atmosphere, spectra and comp. 80−41680
primary nucleon spectra from atmospheric γ-ray and muon data 79−44320
proton flares, fast particles flight time from polar cap absorpt. effects 77−17469
proton flux increases, rel. to solar flares and storm sudden commencements 77−9637

geophysical aspects of cosmic rays continued
proton streams after interplanetary magnetic sector boundary, effect on troposphere 79—53491
protons, as extraterrestrial source of atmospheric water vapour, Sun-weather relationships appls. 78—69416
protons, low-energy events, assoc. with mag. sector boundaries 77—45265
protons, pitch angle distrib. in high-latitude magnetotail during 1970 April 16 solar proton event 79—53670
protons in plasma sheet boundary during substorm expansion phase 79—35062
radiation belt around Earth, electron energies above 100 MeV, produced by primary cosmic rays 78—36409
radioactive particle production in atmosphere, external environmental radiation levels 78—9001
radiofrequency noise 'absorbed' by E-region plasma waves 80—82139
radiowave absorption ionosphere, impulsive quasi-periodic variations 80—105116
recurrent Forbush decreases and solar active regions rel. to M-regions 78—96367
recurrent particle streams at 1 AU 79—96867
sea level ionisation meas. in 900 l chamber 79—35081
sea level muon spectrum, Bugaev model 77—82094
sea level muon spectrum, Cocconi-Koester-Perkins model calcs., using nucleon spectrum 77—49258
sea level muon spectrum and primary nucleon spectrum, Cocconi-Koester-Perkins model 79—84612
sea-level flux determination for heavy cosmic-ray particles 79—29956
sea-level muon spectra, Cocconi-Koester-Perkins model 79—48634
sea-level muon spectra, model using kaon-pion ratio 78—93064
seawater and atm. surface layer gamma radiation field rel. to cosmic ray neutrons *(Russian)* 79—39746
secondary electron fluxes at equator, Kosmos-428 data 78—45168
secondary gamma-rays, energy spectra rel. to atmos. depth 79—58205
secondary protons, fluxes above 500 MeV at 200-300 km altitudes 77—64497
semidiurnal anisotropy, latitude dependence 79—48631
short period variations, 2-60 cycles/hr., possible meteorological variations 77—53371
short-term cosmic ray fluctuations, time anal. 80—67483
snow gauge, cosmic ray, construction, characts., snow-water equivalent meas. *(Japanese)* 78—69498
solar activity, cosmic-ray variations, and neutrino fluxes, review 79—84599
solar cosmic rays production rate, influence on terrestrial life 79—92735
solar cosmic-ray fluxes in high-latit. magnetosphere, isotropic diffusion model calc. 77—64531
solar electron streams, excitation of ionospheric radio noise 79—62646
solar flare particles, possible cause of ancient climatic and biological catastrophes 77—78587
solar flare protons, rel. to August 1972 polar cap absorpt. event, auroral diagnostics 77—29567
solar flares near-Earth radiation hazard, dosage estimation technique 80—67482
solar particles, spectrum formation near Earth, propagation and acceleration *(Russian)* 80—4211
solar proton albedo neutron flux north-south asymm. meas. 79—75061
solar proton event, 1972 August 4, influence on stratospheric O_3 78—7732
solar protons in magnetosphere (1971 September 1-16) 79—2446
solar protons in polar regions of magnetosphere (August 1970) 78—16256
south-north asymmetry in high latit. magnetosphere, 1969-77 period 79—84600
splash and re-entrant albedo electrons, energy spectra 78—69630
stratosphere, cosmic ray and pressure oscills., balloon obs. *(Japanese)* 80—31182
stratosphere, primary-electron spectrum above 3 GeV meas. 77—53374
stratosphere cosmic rays, eleven-year cycle 80—4212
stratosphere obs., evidence for interplanetary modulation processes 80—101508
stratospheric cosmic rays height-intensity distrib., meson decay effect 79—12364
stratospheric superfamily with $\Sigma E_{\gamma} \sim 2.10^{15}$ eV 79—2451
supernova, nearby, cosmic radiation, effects on terrestrial atmosphere 80—94584
temperature variations, spectrographic obs. of secondary cosmic rays 78—69628
time correlation of muon pairs and multiple hadron production 79—80178
tridiurnal intensity variations, theory 77—33305
turbulent diffusion, partially averaged field approach 78—53776
two year variations in Earth atm., sonde obs. 80—101511
ultraheavy nuclei, errors due to geometically forbidden light nuclei identification as re-entrant albedo particles 77—37489
underground muons, response functions for different depths 80—82160
underground obs. of fluctuations, nonlinearities effect on power spectrum 80—41679
underground observations, difference coupling coeffs. and difference meteorological coeffs. 78—28464
underground observations, spectrographic method, medium to high energy range 78—32307
$p/\bar{p}$ flux ratio at top of atmosphere 78—40783
$\pi^{\pm}$ charge ratio in atmosphere 78—28463
^{7}Be production in atm. and transport from Sun, tracer for terrestrial-solar relationship 80—98525
^{7}Be production in troposphere, mean residence time calc. 78—85633
^{10}Be deposition rates at Earth surface, seasonal vars. 80—26707
^{10}Be in marine sediments rel. to geophysical events and cosmic ray var. 79—29748
^{14}C form. in atm., diffusion distrib. 80—101510
^{14}C in atmosphere content variation, past geomagnetic and cosmic ray intensity variations 78—61691
^{14}C in tree rings, climatic vars. record rel. to solar variability 80—101424
^{14}C, production rel. to cosmic rays and solar activity cyclic vars. 79—16776
^{41}Ca production in Earth surface layers, possible use for radioactive dating 79—21063
O_3 levels in stratosphere, solar activity, cosmic rays effects 77—53362

geophysical equipment
see also atmospheric measuring apparatus; geophysical prospecting; geophysical techniques; meteorological instruments; oceanographic equipment; seismometers
absolute vector magnetometer 79—16703
AC demagnetisation apparatus, palaeomagnetic research appl. 78—85733
additive colour viewer, for inexpensive remote sensing 79—29897
aerial lenses, for multispectral photographs from high altitudes 79—35868
aerial multispectral-photographic lenses, Pinatar 4/125, manufacture *(German)* 78—4717
aerial photographic equipment developments, aerial survey camera and navigation telescope 77—66997
aerogravimetric apparatus, for gravity meas. from aeroplane *(Russian)* 78—40704
air gun array, high resolution or deep penetration survey, characts. 80—12557
airborne IR line-scan, tangent sweep time base for recording of data, cct. 77—9525
airborne IR scanners, temp. calibration 80—41572
airborne lidar system for geophysical and atmospheric expts. *(Italian)* 80—109277
airborne microwave radiometer, stepped-frequency, 4.5 to 7.2 GHz, remote sensing appl. 79—80062
airborne multicoil EM survey system for resistivity mapping 78—77348
airborne phoswich detector system for U exploration 79—53576
airguns, linear arrays, signature and amplitude 78—69297
analytical plotters, photogrammetric appl., development progress and advantages 78—40710
analytical plotters, photogrammetric appl., future prospects 78—40708
analytical plotters, props. and software aspects, photogrammetric appl. 78—40709
analytical stereoplotter, OMI AP/C4, photogrammetric appl., features 78—40715
analytical stereoplotter, TRASTER 77, photogrammetric appl., features 78—40712
analytical stereoplotting system, C-100 PLANICOMP, features 78—40711
Ancona plano-altimetric network, strain meas. 77—86742
ARAKS experiment, picture tube with curved microchannel plates, appl. *(French)* 78—40671
array antennas radiometric earth and atmospheric sensing systems for large structures 77—41281
aspect sensor, for small space vehicles 77—45279
automatic AF demagnetiser for igneous rock specimens 79—25347
automatic digital magnetic recording system in Tihany Observatory 79—39989
automatic drafting system, appl. to problems of geodesy *(German)* 78—15952
automatic spinner magnetometer for rock specimens 80—101455
automtic optical plumbline requirements and design *(German)* 77—70877
balloon data storage, prior to transmission to ground via satellite 80—46263
bedload transport oscillations, circuit for acoustic detect. 77—45168
bore-hole strainmeter, Earth strain meas. at Matsushiro Observatory and seismic waves response *(Japanese)* 79—96745
borehole equipment for temp. and heat flow meas. in Ukraine *(Russian)* 77—91294
borehole extensometers, suggested methods for monitoring rock movements 79—84512
borehole flow, instrument for simultaneous meas. of axial and radial components 79—80051
borehole probe with LED for γ-ray spectrum stabilisation 79—45552
bubble tiltmeter use as horizontal seismometer, comment 80—21839
C-CD digital image store for Earth resource surveying 79—34964
C-CD space-borne Earth imager, high resolution, features 79—35097
Cactus accelerometer on Castor satellite, flight results synthesis for accels. below 10^{-9}g 80—77251
camera, remote sensing, film and solid-state-array types comparison w.r.t. imagery 78—4723
Camkometer, in situ soil testing pressuremeter 79—8717
Canadian magnetic observatories, annual report for 1973 77—45183
Canadian Magnetic Observatory Network, annual report (1977) *(French, English)* 80—72418
carbonate mineral identification by CO_2 evolution on heating 80—90248
cavity pyrheliometers, appl. to solar const. accurate determs. 79—2341
colour plotter system, application to computer graphics 80—4130
colour plotter system for computer graphics output, appls. in geoscience 80—98467
coordimeter, two-dimens. for displacement meas. in rock masses 79—35016
core drilling equipment for permafrost regions *(French)* 80—77140
crustal tilt meter, long water tube instrument for earth tide meas. 79—100959
cursor, aided-track, for improving digitising accuracy 79—29899
cylindrical jack for surface rock stress meas. 77—9575
data logger, portable, for ground surveys 80—26615
decrepitometric recorder with electronic filter *(French)* 79—48571
deep EM sounding of Earths crust, pulsed MHD generator 79—48589
deep ocean seamount detection using reconnaissance sonar 78—69551
depth measuring apparatus for borehole logging 79—5643
DGU-2 curve plotter, appl. to geophysical data real-time processing 80—36422
differential capacitance displacement transducer with low power lock-in amplifier 77—49710
differential rectifiers, digitally controlled, for photogrammetry *(German)* 77—60495
digital bandpass filters, filter type and operator parameters selection for instrumental realisation *(Russian)* 79—74984
digital recording field system for geomagnetic telluric-array studies 79—62605
digital voltmeter, for soil bulk resistivity meas. 78—24381
discharge transient recorder for induced polarisation meas. 78—65398
distance measurement device, electro-optical, appl. to water levels obs. *(German)* 78—69280
divided-bar apparatus for thermal conductivity measurements on saturated rocks at permafrost temperatures 79—84232
Doppler receiver, dual freq., for NAVSTAR Global Positioning System satellites, accuracy 79—100803

geophysical equipment continued
drawing instruments, electronically controlled, appl. to Digital Terrain Model *(German)* 78−20348
dynamic hydrothermal experimental system, for seawater-basalt reactions study 79−5686
Earth Observation satellite programmes 77−29631
Earth resources survey sensor, calibration linear photodiode array in push-broom scan mode, satellite appl. 80−56693
Earth strain meas. with laser interferometer *(Japanese)* 77−81783
Earth tide recorder photoelec. compensation method to acquire data 80−77129
electric soil moisture gauges, testing procedure 77−78481
electrode arrays comparison for induced polarization and apparent resistivity responses 79−58107
electrode arrays for Earth induced polarisation (IP) sounding, effects of EM coupling over uniform half-space 80−101324
electron system for image transformation and coding in conventional colours 80−4117
electronic alpha cups for U exploration 78−7781
electronic tachymetry, ten years of Zeiss equipment *(German)* 79−34999
electrooptical distance meas. instruments, Zeiss ELDI 2 type, error anal. *(German)* 79−21081
electrostatic accelerator, appl. to ^{36}Cl anal. in environmental water samples 79−20895
ELWAAG automatic hydrostatic system for geodetic height meas. *(German)* 79−88511
EM depth sounding systems, detectability analysis 77−91295
EM field, conf., Hurbanovo, Czechoslovakia (Oct. 75) 79−39646
EM sounding system, multifrequency, topographic and misorientation effects study 80−101451
emission spectrographic analysis system, minicomputer based, using scanning microphotometry 80−22436
N.W.Europe gravity base network, for gravity and altitude vars. meas. *(German)* 78−15948
extended-range three-wavelength distance measuring instrument design 79−80053
extensometer, magnetic cantilever, design and development 79−84511
feature identification and location experiment FILE, sensors 80−56657
field averaging spectrograph camera for remote sensing 77−45161
flexure torsion apparatus, for internal friction Q-factors meas. in brittle materials 77−27499
flowmeter, flumes and weir, construction error compensation, computer anal. 78−30387
flowmeter, open channel acoustic flowmeter, error sources and calibration 78−30389
flowmeters, Price and Pygmy current meter traverses, error sources 78−30385
flowmeters, V-notch weir, approach channel and sedimentation effects 78−30386
fluid tube tiltmeters, thermally induced errors 78−36303
fluxgate magnetometry, review 79−35800
Fourier transform IR spectrometer, for satellite, optical design problems *(German)* 78−86360
gamma-ray detectors, airborne, fields of view 80−51555
gamma-ray spectrometric logging and surface exploration equipment calibration 78−85706
geodesy, measurement and instrumentation techniques *(German)* 77−33219
geodetic instruments, periodic errors determ. via spectral anal. *(German)* 77−87131
geodetic level testing, vertical and horizontal settings 77−29489
geodetic levels with compensators, systematic errors, new instrumental development *(German)* 77−2289
geomagnetic monitoring system for International Magnetospheric Study 79−29882
geophones, electromechanical feedback for low freq. equipment *(Russian)* 79−62618
GEOS, Europe's first geosynchronous scientific satellite 77−37495
GEOS, IUF, and METEOSAT ground stations, weather obs., Earth exploration *(German)* 77−56763
Geos 3 tracking systems, intercomparison 80−4227
GEOS characts. *(German)* 77−82105
geothermal field station GS-1 with thermoquartz resonators, description *(Russian)* 78−93000
geothermal logging instrumentation, borehole measurements, developments 80−61909
geothermal well logging instrumentation, hybrid microcircuit design, performance 79−96845
geothermal well logging using 300°C hybrid IC 77−73895
geothermal well-logging, high temp. instrum., passive components fabrication 80−40266
glacier sounder, appl. to gravity surveys in glacier-covered regions 79−16697
Goddard laser systems and their accuracies 77−64482
gradient magnetometers, appl. to induced elec. currents meas. in Alaska oil pipeline 80−98231
graduated circles, horizontal and vertical, determ. of micrometer errors and short period errors *(German)* 78−45038
graphics computing system linked with signal enhancement seismograph, description and application 80−4131
gravimeter, LaCoste and Romberg, vibr. characts. *(Japanese)* 78−65400
gravimeter of Gs-11/12 type adapted to seismometer operation *(German)* 80−31127
gravimeters, sensitivity determ. rel. to gravity tidal changes at Poltava *(Russian)* 78−88782
gravimeters in artificial Earth satellites, basic mechanical principles *(German)* 80−101461
gravimetric networks, adjustment *(German)* 79−44084
gravity corer for sampling lake sediment-water interface 79−88512
gravity gradiometer, moving-base, surveys and interpretation 78−77344
gravity gradiometers in artificial Earth satellites, basic mechanical principles *(German)* 80−101461
gravity meters, quartz, terrestrial, microseisms influence on reading, mechanism *(Russian)* 79−39967
gravity networks, optimisation *(German)* 78−15950
ground receiving system, Earth survey data, facsimile features 77−82012
groundwater sampling procedure 77−41215
gyrostabiliser, single-axis with pneumatic stabilising circuit, description and appl. *(Russian)* 77−26283

geophysical equipment continued
halfsecond levels, investigations using atuomatic comparator *(Russian)* 78−40675
HF EM induction profiling instruments, for boreholes in underground mines *(Polish)* 80−51547
high temperature electronics for geothermal energy 80−11997
high temperature MOSFET characteristics for geothermal instrumentation, up to 300°C 78−73553
high-pressure apparatus for investigation of rocks and minerals physical props. *(Russian)* 77−70850
high-pressure apparatus for rocks elasticity and density simultaneous meas. *(Russian)* 77−70851
high-temperature creep and relaxation meas. device, appl. to mantle peridotite meas. 80−17256
horizontal pendulum tiltmeters, recording device 78−40679
hot water drill, open circuit, for hole drilling in cold glaciers 78−65402
HS plexiglass flumes, for open channel flows meas. 77−62321
from Hungary, prospecting appl. 78−7787
hybrid ICs, geothermal well logging instrumentation appls. for 300°C operation 78−3976
hydraulic conductivity meas. apparatus for frozen soils 77−45035
hydraulic electronic instrumentation, rain models, sediment transport *(Italian)* 77−91334
hydrology instrumentation, review *(French)* 79−39979
hydrostatic levelling, automatic precision instrument for geodesy *(German)* 77−29514
IAS triangulation camera *(French)* 77−33192
imaging photon detectors 80−86405
induction logging probes for rock forms. elec. parameters determ., number and type choice *(Russian)* 79−39969
induction-logging tools, sonde eccentricity effect on response 79−12300
inertial rotation sensors for surveying and geophysical meas. 80−12571
interpretation system for resistivity soundings over horizontal strata 78−45014
IR Fourier spectrometer for space appl., thermal behaviour *(German)* 79−35091
i.r. imaging, airborne system resolution, object contrast depend. 77−2285
IR line scanner, Reconofax XIII A, improved recording system using LED 79−25335
IR radiation detector, for minerals post-shock temps. meas. 79−92527
IR sensor systems, interfering space radiation background 77−22011
IR system performance in airborne environment 78−82039
JMA seismic network, epicentre detect. capability simulation for local earthquakes *(Japanese)* 79−96844
Kodak LR 115 dielec. track detect., applicability as α-particle detector *(Czech)* 79−8711
LaCoste and Romberg inertial navigation system for gravity meters 77−82022
LANDSAT satellites 77−56812
Landset filters for rock type discrimination assessment using laboratory spectra information 79−16791
laser extensometer, comparative anal. with rod extensometers 77−64452
laser gyroscope, passive ring resonator, for inertial rot. meas. 77−58352
laser interferometer, 500-m base, Earth surface deform. detect. 80−105087
laser interferometer with path difference up to 1 km, geophysical appl. 78−61616
laser microprobe system for spectrochemical anal. *(Italian)* 77−25323
laser remote sensing system, heterodyne reception airborne CW CO_2 lasers 78−40676
Laterolog 7 resistivity logging, field tests 78−61574
Laterolog borehole resist. logging device, function and applications 80−85755
lava temp. meas. techniques and apparatus on Etna 77−25800
lensless scanning telescope, MTF 80−58655
line scanning sensor, spatial filtering design 79−53527
linear multichannel systems employed in regular waves separation, efficiency comparative anal. *(Russian)* 79−39922
lysimeter, plastic, suction, for sampling percolating soil water 77−29498
magnetic sensor, high permeability metal core solenoid absolute sensitivity calibration 80−31133
magnetometer, appl. of Nb SQUID 77−22583
magnetometer, quantum, using alkali metal-He 80−17965
magnetometer, RF SQUID, construction, geomag. microfluctuation meas. appl. *(Japanese)* 79−5641
magnetometer, ring-core type, high sensitivity, for balloons, high-altitude mag meas. *(Japanese)* 80−94608
magnetometer, undersea, for meas. transient mag. field horizontal components *(French)* 78−40670
magnetometer (quartz H type), calc. formula for horiz. component 80−105062
magnetometer array, two-dimensional, for ground-based obs. of auroral zone elec. currents. 80−90245
magnetometer detector types, study and comparison *(Spanish)* 78−4008
magnetometers, absolute variometers in marine sounding 79−62600
magnetometers, induction-coil, optimisation theory at audio and higher freqs. 79−85156
magnetometers, RF-driven SQUID, rock magnetism and palaeomag. appls. 77−45201
magnetostatic variometers, selection of separation distance 77−13129
magnetostriction appls. in geodesy and instrumental geophysics *(French)* 78−12004
magnetotelluric signals digitization equipment *(French)* 77−87092
marine deep seismic sounding system 77−87083
marine spring gravimeter, GMN automatic equipment *(Russian)* 77−45197
mass spectrometer, solid-source, appl. to Rb-Sr dating of rocks 77−70840
measuring equipment, metrological provisions, oil, natural gas reserves appl. 78−93002
microcapacitive transducer for geophysical appls. *(Rumanian)* 79−58121
microprocessor-based system for surveying data acquisition and processing 79−29913
microscope photometer/semiautomatic image anal. instrument system for morphometric and photometric value meas. 80−82815
mini-SOSIE, for land seismology 77−21917
Mini-Sosie high resolution seismic reflection system, operational principles 78−85707
miniature radio interferometer terminals, for Earth surveying 79−100805

geophysical equipment continued
minicomputer based system for marine seismic data acquisition 77—82072
Mossbauer gravimeter 77—37444
MPP-1 stationary precision proton magnetometer, errors and calibration 79—53535
Multi-detector Electro-optical Imaging Scanner for aircraft remote sensing 80—82085
multi-frequency EM system, numerical modelling 80—56623
multi-wavelength distance measuring instrument 77—29484
multichannel radiometer, programmable, for Earth remote sensing 80—77253
multichannel spectrometer, for remote sensing multispectral information volume optimisation 80—4118
multichannel telemetry system, design, seismic data processing *(Chinese)* 79—21033
multicoil II airborne EM system 80—51554
multifrequency airborne EM system, for Earth conductivities mapping 79—5446
multispectral camera, use on Soyuz 22 spacecraft 78—40794
multispectral linear arrays, alternative to LANDSAT D thematic mapper 80—4153
multispectral projector, colour synthesis instrument for evaluating multispectral photographs 78—40688
multispectral scanner, for remote sensing, parametric model 80—77261
multispectral scanner, high resolution, for Earth obs., optical design 80—82174
multispectral scanner system, empirical study of parameters 77—56743
multispectral sensor for satellite, analytical design 80—77262
navigational sextant, hand-held SPT-2, construction features 79—32027
NAVSTAR, satellite Global Positioning System 79—101042
neutron moisture gauge for permafast regions *(Chinese)* 79—34997
Nimbus-6 instrument for Earth radiation budget expt. 77—41106
nonimaging airborne geophysical and miscellaneous systems 77—56777
nuclear and acoustic logger for cased well and open hole studies 77—87098
nuclear borehole logging system 79—25353
oil, exploration and exploitation instrumentation 79—34982
optical filters for image processing, apodisation for distortion reduction *(Russian)* 77—9564
optical reimaging system, out-of-field radiation analysis 78—59117
optical sensor array systems for astronomic longitude determ. 77—82023
optical systems, high-precision compensated levels, geodetic appl. 80—101813
optical universal stage, appl. to Saxony Granulites petrofabric anal. 80—21740
optical-mechanical scanners for Earth observation *(Russian)* 78—96321
optimum multichannel filters used in seismic surveys theory *(Russian)* 79—39921
opto-electronic device for aerial colour photograph interpretation *(Russian)* 80—61920
optoelectronic analyzer for seismic data processing *(Russian)* 77—29516
oscillograph for ground porosity depth meas. using reversible counter with digital indication *(Russian)* 77—41209
PAG-5 air and marine proton magnetometer *(Russian)* 77—60489
Penning source, continuous discharge, with 50 Å to 300 Å emission lines 79—50363
petroluem industry, implementation guidelines for promotion of electronics in oil and gas sector 79—80039
phoswich battery operated portable detector for field monitoring of transuranic contaminants 79—683
photoelectric inclinometer, sensitivity stabilization by negative feedback *(Russian)* 78—4012
photoelectric inclinometers with photoresistors in transducers *(Russian)* 78—4013
photogrammetric camera, distortion calibration using star images 79—35881
photomapping, Gestalt computer-controlled system features 78—40714
photometric analyser for crystallographic orientations in rock thin sections, microprocessor controlled 80—41560
piezoelectric sensor element for press. meas. in soil pores *(Polish)* 79—25363
pinch-off device, for noble-metal tubes cold-weld sealing 80—41556
Ploskii Tolbachik volcano, night observations *(Russian)* 79—84205
polished metal sphere and microaccelerometer, for absolute meas. of Earth's radiation balance *(French)* 79—29900
pore pressure transducer, appl. to Kayenta sandstone mechanical props. meas. 78—81150
porous cup samplers for soil water, nearby water regimes 77—66942
portable T-MP field proton magnetometer for high accuracy geomag. field meas. 77—29467
position indicator with freq. data transmission for distance meas. *(Russian)* 77—65019
precision comparator, Zeiss PK-1, accuracy, appls. *(German)* 79—97359
probes with semiconductor temp. sensors for sediments thermal cond. meas. *(Russian)* 78—65431
profilograph, for rock joints roughness determ. 78—96315
proton magnetometer, synchronous polarisation method advantages *(Russian)* 77—60482
proton magnetometers, toroidal sensor directivity characts. *(Russian)* 77—60483
proton microprobe, X-ray and γ-ray, appls. 79—48010
radar systems, space based, development, appl. 78—81525
radioactivity detector immersed in extensive liquid, sensitivity determ. *(Rumanian)* 77—26950
radiometer, polarisation effects meas. using partially polarized light 79—49266
radiometer for Earth radiation meas., fused silica filter performance 80—87473
radiometric field instruments, experiences with concrete calibration sources 79—5633
rain gauge, quick response, water drop counting type 79—5647
rainfall simulator, portable, for soil erosion studies in difficult terrain 78—20537
reaction cell, for hydrothermal soln. equipment 80—41555
receiving optical antenna, sensitivity to scatt. aerosol particle, laser location of atm. aerosols 77—70847
recording device for ground freezing vel. meas. *(Japanese)* 77—82033
recording system for mag. pulsation obs., first results from Alibag 79—88488

geophysical equipment continued
remote sensing, sensors and detectors in NASA's future mission 79—5656
remote sensing, sensors and sensing vehicles review 77—2286
remote sensing from space, microwave, synthetic-aperture radar systems and Spacelab expts. 80—36409
resistivity surveying, apparatus, interpretation, undergrad. fieldwork 78—49623
rock deformation system, anal. of microacoustic signals assoc. with rock fracture 78—32070
rock elastic wave absorption meas. and recording instrument *(Russian)* 79—29891
rock fracture measurement in laboratory, under geological conditions 80—46171
rock mechanics testing, lateral deform. gauge 79—57163
rock melting drills, thermal analysis 77—17258
rock structure monitoring instrumentation 78—7790
rocks hardness and abrasiveness meas. apparatus, suggested methods of use 78—96313
rod mill, for wet grinding of igneous rock at temps. up to 400°C 80—37012
sampler for ephemeral wadi floods 80—98493
satellite IR radiometer, calibration 80—101440
satellite laser ranging system 79—39994
satellite telemetering system, NOAA 80—56592
sediment magnetisation studies, high-press. cell for chem. demagnetisation 80—31126
seismic broadband recording and data processing system 77—49173
seismic field recorder, dedication of micro-computer to signal selection 77—82073
seismic observation network *(Japanese)* 78—28341
seismic receivers, cable and amplifier system, freq. characts. *(Russian)* 79—84529
seismic recording channel, input cct. parameters matching *(Russian)* 79—39920
seismic signal detect. system *(Russian)* 77—29515
seismic vibrator (electromagnetic), characts. for self-excited regime 80—90262
seismic vibrator signals, non-sinusoidal, theory 80—82086
seismic wide-band recorders specification 79—39908
seismoacoustic station ASS-1, construction, operation principles *(Polish)* 78—24377
seismological investigation, possibilities in development of equipment 77—53228
seismological observatories and seismic instrument construction in Poland *(Polish)* 77—21911
seston (particulate matter) traps for lakes and relocation system 79—74964
shear wave generator in borehole, construction, expt. results 78—40692
shear wave transducer for use in marine sediment studies 78—63257
signal amplitude digital auotmatic control system, instrumental realisation algorithm *(Russian)* 79—39924
'smart sensors', role in remote sensing of Earth from space, book 80—62402
Smithsonian Astrophysical Observatory laser tracking systems 77—64481
snow gauge, cosmic ray, construction, characts., snow-water equivalent meas. *(Japanese)* 78—69498
snow melt calorimeter *(Japanese)* 78—88934
soil, neutron moisture meter calibration, neutron absorpt. cross section meas. 77—9545
soil freq. shift dielectric 78—53739
soil moisture meter, development *(Japanese)* 78—88935
soil resistance meter, geological and archaeological applications *(German)* 78—57361
soil temperature measuring system and data for Whiteshell Nuclear Resea-ch Establishment 79—48590
solar-radiation meter, automatic 80—89592
sonar, fibre optic system, geological and hydrographic survey applications 78—88947
sonobuoys, data comparison with ocean bottom seismograph rel. to Texas shelf zone crustal struct. 79—5462
Space Borne Event Timer, NASA laser ranging system, meas. of Earth movement along San Andreas Fault 80—61984
spaceborne laser ranging system, SPEAR, for measuring intersite distances on Earth 78—3978
specific resistivity meter with logarithmic output for rock samples 79—35781
Spectral Infrared Experiment equipment and objectives 78—81456
spectroradiometer, lone wavelength Exotech model 20C, Earth reso[illegible] remote sensing appl. 79—88474
spectroradiometer for airborne remote sensing 78—88943
spectroradiometer for reflectance measurements 80—56658
spindle stage, turning point for optical crystallography 78—[illegible]02
SQUID, for magnetic field and spatial gradient meas., des[illegible] and advantages 77—26369
SQUID arrays, for mag. field meas., geophysical, biom[illegible]ical appls. 78—32830
SQUID magnetometers, dewar systems design 80—101462
step-stare spaceborne optical system image motion compensation 80—90322
stereo side-looking radar, accuracy anal. 80—56646
STEREOMETROGRAPH model G with [illegible] motor drive 77—66996
strain meter, He-Ne laser, I_2-stabilised, with long path interferometer, optical feedback effect 77—9544
stress gauge, meas. in N.China *(Chinese)* 79—88312
strong motion accelerographs, characts. of EM starters 78—65396
submarine devices, habitable, use in marine geology *(Russian)* 79—88502
superconducting magnetic gradiometer, LF noise spectra 77—33203
superconducting magnets, appl. to minerals mag. separation *(Czech)* 78—88923
superconductive gradiometers, for measuring magnetic effects of geophysical origin 80—101463
superconductive magnetic gradiometer for meas. of mag. gradients from ocean waves 79—29867
surveying instruments, JENA Autocollimation Outfit 77—82030
Switzerland geomagnetic survey instrumentation and results *(French)* 78—15966
Talyvel electronic level, temp. effects *(German)* 78—45037
temperature and pressure transducers with ground-level tape recorder, hydrodynamic logging in boreholes *(Russian)* 78—53761

geophysical equipment continued
temperature gradients continuous logging system 77–82052
temperature indicators for geothermal well logging 80–56659
temperature wave generator for diurnal temp. wave propag. simulation 78–85735
terrain profiler, pulsed GaAs laser system 77–91297
terrain profiler, pulsed GaAs laser system 78–49145
texture goniometer for analysis of rocks 80–26630
thematic mapper, time-delay and integration CCD imager appl. 79–35098
Thematic Mapper of Landsat-D, optical component design 80–77260
Theo 002 Universal Theodolite for geodetic astronomy 77–82028
THEO 020 A universal theodolite for surveying 77–82029
theodolite, reduction of influence of vertical axis error on horizontal angle meas. *(German)* 79–44278
theodolite, THEO 080 A, with attachable circular compass 80–56634
theodolite, type 2T, highly unified instrum. 80–13120
theodolite standardised series, specification 78–73543
theodolites, electrooptical and microprocessor-based *(Czech)* 78–77860
thermal conductivity apparatus for sedimentary rocks, using needle probe and microcomputer control 79–100970
thermal conductivity measurement of soil by probe method, minimisation of errors 77–17259
thermistor probes for groundwater filtration rate meas. *(Polish)* 77–70872
thermograph for soil temp. meas. 78–4005
thermomagnetometers, for rocks remanent mag. meas. 78–85719
tide-recording equipment, phototransducers emission source light output ratio stabilisation *(Russian)* 78–88949
tilt gauge, based on Hg pool 78–88931
tilt meter at Berezovaya Rudka station, obs. and sensitivity vars. *(Russian)* 78–88783
tilt meters, photoelectric, with negative feedback, block diagrams anal. *(Russian)* 78–88948
tiltmeter, two-fluid, for precision levelling 77–21919
tiltmeter for long-baseline operation 78–81440
time digitiser for laser ranging, ps. resolution, built in CAMAC minicrate 78–36301
TOPOCART-ORTHOPHOT C system for prod. of stereo orthophotos 77–66994
TOPOMAT all-automatic photogrammetric system for aerial photography 77–66993
trace elements in rocks, analysis by direct-reading spectrometer 78–85738
transistor sensors for electrical temp. meas. *(German)* 79–30468
TRG-1 Earth tide meter, possible non-linear effects 78–45018
triaxial loading apparatus, for determ. of time-depend. behaviour of rock 77–9538
triaxial strain cell for rock stress meas. 77–9574
universal stereoplotter, US-1, photogrammetric appl., features 78–40713
vector aeromagnetometer instrument set, accuracy in bench tests 78–45016
vector aeromagnetometer instrument system, design principles 78–28335
vector EM system, magnetic field measurements, field applications 79–84499
vector magnetometer stabilisation using independent servo system 78–77355
Verbaandert-Melchior horizontal pendulum tidal anal. results *(French)* 77–17013
vertical automatic profiling system for lakes temp. and current meas. 78–36327
visible IR spectrometer, on Skylab, for Earth surface remote sensing 77–60567
wide-band optical-mechanical system for measuring rock acoustic emissions at high temp. and press. 78–1525
wire strainmeter 77–41178
wire-line core barrels for exploratory drilling 80–98482
X-ray fluorescence analyser for in situ Au trace anal. 78–49160
X-ray powder camera, for low temp. photography 79–58099
Zeiss Stereotop, appl. to Landsat imagery planimetric restitution 80–56648
zoom height finder for height meas. from satellite images 78–36308
Zoom Transfer Scope, data transfer system for maps 80–8450
Ge intrinsic detector, use in borehole sonde for U exploration 77–9547
Ge(Li) and intrinsic Ge detectors in borehole sondes for U and coal exploration 77–37442
[illegible]e magnetometer, optically pumped *(Japanese)* 80–8434
7[illegible]-^{241}Am monitor for in situ soil surface and pond bottom assay
Rn-[illegible]9546
SiO$_2$-O[illegible]onitor for earthquake prediction research 78–73532
U boreh[illegible]/SiO$_2$ load bearing optical cable, geophys. appls. 80–91923
^{252}Cf sour[illegible]ogging system, delayed neutron activation anal. method using
U deposits, i[illegible] 79–53569
77–37440 [illegible]u assay logging system using delayed fission neutrons

geophysical prospecting
see also minerals
acoustic log primary si[illegible]ls recording, synchronous orthogonal detect. appl. *(Russian)* 79–[illegible]98
acoustic logging, channel r[illegible]irements for elastic waves recording *(Russian)* 79–39955
acoustic logging, elastic props. [illegible] near-hole bed-zone and profile lengths *(Russian)* 79–39938
acoustic logging, errors of statistica[illegible]signal processing *(Russian)* 79–39939
acoustic logging, optical filtering appl. [illegible] data processing *(Russian)* 79–39942
acoustic logging, phase-freq. charact. effect [illegible]n transmission accuracy of analogue signals *(Russian)* 79–39940
acoustic logging data, on-line computer interpretation techniques 80–90239
acoustic reflection in discrete layered media, structure estimation accuracy 79–23108
acoustic sounding of ocean-bottom subsurface layered media, spatial parameter estimation 80–77134
acoustic wave log, data interpretation *(Russian)* 79–84539
aerial electroprospecting, transducer interference analysis *(Russian)* 77–56766
aerial prospecting magnetometer cable length optimisation *(Russian)* 77–73881

geophysical prospecting continued
aerial radiometric data anal. using line-intensity estimation code MAZAS 79–62627
aeromagnetic data, diurnal drift removal by least squares 79–53529
aeromagnetic survey of sedimentary cover thickness, using 1-D spectral anal. 80–77138
aeromagnetic surveys, bicubic spline interpolation 80–17405
air gun array, high resolution or deep penetration survey, characts. 80–12557
air-gun arrays, efficient design 77–41193
air-gun arrays for marine prospecting, acoustic wave radiation 77–39177
airborne EM meas., use of decay patterns in anomaly classification 77–17224
airborne gamma-ray spectrometry data processing using multivariable statistical analysis 79–35004
airborne radiometric data inversion, radioactive elements conc. mapping 78–77347
airborne radiometry, statistical noise reduction 77–17220
airborne wave tilt meas. for reconnaissance mapping at poorly cond. areas 77–78473
airguns, linear arrays, signature and amplitude 78–69297
alpha activity of natural samples, appl. of Kodak LR 115 dielectric track detector *(Czech)* 79–8711
analysis of statistical distribs. rel. to seismic exploration for bauxite *(Russian)* 77–9561
anomalies of mag. and gravity field, anal. by unitary method 80–89932
anomaly detection, FORTRAN IV programs for statistical method appl. *(Rumanian)* 77–41214
apparent resistivity and Laterlog 7 sonde results 78–44759
apparent resistivity curve standardization 77–21675
apparent resistivity data interpretation, Apodi Valley, Brazil 78–3712
applied geophysics, conf., Oulu, Finland (Jan. 1978) 79–58105
applied inverse problems, book 79–49017
artificial premagnetization method, theory, ore prospecting appl. 79–39876
Asama volcano, Japan, in situ gamma ray radiometry appl. *(Japanese)* 79–66824
Athabasca oil sand behaviour under cyclic and uniaxial loading and hydrostatic press. 79–48468
base metal exploration with rapid pyroclastic mapping 77–53052
bauxite, increasing contrast of secondary scatt. aureoles *(Russian)* 77–29299
Black Sea continental platform, seismic prospecting method appl. *(Rumanian)* 78–20564
borehole acoustic logging, calc. of transient acoustic waveform 80–72640
borehole acoustic velocity measurement system, within or between boreholes 80–51557
borehole activation analysis, neutron energy distrib. in low-porosity rock 77–64286
borehole capture gamma-ray anal., optimal size ^{252}Cf neutron source 79–29890
borehole casing perforation by liquid metal jet, nozzle design, theory *(Russian)* 78–51216
borehole EM wave exploration, digital holography technique appl. *(Chinese)* 80–82080
borehole explosions, mechanical impulse of plates *(Russian)* 79–62455
borehole gravimetry, estimation of dip and lateral extent of beds 78–7782
borehole logging, minicomputer appl. *(Russian)* 79–84538
borehole radar exploration in coal seams 78–28235
borehole soundings, asymptotes of extreme curves *(Russian)* 79–88499
borehole temperature gradients, continuous logging, deconvolution 77–91288
borehole-layer system, neutrons elastic and nonelastic scatt. on nuclei of rock-forming elements 78–61582
Bouguer reduction of gravity anomalies using log data *(Russian)* 79–84082
S.Brazil, structural mapping, mineral deposits rel. to tectonics 77–81855
bright spot zones, simple upgrade 78–3965
Canadian Cordillera geomag. transition anomaly, lateral cond. changes 77–64200
Canadian deposits, reconnaissance programme *(French)* 78–88827
Canadian mineral occurrence index 77–53205
Cerro Impacto, Venezuela, thermoluminescence radiation dosimetry appl. to Th prospecting 78–32244
coal, seismic respons of carboniferous rock, synthetic seismograms 78–69293
coal analysis by neutron-capture gamma-ray meas. in boreholes 79–52853
coal banding-plane indicator, magnetic susceptibility anisotropy meas. 78–77221
coal fields of India, seam thickness by elec. and γ-logging 80–51394
coal formations seismic tracing, interference waves appl. *(Russian)* 79–74858
coal prospecting by seismic profiling, new technique testing 80–17404
coal seam, EM modelling of refls. in in situ gasified section 77–41212
coal seam depth determ. by elec. method *(Spanish)* 78–45031
coal seams, synthetic seismogram calc. with reflectivity method 79–74844
coal seams with discontinuities, SH channel wave attenuation 78–69292
coal seismic prospecting, approx. diffr. theory for transparent half-planes 80–89974
coaxial coils, for signalling between surface and buried coils, max. induced voltage calc. 79–12299
E.Colorado, electrical and seismic sounding of low-resistivity low-velocity materials 78–3711
common depth point survey data, vel. characts. determ., refl. interfaces inclination angles *(Russian)* 78–53753
common depth point survey technique appl. in permafrost conditions *(Russian)* 78–53751
common depth point technique efficiency for inclined reflecting surfaces *(Russian)* 79–84527
conducting cylinder inside shell, EM response 77–64198
conducting sphere in mag. dipole field, general soln. 80–3921
conductive overburden effect on transient EM response of sphere 77–64197
conductivity determ. using single superconducting coil 77–41184
conductor depth estimation using EM transients 77–64195
conference, Nov. 1979, New Orleans, USA 80–81891
continental basement exploration by seismic reflection profiling 78–96172

geophysical equipment continued
- temperature gradients continuous logging system 77—8[illegible]
- temperature indicators for geothermal well logging 80—38835
- temperature wave generator for thermal temp. wave probing (Russian) 78—35735
- terrain profiler, pulsed GaAs laser system 77—90202
- terrain profiler, pulsed GaAs laser system 78—60141
- texture goniometer for analysis of rocks 80—28630
- thematic mapper, time-delay and integration CCD sensors [illegible] 78—53098
- Thematic Mapper of Landsat-D, surface component design 80—72262
- Theo 002 Universal Theodolite for geodetic surveying 77—82025
- THEO 020 A universal theodolite for surveying 77—82029
- theodolite, reduction of influence of vertical axis error on horizontal angle meas. (German) 77—84276
- theodolite, TM1D and A. with attachable distance meters 80—56816
- theodolite, type [illegible], highly sealed [illegible] 80—[illegible]
- theodolite [illegible] survey specifications 80—[illegible]
- theodolites, electro-optical and microprocessor-based [illegible] 78—78860
- thermal conductivity apparatus for sedimentary rocks, using needle probe and microcomputer control 79—[illegible]
- thermal conductivity measurement of rocks by probe method, minimization of errors 77—13393
- thermistor probes for groundwater filtration rate meas. (Polish) 77—70877
- thermocouple for soil temp. meas. 78—4[illegible]
- thermomagnetometer, for rock remanent mag. meas. 78—8[illegible]
- tide-recording equipment, [illegible] (Russian) 78—88949
- tilt gauge, based on [illegible] 77—88[illegible]
- tilt meter at [illegible], [illegible] obs. and sensitivity tests (German) 78—89785
- tilt meters, photoelectric, with negative feedback, block diagrams and [illegible] (Russian) 78—88948
- tiltmeter, two-axis, for precision levelling 77—21910
- tiltmeter for long-baseline operation 78—81640
- time digitizer for laser ranging, [illegible] CAMAC [illegible] rate 78—36391
- TOPOCART-ORTHOPHOT B system for prod. of [illegible] 77—66994
- TOPOMAT all-automatic photogrammetric system for aerial photography 77—66993
- trace elements in rocks analysis by direct-reading spectrometry 78—35735
- transient sensors for electrical [illegible] meas. (Japanese) 78—[illegible]
- TRG-1 earth tide meter, possible [illegible] effects 78—[illegible]
- triaxial loading apparatus for studies of time-dependent behaviour of rocks 77—9578
- [illegible] 77—[illegible]
- universal stereoplotter DS-1, photogrammetric appl. features 77—[illegible]
- vector aeromagnetometer [illegible] 78—45016
- vector aeromagnetometer [illegible] system, design [illegible] 77—[illegible]
- vector EM system, magnetic field measurements, field [illegible] 77—33493
- vector magnetometer stabilization [illegible] 78—77353
- [illegible] (German) 77—[illegible]
- vertical automatic profiling system for water temp. and current meas. 78—35329
- visible IR spectrometer [illegible] for Earth surface remote sensing 77—[illegible]
- wide-band opto-mechanical system for monitoring rock [illegible] of high temp. and press. 78—[illegible]
- wire [illegible] 77—41178
- [illegible] for exploratory drilling 80—[illegible]
- X-ray fluorescence analyser for [illegible]
- X-ray [illegible] camera, for low temp. photography [illegible]
- Zeiss Stereotop, appl. to Landsat imagery [illegible] 80—56668
- zoom [illegible] for [illegible] 78—[illegible]
- Zoom Transfer Scope, data transfer system for maps [illegible]
- Ge [illegible]
- Ge(Li) and intrinsic Ge detectors in borehole [illegible] for U [illegible] exploration 77—37[illegible]
- [illegible] magnetometer, optically pumped (Japanese) 80—8434
- [illegible]
- SiO [illegible] for earthquake prediction research 78—[illegible]
- U [illegible] 80—[illegible]
- U deposits [illegible] logging system using [illegible] 77—[illegible]

geophysical prospecting
- see also minerals
- acoustic [illegible] (Russian) 7[illegible]
- acoustic logging [illegible] 79—[illegible]
- acoustic logging [illegible] (Russian) 79—[illegible]
- acoustic logging [illegible] 79—[illegible]
- acoustic logging [illegible] 79—[illegible]
- acoustic logging [illegible] (Russian) 79—[illegible]
- acoustic logging [illegible] 80—[illegible]
- acoustic reflection in discrete layered media [illegible] 79—23109
- acoustic sounding of [illegible] parameter estimation 80—77134
- acoustic wave [illegible] data interpretation (Russian) [illegible]
- aerial electromagnetic [illegible] interference analysis [illegible] 77—16708
- aerial [illegible] 77—[illegible]

geophysical prospecting continued
- aerial radiometric data anal. using [illegible] MAZAR 79—[illegible]
- aeromagnetic data, magnetic field [illegible] least squares 79—33508
- aeromagnetic survey [illegible] 80—77129
- [illegible] 80—[illegible]
- [illegible] 80—[illegible]
- [illegible] 77—[illegible]
- [illegible] 77—28177
- [illegible]
- [illegible]
- [illegible]
- [illegible]
- [illegible]
- [illegible]
- [illegible]
- [illegible] 79—[illegible]
- [illegible]
- [illegible] Brazil 79—[illegible]
- [illegible] 79—38105
- [illegible]
- [illegible]
- [illegible]
- [illegible]
- [illegible] 79—29299
- [illegible] 78—[illegible]
- borehole acoustic logging [illegible] 80—77640
- borehole acoustic velocity measurement system [illegible] 80—[illegible]
- borehole [illegible] 77—[illegible]
- borehole [illegible] 78—[illegible]
- borehole [illegible] 79—[illegible]
- borehole [illegible] 80—[illegible]
- borehole [illegible] 79—62455
- borehole [illegible] 78—[illegible]
- borehole [illegible] 79—[illegible]
- borehole [illegible] 79—98499
- borehole [illegible] 79—[illegible]
- [illegible]
- [illegible] (Russian) [illegible]
- [illegible] 77—61835
- [illegible]
- [illegible]
- [illegible] 78—33827
- [illegible]
- [illegible]
- [illegible]
- [illegible]
- [illegible]
- [illegible] 80—51334
- [illegible] 79—[illegible]
- [illegible] 80—17604
- [illegible] 77—41212
- [illegible] 79—[illegible]
- [illegible] 80—[illegible]
- [illegible] 78—69292
- [illegible] 80—[illegible]
- [illegible]
- [illegible]
- [illegible]
- [illegible]
- [illegible]
- [illegible] 77—[illegible]
- [illegible] 79—[illegible]
- [illegible]
- [illegible] 77—[illegible]
- [illegible] 80—[illegible]
- [illegible]